Materials Science, Computer and Information Technology

Edited by
S.Z. Cai, Q.F. Zhang, X.P. Xu, D.H. Hu and Y.M. Qu

TRANS TECH PUBLICATIONS

Materials Science, Computer and Information Technology

Edited by
S.Z. Cai
Q.F. Zhang
X.P. Xu
D.H. Hu
Y.M. Qu

Materials Science, Computer and Information Technology

Selected, peer reviewed papers from the
2014 4th International Conference on
Materials Science and Information Technology
(MSIT 2014),
June 14-15, 2014, Tianjin, China

Edited by

S.Z. Cai, Q.F. Zhang, X.P. Xu, D.H. Hu and Y.M. Qu

Copyright © 2014 Trans Tech Publications Ltd, Switzerland

All rights reserved. No part of the contents of this publication may be reproduced or transmitted in any form or by any means without the written permission of the publisher.

Trans Tech Publications Ltd
Churerstrasse 20
CH-8808 Pfaffikon
Switzerland
http://www.ttp.net

Volumes 989-994 of
Advanced Materials Research
ISSN print 1022-6680
ISSN cd 1022-6680
ISSN web 1662-8985

Full text available online at *http://www.scientific.net*

***Distributed** worldwide by*

Trans Tech Publications Ltd
Churerstrasse 20
CH-8808 Pfaffikon
Switzerland

Fax: +41 (44) 922 10 33
e-mail: sales@ttp.net

and in the Americas by

Trans Tech Publications Inc.
PO Box 699, May Street
Enfield, NH 03748
USA

Phone: +1 (603) 632-7377
Fax: +1 (603) 632-5611
e-mail: sales-usa@ttp.net

Preface

It is our pleasure to welcome you to the 2014 4th International Conference on Materials Science and Information Technology (MSIT 2014) in Tianjin, China. MSIT 2014 is the first conference dedicated to issues related to Materials Science , Mechatronics, Manufacturing Technology, Control, Measurement and Monitoring, Information Technology， Computer Engineering and Applied Computing Methods, Energy and Environmental Engineering. A major goal and feature of it is to bring academic scientists, engineers, industrial researchers together to exchange and share their experiences and research results about most aspects of Materials Science , Mechatronics, Manufacturing Technology, Control, Measurement and Monitoring, Information Technology， Computer Engineering and Applied Computing Methods, Energy and Environmental Engineering, and discuss the practical challenges encountered and the solutions adopted.

We hope you will have a technically rewarding experience, and use this occasion to meet old friends and make many new ones. Don’t miss the opportunity to explore in Tianjin, China. And don’t forget to take a sample of the many and diverse attractions in the rest of the China.

MSIT 2014 promises to be both stimulating and informative with a wonderful array of keynote and invited speakers from all over the world. Delegates will have a wide range of sessions to choose from and will have a difficult decision in deciding which sessions to attend.

The program consists of invited sessions, and technical workshops and discussions with eminent speakers covering a wide range of topics in Materials Science , Mechatronics, Manufacturing Technology, Control, Measurement and Monitoring, Information Technology， Computer Engineering and Applied Computing Methods, Energy and Environmental Engineering. This rich program provides all attendees with the opportunities to meet and interact with one another. We hope your experience with MSIT 2014 is a fruitful and long lasting one. With your support and participation, the conference will continue its success for a long time.

We would like to thank the organization staff, the members of the program committees and reviewers. They have worked very hard in reviewing papers and making valuable suggestions for the authors to improve their work. We also would like to express our gratitude to the external reviewers, for providing extra helps in the review process, and the authors for contributing their research result to the conference. Special thanks go to TTP Publisher.

We wish all attendees of MSIT 2014 an enjoyable scientific gathering in Tianjin, China. We look forward to seeing all of you next year at the conference.

Program Committee Chair

Dr. S. Z. Cai

Table of Contents

Preface

Chapter 1: Advanced Materials Science, Chemical Engineering and Processing Technologies

High Value Added Utilization of Vanadium Slag
T. Du, X. Fang and X.P. Zhang 3

Preparation of Zeolite 4A Using Laterite Nickel Slag and the Characteristic Study of CO_2/N_2 Separation
T. Du, S.L. Li and F. Yang 7

Bi_2S_3 Nanoflowers Synthesized via Hydrothermal Method
X.L. Chen and Y.P. Ji 11

Study of Oxidation Degradation Eosin by Ferrate
D.S. Li and X.L. Chen 15

The Relationship between Calcium Hydroxide Concentration in Pore Solution and the Strength of Stabilized Soils
L. Dai and X.X. Deng 19

Development and Application of the Screw Separator
J.B. Yin, J. Lu, L. Zhao and S.S. Wang 23

On Laser Shock Processing to Improve Hot Corrosion Resistance of In718 Superalloy
Y.C. Bai, Y.Q. Hua, Z. Rong, Q. Xue and R.F. Chen 27

Extraction and Purification of Fluorene from Wash Oil
Y.S. E 31

Microwave Hydrothermal Synthesis and Characterization of In_2O_3 Nanocrystalline
Y.Y. Hu, W.X. Ye, J. Lei, Q.X. Zhu, W.Q. Xiong and X.H. Liao 35

Synthesis of High-Strength and Water-Resistant Phosphogypsum Small Hollow Block
H.B. Xie, W.B. Ma and C.T. Ye 39

Study on Laser Micro Shock Effect on Electrical Resistivity of Nanometer Copper Film
Q. Xue, Y.Q. Hua, Y.C. Bai, R.F. Chen and H.X. Liu 45

Effect of Process Parameters on Residual Stress Distribution during Direct Laser Metal Deposition Shaping
H. Wang 49

Plasma-Induced Degradation of Benzene in Aqueous Solution
H.L. Qi, K. Gai and D.P. Ma 55

Liquid Phase Rhodamine Boxidation Induced by Plasma with Glow Discharge Electrolysis
K. Gai, H.L. Qi, D.P. Ma and Y.Q. Zhang 60

The Preparation of ZnO: Al Thin Films on Flexible Substrates by Magnetron Sputtering Method
X.J. Wang 65

Analysis Analysis and Suggestions on Device Clamp Screw Fracture of 110kV Transmission Line
X.X. Xu, W.Y. Li, G.X. Zhang, Y.T. Feng, H. Ke, Q. Wang and H.X. Cui 69

Ply Thickness' Effect on Composite Laminate under Low-Velocity Impact
X.C. Luo, T. Zhang and Q.S. Wang 74

Study on the Synthesis of Ethylene Glycol by Catalytic Hydrolyze of Ethylene Carbonate
M. Zhang 79

Efficient Synthesis 2,3-Dihydroquinazolin-4(1H)-Ones Using Coconut Shell Char Sulfonic Acid as a Reusable Catalyst in Ethanol
X.Y. Liu and Z.G. Yang 83

Study on the Urea Demand Model of SCR Control Technology
Z.L. Liu and D. Wa 87

Effect of Sodium Methylacrysulfonate upon the Molecular Weight and Performance of Polycarboxylate Superplasticizer
L. Xiong, G.J. Zheng, Y. Bi, C.F. Fu and S.F. Wang 91

Influence of the pH Value on the Water-Reducing Performance of Polycarboxylate-Based Superplasticizers at Room Temperature
J.W. Wang, G.J. Zheng, S.F. Wang, C.F. Fu and Y. Bi 97

Preparation and *In Vitro* Release Behaviors of Paclitaxel-Loaded Pluronic F87/Poly(Lactic Acid) Nanoparticle
Z.L. Li, Y.S. Huang, X.Y. Xiong, Y.C. Gong and Y.P. Li 102

Application of High-Efficiency Reverse Osmosis Technology in Reclaimed Water Treatment in Power Plants
X. Long, Q. Zhu, X.Y. Wang and J.H. Shi 108

Measurement of Ultra Low Sulfur in IN718 by Using Infrared Absorption Method
P.R. Zalupski and F.Y. Liu 115

The Synthesis and Characterization of Polyphenylene Vinylene (PPV) Derivatives with Alkoxy Branched Chains
X.Z. Zhang and Y.W. Wang 121

Comparison and Characterization of Two Preparation Methods of Graphene Oxide
H.B. Liu, W.Y. Zhang, F. Lin and H.D. Cao 125

Detection of Phase Purity of Sr_2FeMoO_6 by Raman Spectroscopy
Z.F. Xu, Q. Zhang and S.J. Yuan 130

A Novel Environment Friendly Material: Sucrose Char Sulfonic Acid Catalyzed Three-Component Mannich Reaction
Y.Y. She, X.Y. Liu and Z.G. Yang 134

Investigation of Sewage Sludge Anaerobic Digestion Performance Using Peracetic Acid as a Pretreatment
N. Wei 138

Synthesis and Characterization of Sulfonated Poly(Arylene Ether Sulfone) Multiblock Copolymers for Proton Exchange Membrane
T. Xue, Z.X. Hu and S.W. Chen 142

Study on Carbon and Sulfur Detection by Using Infrared Absorption Method
M.R. Bayati and P.Y. Wei 146

Effects of the Carboxyl Density on the Properties of Polycarboxylate-Type Superplasticizer
C.F. Fu, G.J. Zheng, K.L. Li, Y. Bi and L. Xiong 151

Preparation of Copolymer Modified with Oxidized Starch and Dispersion Ability for Ferric Oxide
J.C. Xu, X.S. Rong, X.R. Guo and F.X. Qiu 156

Corrosion Inhibitor Polymer Modified with Acid Activated Attapulgite: Preparation and Performance of Dispersing Ferric Oxide
J.C. Xu, X.S. Rong, X.R. Guo and F.X. Qiu 160

Preparation of a Novel Magnetic Stir Bar for the Pretreatment of the Plasticizers in Lake Water
R. Feng 164

Simulation of CVD Diamond Film Growth by Method of Revised KMC
L.Z. Zhang and F.Z. Wang 168

Relaxation Properties of the Solid Propellant Based on Hydroxyl-Terminated Polybutadiene
Z.M. Xie, S.C. Chen and Y.S. Wang 172

Effect of Fiber's Surface Pretreatment on the Interfacial Bonding Strength between Steel Fiber and Resin
H. Yang, J.H. Zhang, G.Y. Sun and Y. Zhang 177

Synthesis Alloy and Composite Materials of Nano-Silver-Nickel
W.J. Cui, L. Wang, J.W. Fu and D.Y. Zhao 181

Synthesis and Phase Behavior of a New Thiophene Monomer as Nematic Liquid Crystal
L. Wang, Y.J. Xie, X.X. Zhang and J.S. Hu 185

Synthesis of Novel Cationic Asphalt Emulsifier and its Investigation by Online FTIR Spectrophotometry
M.J. Sun, L.S. Shi, Z.Y. Jin, N. Li and X. Tao 189

Original Silk Pre-Oxidation Treatment of Carbon Fiber from Coal Tar Pitch
X.F. Zhao, Y.F. Wen, T. Qi, S.Q. Lai and L.J. Gao 194

4
X.E. Zhao 199

New Seawater Flocculants
J.A. Hao, B. Yang, X.Q. Zhang, A.J. Zhang, T.X. Jiang, X.Z. Zhang, J. Wang and Y.S. Zhang 203

Research on the Corrosion Resistance of Tinplate with Reflowing Technology
C.Q. An, C.M. Liu, H. Wang and S.D. Zhang 208

Effect of Ferrite Volume Fraction on Mechanical Properties of X80 Pipeline Steel
J. Liu, G. Zhu and W. Mao 212

Computer Simulation: A Tool for Researching the Basic Physical Properties of NiAl and Ni_3Al
C. Xu and D. Chen 216

Newly Determined Crystal Structure and Optical Property of the Intermetallic NiAl and Ni_3Al Alloys: A First-Principles Computer Simulated Investigation
C. Xu and D. Chen 220

TiO_2-Based Composite Film for the Photodegradation of Methyl Green
N. Song, F. Li and M.M. Yao 224

Synthesis and Characterization on a Kind of Polycarboxylate Superplasticizer
X. Li, G.J. Zheng, Y. Bi, C.F. Fu, M.H. Yuan and S.F. Wang 228

Synthesis for an Amide-Ester Type Polycarboxylate Superplasticizer and its Application in Concrete
C. Sun, G.J. Zheng, Y. Bi and H. Zhou 233

High Cycle Fatigue Performances of Advanced High Strength Steel CP800
L.M. Gui, X.C. Jin, H.T. Li and M. Zhang 238

Preparation and Dielectric Property of Ag/PVDF Composite Film
Y.J. Wang, J.W. Zhai, F.F. Wang and C.G. Feng 242

Microstructure and Wear Resistance of $Cu_{0.9}$NiAlCoCrFe High Entropy Alloy Coating on AZ91D Magnesium Alloys by Laser Cladding
K.J. Huang, Y.Y. Wang and X. Lin 246

Temporal and Spatial Characterizations of Zn Ions in Plasma by Pulsed-Laser Ablation of Zinc Metal in Vacuum Condition
Y. Jiao 251

Lignite-Fired CFB Boiler SO_2, NO Emission Control Technology Research
J.M. Yang, B.Z. Wang and W. Wang 256

Laying the Ground of Indoor Restrooms by Using Foam Glass and Waterproof Coating
S.M. Shi 260

Influence of Mo Addition on a Nickel-Base Single Crystal Superalloy
K. Zhao 264

Superhydrophobicity of Silicon-Based Microstructured Surfaces
G. Li 267

Research on Erosion Resistance of TiB_2 Ceramic Particle Reinforced MMC Coating
J.J. Fang, Y.J. Song and Z.X. Li 270

The Application of New Material in Industrial Design
L.L. Wang, T.T. Xie and Y.J. Liu 276

Spherical $SrCO_3$ Nanopowder Synthesized by Super Gravity Method
Z.S. Yang, J.H. Jin, B. Li, X.W. Zou Qi and Y.Z. Gang 280

Synthesis of a Novel Donor Unit for Organic Light-Emitting Materials: 10-octyl-3,7-di(thiophen-2-Yl)-10H-Phenothiazine
Z.B. Tang, X.X. Sun, L.P. Miao and H.Y. Shen 284

Current Situation and Latest Development of Intelligent Materials
G.M. Lin, F. Yuan and Y.H. Li 288

Synthesis of a Novel D-A Type Molecule Based on Carbazole Unit for Organic Light-Emitting Material Applications
Z.B. Tang, X.X. Sun, H.W. Yan and L.P. Miao 292

Growth Behavior of WC Grains in Ni_3Al Matrix during Liquid Phase Sintering
W.B. Zhang, W. Peng, J.Z. Long and X.Y. Wei 297

Synthesis and Characterization of Nano Melamine Phosphate
Z.Z. Wang and S.H. Xu 301

Preparation and Characterization of Transparent Oxyfluoride Tellurite Glass-Ceramics Containing CaF_2 Nanocrystals
Z.X. Hou, H.X. Li, S.H. Wang, M.H. Wang and X.D. Hu 305

Influence of Electrolysis and Plasma Polishing on Surface Properties of SUS304 Stainless Steel
X.M. Zong, J. Wang, Y.F. Wang and J.F. Liu 308

Effect of Initial Concentration of Cu^{2+} on the Adsorption Performance of Hydroxyapatite
Y.T. Guan, S.H. Wang, M.H. Wang, Z.X. Hou, X.D. Hu, H. Wang, H.L. Fan and N. Zhang 312

$Li_{0.95}Na_{0.05}Ti_2(PO_4)_3$/C with Good Performance as Anode Material for Aqueous Rechargeable Lithium Batteries
J. Zhu, Y.G. Liu, Q.Q. Tian, L. Wang and J.L. Cao 316

Effect of Melting Temperature on Microstructure of *In Situ* TiC/Al Composite and Formation Mechanism of TiC
H.L. Yuan, Z.H. Zhou, Z.H. Wang, Z.J. Zhong, X. Zhang and X.F. Xue 320

Effect of Cr on Microstructure and Mechanical Properties of Al–3.2Mg Alloys
Z.J. Zhong, Z.H. Zhou, Z.H. Wang, X. Zhang, H.L. Yuan and X.F. Xue 325

Research on Preparation of Aluminum-Metal Coating and its Microstructure by Melting-Casting
X.F. Xue, Z.H. Zhou, Z.H. Wang, J. Shao, H.L. Yuan and Z.J. Zhong 331

Research Progress of Graphene-Based Composites in Supercapacitor
Z.X. Hou, G.B. Li, S.H. Wang, M.H. Wang, X.D. Hu, Y. Zhou and S.M. Li 337

Dielectric Barrier Discharge Plasma Reduced Pt Catalysts Supported on Activated Carbon and their Electrocatalytic Activity
L.B. Di 340

Preparation of Au/P25 Catalysts for Removal of CO by Dielectric Barrier Discharge Plasma
L.B. Di 344

Kinetics of Inverse Emulsion Copolymerization of Dimethyl Diallyl Ammonium Chloride and Acrylamide
X.N. Wang, R.Z. Zhang and N.S. Jin 348

Research of Formation Mechanics on Nanostructured Chips by Multi-Deformations Based on Finite Element Method
C.L. Wu, Z.R. Wang and W. Zhang 352

Single Frequency LD-Pumped 2.09 μm Cr, Tm, Ho: YAG Microchip Laser
Y.M. Nie, Y.K. Guo, X. Ding and M.M. Guo 356

Review and Prospect on Tear Damage Research for High-Performance Flexible Fiber-Reinforced Composite Material
S. Cao, L.B. Liu, H.D. Xiao and M.Y. Lv 360

Influence of Volume Fraction of Piezoelectric Ceramics on Poperties of PZT672/Epoxy1-3 Piezocomposite
B. Zhang, L.K. Wang, L. Qin, C. Zhong, D. Long and J.J. Liu 364

Luminescence Properties of Rare-Earth Co-Doped Phosphate Glasses for White Light Emitting Diodes
G.H. Chen, X.L. Kang and Y. Yang 369

Monolithic Porous Graphene/Poly(Vinyl Alcohol) Gels: Preparation, Structure and Dye Adsorption
P. Wang and Y.P. Guo 373

Research Progress for High Strength Structural Steel and Key Issues of Application in Seismic Zone
L.X. Ji and T. An 379

Luminescent Properties of $Ca_{1-x}Ba_xSnO_3$: Eu^{3+}, Dy^{3+} Composites Prepared by Coprecipitation
L.M. Dong, F. Lv, Q. Li, Z.D. Han and X.Y. Zhang 383

Study of Dislocation Densities of Thick GaN Films
Y.G. Li, X.Q. Xiu, X.M. Hua, S.Y. Zhang, S.P. Gu, R. Zhang, Z.L. Xie, B. Liu, P. Chen, P. Han and Y.D. Zheng 387

The Luminescence Properties of Green YPO_4: Tb^{3+},Ce^{3+} Phosphors for WLED
J. Li, L.M. Dong, Q. Li and Z.D. Han 391

Preparation and Luminescent Properties of Single White $Ca_2MgSi_2O_7$: Eu^{3+}, Ce^{3+}, Tb^{3+} Phosphor for WLED
X.Q. Zhang, L.M. Dong, X.C. Tang, Q. Li and Z.D. Han 395

The Temperature Control of the Preheating Tank in the Procedure of Chloroacetic Acid's Crystallization
Z.F. Wang, C.Y. Liu, X.L. Song and Y.X. Gao 399

Effects of $SnCl_4$ Concentration on the Properties of Electroless Deposited Ni-Sn-P Coatings
X.R. Wang, W.T. Wang and B. Yang 403

Application of Environmental Rubber in Concrete Road Engineering
R. Yang 407

Hot Water Extraction of Corncob Hemicelluloses to Prepare Composite Films
Q.X. Yu, G. Yu, Y.D. Zhang, Y.F. Liu, H.S. Wang and F.Q. Chu 412

Analysis of the Atmospheric Particles Governance Based on Aerosol Hygroscopicity
T.Y. Sun, Q.Y. Wang, J. Zhang and J.X. Ren 416

Effect of Ni on Corrosion Resistance of Weathering Steels in Wet/Dry Environments
R. Liu, X.P. Chen and Q.N. Shi 420

Corrugated Waist Rail Microstructure Evolution Simulation
J.H. Ma, B. Tao and X.H. Yao 425

The Recrystallization of Corrugated Waist Rail in the Rolling Process
J.H. Ma, B. Tao and X.H. Yao 429

Behavior of Geosynthetic Clay Liners due to the Migration of Heavy Metal
J.J. Fan 433

Study on the Morphology and Thermal Stability of Li_2SrSiO_4: Tb^{3+} Materials
P.L. You 437

Study on CO_2 Adsorption of Halloysite Modified by Silane Coupling
H.L. Zhang, X.Y. Lai and H.J. Wu 441

Electrochemical Behavior of the Initial Atmospheric Corrosion of 2Cr13 Steel in Guiyang City Atmosphere
L.Y. Li and Y.N. Hu 446

The Difficulties of Dyeing of Flax Fiber and the Improving Method
Q.Y. Zhang, Z.D. Liu, Y. Zhang and L.B. Xu 450

Spatial Distribution of Heavy Metal in Urban Soil of China
X.X. Li 454

Research on Chloride Appropriate Dosage for Incorporated Accelerated Corrosion
Q.X. Liu and S.L. Zhan 458

Effects of Feed Rate and pH Value on the Physical and Electrochemical Properties of $LiNi_{0.4}Co_{0.2}Mn_{0.4}O_2$ Cathode Material for Lithiumion Battery
F. Du and L.F. Peng 462

Optical Absorption Study of Ar^+ Implanted $SrTiO_3$ Single Crystals
Y.S. Wang, M.J. Zhang, Y.D. Gao, D.F. Liu, Y.W. Chen and P.F. Wang 467

Au Nanoparticles Prepared by Microwave Irradiation
Y. Qiao and A.N. Jiang 471

Test and Research on Controlled Cooling Technology for High Carbon High Silicon Wire Rod of S87B
L. Zhang, J.L. Sun, Y. Li, J. Cui and F. Zhang 475

Simultaneous Determination of Ruthenium, Zinc and Zirconium in Waste Zirconium Dioxide Loaded Ruthenium-Zinc Catalysts Using Inductively Coupled Plasma Optical Emission Spectrometry
X.J. Wei and J.M. Pan 480

Propagation Characteristics of Seismic Waves Taking Stratigraphic Composition into Consideration
B.B. Xu, K. Nakai and T. Noda 484

Effect of SO_2 on Mn-Mg-O_x Catalyst Treated by Non-Thermal Plasma for NO Catalytic Oxidation
R.Y. Lai, X.L. Tang, H.H. Yi, K. Li, Y. Xiang and X. Sun 490

Synthesis and Characterisation of a Novel Thermoresponsive Dendronized Monomer Bearing Azobenzene Moiety
C.A. Yang, W.J. Xiao, E.X. Liang, Y. Lu and G.Y. Li 494

Temperature Controlled Dispersion of Multi-Walled Carbon Nanotubes in Water with Poly[(N-Isopropylacrylamide)-Co-(Ionic Liquid)]
W.J. Xiao, C.A. Yang, J.J. Peng, J.Y. Li and Y. Bai 498

Rapid Repair of Titanium Aero Structure with Cracks
Y.S. Guo and Y. Zhang 502

Determination of Novel Brominated Flame Retardants in Flexible Polyurethane Foam by GC-MS
Y.J. Chen, P.G. Dai, L.Z. Peng, C. Du and S.J. Liang 506

Affect of Brominated Flame Retardant on the Flexible Polyurethane Foam
Y.J. Chen, L.Z. Peng, P.G. Dai, D.L. Li and L.J. Wu 511

Effect of Reinforcement Addition on Microstructure and Mechanical Properties of Al Matrix Composites
G.J. Ma, Y.T. Ding and P.P. Jin 515

Preparation and Properties of Complex Antioxidants LDPE Antioxidant Film
H. Yang, L. Li, F.X. Yang, Y.Y. Zhou, L.J. Ou and S.F. Hu 519

Photo-Switchable Binding between a Photochromic Calix[4]Arene Derivative and Lanthanum Ions
Z.L. Liu, X.H. Li and Z.N. Yu 523

Highly Efficient Photodegradation of MO Dye by TiO_2 Nanoparticles
X.Z. Fang and L.S. Gao 527

Preparation of Visible-Light Active Mn-Doped TiO_2 Photocatalyst and its Photodegradation of Methylene Blue from Solution
Y. Chen and X.J. Ma 531

Adsorption and Inhibitive Properties of 1-phenylaminomethyl-benzimidazole on Corrosion of Mild Steel in Hydrochloric Acid
T.J. Su and K.H. Li 536

Progress in Preparation of Nano-Sized Magnesium Hydroxide from Concentrated Seawater and Brine
H.H. Wu, C.J. Gao, B.J. Luo, D. Wu, S.Y. Lu and X.P. Huang 540

The Network Prediction of Hot Temperature Flow Stress and Dynamic Recrystallization of AZ61 Alloy
Q. Li, W.J. Liu, R.J. Cheng, C. Li, S. Jiang, S.Q. Luo, X.Q. Jiang and F.S. Pan 544

The Finite Element Simulation of Thermal Deformation and Microstructure Evolution Forecast of AZ61 Alloy
Q. Li, W.J. Liu, R.J. Cheng, C. Li, S. Jiang, S.Q. Luo, X.Q. Jiang and F.S. Pan 548

Research Progress of Tungsten Nanorods and Nanoplatelets
A.M. Jiang, X.Q. Jiang, J. Yang, R.J. Yang and R. Yu 552

A Method for Scale-Up of Grooved Nanofibers via Flat Off-Centered Core-Shell Structure Spinneret
H.H. Wu, X.H. Meng and Y.C. Zeng 556

The Preparation and Characterization of Polybenzoxazole Copolymerized with Multiwalled Carbon Nanotube via Direct Friedel-Crafts Acylation
Y. Chen, J. Qian, Q.X. Zhuang and Z.W. Han 560

Different Chemical Oxidant of Benzene Series Pollution Site Repair Effect
D.L. Li, X.L. Fang, M.D. Yu, H. Lv and Y. Yang 564

Design, Synthesis and Anticancer Activity of 4-Morpholinothieno[3,2-*D*]-Pyrimidine Derivatives Bearing Chromone Moiety
C.Y. Sun, C. Chen, C.J. Wu, P.W. Zheng and W.F. Zhu 568

Vertical Flow Constructed Wetland Spherical Light Ceramsite Substrate Nitrogen Factor Research
Y. Yu, H.J. Yu and T. Jiang 572

Effect of Post-Weld Heat Treatment on Carbide Precipitation and Impact Properties of Coarse-Grained Heat-Affected Zone of Q690 Steel
Z.S. Li, S.L. Li, L. Tian, X.H. Zhang and J.Z. Liu 576

Preparation of Polypropylene/Sisal Fiber Composites and Study on the Fiber Orientation
R.Y. Chen, Z. Huang, W. Zou, H.C. Zhang and J.P. Qu 581

Mechanical Properties of Chopped Carbon Fiber Reinforced PBS/CF Composites
W. Li and J.P. Qu 587

Study on Optimization of Degradation of Landfill Leachate by Electrochemical Oxidation Process with Response Surface Methodology
Y. Yu, H.J. Yu and Y.P. Zhao 591

Experimental Research on Silicon-Based Composite Resistance Characteristic under Thermal Load
Z.H. Du, X.F. Hu, M. Wei, L. Wang and B.F. Ren 595

Electrical Simulation Experiment and the Analysis of Thermal Conductivity of Materials
W.B. Li, Y.G. Jin, S. Yin and P.Y. Chen 599

Study on the Impact of DO and Organic Matter on Aerobic Granular Sludge Treating Municipal Sewage
Y. Yu, H.J. Yu and C.C. Ma 603

Flame Retardancy Finishing on Wool Fabric via Sol-Gel Method
W. Zhang, Q.H. Zhang, G.Q. Chen and T.L. Xing 607

Minimum Particle Diameter of the Vanadium/Iron Co-Doped Nano TiO_2 Transparent Hydrosol at Room Temperature
L. Li, W.M. Zhang, H.Y. Zhang, Z.H. Xu, S. Wang, X.W. Li and G.Y. Dong 611

Design of the Portable Detector for Formaldehyde
L. Fu and X.W. Fu 615

Numerical Simulation of the Nanofluid Phase Separation by Lattice Boltzmann Method
S.G. Yao, X.W. Jia, C.J. Zhou and Y.H. Nie 619

The Emission Property of Phosphors LEDs Based on ZnCuInS/ZnSe/ZnS Quantum Dots
K. Bi, W.Y. Liu, T.Y. Xu, T.Q. Zhang and Y. Zhang 623

The Synthesis of Ionic Liquid Crystal Polymer and the Study of as Chromatographic Stationary Phase
S. Fu and J. Zhang 626

Research on Properties of CB/EVA Semiconductive Shielding Composites
B.Z. Han, C.Y. Li, C.C. Zhang and C.M. Li 629

Hygrothermal Ageing Modeling and Numerical Testing of Unidirectional Polymeric Composites
B. Imran Shaban and Y. Zhao 634

Attenuation Characteristics of Ultrasonic Velocity and Acoustic-Based TC4 Alloy Uniformity Nondestructive Evaluation
G.H. Wu, Y.F. Lu, Y.X. Huang and W. Wu 638

Preparation and Application of Blocked & Crosslinked Waterborne Polyurethane Microemulsion as Paper Strengthening Agent
X.J. Lai, M.N. Gong and L. Wang 644

The Fatigue Life Prediction for EB-PVD Thermal Barrier Coating
Y. Hao and H.Y. Qi 648

Research on Performance Features of Shape Memory Alloys
G.M. Lin and Y.H. Li 652

Structural and Optical Properties of Al Co-Doped ZnCoO Thin Film
P. Cao and Y. Bai 656

The Most Probable Mechanism Function of PVC Thermal Decomposition
N. Xu, G.C. Li and R.F. Guan 660

Preparation of Polyacrylic Acid/Rice Straw Composite Superabsorbent and the Loading and Release Properties for Urea
F. Zhang, G. Tang, S.T. Yu, G.H. Hou and N. Xu 665

Low-Temperature Catalytic Combustion of VOCs over MnO_x–ZnO Mixed Oxides Supported on Cordierite Ceramic
Q. Huang, Y.W. Chen, S.B. Shen and M.D. Chen 671

Ionic Liquid [Bmim]OH Grafted Catalyst for Cycloaddition of Carbon Dioxide
X.L. Zhang and D.F. Wang 676

The Molecular Orientation in Monomolecular Layer of Phthalocyanine and Porphyrin Derivatives
C.P. Zhang, H.M. Guo, H.N. Cui, H.S. Wang and S.Q. Xi 680

Research on Grinding Ti6Al4V Alloy with Inner-Lubricating Wheel
W.G. Huo, X.Y. Zhang, Q.Y. Dong, L.R. Cai and J. Shao 684

The Studies of ScB_2 (0001) Surfaces from the First-Principles
H. Zhao and Q. Han 688

Synthesis and Fluorescence Study of Cobalt(II) Deuteroporphyrin Dimethyl Ester
C.M. Yu and B.C. Hu 694

A Study of the Effect of Starch in Polymer Blends of Carboxymethyl Cellulose and Chitosan
N. Keungputpong, N. Matchariyakul and S. Tiptipakorn 697

A New Type Aluminum Alloy Backup Frame of FAST Project
B.Q. Zhao, Q.M. Wang, Q. Zhao, X.D. Gu and J.W. Hu 701

Changes in Water Adsorption Desorption Isotherms of Cement Mortars Caused by Carbonation Coupled with Humidification-Drying Cycles
T.P. Son 705

Research Progress of Sintered Wall Material Products Synchronous Cutting Machine
H.M. Liu, C.Q. Wu, X. Zhang and Y.B. Xu 710

The Higher Order Crack Tip Fields for Anti-Plane Crack in Linear Functionally Graded Piezoelectric Materials
Y. Dai, X. Chong and S.M. Li 715

The Crack Tip Fields for Anti-Plane Interfacial Crack between Functionally Graded and Homogeneous Piezoelectric Materials
Y. Dai and X. Chong 719

The Preparation and Detection of Quality Standard about Houttuynia Spray
T. Xia, Q.D. Chen, J.K. Wang, J. Zeng and J.Y. Guo 723

Ethylene Oligomerization by Ni(II) Complex Based on Peptide
W. Bai, C.G. Cao, H.X. Pei, K.H. Hu, H. Zhou, M. Peng, T. Jiang and J.Y. Dong 727

Synthesis of Nickel(II) Complexes and its Application to Ethylene Oligomerization
J.B. Kou, S.N. Zhao, C.G. Cao, H. Zhou, K.H. Hu, M. Peng, G.S. Su, T. Jiang and J.Y. Dong 731

***In Situ* Formation of Insect Repellent Delivery System**
D.R. Lin and L.J. Hu 735

Structure of Bridged Silsesquioxane Material Bearing a Pendant Dodecylamine
D.R. Lin and L.J. Hu 739

Hedgehog Buckyball: High-Symmetry Complete Polyhedral Oligomeric Silsesquioxanes (POSSs) Characterized by UV-MALDI-TOF Mass Spectrometry
D.R. Lin and L.J. Hu 743

Effect of Temperature on the Growth and Biochemical Composition of *Sargassum muticum*
C.Y. Yuan, S. Yang, Y. Wang and Q.M. Cui 747

Numerical Simulation of Cr12MoV Steel during Quenching Process
W. Zhang, Z.D. Qu, X.H. Deng and X.W. Duan 751

Effect of NH4Cl Flux on Structural and Luminescent Properties of CaS: Eu^{2+} Phosphors
Y.J. Zhang, J. Zhao, D.J. Wang and J. Ma 755

Preparation and Properties of Multi-Elements Doped Perovskite-Type Mixed Conductors for IT-SOFC Cathodes
J. Fu, J. Zhao, Y. Fu and R.R. Li 759

Research on Microstructure and Properties of Plasma Powder Spray Welding Layer Based on 3D Printing
E. Meheretu, Z.M. Wang and H.C. Han 763

The Bioactivity of Gradient Composite Bioceramic Coating with Two Kinds of Rare Earth Oxide Fabricated by Wide Band Laser Cladding
P.Z. Jiang, Q.B. Liu, L.Y. Zhang, H.B. Jiang and Z. Zhang 767

Discussions on the Pretreatment of the Air-Conditioning/Cotton Blended Fiber – The Application of Tea Saponin
Y.J. Zhang and Y.Y. Zhang 771

Effect of Mixed Multiple Rare Earth Oxide on the Microstructure of Bioceramic Coating Prepared by Wide Band Laser Cladding
Z. Zhang, Q.B. Liu, L.Y. Zhang, H.B. Jiang and P.Z. Jiang 775

The Chemistry Model of Ion-Ion Interaction Energy of Full Ionized Hydrogen Plasma
L.S. Guo, X.R. Zheng and Z.R. Wu 779

Study on Catalyst for Catalytic Ozonation to Leachate and Catalytic Process
B.J. Jiang, Z.J. Tian and J.M. Jiang 783

Carbon Nanotubes-Assisted Fabrication of TiO_2 Nanocomposite Film for Optimum Electrochromic Application
S.P. Liu, W. Wang, L.L. Cui and H.N. Guan 789

Evaluation the Effect of Anti-Oxidation of Chondroitin Sulfate
L.P. Xu and X. Wang 793

On Pretreatment Experimental Study of High Strength Gypsum by Yunnan Phosphorus Gypsum
S.C. Quan, Z.M. Zhao, R. Tian and S. Han 797

Research on the Treatment of the Yellow River Micro-Polluted Water in Shanxi by Ozone-Activated Carbon Process
X.B. Tang, J.F. Zou, K.F. He, J. Liu, J.J. Zhou, F.J. Wang, Y.X. Yuan and J.G. He 803

Dye Adsorbent Prepared by Crosslinking of Poly(γ-glutamic acid) and Gelatin
W. Wang, S.P. Liu, H.N. Guan, J.Z. Liang and C. Tan 809

Study on the Growth Model of Expandable Graphite
F. Ye, C.G. Zhu and Z.H. Zhang 814

Coupled Hydrogen and Oxygen Isotope Analyses for the Mainstream of Poyanghu Lake (Jiangxi Province) and their Environmental Implications
D.R. Lai, A.D. Wang, C.G. Li, Y.P. Chen, Z.B. Yan and J.J. Wan 820

Experimental Study the Affection of the Dust Emission on Sand Stockpile by the Height of Windbreak Wall and Wind Speed
Z.Q. Liu, L.Y. Ma and X.Y. Zhao 823

Adsorption Removal of Phosphorus from Wastewater by Steel Slag Filter Material
J.T. Wang, Y.Z. Yu and L.L. Gao 827

Simulation of Vapor Absorption of Aqueous Libr Solution on Alternate Heat and Mass Transfer Surfaces of Corrugated Plates and Mesh Pecking
R.B. Cao, Y.P. Chen and J.F. Wu 831

A Novel Multilayer Structure with Frequency Selected Surface for Electromagnetic Compatibility
J. Li and D.L. Xu 837

Study on Processing Technology of Brewer's Grains on Acid Dye Brilliant Cresyl Blue Wastewater
Y.H. Jiang, X.L. Jiang and C.G. Cai 841

A New Harmless Disposal Method of Aluminium Phosphide Residue
X.C. Wang, D. Li, S.L. Duan, D.B. Li and X.L. Qi 845

Experimental Study on Sewage Treatment by Vortex-Grid Flocculation Technology
F.P. Hu, H.H. Li, L.Y. Wang, Z.G. Tong, Q. Zhang and H.L. Dai 849

Study on Removing Atrazine and Chlorothalonil in Raw Water in Reservoirs in North China by PAC Adsorption and Enhanced Coagulation
J.F. Zou, X.B. Tang, M. Yu, J.J. Zhou, F.J. Wang, J.G. He and Y.X. Yuan 853

Modified Reduced Graphene Oxide with Enhanced Solubility and Conductivity and its Application
X.P. Zeng 859

Aero-Optical Effects of Mc=0.5 Supersonic Mixing Layer
L.F. Tian, S.H. Yi, Y.Z. Zhu, Y.X. Zhao and L. He 863

Simulation Realization of Frequency-Variable and Speed-Adjustable System Based on Vector Control
Y. She 867

Research Status and Application Prospect of Deep Cryogenic Treatment Technology on Cemented Carbide
T.H. Guan, H.M. Liu, Y.B. Xu, C.Q. Wu and Y. Lv 871

Chapter 2: Applied Mechanics, Construction and Testing Technologies

The Fatigue Performance Evaluation of Pressure Vessel Steel Using Modified Staircase Method
H. Xue, R.F. Li, L.X. Wu, W.J. Peng and J.Q. Huang 879

The Welding Residual Stress Analysis on High Performance Bridge Steel with Different Testing Method
H. Xue, R.F. Li, L. Yu, D. Liu and W.J. Peng 883

A Study on the Sample Overheat Phenomenon of Fatigue Test
H. Xue, J. He, J.Q. Hu, L.X. Kuang and W.J. Peng 887

Numerical Simulation Study of Stress-Magnetization Effect on Different Notch Steel Specimens
X.W. Xi, S.K. Ren and Y. Huang 891

Study on Factors of Axial Crushing of Thin-Walled High-Strength Steel Sections Used in Passenger Car
G.F. Zhao, Y.W. Hu, X. Cheng and K. Xiao 898

Study on the Borehole Stability in Liulin Coal Reservoirs
L.Y. Song, L.J. Xiao, J.W. Wang, J. Zhang and T.L. Zhuang 903

An Improved CEM with Regard to the Crack-Tip
Y.S. Lin 908

Efficiency Prediction of Limestone-Gypsum Wet Desulphurization Based on Support Vector Machine
J.M. Yang, B.S. Sun and N.Z. Qi 913

Research on Failure Mechanism Consistency in Accelerated Wear Test of Metal Materials
X.B. Ma and B. Cheng 918

Stability Analysis of Single-Pier Variable Cross-Section Box-Girder Continuous Bridge
G.S. Yin, J. Bai and J.J. Feng 923

Effect of Convex Platform on Stress Distribution in Nickel-Based Superalloy Plate Produced by Vacuum Countergravity Casting
C.M. Zou, S.Q. Su, H.W. Wang and Z.J. Wei 927

Calculation about Stress Concentration Coefficient of Welded Cruciform Joints of Magnesium Alloy Based on FEM
B.L. He, Y.X. Yu, X.D. Zhang and S.S. Xia 931

Finite Element Calculation about Stress Concentration Coefficient of Welded Butt Joints of Magnesium Alloy
Y.X. Yu, B.L. He, X.D. Zhang and S.Y. Lei 935

Effect Study of Water on the Mechanical Behavior of Gangue in Chongqing Tongliang Mine
Y.J. Zang 939

Experimental Research on Tensile Strength of Out-of-Plane Composite Joints for Integrated Composite Cabins
D.H. Zhang, X.H. Zhou and L.W. Zhou 943

Modeling and Simulation Analysis on Building Temperature and Toughness
Q. Zhang 947

Relationship Modeling between Tensile Strength of Steel Building and Temperature
Q. Zhang 951

Study on the Affects of Partition of the Parallel and Cross Tunnel Adjacent Construction
W. Zheng and L. Gao 954

The Application of MASW Method on the Studying of the Vibrations in Civil Engineering
K. Luo 958

Experiment Research on Mechanical Properties and Penetration Performance of UHMWPE Fiber Concrete
Y.W. Zhang, L.H. Yan, L. Zhu, S. Zhang and L.F. Li 961

Treatment of Simulated Acid Mine Drainage by Permeable Reactive Barrier: Column Study
C.F. Cai, F.Z. Qi, X.L. Lin and L. Jiang 966

New Method to Predict the Bearing Capacity and End-Bearing Ratio of Friction-Type Long Pile
Z. Qian and K.H. Wang 970

Research on the Succession of *Artemisia ordosica* Community in Mu Us Sandy Land
J.H. Zhang 975

Research on Performance of Coupled Heat Pump System with Different Backfill Material
J. Liu 978

Numerical Simulation of the Kinetic Energy Projectile Oblique Penetration into the Concrete
J. Chen and X.J. Ye 982

Analysis on Aerostatic Stability for Jianghai Direct Ship Channel Bridge in Finished Stage
L. Yu, S. Wang, Y.Y. Che and G.H. Zhao 986

Chapter 3: Bio- and Medicine Research

Spectrophotometric Method for the Assay of Norfloxacin Lactate
Y.H. Lei 993

Co-Expression of Threonine Dehydratase and Acetolactate Synthase in Escherichia Coli for L-Isoleucine Production
J. Wang, J.K. Sun and Q.Y. Xu 997

Developing a Sensitive Reporter System for Monitoring of Pancreatic and Duodenal Homeobox Gene 1 (Pdx1) and Neurogenin 3 (Ngn3) – Mediated Transdifferentiation from Human Hepatic Cells into Insulin-Producing Beta-Like Cells
C. Xie, W. Donelan, S. Lu and L.J. Yang 1003

A Method for the Determination of Atropine in Pharmaceutical Preparation Using CE-ECL
Q. Xiang, X.D. Yang and Y. Gao 1007

Effect of Natural Clarifying Agents ZTC1+1 II on Purification of *Angelica* Polysaccharides
C.L. Li, Y. Men, L. Yang, A.M. Yang and Q. Shang 1011

Effect of Ginkgo Biloba Extract on Contractility Enhancement of Diaphragm of Rats with Type 2 Diabetes
X.S. Li, R.Y. Wu and Y. Hu 1015

Study on Degradation of Radix Isatidis Polypeptide in Artificial Gastrointestinal Environment
N. Nan and X.J. Liu 1020

Repetitive-Element PCR Technology for Identification of Mulberry Pathogens
G. Li, H.Z. Song, J. Wang and F.A. Wu 1025

Optimum Process for Extraction of Total Flavonoids from Castor Leaves by Orthogonal Test
Y.H. Jiang, X.L. Jiang and C.G. Cai 1029

Comparative Bioenergetics of Diploid and Triploid Pacific Oysters *Crassostreas gigas* at Different Temperatures
X.Y. Li and Z.M. Zhou 1033

Prognostic Significance of Glycoprotein 96 in Human Hepatocellular Carcinoma
X.P. Wang, H.P. Lin, B. Xu, K.P. Zhang, J.G. Fang and Y.X. Yang 1037

An Evaluation of the Potential for Pharmacokinetic Interaction between Tramadol and Cytochrome P450 2D6 Inhibitor Promethazine
P. Liu, L. Sun, J. Zhang and R.C. Guo 1041

Effect of Crude Polysaccharides from *Discorea bulbifera* L. on the Liver in the Mice Bearing U14 Cervical Carcinoma
H.X. Cui 1044

Design, Synthesis, and Biological Evaluation of Sorafenib Analogs Bearing a Sulfonylurea Unit as Novel VEGFR2 Kinase Inhibitors
W.F. Zhu, C.J. Wu, S. Xu, W. Li, H.H. Fang, Z.C. Chen, X.H. Tu and P.W. Zheng 1048

The Effects of the Film Made by Citral β-Cyclodextrin Inclusion Complex Combined with Chitosan on Fresh Beef
H.J. Chen, F.X. Yang, L.J. Ou, D.X. Zhou and L. Li 1052

Polysaccharide from Eucheuma Gelatinae Enhance Immunocompetence against Murine H22 Tumor *In Vivo*
J. Tang, Z. Kong, D.Y. Liu and A.J. Liu 1056

Analysis of Paclitaxel in Pharmaceutical Injection by Ultra Performance Convergence Chromatography
X. Gong, X.B. Huang, Y.H. Wei, N.L. Qi, L.J. Lin and Y.Y. Liu 1060

Study on the Genotoxicity of Organic Extracts of the Water from a Reservoir by Using Comet Assay
J.T. Wang, Y.Z. Yu and X. Li 1064

Wireless Power Transmission System of Radio-Telemetry System for Physiological Parameters Detection
Z.W. Jia, H.R. Ren and G.Z. Yan 1068

Study on Degradation of Traditional Chinese Medicine Wastewater with Cu/Cu_2O Composite Photocatalyst
C.H. Yuan 1073

Design Consideration of a Health-Information-Technology-Supported Intelligent Urinalysis System
T. Dong 1077

An Improved Medical Image Fusion Method Based on Nonsubsampled Contourlet Transform
Y.C. Yang, J.W. Dang and Y.P. Wang 1082

Interactive Medical Image Segmentation Method with only Positive Label Examples
C.G. Zhang, Y. Zhang and X.H. Zhang 1088

The Influence of Perceptual Load on Inhibition of Return
X.J. Liu, Z.H. Fan and J.Z. Zhou 1093

The Design and Application of the Information Management Platform for the Prevention and Control of AIDS on the Basis of the Residents' Health Records
S.H. Shi and S.W. Xiong 1097

Mobile Nurse Information System with Efficient Physiological Monitoring for Patient
F. Wu and H. Wang 1103

College Female Students' Physical Health Evaluation Index Correlation Research Based on the PDCA Cycle Model
J. Shou 1107

The Risk Factors for Pediatric Care and Preventive Measures
L.B. Liu 1111

Design and Evaluation of the Primers for Rift Valley Fever (RVF) Virus RT-PCR Detection
Z.X. Yang, B. Wang, Q.M. Xu, X.P. Yao, L. Zhu, Z.W. Xu, K.Y. Wang, G.L. Li, S.Z. Peng and Y. Wang 1115

Detection on the Pulse Signal of Human Body Based on Piezoelectric Impedance Technique
J. Zhang, B.Z. Guo and H.M. Tang 1120

Chapter 4: Resource, Energy and Electronic Development, Environmental Engineering

The Making of Mathematical Models for Ecological Cities
Y. Xu 1127

Multilayer Architecture on Urban Public Crisis Decision Support System
Y.C. Ren 1131

Accurate Calculation Receiving Power of the Electromagnetic Wave Scattering between Two Stations on Sea Surface
X.M. Li, T.L. Dong and G.M. Huang 1135

Simulation and Analysis for Damage of Certain Electrical Power Equipment in Battlefield
X.Y. Yang, Q.S. Ma, P.Y. Cheng, Q. Zhang and L. Zhang 1141

Application Research on Technique of Re-Entry Old Wells in Sulige Area
Y.F. Xue, Z.Y. Zhu and D. Li 1146

Unsteady Heat Transfer Analysis: Saving-Energy and the Regionalism Design on Air-Conditioning System for Car
L. Ouyang and D. Li 1150

Constructing of Low Carbon Ecological Index System for Planning: Liaobin New Town as an Instance
J.C. Yuan, S. Chen, M.Z. Huang and L. Fang 1157

Ballast Water Discharge and the Influence of Seawater Environment
X.Y. Li, S. Liu and Z.M. Zhou 1161

A High-Order CMOS Bandgap Voltage Reference
Q.N. Zhou, Y.S. Li, J.Z. Lin, H.J. Li, C. Li, Y. Pang, G.Q. Li, X.M. Cai and Q. Li 1165

Multistage Amplifier Using Dual-Miller with Nulling-Resistor and Dual-Feedforward Structure
Q.N. Zhou, Q. Li, J.Z. Lin, H.J. Li, C. Li, Y. Pang, G.Q. Li, X.M. Cai and Y.S. Li 1169

Photovoltaic Inverter Output Current Research of Adaptive Active Harmonic Compensation Device
F.J. Chang, H.Q. Ma, C. Cui and J. Zhang 1173

A New Optimal Method for Load Transfer in Power Distribution Network
Q. Wang, L. Yao and Z.L. Zhang 1177

Reliability Evaluation for Distribution System Including Protection System Failures
Z.L. Zhang, L. Yao and Q. Wang 1181

The New Technology of PV Power Generation System Based on Extremum Seeking Control
J.Y. Shi, K. Zhang and Y.G. Zhang 1185

Evaluation of the Yangtze River Littoral Wetland Soil with Total Organic Carbon
Z.W. Luo and X. Wang 1189

Public Greenbelt Layout Optimization for Ecological Civilization City Construction
C.G. Chang, M.H. Qi, W. Li and K. Yin 1192

Design, Simulation and Experiment of Polarization Transformers Based on Twisted Chiral Metamaterials
Z. Yang, Z.S. Jing, Q.Y. Su, G.W. Qin and Z.L. Zhou 1196

The Research of Atmospheric Pressure Cold Plasma Jet Generated by Auto-Excited-Pulsed DC Discharge
Y.L. Hu, Q. Wang and Z.Q. Chen 1200

The Research of Hybrid Genetic – Particle Swarm Optimization Algorithm Based Reconfiguration of the Electric Distribution Network
X.N. Zhou, D.P. Ke, Y.Z. Sun and L.Y. Xu 1204

Effects of Geomembrance on the Contaminant Transport in Compacted Clay Liner System
J.J. Fan 1208

The Higher Order Crack-Tip Fields for Anti-Plane Crack in Exponential Functionally Graded Piezoelectric Materials
Y. Dai, X. Chong and S.M. Li 1212

The Effects and Countermeasures of Low-Carbon Economy on China's International Competitiveness of Industries
J.B. Hu 1216

The Application of Transformer Protection in 220KV Substation
W.L. Peng, W.L. Bian and M. Wang 1220

Analysis of Data Center Power System
H. Song and Z.T. Wang 1224

Urban Ecological Environmental Quality Evaluation System Research
X.X. Li 1228

Eco-Environmental Construction in Zhengzhou
X.X. Li 1232

The Influence of Lanzhou Reach of Yellow River to Temperature-Humidity Effect on Surrounding Lawn and Brick Underlying Surface
G.C. Liu, Y. Huang and S.Q. Gao 1236

Study of Morphological Changes Induced by Man-Made Coastal Project
T. Xu 1240

Simulation of Salinity Changes Induced by Man-Made Sea Embankment
T. Xu 1244

Forecast of Energy Consumption and Carbon Emission of Urban Traffic by Using System Dynamics
Y. Zhang, L.J. Wan, L. Zhang and D.X. Cheng 1248

Study on Feasibility of Concentrated Activated Sludge Reflow of Biochemical Pool of Small-Sized Wastewater Plant
Y.C. Guo and Y. Chen 1252

Analysis on Fluctuation Characteristics of Wind Power
Y. Wang 1256

Partial Discharge Characteristics Research Based on RVM
Y.H. Meng, H.Q. Li and Y. Hu 1260

Regional Water Resource Utilization Evaluation and Influential Factors Analyses
Y.Y. Wang and X.P. Hu 1264

Mineralizaton Process of the Bauxite in WZD Area
T. Cui 1269

Inhibiting Effect of Nonlinear Shielding Layer on Electrical Tree Propagation inside Insulation Layer of High-Voltage Cable
C.M. Li, B.Z. Han, L. Zhao and C.P. Yin 1273

The Power Supply Area Divided Based on Improved Voronoi Diagram
L. Liu, X.B. Tang, C.H. Zhao, Z.Y. Sha and X. Chen 1278

Investigation on the Energy Efficiency of Innovative Hybrid Impact Hydroforming
S.H. Wang, L.H. Lang and L.J. Lin 1282

Investigation on Nutrient Loads of Lake Taihu in China
H. Wang, K. Xia, B. Li and Y.Y. Zhou 1286

The Soil Enzyme Activities with Age of Tea in Three Gorges Reservoir Area
L.P. Zhang, G.M. Jia and Y. Xi 1292

Temperature Effect on the Hypergene Mineral Formation Process (The Case of Tailing Dumps of Komsomolsky Tin-Ore District)
V. Zvereva, A. Kostina and K. Frolov 1297

Evaluation of Technogenous Processes Proceeding in Tailing Dump of the Central Concentrating Mill of Dal'Negorsk District and their Effect on the Hydrosphere with Method of Physicochemical Modeling
V.P. Zvereva, A.I. Lysenko and A.M. Kostina 1301

Some Ecological Problems of Development of Mineral Raw Materials in Amurskaya Oblast'
L.T. Krupskaya, V.P. Zvereva and O.O. Panfilov 1305

Study on Sewage Treatment Process in Stone Production
M. Zhao, W.W. Guo, Q. Xiao and J. Zhang 1309

Accumulation of Chromium in *Vetiveria zizanioides* Assisted by Earthworm (*Eisenia foelide*) in Contaminated Soil
K. Zhang, Q. Chen, H.B. Luo and X.T. Li 1313

Study on Response of *Cyperus alternifolius* to Cr(VI) and Ni Combined Pollution
M.C. Liu and W. Zhou 1319

A Research of Environment Management Policy Based on the Externality Theory
H.C. Che and F. Cao 1324

Research on the Simulation and Realization Approach of Urban Low-Carbon Transport
X.L. Gao, T.J. Hu and P. Peng 1328

The Spatial Effect Identification of Pollution Treatment Investment in China
L.X. Huang and M. Liu 1333

Characteristics of Heavy Atmospheric Particulate Pollution under Beijing Fog and Haze
J.X. Liu, P. Yang, A.G.D.M. Liu and J. Liu 1338

Urban River Water Purification Experiment by Strengthening Ecological Engineering Methods
S.H. Yin, Y.C. Wang, W.Q. Peng, Y.L. Du, B. Gao, J.J. Gao, H.D. Zhou, Q.Y. Meng and Q.J. Li 1341

The Combinatorial Prediction about Chaotic Times Series of Natural Circulation Flow under Rolling Motion
C. Yuan, Q. Cai, G. Liu and F. Yan 1348

A Rapid Determination Method of ^{40}K Concentration in the Soil
W.W. Lu, H.G. Yue, J. Li and Y.X. Zhang 1352

Effect of Hg in Jiaozhou Bay Waters-Settling Process
D.F. Yang, F.Y. Wang, H.Z. He, Y.F. Wu and S.X. Zhu 1356

The High Resolution Sequence Stratigraphic Isochronous Framework in Threezhao Peripheral Zone
Z. Na, C.Z. Liu and P. Li 1359

Use Horizontal Aeration Method to Treat Organic Pollution in Soil
L.Y. Xu 1364

Study on Identification Method of Fructus Lycii Origin by Mineral Elements
Y.P. Pang, K. Liu, Z.L. Zhao and X.T. Li 1368

Establishment of Models for Tight Sandstone Formation Evaluation in the Ordos Basin of Northwest China
X.L. Wei, J. Li, R. Xu and L.L. Zhi 1372

The Research and Application of Multiple Collaborative Anti-Sloughing Drilling Fluid
M.T. Jiang, H.Y. Wei, Y.H. Li and W.Z. Shi 1376

Vertical Zonation in Penecontemporaneous Period of the Bauxite in WZD Area
T. Cui 1380

Preservative Features of the Fossils in Bauxite Deposit of WZD Area, Northern Guizhou, China
T. Cui 1384

Characteristics of Interlayers in Bauxite Deposit of WZD Area, Northern Guizhou, China
T. Cui 1388

Research Progress of Bauxite in WZD Area, Northern Guizhou, China
T. Cui 1392

Evaluation Method of Coral Reef Integrity: RMDI and Coring Rate Comparative Analysis Method
J.C. Wang, C.Y. Wang and Z.Q. Han 1396

Special Structure and its Geological Significances of WZD Bauxite
T. Cui 1400

Analysis on Oxidized and Reduced Conditions in Penecontemporaneous Period on the Bauxite in WZD Area
T. Cui 1404

Beneficiation of a Low-Grade Barite Ore in Myanmar
T.T. Li, S.Q. Liu, Y. Zhao and H.J. Wang 1408

Research on the Flotation of Low Grade Copper-Nickle Ore
Z.B. Deng, T. Xiong, X. Wang, Q.Y. Zhao, X. Xie and X.W. Lv 1411

Concentration and Distribution of Cr, Pb and Zn in the Jurassic Coals from Northern Shaanxi and Ningxia, China
H. Wang, M.L. Du and G.T. Zhang 1415

The Quantitative Model Research of Impact of Water Level Changes on Channel Capacity
T. Liu, L. Yao and C. Zhao 1419

Porosity Inversion under the Sequence Stratigraphy Framework
W. Yang and M.Y. Hu 1424

Analysis on Acidity and Alkalinity of Metallogenetic Environment in Penecontemporaneous Period on the Bauxite in WZD Area, Northern Guizhou, China
T. Cui 1428

Chapter 5: Advanced Technologies in Modelling, Simulation and Optimization, Computation Methods and Algorithms, Intelligent Engineering Applications

An Optimal Algorithm for Estimating Fundamental Matrix by Removing the Outliers
L.Q. Guo, J.B. Liao, F.P. Zhong, X. Yu and J. Tao 1435

Complex Network Optimization Research of Personalization-Based Recommendation Algorithm
C.X. Gao and C.P. Qi 1441

Algorithm Study and Application of Personalized Intelligent Recommendation Engine
G.L. Pu 1445

Research on Marine Fuel Boiler Drum Water Level Model and Dynamic Analysis
M. Zhu 1449

Studies on Broad-Sense Sample Method in Data Mining
Y. Tang 1453

The Application of Maximum Differential Algorithm in Adaptive Ocean Sampling
Y. Wang, C.S. Wu and Y.Q. Shi 1456

Parameter Estimation for Wiener Systems with Preload Nonlinearities
Y.X. Ni and J.D. Cao 1460

A Vertical Handoff Decision Algorithm Based on QoS Evaluation
Y. Tao and K. Zhou 1464

A Video Digital Watermarking Algorithm Based on Chaotic Maps
Y.W. Li 1469

Zero Watermarking Method Based on Enhanced Bit-Plane
J. Zhao, B.F. Yang and X.Y. Wu 1473

Research on Simulation of Modern Storage System with Flexsim
Q.T. Han 1477

Study on Application of Vendor Managed Inventory Model
Q.T. Han 1481

Research on Material Inventory Model and Application
Q.T. Han 1485

A Fuzzy Clustering Algorithm of Automatic Classification Based on EnFCM
H.W. Han, L. Tian and J.Q. Miao 1489

Knowledge Representation of Art Patterns Based on the Calculation Mental Image
S.R. Kuang 1493

Improved Software Cost Estimation Method Based on COCOMO Model and Linear Regression
H. Yang 1497

Research on Improved Staged Software Cost Estimation Method Based on COCOMO Model
H. Yang 1501

Analysis of Knowledge Fusion System Model Based on Ontology and Multi-Agent Theory
L. Lei and M. Zhang 1505

Research on Classification and Encoding of Digital Cultural Relics
L. Lei and M. Zhang 1509

An OCL-Based Formal Model for Cloud Forensics
J. Wang, Z.M. Tang and X.L. Jin 1513

Research on Customers Churn Prediction Model Based on Logistic
M. Jiang, N. Chu and X.M. Bi 1517

Site Selection of Customer Operation Center for Pull and Drag Transportation Based on the Analytic Hierarchy Process
X.Q. Luo and X.Y. Yin 1522

Research on the Layout of Integrated Freight Hub Based on Two-Stage Model
Y.Y. Chen and T.X. Liu 1526

The Optimization of Logistics and Distribution
W. Xiong and L.Y. Zhang 1532

Research on Rough Set Theory-Based Customer Division
G.J. Song, X. Cao and X.Y. Wang 1536

A K-Nearest-Neighbour Based Classifier for Securities Text Categorization
T.B. Liu 1541

Research of Intelligent Warehouse Layout Base on Genetic Algorithm and Dynamic Programming
L.Q. Yang and Q. Yan 1547

A Generalized Attributes Significance Measure Method
F.C. Li, M. Li and S. Liu 1551

A Fusion Method of Point-Cloud Based on Parallel Estimation of Distribution Algorithm
Z.T. Jiang, L. Zhou and L. Zhou 1555

Bacteria Genome Compression Based on the Weighted Context Model
M. Chen, X.M. Jia and L. Liu 1561

Research on Blind Source Separation Algorithm Based on Particle Swarm Optimization
H. Zhou, C.Z. Chen, X.M. Sun and H. Liu 1566

The Data Mining Technology of Particle Swarm Optimization Algorithm in Earthquake Prediction
X.Y. Zhang, X. Li and X. Lin 1570

An Improved Weighted Centroid Localization Algorithm Based on RSSI
C.L. Liu and Z. Li 1574

A Parallel Implementation of the K-Means Algorithm Based on MapReduce
W. Yan, J. Zhou, Q. Huang and L. Shi 1578

A Inflexion Nonlinear Global Particle Swarm Optimization (PSO) Algorithm
L.X. Lv and X.Y. Lin 1582

The Research of Improving Clothing Crossing-Selling Based on Apriori Arithmetic
C. Zhang, Y. Liu, F.S. Sun and L. Yao 1586

Research of Propagation Behavior on Tibetan Network Public Sentiment
Y.X. Li, A.L. Wu and Y.N. E 1590

Research on Anti-Plagiarism in the Education Informatization Background
B. Fu and B.G. Xie 1594

Towards the Evaluation of Suffix Trees
X.P. Wang 1598

Research of Geomagnetic Matching Algorithm Based on Artificial Fish Swarm Searching Strategy
X. Li and Z.L. Zhu 1602

Given the Principal Disjunctive Normal Form of Simple Proposition Formula
Z.J. Chen, H.Z. Shi and Y.J. Liu 1607

Online Long-Term Object Tracking Based on Compressed Haar-Like Features via Sparse Representation
M. Zhao, L.P. Wang and L.P. Zhang 1610

A New Virtual Visual Servo Algorithm
M. Li, X.N. Wang and J. Zhu 1615

A Path Planning Algorithm Based on the CNN Model under the Curvature Constraint
S.J. Wang, X.N. Wang and J. Ping 1621

Niche Brain Storm Optimization Algorithm for Multi-Peak Function Optimization
H.J. Zhou, M.Y. Jiang and X.Y. Ben 1626

Research on the Validation Method of Product Data Quality
P. Wang and B. Wang 1631

Stock Price Prediction Model Based on IWO Neural Network and its Applications
H. Liu and X.Y. Lv 1635

An Interval Slope Approach to Fuzzy C-Means Clustering Algorithm for Interval Valued Data
Y. Jin and J.H. Ma 1641

Stock Price Prediction Model Based on BA Neural Network and its Applications
X.Y. Lv, S.L. Sun and H. Liu 1646

A Fast Locating Algorithm of Vehicle License Plate under Complex Scenes
Y. Lei and Y. Zhang 1652

A Multidimensional Model of Data Warehouses
Z.Y. Chen and T.X. Zhao 1657

Architecting Service-Oriented Publish/Subscribe Applications: Data Model and Matching Algorithm
B. Dong 1660

Research on Psychology Data Clustering Algorithm Based on CUDA
L.L. Dong, Z.S. Ma, W. Dong and X. Zhang 1664

Cell Selection Algorithm Based on Coordinated Beamforming
Z. Liang, Y.B. Li and F. Ye 1671

Research on Sub-Band Synthesis Algorithm of MIMO-SAR
Y.A. Xie and Z.M. Tan 1676

Comprehensive Similarity Measurement Model Based on Three Algorithms
N. Liu, B.L. Long, X.K. Zheng, L.F. Han, T. Qu and B.J. Cui 1680

Mean Evolutionary Algorithm Based on Intermediate Value Theorem of Continuous Function
Y.C. Tan, C.S. Deng and Y. Liu 1686

Meta-Analysis and Evaluation of Visualization Support to Decision Trees Classification
Z.Y. Chen and T.X. Zhao 1692

Allocation Scheme of Short Training Sequence Based on OFDM-PON
S.L. Guo, X. Chen, C.X. Xu, Y. Jiang and Y.C. Li 1695

Three-Dimensional Yarns Modeling for Tufted Carpet Simulation
J.H. Li, G.F. Chen, Q.Q. Huang and X. Wei 1700

Decision Making Support Model for the Incident Emergency Management of Migrant's Group Based on CBR
D.H. Zhang, L. Cheng, R.W. Wu, J. Wang and J.Y. Liu 1704

Equivalent Integral Equations of the Static Schrödinger Equation by Variation of Constants Method
S. Zhang, B. Cai and D. Wang 1712

Kink-Type Solutions of the MKdV Lattice Equation with an Arbitrary Function
S. Zhang, Y.Y. Zhou and B. Cai 1716

An Improvement of the Method for Paraphrase of Chinese Double Negation
Z.J. Wang, S.J. Zhang, Y.F. Gao, Y.F. Lin and Z.J. Wang 1720

Water Fluid Simulation with an Improved SPH Method
X. Zhao 1724

Analysis of Convergence Rate for Improved Generalized Ant Colony Optimization Algorithm
D.Y. Zhang and H. Zhao 1728

Convergence Speed of Multi-Objective Generalized Ant Colony Optimization Algorithm
D.Y. Zhang and P. Fu 1732

The Applications Based on the Rough Set Theory Algorithms to Determine the Weight
N.N. Chen 1736

Takeoff Performance Algorithms Analysis of EFB Based on iOS
J. Lu, Q. Li, B.B. Zhao, F. Xiao and W.Y. Qiu 1739

Region Analogy-Based Quantization Method for Numerical Data
Y.D. Sun 1743

Application of Improved ANT Algorithm to Planning of Anti-Ship Cruise Missile Route
Y.T. Yu and Y. Ding 1747

Application of Improved Intuitionistic Fuzzy for Sea-Battlefield Situation Assessment
Y.T. Yu and Y. Ding 1751

Imbalanced Data Classification Using Cost-Sensitive Support Vector Machine Based on Information Entropy
W. Duan, L. Jing and X.Y. Lu 1756

Develop Local Fuzzy Classifier to Modify Low-Confidence Output of Global Classifier
P. Ling, X.S. Rong, Y.Q. Dong and G.S. Hao 1762

The Improved Algorithm about Binocular Vision of Flexible Structure in On-Orbit Modal Identification
Y. Zhao, J.B. Gao, C. Xu and C.F. Zhang 1766

An Algorithm of Uncertain Reasoning Considering Subjective Factors
Y.H. Han, K.T. Chen, H. Shao and L. Du 1770

A Fuzzy Clustering Algorithm of Web Customers Based on Attributes Reduction
H.X. Wan and Y. Peng 1775

The Application of Graph Model in the Cultural Archives
P. Sun 1779

Deobfuscate Non-Returning Calls and Call-Stack Tampering in Instruction Traces
J. Qiu, X.H. Su and P.J. Ma 1782

Constructing Attractors via the Improved Eugenics Genetic Algorithm
L.M. Du, F.Y. Wang and Z.Y. Han 1786

Comparison Results between Jacobi and USSOR Iterative Methods
T. Zhou and S.G. Zhang 1790

Convergence Results of the Improving Modified Gauss-Seidel (IMGS) Iterative Method for a Symmetric Positive Definite Matrix
S.G. Zhang and T. Zhou 1794

A Fast Algorithm for Computing the Determinants of the Heptadiagonal Matrices
X. Li and L. Yang 1798

Two-Parameter Conjugate Gradient Projection Method and its Application
H.F. Cui 1802

Generalized J Sets Based on Periodic Orbit and Attract Time
L.M. Du, F.Y. Wang and Z.Y. Han 1806

Static Fault-Tolerant Strategy for High Performance Computing Platform
Y. Sun and J. Liu 1810

Prediction of Mine Inrush Water Based on BP Neural Network Method
A.J. Shao, Q.X. Meng, S.W. Wang and Y. Liu 1814

Fuzzy Comprehensive Evaluation Model of Selecting Football Coach
C.J. Rao and J.H. Dong 1821

Calculation of Dynamic Stress Intensity Factor by the Boundary Element - Laplace Transform Method
W. Zhang 1825

Point Rupture Solutions of a Singular Quasilinear Elliptic Equation Arise from Non-Newtonian Fluids
Z.J. Cui, M.Y. Xu and R. Zhang 1829

Application of Ant Colony Algorithm to the Hierarchical Routing in Wireless Sensor Networks
L. Sang and D. Long 1833

Study on the Optimization of Data Mining in Big Data
G. Xin and H. Yan 1837

Design and Implementation of Instruction Expert System Based on Improved Genetic Algorithm
D.Q. Wu and S.S. Wang 1841

Investor Selection Model under Uncertain Information Environment
C.J. Rao and C. Wang 1845

A Novel Multiobjective Memetic Algorithm Based on IWO-DE and its Application in Nutrition Decision Making Problem
G.P. Wang, M. Zhang and W.W. Zhao 1849

An Improved Genetic Algorithm for Text Clustering
S.D. Yu, Y. Ding, X.C. Ma and J. Sun 1853

Applied Technology with a Modified Sixth-Order Convergent Iterative Method for Solving Nonlinear Equations
L. Fang, Y. Li, H.Q. Wang and R. Chen 1857

Research on Improved AES Encryption Algorithm
Z.H. Yang, N. Li, L.Y. Liu, R.J. Qi and L.L. Yu 1861

CMA Blind Equalization with Quasi-Newton Algorithm in Underwater Acoustic Channels Based on Simplified Cost Function
Y. Xiao and R. Ruan 1865

The CPML for Hybrid Implicit-Explicit FDTD Method Based on Auxiliary Differential Equation
Y.F. Mao, P.H. Huang and L.G. Ma 1869

Parameters of Support Vector Machines Model Optimized Method Based on Genetic Algorithm
Y.Z. Xie, Z.G. Wang and X.W. Dai 1873

Robust Exponential Stability of Stochastic Discrete-Time BAM Neural Networks with Markovian Jumping Parameters and Delays
L.D. Guo, J. Nie and Y.S. Zhang 1877

A Correlation Coefficient Estimation Algorithm Based on Subspace Decomposition
N. Wu, W.J. Si and S.H. Jiao 1883

A Multi-Objective Coordinative Optimization Model and its Cultural Immune Algorithm
C.G. Chang, W. Li, K. Yin and M.H. Qi 1887

The Implement of Parcel Sea Map Automatic Mapping Algorithm
D.R. Song, K. Cao and Y. Hao 1891

A New Network Traffic Classification Method Based on Optimized Hadamard Matrix and ECOC-SVM
H.Z. Wang and L.H. Yan 1895

A Novel Blind Watermark Extraction Algorithm Based on Nonsubsampled Contourlet Transform
L. Feng, X.F. Shi, H.Y. Chen, Y.H. Li and Y.L. Zhang 1901

An Improved Algorithm for Multi-Tag Anti-Collision in RFID System
Y.R. Zhao and W.L. Miao 1905

Numerical Simulations of Two Four-Petal Gaussian Beams Propagating in Strongly Nonlocal Media
Z.F. Yang 1909

An Approach for Sentiment Tendency Analysis on Comment Text
M. Li, M.D. Chen and X.B. Li 1913

Extending the α-Algorithm to Mine Repetitive Task Based on Complex Structure
H. Li, Y. Wei, X.H. Ye, S.W. Yao and J. Yang 1918

Process Mining: Overview and Comparative Analysis of the Mining Algorithms
H. Li, Y. Wei, L. Liu, S.W. Yao and J. Yang 1924

A P2P Resource Management Model Based on Cloud Computing
Y. Lu and G.F. Liu 1930

Architecture Research and Design of Cloud Computing Service Based on REST
K. Huang 1934

High Precision Data Processing Method Based on the Complex-Step Differentiation
F.L. Tan, Y.K. Guo, Y.M. Nie and F. Sun 1938

Routing Algorithm with Energy-Efficient and High Quality of Clusters in Wireless Sensor Network
Y.H. Yi and R.L. Wang 1942

DSP Memory Allocation Strategy Based on Greedy Algorithm
Y.H. Fan, X.F. Ma, J.S. Jiang, X.M. Xu, Q.Y. Hao and P. Zhang 1946

Research on an Embedded Ultra-Low-Bit-Rate Speech Coding Algorithm
Y. Li, Y.H. Fan, F. Yuan and X.M. Xu 1951

Research on Materialized Views under Disk-Space Constraint in Data Warehouse
L. Ma 1955

Review of Otsu Segmentation Algorithm
Y.X. Dong 1959

Non-Linear Least Squares Large Misalignment Estimation in Transfer Alignment
Y. Lu and X.H. Cheng 1962

Singularly Perturbed Systems with Diffusion and Time Delay
C.Y. Wang, Q. Dou and X.W. Li 1969

An Algorithm of DOA Estimation in Linear Canonical Transform Domain
H. Zhao, Y.H. Zhang and H.H. Li 1973

Computerized Simulation of Board-Level EMC in High-Speed PCB
X.Z. Wu, C. Zhang, S.F. Yang and L.Q. Zhao 1977

On Application of Texture Mapping Technology in Simulation
W. Zhang, C.H. Zhang and Y. Zhang 1981

The Discussion on the Improved Association Rules Algorithm in Data Mining
T. Wen, L. Sun and L. Zhu 1985

An Information Classification Optimization Model Based on Improved Ant Colony Algorithm
C.M. Hao 1989

Simulation Analysis of a Statistical Model for Herd Mentality Trend
S.Y. Pan 1993

Virtual Simulation of Aerobics Movement Based on Vision
X.H. Wang 1997

The Research of Key Data Classification Optimal Mining Methods for Massive Data
Y.Y. Li and Y.Z. Wang 2001

Group Customer Special Line Correction Algorithm Design and Application Based on PTN Technology
H.J. Zhu and D.F. Li 2004

Position Mobil Information Encryption Algorithm Based on Key Attributes of Reduced Rank Agent under Cloud Storage
H.L. Guo and H.L. Yu 2008

Network Intrusion Detection Model Based on Genetic Algorithm Optimizing Parameters of Support Vector Machine
C. Liu 2012

A New Method of Face Modeling with Construction of Local Texture Model
J.B. Shan, W.W. Jiang and S.L. Mu 2016

Simulation of Data Mining System Design in Database
R.Y. Zheng 2020

Analysis on Digital Signal Processing and Algorithm Based on Coherent Light
Y. Xing, L. Zhang, Z.Y. Cheng and K. Gu 2024

A New Improved Attribute Weight Algorithm Based on Rough Sets Theory for One Command Information System
S.M. Yang, Y.M. Yan, K. Wang and Z.Y. Xie 2029

Research on Leaning and Evolutionary Algorithm of Agent for Task Oriented
G.F. Xu and Y.W. Cai 2033

Research on Modeling of Brain Function Network in Major Depressive Disorder
L.M. Niu, H. Guo and J.J. Chen 2037

A Classification Algorithm of Moving Military Vehicle
Y.F. Ma and F. Chen 2043

Analysis of Fuzzy Clustering for the Adoption in Data Mining
Y.J. Wang 2047

Joint Spectrum and Power Allocation for Femtocell Based on Graph and Game Theory
Y. Wang and Q. Zhu 2051

The Research and Application of Data Glove in Virtual Interaction System
Y.X. Xu and X. Zhu 2057

Brief Report of Implementation of T9 Input with Python and Evaluation
Y.J. Wang 2062

Simulation Analysis of Mind Sports Games Based on Artificial Intelligence
G.W. Cui and X.Q. Li 2065

Genetic Algorithm Design on Scalable Data Mining of Cultural Industry
H.W. Xue 2070

Simulation Study of Waveform Variation of Fixed Assets Based on Logical Database Structure
S.P. Liu 2075

The Research of Data Mining Based on Neural Networks
Q. Guo and J. Niu 2080

Towards the Simulation of Evolutionary Programming
X.W. Li, L. Zhou and L.H. Yuan 2084

Based on Canny Operator with Regional Growth Combined Research on Accurate Image Segmentation Algorithm
J.Q. Miao 2088

Studying Sensor Networks and Multicast Algorithms with TACKY
C.C. Xu 2093

The Analysis and Realization of Interpreter Language in Nuclear Industry
Z. Zhang, H.B. He and H.L. Lu 2097

Time Prediction Based on Process Mining Taking Concept Drift into Consideration
F.F. Huang, L.Q. Zhang and Z. Li 2101

SBN Constructing Algorithm Based on Extended MEBN
S. Ge and X.Z. Xia 2106

A Mobile-Terminal-Oriented and Mobile-Cloud-Computing-Based Localized Scheduling Algorithm
R.X. Liu, Y.H. Zhang and Y. Tang 2111

Research of the Ubiquitous English Learning Based on Cloud Computing
S. Han and X.D. Zhang 2115

Simulation of Neural Network Recognizing Isolated Words under MATLAB Environment
F. Zhao 2119

The MapReduce Parallel Study of KNN Algorithm
C.Y. Wang and X.F. Zhou 2123

Software Structural Stability Evaluation Method Based on Motifs
C. Shan, L. Huang, C.Z. Hu, X.L. Zhao and J.S. Ma 2128

Locating Method for Character 2D Barcode
Z. Liu, S.C. Yin, S.C. Ye and H.R. Zheng 2135

Research on Motion Model of "Wind-Blowing & Trees-Swinging" and "Leaves-Falling & Branches-Broken" Based on Fractal Theory
H.Q. Liu, J. Wang and L.P. Feng 2139

Algorithm of Representing and Preparing for Resources in EEM
Q. Yu, T. Li, X. Zhang, Y. Lin, Y. Yu and N. Zhao 2144

Research of Computer Forensics Based on Benford's Law
M.J. Shan 2148

Using Zipf Distribution to Predict Popularity Data for Storage Systems
Y. Yang, W.Y. Li, M.N. Zhang, X.M. Ding and J. Dai 2152

A Method for Transforming the Online Handwritten Mathematical Formula into MathML
D.Q. Fu, W.Y. Zhang and S.T. Jhang 2156

Adaptive Bit Allocation Algorithm for OFDM System
W. Wei and W.D. An 2161

Stepped Cooling Control Model Based on Optimal Algorithm
Z.W. Yan, H.A. Bu, G.S. Ma and D.H. Zhang 2165

Cluster Center Initialization Parallel Algorithm for K-Means Algorithm
B. Yan, Y. Zhang, H.Y. Su and H. Zheng 2169

Study for Embedded Colony Algorithm Based on Morphological Technology
K.Y. Chen, X.Y. Zheng and H. Yu 2173

A Semantic Retrieval Method Based on Ontology
Q. Shen and M. Zhang 2179

Using PROSEPCT and SVM for the Estimation of Chlorophyll Concentration
J. Lv, F.L. Deng and Z.G. Yan 2184

Distributed Collaborative Filtering Recommendation Model Based on Expand-Vector
Y. Zhu, H.Y. Su, C.Q. Wang, B. Yan and H. Zheng 2188

Improved Ant Colony Algorithm Based on PSO and its Application on Cloud Computing Resource Scheduling
H. Yang 2192

Study on Traveling Salesman Problem Based on the Improved Chaos Ant Colony Algorithm
H. Yang 2196

An Improved Scheduling Algorithm for Cloud Storage
P. Wang 2200

A New Spatial Correlation Model Based on the Distributed RC-$_{\prod}$ Model
X.X. Liu, J.B. Shao and L.L. Zhao 2204

Study on Modeling of the Minimum Lethal Dose while Rescue Poisoning
C.X. Zhao, Y. Jiang, H. Yang and M.T. Cui 2208

Maneuvering Target Tracking Algorithm Based on Particle PHD Filtering
S. Gao, C.B. Chen and Q. Gong 2212

Applying Grey System Theory in an Ideological and Political Education Course
M. Zhang 2216

Ideological and Political Education Linear Regression Theory
M. Zhang 2220

An Improved Genetic Algorithm in Vehicle Dispactcher
S.H. Zhu and P. Tang 2223

Research on Robustness of Typically Opportunistic Network Routing Algorithm under Flooding Attack
G. Yu, D.F. Yuan, Y. Cui, Y.D. Wang and P. Zong 2227

A Localization Algorithm Research to Eliminate the Indoor NLOS Error
J.Z. Dong, Y.W. Wang, F. Wei and J. Yu 2232

Communication Network Alarm Correlation Based on the Confidence Fusion Algorithm
H.S. Gao and Y.M. Li 2237

A Purchase Prediction Based on Collaborative Filtering Algorithm
Z. Fu and L.F. Zhou 2241

K-Means Clustering Algorithm Method Based on Shuffled Frog Leaping Algorithm
Z. Tang and K. Luo 2245

A Modified Regularized Super-Resolution Reconstruction Algorithm
Q. Xie and W.Y. Chen 2250

Simulation of Whole Movement Process of Muzhuping Landslide with DDA and Prediction of Surge
Z.H. Dong, X.L. Ding, A.Q. Wu and B. Lu 2254

State-Space Model and Simulation for Dynamic Stall
W.D. Lei, G.C. Hu and Q. Liu 2258

CFD Simulation of Gas Distributor with Two Chambers
D.F. Zhao and F.G. Liu 2264

Ratio Based Weapon System of Systems Capability Gaps Assessment Method Research
X.X. Zhang, K.W. Yang, B. Zhang and J. Jiang 2268

Study on an Improved Median Filtering Algorithm
H. Zhang, M. Gao and H.L. Ren 2273

The Application of Cross-Correlation Algorithm in CSAMT Received Data Processing
Z.P. Zhou, Y. Zhu and T.H. Wang 2278

Assignment Performance at Beijing South Railway Station Based on Anylogic Simulation
Y.J. Liang and Z.Z. Yuan 2283

Study of Storm Surge Numerical Simulation in the Bohai Sea
Y.Q. Zhang, Q.L. Leng, Z.J. Hu, Z.C. Zhu, W.J. Zhang and S.H. Bian 2288

A Method of Domain Compound Concept Extraction Based on Multilevel Filter
B. Wu and L.B. Ouyang 2292

Design and Realization Based on Cloud Stack Hybrid Cloud Computing Platform
P. Cheng and H. Qu 2297

A Particle Swarm Optimization Algorithm Based on Simulated Annealing
Z.C. Yan and Y.S. Luo 2301

The Gray Relation Analysis of Non-Coal Mine Accidents Causation
X.Y. Meng, R.H. Chen and S.B. Wang 2306

Research on Algorithm of Video Segmentation Based on Self-Adaptive Single Gaussian Model
Y. Zhu, D.H. Wang and J.L. Liu 2310

Research on the Evaluation Method of OSHMS Performance Based on Fuzzy Theory
H.M. Zhou and D.T. Hu 2314

Parallel Sets Based on the Improved ACLEARCR Algorithm
H.K. Zhang, N.W. Sun, C. Zhang, T.T. Jiang and C.H. Dai 2318

Evaluation of Ground Thermal Infrared Camouflage Using Pure Technical and Pure Scale Dynamic DEA Model
L. Li, X.L. Lv, B.Z. Li, X.P. Li and H.X. Wang 2323

2D Numerical Simulation of Termal Discharge in Coastal Area
T. Xu 2328

Study on Settlement Process of Dredger under Current Force
T. Xu, Z. Xiao and L.C. Sun 2332

The Effect of Enterprise Business Process Reengineering Fuzzy Comprehensive Evaluation
S. Ling and C.Y. Ye 2336

A New Highway Safety Model Based on Cellular Automata
L.X. Li 2340

A Model for Seat Allocation of Railway Passenger Transport Based on OD's Priority
Y.T. Zhu, F.Z. Wang, X.H. Shan and X.Y. Lv 2344

IBC-Based Authentication Protocols and a Method of Data Sharing for Cloud Systems
K.K. Chen, C.L. Cao, J.Y. Liu and R. Zhang 2349

J-Integral Computation in Mixed Mode I and II
Y.M. Cai, F.Y. Zhang and Y.J. Xie 2356

A Kind of MSD Performance Compensation Method Based on the Strategy of Sliding
D.X. Zhu, G. Fu and Q. He 2360

Research on Phase Locked Loop Software Parallel Processing Methods
R.L. Li, G. Fu, Y.J. Wu and L.P. Wang 2364

An Algorithm to Control Watermarking Capacity Using PSNR
Y. Xing and D.S. Wang 2368

Simulation of Dynamic Compaction on Soft Soil Foundation
Y.L. Pang and D.M. Dai 2373

Look the Partial Equilibrium with the Global Optimum from the Problem of the Shortest Circuit for Three Villages
X.W. Jiang, Y. Hu, Y.T. Yang and T. Luan 2377

Adaptive Discriminant Linear Local Tangent Space Alignment Algorithm on Face Recognition
Y.X. Lv, Y.N. Deng, Y. Shi, Q. Li and W. Peng 2381

Research on the Traffic Rules of the Freeway
Y.X. Jiang 2385

A Collision Detection Algorithm Using AABB and Octree Space Division
H.Y. Wang and S.G. Liu 2389

A Visual Hiding Algorithm Based on Human Visual System
R. Dong and D.S. Wang 2393

Augmented Lagrangian Method for Nonlinear Programming with many Complex Constraints
X.W. Jiang, Y.T. Yang and Y.L. Lu 2398

Consensus Equilibrium Point Analysis for Heterogeneous Multi-Agent System in Undirected Graph
Y.J. Sun, G.L. Zhang and J. Zeng 2402

A Projected Conjugate Gradient Method for Box-Constrained Optimization
T.F. Li, Z.Y. Liu and Z.B. Du 2406

Decomposition of New Construction Land Quota in Rural Land Based on AHP
X.W. Cai, H.Y. Wang, Y. Sun and C.H. Gao 2410

Design and Implementation of General High-Speed Data Storage System
G. Fu, W.J. Geng and R.L. Li 2414

Research on Software Algorithm Capture of Spread Spectrum TT&C Signals
R.L. Li, G. Fu and G.Z. Wu 2418

Improved Genetic Algorithm in Vehicle Management
S.H. Zhu and T. Kuang 2422

Detecting Epistasis by LASSO-Penalized-Model Search Algorithm in Human Genome-Wide Association Studies
Z.H. Zhou, G.X. Liu, L.T. Su, L. Han and L. Yan 2426

A Fuzzy Clustering Algorithm Based on Parameter Optimization in Large Transaction Database
W. Su, X. Zhang and J.J. Xu 2431

A Hybrid Approach for Critical Technology Identification
C.Y. Li, J. Jiang and M.J. Li 2438

Coupling Sentiment Dictionary and SVM Classification for Text Orientation Analysis
M.Z. Gao, F.F. Li, Z.Y. Ding and W.D. Xiao 2444

Research on the Optimization of the Storage Strategy of HDFS
H. Cao 2450

Research on Packet Encryption Algorithm in the Cloud Storage
H. Cao 2454

ZFDV: Zoom Financial Data Visualization in the Era of Big Data
T.T. Jiang, Q.G. Wang, H.K. Zhang, W.D. Xiao, C. Zhang and B. Ge 2457

A New Analysis of the Iterative Threshold Algorithm for RPCA by Primal-Dual Method
R.Y. Fan, H.X. Wang and H. Zhang 2462

Robot Path Planning Based on Artificial Fish Swarm Algorithm under a Known Environment
J. Wang and L.J. Wu 2467

A Study of the Keep-Right-Except-to-Pass Traffic Rule on Cellular Automata
W.B. Cao 2470

Probabilistic Model Checking by Model Equivalent Reduction and Abstraction
Z.L. Bai, L.Y. Xu and Z.S. Yu 2474

Computing Volumes Surrounded by a Quadric Surface and a Plane with MATLAB
Q.L. Yin 2480

A New Defogging Algorithm Based on Atmospheric Degradation Physical Model
X.G. Li 2484

The Evaluation of Teaching Quality Based on Fuzzy Method
J. Zhu, J.Y. Tian, J.H. Hao and S.Y. Zhang 2488

Identical Distributed Pairwise NQD Random Variables Sequences with a Novel Mutation Operator
J. Cao, G. Li and C.R. Ma 2491

Improving Performance of Wireless-Optical Broadband Access Network by Interpolation Algorithm of Zadoff-Chu Sequence
J. Cao, C.R. Ma and X.J. Hu 2495

Image Fusion Algorithm by Improved Chaos Immune Genetic Algorithm in Multi-Wavelet Transform Domain
J. Cao, T.F. Li and Y.P. Gao 2499

Interpolation Algorithm Application Using Neural Networks for Flywheel Energy Storage System
S.S. Wan, J. Cao, Q.S. Zhu and C. Yan 2503

The Application of Correlation Dimension in the Multi-Objective Comprehensive Evaluation of the Large Complex Equipment Procurement Scheme
Y.X. Yang, F.J. Wei and F. Wang 2507

Modeling and Simulation of Vehicle Traffic Detection System Based on Ground Sense Coil
J.W. Ju, J.Y. Liu, W. Yang and N. Liu 2511

Efficient Simulation for Dynamic Systems with Discontinuities
Q. Yuan 2515

Optimization Model and Algorithm for Responsive Closed-Loop Supply Chain Logistics Network with Direct Shipment under E-Commerce
J. Liu, Q. Li and H.W. Wu 2519

Tabu Search for Bus Crew Scheduling with Feasible Sets of Shifts
J. Wang, J.H. Ma, W. Guan and H.T. Gu 2523

Modified Harmony Search Algorithm for Unconstrained Numerical Optimization Problems
H.G. Xia and Q.Z. Wang 2528

A Modified Harmony Search Algorithm for Numerical Optimization Problems
H.G. Xia and Q.Z. Wang 2532

Modified Differential Evolution Algorithm for Numerical Optimization Problems
H.G. Xia and Q.Z. Wang 2536

People Counting Based on the Moving Feature of the Mass
P.Z. Qiao, T. Li, T. Xiang and X.Z. Zhang 2540

A Cloud Storage Encryption Scheme Based on Separated Key and Encryption Policy
P. Wang, F.Z. Zhang and C.L. Han 2543

Method Based on the Minimum Deviation for Multi-Attribute Decision-Making and its Application
H.A. Zhou 2547

Orthogonal Semi-Supervised Marginal Fisher Analysis
X.Z. Liang and Y.E. Lin 2551

Simulation Research on GM Navigation Based on AFSA
Z.L. Zhu, G.L. Yang, J. Li, S.J. Yang and Y.Y. Liu 2555

Currency Crisis Prediction Using Wavelet-Based Support Vector Machine
Q.L. Zhang 2560

An Improved Speech Enhancement Algorithm Based on Wiener-Filtering
Y.H. Liu, D.M. Zhou and J. Di 2565

Research of License Plate Recognition under Complex Environment
F. Gao, Z.J. Dai, K. Zhou and Y.P. Dai 2569

Hidden Markov Modeling for Nakagami Fading Channel
Y.H. Yang, L.F. Wang and Y.P. Sun 2576

Application of Multipurpose Decision Making Problem with AHP and Rectilinear Norm in Old Town Renewal Proposals
B.J. Zhang 2580

Application with AHP in Assessment of House Plans
B.J. Zhang 2588

Algebraic Immunity, Correlation Immunity and other Cryptographic Properties of Quadratic Rotation Symmetric Boolean Functions
J.L. Huang, Z. Wang and M.R. He 2593

Relations among E-Derivative, Derivative, Algebraic Degree, Correlation Immunity and Annihilators for H Boolean Functions
J.L. Huang, Z. Wang and J. Li 2599

Moving Vehicle Detection Scheme Using Edge Information and Background Subtraction in YCbCr Color Space
W.X. Yu and J. Su 2605

A Hybrid 2-Population Genetic Algorithm for the Job Shop Scheduling Problem
Z. Xu, R. Wang and Z.M. Wang 2609

Robust Principal Component Analysis Algorithm Based on Nonparametric Correlation Coefficient Matrix
N. Zhao and H.Y. Shao 2613

Design Modeling and Simulation by Interpolation Algorithm of Zadoff-Chu Sequence
S.S. Wan, Q.S. Zhu and J. Cao 2617

Particle Swarm Optimization by Improved Chaos Immune Genetic Algorithm
S.S. Wan, J. Cao and Q.S. Zhu 2621

The Research of Financial Risk Warning Model about Real Estate Enterprises in China
X.R. Tian, H.D. Jiang and J.L. Liu 2625

Prediction Model of Aerosol Fire Extinguishing Agent Performance Based on Combination of Genetic Algorithm and Back-Propagation Neural Network
Z.J. Chen, C.G. Zhu and Z.H. Zhang 2629

$F_P+vF_P+v^2F_P$
L. Chen and M.J. Shi 2634

Dynamic Network Model Analysis Based on Communication Network
N.Q. Yuan, T. Jiang, S. Bai, H. Sun and J.M. Zhao 2639

The New Class of Laplacian Integral Graphs
S.F. Lu and J.Y. Zou 2643

An Efficient Methodology for Estimating Interconnect Crosstalk Noise in Deep-Submicron Technologies
X.X. Liu, J.B. Shao and L.L. Zhao 2647

Feature-Based Real-Time Visual SLAM Using Kinect
Y. Song and B. He 2651

Research Progress in Topological Relations of Objects with Holes
S. Di, J.M. Zhang, Y.F. Shi and L.L. Zhang 2655

Complexity Research on Second Class Orthogonal Weight Function Neural Networks
D.Y. Zhang and R. Zhao 2659

Research of the First Kind of Padé Weight Function Neural Networks
D.Y. Zhang and Y. Xu 2663

Time Complexity Research on the Second Type Neural Networks of Padé Weight Functions
D.Y. Zhang and L. Yang 2667

Research on Safety Comprehensive Assessment Method for Air Traffic Control Based on RBF Neural Network
X.S. Gan and H.P. Li 2671

On the Application of Ant Colony Neural Network for the Highway Traffic Safety Facilities System
G.L. Jia, R.G. Ma and Y.J. Deng 2675

Numerical Simulation of Cook-Off for Passive RDX
C. Chen, W.B. Li and J. Liu 2679

Traffic Flow Prediction with few Data Using Fuzzy Neural Network Method
W. Zhou and X.X. Wang 2684

The Evaluation to Influence Factors of Concrete Durability Based on Grey Correlation Degree Method
X.P. Su and H.Y. Sun 2688

Camshift Algorithm Based on Multi-Features, and its Further Improvement Study
J.H. Lin and G. Fu 2693

Study of Numerical Simulation of RF Wave in Magnetized Plasma
J.F. Jiang, Z.H. Jiang, X.F. Sun and W.X. Guo 2697

Research on Workpiece Deformation in Electromagnetic Forming Process with Finite Element Method
C. Peng, L. Qiu, K.S. Gong and D.J. Wang 2702

Research on Learning Algorithm of RBF Neural Network Based on Extended Kalman Filter
X.S. Gan and H.L. Gao 2705

Interpolation Algorithm Application of Zadoff-Chu Sequence Using Neural Networks
J. Cao, Y.B. Li and C. Yan 2709

Comparison on Turnovers of Agricultural Products Futures Based on Hilbert-Huang Transform
Q.B. Han and H.L. Shi 2713

From Epanechnikov Mixture Model to Rule-Centered Fuzzy Model and its Application to Stock Index Prediction
Q.L. Zhang 2719

A Multifactor Grey Forecasting Model of Agriculture Output Value
W.Z. Chen and L.J. Liang 2723

Research on Software Demodulation of PCM/FM Algorithm Based on MSD
G. Fu, Y.J. Wu, R.L. Li and L.P. Wang 2727

Mixed Features Based Improved Human Action Recognition Algorithm
H.L. Jia and K. Cao 2731

Knowledge-Based Fuzzy Diagnostic Model
H.W. Lv, X.K. Li and K. Wang 2735

Chapter 6: Advanced Technologies in Mechanical Engineering, Mechatronics, Automation, Measuremant, Control and Manufacturing Technology

Design and Simulation for New Type Pulley Straightening Machine Based on Pro/E
J.H. Geng, B. Yu and B. Fan 2741

Based on the Modeling and Simulation Analysis of the Spray Pump of Soildworks
D.D. Jiang, Z.B. Zhou, J. Xu, L. Chen and M. Li 2745

Study on the Statics Analysis of Promoting the Drilling Efficiency of PDC Anchor Bit
Y. Li, Y.F. Song and Y.L. Mao 2749

Impact of Tooth Shape Parameters on Strength Safety Coefficient of Herringbone Planetary Train
Z.B. Zhu, C.Q. Shu, Y.L. Xu, C. Li and M. Yin 2753

Design of Monitoring System for Hydraulic Support Based on LabVIEW
S.S. Tang and C.K. Wei 2758

Research of Laser Induced Fluorescence Detection Techniques Based on Microfluidic Devices
Y.Q. Cheng, C.L. Guo, B. Zhao and L. Yang 2761

Detecting Ultra Low Carbon and Sulfur Contents in Steel by Using Infrared Absorption Method
M.R. Bayati and P.Y. Wei 2764

Research Progress of Detection Method of Sulfur in Iron-Base Alloys
M.R. Bayati and P.Y. Wei 2768

Experimental Study on Active Vibration Control of Flexible Manipulator Based on Improved PPF Algorithm
F. Du and T.B. Ma 2774

The Wind and Light Power Supply System Controller in the Mobile Base Stations
H. Ma 2778

Study on Dynamic Mechanism of LOGINK Service Innovation Based on System Dynamics
L.L. Li, S.W. Ji and L.S. Wang 2782

Numerical Simulation of the Kinetic Energy Projectile Deflected by Targets Moving along Transverse Direction
J. Chen and X.J. Ye 2787

City Sludge's Differential Scanning Calorimetry Analysis
L. Yang and S.H. Lin 2791

Research on the Regionalism Air-Conditioning System Design of Car and Saving Energy
L. Ouyang and D. Li 2796

Design of the Hydraulic System for Carrying Manipulator with 6-DOF
M. Wang, C.D. Wang, H. Zheng and G.F. Fan 2802

Simulation and Study of SPWM Variable-Frequency Drives of Asynchronous Motors Based on Aerostatic Guide Way
W. Long, Y. Liu, X.L. Zhang and T.Y. Wang 2807

Implementing Lean Techniques on the Shop Floor Improvement of a Delivery Company
J. Shay and P.I. Shieh 2811

Research on Direct Torque Control Adaptive Fuzzy Neural Network Controller of Permanent Magnet Synchronous Motor
C.F. Lu and H.B. Yu 2815

The Series and Parallel Energy Storage System Based on Super Capacitors
K. Zhao, Y.B. Zhang and B. Yu 2820

Nonsmooth Bifurcations in a Cracked Rotor-Active Magnetic Bearings System
F.H. Yang and H.Z. Tong 2825

Modeling and Analysis of Arresting Property of EMAS
H.H. Zhao and H.B. Yu 2829

Comparison Research on Aerodynamic Drags and Pressure Coefficients of Reference Car Models in Automotive Wind Tunnel
Y.C. Zhang, W. Ding, Z. Zhang and J. Li 2834

Performance Analysis and Simulation Study of Boiler-Turbine Coordinated Control System
Y.Y. Jiang and D.F. Wang 2839

Exploration on the Dual Spool Design of Rotary Hydraulic Valve
L.J. Qiu and S.Y. Xu 2845

Computing Method of Auto-Rotated Precision Index of Gun Barrel Based on Exterior Ballistic Computation
Y.D. Yang, J.S. Ma and C.Z. Jia 2849

Parameter Matching and Simulation Analysis on Power System of Plug-In Hybrid Vehicles
D. Ji, H.F. Zhang and J. Yang 2854

Buckling Stability Analysis of Parallel Micro-Spring
J. Zhang, L. Sui, X.H. Guo and G.H. Liu 2859

Passivity-Based Control of Motor for Reaction Wheel
R.L. Yu and J. Jin 2865

The Study of Mine Explosion-Proof Enclosure Design and Optimization
Q.L. Zhang and S.J. Yang 2869

Research for Guide Groove Configuration of Rotary Valve
S.Y. Xu 2874

A Study of Influence of Shape Technique on Radar-Scattering Characteristic for Tank Turret
Y. Ma, W.D. Xu, F.M. Shi, J. Liu, F. Lu and L.Y. Zhu 2878

Feasibility Investigation for Visible-Laser Compatible Camouflage Thin Film
L.Y. Zhu, W.D. Xu, A. Wan, Z.Y. Zeng and Y. Ma 2882

PWM Control for Actively Clamped Resonant DC-Link Inverter on Soft-Switching
Y. She 2886

Design Improvement on Shipping Container Spraying Production Line
S.O. Okorie and J. Shi 2890

Overview of the Control Methods for LTCC Substrate Shrinkage
X.D. Liu, S.H. Wang, Z.X. Hou, D. Zhou and L.Q. Yang 2895

Research on Fault Diagnosis Method for Crankshaft of Drilling Pump Based on Operational Deflection Analysis
F.F. Bie, J.F. Pei and F.X. Lv 2899

Hydraulic Vibration Exciter and Hydraulic Circuit Design Research
J. Yang 2904

Path Planning for Circular Cutter Envelop Milling of Steam Turbine Blade
J.J. Wang, K. Wang and Q. Wu 2908

Improving Design of Cup Conveying Part for Sealing Machine Based on PLC
L.A. Pan, Q.L. Du and Y.L. Wu 2913

Research on the Optimal Design and Gear Modification of Gearbox of a Wind Turbine Based on the Virtual Prototype
H.B. He, H.Y. Li, J. Yang, G.C. Lu and T. Gu 2917

Thermal Structure Coupling Analysis of Lathe Built-In Electric Spindle under Intermittent Load
K. Wang, J.H. Liu, G.K. Wu and X.W. Sun 2922

Analysis of Impact of Driving Amplitude on Resonance Frequency of Silicon Microgyroscope
S.D. Jiang, Y. Su, Q. Shi and A.P. Qiu 2926

Research on Credit Evaluation and Verification Model in Equipment Manufacture Industry
L.F. Zhao and S.H. Zhou 2931

The Improvement for the Structure of the Coil Transporters and its FEA
Q. Wang, Y. Sun, Z. Li, X.Q. Peng and B. Han 2935

The Influence of Diamond Graver's Edge Radius in Diffraction Grating Scoring Process
P. Sun, H.W. Wang, X.Y. Zhang, L.M. Qiao and X.L. Wei 2939

Stress Characterization and Mechanical Analysis for Supporting Leg of SiGe/Si MQWs Based Bolometer
B. Jiang, T. Dong, Y. He and Y. Su 2943

Analysis of Aircraft Hydraulic System Failures
W.G. Zhang and G.M. Lin 2947

Design and Realization of Remote Control UAV's Flight Controller
Y. Tian, H.D. Deng and H.Y. Zhuang 2951

Study of AT Based on the Lever Method
J.J. Li and J.H. Li 2955

Design and Analysis of Hydraulic Piston Structure Exciter
S.J. Wang and K.L. Yu 2959

Design of Underground Gas Concentration and Humidity Monitoring System Based on RS-485
Y.H. Long 2962

Adaptive Controller for ROV Based on Hybrid Theory
Y.H. Xie 2965

Data Storm Monitoring System of Large Power Industrial Control Network under Non Uniform Format
L. Liao, Y.H. Huang and C.J. Zhao 2970

Design and Calculation of a New Type of Elastic Gear Coupling and Finite Element Analysis
F. Chen, Z.F. Li and Y.X. Liu 2975

Study of Sub-Synchronous Control Interaction (SSCI) Based on the Test Signal Method
B.F. Gao, J. Liu and S.Q. Zhao 2980

Estimation of a State Vector of an Inertial Unit
H.P. Zhang, P. Pei, R. Ceschi and O. Rabreau 2985

Study of a Predictive Compensator for Internet-Based Remote Vehicle Steering Control
M.G. Zhong and H.C. Hong 2990

Research on Auto-Test System of Telescope Laser Indicator
N. Zhou, Y.H. Li and X.Y. Li 2995

The Development of Underground Personnel Data Terminal Based on RSSI Location
H.Y. Li and C.Z. Chen 2999

The Design of Embedded Video Monitoring System Based on DSP Processor
W.B. Hu 3003

A Calibration Method of Binocular Stereo Vision System Based on Halcon
Z.X. Zhang and Z.D. Zhu 3007

The Brief Introduction of Several Common Subway Shock Absorber Fasteners in China
H.P. Luo, D.J. Cai, M.L. Liu and P. Wang 3011

Design of the Improved Accompanying Temperature Logger
J. Guo, S.Y. Liang and Z.T. Yin 3015

Coiling Tension Control System of PID Simulation
Z.C. Wang, Y. Ding, H.Y. Zhao and X.D. Hu 3019

Structure Principle and Measurement Index of New Energy Reclaiming Suspension
J. Bai, Y.Z. Guo and M. Peng 3025

Method Research on Bending Fatigue Test of Vehicle Steering Wheel
X.J. Xu and L. Tian 3029

The Method of the Abnormal Sound Detection for Final Drive Based on DSP Technology
X.J. Xu and Z.G. Fang 3033

The Multi-Body Dynamics Contact Simulation on Transmission Gears
X.H. Deng 3037

Analog Circuit Parameters Measurement System Based on Multiplier
Y.X. Wang and M. Hu 3041

Numerical Simulation of Skid Steer Loader Steering Characteristic
F. Ren, X.H. Liu, J.S. Chen, P. Zeng, X.F. Jia and Q.M. Wang 3045

A Improvement of the Keep-Right-Except-to-Pass Rule in the Model of Modified CA (Cellular Automata)
Y. Ma 3050

Design and Implementation of Remote Control System Based on Embedded Mobile Network
J.X. Wei 3054

Vibration Analysis of Cable Suspended Parallel Mechanisms with Dynamic Base Platforms
Y.P. Hu and L.M. Tao 3058

The Design of Monitoring System in Large Hydraulic Press Aiming at the Precise Closed-Loop Control
H. Du, B. Huang, L. Wang and S.M. Chen 3062

Based on the Geostress to Research Slope Stability in the Deep Open Pit
Q.W. Li, L. Qiao and L. Chen 3070

Improvements on Structural Static Pushover Analysis Method in High-Rise Building Structure
M. Yu, Z.H. Dai and G.J. Hu 3075

Dynamics Analysis of Manipulator in the Hot Line
D.D. Zhang 3079

Design and Implementation of Driving Mechanism on Software Aerospace Measurement and Control System
G. Fu, M.X. Kou and R.L. Li 3084

Research on Workshop Layout Based on SLP and Witness
Q. Cheng, T.M. Guan, L. Sun and F.B. Jing 3088

Study on the Voltage Measurement in a Battery Manage System Based on LTC6802
Y.W. Zhu and B. Shi 3092

Research on Multistage Horizontal Well Fracturing in the East of Sulige Gas Field
Y.F. Xue, D. Li and Z.Y. Zhu 3096

Numerical Analysis of Heat and Mass Transfer Performance of the Packed-Type Parallel Flow Dehumidifier
R.H. Zhang, Z.Y. Wang and R.P. Niu 3100

A Novel Vertical Lift Machine and its Precise Pose Control
X.B. Liu, X.F. Wei, X.D. Yuan and W. Ni 3105

Investigation on Flat Wheel In-Suit Measuring System and Errors Compensation for Wheel Radius under Aspheric Grinding Process
F.M. Nie, Z.G. Li and Q.T. Wu 3110

An Intelligent Fault Monitoring System for Hydraulic Excavator
L. Ni, X.S. Chen, A.L. Wang and S.K. Cao 3114

Modeling and Simulation of Feed Drive System Vibrations Based on Dual Inertia System
L. Luo, W.M. Zhang and Y.L. Zhang 3117

Comparative Study of Moving Target Analysis System
M. Feng and H.C. Du 3122

The Injection Mold Design of Clamshell Phone Upper Cover
G.D. Liang and J.H. Liu 3127

Based on PMAC Control 4-DOF Manipulator
J.W. Fan, Y.J. Liu, L. Chen and C. Liu 3132

Development of a Rotary Drilling Mechanism for Impregnated Diamond Bits
Z.T. Li, Y.Z. Ma and K. Itakura 3136

Studies on Backward Median Current Waveform Control Research in Pulsed MIG Welding
Q. Zhu, J.X. Xue, X.L. Zhang, C.W. Dong, Z.S. Chen, Z.H. Li and P. Yao 3140

Soil Moisture Monitoring System Based on RS485 Bus
L. Wang 3145

The Finite Element Analysis of the Large-Diameter Composite Slurry Valve Gate
J. Wu, Z.M. Yang and D.Z. Wang 3149

Fit Degree Calculation of an Aircraft Part Manufacturing Process
X.F. Huang, F. Zhu and N. Wei 3153

Fuzzy Adaptive PID Controller Optimization Design in Temperature Control System
X.P. Li and L.Z. Chen 3157

Research on the Correction of Regeneration Opportunity of DPF Using GW4D20 Engine
S.J. Qiao and Y. Liu 3161

Dynamic Characteristics of Arch Steel Tower in Construction Stages
L. Yu, Y.Y. Che, S. Wang and G.H. Zhao 3165

Inhibition of Return Effect Reversed by Perceptual Load
X.J. Liu, Z.H. Fan and J.Z. Zhou 3169

Brushless DC Motor Speed Control System Based on Fuzzy PID Control
Y.H. Zhang and L.P. Song 3172

Research on Algorithm to Improve Performance of Multi-Wheel Steering Control System
S.S. Wan, J. Cao, Q.S. Zhu and C. Yan 3177

Research on Image Vectorization Based on Dual-Thumb Pneumatic Flexible Robot Hand
S.S. Wan, J. Cao, Q.S. Zhu and C. Yan 3181

Based on ANASYS with Finite Element Analysis and Calculation of Cracked Pipeline
X.M. Zhu and Y.P. Lv 3185

Simulation Study of Magnetic Memory Signal Correlation Effect of Dual Defects by ANSYS
X.W. Xi, S.K. Ren, Y.F. Zhang and Y. Huang 3189

Temperature Control Features and Simulation Research on High and Low Gimbals
Z.J. Xiao, X.X. Guo, H.B. Zhu, Z.G. Xu and Z.Y. An 3195

Prediction System Design on Noise Airworthiness Compliance
G.H. Yan, S.Q. Liu and W.Q. Song 3199

Separating the Time Field Signal of Rotor Unbalance Vibration Based on EMD Method
S.H. Zhang, X.W. Guo and Z.M. Zhang 3204

Application of Rapid Prototyping Technology in Product Design
D.T. Li, Z. Zhang, J.W. Deng, M.Y. Huang, X.F. Wan and H.J. Ni 3208

AHP Effectiveness Evaluation of Electronic Warfare Command and Control System under Complex Electromagnetic Environment
G.S. Wang and Z.F. Qi 3212

Design of Quadrotor's Control System Based on DSP
Q. Lv, P.P. Ni, G.S. Wang and F. Liu 3216

Fault Diagnosis of Rolling Bearing Based on MED and Morphological Filtering
S.K. Liu, G.J. Tang and B. Pang 3220

Transform a Mechanical Testing Machine into High-Temperature Disk Spring Stress Relaxation Test Equipment
X.Y. Zhou and Y.Z. Yu 3224

Vista of Silt Brick Cutting Machine Development Situation
Z. Zhou, Y. Lv, H.J. Ni and C.Q. Wu 3228

The Design of the Single-Phase Inverter Based on DSP (TMS320F2812)
Z.X. Zhou and J.E. Huang 3231

LDO of High Power Supply Rejection with Two-Stage Error Amplifiers and Buffer Compensation
Y.T. Chang, Y.D. Shiau, P.C. Wu, R.H. Xue and P.Y. Cheng 3236

The Research of Numerical Control Transformation Based on Turbo PMAC
H.C. Sun, L.N. Li and S.P. Deng 3240

Rotor Local Rubbing Fault Feature Analysis Based on Teager-Huang Transform
S.K. Liu, G.J. Tang and B. Pang 3244

Coupled FE-SPH Simulation of a High-Speed Grinding Process Using a Multiple-Grain Model
R.D. Shen, X.M. Wang and C.H. Yang 3248

Sensorless Control of Switched Reluctance Motors Based on Pulse Injection, Position Sectors Divided and Variable Thresholds
Z.F. Jia, D.A. Zhao and Y.Y. Zhao 3252

Research on the Static Cushioning Property of Folding Corrugated Cushions
Y.M. Qi and W.H. Gao 3258

Interesting Packaging Structure Design of Children's Biscuits
Y.M. Qi and W.H. Gao 3262

Study on Axis Calibration Method of the Coordinate Measurement System Based on Binocular Vision
Z.M. Zhang, S.H. Zhang and Y.N. Yu 3266

Research on Cantilever Used for Thermal Flow Meter as Switch
Z.L. Zhang, Y.Q. Wu and C.M. Liu 3270

The Design of Multichannel Marine Seismic Acquisition Unit Based on ADS1282
Z.L. Zhang, Y. Zhang and P. Chen 3274

Complicated Manufacturing System Dynamic Measure-Control and Intelligence Diagnosis
J. Ma, W.W. Li and P.T. Liu 3278

Communication Module Design of Offshore Drilling Platform Cleaning Robot
Y.X. Jiang, J.F. Liu, X.H. Zhang and Y.L. Zhao 3282

Design of Pneumatic Parachute-Packing Machine
Y.F. Wang, S.P. Deng, B. Chen and L.L. Zhang 3286

Development of G-Code Based on PMAC in CNC Machining Center
C.C. Cao, Q.H. Sun, S.P. Deng and Y. Zhou 3290

Research on Automatic Changing Film Mechanism of $PM_{2.5}$ Sampler
Y. Mei, S.P. Deng, K. Yang, W.F. Zhou and J.T. Wu 3294

Design of Shock-Absorbing System for Disaster Rescue Robot
L. Xie and Y.M. Qi 3298

Failure Analysis and Preventive Measures of Cooling Tower Fan Gearbox
J.P. Chen, Y.L. Wang, C.X. Zhao and X. Li 3302

Application of Viscous Pressure Forming in Aeronautics and Astronautics
J.G. Li, J.G. Zhang, J.P. Liu, R.F. Zhao, Y. Li, Y.C. Li, S.X. Yu and Z.J. Wang 3306

Methods of Metal Parts Unfolding
Y. Li, J.G. Zhang, J.G. Li and Y.C. Li 3310

Equipments of Pulsed Welding System and its Application
L.Y. Lou and Y. Gao 3314

Reviews on Automobile Abnormal Sound Fault Diagnosis
G.L. Tan, D.H. Miao, Y.M. Qi and S.P. Deng 3319

Research on Disassembling Equipment for Construction Machinery Hydraulic Cylinder
X.H. Zhang and J.X. Zhang 3323

Stiffness Modeling and Sensitivity Analysis for Worm Geared Transmission
L. Han and H.J. Qi 3328

Theoretical Surface Roughness Model in High Speed Face Milling
T. Zhang, G.H. Li and L. Han 3331

An Analysis of Electric Inertia Simulation Method on the Test Platform of Electric Bicycle Brake Force
Z.X. Yu and H.B. Yu 3335

A Simple Criterion for Robust Stabilization Design of Interval Time-Delay Systems
C.H. Lee and P.S. Liao 3340

Optimization of Operation Frequency in the Evaluation of TBCs Using Microwave Technique
Y.E. Yang and G.M. Zhang 3344

Damage Detection of the Honeycomb Sandwich Panel Based on Frequency Dactylogram
G.C. Li, Y.Q. Li and Y.L. He 3349

The Research of Fluid in the Cross Micro-Channel
J.Y. Li, W. Zhou, X. Zhang, Y.F. Jiang, L. Yang and S.X. Zhang 3354

Research to the Model Design of Real Platform Based on the Simulating Network
G.Q. Liu 3359

Fatigue Loads Prediction Based on a Hybrid Road Approach
Y.H. Mei and Q.S. Xie 3363

Assessing the Harmonic Emission Level Based on Partial Least-Squares Regression with Data Envelopment Analysis
X. Li, M.Y. Chen and Y.W. Zheng 3367

Software Design of Micromouse Dash Motion
H.M. Zhang, L.S. Peh and Y.H. Wang 3371

Double DSP Communication Based on CAN Bus Interface
H.D. Deng and Z. Yan 3375

Aerospace Test and Launch Process Dynamic Management System Based on the Network Diagram Method
Y. Wang, H. Wang and Y. Li 3379

Research to the Development of Network-Anticipated Controlled System Based on Arbitrary Bounded Packet Loss
G.Q. Liu 3382

Flatness Feed-Forward Control Model Based on Neural Networks
Z.W. Yan, H.A. Bu, D.H. Zhang and J. Sun 3386

The Design of Greenhouse Environment Monitoring System Based on ZigBee
G.S. Chen, Z.S. Wang and X. Shang 3390

The Design of Portable Granary Thermometer
G. Qin and D.Q. Cui 3394

Research and Design of Light Moisture Tester
Y.P. Tang 3399

Software System for Unmanned Surface Vehicle Using PCI8602
X. Shi, S.M. Wang, Z. Xu and Q.Y. He 3407

Research on Integrated Application of Multi-Display Technology in the Mobile Terminal
X.M. Mao and J.G. Liu 3411

Design of Remote Monitoring System of Temperature and Humidity Based on Internet of Things Technology
L. Wang 3415

The Design of Intelligent Home Furnishing System of Internet of Things
L. Wang 3419

Transmission Delay Monitoring Method in Intelligent Substation
X.H. Song, Z.Z. Guo and G.B. Li 3423

Study of Maximum Power Point Tracking Control Based on GRNN Neural Network
K. Liu, T.Z. Ji, X.Y. Li, X.F. He and M. Zhang 3427

Arrangement of Sensor Nodes for Wireless Sensor Network in Aquatic Products Breeding
B. Shi, S.K. Xu and J.M. Jiang 3433

A Platform of Lightning Protection Business Based on Tablet-PC
Y.H. Zhang, J.C. Zhou, X. Jiao, J. Zhou and Q.F. Zeng 3437

Prediction and Analysis of Safety Production Accident in Mining Based on the GM(1,1)
C.F. Jiang, K.P. Hou and H.F. Sun 3443

A Production Planning and Scheduling Process Study Based on Dynamic Information Feedback
Q. Yang and Y.H. Ni 3447

The Key Technology Research on Information Acquisition about Tropical Crop Production Environment
L.L. Wang, K. Lu, H.X. Luo and J.H. Fang 3452

Flow Field Simulation in Water Washing Tank of Explosion-Proof Diesel
R.S. Long, Z.S. Lian, S.N. Sun and Q.L. Wang 3456

Research on Jet Current Field Characteristic under Waves by Numerical Modelling in Flowing Ambient Fluid
M.C. Li, Q. Si and Y. Wang 3460

Feedforward Improved PID Algorithm to Control the Smart Car
Y.H. Xie and X.Q. Liu 3464

Evaluation of Various Turbulence Models in Predicting Airflow and Turbulence around a Generic Vehicle Model
C. Wu, Y.P. Wang and X. Yang 3468

Ground Simulation Method for Envelope Performance of Airship in near Space
L.B. Liu, P.P. Mi, S. Cao and M.Y. Lv 3473

Based on 3-D Modeling and Value Simulation of the Intake System in CNG
J.H. Li and J.J. Li 3477

The Metabolic GM (1,1) Prediction of the Absolute Gas Emission Quantity in a Certain Mine
X.Y. Meng, R.H. Chen and S.B. Wang 3480

Numerical Analysis of the Wind Tunnel Effect on the Chinese Kang in the Northern China
Z.L. Lu, Y.H. Xu, H.L. Wang and D.D. Xi 3485

Photometric Data Procession of the Swift/UVOT Instrument
X.P. Li, C. Yang, L. Zhou and H.T. Yang 3489

Process Simulation and Parametric Analysis of Gas Fractionation Unit
Q.R. Li, P. Li and P. Zhang 3493

Design and Simulation of Airborne Circular Omni-Directional Slot Antenna
L. Ren, Y.Z. Zhu, D. Su and X. Deng 3497

Based on Small Current Grounding Fault Analysis and Testing
H.L. Lv 3501

Prediction Model of Silicon Content in Blast Furnace Hot Metal Based on Artificial Neural Network and Genetic Algorithm
Y.H. Cheng, C.W. Niu and Y.X. Zhang 3505

Comparison of Two Computing Method on Thermal Conductivity of Aluminum Nitride
X.M. Cai, Q.N. Zhou and J.M. Wang 3509

Numerical Simulation and Experimental Study on Thawing Time of Cylindrical Frozen Food
A.M. Ji, X.C. Niu, B.N. Tang and F.L. Li 3513

Chapter 7: Communication, Signal and Image Processing, Data Acquisition and Recognation Technologies

A Modified DFT-Based Channel Estimation Method for OFDM-RoF System
L.Q. Huang, P. Zhang and G. Yang 3521

Dual Station Based Bearings-Only Tracking Using Unscented Filter
H.W. Quan, J.H. Li and M.S. Chen 3526

Mobile Wireless Communications Device with Buffered Cock Distribution Network
J.P. Jia, C.S. Wu, J.W. Chen and Y.Q. Shi 3530

POS Supported ADS40/80 Imagery Direct Geo-Positioning and Positioning Accuracy Optimization
Y. Zhang, T. Wang, W.F. Feng, Y.H. Fan and J. Rui 3534

The CDMA Spread-Spectrum Cell Mobile Communication Uplink System with Cooperative Diversity
H.C. Liao 3540

3D Facial Shape Reconstruction from a Single Frontal Image
Q. Ma 3544

Processing and Mosaicing System of Civil Unmanned Aerial Vehicle Remote Sensing Image
Y. Yang, L.J. Wang and L. Yang 3548

Image Retrieval Based on Color Histogram of Saliency Map
J.F. Wu, X.Q. Lv, W.L. Yang, Y. Tao, J. Zhang and S. Yang 3552

Beamforming with Kerdock Codes in LTE System for High-Speed Railway
Z.H. Yang, L.J. Wang and Z.K. Fang 3556

A Chaotic Image Encryption Algorithm Based on a Dynamical Feedback Operation
G.S. Gu, J. Ling, G.B. Xie and Y.Y. Ou 3561

The Application of the Movement Video Analysis Technology in the Sports Area
X. Xiao 3567

Anti-Counterfeiting Technologies for Digital Halftone Images Based on Moire Methods
J.H. Ge, J. Pan and M.X. Li 3571

Method Research on Based-Static Motion Image Retrieval
S.Y. Sun and C.S. Wu 3575

Relevance Feedback Based on Particle Swarm Optimize Weight-Vector for Image Retrieval
F.Y. Lv, X.H. Yang and D.F. Li 3579

Design of Optical Fiber Transmission System Based on Absolute Polar Duty Cycle Division Multiplexing (APDCDM)
X.Q. Chen and L. Tang 3583

Target Tracking Based on Improved Camshift and Kalman Filter
L.Y. Ban, Y.H. Han and Y.H. Wu 3587

Sensing Matrix Setting in Cognitive Radio Networks
X.Z. Chen and B.D. Chen 3591

Wavelet De-Noising Based on Genetic Adaptive Threshold Algorithm
G.W. Wu and C.M. Wang 3595

3D Graphical Representation of Protein Sequences Based on Conformational Parameters of Amino Acids
Q.J. Xiao and Z.G. Deng 3599

Adaptive Image Feature Reduction for Object Tracking
C. Lin and C.M. Pun 3605

Research on Blind Signal Extraction Based on Normalized Kurtosis
Y.J. Zhao 3609

Extraction of Signals with Reference
Y.J. Zhao and H.N. Jiang 3613

Research on the Optimal Classification Method for Remote Sensing Image Based on the Gabor-PCA Analysis
J.H. Yang, L.G. Wang and J.X. Qian 3617

Orthogonal Discrete Frequency-Phase Waveform Design Based on Hybrid Chaos for MIMO Radar
Y.N. Xie and J.J. Wang 3621

The Communication Capability of Shipboard Radio Based on Path Loss
X.G. Huang, A.M. Zhu and S.J. Yao 3625

Study of Synchronization Strategy Based on Timestamp
L. Xu 3629

Research on Multi-Sensor Data Aggregation Based on Clustering Analysis and Correlation
X.C. Dang, Q. Gao and Z.J. Hao 3633

Automatic Registration between High Resolution SAR Image and GIS Road Network Based on Pairwise Constraint and ICM Optimization
H.G. Sui, F. Hua, G. Chen and C. Xu 3639

Semi-Automatic Extraction Method for Low Contrast Road Based on Gabor Filter and Simulated Annealing
G. Chen, H.G. Sui, L. Dong and H. Sun 3644

Multi-Threshold Image Segmentation Based on Improved Particle Swarm Optimization and Maximum Entropy Method
Y.T. Lu, W.L. Zhao and X.B. Mao 3649

Speech Enhancement Based on EMD and Wavelet Threshold in Noisy Environments
Z.Q. Chen, D.X. Zhang and D.L. Yuan 3654

Study of SC-FDMA Reduce PAPR Based on the Power Line Carrier Communication
G.J. Gong, D.K. Hao, Y. Zhang, J. Lu and G. Xu 3658

An Improved Image Stitching Algorithm
D. Li 3663

Speech Airflow and Air-Pressure Signal Editing Platform
S.L. Lv and Y.S. Jin 3667

Modeling Difficult-to-Measure Process Parameters Based on Intrinsic Mode Functions Frequency Spectral Features of Mechanical Vibration and Acoustical Signals
J. Tang, Z. Liu, Y.J. Wu and L.J. Zhao 3671

Image Retrieval of Self-Adapt Distance Measure Based on SLLE
X.F. Wang, H.N. Zhang, X.R. Qiu, J.P. Song and K.X. Zhang 3675

Study on Deep Structure of Extreme Learning Machine (DS-ELM) for Datasets with Noise
M.M. Ma and B. He 3679

Design of 2_DOF Simulation Platform for the Testing of Airborne Laser Communication APT System
L.X. Meng, D.X. Zhao, Y.Y. Bai and L.Z. Zhang 3683

The Method of Optimal Group Based on the Kernel Density Estimation and the Close Degree
F. Ye, X. Wang, D.H. Peng and C.H. Jiao 3689

Research of Frequency-Hopping Communication for Arbitrary Array Based on Adaptive Beam-Forming
C.L. Qiao, H.D. Quan and P.Z. Cui 3693

Research on Fabric Image Acquisition Based on Compressed Sensing
J.C. Dong, S.Q. Guan and L.L. Chen 3698

Adaptive Equalization with Variable Step Size Algorithm Based on Gradient for HF Channel
F.F. Han and Z.H. Lin 3702

Joint Estimation of Doppler and Time Delay of Wideband Echoes for LFM Pulse Radar Based on Fractional Correlation in Impulse Noise Environment
L. Li 3706

Parameter Estimation Based on Fractional Correlation under Alpha-Stable Distribution Noise Environment in Bistatic MIMO Radar System
L. Li 3710

Multi-View Video Coding Based on Video Correction
T. Yan, X.X. Zhou, W.T. Luo, Z.L. Liu and P.D. Zhang 3714

De-Noising of Underwater Acoustic Weak Signals Based on Compressed Sensing Technique
L.L. Zhao and X.W. Dai 3718

A Beam Forming Method Based on Amplitude Weighting of Uniform Circular Array
J.L. Wang, Y.Q. Fu and X. Liu 3722

Impulse Noise Suppression Method for Telemetry Signal by Multi-Scale Median Filtering
X.F. Liu 3726

Research on Color Vegetable Diseases in Greenhouse Image Pretreatment and Extraction Method
X.L. Luo 3730

An Infrared and Visible Images Fusion Algorithm Based on Wavelet Multi-Resolution Decomposition
L.K. Liu and Z.J. Wu 3734

Simulation Research on Rolling Element Bearing Fault Signal Extraction Based on Blind Source Separation
Y.X. Zhang, J.P. Zhu and S. Zhang 3738

The Improved Membership Matrix Initialization Method of FCM for Image Segmentation
Z.J. Wu and L.K. Liu 3743

Discovering Frequent Itemsets an Improved Algorithm of Bit Vector and Graph
N.L. Liu 3747

An Improved Otsu Image Segmentation Algorithm
Y.X. Dong 3751

Radar Compressed Sensing Imaging Method with Two-Dimensional Separable Sampling
S.H. Jiao, L. Tang, X. Liu and H. Qi 3755

A MMSE Channel Estimation Method in QC-LDPC Coded OFDM Systems
G. Sangirov, Y.Q. Fu and Y. Fang 3759

Novel Infrared and Visible Images Fusion Algorithm Based on NSCT
H.F. Tan, T.W. Luo, J.J. Zhu, G.Z. Li and Q.X. Zhang 3763

A Novel Text Extraction Method from Pure Text Images Using Morphological Operations
X.Q. Chen, B. He, G.C. Wang and Y.X. Li 3768

Long-Range Communication Scheme Based on Majority Combing
Y. Peng, X. Huang, L. He and Y.P. Cui 3773

Electromagnetic Scattering from Perfectly Conducting Periodic Rough Surfaces Using Improved Complex Images Method
L. Li and W.C. Zheng 3777

Application and Analysis of the Full-Wave Band CCD System in Image Interpretation Technology
W. Han, J. Xie, J.H. Bao, M. Zhao, X.Y. Fan and F. Guo 3782

An Improved DFT-Based Channel Estimation Algorithm for OFDM System on Time-Varying Multipath Fading Channels
X.L. Ma, T.L. Fan and Y.F. Du 3786

Flattop Broadband Wavelength Conversion Based on Cascaded Second-Harmonic Generation and Difference Frequency Generation in Step-Segmented Quasi-Phase Matched Gratings
H.D. Wu, J.S. Guo, Y.W. Wu and Z.X. Wang 3790

Investigation of Efficient Wavelength Conversion Based by Difference Frequency Generation in Step-Segmented Quasi-Phase Matched Gratings
J.S. Guo, H.D. Wu, Y.W. Wu and Z.X. Wang 3794

Wavelet Transform Adjustment Method Study in Color Image Enhancement
Z.G. Zhang, S.Q. Yan and P. Geng 3798

Accurate Detection of Fault Signal in Large-Scale Communication
N. Shu 3802

Long Reach 10-Gbps WDM-PON Based on Carrier Distribution and Coherent Detection for Upstream Transmission
J.H. Liu, Y.P. Ma, S.R. Ren, Y. Yang and B. Zhang 3806

Analysis on Signal Extraction under Sudden Changing Noise Interference Based on Time Frequency Analysis
S.H. Nie 3810

Application and Research of Data Mining Technology in Communication Network Environment
Z. Zhang 3814

Study on Optimal Design Approach of One-Card under Multi-Signal Conflict
H.J. Zhu and Z. Wang 3818

Design and Simulation of Wireless Communication System Channel in Coal Mine Based on OFDM Technology
R.H. Ma 3823

Astronomical Image Matching Based on the Cross-Correlation Algorithm
J.J. Sun 3827

Dynamic Simulation of TT&C Signal Based on VFD Filter
W.G. Yang, W. Li and J. Zhao 3834

Enhancement Algorithm of Color Fog Image Based on the Adaptive Scale and Multi-Parameter Correction
Y. Gao, L.J. Yun, J.S. Shi and F.Y. Cheng 3838

3-D Reconstruction of Image Sequence Based on Independent Three-View
C. Li, H.R. Zhao and G. Fu 3844

Study on Enhancing Terminal Identification in Track and Field Using Digital X-Ray Photography Image
G.J. Lai 3851

Track and Field Image Segmentation Technology of Automatic Multi-Threshold Block Sampling Based on Matlab
A.L. Yu 3856

The Design of Image Acquisition System Based on CMOS Image Sensor USB Interface
Z.Y. Hu and L. Li 3861

Locating Method of DPM 2D Barcode Image
H.R. Zheng, B. Shan and Z. Liu 3865

The Simulation of DS-UWB RAKE Receiver over the Multipath Channel
K. Zhang, Y. Cao, C.F. Li and W.Y. Liu 3868

Video Sequences Foreground Enhancement Using Hidden Markov Model
D.Y. Lv, D.Y. Liu, Z.P. Huang, N.H. Yu and J.K. Wu 3872

The Study of a Fast Sub-Pixel Registration Method for Remote Sensing Image
C. Zhou, J.H. Zhou and D.H. Fan 3877

The Study of Combination Filtering for Removing Mixed Noise of Remote Sensing Image
C. Zhou, J.H. Zhou and D.H. Fan 3881

Hyperspectral Image Classification via Discriminative Sparse Representation with Extended LBP Texture
Y.M. Ren, Y.N. Zhang and W. Wei 3885

Channel Reservation Strategies for Multiple Secondary Users in Cognitive Radio Networks
Q. Peng, Y. Jiang, G. Liu, F. Cui, G.B. He and W.M. Wu 3889

New Enhancement Algorithm of Infrared Images Based on Dual Threshold of the Exponential Transform
J. Lv, J. Lv, C.F. Wu, Y. Zhou, F.P. Sun and K. Che 3893

Novel Single Image Dehazing Algorithm
J.P. Chen, D.Y. Bi, C. Liu and Z.L. Fan 3898

Simulation and Application of Space-Time Coding in OFDM System in Coal Mines
J.X. Wei and C. Sun 3902

Digital Image Technology Mineral Feature Extraction Method Research
J. Peng and D.B. Li 3906

Image Compression Technology Reseach Based on Lifting Wavelet Transform
R. Guo, Y.F. Li and F. Liu 3910

Optimization of Traffic Signal Timings Based on Surrogate Measures of Safety
Y. Zhang, C.C. Zheng, L. Zhang, X.R. You and D.X. Cheng 3915

Research on the Key Technology of Laser Engraved Image
S.Q. Zhang, D.M. Zhang and Q.H. Feng 3919

Study of PCM/FM Telemetry Sequence Soft Demodulation
D.X. Zhu, G. Fu and Y. Feng 3922

Study of Reentry Telemetry Signal in the Environment of Soft Demodulation
G. Fu, M. Tao and Q. He 3926

Research on Continuous Phase FM Signal Demodulation Based on STFT
Y. Feng, G. Fu, R.L. Li and L.P. Wang 3930

An Adaptive Filtering Method for Chirp Signal Based on FRFT
Y.J. Wu, G. Fu and G. Cheng 3934

Research on FM Telemetry Software Demodulation Algorithms
G. Fu, Y.J. Wu, R.L. Li and L.P. Wang 3938

Performance Analysis on Three Methods for Chirp Signal Parameters Estimation Based on FRFT
Y.J. Wu, G. Fu and P. Yu 3942

Group Sparsity Regularization Based Compressed Sensing MR Image Reconstruction
X. Jin, M.F. Jiang and J. Feng 3946

Pulse Coding Soft FM Telemetry Signal Demodulation
Y.J. Wu, G. Fu and G. Cheng 3952

Design of High-Speed Data Collector of Blast Wave Signal Based on the Post-Trigger Principle
X.G. Tang 3956

On Matlab's Simulations in Underground Mobile Multipath Channel
J.X. Wei 3960

Clutter Modeling and Characteristic Analysis for Airborne MIMO Radar
L. Hao, Y.S. Zhang, Z. Li and J. Xu 3963

Recognition of Paper Currency Research Based on AGA-BP Neural Network
X. Xiao, Q.H. Wu and Y. Zhang 3968

Wavelet De-Noising Algorithm Based on OpenCV for Images Edge Detection
Y.F. Ma and S.G. Liu 3973

A New Method of Multi-Component Chirp Signal Array Detection
G. Fu, Y.J. Wu and H.T. Tao 3977

Demodulation Method of Telemetry Signal Based on Virtual Radio
X.L. Yao, G. Fu and R.L. Li 3981

Multi-Frequency Estimates Based on IIR Adaptive Frequency Estimator
M.X. Kou, J.H. Lin and G. Fu 3985

Detection and Parameter Estimation of Chirp Signal Based on Time-Frequency Analysis
G.Z. Wu, G. Fu and Y.J. Wu 3989

Parameters Estimation and Waveform Reconstruction of Chirp Signal Based on FRFT
Y.J. Wu, G. Fu and F. Liu 3993

Research on Demodulation of Pulse Code Modulated Signal Based on Instantaneous Frequency Measurement
G. Fu, Y.J. Wu and Y. Feng 3997

LFM Signal Detection Method Based on Fractional Fourier Transform
Y.J. Wu, G. Fu and Y.M. Zhu 4001

Interference Suppression of VLF Communications in Atmospheric Noise
Y.J. Wu, G. Fu and W.J. Geng 4005

Research on Joint Time-Frequency Analysis Methods of Adaptive Radar Signal
Q. Xing, W.G. Zhu, Y. Bo and K. Wang 4009

A Study on Same-Beam Interferometry in Deep Space
X.Y. Wang, J.C. Hong and K. Hu 4014

The Application and Simulation of OFDM Technology in Power Line Communication
Y.W. Chen, B. Xu and J.H. Hao 4019

Research on Demodulation of High Bit Rate Telemetry Signal in FM Baseband
L. Yi, G. Fu and G.Z. Wu 4023

Study on Identification Method of Zherong Radix Pseudostellariae with Near-Infrared Spectroscopy
Y.P. Pang, K. Liu, L.Y. Xia and S.L. Yu 4028

Color Image Segmentation Based on Secondary Watershed and GrowCut Algorithm
J.M. Chen and H.Y. Lu 4032

Tracking Optimization of FH Signal Based on Wiener Filtering
Q. He, G.Z. Wu and Y.J. Wu 4038

Detection of Nonlinear Frequency Modulated Signal Based on Fractional Fourier Transform
Y.J. Wu, M. Tao and M.Q. Zhou 4042

Detection of Chirp Signal with Time-Varying Amplitude Based on FRFT
Y.J. Wu, R.L. Li and X. Wang 4046

Analysis on Ranging and Velocity Measurement Performance of DS/FH Hybrid Spread Spectrum Signal
Y.J. Wu, X.L. Yao and J. Xia 4050

Research of Image Denoising Method about Wavelet Transform with Neighborhood Average
C. Huang 4054

Application and Debugging of All-Digital Frequency Synthesizer
H.B. Fan, X. Meng and J.M. Hou 4058

Electronic Satellite Scheduling Problem and its Heuristic Method
J.C. Li, L.N. Xing, Y.W. Chen and X.Y. Wei 4062

Recent Improvements in Image Retrieval
Y.S. Zeng and X.L. Ying 4069

Mineral Belt Image Segmentation Using Firefly Algorithm
L.F. He, X. Tong and S.W. Huang 4074

The Hidden Terminal Problem of 802.11 MAC and 802.15.4 MAC Protocols Based on NS2 Platform
D. Qiu and Y.X. Yang 4078

Research on Halftone Technique of Digital Images
W.B. Dai, L. Chen, X.W. Zhang, L. Wang, S.Y. Nie, K.J. Yang and Y.W. Wang 4082

Research and Implement of Digital Image Watermark Based on DCT
L.Y. Liu 4086

Face Recognition Based on Gabor Filter and Improved Linear Local Tangent Space Alignment Algorithm
X.Y. Xu, J.Y. Liu, Y. Shi and T. Deng 4091

A New Way to Optimize LDPC Code in Multiple Access Channel
J.X. Zhang 4095

A Study and Design of Compressed Encoder Based on Neural Network for Remote Sensing Image
L. Tao, W.L. Li, Y.Y. Yu, J. Kang and J. Yang 4100

A New Method of Image Matching in a Vision-Based Mobile Robot System
C.Z. Cao, W.Z. Gao and H.J. Li 4104

The Research of Starry-Sky Image Bright Stray Light Background Suppression Method
S.J. Guo and Z. Wang 4107

Body Surface to External Channel Modeling
Y.H. Yang, L.F. Wang, D.Y. Shen and M. Yang 4111

Research and Solution on Bottleneck Problem in Zigbee
J.P. Zhang and X.L. Zeng 4115

A Image Decomposition Method Based on Euler Mapping for Face Recognition
Z.K. Li and Y. Wang 4119

Color Space Comparison between RGB and HSV Based Images Retrieval
C.H. Su, H.S. Chiu, J.H. Hung and T.M. Hsieh 4123

Blind Detection of Copy-Move Forgery in Digital Images Based on Dyadic Wavelet Transform
R.F. Zhang, H.M. Ye, Z.H. Song and M. Wang 4127

The Realization of Receiving and Reporting the HARQ-ACK Information in LTE System
P. Sun, J. Yang, Y.J. Chen and C. Zhou 4132

NSCT-Based Image Enhancement Combing Homomorphic Filtering with Fuzzy Theory
K. Wen, B. Sun and J. Yang 4136

Realization of Book Locating by RFID Technology in Mobile Phone Libraries
Y.P. Wang 4140

Design of a Novel Variable Bit Rate Video Traffic Prediction Model Based on Neural Networks
Z.Z. Lian, H.Z. Wang and D.H. Li 4143

The Application of Physical Layer Network Coding in the UAVs
Z.M. Yang, Y.J. Hu, C.L. Wang and Q.S. Yuan 4147

Study on the Implementation of RAKE Receiver in 4G System
H.Y. Fu, C.R. Zhu and X.D. Jia 4152

The Research of M-Learning Platform Based on 4G Network
H.Y. Lin and Y.J. Wang 4157

3D Human Body Data Acquisition and Fit Evaluation of Clothing
Z. Wang, Y.Q. Zhong, K.J. Chen, J.Y. Ruan and J.C. Zhu 4161

Design and Implementation of Telemetry Data Post-Processing System
X.C. Wu, G. Fu and R.L. Li 4165

An Energy-Efficient Three-Dimensional Positioning Technology for Underwater Acoustic Wireless Sensor Network
X.Y. Wei, C. Zhu and S.D. Qiao 4169

Electric Power Communication Network Alarm Data Acquisition System Based on CORBA Northbound Interface
Y.J. He, Y. He, P. Peng and R. Chen 4175

Robustness Analysis of Telecommunications Customer Service System
B. Wu 4179

A Novel Public Key Image Cryptosystem Based on Elliptic Curve and Arnold Cat Map
L.J. Chen and A.D. Shen 4183

Research on Adaptive Face Gender Recognition Based on Compressive Sensing
L. Zhang 4187

The Application of a New Demodulation Technology in the Telemetry System
M. Tao, G. Fu and G.Z. Wu 4191

Digital Signal Processing Approach of Dithered RLG Based on IFIR Digital Filter
K. Zhang, G.L. Yang, W.Z. Zheng and R.D. Ma 4195

A New Framework for Churners' Influence Analysis Using Call Data Records
O.O. Georges, S.Q. Cai and Q. Yuan 4200

A Robust Image Preprocessing Algorithm for Face Recognition
Y. Wang and Z.K. Li 4205

Feature Representation Method Based on Kirsch Masks Filter for Face Recognition
Z.K. Li and Y. Wang 4209

Chapter 8: General Principles of Information Technology, WEB and Networks Engineering, Information Security, E-Engineering, Software Application and Development

Research to Household Sub-Network Development Based on Bluetooth Control Technology
L. Qian 4215

The Archives Management in the Environment of Office Automation
H.Q. Zhou and L. Huang 4219

Analysis of Application of Digital Media Arts
S. Nie and Y. Liu 4223

Discussion on the Digital Cinema Technology and its Development Trends
S. Nie and Y. Liu 4226

Application of Virtual Reality in Forestry
W. Dong and W.J. Gu 4229

Optimized Analysis of Cyber Topology Based on Reliable Restraint
H. Yan 4233

Application of Complex Network Theory in Computer Network Topology Optimization Research
Z.K. Wang 4237

Research on the Model Based on Multiple Websites Browsing Behavior
Z.H. Li and L.C. Zheng 4241

LAN Security Strategy Based on AES
J.W. Chen, C.S. Wu, J.P. Jia and Y.F. Zhang 4245

A Radio Link Logical Relationship between and One Network Apparatus
C.S. Wu 4249

Real-Time Cluster Resources Scheduling Strategy in WIA-PA Networks
Y.P. Sun, M.J. Fang and J.H. Sun 4253

Research on Security Issues of the Internet of Things
X.F. Wang 4261

Research on Network Control Based on QoS of the Network
Y. Zhou 4265

Research on Computer Cluster Load Balancing Mechanism
X.Y. Li and T.T. Jiang 4269

Improvement of Cluster-Head Selection Mechanism Based on LEACH Protocol in Wireless Sensor Networks
S.P. Fan, X.D. Zhang and H.L. Wang 4273

The Development of Interactive Marine Incinerator Operational Training System Based on Web3D
W.L. Yao 4277

A Review of Cluster Based Routing Protocols in Wireless Sensor Networks
J. Wu and G.Z. Hou 4281

Analysis of the Technologies for Host and Port Scanning
N.F. Zhu, Y. Zhou, W. Wang and L. Lou 4286

The Application of Multicarrier Code Division Multiple Access System in the Internet of Things
H.C. Liao 4290

Improved Ant Colony Algorithm and its Application on the Routing Selection of Stable Clusters in Wireless Sensor Networks
H. Yang 4294

Research the Architecture of a New Leisure Agriculture Intelligent System Base on the Internet of Things
Y.G. Lin 4298

Technical Framework and Functional Framework on Sports E-Government Platform
L.X. Wang and L.G. Zhao 4302

Design and Implementation of Portable Software System
X.Y. Chen, H.L. Wan and M.H. Guo 4306

Design and Analysis of a Reliable Group Signature Scheme Based on Discrete Logarithm
H.L. Wan, G.J. Song and Y.H. Chen 4310

The Solution of Safety of Electronic Cash in E-Commerce under Cloud Computing Environment
S.J. Gong and L.P. Zeng 4314

On the China Tourist Hotel E-Business Management
F.L. Liu 4318

Design and Implementation of Web Extraction System of Ceramic Products' Information in the Business Website
M.Q. Zhan and R.H. Lu 4322

An Improvement for Fully Homomorphic Encryption over Integers with Shorter Public Keys
Z.T. Jiang and X.T. Huang 4326

Design and Implement an Application Development Platform Based on Open Source Technology
T.B. Liu 4332

Research on Network Management Network
L.R. Wang, C.S. Wu, S.C. Zhao and F.H. Liu 4338

The Application Research of Lightweight J2EE Security Framework
A.M. Hu 4342

The Solution of P-Teredo Service Traversing Symmetric NAT
F.Y. Xia 4346

Design and Implementation of Dynamic Web Services Publishing Software Based on CXF
C. Shan, L.X. Wu, Y. Yang and J.F. Xue 4350

The Design and Implementation of Micro Player
H.E. Chen 4355

The Application of Digital Information Technology in the Volleyball Game
Z. Bai and Q. Zhang 4358

The Application of Computer Digital Simulation Technology in the Technical Structure Study of the Martial Arts
M.H. Gao 4362

The Application of Computer Numerical Simulation in the Sports Science Study
S.G. Yi Qin 4367

Security Protection Model of QR Code Scanning Software
L. Zhu 4371

Based on SVM Tibetan Web Public Opinion Sentiment Classification
Y.X. Li, Z.J. Zheng and Y.N. E 4375

Web-Based Data Translation for a Resource Management Grid
L. Zhang 4379

Design and Implement of Decision Support System in the Ceramic Information Technology Integration Service Platform
H. Huang, Y.L. Zhang and M. Zhang 4383

Design of Campus E-Commerce Platform Based on MVC Model
S. Zhao, Y.D. Sun and X.K. Shi 4388

The Study on the Improvement of Observer Pattern Based on .net Framework
Z.J. Fan 4392

Design and Implementation of an Intelligent Cross-Platform IaaS
F. Guo, Q. Du and J. Yang 4396

A Network Information Filtering Method Based on Node Energy Transfer
J. Liu 4400

Improved HEED Based Trust Routing Algorithm for WSNs
J.W. Wang and W.Y. Sun 4405

Self-Certified Ring Signcryption Scheme Based on Discrete Logarithm Problem
H.S. Qin, Z.X. Jiang, M.K. Geng, J. Luo and S.L. Zhou 4409

Research on Ontology Based Government Affair Workflow
S.X. Wang and Z.Q. Wang 4413

The Robustness and Mutual Information Entropy of Random Modular Boolean Networks
N. Zhao, B.H. Guo and F.C. Meng 4417

Research and Design of Network Instruction Interaction Mode
C. Liu 4421

Research on TCP Congestion Control Mechanisms
S.G. Zhang, Q.Y. Sun, Q.H. Gao, M. Wang and Y. Zhang 4427

Research on Forensics Method Based on Log on SaaS
G. Zeng 4432

Complexity Analysis of Neural Network Using First Category Orthogonal Weight Functions
D.Y. Zhang and J.H. Zhan 4437

Crowdsourcing Software Development Process Study on Ultra-Large-Scale System
X.L. Xu and Y. Wang 4441

The Implement of a Linux Database Data Processing Mechanism Based on Cache
Y.J. Zhang and C.H. Li 4447

Experimental Data Publishing Based on Browser/Server for Neutral Beam Injection in EAST
R. Zhang, C.D. Hu, P. Sheng, X.D. Zhang, Y.Z. Zhao, D.Y. Wu, Q.L. Cui and Y.L. Lin 4452

Three Networks Convergence Analysis Based on SWOT Theory
R. Zhang and Y. An 4456

The Research of Multi-Network Switching Model for Power Communication Network Based on Analytic Hierarchy Process
G.J. Gong, G.L. Song, D.K. Hao, J.H. Hao and G. Xu 4461

Active Online Thematic Map Cartography Based on Network
D.G. Su, L. Wang, X.M. Cui and D.B. Yuan 4466

Study on One Generating Method of Digital Painting Patterns
W.D. Xu, J.F. Qin, J.S. Zhu and X.L. Lu 4470

A Wavelet Kernel-Based Support Vector Machine for Communication Network Intrusion Detection
Y. Zhan 4474

The Attendance Management System Based on Micro-Cellular and GIS Technology
J.F. Zhu, F. Wang and K. Zhang 4478

A Prevention Scheme for Black Hole Attack Based on NS2
X.J. Meng, D.Y. Lin, D.Q. Lin and R. Hua 4482

Design and Implementation of a Software Automation Development Framework for Management Information System
X. Cheng and X.X. Qiu 4488

Study on the Adaptive Congestion Control Algorithms for Wireless Sensor Networks
Z.J. Zhang and Z.X. Xie 4493

An Approach to Describing Software Logic Model
X.G. An 4497

Software Platform of Home-Based Community Care for the old Based on jQuery Mobile
H.M. Xin, S.W. Li and M.Z. Fu 4501

Design and Implementation of Personalization Recommendation System in Mobile E-Commerce
J.F. Miao 4506

A Novel Feature Selection Method Based on Principal Component Analysis for Network Traffic Classification
H.Z. Wang, J.P. Zhang and Z.Y. Shang 4510

A Security Compliance Based Mobile User Authentication Scheme
Y.F. Yuan, L.Z. Liu and C.Y. Han 4514

An IPv6 Security Multicast System Based on CA Authentication
J.B. Li, X.P. Li, F. Yang and Q.K. Dong 4519

Research on SIQRS Spreading Dynamic Model with Feedback Mechanism on Scale-Free Networks
T. Li, Y.M. Wang and Y.P. Yang 4524

Research on Web Service-Oriented Access Control Model
M. Liu, L.Z. Liu and Y. Zhang 4528

Network Security Technology Research in the Process of Art E-Commerce Transactions
Y.L. Li 4533

The Application Design of Personalized Recommendation System Based on Data Mining to E-Commerce
L. Sun 4538

Research on Combine White-Box Testing and Black-Box Testing of Web Applications Security
J. Fan, P. Gao, C.C. Shi and N.G. Li 4542

Performance Comparison Based-RSSI for Sensor Networks in Different Environments
Y. Feng and B. Yi 4547

Research of Virtual Simulation Scenario Editor for Earthquake Tabletop Exercise
B.J. Zhou, Q.L. Jia and K. Cen 4551

HIPPO: An Adaptive, Scalable, Hierarchical P2PLive Streaming System
K. Lei, L.H. Li, C. Peng and L.Y. Yu 4556

About the Requirement Analysis Changes of ERP Software Project
W.J. Liu, Y.Y. Song, M. Zhao, P. Wang and X. Wang 4562

The Study on Optimization of Energy Consumption for Nodes ZigBee Wireless Sensor Networks Based on Library Information Service
J.S. Zhang, B. Sun and D.M. Liu 4566

On the Model Analysis of Wireless Sensor Networks Based on Library Information Service
D.M. Liu and J.S. Zhang 4570

Comparative Study of Construction and Operation of the Domestic Famous Park Platform
Y. Wu, T. Xu, Y.X. Fang and S.H. Fan 4573

Discussion on the Micro-Blog Information Resources in Disseminating the Local Image
Z.X. Luo and S.Y. Li 4577

Design of Multi-Functional Gateway in Mine Internet of Things
Y.Q. Su, Y. Liang and Z. Xu 4581

The Research and Design Based on IntelliJ IDEA+Oracle Measuring Management System
L. Zhu, L. Bai and R.Y. Zheng 4585

Analysis of Conflict Resolution Model in Campus WLAN Wireless Network
H.J. Zhu and R. Wang 4590

Large-Scale Data Mining and Distributed Processing in Big Data Internet
C.Z. Xing 4594

Design of Smart Household Monitoring Platform Based on Internet of Things
Y. Xu 4598

GNS-Based Simulation and Analysis of OSPFv2 Neighbor Authentication
X.H. Li, R.L. Zhang, Y.J. Wang, L. Yang, J. Nie and Q.Y. Yang 4603

Study on the Design of Mobile Digital Library Based on 3G Mobile Internet Technology
J. Zhao 4608

Research on Key Technology of Web Network Based on Mobile Computing
R. Deng 4612

Jess-Based Argumentative E-Commerce Negotiation System
W. Zhang, Y.N. Zhang, S.S. Guo and X.Z. Ma 4617

The Application Research of Information System in the Information Pipe
Z.J. Huang 4621

Research on the Information Push System Using Case-Based Reasoning
H.L. Shen and L.P. Fu 4625

Analysis of Wireless Mesh Network Routing
X.L. Tan, J. Zhou and W.B. Wang 4629

Research of Ad Hoc Network Routing Based on NS2 by Performance Comparison
X.L. Tan, J. Zhou and W.B. Wang 4633

Research of the Computer-Aided-Translation Software
S. Han and X.D. Zhang 4637

Design and Realization of Alfresco Database of the Micro-Information System
X.Y. Yan, Z.P. Lin, X.M. Zhang and W.C. Yang 4643

An Improved RBAC Model and its Application in Development of Information System
W.L. Song, H.F. Zhang, W.F. Wu and W.J. He 4650

Research on ASP.NET-Based Task Management Platform
F.W. Wang, Z.H. Xing and C. Liu 4654

Research on Application Technology of Body Area Network and the Internet of Things Connection
X.F. Liu and C. Liu 4657

A SVM Reliability Evaluation Framework for the Component-Based Web System
P. Nie 4660

The Design and Realization of Virtual Editing Environment for News Release
C.J. Wang 4665

Reliable Node Based Multipath QoS Routing Protocol on Opportunistic Networks
X.B. Ma, L.T. Wang and Z.C. Ouyang 4669

Privilege Separation in Browser Extensions Based on Web Workers
C.M. Yu, J.H. Sun, H. Chen and X.H. Xu 4675

Bayesian Inference of Information Theoretic Metrics of Anonymity
H.R. Pei, Z.J. Wang and Y. Wang 4680

Software Safety Analysis Based on Multiple State Transition
Y.L. Wang, J.L. Xiao, Y.K. Liu, T.Q. Li and W. Wu 4684

Security Framework Based on SDN
Y. Yu, Y.N. Wang and W. Yang 4690

Research of Application of 3D Pipeline in Mobile E-Commerce
J.Q. Zhang, P. Wu, T. Yu, Q.Q. Cao and F. Xiong 4694

Research on the Structure of Authentication Protocol Analysis Based on MSCs/Promela
C. Zhang and Y. Wang 4698

Hot News Recommendation System across Heterogonous Websites Using Hadoop
S.W. Xu and Z.Y. Xia 4704

On the Process Modeling of Software Crowdsourcing Based on Competitive Relation
X.L. Xu and Y. Wang 4708

On Application of E-Government 2.0 in Basic Public Services
Y.H. Hua, P.F. Li, Z.J. Wang and B.F. Liu 4713

The Big Data how to Influence the Development of E-Government
B. Li, B.F. Liu and N.X. Liu 4717

Design and Implementation of Topology Management Based on EPON Network Management System
Z.G. Yang, D.F. Liu and Y. Gao 4723

The Research and Application Based on Competitive Scheduling Mechanism in Mine Based Wireless Mesh Networks
Q. Shen 4727

Study on the Technologies of Operating System Scanning
N.F. Zhu, Y. Zhou, L. Lou and W. Wang 4733

Design and Implementation of IPv6 Border Router for Wireless Sensor Networks
H. Wang, B.G. Wang, S.Q. Zhao and X.F. Lv 4737

Design and Realization of On-Line Uyghur Handwritten Character Collection System
H. Dilmurat and K. Ubul 4742

Researching of Project Management Information Systems Based on WBS
W.Y. Du 4747

Research of Access Control Models in Personal Networks
Y.L. Zhao and C.F. Jiang 4751

Research of Trust Model for File-Sharing System
C.F. Jiang and W. Xu 4755

Research and Implementation of Image Transmission Key Technological Based on WSN
Z.S. Wang and D.L. Huang 4759

Research on User Behavior Analysis Engine System
S.H. Zhu and P. Tang 4763

Resource Sharing between Social Network and UPnP Network
H.L. Jia, Y. He, C.C. Zhang and L. Chen 4767

Research and Design on P2P Business Process Execution Framework for Workflow Management Systems
T. Wu 4771

Research on a Theatre Recommendation System
Y.L. Li, Y. Li, W. Jiang and Z. Zhou 4775

The Analysis of Constructing Fully Homomorphic Encryption over Integers
L. Jin and X.X. Song 4780

Latent Semantic Index Applied in Question-Answering System about Agriculture Technology
L.Y. Cao, X.X. Zhang, X.H. San and G.F. Chen 4785

Creating a New Combined Influence Measure: An Analysis of the Citation Network
R. Deng 4789

OpenFlow-Based Global Load Balancing in Fat-Tree Networks
Y.W. Wu and W. Zhang 4794

Research on the Cloud Services Plat Form Architecture of Digital Library Based on Cloud Computing Technology
S.H. Zhu and T. Kuang 4799

Data Integration in B2B E-Commerce
Y. Zhang 4802

Election System Based on Prior Knowledge
G.D. Wu and Z.Y. Liu 4806

Audio and Video Media Asset Management System Based on Cloud Storage
C. Li, S.X. Cao and L.J. Yang 4811

Resource Query Mechanism Research of Structured P2P Network Based on Node Interest Community
J.L. Jiao and M.Z. Zhang 4815

Research on Accounting Decision Support System Based on Data Warehouse and Data Mining
Z.W. Li and D. Bai 4819

Design of Mobile Police Store System Based on the Technology of Information Security
X.Y. Zhang, H.Z. Ji and M. Li 4823

A Study on Security Mechanism for Resource Identifiers in Ubiquitous Network
M.L. Jiang, F. Cheng and P. Zhang 4827

Research of Wireless Sensor Network Intrusion Detection Based on Ant-Miner
T. Liu, S.Y. Liu, D. Wei and J. Cui 4832

A Fuzzy Trust Model for Public Key Distribution in Body Area Networks
G.W. Wu, Z.S. Liu and P. Pirozmand 4837

Exploration and Implementation of Electronic Lottery Distribution System Based on Struts Framework
R.J. Zhang and Y. Xiao 4841

Topic-Oriented Information Retrieval
L. Li, W.J. Li and Y.Y. Fan 4845

Representing and Preparing for Resources in EPM's Execution Model
Q. Yu, T. Li, X. Zhang, Y. Lin, Y. Yu and N. Zhao 4851

Application of Gis in Environmental Impact Assessment
D.Q. Chen 4855

Remote Maintenance System Based on Browser\Server and VIRTOOLS
T. Yuan, C.D. Yang and B. Shen 4861

Improved XFBT: A Low-Power Topology of Network-on-Chip
H.B. Chen and C. Li 4865

A Database Grid Service with a Novel Mutation Operator
J. Cao, Y.B. Li and C. Yan 4869

Research on Algorithm to Improve Performance of Wireless-Optical Broadband Access Network
J. Cao, Y.B. Li and C. Yan 4873

Research on Image Vectorization Based on Fuzzy Neural Network and Expert System
S.S. Wan, J. Cao and Q.S. Zhu 4877

Research on Social Engineering in Network Security
G. Chen, J. Yang and J.P. Cai 4881

Network Security Situation Awareness Based on Multi-Source Data Fusion
G. Chen, J.P. Cai and J. Yang 4885

Research on Mobile E-Commerce in 3G Environment
Y. Luo and B. Gui 4889

Research and Analysis Process of Android Communication Platform in AIDL Model
A.M. Hu 4893

Push Technology Based on Analytic Hierarchy Process
Z. Liu, X.C. Xia and Y. Li 4897

Information Management of Digtal Libirary Based on Data Mining
S.Y. Huang 4902

Research on E-Government Model Based on Big Data
Y.Q. Lu 4905

Internet Public Opinion Recognition and Tracking Based on Web Mining
H.L. Shen and F.X. Bao 4909

Data Redundancy Replication Strategy Based on Relevant Failure in Cloud Environment
L. Liu, D. Li, C. Shen and W.B. Zhou 4913

Research and Implementation of Oracle Database Synchronization Timing
J.F. Wang, Z.F. Shi, Z. Qu and S.S. Li 4917

User Behavior Prediction Analysis Based on Time Context
W. Gu and L.J. Chen 4920

Research of the Minimum Vertex-Cover Solutions on the Tree and Lattice Structures
Y.J. Zhang, W. Wei and T. Wang 4926

Research on Multi-Channel Network Information Interactive Technology
X.H. Wang, J.Q. Zhang and C.C. Ou 4930

Collective Communication Optimization for Solving Linear Algebraic Equations
X.G. Ren, W.H. Zhou and J. Chen 4934

Trusted Software Architecture Evolution Based on Graph Transformation Rule
H.W. Jiang and R.L. Wang 4940

The Method Research of Environmental Noise 3D Graphic Expression Based on CityEngine
X.L. Liu, X.Y. Yang and T. Zhu 4945

Study on CDIO Talents Training System Based on the Internet of Things and Cloud Computing in Big Data Era
H. Yan and H.Y. Hu 4949

Research on Setting Strategy of Area Router Based on Scale-Free Internet
J.Q. Song 4953

Information Construction of Chinese Local Government in the Era of Big Bata
Y.H. Hua, Z.J. Wang, M.L. Geng and B.F. Liu 4957

Realization of RIP Module on GPON OLT System
W.H. Kang, X.H. Huang, S.C. Zhang and X.Y. Zhang 4962

The Study of iPark Cloud Platform Construction and Application Modes
T. Xu, Z.G. Zhang, Y. Wu, Q. Pan and S.H. Fan 4966

Research on APT and its Secrutiy Protection
G. Chen, C.L. Yang, J. Yang and J.P. Cai 4970

Data Mining Technology Applied in Network Security
Z.Y. Wang, B.Z. Wang and Y.D. Wang 4974

The Optimized Evaluating Model and Method of Transaction Credit for E-Commerce
X.K. Liang and L.M. Tao 4980

Research and Implement of Micro-Blog Social Network System Based on Users' Association Analysis
H. Chen 4985

Chinese-Uyghur Sentences Alignment Using Multiple Clues
S. Maimaitimin and M. Hou 4990

E-Commerce Personalized Recommendation
Y. Zhang 4996

Research of the Issues Based on Trusted Cloud Security
Y. Huang, X.Q. Ma, Y.Y. Liu and D.N. Li 5000

The Application Based on the Internet of Things and Cloud Computing
Z.N. Liao and Y.R. Hu 5004

Research on the Security of the Digital Learning Resources Library Based on Cloud Storage
H. Cao 5007

Coaches Ranking: A Time-Irrelevant Data Mining Solution with Flexibility and Objectivity
Y.Y. Chen, M.J. Zhang, Z. Shen and J.X. Chen 5010

Ontology of Aircraft Carrier Geographic Information
Z.L. Shi, D.Q. Tang, Z. Tan and G.F. Wang 5014

Chapter 9: Advanced Information and Innovative Technologies for Management, Logistics, Economics, Education, Assessment

Study on Utilizing Foreign Direct Investment in Underdeveloped Areas
J.B. Hu 5023

Analysis of Reliability and Validity in Computer Assisted English Teaching Test
X.W. Zou, X.L. Wang and Y. Wang 5029

Comparative Analysis of the Professional Situations and System of Television Basketball Commentator in China and America
Y.W. Fan and X. Fan 5033

The Impact of RMB Appreciation on the Sporting Goods Industry and Countermeasures
Y.W. Fan and X. Fan 5037

Analysis of Things Technology to Promote the Dynamic Alliance Virtual Performance Evaluation
H.X. Zhang and Q. Zhang 5041

Research on Dynamic Relation Model of LOGINK Service Innovation
T.T. Huang, S.W. Ji and L.S. Wang 5045

The Research on Visual Simulation Technology Applied in College English Teaching
M. Zhao and W. Zhang 5049

The Application of Modern Information Technology in Competitive Sports
B. Xiao 5053

Based on Project-Driven ASP.NET Teaching Research and Exploration
W.D. Zhao and H.Y. Zhou 5057

Application Development of Student Score Analysis System for Secondary School Based on Standard Score
W.D. Zhao and Y.D. Zhang 5062

Research of Current Situation and Risk of Bitcoin
Y.Q. Lu 5066

Risk Analysis of a Large-Scale Construction Project
W.J. Dai 5070

Internet Financial Credit Evaluation for the Small and Medium Enterprises
Y.Q. Lu 5075

College Aerobics Curriculum System Construction in Perspective of Systems Theory
Y. Zhang 5078

Development of Logistics Bases in China - A Case Study of Jiangxi Yinyan Logistics Base
W. Xiong and M. Zhang 5082

Discussion of Chinese Industry Information Service Transformation
S.J. Mao and L.Y. Zhang 5086

Distribution Research of Survival Road for Local Retail Businesses in Relatively Backward Areas - A Case Study on Luoyang Dazhang
W. Xiong and M. Zhang 5090

Statistical Analysis on Primary and Secondary School Digital Disaster Education in China
S.J. Mao 5094

Fashion Design Professional Basis Based on Design Process
T. Guo 5098

Research on Development and Application of Computer Supplementary Software in PE Teaching of Higher Education
Y.H. Qiu, Y.M. Wang and K. Hu 5102

Constructing Micro-Teaching Experimental Environment with Information Technology
J.X. Wang and S.Q. Ma 5106

The Study of Risk Management of Government IT Service Outsourcing
B. Liang, H.F. Liu, G.N. Geng and G. Yang 5112

A Spectrum of Findings: Mechanisms for Third-Party Evaluation of the Quality on the Application-Oriented Undergraduate Teaching
L. Lei and J. Peng 5116

Research on Design & Application of Multimedia CAI Courseware for Technique Teaching in Physical Education Courses
Y.H. Qiu, G.Z. Ou and J. Huang 5120

Economic Analysis and Governance Countermeasure of Overload and Out-of-Gauge on the Highway
L.J. Zhou 5124

Governance Mechanism of Rural Population Hollowing under the Background of Balancing Urban and Rural Development
F.J. Song, D.Q. Wang and S.Q. Tian 5128

The Application of Factor Analysis in the Study on Cultural Industry Competitiveness Evaluation Index System
P. Sun 5132

Research on Rapid Bidding of Forgings
F. Gu 5136

Study on Evaluation Index System and Methods of Vendor Selection
C.J. Rao and J.H. Dong 5140

Analyze the Combination of National Symbols and Design Aesthetics
Y.Y. Chen 5144

Application of Game Theory in Mode Selection of Combined Training of the Postgraduate
T.Y. Guo, J.J. Li, B. Ma, J.X. Pian, H.C. Wang and F.Y. Han 5148

The Revelation from MOOCs on our Country's Remote Education
J.F. Wang 5152

The Coupling Relationship between Information Technology Level and Public Transportation: A Case Study of Cities in Guangdong
M.X. Zhao, Q. Gu, Y. Duan and J.Y. Liang 5157

The Research of Building CAI Table Tennis Teaching System
B.W. Zhang 5165

Construction the Bottleneck and Countermeasures of BIM High-End Talent Cultivation in Colleges and Universities
B.K. Qi and H. Xue 5169

Purchase Cost Control in Electronics Manufacturing Service (EMS) Corporations
D.X. Lin, Z.Y. Lu and L. Ma 5173

The Application of the Multimedia Technology in College Physical Teaching Reform
J.H. Shi 5178

Prediction of Cigarette Sales Amount and Average Price Based on Lunar Calendar
X. Yang 5182

The Study of SWOT Analysis and Countermeasures on Developing Tourism Resources in Xinxiang City
X.X. Li 5186

Marxist Philosophy in Object-Oriented Practical Education
M. Zhang 5189

The Application of Basketball Zone Defense Tactics
B. Gao, Z.L. Zhao and M.M. Zhang 5193

The Study of Interactive Relationship between Urban Construction Area and Road Area
S.S. Zhang and Z.Z. Yuan 5197

Rethinking on Social Responsibility Accounting Information Disclosure of Public Hospitals in China
W. Tan and Q.L. Yang 5201

Research on Corporate Social Responsibility to Employees Voluntarily Assume
Y.H. Li and Y. Wang 5205

The Research of the Second Class Credit in the Credit System
S.L. Yao and S.T. Wang 5209

Research on the Multidimensional Teaching Goal Setting and Implementation of Exhibition Lighting and Illumination Design
Q. Gong 5213

A Discussion about Economic Theory Used in Safety Investment of Petrochemical Enterprises
X. Dong and S. Hu 5217

Analysis of Digital Electronic Teaching in Higher Vocational Colleges - Cultivating and Stimulating Learning Motivation
Y.H. Li 5221

The Application of Project Driven Teaching Method in Win Server 2008
C.B. Yin, D.L. Lin and P. Ren 5224

Application of the Multi-Level Fuzzy Comprehensive Evaluation Method to Software Companies' Choice of Competitive Strategies
W.D. Zhang, Z.X. Jiang, Y.Z. Li and S. Zhang 5228

Analysis of Low Carbon Development Path for Coal Industry of Multiagent Network Structure under Carbon Tax Background
L.H. Wang, X. Li, Y.J. Yuan and Q.X. Cai 5232

The Enterprise Oriented Computer Graphic Design Courses Construction of Practice Teaching System
E.J. Bai and D.L. Lin 5237

Quasiconvex Cash Subadditivity Risk Measure for Portfolios
H.W. Liu and C.B. Xiao 5241

An Analysis of Characteristics and Purchase Predisposition of Consumer of Urban Community Commercial Service
Q.F. Geng 5245

An Evaluation Index System of Physical Education Quality Based on Analytic Hierarchy Process Model (AHP)
W.Y. Chen and J.B. Hu 5250

Experience and Enlightenment of American Internet Finance Supervision
J.B. Hu 5254

Influential Factors of College Students' Mobile Phone Recycling Behaviors
Y.Y. Wang and B.Q. Ma 5258

Application of Cooperative Project Teaching Method in the Program Design Teaching
S.Q. Sun, C.B. Yin and Y.M. Su 5263

A Discussion on the Construction of Information Integration Based on the Integrated Development and Management of International River
S.Z. Guo, Q.P. Wang and M.M. Hou 5267

The Research on Site Selection of Urban Infrastructure towards the Major Function Zoning
S.P. Zhang and H.R. Li 5273

Comparative Study of R&D Spillover Effect for High Technology Industry and Traditional Industry
F.J. Meng 5278

A Study on Web-Based EVP Teaching Platform
W.J. Zhang 5282

Research on Evaluation Index System of Risk Management Capacities of Private Banks in China
L. Yang and F.P. Wu 5286

The Research and Practice of Network Teaching Pattern
L.L. Zhao, Q.Y. Sun, X.X. Liu and Q.H. Gao 5290

Technical Risk Assessment of Large-Scale Construction Project Based on Triangle Whitening Weight Function
W. Ma 5294

Design of Expressway Construction Safety Evaluation System Based on AHP
H.L. Guo, Z.N. Wang, L.X. Zhang and L. Xiao 5300

Design and Implementation of Teacher-Student Interactive Platforms in the Campus Network Based on UML
Y.L. Cheng and Y.H. Zhang 5304

Research on Distribution Issues of Book Chain Taking Xinhua Bookstore as an Example
W. Xiong and M. Zhang 5311

Research on Methods of Distribution Center Facility Siting
W. Xiong and L.Y. Zhang 5315

Study on Classification of Body Shape and Size Grading on Young Women of Quanzhou District
C.Y. Huang 5319

City Waterfront Landscape Post Assessment Based on System Dynamics
L. Zhao and C. Gui 5323

The Modeling of Buildings Cost Assessment Expert System with Differences
H.W. Yin 5327

Research on the Organization Operation Mode of the Hong Kong-Zhuhai-Macao Bridge Based on VSM
G. Sheng and J.Q. Yu 5331

Physiological Mandarin Speech Corpus for the International Preparatory Students in China: Design and Initial Application
X.P. Du, W.P. Zhang, Y.F. Hou and J.G. Wei 5336

Construction and Implementation of the Network Teaching System of Mechanical Design Basic Course Based on Web
M.C. Ran and M. Xia 5341

The Application of Multimedia Technology in Medical Information Management
J. Niu and Q. Guo 5345

Cultivating College Students' Information Literacy under Network Environment
A. Wang and X.Q. Zhang 5349

Application of Virtual Technology in Medical College
L.R. Shen 5353

Research on Cloud Computing-Based Virtual Logistics Enterprise Performance Management
H.X. Zhang and X.D. Zhang 5357

Design and Implementation of Real Estate Sales System Based on B/S
X.Y. Zhu 5361

The Design of Finance Assistant Management System for the Modern Enterprise Management by Using Computer
G. Liu and H.B. Zhang 5364

Design and Realization of Computer Teaching Room Based on VMware Visualization Technology
H.C. Shao 5369

Construction of Evaluation Index System for Finnish Design Policy
C.J. Chen, F. Hai and D.J. Yu 5373

Process and Technology Research on Information Management of Agricultural Disaster Prevention and Reduction
Y.H. Wu and W.L. Liu 5378

Research on Information Management Frameworks of Agricultural Disaster Prevention and Reduction
R.R. Deng and Y.H. Wu 5382

Internet Financial Innovation Based on Enterprise Growth Cycle for the Small and Medium Enterprises
Y.Q. Lu 5386

Impact of Digital Technology on Architectural Design Teaching
F.D. Yu 5390

Study on the Landscape Pattern Change of Haikou City Based on GIS
F.X. Wang and W.H. Liu 5394

Design of Information Disclosure Platform in Engineering Based on Reliability Model
Q.F. Meng, Z.Q. Feng, Z. Li and S.G. Hao 5398

The Research on Statistical Characteristics of China Civil Aviation Network
H.G. Yao 5403

Application of Digital Media Technology in Exhibition Design for the Geological Museum
K.F. Zhou and J.S. Wang 5407

Application of Information Visualization in Museums' Display and Design
J.M. Hu 5411

Based on Computer Network Security in Financial Informationization Construction of Colleges and Universities
S.Z. Wu 5415

Study on Application of Database Synchronization Technology in the CDIO Teaching System Based on Android
H.Y. Hu and H. Yan 5419

A Comprehensive Experimental Practice for Ship Bridge Resource Management Training Based on Ship Handling Simulator
Y.F. YANG and M.K. Feng 5423

Research on the Platform of 3D Information Management for the Ordnance Maintenance Equipment
Z.Y. Cheng, R.Y. Xie, L. Qiu, X. Zhou and C.F. Yu 5427

Study on Fire Safety of Building External Thermal Insulation Materials
L. Yang 5431

Analysis and Control of the Pollution Problem in the Process of Wheat Anther Culture
X. Yang, D. Wang, L.Q. Zhang, H.P. Chang, C.L. Liu, H.P. Han, W.H. Xing and S.J. Wang 5435

The Research of Wisdom Campus Construction and Development Based on Internet of Things
Y.P. Wang 5439

Review of the Integrated Researches on Internet of Things and GIS in Fire Emergency Plan
L.J. Yu, H. Wei, Z.Z. Zheng, Y.L. Liu, T.H. Chi and L. Peng 5444

Analyses of the Model Design of Urban Emergency Management System
X.M. Wang and Y. Lv 5448

Inventory Information Management of Logistics Supply Chain
Z.J. Zhuang 5453

The Design of Transaction Condition Expert Evaluation System for the Logistics Online Retailers
J.H. Geng 5457

Application of Visual Correction on Physical Training
Q. Zhai 5461

Monitoring System of High-Power Project Control Network Data Storm under Non-Uniform Format
J. Liu, Y. Dai and J.J. Chen 5464

The Research on the Six Sigma Management Integrated System Design Based on Minitab/DDE
T.H. Huang, S.H. Fan and L.J. Dong 5468

Research on the Specialization and Theory of Building Engineering
Z.J. Zhang 5472

The Construction of the Agricultural Products Traceablity Code System Based on a Type of Barcode Technology
Y. Zhao and G. Zheng 5476

Research on Designing the Information Management Platform of Physical Education Based on B/S Model
G.Y. Wang 5481

Study on the Construction of Linguistics Examination Database Based on Computer Network Technology
Y. Zhang 5486

Research and Implementation of Groundwater Management Information System Based on J2EE
D.M. Ma, H.P. Zhang, H.D. Xue and T. Zhang 5491

Research of the Multimodal English Teaching in the Cloud Computing Environment
S. Han and X.D. Zhang 5495

Research of Public Service Platform Based on Cloud Computing for Middle Size Enterprises
C.X. Wang, Y. Guo and X.G. Guo 5498

Design and Implementation of Agricultural Logistics Distribution Vehicle Scheduling System Based on LBS
R. Ma, G.Z. Xie and C. Zhang 5504

Spatial Characteristic Indicator of Pedestrian Facilities for Evacuation
M. Li, H. Yue, B.Y. Zhang and X.Y. Mi 5508

Frame Research of the Building Information Model in Project Management Information System
X.S. He, X.N. Yu and X.Z. Ma 5512

Study on Architecture of Power Marketing Management Information System Based on Web Service
Q. Zhang 5516

Analysis and Design of Supply Chain Inventory Management System under Internet of Things Environment
Z.P. Peng 5520

A Study on the Data Design of Residents Electronic Health Records System
N. Liu 5524

Research on Emotional Interaction Design of Mobile Terminal Application
X.M. Mao 5528

Intelligent Classroom Attendance Checking System Based on RFID and GSM
H. Chen 5532

Inflation Forecast Based on BP Neural Network Model
Y.C. Wen, L.N. Tan and H.L. Wu 5536

Research on Related Model for Urban Public Crisis Handle Mechanism
Y.C. Ren 5540

Study on the Effectiveness Evaluation of Missile and Artillery Air Defense Group
P.C. Zhang, Y.Z. Cheng, W. Mei and B.Q. Cao 5544

Optimal Design for the Manufacturing/Remanufacturing Integrated Logistics Network under Fuzzy Environment
L.G. Sun and Z. Zhang 5547

Application Research of Growth Management Model of Crop
J.F. Liang, Y.Q. Wang, L.L. An and X.N. Liu 5551

Fuzzy Mathematics Theory in Logistics Center Address Selection of Application
H. Yu and K. Zhang 5555

Merging Unit Performance Evaluation of Intelligent Substation Based on the Triangular Fuzzy Number
H.T. Liu, M.Y. Huang and Y.H. Zhang 5559

Research on Travel Time Prediction under the Condition of Urban Rainstorm in Overpass Area
S. Bi, Z.C. Zhao, G. Wang, L. Kong, Q. Diao, C.W. Han and D.H. Sun 5565

Application of Information Technology in Engineering Thermodynamics
J. Li and J. Wei 5571

Wastewater Management in Shanghai
J.C. Kang, H. Lin, J. Zhu and G.D. Yan 5575

The Implementation of Network Teaching Resources Sharing Center Based on Google Cloud
H.E. Chen 5580

Study on the Environment Tax Realize Ecological Compensation in China
L.Y. Xu 5584

Analysis and Design on Sports Meeting Information System
L.H. Chen and T.Z. Niu 5588

Green Management of Tourist Attractions Region under the Background of Circular Economy
F.L. Liu 5592

Research on Health Risk Assessment Methodologies of Municipal Solid Waste Landfill
H.J. Zhang, X.H. Liu, S.J. Wang, L. Fang and L.H. Zhang 5596

Effect of Hg in Jiaozhou Bay Waters - The Vertical Variation of the Hg Content
D.F. Yang, S.X. Zhu, F.Y. Wang, X.Q. Yang and Y.J. Wu 5601

Design and Implementation Based on Java EE Student Attendance System
Z.H. Zhao and Y.B. Chen 5605

Research on Design of Modern Warship Networked Fighting Simulation System
Y.H. Wang, J.Z. Mao and Z.H. Xiu 5609

Application of Reusable Framework Technology on the Workflow System
C.Y. Xue 5614

Research on the SWIM System and its Development
X.H. Zhang, J. Huang and J. Xu 5619

The Study of Bus Transit Network Design Methods for Different Sized Cities
W.Y. Tu, J.H. Ma, W. Guan and X.J. Chen 5624

Research of Agricultural Information Management and Retrieval
J.F. Liang, C. Jin, L. Zhang and X.N. Liu 5630

Term Structure of Interest Rates with B-Spline Model during the Money-Shortage-Event in China
P. Zheng, L.Q. Yang and Z.N. Dai 5634

CHAPTER 1:

Advanced Materials Science, Chemical Engineering and Processing Technologies

Advanced Materials Research Vols. 989-994 (2014) pp 3-6
© (2014) Trans Tech Publications, Switzerland
doi:10.4028/www.scientific.net/AMR.989-994.3

High Value Added Utilization of Vanadium Slag

DU TAO[1, a], FANG XIN[2, b], ZHANG XINPU[3, c]

[1]State Environmental Protection Key Laboratory of Eco-Industry, Northeastern University, Shenyang, 110819, China

[2]State Environmental Protection Key Laboratory of Eco-Industry, Northeastern University, Shenyang, 110819, China

[3]State Environmental Protection Key Laboratory of Eco-Industry, Northeastern University, Shenyang, 110819, China

[a]email: dut@smm.neu.edu.cn, [b]email: fang_xin1990@163.com, [c]email: 825264510@qq.com

Keywords: Vanadium Slag; Vanadium Titanium Catalyst; Zeolite 4A; Adsorption

Abstract. Vanadium slag is a kind of common furnace slags in the metallurgical field that contains rich vanadium oxides and iron oxides. The high value added utilization of vanadium slag was exploratory studied in this paper. Under the existing experimental conditions, chemical reactions conducted between vanadium slag and concentrated sulfuric acid. Vanadium titanium catalyst was prepared with the lixivium(whose main ingredients were 44.42% of V_2O_5 and 29.36% of TiO_2), which could meet the demand of industrial production; zeolite 4A was prepared creatively with leach residue of vanadium slag for the first time and its feasibility in CO_2 capture was verified via detecting the CO_2/N_2 adsorption capacity. It is feasible to recycle solid wastes efficiently, reduce the environmental pollution and promote the development of CO_2 reduction technology by this means.

Introduction

Vanadium slag is a kind of furnace slags that contains rich vanadium oxides and iron oxides, whose vanadium content largely depends on the contents of vanadium and impurity elements(Si, Mn, Ti, Cr, etc.) in the molten iron[1]. Currently, its main application lies in extracting the vanadium in it, but problems such as after baking, high energy consumption and environmental pollution still exist.

In terms of vanadium extraction. Peng Yi, Zhu Shengyou et al.[2] proposed a method via calcium roasting, which avoided the environmental pollution during the decomposition of sodium salt. LU Zhao-ling[3] reported a process of direct acid leaching of vanadium, whose leaching rate of vanadium reached 80%. FENG Qi-ming[4] researched the influence factors in high pressure acid leaching of vanadium and found that oxidizing agent would play a promoting role in the process.

In recent years, extensive research has been devoted recently to CO_2-capture techniques because of growing concerns with respect to greenhouse gas emissions[5][6]. Zeolite molecular sieves are those natural and synthetic crystalline aluminosilicates with molecular sieving effect[7]. Various cheap raw materials were used in preparation of zeolite. Xu Guoxiang et al.[8] provided the methods to prepare zeolite by alkali fusion, Wu Qisheng et al.[9] took coal series kaolinite as the principal raw material. Moreover, raw materials in relevant studies involved coal gangue, oil shale, etc.

Although there have been some new processes related to acid leaching of vanadium, no similar report exists in direct acid leaching for vanadium slag as well as in synthesizing zeolite with vanadium slag. In this study, vanadium slag of BOF(Basic Oxygen Furnace) from Panzhihua was taken as the raw material and leached directly via acid leaching. Then, vanadium titanium catalyst would be prepared with the lixivium and zeolite 4A would be prepared with the SiO_2-rich leach residue via alkali fusion-hydrothermal method as well. In summary, vanadium slag could be utilized efficiently and profitably with this approach.

Experiments

In acid leaching of vanadium slag, vanadium slag of BOF from Panzhihua was taken as the raw material and the other chemicals used were analytically pure. To begin with, the vanadium slag was levigated and placed in a customized round-bottomed flask. A certain amount of sulfuric acid, whose concentration is 50%, was injected in the flask until the liquid-solid ratio reached 3:1. Then, the mixed solution was heated and stirred under 140℃ for 3.5h. The above reactant, after the reaction, was filtered for two times and residue get in filtration was put into the drying oven and weighed.

In preparation of vanadium titanium catalyst, hydrogen peroxide was gradually added in 50mL prepared solution(concentration of vanadium ion was 0.260mol/L) until the lixivium was near colorless. Then, aqueous ammonia was added dropwise after 10 minutes' standing each time so that the reactions could proceed adequately. The pH was adjusted and the first precipitates were filtered, dried and calcined after 1h of stewing. At the same time, aqueous ammonia was continuously added into the filtrate until the pH reached 8. Finally, the filtrate was filtered and dried under 100℃ for 3h and the second precipitates was put in high-temperature furnace to roast under 600℃ for 1h.

In the preparation of zeolite 4a with leach residue, residue from acid leaching of vanadium slag was used in preparing zeolite 4A. $NaAlO_2$ was taken as aluminum source and NaOH was added according to the alumina ratio of 2, NaO_2/SiO_2 ratio of 3.5. Next, the liquor was stirred evenly in porcelain boat and put in high-temperature furnace to roast under 600℃. Water and certain quantity of $sNa_2Al_2O_4$ were then added. The mixture was stirred, moved into stainless steel reactor and sealed. In drying oven, precipitation crystallization proceed at 95℃ for 12h. Finally, the mixture was filtered and washed until neutral. Since then, zeolite product was obtained after dried at 100℃.

Results and Analysis

According to X-ray fluorescence spectroscopies of the first precipitate and the second precipitate(Table1), there are greater contents of vanadium and titanium while no much iron in the first precipitates under stronger acidity. By contrast, there are greater contents of iron oxide and manganese oxide while no much oxide of vanadium and titanium in the second precipitates.

Table1 Chemical Compositions of Precipitated Materials（mass, %）

Chemical Composition	V_2O_5	TiO_2	Fe_2O_3	Cr_2O_3	Al_2O_3	MnO	Others
Content(The first precipitates）	44.42	29.36	12.47	6.43	3.34	2.73	1.25
Content(The second precipitates）	14.24	12.47	39.46	1.46	2.37	28.77	1.23

Fig.1 is the XRD patterns of precipitates. There are apparent characteristic peak of rutile TiO_2 and tiny diffraction peak of V_2O_5 in both patterns, which indicates vanadium, at the moment, might exist in the forms of polymer, monomer or amorphous state. It might also be that polymer of the V_2O_5 crystal here is tiny in size and small in quantity so the diffraction peak detected by XRD appears pretty weakly[10]. No obvious diffraction peak of iron oxide or manganese oxide could be found in each pattern, which indicates there are less impurity contents in products.

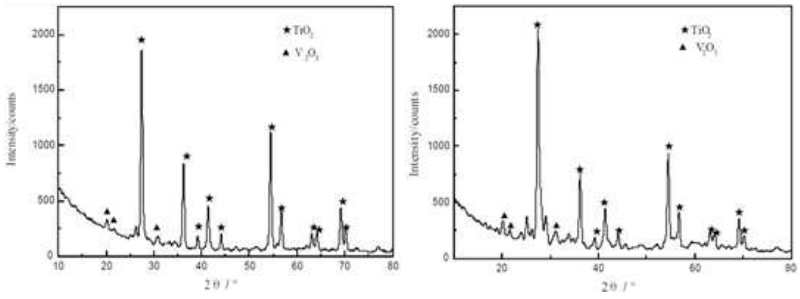

the first precipitates　　the second precipitates

Fig.1 XRD Patterns of Precipitates

The prepared zeolite 4A was analyzed via X-ray fluorescence spectroscopy(as shown in Table2). On the basis of contents of SiO_2, Al_2O_3 and Na_2O in Table2, the ratio of these three parameters is

close to 1:1:1, which is extremely analogous with the chemical formula of zeolite 4A. It can be seen that we have successfully prepared zeolite 4A via the means offered in this paper.

Table2 Chemical Compositions of Zeolite 4A (mass，%)

Chemical Composition	SiO_2	Al_2O_3	Na_2O	Fe_2O_3	CaO	TiO_2	MnO	Others
Content	32.8	28.7	17.8	9.8	3.8	3.1	2.5	1.5

Furthermore, we detected the obtained zeolite 4A via SEM(as shown in Fig.2). The SEM images demonstrate the synthetic zeolite 4A has formed intact cubic crystal and the particle size of samples is 5μm or less. The finished zeolite 4A exhibits uniform particle size and intact crystal of regular hexahedron structure, which is consistent with literature reports. Moreover, the SEM images intuitively reflect the crystallinity of products and indicate the obtained zeolite 4A enjoys high purity and uniform particle size.

In order to analyze the CO_2/N_2 separating property, we utilized Agilent 409 PC thermogravimetric analyzer to measure its adsorption curves under the temperature of 60℃ and 30℃(as shown in Fig.3). Fig.3(A) shows the CO_2/N_2 adsorbing capacity of obtained zeolite 4A at 60℃ under normal pressure, which is respectively 2.402mmol/g and 0.446mmol/g. Fig.3(B) exhibits that, at 30℃ under normal pressure, its CO_2 adsorbing capacity is 3.772mmol/g and N_2 adsorbing capacity is 0.568mmol/g. It can be seen from Fig.3 that huge gap exists between its adsorbing capacities of the two kinds of gasses. We could also figure out by comparing the two figures that the falling range of CO_2 adsorbing capacity is much larger than the other one when the temperature rises from 30℃ to 60℃. In other words, impact effects of temperature are different to adsorbing capacities of CO_2/N_2: the obtained zeolite 4A shows better CO_2/N_2 adsorbing capacity at 30℃ compared to that at 60℃.

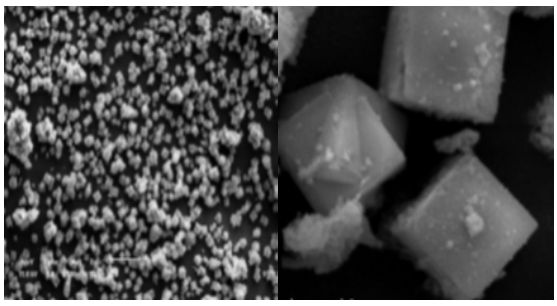

Fig.2 SEM Images of Zeolite 4A

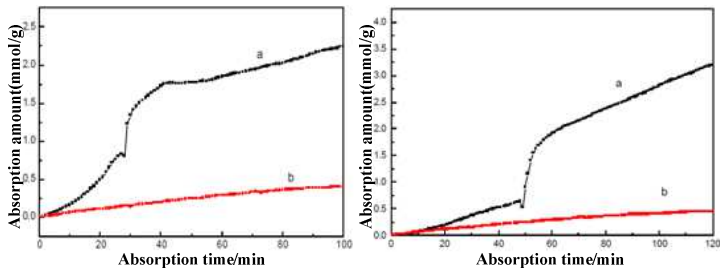

Fig.3 CO_2(a) and N_2(b) Adsorption Isotherms on Zeolite 4A at 60℃(A) and 30℃(B)

Conclusions

In this paper, we exploratory studied on the high value added utilization of vanadium slag.

1) Chemical reactions conducted between vanadium slag and concentrated sulfuric acid. According to XRD analysis, main ingredients in the first precipitates are 44.42% of V_2O_5 and 29.36% of TiO_2 and there are less impurity contents in products.

2) Zeolite 4A is prepared with the leach residue of vanadium slag, which has opened a totally new channel in zeolite preparation. By means of analyzing the adsorption curve of zeolite 4A, it could be found that the CO_2/N_2 adsorbing capacity of it, at 30℃ under normal pressure, is respectively 3.772mmol/g and 0.568mmol/g and thus its feasibility in CO_2 capture has been verified.

3) The utilization of vanadium slag offered in this paper could well solved the problems such as after baking, high energy consumption, environmental pollution, etc. It is achievable to recycle solid wastes efficiently, reduce the environmental pollution and promote the development of CO_2 reduction technology.

Acknowledgement

In this paper, the research was sponsored by the Natural Science Foundation of Liaoning Province (Project No. 201102069).

References

[1] HUANG Dao-xin, CHEN Hou-sheng. Vanadium extracting and steelmaking [M]. Beijing: Metallurgical Industry Press, 2000.(in Chinese)

[2] R R Moskalyk, A M Alfantatazi. Processing of vanadium: a review[J]. Minerals Engineering, 2003, 16(9): 793-805.

[3] LU Zhao-ling. Investigation and industrial practice on extraction of V_2O_5 from stone coal containing vanadium by acid process[J]. Hydrometallurgy of China, 2002, 21(4): 175-183. (in Chinese)

[4] FENG Qi-ming, HE Dong-sheng, ZHANG Guo-fan, OU Le-ming, LU Yi-ping. Effect of vanadium oxidation and conversion on vanadium leaching in extraction process of vanadium from stone coal[J]. The Chinese Journal of Nonferrous Metals, 2007, 17(8): 1348-1352. (in Chinese)

[5] WANG Hong, XU Hui-bi, ZHENG Chu-guang, QIU Jian-rong. Temperature dependence on reaction of $CaCO_3$ and SO_2 in O_2/CO_2 coal combustion[J]. Journal of Central South University: Science and Technology, 2009, 05:845-890.

[6] Rajender Gupta, Rachid B Slimane, Alan E Bland, Ian Wright. Progress in carbon dioxide separation and capture: A review[J]. Journal of Environmental Sciences, 2008, 01:14-27.

[7] WANG Zun-ming, YANG Zan-zhong. Review on synthesis methods of zeolites from coal fly ash[J]. Bulletin of the Chinese Ceramic Society, 2008, 27(3): 552-555. (in Chinese)

[8] XU Guo-xiang, FAN Li-hua, LI Xue-yu, ET al. Synthesis of zeolite with fly ash and its application[J]. Industrial Minerals & Processing, 2006, 35(9): 32-34. (in Chinese)

[9] WU Qi-sheng, LI Shui-ping, SU Shasha. Preparation of 4A zeolite molecular sieve from Xuzhou coal-measure kaojin[J]. Chemical Industry and Engineering Progress, 2009, 28(1): 130-134. (in Chinese)

[10] Delaigle R, Eloy P, Gaigneaux E M. Necessary conditions for asynergy between Ag and V_2O_5 in the total oxidation of chlorobenzene[J]. Catal. Today, 2011, 175(1):177-182.

Advanced Materials Research Vols. 989-994 (2014) pp 7-10
© (2014) Trans Tech Publications, Switzerland
doi:10.4028/www.scientific.net/AMR.989-994.7

Preparation of Zeolite 4A using Laterite Nickel Slag and the Characteristic Study of CO_2/N_2 Separation

Tao DU [1, a], Shenglu LI [2, b], Fan YANG[3, c]

[1]State Environmental Protection Laboratory of Eco-Industry, Shen Yang 110819

[2]School of Material and Metallurgy, Northeastern University, Shen Yang 110819

[3]School of Material and Metallurgy, Northeastern University, Shen Yang 110819

[a]email: dut@smm.neu.edu.cn, [b]email: 511920551@qq.com, [c]email: 895142996@qq.com

Keywords: Laterite nickel slag; Zeolite 4A; Crystallinity; separation of CO_2/N_2

Abstract. Laterite nickel ore is a kind of abundant and low-cost ore. In order to obtain the cheap and high-performance adsorption material, this paper addresses that Zeolite 4A was synthesized by laterite nickel slag, based on two-step hydrothermal synthesis procedure and alkali-melting process. The crystallization degrees of different kinds of Zeolite 4A were explored under different ratios of the reactants. Optimal condition was found out for synthesis of Zeolite 4A, including the ratios of the reactants. Finally, Zeolite 4A obtained under the optimal condition was tested by XRF, NOVA 1200e physical adsorption analyzer, and SEW separately, which confirmed its high purity and complete crystals. Finally, separation of CO_2/N_2 by Zeolite 4A using STA409PC Physical adsorption instrument was studied, revealing good adsorption selectivity which became lower with rising temperature.

Introduction

With the increasing consumption of fossil fuels, CO_2 emission is rising rapidly, resulting in serious global warming. Therefore, Carbon capture and storage plays an important role in the protection of environment. Meanwhile, it is also vital for humans to study and exploit adsorption material which is high-performance, cheap, and green. Zeolite 4A consisting of polyhedron is a kind of adsorption materials which are synthesized by cheap and industrial waste materials[1]. As crystal of Zeolite A contains huge coulomb field and polarity effect, Zeolite 4A has strong adsorption capacity which can absorb a great number of molecules and ions of small diameter less than 0.4nm[2]. Now, there are no reports Zeolite synthesized by laterite nickel slag. In the case of adding $NaAlO_2$ as aluminum source, this paper developed a new process to synthesize Zeolite using laterite nickel slag as silicon source, combined with two-step hydrothermal synthesis procedure[3] and alkali-melting process[4]. That process not only made full use of silicon in laterite nickel slag, but also got high purity Zeolite 4A.

Preparation of Zeolite 4A

After magnetic separation, laterite nickel slags mainly include SiO_2 with a few impurities. The main ingredients were presented in Table 1.

Table 1 Chemical composition of laterite nickel slag

Ingredients	SiO_2	Fe_2O_3	MgO	Al_2O_3	K_2O	Others
Percentage(%)	83.84	4.59	2.79	2.25	1.30	5.23

When materials were acquired, the preparation steps for Zeolite were as following:

(1)Make the laterite nickel slags after magnetic separation pass through 200 mesh sieve, the finer slag, the higher hydrothermal degree;

(2)Regarding sodium hydroxide as activator, the raw materials are calcined at 500 °C where crystallinity reaches the maximum for 2h[5];

(3)Add a certain proportion of deionized water and stir, then filter;

(4)Mix a specific ratio of $NaAlO_2$ to the extracted liquid slags to adjust Si/Al molar ratio;

(5)Add distilled water, and stir it 3h to be uniform with magnetic stirrer for further refined of materials and uniform distribution of water, and then plasticity index of mixture increase obviously, good for nucleation of Zeolite[6];

(6)Crystallize at constant temperature for 8h in 100°C dry box;

(7)Wash the crystalline product thoroughly until the filtrate pH reaches 9-10[7], and then dry it at temperature of 80°C in oven and ground it to pieces, namely Zeolite 4A.

Results and discussions

The concentration of NaOH, has immense impact on the crystalline product during the process of crystallization. NaOH not only is used in forming alkaline condition which compensates for excessive negative charge in Zeolite, but also take part in the synthesis of the Zeolite 4A directly in the hydrothermal system involving laterite nickel slag, $NaAlO_2$, sodium hydroxide and water[8].

In order to analyze the impact of H_2O/Na_2O on crystallization of Zeolite 4A, various kinds of Zeolite 4A, in the phase region generated Zeolite 4A, were integrated in different H_2O/Na_2O ratio, under the conditions: $n(SiO_2/Al_2O_3)$=2.4, $n(Na_2O/SiO_2)$=1.4. The ratios of H_2O/Na_2O were 45, 60, 75, 85, 110, 155, 200. Samples were named Al, A2, A3, A4, A5, A6, A7, and the corresponding crystallinity degrees were 92.7, 84.1, 89.7, 88.8, 93.9, 40.7, 22.3(%).

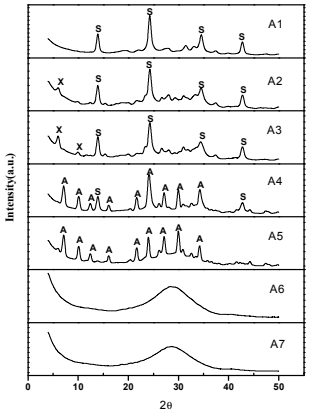

Fig.1 XRD patterns of 4A zeolites synthesized with different H_2O/Na_2O

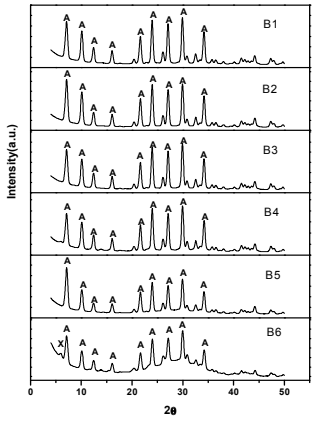

Fig.2 XRD patterns of 4A zeolites synthesized with different SiO_2/Al_2O_3

XRD patterns of 4A zeolites synthesized with different H_2O/Na_2O are shown in Fig. 1. Comparing these seven XRD patterns, it was showed that the higher alkalinity is, the more stable Sodalite is; Zeolite A is stable in a certain low alkalinity; when alkalinity is too low, it is not enough to synthesize Zeolite, but SiO_2. Hence, the optimum H_2O/Na_2O ratio of reaction is 110, with the highest crystallization accounting for 93.9%.

In general, under the other constant conditions, the higher silica-alumina ratio, the slower the crystallization does, and vice versa[9].

To study the effect of SiO_2/Al_2O_3 on crystallization of Zeolite 4A, the other reaction parameters were set as follows: $n(Na_2O/SiO_2)$=1.4, $n(H_2O/Na_2O)$=110. With the conditions, the $n(SiO_2/Al_2O_3)$ was set as follows: 1.5, 2, 2.5, 3, 3.5, 3.8, samples were B1, B2, B3, B4, B5, B6 respectively, and the corresponding crystallinity degrees were 96.1, 97.7, 96.0, 96.2, 96.9, 93.9(%).

Varying the quantity of $NaAlO_2$ to change SiO_2/Al_2O_3 relatively, XRD patterns of the productions were shown in Fig. 2. As seen in the picture, the characteristic peaks of Zeolite was the strongest and the most complete among all the characteristic peaks and the diffraction peak was clear and regular when $n(SiO_2/Al_2O_3)$ =2.0, which confirmed that the crystallization Zeolite 4A was the best at this time, corresponding with the result of experiment. Thus, the best SiO_2/Al_2O_3 ratio was 2.0.

In the process of crystallizing molecular sieve, Alkali participates in the system of aluminate and silicate ions in polycondensation reaction and improves the efficiency of crystalline reaction and

saves synthetic time [10]. The increasing sodium hydroxide can improve the dissolving capacity of water, which can increases the dissolution rate and concentration of silicate and aluminate ions in the reaction system and be good for zeolite's growth. So it is supposed to add sodium hydroxide in the preparation of molecular sieve.

For the purpose of researching the effect of Na_2O/Al_2O_3 on crystallization of Zeolite 4A, in the phase region generating Zeolite 4A, reactants condition was set: $n(SiO_2/Al_2O_3)$=2.0, $n(H_2O/Na_2O)$=110. The samples, namely C1, C2, C3, C4, C5, C6 with corresponding crystallinity degrees: 95.7, 95.8, 97.7, 96.1, and 96.3(%) under the condition that Na_2O/SiO_2 ratios were 1.2, 1.3, 1.4, 1.5, 1.6 correspondingly.

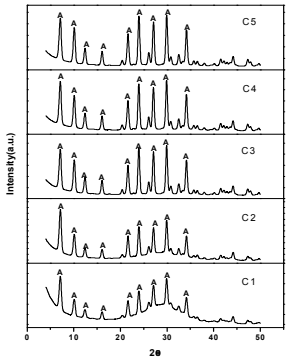

Fig.3 XRD patterns with different Na_2O/SiO_2

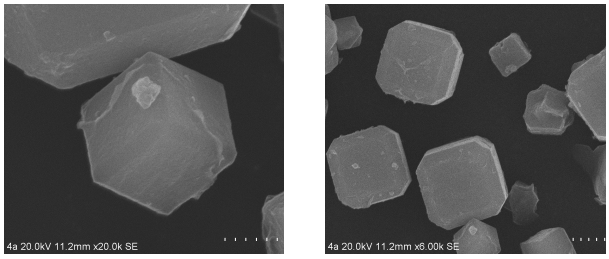

Fig.4 SEM images of zeolite 4A

Adjusting the amount of sodium hydroxide, Na_2O/SiO_2 ratio was changing simultaneously, which was depicted in Fig.3. Comparing the peaks, it is obvious that relative crystallinity increased to 97.7% along with Na_2O/SiO_2 ratio ranging from 1.2 to 1.4. Meanwhile, the characteristic peaks are stronger and stronger, and the strengths of diffraction peaks are higher and higher. But, after 1.4, the higher the Na_2O/SiO_2 ratio was, the lower the relevant crystallinity was. Consequently, the optimum n(Na_2O/SiO_2) was 1.4.

Characterization of Zeolite 4A

The XRF of Zeolite 4A showed that SiO_2/Al_2O_3 ratio was 1.94, closing to the best ratio confirmed by experiment: $n(SiO_2/Al_2O_3)$=2.0, which was corroborated silicon and aluminum had almost sufficient reaction. In addition, the product had few impurities, especially the contents of Fe_2O_3 and MgO, so the purity of Zeolite 4A was very high.

This experiment measured the specific surface area of Zeolite 4A using NOVA 1200e physical adsorption analyzer. The BET surface area of Zeolite 4A and Commercial Zeolite A were respectively 31cm^2/g and 300cm^2/g. The reason lay in pores of Zeolite 4A contracted so many that N2 molecules couldn't enter into it at 77K temperature.

SEM photographs in Fig.4 depict that 4A molecular sieves are typical cubic morphology and crystals are relatively complete, uniform dispersion and high purity, which corresponded with Zeolite 4A synthesized by Liu Liying[11] using fly ash.

The Separation of CO2/N2 of Zeolite 4A

Sorption isotherms were tested by STA409PC Physical adsorption instrument produced by NETZSCH at 30°C and 60°C respectively, which could show the adsorption capacity of Zeolite 4A to CO_2 and N_2, and judge the separation performance of CO_2/N_2 of Zeolite 4A further.

As is depicted in Fig.5, CO_2 and N_2 adsorption capacity of Zeolite 4A are 3.803mmol/g and 0.389mmol/g at atmospheric pressure and 30°C respectively, which reveals Zeolite 4A having a high adsorption selectivity on CO_2/N_2.

As is subtly portrayed in Fig.6, at 60°C and atmospheric pressure, adsorption capacity of Zeolite 4A to CO_2 and N_2 are 2.939mmol/g and 0.964mmol/g respectively, which indicates adsorption capacity to CO_2 is also much larger than that to N_2. Compared with the condition of 30°C, the adsorption capacity to CO_2 at 60°C is lower obviously. But the adsorption capacity to N_2

at 60°C is higher. Wherefore, as the temperature rises, the adsorption selectivity on CO_2/N_2 of Zeolite 4A gets down.

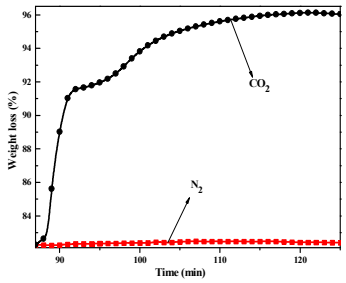

Fig.5 Adsorption isotherms of 4A at 30°C

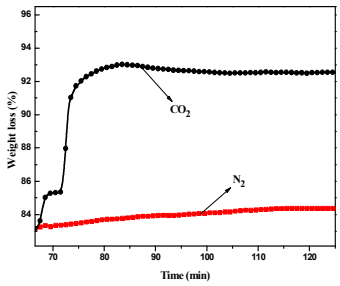

Fig.6 Adsorption isotherms of 4A at 60°C

Conclusions

(1)The optimal conditions of synthesizing Zeolite 4A using methods which associate two-step hydrothermal synthesis procedure with alkali-melting process are as follows: $n(SiO_2/Al_2O_3)=2$, $n(Na_2O/SiO_2)=1.4$, $n(H_2O/Na_2O)=110$.

(2) SiO_2/Al_2O_3 ratio was 1.94, which shown silicon and aluminum had almost sufficient reaction. The BET surface area of Zeolite 4A was 31cm^2/g. Zeolite 4A synthesized under the optimal condition has complete morphology and high purity.

(3) Zeolite 4A has a high adsorption selectivity on CO_2/N_2 at atmospheric pressure and 30°C. With the temperature rising, this performance weakens.

References

[1] Liu Yan, Ma Yi, Li Yan, Xing Cunzhang, Lü Hailiang. Zeolite synthesis from coal fly ash[J], COAL CONVERSION, 2007, 30(2), 91-95.

[2] Sun Xia. Zeolite NaA and NaX synthesis from fly ash and their adsorption of heavy metal ions in wasterwater [D]，Nan Jing：Nan Jing University of Science&Technology，2007

[3] Hollman G G,Steenbruggen G, Janssen-Jurkovicova M. A Two-step Process for the Synthesis of Zeolites from Coal Fly Ash[J]. Fuel, 1999, 78(10): 1225-1230.

[4] Molina A , Poole C. A Comparative Study Using Two Methods to Produce Zeolites from Fly Ash[J]. Minerals Engineering, 2004, 17(2): 167-173.

[5] MA Hongchao, YAO Quantong, FU Yinghuan, et al. Synthesis of Zeolite of Type A from Bentonite by Alkali Fusion Activation Using Na2CO3[J], Ind. Eng. Chem. Res, 2010, 49: 454-458.

[6] KEKA OJHA, NARAYAN C PRADHAN, AMAR NATH SAMANTA. Zeolite from fly ash: synthesis and characterization[J], Bull. Mater Sci, 2004, 27(6): 555-564.

[7] ZENG Zhengzhong, Li Bo, NAN Zhongren. Aging Time and Ash-Water Rate Affected to Fly Ash Synthesized A Type Zeolite [J], Coal Science and Technology, 2009, 37(4): 124-128.

[8] V.J. Inglezakis. The concept of “capacity” in zeolite ion-exchange systems[J], Colloid Interface Sci, 2005, 281: 68-79.

[9] ZHAO Xiufang. Technology research of 13X molecular sieve[D], Chang Sha, Zhong Nan University, 2004: 4-5.

[10] JIANG Rongli, KONG Deshun, XIA Xiaobo, CHEN Wenlong. Synthesis of 13x molecular sieve in the hydrothermal reaction system of metakaolinite–alkali–sodium silicate [J], JOURNAL OF THE CHINESE CERAMIC SOCIETY, 2008, 36(6): 832-836.

[11] Liu Liying, Singh Ranjeet, Xiao Penny. Zeolite synthesis from waste fly ash and its application in CO2 capture from flue gas streams[J], 2011, 17(5): 795-800.

Advanced Materials Research Vols. 989-994 (2014) pp 11-14
© (2014) Trans Tech Publications, Switzerland
doi:10.4028/www.scientific.net/AMR.989-994.11

Bi_2S_3 nanoflowers Synthesized via Hydrothermal Method

Xiliang CHEN [a], Yanpei JI[b]

Applied Chemistry Research Center, Yellow River Conservancy Technical Institute, Kaifeng 475003

[a]email: cxliang2006@163.com

[b]email: 875521665@qq.com

Keywords: Bismuth sulfide, hydrothermal, Preheating

Abstract. Bi_2S_3 flowerlike patterns were synthesized via a facile hydrothermal approach without using any surfactant and acid. The morphology, structure, phase composition, of the as-prepared Bi_2S_3 products were characterized using scanning electron microscopy, X-ray diffraction, high-resolution transmission and electron microscopy, respectively. The experimental results showed that the product possesses good distribution of morphology, well crystallized nanostructure.

Introduction

Semiconducting chalcogenides are materials which have attracted a great deal of interest. Bismuth sulfide (Bi_2S_3) is one of these materials which belongs to the family of main group metal chalcogenides A2VB3VI (A=As, Sb and Bi; B=S, Se and Te), an important class of semiconductors with numerous applications including photovoltaics, thermoelectrics and IR spectroscopy [1-3]. Recently, Bi2S3 nanoparticles have been found to be a promising imaging agents in X-ray computed tomography, electrochemical hydrogen storage and photosensor [4-6].

There have been several recent reports on synthesis of Bi_2S_3 nanostructures. The lamellar crystalline structure of Bi_2S_3 gives rise to the development of different 1D nanostructure under certain growth conditions [7]. Nanowires, nanorods, nanotubes, and nonoribbons have been produced by solvothermal or hydrothermal process [7-10], microwave irradiation approach [11], ultrasonic method [12], template-assisted pressure-injection technique [13] and so forth. More complex morphologies of Bi_2S_3 have been made by employing the soft template effects [14-17]. Since the physical properties and performance of Bi_2S_3 nanostructures could be tuned by different dimensions morphologies, it is attractive to realize the facile synthesis of Bi_2S_3 nanostructures with controlled morphologies.

Hydrothermal approach is an effective and economical method, which has been applied to prepare Bi_2S_3 with different structures by varying the reaction conditions. Na_2S, CS_2, sodium thiosulfate and dithiocarbamate have been used to react with bismuth salt at an elevated temperature and pressure. Phuruangrat et al. [10] has prepared Bi_2S_3 nanorods via hydrothermal method with bismuth nitrate and thiourea (NH_2CSNH_2) as starting reagents in acid solution without any surfactant. Acid concentration in the reaction plays an important role in controlling the morphologies of Bi_2S_3 nanostructures. In acid-free solution, the product obtained through hydrothermal process was irregular in shape [18]. On the contrary, the introduction of too much amount of acid results in the appearance of Bi_2S_3 nanoparticles [19, 20] because of dissolving of Bi_2S_3. It is not easy to control the morphology and crystalline of the product since the morphology of the product is quite sensitive to the acid. The acidity should be altered very carefully to obtain the desired nanostructures. Furthermore, the acid used in the reaction usually involves nitric acid and hydrochloric acid, which is contaminative to the environment. Therefore, the development of facile

and environmental friendly strategies without using contaminating acid for synthesis of Bi_2S_3 nanostructures is deemed necessary.

In this article, Bi_2S_3 were prepared by hydrothermal methods. The mixture of $Bi(NO_3)_3 \cdot 5H_2O$ and NH_2CSNH_2 solutions was preheated firstly and then hydrothermally processed in an autoclave. Through this method flowerlike Bi_2S_3 were synthesized without using any acid.

2. Experimental

All reagents were analytical grade and used as received without any further purification. To produce nanostructured Bi_2S_3, 2 mmol $Bi(NO_3)_3 \cdot 5H_2O$ and 6 mmol NH_2CSNH_2 powders were dissolved in 25 and 5 mL distilled water, respectively. Subsequently, the thiourea solution was added into the bismuth nitrate suspension under vigorous stirring. At this stage, the color of the solution turned from white to light yellow. The mixture was thoroughly mixed by stirring at 60 °C for 20 minutes before transferred into a Teflon-lined stainless-steel autoclave. The autoclave was sealed and maintained at 160 °C for 15 hours and then cooled to room temperature naturally. Finally, black precipitates were produced, which were separated, washed and dried, for further analysis.

The products were characterized extensively for morphology, phase, and growth direction by using scanning electron microscopy (SEM, JEOL, JSM-5600LV, Japan), X-ray powder diffraction (XRD, X'Pert Pro), selective area electron diffraction (SAED) and high resolution TEM (HRTEM, JEM-2010CXII).

3. Results and discussion

Fig.1 shows the XRD pattern of the as-prepared Bi_2S_3 products. All reflections in Fig.1 can be indexed to a pure orthorhombic phase bismuth sulfide (JCPDS file 65-2431) with lattice parameter a=11.29 Å, b=3.978 Å, c=11.15 Å. No characteristic of other impurities ($BiONO_3$, Bi_2O_3 and Bi, etc.) were observed. The intense diffraction peaks in Fig.1 indicates that the product should be well crystallized. This is further demonstrated by HRTEM and ED analysis.

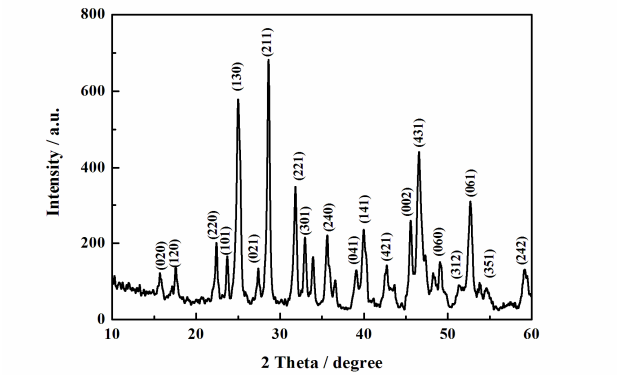

Fig.1 XRD patterns of Bi_2S_3 powder prepared in acid-free solution

Fig. 2(a) is typical SEM images of Bi_2S_3 synthesized by combination of preheating and hydrothermal process. SEM images of the as-prepared Bi_2S_3 nanostructures demonstrated that the sample is composed of flowerlike patterns in a well organized way. The typical size of the nanoflower is about 6 μm in diameter. As shown in Fig. 2(b), Bi_2S_3 nanoflower is constituted of nanorods with a diameter 50-100 nm and up to 1-2 μm long. These nanorods are all smooth, clean and without any amorphous phase in surface. Electron diffraction (ED) patterns of the Bi_2S_3 in Fig. 2(c) indicates that the nanorod is a single crystal and predominately grows along the [001] direction. The conclusion is also supported by the HRTEM observations in Fig. 2 (d), in which the clearly observed lattice fringes reveal that the Bi_2S_3 nanorods in the flowerlike patterns are highly crystalline. The crystal planes, parallel and perpendicular to the rod axis, having spacing of 0.8 and

0.4 nm, which match well with the separations between the neighboring lattices of (110) and (001) planes, respectively. This result further verifies that the preferential growth occurred along the [001] direction.

Thiourea has been used as sulfur source to control the morphological evolution of metal sulfides in the solution phase. As we know, $Bi(NO_3)_3$ has a strong tendency to hydrolyze in neutral solution and generate white $BiONO_3$ precipitation. As the addition of thiourea, thiourea coordinates to bismuth ions to form complexes, prevents the explosive production of bismuth sulfide and benefits the oriented growth of final nanorods. The H_2S generated by thiourea decomposition at high temperature will act with Bi^{3+} and produce Bi_2S_3. The generation of nanorods may involve the formation of "growing seeds" during the decomposition of the precursors, followed by the production of crystalline nanonuclei and preferential growth of [001]-oriented Bi_2S_3 nanorods. Bi_2S_3 precursor forms by preheating the reagents [22] at the first step. It is gradually crystallized by hydrothermal treating and act as the crystalline nuclei. Bi_2S_3 nanoparticles deposited from supersaturated solution grew on these nuclei cites gradually to form nanorod at a prior growing direction. In solution without preheating, however, the formed $BiONO_3$ precipitation will react with NH_2SCNH_2 to form irregular nanostructures. It may be attributed to fact that the Bi_2S_3 nanoparticles mushroomed under high temperature and pressure.

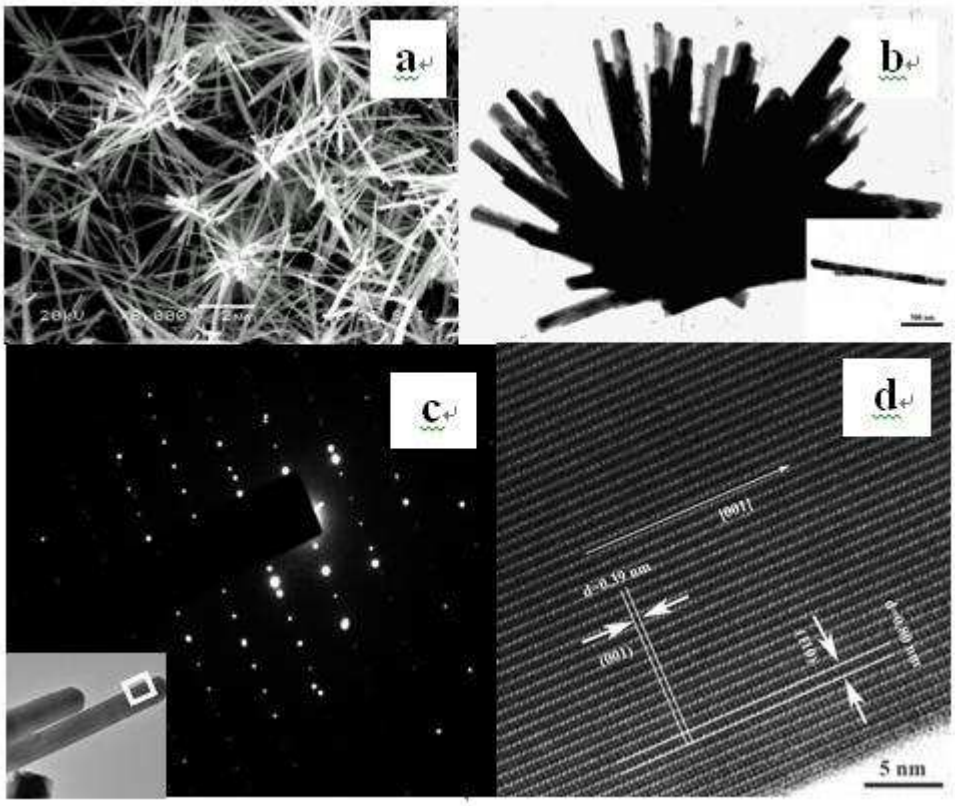

Fig. 2 (a) SEM image of the Bi_2S_3 flower pattern prepared in acid-free solution for 15 h (b) TEM images (c) is the ED pattern (d) HRTEM images.

Conclusion

In summary, preheating effect on the morphology of Bi_2S_3 nanostructures synthesized by hydrothermal method has been investigated. It provides a more controllable and environmentally friendly way to the Bi_2S_3 synthesis without using any surfactant or acid.

Acknowledgement

This work was financially supported by Natural Science Foundation of the Education Department of Henan Province (14B150008) and Foundation of Yellow River Conservancy Technical Institute (2013KXJS009).

References

[1] B.B. Nayak, H.N. Acharya, G.B. Mitra, B.K. Mathur, Thin Solid Films 105 (1983) 17-24.
[2] H. Cui, X. Liu, X. Li, J. Wang, F. Han, X. Zhang, et al., J. Solid State Chem. 177 (2004) 4001-4006.
[3] B. X. Chen, C. Uher, Chem. Mater, 9: 1655-1658, 1997.
[4] Rabin, O; Perez, J. M.; Grimm, J; Wojtkiewicz, G; Weissleder, R. Nat. Mater. 2006, 5, 117.
[5] B. Zhang, X.C. Ye, W. Y. Hou, Y. Zhao, Y. Xie, J. Phys. Chem. B, 110: 8978-8985, 2006.
[6] R. R. Ahire, N. G. Deshpande, Y. G. Gudage, A. A. Sagade, S. D. Chavhan, D.M. Phase, Ramphal Sharma, Sensors and Actuators A, 140: 207-214, 2007.
[7] Yue Wang, Jing Chen, Peng Wang, Ling Chen, Yu-Biao Chen, Li-Ming Wu, J. Phys. Chem. C, 113: 16009-16014, 2009.
[8] Gangqiang Zhu, Peng Liu, Jianping Zhou, Xiaobing Bian, Xiaobo Wang, Jiao Li, Bin Chen, Materials Letters 62 (2008) 2335-2338.
[9] Mingwang Shao, Wu Zhang, Zhengcui Wu, Youbao Ni, Journal of Crystal Growth 265 (2004) 318-321.
[10] Anukorn Phuruangrat, Titipun Thongtem, Somchai Thongtem, Materials Letters 63 (2009) 1496-1498.
[11] Rong He, Xuefeng Qian, Jie Yin, Zikang Zhu, Journal of Crystal Growth 252 (2003) 505-510.
[12] Guangjian Xing, Zhenjian Feng, Guanghua Chen, Wang Yao, Xuemei Song, Materials Letters 57 (2003) 4555-4559.
[13] Nikolay Petkov, Ju Xu, Michael A. Morris, Justin D. Holmes, J. Phys. Chem. C 2008, 112, 7345-7355.
[14] Jiang, J.; Yu, S. H. Chem. Mater. 2005, 17, 6094-6100.
[15] Lu Tian, Han Yao Tan, and Jagadese J. Vittal, Crystal Growth & Design, 8(2): 734-738, 2008.
[16] Jing Tang and A. Paul Alivisatos, Nano Letters, 6(12): 2701-2706, 2006.
[17] Lianshan Li, Ruiguo Cao, Zhijian Wang, Jingjian Li, and Limin Q, J. Phys. Chem. C 2009, 113, 18075-18081
[18] Lu J, Han Q, Yang X, Lu L, Wang X. Mater Lett 2007;61:3425-8.
[19] Dong L, Chu Y, Zhang W. Mater Lett 2008; 62: 4269-72.
[20] Lihong Dong , Ying Chu , Wei Zhang, Materials Letters 62 (2008) 4269-4272
[21] Juan Lu, Qiaofeng Han, Xujie Yang, Lude Lu, Xin Wang, Materials Letters 61 (2007) 3425-3428
[22] Xuebo Caoa, Xianmei Lana, Cui Zhaoa, Wenjun Shena, Dan Yaoa, Weijian Gao, Journal of Crystal Growth 306 (2007) 225-232.

Advanced Materials Research Vols. 989-994 (2014) pp 15-18
© (2014) Trans Tech Publications, Switzerland
doi:10.4028/www.scientific.net/AMR.989-994.15

Study of oxidation degradation eosin by ferrate

LI DangSheng[1a], CHEN XiLiang[1b]

Applied Chemistry Research Center, Yellow River Conservancy Technical Institute, Kaifeng 475003

[a]email: lidangsheng2002@163.com,

[b]email: cxliang2006@163.com

Keywords: eosin, ferrate, oxidation, pH

Abstract. This paper presents a comparative study of the performance of ferrate (VI) towards wastewater treatment. The effects of solution pH, reaction temperature and amount of ferrate on the eosin removal rate were investigated. Results demonstrated that increasing the amount of ferrate (VI) and low acidity leads to good removal performance of ferrate towards eosin. So ferrate (VI) is an effective reagent for dyes treatment. The reaction temperature, however, has little influence on the removal rate which may be due to the degradation effects of ferrate at elevated temperatures.

Introduction

Potassium ferrate, K_2FeO_4, is a strong and environmental friendly oxidant [1]. It has been attracting more and more research interest during the past decades. The redox potential of ferrate (VI) ions is as high as 2.2V and 0.72V under the acidic and basic conditions, respectively[2]. Ferrate is attracting growing attention for several water treatment applications because of the reagent's selective oxidizing properties. Additionally, the product of ferrate oxidation reaction is considered to be ferric hydroxide, which is useful coagulant and will enhance the water remediation performance. So it is a promising chemicals for treatment of waste water. The instability of ferrate solutions has limited its use in field treatment applications, but recent efforts are focused on developing technologies for on-site ferrate generation. The loss of ferrate due to the degradation during the storage and transport process would be avoided.

In recent years, various accelerated energy consumption and the unabated release of toxic agents into the air and water has led to such adverse effects as pollution-related disease and global warming. So, it is urgent to develop clean and safe chemical technologies, materials and process for environmental remediation. Eosin is an important acidic dye used as indicator. It dissociates in water into ions. Its negative ion, which is acidic in nature, readily combines with positively charged regions of cellular, macromolecules, proteins, colouring them a variety of hues, ranging from pink to red to orange.

In this article, eosin was used as a model pollutants. The oxidation effects of ferrate to eosin was investigated. Factors, such as pH value, temperature, the amount of ferrate, and so forth, that influence the reaction rate was explored.

Experiment sections

Experimental materials

K_2FeO_4 was prepared according to Delaude et al. [3], yielding a material with an iron content was 86%. Other chemicals were of high purity and were used as received.

Degradation test

The absorb spectrum of ferrate solution and eosin solution was obtained with UV/vis spectroscopy. The concentration of ferrate solution was further determined by UV/vis spectroscopy at 510 nm where the solutions possess a maximum absorbance. The relations between absorbance and concentration has been detailed described in Ref [2].

The eosin solutions were prepared by dissolving eosin samples into distilled water. The effect of pH, temperature and amount of ferrate solutions to the was investigated. The pH value of the sample was adjusted by adding diluted sulphuric acid. After a certain reaction time, excess sodium sulfite solution was added to the reaction solution. Because the sodium sulphite is a strong reducing agent, the excess ferrate in the solution will be reduced by the sodium sulphite. Otherwise, the remaining ferrate solution will affect the determination of the concentration of eosin. Because their maximum absorption wavelength is relatively close to each other. Then by measuring the absorbance of the solution, the content of eosin in solution was determined.

Results and discussions

As shown in Figure 1, the UV-vis curve is the absorption spectrum of the eosin solution. At 515nm, there is a maximum absorption peak. According to the literature, the absorption peak was assigned to the characteristic absorption peak of eosin, which can be used as a qualitative description of eosin solution. In the following discussion, all the absorbance measurements were performed at this wavelength.

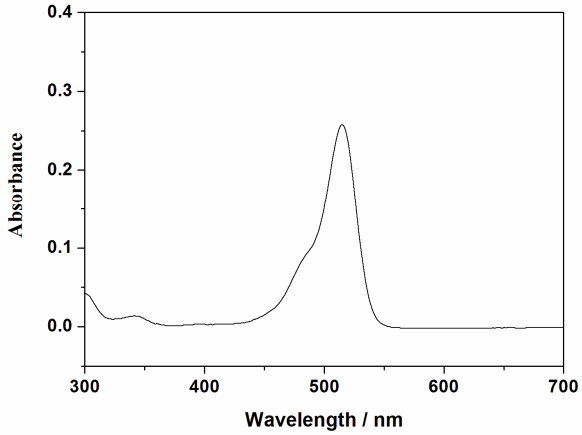

Fig.1 UV-vis spectrum of eosin solution

Figure 2 shows the effects of the ferrate amount to the eosin removal performance as a function of reaction time. As can be seen from the figure, regardless of the added ferrate amount, the reaction is carried out quickly. Within 2 minutes, the solution between eosin and ferrate has been reacted adequately. As the reaction time prolonged from 2 to 15 minutes, although the of removal eosin further increases, but the magnitude of the increase is very low. In addition, with the increasing amount of ferrate, the eosin removal rate increased steadily with the same reaction time. When adding 8mL ferrate solution into 50mL of the reaction solution, the eosin removal was up to 80%, indicating a strong removal performance of ferrate to eosin dye.

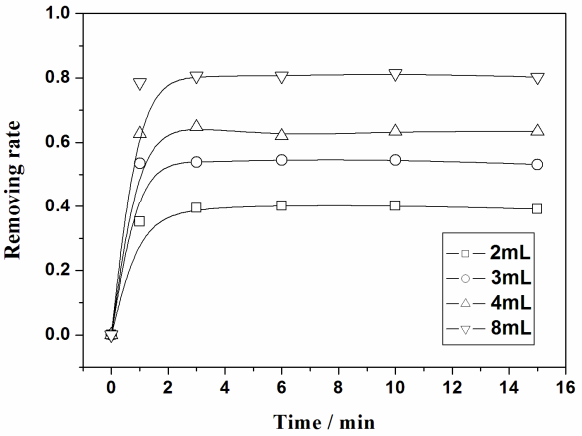

Fig.2 Fe (VI) amount effect to the eosin removal rate of Fe (VI) solutions

Figure 3 shows the effects of the solution pH on the removal performance of ferrate to eosin. As can be seen from the figure, with the decreasing of the pH value, eosin removal rate increased significantly. At the reaction time of 2 minutes, if the pH of the solution is 5, eosin removal rate can be 40%, and when the pH of the solution is reduced to 3, then the removal rate of eosin was up to 90%. This is mainly due to higher ferrate oxidation potential and thus the oxidation capability in acidic solution. According to the results reported in the literature, under acidic conditions, ferrate possesses the highest oxidation potential as we known. While under alkaline conditions, the oxidation potential reduced to 0.72V. Thus, reducing the pH is a good method to improve the ferrate oxidation property.

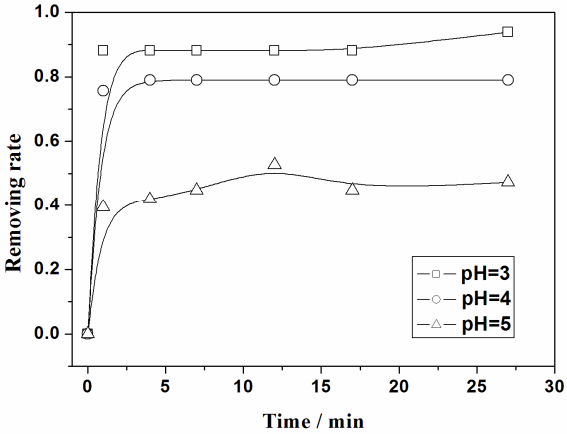

Fig.3 pH value effect to the eosin removal rate of Fe (VI) solutions

Figure 4 is the effect of reaction temperature on the removal of eosin. As can be seen from the figure, at the temperature range from 20 degrees to 50 degrees, the effect of temperature on the reaction is not very notable. Generally, the reaction speed will accelerate as the reaction temperature increases. However, due to the degradation of the ferrate as the temperature rises, the concentration of the ferrate solutions reduces resulting in the oxidation capability decrease. Especially under conditions of 50 degrees, it can be seen clearly from the figure that as the reaction time extended, the removal performance of ferrate to eosin decreases. For one hand, ferrate is unstable at high temperatures, it will degrade partly. For the other hand, the solution evaporated seriously at high temperature, resulting in the concentration of eosin solution raising.

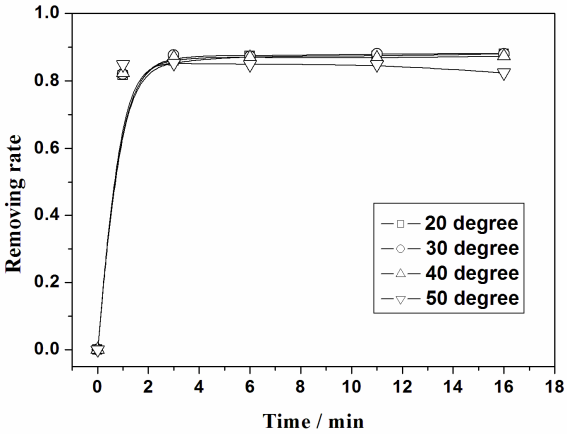

Fig.4 Reaction temperature effect to the eosin removal rate of Fe (VI) solutions

Conclusions

This paper studies the oxidation removal effects of ferrate towards eosin dye. The study found that with the increasing amount of ferrate, eosin removal steadily improved. Lowering the pH of the reaction system, the oxidation ability of ferrate can significantly improved, so that eosin removal increases. The effect of reaction temperature on the removal of eosin was not significant, mainly due to the temperature rise associated with the evaporation of solution and the degradation of ferrate solution. In short, ferrate is an excellent water treatment agent, which can be used to effectively remove dyes in the wastewater.

Acknowledgements

This work was financially supported by Natural Science Foundation of the Education Department of Henan Province (13B150132, 14B150008) and Foundation of Yellow River Conservancy Technical Institute (2013KXJS009).

References

[1] D. S. Li, X. L. Chen. Advanced Material Research, 2012, 554-556: 632-635

[2] H D Jia, X L Yang, Y Yang. Analytical chemistry, 1999, 27(4): 617-619.

[3] Delaude, L & Laszlo, P. A novel oxidizing regent based on potassium ferrate, J. Org. Chem. 1996, 61, 6360-6370

Advanced Materials Research Vols. 989-994 (2014) pp 19-22
© (2014) Trans Tech Publications, Switzerland
doi:10.4028/www.scientific.net/AMR.989-994.19

The relationship between calcium hydroxide concentration in pore solution and the strength of stabilized soils

Lei DAI[1, a], Xiaoxuan DENG[2, b]

[1] Beijing Building Materials Academy of Sciences Research, Beijing, 100041, China

[2]Building Materials Institute China Academy of Building Research, Beijing, 100013, China

[a]email: dailei@bmt-bj.com, [b]email:xiaoxuandeng@foxmail.com

Keywords: Calcium hydroxide concentration; Pore solution; Strength; Stabilized soils

Abstract. Under the same cement content, the stabilized soils, made of the soils with similar physical properties, may be significant difference in the strength. In this research, three groups of soils were selected, and the soils in each group are similar in physical properties. Strength and ions concentration in pore solution of the stabilized soils were investigated. The result reveals that calcium hydroxide (CH) concentration in pore solution of the stabilized soils might not reach to saturation due to soil consuming Ca^{2+} and thus cause calcium silicate hydrates gels (C-S-H) and calcium aluminates hydrates gels (C-A-H) to form less. The cementitious hydrates are the main strength contributors of the stabilized soils. The Strengths of stabilized soils, the soils bearing similar physical properties, were almost identical as long as the CH concentrations in pore solution were saturated. The effect of chemical factors of soil on the strength of stabilized soil can be briefly attributed to the change of CH concentration in pore solution, and be further attributed to the influence of CH concentration on the amount of C-S-H and C-A-H formed in stabilized soils.

Introduction

Cement based stabilizer (Portland cement or that composed mainly from Portland cement) is well-established technique in subgrade stabilization [1-5]. Stabilized soils, under the same cement content, which are composed of the stabilizer and the soils bearing similar physical properties, exhibit significant differences in strength, even the strength of stabilized soils made of the soil with better physical properties is lower than that of the one made of the soil with worse physical properties [2,6]. Obviously, there must be some other factors that affect the strength of stabilized soils except for physical properties of soil.

After cement is mixed with clay, cement hydration mainly produces CH, C-S-H and C-A-H, and Ca^{2+} provided by CH is absorbed by soil until reaching saturation point, then pozzolanic reaction happens between the remaining CH and silica and alumina dissolved from the clay lattice to form additional cementitious material (C-S-H and C-A-H)[7,8]. The strength differences in stabilized soils are decided by the amount of hydrates produced by the pozzolanic reaction, the more CH participate in the pozzolanic reaction, the more hydrates are formed, and the higher strength of stabilized soil is obtained. However, the investigation cannot satisfactorily explain that soils bearing similar physical properties are significant difference in the strength of stabilized soil in the same cement content.

Cement can normally hydrate in different clay types, while the clays are different in the absorption amount of Ca^{2+} [9]. The soil is composed of kaolinite and illite, consuming less Ca^{2+} than that is composed of montmorillonite, therefore the strength of the stabilized soil is higher [10]. Additionally, other cations in soils, like Na^{+} and K^{+}, exchange with Ca^{2+} come from cement hydration, the more cation exchange capacity (CEC) of soils are, the lower strength of stabilized soils are obtained, and vice versa [11-14]. If organism in soil absorbs Ca^{2+} to exceed a certain degree, then the stabilized soils will not obtain adequate strength [15, 16]. It was reported that CH in stabilized soils might not be saturated, under the conditions, the soil further absorbing Ca^{2+} from cement hydrates would decrease the amount of cemetitious hydrates produced by the reaction between CH and soil, such as C-S-H and C-A-H etc., therefore, the same amount cement might not

produce the same amount of hydrates and obtain the same strength in the stabilized soils that were made of similar physical properties [6]. Nevertheless, the investigation does not provide enough proofs; moreover, it is still unclear the effect of chemical factors of the soils on the hydrates growing and compressive strength.

Test results

The specimens were made by mixing the soils (BT, TT2, WT, TT1, NT and GT) and different cement content (aw, aw=6, 8, 10, 12, 15, 18, 20, 22, 25, 28 and 30% of wet soil weight), and the specimens were named as BS, TS2, WS, TS1, NS and GS correspondingly. Relationship between the unconfined compressive strength of specimens (qu) and aw are shown in Fig.1, which reveals that qu increases slowly, as aw increases, until aw reaches the turning point indicated with arrow in Fig. 1 (named aw′), then the increment of qu produced by unit cement content increases obviously. As can be seen in Fig.1, although the soils with similar physical properties were mixed with equal cement content, the corresponding stabilized soils indicate significant differences in strength. Fig.1(a) indicates when BT and TT2 are both mixed with the same cement content (aw = 15 %), the strength of BS is one time higher than that of TS2, as aw＜aw′ , the strength increment of BS and TS2 produced by unit cement content are different, while aw＞aw′ , that of the two stabilized soils become almost identical. The similar phenomena are observed in Fig.1 (b) and Fig.1 (c).

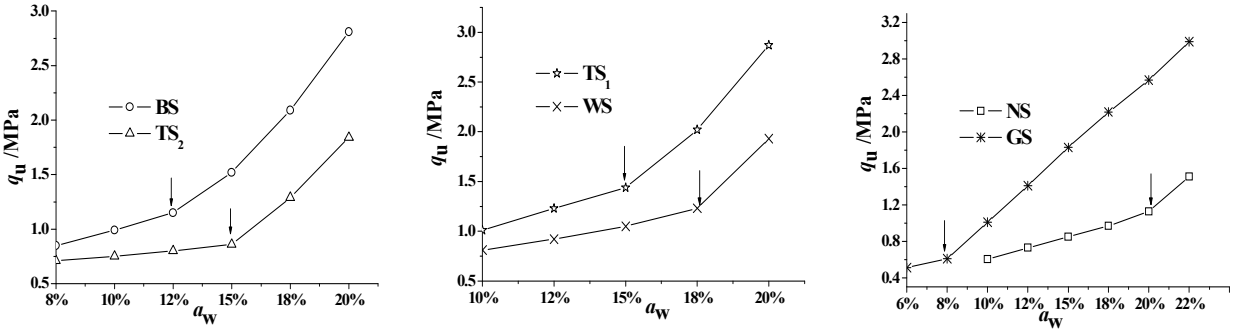

(a) (b) (c)

Fig.1 Unconfined compressive strength for stabilized soils

Table1 Ions concentration in pore solution and pH value of soils in different cement content(mmol/l)

Soil	Cement (%)	pH	K^+	Na^+	Ca^{2+}	Al^{3+}	OH^-	S^{2-}	Si^{2-}	K^++Na^+
BT	10	12.4	8·785	25·800	2·919	0·247	41·782	0·498	0·708	34·585
BT	12	12.6	12·985	33·896	2·089	0·300	73·93	1·003	1·022	46·880
BT	15	13.1	19·718	68·652	1·672	0·378	155·89	1·441	0·470	88·370
TT_2	12	12.1	2.033	14.057	5.701	0.571	19.461	4.056	1.908	16.090
TT_2	15	12.3	3.021	22.074	4.728	0.549	35.894	4.297	1.267	25.725
TT_2	18	12.7	9.964	46.017	3.546	0.489	90.894	5.066	0.787	55.980
WT	12	12.0	29.297	57.991	2.660	2.500	37.024	0.656	0.473	87.289
WT	15	12.4	44.967	65.809	2.363	3.755	59.106	0.918	0.180	110.78
WT	18	12.8	69.346	91.596	1.961	8.125	127.34	1.070	1.096	160.94
TT_1	15	12.2	7.095	31.465	2.924	2.632	46.888	7.589	1.296	38.56
TT_1	18	12.5	8.672	56.704	2.727	3.669	62.011	7.292	2.307	65.376
TT_1	20	12.8	19.485	90.661	1.904	7.821	152.00	6.042	1.808	110.15
NT	18	12.1	2.374	20.965	4.719	0.266	25.259	1.094	0.470	23.34
NT	20	12.3	4.910	24.196	3.839	0.374	43.806	1.208	0.337	29.11
NT	22	12.6	9.495	36.600	2.997	0.579	92.612	1.390	0.655	46.09
GT	6	12.3	0.913	5.607	2.989	0.923	46.447	0.141	0.363	6.520
GT	8	12.5	2.297	9.561	2.348	2.168	73.688	0.405	0.664	11.858
GT	10	13	4.567	20.426	1.679	3.658	156.93	0.588	0.440	24.993

Specimens were selected from each series of stabilized soils and were stabilized with three cement contents that were changed around aw′ , (as seen in Fig. 1, the aw′ of BS is 12%, and that of TS2, TS1, WS, NS and GS are 15%, 15%, 18%, 20% and 8%, respectively). Pore solutions

of the specimens were extracted, and pore solution's analysis are shown in Table 1, in each series, the pH and the concentration of OH^-, K^+ and Na^+ increase as cement content increasing, while the concentration of Ca^{2+} gradually reduces. Other ions concentration, such as Al^{3+}, SO_4^{2-} and SiO_4^{4-}, irregularly change.

The strength of BS is higher than that of TS2 under the same cement content, as shown in Fig.1(a), correspondingly, the pH and concentration of OH^-, K^+ and Na^+ of BS are higher than that of TS2, while the concentration of Ca^{2+} of BS is lower than that of TS2, as shown in Table 1. The similar phenomena can be observed from TS1 and WS, GS and NS in Fig.1 and Table 1.

The soils bearing similar physical properties may be different in chemical properties, such as cation exchange capacity and pozzolanic reactive ability, thus their Ca^{2+} consumption ability are different, which causes the amount of C-S-H and C-A-H produced in the stabilized soils to be different and thus produces different strengths of the stabilized soils, as the same cement content is added. For example, pH of BT is higher than that of TT2 (as shown in Table 1), thus CH concentration in pore solution of BS is higher than that of TS2 at equal cement content, and the strength of BS is higher than that of TS2. Similarly, although TT1 and WT are homogeneous in pH, cation exchange capacity and the amount of available silicon and alumina of WT are much higher than those of TTI, therefore CH concentration in pore solution of TS1 is higher than that of WS at equal cement content, and the amount of C-S-H and strength of TS1 are higher than that of WS. If sufficient cement is added to stabilize soils with similar physical properties, its hydration will produce enough CH to ensure CH saturated in pore solution of the stabilized soils. Under such conditions, soil consuming Ca^{2+} may only reduce the amount of CH instead of the amount of C-S-H; therefore, equal cement content could produce the same amount of C-S-H, and achieve the same strength of the stabilized soils. Fig. 1 shows that the strength increasing rates of specimens in each group are almost identical after cement content exceeding aw′ (CH saturation point of the stabilized soils). Specially, as shown in Fig.4, the specimens, treated to the CH saturated point, their strength increasing rules of stabilized soils in each group do represent the homogeneous strength development tendency.

Above results reveal an important fact, although there are many chemical factors affecting the strength of stabilized soils, which are different in different soils, the influences of different chemical factors on the strength of stabilized soils can be attributed to the influence on CH concentration in stabilized soils, and further be attributed to the influence of the CH concentration on the amount of C-S-H and C-A-H. Therefore, the adverse effects of different chemical factors of soils can be counteracted by increasing the CH concentration of stabilized soils.

Conclusions

1. Under the influence of physical and chemical factors of soil, soil may consume a lot of Ca^{2+} produced by stabilizer, which results in CH concentrations in pore solution of stabilized soils are under saturated. Thus the amount of C-S-H and C-A-H become less. The soils bearing similar physical properties may be significantly different in Ca^{2+} consumption, consequently, the amount of C-S-H and C-A-H generated by equal amount of cement may also have great difference, which causes the great difference in the strength of stabilized soils.;2. As long as CH concentration in pore solution of stabilized soils is saturated, C-S-H and C-A-H may normally form, as a result, equal amount of cement may produce equal amount of hydrates, and make the stabilized soils made of the soils bearing similar physical properties obtain the same strength.;3. CH concentrations in pore solution of the stabilized soils represent significant differences for the soils are very different in chemical factors, such as CEC and pozzolanic reaction, which lead to the variation in the consuming amount of Ca^{2+} provided by cement hydration and the formation amount of cementitious materials, like C-S-H and C-A-H.

References

[1] Mitchell, J.K., 1976. The Properties of Cement-Stabilized soils, Proceeding of Residential Workshop on Materials and Methods for Low Cost Road, Rail, and Reclamation Works. Leura, Australia.

[2] Bell, F G., 1996. Lime stabilization of clay minerals and soils. Engineering Geology 42, 223-237.

[3]Lorenzo, A.L., Bergado, D.T., 2004. Fundamental parameters of cement-admixed clay—new approach. Journal of Geotechnical and Geoenvironmental Engineering ASCE 130 (10), 1042–1050.

[4] Aydın Kavak, Gökhan Baykal, 2012. Long-term behavior of lime-stabilized kaolinite clay. Environ Earth Sci 66:1943–1955

[5] M. Afiabi, S. Wild (1986) J Mater Sci 21:497. doi:

[6] Huang X., 1997. On Suitability of Stabilizer Based on Chemical Analysis of the liquid from Stabilized soils//Proc. of 14th Int. Conf. SMFE, 1613-1616(in Chinese).

[7] Saitoh S, Suzuki Y., 1985. Hardening of Soil Improved by Deep Mixing Method. Proc. of 11th Int. Conf. SMFE, 1745-1748(in Japanese).

[8] Wang L. (2002) Cementitious Stabilization of Soils in the Presence Of Sulfate, PhD Thesis, Louisiana State University. Baton Rouge.

[9] Tsuki Kawamula, 1969. The interaction of selenium and clay mineral. Civil Engineering Committee 169(in Japanese).

[10]Croft J B., 1967. The Influence of Soil Mineralogical Composition on Cement Stabilization. Geotechnique117, 119-135.

[11]Yasuo Nakatsuka, 1986. The influence of cations exchange capacity (CEC) on strength of stabilized seabed silts. Proc. of the 41th Conf. of Japan Civil Engineering Committee13, 219-220(in Japanese).

[12] Mitsnnori Kawamuka, 1971. Influence of Exel-Augeable Cations(Na^{+}, Mg^{2+}, Ca^{2+}) Held on Bentonite on the Bentonite-Cement Interaction. Japan Civil Engineering Committee 192.

[13]Waddah S. Abdullah, Khalid A. Alshibli, Mohammed S. Al-Zou'bi, 1999. Influence of pore water chemistry on the swelling behavior of compacted clays. Applied Clay Science15, 447-462.

[14]Boardman DI, Glendinning S., Rogers CDF, 2001. Development of stabilisation and solidification in lime–clay mixes. Géotechnique51, 533-543.

[15]Junichi Kasai, 1979.Chemical improvement for Soil. Default Sementoenwari9 (391), 112-129 (in Japanese).

[16] Maclean D J., 1997. The influence of organism on cement stabilized soils. The Proc. of 5th Int. Conf. SMFE 2, 269-275.

Advanced Materials Research Vols. 989-994 (2014) pp 23-26
© (2014) Trans Tech Publications, Switzerland
doi:10.4028/www.scientific.net/AMR.989-994.23

Development and Application of the Screw Separator

Jingbo YIN [1, a], Jing LU [2, b], Li ZHAO[3, c], Sansi WANG[4,d]

[1]Shandong Water Polytechnic Rizhao,Shandong, 276826,China

[2] Rizhao DongGangDistrict people's hospital Rizhao,Shandong, 276826,China

[3]Shandong Water Polytechnic Rizhao,Shandong, 276826,China

[4] Shouguang City people's hospital Weifang,Shandong, 262700, China

[a]email: yinjb_2008@163.com, [b]email:59084998@qq.com [c]email:zhaoli_200909@126.com
[d]email:798858976@qq.com

Keywords: screw separator; development; application

Abstract. This article describes the research and development with the international advanced level of the screw separator, mainly used for the cleaner tailings fiber and the wastewater recycling and the use of stand-alone concentrated effect, into the plasma concentration of more than 0.5%, themaximum slurry concentration up to 60%, the device uses a unique control mechanism, without the power consumption will be able to achieve the automatic control of the plasma concentration, can efficiently remove moisture, recycled fiber, conservation of resources.

1Overview

In pulping process,it will produce a certain amount of waste residue, also known as tailings. The tailings contain a large number of moisture content and fiber. Now, stacked tailings of many enterprises are in the outdoor. Severe pollution caused by a lot of stacked tailings, which don't do process.Loss of water and fiber caused great waste to the enterprise. To draw lessons from foreign advanced technology, it will design and develop the screw separator with advanced level at home and abroad, mainly used for the cleaner tailings fiber and the wastewater recycling. The current domestic pulp manufacturers don't do process tailings, direct discharge away, which is no processing equipment. So the development of the screw separator will fill the domestic blank.

2 Introduction of the equipment

2.1 Structure

As shown in figure 1, the machine is made up of feeding mouth, motor, reducer, rack, filter drum, screw axis, automatic discharging export control mechanism, wastewater, etc. Contact with the plasma, the liquid parts adopt stainless steel manufacturing.

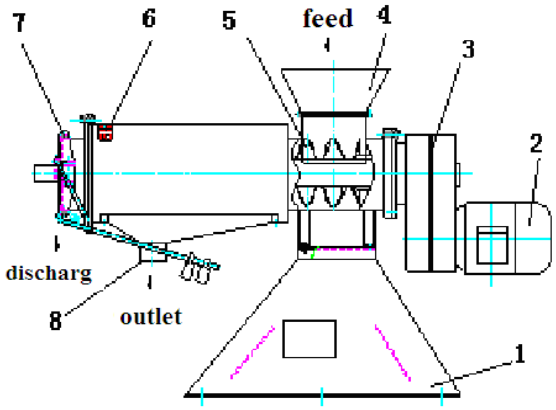

1-frame; 2- motor; 3-reducer; 4-feeding mechanism; 5-screw spindle; 6-filter drum; 7-discharging control mechanism; 8-outlet

Fig.1. Results structure of the screw separator

(1)Rack

Frame is composed of steel and steel plate welding. The frame is the matrix of the equipment, so it is the main supporting role. According to the 3 d model for the stress analysis of the whole machine to determine the center of gravity of the machine parts, and then designs as shown in the frame structure, ensure the stability and reliability of the equipment work.

(2)Screw Axis

Spiral shaft is composed of spiral pipe and spiral blade, the shaft top, which is all made of stainless steel materials. Equal pitch of the helical blade, and it is such as diameter, pulp from into pulp after entering the spiral filter press, box through the rotation of the screw axis, driven pulp movement forward. At the same time the pulp is for extrusion, and dehydration.

Screw axis and the connecting way of reducer is straight plug-in, which reduces intermediate links, ensures the installation precision and improves the transmission efficiency.

(3)The Filter Drum

Water drum filter consists of flange, filter plate, steel plate, such as stainless steel welded together. The pressure of the filter drum gradually increase from the inlet to the discharging mouth, so the center of the filter drum flange changed gradually from the beginning to the end. Screw axis of slurry squeezing out water drums filter after dehydration, drum filter using slotted screen.The size of the gap according to the concentration of the slurry, generally from 0.2 mm to 0.2 mm.

(4)Part of the Control

Control part consists of discharging plate, connecting rod, a heavy hammer, chain plate, pin, etc, is a special kind of linkage. Through the gravity of the hammer, to adjust the opening degree of discharging plate, the plate opening is smaller, the greater the pressure of the pulp, the smaller the slurry concentration. On discharging plate opening, the greater the pulp you less pressure, the slurry concentration. according to the concentration of slurry to adjust heavy hammer position, to control the pulp out of the slurry concentration[1].

(5)Device of the Transmission

Transmission device is to choose the structure of motor and speed reducer. The compact structure, transmission cumulative error is small and little vibration. At the same time installation space is small and saves the area.

2.2 The main technical parameters

Model: SP260, into the slurry concentration above 0.5%; The plasma concentration of 30%~60%; Production capacity is 6~8 $t \cdot d^{-1}$; Screw specifications phi 260 mm; Screw speed 50 $r \cdot min^{-1}$; The motor power 7.5 kw; Overall dimensions1720mm×660 mm×1900 mm; Equipment weight 550 kg.

2.3 The Principle of Work

As shown in figure 1, screw press filter consists of inlet, motor, reducer, rack, filter drum, screw axis, automatic discharge control mechanism, and other components of the waste water outlet, separation, dehydration, filtering, and the integrated use of extrusion technology. Feed concentration for more than 0.5%, according to the different of a slurry of plasma concentration can reach 60%, the highest realizes one machine can, is the present domestic very advanced solid-liquid separation equipment, can be used for the separation of a variety of materials, such as fiber, plastic, minerals, sludge, etc., mainly used for pulp and paper, sewage treatment, agriculture, food industry, such as domain, application scope is very broad.

Tailings from the slag separator into the screw pressure filter, screws spindle drive tailings with spiral blade forward movement and distribution on the axis of the auger spiral blade has a certain compression ratio. At the same time it improves the pressure of the front, forcing the moisture in the material under the action of pressure and filter out filter drum, out of a drain. Work is continuous press filter, the material is pumped through the body, front mounting pressure, when the big to a certain degree, is to open discharge outlet, squeeze, achieve the goal of extruded material. In order to grasp discharging speed and water content, it can adjust the host at the bottom of the counter weight (weight), in order to achieve satisfaction proper discharge concentration[2].

2.4 Technical Characteristics

(1)Into the pulp concentration is 0.5% more than without preconcentration, thus saving the water resource;

(2)Can be used for the separation of various solid structure, such as fiber, plastic, minerals, etc.;

(3)Stand-alone generate solid dryness up to more than 60%, this is does not have the similar equipment at home, the highest domestic enrichment equipment stand-alone dryness in about 28% or so;

(4)After the separation of solid dryness can adjust;

(5)Even particle size less than screen hole, the particle can be filtered out;

(6)Easy to install, operate and maintain, the screw has self-cleaning function;

(7)The space is little, installation without operators;

(8)Low investment cost, operation cost is low;

(9)Screw press filter uses a special link mechanism, by weight of weight of pulp out of the automatic control of dryness, change of the paste extrusion, in order to obtain different degree of dry solid. The control mechanism without hydraulic, pneumatic control, don't need any energy consumption, saving power consumption. At the same time, the single machine to more machine can realize the function, truly a multi-usage, reduce the production cost, save the water;

(10)The device has the function of overload protection.

3 The Flow of Process

In waste-paper deinking production line, for example, its production process flow diagram for[3]:

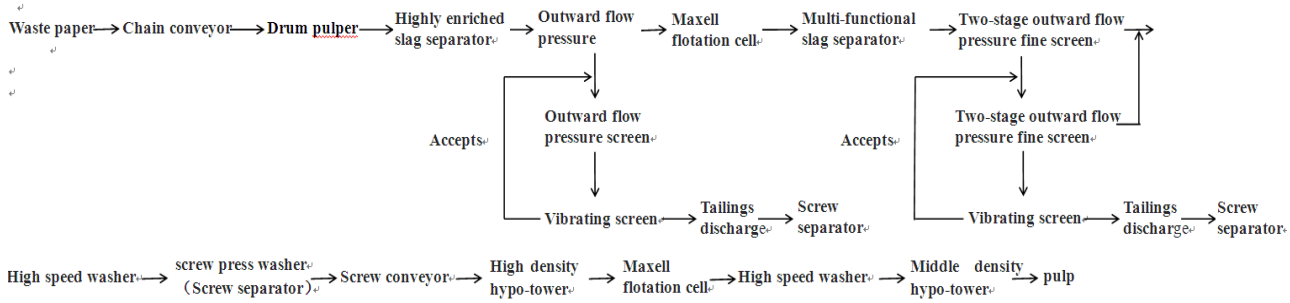

Fig.2. Waste-paper deinking production line flow chart

Can be seen from the above process, the spiral press filter installation is simple, which just puts the discharge of tailings to the screw press filter. In addition, the screw press filter can also be used in the mainstream line alternative helix crowded pulp machine, especially in non-wood fiber (cotton, bamboo, cotton, etc.) production line in the enrichment effect, which is better than spiral syrupcrowede confidential[3].

4 The Compare of Screw Press Filter and the Helix Crowded Pulp Machine

Helix crowded pulp machine is the wide application of an enrichment equipment, its different with spiral press filter is:

4.1 Screw press filter with helix crowded pulp machine are made of screw extrusion materials, action principle is the same. Due to the complex helix crowded pulp machine structure, big volume, heavy, the smallest screw phi 450 mm diameter, production capacity of 40 ~ 50 t/d, it is used in the mainstream line. Screw press filter for phi 260 mm diameter, production capacity of 6 ~ 8 t/d, apply to the tailings concentrated, mainly used in the end production line[4].

4.2 Screw press filter with helix crowded pulp machine control system is different. Four pneumatic cylinder helix crowded pulp machine by controlling the size of the discharging mouth to control discharge concentration. Pressure filter is established by the host at the bottom of the counter weight (weight) to control the pulp concentration. The position of the moving heavy

hammer, adjust the size of torque, control the discharging mouth opening degree and the extrusion pressure, reach the purpose of extruded materials, so as to control the size of the plasma concentration of[5].

5 Conclusion

Screw press filter of different pulp, pulp density is different, the cotton fiber, cotton stalk, and wood pulp pulping tailings for enrichment, the plasma concentration can reach 60%, even higher, to the tailings concentration, paper pulp slurry concentration can reach 30-40%. Screw press filter after successful development, the first in shandong gaomi paper mill trial, after more than half a year of operation practice proves that spiral press filter running effect is good. The tailings fiber and waste water recycling, saves a lot of resources for the enterprise, reduces the production cost, brings the good economic benefits. Now, the equipment has been concentrated in shandong JiaHe group compound fertilizer raw material used in production lines.

Next, we will develop a screw press filter series products, expand product specifications, to meet the market demand.

Add: three-dimensional figure spiral filter press

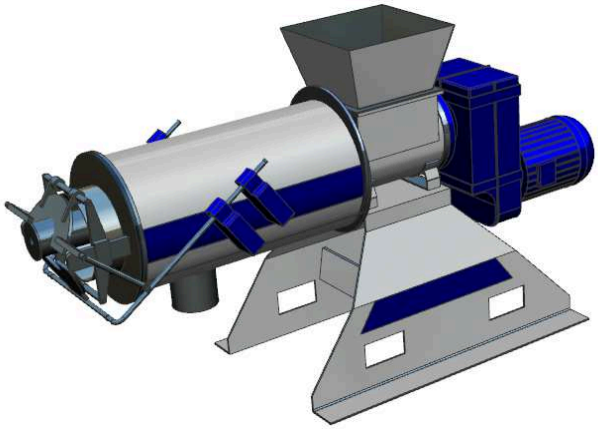

References

[1] Huang Shimao. Pulp and paper processing equipment [M]. Beijing: chemical and industrial press, 2002.

[2] King oak. Mechanical design [M]. Beijing: Beijing university of aeronautics and astronautics press, 2011.

[3] Zhao Li. Development and application of the high speed pulp washing machine [J]. Journal of China papermaking. 2005.8

[4] Zhao Li, Guo Lei.Countries on the basis of UG6.0 helix crowded pulp machine 3 d modeling design [J]. Journal of paper and paper. 2012.8

[5]YIN Jingbo, LI Zongyu.improvement design of screw shaft structure of a single-screw puple extruding machine[J].Forestry Machinery and Woodworking Equipment.2009.3

Advanced Materials Research Vols. 989-994 (2014) pp 27-30
© (2014) Trans Tech Publications, Switzerland
doi:10.4028/www.scientific.net/AMR.989-994.27

On laser shock processing to improve hot corrosion resistance of In718 superalloy

Yuchuan Bai[1a], Yinqun Hua[2,b,*], Zhen Rong[2]，Qing Xue[1]，Ruifang Chen[1]

[1]School of Mechanical Engineering, Jiangsu University, Zhenjiang Jiangsu 212013, China;

[2]School of Material Science and Engineering, Jiangsu University, Zhenjiang Jiangsu 212013, China

[a]e-mai: huxinzhuying@sina.cn, [b]e-mai: huayq@ujs.edu.cn.

* Corresponding author

Key words: Hot corrosion; Laser shock processing; In718 superalloy

Abstract: The aim of this research is to improve the hot corrosion resistance of In718 superalloy by laser shock processing. Specimens were treated by laser shock processing on the whole surface. The hot corrosion resistance beneath molten Na_2SO_4 under 900 ℃ was investigated. The effects of laser shock processing impacts on residual stress, surface microstructure and microstructure after hot corrosion test were investigated. Results show that 3 times laser shock processing can induce -400 MPa compressive residual stress. The microstructure was characterized by highly tangled and dense dislocations and a large number of twins. The average corrosion rate of In718 superalloy treated by laser shock processing is about 50 % lower than that of the untreated superalloy.

Introduction

Laser shock processing (LSP) is one of the most important surface modification techniques. Due to the interaction between high power density (GW/cm^2) laser beams and the surface of alloys, a high pressure shock wave was generated. The high level pressure causes a strong plastic deformation on the surface, which leads to a compressive residual stresses of several hundred MPa [1]. And the grain is refined owing to the dynamic recrystallization. Meanwhile, a larger number of microstructure defects, such as dislocation and twins, are induced on the surface layer.

In718 superalloy has a good comprehensive mechanical property, hot corrosion resistance, and oxidation resistance in the medium microtherm. It is widely used in turbine engine, advanced ship engine. In recent years, many researches have been done on the improvement of alloy's mechanical properties and electrochemical corrosion resistance. J.Z. Lu et al. concluded that compressive residual stress and grain refinement during LSP improved the stress corrosion cracking (SCC) resistance [2]. C. H. Zhou et al. improved hot corrosion resistance of alloys by nano crystallized and the micro crystallized coating [3]. However, the hot corrosion behavior of alloys treated by LSP is rarely involved. This study is trying to figure out the LSP's effects on the hot corrosion resistance of In718 superalloy under 900℃.

Experiment

The alloy used in this experiment is In718 superalloy, whose chemical composition (wt.%) is: Cr-20, Mo-3.3, Al-0.5, Ti-0.75, Nb-5, Ni-55, C-0.05 and balanced Fe. The material was cut into rectangular specimens of 15 mm × 15 mm × 2 mm in size.

The LSP experiments were carried out by a Q switched Nd: glass high power laser. The residual stresses were tested by applying standard X-ray diffraction (XRD) techniques. Transmission electron microscope (TEM) was used to observe the microstructure of the laser treated layer.

The specimens treated by LSP and prepared salt were put into a large Al_2O_3 crucible, which was then placed in an chamber electric furnace under 900 ℃. All the specimens were surrounded by an atmosphere consisting of Na_2SO_4 molten salt and air at the test temperature for 20 hours. The initial and final weights of the specimens were measured to assess the corrosion level. The surface morphology was characterized by scanning electron microscope (SEM) equipped with energy dispersive spectrum (EDS). The phases were identified by X-ray diffraction (XRD).

Results

Specimens treated by LSP from 1 to 3 times maintained an average compressive residual stress of -280 MPa, -360 MPa and -400 MPa, respectively. High level compressive residual stresses maintained within 250 μm from the top surface. The cross section of the alloy was observed by metallurgical microscopy. Figure.1 shows the typical TEM images of the substructures effected by LSP in the top surface layer of In718 superalloy. Fig.1 (a) is the image of highly tangled and dense dislocation. Fig.1 (b) is a lager number of typical mechanical twins.

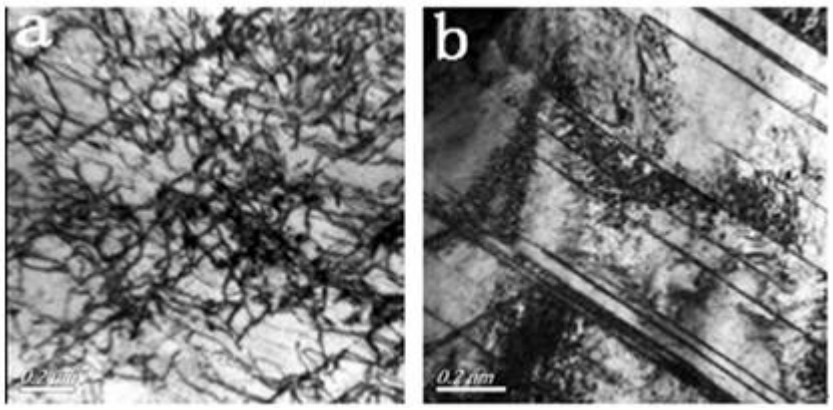

Fig.1. Typical substructure of the top surface after LSP

(a) dislocation (b) mechanical twins

As is shown in Fig.2, all of the specimens were layered to three layers after hot corrosion test. However, the depth of corrosion layers was quite different. From Fig.2 (a), specimens untreated by LSP have an corrosion depth about 30μm. The outer layer has been cracked and the grains were not homogeneous, its inner corrosion layer is very deep. The interface of oxidate film and substrate is wave shaped and has holes in it. While Fig.2 (b) shows specimens treated by 3 times LSP have an corrosion depth about 20μm. The corrosion layer has a good adherence with the substrate and the grains are tiny homogeneous. The interface is much smooth and has less holes. From the corresponding EDS of the inner layer, both of the specimens are rich of Cr in this exact layer.

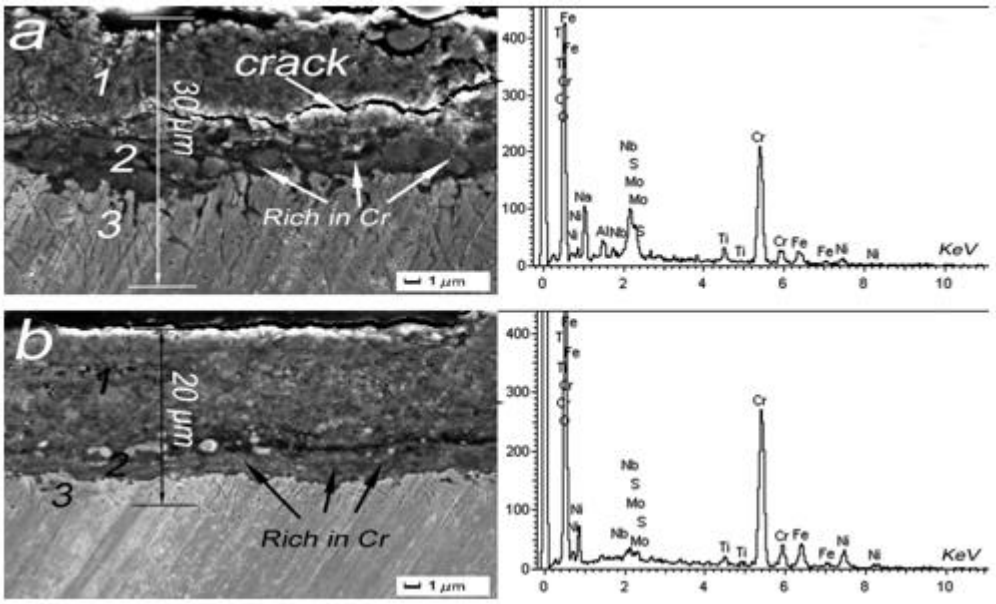

Fig.2. The section morphology of corrosion layers and their EDS of the inner layers

(a) specimen untreated by LSP (b) specimen treated by 3 times LSP

According to the phase analysis, the outer layer corrosion products are very complicated. The inner layer corrosion products mainly consist of (Cr, Fe)$_2O_3$, Fe(Cr,Al)$_2O_4$, NiCr$_2O_4$, Al$_2O_3$. The inner corrosion layer corrosion products mainly consist of (Cr, Fe)$_2O_3$, Al$_2O_3$. Normally, oxidates such as Cr$_2O_3$, Al$_2O_3$ grow slowly and have good stabilities at high temperature [4].

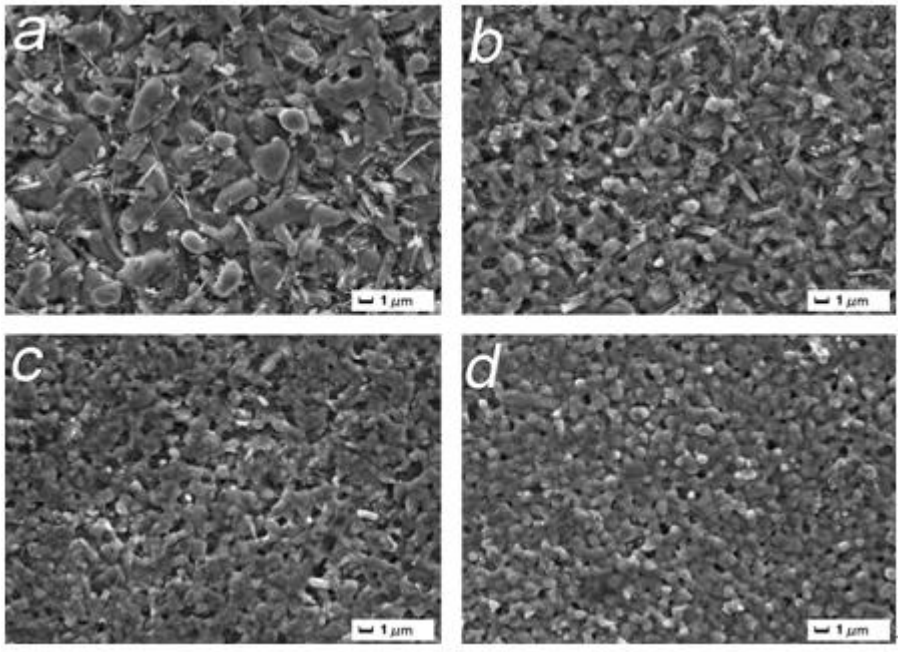

Fig.3. Hot corrosion morphology of In718 superalloy

(a) 0 LSP, (b) 1 LSP, (c) 2 LSP, (d) 3 LSP

Fig.3. shows the hot corrosion morphology of In718 superalloy. With the increase of LSP times, the corrosion products turned to be tiny homogeneous, the continuity was getting better. Corrosion products of untreated specimens are several times bigger than those treated specimens. The tiny homogeneous corrosion products will be beneficial for the dispersion of the corrosion stress.

After corrosion in molten Na$_2$SO$_4$ for 20 h, the average corrosion rate of specimens untreated by LSP was 0.88 (mg/cm^2·h), while the average corrosion rate of specimens treated by 1 time LSP was 0.65 (mg/cm^2·h), which is 35.4 % lower. The average corrosion rate of specimens treated by 2 times LSP was 0.60 (mg/cm^2·h) , which is 46.7 % lower than that of the untreated specimens. And the average corrosion rate of specimens treated by 3 times LSP was 0.57 (mg/cm^2·h) , which is 54.4 % lower than that of the untreated specimens. Therefore, LSP has beneficial effects on the hot corrosion resistance of the In718 superalloy.

4. Discussion

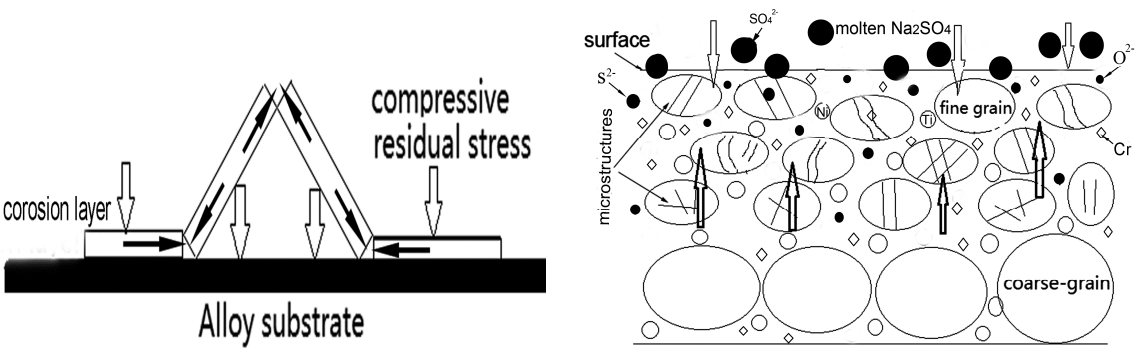

(a) compressive residual stress effect (b) microstructure effect

Fig. 4. Schematic of the LSP effect on hot corrosion behavior

We have shown that the interaction between laser pulse and the surface of In718 superalloy could lead to a high level compressive residual stress in the surface and depth direction. There is serious stress corrosion in the hot corrosion test. As is shown in Fig.4 (a), compressive residual stress in the surface direction can delay crack initiation of the corrosion layer and compressive residual stress in the depth direction can slow down the growth of microcrack on the specimen surface [5].

According to the oxide film mass transfer experiments [6], dislocation and grain boundary diffusion was significantly faster than the lattice diffusion. As is shown in Fig.4 (b), in the corrosion process, these microstructures induced by LSP added the paths of element diffusion. Self-healing capability of the oxidation films was improved. Moreover, the nucleation energy reduced in the crystal defects, so oxidation film can be more easily nucleated in these places. The growth stress was released, which also makes a better adhesion with the alloy substrate.

5. Conclusions

The following conclusions can be drawn from this research:

1) With the increase of laser shock times, the corrosion lightened. After corrosion for 20 h at 900 ℃, the average corrosion rate of In718 superalloy treated by laser shock processing was about 50 % lower than that of the untreated superalloy.

2) The grain refinement and microstructures in it add the element (Cr, Ti etc.) diffusion paths. Self-healing capability of the oxidation films were improved. The tiny homogeneous oxidation layer with a good plasticity was formed in a short time. The high level compressive residual stress in the LSP treated layer can increase the adhesion of the corrosion layer. It works for the balance of the corrosion stress.

Acknowledgments

The authors acknowledge this work was supported by the National Natural Science Foundation of China (No.51175234) and the Heights Talent Support Programs in Six Industrial Fields in Jiangsu Province (No. 2011-JXQC069).

References

[1] Zongbao Shen, et al., An experimental study of overlapping laser shock micro-adjustment using a pulsed Nd:YAG laser, Optics & Laser Technology, 54 (2013), pp. 110–119.
[2] J.Z. Lu, et al., Effects of laser peening on stress corrosion cracking (SCC) of ANSI 304 austenitic stainless steel. Corros. Sci. 60 (2012), pp. 145–152.
[3] C. H. Zhou, et al., Comparison of the hot corrosion of nanostructured and microstructure thermal barrier coatings. Materials and Corrosion, 2012, 63, No. 9999.
[4] Z.M. Li , et al., Microstructure and oxidation resistance of magnetron-sputtered nano crystalline NiCoCrAlY coatings on nickel-based superalloy, J. Alloys Compd. 505 (2010), pp. 675–679.
[5] Zhang XC, et al. Effect of graded interlayer on the mode I edge delamination by residual stresses in multilayer coating-based systems. Appl. Surf .Sci. 254 (2008), pp.1881–9.
[6] Graham M J, Hussey R J. Analytical techniques in high temperature corrosion, Oxid. Met. 44 (1/2) (1995), pp.339-374.

Advanced Materials Research Vols. 989-994 (2014) pp 31-34
© (2014) Trans Tech Publications, Switzerland
doi:10.4028/www.scientific.net/AMR.989-994.31

Extraction and Purification of Fluorene from Wash Oil

Yongsheng E

Department of Biomedical and Chemical Engineering, Liaoning Institute of Science and Technology, Benxi Liaoning, 117022, China

email: eys73@126.com

Keywords: Fluorene; Extraction; Purification

Abstract: Fluorene is a basic chemical raw material, which has wide applications.This paper introduces the current fluorene technology of extration and purification from wash oil. Use the after-cut of wash oil as raw material, get fluorene by distillation and solvent crystallization. The content of fluorene is higher than 97%.The total yield is 72.24%, which is higher than current domestic production levels.

1 Introduction

Fluorene is a basic chemical raw material, which is mainly used for preparation of medicines, synthesizing dyes and accessory ingredients etc. It is really worthwhile expanding the market[1].

The production methods of fluorene are divided into two kinds of synthesis and extraction in general. Due to the high cost and serious pollution of synthesis, all fluorene products are extracted from coal tar[2]. Fluorene are mainly distributed in the wash oil of coal tar, the mass fraction is about 10%. The study about extraction and purification of fluorene from the wash oil has important significance.

Extraction and purification of fluorene from wash oil have cooling crystallization method and solvent crystallization method[3]. Cooling crystallization method is through cooling fluorene fractions and crystallizing without solvent, the concent of fluorene product is 85%. Solvent crystallization method is through adding solvent in the crystallization process, thus the concent is higher than 95%[4]. Because fluorene product has high purity and good quality by solvent crystallization method, thus it becomes the main method for producing fluorene[5]. This paper will do detailed study to solvent crystallization method.

2 Experiment

2.1 raw material

The after-cut of wash oil, the composition are shown in Table 1

Table 1 Composition of the after-cut

Component	*acenaphthene*	*diphenylene oxide*	*fluorene*	**others**
Content [%]	15	30	38	17

2.2 The experimental equipment

Efficient distillation column, φ100 × 2500, triangular spiral filler, the number of measured plate is 85.

A crystallization device.

The results are analyzed by a gas chromatograph.

2.3 The experimental procedure

Take the after-cut of wash oil 40kg, which is distillated in the distillation column of plate number 85. When the reflux ratio is 5:1, 10:1 or 15:1, we cut a fraction every 2-3℃, test its purity and calculate yield. According to the results, we choose suitable distillation rang and reflux ratio.

Use ethanol, toluene or xylene to purify fluorene fractions above by crystallization. Change solvent ratios and crystallization temperature to observe the changes in quality and yield of fluorene. We require the content of fluorene products is more than 97%.

3 Results and discussion

3.1 the distillation of after-cut

Take the after-cut of wash oil 40kg, distill, the experimental results are shown in Table 2.

Table 2 The experimental results of distilling the after-cut

Serial Number	Distillation Range [℃]	Reflux Ratio	Weight [kg]	Content [%]	Fractions species
1	280-283		3.4	25.4	Before-cut
2	283-285		4.2	39.92	Main distillate fraction
3	285-287		5.12	59.15	Main distillate fraction
4	287-290	5：1	4.56	66.76	Main distillate fraction
5	290-292		4.7	65.59	Main distillate fraction
6	292-294		2.5	58.32	Main distillate fraction
7	294-297		3.2	35.35	After-cut
8	283-285		5	44.29	Main distillate fraction
9	285-287		5.52	65.51	Main distillate fraction
10	287-290	10：1	4.16	71.81	Main distillate fraction
11	290-292		4	70.95	Main distillate fraction
12	292-294		3.2	64.15	Main distillate fraction
13	294-297		2.4	38.21	After-cut
14	283-285		4.47	45.37	Main distillate fraction
15	285-287		5.26	65.67	Main distillate fraction
16	287-290	15：1	4.7	72.02	Main distillate fraction
17	290-292		4.5	71.39	Main distillate fraction
18	292-294		3.2	63.66	Main distillate fraction

It can be seen from the experimental results, the content and quantity of fluorene fractions are different with the different reflux ratio and distillation range. The suitable distillation range is 283℃ ~ 294℃.

These main distillate fractions every reflux ratio are mixed, we will obtain the entire quantity of fluorene fractions, and may calculate the yield and content of the main distillate fraction every reflux ratio. The results are shown in Table 3.

Table 3 The results of the mixed main distillate fractions

Serial Number	Distillation Range [℃]	Reflux Ratio	Weight [kg]	Content [%]	Yield(%)
1	283-294	5：1	21.08	58.30	80.85
2	283-294	10：1	21.88	62.65	90.18
3	283-294	15：1	22.13	63.79	92.87

It can be seen from table 3, the weight, content and yield of fluorene fractions are different with the different reflux ratio. When the reflux ratio is 5:1, the producing speed increases and energy consumption reduces, but the content and yield are low. When the reflux ratio is 15:1, the content and yield of flourene fractions are high, but the production efficiency is low and energy consumption becomes large. We should comprehensively consider these factors, choose appropriate reflux ratio. According to the above results, we select the reflux ratio of 10:1, thus, we can get the flourene fractions, its content is 62.5% and its yield is up to 90.18%.

3.2 the solvent crystallization of flourene fractions

Take flourene fractions above, its content is 62.5%, crystallize with different solvent, the experimental results are shown in Table 4.

Table 4 The experimental results of solvent crystallization

Serial Number	Solvent Species	Solvent and fraction ratio	Crystallization Temperature (℃)	Content [%]	Yield [%]
1	ethanol	0.8：1	25	88.15	84.51
2	toluene	0.6：1	25	92.47	80.21
3	toluene	0.8：1	25	95.26	78.54
4	toluene	1：1	25	96.38	74.28
5	xylene	0.6：1	25	94.21	81.25
6	xylene	0.8：1	25	97.45	80.11
7	xylene	1：1	25	97.89	75.69
8	xylene	0.8：1	20	93.84	83.57
9	xylene	0.8：1	23	95.73	81.49
10	xylene	0.8：1	28	97.69	76.38
11	xylene	0.8：1	30	97.92	73.24

It can be seen from the experimental results, due to poor solubility, ethanol is not suitable as the crystallization solvent of fluorene fractions. In the same amount of solvent and crystallization temperature conditions, the yield and quality using xylene as solvent is better than using toluene, therefore, we choose xylene as crystallization solvent of fluorene fractions.

It can also be seen from Table 4, a large proportion of the solvent and a high crystallization temperature will improve the quality of fluorene, but the yield is low. On the contrary, a small proportion of the solvent and a low crystallization temperature will increase yield of fluorene, but the quality is poor.

According to the results shown in Table 4, we select the solvent and fluorene fractions ratio of 0.8:1, the crystallization temperature of 25℃, which are more suitable crystallization conditions. Thus, we can get fluorene product whose content is 97.45% and yield is 80.11%.

The total yield of two steps is 72.24%.

4 Conclusion

4.1 First, the after-cut of wash oil is distillated in the distillation column of plate number 85, the reflux ratio is 10:1, the range of distillate temperature is between 283 ℃ and 294 ℃. The content of fluorene fractions is 62.65% and the yield is 90.18%.

4.2 Second, use xylene as solvent to purify fluorene fractions. The solvent and fluorene fractions ratio is 0.8:1, the crystallization temperature is 25℃, content is 97.45% and yield is 80.11%. The total yield of two steps is 72.24%.

References

[1] Lv Miao, Yi Ding, Wang Renyuan. Study on Fluorene Extraction from Acenaphthylene Oil [J]. Fuel ＆ Chemical Processes. 2005,36 (5) :38-40.

[2] Liang Xiaoqiang. Fluorene and Dibenzofuran from Gas Absorber Oil [D]. Taiyuan University of Technology Master thesis.

[3] JIA Chunyan, YIN Qiuxiang, ZHANG Meijing, WANG Jingkang. Purification of fluorene by melt crystallization [J]. Journal of Chemical Industry and Engineering (China). 2007,58(9):2266-2269.

[4] Xiao Ruihua. Coal Tar Chemical Engineering(the Second Edition) [M]. Metallurgical Industry Press. 2009.2.1:199-202.

[5] Gong Junku. Research on producing high purity fluorene using solvent crystallization [J]. Fuel ＆ Chemical Processes. 1998,29 (4) :213-215.

Advanced Materials Research Vols. 989-994 (2014) pp 35-38
© (2014) Trans Tech Publications, Switzerland
doi:10.4028/www.scientific.net/AMR.989-994.35

Microwave Hydrothermal Synthesis and Characterization of In_2O_3 Nanocrystalline

Yinyin HU, Wenxiang YE，Jian LEI , Quanxin ZHU, Wanqing XIONG and Xue-Hong LIAO*

Hubei Key Laboratory of Preparation and Application of Catalytic Materials，The College of Chemical Engineering, Huanggang Normal University, Huanggang, 438000, Hubei, P.R.China

Email:liaoxuehong@sohu.com

Keywords: Microwave-hydrothermal method; synthesis; Indium oxide; nanopowder.

Abstract: In_2O_3 nanopowder was successfully synthesized using microwave-hydrothermal method; by a very simple fast reaction between $InCl_3$ and urea in aqueous solution contain 1% polyethylene glycol. The products were characterized by the techniques of X-ray diffraction (XRD), Scanning electron microscope (SEM) and Fluorescent spectrum. The result shows that as-prepared In_2O_3 nanopowder is cubic phase, the morphology is square composed of many particles.

1 Introduction

In_2O_3 is an important functional material which has a wide band gap, small resistivity and high catalytic activity. It is a kind of n-type semiconductor. Because In_2O_3 material has showed good gas-sensing properties for oxidizing and reducing gases, and is widely used in gas sensors[1].

Indium oxide and indium hydroxide is important semiconductor material, the block In_2O_3 has no fluorescence properties at room temperature. However, when the size reduced to the nanoscale, as a result of the existence of crystal aerobic hole, it has good fluorescence properties. The direct band gap width of In_2O_3 is 3.6 eV, indirect band gap is 2.6 eV, In_2O_3 is a kind of wide band gap transparent semiconductor materials. Bulk phase indium oxide is a larger third-order nonlinear vibration of non-oblique inorganic materials, But when the particle size decreases, especially after nanoparticlization, as nanoparticles have larger surface area. There are a large number of atoms, or ions in particle surface show that the larger surface activity, so they are sensitive to the external environment[2]. By changing the environment around the particles, the optical properties of the particles will have great changes. There have been many past literature reported In_2O_3 nanostructures with good photoluminescence properties. For example, Yang etc found that the emission wavelength of In_2O_3 nanosphere and nanoclusters is 416 nm and 439 nm. Zhang etc reported indium oxide nanoparticles under UV irradiation has distinct emission peaks at 480 nm and 520 nm[3]. Qian etc found that the emission wavelength of In_2O_3 nanocubes is 378 nm, 378 nm, 420 nm, and the emission wavelength of In_2O_3 nanofibers is 450 nm.

The nanometerIn_2O_3 is a new type of inorganic materials, which is applied widely. Due to the fine particle size of particles, nanometer materials produced surface effect, quantum size effect, small size effect and macroscopic quantum tunneling effect what bulk material does not have. Because the nanometer indium oxide has many excellent properties, the preparation of nanometer In_2O_3 becomes one of the hot research in China in recent years [4] .

In this paper, nanometer In_2O_3 was synthesized using Microwave-hydrothermal method. It was characterized by the techniques of X-ray diffraction (XRD), and a preliminary discussion of the formation mechanism of indium oxide particles.

2 Experimental section

2.1 Instruments and reagents

Chempower microwave synthesizer（Zhichun, Shanghai Scientific Instrument Co.,Ltd) was used. Powder XRD was used to characterize the sample. Data were collected on a Rigaku

D/max-2500V/PC X-ray diffractometer(Japan). The morphology and size were determined by SEM. The SEM images were recorded on a Quanta 200 FEG field emission scanning electron microscopy (USA). Cary Eclipse fluorescence spectrometer(USA Varian Company) was used for monitoring the fluorescent spectrum of as-prepared sample.

All the reagents used were of analytical purity. Doubly distilled water was used throughout the experiments.

2.2 Synthesis of In_2O_3 nanopowder

Put 0.3g $InCl_3$ and 0.4g urea in the microwave hydrothermal reaction bottle, 10mL 1%PEG solution was added, sealed bottle and put it in the microwave reaction apparatus. At 120 ℃, microwave reactor 180 minutes. When the reaction was ended and cool down naturally to the room temperature. Then the precipitate was centrifuged, washed with the distilled water and dried at 60 ℃ in the vacuum for 4 h, the power was sintered at 773 K for 2 h. The final product was collected for the characterization.

3. Results and discussion

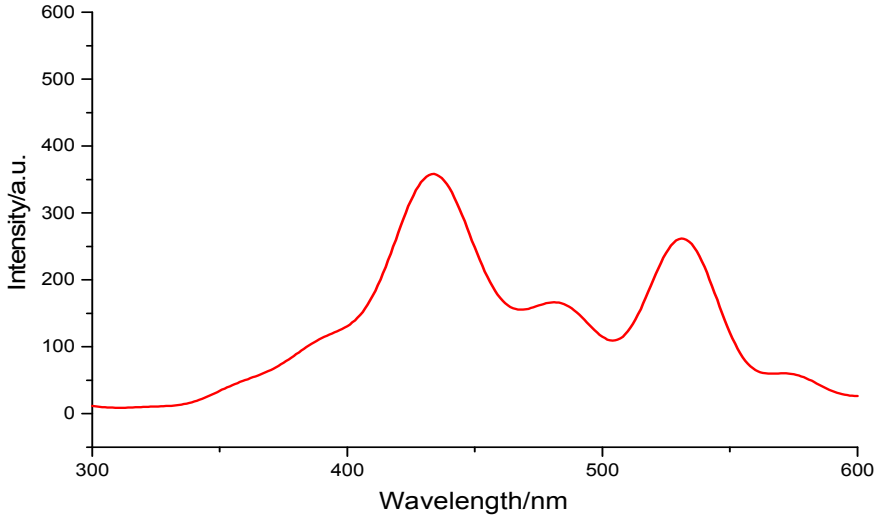

Fig.1 Fluorescent spectrums of sample

Figure 1 shows that at 435 nm and 530 nm, samples have strong fluorescence emission. Known by the SEM image, the product is a cubic structure. the block In_2O_3 has no luminescent properties. And different methods for preparing nanometer In_2O_3 particles have different emission spectra. Indicating their photoluminescence properties may be affected by the dimensions, shape and size. Compared with the literature [2], the strongest absorption peak of the sample is 435nm, slightly red shifted.

Figure 2 is a scanning electron micrograph of the sample. It is evident from the figure that sample particle is tetragonal structure, and its shape is very regular, angular. Because of reunion, some part seems to be the large square.

Fig.3 is the X-ray diffraction patterns of as-prepared samples. The result shows that In_2O_3 product is cubic structure. The intensity of the diffraction peak is higher declares that product has good crystallinity.

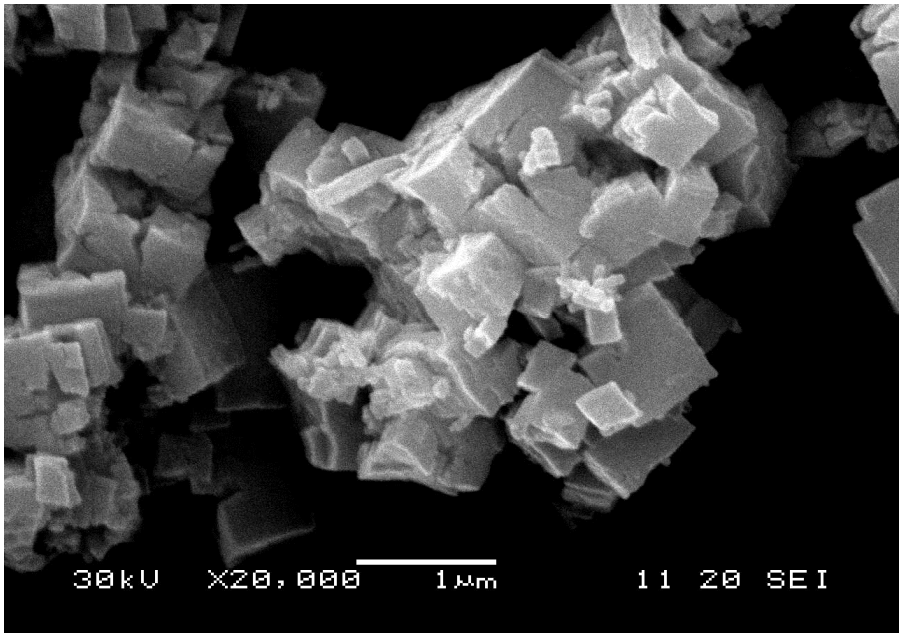

Fig.2 Scanning electron micrograph of as-prepared sample

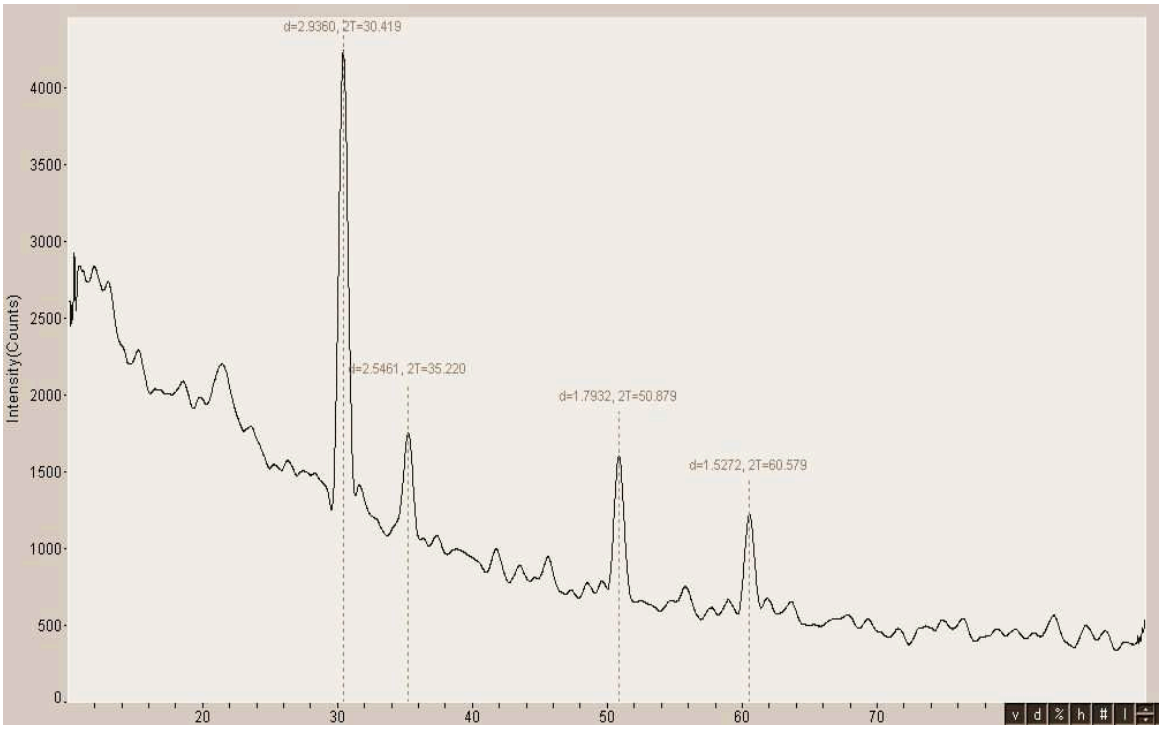

Fig.3 The X-ray diffraction patterns of as-prepared samples

Under the condition of microwave reaction, $InCl_3$ releases In^{3+} which combines with OH^- which urea releases. Producing predecessor $In(OH)_3$. PEG in the reaction is a surface active agent, serving as dispersion. Precursor decomposes at a high temperature, to produce In_2O_3 pale yellow powder.

$$In^{3+} + OH^- \rightarrow In(OH)_3$$

$$In(OH)_3 \rightarrow In_2O_3 + H_2O$$

In the process, the influence of the temperature may be reflected in two aspects. Firstly, under the high temperature calcination, due to the loss of lattice oxygen, indium oxide can form the stoichiometric oxide. Indium oxide bulk phase produces oxygen vacancy and free electrons. In the process of gas sensitive response, is a important factor to affect gas sensitive performance. Secondly, the calcination temperature is different, the size and the crystallisation degree of In_2O_3 will be affected [5].

4 Conclusions

Under the microwave hydrothermal conditions, white fine powder $In(OH)_3$ was prepared by $InCl_3$ and urea in PEG aqueous solution. Unde the high temperature calcination, the predecessor decomposed, producing In_2O_3 light yellow crystal. The shape is more regular, and is tetragonal structure. There was a strong fluorescence emission at 435 nm and 530 nm, compared with the literature, slightly red shifted.

Acknowledgments: This work is supported by Functional Materials Research Team of Huanggang Normal University.

References

[1] J Xu, X Wang, G Wang, et al, In_2O_3 nanomaterials of hydrothermal synthesis, structure characterization and its gas sensitive properties:Journal of Sensors and Actuators, 2007,20（1）:1
[2] C Wang, Controlled synthesis and characterization of nanostructured indium oxide [doctor thesis], Shangdong: Shandong University, 20090410
[3] L Zheng, X Wu, Study on the Preparation of indium oxide nanoparticles: Guizhou Chemical Industry 2005,30（3）：25
[4] J Zhou, D Jia, J Liu. Low heatsolid-state reaction and opticalproperties of copper sulfide nanorods. Chemical Journal of Chinese Universities, 2005，26（4）：620—622.
[5] G Zhu, H Xu, Hydrothermal synthesis of monodispersed nanometer indium tin oxide powder, Journal of Inorganic Materials, 2005,20（2）：13-14

Advanced Materials Research Vols. 989-994 (2014) pp 39-44
© (2014) Trans Tech Publications, Switzerland
doi:10.4028/www.scientific.net/AMR.989-994.39

Synthesis of High-strength and Water-resistant Phosphogypsum Small Hollow Block

Hongbo XIE [1,2,3,a], Weibin MA [1,b] ,Cantao YE[1,c]

[1]CAS Key Laboratory of Renewable Energy,Guangzhou Institute of Energy Conversion，Chinese Academy of Sciences, Guangzhou 510640，China；

[2]University of Chinese Academy of Sciences，Beijing 100049，China；

[3]GuangDong Building Material Research Institute，Guangzhou 510160，China；

[a]emali:gdbuilding@163.com, [b]email: mawb@ms.giec.ac.cn, [c]email: yect@ms.giec.ac.cn

Key words: Phosphogypsum; Softening coefficient；Balling; Cement coating;Small hollow block

Abstract. The non-calcined phosphogypsum was modified and purified by quicklime, aged, treated by balling and cement coating, and then mixed with an appropriate amount of water, the cementitious material, gravel and so on. After using the vibration pressure molding process and the nature curing, the prepared high-strength and water-resistant phosphogypsum small hollow block can produce a softening coefficient of 0.82 and a compressive strength of 7.5 MPa, and the other properties meet the MU7.5 grade requirements of normal concrete small hollow block on the GB 8239-1997, which broadens the application range of phosphogypsum small hollow block, and may provide a new way to solve the comprehensive utilization of phosphogypsum.

Introduction

Phosphogypsum is industrial byproducts of phosphoric acid production process emission, and producing of 1t phosphoric acid will discharge about 5t phosphogypsum. With industrial development, China has accumulated stockpiles of several gigatons phosphogypsum, and the annual phosphogypsum emissions have more than 50 million tons, but its utilization rate is only 20%. Phosphorus chemical phosphogypsum piles up like a mountain, encroaches the fertile land, pollutes the environment, and causes the nuisance. In order to solve the hard bottleneck problem in the use of phosphogypsum, the development and application of phosphogypsum are imminent, but more difficult [1,2]. Currently the mature phosphogypsum application process technology in the implementation process will consume a certain amount of energy in China, for example calcining of the raw material in the production process and autoclave curing of phosphogypsum products will consume a lot of fuel coal and hydropower resources, which is contrary direction of the world's low-carbon economy and low-carbon building materials [3,4].

In this paper, non-calcined gypsum is used as the main raw material, followed by the modified impurity, aging, balling, cement coating process, the vibration compression molding, the nature conservancy and other process steps are used, and a high water resistance phosphogypsum blocks are produced. Their various performance indicators have reached the MU7.5 grade requirements of normal concrete small hollow block on the GB 8239-1997. And because its production process does not need the calcined gypsum and autoclave curing of phosphogypsum blocks, compared with the traditional method to produce gypsum products [3,4], the small hollow block production process is more energy efficient, consistent with the direction of Chinese current the development of low-carbon, friendly environment, energy-saving building materials, and also provides a new way to solve the problem of comprehensive utilization of phosphogypsum.

1 Experiment

1.1 Raw materials

(1) Phosphogypsum is purchased from the discharged phosphogypsum yard of a phosphoric acid production enterprise in Zhanjiang City, Guangdong Province, China, and its composition is shown in Table 1.

Table 1 Chemical composition of phosphogypsum

SO_3	Al_2O_3	CaO	MgO	SiO_2	Fe_2O_3	P_2O_5	F^-	ignition loss	crystal water	PH
38.28	0.82	29.42	0.53	10.36	1.49	1.95	0.25	17.62	16.90	4.8

(2) Quicklime is purchased form a quicklime factory in Pingnan City, Guangxi Province, China. Quicklime is grounded to 200 mesh with sieve residue less than 15%, the effective CaO content is greater than 80%, digestion time is 3~4 min, digestion temperature is 90 ℃, and quicklime is rapidly digested lime.

(3) Cementitious materials are P.O 42.5R Conch, China.

(4) Gravel is from sand and stone market in Zhanjiang City, Guangdong Province, China.

1.2 Experimental method

(1) modifying of phosphogypsum: a certain amount of gypsum and quicklime are dryly mixed, kept stirring, sprayed with water mist, aged 1 days to make the quicklime fully digest and react sufficiently with harmful impurities of phosphogypsum, and the modified phosphogypsum powder is prepared.

(2) Preparation of phosphogypsum ball: the modified phosphogypsum powder balls via a ball machine, and phosphogypsum ball is obtained; and on this basis of its parcel handling of cement, cement coated phosphogypsum ball is obtained.

(3) Sample preparation and performance test: The above modified phosphogypsum powder, phosphogypsum ball, cement coated phosphogypsum ball, cement and gravel are mixed with a certain amount of water, added into block machine, made small hollow block size of 390mm × 190mm ×190mm, aged for conservation under natural conditions, and tested the performances. All performance tests are in accordance with the test methods for normal concrete small hollow block on the GB 4111-2013[5,6].

2 Results and analysis

2.1 Effect of quicklime addition on the modification of phosphogypsum and performance of small hollow block

From the phosphogypsum component analysis, as shown in Table 1, phosphogypsum contains a certain amount of soluble phosphorus (as P_2O_5) and soluble fluorine (in F^- meter), if the impurity processing of these soluble impurities are not carried out, it will adversely affect the performance of phosphogypsum small hollow blocks, especially the compressive strength and softening coefficient [7,8]. Quicklime was added to impurity and fully mixed with phosphogypsum by adding an appropriate amount of water, the soluble impurities were transformed into insoluble or poorly soluble substances by chemical reaction, which eliminates the effect of the soluble impurities on performance of phosphogypsum blocks, the involved chemical reactions are:

$$CaO + H_2O = Ca(OH)_2$$

$$3Ca(OH)_2 + P_2O_5 = Ca_3(PO_4)_2 \downarrow + 3H_2O$$

$$2F^- + Ca^{2+} \rightarrow CaF_2 \downarrow$$

Calculated from the above reaction formula, in order to enable soluble phosphorus and fluorine of phosphogypsum completely convert to insoluble or poorly soluble material, the additive amount of quicklime was about 3%.

Meanwhile, in order to investigate the quicklime addition on properties of phosphogypsum small hollow blocks, 1%, 2%, 3%, 4%, 5%, 6% quicklime (relative phosphogypsum mass) was modified, aged for 1 days, phosphogypsum small hollow block samples were obtained by using vibration compression molding with the ratio of the modified phosphogypsum powder, cement and gravel of 5:1:4, 10% water, the pressure of 15MPa, and natural curing after ejection for 28 days, the compressive strength and softening coefficient are measured, the test results are shown in Fig.1 and Fig.2.

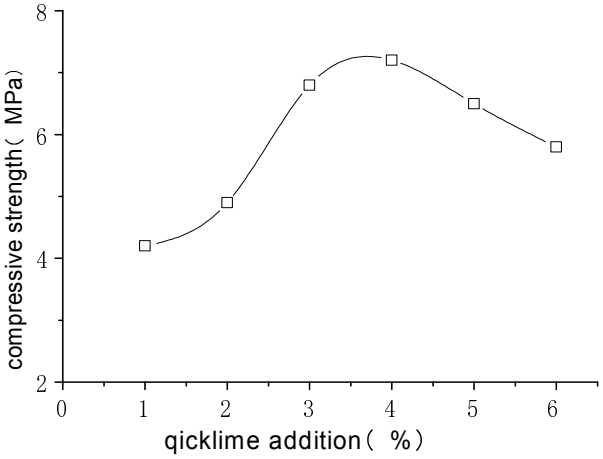

Fig.1. Effect of quicklime addition on the compressive strength of block

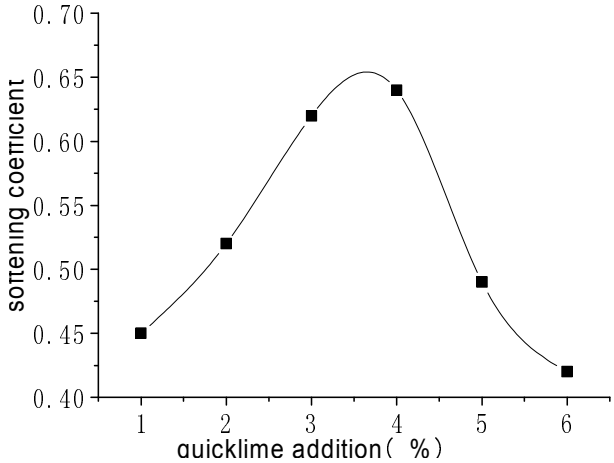

Fig.2. Effect of quicklime addition on the softening coefficient of block

Fig.1 and Fig.2 show that the compressive strength and softening coefficient of phosphogypsum small hollow blocks increased first and then decreased with the increasing of the amount of quicklime. When quicklime was less than 3%, the compressive strength and softening increased significantly, when it is 4%, two performance index reached maximum, then decreased with the increasing of the amount of quicklime. And it can be seen from Fig.2 that when the amount of quicklime was over 4%, the softening coefficient of phosphogypsum small hollow blocks significantly decreased. The reason may be that when the amount of quicklime is less than 3%, the soluble phosphorus and fluorine impurities of phosphogypsum could not completely be converted to insoluble or poorly soluble substances, leading to the compressive strength and softening coefficient of resulting small hollow block low; if quicklime was greater than 4%, although the soluble phosphorus and fluorine impurities of phosphogypsum have been converted to insoluble or poorly soluble substance, there is quicklime participate in the reaction (or known as f-CaO), the compressive strength of prepared phosphogypsum small hollow blocks decreased due to residues of these quicklime, and the block body will swell after soaking in water, resulting in softening coefficient blocks significantly lower. So the ideal dosage of quicklime was 4%, slightly larger than the previous calculation results, which can be considered that part of the acid-base neutralization reaction was involved, and the compressive strength and softening coefficient of phosphogypsum small hollow blocks were 7.2 MPa and 0.62, respectively.

2.2 Effect of phosphogypsum treatment on the properties and morphology of phosphogypsum small hollow blocks

As is known from the previous experiment, when the amount of quicklime was 4% of phosphogypsum, the compressive strength and softening coefficient of phosphogypsum small hollow blocks were 7.2 MPa and 0.62, respectively if the materials were mixed in powder, the compressive strength had reached standard requirements of normal concrete small hollow block on the GB 8239-1997, but their softening coefficient was still low. In order to improve the softening

coefficient of phosphogypsum small hollow blocks, the modified phosphogypsum was balled into phosphogypsum powder, coated with cement, and the prepared phosphogypsum balls and cement coated phosphogypsum balls are shown in Fig.3 and Fig.4, respectively. And referring to the molding process and formula described in 2.1, phosphogypsum small hollow blocks were prepared, maintained to the age, the softening coefficient and compressive strength were tested. The compressive strength and softening coefficient of phosphogypsum small hollow blocks obtained with different treatment process are shown in Fig.5 and Fig.6.

Fig.3. Phosphogypsum balls

Fig.4. Cement coatedphosphogypsum balls

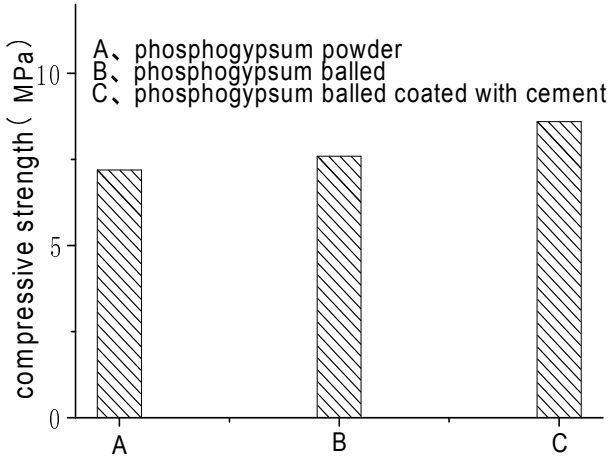

Fig.5. Effect of treatment process on the

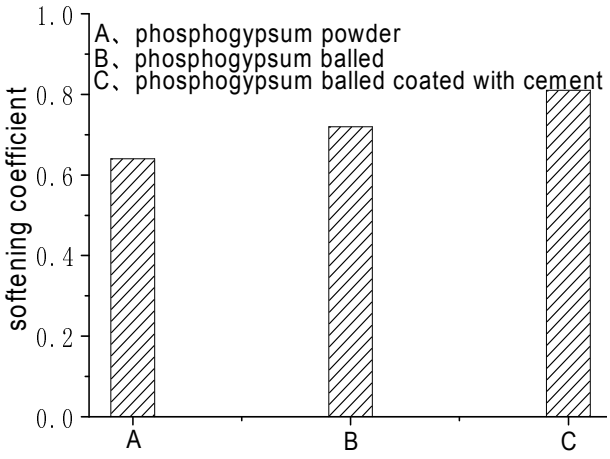

Fig.6. Effect of treatment process on the softening coefficient

Fig.5 and Fig.6 show that the compressive strength and softening coefficient of the obtained modified phosphogypsum small hollow block powder after balled and cement coated were improved, and its compressive strength and softening coefficient were 7.2 MPa and 0.66, respectively, compared with 7.6 MPa and 0.74 before balling; based on balling, the compressive strength and softening coefficient of the obtained phosphogypsum small hollow blocks after coated with cement dramatically increased to8.6 MPa and 0.82, respectively, compared with 7.2 MPa and 0.64 before balling, which has basically met the requirements of normal concrete small hollow block on the GB 8239-1997 standard MU7.5 grade index, indicating the compressive strength and softening coefficient of phosphogypsum small hollow blocks after modified, balled and coated with cement could be significantly improved. The main reason is that the surface of phosphogypsum just treated by balling is very rough (Fig.3), and there is a gap between the crystal for the phosphogypsum small hollow blocks through hydration reaction (Fig.7), the moisture easily penetrated the inside of ball, and the gypsum dissolved, resulting in a softening coefficient and strength decreased low; the surface of the phosphogypsum ball coated with cement became

relatively smooth (Fig.4), the surface of the phosphogypsum ball coated with cement after hydration reaction had no voids (Fig.8), effectively blocking the invasion of moisture, thereby improving the compressive strength and softening coefficient of phosphogypsum small hollow blocks.

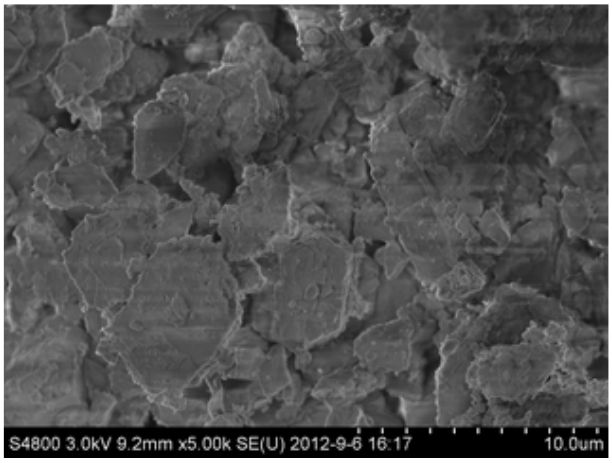

Fig.7. SEM images of the surface of phosphogypsum blocks

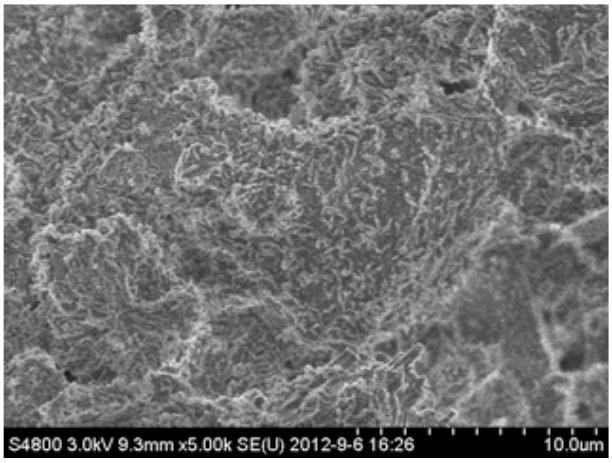

Fig.8. SEM images of the surface of phosphogypsum blocks coated with cement

2.3 Analysis of water-resistant and high-strength phosphogypsum small hollow blocks

With the above modification process and the molding process, the obtained phosphogypsum small hollow blocks tested with the Chinese statutory construction material product quality inspection institutions, their performance indicators are shown in Table 2.

Table 2 Test results of phosphogypsum blocks

Test items		Unit	Test results	Judgement
Compressive strength		MPa	8.60	According to the requirements of the standard GB 3289-1997
Core ratio		%	42	
Frost resistance	Mass loss	%	1.5	
	Strength loss	%	22.8	
Comparatively percentage of moisture		%	38.0	
Radionuclide Specific activity	^{226}Ra	Bq/kg	50.72	According to the requirements of the standard GB 6566-2010
	^{232}Th	Bq/kg	32.60	
	^{40}K	Bq/kg	753.58	
Building material standard request	I_{Ra}	---	0.25	
	I_r	---	0.44	
Softening coefficient		--	0.82	According to the requirements of the general concrete products

As can be seen from Table 2, the performance such as compressive strength drying shrinkage, and softening coefficient of the prepared phosphogypsum small hollow blocks with the above ratio met the MU7.5 grade requirements of normal concrete small hollow block on the GB 3289-1997; as can be seen from Table 2, development and production of radioactive phosphogypsum bricks met the main building material requirements of limited building radionuclide on the GB 6566-2010. Comprehensive analysis of the performance indicators of phosphogypsum small hollow block shows that the water was not only high-strength phosphogypsum small hollow blocks could be widely used in interior and exterior walls of buildings, but also could replace the ordinary the

general concrete products used in cable trenches, guide ditches and other municipal projects, thus expanding their application scope, which will provide a new way to solve the comprehensive problem of phosphogypsum for the further utilization .

3 Conclusion

(1) Phosphogypsum was modified by the use of quicklime, followed into a ball, coated with cement, aged, which not only effectively removed soluble phosphorus, fluorine and other impurities on the adverse effects of phosphogypsum small hollow blocks, but also significantly improved the compressive strength and softening coefficient and other properties of phosphogypsum small hollow blocks.

(2) The mixed raw material ratio of modified, balled, cement coated phosphogypsum: gravel: cement of 50:40:1, 10% water, pressure of 15 MPa, and vibration compression molding was used, the nature conservancy maintained to 28 days after stripping, the performance targets of prepared phosphogypsum bricks had met or exceeded the standard MU7.5 grade index requirements of normal concrete small hollow block GB 8239-1997.

(3) The prepared phosphogypsum small hollow blocks belonging to the new building materials, had high strength and water resistance, which provided a new way to solve the comprehensive problem of phosphogypsum for the further utilization.

Acknowledgement

In this paper, the research was sponsored by the High-tech Industrialization Projects Foundation of Guangdong Province (Project No. 2010B010900049).

References

[1] Qinjun Fang. The Study on Comprehensive Utilization of phosphogypsum. China Resources Comprehensive Utilization, In Chinese 2010,28 (3) :23-25.

[2] Singh M. Treating waste phosphogypsum for cement and plaster manufacture. Cement Concrete Research 2002;32:1033-8.

[3] CIVIL ENGINEERING AND; Danzong Li phosphogypsum Preparation Process of Building Gypsum. New Building Materials,In Chinese 2007, (7): 48-52.

[4] Yang; Young three available; Zhou Yongbo, etc. High ash autoclaved brick phosphogypsum Water Development . Nonmetal mines, In Chinese 2010, 33 (2): 41-43.

[5] Yang Min, Qian Jueshi, Pang Ying. Activation of fly ash-lime systems using calcined phosphogypsum. Construction and Building Materials 2008;22:1004-8.

[6] Test methods for normal concrete small hollow blocks. GB/T 4111-2013, General Administration of Quality Supervision, Inspection and Quarantine of PR China, Beijing; 2013.

[7] Supply Mechanism. Composite modified gypsum cement Coagulator doing research [D]. Chongqing University, 2010.

[8] Kumar Sunil. A perspective study on fly ash-lime-gypsum bricks and hollow blocks for low cost housing development. Construction and Building Materials 2002;16(3):519-25.

Advanced Materials Research Vols. 989-994 (2014) pp 45-48
© (2014) Trans Tech Publications, Switzerland
doi:10.4028/www.scientific.net/AMR.989-994.45

Study on laser micro shock effect on electrical resistivity of nanometer copper film

Qing Xue[1], Yinqun Hua[2,a,*], Yuchuan Bai[1], Ruifang Chen[1], Haixia Liu[2]

[1]School of Mechanical Engineering, Jiangsu University, Zhenjiang Jiangsu 212013, China;

[2]School of Material Science and Engineering, Jiangsu University, Zhenjiang Jiangsu 212013, China

[a]e-mai: huayq@ujs.edu.cn.

Keywords: Nanometer copper film; Laser micro shock processing; electrical resistivity

Abstract: The aim of this research is to improve the electrical performance of the nanometer copper film by laser micro shock processing. The nanometer copper film was prepared by the magnetron sputtering. The mechanism of laser micro shock processing effect on electrical resistivity, hardness and elastic modulus was investigated. The results show that the electrical resistivity of copper film after laser micro shock reduced by 22.5 % on average. And, the hardness and the elastic modulus increased by 38.5 % and 45.2 % on average, respectively. According to our research, we conclude that, the existence of a large number of twin, twin boundary, fault and the grow up grain are the main factor of the improvement of the electrical performance; and the existence of twin, stress concentration holes and fault are the key to improve its mechanical properties.

Introduction

Laser shock processing (LSP) is one of the most important surface modification technologies. It has been widely used in surface improvement of metal materials [1]. At present, with the rapid development of Micro/nano device, mechanical strength of the device materials and integrated electronic attachment material has become a research focus at home and abroad [2]. In this paper, the nanometer copper film prepared with on the magnetron sputtering was treated by laser micro shock processing, aiming to explore the application prospect of laser shock processing technology in nanometer thin film materials. In previous studies [3] we have shown that a large number of abundant twin, fault, space and a small amount of dislocation can be produced by laser micro shock processing. Also, we observed the grain growth phenomenon. The key point of this article is to expound the mechanism of laser micro shock processing impact on the thin film's electrical and mechanical performance.

Experiment

The copper thin film materials preparation has been detailed in our previous article. [4]. The film was prepared on JGP560CVI ultra high vacuum multifunctional magnetron sputtering equipment. The experiment was conducted on neodymium glass high power laser.

Nanoindentor produced by Hysitron company was used in this experiment. The hardness and elastic modulus of the nanometer copper film were tested by the method of nanoindentation. The device can record the load-displacement curve. Actually, the curve contains the deformation information in different depth in the indention process. So the hardness and elastic modulus in different depth can be calculated according to the curve. Computation formula of the elastic modulus is as follows [5]:

$$E_r = \frac{\sqrt{\pi}}{2}\frac{S}{\sqrt{A}} \tag{1}$$

where A is the elastic contact area, S is the initial unloading stiffness. In addition, equation (2) can be obtained by definitions of hardness of materials:

$$H = \frac{P_{\max}}{A} \qquad (2)$$

where P_{max} is the load, H is the hardness of the measured material.

According to elastic modulus E_r and hardness H in equation (1) and (2), we calculate the hardness and elastic modulus of the sample under various states of each test point, and then averaged.

Nanoindentation test were carry out in both the LSP impact area and none LSP impact area of sample C1, C2, C3, C4 and C5. The load - displacement curves for samples were obtained. The electrical resistivity test were carried out by a SZ - 82 digital four point probe tester at room temperature (293 K) at 5 points on each sample, of which take the average result was taken to be the object value.

Results

According to the data tested in the load - displacement curve and the calculated equation (1), (2), the hardness and elastic modulus in LSP impact areas and none LSP impact areas were shown in Fig. 1. As is shown in Fig. 1(a), hardness of nanometer copper films after LSP have been increased by 38.5 % on average. As is shown in Fig. 1(b), elastic modulus of samples after LSP have been increased by 45.2 % on average. The results show that the LSP improved the mechanical properties of nanometer copper films effectively.

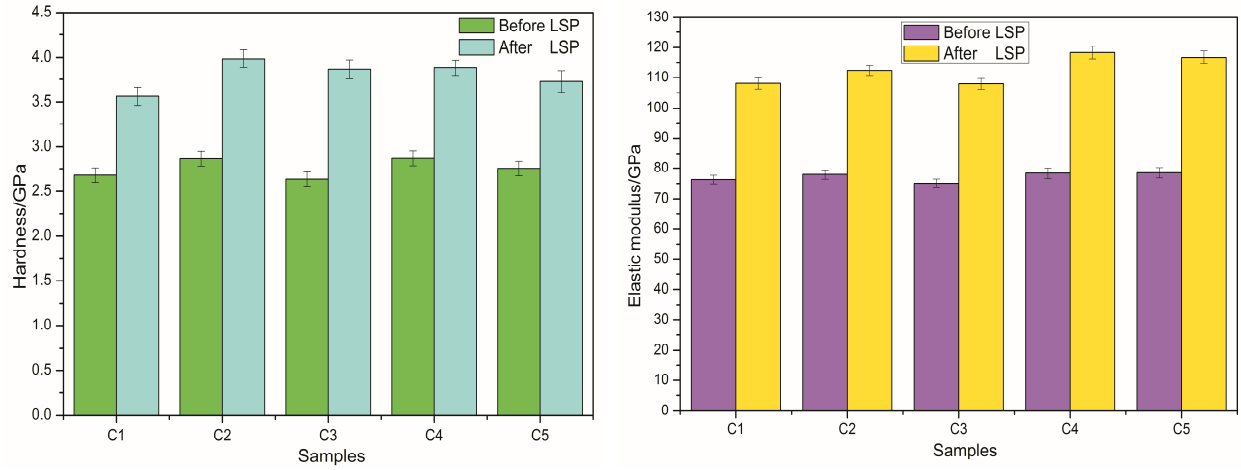

(a) (b)

Fig. 1 Hardness (a) and elastic modulus (b) of nanometer copper films before and after LSP

Electrical resistivity of nanometer copper film is 1.112×10^{-8} Ω·m on average and coarse grained copper is $(1.691\pm0.020)\times10^{-8}$ Ω·m [oxygen free high conductivity copper (OFHC) is $(1.672\pm0.020)\times10^{-8}$ Ω·m]. This suggests that the electrical resistivity of nanometer copper film produced by the magnetron sputtering in the optimized parameters can be lower than that of OFHC.

After LSP, the electrical resistivity of the five samples above was tested according to the above method. The results are shown in Fig. 2. The experimental results show that the electrical resistivity of nanometer copper film after LSP is 0.8576×10^{-8} Ω·m on average. The electrical resistivity declines in different degrees rather than rises, with the electrical resistivity decreasing by 22.5 % on average, falling by 25.6 % to the utmost.

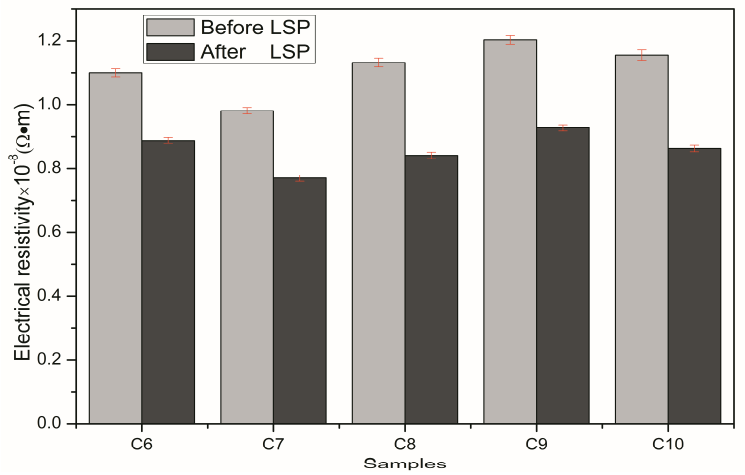

Fig. 2 Electrical resistivity of nanometer copper films before and after LSP

Discussion

Fig. 3 shows the TEM image of copper thin film without LSP. As we can see from Fig. 3 (a), the grains of copper thin film are in a quasi-static and the primary twins were overlapped with another grain (region A). Fig. 3 (b) is the detail view of B region in Fig. 3 (a). It clearly shows the quasi-static grain. A high level stress induced by LSP will make it continue grow up [5].

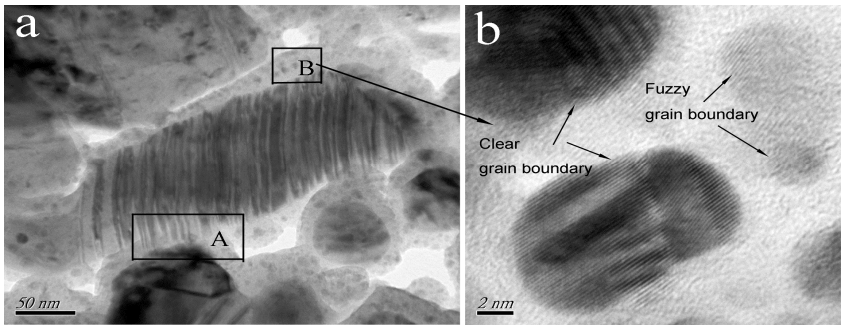

Fig. 3 TEM image of copper thin film without LSP

(a) quasi-static grain and the primary twin (b) detail view of B region in Fig. 3 (a)

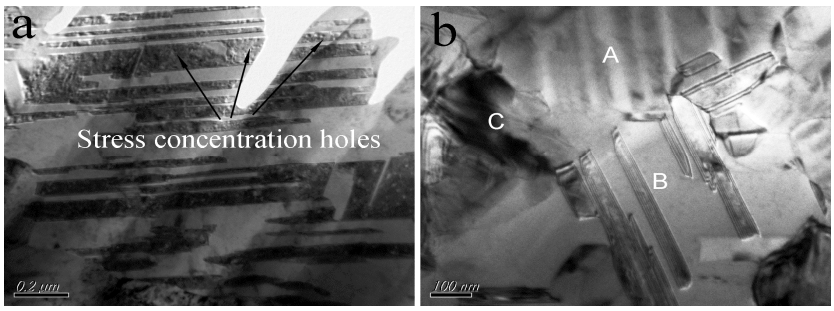

Fig. 4 TEM image of copper thin film after LSP. (a) The transgranular growth twin and the stress concentration holes (b) twin and dislocation

The TEM image of copper thin film after LSP has been shown in Fig. 4. Fig. 4 (a) is the transgranular growth twin and the stress concentration holes. From Fig. 4 (b), we can observe primary twin organization with fuzzy grain boundary in A region. There are complete twin organizations in B region, with very instinct grain boundary. A large amount of dislocation can be found in C region. We found that dislocation can rarely be found in the organization after LSP. Where there is an obvious twin produced, there is no dislocation, and where there is no twin produced, there is a little amount of dislocation. It means that the consistency of the lattice structure is not easy to produce dislocation defect within a single element metal film.

After LSP, the biggest characteristic of the copper thin film organization change is the slip deformation. As we all know, the dislocation slip is one of the line slip deformation, which needs very small energy compared with the surface sliping deformation. Although we found the grains have a grow up phenomenon, the substructure in the twin are very small and the width of the twin is only a few nanometers to tens of nanometers. Coherency distortion of the twin enhances the material's ability to resist deformation, the hardness and elastic modulus. The existence of the stacking fault also improves the material's mechanical properties. A large number of vacancy defects form in the process of atomic plane slip. These vacancy defects are equivalent to the dislocation tangles and played an important role of "pinning" in the deformation process. Their existence will improve the nanometer copper thin film's mechanical properties, too.

Data show that the room temperature resistivity of copper in the grain boundary and in the stacking fault is 3.6×10^{-16} Ω·m and 3.4×10^{-17} Ω·m [6]. Resistivity of coherent twin boundary is about half of that of stacking fault, i.e. 1.7×10^{-17} Ω·m for the copper [7]. Resistivity introduced by twin boundary is far less than that introduced by grain boundary, so we can think that the increase in the total resistivity comes mainly from the grain boundary and the high density of twin boundary.

5. Conclusions

Through the experimental study and theoretical analysis, the following conclusions can be drawn:

1) The electrical resistivity of nanometer copper film after LSP, instead of increase, is reduced by an average of 22.5 %. After LSP, the hardness and elastic modulus of the nanometer copper film increase by 38.5 %, 45.2 %, respectively;

2) The existence of a large number of twin, twin boundary, fault and the grain growing up are the main factor of the improvement of the electrical performance. The existence of twin, vacancies and fault are the key to improve the mechanical properties.

Acknowledgments

The authors acknowledge this work was supported by the National Natural Science Foundation of China (No.51175234) and the Heights Talent Support Programs in Six Industrial Fields in Jiangsu Province (No. 2011-JXQC069).

References

[1] Liu Yunxun, et al., Surface morphology and Deformation mechanism of 304 stainless steel treated by laser shock peening, Chinese J. Laser 40 (2013) 1-8 (In Chinese).
[2] Eduardo, M.Bringa, Alfredo Caro, Ultrahigh strength in nanocrystalline materials under shock loading, Science 16 September 309 (2005) 1838-1841.
[3] Yinqun Hua, et al., Study of substructure in nanometer copper thin films treated by laser shock processing. Chinese Optics Letters, 11 (2013) 031402-031404.
[4] C. Rubio-González, et al., A. Banderas, J.Porro, M. Morales, Effect of an absorbent overlay on the residual stress field induced by laser shock processing on aluminum samples, Appl. Surf. Sci. 252 (2006) 6201–6205.
[5] L.Lu, M.L.Sui, Lu, Superplastic Extensibility of Nanocrystalline Copper at Room Temperature, Science 287 (2002) 1463-1465.
[6] K.M.Mannan, K.R.Karin, Phys F: Metal Phys,5 (1975) 1687.
[7] I. Nakamzchi, Electrical resistivity and grain boundaries in metals, Materials Science Forum 47 (1996) 207-209.

Advanced Materials Research Vols. 989-994 (2014) pp 49-54
© (2014) Trans Tech Publications, Switzerland
doi:10.4028/www.scientific.net/AMR.989-994.49

Effect of Process parameters on Residual Stress Distribution During Direct Laser Metal Deposition Shaping

Hao WANG[1,a]

[1]Drilling & Production Technology Research Institute of Liaohe Oilfield Company China National Petroleum Corporation, Panjin 124010, China

[a]whprettymouse1981@126.com

Keywords: Laser metal deposition shaping; Numerical simulation; Process parameters; Residual stress

Abstract. In order to improve the quality of sample and decrease the stress during process, it is important to study the residual stress distribution during direct laser metal deposition (LMDS) process. In this paper, according to the "element life and death" technique of finite element method ,with APDL, we simulated the effects of Laser power, scanning velocity, substrate preheat temperature and powder addition speed in top layer of samples residual stress distribution during whole LMDS process are studied. The residual stress distribution under different process parameters is researched in detail. Using the same process parameters, the simulation results show good agreement with the features of sample which fabricated by LMDS.

Introduction

Laser metal deposition shaping (LMDS) technique has been widely used in many industrial applications such as aerospace，automobile，weapons and so on [1][2]. LMDS accumulates metal powder materials according to two-dimensional profile information one layer off another, and finally the three-dimensional solid parts are formed in substrate, with the laser cladding method. And it's a fusion and solidification process essentially, which involves complicated interactions between the laser beam, metal powders, the base material (substrate), and processing gases. Typical physical phenomena in laser cladding include laser-powder interactions, heat transfer, fusion, and solidification. There are approximately variables which strongly influence the characteristics of the clad part. These variables include actual laser power, spatial distribution (model) of the laser beam, powder delivery gas flow, powder feed rate, material parameters, powder parameters, powder carry method, height increment per layer, percentage overlap between tracks, and tool-path patterns. Some of these processing parameters are strongly coupled with each other. These processing parameters are necessary to obtain the desired dimensional accuracy and material integrity of laser clad parts. Process optimization requires both theoretical and experimental understanding of the associated physical phenomena.

In the past decades, many analytical and numerical LMDS models have been developed by researchers, revealing the temperature gradient [3]-[10], as human people difficult to measure many of the physical phenomena, directly. Recently, three-dimensional laser forming simulations have been conducted using commercial FEA software or manual programming. Long et al [7][10] developed a three-dimensional dynamics stress field under different scanning method and substrate preheat temperature during multi-track & multi-layer laser metal deposition shaping(LMDS) process with ANSYS parametric design language (APDL).In their work, a multi-track & multi-layer part was deposited on a substrate，and the temperatures of those nodes in molten pool were set as the melting point at each incremental step.

In this paper, according to the "element life and death" technique of finite element method, with APDL, we simulated the effects of Laser power, scanning velocity, substrate preheat temperature and powder addition speed in different top layer of samples reciprocating scanning method to residual stress distribution during whole LMDS process. The residual stress distribution under different process parameters are studied in detail. With the same process parameters, the samples fabricated by LMDS show good agreement with the simulation results.

Model of finite element method

As shown in Fig.1 based on “birth and dead element” technique ,we built the model of finite element method of LMDS with APDL(ANSYS Parametric Design Language).

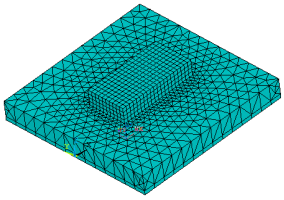

Fig.1. The FEM model

The overall computational domain size is 20mm*10mm*4mm in X, Y and Z. The size of grid is 1mm*1mm*1mm, and the element is SOLID5. The metal material of both the clad and substrate are TC4 (Ti-6Al-4V). The chemical compositions are listed in Table 1, and its partial thermo-physical parameters are listed in Table 2.

Table 1 Chemical compositions of TC4

Chemical compositions	H	O	Al	N	C
Percent/*w*	≤0.009	≤0.16	≤6.02	≤0.027	≤0.056
Chemical compositions	V	Si	Fe	Ti	
Percent/*w*	≤4.00	≤0.039	≤0.15	bal	

Table 2 Partial thermo-physical parameters of TC4

Temperature （°C）	20	200	400	600	1530	1650	2000
Heat transfer coefficient （W/°C *m）	17	15	15	16	20	20.5	21
Specific heat (J/kg*°C)	500	580	595	615	760	840	730
Density（kg/m3）	4420	4420	4420	4420	4420	4420	4420
Elastic modulus (Pa)	1.2E11	1.1E11	0.88E11	0.7E11	0.035E11	0.03E11	0.001E11
Linear expansion coefficient (1/°C)	0.9E-5	0.965E-5	1.107E-5	1.004E-5	1.005E-5	1.006E-5	1.008E-5
Poissonratio (PRXY)	0.3	0.31	0.325	0.342	0.38	0.384	0.39

Simulation results and analysis of the Residual stress distribution

In this model, we set the processing parameters as follows: the laser power is 2000W, the radius of the beam is 1mm, the scanning velocity is 5mm/s, the scan pitch is 1mm, the environmental and substrate preheating temperature both are 20°C. The whole process lasts for 360 seconds. (Processing time 160s + cooling time 200s). The process parameters are listed in Table 3.

Table 3 Parameters table

Laser power （w）	Scanning velocity （mm/s）	Substrate temperature (℃)	Powder feed rate （g/min）
2200	6.25	350	5
2119	6	300	4
2000	5	200	3
1881	4	50	2
1800	3	20	1

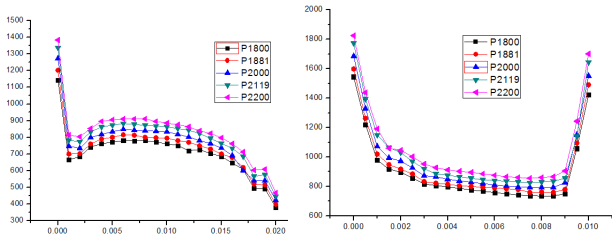

(a) On X-ray (b) On Y-ray

Fig.2. The residual stress distribution on different directions of top layer under different Laser powers

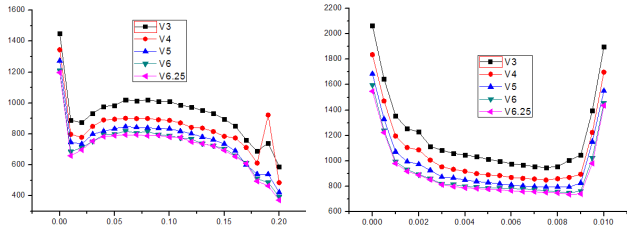

(a) On X-ray (b) On Y-ray

Fig.3. The residual stress distribution on different directions of top layer under different scanning velocity (a) On X-ray (b)

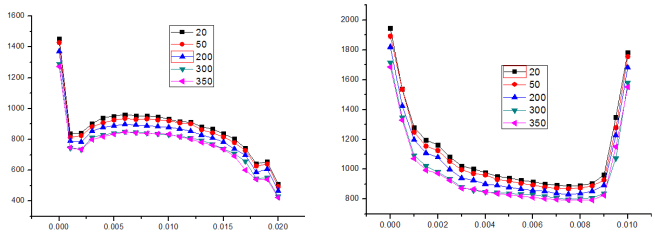

(a) On X-ray (b) On Y-ray

Fig.4. The residual stress distribution on different directions of top layer under different substrate preheating temperature

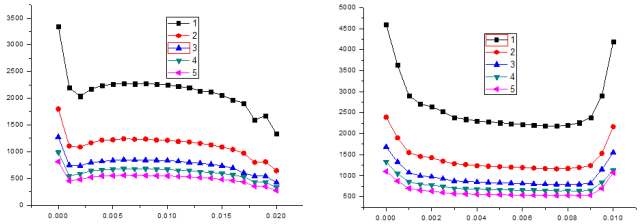

(a) On X-ray (b) On Y-ray

Fig.5. The residual stress distribution on different directions of top layer under different powder speed rate

It is shown that the X-ray and Y-ray residual stress distribution on each top layers under different process parameters in Fig.2. We can see the X-ray and Y-ray residual stress were strong in ends of the sample. Because of The laser scanning from left side of top layer to start, as the scan in the right side of third layer had just finished, the temperature gradient changed gently. Distribution of residual stress under different process parameters in middle of each layers of piece is small. Because the temperature gradient changes greatly at starting point of top layer, the residual stress is centralized. The residual stress on the top layer rises with ascending of laser power.Similarly，in Fig3-5, we can discover that the residual stress on the top layer reduces with ascending of scanning velocity; The residual stress on the top layer reduces with ascending of substrate preheating temperature; The residual stress on the top layer reduces with ascending of powder speed rate.

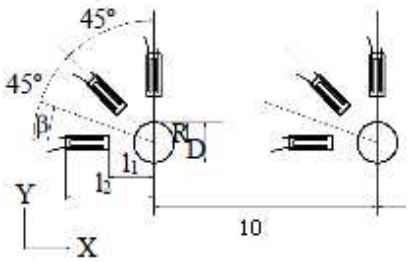

Fig.6. The schematic of residual stress testing

Comparisons to experimental results

For detected the residual stress distribution in the sample, for compare with the numerical results, we used the same processing parameters. We measure the residual stress with blind-hole method[11]. The experimental procedure is that:

For the strain slice connected tightly with sample, we should be pre-processing the sample before pasting strain slice on the sample.

The strain slice pasting as in Fig.6 shown.

To avoid the effects of drilling thermal, we measured the strain with average method. We should that read the strain values and average them every 5 minutes, after drilled at least 40 minutes.

We obtained the fixed-point measuring result of residual stress variations at the ends and middle points on the top of the sample as in Fig.7-14 shown.

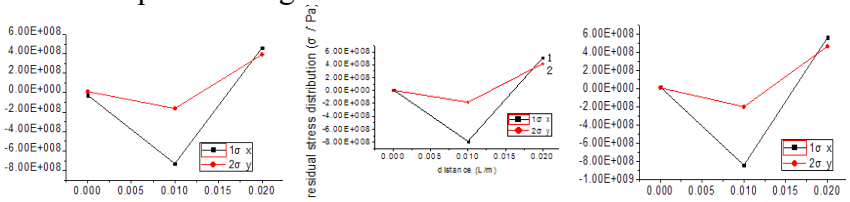

(a) P=1800w (b) P=2000w (c) P=2200w

Fig.7. The residual stress distribution under different Laser power on X-ray of surface of samples

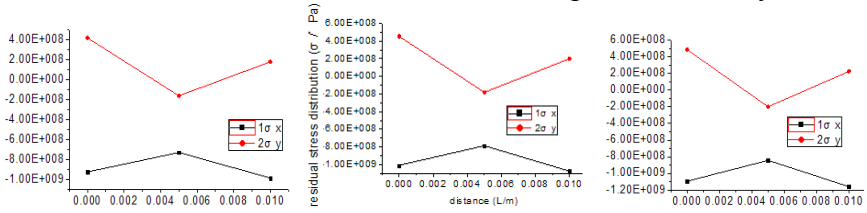

(a) P=1800w (b) P=2000w (c) P=2200w

Fig.8. The residual stress distribution under different Laser power on Y-ray of surface of samples

In Fig.7 shown that The residual stress distribution under different Laser Powers on X-ray of surface of samples. we can see under Laser Power 2000W and Laser Power 2200W (In Fig 7(b)and (c)), Both of the residual stress distribution in the top of sample are similar. The σ_y change amplitude is small, both are tensile stress and change from 0 to max at the middle point, and getting smaller to 0, then getting to shrinkage stress and the value of the stress getting larger. We can explain about σ_x in this way, but x- change amplitude just than more σ_y larger. In Fig.8(a) shown, x is mainly shrinkage stress. At the middle point, it is minimum value, then it getting larger. but σ_y was just contrary to σ_x, mainly tensile stress, at the middle point ,it is minimum value. it is similar to the Fig.2(a).We able to explain about Fig.8， It similar to the Fig.2(b).

In the same way we can explain about Fig 9-14.

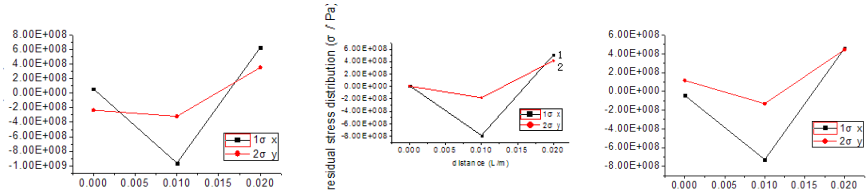

(a) V=3mm/s (b) V=5mm/s (c) V=6.25mm/s

Fig.9. The residual stress distribution under different scanning velocity on X-ray of surface of samples

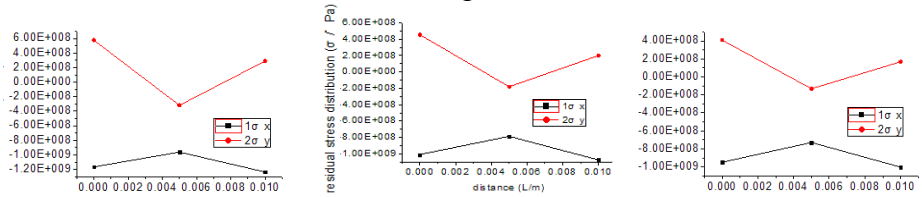

(a) V=3mm/s (b) V=5mm/s (c) V=6.25mm/s

Fig.10. The residual stress distribution under different scanning velocity on Y-ray of surface of samples

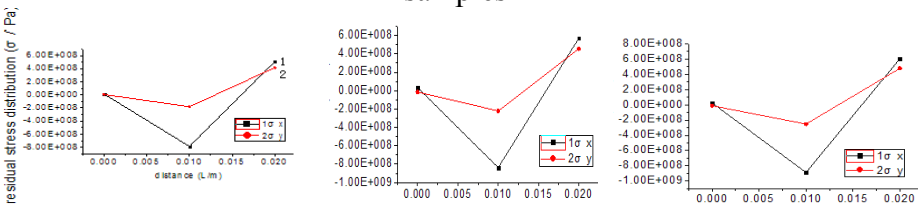

(a) 20°C (b) 200°C (c) 350°C

Fig.11.The residual stress distribution under different substrate preheating temperature on X-ray of surface of samples

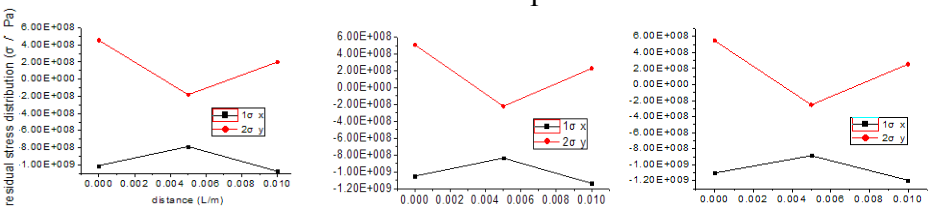

(a) 20°C (b) 200°C (c) 350°C

Fig.12.The residual stress distribution under different substrate preheating temperature on Y-ray of surface of samples

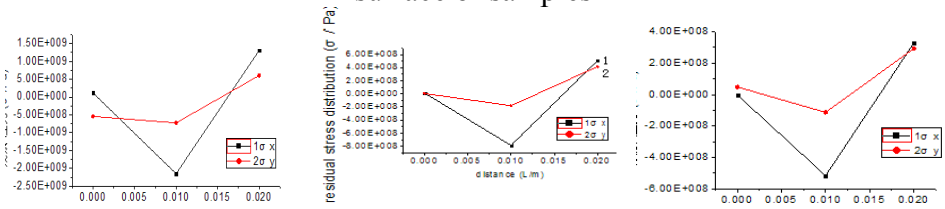

(a) 1g/min (b) 3g/min (c) 5g/min

Fig.13. The residual stress distribution under different powder addition speed on X-ray of surface of samples.

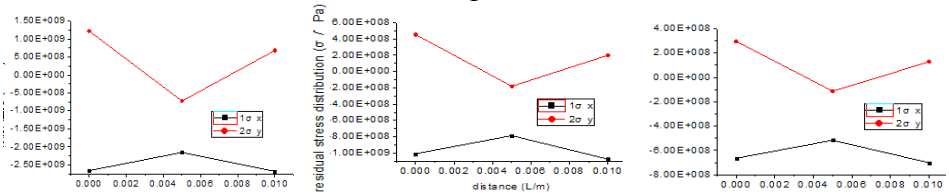

(a) 1g/min (b) 3g/min (c) 5g/min

Fig.14. The residual stress distribution under different powder addition speed on Y-ray of surface of samples.

Conclusions

According to the “element life and death” technique of finite element method ,with APDL, we simulated the effects of different process parameters to residual stress distribution during whole LMDS process are studied. The residual stress distribution under different scanning methods is researched in detail.

The residual stress on the top layer reduces with ascending of scanning velocity; The residual stress on the top layer rises with ascending of laser power; The residual stress on the top layer reduces with ascending of substrate preheating temperature; The residual stress on the top layer reduces with ascending of powder speed rate.

Using the same process parameters, the simulation result show good agreement with the features of sample which fabricated by LMDS.

References

[1] Zuo TieChuan Chen Hong. Green Manufacture in 21Century ——Laser Manufacturing Technology and Application. [J] Chinese Journal of Mechanical Engineering. 2009,45(10):106-110.

[2] Yao Shan， Zeng Feng et al. New Laser Rapid Prototyping Method and It’s Applications Chinese Journal of Mechanical Engineering. 2007,43(5):230-234.

[3] LABUDOVIC M, HU D, KOVACEVIC R. A three dimensional model for direct laser metal powder deposition and rapid prototyping [J]Journal of materials science, 2003, 38(1): 35-49.

[4] MAZUMDER J. Overview of melt dynamics in laser processing [J]. Optical engineering, 1991, 30(1208).

[5] Jia Wen -Peng,,Lin Xin,Chen Jing,et al. Numerical Simulation for Temperature/strees Field of TC4 Titanium Alloy Hollow Blade during Laser Rapid Forming Process[J].CHINESE JOURNAL OF LASERS, 2007, 34(009): 1308-1312.

[6] Long Ri-Sheng Liu Wei-jun et al. effects of scanning methods on thermal stress during laser meter deposition shaping. Chinese Journal of Mechanical Engineering.2007，43（11）：74-80.

[7] Xi Ming-Zhe，Yu Gang. Numerical Simulation for the Transient Temperature Field of 3D Moving Laser Molten Pool[J].CHINESE JOURNAL OF LASERS, 2004, 31(012): 1527-1532.

[8] Xin Wang, Ping Xiao Characterisation of ceramic coatings sintering using residual stress measurements. Journal of the European Ceramic Society24 (2004) 283–288.

[9] Tabernero, I. (2011). Evaluation of the mechanical properties of Inconel 718 components built by laser cladding. International Journal of Machine Tools and Manufacture. International Journal of Machine Tools & Manufacture 51(2011) 465–470.

[10] LONG Risheng, LIU Weijun, XING Fei, et al. Effects of substrate preheating on thermal stress during laser metal deposition shaping[J]. Journal of Mechanical Engineering,2009，45(10)：241-247.

[11] YANG Jian CHEN Jing et al. Experimental Study on Residual Stress Distribution of Laser Rapid Forming Process.[J]Rare Metal Materials and Engineering. 2004,33(12):1304-1307.

Advanced Materials Research Vols. 989-994 (2014) pp 55-59
© (2014) Trans Tech Publications, Switzerland
doi:10.4028/www.scientific.net/AMR.989-994.55

Plasma-induced degradation of benzene in aqueous solution

Huili Qi[a], Ke Gai[b], Dongping Ma[c]

College of Chemistry and Chemical Engineering, Longdong University, Qingyang, 745000，China

[a]email:qihuili33@sohu.com, [b]email:gaike310@sohu.com, [c]email:mdp_725@163.com

Keywords: Benzene; Plasma; Glow Discharge Electrolysis; Hydroxyl Radicals

Abstract. Removal of benzene and effects of various parameters on the removal efficiency in the aqueous solution with plasma are studied. Results indicated that the degradation rate can be considerably raised by prolonging the discharge time, removal proceeded faster when the treatment was conducted in alkaline or acidic than in neutral media. Fe^{2+} shows an evident accelerated effect on the benzene elimination, and the presence of H_2O_2 benefited the degradation. It is demonstrated that the hydroxyl radicals were the most responsible oxidants in the benzene degradation. The major intermediate products resulted from the degradation were identified by an HPLC analysis and a degradation path way was proposed.

Introduction

Volatile organic compounds (VOCs), emitted from chemical, petrochemical, and related industries, have received increased attention in recent years. Benzene, one of the most prevalent VOCs, is a naturally occurring aromatic compound present in petroleum fuels and is a frequent contaminant in both surface and subsurface environments. When benzene diffuses into the environment, it poses great threats to human health, such as drowsiness, dizziness, unconsciousness, and an increased risk of cancer [1]. Because of its high toxicity, confirmed carcinogenicity, and environmental persistence, it is regarded as the priority hazardous substance [2]. The development of an efficient, mild and cost-effective technology for benzene degradation in the ambient environment is absolutely necessarily.

Several advanced oxidation process, such as ultraviolet photolysis, TiO_2-based photocatalytic oxidation, direct ozonation, electron beam and various combinations of radiation are currently under development [3,4]. In this process, the attention has been focused on hydroxyl radical, since the most powerful oxidizing species are in fact the hydroxyl radical. The hydroxyl radical reacts strongly with all organic substances usually by hydrogen abstraction.

Contact glow discharge electrolysis (CGDE) is a novel type of electrochemical process in which plasma was directly produced by the electrical discharge against water. Because of its high efficiency, high amenability to automation and environmental compatibility in which high energy of plasmas, CGDE were directly produced by the water discharge were mostly utilized for the destruction of hazardous organics in the aqueous solution. In this process, $HO\cdot$ radical are produced electrochemically in an anodic reaction directly from water. By using the electrochemical production of hydroxyl radicals, no addition of chemical substances is necessary and the process can be performed at affordable costs, determined mainly by the power required for driving the electrochemical process and without the common AOP drawbacks. The mechanism of producing plasmas in this process has been studied by M. A. Malik and so on [5-7]. Recently, there were several reports [8-10] on the degradation of certain organic target compounds dissolved in water by use of contact glow discharge. All these investigations confirm that contact glow discharge plasma was a prospective process for the degradation of toxic substances.

In the present paper, benzene was chosen as a model pollutant dissolved in potassium sulfate by means of glow discharge electrolysis under water in order to further study the degradation behavior of benzene, focusing on the reaction kinetics and the mechanism aspects.

1. Experimental

The experimental apparatus consists of a reaction cell and a high voltage power supply as showed in Figure1. The experimental apparatus is schematically identical to that mentioned in the literature [10]. It consists of a reaction reactor and a high voltage power. The electrode system consisted of a platinum wire anode (I.D. 0.5 mm) and a stainless steel rod (I.D. 0.5 cm) cathode with an electrode distance of 3 cm. The anode was encased in a glass tube located in the bottom center of a glass cylinder reactor (inner diameter=6.5 cm, length=20 cm), with the needle tip protruding 1 mm from the glass tube. The cathode was inserted through the top of the reactor. In addition, the reaction cell was coated by a water jacket, in which the temperature was controlled at room temperature. A positive high voltage was applied to the needle anode by a WYJ-1000V2A dc power unit produced by Shanghai Changjiang Electron Instrument Company providing voltage of 0-1000 V and current output of 0-2 A.

The benzene solution was prepared by dissolving analytical grade benzene in a potassium sulfate solution ($1g \cdot L^{-1}$). The pH of the aqueous solution and electric conductivity were adjusted with dilute sodium hydroxide, dilute sulfuric acid and potassium sulfate to the expected value. During the reaction, a small portion of the solution (0.025 ml) was periodically sampled out from the sampling port with a finnpipette made by Thermo Electron Corporation to measure the reduction of benzene immediately by a UV-V spectrophotometer (SPECORD50, Analytic Jena) and HPLC (LC-10AT vp, Shimadzu Company) respectively.

The experiments were performed under the conditions as follows: volume of electrolyte, 200 ml; initial concentration of benzene, 100 $mg \cdot L^{-1}$; voltage, 700 V; initial pH, 6.89; temperature, 298K. The maximum absorption wavelength is 194 nm. These are referred as the “standard conditions” or otherwise specified.

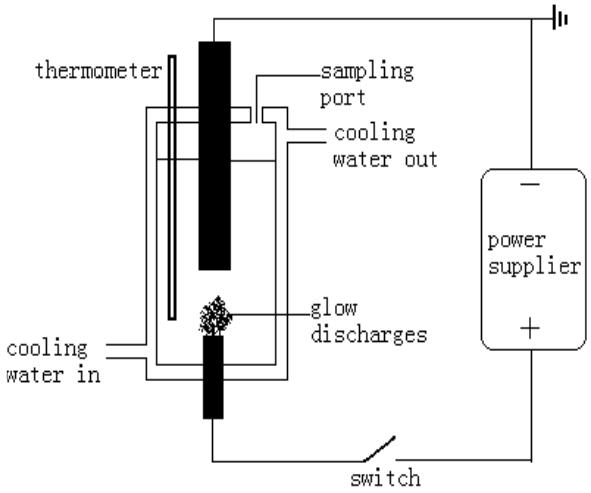

Fig.1. Scheme of the experimental apparatus

2. Results and discussion

2.1 Removal of the benzene

The oxidative degradation of benzene proceeded abruptly when glow discharge electrolysis was carried out on the solution containing it. Figure 2 exhibits the time profile of benzene removal under 700V. The initial concentration(c_0) of benzene was 100 $mg \cdot L^{-1}$. It can be seen that the benzene removal increases with the discharge time. This indicates that glow discharge electrolysis is a very efficient tool for benzene degradation because generally the pollutant cannot be completely removed in other processes.

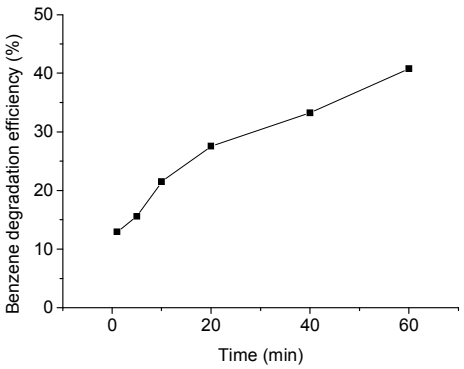

Fig. 2. Time profile of benzene degradation

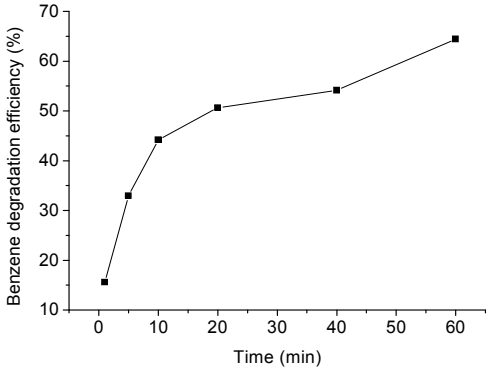

Fig. 3. Accelerating effect of H_2O_2 on benzene degradation

2.2 Effects of and hydrogen peroxide

In order to investigate the role of H_2O_2 in removing benzene from the aqueous solution, H_2O_2 (100 mg·L^{-1}) was added into the benzene solution respectively. Figure 3 shows the concentration of the benzene at reaction time from 1 to 60 minutes. Obviously, the removal efficiency of 100 mg·L^{-1} with H_2O_2 is higher than without H_2O_2. It is also observed that the higher H_2O_2 concentration is beneficial to removel of organic compounds. It may be explained that the concentration of HO· is increased when H_2O_2 was added into the benzene solution.

2.3 Accelerated effect of ferrous ions

It is well known that the ferrous ion could react with hydrogen peroxide and produce hydroxyl radicals with powerful oxidizing abilities to degrade organic pollutants. Hickling et al found that the primary yield of oxidizing species was about four times larger than the case without ferrous ion in the solutions [11]. This can be achieved by Fenton's reaction, therefore, some ferrous sulfate was added into the solution and results were shown in figure 4. The initial concentration of benzene was 100 mg·L^{-1}, pH value was 6.89 and applied voltage was 700V. It can be seen that Fe^{2+} has an evident catalytic effect when its concentration is more than 2×10^{-3} mol·L^{-1}. Therefore, 2×10^{-3} mol·L^{-1} is the optimum concentration of the catalyst under experimental conditions.

The reason is as follows:

$$H_2O_{gas} - e \rightarrow H_2O^+_{gas}$$

$$H_2O^+_{gas} + (n+1)\,H_2O \rightarrow H_3O^+ + (n+1)\,HO\cdot + n\,H\cdot$$

$$HO\cdot + H\cdot \rightarrow H_2O$$

$$2HO\cdot \rightarrow H_2O_2$$

$$Fe^{2+} + H_2O_2 \rightarrow Fe^{3+} + HO\cdot + OH^-$$

$$Fe^{2+} + HO\cdot \rightarrow Fe^{3+} + OH^-$$

$$OH\cdot + H_2O_2 \rightarrow H_2O + HO_2\cdot$$

$$Fe^{3+} + H_2O_2 \rightarrow Fe^{2+} + HO_2\cdot + H^+$$

$$OH\cdot + H_2O_2 \rightarrow H_2O + HO_2\cdot$$

From the above reactions, it can be found that in the presence of Fe^{2+}, the H_2O_2 produced by the discharge was converted to HO· again, which in turn, accelerates the degradation. In addition, it was found that the most favorable pH is 5.6 in the presence of Fe^{2+}, this maybe due to the synergistic effects of the coagulation action of $Fe(OH)_3$ produced by the induced reaction.

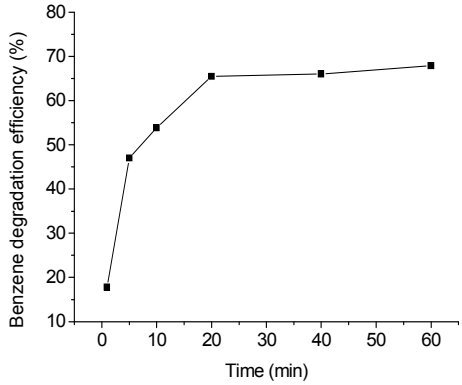

Fig. 4. Effects of ferrous sulfate（2×10^{-3} mol·l^{-1} $FeSO_4$）

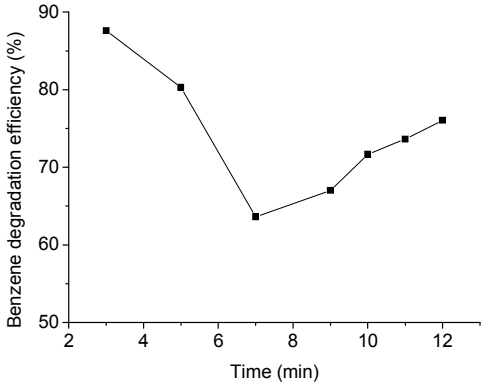

Fig. 5. Effects of pH on benzene removal

2.4 pH Effects

Since the pH often plays an important role in the wastewater treatment, we studied the effects of initial pH on the degradation of benzene. Figure 5 shows the results of a series of experiments at different pH at given reaction time 30min. The initial conditions for the model were as follows: benzene concentration (c_0) was 100 $mg \cdot L^{-1}$ and applied voltage was 700V. A faster benzene removal rate can be achieved for a relatively higher alkalinity or acidity. As we already know, the oxidative ability of plasma is stronger in acidic conditions. When the solution was basic, the amount of the plasma is increased and the charge distribution of the reactant changes, which makes it favorable to attack of the OH· free radicals. Because most of the wastewater is acidic or basic, it does not need pH adjustment.

2.5 Intermediate products and degradation mechanism

In order to obtain the reaction path, a series of experiments were carried to determine the intermediates by HPLC under normal conditions, that is, without any other substance added (Fig. 6). By the detailed analysis of the intermediate products and kinetic consideration, it was proposed that the reaction of benzene with the hydroxyl radical might lead to the formation of methanoic acid, acetic acid, oxalic acid and so on as the primary products. In the end, all of the carboxylic acids were decomposed into inorganic carbon, which might exist as bicarbonate or carbon dioxide. These results were in agreement with that of references [9,10].

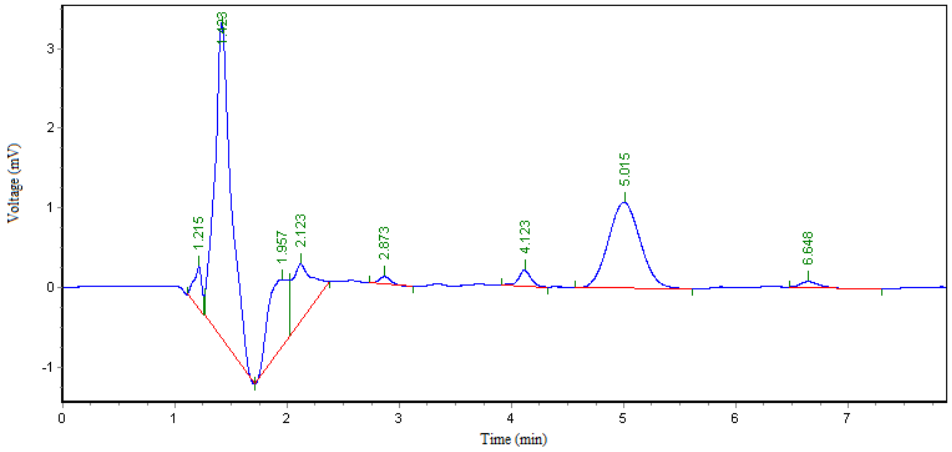

Fig. 6 HPLC chromatogram of intermediate products at 10 minutes of degradation.

The operating conditions: Column, Luna 5u C18; Mobile phase, acetonitrile-phosphate suffer (20 %) =40:60(V/V); Pressure, 14.2 M Pa; Wavelength, 254 nm; Flow rate: 1.0 ml/min.

Based on previous studies [9,13] and the above discussion, a possible mechanism for the benzene degradation with CGDE can be proposed(Scheme 1).

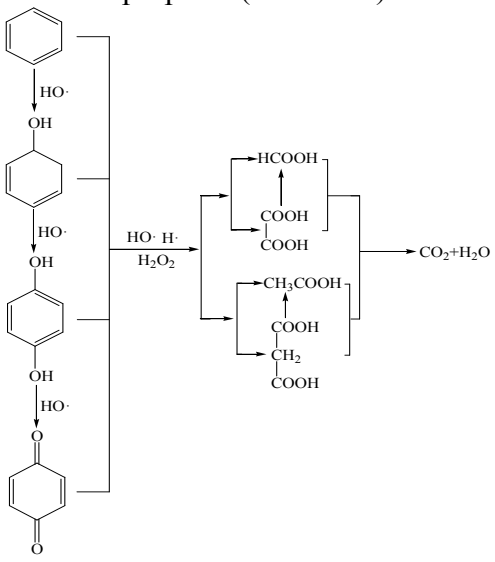

Scheme 1. The mechanism for the benzene degradation with CGDE.

3. Conclusion

From the above experiments, the following conclusions can be drawn:

i) Benzene can be rapidly and exhaustively degraded by glow discharge electrolysis in water. The final product was inorganic carbon.

ii) Faster benzene removal rate can be achieved for a relatively higher alkalinity or acidity.

iii) The degradation can be greatly accelerated in the presence of Fe^{2+} and H_2O_2.

These wonderful results suggest that glow discharge electrolysis is an efficient tool for degradation of benzene, and further study is under way.

Acknowledgment

In this paper, the research was sponsored by the School of GANSU Province Graduate Student Teacher Research Item Project Stake (Project No. 121003), the Applied Chemistry Key Subject of Gansu Pronvince (Project No. GSACKS20130113), and the Youth Technology Innovation Projects of Longdong University (Project No. XYZK1013).

References

[1] J. Karuppiah, E. L. Reddy, P. M. K. Reddy, B. Ramaraju, R. Karvembu, C. Subrahmanyam. Abatement of mixture of volatile organic compounds (VOCs) in a catalytic non-thermal plasma reactor [J]. J. Hazard. Mater., 2012 237-238 283-289.

[2] Priority Pollutants, Code of Federal Regulations, Title 40, U.S. Environmental Protection Agency, U. S. Government Printing Office: Washington, DC, 1996, Chapter 1, Part 423, App. A.

[3] C.W. Kwong, Christopher Y.H. Chao, K.S. Hui, M.P. Wan. Removal of VOCs from indoor environment by ozonation over different porous materials [J]. Atmos. Environ., 2008 42 (10) 2300-2311.

[4] Sun Y., Zhou L., Zhang L., Sui H. Synergistic effects of non-thermal plasma- assisted catalyst and ultrasound on toluene removal [J]. J. Environ. Sci., 2012 24 (5) 891-896.

[5] M. A. Malik, A. Ghaffar, S. A. Malik. Water purification by electrical discharges [J]. Plasma Sources Sci. Technol., 2001 10 (1) 82-91.

[6] Y. Chen, X. Zhang, Y Dai, W Yuan. Pulsed high-voltage discharge plasma for degradation of phenol in aqueous solution [J]. Separation and Purification Technology, 2004 34 (1-3) 5-12.

[7] H. V. María, R. Molina, H. Schikora, M. Müller, J. M. Bayona. Removal of priority pollutants from water by means of dielectric barrier discharge atmospheric plasma [J]. J. Hazard. Mater., 2013 262 664-673.

[8] C. Lee, Y. Lee, J. Yoon. Oxidative Degradation of Dimethyhulfoxide by Locally Concentrated Hydroxyl Radicals in Streamer Corona Discharge Process [J]. Chemosphere, 2006 65 (7) 1163-1170.

[9] L. C. Lei, Y. Zhang, X. W. Zhnng, et al. Using a novel pulsed high-voltage gas-liquid hybrid discharge continuous reactor for removal of organic pollutant in oxygen atmosphere [J]. J.Electrostat., 2008 66 (1-2) 16-24.

[10] K. Gai. Anodic oxidation with platinum electrodes for degradation of p-xylene in aqueous solution [J]. Journal of Electrostatics, 2009 67 (4) 554-557.

[11] A. Hickling, M. D. Ingram. Glow-discharge electrolysis [J]. J. Electroanal. Chem., 1964, 8 (1): 65-81.

Advanced Materials Research Vols. 989-994 (2014) pp 60-64
© (2014) Trans Tech Publications, Switzerland
doi:10.4028/www.scientific.net/AMR.989-994.60

Liquid phase Rhodamine Boxidation induced by plasma with glow discharge electrolysis

Ke Gai[a], Huili Qi[b], Dongping Ma[c], Yuquan Zhang[d]

College of Chemistry and Chemical Engineering, Longdong University, Qingyang, 745000，China
[a]email:gaike310@sohu.com, [b]email:qhl725@sohu.com, [c]email:mdp_725@163.com,
[d]email:357767938@qq.com

Keywords: Rhodamine B; plasma; glow discharge; degradation; hydroxyl radicals

Abstract. Exhaustive Rhodamine B oxidation by means of contact glow discharge plasma in aqueous solution has been investigated. The rate of degradation in different conditions such as pH, H_2O_2, Fe^{2+}, n-butanol, and other factors affecting was studied. The results showed that, there are faster removal rate when the solution was in a relatively higher acidity; H_2O_2 presence can improve the efficiency rate.Fe^{2+} can promote reaction. Radical scavenger, n-butanol, inhibits the Rhodamine B removal significantly. Some major intermediate products were detected by HPLC and GC-MS, respectively.

1. Introduction

Rhodamine B（RhB) is a cationic very stable dye. It has the xanthene structures and often as cationic molecular model of refractory organic pollution. Because it`s stability and the dyeing ability， RhB is widely used in industry and will cause great damage to the water environment[1-2].The treatment of wastewater containing RhB is very important. Because many anti microbial degradation of dye，the study of many physical and chemical treatment of wastewater containing such aselectrochemical oxidation, ozonation and biological treatment etc[3-5].

The most suitable alternative method is advanced oxidation processes (AOP), since the most powerful oxidizing species in this process are in fact the hydroxyl radical. The hydroxyl radical reacts strongly with organic substances. In this process, HO·radical are produced electrochemically in an anodic reaction directly from water which has to be treated [6] as follows:

$$H_2O - e \rightarrow H_2O^{+} \rightarrow HO\cdot + H^{+}$$
$$2HO\cdot \rightarrow H_2O_2$$
$$H_2O_2 \rightarrow O_2 + H_2O$$
$$O_2 + H_2O + 2e \rightarrow H_2O_2 + 2OH^{-}$$
$$OH^{\cdot} + H_2O_2 \rightarrow H_2O + HO_2^{\cdot}$$
$$H^{+} + OH^{-} \rightarrow H_2O$$

By using the electrochemical production of hydroxyl radicals, no addition of chemical substances is necessary and the process can be performed at affordable costs, determined mainly by the power required for driving the electrochemical process and without the common AOP drawbacks. Most of the researches focus on dissolved easily and low toxic substances, some of them attempted to design complex apparatus including costly diamond anodes for the COD removal from several industrial wastewaters [7-8].

Removal of RhB and effects of various parameters on the removal efficiency in the aqueous solution with plasma are studied. The anodic contact glow discharge plasma may be promising since it doesn't need any evacuating system or special power source. The mechanism of producing plasmas in this process has been studied by M. A. Malik and so on [9-11]. Recently, there were several reports on the degradation of certain organic target compounds dissolved in water by use of contact glow discharge. These reports concerned chlorophenols [12], aniline [13], phenol [14], azobenzene [15], auramine [16] and so on. All these investigations confirm that contact glow discharge plasma was a prospective process for the degradation of toxic substances. In the present paper, RhB was chosen as a model pollutant dissolved in potassium sulfate by means of glow

discharge electrolysis under water in order to further study the degradation behavior of organic compounds.

2. Experimental

The experimental apparatus was comprised of a reaction cell and a high voltage power supply as illustrated in Fig. 1. The anode from which the glow discharges emitted was a pointed platinum wire (I.D. 0.3 mm) encased in a glass tube located in the bottom center of a cylinder reactor, with the needle tip protruding 1 mm from the glass tube. The cathode was a stainless steel rod placed in the opposite position of the anode. A positive high voltage was applied to the needle anode by a WYJ-1000V2A dc power unit providing voltage of 0-1000 and current output of 0-2 A （VWYJ-1000V2A）. In addition, the reaction cell was coated by a water jacket, in which the temperature was controlled at the room temperature. When the glow discharge electrolysis began, a lot of heat was produced, which can convert the solution. Therefore, no other system was employed to stir the solution.

RhB was dissolved in an aqueous potassium sulfate solution (2g/L). The pH of the solution was adjusted with dilute sodium hydroxylate and dilute sulfuric acid to the expected value. During the reaction, a small portion of the solution (0.025ml) was periodically sampled out from the sampling port to measure the reduction of RhB immediately by UV spectrometer (SPECORD50) and high performance liquid chromatography (LC-10ATvp).

The experimental conditions usually employed were: electrolyte, 150mL; voltage, 600V; temperature, 298K. The maximum absorption wavelength is 554nm.These are refered as the “standard conditions” or otherwise specified.

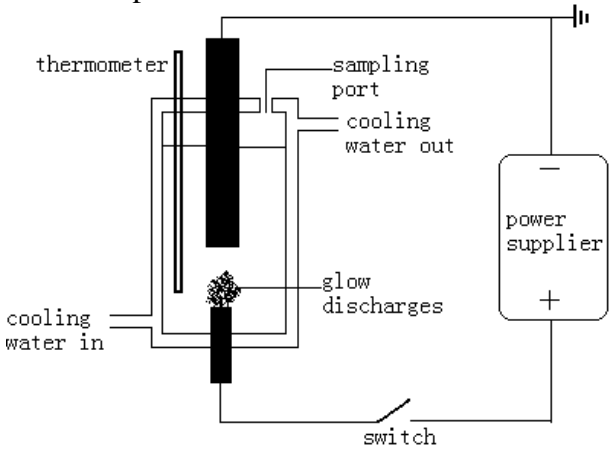

Fig. 1. Scheme of the experimental apparatus

3. Results and discussion

3.1 The characteristic curve of current vs. voltage

In order to clarify the glow discharge electrolysis underwater, a characteristic curve of current vs voltage was presented in Fig.2. A 150ml solution containing 2g/L K_2SO_4 and 100mg/L RhB was used for degeadation under defferent voltage. From the curve, it can be found that the current increased almost proportionately with the increase of the applied voltage in 0～250V, suggesting that the electrolysis observe the ohm’s law in this stage. The reaction was mainly attributed to the oxidation of water at the anode and reduction at the cathode. When the applied voltage is over 320V, the current decreased with the increasing of the voltage, this can be explained by the fact that a lot of heat was produced near the tip of the anode, making the water surrounding the anode vaporization and the current decreased because the water vaper is dielectric. From the experiment, it was found that there is almost no signs of the melting of the anode even the applied voltage increased to 700V, proving that the glow discharge electrolysis under water can widen the applied voltage range.

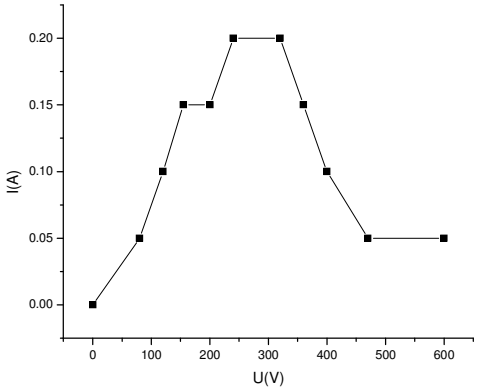

Fig. 2. The characteristic curve of current vs voltage

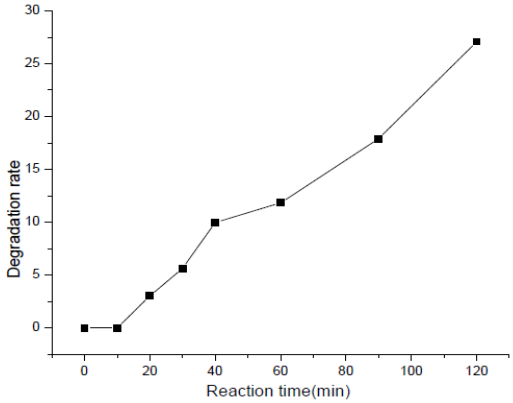

Fig. 3. Time profile of RhB degradation

3.2 RhB removal

The oxidative degradation of RhB proceeded abruptly when glow discharge electrolysis was carried out on the solution containing it. Fig. 3 exhibits the time profile of RhB removal under 600V. It can be seen that the RhB removal increases with the discharge time. This indicates that glow discharge electrolysis is a very efficient tool for RhB degradation because generally the pollutant cannot be completely removed in other processes. The degradation rate was calculated by the following formula:

$$\text{Elimination rate} = \frac{\text{concentration(initial)} - \text{concentration (treated)}}{\text{concentration (initial)}}$$

3.3 Effects of and hydrogen peroxide（30%）

In order to investigate the role of H_2O_2 in removing RhB from the aqueous solution, 5 mL H_2O_2 were added to 150ml solutions of RhB, respectively, to study the RhB degradation behavior. Fig. 4 indicates the elimanation rate of the RhB in the presence of H_2O_2 at reaction time 120 minutes. The results show that the removal efficiency of RhB with hydrogen peroxide is higher than without hydrogen peroxide. It may be explained that the concentration of HO· is increased when H_2O_2 was added into the RhB solution and hydroxyl radical is the most responsible oxidant in the degradation of RhB.

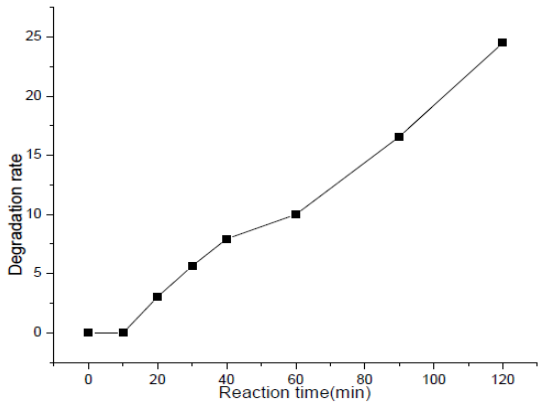

Fig. 4. Accelerating effect of H_2O_2 on RhB degradation

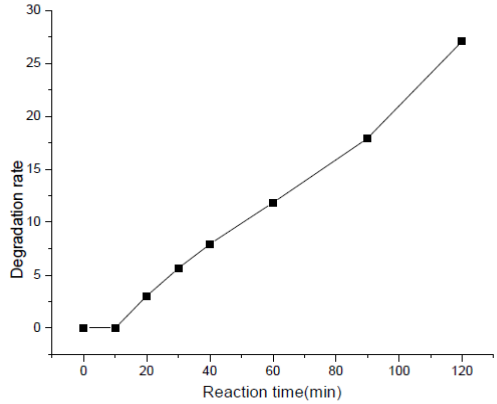

Fig. 5. Effects of ferrous sulfate（0.4mL10% Fe^{2+}）

3.4 Effects of ferrous sulfate

Fig.5 shows the removals of RhB in the presence of ferrous sulfateduring 120 minutes of treatment. The results show that Fe^{2+} has a obvious catalytic effect for RhB degradation. The rapid increase in the reaction rate upon the addition of $FeSO_4$ may be attributed to the Fenton's reaction. In the presence of Fe^{2+}, the H_2O_2 produced by the discharge was converted to ·OH again, thus accelerating the degradation velocity [17-18]. Therefore, the amounts of hydroxyl radicals which are available for the reaction with RhB.

3.5 pH Effects

Special attention was paid to investigate the effects of solution pH on RhB degradation, since the pH often plays an important role in the wastewater treatment. Fig.5 shows the results of a series of experiments at different pH. Faster RhB removal rate can be obtained in a relatively higher acidity than in neutral conditions and alkalinity. This maybe presumed that more ·OH was produced in CGDE under acidity conditions. Because a lot of industrial wastewater is acidic, the treatment of wastewater does not need pH adjustment in the plasma process.

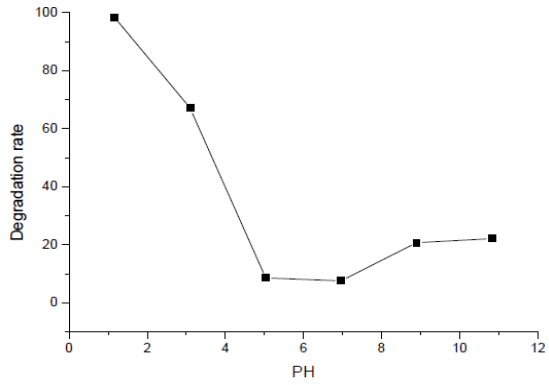

Fig. 6. Effects of pH on RhB removal

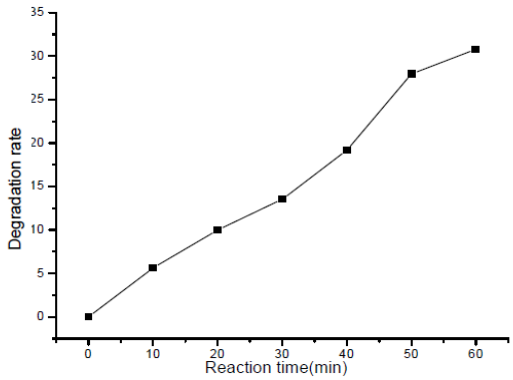

Fig.7. Effects of n-butanal(0.4mL)

3.6 Effects of n-butanol

Fig.6 shows the removals of RhB in the presence of n-butanol during 60 minutes of treatment. The results show that n-butanol has a strong inhibition effect on RhB degradation. As well known that n-butanol reacts with hydroxyl radical with a high rate constant (10^8 L·mol^{-1}·s^{-1} [4]). Therefore, the amounts of hydroxyl radicals that are available for the reaction with RhB are lower in the presence of n-butanol than those without n-butanol.

3.7 Intermediate products

For better understanding the degradation mechanism, HPLC and GC-MS were used to determine the intermediate products formed during degradation process. The major intermediate products identified by GC-MS were benzoic acid, paradioxybenzene, benzoquinone, benzene and some other products. As the treatment went on, some carboxylic acids such as formic, oxalic and malonic acids etc. were formed. In the end, all of the carboxylic acids were decomposed to inorganic carbon, which might exist as bicarbonate or carbon dioxide.

4. Conclusion

RhB can be rapidly and exhaustively degraded by glow discharge electrolysis under water. The final products were inorganic carbon and inorganic nitrogen. Faster RhB removal rate can be achieved in relatively higher acidity. The degradation can be greatly accelerated in the presence of Fe^{2+} ion and H_2O_2 and can be inhibited in the presence of *n*-butanol. All the experimental results show that the hydroxyl radicals are the most responsible oxidants for RhB degradation in glow discharge electrolysis under water. Therefore, glow discharge electrolysis under water is an efficient method for RhB degradation.

Acknowledgement

In this paper, the research was sponsored by the School of GANSU Province Graduate Student Teacher Research Item Project Stake (Project No. 121003), the Applied Chemistry Key Subject of Gansu Pronvince (Project No. GSACKS20130113), and the Youth Technology Innovation Projects of Longdong University (Project No. XYZK1013).

References

[1] Jincai Z, Taixing W, Kaiqun W, et al. Degradation of the cationic dye rhodamine B in aqueous anionic surfactant/TiO_2 dispersions under visible light irradiation [J]. Environ. Sci. Tecnnol., 1998 32 2394-2400.
[2] Hongbin Li, Lianjie Zhu, Chunyan Ma. TiO_2 hollow microspheres: synthesis, photocatalytic activity, and selectivity for a mixture of organic dyes [J]. Monatshefte fur Chemie, 2014 1 29-35.
[3] Zhao J C, Lei P X. Degradation of dye pollutants by immobilized polyoxometalate with H_2O_2 under visible-light irradiation [J]. Envion. Sci. Techonl., 2005 39 8466-8474.
[4] V. Abramov, O. Abramov, A. Gekhman, V. Kuznetsov, G. J. Price. Ultrasonic intensification of ozone and electrochemical destruction of 1,3-dinitrobenzene and 2,4-dinitrotoluene [J]. Ult. Sonochem., 2006 13 303-307.
[5] T. Essam, M. A. Amin, O. Tayeb, B. Mattiasson, B. Guieysse. Sequential photochemical-biological degradation of chlorophenols [J]. Chemosphere, 2007 66 2201-2209.
[6] B. Marselli, J Garacia-Gomez, P. A. Michaud. Electrogeneration of Hydroxyl Radicals on Boron-Doped Diamond Electrodes [J]. J. Electrochem .Soc. 2003 150D 79-83.
[7] N. Katsuki, E. Takahashi, M.Toyoda, T. Kurosu, M. Iida, S. Wakita, Y.Nishiki, T. Shimamune, Water electrolysis using diamond thin-film electrodes [J]. J. Electrochem. Soc., 1998 145 2358-2362.
[8] M. A. Rodrigo, P. A. Michaud, I. Duo. Oxidation of 4-Chlorophenol at boron-doped diamond electrode for wastewater treatment [J]. J. Electrochem. Soc., 2001 148 60-64.
[9] M. A. Malik, A. Ghaffar, S. A. Malik. Water purification by electrical discharges [J]. Plasma Sources Sci. Technol., 2001 10 82-91.
[10] M. M. Kuraica, B. M. Obradovic, D. Manojlovic, D. R. Ostojic. Ozonized water generator based on coaxial dielectric-barrier-discharge in air [J]. J. Puric. Vacuum., 2004 73 705-708.
[11] Chen Y, Zhang X, Dai Y, Yuan W. Pulsed high-voitage discharge plasma for degradation of phenol in aqueous solution [J]. Sep. & Pur. Technol., 2004 34 5-9.
[12] M. Tezuka, M. Iwasaki. Plasma induced degradation chlorophenols in aqueous solution [J]. Thin Solid Films, 1998 316 123-126.
[13] M. Tezuka, M. Iwasaki. Plasma-induced degradation of aniline in aqueous solution [J]. Thin Solid Films, 2001 386 204-207.
[14] Gao J, Liu Y, Yang W, Pu L, Yu J, Lu Q. Oxidative degradation of phenol in aqueous electrolyte induced by plasma from a direct glow discharge [J]. Plasma Sources Sci. Technol., 2003 12 533-538.
[15] Gai K, Dong Y. Plasma induced degradation of azobenzene in water [J]. Journal of the Chinese Chemical Society, 2005 52 273-276.
[16] Gai K, Dong Y. Liquid phase auramine oxidation induced by plasma with glow discharge electrolysis [J]. Plasma Sources Sci. Technol., 2005 14 589-593.
[17] A. Hickling, J. K. Linacre. The anodic oxidation of ferrous sulphate [J]. J. Chem. Soc., 1954 (2) 711-719.
[18] H. A. Dewhurst, J. F. Flagg, P. K. Watson. Oxidation of aqueous ferrous sulfate by glow discharge [J]. J. Electrochem. Soc., 1959 106 366-367.

Advanced Materials Research Vols. 989-994 (2014) pp 65-68
© (2014) Trans Tech Publications, Switzerland
doi:10.4028/www.scientific.net/AMR.989-994.65

The preparation of ZnO: Al thin films on flexible substrates by magnetron sputtering method

Wang XiaoJing

College of electronics & information engineering, Wuhan Textile University ,Wuhan 430074,China

wxjisme@126.com

Keywords: ZnO:Al; Magnetron Sputtering; Buffer layer;Structure and properties

Abstract. ZnO: Al film was deposited on TPT substrate with SiO_2 buffer layer by RF magnetron sputtering. The obtained film had a hexagonal structure and highly (002) preferred orientation. The lattice constant distortion of the film with buffer layer was decreased and the compressive stress was 0.779GPa. The carrier concentratio reached to $3.15\times10^{+20}$/cm3. The resistivity of ZAO film with SiO_2 buffer layer was about 9.2×10^{-3} Ω·cm and the average transmittance was over 72% in the range of 380~900nm.

Introduction

ZnO: Al (ZAO) transparent conductive thin films on flexible substrates are a hot subject of research for their special advantages including light weight, easy bending and resistant to impact damage [1-2], which are important for the applications in some devices such as flexible solar cells and flexible touch screens. ZAO thin films on some flexible materials are almost deposited at low temperature（ < 200℃）due to the poor high-temperature characteristics of these flexible substrates, including PET [3], PC [4], PI [5], PPA [6], Teflon [7], PES[8] and so on. Since the resistivities of ZAO films on flexible substrates are high, in the quantity of 10^{-2}~10^{-3}Ω·cm[9-10], they need to be improved especially for the industrial application in solar cells and other devices. There are several methods to improve the conductivity of ZAO films, such as increasing the film thickness, adjusting the deposition parameters , adopting a buffer layer between the flexible substrate and the ZAO films . The last one is an effective way to improve the conductivity of the ZAO films and will not be damaged to the optical properties of the films. Various kinds of buffer layers have been introduced in ZnO film growth, such as ZnO[11], Al_2O_3[12] , MgO[13] and SiOx[14].

The deposition of ZAO films on transparent TPT substrates by RF Magnetron Sputtering method has been successfully prepared by our group [15].In this paper, we reported the preparation of high conductivity of ZAO thin film on transparent TPT substrate by introducing a SiO_2 buffer layer and studied the influence of buffer layer on the structural, optical and electrical properties of AZO films.

Experimental procedure

The ZAO thin films were deposited on transparent TPT substrate by RF magnetron sputtering system from a ZnO: 2.0 wt % Al_2O_3 target (purity: 99.99%). The substrate with thickness of 50μm was ultrasonically cleaned in acetone and then in ethanol for 15 min respectively before it was loading into the deposition chamber. The distance between the target and substrate was about 50 mm. Before the deposition of ZAO thin films, SiO_2 buffer layers were deposited using a SiO_2 target (purity: 99.99%) by RF magnetron sputtering at room temperature with 0.5 Pa of deposition pressure and 300W of RF power. For the purpose of comparison, the ZAO films without buffer layers were also deposited on TPT substrates. The ZAO films were grown at room temperature (about 25℃) for 180 min with the flow rate of Ar of 20 sccm, the deposition pressure of 1.0 Pa and the RF sputtering power of 120 W.

The structure properties and surface compositions of the ZAO films were analyzed with X-ray diffraction (XRD, X'Pert PRO, λ=0.154 nm) using Cu-Kα radiation and field-emission scanning electron microscopy (FE-SEM, Sirion 200) . The transmittances of the films were measured by spectrophotometer (UV, Lambda 35) in the range of 380~900 nm and the electrical properties were characterized by a Hall Effect Measurement System (Lakeshore MODEL 642) at room temperature.

Results and discussions

Structure properties

Fig.1 shows XRD patterns of ZAO films. The ZAO film without buffer layer had a diffraction peak at 2θ about 34.22° and the film with SiO_2 layer had a diffraction peak at 2θ about 34.25°, which is associated with the (002) plane of hexagonal phase ZnO and implied that the prepared films had a c-axis preferred orientation. The average grain sizes were derived by Scherrer equations as follows:

$$D = \frac{0.9\lambda}{\beta \cos\theta} \tag{1}$$

where λ is the X-ray wavelength (0.154 nm), θ is the Bragg angle, and β is the FWHM of the (002) diffraction peak. The grain size of ZAO film is 68.26nm for sample without buffer layer and 60.15nm for those with buffer layer.

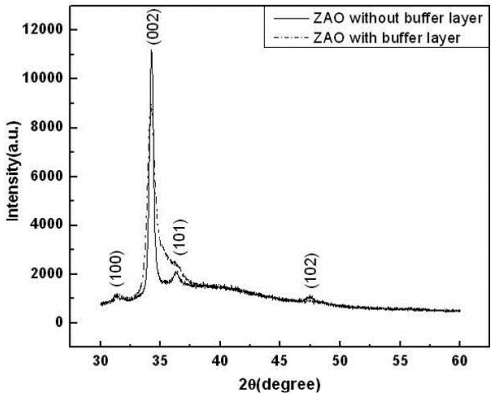

Fig.1. XRD patterns of ZAO thin films

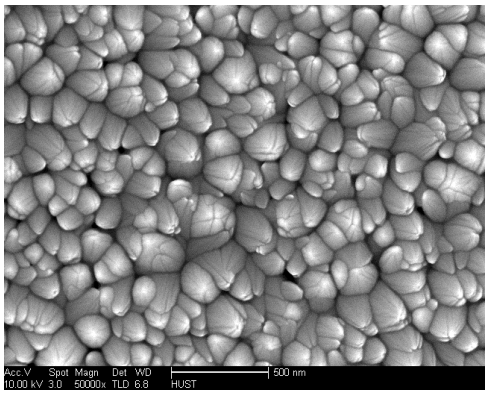

Fig. 2. SEM images of ZAO thin films with SiO_2 buffer layer

The SEM image of theZAO thin film was shown in Fig. 2. It was observed that the ZAO films consisted of some columnar structured grains. The ZAO film was compact. The deposition rate of the ZAO film with buffer layer was about 5.4nm/min.

The strain along c-axis orientation was derived by the formula [16]:

$$\varepsilon_{zz} = \frac{c - c_0}{c_0} \times 100\% \tag{2}$$

where c is lattice constant calculated from XRD result, c_0 (0.521nm) is unstrained lattice constant measured from ZnO powder. The stress parallel to the ZAO film surface was calculated by the following formula [17] :

$$\sigma_{film} = \frac{2c_{13}^2 - c_{33}(c_{11} + c_{12})}{2C_{13}} \times \frac{c_{film} - c_0}{c_0}, \tag{3}$$

where c_{ij} is elastic constants， the data have been used : c_{11} =208.8, c_{33} =213.8, c_{12} =119.7, c_{13} =104.2GPa. The stress in the film with buffer layer is -0.654GPa, where negative sign corresponds to compressive stress. These may be due to the following two reasons : one is intrinsic stress caused by impurities and defects; the other is thermal expansion coefficient mismatch between the film and the substrate.

Electrical properties

The electrical properties of the ZAO films were measured by Hall Effect Measurement System. The lowest resistivity was $9.2\times10^{-3}\Omega\cdot$cm with a carrier concentration of $3.15\times10^{+20}/cm^3$ and hall mobility of $3.5cm^2/(VS)$.

Optical properties

Fig. 3 shows the optical transmittances of the ZAO films including the TPT substrates. It was seen that the transmittances of the ZAO films on TPT substrates were over 65% in the visible region, and the average transmittances of the two films were over 72% in the range of 380~900nm. The absorption edge of the ZAO film with buffer layer was shifted to the higher energy. It is attributed to the Burstein-Moss effect [30], which is the blue shift of the absorption edge with increasing carrier concentration. The transmittance of the ZAO film with buffer layer was a little higher than that of the film without buffer layer. It is mainly because that the latter was thicker than the former at different film deposition rate.

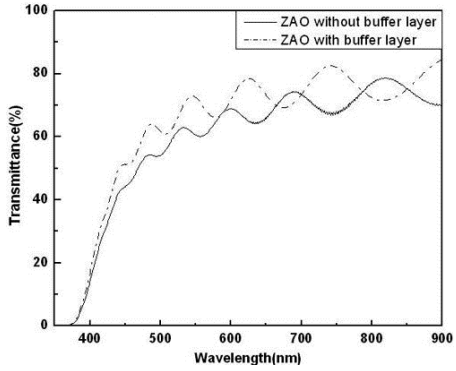

Fig. 3. Transmittance curves of ZAO thin films on TPT substrates

Conclusions

ZAO thin films with SiO_2 buffer layer were prepared on TPT substrate by magnetron sputtering. XRD and SEM measurements revealed that the films were highly c-axis oriented. The resistivity of ZAO film with SiO_2 buffer layer was $9.2\times10^{-3}\ \Omega\cdot$cm with a carrier concentration $3.15\times10^{+20}/cm^3$. The optical transmittance of the ZAO film was over 72% in the range of 380~ 900nm.

References

[1] T.T. Guo,G.B.Dong,F.Y.Gao,Y.Xiao,Q.Chen,X.G.Diao:Appl. Surf. Sci.282(2013),p.467
[2] C. Oliveira, L. Rebouta, T .D. Lacerda-Arôso, S. Lanceros-Mendez , T. Viseu, C. J. Tavares, J. Tovar, S. Ferdov, E. Alves:SThin Solid Films 517(2009),p 6290
[3] S. Fernandez, F.B. Naranjo: Sol. Energy Mater. Sol. Cells 94(2010),p157
[4] Y.D. Liu, Q.Li, H.L. Shao, Properties of ZnO:Al films deposited on polycarbonate substrate. Vacuum 83(2009),p1435
[5] X.T. Hao, J. Ma, D.H. Zhang, Y.G. Yang, H.L. Ma , C.F. Cheng, X.D. Liu,: Mater. Sci. Eng., B 90(2002),p50
[6] H.L. Ma, X.T. Hao, J. Ma, Y.G. Yang, S.L. Huang, F. Chen, Q.P. Wang, D.H. Zhang:Surf. Coat. Technol. 161(2002),p 58
[7] Y.Y. Liu, Y.Z.Yuan, C.F. Li, X.U. Gao, X.Z. Cao, J.B. Li:Mater. Lett. 62 (2008),p 2907
[8] Y.C. Lin, M.Z. Chen, C.C. Kuo, W. T. Yen:Colloids and Surfaces A: Physicochem. Eng. Aspects 337(2009),p52

[9] S. Fernández, A. Martínez-Steele, J.J. Gandía, F.B. Naranjo:Thin Solid Films 517(2009),p 3152
[10] W.F. Liu, G.T. Du, Y.F. Sun, J.M. Bian, Y. Cheng, T.P. Yang, Y.C. Chang, Y.B. Xu: Appl. Surf. Sci.253 (2007) ,p2999
[11] C.Y. Hsu, T.F. Ko, Y.M. Huang:J. Eur. Ceram. Soc. 28(2008),p3065
[12] Z.L. Pei, X.B. Zhang, G.P. Zhang, J. Gong, C. Sun, R. F. Huang, L. S. Wen: Thin Solid Films 497(2006),p20
[13] M. Fujita, N. Kawamoto, M. Sasajima, Y.J Horikoshi:J.Vac. Sci.Technol. B 22(2004),p1484
[14]D. A .Byung , G. K.Young, H. O. Sang, J. H .Song, H. J. Kim:Thin Solid Films 517(2009),p6414
[15] X. J. Wang, Q. S. Lei, W. Xu, W. L. Zhou, Yu J: Mater. Lett.63(2009),p1371
[16] H.C. Ong, A.X.E. Zhu, G.T. Du:Appl. Phys. Lett. 80(2002),p941
[17] R. Cebulla, R. Wendt, K. J.Ellmer:J.Appl. Phys. 83(1998),p1087

Advanced Materials Research Vols. 989-994 (2014) pp 69-73
© (2014) Trans Tech Publications, Switzerland
doi:10.4028/www.scientific.net/AMR.989-994.69

Analysis Analysis and Suggestions on Device Clamp Screw Fracture of 110kV Transmission Line

Xuexia XU[1, a], Weiyong LI[2,b], Guangxing ZHANG[1,c], Yanting FENG[1,d], Hao KE[1,e], Qiang WANG[1,f] , Hongxia CUI[1,g]

[1]Bureau of Boiler Inspection, State Grid Hebei Electric Power Research Institute, Shijiazhuang, 050021, China

[2]Department of Materials and Technology, Hebei College of Industry and Technology, Shijiazhuang, 050016, China

[a]email: xuxuexia2008@163.com, [b]email:13933882838@139.com, [c]email:hepri-zhanggx@he.sgcc.com.cn, [d]email:13503206410@139.com, [e]email:hepri-kehao@he.sgcc.com.cn, [f]email:hepri-wangq1@he.sgcc.com.cn, [g]email:hepri-chx@he.sgcc.com.cn

Keywords: Screw; device clamp; fracture; transmission line.

Abstract. Fracture failure analysis on device clamp screws of one 110kV transmission line has been carried out based on results of macro-observation, pre-tightening test, mechanical property examination, chemical composition analysis, microstructure observation, SEM observation and EDAX analysis. It is concluded that the main reason of the screw fracture lies in misuse material and improper heat processing which led to material degradation. Suggestions are put forward finally.

Introduction

Device clamp was a kind of connection fitting used to fix mother conductor and terminal outgoing. As one of power fittings, device clamp plays an important role in guaranteeing safe and stable operation of high and super high voltage transmission lines [1] [2]. Device clamp failure will cause severe electric network accidents and failure analysis is necessary and instructive to avoid similar events [3] [4] [5].

The failure causes of device clamp of one 110kV transmission line were discussed in this paper and measurements were provided. The failure crack happened to the strain clamp on A-phase of 158-5 knife switch whose screws cracked, and overheating temperature was as high as 360^{o}C under 80A electric current. The screw dimension was M10 and its material was austenite stainless steel with minimum tensile strength of 700MPa according to GB/T 3098.6-2000.

Experimental Observation and Analysis

The dimension of the screw was measured to be M10. It can be consumed that the screw was processed by upset forging according to the metal flow in the screw section and the thread was processed by squeezing as shown in Fig.1 (a) and (b).

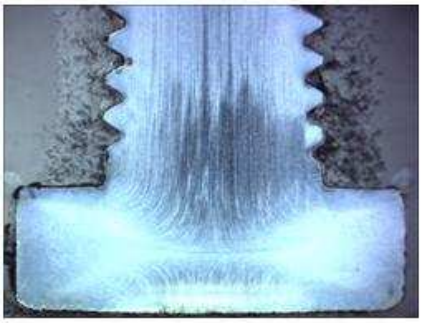

(a)The metal flow in the screw section

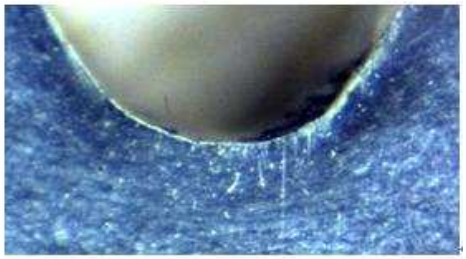

(b)The metal flow in the screw end

Fig.1 The macro morphology of the metal flow in the screw

The fracture morphology of the failure screw was observed by stereomicroscope. Old fracture section was found in the fresh fracture, meaning that crack defect had existed before the screw fracture. The morphology was shown in Fig.2.

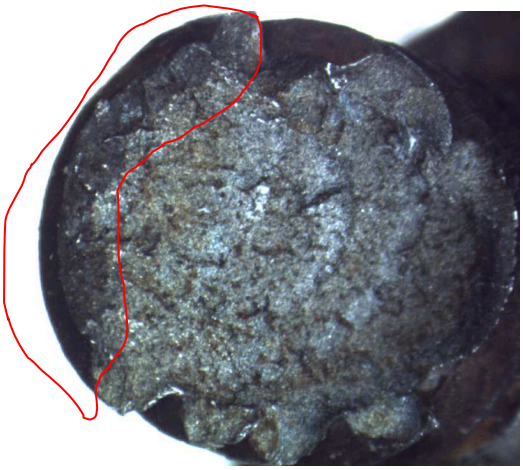

Fig.2 The origin defect in the screw fracture

The unbroken screw was fastened on the test table and the test was carried out by torque wrench and load measurement equipment. When the single nut was pre-tightened, the thread was easily damaged due to the engagement between screw and led to nut slippage as shown in Fig.3. During the pre-tightening test for single screw, the phenomenon happened twice with driving torque of 60Nm and pre-tightening load of 885N which far below fracture load, meaning that nut tightening was impossible to result in screw broken.

Fig.3 The engagement area between screw and nut

The pre-tightening test result was given in table.1.

Table.1 Pre-tightening test result of the unbroken screw

Serial number	Torque(Nm)	Voltage of sensor(V)	Pretightening load(N)	Remarks
1	40	0.256	796.4	/
2	60	0.281	885.7	Thread cracking noise
3	70	0.296	939.3	Thread slippage

The result of mechanical properties test was illustrated in table.2 it can be found that the tensile stress of the screw meet the standard for A2-70 stainless steel of 700MPa,, whereas its percentage elongation after fracture was lower than the standard requirement of 4mm. Therefore, the mechanical properties of the tested screws didn't accord with the relevant standard requirement.

Table.2 The mechanical properties of the screws

Sample number	Original length(mm)	Length after fracture(mm)	Elongation after fracture(mm)	Maximum tensile load(N)	Tensile stress(MPa)
1	49.9	52.8	2.9	51.22	883
2	49.8	52.8	3	53.55	923
3	49.8	50.8	1	46.68	805

In addition, original crack was found at the end of the screw of sample 3 as indicated in Fig.4 that showed the process of these screws was improper.

Fig.4 The original defect on the tensile fracture pf the screw(circled area by the red line)

The chemical composition of the screw was analyzed by ARL 3460 direct-reading spectrometer in order to examine the material. The result was given in table.3.

Table.3 The result of chemical composition analysis of the screw

Element	C	Si	Mn	S	P	Cr	Ni	V	Cu
Mass percentage(%)	0.03	0.43	17.93	0.012	0.061	7.07	0.12	0.01	0.16

It can be seen from table.3 that the material was not austenite stainless steel but that substitued Ni by Mn. Therefore the material doesn't meet with the requirement of GB/T 3098.6-2000 for A2-70 stainless steel(C<0.1%,Si<1%,Mn<2%,P<0.05%,S<0.03%,Cr=15~20%,Ni=8~19%,Cu<4%).

The microstructure of the screw was illustrated in Fig.5. It can be found to be austenite microstructure.

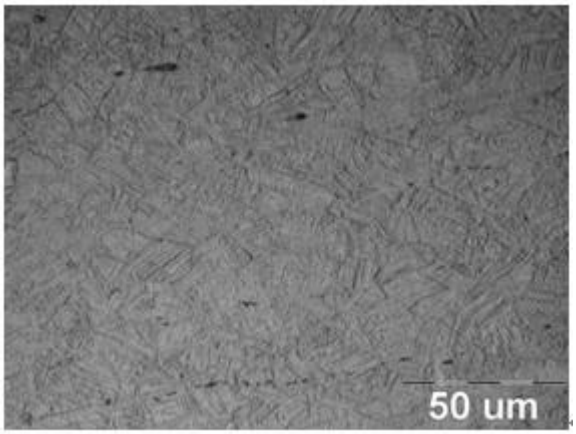

Fig.5 Metallurgical microstructure of the screw

The original crack of the screw fracture was observed by SEM and it was seen thick oxides covered there as shown in Fig.6 (a) and (b).

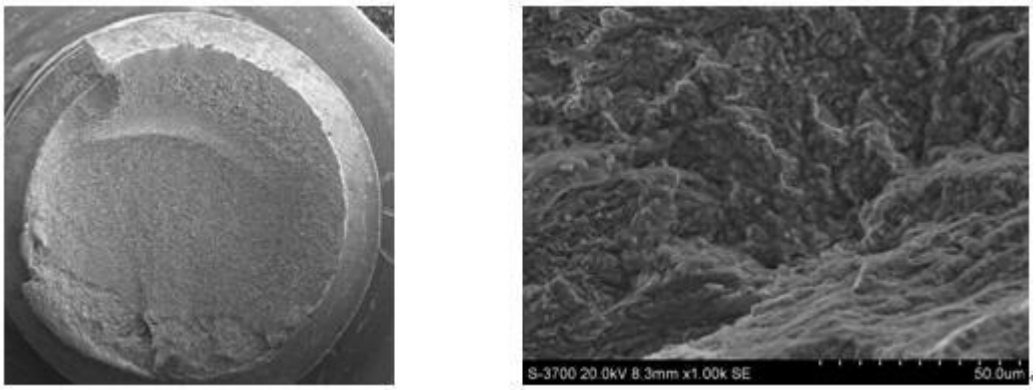

(a) SEM of the failure screw fracture (b) Thick oxides on the original crack area

Fig.6 SEM morphology of thick oxides covering the original crack area

EDS analysis examined high quantity sulfur whereas no element usually contained in water such as Cl, Na, Ca as shown in Fig.7 and table.3.

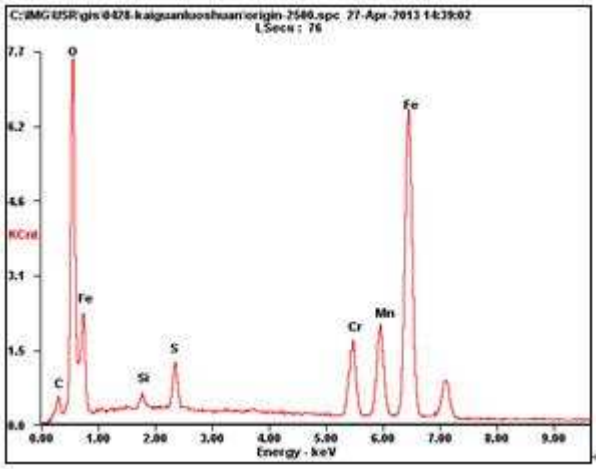

Fig.7 EDS analysis of the original crack fracture

Table.3 EDS quantity analysis result of original crack area

Element	C	O	Si	S	Cr	Mn	Fe
Mass percentage(%)	0.05	24.15	0.83	2.34	7.48	11.92	53.24

In addition, SEM observation on the fracture of crack propagation area exhibited characteristics of dimple fracture shown in Fig.8.

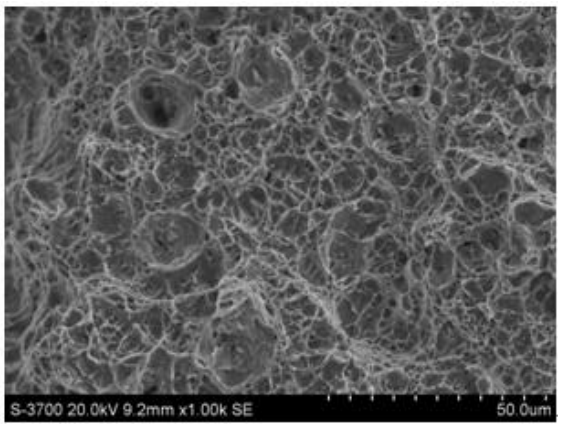

Fig.8 SEM of dimple fracture of crack propagation area

The fracture screw remained on the apparatus was examined by SEM and it was also found there existed old crack, and the fresh fracture was characterized by intergranular fracture as illustrated in Fig.9.

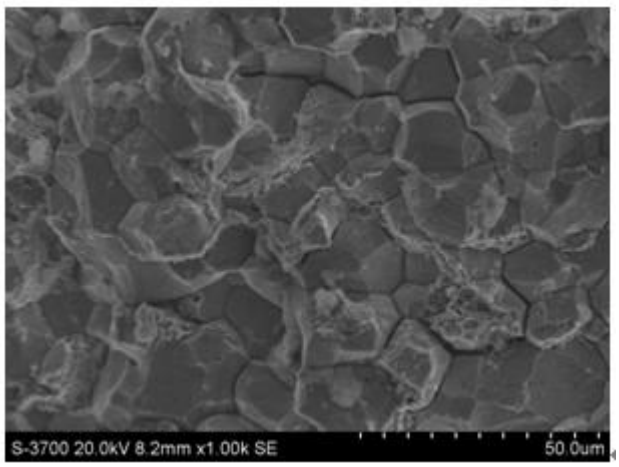

Fig.9 SEM fracture of the broken screw remained on the apparatus

Discussion

Macro-observation showed that the pre-tightening load of single screw was far below its fracture load, so the old fracture was not due to over-high pre-tightening load. Neither mechanical properties nor chemical composition met with the requirement of relevant standards. Although sulfur was examined in original crack area, no features of stress corrosion being found and compressive stress due to squeezing processing denied the possibility of stress corrosion. All the failure screws expressed characteristics of inter-granular crack the screw except old crack area, meaning that the improper heat treatment was carried out or temper brittleness happened during the subsequent processing.

Conclusion and Suggestion

Misuse of material and improper hardworking process contributed to the screw failure. It was suggested the screws be replaced and acceptance inspection be carried out on the new screws to ensure their qualification.

References

[1] Wei Fan, Shaoyu Chen, Chunhu Lan. Analysis and Improvement Measurements for Oxidation of Terminal Connector Used for Overhead Lines[J]. Corrosion & Protection, 2012, 33(9): 826-828.
[2] Xian Xu, Guozhong Wu, Yanrong Bao, et al. Analysis on Fracture Fault of Aluminum Device Clamp in Substation[J]. Hot Working Technology, 2012, 141(7): 191-192.
[3] Xu Xuexia, Ouyang Jie, Feng Yanting, et al. Analysis on Crack Failure of Terminal Connector[J]. Hot wording technology. 2011,40(13): 160-163.
[4] Ming Fan, Qiangfeng Xia, Yewei Tu, et al. Analysis on a Cleat Failure of 220kV Fixture Wire[J]. Zhejiang Electric Power, 2013, 32(8): 29-32.
[5] Jiarui Hu, Yi Xie, Chun Liu, et al. Analysis on Typical Defect of Stain Clamp, North China Electric Power, 2013(4): 34-37.

Advanced Materials Research Vols. 989-994 (2014) pp 74-78
© (2014) Trans Tech Publications, Switzerland
doi:10.4028/www.scientific.net/AMR.989-994.74

Ply Thickness' Effect on Composite Laminate under Low-velocity Impact

Xiangcheng LUO[1,a], Tao Zhang[2,b], Qingshan WANG[3,c]

[1]College of Mechanical and Electrical Engineering, Harbin Engineering University, Harbin 150001, China

[2]College of Mechanical and Electrical Engineering, Harbin Engineering University, Harbin 150001, China

[3]College of Mechanical and Electrical Engineering, Harbin Engineering University, Harbin 150001, China

[a]email:luoxiangcheng@yeah.net, [b]email:1228707501@yeah.net, [c]email:wangqingshanxlz@hotmail.com

Keywords: Laminate; Ply thickness; Dynamic Response; Low-velocity Impact

Abstract. Based on the two-dimensional Hashin failure criteria and the introduction of material degradation damage factor, low-speed impact model of composite laminated plate was established by ABAQUS with fiber and matrix's failure modes being taken into consideration. The mode is verified by referring to Karakuzu test. Next, it analyzes single ply thickness' effect on laminated plate's response and damaged under low-velocity impact. The result shows that with the thickness increasing, impact contact time and laminated plate impact point's deflection displacement reduce, while the impact force and volatile shocks are more obvious.

Introduction

Composite laminated plate with excellent mechanical properties, has been widely applied in aerospace and ship, etc. Laminated plates in low-velocity impact injury prone to failure under the action of the internal material to induce the degradation of its mechanical performance, reduces the safety of the structure. Research that aimed at low-velocity impact damage characteristics of laminated plates, domestic and foreign scholars have done much work in both experiment and numerical simulation. Through the work of Moura [1], damage prediction of the carbon/epoxy laminated plates under low-velocity impact was carried out with experimental and numerical method, the numerical results of degradation damage shape and distribution direction are in good agreement with the experiment. Low-velocity impact test and numerical simulation of the laminated plates were done by Choi [2], etc, the relationship between matrix failure and layered is analyzed. Researchers considered that the impact of the laminated plates' initial damage form is the matrix failure. Shi [3], etc, had studied the damage of laminated plates under different impact speed by establishing a 3D model, the model accorded with the Hashin failure criterion based on stress and uses cohesive unit to simulate the stratified, and Shi also analyzed the differences of numerical and experimental results. By using finite element method, Wu [4] regarded the low-velocity impact process as a reference and investigated the interference of medium plate under low-velocity impact of composite material plate with SMA volume effect on shock response of the situation. So Wu deemed that if the content of SMA volume increase, low-velocity impact damage resistance of the composite material plate would improve. Low-velocity impact model was established and the laminated plate impact damage factors was analyzed by Fuoss [5], finding the maximum impact plays a bigger role, however, the model stiffness degradation failure caused by material was not took into account, gradually leading to the bias between numerical results and experimental results. Karakuzu [6] carried out the low-velocity impact test of glass fiber/epoxy resin composite material, analyzed tha impact damage characteristics of composite material plate under different impact energy, quality, speed, and established three-dimensional model for numerical simulation, the results are agreed with the experimental results. Referring to Karakuzu's experiment, this work is based on the Hashin failure criterion and introduces the material degradation damage factor, uses

ABAQUS to establish two-dimensional composite laminated plate's low-velocity impact model, tests and verifies the rationality of the model, finishes the related impact numerical simulation by using the model, provides relevant basis and conclusion as reference for the engineering application of composite laminated plate.

Material Failure Criterion

Among failure criteria of composite laminated plate's ply, maximum stress theory, maximum strain theory, rule of Tsai-Hill, Hoffman criteria, Tsai-Wu tensor rule are commonly used. Because the material failure mode and mechanism of the criterion is not added to the material failure conditions, these criteria have nothing to do with the pattern of rule. Ignoring the stress between the middle laminated plate failure process and considering the failure modes and mechanism of material, the rule of two-dimensional Hashin process is applied to determining the damage impact on laminated plates, and its expression is shown in table 1. Type: σ_1, σ_2, τ_{12} are the normal stress and shear stress of composite laminated plate's ply; X_t and X_c are the ply's longitudinal tensile and compression strength; Y_t and Y_c are the ply's transverse tensile and compression strength; S_{12} is shear strength of the ply on direction 1-2.

Tab.1. Hashin failure criteria

Failure mode	expression
Fiber tensile failure	$\left(\frac{\sigma_1}{X_t}\right)^2+\left(\frac{\tau_{12}}{S_{12}}\right)^2\geq 1 \quad \sigma_1\geq 0$
Fiber compression fracture	$\left(\frac{\sigma_1}{X_c}\right)^2\geq 1 \quad \sigma_1\leq 0$
Substrate tensile or shear failure	$\left(\frac{\sigma_2}{Y_t}\right)^2+\left(\frac{\tau_{12}}{S_{12}}\right)^2\geq 1 \quad \sigma_2\geq 0$
Matrix compression or shear failure	$\left(\frac{\sigma_2}{Y_c}\right)^2+\left(\frac{\tau_{12}}{S_{12}}\right)^2\geq 1 \quad \sigma_2\geq 0$

Material Degradation Rule and Unit Removing

In the process of low-velocity impact, once the unit stress in the laminated plates meets one of the failure criteria in table 1, failure of materials will lead to the performance deterioration. Accordingly, the rigidity of unit's material should be reduced. The model is using the material degradation form of ABAQUS software [7].By introducing a simple linear elastic model based on energy, when the accumulation of material damage energy meets the initial damage threshold and attains to destructive critical threshold (breaking energy), material will reduce along with stress-strain relationship curve of the linear softened definition, in material damage evolution stage.

Materials are set as linear elastic before the initial damage does no happen. After damage, material constitutive relation is as follows:

$$\sigma = C_d\varepsilon \tag{1}$$

In the type(1): ε is strain for material. Damage stiffness matrix representation C_d is as follows:

$$C_d=\begin{bmatrix}(1-d_f)E_1 & (1-d_f)(1-d_m)E_1 & 0\\ (1-d_f)(1-d_m)E_2 & (1-d_m)E_2 & 0\\ 0 & 0 & (1-d_s)GD\end{bmatrix} \tag{2}$$

In the type(2): $D=1-(1-d_f)(1-d_m)\nu_{12}\nu_{21}$. d_f, d_m, d_s are variables of fiber, matrix, the shear damage under the current status respectively. d_f, d_m, d_s are gained from Hashin damage variables of four damage modes, the concrete expressions are as follows:

$$d_f=\begin{cases}d_f^{\,t} & (\hat{\sigma}_{11}>0)\\ d_f^{\,c} & (\hat{\sigma}_{22}<0)\end{cases} \tag{3}$$

$$d_m = \begin{cases} d_m{}^t & (\hat{\sigma}_{22} > 0) \\ d_m{}^c & (\hat{\sigma}_{22} < 0) \end{cases} \tag{4}$$

$$d_s = 1-(1-d_f{}^t)(1-d_f{}^c)(1-d_m{}^t)(1-d_m{}^c) \tag{5}$$

In the process of low-velocity impact, if both fiber and matrix of a unit within a ply lost bearing capacity, it means that the ply is broken and that unit should be removed from the model.

The Establishment of the Model

Referring to the test of Karakuzu, laminated board size is 76.2mm×76.2mm. Thickness of a single ply: d_0=0.36mm, a total of 8 layers. Ply in the form: [0°/30°/60°/90°]s. Composite laminated plate material parameters and mechanical performance parameters are shown in table 2 and 3. Finite element analysis software ABAQUS is used to analyze the composite laminated plate's low-velocity impact mode. Since the ratio of laminated plate's width and thin is more than 10, it's a thin-walled structure. Then laminated plate is described as a 4 nodes first-order reduced integral shell unit (S4R) with an control hourglass, and the influence of shear deformation is took into consideration, so the computer can obtain higher accuracy of the results while saving calculating cost. Considering the more violent grid deformation of impact center during impact, the center regional grid is refined in meshing phase to improve the calculation accuracy. The center grid size is 1 mm×1 mm, mesh size's transition between center regional and border area guarantees the quality of the grid and reduces the computing time. Laminated plate's boundary setting refers to Karakuzu test, bordering around the ground constraints, which restrict only three direction of the displacement of edges and not restrict rotational degree of freedom.

Tab.2. Mechanical properties of the composite laminate

ρ (g/cm^3)	E_{11} (GPa)	E_{22} (GPa)	G_{12} (GPa)	v_{12}
1.83	40.51	13.96	3.10	0.22

Tab.3. Mechanical properties of the composite laminate

X_T (MPa)	X_C (MPa)	Y_T (MPa)	Y_C (MPa)	S_1 (MPa)	S_{12} (GPa)
783.30	298.00	64.00	124.00	38.00	69.00

The punch model is 12.7 mm steel hemispherical punch. The simulation aims mainly at investigating the dynamic response of the impact process and damage evolution characteristics, moreover, the stiffness of the punch is much bigger than laminated plate's, so the unit type is two-dimensional analytical rigid body without considering deformation of the punch. By setting reference point and exerting quality and speed on the reference point according to the formula $E=mv^2/2$, punch head is imposed with impact energy. The contact between the punch and laminated plate is hard contact and it can cause contact element failure, so the ordinary hard contact algorithm is adopted. Composite laminated plate low-velocity impact finite element model is set up as shown in figure1.

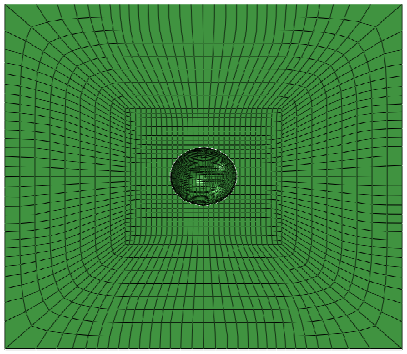

Fig.1. FEM model of composite laminates

The Model Validation

Referring to the test, 5 test cases are selected: 5kg-10J, 5kg-20J, 5kg-30J, 10kg-20J, 15kg-30J, respectively mark as impact conditions 1, 2, 3, 4, 5, that are divided into two groups: the same impact velocity and the same impact quality, and finish laminated plates low-velocity impact numerical simulation. The parameters of working conditions shows in table 4.

Tab.4. Different impact test cases

Impact energy	Under the same impact velocity (2m/s) the impact of the quality/kg	Under the same impact mass (5 kg) of impact velocity/(m/s)
10	5	2
20	10	2.828
30	15	3.464

In order to verify the correctness of the finite element model of low-velocity impact, comparison results under various impact conditions in this paper is given. figure 2 shows impulse response processing curves of numerical simulation, the experimental value and Karakuzu numerical simulation.

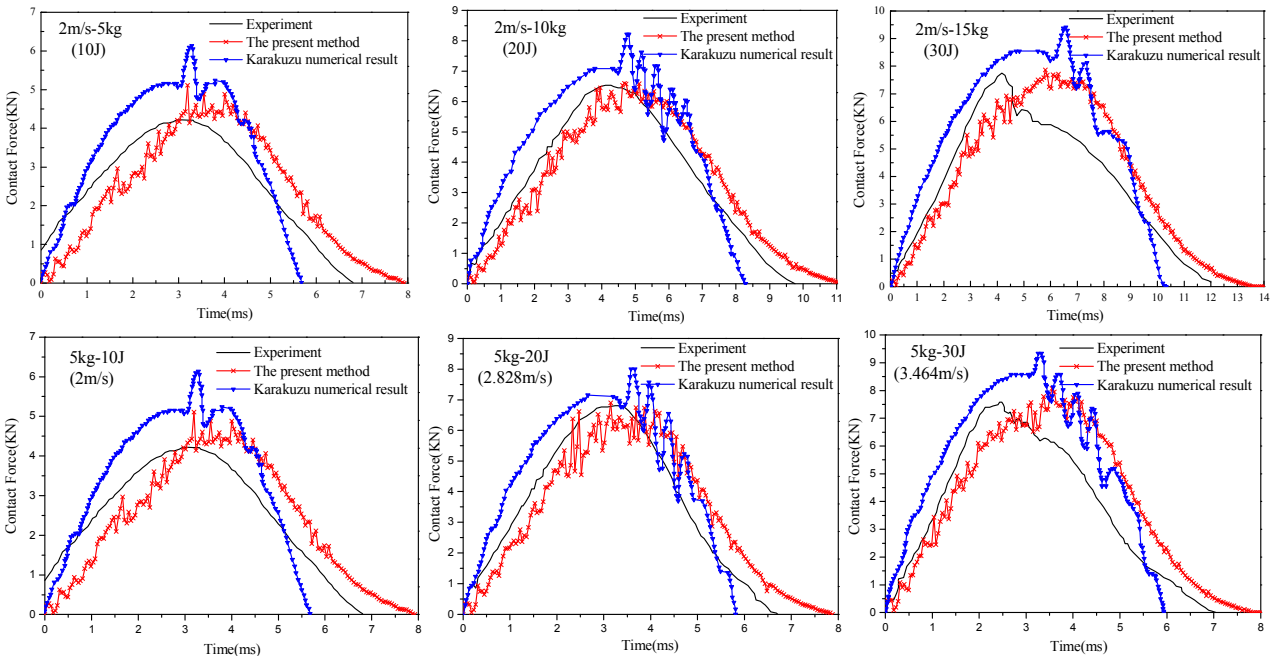

Fig.2. Comparison of impact force-time curves

Ply Thickness' Effect on Shock Response

In the optimization design of the composite material plate performance, in order to avoid the waste of material and maintain specific intensity and specific stiffness properties of the laminated plates, ply should not be too thick. And the thickness of laminated plates should not be too thin to keep the compressive strength, so the selection of ply thickness is very important.

Under impact condition 4, the ply thickness' influence on impact damage properties is explored by changing the ply thickness d_0. Shock responses of laminated plates ply with thickness of 0.12 mm, 0.24 mm, 0.36 mm, 0.48 mm, 0.60 mm are investigated. When d_0=0.12mm the thickness is too thin to offer sufficient strength. Then deformation of laminated plate's impact area is too large in impact process, the compressive failure damage of spreading layer's fiber and material occurs, so laminated plate is not able to resist impact of the punch. Figure 3 shows the impact-time curves of the other four sets' layer thickness. As shown in the diagram, when d_0=0.24mm, impact rises gradually and reduces gradually to zero after meeting the peak, and there is an obvious bending deformation on laminated plate impact area. As the layer thickness of laminated increase, ensemble strength of plate increases, resistance to shock increases while impact contact time decreases, and the impact increases, the impact amplitude fluctuation also increase gradually.

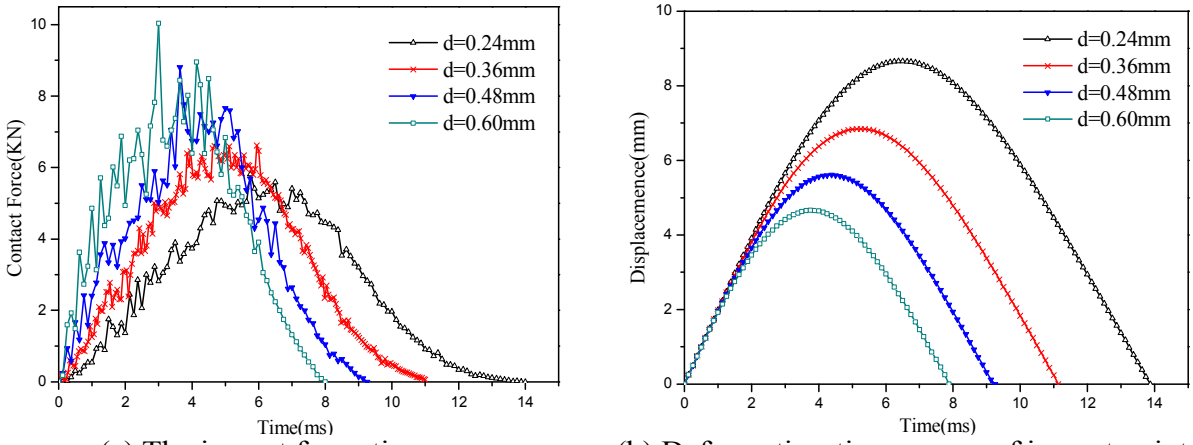

(a) The impact force-time curves (b) Deformation-time curves of impact point

Fig.3. The numerical results

Conclusion

Based on the two-dimensional Hashin failure criteria and the introduction of material degradation damage factor, low-velocity impact model of composite laminated plate was established by ABAQUS. After the accuracy of laminated plates model's impact dynamic response and damaged under low-velocity are verified, a thorough research of the ply thickness' effect on the impact response under low-velocity is carried out. The result shows that and laminated plate overall strength is not enough to resist impact if ply thickness is too thin, and with the thickness increasing, impact contact time and laminated plate impact point's deflection displacement reduce, while the impact force and volatile shocks are more obvious.

Reference

[1]. De Moura M, Marques A T. Prediction of low velocity impact damage in carbon–epoxy laminates[J]. Composites Part A: Applied Science and Manufacturing, 2002, 33(3): 361-368.

[2]. Choi H Y, Wu H Y T, Chang F K. A new approach toward understanding damage mechanisms and mechanics of laminated composites due to low-velocity impact: Part II—analysis[J]. Journal of Composite Materials, 1991, 25(8): 1012-1038.

[3]. Shi Y, Swait T, Soutis C. Modelling damage evolution in composite laminates subjected to low velocity impact[J]. Composite Structures, 2012, 94(9): 2902-2913.

[4]. Yongdong Wu, Weifang Zhong, Qing Zhu. Research on the low velocity impact response of SMA hybrid composite plate[J]. Journal of vibration and shock, 2004, 23(1): 70-73.

[5]. Fuoss E, Straznicky P V, Poon C. Effects of stacking sequence on the impact resistance in composite laminates—Part 1: parametric study[J]. Composite Structures, 1998, 41(1): 67-77.

[6]. Karakuzu R, Erbil E, Aktas M. Impact characterization of glass/epoxy composite plates: an experimental and numerical study[J]. Composites Part B: Engineering, 2010, 41(5): 388-395.

[7]. ABAQUS 6.10-1 Documentation. Abaqus analysis user's manual; 2010. p.(21.3.1-1) –(21.3.2-4).

Advanced Materials Research Vols. 989-994 (2014) pp 79-82
© (2014) Trans Tech Publications, Switzerland
doi:10.4028/www.scientific.net/AMR.989-994.79

Study on the Synthesis of Ethylene Glycol by Catalytic Hydrolyze of Ethylene Carbonate

Min Zhang[1, a]

[1]Secondary College of Textile and Dye Engineering, Nantong Textile Vocational Technology College, Nantong, 226007, China

[a] zhangmin@nttec.edu.cn

Keywords: Ethylene carbonate; Catalytic hydrolyze; Ethylene glycol; Water ratio.

Abstract. The process for ethylene glycol (EG) by catalytic hydrolysis of ethylene carbonate (EC) was studied. The influencing factors of the reaction products were studied which include the reaction temperature, the mole ratio of H_2O to EC, the mass fraction of the catalyst and the reaction time. The optimal conditions were identified as follows: the reaction temperature is 140-145℃, n(H_2O) :n(EC) = 2.0-2.5 : 1, the catalyst of Al_2O_3 is about 2.0wt%, the reaction time is about two hours. Under the above conditions, EC can be completely hydrolyzed and the selectivity of EG is above 98%.

Introduction

Ethylene glycol (abbr. EG) is an important organic chemical material. It is widely used to produce antifreeze agent, polyester fiber, lubricants, unsaturated polyester resin, explosives and non-ionic surfactants etc. . In recent years, the total demand of ethylene is rising gradually in the world, it has become the third large variety of series products of ethylene after polyethylene, polyvinyl chloride (PVC). [1]

At this stage, the large-scale industrial production of ethylene glycol adopts the direct hydration method of ethylene oxide (abbr. EO), the disadvantages of this process mainly includes as follows: the mole ratio of H_2O to EO is very high, the process flow is longer, the selectivity of MEG is lower. In the process the energy consumption of the devices is more, the most of the energy is used to evaporate water of the products [2, 3]. In recent years, in order to improve the selectivity of the end product EG and reduce energy consumption, the researchers have constantly developed new EG synthesis processes, the new processes are mainly catalytic hydration of EO, the process of ethylene carbonate (EC), the syngas method and formaldehyde or methanol synthesis method, etc. The process of catalytic hydrolyze of ethylene carbonate among them is considered to be one of the promising methods of industrialization, because it has many advantages including the higher selectivity of EG, the lower mole ratio of water to EC (hereinafter referred to as water ratio) , mild reaction condition, lower energy consumption, Less investment and so on[4]. Now the companies which have much deeper research on the method are mainly American Halcon-SD, Nippon Shokubai, Mitsubishi Chemical Corporation, Japan. The difference lies primarily in the choice of catalyst among the research process of three companies.

The synthesis process of ethylene glycol by catalytic hydrolyze of ethylene carbonate mainly consists of two steps, esterification and hydrolysis. In the two reactions above, the first step is the synthesis of EC by the reaction of carbon dioxide with ethylene oxide under the action of catalyst. The second step is the synthesis of EG by the catalytic hydrolysis of EC. And the research on the first esterifiable process is fairly mature and it has been industrialized, but study on the second hydrolyzed research is still not successful. This paper is just researching for synthesis of EG by catalytic hydrolysis of EC as material.

In recent years, domestic Nanjing University of Technology has been engaged in related research for the second step hydrolysis reaction. This paper is based on the previous studies[5,6] to further optimize the reaction conditions for EG synthesis process by this method, active aluminum oxide has been chose as catalyst, The influence of reaction factors such as reaction temperature, water ratio,

catalyst dosage, reaction time has been investigated and the optimal reaction conditions have been obtained.

Experiment Part

Raw Materials and Main Equipments

Ethylene carbonate, no less than 99.5%, Nantong Merck chemicals co., LTD. Ethylene glycol, AR, Shanghai Ling Feng chemical reagents co., LTD. Activated alumina γ -Al_2O_3. Three-necks flask, 250 mL. Type of WT – 100B temperature programmed controller, plant of southeast university. Analytical balance, Shanghai Jingke co., LTD. Type of SP-6801 GC, Shandong Lunan Ruihong chemical instruments co., LTD.

Analysis Conditions and Analysis Methods of Gas Chromatographic

Analysis conditions of gas chromatographic are as follows : the column is a stainless steel packed column whose length is 2 meters, diameter is 4 mm x 1 mm, packing inside is GDX-103. carrier gas is H_2, the pressure before the column is 0.06 MPa, thermal conductivity cell detector, bridge flow is 125 mA, gasification chamber temperature is 250℃, the detector temperature is 250℃, column temperature is 220 ℃, sample size is 1.0 μL.

Analysis methods are as follows: product qualitative analysis is carried out by the comparison with standard substance. The different solubility standard solutions are analyzed by GC, and relative mass correction factor of each composition are calculated, and then the conversion of EC and selectivity of EG are calculated by the area normalization method.

Determination of Relative Mass Correction Factor

The quantitative analysis of GC is done by the proportion of weight of each composition or concentration in the carrier gas to the detector response value, and because the same detector has different response value with different material, the peak areas measured are often not equal with the same amount of two different materials. So the correction factor is required to add. Relative mass correction factors of various compositions are determined and shown in the following table in this experiment.

Table1. Relative mass correction factor of several chemicals

Chemicals	H_2O	EG	DEG	EC
f_m'	1.000	2.003	2.087	2.466

Results and Discussion

Effect of Reaction Temperature

Reaction conditions: water ratio is 2.0, the dosage of catalyst is 2% of the total amount of EC and water (by mass, the same below), reaction time is 2h. According to EC 44g, H_2O 18g, Al_2O_3 catalyst 1.25g, reaction time 2 hours in each experiment, the effects of different reaction temperature on the reaction product are discussed, the experimental results are shown as Fig.2.

Fig. 2 shows, when temperature is 120 ℃, the conversion rate of EC is only 55%, when the temperature is higher than 140 ℃, the conversion rate of EC reaches 100%. And when the temperature is higher than 140 ℃, the selectivity of EG will decrease. When the temperature rises to 170 ℃, the selectivity of EG reduced to 90%. This is mainly due to acceleration of the decomposition rate of EC[7]. When temperature is higher than 150 ℃, EO produced by the decomposition of EC and EG will continue reaction to transform into diethylene glycol. Therefore, in the process the reaction temperature should be controlled in 140-145 ℃, and keep stirring to avoid increase of the decomposition of EC because of over-high local temperature.

Effect of Water Ratio

Reaction conditions: According to reaction temperature 140℃, the dosage of catalyst 2%, reaction time 2h, the effects of different water ratios on the reaction product are discussed. The experimental results are shown as Fig. 3.

Fig.3 shows, when water ratio is 2.0 or higher, conversion of EC and selectivity of EG are both 100%, but energy consumption will increase with the increase of water ratio. When the water ratio is 1.5, water is 0.8wt%, ethylene glycol is 23wt%, there are EC and DEG besides water and EG in the product by GC. This shows that EC has not fully hydrolyzed and there are by-products DEG generated. Therefore, the experimental result shows that water ratio should be controlled in 2.0 ~ 2.5.

Effect of Catalyst Dosage

Reaction conditions: reaction temperature is 140℃, water ratio is 2.0, reaction time is about 2h, and the influence of catalyst dosage on the experimental product is discussed by changing its dosage. The experimental results are as Fig.4.

Fig. 4 shows, when the catalyst dosage is less than 2.0%, there are still EC un-reacted in product, and with the increase of catalyst dosage, conversion rate of EC will increase gradually, when the catalyst dosage is 2.0% or higher, conversion rate of EC reaches 100%, but with the increase of catalyst dosage, the selectivity of EG will decline. Therefore, the experimental results show that the catalyst dosage should be controlled at about 2%.

Effect of Reaction Time

Reaction conditions: Reaction temperature is 140℃, water ratio is 2.0, the catalyst dosage is 2%, the influence of reaction time on the experimental product is discussed by changing the length of reaction time. These situations are discussed when the reaction time is respectively 1.0h, 1.5h, 2.0h, 2.5h, 3.0h, the experimental results are as follows.

Fig. 5 shows, when the reaction temperature is 140℃, the reaction time is 2h, both the conversion rate of EC and the selectivity of EG are 100%. When the reaction time is more than 2h, the selectivity of EG will decrease, when the reaction time is 3h, the selectivity of EG is 95%. Therefore, the appropriate reaction time should be controlled for about 2 hours.

Conclusions

(1) When temperature is below 120℃, the conversion rate of EC is lower. When temperature is above 150℃, the decomposition rate of EC is fast, this will lead to the selectivity of EG decrease gradually. So reaction temperature should be controlled between 140℃ and 145℃.

(2) Water ratio can be reduced to about 2.0, close to the theoretical value in this process of the synthesis of ethylene glycol. Compared with the direct hydration process in the current, water ratio decreases significantly, which will greatly reduce the energy consumption needed to evaporate the moisture in the subsequent purification of ethylene glycol.

(3) The study of the effects of the amount of catalyst and reaction time on the product shows that the amount of catalyst should be controlled in 2%, it is appropriate that reaction time should be controlled for about two hours. At this point, EC conversion rate and EG selectivity are both 100%.

(4) According to the study on the influence of reaction temperature, water ratio, amount of catalyst and reaction time on the reaction, the optimum reaction conditions of this process are as following: reaction temperature is between 140℃ and 145℃, water ratio is between 2 and 2.5, mass fraction of catalyst is about 2%, reaction time is about 2h, conversion rate of EC is 100%, selectivity of EG is more than 98%.

Acknowledgement

This work is sponsored by the grant No. FYKY/2013/16 from Science and Technology Program of Nantong Textile Vocational Technology College.

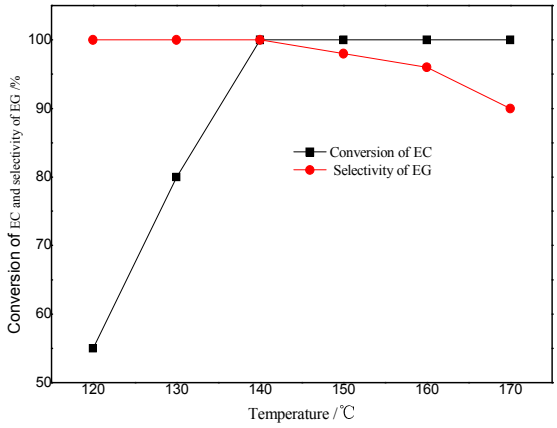

Fig.2 Effect of reaction temperature

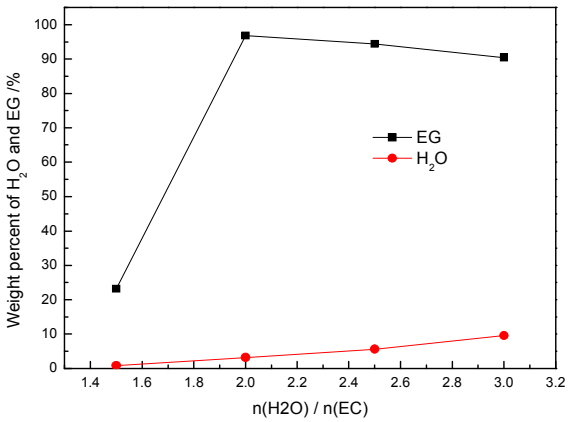

Fig.3 Effect of n (H2O)/n (EC)

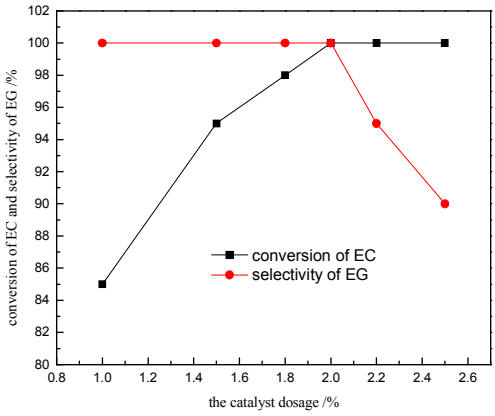

Fig.4 Effect of the catalyst dosage

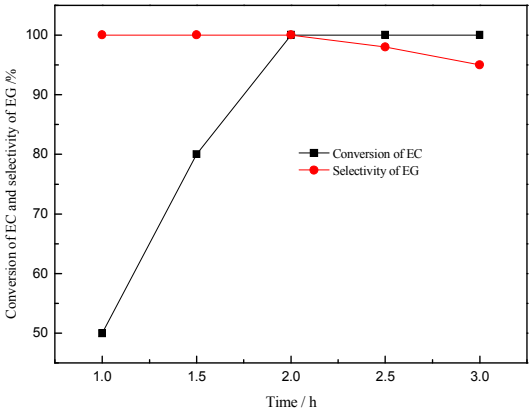

Fig.5 Effect of reaction time

References

[1] DAI Houliang, YAO Huqing, OUYANG Pingkai. Producing technology and suggestion on synthesis of ethylene oxide/ethylene glycol. MODERN CHEMICAL INDUSTRY, 2005, 25(12): 11-16.

[2] Zhu Lingjun, Wang Shurong, Ge Xiaolan, et al. The Structure Morphology and Catalytic Performance of a Silica Supported Cu Catalyst for Ethylene Glycol Synthesis [J]. Adv Mater Res, 2011(217):1070-1074.

[3] van Hal J W, Ledford J S, Zhang Xiankttan. Investigation of Three Types of Catalysts for the Hydration of Ethylene Oxide (EO) to Monoethylene Glycol (MEG) [J]. Catal Today, 2007, 123(1): 310-315.

[4] China Academy of Sciences Lanzhou Institute of Chemical Physics. Preparation method of ethanol by hydrolysis of ethylene carbonate: China, 200510129880.3 [P]. 2007-06-13.

[5] Shen Wenbin, Zhu Weiguang, Liu Dinghua, Liu Xiaoqin. Heterogeneous Hydrolysis of Ethylene Carbonate to Ethylene Glycol Catalyzed by γ-Al_2O_3. Petrochemical Technology, 2012, 41(9): 1005-1010.

[6] He Tao, Liu Dinghua, Liu Xiaoqin. Catalytic hydrolyzation of ethylene carbonate to ethylene glycol. Chemical Industry and Engineering Progress, 2008, 27(11): 1808-1811.

[7] Chen Lantian, Gong Tao, et al.. Evaluation on pyrolysis performance of byproduct low carbon hydrocarbons and low octane number oils from refinery. Petrochemical Technology & Application, 2008, 26(3): 216-217.

Advanced Materials Research Vols. 989-994 (2014) pp 83-86
© (2014) Trans Tech Publications, Switzerland
doi:10.4028/www.scientific.net/AMR.989-994.83

Efficient synthesis 2,3-dihydroquinazolin-4(1H)-ones using Coconut shell char sulfonic acid as a reusable catalyst in ethanol

Xuanyan LIU[1,a], Zhigao YANG[2,b]

[1]Hunan Chemical Vocational and Technical College, Zhuzhou, 412004, China

[2]The NO1 Middle School of Ningxiang, Ningxiang, 410600, China

[a]liuxuanyanlz@163.com, [b]183362662@qq.com

Key words: CSCSA; Biginelli reaction; heterogeneous catalysts; Di-hydropyrimidin

Abstract. 3,4-Dihydropyrimidin-2(1H)-ones derivatives were synthesized in moderate to high yields in one-pot three component reaction from the corresponding aldehydes, 1,3-dicarbonyl compounds and urea, Coconut shell char sulfonic acid (CSCSA) used as a reusable, and efficient catalyst. Compared to the classical acid catalyst, This new protocol for the Biginelli reaction includes the following important features: excellent yields, non-toxic, inexpensive and easily available reagent.

Introduction

3,4-Dihydropyrimidinones (DHPMs) have been reported to possess diverse biological activities, including antiviral, antitumour, antibacterial activities. Functionalized dihydropyrimidinones have been used as potent calcium channel blockers and neuropeptide Y antagonist. Furthermore, several marine alaloids with interesting biological activities containing the dihydropyrimidine-5- carboxylate skeleton were isolated recently[1]. The one-pot, three-component Biginelli condensation provides certainly the most efficient access to DHMP derivatives due to its atom economy feature and the availability in this reaction (Scheme1).The original protocol for the DHPMs reported first by Biginelli in 1893[2], consisted of heating a mixture of the three components in ethanol. Due to the importance of DHPMs, many synthetic methods for the synthesis of this heterocyclic scaffold have been developed[3]. Various homogeneous catalysts[4] and heterogeneous catalysts[5] have been used in Biginelli reaction. In addition, Polymer-supported ionic liquids[6] and microwave irradiation[7] towards Dihydropyrimidinones also have been employed. The discovery and introduction of milder, faster, eco-friendly conditions resulting in high yields whilst using inexpensive reagents are in great demand.

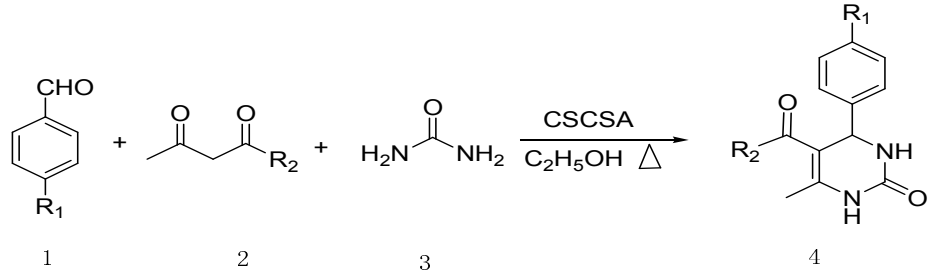

1 2 3 4

Scheme 1. Bilginelli reaction catalyzed by CSCS

Recently, carbon-based solid acids, a novel and inexpensive solid acid with mild acidity, has emerged as a substituted for conventional acidic catalysts in different areas of organic synthesis: esterification, hydrolysis, hydration, etc[13]. This heterogeneous catalyst can be readily recycled and reused through simple filtration, washing and desiccation. Recently we reported the bamboo char sulfonic acid for acid catalyzed reaction of Claisen-Schmidt condensation between benzaldehyde and acetophenone[14]. Here, we report a clean and single-step multi-component reactions of β-ketoesters 1,aldehydes 2 and urea 3 (Scheme 1) in ethanol over CSCSA with high yields.

Experimental

A. Preparation and recycling of CSCSA.CSCSA was prepared according to Xu Qiong's procedure[14]. The catalyst was separated in the first stage of the above work up procedure. The residue was washed with acetone and dried at 100℃ for 5 h to give pure CSCSA for further runs.

B. General procedure for one-pot three-component Biginelli reaction. A solution of ethyl acetoacetate (2 mmol), aldehyde (2 mmol), urea (3 mmol) and CSCSA (20 mol %) in ethanol (5 ml) was heated under reflux for 5-8 h. Upon completion of the reaction, CSCSA then filtered off and the solution poured into crushed ice with stirring. The crude product was filtered, washed with 95% ethanol, dried and recrystallised from hot ethanol to give product 4. Some typical compounds are fully characterised by 1H NMR spectroscopy.

C. Spectral data of typical products. Ethyl\6-methyl-2-oxo-4-phenyl-1,2,3,4-tetrahydro -pyrimidine-5-carboxylate[1H NMR (500 MHz; $CDCl_3$; Me4Si): δ 7.34-7.28(m, 5H, J=4.0 Hz), 5.65 (s, 1H), 5.42 (d, 1H, J=3.0Hz), 4.10-4.09 (m, 2H, J=3.5 Hz), 2.38 (s, 3H), 1.19-1.18 (t, 3H, J=7.5 Hz)]; 5-acetyl-6-methyl-4-phenyl-3,4- dihydropyrimidin-2(1H)-one[1H NMR (500 MHz; $CDCl_3$; Me_4Si): δ 7.34-7.28(m, 5H, J=4.0 Hz), 5.70 (s, 1H), 5.42 (d, 1H, J=3.0Hz), 2.38 (s, 3H), 2.14 (s, 3H)]; Ethyl\4-(4-methoxyphenyl)-6-methyl-2-oxo-1,2,3,4-tetrahydropyrimidine-5-carboxy-late[1H NMR (500 MHz; $CDCl_3$; Me_4Si): δ 7.26-7.24(d, 2H, J=8.5Hz), 6.86-6.84(d, 2H, J=9.0 Hz), 5.76 (s, 1H), 5.37 (d, 1H, J=2.5Hz), 4.11-4.07 (m, 2H, J=4.5 Hz), 3.80 (s, 3H), 2.35 (s, 3H), 1.20-1.18 (t, 3H, J=7.0 Hz)]; 5-acetyl-4-(4-methoxyphenyl)-6-methyl-3,4-dihydropyrimidin-2(1H)-one[1H NMR (500 MHz; $CDCl_3$; Me_4Si): δ 7.24-7.22(d, 2H, J=8.5Hz), 6.88-6.86(d, 2H, J=9.0 Hz), 5.81 (s, 1H), 5.41 (d, 1H, J=2.5Hz), 3.81 (s, 3H), 2.36 (s, 3H), 2.12(s, 3H)]; Ethyl\6-methyl-4-(4-nitrophenyl)-2-oxo-1,2,3,4- tetrahydropyrimidine-5-carboxylate[1H NMR (500 MHz; $CDCl_3$; Me_4Si): δ 8.21-8.20(d, 2H, J=9.0Hz), 7.54-7.53(d, 2H, J=8.5 Hz), 5.76 (s, 1H), 5.54 (d, 1H, J=3.0Hz), 4.14-4.12 (m, 2H, J=6.0 Hz), 2.39 (s, 3H), 1.22-1.20 (t, 3H, J=7.0 Hz)]; Ethyl\4-(4-chlorophenyl)-6-methyl-2-oxo-1,2,3,4- tetrahydropyrimidine-5-carboxylate[1H NMR (500 MHz; $CDCl_3$; Me_4Si): δ 7.30-7.29(d, 2H, J=8.5Hz), 7.25-7.24(d, 2H, J=8.5 Hz), 5.82 (s, 1H), 5.39-5.38 (d, 1H, J=2.5Hz), 4.14-4.12 (m, 2H, J=6.0 Hz), 2.35 (s, 3H), 1.20-1.19 (t, 3H, J=7.0 Hz).

Results and discussion

The results of optimization experiments for the three component Biginelli condensation involving ethylacetoacetate, benzaldehyde and urea with CSCSA as catalysts are presented in Table 1. Entries 1-3 show the effect of various solvents, amounts of catalysts and different common sulfonic groups catalysts on the yield of the reaction. Although CH_3CN and toluene afforded the product in high yields, we chose ethanol for its cheapness and environmental acceptability. The amount of catalysts used equaled acid capacity of CSCSA (entries 3). It is clearly that the yield of DHPMs in the presence of CSCSA is higher than resin. Although sulfamic acid afforded the product in high yields, but high catalytic activity, low toxicity, moisture and air tolerance make CSCSA catalysts attractive.

Encouraged by the remarkable results obtained in the above reaction conditions and in order to show the generality and scope of this new protocol, we further surveyed the scope of benzaldehyde and β-ketoester in the direct Biginelli reactions in the presence of 20 mol % CSCSA as the catalyst and the results were summarized in Table 2.

All the aldehydes studied were smoothly converted to their corresponding 3,4-dihydropyrimidin-2(1H)-ones in excellent yield, which were identified by comparing their spectral data(1H NMR) with those of authentic samples. The use of methyl acetoacetate and acetyl acetone as 1,3-dicarbonyl moieties in place of ethyl acetoacetate also gave similar results, but 1,1,1-Trifluoroacetylacetone was in very low yield.

Finally, the recycling performance of CSCSA was investigated using the three-component Biginelli reaction. The yields of DHPMs were 87.6%, 85.6% and 84.4% respectively, which showed good reusability of this catalyst.

Table 1 CSCSA catalyzed condensation of benzaldehyde, ethylacetoacetate and urea[a]

entry	catalyst	Catalyst/mol%	solvent	Yield/%[b]
1	CSCSA	10	ethanol	57.1
	CSCSA	10	ethanol	77.2
	CSCSA	20	ethanol	87.6
	CSCSA	30	ethanol	88.7
2	CSCSA	20	CH_2Cl_2	39.8
	CSCSA	20	THF	76.3
	CSCSA	20	CH_3CN	85.2
	CSCSA	20	Toluene	88.9
	CSCSA	20	H_2O	33.8
3	paratoluenesulfonic acid	20	ethanol	83.6
	sulfamic acid	20	ethanol	92.7
	resin	20	ethanol	76.2

[a]Reaction conditions benzaldehyde(2mmol), ethylacetoacetate (2 mmol) , urea(3 mmol), refiux; [b]Isolated yields.

Tabe 2 CSCSA catalyzed synthesis of different dihydropyrimidinones[a]

Entry[b]	R_1	R_2	Yield/%[c]	reported
1	-H	$-OC_2H_5$	87.6	[9],[11],[10],[11]
2	-H	$-OCH_3$	91.7	[10],[12]
3	-H	$-CH_3$	73.2	[10],[12],[13]
4	-H	$-CF_3$	42.0	[15]
5	$-OCH_3$	$-OC_2H_5$	74.3	[9],[10],[12],[14]
6	$-OCH_3$	$-OCH_3$	84.4	[10],[13]
7	$-OCH_3$	$-CH_3$	70.1	[10],[12],[13]
8	$-OCH_3$	$-CF_3$	44.1	[15]
9	$-NO_2$	$-OC_2H_5$	91.8	[9],[10],[13],[14]
10	$-NO_2$	$-OCH_3$	84.3	[10],[12]
11	$-NO_2$	$-CH_3$	80.4	[10],[12]
12	$-NO_2$	$-CF_3$	49.5	[15]
13	4-OH, 3-OCH_3	$-OC_2H_5$	84.3	[16]
14	4-OH, 3-OCH_3	$-OCH_3$	82.1	--
15	4-OH, 3-OCH_3	$-CH_3$	80.2	--
16	4-OH, 3-OCH_3	$-CF_3$	40.7	[15]
17	-Cl	$-OC_2H_5$	86.2	[9],[11],[10],[11]
18	-Cl	$-OCH_3$	87.7	[10],[13],[14]
19	-Cl	$-CH_3$	83.7	[10],[12]
20	-Cl	$-CF_3$	47.7	--
21	-OH	$-OC_2H_5$	85.1	[7b],[9],[11],[12]
22	-OH	$-OCH_3$	86.7	[7b],[9],[11]
23	-OH	$-CH_3$	83.8	[7b],[9],[11],[12]
24	-OH	$-CF_3$	50.8	[7b],[9],[12]
25	$-N(CH_3)_2$	$-OC_2H_5$	76.2	[11],[12]
26	$-N(CH_3)_2$	$-OCH_3$	78.7	[17]
27	$-N(CH_3)_2$	$-CH_3$	73.2	--
28	$-N(CH_3)_2$	$-CF_3$	39.2	--

The weight of catalyst increased slightly and no sulfate ion was detected in reaction mixture after each reaction which indicated that reactants or products may deposit in catalyst. Compared with the traditional solvents and catalysts, the easy recycling performance is also an attractive property of the SCSA for the environmental protection and economic reasons.

Finally, the recycling performance of CSCSA was investigated using the three-component Biginelli reaction. The yields of DHPMs were 87.6%, 85.6% and 84.4% respectively, which showed good reusability of this catalyst. The weight of catalyst increased slightly and no sulfate ion was detected in reaction mixture after each reaction which indicated that reactants or products may deposit in catalyst. Compared with the traditional solvents and catalysts, the easy recycling performance is also an attractive property of the SCSA for the environmental protection and economic reasons.

Conclusion

In summary, we herein described an originally and effectively CSCSA catalyzed protocol for the construction of DHPMs via three-component direct Biginelli reaction. This procedure offers several advantages including inexpensive catalyst, excellent yields, clean reaction, easily available reagent, which make it a useful and attractive strategy for the multi-component reactions of combinational chemistry. Current efforts in our research group are attempting to expand the application of CSCSA in other reactions. Therefore, we believe that the work reported here would have potential application in green chemistry.

Acknowledgement

The authors would like to thank the Hunan Provincial Department of education science research project (No 12C044) for fund support.

References

[1] (a) K. S. Atawal, G. C. Rovnyak, B. C. O. Reilly, J. Schwartz, J. Org. Chem. 1989, 54, 5859; (b) C. O. Kappe, W. M. F. Fabian, M. A. Semones, tetrahedron 1997, 53, 2803.
[2] R. Biginelli, Gazz. Chim. Ital. 23 (1893) 360.
[3] C.O. Kappe, Acc. Chem. Res. 33 (2000) 879.
[4] (a) Y. Ma, C.T. Qian, L.M. Wang, et al. J. Org. Chem. 65 (2000) 3864; (b) A. Debache, B. Boumoud, M. Amimour, et al. Tetrahedron Lett. 47 (2006) 5697.
[5] H. X. Lin, Q. J. Zhao, B. Xu, , et al. Chinese Chemical Letters. 18 (2007) 502-504.
[6] Z. T. Wang, S. C. Wang, et al. Helvetica Chimica Acta-Vol.88(2005).
[7] V. R. Choudhary, V.H. Tillu, V.S. Narkhede, et al. Catal. Commun. 4 (2003) 449.
[8] (a) A.Takagaki, M. Toda, M. Okamura, et al. Catal today. 2006, 116, 157-161; (b) M. Hara, T. Yoshida, A. Takagaki, , et al. Angew. Chem. Int. E2004, 43, 2955.
[9] Q. Xu; Z.G. Yang; D.L. Yin; , et al. Catal. Commun.2008, 9,1579.
[10] P. Salehi, M. Dabira, M. A. Zolfigol, et al. Tetrahedron Lett. 44 (2003）2889-2891.
[11] I. Suzuki, Y. Suzumura, K. Takeda. Tetrahedron Lett. 47 (2006) 7861-7864.
[12] S. L. Jain, J. K. Joseph, S. Singhal, , et al. J. Mol. Catal. 268(2007) 134-138.
[13] J. Azizian, A. A. Mohammadi, A. R. Karimi, et al. Applied Catalysis. 300(2006) 85-88.
[14] M. M. Heravi, K. Bakhtiari, et al. catal commun. 7 (2006) 373-376.
[15] V.I. Saloutin, Y.V. Burgarta, O.G. Kuzuevaa, et al. Journal of Fluorine Chemistry 103 (2000) 17-23.
[16] G. Maiti, P. Kundua, C. Guin. Tetrahedron Letters. 44 (2003) 2757–2758.
[17] E. Rafiee, F. Shahbazi. Journal of Molecular Catalysis A: Chemical 250(2006) 57–61.

Advanced Materials Research Vols. 989-994 (2014) pp 87-90
© (2014) Trans Tech Publications, Switzerland
doi:10.4028/www.scientific.net/AMR.989-994.87

Study on the Urea Demand Model of SCR Control Technology

Zhilin Liu, Da Wa

Agricultural and Animal Husbandry College of Tibet University, Linzhi, Tibet, China, 860000

linlin0324ok@126.com

Keywords: SCR; Urea; Emission control.

Abstract. In this paper, the NOx emission of original diesel engine and the urea supply model of SCR system under different working conditions of ESC were obtained according the requirement of GB17691-2005[1]. Then the model of urea demand was established, and the comparison was made with the actual urea supply. In addition, the causes of the differences between them were analyzed.

Introduction

In recent years, the rapid development of China's automotive industry has made great contributions to the economic construction of our country, however, its pollution problems have become increasingly prominent, emission control technology of automobile are increasingly widespread attention from all sectors of society [2][3][4]. In order to meet the reality of China's national conditions, many automobile manufacturers and R & D department has find a suitable for China's national conditions of the diesel engine emission control technology---- selective catalytic reduction (SCR) technology, this technology can effectively overcome the influence of sulfur content in diesel oil, thus favored.

SCR technology's reducing agent is urea solution which concentration is 32.5% (mass ratio), spray urea solution into automobile exhaust, it will create NH_3 after hydrolysis at high temperature and under the action of a catalyst, then the NH_3 can react with NOx generated in exhaust, produce water and CO_2, reduce the pollution of the air. The research content of this paper is urea demand model of SCR technology.

Calculation of the theoretical urea solution demand

Assuming you can obtain unit time (usually in hours) parameters of diesel such as exhaust temperature, exhaust back pressure and exhaust mass flow, after conversion to obtain NOx emissions per unit time as A mol.

1mol NOx requires 0.5mol urea. The molecular weight of urea was 60g/mol, concentration of urea aqueous solution is 32.5%, then 1mol urea can be formulated as 60/0.325=184.6 grams' urea solution. Urea aqueous solution's density is 1.09kg/L, so you can obtain 184.6 * 10-3 /1.09 =0.169 L urea aqueous solution when 1mol urea used.

In summary, if eliminate 1 mol NOx, we should use 0.169/2=0.0845L urea aqueous solution. Therefore, the elimination of A mol NOx , 0.0845*A L urea aqueous solution will be required.

Diesel engine NOx emission test

If establish a suited urea demand model for the diesel engine, you should according to the emission characteristics of engine. European steady thirteen conditions test method (ESC) is a standard

method for the determination of diesel engine emission performance, so we used ESC method in our test.

The concentration of NOx can be obtained under different ESC conditions for a diesel engine made in China by ESC method as shown in figure 1.

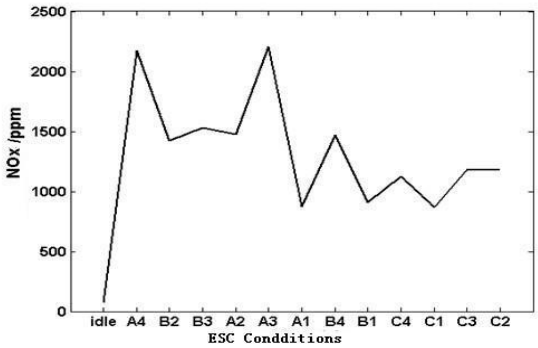

Figure 1 The situation of NOx concentration in original diesel emission experiment

Based on the measured data of each condition test (NOx emission value, gas flow, fuel consumption and exhaust temperature), we can obtain the calculation value of NOx emission is 6.24g/(kw.h) after calculation of standard method. It proves that the tested diesel engine meets national standard Ⅲ because its value less than 6.5g/(kw.h).

Model of theoretical urea aqueous solution demand

The concentration of NOx was obtained by ESC test, then NOx volume flow can get through the calculation of the total exhaust. The amount of air and fuel consumption has been obtained by ESC test. From the mass conservation law we can get exhaust consumption in unit time, then calculate NOx molar flow by exhaust parameters.

Assume that the consumption of air and diesel oil to diesel engine in unit time and a certain condition respectively are Ma and Mo, we can obtain the medium into diesel engine in unit time:

$$M_{in} = M_a + M_o \tag{1}$$

The import and export of medium for the diesel engine should be equal by mass conservation law, that is:

$$M_{in} = M_{out} \tag{2}$$

The diesel engine medium (air and diesel) are discharged in the form of exhaust, that is to say, the amount of air and fuel consumption into diesel are equal to the exhaust volume of the diesel engine per unit time, that is:

$$M_a + M_o = M_{ex} \tag{3}$$

Set in this condition, the exhaust's temperature is T through catalyst, the exhaust back pressure is P (absolute pressure), exhaust molar mass is M=29g/mol, from gas state equation [4], we can get that:

The volume flow of diesel exhaust in unit time (unit: m3/h)

$$\mathrm{Q} = \frac{\mathrm{m} \times \mathrm{R} \times \mathrm{T}}{\mathrm{M} \times \mathrm{P}} \tag{4}$$

Under this condition, the concentration of NOx in the exhaust is A ppm, The pressure and temperature respectively are P_0 and T_0 under standard conditions. Then the volume flow of NOx in unit time can be obtained under standard conditions.

$$Q_S = \frac{T \times P_0}{T_0 \times P} \times Q \times A \tag{5}$$

The molar volume of the gas is V=22.4 L/mol = 0.0224 m3/mol under standard conditions, then the molar flow of NOx in unit time (unit: mol/h) can obtained:

$$Q_M = \frac{Q_S}{V} = \frac{1000 \times Q_N}{22.4} \tag{6}$$

Calculation of theoretical urea aqueous solution demand shows that per mole NOx consumes 0.0845 L urea aqueous solution, therefore, demand for urea solution, namely urea supply flow (unit: L/h)

$$Q_L = 0.0845/Q_M \tag{7}$$

Put the test data measured into formula (1) ~ formula (7), we can obtain theoretical urea solution demand for remove NOx completely under ESC different conditions as shown in table 1.

Table 1 Theoretical urea solution demand

ESC Conditions	Idle	A4	B2	B3	A2	A3	A1	B4	B1	C4	C1	C3	C2
Flow (L/h)	0.04	5.42	3.34	4.60	2.24	4.39	1.17	5.39	1.68	4.83	2.07	4.35	3.50

Comparison of theoretical urea solution demand and actual measurement

The urea flow sensor is installed in the nozzle of urea, still do engine test according to ESC , the actual flow of urea aqueous solution can be obtained as shown in table 2.

Table 2 Actual measured urea solution amount

ESC Conditions	Idle	A4	B2	B3	A2	A3	A1	B4	B1	C4	C1	C3	C2
Flow (L/h)	0	3.16	1.79	2.38	1.89	2.76	0.44	2.16	0.96	1.34	0.59	1.72	1.44

The comparison of theoretical and actual aqueous urea solution demand as shown in figure 2.

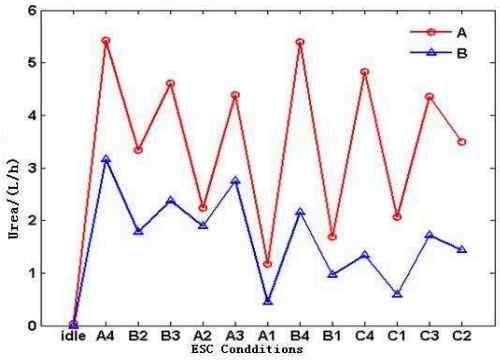

A- Theoretical demand,B-Actual injection

Figure 2 Theoretical and actual urea solution

Conclusion and discussion

From the comparison and analysis above: the trends of theoretical demand and actual injection for urea are nearly the same, which proved that the model is feasible in some extent.

However, there are some differences between them. Analysis of the causes of these differences, there may be the following three aspects:

1. The control goal of SCR system is based on the national emission standard III to national emission standard IV, so its control strategy is also based on that goal to supply urea, which determines the urea supply and NOx emissions is impossibly 1:1, therefore, differences will produce between theoretical and actual urea solution;

2. The performance of the catalyst is limited. If increase the injection of urea solution (equivalent to the increase NH_3), the conversion efficiency of NOx will be improved definitely. However, leakage of NH_3 will be increased if beyond the processing capacity of the catalyst, also does not meet the emission regulations. Therefore, performance of the catalyst also may be an important reason for these differences.

3. Error measurement and calculation. This error is inevitable, but little effect, can not be considered.

Acknowledgment

This article is supported by “Higher education institution Education Reform project of Xizang Autonomous Region --- Reform of Engineering Practice Teching System of Mechanical Courses of Tibeet Higher Education Institution” and “Higher education institution project of Xizang Autonomous Region---Comprehensive Reform Pilot of Hydraulic and Hydropower Engineering ”.

References

[1] State Environmental Protection Administration of China, General Administration of Quality Supervision, Inspection and Quarantine of the PRC. GB17691-2005: The emission limits and measurement methods for automotive compression ignition, gas fuel ignition engine and automobile exhaust, Beijing, 2005.

[2] Jun Qin, Lin Lv. Study on the route of China IV heavy-duty diesel engine technology, Journal of Engine information for vehicle, 2007, 5(4) : p.4-9.

[3] Hong He, Duan Weng. Overview of technology to diesel engine emission control, Journal of Environmental Science, 2007, 28(6) : p.1169-1171.

[4] Giuseppe Gulino,Ricardo Vieira,Julien Amadou. C_2H_6 as an active carbon source for a large scale synthesis of carbon nanotubes by chemical vapour deposition, Journal of Applied Catalysis 2005(279) : p. 91-95.

[5] Qinsheng Fu, Yaling He. Foundation and application of thermal, Beijing: Machinery Industry Press, 2006 : p.57-59.

Advanced Materials Research Vols. 989-994 (2014) pp 91-96
© (2014) Trans Tech Publications, Switzerland
doi:10.4028/www.scientific.net/AMR.989-994.91

Effect of sodium methylacrysulfonate upon the molecular weight and performance of polycarboxylate superplasticizer

Long xiong[1, a], Guangjun Zheng[2,b], Yao Bi[3,c] , Chengfei Fu[4,d] and Shaofeng Wang[5,f]

[1]China Construction Ready Mixed Concrete Co. Ltd, Wuhan 430205, China,

[2] China Construction Ready Mixed Concrete Co. Ltd, Wuhan 430205, China,

[3] China Construction Ready Mixed Concrete Co. Ltd, Wuhan 430205, China,

[a]xionglong1987@126.com, [b]27307274@qq.com, [f]2505652111@qq.com

Keywords: Sodium methylacrylsulfonate; Molecular weight; Monomer conversion;

Abstract. The effect of sodium methylacrysulfonate (SMAS) upon the molecular weight, molecular weight distribution and polycarboxylate (PCE)'s dispersion and dispersion-retaining ability were investigated by Gel permeation chromatography (GPC) and test of the fluidity of cement pastes. The results showed that the dosage of SMAS was inversely proportional to the molecular weight of polycarboxylate, and a cubic equation relationship existed between the molecular weight of the polycarboxylate and the reciprocal of SMAS dosage. There was an optimum middle dosage of sodium methylacrysulfonate which could control the molecular weight polycarboxylate, and then affect its dispersion and dispersion maintain performance. The effect of sodium methylacrysulfonate on the monomer conversion rate was also systematically discussed by means of high performance liquid chromatography (HPLC).

Introduction

Polycarboxylate superplasticizer was most favored to industry due to its chemical structure which has the potential to design to meet specific needs in various applications [1-3]. The comb-type structure of PCE consists of several functional groups such as sulfonic acid group, carboxyl group, amino group and PCE long- chain [4-5]. The density and types of the functional groups and the molecular weight and distribution significantly affect the achievement of steric exclusion and electrostatic repulsion, thus definitely influence the dispersion water-reducing properties [6-8].

SMAS is frequently used as an co-monomer in the synthesis of polycarboxylate superplasticizer. It can not only adopt sulfonic acid group with the effect of water reduce, but also have the ability to control the molecular weight and molecular weight distribution due to its chain transfer effect[. Therefore, grasp the impact of such comonomer on the polymerization process of polycarboxylate is of great significance.

In this study, PCE was obtained by the polymerization of TPEG, SMAS and AA, initiated ammonium persulphate. The effect of SMAS dosage on the molecular weight and molecular weight distribution of the synthesized PCE, monomer conversion as well as the PCE's dispersion and dispersion-retaining ability was systematically investigated.

1 Experimental

1.1 Synthesis of PCE

The PCE was synthesized according to previous study by aqueous free radical copolymerization of acrylic acid (AA), SMAS and polyoxyethylene ether (TPEG-2400). Ammonium persulphate (APS) was used as initiator. 100g water and 150g TPEG-2400 were added to a 500ml four-necked flask equipped with a condenser, a nitrogen inlet and a stirring bar afterwards and stirred for 15min to give a homogeneous solution. The solution was gently heated to 60°C and 16.2g AA with 45g water and

amount of SMAS with 55g water was then added to the flask under a fixed feeding rate. After complete the feeding process, the mixture was stirred for several hours under the same temperature. At the end, the pH was adjusted to 7 with 30wt% NaOH and the PCE was acquired.

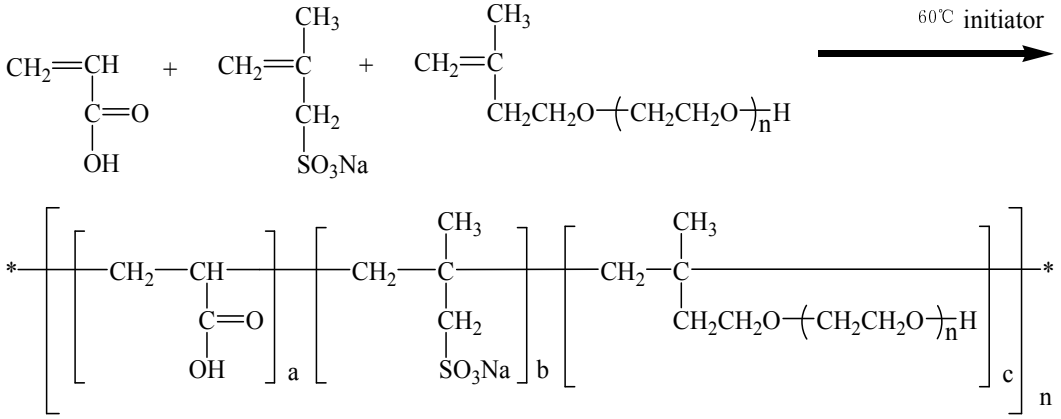

Fig. 1 Reaction equation of the polycarboxylate

1.2 The test of monomer conversion

The monomer conversion of PCE was measured by chromatography system (HPLC, Agilent 1100; Column, SinoChrom ODS-BP (C18) 5μm, 4.6mm × 200mm; detector, λ-35 -type UV spectrum, PE company, USA).

Weigh the test sample superplasticizer 0.10g ~ 0.25g, diluted with the mobile phase to 25mL, filtrated with the 0.45μm filter membrane and chromatographic analysis with external standard method.

1.3 Gel permeation chromatography (GPC)

Molecular weight of PCE was measured by gel permeation chromatography (GPC, Waters 150C, USA), using the solution of methanol and buffer solution (1/2, v/v) as the eluent (Column, PL aquagel, mix/m, 7.8*300 mm, Agilent1100, Agilent Company, USA). The buffer solution was Na2B4O7/KCl aqueous solution (pH = 8). Narrow polyethylene glycol (PEG) was used as calibration standards. The GPC detector included the refractive index.

1.4 Mini slump test

Test of the fluidity of cement pastes added with superplasticizer was under the national standard GB 8077-2000 “methods for testing uniformity of concrete mixture” and the cement used for the test was HUAXIN P·O 42.5, the w/c ratio was 0.29 and the dosage of the PCE was 0.15% (by percent Weight based on solids cement).

2 Experimental results and analysis

2.1 The effect of SMAS dosage on the molecular weight and molecular weight distribution of PCE

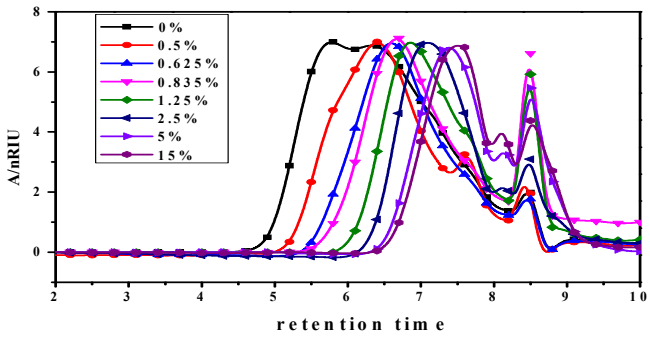

Fig. 2 GPC of PCE with different SMAS dosage

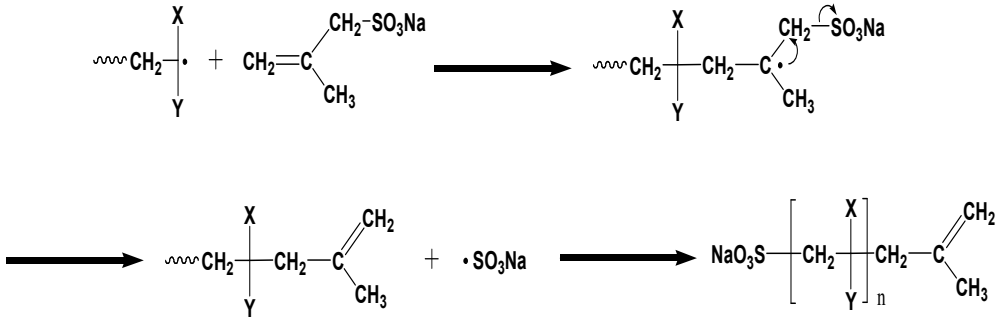

Fig. 3 The chain transfer mechanism of SMAS

The molecular weight and distribution is an important element to the performance of PCE. as can be seen from Fig. 2 and table 1 , the molecular weight of PCE is relatively large (about 230,000) and presents broad molecular weight distribution （DPI = 12.4）and multiple decentralized state in the case of no or small amount of SMAS（0.5% of the total mass of the TPEG-2400 and acrylic acid）, while the molecular weight tend to smaller and the molecular weight distribution of polycaprolactones gained tent to narrow in the case of Further adding of SMAS. This is attributed to the obvious effect of chain transfer of SMAS which belong to the allyl thiosulfate compound. The chain transfer mechanism of SMAS presented in fig. 3

Table 1 The calculated result of fig. 2

SMAS（%）	Mw	Mn	DPI	Mp
0	234256.2	10928.2	12.4	209122.1/50338.5
0.5	115918.5	18588.9	6.2	40506.1
0.625	61284.3	13314.7	4.6	28122.3
0.835	55601.7	12901.6	4.3	24319.4
1.25	52219.6	13287.9	3.9	22787.7
2.5	35553.7	10928.2	3.2	16110.2
5	17020.6	8017.8	2.1	9113.8
15	11038.1	6598.0	1.7	5400.7
25	7061.8	5023.3	1.4	2916.8
35	6608.9	4914.9	1.3	1715.9

2.2 The mathematical fitting model between SMAS dosage and molecular weight

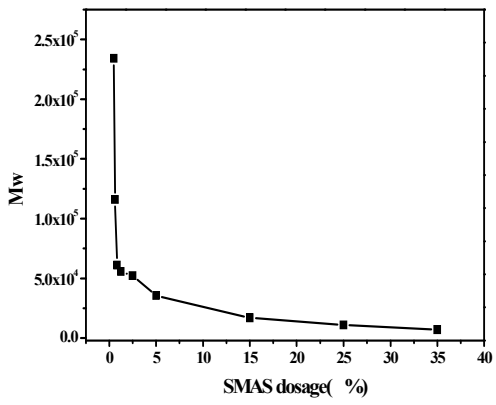

Fig. 4 Relationship between SMAS dosage and Mw

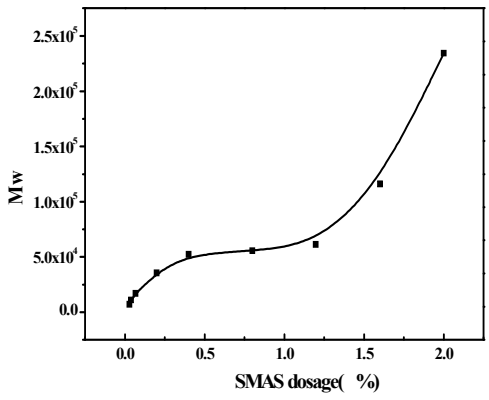

Fig. 5 Relationship between Mw and the reciprocal of SMAS dosage

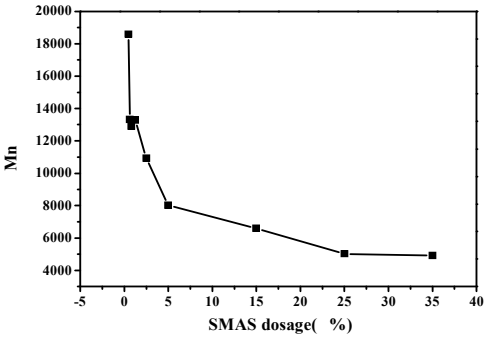

Fig. 6 Relationship between SMAS dosage and Mn

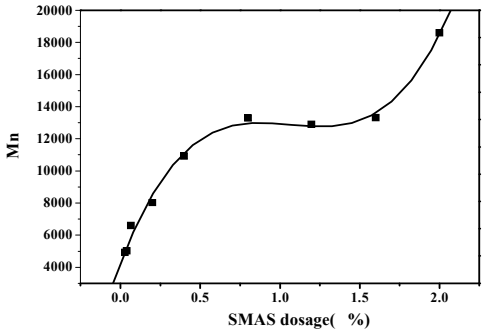

Fig. 7 Relationship between Mn and the reciprocal of SMAS dosage

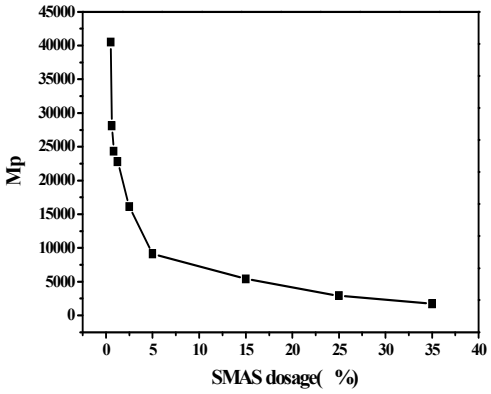

Fig. 8 Relationship between SMAS dosage and Mp

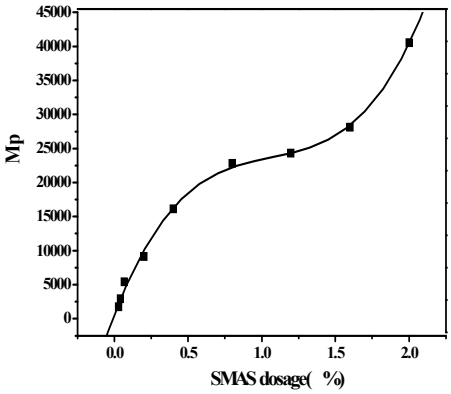

Fig. 9 Relationship between the reciprocal of SMAS dosage and Mp

Fig. 4, Fig. 6 and Fig. 8 was made according to the SMAS dosage and molecular weight (Mw, Mn and Mp) from the date of table 1. Fig. 5, Fig. 7 and Fig. 9 was gained by plotting and polynomial fitting according to the reciprocal of SMAS dosage and molecular weight (Mw, Mn and Mp). The mathematical fitting formula was listed in table 2

It can be seen from the Fig. 4, Fig. 6 and Fig. 8, the molecular weight is inversely proportional to the amount of the SMAS dosage. Fig. 2.5, Fig. 7, Fig. 9 and table 2 display a cubic equation relationship between the molecular weight of the polycarboxylate and the reciprocal of SMAS dosage.

Table 2 The mathematical fitting model

	Polynomial	The correlation coefficient（R^2）
Mw	Y= 100469X3 – 240107X2 + 194124X + 4094.4	0.9988
Mn	Y= 7893.4X3 - 25252X2 + 26048X + 4247.2	0.9936
Mp	Y = 15234X3 - 48576X2 + 56074X + 668.3	0.9977

Wherein Y represents molecular weight of polycarboxylate superplasticizer; X represents the reciprocal of SMAS dosage

2.2 The effect of SMAS dosage on the PCE's dispersion and dispersion-retaining ability.

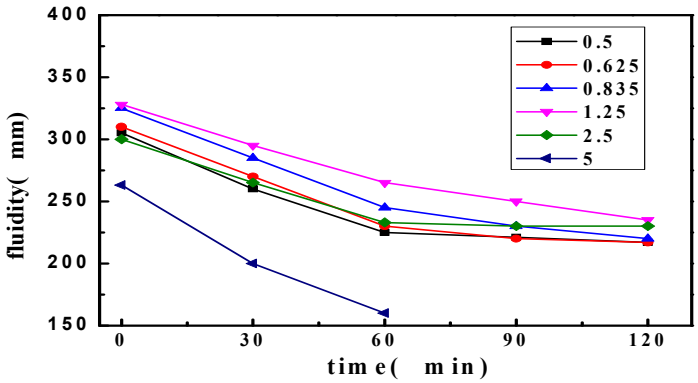

Fig. 10 Fluidity of the cement paste of PCE with different SMAS dosage

As can be showed from Fig. 10, the fluidity of the cement paste increase as the SMAS dosage increase and then decrease when the SMAS dosage continue to increase. The dates of the fluidity-loss within different time also show the same tendency. This is mainly due to that SMAS can control the molecular weight of polycarboxylate as discussion of 2.1, and then affect its dispersion and dispersion maintain performance. Therefore，there was a optimum middle dosage of SMAS. It can be ascribed that under this optimum middle dosage of SMAS, the molecular weight can reach a relatively optimum value, which can benefit the PCE's electrostatic repulsion of electric charges and the steric hindrance[9].

2.2 Effect of SMAS dosage on the monomer conversion

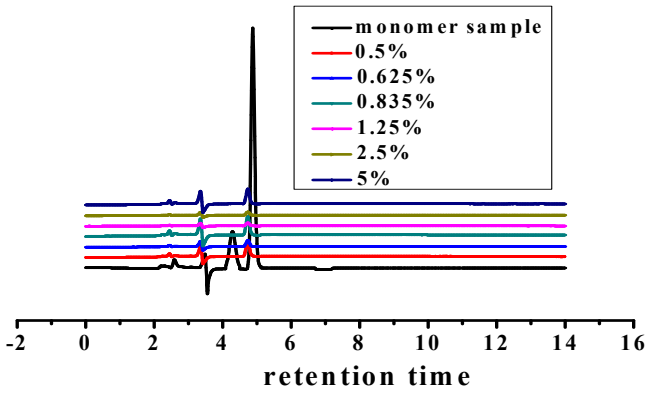

Fig. 11 The HPLC of monomer sample and PCE with different SMAS dosage

Table 3 The calculated results of Fig. 11

SMAS dosage	0.5%	0.625%	0.835%	1.25%	2.5%	5%
monomer conversion	99.11%	98.80%	99.55%	99.49%	98.52%	99.45%

According to Fig. 11, the monomer sample of SMAS and AA response to the peak at 4.3 and 4.9 minutes, respectively [10]. While there are no response peaks at 4.3 min and 4.9 min for the PCE sample of different SMAS dosage, which means SMAS and AA almost completely react. Table 3 also shows that SMAS does not affect the rate of monomer conversion.

3 Conclusion

This work confirms that SMAS has obvious effect of chain transfer. The molecular weight of PCE is inversely proportional to the amount of SMAS dosage. More precisely speaking, molecular weight of PCE and the reciprocal of SMAS dosage abide by the cubic polynomial fitting mathematical model. SMAS dosage decide the molecular weight of PCE and then affect its dispersion and dispersion maintain performance. A optimum middle dosage of SMAS exist which make the molecular weight can reach a relatively optimum value and benefit the PCE's dispersion and dispersion-retaining ability. The results of HPLC prove that SMAS does not cause the slightest impact on the rate of monomer conversion.

References

[1] Houst.Y. F, Bowen. P, Perche. F, et al. Design and function of novel superplasticizers for more durable high performance concrete (superplast project) [J]. Cement and Concrete Research. 2008, 38(10): 1197-1209.
[2] Ran. Q, Somasundaran. P, Miao. C, et al. Effect of the length of the side chains of comb-like copolymer dispersants on dispersion and rheological properties of concentrated cement suspensions [J]. Journal of Colloid and Interface Science. 2009, 336(2): 624-633.
[3] Bouhamed. H, Boufi. S, Magnin. A. Dispersion of alumina suspension using comb-like and diblock copolymers produced by RAFT polymerization of AMPS and MPEG [J]. Journal of Colloid and Interface Science. 2007, 312(2): 279-291.
[4] Winnefeld. F, Becker. S, Pakusch. J, et al. Effects of the molecular architecture of comb-shaped superplasticizers on their performance in cementitious systems [J]. Cement and Concrete Composites. 2007, 29(4): 251-262.
[5] Papayianni. I, Tsohos. G, Oikonomou. N, et al. Influence of superplasticizer type and mix design parameters on the performance of them in concrete mixtures [J]. Cement and Concrete Composites. 2005, 27(2): 217-222.
[6] Plank. J, Dugonjić-Bilić. F, Lummer.N. R. Modification of the molar anionic charge density of acetone–formaldehyde–sulfite dispersant to improve adsorption behavior and effectiveness in the presence of CaAMPS®-co-NNDMA cement fluid loss polymer [J]. Journal of Applied Polymer Science. 2008, 111(4): 2018-2024.
[7] Yamada. K, Takahashi. T, Hanehara. S, et al. Effects of the chemical structure on the properties of polycarboxylate-type superplasticizer [J]. Cement and concrete research. 2000, 30(2): 197-207.
[8] Kinoshita. M, Nawa. T, Iida. M, et al. Effect of chemical structure on fluidizing mechanism of concrete superplasticizer containing polyethylene oxide graft chains [J]. ACI SPECIAL PUBLICATIONS. 2000, 195: 163-180.
[9] Li. S, Yu. Q, Wei. J, et al, Effects of molecular mass and its distribution on adsorption behavior of polycarboxylate water reducers, Journal of the Chinese Ceramic Society, 1 (2011) 81-83.
[10] Guo. L, Wang. S, Zhang. A, et al. Determination of residual monomers in polycarboxylate superplasticizer using high performance liquid chromatography [J]. Journal of Wuhan University of Technology--Materials Science Edition. 2011, 26(3): 439-442.

Advanced Materials Research Vols. 989-994 (2014) pp 97-101
© (2014) Trans Tech Publications, Switzerland
doi:10.4028/www.scientific.net/AMR.989-994.97

Influence of the pH value on the water-reducing performance of polycarboxylate-based superplasticizers at room temperature

Jinwen Wang[1, a], Guangjun Zheng[1, b], Shaofeng Wang[1], Chenfei Fu[1], Yao Bi[1, c]

[1] Department of Technology Center, China State Construction Ready Mixed Concrete CO., LTD, Wuhan, 430074, China

[a] email: wangjinwench@163.com, [b] email: jaylia08@hotmail.com, [c] email: freddiebee@163.com

Keywords: Superplasticizers, Water-reducing Performance, pH Value, Room Temperature

Abstract. In order to study the effect of the pH value of reaction system on the properties of polycarboxylate-based superplasticizers (PC) and on the cement workability, the PC are synthesized in different pH environments from 3 to 11 at room temperature. The results show the water-reducing performance of PC can be tuned by controlling the pH value of reaction system at room temperature, which affects not only the efficiency and rate of redox initiator systems but also the reactivity of active monomers.

1. Introduction

Superplasticizers, such as sulfonated melamine formaldehyde (SMF) condensate, sulfonated naphthalene formaldehyde (SNF) condensate and acrylic polymer (AP), are incorporated in concrete mainly to modify its workability in the fresh state, and to yield high concrete strength and durability at low water/cement ratios [1][2]. Nowadays, superplasticizers are absolutely necessary for the production of high performance concrete, and are known as the fifth component of concrete, besides cement, sand, gravel and water [3]. Recently, polycarboxylate-based superplasticizers have been developed and commonly used in the construction industry, due to their outstanding water reducing ratio, high workability retention at small dosages, and excellent compatibility[4][5].

The effects of the superplasticizers on the properties of cementitious system depend on various designs of molecular structures. Apart from the functional groups and chemical configuration, the molecular weight and its distribution of superplasticizers have a significant impact on the properties of concrete [6]. Up to now, most of the research focuses on the effect of initiator concentration, reaction temperature and time, the feeding methods, and monomer proportion on the performance of water-reducing agent[7][8]. However, very few researches concern about the change of the pH value during the polymerization reaction. Since the pH value of reaction system affect not only the efficiency and rate of redox initiator systems but also the reactivity of active monomers, the chain structure and molecular weight distribution of the superplasticizers can undergone a corresponding change [9].

In this paper, the pH value of reaction system has successfully been controlled by the addition of sodium hydroxide solution and acrylic acid monomer. The addition of sodium hydroxide solution causes the increase of the pH value by neutral reaction with acrylic acid, whereas the addition of acrylic acid decreases the pH value by the increasing concentration of hydrogen ions. The relationship between the pH value of reaction system and water-reducing performance of PC has been investigated by evaluating the workability of cement paste.

2. Experimental

2.1 Raw materials

The cement used is commercially available normal Portland cement from Huaxin cement factory in china. The specific characteristics of raw materials are shown in *Table 1*.

The Polyether Macromer (F108) is obtained from Liaoning Kelong Fine Chemical Co., Ltd. Acrylic acid (AA), sodium methallyl sulfonate (SMS), hydrogen peroxide (H_2O_2), ascorbic acid (Vc) and sodium hydroxide (NaOH) are purchased from Sinopharm Chemical Reagent Co., Ltd. All the

copolymerization reactions are carried out in an aqueous medium at room temperature for 2 hours using hydrogen peroxide as an initiator and ascorbic acid as an activator, respectively, under a nitrogen gas atmosphere. The polymer solutions have a solids content of 40 wt%, determined by oven drying method. The pH value of reaction system is adjusted by the addition of sodium hydroxide solution and acrylic acid monomer. PC3 stands for the PC synthesized at the pH value of 3 and the PC9 stands for the PC synthesized at the pH value of 9.

Table 1 Characteristics and Chemical compositions of raw materials

Materials	Chemical compositions (%)							Specific surface (m^2/kg)
	SiO_2	Al_2O_3	Fe_2O_3	CaO	MgO	SO_3	Loss	
Cement	22.1	6.08	3.04	58.6	3.32	2.08	2.38	346

2.2 Evaluation

The cement pastes are prepared at a water to cement ratio (w/c) of 0.29 with the PC dosage of 0.15% against the mass of cement using an epicyclical mixer. The spread diameter of the cement cake is measured, which is used for measuring its fluidity. The cement paste is monitored over time to determine paste loss, and measurements are made every 30 min up to 120 min.

Molecular weights (Mw, Mn) of synthesized PCs are determined by gel permeation chromatography (GPC) using 0.1mol/L buffer solution of phosphoric acid as a mobile phase at a flow rate of 1.0 mL/min.

The IR spectrum analysis are determined with AVATAR-370 infrared spectroscopy (Thermo Nicolet Company, US) working at a resolution of 4 cm^{-1} and an accumulation of 32 scans. The spectra are recorded from KBr pellets, weighing 300 mg of KBr and 1 mg of admixture.

3. Results and discussion

3.1 Characterization of synthesized PCs by the FT-IR spectrum

The infrared spectrum for the PCs at different pH value of reaction system are given in *Fig.1*, as the FTIR spectrum has been proved to be a useful tool to effectively character the functional group of polymer [10]. It can be found that the absorption band in 3433 cm^{-1} corresponds to the stretching vibration of hydroxyl groups. The band at 2877, 1458, 1352 cm^{-1} arises from the C–H stretching and bending vibration in the methylene group. The absorption bands appear at 1107 cm^{-1} assigned to stretching vibrations of the characteristic absorption peaks of ether groups in the polyether side chain. Absorption bands at 1643 and 951 cm^{-1} could be assigned to the stretching vibrations of carbonyl groups.

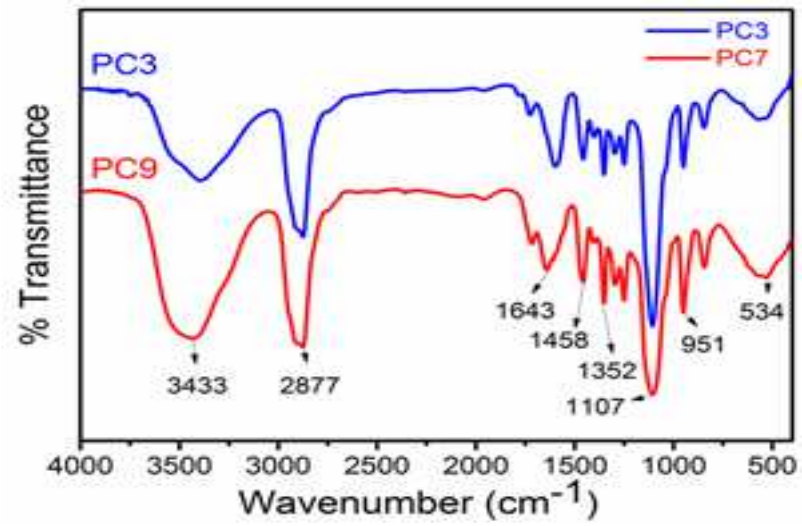

Fig.1 The infrared spectrum for the PCs at different pH value of reaction system

According to the result of the FT-IR spectrum, it is obviously proved the functional groups have been successfully copolymerized to the molecular structure of PCs. However, the PCs synthesized at different pH value of reaction system is not shown much difference in the whole spectrum, except for little varied intensity of peaks in some groups, which can easily be deduced those PCs have similar functional groups.

3.2 The molar masses and polydispersities of PCs synthesized at different pH

As the pH value of reaction system affect not only the efficiency and rate of redox initiator systems but also the reactivity of active monomers, the molecular weight and its distribution of the PCs will make a big difference. The molar masses and polydispersities of PCs synthesized at different pH are shown in *Fig.2* and the statistical data are displayed in *Table 2*. The polydispersity index (PDI) is obtained by dividing the weight average molecular weight (Mw) by the number average molecular weight (Mn). It describes the uniformity of a polymer with respect to molecular mass distribution. It can also be seen that polymer molecules with higher molecular weight elute earlier from the chromatography column.

Since the synthesis conditions remained the same for all polymerizations, apart from the pH value of reaction system being varied, the mean polymer weights decrease accordingly from PC3 to PC9. It appears to be obvious that PC3 has a much lower polydispersity than PC9. The initiator and monomers possess higher reaction activity under acidic conditions, which are rapid and dramatic in initiating the polymerization, resulting smaller molecular weight and wider distribution than alkaline environment. The both of the PCs were shown only small amounts of unreacted monomers or by-products formed can be observed at higher elution times.

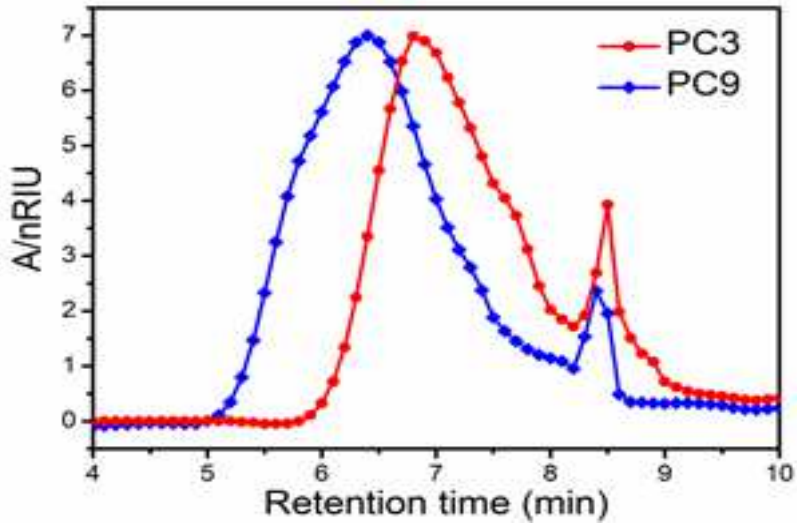

Fig.2 GPC spectrum of different PCs synthesized at the pH value of 3 and 9.

Table 2 Molar masses and polydispersities of PCs synthesized at different pH

Sample	Mw	Mn	DPI
PC3	17020.6	8017.8	2.1
PC9	52219.6	13287.9	3.9

3.3 Effect of different PCs on dispersion of cement pastes

The effect of PCs synthesized at the pH value of reaction system on the fluidity of cement paste is shown in *Fig.3* as a function of pH value and time elapsed. It is can be seen the initial fluidity of the cement pastes is decreased with the increasing pH value of reaction system, which is largely reduced from 330 mm to 140 mm. However, the fluidity retention capacity of the cement pastes is shown an obviously contradictory trend.

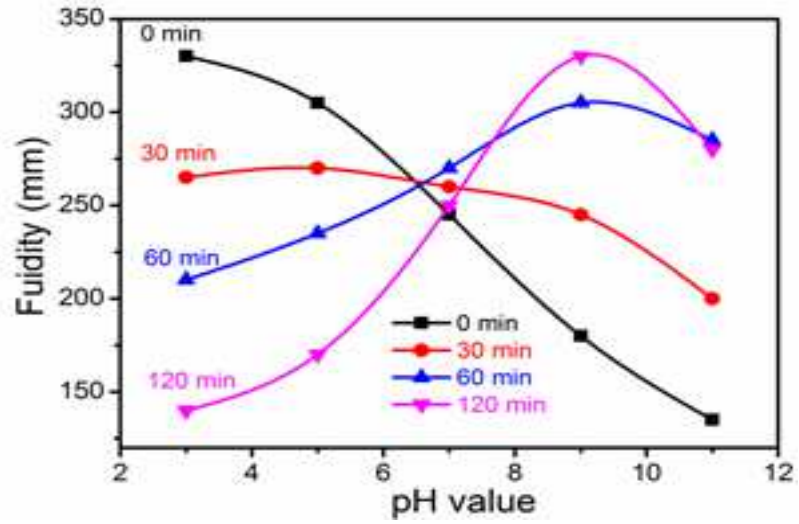

Fig.3 Effect of the pH value of reaction system and time elapsed on fluidity of cement pastes.

Fluidity loss of cement pastes could result from the drop of dispersive capacity caused by the vanishing of PCs with time elapsed. The more amount of adsorption of PCs on the surface of cement particles is, the better fluidity of cement paste is and the less amount of the rest of PCs in solutions at the same time is, which will decrease the ability of fluidity retention. Since the adsorption rate of PCs with higher molecular weight is slower than the lower ones, the corresponding cement pastes possess smaller initial fluidity but higher the fluidity retention capacity. As the molecular weight increasing, the initial fluidity of the cement pastes become smaller and the fluidity retention capacity become larger, it is likely that the adsorption of PCs with wider molecular weight distribution are more durable.

4. Conclusions

In summary, not only the effect of the pH value of reaction system on the molecular weight and its distribution of PCs, but also the corresponding dispersion and workability behavior of cement paste are investigated systematically in this paper. The results show that the PCs synthesized at the higher pH value of reaction system possess higher molecular weight and wider distribution, resulting in smaller initial fluidity but higher fluidity retention capacity. Since tuning the water-reducing performance of PCs by controlling of the pH value of reaction system at room temperature is simple and effective in this redox initiator system, this method has tremendous potential to be applied in laboratorial and industrial synthesis.

5. Reference

[1] Mollah. M, Adams. W. A review of cement superplasticizers interactions and their models [J]. Advances in Cement Research, 2000, 12(4):153-161.
[2] Janowska E. The effect of superplasticizers' chemical structure on their efficiency in cement pastes [J]. Construction and Building Materials, 2013(38):1204-1210.
[3] Collepardi M, Valente M. Recent development in superplasticizers 8th CANMET/ACI International Conference on Superplasticizers and Other Chemical Admixtures In Concrete [C].American Concrete Institute,2006(239):1-14
[4] Habbaba A, Plank J. Interaction between polycarboxylate superplasticizers and amorphous ground granulated blast furnace slag [J]. Journal of the American Ceramic Society, 2012, 93:2857-2863
[5] Alone M, Palacios M, et al. Compatibility between polycarboxylate-based admixtures and blended-cement pastes [J]. Cement and Concrete Composites, 2013, 35(1):151-162.
[6] Pang L, Zhou X. Research of polyocarboxy acid water-reducer with modified polyether and its effect on concrete's workability [J].Advanced Materials Research, 2011, 250:2032-2035.

[7] Yves F. Design and function of novel superplasticizers for more durable high performance concrete [J]. Cement and Concrete Research, 2008, 38(2):1197-1209
[8] Chongzhi L, NaiQian F, et al. Effects of polyethylene oxide chain on the performance of polycarboxylate-type water-reducers [J]. Cement and Concrete Research, 2005, 35(4):867-873.
[9] Ohta A, Sugiyama T. Study on the dispersing effect of polycarboxylate-based dispersant [J]. Cement Science and Concrete Technology, 1999(53):7-12.
[10] Yamada K, Takahashi T, et al. Effects of the chemical structure on the properties of polycarboxylate-type superplasticizers [J]. Cement and Concrete Research, 2000, 30(2):197–207.

Advanced Materials Research Vols. 989-994 (2014) pp 102-107
© (2014) Trans Tech Publications, Switzerland
doi:10.4028/www.scientific.net/AMR.989-994.102

Preparation and in vitro release behaviors of paclitaxel-loaded Pluronic F87/Poly(lactic acid) Nanoparticle

Ziling Li[1, a], Yousheng Huang[2, b], Xiangyuan Xiong[1,c *] ,Yanchun Gong[1,d], Yuping Li[1,e]

[1]School of Life Science, Jiangxi Science & Technology Normal University, Nanchang,330013 China

[2] Analytical and Testing Center of JiangXi Province,Nanchang 330029,China

*Corresponding Author

[a] lzlowen2010@gmail.com, [b] yshuang0526@163.com, [c]xyxiong@gmail.com, [d]spoilming@163.com,[e]1404543371@qq.com

KeyWords: block copolymer; Pluronic F87; PLA; paclitaxel; in vitro release

Abstract: Pluronic F87/Poly(lactic acid)block copolymer (PLA-F87-PLA) was synthesized by bulk polymerization. Paclitaxel-loaded PLA-F87-PLA nanoparcticles were prepared by a dialysis method. The loading efficiency was determined by UV. The results showed that the loading efficiency of paclitaxel for PLA-F87-PLA nanoparticles was 69%. In vitro release behavior of paclitaxel-loaded PLA-F87-PLA nanoparticles was studied by HPLC. In vitro release behavior showed an initial rapid release followed by a slow release. The biocompatibility of nanoparticles was measured by MTT. The viability of paclitaxel-loaded PLA-F87-PLA nanoparticles was less than that of free paclitaxel. The results indicated that PLA-F87-PLA copolymer has good biocompatibility.

Introduction

Biocompatible amphiphilic copolymers are able to self-assemble into nanoparticles with different morphologies in aqueous solution. Drug can be entrapped within the nanoparticles. Hydrophilic segments in surface can protect the drug would not be destroyed. Therefore, the method has been widely used to application of drug delivery stystems[1-3].

Paclitaxel is a natural anti-cancer drug extract from Taxus plant. It has a good effection on breast cancer, ovarian cancer, liver cancer and other cancers. Because the water solubility of paclitaxel is extremely low, the administration in clinical adopts injection mode. Paclitaxel was dissolved in the mixture of polyoxyethylene castor oil and ethanol solution and administration. However, polyoxyethylene castor oil is easy to cause serious adverse effects so that clinical application is limited. To avoid the negative effects, a variety of carriers were used to loaded paclitaxel, which is widely applied in current research, such as liposome[4], chitosan[5], Polymeric micelles[6] and so on.

Poly(ethylene oxide)-poly(propylene oxide)-poly(ethylene oxide) (PEO-PPO-PEO) triblock copolymer is an important amphiphilic molecules, commercially available as Pluronics. The U.S. Food and Drug Administration (FDA) has approved its application in food additives and pharmaceutical ingredients [7-9]. PLA is a well-known biodegradable and biocompatible polyester. Its degradation products are carbon dioxide and water, which can be excreted through the kidneys in human body.

Thus, in this study, PLA-F87-PLA block copolymer was synthesized. The block copolymer can be used as carrier material. Paclitaxel-loaded PLA-F87-PLA nanoparcticles were prepared by a dialysis method. The morphology of the nanoparticles and their in vitro release behaviors were studied.

Materials and Methods

Materials

Pluronic F87 ($\overline{Mn}$ 7700, 70wt% PEO) was kindly supplied by BASF Corporation. L-lactide and stannous octoate [$Sn(Oct)_2$] was purchased from Sigma-Aldrich. Paclitaxel was kindly supplied by Fujian Nanfang Biotechnoloty. MTT was purchased from Solarbio and used as received.

Dulbecco's Modified Eagle's Medium(DMEM) was purchased from Gibco and used as received. All other chemicals were of reagent grade. Human ovarian cancer cells OVCAR-3 was purchased from CICAMS.

Synthesis of PLA-F87-PLA block copolymers

PLA hydrophobic chains were attached to both ends of Pluronic F87 using $Sn(Oct)_2$ as the catalyst to obtain amphiphilic block copolymers PLA–F87–PLA. The synthesis procedure of PLA–F87–PLA is described as follows. A round bottom flask with a stopcock was heated to remove the moisture under reduced pressure. After being cooled to room temperature, argon was introduced into the flask. After this, LA and F87 were added and heated to form a well-mixed molted phase. $Sn(Oct)_2$ was added to the flask under argon environment when the mixture was cooled. The vacuum-purge cycle was repeated to remove oxygen in the flask, and the mixture was heated to 160 °C. After being stirred for 15 h, the reaction product was cooled to room temperature. The product was dissolved in methylene chloride and precipitated once in 10-fold volume of cold methanol and once in 10-fold volume of cold diethyl ether. The white product was filtered and dried overnight under vacuum.

Preparation of PLA-F87-PLA nanoparticles

PLA-F87-PLA block copolymer was dissolved in THF and then the polymer solution was added drop wise to ultra pure water. The polymer aggregates solution was dialyzed against ultra pure water for 5 h using a cellulose membrane tubing (molecular weight cut-off 12,000 – 14,000 Da) to remove THF from the solution. The water was exchanged at intervals of 1 h and the final concentration of PLA-F87-PLA aggregates is about 0.1 wt %.

Preparation of paclitaxel-loaded PLA-F87-PLA nanoparticles

PLA-F87-PLA block copolymer and hydrophobic drug paclitaxel were dissolved in THF and then the solution was slowly added drop wise to the ultra pure water under gentle stirring. The drug-loaded polymer aggregates in water were against distilled water using dialysis membrane to remove THF and excess drug molecules outside the particles. Finally, the paclitaxel-loaded PLA-F87-PLA nanoparticles was prepared.

Transmission electron microscope

TEM was performed on a HITACHI H-600 electron microscope at an acceleration voltage of 75 kV. The copper grid (300 meshes) with a carbon film was used. A drop of PLA-F87-PLA nanoparticles solution dripping on the sealing membrane to form a droplets. The copper grid was immersed in the droplets for 3 min and then removed the solution from the edge using filter paper. A drop of sodium phosphotungstate (2 wt %) was placed on the copper grid for 2 min. The copper grid was then dried overnight at room temperature before measurement.

Paclitaxel Loading Study

In order to determine the loading efficiency and loading capacity, a small amount of paclitaxel-loaded PLA-F87-PLA nanoparticles solution was lyophilized and then dissolved with THF. Using a Lambda 35 UV-Vis spectrophotomete determined paclitaxel content. The detection wavelength was 252 nm (paclitaxel characteristic absorption peak at 252nm wavelength).Using THF as the blank control. The loading efficiency and loading capacity of paclitaxel into PLA-F87-PLA nanoparticles were calculated as follows:

$$\text{loading efficiency} = \frac{\text{paclitaxel in nanoparticles (mg)}}{\textit{Total}\ \text{paclitaxel in fomulation (mg)}} \quad (1)$$

$$\textit{loading}\ \text{capacity} = \frac{\text{paclitaexl in nanoparticles (mg)}}{\text{nanoparticles recovered (mg)}} \quad (2)$$

In vitro release study

Paclitaxel-loaded PLA-F87–PLA nanoparticles solution was added into the dialysis membrane and then placed in 0.01 M phosphate-buffered saline (PBS, pH 7.4) aqueous solution. The whole solution was then placed in a shaking water bath at 37◦C for the drug-release study. At predetermined time intervals, taking 5 ml released paclitaxel solution outside the dialysis membrane while adding 5 ml fresh PBS replacement to maintain the volume of the release sample. The

released paclitaxel solution was measured by HPLC to determine the concentration of paclitaxel. An AGilent HPLC Series 1100 equipped with a UV-Vis detector, connected with a zorbax Eclipse XDB-C18 column. Chromatographic conditions as follows: Acetonitrile/PBS aqueous solution (50:50 v/v) as the mobile phase. Flow rate was1.0ml/min. Detection wavelength was 227 nm. Column temperature was 30 ◦C.

In vitro cytotoxicity study

OVCAR-3 cells were cultured in DEME supplemented with 2.0mM glutamine, 10% fetal bovine serum, 100ug/ml streptomycin sulfate and 100U/ml penicillin at 37 ^{0}C in humidified 5% CO_2. OVCAR-3 cells were seeded on 96-well culture plates at a cell density of 2.5×10^5 L^{-1} and cultured for 8h. Following this, the medium was removed and cells were incubated with PLA-F87-PLA nanoparticles solution and paclitaxel-loaded PLA-F87-PLA nanoparticles at paclitaxel concentrations between 0.1 and 10mg/l for 24h. Following this, 20ul MTT solution (5g/l) was added to each well and incubated for 4h under normal growing conditions. Then all media was removed and 150ul dimethylsulfoxide(DMSO) was added. After shaking the plate for 10 min, the absorbance was determined at 492nm using a microplate reader(Thermo Labsystems MK3). The cell viability was calculated as follows:

$$\text{Viability}(\%)=(\frac{A_{test}}{A_{control}})\times100\%$$

Where A_{test} and $A_{control}$ are the absorbance of surviving cells treated with nanoparticles and untreated cells, respectively.

Results and Discussion

synthesis and characterization of PLA–F87–PLA block copolymer

The amphiphilic block copolymers PLA–F87–PLA were synthesized by ring opening polymerization of the monomer L-lactide using F87 as the initiator and $Sn(Oct)_2$ as the catalyst via co-ordination polymerization mechanism. The polymer structure and molecular weight were characterized by ^{1}HNMR. Figure 1 shows a ^{1}HNMR spectrum of a typical PLA-F87-PLA in $CDCl_3$. The small peak at δ of 4.30 ppm belongs to methylene protons of the PLA-CO-OC$\underline{H_2}$-CH_2-O-PEO segment. It was indicated that the PLA-F87-PLA block copolymer was synthesized successfully. According to the ^{1}HNMR spectrum, the number-average molecular weight ($\overline{M}$n) of the PLA-F87-PLA copolymer was 21400.

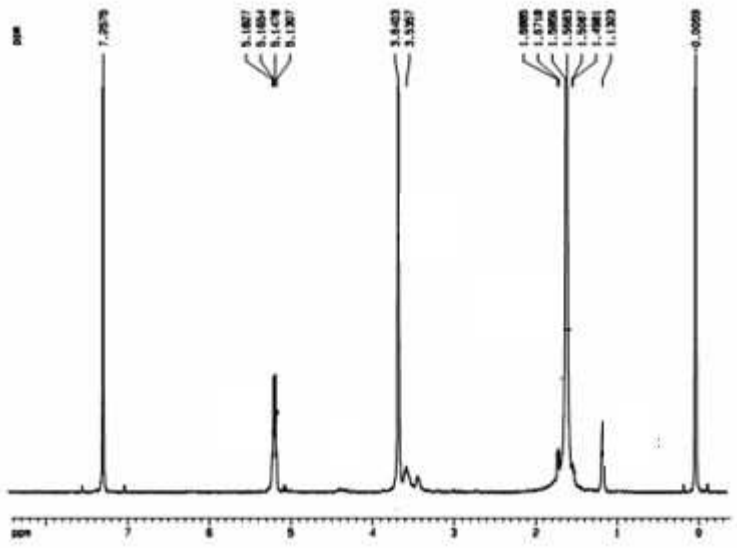

Figure 1 ^{1}H NMR spectrum of PLA-F87-PLA

Characterization of nanoparticles

The particles size and size distribution of PLA-F87-PLA nonoparticles and paclitaxel-loaded PLA-F87-PLA nonoparticles were determined by DLS method using PSS Particle Sizing Systems. The figure 2 shows the intensity-weight Gaussian distribution of PLA-F87-PLA nonoparticles. It was

observed that the PLA-F87-PLA nonoparticles showed a single, narrow distribution. The particle size of PLA-F87-PLA nanoparticles was 175nm.

The morphology of PLA-F87-PLA nanoparticles was examined by TEM. The nanoparticles was negatively stained by sodium phosphotungstate. Figure 3 shows the TEM pictures of PLA-F87-PLA nanoparticles. It was shown that PLA-F87-PLA nanoparticles is spherical core-shell micelles

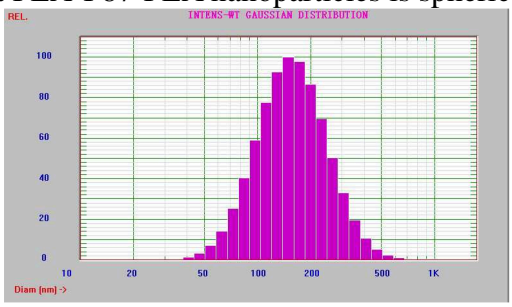

Figure 2 The intensity-weight Gaussian distribution for PLA-F87-PLA nanoparticles

Figure 3 Transmission electron microscopy images of PLA-F87-PLA nanoparticles

Paclitaxel-release study

Paclitaxel–release study from PLA-F87-PLA nanoparticles was performed in PBS solution at 37℃. The loading efficiency and loading capacity of paclitaxel for PLA-F87-PLA was 69% and 9.3%, respectively. Figure 4 shows the drug-release profiles of paclitaxel-loaded PLA-F87-PLA nanoparticles. This study suggested that paclitaxel-loaded PLA-F87-PLA nanoparticles presented an initial rapid release of the front 20h, and then shows a slow release within a time of up to about 4d, and only about 20% of paclitaxel loaded in PLA-F87-PLA was released. Part of the hydrophobic paclitaxel could forms aggregates due to the hydrophobic interaction within the PLA core of PLA-F87-PLA nanoparticles, thus resulting in their non-diffusible property.

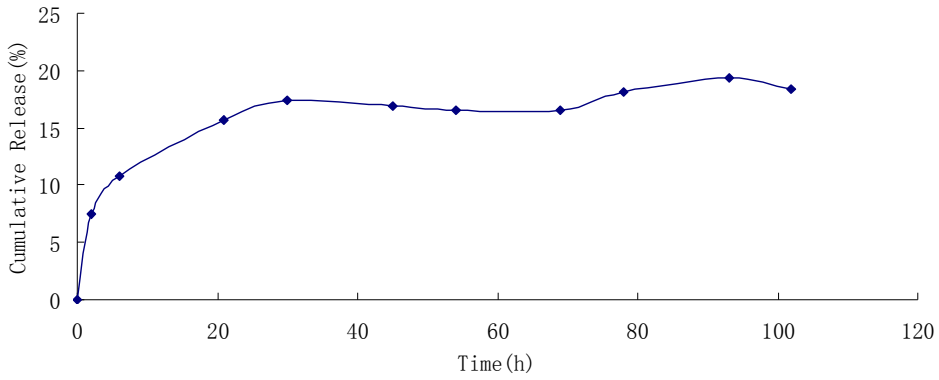

Figure 4 The release behaviors of pacliaxel-loaded PlA-F87-PLA nanopariticles

Cell cytotoxicity

The cytotoxicity of paclitaxel-loaded PLA-F87-PLA nanoparticles was evaluated using MTT assay. Figure 5 shows the viability of OVCAR-3 cells treated with paclitaxel-loaded PLA-F87-PLA nanoparticles and free paclitaxel. The data were analyzed by t test. The P values were 0.002, 0.04 and 0.04, respectively. They were less than 0.05. Results show that there is statistically significant

correlation between paclitaxel-loaded PLA-F87-PLA nanoparticles and free paclitaxel. Besides, it can be seen from figure 5 that the viability of paclitaxel-loaded PLA-F87-PLA nanoparticles was less than free paclitaxel and the viability of paclitaxel-loaded nanoparticles decrease with the increasing paclitaxel concentrations. This study suggests that the ability to kill cancer cells for paclitaxel-loaed PLA-F87-PLA nanoparticles is stronger than that for free paclitaxle.

In addition, in order to validate the cytotoxicity of blank PLA-F87-PLA nanoparticles, PLA-F87-PLA nanoparticles (115mg/L) was used to treated OVCAR-3 cells. The viability of OVCAR-3 was 76%. PLA homopolymer and Pluronic F87 are well-known biocompatible polymers. The earlier results indicate that PLA-F87-PLA block copolymer also has good biocompatibility..

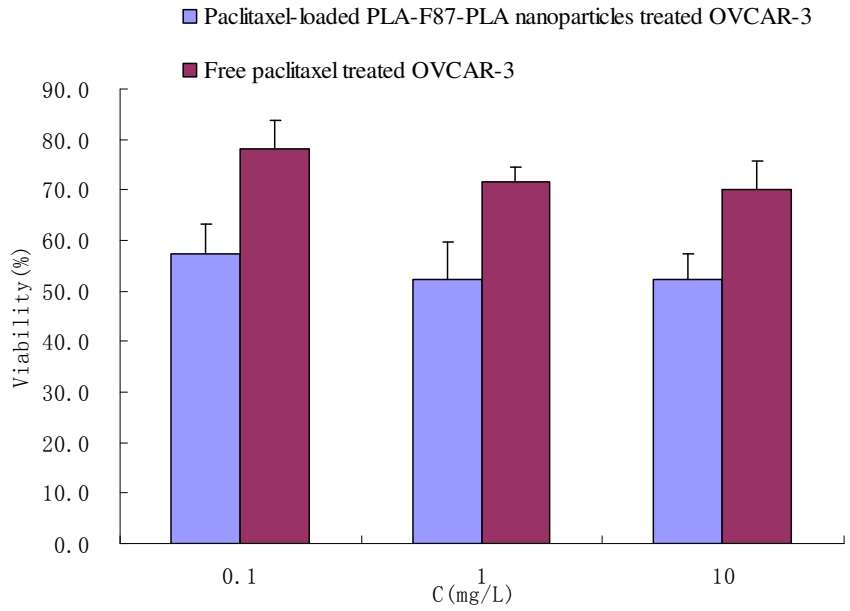

Figure 5 Cytotoxicity of OVCAR-3 cells treated with paclitaxel-loaded PLA-F87-PLA nanoparticles and free paclitaxel

Conclusions

In this study, PLA-F87-PLA copolymer was synthesized. The self-assembling behaviors of PLA-F87-PLA in aqueous solutions were examined. The release of paclitaxel loaded in PLA-F87-PLA nanoparticles shows an initial burst release in the front 20h, and followed by a slow release, only about 20% paclitaxel was released. PLA-F87-PLA copolymer was found to have good biocompatibility by MTT assay using human ovarian cancer cells OVCAR-3. The study of PLA-F87-PLA copolymer on the application of drug delivery systems is on progress.

Acknowledgement

In this paper, the research was sponsored by the National Natural Science Foundation of China (No. 21264009 and 31360376); Natural Science Foundation of Jiangxi Province (No. 20132BAB206034); Scientific and Technological Landing Project of Higher Education of Jiangxi Province (No. KJLD13071)

References

[1] Xiong XY, Li YP, Li ZL, et al. Vesicles from Pluronic/poly(lactic acid) block copolymers as new carriers for oral insulin delivery[J].. J Control Release. 2007;120(1-2):11-17.

[2] Fabienne Danhier, Nathalie Lecouturier, Benoît Vroman.et al Paclitaxel-loaded PEGylated PLGA-based nanoparticles: In vitro and in vivo evaluation[J]..Journal of Controlled Release.2009,133:11–17

[3] Soo Young Lee, Hoon Hyuna, , Ju Yong Youn et al. Preparation of nano-emulsified paclitaxel using MPEG–PLGA diblock copolymers. Colloids and Surfaces A, Physicochem. Eng. Aspects 2008,313–314:126–130

[4] XIN ShCh, WU XR,ZHOU LZh. Preparation of magnetic solid liposome nanoparticles of paclitaxel[J]. Acta Pharmaceutica Sinica 2006, 41 (10) : 933 - 938
[5] Jong-Ho Kim, Yoo-Shin Kim, Sungwon Kim et al.Hydrophobically modified glycol chitosan nanoparticles as carriers for paclitaxel[J].. Journal of Controlled Release.2006,111: 228–234
[6] WANG YZh, FANG XL Li YJ,et al. Preparation, character ization of paclitaxel2loaded Pluron ic P105 polymer ic m icelles and in vitro reversal of multidrug resistant tumor[J] Acta Pharmaceutica Sinica 2008, 43 (6) : 640 - 646
[7] X. Y. Xiong, K. C. Tam, L. H. Gan. Polymeric Nanostructures for Drug Delivery Applications Based on Pluronic Copolymer Systems[J]. Journal of Nanoscience and Nanotechnology.2006,.6:2638–2650,
[8] J.R. DesNoyer, A.J. McHugh.The effect of Pluronic on the protein release kinetics of an injectable drug delivery system[J].. Journal of Controlled Release. 2003,86:15–24
[9] Alexandre Marin, Hao Sun, Ghaleb A. Husseini et al. Drug delivery in pluronic micelles: effect of high-frequency ultrasound on drug release from micelles and intracellular uptake[J].. Journal of Controlled Release. 2002,84:39–47

Advanced Materials Research Vols. 989-994 (2014) pp 108-114
© (2014) Trans Tech Publications, Switzerland
doi:10.4028/www.scientific.net/AMR.989-994.108

Application of High-Efficiency Reverse Osmosis Technology in Reclaimed Water Treatment in Power Plants

Xiao Long[1,a], Qing Zhu[2,b], Xiaoyi Wang[3,c], Jinhong Shi[3,d]

[1]State Grid Hebei Electric Power Research Institute, Shijiazhuang, 050021,China

[2]Electric Power Research Institute, Shanghai Municipal Electric Power Co., Shanghai, 200437,China

[3]Hebei Huadian Shijiazhuang Yuhua Thermal Power Co., Ltd., Shijiazhuang, 051430,China

[a]email:13832168901@126.com@163.com, [b]email:wingandlionjiji@126.com, [c]email:4500566@qq.com, [d]email:shijinhong@chdyh.com

Keywords: Reclaimed Water Reuse; High-Efficiency Reverse Osmosis; Power Plant

Abstract. Because of the poor quality of the operational water (urban reclaimed water) of one power plant in Hebei, China, a high-efficiency reverse osmosis (HERO) system with foreign patents is utilized for advanced treatment of the reclaimed water. The influence of the main factors (including the alkalinity and the suspended solid content of the feed water, the flux, and the pH of the concentrated water) on the performance of the HERO system were studied. The high alkalinity (high concentration of carbonate) of the feed water resulted in HERO scaling, and the low alkalinity caused the penetration of hardness through the weak acid ion exchangers and, therefore, also caused HERO scaling. The high suspended solid content of the feed water caused rapid decrease in the product flux of HERO. The low concentrated water flux also decreased the product flux. As the pH of the concentrated water became higher, the stability of the HERO operation increased. Based on the pH endurance of the membranes and the characteristic of the high-pH operation of the HERO system, the water production was basically stable when the pH of the concentrated water lay between 10.5 and 10.8. Affected by the ammonia in the reclaimed water, the pH of the product water was higher than that of the feed water. The pH of the feed water was higher than that of the concentrated water. When the pH of the concentrated water was above 10.8, the pH values were close to one another. The results of the chemical cleaning experiments indicated that hardness, phosphorus, ammonia, silicon dioxide, and iron ions were the main influencing chemical factors of HERO, in which the former three formed a sediment of magnesium ammonium phosphate, and the latter two formed an iron silicate sediment.

One thermal power plant in Hebei, China consists of 2×300 MW sub-critical heat-supply units, and reclaimed water from a sewage treatment plant is utilized as the source of the thermal network replenishment and chemical make-up water. Most wastewater that enters this sewage treatment plant comes from the industrial processes and the quality of the wastewater changes greatly with the change in the seasons. Taking into consideration that water contains abundant organic compounds, surfactant, and ammonia nitrogen, the combined techniques of lime treatment and high-efficiency reverse osmosis (HERO) are utilized to treat the reclaimed water. The system has been operating for nearly three years. The HERO technology performance shows that it has its own characteristics that are much different from the conventional reverse osmosis.

1 Process and characteristics of HERO

The HERO process in the advanced treatment of the reclaimed water is shown as follows: product water of lime treatment→ high-efficiency filters→ sodium cation exchangers→ weak acid

cation exchangers→ acid dosing→ decarbonators→ sodium hydroxide dosing→ HERO→ product water sent to the thermal network replenishment and chemical make-up water systems.

Throughout the entire process, the suspended solid content of the product water from lime treatment is reduced by the high-efficiency filters. Then, hardness is completely removed by the sodium cation exchangers and weak acid cation exchangers. After acid dosing, carbon dioxide is removed by the decarbonators. The pH is further adjusted to the range from 10.0 to 11.0 by sodium hydroxide dosing, and the water enters the reverse osmosis system. Finally, softened water with high pH is produced and sent to the users.

HERO is a technology with foreign patents, and the system in this power plant was the first system in China that applies HERO for reclaimed water treatment. The main feature of HERO is that the operational recovery rate could increase to 90% or higher. The system is less prone to scaling and fouling, and the membrane flux is much higher than that of the conventional reverse osmosis, which means that HERO produces much higher amount of product water than the conventional reverse osmosis, using the same amount of membrane modules. In addition, the scale inhibitor dosing is not required in the HERO system operation. Only the sodium hydroxide dosing is performed to maintain a high pH value.

The 90% recovery rate indicates that the feed water of the reverse osmosis system is concentrated 10 times before being discharged. This concentration rate is obviously much higher than that of the conventional reverse osmosis in which the feed water is normally concentrated four times. The reasons for the high recovery rate of HERO are as follows:

(1) Hardness, multivalent ions (such as iron, barium, and strontium), and carbonate alkalinity are thoroughly removed by the pretreatment from the feed water using reverse osmosis; thus, carbonate, sulfate, and hydroxide scales do not exist in the concentrated water.

(2) Because the solubility of silicon increases with the increase in pH under alkaline conditions, the scaling limit of silicon is also significantly raised in HERO. During the HERO operation, the solubility of silicon in the concentrated water could be increased to 350 mg/L without scaling, whereas in the conventional reverse osmosis system, scale inhibitor dosing is carried out to avoid silica scaling once the silicon content of the feed water reaches 25 mg/L.

(3) The propagation of microbes in the reverse osmosis system stops when the pH is above 10.0; therefore, breeding of microbes in the reverse osmosis membranes is prevented.

(4) The charge status on the surfaces of the particles and organic compounds changes under high pH conditions, and the repulsive forces between them and the membranes are enhanced; thus, the tolerance of HERO for organisms and SDI is higher. Organics have been reported to be emulsified or saponified under high pH conditions [1] and are less prone to adhere to reverse osmosis membranes.

After the influence of all the scaling and fouling factors of the reverse osmosis are alleviated or even eliminated by the pretreatment and adjustment of high pH, HERO could obtain a higher recovery rate.

2 Quality and characteristics of the reclaimed water

Based on the long-term monitoring of the water quality and the performance of HERO in the recent three years, we found several characteristics of the product water from the sewage treatment plant as follows:

(1) The quality of the product water from the sewage treatment plant fluctuated greatly. The alkalinity fluctuated in the range of 2 mmol/L to 10 mmol/L, and the conductivity of the feed water from the reverse osmosis fluctuated in the range from 2,000 μS/cm to 3,000 μS/cm. The suspended solid content stayed low from June to September; thus, the performance of the lime coagulation treatment was good, and the turbidity of the product water from the lime treatment was low.

(2) The organics, ammonia nitrogen, and surfactant contents were comparatively high, and so was the chroma. The COD_{Cr} content was in the range from 80 mg/L to 200 mg/L most of the time. The ammonia nitrogen was usually in the range from 50 mg/L to 80 mg/L. Large amount of bubbles and foams existed in both the product water from the lime treatment and the concentrated water

from the reverse osmosis. The anionic detergent content was in the range from 0.08 mg/L to 0.32 mg/L, and the chroma was generally in the range from 50 degrees to 190 degrees.

(3) The suspended solid content also fluctuated greatly, and some materials in the water caused bad performance in the coagulation of the lime treatment and high turbidity of the product water (sometimes higher than that of the feed water, and this case occurred in every season). The temperature of the product water of the sewage treatment plant was generally above 17 ℃ even in winter; hence, the influence of low water temperature on the coagulation performance could be ruled out.

(4) The chloride and sulfate contents were comparatively high. The former was in the range from 200 mg/L to 400 mg/L, and the latter was in the range from 300 mg/L to 500 mg/L.

3 Application of HERO

Because of the poor quality of the reclaimed water, HERO was applied to perform advanced treatment in the power plant in Hebei. The debugging of the HERO system started in September 2009, and reliable operation was achieved after a series of optimizations. Currently, the product water of HERO is directly utilized as the feed water of the make-up water treatment system, which consists of the treatment of conventional reverse osmosis (recovery rate of up to 90% without the dosing of scale inhibitor, fungicide, and reductant) and the mixed ion exchangers. During winter, the product water of HERO was directly utilized for thermal network replenishment. The quality of the feed and product water of HERO in October 2009 are shown in Tables 1 and 2.

Table 1 Quality of the feed water of HERO (before sodium hydroxide dosing)

Items		Results (mg/L)	Results (mmol/L)	Items		Results (mg/L)	Results (mmol/L)
Cations	K^+	20.0	0.51	Anions	Cl^-	248.2	7.00
	Na^+	373.8	16.25		$1/2SO_4^{2-}$	510.4	10.63
	$1/2Ca^{2+}$	0.0	0.00		HCO_3^-	31.7	0.52
	$1/2Mg^{2+}$	0.0	0.00		$1/2CO_3^{2-}$	0.0	0.00
	NH_4^+	80.00	0.88		NO_2^-	19.0	0.41
					NO_3^-	8.2	0.13
					F^-	3.8	0.04
	Total	473.8	18.20		Total	821.3	18.73
Items		Results ($CaCO_3$)/(mg/L)	Items	Results (mg/L)		Items	Results (mg/L)
Total Hardness		0.0	Total Silicon	19.8		Sr	0.017
Permanent Hardness		0.0	Active Silicon	18.6		Total Alkalinity	26.0
Temporary Hardness		26.0	Carbon Dioxide	11.44		Total Acidity	13.0
Negative Hardness		0.0	COD_{Mn}	20.3		pH	7.57

Table 2 Quality of the product water of HERO

Items		Results (mg/L)	Results (mmol/L)	Items		Results (mg/L)	Results (mmol/L)
Cations	K^+	0.9	0.02	Anions	Cl^-	22.7	0.64
	Na^+	19.0	0.83		$1/2SO_4^{2-}$	2.2	0.05
	$1/2Ca^{2+}$	0.0	0.00		HCO_3^-	0.0	0.00
	$1/2Mg^{2+}$	0.0	0.00		$1/2CO_3^{2-}$	33.6	1.12
	NH_4^+	30.0	1.65		NO_2^-	0.1	0.003
					NO_3^-	0.4	0.006
					F^-	—	—
	Total	49.9	2.50		Total	59.0	1.82
Items		Results ($CaCO_3$)/(mg/L)	Items	Results (mg/L)		Items	Results (mg/L)
Total Hardness		0.0	Total Silicon	0.6		Sr	＜0.010
Permanent Hardness		0.0	Active Silicon	0.6		Total Alkalinity	56.1
Temporary Hardness		0.0	Carbon Dioxide	0.0		Total Acidity	0.0
Negative Hardness		56.1	COD_{Mn}	0.9		pH	10.9

3.1 Parameters of the HERO equipment

The HERO system in the power plant consists of two stages between which the ratio is 28:6. Stage 1 is divided into three units where each unit is composed of 28 membrane pressure vessels, and each vessel contains eight Dow BW30-440i reverse osmosis membrane modules (224 membrane modules for every unit). Stage 2 is divided into three columns where each unit is composed of six membrane pressure vessels (identical with those in Stage 1; hence, 144 membrane modules exist for the whole stage). According to the original design, the number of columns in the Stage 2 operation is equal to that of the units in Stage 1. Five degassing pumps (designed output = 325 t/h) are installed on the feed water side, five high-pressure pumps (one is a variable-frequency pump) are installed for each unit in Stage 1 and five for the entire Stage 2. Two security filters with 10-μm filter cartridges are also installed.

3.2 HERO operation

After three years of operation and optimization, we found that under current conditions of the reclaimed water and the configuration of the membrane modules, the product water flux of each unit in Stage 1 changed in the range from 180 t/h to 250 t/h with the change in the water temperature under stable and constant operation. The maximum stable product water flux of each unit in summer was 250 t/h at a concentrated water flux of approximately 84 t/h; hence, we conclude that the recovery rate of Stage 1 was approximately 65% to 75%. The product water flux of Stage 2 was approximately 50 t/h to 60 t/h at a concentrated water flux of approximately 82 t/h (only part of the concentrated water in Stage 1 entered Stage 2, whereas the rest was directly drained off via bypass); thus, we conclude that the recovery rate of the entire HERO was approximately from 76% to 81%. So far, two off-line and several on-line chemical cleaning processes have been conducted in HERO, and the system has maintained a very good operational performance. However, during the periods when the water quality fluctuated because of the effect of the high turbidity of the feed water in HERO caused by the poor coagulation performance of the lime treatment system, the product water flux of HERO sharply decreased.

4 Analysis and discussion of the results

4.1 Influence of alkalinity on HERO

The influence of alkalinity on the HERO system is mainly manifested in two directions: the effect on the weak acid cation exchangers and the influence on the operation of HERO.

(1) Effect on weak acid cation exchangers

As the final barrier before HERO, the weak acid cation exchanger must completely remove the hardness of the feed water. Under current conditions of the water quality, the scaling caused by the leakage of hardness imposes much heavier effect on the product water flux than the contamination of organics; therefore, the hardness of the product water in the weak acid cation exchangers should be strictly controlled and monitored. Currently, the operation standard is set to 10 μmol/L.

Compared with strong acid resins, the weak acid resins can only remove the hardness lower than the alkalinity (called temporary hardness) and are not capable of removing the permanent hardness. Thus, sodium cation exchangers are required to remove most of the hardness to ensure that the remaining hardness (entering the weak acid cation exchangers) is lower than the alkalinity. The quantity of acid dosing in the product water from the lime treatment is also adjusted to keep the alkalinity in an appropriate range and avoid both the scaling of the system before the weak acid cation exchangers caused by high alkalinity and the leakage of hardness caused by low alkalinity. Currently, the alkalinity of the feed water in the weak acid cation exchangers is controlled in the range from 1.2 mmol/L to 1.5 mmol/L, and the hardness is controlled below 1 mmol/L.

(2) Influence on the operation of HERO

Because of the fluctuations in the quality of the reclaimed water, sometimes the alkalinity of the feed water in the weak acid cation exchangers reaches very high levels. Considering that the exchange capacity is normally high and the hardness of the product water in the sodium cation exchangers is controlled to be low, the weak acid cation exchangers show good performance

without losing their effectiveness even if the pH of the product water reaches 8.5 or higher and the product water contained much more carbonate.

For example, we have observed once during the operation of HERO that the inlet pressure of Stage 2 rose sharply from 2.60 MPa to 2.80 MPa. At that time, the alkalinity of the reclaimed water was very high, and the alkalinity of the product water in the sodium cation exchangers reached 9.0 mmol/L, causing high alkalinity in the product water in the weak acid cation exchangers. Thus, the carbonate was not thoroughly removed even though the decarbonators were operating at full load. In such a case, we speculated that carbonate scaling had occurred in the membranes in Stage 2. Therefore, on-line pickling was conducted, and the inlet pressure in Stage 2 was reduced to 2.55 MPa.

From the above example, supplying total hardness-free feed water to HERO is impossible. Scaling of the membranes in Stage 2 would occur rapidly if the system operates under the conditions of high feed water alkalinity and high pH. Therefore, the alkalinity (carbonate content) of the feed water must be strictly controlled.

4.2 Influence of suspended solids on HERO

The applied specialized fabrication process enables the membranes of HERO to endure higher SDI based on our long-term observation of the operation. The main factor that contributes to the high SDI that HERO can deal with should be the colloid and not the suspended solids.

Ultrafiltration devices are not applied in the pretreatment system of HERO. Only variable-pore micro filters of the lime treatment system and high-efficiency filters are utilized for filtering. The SDI of the feed water of HERO is continuously measured, and the results indicate that in most cases, the SDI reaches the limit value of 6.7, which means it is too high to measure. Generally, the solid materials on the diaphragms are visible, and in a few cases, the diaphragms are pierced by suspended solid particles, which shows that suspended solids, colloids, and other SDI-related materials are not effectively removed from the reclaimed water after the lime treatment and high-efficiency filtering. Constant excessively high SDI could impose negative influence on the stability of the HERO operation. In particular, when the content of the suspended materials is high, the product water flux of HERO drops significantly. When the turbidity of the feed water of HERO is below 1NTU, HERO maintains a stable operation even if the SDI cannot be measured. When the turbidity of the feed water exceeds 5NTU, the product water flux begins to decrease significantly; when the turbidity reaches 8NTU to 10NTU because of the “sediment upturning” of the clarifier in the lime treatment system caused by water quality fluctuation, the product water flux drops sharply (e.g., the flux of a unit dropped from 178 t/h to 167 t/h within one day). Although specialized processes of water softening and high pH adjustment are adopted in HERO, fouling of suspended solids is still not well prevented; therefore, the turbidity or the suspended solid content of the feed water of HERO must be strictly controlled.

4.3 Influence of the concentrated water flux on HERO

As the concentrated water flux of the membrane modules becomes lower, the recovery rate becomes higher, and the operational energy consumption is reduced. On the other hand, guaranteeing a certain concentrated water flux is extremely important to maintain a stable operation of HERO. The contaminants in the concentrated water could be effectively entrained and discharged to reduce the contamination of organics and microbes only when the turbulent layer is sufficiently thick. The thickness of the laminar layer could be reduced to weaken the concentration polarization on the membrane surface and thus decrease the content of the insoluble salts and avoid pollution of inorganic precipitate[2]-[5].

HERO did not comply with the requirements of the DOW membrane technical manual because of the specialized fabrication process it applied. The operation of HERO has been continuously optimized; the concentrated water flux of each unit in Stage 1 has been figured out to be above 84 t/h and that of Stage 2 should be above 82 t/h. If the flux does not reach these values, the product water flux of HERO would be affected. Stage 2 consists only of 144 membrane modules. In view of the current water quality, the membrane flux in Stage 2 is reduced to ensure the stability of the operation. A direct drainage pipe for the concentrated water of Stage 1 is added, and part of the

concentrated water is directly discharged through this pipe. With the installation and utilization of the direct drainage pipe, the operational burden of Stage 2 is reduced, and the concentrated water flux in Stage 1 increases; therefore, the stabilities of Stages 1 and 2 are both reinforced.

After the adjustment was performed, sufficient concentrated water flux is guaranteed, and the deposition rate of the contaminants on the membrane surface is effectively lowered (especially when high suspended material content resulting from the fluctuations of the reclaimed water occurred). The operation of the entire HERO is further stabilized.

4.4 Influence of pH on HERO

In the early operational period of HERO, the pH of the concentrated water was controlled from 9.5 to 10.0. In the winter of 2009, we found that the performance of the biochemical treatment of the sewage treatment plant was not sufficiently good because of the low water temperature; thus, the content of the organics of the reclaimed water for the power plant reached a higher level (the COD_{Cr} of the feed water in HERO was in the range from 150 mg/L to 180mg/L), which finally caused the gradual decline of the product water flux. As continuous adjustments were performed, we found that the decline in the product water flux became slower as the pH of the concentrated water increased. Finally, the pH was adjusted to 10.5–10.8, and the product water flux of HERO stopped declining and remained basically stable.

Because of the influence of ammonia nitrogen in water, the pH of the product water of HERO is higher than the pH of the feed water, and the pH of the feed water is higher than the pH of the concentrated water. The limiting pH of the long-term operation of DOW membranes is 11.0. Hence, the pH of the concentrated water was controlled below 10.8 because the pH of the product water was already very close to 11.0 at the same time.

Maintaining a high concentrated water pH has been shown to reduce effectively the effect of organics and maintain the product water flux of HERO.

4.5 Analysis of the results of chemical cleaning

At the end of 2010, an on-line chemical cleaning was conducted on HERO. The process included ①pickling (HCl pH=2), ②acid soaking, ③water rinsing, ④alkaline cleaning (NaOH + sodium dodecyl benzene sulfonate, pH=12), ⑤alkaline soaking, ⑥water rinsing, and ⑦re-pickling. Measurements by the inductively coupled plasma atomic emission spectroscopy were conducted to determine the contents of the different elements in the effluent, and the results are shown in Table 3.

Table 3 Contents of different elements in the effluent of chemical cleaning (mg/L)

Coefficients	Oxides	Effluent of pickling, 3rd column	Effluent of alkaline soaking, 3rd column (acid dosed and filtered)	Effluent of alkaline soaking, 2nd column (acid dosed and filtered)	Effluent of alkaline soaking, 4th column (acid dosed and filtered)	Effluent of alkaline soaking, 4th column (acid dosed and filtered)
1.21	K_2O	7.801	3.062	2.525	3.389	3.54
1.35	Na_2O	118.5	994.1	752.0	1001.0	984.3
1.40	CaO	9.610	0.2761	0.5505	20.16	7.923
1.67	MgO	2.782	0.0207	0.0350	1.351	2.114
1.28	CuO	0.0138	0.0015	0.0130	0.0172	0.0142
1.43	Fe_2O_3	259.1	10.73	11.76	40.29	26.19
1.25	ZnO	1.414	0.0002	0.0375	0.1333	0.0426
2.14	SiO_2	199.9	108.7	87.44	168.7	157.4
1.89	Al_2O_3	6.863	0.9640	0.6621	1.602	1.298
1.67	TiO_2	4.413	—	0.8741	3.507	2.398
2.50	SO_3	4.856	158.6	111.4	189.7	186.3
2.29	P_2O_5	0.933	9.233	9.195	10.87	17.31
1.58	MnO_2	1.847	0.0248	0.0295	0.1330	0.0519

The data in Table 3 indicate the following:

(1) P_2O_5 (or phosphorus-containing substance on the membrane surface) dissolved under alkaline conditions. After the acid dosing was carried out, part of P_2O_5 precipitated and was filtered out.

(2) From the data of the pickling and alkaline cleaning in the third column, most of the iron still existed in the form of ions. The colloidal iron content was low, indicating that iron leakage from the weak acid cation exchangers occurred.

(3) From the data in the third column, the total silicon content on the membrane surface was higher than 300 mg/L, indicating that the concentrated water flux was not sufficient, and silicon deposition occurred. Heavy deposition of iron silicate was also observed either because of the low pH or the excessively high iron content.

(4) From the data in the third and the fourth columns, the calcium content of the feed water of HERO was high, indicating that calcium was not effectively removed by the weak acid cation exchangers. The water rinsing in the fourth column after pickling was not thorough, and re-pickling after alkaline cleaning was necessary.

(5) From the data in the fourth column, part of the iron in the fourth column had already precipitated when alkaline cleaning was performed.

4.6 Advantages of HERO in reclaimed water treatment

For the conventional reverse osmosis system, periodic chemical cleaning is necessary to deal with the reclaimed water to mitigate the effect of organic matters and other fouling substances. In addition, ultrafiltration devices must be utilized; thus, problems of higher space demand, higher operational cost, and ultrafiltration fouling emerge. Compared with the conventional reverse osmosis system, the operation stability of HERO is much higher, the frequency of chemical cleaning is much lower, and the recovery rate is higher. In addition, no ultrafiltration system is needed. Therefore, the space demand and operational cost could be greatly reduced.

5 Conclusions

(1)The HERO system has shown strong advantages in treating reclaimed water with poor quality. It could be operated under conditions of high organic matter content and high SDI, and could achieve obvious economic benefits in terms of reclaimed water treatment.

(2)The alkalinity, content of suspended solids, concentrated water flux, and pH were the most significant factors that influenced the operation of the HERO system.

(3)The hardness and phosphorus, silicon, and iron contents were the most significant factors that influenced the fouling of the HERO system. These parameters of the feed water in HERO must be strictly controlled.

Reference

[1] Wenzhong Chen, Application of High Efficiency Reverse Osmosis Technology in Boiler Makeup Water Treatment, Thermal Power Generation, 2009, 38(6) 91-98.

[2] Dawei Jin, Optimized Design of Reverse Osmosis System, Press of Chemical Industry, Beijing, 2006.

[3] Liu, F.N., Zhang, G.L., Meng, Q., Zhang, H.Z., Performance of nanofiltration and reverse osmosis membranes in metal effluent treatment, Chinese Journal of Chemical Engineering, 2008, 16(3), 441-445

[4] Jehad Abbadi, Rinad Saleh, Sameh Nusseibeh, Muhannad Qurie, Mustafa Khamis, Rafik Karaman, Laura Scrano and Sabino Aurelio Bufo, Microbial Removal from Secondary Treated Wastewater Using a Hybrid System of Ultrafiltration and Reverse Osmosis, Journal of Environmental Science and Engineering,2012, A 1, 853-869

[5] Yi, L.L., Jiao, W.T., Chen, X.N., Chen, W.P., An overview of reclaimed water reuse in China, Journal of Environmental Sciences, 2011,23(10), 1585-1593

Advanced Materials Research Vols. 989-994 (2014) pp 115-120
© (2014) Trans Tech Publications, Switzerland
doi:10.4028/www.scientific.net/AMR.989-994.115

Measurement of Ultra Low Sulfur in IN718 by using Infrared Absorption Method

Zalupski, P.R., Fengyan Liu

Department of Chemistry, Loyola University of Chicago, Chicago, IL 60626, United States

fengyanliu8105@sina.com

Keywords: Infrared absorption method, IN718, ultra low sulfur.

Abstract. The paper introduces an experimental process on measurement of ultra low sulfur in IN718 by using infrared carbon sulfur analyzer. The experimental data shows that, infrared absorption method can be used to analyze and measure the ultra low sulfur in IN718, and the precision and accuracy of this method meets the requirement of ASTM E l019-2000. It can be concluded that it is a feasible method in practice.

Introduction

Superalloy INCONEL 718（IN718）has been applied in making aircraft engine for half a century. Since 1960s, after INCO Huntington Alloys (now Special Metals Co．)has been invented and applied for manufacturing turbine parts, IN718 has become the most widely applied nickel-base Superalloy in the development history of aircraft engines. The unique alloy component design of IN718 allows it to have excellent comprehensive performances, such as high strength, creep resistance, and fatigue endurance. Many parts of modern aircraft engines, such as turbine discs, blades, cartridge receivers, axles, stators, obturage, supporters, pipelines, fastening pieces, are made from IN718.

In recent years, along with the increasingly higher demand on performance and efficiency of turbine engines, the working temperature of engines has been increasing constantly. IN718 alloy materials with high degree of cleanliness are used for manufacturing the key parts of engines [1]. IN718 alloy materials with high degree of cleanliness have a very strict demand on chemical components and their sulfur contents have to be controlled at S:1μg/g~10μg/g. Since sulfur in IN718 is taken as impurities, which may easily become the occurrence place and extending channel of endurance cracks. In addition, these impurities may become crystallization nuclei, which may lead to performance degradation of alloys[2][3]. Therefore, accurate analysis of the content of Ultra-low sulfur in IN718 has become an important link in the quality control process.

Currently, the standard methods of using infrared absorption to measure the sulfur content in alloys mainly include ISO 15350[4], ASTM E1019[5], etc. However, the analytical range of above methods (S ＞5μg/g) can not meet actual demand.

To meet the requirements of the market on higher quality and diversified products of IN718, the application of the Ultra-low sulfur （S:1μg/g~10μg/g）IN718 will become a development trend. Accordingly, the corresponding analytical technology should be developed for providing support.

By selecting infrared carbon sulfur analyzer as analytical instrument, and through experiments on relevant factors such as combustion conditions and blank control, this study has worked out the best analyzing conditions of sulfur（S:1μg/g~10μg/g）in IN718 and established an analytical method. The method has been used for measuring ultra-low sulfur, and the result is satisfactory.

Selection of analytical and testing conditions

Principle of analyzing Ultra-low sulfur by using infrared absorption method

The sample is placed in a ceramic crucible, and the high-frequency furnace is supplied with oxygen. After combustion in high temperature, the sample is melting, and the sulfur in sample, under the effect of carrier gas, generates sulfur dioxide. After the infrared pool absorbs the infrared energy

with specific wave length, we can calculate the integral value of sulfur dioxide according to the difference of the infrared energies before and after the absorption, and with pure oxygen as reference, and thus calculate the percentage composition of sulfur.

Sample preparation and sample quantity

Samples should be prepared into crumb shape, as fine and small as possible, and they should not be prepared into lump. Special processing and sample container must be used during processing procedure. The processed samples should be immediately put into a grinding mouth bottle so as to avoid greasy dirt and other impurities. When necessary, ether or acetone could be used for cleaning the samples, and then the absolute ethyl alcohol is used to rinse samples and dry it.

Due to the low sulfur content in IN718, ($S \leq 10\mu g/g$), if sample quantity is too less, the sulfur in the sample loses its representativeness, if sample quality is too much, the combustion will not be complete. Usually, the sample of 0.500g will be taken for measurement.

Selection of fluxing agents and their dosage

By examining the effect of various fluxing agents (such as tin grain, tungsten grain, and pure iron) on measurement result, we can conclude that, the different fluxing agents have different effects on the measurement process.

When adding tin grain, the pollution degree of combustion furnace and gas circuit will be increased notably. By selecting tungsten grain as fluxing agent, it can react with oxygen under the temperature of 400 ℃, and generates tungsten trioxide. The oxidation process will release large amount of heat, which immediately raises the temperature of samples in it and causes it to react. Meanwhile, volatilization of tungsten trioxide raises the speed of diffusion of the sulfur, which is conductive to the release of sulfur dioxide and the measurement of sulfur.

Ferric oxide, the product of combustion of iron, is featured with magnetism, and under the condition of high frequency, it can keep the combustion product in a meltdown state, which allows the complete release of SO_2. The disadvantage of pure iron fluxing agent is its high S blank value, usually $S \approx 0.0005\%$.

By summarizing the experiment result, this study selects composite fluxing agents: 2.000g tungsten-tin grain + 0.500g iron.

Experiment on selection of instrument parameters

Gas circuit may have a little amount of remaining SO_2 due to its absorption effect, which may cause variation of analysis results. It is necessary to use oxygen to blow and wash the gas circuit. If the time of the oxygen washing is too short, the effect is small; if the time of oxygen washing is too long, large amount of oxygen will be consumed. Therefore, the proper washing time should be identified. The oxygen washing time of this study is identified as 10 seconds.

The analysis result is directly proportional to the integral value of area of dissolution curve. The integral value of area involves the comparison level of analysis (also called cut-off level). If the cut-off level is set too low, it may cause the time extension of the analysis, and thus affect the blank value in the system. As a result, the precision of the analysis will be compromised. If the cut-off level is set too high, it may shorten the analysis time, which may cause incomplete combustion and incomplete collection of data signal. As a result, it may affect the precision and accuracy of the analysis result.

In the measurement of ultra-low sulfur in IN718, the cut-off level has relatively great influence on the result of the measurement due to relatively low releasing curve. The cut-off level of this study is set to be 4.

Complete collection of measured signals within the shortest analytical time is an indispensable condition for ensuring the precision of analysis. If the preset minimal analytical time is too short, it is likely to cause the loss of partial measured signals, and thus the reduce the analysis precision; if the preset minimal analytical time is too long, it may introduce noise signals, and cause relative high analysis result. It can be seen from the ideal releasing curve illustrated in Figure 1 that, the measured signals are completely collected after 40 seconds of analysis. Therefore, the minimal analytical time is set to be 40 seconds.

Purpose of selecting combustion conditions

The purpose of selecting combustion conditions is to allow the complete combustion and release of sulfur in the samples. Firstly, the ideal releasing curve must occur (see Figure 1). Meanwhile, after meltdown, the bottom of the crucible pot is smooth, and unmelted sample is not found in the molten mass (see Figure 2). If the analytical conditions are not correctly set, the multi-peak curve and trailing curve may occur, which may affect the analytical precision.

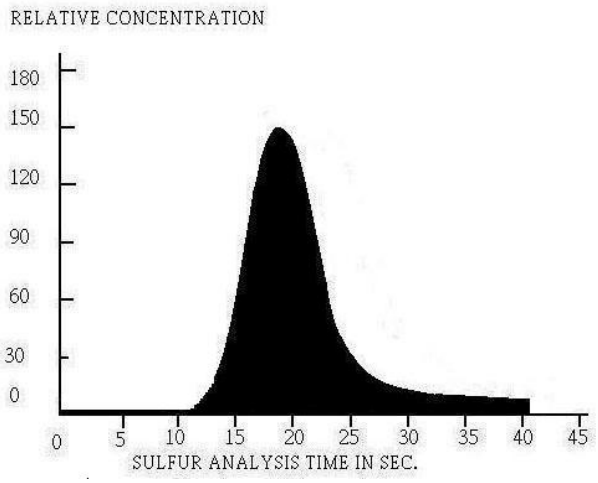

Figure 1 Ideal Releasing Curve

Figure 2 Smooth Bottom of Crucible Pot after Meltdown

Blank Control

If the measurement of ultra-low sulfur content does not deduct blank value, it may cause large error. The contents of ultra-low sulfur（S:1μg/g~10μg/g）in IN718 is in the same order of magnitudes with the sulfur content of fluxing agent and it is important to deduct blank value. Therefore, the measurement and deduction of blank values is a key technology to ensure the precision and accuracy of measurement of ultra-low sulfur in IN718.

Sources of blank values

Blank values mainly come from oxygen, crucible, fluxing agent, combustion system, instrument noise, etc.[6][7].

High purity oxygen is used and the trace amount of remaining SO_3 and SO_2 are absorbed by Soda asbestos. After measurement, the system blank in oxygen S＜0.3μg/g.

For the measurement of ultra low sulfur in IN718, blank processing of crucible is very important. This paper uses LECO special crucible, and it is heated in muffle furnace at 1000℃ for 4 hours, and cooling down to 200℃, and placed into dryer for storage. Before use, it needs to be heated in the muffle furnace at 1000℃ for 15 minutes and then taken out. After its color turns into white, the sample and the fluxing agent are placed into a processed crucible and they are kept in muffle furnace or resistance furnace at 420℃ for 5～10min. After processing, the blank value can be effectively reduced, and after the measured blank value S＜0.3μg/g.

Blank value brought by combustion system is caused by the imbalance of the adsorption and desorption of the whole system to sulfur. When the adsorption exceeds desorption, the measured result is relatively too low; when desorption exceeds adsorption, the measured result is relatively too high. Usually, preburning of 10 waste samples could reach the balance between adsorption and desorption.

It can be seen from the releasing curve (vertical coordinate is the relative concentration), the peak value of ultra-low sulfur release is usually no more than 200. Instrument noise may affect the measuring result. Usually it is reduced by selecting the above mentioned cut-off level and minimal analytical time.

In tungsten-tin grain fluxing agent, the sulfur blank S≈1μg/g. In pure iron fluxing agent, the sulfur blank S≈5μg/g.

Measurement of total blank value

There are three methods to measure blank values: cycle measurement[8], direct measurement[9] and indirect measurement[9].

Method of total blank value deduction

The total blank value measured by using cycle measurement method is entered into blank value field, and the instrument will make a automatic deduction.

Analysis and discussion of the experiment

Measurement of total blank value

This study uses cycle measurement method to measure the total blank value of sulfur[8].

Two standard substances of AR 673 [S:0.0011±0.0002] and LECO 502-348 [S:0.0008±0.0001] are selected, and 2.000g of tungsten-tin fluxing agent and 0.500g of pure iron fluxing agent are put into crucible. Parallel measurements of samples are conducted for 9 times according to the operation procedure. And the measurement result of the second time is illustrated in the Table 1.

Table 1. Second measurement result of the blank value %

	Blank value
Measured value	0.00010, 0.00009, 0.00013, 0.00011, 0.00008 0.00012, 0.00014, 0.00012, 0.00010
Average measured value	0.00011
Standard deviation	0.0000194
RSD	17.6

It can be seen from table 1, RSD=17.6, and the total blank value is stable. The total blank value of S:0.00011% is entered into the blank value field of the instrument, and the automatic deduction will be performed by the instrument.

Experiment on precision and accuracy

In order to examining the precision and accuracy of analysis, a standard substance AR 673(S:0.0011±0.0002%) calibration instrument is selected. The calibration result is illustrated in the Table 1. The measurements for additional three types of standard substances of ultra-low sulfur, and parallel measurement of each standard substance will be performed 9 times according to analytical procedure. The analytical result is illustrated in table 3.

Table 2 Result of Instrument Calibration

	AR 673
Standard value	0.0011±0.0002
Measured value	0.00105, 0.00112, 0.00109, 0.00115, 0.00107 0.00103, 0.00108, 0.00121, 0.00110
Average measured value	0.0011
Standard deviation	0.000055
RSD	4.96

Table 3 Precision and accuracy of standard substance measurement %

Standard substance	LECO 502-348	YSBC20171	Pure iron 4#
Standard value	0.0008±0.0001	0.00055	0.00045
Measured value	0.00089, 0.00080, 0.00077 0.00075, 0.00099, 0.00081 0.00088, 0.00093, 0.00083	0.00043, 0.00039, 0.00052 0.00050, 0.00040, 0.00042 0.00048, 0.00051, 0.00055	0.00037, 0.00034, 0.00038 0.00039, 0.00049, 0.00046 0.00035, 0.00041, 0.00037
Average measured value	0.00085	0.00047	0.00040
Standard deviation	0.000079	0.000058	0.000050
RSD	9.24	12.3	12.5

The experiment data from Table 2 and Table 3 shows that, the measured value of each analytical result is basically consistent with standard value of standard substance. Furthermore, the different between average value and standard value can meet the requirement of ASTMEl019[5] on analytical precision.

Sample analysis

Parallel measurements of three IN718 samples are performed 9 times separately, and the results are illustrated in the Table 4.

Table 4 Results of the IN718 Sample Measurement

Sample No.	1#	2#	3#
Measured value	0.00115, 0.00131, 0.00100 0.00101, 0.00121, 0.00098 0.00135, 0.00125, 0.00121	0.00066, 0.00077, 0.00087 0.00090, 0.00056, 0.00066 0.00088, 0.00075, 0.00074	0.00035, 0.00044, 0.00050 0.00028, 0.00040, 0.00036 0.00031, 0.00036, 0.00043
Average measured value	0.00116	0.00075	0.00038
Standard deviation	0.000138	0.000115	0.000068
RSD	11.9	15.4	18.0

It can be seen from the data of the Table 4, relative standard deviation is less than 20%, and the analytical precision is relative high, which demonstrates that, the infrared absorption method is a feasible method for analyzing ultra-low sulfur in IN718.

Sulfur Detection Limit

Total blank value of S:0.00011% is entered into the blank value field of the instrument, and the automatic deduction will be performed by the instrument. Then, without adding sample, fluxing agent is added to measure the sulfur content by simulating the analytical conditions, and it is called the measurement of blank value.

Table 5 Measurement of Blank Value

	Measurement of Blank value
Measured value	-0.00002, 0.00003, 0.00002, -0.00003, -0.00003 0.00000, 0.00003, -0.00003, 0.00004
Measued averave blank value $\overline{X}$	0.000001
Standaard diviation S	0.0000293

Sulfur detection limit $= \bar{X} + 3S = 0.0000011 + 3 \times 0.0000293 = 0.00009\%$. It can meet the analysis requirement of ultra-low sulfur（S:0.0001%~0.0010%).

Standard Addition Test

Recovery test is conducted by using standard addition method. Standard substance AR-673 [S:0.0011±0.0002%] is added into 0.200g of 2#IN718, and 0.5000g analytical quantity is entered. The test is performed according to the best condition identified above and the test result is illustrated in the Table 6.

Table 6. Recycled Volume and Recovery Rate

Sn.	AR-673 (S:0.0011±0.0002%) Add on Amount[g]	Added sulfur [μg]	Measured value [%]	Sulfur content [μg]	Recycled Sulfur [μg]	Sulfur recovery rate [%]
1	0.100	1.10	0.00054	2.70	1.20	109.1
2	0.200	2.20	0.00075	3.75	2.25	102.3
3	0.300	3.30	0.00096	4.80	3.30	100.0
4	0.400	4.40	0.00105	5.25	3.75	85.2
5	0.500	5.50	0.00137	6.85	5.35	97.3

In the table 6, the sulfur content in 0.200g of high strength stainless steel is calculated. According to the average value of 0.00075% of 9 times of measurement of 2#IN718 sample analysis, it is calculated as follows: $0.200g \times 0.00075\% = 1.5 \times 10^{-6}g = 1.5\mu g$;

It can be seen from table 6, the recovery rate is between 85% and 110%, which indicates that the accuracy of this method is relative high.

Conclusion

By using Carbon- Sulfur Analyzer, the infrared absorption method is used to analyze ultra-low sulfur, and the sample quantity is 0.500g. Total blank value of sulfur is measured by using cycle measurement method, and the result of 0.00011% is entered into the blank value field of the instrument to automatically deduct the blank. According to the measurement result of IN718, the data is processed. The RSD is between 7% and 17%, and the detection limit of this method is 0.00009%. The analysis result of this method meets the requirement of ASTM E 1019 on analysis precision and accuracy, and it is feasible in practice.

References

[1] Qi Huan, University of Michigan-Shanghai Jiao Tong University Joint Institute, Materials Engineering 2012.8, 92-100.

[2] Dong J X, Xie X S, Thompson R G, The influence of sulfur on stress-rupture fracture in INCONEL 718 superalloys Science. 2000 September; vol. 31A, no. 9: 2135-2144.

[3] Masatake Yamaguchi, Motoyuki, Hideo Kaburaki, Grain boundary decohesion by impurity segregation in a nickel-sulfur system, Science 307,393(2005).

[4] ISO 15350-2000 Steel and iron - Determination of total carbon and sulfur content - Infrared absorption method after combustion in an induction furnace (routine method).

[5] ASTM E1019-11 Standard Test Methods for Determination of Carbon, Sulfur, Nitrogen, and Oxygen in Steel, Iron, Nickel, and Cobalt Alloys by Various Combustion and Fusion Techniques.

[6] Yingyou Yang, Infrared absorption method for the determination of ultra low sulfur superalloy, Steel Technology, 1996,4(52).

[7] Ying Chen, The factors affecting of low carbon and sulfur with high-frequency infrared analysis, PTCA（PART B: CHEMICAL ANALYSIS）Vol.40 No.5 May 2004, 279.

[8] Jianhuan Wei, Huafeng Sun, Shengjie Yang, the cycle measurement of sulfur blank value with the CS-444 infrared ray carbon sulfur analyzer, Advanced Materials Research, Vals.399-401(2012) 2173-2176.

[9] Yingyan Tian, and Fanxiu Ye, and Yongxiang Shen, Monograph of Carbon and Sulfur Analysis, Metallurgical Industry Press, 2010, 21.

Advanced Materials Research Vols. 989-994 (2014) pp 121-124
© (2014) Trans Tech Publications, Switzerland
doi:10.4028/www.scientific.net/AMR.989-994.121

The Synthesis and Characterization of Polyphenylene Vinylene (PPV) Derivatives with Alkoxy Branched Chains

Zhang Xiao-zhoua, Wang Yu-weib

College of Materials Science and Engineering, Qiqihar University, Qiqihar, 161005,China

aemail: zhangxzh-n@163.com, bemail:wyw032378@163.com

Keywords: poly(p-phenylene vinylene); dehydrochlorination; luminescence polymer; fluorescence spectra

Abstract. Polyphenylene vinylene derivatives with various alkoxy branched chains, including PMOBOPV,PMOCOPV,iso-PMOCOPV and PMODOPV,were synthesized via a dehydrochlorination route,and characterized by FTIR,HNMR,DSC,TGA,UV-Visible and fluorescence spectroscopy. The result indicated that as-prepared polymers were of remarkable thermal stability and solubility in common solvent with the maximum UV absorption peak at ~492nm and light emission at ~555 nm.

Introduction

Conjugated organic polymers are a class of materials which possess not only the electrical and optical properties of traditional semiconductors, but also the mechanical and processing advantages of polymers. Among these, polyphenylene vinylene or PPV is studied intensively due to its strong photoluminescence (PL) at a wavelength ~2.2eV, which are very useful in photoelectronic applications, such as light emitting diode, first reported by Burroughes in 1990[1-3]. However, PPV with an unfunctionalized form is not readily put in liquid form, either by melting or by dissolving volatile solvents in a process to fabricate PPV-based films and fibers because of strong interactions between chains[4]. A resolution for the intractability is to add alky or alkoxy side chains to PPV backbones, which reduces the melting point of PPV and makes it more compatible with organic solvents. By increasing the length of side chains, the PL intensity can be enhanced because the long side chain prohibits the mobility of excitons towards recombination centers. Additionally, groups introduced in 2- and 5- positions with different structures decrease the crystallization of polymers and morphological defects[5]. However, it remains challenging to prepare PPV derivatives with a good solubility, controllable molecular weight (MW) and narrow MW distribution. Heeger et al. reported a dehydrochlorination process to synthesize soluble copolymer of PPV with short steps and facile operations[6].

In this work, four PPV derivatives were prepared by the dehydrochlorination of p-hydroxyanisole, which consist of a methoxyl group in position[2]and different alkoxy substitutes in position [5]. The influence of reaction conditions on the polymer yield is discussed. In this work, absolute AlCl3 was used as a Lewis acid catalyst to improve the yield and selectivity of chloromethylation. Moreover, the impact of alkoxy side chains on the propertie of as-prepared polymers, such as solubility, thermal stability and luminescence, are investigated.

Experiment

Measurement.1HNMR spectra were collected on a Bruker Avance 400 spectrometer with chloroform-d as solvent and tetramethylsilane as internal standard. FTIR spectra were recorded on a PerkinElmer Spectrum One B spectrometer. Thermogravimetric analyses (TGA) were conducted on a PerkinElmer Pyris Diamond thermogravimetric analyzer in a temperature range from 20 to 500 °C at the heating rate of 20 °C/min and calcined Al2O3 powder as the standard reference under nitrogen atmosphere. The molecular weight of PPV derivatives was measured by GPC (Waters 1515

GPC instrument, using styragel-1000 columns and tetrahydrofuran as a mobile phase). UV-Visible spectra were obtained on a Perkin-Elmer Lambda 35 Spectrometer in chloroform solution. Photoluminescence spectra were measured by a Hitachi F24500 fluorescence spectrometer in chloroform solution.

Reaction Equitions.

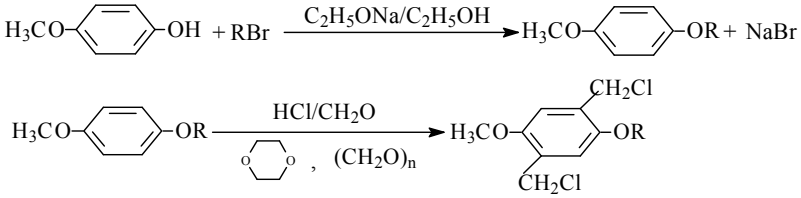

(R=n-C4H9, n-C8H17, iso-C8H17, n-C12H25)

Materials 1-methoxyl-4-alkoxy benzene(I). 0.05 mol p-hydroxyanisole and CH3CH2ONa/CH3CH2OH solution in a 250 ml were added into a four-neck flask (250 ml) equipped with a condenser and stirrer, and reacted at 80 °C in N2 under reflux for 90 min. A yellow solution was obtained and cooled to 20 °C. Then bromoalkane (n-Butyl bromide, n-Octyl bromide, i-Octyl bromide or n-Dodecyl bromide) were added dropwise into the yellow solution and reacted at 80 °C in reflux conditions for 5 h. After reaction, a reduced pressure distillation was used to separate EtOH from the red-brown solution obtained. The remnant were dissolved in 15% KOH solution and then extracted by ethyl ether. The oil layer was washed by 30 °C distilled water twice, heated to evaporate ethyl ether and dried by absolute MgSO4. The product I obtained was a yellowish solid in room temperature. The yield are 48, 57, 76 and 62%(wt) while using n-butyl bromide, n-octyl bromide, i-octyl bromide or n-dodecyl bromide to conduct the substitution reaction.

1,4-dichloromethyl-2-methoxyl-5-alkoxyl benzene (II). To as-synthesized I in a ice bath was added 50 ml 1,4-dioxacyclohexane, certain amount of formaldehyde, concentrated HCl and paraformaldehyde (the molar ratio of I, formaldehyde and concentrated HCl was ~ 1:10:10). The mixture was transferred to a four-neck flask, refluxed at 90 °C in the presence of absolute AlCl3 for 5 h, and then cooled to room temperature. A rotatory evaporation process was used for the removal of 1,4-dioxacyclohexane. The remant was treated by crystallization and a followed recrystallization in a mixture of n-heptane and ice methanol with a volume ration of 1:1. The white II powder could be obtained after separated from the solution by filter, washed by ethanol and dried in vacuums. The yield were 58,52,65 and 61%(wt) for 1,4-dichloromethyl-2-methoxyl-5-n-butyloxybenzene,1,4-dichloromethyl-2-methoxyl-5-n-Octyloxybenzene,1,4-dichloromethyl-2-methoxyl-5-i-octyloxybenzene,and1,4-dichloromethyl -2-methoxyl -5-dodecoxybenzene, respectively.

Poly (2- methoxyl-5-alkoxyl p-phenyl vinylene)(III). To a solution of 0.0025 mol II in 10 ml tetrahydrofuran(THF), was added dropwise a fresh potassium t-butoxide THF solution [(CH3)3COK:THF=1:1.6 (mole ratio)] in a three-neck flask (25 ml). The mixture was refluxed with N2 protection at 66 °C for 2 h. The color of solution changed gradually from colorless to yellow and to dark orange. Then 10 ml methanol was added to the mixture and reacted for 10 min. THF was removed by rotatary evaporation, and the III powder was washed successively with absolute ethanol and distilled water and separated by vacuum filtrations. The yield is 49% for poly (2-methoxyl-5- Butoxyl p-phenyl vinylene) (PMOBOPV, orange red), 54% for poly (2- methoxyl-5-octoxyl p-phenyl vinylene) (PMOCOPV, orange red),56% for poly (2- methoxyl-5- isooctoxyl p-phenyl vinylene) (iso-PMOCOPV, red) and 51% for poly (2- methoxyl-5- dodecoxyl p-phenyl vinylene) (PMODOPV, dark red).

PMOBOPV：1 HNMR，δ1.29 ~ 1.63（4H，methene），δ0.97（3H，methyl），δ4.68（2H，ethylene），δ6.98（2H，aromatic protons），δ7.26（3H，-OCH3），δ3.89（2H，-OCH2）；PMOCOPV：1 HNMR，δ1.22 ~ 1.80（12H，methene），δ0.88（3H，methyl），δ4.57（2H，ethylene），δ6.86（2H，aromatic protons），δ7.15（3H，-OCH3），δ3.89（2H，-OCH2）；iso-PMOCOPV:1 HNMR，δ1.18 ~ 1.80（9H， methene），δ0.82（6H，methyl），δ4.66（2H，ethylene），δ6.83（2H，aromatic protons），δ7.14（3H，-OCH3），δ3.69（4H，-OCH2）；PMODOPV:1 HNMR，δ1.26 ~ 1.77（18H，methene），δ0.89（3H，methyl），δ4.55（2H，ethylene），δ6.83（2H，aromatic protons，δ7.26（3H，-OCH3），δ3.92（2H，-OCH2）.

Results and Discussion

Substituent groups and solubility. To PPV derivatives with alkoxyl branched chains, the length of branched chains is helpful for the enhancement of solubility. Compared with PMOBOPV, PMOCOPV, and iso-PMOCOPV, PMODOPV (containing dodecoxyl groups) could be dissolved into THF faster. Since branched chains decrease the degree of order of the main chain in a polymer; asymmetric branched chains diminished the interaction between chains of PPV macromolecules, which contribute to a higher solubility of polymers in solvents. Therefore, the larger solubility of PMODOPV is attributed to its longer branched chains (dodecoxyl groups), worse symmetry due to different lengths of branched chains on 2-and 5- positions and lower crystallinity among four polymers. Additionally, it was found that four polymers could be dissolving in other solvents such as chloroform, tetrachloromethane, and toluene.

Molecular weight of polymers. GPC analysis revealed that the number average molecular weight (Mn) and weight average molecular weight (Mw) of the polymers are ~50000 with a polydispersity index (PDI) ~1 as shown in Table1. Such uniform molecular weight distributions are helpful for the fabrication of optical film.

Thermal stability of polymers. The thermogravimetric (TG) curves of four polymers are shown in Fig. 3. iso-PMOCOPV and PMOCOPV have similar TG curves with an initial thermo- decomposed temperature ~328 °C, which is close to that of PMOBOPV (~333 °C). By contrast, the initial thermo- decomposed temperature of PMODOPV is 159 °C, much lower than others. It implies that the increasing length of substituent groups detrimentally affects the thermal stability of polymers.

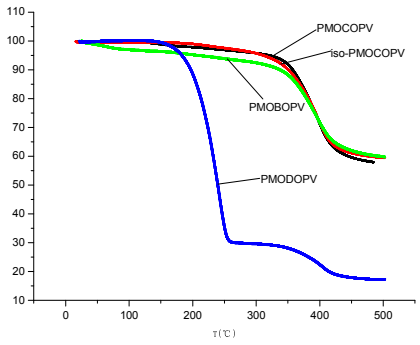

Table1. Molecular weight of polymers

Polymer	Mn	Mw	PDI
PMOBOPV	47214	47532	1.001
PMOCOPV	43339	48013	1.108
iso-PMOCOPV	55374	57362	1.036
PMODOPV	49215	51595	1.048

Fig.3. TG curves of different polymers

UV/visible absorption spectrum. The absorption peaks of UV/visible of polymers are determined by the length of conjugated chains and the electron effect of substituent groups in the benzene ring. Different side chains vary the bandgap, electron affinity, and ionization potential of polymers. For example, alkyl group, alkoxy group and other electron-donor group in the benzene ring can decrease the bandgap of PPV and cause an absorption redshift8. In this work, the maximum absorption is at 438 nm, 492 nm, 487 nm, and 492 nm for PMOBOPV, PMOCOPV, iso-PMOCOPV

and PMODOPV, respectively. Such an observation is consistent to the previous report that the absorption peak of PPV shifts from 420 nm (without substituents) to 490 nm (with alkoxy substituents).9These shifts are explained as being a result of the inductive electron withdrawing properties of the fluorine substitution leading to reduced electron density in the conjugated polymers and leading to an increase in the HOMO-LUMO band gap.The number of carbon atoms has no effect on the absorption spectrum if the side chain contains more than 5 carbon atoms.

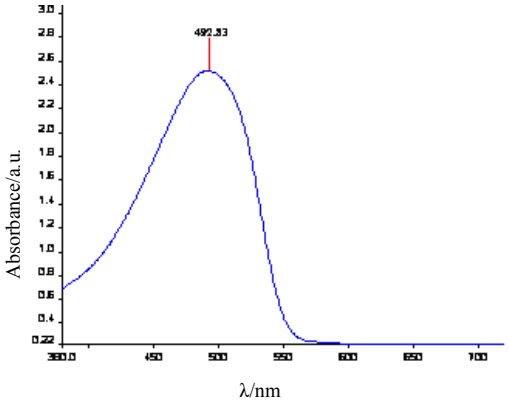

Fig.4. UV-Visible absorption spectrum of iso-PMOCOPV

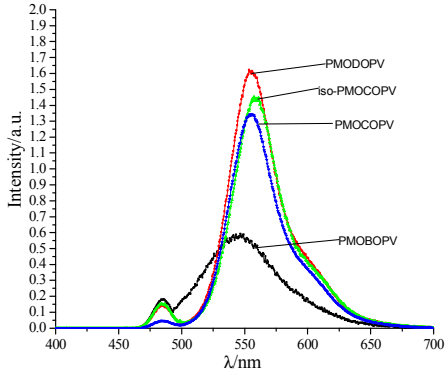

Fig.5. PL spectra of different PPV derivatives

Photoluminescence. The PL spectra of the dilute solutions of PPVs are shown in Fig. 5. The maximum emission of PMOBOPV occurs at 548 nm. PMOCOPV, iso-PMOCOPV and PMODOPV exhibit similar PL spectra with maximum emission at ~555 nm. Such a result indicates that the length of branched chains has little effect on the PL spectra of PPV with alkoxy substituents. Compared with the maximum emission (~540 nm) of PPV without substituents,6 red shifts were observed in PL spectra as shown in Fig. 5. It could be resulted from two reasons: the first, these PPV derivatives have longer conjugated chains. The dislocation π electrons can be excited by a relatively lower energy and cause red shifts in PL spectra; the second, an alkoxy substituent is of lone pair electrons and the π electron cloud approximately parallels a π orbit of the benzene ring. Such a structure is helpful to share π-electron conjugation and expand conjugated π systems, which causes red shifts in PL spectra.

Conclusions

In this work, four polymers, PMOBOPV, PMOCOPV, iso-PMOCOPV and PMODOPV, were synthesized by a strong base induced dechlorination process and characterized. The optimal conditions were 16:1:7 in the molar ratio of AlCl3/double ether/paraformaldehyde for the dechlorination reaction, and 2.6:1 in the ratio of potassium tert-butoxide/chlorben for the polymerization reaction. These PPV derivatives reveal good thermal stability, solubility in common organic solvents, and strong absorption and emission properties.

Reference

[1] Burroughes J H, Bradley DDC, Brown AR, et a1. Light-emitting diodes based on conjugated polymers [J]. Nature, 1990, 347:539~541.

[2] Hong-Ku Shim, Jung-Il Jin. Light-Emitting Characteristics of Conjugated Polymers[J]. Advances in Polymer Sience, 2002, 158:195~197.

[3] C. L. Gettinger, A. J. Heeger, J. M. Drake and D. J. Pine J. Chem. Phys. 1994, 101,1673-1678.

[4] Wang J Y, Li Y K, Hu W X, et a1. The synthesis and electronic characteristics of poly(p-Phenylene vinylene) [J]. Chin. Chem. Lett., 1998, 9(1) :75~77.

[5] Wang J Y, Li Y K, Hu W X, et al. The synthesis of soluble copolymer of poly(p-Phenylene Vinylene) [J]. Chin. Chem. Lett., 1998, 9(1):79~81.

[6] Braun D., Heeger A. J. .Electroluminescence from light-emitting diodes fabricated from conducting polymers[J]. Thin Solid Films, 1992, 216:96~102.

Advanced Materials Research Vols. 989-994 (2014) pp 125-129
© (2014) Trans Tech Publications, Switzerland
doi:10.4028/www.scientific.net/AMR.989-994.125

Comparison and Characterization of Two Preparation Methods of Graphene Oxide

Hongbo Liu [1,a*], Wuying Zhang[1], Feng Lin[1,b], Hongda Cao[1,2]

[1]School of Applied Chemistry and Biological Technology, Shenzhen Polytechnic, Shenzhen 518055, People's Republic of China

[2]Harbin Institute of Shenzhen Graduate School, Shenzhen 518055, People's Republic of China

[a]lhb206@163.com, [b]lfeng00@yahoo.com.cn

Keywords: preparation, characterization, method, graphene oxide

Abstract. The graphene oxides were prepared form graphite by thermal expansion and ultrasonic dispersion. The structure of graphene oxides was characterized by Fourier transform infrared spectrometer (FTIR), scanning electron microscope (SEM), X-ray diffraction (XRD) and Raman spectra. The difference of structure of graphene oxides by two preparation methods was compared. The measurement of FTIR and XRD showed the graphite was completely oxidized. The graphene oxide prepared by thermal expansion would lose large number of active functional groups, such as hydroxyl, carboxyl group, et al. However, the graphene oxide prepared by ultrasonic dispersion can retain these active functional groups. These active functional groups will be benefit to chemically modify the graphene oxides and prepare the polymer/graphene nanocomposites.

Introduction

Graphene sheets have attracted tremendous attention from both the theoretical and experimental scientific communities in recent years, due to its unique physical properties like superior mechanical properties, flexibility, high specific surface area, extraordinary thermal conductivity and excellent electronic transport properties [1,2].

Graphene, as the thinnest material known in the universe, is a single-atom-thick sheet of sp2-bonded carbon atoms in a hexagonal two-dimensional lattice. The promising mechanical, electrical, optical, thermal and magnetic properties of graphene have "led to the creation of a new and exciting 'laboratory' for the study of fundamental science." Graphene as a nanofiller, may be preferred over other conventional nanofillers. It has found applications as the key filler among the carbon-based nanofillers owing to high surface area, aspect ratio, tensile strength, thermal conductivity and electrical conductivity, flexibility, transparency [3,4].

When the graphene was dispersed in polymer as nanofiller, the polymer/graphene nanocomposites show superior mechanical, thermal, gas barrier, electrical and flame retardant properties compared to the neat polymer. However, the improvement in the physicochemical properties of the polymer/graphene nanocomposites depends on the distribution of graphene layers in the polymer matrix as well as interfacial bonding between the graphene layers and polymer matrix. Interfacial bonding between graphene and the host polymer dictates the final properties of the graphene reinforced polymer nanocomposite [4-8].

It is well known that the graphene is not compatible with organic polymers and it is difficult to form polymer/graphene nanocomposites. The graphene are heavily oxygenated to prepare the graphene oxide sheets. In contrast, the graphene oxide can alter the van der Waals interactions significantly and be more compatible with organic polymers because of its bearing hydroxyl, epoxide, diols, ketones and carboxyls functional groups [9-12]. For this reason, the graphene oxide has attracted considerable attention as a nanofiller for polymer nanocomposites. The surface chemical modification of graphene is an essential step for obtaining a molecular level dispersion of individual graphene in a polymer matrix [13].

Several preparation methods of graphene oxide were developed and researched in recent years, such as ultrasonic dispersion, thermal expansion, mechanical stripping, et al. The structure and properties of graphene oxide are different by those preparation methods. The structure and properties of graphene oxide will effect the surface chemical modification and the dispersion in the organic polymers. Then, it is important that the structure and properties of graphene oxide by different preparation methods are characterized. In this paper, the graphene oxide was prepared by ultrasonic dispersion and thermal expansion, its structure and properties were measured.

Experimental

Materials

Graphite, concentrated sulfuric acid, hydrogen peroxide, hydrochloric acid, potassium permanganate, sodium nitrate and barium chloride were supplied by Guangzhou Chemical Reagent Co., Ltd. N-methylpyrrolidone(NMP), N,N-dimethyl-formamide(DMF), acetone, dimethylbenzene were purchased from Shenzhen Baoyu Chemical Reagent Company. All the materials in this study were used as received without further purification.

Preparation of graphite oxide

The concentrated sulfuric acid（115ml，98%）and sodium nitrate（$NaNO_3$, 2.5g）were added in the beaker and were stirred under ice bath. Then the graphite was added when the temperature was below 5℃ in system and still stirred 30min. The potassium permanganate (15g) was slowly added and still stirred 60min under ice bath. The beaker was placed in constant temperature water bath at 40℃ and still stirred 30min, and the 220mL deionized water was added in the beaker. The temperature was controlled under 90℃. The hydrogen peroxide (5%，35ml）was added, and the color of solution was changed from brown black to light brown. The product was filtered and washed by 5% hydrochloric acid until the SO_4^{2-} didn't detect by barium chloride solution. Then the product was washed by deionized water and dried in the oven at 50℃.

Preparation of graphene oxide

The graphene oxide was prepared by ultrasonic dispersion and thermal expansion. The first method, the graphite oxide was placed in pipe furnace under nitrogen protection, and the temperature rise to 1050℃ for 1-2min. The graphene oxide was kept in the oven at 50℃. The second method, the graphite oxide was ultrasonic dispersed in water N-methylpyrrolidone (NMP), N,N-dimethyl-formamide(DMF), acetone and dimethylbenzene .

Measurement

The graphite oxide and graphene oxide were measured by Fourier transform infrared spectrometer (Analect RFX-65A, FTIR), scanning electron microscope (Hitachi S-3000H, SEM), X-ray diffraction (XRD-6100) and Raman spectra (Advantage 532).

Results and discussion

The FTIR spectra of graphite oxide is shown in Figure 1, There existed evident absorption peaks of C=O at 1720cm-1. The absorption peak of OH was at 3600 cm-1 and 1400cm-1. The stretching vibration peak of C-OH was at 1214cm-1, and the characteristic peak of C-O was at 1053cm^{-1}. The results in Fig. 1 showed that the graphite was oxidized.

The XRD of graphite and graphite oxide were showed in Fig. 2. The X-ray diffraction spectra of graphite showed that the diffraction peak was at 26.5°. The interplanar crystal spacing of graphite was 0.34nm by Bragg equation. The X-ray diffraction spectra of graphite oxide showed the peak of 26.5°was disappeared and the diffraction peak occurred at 10°, and the interplanar crystal spacing of graphite oxide was 0.94nm. The results accorded with the literature, and those proved that the graphite was completely oxidized.

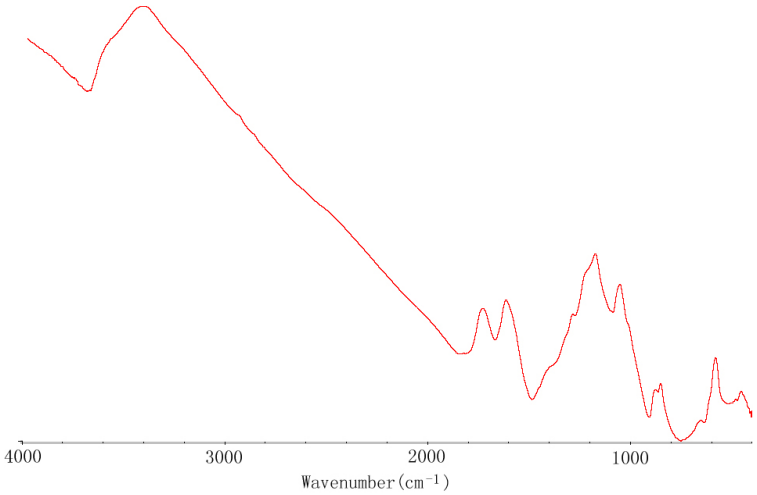

Fig. 1 The FTIR of the graphite oxide

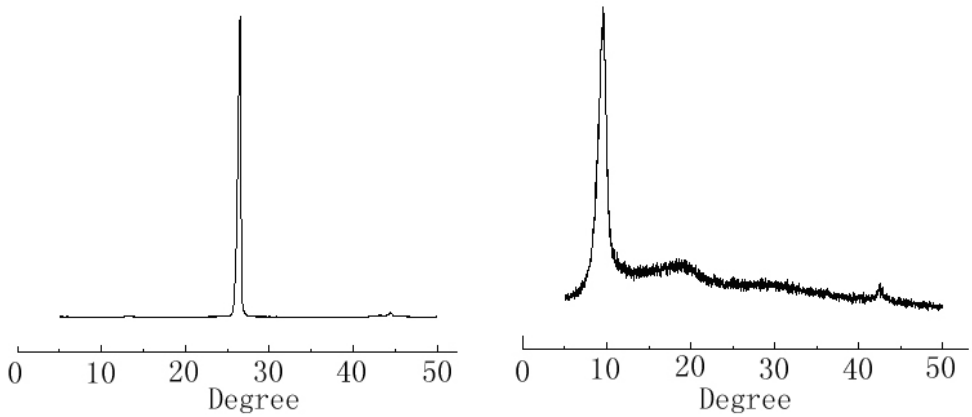

Fig. 2 The XRD of graphite and graphite oxide

The most important feature of two preparation methods of graphene oxide was the graphene oxide prepared by thermal expansion would lose large number of active functional groups, such as hydroxyl, carboxyl group, et al. The decrease of active functional groups in graphene oxide was disadvantage to chemical modification. However, it must choose the appropriate solvent to prepare graphene oxide by ultrasonic dispersion. The preparation of graphene oxide by ultrasonic dispersion indicated that the graphite oxide can be easily dispersed in water, N-methylpyrrolidone (NMP) and N,N-dimethyl-formamide (DMF), and dispersed solution stability was formed. But it was difficult to disperse in acetone and dimethylbenzene. The Raman spectra of graphene oxide were shown in fig. 3.

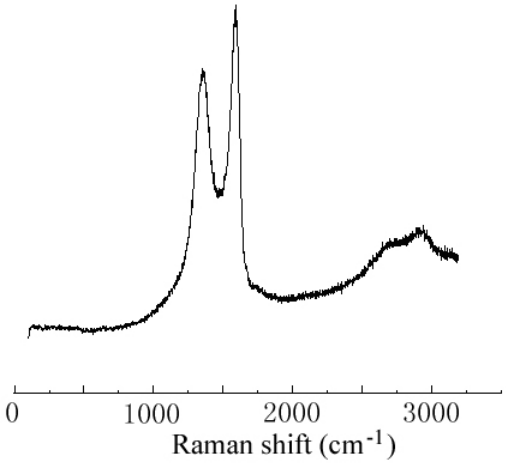

Fig. 3 The Raman spectra of graphene oxide

The graphene oxide prepared by ultrasonic dispersion and thermal expansion were characterized by XRD and SEM, and the measurement were shown in figure 4, figure 5, figure 6 and figure 7. The

structure of graphene oxide by two different preparation methods was significant difference. The diffraction peak of graphene oxide prepared by ultrasonic dispersion was 10°, but the diffraction peak of graphene oxide prepared by thermal expansion occurred at 20-30°. The SEM spectra indicated that the degree of separation was different. Generally, the degree of separation of graphene oxide prepared by ultrasonic dispersion was better than that of prepared by thermal expansion.

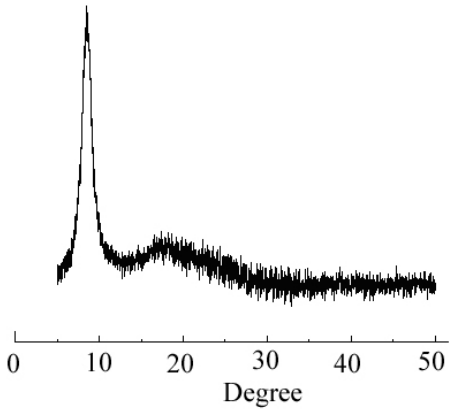

Figure 4 The XRD of graphene oxide prepared by ultrasonic dispersion

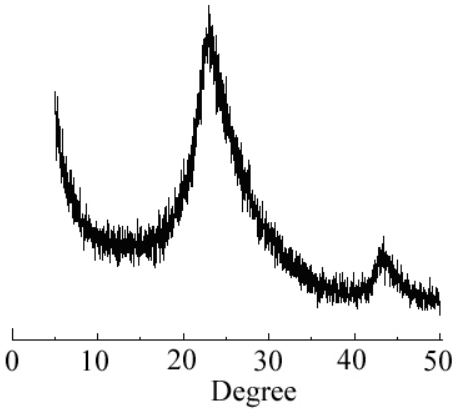

Figure 5 The XRD of graphene oxide prepared by thermal expansion

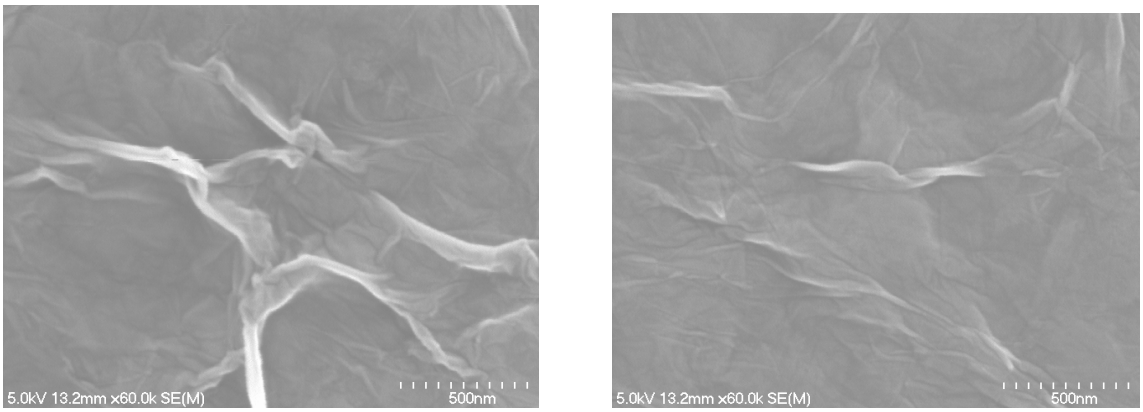

Figure 6 The SEM of graphene oxide prepared by ultrasonic dispersion

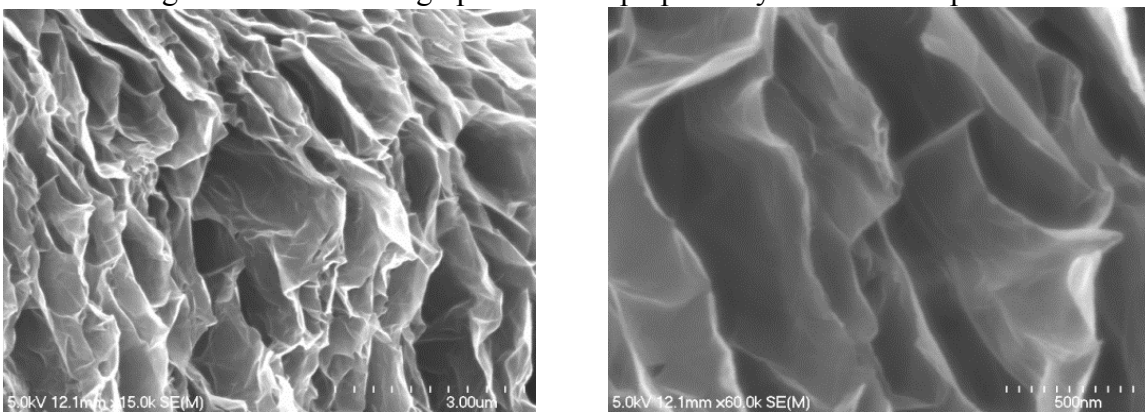

Figure 7 The SEM of graphene oxide prepared by thermal expansion

Conclusion

Some graphene oxides were prepared by thermal expansion, and other graphene oxides were prepared by ultrasonic dispersion in solvent, such as water, N-methylpyrrolidone (NMP), N,N-dimethyl-formamide (DMF), acetone, dimethylbenzene. The FTIR and XRD of the graphite oxide were measured, the results showed the graphite was completely oxidized. The Raman spectra, XRD and SEM of graphene oxides were tested. The results indicated that the structure of graphene oxides prepared by ultrasonic dispersion and thermal expansion was different. Those differences would

effect the chemical modification of graphene oxides. More work will do about the chemical modification of graphene oxides and the preparation of polymer/graphene nanocomposites.

Acknowledgements

This work was financially supported by the Shenzhen Science and Technology Foundation (JCYJ20120617140951133).

References

[1] K. P. Loh, Q. L. Bao, P. K. Ang, et al: J. Mater. Chem. Vol. 20 (2010), p.2277
[2] V. Nalla, L. Polavarapu, K. K. Manga: Nanotechnol. Vol. 21 (2010), p.415203
[3] K.P. Pramoda, H. Hussain, H.M. Koh, et al: J. Polym. Sci. Part A: Polym.Chem. Vol. 48 (2010), p. 4262
[4] T. Kuilla, S. Bhadra, D. Yao, et al : Prog. Polym. Sci., Vol. 35 (2010), p.1350
[5] S. Ansari, E.P.Giannelis: J. Polym. Sci. Part B: Polym. Phys. Vol. 47 (2009), p. 888
[6] T. Ramanathan, A.A. Abdala, S. Stankovich, et al: Nat. Nanotechnol. Vol. 3 (2008), p. 327
[7] Y.R. Lee, A.V. Raghu, H.M. Jeong, et al: Macromol. Chem. Phys. Vol. 210 (2009), p. 1247
[8] Y. Xu, Y. Wang, L. Jiajie, et al: Nano. Res. Vol. 2 (2009), p.343
[9] H. Becerril, J. Mao, Z. Liu, et al: ACS Nano. Vol. 2 (2008), p. 463
[10] A.K. Dikin, S. Stankovich, E.J. Zimney, et al: Nature. Vol. 448 (2008), p.457
[11] L. Vickery, A.J. Patil, S. Mann: Adv. Mater. Vol.21 (2009), p. 2180
[12] M.J. McAllister, J.L. Li, D.H. Adamson, et al: Chem. Mater. Vol.19 (2009), p. 4396
[13] S. Stankovich, D.A. Dikin, G.H.B. Dommett, et al: Nature. Vol.442 (2006), p. 282

Advanced Materials Research Vols. 989-994 (2014) pp 130-133
© (2014) Trans Tech Publications, Switzerland
doi:10.4028/www.scientific.net/AMR.989-994.130

Detection of Phase Purity of Sr_2FeMoO_6 by Raman Spectroscopy

Zhenfeng Xu[1, a], Qin Zhang[2, b],Suojia Yuan[2]

[1]Academic Affairs Office of Shandong Jiaotong University,
Jinan, 250357, People's Republic of China

[2] School of Science, Shandong Jiaotong University,

Jinan, 250357, People's Republic of China

[a]email: zhenfengxu@163.com, [b]email:zhangqin@sdjtu.edu.cn

Keywords: Raman Spectroscopy; Sr_2FeMoO_6

Abstract. The micro-Raman technique is used to examine the phase purity of Sr_2FeMoO_6 compound in this work. It is found that the Raman spectra of Sr_2FeMoO_6 compound without impurity consists of the peaks at about 440cm^{-1} and 620cm^{-1}. The broad peak and shoulder at 820-890cm^{-1} in the Raman spectra is assigned to the most common impurity $SrMoO_4$ and some other unidentified co-existing phases, which is approved by the results of X-ray diffraction.

Introduction

Double perovskite compound $A_2BB\acute{}O_6$ with A an alkaline earth and B, Ḃ two different transitional metals has been most studied since the discovery of large room-temperature low field magnetoresistance in Sr_2FeMoO_6 [1]. Crystal structure of Sr_2FeMoO_6 is known as cubic [2]or tetragonal [3] with the regular arrangement of the alternating FeO_6 and MoO_6 octahedra. Depending on the size of the A cations, the structure has been described as cubic (Ba_2FeMoO_6, crystal symmetry $Fm\bar{3}m$), tetragonal (Sr_2FeMoO_6, crystal symmetry $I4/m$) or monoclinic lattice (Ca_2FeMoO_6, crystal symmetry $P2_1/n$) [4, 5]. Band-structure calculations show that Sr_2FeMoO_6 is a half−metal [1], where the Mo t_{2g} spin-down sub-band (hybridized with the Fe t_{2g} spin-down sub-band) crosses the Fermi level, while the spin-up sub-band, essentially composed of Fe t_{2g} and Fe e_g states, is separated by an insulating gap.

For the potential application of Sr_2FeMoO_6 in spin devices, both large magnetoresistance and high Curie-temperature (T_C) are required. As reported in ref [6], the low-field magnetoresistance of Sr_2FeMoO_6 decreases linearly with the increasement of the concentration of anti-site defects (amount of Fe on Mo site or Mo on Fe site). Meanwhile, Park [7] and Aguilar [8] reported that anti-site defects could lower T_C of Sr_2FeMoO_6 to large degree. Therefore, anti-site defects bring large effects on the magnetic properties of Sr_2FeMoO_6. In order to obtain the Sr_2FeMoO_6 compound with higher degree of ordering (1-AS), researchers improves the preparation process of Sr_2FeMoO_6 little by little. Furthermore, doping method is also introduced to enhance the degree of ordering of Sr_2FeMoO_6 [9,10]. As a matter of fact, besides the factors mentioned above, purity of the compound is another important factor that affects on the degree of ordering. The lower the purity, the lower the degree of ordering. Generally, X ray diffraction is the most-common used method to detect the purity of the compound. Meanwhile the micro-Raman technique is also an useful method to analyze the phase of the ceramic compound. However, Raman spectra of Sr_2FeMoO_6 is rarely reported up to date. In this work, we synthesized Sr_2FeMoO_6 compound and detected the Raman spectra of the compound. It is found that the main Raman spectra of Sr_2FeMoO_6 consists of the peaks at about 420cm^{-1} and 620cm^{-1}, the spectra of the common impurity $SrMoO_4$ appears at about 840cm^{-1}.

Experimental

Polycrystalline Sr_2FeMoO_6 (SFMO) compounds were prepared by standard solid-state reaction. Stoichiometric powders of $SrCO_3$, MoO_3 and Fe_2O_3 were mixed, ground and fired at 900 ℃ for 5

hours in air. The pre-reacted mixture was then finely ground, pressed into pellets and sintered at 1280 ℃ in a stream of 5% H_2/Ar gas. The flow of the gas is controlled at 50mL/min and 30mL/min, the as-prepared compound is named as SFMO A and SFMO B.

Phase purity of the compounds was examined by X-ray diffraction (XRD) and micro-Raman technique. X-ray diffraction was carried out using a Bruker D8 Advance diffractometer with the 2θ range of 15˚-100˚. Raman spectra was measured on FTIR-7600 spectrometer with infrared emitter.

Results and discussion

Figure 1 (a) presents the XRD pattern of SFMO A compound. Evidently, SFMO A compound is of single phase without detectable impurity phases. The crystal symmetry is tetragonal lattice and the space group is I4/m. Owing to the ordering arrangement of Fe and Mo on B and B́ sites in perovskite structure, the superstructure reflection (101) at ~19˚is observed in our pattern. The Raman spectra of the phase-pure SFMO A compound was measured and the spectra is shown in Fig. 1(b). Two weak peaks are found at 440cm^{-1} and 620cm^{-1} respectivelly, and these two peaks should be assigned to Sr_2FeMoO_6 compound considering the nature of single phase of SFMO A compound. As reported by Son et al [11], the Raman spectra of Sr_2FeMoO_6 compound consists of the peaks and shoulders at about 770cm^{-1}, 620cm^{-1}, 440cm^{-1}, 390cm^{-1}, 290cm^{-1} and 210cm^{-1}, which is consistent with our results.

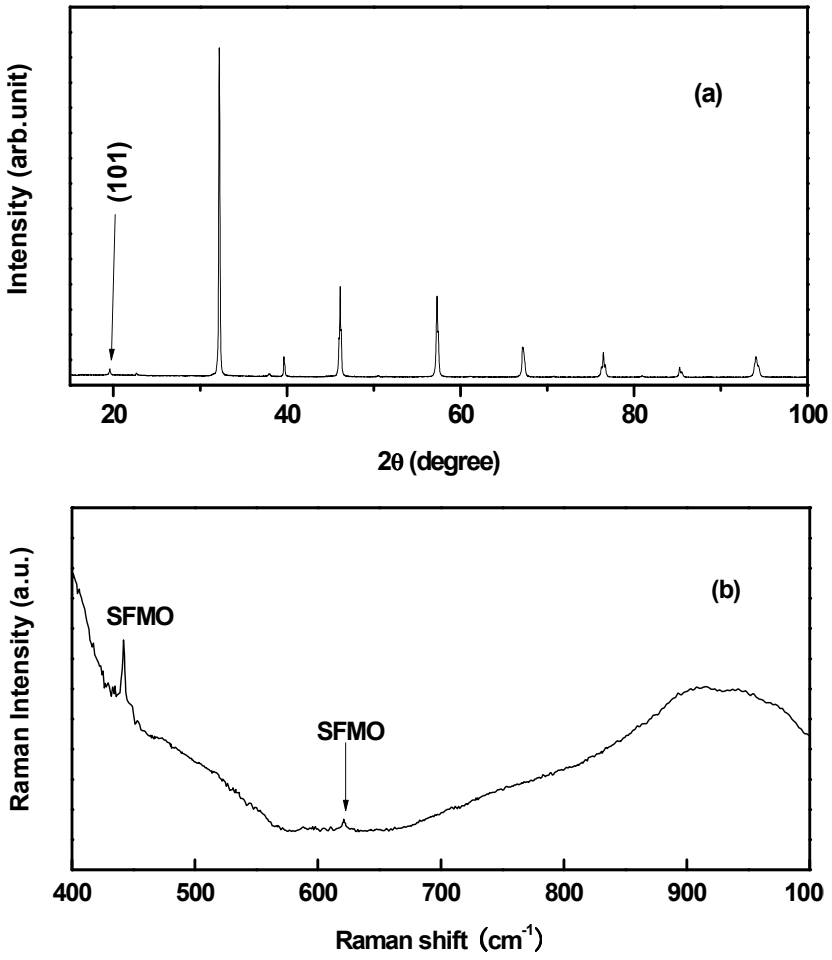

Figure 1 X-ray diffraction pattern (a) and Raman spectra (b) of SFMO A compound

Raman spectra of SFMO B compound is shown in Fig. 2(a). Different from the Raman spectra of SFMO A compound, another broad peak and shoulder at 820-890cm^{-1} are found besides the peaks at 440cm^{-1} and 620cm^{-1}. According to the results reported in ref [11], the peaks at 882.3cm^{-1}, 840.1cm^{-1} and 789cm^{-1} should be assigned to $SrMoO_4$, and other wide peaks and shoulders

probably due to $SrFeO_3$ and other unidentified co-existing phases. Therefore, the wide peak and shoulder observed in Fig. 2(a) maybe from $SrMoO_4$ and other unidentified co-existing phases. Consistent with the results of Raman spectra, besides the peaks from Sr_2FeMoO_6 double perovskite, the characteristic peak of $SrMoO_4$ at 27.5° is clearly observed in the XRD pattern of SFMO B compound (Fig. 2(b)).

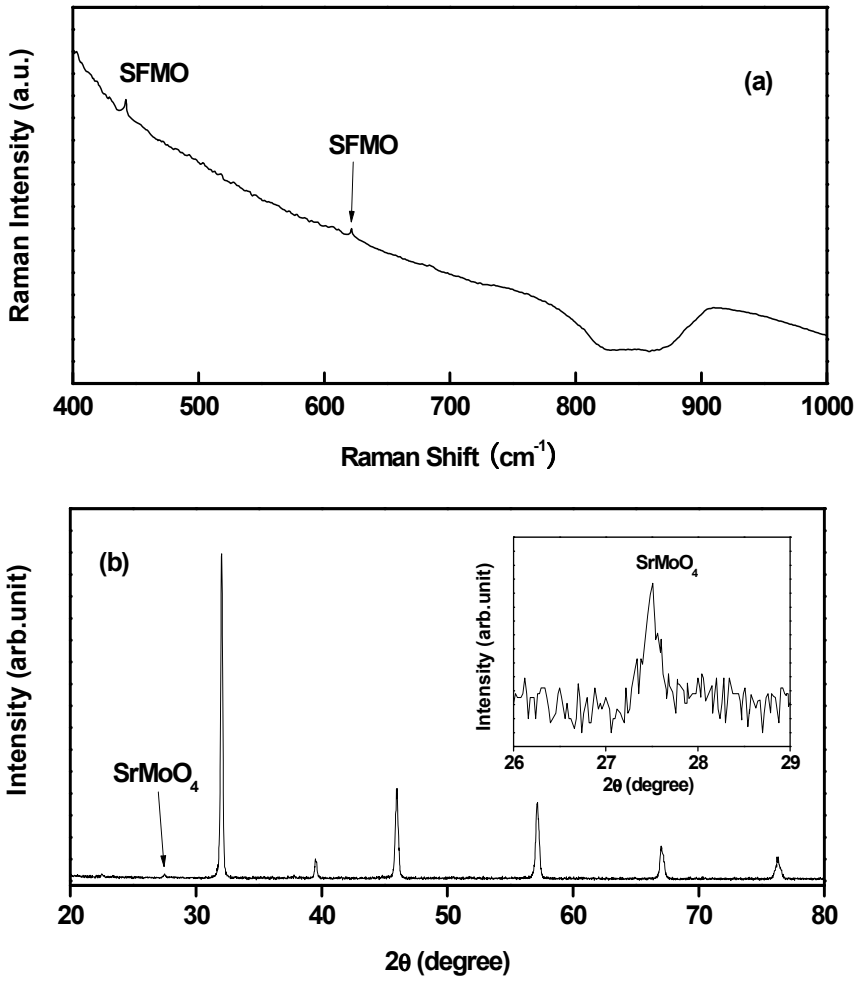

Figure 2 Raman spectra (a) and X-ray diffraction of SFMO B compound with impurity. Inset in (b) shows the enlarged pattern around 27°.

Conclusion

Both micro-Raman and X-ray diffraction technique are used to examine the phase of Sr_2FeMoO_6 compound. Consistent with the results of X-ray diffraction, the Raman spectra of phase-pure Sr_2FeMoO_6 consists of the peak at 440cm^{-1} and 620cm^{-1} with weak intensity. The Raman spectra of Sr_2FeMoO_6 compound with impurity is also examined in this work, it is found that another broad peak and shoulder at 820-890cm^{-1} is observed besides the peak at 440cm^{-1} and 620cm^{-1}, which is assigned to $SrMoO_4$ and other unidentified co-existing phases.

Acknowledgement

This work is supported by the National Natural Science Foundation of China (Grant No. 11304182).

References

[1] K.-I. Kobayashi, T. Kimura, H. Sawada, K. Terakura, Y. Tokura, Nature vol. 395 (1998) p. 677.

[2] F. K. Patterson, C. W. Moeller, and R. Ward, Inorg. Chem, vol.2, (1963) p.196.

[3] F. S. Galasso, F. C. Douglas, and R. J. Kasper, J. Chem. Phys, vol.44, (1966) p.1672.

[4] C. Ritter, M.R. Ibarra, L. Morellon, J. Blasco, J. García, and J.M. De Teresa, J. Phys.: Condens. Matter, vol.12 (2000) p.8295.

[5] R.P. Borges, R.M. Thomas, C.Cullinan, J.M.D. Coey, R. Suryanarayanan, L. Ben-Dor, L. Pinsard-Gaudart, A. Revcolevschi, J. Phys.: Condens. Matter, vol.11 (1999) p.L445.

[6] M. García-Hernández, J.L. Martínez, M.J. Martínez-Lope, M.T. Casais, and J.A. Alonso, Phys. Rev. Lett, vol.86, (2001) p.2443.

[7] B.J. Park, H. Han, J. Kim, Y.J. Kim, C.S. Kim, B.W. Lee, J. Magn. Magn. Mater. vol.272–276 (2004) p.1851.

[8] B. Aguilar, O. Navarro, M. Avignon, J. Microelectron. vol.39, (2008) p.560.

[9] Q. Zhang, G.H. Rao, Y.G. Xiao et al, Appl. Phys. A vol.84 (2006) p.459.

[10] X.M. Feng, G.H. Rao, G.Y. Liu, H.F. Yang, W.F. Liu, Z.W. Ouyang, L.T. Yang, Z.X. Liu, RC Yu, C.Q Jin, and J.K. Liang, J. Phys.: Condens. Matter, vol.14, (2002) p.12503.

[11] L.H. Son, N.X. Phuc, P.V. Phuc, N.M. Hong, L.V. Hong, J. Raman Spectrosc. vol.32 (2001) p.817.

Advanced Materials Research Vols. 989-994 (2014) pp 134-137
© (2014) Trans Tech Publications, Switzerland
doi:10.4028/www.scientific.net/AMR.989-994.134

A Novel Environment Friendly Material:Sucrose char sulfonic acid catalyzed Three-component Mannich reaction

Yuanyuan SHE[1,a], Xuanyan LIU[1], ZhigaoYANG[2]

[1]Hunan chemical vocational technology college, Zhuzhou 412004, China

[2]Hunan province ningxiang county long the first senior middle school, Changsha 410660

[a]email: yuanyuans_0@163.com

Key words: sucrose; solid sulfonic acid; β-amino ketone; Mannich; 2-Acetylpyrazine.

Abstract: Sucrose char sulfonic acid(SCSA) efficiently catalyzed the one-pot, three-component Mannich reaction of ketones, aromatic aldehydes and different amines in ethanol at 30℃ and afforded the corresponding β-amino carbonyl compounds in good to excellent yields . This method provides a novel and improved modification of the three-component Mannich reaction in terms of mild reaction conditions , clean reaction profiles and a simple workup procedure.

Introduction

The Mannich reaction is one of the most important fundamental carbon-carbon bond-forming reactions in organic chemistry for the preparation of secondary and tertiary amine derivatives [1]. The products of Mannich reaction are mainly β-amino carbonyl compounds and 1, 2-amino alcohol derivatives, which are valuable synthetic intermediates for the synthesis of drugs and biologically active compounds.[2] Though the study on Mannich reaction has developed over the past decades[3], the most straightforward and atom-economic route to β-amino carbonyl compounds is the direct three-component reaction[4] of aldehydes,amines and ketones. Solid sulfonic acid catalysts such as sulfonic acid resin,PS-SO_3H[5]and sulfonic groups functionalized silica materials[6]are always as an alternative for sulfuric acid. Recently,carbon-based solid acids,a novel and inexpensive solid acid with mild acidity,has emerged as a substituted for conventional acidic catalysts in different areas of organicsynthesis: esterification, hydrolysis, hydration,etc.[7] We reported the bamboo char sulfonic acid for acid catalyzed reaction of Claisen-Schmidt condensation between benzaldehyde and acetophenone[8].A series of biomass char sulfonic acid using saccharide molecules, bamboo sawdust,pine needles, etc. as raw materials have been prepared in our laboratory. High catalytic activity, low toxicity, moisture and air tolerance make biomass char sulfonic acid catalysts attractive.We report herein full details of a novel, convenient, and simple procedure to realize a one-pot three-component reaction of aldehydes,amines and ketones used sucrose char sulfonic acid as a green catalyst for the preparation of β-amino carbonyl compounds in ethanol.

Experimental

SCSA was prepared according to Xu Qiong's procedure[8]. The catalyst was separated in the first stage of the above work up procedure. The residue was washed with acetone and dried at 100℃ for 5 h to give pure SCSA for further runs.

A mixture of aromatic aldehyde, (2.0 mmol), amines (2.0 mmol), cyclohexanone (6.0 mmol) or 2-Acetylpyrazine. (2.0 mmol) and catalyst were stirred in anhydrous Ethanol (5 ml) at 30℃. After the reaction was completed, the mixture was cooled and then filtered to separate the solvent. The solid was washed twice with anhydrous ethanol and dissolved in CH_2Cl_2. Catalyst was removed by filtration., and filtrate was evaporated under vacuum condition. The crude product was purified via recrystallisation from anhydrous Ethanol to give the resulting product 4.

Spectral data of new products. 3-phenyl-3-(phenylamino)-1-(pyrazin-2-yl)propan-1-one (Table2,entry1),mp152-153℃,1HNMR(500MHz;$CDCl_3$;Me_4Si):δ9.23(d,1H,J=1.5Hz),8.79(d,1H,J=2.5Hz),8.69-8.68(m,1H,J=4.0Hz),7.48-7.46(m,2H,J=7.0Hz),7.36-7.33(m,2H,J=8.0Hz),7.26-7.23(m,1H,J=7.5Hz),7.11-7.08(m,2H,J=7.5Hz),6.68-6.65(m,1H,J=7.5Hz),6.56-6.54(m,2H,J=8.0Hz),5.09-5.

07(m,1H,J=5.0Hz,8.0Hz),4.63(s,1H),3.74-3.63(m,2H);3-(p-toluidino)-3-phenyl-1-(pyrazin-2-yl)propan-1-one(Table2,entry2),mp152-153℃;1HNMR(500MHz;$CDCl_3$;Me_4Si):δ9.19(d,1H,J=1.5Hz),8.76(d,1H,J=2.5Hz),8.65(m,1H,J=4.0Hz),7.44-7.42(m,2H,J=1.5Hz),7.32-7.29(m,2H),7.23-7.20(m,1H,J=7.5Hz),6.88-6.86(m,2H,J=1.5Hz),6.46-6.43(m,2H,J=8.5Hz),5.04-5.01(m,1H,J=5.0Hz,8.5Hz),3.67-3.59(m,2H),2.16(s,3H);3-(4-chlorophenylamino)-3-phenyl-1-(pyrazin-2-yl) propan-1-one (Table 2, entry 3), mp153-154℃,1HNMR(500MHz;$CDCl_3$; Me_4Si):δ9.21(d,1H,J=1.5Hz),8.78(d,1H, J=2.5Hz),8.66-8.65(m,1H,J=4.0Hz),7.42-7.40(m,2H,J=2.0Hz),7.33-7.32(m,2H,J=2.0Hz),7.26-7.22(m,1H,J=7.0Hz),7.02-6.99(m,2H,J=4.0Hz),6.46-6.45(m,2H,J=5.5Hz),5.00-4.98(m,1H,J=5.0Hz,8.5Hz),4.68(s,1H),3.72-3.58(m,2H);3-(4-nitrylphenylamino)-3-phenyl-1-(pyrazin-2-yl)propan-1-one (Table 2, entry4),mp127-128℃,1HNMR(500MHz;$CDCl_3$;Me_4Si):δ9.24-9.22(d,1H,J=1.5Hz),8.80(d,1H,J=2.0Hz),8.67-8.65(m,1H,J=4.0Hz),8.00-7.99(m,2H,J=9.0Hz),7.41-7.40(m,2H,J=2.5Hz),7.36-7.33(m,2H,J=5.0Hz),7.28-7.25(m,1H,J=4.0Hz),6.51-6.49(m,2H,J=9.0Hz),5.50(s,1H),5.14-5.12(m,1H,J=7.5Hz),3.83-3.60(m,2H),3-(4-methoxyphenyl)-3-(phenylamino)-1-(pyrazin-2-yl)propan-1-one(Table2,entry5),mp138-139℃;1HNMR(500MHz;$CDCl_3$;Me4Si):δ9.19(d,1H,J=3.5Hz),8.75(d,1H,J=2.5Hz),8.65(m,1H,J=3.5Hz),7.36-7.34(m,2H,J=9.0Hz),7.08-7.05(m,2H,J=7.5Hz),6.85-6.83(m,2H,J=8.5Hz),6.65-6.62(m,1H),6.54(m,2H,J=1.0Hz),5.02-5.00(m,1H,J=1.0Hz,8.0Hz),3.76(s,3H),3.70-3.61(m,2H),3-(p-toluidino)-3-(4-methoxyphenyl)-1-(pyrazin-2-yl)propan-1-one(Table2,entry6),mp139℃;1HNMR(500MHz;$CDCl_3$;Me4Si):δ9.18(d,1H,J=1.5Hz),8.74(d,1H,J=2.5Hz),8.64(m,1H,J=4.0Hz),7.35-7.32(m,2H,J=9.0Hz),6.88-6.87(m,2H,J=1.5Hz),6.84-6.82(m,2H,J=8.0Hz),6.46-6.44(m,2H,J=8.5Hz),5.03-5.00(m,1H,J=5.5Hz),3.76(s,3H),3.63-3.36(m,2H,J=8.0Hz),2.16(s,3H);3-(4-chlorophenylamino)-3-(4-methoxyphenyl)-1-(pyrazin-2-yl)propan-1-one(Table2,entry7),mp140℃;1HNMR(500MHz;$CDCl_3$;Me4Si):δ9.20-9.19(d,1H,J=1.5Hz),8.76(d,1H,J=2.5Hz),8.65-8.64(m,1H,J=4.0Hz),7.34-7.31(m,2HJ=9.0Hz),7.02-6.99(m,2H,J=4.0Hz),6.84-6.83(m,2H,J=9.0Hz),6.46-6.45(m,2H,J=5.5Hz),5.03-5.00(m,1H),3.76(s,3H),3.69-3.56(m,2H);3-(4-nitrylphenylamino)-3-(4-methoxyphenyl)-1-(pyrazin-2-yl)propan-1-one(Table2,entry8),mp121-122℃;1HNMR(500MHz;$CDCl_3$;Me_4Si):δ9.10(d,1H,J=1.5Hz),8.76(d,1H,J=2.5Hz),7.97-7.91(m,2H,J=7Hz),7.45-7.43(m,2H,J=9Hz),7.37-7.32(m,2HJ=9.0Hz),6.89-6.86(m,2H,J=1.5Hz),6.84-6.82(m,2H,J=8.5Hz),6.68-6.63(m,2H,J=2.5Hz),5.29-5.26(m,1H),3.76(s,3H),3.67-3.62(m,2H);3-(4-nitrophenyl)-3-(phenylamino)-1-(pyrazin-2-yl)propan-1-one(Table2,entry9),mp133-134℃;1HNMR(500MHz;$CDCl_3$;Me_4Si):δ9.23(d,1H,J=1.5Hz),8.82-8.72(m,1H,J=2.5Hz),8.67(d,1H,J=1.5Hz),8.19-8.18(m,2H,J=8.5Hz),7.66-7.65(m,2H,J=9.0Hz),7.27(d,1HJ=1.5Hz),7.10-7.07(m,2H,J=2.5Hz),6.70-6.67(m,1H,J=6.0Hz),6.49-6.47(m,2H,J=8.5Hz),5.15-5.14(m,1H,J=5.0Hz),4.74(s,1H),3.73-3.63(m,2H,J=5.0Hz,);3-(p-toluidino)-3-(4-nitrophenyl)-1-(pyrazin-2-yl)propan-1-one(Table2,entry10),mp151-152℃;1HNMR(500MHz;$CDCl_3$;Me_4Si):δ9.22(d,1H,J=1.5Hz),8.79(d,1H,J=2.5Hz),8.66(m,1H,J=1.5Hz),8.19-8.16(m,2H,J=2.5Hz),7.66-7.63(m,2H,J=4.0Hz),7.26-7.24(m,1H,J=5.5Hz),7.22-7.19(m,1H,J=6.5Hz),6.91-6.88(m,2H,J=4.0Hz),6.42-6.39(m,2H,J=2.0Hz),5.12-5.10(m,1H,J=7.5Hz),4.56(s,1H),3.71-3.62(m,2HJ=5.0Hz,),2.16(s,3H);3-(4-chlorophenylamino)-3-(4-nitrophenyl)-1-(pyrazin-2-yl)propan-1-one(Table2,entry11),mp148-149℃;1HNMR(500MHz;$CDCl_3$;Me_4Si):δ9.23(d,1H,J=1.0Hz),8.81-8.80(d,1H,J=2.5Hz),8.67-8.66(m,1H,J=3.5Hz),8.20-8.18(m,2H,J=6.0Hz),7.63-7.62(d,2H,J=9.0Hz),7.05(m,2H,J=2.0Hz),6.42-6.40(m,2H,J=4.0Hz),5.10-5.07(m,1H,J=3.0Hz),4.78(s,1H),3.73-3.62(m,2H,J=14.0Hz);3-(4-chlorophenylamino)-3-(4-nitrophenyl)-1-(pyrazin-2-yl)propan-1-one(Table2,entry12),mp159-160℃;1HNMR(500MHz;$CDCl_3$;Me_4Si):δ9.25-9.24(d,1H,J=1.0Hz),8.84-8.83(d,1H,J=2.5Hz),8.68-8.67(m,1H,J=4.0Hz),8.41-8.39(m,2H,J=8.5Hz),8.23-8.22(m,2H,J=3.5Hz),8.02-8.01(m,2H,J=6.0Hz),6.64-6.62(m,2H,J=9.5Hz),5.68(s,1H),5.20-5.18(m,1H,J=3.0Hz),3.83-3.68 (m,2H,J=7.0Hz)

Results and discussion

Initially, the three-component Mannich reaction of benzaldehyde(2.0 mmol) , aniline(2.0 mmol) , and cyclohexanone(6.0 mmol) was examined(Scheme 1). Several solvents were screened in the model reaction. The results of extensive acid and solvent screening and optimization are shown in Table 1. Interestingly, the Mannich reaction showed an intriguing solvent effect, In ethanol gave a yield of 91%(entry 1) which was higher than that in CH3CN, ethyl acetate, CH2Cl2 . And we

pleasantly surprised found that Mannich reaction with solvent-free and in water gave the yield which was slightly lower than in Ethanol (entres 6, 10) .

We also screened different common sulfonic groups catalysts for their ability to catalyzed the three-component Mannich type reaction. The amount of catalysts used equaled acid capacity of SCSA. Results are depicted in Table 1(entries 1-5). It is clearly that the yield of Mannich base in the presence of sucrose char sulfonic acid is higher than that of either typical acid catalyst, This novel catalyst are high activity, simplicity of preparation method, low cost, wide availability of raw materials which can be a benefit for its extensive application in organic synthesis reactions.

Table 1 Influence of catalysts and solvent on the Mannich reaction of aromatic aldehydes, aromatic amines and cyclohexanone [a]

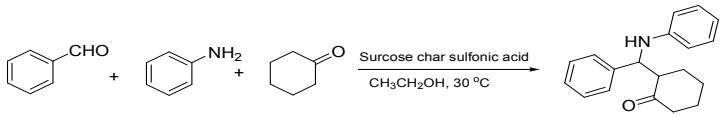

entry	catalyst	solvent	**I**solated yield/%
1	SCSA	Ethanol	91
2	sodium bisulfate	Ethanol	83
3	sulfamic acid	Ethanol	87
4	sulfonic resin	Ethanol	69
5	paratoluenesulfonic acid	Ethanol	84
6	SCSA	None	86
7	SCSA	Ethyl acetate	68
8	SCSA	CH_2Cl_2	57
9	SCSA	CH_3CN	56
10	SCSA	water	79

[a] Benzaldehyde(2.0 mmol) , aniline(2.0 mmol) , and cyclohexanone(6.0 mmol), 4% mol catalyst, r.t. 6 h

Encouraged by the remarkable results obtained with the above reaction conditions, and in order to show the generality and scope of this new protocol. We further surveyed the scope of arylaldehydes and amines in the direct Mannich reactions in the presence of 8 mol % SCSA as the catalyst and the results were summarized in Table 2. Table 2 clearly demonstrates that SCSA are excellent catalysts for Mannich reactions in ethanol. Thus, a variety of aromatic aldehydes and amines, including electron-withdrawing and electron-donating groups, were tested using our new method in ethanol in the presence of SCSA. In Table 2, it seemed that there was no remarkable electronic effect from the substituents at aldehyde moiety, since aryladehydes with both electron-donating groups like $-OCH_3$ (Table 2, entries 5-8,) and electron-withdrawing groups like $-NO_2$ (Table 2, entries 9-12) could be applied as efficient candidates for the direct Mannich reaction at 30℃ to offer the expected β-amino carbonyl compounds good yields. The scope of our method was extended to other amines. In the case of amines having an electron-donating group, such as 4-methylaniline(entry 2), the corresponding β-amino carbonyl compounds were obtained good yields. Furthermore, amines with electron-withdrawing groups, such as 4-nitrylaniline(entry 4) gave the desired product in low yield.

Table 2 One-pot three-component Mannich reaction of aromatic aldehydes, aromatic amines and 2-Acetylpyrazine in sucrose char sulfonic acid catalytic system

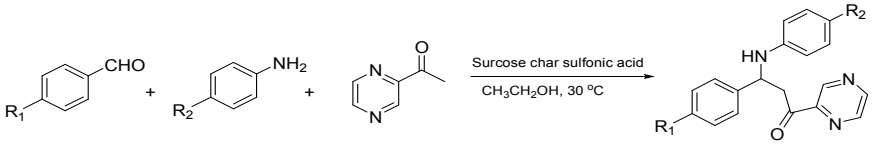

entry	R_1	R_2	Isolated yield/%
1	-H	-H	67
2	-H	- CH_3	73
3	-H	- Cl	59
4	-H	- NO_2	45
5	-OCH_3	-H	55
6	- OCH_3	- CH_3	74
7	- OCH_3	- Cl	48
8	- OCH_3	- NO_2	33
9	-NO_2	-H	69
10	- NO_2	- CH3	67
11	- NO_2	- Cl	57
12	- NO_2	- NO_2	66

Reaction conditions : aldehyde (2.0mmol), amine (2.0 mmol), 2-acetylpyrazine (2.0 mmol), catalyst(4 mol %), CH_3CH_2OH (3 ml), 30 ^oC

Finally, the recycling performance of SCSA was investigated using the three-component Mannich reaction of benzaldehyde, aniline and cyclohexanone. The yields of Mannich base were 91%, 88 %, 87%and 86%. respectively, which showed good reusability of this catalyst. The weight of catalyst increased slightly and no sulfate ion was detected in reaction mixture after each reaction which indicated that reactants or products may deposit in catalyst . Compared with the traditional solvents and catalysts, the easy recycling performance is also an attractive property of the SCSA for the environmental protection and economic reasons.

Conclusion

In summary, we herein described an originally and effectively SCSA catalyzed protocol for the construction of β-amino ketones via three-component direct Mannich reaction. The merit of this methodology is simple, mild, efficient and the raw materials are cheap . Therefore, we believe that the work reported here would have potential application in green chemistry.

Acknowledgements

In this paper, the research was sponsored by the Nature Science Foundation of Hunan chemical vocational technology college (Project No.hnhyB007) .

References

[1] (a) M.Arend, B.Westermann,N. Risch, Angew. Chem. Int. Ed. 37, (1998) 1044; (b) S. Kobayashi, H. Ishitani, Chem. Rev. 99 (1999) 1069; (c) A. Cordova, Acc. Chem. Res. 37 (2004) 102.
[2] (a) Muller, R.; Goesmann, H.; Waldmann, H. Angew. Chem., Int. Ed. 1999, 38, 184
[3] (a) Josephsohn,N.S.; Carswell, E.L.; Snapper, M.L.; Hoveyda,A.H.*Org. Lett*. **2005**, *7*, 2711. (b) Urbaniak,M.;Iwanek,W.*Tetrahedron* **2006**, *62,* 1508. (c) Hasegawa,A.; Naganawa,Y.; Fushimi, M.; Ishihara,K.; Yamamoto,H.Org. Lett., **2006**, *8*, 3175; (d) Yi,W.B.; Cai, Ch. *J. Fluorine Chem.* **2006**, *127*, 1515; (e) Fang, D.; Luo, J.; Zhou, X. L.; Liu, Z.L. *Catalysis Lett*, **2007**, *116*, 76
[4] (a) Ollevier,T.;NadeauE.;Guay-BeginA.Tetrahedron Lett.2006,47,8351;(b)Azizi,N.; Torkiyan,L.; Saidi, M. R. Org. Lett., 2006, 8 ,2079; (c) Hirose,T.; Sunazuka, T.;Yamamoto,D.;Kaji E.;Omura S. Tetrahedron Lett. 2006, 47, 6761; (d) Wu, M.;Jing, H.W.;Chang,T. Catal. Commun. 2007, 8, 2217
[5] Iimura, S.; Nobutou, D.; Manabe, K.; Kobayashi, S. Chem. Commun. 2003, 1644
[6] Hui Wu, Yang Shen, Li-yan Fan. Tertahedron. 2007, 63, 2404
[7] (a)Atsushi Takagaki , Masakazu Toda , Mai Okamura , Junko N. Kondo , Shigenobu Hayashi , Kazunari Domen , Michikazu Hara*; catal today. 2006, 116, 157-161; (b) Michikazu Hara,* Takemi Yoshida, Atsushi Takagaki, Tsuyoshi Takata, Junko N. Kondo, Shigenobu Hayashi, and Kazunari Domen. Angew. Chem. Int. Ed. 2004, 43, 2955
[8] Qiong Xu,; Zhigao Yang ;Dulin Yin ; Feng Zhang. Catal. Commun.2008, 9,1579

Advanced Materials Research Vols. 989-994 (2014) pp 138-141
© (2014) Trans Tech Publications, Switzerland
doi:10.4028/www.scientific.net/AMR.989-994.138

Investigation of sewage sludge anaerobic digestion performance using peracetic acid as a pretreatment

Na Wei

School of Civil Engineering and Architecture; Wuhan Polytechnic University, Wuhan, 430023,

email: weina31@126.com

Keywords: Peracetic acid, sewage sludge, pretreatment, biomass material

Abstract: Sewage sludge is difficult to degrade in anaerobic digestion systems and pretreatments have been shown to speed up the hydrolysis stage. In this paper sludge anaerobic digestion experiments with peracetic acid as a pretreatment were carried out and the effects of acid pretreatment using peracetic acid on subsequent digestion were investigated. It has been proved that this treatment effectively leads to a solubilisation of organic material and thus leads to a increase of soluble chemical oxygen demand(SCOD) and volatile fatty acids(VFA)concentration. Besides, the SV of sludge was reduced and the settling characteristics of sludge were improved. But high dosage of peracetic acid lead to a decrease in biogas production and the proper dosage was 20 g/kg DS. It can be concluded that sludge anaerobic digestion with peracetic acid pretreatment is an effective method for biomass material transformation.

Introduction

Sewage sludge is the main waste from the urban wastewater treatment process and the amounts of this residue are increasing in many parts of the world[1]. So far, sewage sludge has been disposed off by some methods, such as soil application [2][3], anaerobic digestion[4] and landfilling [5]. As one kind of biomass materials, sludge anaerobic digestion produces biogas and reduces the amount of organic matter. Treatment of sewage sludge via anaerobic digestion has been carried out widely and technology has recently received increased interest in many countries due to the renewable energy it can produce.

However, anaerobic digestion has some limitations, such as the length of time it takes for the sludge to be digested and the ineffectiveness of totally breaking down the solids. Various pretreatment technologies have been suggested in the literature as solutions for overcoming these limitations and for improving the biogas production rate [6-8]. Methods that were previously studied include chemical, mechanical and thermal treatments [9-10]. In the past, several oxidants have been applied to break down sewage sludge, although only few have been combined with anaerobic digestion [11]. Peracetic acid is an useful oxidant and it has many applications in the medical and food industry as a disinfectant and in water purification as an oxidizing agent. The main advantage is that no toxic degradation products are formed.

In this paper, the effect of peracetic acid on anaerobic digestion of sewage sludge was studied. The objectives of this research were finding out the function of peracetic acid pretreatment on anaerobic digestion of sewage sludge and bio-hydrogen production. Besides, the settling characteristics of sludge were also examined.

Materials and Methods

Sludge sample:The sewage sludge used was collected from the Wastewater Treatment Plant of Hanxi, Wuhan city and stored at 4℃ before use. The main characteristics of sludge are listed in Table 1.

For the treatment, a 1L sludge sample was introduced in a breaker, and an appropriate amount of peracetic acid was added. A dose range between 10 and 60g peracetic acid /kg dry solids(DS) was applied to the sludge. The sludge was gently stirred by a magnetic stirrer during the reaction. A

Table 1. Main characteristics of the sewage sludge.

Moisture %	Total solid(TS) mg/L	PH	Organic matter %
98.5	20200	7.07	79.5

release of soluble chemical oxygen demand (SCOD) due to this stirring was not expected because of its gentle nature.

Compositional analysis: The following components were analysed before and after pretreatment: SCOD, and concentration of volatile fatty acids(VFA). SCOD and DO were analyzed using a HACH DR/2000 spectrometer(Hach Company, USA). VFA concentrations were analyzed by a High Performance Liquid chromatograph(GP40, Dionex, CA) with an absorbance detector(AD20, Dionex) and a 300 mm-7.8mm Metacarb 67H column(Varian, CA) using 0.05 M H2SO4 as mobile phase.

The settling characteristics of sludge: Settling velocity(SV) is one of sludge's most important settling parameters in routine process control. SV was calculated as the volume ratio of concentrated sludge to the initial sample after 30min settlement in a 100ml measuring cylinder.

Results and Discussions

Variation of SCOD and VFA concentration： Fig. 1 shows the effect of the peracetic acid treatment on the SCOD concentration in the sludge. As organic matter in the sludge was degraded during the treatment, with the increase of peracetic acid dosage, a obvious increase of SCOD was noticed. However, for the dosage of 40 and 60g/kg DS, the concentration of SCOD decreased after 3h treatment. This may be attribute to the oxidation reaction between the liquid organic matter in sludge and incompletely reacted peracetic acid. It can be concluded that high concentration of peracetic acid is not needed and it may even affect the methane yield in anaerobic digestion as the decrease of SCOD in sludge. In this experiment, the economic dosage of peracetic acid was 20g peracetic acid/kg DS. After 12h treatment, the VFA concentration of sludge in the dosage of peracetic acid of 10g/kg DS, 20g/kg DS, 40g/kg DS, 60g/kg DS was 675mg/L, 993mg/L, 4653 mg/L and 8910mg/L. The large increase in VFA concentration is due to the partial oxidation of organic matter to VFAs. It appears that the oxidative strength of the treatment is sufficient to result in an effective oxidation. Besides, the large increase in VFA concentration is also due to the addition of peracetic acid mixture.

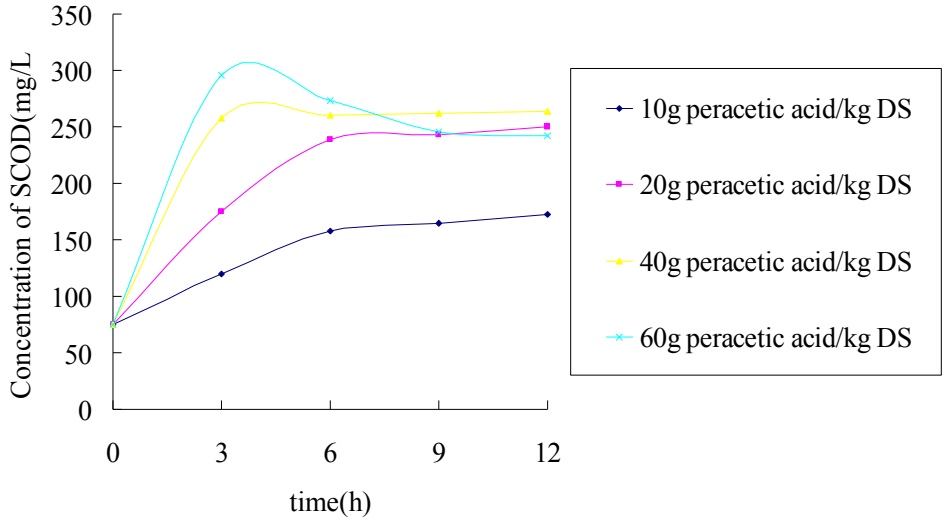

Fig. 1 SCOD of treated sludge as a function of time

Methane yield in anaerobic digestion： Fig.2 shows the biogas production (in mL/L) at the dosage of 20g/kg DS as a function of time. Methane production, the major result of anaerobic

digestion, was markedly increased. However, applying high dosage even leads to a significant lower biogas produciton. Although higher concentrations leads to a high sludge sulubilisation and hence a large availability of highly biodegradable organic matter, these soluble organics are not further converted into extra biogas. Thus, high dosage of peracetic acid was not needed for sludge anaerobic digestion.

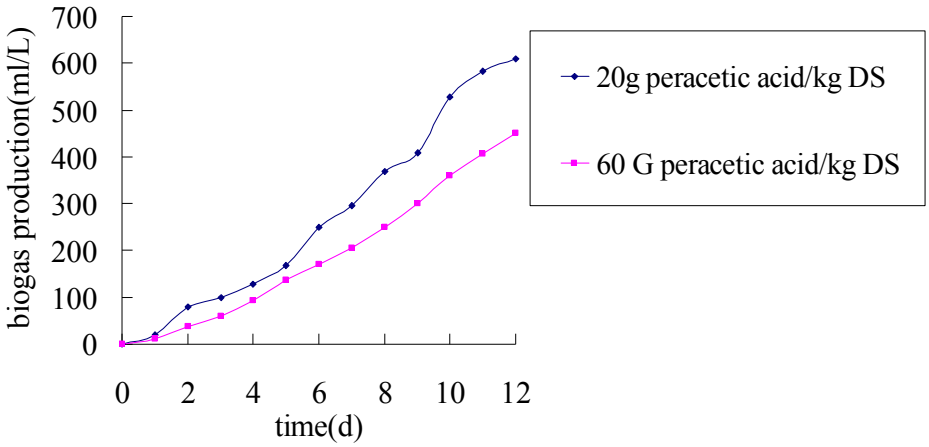

Fig.2 Biogas production of sludge as a function of time

Effect of ultrasonic pretreatment on sludge settling characteristics： In order to evaluate effect of the ultrasonic pretreatment on sludge settling characteristics, one parameters of sludge, namely, SV was studied. Fig.3 shows the trend of changes of SV of treated(with the dosage of 20g/kg DS) and untreated slduge. According to this graph, sludge using ultrasonic waves reduces SV and therefore, improves the settling characteristics of the sludge.

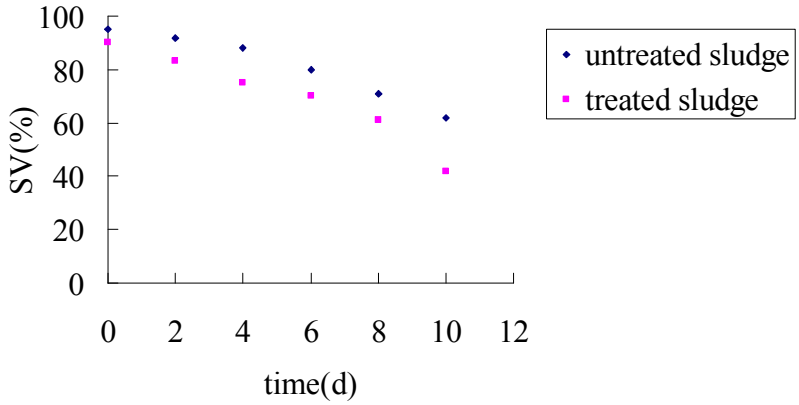

Fig. 3 SV of treated and untreated sludge as a function of time

Conclusions

1. The pretreatment of sludge by peracetic acid has a significant effect on the sludge biodegradability during the anaerobic digestion that increases the SCOD and VFA concentration as well as biogas generation.

2. The settling characteristics of sludge was also improved.

3.The higher dosage of peracetic acid may lead to lower biogass production and a proper dosage was 20g/kg DS.

Acknowledgement

In this paper, the research was sponsored by the Introduced Talent Support Project of Wuhan Polytechnic University, China(Project No.2010RZ08) the Scientific Technology Research Project of Education Department of Hubei Province, China (Project no.Q20131701).

References

[1] Magdalena S.; Morgan F., Michael M., William, A. P., Jefferson T. Environmental assessment of supercritical water oxidation of sewage sludge [J]. Resources, Conservation and Recycling, 2004 (41) 321-338.

[2] MLimin Ma, Houran Sun, Ling Chen, Jian Zhao. Relation between heavy metal fraction in soils and plants enrichment in pilot scale experiment on land application of sewage sludge [J]. Food, Agriculture and Environment. 2011:9 (3-4) 967-973.

[3] Osmetullah Arvas, Seyda Zorer Celebi, lbrahim Hakki Yilmaz. The effect of sewage sludge and chemical fertilizer on natural pasture's yield and botanical composition [J]. Food, Agriculture and Environment. 2011:9 (2) 525-530.

[4] lgoni A.H., Abowei M.F.N., Ayotamuno J.M., Eze C.L. Effect of total concentration of municipal solid waste in anaerobic batch digestion on the biogas produced [J]. Food, Agriculture and Environment. 2007:5 (2) 333-337.

[5] Inga Herrmann, Malin Svensson, Holger Ecke, Jurate Kumpiene, Christian Maurice, Lale Andreas, Anders Lagerkvist. Hydraulic conductivity of fly ash-sewage sludge mixes for use in landfill cover liners [J]. Water Research. 2009: 43(14), 3541-3547.

[6] Lise Appels, Jan Degreve, Bart Van der Bruggen, Jan Van lmpe, Raf Dewil. Influence of low temperature thermal pre-treatment on sludge solubilisation, heavy metal release and anaerobic digestion [J]. Bioresource. Technology]. 2010:101(15): 5743-5748.

[7] Wouter Ghyoot, Willy Verstraete. Anaerobic digestion of primary sludge from chemical pre-precipitation [J]. Water. Science and Technology. 1997:36(6-7) 357-365.

[8] Tiehm A., Nickel K., Zellhorn M., Neis U. Ultrasonic waste activated sludge disintegration for improving anaerobic stabilization [J]. Water Research.2001: 35(8): 2003-2009.

[9] Mavi Climent, Ivet Ferrer, Ma del Mar Baeza, Adriana Artola, Felicitas Vazquez, Xavier Font. Effects of thermal and machanical pretreatments of secondary sludge on biogas production under thermophilic conditons [J]. Chemical Engineering Journal. 2007:133(1-3): 335-342.

[10] Raf Dewil, Lise Appels, Jan Baeyens, Jan Degreve. Peroxidation enhances the biogas production in the anaerobic digestion of biosolids [J]. Journal of Hazard Materials. 2007: 146(3): 577-581.

[11] Cigdem Eskicioglu, Audrey Prorot, Juan Marin, Ronald L. Droste, Kevin J. Kennedy. Synergetic pretreatment of sewage sludge by microwave irradiation in presence of H_2O_2 for enhanced anaerobic digestion [J]. Water Research. 2008: 42(18): 4674-4682.

Advanced Materials Research Vols. 989-994 (2014) pp 142-145
© (2014) Trans Tech Publications, Switzerland
doi:10.4028/www.scientific.net/AMR.989-994.142

Synthesis and characterization of sulfonated poly(arylene ether sulfone) multiblock copolymers for proton exchange membrane

Tong Xue, Zhaoxia Hu, Shouwen Chen*

School of Environmental & Biological Engineering, Nanjing University of Science & Technology, Nanjing 210094, China

email: chensw@mail.njust.edu.cn

Keywords: multiblock copolymers; sulfonated poly (arylene ether sulfone); oligomers

Abstract. A series of multiblock copolymers based on sulfonated poly (arylene ether sulfone) (bSPAES-SF) with highly rigid hydrophilic sulfonate blocks and flexible hydrophobic blocks were successfully synthesized by the condensation of sulfonated decafluorobiphenyl-terminated oligomers and the hydroxyl-terminated oligomers. The former oligomers were sulfonated by fuming sulfonic acid. The bSPAES-SF membranes with IEC of 1.26-1.70 mmol/g exhibited high proton conductivity, hydrolytic and dimensional stability.

Introduction

In recent years, polymer electrolyte membrane fuel cells (PEMFCs) have drawn considerable attention as clean energy sources for portable devices, stationary power sources and hydrogen energy vehicles due to the high energy efficiency and environmental friendliness.[1] Polymer electrolyte membrane (PEM) is one of the key component of PEMFC system, which conducts protons from anode to cathode and avoids fuel and oxidizing agent from mixing.

Sulfonated aromatic hydrocarbon polymers as alternative materials have been intensively studied in the past decades.[2] However, most of the developed hydrocarbon-based PEMs suffer from dilemma of the basic properties for PEMs of ion exchange capacity (IEC), water uptake and proton conductivity. Recently, there are a handful of reports on the hydrocarbon polymers with high locally concentrated sulfonic acid groups. The as-prepared PEMs showed enhanced nano-scale phase-separation morphology and improved proton conductivity at moderate IEC levels which was a great advantage in PEMFCs application.[3]

In this report, we prepared a series of PEMs derived from multiblock copolymers of sulfonated poly (arylene ether sulfone) (bSPAES-SF) with highly sulfonated hydrophilic blocks simply sulfonated by fuming sulfonic acid. Their characterizations, fundamental physical properties and hydrolytic stability were investigated.

Experimental

4,4'-Difluorodiphenyl sulfone (DFDPS), 4,4'-biphenol (BP), 9,9-bis(4-hydroxyphenyl) fluorene (BHPF) were recrystallized from toluene, acetone and ethanol-water mixture before use, respectively. Dimethyl sulfoxide (DMSO) was dried over CaH_2 and distilled under reduced pressure and stored over 5 Å molecular sieve, while toluene and cyclohexane were dried over P_2O_5 and stored over sodium prior to use. Potassium carbonate was dried at 120^{o}C for 6 h under vacuum before use. Fuming sulfuric acid (SO_3, 20%) and other reagents were used as received.

The synthetic route of the multiblock copolymers was illustrated in Scheme 1. The copolymers were named as bSPAES-SF(m/n), where m and n refer to the block length of the hydrophilic and hydrophobic blocks, respectively. The hydrophobic, DFBP-terminated hydrophilic blocks (or oligomers) and the final multiblock copolymers were synthesized by the nucleophilic substitution reaction. The DFBP-terminated oligomers were sulfonated by fuming sulfuric acid (10%) at 100 ^{o}C for 20 hrs and purified by salting out method. The bSPAES-SF membranes (about 50 μm) were prepared by solvent casting method in DMSO solution and proton exchanged with 2 M HCl.

^{1}H NMR, reduced viscosity (η_r) , mechanical tensile tests, SEM, Water uptake (WU), the dimensional change, IEC, proton conductivity (σ) and hydrolytic stability were measured according to the method described elsewhere [4].

Results and discussion

The synthetic route for oligomers and multiblock copolymers is shown in Scheme 1. Post sulfonation method has been used to prepare hydrocarbon PEMs, but the inevitable polymer degradation could cause deterioration of mechanical strength of the as-obtained membranes.[5] To avoid this, the sulfonation of oligomers was carried out instead of the copolymers. Sakaguchi et al. studied the sulfonation of fluorine-containing poly(arylene ether ketone) copolymers by using concentrated sulfuric acid as the sulfonating reagent.[6] In this case, the sulfonation reaction was conducted by using fuming sulfuric acid as the sulfonating reagent and carried out at 100°C through electrophilic substitution reaction. Figure 1 shows the ^{1}H NMR spectra of the hydrophilic oligomers after the sulfonation reaction. It indicated that the substitution reaction occurred on the positions of fluorene moieties, both the pendant and backbone phenyl rings due to the relatively higher electron density as reported by [3]. For the hydrophobic oligomers, the block length (5, 10 and 15) was controlled by varying the molar ratio of starting materials of DFDPS and BP. The reduced viscosities of the copolymers were in the range of 1.1-1.5 dL/g, indicating the rather high molecular weight of the copolymer products. Transparent, tough and flexible membranes were successfully obtained through solvent-casting method.

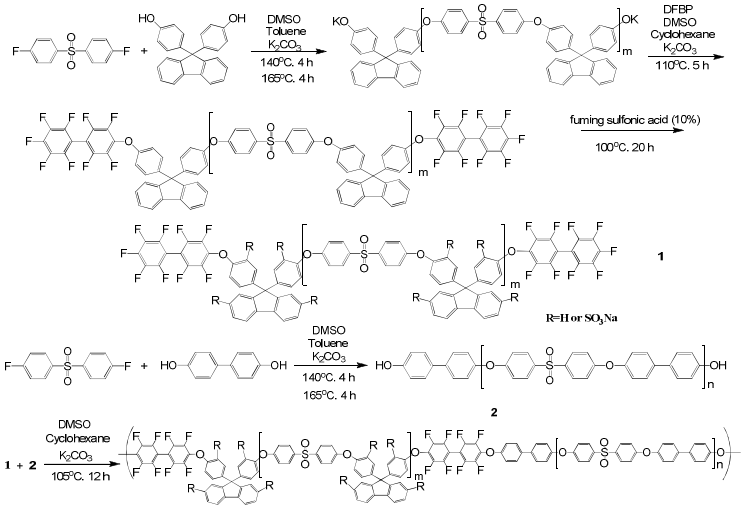

Scheme 1. Synthetic route of bSPAES-SF copolymers.

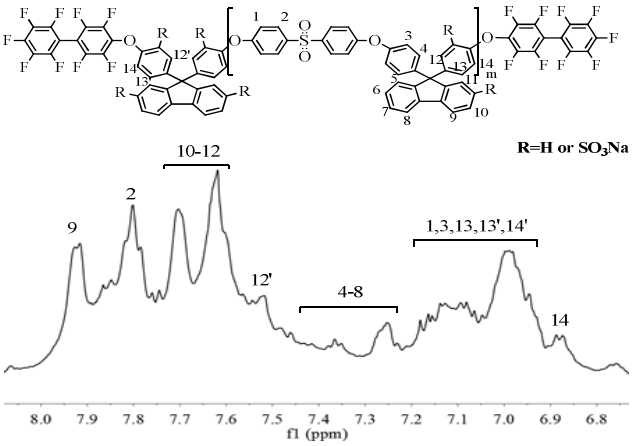

Figure 1. ^{1}H NMR spectra of sulfonated oligomers (m=5).

Figure 2 shows the SEM images of bSPAES-SF(5/10). Smooth and uniform surface and fracture surface were observed for the membranes, indicating their homogenous morphology in the micrometer scale.

Table 1 summarized the physical properties of the obtained bSPAES-SF membranes. IEC is an important property parameter for the PEMs because it is the indicator of the ionic group content inside the membrane matrix and closely related to the absorbed water, membrane swelling and proton conduction. As shown in Table 1, the titration IECs of the obtained bSPAES-SF membranes were 1.12, 1.26 and 1.70 mmol/g.

Obviously, the water uptakes are closely related to the IEC values and temperature as

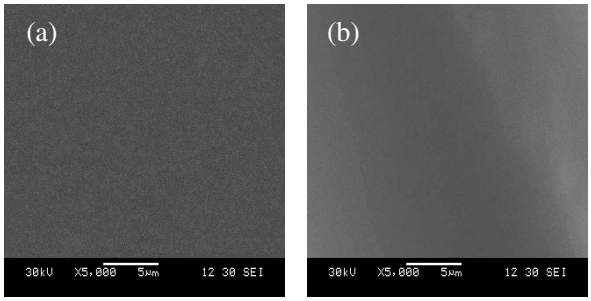

Figure 2. SEM micrographs of multiblock membranes (a) bSPAES-SF (5/10) in plane direction. (b) bSPAES-SF (5/10) in section direction.

reported [8]. For example, the membrane of bSPAES-SF(5/5) displayed 2.2-2.3 times water uptakes of that for bSPAES-SF(5/15). Based on the comparison of the average water molecules absorbed per sulfonic acid group, λ, it is also found that the λ value also increased with the IEC, it was about 25% larger for bSPAES-SF(5/5) than that for bSPAES-SF(5/10) and 60% larger than that for bSPAES-SF(5/15). Considering the same hydrophilic and hydrophobic block structures, the difference in λ could be caused by the different block length of hydrophobic blocks. For the hydrophobic blocks with larger block length, the enhanced hydrophobic nature can weaken the water affinity of the membrane matrix, resulting in the reduced water absorbing capacity.

Table 1. Physical properties of the prepared bSPAES-SF membranes

Copolymer	η_r	IEC[a]	*WU*/%		λ^b	Δl_c/%		Δt_c/%		Y_M	E_B	*WL*	Tough-ness
	/dLg^{-1}	/mmolg^{-1}	30°C	80°C		30°C	80°C	30°C	80°C	/GPa	/%	/%	
bSPAES-SF(5/5)	1.5	1.7	48	72	16	8.4	14.4	17.5	24.9	\[c]	\[c]	1	V
bSPAES-SF(5/10)	1.1	1.26	28	37	12	3.2	7.0	10.2	16.1	0.9	23	0.4	V
bSPAES-SF(5/15)	1.2	1.12	21	31	10	2.7	5.1	4.6	11.6	1.1	29	0.6	V
Nafion 112	1.2	0.89	33	42	20	12	12	13	15	0.2	410	\	\

[a] Titration value; [b] at 30 °C; [c] not measured.

The through-plane and in-plane dimensional change was listed in Table 1. All the bSPAES-SF membranes exhibited obvious anisotropic swelling behavior in water with about one time larger through-plane dimensional changes than the in-plane ones. The preferable alignment of polymer chains in the plane direction due to the existence of rigid and bulky fluorenyl moieties in the polymer backbone could be responsible for it as reported.[3] In addition, in the in-plane direction, the dimensional changes (2.7-8.4%) were much smaller or slightly larger (for bSPAES-SF(5/5)) than Nafion 112 (12.0%) at 80oC although they had higher IECs, indicating their good dimensional stability. This will be favorable for the long term stability of the membrane-electrode-membrane assembly under changing operating conditions.

Table 1 lists the Young's modulus(YM), elongation at break point(EB), weight loss and toughness of the membrane after the hydrolytic test of the obtained bSPAES-SF membranes. During the test, the bSPAES-SF(5/5) was too brittle to be measured at dry state although the copolymer showed relatively higher η_r value (1.5 dL/g) than the other two copolymers. On the other hand, for the membranes of bSPAES-SF(5/10) and bSPAES-SF(5/15), they displayed Young's modula about 0.9-1.1 GPa and elongation at break point of 23-29%, suggesting the quite good mechanical strength. A slightly improvement in the mechanical strength with the increase in the block length of hydrophobic block was observed. It suggested that the appropriate structural design of the hydrophobic block are important to get tough and flexible membranes.

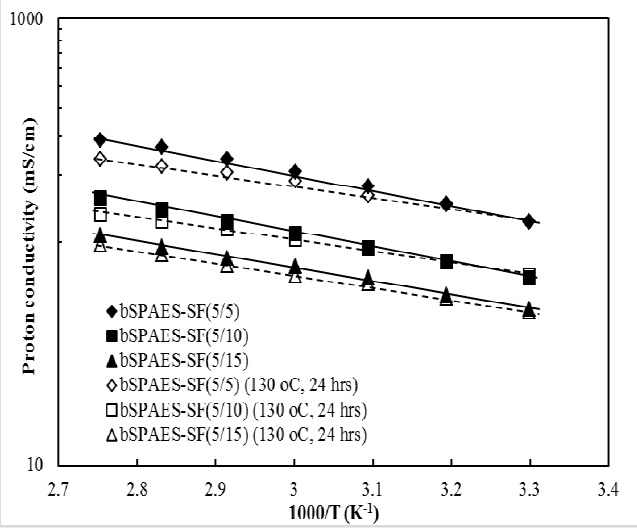

Figure 3. Temperature dependence of proton conductivity for the obtained bSPAES-SF membranes.

Proton conductivity is one of the most important property parameters to evaluate membrane performance. Figure 3 shows the temperature dependence of the proton conductivity for the obtained bSPAES-SF membranes in water. Membrane with higher IEC exhibited higher proton conductivities. For example, the membrane of bSPAES-SF(5/5) exhibited proton conductivity of 153 mS/cm at 30°C, and reached the maximum of 286 mS/cm at 90°C. Clearly, all the membranes showed Arrhenius-type temperature dependant proton conductivity behavior. According to

Arrhenius equation, the calculated activation energy of the obtained bSPAES-SF membranes were in the range of 11.50-12.76 kJ/mol, which is a little higher than the reported value of Nafion 117 (9.57 kJ/mol).[9]

The hydrolytic stability was simply evaluated by treating membrane samples in pressurized water at 130^{o}C for 24 hrs. After the treatment, all the bSPAES-SF membranes maintained original shape and could be bent and folded back without fracture, even for the membrane of bSPAES-SF(5/5) which is fragile at dry state. Weight losses no more than 1.0% were found for the obtained membranes, indicating the good integrity of the membranes under harsh conditions. From Figure 3, it is clearly noted that after the treatment, the membranes still kept high proton conductivities. For example, the membrane of bSPAES-SF(5/5) exhibited proton conductivity of 177 mS/cm and 162 mS/cm before and after the treatment at 50^{o}C.

Conclusions

A series of novel PEMs based on sulfonated poly(arylene ether sulfone) multiblock copolymers with high local ionic group concentration were successfully prepared from hydrophobic and post-sulfonated hydrophilic oligomers. The sulfonation reaction of the oligomers were carried out smoothly by fuming sulfonic acid at 100^{o}C. The obtained bSPAES-SF membranes (1.12-1.70 mmol/g) were ductile, exhibited moderate water uptakes, high proton conductivity, good dimensional and hydrolytic stability.

Acknowledgement

This work was financial supported by, or in part by, the National Natural Science Foundation of China (21006052, 21276128), Basic Research Program of JiangSu Province of China (BK2011713), the Scientific Research Foundation for the Returned Overseas Chinese Scholars, the Fundamental Research Funds for the Central Universities (30920130121014).

References

[1] Amrit Chandan, Mariska Hattenberger. High temperature (HT) polymer electrolyte membrane fuel cells (PEMFC)-A review [J], Journal of Power Sources, 2013 (231) 264-278.

[2] Zhaoxia Hu, Yan Yin, Kazuaki Yaguchi. Synthesis and properties of sulfonated multiblock copolynaphthalimides [J] Polymer, 2009 (50) 2933-2943.

[3] Byungchan Bae, Takayuki Hoshi. Block Poly(arylene ether sulfone) Membranes for Fuel CellApplications via Oligomeric Sulfonation [J] Macromolecules, 2011 (44) 3884-3892.

[4] Shouwen Chen, Kangcheng Chen. Poly(sulfonated phenylene)-block-poly(arylene ether sulfone) copolymer for polymer electrolyte fuel cell application [J] Polymer, 2013 (54) 236-245.

[5] Elif Erdal Unveren, Tuba Erdogan. Role of post-sulfonation of poly(ether ether sulfone) in proton conductivity and chemical stability of its proton exchange membranes for fuel cell [J] international journal of hydrogen energy, 2010 (35) 3736-3744

[6] Yoshimitsu Sakaguchi, Atsushi Kaji. Polymer electrolyte membranes derived from novel fluorine-containing poly(arylene ether ketone)s by controlled post-sulfonation [J] Polymer, 2012 (53) 4388-4398

[7] Aruna Kumar Mohanty, Ershad Ali Mistri. Synthesis and characterization of novel fluorinated poly(arylene ether sulfone)s containing pendant sulfonic acid groups for proton exchange membrane materials [J] Journal of Membrane Science, 2012 (409) 145-155

[8] Chengsong Ma, Lei Zhang. An investigation of proton conduction in select PEM's and reaction layer interfaces-designed for elevated temperature operation [J] 2003 (219) 123-136

Advanced Materials Research Vols. 989-994 (2014) pp 146-150
© (2014) Trans Tech Publications, Switzerland
doi:10.4028/www.scientific.net/AMR.989-994.146

Study on Carbon and Sulfur Detection by Using Infrared Absorption Method

Bayati, M.R., Pengyi WEI

Department of Materials Science and Engineering,

North Carolina State University, Raleigh, NC 27695, United States

email: pengyiwei5101@sina.com

Keywords: Infrared Absorption Method; Detection; Carbon; Sulfur

Abstract. This paper focuses on discussing the principle of detecting carbon and sulphur by using infrared absorption method, characteristics of high-frequency heating, system blank value, and method for detecting trace carbon and sulphur.

Introduction

Chemical composition analysis of metal materials is an important way of evaluating the quality of materials, and currently, the composition of metal materials is measured by practical methods such as standard method and routine analysis method. When applying above methods, analysts often meet some difficulties and it is necessary to understand some principles. This paper focuses on discussing the principle of detecting carbon and sulphur by using infrared absorption method, characteristics of high-frequency heating, system blank value, and method for detecting trace carbon and sulphur.

Principles

Special analyzer integrated with gas absorption pool and high temperature furnace (usually using high frequency induction furnace) is a device specially used for detecting carbon and sulphur contents in steel and non-metallic materials by using infrared spectral absorption method. After heating and melting in high temperature, carbon (or sulfur) in the samples oxidizes in oxygen to generate CO_2 or SO_2. The contents of carbon/sulfur can be detected by using infrared absorption method.

Put the sample and fluxing agent into the porcelain crucible. When the sample is fused in the oxygen flow with high frequency induction heating, the carbon is oxidized into CO_2 and the sulphur is oxidized into SO_2, both of which are sent into the infrared analyzer. Since CO_2 and SO_2 can absorb specific wavelength of infrared, which leads to attenuation of infrared intensity, there is a function relationship between the attenuation of infrared intensity and the change of concentration of CO_2 and SO_2. The contents of carbon and sulphur can thus be measured according to the changes of the infrared intensity.

See Figure 1 for process diagram of carbon sulfur analyzer by using high frequency induction heating—infrared absorption method

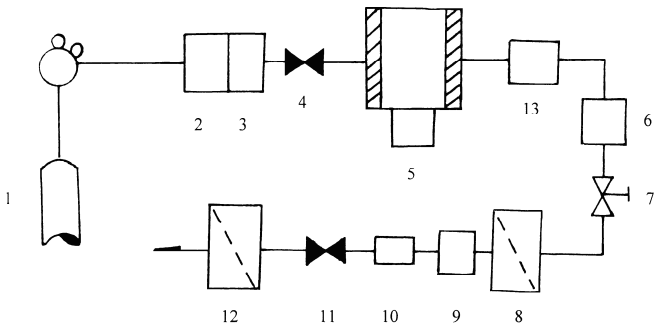

Figure 1 Process diagram of carbon sulfur analyzer by using high frequency induction heating—infrared absorption method

In the Figure 1: 1—Oxygen; 2—Soda asbestos; 3,6—Anhydrous magnesium perchlorate; 4,11—Flow controller; 5—High frequency induction heating furnace; 7—Flow control valve; 8—SO_2 infrared detector; 9—CO, SO_2 catalytic converter; 10—SO_3 absorber; 12—CO_2 infrared detector; 13—Filter.

Characteristics of high frequency heating

Principles

According to the Faraday's law of induction, when current passes a metal conductor in a high frequency alternating electric field, the metal conductor surface will generate powerful induced current. According to Joule-Lenz's law, alternating magnetic field will make the current in a conductor to flow through the surface of the conductor, causing skin effect. Instantaneous electric current density is proportional to the frequency. The higher the frequency is, the higher the intensity of the induced current will be concentrated in the surface of the conductor, namely, more serious skin effect. Reduction of effective conductive surface increases the resistance, which leads to rapid increase of the temperature of the sample metal conductor. As a result, the metal samples under oxygen-enriched state burns rapidly.

Advantages

We all know that, to detect the carbon and sulphur contents in steel by using combustion method, we must firstly make a complete combustion of the sample; especially when detecting sulfur, the detection is achieved through the detection of SO_2. Therefore, after combustion, it is better to generate more SO_2 but less SO_3 as far as possible, which is mainly determined by the heating temperature. Theoretically, proportion of SO_3 generation is higher than 15% when the temperature is lower than 1300℃; while when the temperature is higher than 1500℃, the ratio of SO_3 generation will be lower than 3%. The temperature of high frequency combustion method can reach 1400-1600℃.

Hence, the detection of carbon and sulphur by using Infrared Absorption is usually conducted by connecting with high frequency induction combustion method, so as to meet requirements of fast and accurate detection.

Detection of trace carbon and sulfur

Important Notice

Trace sulfur and carbon detection refers to the detection of $\mu g.g^{-1}$ level carbon and sulfur contents. Attention must be paid to the following aspects: ①stabilize and reduce system blank values: ②accurately measure blank values: ③Calibrate equipment; ④prepare the analysis of samples.

System blank value and its processing

When detecting ultra-low carbon/sulfur contents by using infrared spectral absorption method, there are trace carbon and sulfur elements in crucible, fluxing agent, and oxygen, which may affect the background of analyzing low content carbon and sulfur samples. All of these impacts are called system blank value.

The processing method is described as follows:

① Crucible: During making, sintering, packing and shipping processes, residuals of carbonate, sulfate, organic matters and moistures may remain stay on the surface. Thus the combustion process may generate CO_2, SO_2 and moisture. CO_2 and SO_2 entering into absorption pool may lead to the analysis results of carbon and sulphur contents higher than the actual contents; the moisture discharged during the combustion process may be condensed in the cold gas pipelines, and the moisture may cause CO_2, SO_2 or SO_3 to generate carbonic acid, sulphurous acid, sulfuric acid, which are adsorbed in the gas pipeline and thus cause the analysis results lower than the actual value. In addition, if moisture enters into absorption pool along with the gas to be analyzed, it may lead to detection result higher than actual value due to the similar infrared absorption wavelength between the gas and the SO_2. In summary, above reasons may affect the accuracy of carbon and sulfur analysis result. According to the provisions of international standard of ISO9556[1] and ISO4935[2], before use, crucible should be place in the high temperature furnace for burning with no less than 2h under the temperature of 1100℃ with the gas and oxygen flow. And then it is placed into a dryer for cooling and for future use. The time of storage in the dryer should be no more than 72h. When detecting low content carbon and sulfur, the crucible should be burned in oxygen flow under the temperature of 1350℃. If there is no available special crucible burning furnace, or if a temporary detection of low carbon and low sulfur samples is required, the same amount fluxing agent with samples to be measured can be put into crucible, and they are burned in high frequency furnace. Immediately after cooling down, they can be used for sample detection. This type of crucible is also called bottomed crucible, and the blank value obtained from this type of crucible is more stable than previous one. The experimental result shows that, the blank value after burning of crucible is significantly reduced. (See table 1)

Table 1. Blank values of crucibles with different crucible processing methods

Crucible processing methods	Weight of Tungsten granular (g)	Value input into PC (g)	Measured value of carbon (w/%)	Measured value of sulphur (w/%)
Unburned crucible	1.50	1.50	0. 014 8 0. 013 7 0. 012 3	0. 000 08 0. 000 10 0. 000 09
Burned crucible under the temperature of 1300℃	1.50	1.50	0. 000 41 0. 000 37 0. 000 39	0. 000 00 0. 000 01 0. 000 01
Bottomed crucible	1.50	1.50	0. 000 40 0. 000 36 0. 000 39	0. 000 01 0. 000 00 0. 000 01

②fluxing agent: Pure tungsten granular is used as fluxing agent during the detection of trace carbon and sulfur contents [3]. Before use, the adsorbed impurities (e.g., CO_2, SO_2, H_2O) should be removed. Tungsten granular can be firstly placed into drying oven and heated to the temperature 300℃ for 1h. After drying, it is taken out and put into a dryer for cooling. Then it is put into a grinding mouth bottle for future use. A good habit of timely sealing the cover of the tungsten granular container after taking out of tungsten granular shall be established. When analyzing, the volume of fluxing agent should be maintained constant, so as to eliminate the impact of unstable blank values caused by the different volume of fluxing agent. If using other fluxing agents or mixed fluxing agents, the volume of each time should be maintained constant. The experimental result shows that, the blank value of tungsten granular after drying is significantly reduced. (See table 2)

Table 2. Blank values of tungsten granular after different processing methods

Crucible processing methods	Weight of Tungsten granular (g)	Value input into PC (g)	Measured value of carbon (w/%)	Measured value of sulphur (w/%)
Unbaked tungsten granular	1. 50	1. 50	0. 000 77 0. 000 75 0. 000 83	0. 000 02 0. 000 01 0. 000 02
Baked tungsten granular under 300℃	1. 50	1. 50	0. 000 33 0. 000 30 0. 000 31	0. 000 01 0. 000 00 0. 000 00

③Oxygen: According to the stipulation of international standards of ISO9556[1] and 1SO4935[2], the oxygen purity should be at least 99. 5%, but the oxygen used for trace carbon and sulfur detection is high purity oxygen, with the purity of 99. 99%. The oxygen could be purified by using purification device before it enters into the analyzer. The purification devices of various models of Infrared carbon sulfur analyzer could be divided into two types: absorption, and heating-decomposition-absorption. Absorption makes use of the nature of CO_2 and SO_2, Namely, both two types of gases are acidic oxides, which can react with alkali as follows:

$$CO_2 + 2NaOH = Na_2CO_3 + H_2O$$

$$SO_2 + 2NaOH = Na_2SO_3 + H_2O$$

By making use of above features, the acidic materials such as CO_2, SO_2 could be removed from oxygen. Meanwhile, the desiccants such as anhydrous magnesium perchlorate could be used for removing moisture from oxygen. Heating-decomposition-absorption method is to heat the oxygen to 450℃. Catalyzed by catalyst（such as copper oxide）, hydrocarbon is decomposed into CO_2 and water, and the alkaline substances and desiccant are used to purify oxygen.

When detecting trace sulfur, the pressure of bottled oxygen should not be too low. When the pressure of bottled oxygen is reduced to below 50kg.cm^{-2}, moisture content in the gas will be increased dramatically. When using such oxygen to analyse samples, the magnesium perchlorate in test tube may change color due to deliquesce, and it may cause ossification of indicator, which may lead to inconsistent results of low sulfur detection. Therefore, when analyzing low sulfur samples, the pressure of bottled oxygen should be higher than 880kg.cm^{-2}. The blank values of regular oxygen and high purity oxygen are illustrated in the Table 3.

Table 3. The blank values of regular oxygen and high purity oxygen

Types of oxygen	Weight of Tungsten granular (g)	Value input into PC (g)	Measured value of carbon (w/%)	Measured value of sulphur (w/%)
Regular oxygen	1. 50	1. 50	0. 000 80 0. 000 84 0. 000 79	0. 000 03 0. 000 09 0. 000 02
High purity oxygen	1. 50	1. 50	0. 000 67 0. 000 69 0. 000 64	0. 000 01 0. 000 03 0. 000 00

④Correct detection of blank values: when detecting trace carbon and sulfur in steel, sometimes, system blank value is almost the same with the sample analysis value, even higher than sample analysis value[4]. Therefore, the correct use of blank value method will directly affect the accuracy of the analytical result of trace carbon and sulfur contents in samples. In order to obtain accurate blank value, firstly, the crucibles with the same batch of processing are used with adding fixed amount of fluxing agents; secondly, when detecting blank value, input value should be consistent with the weight of samples to be analyzed; thirdly, the analysis conditions of two analyses should be maintained basically same, especially the same combustion temperature. In detecting blank value and analyzing sample, if the difference of combustion temperature is too large, then the differences of introduced blank values will also be large. Since if the combustion temperature is high, the carbon and sulfur elements of the crucibles materials will be gradually released during the analysis

process, and the CO_2, SO_2 gases deeply absorbed in the tube wall will also be released along with the increase of temperature and the extension of combustion time, and thus the blank values will be increased. Fourthly, the sulfur blank value cyclic detection method [5] is used to correctly measure the total sulfur blank value. The blank value is input into the blank value field of the analyzer, and the analyzer will automatically deduct the blank value during the detection process.

⑤Equipment Calibration: Consensus has been reached that accurate analysis method should take pure compound as the calibration benchmark. International standards ISO 9556 takes sucrose, sodium carbonate, barium carbonate as standard substances of carbon for calibration: ISO 4935 takes potassium sulphate as the standard substance of sulfur for calibration. Although using pure compound is a good way of linear calibration for analyzer, but in practice, the deviation of calibration coefficient has occurred during the analysis process of metal materials such as steel. Since the combustion release of pure compound is different from that of steel, it is not suitable for the analyzer calibrated with pure compound to detect the low content steel. Experience shows, for analyzing a type of material, same materials should be applied for standard substance calibration, and first level standard substance produced recently should be chosen, In addition, it must follow the principle of using high quality standard to calibrate the low one, namely, high quality low-carbon and low-sulfur samples with high contents are used to calibrate and then the low-carbon and low-sulfur samples with relatively lower contents are measured. Both samples have the same matrix components. When conducting detection, it is necessary to pay attention to the consistency of the analysis conditions between the standard substance and samples.

⑥Environmental requirements: Environment temperature and humidity affects the accuracy of analysis result of trace carbon and sulfur contents. In winter, when the temperature is low, it is found that low content sulfur may not be detected or the result of the detection is significantly lower than the actual value. To solve this problem, we may increase the room temperature and firstly burn a couple of waste samples so as to increase the temperature of furnace end, and then conduct the detection of samples. When environmental humidity increases, the moisture in the atmosphere may enter or be absorbed on the tube wall, on surface of stainless strainer, cylinder surface, and gas pipeline wall surface. When sample is burning and releasing heat, it enters into test tube along with gas to be analyzed or condenses at somewhere with low temperature, which will definitely affect the accuracy of analysis. Therefore, when detecting trace carbon and sulfur sample, the room temperature must be maintained at about 25℃, with the relative humidity lower than 60%. Usually, the crucible bracket is raised to its up limit, the pipeline is sealed, so as to prevent atmosphere from entering into the crucible. Sample should be quickly put into place, without being exposed to the air for too long time. Analysis and test of chemical elements of materials involves many contents and many methods, and it is also affected by complicated factors. As an analyst, we should master the professional skills and operate rigorously so as to obtain correct analysis results.

References

[1] ISO 9556 Steel and iron - Determination of total carbon content - Infrared absorption method after combustion in an induction furnace.

[2] ISO 4935 Steel and iron--Determination of sulfur content--Infrared absorption method after combustion in an induction furnace.

[3] Ashino T.; Takada K.;Morimoto Y.;Abiko K. Determination of trace amounts of sulfur in high-purity iron by infrared absorption after combustion: Selection and pre-treatment of reaction accelerators, Physica Status Solidi. A, Applied Research. 2002, 189, 1, 123-132.

[4] Kunio Takada, Tetsuya Ashino, Yukitoshi Morimoto, Hisao Yasuhara, Mayuko Kurosaki and Kenji Abiko, Determination of Trace Amounts of Sulfur in High-Purity Iron by Infrared Absorption after Combustion: Removal of Sulfur Blank, Materials Transactions, JIM, Vol,41,No. 1(2000). 53 to 56.

[5] Jianhuan Wei, Huafeng Sun, Shengjie Yang, the cycle measurement of sulfur blank value with the CS-444 infrared ray carbon sulfur analyzer, Advanced Materials Research, Vals.399-401(2012).2173-2176.

Advanced Materials Research Vols. 989-994 (2014) pp 151-155
© (2014) Trans Tech Publications, Switzerland
doi:10.4028/www.scientific.net/AMR.989-994.151

Effects of the Carboxyl Density on the Properties of Polycarboxylate-type Superplasticizer

Chengfei Fu[1, a], Guangjun Zheng[1,b], Kangling Li[1,c], Yao Bi[1,d], Long Xiong[1,e]

[1]China Construction Ready Mixed Concrete Co. Ltd, Wuhan 430205, China

[a]fuchengfei0816@163.com, [b]zhengguanjun@cscec.com, [c]houziaidy@163.com, [d]freddiebee@163.com, [e]xionglong1987@126.com

Keywords: carboxyl density; molecular weight; monomer conversion; dispersion ability

Abstract. The effect of carboxyl density (the ratio of acrylic acid and polyoxyethylene ether) upon the performance, molecular weight, and monomer conversion rate of polycarboxylate (PCE) were investigated by slump test, Gel Permeation Chromatography (GPC) and High Performance Liquid Chromatography (HPLC), respectively. The results showed that with carboxyl density increased from 2:1 to 7:1, molecular weight of PCE increased from 7968.5 to 13930.1 and the molecular weight distribution coefficient increased from 1.5 to 2. The HPLC date indicated carboxyl density does not affect the rate of monomer conversion. Test of the fluidity of cement pastes displayed that as carboxyl density was 4.0:1, PCE show the optimal dispersion and dispersion-retaining ability.

Introduction

Polycarboxylates (PCE) are commonly used as superplasticizers to disperse cement particles in concrete and mortar [1]. The research and development of polycarboxylic acid type water-reducers has been one of important direction in concrete admixtures because of their excellent water-reducing rate [2-5]. Currently, it's well known that the dispersing mechanism of these superplasticizers is generally thought to be related to the adsorption of the polymer backbone via carboxylic functional groups and the steric hindrance effect generated by PEG side chains [6]. The dispersion of polycarboxylate superplasticizer for cement was based on their molecular structure[7]. In previous studies, the dispersive force of PCE molecules often was correlated with their anionic charge density calculated from the chemical formula[8]. But because these PCE were polymers with wide molecular weight distribution and it was not easy to characterize their chemical structures, many studies did not concern about the chemical structures of PCE were not analyzed in detail.

To profoundly understand the molecular structure of PCE, specially the charge density of PCE , with their performance in cementitious systems. The dispersion properties of PCE on cementitious systems at different charge density was studied, and then the rate of monomer conversion and the molecular weight was discussed when the charge density of PCE was changed.

1 Experimental

1.1 Synthesis of PCE

The PCE was synthesized according to previous study by aqueous free radical copolymerization of acrylic acid (AA), sodium methylacrysulfonate (SMAS) and polyoxyethylene ether (TPEG-2400). 100g deionized water and 150g TPEG-2400 were added to a 500ml four-necked flask equipped with a condenser, a nitrogen inlet and a stirring bar afterwards and stirred for 15min. The solution was gently heated to 60°C. 1.5g of Ammonium persulphate (APS, initiator) was dissolved in 45 ml deionized water. This solution was designated as Solution I. Separately, variable amount of AA and 0.8g of SMAS (chain transfer agent) with 55g water was then dissolved in 55 ml deionized water. This solution was designated as Solution II. Using two peristaltic pumps, Solutions I and II were fed separately and continuously into the vessel over the periods of 75 min (Sol. I) and 60 min (Sol. II).

After complete the feeding process, the mixture was stirred for several hours under the reaction temperature. At the end, the pH was adjusted to 7 with 30wt% NaOH and the PCE was acquired.

1.2 Testing of monomer conversion

The monomer conversion of PCE was measured by chromatography system (HPLC, Agilent 1100; Column, SinoChrom ODS-BP (C18) 5μm, 4.6mm × 200mm; detector, λ-35 -type UV spectrum, PE company, USA).
Weigh the test sample superplasticizer 0.10g ~ 0.25g, diluted with the mobile phase to 25mL, filtrated with the 0.45μm filter membrane and chromatographic analysis with external standard method.

1.3 Gel Permeation Chromatography (GPC)

Molecular weight of PCE was measured by Gel Permeation Chromatography (GPC, Waters 150C, USA), using the solution of methanol and buffer solution (1/2, v/v) as the eluent. (Column, PL aquagel, 7.8*300 mm, Agilent1100, Agilent Company, USA). The buffer solution was $Na_2B_4O_7$/KCl aqueous solution (pH = 8). Narrow polyethylene glycol (PEG) was used as calibration standards. The GPC detector included the refractive index.

1.4 Mini slump test

Testing of the fluidity of cement pastes was under the national standard GB 8077-2000 “methods for testing uniformity of concrete mixture” and the cement used for the test was HUAXIN P·O 42.5, the w/c ratio was 0.29 and the dosage of the PCE was 0.15% (by percent Weight based on solids cement).

2 Experimental results and analysis

2.1 The effect of carboxyl density on the molecular weight of PCE

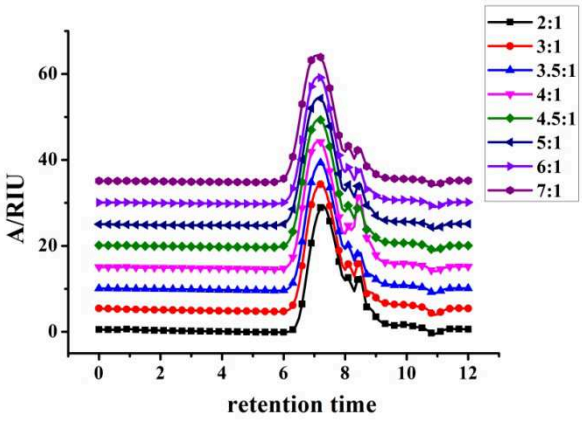

Fig. 2.1 GPC of PCE with different carboxyl density

As can be seen from the GPC results of PCE with different carboxyl density showed in Fig. 2.1 and table 2.1, the molecular weight of PCE become larger and present more broad molecular weight distribution when the carboxyl density increase.

Table 2.1 The calculated result of fig. 2.1

carboxyl density	Mw	Mn	DPI.	Mp
2:1	7968.5	5313.9	1.5	2841.9
3:1	9669.4	5816.6	1.7	3784.8
3.5:1	9949.8	5893.4	1.7	3784.8
4:1	10986.1	6220.9	1.8	5040.4
4.5:1	11797.5	6351.7	1.8	3784.8
5:1	11910.2	6377.4	1.9	5040.4
6:1	11851.2	6360.2	1.9	5040.4
7:1	13930.1	6798.8	2.0	5040.4

This may be caused by two reasons: 1) as the increased of carboxyl density, the charge in the molecular main chain of PCE increase, resulting in the repulsion between the functional groups increases. Wherefore, the molecule stays more open, display larger molecular volume, and show smaller elution volume of the gel permeation chromatogram. Eventually, the greater the molecular weight is calculated out. 2) Since the total molar mass unchanged, thereby the amount of TPEG decrease as the increased of AA. From this, it can be speculated that TPEG possess some certain chain transfer effect.

2.2 Effect of carboxyl density on the monomer conversion of PCE

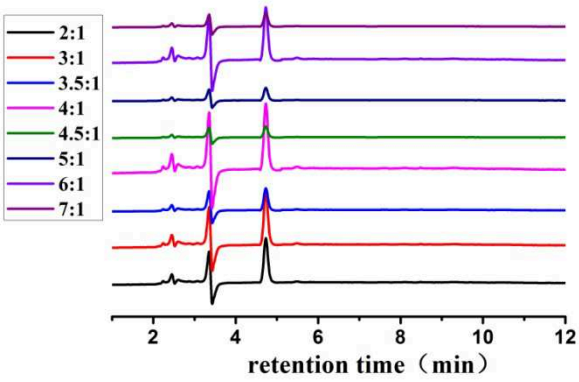

Fig. 2.3 HPLC of PCE with different carboxyl density

Table 2.2 The calculated results of Fig. 2.3

Carboxyl density	2:1	3:1	3.5:1	4:1	4.5:1	5:1	6:1	7:1
Monomer conversion（%）	98.2	99.1	98.8	99.5	99.5	98.5	99.4	98.6

Fig. 2.3 and Table 2.2 show the monomer conversion in the polymerization process of PCE with different carboxyl density. As shown from the results that SMAS and AA almost completely react, which means carboxyl density does not affect the rate of conversion of monomer.

2.3 The effect of carboxyl density on the performance of PCE

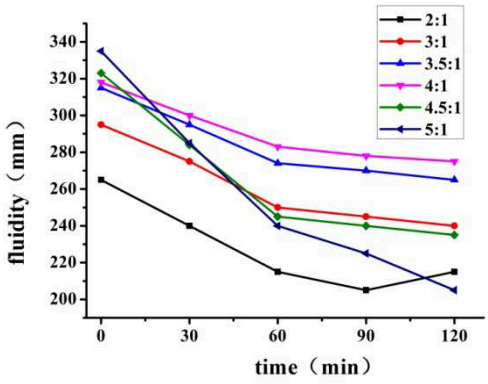

Fig. 2.4 The effect of carboxyl density on the cement paste fluidity over time

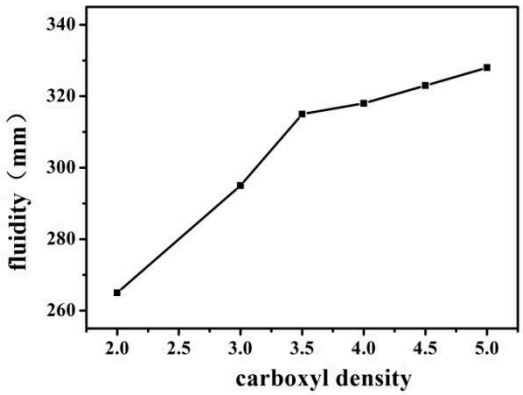

Fig. 2.5 Effects of carboxyl density on initial dispersion performance of PCE

Fig. 2.4 and displays the effects of the carboxyl density on the dispersion capacity and the dispersion retention capacity. Fig. 2.5 displays the effects of the carboxyl density on initial dispersion performance of PCE. It can be seen that when the molar ratio of AA and TPEG-2400 increase from 2:1 to 3.5:1, the fluidity of cement pastes quickly lose from 265mm to 315mm. This tendency would slow down with the further increasing of carboxyl density. The results show that the carboxyl density make a tremendous impact on the dispersant of PCE. It can be ascribed to that AA can provide carboxyl which is of great important to electrostatic repulsion and adsorption capacity acting on the surface of cement particles. As the carboxyl density is low, the electrostatic repulsion and adsorption capacity are insufficient to make a more powerful dispersant in cement. However, the electrostatic repulsion and adsorption capacity are saturated when the carboxyl density is more than 3.5:1.

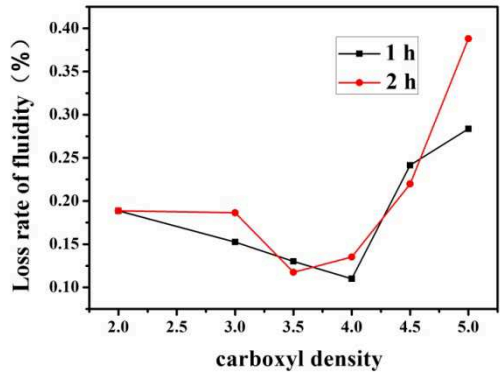

Fig. 2.6 The effect of carboxyl density on the loss rate of the cement paste fluidity

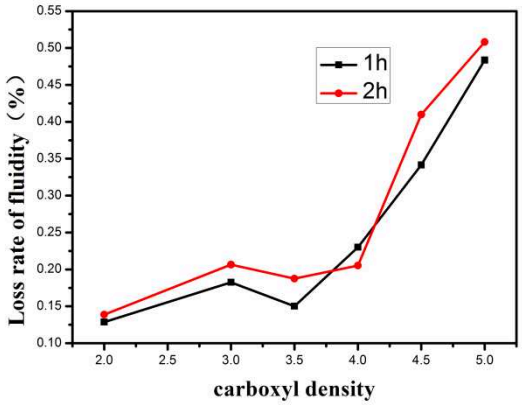

Fig. 2.7 The effect of carboxyl density on the loss rate of the concrete fluidity

The effect of carboxyl density on the loss rate of the cement paste fluidity has been investigated and the results are shown in Fig. 2.6. According to the data above, the PCE exhibits the optimal dispersed retention with the carboxyl density of 4:1. This means the carboxyl density of 4:1 could provide the suited charge density which can benefit the maintenance of electrostatic repulsion. The effect of carboxyl density on the loss rate of the concrete has been investigated and the results are shown in Fig. 2.7. According to the data above, the PCE exhibits the optimal dispersed retention with the carboxyl density of 3.5:1 when it was used in the concrete. the rate of loss of the fluidity on concrete is much greater than on cement.

Conclusion

Based on the research on the molecular weight and monomer conversion by Gel Permeation Chromatography (GPC) and High Performance Liquid Chromatography (HPLC), It was found that the molecular weight of PCE become larger and present more broad molecular weight distribution when the carboxyl density increase. The HPLC date indicated carboxyl density does not affect the rate of monomer conversion. The cement paste fluidity and concrete fluidity when added the PCE show that the loss rate of the fluidity Showing a gradually increasing trend overall. take into account the dispersion and dispersion-retaining ability, it was proposed that the optimal carboxyl density was 4.0:1.

References

[1] Vangi S. Ramachandran, Concrete admixtures handbook: properties, science, and technology[M]. William Andrew, 1995.

[2] Lange A, Hirata T, Plank J. Influence of the HLB value of polycarboxylate superplasticizers on the flow behavior of mortar and concrete[J]. Cement and Concrete Research, 2014, 60: 45-50.

[3] Lei L, Plank J. Synthesis and Properties of a Vinyl Ether Based Polycarboxylate Superplasticizer For Concrete Possessing Clay Tolerance[J]. Industrial & Engineering Chemistry Research, 2013.

[4] Schmidt W, Brouwers H J H, Kühne H C, et al. Influences of superplasticizer modification and mixture composition on the performance of self-compacting concrete at varied ambient temperatures[J]. Cement and Concrete Composites, 2013.

[5] Perrot A, Rangeard D, Picandet V, et al. Hydro-mechanical properties of fresh cement pastes containing polycarboxylate superplasticizer[J]. Cement and Concrete Research, 2013, 53: 221-228.

[6] Lange A, Plank J. Study on the foaming behaviour of allyl ether-based polycarboxylate superplasticizers[J]. Cement and Concrete Research, 2012, 42(2): 484-489.

[7] Yamada K, Takahashi T, Hanehara S, et al. Effects of the chemical structure on the properties of polycarboxylate-type superplasticizer[J]. Cement and concrete research, 2000, 30(2): 197-207.

[8] Plank J, Sachsenhauser B. Experimental determination of the effective anionic charge density of polycarboxylate superplasticizers in cement pore solution[J]. Cement and Concrete Research, 2009, 39(1): 1-5.

Advanced Materials Research Vols. 989-994 (2014) pp 156-159
© (2014) Trans Tech Publications, Switzerland
doi:10.4028/www.scientific.net/AMR.989-994.156

Preparation of Copolymer Modified with Oxidized Starch and Dispersion Ability for Ferric Oxide

Jicheng Xu[1, 2], Xinshan Rong[1], Xiaorui Guo[3] and Fengxian Qiu[3,a*]

[1] School of Environment and Safety Engineering, Jiangsu University, Zhenjiang 212013, China

[2] Department of Chemical Engineering, Zhenjiang College, Zhenjiang 212003, China

[3] School of Chemistry and Chemical Engineering, Jiangsu University, Zhenjiang 212013, China

* fxqiu@ujs.edu.cn

Keywords: Copolymer; Oxidized Starch; Dispersing Ferric Oxide

Abstract. A series of copolymers modified with oxidized starch containing maleic anhydride (MA), styrene sulfonic sodium (SSS) and oxidized starch (OS) were synthesized by the free-radical polymerization. The polymerization is initiated by ammonium persulfate. The effects of content of monomer and initiator, reaction time, reaction temperature on dispersion ability for Fe_2O_3 were investigated by single factor experiment. The dispersion ability for Fe_2O_3 measured through UV spectroscopy was studied. The experimental results show that the copolymer has good dispersion ability for Fe_2O_3 when the mass proportion of monomers is OS:SSS:MA = 1:3:1, the mass fraction of initiator in total monomers is 10 %, reaction time is 5 h, and the reaction temperature is 70 ^oC. The morphology of the copolymer was observed by scanning electron microscope (SEM). The experimental results indicate that the prepared copolymer modified with oxidized starch could be used in the corrosion inhibitor of high temperature water.

Introduction

Recent years, the consumption and pollution of industrial water increase significantly with the rapid development of modern industry, which intensifies shortage of fresh water resource [1]. Internal corrosion of metallic pipes is ubiquitous in drinking water distribution systems [2]. Corrosion scales formed by the accumulation of corrosion products could serve as the breeding ground for microbes and sinks for heavy metals or other contaminants [3]. Ferric oxide deposited cause technical and economical problems such as decreased system efficiency and increased chemical cleaning frequency. On the other hand, ferric oxide deposited on the surface of the recycling cooling water system will not only reduce the heat transfer efficiency, but also lead to breed iron bacteria, which cause corrosion under the scale. So, inhibiting and dispersing ferric oxide deposition becomes very important to the cooling water system.

Copolymers have been applied widely in circulating cooling water treatment contribute to their excellent performances such as inhibiting formation of calcium carbonate scale and dispersing ferric oxide (Fe_2O_3) in water [4]. Among carbohydrate polymers, starch was mainly composed of polyhydric glucose unit. The starch derivants with good performance and multi-varieties could be obtained by chemical, physical or biological deep-processing methods [5].

In this paper, a novel environmentally friendly non-phosphorus copolymer (MA-SSS-OS) was prepared by a free radical solution polymerization with maleic anhydride (MA), styrene sulfonic sodium (SSS) and oxidized starch (OS) as monomers, ammonium persulfate as initiatora. The dispersion ability for Fe_2O_3 measured through UV spectroscopy was studied. To the best our knowledge, this is the first time that dispersing ferric oxide of copolymer modified with oxidized starch is reported.

Experimental section

Synthesis of copolymer modified with oxidized starch. A certain amount of maleic anhydride (MA) was dissolved into appropriate deionized water in a four-necked flask encircled with

water-bath at 80°C. Then, styrene sulfonic sodium (SSS) and the ammonium persulfate initiator were added in turn under ambient pressure, the polymerization was carried out at 80°C for 2h. After that, a copolymer MA-SSS was obtained.

A certain amount of oxidized starch (OS) was dissolved into deionized water containing to acetic acid in a four-necked flask encircled with water-bath at 80°C and the solution was stirred for about 2h. Then, the solution was added into the above copolymer. The mixture was stirred for about 5h and was filtered. The sample was heated at 55°C under vacuum for 2h to remove residual solvent. The copolymer (MA-SSS-OS) modified with oxidized starch was obtained.

Dispersion ability for ferric oxide. The dispersion ability for ferric oxide measured through UV spectroscopy as follows: the mixture containing 1.5 mL $CaCl_2$ solution ($0.15mol \cdot L^{-1}$) and 2.5mL $FeSO_4$ ($0.009mol \cdot L^{-1}$) was prepared. To each 100 mL portion of solution, different quantities of the copolymers were added and treated as the test solution. The other portion without the copolymer served as the blank. The pH was maintained at 9 and the temperature at 50°C. After the test period of 5h, the supernatant solutions were analyzed for iron ion retained in the solution at the wavelength of 420nm. The ultimate dispersion ability for ferric oxide (η) was obtained by the formula as below:

$$\eta = \frac{T_0 - T_2}{T_0 - T_1} \times 100\% \qquad (1)$$

where T_0 was the transmittance without heating and copolymer in the solution for 5h; T_1 was the transmittance without copolymer in the solution after heating for 5h; T_2 was the transmittance in presence of copolymer after heating for 5h.

Results and discussion

Effect of mass ratio of OS:SSS on the dispersion ability for ferric oxide. The effect of the mass ratio of OS and SSS on the dispersion ability for ferric oxide (η) was obtained at the fixed reaction time 5 h, temperature 70°C, OS:MA = 1:1(mass ratio) and the amount of initiator 10 %. The results are listed in Table 1.

Table 1. The effect of mass ratio of OS to SSS on dispersion ability for ferric oxide

OS:SSS	1:2	1:2.5	1:3	1:3.5	1:4
η (%)	57.14	66.40	98.80	82.14	76.00

As can be seen from Table 1, the η value increases with increasing mass ratio of OS:SSS. When the mass ratio of OS:SSS is 1:3, the MA-SSS-OS has the highest dispersion ability for Fe_2O_3, and the η value is 98.80%. However, with the mass proportion of OS and SSS further increasing, the η value decreases. Hence, the mass proportion of OS and SSS of 1:3 is chosen for the preparing copolymer in this reaction system.

Effect of mass ratio of OS:MA on the dispersion ability for ferric oxide. The effect of the mass ratio of OS and MA on the dispersion ability for ferric oxide was obtained at the fixed reaction time 5 h, temperature 70°C, OS:SSS=1:3(mass ratio) and the amount of initiator 10 %. The results are listed in Table 2.

Table 2. The effect of mass ratio of OS to MA on dispersion ability for ferric oxide

OS:MA	1:0	1:0.5	1:1	1:1.5	1:2
η (%)	65.87	87.70	98.80	76.98	56.35

As shown in Table 2, the η value increases with increasing mass ratio of OS:MA. When the mass ratio of OS:MA is 1:1, the MA-SSS-OS has the highest dispersion ability for Fe_2O_3, and the η value is 98.80%. However, with the mass proportion of OS and MA is further increasing, the η value decreases. Hence, the mass proportion of OS and MA of 1:1 is chosen for the preparing copolymer in this reaction system.

Effect of reaction time on the dispersion ability for ferric oxide. The effect of the reaction time on the dispersion ability for ferric oxide was obtained at the fixed temperature 70°C, OS:SSS:MA=1:3:1(mass ratio) and the amount of initiator 10 %. The results are listed in Table 3.

Table 3. The effect of reaction time on dispersion ability for ferric oxide

Time (h)	3	4	5	6	7
η (%)	58.85	72.18	98.80	97.62	92.86

As shown in Table 3, the η value increases with increasing reaction time. When reaction time is 5h, the MA-SSS-OS has the highest dispersion ability for Fe_2O_3, and the η value is 98.80%. So, 5h is the best reaction time.

Effect of amount of initiator on the dispersion ability for ferric oxide. The effect of the amount of initiator on the dispersion ability for ferric oxide was obtained at the fixed reaction time 5 h, temperature 70°C and OS:SSS:MA=1:3:1 (mass ratio). The results are shown in Table 4.

Table 4. The effect of amount of initiator on dispersion ability for ferric oxide

Initiator (%)	4	6	8	10	12
η (%)	68.65	74.60	92.86	98.80	93.65

As can be seen from Table 4, the η value increases with increasing amount of initiator. At the amount of initiator is 10%, the polymer OS-SSS-MA has the highest dispersion ability for Fe_2O_3, and the η value is 98.80%. From the obtained results, the dispersion ability for Fe_2O_3 changes little after the amount of initiator is higher than 10%.

Effect of reaction temperature on the dispersion ability for ferric oxide. The effect of the reaction temperature on the dispersion ability for ferric oxide was obtained at the fixed time 5h, OS:SSS:MA=1:3:1(mass ratio) and the amount of initiator 10 %. The results are listed in Table 5.

Table 5. The effect of reaction temperature on dispersion ability for ferric oxide

Temperature (°C)	50	60	70	80	90
η (%)	64.21	73.41	98.80	89.52	80.16

As shown in Table 5, the η value increases with increasing reaction temperature. When reaction temperature is 70 °C, the MA-SSS-OS has the highest dispersion ability for Fe_2O_3, and the η value is 98.80%. Then the dispersion ability for ferric oxide of the copolymer decreases with increasing reaction temperature.

In conclusion, the optimum condition of preparing copolymer is: the mass proportion of monomers is OS:SSS:MA=1:3:1; the mass fraction of initiator in total monomers is 10 %; reaction time is 5 h and the reaction temperature is 70 °C. At the optimum condition, copolymer has the highest dispersion ability for Fe_2O_3 and the value is 98.80 %. The obtained results indicate that the copolymer is efficient Fe_2O_3 dispersion agent and could be used in the system of high hardness water.

SEM micrographs of OS and copolymer. The SEM micrographs of the OS (a) and prepared copolymer (b) are shown in Figure 1. In most cases, surface morphology of materials is of great importance for many technical applications requiring well-defined surfaces or interfaces. The SEM micrograph of OS (Figure 1(a)) shows regular spherical shape. After copolymerization, the copolymer has regular rhombohedron shape. (Figure 1(b)). It might be attributed to the polar difference between OS and copolymer and the destruction of the intermolecular hydrogen bonds and the crystalline regions of OS, which indicates intuitively that the copolymer side chains are introduced into OS main chains.

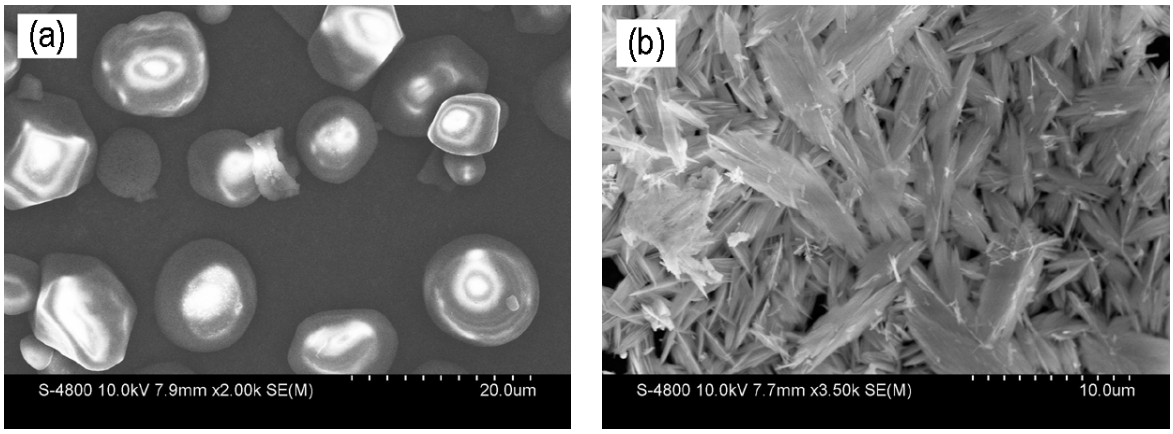

Fig.1. SEM micrographs of OS (a) and copolymer (b)

Conclusions

A novel copolymer modified with oxidized starch was prepared. The optimal condition for the preparation of copolymer is: a OS:SSS mass ratio of 1:3, a OS:MA mass ratio of 1:1, a mass fraction of initiator of 10 %, a reaction time of 5 h and a reaction temperature of 70 ^{o}C. At the optimum condition, copolymer has the highest dispersion ability for Fe_2O_3 and the value is 98.80 %. The SEM micrograph of copolymer indicates that after copolymerization, the copolymer has regular rhombohedron shape. The obtained results indicate that the copolymer is efficient Fe_2O_3 dispersion agent and could be used in the system of high hardness water.

References

[1] Y. Xu, L.L. Zhao, L.N. Wang, S.Y. Xu, Y.C. Cui, Synthesis of polyaspartic acid–melamine grafted copolymer and evaluation of its scale inhibition performance and dispersion capacity for ferric oxide, Desalination 286 (2012) 285-289.

[2] F. Yang, B. Shi, J. Gu, D. Wang, M. Yang, Morphological and physicochemical characteristics of iron corrosion scales formed under different water source histories in a drinking water distribution system, Water Res. 46 (2012) 5423-5433.

[3] V.N. Rajakovic-Ognjanovic, B.N. Grgur, Corroded scale analysis from water distribution pipes, Hem. Ind. 65 (2011) 507-515.

[4] X.X. Gu, F.X. Qiu, X. Zhou, J. Qi, Y. Zhou, D.Y. Yang, Q. Guo, X.R. Guo, Preparation and application of polymer as inhibitor for calcium carbonate and calcium phosphate scales. Int. J. Polym. Mater. 62 (2013) 323-329.

[5] B. Kaur, F. Ariffin, R. Bhat, A.A. Karim, Progress in starch modification in the last decade, Food Hydrocolloid. 26 (2012) 398-404.

Advanced Materials Research Vols. 989-994 (2014) pp 160-163
© (2014) Trans Tech Publications, Switzerland
doi:10.4028/www.scientific.net/AMR.989-994.160

Corrosion Inhibitor Polymer Modified with Acid Activated Attapulgite: Preparation and Performance of Dispersing Ferric Oxide

Jicheng Xu[1, 2], Xinshan Rong[1], Xiaorui Guo[3] and Fengxian Qiu[3,a*]

[1] School of Environment and Safety Engineering, Jiangsu University, Zhenjiang 212013, China

[2] Department of Chemical Engineering, Zhenjiang College, Zhenjiang 212003, China

[3] School of Chemistry and Chemical Engineering, Jiangsu University, Zhenjiang 212013, China

* fxqiu@ujs.edu.cn

Keywords: Attapulgite; Corrosion Inhibitor; Dispersing Ferric Oxide

Abstract. The corrosion inhibitor modified with acid activated attapulgite (CIATP) was prepared with acid activated attapulgite (HATP), styrene sulfonic sodium (SSS), maleic anhydride (MA) as monomers, water as solvent and ammonium persulfate as initiator. The effects of mass ratio of monomer, reaction temperature, the content of initiator and reaction time of preparing CIATP were investigated. The influences of the prepared CIATP concentration, time, pH and temperature of the system on the dispersing ferric oxide efficiency were also investigated. The obtained results showed that the prepared CIATP had excellent efficiency of dispersing ferric oxide, and nearly 98.98 % of dispersing ferric oxide efficiency was obtained. The experimental results indicate the corrosion inhibitor CIATP could be used in the corrosion inhibitor of high temperature water.

Introduction

At the present time, some of the demand for better utilization of the limited water supplies is due to population growth and increasing development [1]. Scale formation is a serious problem encountered in many industries including oil or gas production, water transport, power generation and batch precipitation [2]. Ferric oxide deposited on the surface of the recycling cooling water system will not only reduce the heat transfer efficiency, but also lead to breed iron bacteria, which cause corrosion under the scale. The most common and effective scale control method is the use of scale inhibitors. Copolymer has been used satisfactorily as a specific scale inhibitor in the circulating cooling water systems, because of its strong complexation of functional groups and superior dispersion characteristic of macromolecule [3]. Attapulgite (ATP) is a kind of crystalline hydrated magnesium aluminum silicate with unique three dimensional structures and has a fibrous morphology with exchangeable cations and reactive -OH groups on its surface [4].

In this work, corrosion inhibitor (CIATP) was synthesized with acid activated attapulgite (HATP), styrene sulfonic sodium (SSS), maleic anhydride (MA) as monomers, water as solvent, ammonium persulfate as initiator by the free-radical polymerization. The conditions of preparing CIATP and performance of dispersing ferric oxide were investigated.

Experimental section

Preparation of corrosion inhibitor polymer modified with acid activated attapulgite (CIATP). The ATP (10.0g) was deposed in HCl (100mL, 2.0mol/L) in a flask, and stirred magnetically for 30min at 30^{o}C. Then, the solution was vibrated with the aid of ultrasonic instrument for 10min. After removing the supernatant, the residue was centrifuged and washed with distilled water several times until pH =7 and drying under vacuum at 105 ^{o}C. After grinding, the acid activated attapulgite (HATP) solid was obtained and stored in desiccator. A certain amount of HATP was dissolved in 15 mL of water solution in a four-necked flask encircled with water-bath at 80 ^{o}C and the solution was stirred for about 2h. Then, SSS, MA and initiator ammonium persulfate mixed solution was dropped slowly, and the reaction was left for 5 h under slow agitation. The corrosion inhibitor polymer CIATP was obtained by evaporation- crystallization process.

The performance of dispersing ferric oxide. The dispersion ability for ferric oxide measured through UV spectroscopy as follows: the mixture containing 1.5 mL CaCl2 solution (0.15mol·L-1) and 2.5mL FeSO4 (0.009mol·L-1) was prepared. To each 100 mL solution, different quantities of the copolymers were added and treated as the test solution. The other portion without the copolymer served as the blank. The pH was maintained at 9 and the temperature at 50°C. After the test period of 5h, the supernatant solutions were analyzed for iron ion retained in the solution at the wavelength of 420nm. The ultimate dispersion ability for ferric oxide (η) was obtained by the formula as below:

$$\eta = \frac{T_0 - T_2}{T_0 - T_1} \times 100\% \quad (1)$$

where T_0 was the transmittance without heating and copolymer in the solution for 5h; T_1 was the transmittance without copolymer in the solution after heating for 5h; T_2 was the transmittance in presence of copolymer after heating for 5h.

Results and discussion

Effect of HATP content on the performance of dispersing ferric oxide. Fixed SSS:MA=3:1 (mass ratio), reaction time of 4 h, the reaction temperature of 80oC and the content of initiator 12.0 %, effects of the HATP content on the performance of dispersing ferric oxide are listed in Table 1. The dispersing efficiency of 85.27 % to Fe_2O_3 is obtained when the content of HATP is 11.0 %. This is mainly because graft copolymerization between HATP and organics exist the saturation adsorption quantity; if it is exceeded, the redundant HATP would suspend in the copolymerization system and solutions. Therefore, the chosen content of HATP is 11.0 % in the experiment.

Table 1. The effect of the HATP content on the performance of dispersing ferric oxide

HATP (%)	4.0	7.0	11.0	14.0	17.0
η (%)	48.74	66.77	85.27	53.61	42.32

Effect of mass ratio of HATP:SSS on the performance of dispersing ferric oxid. Fixed the content of HATP of 11.0 %, HATP:MA=1:1.7, reaction time of 4 h, the reaction temperature of 80°C and the content of initiator 12.0 %, effect of mass ratio of HATP:SSS is shown in Table 2. When the HATP:SSS is 1:4, the corrosion inhibitor has the best performance of dispersing ferric oxide. Hence, the HATP:SSS of 1:4 is chosen for further experiments.

Table 2. The of mass ratio of HATP:SSS on the performance of dispersing ferric oxide

HATP:SSS (mass ratio)	1:3	1:4	1:5	1:6	1:7
η (%)	70.85	85.27	82.45	69.28	65.52

Effect of the mass ratio of HATP:MA on the performance of dispersing ferric oxide. Fixed the content of HATP of 11.0 %, HATP:SSS=1:4, reaction time of 4 h, the reaction temperature of 80°C and the content of initiator 12.0 %, effect of the mass ratio of HATP:MA is shown in Table 3. The dispersing efficiency of 85.27% to Fe_2O_3 is obtained when the mass proportion of HATP:MA is 1:1.3. Hence, the HATP:MA of 1:1.3 is chosen in the experiment.

Table 3. The effect of the mass ratio of HATP:MA on the performance of dispersing ferric oxide

HATP:MA (mass ratio)	1:1	1:1.3	1:1.7	1:2	1:2.3
η (%)	42.63	85.27	82.45	51.72	42.95

Effect of mass content of initiator on the performance of dispersing ferric oxide. Fixed the content of HATP of 11.0 %, HATP:SSS:MA=1:4:1.3, reaction time of 4 h and the reaction temperature of 80°C, effect of mass content of initiator is shown in Table 4. At the content of initiator is 10.0 %, the corrosion inhibitor shows the best performance of dispersing ferric oxide, then the dispersing ferric oxide efficiency of the corrosion inhibitor decreases with increasing content of initiator. This is mainly because the initiator content is too little, the relative molecular

weight of the corrosion inhibitor is too big and the molecular chain of the corrosion inhibitor is too long. The carboxylic acid group on either side of the molecular chain can absorb more ferric oxide, and influence the performance of dispersing ferric oxide. Hence, the content of initiator of 10.0 % is chosen in the experiment.

Table 4. The effect of mass content of initiator on the performance of dispersing ferric oxide

Mass content (%)	6.0	8.0	10.0	12.0	14.0
η (%)	38.53	65.83	86.52	85.27	78.06

Effect of reaction temperature on the performance of dispersing ferric oxide. Fixed the content of HATP of 11.0 %, HATP:SSS:MA=1:4:1.3, reaction time of 4 h and the content of initiator 10.0 %, effect of reaction temperature is shown in Table 5. The highest dispersing efficiency of 90.60 % to Fe_2O_3 is obtained when the temperature is 60 ^oC. Hence, the reaction temperature of 60 ^oC is chosen in the experiment.

Table 5. The effect of reaction temperature on the performance of dispersing ferric oxide

Temperature (^oC)	50	60	70	80	90
η (%)	59.87	90.60	77.12	66.14	64.89

Effect of reaction time on the performance of dispersing ferric oxide. Fixed the content of HATP of 11.0 %, HATP:SSS:MA=1:4:1.3, reaction temperature of 60^{o}C and the content of initiator 10.0 %, effect of reaction time is shown in Table 6. When the reaction time is 5h, the corrosion inhibitor has the highest dispersing ferric oxide efficiency which the value is 94.65%. With the extension of reaction time, dispersing ferric oxide efficiency of the corrosion inhibitor changes little. Therefore, 5 h is the balance point of copolymerization, and is chosen in the experiment.

Table 6. The effect of reaction time on the performance of dispersing ferric oxide

Time (h)	2	3	4	5	6
η (%)	47.65	79.94	93.73	94.65	94.57

In conclusion, the optimum conditions of preparing CIATP are obtained as follows: the content of HATP of 11.0 %, ATP:SSS:MA=1:4:1.3 (mass ratio), reaction temperature of 60 oC, the content of initiator in total monomers 10.0 % and reaction time of 5 h.

Influence of the CIATP concentration on the dispersing ferric oxide efficiency. The influence of the CIATP concentration on the dispersing ferric oxide efficiency is shown in Figure 1(a) at the fixed the temperature of 50^{o}C, the time of 5 h, Fe^{2+} concentration of 0.01 mol/L and the pH value of 9.0. When the CIATP concentration is 0.16 g/L, the highest dispersing ferric oxide efficiency is reached; and the value is 95.86 %. However, the dispersing ferric oxide efficiency decreases when the CIATP concentration is beyond 0.16 g/L. This is mainly because the CIATP contains hydroxide radical and is able to coordinate with metal ions to generate stable complex, thereby preventing ferric oxide from precipitation. Moreover, the CIATP contains carboxyl and sulfonic acid groups; these active groups can bond with Fe^{2+} in the solution to form chelates which can be adsorbed on the surface of the corrosion inhibitor. With the increase of the CIATP concentration, the bond of corrosion inhibitor with the Fe^{2+} ions increases; and the dispersing ferric oxide efficiency increases. When the CIATP concentration is beyond the optimal value; such as 0.16 g/L in this experiment condition, the Fe^{2+} ions in the solution almost are chelated. The dispersing ferric oxide efficiency does not increase, but also the efficiency decreases, which is due to the flocculation of the copolymer by the polarity action of active groups.

Influence of time on the dispersing ferric oxide efficiency. Fixed the temperature of 50 ^oC, the CIATP concentration of 0.16 g/L, the Fe^{2+} concentration of 0.01 mol/L and the pH value of 9.0, the influence of time on the dispersing ferric oxide efficiency is shown in Figure 1(b). When the time is 3 h, the CIATP has the highest dispersing ferric oxide efficiency; and the value is 98.07 %. After 8 h, the dispersing ferric oxide efficiency is stable. This may be due to the fact that at a certain time, the reaction of dispersing ferric oxide has completely finished, so there is a little effect even with the extension of bath time.

Influence of temperature and pH on the dispersing ferric oxide efficiency.

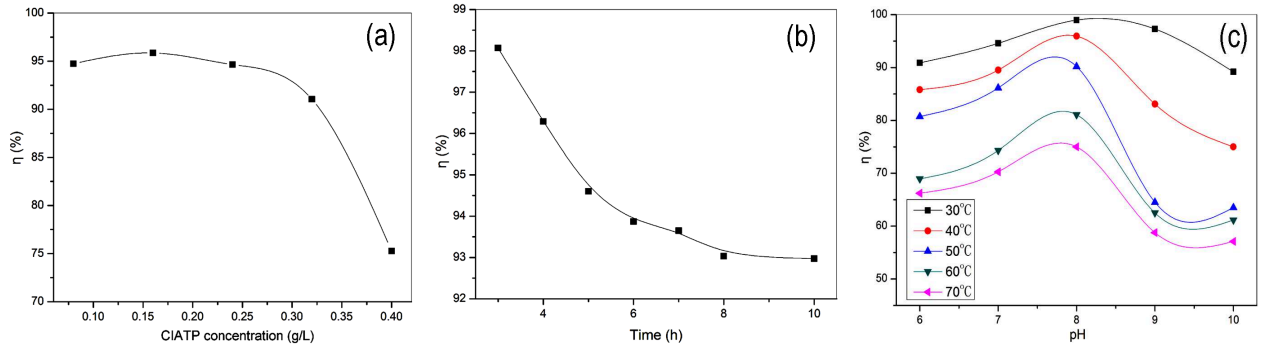

Fig.1. The experimental results

Fixed the time of 5 h, the CIATP concentration of 0.16 g/L, the Fe2+ concentration of 0.010 mol/L, influences of temperature and pH on the dispersing ferric oxide efficiency are shown in Figure 1(c). With temperature rising, the dispersing efficiency decreases. This can be ascribed that with the increase of water temperature, microcrystal particles move more quickly and the speed of particle colliding with each other is even faster, which accelerates the formation of scale easily. From the Figure 1(c), the dispersing ferric oxide efficiency increases steeply with increasing of pH value of the solution from 6.0 to 8.0. Then, the dispersing ferric oxide efficiency decreases with the increase pH value of the solution, which indicates that the dispersing ferric oxide efficiency for the CIATP is influenced greatly by the system acidity. The results show that the groups on the CIATP, such as carboxyl, phosphite and sulfonic acid groups have better dispersing ferric oxide efficiency in basic solution than that in acidic solution. When pH value of the solution is 8.0, the CIATP has the highest dispersing ferric oxide efficiency, and the value is up to 98.98%.

Conclusions

A novel corrosion inhibitor polymer modified with acid activated attapulgite (CIATP) was prepared by a free radical solution polymerization. The optimum conditions of preparing CIATP were obtained as follows: the content of HATP of 11.0 %, ATP:SSS:MA=1:4:1.3 (mass ratio), reaction temperature of 60oC, the content of initiator in total monomers 10.0 % and reaction time of 5 h. The dispersing ferric oxide efficiency was investigated and the result was up to 98.98%. The experimental result shows that the prepared corrosion inhibitor CIATP has a high capacity of dispersing ferric oxide and could be used in the corrosion inhibitor of recycled water.

References

[1] Y. Xu, L.L. Zhao, L.N. Wang, S.Y. Xu, Y.C. Cui, Synthesis of polyaspartic acid–melamine grafted copolymer and evaluation of its scale inhibition performance and dispersion capacity for ferric oxide, Desalination 286 (2012) 285-289.

[2] F. Yang, B. Shi, J. Gu, D. Wang, M. Yang, Morphological and physicochemical characteristics of iron corrosion scales formed under different water source histories in a drinking water distribution system, Water Res. 46 (2012) 5423-5433.

[3] V.N. Rajakovic-Ognjanovic, B.N. Grgur, Corroded scale analysis from water distribution pipes, Hem. Ind. 65 (2011) 507-515.

[4] X.X. Gu, F.X. Qiu, X. Zhou, J. Qi, Y. Zhou, D.Y. Yang, Q. Guo, X.R. Guo, Preparation and application of polymer as inhibitor for calcium carbonate and calcium phosphate scales. Int. J. Polym. Mater. 62 (2013) 323-329.

[5] B. Kaur, F. Ariffin, R. Bhat, A.A. Karim, Progress in starch modification in the last decade, Food Hydrocolloid. 26 (2012) 398-404.

Advanced Materials Research Vols. 989-994 (2014) pp 164-167
© (2014) Trans Tech Publications, Switzerland
doi:10.4028/www.scientific.net/AMR.989-994.164

Preparation of a novel magnetic stir bar for the pretreatment of the plasticizers in lake water

Rui Feng

Department of Public Teaching, Nanyang Medical College, Henan 473061, China

fengrui20032006@163.com

Keywords: Stir bar; Plasticizer; Polymerization; High performance liquid chromatography

Abstract. An in-situ polymerization method was used for the preparation of a novel stir bar based on neodymium magnet ($Nd_2Fe_{14}B$) powders. The processes were carried out by several steps including the enwrapping of $Nd_2Fe_{14}B$, the modification of the enclosed $Nd_2Fe_{14}B$, and the form of organic polymers on the surface of the modified powders. It was successfully used to enrich the plasticizers in water sample by stir bar sorptive extraction (SBSE). The experimental conditions for SBSE, such as the choice of extraction sorvents, salt concentration, extraction and desorption time were optimized in detail. Coupled to high performance liquid chromatography (HPLC), the recoveries of dibutyl phthalate (DBP), dimethyl phthalate (DMP), diethyl phthalate (DEP) were 89.2%~92.1%**,** 91.9%~96.6% and 94.3%~96.7%, respectively; the linear relationships between the concentration 5 μg/L and 800 μg/L for DBP were obtained; the limits of detection ranged from 0.09 μg/L to 0.21 μg/L in the optimal conditions.

Introduction

Food, beverage and bottled water are generally the major sources of human exposure to PAEs due to the wide addition during their industrious production [1]. Effectively detection and supervision of the composition and content in different samples is very important and necessary, current research efforts are directed towards the development of simple and sensitive analytical methods, capable of accurately determining the trace quantities of PAEs in different complex samples. Some preconcentration techniques were generally selected as the sample preparation procedures, based on liquid-liquid extraction, solid-phase extraction (SPE), and solid-phase microextraction (SPME), followed by gas chromatography (GC), liquid chromatography (LC), capillary electrophoresis (CE), or gas chromatography and mass spectrometry (GC-MS) [2-4]. SBSE, as well as SPE or SPME, are popular sample preparation techniques based upon sorptive extraction. It integrates extraction and stirring in the same device, avoiding potential analytes losses due to the introduction of an external stirring device. In this paper, a common stir bar based on organic-based polymers was initially fabricated by bulk polymerization. The obtained magnetic stir bar was applied to preconcentrate and determine some typical PAEs such as DBP, DEP and DMP (see **Fig.1**) in the lake water by HPLC, and better recoveries in three spiked levels were obtained under the optimal conditions.

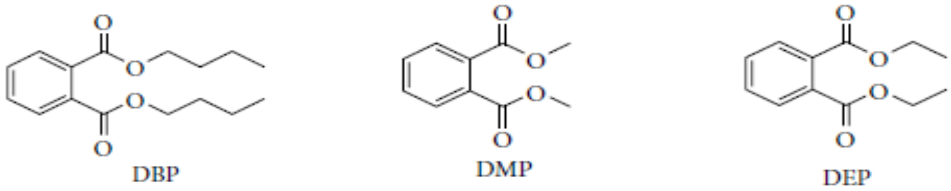

Fig.1. The molecular structures of the studied PAEs

Experimental

Instrument

HPLC experiments were carried out by a P1201 HPLC system (Elite Analytical Instrumental Co. Ltd., Dalian, China), equipped with an injector with a 20 μL quantitative tube (Rheodyne 7725i), and a detector with a changeable ultraviolet-visible wavelength in the range of 190-700 nm. A chromatographic column packing with ODS-C_{18} (150 ×4.6 mm，5 μm) was used as the stationary phase and a binary solvent of ACN/H_2O (V/V=80/20) was used as the mobile phase，the flow rate is 1ml/min, the detection wavelength was set at 224nm, detection was carried out at room temperature. Quanta 200 Scanning Electron Microscopes (FEI，Hillsboro，Oregon，USA）, magnetic separation rack(Zhengzhou Innosep Biosciences Co. Ltd.), HH-4 thermostat water bath (Henan Zhicheng Scientific Development Co.Ltd.), a BOS60-S Electric Mixer with digital screen（Jinghua Huaou Experimental Instrument Factory).

Materials and Chemicals

99.5% α-methacrylic acid（MAA）, 98% γ-methacryloxypropyltrimethoxysilane (MPTMS), 98% ethylene dimethacrylate (EDMA), tetraethyl orthosilicate (TEOS), 99.5% acetone, methanol (MeOH), acetonitrile (ACN), toluene, CH_3COOH, NaCI, CH_3CI were purchased from Beijing Bailingwei Chemical Reagent Company and Tianjing Chemical Reagent Company, China. 2, 2-azobisisobutyronitrile (AIBN, analytically pure) was purchased from Tianjin Guangfu Fine Chemical Research Institute; EDMA were extracted with 5%-10% aqueous sodium hydroxide and water before use. 99.5% dibutyl phthalate (DBP), 99.5% dimethyl phthalate (DMP), 99.5% diethyl phthalate (DEP) were purchased from Sinapharm Chemical Reagent Beijing Co.,Ltd. Rb-Fe-B (sintered NdFeB magnet), with positive component ratio of Nd to Fe in the main phase $Nd_2Fe_{14}B$ 1 to 7, density is ≥ 7.5, remanence induction strength classically 12.5 kilogauss (KG)s, and particle size ≤ 30 μm, was provided by Beijing Zhong Ke San Huan Hi-tech Co., Ltd. Other reagents are analytically pure and water used in the experiment was double distilled water.

Results and discussion

Preparation of the magnetic stir bar

The preparation of the monolithic stir bar was carried out step by step as follows [5]: Firstly, the purchased magnetic powder was immersed in acetone and alkaline solution for 30 min, respectively, to remove the organic compounds from the surface, followed by vacuum drying for further use. The monolithic stir bars were synthesized by thermal polymerization in the glass tube using the modified $Nd_2Fe_{14}B$ magnetic particles as the starting materials. Twenty grams of the pretreated dried magnetic powder was put into 50 mL acetone and 4 mL distilled water, 5 mL ammonia solution and 5 mL TEOS were added dropwisely while stirring (500 rpm) at room temperature, then stirred for additional several hours. Magnetic powders were collected using magnetic separation rack, washed with distilled water and vacuum dried at 120 °C to obtain SiO_2 coated magnetic powders for next modification. γ-MAPS (20 mmol/L) was put into toluene to make 10% (v/v) solution, and 20 g magnetic powder was put into this solution in a conical flask to be shaken for 2 h in order to obtain more unsaturated double bonds on the surface of the enclosed magnetic powders. Finally, the monoliths were formed on the surface of $Nd_2Fe_{14}B@SiO_2$ by the copolymerization of vinyl end groups with functional monomer, BMA, EDMA, AIBN.

It should be noted that the modified $Nd_2Fe_{14}B@SiO_2$ microparticles can be further cross-linked due to the broken vinyl end groups during thermal polymerization, so as to form a magnetic monolithic bar in the glass tube in situ. Finally, MAA (4 mmol, 0.341 mL) were dissolved into 5 mL chloroform, ultrasonic vibrated for 15 min, and then filled with nitrogen following by 30 min standing for molecular self-assembling. After that, EDMA (30 mmol, 5 mL) and ethyl cellulose (EC) (0.1 g) (accounts for 1% of the total volume) were added, ultrasonic vibrated until EC was fully dissolved, and then added with AIBN (0.03 g). The prepared solution (480μL) and the modified magnetic powder (2.48 g) were filled into a glass tube (0.4 cm in diameter, 8 cm in length) in 6 times (solution was filled before the magnetic powders). The filled glass tube was ultrasonic

vibrated for 10 min to increase the compaction degree. Then the tube was sealed with rubber plug, and incubated for 42 h in 80 °C water bath. After thermal polymerization, the glass tube was cracked and the the resulted stir bar was cut into several parts with a length of 1 cm. The magnetic stir bar self stirred for 12 h in methanol/acetic acid (v/v=9:1) solution, and the solution was changed every 3 h. Then, the stir bar self stirred for 6 h in pure methanol solution, and the solution was changed every 2 h, until no impurity peak can be detected.

Optimization of SBSE Extraction

Optimization of SBSE procedure was carried out in a 5 mL vial sealed with a silicone-rubber septum cap at a constant stir speed of 400 rpm. It was accomplished by directly insert a prepared stir bar in 0.5 μg/mL DBP standard solution for this investigation. Moreover, the desorption was carried out by moving the stir bar in a 1 mL vial, followed by the addition of 200 μL desorption solvent and ultronsonication about 20 min. Evaluation of the extraction parameters in different conditions was carried out using HPLC peak area which indicated the analyte concentration. Extraction and elution reagents, stirring rate, extraction and elution time, salt concentration and pH were, respectively, optimized for the SBSE procedure in detail. The final optimal condition was finally selected as follows: water is selected the optimal extraction solution, compared with hexane, toluene, chloroform and ACN, and extraction time 70 min, 15% (w/w) NaCl was selected as the optimal salt concentration, 200 μL ACN as desorption solution, ultrasonic, and desorption for 20 min.

The absorption curve of the prepared stir bar

The extraction amount of the stir bar was investigated using a series of DBP standard solutions in the range of 5-2500 μg/L. As shown in **Fig.2**, it indicated that the peak area of DBP increased continuously along with the increase of concentration for the resulted stir bar. Overall, the extraction reached equilibrium when the concentration was up to 800 μg/L, with a BPA peak area about 400 mV·s or so.

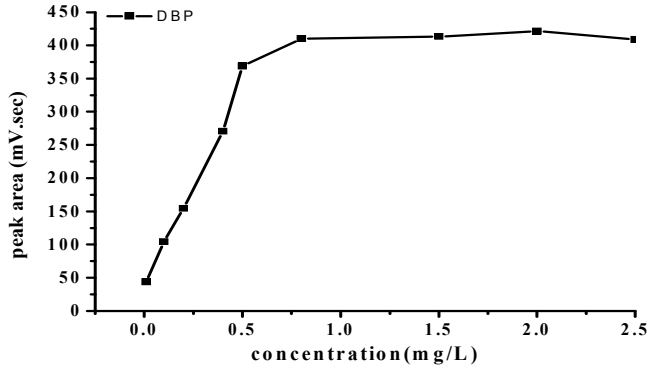

Fig.2. DMP adsorption curve of stir bar in the concentration range of 0-2.5 mg/L

The calibration curve was constructed using the areas of the chromatographic peaks measured (y) at different increasing levels (x) for the mixture of DBP, DEP and DMP. Good linearity was observed for three analytes, respectively, in the selected concentration range of 5-800 μg/L. The regression equations and limited of detection (LOD, 3S/N) were calculated as follows: y_{DMP}=89.895x+13.11 (R=0.998, LOD=93 ng/L); y_{DEP} =84.573x+11.3 (R = 0.996, LOD=150ng/L); y_{DBP} =85.527x+8.5813 (R=0.998, LOD=210 ng/L).To demonstrate the suitability and potential application of the developed SBSE-HPLC method for real analysis, the recovery experiments were carried out by spiking three different levels of the mixture of DBP, DEP and DMP into the bottled water. The accuracy and precision of the method were assessed by performing analyses of spiked samples in five replicates. Higher relative recoveries in the range of 91.9-96.6%,94.3-96.7% and 89.2-92.1% for DMP, DEP and DBP were obtained at three spiked concentration of 100, 200 and 400 μg/L, respectively, corresponding to their relative standard deviations (RSD, n = 5) of 2.5-4.1%,

3.2-5.4% and 2.9-4.7% accordingly. The relative chromatograms were shown in Fig.3, the real sample of lake water (c) was detected by HPLC, but no PAEs was found compared with the retention time of the mixed standards of DBP, DEP and DMP (b). It should be noted that some peaks from impurities were removed after the real sample were pre-concentrated by SBSE procedure (see b). Furthermore, after the spiked sample was subject to the SBSE (a) procedure, the sensitivities for three analytes were greatly enhanced owing to the enrichment of the stir bar.

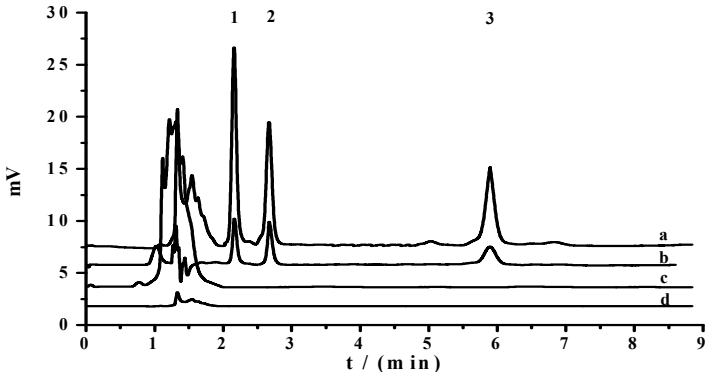

Fig.3. HPLC chromatograms of lake water sample

(a) lake water spiked with 0.1mg/L DMP, DEP and DBP, respectively; (b) 0.1mg/L mixed standards of DMP, DEP and DBP; (c) lake water; (d) lake water after pretreatment by SBSR; Peak identification: 1.DMP, 2.DEP, 3.DBP.

Conclusions

A novel stir bar based on organic polymers was successfully prepared and used for the detection of typical PAEs coupled to HPLC. It will potentially be used for the pretreatment of general samples in the application of SBSE techniques in the future.

References

[1] Xiaojia Huang, Ningning Qiu, Dongxing Yuan, Qingmei Lin. Preparation of a mixed stir bar for sorptive extraction based on monolithic material for the extraction of quinolones from wastewater[J]. Journal of Chromatography A, 2010 (1217) 2667–2673.

[2] Junko Nishioka,Chihiro Iwahara,Mikiko Kawasaki,Fumiko Yoshizaki,Hitoshi Nakayama,Kenji Takamori,Hideoki Ogawa,Kazuhisa Iwabuchi. Di-(2-ethylhexyl) phthalate induces production of inflammatory molecules in human macrophages [J]. Inflammation Research, 2012(61)69–78.

[3] Feng Zeng, Kunyan Cui , Zhiyong Xie, Min Liu, Guoquan Sun, Yujun Lin, Danling Luo and Zunxiang Zeng. Phthalate esters (PAEs): emerging organic contaminants in agricultural soils in urban areas around Guangzhou, China [J]. Environmental Pollution, 2008 (156) 425–434.

[4] Rawi Ramautar, Gerhardus J. de Jong and Govert W. Somsen. Developments in coupled solid-phase extraction-capillary electrophoresis 2009–2011[J]. Electrophoresis, 2012 (33)243–250.

[5] Kunfeng Liu, Rui Feng, Yuping Zhang, Jun Chen, Lianyang Bai. Selective solid-phase extraction of bisphenol A using a novel stir bar based on molecularly imprinted monolithic material [J]. Journal of Chinese Chemical Society, 2014 (61) 420-424.

Advanced Materials Research Vols. 989-994 (2014) pp 168-171
© (2014) Trans Tech Publications, Switzerland
doi:10.4028/www.scientific.net/AMR.989-994.168

Simulation of CVD diamond film growth by method of revised KMC

Li-zhu Zhang[1,a], Fu-zhong Wang[2,b]

[1]School of science, Tianjin University of Technology and Education, Tianjin, 300220, China

[2]Department of Physics, Tianjin Polytechnic University, Tianjin, 300387, China

[a]zlzjcb@163.com,[b]wangfuzhong@163.com

Keywords: simulation, Chemical Vapor Deposition diamond film, Kinetic Monte Carlo method

Abstract. The growth of CVD diamond film was simulated by using revised KMC method. The simulation was conducted at CH_3 radical concentration (0.01%-0.03%) and atomic hydrogen concentration (0.01%-0.5%). The results showed that: The CVD diamond film growth under revised KMC method is superior, which is in good agreement with the experimental results. The concentration of CH_3 ([CH_3]) and the concentration of atomic H ([H]) can produce important effects on the film deposition rate, surface roughness and the concentration of atom H embedded in the film.

Introduction

CVD (Chemical Vapor Deposition) diamond film is a material of many unique properties. These properties have created potential opportunities for diamond film in mechanical, electronic, thermal, optical and chemical applications among others [1][2][3]. Even though quick progress has been made in the CVD diamond film growth [4] [5], however, the growth mechanism of diamond film is not well understood yet, especially the precise relationship between processing conditions [6].

In our previous study, the growth of CVD diamond film in C-H system and C-H-Cl system was simulated by using revised Kinetic Monte Carlo (KMC) method [7][8]. In the article, the growth of CVD diamond film will be simulated under a new process.

Method

Diamond film is usually deposited at sub-atmospheric pressure (20 Torr). The typical deposition conditions are as following: A feed gas of H_2 containing a small fraction of hydrocarbon precursor (often 1% CH_4 by volume) is supplied to the growth reactor and activated by exposure to a heat source. The growth substrate is in contact with this activated gas and diamond deposition occurs mainly by the reaction of the substrate with H, C, CH, CH_2, C_2 and C_2H_2 etc. according to a set of chemical reactions. These chemical reactions are all included in a certain chemical reaction model [9] we term it as B-S model hereafter.

The film growth simulation starts on an H-passivated diamond substrate. All lattice sites are fixed at their diamond cubic positions. The temporal evolution of the diamond surface is simulated by means of a modified KMC method [8]. Within this method, one surface reaction is allowed to take place at one surface site during each time step. At each time step, a chemical reaction is selected among all possible reactions, which can occur under B-S model [9]. After a reaction has occurred, the total number of possible reactions is updated and the procedure is repeated. Traditional CVD diamond film growth process conditions are as following: Substrate temperature T_s=1200K, concentration of atom hydrogen [H] =0.2%, [H_2] =88.9%, [CH_3] =0.02%, [C_2H_2] =0.2%, and P=20Torr. We call this the standard case.

In the paper, we introduce a new growth process of CVD diamond film. The new growth model is carried out as follows: at first, the concentration of CH_3 and C_2H_2 is set to 0.006% and 0.07%, much lower than those in standard case, respectively. Other parameters are in the same value with the standard case. In the whole process, we assume that all the parameters in this step are invariable. CVD diamond film grows in such condition for a period of time (usually the time of some islands formed on the growth surface). Then the concentration of CH_3 and C_2H_2 is increased to standard case.

The film is allowed to grow in the z-direction while periodic boundary conditions are applied in the x and y directions in order to avoid the film edge affects. The size of the computational lattice in x-y plane, where $d_{(u\ v\ w)}$ is the spacing of the (u v w) diamond planes. The substrate used in this study is partially shown in Fig. 1.

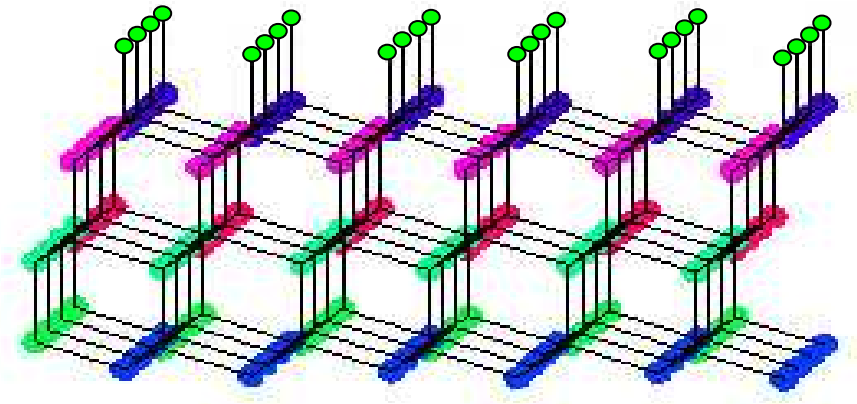

Fig.1 Part of the diamond substrate for CVD diamond film growth

Influence of [CH_3] on film deposition

Keep all the other parameters constant and set [CH_3] = 0.01%, 0.02% and 0.03%, respectively. The effect of [CH_3] on the film deposition rate is examined (see Fig. 2). This plot shows that the deposition rate of diamond film will increase if the [CH_3] is elevated. Since as the main growth CVD diamond film, increasing [CH_3] means the enhancing of the adsorption of CH_3 to the growth surface, which will definitely speed up the film deposition.

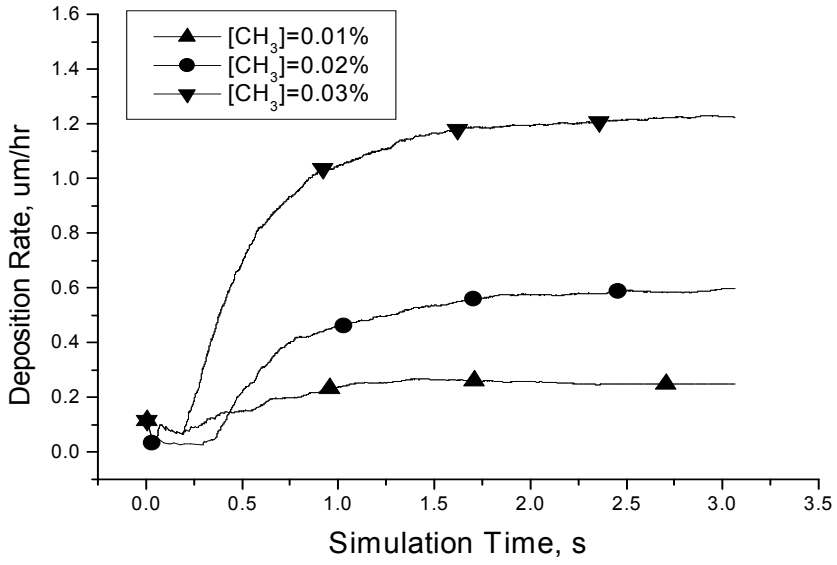

Fig. 2 Variation of deposition rate at different [CH_3] with deposition time

Influence of [H] on film deposition

Fig.3 shows the effect of [CH_3] on the film surface roughness. In the work, increasing the [CH_3] will make the film surface coarser. So from the simulation result, we can draw a conclusion: the higher the deposition rate, the coarser the diamond film, which is in good agreement with the prediction of reference [9].

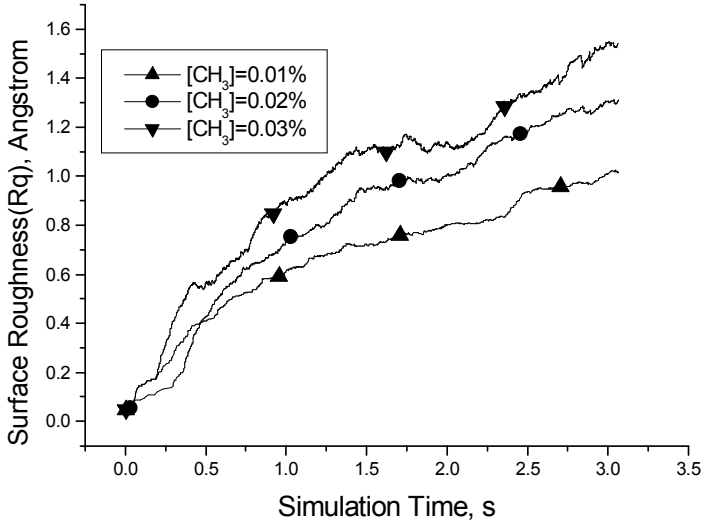

Fig. 3Variation of film surface roughness at different [CH3] with deposition time.

The influence of [CH_3] on the concentration of atom H embedded in film is shown in Fig. 4. Even though there is hardly the atom H embedded in the film in the first stage of the two-step model, however, the lower deposition rate in this stage limits its further application. From the second stage, we can find that the concentration of atom H embedded in the film increases with [CH_3]. This can be due to the indirect influence of [CH_3] on film deposition rate.

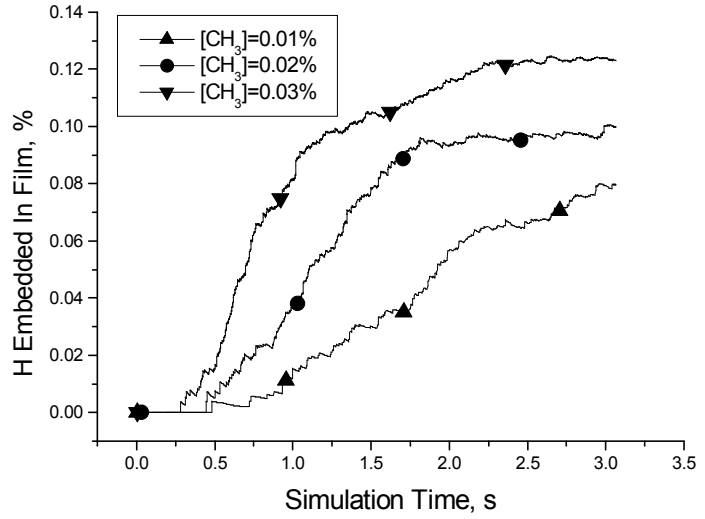

Fig. 4 Influences of [CH3] on the concentration of atom H embedded in film.

Keep all the other parameters constant and set [H] =0.01%, 0.05%, 0.1%, 0.2%, 0.3% and0.5%, respectively. The effect of [H] on film deposition rate is shown in Fig. 8. The deposition rate increases with [H] at first, then it decreases with the increasing [H]. Because too much atomic hydrogen causes unnecessarily strong abstraction, the formation of dimers will increase, which results in the deterioration of diamond film quality. So [H] =0.1% seems the optimal value in the present study. For each [H] value, the deposition rate of the new model is obviously higher than that of standard case.

Table 1 depicts the influences of [H] on film surface roughness and atom H embedded in film, respectively. It can be found that as the increasing of [H], the film becomes coarser. Even though when [H] equals to 0.02%, the film has smoother surface and less atom H embedded. However, its lower deposition rate at this [H] limits its further application. The variation tendency of Table 1 indicates that the concentration of atom H embedded in film is in proportional with the deposition rate.

Table 1 Influences of [H] on film deposition rate and surface roughness

H Concentration (%)	Deposition Rate(μ m/h)	Surface Roughness(Angstrom)
0.01	0.19	0.68
0.05	0.56	1.09
0.1	0.75	0.98
0.2	0.64	1.31
0.3	0.52	1.17
0.5	0.49	1.05

Conclusions

From the present simulation experiments of CVD diamond film growth, following conclusions can be drawn:

(1) The concentration of CH_3 can also influence the growth of CVD diamond film. The higher the concentration of CH_3, the faster the film growth, and the worse the film quality.

(2) Increasing the concentration of atom H can to some extent speed up film deposition rate, however, too much atom H on the contrary will hinder film grow and make the film coarser, therefore the concentration of atom H should be controlled to a constant value, in our simulation, 0.1% atom H is desirable.

Acknowledgements

This work was supported by the Tianjin application fundamental and frontier technology research projects（14JCYBJC17100）and Tianjin University of Technology and Education research projects (KJY1313).

References

[1] Y. Mitsuda and K. Kobayashi: Thin solid Films 345 (1999), p. 55

[2] K. V. Ravi: Mater. Sci. Eng. B 19 (1993), p. 203

[3] W. Yarbrough and R. Messier: Science .247 (1990), p. 688

[4] F. C. Hong, G. Liang, J. Wu, D. Chang and H. Hsieh: Appl. Phys. Lett. 63, 23 (1993), p. 3149

[5] J. C. Angus and C. C. Hayman: Science. 241 (1988), p. 913

[6] X. Z. An, Y. Zhang, G. Q. Liu, X. G. Qin, F. Z. Wang and S. X. Liu: Chinese Physics Letters.19,7 (2002), p. 1019

[7] F. Silva, X. Bonnin, J. Scharpf, A. Pasquarelli, Diamond Relat. Mater. 19 (2010), p.397.

[8] H. Yamada, A. Chayahara, Y. Mokuno, S.I. Shikata, Diamond Relat. Mater. 18 (2009), p.117.

[7] X. Z. An: Ph.D. thesis, University of Science & Technology, 2002

[8] Y. Zhang: Ph.D. thesis, University of Science & Technology, 2001.

[9] C. C. Battaile, D. J. Srolovitz, I. I. Oleinik, D. G. Pettifor, A. P. Suton, S. J. Harris and J. E.Butler: J. Chem. Phys. 111,9 (1999) , p.4291

Advanced Materials Research Vols. 989-994 (2014) pp 172-176
© (2014) Trans Tech Publications, Switzerland
doi:10.4028/www.scientific.net/AMR.989-994.172

Relaxation properties of the Solid Propellant Based on Hydroxyl-Terminated Polybutadiene

Zhimin Xie[a], Sichi Chen[b], Youshan Wang[c]

National Key Laboratory of Science and Technology on Advanced Composites in Special Environment, Center for Composite Materials, Harbin Institute of Technology, Harbin 150001, P.R. China

[a]xiezhm@hit.edu.cn, [b]csc0000000@163.com, [c]wangys@hit.edu.cn

Keywords: HTPB; Propellant; Relaxation; Master curve; Transformation relation

Abstract. The polymer-based propellant is a typical viscoelastic material. Better understanding of the relaxation properties of the propellant in the storage conditions is of great importance for predicting the lifetime. Due to the component complexity of the composite propellants, the transformation relation between the relaxation modulus and the complex modulus may not be suitable for all kinds of propellants. In the present work, we focused on the transformation of the relaxation modulus and complex modulus for the HTPB propellant. The master curves for the relaxation modulus and the storage modulus of the aged/unaged HTPB propellants were obtained by performing the stress relaxation tests and DMA tests, respectively. It was found that there existed a great difference in the double logarithmic plot between relaxation modulus and storage modulus master curves. Moreover, the testing results for the relaxation modulus and the storage modulus were well fitted by an empirical transformation relation with three segment-related coefficients. These three coefficients were determined by using the unaged samples, and then were applied to estimate the relaxation modulus of the aged samples. A good agreement between the calculation and the experimental results was also found, revealing that the three coefficients were insensitive to the aging time.

Introduction

The solid propellant based on the hydroxyl-terminated polybutadiene (HTPB) usually contains the ammonium perchlorate (AP), aluminum powder (Al) solids and additives, e.g. plasticizers. The combination of the polymer degradation due to the oxidizability of AP and the diffusion of the plasticizers in the storage condition may deteriorate the physical properties of the propellant [1,2]. The polymer-based propellant is a typical viscoelastic material. Therefore, better understanding of the relaxation properties of the propellant in the storage conditions is of great importance for predicting the lifetime. Two experimental methods, quasi-static extension and dynamic mechanical analysis (DMA), are commonly used to measure the relaxation properties of the viscoelastic materials [3-5]. The relaxation modulus in time domain and the complex modulus in frequency domain can be obtained by the two means, respectively. Compared with the time-consuming measurement for the relaxation modulus, the DMA testing for the complex modulus costs less time. It has been accepted that there exists a transformation relation between the relaxation modulus and the complex modulus [6]. Thus, the relaxation modulus may be easily estimated by conducting DMA tests based upon the transformation relation. Shen [4] presented an approximate relation between the storage modulus and relaxation modulus in terms of the HTPB propellants. However, there was a large deviation between the calculations and the test results when the expression was applied. Zhang [5] proposed a simplified transformation formula for the Nitrate Ester Plasticized Polyether (NEPE) propellant, and discussed the evaluation method for the NEPE aging under an assumption that there was a constant difference between the static relaxation modulus and the dynamic storage modulus. Due to the complexity of the composite propellants, the transformation formula may not be suitable for all kinds of propellants. In the present work, we focused on the transformation of the relaxation modulus and complex modulus for the HTPB propellants.

Relation of relaxation modulus to complex modulus

According to the linear theory of viscoelasticity, the transformation relation of the relaxation modulus $E(t)$ to the complex modulus $E(\omega)$ is expressed [6] as,

$$E'(\omega) = E_e + \omega\int_0^\infty \left[E(t) - E_e\right]\sin\omega t dt\,, \tag{1}$$

$$E''(\omega) = \omega\int_0^\infty \left[E(t) - E(\infty)\right]\cos\omega t dt\,, \tag{2}$$

where Ee is the equilibrium modulus; $E'(t)$ and $E''(t)$ are the dynamic storage modulus and loss modulus, respectively. Furthermore, one may get the following formulas by means of the Fourier transform, i.e.

$$E(t) = E_e + \frac{2}{\pi}\int_0^\infty \frac{1}{\omega}\left[E''(\omega)\right]\cos\omega t d\omega\,, \tag{3}$$

$$E(t) = E_e + \frac{2}{\pi}\int_0^\infty \frac{1}{\omega}\left[E'(\omega) - E_e\right]\sin\omega t d\omega\,. \tag{4}$$

Thus the static relaxation modulus $E(t)$ can be calculated if the complex modulus $E(\omega)$ is known. However, Eq.(3) and Eq.(4) are simple transformation relations mathematically. In practice, this set of relationships is not applicable so that some approximate transformation formulas are often used as follows [7],

$$E(t) = E'(\omega) - 0.4E''(0.4\omega) + 0.014E'(10\omega)|_{\omega=1/t}\,. \tag{5}$$

In view of the difference in the master curves between the storage modulus and the relaxation modulus for the HTPB propellant, Shen [4] proposed an exponential function of $a\exp[\pm(b\pm c\log t)]$ to modify the transformation relation. The approximate formula was then obtained as [4],

$$E(t) \approx 0.282\exp\left(-0.108 + 0.015\log t\right)E'(\omega)|_{\omega=1/t}\,. \tag{6}$$

It was found that the deviation cannot be neglected in some cases, which may attribute to the assumption that there was a constant difference in the master curves between the storage modulus and the relaxation modulus. In the present work, a term of $a+(b\log t/t_0)^c$ with three constants was incorporated into the transformation relation, and a segmented correction method was used to fit the measured curves.

Experimental

The aging experiments were performed in an oven with an electric heating oil bath, model DU-288. To evaluate the effects of aging on the relaxation properties, the samples were aged for 30 days at 50°C. The unidirectional tensile stress relaxation tests were conducted according to the Chinese Standard QJ 2487-1993 with an Instron Tester, Model 3365 at 70°C, 50°C, 20°C, 0°C, -20°C and -40°C. The initial strain was set to 5%. The acquisition time for the relaxation force is 2-1000s.

The dynamic complex modulus was measured by means of a commercial dynamic mechanical analyzer (TA Instruments, DMA Q800, USA), using rectangular specimens of about 35mm in length, 13mm width and 3mm thickness, and operated in the single cantilever mode. The scanning temperature ranges from -60°C to 60°C every 5°C at frequency of 1, 2, 4, 8, 16Hz.

Results and discussion

The relaxation modulus master curves of the aged/unaged HTPB propellants in the double logarithmic plot are shown in Fig.1. The storage modulus of the aged/unaged HTPB propellants at different frequencies was measured, and then the storage modulus master curves at the reference temperature of 20°C were obtained by performing the time-temperature superposition (TTS) procedure based on the principle of the equivalence of time and temperature, as shown in Fig.2, where a_T is a shift factor, T_s and T are the reference temperature and the test temperature, respectively.

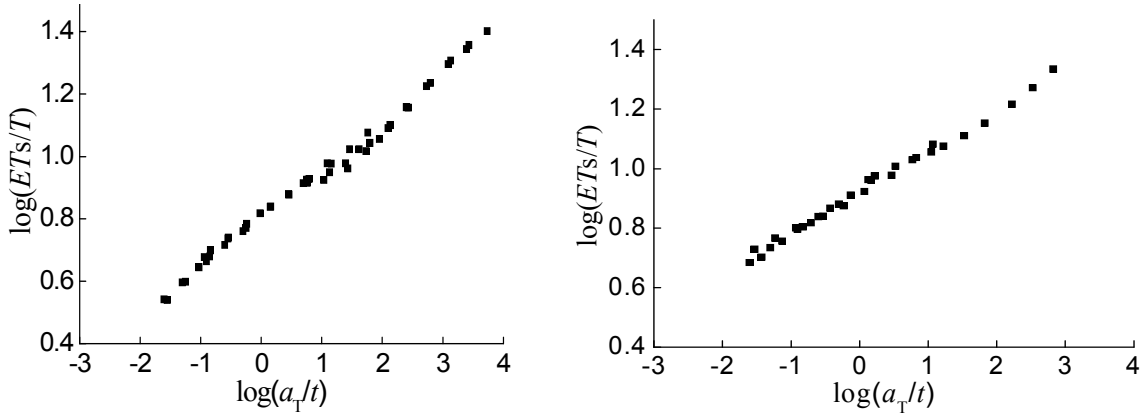

Fig. 1 The relaxation modulus master curves of unaged (Left) and aged (Right) propellants.

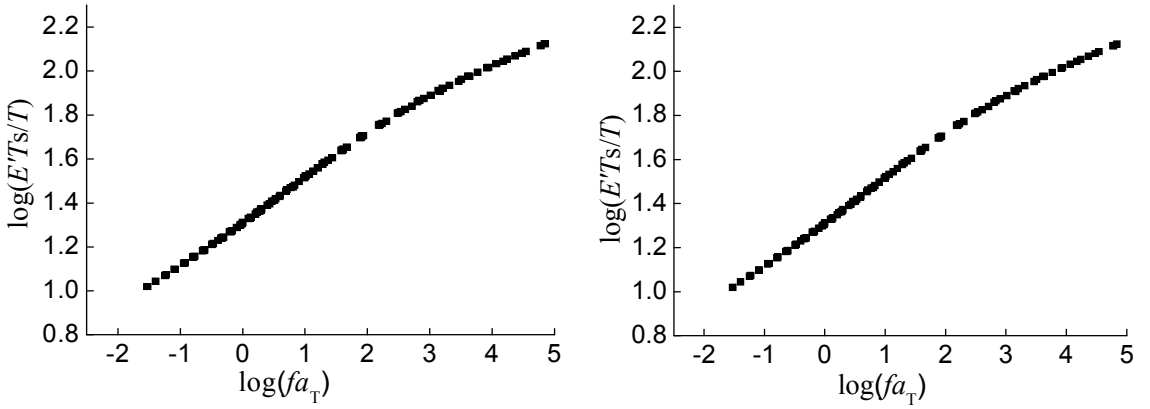

Fig. 2 The storage modulus master curves of unaged (Left) and aged (Right) propellants.

The same trends as reported by Ref.[4,5] were found for the relaxation modulus in time domain and for the storage modulus in frequency domain from Fig.1 and Fig.2. The relaxation modulus master curves differ from the storage modulus master curves in the vertical direction. In order to achieve a more reliable transformation relation of the relaxation modulus with the complex modulus, we shifted the storage modulus master curve downwards by a distance of d, and kept the relaxation modulus master curve and the storage modulus master curve to be located on the same beginning point, as illustrated in Fig.3.

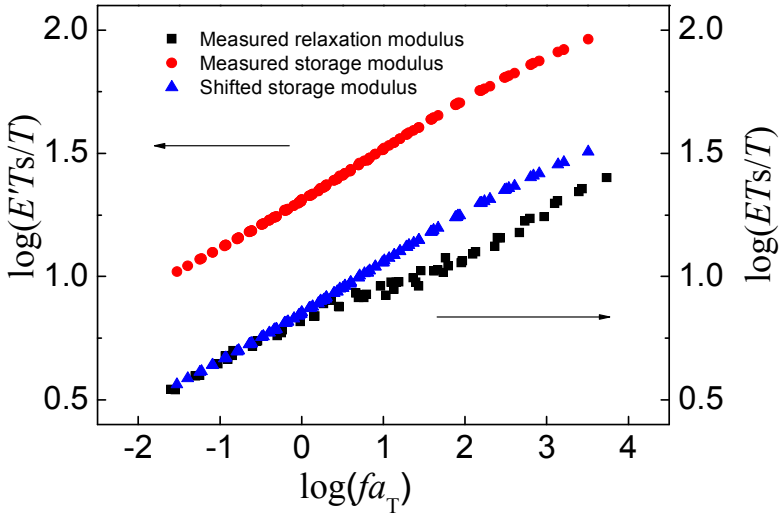

Fig. 3 The comparison to the master curves between the relaxation modulus and the storage modulus

By introducing the term of $a+(b\log t/t_0)^c$, the transformation relation becomes,

$$E(t)\approx\left[a+\left(b\log\frac{t}{t_0}\right)^c\right]E'(\omega)+d\,. \tag{7}$$

The three constants in the above formula were determined for the unaged HTPB propellants by a least square procedure over a three-segment fit. The three segments range -2-0, 0-2 and 2-4 in the horizontal axis of the master curve in Fig.4. The three coefficients *a*, *b* and *c* are different in three regions, as listed in Table 1. Therefore, three modified functions in the three segments can be reached easily. The constant *d* was determined by computing the vertical difference between the two master curves of the relaxation modulus and the storage modulus in Fig.4. The relaxation modulus calculated by using Eq.(7) was in agreement with the results measured by DMA, as indicated in Fig.4.

Table 1 The coefficients in three regions

$\log(f\,a_T)$	*a*	*b*	*c*
-2-0	1.106	-0.113	1.039
0-2	0.924	0.156	1.146
2-4	0.917	0.142	1.076

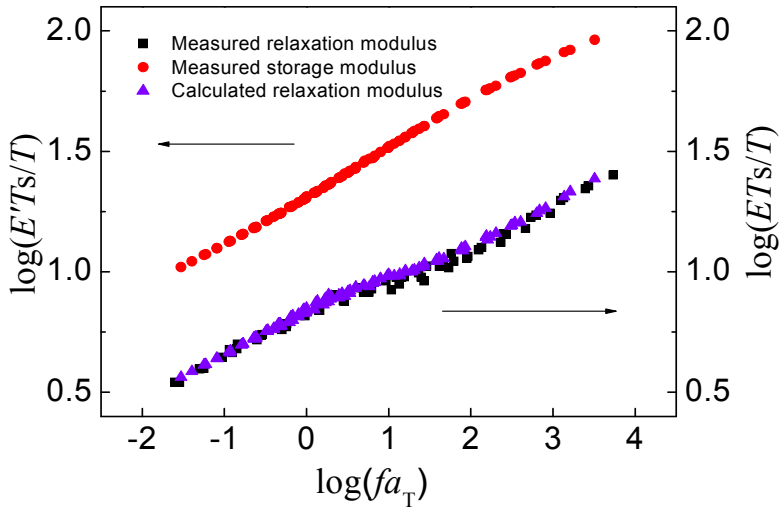

Fig. 4 The calculated relaxation modulus of unaged propellants and experimental data

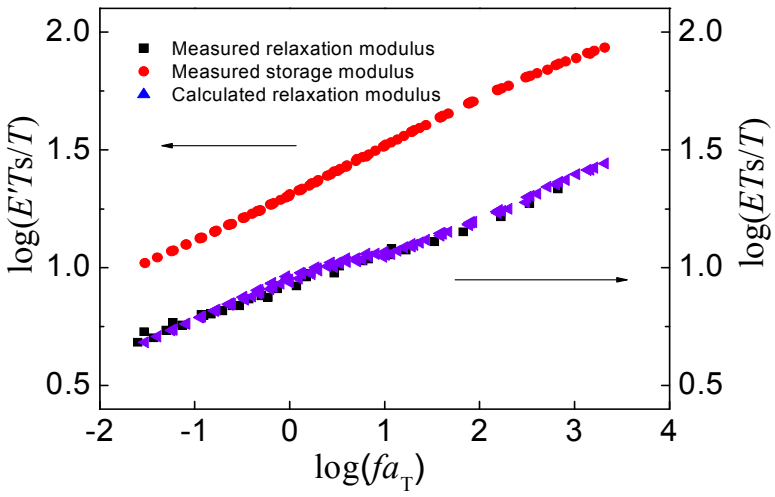

Fig. 5 The calculated relaxation modulus of aged propellants and experimental data

The three coefficients *a*, *b* and *c* were determined by using the unaged HTPB propellant samples, and then applied to Eq.(7) to estimate the relaxation modulus of the aged samples. A good agreement between the calculation and the experimental results was also found as shown in Fig.5, revealing that the three coefficients were insensitive to the aging time.

Conclusions

The master curves for the relaxation modulus and the storage modulus of the aged/unaged HTPB propellants were obtained by performing the stress relaxation tests and DMA tests, respectively. It was found that the relaxation modulus in time domain had the same trend as the storage modulus in frequency domain. There existed a great difference in the double logarithmic plot between the relaxation modulus and storage modulus master curves. Moreover, the testing results for the relaxation modulus and the storage modulus were well fitted by an empirical transformation relation with three segment-related coefficients. These three coefficients were determined by using the unaged samples, and then applied to estimate the relaxation modulus of the aged samples. A good agreement between the calculation and the experimental results was also found, revealing that the three coefficients were insensitive to the aging time.

References

[1] L. Gottlieb, S. Bar. Migration of plasticizer between bonded propellant interfaces [J]. Propellants Explosives, Pyrotechnics. 2003 28 (1) 12-17.

[2] J. Libardi, S.P. Ravagnani, A.M.F. Morais, A.R. Cardoso. Diffusion of plasticizer in a solid propellant based on hydroxyl-terminated polybutadiene [J]. Polímeros. 2010 20 (4) 241-245.

[3] D.M. Husband. Use of dynamic mechanical measurements to determine the aging behavior of solid propellant [J]. Propellants Explosives, Pyrotechnics. 1992 17 (4) 196-201.

[4] T.F. Shen, M. Gao, B.H. Zhao. Engineering methods for the transform inversion of stress relaxation modulus and complex modulus [J]. Acta Armamentarii,1995 (3) 40-44.

[5] H. Zhang, A.M. Pang, S. Peng. Nondestructive assessment approaches to storage life of solid propellants(II)-Master curve of dynamic mechanical property surveillance method [J]. Journal of Solid Rocket Technology, 2006 29 (3) 190-194. (In Chinese)

[6] R.M. Christensen. Theory of Viscoelasticity [M]. 1982.

[7] K. Ninomiya, J.D. Ferry. Some approximate equations useful in the phenomenological treatment of linear viscoelastic data [J].Journal of Colloid Science. 1959 14 (1) 36-48.

Advanced Materials Research Vols. 989-994 (2014) pp 177-180
© (2014) Trans Tech Publications, Switzerland
doi:10.4028/www.scientific.net/AMR.989-994.177

Effect of fiber's surface pretreatment on the interfacial bonding strength between steel fiber and resin

Hao Yang[1, a], Jianhua Zhang[2, b*], Guoyan Sun[3, c] and Yi Zhang[4, d]

[1, 2, 3, 4] Key Laboratory of High-efficiency and Clean Mechanical Manufacture (Shandong University), Ministry of Education, Jinan 250061, China;

[a]yanghao_sdu@163.com, [b]jhzhang@sdu.edu.cn, [c]sunguoyan2012@126.com, [d]zhangyi.sdu@163.com

Keywords: Steel fiber, surface pretreatment, interfacial bonding strength, pull-off test.

Abstract. For the characteristic that the mechanical properties of resin composite are lower than cast iron, steel fibers are used to improve its properties in this paper. A weak interfacial bonding strength between steel fibers and resin indicates that steel fibers' property cannot perform well in the polymer. In order to improve the interfacial bonding strength, four methods of surface treatment, phosphating, acid pickling, oxidation, and coupling are applied to steel fibers, and the corresponding pull-off tests are carried out to compare with untreated steel fibers. Research results show that the maximum interfacial bonding strength is increased by 45.1% after coupling treatment.

Introduction

With the development of engineering technology and increasing awareness of environment protection, some traditional metal materials are gradually replaced by advanced materials. Resin mineral composite is attractive due to its recyclability and easy process-ability and is superior in its good damping vibration attenuation and thermo stability, which is appropriate to manufacture basic parts of high-speed and precise machine tool, armarium, laser machinery[1,2], etc. However, the mechanical property of resin mineral composite is poor compared with cast iron, and fibers are considered to be used to improve its mechanical property. V.E. Yudin[3] and Hui Guo[4] studied the properties of carbon fiber reinforced resin composites and Ehsan Moaseri [5] used a microwave-assisted approach to enhance the interactions between carbon fiber and epoxy resin.

Resin matrix exhibits weak interfacial adhesion with most fibers due to low surface energy and chemically inert surfaces. Meng L [6] found that the maximal interlaminar shear strength and interface shear strength of carbon fiber/epoxy resin composite treated by supercritical water and hydrogen peroxide systems increased by 13.4% and 29.6% respectively compared with untreated carbon fibers. Hassan R M [7] and Abdel-Hamid M I [8] investigated the oxidation mechanism of chromic acid and found that oxidation treatment increased the number of function groups on the surface.

In this paper, four methods of surface treatment, phosphating, acid pickling, oxidation, and coupling are applied to steel fibers.

Experiments

Surface treatment methods

304 stainless steel fibers with average diameter of 0.2 mm were selected, and they were rinsed by ultrasonic cleaning for 15 minutes before surface treatment.

Phosphating treatment: The Phosphating reagent was mixed by 38.5% (v/v) phosphating liquid and 61.5% (v/v) H_2O. The fibers were immersed in the reagent at 45℃ for 8 minutes, and then dry in air.

Pickling treatment: A compounded pickling reagent, mixed by 15.3% (w/w) HNO_3, 2.0% (w/w) HF and 82.7% (w/w) H_2O, was used for test. The fibers were immersed in the reagent at 55℃ for 10 minutes, and then flush with water and dry in air.

Oxidation treatment: A chromic acid, mixed by 4.4% (w/w) $K_2Cr_2O_7$, 88.5% (w/w) H_2SO_4 and 7.1% (w/w) H_2O, was used for test. The fibers were immersed in the reagent at 70℃ for 5 minutes, and then flush with water and dry in air.

Coupling treatment: The coupling reagent was mixed by 59.1% (v/v) C_2H_5OH, 31.8% (v/v) H_2O and 9.1% (v/v) silane coupling agent. The pH value of the coupling reagent was kept between 4 and 6 by acetic acid. After 48h hydrolyzing at room temperature, the fibers were immersed in the reagent for 90-s then dry at 120℃ for 15 minutes.

Pull-off test of single steel fiber

The cylinder specimen is ø 14.4mm×8mm. The initial distance between clamps is 60mm and the speed is 1mm/min.

Results and discussion

Table 1 shows the results of pull-off tests of single steel before and after surface treatment, and Fig. 1 shows the average value of pull-off tests of single fiber.

Table 1 Maximum interfacial strength and residual strength of single steel fiber by different treatment methods

Treatment method	Maximum interfacial strength/residual strength(N)				
Untreated	32/10	26/12	34/12	32/12	40/14
Phosphating	36/20	30/14	34/18	28/18	36/20
Pickling	38/28	34/28	34/26	38/26	36/26
Oxidation	42/18	40/18	40/20	44/18	40/16
Coupling	46/16	46/14	58/24	44/16	44/16

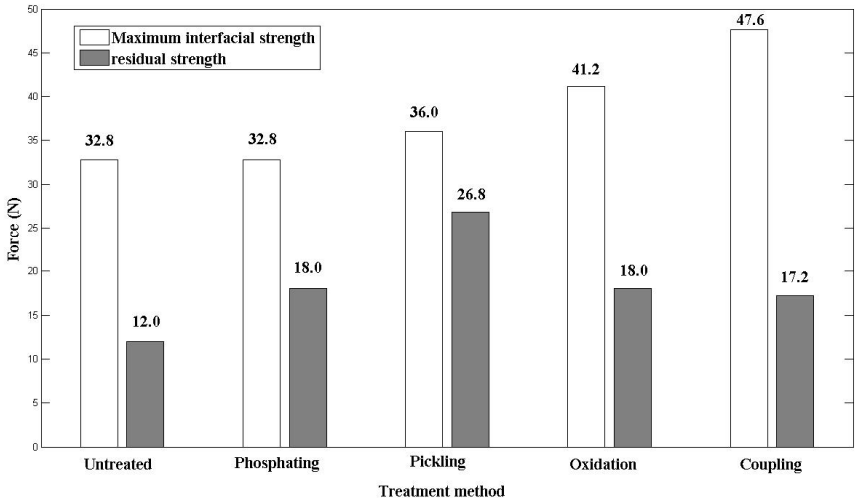

Fig. 1 Comparison of different maximum interfacial strength and residual strength of single steel fiber by different treatment methods

After phosphating treatment, a phosphating coating was added on the surface of steel fiber. The phosphating coating is composed of different phosphatic crystals, and tiny cracks exist among these phosphatic crystals [9]. These tiny cracks hinder fiber's pull-off from resin matrix after interfacial disbonding and cause the residual strength to increase.

The surfaces of steel fibers after pickling treatment were observed by microscope. Fig. 2 shows, corrosion pit spread all over the steel fiber surface while untreated fiber surface is smooth with shallow longitudinal grooves [8]. Fiber surface covered with corrosion pits increase the mechanical interlocking force with resin matrix, which result in a higher maximum interfacial strength and residual strength. Fig. 1 shows that the residual strength increases by 123% compared with untreated surface, and the maximum interfacial strength increases by 9.8%.

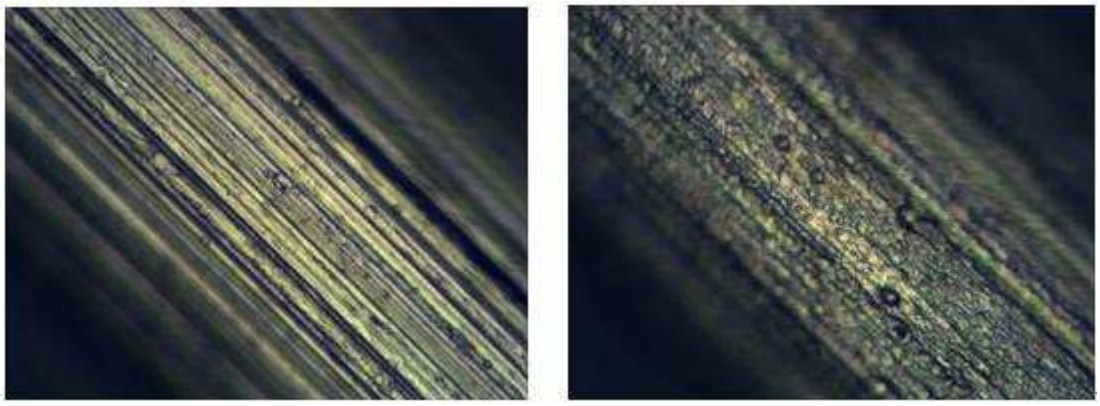

(a) (b)

Fig. 2 Microphotograph of steel fiber surface: (a) untreated, (b) pickling treatment.

Fig. 3 and Fig. 4 show the pull-test result of untreated and pickling single steel fiber, respectively.

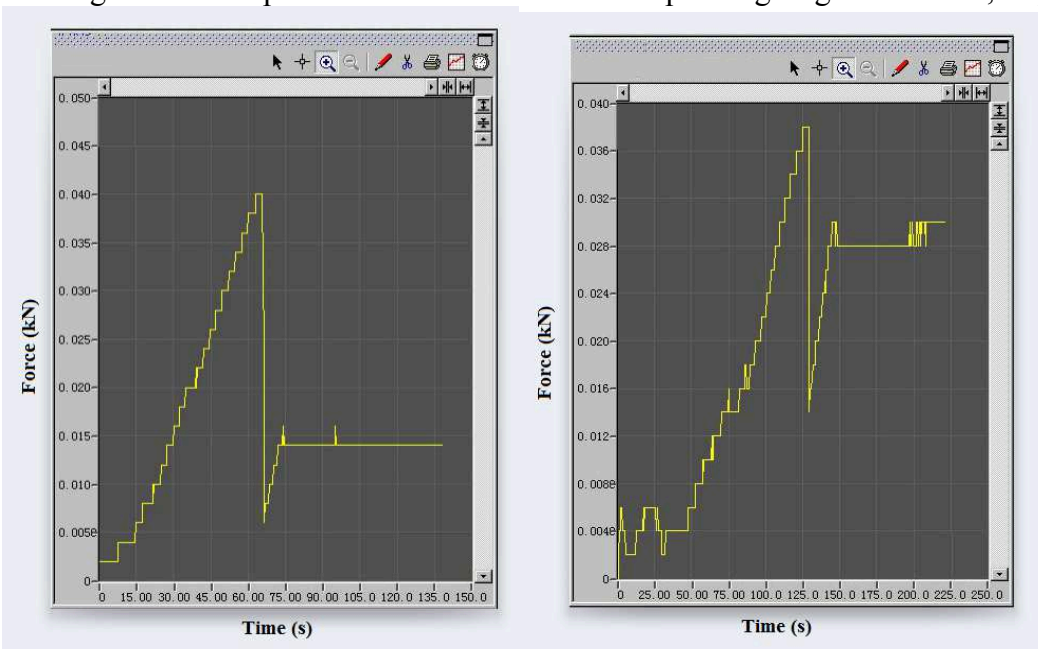

Fig. 3 Pull-off test result of untreated single steel fiber

Fig. 4 Pull-off test result of pickling single steel fiber

Oxidation treatment process uses chromium as intermediate product to trigger hydrolysis reaction on steel fiber surface, and further be oxidized into function groups. Fig. 1 shows, the maximum interfacial strength increases by 25.6%. This potentiation is mainly because oxidation treatment increases the number of function groups on steel fiber surface, such as hydroxyl groups and carboxyl groups [10]. The increasing function groups result in an increase of superficial wettability as well as surface free energy.

Fibers after coupling treatment perform the most considerable property among the four treatments, with 45.1% increase of the maximum interfacial strength. A strong chemical bonding is created between steel fiber surface and silane coupling agent, and silane coupling agent plays an important role in bridging between steel fiber and resin matrix [11, 12]. With the increase of reaction time, a strong interpenetrating layer has been formed, which increases the maximum interfacial strength between steel fiber and resin matrix.

Summary

Four different surface treatment methods are adopted to investigate the potentiation of interfacial bonding strength between steel fiber and resin. The following conclusions are derived from the experimental results.

The pull-off test of single steel fiber shows different degrees of increase in steel fiber's maximum interfacial strength compared with untreated steel fiber. Oxidation and coupling treatment perform a prominent increase of 25.6% and 45.1% respectively.

The residual strength improves obviously after all the four surface treatment, especially for the fibers after pickling, because the corrosion pits on fiber surface increase its mechanical interlocking force with resin matrix.

Acknowledgements

This research is supported by the National Natural Science Foundation of China (Grant No. 51175308) and the National Science and Technology Major Project of China (Grant No. 2012ZX04010032).

References

[1] Wong K H, Syed Mohammed D, Pickering S J, et al. Effect of coupling agents on reinforcing potential of recycled carbon fibre for polypropylene composite[J]. Composites Science and Technology, 2012, 72(7): 835-844.

[2] Fuad M Y A, Ismail Z, Ishak Z A M, et al. Application of rice husk ash as fillers in polypropylene: effect of titanate, zirconate and silane coupling agents[J]. European Polymer Journal, 1995, 31(9): 885-893.

[3] Yudin V E, Goykhman M Y, Balik K, et al.Carbonization behaviour of some polyimide resins reinforced with carbon fibers[J]. Carbon, 2000, 38(1): 5-12.

[4] Guo H, Huang Y, Liu L, et al. Effect of epoxy coatings on carbon fibers during manufacture of carbon fiber reinforced resin matrix composites[J]. Materials & Design, 2010, 31(3): 1186-1190.

[5] Moaseri E, Maghrebi M, Baniadam M. Improvements in mechanical properties of carbon fiber-reinforced epoxy composites: A microwave-assisted approach in functionalization of carbon fiber via diamines[J]. Materials & Design, 2014, 55: 644-652.

[6] Meng L, Fan D, Zhang C, et al. The effect of oxidation treatment with supercritical water/hydrogen peroxide system on intersurface performance for polyacrylonitrile-based carbon fibers[J]. Applied Surface Science, 2013, 273: 167-172.

[7] Hassan R M, Ahmed S M, Fawzy A, et al. Acid-catalyzed oxidation of carboxymethyl cellulose polysaccharide by chromic acid in aqueous perchlorate solutions. A kinetics study[J]. Catalysis Communications, 2010, 11(7): 611-615.

[8] Abdel-Hamid M I, Ahmed G A W, Hassan R M. Kinetics and mechanism of oxidation of poly (vinyl alcohol) macromolecule by chromic acid in aqueous perchloric acid[J]. European polymer journal, 2001, 37(11): 2201-2206.

[9] Fouladi M, Amadeh A. Effect of phosphating time and temperature on microstructure and corrosion behavior of magnesium phosphate coating[J]. ElectrochimicaActa, 2013, 106: 1-12.

[10] Panas I, Svensson J E, Asteman H, et al. Chromic acid evaporation upon exposure of Cr< sub> 2</sub> O< sub> 3</sub>(s) to H< sub> 2</sub> O (g) and O< sub> 2</sub>(g)–mechanism from first principles[J]. Chemical physics letters, 2004, 383(5): 549-554.

[11] Han S H, Oh H J, Kim S S. Evaluation of fiber surface treatment on the interfacial behavior of carbon fiber-reinforced polypropylene composites[J]. Composites Part B: Engineering, 2014.

[12] Choi M H, Jeon B H, Chung I J. The effect of coupling agent on electrical and mechanical properties of carbon fiber/phenolic resin composites[J]. Polymer, 2000, 41(9): 3243-3252.

Advanced Materials Research Vols. 989-994 (2014) pp 181-184
© (2014) Trans Tech Publications, Switzerland
doi:10.4028/www.scientific.net/AMR.989-994.181

Synthesis alloy and composite materials of nano-silver-nickel

Wenjing Cui[1,a],Lin Wang[2,b],Jingwen Fu[3,c],Dongyu Zhao[1,2,d,*]

[1] Key Laboratory of Chemical Engineering Process & Technology for High-efficiency Conversion,

College of Heilongjiang Province, Harbin, China

[2] School of Chemistry and Materials Science, Heilongjiang University, Harbin, China

[a]317583421@qq.com,[b]973196253@qq.com, [c]591641326@qq.com, [d]zhaodyu@aliyun.com

Keywords: nano silver-nickel alloy; hydrazine hydrate; liquid-phase reduction; polyaniline; conductive composites.

Abstract. In this research, Silver—nickel alloy nanocomposites has been synthesized by reducing mixture solution of Ni^{2+}, Ag^{+} with hydrazine hydrate as reducer and OP-10 as surfactant. Silver—nickel alloy nano-composites were characterized by FT-IR, XRD, SEM. And the electrochemical properties of the samples were studied by cyclic voltammetry. Ag-Ni/PANI composites were prepared by in-situ synthesis and emulsion polymerization, and the effect of conduction on the conductivity was investigated including content of alloy. The detailed analysis of the synthesis conditions shows that the reduction takes place in alkaline environment and low-temperature is propitious to generate alloy solid-solution grain. Composites prepared by emulsion polymerization in acidic aqueous solutions synthesis of polyaniline shows higher conductivity than pure polymer, due to the strong interaction between alloy particles and doping PANI.

Introduction

The range of properties of metallic systems can be greatly extended by taking mixtures of elements to generate intermetallic compounds and alloys [1]. In many cases, there is an enhancement in specific properties upon alloying, due to synergistic effects. The rich diversity of compositions, structures and properties of metallic alloys, has led to widespread applications in electronics, engineering and catalysis. The desire to fabricate materials with well defined, controllable, properties and structures, on the nanometre scale, coupled with the flexibility afforded by intermetallic materials, has generated interest in bimetallic alloy clusters, or ‘‘nanoalloys’’. Such clusters have been studied in colloidal solutions, in the solid state, on solid supports and in molecular beams [2-6].

Polyaniline is one of the most important conducting polymers (Trivedi, 1997). It is the first conducting polymer to be commercialized and now has applications ranging from batteries (Osama et al., 1992) to biosensors (Kim et al., 2000). Most polyaniline syntheses are carried out using aniline hydrochloride solution or a mixture of an aniline monomer and a dilute hydrochloride acid (Stejskal and Gelberg, 2002) [7-8]. Nowadays, composite materials give rise to numerous studies with a view to improving their mechanical, thermal, optical and other properties, which hold promise for novel technological applications.

Experimental

Preparation of nano-silver-nickel alloy. Ailver nitrate was obtained from Tianjin Xianshugu industrial park. Nickel sulfate was obtained from Tianjin chemical Regent Ltd. A quantity of silver nitrate and nickel sulfate solids were dissolved, and then mixed into a large beaker ultrasound. NaOH was added to adjust pH, and OP-10 was added as modifying agent. The mixture reactant was placed in 500ml three-necked flask, then hydrazine hydrate was added as reducing agent. Black powder was synthesized after been washed with distilled water, ethanol and acetone.

Preparation of nano-silver-nickel alloy/polyaniline composites. 50ml APS solution was added to a mixed solution of aniline hydrochloride and the microemulsion of nano silver-nickel alloy, then ultrasonic vibration 15 min. The solution was controlled to reaction at 0~5℃/4h. The reaction stopped, the solution was added large volume of acetone and washed several times with distilled water, ethanol and acetone.

The mixture was put into a vacuum oven at 50℃/24h.

Results and discussion

Silver-nickel alloy were determined by X-ray diffraction. Fig.1 showed characteristic peaks of 2θ = 38.08 °, 44.38 °, 51.8 °, 64.42 °, 77.4 ° and 81.5 °, the map contains all the characteristic peaks of silver and nickel. Silver nickel metal alloying has occurred compare with binary phase diagram of silver-nickel alloy. The peak of 2θ = 38.08 ° was larger than the corresponding peak of metal Ag, and the peak of 2θ = 44.38 ° was smaller than the corresponding peak of metal Ni, which showed that solids of Ag and Ni were mutual dissolved. Width phenomenon occurred on the XRD peak, the particle size of the sample smaller in alloying process. Figure 2 showed amorphous black sheet of nickel-silver alloy nanoparticles, and the average particle size about 50 nm.

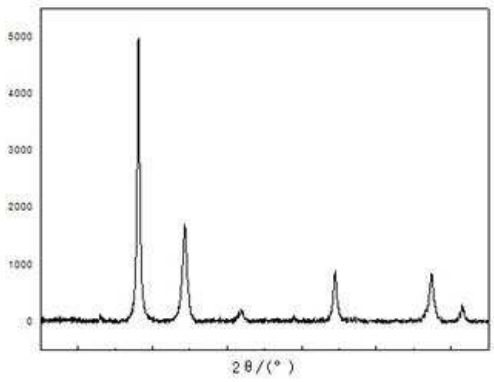

Fig. 1 XRD patterns of Ag-Ni particles

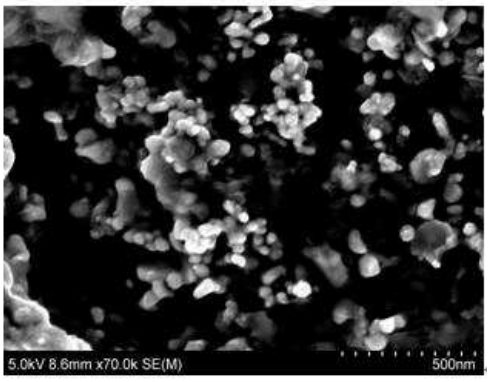

Fig. 2 SEM image of Ag-Ni alloy particles

Figure 3 showed XRD comparison chart of Ag-Ni alloy, Ag-Ni alloy/PANI composites and pure PANI. C showed the XRD patterns of pure nano-silver-nickel, the characterized peaks 2θ=38.08°, 44.38°, 51.8°, 64.42°, 77.4°, 81.5°; b showed the XRD patterns of pure polyaniline, the characterized peaks around 2θ=25°, and the strength relative weak; a showed the XRD patterns of nano-silver-nickel alloy/polyaniline composites, it can be seen that the eristic lines containing both all the diffraction peaks of silver-nickel and a wide area of the characteristic diffraction peaks of polyaniline. It showed that nano-silver-nickel alloy particles were contained in the composite materials.

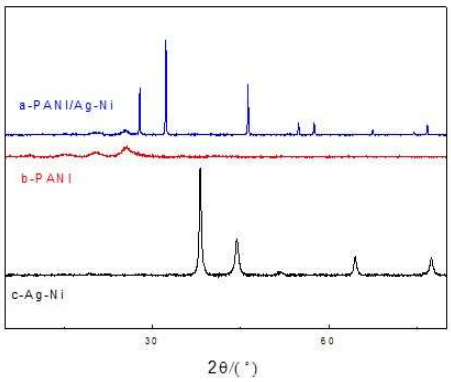

Fig. 3 XRD patterns of (a) Ag-Ni alloys (b) Ag-Ni/PANI composites (containing 25 wt % Ag-Ni alloys) (c) neat PANI

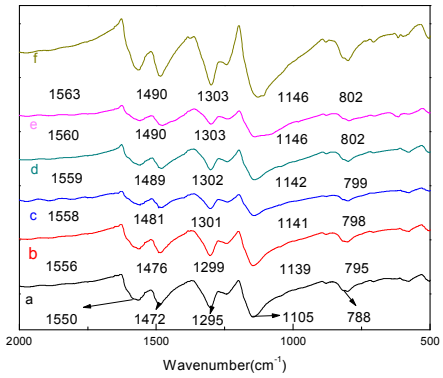

Fig. 4 FT-IR spectra of prepared with different Ag-Ni/PANI ratios(wt%) a) 0, (b) 5; (c) 10; (d) 15; (e) 20; (f) 25

Figure 4 showed the FTIR map of the different content of nano-silver-nickel alloy polyaniline nanocomposites. The contrast pattern can be clearly seen that the spectra of Ag-Ni/PANI and polyaniline were similar, which can be seen the surface of nano-alloy particles wrapped polyaniline. The characteristic peaks showed that the absorption peak of the composite material increased with the nano-metal content increased. Infrared absorption was occurred blue shift, which indicated that the strong chemical interactions existed between the nano-alloy and polyaniline.

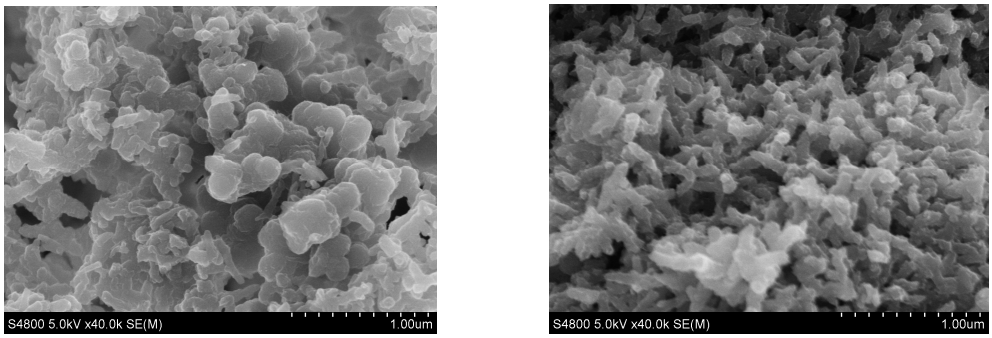

(a) (b)

Fig. 5 SEM of neat PANI (a) and the Ag-Ni/PANI composites (b)

Figure 5(a) showed the amorphous sheet of pure PANI, and the particle size distribution in the 0.1 μm-0.5 μm. Figure 5(b) showed the SEM photograph of nano-Ag-Ni alloy / PANI composites, it can be seen, PANI and nano-alloy composites particles from the amorphous sheet into rod, particle size about 0.1 μm, and about 4-8 μm in length. The SEM photograph and XRD analysis showed that the composite structure of the nano silver-nickel alloy particles were wrapped by PANI, the particles increase, and orderly rod, which was due to the polyaniline and nano alloys particles were bonded, the of nano-alloy particles were hinded agglomeration by the PANI adsorbed on the surface.

Acknowledgments

The work was supported by Harbin Scientific and Technological Special Fund for Innovative Talents (Grant Num 2012RFXXG093) and the Scientific Research Project for Heilongjiang Provincial Education Committee (Grant Num 11551328).

References

[1] W.B. Pearson, The Crystal Chemistry and Physics of Metals and Alloys, Wiley, New York, 1972.
[2] S. Giorgio, H. Graoui, C. Chapan, C.R. Henry, in: P. Braunstein, L.A. Oro, P.R. Raithby (Eds.), Metal Clusters in Chemistry, vol. 2, Wiley–VCH, Weinheim, 1999, p. 1194.
[3] H. Mori, M. Komatsu, K. Takeda, H. Fujita, Phil. Mag. Lett. 63 (1991) 173.
[4] W. Biuwen, F. Vanhoutte, F. Despa, S. Bouckaert, S. Neukermans, L.T. Kuhn, H. Weidele, P. Lievens, R.E. Silverans, Chem. Phys. Lett. 314 (1999) 227.
[5] B. Pauwels, G. Van Tendeloo, E. Zhurkin, M. Hou, G. Verschoren, L.T. Kuhn, W. Bouwen, P. Lievens, Phys. Rev. B 63 (2001) 165406.
[6] J. Jellinek, E.B. Krissinel, in: J. Jellinek (Ed.), Theory of Atomic and Molecular Clusters, Springer, Berlin, 1999, p. 277 (and references therein).
[7] Baker, J.C., 1995. The clinical manifestation of bovine viral diarrhea infection. Vet. Clin. N. Am.: Food Anim. Pract. 11, 425–445.
[8] S. L. Gonzalez-Cortes, S. M. A. Rodulfo-Baechler, A. Oliveros, J. Orozco, B. Fontal, A. J. Mora, G. Delgado, React. Kinet. Catal. Lett. 2002, 75,3.

Advanced Materials Research Vols. 989-994 (2014) pp 185-188
© (2014) Trans Tech Publications, Switzerland
doi:10.4028/www.scientific.net/AMR.989-994.185

Synthesis and Phase Behavior of a New Thiophene Monomer as Nematic Liquid Crystal

Lin WANG[1, a], Yujiao XIE[2, b], Xingxing ZHANG[3, c], Jianshe HU[*4, d]

[1]Department of Chemistry, College of Science, Northeastern University, Shenyang 110004, China

[2]Department of Chemistry, College of Science, Northeastern University, Shenyang 110004, China

[3]Department of Chemistry, College of Science, Northeastern University, Shenyang 110004, China

[4]Center for Molecular Science and Engineering, College of Science, Northeastern University, Shenyang 110004, China

[a]E-mail: 543166250@qq.com; [b]E-mail:1499317854@qq.com; [c]E-mail:2549164606@qq.com; [d]E-mail: hujs@mail.neu.edu.cn;

Keywords: Thiophene; Liquid Crystal; Synthesis; Phase Behavior

Abstract. The synthesis of a new liquid crystal thiophene monomer of (*E*)-4-(6-(3-(thiophen-3-yl)-acryloyloxy)hexyloxy)biphenyl-4'-ethylbenzoate (LC-M) is presented. The chemical structure of this monomer and intermediate compounds was characterized by FT-IR and ^{1}H-NMR. The phase behavior was investigated by polarizing optical microscopy and differential scanning calorimetry. LC-M showed nematic threaded and schlieren textures on heating and cooling cycles.

Introduction

In recent year, the organic conjugated materials have attracted more and more interest due to their excellent electrical and optoelectric properties [1-3], and many important potential applications in various areas such as organic thin-film transistors [4], solar cells [5], organic light-emitting diodes [6], sensor arrays [7], large-area plastic displays [8], and power transmission devices [9]. Today, the thiophene derivatives occupy an important position in the study of the organic conjugated materials. Functionalized thiophenes based molecules are being shown to be the potential candidates for high end applications [10] [11]. From a scientific and industrial point of view, the liquid crystalline (LC) thiophene derivatives are fascinating because they combine the electrical properties of thiophene with the optical properties of conventional LC materials. These properties are expected to be controllable through the spontaneous orientation of mesogenic group in side chain to enhance the main chain thiophene coplanarity.

In this study, a new nematic thiophene monomer containing long flexible spacer length between thiophene and mesogenic unit was prepared and characterized. The phase behavior was investigated with polarizing optical microscopy (POM) and differential scanning calorimetry (DSC).

Experimental

Materials. All chemicals were obtained from the indicated sources and used as received. 4-Ethylbenzoic acid (Beijing, China), 1,6-dibromohexane (Shenyang, China), and 4,4′-dihydroxybiphenyl (Sigma-Aldrich) were used as received. Potassium (*E*)-3-(thiophen-3-yl)acrylate were obtained from Chemistry Laboratory Center in Northeastern University of China. All other solvents and reagents used were purified by standard methods.

Measurements. FT-IR spectra were measured on a PerkinElmer spectrum One (B) spectrometer (PerkinElmer, Foster City, CA). ^{1}H-NMR spectra were obtained using a Bruker Avance 400 (Bruker, Swiss) high resolution NMR spectrometer, and chemical shifts were reported in ppm with tetramethylsilane (TMS) as an internal standard. The characteristic optical textures were observed with a Leica DMRX POM (Leica, Germany) equipped with a Linkam THMSE-600 (Linkam, United Kingdom) cool and hot stage. The thermal properties were determined with a Netzsch DSC 204 (Netzsch, Hanau, Germany) equipped with a cooling system at a heating and cooling rates of 10^{o}C/min in a nitrogen atmosphere.

Synthesis of liquid crystal thiophene monomer. The typical synthetic route of the thiophene monomer is outlined in Scheme 1.

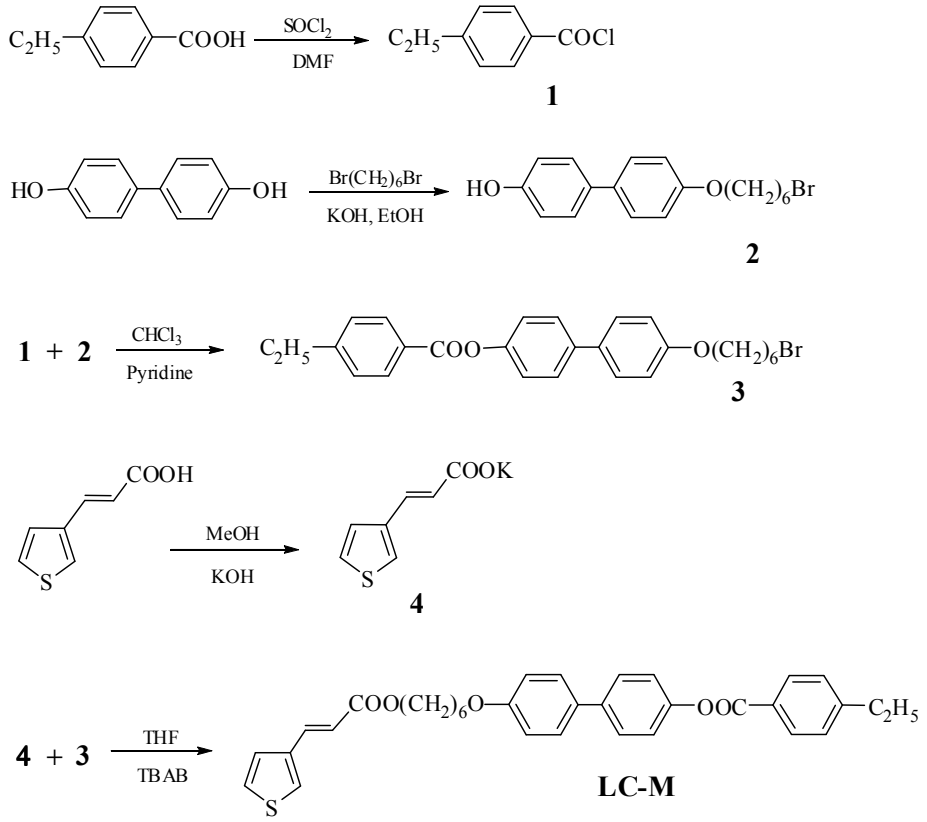

Scheme 1 Synthetic route of LC-M

4-(6-bromohexyloxy)biphenyl-4'-ol (2). 4-(6-Bromohexyloxy)biphenyl-4'-ol (2) was prepared according to the method reported by Hu and coworkers [12]. Yield: 63%, mp: 133°C. IR (KBr, cm^{-1}): 3388 (–OH); 2933, 2860 ($-CH_2-$); 1611, 1501 (Ar–), 1247 (C–O–C); 515 (C–Br). ^{1}H-NMR (δ, ppm from TMS in $CDCl_3$): 1.28–1.87 [m, 8H, $-OCH_2(C\underline{H}_2)_4CH_2Br$], 3.58 (t, 2H, $-C\underline{H}_2Br$), 4.14 [t, 2H, $-OC\underline{H}_2-$], 6.89–7.70 (m, 8H, Ar–H), 9.45 (s, 1H, –OH).

4-(6-bromohexyloxy)biphenyl-4'-ethylbenzoate (3). The compound **1** (8.4g, 0.05mol), dissolved in 10mL of chloroform, was added dropwise to a stirred solution of the compound **2** (17.4g, 0.05mol) in 250mL of chloroform and 8mL of dry pyridine. The reaction mixture was stirred at room temperature for 2h, and followed by refluxing at 65°C for 24h. The resulting mixture was cooled to ambient temperature. After evaporation of the solvent under reduced pressure, the crude product was precipitated by adding methanol to the residue and recrystallized with ethanol/acetone (1:1). Solid **3** was obtained. Yield: 65%, mp: 124°C. IR (KBr, cm^{-1}): 2977, 2856 ($-CH_2-$, $-CH_3$); 1727 (C=O); 1605, 1496 (Ar–), 1257 (C–O–C); 519 (C–Br). ^{1}H-NMR (δ, ppm from TMS in $CDCl_3$): 1.30 (t, 3H, $-C\underline{H}_3$), 1.37–1.85 [m, 8H, $-CH_2(C\underline{H}_2)_4CH_2-$], 2.71 (m, 2H, $-C\underline{H}_2CH_3$), 3.57 (t, 2H, $BrC\underline{H}_2-$), 4.15 [t, 2H, $-(CH_2)_5C\underline{H}_2O-$), 7.01–8.18 (m, 12H in aromatic).

(E)-4-(6-(3-(Thiophen-3-yl)acryloyloxy)hexyloxy)biphenyl-4'-ethylbenzoate (LC-M). The compound **3** (4.8g, 0.01mol), potassium (*E*)-3-(thiophen-3-yl)acrylate (1.92g, 0.01mol), and tetrabutyl ammonium bromide (0.2g) were dissolved in 200mL of dry tetrahydrofuran (THF). The reaction mixture was stirred for 48 h at 60°C under nitrogen conditions. The resulting solution was filtered. After THF was removed by evaporation, the residue was poured into 150mL of cold water, and the precipitate was filtered. The crude product was washed several times with water, recrystallized from acetone, and purified by column chromatography (silica gel, dichloromethane). Yield: 76%. mp: 94°C. IR (KBr, cm^{-1}): 2927, 2856 ($-CH_2-$, $-CH_3$); 1728, 1711 (C=O); 1635(C=C); 1605, 1495 (Ar–), 1257 (C–O–C and C-S). ^{1}H-NMR (δ, ppm from TMS in $CDCl_3$): 1.31 (t, 3H, $-C\underline{H}_3$), 1.56–1.86 [m, 8H, $-CH_2(C\underline{H}_2)_4CH_2-$], 2.71 (m, 2H, $-C\underline{H}_2CH_3$), 4.04 (t, 2H, $-COOC\underline{H}_2-$),

4.16 [t, 2H, −$(CH_2)_5C\underline{H}_2O$−), 6.29 (d, 1H, −C<u>H</u>=CHCOO−), 7.69 (d, 1H, −CH=C<u>H</u>COO−), 6.99–8.18 (m, 15H in thiophene and aromatic).

Results and discussion

Optical textures. The optical textures of the thiophene monomer LC-M were observed by POM with hot stage. The visual observations under POM showed that LC-M revealed enantiotropic nematic phase on heating and cooling cycles. When LC-M was heated to 90°C, the sample melted and the threaded texture gradually appeared, and the texture disappeared at 178°C. Cooling isotropic state, the schlieren texture slowly appeared at 178°C, and crystallized at 67°C. Optical textures of LC-M are shown in Figure 1 (a) and (b).

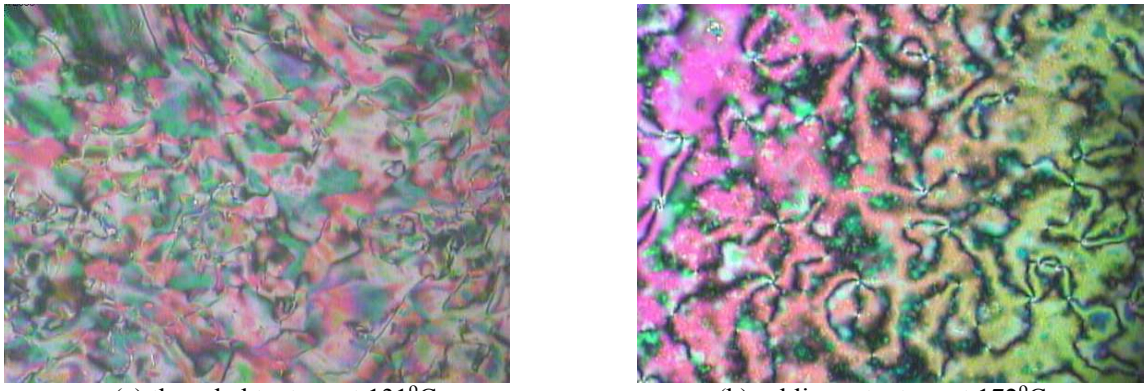

(a) threaded texture at 131°C (b) schlieren texture at 172°C

Fig.1. Optical textures of LC-M (200×)

Thermal properties. The thermal properties of LC-M were investigated with DSC. The DSC curves, obtained on the second heating and cooling scans, are shown in Figure 2.

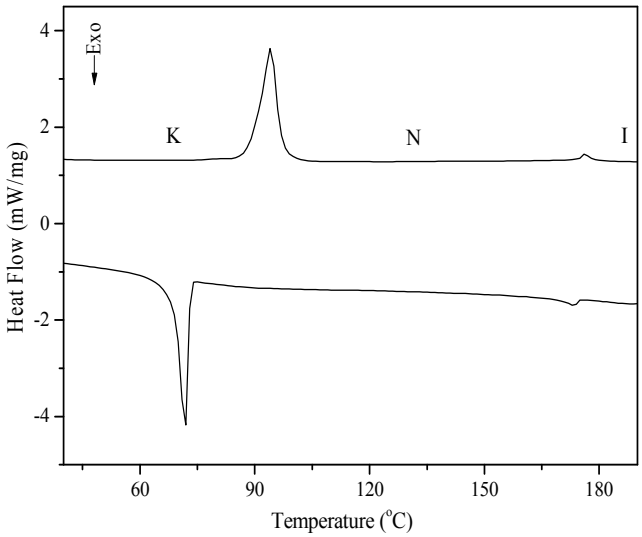

Fig.2. DSC curves of LC-M

DSC heating curve of LC-M showed a melting transition at 94.2°C and a nematic to isotropic phase transition at 176.2°C. The mesophase temperature range was 82°C. On cooling, two exothermic peaks were seen, which represent an isotropic to nematic phase transition at 173.4°C, a nematic to crystallization transition at 71.7°C. All phase transitions were reversible and did not change on repeated heating and cooling cycles, the phase transition temperatures noted in DSC curves were in agreement with the phase transition temperatures observed by POM.

Conclusion

We reported a new thiophene monomer as nematic liquid crystal. LC-M exhibited the threaded texture and schlieren texture of a nematic phase. Its melting temperature and isotropic or clearing temperature were 94.2^{o}C and 176.2^{o}C, respectively. The mesophase temperature range was 82^{o}C.

Acknowledgement

In this paper, the research was sponsored by Fundamental Research Funds for the Central Universities (N130205001 and N110705001) for financial support of this study.

References

[1] Sonmez G, Meng H, Zhang Q, Wudl F. A highly stable, new electrochromic polymer: Poly(1,4-bis(2-(3′,4′-ethylenedioxy)thienyl)-2-methoxy-5-2″-ethylhexyloxy benzene) [J]. Adv Funct Mater. 2003, 13(9): 726–731.
[2] Friend RH, Gymer RW, Holmes AB, et al. Electroluminescence in conjugated polymers [J]. Nature 1999, 397(6715): 121−128.
[3] Huitena HEA, Gelinck GH, van der Putter JBP, et al. Plastic transistors in active-matrix displays -The handling of grey levels by these large displays paves the way for electronic paper [J]. Nature 2001, 414(6864): 599-600.
[4] Sokolov AN, Roberts ME, Bao, ZA. Fabrication of low-cost electronic biosensors [J]. Mater. Today 2009, 12(9): 12-20.
[5] Peet J, Kim JY, Coates NE, et al. Efficiency enhancement in low-bandgap polymer solar cells by processing with alkane dithiols [J]. Nat. Mater. 2007, 6(7): 497-500.
[6] Giovanella U, Pasini M, Freund C, et al. Highly efficient color-tunable oled based on poly(9,9-dioctylfluorene) doped with a novel europium complex [J]. J. Phys. Chem. C 2009, 113(6): 2290-2295.
[7] Crone BK, Dodabalapur A, Sarpeshkar R, et al. Organic oscillator and adaptive amplifier circuits for chemical vapor sensing [J]. J Appl Phys. 2002, 91(12): 10140-10146.
[8] Dimitrakopoulos CD, Malenfant PRL. Organic thin film transistors for large area electronics [J]. Adv Mater. 2002, 14(2): 99-117.
[9] Sekitani T, Takamiya M, Noguchi Y, et al. A large-area wireless power-transmission sheet using printed organic transistors and plastic MEMS switches [J]. Nat Mater. 2007, 6(6): 413-417.
[10] Lungenschmied C, Bauer S, Schwödiauer R, et al. Real-time in-situ observation of morphological changes in organic bulk-heterojunction solar cells by means of capacitance measurements [J]. J Appl Phys. 2011, 109(4): 044503-044507.
[11] Ichikawa M, Yamamura K, Jeon HG, et al. Effects of volatile additives in solutions used to prepare polythiophene-based thin-film transistors [J]. J Appl Phys. 2011, 109(5): 054504-054509.
[12] Hu J S, Li Q, Liu Y N, Song Y T. New chiral liquid crystal monomers and cholesteric polyacrylates: synthesis and characterization [J]. Liq cryst. 2013, 40(8): 1095-1104.

Advanced Materials Research Vols. 989-994 (2014) pp 189-193
© (2014) Trans Tech Publications, Switzerland
doi:10.4028/www.scientific.net/AMR.989-994.189

Synthesis of novel cationic asphalt emulsifier and its investigation by online FTIR spectrophotometry

Meijie Sun, Laishun Shi [a], Zheying Jin, Na Li, Xiang Tao

School of Chemistry and Chemical Engineering, South Campus, Shandong University, Jinan 250061, P. R. China

[a]LSHUNSH@sdu.edu.cn

Keywords: asphalt; emulsifier; nonylphenol polyoxyethylene ether; synthesis; online FTIR

Abstract. A novel cationic asphalt emulsifier of N-(3-polyoxyethylene nonyl phenyl ether (10)-2-hydroxyl) propyl-N,N,N- triethyl ammonium chloride was synthesized by nonylphenol polyoxyethylene ether (NP-10), epichlorohydrin and triethylamine. The optimum reaction condition was obtained. The yield reaches 48.72% at the optimum conditions of the feedstock mole ratio of NaOH to NP-10 1.0, the mole ratio of epichlorohydrin to NP-10 1.2, the mole ratio of triethylamine to NP-10 1.2, reaction temperature 70℃, and reaction time 8 h. The structure of the emulsifier was identified by FTIR. The synthesis process was monitored by online FTIR technique and the intermediate was detected. Based upon the experimental data, a plausible reaction mechanism was proposed for the reaction. The emulsifier belongs to slow-set asphalt emulsifier.

Introduction

Asphalt emulsifier is divided into cationic, anionic, nonionic and amphoteric according to the different charges [1,2]. Negm [3] synthesized a series of cationic surfactants with benzaldehyde, p-aminopyridine, xylene, 1,2-dibromoethane, 1,6-dibromohexane and 1,12-dibromododecane. Two kinds of Gemini cationic asphalt emulsifier were synthesized by the reaction of octadecyl amine, octadecyldimethyl tertiary amine and epichlorohydrin[4]. Li [5] synthesized an asymmetric Gemini cationic surfactants, characterized its structure and discussed the affect factors of stability. Banno [6] synthesized novel cationic surfactants which have biodegradability and chemical recyclability green sustainable. Slow-set asphalt emulsifier is a key material for slurry seal [7,8].

In previous papers, we have synthesized different kinds of asphalt emulsifiers [4,9,10]. A novel cationic asphalt emulsifier was synthesized in this paper. The synthesis process was monitored by online FTIR technique and the intermediate was detected. Based upon the experimental data, a plausible reaction mechanism was proposed for the reaction.

Experimental

Materials. Nonylphenol polyoxyethylene ether was technical grade and obtained from Nanjing Gutian Chemical Co., Ltd, Nanjing, China. All the other reagents were of analytical reagent grade and used without further purification. The asphalt used was AH-90, which was provided by Shengli Refinery of Qilu Petrochemical Company, Zibo, China. The mineral aggregate was the mixture of different size of marble stone.

Synthesis of asphalt emulsifier.

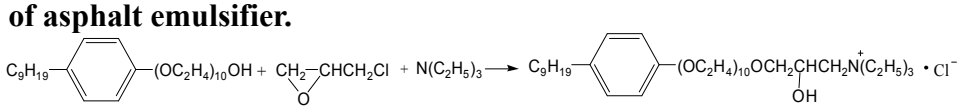

(R1)

NP-10 (66.0 g, 0.1 mol), NaOH (4.0 g, 0.1 mol) and 30 mL isopropanol were added in a three-necked flask. Epichlorohydrin (11.10 g, 0.12 mol) was added dropwise. Triethylamine (12.15 g, 0.12 mol) was added dropwise and stirred for 8 h at 70℃ in a water bath.

The yield of product. The yield (Y_1) of product was measured by bromophenol blue two-phase titration method. 2.0000 g sample was weighted and dissolved in distilled water, and transferred to a 100 mL volumetric flask. Then, 10mL of the sample solution was measured by a pipette and placed

in a stoppered graduated cylinder. 1mL 10% sodium carbonate solution and 0.2 mL of bromophenol blue indicator were added. The stoppered graduated cylinder was shaken well. Then 10 mL 1,2-dichloroethane was added. The mixed solution was titrated with standard sodium dodecyl sulfate solution. The endpoint of the titration was identified as the blue color of lower solvent phase completely disappeared.

$$Y_1 = \frac{C \times V_1 \times 10^{-3} \times 10}{n \times m_1} \times m \times 100\%$$

where, Y_1—means the yield of product, %.

V_1—means the consumed volume of sodium dodecyl sulfate standard solution, mL.

C—means the concentration of sodium dodecyl sulfate standard solution, mol/L.

m—means the total mass of sample, gram.

m_1—means the mass of sample to be titrated, gram.

n—means the mole of NP-10, mol.

FTIR analysis. FTIR spectra were recorded from 400 to 4000 cm^{-1} wavenumber range with averaging 32 scans at a resolution of 4 cm^{-1} on a Bruker Tensor-27 FTIR spectrophotometer.

Online FTIR analysis. The online FTIR analysis was performed on a ReactIR 4000 spectrophotometer (Mettler-Toledo AutoChem, Inc., USA). FTIR spectra were recorded from 650 to 4000 cm^{-1} wavenumber range at a resolution of 8 cm^{-1}. NP-10 (66.0 g, 0.10 mol), NaOH (4 g, 0.1 mol) and 160 ml isopropanol were added in a three-necked flask. The solution was stirred and heated to 70℃ in a water bath. The detector of the online FTIR analysis system was immersed in the solution during the reaction to record the 3D online FTIR spectra. Epichlorohydrin (11.10 g, 0.12 mol) was added dropwise after 8 min. Triethylamine (12.15 g, 0.12 mol) was added dropwise after 15 min. The magnetic stirrer was under operation during the online FTIR measurement.

Preparation of bituminous emulsion.12.5 g emulsifier of product was dissolved in 200 mL water. The pH value was adjusted to 2.0 by adding hydrochloric acid, then the solution was heated to 60℃. 300 g AH-90 asphalt was heated to 120℃. The bituminous emulsion was prepared by mixing the aqueous solution containing emulsifier and asphalt in a colloid mill for 1 min.

Mixing experiment. Mineral aggregate (100 g), cement (1 g) and water (8 g) were mixed. Bituminous emulsion (10 g) was then added, and the mixture was stirred at 60 revolutions per minute. The mixing time was recorded by observation of the mixing performance.

Results and discussion

Synthesis route optimization

Reaction time. The reaction conditions were as follows: reaction temperature 70℃, the mole ratio of NaOH to NP-10 1.0, the mole ratio of epichlorohydrin to NP-10 1.2, the mole ratio of triethylamine to NP-10 1.2. Figure 1 represents the yield (Y_1) of product versus reaction time. As shown in Fig. 1, the yield increases with the reaction time, and levels off after 8 h. Therefore, the optimum reaction time is 8 h.

Reaction temperature. The reaction conditions were as follows: reaction time 8 h, the mole ratio of NaOH to NP-10 1.0, the mole ratio of epichlorohydrin to NP-10 1.2, the mole ratio of triethylamine to NP-10 1.2. Figure 2 represents the yield versus reaction temperature. As shown in Fig. 2, the yield increases with reaction temperature, and levels off after 70℃. Therefore, the optimum reaction temperature is 70℃.

The dosage of NaOH. The reaction conditions were as follows: reaction temperature 70℃, reaction time 8 h, the mole ratio of epichlorohydrin to NP-10 1.2, the mole ratio of triethylamine to NP-10 1.2. Figure 3 represents the yield versus the mole ratio (m) of NaOH to NP-10. As shown in Fig. 3, the yield increases with the mole ratio (m) of NaOH to NP-10, and levels off after 1.0. Therefore, the optimum the mole ratio (m) of NaOH to NP-10 is 1.0.

The mole ratio of epichlorohydrin to NP-10. The reaction conditions were as follows: reaction temperature 70℃, reaction time 8 h, the mole ratio of NaOH to NP-10 1.0, the mole ratio of

triethylamine to NP-10 1.2. Figure 4 represents the yield versus the mole ratio (n) of epichlorohydrin to NP-10. As shown in Fig. 4, the yield increases with the mole ratio (n), and levels off after 1.2. Therefore, the optimum the mole ratio (n) of epichlorohydrin to NP-10 is 1.2.

The mole ratio of triethylamine to NP-10. The reaction conditions were as follows: reaction temperature 70℃, reaction time 8 h, the mole ratio of NaOH to NP-10 1.0, the mole ratio of epichlorohydrin to NP-10 1.2. Figure 5 represents the yield versus the mole ratio (r) of triethylamine to NP-10. As shown in Fig. 5, the yield increases with the mole ratio (r), and levels off after 1.2. Therefore, the optimum the mole ratio (r) of triethylamine to NP-10 is 1.2.

Overall speaking, the optimum reaction conditions are as below: reaction temperature 70℃, reaction time 8 h, the mole ratio of NaOH to NP-10 1.0, the mole ratio of epichlorohydrin to NP-10 1.2, the mole ratio of triethylamine to NP-10 1.2. The yield reaches 48.72% at the optimum reaction conditions.

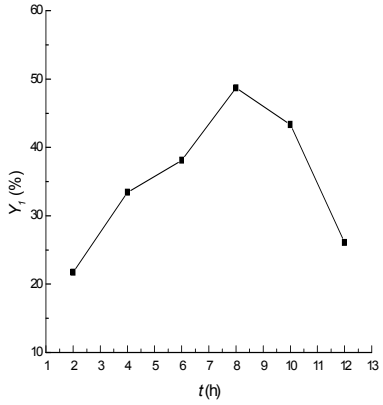

Fig.1 Yield versus reaction time

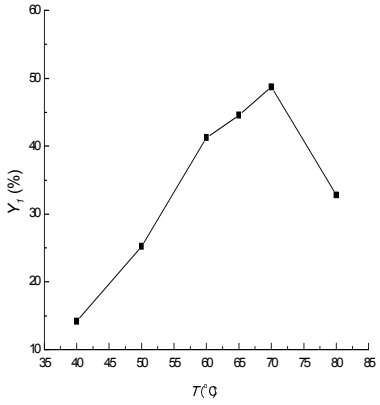

Fig.2 Yield versus temperature

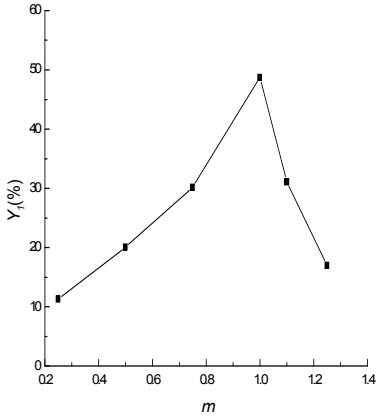

Fig.3 Yield versus the mole ratio (m) of NaOH to NP-10

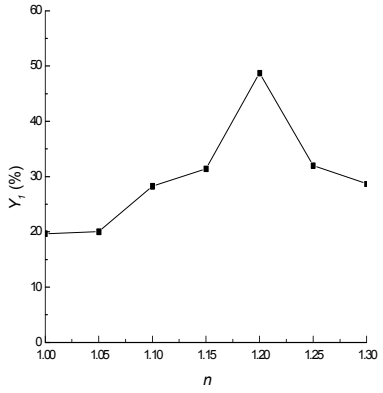

Fig.4 Yield versus the mole ratio (n) of epichlorohydrin to NP-10

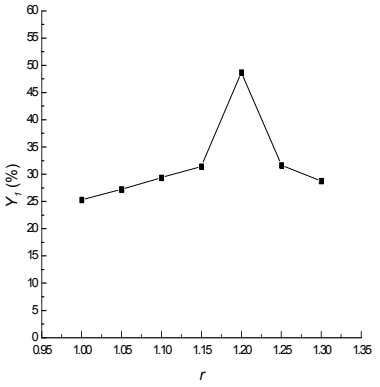

Fig.5 Yield versus the mole ratio (r) of triethylamine to NP-10

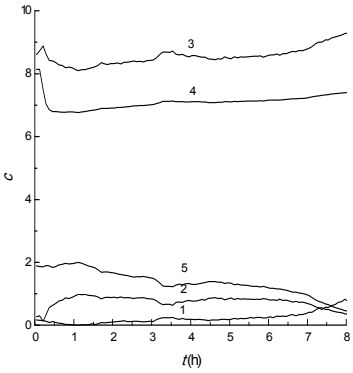

Fig. 6 Relative concentration of component 1-5 versus time

FTIR characterization. In the FTIR spectrum of product, the absorption at 3404 cm^{-1} is assigned to the O-H stretching. The absorption at 3050 cm^{-1} is assigned to the C-H stretching, which is attributed to benzene. The absorption at 1604 cm^{-1}, 1578 cm^{-1}, 1505 cm^{-1} and 1460 cm^{-1} are assigned to benzene skeleton vibration. The absorptions at 1348 cm^{-1} is assigned to O-H out-plane bending vibration. The absorption at 1250 cm^{-1} is assigned to Ar-O-C asymmetrical stretching vibration. The absorption at 1184 cm^{-1} is assigned to C-N stretching. The absorption at 1106 cm^{-1} is assigned to C-O stretching. The absorption at 949 cm^{-1} is assigned to O-H out-plane bending vibration. Therefore, the FTIR spectrum agrees with the chemical structure of the target product.

Online FTIR Analysis. The reaction was monitored by online FTIR technique. Five components were detected automatically during the online FTIR analysis. Its FTIR spectra were obtained. In the

FTIR spectrum of component 1, the absorptions at 1654 cm^{-1}, 1543 cm^{-1}, 1505 cm^{-1} are assigned to benzene skeleton vibration. The absorption at 1316 cm^{-1} is assigned to O-H plane bending vibration. The absorption at 1250 cm^{-1} is assigned to Ar-O-C asymmetrical stretching vibration. The absorption at 1108 cm^{-1} is assigned to C-OH stretching. The absorption at 1067 cm^{-1} is assigned to C-O-C stretching. The absorption at 952 cm^{-1} is assigned to vibration in ring. The absorption at 679 cm^{-1} is assigned to C-Cl stretching. Therefore, component 1 obtained by online FTIR should be the intermediate 1 as shown in Scheme 1.

In the FTIR spectrum of component 2, the absorptions at 1654 cm^{-1} and 1505 cm^{-1} are assigned to benzene skeleton vibration. The absorptions at 1292 cm^{-1} and 1049 cm^{-1} are assigned to Ar-O-C stretching vibration. The absorptions at 1257 cm^{-1}, 950 cm^{-1} and 793 cm^{-1} are assigned to epoxy C-O stretching vibration. The absorption at 1148 cm^{-1} is assigned to C-O-C stretching. The absorption at 732 cm^{-1} is assigned to methylene plane swing vibration. Therefore, component 2 obtained by online FTIR should be the intermediate 2 as shown in Scheme 1.

In the FTIR spectrum of component 3, the absorption at 1349 cm^{-1} is assigned to O-H plane bending vibration. The absorptions at 1266 cm^{-1} and 1063 cm^{-1} are assigned to Ar-O-C stretching vibration. The absorption at 1086 cm^{-1} is assigned to C-OH stretching. The absorption at 949 cm^{-1} is assigned to vibration in ring. The absorption at 852 cm^{-1} is assigned to C-Cl stretching. Therefore, component 3 agrees with the chemical structure of the target product.

In the FTIR spectrum of component 4, the absorptions at 1245 cm^{-1} and 952 cm^{-1} are assigned to epoxy C-O stretching vibration. The absorption at 1124 cm^{-1} is assigned to C-O-C stretching. The absorption at 816 cm^{-1} is assigned to C-Cl stretching. Therefore, component 4 obtained by online FTIR agrees with the chemical structure of epichlorohydrin.

In the FTIR spectrum of component 5, the absorptions at 1650 cm^{-1}, 1558 cm^{-1} and 1506 cm^{-1} are assigned to benzene skeleton vibration. The absorption at 1314 cm^{-1} is assigned to O-H plane bending vibration. The absorptions at 1269 cm^{-1} and 1065 cm^{-1} are assigned to Ar-O-C asymmetric stretching vibration. The absorption at 1160 cm^{-1} is assigned to C-O-C stretching. The absorption at 1108 cm^{-1} is assigned to C-OH stretching. The absorption at 947 cm^{-1} is assigned to vibration in benzene ring. Therefore, the spectrum of component 5 agrees with the chemical structure of NP-10.

Figure 6 gives the relative concentration (c) of component 1-5 versus reaction time. As shown in Fig. 6, the relative concentration of component 1 increases slightly with reaction time. Therefore, we can ascertain that component 1 should be the intermediate 1 as shown in Scheme 1 according to the changing trend of concentration and the online FTIR spectrum.

The relative concentration of component 2 increases gradually with reaction time. Then the relative concentration of component 2 keeps constant. Finally the relative concentration of component 2 decreases slightly. Therefore, we can ascertain that component 2 should be the intermediate 2 as shown in Scheme 1 according to the changing trend of concentration and the online FTIR spectrum. The relative concentration of component 3 increases on the whole. Therefore, we can ascertain that component 3 should be the product according to the changing trend of concentration and the online FTIR spectrum. The relative concentration of component 4 decreases gradually with reaction time, then keeps constant. Therefore, we can ascertain that component 4 should be epichlorohydrin according to the changing trend of concentration and the online FTIR spectrum. The relative concentration of component 5 decreases gradually with reaction time. Therefore, we can ascertain that component 5 should be NP-10 according to the changing trend of concentration and the online FTIR spectrum.

Synthesis reaction mechanism. For reaction (R1), we proposed a Scheme 1 as shown in reactions (R2-R6), based upon the spectra obtained by online FTIR and the concentration changing trends of the five components in Fig. 6. Alcohol anion is formed by ionization from NP-10 in alkaline condition (reaction R2). The alcohol anion is a strong nucleophile, and attacks the less substituted carbon atom of epichlorohydrin in an S_N2 reaction (reaction R3). The intermediate 1 is formed. The intermediate 2 is obtained by the cyclization reaction of intermediate 1 (reaction R4). Triethylamine has strong nucleophilicity. Then, the product is formed by triethylamine attacking the less substituted carbon atoms of epoxy group (reaction R5-R6).

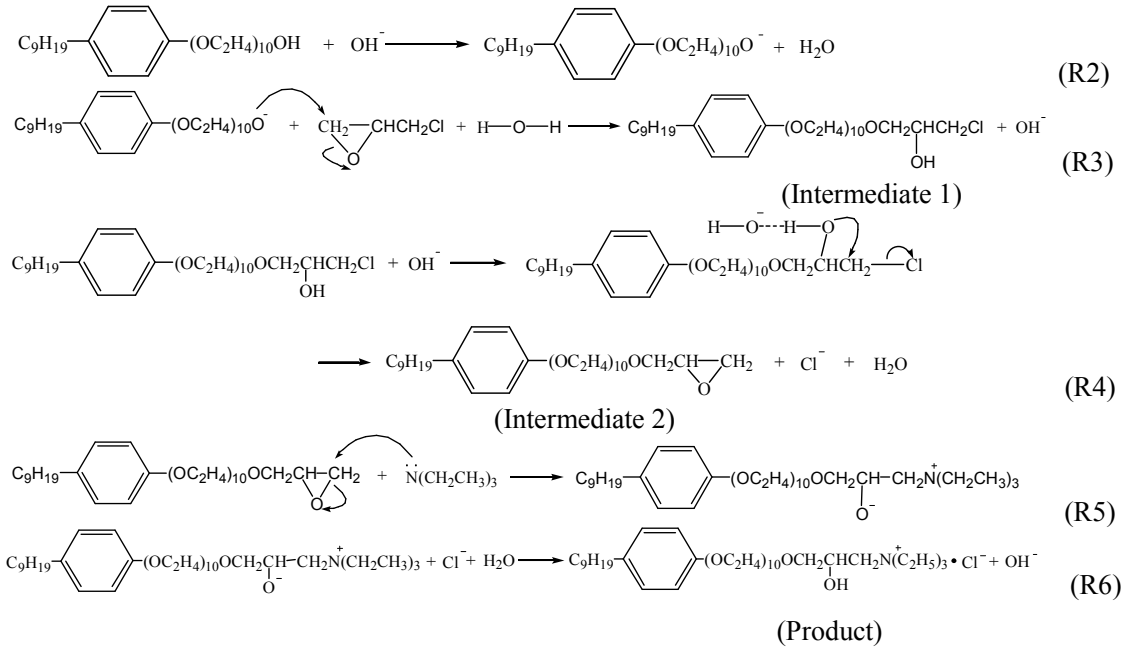

Scheme 1 Synthesis reaction mechanism

Mixing performance. The emulsifier has excellent emulsifying ability to asphalt. The mixing time was over 120 s, which indicated that the emulsifier belongs to slow-set asphalt emulsifier. It can be designed to perform in a wide variety of applications including slurry seal and solventless cold mix applications, for example recycling and base stabilization in asphalt pavement construction.

Conclusion

A novel cationic asphalt emulsifier was synthesized by nonylphenol polyoxyethylene ether, epichlorohydrin and triethylamine. The optimum reaction condition was obtained. The synthesis process was monitored by online FTIR technique and the intermediate was detected. Based upon the experimental data, a plausible reaction mechanism was proposed for the reaction. The emulsifier belongs to slow-set asphalt emulsifier.

Acknowledgement

The authors would like to thank the financial support from the Shandong Provincial Science and Technology Project (No. 2012GGX10708).

References

[1] K. Isobe, R. Tamaki: U.S. Patent 6,114,418. (2000)
[2] P. R. J. Blanpain, J. W. Creak, G. F. Mori, et al: U.S. Patent 4,997,868. (1991)
[3] N. A. Negm, M. A. El-Hashash, D. E. Mohamed: J. Surfactants Deterg. Vol. 16(2013), p.733
[4] L. Shi, Y. Zhao: Petroleum Asphalt Vol. 24(2010), p.66.
[5] H. P. Li, H. Zhao, K. Liao: Energy Sources, Part A Vol. 35(2013), p.2285
[6] T. Banno, K. Toshima, K. Kawada, et al: J. Surfactants Deterg. Vol. 12(2009), p.249
[7] W. A. Mclntosh: Industrial & Engineering Chemistry Vol. 44(1952), p.1656
[8] X. Zhi, W. Wang, Y. Tsai: Journal of Central South University Vol. 19(2012), p.2394
[9] C. Huai, L. Shi, N. Li: Res. Chem. Intermed. Vol. 39(2013), p.597
[10] X. Tao, L. Shi, M. Sun, N. Li: Advanced Materials Research Vol. 909(2014), p.72

Advanced Materials Research Vols. 989-994 (2014) pp 194-198
© (2014) Trans Tech Publications, Switzerland
doi:10.4028/www.scientific.net/AMR.989-994.194

Original Silk Pre-oxidation Treatment of Carbon Fiber from Coal Tar Pitch

Xuefei ZHAO[1, a], Yifan WEN[2, b], Tao QI, Shiquan LAI, Lijuan GAO

[1]School of Chemical Engineering, University of Science and Technology Liaoning, Anshan, 114051, China

[2]School of chemical engineering, University of Science and Technology Liaoning, Anshan, 114051, China

[a]email: zhao_xuefei@sohu.com, [b]email:wenyifanjiayou@163.com

Keywords: Coal Tar Pitch; Carbon Fiber; Pre-oxidation Treatment

Abstract. In the preparing process of carbon fiber, the fiber mechanical performance is affected by the pre-oxidation condition. In this paper the pre-oxidation technology condition of the original silk is researched, and the functional group in the molecule and the process of thermal gravimetric of the original silk and pre-oxidized silk are investigated by the method of infrared spectroscopy analysis and thermal gravimetric analysis. The IR analysis shows that associated hydroxyl is disappeared, Ar-H is decreased substantially, and methyl and methylene of the ring structure are changed greatly in the molecule of pre-oxidized silk. The TG analysis shows that the first weight loss temperature is increased, weight loss temperature range is moved to the higher temperature direction, the total weight loss rate is decreased, and weight loss velocity is decreased substantially. The mechanical performance of carbon fiber is affected by the pre-oxidation heating rate. When pre-oxidation heating rate is 1.5℃/min, the breaking strength of carbon fiber is 1195.84Mpa and the Young's modulus is 80Gpa.

Introduction

The coal tar pitch-based carbon fiber is a new kind of chemical material developed in the 1960s. Because of the excellent properties of high strength, high modulus, corrosion resistance, high temperature resistance, fatigue resistance, creep resistance and high thermal conductive, the carbon fiber has been widely applied in aerospace, sports, and medical supplies, automotive and construction industries [1-3]. The manufacture and application research of coal tar pitch-based carbon fiber in China is still in the stage of development, the product property is not stable, and the scale of production is too small to meet the demand of the market [4][5].

The original silk must be pre-oxidized treatment and can't be directly carbonized at high temperature because the original silk is thermoplastic material. asphalt macromolecule can form not-melting and cross-linking structure by being cross-linked in the air, O_2, O_3, CO_2 and other oxidizing atmosphere, keeping the fiber morphology and properties in high temperature carbonization [6].

The IR and TG of the homemade original silk and the pre-oxidized silk are researched by comparison in this paper. The effect of preparation condition on carbon fiber performance is discussed, combined the technology condition of the original silk pre-oxidation and carbonization treatment. The technology parameters are provided for the process of making carbon fiber.

1. Experimental Research Methods

(1) The property of coal tar pitch and the size of original silk such as table 1.

Tab.1. The properties of coal tar pitch and the size of original silk

soft point/℃	coking value/%	QI*/%	TI**/%	original silk size/ μm
275	76.45	5.96	53.91	14.92

* QI: quinoline insoluble, ** TI: toluene insoluble

(2) The condition of pre-oxidation and carbonization

The original silk is placed in the pre-oxidation furnace. The pre-oxidation of the original silk is been doing at the condition of given atmosphere quantum (air flow), according to fixed heating rate and treatment time.

The pre-oxidized silk is carbonized in the carbonization furnace, with 60 ml/min flow into the nitrogen protection, according to certain carbonization heating rate; the terminal temperature carbonization is 1000℃.

(3) The method of sample characterization

The obtained sample of experiment is characterized with the IR (instrument model: WQF-200, Beijing, China), the TG (instrument model: Diamond TG/DTG, America), the SEM (instrument model: Jnsl-5600VL，EJOL, Japan). The mechanical property of carbon fiber is detected by YG004D strength tester.

2. Results and Discussion

2.1 The IR discussion of the original silk and the pre-oxidized silk [7]

The IR of the original silk and the pre-oxidized silk is shown in figure 1.

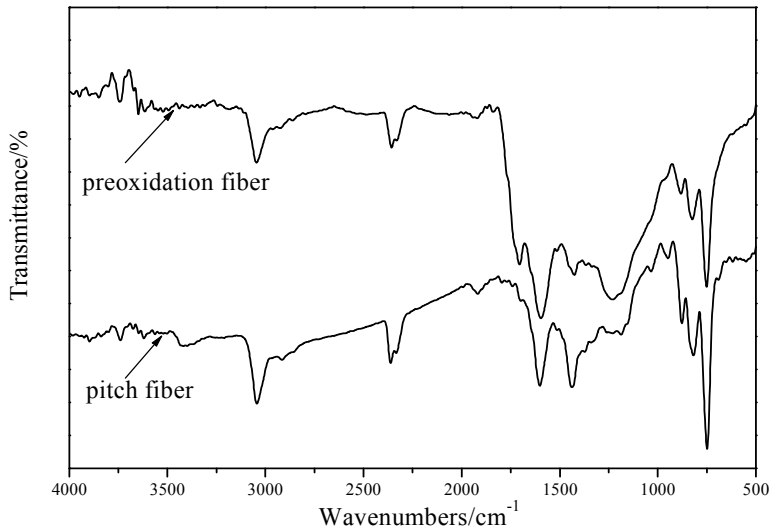

Fig.1. The IR of the original pitch silk and the pre-oxidized silk

The IRs between the original silk and the pre-oxidized silk have obvious difference from figure 1. After the original silk is pre-oxidized, the 3396-3432cm^{-1} absorption peak tends to disappearance. The result shows that the hydrogen bond associated –OH, -NH- are decreased, disappeared finally in the original silk, as the reaction progresses. Strength of the 2920cm^{-1} absorption peak is

weakened, which indicates the -CH_2- and -CH_3 are reduced. Strength of the 1710cm^{-1}, 1220cm^{-1} absorption peak is increased. The phenomenon indicates that carboxyl is increased. Strength of the 945$cm^{-1}$and 882-730cm^{-1} is weakened, which shows that the deformation vibration of the external plane of aryl or the aromatic ring substituents is weakened.

The IR information shows that the chemical structure of pitch is changed, aliphatic hydrocarbon and the aromatic ring substituents are decreased, associated hydrogen bond is disappeared, and the carboxyl is generated after pre-oxidation.

2.2 The TG of the original silk and the pre-oxidized silk

Under the heating rate of 10℃/min, the terminal temperature weightlessness of 1000℃ condition, TG and DTG experimental results are shown in figure 2 and figure 3.

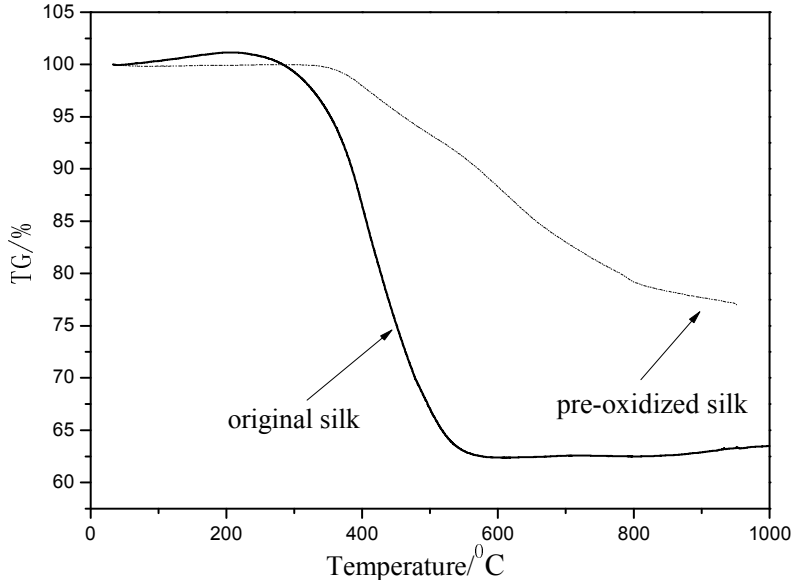

Fig.2. The TG curves of the original silk and the pre-oxidized silk

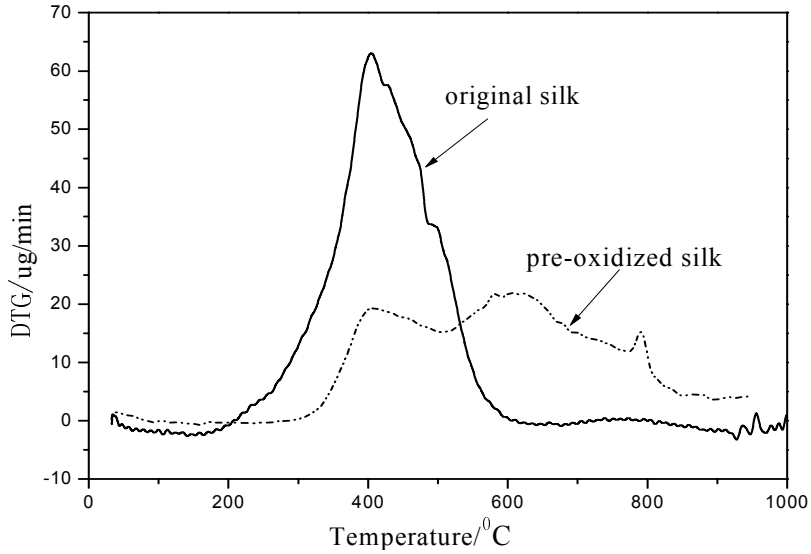

Fig.3. The DTG curves of the original silk and the pre-oxidized silk

By comparing the TG curves of the pre-oxidized silk with the TG curves of the original silk from figure 2, their characteristics of heat weight loss have been greatly changed. The first weight loss temperature of the pre-oxidized silk is increased obviously (the pitch fiber is 291℃, the pre-oxidized silk is 350℃); After the original silk is pre-oxidized, weight loss temperature range is moved to the high temperature direction, the original silk is 291-580℃, and the pre-oxidized silk is 350-950℃; total weight loss rate is decreased (total weight loss rate of the original silk and the pre-oxidized silk respectively is 36.5% and 23.1%); maximum weight loss velocity is decreased substantially after the original silk is pre-oxidized from figure 3.

The experimental results show that, the cross-linking poly-condensation reaction is occurred between pitch molecules after the original silk is pre-oxidized, and then a kind of net structure with thermosetting is generated, the molecular size and the structure of the poly-condensation of which have a major impact on mechanical properties and chemical activity.

2.3 The influence of pre-oxidation treatment condition on the mechanical properties of carbon fiber

The heating rate, terminal temperature and air flow of pre-oxidation have important influence. The condition of pre-oxidation and carbonization such as table 2. The influence on mechanical properties of pre-oxidation heating rate is showed in figure 4.

Tab.2. The pre-oxidation and carbonization conditions of the original silk

Sample	Pre-oxidation heating rate ℃/min	Terminal pre-oxidation temperature/℃	Carbonization heating rate ℃/min	Terminal carbonization temperature /℃
$CF_{0.2}^{0.5}$-08-5	0.5	320	5	1000
$CF_{0.2}^{1.0}$-08-5	1	320	5	1000
$CF_{0.2}^{1.5}$-08-5	1.5	320	5	1000
$CF_{0.2}^{2}$-08-5	2	320	5	1000
$CF_{0.2}^{2.5}$-08-5	2.5	320	5	1000

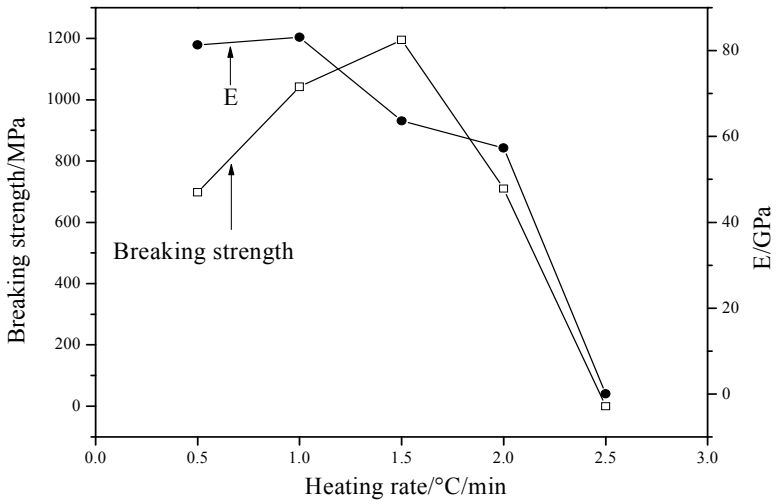

Fig.4.The influence of preo-xidation heating rate on mechanical properties of carbon fiber

The breaking strength and the Young's modulus of carbon fiber are importantly affected by pre-oxidation heating rate from figure 4. The improvement of breaking strength is affected by the pre-oxidation heating rate, when the pre-oxidation heating rate is too slow, the cross-linking reaction rate too slow , the small weight molecular resin molecules are formed in the original silk molecules and the defects would be shown on the pre-oxidized silk after carbonization ,such as 0.5℃/min, the breaking strength of carbon fiber is 697.70MPa. With the improvement of pre-oxidation heating rate, the breaking strength of carbon fiber is enhanced unceasingly, when the pre-oxidation heating rate is 1.5℃/min, the breaking strength reached the maximum 1195.84Mpa, such as figure 5; Because of the adhesion phenomenon between the original silk, when the pre-oxidation heating rate is continued to rise, the breaking strength of carbon fiber is decreased obviously. The influencing trend of the pre-oxidation heating rate on the Young's modulus is equal

to that of the breaking strength of carbon fiber, the Young's modulus is maximum, when the pre-oxidation heating rate is 1.0℃/min.

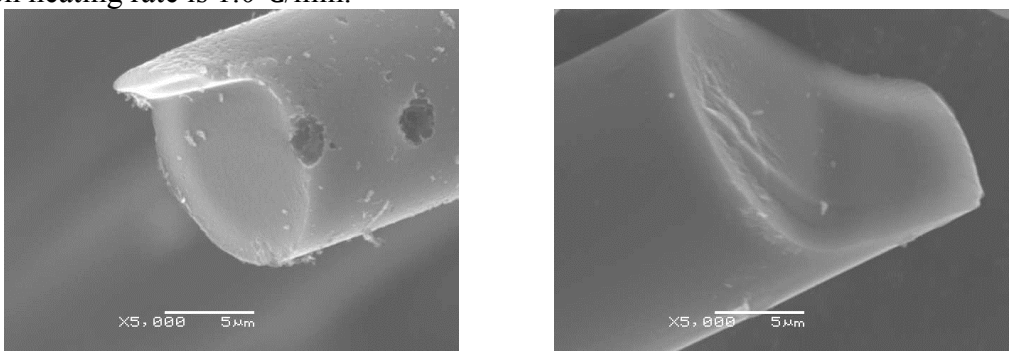

(a)0.5℃/min (b)1.5℃/min

Fig.5. The carbon fiber SEM images from the different pre-oxidation heating rate

3. Conclusions

(1) The IR information shows that the chemical structure of the original silk is changed, aliphatic hydrocarbon and the aromatic ring substituents are decreased, associated hydrogen bond is disappeared, and the carboxyl is generated.

(2) After the original silk is pre-oxidized, the first weight loss temperature of the pre-oxidized silk is increased obviously, weight loss temperature range is moved to the high temperature direction, total weight loss rate is decreased, and the velocity of weight loss is decreased substantially.

(3) The breaking strength and the Young's modulus of carbon fiber are importantly affected by pre-oxidation heating rate, the mechanical properties of the carbon fiber are affected by the pre-oxidation heating rate, and the appropriate pre-oxidation heating rate is 1.5℃/min.

References

[1]Li wei, Guo Quanfeng, Application of carbon fiber composites to cosmonautic fields. [J]. Chinese Optics, 2011, 4(3):201-212.

[2]Mao Dejun, Production and application of pitch-based carbon fiber. [J]. Oil refining and Chemical Industry, 2002, 13 (4):3-4.

[3]Ma Yunzhi, Development and application of pitch-based carbon fiber. [J]. Textile Economy Shandong, 2006, 3:74-76.

[4]Zou Zuqiao, Liu Lang, Preparation of general pitch carbon fiber from coal. [J]. Coal Conversion, 1998, 21 (2):87-89.

[5]Zhang Shaocheng, Han Baolian, Brief study on market and production situation of pitch-based carbon fiber. [J]. Coal Chemical Industry, 2001, 3:21-22.

[6]Wang Maozhang, He Fu, Production, property and application for carbon fibers. [J]. Science Press, 1984.

[7]Liu Xinwei, He Yingchun and so on, Non-melten treatment of coal pitch fibers. [J]. Carbon Fiber, 1992:8-14.

Advanced Materials Research Vols. 989-994 (2014) pp 199-202
© (2014) Trans Tech Publications, Switzerland
doi:10.4028/www.scientific.net/AMR.989-994.199

Study on the pathway of CS Stimulant with $KMnO_4$ Solution

Xiao'en Zhao

[1] The Engineering University of CAPF Training Department, Xi'an, P.R.China, 710086

wanghe717@163.com

Keywords: CS; KMnO4 Solution; pathway

Abstract: On base of the main decomposition approaches for CS, the decontamination pathway on CS stimulant with $KMnO_4$ solution was studied through the UV tests. In this paper, with the purpose of safe decontamination for environment, KMnO4 solution has been chosen to change the CS into non-toxic and non-irritating substances with boric acid as catalyst by oxidation-reduction reaction. The results of test showed that KMnO4 solution at the low concentration can finish the effective and safe decontamination of CS in a short time, which was also in accordance with the requirements of human security.

Introduction

There are three main decomposition approaches for CS, namely pyrolysis, alkaline hydrolysis and redox [1]. limited to stable chemical structure, CS does not break down below 400℃, so pyrolysis can not be used for environmental decontamination; Alkaline hydrolysis belongs to a reversible reaction, whose rate is usual slow that means alkaline hydrolysis is incompatible with the goal of rapid decontamination equally while it only plays a part in a strong alkaline solution. Redox makes use of some strong oxidizability to finish the decontamination of CS and change it into some substances with non-toxic and non-irritating, which is thought of an ideal way among three approaches. As a strong oxidizability, the decontamination pathway on CS for $KMnO_4$ solution was studied through UV tests.

Principle

Although $KMnO_4$ owns strong oxidizing property, its solution with low concentrations can directly act on the human body as a common form of disinfection reagents, which has been reported in clinical application [1, 2]. Therefore, $KMnO_4$ can guarantee the security as environmental decontamination agents. According to the equation of redox reaction, $KMnO_4$ can convert CS into two kinds of byproduct named Pro-chlorophenyl two hydroxy succinic nitrile and manganese dioxide, which were both non-toxic and no stimulating for environment. From the reaction kinetics, the oxidation ability of $KMnO_4$ enhanced a certain degree in acid-catalyzed conditions [3], so using boric acid as a catalyst in the experiments can increase the reaction rate. Boric acid belongs to a kind of tribasic weak acid, it was used to disinfection for clinical wound. Boric acid regulate to the PH value of reaction conditions as a cataelonlyst so that the $KMnO_4$ can better play its oxidation in the weakly acidic environment.

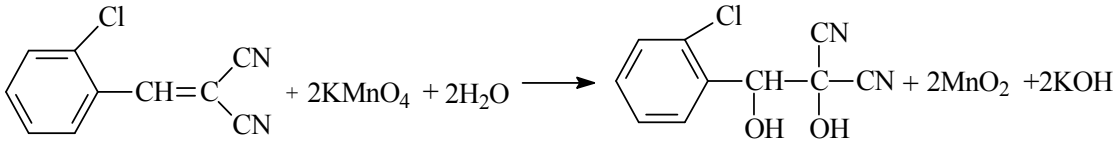

(1)

$$4H_3BO_3+2KOH \longrightarrow K_2B_4O_7+7H_2O \quad (2)$$

TEST

Instruments and medicines

The main instrument used in the experiment were followed: KDM model thermostat water bath (Shandong Province the Juancheng bright instrument Co. Ltd.), JJ model precision increase power electric mixer (Shanghai Pudong Physical Optics Instrument Factory), 1/10000 analytical balance (Swiss Mette Le), vacuum pumps, ball-type water condenser, vacuum distillation head, mouth round bottom flask, three round-bottomed flask, separating funnel, conical bottles, beakers, thermometers and other commonly used laboratory instruments. Chemicals used in the tests were shown in Table 1

Table 1 Characteristics of chemicals used in the test

Chemicals	Formula	Molecular weight g/moL	Product Specifications
CS	$C_{10}H_5N_2ClC_{10}H_5N_2Cl$	188.5	98.9%
Acetone	$C_3H_6OC_3H_6O$	58.0	AR
KMnO4	$KMnO_4$	54.9	AR
Boric acid	H_3BO_3	61.8	AR

Experiment steps

Since CS is almost insoluble in water (solubility of ≤0.01%), acetone should be used as a cosolvent (solubility ≥ 56%) to make sure that CS full contact with the KMnO4 solution. The specific operation should obey as following steps: take appropriate ball CS with medication spoon and press it into powder, then dissolve in acetone by the ratio of 1:1. Operation in the whole process should be pay attention to prevent the CS particles dispersing into the air to cause pollution. Add $KMnO_4$ solution with concentration of 0.02% and excess CS-acetone solution into a 1000ml flask with thermometer and blender, heated and kept the temperature at 30℃. Start the blender immediately after adding boric acid and began to count, and stop stirring after 10min. The reaction rate increased with adding into catalyst, and the mixed solution in the flask was at the state of brown and muddy until the reaction has been accomplished. Reactants must last for 0.5h, when the bottom of the flask appeared with a large number of brown floccose precipitations, which was regarded as manganese dioxide by analysis. Because of its little particle size, manganese dioxide was easy to complex with water, so the floccose precipitation observed is a kind of hydrated manganese dioxide. Hydrated manganese dioxide has a high adsorption capacity, and also includes a small amount of untreated CS.

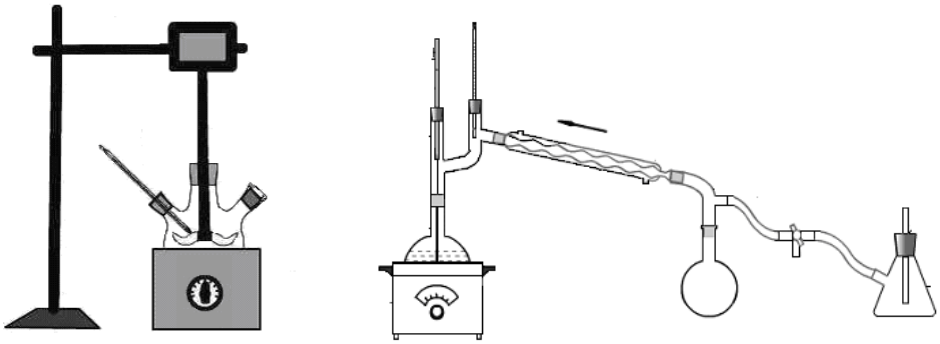

Figure1 Testing apparatus and procedure

Floccose precipitation was usually got rid of by the way of filtration. Due to containing unreacted CS, the residue after separation on the filter paper required to be rinsed three times with acetone at least, and each wash solution need to be collected together retention, in which the

concentration of CS measured. Co solvent acetone in lotion as well as reaction vessel can be removed by vacuum distillation method and reuse in the next tests.

Decontamination effect

The decontamination effect can be weighted up by the reaction conversion rate of CS. in order to estimate the CS conversion rate, it can get the content of unreacted CS by measuring the concentration of CS in the filtrate, which is calculated as follows:

$$\eta = \frac{m_1 - m_2}{m_1} \times 100\% \quad (3)$$

Where, η—*CS* conversion rate, %; m_1—as the quality of the reactants, g; m_2 —remaining CS response quality, g.

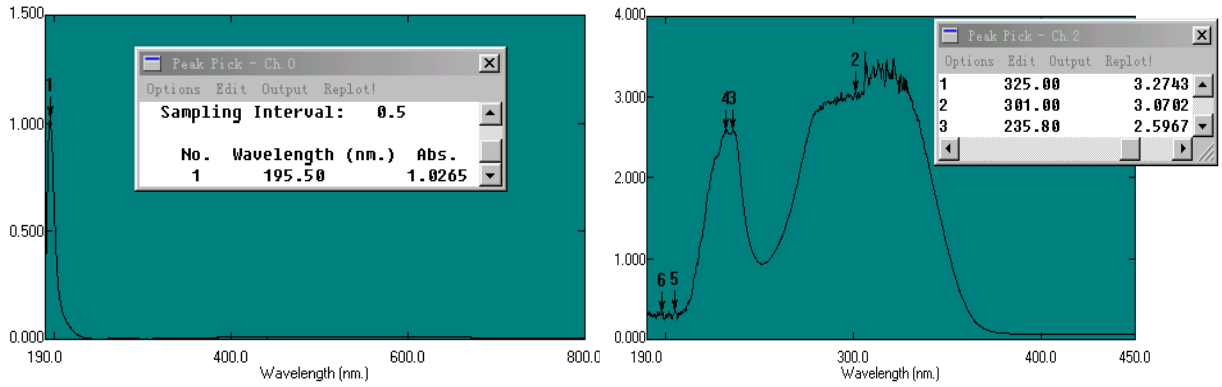

(A) $KMnO_4$ solution (B) CS-acetone

Figure2 UV absorption spectra

The concentration of CS in the acetone solution should be measured according to the working curve of absorbance after washing. A UV spectrophotometer was used to measure the absorbance (A) from CS-acetone solution and $KMnO_4$-acetone (boric acid content is so low that it can be ignored), as shown in Figure 2. By comparison, it can be seen that the $KMnO_4$-acetone solution can not form a shield for the absorption peak of the CS, so the working curve can wavelength of 301nm at the absorption peak.

First, Absorbing the CS standard solution 0, 0.50, 1.00, 3.00, 5.00, 7.00, 10.00ml into 50ml color comparison tube and numbered separately; second, adding acetone to 25ml along the wall of the color comparison tube and then mixed. After placing it for 15min, measured its absorbance at a wavelength of 301nm with the cuvette of 30mm optical distance, and take acetone as the reference solution.

According to the Lambert—Beer Law:

$$A=lg1/T=abC \quad (4)$$

Where, *A*—absorbance, *T*—transmittance, *a*—absorptivity, *b*—the thickness of the absorption fluid layer, *C*—concentration of the solution.

When *B* is fixed, then *A* can be given:

$$A=lg1/T=KC \quad (5)$$

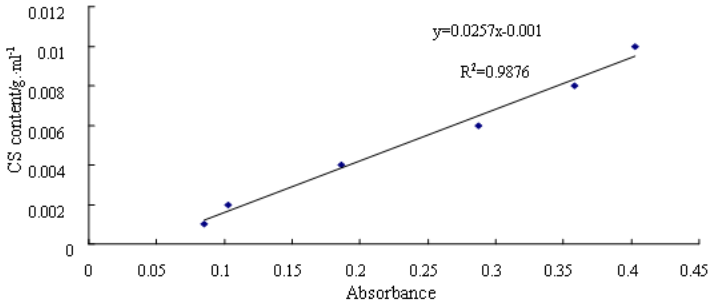

Figure 3 Standard curve

A series of CS-acetone solution with different concentrations were prepared and measured the absorbance (A) at each concentration (C) of 301nm. Corresponding to the CS content as abscissa and absorbance for ordinate, the standard curve was designed as shown in Figure 2.

Conclusions

As a friendly environment decontamination agent, low concentration of $KMnO_4$ can not only carry out rapid decomposition of CS solution but also ensure the safety of users, which has the advantages of shorter onset time and a wide temperature range of options.

Acknowledgement

In this paper, the research was sponsored by the Nature Science Foundation of Shaanxi Province (Project No. 2014JM7284) and the Post-doctoral Science Foundation of China (Grant No. 2012M521945).

References

[1] S.Varma, PJAHolt. Severe cutaneous reaction to CS gas[J]. 2011 Blackwell Science Ltd. Clinical and Experimental Dermatology, 2009, 26(3): 248–250.

[2] Diao hongxing, Huang wanying, Tang Xinlan. Discussion on the suitable concentration of KMnO4 collyria in the clinic[J]. Chinese pharmacy, 2005, 16(19): 1488–1489.

[3] Peter G. Blain. Tear Gases and Irritant Incapacitants 1-Chloroacetophenone, 2-Chlorobenzylidene and Dibenz[B,F]-1,4-Oxazepine Malononitrile[J].Toxical Rev, 2003, 22(2): 103–110.

[4] Davey1 and IKMoppett. Case Report Postoperative complications after CS spray exposure [J].Anaesthesia, 2004, 59: 1219–1220.

[5] Wang Chunyao, Song Guoying, Xing Jinshan. Study on inhalation toxicity experiments of FKB07 CS (CN) Anti-Robbery tear devices[J]. Chinese public health, 2003, 19(3): 343–345.

Advanced Materials Research Vols. 989-994 (2014) pp 203-207
© (2014) Trans Tech Publications, Switzerland
doi:10.4028/www.scientific.net/AMR.989-994.203

New Seawater Flocculants

Jian'an Hao[a], Bo Yang[b], Xiao Qing Zhang[c], Ai Jun Zhang[d], Tian Xiang Jiang[e], Xiu Zhi Zhang[f], Jing Wang[g] and Yu Shan Zhang[h]

The Institute of Seawater Desalination and Multipurpose Utilization, SOA Tianjin 300192, China

[a]phoenix328@hotmail.com, [b]yangbo82@21cn.com, [c]radicle@163.com, [d]meimei842858@163.com, [e]87898135@163.com, [f]zhang-xiuzhi@eyou.com, [g]wang_nana@163.com, [h]yushanzhang@hotmail.com

Yushan Zhang, Jian'an Hao and Bo Yang contributed equally to this article

Keywords: Seawater treatment; New seawater flocculants; Multi-effect

Abstract This paper introduces new seawater flocculants. Ferric sulfate solution and polysilicic acid were mixed. After standing and curing, polymeric ferric silicate sulfate was obtained. The optimum preparation process was explored. When Fe/Si=10:20, curing pH in the range of 1.0 to 3.0, flocculants had best flocculating activity. The polymeric ferric silicate sulfate solution and 200 μg/L chitosan solution were mixed to make composite flocculants. Flocculating activity assessments were studied. When pH in the range of 6.0 to 10.0, temperature in the range of 10 ℃to 40 ℃, flocculating activity could be stable. Total phosphorus (TP) and total organic carbon (TOC) removal rates of new flocculants were higher than 80% while algae and bacteria removal rates of new flocculants were all higher than 90%. These flocculants were multi-effect seawater flocculants.

Introduction

Flocculation (in polymer science): Reversible formation of aggregates in which the particles are not in physical contact [1]. Floccunlant is a chemical for producing flocculation of suspended particles, as to improve the plasticity of clay for ceramic purposes. Flocculants are widely used in chemical industry, mining, environmental protection and other fields [2] [3] [4]. In the process of water treatment, flocculants could improve the effect of sedimentation of fine solid [5]. In recent years, along with the development of social economy and population increase, water pollution has become a serious problem. And so on, the treatment of polluted water has become a hotspot. At present, there are multiple ways in water treatment, such as biochemistry, ion exchange, adsorption, chemical oxidation, electro dialysis, etc. But the flocculation process has been confirmed as a widely used water purification process due to its simple operation and low cost [6].

Inorganic flocculant is the most commonly used flocculant. There are two main types: iron and aluminum. According to their molecular weights, they can be divided into two categories, low molecular type and polymer type. Inorganic low molecular flocculant was applied earlier. Now this kind of flocculant is still widely used in the treatment of wastewater. But the effect of them is not ideal in some situations because of its corrosion effect [7]. Inorganic polymer flocculant was invented in 1960's on the basis of the traditional Inorganic low molecular flocculant. This kind of flocculant mostly contains hydroxyl complex ion and bridged poly nuclear complex. These constructions make them huge inorganic polymer compounds. Inorganic polymer flocculants have better flocculating abilities and have become mainstream flocculation reagents [8]. Production and application of inorganic polymer flocculants have a considerable scale in Japan, Russia and Western Europe. Inorganic polymer flocculants accounted for 30%~60% of the total output of flocculants. In recent years, development of polymeric aluminum, iron, silicon, and various kinds of composite inorganic flocculant has become hotspots. Inorganic polymer flocculant varieties have gradually formed series [9].

Seawater desalination is a sunrise industry and has good prospect. Seawater quality defines the efficiency of seawater desalination. However, at present there is not seawater flocculants in the market. Therefore, in this article, we developed new types of flocculants. At the same time, the related functions were studied.

Methods

Flocculating Activity Test

Flocculating activity test was taken by six electric blender. 1 L seawater was put in every beaker. One beaker was control. The other five beakers were added samples. Flocculating process was divided into three phases. In rapid mixing stage, stir speed was 200 rpm and the process lasted 2 min. In slow mixing stage, stir speed was 30 rpm and the process lasted 25 min. In reaction stage, stir was stopped and reaction system stood for 15 min. Supernatant at the top of the solution was taken to measure the residual turbidity.

Flocculating active ratio= (A-B)/A × 100%

A: residual turbidity of control B: residual turbidity of sample

Preparation of Poly Ferric Sulfate (PFSS)

According to different Fe/Si mole ratio, polysilicic acid was slowly added to 20 mL 0.3 mol/L (Fe^{3+} concentration) ferric sulfate solution under magnetic stirring. The constant volume of the solution was 100 mL and final concentration of Fe^{3+} was 0.06 mol/L. Stir was continued and then the solution stood at room temperature for 5 h. At last liquid PFSS was made.

Preparation of Composite Flocculant

Liquid polysilicic acid ferric sulfate was mixed with chitosan solution and stirred at room temperature for 1 h. At last composited flocculant was made.

Flocculating Activity Evaluation

Influences of different pH values and environment temperatures were measured. Removal rates of total phosphorus (TP), total nitrogen (TN), total organic carbon (TOC), bacteria and algae were measured to evaluate the effects of this complex flocculant.

Results and Discussions

Preparation of Poly Ferric Sulfate (PFSS)

Flocculating activity test described in the previous chapter was used. Concentration of Fe^{3+} was 0.03 mol/L. Effects of different Fe/Si ratio on PFSS flocculation were shown in Fig.1.(a). Effects of different curing pH on PFSS flocculation were shown in Fig.1.(b).

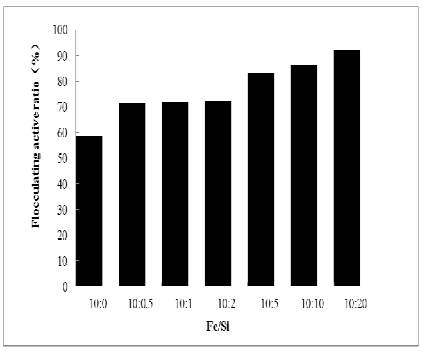

(a) Influence of different Fe/Si mole ratio

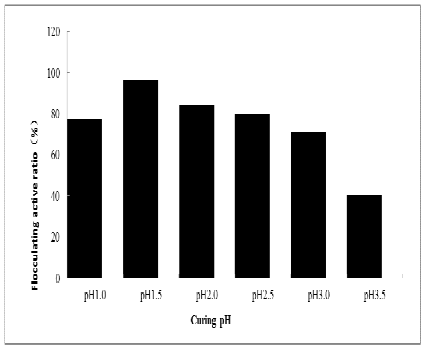

(b) Influence of different curing pH

Fig.1. Preparation of PFSS

As shown in Fig.1.(a), flocculating activity of PFSS gradually increased with the increase of Fe/Si mole ratio. When Fe/Si = 10:0.5, flocculating active ratio was above 70%. When Fe/Si=10:20, flocculating active ratio reached 95.6% and the residual turbidity was below 2 NTU.

As shown in Fig.1.(b), pH in the range of 1.0 to 3.0, flocculating activity of PFSS kept above 85%. When pH beyond 3.0, a large amount of precipitations occurred, and flocculating activity dropped rapidly.

When the silicic acid polymerized, three-dimensional structure could be loops and nets. The structure led to strong adsorption bridging activity. While polysilicic acid and ferric salt hydrolyze in aqueous solution, a series of positive charge hydrolysis hydroxyl ions were formed and strong abilities of charge neutralization occurred. The combination of polysilicic acid and ferric salt could produce a synergistic effect. Experiments found that turbidity removal rate of this new type of flocculant can reach above 90%.

In addition to these experiments, pH value of polysilicic acid, PFSS curing time, concentration of Fe^{3+} and other parameters that may affect the preparation of PFSS were studied (data not shown). We found that these factors were not main factors affected flocculating effects. In addition, tenfold concentration PFSS could maintain its flocculating activity after a few months. So the initial preparation process had overcome the low concentration and stability compared with the traditional process.

Preparation of Composite Flocculant

Flocculating activity test described in the previous chapter was used. Fe/Si=10:20，Concentration of Fe^{3+} was 0.03 mol/L. Flocculating activities of different concentration of chitosan composited with PFSS were shown in Fig.2..

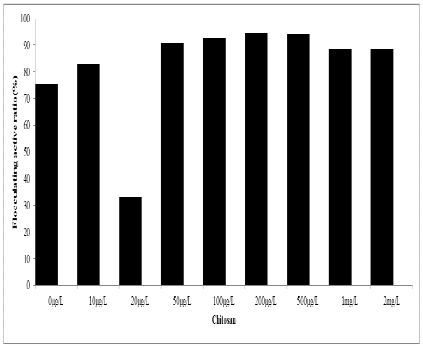

Fig.2. Preparation of composite flocculant

Chitosan had obvious effects on flocculating activity. With the addition of chitosan, velocity of precipitation accelerated, the turbidity removal rate of composite flocculant increased significantly. When the concentration of chitosan reached 200 μg/L, the flocculating active ratio could reach 97%.

There were a large number of free amino groups on the molecular chain of chitosan. When chitosan was protonated in acid solution, a large number of positive charges appeared on the chitosan chain. This kind of chitosan became a typical cationic flocculant. PFSS composited with chitosan could play advantages of both. Dosage of PFSS and chitosan could be reduced under the premise of maintaining efficacy.

Flocculating Activity Evaluation

Influences of different pH values were measured and shown in Fig.3.(a). Influences of different environment temperatures were measured and shown in Fig.3.(b).

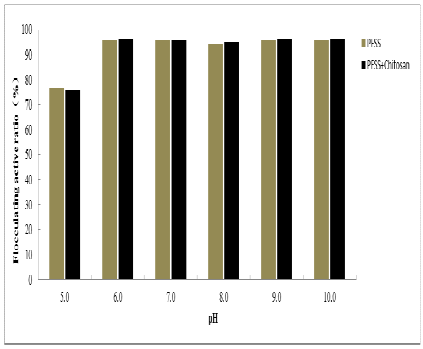

(a) Influence of pH

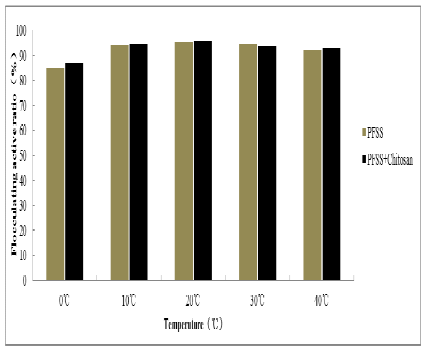

(b) Influence of temperature

Fig.3. Assessment of flocculating conditions

Different pH values had little impact on flocculating activity. When pH=5.0, the flocculating active ratios of both flocculants were all between 70%-80%. When pH varied from 6.0 to 10.0, the flocculating active ratio of both flocculants were all above 94%. This test suggested PFSS and composited flocculant both had tolerance toward variation of pH values.

Different temperatures had little impact on flocculating activity. When temperatures varied from 0 ℃ to 40 ℃, the flocculating active ratios of both flocculants were all above 80%. This test suggested PFSS and composited flocculant both had tolerance toward variation of temperatures.

Removal rates of total phosphorus (TP), total nitrogen (TN), total organic carbon (TOC), bacteria and algae were measured to evaluate the effects of flocculants. The result was shown in Fig.4..

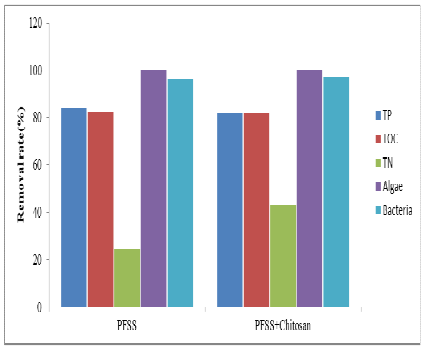

Fig.4. Assessment of flocculating activities

As shown in Fig.4., removal rates of TN were all below 60% while the removal rates of TP, TOC, bacteria and algae were all above 75%. Especially the removal rates of bacteria and algae could reach 90%. The results suggested both PFSS and composited flocculant were multi-effect flocculants.

Conclusion

This article summarizes a method for preparing new seawater flocculants. The optimum conditions of preparing PFSS: Fe/Si=10:20, curing pH 1.0-3.0. The composited flocculant was made by mixing PFSS with 200μg/L chitosan. Both flocculants had stable activities while pH varied from 6 to 10 and temperatures varied from 10℃ to 40℃. Moreover, both flocculants could remove TP, TOC, algae and bacteria from seawater.

Acknowledgement

In this paper, the research was sponsored by the Marine nonprofit and special research funding (201105026), Tianjin marine science and technology project (KJXH2011-01). The corresponding author is Yu Shan Zhang.

References

[1] Stanislaw Slomkowski, José V. Alemán, Robert G. Gilbert, Michael Hess, Kazuyuki Horie, Richard G. Jones, Przemyslaw Kubisa, Ingrid Meisel, Werner Mormann, Stanislaw Penczek, Robert F. T. Stepto, Terminology of polymers and polymerization processes in dispersed systems (IUPAC Recommendations 2011) [J]. Pure and Applied Chemistry, 2011 83 (12) 2229–2259.

[2] Zhonglian Yang, Xiwu Lu, Baoyu Gao, Yan Wang, Qinyan Yue, Ting Chen. Fabrication and characterization of poly (ferric chloride)-polyamine flocculant and its application to the decolorization of reactive dyes [J]. Journal of Materials Science, 2014 49(8) 3196-3204.

[3] Lin Yu, Jianwei Guo, Guobin Yi and Qian Yu. Application of Flocculant and Coagulant to Coal Slime Water [J]. Advanced Materials Research, 2013 781-784 2170-2173.

[4] Lianghua Lu, Zhida Pan, Nan Hao, Wenqing Peng. A novel acrylamide-free flocculant and its application for sludge dewatering [J]. Water Research, 2014 57 304–312.

[5] Liu XX, Yang ZL, Gao BY, Wang Y, Yue QY, Li Q. Coagulation characteristics of polyferric chloride-poly (epichlorohydrin-dimethylamine) composite flocculant for simulated water treatment [J]. Huan Jing Ke Xue, 2013, 34(9) 3493-3501.

[6] LI Xiao-mei, Zeng Shi-dong. Types and Development Prospects of Water Treatment Flocculants [J]. Xian Dai Nong Ye Ke Ji, 2013, 24 242-243.

[7] Meng Ge, Liu Guo-bin, Li Ping, Yang Shuang-chun. Research Progress in Ferrite Series Inorganic Polymer Cationic Flocculants [J]. Contemporary Chemical Industry, 2013 12 1684-1686.

[8] Zheng Huali, Liu Kewan. Progress in researches on inorganic polymer composite flocculants and developing trend [J]. Technology of Water Treatment, 2004, 30(6) 315-319.

[9] Mao Yan-li, Zhang Yan-feng, Luo Shi-tian,Yan Yong-sheng. Advances in FLocculation Mechanisms and Research of Water-treatment Flocculants [J]. Journal of Huazhong University of Science and Technology (Urban Science Edition), 2008 25(2) 78-82.

Advanced Materials Research Vols. 989-994 (2014) pp 208-211
© (2014) Trans Tech Publications, Switzerland
doi:10.4028/www.scientific.net/AMR.989-994.208

Research On The Corrosion Resistance Of Tinplate With Reflowing Technology

Chengqiang AN[1,2,a], Chunming LIU[1], Hao WANG[2], Shudi ZHANG[1,2,b]

[1]School of Materials & Metallurgy, Northeastern University, Shenyang 110819, China
[2]School of Environmental and Chemical Engineering, Shenyang Ligong University, Shenyang 110159, China
[a]email: acq306@163.com, [b]email: zhangshudi@163.com

Keywords: Corrosion resistance; reflowing technology; tinplate

Abstract Reflowing technology was used to further improve the corrosion resistance of tinplate. Through one-factor experiment, the effects of heating power, heating time, quenching water temperature on the corrosion resistance of tinplate were investigated. The results showed that heating power and time of reflowing had effects on the corrosion resistance of tinplate; The corrosion area of tin layer surface was gradually reduced with the decrease of quenching water temperature, and its corrosion resistance was enhanced. The optimum process was determined as follows: heating power is 410W, heating time is 9s, and the range of quenching water temperature is from 30℃ to 50 ℃.

Introduction

In modern industrial production, tinplate was usually coated with commercially pure tin on both sides of the cold-rolled carbon steel sheet. Tin-plated layer showed good weldability, electrical conductivity, low melting point, strength and punching performance, therefore，tinplate was widely used in the package of electronics and chemical products, also in food canning industry [1-6]. Tin had a tendency to grow whisker under humid conditions, in order to prevent the growth of whisker, reflowing process was often used. Reflowing technology could has a good fluidity of tin solder, and it also could significantly improve bonding strength [7, 8].Suitable reflowing time and temperature could make the grain size of alloy layer on tinplate increase, and also the corrosion resistance would be enhanced[9-11]. In this paper, using reflowing technology, through one-factor experiment, the effects of heating power, heating time, quenching water temperature on the corrosion resistance of tinplate were studied, then the optimum process was finalized.

Experimental

Test specimens was secondary cold-rolled sheet, the anode was titanium. The test piece was heated to a temperature above the melting point of tin by reflow device, the tin layer was melted , then immediately immersed in water to cool it, making it a lustrous tinplate, this was reflowing technology.

Referring to GB / T 6461-2002 " *Assessment and rating on the specimen of metals and other inorganic coatings based on metals after the corrosion test* ", model DCTC1200P salt spray chamber was used to make a salt spray experiment with the specimens.

In the test, the scanning speed of the potential is 0.005V / s; when testing AC impedance, the working potential of sample was kept at the self-corrosion potential , the sine wave signal amplitude was 5mV; the range of scanning frequency was 10mHz ~ 100KHz, scanning speed was 0.01V / s.

For electroplating, coating appearance was an important index to evaluate the quality of coatings. By visual observation method, we could observe the coating , whether there was uniform, peeling, leak-plated, bright, burning, dendritic crystal and other phenomenon, and make a preliminary judgment on the merits of coating.

Results and discussion

Effects of reflowing power on corrosion resistance

Since the melting point of tin was 232 ℃, so the temperature selected in this experiment were higher than 232 ℃. Through exploratory test, the reflowing time was set at 10s. Under other conditions being equal, the tinplate was reflowed at different power, the corrosion morphology of tinplate was analyzed by neutral salt spray corrosion test, the results were shown in Figure 1.

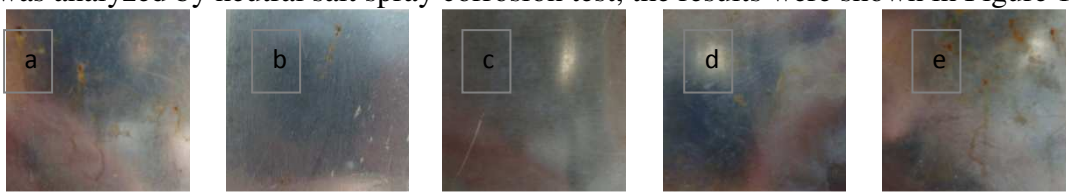

Fig.1.
The corrosion morphology of tin layer at different reflow power
(a) 350W；(b)380W；(c)410W；(d)450W；(e)480W

As we could see from Figure 1: When reflowing the tinplate, heating temperature exceeded the melting point of 232 ℃, the surface of the tinlayer was instantaneously melted, the molten liquid tin flowed into flat rapidly, then it could get a smooth and lustrous surface. When the power was 410W, the flow ability of liquid tin was improved, tinplate reflowed more fully, when reaching full reflowing state, the leveling effect of molten tin layer was more evident, a smooth and shiny tin surface formed (Fig. 1 (c)). However, when the heating power was greater than 410W, the molten tin layer would react with oxygen rapidly, so that the surface morphology of tinplate was destroyed.

Effects of reflowing Power on electrochemical properties

Under different reflowing power, Tafel polarization curves of pure tinlayer corrosion resistance on tinplate were shown in Fig.2, also the corrosion current, corrosion potential and polarization resistance of tinplate were shown in Table 1. It is showed that: with the increase of the reflowing power, the tinplate corrosion potential had a obvious tendency to move forward[12, 13], at the same time, the surface state of tinplate and the structure of tin layer were destroyed ,so ,in the terms of process parameters settings, we must do as much as possible to prevent the generation of

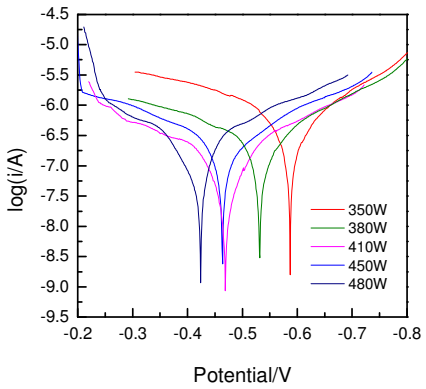

Fig.2Tafel curves at different reflowing power

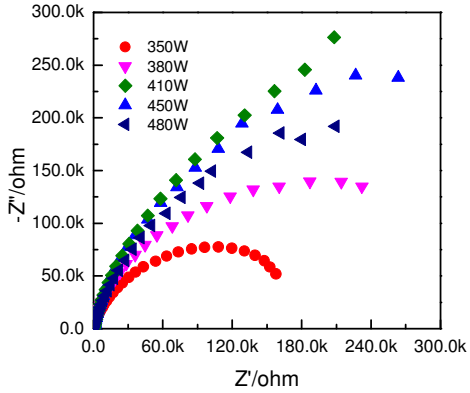

Fig.3EIS spectra at different temperatures

high-temperature oxidation layer.

Under different reflowing power, EIS spectra of pure tin layer corrosion resistance on tinplate were shown in Fig.3. Fig.3 showed that: with the increase of the reflowing power, the impedance radius of tinplate became large, that was to say, the polarization resistance and impedance value became larger, the corrosion resistance was also improved; when reflowing power was above 410W, impedance radius became smaller, and corrosion resistance decreased.

Table 1 The relationship between different parameter of molten tinplate

Reflowing power /W	Corrosion potential /V	Corrosion current /A	Polarization resistance /Ω/cm^2
350	-0.587	4.989×10^{-7}	83913.4
380	-0.532	2.965×10^{-7}	215489.0

410	-0.469	1.066×10^{-7}	471060.2
450	-0.464	3.014×10^{-7}	146627.8
480	-0.424	2.204×10^{-7}	149458.4

Effects of reflowing time on corrosion resistance

When the reflowing power was 410W, at different time, then corrosion morphology of tinplate was analyzed by using neutral salt spray corrosion test , it was shown in Fig.4.

Fig.4 Corrosion morphology of tinplate tin layer under different reflowing time

(a)5s；(b)7s；(c)9s；(d)11s；(e)13s

From Fig. 4 ,it could be seen: when the reflowing heating time was 9s, the flow ability of liquid tin improved, tinplate reflowed more fully ,when achieving the state of full reflowing, the leveling effect of molten tin layer was more obvious, forming a smooth and lustrous tin surface

Effects of reflowing quenching water temperature on corrosion resistance

In order to study the effects of different quenching water temperature on corrosion resistance of tinplate in reflowing technology, under the conditions that reflowing power of 410W, reaction time of 9s, after reflowing treatment, the tinplate was quenched into water of 20 ~ 80 ℃,then made

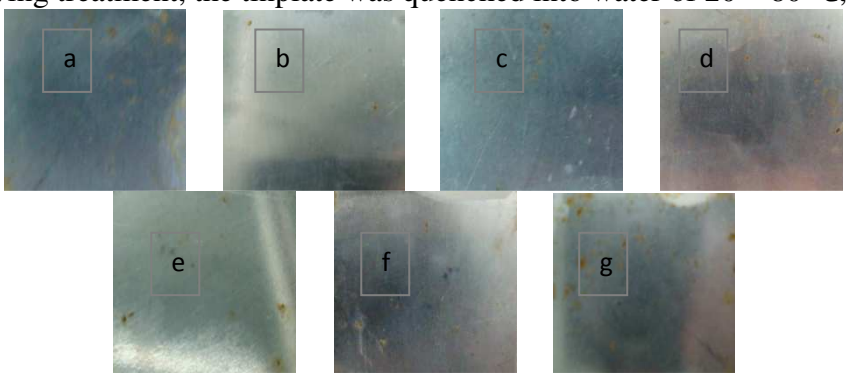

Fig.5 Corrosion morphology of tinplate at different quenching water temperature

(a)20℃；(b)30℃；(c)40℃；(d)50℃；(e)60℃；(f)70℃；(g)80℃

neutral salt spray corrosion test on it, and observed corrosion morphology of the surface.

It could be seen from Fig.5, when the quenching water temperature was 30 ~ 50 ℃ there were small corrosion area, low porosity and good corrosion resistance. within a certain range ,the nucleation rate of metal crystallization increased with the rising of supercooling degree, so the decrease of quenching water temperature could increase the nucleation rate of the tin layer crystallization, and the crystallization was more compact, which was conducive to reducing the probability of exposure of the iron matrix, improving the corrosion resistance of tinned steel sheet.

Conclusion

Reflowing heating power and time had influence on the corrosion resistance of tinplate . With the increased reflowing power or extended time, the corrosion area of tinplate surface decreased, the corrosion current and corrosion potential significantly reduced and moved forward, and thus improved its corrosion resistance.In the reflowing technology, when the quenching water temperature was different, due to the different supercooling degree of tin layer crystallization, the impact on the corrosion resistance of tinplate was different. With the decrease of quenching water temperature, the corrosion area of tinplate surface was gradually reduced, it indicated that the number of pinholes had a tendency to decrease, and its corrosion resistance improved.

Acknowledgement

In this paper, the research was especially thank for Pro. Chunming LIU , Associate Pro. Shudi ZHANG, and Hao WANG.

References

[1] Shu Cao, huanqin Zhou, weijian Hu.The production technology and new developments of tin plating steel[J].Shanghai Metal,1994,16(2):1-6.

[2] Zumelzu E, Cabezas C. Observations on the influence of microstructure on electrolytic tinplate Corrosion [J].Mater Charact,1995,34(2):143-148.

[3] Katemann B B, Inchauspe C G, Castro P A,et al. Precursor sites for localised corrosion on lacquered tinplates visualised by means of alternating current scanning electrochemical microscopy[J].Electrochim Acta, 2003, 48(9): 1115-1121.

[4] Arenas M A, Conde A, de Damborenea J J. Cerium: a suitable green corrosion inhibitor for tinplate [J].Corros Sci,2002,44(3):511-520.

[5] Xiaobo Zhang.Reflowing treatment process of tin layer in tinplate production[J]. Design and Research of Nonferrous Metallurgy,2001,2(1):25-27.

[6] Carano M. Tin Plating[J]. Plating and Surface Finishing,1998,85(11):66-67.

[7] Anqiang He Qi Liu Douglas G. Ivey. Electrodeposition of tin:a simple approach[J]. Mater Electron, 2008,19:553-562.

[8] R.Sekar C. Eagammai Sobha Jayakrislman. Effect of additives on electrodeposition of tin and its struetural and corrosion behaviour[J].J Appl Eleetrochem, 2010,40:49-57.

[9]Jiugui Huang,Ning Li,Limin Jiang,etc.Effect of reflowing conditions on alloy layer organization and corrosion resistance of tinplate[J]. Shanghai Metal,2004,26(3):19-22.

[10] Yijun Du, Yong Sun,Li Shen,etc. Effect of reflowing treatment on tinplate[J]. Electroplating&Environmental,2005,25(4):6-8.

[11] Zhen Zheng, Jiugui Huang,Binghu Li,etc. Impact of reflow process on the tin plate porosity [J]. Material Protection,2012, 45(9): 35-38.

[12] Ning Li,Zhenmo Wang,Deyu Li. Research on high temperature oxidation of tinplate [J]. Journal of Iron and Steel Research,2000,12(4):47-50.

[13] Qiliang Zhou translate.Tinplate Guide[M].Beijing: Metallurgical Industry Press,1989.

Advanced Materials Research Vols. 989-994 (2014) pp 212-215
© (2014) Trans Tech Publications, Switzerland
doi:10.4028/www.scientific.net/AMR.989-994.212

Effect of Ferrite Volume Fraction on Mechanical Properties of X80 Pipeline Steel

J. Liu [1, a], G. Zhu [1, 2, b], W.Mao [1, 3, c]

[1] School of Materials Science and Engineering, University of Science and Technology Beijing, Beijing, 100083, China

[2] Anhui University of Technology, Anhui, 243000, China

[3] State Key Laboratory for Advanced Metals and Materials, University of Science and Technology Beijing, Beijing, 100083, China

[a]email: ljustb@163.com, [b]email: zhugh@ahut.edu.cn, [c]email: wmmao@ustb.edu.cn

Keywords: X80 Pipeline Steel; Bainite/Ferrite Two Phases; Plasticity; Work Hardening; Strain Distribution

Abstract. The effect of volume fraction of ferrite on the mechanical properties including strength, plasticity and wok hardening was systematically investigated in X80 pipeline steel in order to improve the plasticity. The microstructures with different volume fraction of ferrite and bainite were obtained by heat-treatment processing and the mechanical properties were tested. The work hardening behavior was analyzed by C-J method. The results show that the small amount of ferrite could effectively improve the plasticity. The work hardening ability and the ratio of yield/tensile strength with two phases of ferrite/bainite would be obviously better than that with single phase of bainite. The improvement of plasticity could be attributed to the ferrite in which more plastic deformation was afforded.

Introduction

In order to improve the application safety of pipeline steels, especially applicable in the case of bad geological conditions such as landslide and earthquake, etc, it is very increasingly interested that to enhance the plasticity of high-strength pipeline steels [1] [2]. The plasticity enhancement of pipeline steels is currently developed by introducing of soft ferrite phase based on the physical principle of dual-phase steels applicable to auto manufacturing [3] [4] [5] [6]. However, it should be noted that there are two intrinsic difference in two steels of pipeline and dual phase steels, firstly the ferrite is small volume fraction of about 10-20% in pipeline steels [6] whereas ferrite is 70-80% in dual phase steels [7]; sencondly ferrite and bainite are phase components in pipeline steels whereas ferrite and martensite are phase components in dual phase steels [8]. It is required to understand the effect of ferrite volume fraction on the mechanical properties of high strength pipeline steels. In the present work, the volume fraction of ferrite was introduced in commercial X80 pipeline steel. The yield/tensile strength and plasticity were systematically investigated experimentally. The work hardening behavior was analyzed by C-J method was investigated.

Experiments

Commercial X80 line pipe steel was used as experimental material. The composition of the steel was listed as table 1.

Table 1 The composition of the experimental steel

C	Si	Mn	Cr	Nb	Ni	Cu	Mo
0.038	0.237	1.94	0.025	0.069	0.245	0.179	0.31
P	S	V	Ti	Al	W		
0.01	0.0009	0.006	0.011	0.018	0.069		

The specimens were reheated to different temperature and hold for different time in order to obtain different ferrite volume fraction. The samples were then quenched by oil at about cooling rate of 30℃/s in order to promote phase transformation of austenite to bainite. The heat-treatment processing was shown in figure 1. The Ac1 and Ac3 temperatures were measured by Gleeble 3500. The samples were made as standard specimens for mechanical properties measurement. The microstructures of the samples were observed in Olympus X51 optical metallography. The mechanical properties were measured in CMT4150 materials test.

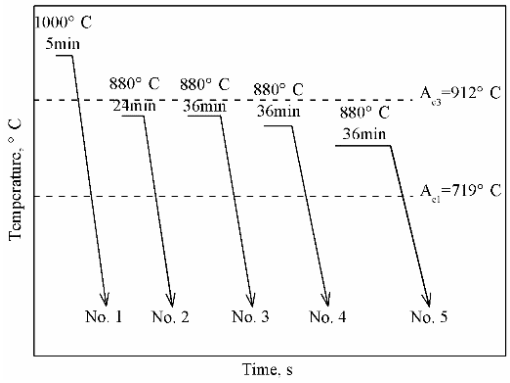

Fig. 1. The heat-treatment processing

Results and Discussion

The microstructure of the sample No.1 which was reheated to 1000℃ hold 5 minutes and then quenched was shown in figure 2(a). It could be seen that almost fully bainite microstructure was obtained. The microstructures of samples with different heat treatment processing would be two phase components of ferrite and bainite as typically shown in figure 2(b). The volume fraction of ferrite with different heat treatments was listed in table 2.

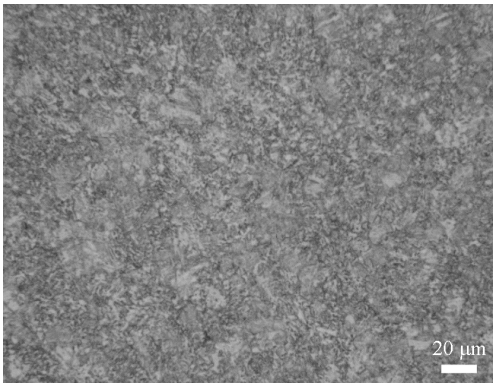

(a) Microstructure of the sample No. 1

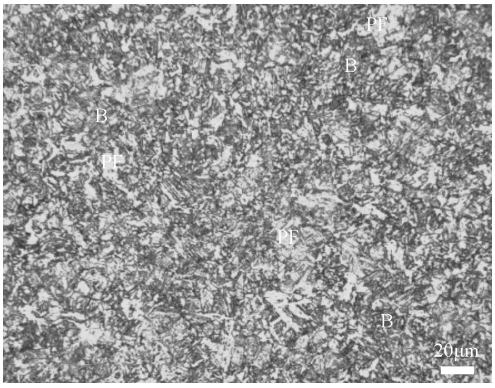

(b) Typical microstructure of bainite/ferrite two phase

Fig. 2. Typical microstructures of the samples after heat-treatments

Table 2 Volume fraction of the samples after different heat-treatments

Steel	No. 1	No. 2	No. 3	No. 4	No. 5
Volume of ferrite, %	<2%	5.11%	15.68	20.04	30.58

The stress-strain behavior of all samples exhibited continuous yield. The mechanical properties as the function of volume fraction of ferrite was shown in table 3. It could be seen that the yield/tensile strength would be decreased as the volume fraction of ferrite increased but the elongation would be enhanced. It should be noted that the yield and tensile strength could be still about 600MPa and 820MPa respectively when the ferrite volume fraction reached to 15.68%. The yield and tensile strength were decreased about 5.9% and 6.1% respectively. However, the uniform elongation was increased up to 32.4%. It is applicable to improve anti-deformation ability by introducing small volume fraction of ferrite.

Table 3 Volume fraction of the samples after different heat-treatments

Steel	True stress/strain						
	R_m, MPa	$R_{0.2}$, MPa	$R_{0.2}/R_m$	HV	ε_u	ε_t	Z, %
No. 1	875.62	636.81	0.727	295.30	0.0377	0.1441	81.63
No. 2	856.31	630.91	0.737	277.55	0.0475	0.1532	85.03
No. 3	821.86	598.93	0.729	261.25	0.0499	0.1587	84.17
No. 4	805.77	561.38	0.697	260.32	0.0631	0.1825	84.48
No. 5	776.62	482.22	0.621	255.93	0.0688	0.1739	83.65

According to A. Kummar and A. Bag's work [8] [9], the work hardening could be divided into three stage during deformation processing in two phase steels. The first stage is homogenous plastic deformation occurred only in soft phase (m_I), the second stage is inhomogeneous plastic deformation occurred in soft phase because the restraint of the hard phase without plastic deformation (m_{II}) and the third stage is soft and hard phase coordinated deformation (m_{III}). C-J analysis method [10] was applied in the present work for investigation of the effect of ferrite volume fraction of work hardening behavior. There was no m_I stage could be found in all of the samples which could be due to small amount of ferrite volume fraction and very small grain size. When ferrite grain size is small enough, the deformation could not be homogeneous because interface impede of phase boundaries. Only one stage could be observed in full bainite microstructure as shown in table 4. The stage of m_{II} and m_{III} could be observed as shown in table 4, which implied that the plastic deformation firstly occurred in ferrite. As shown in table 4, the m_{III} stage always occurred at the strain larger than 0.002%, which implied that the plastic deformation occurred after macro yield. As the volume fraction of ferrite increased, the start strain where the m_{III} stage starting would be increased. The plastic deformation was firstly occurred in ferrite to give plasticity and then when the stress accumulation at the phase boundaries was overcome the yield stress for bainite, the plastic deformation was occurred in bainite resulting in different work hardening behavior. It could be concluded that the improvement of plasticity could be attribute to the prior deformation in ferrite.

Table 4 The stress exponent of m_{II} and m_{III} stage, and the start stress and strain where the m_{III} stage starting

Steel	m_{II}	m_{III}	$m_{II} \rightarrow m_{III}$	
			σ_{tr}, MPa	ε_{tr}, %
No. 1	-	13.28	-	-
No. 2	8.58	13.61	689.78	0.0040
No. 3	10.83	12.46	666.60	0.0042
No. 4	7.72	11.84	641.97	0.0062
No. 5	7.58	14.50	713.36	0.0315

Summery

The improvement of plasticity could be obtained by introducing soft ferrite in X80 pipeline steel. Although the yield and tensile strength would be decreased by introducing the ferrite, the plastic elongation would be obviously increased. The two stage work hardening behavior could be observed in ferrite/banite two phase microstructure instead of only one stage work hardening in full bainite microstructure. This resulted improvement of yield/tensile strength ratio. The plasticity enhancement of ferrite/bainite pipeline steel could be attributed to the prior deformation in ferrite.

Acknowledgement

The authors gratefully acknowledge financial support from the National Natural Science Foundations of China (Grant No. 51071026) and Ministry of Education of the People's Republic of China.

References

[1] Schwinn V, Fluess P, Liessem A, et al. Concepts of grade X100 for high toughness and strain based design application, The Eighteenth International Offshore and Polar Engineering Conference. 2008.

[2] Endo S, Ishikawa N, Development of high strength line pipes with excellent deformability, Proceedings of the International Seminar on Application of High Strength Line Pipe and Integrity Assessment of Pipeline. 2006.

[3] Xiaoyong Zhang, Huilin Gao, Xueqin Zhang, et al. Effect of volume fraction of bainite on microstructure and mechanical properties of X80 pipeline steel with excellent deformability [J]. Materials Science and Engineering A, 2012 (531) 84-90.

[4] Fengliang Tan, Qingyou Liu, Ting Lei, et al. Ferrite Evolution During Isothermal Process in a High Deformability Pipeline Steel [J]. Journal of Iron and Steel Research, International, 2013 (7) 89-93.

[5] Xiaofei Zheng, Yonglin Kang, Deliang Meng, et al. Effect of cooling start temperature on microstructure and mechanical properties of X80 high deformability pipeline steel [J]. Journal of Iron and Steel Research, International, 2011 (10) 42-71.

[6] Jinqiao Xu and so on. Understanding variability in mechanical properties of hot rolled microalloyed pipeline steels: Process–structure–property relationship [J]. Materials Science and Engineering A, 2013 (574) 94-103.

[7] Yasuhiro Shinohara, Eiji Tsuru, Hitoshi Asahi. Development of high-strength steel line pipe for SBD applications [J]. International Journal of Offshore and Polar Engineering, 2008 (3) 220-224.

[8] Anand Kumar, Shashi B. Singh, K K Ray. Influence of bainite/martensite-content on the tensile properties of low carbon dual-phase steels [J]. Materials Science and Engineering A, 2008 (474) 270-282.

[9] Asim Bag and so on. Influence of martensite content and morphology on tensile and impact properties of high-martensite dual-phase steels [J]. Metallurgical and Materials Transactions A, 1999 (5) 1193-1202.

[10] C Crussard. Relationship Between Exact Form of Tensile Curves of Metals and Accompanying Changes in Their Structure [J]. Revue de Metallurgie, 1953 (50) 697-710.

Advanced Materials Research Vols. 989-994 (2014) pp 216-219
© (2014) Trans Tech Publications, Switzerland
doi:10.4028/www.scientific.net/AMR.989-994.216

Computer Simulation: A Tool for Researching the Basic Physical Properties of NiAl and Ni_3Al

Chao XU [1, a] and Dong CHEN[2, b,*]

[1] Henan Xinyang Power Supply Company, Xinyang 464000, China

[2] College of Physics and Electronic Engineering, Xinyang Normal University, Xinyang 464000, China

[a] email: sandy1166@126.com

* Corresponding author: Dong CHEN [b] email: chchendong2010@163.com

Keywords: Computer simulation, Elastic constants, Band structure, Bulk modulus

Abstract. The crystal structures, lattice parameters, volumes, elastic constants, bulk moduli and shear moduli of the binary NiAl and Ni_3Al alloys have been predicted by taking the first-principles plane-wave method in combination with ultra-soft pseudo-potentials. Also the pressure dependence of C_{ij}, B and G are described and quantitatively discussed. The calculated results agree with the experimental data. The elastic constants obtained from our calculations meet their mechanical stability criteria. The DOS results show that the strong Ni-Al interaction plays an important role in the chemical bond of the Ni-Al alloys. Our predictions should be testified by the experimental investigations.

Introduction

The high melting point intermetallics NiAl and Ni_3Al have outstanding physical and mechanical properties [1]. Advanced Ni-Al alloys for structural applications in energy conversion systems are currently under development [2]. NiAl and Ni_3Al super alloys have been widely used for turbine blades, structural applications and engines for space projects due to their high strength, unique mechanical property, elevated thermal stability and good corrosion resistance under extreme conditions [3, 4]. Ni-Al binary systems have also been used as nuclear reactors due to the low density, low weight and high melting point [5, 6]. Besides, NiAl is an excellent alumina-scale former with good thermo-mechanical properties and it has been carefully used in a wide range of modern industry [7, 8]. NiAl crystallize in cubic structure (space group: *PM-3M*). The Ni and Al atoms occupy the (0.5, 0.5, 0.5) and (0, 0, 0) Wyckoff positions, respectively [9]. The Ni_3Al alloy has a face-centred cubic lattice (space group: 221). Different atoms occupy the Ni (0.5, 0, 0.5) and Al (0, 0, 0) sites. The lattice parameters of Ni_3Al are a=b=c=0.3568nm [10].

Shang et al. [11] have investigated some fundamental thermal properties (thermal expansion coefficient, bulk modulus, entropy, enthalpy and heat capacity) of Ni and Ni_3Al through the first-principles projector-augmented wave method. Saadi et al. [12] have determined the structure and surface composition of the NiAl (110) and Ni_3Al (111) at conditions relevant for metal dusting. The elastic anisotropy and phonon focusing of NiAl have been predicted using ultra-soft pseudopotentials within the framework of density functional theory [13]. Recently, the structural, elastic and electronic properties of NiAl with rare earth element Ce have been obtained by using first-principles calculations [14]. Generally speaking, the physical properties of NiAl and Ni_3Al have been widely studied by different experiments and theoretical works. Nevertheless, the band structure and density of states are less investigated, especially at high pressures.

The aim of this paper is to predict the electronic structures (band structure, DOS) of NiAl and Ni_3Al through first-principles calculation. The detailed bonding interactions in these alloys are also analysed in this work. This paper is organized as follows. The computational details are given in the following section, i.e. Section 2. Section 3 describes the calculated results and the corresponding discussions. At first, we describe the crystal structure and elastic constants of NiAl and Ni_3Al. Then,

we show the DOS and band structure to analyse the chemical bonding of the two alloys. Finally, some brief conclusions are illustrated in Section 4.

Crystal structure and calculation scheme

In our computations we used the first-principles density functional theory. Namely, the structural and elastic properties were predicted within the plane-wave pseudo-potential method [15]. A plane-wave cutoff energy of 330eV was used in our scheme. According to the Monkhorst-Pack girds [16], the k-point meshes of 10×10×10 and 8×8×8 were used for NiAl and Ni_3Al, respectively. The Perdew-Burke-Ernzerhof (PBE) functional was applied to the exchange-correlation relationship [17]. The Al-$3s^2 3p^1$ and Ni-$3d^8 4s^2$ states are treated as valence electrons. The convergence of total energy was set to be 10^{-6}eV/atom.

Results and discussions

Appling the above-mentioned plane-wave pseudo-potential method, the computed lattice parameter a, cell volume V, elastic constants C_{ij}, bulk modulus B and shear modulus G of NiAl and Ni_3Al at different pressures are listed in Table 1.

Table 1. Lattice constant, cell volume, elastic constants, bulk modulus and shear modulus of NiAl and Ni_3Al under pressures.

	P /GPa	a /nm	V /Å^3	C_{11} /GPa	C_{12} /GPa	C_{44} /GPa	B /GPa	G /GPa
NiAl	5	0.2871	23.68	184.85	169.67	110.33	174.73	43.22
	15	0.2823	22.51	224.19	210.20	140.33	214.86	51.63
	25	0.2784	21.58	266.83	250.33	169.26	255.83	62.04
	35	0.2751	20.81	307.66	288.57	195.59	294.93	71.71
	0 [1]	0.2900	24.38	198.00	137.00	116.00	157.33	--------
Ni_3Al	5	0.3549	44.71	296.71	151.11	64.23	199.64	67.53
	15	0.3497	42.76	356.16	189.31	74.85	244.93	78.17
	25	0.3456	41.29	391.49	218.85	75.74	276.41	79.81
	35	0.3418	39.95	449.11	255.86	85.37	320.28	89.71
	0	0.3572[18]	45.57[3]	225.30[3]	157.60[3]	121.10[3]	180.20[3]	72.90[3]

The lattice constants and elastic moduli of NiAl and Ni_3Al are listed in Table 1. As it can be seen in Table 1, the calculated lattice constants agree well with the experimental data [1, 18]. The maximum relative errors for lattice parameter and bulk modulus are 1.0% and 9.9%, respectively. This is within the general accuracy of GGA for lattice constant (usually 1～2%) and bulk modulus (5～10%). This has proven the reliability of our calculation. As shown in Table 1, the elastic constants C_{ij}, B and G increase with applied pressure, but the slopes are different. The elastic constant C_{11}, which corresponds to the longitudinal wave v_{p1} propagated along [001], increases dramatically with the increasing temperature. C_{44} increases slowly with the elevated temperature, which indicates that the velocity of shear wave v_{s1} propagated along [110] or [001] will be faster as the pressure increases. For the cubic NiAl and Ni_3Al alloys, the mechanical stability rules are $C_{44}>0$, $C_{11}-C_{12}>0$ and $C_{11}+2C_{12}>0$ [19]. All the elastic constants listed in Table 1 satisfy these rules, which indicate that the two alloys are mechanically stable in the pressure range of 5—35GPa.

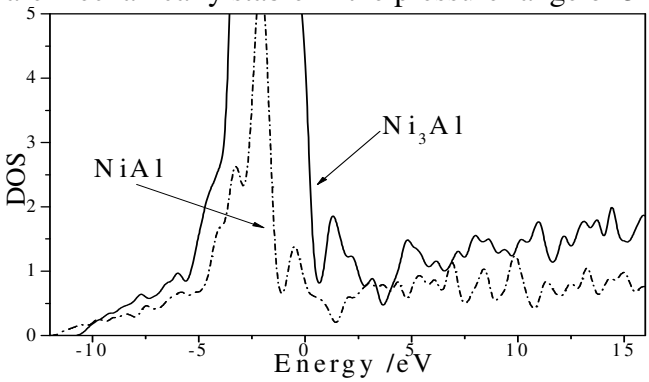

Fig. 1. Total density of state (TDOS) for NiAl (dotted line) and Ni_3Al (dashed line) at 15GPa.

The calculated TDOS of NiAl and Ni_3Al are plotted in Fig. 1. The origin of the energy is located at the Fermi energy level E_F. There is no gap at 0eV, which indicates that NiAl and Ni_3Al belong to metallic materials. The DOS of NiAl is broader than that of Ni_3Al, which reflects that the electrons in Ni_3Al are more localized than the electrons in NiAl. There is no gap appears in the whole energy region, which shows the strong Ni-Al interactions in these alloys. The DOS at E_F are 0.82 and 4.19 for NiAl and Ni_3Al, respectively. The corresponding electronic specific heat coefficients γ are 1.93 and 9.88 J/mol·cell·K^2 ($\gamma=nk_B^2\pi^2/3$, where k_B is the Boltzmann's constant [20]).

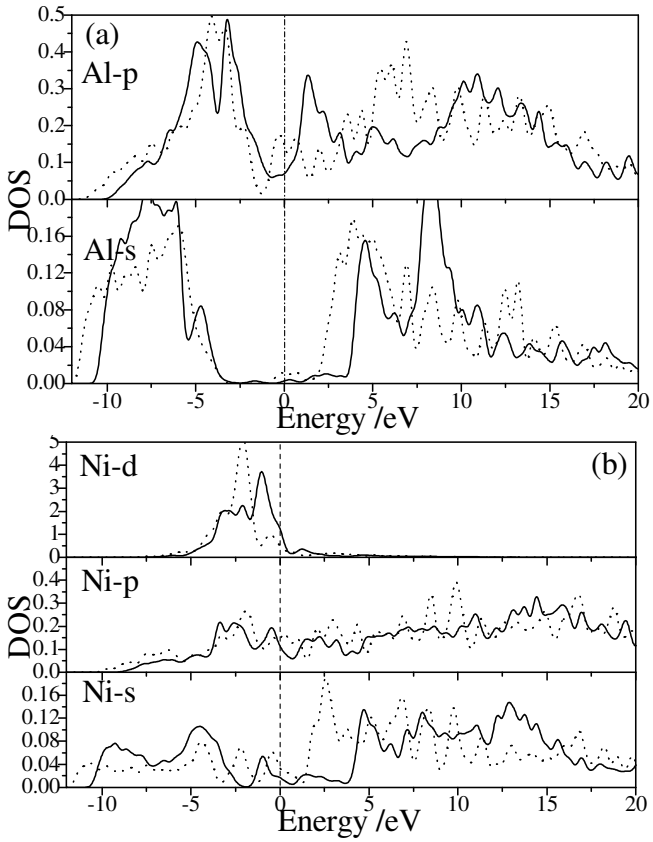

Fig. 2. Spin-averaged density of state projected on to the (a) Al and (b) Ni atoms.

In Fig. 2, the valence band can be clearly divided into two regions, namely the lowest region (below -5eV) and the lower region (-5---0eV). The lowest region is mainly composed of the Al-s and Ni-s bands. The lower region is mainly contributed by the Ni-d, Ni-p and Al-p states. The Ni-d band is much stronger than the other bands. The DOS at E_F is mainly contributed by the Ni-3d state, which is not entirely filled. The conduction band is contributed by the Ni-p, Ni-s and Al-p bands. NiAl is more stable than Ni_3Al, the stability of the Ni-Al compound decreases with the Ni concentration. More importantly, the DOS of NiAl and Ni_3Al are similar with each other.

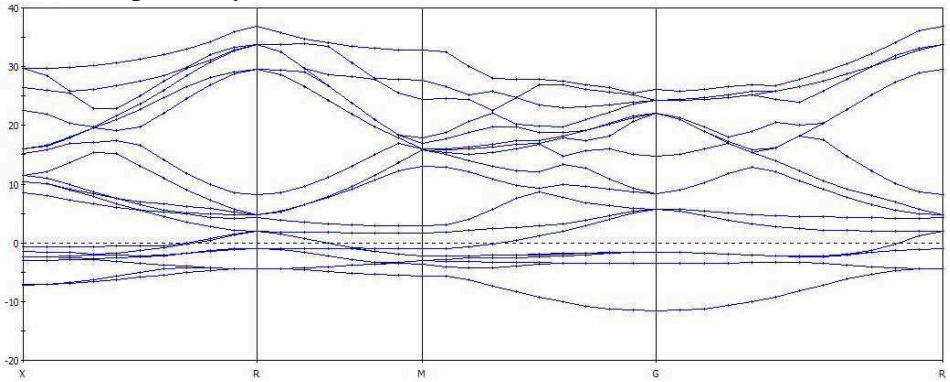

Fig. 3. Calculated electronic band structure of NiAl at 15GPa.

Figs. 3 and 4 show the calculated band structures of NiAl and Ni_3Al along the select high symmetry points X, R, M and G (Γ point), respectively. The band structure curves drawn in Fig. 4are very similar to those of Hussain et al. [10] and Rhee et al. [21]. The energy gap, defined as the difference between the energies of the conduction band and valence band, does not exist in these two compounds, because we could not observe any gap in Figs. 2 and 3. This is also in agreement with the fact that NiAl and Ni_3Al have metallic characters. The densities of states are concentrated in the energy range of -5—0eV (the reciprocal lattice of W to K), which indicates that most bands are not in the centre Γ point.

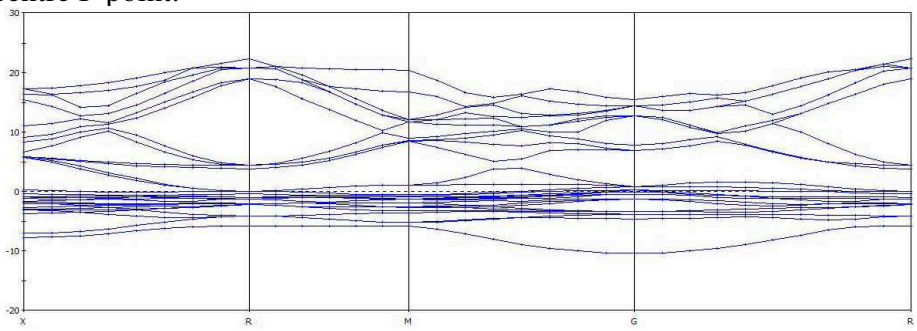

Fig. 4. Band structure of Ni_3Al along some high symmetry points (at 15GPa).

Conclusions

In this work, the first-principles calculations have been performed to study the binary NiAl and Ni_3Al alloys on the structural, elastic and electronic properties in the pressure range of 5—35GPa. The calculated results agree well with the experimental data. The two alloys are mechanically stable under different pressures. All the elastic constants and elastic moduli increase with applied pressure, but the slopes are different. The DOS shows that the band near the Fermi energy are highly localized, which is mainly contributed by the Ni-3d band. The conduction band is completely delocalized. Generally speaking, our predictions need to be verified by the other investigations

References

[1] G. Frommeyer, R. Rablbauer and H.J. Schäfer: Intermetallics Vol. 18 (2010), p. 299
[2] A. Misra, R. Gibala and R.D. Noebe: Metall. Mater. Trans. A Vol. 30A (1999), p. 1003
[3] H. Hou, Z. Wen, Y. Zhao, L. Fu, N. Wang and P. Han: Intermetallics Vol. 44 (2014), p. 110
[4] H. Yasuda, T. Takasugi and M. Koiwa: Acta. Metall. Mater. Vol. 40 (1992), p. 381
[5] Y. Wang, Z.K. Liu and L.Q. Chen: Acta Mater. Vol. 52 (2004), p. 2665
[6] S. He, P. Peng, L. Peng, Y. Chen, H. Wei and Z. Hu: J. Alloys Compd. Vol. 597 (2014), p. 243
[7] Z.F. Zhang, B. Gleeson, K. Jung, L. Li and J.C. Yang: Acta Mater. Vol. 60 (2012), p. 5273
[8] N.P. Padture, M. Gell and E.H. Jordan: Science Vol. 296 (2002), p. 280
[9] J.Q. He, Y. Wang, M.F. Yan, Y. Yang and L. Wang: Comput. Mater. Sci. Vol. 50 (2010), p. 545
[10] A. Hussain, S. Aryal, P. Rulis, M.A. Choudhry, J. Chen and W.Y. Ching: J. Alloys Compd. Vol. 509 (2011), p. 5230
[11] S.L. Shang, Y. Wang, D.E. Kim and Z.K. Liu: Comput. Mater. Sci. Vol. 47 (2010), p. 1040
[12] S. Saadi, B. Hinnemann, C.C. Rappel, S. Helveg, F. Abild-Pedersen and J.K. Nørskov: Surf. Sci. Vol. 605 (2011), p. 582
[13] H.Z. Fu, Z.F. Hou, J. Fu and Y.M. Ma: Intermetallics Vol. 42 (2013), p. 156
[14] Y. Wang, J.Q. He, M.F. Yan, C.Q. Li, L. Wang and Y. Zhou: J. Mater. Sci. Technol. Vol. 27 (2011), p. 719
[15] N. Troullier and J.L. Martins: Phys. Rev. B Vol. 43 (1991), p. 2006
[16] H.J. Monkhorst and J.D. Pack: Phys. Rev. B Vol. 13 (1976), p. 5188
[17] J.P. Perdew, K. Burke and M. Ernzerhof: Phys. Rev. Lett. Vol. 77 (1996), p. 3865
[18] P.M. Rao, S. Suryanarayana, K.S. Murthy and S.N. Naidu: J. Phys.: Cond. Mat. Vol. 1 (1989), p. 5357
[19] S. Yip, J. Li, M. Tang and J. Wang: Mater. Sci. Eng. A Vol. 317 (2001), p. 236
[20] J.W. Oh, C.Y. Kim, K.S. Nahm and K.S. Sim: J. Alloys Compd. Vol. 278 (1998), p. 270
[21] J.Y. Rhee, B.N. Harmon and D.W. Lynch: Phys. Rev. B Vol. 55 (1997), p. 4124

Advanced Materials Research Vols. 989-994 (2014) pp 220-223
© (2014) Trans Tech Publications, Switzerland
doi:10.4028/www.scientific.net/AMR.989-994.220

Newly Determined Crystal Structure and Optical Property of the Intermetallic NiAl and Ni_3Al Alloys: A First-Principles Computer Simulated Investigation

Chao XU [1, a] and Dong CHEN[2, b,*]

[1] Henan Xinyang Power Supply Company, Xinyang 464000, China

[2] College of Physics and Electronic Engineering, Xinyang Normal University, Xinyang 464000, China

[a] email: sandy1166@126.com

* Corresponding author: Dong CHEN [b] email: chchendong2010@163.com

Keywords: Computer simulation, Lattice constant, Reflectivity, Dielectric function

Abstract. Using quantum mechanics plane-wave approach based on the density functional theory, the lattice constants of Ni_xAl at different Ni concentrations (x=1, 3) are predicted. Optical properties such as dielectric function, energy loss function and reflectivity are also investigated. Results show that with the increase of Ni constituent, the location of the peak in loss function moves to the lower energy region, but the peak height increases. At 0eV, the reflectivity increases rapidly with the Ni concentration. The reflectivity of NiAl and Ni_3Al are pronounced in the UV region (not in the visible light region). The dielectric properties, namely the real and imaginary parts of the dielectric function, changed significantly with Ni constituent.

Introduction

Ni-Al constructional alloys play an important role for a wide range of technical applications due to their good corrosion resistance and enhanced strength under extreme conditions [1-3]. To protect engine components made from different alloys from thermo-mechanical failure, the high-temperature Ni-Al binary alloys have been developed to improve their high-temperature hardness at elevated temperatures [4]. The NiAl alloys reveal several interesting properties including low density (about 6 g/cm^3), high melting temperature (1911K) and good oxidation resistance up to 1573K, as well as excellent thermal conductivity [5]. Recently, the laser post-ionisation measurement [6] reflects that the excitation energy, the electron configuration and the band structure have significant effects on the formation of an excited Ni/Al atom [7]. As we all know, the NiAl alloy has a body-centred cubic structure (space group: 221), the Al and Ni atoms occupy the (0, 0, 0) and (0.5, 0.5, 0.5) Wyckoff sites, respectively [8]. Ni_3Al crystallizes in the face centred cubic lattice (space group: 221), different atoms occupy the Ni (0.5, 0, 0.5) and Al (0, 0, 0) positions [9].

The equilibrium lattice parameters, lattice constants, cohesive energies, effective formation energies and self-diffusions in NiAl and Ni_3Al have been determined by molecular dynamics [10] and the analytical embedded atom method [11]. Generated by modifying the aluminium content in Ni_3Al, Takizawa et al. [12] have obtained the $L1_0$ structure of NiAl and have investigated the large distortion in its *c*-axis. Tang et al. [13] have studied the growth behaviour of Ni_3Al layer (shape evolution, growth kinetics) in the β/γ couple of Ni-Al alloys. More importantly, the growth of layers or the formation of ordered 2D over-layers of the Ni-Al binary alloys have been carried out for the Ni (111) [14], NiAl (110) [2], Ni (100) [3] and Ni_3Al (100) planes [3]. Generally speaking, most works are concentrated on the mechanical, physical and thermal properties of NiAl and Ni_3Al. The optical properties of these compounds are less studied. It is worthy of note that the optical properties of metals are directly related to their fundamental properties such as band structures, defects, lattice vibrations and magnetic excitations. Therefore, it is very important to obtain the optical properties of NiAl and Ni_3Al alloys.

The purpose of this study is to investigate the optical properties of Ni-Al based alloys and to determine the fundamental properties which is related to optical properties. The rest of this paper is organized as follows. Section 2 describes the calculation methodology of this work. Section 3 introduces the calculated results and discussions. Finally, I conclude the paper in Section 4.

Crystal structure and calculation scheme

In our computations we used the first-principles density functional theory. Namely, the structural and elastic properties were predicted within the plane-wave pseudo-potential method [15]. A plane-wave energy cutoff of 330eV was used in our scheme. According to the Monkhorst-Pack girds [16], the k-point meshes of 10×10×10 and 8×8×8 were used for NiAl and Ni_3Al, respectively. The Perdew-Burke-Ernzerhof (PBE) functional was applied to the exchange-correlation relationship [17]. The Al-$3s^2 3p^1$ and Ni-$3d^8 4s^2$ states are treated as valence electrons. The convergence of total energy was set to be 10^{-6}eV/atom.

Results and discussions

Firstly, we have investigated the lattice constants. The computed lattice constants of NiAl and Ni_3Al are 0.2901nm and 0.3580nm, respectively. This is in excellent agreement with the experimental data (0.2880nm for NiAl [18] and 0.3572nm for Ni_3Al [19]). Through the above-mentioned first-principles method, we have calculated and plotted the reflectivity of NiAl and Ni_3Al in Fig. 1.

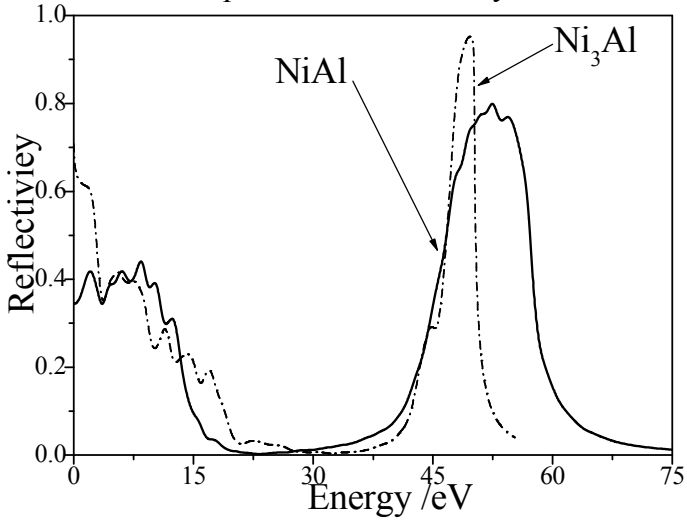

Fig. 1. Optical reflectivity *R* of the NiAl and Ni_3Al alloys.

Then, the optical reflectivities *R* were calculated and drawn in Fig. 1. The optical reflectivity can be determined by the relationship $R=[(n-1)^2+k^2]/[(n+1)^2+k^2]$ [20], where *n* and *k* are the reflective index and extinction coefficient, respectively. The reflectivity spectra shows moderate values near 4.5—12.4eV, the average *R* reaches up to 40%, almost 1/2 visible light is reflected, the materials have metal reflection characters. At 0eV, the first edge values of *R* are 34.6% and 70.7% for NiAl and Ni_3Al, respectively. The main peaks of the curves appear at 45—52eV, which reflects that *R* is more pronounced in the UV region. Besides, the maximum values of *R* are 79.7% and 95.2% for NiAl and Ni_3Al, respectively.

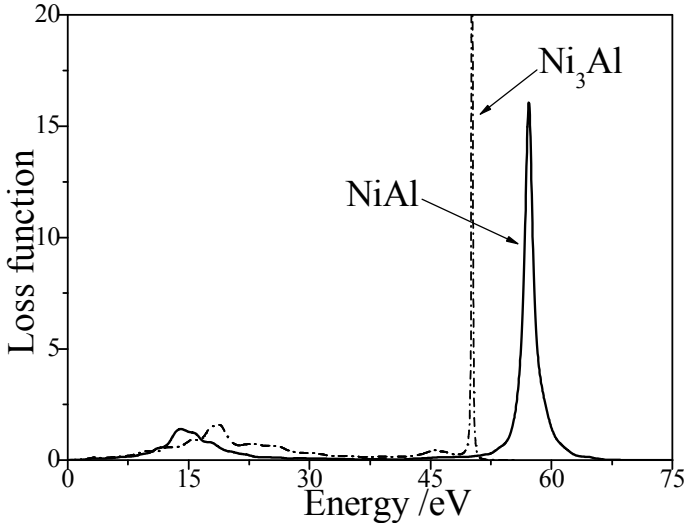

Fig. 2. Energy loss function L of the NiAl and Ni_3Al alloys.

The energy loss function L is an important index which describes the energy loss of a fast electron traversing in a solid [21]. The calculated loss function of NiAl and Ni_3Al are plotted in Fig. 2. The main peak in L spectra represents the plasma resonance, which means a collective oscillation of the valence electrons. The main peak corresponds to the plasma frequency ω_P. The peaks locate at 58 and 47eV for NiAl and Ni_3Al, respectively. At these energies the real part of the dielectric function vanishes. The location of the peak decreases with the Ni concentration, while the peak height increases with the Ni concentration.

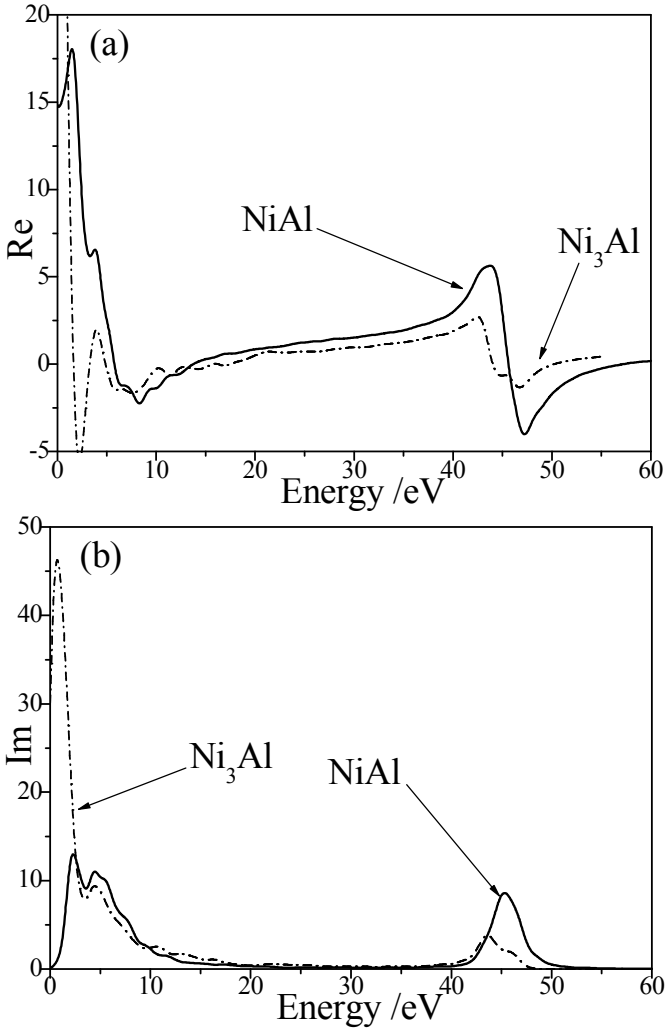

Fig. 3. Calculated (a) real and (b) imaginary parts of dielectric function of NiAl and Ni_3Al.

As the bridge between microcosmic physics process of electrons emission and the macroscopic electronic structures, dielectric function response the band structure and other spectral information of solids [21]. The dielectric function ε can be determined by $\varepsilon=\varepsilon_1+i\varepsilon_2$, where ε_1 and ε_2 are the real part and the imaginary part of the dielectric function, respectively [22]. The real parts of the dielectric functions of NiAl and Ni_3Al are shown in Fig. 3(a). The static dielectric constant $\varepsilon(0)$ and the high-frequency dielectric constant $\varepsilon(\infty)$ can be obtained at 0eV and the energy limit ∞, respectively. Therefore, $\varepsilon(0)$ and $\varepsilon(\infty)$ are 14.88 (129.58) and 0 (0) for NiAl (Ni_3Al), respectively. In Fig. 3(b), the imaginary parts increases from 0eV, which shows that the energy band gap of the two alloys are 0eV (metallic characters).

Conclusions

We studied the optical properties of Ni-Al binary alloys by using the first-principles plane-wave method with the famous PBE exchange-correlation functional. The calculated lattice constants are in good agreement with the experimental data. The static dielectric constant increases rapidly with the Ni concentration. The Ni constituent can also significantly influence the optical dielectric function. The location of the peak in the loss function decreases with the Ni concentration, while the peak increases with the Ni concentration. The reflectivity indicates that *R* is more pronounced in the UV region (not in the visible light region). As a metal, Ni-Al alloy has a suitable band gap of 0eV.

References

[1] E.I. Isaev, A.I. Lichtenstein, Y.K. Vekilov, E.A. Smirnova, I.A. Abrikosov, S.I. Simak, R. Ahuja and B. Johansson: Solid State Commun. Vol. 129 (2004), p. 809
[2] Y. Han, B. Ünal and J.W. Evans: Phys. Rev. Lett. Vol. 108 (2012), p. 216102
[3] M. Tan and B.V. King: Phys. Rev. B Vol. 73 (2006), p. 075414
[4] Q. Wu, S.S. Li, Y. Ma and S.K. Gong: Vacuum Vol. 93 (2013), p. 37
[5] T. Czeppe and S. Wierzbinski: Int. J. Mechan. Sci. Vol. 42 (2000), p. 1499
[6] K.M. Downard: Euro. J. Mass Spectrom. Vol. 13 (2007), p. 177
[7] M. Tan and B.V. King: Appl. Surf. Sci. Vol. 203-204 (2003), p. 248
[8] J.Q. He, Y. Wang, M.F. Yan, Y. Yang and L. Wang: Comput. Mater. Sci. Vol. 50 (2010), p. 545
[9] A. Hussain, S. Aryal, P. Rulis, M.A. Choudhry, J. Chen and W.Y. Ching: J. Alloys Compd. Vol. 509 (2011), p. 5230
[10] B.J. Alder and T.E. Wainwright: J. Chem. Phys. Vol. 31 (1959), p. 459
[11] S. Yu, C.Y. Wang, T. Yu and J. Cai: Physica B Vol. 396 (2007), p. 138
[12] S. Takizawa, S. Miura and T. Mohri: Intermetallics Vol. 13 (2005), p. 1137
[13] S. Tang, J.C. Wang, G.C. Yang and Y.H. Zhou: Intermetallics Vol. 19 (2011), p. 229
[14] S. Le Pevedic, D. Schmaus and C. Cohen: Surf. Sci. Vol. 601 (2007), p. 395
[15] N. Troullier and J.L. Martins: Phys. Rev. B Vol. 43 (1991), p. 2006
[16] H.J. Monkhorst and J.D. Pack: Phys. Rev. B Vol. 13 (1976), p. 5188
[17] J.P. Perdew, K. Burke and M. Ernzerhof: Phys. Rev. Lett. Vol. 77 (1996), p. 3865
[18] H.Z. Fu, Z.F. Hou, J. Fu and Y.M. Ma: Intermetallics Vol. 42 (2013), p. 156
[19] H. Hou, Z. Wen, Y. Zhao, L. Fu, N. Wang and P. Han: Intermetallics Vol. 44 (2014), p. 110
[20] M. Jafari, H. R. Hajiyani, Z. Sohrabikia and H. Galavani: Comput. Mater. Sci. Vol. 77 (2013), p. 224
[21] X. Yu, Y. Du, B. Chang, Z. Ge and H. Wang: Optik Vol. 124 (2013), p. 4402
[22] J.D. Sharma, M. Sharma, N. Kumar and P.K. Ahluwalia: J. Phys.: Conf. Ser. Vol. 472 (2013), p. 012010

Advanced Materials Research Vols. 989-994 (2014) pp 224-227
© (2014) Trans Tech Publications, Switzerland
doi:10.4028/www.scientific.net/AMR.989-994.224

TiO_2-based composite film for the photodegradation of methyl green

Na Song, Fang Li, Ming-ming Yao

[b] Key Laboratory of Chemical Sensing & Analysis in Universities of Shandong, School of Chemistry and Chemical Engineering, University of Jinan, Jinan 250022, China

email, yaomm4364@sina.com; chm_lif@ujn.edu.cn

Keywords: TiO_2-based; Composite film; photodegradation

Abstract. A simple process was developed for preparation of highly photoactive Fe and S codoped TiO_2-SiO_2-ZnO composite film. The Brunauer–Emmett–Teller (BET) surface area results showed that the specific surface area of the composite TiO_2 sample was 432.5m^2g^{-1}, while that of the pure TiO_2 was 103.4m^2g^{-1}. The diffuse reflectance measurements exhibited an extension of light absorption into the visible region for the composite TiO_2. The photoluminescence (PL) spectra analysis indicated that the electron-hole recombination rate was effectively inhibited in the composite TiO_2. The photocatalytic activities of the TiO_2 films were evaluated by the photocatalytic decomposition of methyl green in aqueous solution. The composite TiO_2 film exhibited excellent photocatalytic activities compared to pure TiO_2 film.

Introduction

The reuse and recycling of wastewater effluent is rapidly growing due to limited fresh water supply in the world. However, it is difficult to remove them by traditional pollutant treatment methods. Semiconductor heterogeneous photocatalytic oxidation process is a popular technique that has great potential to remove organic dyes in wastewater. Among various semiconductors, titanium dioxide is considered as the most useful photocatalyst owing to its long-term stability, lowtoxicity, chemical and biological inertness, controllable structure and morphology, strong oxidizing power, as well as its low cost [1-3].

In this paper, we report the Fe and S codoped TiO_2-SiO_2-ZnO composite films with an attempt to increase the specific surface area of the TiO_2-based photocatalyst, extend light absorption of TiO_2 into the visible region and reduce the rapid recombination of photogenerated electron and holes. We have investigated the effect of the co-modifying on the photocatalytic degradation of methyl green.

Experimental

All chemicals used in this study were analytically pure. TiO_2 colloid or SiO_2 colloid was prepared through the sol-gel method [4, 5]. TiO_2-ZnO composite colloid was prepared by the following method. 1mL tetrabutyl titanate ($TiO(C_4H_9O)_4$) was added dropwise to 20mL absolute ethanol in a clean vessel, and 20 mL 0.2M nitric acid contained 100mg zinc nitrate were added to the above solution under vigorous stirring. After 24h aging, the composite colloidal TiO_2-ZnO could be obtained. TiO_2-SiO_2 composite colloid was prepared by mixing TiO_2 and SiO_2 colloid in a 2/1 in volume ratio under strong stirring. After 24h aging, the composite colloidal TiO_2-SiO_2 could be obtained. TiO_2-SiO_2-ZnO composite colloid was prepared by mixing colloidal TiO_2-ZnO and SiO_2 in a 2/1 in volume ratio under strong stirring.

All sol-films were coated on the surface of a glass substrate by the controllable dip-coating device in the atmosphere. 5.0×10^{-3} mol dm^{-3} iron nitrate aqueous solutions or 5.0×10^{-3} mol dm^{-3} carbamide ($CS(NH_2)_2$) aqueous solutions was doped into the surface layer of TiO_2 gel-film, respectively. The surface doped TiO_2 composite films were calcined in air at a rate of 5℃/min up to 450℃ and were left to stay in the furnace for 1 h for organics removal.

The photodegradation activity of the photocatalyst was studied with TU-1901 UV-Vis spectrometer. The Brunauer-Emmett-Teller (BET) surface area of the TiO_2 powders was analyzed by nitrogen adsorption/desorption apparatus (ASAP 2020). UV-Vis diffuse reflectance spectra of the

film was recorded on a UV–Vis spectrophotometer with an integrating sphere accessory (IS19-1) using blank glass plate as a reference. The recombination of electron-hole in the sample was studied by the photoluminescence (PL) emission spectra, recorded at room temperature by a FLS 920 spectrometer with a 300-nm line of 450 W xenon lamp as excitation source.

Results and discussion

Methyl green (MG) is a recalcitrant organic dye. Figure 1 shows UV–Vis absorption spectra (a) and degradation rate (b) of MG solutions using pure TiO_2 film, TiO_2-SiO_2 film, TiO_2-SiO_2-ZnO film, Fe doped TiO_2-SiO_2-ZnO film and Fe/S codoped TiO_2-SiO_2-ZnO film on common glass substrates under UV-lamp irradiated with wavelength of 365 nm for 45 min. The degradation rates of pure TiO_2 film is 21%; TiO_2-SiO_2 film 38%; TiO_2-SiO_2-ZnO film 41%; Fe doped TiO_2-SiO_2-ZnO film 47%; and Fe/S codoped TiO_2-SiO_2-ZnO film 59%. Obviously, the Fe/S codoped TiO_2-SiO_2-ZnO composite photocatalysts in MG dye aqueous solutions exhibit highest photocatalytic activity in all samples.

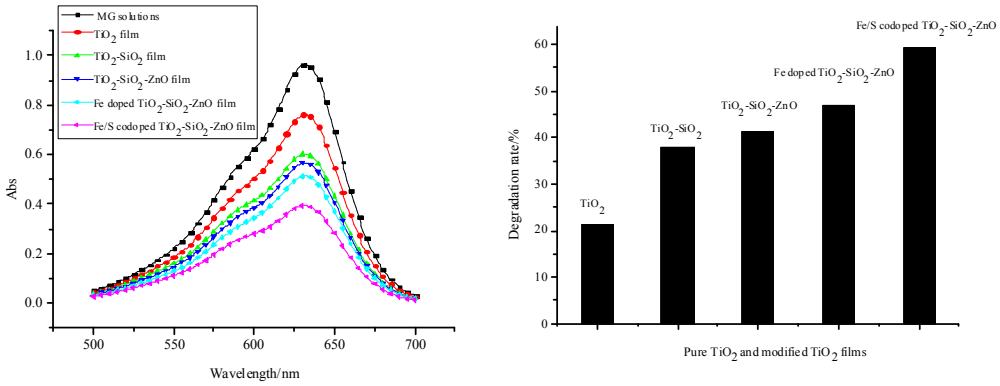

(a) (b)

Fig.1. Absorption spectra (a) and degradation percentage (b) of MG solutions using pure TiO_2 and modified TiO_2 films on glass substrates after irradiated for 45 min

Figure 2 shows N_2 adsorption/desorption isotherms of the pure TiO_2, TiO_2-SiO_2, TiO_2-SiO_2-ZnO, and Fe/S codoped TiO_2-SiO_2-ZnO powders calcined at 450°C in air for 1.0 h. BET surface areas can be determined using nitrogen adsorption and desorption isotherms. From Fig. 2, the isotherms of the four samples exhibit hysteresis loops at high relative pressures from 0.4 to 0.8. It is evident that with the same relative pressure Fe/S codoped TiO_2-SiO_2-ZnO samples have highest adsorption quantities as well as highest surface area in all samples. In our case, the specific surface area of Fe/S codoped TiO_2-SiO_2-ZnO sample was determined to be 432.5 $m^2\ g^{-1}$, compared with pure TiO_2 103.4 $m^2\ g^{-1}$, TiO_2-SiO_2 388.1 $m^2\ g^{-1}$, and TiO_2-SiO_2-ZnO 413.8 $m^2\ g^{-1}$. The large specific surface area is favorable to the photocatalytic degradation, so the Fe/S codoped TiO_2-SiO_2-ZnO film exhibits highest photocatalytic activity in all samples.

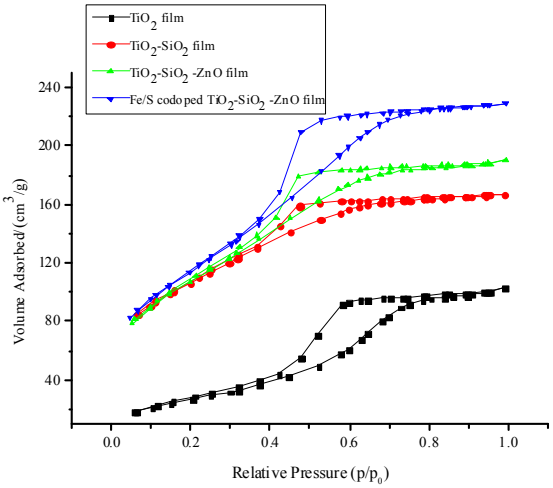

Fig. 2. N_2 adsorption/desorption isotherms of pure TiO_2 and modified TiO_2 samples

Photoluminescence emission is useful to understand the fate electron-hole pairs in semiconductor particles. The PL emission spectra of pure TiO_2, TiO_2-SiO_2, TiO_2-SiO_2-ZnO, and Fe/S codoped TiO_2-SiO_2-ZnO films are examined in the wavelength range of 325–500 nm in Figure 3. It shows that the position of the peaks about 375 nm due to the emission of the band gap transition is similar while PL intensities are different for three samples. The PL intensity of Fe/S codoped TiO_2-SiO_2-ZnO film is the lowest among all samples, indicating the recombination of electron and hole is effectively prohibited compared with other samples. Lowest recombination of electron and hole can result in highest photocatalytic activity of Fe/S codoped TiO_2-SiO_2-ZnO film.

UV–vis diffuse reflection spectra of pure TiO_2, TiO_2-SiO_2, TiO_2-SiO_2-ZnO, and Fe /S codoped TiO_2-SiO_2-ZnO films are shown in Figure 4. It can be seen that the absorbance onset of Fe /S codoped TiO_2-SiO_2-ZnO film red shift to more than 500nm. As a result, more photogenerated carriers can join in the degradation reaction; leading to enhance the photocatalytic activity of the multi-modified TiO_2 film. Considering the above discussion, the enhanced photocatalytic activity of the Fe/S codoped TiO_2-SiO_2-ZnO film is attributed to factors such as improved optical absorption property and improved lifetime of the charge carriers.

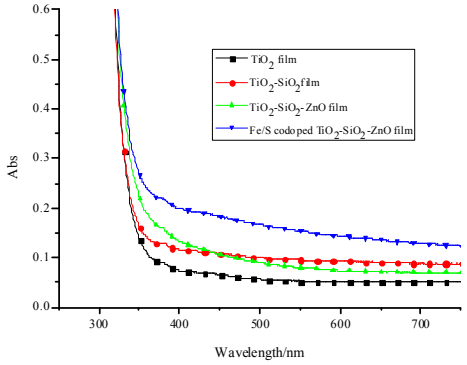

Fig. 3. Photoluminescence spectra of pure TiO_2 and modified TiO_2 films

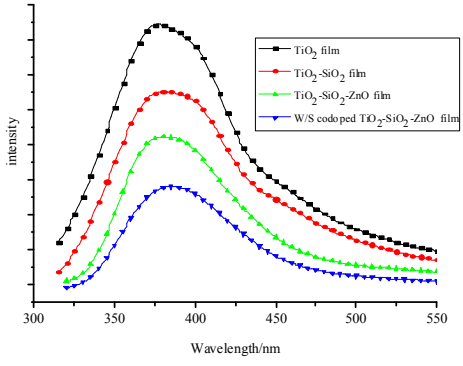

Fig. 4. Diffuse reflection UV-vis absorption spectra of pure TiO_2 and modified TiO_2 films

Conclusions

Fe and S codoped TiO_2-SiO_2-ZnO composite films were successfully prepared by composite semiconductor and metal or non-metal codoping in our experiment. Enhanced photocatalytic activity for the photodegradation of methyl green dye was observed for the modified TiO_2 composite film. In the system, obviously red shift and improved lifetime of the charge carriers may promise a potential application for TiO_2 film in visible light or solar light.

Acknowledgements

This work was financially supported partially by National Natural Science Foundation of China (Grant No. 51102114), Shandong Provincial Natural Science Foundation, China (ZR2012BM009).

References

[1] A. Charanpaharia, S.S. Umarea, S.P. Gokhaleb, V. Sudarsanc, B. Sreedhard and R. Sasikalac: Appl. Catal. Vol. 443-444 (2012), p.96

[2] K. Li, Y. He, Y.L. Xu, Y.L. Wang and J.P. Jia: Environ. Sci. Technol. Vol. 45 (2011), p.7401

[3] F. Li, L.X. Guan, M.L. Dai, J.J. Feng and M.M. Yao: Ceram. Int. Vol. 39 (2013), p. 7395

[4] N. Zhao, Y. Yao, J.J. Feng, M. M. Yao and F. Li: Water Air Soil. Pollut. Vol. 223 (2012), p. 5855

[5] Y. Yao, N. Zhao, J.J. Feng, M.M. Yao and F. Li: Ceram. Int. Vol. 39 (2013), p.4735

Advanced Materials Research Vols. 989-994 (2014) pp 228-232
© (2014) Trans Tech Publications, Switzerland
doi:10.4028/www.scientific.net/AMR.989-994.228

Synthesis and Characterization on a kind of polycarboxylate superplasticizer

Xing Li[1, a], Guangjun Zheng[1,b], Yao Bi [1], Chengfei Fu[1], Minghua Yuan[1] and Shaofeng Wang[1]

[1] China Construction Ready Mixed Concrete Co. Ltd, Wuhan 430205, China,

[a]leexingbridge@yeah.net, [b]27307274@qq.com

Keywords: polycarboxylate superplasticizer, density of carboxyl, fluidity of cement paste, concrete slump

Abstract. This study was undertaken to evaluate a new kind of polycarboxylate superplasticizer. Used polyoxyethylene ether (TPEG), acrylic acid (AA) as the monomer, ammonium persulfate (APS) as initiator, thioglycolic acid (TGA) as chain transfer agent, synthesised polycarboxylate superplasticizer with high water reducing rate. The effect of admixtures on fluidity and concrete slump were discussed in this paper. The structure of carboxylic acid water reducing agent was characterized by IR spectra and Gel permeation chromatography.This investigation also evaluated the influence of different serials of polyoxyethylene ether (TPEG), the dosage of acrylic acid (AA) and ammonium persulfate (APS).

Introduction

Polycarboxylate Superplasticizers are widely used in concrete today to increase the workability of fresh concrete as well as decrease the water requirement to achieve a given workability,they can reduce the hydration heat,increase the fluidity,lead to higher strength and better durability of the hardened products[1].

Polycarboxylate superplasticizers are considered the most potential category of polymeric dispersants. In terms of chemical structure,these polymers have lots of advantages: better fluidity and slump flow with low dosage of PCs, wide adaptability for cement,higher water-reducing efficiency,large freedom of molecular structure,more synthesis technology,more room for improvement[2-4]. The research and application of Polycarboxylate superplasticizers is just a decade. Researches focus on the choice of reaction monomer,synthesis temperature,initiator species,adjustment of process conditions,reduction of engineering cost and control of product prices,etc [5-6]. We have less understanding and cognition on relationship between PCs structure and dispertion properties,rheological properties and hydration theory as well as practical application in construction[7].

This paper had synthesized a series of polycarboxylate superplasticizaers in different pH .Different kinds of Isoamyl alcohol polyoxyethylene ether(TPEG) and different dosage of acrylic acid were used as monomer, ammonium persulfate (Aps) was used as initiator, TGA used as chain transfer agent. The influence of monomer type, carboxyl density , initiator dosage, chain transfer agent dosage and pH on dispersion property of superplasticizer was studied through the fluidity of cement paste and concrete slump flow .

Experimental

1.1 Chemicals and Equipment.

Prenyl alcohol ethoxylates (TPEG, Liaoning Kelong Chemical Co. LTD), Acrylic acid (AA,Wuhan Zhonghua Yongye Chemical Co. LTD), Ammonium persulfate (Aps, Shanghai degussa-aj chemical Co. LTD), Chain transfer agent (TGA, Changzhou Yurong Chemical Co.LTD)

,sodium hydroxide(NaOH),HuaXin cement,P.O42.5，WuGang II flyash,WuXin S95 silica fume. Cement paste mixer,NJ-160A,WuXi JianYi equipment Co. LTD ; Single horizontal-axis laboratory concrete mixer,HJW-60,ShenYang JuLin equipment Co. LTD.

1.2 Synthesis Process.

Put a flask within water and TPEG into water-bath heater, and stirried until the end of experiment; wait until TPEG dissolved, then add ed the APS at 60^{o}C, and dripped the AA and TGA solution; keep heating for certain hours, then decreased temperature; added the sodium hydroxide and water, and adjusted pH of the new product about 7; The new product would been gotten and its solid content was 40%.

1.3 Measurement.

The fluidity of cement slurry was tested according to Chinese Standard (GB/8077-2000).The water-cement ratio is 0.29,PCs dosage is 0.13%.

1.4 GPC Analysis method

The average of molecular mass and distribution of the new product was determined by gel permeation chromatography (GPC) using an Agilent-1100 chromatographic apparatus equipped with PL AQUAGEL-OH mixed 8μm, as well as a detector (Agilent-1100 VWD). The sample was analyzed using a 0.1mol/L of phosphate buffer solution. The standard material is PEG from UK Polymer lab

1.5 FT-IR Analysis method

The reaction product is distilled under reduced pressure，when the liquid is reduced to a certain extent,poured the solution into the beaker.It is precipitated,dissolved,washed and filtered by Isoropyl alcohol. Isoropyl alcohol is volatilized at 50℃,then dry to powder until constant weight at 85℃ .Presseed 1mg PCs and 100mg KBr into transparent sheet, wave at between 400-4000 cm^{-1} for 50 times.

Results and Discussion

2.1 Determination of monomer type

F108 and TJ-188 are synthesised by imported initiator, while F1088 and TJ-188C are synthesised by domestic initiator. The front two kinds of monomers are more active than back ones. The table shows F108 is more suitable for this method.

Table.1 Fluidity of cement paste with different monomer condition of PCs

Type	Fluidity of cement paste(mm)	Slump flow(mm)
F108(Liaoning Kelong Chemical Co. LTD)	260	230/560
F1088(Liaoning Kelong Chemical Co. LTD)	240	220/520
TJ188(ShangHai TaiJie Chemical Co. LTD)	250	230/540
TJ188C(ShangHai TaiJie Chemical Co. LTD)	235	225/515

2.2 Determination of carboxylic acid Dosage

Figures 1 and 2 are efforts of cement paste and concrete with different carboxylic acid dosage. We can see from the figures, with the carboxyl density increased from 1.5 to 3.8, the fluidity of cement paste increase gradually. When the carboxyl density exceeds 3.8, PCs are adsorbed to saturation on the surface of cement particles. While the carboxyl density increases, PCs absorb rapidly, it leads to slump loss of concrete. Less carboxyl density can cause poor adsorption capacity, PCs can't adsorb on the surface of cement particles effectively, the steric effects can't fully work, the fluidity of cement paste is small. When carboxyl density increases, the content of -COO- side chain increases, lead to more anionic charge density and larger electrostatic repulsion, add adsorption on cement particles, Dispersion performance was improved[8].

More carboxyl density caused higher adsorbtion ability , however, this decreases its branched chain density. The number of branched chain on the cement particle reduces, so its space steric hindrance weakens to some extent. Therefore the dispersion effect decreases. Figure 2 shows that the fluidity of cement paste can be achieved when carboxyl density is 3.8.

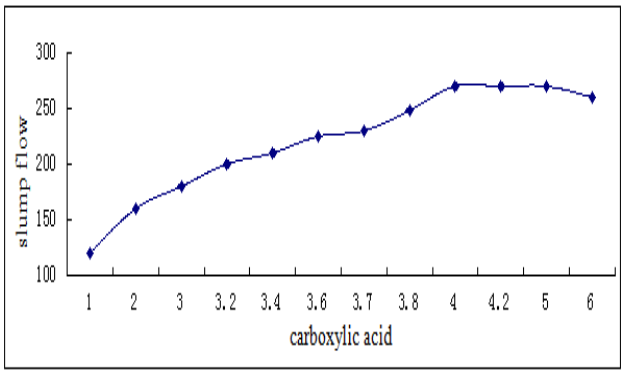

Fig.1 Fluidity of cement paste with different carboxylic

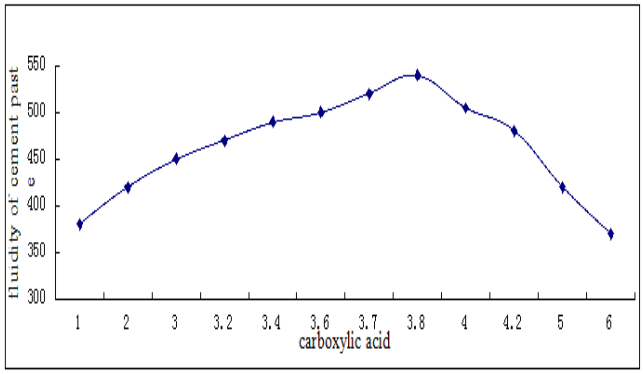

Fig.2 Slump flow with different density of carboxylic

2.3 Determination of initiator Dosage

We can see from figure 3 and 4, with all other conditions being equal, concrete has the best dispertion performance when the dosage of initiator is 0.35mol. This is because low dosage of initiator causes little active centre, reaction is not complete; as high dosage of initiator causes too many active centre, the molecular weight is too small to the disadvantage of space steric hindrance.

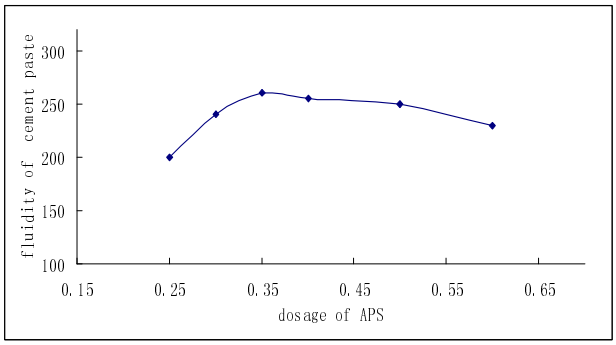

Fig.3 Fluidity of cement paste with different density of initiator

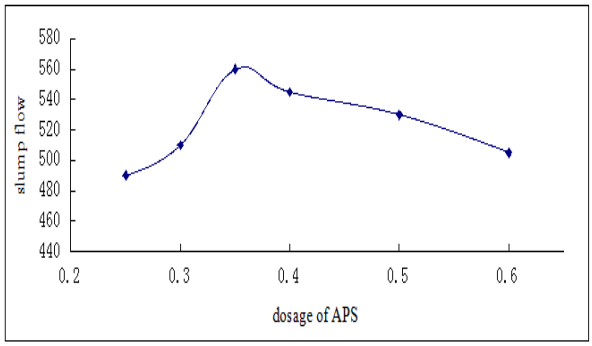

Fig.4 Slump flow with different density of initiator

2.4 pH effect on the performance of cement paste and concrete

We can conclude from Fig. 5 and 6, PCs impact little on the fluidity of cement paste and dispertion of concrete when pH changes between 3-9. Alkali aggregate reaction won't occur in this pH range.

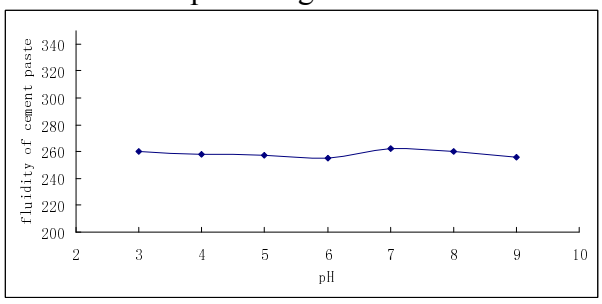

Figure 5.pH effect on the performance of cement paste

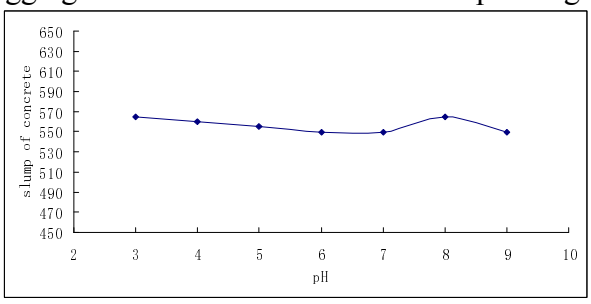

Figure 6.pH effect on the performance of concrete

2.5 GPC Analysis

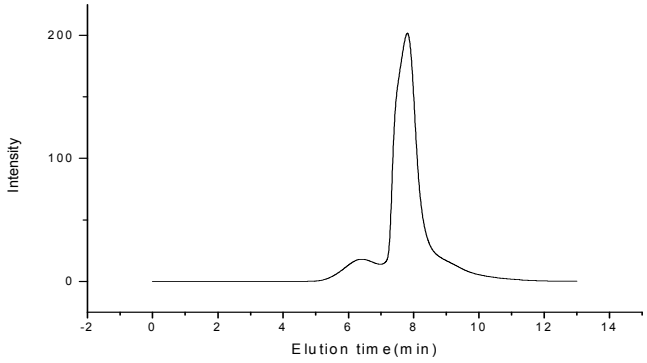

Fig.7 Molecular mass distribution of PCs

The molecular weight and distribution is an important element in evaluating the performance of PCs. High average molecular weight of PCs leads to higher absorption on the surface of cement .Higher molecular weight of PCs adsorb on the surface of cement particles preferentially; with its adsorption capacity on the surface of cement particles increase, the fluidity of concrete increases. The concrete can entrain large amount of air content if the molecular is too small, moreover, it causes faster slump loss and lower strength of concrete; The adsorption amount decreases when the molecular is large , it reduces the dispersion of concrete. Therefore, the best dispersion can be achieved when the molecular weight of PCs is within an appropriate range. Fig. 7 may have an intuitive understanding of its molecular weight distribution, it has narrow Fig. 7 may have an intuitive understanding of its molecular weight distribution, narrow molecular weight distribution of the molecular weight[9-10] .

2.6 FT-IR Analysis

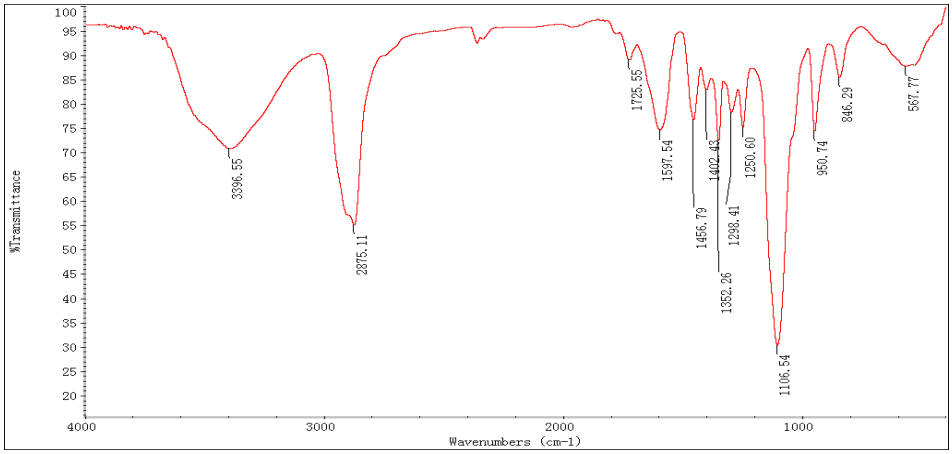

Fig. 8 IR of spectra of PCs

Fig. 8 shows that the wide peaks vary form 3350 cm^{-1} to 3400 cm^{-1} was due to the stretching vibration of O-H bond. The peaks at 2875 cm^{-1}, 1456 cm^{-1}, 1298 cm-1,1250 cm^{-1}, and 950cm^{-1} were the characteristic of absorption peaks of the polythethylene axide group (CH_2CH_2O). The typical absorption peak of the stretching vibration of C-O-C structure was detected at 1106 cm-1 and 1110 cm^{-1}. The characteristic of absorption peak of the COO- group appeared at 1725 cm^{-1} and 1456 cm^{-1}. And the absorption peak of the C=O in the ester bond was detected at 1725 cm^{-1}. It was declared that the sample was synthesized with different monomers which were referred to from Chapter 1.1 by IR analysis.

Conclusion

By discussing various factors that impact the performance of PCs, we confirm a suitable process conditions which a new type of polycarboxylate superplasticizer with high dispersibility was synthesized . The influencing factors of reaction include proportion of acid, initiator concentration, pH and additive. The fluidity of cement paste and slump flow of concrete can achieve 275mm and 570mm. It is possible to realize industrial production.

References

[1] J. Witt, J. Plank, A Novel type of PCE possessing Silyl Functionalities, In print.

[2] E.Sakai, A.Ishida, A.Ohta, New trend in the Development of Chemical Admixtures in Japan, J. Adv. Concr. Technol.4(2006)211-223

[3] K. Magarotto, I. Torresan,N.Zeminian, Effect of Alkaline Sulfates on Performance of Superplasticizers Superplasticizers.Vol.2.Durban, South Africa, May11-16(2003)569-580.

[4] K.Yamada,S.Ogawa, S, Hanebara, Controlling of the Adsorption and Dispersing Force of Polycarboxylate type Superplasticizer by Sulfate ion Concentration in Aqueous Phase, Cem. Concr. Res.31(2001) 375-383.

[5] S. Li, Q. Yu, J. Wei, et al, Effects of molecular mass and its distribution on adsorption behaviorof polycarboxylate water reducers, Journal of the Chinese Ceramic Society, 1 (2011) 81-83.

[6] A. Lange A., J. Plank, Study on the Foaming Behaviour of Allyl Ether-Based Polycarboxylate Superplasticizers, Cem. Concr. Res. 42(2012)484-489.

[7] T. Hirata, A. Lange , J. Plank, "Copolymer for dispersant for cement and cement coposition", EP 12 162 379.7(2012)

[8] C. Li, H. Wang, H. Wu, et al, Synthesis and performance a slowly-released type polycarboxylic water-reducers, Baton Chinese Edition-ready-mixed Concrete, 10 (2010) 27-28.

[9] Z. Wang, Polycarboxylate Superplasticizer--Preparation Performance and Application, China Building Industry Press, Beijing, (2009) 153-201.

[10] S. Li, Q. Yu, J. Wei, Effect of molecular structure of polycarboxylate water reducers on hydration of cement, Journal of the Chinese Ceramic Society, 4 (2012) 614-618.

Advanced Materials Research Vols. 989-994 (2014) pp 233-237
© (2014) Trans Tech Publications, Switzerland
doi:10.4028/www.scientific.net/AMR.989-994.233

Synthesis for an Amide-ester Type Polycarboxylate Superplasticizer and its application in concrete

Chong Sun[1, a], Guangjun Zheng[1, b], Yao Bi[1, c], Hui Zhou[1, d]

[1] China Construction Ready Mixed Concrete Co. Ltd, Wuhan 430205, China

[a]253186118@qq.com, [b]chenzhengjiwit@yahoo.cn, [d]87404692@qq.com,

Keywords: Modification; Mannich reaction; amidation; esterification; superplasticizer; synthesize

Abstract. A new type of amide-modified polycarboxylate superplasticizer was synthesized by a two-step method: Firstly, a mixture of amidated and esterified products reacted by maleic anhydride and 2-aminoethanol was modified through Mannich reaction. Then, the modified product was reacted with Prenyl alcohol polyethenoxy ether (TPEG), acrylic acid and other monomers to obtain an amide-structured polycarboxylate superplasticizer. The molecular weight and molecular weight distribution were measured by Gel permeation chromatography (GPC). Lastly, the optimum AA to modified product ratio, initiator dosage and reaction time were determined by cement mortar test. The concrete application performance showed that the synthesized superplasticizer could improve the fluidity of the concrete and maintain the slump loss as well. The introduction of modified PCE has no harm for the concrete strength.

Introduction

Nowadays, superplasticizer has been an essential component in cement admixtures for the superior performance it endows to concrete or other cement materials. Among those superplasticizers, polycarboxylate-type (PCE) superplasticizer was most favored to industry due to its high water-reduction ratio and flexibility in chemical structural design [1]. The special chemical structure of PCE has the potential to be modified which can be easily designed to meet specific needs in various applications [2-6].

Researchers have already used the products reacted by maleic anhydride and 2-aminoethanol as the monomer to polymerize with other functional monomer to obtain PCE [7]. The main drawback for this method is that the inefficient use of the esterified product acquired from the amidation-esterification process as the performance of the PCE mostly relied on the amidated product. It has to be noted that even use highly efficient amidation catalyzer, high degree of amidation still can't be achieved.

In this study, in order to provide the PCE with better dispersion ability and to overcome the large time spans between the production of concrete and incorporation thereof which often leads to server slump loss[8], Mannich reaction was chosen to modify the esterified product with a functional monomer to give fully use of the amidation-esterification product. Then, the modified product (M) was polymerized with other monomers to obtain the modified PCE. The optimum condition for the polymerization was determined and the performance in concrete of the modified PCE was measured, in comparison with other samples, the modified PCE showed good dispersion and slump-retaining ability.

Materials and methods

Chemicals and materials. The maleic anhydride (MA), acrylic acid (AA), sodium hydrate, sodium methylacrylsufonate (SMAS), ammonium persulphate (APS) and thioglycollic acid (TGA) are all industrial grade. TPEG (M_n=2400) was obtained from. 2-aminoethanol, 4-dimethylaminopyridine (DMAP), functional monomer A, polyoxymethylene and propionic acid are all commercially available in analytical grade.

Modification of amidated and esterified products. At first, an amount of 2-aminoethanol was added to a 500ml four-necked flask equipped with a condenser and a stirring bar. Then, propionic acid was added to the flask to fully neutralize the solution and the mixture was heated to 60°C in water bath. Finally, MA and DMAP were added to the mixture to react for 2h and product was withdrawn from the reactor. The esterify ratio was measured as the given literature.

According to the obtained data, monomer A and polyoxymethylene were then added to the flask to react for 2 more hours under 80°C to give the modified product(M). Figure 1 was the general equation for the reaction:

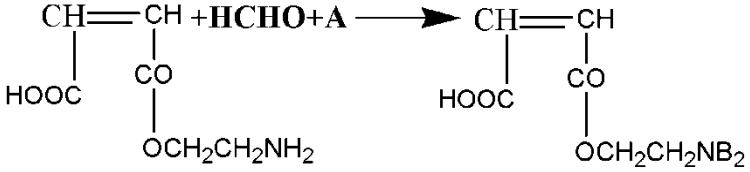

Fig.1 Reaction equation for modification

Synthesis of the modified PCE. An amount of M, AA, SMAS and TGA was mixed in water to give a 20wt% solution. 150g TEPG and water was added to a 500ml four-necked flask equipped with a condenser, a nitrogen inlet and a stirring bar afterwards and stirred for 15min to give a homogeneous solution. The solution was gently heated to 60°C and the monomer solution and APS solution(20%wt) was then added to the flask under a fixed feeding rate. After complete the feeding process, the mixture was stirred for several hours under the same temperature. At the end, the pH was adjusted to 7 with 30wt% NaOH and the PCE was acquired.

Measurements. Molecular weight of PCE was measured by gel permeation chromatography (GPC, Waters 150C, USA), using the solution of methanol and buffer solution (1/2, v/v) as the eluent. (Column, PL aquagel mix/m, 7.8*300 mm, Agilent1100, Agilent Company, USA). The buffer solution was $Na_2B_4O_7$/KCl aqueous solution (pH = 8). Narrow polyethylene glycol (PEG) was used as calibration standards. The GPC detector included the refractive index.

Test of the fluidity of cement pastes added with superplasticizer was under the Chinese National Standard (GB 8077-2000) "Methods for testing uniformity of concrete mixture" and the cement used for the test was HUAXIN P·O 42.5, the w/c ratio was 0.29 and the dosage of the PCE was 0.13% (by percent Weight based on solids cement).

Concrete performance was measured following the Chinese National Standard (GB 8077-2008) "Concrete admixtures" and the material proportion was shown in Table 1, the dosage for the PCE was 1.8%.

Table 1 Material proportion for the concrete test

Water (kg/m^3)	Cement (kg/m^3)	Fly ash (kg/m^3)	Slag (kg/m^3)	Sand (kg/m^3)	Gravel (kg/m^3)	PCE dosage (%)
155	210	90	80	760	1080	1.2

Results and discussion

Effect of AA to modified product (M) ratio on the property of the PCE. The AA to M's ratio directly affects the charge density on the polymer chain which determines the PCE's dispersion ability so it was discussed at first. The effect of AA to modified product (M) ratio on the fluidity of cement paste was shown on Figure 2.

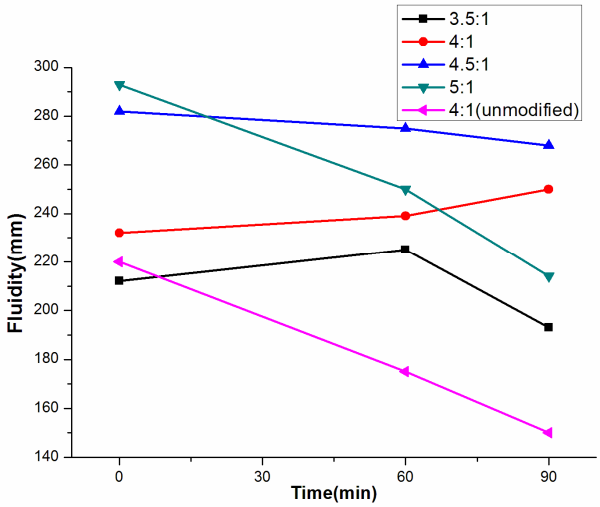

Fig. 2 Effect of the AA to M's ratio on the fluidity of cement pastes

According to Figure 2, the initial fluidity of the cement paste increase as the AA to M's ratio increase and it's obvious that PCE synthesized by M showed better dispersion ability. This is because the modified product can hydrolyze in alkaline environment and then provide better dispersion and fluidity retaining ability. When the ratio was 4.5:1, the PCE showed good initial fluidity and no slight lose on fluidity was observed within 1 hour. This means under this ratio, the charge distribution on the side chain of the PCE can reach a relatively optimum value, which can benefit the PCE's electrostatic repulsion of electric charges and the steric hindrance [9]. When the ratio above 4.5:1, the initial fluidity kept on increasing while obvious lose was taken place. This can be ascribed to two reasons: 1. The PCE can absorb faster under higher AA to M's ratio which will lead to fluidity lose caused by the hydration of the cement. 2. The number of amide group and the ester group will decrease as the increase of the AA to M's ratio which will affect its ability to retain fluidity.

Effect of the dosage of initiator on the property of the PCE. The effect of the dosage of initiator on the dispersing effectiveness of the PCE was shown in Figure 3.

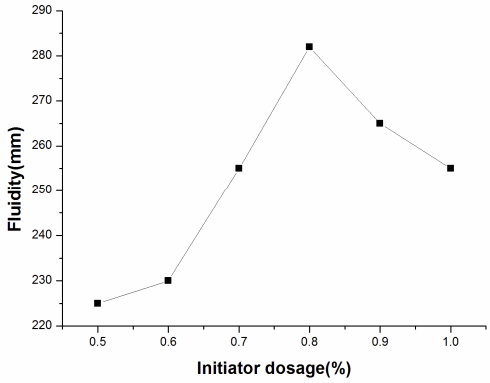

Fig. 3 Effect of the dosage of initiator on the fluidity of cement pastes

As shown in Figure 3, the fluidity increase as the initiator dosage increase and the best dosage for the initiator was 0.8wt% to all monomer. The fluidity of the cement paste decrease as the dosage exceed 0.8wt%. This is attributed to the higher molecular weight of the PCE synthesized under lower initiator concentration which has poor dispersion ability and the lower molecular weight of the PCE synthesized under higher initiator concentration which impedes the ability of steric hindrance[10].

Effect of the reaction time on the property of the PCE. Figure 4 presents the evolution of fluidity with reaction time for PCE synthesized under the AA to M's ratio was 4.5:1.

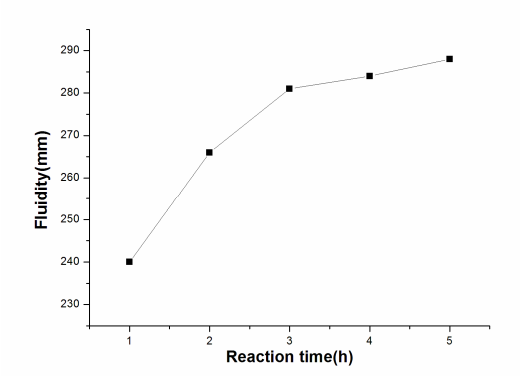

Fig. 4 Effect of the reaction time on the fluidity of cement pastes

The data suggests that the optimum reaction time for the polymerization was 3 hours which gives the PCE favorable dispersion ability. This is mainly due to the low reaction activity of the maleic anhydride and its derivants. If the reaction time is short, the monomer conversion will be affected thus will reduce the PCE's dispersion ability. If the reaction time is too long, no distinct improvement in dispersion ability can be seen. Considering the energy consuming cost and the efficiency, we selected 3 hours as the optimum reaction time.

Molecular weight and molecular weight distribution for the PCE. The plot of molecular weight and molecular weight distribution (MWD) of the modified PCE was shown in Table 3 and Figure 5.

Table 2 Molecular weight and its distribution for the modified PCE

sample	M_n (g/mol)	M_w (g/mol)	M_p (g/mol)	MWD
Modified PCE	35553.7	10928.2	16110.2	3.2

In Figure 5, despite a negative peak corresponded to solvent, only one sharp peak can be seen which indicates almost no unreacted monomer remained in the final product. On the other hand, it proves that the modified product has sufficient polymerization activity and capable of forming the amide-structural PCE.

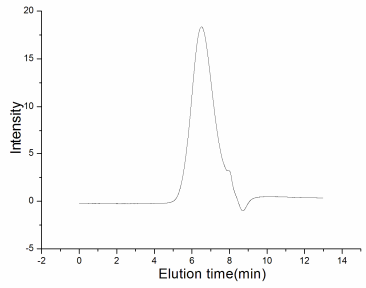

Fig. 5 Molecular weight and its distribution for the modified PCE

Concrete application test. For the better use of our modified PCE, concrete application test was utilized and the results were shown in Table 2.

Table 3 Application performance of modified PCE in concrete

sample	(slump/spread)/mm		Compressive strength (MPa)	
	Initial	1h	7d	28d
1	230/560	210/510	25.5	37.1
2	235/605	220/570	25.8	38.9
3	250/600	225/590	25.2	38.2

*Sample 1 is the conventional PCE supplied by our own admixture department, sample 2 is the modified PCE and sample 3 is the S-95 PCE supplied by Nippon Shokubai Co., Ltd.

From the table 2, the fresh concretes mixed with modified PCE and S-95 both exhibited a good slump and slump retention behavior under the same dosage. Our modified PCE has comparable initial dispersion ability to S-95 while a bit of worse in slump retention ability. At the same time, the adding of modified PCE has no harm to concrete's early strength while exhibits higher 28d strength. One of the reasons was our modified PCE has a notable complexation behavior, which endows the hydration products a more dense structure.

Conclusions

With AA to M's ratio of 4.5:1, initiator dosage at a dosage of 0.8wt% and the reaction time of 3 hours, a modified PCE with good flow property and slump retaining ability was successfully synthesized.

GPC measurement showed that the modified product had a desirable polymerization activity and no monomer residual was observed.

The concrete test accorded well with the cement pastes fluidity results. The modified PCE showed good dispersion and slump-retaining ability and may provide extra strength upon 28 days.

References

[1] K. Yamada, T. Takahashi, S. Hanehara, M. Matsuhisa, Effects of the chemical structure on the properties of polycarboxylate-type superplasticizer, Cement and Concrete Research, 30 (2000) 197–207.

[2] L. Patural, P. Marchal, A. Govin, P. Grosseau, B. Ruot, O. Deves, Cellulose ethers influence on water retention and consistency in cement-based mortars, Cement and Concrete Research, 41 (1) (2011) 46–55.

[3] D.F. Zhang, B.Z. Ju, S.F. Zhang, J.Z. Yang, The study on the synthesis and action mechanism of starchsuccinate half ester as water-reducing agent with super retarding performance, Carbohydrate Polymers, 71 (1) (2008) 80–84.

[4] K.H. Khayat, Z. Guizani, Use of viscosity modifying admixtures to enhance stability of fluid concrete, Aci Materials Journal, 94 (4) (1997) 332–340

[5]Z.J. Jiang, Y.H Fang, Q.R Wen, X.Q Guo, Preparation of a new type of amphoteric polycarboxylate superplasticizer, New Building Materials, 8(2011) 47-49

[6] Y. Bao,J. He, and Y. Li, "Synthesis of novel hyperbranched poly(ester-amide)s based on acidic and basic amino acids via "AD + CBB" couple-monomer approach, Polymer, 53, 145–152, 2012

[7] N. Feng, H. Ye, The technical characteristics of the R & D of high performance concrete and Countermeasures, China Concrete and Cement Products, 3 (2008) 2-4.

[8] I. Papayianni, G. Tsohos, N. Oikonomou, and P. Mavria, "Influence of superplasticizer type and mix design parameters on the performance of them in concrete mixtures" Cement and Concrete Composites, 27(2), 217–222,2005

[9] K. Yoshioka, E. Sakai, M. Daimon, Role of steric hindrance in the performance of superplasticizer for concrete, Journal of the American Ceramic Society, 80 (1997) 2667–2671

[10] W.J. Guo, N. Sun, J.J. Qin, J. Zhang, M.S. Pei and Y.F. Wang, Synthesis and properties of an amphoteric polycarboxylic acid-based superplasticizer used in sulfoaluminate cement, journal of applied polymer science, 125 (2012) 283–290.

Advanced Materials Research Vols. 989-994 (2014) pp 238-241
© (2014) Trans Tech Publications, Switzerland
doi:10.4028/www.scientific.net/AMR.989-994.238

High Cycle Fatigue Performances of Advanced High Strength Steel CP800

GUI Longming,[1, a], JIN Xiaochun[1,b], LI Hongtao[2], ZHANG Mei[2,c*]

[1] Technical Center, Shanghai Huizhong Automotive Manufacturing Co. Ltd.

No.1493, S. Pudong Road, 200122 Shanghai, China

[2] School of Materials Science and Engineering, Shanghai University, 200072 Shanghai, China

[a]guilongming@shac.com.cn, [b]jinxiaocun@shac.com.cn, [c*]zhangmei3721@shu.edu.cn

* Corresponding author

Keywords: High cycle fatigue (HCF); Fatigue strength; Staircase (SC) test; S-N curve; Advanced high strength steel; CP800

Abstract. A low carbon content and improved steel making practices have imparted advanced high strength steel (AHSS) CP800 with superior combination of strength, ductility and weldability. Its performance in fatigue, however, is not well understood. Stress-controlled high cycle fatigue (HCF) tests were conducted to obtain stress vs. fatigue life curve (S-N curve), and the fatigue limit of CP800. The follow HCF performances were obtained. $\sigma_{0.1} = 476MPa$, SRI1=1940MPa, b=-0.09972, $Nc_1=2.89\times10^6$, and $R^2= 0.88$. The collected material data are used as a basis of comparison of CP800 with more common grades of structural steel. CP800 steel shows high strength, comparable ductility, and high fatigue limit level. The test results indicate that compare to that of lower strength common grades of structural steels, CP800 steel has a much higher fatigue endurance limit (say, 476MPa), about 0.6 of its tensile strength (TS). Thus, provides a distinct advantage.

Introduction

Fatigue is the progressive and localized structural damage that occurs when a material is subjected to cyclic loading, the most important failure mode for mechanical components under cyclic loads, and problem for many types of structures. As the century progressed, more and more failures of components subjected to repeated loads were recorded. Today, structural fatigue has assumed an even greater importance as a result of the ever-increasing use of high-strength materials and the desire for higher performance from these materials [1-2].

Compared to conventional structural grade steels, CP800 provides superior strength, comparable ductility [3-4], as well as improved weldability [5]. The improved performance of CP800 is achieved through lower levels of carbon and other elements, in conjunction with advanced steel making practices. As a result of the improved performances of advanced high strength steel CP800, it is rapidly gaining popularity for use in car manufacturing. However, utilizing the benefits of CP800 with higher yield strength (say, higher than 680 MPa) may not be possible under current design standards because the fatigue limit state is likely to control the design [1]. Research on CP800 has mainly focused on mechanical properties and weldability [3-4]. Little attention has been paid to its fatigue properties. The work presented is aimed at investigate the fatigue properties of CP800 for component life prediction purpose. The fatigue performance of CP800 steel is compared to other grades of structural steels including TL1114, S500MC, and TRIP600-SH steel, commonly used in modern car structures.

Material and Experimenal

Material. The sheet steel investigated is CP800 with a thickness of 3.5mm. Its chemical composition in mass percent is 0.06C-1.71Mn-0.45Si-0.11Ti.

Test method and equipment. HCF tests were carried out on ZWICK-100KN HCF test machine. Using a stress ratio of 0.1(R= 0.1). HCF tests were done according to nation standard of China GB/T 3075-2008[6]. The specimen size of HCF test is presented in Fig.1, with a guage length of 42mm and width of 10.5mm. The specimen is parallel to the rolling direction of the sheet.

Fatigue strength is obtained with staircase test method. High-cycle fatigue data are usually presented as a plot of stress, S, versus the number of cycles to failure, N. A log scale is used for both of the stress and the number of cycles. Here afterward, the value of stress, S, is chosen to be the maximum stress, S_{max}. The fatigue life is the number of cycles to failure at a specified stress level, while the fatigue strength (also referred to as the endurance limit) is the stress below which failure does not occur. As the applied stress level is decreased, the number of cycles to failure increases.

S-N curve and parameter SRI1, b, N_{C1} is illustration in Fig.2. Here, SRI1 is the intercept of the diagonal line to Y axis, b is the slope of the diagonal line, and Nc_1 is fatigue life of the intersection point of two lines, the slope of the horizon line (b_2) is 0.

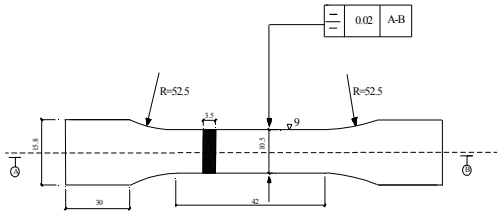

Fig. 1 Specimen of HCF test

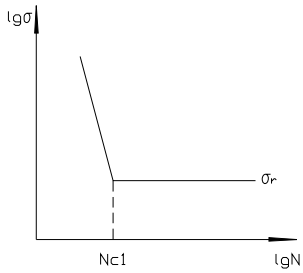

Fig. 2 S-N curve and HCF test parameters

Results and discussion.

HCF test data. Table 1 listed the HCF test data of steel CP800.

S-N curve. S-N curve drawn on the basis of HCF test data is shown in Fig. 3. From the linear regression of the diagonal curve on the S-N digram, parameters of fatigue characteristics such as SRI1, σ_r, N_{C1} and b were obtained as follow.

Table 1 High cycle fatigue test data of CP800 (R= 0.1)

Stress	N 10^5			N_{mean} 10^5
（MPa）	1	2	3	
600	0.82	0.87	1.09	0.93
560	1.55	1.73	2.72	2.00
520	3.56	6.58	9.86	6.67
480	10.2	11	100	40.40
440	100	100	100	100

Diagonal line:

$$Y=3.28771+(-0.09972)X$$

$$R^2 = 0.88335832$$

$$\lg(\sigma_{0.1}) = 3.28771 + (-0.09972)\lg N$$

Slope: b = - 0.09972

When: $\lg(\sigma_{0.1}) = 3.28771$

Intercept of the diagonal part of the curve to Y axis: SRI1=1940MPa

$$Nc_1 = 2.8886\times10^6$$

Thus, fatigue properties of CP800 of the diagonal line fit the following equation.

$$\sigma_{0.1} = 1940 - 0.09972\lg N$$

Test data drawn on the basis of staircase test results of CP800 in HCF test is shown in Fig. 4. So the fatigue strength of CP800 is obtained with the following calculation. The fatigue strength $\sigma_{0.1}$ at stress ratio 0.1 of CP800 is 476MPa.

$$\sigma_{0.1} = \frac{440\times3+480\times5+520\times2}{3+5+2} = 476$$

$$\sigma_{0.1} = 476MPa$$

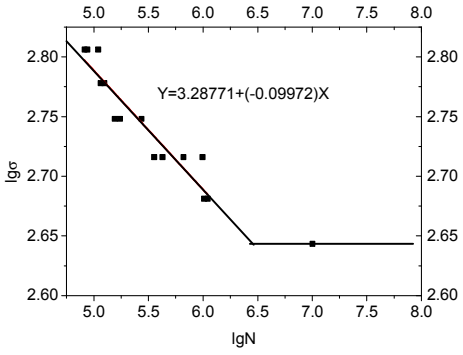

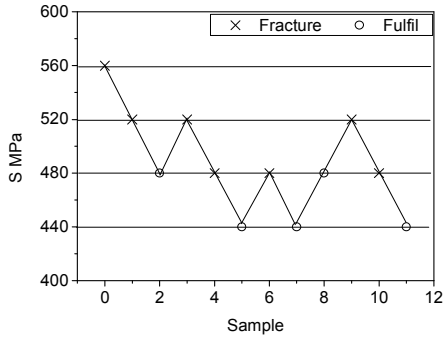

$N_0=10^7$，ΔS=40MPa，×-fracture, O-runout

Fig. 3 S-N curve of steel CP800 Fig. 4 Stair case test results of CP800

Comparison of HCF properties of CP800 to other steels. The comparison of HCF properties of CP800 to other steels such as TL1114, TRIP600-SH and S500MC is listed in Table 2.

It is found that the fatigue strength $\sigma_{0.1}$ of steel CP800 is 476MPa, much larger than that of steel TL1114 and TRIP-SH[7], and also larger than S500MC[8]. It indicates that CP800 has much better HCF properties. Thus CP800 can be chosen to use in lightweight car application purpose.

For a large number of steels, there is a direct correlation between tensile strength and fatigue strength; generally, higher-tensile-strength steels have higher endurance limits. The endurance limit is normally in the range of 0.35 to 0.60 of the tensile strength (TS).

Table. 2 Comparison of high cycle fatigue properties of different steels

Steel	SRI1 /MPa	Slope b	Nc_1 $\times10^6$	$\sigma_{0.1}$ MPa
CP800	1940	-0.09972	2.89	476
S500MC	1613	-0.08933	2.03	471
TRIP600-SH	774	-0.0398	11.7	405
TL1114	1193	-0.06896	7.59	400

Microstructure and mechanical properties on fatigue performance. The microstructure appearance of longitudinal specimen of steel CP800 is shown in Fig. 5. It is clear that fine second phases uniformly distributed on the polygonal ferrite matrix.

The stress-strain curves of CP800 are shown in Fig. 6, showing a yield strength (YS) of 750MPa, tensile strength (TS) 800MPa and total elongation (TE) 17%. Homogeneous microstructure of CP800 is benefit to obtain good combination of strength, ductility and fatigue properties. This causes the steel has a high fatigue strength of 476MPa.

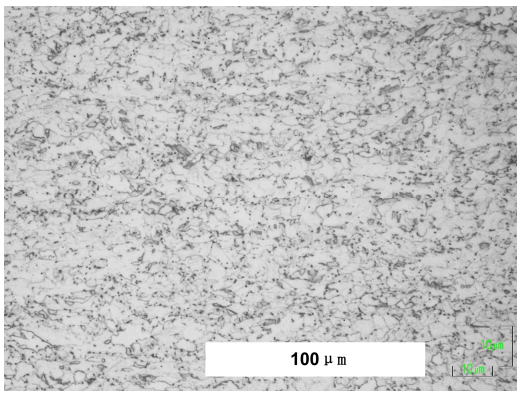

Fig. 5 Microstructure

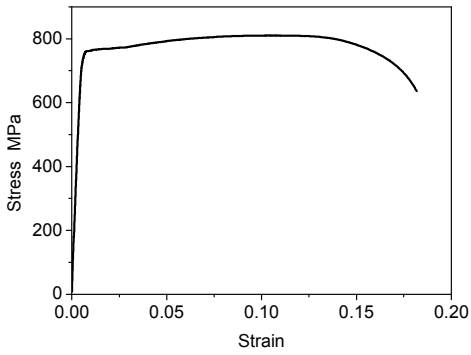

Fig. 6 Stress versus strain curve

Conclusions

The studied AHSS CP800 has a quite large fatigue strength of 476MPa at R=0.1, which is about 60% of its TS. Indicates that the studied steel CP800 has good fatigue property. The HCF performance of CP800 are listed as follow:

$\sigma_{0.1} = 1940 - 0.09972\lg N$

SRI1=1940MPa, b= - 0.09972, $N_{C1}= 2.89\times10^6$, R^2 = -0. 88335832

Acknowledgements

The authors are grateful for the financial supports from Sciences and Technology Development Foundation of Shanghai Automotive Industry (Grant No.1201), and the National Natural Sciences Foundation of China (Grant Nos. 50934011 and 50971137).

*** Corresponding author**

ZHANG Mei, Doctor. Email address: zhangmei3721@shu.edu.cn.

References

[1] www.asminternational.org. Elements of Metallurgy and Engineering Alloys (#05224G) p.243-246

[2] T. Yokoi, K. Kawasaki, M. Takahashi: Fatigue properties of high strength steels containing retained austenite[J]. JSAE Review, 1996, 17(2): 210-212.

[3] W.M. Zeng, Study of Rolling Process with Physic Simulation on Ultra-High Strength low-alloy complex phase Steels [D]. Master degree thesis, Shanghai University, 2011

[4] M. Zhang, C.B. Huang, W.M. Zeng, R.Y. Fu, L. Li: Materials Science Forum Vol. 762 (2013), p. 128

[5] M. Zhang, Q.S. Li, C.B. Huang, R.Y. Wu, R.Y. Fu, L. Li and P. Fang: Advanced Materials Research Vol. 634 (2013), p. 2899-2903.

[6] GB/T3075-2008 Metallic materials-Fatigue testing-axial-force-controlled method[S]. in Chinese.

[7] Y. Su, M. Zhang, R.Y. Fu, L. Li: Heat treatment of metal, 2008, 33(8): 25-29.

[8] M. Zhang, Y.X. Ning, J. Zhang, Z. Wan, T. Wang, L. Li: Shanghai metal, 2014,(1),11-13,17.

Advanced Materials Research Vols. 989-994 (2014) pp 242-245
© (2014) Trans Tech Publications, Switzerland
doi:10.4028/www.scientific.net/AMR.989-994.242

Preparation and Dielectric Property of Ag/PVDF Composite Film

Yajun WANG[a], Jianwen ZHAI[b], Fangfang WANG[c] and Changgen FENG[d]

State Key Laboratory of Explosion Science and Technology, Beijing Institute of Technology, Beijing 100081, China

[a]yajunwang@bit.edu.cn, [b]zhaijw121@sina.com, [c]wangff_bit@163.com, [d]cgfeng@wuma.com.cn

Keywords: nano Ag; PVDF; dielectric constant; energy storage density

Abstract. Conductive particle fillers could improve the dielectric properties of the polymer matrix. By solvent casting method, different volume fraction of nano silver particles were added into the PVDF film to prepare Ag/PVDF composite film so as to increase the dielectric properties of the materials. SEM was used to analyze the microstructure of the films. SEM images show that nano Ag filler particles were uniformly distributed throughout the whole matrix of the composite films. Dielectric property tests show that with the increase of nano Ag content, the dielectric constants of the composites increase first and decrease later while the dielectric losses decrease first and increase later. In the case of the optimal 17vol% Ag content, the dielectric constant of the composite film is the highest (14.5 at 100 Hz) with lower dielectric loss, and the energy storage density is relatively high (0.340 $J \cdot cm^{-3}$).

Introduction

Due to the excellent piezoelectric and dielectric properties, poly(vinylidene fluoride) (PVDF) and its copolymers have been studied widely over the last several decades [1,2]. There are several researches showing that the conductive metal (such as Pt, Pd, Ag, Al, Cu, Ni, Fe, and carbon nano tube [3]) and metal halide fillers ($BiCl_3$ [4], NaCl [5], $CuCl_2$ [6], LiCl [7]) could modify significantly the structure and physical properties of the polymer matrix, such as PVDF.

Adding of a small amount of conductive particles to the polymer matrix could effectively increase the dielectric constant of the substrate, and low content conductive particles/polymer matrix composite film can maintain good mechanical properties. In the present paper, nano Ag particles (diameter d=50 nm) was chosen as the conductive material, and Ag/PVDF two-phase composite films were prepared. By SEM analysis and dielectric property tests, the optimum nano Ag powder adding amount will be obtained. According to the literatures, percolation threshold of nano silver powder is about 17vol%. Therefore, in the paper, the contents of added nano-Ag powder are 15vol%, 16vol%, 17vol%, and 18vol%, so as to get the appropriate amount of nano-Ag powder.

Experiment

PVDF films doped with different amounts of nano Ag as filler were prepared by solvent casting method. Nano Ag powder was purchased from Beijing DK Nano Technology Co., Ltd., China, and PVDF, Shanghai 3F New Material Co., Ltd., China. The PVDF powder and different volume fraction of Ag filler, which were 15vol%, 16vol%, 17vol%, and 18vol% respectively, were dissolved in dimethylformamide (DMF) respectively, stirred for 30 min, then Ag solutions were added into PVDF solution with an appropriate velocity, stirred for 6 h to form the uniform mixtures. The mixtures were cast on glass dishes and kept in vacuum oven at 70 ℃ for 20 h to remove the solvent completely.

The surface morphology was measured by a Scanning Electron Microscope (BACPC S-4800, Hitachi, Japan). The dielectric properties of the films were measured by an impedance analyzer (HP4192A, NOVOCONTROL GmbH, Germany). The electrical strength measurement was performed on CS2671A (Nanjing Changsheng Instrument Co., Ltd., China).

Results and Discussion

Scanning Electron Microscope (SEM). Fig.1 shows the surface morphology of the PVDF films doped with different fraction of Ag particles. It can be found that Ag particles are uniformly distributed throughout the PVDF matrix. When the volume fraction of nano Ag is 16%, inter-particle spacing is big with sparse particle distribution; While in the case of 17vol% of Ag, the inter-particle spacing is small and the film surface becomes rough with some small aggregation.

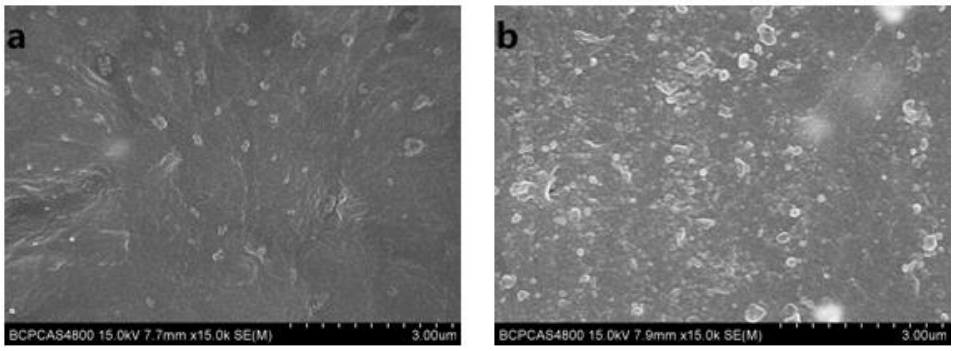

(a) 16 vol%-Ag/PVDF (b) 17 vol%-Ag/PVDF

Fig.1 SEM images of Ag/PVDF composite films

Dielectric Properties. The appropriate amount of nano silver can not only achieve good dielectric properties, but also keep good mechanical properties of polymer matrix. According to percolation theory, for conductive particles/polymer composites, when the content of particles is close to the percolation threshold, the dielectric properties will change exponentially. Therefore, nano Ag/PVDF composite films with 15vol%, 16vol%, 17vol%, and 18vol% Ag were prepared to determine the appropriate amount of silver. Fig.2 shows the dielectric properties of Ag/PVDF composite films with frequency.

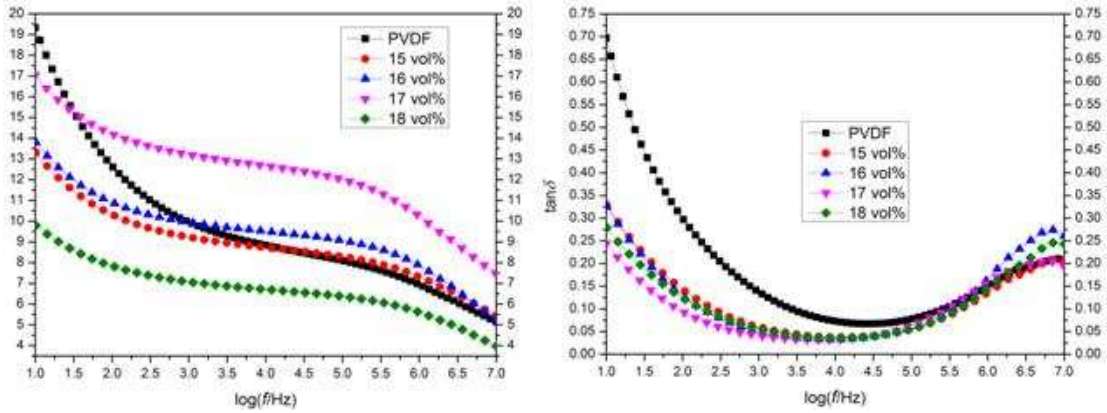

Fig.2 Frequency dependence of dielectric properties of Ag/PVDF composite films at room temperature

As can be seen from Fig.2, the change of dielectric constant of composite film with frequency is diffrent from that of pure PVDF. Dielectric constant decreased with increasing frequency more slowly, and the change of dielectric constants is the same for diffrent Ag contents, namely decreased with increasing frequency. At the same time, compared with pure PVDF, the change of dielectric constants is also different with different amounts of nano Ag added. When the amount of Ag is little or much, the dielectric constants of composites are lower than that of pure PVDF, while for addition amount of 17 vol% nano Ag, the dielectric constant of the composite is maximum. When the amount of nano Ag powder is less than 17 vol%, at the same frequency, dielectric constant increases with the increase of Ag nanoparticles, while the dielectric constant rapidly decreases when Ag content is greater than 17vol%.

From Fig.2 it could be seen that dielectric losses of all Ag/PVDF composite films are less than that of pure PVDF over a wide frequency range (10–10^6 Hz), and increase first and decrease later with the

increase of frequency. The lowest loss is about 0.05 at the frequency of 10 kHz. And there are little differences among the losses of composites with different Ag content. At the frequency range of 10–10^4 Hz, when the amount of nano Ag powder added is less than 17vol%, the loss of Ag/PVDF composites decreased with increasing Ag powder; And when the frequency is greater than 10 kHz, the losses of the films are the same.

Optimal Ag Content. According to percolation theory, in the conductive particle/polymer composite system, when the conductive filler content is close to the percolation threshold, the electrical performance will change abruptly, such as the dielectric constant. Accordingly, to determine the appropriate amount of Ag nanoparticles, Ag/PVDF composites with different Ag content were prepared. Fig.3 compares the dielectric properties nano Ag/PVDF composite films with 15vol%, 16vol%, 17vol%, and 18vol% Ag at 100 Hz.

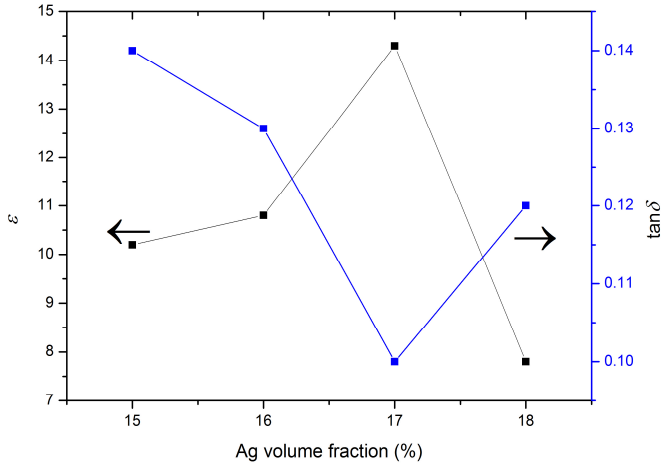

Fig.3 Dielectric properties of Ag/PVDF composite films with Ag content at 100 Hz

Fig.3 shows that with increasing the amount of Ag nanoparticles, the dielectric constant of Ag/PVDF composite films increase first and decrease later while dielectric loss being opposite; When the content of Ag nanoparticles was 17vol%, the dielectric constant reaches the highest while dielectric loss the lowest. Thus, it is determined during the experiment that 17vol% is the optimum content of nano Ag powder.

Dielectric Strength and Energy Storagy Density. Table 1 gives the dielectric strength of Ag/PVDF composite files with different Ag content. According to Fig.2, dielectric constants of 15vol%–18vol% Ag/PVDF at 100 Hz are 10.3, 10.5, 14.5, and 7.8 respectively. By the following equation $W = \frac{1}{2}\varepsilon_0 \varepsilon E_{bd}^2$ (W, ε_0, ε, and E_{bd} are energy storagy density, vacuum dielectric conatant, dielectric conatant, and breakdown voltage respectively), energy storagy density of Ag/PVDF films could be calculated shown in Table 1.

Table 1 Dielectric strength and energy storagy density of Ag/PVDF films at 100 Hz

Content of Ag	Breakdown voltage [kV]	Thickness [mm]	Dielectric strength [kV·mm^{-1}]	Energy storagy density [J·cm^{-3}]
15 vol% Ag	3.68	0.0398	92.46	0.389
16 vol% Ag	3.52	0.0434	81.11	0.305
17 vol% Ag	4.44	0.0610	72.79	0.340
18 vol% Ag	3.81	0.0644	59.16	0.121

It can be seen from Table 1 that with the increase of Ag content, although the dielectric constant increased to some degree, the dielectric strength and the energy storage density decreased. In the case of the optimal Ag content 17 vol%, the dielectric constant is the highest (14.5) and the energy storage density is relatively high (0.340 J·cm^{-3}).

Conclusion

Conductive particle/polymer composites nano Ag/PVDF were prepared with Ag volumme content of 15%, 16%, 17%, and 18% according to percolation theory. The microstructure analysis and dielectric property tests were performed. SEM images show that filler particles nano Ag were uniformly distributed throughout the whole matrix of the composite films. Dielectric property nanalysis show that with the increase of Ag content, the dielectric constants of the composites increase first and decrease later while the dielectric losses decrease first and increase later. In the case of 17vol% Ag content, the dielectric constant of the composite is the highest (14.5 at 100 Hz) with lower loss, and the energy storage density is relatively high (0.340 $J \cdot cm^{-3}$).

Acknowledgement

This paper is supported by the project of State Key Laboratory of Explosion Science and Technology (Beijing Institute of Technology, China) (No.YBKT14-09) and the Basic Research Foundation of Beijing Institute of Technology, China (No.20120242013).

References

[1] T. Hattori, M. Kanaoka and H. Ohigashi: J. Appl. Phys. Vol. 79 (1996), p. 2016

[2] B. Ploss, R. Emmerich and S. Bauer: J. Appl. Phys. Vol. 72 (1992), p. 5363

[3] Z.M. Dang, Y.J. Li, and M. Xu: Appl. Phys. Lett. Vol. 89 (2006), p. 72902

[4] Y.J. Wang, F.F. Wang, and L.J. Xu: Adv.Mater. Res. Vol. 804 (2013), p. 74

[5] I.S. Elashmawi: Cryst. Res. Technol. Vol. 42 (2007) p. 389

[6] A. Tawansi, M.I. Ayad and E.M. Abdel-Razek: J. App. Poly. Sci. Vol. 72 (1999), p. 771

[7] I.S. Eleshmawi: J. Elas. Plast. Vol. 40 (2008), p. 211

Advanced Materials Research Vols. 989-994 (2014) pp 246-250
© (2014) Trans Tech Publications, Switzerland
doi:10.4028/www.scientific.net/AMR.989-994.246

Microstructure and Wear Resistance of $Cu_{0.9}NiAlCoCrFe$ High Entropy Alloy Coating on AZ91D Magnesium Alloys by Laser Cladding

Kaijin Huang[1,2,3,4,a] , Yuyue Wang[1,b] and Xin Lin[3,c]

[1:]State Key Laboratory for Mechanical Behavior of Materials,Xi'an Jiaotong University,Xi'an 710049, P.R.China

[2:] State Key Laboratory of Materials Processing and Die & Mould Technology, Huazhong University of Science and Technology, Wuhan 430074, P.R.China

[3:] State Key Laboratory of Solidification Processing, Northwestern Polytechnic University, Xi'an 710072, P.R.China

[4:]State Key Laboratory of Advanced Processing and Recycling of Non-ferrous Metals,Lanzhou University of Technology, Lanzhou 730050, P.R.China

[a]email: huangkaijin@hust.edu.cn, [b]email: wangyy@mail.xjtu.edu.cn, [c]email: xlin@nwpu.edu.cn

Keywords: Laser cladding; High entropy alloy coating; Wear; Magnesium alloy

Abstract: To improve the wear properties of AZ91D magnesium alloys, a $Cu_{0.9}NiAlCoCrFe$ high entropy alloy (HEA) coating was fabricated on AZ91D magnesium alloys by laser cladding using prealloyed $Cu_{0.9}NiAlCoCrFe$ powders. The microstructure of the HEA coating was characterized by OM, SEM and XRD. The wear resistance of the HEA coating was evaluated under dry sliding wear test condition at room temperature. The results show that the HEA coating mainly consists of a simple BCC solid solution phase. The HEA coating exhibits excellent wear resistance. The main wear mechanisms of the HEA coating and the AZ91D substrate were different, the former dominated by oxidative abrasive wear and the latter suffered from both adhesive and abrasive wear.

1. Introduction

High entropy alloys (HEAs) including at least five principal elements in equimolar or near-equimolar ratios were reported by Yeh in 1995 for the first time. Literatures had shown that HEAs formed simple body center cubic (BCC) and/or face center cubic (FCC) solid-solution phases identified by X-ray diffraction (XRD) patterns [1-2]. HEAs exhibites many advantages in application such as high wear resistance [1-2], excellent corrosion resistance [3], outstanding oxidation resistance [4], low electrical and thermal conductivity and low coefficient of thermal expansion [5]. The microstructure characteristic of HEAs results in four main effects including high entropy, severe lattice distortion, sluggish diffusion and cocktail effect [2], which is different from conventional alloys such as Fe, Al, Cu, Ti, Mg, Ni-based alloys and intermetallic compounds such as Ti-Al, Ni-Al, and Fe-Al.

Up to date, plenty of technologies, for instance, vacuum arc melting[1], hard surface welding (tungsten inert gas (TIG)[6] and gas tungsten arc welding (GTAW)[7]), mechanical alloying[8], thin-film coating deposition (reactive DC sputtering)[9], thermal spray [4], and laser cladding [10-13] have been applied to produce HEAs or high-entropy alloy coatings. Among these technologies, laser cladding has attracted growing interest in recent years because of its advantages such as fast heating and cooling, uniform and dense cladding, and low dilution [12, 13]. Researchers mainly focused on microstructures and properties of laser cladding coatings on Ti-6Al-4V [10] and carbon steel [11-13]. However, it's very difficult to obtain good quality laser-clad coatings fabricated on pure magnesium substrate [14,15] as a result of the low melting and boiling point of magnesium. Consequently, few literatures were reported.

Magnesium alloys are widely used in many fields such as automotive, communication, electron, and aerospace. However, low surface hardness and poor corrosion resistance have hindered its widespread. A number of surface modification techniques, for example, electrochemical plating, conversion coating, anodizing, gas-phase deposition process and organic coating, have been used to improve its wear and corrosion resistance. However, all these techniques have their own drawbacks and are not able to fulfill the goal mentioned above. Thus, it's very urgent to develop a better, simpler and cheaper coating technology on magnesium substrate.

Surface engineering technique, namely laser cladding, has drawn considerable attention in recent years for the enhancement of the wear resistance and corrosion properties of magnesium alloys[16]. For example, Zr-based amorphous composite coatings were fabricated on pure magnesium substrate successfully by laser cladding to improve property. Furthermore, this kind of coating also has promising application in various industries owing to amorphous phase with high corrosion resistance and nano-crystalline and/or microcrystalline with eminent wear resistance [16]. To the best of our knowledge, no literature has reported the $Cu_{0.9}$NiAlCoCrFe high-entropy alloy coating fabricated by laser cladding on AZ91D magnesium alloys.

In this paper, a $Cu_{0.9}$NiAlCoCrFe high-entropy alloy coating on AZ91D magnesium alloys was fabricated by laser cladding. What's more, microstructures and wear behaviors of the coating were studied in this study.

2. Experimental methods and materials

The prealloyed $Cu_{0.9}$NiAlCoCrFe powder was prepared by argon gas atomization of the $Cu_{0.9}$NiAlCoCrFe melt, which was produced by using elemental metals (Cu 99.9%, Ni 99.95%, Al 99.8%, Co 99.95%, Cr 99.8% and Fe 99.9%). Particle size and purity of the prealloyed $Cu_{0.9}$NiAlCoCrFe powder were 48-75μm and 99 wt.%, respectively. Laser cladding of the prealloyed $Cu_{0.9}$NiAlCoCrFe powder was conducted approximately 1mm thick on AZ91D magnesium alloys with the size of 100mm×50mm×10mm by pasting binder. Afterwards, a high power Rofin TR050 CO_2 laser was employed to track melting under the 99.999% Ar-shielding atmosphere. The laser spot diameter and laser power were kept constant at 4mm and 3000W, respectively, and laser scanning velocity of 10mm/s and 25% track overlapping condition was adopted.

Phases of the coating were determined by an X-ray diffraction (XRD) with Cu-K_α radiation at 40 kV and 30mA (X' Pert PRO). Microstructure of the cross-section coatings etched by alcohol solution with 4% of nitric acid (volume fraction) and etched by aqua regia solution was examined by an Axiovert 200MAT optical microscope (OM) and a Quanta 400 scanning electron microscope (SEM) with an energy dispersive X-ray spectroscopy (EDS), respectively. A micro-hardness tester (MICROMET 3) using a test load of 100g and a load-well time of 15s was employed to measure the microhardness of the cross-section coating.

The dry sliding wear resistance of the HEA coating was evaluated using a block-on-ring dry sliding wear tester at room temperature. The cladded specimens for the wear test were cube blocks with dimensions of 10mm×10mm×10mm, which were slid against a rotating ring of hardened bearing steel AISI52100 (Fe-1.0C-1.5Cr-0.25Si-3.0Mn) with a hardness of 60HRC ($HV_{0.1}$700). The test load used was 98N. The relative sliding speed was at 0.4187m/s. The wear test cycle lasted for 75min and the corresponding total wear sliding distance was 1884 m. The as-received AZ91D magnesium alloys was selected as the reference materials for all wear tests. Each test was repeated three times. The wear weight loss was measured using an electronic balance (Bartorius BS110) with an accuracy of 0.1mg.The surface morphologies of the worn specimens were examined by a Quanta 400 SEM with an EDS.

3 Results and Discussion

3.1 Microstructure

Figure 1(a) shows the OM image of the $Cu_{0.9}$NiAlCoCrFe high-entropy alloy coating on AZ91D magnesium alloys. The interface between the laser-clad high-entropy alloy coating and the AZ91D substrate is in good condition, indicating an excellent metallurgical bonding between the laser-clad coating and the substrate. Furthermore, it is found in Figure 1(b) that the coating has a fine microstructure with many small long rod-shaped patterns, which may be explained that heating and cooling effect during laser cladding is too fast for them to grow up. Table 1 is the EDS results of the $Cu_{0.9}$NiAlCoCrFe HEA coating. The results show that the chemical compositions of different positions are not close to the designed compositions and copper segregation of different degrees were observed in intragranular (position 2) and in intergranular (positions 1,3 and 4). That is to say, Cu element is easy to segregate in the Cu-Ni-Al-Co-Cr-Fe HEA system and this phenomena was proved by many researchers[15,17-18].

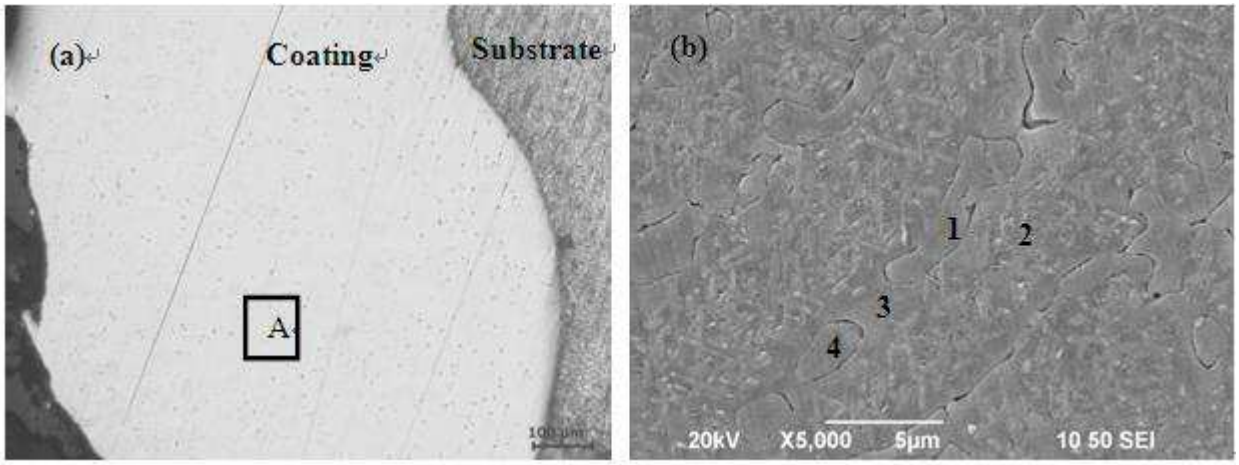

Fig.1 The morphologies of the laser-clad $Cu_{0.9}NiAlCoCrFe$ HEA coating: (a)OM image,(b)SEM image in area A.

Table 1 EDS results of the laser-clad HEA coating (wt.%)

Element	Al	Cr	Fe	Co	Ni	Cu
Point 1	6.01	8.79	12.03	11.98	14.70	46.49
Point 2	8.78	13.47	17.72	20.13	17.83	22.07
Point 3	8.94	12.65	16.05	17.70	19.34	25.32
Point 4	7.81	11.54	14.32	14.87	18.32	33.14
Raw powders	8.54	17.26	18.18	19.47	18.34	18.21

According to the Gibbs free energy formula: $G_{mix}=H_{mix}-TS_{mix}$, the higher mixing entropy, the lower system free energy. Thus, it is not strange that when segregation is smaller in the alloy because the solid solution is easier to form compared with the intermetallic compounds or the other ordered phase. Based on the data of reference [19], the enthalpy the Cu and Ni, Cu and Al, Cu and Co, Cu and Cr, Cu and Fe, Ni and Al, Ni and Co, Ni and Cr, Ni and Fe, Al and Co, Al and Cr, Al and Fe, Co and Cr, Co and Fe, Cr and Fe mixture are +4 kJ/mol,-1 kJ/mol,+6 kJ/mol,+12 kJ/mol,+13 kJ/mol,-22 kJ/mol,0 kJ/mol,-7 kJ/mol,-2 kJ/mol,-19 kJ/mol,-10 kJ/mol,-11 kJ/mol,-4 kJ/mol,-1 kJ/mol and -1 kJ/mol, respectively. Therefore, the mixing entropy in Cu-Ni, Cu-Co, Cu-Cr and Cu-Fe is insufficient to balance the huge mixing enthalpy between them. Thus, Ni, Co, Cr and Fe would seriously prevent the existence of Cu, and Cu (positions 1,2,3 and 4) appeared segregation.

Analytical results of XRD (Figure 2) confirmed that the laser-clad coating is a simple BCC solid solution. The results also prove that a laser-clad $Cu_{0.9}NiAlCoCrFe$ high-entropy alloy coating is successfully fabricated on AZ91D magnesium alloys by laser cladding. The formation of simple solid solution is attributed to the high mixing entropy. According to Boltzmann's hypothesis, high mixing entropy of solid solution with multi-principal elements will lower the tendency of ordering and segregation [20]. For the alloy $Cu_{0.9}NiAlCoCrFe$ in the experiments, its mixing entropy $\Delta Sm=Rln(n)=Rln6=1.79R$, (R: gas constant; n: the number of elements), is much higher than the formation entropy of intermetallic compounds or ordered phases. Thus, $Cu_{0.9}NiAlCoCrFe$ multi-element alloy is more likely to form solid solution rather than intermetallic or ordered phases.

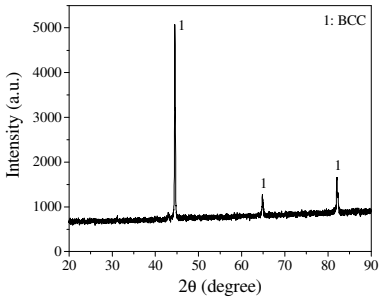

Fig.2 XRD patterns of the laser -clad HEA coating

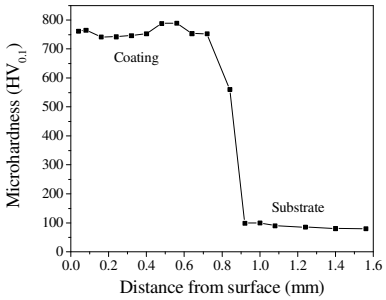

Fig.3 Microhardness of the laser -clad HEA coating

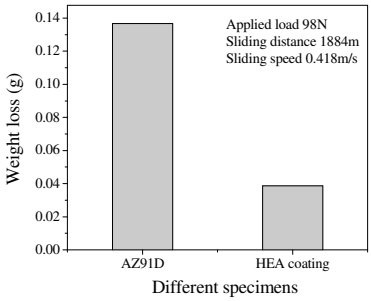

Fig.4 Weight loss of different specimens

3.2 Microhardness

Figure 3 presents the microhardness of the $Cu_{0.9}$NiAlCoCrFe HEA coating as a function of distance from the laser-clad surface. The results indicate that the microhardness of the HEA coating was about 7 times higher than that of the AZ91D substrate, and is bigger than that of the CuNiAlCoCrFe HEA (HV420) and the $Cu_{0.5}$NiAlCoCrFe HEA (HV458) [17], which were fabricated by cast process. The reason is that, under the effect of rapid heating and rapid cooling of the laser beam, the microstructure became very fine and is benefical to improve the microhardness of the HEA coating due to the fine-grained strengthening effect. In addition, the differences among atomic sizes (Table 2) of elements makes the lattice distortion more severe, which also enhance the solid-solution strengthening effect. The high microhardness of the coating will be beneficial to improve the wear properties of the HEA coating.

Table 2 Atomic sizes of different elements

Element	Al	Cr	Fe	Co	Ni	Cu
Atomic size (nm)	0.143	0.125	0.124	0.125	0.125	0.128

3.3 Wear resistance

Figure 4 shows the wear test weight loss results of the laser-clad $Cu_{0.9}$NiAlCoCrFe HEA coating specimen and the uncoated AZ91D specimen under dry sliding wear test condition at room temperature. The results show that the wear resistance of the laser-clad $Cu_{0.9}$NiAlCoCrFe HEA coating was superior to that of the AZ91D substrate, and the weight loss of the former was about three times less than that of the latter. The wear-resistance results of different specimens are consistent with the corresponding microhardnesses of different specimens (Figure 3), and the higher microhardness, the better wear resistance.

A study of the worn surfaces of these two specimens showed that both surfaces displayed a plough-shaped appearance with fairly long continuous grooves. This indicates that the laser-clad $Cu_{0.9}$NiAlCoCrFe HEA coating can be deformed plastically and can keep up with plastic strains. The study also showed that the uncoated AZ91D specimen suffered from abrasive wear as well as adhesive wear. The latter is proved by the features of some elongated pockmarks (Figure 5a). In addition, microcracks had developed at the heavily deformed edges. A combined action of abrasive and adhesive wear together with edge cracking had caused a high wear rate (30.38μg/s). On the other hand, the dominant wear mechanism of the laser-clad specimen was oxidative abrasive. This is proved by the clear furrows with a great amount of wear oxide debris (Figure 5b). The results of EDS analysis (Table 3) of the worn surfaces showed that most of the wear debris was iron oxides mixed with elements of the laser-clad $Cu_{0.9}$NiAlCoCrFe HEA. According to Figure 3, the microhardness of the HEA coating is higher than that of the steel ring tool, thus, the steel ring tool material could be sheared off, and the wear debris would be smeared over the coated surface. Of course, sliding actions would cause the worn-off Fe debris suffered elevated temperature oxidation and formed iron oxides with the laser-clad $Cu_{0.9}$NiAlCoCrFe HEA under the dry wear test condition. This oxide debris would act as abrasive and resulted in the damage of the laser-clad $Cu_{0.9}$NiAlCoCrFe HEA coating. However, considering that a three-body wear mechanism was taking effect, a low wear rate of 8.58μg/s was obtained. As for the uncoated AZ91D specimen, only a small quantity of Fe oxide particles were detected on the worn surface (Figure 5a and Table 3) because its microhardness is lower than that of the test ring material.

Table 3 EDS results of the worn surfaces of the uncoated AZ91D and the laser-clad specimen (wt. %)

Samples	Position	C	O	Mg	Al	Zn	Fe	Ni	Cu	Cr	Co	Mn
AZ91D	1	2.26	6.46	83.80	6.78	0.70	–	–	–	–	–	–
AZ91D	2	1.80	44.68	1.25	1.30	0.17	50.80	–	–	–	–	–
Coating	1	1.04	8.96	-	8.72	–	17.77	14.96	15.64	15.25	17.66	–
Coating	2	1.46	32.54	-	2.38	–	36.74	4.76	6.85	7.22	8.05	–
AZ91D	Raw	–	–	90.16	8.95	0.63	–	–	–	–	–	0.26

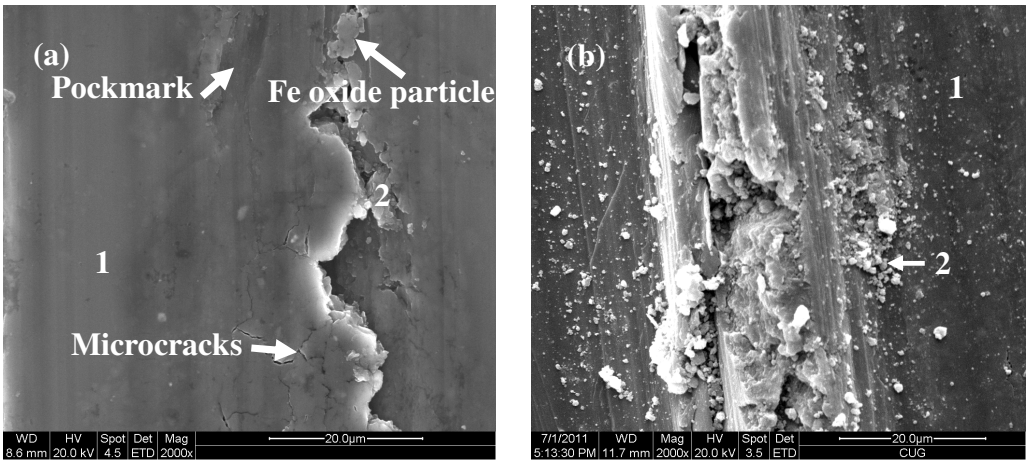

Fig.5 Worn surfaces of (a) uncoated AZ91D specimen, (b) laser-clad specimen

5. Conclusions

(1) A high wear resistant $Cu_{0.9}$NiAlCoCrFe HEA coating can be fabricated on AZ91D magnesium alloys by laser cladding using prealloyed $Cu_{0.9}$NiAlCoCrFe powders.The coating mainly consists of a simple BBC solid-solution phase.

(2) Under dry sliding wear conditions, the wear resistance of the laser-clad $Cu_{0.9}$NiAlCoCrFe HEA coating was considerably higher than that of the uncoated AZ91D magnesium alloys, and the weight loss of the latter was about three times higher than that of the former. The main wear mechanism of the HEA coating was dominated by oxidative abrasive wear.

Acknowledgements

This work was supported by the Fund (20121204) of the State Key Laboratory for Mechanical Behavior of Materials in Xi'an Jiaotong University, the Fund (SKLSP201108) of the State Key Laboratory of Solidification Processing in NWPU, and the Fund of State Key Laboratory of Advanced Processing and Recycling of Non-ferrous Metals in LUT.

References

[1]M.R.Chen, S.J.Lin, J.W.Yeh, S.K.Chen, Y.S.Huang and M.H.Chuang: Metall. Mater. Trans. A Vol.37(2006),p.1363

[2]W.Y.Tang, M.H.Chuang, H.Y.Chen and J.W.Yeh: Adv. Eng. Mater. Vol.11(2009), p.788

[3]C.P.Lee, C.C.Chang, Y.Y.Chen, J.W.Yeh and H.C. Shih: Corros. Sci. Vol.50(2008), p.2053

[4]P.K.Huang,J.W.Yeh,T.T.Shun and S.K.Chen: Adv. Eng. Mater. Vol.6(2004), p.74

[5]H.P.Chou, Y.S.Chang, S.K.Chen and J.W.Yeh: Mater. Sci. Eng. B Vol.163(2009), p.184

[6]K.C.Hsieh, C.F.Yu, W.T.Hsieh, W.R.Chiang, J.S.Ku, J.H.Lai, C.P.Tu and C.C.Yang: J. Alloys Compd. Vol.483(2009), p.209

[7]Y.C.Lin and Y.H.Cho: Surf. Coat. Technol. Vol.202(2008), p.4666

[8]S.Varalakshmi, M.Kamaraj and B.S.Murty: J. Alloys Compd. Vol.460(2008), p. 253

[9]T.K.Chen, M.S.Wong, T.T.Shun and J.W.Yeh: Surf. Coat. Technol. Vol.200(2005), p.1361

[10]C.Huang, Y.Z.Zhang, R.Vilar and J.Y.Shen: Mater. Des. Vol. 41(2012), p.338

[11]H.Zhang, Y.Pan and Y.Z.He: Surf. Coat. Technol. Vol.205(2011), p.4086

[12]X.W.Qiu and C.G.Liu: J.Alloys Compd. Vol.553(2013), p.216

[13]X.W.Qiu, Y.P.Zhang, He Li and C.G.Liu: J.Alloys Compd. Vol.549(2013), p.195

[14]T.M.Yue, H.Xie, X.Lin, H.O.Yang and G.H.Meng: Entropy Vol. 15(2013), p.2833

[15]T.M.Yue, H.Xie, X.Lin, H.O.Yang and G.H.Meng: J.Alloys Compd. Vol.587(2014), p.588

[16]T.M.Yue, Y.P.Su and H.O.Yang: Mater. Lett. Vol.61(2007), p.209

[17]C.C.Tung, J.W.Yeh, T.T. Shun, S.K. Chen, Y.S. Huang and H.C. Chen: Mater.Lett. Vol.61(2007), p.1

[18]C.J. Tong, Y.L. Chen, S.K. Chen, J.W. Yeh, T.T. Shun, C.H. Tsau, S.J. Lin and S.Y. Chang: Metall. Mater. Trans. A Vol.36(2005), p.881

[19]A. Takeuchi and A.Inoue: Mater. Trans. Vol.46(2005), p.2817

[20]J.W.Yeh: Ann. Chim.-Sci. Mat. Vol.31(2006), p.633

Advanced Materials Research Vols. 989-994 (2014) pp 251-255
© (2014) Trans Tech Publications, Switzerland
doi:10.4028/www.scientific.net/AMR.989-994.251

Temporal and spatial characterizations of Zn ions in plasma by pulsed-laser ablation of zinc metal in vacuum condition

Yang Jiao

College of Physics and Electronics, Shandong Normal University, Jinan, 250014, China

email: sdujy@163.com

Keywords: Laser plasma; Optical emission

Abstract. Plasma emission spectroscopy was used to study the evolution behavior of the Zn ions in the plasma produced by nanosecond pulsed laser beam irradiating on pure zinc metal targets. The measurements indicated that the hotter and denser region in the plasma was located at about 0.75mm from target surface and presented at delay time 250 ns with respect to the laser pulse. Compared to Zn atoms in the plasma expansion, the results reveal that Zn ions are characterized by weaker intensity in spatial profiles and shorter lifetime in temporal evolution, while, much higher brightness of Zn ions can been observed in early-state plasma emission.

Introduction

Pulsed-laser ablated plasma emission spectroscopy (PLAPES) has long been used as a very promising technique for real-time detection of multiple elements and determining the composition of materials in any physical state, including solids, liquids and aerosols [1-4]. Moreover, the deposition parameters of high quality films prepared using pulsed laser deposition (PLD) method can also be effectively controlled by PLAES [2-6]. Despite its versatility and wide applicability, however, it is well known that the plasma emission spectroscopy is not sensitive to accuracy, precision, limit of detection, etc., compared to some other established methods of chemical analysis.

The improvement of these applications has been proposed at the region of higher temperature and density plasma, which is highly related to the ablation process, the aerosol transport and the vaporization, atomization and ionization within the plasma. The enhancement of spectral lines, especially the spectral emission from multi-charged ions can be obtained at this region [4-6]. Recently, detailed characterization of ions in plasma by laser beam ablated metal has been provided to give very important and useful information for improving the analytical sensitivity and capability of PLAPES [3-7].

In this paper, we used plasma emission spectroscopy method to study the spatial and temporal evolution of Zn atoms and ions at the hot and dense region in the plasma by the interaction of a high intensity laser beam with the pure zinc metal. This suitable region can be deduced on the basis evolution of plasma parameters (electron temperature and density). The aim of the present work is to investigate the distinctions in intensities of spectra lines from atoms and ions in plasma expanding procession, by taking advantage of their different spatial and temporal evolution characteristics.

Experimental setup

The experimental scheme used for this work is similar to that described in previous studies [7-10]. Briefly, a laser beam from a Nd:YAG laser (Quanta Ray, Spectra Physics) was focused through a quartz lens (111 mm focal length) on a pure (99.99%) zinc metal target located inside a vacuum chamber (10-6 Torr) to ignite a plasma. The laser beam was operated in fundamental IR (1064 nm) modes with 5 Hz repetition rate and the pulse width of 10 ns. The spatial visible image of expanding plasma produced by four different laser intensities were given in Fig.1, which were recorded by digital camera. A spectrometer equipped with 1200/mm grating (blazed at 500 nm) was employed to disperse the plasma emission, and covering the spectral range of 180-850 nm at

0.05nm wavelength resolution. The emission spectra lines from the expanding plasma was detected by a time-gated intensified charge-coupled device (ICCD) (DH740-18F-03, Andor Technology) at different time delays with respect to the ablating laser pulse. A four channel digital delay generator (DG535, Stanford Research Systems) was employed to delay the time gate of the ICCD (t=10ns) with respect to the laser pulse. An optical signal from the scattered pump light was used as a master trigger for the delay generator. The zinc metal sample was mounted on a three-dimensional sample stage, which was rotated to keep a fresh surface for each laser beam.

Results and discussion

Before discussing the characterizations of the plasma emission spectroscopy of Zn atoms and ions, the evolutions of plasma parameters, electronic temperature (T_e) and density(N_e), should be analyzed to find out hot and dense region in plasma expanding. Therefore, the representative spectral lines of Zn atoms and ions can been easily and clearly observed at this suitable location.

The approximate excitation temperature was determined by the well-known Boltzmann plot method [8-10, 12, 13] under the assumption of local thermodynamic equilibrium (LTE).

$$\ln(I\lambda/Ag_m)=-E_m/kT_e+B. \quad (1)$$

Where I, λ and A refer to the relative integrated intensity, the wavelength and the spontaneous emission rate, respectively, g_m is the statistical weight factor for the excited state, E_m is the energy of the excited state, k is the Boltzmann constant, and B is a constant parameter for all ion lines considered. In present work, five spectral lines of Zn atoms at 330.26nm, 334.50nm, 472.21nm, 481.05nm, and 636.2nm were selected to evaluate the electron temperature. The spectroscopic constants of these spectral lines can be obtained from Ref. [11].

A representative Boltzmann plot for the determination of electron temperature at a distance of 5mm from the target surface for the case of the laser pulse intensity ~ 1.87GW/cm^2 was shown in Fig.2. The slope of the linear fit is inversely proportional to the electron excitation temperature. The data were fitted by a least-squares approximation with a result electron temperature of 0.45eV.

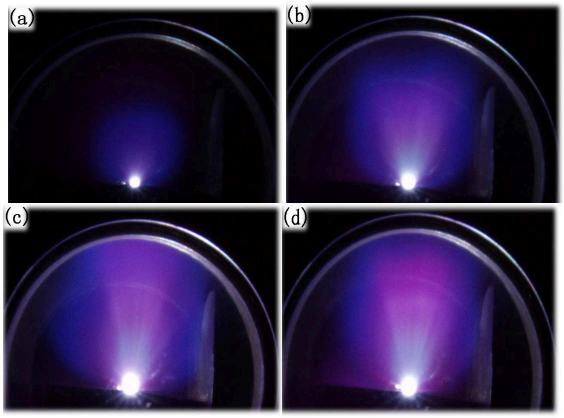

Fig.1 The representative emission images of expanding plasma produced by laser ablating pure zinc metal target, captured by a digital camera.(size of every one is 5cm ×5cm) (laser intensities were fixed at 0.63, 1.21, 1.87, 2.45GW/cm^2).

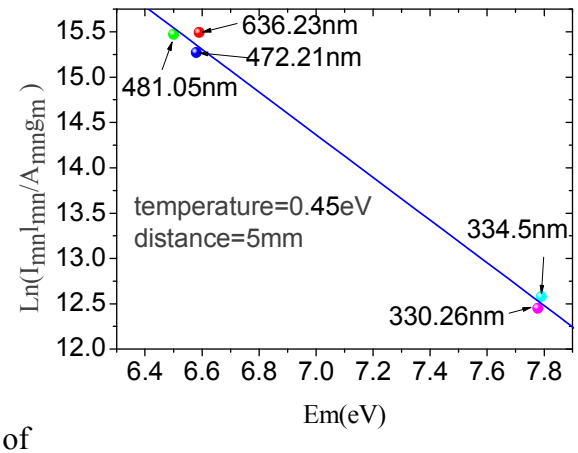

Fig.2 Boltzmann plot for determining the electronic temperatures. Laser irradiation used 1.87 GW/cm^2.

Additionally, the full width at half maximum ($\Delta\lambda_{1/2}$) of Stark broadened profile from well-isolated spectral lines is related with the electron density N_e in plasma through the following relation [8-10, 12, 13],

$$N_e=(\Delta\lambda_{1/2}/2W)\times10^{16}\text{cm}^{-3}, \quad (2)$$

where W is an electron impact parameter, which is weakly related to different temperature. For the evaluation of N_e, in the present work, the Stark broadened FWHM of Zn ions at 334.50 nm was used to determine the electron density. We have used W=0.0327 nm with the increase of temperature in a range of 40000~80000K [22].

Figure 3(a) and (b) illustrate the spatial dependence of electron temperature and density of plasma by four laser intensities ablating on Zn target. As shown, the curves of electron temperature and density versus distance from target surface show very similar behavior. For example, at laser intensity of 1.87 GW/cm^2, N_e first linearly increases from 4×10^{17} cm^{-3} at 0.25mm to a maximum of 5.12×10^{17} cm^{-3} at 0.75mm, and then drops to 1.3×10^{17} cm^{-3} at 3mm, subsequently remains practically constant for longer distance. The spatial profiles of electron temperature and density clearly indicate that the maximal value of T_e and N_e (the peak temperature and density) locates at the 0.75mm from Zn target surface, although the values depend on the laser intensities. As following discussion about the spatial profile of Zn atoms and ions spectral lines, the detection region should be located around 0.75mm from target surface, where plasma temperature and density are higher than other place.

Compared to the spatial profile of T_e and N_e as a function of the distance, in Fig.3(c) and (d), similar analyses were also performed for the temporal evolution of the electron temperature and density at 0.75mm distance from the target surface. We measured the spectral lines with a constant gate width (t=10 ns) but different delay times (50~850 ns) with respect to the laser pulse. In the early stage, it is noteworthy that electron temperature and density first increase up to maximum values at delay time around 250 ns and then decrease at the later stage of plasma expansion. From the results given above, combined with the spatial profiles of peak temperature and density at 0.75mm from target surface in experimental studies, the plasma is also characterized by temporal profiles of peak temperature and density at delay time of 250 ns in the earlier stage of expansion process. Owing to stronger plasma shielding and absorption at high laser intensity, more absorbed energy from laser irradiance can be released quickly in the early-stage evolution of the plasma, therefore the hot and dense particle cloud become more reactive in the earlier evolution of the plasma [6-9]. The conclusions are in agree with that of recent studies on laser ablation of SiC and KTP targets [8, 9], although the values of space and temporal regions are slightly different from our present work.

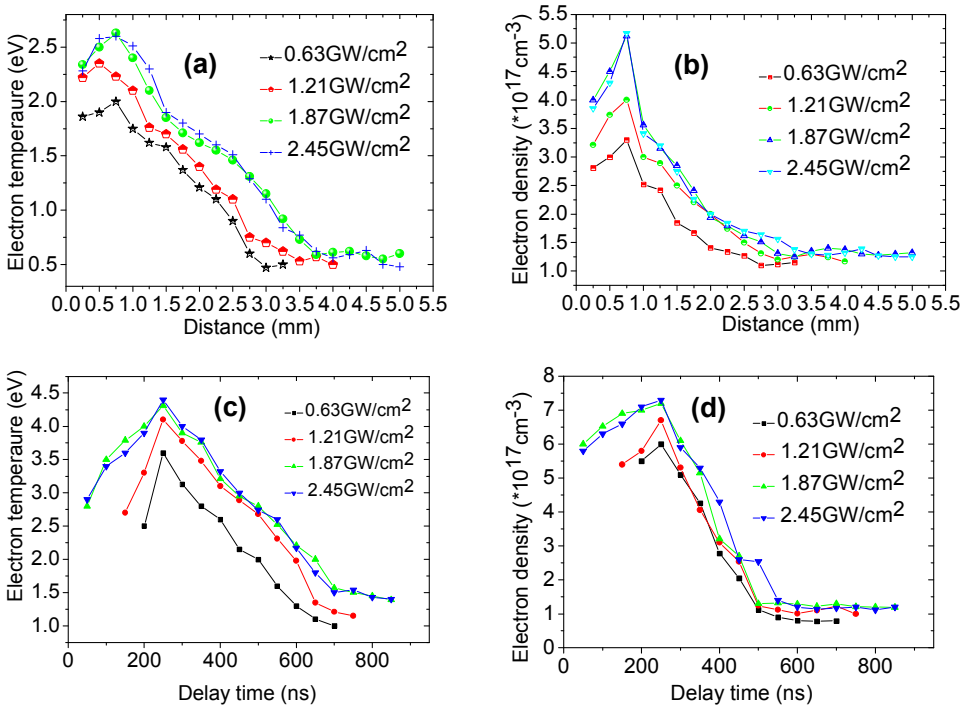

Fig. 3 (a) and (b) show electron temperature and density as function distance from the target surface at four different laser intensities. The temporal evolutions of electron temperature and density of the expanding plasma were displayed in (c) and (d).

Figure 4 shows four well-isolated spectral images (upper panel) and lines (lower panel), emitted from Zn atoms (at 468.01nm, 472.21nm, 481.5nm) and single-charged Zn ion (at 491.16nm), respectively, which were detected at 0.75 mm from target surface by using time integrated CCD chip. The incident power was fixed at 2.45 GW/cm^2. It should be pointed out that the spectral lines of other Zn atoms, such as 307.5nm, 692.83nm, 693.84nm, 694.3nm were also observed at our experiment. While, some of these spectral lines are likely interfered by each other, and the average intensities of these spectral lines are much lower than that selected in Fig.4. Moreover, the emission lines from multi-charged Zn ions (except for single-charged at 491.16nm in Fig.4) can not clearly detected by present detection system (180-850nm) any more. As seen from Fig.4, the intensities of Zn atoms spectral lines are much higher (almost a factor of 4 to 12 times) than that Zn ions at 491.16nm, which confirms that the number of Zn atoms in plasma by laser ablated zinc metal is much larger than Zn ions.

To provide crucial information for improving the analytical capability of PLAPES, the temporal evolution of the Zn ions in the plasma expanding should be taken in to consider. Figure 5 shows the emission spectral lines of Zn atoms and ions at different delay time (gate width of 10 ns) with respect to the laser pulse, measured at 0.75 mm from the target surface. It is interesting to see that the lifetime scale (~300ns) of the line at 491.16 nm from Zn ions is much shorter than that (longer than 800 ns) for Zn atoms spectral lines. However, at the early stage evolution(less than 150ns), compared to Zn atoms, higher intensities spectral line for Zn ions at 491.16 nm ((up to three times than Zn atoms spectral lines) were presented. Considering that the most absorbed energy from laser irradiance was released at delay time 250 ns in our experiment, dense Zn ions should be formed directly by the laser- zinc metal interaction, and Zn atoms are partly produced by this process. The absorbed laser energy by plasma shielding can not provide more Zn ions at late-stage plasma expansion, because higher energy must be required for ionization (transition from atoms to ions), while a lot of Zn atoms are present at this time region by electron-ion inverse bremsstrahlung process and the collision within neutral. The understanding of the characteristics of Zn ions in the plasma expanding by laser ablating pure zinc metal will be very important for remote material analysis by plasma emission spectroscopy.

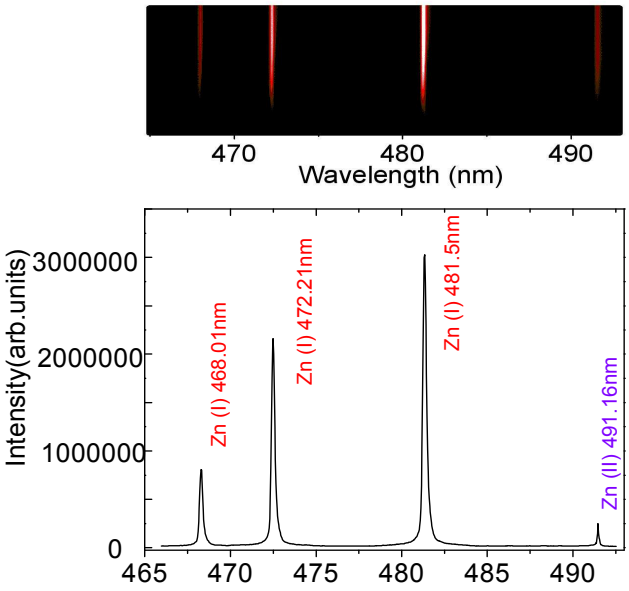

Fig. 4 The spatial evolutions of the representative well-isolated spectral images (up panel) and lines (down graph) taken from Zn atoms and ions in the expanding plasma produced by 2.45 GW/cm^2 laser irradiations.

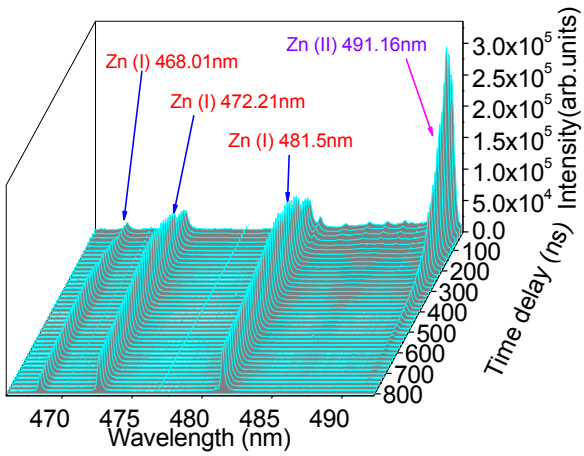

Fig. 5 The early-stage evolution of the emission spectra lines from Zn atoms and ions versus delay time (gate width of 10 ns) with respect to the laser pulse, measured at 0.75 mm from the target surface.

Conclusion

In summary, detailed analyses of the spatial and temporal dependence of Zn ions spectral line in plasma produced by ablation of pure zinc metal were reported. The plasma with the spatial profiles of peak temperature and density at 0.75mm from target surface and temporal profiles of peak Te and Ne at delay time of 250 ns with respect to laser pulse have been discussed. Compared to Zn atoms, our results revealed that Zn ions in the plasma are characterized by weaker intensity in spatial resolved profiles and shorter decay times in temporal evolution, but higher bright in early-state plasma expansion.

Acknowledgement

In this paper, the research was sponsored by the Shandong Province Middle-Aged and Young Scientists Research Awards Fund (Grant No. BS2012CL033) and Shandong Province Post Doctoral innovation foundation (No. 201302019).

References

[1] A.A.I. Khalil and N. Sreenivasan: Laser, Phys. Lett. Vol. 9 (2005), p. 445

[2] S.V. Popruzhenko, D.F. Zaretsky and D. Bauer: Laser Phys. Lett. Vol. 5 (2008), p. 631

[3] R.F.Z. Lizarelli, M.M. Costa, E. Carvalho-Filho, F.D. Nunes and V.S. Bagnato: Laser Phys. Lett. Vol. 5 (2008), p. 63

[4] J. Ben Ahmed, Z. Ben Lakhdar and G. Taïeb: Laser Phys. Lett. Vol. 1 (2004), p. 542

[5] G. Abdellatif and H. Imamb: Spectrochim. Acta Part B. Vol. 57 (2002), p. 1155

[6] B. Wu: Appl. Phys. Lett. Vol. 93 (2008), p. 101104

[7] J. Siegel, G. Epurescu, A. Perea, F.J. Gordillo-Vázquez, J. Gonzalo and. C.N. Afonso: Opt. Lett. Vol. 29 (2004), p. 2228

[8] M. Chen, X. Liu, M. Zhao, C. Chen and B. Man: Phys. Rev. E Vol. 80 (2009), p. 016405

[9] M. Chen, X. Liu, M. Zhao and Y. Sun: Opt. Lett. Vol. 17 (2009), p. 2682

[10] H. Qi, Y. Sun, X. Liu, X. Hou and Y. Li: Laser Phys. Lett. Vol. 4 (2007), p. 212

[11] W.L. Wiese and G.A. Martin: *Atomic Transition Probabilities* (National Stand, Washington 1969).

[12] J. Gordillo-vazquez, A. Perea. J.A. Chaos, J. Gonzalo and C.N. Afonso: Appl. Phys. Lett. Vol. 78 (2001), p. 7

[13] Y. Zhao, S. Singha, Y. Liu and R. J. Gordon: Opt. Lett. Vol. 34 (2009), p. 494

[14] G. Bekfi: *Principles of Laser Plasmas* (Wiley, New York 1976)

Advanced Materials Research Vols. 989-994 (2014) pp 256-259
© (2014) Trans Tech Publications, Switzerland
doi:10.4028/www.scientific.net/AMR.989-994.256

Lignite-fired CFB boiler SO_2, NO emission control technology research

Jianmeng Yang[1, a], Bizheng wang[1,b] and Wei Wang [1,c]

[1] North China Electric Power University, Hebei Baoding071003, China

[a] yjm8123445@126.com

[b] bb1096422360@hotmail.com

[c] 527783602@qq.com

Keywords: Circulating fluidized bed. bed pressure. lignite combustion. SO2; NO; combustion adjustment.

Abstract: For study on SO2 and NO emission characteristics of circulating fluidized bed boiler experiments were carried out in a 300MW circulating fluidized bed boiler. In these experiments, the variables were the amount of limestone and bed temperature. While conducting the test, the reasons for the changes in emission were analyzed, and some advices about combustion adjustment were proposed.

Introduction

GB13223-2011 implemented from January 1, 2012, the emission concentration of SO_2 and NO circulating fluidized bed boiler this standard has more stringent requirements, the provisions of its emissions should not exceed 200mg/m^3. In the circulating fluidized bed boiler in actual operation, some factors that influence on SO_2 and NO emission is different, even contradictory[1]. Therefore, how to control these two kinds of emissions is an unavoidable problem in the process of the development of circulating fluidized bed combustion technology. This paper studied the problem, and put forward some optimization measures.

Research Process

Object Of Study And Research Process

The test of boiler is circulating fluidized bed No. 1 boiler from Yunnan. This is the use of technology for the design and manufacturing of ALSTOM company. Boiler is a subcritical pressure, natural circulation, single cylinder, the balance of circulating fluidized bed boiler ventilation, fueled with lignite. Boiler with maximum continuous load (BMCR condition) as design parameters, maximum continuous evaporation capacity of the boiler is 1025t/h. Unit load is 300MW and rated capacity is 934.8t/h.

In the design of combustion of coal and checked coal, limestone into the design of Ca/S molar ratio of 2, the dry flue gas oxygen content is 6%, SO_2 emission concentration is less than 400 mg/Nm^3.

Study on the test method of the industry, the test process as follows:

(a) In tail flue outlet with Fourier transform infrared gas analyzer and electrochemical oxygen analyzer for direct measurement of NO concentration in flue gas, SO_2 and O_2 concentration.

(b) CFB boiler test is divided into three parts. The first part is to make the bed temperature were stable at 785℃,800℃,805℃ and 815℃, keeping other relevant data such as the amount of limestone, bed pressure, load, oxygen and other conditions do not change, the acquisition of N_2O and SO_2 emission concentration.

Coal and Sorbent Of The Test

Blended coal used in the experiment is Buzhaoba coal and Xinshao coal blended in a 1:1 ratio blended coal. Table 1 shows the coal of the test.

Table 1 Test coal Overview

Test items	Test results
M_t(%)	44.68
A_{ar}(%)	12.22
V_{ar}(%)	24.87
FC_{ar}(%)	18.23
C_{ar}(%)	24.75
H_{ar}(%)	2.11
N_{ar}(%)	0.48

Limestone were used in each experiment from the same origin, were maintained in diameter 3mm, Table 2 is an overview of test limestone.

Table 2 Limestone profile test

SiO_2	1.0%
Al_2O_3	0.14%
Fe_2O_3	0.18%
CaO	55.11%
MgO	0.56%
SO_3	<0.15%
Mt	0.23%
LOI	41.32%

Research Results And Analysis

Effects of the bed temperature on the concentrations of SO2 and NO emissions

The test load is 300MW, limestone amount of 100t/h, oxygen control at 2.0%, the bed pressure stabilized at 6.3KPa. The results show in the Figure 1.

Effects of bed temperature on SO_2 emissions concentrations

Figure 1 shows that, with the gradual rise in bed temperature between 770℃~ 815℃, the concentration of SO_2 emissions also increase. This conclusion results contrast with many studies .This is because the test plant at high altitude, air pressure and density are relatively low, resulting in reduced fuel combustion reaction speed, air and flue gas volume expansion, and limited the furnace space, making the flue gas residence time in the furnace becomes shorter, burning incomplete. In the test conditions, to maintain a certain amount of coal, relatively low combustion temperature, combustion of lignite was not yet fully brought out the furnace flue, although circulating fluidized bed combustion boiler materials will cycle, but still inevitably causing sulfur incomplete combustion, making the low flue gas SO content. As the combustion temperature gradually increased, more and more fuel combustion, emissions of SO_2 concentrations increased accordingly.

Table 3 shows the test results of slag samples under different bed temperature:

Table 3 Slag sample test results

Bed temperature(^oC)	785	800	805	815
Fly ash slag combustibles(%)	1.50	1.28	1.11	0.93

It can be found, as the bed temperature rises, fuel ash content decreased. It shows the extent of coal getting high.

Effects of bed temperature on the concentration of NO emissions

With the bed temperature high, NO emission concentrations continue to rise. When fuel combustion, there are two main ways the conversion of fuel N. One is to generate NO, the other is generated N_2O. Particular reaction process is as follows:

$$HCN + O \rightarrow NCO + H \quad (1)$$

$$HCN + OH \rightarrow HNCO + H \quad (2)$$

$$HNCO + OH \rightarrow NCO + H_2O \quad (3)$$

$$NCO + NO \rightarrow N_2O + CO \quad (4)$$

$$NCO + NO \rightarrow N_2 + CO_2 \quad (5)$$

$$NCO + O \rightarrow NO + CO \quad (6)$$

$$NCO + OH \rightarrow NO + CO + H \quad (7)$$

As the bed temperature increased, the degree of coal volatiles also continues to deepen, the amount of HCN and NH_3 are also increasing. Studies show that when the bed temperature is less than 600℃, the HCN oxidation reaction is carried slowly. With the temperature increase, the reaction get much faster. As can be seen from the above reaction, HCN can either generate NO, also can generate N_2O. Since both N sources are volatile N, so the ratio of NO and N_2O is the shift in the relationship. When the bed temperature is gradually increasing, the reaction (4) is suppressed, the reaction (6) is strengthened, so in this case the concentration of NO emissions continue to rise with the bed temperature.

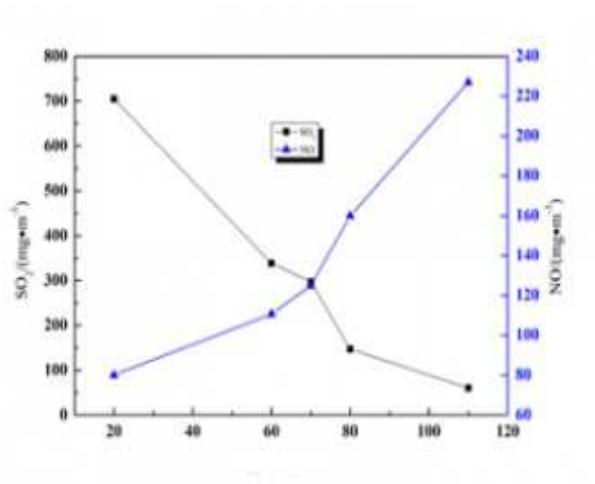

Figure 1 Effects of bed temperature on the concentrations of SO_2 and NO emissions

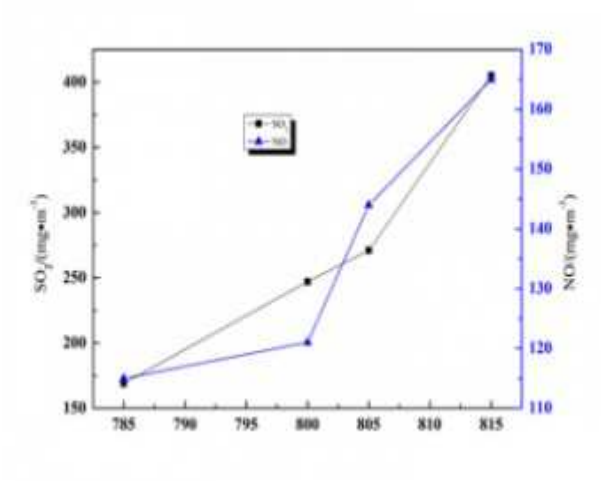

Figure 2 Changes affect the amount of limestone on NO and SO_2emissions

Impact of changes in the amount of limestone

The test load is 300MW, bed temperature control 835℃, oxygen stable at 2.3%. The test result shown in Figure 2.

Affect the amount of limestone concentration of SO_2 emissions

As can be seen from Figure 2, the amount of coal remain unchanged, increase the amount of limestone, the concentration of SO_2 emissions show a downward trend. Increasing the amount of limestone calcium sulfur ratio becomes large, which makes the desulfurizing agent to capture more SO_2, thereby increasing desulfurization efficiency. But it is worth noting that with the increase in the amount of limestone desulfurization efficiency of growth will gradually slow down. In Figure 2, when the amount of limestone increased from 20t/h to 80t/h, the SO_2 emissions decreased 700 $mg \cdot m^{-3}$ to 100 $mg \cdot m^{-3}$, the rate of decrease approaching 10mg/t, but when the amount of limestone from the 80t/h increased to 110t / h, SO_2 fell only about 50mg, decreased rate of 1.8mg/ t. Decline in SO_2 slows. Considering the increasing amount of limestone, will increase the operating costs of power plant, so the amount of limestone should not exceed 80t/h.

Affect the amount of limestone concentration of NO emissions

For the emission concentration of NO increased with increasing the amount of limestone, some scholars believe is the impact of desulfurization, $CaSO_4$, on the reaction of NH_3-NO[3]. However, according to recent research, it shows that this argument is not comprehensive. After an increase in the amount of limestone, the furnace has a lot of CaO exist, and CaO fuel nitrogen is converted to NO strong catalyst[4]. Although CaO for CO and H have catalytic reduction of NO, the impact of the latter is less than the former, so the increase in the amount of limestone, NO emissions increased. In addition, there are scholars believe that limestone can also catalyze HCN and NH_3 generate NO, thereby inhibiting the volatile N to N_2O change, while also increasing the amount of NO generation[5].

Combustion Adjustment Programs

When the bed temperature changes, SO_2 and NO emission concentrations were increased. When the bed temperature at 790℃or less, SO_2 emission concentration less than 200 $mg \cdot m^{-3}$ and NO less than 125 $mg \cdot m^{-3}$. Therefore, we can try to make the bed temperature lower, but when the bed temperature too low, it will make the boiler output decline. However, within the scope of the study, the main-steam flow varies only with the bed temperature changes, smaller changes between 947.51t/h to 963.8t/h, therefore when the bed temperature dropped to 785℃ impact on boiler output is not great, bed temperature control can be considered at about 785℃, in order to reduce the concentration of pollutants discharged as possible.

In the test, with the increase in the amount of limestone, and the concentration of SO_2 emission reduction, the concentration of NO emission increase. According to GB13223-2011 thermal power plant air pollutant emission standards, SO_2 emission concentration should be controlled at 200 $mg \cdot m^{-3}$ or less, so the amount of not less than limestone 75t/h. Although limestone continues to increase, SO_2 emissions will significantly reduce the concentration of smaller changes in the concentration of NO emissions, considering the desulfurization economy, limestone amount held in the 80t/h more appropriate.

References

[1] Yin Li-bao, Yan Wei-ping, Ye Xue-min, etc. Comparative Study on N_2O Emission Reduction Technologies for Circulating Fluidized Bed Boilers[J]. Boiler Manufacturing,2003,1(1)：7-9

[2] MA Shuang-chen. Experimental Research CFB FGD [D]. Beijing, North China Electric Power University, 2002

[3] Li Xuan-tian, Luo Zhong-yang, NI Ming-jiang, Cen Ke-fa, etc. Research During Coal Combustion Emissions Impact Of Limestone Desulfurization NO_x Pair. Fuel Chemistry and Technology [J], 1991 [1]

[4] Cen Ke-fa. Circulating Fluidized Bed Boiler Design And Operation Theory [M] Beijing: China Electric Power Press, 1998.

[5] B.X.Shen,T.Mi,D.C.Liu,B. Feng,Q.Yao,Franz Winter,N_2O Emission Under Fluidized Bed Combustion Condition,Fuel Processing Technology 84(2003) 13-21.

Advanced Materials Research Vols. 989-994 (2014) pp 260-263
© (2014) Trans Tech Publications, Switzerland
doi:10.4028/www.scientific.net/AMR.989-994.260

Laying the Ground of Indoor Restrooms by Using Foam Glass and Waterproof Coating

Shuomang Shi[1, a]

[1]Southwest Jiaotong University, Chengdu, Sichuan, China

[a]ssmabc@sina.cn

Keywords: Basements, restrooms, furring brick, foam glass, pure acrylic coating, silicon sealant

Abstract

This article presents a new design of waterproof ground for rest rooms in basements by using new materials and new combination. First use cement mortar to paste the waterproof and heat resistance foam glass furring bricks which have low density and high strength on the ground. Then use silicon sealant to fill the gap between the bricks. Roll brush the multifunctional transparent elastic waterproof coating pure acrylic JQ - 168 on the bricks as surface. The combination of the two formed a sealed waterproof ground in indoor restrooms with certain strength and toughness. So this kind of ground surface can have stable and reliable waterproof function when in face of the situation that groundwater upwelling through fissures in concrete created by resistless damage like earthquake and so on.

Research background

Nowadays in China, the use of underground space more and more appear in all kinds of civil and public buildings due to the pressure of population and demand for land conservation, such as subway, underground shopping malls, residential basement, etc. So here come many underground restrooms. A restroom itself is in a moist environment. Cause the ground of restrooms directly contact with water. Also it can be infiltrated by moist air or water from the lower concrete because of the rupture from external force. And the basements are usually immersed in wet soil at the area where groundwater level is higher than average. Therefore, the ground of the basement is bound to waterproof and waterproof processing. The main methods are waterproof coating and using waterproof roll in China. [1]But once the water-resisting layer is damaged due to external factors such as earthquakes the function of waterproof is gone. So it demands that indoor waterproofing methods can compensate the water proofing property losses due to the structure failure. At present people use porcelain bricks and Mosaic on the ground on most of the floor. And lay waterproof roll under them. But the function of waterproof will be lost if the layer was damaged with structure failure. Considering this, we are using waterproofness and toughness of foam glass with silicon sealant and transparent waterproof surface coating to make the inner defensive line of a restroom underground.

Materials

Foam glass: Foam glass refers to the evenly mixing material made of various kinds of waste mineral residue by adding an appropriate amount of foaming agent, flux and various kinds of modified additives mixtures. They can be transformed into porous glass after preheating, melting, foaming and cooling technology. Inside the foam glass there are numerous small, uniform, connected or closed pores, so this is a uniform system of gas phase and solid phase. The microstructure is shown in Fig.1. The volume of pore makes up 50%-95% of the total. And the diameter of the pores range from 0.5 - 5mm. Foam glass has low density, large closed porosity,

Low thermal expansion coefficient, low coefficient of thermal conductivity, stable thermal performance, nonflammable, long-life, strong corrosion resistance, and many other advantages. [2]

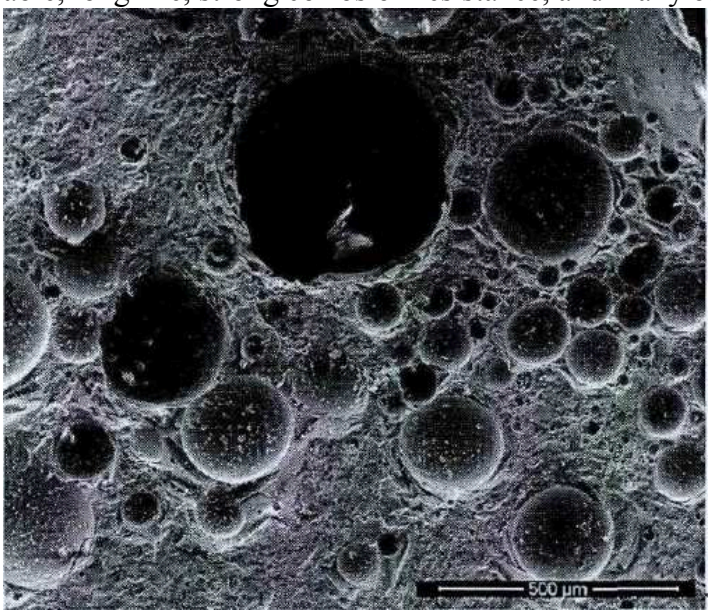

Fig.1. The microstructure of foam glass

The multifunctional transparent elastic waterproof coating JQ - 168: It is made of pure acrylic as the main raw material, mixed with a certain proportion of cationic surfactant, coupling agent. The coating is non-toxic, tasteless, and nonflammable. (Features are shown in Table.1) Its liquid is white uniform paste without aggregation and will become colorless and transparent after condensation. It has excellent waterproofness, tenacity and weather resistance. [3] The microstructure of pure acrylic is shown in Fig.2.

Table.1. Features of pure acrylic

Features of pure acrylic	
Appearance	milky white liquid
Dry time of surface/h	≦4
Time of absolutely dry/h	≦12
Tensile strength/Mpa, 20°	≧300%
Impervious(0.3Mpa, 600min)	None
Cohesiveness/Mpa	≧02-0.3
Heat resistance(852 C,5h)	No flowing air bubbles
Freezing and thawing cycles(10)	normal

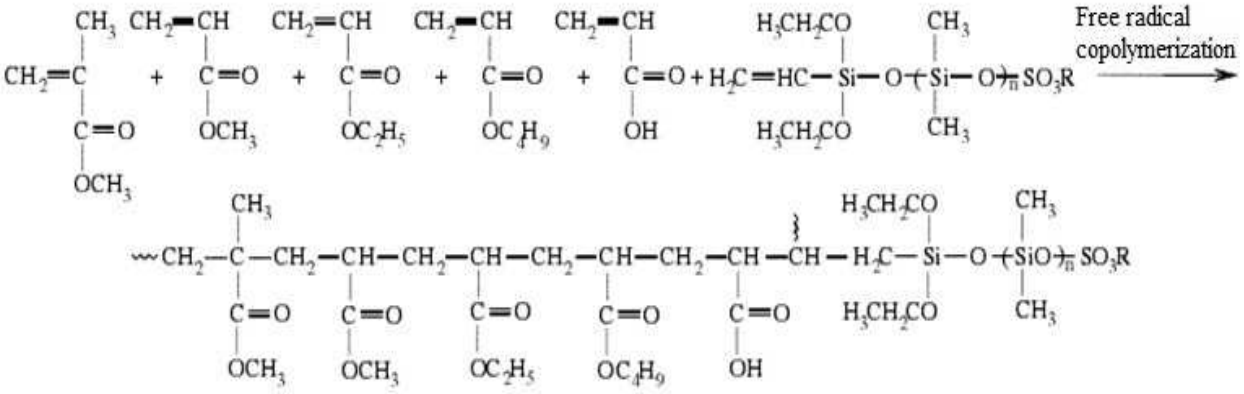

Fig.2. Microstructure of pure acrylic

Construction principle and methods

Structure principle: This scheme takes advantage of the two kinds of waterproof materials synthesis as a whole. Firstly we make foam glass into a certain specifications of the watertight ground brick for the convenience of use and arrangement for the convenience of use and arrangement. We use cement mortar set the bricks on the ground as the main body of the waterproof. Then we use silicon sealant to fill the gaps between the bricks to make the bricks into a whole and let the surface be flat. Secondly we brush a layer with certain thickness of pure acrylic coating on them. [4]So the bricks and the layer form a seal inside which can bear and resist the water in the inner space and prevent the moisture from the concrete outside it. So the inner space can be prevented from water seepage and leaking.

Construction method:

a) Apply cement mortar evenly on the concrete ground. Lay prefabricated foam glass bricks with standard 50cmx50cmx2cm and leave 3-5mm wide gaps between them.

b) Clean up the gap of cement mortar with scraper become to a depth of about 9-10 mm gap.

c) Inject silicon sealant after cement mortar's solidification. Scrape the surface till smooth and flat. Repeat this step 3 times to ensure the Inject silicon full of gaps without air.

d) Brush or spray pure acrylic coating JQ-168 on bricks and silicon sealant with a thickness of 1.2-1.5mm. Brush a second layer after the solidification of the previous level. Repeat this till 3 times to get a thick transparent elastic waterproof layer.(The schematic and design sketch ore shown in Fig.3 and Fig.4)

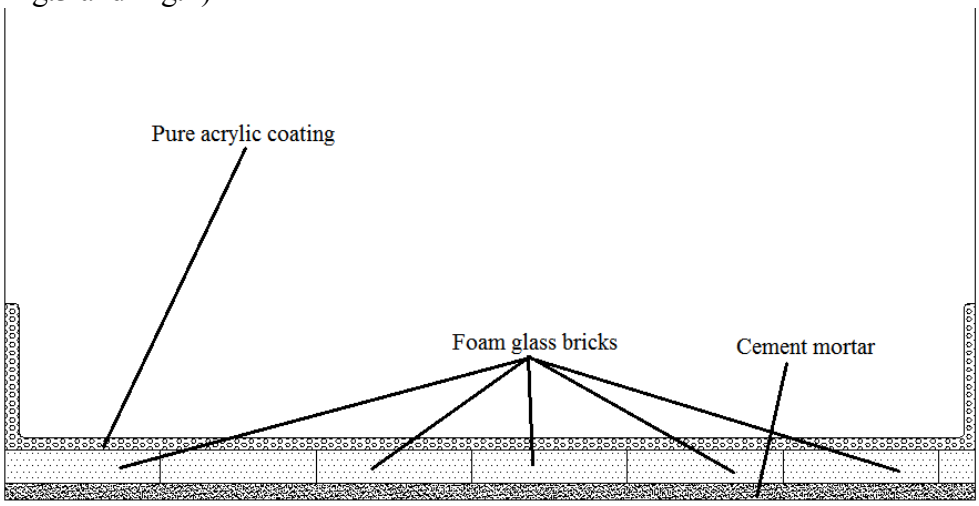

Fig.3. Schematic of the design

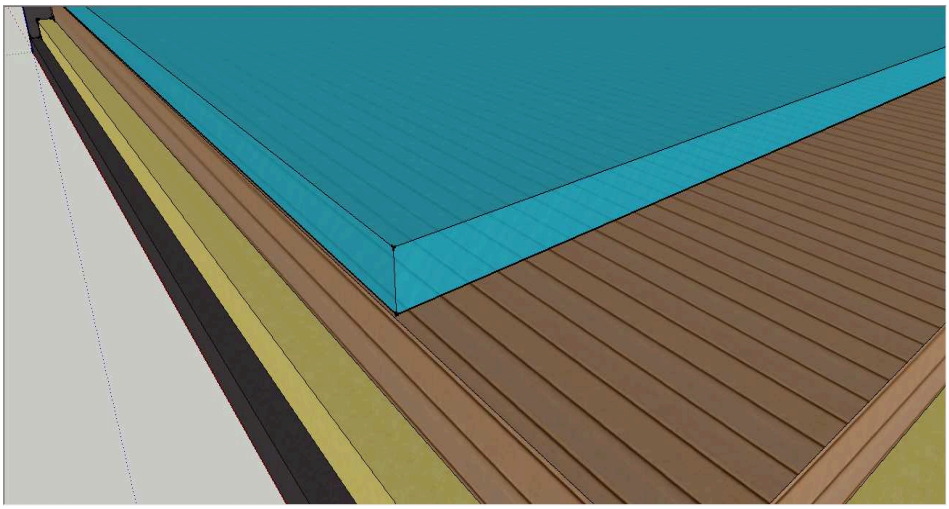

Fig.4. Design sketch

Characteristics and the advantages and disadvantages analysis

Characteristics of materials: The main body foam glass is a kind of inorganic non-metallic material after high temperature foaming. It has properties of fire prevention, waterproof, non-toxic, corrosion resistance, moth-proofing, not aging, no radiation, insulation, anti-magnetic wave, antistatic, high mechanical strength and a good bond to all kinds of cement. Besides the raw material of foam glass is wasted glass and industry residue. These avoid the waste of heat and a large number of manpower and material resources waste in the aspect of production material to let secondary utilization of the waste possible. This can have the effect of energy conservation and emissions reduction, in line with the requirements of global low carbon emissions. On the other hand foam glass itself is colorless or translucent white for porosity reasons. So when the production it can be mixed with pigment to form all kinds of patterns and decoration [5]. With the transparent coating on the top it can achieve the aesthetic of interior decoration and design requirements.

Defect analysis: The construction steps are a little bit complicated. During the process we have to wait for the consolidation of the cement to inject silicon sealant, and the consolidation of the previous waterproof coat to brush the next level. All these will lead a waste of time. What's more it calls for strict demand. During the process a light touch or disturb will cause the surface no longer a flat one and that will cause an excessive loss while using in the future which would lead to a partial failure.

Conclusion

This design uses a new type of combination which uses low-cost environmental protection material foam glass as bricks and multifunctional transparent elastic waterproof coating as surface, offers an effective solution for the demand of waterproof in places where contact water a lot.

In the aspect of function it can satisfy the waterproof and moisture-proof requirements of civil space. In the aspect of exterior it can be beautiful and has the function of decoration. Adding the good carrying capacity, corrosion resistance and durability, it can be the first choice when it comes to a waterproof inner space.

References

[1] Information from http://baike.baidu.com.
[2] The properties of the foam glass and application in civil engineering exploration-Fanying Kong, Jian Gao, 2004, 31(9), 104~105 (In Chines)
[3] Pure acrylic multifunctional transparent elastic waterproof coating application in exterior wall waterproof engineering-Zhiyuan Chen, Shuxiong He, 2003, 1004-1672(2003)04-0049-02 (In Chinese)
[4] Waterproof foam glass materials – Japanese, 59-207855(In Chinese)
[5] Preparation and Properties of Foam Glass, Bo Chen, 2012(In Chinese)

Advanced Materials Research Vols. 989-994 (2014) pp 264-266
© (2014) Trans Tech Publications, Switzerland
doi:10.4028/www.scientific.net/AMR.989-994.264

Influence of Mo addition on a nickel-base single crystal superalloy

Kai Zhao [1, a]

[1]School of Metallurgical and Materials Engineering, Chongqing University of Science and Technology, Chongqing, 401331, China

[a] tony_zk@163.com

Keywords: superalloy; Mo; lattice misfit; creep rupture strength

Abstract. The influence of minor Mo addition on the lattice misfit and creep rupture strength of a new single crystal superalloy have been investigated. It was shown that Mo can reduce the lattice misfit; increase the tendency of forming TCP phase; extend the time to material failure.

Introduction

Mo is one of the main refractory strengtheners in nickel-base superalloys. Since high temperature creep was generally diffusion controlled, additions of Mo were quite effective in reducing creep rates because Mo diffused very slowly in nickel. Mo was found to have a similar effect as rhenium in a fourth generation single crystal superalloy—TMS-162, in which the effects of tantalum and niobium additions were not so significant. These were also considered to be attributed to the increase of the magnitude of the lattice misfit, which was believed to be beneficial because of stronger γ/γ′ interfaces [1]. Mo markedly increased the γ′ phase solvus temperature; correspondingly, the weight fraction of γ′ phase increased with Mo additions. Lattice parameters of both the matrix and the γ′ phase were increased markedly by Mo [2]. Mo additions were also very effective in reducing the coefficients of thermal expansion [3].

However, more Mo additions resulted in the degeneration of mechanical properties due to the precipitation of topologically closed packed (TCP) phases. Accordingly, reducing the Mo content by only 0.73 mass% increased the creep rupture life by a factor of three, because the precipitation of TCP phase was eliminated [4].

Mo oxidizes rapidly at elevated temperatures. The complexity of the problem resides in the volatility of Mo trioxide, the end product of the oxidation reaction, which prevents the possible formation of protective oxides. At about 770℃ the rate of evaporation of Mo trioxide equals its rate of formation and, as temperature increases, the volatilization rate becomes extremely rapid [5]. Also, some authors [6-9] suggested that Mo was detrimental to hot corrosion resistance of simple ternary nickel-base superalloys. However, it was reported that Mo significantly reduced the amount of hot corrosion attack at 870℃ for the aluminum-containing alloys. For the titanium-containing alloys tested at 870℃ and all alloys exposed at 980℃, Mo exerted little influence on hot corrosion behavior [10]. Zheng et al. [11] thought that Mo may accelerate acid fluxing action, which may result in the catastrophically accelerating effect. Generally, the Mo content in nickel-base superalloys is less than 2 mass%.

Several research investigations have studied the influence of Mo on the microstructure and creep properties of nickel-base superalloys [12-13]. Most of the previous studies were concerned with the superalloys bearing high Mo contents. In present paper, we will focus on the lattice misfit and creep rupture strength of a new single crystal superalloy with minor Mo addition.

Experimental procedure

Three experimental superalloys have been used in this study. Nominal chemical compositions of these alloys are listed in Table 1.

Table 1 Nominal compositions of the experimental alloys (mass %)

Alloys	Cr	Mo	W	Al	Ta	Ni
1	9	-	8	5.4	10	Bal.
2	9	0.4	8	5.4	10	Bal.
3	9	1.2	8	5.4	10	Bal.

Samples used for experiments were vacuum induction melted and fabricated using standard directional solidification casting procedures; materials were supplied as 10 mm diameter cylindrical bars with orientations within 5° of the [001] orientation. Samples were given the following heat treatments: 1320℃/5h+1100℃/4h +870℃/20h, followed by air cooling.

Specimens were mechanically polished and then electronically etched (2V d.c. and 0.2 A) by 21 ml H_3PO_4+17 ml H_2SO_4+12 ml H_2O. Specimens were observed by using a JEOL-JSM6060 scanning electron microscope (SEM).

Results and discussion

1. On the lattice misfit

Fig. 1 summarized the dependence of the lattice misfit on Mo content in nickel-base superalloys. Mo was found to reduce the lattice misfit, although data were somewhat different in different alloying systems [14-17].

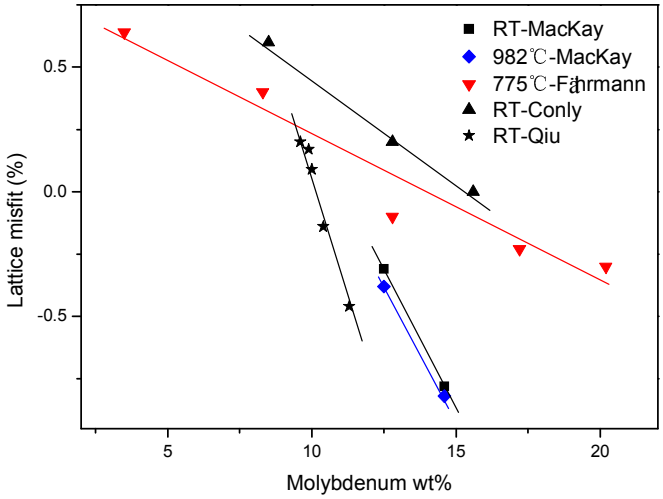

Fig. 1 Lattice misfit as a function of molybdenum contents.

2. On microstructure stability

Mo was the strongest for the tendency of forming TCP phase, rhenium, tungsten, and chromium the second place, and cobalt and niobium the weakest. However, no TCP phase was observed in the alloys bearing 12.5 wt% Mo [16]. In the present three alloys, TCP phases were observed in Alloy 3, which mainly distribute in the dendritic core. Alloy 1 and 2 contained no TCP phase.

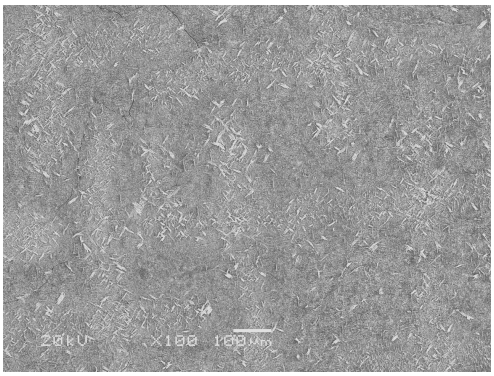

Fig. 2 TCP phases precipitated in Alloy 3 (1100 ℃/600 hours).

3. On stress-rupture properties

Fig. 3 shows the creep rupture strengths of the three experimental alloys. Increasing the Mo content substantially extended the time to material failure, except of 1100 ℃/137 MPa.

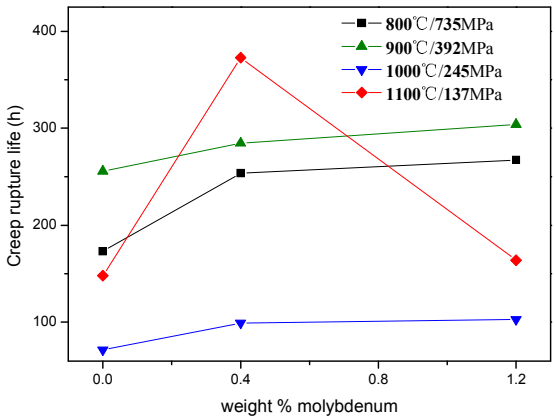

Fig. 3 Creep rupture life as a function of molybdenum contents.

Summary

The influence of minor Mo addition on the lattice misfit and creep rupture strength of a new single crystal superalloy have been investigated. It was shown that Mo reduced the lattice misfit. Mo was the strongest for the tendency of forming TCP phase. Increasing the Mo content substantially extended the time to material failure, except of 1100 ℃/137 MPa.

Acknowledgement

This research is funded by Natural Science Foundation Project of CQ CSTC2012jjA1491 and Research Foundation of Chongqing University of Science & Technology (No. is CK2011B18).

References

[1] Y. Koizumi, T. Kobayashi, T. Yokokawa, M. Osawa, H. Harada, Y. Aoki, M. Arai: J. Japan Inst. Metals Vol.68(2004), p.206-209.
[2] W.T. Loomis, J.W. Freeman, D.L. Sponseller: Metall. Trans. Vol.3(1972), p.989-1000.
[3] M. Ⅲ Hugh, D.L. Sponseller, M. Semchyshen: Metall. Trans. A, Vol.6(1975), p.477-485.
[4] R.A. Mackay, L.J. Ebert, in: *Proc. 5th Int. Symp. On Superalloys*, edtied by M. Gell, C.S. Kortovich, R.H. Bricknell, W.B. Kent, J.F. Radavich, AIME, New York (1984), p.135-144.
[5] J.J. Harwood, in: *The Metal Mo*, Ohio ASM (1956), p.421.
[6] P.A. Bergman, C.T. Sims, A.M. Beltran, in: *Hot corrosion problems associated with gas turbines*, ASTP STP 421, Amer. Soc. Testing Materials (1967), p.38-63.
[7] R.W. Hardt, J.R. Gambino, P.A. Bergman, in: *Hot corrosion problem associated with gas turbines*, ASTM Spec. Tech. Publ. 421 (1967), pp.64-83.
[8] A.U. Seybolt, P.A. Bergman, M. Kaufman, in: *Hot corrosion Mechanism Study, Final Report*, Research and Development Center, General Electric Company, Schenectady, New York, (1967), Navy Contract No.N600(61533)65595.
[9] K.H. Ryan, J.R. Kildsig, P.E. Hamilton, in: *Investigation of hot corrosion of nickel-base superalloys used in gas turbine engines*, AFML-TR-67-306, (1967).
[10] M. Ⅲ Hugh, D.L. Sponseller, M. Semchyshen: Metall. Trans. A Vol.5(1974), p.673-683.
[11] Y.R. Zheng, D.T. Zhang, in: *Color Metallographic Investigation of Superalloys and Steels*, National Defence Press of Technology, Beijing (1999), pp. 8.
[12] W.Y. Ma, Y.F. Han, S.S. Li, Y.R. Zheng, S.K. Gong: Acta Metall. Sinica, Vol.42(2006), p.1191-96.
[13] W.T. Loomos, J.W. Freeman, D.L. Sponseller: Metall. Trans. Vol.3(1972), p.989.
[14] M. Fährmann, P. Fratzl, O. Paris, E. Fährmann, W.C. Johnson: Acta Metall. Mater. Vol.43(1995), p.1007-122.
[15] J.G. Conly, M.E. Fine, J.R. Weertman: Acta Metall. Vol.37(1989), p.1251-63.
[16] R.A. MacKay, M.V. Nathal, D.D. Pearson: Metall. Trans. A, Vol.21(1990), p.381-388.
[17] Y.Y. Qiu: Scripta Metall. Mater. Vol.33(1995), p.1961-68.

Advanced Materials Research Vols. 989-994 (2014) pp 267-269
© (2014) Trans Tech Publications, Switzerland
doi:10.4028/www.scientific.net/AMR.989-994.267

Superhydrophobicity of silicon-based microstructured surfaces

Gang Li

School of Mechatronic Engineering, East China Jiaotong University, Nanchang 330013, China

ligang0794@163.com

Keywords: Superhydrophobicity; Wettability; Contace angle; Microstructure

Abstract. Here, a simple method was presented for fabricating superhydrophobic silicon surfaces. Square-pillar-array samples were fabricated on silicon substrates by using the femtosecond laser micromachining technology. We measured the static and dynamic contact angles for water on these surfaces. The contact angles and the rolling angles on the silicon surfaces were measured through an optical contact angle meter. Wettability studies revealed the films exhibited a superhydrophobic behaviour with a higher contact angle and lower rolling angle-a water droplet moved easily on the surface.

Introduction

Wettability is important for solid surface. A surface having water contact angle greater than 150°is commonly called super-hydrophobic. An example of a naturally occurring superhydrophobic surface is the lotus leaf. Upon landing on the surface of a lotus leaf, water beads up to form nearly spherical drops that immediately roll off. Surperhydrophobic materials have attracted much attention due to their potential applications in microfluidic devices where contact with water is detrimental to performance or durability. The decreased contact area between water and solid surfaces in superhydrophobic samples reduces effects such as anticontamination[1], self-cleaning[2,3] and friction of bearing lubrication.

The wettability of a surface depends on both its chemical compositions and surface roughness. Although lowering the surface energy of a substrate decreases its wettability, the water contact angles on smooth hydrophobic surfaces are not exceeding 120°, even when coated with a monolayer of perfectly close-hexagonal-packed-CF3 groups[4]. Inspired by the morphology of the lotus leaf, engineers are trying to mimic nature and produce artificial superhydrophobic surfaces. Some of the numerous approaches employed in the preparations of superhydrophobic surfaces include nanosphere lithography[5], plasma lithography[6], nanoimprint lithography[7], soft lithography technology [8] and multibeaminterference lithography[9], but these mothods are high cost and complicated. Here we have fabricated microstructure surfaces on by a novel femtosecond laser micromachining technology. The wettability of these fabricated superhydrophobic surfaces is studied in detail.

Experimental

Fabrication of silicon-based microstructured surfaces

The substrates with used in experiments were p-type (100) orientated silicon wafers with resistivity of 15-25 Ω.cm. In order to remove chemical impurities and particles, the wafers were cleaned by standard RCA cleaning procedures before micromachining. Fabrication of microstructures was completed by a femtosecond laser micromachining system. The correlative laser parameters are listed as follows: laser wavelength, λ=800 nm; selected laser energy density, U=2.5 J/cm2; and laser scanning velocity, υ=0.4 inch/s. The fabricated microstructures on the surfaces are square-pillar-array structures. The predesigned geometric parameters of the microstructures before fabrication are listed as follows: the upside lengths a of the pillars, the heights h of the pillars, and the spaces b of the pillars.

Characterization

Morphologies of these fabricated superhydrophobic surfaces were examined thermal field scaning electron microscopy (SEM, JEOL，JXA-840, Japan). The WCA were measured by an optical contact angle meter (Dataphysics, OCAH200, Germany) at room temperature after SEM observation. The contact angles for five different positions of the sample were measured and the average was adopted.

Results and discussion

SEM images of the silicon surface with the periodic square-pillar-array microstructure fabricated by femtosecond laser was shown in Fig. 1. It was evidently seen from the observed SEM images that the surface quality of silicon surface with the square-pillar-array structure was very good and distributed periodically on the surface. There weren't almost surface collapse and deformation phenomena on the surface. Uneven surface of the sample with smaller irregular structure, and some reaching the nanometer scale can be seen in Fig. 1. This is due to laser interaction with the silicon surface and the photon avalanche ionization caused by the nonlinear absorption on the material surface, leading to permanent damage and forming a large number of irregular fine structure on the square-pillar-array surface.

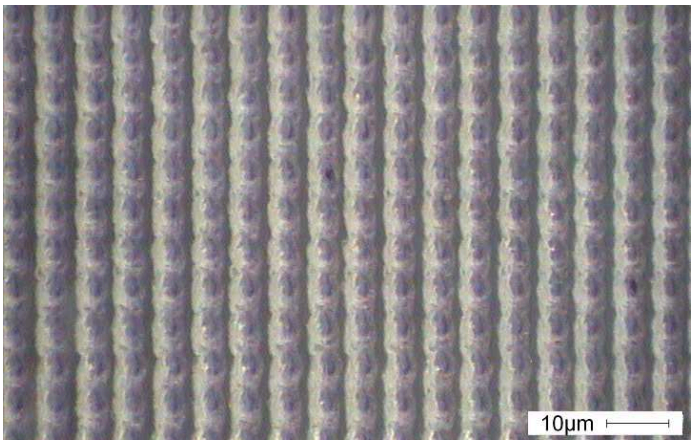

Fig. 1 SEM image of the surface of the square-pillar-array structure

Contact angle measurements

Contact angle measurement is probably the most common method of solid surface tension measurement. One of the most frequently used methods of contact angle assessment is the sessile drop technique. To compare the wettability of smooth silicon surface with that of silicon surface with square-pillar microstructure, the static contact angle of water on both surfaces were measured using the sessile droplet method and the results were shown in Table 1.the results showed that the smooth surface was hydrophobic (CA=99.2°) and the textured surface was superhydrophobic (CA=159.3°). The shape of water droplet on the both surfaces showed in Fig.2. It was clearly seen that the droplet sit on the peak of the roughness (Fig. 2b) and the light could pass through the space in the depressions of the rough surface, which indicated that a composite surface was formed on the textured silicon surface.

Cassie and Baxter[10] studied abundant superhydrophobicity in nature, they put forward a concept of composte contact. It is assumed that the liquid forms composite surface on the rough substrate as shown in Fig.2b, i.e. if microstructured surface is hydrophobic enough, the liquid does not fill the grooves on the rough surface and the droplet is just sitting on the air and protruded surface.

Cassie and Baxter also obtained the equation, which adapts to any composite surface contact from a thermodynamic point of view.

Table 1 Contact angle of surface of the as-fabricated samples (°)

samples	Contact angle θ/°					Average θ/°
	1	2	3	4	5	
Smooth silicon surface	94.9	96.6	104.9	97.5	102.2	99.2
Microstructure surface	159.6	158.2	156.9	160.4	161.5	159.3

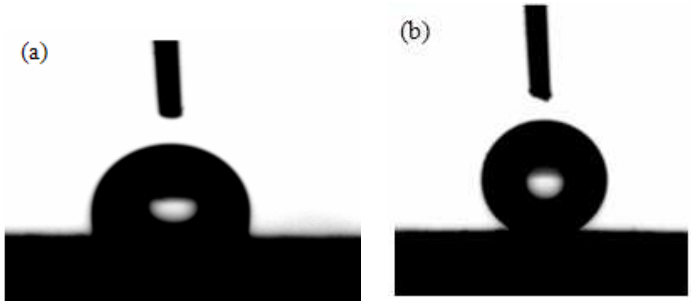

Fig. 3 Photographs of water droplets on the sample surface of (a) the smooth silicon surface, and (b) the square-pillar microstructure silicon surface

$$\cos\theta^* = f_1 \cos\theta_1 + f_2 \cos\theta_2, \quad (1)$$

Where θ^* is the apparent contact angle of the composite surfaces, θ_1 and θ_2 are the intrinsic contact angles of two materials, respectively, and f_1 and f_2 are the fractions of two materials of the compostie surfaces ($f_1 + f_2 = 1$).

When one of these two materials is air, whose contact angle for water is 180°, eq. (1) are can be transform as follows,

$$\cos\theta^* = f_1(\cos\theta_1 + 1) - 1, \quad (2)$$

Equations (1) and (2) are the formulaic expressions of Wenzel's and Cassie's classical wetting theories. In addition, de Genne et al. proposed another wetting mode, i.e., the Cassie impregnating wetting state where crannies of the solid are wetted with liquid and the solid convexities are dry. The Cassie impregnating wetting regime is described with equations that are different from the Wenzel and Cassie heterogeneous ones. In this regime, when the Young's angle is less than a critical value calculated by the equations, the liquid film impregnates the texture; however, remaining islands emerge above the "absorbed" liquid film.

Conclusion

The textured surface with periodic square-pillar-array microstructure been fabricated with different parameters by a novel femtosecond laser. The wettability of such square-pillar-array samples was investigated. The microstructured surface showed superhydrophobic with higher contact angle and lower rolling angle. The results showed that these discrete pillars formed microstructure in the surface, which was strongly affected the contact angle and the rolling angle. On the basis of this sutdy, superhydrophobicity of silicon-based microstructured surfaces using femtosecond laser may have strong potential applications in the future.

Acknowledgments

This material is based upon work supported by the Natural Science Foundation of Jiangxi Province (No 20122BAB206029), the International Science and Technology Cooperation Project of Jiangxi Province (No. 20121BDH80016).

References

[1] R Furstner, W Barthlott, C Neinhuis: Langmuir, Vol. 21(2005), p.956
[2] Y Cheng and D E Rodak: Appl. Phys. Lett., Vol. 86(2005), p.144101
[3] T L Sun, L Feng, X F Gao: Acc. Chem. Res., Vol. 38(2005), p.644
[4] R Blossey: Nat. Mater., Vol. 2(2003), p.301
[5] J Y Shiu, C W Kuo and P Chen: Chem. Mater., Vol. 2(2004), p.561
[6] N Vandencasteele, H Fairbrother and F Reniers: Plasma Process. Polym., Vol. 2(2005), p.493
[7] A Pozzato, S Dal Zilio, G Fois: Microelectronic Engineering, Vol. 83(2006), p. 884
[8] G Li, ZG Li, LM Lu: Journal of Wuhan University of Technology-Materials Science Edition, Vol. 27(2003), p. 138
[9] D Wu, QD Chen, H Xia: Soft Matter, Vol. 2(2010), p. 263
[10] ABD Cassie and S Baxter: Trans. Faraday. Soc. Vol. 40(1944), p. 546

Advanced Materials Research Vols. 989-994 (2014) pp 270-275
© (2014) Trans Tech Publications, Switzerland
doi:10.4028/www.scientific.net/AMR.989-994.270

Research on Erosion Resistance of TiB_2 Ceramic Particle Reinforced MMC Coating

Fang Jianjun[1, a], Song Yunjing[1] and Li Zhuoxin[2]

([1.] New Energy Training Department of State Grid Technical Institute, No. 500, South Erhuan Road, Jinan City, Shandong Province, 250002;

[2.] Material School of Beijing University of Technology, No. 100, Pingleyuan, Chaoyang District, Beijing City, 100025)

Keywords: TiB_2, metal matrix composite (MMC), erosion resistance

Abstract. The research uses electric arc spraying with low cost and convenient operation to prepare four TiB_2 particle reinforced composite coatings with high bonding strength and uniform tissue. It makes comparative study on elevated temperature erosion actions of coating and 45CT of electric arc spraying. The results indicate the coating has excellent erosion wearing resistance. TiB_2 particles in M-TiB_2 coating have small size, have good unity with metallic matrix, and are distributed on metallic matrix with high hardness relatively uniformly, and porosity of coating is low. The coating has excellent erosion resistance.

1 Foreword

Erosion wear is material loss phenomenon caused by small particles of liquid or solid impacting material surface by certain speed or angle, and measurement system of erosive quantity has different theoretical models depending on plastic or crisp material; factors that influence erosion wear mainly include various aspects such as particle property, environmental factor and material property. By comparing with welding and other surface technologies, electric arc spraying has various advantages high efficiency, low cost, simple operation, low toxicity of generated gas and especially suitable for site operation with narrow space[1].

Previous research has proven that erosion resistance of metallic matrix ceramic composite coating is better than that of metallic coatings such as self fluxing alloy [2-3]. One of important background of the subject to study metal matrix composite coating that contains TiB_2 is to solve pipe erosion problem of coal fired boiler, so the chapter makes erosion resistance test on developed MCW series four coatings (304L-TiB_2, 304L-TiB_2/Al_2O_3, NiCr-TiB_2/Al_2O_3 and NiCr-TiB_2) with good comprehensive properties, compares them with 45CT coating, and studies erosion resisting mechanism of coating.

2 Experiment process

Elevated temperature erosion wearing test is made on GW/CS-MS device researched by Army Equipment Repair Surface Engineering Research Center by referring to ASTM G76-95 standard. Fuel gas fly ash abrasive grain erosion, and its working schematic diagram is shown in Fig. 1. Test conditions are shown in Table 1.

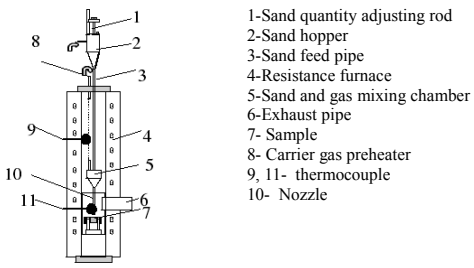

Fig.1 Structure schematic diagram of GW/CS-MS erosion wear device under elevated temperature

Table 1 Experimental conditions of erosion test

Temperature (℃)	25		500		650	
Erosion angle (°)	30	90	30	90	30	90
Erosion particle mass (g)	100	100	100	100	100	100
Erosion time (s)	360-480					
Erosion particle speed (m/s)	40-60					
Erosion particle	Power plant fly ash					

arc spraying erosion sample to researched four cored wires on 20G matrix. Use JZY-250 type electric arc spraying equipment to prepare coating. Select 20 steel as matrix. electric arc spraying technological parameters: Electric arc voltage is 28-32V, working current is 150-200A, compressed air pressure is 0.5-0.65 MPa, and distance is 100-200 mm. Aluminizing agent formula [4] is (15% Al powder + 85% Al_2O_3 + 0.5% NH_4Cl + 0.5% KHF_2), aluminizing technology is 900℃×2h, and aluminizing layer thickness is about 100 μm. Morphology of fly ash grain is shown in Fig.2.

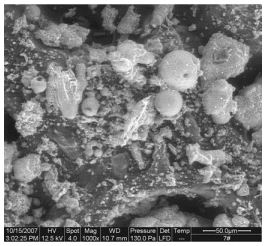

Fig.2 Morphology of fly ash

3 Results and analyze

Erosion test results of TiB_2 ceramic particle reinforced metal matrix composite coating and commercial coating 45CT prepared by electric arc spraying are shown in following Fig. 3.

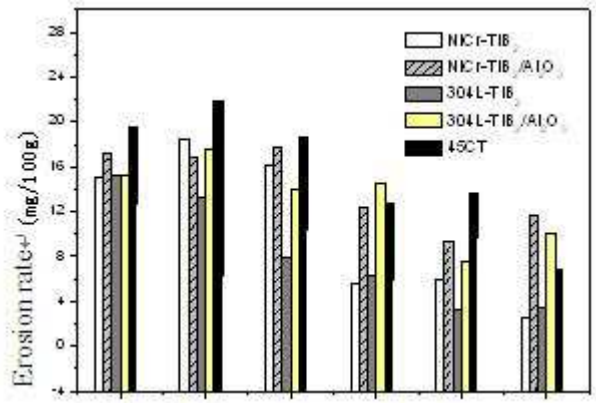

Fig.3 Erosion loss of coatings

It can be seen from the figure that, erosion resistance of TiB_2 ceramic particle reinforced metal matrix composite coating prepared by electric arc spraying is better than 45CT coating in general. According to erosion rate, with change of attack angle, block material is divided into two types, i.e., erosion damage of plastic material and crisp material (Fig. 4).

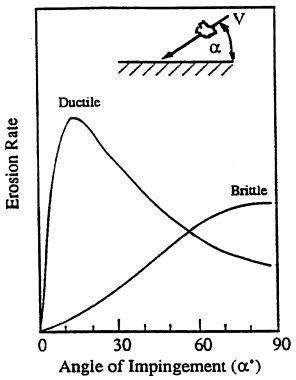

Fig. 4 Relation between erosion rate and erosion angle of both ductile and brittle materials under ideal status

4.1 Influence of erosion angle and temperature on NiCr-TiB_2 composite coating erosion property

Fig. 5 shows erosion test results of coating under different conditions, and Fig. 6 shows coating surface before erosion.It can be seen from Fig. 5, erosion loss of NiCr-TiB_2 composite coating under room temperature and both 30° and 90° is more than that under elevated temperature. Coating under room temperature erosion shows crisp feature (Fig. 7), and surface under 30° erosion shows large quantity of slight crisp cracks. Many plastic rolled protruding crescent lips occur along erosion direction of fly ash particle, after erosion continues, such rolled crescent lips will have crisp collapse. Main damage mechanism of coating is chipping and soyabean residue shaped crisp collapse. Surface of NiCr-TiB_2 composite coating under room temperature and 90°erosion is full of erosion pits, and these damages don't have direction under 30° erosion. Serious loss under 90° erosion is mainly caused by knocking peeling of large flat particle (Fig. 8). According to Suh's [5] delamination wearing theory, under continuous impact load function of abrasive grain, erosion wear process of material can be regarded as generation, growth, expansion, breakage of material sub-surface slight crack, which form stripe abrasive dust and removes from the matrix.

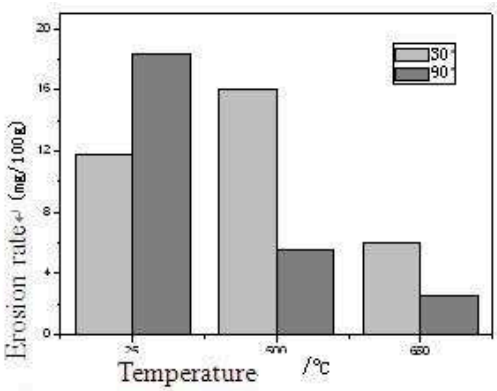

Fig. 5 Erosion results of NiCr-TiB_2 coating under different attack angles and temperatures

Fig.6 Surface of composite coating after mechanic grinding without erosion

(a) Erosion surface (b) Magnification of Fig. a

Fig.7 Erosion surface of NiCr-TiB_2 composite coating under 30° incidence at room temperature

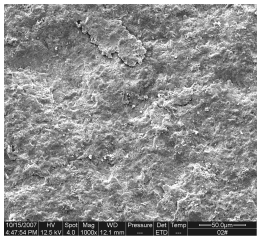

Fig.8 Erosion surface of NiCr-TiB_2 composite coating under 90° incidence at room temperature

Influence of temperature. Fig. 9 is surface morphology ofNiCr-TiB_2 composite coating under 500℃ and 30° erosion.

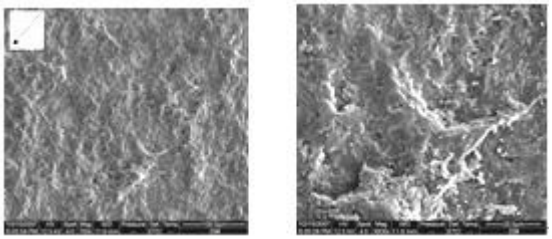

(a) Erosion surface (b) Magnification of Fig. a

Fig.9 Erosion surface of NiCr-TiB_2 composite coating under 500℃ and 30° incidence

Fig. 10 shows surface morphology of NiCr-TiB_2 composite coating under 500℃ and 90° erosion. Under room temperature and 90° erosion, NiCr-TiB_2 composite coating shows feature of crisp collapse of large material, after 500℃ and 90° erosion, indentation of surface is small, and is relatively shallow.

It can be seen from Fig. 11, surface of NiCr-TiB_2 composite coating after 650℃ erosion has very small damage and less material loss. Bitter, etc [6, 7] have two explanation on this. One party considers under elevated temperature material surface forms oxide film, and formation of oxide film improves erosion wear resistance of material; another party considers, with increase of temperature, plasticity of material increases, and wearing resistance adds.

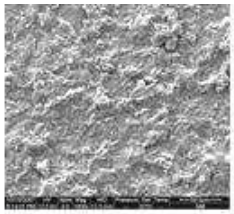

Fig. 10 Surface morphology of NiCr-TiB_2 composite coating under 500℃ and 90° erosion

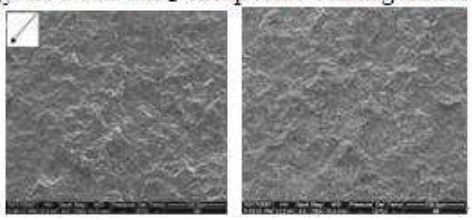

(a) 30° erosion (b) 90° erosion

Fig.11 Surface Morphology of NiCr-TiB_2 composite coating surface under 650℃ and different-angle erosion

Erosion property of 45CT coating

45CT coating is commercial coating material that is widely used in antisepsis and erosion of coal powder boiler pipe, and its erosion rate in test of the research is the highest. Fig. 12 is erosion surface of 45CT coating. Furrow, crack and chipping pit of coating surface caused by erosion particle can be observed under small amplification factor, and this indicates coating material loss is serious. 45CT coating is crisp, surface under 90° erosion finds large quantity of crisp exfoliating, and erosion surface has serious impact by particle.

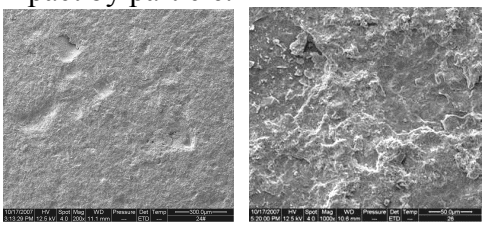

(a) Under room temperature 30° erosion (b) Under 500℃ and 90° erosion

Fig. 12 Erosion Damage surface of 45CT coating

4 Conclusions

Erosion resistance of electric arc spraying TiB_2 particle reinforced composite coating is better than that of 45CT coating, under various erosion conditions, erosion resistance of NiCr-TiB_2 coating is the best. Under elevated temperature, tenacity of coating increases, and whether combination firmness of ceramic phase and metal adhesion phase is main cause that influences improvement of its elevated temperature erosion wear resistance.Coating with same metal adhesion phase matrix, hardness and porosity of coating, distribution of TiB_2 matrix ceramic phase and combination property with metal adhesion phase decide erosion property of MMC coating.

References

[1] P. Kulu and J. Hailing. Recycled Hard Metal-Base Wear-Resistant Composite Coatings. Journal of Thermal Spray Technology. 1998, 7 (2): 173-178

[2] Deng Shijun. Hot Painting High Performance Ceramic Coating. Material Protection. 1999, 32 (1): 31

[3] D. W. McKee. The Oxidation of Dispersed Refractory Metal Compounds and Their Behavior As Carbon Oxidation Catalysts. Carbon. 1986, 245 (3): 331-336

[4] Qu Jingxin, Wang Honghong. Surface Engineering Manual. Beijing: Chemical Industrial Press. 1998: 589

[5] A. V. Levy. Solid Particles Erosion and Erosion-Corrosion of Materials. Ohio: ASM International. 1995: 73-170

[6] Jiang Jianmin, Fu Binyou, He Dingyong, etc. Relation between Hardness and Wearing Resistance of electric arc spraying coating. The Ninth International Hot Painting Seminar. Beijing. 2006

[7] S. Economou, M.De Bonte, J. P. Celis, et al. Tribological Behaviour of TiC/TaC Reinforced Cermet Plasma Sprayed Coatings Tested Againt Sapphire. Wear.1995, 185 (1-2): 93-110.

[8] M. Mohanty and R. W. Smith. Sliding Wear Behavior of Thermally Sprayed Cr_3C_2/NiCr Wear Resistant Coating. Wear. 1996, 198 (1-2): 251-266

[9] Xu Runsheng. Research and Application of High Speed Flame Painting Fe-15Al/45 Cr_3C_2 Composite Coating. Doctoral Dissertation of Armored Engineering Institute. 2005: 90-110

[10] C. C. Degnan and P. H. Shipway. A Comparison of the Reciprocating Sliding Wear Behaviour of Steel Based Metal Matrix Composites Processed from Self-propagating High-temperature Synthesised Fe-TiC and Fe-TiB2 Masteralloys. Wear. 2002, 252 (9-10): 832-841

Advanced Materials Research Vols. 989-994 (2014) pp 276-279
© (2014) Trans Tech Publications, Switzerland
doi:10.4028/www.scientific.net/AMR.989-994.276

The Application of New Material in Industrial Design

Lili Wang[1, a *], Tongtong Xie[1, b] and Yujie Liu[1, c]

[1]School of Mechanical Engineering, Shenyang University, Shenyang, Liaoning Province, China

[a]1873666706@qq.com, [b]1052588325@qq.com, [c]2035950162@qq.com

Keywords: Industrial design, Gray theory, New material

Abstract. Material is the carrier of all industrial design, which is inseparable with. Material is the material basis for human survival and development and new materials is a foundation for future world. With the development of science and technology and rapidly changing times, people have developed more new material on the basis of traditional materials. Based on gray theory of new materials evaluation system, the paper made an analysis and research on a representative of the new materials.

Introduction

Industrial design is a integrated product of technology, art and economic with the development of high civilization. International Council of societies of industrial design made a definition to industrial design that under "the mass produced products", with training, technology, knowledge, experience, and visual feeling of the materials, structures, patterns, color, surface processing, as well as decorated with new quality and qualifications, above all are called industrial design. Industrial design can be divided into two areas of generalized and narrow. Generalized industrial design includes industrial product design, visual communication design and environmental art design, and so on. Narrow meaning industrial design refers to industrial product design as the main research content of the system design[1].

New Materials and Modeling Design of Product

The relationship between new materials and product design is mutual stimulation and promote each other. The emergence of new materials provides a wide design possibility for product design and product design technology is boosting the material development [2].

In the trend of further electronic product, integration, miniaturization, the use of new materials has the potential possibility to break through the traditional structures, and might even lead to a revolution of materials and technology, and to generate a new product designs style. Different materials have different styling potential possibility, as well as visual, tactile feeling contrast with, imagination and reality, fusion of hard and soft, the creative combination of materials and processes, greatly expanding the expressive power of traditional materials.

Adapted to the function at the same time, new material should have also good tactile textures and better interoperability. Through the use of new materials, the design should be given the product a new maximum glamour [3]. For designers, they should be concerned about modeling design of product at the same time, research on physical, chemical characteristics and properties of the materials, in order to better achieve the product functional and emotional function.

The Classification New Material

Material can be classified from the structure, composition, function and application fields, such as a variety of classified angle. The article made a main study to structural materials and functional materials.

New Modeling Structure Material. New modeling structure material, have many kinds, such as a new type of metal materials, new high polymer material, new type of composite materials, a new type of glass material and so on. Some new materials were introduced here.

New Metal Material. At room temperature, the strength of metal plastic is similar to the ultra-high-strength of aluminum-magnesium alloy. Metal plastic have performance of surplus plastic in boiling water, and low temperature ductility and good wear resistance, and corrosion resistance. With a lower than boiling water temperature of the glass transition temperature, metal material can be formed, such as tensile, compression, bending, deformations in the water of around 100 degrees centigrade. It looks like a regular cast iron, which luster is dim. It has hardness, wear resistance, high density at room temperature. Metal material has long service life, and easy to recycle, and environment-friendly.

New Glass Material. For example, nanometer diamond glass, is a kind of new glass material which surface is a layer made up of carbon. The material is hard, crystal clear like a mirror and very metallic.

New-type Ceramic Material. Foamed ceramic material is a shape resembling a porous foam ceramics. This high-tech ceramic has a three dimensional-connected duct, while the shape, whole size, permeability, surface area and chemical properties can be suitably adjusted. As a new type of inorganic non-metallic filter materials, ceramic foam have many advantages such as light weight, high strength, high temperature resistance, corrosion resistance and simple regeneration , long service life and good filtration and adsorption properties and so on. It has properties of simple operation, energy savings, low cost, and filter effects. Ceramic foam can be widely used in metallurgy, chemical industry, light industry, food, environmental protection, energy conservation and other areas [4].

New Type Function Material. New type functional materials is a kind of high and new type material that has special function of electric, magnetic, optical, thermal, acoustic, mechanical, chemical, and biological properties and transformation functions, perception of information and energy. It can be achieved, measurement, display, control, and transformation of non-structural material. In addition to information, energy, nanotechnology, biomedical materials, new type function material include high-temperature superconductivity material, magnetic materials, diamond films, and so on. Typical materials have self-healing functionality, high performance nanometer rare earth permanent magnet materials, memory glass, and so on.

Example analysis

Nanometer diamond glass material has physical performance of hard texture, wear resistant, anti-scratch, anti-contamination, light weight, fire resistant, lower expansion and contraction rates. Nanometer diamond glass material has chemical performance of resistant to mild acids, weak base, oxidation.

According to the various properties of the new materials and their application in products, it can be predicted that the material will be suitable for the outer surface of household appliances, such as refrigerators, freezers, microwave ovens. Application of evaluation method of gray theory, the paper made a study to the application in the evaluation.

Building of Evaluation Index to Nanometer Diamond Glass. By analyzing the factors of physical properties, chemical properties, processing characteristics, material appearance, and tactile experience, psychological attributes, and price factors, and environmental factors, the paper established of materials evaluation indicators, as shown in Figure 1.

Evaluation to the Material of Gray Theory. Grey system theory means that the system is order and whole function, although its behavior unclear, the data is complex. The theory takes small sample, dim information, and uncertainty system as the object of study. By analyzing the known information about the generation, development, the theory extracts the valuable information and makes the gray system of the factors from dim to clear, from little to more, and make the correct understanding and effective application to the system [5].

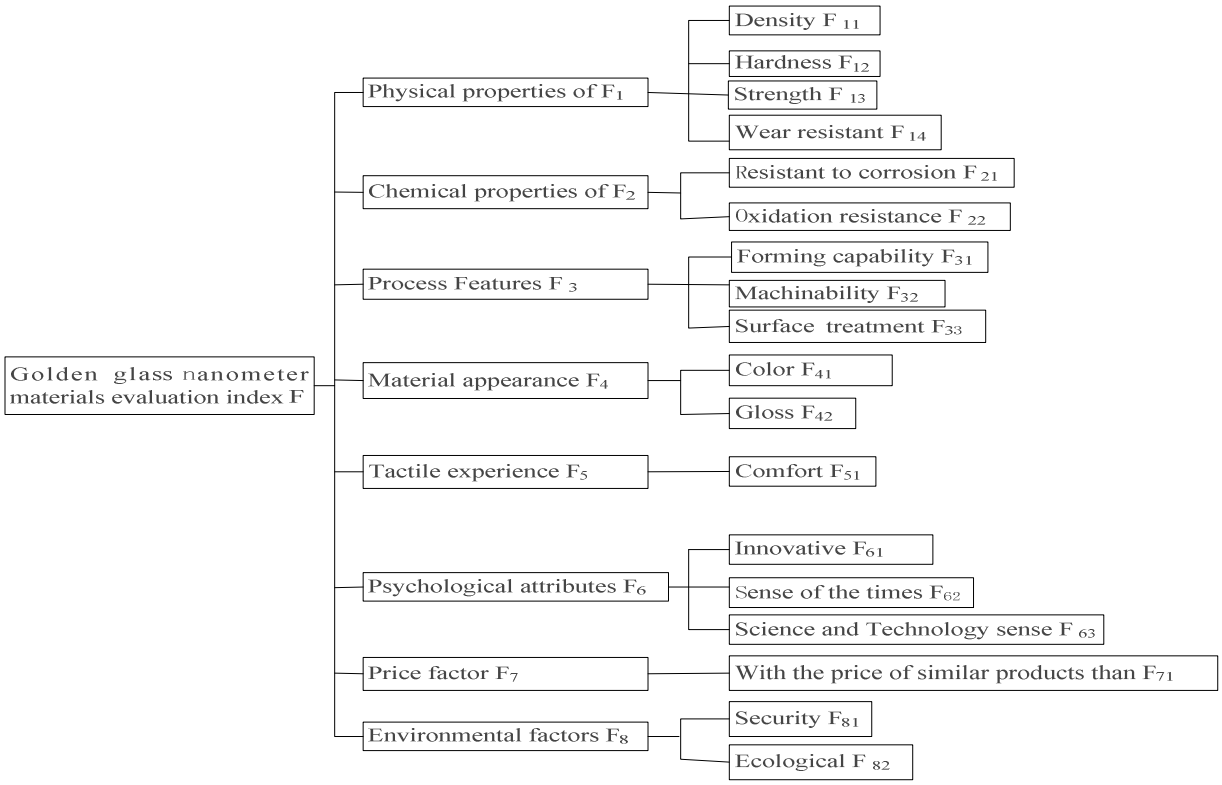

Fig.1 Evaluation index of nanometer diamond glass

The evaluation indicators at different levels are divided into 7 classes. The standards of grading are drawn up with the score of 9, 7, 5, and 3. When the target level is between two adjacent levels, the score of 8, 6, 4 are defined. Invitation to 5 industrial designers is invited to make an evaluation to materials. The steps are as follows:

Identifying weight vector of evaluation indicators.

$W = (0.211,0.087,0.0\ 62,0.188,0\ .137,0.162\ ,0.050,0.1\ 03)$, $W_1 = (0.104,0.325,0.175,0.396)$, $W_2 = (0.405,0.595)$, $W_3 = (0.421,0.367,0.212)$, $W_4 = (0.356,0.644)$, $W_5 = (1)$, $W_6 = (0.335,0.431,0.234)$, $W_7 = (1)$ $W_8 = (0.591,0.409)$.

Evaluators score and establish evaluation sample matrix, as shown in table 1.

Table 1 Materials evaluation sample

	F_{11}	F_{12}	F_{13}	F_{14}	F_{21}	F_{22}	F_{31}	F_{32}	F_{33}
E_1	5	8	6	8	6	8	4	4	5
E_2	6	7	7	9	5	7	6	3	4
E_3	6	8	8	9	5	7	4	6	6
E_4	7	8	7	8	6	8	5	4	5
E_5	6	7	6	9	5	7	5	5	6
	F_{41}	F_{42}	F_{51}	F_{61}	F_{62}	F_{63}	F_{71}	F_{81}	F_{82}
E_1	7	9	7	6	7	9	4	6	5
E_2	8	8	8	5	6	8	3	8	4
E_3	8	8	6	7	6	7	3	7	6
E_4	7	9	7	7	7	9	4	8	6
E_5	6	9	7	6	5	8	4	7	5

Determine the gray class.

Set up “excellent, good, medium, poor”4 evaluation level in class. Corresponding gray number and whitening weight function is: the first gray class is “excellent”(e=1), gray number $\otimes_1 = [9,\infty]$,whitening weight function f_1; the second gray class is “good” (e=2), gray number $\otimes_2 = [0,7,14]$, whitening weight function f_2; the third gray class is “medium” (e=3), gray

number $\otimes_3 = [0,5,10]$, whitening weight function f_3 ; the fourth gray class is "poor" (e=4), gray number $\otimes_4 = [0,3,6]$, whitening weight function f_4.

Calculating the number of gray evaluation.

Evaluation of the material F11 (density) belong to class e evaluation of ash gray evaluation $X_{11e}^{(1)}$:

e=1, $X_{111}^{(1)} = \sum_{k=1}^{5} f_1(d_{11k}^1) = 3.33$; the same way: e=2, $X_{112}^{(1)} = 4.286$; e=3, $X_{113}^{(1)} = 4$; e=4, $X_{114}^{(1)} = 0.333$.

For indicators F_{11}, overall gray evaluation factor for: $X_{11}^{(1)} = X_{111}^{(1)} + X_{112}^{(1)} + X_{113}^{(1)} + X_{114}^{(1)} = 11.952$.

Vector and matrix of gray evaluation.

On the indicators F_{11}, in the first paragraph that the e evaluation of gray class of gray for evaluation $r_{11e}^{(1)}$:

$e=1$, $r_{111}^{(1)} = \frac{X_{111}^{(1)}}{X_{11}^{(1)}} = \frac{3.333}{11.952} = 0.297$; the same way: $e=2$, $r_{112}^{(1)} = 0.359$; $e=3$, $r_{113}^{(1)} = 0.335$; $e=4$, $r_{114}^{(1)} = 0.028$.

Evaluation indicators F_{11} for the gray of gray class evaluation vector:

$r_{11}^{(1)} = \left(r_{111}^{(1)}, r_{112}^{(1)}, r_{113}^{(1)}, r_{114}^{(1)}\right) = (0.279,0.359,0.335,0.028)$, the same way: $r_{12}^{(1)}$, $r_{13}^{(1)}$, $r_{14}^{(1)}$, $r_{21}^{(1)}$, $r_{22}^{(1)} \ldots r_{81}^{(1)}$, $r_{82}^{(1)}$, get gray evaluation matrix $R_i^{(1)}$.

Comprehensive evaluation to F_i:

$B_1^{(1)} = W_1 \bullet R_1^{(1)}$, $B_2^{(1)} = W_2 \bullet R_2^{(1)} \ldots B_8^{(1)} = W_8 \bullet R_8^{(1)}$.

Comprehensive evaluation to F:

$B^{(1)} = W \bullet R^{(1)} = (0.316,0.383,0.373,0.186)$.

Calculating the evaluation value.

$F^{(1)} = B^{(1)} \bullet C^T = (0.316,0.383,0.373,0.186) \times (9,7,5,3)^T = 7.948$.

The figures prove the gray comprehensive evaluation of nanometer diamond glass material value is higher and it should be used in household appliances, such as refrigerators, freezers, microwave ovens and outdoor surfaces.

Conclusion

Product forming design is based on the present and future-oriented design. In the design, selection of materials and material properties analysis become important part of product design. By evaluation of gray theory, the paper made a representative studies to the new material, and verified if the materials are suitable for product design.

References

[1]Yuanlong Gui, Xiangrong Xu, Industrial design materials and process, Beijing Institute of Technology, 2007.9. (In Chinese)

[2] Shuyao Liu, New materials and product design research, in: Hefei University of Technology, Anhui, 2009. (In Chinese)

[3] Jianying Lao, Product design, new material in the Applied Research--Based on ceramic materials, modern furniture design Explore, in: Donghua University, Shanghai, 2012(In Chinese)

[4] Jinfa Huang, Xiaozhen Zhang, Yueming He:China Ceramic, (2008). (In Chinese)

[5] Jianning Su, Heqi Li: Journal of Gansu University of Technology, (2003). (In Chinese)

Advanced Materials Research Vols. 989-994 (2014) pp 280-283
© (2014) Trans Tech Publications, Switzerland
doi:10.4028/www.scientific.net/AMR.989-994.280

Spherical SrCO3 nanopowder synthesized by super gravity method

Zhanshou Yang [1,a], jianhua Jin[2,b],bo Li[1,c],Xinwu Zou Qi[1,d] , Youzhi,Gang[1,e]

[1]Qinghai Institute of Salt Lake, Chinese Academy of Science, Xining, 810008, China

[2]Qinghai university fou nationalities, Xining, 810007, China

[a]email:yangzhanshou@126.com, [b]email:jinjianhua_94@163,

[c]email:1142025301@qq.com,[d]email:409222710.com,[e]email:651992456@qq.com

Keywords: $Sr(OH)_2$,$SrCO_3$, Nanopowder, Super gravity

Abstract: $SrCO_3$ were synthesized using $Sr(OH)_2$ solution and CO2 in super gravity reactor of carbide. It studied $SrCO_3$ powder morphology by the dosage of the appearance agent Ethylene Diamine Tetraacetic Acid(EDTA), material flow and flow velocity and the speed of the rotating packed bed. Samples were characterized using X-ray powder diffraction (XRD) and scanning electron microscope(SEM). These products were found to be orthorhombic SrCO3 nanoparticles with 90–110 nm ranges.

1.Introduction

SrCO3 is an important chemical raw material, be used as additive production of color TV picture tube and as ferrite Production [1-2], small dc motor has been widely used in the production of special glass, dye, paint, fireworks, strontium and other metal strontium metal compounds [3-4]. Nanoscale SrCO3 ultrafine particles, the crystal structure of the surface electronic structure changes, the quantum size effect, small size effect, surface effect and macroscopic quantum effect, made of nanoscale SrCO3 product has high permeability, low loss, high saturation magnetization, such as performance, also used for chemical sensors [5] and [6] of catalyst

1.Introduction

$SrCO_3$ is an important material in the production of glass for color television tubes and ferrite magnets for small DC motors[1-2],and also used in the production of iridescent and special glasses， pigments,driers,paints,pyrotechnics,catalysts and chemical sensors [2].Nanoscale SrCO3 ultrafine particles made change the crystal structure of the surface electronic structure. It own the quantum size effect, small size effect, surface effect and macroscopic quantum effect.Nanoscale SrCO3 manufactured products with high magnetic permeability, low loss, high saturation magnetization intensity and other performance[3].

At present, a variety of methods for the fabrication of $SrCO_3$ such as self-assembled monolayers,ion entrapment method,hydrothermal method, micro-emulsion mediated solvothermal method,homogeneous precipitation by enzyme-catalyzed reaction, biological synthesis using the fungus fusarium oxysporum have been reported[4-5]. Du[6] reported the synthesis of mesoporous SrCO3 spheres by using SrCl2·6H2O, NaOH, and CO2 in1,1,1,3-3-tetramethyl-guanidinium lactate. This work synthesized SrCO3 nanopowder with spherical morphology in super gravity reactor using hydroxide strontium solution and CO2.This method is simple,fast,low-cost and suitable for large-scale production of $SrCO_3$ nanostructures with spherical morphology.

2Experimental

All chemicals used were analytical grade reagents and used as received without further purification. All experiments were conducted under air atmosphere.

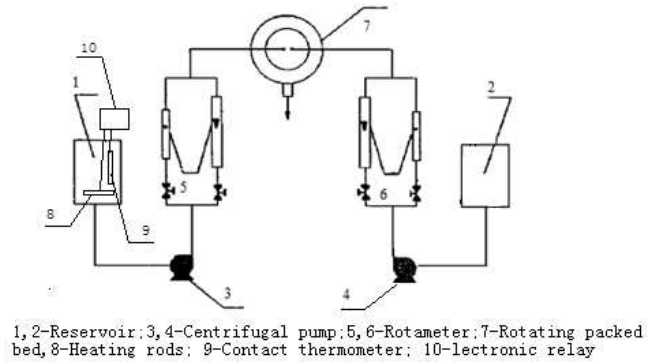

Fig.1 Diagram of experimental device

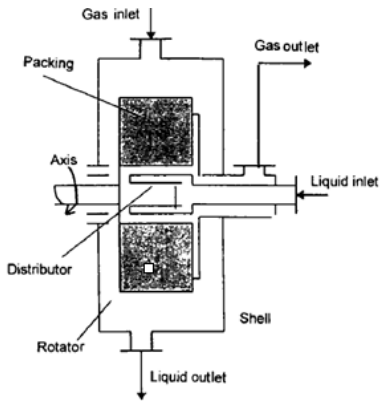

Fig.2 Schematic of rotating packed bed

Fig.1 is super gravity after reforming reactor, increasing the heater, contact thermometers and electronic relay. heating rods heat materials within the reservoir ,contact thermometer testing raw material liquid temperature snd electronic relay to control its temperature. reaction temperature is invariable and can make the uniform concentration of feed solution with no concentration gradient.Contact the temperature of the thermometer is 60 ℃ and add 1000 ml of distilled water in reservoir 1 whit turning on the electronic relay.After a certain time, the temperature of the distilled water achieve 60℃,join $Sr(OH)_2 \cdot 8H_2O$(130g) in the reservoir 1 and stir to dissolve.Solution was added EDTA(59g) after Completely dissolved Sr(OH)2 and stirring dissolved to make Configuration fluid materials.

The Sr (OH) 2 solution made from feeding pump the storage tank 1 through pump 3 by regulating the flow of rotameter 5 to control solution. It enter from figure 2 into the inlet into the rotating packed bed and carbon dioxide enter from the air tank by the pressure reducing valve flow in figure 2 to unreacted carbon dioxide vent discharge from figure 2.

FM instrument were adjusted to control the speed of the rotating packed bed after raw material into the super gravity reactor.Liquid was forced the action of centrifugal force along the packing porosity by the rotor to the rotor outer rim around the inner flow, and during time, raw material liquid are mixing reaction in packing layer. Raction products were made finally influx to the shell in the outer packing to get slurry by super gravity. Slurry was be disposed by centrifugal and washing by anhydrous ethanol.It was characterized using XRD and SEM.

2. Results and discussion

2.1 Reaction principle

Hydroxide strontium solution reacts with CO2 in the water phase and reaction is as follows:

$$Sr(OH)_2+CO_2=SrCO_3+H_2O$$

2.2 The influence of flow rate and rotating speed on nanopowder

Rotameter sets raw material liquid flow rate of 200 ml/l and CO_2 flow rate of 2 l/min adding a certain amount of morphology to react.FM frequency was 13Hz,20Hz, 25Hz, 30Hz, 35Hz and 40Hz,respectively.It corresponds to speed 780 r/min,1080 r/min,1200 r/min,1500 r/min,1800 r/min , 2100 r/min and 2400 r/min, respectively.strontium carbonate slurry was centrifugal separate by under different rotational speed to get samples that was washed by ethanol,and than ultrasonic dispersion for SEM analysis.fig. 3 was shown that from A-1 to A-5 in fig.3 was SEM analysis picture after the different rotational speed of rotating packed bed. It can draw the conclusion that the rotational speed between 780-2100 r/min get spherical strontium carbonate powder material that the granularity and the dispersivity is good. from A-6 to A-7 in fig.3 is SEM analysis of pictures,if rotating speed is more than 2100r/min, spherical particles was broken and reunited, the particle size is not uniform.The rotating bed inner pressure was increased while the rotating bed speed was increasing to lead to inner cavity by the nozzle spray sprinkled on the rotor point. The rotor circumferential velocity was increased by into liquid under the effect of the filler inside the rotor, that it can the liquid turbulent degree increases and the fluid shear force quickly. The centrifugal

force will have just generated in the process of it to the rotor outer spherical powders were shattered by subsequent liquid again with the rotating packed bed cutting of high speed spinning and scattered. Therefore, the speed of the rotating packed bed is less than 2100 r/min in the preparation of strontium carbonate powder materials.

Flow of carbon dioxide has a major impact for the strontium carbonate powder morphology. From B-1 to B-2 in fig.3 get analysis of the SEM images by hydrogen strontium oxide solution flow rate for 200ml/min, the flow rate of the carbon dioxide for 9l/min and rotating packed bed is 1080 r/min,which the spherical particles is broken and reunited, the particle size is not uniform.It do the single factor experiment to the above enumerated different rotation speed after the flow of hydroxide strontium solution for 200ml/min and the flow carbon dioxide for 9l/min. All samples was analyzed by SEM and other SEM images is without insert for limited the article number.SEM images are similar with B-1 and B-2 and to get the spherical strontium carbonate powder particles has been broken.

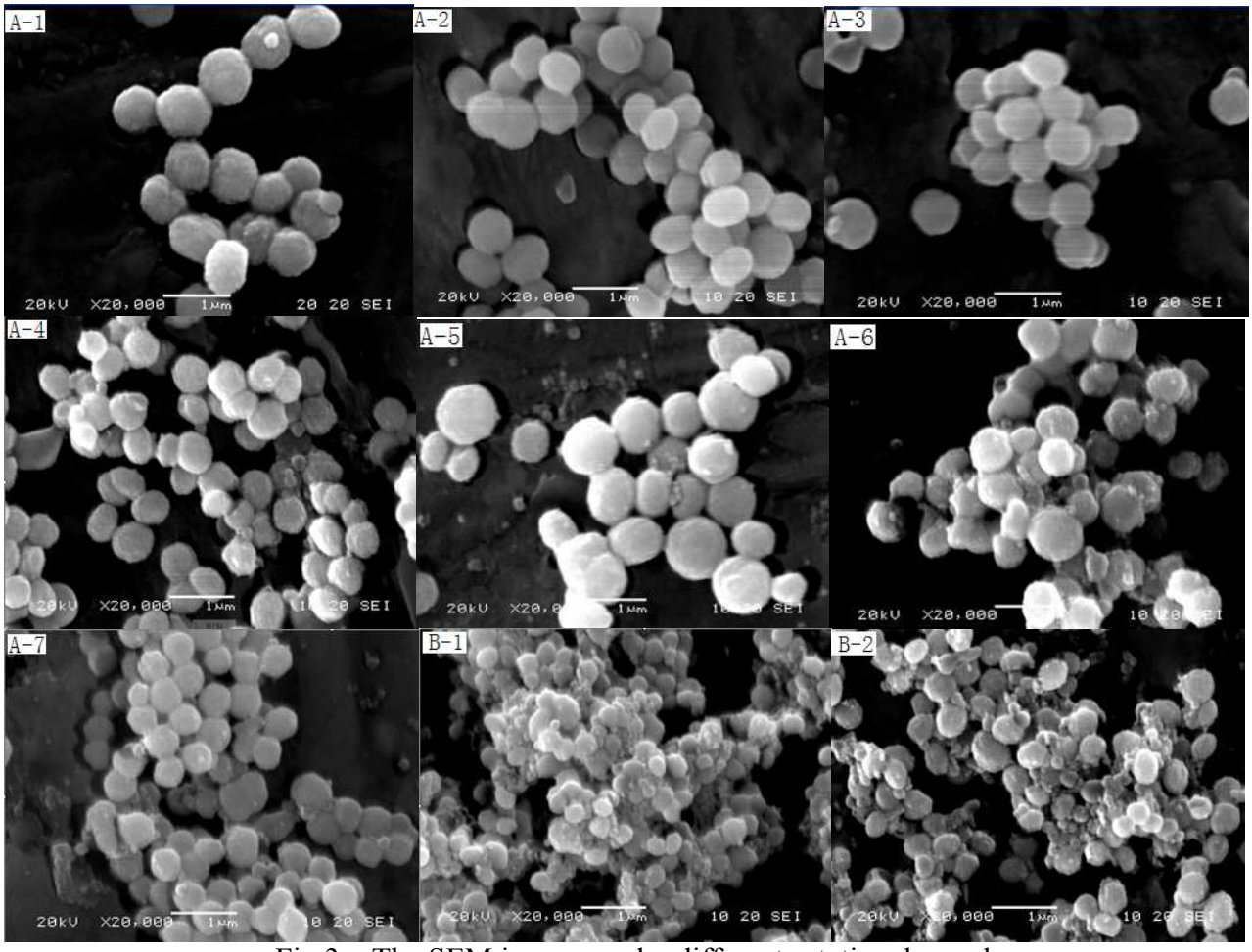

Fig.3 The SEM images under different rotational speed

2.3 The influence of morphology agent for $SrCO_3$ powder

EDTA is an effective for complexant Sr^{2+},EDTA can form the stable Sr-EDTA complexes with Sr^{2+}. Carbon dioxide react with water to form carbonic acid root when bubbled into carbon dioxide, at the same time, Sr^{2+} will release from the Sr-EDTA complexes to form SrCO3. The chemical reaction principle is as follows:

$$Sr^{2+} + EDTA \rightarrow Sr\text{-}EDTA \qquad Sr\text{-}EDTA + CO_3^{2-} \rightarrow SrCO_3 + EDTA$$

The different n_{Sr2+}/n_{EDTA} molar ratio was synthesized by hydroxide strontium solution flow rate of 200ml/l, CO2 flow rate of 2l/min and the speed of 1500 r/min to choose the mole ratio of 0.25 and 0.5 for experiments,respectively.EDTA had a greater influence on the morphology of strontium carbonate. Mole ratio was 0.25 by SEM image contrast synthetic powder morphology which was no rules. Mole ratio was 0.5 to obtain spherical nanometer strontium carbonate powder materials.

EDTA control the release rate of Sr^{2+} to contribute to separation the nucleation and growth of two phase.Mole ratio is small, which can not effectively control the release rate of $Sr2^{+}$ to lead to without separation nucleation and growth.

2.4 The XRD analysis of the sample

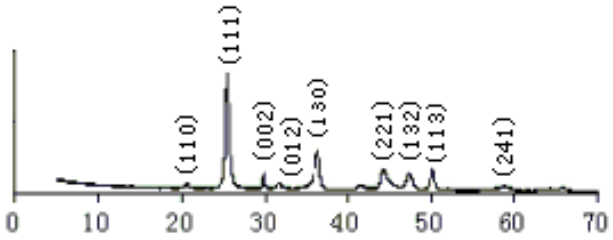

Fig.4 XRD patterns of $SrCO_3$

Typical XRD patterns of the as synthesized $SrCO_3$ nanopowder are shown in Fig.4,which is n_{Sr2+}/n_{EDTA} value equal to 0.5, the rotating speed of 1500 r/min, flow rate of 200 ml/l $SrCO_3$ solution and CO2 flow rate of 2l/min.All diffraction peaks were identified to be orthorhombic $SrCO_3$-compared to the JCPDS No. 05-0418(a=5.1039A，b=8.4022A,c=6.0210A,$\alpha=\beta=\gamma=90^{o}$). Slightly broadened diffraction peaks with 2θ(°) of 20.34, 25.39, 29.63, 31.75, 36.52, 44.47, 47.18, 50.08 and 58.63 were readily indexed as the(110), (111), (002), (012), (130), (221), (132), (113)and(241).

3 Conclusion

Spherical $SrCO_3$ nanopowder were successfully synthesized by the super gravity reactor.Raw materials is the $Sr(OH)_2$, CO2 and EDTA.For the best reaction conditions is that hydroxide of strontium solution temperature was 60℃ and the flow rate was 200 ml/min, joining n_{Sr2+}/ n_{EDTA} is equal to 0.5,the flow rate of CO_2 was 2l/min, the speed of the rotating packed bed was 1500 r/min. Samples were characterized using XRD and(SEM). These products were found to be orthorhombic SrCO3 nanoparticles with 90–110 nm ranges.

References

[1]Shenzhong Li, HuiZhang,etal. Hydrothermal synthesis of flower-like $SrCO_3$ nanostructures, Materials Letters 59(2005)420–422.

[2]Ming-Guo Ma, Ying-Jie Zhu, Microwave synthesis of SrCO3 one-dimensional nanostructures assembled from nanocrystals using ethylenediamine additive,Materials Letters 62(2008)2512 – 2515.

[3]Titipun Thongtem, Narongrit Tipcompor,etal.Characterization of SrCO3 and BaCO3 nanoparticles synthesized by sonochemical method,Materials Letters 64 (2010)510-512.

[4]George Owusu,ohn E.Litz,Water leaching of SrS and precipitation of SrCO3 using carbon dioxide as the precipitating agent,Hydrometallurgy 57(2000) 23–29.

[5]Lishuo Li,Rongyi Lin,Crystallization control of SrCO3 nanostructure in imidazolium-based temperature ionic liquids,Materials Research Bulletin 47(2012)3100–3106.

[6]Mohammad Amin Alavi,Ali Morsali, etal.Syntheses and characterization of Sr(OH)2 and SrCO3 nanostructures by ultrasonic method,Ultrasonics Sonochemistry 17(2010)132-138.

Advanced Materials Research Vols. 989-994 (2014) pp 284-287
© (2014) Trans Tech Publications, Switzerland
doi:10.4028/www.scientific.net/AMR.989-994.284

Synthesis of a novel donor unit for organic light-emitting materials: 10-octyl-3,7-di(thiophen-2-yl)-10H-phenothiazine

TANG Zebiao[1,a], SUN Xiaoxia[1,b*] MIAO Leping[1,c], SHEN Huayin[1,d]

[1]Jiangxi Key Laboratory of Organic Chemistry, Jiangxi Science and Technology Normal University, Nanchang 330013, People's Republic of China

[a]tangzebiao88@163.com; [b]sunxiaoxia77@126.com; [c]miaoleping@163.com; [d]shenhuayin49565880@163.com

Keywords: donor unit; organic molecule; light-emitting material

Abstract. A novel electron donor unit based on phenothiazine has been designed and constructed. The target compound 10-octyl-3,7-di(thiophen-2-yl)-10H-phenothiazine was easily synthesized in high yields with a milder and efficient route via the Suzuki coupling reaction. Optical spectra show that, from the solution to the solid state, both the absorption and fluorescence spectra of the target compound are small blue-shifted. Moreover, the fluorescence spectra exhibit the emission maxima of the target compound ranging from 485 nm to 496 nm, which belongs to blue-green light region. As expected, the target compound should be a promising donor to construct D-A type materials for applications in organic light-emitting diodes (OLEDs).

Introduction

The D-A type molecules have attracted much academic and technological research attention during the past decade because of their great potential applications as photoactive materials in molecular electronics, such as biochemical fluorescent technology,[1] electrogenerated chemiluminescence,[2] organic light emitting diodes (OLEDs),[3] and photovoltaic cells.[4] Compared to other materials, the donor-acceptor materials have an advantage on their physical properties easily being tuned over a wide range by appropriate chemical modification to the structures of donors or acceptors.[5] Recently, Donor-acceptor (D-A) molecules are of great interest as light-emitting and electroluminescent multifunctional materials for organic light-emitting diodes (OLEDs).[6] To make a improvement of the property of OLEDs, the feature of emissive materials we desired should be highly capable of accepting both electrons and holes while exhibiting high luminescence quantum yield.[7] That's to say, we should explore a new molecular design approach to combine distinct electron-donating and electron-accepting units into a suitable emissive D-A molecule to improve functions of OLEDs. A plenty of carbazole, triarylamine and their derivatives have been extensively studied as electron donors in emissive materials in OLEDs.[8] Although triarylamine and carbazole designed as a donor for many D-A molecules have been explored in OLEDs, phenothiazine and phenoxazine are potentially better electron donors , due to their 0.7 eV lower ionization potentials and more stable radical cations.[9] These results motivate us to design new donors based on phenothiazine and its derivatives for D-A type materials in OLEDs.

Herein, we design and synthesize a novel donor based on phenothiazine to construct D-A type molecules through a Suzuki reaction, The optical properties in solution and in the state were characterized by means of UV-vis and fluorescence spectroscopy, which exhibit that 10-octyl-3,7-di(thiophen-2-yl)-10H-phenothiazine should be promising candidates for light-emitting diodes because of its relatively good electronic and optical properties.

Experimental Section

Characterization: ^{1}H NMR and ^{13}C NMR spectra were collected on a Bruker AM-400WB spectrometer in chloroform-d as solvent and tetramethylsilane (TMS) as the internal standard. The mass spectra were obtained by using a Bruker Daltonics Autoflex II TOF system. FT-IR spectra were

recorded using a Bruker Vertex 70 FT-IR spectrometer with samples in KBr pellets. Materials: Diethyl ether and tetrahydrofuran (THF) were dried over sodium benzophenone and distilled under argon atmosphere before use. $CHCl_3$ and DMF were dried over CaH_2 and then distilled under nitrogen atmosphere and deoxygenated by purging with nitrogen for 30 min before use in monomer synthesis. Films were easily formed by spin coating from PMMA-THF solution (1 mg ml-1, quartz substrate). Other chemicals were purchased from Acros and used without further purifications.

2.1 Synthesis of 3,6-dibromo-9-octyl-9H-carbazole 1

3,6-dibromo-9H-carbazole (2.0 g, 6.15 mmol) and 1-bromooctane (1.43 g, 7.38 mmol) were dissolved in DMSO (40 ml) and stirred for 30 min at room temperature, A sodium hydroxide solution (5 ml, v: 50%) was slowly added and then stirred for overnight at room temperature. Then the reaction mixture was poured into water. The precipitate was filtered, repeatedly washed with distilled water and dried under vacuum. The product was obtained as off-white solids without further purifications. Yield: 2.3 g, (86 %). 1H NMR (400 MHz, $CDCl_3$, ppm): δ= 8.08 (s, 2H), 7.48 (d, J=8.8 Hz, 2H), 7.20 (d, J=7.2 Hz, 2H), 4.16 (t, J=6.8 Hz, 2H), 1.74 (d, J=6.4 Hz, 2H), 1.23−1.15 (m, 10H), 0.79 (t, J=6.4 Hz, 3H). 13C NMR (100 MHz, $CDCl_3$): δ 138.00, 127.76, 122.27, 111.03, 109.01, 42.06, 30.69, 28.15, 27.72, 26.11, 21.54, 13.04 (ppm).

2.2 Synthesis of 9-octyl-3,6-di(thiophen-2-yl)-9H-carbazole M1

A mixture of 3,6-dibromo-9-octyl-9H-carbazole (0.50 g, 1.14 mmol), tributyl(thiophen-2-yl)stannane (1.07 g, 2.86 mmol), and $Pd(PPh_3)_2Cl_2$ (0.09 g, 0.13 mmol) in dry toluene (30 ml) was stirred at 115 ℃ under N_2 for 24 h. After cooling the mixture to the room temperature, the solvent was directly removed, The crude product was purified using column chromatography on a silica gel with petroleum ether as the eluent. The product was obtained as white solid. Yield: 0.40 g, (78%). 1H NMR (400 MHz, $CDCl_3$, ppm): δ= 8.27 (s, 2H), 7.66 (d, J=8.0 Hz, 2H), 7.30 (t, J=7.4 Hz, 4H), 7.19 (d, J=5.2 Hz, 2H), 7.04 (s, 2H), 4.22 (t, J=7.0 Hz, 2H), 1.81 (t, J=6.6 Hz, 2H), 1.31−1.15 (m, 10H), 0.80 (m, 3H). 13C NMR (100 MHz, $CDCl_3$): δ 144.54, 139.21, 127.06, 124.70, 123.37, 122.52, 122.03, 120.94, 116.90, 108.15, 42.01, 30.72, 28.30, 27.89, 26.96, 21.55, 13.05 (ppm).

Results and Discussion

3.1 Synthetic Design

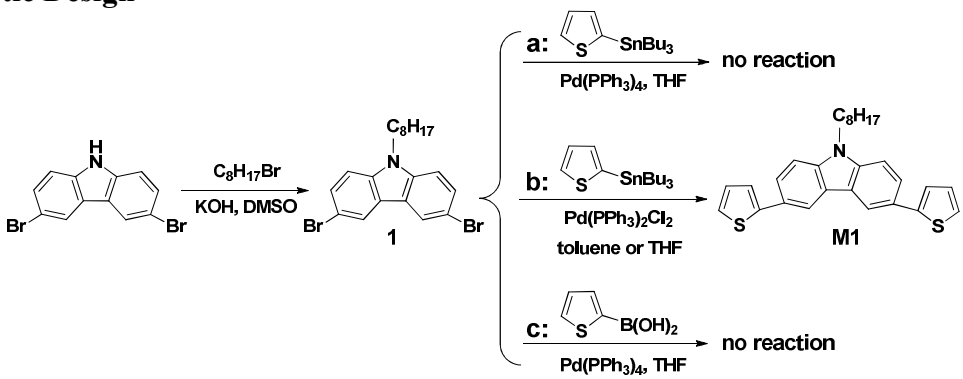

Scheme 1 The synthesis of acceptor monomer **4**

The target compound M1 was synthesized via the Still coupling reaction as illustrated in Scheme 1. First, 3,6-dibromo-9H-carbazole reacted with 1-bromooctane in DMSO under a milder reaction condition and a simple purification process to give **1** in 86% yield. Then, a reaction of 3,6-dibromo-9-octyl-9H-carbazole with 3.0 equiv. of tributyl(thiophen-2-yl)stannane and $Pd(PPh_3)_2Cl_2$ as a catalyst to afford **M1** in 78% yield, which was adopted after a, b and c reaction route selections.

The organic molecule 5,5'-(9,9-dioctyl-9H-fluorene-2,7-diyl)bis(thiophene-2-carbal dehyde) are successfully synthesized over four steps from readily available starting materials, which was freely soluble in most common organic solvents so that it should be a intermediate used to form new

donor-acceptor type oligomers. In view of their relatively good electronic and optical properties, we believe such materials should be promising candidates for light-emitting diodes, field-effect transistors or photocells.

Table1 The synthesis of Compound **3**

Entry	Reagent	solvent	catalyst	Yield (%)
1	Thiophen-2-ylboronic acid	THF	$Pd(PPh_3)_4$	0
2	Tributyl(thiophen-2-yl)stannane	THF	$Pd(PPh_3)_4$	0
3	Tributyl(thiophen-2-yl)stannane	THF	$Pd(PPh_3)_2Cl_2$	48
4	Tributyl(thiophen-2-yl)stannane	toluene	$Pd(PPh_3)_2Cl_2$	78

3.2 Optical properties

The electronic spectra of the compound **M1** were recorded in THF solutions and as PMMA thin films on quartz substrates as shown in Table 2. Fig. 1 shows the UV-vis absorption spectra and fluorescence emission spectra of compound **M1** measured in THF solutions and PMMA thin films. Films were easily formed by spin coating from PMMA-THF solutions (1 mg ml^{-1}, quartz substrate). The absorption spectra (Fig. 1 a) of compound **M1** exhibit two absorption bands in solution, also reveal similar trends in the solid state. Obviously, both of them exhibit the absorption bands at 292-354 nm, which attribute to the localized π-π* transition. In both states, it cannot bring obvious shift of the absorbance band at around 293 nm. However, the absorption band in the solid state exhibit a small blue shift (10 nm), compared to the absorption band at 354 nm in solution. Optical band gaps (Table 2) in solution and solid state were approximated by extrapolation of the low-energy side of the absorption spectra to the baseline.[10] In our expectations, the energy band gaps of compound **M1** is similar, either in solution or in the solid state.

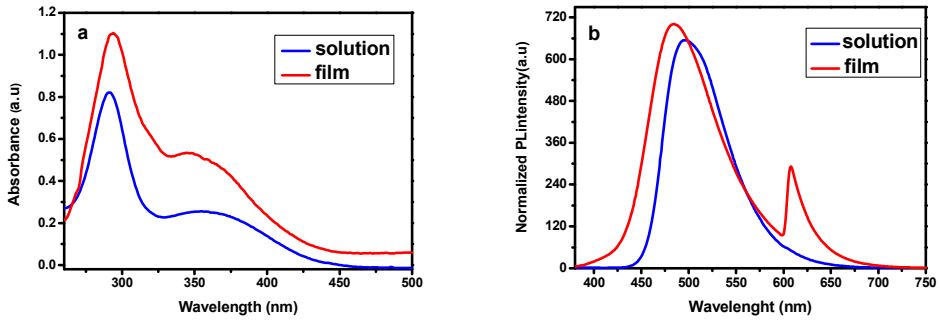

Fig. 1 (a) Absorption and (b) fluorescence spectra of compound **M1** in THF (10^{-5} M) and in PMMA-film.

Table 2 Optical data for compounds **M1**

	Solution				**Film**[d]			
Compds	λ_{abs}[a] /nm	λ_{lum}[b] /nm	Stokes shift/nm	λ_{onset}[a] /nm (Eg[c] /eV)	λ_{abs}[e] /nm	λ_{lum}[b] /nm	Stokes shift/nm	λ_{onset}[a] /nm (Eg[c] /eV)
3	292,354	496	142	434 (2.86)	294, 344	485,608	141	429 (2.89)

[a]Measured in a dilute THF solution (1×10^{-5} M). [b] Excited at the absorbance maxima. [c]Estimated from the onset of absorbance ($E_g=1240/\lambda_{onset}$). [d]Film were drop cast from PMMA-THF solution (1 mg ml^{-1}, quartz substrate). [e]Reported values are the absorbance maxima.

The fluorescence spectra of the compound **M1** have well-resolved vibronic structures in dilute THF solutions and in the solid states, as shown in Fig. 1b. In the solid state, the fluorescence spectra of compound **M1** exhibit an emission maxima at 485 nm with a shoulder at 608 nm, which is relatively small blue-shifted, compared with the emission maxima observed in solution. The phenomenon of blue shifts of the emission maxima is identical to the optical absorption, which could be explained by noncoplanar phenothiazine impacting the interactions between molecules (packing effect) in the solid state. Furthermore, it is obvious that the Stokes shifts of the compound **M1** are large, taking 142 nm in

solution and 141 nm in the solid state. The fluorescence spectra exhibit that the emission maxima of compound 3 from 485 nm to 496 nm belong to blue-green light range. Thus, the target compounds is expected to be a promising blue-green light-emitting material for applications in organic light-emitting diodes (OLEDs).

Conclusions

In summary, we have successfully designed and constructed a novel electron donor unit based on phenothiazine. The target compound10-octyl-3,7-di(thiophen-2-yl)-10H -phenothiazine was synthesized in high yields over three steps with a milder and efficient route via the Suzuki coupling reaction. Optical spectra show that, from the solution to the solid state, both the absorption and fluorescence spectra of the target compound are small blue-shifted. the fluorescence spectra also exhibit the emission maxima of compound **M1** ranging from 485 nm to 496 nm, which belongs to blue-green light range. In our expectations, the target compound should be a promising donor to construct D-A type materials for applications in organic light-emitting diodes. Furthermore, studies on the constructions of distinct donor-acceptor molecules for high-performance photovoltaic materials in organic light-emitting diodes are ongoing in our group, which will be reported in due course.

Acknowledgements

We are grateful for the financial support of the Science Fund of the Technology Office of Jiangxi, China (20122BAB203017 and 20132BBE50024).

Reference

[1]. Jiao, G. S.; Thoresen, L. H.; Burgess, K. *J. Am. Chem. Soc.* 2003, *125*, 14668-14669.
[2]. Lai, R. Y.; Fabrizio, E. F.; Lu, L.; Jenekhe, S. A.; Bard, A. J. *J. Am. Chem. Soc.* 2001, *123*, 9112-9118.
[3]. Li, J. Y.; Liu, D.; Hong, Z. R.; Tong, S. W.; Wang, P. F.; Ma, C. W.; Lengyel, O.; Lee, C. S.; Kwong, H. L.; Lee, S. T. *Chem. Mater.* 2003, *15*, 1486-1490.
[4]. (a) Tang, C. W.; VanSlyke, S. A.; Chen, C. H. *J. Appl. Phy*s. 1989, *65*, 3610-3616. (b)Zhang, X. H.; Chen, B. J.; Lin, X. Q.; Wong, O. Y.; Lee. C. S.; Kwong, H. L.; Lee, S. T.; Wu, S. K. *Chem. Mater.* 2001, *13*, 1565-1569. (c) Li, J. Y.; Liu, D.; Hong, Z. R.; Tong, S. W.; Wang, P. F.; Ma, C. W.; Lengyel, O.; Lee, C. S.; Kwong, H. L.; Lee, S. T. *Chem. Mater.* 2003, *15*, 1486-1490.
[5]. Sun, X. B.; Liu, Y. Q,; Xu, X. J,; Yang, C.H,; Yu, G,; Chen, S. Y,; Zhao, Z.H,; Qiu, W. F,; Li, Y. F,; Zhu, D. B,; *J. Phys. Chem. B,* 2005, *109*, 21.
[6]. (a) Goes, M.; Verhoeven, J. W.; Hofstraat, H.; Brunner, K. *Chem. Phys. Chem* 2003, *4*, 349. (b) Kulkarni, A. P.; Tonzola, C. J.; Babel, A.; Jenekhe, S. A. *Chem. Mater.* 2004, *16*, 4556. (c) Yan, H.; Lee, P.; Armstrong, N. R.; Graham, A.; Evmenenko, G. A.; Dutta, P.; Marks, T. J. *J. Am. Chem. Soc.* 2005, *127*, 3172.
[7]. Kulkarni, A. P.; Tonzola, C. J.; Babel, A.; Jenekhe, S. A. Chem. Mater. 2004, 16, 4556. (b) Shirota, Y. *J. Mater. Chem*. 2005, *15*, 75.
[8]. Chen, C. H.; Tang, C. W. *Appl. Phys. Lett*. 2001, *79*, 3711. (b) Justin Thomas, K. R.; Lin, J. T.; Tao, Y. T.; Ko, C. W. *J. Am. Chem. Soc.* 2001, *123*, 9404. (c) Morin, J. F.; Drolet, N.; Tao, Y.; Leclerc, M. *Chem. Mater*. 2004, *16*, 4619.
[9]. (a) Kong, X.; Kulkarni, A. P.; Jenekhe, S. A. *Macromolecules* 2003, *36*, 8992. (b) Hwang, D. H.; Kim, S. K.; Park, M. J.; Lee, J. H.; Koo, B. W.; Kang, I. N.; Kim, S. H.; Zyung, T. *Chem. Mater*. 2004, *16*, 1298.
[10]. J. Cao, J. W. K amkf and M. D. Cuetis. *Chem. Mater.,* 2003, *15*, 404.

Advanced Materials Research Vols. 989-994 (2014) pp 288-291
© (2014) Trans Tech Publications, Switzerland
doi:10.4028/www.scientific.net/AMR.989-994.288

Current Situation and Latest Development of Intelligent Materials

Guomin LIN[1,a], Fang YUAN[2,b],Yanhua LI [3,c]

[a]Postgraduate Department, Xijing University, Xi'an, 710123,China

[b]Scientific Bureau,Xijing University, Xi'an, 710123,China

[c]Information and Navigation Institute, Air Force Engineering University, Xi'an, 710077,China

[a]email: gmlin@21cn.com, [b]email:yuanfang@163.com, [c]email:liyanhua108@21cn.com

Key words: Intelligent materials; Self diagnosis; Adaptive; Sensor

Abstract. The background and design idea of the intelligent materials is introduced. Three elements of intelligent materials are given. Then based on classifying of intelligent materials, the features and applications of intelligent materials are researched.Principle and the latest applications of typical intelligent materials such as optical fiber, shape memory alloys, shape memory polymers, piezoelectric, magnetostrictive materials, fluid material and polymer colloid are analyzed simplely. The research difficulties and the future research focuses of intelligent material are pointed out.

Introduction of Intelligent Materials

Intelligent material is the fourth generation materials after the natural materials, polymer materials and artificial materials, it is one of the important development directions of the modern high-tech materials.Concept of intelligent materials was proposed first by Japan scientist in 1989. Intelligent material is called as sensitive material, is combined by sensor or sensing elements with traditional materials. Intelligent materials can feeling the stimuli from environmental then analysis, process, judgment and taking certain measures to moderate response.Idea of intelligent material comes from bionics, its goal is to study a "live" material with variety function similar to the biological therefore intelligent materials must have three essential elements follow as perception, drive and control.

Measure of Intelligent Materials

The measure indicator of intelligent material general used of qualitative indicator, it is measured mainly from following aspects: The perception function which can detect and discriminate outside of stimulus strength.The drive function which can response outside changes.It can select and control response according to set of way.Its reaction compared with sensitive timely and appropriate.It can quickly to recovery to original state after external stimulus elimination.

Classification of Intelligent Materials

Intelligent materials can be divided into intelligent material and non-embedded intelligent material accordance the structure. The embedded intelligent material is made by three kinds of raw materials with sensing, driving sensors and processing functions,it is embedded in the substrate material, sensor collecting and detecting the information from the external environment and control processor incentives driven component performs the appropriate action.The non-embedded intelligent material with intelligent features, can change depending on the environment and time.Intelligent material can be divided into metal intelligent materials, inorganic non-metallic intelligent materials and polymeric intelligent materials according to the sources. Intelligent materials can be divided into optical fiber, shape memory alloys, piezoelectronic materials, magnetostrictive materials and electrostrictive materials etc. according to their different functions. According to the composition of structure intelligent materialscan be divided into driven materials, sensitive materials, substrate material and so on[1].

Function of Intelligent Materials

Intelligent materials have the following functions:A.Sensing function when used as a sensor, it is able to perceive the information from outside or their environmental conditions such as load, stress, strain, vibration, thermal, light, electromagnetic, chemical, nuclear radiation intensity and its variation.B.Feedback function when used as a feedback device,it can compare input information with output information of the system by sensing networks and provide the results to control systems timely and accurately.C.Information identification function and accumulation function,it can identify various types from sensing networks and accumulate the information.D.Response function, it has drive function, according to the external environment and internal conditions change, to make an appropriate response in time dynamically, select and control the response according to the setting of set way and take the necessary action.E.Self-diagnosis function,it can self-diagnose a series of issues such as system failures and misjudgments and correct the issues through comparison and analysis the current situation with the past situation of the system.F.Self-recovery function,it can fix some local damage or destruction after an external stimulus eliminated, and can be quickly restored to its original state through self-breeding, self-growth, in-situ composite mechanism.G.Self-adjusting functions,it can adjust its structure and function automatically in a timely and change their status and behavior, according to the changing external environment and conditions, make material system in an optimal way to proper response to external changes.

Application of Intelligent Materials

Intelligent material is a complex material of system, it collects materials, structures, intelligent processing, implementation systems, control systems and sensing systems in one. Intelligent materials mainly used in the following areas.A.Building area[2]. The fiber with "self-healing" function can feel the information from cracks in concrete and steel corrosion and can bond the cracks in concrete or block the corrosion on reinforcing steel bar automatically.Fiber for binding cracks is made of glass-fiber and polypropylene porous hollow fibers, after mixed in concrete, when it excessive flexed in concrete and is ripped, thereby release chemicals to filling and bonded cracks in concrete.Anticorrosion fiber is placed around steel, when the acidity around the steel reaches a certain value, the fiber coating will be dissolved and release some substances from the fibers to prevent the steel in concrete.B.Aircraft manufacturing.Intelligent materials with "adaptive" function can make a flying aircraft when encounter the vortices or gust, in intelligent materials of wing drive deformation and make the wing shape changes, thus eliminating the effect of vortices or gust, to fly aircraft is able to maintain a steady state. Damage assessment and life prediction of aircraft can be self diagnostic monitoring systems, can judge cumulative damage and structural damage for themselves suddenly, according to the aircraft flight experience and injury data forecast the life of aircraft structures,in the case of security,reduces the grounding repair times and routine maintenance costs significantly, increases the economic benefits of commercial aircraft finally.C. Medical field.Intelligent materials and structures can be used manufacturing artificial limbs with a sense response without the motor control, imitate the smooth movement of muscles of the human body, make use of controllable shape recovery force of intelligent materials, grabs the fragile items deftly.Polymeric intelligent materials with "automatically administer drugs" function can administer drugs automatically according to glucose concentration of human blood.When the glucose concentration is too low, polymers would have collapsed into a small ball, insulin is sealed inside the ball; when glucose concentration at the high level the ball will stretch ribbon, the insulin sealed in small ball is released into the blood, so that the body's blood sugar level is always kept at normal level.D.Military field.Nuclear explosive optic fiber sensors and X-ray optic detectors implanted in the skin of aircraft, can real-time monitoring and early warning of enemy threat, therefore can improve the ability to resistant damage of weapons platform. Intelligent materials can also reduce noise in military systems, intelligent materials coated on the submarine can reduce noise for 60dB and submarine detection time is reduced for100 times.

Design Ideas of Intelligent Material

Design ideals of intelligent materials are relative with the following factors: material development history, influence of artificial intelligent computer, intelligent materials manufacturing, software function material, material aspirations, energy delivery, materials with the timeline. Development and design ideas of intelligent materials should start from two different views, one is the bionic technology, another is structures characteristic of the intelligent material itself.A.Bionic technology.Due to the organism has environmental perception and response, it provides a blueprint for intelligent material design. Intelligent is a characteristic of organisms, the environmental perception and response inspire to explore the adaptive of material systems and structures from bio-science, bio-engineering and approximation to multiple functions of the organism.B.Structure feature of intelligent material itself.Intelligent material structure of total regular is found from the structure characteristics of the intelligent material itself, thus synthesis, processing, design of different properties intelligent materials. Mesoscope dimensions structure plays an extremely important role in the development of intelligent materials, it is a size structure from nanometer to micron, such as the people most familiar with the proteins and enzymes, has a very important physiological function, it belongs to the nano-size of structure material.

Typical Intelligent Materials

At present, intelligent material has been widely used, has formed a separate system according to its intelligent functions. Typical intelligent materials mainly include:optical fiber, shape memory alloy,shape memory polymer,piezoelectronic material,magnetostrictive material, electro-rheological material and polymer colloid.A.Optical fibre.It is used in optical fibers made of glass or plastic, made from the principle of total reflection of light transmission. Conduction losses are far below the wires of the light transmission, therefore,it can be applied in long distance information transmission.B.Shape memory alloys[3].It is heated to a critical temperature above for shape memory heat treatment, formed martensite phase after rush cold, then exert a deformation, shape memory alloy is heated to critical temperature above again, makes crystal phase reverse shift, make the cryogenic martensite phase inverse becomes high temperature austenitic phase and recovery to inherent shape before deformation or return to martensite phase through internal elastic energy is released in follow-up cooling.C.Shape memory polymers[4].It is using modern high-molecular theory in physics and polymer synthesis and modification, molecular combinations of common polymer materials acquired and modified polymers of the kind, with characteristics of plastic and rubber. The relationship between polymer deformation and temperature (refer with Fig.1); the stress-strain curve of high elastic deformation(refer with Fig.2).D.Piezoelectronic material[5].It is a material with piezoelectrnoic effect. When a mechanical deformation is exerted on piezoelectronic materials, an electromotive force is produced in its internal, when the voltage is applied, materials produces a mechanical deformation and change size.Piezoelectronic materials includes piezoelectronic crystal, piezoelectronic fiber,piezoelectronic ceramics,piezoelectronic polymers, piezoelectronic composites etc.Piezoelectronic intelligent materials can be rapidly transformed into electrical signals or transforming the electrical signal into a vibration signal[6].E.Magnetostrictive materials.It is a material within the small magnetic domain deflected by external magnetic field and thereby causing material along the direction of the magnetic field orientation contingency stretch.F.Electro rheological materials.It is a suspension system comprised of electrolyte particles with high dielectric constant and low conductivity spread in insulating liquids of low dielectric constant, it can respond and reversible electric field rapidly.G.Aggregate colloid.It is a homogeneous mixture,it contains two different phases substance,dispersed and continuous. Former is made of tiny particles or droplets, 1~100nm in diameter; the latter is a continuous state of liquid.Aggregate colloid is polymers as the main components which is a typical of the intelligent polymer materials.Chemical energy transformed into mechanical energy to each other in aggregate colloid.

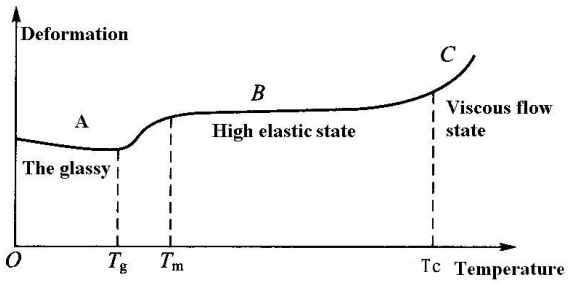

Fig.1. Relationship between polymer deformation and temperature

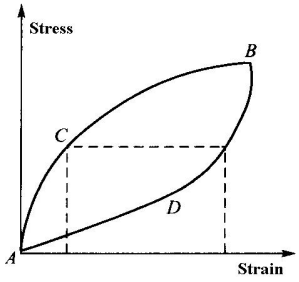

Fig.2. Stress-strain curve of high elastic deformation

Conclusion

Development and widely application of intelligent materials will result in a major revolution in materials science. Intelligent material is an open system that relies on continuous input energy or substance to dynamically adjust the adaptive capacity of outside from the surroundings to maintain its activity similar to organisms, therefore, the primary research difficulty of intelligent materials is energy conversion and storage; another difficulty is that upgrades ability of intelligent materials such as self learning, self judgment and self upgrade. Intelligent materials research focuses on the following aspects future: study of bionics theory on conceptual design of intelligent materials; study of intelligent material intrinsic properties and evaluation system of intelligent quotient; study of dissipative structure theory applied in intelligent materials; principles of complex integration and design theory of intelligent materials; nonlinear theory of integrated intelligent structure; humanoid intelligent control theory.

References

[1] PENG Yangxing,HU Jianming. Principles and Applications of Fiber Grating Sensor [J].Journal of Chongqing Normal University, 2009 (04): 64-68

[2] LI Bing. Development of Shape Memory Alloy Materials [J]. Metal World, 2005 (12): 26-29

[3] ZHANG Guanglei, DU Yanliang. Intelligent Materials and Structural Systems [M], Beijing: Beijing University Press, 2010.8

[4] WANG Kun. Development of Shape Memory Polymer Composites [J]. Materials Review, 2012 (10): 76-69

[5] ZHU Haixia. Vibration Active Control System Based on Piezoelectric Element [J]. Journal of Chongqing Institute of Technology: 2009 (2): 131-135

[6] PEI Xianru, GAO Hairong. Present Situation of Research and Application of Piezoelectric Materials [J]. Anhui Chemical, 2010 (03): 15-18

Advanced Materials Research Vols. 989-994 (2014) pp 292-296
© (2014) Trans Tech Publications, Switzerland
doi:10.4028/www.scientific.net/AMR.989-994.292

Synthesis of a novel D-A type molecule based on carbazole unit for organic light-emitting material applications

TANG Zebiao[1,a], SUN Xiaoxia[1,b*],YAN Hewei[1,c], MIAO Leping[1,d]

[1]Jiangxi Key Laboratory of Organic Chemistry, Jiangxi Science and Technology Normal University, Nanchang 330013, People's Republic of China

[a]tangzebiao88@163.com; [b]sunxiaoxia77@126.com; [c]yanhewei1990@163.com; [d]miaoleping@163.com

Keywords: carbazole unit; donor-acceptor; molecule; organic light-emitting

Abstract. A novel D-A type molecule based on carbazole central core and aldehyde terminal groups has been designed and synthesized. Optical properties of the resulting compounds were examined by means of UV-vis and fluorescence spectroscopies. It shows that, the absorption and fluorescence spectra of M2 are large red-shifted relative to M1 in both states, whereas the absorption maximum and emission maxima of M1 and M2 are small blue-shifted, from solution to the solid state. The fluorescence spectra exhibit that the emission maxima of the compounds which range from 419 nm to 472 nm belong to blue light region. As expected, the target compounds should be a promising pure blue light-emitting material for applications in organic light-emitting diodes (OLEDs).

Introduction

Conjugated organic polymers and molecules have attracted a variety of attention during the past decade due to their potential optoelectronic applications in organic light-emitting diodes (OLEDs), organic field effect transistors (OFETs) and organic photodiodes (OPVs) etc.[1] Organic molecules are of great advantages on their clear molecular structure, fixed molecular weight and higher purity, which receive a significant amount of interest by researchers currently.[2] Especially, those with donor-acceptor (D-A) architectures, play an key role in organic materials leading to desirable semiconductor properties for electrical and optical applications. As a result of their properties easily being tuned over a wide range by appropriate chemical modification to the structures of donors or acceptors, donor-acceptor (D-A) organic molecules could be used as light-emitting materials for organic light-emitting diodes (OLEDs).[3] These materials we desired should be donor-acceptor materials that combine high fluorescence quantum yields with low ionization potential or high electron affinity. Thus, exploring new synthesis and investigation of conjugated D-A molecules are essential to improve the electronic and optoelectronic properties of these materials and turn improvement of the performance of the devices.[4]

Conjugated donor-acceptor molecule systems based on thiophene, carbazole, fluorene, or phenothiazine are among the most promising materials for the development of new generation, highly efficient OLEDs devices.[5]

Carbazole and its derivatives, due to their properties of rigid plane, long conjugation length, good hole transporting properties and charge transporting compounds creating free carriers in the visible region through the photo-carrier generation process, are usually chosen to construct donor-acceptor (D-A) organic molecules used in OLEDs.[6] In the context of these, it affords us a motivation to design new molecules based on carbazolyl groups for OLEDs applications.

In this article, we design and synthesize a novel conjugated organic molecule based on carbazole unit as a donor and aldehyde groups as an acceptor to investigate electronic and optical properties of light-emitting materials in OLEDs. The optical properties in solution and in the state were characterized by means of UV-vis and fluorescence spectroscopies, which exhibit that the target compounds should be promising candidates for organic light-emitting diodes because of their relatively good electronic and optical properties.

2 Experimental Section

Characterization: ^{1}H NMR and ^{13}C NMR spectra were collected on a Bruker AM-400WB spectrometer in chloroform-d as solvent and tetramethylsilane (TMS) as the internal standard. The mass spectra were obtained by using a Bruker Daltonics Autoflex II TOF system. FT-IR spectra were recorded using a Bruker Vertex 70 FT-IR spectrometer with samples in KBr pellets. Materials: Diethyl ether and tetrahydrofuran (THF) were dried over sodium benzophenone and distilled under argon atmosphere before use. $CHCl_3$ and DMF were dried over CaH_2 and then distilled under nitrogen atmosphere and deoxygenated by purging with nitrogen for 30 min before use in monomer synthesis. Other chemicals were purchased from Acros and used without further purification. Films were easily formed by spin coating from PMMA-THF solution (1 mg ml^{-1}, quartz substrate). Other chemicals were purchased from Acros and used without further purifications.

Synthesis of 5,5'-(9-octyl-9H-carbazole-3,6-diyl)bis(thiophene-2-carbaldehyde)(M2)

9-octyl-3,6-di(thiophen-2-yl)-9H-carbazole (0.84g, 1.89 mmol) and DMF (4.0 ml) was dissolved in 1,2-dichloroehane (30 ml) and Phosphorus oxychloride (6 ml) was added dropwise, keeping the reaction temperature below 5 ℃ . After $POCl_3$ added completely, the reaction solution was stirred at reflux for 12h. Then the mixture was poured into a cooled saturated sodium bicarbonate solution, neutralized with odium bicarbonate solution, extracted with dichloromehane and washed with saturated brine. The organic layer separated and dried over anhydrous magnesium sulfite. The crude product was purified using column chromatography with petroleum ether/dichloromethane (11:1, v/v) as the eluent. The product was obtained as yellow solids. Yield: 0.8 g, (84%). 1H NMR (400 MHz, $CDCl_3$, ppm): δ= 9.89 (s, 2H), 8.39 (s, 2H), 7.79 (d, J = 10.1 Hz, 4H), 7.54–7.34 (m, 4H), 4.29 (t, J = 6.6 Hz, 2H), 1.87 (s, 2H), 1.43–1.17 (m, 10H), 0.85 (t, J = 6.2 Hz, 3H). 13C NMR (100 MHz, $CDCl_3$): δ 181.57, 154.67, 140.52, 136.80, 123.97, 122.16, 117.65, 108.74, 42.50, 30.73, 29.90, 28.26, 26.23, 21.56, 13.03 (ppm).

3 Results and Discussion

3.1 Synthetic Design

In our previous report, compound M1 has been synthesized in an acceptable yield via the Still coupling reaction after multiple reaction route selections. In this article, we construct the target compound M2 by using compound M1 as the raw material via the Vilsmeier-Haack reaction, as illustrated in Scheme 1. Firstly, a reaction of 3,6-dibromo-9H-carbazole with 1-bromooctane in DMSO under a mild reaction condition and a simple purification process gave 1 in 86% yield. Then, 3,6-dibromo-9-octyl-9H-carbazole and 2.5 equiv. of tributyl(thiophen-2-yl)stannane reacted in toluene used $Pd(PPh_3)_2Cl_2$ as a catalyst to afford M1 in a yield of 78% . In the last step, DMF and $POCl_3$ were used to give the target compound M2 in 84%yield.

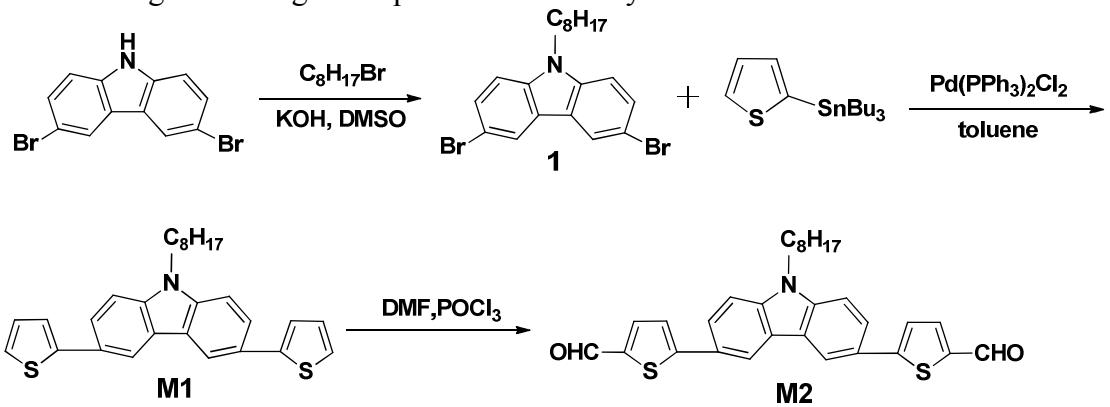

Scheme 1 Synthesis of compound M1 and M2

The target compound M2 5,5'-(9-octyl-9H-carbazole-3,6-diyl)bis(thiophene-2- carbaldehyde) was successfully synthesized from readily available starting materials, which was freely soluble in most

common organic solvents so that it could be a promising candidate for organic donor-acceptor type materials, so as to explore their electronic and optical properties for light-emitting diodes.

3.2 Optical properties

The electronic spectra of compounds M1 and M2 were recorded in THF solutions and as PMMA thin films on quartz substrates as shown in Table 1. Fig.1 and Fig.2 show the UV-vis absorption spectra and fluorescence emission spectra of M1 and M2 measured in THF solutions and PMMA thin films. Films were easily formed by spin coating from PMMA-THF solutions (1 mg ml^{-1}, quartz substrate). The absorption spectra (Fig.1a) of M1 exhibit three absorption bands in both solution and solid state, the absorption band ranges from 257 nm to 313 nm is attributed to the localized π-π* transition. However, the absorption spectra (Fig.2a) of M2 exhibit only one obvious absorption band in both states, the absorption band at 393-395 nm is assigned to an intramolecular charge transfer (ICT) between the aromatic ring donor part and the acceptor end groups.[7] Compared with M1 in solution and in the solid state, respectively, M2 exhibits a large bathochromic shift (81 nm and 82 nm) of the absorbance maximum (Fig.1a, Fig.2a), which is resulted from aldehyde groups taking part in the conjugation as an electron-withdrawing unit and the great stabilization of the LUMO by the electron-withdrawing groups.[8] Furthermore, both M1 and M2, from the solution to the solid state, it cannot bring large shift of the absorbance band. Optical band gaps (Table 1) in solution and solid state were approximated by extrapolation of the low-energy side of the absorption spectra to the baseline.[9] In our expectations, the energy band gaps of compounds decrease in the order, M1>M2, either in solution and in the solid state.

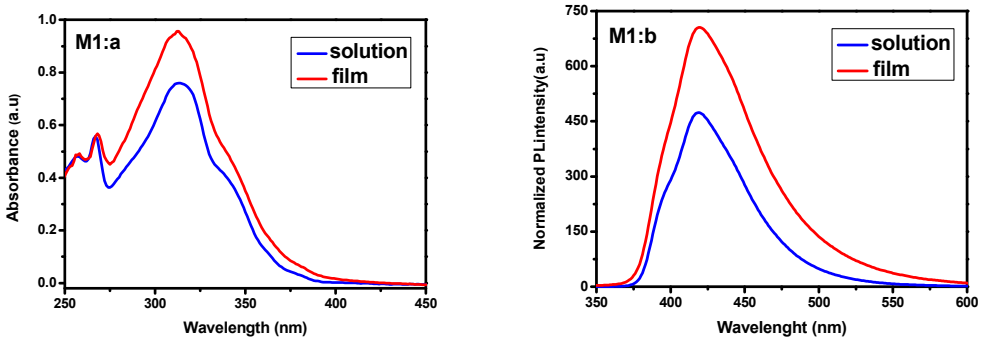

Fig. 1 (a) Absorption and (b) fluorescence spectra of M1 in THF (10-5 M) and in PMMA film.

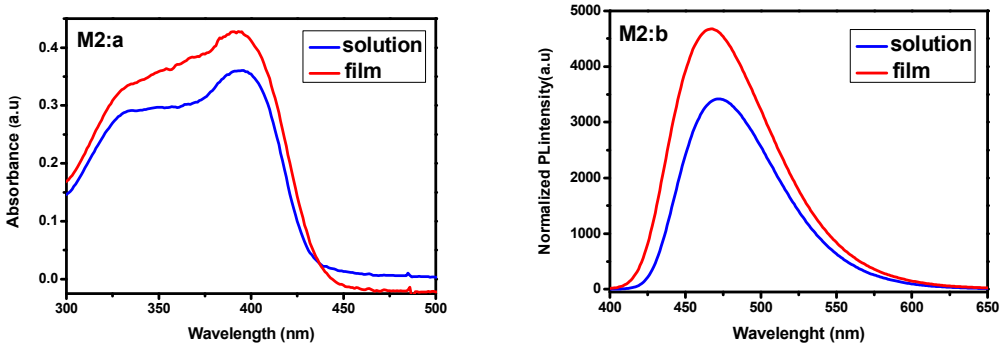

Fig. 2 (a) Absorption and (b) fluorescence spectra of M2 in THF (10^{-5} M) and in PMMA film.

The fluorescence spectra of the compounds have well-resolved vibronic structures in dilute THF solutions, as shown in Fig.1b and Fig.2b. The fluorescence spectra of M2 exhibit an emission maxima at 472 nm, which is relatively large than that of M1. Meanwhile, a bathochromic shift (48 nm) of emission maxima of M2 is more clearly observed in the solid state (Fig.1b and Fig.2b). The phenomenon of bathochromic shifts of the emission maxima is identical to the optical absorption in both states. It is easily obtained that the Stokes shifts of the compounds are relatively large, ranging

from 77 to 106 nm in solution and from 74 to 105 nm in the solid state. Not only M2 has the smallest Stokes shift and M1 has the largest one, either in solution or in the solid state, but also the Stokes shifts of both M1 and M2 in solution are larger than that in the solid state. The reason could be that the dipole moment of M2 in the solid state is much smaller than that of M1 in solution, and the emitting state of the later would be more stabilized by the ICT.10 From the solution to the solid state, the absorption and fluorescence spectra of the compounds are close and some are even blue-shifted (Table 1), which could be explained by the fact that the octyl side chain in the 9-position of the carbazole rings is not optimum charge transport in the solid state.11 The fluorescence spectra exhibit that the emission maxima of M1 and M2 from 419 nm to 472 nm belongs to blue light region. Thus, the target compounds are expected to be promising pure blue light-emitting materials for applications in organic light-emitting diodes (OLEDs).

Table 1 Optical data for compounds 3 and 4

Compds	**Solution**				**Film**[d]			
	Stokes λ_{onset}[a] /nm				Stokes λ_{onset}[a]/nm			
	λ_{abs}[a] /nm	λ_{lum}[b] /nm	shift /nm	(Eg[c] /eV)	λ_{abs}[e]/nm	λ_{lum}[b]/nm	shift /nm	(Eg[c]/eV)
M1	257,267, 313	419	106	375 (3.31)	258,268, 312	419	105	375 (3.31)
M2	395	472	77	432 (2.87)	393	467	437	437 (2.84)

a Measured in a dilute THF solution (1×10-5 M). b Excited at the absorbance maxima. cEstimated from the onset of absorbance (Eg = 1240/λonset). d Film were drop cast from PMMA-THF solution (1 mg ml-1, quartz substrate). e Reported values are the absorbance maxima.

4. Conclusions

In summary, we have successfully designed and constructed a novel D-A type molecule based on carbazole central core as an electron donor and aldehyde terminal groups as an electron acceptor. The target compound M2 5,5'-(9-octyl-9H-Carbazole- 3,6-diyl)bis(thiophene-2-carbaldehyde) was synthesized via the Vilsmeier-Haack reaction from readily available starting materials. Optical properties of the resulting compounds were examined by means of UV-vis and fluorescence spectroscopies. It shows that, the absorption and fluorescence spectra of M2 are large red-shifted relative to M1 in both states, whereas the absorption maximum and emission maxima of M1 and M2 are small blue-shifted, from solution to the solid state. The fluorescence spectra exhibit that the emission maxima of the compounds which range from 419 nm to 472 nm belong to blue light region. As expected, the target compounds should be a promising pure blue light-emitting material for applications in organic light-emitting diodes (OLEDs) and further experiments on electroluminescent properties and film morphology are in progress.

Acknowledgements

We are grateful for the financial support of the Science Fund of the Technology Office of Jiangxi, China (20122BAB203017 and 20132BBE50024).

Reference

[1]. Zen, A.; Pingel, P.; Neher, D.; Grenzer, J.; Zhuang, W.; Rabe, J.P.; Bilge, A.; Nehls, B. F.; Farrell, T.; Scherf, U.; Grozema, F. C.; Sibbeles, L. D. A. *Chem. Mater*. **2007**, *19*, 1267.
[2]. (a) Li, Y. W.; Guo, Q.; Li, Z. F.; Pei, J. N.; Tian, W. J. *Energy Environ. Sci*. **2010**, *3*, 1427. (b) Roquet, S.; Cravino, A.; Leriche, P.; Alévêque, O.; Frère, P.; Roncali, J. *J. Am. Chem. Soc.* **2006**, *128*, 3459. (c) Ripaud, E.; Rousseau, T.; Leriche, P.; Roncali, J. *Adv. Energy Mater.* **2011**, *1*, 540.
[3]. (a) Goes, M.; Verhoeven, J. W.; Hofstraat, H.; Brunner, K. *Chem. Phys. Chem* **2003**, *4*, 349. (b) Yan, H.; Lee, P.; Armstrong, N. R.; Graham, A.; Evmenenko, G. A.; Dutta, P.; Marks, T. J. *J. Am. Chem. Soc.* **2005**. *127*, 3172.
[4]. Kong, X.; Kulkarni, A. P.; Jenekhe, S. A. *Macromolecules.* **2003**. *36*, 8992.
[5]. Tacca A, Po R, Caldararo M, et al. *Electrochimica acta*, **2011**, *56*, 6638-6653.
[6]. Zhou H, Zhou F, Tang S, et al. *Dyes and Pigments*, **2012**, *92*, 633-641.
[7]. (a) H. Meier, Angew. *Chem., Int. Ed.*, **2005**, *44*, 2482; (b) A. R. Katritzky, D.W. Zhu and K. S. Schanze, *J. Phys. Chem.*, **1991**, *95*, 5137.
[8]. J. Casado, T. M. Pappenfus, L. L. Miller, K. R. Mann, E. Orti, P. M. Viruela, R. Pou-Ame´rigo, V. Herna´ndez and J. T. Lo´pez Navarrete, *J. Am. Chem. Soc.*, **2003**, *125*, 2524.
[9]. J. Cao, J. W. Kamkf and M. D. Cuetis. *Chem. Mater.* **2003,** *15*, 404.
[10]. W. J. Yang, D. Y. Kim, M. Y. Jeong, H. M. Kim, Y. K. Lee, X. Fang, S.J. Jeon and B. R. Cho. *Chem. Eur. J.* **2005**, *11*, 4191.
[11]. H. E. Katz, Z. Bao and S. L. Gilat, Acc. *Chem. Res.*, **2001**, *34*, 359. (b) A. Babel and S. A. Jenekhe, *Synth. Met.*, **2005**, *148*, 169.

Advanced Materials Research Vols. 989-994 (2014) pp 297-300
© (2014) Trans Tech Publications, Switzerland
doi:10.4028/www.scientific.net/AMR.989-994.297

Growth Behavior of WC Grains in Ni_3Al Matrix during Liquid Phase Sintering

Weibing Zhang[1,2,a], Wen Peng[1,2,b], Jianzhan Long[1,2,c], Xiuyu Wei[1,2,d]

[1] State Key Laboratory of Cemented Carbide, Zhuzhou 412000, China

[2] Zhuzhou Cemented Carbide Group Corp. Ltd., Zhuzhou 412000, China

[a]email: zhangmm-5625@163.com, [b]email: 1335030041@qq.com

[c]email: 281264623@qq.com, [d]email: 17456421@qq.com

Keywords: Grain growth; WC–Ni_3Al; Grain shape; Sintering

Abstract. Growth behavior of WC grains with two different sizes of 10 μm and 4 μm in the same liquid matrix has been studied in the WC–40vol.%Ni_3Al system. The samples were sintered under a carbon saturated condition. Surfaces of the coarse WC grains are strongly micro-faceted and stepped. With the increase of sintering time, the average size of the fine WC grain increases continuously and very large plate-like triangular prismatic WC grains appear. The present investigation thus shows that the growth behavior of fine WC grain is affected by lower solubility of W in Ni_3Al matrix and the abnormal growth of WC grains is suppressed. However, the growth behavior of coarse WC grain is governed only by the difference in energy between the facets.

Introduction

WC-Co cemented carbides [1] are the most important commercial grades of WC cemented carbides, which are widely used in metal cutting, molds, mineral and petroleum industries. However, the favorable mechanical properties of WC-Co cemented carbides are significantly degraded at elevated temperature. Moreover, WC-Co cemented carbides exhibit poor resistance to corrosion resistance in aqueous and acidic environments. Meanwhile elemental cobalt has environmental toxicity when present as fine particulates.

As we all know, the improved properties [2] of hard metals can be achieved by appropriate modification of microchemistry (e.g. the composition of the binder), besides optimizing of the microstructure (e.g. the WC grain size). In order to overcome the shortcomings of WC-Co cemented carbide, recently, Ni_3Al has attracted considerable attention among intermetallic compounds as the new potential binders in WC-based composites due to their certain combination of properties [3-5] such as strength increasing with temperature rising to a maximum at 700-800 ℃, good oxidation resistance and good resistance to aqueous acidic corrosion environments. Thus significant research efforts [3, 5-8] have been made to replace Co with Ni_3Al as the binding metal and some helpful property data have been obtained. Nevertheless the mechanism of WC morphology transformation is still not clear.

As we all know, the WC grain shape is an important parameter to control during sintering since it influences the mechanical properties of the tools. However, little experimental work has been devoted to the effect of the Ni_3Al binder on the WC morphology in WC-Ni_3Al composites. Any theoretical or experimental data should help in understanding the factors influencing the WC morphology during sintering. In this work, the morphology of WC grain is examined in WC-36 vol% Ni_3Al alloy with different sintering time.

Experimental

The starting materials were medium WC powders (4 μm), coarse WC powders (10 μm) and the homogeneous WC+Ni3Al (20 μm) prealloyed powders, as shown in Fig. 1. The WC+Ni3Al prealloyed powders were produced in vacuum heat treatment furnace by reaction synthesis of pure carbonyl Ni, analytical reagent Al and WC powders (10 μm) at 1100-1200℃ using the processing

conditions described in detail in Ref.[9]. Conventional Co powders (1.5 μm) were adopted in this study.

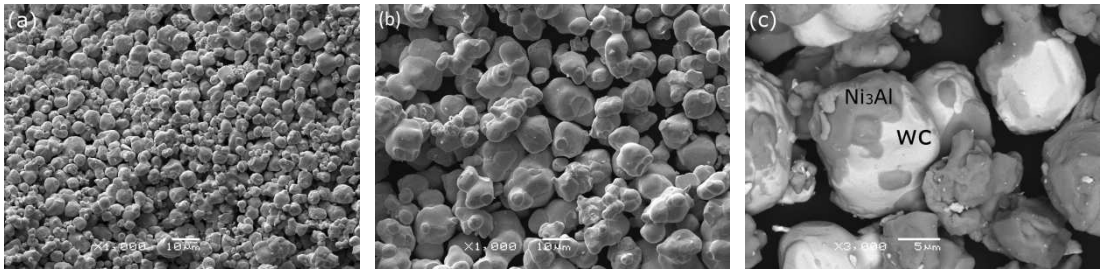

(a) medium WC powder, (b) coarse WC powder, (c) WC+Ni3Al prealloyed powder.

Fig.1. SEM images

Powder technology was used to manufacture the WC-36 vol% Ni3Al composites. Since the medium-grain powders tend to grow stronger than coarser-grain powders, in order to promote WC grain growth and obtain better observation, coarse WC (10 μm) and medium WC (4 μm) particles were used simultaneously in the weight ratio of 2:1. The starting materials were milled in ethyl alcohol in a ball mill at the ball-to-powder ratio of 4:1 for 24 h. WC-6 wt%Co balls with Φ10×20 mm were used. The powder mixture was dried under vacuum at 85 ℃ and sieved. The samples were uniaxially cold pressed to bars of 25×8×6.7 mm at pressure of 100 MPa, and then sintered at 6 MPa low-pressure in a sintering furnace (PVA, Germany) with graphite heating elements, for 1 h at 1450 ℃. In order to further investigate the effect of sintering time on WC grain shape, the sintered samples were re-sintered at 1450 ℃ for 8 h again.

The sintered samples were cut, ground and polished and mirror polished with diamond pastes. SEM imaging was performed on etched sections (10 wt% NaOH and K3Fe(CN)6 solution ; 20 s) using a scanning electron microscope (Model JSM-6701F, Jeol, Japan) with an X-ray energy dispersive spectroscopy (EDS) system. The chemical compositions of binder phase were characterized by energy dispersive spectroscopy (EDS). For a clear observation of WC grain shape by scanning electron microscopy, WC grains in the sintered samples were extracted by removing the binder matrix with saturation hydrochloric and Fe3Cl solution in supersonic cleaner (Branson B3500S-MT) for 5 min. The high-magnification WC morphology was measured using transmission electron microscopy (TEM).

Results and discussion

Fig. 2(a) shows the micrograph of the WC-36 vol% Ni3Al compositions sintered at 1450 ℃ for 1 h. Each microstructure belonges to two-phase region consisting of WC and binder γ. In these cases, a bimodal WC grain size distribution is formed during sintering due to two kinds of WC raw materials. WC-36 vol% Ni3Al compositions consist of faceted WC grains embedded in Ni3Al binder. Fig. 2(b) shows the results obtained from re-sintered experiments. It shows that faceted steps on the large WC grains become prevalent in Ni3Al binder.

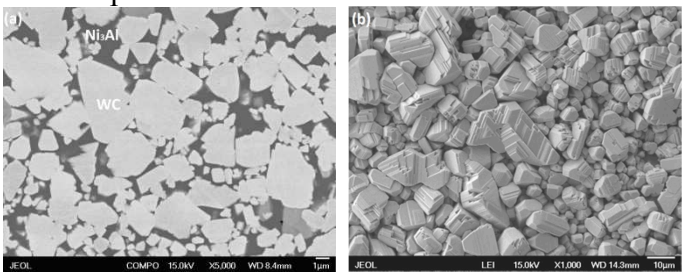

(a)1450 ℃ for 1 h, (b) 1450 ℃ for 8 h (after binder etched)

Fig.2. Micrographs of the WC-36 vol% Ni3Al composites sintered at

Fig.3 shows the WC grains extracted from the WC-36 vol%Ni3Al and WC-36 vol%Co composites sintered at 1450 ℃ for 8 h. The results in Fig.3(a) are direct evidence showing the WC grains in the Ni3Al binder exhibit distinct growth trace and the faceted steps on the surface begin to

appear. Generally, the shape of WC grain becomes rounder in the Ni3Al binder and the degree of faceted shape becomes weaker compared with that in Co binder(Fig.3(b)).

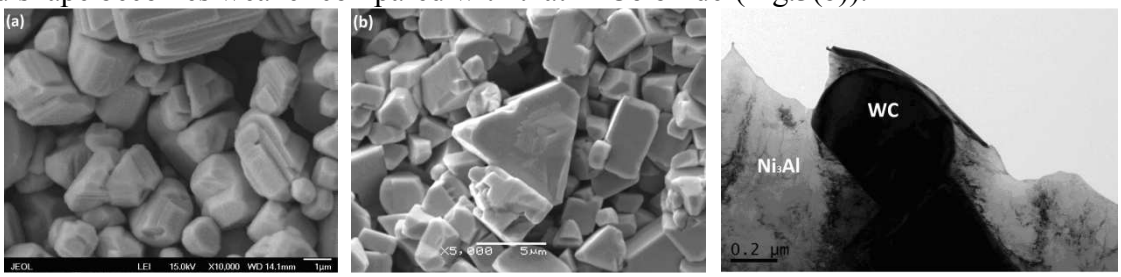

(a)WC-36Ni3Al, (b) WC-36Co. (c) TEM image of WC grains in WC-36Ni3Al

Fig.3. The WC morphology extracted from the composites with different binder metals. All the samples were re-sintered together at 1450 ℃ for 8 h(after binder etched).

Fig.3(c) shows TEM image of WC grains re-sintered at 1450 ℃ for 8 h. Generally, the WC grain in WC-Co composites has three long facets and three short facets and sharp corners. However, round grains in WC-36 vol%Ni3Al composites are more often observed in the largest grains of the Ni3Al binder alloys.

The W contents in the binder were examined by EDS. The results show that the W content in Co binder phase is approximately 22.4 wt% and that in Ni3Al binder phase is approximately 9.0 wt%. From the EDS microanalyses results obtained so far, it is reasonable to suggest that the amount of W dissolved in the Ni3Al binder metal is lower than that found for pure Co binder metal.

WC crystal has a $P_{\bar{6}}m2$ crystal symmetry [10]. The cell dimensions are a=0.2906 nm and c=0.2837 nm with c/a=0.976. The carbon atoms take the asymmetric position of (1/3, 2/3, 1/2) in the unit cell and this asymmetric occupation of carbon atoms divides the prismatic planes into two different families of planes with different atom arrangements. The structure of WC contains three kinds of dense planes formed, namely $\{0001\}$ and two different prisms planes $\{10\bar{1}0\}$ and $\{01\bar{1}0\}$.

These two families of prismatic planes can have a different affinity to carbon because W atoms on each plane have a different number of W–C bonds [11]. The planes with high affinity to carbon grow preferentially in the saturated carbon conditions and disappear finally leaving triangular prism in shape.

In case of the $\{10\bar{1}0\}$ planes all W atoms on the surface form only two W-C bonds, whereas in case of $\{01\bar{1}0\}$ planes four W-C bonds are formed on the surface. The planes with two bonds left have a higher surface energy than those with four, that is responsible for the characteristic trigonal shape of the WC formed during liquid phase sintering.

The shape change of WC grain in WC-36 vol%Ni3Al composites is possiblly attributed to the change of the solubility of W in binder. As for WC-Co cemented carbide, the carbon content in cemented carbide plays an important role on WC grain growth [12] and shape of WC [11]. However, the solubility of W in cobalt increases with decreasing carbon content and has been reported to vary, accordingly, between 2 and 15 wt% at 1250°C [13]. However, there is significantly lower solubility of W in Ni3Al in comparison with the solubility of that in cobalt [14]. The solubility of WC of Ni3Al was found to be 3-4 at.% at 1500°C [15]. It is likely that the lower solubility of W in binder will result in slowing down solution/re-precipitation processes during sintering. So the WC grain growth is inhibited and finer small WC grain will exist in Ni3Al rich binder alloys. However, when given enough sintering time, one of two families of prismatic planes will grow preferentially and/or more rapidly and the steps will form.

Conclusion

(1) The WC grains in the Ni3Al binder become rounder compared with that in Co binder. The dependence of WC grain shape on the Ni3Al content is attributed to the different solubility of W in binder.

(2) With the increase of sintering time, surfaces of WC grains are strongly micro-faceted and stepped.

References

[1] Correa E, Santos J, Klein A. Microstructure and mechanical properties of WC Ni–Si based cemented carbides developed by powder metallurgy. International Journal of Refractory Metals and Hard Materials. 2010;28:572-5.

[2] Ahmadian M, Chandra T, Wexler D, Calka A. Effect of Boron on the WC Morphology in Sub Micron Tungsten Carbide-Aluminide Composites. Materials Science Forum. 2007;561-565:675-8.

[3] Tiegs T, Alexander K, Plucknett K, Menchhofer P, Becher P, Waters S. Ceramic composites with a ductile Ni3Al binder phase. Materials Science and Engineering: A. 1996;209:243-7.

[4] Ahmadian M, Wexler D, Chandra T, Calka A. Abrasive wear of WC–FeAl–B and WC–Ni3Al–B composites. International Journal of Refractory Metals and Hard Materials. 2005;23:155-9.

[5] Becher PF, Plucknett KP. Properties of Ni3Al-bonded Titanium Carbide Ceramics. Journal of the European Ceramic Society. 1998;18:395-400.

[6] Plucknett KP, Tiegs TN, Becher PF, Waters SB, Menchhofer PA. Ductile intermetallic toughened carbide matrix composites. Wiley Online Library; 1996. p. 314-21.

[7] Almond E, Roebuck B. Identification of optimum binder phase compositions for improved WC hard metals. Materials Science and Engineering: A. 1988;105:237-48.

[8] Talanova GV, Padalko AG, Panov VS, Veselov AN, Shvorneva LI. Effect of barothermal processing on the structure and properties of a WC-Ni3Al alloy. Inorganic Materials. 2008;44:244-7.

[9] Long J-z, Zhang Z-j, Xu T, Peng W, Wei X-y, Lu B-z, et al. WC–Ni3Al–B composites prepared through Ni+Al elemental powder route. Transactions of Nonferrous Metals Society of China. 2012;22:847-52.

[10] Herber R P, Schubert W D, Lux B. Hardmetals with “rounded” WC grains[J]. International Journal of Refractory Metals and Hard Materials, 2006, 24(5): 360-364.

[11] Kim S, Han S H, Park J K, et al. Variation of WC grain shape with carbon content in the WC–Co alloys during liquid-phase sintering[J]. Scripta materialia, 2003, 48(5):635-639.

[12] Konyashin I, Hlawatschek S, Ries B, et al. On the mechanism of WC coarsening in WC-Co hardmetals with various carbon contents[J]. International Journal of Refractory Metals and Hard Materials, 2009,27(2):234-243.

[13] Fernandes C, Senos A. Cemented carbide phase diagrams: A review[J]. International Journal of Refractory Metals and Hard Materials, 2011, 29(4):405-418.

[14] Tiegs T, Menchhofer P. Hardmetals based on Ni3Al as the binder phase[J]. P/M in aerospace, defense and demanding applications-1995, 1995, 211-218.

[15] Panov V, Gol’dberg M. Interaction of tungsten carbide with aluminum nickelide Ni3Al[J]. Powder Metallurgy and Metal Ceramics,2009, 48(7):445-448.

Advanced Materials Research Vols. 989-994 (2014) pp 301-304
© (2014) Trans Tech Publications, Switzerland
doi:10.4028/www.scientific.net/AMR.989-994.301

Synthesis and Characterization of Nano Melamine Phosphate

Zhengzhou WANG[1,2 a], Shaohong XU[1]

[1] School of Materials Science and Engineering, Tongji University, Shanghai 200092, China

[2] Key laboratory Advanced Civil Engineering Materials, Ministry of Education, Tongji University, Shanghai 200092, China

[a]email: zwang@ tongji.edu.cn

Keywords: Solvothermal synthesis; Characterization; Nano melamine phosphate

Abstract. Nano melamine phosphate (NMP) flame retardant was synthesized by means of a solvothermal method, and was characterized by Fourier transform infra-red spectroscopy, X-ray diffraction, and scanning electron microscopy. Effects of reaction temperature and reaction time on the morphology of reaction products were investigated. It was observed that the morphology of the products changes greatly as reaction temperature or reaction time changes.

Introduction

There are increasingly concerns about the use of halogen-containing flame retardants because they can produce a lot of smoke and toxic gases on heating or during fires. In recent years, researchers pay more attention to intumescent flame retardation (IFR) of polymers. Generally, an IFR system usually consists of three components, i.e. an acid source, e.g. ammonium polyphosphate (APP) and melamine phosphate (MP), a carbon source, such as pentaerythritol (PER) and pentaerythritol derivatives, and a blowing agent, e.g. melamine (MEL). MP is a commonly used IFR flame retardant, and it exerts an excellent flame retardant role in many polymers, e.g. poly(vinyl alcohol), polylactide, polypropylene, polyamide, epoxy resin, and so on [1-5]. However, the particle size of the commonly used MP products is at the micro scale, and the addition of MP into polymers usually deteriorates mechanical properties of the filled polymers.

In the present work, nano melamine phosphate (NMP) was first synthesized by using a solvothermal method. To our knowledge, there are no reports on the preparation of NMP previously.

Experimental

Materials

Phosphorus acid (85%), sodium dodecyl sulfate (SDS) and benzene were all analytical reagents, obtained by Sinopharm Chemical Reagent Co. Melamine was bought from Anhui Hongsifang Company.

Synthesis of NMP

Nano MP (NMP) particles were prepared by using a solvothermal method. Firstly, melamine (12.6g, 0.1 mol), phosphorus acid (11.5g, 85%, 0.1 mol), 0.48 g SDS, and 200 ml benzene were placed in a teflon-lined cylinder (autoclave). After 30 minutes of stirring, the closed autoclave was placed inside a furnace at a preset temperature (120-180°C) and heated for 1-5 h. The chamber was left overnight to cool. The white precipitate was filtrated and washed with water. Final product was dried in a vacuum oven at 80 °C for 48 h.

Characterization

The Fourier transform infrared (FTIR) spectra of samples were recorded by using a spectrophotometer (Equinoxss/Hyperion 2000, Bruker, Gemany). The X-ray diffraction (XRD) data were obtained at room temperature by using an X-ray diffractometer (D/max2550VB3+/PC, Rigaku International Corporation). The morphology of nano powders was investigated by a scanning electron microscope (S4800, Hitachi, Japan).

Results and Discussion

Fig. 1 shows FTIR spectrum of nano MP (NMP) prepared by means of a solvothermal method at 150 °C for 3h. The peaks at 3400 cm^{-1} and 1050 cm^{-1} are the absorptions from OH. The absorptions at 3140 cm^{-1} and 1664 cm^{-1} are assigned to stretching vibration and deformation vibration of NH_2, respectively. The 1559 cm^{-1} and 1515 cm^{-1} peaks are the typical absorptions of triazine rings. The absorptions at 1245 cm^{-1}, 1100 cm^{-1} and 950 cm^{-1} are attributed to absorptions of P=O, P-O and P-OH groups, respectively [6,7].

XRD patterns of NMP are shown in Fig. 2. The main diffraction peaks at 12.2º, 19.0º, 22.2º, 24.5º, and 26.3º in Fig. 1B can be indexed as the (110), (120), (1-20), (220), and (030) planes of MP, respectively, which are in agreement with the literature (JCPDS 44-1707).

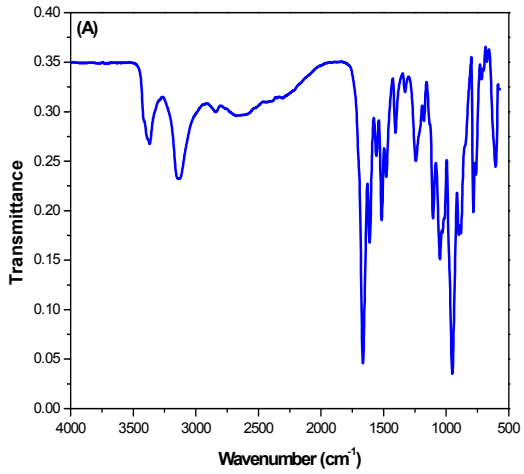

Fig.1 FTIR of NMP

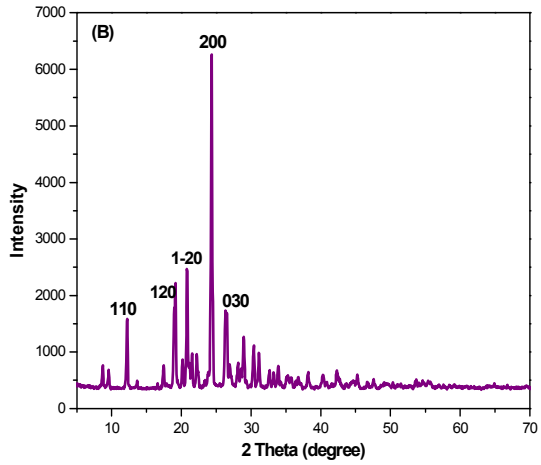

Fig.2 XRD of NMP

The morphology of the NMP particles was further observed by SEM. Fig. 3 shows the SEM images of reaction products prepared at different reaction temperatures for 3h. As can be seen from Fig. 3A and Fig. 3B, the size of particles prepared at 120 ºC and 150 ºC is at the nano scale (below 100 nm). When the reaction temperature is 180 ºC, the shapes of reaction products become irregularly rod-like and their diameters reach up to several hundred nano meters (Fig. 3C).

As for the effect of reaction time on the morphology of the reaction products, it was observed from Fig. 4A and Fig. 4B that the particle size of the products prepared at 150 ºC for 1h and 3h is also below 100 nm. A further increase of reaction time to 5h leads to a great increase particle size and a change in shape. The products become rod-like in shape, with a diameter of 100-200 nm and a length up to 1 mm as shown in Fig. 4C. Our results agree well with the previous reports where researchers in the preparation of titanium dioxide (TiO_2) nano powders by the solvothermal method found that the average particle size increased with an increase in the reaction temperature and reaction time [8,9]. In hydrothermal or solvothermal synthesis, there are many factors affecting crystal growth and morphology, such as characteristics of reactants and reaction conditions [10,11]. It was reported that the crystal growth and morphology evolution are possibly controlled by the well-known Ostwald ripening process [12], namely the dissolution of fine particles and their redeposition on larger particles. In this study, Ostwald ripening may be a dominant mechanism of the formation of NMP. At lower temperatures or shorter reaction time, the shape of NMP particles is spherical, with a diameter of about 50 nm. When the reaction temperature increases or the reaction time is prolonged, the fine spherical NMP particles may undergo aggregation due to higher free energy as shown in Fig. 4C and Fig. 4C.

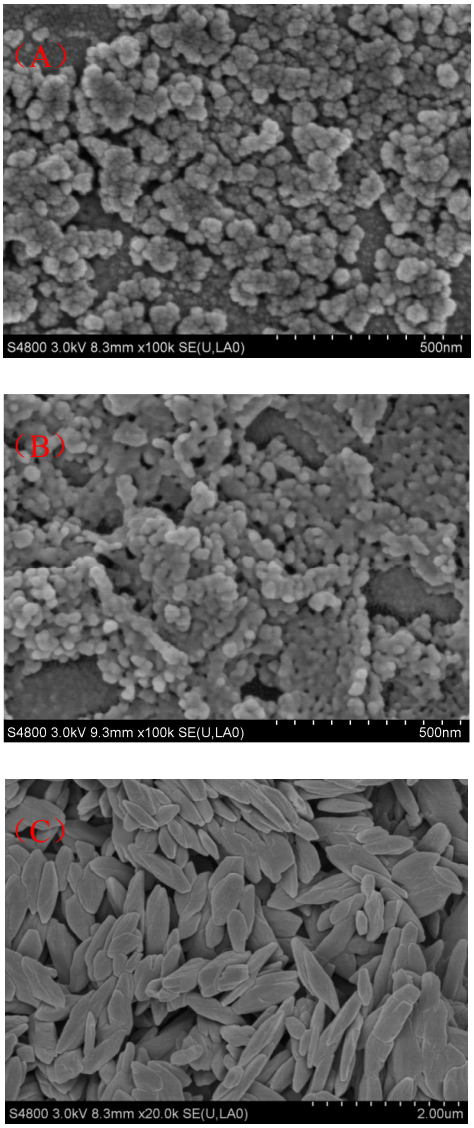

Fig. 3 SEM of MP prepared at different temperatures, (A) 120 ℃; (B) 150 ℃; (C) 180 ℃

Conclusion

In this work, nano melamine phosphate (NMP) was synthesized by a solvothermal method, and it is found that reaction temperature and reaction time have a great influence on the particle size of the product. The suitable reaction conditions for the preparation of NMP are 120-150 ºC and 1-3 h.

Acknowledgement

This work is supported by the National Natural Science Foundation of China (Project Nos. 21174106 and U1205114/L11).

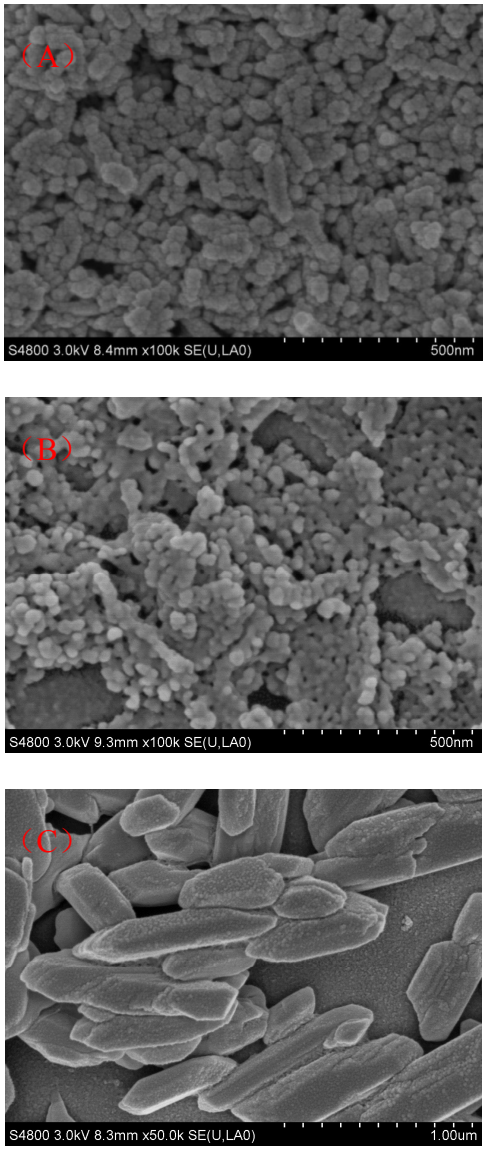

Fig. 4 SEM of MP prepared at different times, (A) 1h; (B) 3h; (C) 5h.

References

[1] Guo D., Wang Q., Bai S. B., *Polym. Adv. Tech.*, 2013, 24(3):339-47.
[2] Song L., Xuan S. Y., Wang X., Hu Y. *Thermochimica Acta*, 2012, 527: 1-7.
[3] Fu X. M., Liu Y., Wang Q., Zhang Z. J., Wang Z. Y., Zhang J. Z. *Polym. Plast.Tech. Eng.*, 2011, 50(15):1527-1532.
[4] Salaün F., Lewandowski M., Vroman I., Bedek G., Bourbigot S., *Polym. Degrad. Stab.*, 2011, 96(1,):131-143.
[5] Lv P., Wang Z. Z., Hu K. L. Fan W. C., *Polym. Degrad. Stab*., 2005, 90(3): 523-534
[6] Balabanovich AI, Prokopovich VP. Thermochimica Acta, 2006, 76:169-178.
[7] Levchik SV, Balabanovich A I, Levchik GF, Costa L. Fire Mater., 1997, 21:75-83.
[8] Pookmanee P, Ninsonti H, Sangsrichan S, Adv. Mater. Res., 2010, 161:93-94.
[9] Pookmanee P, Phiwchai I, Yoriya S, et al. Ferroelectrics, 2013, 457:30-38.
[10] Wang W, Xu C, Wang G, Liu Y, Zheng C, Adv. Mater., 2002, 14: 837-840.
[11] Yu SH, Biao L, Mo MS, Huang JH, Liu XM, Qian YT, Adv. Funct. Mater., 2003, 13:639-647.
[12] Upendra AJ, Lee JS. Small, 2005, 1:1172-1176.

Advanced Materials Research Vols. 989-994 (2014) pp 305-307
© (2014) Trans Tech Publications, Switzerland
doi:10.4028/www.scientific.net/AMR.989-994.305

Preparation and Characterization of Transparent Oxyfluoride Tellurite Glass-ceramics Containing CaF_2 Nanocrystals

Zhaoxia Hou[1,a], Hangxin Li[1,b], Shaohong Wang[1], Meihan Wang[1], Xiaodan Hu[1]

[1]Liaoning Province Key Laboratory of New Functional Materials and Chemical Technology, Shenyang University, Shenyang 110044, China

[a]email:Luckyxia2007@126.com,[b]email:lihangxin@126.com

Keywords: Tellurite; Glass-ceramics; CaF_2 Nanocrystals

Abstract. Transparent oxyfluoride tellurite glass-ceramics containing CaF_2 nanocrystals were prepared by high temperature melting method. The glass-ceramics were characterized by Differential scanning calorimetry, X-ray diffraction and scanning electron microscope, respectively. The results showed that the CaF_2 nanocrystals were spherical and the average size was found to be 60 nm.

Introduction

Tellurite glasses have more advantages than silicate and borate glasses because of the physical properties such as low-melting temperature, high-refractive index, high-dielectric constant and good infrared transmissivity. Oxyfluoride Tellurite Glass-ceramics is a new type of material which based on tellurite glass and nanocrystals separated out in the substrate material. Due to the unique properties, tellurate glass-ceramics have great application potential in the fields such as pressure sensors, data storage, optical displays, optical amplifiers or as new laser hosts, optical modulators, and optical memory storage systems[1-4]. Nowadays, fluoride oxide tellurite glass and glass-ceramics become a hot research topic domestically and abroad[5-7].

Experiments

The oxyfluoride tellurite glasses used in this work were prepared with the following composition in mol%: $60TeO_2$-$15Al_2O_3$-$15CaF_2$-10NaF by using high purity TeO_2 (99.99%), Al_2O_3 (99.99%), CaF_2 (99.99%) and NaF (99.99%)) as raw materials. Batches of about 100 g of staring materials were fully mixed and melted in covered corundum crucibles at 1100 ℃ for 30 min in air. The melts were poured onto a preheated stainless steel plate followed by annealing at 200 ℃ for 2 h, and then cooled down to room temperature. The glass samples turned yellow. The obtained glass samples were then respectively polished and heat treated at 550℃ for 2 h, 3 h and 4 h to prepare transparent GC1, GC2 and GC3 samples.

GC sample	Heating temperature	Holding time
GC1	550℃	2h
GC2	550℃	3h
GC3	550℃	4h

Differential scanning calorimetry (DSC) experiment was carried out on the powder glass sample at a heating rate of 10K/min. X-ray diffraction (XRD) measurements were performed on a Philips Model PW1830 diffractometer with $CuK_{á}$ radiation. The microstructures of the samples were studied by scanning electron microscope (SEM).

Results and discussion

DSC curves were showed in Fig.1. Based on the DSC curve showed in Fig.1, there was a intense endothermic peak at 470 ℃ and exothermic peak at 550℃, so Tg(glass transition temperature) and Tx(glass crystallization temperature) were found to be 470 ℃ and 550 ℃.

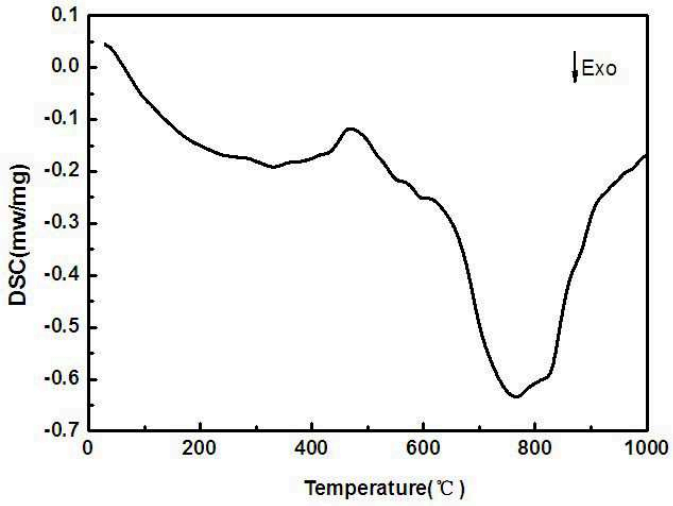

Fig.1. DSC curves of tellurite glass

It is observed that the GC1 is completely amorphous with no diffraction peaks. After crystallized by thermal treatment at 550 ℃ for 3 h or 4 h, the XRD profiles show intense diffraction peaks, which could be all assigned to the well crystallized cubic CaF_2 phases (JCPDS Card No. (35-0816)[8-9]. Diffraction peaks of GC3 are more acute than GC2.

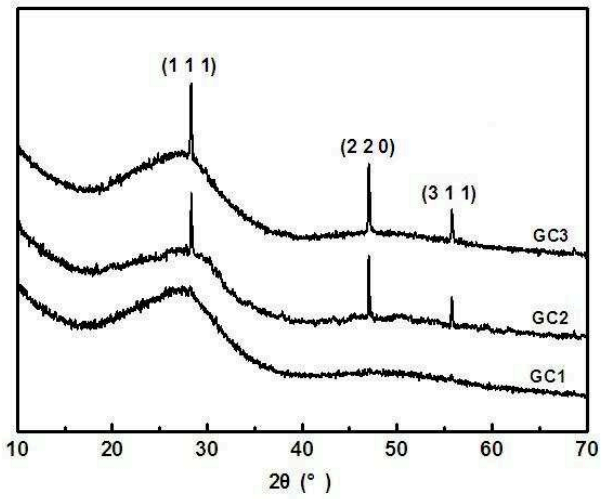

Fig.2. XRD patterns of glass-ceramics

The morphologies of GC were showed in Fig. 3. It can be seen that spherical-like parcels homogeneously dispersed in the amorphous glasses. The SEM image reveals that the nanocrystals distributed evenly in GC2 and the aggregation of nanocrystals appears in sample GC3.The average size of the nanocrystals was estimated from the line broadening of the XRD peaks and Scherrer's equation[10]:

$$d = 0.89\lambda / \beta \cos \theta_B$$

the average particle size was calculated to be 60 nm.

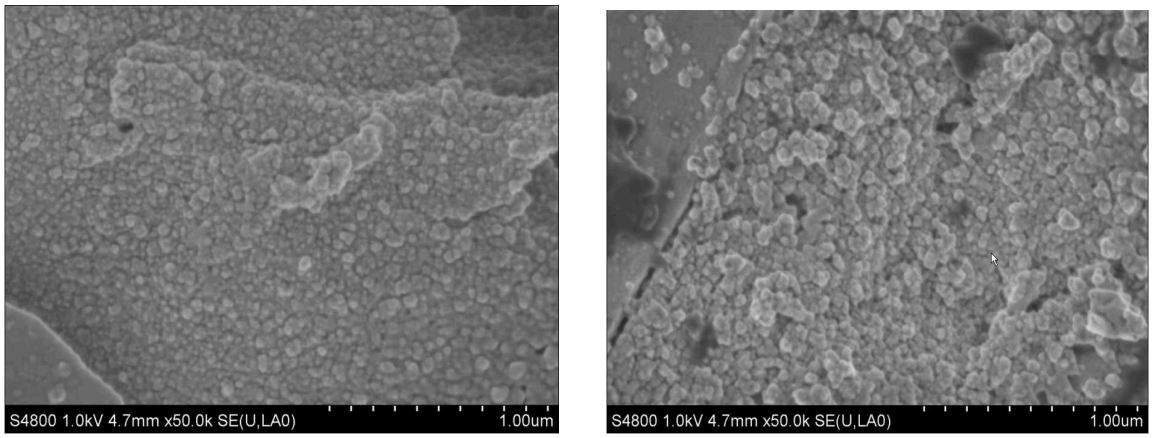

Fig.3. SEM images of sample GC2 and GC3

Conclusion

In this paper, transparent oxyfluoride tellurite glass ceramics containing CaF_2 nanocrystals were prepared by high temperature melting method. Tg(glass transition temperature) and Tx(glass crystallization temperature) were found to be 470 ℃ and 550 ℃. With the increase of the holding time, the diffraction peaks of CaF_2 nanocrystals became sharper. The nanocrystals were spherical and the average size was calculated to be 60 nm.

Acknowledgement

This work was financially supported by the Program for Liaoning Excellent Talents in University of China (no. LJQ2011125), Program for Liaoning Nature Science Foundation of China (no. 20102156), Program for Liaoning Scientific Research in University of China (no. L2010371).

References

[1] Marian Kubliha，Viera Trnovcova，Ivan Furar,et al. Journal of Non- Crystalline Solids, Vol.355(2009),p.2035.

[2] Xueying Wang，Hai Lin，Changmin Li，et al. Measurement Science and Technology, Vol.18(2007),p.1348.

[3] K Shinozaki, T Honma, K Ohishi, T Komatsu. Optical Materials,Vol.33(2011),p.1350.

[4] W J Zhang, Q J Chen,Q Y Zhang,et al. Journal of Non-Crystalline Solids, Vol.357(2011),p.2278.

[5] Qiao Xvsheng, Fan Xianping, Wang Jin. Journal of non-crystalline solids, Vol.31(2005),p.357.

[6] Arnab Ghosh, Radhaballabh Debnath. Optical Materials,Vol.31(2009), p.604.

[7] Angelos G, Kalampounias, Bull. Mater. Sci.,Vol.31(2008),p.781.

[8] Y Kishi, S.Tanabe, J.Alloye Compd, Vol.408(2006),p.842.

[9] L Zhou, D Chen, W Luo, Y Wang, Y Yu, F Liu, Mater,lett.Vol.61(2007), p.3988.

[10] Vinay Kumar, Ravi Kumar, S P.Lochab, Nafa Singh, J Phys, Appl.Phys, Vol.39(2006), p.5137.

Advanced Materials Research Vols. 989-994 (2014) pp 308-311
© (2014) Trans Tech Publications, Switzerland
doi:10.4028/www.scientific.net/AMR.989-994.308

Influence of Electrolysis and Plasma Polishing on Surface Properties of SUS304 Stainless Steel

Xuemei ZONG [a],Ji WANG[b],Yanfei WANG [c],Jianfei LIU [d]

Jiangsu Xuzhou Construction Machinery Research Institute, Xuzhou 221004, China

[a]email:zongxuemei@139.com, [b]email:wangji8110@126.com, [c]email:wangyfmeng2010@163.com, [d]email:jf_liu@163.com

Keywords: Electrolysis and Plasma Polishing; Stainless Steel; Roughness; Corrosion Resistance

Abstract. Polishing was performed by using a self-made 40kw electrolysis and plasma polishing machine, and the test specimens were SUS304 stainless steel sheets. Roughness, micro-morphology, surface chemical composition and corrosion resistance of the specimens were analyzed. The results show the surface roughness value decreases quickly from R_a=0.573μm to R_a=0.115μm in first 10 minutes polishing. After 30 minutes polishing, the surface roughness value decreases to R_a=0.066μm. Microdefects on the surface are removed obtaining the smooth surface and Cr content of the surface increases slightly as well as the other elements content is nearly unchanged after the polishing, so the corrosion resistance measured by electrochemical analyzer is improved.

Introduction

Electrolysis and plasma polishing (EPP) is a new green polishing technique which can be applied in polishing metal workpieces. This processing technique with the characteristics such as polishing no mechanical stresses, high machining efficiency and high uniform polishing quality can polish the workpieces with complex shape. Polishing solution of EPP is salt solution with low concentration (3-6wt%)[1], which is non-pollution and recycling, therefore it can solve the pollution problems brought by electrolytic polishing and chemical polishing[2]. The method can be widely used in polishing, removing burr and oxidation layer, cleaning welding seam and surface stain, and so on. It can play an important role in machinery manufacturing, aviation industry, ship building, chemical industry, food industry, etc.

Mechanism

The workpiece soaked into the polishing solution is linked with DC power positive pole. Meanwhile, polishing solution and polishing cell is linked with negative pole (see Fig.1). At the beginning, because of instantaneous short circuit of the system, a large amount of heat quantity is released so that the solution is evaporated to form a gas layer, which will segregate the workpiece and the polishing solution completely. Discharge channel will be formed in the gas layer under voltage application. The collision between electrons and positive ions moving with high speed in discharge channel produces a large amount of heat energy to the workpiece surface, with heat radiation and gas expansion energy. The involving energy removes the surface melt rapidly. In the convex zone on the undulate surface, the gas layer is thinner, which causes stronger electric field, and electrons with higher speed will reach the surface rapidly, so discharge channel will preferentially form in the convex zone, and material in this location is removed earlier and more.

Experiment

Polishing was performed by using a self-made 40kw EPP machine and ammonium sulfate solution with concentration 0.4% was chose as polishing solution, solution temperature was kept in the range of 79^{o}C-81^{o}C. The material during the polishing was SUS304 stainless steel and was cut into test specimens of 50×20×1.8mm^3. Polishing voltage was 280V. Polishing lasted about 40 minutes. The surface properties before and after polishing were analyzed.

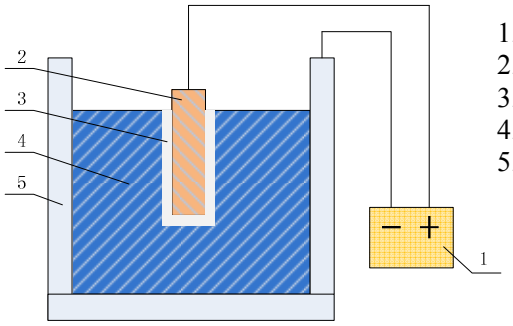

Fig.1. Schematic of EPP

Results and Discussion

Roughness. The initial roughness of the specimens is R_a=0.573μm. Roughness was measured at short intervals during the polishing to obtain the curve of surface roughness with polishing time, as shown in Fig.2. In the first ten minutes, the roughness value decreases quickly from R_a=0.573μm to R_a=0.115μm. While the roughness value decreases to R_a=0.066μm after subsequent 30 minutes, and roughness gradient is small. The larger initial roughness is, the faster roughness decreases. Larger roughness means larger difference of electric field between convex and concave during the polishing, discharge channel forms more easily in the convex places, and more material is removed here, so roughness value decreases faster. Oppositely, difference of electric field is insignificant in flat surface, so the roughness change is small correspondingly.

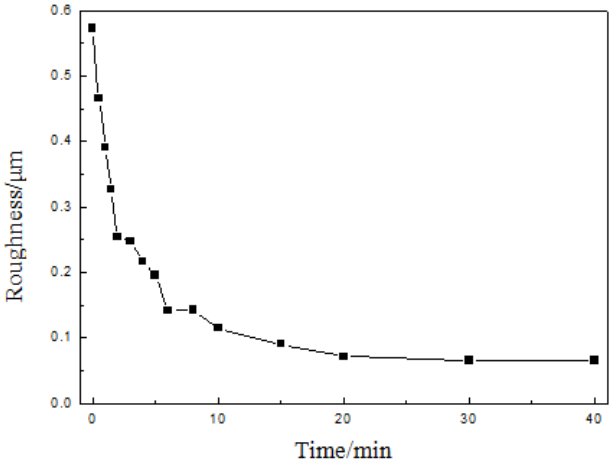

Fig.2 Curve of roughness with polishing time

Micro-morphology. The surface outline of the specimens before and after polishing is measured, as shown in Fig.3. The initial outline curve fluctuates in the range of 5μm. After 10 minutes polishing, sharp location of surface outline is disappeared, the outline curve fluctuates in the range of 1μm and surface is smooth, which is one of the reasons obtaining mirror surface [3]. Fig.4 shows the initial and polished SEM micro-morphology. The specimens are cleaned by acetone before being examined. By looking at the SEM micro-morphology (500x), we can see there are many convexities distributing on the surface of the initial specimen obviously, and after 10 minutes polishing, the convexities are disappeared. Grain boundary is also clear and no corrosion micro-pits on the surface of the polished specimen. The results show the microdefects of the surface can be removed well by EPP.

Surface Chemical Composition. During the polishing, the chemical reactions occur between gas and workpiece, which leads to the change of chemical composition of surface inevitably. The initial and polished chemical composition is analyzed by EDS, as shown in Fig.5. After 10 minutes polishing, the mass percentage and atomic number percentage of Cr increase slightly, but the percentage of other chemical elements almost remains unchanged. This phenomenon depends on

high inertia of Cr, and chemical reaction is preferential to occur between gas layer and low inertia elements such as Fe. The reaction products adhering to the surface are removed by discharge, leading to the relative increase of Cr, which is beneficial for improving corrosion resistance of the stainless steel, as enough Cr in steel is easy formed passivation layer on surface to protect steel from oxidation [4].

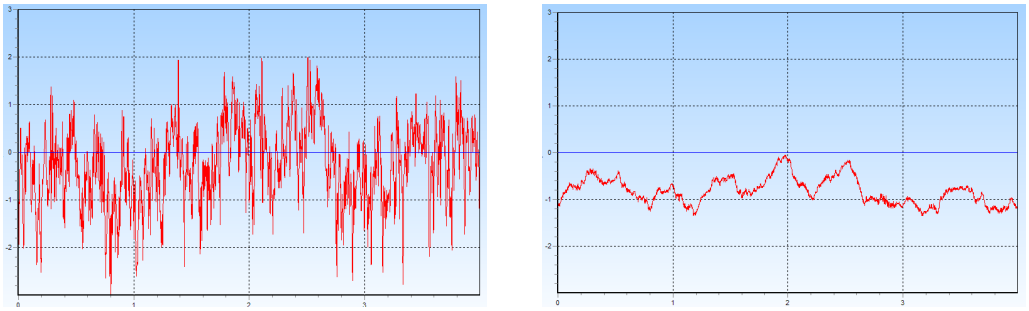

(a) Initial outline (b) Polished outline

Fig.3. Surface outline before and after polishing

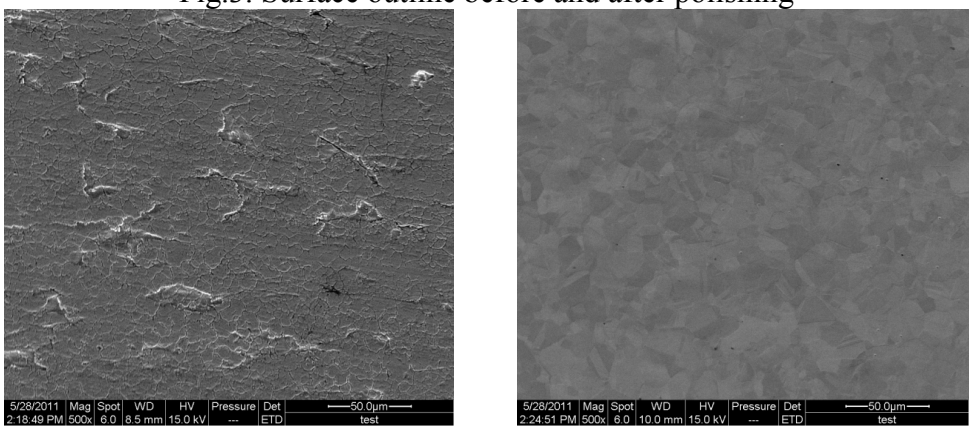

(a) Initial micro-morphology (500x) (b) Polished Micro-morphology (500x)

Fig.4. SEM micro-morphology before and after polishing

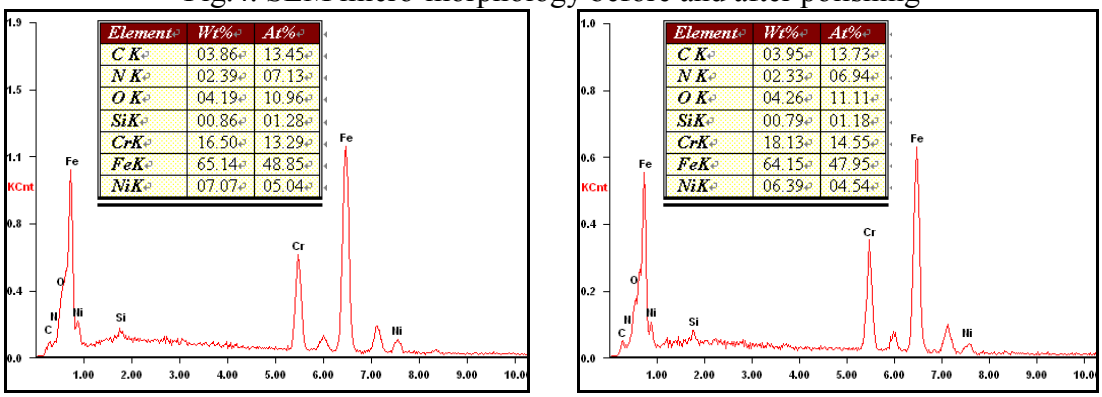

(a) Initial specimen (b) Polished specimen

Fig.5. Change of chemical composition before and after polishing

Corrosion Resistance. The corrosion resistance of the specimens before and after polishing were measured in NaCl solution with concentration 0.9% by electrochemical analyzer. The scanning speed of the polarization curve was 5mV/s, and the scanning margin is the open-circuit-potential plus or minus 0.25V. The corrosion potential E_{corr} and current density J_{corr} can be obtained through polarization curve in test. The more the E_{corr} offsets towards positive direction, the smaller corrosion tendentiousness is. The smaller corrosion current I_{corr} is, the lower rate of corrosion is [5]. The polarization resistance R_p is given by

$$R_p = \frac{b_a b_c}{2.303(b_a + b_c) J_{corr}} \tag{1}$$

where b_a and b_c are positive Tafel gradient and negative Tafel gradient, respectively.

Fig.6 shows the polarization curves before and after polishing. The polarization curve of the polished specimen offsets towards right obviously. The parameters of b_a, b_c, E_{corr}, I_{corr} can be got by fitting polarization curves before and after polishing, as shown in Table 1. Solving equation (1) with above parameters, polarization resistances R_p are fixed.

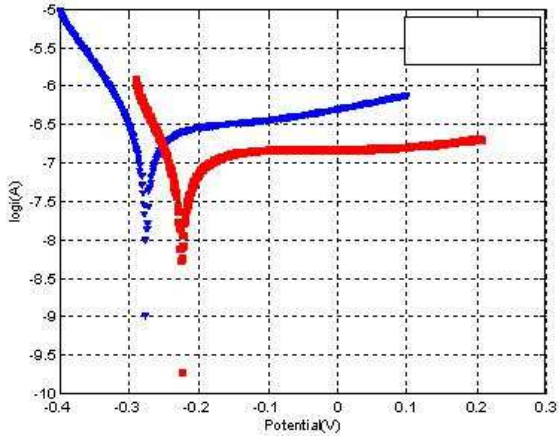

Fig.6 Polarization curves before and after polishing

Table 1. Polarization curve -fitting results before and after polishing

Specimen	E_{corr} (V)	I_{corr} (μA)	b_a	b_c	R_p(Ω)
Inintial	-0.276	2.786e-7	1.337	12.786	110500.4
Polished	-0.224	8.611e-8	1.215	0	247452.0

As observed in Table 1, the corrosion potential of the polished specimen offsets towards positive direction more than the initial specimen's, while the corrosion current is found to be smaller. The results just show the surface corrosion resistance is improved indeed after EPP. On the one hand, the increase of Cr content is beneficial to improve corrosion resistance as discussed above. On the other hand, the surface is smooth after the polishing and microdefects are removed, which prevent corrosion propagation happening on the surface and decrease the corrosion inducements.

Conclusion

SUS304 stainless steel sheets were polished using the new technique of EPP. Surface properties are improved after polishing.

(1) Surface roughness value decreases from R_a =0.573μm to R_a =0.066μm after 40 minutes.
(2) Microdefects on surface are removed well obtaining mirror surface.
(3) The mass percentage and atomic number percentage of Cr increase slightly.
(4) According to electrochemical analyzer, surface corrosion resistance is improved after polishing.

References

[1] Wang J, Suo L C，Guan L L, et al. Analytical Study on Mechanism of Electrolysis and Plasma Polishing [J]. Advanced Materials Research, 2012(472-475):350-353.

[2] Cecil A, Coutinho A, Subrhamanya R M, et al. Novel Ceria-polymer Microcomposites for Chemical Mechanical Polishing [J]. Applied Surface Science, 2008(255):3090-3096.

[3] Xiaoyu Wang, Yong Jia, Baikun Shi. Process of Mirror Surface Grinding [J]. Mechanical Engineer, 2011(11):156-159.

[4] Evans C J, Paul E, Dornfeld D, et al. Material Removal Mechanisms in Lapping and Polishing [J]. CIRP Annals-Manufacturing Technology, 2003, (52):611-633.

[5] Chunan Chao. Theory of Corrosion Electrochemical [M], Beijing: Chemical Industry Press. 2008:99-176.

Advanced Materials Research Vols. 989-994 (2014) pp 312-315
© (2014) Trans Tech Publications, Switzerland
doi:10.4028/www.scientific.net/AMR.989-994.312

Effect of initial concentration of Cu^{2+} on the adsorption performance of hydroxyapatite

Yutong Guan[1a], Shaohong Wang[1b], Meihan Wang[1], Zhaoxia Hou[1], Xiaodan Hu[1], Hao Wang[1] Hailin Fan, Ning Zhang[2]

Liaoning Province Key Laboratory of New Functional Materials and the Chemical Technology,Shenyang University, Shenyang 110044, China

Liaoning Province Key Laboratory of Advanced Materials Technology,Shenyang University,Shenyang 110044,China

[a]email: xcvcvb@126.com [b]email: wang-sh@tsinghua.edu.cn

Keywords: Hydroxyapatite; Initial Concentration; Copper Ion; Adsorption;

Abstract: Hydroxyapatite (HAP) is an effective adsorbent for removing heavy metal ions. In this study, HAP was prepared by sol-gel method and used for removing Cu^{2+} from aqueous solution. Initial concentration of Cu^{2+} in the aqueous solution was evaluated as an important parameter determining uptake. The removal efficiency and the adsorption capacity of HAP for Cu^{2+} were investigated. EDS analysis indicated the presence of Cu^{2+} on the HAP surface.

Introduction

Heavy metals pollution is a worldwide environmental problem. The hazardous heavy metals are not biodegradable and tend to accumulate in living organisms, causing various diseases and disorders[1,2]. Therefore, effective strategies for removing heavy metal ions from water and various industrial effluents have attracted considerable research and practical interest[3]. As one of the important toxic heavy metal, copper finds its way to the industrial effluents includes metal cleaning and plating bath, mining, iron and steel production, wood pulp production and fertilizer industry[4,5].

Although previous research has mentioned that HAP had higher efficiency in the removal of heavy metals (Pb^{2+}, Cd^{2+}), little research has investigated the detailed adsorption characteristics of heavy metals removal by HAP[6,7]. Cu^{2+} sorption onto HAP particles has not been studied in detail.

The main aim of this work was to study the efficiency of HAP for Cu^{2+} removal from aqueous solution. Furthermore, we also investigated the influence factor of initial concentration on the removal efficiency of Cu^{2+}.

1. Materials and methods

1.1 Materials

The synthetic HAP was prepared using the standard procedure published in rare metal materials and engineering [8]. The powder was calcined in air at 600°C for 2h. X-ray diffraction (XRD) analysis conformed with the literature and the JCPDS card No. (07-0747). There are no calcium hydroxide and calcium phosphates phase present in the XRD, implying that pure HAP phase was prepared under the present experimental conditions.

The synthetic solution were all prepared by diluting the stock solution (concentration 1000 mg/L) obtained by dissolving $Cu(NO_3)_2$ in deionized water. Before mixing the adsorbent, the pH of each last solution was adjusted to the required value with dilute solutions of 0.1mol/L HNO_3 and 0.1mol/L NH_4OH. All reagents used in this experiment were of analytical grade or better.

1.2 Sorption procedure

Sorption experiments were carried out in batch. The HAP (0.5g) was added into a 100ml metal solutions with the concentration range of 20-200mg/L, was agitated for a specified period of contact time at 600rpm and room temperature. At the end of the adsorption process adsorbent was separated from the solution by centrifuge (TGL-16G). The concentration of Cu^{2+} was measured by atomic

adsorption spectroscopy (AAS, Varian AA220, USA). The copper ions measurements were repeated three times and the results given were the average values. The percentage ions removal by the adsorbent was calculated using the following equation:

$$Y = \frac{C_0 - C_e}{C_0} \times 100\%$$

Where Y is the ions removal, C_0 and C_e are the concentration of metal ions in solution before and after adsorption (mg/L).

The adsorption capacity of HAP was calculated using the general equation:

$$q = \frac{(C_0 - C_e) \times V}{m}$$

Where q is the uptake capacity (mg/g), V is the volume of the solution (ml), m is the amount of the HAP used in the reaction mixture (g).

2. Results and discussion

2.1 Effect of initial concentration of Cu^{2+}

The effect of initial concentration of Cu^{2+} was investigated in the range of 20~200mg/L. the results are presented in Fig.1. The removal efficiency at 240min decreased from 99.64% to 76.68% as Cu^{2+} concentration increased from 20mg/L to 200mg/L. The results indicate that there was a reduction in Cu^{2+} adsorption, owing to the lack of available active points required for the high initial concentration of Cu^{2+}. However, the sorption capacities of the HAP at 240min from increased from 4.18mg/g to 30.17mg/g as Cu^{2+} concentration increased from 20mg/L to 200mg/L (as shown in Fig.2). The reason may be due to increasing the mass transfer driving force.

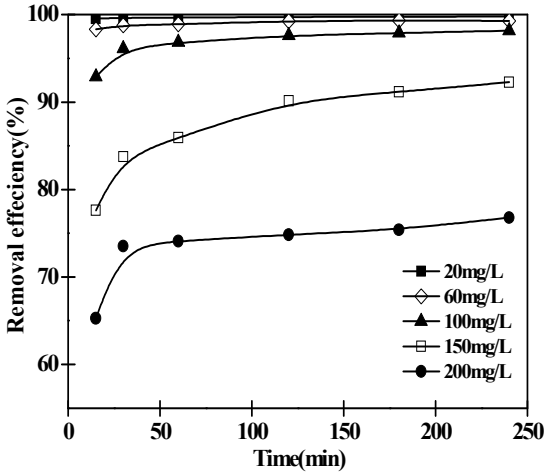

Fig. 1. Effect of initial concentration of Cu^{2+}on the removal efficiency

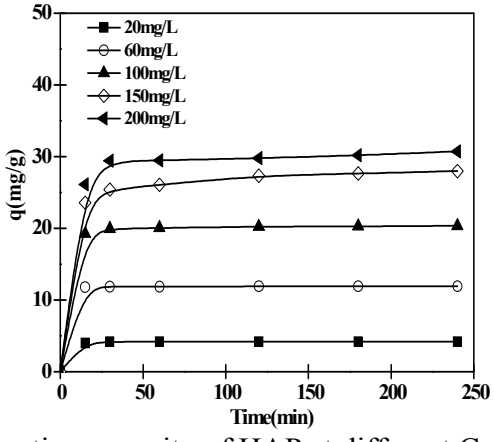

Fig. 2. The adsorption capacity of HAP at different Cu^{2+} concentration

2.2 SEM-EDS analysis

The adsorbent shape and size impact the adsorption capacity of the adsorbent. SEM micrographs of HAP are shown in Fig.3(a). It was observed that the HAP particles are spherical shape with a mean diameter approx. 100nm. This small HAP particles size provides a larger surface area for contaminant adsorption. Fig.3(b) show the micrographs of HAP after the adsorption of Cu^{2+} ions. It can be seen that the HAP became denser and there are some needle-like substance appear. The morphology change of the composite before and after Cu^{2+} treatment indicates the structural changes of the sorbent. The EDS analysis provides direct evidence for the sorption of Cu^{2+} onto the HAP (See Fig.3(c) and (d)).

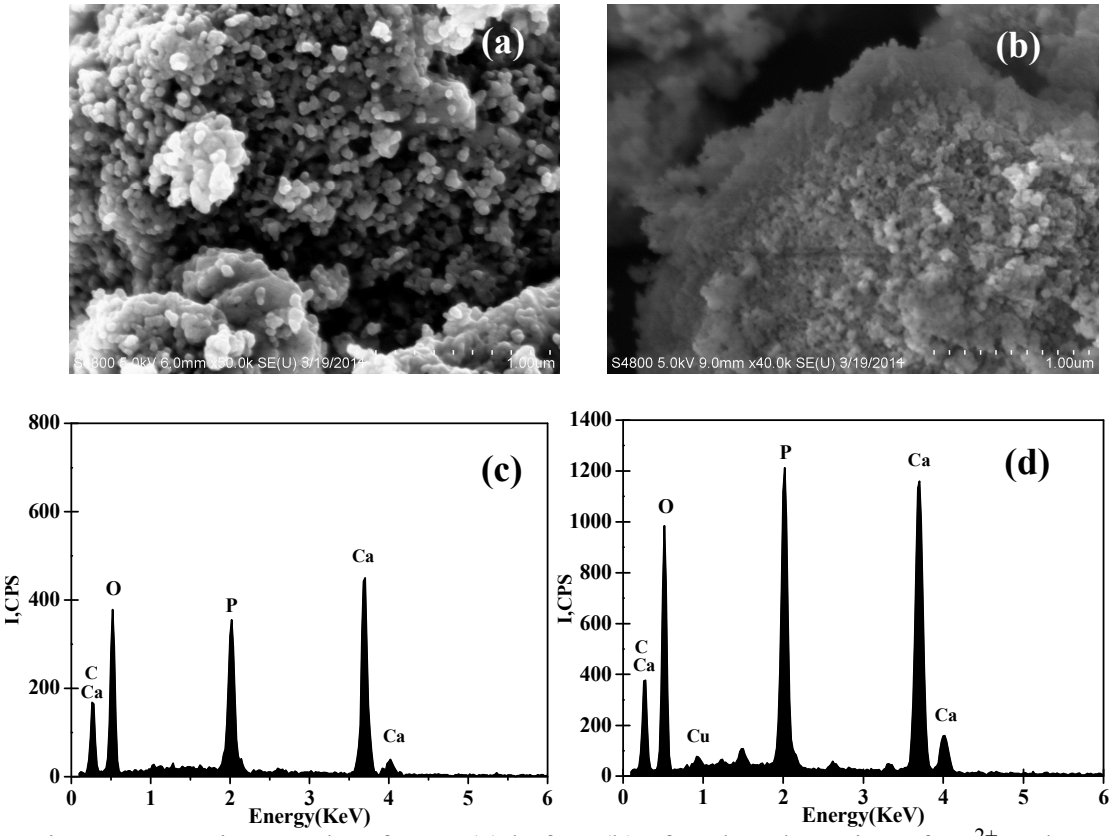

Fig. 3. SEM micrographs of HAP (a) before (b) after the adsorption of Cu^{2+} and EDS analysis of HAP (c) before (d) after the adsorption of Cu^{2+}

3. Conclusions

The present studies clearly reveal that HAP can be used as an effective adsorbent for removing Cu^{2+} from aqueous solution. The sorption performances were affected considerably by the initial concentration of Cu^{2+}. With the increasing of the concentration of Cu^{2+}, the removal efficiency gradually goes down at a specific time. It is speculated that the driving force of adsorption in the process is the concentration gradient. The absorption effect significantly increased due to higher concentration gradient of Cu^{2+}.

Acknowledgement

This work was supported by National Science Foundation of China (NO.51272162), Program for Liaoning Excellent Talents in University (LJQ2011125), Key Laboratory Construction Project in Shenyang City of China (No.F10216100).

References

[1] Majid Aliabadi, Mohammad Irani, Jabir Ismaeili, Saeed Najafzadeh. Design and evaluation of chitosan/hydroxyapatite composite nanofiber membrane for the removal of heavy metal ions from aqueous solution [J]. Journal of the Taiwan Institute of Chemical Engineers, 2014, 45: 518–526.

[2] Suk Hyun Jang, Byung Gil Min, Young Gyu Jeong, et al. Removal of lead ions in aqueous solution by hydroxyapatite/polyurethane composite foams [J]. Journal of hazardous materials, 2008, 152(3): 1285-1292.

[3] Mustafa Ozmena, Keziban Cana, Gulsin Arslana, et al. Adsorption of Cu (II) from aqueous solution by using modified Fe_3O_4 magnetic nanoparticles [J]. Desalination, 2010, 254(1): 162-169.

[4] Mausumi Mukhopadhyay, Noronha S.B., Suraishkumar G.K.. Kinetic modeling for the biosorption of copper by pretreated Aspergillus niger biomass [J]. Bioresource technology, 2007, 98(9): 1781-1787.

[5] Wan Ngah W.S., Hanafiah M.A.K.M.. Biosorption of copper ions from dilute aqueous solutions on base treatedrubber (Hevea brasiliensis) leaves powder: kinetics, isotherm, and biosorption mechanisms [J]. Journal of Environmental Sciences, 2008, 20(10): 1168-1176.

[6] Zhao Xin-Yu, Zhu Ying-Jie, Zhao Jing, et al. Hydroxyapatite nanosheet-assembled microspheres: Hemoglobin-templated synthesis and adsorption for heavy metal ions [J]. Journal of colloid and interface science, 2014, 416: 11-18.

[7] Pandey P. K., Sharma S. K., Sambi S. S.. Kinetics and equilibrium study of chromium adsorption on zeoliteNaX [J]. International Journal of Environmental Science & Technology, 2010, 7(2): 395-404.

[8] Wang Shao-Hong, Wang Hao, Hou Zhao-Xia. Crystal growth and crystallinity of nano-hydroxyapatite prepared by sol-gel [J]. rare metal materials and engineering. 2011, 40: 44-47.

Advanced Materials Research Vols. 989-994 (2014) pp 316-319
© (2014) Trans Tech Publications, Switzerland
doi:10.4028/www.scientific.net/AMR.989-994.316

$Li_{0.95}Na_{0.05}Ti_2(PO_4)_3$/C with good performance as anode material for aqueous rechargeable lithium batteries

Jing ZHU[1,2] Yongguang LIU[2], Qingqing Tian[2] Ling Wang[2] Jilin Cao[1]*

[1] School of chemical engineering, Hebei University of Technology, 300130,Tianjin, China

[2] School of chemical engineering, Hebei United University, Tangshan 063009, China

email:tszhujing@163.com

KeyWords: Aqueous Lithium batteries; anode material; $Li_{0.95}Na_{0.05}Ti_2(PO_4)_3$/C; Carbon coating

Abstract: $Li_{0.95}Na_{0.05}Ti_2(PO_4)_3$/C nanocomposite was prepared by sol-gel method.The structure and morphology of the samples were characterized by XRD, SEM which showed the particles had typical NASICON structure and diameter range from 400~500nm. The electrochemical performance were tested by cyclic voltammetry and galvanostatic charge–discharge. Results show $Li_{0.95}Na_{0.05}Ti_2(PO_4)_3$/C nanocomposite exhibitsmuch better electrochemical performance than bare $Li_{0.95}Na_{0.05}Ti_2(PO_4)_3$.

1.Introduction

The demand for lithium ion batteries for low cost, high safety and high energy density is more and more urgent. Most of the commercial lithium-ion battery uses the organic electrolyte, which is toxic and flammable. During the large-scale use and high rate discharge situation, the overcharge or short circuit will cause the security problems. Additionally, the high price of organic electrolyte, low ionic conductivity and the strict manufacturing requirements, resulting in high cost of the whole battery. Aqueous lithium ion battery can overcome the shortcomings, save the cost and simplify the process. The NASICON-type $LiTi_2(PO_4)_3$ was proposed as an promising anode material for aqueous lithium ion battery. The theory capacity of $LiTi_2(PO_4)_3$ is 138.3 $mAhg^{-1}$,with stable charge discharge platform. But the electrochemical performance is still not satisfactory because of the capacity fading during cycling[1-3]. In this work, Sodium ion was doped to improve the conductivity and carbon used as conducting additive also acts as a coating prohibiting the dissolution of active mass.

2. Experiment

2.1 Preparation of Li0.95Na0.05Ti2(PO4)3/C

The $LiTi_2(PO_4)_3$/C and Na-doped $Li_{0.95}Na_{0.05}Ti_2(PO_4)_3$/C used as anode active material in this work was prepared by sol–gel method accord-ing to reference[1]. Stoichiometric amounts of tetrabutyl orthotitanate，lithium carbonate，sodium carbonate, and ammonium dihydrogen phosphate were used as starting materials; citric acid was adopted as a chelating agent. The sol was dried 140°C for 12 h, heating at 350°C for 2h and 800°C for 12h. The $Li_{0.95}Na_{0.05}Ti_2(PO_4)_3$ was obtained. Then the powder and glucose milled for 12h ,and heating under the protection of nitrogen atmosphere at 700°Cto get $Li_{0.95}Na_{0.05}Ti_2$ $(PO_4)_3$/C.

2.2. Characterization of the prepared anode materials

Crystal structures of the prepared $Li_{0.95}Na_{0.05}Ti_2(PO_4)_3$/C nanocomposite were characterized by X-ray powder diffraction(XRD) using a Bruker Analytical X-ray System with CuKa radiation source. Scanning electronmicrographs(SEM) were obtained on a Hitachi-S4800 scanning electron microscope.

For electrochemical tests, anodes were prepared by pressing a powdered mixture of the sample, acetylene black, and poly(tetrafluoroethylene) (PTFE) in a weightratio of 80:10:10, stainless steel net as current collector. A two-electrode simulated battery consisting of the $LiMn_2O_4$ cathode and the prepared anode was used to test the electrochemical properties of the materials.Galvanostatic charge and discharge were performed on LAND-CT2001 Charge-discharge Test System in aqueous 5M Li_2NO_3 solution of pH=7. Discharge/charge cut-off voltages were set at 0.3 and 1.6 V.

Cyclic voltammetry was carried out with an electrochemical work station (Zahner-IM6e).A saturated calomel electrode (SCE) and a stainless steel mesh were used as reference and counter electrodes, respectively.

3. Results and discussion

SEM micrographs of $Li_{0.95}Na_{0.05}Ti_2(PO_4)_3$ and $Li_{0.95}Na_{0.05}Ti_2(PO_4)_3$/C nanocomposite are shown in Fig. 1. Evidently, the as-prepared materials with uniform particle size by sol-gel method. The size is about 300~400 nm. And The particle size increased to 400~500 nm after carbon coating.

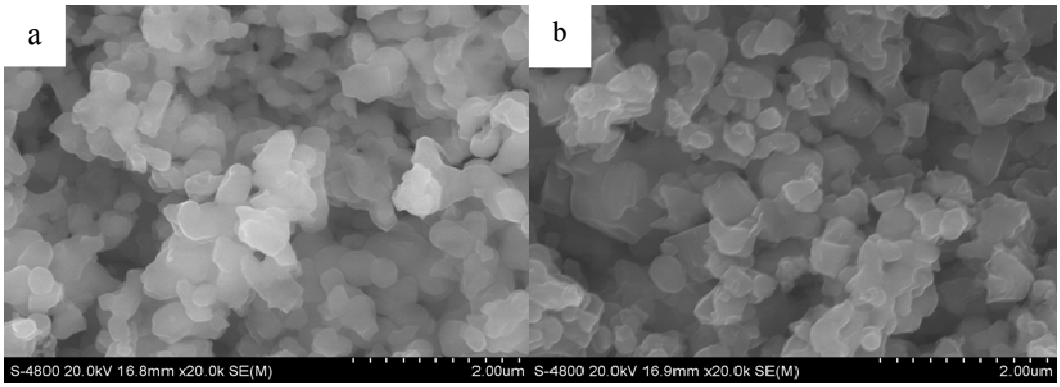

Fig.1 SEM images of $Li_{1-x}Na_xTi_2(PO4)_3$ (a) and $LiTi_2(PO_4)_3$/C(b) samples

The XRD pattern (Fig.2)shows that the characteristic peak positions of both $Li_{0.95}Na_{0.05}Ti_2(PO_4)_3$ and $Li_{0.95}Na_{0.05}Ti_2(PO_4)_3$/C coincide with the standard card. The main peaks are high intensity, narrow half-peak width, which indicated the as-prepared materials described full NASICON structure, polymorph complete development. The diffraction peak intensity of carbon coated materials decreases slightly.

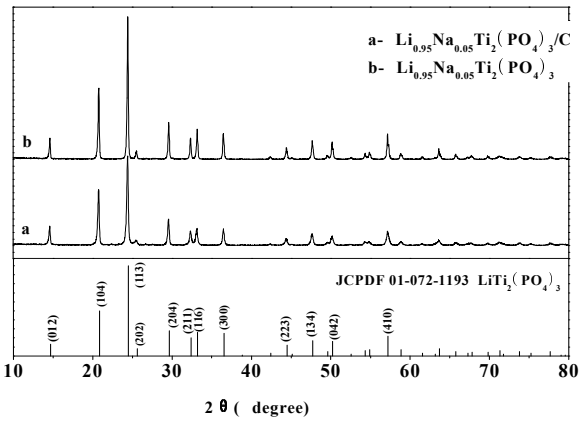

Fig.2 XRD pattern of $Li_{1-x}Na_xTi_2(PO4)_3$/C and $LiTi_2(PO_4)_3$/C samples

Cyclic voltammetry curves of $Li_{0.95}Na_{0.05}Ti_2(PO_4)_3$/C with different scan rates were measured. In order to prevent the hydrogen evolution reaction, scanning potential limitation in -0.8~0.2 V （vs.SCE）,as shown in Fig. 3. Obviously, the nanocomposite present one pair of sharp redox peaks that corresponds to the insertion and extraction of Li ions into and from the $Li_{0.95}Na_{0.05}Ti_2(PO_4)_3$/C structure.With increasing of scanning speed, the shape of peak changed, and the peak current is increased. The oxidation peak and the reduction peak respectively to the positive and negative direction, △U between oxidation potential and reduction potential increases (Figure 3). Shows that the electrode materials have a certain polarization phenomenon. Lithium ions diffusion coefficient in the electrode have great influence on charge discharge performance and battery polarization.

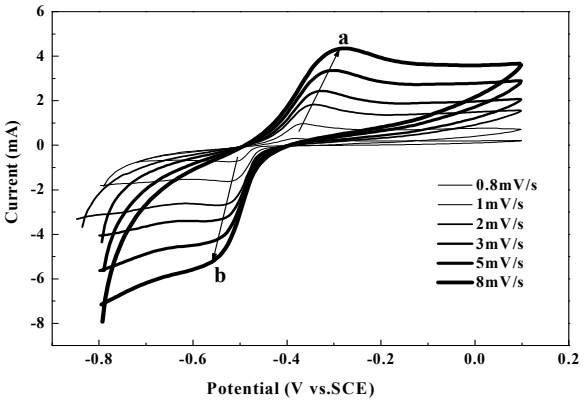

Fig. 3 Cyclic voltammograms of $LiTi_2(PO_4)_3/C$ at different scan rate

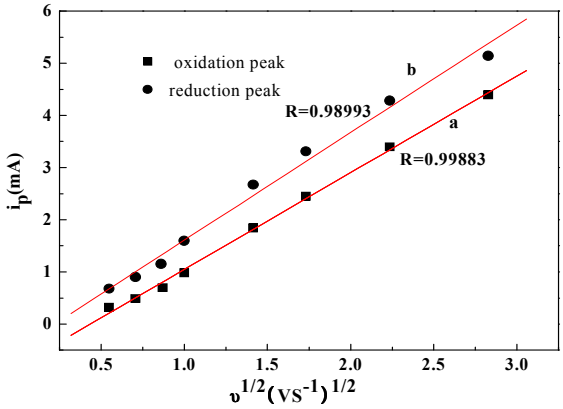

Fig. 4 Relationship of peak current (i_p) vs the square root of scan rate ($\upsilon^{1/2}$)

Relationship between the peak current and the scan rate was shown in Fig. 4. There is a linear relationship between the peak current (i_p) and the square root of the scan rate ($\upsilon^{1/2}$). The diffusion coefficient D_{Li} can be calculated under different peak values. According to Equation: $I_p = (2.69\times10^5)n^{3/2}AC_{Li}^{*}D_{Li}^{1/2}v^{1/2}$

In the experiment A=0.3cm^2，n=2，C_{Li}^{*} is calculated as follows:

$$C^{*}=\frac{n}{V}=\frac{6/6.02\times10^{23}}{1.31\times10^{-27}}=0.761\times10^{4}\ \text{mol/ m}^3$$

According to the Randles Sevcik equation

$$D=\frac{I_P^{\ 2}/v}{2.09^2\times10^{10}\times n^3A^2C^{*2}}$$

The diffusion coefficients of the Li ions were obtained for substitution parameters：4.302×10^{-5}cm^2/s，2.44×10^{-5}cm^2/s，which shows the diffusion coefficients of the oxidation and reduction reaction was basically in the same magnitude. But in the high-speed scanning, the reduction peak of each cycle of the area is larger than the oxidation peak area. The reversibility of material deteriorate in the fast charge-discharge cycle. Dissolution of the electrode material occurs so that the electrolyte becomes yellow, which may be one reason for the fast decay cycle capacity of the material in an aqueous solution. And in the slow scan, the reduction ratio of the peak area of the peaks and the oxidation is nearly equal, indicates that when a small current discharge $Li_{0.95}Na_{0.05}Ti_2(PO_4)_3/C$ material having good reversible deintercalation of lithium.

Fig.5 shows the initial charge-discharge curves of the materials with saturated $LiNO_3$ aqueous solution electrolyte. The initial discharge capacityof $Li_{0.95}Na_{0.05}Ti_2(PO_4)_3$ and $Li_{0.95}Na_{0.05}Ti_2(PO_4)_3/C$ obtained at this condition was 52.9mAh/g,47.6 mAh/g. Fig.6 shows the cyclling performance of $Li_{0.95}Na_{0.05}Ti_2(PO_4)_3$and $Li_{0.95}Na_{0.05}Ti_2(PO_4)_3/C$. The data were obtained at a current density of 0.2mA/cm^2 over the potential range0.3~1.6V.Evdently,discharge capacity of two anode materials were reduced with cycles, but $Li_{0.95}Na_{0.05}Ti_2(PO_4)_3/C$ material capacity fading slowly than $Li_{0.95}Na_{0.05}Ti_2(PO_4)_3$.

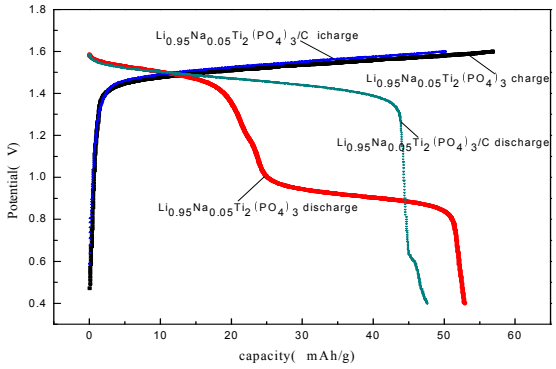

Fig.5 The initial charge-discharge curves of the materials

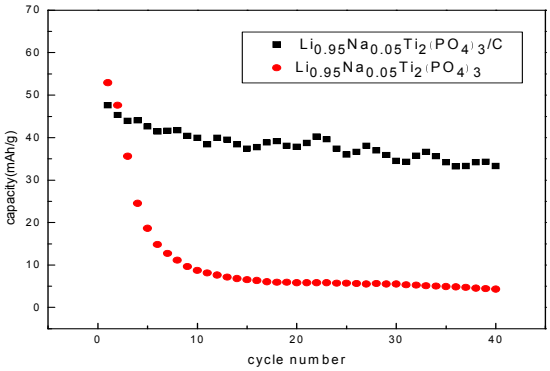

Fig.6 Cycling performance of the materials

The $Li_{0.95}Na_{0.05}Ti_2(PO_4)_3$/C anode materials simulated battery initial discharge capacity of 47.6 mAh/g, after 40 cycles, the discharge capacity of 33.3 mAh • g-1, the capacity retention rate of 70%. Although $Li_{0.95}Na_{0.05}Ti_2(PO_4)_3$ shows hihger capacity of 52.9mAh/g, 4.3 mAh/gremained after 40 cycles, the capacity retention rate of 8%.The possibility of the decomposition of water and the dissolution of $Li_{0.95}Na_{0.05}Ti_2(PO_4)_3$ lead to the capacity fading.

4.Conclusion:

$Li_{0.95}Na_{0.05}Ti_2(PO_4)_3$ prepared by sol-gel method shows completely NASICON structure , the size is about 300~400 nm, the carbon coated particle $Li_{0.95}Na_{0.05}Ti_2(PO_4)_3$/C size increased to 400~500 nm. By comparing the results of CV test, $Li_{0.95}Na_{0.05}Ti_2(PO_4)_3$/C material has good lithium reversible, but in the rapid scanning, Li^+ can not diffuse to the electrode surface, the polarization increases, which may be one of the reasons for capacity fading. Capacity of $Li_{0.95}Na_{0.05}Ti_2(PO_4)_3$/C the first discharge capacity of 47.6 mAh/g after 40 cycles, the discharge specific capacity is 33.3 mAh • g-1, the capacity retention was 70%.

Acknowledgements

This work was supported financially by the Natural Science Foundation of Hebei province (Project No. E2014209303) and Higher school scientific research project of Hebei Province .

References

[1] Wang H B, Huang K L, Zeng Y Q,et al. Electrochemical properties of TiP_2O_7 and $LiTi_2(PO_4)_3$ as anode material for lithium ion battery with aqueous solution electrolyte[J]. Electrochim.Acta, 2007, 52: 3280~3285

[2] Luo Jia Yan, Xia Yong Yao. Aqueous lithium-ion battery $LiTi_2(PO_4)_3/LiMn_2O_4$ with high power andenergy densities as well as superior cycling stability[J]. Adv.Funct.Mater., 2007, 17: 3877~3884

[3] Luo Jia Yan, XIA Yong Yao. Electrochemical profile of an asymmetric supercapacitor using carbon-coated $LiTi_2(PO_4)_3$ and active carbon electrodes [J]. Journal of Power Sources, 2009, 186(1): 224-227.

Advanced Materials Research Vols. 989-994 (2014) pp 320-324
© (2014) Trans Tech Publications, Switzerland
doi:10.4028/www.scientific.net/AMR.989-994.320

Effect of melting temperature on microstructure of in situ TiC/Al composite and formation mechanism of TiC

Huanlong YUAN[1,a], Zehua ZHOU[1,2], Zehua WANG[1], ZhaoJun ZHONG[1], Xin ZHANG[1], Xiaofeng XUE[1]

[1]Institute of Metals and Protection, College of Mechanics and Materials, Hohai University, Nanjing, 210098, China

[2]Changzhou Hohai Science &Technology Research Institute Co. Ltd, Changzhou, 213164, China

[a]email: yuanhuanlong@163.com

Keywords: melting temperature; in-situ; TiC/Al composite; Al_4C_3; Al_3Ti

Abstract. Formation mechanism of TiC in Al matrix at a rather low melting temperature using in situ technology was studied. And effect of the melting temperature on the microstructure of in-situ TiC/Al composite was investigated. The results indicate that, the resultants of TiC and Al_3Ti were found out in the matrix; however, no evidence showed that Al_4C_3, a resultant phase existed probably in TiC/Al composite in accordance with the relative reference, was found out. Compared to the sample of T750, more TiC and less Al_3Ti existed in the sample of T850, and morphography of Al_3Ti changed from block to bar with the increasing melting temperature. The melting temperature affected extremely the reaction speed and the resultants.

Introduction

TiC/Al composite prepared with in situ method has been studied for decades and presents broad applications including in automobile, aerospace and military industries due to its remarkable specific strength, stiffness and modulus [1, 2]. However there is no agreement on mechanism of in situ synthesis of TiC reacted in aluminum melt, though it has been investigated for many years [3]. Kun jiang[4] and M. K. premkumar[5] consider that TiC is formed from the reactants of dissolved carbon and titanium; but some studies[6, 7] support that resultant of TiC derives from the reaction of Al_3Ti and Al_4C_3; meanwhile, some researches[8, 9] think the mechanisms mentioned above exist together. Therefore, there is not an unified theory to explain the formation of TiC in TiC/Al composite.

Brittle Al_3Ti is considered as a harmful phase in the TiC/Al composite because it results severely in low properties of both strength and ductility. According to the reference[10], a proper approach to decrease the amount of Al_3Ti is to increase melting temperature of the TiC/Al composite. When the molting temperature was over 1000℃, Al_3Ti was effectively reduced, and the size of the resultant of TiC was 2-3μm[11]. The brittle phase of Al_3Ti disappeared when the melting temperature was above 1200℃[12]. However, two disadvantages are inevitable using this conventional method: waste of energy and rapid growth of TiC grains at a high melting temperature [13].

This paper presents a fabricating process of TiC/Al composite using in situ technique. The conventional Al-Ti-C mixed powder was used as the reaction system. A special device was designed to introduce the green contacts into the molten. The aim of our research is to discuss the mechanism of the formation of TiC in the system of Al-Ti-C by means of analysis of the change of the microstructure of the composites fabricated at different melting temperature, and effect of the melting temperature on the microstructure of TiC/Al composite was discussed. Two different melting temperatures of 750℃ and 850℃ were considered.

Experimental procedure

Commercial pure aluminum was used as the matrix, titanium powder (99.5% pure, 325 mesh), aluminum powder (99.5% pure, 200 mesh), graphite powder (99% pure, 200 mesh) were considered

as additives for the in situ reaction system. A mixture of powders was pressed into a cylindrical contact with a diameter of 10mm and a height of 10mm at 20MPa, in which the molar ratio of Ti:C was 1:1.2 and the content of aluminum powder was 30wt.%.

A pure aluminum ingot was first molten in a graphite crucible in the furnace, and then the contacts were put into the liquid Alumina. The schematic of the fabricating equipments was shown in Fig.1. After 15min, a stainless steel stirrer was used to improve the uniformity of the melting composite. The melt was held for 10min to release the gas and slag, then the melt was cast into a steel mold preheated to 200℃. The composite samples prepared at 750℃ and 850℃ were designated as T750 and T850, respectively.

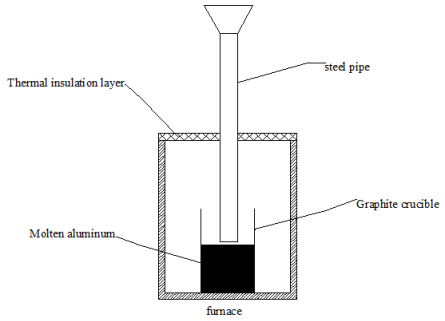

Fig.1Schematic diagrams of fabricating device for in situ TiC/Al composites

The microstructure was investigated by means of the optical microscope (OM), the scanning electron microscope (SEM) equipped with energy dispersive spectroscope (EDS). Phase analysis was performed using X-ray diffraction (scan rate was 0.02^{o}/s).

Results and discussion

In the process, the contacts were rapidly dropped into the liquid Alumina and the in situ reaction took place inside the liquid, and no visible spark appeared.

The XRD pattern (Fig.2) shows that there are four phases in the product of T750 and T850, i.e. Al, Al_3Ti, TiC and C , The emergence of graphite in the sample of T750 and T850 indicates that the reactions has not took place completely, but it worth noting that the amount of graphite is very little in T850. The diffraction peak of Al_3Ti in the T850 is weaker than that in the sample of T750, indicate that the amount of Al_3Ti in the product of T850 is lower.

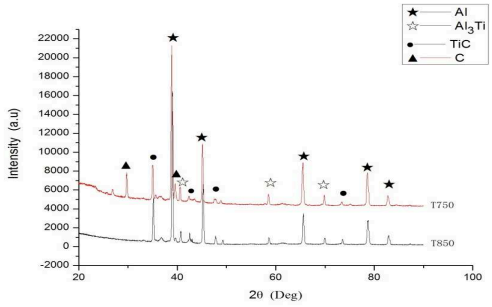

Fig. 2 XRD patterns of the sample T750 and T850

Fig.3 (a) shows the micrograph of sample T850. The grain boundary is clearly delineated by some tiny second phases, it was considered that these tiny particles were pushed by grain boundaries during solidification, Rod-like Al_3Ti was also founded in sample T850 (Fig.4). Combining XRD patterns in Fig. 2 and EDS results in Fig. 5, these tiny particles distributing at the grain boundary were confirmed as the compound of Al_3Ti and TiC.

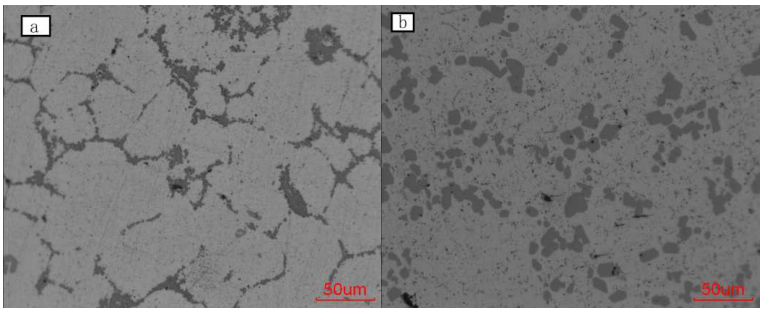

Fig.3 (a) OM micrograph of T850; (b) OM micrograph of T750

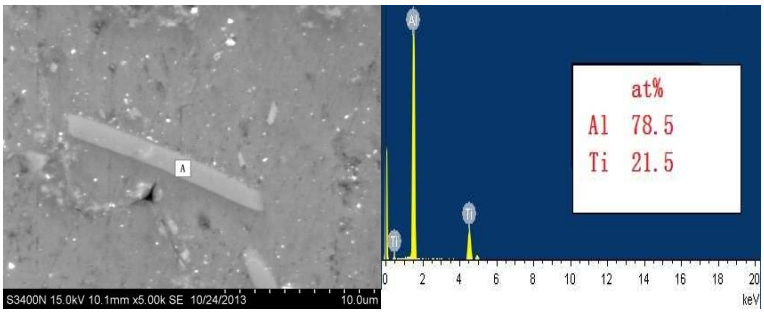

Fig.4 SEM photographs of the rod phase in T850, the composition of A was listed in right table

Fig.3 (b) shows the OM micrograph of T750. It was found that there were many block-like Al_3Ti in the matrix as well as some graphite phase. The interface and the map scanning distribution of elements of the dark zones in sample T750 was shown in Fig.6, Graphite phase was surrounded by a layer which was rich in titanium. It was confirmed as the mixture of Al_3Ti and TiC.

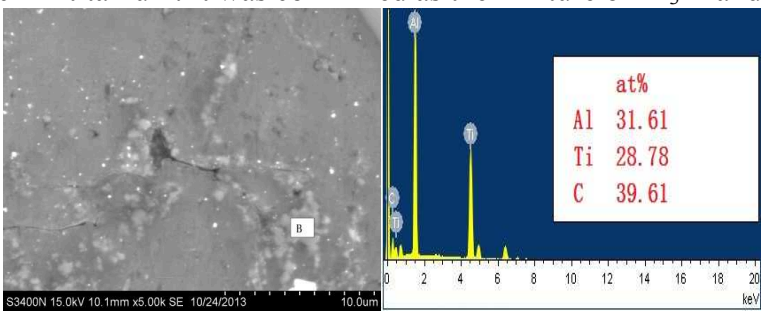

Fig.5 SEM photograph of the phase assemble at the boundary, EDS results of point (B) is listed on the left photograph.

The TiC/Al composite system has been investigated by many researchers, but the mechanism of the reactions is still unknown. Some reactions may take place as the follows equations:

$$Ti(s) + C(s) \rightarrow TiC(s) \quad (1)$$

$$Al(l) + Ti(s) \rightarrow Al_3Ti(s) \quad (2)$$

$$Al(l) + C(s) \rightarrow Al_4C_3(s) \quad (3)$$

$$Al_4C_3(s) + Ti(s) \rightarrow Al(l) + TiC(s) \quad (4)$$

$$Al_3Ti(s) + Al_4C_3(s) \rightarrow Al(l) + TiC(s) \quad (5)$$

$$Al_3Ti(s) + C(s) \rightarrow Al(l) + TiC(s) \quad (6)$$

Reaction (1) would not happen if the temperature under 1873K. In the early stage of the reaction, the temperature was low, the condition of the Thermodynamic was not enough, this reaction is not the main source of the TiC. The Gibbs free energy of reaction (2) is negative. Moreover, it is known that the reaction (2) occurs between 890~990K, and this reaction will release huge energy, the vast heat coming from the reaction (2) would accelerate the formation of TiC, there is no evidence (4) , (5) and (6) which reaction is the source of TiC. For reaction (4), firstly, whether the reaction (4) occur or not depend on the reaction (3), secondly, it is known that at the beginning of the reaction, almost all of the titanium is consumed by the reaction (2). So there is almost no Ti was left for the

reaction (4), the XRD pattern (Fig.2) and EDS indicate that there is no Al_4C_3 exist in the composites, in spite of some articles [14, 15] reported that Al_4C_3 was found in the product of TiC/Al composite. This phenomenon may have three assumptions:

1. The amount of Al_4C_3 is too little to be found.
2. The produced Al_4C_3 has been consumed by other reactions.
3. Al_4C_3 has not been produced.

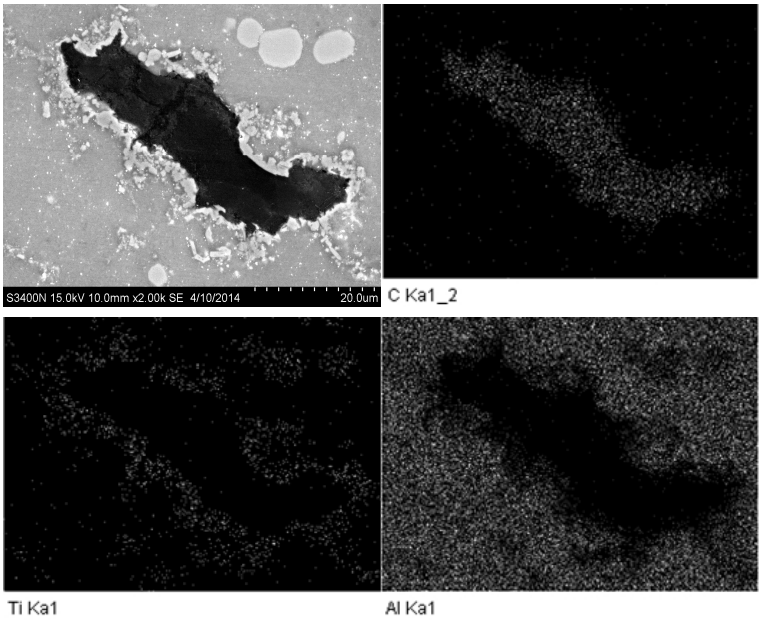

Fig.6 The interface and the map scanning distribution of elements of the black area in T750

There is no sign of Al_4C_3 neither in EDS nor in XRD pattern, so the first assumption is too farfetched; As for the second assumption, for the sample of T750, the melt temperature was only 750℃, and the mojority of the second phases is Al_3Ti, so it is highly unlikely that the reaction completed totally, and this assumption can be denied according to the direct proportional relationship of Al_3Ti and C in T750 and T850. The third assumption is the best answer for the absent of Al_4C_3. In that case, Reaction (6) is the source of TiC. This conclusion can be explained by the information of Fig.6. It is very clear that graphite is surrounded by Al_3Ti and TiC, it seems that the reaction has not totally complete before solidification. Meanwhile, the amount of TiC has increased along with the decrease of Al_3Ti. This fact is confirmed by the XRD pattern (Fig.2) analysis.

The reactions take place once the contacts were introduced into the aluminum melt. Al_3Ti was formed firstly from the reaction between aluminum and titanium, with the help of the huge energy released from the reaction (2), reaction (3) occurs, due to the low melt temperature, the speed of the reaction (2) is slower in T750 than T850, and the ultimate temperature of T750 is lower than T850, the reaction (3) is more completely in T850 , so there is more TiC and little Al_3Ti in T850; the consume of Al_3Ti result in the decrease of the amount of Al_3Ti and the change in morphography of Al_3Ti, this is confirmed by the phenomenon of tiny Al_3Ti and TiC was assembled around the graphite while other Al_3Ti was bigger in size which was far away from the graphite (Fig.6).

Conclusions

TiC/Al composites were successfully fabricated using in situ method, formation mechanism of TiC was investigated, and effect of the melt temperature on the microstructure of the composite was also discussed. The results indicate that two step of the reaction for the formation of TiC are inevitable in low melt temperature, i.e., Al_3Ti was firstly formed, then the reaction between Al_3Ti and graphite occur, this reaction is the source of TiC. When the melt temperature was 750℃, there are a lot of unreacted block-like Al_3Ti in the composite, when the temperature was increased to 850℃, the amount of Al_3Ti decreased and its shape changed into bar-like. In addition, in the whole

process, the resultants of TiC and Al_3Ti were found out in the matrix; no Al_4C_3 phase was found out, which means the study is opposite to some reference. Compared to the sample of T750, more TiC and less Al_3Ti existed in the sample of T850, and morphography of Al_3Ti changed from block to bar with the increasing melting temperature. The melting temperature affected extremely the reaction speed and the resultants.

Acknowledgements

This work is supported by Changzhou Research Program of Application Foundation (CJ20125002, Changzhou city).

Reference

[1] Rohatgi P K. Metal matrix composites[J]. Defence Science Journal, 2013,43(4):323-349.
[2] Travitzky N, Bonet A, Dermeik B, et al. Additive Manufacturing of Ceramic-Based Materials[J]. Advanced Engineering Materials, 2014.
[3] Liu Z, Wang X, Han Q, et al. Synthesis of submicrometer-sized TiC particles in aluminum melt at low melting temperature[J]. Journal of Materials Research, 2014,29(07):896-901.
[4] Jiang K, Liu X. The effect of melting temperature and time on the TiC particles[J]. Journal of Alloys and Compounds, 2009,484(1):95-101.
[5] Premkumar M K, Chu M G. Synthesis of TiC particulates and their segregation during solidification in In Situ processed AI-TiC composites[J]. Metallurgical and Materials Transactions A, 1993,24(10):2358-2362.
[6] Wang Z, Liu X, Zhang J, et al. Reaction mechanism in the ball-milled Al—Ti—C powders[J]. Journal of materials science letters, 2003,22(20):1427-1429.
[7] Kennedy A R, Weston D P, Jones M I, et al. Reaction in Al-Ti-C powders and its relation to the formation and stability of TiC in Al at high temperatures[J]. Scripta materialia, 2000,42(12):1187-1192.
[8] Yang B, Chen G, Zhang J. Effect of Ti/C additions on the formation of Al< sub> 3 Ti of in situ TiC/Al composites[J]. Materials & Design, 2001,22(8):645-650.
[9] Yang B, Wang F, Zhang J S. Microstructural characterization of in situ TiC/Al and TiC/Al–20Si–5Fe–3Cu–1Mg composites prepared by spray deposition[J]. Acta materialia, 2003,51(17):4977-4989.
[10] Jiang Q C, Wang H Y, Guan Q F, et al. Effect of the Temperature of Molten Magnsium on the Thermal Explosion Synthesis Reaction of Al–Ti–C System for Fabricating TiC/Mg Composite[J]. Advanced Engineering Materials, 2003,5(10):722-725.
[11] Liang Y F, Zhou J E, Dong S Q. Microstructure and tensile properties of in situ TiC< sub> $_p$/Al–4.5 wt.% Cu composites obtained by direct reaction synthesis[J]. Materials Science and Engineering: A, 2010,527(29):7955-7960.
[12] Bauri R, Yadav D, Suhas G. Effect of friction stir processing (FSP) on microstructure and properties of Al–TiC in situ composite[J]. Materials Science and Engineering: A, 2011,528(13):4732-4739.
[13] Kim W J, Yu Y J. The effect of the addition of multiwalled carbon nanotubes on the uniform distribution of TiC nanoparticles in aluminum nanocomposites[J]. Scripta Materialia, 2014,72:25-28.
[14] Mazaheri Y, Meratian M, Emadi R, et al. Comparison of microstructural and mechanical properties of Al–TiC, Al–B< sub> 4 C and Al–TiC–B< sub> 4 C composites prepared by casting techniques[J]. Materials Science and Engineering: A, 2013,560:278-287.
[15] Ding H, Liu X. Influence of Si on stability of TiC in Al melts[J]. Transactions of Nonferrous Metals Society of China, 2011,21(7):1465-1472.

Advanced Materials Research Vols. 989-994 (2014) pp 325-330
© (2014) Trans Tech Publications, Switzerland
doi:10.4028/www.scientific.net/AMR.989-994.325

Effect of Cr on microstructure and mechanical properties of Al–3.2Mg alloys

Zhaojun ZHONG[1,a], Zehua ZHOU[1], Zehua WANG[1], Xin ZHANG[1], Huanlong YUAN[1], Xiaofeng XUE[1]

[1]Institute of Metals and Protection, College of Mechanics and Materials, Hohai University, Nanjing 210098, China

[a]Email: zhongzhaojun89@126.com

Key words: Al-3.2Mg alloys; microstructure; alloy element; tensile property

Abstract: Effect of Cr element on microstructure of Al-3.2Mg alloys was investigated using optical microscopy, scanning electron microscopy (SEM) and EDS. Moreover, the tensile and hardness test were carried out. The results show that a minor additive of Cr can refine effectively the secondary dendrite arm spacing and decrease the number of coarse interdendritic structures. In the whole series of the alloys, the secondary dendrite arm spacing of Al–3.2Mg-0.1Cr alloy was the smallest, and the spacing presented an increasing trend with the Cr content. With high levels of Cr, the intermetallic compounds are formed by Cr with Al, Mg and Fe, the shape of the second phase particles were transformed from bulky bone shape to fine bone shape and long striped. The strength and the hardness of Al–3.2Mg alloys were greatly improved when the additions of Cr were 0.05% and 0.1%, but the ductility of the alloys remained at a low level by adding 0.05%Cr. Therefore, combining with the comprehensive properties and the microstructure, the best addition of Cr in the alloy was 0.10% in the whole series.

1. Introduction

Al-Mg series alloys are very important light-weight structure materials among advanced engineering materials, attracting more and more interest due to their remarkable mechanical properties. The alloys have been widely used in aerospace industries, transportation, ship structure, wire and cable fields with respect to their advantages, such as favorable strength, high ductility, low density, good workability and good corrosion resistance, etc [1–3].

Al-Mg series alloys have been widely studied for a long time, Al-3.2Mg alloy belongs to the alloy that can not be strengthened by heat treatment. In general, in order to broaden the application of Al–Mg series alloys, mechanical properties need to be further improved. Currently, micro-alloying and pre-strain have been used to improve the mechanical properties of Al–Mg series alloys. Mg is the main alloying element, the favorable strength of Al-Mg alloy derives from the solid-solution strengthening of magnesium [4]. Other alloying elements such as chromium and zirconium are also very important in strengthening. One approach toward improving the strength of Al-Mg alloys is to add small quantities of Cr. Cr is the common alloying elements in Al-Mg and Al-Mg-Si alloy, because it can improve and enhance the mechanical properties of the alloy [5-7]. While several researchers have indicated that Cr element can increase the strength of Al-Mg alloys, but the relationship between Cr content and the mechanical properties of Al-3.2Mg alloy have not been systematically reported. So this study was attempted to find the optimal formula of alloy content and investigate the effects of Cr on the microstructure and mechanical properties systematically.

2. Experimental

A series of Al-3.2Mg alloys were produced by pure Al, pure Mg and Al-10%Cr master alloy. The normal compositions of the studied alloys are listed in Table 1. The alloys were melted in graphite crucible in an electric resistance furnace, the melting temperature of the alloy was kept at 780 °C and casting was kept at 710 °C. After the process of C_2Cl_6 addition, the alloy melt was held

for 5 min and then cast into an iron mold. The specimens of metallographic analysis were cut from the center of the ingot. Cylindrical tensile specimens were machined from the as-casting specimens.

The Olympus optical microscope (OM, OLYMPUS BX51M, Japan) was used to observe the metallurgical microstructure of the specimens. The micrographs of fractures were observed by scanning electronic microscope (SEM, HITACHI-3400N, Japan) in order to evaluate the fracture mechanisms. Microstructure examination and composition analysis were carried out using scanning electron microscope (SEM, HITACHI-3400N,Japan) coupled with energy-dispersive spectrometry (EDS, Horiba-EX250, Japan).Tensile tests using a tensile test machine (INSTRON-3367, USA) at room temperature. Hardness was determined in HBE-3000A brinell hardness machine.

Table1 Chemical compositions of Al-Mg (-Cr) alloys (mass fraction, %)

Sample No	Mg	Cr	Al
1	3.2	----	Bal
2	3.2	0.05	Bal
3	3.2	0.10	Bal
4	3.2	0.15	Bal
5	3.2	0.20	Bal
6	3.2	0.25	Bal
7	3.2	0.30	Bal

3. Results and discussion

3.1 As-cast microstructures

Fig.1 shows the optical microstructure of the as-cast Al-3.2Mg (-Cr) alloy. As shown in Fig.1(a), dendritic structures can be observed clearly in No.1 alloy, the coarse dendrite was found in cast structure of the Al-3.2Mg alloy. As shown in Fig.1 (b)-(g), it can be seen that the microstructure of the alloys was still the dendritic structures, but the coarse dendritic structure became less. The nano particle size of the measurer analysis software was used to measure the secondary dendrite arm spacing of alloy. As shown in Table 2, the secondary dendrite arm spacing of the as-cast Al-3.2Mg-(Cr) was decreased. Table2 shows that the increase of Cr element from 0.05% to 0.1% can reduce the secondary dendrite arm spacing markedly. However, increasing the percentage of Cr element from 0.15% to 0.3% makes the secondary dendrite arm spacing showing a trend of coarsening. The secondary dendrite arm spacing of No.1 alloy was the largest, and the average size of No.1 alloy was about 17.269 μm. The secondary dendrite arm spacing of No.3 alloy was the smallest, the average size of which was about 14.583 μm. The results show that a minor additive of Cr can refine the secondary dendrite arm spacing effectively and decrease the number of coarse interdendritic structures.

The process of alloy solidification is usually conducted from surface to the center, and the final morphology of grain depends on the front liquid condition of the interface of solidification [8-10]. Dendrites usually appear in the large and wide area of constituent supercooling [11]. Cr element is known to have greater affinity with aluminum. Thus Cr element enters the groups of atoms formed by melt structure and melt energy easily. The structure of the atoms cluster containing Cr is proved to be more stable. What's more, the atoms cluster is easier to grow up to be the basement of the nucleation. Therefore, Cr element can refine the growth of the as-cast grain effectively to some extent. But excessive amount of Cr element would greatly increase the degree of supersaturation of solid solution. It will lower the constituent supercooling of the solidification front in the liquid phase, which will lead the embryos of solidification interface to continue growing in liquid phase. In this way, the bulky dendrite will finally appear in the ingot casting organization [11-14]. At the same time, excess Cr can also form bulky intermetallic compounds. When the bulky intermetallic compounds become nucleation particles, the as-cast organization will coarsen. It is the reason that

increasing Cr from 0.15% to 0.3% makes the secondary dendrite arm spacing showing a trend of coarsening.

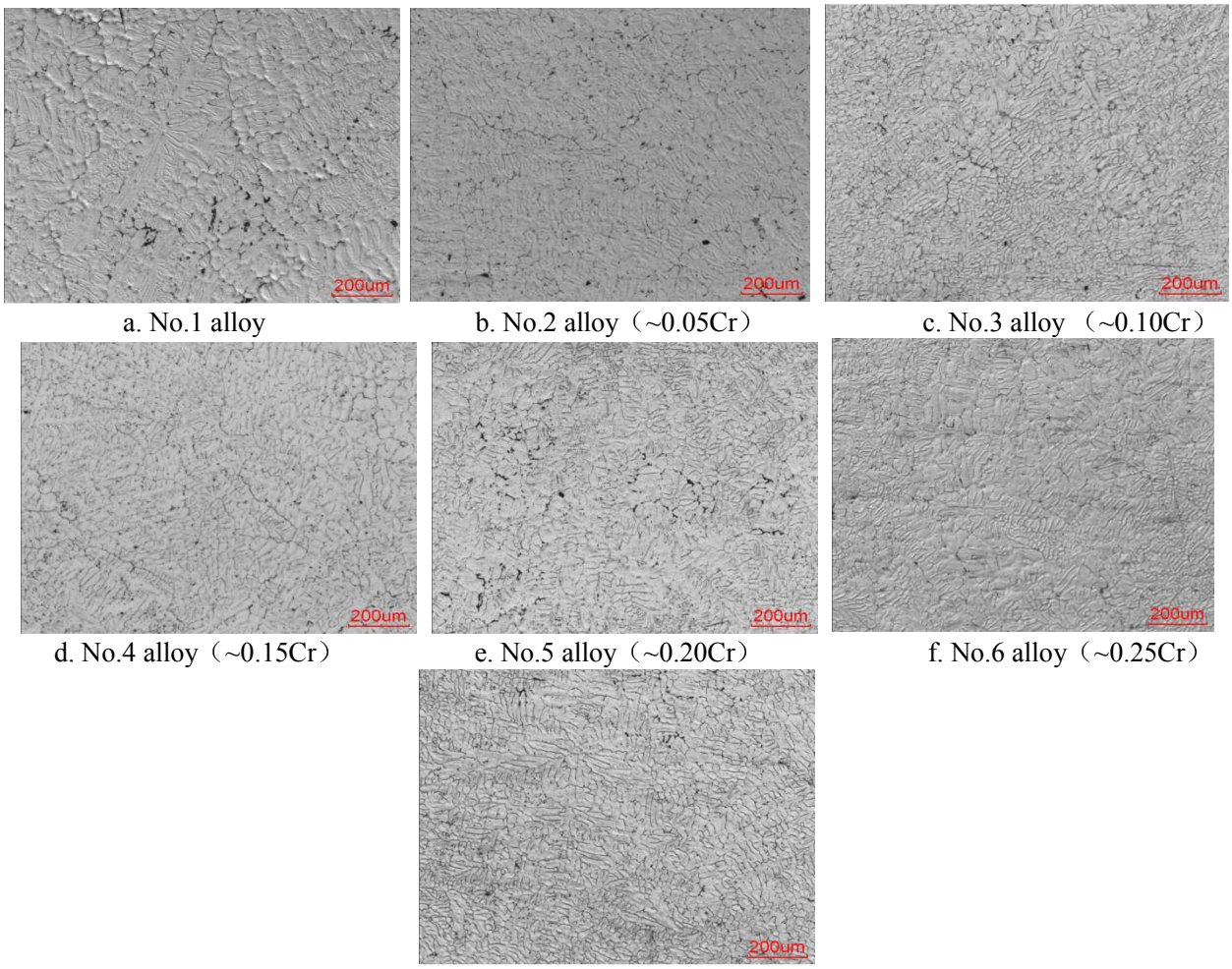

a. No.1 alloy b. No.2 alloy（~0.05Cr） c. No.3 alloy （~0.10Cr）

d. No.4 alloy（~0.15Cr） e. No.5 alloy（~0.20Cr） f. No.6 alloy（~0.25Cr）

g. No.7 alloy（~0.30Cr）

Figure.1 Optical microstructure of the as-cast Al-3.2Mg (-Cr) alloy

Table2 The secondary dendrite arm spacing of Al-3.2Mg (-Cr) alloys

Sample No	1	2	3	4	5	6	7
Size(μm)	17.269	15.349	14.583	15.762	15.442	16.320	16.745

Fig.2 shows the high magnification optical microstructure of as-cast Al-3.2Mg (-Cr) alloy. As shown in Fig.2, the intermetallic compound formed at the grain boundaries as well as around the dendrites. SEM image of as-cast microstructure is shown in Fig.3. Combining with Fig.2 as well as Fig.3, it can be seen that the bone shape second phase particles are found. With high levels of Cr, the shape of the second phase particles were transformed from bulky bone shape to fine bone shape and long striped. But in excess of Cr can also form a small amount of bulky intermetallic compounds. The results of each EDS analyze of the four alloy show that the main elements of the intermetallic compounds are Al, Mg, Fe in No.1, No.2 alloy. And the main elements of the intermetallic compounds are Al, Mg, Cr, Fe in No.7 alloy. It can be deduced that the intermetallic compounds are formed by Cr with Al, Mg and Fe.

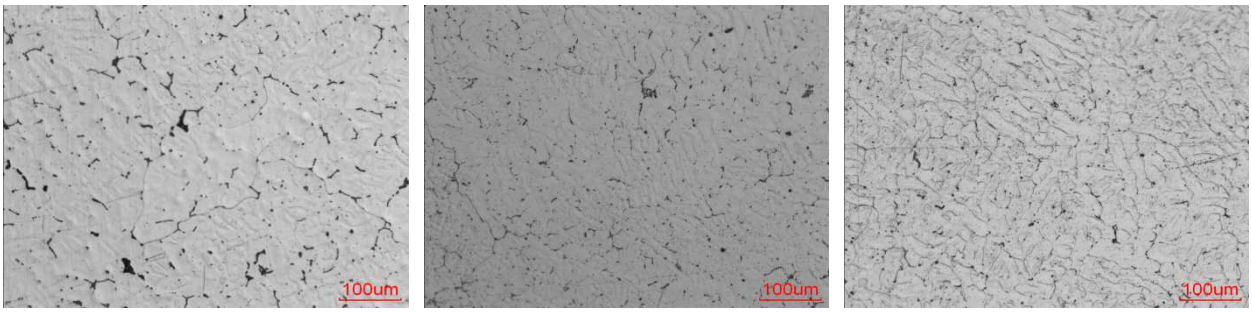

a. No.1 alloy b. No.2 alloy（~0.05Cr） c. No.7 alloy（~0.30Cr）

Figure.2 Optical microstructure of the as-cast Al-3.2Mg (-Cr) alloy

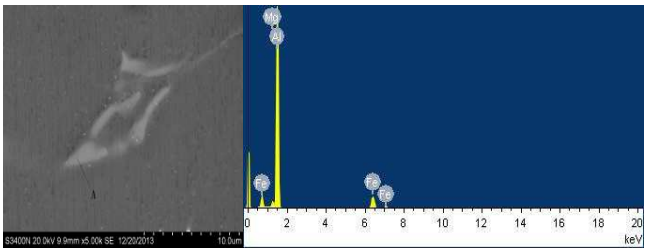

a. No.1 alloy

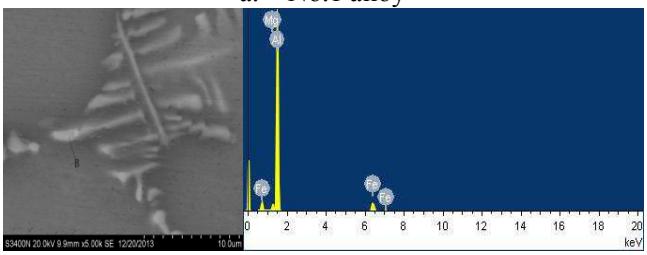

b. No.2 alloy

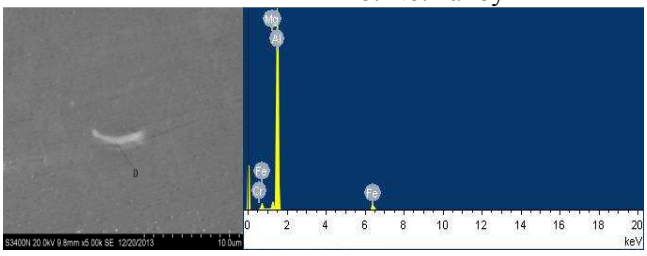

c. No.7 alloy

Figure.3 SEM image of second phase particles and EDS spectrum of particle

3.2 Mechanical properties

Tensile and hardness tests were performed to acquire the effect of Cr on mechanical properties of the cast aluminum alloy. Fig.4 shows the mechanical properties of the as-cast alloys. Both brinell hardness and tensile strength increased with addition of Cr, but the elongation was somewhat decreased. When Cr element content was 0.05% and 0.1%, the brinell hardness and the tensile strength both increased greatly, but elongation was greatly reduced by adding 0.05%Cr. Comprehensive consideration, the best content of Cr to the mechanical properties was 0.10%. The ultimate tensile strength and the tensile strain of the Al-3.2Mg-0.1Cr alloy were 197.7MPa and 37.4%. Compared with Al-3.2Mg alloy (185.5MPa and 39.2%), the tensile strength was increased by 6.6% and the tensile strain was decreased 4.8%.

Combined with optical microstructure and EDS spectrum of particle, the dendrites were refined with the addition of Cr in some degree. With the increase of Cr content, the secondary dendrite arm spacing increased first and then decreased. When the content of Cr element was 0.1%, the secondary dendrite arm spacing was the smallest, and the tensile strength was the largest. With the increase of the secondary dendrite arm spacing, the tensile strength showed a trend of falling. But when the Cr element added too much, the dendrites were coarsen and the coarse grain had more

dislocation pile-up than fine grain, therefore, it was easy to produce larger stress concentration and generate crack initiation, which lead to the decrease of the ductility [15-17].

Part of Cr element can functioned as solution strengthening elements. With the increase of Cr content, the intermetallic compounds are formed by Cr with Al, Mg and Fe. The shape of the second phase particles are transformed from bulky bone shape to fine bone shape and long striped. The fine bone shape and long striped intermetallic compound and the dendrites play a role as barriers to the transmission of the dislocations and hinder the crack propagating [18].

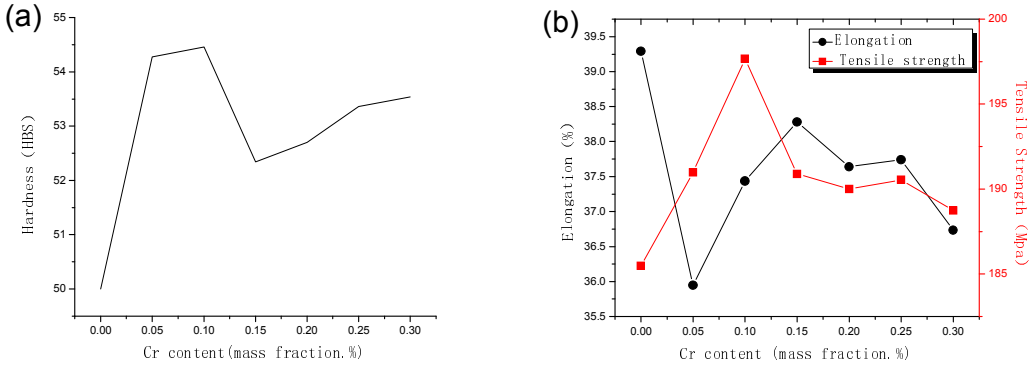

Figure.4 Mechanical properties of studied alloys: (a) Brinell hardness of alloys at different Cr content; (b) Tensile properties of alloys at different Cr content

4. Conclusions

（1）The secondary dendrite arm spacing of the as-cast alloy will decrease with adding a small amount of Cr content. But excessive amounts of Cr element would greatly increase the degree of supersaturation of solid solution, In this way, the bulky dendrite will finally appear in the ingot casting organization.

（2）With increasing Cr content, the shape and size of the second phase are transformed from bulky bone shape to fine bone shape and long striped. But at the same time, excess Cr can also form bulky intermetallic compounds.

（3）Brinell hardness and tensile strength increased with addition of Cr, and the elongation was somewhat decreased. Comprehensive consideration, the best content of Cr was 0.10%.

References

[1] Witkin D, Lee Z, Rodriguez R, et al. Al–Mg alloy engineered with bimodal grain size for high strength and increased ductility[J]. Scripta Materialia, 2003, 49(4): 297-302.

[2] Liu Z, Li Z, Wang M, et al. Effect of complex alloying of Sc, Zr and Ti on the microstructure and mechanical properties of Al–5Mg alloys[J]. Materials Science and Engineering: A, 2008, 483: 120-122.

[3] Peng Y Y, Yin Z M, Nie B, et al. Effect of minor Sc and Zr on superplasticity of Al-Mg-Mn alloys[J]. Transactions of Nonferrous Metals Society of China, 2007, 17(4): 744-750.

[4] Lodgaard L, Ryum N. Precipitation of dispersoids containing Mn and/or Cr in Al–Mg–Si alloys[J]. Materials Science and Engineering: A, 2000, 283(1): 144-152.

[5] Portnoy V K, Rylov D S, Levchenko V S, et al. The influence of chromium on the structure and superplasticity of Al–Mg–Mn alloys[J]. Journal of Alloys and Compounds, 2013, 581: 313-317.

[6] Yongdong H, Xinming Z, Zhiqiang C. Effect of minor Cr, Mn, Zr, Ti and B on grain refinement of as-cast Al-Zn-Mg-Cu alloys[J]. Rare Metal Materials and Engineering, 2010, 39(7): 1135-1140.

[7] Peng G, Chen K, Fang H, et al. Effect of Cr and Yb additions on microstructure and properties of low copper Al–Zn–Mg–Cu–Zr alloy[J]. Materials & Design, 2012, 36: 279-283.

[8] Flemings M C. Solidification processing[J]. Metallurgical transactions, 1974, 5(10): 2121-2134.

[9] Liu X, Zeng M Q, Ma Y, et al. Melting behavior and the correlation of Sn distribution on hardness in a nanostructured Al–Sn alloy[J]. Materials Science and Engineering: A, 2009, 506(1): 1-7.

[10] Wei L Y, Dunlop G L. The solidification behaviour of Mg-Al-rare earth alloys[J]. Journal of Alloys and compounds, 1996, 232(1): 264-268.

[11] Dang J Z, Huang Y F, Cheng J. Effect of Sc and Zr on microstructures and mechanical properties of as-cast Al-Mg-Si-Mn alloys[J]. Transactions of Nonferrous Metals Society of China, 2009, 19(3): 540-544.

[12] Rocha O L, Siqueira C A, Garcia A. Heat flow parameters affecting dendrite spacings during unsteady-state solidification of Sn-Pb and Al-Cu alloys[J]. Metallurgical and Materials Transactions A, 2003, 34(4): 995-1006.

[13] Grugel R N. Secondary and tertiary dendrite arm spacing relationships in directionally solidified Al-Si alloys[J]. Journal of materials science, 1993, 28(3): 677-683.

[14] Veldman N L M, Dahle A K, StJohn D H, et al. Dendrite coherency of Al-Si-Cu alloys[J]. Metallurgical and Materials Transactions A, 2001, 32(1): 147-155.

[15] Xiao D H, Wang J N, Ding D Y, et al. Effect of rare earth Ce addition on the microstructure and mechanical properties of an Al–Cu–Mg–Ag alloy[J]. Journal of Alloys and Compounds, 2003, 352(1): 84-88.

[16] Zou L, Pan Q L, He Y, et al. Effect of minor Sc and Zr addition on microstructures and mechanical properties of Al-Zn-Mg-Cu alloys[J]. Transactions of Nonferrous Metals Society of China, 2007, 17(2): 340-345.

[17] Wang Q G. Microstructural effects on the tensile and fracture behavior of aluminum casting alloys A356/357[J]. Metallurgical and Materials Transactions A, 2003, 34(12): 2887-2899.

[18] Ohamed A M A, Samuel F H. Microstructure, tensile properties and fracture behavior of high temperature Al–Si–Mg–Cu cast alloys[J]. Materials Science and Engineering: A, 2013, 577: 64-72.

Advanced Materials Research Vols. 989-994 (2014) pp 331-336
© (2014) Trans Tech Publications, Switzerland
doi:10.4028/www.scientific.net/AMR.989-994.331

Research on preparation of Aluminum-metal coating and its microstructure by melting-casting

Xiaofeng Xue[1,a], Zehua Zhou[1], Zehua Wang[1], Jia Shao[1], Huanlong Yuan[1], Zhaojun, Zhong[1]

[1]College of Mechanics and Materials, Hohai University, Nanjing, 210098, China
[a]email: xue.xi.aofeng@163.com

Keywords: Melting-Casting; Al_2O_3-metal coating; Microstructure; Element distribution.

Abstract: A sort of Aluminum-metal coating, which is characterized by a bi-layered structure of Fe_2O_3+Cr_2O_3+Al plus NiO+Al layers, was successfully prepared on steel substrate by melting-casting technique. The microstructure, the bonding status of the interface between the coating and the substrate, and the element distribution of the coating were studied. The results indicate that, there is an excellent bonding between the coating and the substrate, and no hole and gap in the composite is found out. Moreover, there is obvious element diffusion in the interface. The coating is composed of block phase, columnar grain, and dendrites. In addition, the elements present a uniform distribution in the interface but an obvious segregation in the middle of the coating.

1. Introduction

In modern industry, many metal components of machinery are often surrounded by some harmful media such as corroded gas, water or chemical medium. They are also suffered from severe wear due to their relative motion. The surface failure is easily caused by the mentioned factors. Correspondingly, low working life or high maintenance cost becomes inevitable [1].

The cermets coating has exhibited excellent properties on resistances against wear and corrosion. Therefore, preparation of cermets coatings on the components is an effective method to reduce wear and corrosion [2]. A number of coating techniques like atmospheric plasma spray [3-4], High Velocity Oxy-fuel [5-6], laser cladding [7], plasma cladding [8], vapour deposition [9-10], and so on, have been investigated to produce cermets coating used in abrasive and erosive wear.

Self-propagating high-temperature synthesis (SHS) is an advanced technology to produce ceramics, cermets and intermetallic materials. Materials prepared by SHS are reported to be purer and require less energy than conventional methods, which are generally energy and time-intensive processes [11-13]. Researchers have tried to obtain ceramic, cermets and intermetallic coatings on metal substrates by SHS. This is a novel coating technology, which combines the fabrication of a material with its coating process. Thick coatings could be produced by it, too [14].

This study was attempted to prepare Al_2O_3 ceramic-metal coating on steel substrate with SHS process at a static condition, which meant that no complicated equipment and strict working conditions were necessary. The morphology, combining condition of interface between the Al_2O_3-metal coating and substrate were investigated in detail, as well as organizations and the distribution of elements in the coating.

2. Experimental method

2.1 Coating preparation

The characteristics of the experimental raw materials are shown in Tab. 1

Table 1 The characteristics of experimental raw materials

Raw material	Fe_2O_3	Cr_2O_3	Al	NiO
Purity（wt.%）	99.0	99.0	99.0	99.0
Particle size（μm）	0.2-0.8	0.5-2.0	4-70	0.3

The ingredient of the SHS system was based on the chemical reaction equations (1)-(3) and a little more Al powders were added to ensure the reaction completely. So the molar ratio of Fe_2O_3: Cr_2O_3: Al was 6:4:21, and the molar ratio of NiO: Al was 3:2. The powders were mixed for 6 hours in a ball-mixed mill. Carbon steel Q235 was used as the substrate with dimension of 50mm×40mm ×6mm and it was sandblasted and cleaned before coating.

$$Fe_2O_3 + 2Al \rightarrow Al_2O_3 + 2Fe \quad (1)$$

$$Cr_2O_3 + 2Al \rightarrow Al_2O_3 + 2Cr \quad (2)$$

$$3NiO + 2Al \rightarrow Al_2O_3 + 3Ni \quad (3)$$

The transition layer and working layer powders were mixed evenly with alcohol respectively, forming a paste. Put the obtained paste transition layer on the pre-treatment steel substrate surface with a thickness of about 5 mm. Bake them in an oven at 100 ℃ for two hours; Put the working layer paste on the above of transition layer with thickness of approximately 22 mm. Then bake them at 100 ℃ for six hours. Then the coated sample was placed in a resistance furnace heated to 500 ℃. Trigger the synthesis reaction system by igniting the magnesium ribbon.

2.2 Analysis and test equipment

The surface morphology and microstructure of the coating, the interface of the coating and substrate were observed by means of Hirox KH-7700 Digital Microscope, Olympus BX51M microscope (OM) and Hitachi S-3400N Scanning electron microscopy (SEM) respectively. The distribution of chemical elements was ascertained with Horiba EX-250 energy dispersive spectrometer (EDS).

3. Results and Discussion

3.1 Morphology of the interfacial region

Fig. 1 shows the interface figure of coating-substrate region after etching. It was clear to find three regions in fig. 1, labeled A, B, C, respectively. The A, B, C regions were analyzed by energy dispersive spectrometer, and the results were shown in Table 2. Point A was mainly composed of Al and O elements. Some Fe, Cr, Ni elements also dissolved in point A. It could be inferred that zone A was Al_2O_3-metal coating. Point B was mainly composed of Fe (53.3 wt. %), Ni and Cr, as well as a small amount of Al and O elements. It could be inferred that area B was the steel substrate, which penetrated a lot of Ni and Cr elements. Therefore, the region B was called the diffusion layer. Point C was mainly composed of Fe (89.52 wt. %), as well as a small amount of Ni, Cr, Al, and O elements. Thus it can be inferred that area C was steel substrate.

Therefore, the area from left to right is steel substrate, diffusion layer and coating, respectively. As can be seen from Fig. 1, the coating combined the substrate well at the interface. Neither cracks nor large pores appeared and the bonding interface was jagged. One of the reasons may be that the surface of steel substrate was uneven itself. The other reason was that micro-melting of a partial substrate occurred. This could be further seen from the data in Table 2. Large numbers of elements spread between A and B region.

Since the reaction system released tremendous heat, which not only made the final product completely in the molten state, but also made steel substrate surface in micro-melting state. At high temperature, Ni and Cr elements were easily to diffuse from coating to the steel substrate, forming the diffusion layer. Further, since the poor wettability of metal and ceramic, metal and ceramic phase separation occurred during solidification process. So the formation of aggregates of metal particles present in the coating.

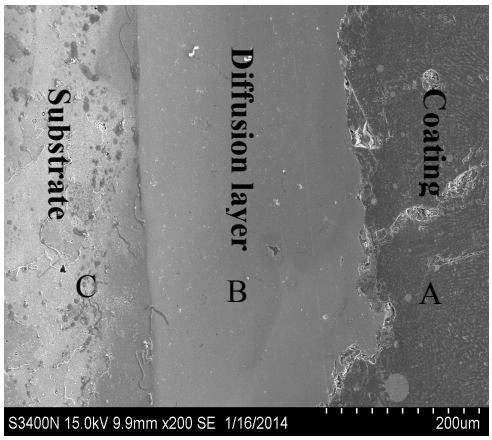

Fig. 1 Interface figure of coating-substrate region after etching

Table 2 EDS results of points A B C in Fig. 2

Elements	A		B		C	
	mass%	at%	mass%	at%	mass%	at%
Al	41.77	41.61	1.94	3.84	2.33	4.56
Fe	8.96	4.32	53.30	50.94	89.52	84.73
Cr	8.56	4.43	15.28	15.67	3.23	3.28
O	25.35	42.61	1.14	3.81	1.25	4.13
Ni	15.36	7.03	28.34	25.74	3.67	3.30

3.2 Microstructure of the coating

Fig. 2 shows the photograph of coating near the interface. From the figure, it can be seen that the coating was relatively dense with almost no pores. The coating had a fine and homogeneous microstructure, only a few metal particles presented in the coating. With increasing distance from the interface of the coating, pores and coarse microstructure began to appear.

Fig. 3 is the SEM of the central coating. It can be seen that the microstructure as a whole showed a certain direction, growing along the direction perpendicular to the interface [15]. However, when growing to a certain extent, the microstructure began to grow in all directions without any regularity. Fig. 4 shows the further amplified columnar grain area. Columnar grains were paralleled to grow in the same direction with uniform thickness. The average thickness of the evenly columnar grain was about 1.5-2 μm. The dendrite arm spacing was about 2.0 ~ 2.5 μm. Another area of the columnar crystals was further amplified in Fig. 5. There were some dendrites appearing in the top of columnar crystals.

Crystallization of the alumina ceramic is also a process of nucleation and growth, just like metal crystallization. The solidification of SHS product is typically a non-equilibrium process [16]. The melting product of complete reaction nucleates firstly on the carbon steel substrate in low temperature. Because of a large undercooling and numerous of nucleation, the nucleus grow rapidly and touch each other. What's more, the timely feeding of products in molten state can get the final products more compact. Thus the small and dense solidification structure without directions is formed. The grain grows along the reverse heat flux extending across the liquid to form columnar crystals. Initially, each dendrite grows in different directions from each other. Only those dendrites growing parallel to the direction of heat flow can be extended forward. The dendrites in unfavorable orientation are not conducive to grow and would be gradually phased out. In this way, the columnar grain structure is gradually formed. Since it is a non-equilibrium process in a rapid cooling speed, and there is still a violent reaction. These factors would disorder the heat flow direction which leads to the columnar crystal growth not in an entirely perpendicular direction to the steel substrate. Since the release of latent heat to the liquid phase during solidification, the liquid in the direction perpendicular to the crystal axis has a negative temperature gradient. Then the crystal axis would appear secondary crystal axis. Similarly, the second crystal axis would grow third crystal axes.

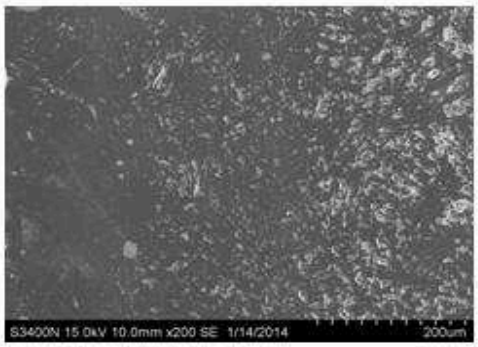

Fig. 2 SEM photograph of coating interface

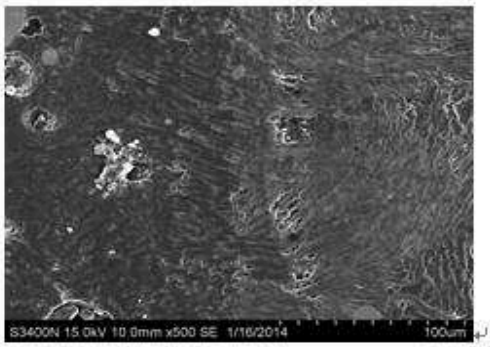

Fig. 3 SEM photograph of the central near the coating

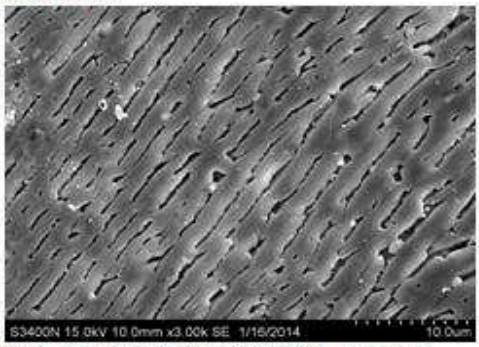

Fig. 4 SEM photograph of the amplified columnar grain

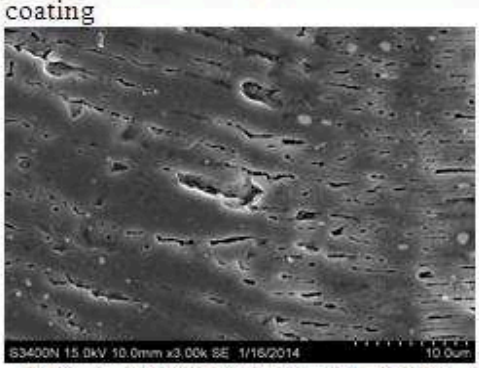

Fig. 5 SEM photograph of the amplified dendrites

3.3 The distribution of elements in the coating

Fig. 6 a) is the SEM photograph of columnar crystal in the middle coating. It can be seen from the figure, there were some bright spots in the internal of the columnar crystals. The columnar crystals and bright spots were analyzed by energy spectrum and the results were shown in Fig. 6 b, c). Combining XRD patterns and data in the table, it can be inferred that the main component of the columnar crystal was Al_2O_3. A small amount of chromium was dissolved in the aluminum. The remainder of chromium and iron aggregated in the form of solid solution.

During the solidification of molten products, alumina is the first to solidify to form a ceramic skeleton because of its highest melting point. Do to the high undercooling, the nucleation rate of metal is extremely high. What's more, the solidified aluminum would block the flow of molten products. In this way, metal elements are too late to escape and forced to dissolve in the ceramics. However, during the process of furnace cooling, staying at high temperature for about an hour provides a good opportunity for the diffusion of elements in solid state due to high temperature.

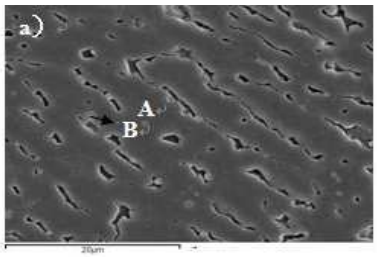

a) SEM photograph of columnar crystal in the middle coating

Elements	Mass%	At%
O	36.11	49.37
Al	60.93	49.39
Cr	2.96	1.25
Total	100.00	

b) EDS analyze of point A

Elements	Mass%	At%
O	27.06	43.61
Al	44.59	42.61
Cr	20.10	9.97
Fe	8.24	3.81
Total	100.00	

c) EDS analyze of point B

Fig. 6 EDS analyze of columnar crystal in the middle coating

4 Conclusions

Al_2O_3-metal coating was successfully prepared on the carbon steel substrate using melting-casting method. The microstructure, the bonding status of the interface between the coating and the substrate, and the element distribution of the coating were studied, and the conclusions were dropped as follows:

(1)The coating combined the substrate well with no significant gaps or holes near the whole interface, mainly in mechanical occlusion and metallurgical combination in certain areas;

(2)The components and pores near the interface of coating distributed evenly, and pores were small shaped in round, showing a typical solidification loose structure;

(3)Columnar grain structure was obvious, and developed dendrite appeared in the top of some coarse columnar crystals;

(4)The metal elements mostly distributed in the grain boundary of massive phase or columnar crystals shaped in spherical.

Acknowledgments

This work was financially supported by the National Natural Science Foundation of China (Grant No. 51379070), the Ministry of Education of China (No. 625010312), and Postgraduates research and innovation projects (CXZZ13_0245).

References

[1] Toma D, Brandl W, Marginean G. Wear and corrosion behaviour of thermally sprayed cermet coatings [J]. Surface and Coatings Technology, 2001, 138(2): 149-158.

[2] Bergmann C P, Vicenzi J. Protection against erosive wear using thermal sprayed cermet: a review [M]. Springer Berlin Heidelberg, 2011.

[3] Zhang J, Wang Z, Lin P, et al. Effect of Sealing Treatment on Corrosion Resistance of Plasma-Sprayed NiCrAl/Cr_2O_3-8 wt.% TiO_2 Coating [J]. Journal of thermal spray technology, 2011, 20(3): 508-513.

[4] Cliche G, Dallaire S. Synthesis and deposition of TiC-Fe coatings by plasma spraying [J]. Surface and Coatings Technology, 1991, 46(2): 199-206.

[5] Sidhu T S, Prakash S, Agrawal R D. Studies of the metallurgical and mechanical properties of high velocity oxy-fuel sprayed stellite-6 coatings on Ni-and Fe-based superalloys [J]. Surface and Coatings Technology, 2006, 201(1): 273-281.

[6] Saha G C, Khan T I, Zhang G A. Erosion–corrosion resistance of microcrystalline and near-nanocrystalline WC–17Co high velocity oxy-fuel thermal spray coatings [J]. Corrosion Science, 2011, 53(6): 2106-2114.

[7] Li J, Yu Z, Wang H, et al. Microstructural characterization of titanium matrix composite coatings reinforced by in situ synthesized TiB+TiC fabricated on Ti_6Al_4V by laser cladding[J]. Rare Metals, 2010, 29(5): 465-472.

[8] Guozhi X, Xiaolong S, Dongjie Z, et al. Microstructure and corrosion properties of thick WC composite coating formed by plasma cladding [J]. Applied Surface Science, 2010, 256(21): 6354-6358.

[9] Roos E, Naga S M, Richter R N, et al. Electron beam physical vapour deposition and mechanical properties of c-ZrO_2-ZTA-coatings on alloy 617 substrates [J]. Ceramics International, 2012, 38(4): 3317-3326.

[10] Li J S, Zhang C R, Li B, et al. Boron nitride coatings by chemical vapor deposition from borazine [J]. Surface and Coatings Technology, 2011, 205(12): 3736-3741.

[11] Varma A, Mukasyan A S. Combustion synthesis of advanced materials: Fundamentals and applications [J]. Korean Journal of Chemical Engineering, 2004, 21(2): 527-536.

[12] Mukasyan A S, White J D E. Combustion joining of refractory materials [J]. International Journal of Self-Propagating High-Temperature Synthesis, 2007, 16(3): 154-168.

[13] Morsi K. The diversity of combustion synthesis processing: a review [J]. Journal of Materials Science, 2012, 47(1): 68-92.

[14] La P, Bai M, Xue Q, et al. A study of Ni_3Al coating on carbon steel surface via the SHS casting route [J]. Surface and Coatings Technology, 1999, 113(1): 44-51.
[15] Niu M, Bi Q, Kong L, et al. A study of Ni_3Si-based composite coating fabricated by self-propagating high temperature synthesis casting route [J]. Surface and Coatings Technology, 2011, 205(17): 4249-4253.
[16] Merzhanov A G. Fundamentals, achievements, and perspectives for development of solid-flame combustion [J]. Russian Chemical Bulletin, 1997, 46(1): 1-27.

Advanced Materials Research Vols. 989-994 (2014) pp 337-339
© (2014) Trans Tech Publications, Switzerland
doi:10.4028/www.scientific.net/AMR.989-994.337

Research progress of graphene-based composites in supercapacitor

Zhaoxia Hou[a], Guangbin Li[b], Shaohong Wang, Meihan Wang,
Xiaodan Hu,Yin Zhou,Siming Li

Liaoning Province Key Laboratory of New Functional Materials and Chemical Technology,
School of Mechanical Engineering, Shenyang University, Shenyang 110044, China

[a]email:Luckyxia2007@126.com,[b]email:sydx07jscl@126.com

Keywords: Graphene; Composite Materials; Supercapacitor

Abstract. In this paper, inorganic/graphene and polymer/graphene composites are mainly introduced. Compared to single component, the inorganic or polymer additions have great improvement on the electrochemical performance and provide the possibility of their application in supercapacitor. The latest application of graphene based composites in supercapacitor is overviewed as well.

Introduction

Graphene is composed of a single layer of carbon atoms connected together in the 2D plane with SP^2 hybrid orbitals. In graphene, each carbon atom forms three π bonds with the nearest three atoms and the formed C-C bond with strong energy has a rigid excellent structure. The excess P electron of each carbon atom perpendiculars to the plane of graphene, overlaps with its counterparts of the surrounding carbon atoms, and forms conjugated π bonds in the vertical of graphene plane. π electrons that can move freely makes graphene a higher electron mobility. Electrode material is the key material of a super capacitor and needed to be higher specific surface area, good conducting electrical conductivity. In general, the commonly used electrode materials are transition metal oxides (MnO, RuO, etc.), conductive polymers (polyaniline, polypyrrole, etc.) and carbon based active material with higher specific surface area (carbon nanotubes, activated carbon, etc.). The excellent properties of graphene will be drowned if it is made to be electrode material and that is to say that the properties of graphene are not fully used. Therefore, to meet the requirements of electrode materials of supercapacitor, graphene based composites with good conductivity and large surface area with the synergistic effect should be developed to really release the excellent performances of graphene.

Application of inorganic/graphene composites in the supercapacitor

$Co(OH)_2$/graphene composites prepared with ethylene glycol as solvent and ammonia as precipitant by the solvent thermal method has a higher capacitance of 518 F/g than the values of 37 F/g of graphite oxide and 25 5F/g of pure Co $(OH)_2$ when the load ratio is 1:10. Moreover, the particles on the surface of the loads and graphite are of the same size and exhibit a uniform distribution. For the Ni $(OH)_2$/ graphene composite material, the ratio of raw material has great influence on the electrochemical properties of the composite. With the concentration increase of $Ni(NO_3)\cdot 6H_2O$, the specific capacitance of composites increases firstly and then decreases, and the maximum capacitance value is 677 F/g. The same tendency of the specific capacitance appears with the increase of reaction time, and it is 688 F/g when the reaction time is 12h[1]. The electrochemical performances of A_3O_4/GNs composites were tested and the specific capacitances of Fe_3O_4/GNs, CO_3O_4/GNs and Mn_3O_4/GNs are 358, 240 and 708 F/g respectively, while the corresponding energy density are 10, 7 and 20 Wh/kg, respectively. After 1000 times of the charge and discharge for the three materials, the capacitors amount to 67.8%, 95.8% and 73% of their previous values. The good electrochemical performance of A_3O_4/GNs reveals has wide application prospect in the field of the supercapacitor [2]. Increases the power density to 5000 W/kg,

the energy density of RuO_2/GR composites can reach to 15.7Wh/kg, while the value of RuO_2 is only 5.8Wh/kg. As shown from the experimental results, the unique particle-lamellar structure of composite can improve the migration rate of ions, increase the energy storage density and exhibit excellent performances of charge discharge [3]. The specific capacitance of graphene/MnO_2 composites which prepared by microwave assisted synthesis method is 310 F/g under the scanning rate of 2mV/s and it is almost 3 times of the values of pure graphene (104 F/g) and pure MnO_2 (103 F/g) [4]. Graphene/MnO_2 composites prepared by electrodeposition method show excellent electrochemical performance and the specific capacitance is 476 F/g at a current density of 1A/g. Increasing the current density to 10A/g, the specific capacitance maintains at 216 F/g and the capacitance retention rate is 88%, which show the good ratio characteristics [5]. Graphene/Ni $(OH)_2$ composite material prepared by hydrothermal method is to deposit single Ni $(OH)_2$ nanosheets directly on the graphene capacitive performance and the specific capacitance can reach to 1335 F/g when charge discharge current density is 2.8A/g. The specific capacitance can remain to about 953F/g even under the high current density of 45.7A/g. In addition, there is no obvious decrease for the capacitance after a cycle of 2000 at 28.6A/g, which shows the excellent energy, power and cycle performances [6]. Nano Co_3O_4/ graphene composites were prepared by the precipitation and heat treatment process and the aggregation of Co_3O_4 nano sheets were effectively inhibited. The charge and discharge tests show that the specific capacitance of Co_3O_4 nano film are 203 F/g at 0.2 A /g and 173 F/g at 1 A /g and the specific capacitance retention rate is 85%. While the nano Co_3O_4/ graphene composites are 338 F/g at 0.2 A /g and 294 F/g at 1 A /g, and the specific capacitance retention rate is 87%. The the electrochemical activity of composites has a significantly improvement [7].

Application of polymer /graphene composites in the supercapacitor

Polymers can be easily attached to the surface or edge of graphene with covalent bond when they are composited with graphene. It breaks the van der Waals force and makes themodified graphene composite with good conductivity and wide application in the supercapacitor [8]. The electrochemical-capacitance performance tests show that the composites of GSP118 prepared with the ratio of graphene oxide: tin dioxide: aniline ratio of 1:1:8 was good electrochemistry performance under a scanning rate of 5mV/s. The specific capacitance of GSP118 composite electrode can reach to 913.4 F/g while the GSP181 is 177.9 F/g and GSP154 is 467.9 F/g [9]. Using aniline and graphene oxide as raw materials and distributing the polyaniline evenly to the graphene layer, polyaniline / graphene composites were synthesized by electrochemical method. Its specific capacitances are 325 F/g at 0.5 A/g and 315 F/g at 1 A/g. After no less than 1000 times of charge and discharge cycles, the specific capacitance retention rate is still as high as 90%. Moreover, the discharge efficiency is extremely high and the electrolyte ions in the electrode are easy to be diffuse and migrate [10].With the aqueous electrochemical deposition of pyrrole monomer, sulfonated graphene, twelve alkyl basic sulfonic acid, sulfonated polymer / graphene composite thin films are prepared. Due to the addition of sulfonated graphene, the conductivity and electrochemical properties of polypyrrole films are significantly improved. When the ratio of sulfonated graphene in composites is 40%, the specific capacitance of the composite films is 285 F/g on the discharge rate of 0.5 A/g [11]. Enhanced electrochemical performance can be obtained by doping PPY with a small amount of GQD（Graphene quantum dots）and the PGQD50（PPY：GQD is 50:1）will be a good candidate for supercapacitor electrode with a competitive specific capacitance of 485 F/g [12]. Graphene/PPy composites that reduced by ethylene glycol exhibit good capacitance performance. In the H_2SO_4 of 1mol/L, the specific capacitance of the composites is 420 F/g at the current density of 0.5A/g. CFGO/PANI composites which prepared by the carboxyl functionalized graphene oxide/polyaniline (CFGO/PANI) show the excellent electrochemical capacitance performance and cycling performance. In the H_2SO_4 of 1mol/L, the specific capacitance of CFGO/PANI reaches to 525 F/g at the current density of 0.3A/g. After 200 cycles of the constant current charge-discharge, the capacitance retention rate is about 91% [13].

Conclusion

Excellent chemical properties, electrical properties and large specific surface area make graphene be potential material in numerous fields in just a few years. Graphene composites not only maintain original performance, but also show the excellent composite effect, which provides the possibility application prospects for graphene composites in supercapacitor.

Acknowledgements

The research was sponsored by the Excellent Talents Program in University of Liaoning Province (No. LJQ2011125) and Key Laboratory Construct Foundation of Shenyang (No. F10-216-1-00).

References

[1] Zhou H. Based on Graphene / hydroxide composite material supercapacitor preparation, properties and mechanism research [D]. Nanjing University of Science and Technology,2013.

[2] Zhang W F. Transition metal oxide / graphite composite materials preparation and invest igation on Supercapacitor properties [D]. Zhejiang University, 2013.

[3] Shao Q, Lin Z F, Liu Q Q, et al. The performance of ruthenium oxide / graphene com posite material supercapacitor [J].Materials and Structures，2013，50（6）：347-352.

[4] Yan J, Fan Z J, Wei T, et al. Fast and reversible surface redox reaction of graphene/M nO_2 composites as supercapacitor electrodes [J]. Carbon, 2010, 48(13): 3825-3833.

[5] Zhao Y Q, Zhao D D, Tang P Y, et al. MnO_2/graphene/nickel foam compositeas high p erformance supercapacitor electrode via a facile electrochemicaldeposition strategy [J]. Materials Letters, 2012, 76: 127-130.

[6] Wang H L, Casalongue H S, Liang Y Y, et al. $Ni(OH)_2$ Nanoplates Grown on Graphene as Advanced Electrochemical Pseudocapacitor Materials [J]. Journalof the American Chemical Society, 2010, 132(21): 7472-7477.

[7] Wang L. Study on Preparation and electrochemical properties of graphene based compos ite electrode materials supercapacitor [D]. Harbin Institute of Technology，2012.

[8] Li G B，Hou Z X，Wang S H, et al. Research progress of graphene-based composites [J]. Ordnance material science and Engineering, 2014, 37（3）.

[9] Jin Y H. Application of graphene and graphene based two component and three componen t for preparing nano composite material in supercapacitor [D]. Beijing University of Te chnology，2013.

[10] Wang H Z，Gao C X，Zhang P, et al. Preparation and electrochemical of graphene / p olyaniline composites［J］Chinese Journal of Chemical Physics，2013, 29(1): 117-122.

[11] Liu A R，Shi G Q . Electrochemical deposition of sulfonated graphene and polypyrrole composite film [C]. 2011 Summary collection of China materials symposium , Beijing.

[12] Kun WU, Sizhe XU, Xuejiao ZHOU et al. Graphene Quantum Dots Enhanced Electroc hemical Performance of Polypyrrole as Supercapacitor Electrode [J]. Journal of electroc hemistry, 2013, 19(4):361-369.

[13] Liu Y. Preparation and properties of graphene / polymer composite material supercapaci tor [D]. Middle and Southern University，2012.

Advanced Materials Research Vols. 989-994 (2014) pp 340-343
© (2014) Trans Tech Publications, Switzerland
doi:10.4028/www.scientific.net/AMR.989-994.340

Dielectric barrier discharge plasma reduced Pt catalysts supported on activated carbon and their electrocatalytic activity

Lanbo Di*

College of Physical Science and Technology, Dalian University, Dalian 116622 (P.R. China)

dilanbo@163.com

*Corresponding author. E-mail address: dilanbo@163.com

Keywords: Pt/C, electrocatalyst, dielectric barrier discharge (DBD), atmospheric-pressure cold plasma, supported metal catalyst

Abstract. Atmospheric-pressure dielectric barrier discharge (DBD) plasma was used to fabricate Pt/C electrocatalysts. The influences of the pretreatment of the activated carbon support and the preparing method on the properties of the Pt/C electrocatalysts were investigated. The composition of the Pt/C samples was characterized by X-ray diffraction (XRD). The electrocatalytic activity of the Pt/C samples was evaluating by measuring the cyclic voltammograms. The results showed that higher dispersion of Pt nanoparticles was obtained on the activated carbon support pretreated by HNO_3, and higher reduction rate of Pt ions was obtained in Pt/C prepared by DBD plasma. As a consequence, the Pt/C samples with the activated carbon support pre-oxidized by HNO_3 and reduced by DBD plasma exhibited the highest electrocatalytic activity.

1. Introduction

Pt-based catalysts were widely employed in fuel cells as cathode electrocatalysts [1]. In order to improve their electrocatalytic activity, many efforts had been attempted, including selection of the supports and the preparing methods. Due to the functional groups on the surface of the supports, metal ions could be adsorbed and intercalated into the sheets and pores to form thermal stable composite materials [2-3]. As for the preparation method, cold plasma reduction had been demonstrated as a facile and green method in catalyst preparation [4-7]. However, these plasma reduction methods were usually operated under low pressure and (or) incorporated with sophisticated discharge systems.

In order to solve these problems, dielectric barrier discharge (DBD) cold plasma was employed. DBD was a simple and easily operated approach for generating atmospheric-pressure cold plasma, and has been used to reduce metal ions [8-9]. However, it has not been reported using atmospheric-pressure DBD cold plasma to prepare supported Pt catalyst on low-cost and easy to get activated carbon.

In this study, high performance Pt/C catalysts were successfully fabricated by a simple and environmentally-friendly DBD plasma reduction method, and the influence of the pretreatment of the activated carbon support was investigated.

2. Experimental

Prior to the Pt/C electrocatalysts preparation, the activated carbon (40-60 mesh, Beijing Guanghua Timber Mill.) was pretreated by two methods. One part of them was washed with deionized water and then dried at 120 ^{o}C for 2 h (denoted as C(W)). The other part was pre-oxidized with 30wt% HNO_3 at 85 ^{o}C for 5 h, and then washed by deionized water and dried at 120 ^{o}C for 2 h (denoted as C(H)).

The activated carbon was impregnated with H_2PtCl_6 (99%, Reagent No.1 Factory of Shanghai Chemical Reagent Co., Ltd, China) solution for 12 h and dried at 100 ^{o}C for 2 h. Then the resultant sample was treated by atmospheric-pressure dielectric barrier discharge (DBD) cold plasma. In order to remove the chloride ions, the Pt/C catalysts prepared by DBD plasma were calcined at 300 ^{o}C in H_2 for 2 h (denoted as Pt/C(H)-PC and

Pt/C(W)-PC). For comparison, Pt/C(H)-C sample was prepared by H_2 calcination at 300 ^oC in H_2 for 2 h. All the loading amounts of metal Pt were 5.0wt% in this study.

The atmospheric-pressure DBD plasma device for preparing Pt/C catalyst was the same as described in our previous paper [10]. Both of the high-voltage electrode and the ground electrode were stainless steel plates (Φ=50 mm). A reaction cell made of quartz was placed between the electrodes. The discharge gap was 4 mm. The plate-to-plate DBD employed in this experiment was powered by a sinusoidal high voltage of 36 kV (peak-to-peak) at a frequency of 14.1 kHz without extra heating (CTP-2000K, Nanjing Suman Electronic Co. Ltd). The mixture of Ar and H_2 with a constant total flow rate of 100 ml·min^{-1} (F_{Ar}: F_{H2} = 1: 1) was used as working gases. The treatment was performed for 6 min.

The composition and crystalline nature of the Pt/C samples prepared by different methods and (or) supported on activated carbon treated by different methods were characterized by X-ray diffraction (XRD) using a DX-2700 diffractometer (Dandong Fangyuan, China) with graphite-monochromatized Cu $K_{\alpha1}$ radiation (λ=1.54178 Å).

Electrochemical measurements were performed with a CHI 600C electrochemical workstation (Shanghai Chenhua Apparatus) at room temperature.

3. Results and Discussion

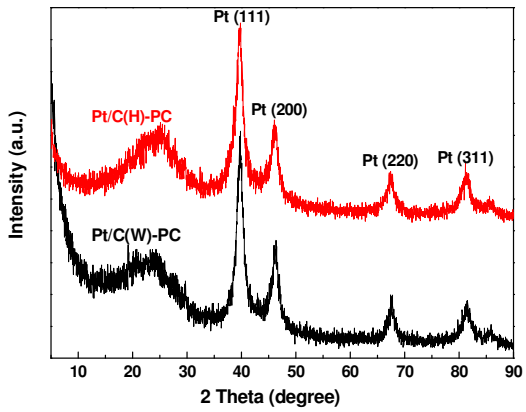

Fig. 1. XRD patterns of Pt/C(H)-PC and Pt/C(W)-PC prepared by DBD plasma with activated carbon treated by water or HNO_3

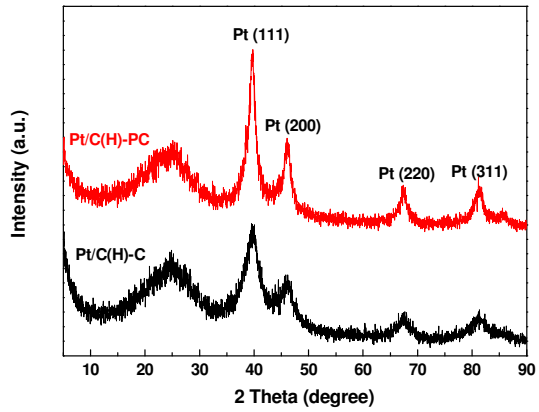

Fig. 2. XRD patterns of Pt/C(H)-PC and Pt/C(H)-C prepared by DBD plasma or thermal reduction

In order to investigate the influence of the pretreatment of the activated carbon support on the properties of the Pt/C catalysts, XRD patterns of Pt/C(W)-PC and Pt/C(H)-PC prepared by DBD plasma with activated carbon treated by water or HNO_3 were shown in Fig. 1. The broad diffraction peaks at 25.0^o for the samples exhibited carbon structure of activated carbon. Peaks associated with Pt (PDF # 04-0802) were observed at 39.8^o (111), 46.4^o (200), 67.8^o (220) and 82.4^o (311) in both of the samples. Compared with Pt/C(H)-PC, agglomeration of Pt nanoparticles appeared for Pt/C(W)-PC. This may be ascribed to the fact that the activated carbon pre-oxidized by HNO_3 was positively charged and the $PtCl_6^{2-}$ ions were uniformly absorbed on its surface, thereby highly dispersed Pt nanoparticles were obtained in Pt/C(H)-PC.

Fig. 2 represented the XRD patterns of Pt/C(H)-PC and Pt/C(H)-C prepared by DBD plasma or thermal reduction. As shown in Fig. 2, the characteristic peaks corresponding to Pt in Pt/C(H)-C were weaker than that in Pt/C(H)-PC, which indicated that a low reduction rate of Pt ions in Pt/C(H)-C was obtained. This may be due to the fact that many oxygen-containing groups were formed on the surface of activated carbon after HNO_3 treatment. These oxygen-containing groups may lead to the low reduction rate of Pt ions [11]. While the Pt/C(H)-PC sample underwent two

reduction processes, DBD plasma reduction and thermal reduction, and therefore a high reduction rate was obtained.

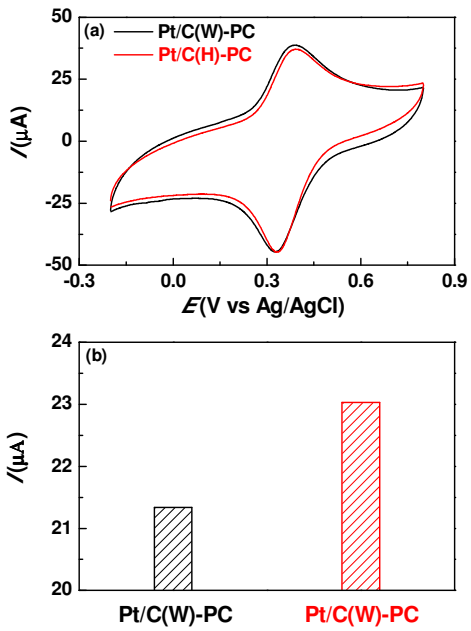

Fig. 3. (a) Cyclic voltammograms of Pt/C(H)-PC and Pt/C(W)-PC and (b) corresponding currents

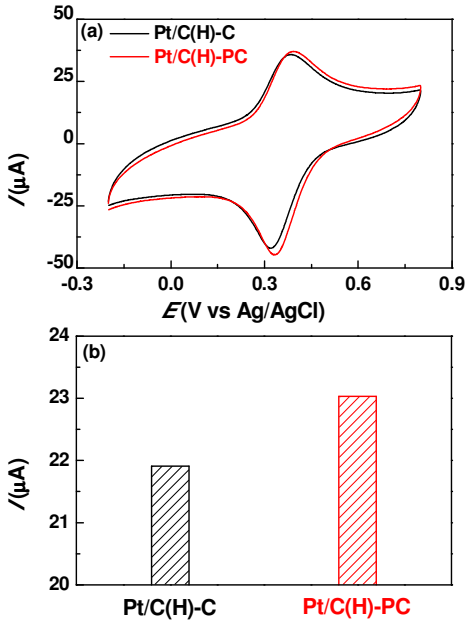

Fig. 4. (a) Cyclic voltammograms of Pt/C(H)-PC and Pt/C(H)-C and (b) corresponding currents

In order to investigate the influence of the pretreatment of the activated carbon support on the electrocatalytic activity of the Pt/C catalysts, cyclic voltammograms of Pt/C(H)-PC and Pt/C(W)-PC and corresponding currents were represented in Fig. 3. It can be seen that high electrocatalytic activity were obtained in both of the two samples, and the Pt/C(H)-PC sample exhibited higher activity than Pt/C(W)-PC, which may be attributed to the small size of Pt nanoparticles (Fig. 1). This indicated that the surface properties of activated carbon played an important role in preparing high dispersion of Pt nanoparticles to obtain high performance Pt/C electrocatalyst.

The cyclic voltammograms of Pt/C(H)-PC and Pt/C(H)-C prepared by DBD plasma and thermal reduction, and corresponding currents were collected and shown in Fig. 4. Pt/C(H)-PC gave an excellent electrocatalytic activity than Pt/C(H)-C, which may be due to the fact that a high reduction rate of Pt ions was obtained in Pt/C(H)-PC (Fig. 2).

In summary, the pretreatment of the activated carbon support play an important role to obtain small size of Pt nanoparticles and atmospheric-pressure DBD plasma was efficient to prepare high performance Pt/C electrocatalyst.

4. Conclusion

High performance Pt/C electrocatalysts were prepared by DBD plasma. The results showed that higher dispersion of Pt nanoparticles was obtained on the activated carbon support pretreated by HNO_3, and higher reduction rate of Pt ions was obtained in Pt/C prepared by DBD plasma. As a consequence, the Pt/C samples with the activated carbon support pre-oxidized by HNO_3 and reduced by DBD plasma exhibited the highest electrocatalytic activity. In conclusion, pretreatment of the activated carbon support play an important role to obtain small size of Pt nanoparticles and atmospheric-pressure DBD plasma was an efficient method to prepare high performance Pt/C electrocatalyst.

Acknowledgements

This work is supported by the Science and Technology Research Project of Liaoning Provincial Education Department (Grant No. L2013464), and the Scientific Research Foundation for the Doctor of Liaoning Province (Grant No. 20131004).

References

[1] Z. H. Zhou, S. L. Wang, W. J. Zhou, G. X. Wang, L. H. Jiang, W. Z. Li, S. Q. Song, J. G. Liu, G. Q. Sun and Q. X. Chem. Commun. (2003) 394-395.

[2] Y. F. Li, Z. Zhou, G. T. Yu, W. Chen and Z. F. Chen, J. Phys. Chem. C 114 (2010) 6250.

[3] X. Y. Liu, C. Y. Mou, S. Lee, Y. N. Li, J. Secrest and B. W. L. Jang, J. Catal. 285 (2012) 152.

[4] J. J. Zou, Y. P. Zhang and C. J. Lui, Langmuir 22 (2006) 11388.

[5] X. Liang, C. J. Liu and P. Kuai, Green Chem. 10 (2008) 1318

[6] K. Qadir, S. Hoon Kim, S. M. Kim, H. Ha and J. Y. Park, J. Phys. Chem. C. 116 (2012) 24054.

[7] V-D. Dao, C. Q Tran, S-H. Ko and H-S. Choi, J. Mater. Chem. A 1 (2013) 4436.

[8] K. Jeon and Z. Lee, Chem. Commun. 47 (2011) 3610.

[9] L. B. Di, X. L. Zhang, Z. J. Xu, K. Wang, Plasma Chem. Plasma P. 34 (2014) 301.

[10] L. B. Di, Z. J. Xu, K. Wang and X. L. Zhang, Catal. Today 211 (2013) 109.

[11] Y. Z. Li, Y. Yu, J. G. Wang, J. Song, Q. Li, M. D. Dong and C. J. Liu, Appl. Catal. B-Environ. 125 (2012) 189.

Advanced Materials Research Vols. 989-994 (2014) pp 344-347
© (2014) Trans Tech Publications, Switzerland
doi:10.4028/www.scientific.net/AMR.989-994.344

Preparation of Au/P25 catalysts for removal of CO by dielectric barrier discharge plasma

Lanbo Di*

College of Physical Science and Technology, Dalian University, Dalian 116622 (P.R. China)

dilanbo@163.com

*Corresponding author. E-mail address: dilanbo@163.com

Keywords: Au, CO oxidation, dielectric barrier discharge (DBD), atmospheric-pressure cold plasma

Abstract. Atmospheric-pressure dielectric barrier discharge (DBD) cold plasma was used to prepare high performance Au/P25 catalysts (Au/P25-P). XRD and UV-Vis DRS spectra for Au/P25 catalysts were performed. The results indicated that the size of Au nanoparticles in Au/P25-P was smaller than that prepared by conventional thermal impregnation method (Au/P25-H). The temperature-dependent CO oxidation was performed to investigate the activity of Au/P25 catalysts. Au/P25-P gave excellent catalytic activity for CO oxidation than that of Au/P25-H. This may be attributed to the smaller size of Au nanoparticles in Au/P25-P.

1. Introduction

Gold nanocatalysts had drawn much research attention since the pioneering work of Haruta in the 80 s of last century [1]. It had been reported that the optimized size of gold nanoparticles in CO oxidation reaction was ~3 nm [2]. However, it was still a challenge to prepare small size of Au nanoparticles.

Recently, atmospheric-pressure cold plasma techniques had attracted significant attention for preparation of supported metal catalysts since they didn't require sophisticated discharge and vacuum systems. Dielectric barrier discharge (DBD) was a simple and easily operated approach for generating atmospheric-pressure cold plasma, and had been used to reduce metal ions [3-4]. For example, Kim et al. [3] prepared supported metal Pt catalyst by using atmospheric-pressure DBD cold plasma to reduce supported Pt metal ions. The plasma catalytic reaction for methane conversion showed positive characteristics to produce light alkanes when Pt catalyst was used after atmospheric-pressure DBD cold plasma treatment. In our previous work [5-6], atmospheric-pressure DBD cold plasma was successfully applied to fabricate Ag/TiO_2 and Pt/TiO_2 photocatalyst. The results showed that the sizes of Ag and Pt nanoparticles in Ag/TiO_2 and Pt/TiO_2 prepared by atmospheric-pressure DBD cold plasma were smaller than that prepared by conventional method, and the photocatalysts exhibited high activity for methylene blue degradation. These results showed that atmospheric-pressure DBD cold plasma does well in fabricating supported metal catalysts with small size of metal nanoparticles.

In this study, Au/P25 catalysts were prepared by atmospheric-pressure DBD cold plasma using Ar and H_2 mixture gases as working gas. The size of Au nanoparticles in Au/P25 prepared by DBD plasma was smaller than that prepared by conventional method, and they gave excellent catalytic activity for CO oxidation.

2. Experimental

Commercially produced TiO_2 powder was obtained from Degussa (P25 powder). Degussa P25 contains 75% anatase and 25% rutile with a specific BET-surface area of 50 $m^2 \cdot g^{-1}$ and primary particle size of 20 nm [7]. The Au/P25 catalysts were prepared by deposition-precipitation with DBD plasma reduction method (denoted as Au/P25-P) and a conventional thermal impregnation method (denoted as Au/P25-H), respectively. A certain amount of $HAuCl_4$ solution (10 $g \cdot L^{-1}$) was first mixed with 2.0 g P25 and 80 ml deionized water, and then a certain amount of urea with a molar ratio of gold to urea at 1/200 was added as the precipitation agent. The mixture was stirred at 80 ^oC for 8 h and aged for 12 h at room temperature. Subsequently, the precipitate was filtrated from the

solution and dried at 80 °C for 6 h. Finally, Au/P25-P was obtained by reducing the powder with atmospheric-pressure DBD plasma. For comparison, Au/P25 by thermal impregnation method was prepared (denoted as Au/P25-H). The P25 powder was impregnated with $HAuCl_4$ solution for 24 h and dried at 100 °C for 2 h. Then it was reduced in flowing hydrogen gas for 2 h to obtain Au/P25-H catalyst.

The atmospheric-pressure DBD plasma device for preparing Au/P25-P was the same as described in our previous paper [8]. Both of the high-voltage electrode and the ground electrode were stainless steel plates (Φ=50 mm). A reaction cell made of quartz was placed between the high-voltage electrode and ground electrode. The discharge gap was 4 mm. The power source (CTP-2000K, Nanjing Suman Electronic Co. Ltd) was capable of supplying a bipolar sine wave output with 0-40 kV peak-to-peak voltage ($U_{p\text{-}p}$) at a frequency of 7.5-30 kHz. The mixture of Ar and H_2 with a constant total flow rate of 100 ml·min^{-1} (F_{Ar}: F_{H2} = 1: 1) was used as working gases. The treatment was performed for 6 min.

The composition and crystalline nature of the Au/P25 samples were characterized by X-ray diffraction (XRD) using a DX-2700 diffractometer (Dandong Fangyuan, China) with graphite-monochromatized Cu $K_{\alpha 1}$ radiation (λ=1.54178 Å). UV-Vis DRS spectra of the Au/P25-P samples were measured by a UV-Vis spectrophotometer (Varian Cary 100, USA) with a $BaSO_4$ plate as the reference.

The temperature-dependent CO oxidation was performed in a quartz tube (4 mm i.d., 6.0 mm o.d.) at atmospheric pressure with 10 mg catalyst. The reaction was started in flowing CO/O_2 mixture (1.0 vol.% CO, 20.0 vol.%O_2, balance N_2) with a 20 ml·min^{-1} flow rate over the temperature range of 30-300 °C. All data were acquired after 30 min reaction time to allow the attainment of steady state. The effluent was then analyzed online by a gas chromatograph (Agilent 7890) equipped with a TDX-01 column and a thermal conductivity detector (TCD).

3. Results and Discussion

The plate-to-plate DBD employed in this experiment was powered by a sinusoidal high voltage of 36 kV (peak-to-peak) at a frequency of 14.1 kHz without extra heating. The voltage waveforms of the plate-to-plate DBD were shown in Fig. 1a. The corresponding Lissajous figure of the plate-to-plate DBD, as indicated in Fig. 1b, gives 65.6 W of the electric discharge power.

Fig. 2 represented the XRD patterns of P25, 2%Au/P25-P and 2%Au/P25-H. After loading Au nanoparticles, the characteristic peaks corresponding to P25 were weakened. Cubic phase of Au (JCPDS card No. 00-004-0784) was observed in both of the 2%Au/P25-H and 2%Au/P25-P samples. The strong characteristic peaks indexed to Au in 2%Au/P25-H may be attributed to the aggregation of Au nanoparticles. Interestingly, these peaks were weakened in 2%Au/P25-P, which indicated that DBD plasma were highly efficient for preparing small size Au nanoparticles.

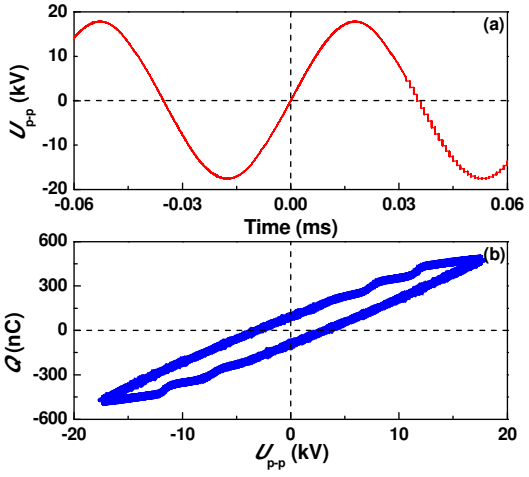

Fig. 1. (a) The waveform of discharge voltage and (b) corresponding Lissajous figure of the DBD for preparation of Au/P25-P

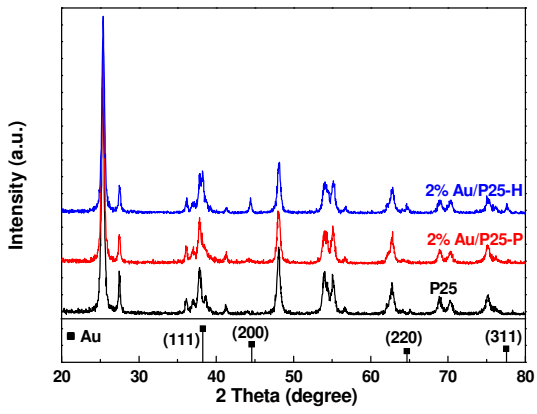

Fig. 2. XRD patterns of P25, 2%Au/P25-P and 2%Au/P25-H

The UV-Vis DRS spectrum for the 1%Au/P25-P sample prepared by atmospheric-pressure DBD cold plasma was shown in Fig. 3. The characteristic absorption around 560 nm was attributed to the surface plasmon resonance peak of the spatially confined electrons in Au nanoparticles [9]. This absorption spectrum indicated that metal Au nanoparticles were present after plasma treatment. Meanwhile, this band was very weak in 1%Au/P25-P compared with previous work, which indicated that small size of Au nanoparticles was obtained by DBD plasma. This was consistent with the results of XRD analysis.

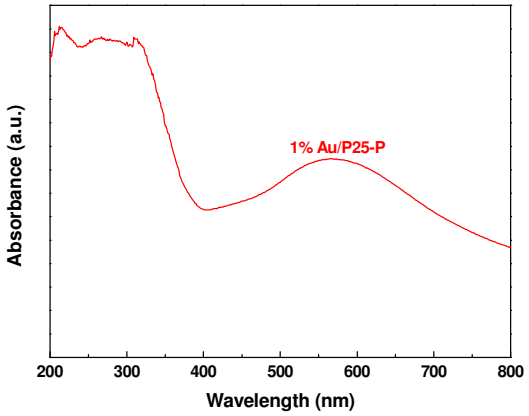

Fig. 3. The UV-Vis DRS spectrum for 1%Au/P25-P prepared by DBD plasma

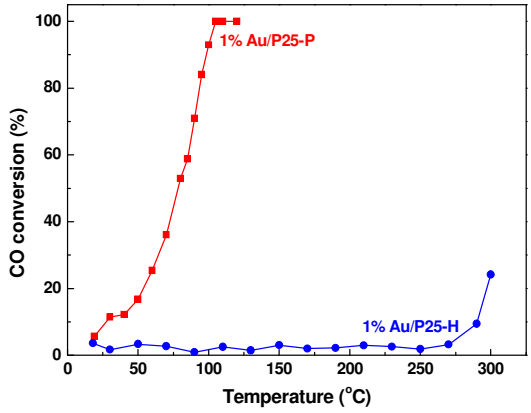

Fig. 4. Catalytic activity for CO oxidation with 1%Au/P25-P and 1%Au/P25-H

Fig. 4 showed the CO oxidation activity of 1%Au/P25-P and 1%Au/P25-H in the temperature range of 30-300 °C. Under the reaction conditions, the CO conversion increased gradually with the increase in temperature. Besides, a sharp increase could be observed for 1%Au/P25-P and the 100% CO conversion temperature was 105 °C, while the CO conversion over 1%Au/P25-H started at about 290 °C. The difference in catalytic activity over 1%Au/P25-P and 1%Au/P25-H may be ascribed to the influence of the size of Au nanoparticles.

In summary, atmospheric-pressure DBD plasma was efficient for preparing high catalytic activity Au/P25 with smaller size of Au nanoparticles. Further progresses will be reported in our future works.

4. Conclusion

High performance Au/P25 catalysts were prepared by atmospheric-pressure dielectric barrier discharge (DBD) cold plasma. The results of XRD and UV-Vis DRS spectra indicated that the size of Au nanoparticles in Au/P25-P was smaller than that for Au/P25-H. The results of the temperature-dependent CO oxidation test exhibited that Au/P25-P gave excellent catalytic activity for CO oxidation than that of Au/P25-H, which may be attributed to the smaller size of Au nanoparticles in Au/P25-P. Atmospheric-pressure DBD cold plasma was efficient for preparing high performance Au/P25 catalysts for CO oxidation.

Acknowledgements

This work is supported by the Science and Technology Research Project of Liaoning Provincial Education Department (Grant No. L2013464), and the Scientific Research Foundation for the Doctor of Liaoning Province (Grant No. 20131004).

References

[1] M. Haruta, N. Yamada, T. Kobayashi, S. Lijima, J. Catal. 115 (1989) 301-309.

[2] M.S. Chen, D.W. Goodman, Science 306 (2004) 252-255.

[3] S.-S. Kim, H. Lee, B.-K. Na, H. K. Song, Catal. Today 89 (2004) 193-200.

[4] K. Jeon and Z. Lee, Chem. Commun. (2011) 47 3610-3612.

[5] L. B. Di, Z. J. Xu, X. L. Zhang, Catal. Today 211 (2013) 143-146.

[6] L. B. Di, X. L. Zhang, Z. J. Xu, K. Wang, Plasma Chem. Plasma Process. 34 (2014) 301-311.

[7] R. I. Bickley, T. G. Carreno, L. Palmisano, R. J. D. Tilley, J. Solid State Chem. 92 (1992) 178-190.

[8] L. B. Di, Z. J. Xu, K. Wang, X. L. Zhang. Catal Today 211 (2013) 109-113.

[9] B. Cojocaru, S. Neatu, E. Sacaliuc-Pârvulescu, F. Lévy, V. I. Pârvulescu, H. Garciac. Appl. Catal. B: Environ. 107 (2011): 140-149.

Advanced Materials Research Vols. 989-994 (2014) pp 348-351
© (2014) Trans Tech Publications, Switzerland
doi:10.4028/www.scientific.net/AMR.989-994.348

Kinetics of inverse emulsion copolymerization of dimethyl diallyl ammonium chloride and acrylamide

Xiaona Wang[1, a], Renzhi Zhang[2, b], Nisha Jin[3, c]

[1]Environmental Management College of China (EMCC), Qinhuangdao 066004, Hebei, China
[2]Environmental Management College of China (EMCC), Qinhuangdao 066004, Hebei, China
[3]Environmental Management College of China (EMCC), Qinhuangdao 066004, Hebei, China
[a]nala1981@163.com, [b]z_renzhi@hotmail.com, [c]jinnisha@126.com

Keywords: Kinetics; Inverse Emulsion Copolymerization; Dimethyl Diallyl Ammonium Chloride;

Abstract. Inverse emulsion copolymerization of DMDAAC with AM has been investigated by the dilatometer technique using the mixture of Span-80 and Tween-80 as the composite emulsifier and 2,2'-azobis(2-methylpropionconidine) dihydro chloride as the initiator. In inverse emulsion copolymerization, the influences of the concentrations of monomers, emulsifier and initiator and initial temperature on polymerization rate and the intrinsic viscosity of polymer have been examined. Its kinetics can be expressed as $R_p \propto [M]^{2.11}[I]^{1.21}[E]^{0.48}$, $[\eta] \propto [M]^{0.87}[I]^{-0.30}[E]^{0.36}$. The overall activation energy for the rate of polymerization was determined with a dilatometer as 20.33 kJ/mol over the temperature range 35-55℃.

1. Introduction

The cationic copolymer of dimethyl diallyl ammonium chloride (DMDAAC) and acrylamide (AM) has the merits of high molecular weight, good water-solubility, wide usable pH range etc. Therefore it is widely used in the areas of oil exploitation, paper making, mining, printing and dyeing of textiles, daily chemical industry and slurry dehydration, etc. Current main method to produce PAM-DMDAAC is solution polymerization [1]. However, at the end of the solution polymerization, the viscosity of the polymer solution is large, and a gel is easily formed. Therefore, it is difficult to produce the polymer with high concentration and high molecular weight [2]. If the product is turned into a powder, the drying process will consume more energy. Agglomeration often happens, and the quality of the product is poor, which is a familiar problem during solution synthesis of polymers. At present, there are many methods to synthesize the polymer; the more successful one is inverse emulsion polymerization, with which the polymer has the merits of high molecular weight and high content. This method solves the problem of solution polymerization. However, a description of the fundamental polymerization kinetics is scarce in the literature [3].

In order to research the free radical copolymerization theoretically, the kinetics studies of inverse emulsion polymerization were made in this work. In this paper the effects of the reaction parameters on the conversion, intrinsic viscosity and polymerization rate were investigated and the dependence of polymerization rate and intrinsic viscosity on monomer, initiator and emulsifier concentrations were determined. Based on the experimental results, the polymerization mechanisms were discussed.

2. Experimental

2.1. Materials

The monomers AM (40% in water), DMDAAC (60% in water) and 2,2'-azobis(2-methylpropionconidine)dihydro chloride (V50) were kindly provided by Binzhou chemical Co. Ltd. (Shandong province, China). The emulsifier is a blend of Span-80 and Tween-80 both provided by Shanghai Guoyao Co. The oil is kerosene which was filtered before use. The

following chemicals obtained from Guangmang Chemical Co. were of analytical-grade and used as supplied: sodium acetate (HCOONa), sodium chloride (NaCl), poly(vinylpyrrolidone) (PVP), N, N, N', N',-tetramethyl-ethylenediamine (TMEDA), ethanol, acetone, ethylene diamine tetraacetic acid (EDTA). Deionized water was used throughout.

2.2. Copolymerization

Varying quantities of the reagents were added to a 500-mL four-neck round bottom flask equipped with an anchor-like paddle stirrer, a thermometer and a nitrogen inlet tube. After purging with N_2 for 30 min and controlling the temperature at 40°C in a water bath, the polymerization was initiated by injecting the initiator into the reaction mixture under stirring and performed for a given reaction time. The reaction time was controlled to give conversions less than 10 wt% to satisfy the differential copolymerization equation. After the desired time the copolymers were separated by precipitation in ethanol and acetone mixture (volume ratio of 1:1), and was washed with fresh acetone. These operations were repeated several times to remove the unreacted monomers. The copolymer was finally dried under vacuum at 40°C to constant weight. The intrinsic viscosity was measured in 1M NaCl aqueous at 30±0.05℃ using an Ubbelhode viscometer. The polymer conversion was recorded as a function of time with a dilatometer, and the polymerization rate (R_p) was obtained from further differentiation. In this paper, the concentrations of initiator and emulsifier are reported as weight percent based on the monomer and the total solution, respectively.

3. Results and Discussion

In this study, the influences of various polymerization parameters, including the initial temperature, and monomer [M], emulsifier [E] and initiator [I] concentrations were investigated systematically. The standard recipe used in this study is given as follows: [M] = 45% of total, n_{AM} / n_{DMDAAC} = 8/2, $T_{initiation}$ = 40℃, [E] =8% of total, [I] = 0.05% (monomer). The amount of each ingredient was kept constant in all experiments excepted as indicated.

3.1. Effect of monomer concentration on copolymerization

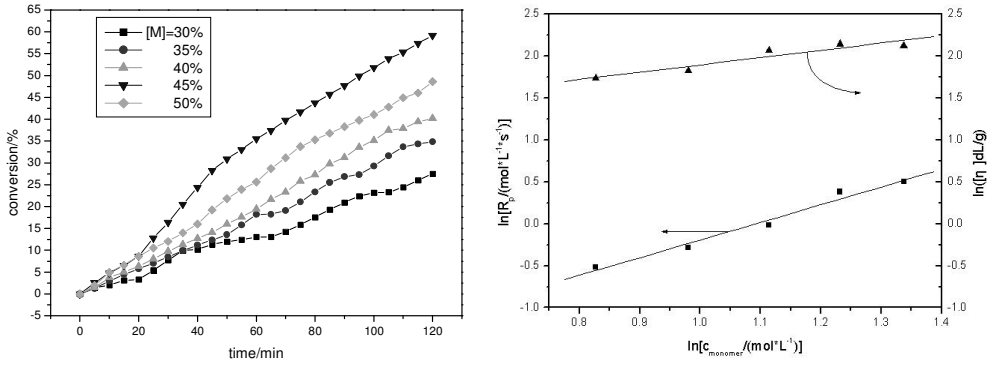

(a) (b)

Fig.1. (a) Conversion vs. time curves at different monomer concentrations; (b) the effect of monomer concentration on polymerization.

Fig. 1 (a) and (b) show the dependence of the conversion on the reaction time at various monomer concentrations and the effect of monomer concentration on polymerization kinetics, respectively. As shown in Fig. 1, conversion, polymerization rate and intrinsic viscosity increase with the increase of monomer concentration. The higher the monomer concentration is, the higher the diffusion rate of monomer to microsphere or free-radical active center is, and then conversion, polymerization rate and intrinsic viscosity increase. The effect of monomer concentration on

polymerization rate and intrinsic viscosity can be calculated as: $R_p \propto [M]^{2.11}$, $[\eta] \propto [M]^{0.87}$. The higher monomer order is due to the fact that the gel effect becomes more and more influential with the increase of monomer concentration.

3.2. Effect of emulsifier content on copolymerization

In the present system, the mixture of Span-80 and Tween-80 is used as a composite emulsifier. Fig. 2 displays the effect of emulsifier content on polymerization. The overall polymerization rate increased with the increase of emulsifier content. The effect of emulsifier content on polymerization kinetics is displayed as: $R_p \propto [E]^{0.48}$, $[\eta] \propto [E]^{0.36}$. Higher emulsifier content causes faster emulsifier adsorption, and hence for a given duration a greater number of smaller particles will be emulsified during the primary emulsifying process. As a result, the total interfacial area will be larger, the capture efficiency of primary radicals will rise and the reaction rate will increase.

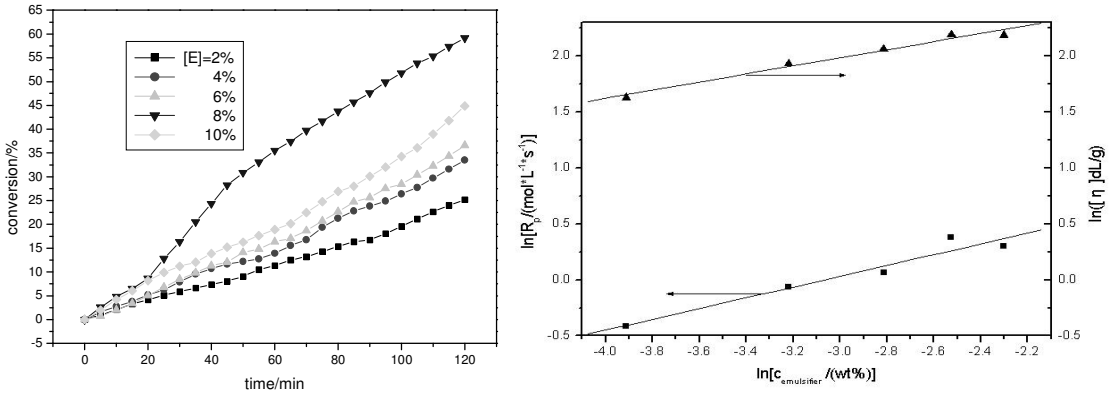

(a) (b)

Fig.2. (a) Conversion vs. time curves at different emulsifier contents; (b) the effect of emulsifier content on polymerization.

3.3. Effect of initiator content on copolymerization

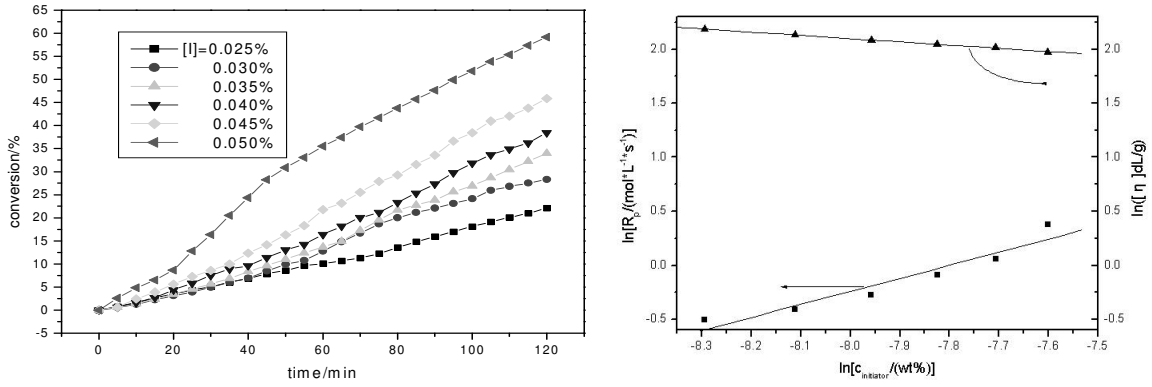

(a) (b)

Fig.3. (a) Conversion vs. time curves at different initiator contents; (b) the effect of initiator content on polymerization.

It was found in Fig. 3 that $R_p \propto [I]^{1.21}$, $[\eta] \propto [I]^{-0.30}$. The overall R_p increases with the increase of initiator content. However, intrinsic viscosity of the polymer formed is found to decreases with increasing initiator content. As the initiator content increases, the rate of free radical formation becomes greater, which leads to faster monomer consumption but also results in a shorter kinetic chain length.

3.4. Effect of polymerization temperature on copolymerization

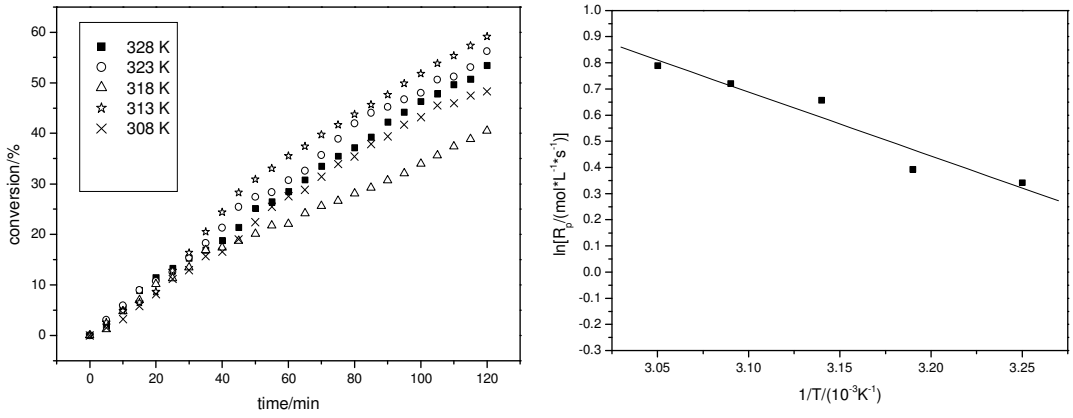

(a) (b)

Fig.4. (a) Conversion vs. time curves at different initial temperature; (b) the effect of initial temperature on polymerization.

The effect of temperature on the polymerization rate is shown in Fig. 4 (b). With increasing temperature, the radical concentration increases, resulting in an increase in the polymerization rate. According to the Arrhenius equation, the overall activation energy of the present polymerization system ([M] = 45% of total, n_{AM} / n_{DMDAAC} = 8/2, [E] =8% of total, [I] = 0.05% (monomer)) is 20.33 kJ/mol calculated by plotting $\ln R_p$ versus 1/T (K) (shown in Fig. 4 (b)). This value corresponds well with the typical activation energies of propagation in free radical polymerization [4][5]. The lower activation energy of polymerization was attributed to the small energy barrier for the absorption of free radicals by latex particles and it was controlled by the initiation and propagation reactions.

4. Conclusion

In this paper, the influences of the concentrations of monomers, emulsifier and initiator and initial temperature on conversion, polymerization rate and intrinsic viscosity of polymer in inverse emulsion polymerization have been examined. The intrinsic viscosity increased with the increasing concentrations of monomers and emulsifier and the decreasing concentration of initiator. The rate of polymerization (R_p) can be represented by $R_p \propto [M]^{2.11}[I]^{1.21}[E]^{0.48}$. The overall activation energy for the rate of polymerization was determined with a dilatometer as 20.33 kJ/mol over the temperature range 35-55℃.

References

[1] Y. Zhang, X. Gu. Research progress in the copolymer of dimethyldiallylammonium chloride and acrylamide[J]. J Fine Chemicals 2002; 19 (9): 521~527.

[2] Yue Q, Li Y, Gao B, Yang Z, Zou X. Study on the inverse emulsion polymerization of PDMDAAC-AM [J]. J Shandong Univ (Natural Sci), 2004, 39 (6): 86-89

[3] Hou S, Ha R. Studies on kinetics of inverse emulsion copolymerization of dimethyl diallyl ammonium chloride and acrylamide [J]. Acta Polymerica Sinica, 1995, 1(3): 349-354.

[4] Behari K, Taunk K, Das R. Polymerization of acrylamide and methacrylamide initiated by a potassium peroxydiphosphate/Mn (II) system[J]. Polymer international, 1998, 46(2): 126-130.

[5] Cowie JMG (1989) In: Allen G, Bevington JC, Booth C, Price C (eds) Comprehensive polymer science, vol. 3. Oxford: Pergamon Press, England.

Advanced Materials Research Vols. 989-994 (2014) pp 352-355
© (2014) Trans Tech Publications, Switzerland
doi:10.4028/www.scientific.net/AMR.989-994.352

Research of Formation Mechanics on Nanostructured Chips by Multi-deformations Based on Finite Element Method

C.L.Wu [1, a], Z.R. Wang [1,b], Wen Zhang[1,c]

[1] School of Mechanical and Automotive Engineering, Xiang Fan University, Xiangfan, China

[a]chunling_wu@126.com, [b] xfuwangzhongren@126.com, [b] zhangwen@126.com

Keywords: large strain machining, rake angle, multi-deformations, FEM

Abstract. Formation of chip is a typical severe plastic deformation progress in machining which is only single deformation stage. The rake angle of tool is governing parameter to create large strain imposed in the chip. Effect of rake angle and deformation times on effective strain, mean strain, strain variety and strain rate imposed in the chip are researched respectively. The result of simulation have shown that the chip with large strain and better uniform of strain along the longitudinal section of chip can be produced with negative rake angle at some lower cutting velocity by multi-deformations in large strain machining.

Introduction

Formation of chip is a typical severe plastic deformation progress in machining with only single deformation stage. Large plastic strain(1-15) can be imposed in the chip by changing the rake angle of tool, with the wore highly strained chips being generated using tools with more negative rake angles. S.Swaninathan[1-2] reported that OFHC chips which were structured by nanoscale equaixed grains with a significant of high-angle grain boundaries can be received at the speed of 0.02m/s with the tool rake angle of -20°. The vickers hardness of the chips were substantially increased from 50 to 155. While at the speed of 0.01m/s with the tool rake angle of -20°, Al6061 chips were structured by nanograins with 75nm. The chip materials with ultrafine grained and high hardness can be produced with negative tool rake angle at some lower cutting velocity.

Since the application of FEM in machining has been receiving much attention since 1970s, FEM has become the main tool for simulation metal cutting progress with result in plastic deformation of metal materials. M.SEVIER[3] studied the influence of the rake angle and friction at the tool-chip interface on the deformation by FEM. They found that the result of FEM on strain, stress, strain rate and machining temperature in the deformation area are consistent with the result of PIV analysis. W.J.Deng[4] analyzed the effect of rake angle on distribution of effective strain imposed in chips by FEM and found that the distribution of effective strain is consistent with microstructure of chips. In this paper, machining model of large negative rake angle and edge radius of tool is established in order to reveal the formation mechanics on nanostructured chips by multi-deformations based on FEM.

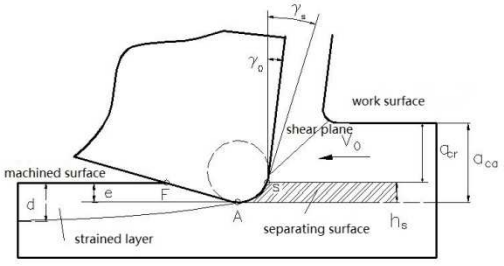

Fig.1 Machining model of large negative rake angle and edge radius of tool

Figure 1 shows the machining model of large negative rake angle and round cutting edge radius of tool. There are three deformation areas during the progress of chip production in the large strain

machining. The chips are produced in the first deformation area under the shear and extraction by large negative rake angle of tool in the large strain machining. In the second deformation area, the chips are undergone extraction and friction from rake flank of tool during they flow along the rake flank and received more sever plastic deformation. In the third deformation area, metal of cutting layer under the shunting point are severely extruded by cutting egde radius of tool, rounded nadir A of cutting edge and sever frictional with rake flank of tool so as to strained larger with sever fibrosis are founded in the work surface which physical and mechanical properties are changed.

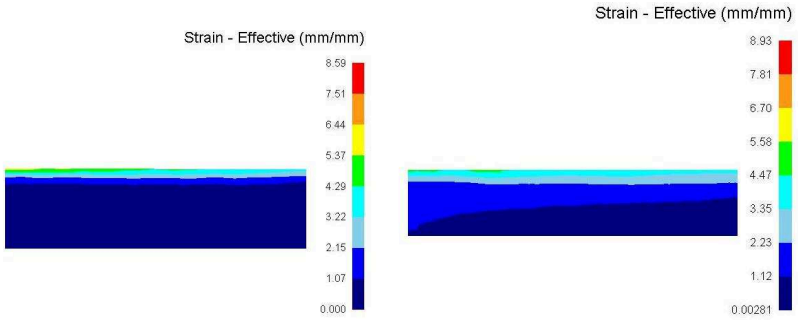

Fig.2 Distribution of effective strain in strained layer

Figure 2 states the distribution of effective strain in strained layer. The height of strained layer is about 0.185mm after the first deformation by the large strain machining with rake angle of -20°. While the height of strained layer is substantially increased from 0.185 to 0.5mm in the third deformation and while the maximum value of effective strain is about 5 in the two deformations. The chip material with larger strain and the improvement of the uniform shear strain distribution in the chip on longitudinal section are produced under the effect of multi cumulative strain.

Result

The simulation of machining was done at the speed of 0.052m/s, with tools of rake angles in the range from 20° to -20° in order to examine the effects of rake angle on the strain, stress and strain rate imposed in the chips and the uniform distribution of shear strain.

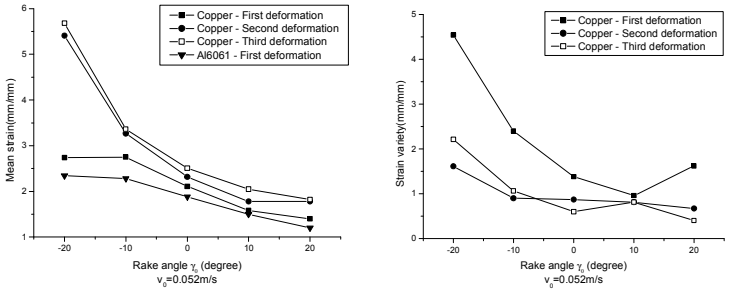

(a) (b)

Fig.3 Influence of rake angle on shear strain of chip (a) rake angle-mean strain. (b) rake angle-strain variety.

Figure 3 states the influence of rake angle on shear strain of chip during three deformation stages. The max of effective shear strain are 2.24, 3.02, 4.26 and 5.34 at the rake angle of 10°, 0°, -10°, and -20° respectively in the first deformation. The thickness of chip and the difference of chip form are increased with the decreased rake angle. With more decrease rake angle of tool, the mean strain and strain variety are a little increased in the range of 20°, 10° and 0°. While at the larger negative rake angle, they are substantially increased. Although compared the first deformation, the max of effective strain are only a little increased with the increase of deformation times at the rake angle of 10°, 0°, -10°, the mean value of effective strain is greatly increased and strain variety is greatly decreased along the longitudinal section of chip in the second and third deformation. The

distributions of shear strain are more uniform along longitudinal section of chip. Especially at the rake angle of $^{-20^{\circ}}$, the max value and mean value of effective strain are increased from 5.34, 2.74 in the first deformation to 7.12, 5.68 in the third deformation respectively and the strain variety is decreased from 4.54 to 2.11. It is showed that with the decrease of rake angle, the mean strain and strain variety are a little increased, but at the more negative rake angle, the mean strain is more substantially increased and strain variety is more decreased. Compared the first deformation, at the rake angle of $^{-20^{\circ}}$, the mean strain of chips are substantially increased and the strain variety are decreased by multi deformation which can improve the uniform distribution of strain and microstructure along the longitudinal section of chip. While the effect of deformation times do little to effective stress of deformation area.

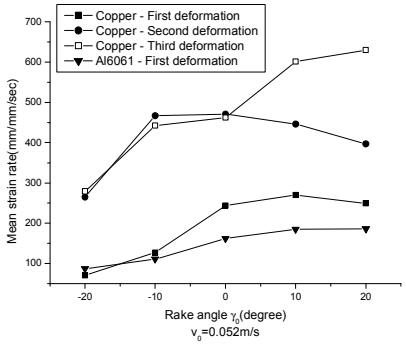

Fig. 4 The effect of rake angle on mean effective strain rate of chips in shear area

Figure 4 shows the effect of rake angle on mean effective strain rate of chips in shear area. With the decreased rake angle, the mean strain rate is decreased at the negative rake angle. Compared the first deformation, the mean effective strain rate are more increased in multi-deformations. At the rake angle of different range, the mean effective strain rate are increased from 249,270,244,127and 70mm/mm/sec in the first deformation to 630,610,462,446 and 279mm/mm/sec in the third deformation at the rake angle of $20°$,10°, 0°, -10° and -20° respectively. It is showed that the strain rate of chips in shear area is higher than the strain rate of material produced by conventionally methods of Severe Plastic Deformation.

Summary

The rake angle of tool is a governing parameter in large strain machining in which chip formation mechanism, strain, strain rate and uniform of strain distribution.

Compared the first deformation, the strain and uniform of strain are improved in the second and third deformation. The increased of deformation times change the machined material to be highly strained material which the chips with larger strain and better uniform of strain can be produced by multi-deformations.

The chip with large strain and better uniform of strain can be produced with negative rake angle at some lower cutting velocity by multi-deformations in large strain machining. The microstructure of chip produced by large strain machining can be greatly fined to be nanoscale which physical and mechanical properties can be substantially improved.

This research is supported by scientific research fund of HuBei provincial education department (No. Q20112602).

References

[1] S.Swaminathan, M.R.Shankar, S.Lee et al. Materials Science and Engineering A:Vol401-411 (2005), p.358

[2] S.Swaminathan, M.R.Shankar, B. C. Rao, et al. Journal of Materials science:Vol.42(2007), p.1529

[3] Sevier Michael, Lee Seongeyl; Shankar M R, and et al. Deformation mechanics associated with formation of ultra-fine grained chips in machining[J]. Materials Science Forum 503-504(2006): 379-384.

[4] Deng W J, Xia W, Li C, Tang Y. Formation of ultra-fine grained materials by machining and the characteristics of the deformation fields[J]. Journal of Materials Processing Technology 209(2009): 4521-4526.

Advanced Materials Research Vols. 989-994 (2014) pp 356-359
© (2014) Trans Tech Publications, Switzerland
doi:10.4028/www.scientific.net/AMR.989-994.356

Single frequency LD-pumped 2.09 μm Cr, Tm, Ho: YAG microchip laser

Yongming NIE[a], Yakun GUO[b], Xin DING[c], Minmin GUO[d]

China Satellite Maritime Tracking and Controlling Department, Jiangyin, 214431, China

[a]email: nwy1986@163.com, [b]email:yimonie@163.com, [c]email:eykiyao@163.com, [d]email: duanfangzhen2005@163.com

Keywords: Lasers and laser optics; Microchip laser; Pumping

Abstract. Single-frequency microchip lasers have been widely used in differential absorption radars, pulse coherent Doppler radars, pumping optical parametric oscillators, and etc. So theoretical analysis and experimental researches on the LD-pumped 2.09 μm microchip laser have important realistic meaning. According to quasi-three-level Cr, Tm, Ho: YAG(CTH:YAG) laser crystal working characteristics, the theoretical expression and relationship curve between the output optical power and 785nm LD-pumped power are obtained by theoretical calculating based on the pumping rate equation. The CTH:YAG crystal with 4mm diameter and 1 mm thickness is used to do experimental test. The corresponding three kinds of particle concentration are 0.85%, 5.9% and 0.36% respectively. When the crystal temperature is controlled at 10 ℃, microchip laser beam output characteristic curve is obtained under different pump spots. The results show that when the pump spot diameter is 75um the maximum single-frequency output power is 32mW and when the pump beam is 100um the maximum single-frequency output power is 30mW. The corresponding optical to optical conversion slope efficiencies are 6.8% and 6% respectively.

Introduction

The single-frequency, diode pumped, and solid-state lasers has been the investigated several decades[1], and the LD-pumped solid-state lasers with wavelength 2μm have been widely used in the areas such as laser medical science, remote sensing, coherent Doppler radar, and differential absorption radar areas [2-5]. Presently, lots of research reports about 2μm microchip lasers have been published [6-8]. There have been a variety of ways to realize 2μm single frequency, for example, Fabry-Perot etalon in the resonant cavity method [9], microchip laser resonant cavity method [10], non-planar ring cavity methods [11], and so on. Simply analyzing all the methods above, it can be easily found that the LD pumped microchip lasers have compact and simple structure characteristics, which is attracting lots of researchers to investigate the microchip lasers. In 1998, Frank F. Heine and his coworkers use external cavity feedback technology to achieve a wavelength tunable single-longitudinal-mode Tm: YAG laser, the wavelength tuning range of which is 15nm and single-frequency output power of 45mW. In 2001, C. Nagasawa and his research team obtained 11mW single longitudinal mode laser output based on a thickness of 0.9mm Tm, Ho: YLF microchip with the 1% output transmittance and 20℃ crystal temperature. In 2009, Beijing Institute of Technology theoretically and experimentally studied the affects of the pumping microchip laser spot size on the single-frequency characteristics in detail [10].

In this manuscript, we make theoretical and experimental investigations on the LD-pumped 2.09 μm microchip laser. Firstly, based on the quasi three-level rate equations the output power and pump power relations of the CTH: YAG laser is deduced and numerical simulation is given. Then, using the LD-pumped 2.09 μm microchip laser with 1mm thickness, the experimental results of the output power and pump power are obtained. At last, conclusions are given.

Principals

In CTH: YAG crystal, the Cr^{3+} and Tm^{3+} are photosensitive ions, and the Ho^{3+} is active ion. Because Cr^{3+} has two very broad absorption bands in the visible optical band, flash lamp is usually used to pump the CTH: YAG crystal. Under the flash lamp pumping condition, Cr^{3+} ion will

produce from $^4A_1$ to $^4T_2$ and $^4T_2$ transitions after absorbing the pumping light. After fast non-radiative relaxation to ^2E state, based on ion-dipole interaction, energy of the Cr^{3+} to ^2E level radiation is transferred to Tm^{3+}, which is transferred from the ground state to the $^3H_4$ state. $^3H_4$ state of Tm^{3+} ion is transferred to $^3F_4$ level through cross relaxation, which has a longer fluorescence lifetime. So the energy can be easily transferred to Ho^{3+} by resonance effect, which can transfer Ho^{3+} from ground state to $^5I_7$. By stimulated radiation, Ho^{3+} is transferred from $^5I_7$ to $^5I_8$ and photons are released, and then laser is generated. If LD pumping form is used, Tm^{3+} can be directly transferred from ground state to $^3F_4$ and the energy is transferred to Ho^{3+} ions, then laser is generated. Because the CTH: YAG crystal has 4nm absorption bandwidth around 785nm and at this wavelength the LD can easily obtain a larger output power at present, 785nm LD pumping technical solution is usually used to pump CTH: YAG or TH: YAG laser to produce a 2.09μm laser. In this case, the impact of the energy transfer between Cr and Tm is little, and the rate equation can only consider the interaction between Tm and Ho. TH: YAG is a quasi-three-level system, according to the reference [12], the rate equation can be written as following.

$$\frac{dN_x}{dt} = R\left(1-(1-f_{Ho})\frac{N_x}{N_{Tm}}\right)-\frac{N_x}{\tau}-k_{\Sigma Ho}N_x^2-\sigma c\left(f_{Ho}(f_u+f_l)N_x-f_lN_{Ho}\right)\Phi \tag{1}$$

where R is the pumping rate, N_{Tm} and N_{Ho} present the Tm and Ho doping concentrations respectively, τ_i present life of the particle energy level i, τ presents the life of laser upper level, k_{ijkl} is the up-conversion coefficient of the energy level i to energy level j and energy level k to energy level l, η_i is cross-relaxation efficiency of energy level i, β_{ij} is spontaneous emission scale factor of the energy level i, f_u and f_l are the upper and lower laser level Boltzmann scores, σ is emission cross section, $f_{Ho}=\frac{N_6}{N_x}$ presents the scale fraction of the total up-level particles of Ho, $k_{\Sigma Tm}$ is the total up-conversion coefficient of Tm, $k_{\Sigma Ho}$ is the total up-conversion coefficient of Ho, Φ is the cavity photon density, and c is the speed of light in vacuum. If laser works in continuous form, $\frac{dN_x}{dt}$ equals zero. The following expression can be obtained.

$$\frac{N_x}{N_{Tm}}=\frac{-(a_2P_1^2+2P_2P_3)\pm\sqrt{\left(a_2P_1^2+2P_2P_3\right)^2-\left(P_1^2-4P_2^2\right)\left(\left(a_1P_1\right)^2-P_3^2\right)}}{2\left[\left(\frac{P_1}{2}\right)^2-P_2^2\right]} \tag{2}$$

where P_p and P_L are the pump power and the output power of the laser, T is the transmittance of the output end, ω_p and ω_L are the radius of pump beam spot and oscillation beam spot, and the significances in detail of the other parameters can be referred to reference [12]. So we will not repeat them here. If another aspect is considered, the laser stability should satisfy the following expression.

$$\frac{N_x}{N_{Tm}}=\frac{(1+r_{HT}\theta)^2N_{Tm}^2-B^2}{\left[2B-2N_{Tm}(1-r_{HT}\theta)\right](\theta-1)N_{Tm}} \tag{3}$$

$$B=\left(1+r_{HT}\theta\right)N_{Tm}-2\left(\theta-1\right)\frac{\frac{\delta}{\sigma l}+f_lN_{Ho}}{f_u+f_l} \tag{4}$$

where δ is single pass loss factor, l is the crystal production, θ is energy transfer coefficients of Tm and Ho, and r_{HT} is the ratio of the concentration of Ho and Tm. Under the steady work condition, expression (2) should be equal to expression (3). After reorganizing, the equation can be obtained as following.

$$\left(\frac{C^2}{4}+a_2C+a_1^2\right)P_1^2-C^2P_2^2+2CP_2P_3-P_3^2=0 \quad (5)$$

According to the theoretical analysis above, the relationship between P_L and P_p can be obtained, as the red curve shown in Fig.2 (a). The black curve presents the experimental relationship between the pumping power and the output power.

Experimentation

The Cr, Tm, Ho doping concentrations of the CTH: YAG crystal used in the experiment are 0.85%, 5.9% and 0.36 % respectively, and the crystal has 4mm diameter and 1mm thickness. The front surface of the crystal is coated with anti-reflection film at wavelength 785nm (T>99%) and high reflection film at wavelength 2.09um (R>99%). The output surface of the crystal is coated with high reflection film at wavelength 785nm (R>93%) and with 1% transmittance film at 2.09um. Under the 785nm LD pumping condition, the experimental absorption coefficient of the crystal is measured 4.3 cm^{-1}. Taking the output surface reflection into account, 1mm thick CTH: YAG crystal absorption rate is about 56%. The experimental setup is shown in Fig.1, which mainly includes a semiconductor laser, focusing system, micro-chip crystal, cooper heat sink, and the infrared filters.

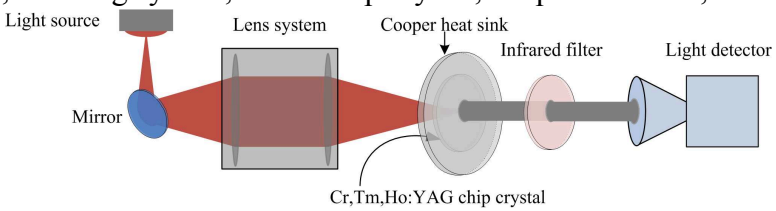

Fig. 1 Sketch of the CTH: YAG micro-chip laser setup

Experimental used pumping maximum power at 785nm is 1.9W, and the light-emitting section is 100um, during which 1:1 and 4:3 focusing systems are used for focusing and the corresponding focused beam diameters is 100um and 75um respectively. Crystal is fixed on the cooper heat sink which is temporal controlled between 10 ℃ and 20 ℃ by a thermoelectric cooler. The infrared filters are used to filter the pump light which is not absorbed. The filter has a high absorption coefficient (T <1%) when the wavelength is shorter than 1um and a high transmittance coefficient (T~90%) when the wavelength is around 2um. A power meter is used to measure the laser output power. The output characteristic curve of the microchip laser at different pumping beam spots when the temperature is 10℃ is shown in Fig.2 (b).

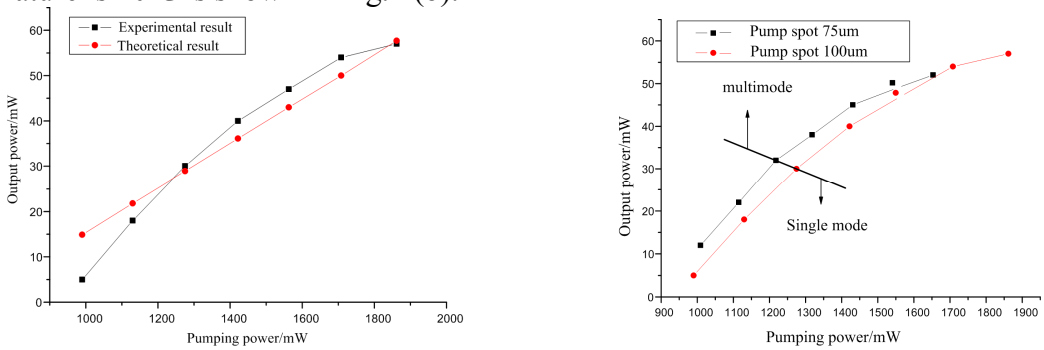

(a) The pumping and the output power (b) Output properties with different beam spots

Fig.2. The theoretical and experimental results

Using a con-focal scanning interferometer, the single-frequency region and multi-longitudinal mode region of the laser are discovered. When the pumping beam spot diameter is 75um, the maximum single-frequency output power is 32mW. When the pumping beam spot diameter is 100um, the maximum output power of the single frequency is 30mW. Correspondingly, the optical to optical conversion slope efficiency is 6.8% and 6% respectively.

Conclusion

In this manuscript, the relationship between the output optical power and 785nm LD-pumped power is obtained by theoretical calculating based on the pumping functions. Then, experimentation is doing to testify the calculating results. The experimental results fit well with the theoretical results and the maximum single-mode output optical power at 2.09μm of the Cr, Tm, Ho: YAG microchip laser is 32 mW .

Acknowledgement

This research was funded by the National Natural Science Foundation of China (NSFC) under grant no.61108089 and no.61107005. The authors acknowledge Doctor Yunshan ZHANG and Yunfei MAO for fruitful discussions.

References

[1] J. J. Zayhowski, A. Mooradian. Single-frequency microchip Nd lasers [J], Opt. Lett., 1989 14(1) 24-26.
[2] L. E. Batay, A. A. Demidovich, A. N. Kuzmin, A. N. Titov, M. Mond, S. Kück. Efficient tunable laser operation of diode-pumped Yb, Tm: $KY(WO_4)_2$ around 1.9μm [J], Appl. Phys. B, 2002 75(4-5):457-461.
[3] G. Galzerano, E. Sani, A. Toncelli, S. Taccheo, M. Tonelli, P. Laporta. Experimental investigation of the 2.1μm single-mode Tm-Ho: KYF laser [J], Appl. Phys. B, 2004 78(6):733-736.
[4] D. Gatti, G. Galzerano, A. Toncelli, M.Tonelli, P. Laporta. Actively mode-locked Tm-Ho: LiYF4 and Tm-Ho: BaY2F8 lasers [J], Appl. Phys. B, 2007 86(2):269-273.
[5] C. P. Hale, J. W. Hobbs, P. Gatt. Broadly tunable master/local oscillator lasers for advanced laser radar applications [C], Proc. of SPIE, 2003 5086:253-263.
[6] J. Sotor, G. Dudzik, K. M. Abramski. Single frequency, monolithic Nd: YVO4/YVO4/KTP diode pumped solid state laser optimization by parasitic oscillations elimination [J], Opt. Comm., 2013 291: 279-284.
[7] J. Z. Sotor, G. Dudzik, A. J. Antonczak, K.M. Abramski. Single-longitudinal mode, monolithic, green solid-state laser [J], Appl. Phys. B, 2011 103(1): 67-74.
[8] Y. Ma, L. Wu, H. Wu, W. Chen, Y. Wang, S. Gu. Single-longitudinal mode Nd:YVO4 microchip laser with orthogonal-polarization bidirectional traveling-waves mode [J], Opt. Express, 2008 16(23): 18702-18713.
[9] P. Laporta, M. Marano, L. Pallaro, S. Taccheo. Amplitude and frequency stabilisation of a Tm–Ho:YAG laser for coherent radar applications at 2.1μm [J], Optics and Lasers Engineering, 2002 37(5): 447-457.
[10] Z. Lin, C. Gao, M. Gao, Y. Zhang, H. Weber. Diode-pumped single-frequency microchip CTH: YAG lasers using different pump spot diameters [J], Appl. Phys. B, 2009 94(1): 81-84.
[11] C. Svelto, I. Freitag, Room-temperature Tm:YAG ring laser with 150mW single-frequency output power at 2.02 μm [J], Electronics Letters, 1999 35(2):152-153.
[12] G. Rustad, K. Stenersen. Modeling of Laser-Pumped Tm and Ho Lasers Accounting for Up-conversion and Ground-State Depletion [J], IEEE J. Quantum Electron., 1996 32(9):1645–1655.

Advanced Materials Research Vols. 989-994 (2014) pp 360-363
© (2014) Trans Tech Publications, Switzerland
doi:10.4028/www.scientific.net/AMR.989-994.360

Review and prospect on tear damage research for high-performance flexible fiber-reinforced composite material

Shuai CAO[1, a], Longbin LIU[1,b], Houdi XIAO[1,c], Mingyun LV[1,d]

[1] School of aeronautical Science and Engineering, Beihang University, Beijing 100191, China

[a]email: caofan1024@126.com, [b]email: longbuaa@sina.com, [c]email: xhdbuaa@126.com, [d]email:lv50@buaa.edu.cn

Keywords: Near Space Airship; Flexible Material; Tear Damage; Space Environment; Multiple Mechanisms Coupling

Abstract. Near space airship increasingly becomes a research hotspot with its inclusive potential military and civilian values. It is necessary to consider single and multiple-coupling space environment effects on evaluating envelope tearing damage mechanisms. The basic characteristics of the space environment and the complexity of tear damage mechanism are introduced, and this presentation also summarizes the research status of the tear damage mechanical mechanism and damage properties under the influence of the multiple space environment factors of high-performance airship envelope. Besides, the main existing problems and prospect in tear damage characterization under real working condition are discussed. The study provides some technical support for high-performance and protecting tearing damage design on airship envelope.

Introduction

With the development of envelope material and solar energy technology, the current ongoing near space airship (floating on the height of 20~30km) projects are practical [1]. many countries such as America, Japan, German, Korea are engaged in studying near space airship. But thermo, temperature, pressure, ozone, UV and other stratospheric environment make it easy to be damaged. Micro cracks or micro holes go expansion, and the result is destruction of envelope material [2].

Considering tear damage mechanical properties, airship envelope material can be seen similar to textile yarn bundle and laminated or coating composite. Combined with flight tests and ground environment chamber simulation tests, there are many researches on macro mechanicals, fatigue life and other aspects to explore the effects of space environment on envelope material [3]. More and more researchers put emphases on micromechanics properties of envelope to reveal its tear failure mechanism under multiple coupling mechanisms and predict fatigue life, which focuses on mesoconstituents of flexibilities and micromechanics characterization and simulation.

Complexities of Airship Envelope Material Tear Damage

Flexible composite material of near space airship envelope is flexible coated fabric or laminated fabric [4]. Its internal reinforced fabric bearing layer and other function layers are combined by coating or laminating adhesive process. Due to fabric bearing layer is one of plain or twill weave, friction and slippage phenomenon occurs when the warp and the weft fiber bundle interact under loading, making its mechanics more complex than other plain or twill weave. In addition, since adhesives substrate plays the role of attaching and bridging, to some extent, function layers elastic-plastic deformation pins down the deformation of bearing layer stretching and bending. Twisted and pre-invaded gum warp and weft yarn bundles add the adhesives friction, making its deformation more complex. From the perspective of meso-tests, it is observed that, yarn bundles fracture caused envelope damage and tearing; the crack tip of tearing appears greater plastic deformation zone than continuum fracture in the course of tearing. It is necessary to take account of such factors as stretch, compression, bending deformation, fracture, friction among layers, substrate crack, benumbing and layered etc. to explore tear mechanism.

Multiple coupling environments in stratosphere make it fatigue and aging; furthermore all constituents go bad and broke one by one. Usually, single or some complex environment not the real space, but the ground simulation tests were adopted to study environment effects on airship envelope material. The differences between simulation environment and real environment add difficulties to analyze its damage and tear. Meanwhile, there are few literatures studying the law of space environment influence on envelope such as surface corrosion, and further researching on failure damage law. However, available information shows that envelope surface deflate, quality impairments, the size and structure local damage because of the vacuum of space environment (≤1.33 mPa) [5]. Affected by ultraviolet ozone factors, high performance yarn bundle presents photolysis; surface morphology change; optical properties; bearing capacity reducing; accelerates aging, degradation and low temperature embrittlement under high and low temperature alternating.

Researches on Mechanical Characteristics of Flexible Material Tear

The particularity of airship envelope molding process and its self-structure makes tear and damage fracture main failure of space airship. Research shows that when the inside and outside overpressure gap reaches certain value, initial defects and micro-cracks begin to expand slowly [6]. Also, it occur that local fiber bundle breakage, matrix cracking and interfacial failure, fiber bundle slippage and reposition in crack tip stress concentration areas, resulting in stress concentration triangle-zone with initial crack damage. In this case, the initial defects and micro-crack stop going spread once overpressure payloads decrease. If the payloads are up to critical value, random crack with a certain shape will expand quickly leading the tear damage of fiber bundles. Initial defects and cracks enlarge dramatically and damage because of pressure resulting from bad working conditions and high-low temperature alternates in a short time. So studies on mechanism of tearing envelope material would lay foundation for optimization of envelope material formation, function design, enhancing its strength and structure layout under complex loads.

The popular ideal fabric reinforced substrate material, PBO, Kevlar and Vectran of near space airship, with the characterization of high strength, light weight, low elongation, corrosion resistance and anti-aging, are weaved as bearing layer of airship envelope. Tear damage strength of textile material is related to singe fiber bundle strength, woven process and substrate features. Although the fiber bundles broke one by one, the crack tip stress spreads out by adjacent bundles shearing, making fiber around the fracture withstanding tensile stress. The number of fiber bundles bearing tensile stress is related to the fiber bundle pitch, the curvature of the fiber, braided angle, cross-sectional shape, fiber twists and other parameters, affecting the tear strength of fabric. Envelope material coating layer (or function layer) not only acts adhesive, air resistance, abrasion resistance and anti-aging but also has great impact on shear properties, limiting the movement of the fiber bundle node, thus affecting tear damage of envelope material.

Tear damage of near space airship envelope is complex. As the stress of envelope material increase to certain value, fiber bundles appear different scales damage in ontology micro-scale and initial crack and defects gradually enlarge. When the stress exceeds the critical breaking strength or elongation, yarn bundle begin to break in succession and slides and relocates in the stress concentration zone, forming triangle stress concentration zone with initial crack and resulting in interface failure and breakage of substrate. With the increase of stress loads, fibers in crack tip zone continuously go fracture. materials go through micro-meso-macro damage, finally get rupture completely. The tearing modal is influenced by components material, coating process, woven forms, interface features and associated with initial defects, crack orientation, environment payloads etc., making it difficult to explore exact mechanism of tear modal.

Envelope structure meso-mechanics can help pursue further study of tear damage mechanism. Scholars develop geometry and mechanical model to investigate envelope mesostructure. Characterization involves in cross-section shape changes and fiber bundle/substrate interface geometry. Researches have presented mosaic, bending and bridging of constituents' structure properties, taking in account fluctuation and pitch in the fiber other factors, to calculate stress and analyze cumulative failure behavioral characteristics. On basis of strain homogenization theory,

effective elastic modulus and thermal expansion coefficient get focus Zhang Yitong etc. put forward fabric oblique heterosexual constitutive equations, studying oblique yarn constitutive behavior under tensile formation. Zhang Chao etc. set method to predict and analyze elastic properties of two-dimensional biaxial woven composite materials based on meso-analysis and volume average method. These efforts provide a valuable reference for studies of coated woven geometric model and mechanical model, but all existing models are mainly applied to predict the elastic properties and strength, not suit for accurate description of envelope tearing.

Studies have shown that overpressure gap induced by sunlight on airship balloon in short time, cause original crack or defects expand and destroy abruptly [7]. Research on airship coating woven tear propagation under biaxial stress and complicated curvature was made. Stress field of envelope material will redistribute randomly. a majority of studies of envelope material tear damage still remain in test observation and qualitative analysis level. However, some researches use material energy function based on random statistical model to express these complicated variation and build crack propagation moldal to predict most likely path of crack propagation via system energy changes. Meanwhile environment adds complexity on material constituents and mechanic parameters. The current on-going projects on coated envelope tear propagation simulation are relatively few. Finite element analysis software usually adopts “life and death cell” method for fiber fracture failure simulation in dynamic simulation. Up to now, there isn’t some method applied to simulate tear propagation under any complex condition to guarantee appropriate accuracy.

Tear Damage Failure Characteristics in Space Environment

The particularity and complexity of space environment make envelope material inevitably bear multiple coupling loads (micro-gravity, high vacuum, ultra high-low alternates, thermal stress fatigue, light aging, ozone, ultraviolet radiation aging, plasma impact etc.) under which material prone to aging, degradation causing envelope and its constituent physical, chemical and mechanical changes and even complete failure. Seldom research on single or multiple effects on envelope material is in progress. Most of researches focus on envelope constituents such as high performance fibers, adhesive substrate layer, and functional layer etc. What’s worse, fewer researchers did tests on multiple coupling loads.. Bending fatigue mechanical properties of fiber bundle under light heat and UV effect got research.

Tamargor etc. employed gravimetric analysis to explore the thermal decomposition characteristics of high performance fiber PBO and used DTG curve to study thermal stability of blend fabric Kevlar/Nomex.. Envelope material appears light aging when working under light, affecting the fiber fracture strength, modulus, breaking elongation, the material composition, surface structure and so on. Day M , Arrieta C etc. carried on outdoor sunlight aging test, researching on light aging strength retention of Nomex and Kevalr49, and discover that illumination damage material mechanics from outside to inside. High strength fiber Kevlar is eager to degradation of the mechanical properties under ultraviolet light. For light and thermal, until now, multiple mechanism experiments only including light aging first and heat aging, heat aging first and light aging have been done, demonstrating that fiber resistance is worse than that in single mechanism environment. Currently, projects on high performance envelope environment resistance are just ongoing. Beihang University, Harbin Institute of Technology, Donghua University has explored some ground simulation environment tests. However, there are many single mechanism environment researches, rather than multiple coupling tests so the effect of multiple coupling environment on high performance envelope tear damage and tear propagation isn’t still evident. Predicts of envelope material tear damage and macro strength are unclear and not quantified. The ongoing application on engineering usually refers to initial extension strength of crack on basis of fracture theory.. Meanwhile, near space environment full of complexity and variation cause envelope tear evolution more unclear.

Prospects

Currently, most of researches on envelope material tear and damage put emphasis on uniaxial / biaxial tensile mechanics. Actually, tensile stress fatigue and bending fatigue further affect tear damage properties under overpressure condition. As usual, the method of continuum macroscopic fracture mechanics and damage mechanics is used to deliver characterizations of envelope tear damage. But, discreteness of bearing fiber and randomness of fracture fiber cause large errors in studying envelope properties by macroscopic fracture mechanics.

On the other hand, new ground multi-mechanism coupling environment simulation test instruments should be developed, making ground environment simulation test equipment to simulate single mechanism or multiple coupling mechanisms. It is valid to verify the tear damage of envelope material in real space environment coupling of multiple factors by means of ground simulation test. During airship envelope works in the space, airbag buoyancy gas such as helium, hydrogen penetrates envelope material through crack. Whereas, the leakage of buoyancy gas accelerate the propagation of initial defects and crack, further affecting fatigue life and stratospheric airship envelope performance. Therefore, in high overpressure condition, failure of airship envelope material must consider the extension response of micro crack or micro holes.

Conclusion

To guarantee airship envelope long-term use and maintain high performance under complex space environment, Studies on envelope material tearing damage should consider thermal stress fatigue caused by temperature variation, thermal cycle, ozone aging, ultraviolet radiation, natural light and so on. Single mechanism and multiple mechanisms should be tested or simulated respectively to explain its function. The damage of envelope material is not a simple plus of several kinds of damage, but a complex coupling of different environment which decide material life.

Except for studies on single mechanism on envelope, as much as possible space environment factors (multiple coupling and interaction of different mechanisms) should be added to develop modal and evolution of envelope damage. Ground environment simulation instruments and device should be set to simulate space environment as real as possible to explore tear damage and accurate characterization methods under the influence of environmental factors.

References

[1] Anthony Colozza. High-Altitude, Long-endurance airships for coastal surveillance: NASA: TM, 2005.

[2] Bai Jiang-bo, Xiong Jun-jiang, Cheng Xu. Tear resistance of orthogonal Kevlar PWF-reinforced TPU film .Chinese Journal of Aeronautics 2011; 24:113-118.

[3] Tan Hui-feng, Liu Yu-xi, Liu Yu-yan, et al. Research progress and requirement analysis of envelope materials for near space airship. Acta Materiae Compositae Sinica, 2012; 29(6): 1-8.

[4] Liu Longbin, Gu Yunchao, Cao Shuai, et al. The research on oblique crack tip deformation field of airship envelope composites based on the digital speckle correlation method [J]. Applied Mechanics and Materials, 2014, 477: 34-38.

[5] Grossman E, Gouzman I. Space environment effects on polymers in low earth orbit. Nuclear Instruments and Methods in Physics Research, 2003; 208(8): 48-57.

[6] Lv Ming-yun, Wu Zi-chun. Thermodynamic model and numerical simulation of high altitude balloon ascending process. Journal of Beijing University of Aeronautics and Astronautics. 2011; 37(5): 505-509.

[7] Liu L B, Liu D X, Lv M Y. A New Design of Inflatable and Lightweight Device for Planetary Exploration [J] . Advanced Materials Research, 2011, 217: 158-162.

Advanced Materials Research Vols. 989-994 (2014) pp 364-368
© (2014) Trans Tech Publications, Switzerland
doi:10.4028/www.scientific.net/AMR.989-994.364

Influence of Volume Fraction of Piezoelectric Ceramics on Poperties of PZT672/Epoxy1-3 Piezocomposite

Bin Zhang[1,a], Likun Wang[1,b], Lei Qin[1,c], Chao Zhong[1,d], Dan Long[1,e] and Jingjing Liu[1, f]

[1]Research Center of Sensor Technology, Beijing Information Science & Technology University, No.35 North Fourth ring road, Chaoyang District, Beijing,100101,China

[a]bin_zhang2011@163.com, [b]wlikun1962@163.com, [c]qinlei110@126.com

[d]zcloverlxm@163.com, [e]llongdan@163.com, [f]lcsljjcg@163.com

Keywords: 1-3 piezocomposite, PZT/epoxy, PZT Volume Fraction

Abstract. PZT672/epoxy 1-3 piezoelectric composites were fabricated by the cut-filling method. The parameters of PZT672/epoxy 1-3 piezoelectric composites varying with different PZT volume fractions have been measured and compared with theoretical values. The results show a good match between theoretical values and measurements. The authors conclude the regular of the properties of composites varying with PZT volume fraction.

Introduction

Piezocomposite is composed by piezoelectric ceramic and polymer phase according to a certain way connected and certain volume or weight ratio[1]. It is a new type material which can greatly improve the piezoelectric properties. 1-3 piezocomposite is the major type of piezocomposites, It consists of the one dimensional connected thin piezoelectric ceramic column paralleled arrangement in the three dimensional connected polymer[2]. It is extensive researched and applied in recent years. 1-3 piezocomposite has the following advantages[3]: low impedance, easier to match with water or human tissue, low Q value, small transverse electromechanical coupling coefficient, good flexibility and high hydrostatic pressure piezoelectric constant. It also can be made into special shape. In addition, it is easier to improve the properties by changing PZT or polymer volume fraction. In this paper, the regular of properties of composites varying with PZT volume fraction will be researched.

Theoretical Derivation of The Properties of 1-3 Piezocomposite

1-3 piezocomposite usually works in thickness vibration patterns, according to the characteristics of thickness vibration mode[4] the properties of 1-3 PZT/epoxy piezocomposite are derivated by e piezoelectric equation[1] and force-electricity boundary conditions. By the constitutive equations of materials[5]:

Piezoelectric phase (1):

$$\begin{cases} S_1^c = \left(s_{11}^{Ec} + s_{12}^{Ec}\right) T_1^c + s_{13}^{Ec} T_3^c + d_{31} E_3^c \\ S_3^c = 2 s_{13}^{E} T_1^c + s_{33}^{E} T_3^c + d_{33} E_3^c \\ D_3^c = 2 d_{31} T_1^c + d_{33} T_3^c + \varepsilon_{33} E_3^c \end{cases} \tag{1}$$

Polymer phase (2):

$$\begin{cases} S_1^p = \left(s_{11}^{Ep} + s_{12}^{Ep}\right) T_1^p + s_{12}^{Ep} T_3^p \\ S_3^p = 2 s_{12}^{Ep} T_1^p + s_{11}^{Ep} T_3^p \\ D_3^p = \varepsilon_{11}^p E_3^p \end{cases} \tag{2}$$

According to the working state of 1-3 piezocomposite, introducing the corresponding physical boundary conditions[6] as Eq. 3:

$$\begin{cases} S_3^c = S_3^p = \overline{S_3} & \overline{S_1} = vS_1^c + (1-v)S_1^p = 0 \\ E_3^c = E_3^p = \overline{E_3} & \overline{T_3} = vT_3^c + (1-v)T_3^p \\ T_1^c = T_1^p = \overline{T_1} & \overline{D_3} = vD_3^c + (1-v)D_3^p \end{cases} \tag{3}$$

Bring Eq. 3 into Eq. 1 and Eq. 2, available elastic constants $\bar{c}_{33}^{E}\ \bar{c}_{33}^{D}$, piezoelectric constant $\bar{e}_{33}\ \bar{h}_{33}$, dielectric constant $\bar{\varepsilon}_{33}^{s}$, piezoelectric isolation rate $\bar{\beta}_{33}^{s}$, piezocomposite density $\bar{\rho}$, thickness electromechanical coupling coefficient $\bar{K}_t$, acoustic impedance $\bar{Z}$ and compressional wave velocity $\bar{v}_t$ expression[6] of 1-3 piezocomposite are simplified as follows Eq. 4 - 13:

$$\bar{c}_{33}^{E} = v\left[c_{33}^{Ec} - 2(1-v)\left(c_{13}^{Ec} - c_{12}^{Ep}\right)^2 \Big/ \left(v\left(c_{11}^{Ep} + c_{12}^{Ep}\right) + (1-v)\left(c_{11}^{Ec} + c_{12}^{Ec}\right)\right)\right] + (1-v)c_{11}^{c} \tag{4}$$

$$\bar{e}_{33} = v\left[e_{33}^{c} - 2(1-v)e_{31}^{c}\left(c_{13}^{Ec} - c_{12}^{p}\right) \Big/ \left(v\left(c_{11}^{p} + c_{12}^{p}\right) + (1-v)\left(c_{11}^{Ec} + c_{12}^{Ec}\right)\right)\right] + (1-v)\varepsilon_{11}^{p} \tag{5}$$

$$\bar{\varepsilon}_{33}^{s} = v\left[\varepsilon_{33}^{Ec} + \left(2(1-v)\left(e_{31}^{c}\right)^2\right) \Big/ \left(v\left(c_{11}^{p} + c_{12}^{p}\right) + (1-v)\left(c_{11}^{Ec} + c_{12}^{Ec}\right)\right)\right] + (1-v)\varepsilon_{11}^{p} \tag{6}$$

$$\bar{c}_{33}^{D} = \bar{c}_{33}^{E} + \bar{e}_{33}^{2} \Big/ \bar{\varepsilon}_{33}^{s} \tag{7}$$

$$\bar{h}_{33} = \bar{e}_{33} \Big/ \bar{e}_{33} \tag{8}$$

$$\bar{\beta}_{33}^{s} = 1 \Big/ \bar{\varepsilon}_{33}^{s} \tag{9}$$

$$\bar{\rho} = v\rho^{c} + (1-v)\rho^{p} \tag{10}$$

$$\bar{K}_t = \bar{h}_{33} \Big/ \left(\bar{c}_{33}^{D}\bar{\beta}_{33}^{s}\right)^{1/2} = \bar{e}_{33} \Big/ \left(\bar{c}_{33}^{D}\bar{\varepsilon}_{33}^{s}\right)^{1/2} \tag{11}$$

$$\bar{v}_t = \left(\bar{c}_{33}^{D} \Big/ \bar{\rho}\right)^{1/2} v \tag{12}$$

$$\bar{Z} = \left(\bar{c}_{33}^{D}\bar{\rho}\right)^{1/2} \tag{13}$$

Series of the above equations, the superscript "-" "c" and "p" express respectively composites, ceramic and polymer material parameters, "t" and "v" express respectively the thickness of piezocomposite and PZT volume fraction.

Fabrication

1-3 piezocomposite is fabricated by the cut-filling method. PZT672(Zhejiang Jiakang Electronics Co, Ltd) is used as piezoelectric function component and epoxy618(China National Chemical Corporation) is used as passive component. PZT672 is a new type of piezoelectric ceramic. It is the favorable material used on sensitive element of ultrasonic transducer. Its detailed properties are shown in Table 1.

Table 1 Properties of PZT672

Material	PZT-672
Q value	247
Electro-mechanical coupling factor K_t	0.48
The quasi-static capacitanceCp(pF)	1754
DepletionD(mU）	15.5
Relative dielectric constant $\bar{\varepsilon}_{33}$	3818
Piezoelectric constant d_{33}（pC/N）	550

PZT672 were cut by automatic scribing machine(DISCO DAD321). Different 1-3 piezocomposite samples were fabricated by changing steps. The PZT volume fractions of 1-3 piezocomposite are varying from 54.76% to 77.76%. The cutting parameters were list in Table 2. Epoxy 618, curing

agent and flexibilizer were mixed by the proportion of 10:1:1. Poured into PZT672 skeleton, solidified for 12 hours in the room temperature. And then the piezocomposite samples were polished with grinding machine(PowerPro3000). The thickness was set to be 0.66 mm. Due to the limitation of precision of the grinding machine, the thickness of samples had a certain difference. The thickness of each sample is shown in Table 2. Finally the electrode was fabricated with magnetron sputtering apparatus(Kurt J.Lasker Inc.). At this point1-3 piezocomposite samples were fabricated completely.

Table 2 Data of fabricated samples

Sample number	Step t(um)	Slit width a (um)	Column width b（um）	PZT Volume fraction v(%)	Thickness h（mm）
1#	250	65	185	54.76	0.65
2#	350	65	285	61.36	0.63
3#	400	65	335	70.14	0.68
4#	450	65	385	73.20	0.64
5#	500	65	435	75.69	0.66
6#	550	65	485	77.76	0.69

Properties Measured

The properties of six samples are measured with impedance analyzer (Agilent4294A). The results are shown in Table 4. The electromechanical coupling coefficient is calculated by Eq. 14. The relative dielectric constant is calculated by Eq. 15. The sound velocityis calculated by Eq. 16. The acoustic impedance is calculated by Eq. 17. In Eq. 14 to 17, f_p expresses parallel resonant frequency.

$$K_t = \sqrt{\pi/2 * f_s/f_p * \tan\left(\pi/2 * (f_p - f_s)/f_p\right)} \tag{14}$$

$$\bar{\varepsilon}_{33} = v\varepsilon_{33}^c + (1-v)\varepsilon_{33}^p \tag{15}$$

$$v_t^D = 2 f_p t \tag{16}$$

$$\bar{Z} = \bar{\rho} v_t^D \tag{17}$$

Table 4 Properties of measured samples

Sample number	h（mm）	f_s (MHz)	Q	f_p (MHz)	$\bar{K}_t$	Z（Mrayl）	$\bar{\varepsilon}_{33}$	V (%)
1#	0.65	2.48	12.96	3.02	0.61	18.5	1707	54.76
2#	0.63	2.55	13.15	3.12	0.62	21.4	2024	66.31
3#	0.68	2.34	13.44	2.9	0.63	22.5	2192	70.14
4#	0.64	2.54	25.4	3.08	0.60	23.3	2228	73.2
5#	0.66	2.52	10.45	3.02	0.59	24.4	2277	75.69
6#	0.69	2.44	15.5	2.9	0.57	25.0	2369	77.76

Results and Discussions

a. PZT volume fraction effects on electromechanical coupling coefficient K_t

Electromechanical coupling coefficient is a physical quantity which represents the conversion capability of mechanical energy and electric energy of piezoelectrics. It is one of the important parameters of piezoelectric material. On the condition of piezoelectric effect, the electromechanical coupling coefficient is equal to the ratio of transformed electrical energy to the mechanical energy. The curve of calculated K_t has been shown in Fig.1and it is compared with measurement curve. Fig. 1 shows that while PZT volume fraction increasing from 40% to 100% the theoretical value slowly increases and reaches the maximum in about 70%, and then slowly falls. In this region, the measurement value is slightly smaller than the theoretical value and they have the same trend, and the deviation is less than 5.8%. Both are far greater than the electromechanical coupling coefficient of single PZT 0.48. The reason for the deviation is that each piezoelectric column is approximated slender column. Its length is much greater than width in theoretical calculation. But the piezoelectric

column cannot achieve the approximate conditions actually. The vibration modal is not entirely the longitudinal vibration of slender column. Therefore its electromechanical coupling coefficient measured is slightly lower than theoretical value.

b. PZT volume fraction effects on the relative dielectric constant $\bar{\varepsilon}_{33}^{s}$

The curves of calculated $\bar{\varepsilon}_{33}^{s}$ changing with PZT volume fraction and the measurement results have been shown in Fig. 2. While PZT volume fraction increasing from 40% to 100% the theoretical value increases linearly. Meanwhile, the measured value also increases linearly and it has the same trend as theoretical value. Measured value is lower than the theoretical value, and the deviation is about 19.9%. The deviation is mainly caused by the high temperature when high energy Ag ions deposited onto the surface of sample in the process of sputtering. It makes the samples at high temperature and the piezoelectric ceramic appears partial depolarization effect. Therefore it makes the relative dielectric constant value lower than expected value.

c. PZT volume fraction effects on the acoustic impedance $\bar{Z}$

Sound velocity is the speed of sound wave propagation in elastic medium. Using Matlab to calculate v_t^D in Eq. 12 and draw the curve changing with PZT volume fraction, and compared it with measurement curve which has been shown in Fig. 3. As we can see, the theoretical value increases slowly with PZT volume fraction varying from 40% to 90%. And it sharply increases when the PZT volume fraction higher than 90%. In the same time, the measured value is close to theoretical value with the same trend, and the deviation is less than 4.41%.

Acoustic impedance is a physical quantity introduced when analyzing acoustics system with lumped parameter. Using Mtalab to calculate $\bar{Z}$ in Eq. 13 and draw the curve changing with PZT volume fraction, and compared it with the measurement curve. The comparison is shown in Fig. 4. The PZT volume fraction varying from 40% to 100% the acoustic impedance also increases linearly. And the measured value is close to theoretical value with consistent trend, and the deviation is no more than 4.38%.

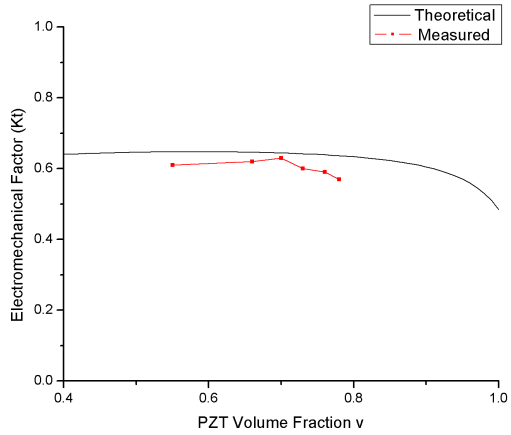

Fig. 1 Electromechanical coupling coefficient

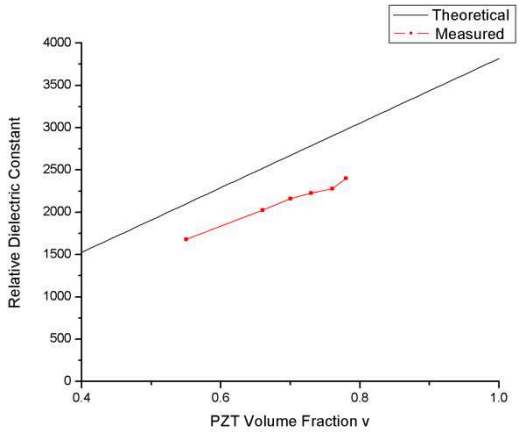

Fig. 2 Relative dielectric constant

By contrasting and discussing the results, measured value is close to theoretical value with consistent trend and also exists a certain deviation. The causes of the deviation are also caused by the following reasons. First, the grinding deviation of the samples can affect the measured deviation. Second, the assumptions of theoretical derivation are the simplify of analytical substance. The third reason is that the theoretical values of properties of PZT672 and epoxy are derived from reference, and a certain difference exists between the theoretical value and the actual value.

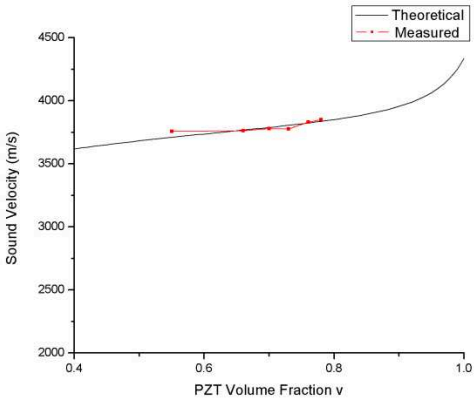

Fig. 3 Sound velocity

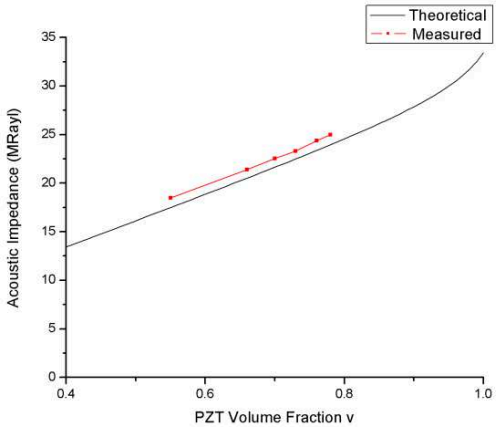

Fig. 4 Acoustic impedance

Conclusions

In this paper, the performance parameters of 1-3 piezocomposite are derived theoretically. Using Matlab to calculate performance parameters and draw the curve changing with PZT volume fraction. Different PZT volume fraction samples are fabricated, and compared the measured value with theoretical value. All the comparison results show that the measured value and the theoretical value have the same trend while the PZT volume fraction varying 54.76% to 77.76%. The electromechanical coupling coefficient reaches the maximum in about 70% volume fraction. The results of this paper provide the reference to choose the piezocomposite PZT volume fraction in practical application.

Acknowledgments

This work was supported by the National Natural Science Foundation of China (No.61302015), the Scientific Research Key Program (No.KZ201110772040) and General Program (No.SQKM201211232022) of Beijing Municipal Commission of Education. The project was also supported by Open Fund of Beijing Key Laboratory of Optoelectronic Measurement Technology (No. GDKF2013004).

References

[1] Guidong Luan, Jinduo Zhang, Renqian Wang, Piezoelectric transducer and transducer array, Beijing University press, 2005 (in Chinese)

[2] Kai Zhang,Yu Lan, Qi Li, Research of 1-3 piezoelectric composite broadband underwater acoustic transducer. Chinese Journal of Acoustics, 2011, 36(6): 631-637 (in Chinese)

[3] Denghua Li, Weijun Ju, Meijuan Jia, Xiaofei Xu, New piezocomposite transducer and its application. Science Press. 2007 (in Chinese)

[4] W.A.Smith. Calculating the Hydrophone Response of Piezoceramic-Rod/Piezopolymer-matrix composites. IEEE Ultrasonics Symposium Proceedings. 1990

[5] H.L.W. Chan, J. Unsworth. Simple model for piezoelectric ceramic/polymer 1–3 composites used in ultrasonic transducer applications. Ultrasonics, Ferroelectrics, and Frequency Control, IEEE Transactions on 1989,36(4): 434-441

[6] Kai Zhang. Research of 1-3 piezoelectric composite acoustic transducer. Harbin Engineering University,2009 (in Chinese)

Advanced Materials Research Vols. 989-994 (2014) pp 369-372
© (2014) Trans Tech Publications, Switzerland
doi:10.4028/www.scientific.net/AMR.989-994.369

Luminescence properties of rare-earth co-doped phosphate glasses for white light emitting diodes

Guo-hua Chen[a], Xiao-ling Kang[b], Yun Yang[c]

School of Materials Science and Engineering, Guilin University of Electronic Technology, Guilin 541004, China

[a] chengh@guet.edu.cn, [b] kxl168@guet.edu.cn, [c] cloud58@guet.edu.cn

Keywords: Glasses; Phosphors; Luminescence; White-light-emitting

Abstract. $Ce^{3+}/Tb^{3+}/Sm^{3+}$ co-doped phosphate glasses were prepared by melt quenching method. The full colors including blue, green and reddish orange emitting were observed simultaneously in the photoluminescent spectra of the glasses at 377 nm excitation, and the combination of these three emitting allows the realization of white light emitting. The CIE chromaticity coordinate (x=0.339, y=0.331) of the emission from the glass is close to the standard white-light illumination (0.333, 0.333). Moreover, the tunable luminescent color and chromaticity parameters could be realized by varying the content of Tb_4O_7 dopant in the glass composition, which is promising fluorescent materials for white light emitting diodes applications.

Introduction

In recent decades, the luminous materials doped with rare earth and transition ions have been studied for color display, temperature sensor, fluorescence labeling, white light simulation [1–5] and so on.

In view of energy and environment problems, it is absolutely necessary to develop pollution-free, cheap, highly efficient white-light-emitting (WLE) materials. It has been found that the

homogenization of the emission in the single phosphor is better compared to that in the mixed phosphors. The product cost of the single phosphor is also lower than that of the mixed phosphors. Thus, it is most valuable to study the single and novel phosphor. In response to these considerable challenges, luminescence glasses could be applied as good potential candidate for developing LEDs devices. Nowadays, some studies have been focused on the possible applications of rare earth ions doped glasses in the fabrication of white LEDs [6−7]. Liang et al. studied the luminescence properties of Tb^{3+}/Sm^{3+} co-doped B_2O_3 – Al_2O_3 – SrO system glasses and glass ceramics [8]. Song et al reported $Tm^{3+}/Tb^{3+}/Mn^{2+}$ co-doped phosphate glass ceramic for enhanced white-light-emitting material [9]. At ultraviolet light excitation, the emission efficiency of the visible light is higher. At ~360 nm light excitation, the materials doped with Tm^{3+}, Tb^{3+}, and Mn^{2+} ions were discovered to be of the blue, green and red phosphors [10−11], respectively. To our best knowledge, no researches on the WLE of $Ce^{3+}/Tb^{3+}/Sm^{3+}$ co-doped strontium zinc phosphate glass have been reported. Hence, in this work, $Ce^{3+}/Tb^{3+}/Sm^{3+}$ co-doped SrO – ZnO – P_2O_5 glass samples were prepared in order to realize the white light emitting and tunable luminescent color.

Experimental procedure

Powders of analytical reagent grade, comprising SrCO3, ZnO, NH4H2PO4 (≥99.5%) and high purity Ce(NO3)3 6H2O, Tb4O7 and Sm2O3 (≥99.99%), were used as the starting materials. The detailed compositions of the glasses are listed in Table 1. The glass batch was melted in a corundum crucible in air at 1230°C for 60 min. Glass melts were poured into a preheated copper mold for quenching. The glass samples were annealed at 480 °C for 2 h to release thermal stress and then cooled to room temperature. For further optical characterization, the bottoms of glass samples were polished carefully to form a mirror surface. The emission and excitation spectra were recorded on FL3-TCSPC fluorescent spectrometer (Horiba Jobin Yvon, France), using Xenon lamp as the

excitation source. All measurements were performed at room temperature. The chromaticity coordinates(x, y) were calculated based on the photoluminescent spectra by using software.

Table1. Composition of the glasses with CeO_2, Tb_4O_7 and Sm_2O_3 added (mol %)

Glass no.	SrO	ZnO	P_2O_5	CeO_2	Tb_4O_7	Sm_2O_3
A	21	42	37	0.1	0	0
B	21	42	37	0	0.125	0
C	21	42	37	0	0	2
D	21	42	37	0.1	0.125	2
E	21	42	37	0.1	0.25	2
F	21	42	37	0.1	0.5	2
G	21	42	37	0.1	0.75	2
H	21	42	37	0.1	1	2

Results and discussions

Fig. 1a shows the emission spectra of glasses A, B and C excited by 377 nm. A wide emission band peaking around 440 nm assigned to the 5d→4f electronic transition of Ce3+ is observed in the photoluminescent spectrum of sample A. For glass B, some characteristic emission occurs from 5D3 (blue) and 5D4 (green) levels to the ground state of Tb3+. The emission bands peaking at 438 and 415 nm are associated with the 5D3→7FJ (J=4, 5) electronic transitions, while the emission lines locating at 620, 582, 545 and 488 nm are due to 5D4→7FJ (J=3, 4, 5, 6) electronic transitions of Tb3+. In the spectrum of sample C, there are three emission lines peaking at 565, 605 and 648 nm originated from 4G5/2→6H5/2, 4G5/2→6H7/2 and 4G5/2→6H9/2 electronic transitions of Sm3+, respectively [13]. Fig. 1b depicts the excitation spectra of glasses A, B and C monitored at 444, 545 and 605 nm, respectively. There is a wide band peaking at 380 nm in the excitation spectrum of sample A. The excitation spectrum of sample B consists of four bands peaking at 350, 369, 377 and 484 nm and they correspond to the electronic transitions of Tb3+ ions from ground state 7F6 to excited states 5D2, 5D3, 5D4 and other higher 4f excited levels, respectively [14]. Three excitation bands peaking at 345, 362 and 375 nm corresponding to the 6H5/2→4K17/2, 6H5/2→4D3/2 and 6H5/2→6P7/2 transitions of Sm3+ respectively are included in the excitation spectra of sample C [15].

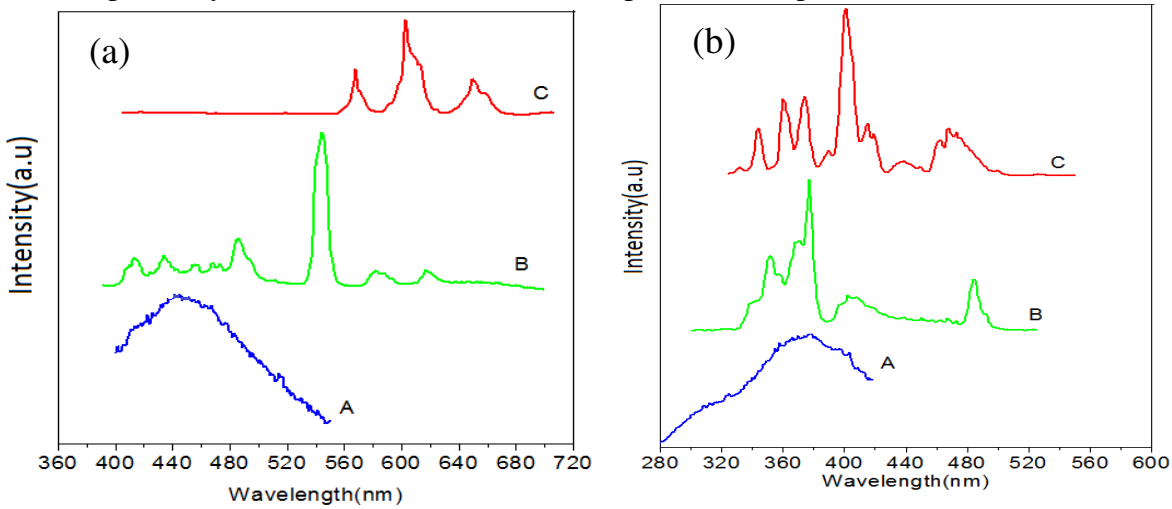

Fig. 1 Emission spectra of glasses A, B and C excited by 377 nm (a) and excitation spectra of glasses A, B and C monitored at 444, 545 and 605 nm (b)

Fig. 2a gives the emission spectra for co-doped glasses D, E, F, G and H excited by 377 nm. For all glass samples, the emission bands peaking at about 437 and 415 nm are ascribed to 5D3→7FJ (J=4, 5) transitions of Tb3+, and the emission bands locating at about 620, 585, 544 and 488 nm correspond to 5D4→7FJ (J=3, 4, 5, 6) transitions of Tb3+, as has been mentioned above [16]. The weak emission

band peaking at 440 nm is assigned to the 5d→4f electronic transition of Ce3+. Besides, the emission lines peaking at 565, 605 and 645 nm originate from 4G5/2→6H5/2, 4G5/2→6H7/2 and 4G5/2→6H9/2 electronic transitions of Sm3+, respectively. The positions of emission peaks are nearly the same for the samples D, E, F and G. Blue, green and reddish orange emission bands are observed in the emission spectra of these four glasses. Spectral comparison in Fig. 2a indicates that the concentration of Tb3+ has an important effect on the luminescence properties of glasses with a certain concentration of Ce3+ and Sm3+. The glass with a higher concentration of Tb3+ exhibits much enhanced green light (544 and 490 nm) and blue light (437 and 415 nm) due to the 5D4 and 5D3 emission of Tb3+. In other words, the increase in the Tb3+ concentration leads to the enhancement of 5D4 and 5D3 emission of Tb3+. With further increase of Tb3+ concentration up to 1mol%Tb4O7 (glass H), the new emission bands locating at about 585 and 620 nm corresponding to 5D4→7FJ (J=3, 4) transitions of Tb3+ occur. Meanwhile, the typical emission lines peaking at 565, 605 and 645 nm originated from 4G5/2→6HJ/2 (J=5, 7, 9) electronic transitions of Sm3+ disappear shown in Fig.2a. A typical excitation spectrum of glass sample G monitored at 444, 545 and 605 nm, respectively, as shown in Fig. 2b. The excitation band monitored at 444 nm is assigned to the 5d→4f electronic transition of Ce3+ and the peak position is located at 377 nm around. In addition, the spectrum monitored at 545 nm consists of five bands peaking at 352, 369, 377 and 484 nm and they correspond to the electronic transitions of Tb3+ ions from ground state 7F6 to excited states 5DJ (J=2, 3, 4) and other higher 4f excited levels respectively. Moreover, there are five excitation bands peaking at 345, 362, 374, 401 and 474 nm in the excitation spectrum monitored at 605 nm. These bands are corresponding to the 6H5/2→4K17/2, 6H5/2→4D3/2, 6H5/2→6P7/2, 6H5/2→4K11/2 and 6H5/2→4I13/2 transitions of Sm3+. Efficient excitation of these kinds of Ce/Tb/Sm co-doped glass with ultraviolet radiation is confirmed here and well fits the requirement of W-LEDs.

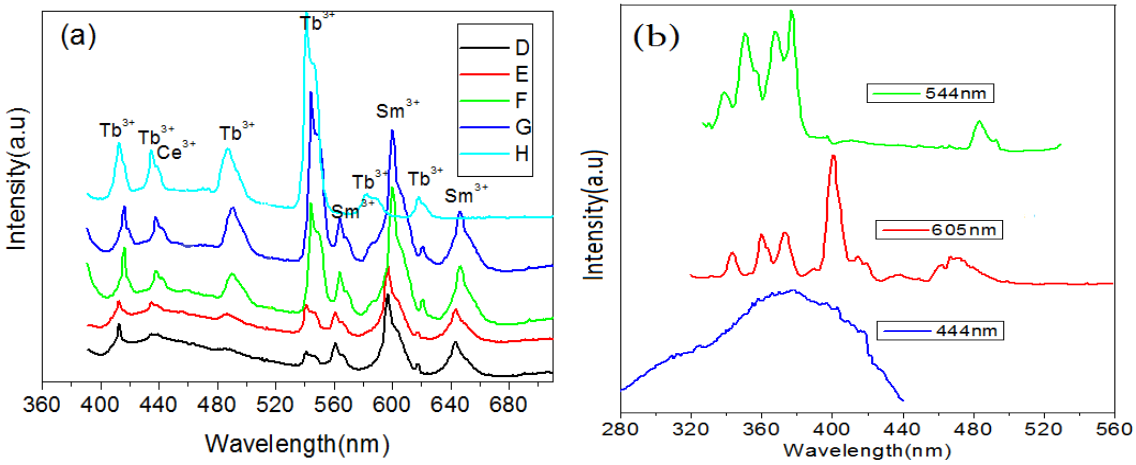

Fig. 2 Emission spectra of glasses D, E, F, G and H excited by 377 nm (a) and a typical excitation spectra of glass G monitored at 444, 544 and 605 nm (b)

The CIE chromaticity diagram for glasses D–H is shown in Fig.3. As seen from Fig.3, at 377 nm excitation, all the co-doped glass samples allow the realization of white light emission mainly due to the mixture of blue, green and red emitting under the same conditions except for glass H. The CIE chromaticity coordinates of the emissions from glasses D-H are (x=0.314, y=0.285), (x=0.316, y=0.292), (x=0.339, y=0.331), (x=0.346, y=0.353) and (x=0.129, y=0.113), respectively. Thus, the luminescent color can be easily altered by varying the content of doped rare earth ions, which realizes the tunable chromaticity parameters and color of these glasses.

Conclusion

Ce3+/Tb3+/Sm3+ co-doped phosphate glasses were prepared by melt quenching method. The full colors including blue, green and reddish orange emitting are observed simultaneously in the emission spectra of the glass samples except for glass sample H, and the combination of these emission bands

allows the realization of white light emitting at 377 nm excitation. Furthermore, the tunable luminescent color and chromaticity parameters could be easily realized by varying Tb4O7 content, which makes the glasses good candidates for WLEDs.

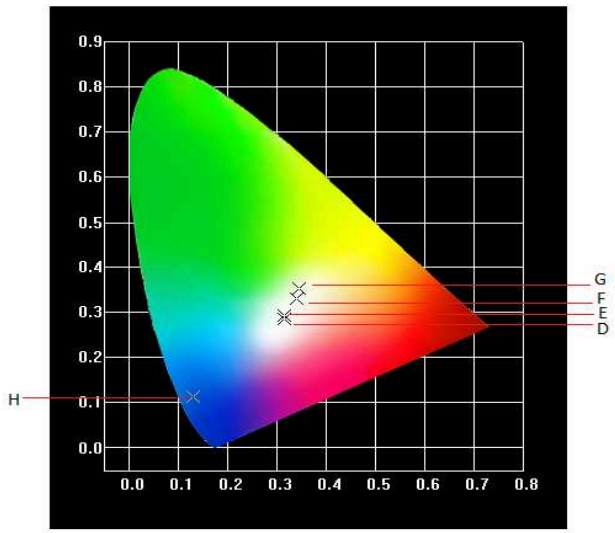

Fig. 3 CIE chromaticity diagram for glasses D–H under 377 nm radiation

Acknowledgements

This work was supported by the Natural Nature Science Foundation of China (51362005), the Natural Science Foundation of Guangxi (2013GXNSFDA019026) and the Program for Postgraduate Joint Training Base of GUET-GLESI (20121225-11-Z).

References

[1] E. Downing, L. Hesselink, J. Ralston and R. Macfarlane: Science, Vol. 273(1996), p1185
[2] S. Das, A.A.Reddy, S.S.Babu and G.V.Prakash: J.Mater. Sci. Vol.46(2011), p7770
[3] J.Burgin, V.Jubera, H.Debeda, B. Glorieux, A. Garcia and C. Lucat: J. Mater. Sci.Vol.46(2011), p2235
[4] L. Tang, H. P. Xia, P. Y. Wang, J. T. Peng, Y. P. Zhang and H. C. Jiang: J. Mater. Sci.Vol.48(2013), p7518
[5] B. Dong, D. P. Liu, X. J. Wang, T. Yang, S. M. Miao and C. R. Li: Appl. Phys. Lett. Vol.90(2007), p18111711
[6] X. L. Liang, Y. X. Yang, C. F. Zhu, S. L. Yuan, G. R. Chen, A. Pring and F. Xia: Appl. Phys. Lett.Vol.91(2007),p0911041
[7] R. F. Wei, H. Zhang, F. Li and H. Guo: J. Am. Ceram. Soc.Vol.95(2012), p34
[8] X. L. Liang, Y. X. Yang, S. F. Wang and G. R. Chen: J. Non-Cryst. Solids.Vol.357(2011), p2255
[9] F. Song, C. G. Ming, L.Q. An, Q. R. Wang, Y.Yu, H. Yu, T.Q. Sun and J. G. Tian: Mater. Lett.Vol.65(2011), p3140
[10] C.Y.Tu, J. F. Li, Z.J.Zhu, Z.Q.Chen, Y.Wang and B.C.Wu: Opt. Comm.Vol.227(2003), p383
[11] H. Lin, E. Y. B. Pun, X. J. Wang and X. R. Liu: J.Alloy. Compd.Vol.390 (2005) , p197
[12] Y. Arai, T. Takahashi and S. Adachi: Opt. Mater.Vol.32(2010), p1095
[13] E. Malchukova, B. Boizot, G. Petite and D. Ghaleb: J. Non-Cryst. Solids.Vol.353(2007), p2397
[14] Tsuboi T. Optical properties of Ce^{3+}/Tb^{3+} co-doped borosilicate glass [J]. Eur. Phys. J.-Appl. Phys.Vol.26(2004), p95
[15] A. Patra, R. Reisfeld and H. Minti: Mater. Lett. Vol.37(1998), p325
[16] P.L. Li, H.Y. Liu, Z.J.Wang, Z.P.Yang, X. Li and Y.M.Yang: Chin. J. Lumin. Vol. 31 (2010), p719

Advanced Materials Research Vols. 989-994 (2014) pp 373-378
© (2014) Trans Tech Publications, Switzerland
doi:10.4028/www.scientific.net/AMR.989-994.373

Monolithic porous graphene/ poly(vinyl alcohol) gels: preparation, structure and dye adsorption

Ping Wang [1] Yuping Guo [1, a]

[1]School of Pharmacy, Jiangxi Science and Technology Normal University,

Nanchang, Jiangxi 330013, China

[a] email: guoyp_2012@126.com

Keywords: porous gels, graphene, graphene oxide, adsorption

Abstract. The porous graphene oxide (GO) gels were prepared using the process of aqueous gel precursor freezing, solvent exchange, and ethanol drying technology. The GO sheets were consolidated by PVA and the obtained GO-PVA gel was reduced by glucose to prepare graphene nanosheet-SA (RGO-PVA) gel. GO-PVA and RGO-PVA gels exhibited the ultra-light densities of 10.52 and 11.24 mg/cm^3, respectively. GO-PVA and RGO-PVA can effectively adsorb the liquids. The less the polarity of the liquid was, the more the adsorption for both GO-PVA and RGO-PVA gels was. The equilibrium and the dynamic adsorption of methylene blue dye were also investigated. The maximum adsorption capacities of dye were 571.4mg/g for GO-PVA and 81.0 mg/g for RGO-PVA at 30 ºC.

1. Introduction

The dye-contaminated wastewater is one of the most serious environmental problems, which are harmful to human beings and toxic to microorganisms [1]. Graphene oxide (GO) has proven to be a highly effective absorbent of methylene blue (MB) and can be used to remove MB from aqueous solution at a huge absorption capacity of 714 mg/g [2]. However, GO is hydrophilic and is hard to separate from water. Since GO has the hydrophilic edges and a hydrophobic basal plane, it can be used in the construction of various supramolecular structures. The hydrogen bonding, static or hydrophobic interactions can make the flexible GO sheets form the 3D monoliths. The formation of 3D monoliths can be realized by adding cross-linkers [3]. Poly(vinyl alcohol) was added as a cross-linker to form a pH-sensitive supramolecular hydrogel with 3D network of GO [4]. Hydrogen bonding between GO sheets and PVA chains is important to form the gels. Single-stranded DNA was also found to be a cross-linker for preparing a GO/DNA composite hydrogel, in which π-π interaction was the dominant driving force [5].In this study, monolithic GO gels were prepared using a freezing, solvent exchange (ice-ethanol) and ethanol drying (FSE) method rather than supercritical drying technology. PVA was used to crosslink GO sheets to form a 3D network. Porous and ultra-light GO gels were obtained, and RGO (reduced GO) gels were also prepared by reduction with glucose. The adsorption behavior of solvents and MB dye by graphene-based gels were investigated to know the new adsorbents well.

2. Materials and methods

2.1. Materials

Natural graphite flakes were provided by Qingdao Tianhe Graphite Co., Ltd, China. The reagents (37.5% HCl, 98% H2SO4, 30% H2O2, and 30% NH3) and the analytical grade reagents (NaNO3, KMnO4, glucose, and ethanol) were obtained from Tianjin Jiangtian Chemical Reagent Co. Ltd. in China. The methylene blue (MB) and PVA were provided by Tianjin Benchmark Chemical Reagent Co., Ltd. Soybean oil was purchased from COFCO Northsea Oils & Grains (Tianjin) Co., Ltd, China.

2.2. Preparation of GO

GO was prepared using the modified Hummers' method [6]. Concentrated H2SO4 (46 mL) and NaNO3 (1 g) were added into an anhydrous beaker at 0 ºC (ice bath), followed by the addition of

graphite (2 g). Then KMnO4 (6 g) was added gradually with stirring while the temperature of the mixture was kept below 20 ºC. The mixture was stirred for 2 h in an ice-bath, and the mixtures reacted for another 1 h at 35 ºC. Distilled water (92 mL) was slowly added to the mixture, and then the temperature was kept at 98 ºC for 15 min. The mixture was then further diluted to 280 mL with distilled water and treated with 30% H2O2. The mixture turned bright yellow. The product was centrifuged and washed with diluted HCl solution and then washed with distilled water to remove the acid.

2.3. Preparation of GO-PVA and RGO-PVA gels

PVA (0.0453 g) was dissolved in distilled water (5mL) at 90oC. 20mL GO dispersion (6.8mg/mL) was added into the PVA solution, and the mixture was shaken violently to form a gel. The mixture was placed at room temperature for 24 h for gelatinization. The gels were frozen for 12 h at -10 ºC. Then the yellow gel was washed several times with ethanol and dried.

The GO-PVA gel was reduced following the method of Ma [7]. Ammonia (30 wt%) solution was added to 50 mL distilled water to adjust to pH 10, and then 2 g glucose was dissolved in the solution, followed by the addition of the dry GO-PVA gel. The mixture reacted for 1 h at 95 ºC in a sealed container. The dark RGO-PVA gel was washed respectively with distilled water and ethanol, and then dried at 50 ºC.

2.4. Scanning electron microscopy (SEM).

The fracture surfaces of GO-PVA and RGO-PVA gels were viewed with a Hitachi S-4800 scanning electron microscope.

2.5. X-ray diffraction (XRD)

GO, GO-PVA and RGO-PVA powders were placed in a sample holder for X-ray diffraction (XRD). XRD patterns were recorded in reflection mode in the angular range of 5-30º (2θ), at ambient temperature, using a Rigaku D/max 2500 v/pc (Japan) operated at a CuKα wavelength of 1.542 Å.

2.6. Apparent density

The apparent density of GO-PVA and RGO-PVA gels, also called bulk density, was defined as the mass of material divided by the total volume occupied [8].

2.7. Ethanol / soybean oil / water adsorption capacity

The dried GO-PVA and RGO-PVA gels (weight = w0) were immersed in ethanol / soybean oil / water for 0.5 h at room temperature. The mixtures were filtered in a funnel under vacuum for soybean oil and gravity for ethanol and water. When there was no more ethanol / soybean oil / water dripping from the filter paper, the gels were weighed (w). The oil adsorption capacity was calculated as follow:

$$\text{Adsorption Capacity} = \frac{w - w_0}{w_0} \qquad \text{Eq. (1)}$$

2.8. MB adsorption experiments

Adsorption experiments were conducted using glass bottles containing 0.3 g L-1 of GO-PVA or RGO-PVA and MB dye (0.1 mmol L−1). The glass bottles were placed on a slow-moving platform shaker and aliquots of approximately 10 mL were taken at different time intervals during the reaction. The MB concentration in the solution were analyzed by UV-Vis spectrometry and relative dye adsorption versus reaction time determined at 30 ºC.

Adsorption isotherm testing showed the concentration of the adsorbent was 0.3 g L−1 and the dye concentrations changed from 0.01 to 0.3 mmol L-1. These experiments were carried out at 30 ºC and all suspensions were shaken on a rotary shaker at 100 rpm for 24 h to reach the adsorption equilibrium.

3. Results and discussion

3.1 SEM

As shown in Fig. 1, the macro-pores led to a 3D network composed of randomly oriented GO sheets. Therefore, it was reasonable to conclude that a loose dynamic GO network existed in the original dispersion of GO sheets owing to the binding interaction [9]. PVA could interact with GO,

owing to the between the oxygen containing groups of GO and PVA. The randomly oriented sheet-like structure of GO gels was consolidated by PVA. The residual oxygen groups of RGO could form the interaction with PVA to maintain the formed 3D network of dark RGO-PVA gel.

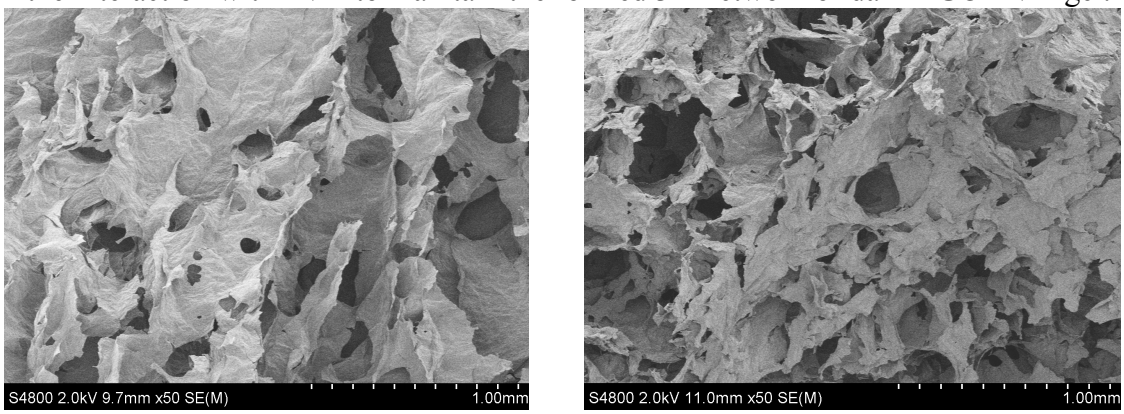

(a) (b)

Fig.1. SEM images of GO-PVA (a) and RGO-PVA (b).

3.2 XRD

Fig. 2exhibits the XRD patterns of GO, GO-PVA and RGO-PVA. According to the Bragg diffraction equation $2d\sin\theta=\lambda$ (λ is the CuKα wavelength of 1.542 Å), the feature diffraction peak of GO at $2\theta = 10.81°$ (001) is observed with interlay space (d-spacing) of 0.82 nm. In GO-PVA, this vale was further increased to 1.04 nm, as the feature diffraction peak of GO shifted to $2\theta = 8.44°$ (001). After exfoliation and reduction of GO-PVA, the regular stacks of GO were destroyed and the diffraction peak became disappeared. Meanwhile, a peak of RGO for RGO-PVA at $2\theta = 21.72°$ was observed, indicating that RGO existed individually and highly disorderly in single or fewer layers [10]

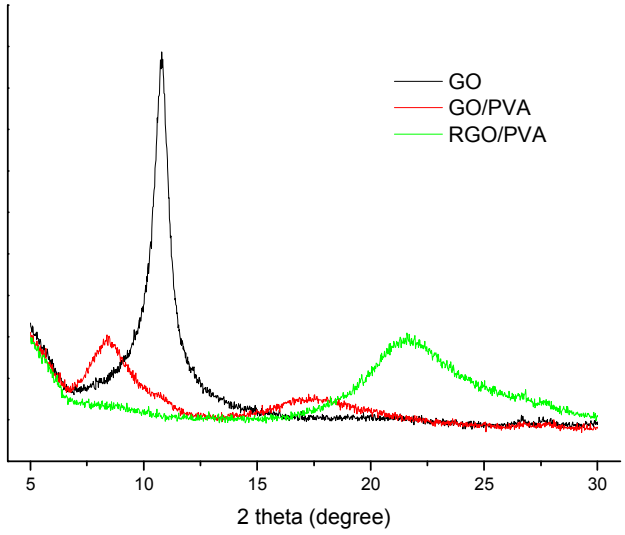

Fig.2. XRD patterns of GO, GO-PVA and RGO-PVA.

3.3. The adsorption of water, ethanol and soybean oil

Table 1 shows the bulk density of GO-PVA and RGO-PVA gels, and the adsorption of water, ethanol and soybean oil. GO-PVA was ultralight with bulk density of 10.52 mg/ cm3, and RGO-PVA was only 11.42 mg/cm3. These macropores of 3D gel network could withhold much liquid. Three liquids with different polarity were adsorbed by GO-PVA and RGO-PVA gels. As listed in Table 1, GO-PVA and RGO-PVA exhibited effective adsorption of the liquids. These macropores could withhold water 37.9-17.5 times, ethanol 40.7-20.6 times and soybean oil 48.7-36.4 times the weight of the gel. The less the polarity of the liquid was, the more the adsorption for both GO-PVA and RGO-PVA gels was. RGO-PVA gel exhibited the soybean oil adsorption as much as 48.7 g/g.

Contrastively, the adsorption capacity of vegetable oil by graphene gel was about 17 times [11]. And silica or rectorite gels absorbed the oils by nearly 15 times [12, 13].

Table 1 Parameters for GO-PVA and RGO-PVA gels

	Bulk density (mg/cm^3)	Water adsorption (g/g)	Ethanol adsorption (g/g)	Oil adsorption (g/g)
GO- PVA	10.52	37.9	40.7	48.7
RGO-PVA	11.42	15.0	20.6	36.4

3.4. Adsorption of MB dye

Fig. 3 illustrates the effects of contact time on adsorption of MB by GO-PVA or RGO-PVA gel. The adsorption of MB by GO-PVA was high and rather fast. At 30 ºC the adsorption equilibrium from the experimental curve reached 120.3 mg g-1 after 2 h for GO-PVA, while for RGO-PVA the amount of dye adsorbed at equilibrium was 71.5 mg/g after 14 h. These facts suggest electrostatic interaction is the primary binding strength between the oxygen containing groups of GO and MB [2], allowing GO-PVA to adsorb more MB than RGO-PVA.

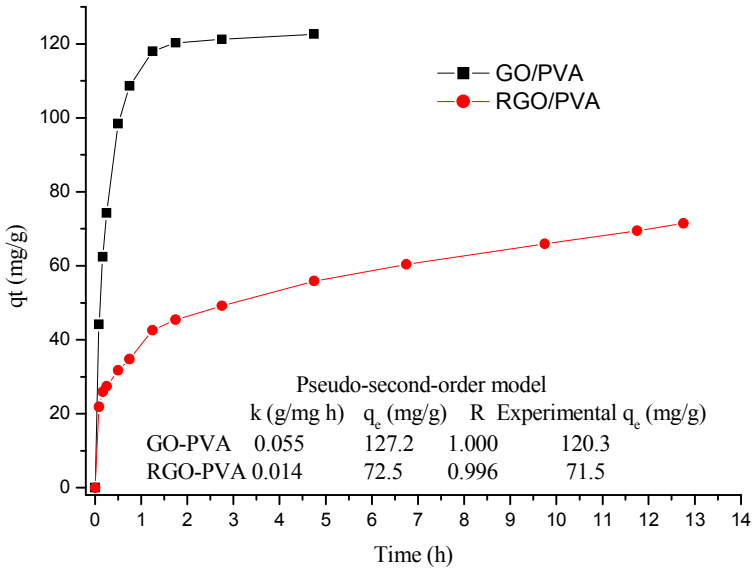

Fig. 3. Effect of contact time on adsorption of MB by GO-PVA and RGO-PVA at 30 ºC. Initial concentration: MB 37.39 mg L-1; GO-PVA or RGO-PVA 0.3 g L-1. The dye adsorption kinetic constants of GO-PVA and RGO-PVA modeled by a pseudo second-order equation were listed in figure.

The kinetic model, pseudo-second-order, was used to investigate the mechanism and rate-controlling step in the overall adsorption process. According to the pseudo second-order model, the amount of dye adsorbed at any time, t (h), is expressed as Eq. (2):

$$\frac{t}{q_t} = \frac{1}{kq_e^{\,2}} + \frac{t}{q_e} \qquad \text{Eq. (2)}$$

where k (mg g-1 h-1) is the second-order rate constant and qt (mg g-1) and qe (mg g-1) represent the amounts of dye adsorbed at any time t (h) and at equilibrium, respectively. The second-order rate constant k and qe can be obtained from the intercept and slope of the line in a t/qt versus t plot. Some kinetic parameters at 30 ºC, estimated from the experimental data and Eq. (1), are listed in Fig. 3. For the adsorption of MB by GO-PVA and RGO-PVA, linear relationships with high correlation coefficients (R > 0.998) between t/qt and t indicated the adsorption process could be well described by the pseudo second-order model. In terms of qe, GO-PVA exhibited better adsorption of MB (127.2 mg g-1) than RGO-PVA (72.5 mg g-1).

The absorption isotherm of MB by GO-PVA is shown in Fig. 4. At low Ce values, the absorption capacities (qe) increase quickly. The qe values increase slowly once Ce is greater than 19.6 mg/L for GO-PVA and 12.6 mg/L for RGO-PVA. The qe value is 573 mg/g for GO-PVA, while the qe value is 79.8 mg/g for RGO-PVA.

Adsorption isotherms are essential for the process of adsorption. The experimental data were applied by the isotherm models of Langmuir Eq. (3). The equations are as follows:

$$\frac{C_e}{q_e} = \frac{1}{bQ_{\max}} + \frac{C_e}{Q_{\max}} \qquad \text{Eq. (3)}$$

where qe (mg/g) is the sorption capacity at equilibrium; Qmax (mg/g) is the maximum adsorption capacity; Ce (mg/L) is the equilibrium concentration in the solution.

The parameters of the Langmuir isotherm are exhibited in Fig. 4. It was found that the adsorption fit this model well. The maximum monolayer adsorption capacities of the adsorbents were 571.4 and 81.0 mg/g for GO-PVA and RGO-PVA, respectively. The Qmax value of GO-PVA is competitive with that of other carbon-based absorbents, such as active carbon (454.2 mg/g) [14] and graphene oxide/calcium alginate composite (181.81 mg/g) [15].

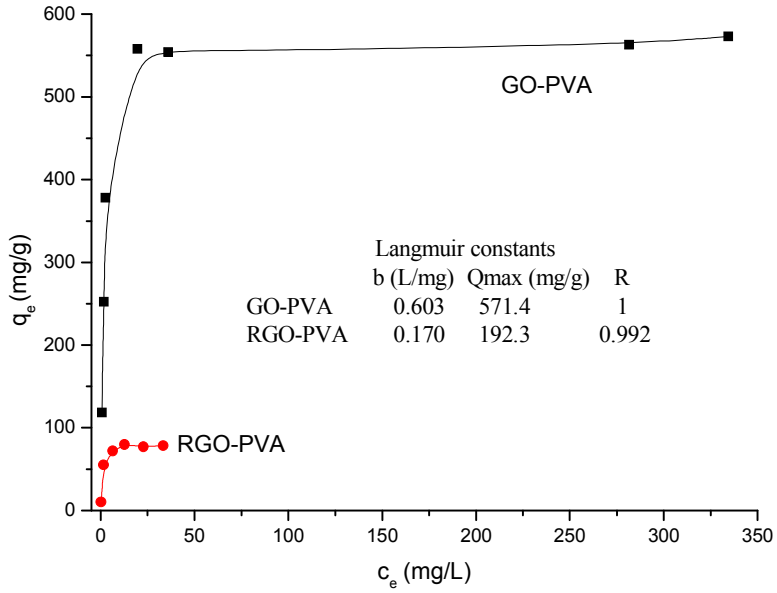

Fig. 4. Adsorption isotherms of MB onto GO-PVA and RGO-PVA at 30 ºC. MB concentrations changed from 0.01 to 0.3 mmol L^{-1}; GO-PVA or RGO-PVA 0.3 g L^{-1}. The Langmuir constants of GO-PVA and RGO-PVA were listed.

4. Conclusion

The ultra-light GO-PVA gel was successfully prepared using a simple process of aqueous gel precursor freezing, solvent exchange (ice-ethanol), and ethanol drying. The 3D porous sheets networks were formed in gels, composed of many macropores, which exhibited low density and high adsorption for water, ethanol and oil. GO-PVA gel with the low density (10.52 mg/cm^3) could respectively withhold water 37.9 times, ethanol 40.7 times and soybean oil 48.7 times the weight of GO-PVA gel, while RGO-PVA gel exhibited lower density (11.42 mg/cm^3), and less water 15.0 times, ethanol 20.6 times and soybean oil 36.4 times. The equilibrium and the dynamic adsorption of MB dye onto the gels were studied. The kinetic process was well described by the pseudo-second-order model. The isotherm adsorption fit well with Langmuir model, and the maximum adsorption capacities were 571.4mg/g for GO-PVA and 81.0 mg/g for RGO-PVA at 30 ºC. GO-PVA and RGO-PVA gel is an efficient adsorbent, which can have potential applications in food, pharmaceuticals, agriculture, cosmetics, pulp and paper, and other industries.

Acknowledgements

This work was supported by the Science and Technology Project of Jiangxi Provincial Office of Education (KJLD12082, GJJ12590, and Innovation Platform "project 311") and Nature Science Foundation of Jiangxi Province (20132BAB 206006) and the National Nature Science Foundation of China (51162011).

References

[1] G. Crini, Bioresour. Technol. 97 (2006) 1061-1085.
[2] S.T. Yang, S. Chen, Y.L. Chang, A.N. Cao, Y.F. Liu, H.F. Wang, J. Colloid. Interf. Sci. 359 (2011) 24-29.
[3] H. Bai, C. Li, X.L. Wang, G.Q. Shi, J. Phys. Chem. C 115 (2011) 5545-5551.
[4] H. Bai, C. Li, X.L. Wang, G.Q. Shi, Chem. Commun. 46 (2010) 2376-2378.
[5] Y.X. Xu, Q. Wu, Y.Q. Sun, H. Bai, G.Q. Shi, ACS Nano 4 (2010) 7358-7362.
[6] J. Cheng, P.W. Zheng, F. Zhao, X.F. Ma, Int. J. Biol. Macromol. 59 (2013) 13-19.
[7] T.T. Ma, P.R. Chang, P.W. Zheng, X.F. Ma, Carbohyd. Polym. 94 (2013) 63-70.
[8] A. Wong, R.K.M. Chu, S.N. Leung, C.B. Park and J.H. Zong, Chem. Eng. Sci. 66 (2011), 55-63.
[9] X. Jiang, Y. W. Ma, J. J Li,. Q. L.Fan, W. Huang, J. Phys. Chem. C 114 (2010) 22462-22465.
[10] W.H. Yuan, B.Q. Li, L. Li, Appl. Surf. Sci. 257 (2011) 10183-10187.
[11] H.P. Cong, X. C. Ren, P. Wang, S.H. Yu, ACS Nano 6 (2012) 2693-2703.
[12] A.V. Rao, N.D. Hegde, H. Hirashima, J. Colloid. Interf. Sci. 305 (2007) 124-132.
[13] P.W. Zheng, P.R. Chang, X.F. Ma, Ind. Eng. Chem. Res. 52 (2013) 5066-5071.
[14] B.H. Hameed, A.T.M. Din, A.L. Ahmad, J. Hazard. Mater. 141 (2007) 819-825
[15] Y.H. Li, Q.J. Du, T.H Liu, J.K. Sun, Y.H. Wang, S.L. Wu, Z.H. Wang, Y.Z. Xia, L.H. Xia, Carbohyd. Polym. 95 (2013) 501-507.

Advanced Materials Research Vols. 989-994 (2014) pp 379-382
© (2014) Trans Tech Publications, Switzerland
doi:10.4028/www.scientific.net/AMR.989-994.379

Research progress for high strength structural steel and key issues of application in seismic zone

Ji Lixia[1,a], An Teng[2,b]

[1.]Department of civil engineering, Graduate School of Southwest Jiaotong University , ChengDu, China,610031

[2.]Department of civil engineering, Graduate School of Southwest Jiaotong University , ChengDu, China,610031

[a.] jilixia_ zq@sina.com [b.]anteng_lj@sina.com

Key words: high strength steel (HSS); recent research progress; seismic; application

Abstract. A review of recent research on mechanical performance of high strength structural steel (HSSS) in the level of both materials and members is presented, including the static material performance, toughness and mechanical property under cyclic loadings of HSSS, buckling and hysteretic behavior of high strength steel columns (HSSC), the ductility and resistance of bolted connection with high strength steel slices etc. Previous research work shows that the application of high strength steel (HSS) is limited in seismic zone .Finally, two design methods of using HSS in seismic zone are proposed based on current seismic design philosophy.

Introduction

HSSS refers to using microalloying and thermo mechanical rolling technology to produce structural steel with high strength (nominal yield strength $f_y \geq 420$ Mpa), good ductility, toughness and processing performance. HSSS has been successfully applied to multiple steel structure engineering at home and abroad, achieving good economic and social benefits. Since the material performance of HSS is significantly different from conventional steel, the applicability of the HSS in using the existing design terms based on the performance of low carbon steel need to be further verified, or put forward a new design method.

The research progress for HSSS

The basic mechanical performance of HSS. Due to the different production processes and microalloying elements, the mechanical properties of HSS have some changes. As shown in figure 1, with the improvement of steel strength, the length of yield platform shortens. When the intensity exceeds 690 Mpa, yield platform disappears. In addition, when steel strength increases, the ultimate strain value corresponding to steel tensile strength decreases gradually.

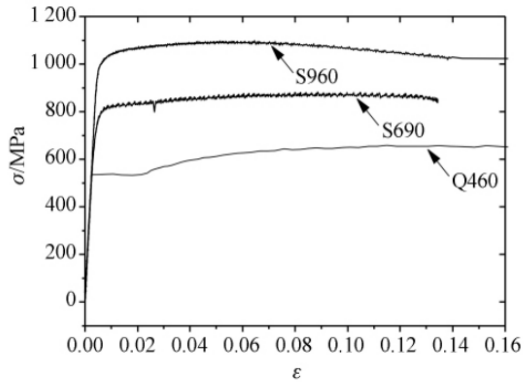

Fig.1 Stress-Strain curves for high strength steels with different grades

In reference [1] the domestic and foreign material datas of HSS are summarized. Through analysis and comparison, it can be concluded that yield ratio of HSS increases with the increase of steel yield strength. When the yield strength exceeds 690 MPa, yield ratio is roughly 0.90~0.95.The yield ratio reflects the margin of strength (MOS) and deformation capacity(DC) of the material, the higher the yield ratio, the lower the MOS and DC. Elongation also has obvious reduction with the increase of yield strength, while the toughness of HSS is better than traditional steel.

The mechanical performance of HSS under cyclic loading. The mechanical properties of steel structure under the action of cyclic loading and monotonic loading are obviously different, and the former research on seismic performance of steel structure has important significance. Figure 2a is the cyclic stress-strain curve of Q460-C steel in the symmetrical sequential loading condition. In figure 2b, the skeleton data points of cyclic stress - strain curve and the skeleton curve simulated by Ramberg-Osgood model compare with steel monotonic tensile curve. It can be seen from figure 2 that the hysteretic curve of this kind of HSS is plump and the HHS has good energy dissipation ability. In addition, material constitutive relation under cyclic loading has obviously changed, and the Ramberg-Osgood model can be well fitted to its skeleton curve. The test results provide the basis for the determination of constitutive model parameters of HSS in the numerical simulation analysis.

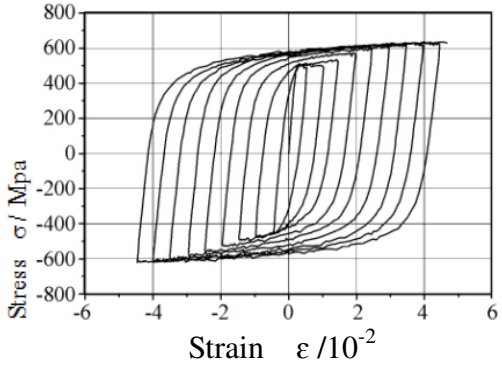

a. Cyclic stress -strain curve

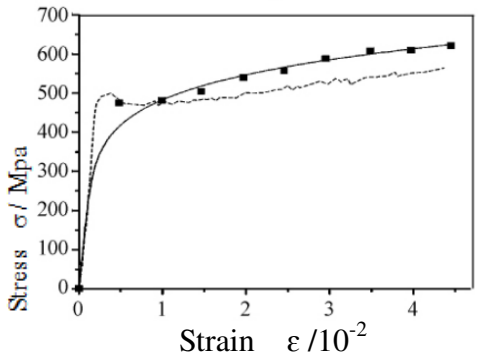

b. Skeleton curve and monotone curve

▪ Skeleton curve data points of cycling test
— Circular skeleton curve
.... Monotonic tensile curve

Fig.2 Cyclic loading test results of Q460-C steel

By cyclic loading test to determine the mechanical properties of the welding connection, it can be found that the maximum intensity of Q460-C welding connection specimens is higher than the parent metal. But the plastic fracture strain is less than the parent metal, and all are broken near the welded seam and heat-affected zone. Hysteresis curve of the welded HSS is still full and it has good energy dissipation capacity [2].

The mechanical properties of HSS at low temperature. The mechanical properties of Q460 - C domestic HSS and its welding connection at low temperature were studied by domestic scholars, including three groups of experiments, namely the basic static tensile, impact toughness and fracture toughness .The study of the yield strength, yield ratio, elongation and other mechanical properties were conducted comprehensively as well. The results show that the domestic HSS has very good impact ductility indicator at normal temperature, but when the temperature is below - 20℃, the toughness decreases significantly, even lower than the relevant standard limits of structural steel in our country.

Overall stability of HSSC under axial compressive force. There are a small amount of experimental researches on overall stability of HSS compression members abroad .The overall stability of five 690 Mpa welded I-shaped cross-section steel column which are unstable around the weak axis and six 690 Mpa welded box section steel column was researched by Rasmussen[3] Usami[4] did research on the overall stability of five 690Mpa welded box section steel column as well.The results show that under the condition of the same axial compressive force, the overall stability coefficient of HSSC is obviously enhanced and significantly higher than that of the

ordinary strength steel column. The existing design method for HSS is too conservative, and when the strength of HSS is more than 690 Mpa , the overall stability coefficient will no longer increase.

Local stability performance of short column of HSS under axial compressive force.

Reference [3] reports the abroad test results of short column of 690 MPa grade HSS, and compares the test results with the limiting value of width-to-thickness ratio in GB 50017-2003 code for design of steel structures. The results show that the limiting value of flange width-to-thickness ratio in GB 50017-2003 is agreed with the test results very well. And the standard still applies to 690 Mpa grade welded steel column of HSS. Tsinghua University [5] did researches on the local stability of thirteen Q460 HSS short column of welded I-shaped cross-section and box section, and compared the test results with calculation methods of local buckling critical stress of box section plate in the GB 50017-2003. Results show that the calculated value of GB 50017-2003 is obviously on the low side, and local stability design of short column of Q460 HSS is too conservative and need to be revised.

Hysteretic performance of bending component of HSS. Studies abroad of hysteretic performance of HSS bending component is very few. Tsinghua University studied on eleven Q460 domestic HSSC of welded I-shaped cross-section and box section under low cyclic loading. Experiment shows that the hysteresis curve of Q460 HSSC is full and the capacity of seismic energy dissipation is good. Furthermore, there is no damage phenomenon of brittle fracture, and width-to-thickness ratio and ratio of axial compression stress to strength of a plate have a significant impact on the seismic performance .The limiting value of width-to-thickness ratio and ratio of axial compression stress to strength of a plate have significant correlation. The calculation formula of the limiting value should be fully aware of the influence of ratio of axial compression stress to strength.

The mechanical performance of shear connection of HSS bolt. Tests on bolt shear connection of nine domestic Q460 steel plate have been carried out by ShiGang[1]. The test results show that the hole wall bearing performance of Q460 steel plate are not well predicted by the design methods of European standard Eurocode 3 and American standard ANSI/AISC360-05.And the calculation results of design are relatively unsafe. There is no mature design method in our country, so new secure design theory and calculation method of HSS shear connection need to be put forward.

The two ideas of the application of HSSS in seismic fortification zone.

With the increase of steel strength, the yield ratio increases while the elongation decreases. As a result, the performance of the HSSS can not meets the requirements of GB 500117—2010 Code for seismic design of building. It can be seen from the mechanical performance index that the steel whose nominal yield strength is higher than 420 MPa can not be used for a seismic structure .And because the only supplement of the Q420 steel in GB 500117—2010 ,the application of the Q460 HSSS and other higher grade steel is restricted.

In order to solve the problems mentioned above, we put forward two kinds of solutions based on the principles of seismic design: one is to improve the seismic action of the HSS structure of poor ductility in the design to insure the reliability of the structure; the other is to set up a special energy dissipation device to consume a large amount of seismic energy under strong earthquakes. So that the situation that HSS structure first yield under strong earthquakes can be avoided.

Improving the seismic action. As shown in figure 3, for a good ductile structure, seismic energy can be dissipated through plastic deformation, so the structure is not severely damaged or collapsed. Therefore, the seismic action of a good ductile structure in design can be reduced appropriately. On the contrary, a structure which has poor ductility should improve the seismic action in design.

Limiting the HSSS to yield. Based on the concept of the capacity design, through the energy consumption after the ductile members yielding to ensure the inductile members are always in the elastic stage under rare earthquakes, therefore the safety of the whole structure can be guaranteed. The research on the examples of seismic damage and the results of theoretical analysis indicate that the shortage of deformation capacity (DC) and energy-dissipating capacity (EDC) is the main reason for the collapse of structure under rare earthquakes [6] .To ensure the HSS structure does not collapse under rare earthquakes, the structure need to have enough DC and can form the effective energy-dissipating mechanism. Semi-rigid joint has good DC and good EDC, therefore the semi-rigid frame structure can be used to ensure the good deformability(as shown in figure 4). The

energy-consuming components as the fuse of the structure first yield under the strong earthquake and dissipate the seismic energy through the plastic deformation, so that the HSS members are in the elastic stage under the strong earthquake.

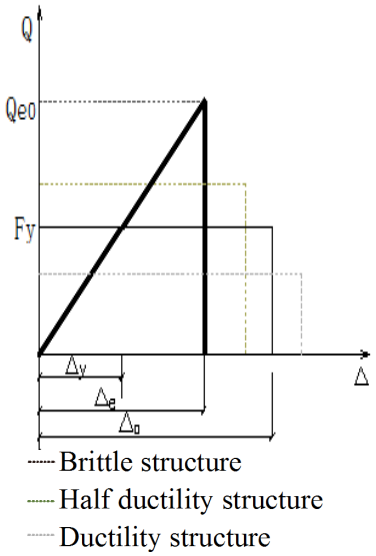

Fig.3 Effect of ductility on requirement of earthquake action

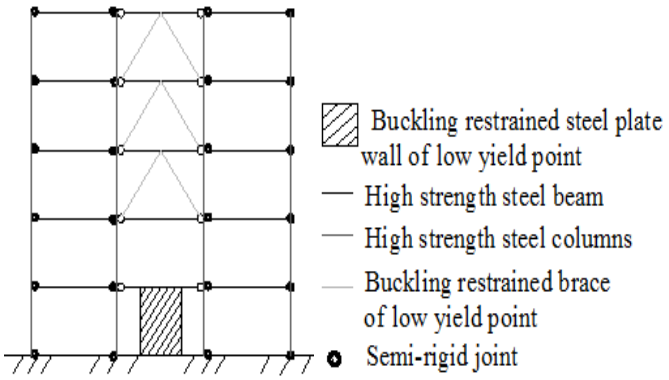

Fig.4 Structural system providing elastic design of HSS member

Conclusion

The existing study results show that HSSS have good mechanical performance, but many design methods of existing specifications are not suitable for HSSS. In addition, the design methods are too conservative and not conducive to advantages in such structural steel. The existing research results have important guiding significance in improving the design method and calculation theory of HSSS .On the basis of the existing research results, the projects need more practical application of HSSS to verify the rationality of the research results and promote new research topics to be presented in the meantime.

References

[1] Ban H. Y，Shi G，Shi Y. J，etal．Research Progress on the Mechanical Property of High Strength Structural Steels[J]．Advanced Materials Research(2011), p.250－253,640－648．

[2] Shi Gang ,Ban Huiyong, Bijlaard F .S .K. Experimental study and finite element analysis on the overall buckling behavior of ultra-highstrength steel compression members with end restraints [J] .China Civil Engineering Journal,Vol. 44(2011), p. 17－25．

[3] Rasmussen K. J. R, Hancock G. J. Tests of high strength steel columns [J]. Journal of Constructional Steel Research, Vol.34(1995),p. 27—52.

[4] Usami T, Fukumoto Y. Local and overall buckling of welded box columns [J]. Journal of the Structural Division, Vol.108(1982), p. 525—542.

[5] Ban H. Y，Shi G，Shi Y. J,Wang Y. Q. Engineering application and recent research progress on high strength steel structures[J]. Industrial Construction ,Vol. 42 No. 1(2012).

[6] Xie Xiaosong.Research and applicationon seismic capability of steel frames with semi-rigid connections[D]．Fuzhou:Fu zhou University(2004)．

[7] Ban H. Y，Shi G，Shi Y. J,Wang Y. Q.Overview of Research Progress for High Strength Steel Structures[J].Engineering Mechanics,Vol.30 No.1 (2013).

Advanced Materials Research Vols. 989-994 (2014) pp 383-386
© (2014) Trans Tech Publications, Switzerland
doi:10.4028/www.scientific.net/AMR.989-994.383

Luminescent Properties of $Ca_{1-x}Ba_xSnO_3$: Eu^{3+}, Dy^{3+} Composites Prepared by Coprecipitation

Limin Dong [1,2,a], Fei Lv [1], Qin Li [1], Zhidong Han [1,2] and Xianyou Zhang [1]

[1] College of Materials Science and Engineering, Harbin University of Science and Technology, Harbin, China

[2] Key Laboratory of Engineering Dielectrics and Its Application, Ministry of Education, Harbin University of Science and Technology, Harbin, China

[a] corresponding author: donglimin@hrbust.edu.cn

Keywords: rare-earth, stannate, coprecipitation

Abstract. A series of Eu^{3+}, Dy^{3+} actived $Ca_{1-x}Ba_xSnO_3$ phosphors were synthesized by coprecipitation method. The structure, morphology and fluorescence property of phosphors were investigated by using X-ray diffraction (XRD), scanning electron microscopy (SEM) and fluorescence spectroscopy. SEM results showed that the as-prepared phosphors are smooth and uniform with the cubic morphology. The incorporation of a small amount of Ba to $CaBaSnO_3$ improved the emission characteristics. Fluorescence spectrum showed the emission intensity is the best with the incorporation of Ba^{2+} (x = 0.3), when calcination temperature is 900℃.

Introduction

White light-emitting diodes (LEDs) are considered to be the fourth generation solid state lighting sources which are following the incandescent, fluorescent and high intensity discharge lamp due to their high efficiency, long lifetime, safety and environmentally friendliness etc [1]. Phosphor is one of the key components in WLED, and the red phosphor has two main purposes [2]. First, by combining the green phosphor with a blue LED chip to produce white light, or fabricated with green as well as blue phosphor to produce white light with near ultraviolet LED chip; Second, for improving the color rendering index or lower color temperature, it is used for compensating the yellow phosphor excited by blue LED chips to produce white light which is in the absence of red. In this case, it is essential to search novel red phosphors for WLED, and the preparation of the red luminescent material with a good performance is the direction of the present study.

Phosphors based on stannate have attracted more and more interest in recent years. Rare-earth stannate is an isometric crystal oxide, with a typical pyrochlore structure. Alkaline earth slant stannate is a composite metal oxide with cubic and perovskite structure. In addition, M^{2+} and O^{2-} constitute the approximate cubic close packing structure [3-6]. So far, the study of $CaBaSnO_3$ is still relatively scarce, which is necessary to conduct a detailed study.

Experimental

$Eu(NO_3)_3$ solution was prepared by dissolving a certain amount of Eu_2O_3 into HNO_3. Then stoichiometric weights of $Ca(NO_3)_2$, $Ba(NO_3)_2$ and $SnCl_4$ were dissolved in water. The flocculent precipitates were obtained after mixing the above solutions under slow titration with ammonia, with the pH of 7. The obtained precipitate was filtered, washed and then dried at 80℃ for 8h. Then the samples were calcined at high temperatures to obtain stannate phosphor powder.

Results and discussion

XRD analysis. The crystal structures of the synthesized samples were determined by powder X-ray diffraction(XRD) using a copper Kα radiation source at 40 kV and 200mA in steps of 0.02. Data were recorded ranging from 10° to 90°.

The XRD patterns of $Ca_{1-x}Ba_xSnO_3$: Eu^{3+}, Dy^{3+} composites which were calcined at 900℃ for 5h is shown in Fig.1, whose reflection peaks can be readily indexed with the cubic perovskite $CaSnO_3$ (JCPDS No. 1-998) [7]. No other phase can be detected, indicating that Ba^{2+} has been dissolved successfully in crystal lattice. And the crystal structure of $CaSnO_3$ is shown in Fig.2, which belongs to the peroskite structure. It can be seen that lattice parameters are a=b=c=7.8900Å and space lattice group is Fm-3m.

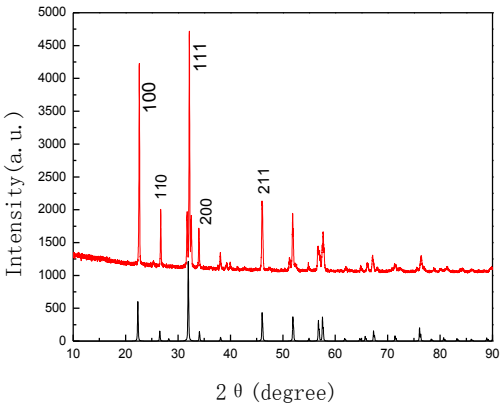

Fig.1 XRD pattern of $Ca_{1-x}Ba_xSnO_3$: Eu^{3+}, Dy^{3+}

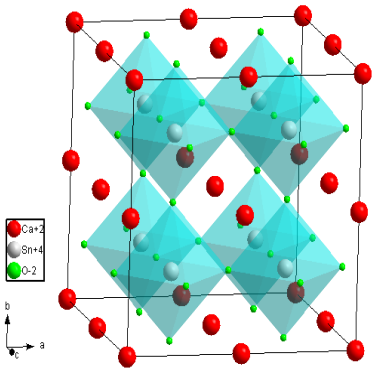

Fig .2 Crystal structure of $CaSnO_3$

Fluorescent properties. Fig.3 shows the room temperature photoluminescence excitation (PLE) (the left half of the curve) and emission (PL) spectra excitated at 395nm and 465nm (the right one).

The excitation spectra of $Ca_{1-x}Ba_xSnO_3$: Eu^{3+}, Dy^{3+} exhibits five obvious excitation peaks located at 361, 383, 395, 415 and 465 nm, which are corresponding to the $^7F_0 \rightarrow {}^5D_4$, $^7F_0 \rightarrow {}^5L_7$, $^7F_0 \rightarrow {}^5L_6$, $^7F_0 \rightarrow {}^5D_3$ and $^7F_0 \rightarrow {}^5D_2$ transitions of Eu^{3+} ion, and the higher excitation peaks are located at 395 nm and 465 nm. The excitation peaks which are located at 395 nm and 465 nm match well with the near ultraviolet LED chip (370 nm to 410 nm) and the blue LED chips respectively. So, it not only can be applied to the near ultraviolet excitation WLED but also can be applied to the blue light excitation WLED.

The emission spectra of $Ca_{1-x}Ba_xSnO_3$: Eu^{3+}, Dy^{3+} exhibits four obvious emission peaks. The peak at 578 nm is due to the magnetic dipole $^5D_0$-$^7F_0$ transition of Eu^{3+}, and the peaks at 589nm and 596nm are due to the magnetic dipole $^5D_0$-$^7F_1$ transition of Eu^{3+}. A broader and stronger emission band with a peak at 613nm is attributed to the $^5D_0$-$^7F_2$ transition of Eu^{3+}. $^5D_0$-$^7F_0$ and $^5D_0$-$^7F_2$ transition emission produced a splitting that is due to $^5D_0$-$^7F_1$ magnetic dipole transition emission of orange color. As the electronic transitions general rule of Eu^{3+} is well known, Eu^{3+} is in the strict inversion center at this time.

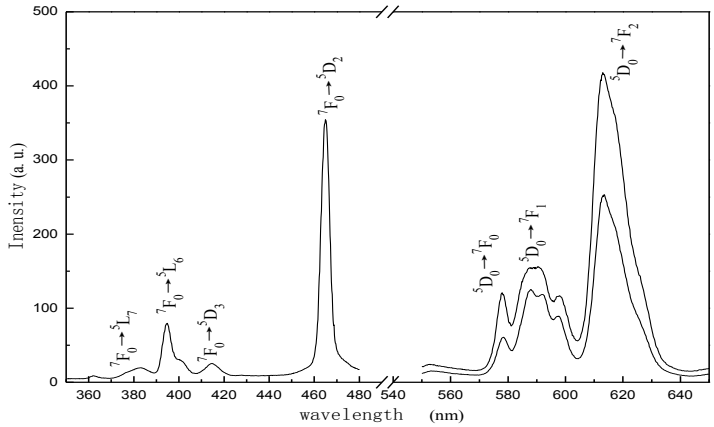

Fig.3 PLE and PL spectra of $Ca_{1-x}Ba_xSnO_3$: Eu^{3+}, Dy^{3+}

The influence of Ba^{3+} concentration. Fig.4 shows the emission spectra of the $Ca_{1-x}Ba_xSnO_3$: Eu^{3+}, Dy^{3+} with various Ba^{3+} concentration.

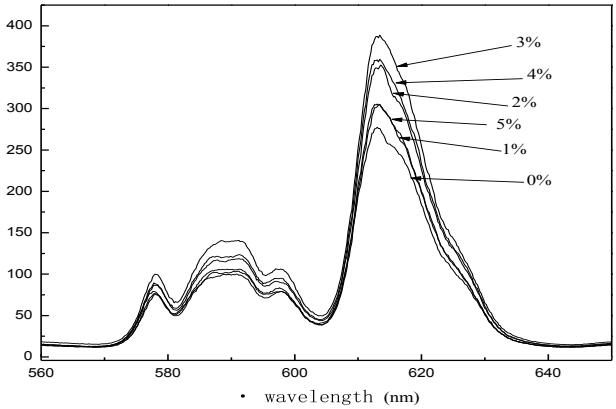

Fig.4 Emission spectra of the $Ca_{1-x}Ba_xSnO_3$: Eu^{3+}, Dy^{3+} with various Ba^{3+} content

As can be seen from Fig.4, with the Ba^{3+} concentration increased, the shape of the emission spectra and emission peak position don't chang, but the luminous intensity of emission peak increase. Compare to the fluorescence properties of undoped Ba^{2+} phosphor, the intensity of each emission peak increases. When the doped concentration of Ba^{2+} is up to 3%, the emission intensity is the best. The reason is the introduction of Ba^{2+} destroys the original Ca_2SnO_3 lattice layout. Since the dopant ions of Ba and Ca are in the same main group with similar nature, solid solution can be more easily formed. While the introduction of Ba resulted in the emergence of new defects and the crystal tends to be deformed. That is beneficial to energy transfer of Eu^{3+} luminescence centers, which will result in a substantial increase in luminescence intensity.

The influence of calcination temperature. Fig. 5 shows the SEM images of samples prepared at different calcination temperatures (800℃, 900℃, 1000℃, and 1100℃).

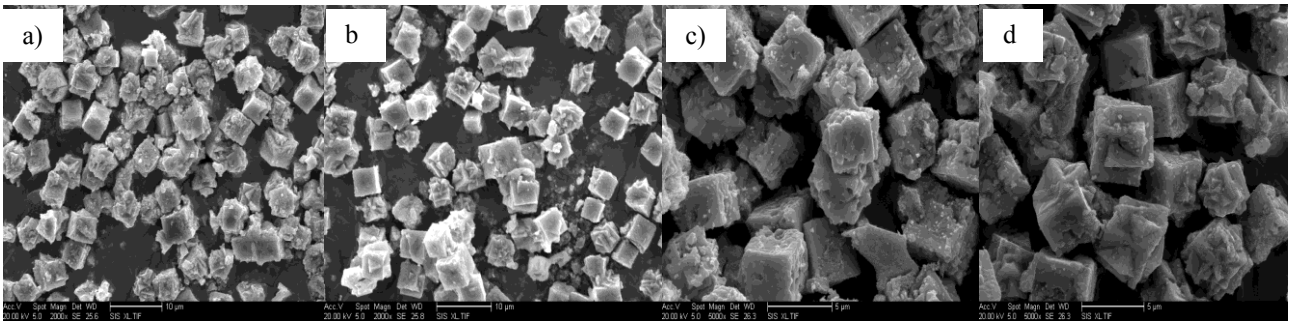

Fig.5 SEM images of $Ca_{1-x}Ba_xSnO_3$: Eu^{3+}, Dy^{3+} at different calcination temperature : (a) 800 ℃; (b)900 ℃; (c) 1000 ℃ and (d) 1100 ℃.

With the calcination temperature increasing, the regularity of surface morphology of samples improved, the morphology changed from irregular to regular and uniform particles consistency improved gradually. When the calcination temperature reaches up to 900 ℃, the particle size and surface smoothness can get the optimal value. But when the calcination temperature is further increased, the prepared samples are irregular and the adhesion and aggregation. This is mainly because that the external high temperature accelerates the grain development of luminescent material fully. With the temperature increasing, the integrity and homogeneity of crystal will obviously increase and the internal defects reduce. However, when the calcination temperature is too high, it makes the grain grow excessively and agglomeration occurs.

The emission spectra of the samples calcined at different temperature are shown in Fig. 6. As can be seen from Fig.6, with the increase of calcination temperature, the shape of the emission spectra and emission peak position don't chang. The main emission peaks are located in 578, 589, 596 and 613 nm respectively. With the increase of the calcination temperature, the fluorescence intensity increases. When the temperature reaches 900℃, maximum emission peak can be found, while with the temperature further increases, the fluorescence intensity decreases. The main reason is that with

the calcination temperature increases, the grain crystallization is improved, the monodispersed crystals generate and the relative luminous intensity increase. But when being calcined at high temperatures, powder agglomeration occurred, resulting in a loss of luminous intensity. Therefore, when the sintering temperature is 900℃, the emission intensity is the best.

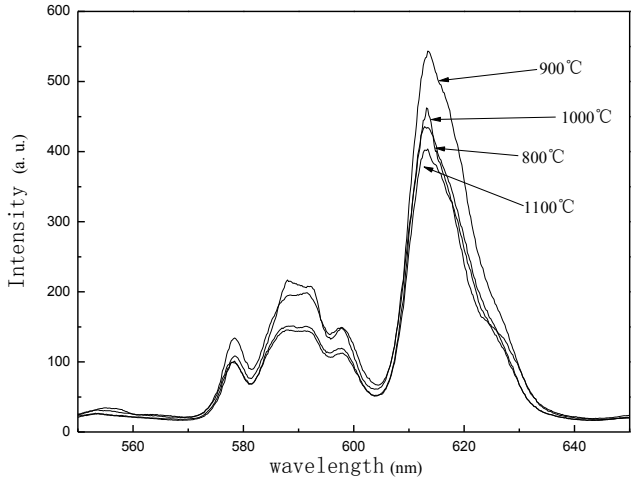

Fig.6 The emission spectrum of the sample calcined at different temperature

Conclusions

A novel red phosphor $Ca_{1-x}Ba_xSnO_3$: Eu^{3+}, Dy^{3+} was prepared by the traditional coprecipitation method. And the structure, morphology and fluorescence properties of the phosphor powders are studied. It was found that the incorporation of a small amount of Ba to $CaBaSnO_3$ improved the emission characteristics. Fluorescence spectrum observations showed that the emission intensity is the best with the incorporation of Ba^{2+} (x = 0.3) and the sintering temperature is 900℃.

Acknowledgements

This work was Innovation Program for new century excellent talents in Heilongjiang provincial university (1251-NCET-014).

References

[1] L Wang. Research and Design about the LED used in Lighting [D]. Zhejiang University, 2004, In Chinese.
[2] Shibao Cheng, Xiaoxia Chen, Chengwu Li. Progress of Research on Red Phosphor [J]. China Chemicals, Chongqing, 400044, In Chinese.
[3] Z. L. Fu, H. K. Yang, B. K. Moon, et al, Synthesis and luminescent properties of europium-activated Ca_2SnO_4 phosphors by sol-gel method [J]. Lumin. 2009, 129: 1669-1672.
[4] H. Hsu, C. L. Liaw, C. H. Lu, Luminescence properties of sol-gel derived $Sr_2(Ce_{1-x}Sn_x)O_4$ blue phosphors[J]. Alloys Comp. 2010, 489: 445-450.
[5] F. Matteucci, G. Cruciani, M. Dondi, G. Baldi, A. Barzanti, Crystal structural and optical properties of Cr-doped $Y_2Ti_2O_7$ and $Y_2Sn_2O_7$ pyrochlores [J], Acta Mater. 2007, 55: 2229-2238.
[6] H G Liu, Y I Lee, W P Qin, K W Jang, S S, Kim X S Feng. Distinct composite structure and properties of $Eu(phen)_2Cl_3(H_2O)_2$ in poly(methyl methacrylate) and polyvinylpyrrolidone. J. Appl. Polym. Sci, 2007, 92 (6): 3524.
[7] Shiying Zhang, Kun Wei. Studyon Luminescence Property of Nanocrystalline Y_2O_3: Eu^{3+} Red Phosphor [J]. Spectroscopy and Spectral Anlaysis, 2004, 24: 407-410.

Advanced Materials Research Vols. 989-994 (2014) pp 387-390
© (2014) Trans Tech Publications, Switzerland
doi:10.4028/www.scientific.net/AMR.989-994.387

Study of dislocation densities of thick GaN films

Yongan Li[1, a], Xiangqian Xiu[1, b], Xuemei Hua[1, c], Shiying Zhang[1, d], Shipu Gu[1, e], Rong Zhang[1, f], Zili Xie[1, g], Bin Liu[1, h], Peng Chen[1, i], Ping Han[1, j], Youdou Zheng[1,k]

[1]Division of Microelectronics, School of Electronic Science and Engineering, Nanjing University, Nanjing, 210093, China

[a]liyongan008@126.com, [b]xqxiu@nju.edu.cn, [c]xmhua@nju.edu.cn, [d]shiyingwl@163.com, [e]gusp@njupt.edu.cn, [f]rzhang@nju.edu.cn, [g]xzl@nju.edu.cn, [h]bliu@nju.edu.cn, [i]pchen@nju.edu.cn, [j]hxhan@jlonline.com, [k] ydzheng@nju.edu.cn

Keywords: GaN, dislocation, thickness, HRXRD, AFM.

Abstract. The dislocation density of GaN thick films has been measured by high-resolution X-ray diffraction. The results show that both the edge dislocations and the screw dislocation reduce with increasing the GaN thickness. And the edge dislocations have a larger fraction of the total dislocation densities, and the densities for the edge dislocation with increasing thickness reduce less in contrast with those for the screw dislocation.

Introduction

GaN has attracted much attention for a wide range of application due to its excellent optoelectronic properties [1]. The defects of the material such as threading dislocations (TDs) have a negative effect on device properties. TDs can act as non-radiative recombinant limiting the efficiencies of light-emitting diodes (LEDs) [2], charged scattering centers reducing carrier mobility [3] and can reduce the leakage current in p-n junctions [4]. The main reason for defect onset is both mismatching of crystal lattice parameters and thermal expansion coefficients between GaN and sapphire used as a substrate. The sustained interest is driven that require the growth of GaN epilayers with ever lower TDs densities for next-generation high-brightness LEDs [5].

Several techniques for the reduction of dislocation density have been proposed for the III-nitride materials [6–11]. Among them, epitaxial lateral overgrowth has been successfully used for the commercialized optical devices. The efforts for further TD reduction have been limited by the additive cost, because it need lithography technique or complicated growth processes.

General, the dislocations in GaN/sapphire originates the interface between GaN and sapphire [12]. And the thicker GaN films would have the lower TDs. However, only few works has been done for the influence of the thickness, where the thickness in those research is only around 20~30μm. In this paper, we have studied the relation between the dislocation densities and the thickness in GaN film with the thickness of several hundred μm. We have also discussed the mechanism among them.

Experimental

In this study, GaN films have been grown by hydride vapor phase epitaxy (HVPE) on sapphire with the thickness of ~670μm. Free-standing thick GaN wafers grown by hydride vapor phase epitaxy and lifted off from the substrate is currently the most feasible way for the substitution of a real bulk material. The growth rate is up to several microns per hour. Here, the edge and screw dislocation densities have been measured by diffuse X-ray scattering from epitaxial layers based on the mosaic crystal approximation was used in [13].

High-resolution X-ray diffraction (HRXRD) measurements have been performed using a PANalytical X'Pert PRO MRD diffractometer and the X-ray radiation is Cu Kα (wave length λ is 0.15406 nm). The rocking curves of reflection (002), (004), (006), (101), (102), (103) are obtained by each measurement.

The sample have been mechanical ground and polished using horizontal rotary grinding machine and single side lapping machine respectively. The film shows a smooth surface with a root mean square surface roughness < 1nm determined by atom force microscope (AFM). Each time, the sample is polished off 70~80μm and HRXRD analysis is performed after each polishing.

Result and Discussion

Fig. 1 is the AFM image of the polished GaN. It can be seen that it is smooth and uniform after the polishing. The RMS roughness is 0.650792nm. It is well-known that both instrumental and sample-related reasons will cause the broadening of the XRD peak. But the instrumental broadening will be negligible by using high-resolution X-ray diffraction.

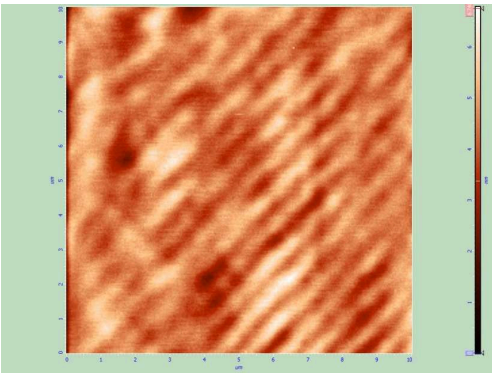

Fig. 1 AFM image of the polished GaN sample

The densities of dislocation of the thicker GaN film are measured by X-Ray Diffraction (XRD) techniques. We can use the following equation to obtain the densities of the screw dislocation Ns [14]:

$$N_S = \frac{\alpha_\Omega^{\,2}}{4.35\mathbf{b}^2} \quad (1)$$

Where b ($|\mathrm{b}|$ = 0.518nm) is the Burgers vector of the screw dislocation.
The densities of the edge dislocation Ne can be obtained by the equation as follow [14]:

$$N_e = \frac{\alpha_\varphi^{\,2}}{4.35\mathbf{b}^2} \quad (2)$$

Where b ($|\mathrm{b}|$ = 0.518nm) is the Burgers vector of the screw dislocation.
Using the method shown in previous report [12], we have obtained the dislocation density variation with the thickness in GaN film, where the screw and edge dislocation density is shown in Fig. 2 and Fig. 3, respectively.

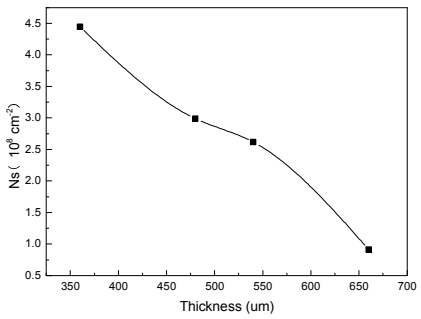

Fig. 2 The screw dislocation density variation with thickness in GaN film

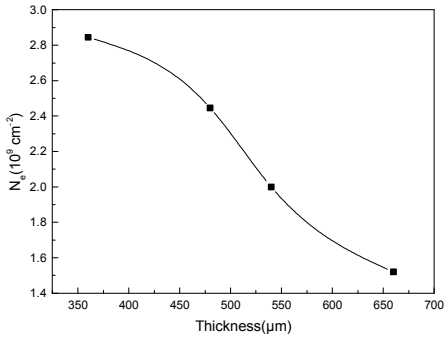

Fig. 3 The edge dislocation density variation with thickness in GaN film

From Fig. 2 and Fig. 3, we can conclude that the densities for the edge and screw dislocation decrease with increasing the GaN thickness, which is in agreement with our impression. We think that the main mechanisms for dislocation densities reduction in films are fusion or annihilation. Dislocations may meet and react with others when they get close proximity during the growth. A fusion happens when two dislocation lines become one dislocation line with the new Burgers vector **b**3 = **b**1 + **b**2. When two dislocations with opposite Burgers vectors react, an annihilation reaction occurs to remove the dislocations entirely [15]. It is found that the line directions for edge and screw dislocations are [0 0 0 1] and 15.6° for the mixed dislocations [15]. The edge-mixed reactions produce the screw dislocations and the screw-mixed reactions produce the edge dislocations. As the film thickness increases, the inclined dislocations move laterally and meet with one another, so the fusion or annihilation will happen.

The results in Fig. 2 and Fig. 3 also demonstrate that the densities for the edge dislocation with increasing thickness reduce less in contrast with those for the screw dislocation: N_{e1} is 1.5201×109 cm^{-2} at 660μm and N_{e2} is 2.8440×109 cm^{-2} at 360μm decreasing by 47.6% while N_{s1} is 9.1280×107 cm^{-2} at 660μm and N_{s2} is 4.4451×108 cm^{-2} decreasing by 80.5%. It can be explained as follows: edge dislocations usually occur during the initial stages of GaN growth when small misoriented GaN islands coalesce to form a continuous thin film. These edge dislocations usually parallel to the c-axis with a small tilt angle, so it is more difficult to meet and fuse for two or more edge dislocations than that of screw dislocations. The screw-edge reactions also have small possibilities because their each Burgers vector is perpendicular and the major fusion for the reduction of the edge dislocation densities are the edge-mixed reactions. On the other hand, the screw dislocations' shape is like half-loops which are extended along the c-axis and they have two screw segments whose line directions are opposite [17]. Two types of screw dislocations exist with Burgers vector **b** = ± [0 0 0 1]. As a result, the screw dislocations can fuse with each other and they also fuse with mixed dislocations through the screw-mixed reactions. For this reason, the reduction of the densities for the edge dislocation is very limited in thicker GaN films compare with screw dislocation densities.

Besides, the edge dislocations have a larger fraction of the total dislocation densities. The edge dislocations possess 86.6% of the all dislocations in 360μm thick while the fraction is 94.4% of total dislocations in 660μm. It should be noted that the variation tendencies of the Fig. 2 and Fig. 3 are inverse correlations which means that the edge dislocation fuse and reduce faster than the screw dislocation. The reason is that faster fusion between edge and mixed dislocations make fewer mixed dislocations available for the screw-mixed fusions. When the mixed dislocation is depleted and no further fusions for the edge dislocations are possible. So the densities for the edge dislocation reduce more slowly when GaN film reaches a certain thickness.

Conclusions

In this paper, the dislocations density of GaN thick films has been measured by high-resolution X-ray diffraction. The results show that the density of edge and screw dislocation decreases with increasing the GaN thickness. It also demonstrates that the densities for the edge dislocation with increasing

thickness reduce less in contrast with those for the screw dislocation. And the edge dislocations have a larger fraction of the total dislocation densities. We have discussed the mechanism of reduction of the dislocations with the thickness. So, HVPE for thick GaN films is a feasible method to reduce threading dislocations.

Acknowledgements

This work is supported by Special Funds for Major State Basic Research Project (2011CB301900, 2012CB619304, 2010CB327504), Hi-tech Research Project (2014AA032605), National Nature Science Foundation of China (60990311, 60906025, 60936004, 61176063), the nature science foundation of Jiangsu province (BK2011010BY2013077，BE2011132).

References

[1] YAMADA T, MUKAI T. Jpn. J. Appl. Phys. 34 (1995), p. 1332- p. 1335
[2] Sugahara T, Sato H, Hao M, et al. Japanese journal of applied physics, 1998, 37(4A), p.398..
[3] Weimann N G, Eastman L F, Doppalapudi D, et al. Journal of Applied Physics, 1998, 83(7), p.3656-p.3659.
[4] Kozodoy P, Ibbetson J P, Marchand H, et al. Applied physics letters, 1998, 73(7), p.975-p.977.
[5] OIDA Technology Roadmap, update 2002, J.Y. Tsao (Ed.), Light Emitting Diodes (LEDs) for General Illumination, Optoelectronics Industry Development Association, Washington, DC
[6] Currie M T, Samavedam S B, Langdo T A, et al. Applied Physics Letters, 1998, 72(14), p.1718-p.1720 .
[7] T. S. Zheleva, O. H. Nam, M. D. Bremser, and R. F. Davis, Appl. Phys. Lett. APPLAB 0003-6951, **71**, 2472 (1997).
[8] S. Tanaka, M. Takeuchi, and Y. Aoyagi, Jpn. J. Appl. Phys., Part 2 JAPLD8 0021-4922, **39**, L831 (1997).
[9] T. Wang, Y. Morishima, N. Naoi, and S. Sakai, J. Cryst. Growth JCRGAE 0022-0248, **213**, 188 (2000).
[10] X. Q. Shen, H. K. Cho, T. Ide, M. Shimizu, and H. Okumura, Jpn. J. Appl. Phys., Part 2 JAPLD8 0021-4922, **41**, L1428 (2002).
[11] T. Akasaka, T. Nishida, Y. Taniyasu, M. Kasu, T. Makimoto, and N. Kobayashi, Appl. Phys. Lett. APPLAB 0003-6951 , 83, 4140 (2003).
[12] N. Kuwano, T. Tsuruda, S. Terao, S. Kamiyama, H. Amano and I. Akasaki, International Scholarly Research Network, ISRN Condensed Matter Physics, 2012, Article ID 184023.
[13] S. Danis, V. Holy, Z. Zhong, G. Bauer, and O. Ambacher, Applied Physics Letters, vol. 85, no. 7, 2004, p.3065–p.3067.
[14] Metzger T, Höpler R, Born E, et al. Philosophical magazine A, 1998, 77(4), p.1013-p.1025.
[15] Mathis S K, Romanov A E, Chen L F, et al. Journal of crystal growth, 2001, 231(3), p.371-p.390.
[16] Liu J Q, Wang J F, Liu Y F, et al. Journal of Crystal Growth, 2009, 311(10), p.3080-p.3084.

Advanced Materials Research Vols. 989-994 (2014) pp 391-394
© (2014) Trans Tech Publications, Switzerland
doi:10.4028/www.scientific.net/AMR.989-994.391

The Luminescence Properties of Green YPO_4: Tb^{3+},Ce^{3+} Phosphors for WLED

Jian Li[1], Limin Dong[1,2,a], Qin Li[1] and Zhidong Han[1,2]

[1] College of Materials Science and Engineering, Harbin University of Science and Technology, Harbin, China

[2] Key Laboratory of Engineering Dielectrics and Its Application, Ministry of Education, Harbin University of Science and Technology, Harbin, China

[a] corresponding author: donglimin@hrbust.edu.cn

Keywords: WLED, Green light-emitting, Rare earth doping, $LnPO_4$.

Abstract. LED as the fourth generation light source has been extensively studied. In order to get a high-performance White Light Emitting Diode (WLED) green phosphor, YPO_4:Ce^{3+},Tb^{3+} was prepared by co-precipitation. It was excited at 380nm. The structure, morphology, fluorescence property and colorimetry of the phosphors were investigated by X-ray diffraction (XRD), scanning electron microscopy (SEM) and fluorescence spectrophotometer. Final results show the optimal concentration ratio are 1:0.05:0.01. The crystal grain of luminescent material is 200 nm. When the bath temperature is 80℃ and calcined at 1000℃ for 3h, the luminescence performance of the luminescent material is excellent.

Introduction

Rare orthophosphate $LnPO_4$ has many prominent advantages, such as high thermal stability, large refractive index and low phonon energy[1,2]. It is widely used in Sensors, ceramic, catalyst carrier and host of fluorescent material[3]. YPO_4 has xenotime structure and assigned to tetragonal crystals. In which Y^{3+} radius is small, rare earth ions can replace the Sites of Y^{3+} without destroying the crystal structure[4,5]. Ce^{3+}, Tb^{3+} co-doped YPO_4 is a commercially efficient green phosphor. Environment of luminescent center ion charge can be adjusted by incorporation of other ions. Since Ce^{3+} 4f layer only has one electron, it has prominent contribution on compensation ion charge environment and sensitizing excited center Tb^{3+}[6].

In a typical process for the synthesis of YPO_4 under high temperature solid state conditions, rare earth oxides and $(NH_4)_2HPO_4$ as raw materials. But the high-temperature lead to P_2O_5 evaporate, causing the ratio of phosphate and rare earth ions can't control. the luminescence properties of phosphors was affected. Precipitation method can solve many problems of solid-phase reactions. Obviously in the solution, it's easy to control the stoichiometric ratio of phosphate and rare earth ions. At the same time it can also make doping ions mixed evenly into the lattice matrix[7].

Experiments

Preparation. The Y_2O_3, Tb_4O_7, $Ce(NO_3)_3$, HNO_3 were selected as the raw material. First, according to the stoichiometric ratio of the elements accurately weighed. In a typical synthesis procedure, Y_2O_3 and Tb_4O_7 were dissolved in HNO_3 with stirring. Diammonium phosphate was dissolved in the as-prepared $Y(NO_3)_3$ and $Tb(NO_3)_3$ aqueous solution under stirring. The mixture was transferred into a flask and stirred at 80℃ in a water bath. Dropwise added the Diammonium phosphate solution. Heavy white precipitate can be seen and continue added until complete precipitation. The resulting precipitate was suction filtered and washed, then placed in a resistance furnace for calcining phosphor obtained.

Characterization. The structures of the phosphor were characterized by X-ray diffractometer (XRD)(Shimadzu, XRD-6000, Cu Ka target) and the morphology of the particles was observed by field emission scanning electron microscope(FE-SEM)(Sirion 200, Philip). The photoluminescence

properties. of the phosphors were studied on fluorescence spectrophotometer (Shimadzu, model RF-5301 PC).

Result and discussion

Structural analysis. Fig. 1 shows the X-ray diffraction (XRD) patterns and crystal structure of $Y_{1-x}PO_4:xTb^{3+}$ and $Y_{1-x-y}PO_4$: xTb^{3+},yCe^{3+}. All the diffraction peaks are in good agreement with the standard positions from the quartet YPO_4 phase(11-0254), and no diffractions from Tb_2O_3 and Ce_2O_3 can be detected, implying the completely substitution of Tb and Ce to Y and without charge compensation.

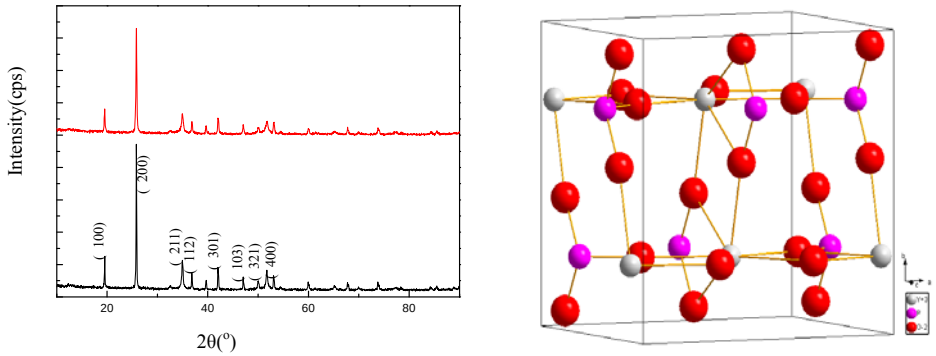

Fig. 1 The XRD patterns and crystal structure of $Y_{1-x}PO_4:xTb^{3+}$ and $Y_{1-x-y}PO_4$: xTb^{3+}, yCe^{3+}.

Fig. 2 shows the XRD patterns of YPO_4:5%Tb^{3+},2%Ce^{3+} calcined at 1000℃ of different time. The shape of the four diffraction peak is almost the same without extra miscellaneous peak. When the calcination time is 1h, the FWHM (Full Width at Half Maximum) is large, which is assigned to inadequate decomposition of organics. Many ions(oxygen ions, hydroxide ions) enter into the crystal interior and combine with lattice point, even destroy the lattice crystal. The sharpness of 2h is higher than 1h. When the calcination time up to 3h, not only the sharpness becomes higher but also the FWHM becomes more narrow. The crystalline phase is fully reflected. With the increasing of the calcination time, the material was burnt. Crystal agglomeration or crystal structure destruction result a significant reduction in the sharpness of the diffraction peaks. So the best calcination time is 3h.

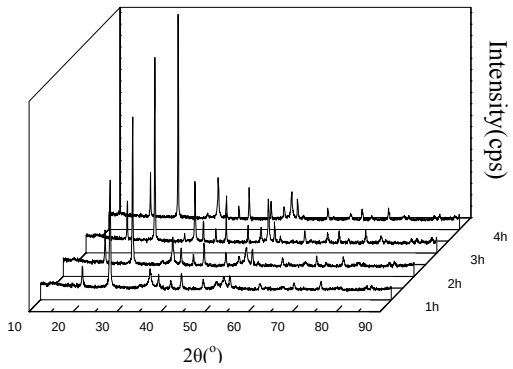

Fig. 2 The XRD patterns of YPO_4:5%Tb^{3+},2%Ce^{3+} calcined at 1000℃ of different time.

Optical characterization

Luminescence performance analysis of $YPO_4:Tb^{3+}$. In order to determine the optimum molar ratio of Tb^{3+}, we designed four horizontal test wherein Tb=x%. All the materials were calcined at 900℃of 3h. From the Fig. 3, the optimal luminescence intensity was Tb=5%.

Luminescence performance analysis of $YPO_4:Tb^{3+},Ce^{3+}$. Fig. 4 shows the excitation and emission spectrum of the prepared samples which are calcined at 1000℃ for 3h.From the excitation spectrum we can see that the peak intensity at 380nm is the strongest. The excitation spectra of

$YPO_4:Tb^{3+},Ce^{3+}$ excited by ultraviolet at 380nm exhibits four obvious excitation peaks which are located at 487, 541, 583 and 620 nm, which are corresponding to the $^4D_3\rightarrow{}^7F_6$,$^5D_4\rightarrow{}^7F_5$,$^5D_4\rightarrow{}^7F_4$ and $^5D_4\rightarrow{}^7F_3$ transitions of Tb^{3+} ion. Among that, the peak at 541 nm is obvious, and the emitting light located in green spectral region[8].

It's easy for Ce^{3+} to absorb energy under UV excitation ,but Tb^{3+} is not. Therefore, the characteristic peaks which is corresponding to the $^2F\rightarrow{}^5D$ transitions of Ce^{3+} ion can be found in the excitation spectrum. Ce^{3+} which can be acted as sensitizer has a good ability to transfer the energy to Tb^{3+} . The characteristic peaks of Tb^{3+} which can be ascribed to $^5D\rightarrow{}^7F_j$(j=6,5,4,3)can be found, whereas Ce^{3+} is not.

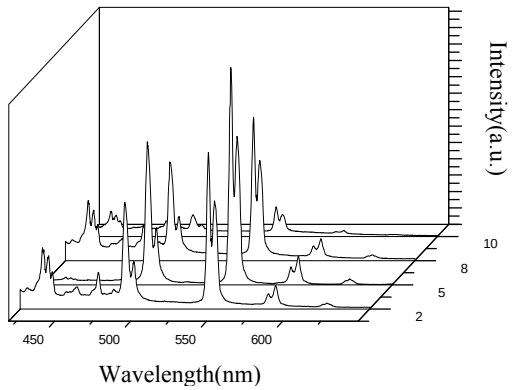

Fig. 3 Luminescence performance analysis of YPO_4:Tb(Tb=2%, 5%, 8%,10%).

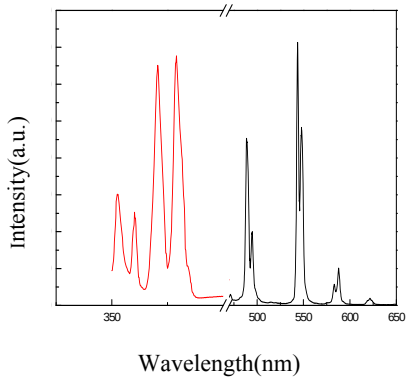

Fig. 4 Excitation(λ_{em}=545nm) and emission(λ_{ex}=380nm) spectrum of material calcined at 1000℃,3h.

The effect of rare earth concentration. Fig.5 shows the emission spectra of YPO_4:0.05Tb:x%Ce. The concentration of Ce^{3+} is 0, 1%, 2%and 4%, respectively. With the concentration of Ce^{3+} increasing, the fluorescence intensity is improved significantly. When the molar ratio of YPO_4: Tb: Ce was set to 100:0.05:0.01, we can get the optimum luminous intensity. In the luminescent material, With the concentration of Ce^{3+} increasing, the energy transfer between Ce and Tb is enhanced. But The concentration quenching occurred when the doping concentration is redundant, and the luminous efficiency dropped.

Concentration quenching,namely with the activator concentration increasing, the luminous efficiency dropped.When the activator reaches a certain value, the interaction between them is enhanced. The probability of non-radiative transition increased result in decreasing of the luminous efficiency.

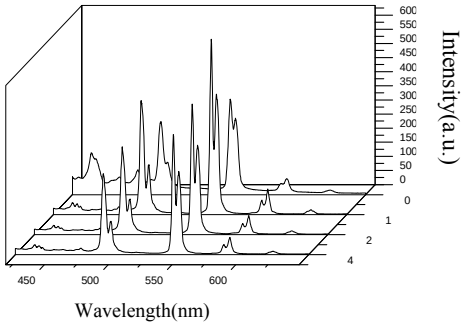

Fig. 5 The emission spectra of YPO_4:0.05Tb^{3+},x%Ce^{3+}.

Morphology analysis. Fig. 6 shows the SEM images of different calcination temperature and the temperature are 900, 1000 and 1100℃ respectively. When the temperature was 900℃, the prepared sample had a relative good morphology, the crystal is not full-grown. The sample under 1000℃ had separated crystal morphology and uniform particles. The particle size is about 200 nm. Fig. 6-c shows the sample calcined under 1100℃. Because of overburning, the lattice crack and crystal phase

liquefaction. This is correspond to the test results of fluorescence intensity. This reflected the effects of morphology on fluorescence performance.

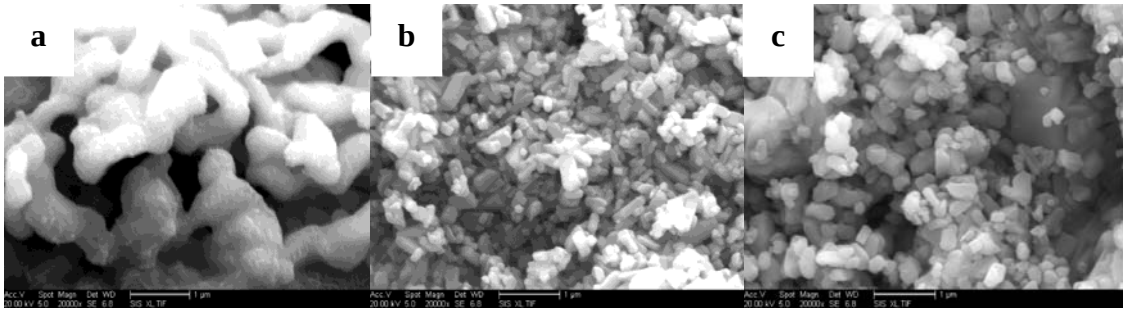

Fig. 6 The SEM images at different temperatures.

Conclusion

A novel green-emitting $YPO_4:Ce^{3+},Tb^{3+}$ phosphor has been synthesized by the traditional coprecipitation method. The excitation spectra of $YPO_4:Tb^{3+},Ce^{3+}$ excited by near-ultraviolet at 380nm. The PL spectra shows that the main emission peak located at 541nm, and the emitting light located in green spectral region. The obtained results show the optimal concentration ratio is 1:0.05:0.01. The crystal grain of luminescent material is 200 nm. When the bath temperature is 80℃ and calcined at 1000℃ for 3h, the luminescence performance of the luminescent material is the best.

Acknowledgements

This work was financially supported by program for new century excellent talents in Heilongjiang provincial university (1251-NCET-014).

References

[1] J. M. Nedelec, C. Mansuy, R. Mahiou. Sol-gel Derived YPO_4 and $LuPO_4$ Phosphors, a spectroscopic study[J]. Journal Molecular Structure. Vol 651-653 (2003), p. 165-170.

[2] R. C. Ropp. Phosphors Based on Rare Earth Phosphates Spectral Properties of Some Rare Earth Phosphates[J]. Electrochem. Soc. Vol 115 (1968), p. 841-845.

[3] A. Leto, F. Piccinelli ,G. Pezzotti ,A. Speghini,. Single Crystal and Nanocrystalline Pr^{3+} Doped $LuPO_4$ Synthesis, Structural Characterization, Photo- and Cathodoluminescence[J]. Materials Research Bulletin. Vol 51 (2014), p. 24–27.

[4] H. Lai, A. Bao, Y. Yang, et al. UV Luminescence Property of $YPO_4:RE(RE=Ce^{3+},Tb^{3+})$[J]. The Journal of Physical Chemistry, Vol 112(1) (2008), p. 282-286.

[5] Y. Lin, J. Fu, et al. Sol–gel Fabrication Patterning and Photo luminescent Properties of $LaPO_4$：Ce^{3+},Tb^{3+} Nano crystal line Thin Films[J]. Chemical Physics Letters. Vol 371 (2003), p. 178-183.

[6] J. M. Nedelec, D. Avignant, P. Mahiou. Soft Chemistry Routes to YPO_4 Based Phosphors: Dependence of Textural and Optical Properties on Synthesis Pathways[J]. Chem Mater. Vol 14 (2002), p. 651-655.

[7] T. Justcl, P. Huppcrtz, W. Mxyr, et al. Temperature-dependent Spectra of YPO_4: Me (Me=Ce, Pr, Nd, Bi)[J]. Journal of Luminescence. Vol 106 (2004), p. 225-232.

[8] H. B. Li, Y. N.Liu, W. G Shu. Research on Preparing Superfine $MgAl_{22}O_{19}:Tb^{3+},Ce^{3+}$[J]. Applied Chemical lndustry. Vol 33(2) (2004), p. 11.

Advanced Materials Research Vols. 989-994 (2014) pp 395-398
© (2014) Trans Tech Publications, Switzerland
doi:10.4028/www.scientific.net/AMR.989-994.395

Preparation and Luminescent Properties of Single White $Ca_2MgSi_2O_7$: Eu^{3+}, Ce^{3+}, Tb^{3+} Phosphor for WLED

Xiaoqi Zhang [1], Limin Dong [1, 2,a], Tang Xincheng[1], Qin Li [1], and Zhidong Han [1,2]

[1] College of Materials Science and Engineering, Harbin University of Science and Technology, Harbin, China

[2] Key Laboratory of Engineering Dielectrics and Its Application, Ministry of Education, Harbin University of Science and Technology, Harbin, China

[a] corresponding author: donglimin@hrbust.edu.cn

Keywords: White light emitting diode, Alkaline earth, Mesosilicate

Abstract. $Ca_2MgSi_2O_7$: Eu^{3+}, Ce^{3+}, Tb^{3+}, a single white Phosphor, was synthesized by the conventional solid-state reaction. The structure, surface morphology and luminescence properties of the prepared samples were investigated to evaluate its potentiality. XRD results confirm the orthorhombic phase of $Ca_2MgSi_2O_7$: Eu^{3+}, Ce^{3+}, Tb^{3+} phosphors. The excitation spectra indicates the phosphor can be excited by 393 nm wavelength. The phosphor exhibits blue light at 467 nm, green light at 588 nm, red light at 618 nm. CIE chromaticity diagram indicates that $Ca_2MgSi_2O_7$: Eu^{3+}, Tb^{3+}, Ce^{3+} exhibits white light. All properties show that the prepared phosphor is a single white phosphor suitable for near ultraviolet excitation which can be applied to new generation white LED lighting.

Introduction

There is a growing worldwide awareness of the need for strengthened environmental and energy protection as people entered the twenty-first century. Currently, the power consumption of lighting can account for 19% of the total power consumption. And the efficiency of incandescent and fluorescent lamps is low, fluorescent lamps also has the problem of environment. WLED have the advantages of lower energy consumption, environmental protection and long lifetime etc[1-3]. The luminescence efficiency has already exceeded that of traditional incandescent lamps and now is competitive with that of fluorescent lamps.

Now, there are three methods to achieve WLED for lighting. One way to produce the white light is to combine the blue GaN chip with yellow phosphor YAG: Ce^{3+}[4]. However, the color quality of these white LEDs has not been fully satisfactory due to the limited white hue tunability, color rendering index, and correlated color temperature. And it is aso difficult to make stable WLED because there are many influencing factors such as the light like drive voltage and coating thickness of phosphor in industrial production. Besides, white light can be produced by mixing blue, green, and red phosphors with near-ultraviolet LED[5-7]. While there is a color reabsorption problem with this approach, it will affect the color reproduction of LED. Single white phosphor does not have the color reabsorption and ratio regulation problems[8], and silicate matrix has a high chemical and thermal stability. $Ca_2MgSi_2O_7$ matrix which can be activated by rare earth ions widely used in the field of LED. Therefore, single white $Ca_2MgSi_2O_7$: Eu^{3+}, Ce^{3+}, Tb^{3+} phosphor has broad application prospects.

Experimental

$Ca_2MgSi_2O_7$: Eu^{3+}, Ce^{3+}, Tb^{3+} phosphors were synthesized by high tempreture solid state method. The raw materials, $CaCO_3$(A.R.), $4MgCO_3 \cdot Mg(OH) \cdot 5H_2O$(A.R.), SiO_2(A.R.), Eu_2O_3(99.99%), Ce_2O_3(99.99%) and Tb_4O_7(99.99%), were mixed thoroughly in stoichiometric proportions, and heated in a temperature range of 950–1250℃ for 2-5h subsequently. Using the XRD study the crystal structure of the sample. The PL spectra of these phosphors were investigated by a Shimadzu, RF-5301PC spectrofluorophotometer. The surface morphology was investigated by a scanning electron microscopy.

Results and discussions

Fig.1 shows the SEM images of $Ca_2MgSi_2O_7$: Eu^{3+}, Ce^{3+}, Tb^{3+} phosphors which are calcined at different tempreture. The calcination temperature of a, b, c, d, is 950℃, 1050℃, 1150℃, 1250℃, respectively. These samples are all held for 4 hours. As shown in Fig.1a, when the calcining temperature is 950℃, the powders are anomalous small particles, the morphology is irregular and the interface between the small particles is not clear. As to 1050℃, the powders is mostly formed crystals, and powder particles distributed uniformly. It presents rules massive structure. But there is still finely particulate. When the calcining temperature rise to 1150℃, powders have clear interface, more complete morphology, smooth surface, and uniform size. While the powders are calcined at 1250℃, the prepared samples are severe adhesion and reunite, and the interface of the powders is not clear. It indicates that when the calcined temperature is too high, the crystal lattice will be cracked and crystalline phase will be liquefied. Therefore, the best sintering temperature is 1150 ℃.

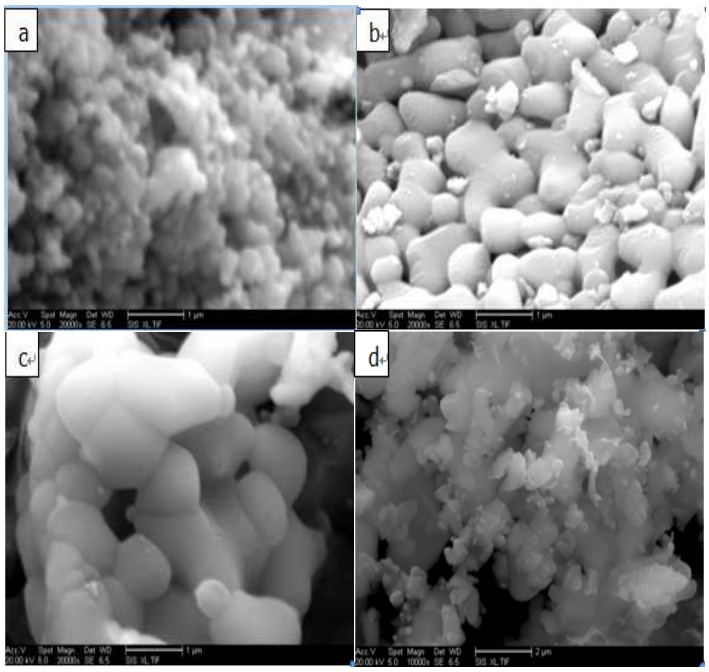

Fig.1 SEM images of $Ca_2MgSi_2O_7$: Eu^{3+}, Ce^{3+}, Tb^{3+} at different calcining temperature a)950℃, b)1050℃, c)1150℃, d)1250℃

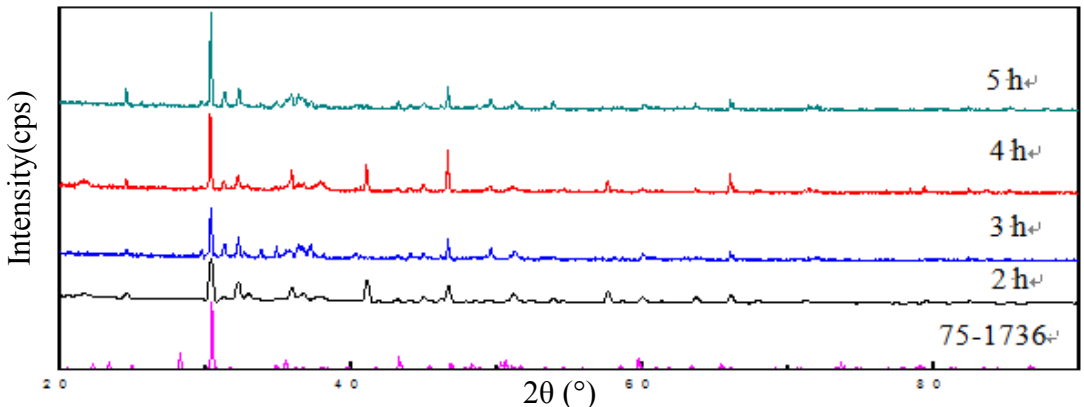

Fig. 2 XRD patterns of $Ca_2MgSi_2O_7$: Eu^{3+}, Ce^{3+}, Tb^{3+} which are held for 2, 3, 4, 5 hours

Fig. 2 shows the XRD patterns of $Ca_2MgSi_2O_7$: Eu^{3+}, Ce^{3+}, Tb^{3+} phosphors sintered for 2,3,4,5 hours. The diffraction peak positions and the relative intensities of the samples match well with the standard XRD patterns of $Ca_2MgSi_2O_7$: Eu^{3+}, Ce^{3+}, Tb^{3+} (PDF75-1736). It indicates that doping with

Eu^{3+}, Ce^{3+}, Tb^{3+} ions do not affect the crystal structure of $Ca_2MgSi_2O_7$. Synthetic samples are tetragonal system, and the space group is P421m(No.113). Diffraction peaks of prepared samples are obvious and relative sharp. With the holding time increased, sharpness of diffraction peaks is increasing and the half peak width is narrowed. When the calcination time is 4h, the diffraction peaks are the sharpest, the half peak width is the narrowest, and impurity peaks are the least. As the holding time further increased, the sharp diffraction peaks become diffuse, and the half peak width broaden. Even the holding time is increasing, the degree of crystallinity does not increase. Therefore, when the calcining time is 4 hours, luminescent material is the best in our experiment.

Curves a in the Fig.3 indicates that the phosphor can be excited by 393nm wavelength. In other words, the phosphor can be excited by NUV InGaN chip. Curves b ,c, d in the Fig.3 show the PL emission spectras of $Ca_2MgSi_2O_7$: Eu^{3+} with Eu^{3+} concentration of 0.5%, 1%, 1.5% when excited at 393nm wavelength. The PL emission spectra (Fig.3) exhibit the emission band peaks are located at 467nm, 588nm, 618nm, which are corresponding to the $^5D_2 \rightarrow {}^7F_0$, $^5D_0 \rightarrow {}^7F_1$, $^5D_0 \rightarrow {}^7F_2$ transitions of Eu^{3+} ion. With the concentration of Eu^{3+} ion further increased, emission peak positions do not change, but the emission intensity increases. When the concentration of Eu^{3+} reach 1%, the phosphors show the highest luminescent intensity. However, when the concentration of Eu^{3+} reach 1.5%, the luminescent intensity of the phosphors dropped. Therefore, the best concentration of Eu^{3+} is 1% in our experiment.

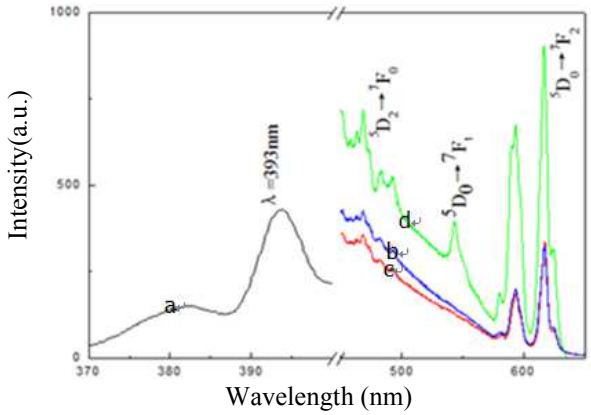

Fig.3 a) Excitation spectra of $Ca_2MgSi_2O_7$:Eu^{3+}, b) c) d) emission spectras of $Ca_2MgSi_2O_7$:Eu^{3+} ， concentration of Eu^{3+} are 0.5%, 1%, 1.5% .

Fig.4 shows PL emission spectrum of $Ca_2MgSi_2O_7$: Eu^{3+}, Ce^{3+}, Tb^{3+} with different doped ion concentration. Curves 1 presents the PL emission spectrum of $Ca_2MgSi_2O_7$: Eu^{3+}, Ce^{3+}, Tb^{3+} and the ratio of Eu^{3+}, Ce^{3+} and Tb^{3+} is 1:1:1.5. Curves 2 presents PL emission spectrum of $Ca_2MgSi_2O_7$: Eu^{3+}, Ce^{3+}, Tb^{3+} and the ratio of Eu^{3+}, Ce^{3+} and Tb^{3+} is 1:1:1. Curves 3 depicts PL emission spectrum of $Ca_2MgSi_2O_7$: Eu^{3+}, Ce^{3+}, Tb^{3+} and the ratio of Eu^{3+}, Ce^{3+} and Tb^{3+} is 1:1.5:1. As we can see from Fig.4, the blue and green emission peak decreased with the concentration of Ce^{3+} reducing, because the reducing concentrations of Ce^{3+} which make transmission of energy between Ce^{3+} and other rare earth ions reduce. When the concentration of Ce^{3+} reduced and the concentration of Tb^{3+} increased, the green emission peak significantly enhanced and the red emission peak significantly decreased. It made luminescent material emits green light instead of white light which we want. In this experiment, the best ratio of Eu^{3+}, Ce^{3+} and Tb^{3+} is 1:1.5:1

All the results calculated from the spectra is plotted in the CIE 1931 chromaticity diagram, as shown in Fig.5. When $Ca_2MgSi_2O_7$ doped with Eu^{3+}, Tb^{3+}, Ce^{3+}, the piont was located at (0.340,0.314). It indicates that $Ca_2MgSi_2O_7$: Eu^{3+}, Tb^{3+}, Ce^{3+} is close to the edge of CIE diagram, which indicates this phosphor emit white light.

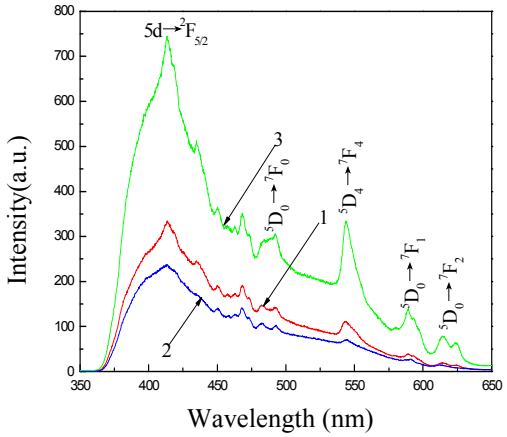

Fig.4 Emission spectras of $Ca_2MgSi_2O_7$ Eu^{3+},Ce^{3+},Tb^{3+}.

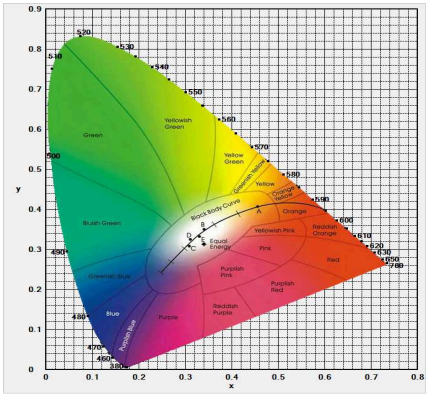

Fig.5 CIE chromaticity diagram of $Ca_2MgSi_2O_7$: Eu^{3+}, Ce^{3+},Tb^{3+}.

Conclusion

In summary, we have successfully prepared a new white $Ca_2MgSi_2O_7$: Eu^{3+}, Ce^{3+}, Tb^{3+} phosphor synthesized by the solid-state reaction. XRD results indicate the prepared phosphor is tetragonal structure. It possesses an ideal spectral feature, which has five main peaks located at 413nm, 492nm, 543nm, 588nm, 614nm. The best molar ratio of Eu^{3+}: Ce^{3+}: Tb^{3+} was set to 1:1.5:1. The CIE coordinates of phosphors can be adjusted by controlling the rare earth ions concentration. The obtained results indicate that $Ca_2MgSi_2O_7$: Eu^{3+}, Ce^{3+}, Tb^{3+} phosphor could be further investigated for its potential application on near-UV excitable WLEDs.

Acknowledgements

This work was financially supported by program for new century excellent talents in Heilongjiang provincial university (1251-NCET-014).

References

[1] D. A. Steigerwald., J. C. Bhat, D Collins., et al. Illumination with solid state lighting technology [J]. IEEEJ. Sel. Top. Quant., 2002, 8(2): 310-320.

[2] Gee J. M., Tsao J. Y., Simmons J. A. Prospects of LED lighting [J]. Proc.of SPIE, 2004, 5187: 227-233.

[3] Y. Narukawa, J Narita, T Sakamoto, et al. Recent progress of high efficiency white LED [J]. Phys Stat, 2007, 204: 2087-2093.

[4] X. Y. Sun, J. H. Zhang, X. Zhang, et al. A Single White Phosphor Suitable for Near Ultraviolet Excitation Applied to New GenerationWhite LED Lighting [J]. Chinese Journal of Luminescence, 2005, 26 (3): 404-406, In Chinese.

[5] Y. Q. Zhai, S. H. Feng, Z. Zhang, et al. Preparation of Orange-red Emitting Phosphors $Sr_2MgSi_3O_9$:Eu^{3+} for White LEDs and Its Photoluminescent Properties [J]. Journal of Hebei University, 2009, 29(6): 609-613, In Chinese.

[6] X. Y. Sun, J. H. Zhang, X. Zhang, et al.. A green-yellow emitting P-Sr_2SiO_4: Eu^{2+} phosphor fornear ultraviolet chip white-light-emitting diode [J]. Rare Earths., 2008, 26(3): 421-424,.

[7] Y. Umetsu, S. Okamoto, H. Yamamoto. Photoluminescence Properties of BaMgSiO: Eu^{2+} Blue Phosphor and BaMgSiO: Eu^{2+}, Mn^{2+} Blue-Red Phosphor under Near-Ultraviolet-Light Excitation [J]. J. Electrochem. Soc., 2008, 155(7): J193-J197.

[8] J. S Kim., P. E Jeon., J. C Choi., H. L Park., S. I Mho., G. C. Kim. Warm white lightemitting diode utilizing a single phase full color $Ba_3MgSi_2O_8$:Eu^{2+},Mn^{2+} phosphor [J].Appl. Phys. Lett., 2004, 84(15): 2931.

Advanced Materials Research Vols. 989-994 (2014) pp 399-402
© (2014) Trans Tech Publications, Switzerland
doi:10.4028/www.scientific.net/AMR.989-994.399

The Temperature Control of the Preheating Tank in the Procedure of Chloroacetic Acid' s Crystallization

Zengfang WANG[1,a], Chaoying LIU[2,b],Xueling SONG[1] and Yuxian GAO[1]

[1] Instituteof electrical engineering, Hebei University of Science and Technology, Shijiazhuang ,China

[2] Polytechnic college, Hebei University of Science and Technology, Shijiazhuang ,China

[a]wzf881207@163.com, [b]liucy@hebust.edu.cn

Keywords: Fuzzy PID control.Smith predictor control.Chloroacetic acid.

Abstract. Based on detailed analysis of crystal process in Chloroacetic Acid(MCA)'s production, a certain control method is exert on it. In order to overcome the time delay ,large inertia, time-varying ,a fuzzy Smith intelligent method is proposed.Simulation results show that this method apparently is superior to the general PID control and Smith control.

Introduction

Adopt method of cooling crystallization in MCA's production,and most of the factories adopt to mixed water in the preheating tank into crystallization reactor jacketed for the material cooling of the reactor.The temperature control of preheating tank need to strictly change according to certain rules[1] .Based on fully understand MCA's crystallization process,design a rational control scheme.Because the preheating tank has the disadvantages of time delay ,large inertia, time-varying,its control effect is often not satisfactory . Therefore, it is very important to seek an effective and accurate method to control the temperature of preheating tank , a fuzzy Smith intelligent method is proposed.Simulation results show that the method can improve the robustness and steady-state accuracy of system.

Crystallization Process and Control Requirements in MCA's Production

Because melting point of different material is different , separate dichloroacetic acid from MCAby method of cooling crystallization[2].According to the process flow diagram of MCA crystallization ,reasonable control scheme is put forward which is shown in Fig. 1.

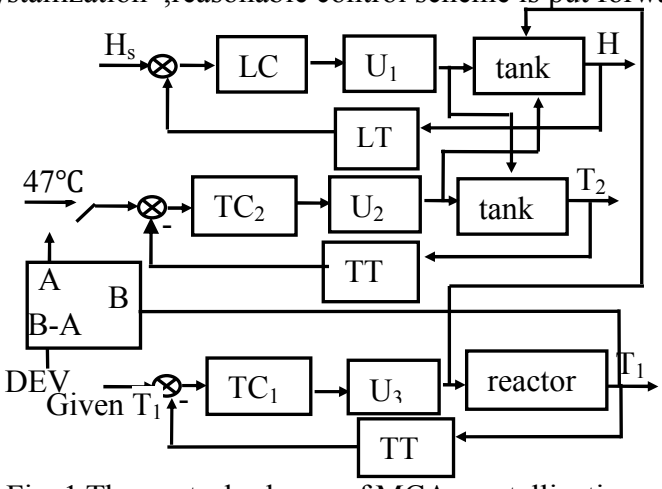

Fig. 1 The control scheme of MCA crystallization

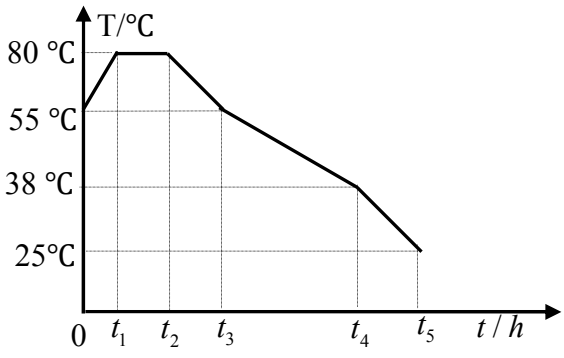

Fig. 2 Material temperature change curve

Crystal process in MCA's production is divided into fifth stages.The temperature variation trend of the material in the crystallization reactor is shown in Fig. 2 .

The first stage($0-t_1$): two-way switch is off,the switch control (LC) 100 ℃hot water to make liquid evel of preheating tank does not exceed the limit .The reactor temperature T1 is given as 80 ℃ make the material quickly heated to 80 ℃.Because of temperature lag,when the reactor temperature

reached 79 ℃, two-way switch connected to given 47 ℃, adjusting the cold water valveU2 for the preheating tank temperature is decreased.Hot water valveU1 opening degree is 40% by manually adjust the valve plug.Like this, not only ensure the accuracy of the temperature, but shorten the crystallization time .

The second stage($t_1 - t_2$):there is a certain amount of hot water in the tank,even if it is injected -15 ℃ cold water, the tank temperature does not drop rapidly .So the temperature of reactor was maintained at 80 ℃, until the temperature of the preheating tank drops to 80 ℃.

The third stage($t_2 - t_3$): there is no crystal production at this stage, so the reactor temperature may drop slightly faster.The preheating tank temperature constant at 47 ℃.The reactor temperature is drop at a rate of 10 ℃/h , until it is decreased to 55 ℃, and then adding crystal seed(0.5kg/m³)[3].

The forthstage($t_3 - t_4$):it is produces a lot of crystals,so the reactor temperature is decreased slowly in case it produce knot wall.At this time two-way switch is turned subtractor, the temperature of preheating tank with the reactor temperature strict control T1-T2 = 8 ± 0.5 ℃, DEV = 8 ± 0.5 ℃.The reactor temperature is drop at a rate of 5 ℃/h , until it is drop to 38 ℃.

The fifth stage($t_4 - t_5$):This stage is not required to consider knot wall phenomenon, the reactor temperature can drop faster.Preheating tank temperature with the temperature of reactor control T1-T2 = 14±2℃.The reactor temperature is drop at a rate of 10℃/h , until the reactor temperature is decreased to 25℃ which to prevent pipe blockage due to temperature fluctuations.

The Temperature Control System for Preheating Tank

The algorithm of improved-type Smith predictor

Smith predictor controller [4]is a algorithm which forecast estimated compensation time lag.In order to overcome the shortcomings of the model error sensitive, C.C.Hang propose an improved-type Smith predictor is shown in Fig. 3.

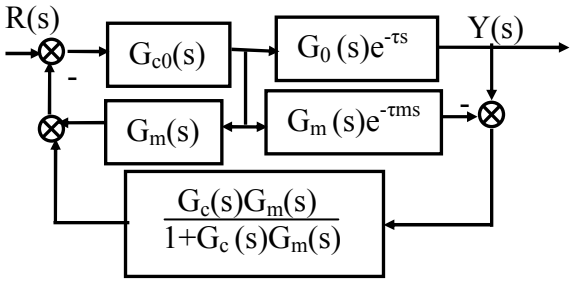

Fig. 3 The structure of the improved-type Smith predictor

It differs from the method of Smith control is more a regulator which feed back transfer function:

$$G_f(s) = \frac{G_c(s)G_m(s)}{1 + G_c(s)\mathrm{G}_m(s)} \tag{1}$$

where, G_c(s) is a PI regulator, G_m(s) is a first-order inertia, regulator integral time constant equal to the time constant of the model, Eq. 1 can be simplified as:

$$G_f = 1/t_f s + 1 \tag{2}$$

Closed loop system transfer function:

$$\frac{Y(s)}{R(s)} = \frac{G_{c0}(s)G_0(s)e^{-\tau s}}{1 + G_{c0}(s)\mathrm{G}_0(s) + \mathrm{G}_{c0}(G_0(s)e^{-\tau s} - G_m(s)e^{-\tau s})\dfrac{1}{t_f s + 1}} \tag{3}$$

Obviously, the improved method is the same with the original Smith predictor which has no effect on the stability of the system,when $G_m(s) = G_0(s), \tau_m = \tau$ .Even if there is an error, as long as appropriate adjustments t_f , Control effect of the system is better.In this paper, the t_f of improved-type Smith predictor is designed by fuzzy control[5].

Design on fuzzy Smith intelligent controller

Fig. 4 shows the structure of the fuzzy Smith intelligent controller for temperature control of preheating tank.

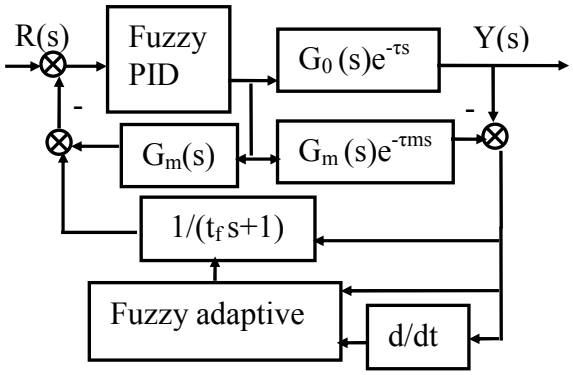

Fig. 4 The structure of the fuzzy Smith intelligent controller

In this paper, t_f is adjusted by fuzzy adaptive mechanism .The error t_e of object output and Smith Predictor output and change in error Δt_e are chosen as inputs to the fuzzy controller, Δt_f is chosen as outputs to modify the parameters t_f . t_f is calculated as follows:

$$t_f(k) = t_f(k-1) + \Delta t_f(k) \tag{4}$$

In order to enhance the robustness of the system , t_f can't be negative which given a minimum.Based on experience, and generally the minimum is $T/4 - T/3$. Δt_f is defined as {-6, +6}, the fuzzy set is {NB，NS，ZO，PS，PB}. The membership function defined as Triangular distribution.

Firstly,setting of t_f to determine the fuzzy control rule. $|\Delta t_e|$ will be large when controlled objects lag time and lag time of predictor are different,but the time constant and the magnification change will not have large $|\Delta t_e|$ .If $|t_e|$ is not too large,and is close to a constant value, it indicates that magnification of controlled objects is charged .Then inertia should not be introduced, should make t_f = 0. Adjusted trend of t_f rely on analysis $|\Delta t_e|$,if it is difficult to determine which parameters change.when $|\Delta t_e|$ is large,need to increase t_f to enhance the stability and robustness of the system;while $|\Delta t_e|$ is small,need to be reduced t_f in order to enhance rapid system.

Based on the above approach of tuning t_f and the past experiences, the control rules for output variables Δt_f is listed in Tables l .

Table 1 The fuzzy rule of Δt_f

Δt_f	Δt_e				
	NB	NS	Z0	PS	PB
t_e	NB PB	PB	PS	PS	PB
	NS PS	NS	NS	Z0	PS
	Z0 PS	Z0	Z0	PS	PS
	PS PS	Z0	NS	PS	PS
	PB PB	Z0	NS	PS	PB

System Simulations and Analysis

The temperature control of preheating tank can be expressed by a time delay plus an inertia input.,the model can be written as the following equation.

$$G(s) = \frac{5.3}{900s+1} e^{-90s} \tag{5}$$

The comparison of simulation results for fuzzy Smith intelligent control , PID control , Smith control are shown in Fig. 5,andFig. 6,respectively,when the model is accurate, the gain K ,the time constant T and the lag time τ are change.The control quality and the robustness of this system apparently are superior to the PID system,especially when model parameters are little uncertain.

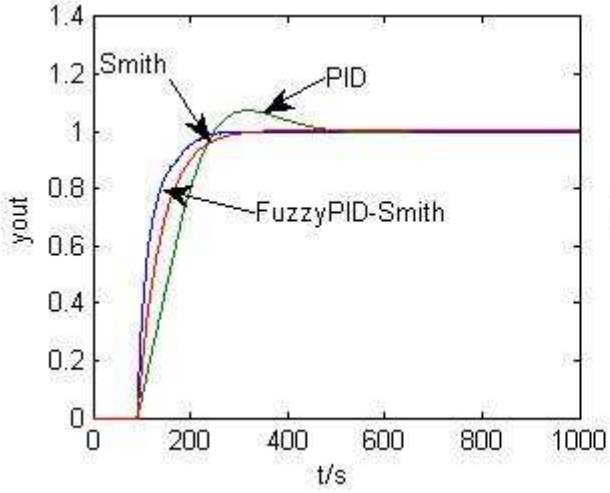

Fig. 5 Simulation results of accurately model

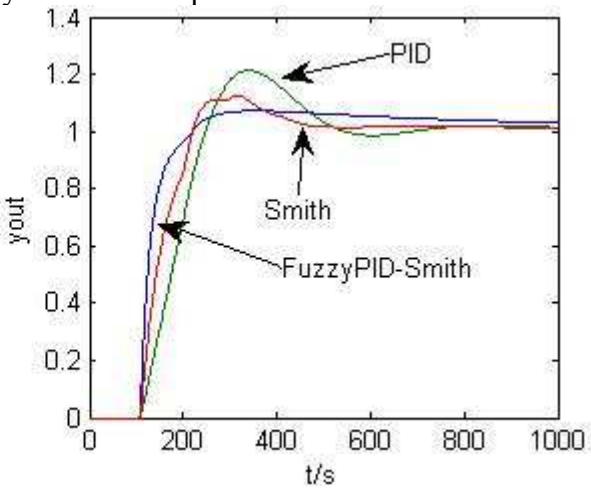

Fig. 6 Simulation results of parameters change

Summary

It is design a rational control schemer for crystal process in MCA's production.In order to solve the control difficulties for preheating tank with long time-delay, large inertia, time-varying ,a fuzzy Smith intelligent control method is proposed in this pape. Combined the fuzzy Smith intelligent control, PID control, with Smith control, this method has improved the dynamic performance of the system, eliminated the steady-state error, and has good adaptability when system model changes.

Acknowledgements

This paper is supported by Institute of electrical engineering, Hebei University of Science and Technology.
Correspondingauthor:Chao-Ying LIU, liucy@hebust.edu.cn

References

[1] Ming Li, Ganping Li and Wei Long. An improvement in the control scheme for the crystallization procedure of MCA' s interval producing process.Journal of Nanchang University,Vol.24(2002).
[2] Haiyan Guo.The study of synthesizing process and crystallizing process on lower unit consumption chloroacetic acid.Dalian: Dalian University of Technology master's degree thesis(2006)
[3] Chaoying Liu,Zheying Song and Xueling Song.Application of Fuzzy decoupling control for penicillin crystallization process.Journal of Hebei University of Technology,Vol.34(2005).
[4] Tan W. Tuning of a modified Smith predict or for processes with time delay . Control Theory & Applications, 2003, 20(2) , p.297-301.
[5] DiLi,YuanpingNi,Zheng Li,HaipengWang.Comparison of Smith Algorithm and Improved-Smith Algorithm in Temperature Control of Beer Fermentation.2010 No.8(Tol.194)

Advanced Materials Research Vols. 989-994 (2014) pp 403-406
© (2014) Trans Tech Publications, Switzerland
doi:10.4028/www.scientific.net/AMR.989-994.403

Effects of $SnCl_4$ concentration on The Properties of Electroless Deposited Ni-Sn-P Coatings

Xiran WANG [1,2,a], Wentao WANG[1,b],Bin YANG[1,c]

[1]School of Materials Science and Engineering, Henan university of science & technology, Luoyang 471023, China;
[2]Henan key laboratory of non-ferrous metal materials science and processing, Luoyang 471023, China)
[a]email: xiranwang1978@163.com, [b]email: 349782812@qq.com, [c]email:Yangbin@163.com

Keywords: Electroless plating; Ni-Sn-P alloy; $SnCl_4$; Alloy properties

Abstract. In this paper, the influence of $SnCl_4$ concentration on deposition rate, tin content, corrosion resistance and surface appearance of the coating are researched respectively. The results show that $SnCl_4$ concentration is increased, deposition rate is increased, then reduced. Tin content in the Ni–Sn–P coatings is increased with increasing $SnCl_4$ concentration in the solutions. However, Ni and P contents in the coating is decreased slightly. The microhardness of plating before and after heat treatment is above 500HV. The hardness will be improved a little after heat treatment. With increasing $SnCl_4$ concentration, the polarization curves slightly move to positive direction and decrease corrosion current, which shows that the introduction of tin tends to enhance resistance corrosion of the coating. When $SnCl_4$ concentration is up to 30g/L, resistant corrosion of the films presents a drop various degrees. The deposits is smooth and uniformity, smooth by SEM and the content of tin is 2.5 to 4.1 percent by EDS.

Introduction

Today the attention to the electroless plating of nickel-based ternary alloys[1-4] has been increased, one of which is Ni-Sn-P alloy. Ni-Sn-P coating has anticorrosion behavior, solderability, better decoration, and so on. Its industrial application is expanding too, such as spaceflight, building, chemical industry, machinery. Because tin has not selfcatalysis, tin ion is regarded as toxic reagent in electroless plating. It can decease the deposition rate, even make it difficultly form coating. So $SnCl_4$ concentration in baths directly affects the tin content, quality, properties of coating. Though a lot of reports [5-7] on this subject and relevant studies have been published, high quality alloy film of Ni-Sn-P obtained should be studied further.

The aim of this review is to obtain good quality of Ni-Sn-P. The effects of $SnCl_4$ concentration in baths on the deposition rate, hardness, corrosion resistance of the deposits is presented. Further -more, the surface morphology and composition of the deposits have also been studied.

Experimental

Sample preparation

Shown in Table 1 are the bath compositions and the operating conditions for the electroless deposition of Ni-Sn-P alloys. $SnCl_4$ concentration in bath is 10g/L, 15g/L, 20g/L, 25g/L, 30g/L, 35 g/L, respectively. All solutions used were freshly prepared using analytical grade chemicals and double-distilled water. Iron samples in a rectangle shape with dimensions of 40mm×15mm×1mm were chosen to be plated. The pre-treatment process of iron substrates is as follows. First, Fe substrate was consecutively degreased in a solution containing 40g/LNa_3PO_4, 40g/L Na_2CO_3 and 30g/L NaOH at 70℃ for 4min, rinsed with deionized water. Secondly, the samples were immersed in hydrochloric acid(hydrochloric acid: water in terms of volume is 1:1) for 30 seconds at room temperature and rinsed with deionized water.

Table1 Bath composition and operating conditions for electroless deposition of Ni-Sn-P alloys

Component	*Values apdoted*
$NiSO_4 \cdot 6H_2O$	30g/L
$C_3H_6O_3$	32.5g/L
$C_4H_4O_6KNa \cdot 4H_2O$	7.5g/L
$C_6H_5Na_3O_7 \cdot 2H_2O$	17.5g/L
$C_4H_6O_4$	16g/L
$NaH_2PO_2 \cdot H_2O$	30g/L
A addition	appropriate amount
pH	5.0
Temperature	90℃
Plating time	1h

The surface morphology and composition of the coating were observed and analyzed with SEM and EDS. The Vicker hardness (Hv) was measured with digital micro-hardness(MH-3), which test-condition is a 0.5N force for 10s. Corrosion test is conducted in 5%NaCl solution with CHI660C electrochemical workstation, which is the plating film as working electrode, high purity graphite works as auxiliary electrode, and saturated calomel electrode (SCE) as reference electrode. The surface of the working electrode is $1cm^2$.

Results and discussion

Effects of $SnCl_4$ concentration on deposition rate and composition of coatings

The effects of $SnCl_4$ concentration in plating solutions on the deposition rate of Ni-Sn-P and its compositions are illustrated in Fig.1 and 2, respectively. Fig.1 shows that deposition rate increases, then decreases with increasing $SnCl_4$ concentration in the solution for a given pH and a given temperature. When $SnCl_4$ concentration is 25g/L, deposition rate is up to $0.098mg \cdot mm^{-2} \cdot h^{-1}$.It is due to the fact that as reactive ion, Sn^{4+} concentration rising is beneficial to improve depositing reaction rate. At the same time, electrode potential of Sn^{4+}/Sn will rise with increasing Sn^{4+} concentration, which is conducive to tin ion deposited. But if $SnCl_4$ concentration was too high, deposition rate is lowered, which is because of tin being not selfcatalysis. Fig.2 shows that tin content in the Ni–Sn–P coatings is increased with increasing $SnCl_4$ concentration in the solutions. However, Ni and P contents in the coating is decreased slightly.

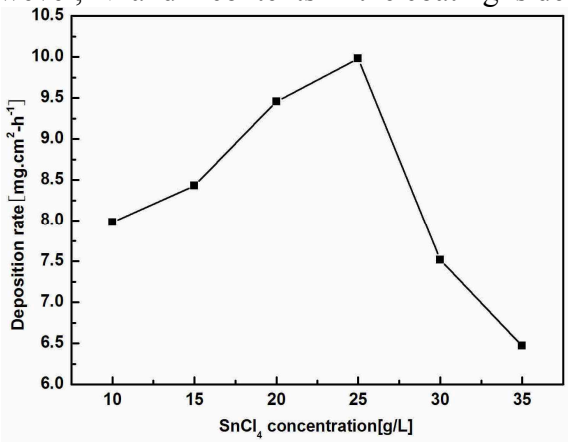

Fig.1 Effect of $SnCl_4$ concentration on deposition rate

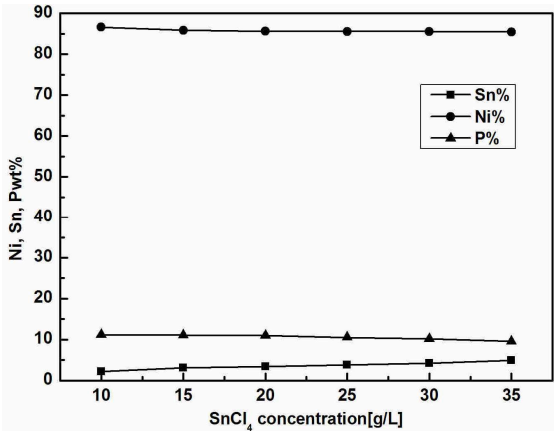

Fig.2 Effect of $SnCl_4$ concentration on coating composition

Effects of $SnCl_4$ concentration on the morphology of the coatings

Fig.4 shows the SEM photograph of the coating surface obtained with different $SnCl_4$ concentration. As showed in Fig.4, the Ni-Sn-P deposits have cell-shaped structure. With increasing $SnCl_4$ concentration, cellular granular of deposits became finer, more homogeneous and rounder, which led to obtaining the film being uniform, compact, and smooth. But if $SnCl_4$ concentration is over

30g/L, the deposits quality has fallen only slightly. Possibly because deposition potentials of Sn^{4+} is greater than that of Ni^{2+}, depositing preferentially tin is bad for depositing Ni and results in organizational segregation. The cells in deposits becomes bigger, as showed as in Fig.3f.

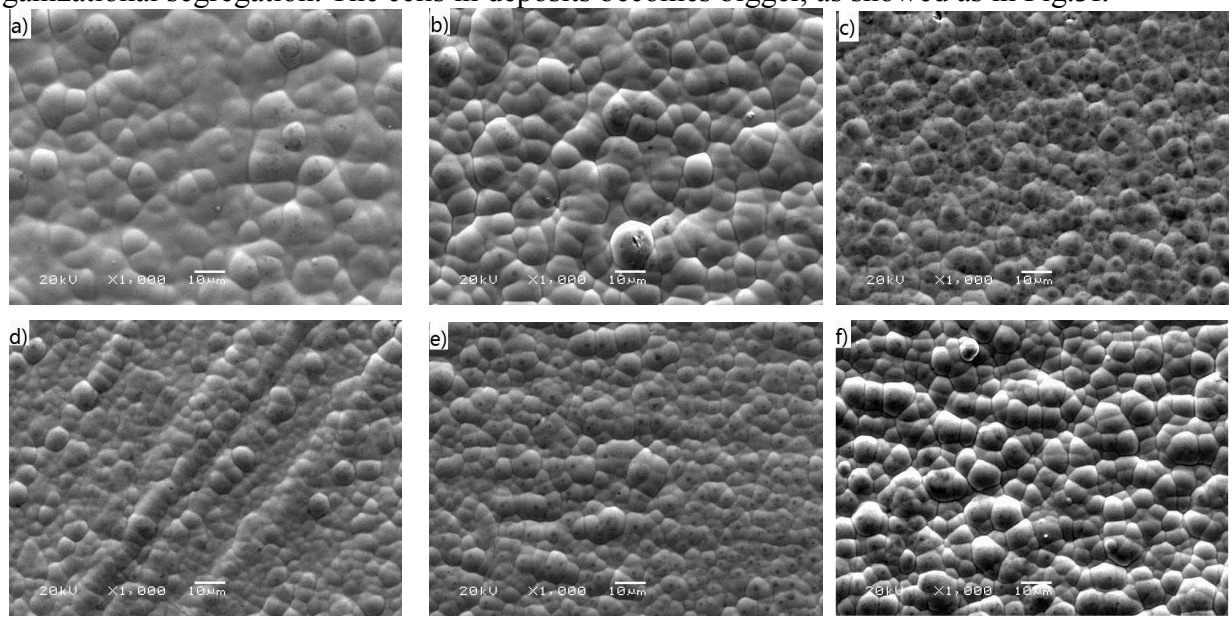

Fig.3 SEM of the film surfaces obtained with different $SnCl_4$ concentration in the solution(a:10g/L $SnCl_4$;b:15g/L$SnCl_4$; c:20g/L $SnCl_4$; d:25g/L$SnCl_4$; e:30g/L $SnCl_4$; f: 35g/L $SnCl_4$)

Effects of $SnCl_4$ concentration on hardeness of deposits

Fig. 4 shows the hardness value (Hv) of the Ni-Sn-P deposit. It is showed that the hardness of the deposits before and after heat treatment are increased, then declined with ascending $SnCl_4$ concentration. Investigated its reason, deposition rate is improved with raising $SnCl_4$ concentration and then the coating thickness increases, as well as the deposit sites grow in number, which causes that the celluar deposited particles become smaller and the film thickness also increases. These makes the deposit hardness increase with raising $SnCl_4$ concentration. However, the deposits quality is deceased when $SnCl_4$ concentration exceeds a specific value, which results in declining the hardness. After heat treatment, new phases in the deposits, such as Ni_3P, Ni_3Sn, have higher hardness and a function of precipitation hardening, improves the resistance of plastic deformation, which leads increasing hardness of deposits after heat treatment.

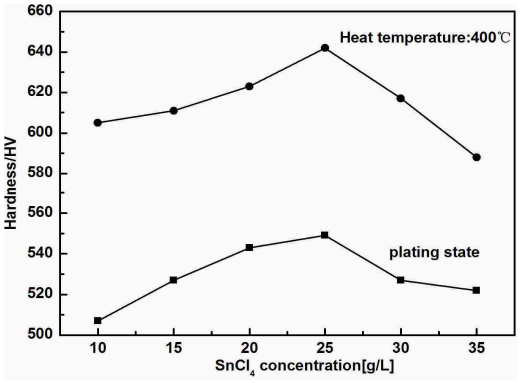

Fig.4 Effect of tin concentration on deposits hardness before and after heat treatment

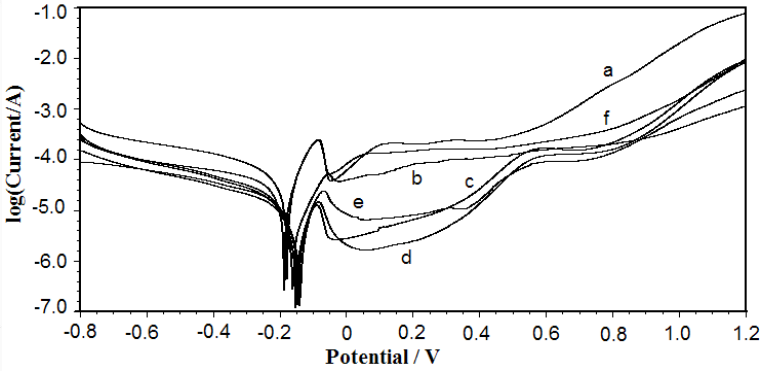

Fig.5 Anodic polarization curves of coatings in 3.5% NaCl solution(a:10g/L$SnCl_4$;b:15g/L$SnCl_4$; c: 20 g/L $SnCl_4$; d:25g/L$SnCl_4$; e:30g/L $SnCl_4$; f:35g/L $SnCl_4$)

Effects of $SnCl_4$ concentration on anticorrosion coating

Fig.5 showed the anodic polarization curves of the coatings in 3.5%NaCl solution. Free corrosion potential and corrosion current of deposits plating state are showed Table 2. As showed in Fig.5 and Table 2. Free corrosion potential varies from -0.187V～-0.138V and free corrosion current ranges from 3.758 e^{-6}～4.998e^{-5}A·cm^{-2}. And these increase firstly and then decrease and show the same trends with deposition rate. With increasing $SnCl_4$ concentration, the polarization curves slightly

move to positive direction and decrease corrosion current, which shows that the introduction of tin tends to enhance resistance corrosion of the coating. Because tin in the films played a sacrificial anode role in corrosion process, their base alloys were effectively protected, resistance corrosion of Ni-Sn-P alloy is improved[8]. When $SnCl_4$ concentration up to 30g/L, the deposits quality is deceased and resistant corrosion of the films presents a drop various degrees.

Table 2 Free corrosion potential and corrosion current of deposits plating state

$SnCl_4$ g/L	E(vs SCE)V	Current/A
10	-0.187	$4.998\times e^{-5}$
15	-0.161	$1.019\times e^{-5}$
20	-0.144	$4.454\times e^{-6}$
25	-0.138	$3.758\times e^{-6}$
30	-0.15	$7.556\times e^{-6}$
35	-0.177	$6.116\times e^{-6}$

Conclusions

Ni-Sn-P alloy with different Sn content are prepared by electrless plating. The results show that with increasing $SnCl_4$ concentration in baths, the deposition rate, hardness, resistance corrosion of the coating show an upward trend. If $SnCl_4$ concentration is too higher, the above will be decreased. After heat treatment, the hardness will be improved a little. The deposition rate tops $9.98mg\cdot cm^{-2}\cdot h^{-1}$, the hardness is above 500Hv, and the highest corrosion current is $4.998e^{-5}$. The content of tin is 2.5 to 4.1 percent in the coatings. Ni-Sn-P alloy the surface morphology of deposits is cystiform structure, smooth, the grain of crystal and good properties.

Acknowledgements

We thank for supporting from Henan key laboratory of non-ferrous metal materials science and processing and SRTP of Henan University of Science & Technology (No. 2012011).

Reference

[1]Hu Yong-jun, Xiong Ling, Meng Ji-long. Applied Surface Science Vol.253(2007),p.5029.
[2]G. Liu, L. Yang, L. Wang, S. Wang, et al. Surface and Coatings Technology,Vol.204(2010),p. 3382.
[3]BalarajuJ N,Millath S,Anjana J.[J].Journal of Alloys and Compounds,436(2007):p319.
[4]Y. Liu, Q. Zhao.Applied Surface Science 228 (2004),p.57–62.
[5]Zhang W X,Jiang Z H,Li G Y,et a1. Surface＆Coating Technology,202(2008):p2570.
[6] Bangwei Z, Haowen X .Mater Sci Eng A 281(2000):p286.
[7]Xia Z P, Lin Y Z Q. Materials Characterization,59(2008):p1324.
[8]Yu J K, Jing T F, Yang J, et a1. Journal of materials processing technology,209(2009):p14.

Advanced Materials Research Vols. 989-994 (2014) pp 407-411
© (2014) Trans Tech Publications, Switzerland
doi:10.4028/www.scientific.net/AMR.989-994.407

Application of Environmental Rubber in Concrete Road Engineering

Rui Yang

JiangSu Jianzhu Institute, Xuzhou, 221116,China

Keywords: Environmental rubber; ANSYS software; Numerical simulation; Ultimate bearing capacity; Secondary development; New materials

Abstract. Environmental rubber concrete is a new building material, which can improve the construction quality of road drainage tube in road engineering and achieve effect of keeping warm and radial anti deformation. In order to study the physical properties of environmental rubber concrete, we use methods of experiment and numerical simulation to test mechanical parameters and effect of thermal insulation of concrete. Through the experiment we obtain the relation between ultimate bearing capacity and temperature. We use the software of ANSYS to secondary development on c numerical calculation, and establish a mathematical model of road drainage tube. Through the numerical simulation we get the temperature distribution and the radial strain nephogram of environmental rubber concrete. It provides a new method to study new materials in road engineering.

Introduction

Environmental rubber concrete is a new building material, due to the double mechanical properties of concrete and rubber, which makes the mechanical properties of the material complicated. ANSYS is professional structural analysis software, which is widely used in the strength calculation and analysis in road engineering [1,2]. In this paper we compare the results of experiment and numerical simulation to study the mechanical properties of rubber concrete[3,4]. The basic process is shown in Figure 1.

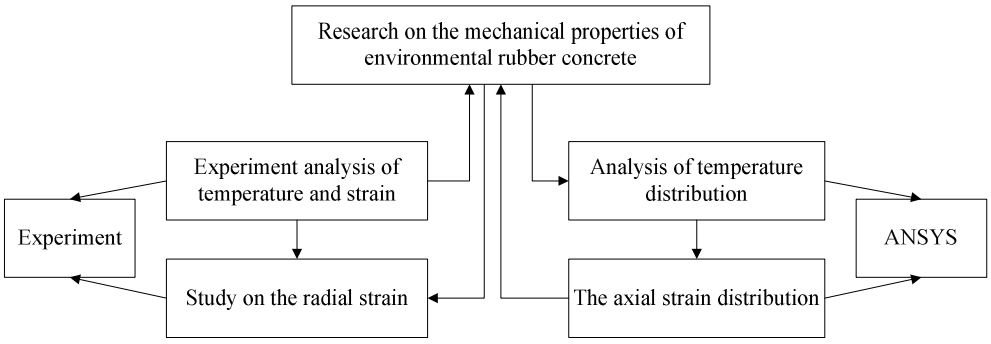

Fig. 1 Flow chart of road environmental rubber concrete

Mathematics Model of Rubber Concrete Road Drainage Pipe and the Design of ANSYS Algorithm

We use mechanics of structure and material to study the mechanics properties of rubber concrete drainage pipeline, and establish reasonable stress and strain model [5, 6]. Assume that the strain of pipeline is *0*, namely $\gamma_{xz}=0,\gamma_{xz}=0$. So the geometric equation can be written as:

$$\begin{cases}\dfrac{\partial b}{\partial z}+\dfrac{\partial c}{\partial y}=0\\ \dfrac{\partial a}{\partial z}+\dfrac{\partial c}{\partial x}=0\end{cases}. \tag{1}$$

If $(a)_{z=0}=0$, $(b)_{z=0}=0$, so we can get:

$$a=-z\frac{\partial c}{\partial x}, b=-z\frac{\partial c}{\partial y}. \tag{2}$$

The three stress zero point in drainage pipe can be written as the partial differential equations as shown in the formula (3).

$$\begin{aligned}\delta_x &= \frac{\partial a}{\partial x}=-z\frac{\partial^2 c}{\partial x^2}\\ \delta_y &= \frac{\partial b}{\partial y}=-z\frac{\partial^2 z}{\partial y^2}\\ \lambda xy &= \frac{\partial a}{\partial y}+\frac{\partial b}{\partial x}=-2w\frac{\partial^2 c}{\partial xy}\end{aligned} \quad . \tag{3}$$

If the value of σ_w can be neglected, the expression of drainage pipe strain can be written as shown in formula (4).

$$\begin{aligned}\delta_x &= \frac{\sigma_x}{E}-\lambda\frac{\sigma_y}{E}\\ \delta_y &= \frac{\sigma_y}{E}-\lambda\frac{\sigma_x}{E}\\ \delta_{xy} &= \frac{2(1+\lambda)}{E}\tau_{xy}\end{aligned} \quad . \tag{4}$$

The stress components can be expressed as:

$$\begin{aligned}\sigma_x &= -\frac{E}{1-\lambda^2}z\left(\frac{\partial^2 c}{\partial x^2}+\mu\frac{\partial^2 c}{\partial y^2}\right)\\ \sigma_y &= -\frac{E}{1-\lambda^2}z\left(\frac{\partial^2 c}{\partial y^2}+\mu\frac{\partial^2 c}{\partial x^2}\right)\\ \tau_{xy} &= -\frac{E}{1+\lambda}c\frac{\partial^2 c}{\partial xy}\end{aligned}. \tag{5}$$

After establishing the stress-strain mathematical model of environmental concrete drainage pipe, we can use ANSYS command stream to develop the model of tress-strain. The main program of command stream is as follows:

```
ET, 1, BEAM3
MP, EX, 1, 207E9
MP, NUXY, 1, 0.3
R, 1, 0.001, 0.020833, 0.05
E, 1, 2 E, 2, 3
EPLOT
ELIST  FINISH  /SOLU
ANTYPE, STATIC
OUTPR, BASIC, ALL
D, 1, UX, 0, , , , , UY, ROTZ
D, 3, UY, 0
F, 2, FY, -200
SOLVE FINISH
/POST1
```

```
PLDISP,2
PRDISP
……
```

Study on the Performance of Rubber Concrete Experiment and Numerical Simulation

In order to verify the effectiveness and reliability of strain-stress mathematical model and the structural analysis algorithm designed in second part, we use the method of materials mechanics and ANSYS numerical simulation to study the performance of rubber concrete materials [7, 8]. By comparing the results of experiment and numerical simulation, it verifies the accuracy of the model.

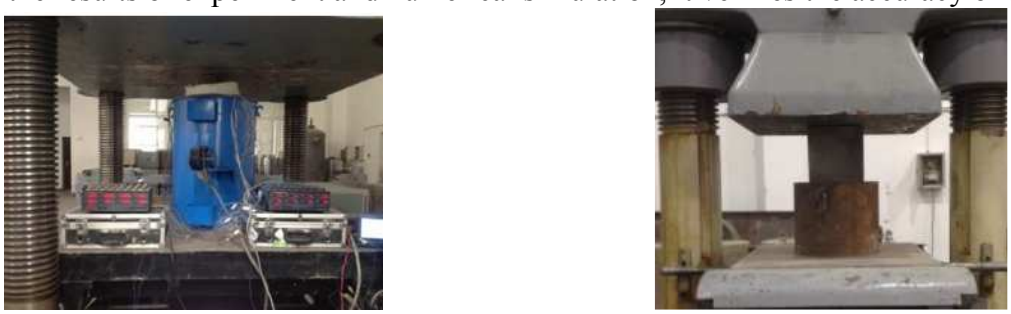

Fig. 2 Experiments of temperature and the tensile

Figure 2 shows studying the mechanical properties of rubber concrete materials by step loading at different temperatures, finally we get the ultimate bearing capacity bearing capacity of rubber concrete materials under different temperature conditions. The results are as shown in Table 1.

Table 1. Results of ultimate bearing capacity

No.	Temperature ($^{\circ}C$)	Ultimate bearing capacity (t)
1	10	185.2
2	20	177.3
3	30	165.8
4	40	158.2

Table 1 shows ultimate bearing capacity of rubber concrete. From the table we can see, the ultimate bearing capacity is different under different temperature, and along with the temperature increasing it gradually decrease. In order to increase the reliability of experimental data, we use ANSYS to do numerical calculation on the mechanical properties of rubber concrete. Firstly we establish mathematical model of drainage tube in road engineering, and modify the model name, do grid division. The structure grid is as shown in Figure 3.

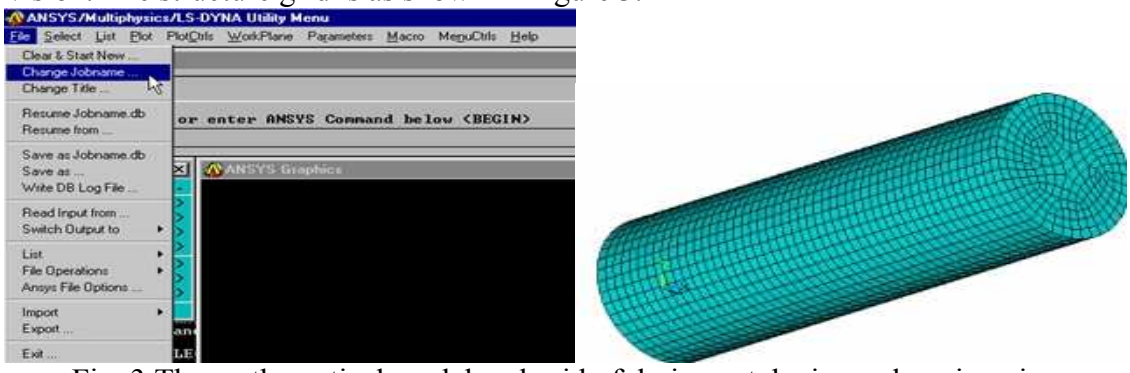

Fig. 3 The mathematical model and grid of drainage tube in road engineering

As shown in Figure 3, after establishing the mathematical model of drainage pipeline we can set the pretreatment process of numerical simulation. The pretreatment includes materials set, boundary conditions loading and calculation initialization. Through calculation we can use Figure 4 to view the ANSYS operation results.

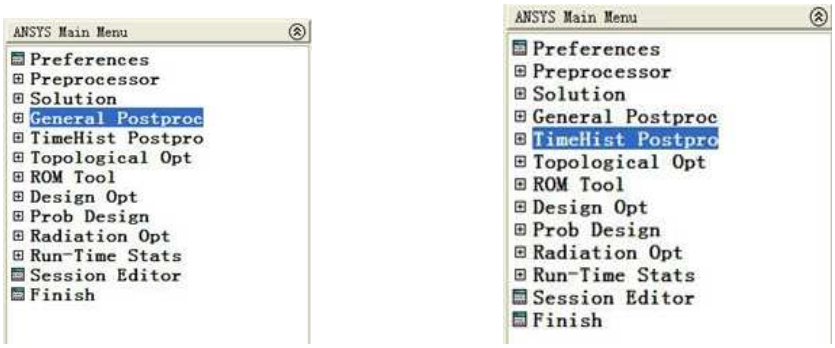

Fig. 4 View window settings of ANSYS calculation result

Figure 4 shows the view setting of ANSYS calculation results. First entering the general-purpose processor or time series processor, we use cloud view, curve drawing and form drawing to display the results [9]. Through the numerical simulation we get the temperature distribution of drainage pipe as shown in Figure 5.

Figure 5 shows the temperature distribution of drainage obtained in road engineering by ANSYS numerical simulation [10]. From it we can see, in the protection of outer rubber concrete layer, heat preservation effect of pipeline is good, tube inside temperature is delaminating and maintains a certain number of value.

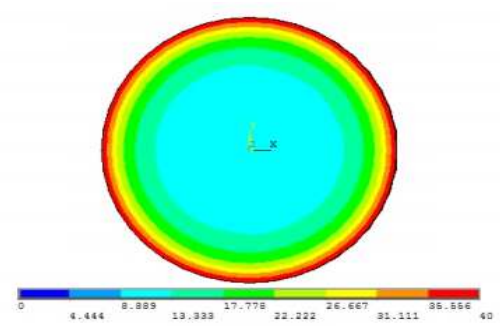

Fig. 5 Temperature nephogram of concrete pipe

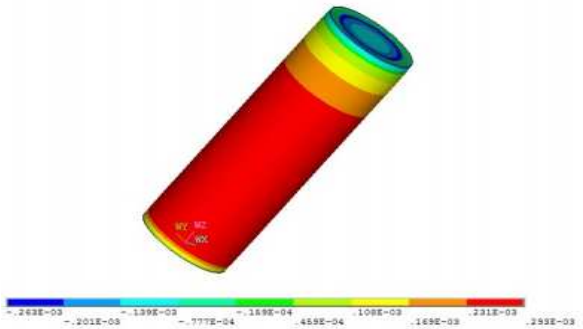

Fig. 6 The radial strain of pipeline

Figure 6 shows the radial stress distribution of road drainage pipe calculated by ANSYS software. From it we can see the radial strain of pipeline is mainly concentrated in the external, internal stress is small, which shows that the rubber concrete protects pipeline effectively and the internal strain of pipeline is reduced to a minimum.

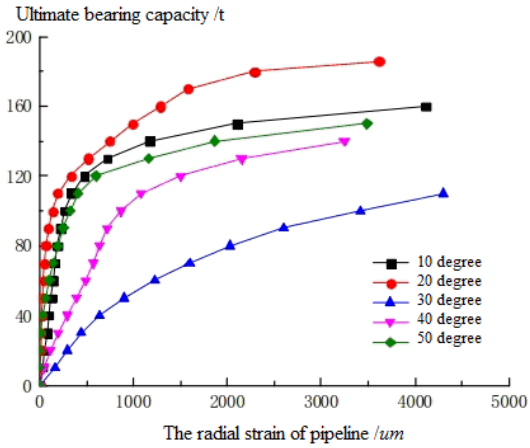

Fig. 7 The calculation results of strain changing with temperature

Figure 7 shows the ultimate bearing capacity curve of the pipeline obtained by ANSYS numerical simulation [11]. From the curve we can see, with the increase of temperature, ultimate bearing capacity of rubber concrete decreases, this is because that the changing temperature changes the mechanical properties of rubber. The numerical results are consistent with the experimental results.

Summary

In this paper we use the experimental methods to test the mechanical properties of environmental rubber, establish mathematical model of rubber concrete, and obtain the mechanical properties curve changing with time by experiment. We use the command stream programming to do secondary development on the performance of ANSYS software, and establish numerical simulation model of road drainage tube. Through the numerical simulation we calculate the temperature distribution and the radial strain nephogram of environmental rubber concrete. By comparing the results of experiment and numerical calculation we obtain the stress-strain nephogram, ultimate bearing capacity changing with time. We find the ultimate bearing capacity decreases with the increase of temperature, and the experiment is consisted with numerical simulation.

Acknowledgments

The work was supported by a provincial project with the project number 2013k4-39 and the project name Research on Application Technology of Rubber Concrete of Environmental Protection in the Road Engineering.

References

[1] Fu Jianhong, Gong Longxiang, Hu Shunqu et al. Analysis of horizontal well casing friction based on ANSYS [J]. Oil drilling production technology, 2010(7): 34-38.

[2] Li Tianning. Key technology practical handbook of modern petroleum drilling engineering [M]. Petroleum industry press, 2010: 22-34.

[3] Zhang Xiaoli, Li Dejian, Li Mingpeng. Application of ANSYS software secondary development [J]. Journal of Chongqing Institute of Technology, 2012(2): 56-59.

[4] Zhao Gaofeng, Song Hongwei.ANSYS secondary development technology and its application in the cavern stability analysis [J]. West China Exploration Engineering, 2011(2): 63-66.

[5] Luo Yangjun, Kang Zhan, Deng Zichen. Topological structure optimization of robust under different conditions [J]. Journal of mechanics, 2011(1): 227-234.

[6] Li Yan, Zan Meisen, Xiong Jingang. Experimental study on the bearing capacity of thin-walled steel tube concrete column compression axis [J]. Theory studying, 2012(11): 47-49.

[7] Teng Jinguang, Yu Tao, Huang Yulong, Dong Shilin, Yang Youfu. Experimental study and theoretical analysis on mechanical performance of the composite column FRP pipe-concrete-steel tube [J]. Steel building structure, 2012, 8(5): 1-7.

[8] Wang Zhibin, Tao Zhong. Bending component performance test on bending component performance test on of FRP-concrete-steel [J]. Industrial construction, 2011, 39(4): 5-9.

[9] Ren Zhigang, Hu Shuguang, Ding Qingjun. Sunshine temperature analysis of steel tube expansion concrete [J]. Journal of Wuhan University of Technology, 2012(11): 99-102.

[10] Ren Zhigang, Hu Shuguang, Ding Qingjun, Lv Linnv, He Yongjia. Thermal strain analysis of steel tubes expansion concrete under seasonal temperature difference [J]. Journal of Wuhan University of Technology, 2011(7): 43-45.

[11] Ren Zhigang, Hu Shuguang, Lu Zhean, Ding Qingjun. Sunshine temperature analysis of double legs round tip shape steel tubular concrete [J]. China Journal of highway and transport, 2012(3): 67-69.

Advanced Materials Research Vols. 989-994 (2014) pp 412-415
© (2014) Trans Tech Publications, Switzerland
doi:10.4028/www.scientific.net/AMR.989-994.412

Hot water extraction of corncob hemicelluloses to prepare composite films

Qingxue Yu[1,2], Guang Yu[1], Yuedong Zhang[1], Yefei Liu[1], Haisong Wang[1a], Fuqiang, Chu[2b]

[1]Key Laboratory of Biofuels, Qingdao Institute of Bioenergy and Bioprocess Technology, Chinese Academy of Sciences, Qingdao 266101, China

[2]Key Laboratory of Paper Science and Technology of Ministry of Education, Qilu University of Technology, Jinan, 250353, China

[a]email: wanghs@qibebt.ac.cn, [b]email: fqchu@126.com

Keywords: hot water extraction; corncob hemicelluloses; composite films

Abstract. In this study, corncob hemicelluloses were extracted by hot water to investigate its potential for film production. Extracted hemicelluloses were mixed with PVA 30 wt%, the prepared films had a smooth, uniform and continuous surface and dense cross section without the phase separation, as characterized by SEM. Besides, the mechanical properties and thermal characteristics tests showed that the films had a tensile strength of 4.6 MPa, elongation at break of 6.4%, and a nice thermally stability.

1. Introduction

Corn planting area in China is widely distributed: northeast, north China, northwest, southwest and southeast etc. Correspondingly, more than ten million tons of corncobs are generated in China every year[1]; these agricultural wastes are renewable, costless and widespread sources of chemicals. But in most cases, the lignocellulosic materials are left unutilized in harvested fields, burned for instance, which not only is an application with low added value but also can cause various environmental problems such as soil and water erosion.

There are many pre-extraction methods of hemicellulose , such as the physical, chemical or biological. As a physical method, hot water treatment shows some unique advantages over others: The whole process is environment-friendly for the reaction media is water and no chemicals, so the corrosion problems are avoided and no specific requirements for equipment[2]. Besides, process structure is simple due to get rid of handling neutralization sludges[3]. In brief, the utilization of hot water method to extract hemicellulose from biomass has broad application prospects. In recent years, increasing studies about the utilization of hemicellulose from agricultural biomass as new films are reported, due to the fact that these feedstock are from renewable and less expensive sources[4]. The hemicellulose films are environmentally friendly, and also naturally biodegradable[5]. It has wide range of potential applications in food packaging and other fields. However, the pure hemicellulose films have some problems in mechanical property. Addition of reinforcing agent and plasticizer can improve the film properties and transfer this potential into reality. Sárossy et al.[6] added sepiolite as reinforcing agent and poly (ethylene glycol) methyl ether (mPEG) plasticizer to rye flour arabinoxylan to enhance the properties of the composite films, and mechanical testing showed increases in film stiffness and strength with the above two additives addition. in order to

develop composite films with corncob hemicellulose and some new reinforcing agent and plasticizer, corncob hemicelluloses were extracted by hot water, then the films on structure, surface and mechanical properties were characterized.

2. Experimental

2.1 Raw material

Corncob were produced in east China, It was first dried in sunlight and then cut into small pieces (2~3 cm), and then the small pieces were milled into 0.18~0.85 mm particle size by a mill, air-dried again and stored until use.

2.2 Analysis of corncob

To analysis of corncob chemical components, the sample was subjected to acid hydrolysis sequentially with 72% and 4% sulphuric acid following standard methods[7]. The compositions of the corncob (%, w/w) are as follows: extract 4.10%, ash 2.15%, Klason lignin 12.50%, acid soluble lignin 1.43%, glucan 32.76%, xylan 34.90%, arabinan 1.08%, and acetyl groups 3.52%.

2.3 Pre-extraction of hemicellulose from corncob

Milled corncob samples and water were mixed in 250mL Parr reactor with the proportions of 1:14 (w/w). The reactor was then sealed and heated to 170 ^{o}C and final temperature was held for 30 min. After the extraction, the liquor were separated by filtration and concentrated to about 50mL under reduced pressure. Sequentially about 150 mL ethanol was added to the concentrated filtrates slowly at room temperature under constant stirring. The precipitated hemicelluloses were recovered by centrifugation, washed with 70% ethanol and freeze-dried.

2.4 Film casting

The ratios of the three components (corncob hemicelluloses, PVA, sorbitol) in composite films were 100:10:10, 100:20:10 and 100:30:10. The solution concentration was 10%. Corncob hemicellulose and sorbitol were mixed with distilled water for 1h at 90 °C under magnetic stirring, and then mixed with PVA solution dissolved in hot water. The film-forming solution was prepared under the heating and stirring at 90 °C for another 1h. Then, the film-forming solution was poured into a Teflon plate. The films were then left to dry under normal room conditions (23 °C, RH 50%) for two days and finally conditioned in a desiccator over magnesium nitrate hexahydrate for a minimum of 48 h prior to analysis.

2.5 Analytical methods

The film thickness was measured by using an Electronic Vernier caliper. The tensile strength and breaking elongation of films were measured using a Universal Testing Machine with a 20N load cell, the films strips were stretched at 20 mm x 6 mm. Microstructure analysis was conducted on a Hitachi S-4800 scanning electron microscope. The film thermal stability was tested with a Rubotherm Thermogravimetric Analyzer. Samples (about 80 mg) were heated from 50 to 600°C at a 10°C/min scanning rate, under nitrogen atmosphere.

3. Results and discussion

3.1 Apparent morphology of films

Fig. 1 The optimal composite hemicelluloses film

With a small amount of PVA and sorbitol, the hemicelluloses can form different films. Film thickness prepared by different amount of PVA showed no significant difference with an average thickness between 0.09~0.12mm. In Fig.1, the color of the composite hemicelluloses film is dark yellow due to a little lignin left. Since it was too fragile when the ratio of PVA to hemicelluloses was under 20%, PVA ratio increased up to 30% to improve the mechanical properties, Taking the cost and practicability into account, the optimal ratio of PVA to hemicelluloses was determined to be 30%.

3.2 Mechanical properties of the optimal films

The films are mainly characterized by their mechanical properties, which includes: tensile strength (TS), elongation at break (E) and elastic modulus (EM). Mechanical properties are an indication of the integrity of films on subjecting to stress conditions. TS is a measurement of film strength and is calculated by dividing the maximum force needed to break the films by the cross-sectional area of the films[8]. Whereas, E-value is an indication of flexibility of films. EM (also known as Young's modulus) is a measurement of stiffness of the films[9].

As the stress-strain curve shown in Fig. 2, the film had a high EM values, indicating that the film had a certain degree of rigidity. With the PVA and sorbitol addition, the composite hemicelluloses film showed a TS of 4.6 MPa, E-value of 6.4%. Mechanical Properties were affected not only by process conditions, but also by different types and compositions of hemicelluloses. In this study, the hemicelluloses used is extracted with hot water method, which was born to have a lower polymerization degree and a shorter molecular chain than hemicellulose extracted by other methods, such as the alkali pretreatment method, then resulting in a lower adhesive strength of intermolecular. So at the macro level, the TS value of films was relatively low.

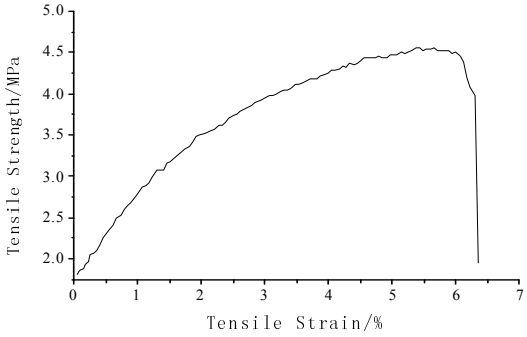

Fig. 2 The stress-strain curve of films

3.3 Microstructure Characteristics

The composite hemicelluloses films were smooth, semitransparent. Fig. 3 shows micrographs of the surface and cross-section areas of films. The outer surface image showed that the films had a uniform and continuous surface, and the cross-section areas showed dense, homogeneous structures without the phase separation. All of this indicated that the hemicelluloses, PVA and sorbitol had a good biological compatibility.

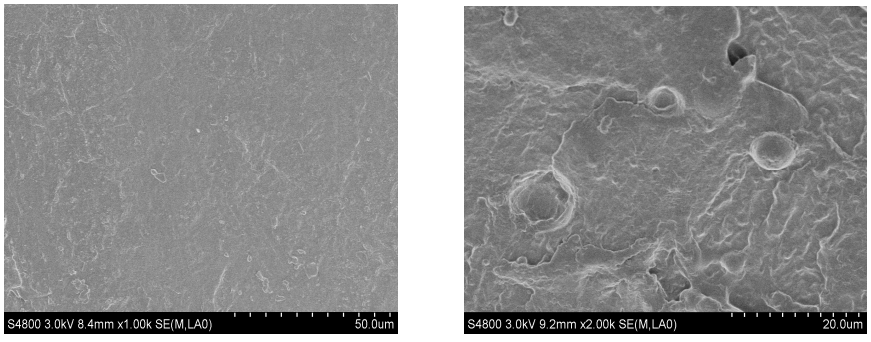

Fig. 3 The surface (left) and cross-section (right) areas SEM images of films

3.4 Thermal Characteristics

The thermogravimetric curves of the composite hemicelluloses films are showed in Fig. 4. The weight loss in the temperature range of 50–190°C was assigned to the evaporation of water from the samples. The decomposition temperature of films began at 190°C, suggesting intercomponent compatibility resulted in a strongly interacting system. The biggest Weightlessness rate range is 210°C ~310°C. These decomposition stages could be ascribed to backbone scission and following fragmentation of hemicelluloses and the additive. This high temperature illustrated that the composite hemicelluloses films is thermally stable.

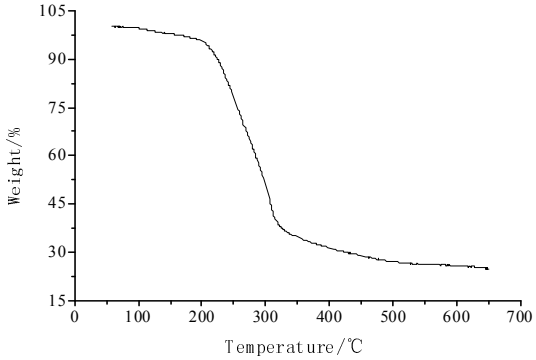

Fig.4 Thermograms of the films

4. Conclusion

Agricultural waste such as corncob can be obtained in large quantities every year. However, most of the corncob is burnt in the fields which can cause environmental problems. Corncob hemicelluloses were extracted by the hot water treatment method and showed that the corncob hemicelluloses has a potential for production of films. Adding 30% PVA and 10% sorbitol to the hemicelluloses, the components can form a continuous films. The composite hemicelluloses films were smooth, semitransparent. In addition, it showed a TS of 4.6 MPa, E-value of 6.4%, and a nice thermally stability.

Acknowledgements

We are grateful for the support of the Natural Science Foundation of China (No. 21206184 and 31370582), the National High Technology Research and Development Program (“863” program) of China (No. 2012AA022301).

References

[1] S. Miura, T. Arimura, N. Itoda, L. Dwiarti, J. B.Feng, C. H. Bin, M. Okabe: J Biosci Bioeng. Vol. 97 (2004), p.153
[2] G. Garrote, H. Dominguez, J. C. Parajo: Originalarbeiten Originals Vol. 57(1999), p, 191
[3] G. Garrote, H. Domınguez, J. C. Parajo: Process Biochem.Vol.36 (2001), p, 571
[4] H. A. Ruiz, M. A. Cerqueira, H. D. Silva, R. M. Rodríguez-Jasso, A. A. Vicente, J. A. Teixeira: Carbohyd Polym Vol.92(2013), p, 2154
[5] S. H. Imam, P. Cinelli, S. H. Gordon, E. Chiellini: J Poly Environ. Vol. 13(2005), p, 47
[6] Z. Sárossy, T. O. J.Blomfeldt, M. S. Hedenqvist, C. B. Koch, S. S. Ray, D. Plackett: Appl Mater Inter. Vol, 4(2012), p, 3378
[7] NREL/TP-510-42618, US: National Renewable Energy Laboratory, 2008
[8] J. H. Han, G. H. Seo, I. M. Park, G. N. Kim, D. S. Lee: J Food Sci. Vol.71(2006),p,290
[9] B. Rajeev, A. Nurulismah, H. Rozman: J Food Sci. Vol. 119(2013), p,707

Advanced Materials Research Vols. 989-994 (2014) pp 416-419
© (2014) Trans Tech Publications, Switzerland
doi:10.4028/www.scientific.net/AMR.989-994.416

Analysis of the atmospheric particles governance based on aerosol hygroscopicity

Tianyu Sun[a], Qingyang Wang[b], Jian Zhang[c] and Jianxing Ren[d]

College of Energy and Mechanical Engineering,Shanghai University Of Electric Power, Yangpu,Shanghai, 200090, China

[a]suntianyu588@126.com,[b]397646509@qq.com,[c]jinhanlin6330@126.com,[d]ren608@163.com

Keywords: Atmospheric particulates; Aerosols hygroscopic; Analysis

Abstract. With the rapid development of economy and the acceleration of the process of city, the problem of the atmospheric particulates is getting more and more serious which has severe impact on human health. Consequently the atmospheric particulates weather management has become a very realistic and an urgent problem to solve. The atmospheric particles mainly consists of water soluble aerosol and non water soluble aerosol. For the water-soluble aerosol should be removed by aerosol hygroscopicity, and for non water soluble aerosol by method of atmospheric water vapor liquefied or artificial humidification, making the small water droplets in the air further increase. So the water vapor can absorb non water soluble aerosol, through the settlement removal.So the utilization of these principles can achieve the purpose of absorbing the atmospheric particulates in the air.

Introduction

Since the 1950s, although the fog-haze phenomenon has often occurred around the world, but in China it happened rarely. However, in recent years in our country the degree and frequency of occurrence in the winter season has increased significantly. Especially in 2013, a wide range of national severe haze caused by concentration of the atmospheric particulates in the air persistently elevated, not only the transportation, but also have a serious impact on public health. Meanwhile, fog-haze also have adverse effects on agriculture. Research shows that too much atmospheric particulates make the decrease of crop yields up to 25%. When he talked about the problem of air pollution control, Premier Li Keqiang emphasized that though the fog-haze problem solving requires a long-term process, but we must do something[1]!

The atmospheric particulates concentration to rise is an anthropogenic pollution phenomenon caused by human economic activity. The green GDP accounting results issued by Ministry of Environmental Protection show that from 2004 to 2009, the cost of environmental pollution has increased from 511.8 billion yuan to 970.1 billion yuan, indicating that China's economic development environment pollution costs continue to rise[2]. At present, in China the cause of atmospheric particulates formation is mainly by industrial sources, most of which are coal-fired industrial and vehicle emissions, in which coal-fired for power generation is the most, taking up about half of the total coal consumption. The eighteen meeting of the Communist Party proposed the development goals of "two hundred years". To achieve these two objectives, we still need to consume large amounts of energy, causing more serious environmental pollution. Therefore, we should vigorously develop new energy technology, pollutant removal technology.

Definition and composition of the atmospheric particulates

The atmospheric particulates are the general term for various solid and liquid particles in the atmosphere. The grains constitutes a large relatively stable suspension system dispersed evenly in the air, namely aerosol system. Particle size is generally in the range of 0.01~100 microns.The main cause of atmospheric particulates problem in our country is serious aerosol pollution. At present, the subjective reasons of formation of atmospheric particulates are pollutant emissions. Therefore we should intensify the control of pollutant emissions and carry out the governance of air pollution.

The atmospheric particulates has very complex composition, including hundreds of particulates, such as mineral grains, salt, sulfate, nitrate, organic aerosol particles. Mineral aerosols (including

soot, dust and urban fugitive dust, etc.) are the largest content of atmospheric particulates component in China, accounting for about 35%. Sulfates and organic carbon aerosols are two other large components, respectively, accounting for about 15%. These three categories of aerosols contribute approximately 70% of the atmospheric particulates mass concentration, while nitrate about 7%, ammonium about 5%, black carbon aerosols only about 3.5%[3]. Therefore, the main component of atmospheric particulates is aerosol particle. When aerosols remain in the atmosphere, it is formed by the nucleation mode particles aerosols through coagulation, aggregation, adhesion and other processes. It absorbs a variety of gaseous and solid pollutants in the air. From the perspective of harm to human health, the particles whose size are larger than 2 μm mainly deposited in the human nose and throat, while those less than 2 μm are mostly deposited in the bronchi and alveoli, causing great harm to the human body, resulting in our more concern[4]. Therefore, the atmospheric particles mainly consists of water soluble aerosol and non water soluble aerosol. For the water-soluble aerosol should be removed by aerosol hygroscopicity, and for non water soluble aerosol by method of atmospheric water vapor liquefied or artificial humidification, making the small water droplets in the air further increase. So the water vapor can absorb non water soluble aerosol, through the settlement removal.

Liquefied conditions of water vapour

Liquefying water vapour need to have sufficiently low temperature heat source. At first the low temperature heat source absorbed the sensible heat, cooled the water droplets to its condensation temperature, then the water vapour become saturated vapor. At this temperature, it continued to absorb its latent heat of condensation, then the saturated vapor convert into fog droplets. This is the general liquefaction of water vapour. Obviously, a sufficiently low temperature heat source is important for liquefying the water vapour[5].

If the temperature of the water vapor is higher than its critical temperature, regardless of how much pressure is applied, it will not be liquefied. So the necessary condition of the liquefaction is the temperature below its critical temperature, while the sufficient condition is that the pressure at the temperature is greater than the saturation vapor pressure. This is because when the water vapor temperature decreases, it will reduce the kinetic energy of molecules, weaken the molecular repulsion; when the pressure increases, it will shorten the distance between molecules, lead the mutual attraction between the molecules increasing. When the mutual attraction is greater than repulsion, in other words, when the attraction plays a leading role, the water vapour will liquefy. Therefore, if the water vapour is at or below its critical temperature, the appropriate increase in pressure will convert it into the liquid from the gas. If the temperature is higher than the critical temperature, the kinetic energy of molecules is large enough to overcome the attraction between molecules. Even if great pressure is applied to shorten the distance between molecules, the repulsive force is greater than intermolecular attraction, so the water vapour cannot be liquefied[6]. Therefore, the liquefied condition of water vapour is at or below its critical temperature.

In conclusion, cooling and pressing are both important and principal physical process to liquefy the water vapour. And, of course, in addition to the temperature and air pressure, air circulation is also influential to liquefaction. The appearence of dew in the summer morning, for instance, is related to whether there was a wind during the night, and dew cannot be formed if it was rather windy last night. It is thus clear that, the more circulation of the air, the less possible that liquefaction will happen.

The feasibility of water-soluble aerosol hygroscopic growth

Study of aerosol hygroscopicity is at the basic position in atmospheric particulate control. Hygroscopicity is the main properties of aerosols, which is the water absorbing capacity of aerosol when the relative humidity of the ambient environment increases. Relative humidity changes are the main factors affecting aerosols hygroscopicity, when the relative humidity reaches the deliquescence point, aerosols absorb a large amount of water leaving the particle size become large. At high relative humidity, hygroscopic aerosols such as small crystals deliquesce into larger droplets as a result of moisture absorption, and then they can be quickly removed from the atmosphere through some methods (such as subsidence)[7].

Fig. 1 was the Cora curve of water-soluble particles hygroscopic growth. Seen from the figure, when ambient vapor pressure is less than the critical value, even though dry hygroscopic particles can grow, they cannot exceed the critical radius scale but only form water vapour. In other words, if the haze drop wants to become droplet through hygroscopic growth, there must be a sufficient degree of supersaturation over the hump, which is not easy to achieve in nature. Therefore, we must conduct hygroscopic growth through artificial means in order to over the supersaturation hump to form droplets.

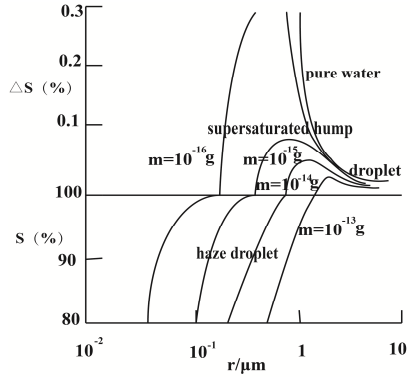

Fig. 1 The Cora curve of water-soluble particles hygroscopic growth

According to article written by GAO Jian et al.[8] published in Inter-comparison of WPS-TEOM-MOUDI and Investigation on Particle Density, we got the particles density within the scope of different size in Shanghai and Beijing.Shanghai inTable 1,for example:

Table 1. The density of particles within different size in Shanghai

The lower limit of particle size/μm	The upper limit of particle size/μm	Density/g.cm^{-3}
0	0.32	0.81
0.32	0.56	6.15
0.56	1.00	1.54
1.00	1.80	1.22
1.80	3.20	0.92
3.20	5.60	2.18
5.60	10.0	1.37

Then according to the size limit, we can calculate the particle average diameter size.According to $V = \frac{1}{6}\pi D^3$ and $m = \rho V$, it can be obtained in Table 2:

Table 2. The mass of particles within different size in Shanghai

The lower limit of particle size/μm	The upper limit of particle size/μm	Density/g.cm^{-3}	Mass/g
0	0.32	0.81	1.74×10^{-15}
0.32	0.56	6.15	2.74×10^{-13}
0.56	1.00	1.54	3.82×10^{-13}
1.00	1.80	1.22	1.75×10^{-12}
1.80	3.20	0.92	7.52×10^{-12}
3.20	5.60	2.18	9.72×10^{-11}
5.60	10.0	1.37	3.40×10^{-10}

Known from the Cora curve, with the increase of particle mass, the critical supersaturated hnmidity goes smaller, making it easier for hygroscopic growth. Mass of the haze particles from the table ranges from 1.74×10^{-15}g to 3.40×10^{-10}g, showing that the need of the critical saturationto is low. Analysis of the measured data shows that the extreme minimum relative humidity for fog existence is 91%[9]. However, when there is more water vapor in the air, some strong absorbent dry aerosol particles will absorb water, grow up. From the observation in North China, we can find that the aerosol particle size after absorb moisture will increase 20% ~60%[10]. Thus, humidification can increase particle size, decrease relative humidity, make it easier to convert into the droplet from the water vapour.

Conclusions

The structure of the energy consumption of China is mainly dominated by coal, fossil energy accounted for 92.7% of overall energy structure. Facing the situation of resource constraint tightens and serious environmental pollution, the transformation of the mode of development, optimizing the energy structure and adjustment of industrial structure is the only way to reduce the frequence of fog haze weather[11]. The eighteen Party's report also pointed out that, "the construction of ecological civilization, is the relationship between people's well-being, concerns national future long-term strategy. Placing the ecological civilization construction in a prominent position, the integration of economic construction, political construction, cultural construction in all aspects and whole process, and strive to build a beautiful China, realize the sustainable development of the Chinese nation."

The atmospheric particles not only have an adverse effect on human health, but also causes atmospheric low visibility, prone to traffic accidents, threat the safety of people. For the removal of atmospheric particulates by cooling, pressure or artificial humidification can make water vapor liquefy, and then increase the particle size, adsorption of non hygroscopic aerosol particles more. But for hygroscopic aerosol particles through the Rescorla curves, when reaching the critical relative saturation wetness, aerosols hygroscopic growth. Finally through the settlement, it achieve the purpose of absorbing the atmospheric particulates in the air.

Acknowledgments

This paper is partly sponsored by Shanghai Engineering Research Center of Power Generation Environment Protection (11dz2281700) and the Key Fund of Shanghai Science Technology Committee (13160501000).

References

[1] Wu Yuping, Zhang Miao, Wei Na, He Wei. Strengthen the comprehensive management of the environment and improving air quality[J].China WTO Tribune, 2013,(2)：81-84

[2] Ai Tieying ."Haze" governance need "combination"[J]. Environmental Economy, 2013,(3)：5

[3] Zhang Xiaoye,Sun Junying,Wang Yaqiang.The thinking about China atmospheric particulates causes and governance[J].Scientia Sinica ,2013,58(13)：1178-1187

[4] Zhang Ning. Advances in the analysis of the research and application of ion chromatography to aerosol water soluble[C].The first academic exchange chromatography in Midwest China Conference,2006：76-82

[5] Miao Hua,Zhang Hua.Process of gas liquefaction[J]. College Physics,2009,(8)：43-45

[6] Zhang Jihuai.Thermodynamic and molecular physics[M].Shijiazhuang:Hebei people's publishing house,1984：40-45

[7] Wang Xuanchen,Jian Hua,Wang Wei.Research status of hygroscopic properties of aerosol particles[J].China Powder Science and Technology,2010,16,(1)：101-107

[8] Gao Jian,Zhou Yang,Wang Jin,et al. Inter-comparison of WPS^{TM}-TEOM^{TM}- MOUDI^{TM} and Investigation on Particle Density[J]. Environmental Science,2007,28(9)：1929-1934

[9] Wu Dui .Re-discussion the difference between the urban's haze and fog[J]. Meteorology,2006, 32(4)：9-15

[10] Pan X L,Yan P,Tang J,et al. Observational study of influence of aerosol hygroscopic growth on scattering coefficient over rural area near Beijing mega-city[J]. Atmospheric Chemistry and Physics,2009,9(19)：7519-7530

[11] Wang Xin,He Qian.The haze weather induced reflection[J]. Ecological Economy, 2013,(4)：18-23

Advanced Materials Research Vols. 989-994 (2014) pp 420-424
© (2014) Trans Tech Publications, Switzerland
doi:10.4028/www.scientific.net/AMR.989-994.420

Effect of Ni on Corrosion Resistance of Weathering Steels in wet/dry Environments

Rui Liu[1,2,a], Xiaoping Chen[2,b] and Qingnan Shi[1,c*]

[1]School of Material Science and Engineering, Kunming University of Science and Technology, Kunming 650093, China;

[2]Centeral Iron and Steel Research Institute, Beijing 100081, China

[a]liurui6699@163.com, [b]chenxiaoping@cisiri.com, *Corresponding author: [c]shikust@vip.163.com

Keywords: Ni element, weathering steel, weight loss, rust, EIS

Abstract: Corrosion behavior of a low alloy steel A with 3% nickel content was studied by a wet/dry cyclic test. A commercial weathering steel Q450NR1 was used for comparison. The classical weight loss method was used to evaluate the weatherability of weathering steel, while the iron rust layers formed on weathering steel were analyzed by using SEM, XRD and electrochemical measurements. The results indicated that the corrosion resistance of steels A was better than that of commercial weathering steel Q450NR1 in the wet/dry cyclic test. The addition of Ni promoted the formation of α-FeOOH so as to improve the resistance of the rust. The EIS results indicated that the charge transfer resistance of steel A was bigger than that of steel Q450NR1.

Introduction

Metal corrosion is a serious problem, which exists in various fields of national economy and national defense construction[1]. So weathering steel has been widely used due to its excellent atmospheric corrosion resistance performance in atmospheres which results from that the alloying elements such as Cu, Cr, Ni, Si, P, etc. in the steel can promote to form a dense and adhesion stability protective film[2]. Nowadays, Ni plays an important role in the corrosion process of structural steel. The steel with Ni can make the selfcorrosion potential move to the positive direction, which increases the stability. The atmospheric exposure research results showed that the corrosion resistance in the sea side environment of the weathering steel with about 4 wt% Ni can be significantly improved[3]. Japanese scholars[4] did the reaches on the corrosion resistance of weathering steel with 3% wt% Ni in the coastal environment and they found that the grain was refined and the density was increased because of the enrichment of Ni in the rust layer. It was difficult for the chloride ion to get through the rust layer to the steel substrate resulting in the reduction of the corrosion rate of the weathering steel. I. Diaz[5] found that weathering steel containing Ni exposured in Marine atmospheric environment of medium chloride ion erosion after a year showed better corrosion resistance, and the higher of the Ni content the better corrosion resistance it had, It was because that the existing of Ni promoted the formation of the nano phase and superparamagnetism α-FeOOH in the inner rust layer, and the particles size of α-FeOOH was less than 15 nm, which can increase the density of the rust layer leading to the improvement of marine atmospheric corrosion resistance.

In this paper, the characteristics of the steel with Ni and conventional weathering steel were investigated in detail after wet/dry corrosion test. And the effect of Ni in improving the corrosion resistance of weathering steel was explored.

Experimental

Composition of tested steels. The steel A with 3 wt% Ni and commercial weathering steel Q450NR1 were used as tested steels and their chemical compositions are given in Table 1.

Table 1 Chemical composition of test materials (wt%)

steel	C	S	P	Mn	Si	Cr	Ni	Cu	Fe
A	0.075	0.0068	0.012	0.80	0.39	0.502	0.193	0.243	rest
Q450NR1	0.081	0.0058	0.0061	0.89	0.40	0.505	2.939	0.272	rest

Periodic immersion wet\dry cyclic corrosion test. The atmospheric corrosion resistance of weathering steels was evaluated through a periodic immersion wet/dry cyclic corrosion test, which was an accelerated corrosion test method under artificially simulated atmospheric environment. There were three parallel samples and the dimension of the sample was 60mm×40mm×5mm. Each cycle of wet/dry cyclic corrosion test lasted for 1 hour and included two stages: (1) immersing the specimens into 2 wt% NaCl aqueous solution for 12±1.5 min (2) drying the specimens immediately after immersion by heating lamps (the surface biggest temperature of the specimens was 70±10℃), subsequently holding the specimens in the testing chamber with a constant humidity of RH 70±5% at 45±2 ℃ totally for 48 min. The total corrosion test lasted for 96 cycles, i.e. 96 h. In this test, 2 wt% NaCl aqueous solutions were used to simulate a marine atmosphere, which is one of the typical atmosphere environments encountered during the application of weathering steels.

A chemical dissolution method was adopted to remove the corrosion layer, i.e. immersing the as-corroded specimen in a vigorously stirred specific diluted hydrochloricacid solution (500 ml HCl+500 ml distilledwater+3.5 g hexamethylenetetramine) for at least 10 min at room temperature[6,7].

Rust analysis. The powdered rust was scraped off from the rusted samples and the powdered rust samples were characterized by means of X-ray diffraction (XRD) to determine its composition. The XRD measurements were carried out using a Rigaku-D/max2000 diffractometer with a Cu Kα target under 50 kV, 250 mA and with a scanning range of 5-40° at a scanning speed of 2° min^{-1}. The rusted samples for cross-sectional analysis were observed using scanning electron microscopy (SEM). SEM observation was performed with a HITACHI_S-4300.

Electrochemical measurements. Polarization measurements were performed with a Model 273A-M398 Potentiostat/Galvanostat at a 0.332mV/s scan rate in 2 wt% NaCl solution while keeping the solution in 30±2 ℃ by using a water bath pot. It used a saturated calomel electrode (SCE) as reference and a Pt counter electrode. The scan range was -250 mV to 250 mV. The steel samples were manually sectioned into coupons of dimensions 10 mm×10 mm×3 mm, which served as the working electrode.

The electrochemical impedance spectroscopy (EIS) measurements were carried out over the frequency rage 100 kHz to 10 mHz with a 5 mV amplitude signal at open circuit potential. Before all the electrochemical experiments were performed, the specimens were kept in the solution for half an hour in order to attain a stable open circuit potential. Electrochemical impedance spectroscopy (EIS) measurements of the bare and rusted steel were carried out in 0.5 wt% NaCl solution.

Results and discussion

Corrosion rate of weathering steel. The corrosion rate of the steels in the artificially simulated marine corrosive atmosphere was determined by weighing the unaffected substrate part of each specimen before and after the tests. The weight loss rate could be determined using the following equation:

$$W = \frac{G_0 - G_1}{S \times t} \quad (1)$$

Where W is the weight loss rate (mg/(cm^2·h)), G_0 is the initial weight of the specimen before corrosion test (mg), G_1 is the weight of the as-corroded specimen after its surface corrosion product was removed (mg), S is the initially total surface area of the specimen(cm^2), t is the test time (h)[8].

Fig.1 presents the corrosion rate of the tested steels. It can be seen clearly that the weight loss of the steel A with 3% wt% Ni is much lower than that of Q450NR1, indicating that the effectiveness of Ni for using in salt-rich environment.

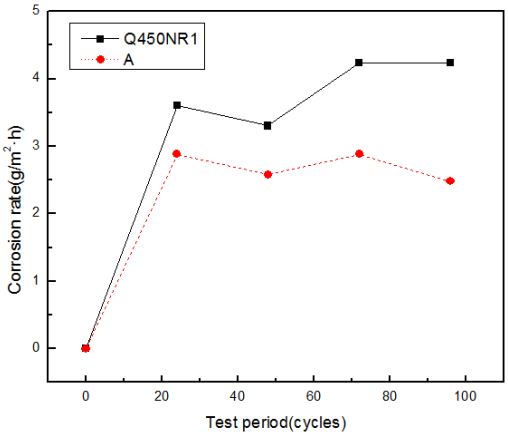

Figure 1.The corrosion rate of the tested steelswet/dry cycles

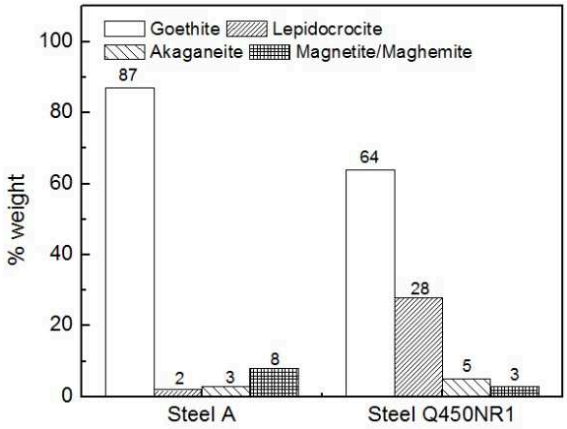

Figure 2. XRD semiquantitative analysis of corrosionproducts formed on steel A and Q450NR1

Composition and structure of rust layer. It can be seen from the XRD that patterns of the rust layers formed on the two steels after periodic immersion wet/dry cyclic corrosion for 72 h, crystalline corrosion products were formed. The rust layers consist of maghemite (Fe_2O_3), magnetite(Fe_3O_4), lepidocrocite(γ-FeOOH), goethite(α-FeOOH) and akaganeite(β-FeOOH). Fig.2 shows the constituents of steel A and Q450NR1 from a semiquantitative analysis. From this results it can be concluded that the additions of Ni could greatly promote the transformation of lepidocrocite(γ-FeOOH) to goethite(α-FeOOH). It has been reported that goethite (α-FeOOH) is non active in the corrosion process, and the γ-FeOOH phase acts as the oxidation agent that accelerates corrosion in a chloride-free environment[9,10]. Furthermore, the addition of Ni decrease the content β-FeOOH which plays the primary role in accelerating the corrosion rate[11].

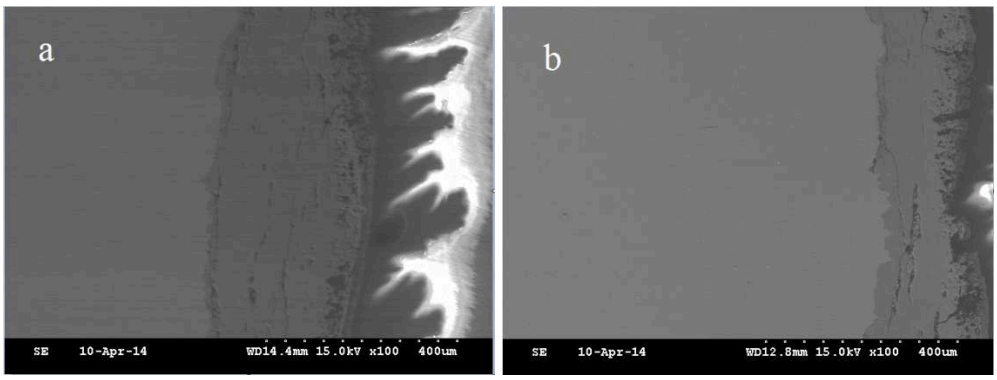

Figure 3. The cross-sectional morphologies of rust layers: (a) Steel Q450NR1 (b) Steel A

The cross-sections of the steels after 72 cycles of accelerated tests were observed by SEM, as shown in Fig.3 (a) and (b). It shows that the rust layers in these test steels all contain voids and /or micro-cracks. Both of them are composed of two parts: the loose outer layer and the dense inner layer. However, the inner rust layer of steel A is denser while the voids and micro-cracks are fewer. Meanwhile, the thickness of the rust layer of steel A is about 200-300μm thinner than that of steel Q450NR1 (400-500μm).

Electrochemical measurements. Fig.4 illustrates the polarization curves of the bare steel A and Q450NR1 in NaCl solution. It can be seen clearly that the selfcorrosion potential of the steel A is higher than steel Q450NR1. It indicates that the corrosion of steel A is harder to occur.

The Nyquist impedance plots of the two bare steels are shown in Fig.5, which show a well defined semicircle. The semicircle diameter of steel A is larger than that of Q450NR1 which means that the corrosion resistance of bare steel A is higher than that of bare Q450NR1.

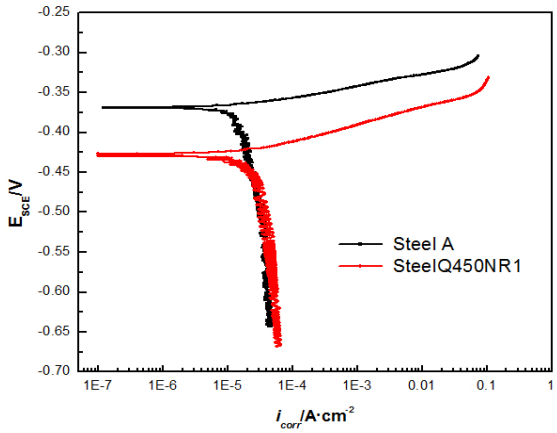

Figure 4. The polarisation of the bare steel of steelA and steel Q450NR1

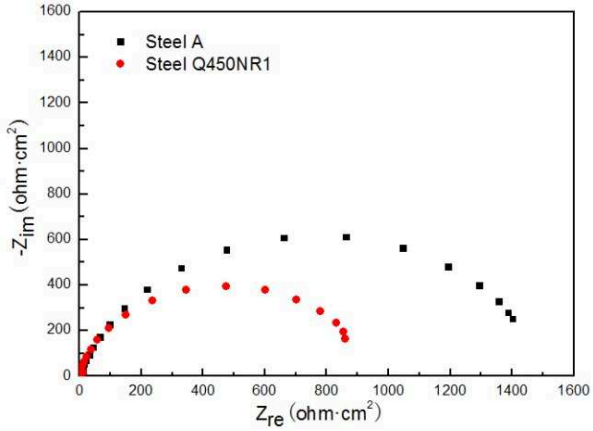

Figure 5. EIS for pre-corroded samples in a 0.5 mass% NaCl aqueous solution

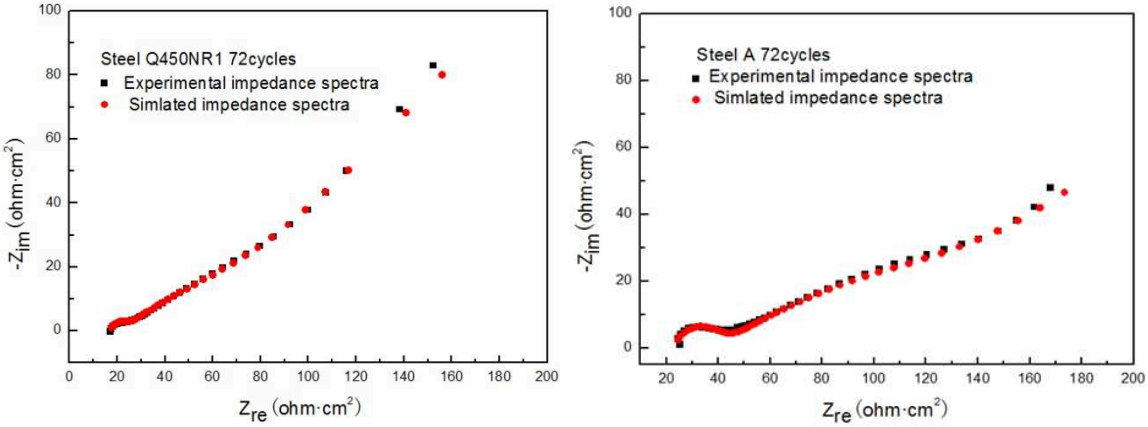

Figure 6. EIS of steel Q450NR1 and A that were subjected to a wet/dry cyclic test for 72cycles

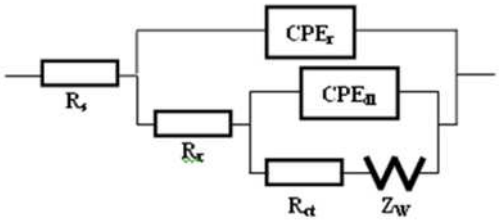

Figure 7. Equivalent circuit for specimens immersed in a 0.5 mass% NaCl solution

Fig.6 shows the Nyquist diagrams of steel A and Q450NR1 that were subjected to a wet/dry cyclic test for 72 cycles. The diagrams of the two steels are consisted of a depressed semicircle at the high frequency region and a long tail at the low frequency region. As can be seen in Fig.6, the impedance data can be well fit, marked by the rounded points, using the equivalent electrical circuit (as shown in Fig.7). There is no obvious interface between the outer rust layer and the inner rust layer. Besides, the inner rust layer can transform into the outer layer as the corrosion proceeds. So, for EIS fitting, it is considered the two layers as a whole. In this case, R_r and CPE_r represente the resistance and capacitance represente the rust layer, respectively. R_{ct} modeled the charge transfer resistance, CPE_{dl} describe the double layer capacity and W is used to model semi-infinite linear diffusion. The R_{ct} value of steel Q459NR1 is 125.2 Ω, while that of steel A is 186.4 Ω. The R_{ct} value of steel A increased to a certain degree, which implied that the charge transfer between the rust layer and the solution became more difficult. This can attribute to the increasement of the chemical activity stability α-FeOOH and the decreasement of the opposite effect γ-FeOOH, according to the XRD analysis above.

Conclusion

The weatherability of two weathering steels in wet/dry environments was discussed and the effect of Ni was clarified. The following conclusions can be drawn. The Ni can improve the corrosion resistance of the weathering steel obviously. It can improve the selfcorrosion potential of the bare steel. The addition of Ni can greatly promote the formation of chemical activity stability goethite (α-FeOOH), which increases the transfer resistance of charge and promotes the formation of a denser and adhesion rust layer, although there are the same crystalline corrosion products in the rust layer of different test steels.

Acknowledgements

This work was supported by the National Key Basic Research and Development Programme of China (No. 2014CB643300).

References

[1] Chunan Cao: The corrosion of materials of in natural environment of china(2005)

[2] Y.S.Choi, J.J.Shim, J.G.kim: Corrosion Engineering Section, vol. 61 (2005) no. 5, p.490-491.

[3] Lihong Liu, Huibin Qi, Yanping Lu, et al: Corrosion Science and Protection, vol. 15 (2003) no.2, p. 86-89.

[4] Hiroshi Kihira, Satoshi Ito, AhigeruMizoguchi, et al: Corrosion Engineering, vol. 49(2000), no. 1, p. 30.

[5] I. Diaz, H. Cano, D. de la Fuente, et al: Corrosion Science, vol. 76(2013), p. 348-360.

[6] J.G Castana, C.A. Botero, A.H. Restrepo, et al: Corrosion Science, vol.52 (2010), p. 216-223.

[7] Y.T. Ma, Y. Li, F.H. Wang: Corrosion Science, vol. 52(2010), p. 1796-1800.

[8] YuhaiQian, Chaohui Ma, Dun Niu, et al: Corrosion Science, vol. 74(2013), p. 424-429.

[9] M. Yamashita, H. Miyuki, Y. Masuda, et al: Corrosion Science, vol. 36(1994), p. 283-299.

[10] I.Suzuki, Y. Hashimoto: Journal of the Electrochemical Society,vol.127 (1980) no. 5, p.2210-2215.

[11] Yutai Ma, Ying Li, Fuhui Wang: Corrosion Science, vol. 51(2009), p. 1725-1732.

Advanced Materials Research Vols. 989-994 (2014) pp 425-428
© (2014) Trans Tech Publications, Switzerland
doi:10.4028/www.scientific.net/AMR.989-994.425

Corrugated Waist Rail Microstructure Evolution Simulation

MA Jin-Hong[1,a,] TAO Bin[1],YAO Xiao-Han[1]

College of Metallurgy and Energy, Hebei United University,Tangshan, 063009, China

[a]email: majinhong@126.com

Keywords: Microstructure; Corrugated Waist Rail;Rolling Process Simulation; DEFORM-3D

Abstract. Applying the research result of the whole corrugated web H-beam to rail structure, a new kind of rail structure, the corrugated web rail was generated. The special structure rail was successfully rolled in the Research Mill Institute of Yanshan University. Based on the finite element analysis software DEFORM-3D, the rolling process of corrugated waist rail is simulated. The miscrostructure evolution of rolling corrugated waist rail is analysed. The relationship between miscrostructure evolution and deformation are also analysed.

Introduction

The research result on the whole corrugated web H-beam is applied to rail structure[1][2], thus, a new kind of rail structure, which is corrugated web rail, is developed. The corrugated web rail is one important way to improve the economic properties of classical rail, and it has great significance on the economy and science. The research on the corrugated web rail is initiative in the world. The corrugated web rail has been successfully rolled in the Rolling Mill Research Institute of Yanshan University[3][4]. This is shown as Fig.1. Because forming corrugated web rail is complex, the corrugated web rail is only formed by the last pass. The corrugated waist rail has the characteristic of higher strengthen and stiffness. The rolled corrugated waist has the characteristic of higher productivity and higher precision.

FEM Model

The rolling simulation model is set up according to 18kg/m traditional rail. In rolling experiment, because the height of the vertical roller is small, the part of rail base of rolling piece was cut out to meet with the experiment condition. Before the last pass, the flange and web have been rolled down in the roughing stand and flanges edged respectively. The profile curves of upper and lower horizontal rollers for forming corrugated rail web are shown in the Fig. 2. The lower roller should be rotated with the degree of 180 / z, where z is the teeth number of the tooth-shaped roller, then the teeth of the upper roller and lower roller are matched correctly. The diameter of pitch circles is 269mm, the diameter of the addendum circle is 278mm and the diameter of the root circles is 260mm. The profile curve of each tooth is made up by three segments tangent arcs, two arcs diameters are 14.02mm and one is 22.68mm. The teeth number of these tooth-shaped rollers is 18. The profile of each tooth is also shown in Fig. 2. The phase angle degree of each tooth is 20°. The rolling model is shown in Fig. 3.

Microstucture Simulation Analysis in the Rolling Process

P1, P2 two points are selected from the corrugated waist rail, P1 is in the corrugated rail waist, P2 in corrugated rail waist on the junction of two wave. Applied Microstructure module of

DEFORM-3D, two points of microstructure are simulated. Variety of microscopic characteristics are shown in Fig.4. Grain size change in the rolling process is shown in Fig.5.

As shown in two figure of Fig.5, the first picture is grain, the second is grain and boundary, the third is grain boundary, the fourth is dislocation density.

As can be seen from Fig.5, dislocation density of P1 is bigger than that of P2, more grain boundary and grain size is smaller. Grain size difference of P2 is not bigger. The deformation of rail base is the least. The deformation of rail waist is bigger. But this is less than that of rail head. Therefore, the microstucture property of rail head is the best after the rolling process.

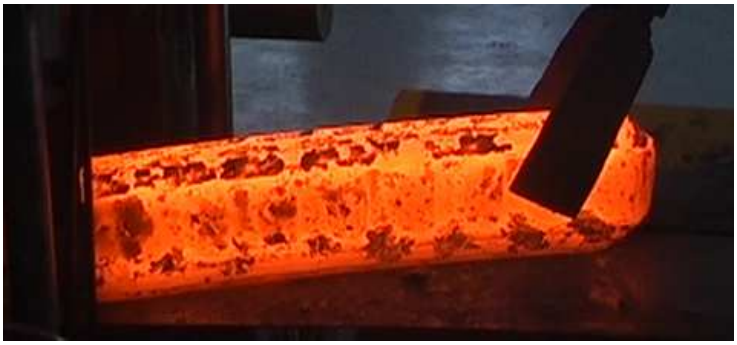

Fig.1 Workpiece after rolling

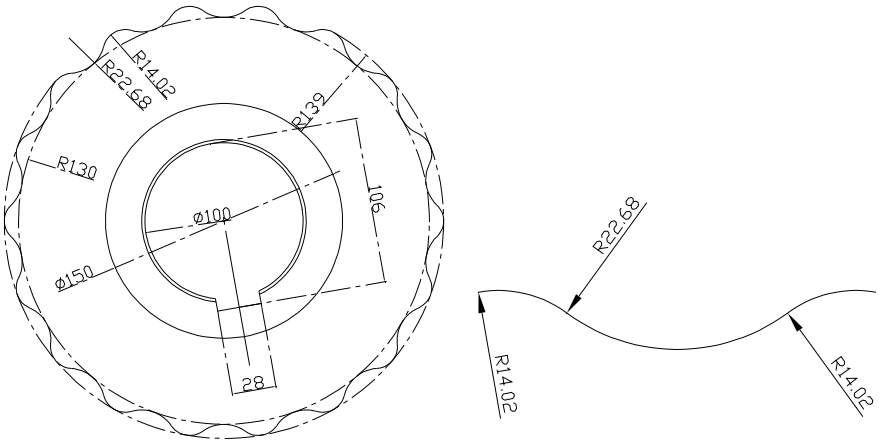

Fig.2 Profile curves of tooth-shaped roll

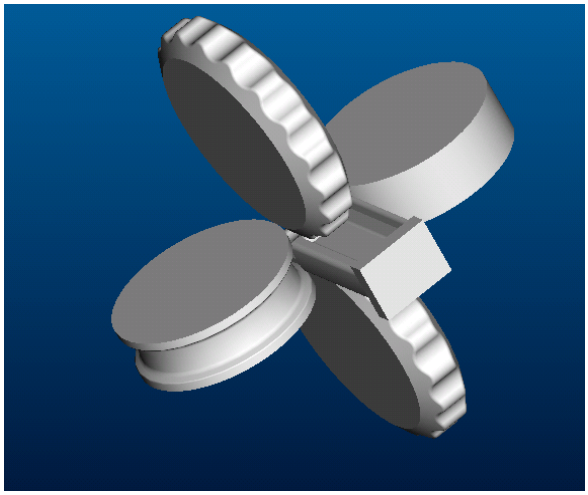

Fig.3 Rolling model

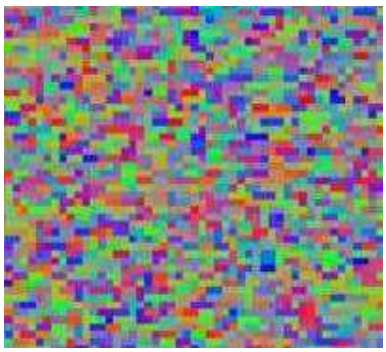

(a)Crystal orientation

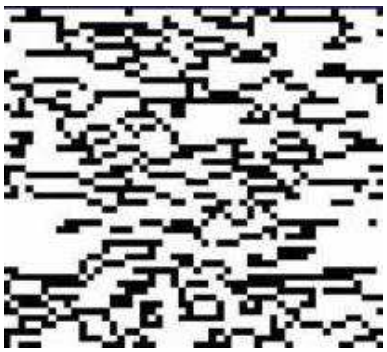

(b)dislocation density

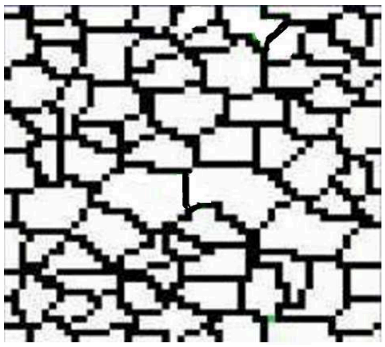

(c)grain boundary

(d)grain orientation ang boundary

Fig.4 Icons displays of different microstructure properties

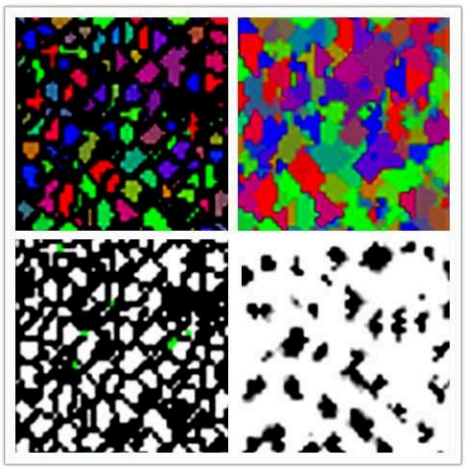

（a）P1

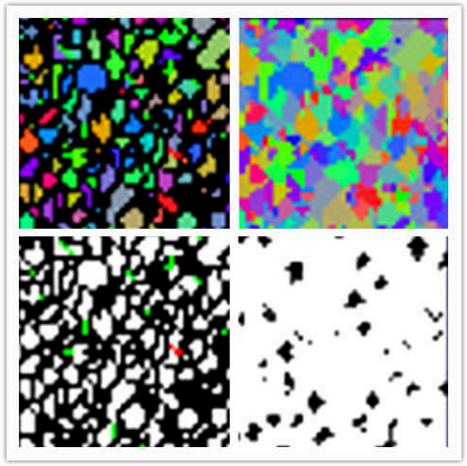

（b）P2

Fig.5 Changes in the process of rolling grain

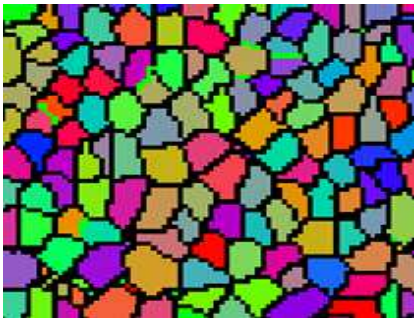

P1

P2

Fig.6 Grain structure and grain size of P1, P2 point

As can be seen fromFig. 6 , the grain size of P1 is 23.1 μ m, the grain size of P2 is 24.6 μ m. The grain size of rail head is the smallest, that of rail waist is the second and that of rail head is the biggest. The grain size of rail waist , rail head is smaller than that of rail waist of two wave link parts.

In the actual production of the corrugated waist rail , at the last pass of rolling traditional rail, a pass of rolling corrugated waist rail is increased. The deformation of rolling corrugated waist rail is bigger than that of rolling traditional rail. This lead to grainof corrugated waist rail is smaller than that of traditional rail. Whereas, because of smaller deformation in rail head and rail base, there are not bigger difference in the grain size of rail head and rail base between the two kind of rail.

Roller profile with corrugated waist rail is complicated in shape. Because of rolling rail waist complex, the deformation amount and deformation force in the elongation direction are different. The microstructures and mechanical properties of the corrugated waist rail after rolling is uneven.

The recrystallization of metals, usually nucleation at maximum distortionin caused by the plastic deformation, such as the grain boundaries, deformation band, area with large inclusion etc. In the deformation zone, when the strain reaches the critical strain, dynamic recrystallization will occur.

After recrystallization, due to internal stress generated by plastic deformationcan be eliminated completely and finally metal tends to a stable state. Between the frame, the metal will not be deformed. When the strain is larger than the critical strain but less than the peak strain, after a period of time, static recrystallization will occur. When the strain is larger than the peak strain but less than the steady-state strain,static recovery and metadynamic recrystallization accompanied by static recrystallization will occur,.when the strain is bigger than steady state strain, metadynamic recrystallization and a small portion of static recovery will occur.

Conclusion

In the production of corrugated waist rail process, in order to improve the mechanical properties, the reduction must be increased and other factors should be taken into consideration. The grain size emerging larger temperature region and rolling velocity region of the rail head should be avoid. To make new rolling rules, the relationship between the matching speed and rolling schedule should be taken into consideration and the factors of rolling temperature, finishing temperature should be also considered.

References

[1]Wenzhi Zhang ,Yanwen Li, Qingtian Zhou,et al. Hot rolling technique and profile design of tooth shape rolls-Development and research on H-beam with wholly corrugated web(WCW)(1).Journal of Materials Processing Technology, 2000,101 (1-3):111-115.

[2]Wenzhi Zhang ,Yanwen Li, Qingtian Zhou,et al. Buckling strength analysis of the web of WCW H-beam Development and research on H-beam with wholly corrugated web(WCW)(2).Journal of Materials Processing Technology,2000,101 (1-3):116-119.

[3] Bo.Wu，Fuqing Chang,Wenzhi Zhang. ng. Stress Analysis of Corrugated Waist Rail. Journal of Yanshan University.2003,27(3):278-282.

[4] Jinhong Ma，Wenzhi Zhang ,WeiChen. Numerical simulation and experimental study on corrugated waist rail with universal rolling .Journal of Plasticity Engineering. 2009,16(1):120-124.

Advanced Materials Research Vols. 989-994 (2014) pp 429-432
© (2014) Trans Tech Publications, Switzerland
doi:10.4028/www.scientific.net/AMR.989-994.429

The Recrystallization of Corrugated Waist Rail in the Rolling Process

MA Jin-Hong[1,a,] TAO Bin[1],YAO Xiao-Han[1]

College of Metallurgy and Energy, Hebei United university,Tangshan, 063009, China

[a]email: majinhong@126.com

Keywords: Recrystallization;Corrugated Waist Rail;Rolling Process Simulation; DEFORM-3D

Abstract. The corrugated waist rail has been successfully rolled in the Mill Research Institute of Yanshan University.Based on commercial FE software of DEFORM-3D, the recrystallization in the rolling process of corrugated waist rail was simulated, the factors affect the recrystallization are analyzed. The different reduces and rolling speed that affect the recrystallization are also analyzed.

Introduction

With the continuously increasing train speed and flow, It is of increasingly stringent requirements about heavy rail . In order to improve the performance and service life of the rail, a new kind of rail structure, corrugated web rail, is developed. The corrugated waist rail has been successfully rolled in the Mill Research Institute of Yanshan University[1], the rolled product is shown in Fig.1. It has been already tested that the mechanical properties of this kind of special structure rail are better than those of the ordinary structure rail. The new structure heavy rail is superior to the ordinary rail on rail waist lateral bending and longitudinal stability[2]. The dynamic properties are also improved[3][4].

Fig.1 The corrugated web rail

FEM model

The rolling simulation model is set up according to18kg/m traditional rail. In rolling experiment, because the height of the vertical roller is small, the part of rail base of rolling piece was cut out to meet with the experiment condition. Before the last pass, the flange and web have been rolled down in the roughing stand and flanges edged respectively. The profile curves of upper and lower horizontal rollers for forming corrugated rail web are shown in the Fig. 1. The lower roller should be rotated with the degree of 180 / z, where z is the teeth number of the tooth-shaped roller, then the teeth of the upper roller and lower roller are matched correctly. The diameter of pitch circles is 269mm, the diameter of the addendum circle is 278mm and the diameter of the root circles is 260mm. The profile curve of each tooth is made up by three segments tangent

arcs, two arcs diameters are 14.02mm and one is 22.68mm. The teeth number of these tooth-shaped rollers is 18. The profile of each tooth is also shown in Fig. 2. The phase angle degree of each tooth is 20°. The rolling model is shown in Fig. 3.

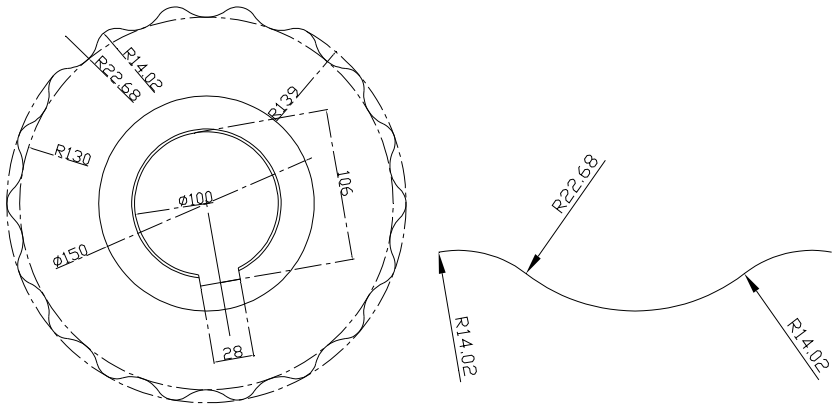

Fig.2 Profile curves of the tooth-shaped roll

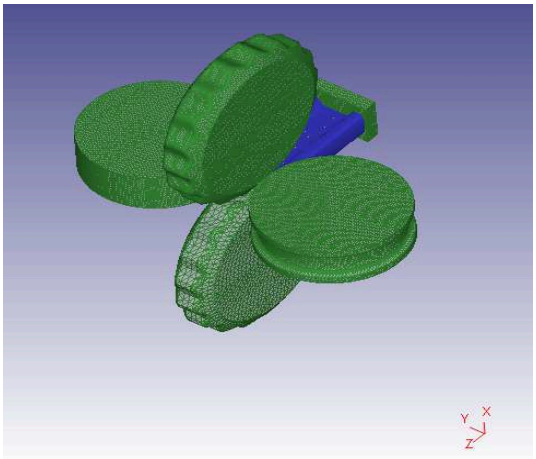

Fig.3 FEM model

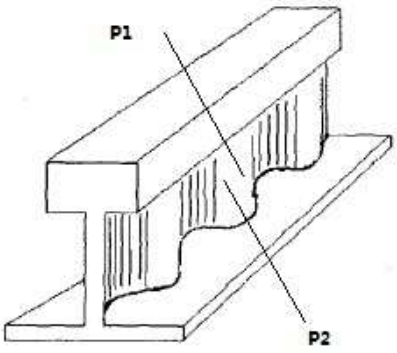

Fig.4 P1and P2 of corrugated rail waist rail

Simulation result and analysis

Deformation degree, deformation speed, temperature and structure evolution are coupled together by DEFORM-3D software. The simulation results, such as average grainsize, volume fraction of dynamic recrystallization and static recrystallization volume fraction ,etc. are analyzed.

In the corrugated waist rail stretch , one point P1 is picked from the wave peak , the other point P2 is picked from the two peak junction , as shown in Fig.4.

Different deformation degree influence

In order to more directly express the rolling piece grain change when increases the reduction, picking the same point at the corrugated waist rail rail waist as the observation point, using point tracing method in the post-processing, tracking the point in the relative reduction of 8% and relative reduction of 10%, grain size change and dynamic recrystallization volume fraction change.

Grain size curves and the dynamic recrystallization volume fraction curves with different relative reduction conditions of P1 is shown in Fig.5 and Fig.6 .

As can be seen from the Fig. 5 and Fig.6 can be seen in the relative reduction of 10%, P1 point and P2 point of grain grain changes little, about 1.2 um . The relative reduction is 8%, the grain and P2 grain size change P1 point is small, it is about 1.25um Thus it can be seen that the relative

pressure increases, the grain size decreases. With the increase of reduction ratio, the strength ,toughness and uniformity can be improved .

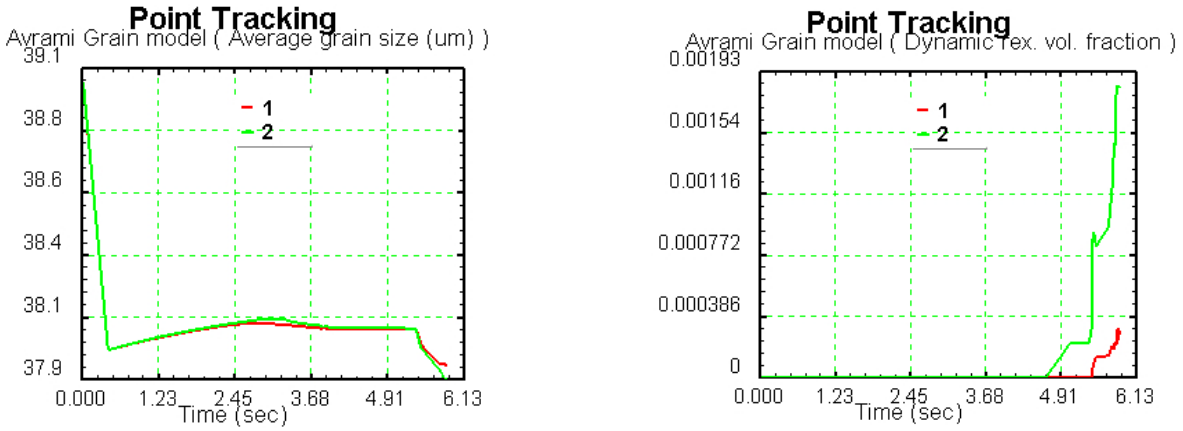

(a)average grain size (b) dynamic recrystallization volume fraction

Fig.5 Parameter changes in rolling（10%）

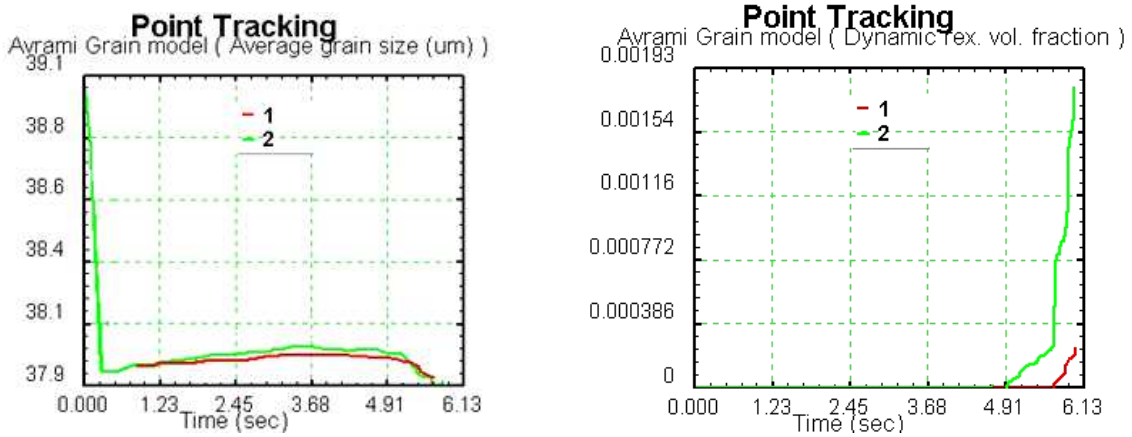

(a)average grain size (b) dynamic recrystallization volume fraction

Fig.6 Parameter changes in rolling（8%）

Different rolling speed influence

At the condition of original reduction, the rolling speed increase to the double, as shown in Figure 20 the rolling process of corrugated waist rail is simulated. The rolling speed is set to 480mm/s, the same P1, tracking the parameters of this point is shown as Fig.7.

As shown in Fig.7, the average grain size of workpiece P1 point changes from 39 um to 37.94 um , the average grain size of P2 points changes from 39 um to 37.9 um .The grain size change is not obvious, the dynamic recrystallization time and is shorter than that of Fig.8 . At less than 2.45s, P1 point began to static recrystallization.

As can be seen from Fig.7 and Fig.8, it is the most obvious change of average grain size. when the rolling speed is 240mm/s, the average grain size is 67.3 μ m. When the rolling speed twicely increased, the average grain size is 37.9 μm. It is shown that the increasement of rolling velocity ,The refinement degree has a certain influence. After rolling velocity, shorten the time of dynamic recrystallization, but it increases the equivalent strain, deformation temperature is lower, so the grain size decreases. Rolling speed changes can also cause the change of plastic strain and temperature, which leads to the different microstructure evolution, grain size change. Thus, in metal rolling process, the rolling speed change can lead to change of the temperature of workpiece, the equivalent plastic strain and the dynamic recrystallization time .

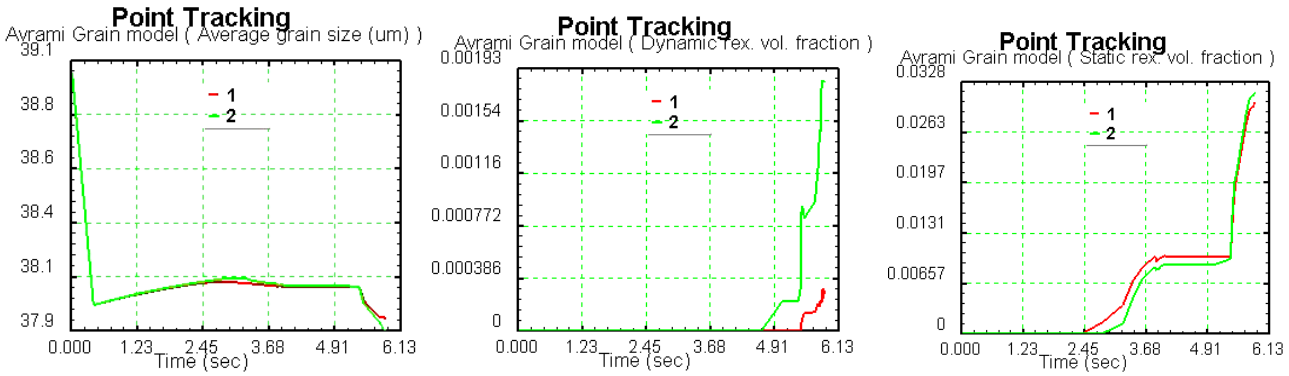

(a)average grain size (b) dynamic recrystallization volume fraction (c)static recrystallization volume fraction

Fig.7 Several parameter changes in rolling(240 mm/s)

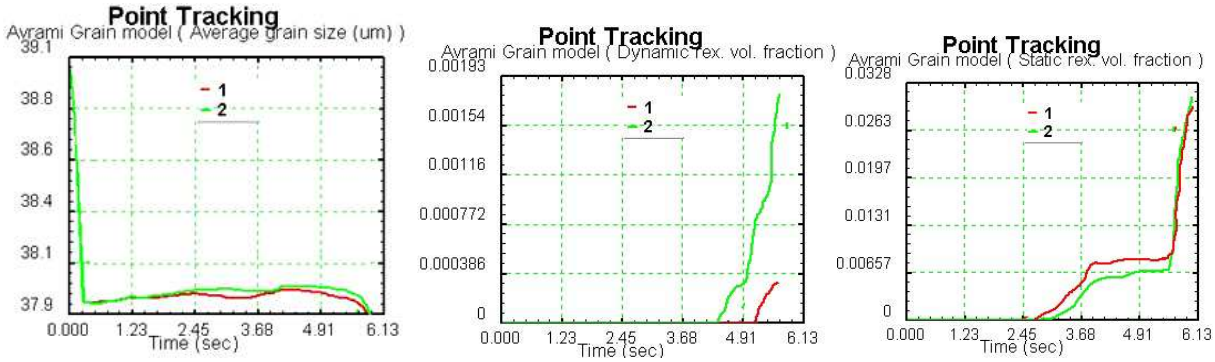

(a)average grain size (b) dynamic recrystallization volume fraction (c)static recrystallization volume fraction

Fig.8 Several parameter changes in rolling (480m/s)

Conclusion

Without changing the rolling speed, increasing the reduce can make the grain size smaller. Increasing the rolling speed, the grain can be refined.

References

[1]XU Xiumei, ZHANG Wenzhi, XIE Hongbiao. Simulation and experimental study on rolling process of corrugated rail waist rail. China mechanical engineering,2005,16(12):1103-1106

[2]WU Bo, CHANG Fuqing, ZHANG Wenzhi. Stress analysis for corrugated waist rail. Journal of Yanshan University, 2003,27(3):278-282

[3] Wu bo, Fuqing Chang and Wenzhi Zhang. Stress Analysis of Corrugated Waist Rail. Journal of Yanshan university, 2003,27(3):278-282.(In Chinese)

[4] Yanwen Li, Wenzhi Zhang et al.. Buckling strength analysis of the web of WCW H-beam-Development and research on H-beam with wholly corrugated web(WCW)(2).Journal of Materials Processing Technology,2000,101(1-3):116-119

Advanced Materials Research Vols. 989-994 (2014) pp 433-436
© (2014) Trans Tech Publications, Switzerland
doi:10.4028/www.scientific.net/AMR.989-994.433

Behavior of geosynthetic clay liners due to the migration of heavy metal

Fan Jingjing[1, a *]

[1.] Changsha Environmental Protection Vocational College, Jing Gui Rd, Changsha, Hunan, 410004, China

[a] fjj-07@163.com

Keywords: Behaivor, Geomembrance, GCL, Liner system, Migration

Abstract. To protect the underlying soil and groundwater from landfills, the landfills are commonly lined with layered liner systems. Geosynthetic clay liners (GCL) have been increasingly used in the landfill liner systems to substitude the traditional compacted clay liners (CCL) because of their low cost, easily construction behavior and low leakage rate. To study the behavior of the GM+GCL liner system used in China due to the migration of Pb^{2+}, we introduce in detail GM+GCL liner systems proposed by the Chinese specification. Then one dimensional finite layer model is used to investigate the anti-pollution behavior of the CM+GCL composite liner systems, with the focuses on the heavy metal Pb^{2+}. It could be concluded that the main migration way through the GM+GCL composite liner system is that the transport of Pb^{2+} through a GM+GCL composite liner system of a landfill cover takes place primarily through the holes in the GM. The findings provide useful reference for preventing, controlling and treating groundwater pollution in the GM+GCL liner system technically and scientifically.

Introduction

According to a recent report, there are 1.2 billion people lack access to clean drinking-water and there are about 2.6 billion have few or no sanitation services[1]. The groundwater is one of the most significant sources of drinking-water. More than 20% of the total drinking-water supply in China is provided by the groundwater in the past thirty years. And there are about 50% of the drinking-water supply is attributed to groundwater in the US. However, the municipal landfills press a great threat to the groundwater due to contamination. In the present, landfilling is main treatment method for municipal solid wastes in China. Consequently, the pollution of groundwater due to landfilling should be assessed analytically[2-3].

To protect the underlying soil and groundwater from landfills, the landfills are commonly lined with layered liner systems. Geosynthetic clay liners (GCL) have been increasingly used in the landfill liner systems to substitude the traditional compacted clay liners (CCL) because of their low cost, easily construction behavior and low leakage rate [4-5]. A number of countries have published technique standards of the GM+GCL composite liner system in accordance to their scientific investigation and practical experience. The Chinese specification (CJJ113-2007) [6-7] specifies a suggestion that recommends the use of GM+GCL composite liners, as shown in Fig 1. The thickness of the GM is 1.5mm. And the thickness of the GCL is 13.8mm. The permeability of the GCL is required to be lower than 5×10^{-11} m/s.

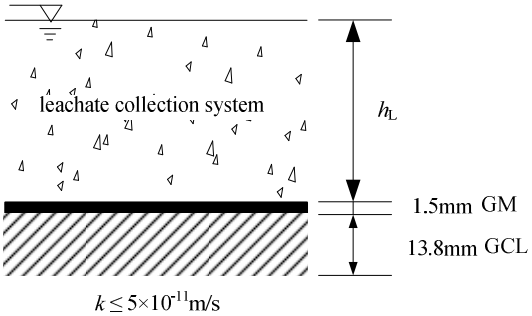

Fig 1 The GM+GCL liner system

In order to investigate the behavior of the GM+GCL composite liner system, an analytical model for the pollutant advection-dispersion-adsorption through the GM+GCL composite liner system is needed. Analytical models for pollutant advection-dispersion through layered liner system have usually been established numerically due to their complicated mathmatical equations. Rowe [5] conducted a comparative study among 3 kinds of composite liner system in the landfill, including GM+CCL, GM+GCL and the double-layered lined system. Xie [8] developed a one-dimensional mathmatical model for pollutant dispersion and advection through a GM+GCL composite liner system to make a comparative study between the behavior of the GCL and the CCL (compacted clay liner). Zhang et al. [9] established a mathmatical model for pollutant migration through a multi-layered landfill bottom liner system by the finite difference method.

Previous reports mainly studied the seepage performance of the GM+CCL composite liner systems according to various kings of structures. The behavior of GM+GCL liner system under the migration of Pb2+ is rarely studied. To study the behavior of GM+GCL liner system, we established a analytical model on the leakage behavior of the GM+GCL composite liner system.

Analytical model

Chinese standard - Technical code for liner system of municipal solid waste landfill- CJJ113-2007 [7] proposed a composite liner system. The high-density polyethylene geomembrance and the compact clay layer liner system is composed of a compact clay layer with a thickness of 0.75m covered by the high-density polyethylene geomembrance with a thickness of 1.5 mm. The coefficient of hydraulic conductivity of the CCL should be less than 1×10^{-9}m/s.

The assumed landfill model has a total length of 150 m in the direction parallel to the flow of the undergroundwater. The pollutant of heavy metal Pb^{2+} is included. The Pb^{2+} is a common kind of heavy metal contaminant in the leachate collection system. The concentration of Pb^{2+} can be assumed as 2 mg/L [8]. Baed on the drinking water standards of the US, the maximum contaminant level (MCL) for Pb^{2+} is suggested to be 0.01 mg/L. Then we could obtain the relative critical concentration of Pb^{2+} by subdivede the initial concentration to the MCL, which is 0.005. The pollutant characteristics are calculated based on Rowe [10-11]. The diffusion coefficient of GM is 7.2×10^{-15} m^2/s. The hydraulic conductivity of GCL is 5×10^{-11} m/s. The hydraulic head is 0.3m as specified in the standards.

Analysis results and discussion

The concentration versus time curves are shown in Fig 2. The location of concentration of Pb^{2+} is at the bottom of the GCL. This picture shows that the concentration of the Pb^{2+} at the bottom of the GCL grows with the growth of time. The concentration adds gradually in the time analysed.

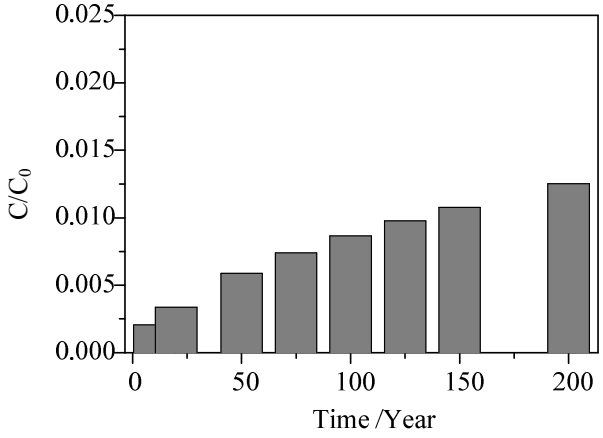

Fig 2 The concentration-time curves at the bottom of GCL

To study the influence of the hydraulic head on the migration of the contaminant, we change the hydraulic head from 1.0m to 10m and re-perform the analysis. The results are shown in Fig 3. For the hydraulic head of 1.0m, the concentration grows gradually. The initial concentration is 0.007 at year 10. The maximum concentration for Pb^{2+} is 0.042, as shown in Fig 3(a). For hydraulic head of 5.0m, the initial concentration is 0.126 at year 10. Then the concentration increase gradually during the time analyzed. The maximum concentration for hydraulic head of 5.0m is 0.54, as shown in Fig 3(b). For hydraulic head of 10m, the initial concentration is 0.4 at year 10. Then the concentration grow rapidly before year 50. After year 50, the curve goes flat because the concentration attains its critical value, which shows clearly the transportation of the contaminant is fast in the early stage of the establishment of the municipal waste landfill. The maximum concentration for hydraulic head 10m is 0.97 for Pb^{2+} at year 150.

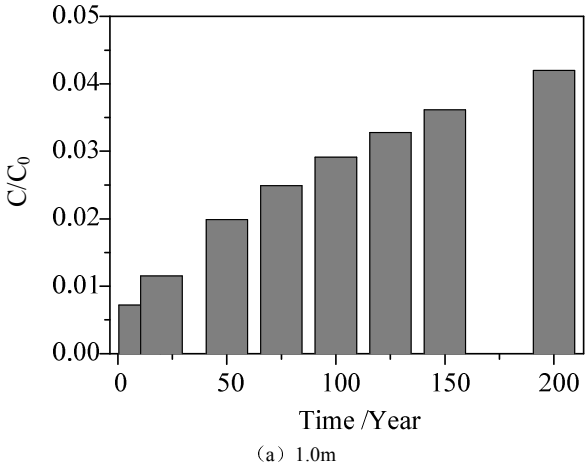

（a）1.0m

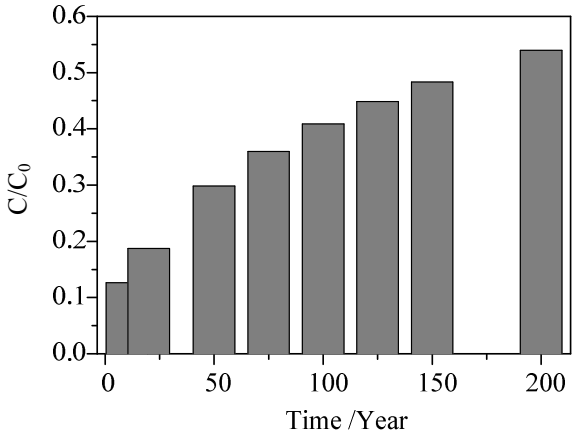

（b）5.0m

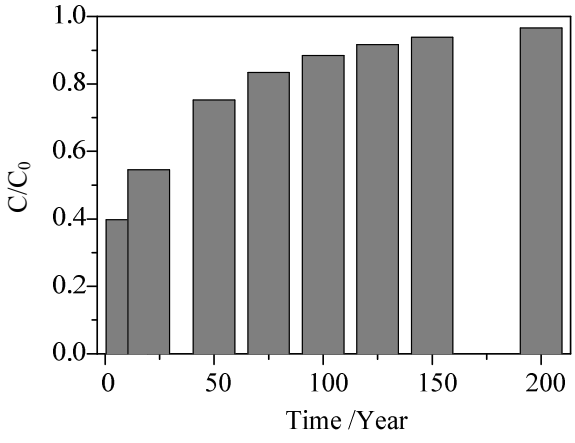

（c）10.0m

Fig 3 The concentration-time curves for different hydraulic head

The values of concentration for Pb^{2+} is listed in Table 1. The concentration increases with the hydraulic head. At year 10, the concentration grows from 0.002 to 0.398 when the hydraulic head increases from 0.3m to 10m. At year 100, the concentration grows from 0.009 to 0.884 when the hydraulic head increases from 0.3m to 1.0m, which indicates that the hydraulic head is an important factor influencing the concentration of Pb^{2+} at the bottom of GCL.

Table 1 The values of concentration for Pb^{2+}

Year	Hydraulic head /m			
	0.3	1.0	5.0	10.0
10	0.002	0.007	0.126	0.398
20	0.003	0.012	0.187	0.546
50	0.006	0.020	0.298	0.752
75	0.007	0.025	0.360	0.834
100	0.009	0.029	0.408	0.884
125	0.010	0.033	0.449	0.916
150	0.011	0.036	0.483	0.939
200	0.013	0.042	0.540	0.965

Summery

The effects of the GM+GCL on the anti-pollution behavior of the composite liner system is studied. Parametric analysis for the Pb^{2+} and the hydraulic head are the focus of the study. The conclusions can be summarized are as follows. 1) The concentration of Pb^{2+} at the bottom of GCL increases with the increase of time. 2). The concentration of Pb^{2+} increases with the increase hydraulic head. At year 100, the concentration grows from 0.009 to 0.884 when the hydraulic head increases from 0.3m to 1.0m, which indicates that the hydraulic head is an important factor that should be considered in the design of GM+GCL composite liner system.

References

[1] Liu CL, Zhang FE, Zhang Y, etc. Experimental and numerical study of pollution process in an aquifer in relation to a garbage dump field. Environmental Geology 2005, 48(8):1107-1115.
[2] Fan, JJ. Pollutant Migration in the GM+CCL Liner System Considering Leachate Mound. Electronic Journal of Geotechnical Engineering. 2013. Vol 18.
[3] Fan, JJ. Leakage performance of the GM+CCL liner system for the MSW Landfill. The Scientific world Journal. 2014.
[4] Dickinson S, Brachman RWI: Assessment of alternative protection layers for a geomembrane - geosynthetic clay liner (GM-GCL) composite liner. Canadian Geotechnical Journal 2008, 45(11):1594-1610.
[5] Rowe RK, Nadarajah P: An analytical method for predicting the velocity field beneath landfills. Canadian Geotechnical Journal 1997, 34(2):264-282.
[6] Xie HJ, Lou ZH, Chen YM, et al.: An analytical solution to contaminant advection and dispersion through a GCL/AL liner system. Chinese Science Bullutin 2011, 56:811-818.
[7] Technical code for liner system of municipal solid waste landfill, 2007, China Architecture & Building Press: Beijing.
[8] Chen, Y., et al., An analytical solution for one-dimensional contaminant diffusion through multi-layered system and its applications. Environmental Geology, 2009. 58(5): p. 1083-1094.
[9] Zhang J L, Luan M T, Yang Q. Two-dimensional numerical analysis of landfill contaminant migration considering non-linear adsorption. Chinese Journal of Geotechnical Engineering, 2008, 30: 354–360
[10] Rowe, R., R. Quigley, and R. Brachman, Barrier Systems for Waste Disposal Facilities. 2004, London and New York: Spon Press.
[11] Jie YX, Peng T, Fu ZB, et al. A study on the permeability of geosynthetic clay liners. China Civil Engineering Journal, 2009, 42: 92–97

Advanced Materials Research Vols. 989-994 (2014) pp 437-440
© (2014) Trans Tech Publications, Switzerland
doi:10.4028/www.scientific.net/AMR.989-994.437

Study on the Morphology and Thermal Stability of Li_2SrSiO_4: Tb^{3+} Materials

Panli You

Xichang College, Xichang 615013, PR China

youpanlizb@163.com

Keywords: Luminescence, Li_2SrSiO_4:Tb^{3+}, Thermal stability, Morphology

Abstract: A series of Tb^{3+}-doped Li_2SrSiO_4:Tb^{3+} phosphors were prepared by high temperature solid state reaction. The morphology and the thermal stability of Li_2SrSiO_4:Tb^{3+} phosphors were discussed by SEM and PL measurements, respectively. The results showed that the morphology of Li_2SrSiO_4:Tb^{3+} was changed from flower-like to rod-like with increasing Tb^{3+}-doped content. Moreover, the emission intensity measured at 350 ^{0}C almost maintain with constant compared with that measured at room temperature. The results showed that Li_2SrSiO_4:Tb^{3+} phosphor might be a potential phosphor for white light-emitting diodes.

Introduction

White light-emitting diodes (LEDs) are the promising new emitting light source for common illumination because of low energy consumption, long lifetime and environment-friendliness. Tb^{3+}-doped materials have been widely applied in LEDs, FEDs as bright green emitting phosphors [[1]-[7]]. The luminescent properties of Tb^{3+}-doped phosphors could be adjusted by the turning the concentration of Tb^{3+}-doped and the matrix compositions [[8][10]].

The crystal structure of Li_2SrSiO_4 was trigonal with space group $P3_121$, Z = 3, unit-cell dimensions a = 5.02281(4) Å and c = 12.45520(8) Å, and V = 272.129(3) Å ^{3} [[11]]. The Sr atoms are located at outside space of the network and the channels formed by two [SiO4] and three [LiO4] tetrahedral units along (100) and (010). The Sr atoms are directly coordinated by eight oxygen atoms with the average bond length of Sr–O of about 2.628 Å [[12]]. The effect of Tb^{3+}-coped concentration on the crystal structure, emission peak position and intensity as well as the Commission International del'Eclairage (CIE) were discussed in our research[[4]]. However, the morphology and the thermal stability of Li_2SrSiO_4:Tb^{3+} phosphors are very importance for the practical application.

In this paper, Tb^{3+}-coped Li_2SrSiO_4:Tb^{3+} phosphors were synthesized by the solid-state reaction. The morphology and the thermal stability of Li_2SrSiO_4:Tb^{3+} phosphors were discussed by SEM and PL measurements, respectively. The result showed that the morphology of Li_2SrSiO_4:Tb^{3+} was changed from flower-like to rod-like with increasing Tb^{3+}-doped content. Moreover, the emission intensity measured at 350 ^{0}C almost retained as high as that measured at room temperature.

Experimental

The Li_2SrSiO_4:Tb^{3+} phosphors were synthesized by the solid-state reaction. Analytical reagent $SrCO_3$, SiO_2, Li_2CO_3 and high purity Tb_4O_7 (99.99 %) were used as the raw materials. The mixed powders according to stoichiometric ratio were preheated in air at 600 °C for 2 h, and then calcined at 900 °C for 4 h in a reducing atmosphere of 95% N_2-5% H_2.

The phase analysis of Tb^{3+}-doped Li_2SrSiO_4 phosphors was characterized by X-ray powder diffraction (XRD, X'Pert MPD 3kW, Philips, Eindhoven, The Netherlands). The morphology of as-prepared sample was examined by means of scanning electron microscopy (SEM，Hitachi, S-4800). Photoluminescence (PL) properties were measured by using a Hitachi F-7000 fluorescence spectrometer equipped with a 150 W-xenon lamp (excitation and emission slits: 2.5 nm; voltage:

500 V). Temperature-dependent measurements were performed using a self-made high-temperature cell for temperature above room temperature. The decay times of $Li_2SrSiO_4:Tb^{3+}$ phosphors were also obtained by time-resolved phosphor luminescence lifetime (short) model. All the properties of the phosphors were performed at room temperature.

Results and discussion

1 Crystal structure and phase analysis

Fig. 1 shows the XRD patterns of Li_2SrSiO_4:1%Tb^{3+} phosphors. The diffraction peaks were indexed by Li_2SrSiO_4 (JCPDS card No. 055–0217) and no impurity phase was detected. The result agreed with the previous reports [[4],[13]].

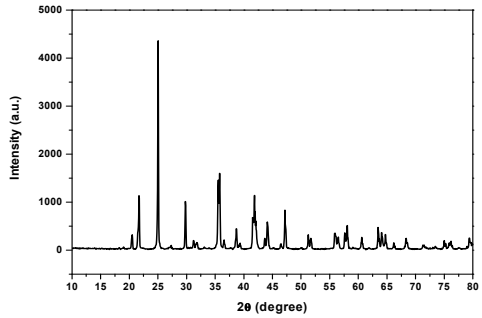

Fig. 1 The XRD patterns of Li_2SrSiO_4:1%Tb^{3+} phosphors

2 SEM analysis

The morphologies of $Li_2Sr_{1-x}SiO_4$:x Tb^{3+} (x = 1%, 4% and 20%) samples are shown in Fig. 2，respectively.

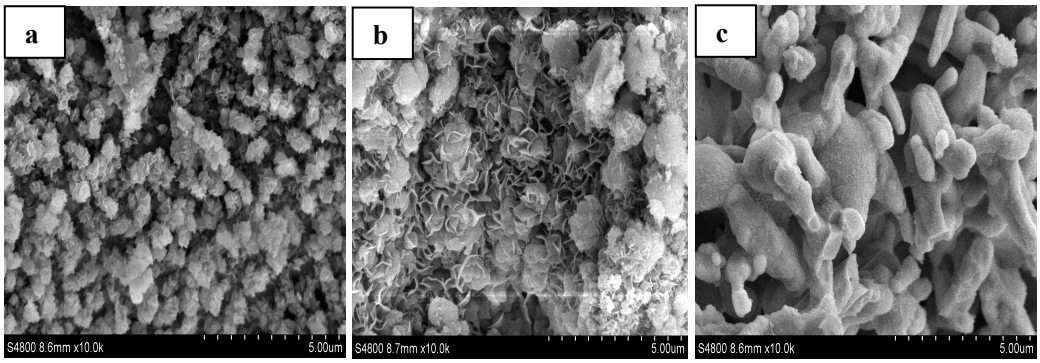

Fig. 2 SEM images of the $Li_2SrSiO_4:Tb^{3+}$, a: 1%, b:4% and c: 20% of Tb^{3+} content

It is clearly observed that the morphologies of $Li_2SrSiO_4:Tb^{3+}$ phosphors were affected by the Tb^{3+}-doped content. As shown in Fig. 2, a uniform flower-like morphology with mean size 1 μm was displayed as adding 1% Tb^{3+}- doped, and then the size of the crystalline grains was increased (about 2 μm) with using 4% Tb^{3+} content. The rod-like morphology with the diameter of about 0.5 μm and the length of 3 μm was presented in 20% Tb^{3+}- doped $Li_2SrSiO_4:Tb^{3+}$ phosphor.

The morphology change with the increase of Tb^{3+}-doped content may be contributed to the preferable growth due to the smeller ion radii of Tb^{3+} compared with that Sr^{2+} in $Li_2SrSiO_4:Tb^{3+}$ phosphor.

3 The thermal stability

The thermal stability of phosphor is required to prevent the changes in chromaticity and brightness of LEDs. The temperature-dependent luminescence properties of $Li_2SrSiO_4:Tb^{3+}$ measured in the range of 25 – 350 ^{0}C were investigated respectively, and the results were presented in Fig. 3.

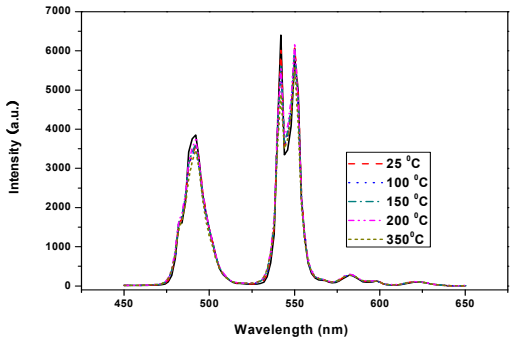

Fig. 3 The temperature-dependent emission spectra of $Li_2SrSiO_4:Tb^{3+}$

It is obviously found that the emission intensity of $Li_2SrSiO_4:Tb^{3+}$ phosphor almost keep constant with increasing the temperature from 25 ^{0}C to 350 ^{0}C. The results indicated that the thermal stability of $Li_2SrSiO_4:Tb^{3+}$ phosphor was very good suitability for use in LEDs. The excellent thermal stability may be ascribed to rigid structure of [SiO4] and [LiO4] tetrahedral network in the Li_2SrSiO_4 host lattice [[12],[13]] as well as the transition feature of Tb^{3+} .

4 Decay lifetime

Effect of Tb^{3+}-coped concentration on the decay time of $Li_2SrSiO_4:Tb^{3+}$ was investigated. The decay curves and fitted lifetimes of Tb^{3+} emission (542 nm) under excitation at 243 nm for $Li_2Sr_{1-x}SiO_4:xTb^{3+}$ (x = 1%, 4% and 20%) were exhibited in Fig. 4, respectively.

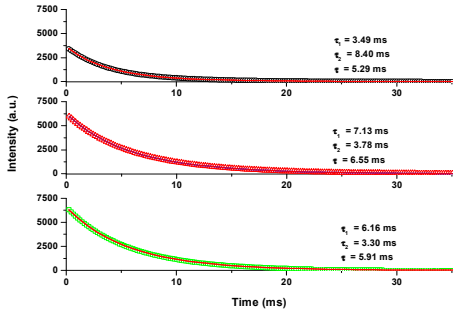

Fig. 4 The decay curves and the fitted lifetime for $Li_2Sr_{1-x}SiO_4:xTb^{3+}$ (x = 1%, 4% and 20%), respectively.

The decay curves could be well fitted by a bi-exponential function [[14]]:

$$I(t) = A_1 \exp(-t/\tau_1) + A_2 \exp(-t/\tau_2) + I_0 \quad (1)$$

Where I_0 and I are the luminescence intensities at time 0 and t, respectively; τ_1 and τ_2 are two components of the luminescence lifetime, and A_1, A_2 are the fitting parameters. Using equation (1), the fitting values in $Li_2Sr_{1-x}SiO_4:xTb^{3+}$ (x = 1%, 4% and 20%) are (τ_1 = 3.549 ms，τ_2 = 8.40 ms; A_1 = *2935.93, A_2 = 705.85*),（τ_1 = 7.13 ms, τ_2= 3.78 ms; A_1 = *4468.42, A_2 = 1765.58*）and （τ_1 = 6.16 ms, τ_2 = 3.30 ms; A_1 = *5588.79, A_2 = 1011.93*）corresponding to 1%, 4% and 20% of Tb^{3+}-doped concentration, respectively.

The two lifetime τ_1 and τ_2 represent the two processes of radiative transition and energy transfer in $Li_2Sr_{1-x}SiO_4:xTb^{3+}$ phosphors. The average lifetime was τ = 5.29, 6.55 and 5.91 ms in turn for 1%, 4% and 20% Tb^{3+} in terms of the following equation [[15]].

$$\tau = (A_1\tau_1^2 + A_2\tau_2^2)/(A_1\tau_1 + A_2\tau_2) \quad (2)$$

The decay lifetime varied with increasing Tb^{3+}-doped amount might be explained by the non – linear resonant energy transfer theory reported by Hayakawa [[16],[17]]. For the lower Tb^{3+} doped content, the decay lifetime increased with increasing the concentration of Tb^{3+} dopant. However, for the higher Tb^{3+} doped amount, the decay lifetime decreased with increasing the concentration of Tb^{3+} dopant due to non – linear resonant energy transfer.

Conclusion

The Tb^{3+}-doped $Li_2SrSiO_4:Tb^{3+}$ phosphor was synthesized by high temperature solid state reaction. The morphology, the thermal stability and decay lifetime of $Li_2SrSiO_4:Tb^{3+}$ phosphors were discussed by SEM and PL measurements, respectively. The results showed that the morphology of $Li_2SrSiO_4:Tb^{3+}$ was changed from flower-like to rod-like with increasing Tb^{3+}-doped content. Moreover, the emission intensity almost maintained a constant as increasing the temperature from 25 ^{0}C to 350 ^{0}C. The decay curves could be well fitted by a bi-exponential function, and the corresponding decay lifetime in $Li_2SrSiO_4:Tb^{3+}$ phosphor was 5.29 ms, 6.55 ms and 5.91 ms for 1%, 4% and 20% Tb^{3+}, respectively. The results showed that $Li_2SrSiO_4:Tb^{3+}$ phosphor can be a potential phosphor for white light-emitting diodes.

Acknowledgements

This work was financially supported by the National Natural Science Foundation of China (61368007) and the specialized research fund for the Doctoral Program of Xichang College (13BQZ03). The authors would like to thank Guangfu Yin and Lijuan Liu of Sichuan University for their support and encouragement.

References

[1] D. Hreniak, W.Strek, P. Mazur, et al., Optical mater.,2004,26:117-121
[2] S. Chen, Y.H. Wang, J. Lumin., 2014, 150 :46-49
[3] Z.J. Wang, P.L. Li, Z.P.Yang, Q.L. Guo, Optics Commun., 2014, 321:100-103
[4] P.L. You, Advance mater. Res., 2014, 919-921:2052-2056
[5] Z.F. Yang, Y.H. Hu, L. Chen, et al., J. Lumin., 2014, 153:412-416
[6] S.J. Jia, L.H. Huang, D.L. Ma, et al., J. Lumin., 2014, 152:241-243
[7] J.T. Ingle, A.B. Gawande, R.P. Sonekar, et al., J. Alloys Compds., 2014, 585: 633-636
[8] Y. Kojima, M. Numazawa, T. Umegaki, J. Lumin., 2012, *132:2992-2996*
[9] N.M. Zhang, C.F. Guo, H. Jing, Spectrochimica Acta Part A: Molecular and Biomolecular Spectroscopy, 2013, 116:556-561
[10] L.X. Song, P.F. Du, Q.X. Jiang, et al., J. Lumin., 2014,150: 50-54
[11] M. P. Saradhi, U.V. Varadaraju, Chem. Mater., 2006, 18:5267-5272
[12] H. Yoshinori, I. Tomoyuki, M. Koichi, et al., Powder Diffr. 2010, 25: 4-8
[13] P.L. You, G.F. Yin, X.C. Chen, et al., Opt. Mater., 2011, 33, 1808-1812
[14] G. Blasse, B.C. Grabmaier, Lumin. Mater., Springer-Verlag:Berlin, 1994
[15] S. Mukarami, H. Markus, R. Doris, et al., Inorg. Chim. Acta., 2000, 300-302: 1014-1021
[16] T. Hayakawa, N. Kamata, K.Yamada, J. Lumin., 1996, 68, 179-186
[17] J.K. Krebs, Z.J. Barninger, J. Lumin., 2010, 130,1305-1307

Advanced Materials Research Vols. 989-994 (2014) pp 441-445
© (2014) Trans Tech Publications, Switzerland
doi:10.4028/www.scientific.net/AMR.989-994.441

Study on CO_2 Adsorption of Halloysite Modified by Silane Coupling

Huali Zhang[1,a], Xiaoying Lai*[1,b], Hanjun Wu[2,b],

[1]National Engineering Research Center of Phosphato Resources Development and Utilization, Wuhan Institute of Technology, Wuhan, Hubei430074, PR China

[2]School of Chemical Engineering & Pharmacy, Wuhan Institute of Technology, Wuhan, Hubei430074, PR China

[a]zhanghl413@126.com, [b]4351842@qq.com, [c]wuhj1204@126.com

*Corresponding author

Keywords: halloysite silane coupling modifying adsorption CO_2

Abstract. The natural halloysite as the main raw material, removing the kaolinite, the quartz, feldspar and other impurities through purification. The purified halloysite was roasting activation pretreatment, in order to enhance surface porosity and reaction activity, and then was made of halloysite composite by modifying through the use of silane coupling agent. The samples were characterized by XRD, FESEM, BET, FT-IR and other chemical analysis method. The weight percentage of CO_2 which were adsorbed by the modified halloysite increased from 3.13% to 13.92%.

Introduction

Recently, global warming and a series of environmental problems caused by a great amount of CO_2 have become the focus in the world[1-2]. Simultaneously, CO_2 is a kind of carbon resource which used as a synthetic organic compounds and fuel for various aspects of national life[3-4]. No matter committed to reducing the content of CO_2 in atmosphere, or to use,separation and recovery of CO_2 is a crucial step.

Now, the methods of trapping and separating CO_2 include adsorption method, membrane separation method, solvent adsorption method and low temperature distillation method[5-6]. Adsorption is a kind of very promising method of separating CO_2[7]. Recently, the popular porous solid adsorbents of CO_2 include metallic-rectangular organic compounds[8-9], zeolites molecular[10], amino-modified mesoporous materials[11-12] and so on. Currently the metallic-rectangular organic compounds are still in research phase and have a certain distance from the large-scale industrial application; zeolites molecular have large adsorption amount of CO_2 at room temperature and good adsorption selectivity, but the capability of adsorbing CO_2 will decrease rapidly under trace water or SO_x conditions; amino-modified mesoporous material receive more and more concerns because of its fine adsorption selectivity in the presence of water. However, the research more of that are amino-modified mesoporous materials, amino-modified resin and amino-modified activated carbon, studies about CO_2 adsorption by natural mineral materials were not reported.

In this paper, halloysite was thermal activated to enhance its surface activity, then choice of silane coupling agent on the impregnation and modification to produce natural mineral based solid alkaline sorbent. The structure, thermal property, and pore size distribution of materials in different stages were characterized by XRD, FT-IR, TG/DSC, BET, and the CO_2 adsorption capacity of the modified material were determined by gravimetric analyzer.

Experimental

Raw and Reagent. Halloysite raw ore was provided by lincang Yunnan Province, r- aminopropyl triethoxy silane, polyacrylamide, and hexametaphosphate were purchased from Compton, Guali fine chemical plant in xiaoshan Hangzhou, and haijing fine chemical plant in hebei Tianjin separately .

Activation of halloysite. (1) Purification of halloysite. Steps of purification: adjust the system's pH value, added a certain amount of dispersant, centrifuging under specified speed, and then obtained the relatively pure **7Å** halloysite product. Technological process: ① Halloysite raw ore was

assigned to slurry which the weight ratio was 15%, and then mixed by high-speed stirrer at rotating speed 8000r/min for 1 h. ② Halloysite slurry was sift by 100 mesh screen after dispersed uniformly. ③ The below-sift slurry standing for 6 h, the suspension in upper layer was collected by centrifuge, and drying 12 h at 95 ℃, scattered by universal grinder. ④ The power in step ③ was assigned to slurry, adjusted its pH value, and then added appropriate content dispersant, mixed by high-speed stirrer for 2 h. ⑤ Placed suspension at centrifuge at a certain speed, removed the sediment in lower layer, placed suspension in upper layer at centrifuge at the speed of 3800r/min for 5 min. ⑥ The sediment in step ⑤ were drying 12 h at 95 ℃, and then obtained high purity 7Å halloysite product.(2) Calcination of halloysite. A certain amount of purified halloysite was placed at SX2-1-10 electric furnace in a certain temperature for 2 h, cooled to room temperature,and made the phase, morphology and elemental analyses.

Preparation of modified halloysite. 100mL ethanol which contain 2mL water placed in conical flask, added 3 mL γ-aminopropyltriethoxysilane, dispersed for 20 min by ultrasonic apparatus, added 2 g halloysite power after calcined for 2 h, mixing and refluxing in water bath in 80 ^{o}C for 6 h, filtered,and then the samples of halloysite modified by silane coupling agent were prepared after baking in 50 ℃ and grinding.

Performance testing of CO_2 adsorption. A certain amount of need checking samples were placed at sample chamber. Pumped in nitrogen gas for 60 min, flow rate at 50 mL/min, and hearting, hearting rate at 10℃/min, heated up to a certain temperature(70~80^{o}C), activated in vacuum condition (vacuum pressure:40KPa), and then cooling, pumped in CO_2(flow rate at 40mL/min) when the system at room Temperature, and stoped at the standard atmosphere(100KPa), adsorbed continuously for 2 h, when adsorption reach to be saturated, reaction finished.

Assuming that original quality of samples were m, the mass percentage reduced by a in the first stage and increased by b in the second stage, then the mass percentage of CO_2 adsorption:

$$\frac{\text{Quality after adsorption}}{\text{Quality before adsorption}} = \frac{m \times b}{m \times (1-a)} = \frac{b}{1-a} \qquad \text{(Type1)}$$

Result and discussion

Activation of halloysite. Fig.1 shows the XRD patterns of crude and pure halloysite. It showed that many diffraction peaks of impurities such as quartz (some characteristic peaks at 0.420nm and 0.3332nm), feldspar (some characteristic peaks at 0.37746nm, 0.34662nm and 0.42169nm), gibbsite (some characteristic peaks at 0.4834nm and 0.3562nm) were appeared in the XRD patterns of crude and pure halloysite. The purity of halloysite after purified was above 98%, and its characteristic peaks appeared at 0.73971nm, 0.44554nm and 0.36429nm. The type of halloysite in lincang Yunnan Province was 7Å (7.25~7.40Å). And it also showed that the polarization of diffracted beams of (02) and (11) were stronger than that of (002) while smaller than that of (001) under the temperature between 20 ℃ and 30℃, $I_{(02)} \sim \frac{I_{(001)} + I_{(002)}}{2}$, there is obvious division in diffracted beams of (13) and (20). This deposit should be classified as the type of coexistence with kaolinite and halloysite[16-17].

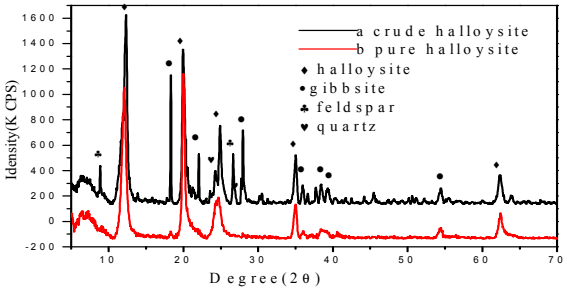

Fig.1 The XRD of crude and pure halloysite

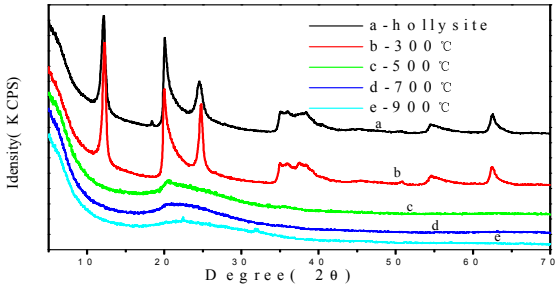

Fig.2 The XRD of halloysite at different temperatures

Fig.2 shows the XRD spectrum of halloysite which were calcined at different temperature, a was x-ray diffraction patterns of halloysite, b, c, d and e were halloysite calcined at 300℃, 500 ℃, 700 ℃, and 900 ℃ for 2h separately.

Fig.2 shows that adsorbed water was disappeared, nanometer channel and structure become fatherly dredging and close respectively, which lead to diffraction peaks shifts of (001) and (002) toward high angle, peak pattern become sharp and relative intensity was enhanced. There wasn't obvious diffraction peak but amorphous state when the calcining temperature was above 500 ℃. So the future calcination test experimented at 300 ℃.

Fig.3 shows the FESEM picture of purified halloysite and halloysite calcined at 300 ℃ for 2h. Picture a and b were respectively the FESEM picture of purified halloysite and halloysite calcined at 300 ℃ for 2h.

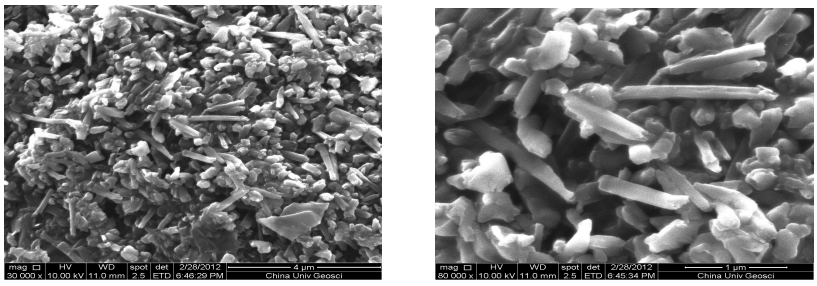

a The purified halloysite

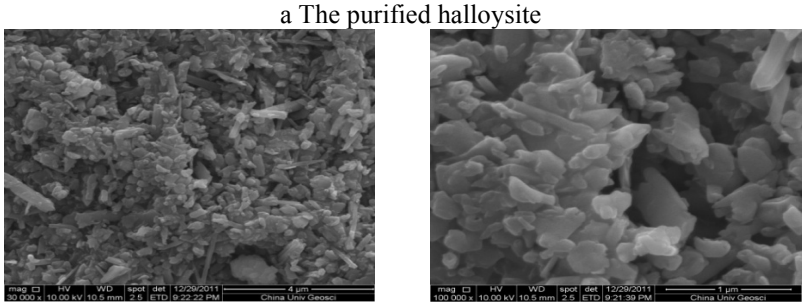

b The calcined halloysite under 300 ℃for 2h

Fig.3 The FESEM of the purified and calcined halloysite

The SEM analysis shows that surface morphology of halloysite original sample were tubular,the length of the tube is 0.5-2um. When calcined at 300℃, the halloysite only removed adsorbed water and crystal water that have no effect on the basic structure. The microstructure had little change and still keep tubular structure, but the length of the tube was 0.3-1um shorter. The fracture of the tubular structure would inevitably result in specific surface area and pore volume increase, and then enhanced the adsorption property of samples, which will conducive to subsequent trials.

Preparation of modified halloysite. Halloysite after activation, although the porosity and the active center density can be increased, enhanced the interaction force with the adsorbed substance, the selectivity of adsorption can not effectively to change. In order to improve the selectivity, halloysite was activated by silane coupling. The infrared spectra of hollysite modified by γ-aminopropyltriethoxysilane is showed in Fig.4, a is the calcined hollysite; b is modified hollysite; c is the silane coupling.

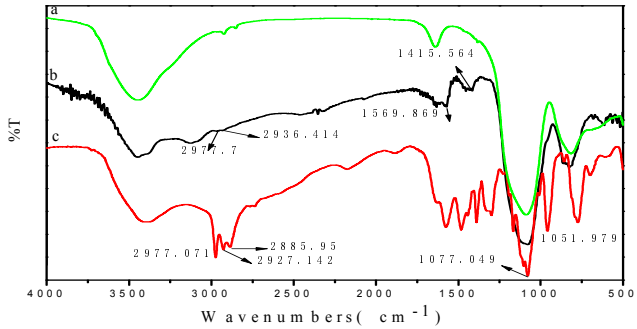

Fig.4 The IR analysis of halloysite modified by silane coupling

The curve a in Fig.4 shows that the bands at 2977.07 cm^{-1} and 2885.95 cm^{-1}, 2927.14 cm^{-1}, 1077.049 cm^{-1} were stretch vibration absorption spectra of C-H bond of -C-CH_3, C-H bond of -C-CH_2-C-, Si-O bond of γ-aminopropyltriethoxysilane respectively.

Fig.4 shows that compared with the infrared spectra curve of unmodified halloysite, the modified by γ-aminopropyltriethoxysilane has extra characteristic absorption peaks 2977 cm^{-1}, 3936 cm^{-1}, 1569 cm^{-1}, 1415 cm^{-1} and 1051 cm^{-1} , the characteristic absorption peaks 2977 cm^{-1} and 3936 cm^{-1}, 1569 cm^{-1}, 1415 cm^{-1} created by the vibration of C-H bond of -C-CH_2- and -CH_3- respectively. This means that there were -C-CH_2- and -CH_3- in modified halloysite samples. The characteristic absorption peaks 1051 cm^{-1} created by the vibration of Si-O bond.

Fig.4 also shows that absorption peaks created by the vibration of Si-O was 1051cm^{-1}, in infrared spectra curve of γ-aminopropyltriethoxysilane. While, in the infrared spectra curve of modified sepiolite, absorption peaks created by the vibration of Si-O bond are 1077 cm^{-1}. The bands between 400-1100 cm^{-1} were stretch vibration absorption spectra of Si-O bond, compared to other two peaks, the peak intensity became stronger, the peak pattern became wider.

Therefore, under the above experimental condition, there was alkyl group in the modified halloysite samples, and the vibration absorption enhanced, γ-aminopropyltriethoxysilane was successfully grafted onto the surface of halloysite. The organic modification of halloysite was realized

Tests on CO_2 adsorption properties

(1)Tests on specific surface area and pore volume

Table 1 lists the pore parameters of calcined halloysite and calcined halloysite modified by silane coupling agent.

Table1 The pore parameter of calcined halloysite and modified by silane coupling

sample	BET(m^2/g)	V_{sp}（cm^3/g）	D_p（nm）	S_{BET}（m^2/g）		V_{sp}（cm^3/g）	
				0-2nm	2-50nm	0-2nm	2-50nm
calcined	37.0370	0.109641	11.84320	0.643	33.561	0.0003100	0.1037
modified	29.1663	0.089684	12.29967	2.123	25.337	0.000988	0.083768

Table 1 shows that the specific surface of modified halloysite decreased from 37.0370 m^2/g to 29.1663 m^2/g. The pore volume of modified halloysite also decreased from 0.109641cm^3/g to 0.089684cm^3/g, while the pore size of modified sepiolite increased from 11.84320nm to 12.29967nm.

After modification, both pore area and pore volume of halloysite are larger than that of before in the micropore scope of 0 to 2 nm. Pore area of halloysite increased from 0.6430m^2/g to 2.123m^2/g, and pore volume of halloysite increased from 0.0003100cm^3/g to 0.000988cm^3/g. While, in the micropore scope of 2 to 50 nm, pore volume of modified halloysite decreases from 0.1037cm^3/g to 0.083768cm^3/g, pore area of modified halloysite decreases from 33.5610 m^2/g to 25.337m^2/g. The increasement of surface area and volume of modified halloysite contributes to the improvement of adsorbing capacity of CO_2.

(2)Tests on CO_2 adsorption properties. Fig.5,6 respectively for sample adsorption CO_2 thermogravimetric curve, stage a on behalf of vacuum pumping stage, b stage as CO_2 adsorption.

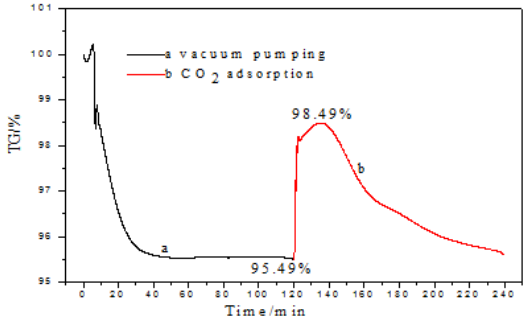

Fig.5 The thermogravimetric curve of calcined halloysite

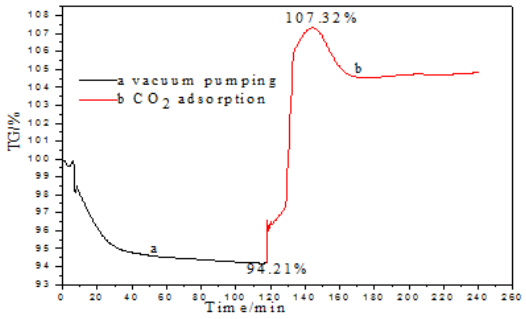

Fig.6 The thermogravimetric curve of modified halloysite

As you can see from Fig.5, in the a stage, quality changes continuously decreased to 95.49%; b stage, the mass percentage of samples rapidly increased to 98.49%, the maximum adsorption capacity of CO_2, followed by a fall and rise, basically in the dynamic adsorption equilibrium. See from Fig.6, in the a stage, the decline in the quality of samples have small fluctuations, the percentage dropped to

94.21%; in the stage of CO_2 adsorption, the percentage quickly up to a maximum of 107.32%, then decreased, and then in a platform, the degree of quality changes very little.

By using Type 1, the mass percentage of CO_2 adsorption had been calculated to be 3.13% and 13.92% respectively pre and post the modification.

Conclusion

(1) After purification, there is a apparent decrease in impurity peaks of gibbsite, quartz, feldspar and illite. Refined halloysite sample with the purity over 98% are obtained. (2) By the XRD analysis of halloysite which were calcined at different temperature, halloysite should be calcined at 300 ℃. When calcined at 300 ℃ for 2h, the microstructure had little change and still keep tubular structure, but the length of the tube was 0.3-1um shorter. The fracture of the tubular structure would inevitably result in specific surface area and pore volume increase, and then enhanced the adsorption property of samples,which will conducive to the further organic modification. (3) Halloysite modified by ethanolamine acetate ionic liquid silane coupling shows a decrease in pore area and pore volume and an increase in pore size. The adsorption amount of CO_2 at room temperature and pressure increases from 3.13% to 13.92%, showing a great improvement of the adsorbing capacity of CO_2 in modified halloysite.

*Corresponding author. E-mail:4351842@qq.com. Tel. 027-87446589. Majoring in energy and environmental sustainability. Supported by Natural Science Foundation of China(71303180).

References

[1] DING Zurong. ECOLOGY AND ENVIRONMENTAL SCIENCES, 2008,17(3):1290-1295.
[2] IPCC. Special Report: on Carbon Dioxide Capture and Storage. 2007
[3] CHENG Zhongming, LI Chuanhua, LING Hai, et al. Fine Chemical Intermediates, 2001, 31(5): 9-11.
[4] YE Endong, LI Guihua, WANG Lijuan. Panzhihua Sci-Tech & Information[J], 2001, 26(2): 30-34.
[5] P. H. M. Feron, A. E. Jansen. The Production of Carbon Dioxide from Flue Gas by Membrane Gas Absorption[J]. Energy Conversion and Management, 1997, 38(1):93-98.
[6] ZHAO Huiling, HU Jun, WANG Jianjun, et al. Acta Physico-Chimica Sinica, 2007, 23(6): 801-806.
[7] Xiao Y, Low B.T, Hosseini S. S, et al. The strategies of molecular architecture and modification of polyimide-based membranes for CO_2 removal from natural gas—A review[J]. Progress in Polymer Science, 2009, 34(6):561-580.
[8] ZHOU Yuanjing, YANG Mingli, WU Kai, et al. Journal of Materials Science and Engineering, 2007, 25(2): 307-312.
[9] Stuart L. J. Metal-organic frameworks[J]. Chemical Society Review, 2003, 32(18): 276-288.
[10] Jadhav, P. D., Chatti, R. V., Biniwale, R. B.. et al. Monoethanol amine modified zeolite 13X for CO_2 adsorption at different temperatures[J]. Energ Fuel, 2007, 21, 3555-3559.
[11] Xu X. C., Song C. S., Miller B. G., et al. Adsorption separation of carbon dioxide from flue gas of natural gas-fired boiler by a novel nanopomus molecular basket adsorbent[J]. Fuel Processing Technology, 2005, 86(14-15): 1457-1472.
[12] Hiyoshi N., Yogo K., Yashima T. Adsorption of carbon dioxide on amine modified SBA-15 in the presence of water vapor [J]. Chemistry Letters, 2004, 33(5):510-511.
[13] ZHAO Chuanwen, CHEN Xiaoping, ZHAO Changsui. CIESC Journal, 2008, 59(9): 2329-2333.
[14] THOMAS. Carbon dioxide capture for storage in deep geologic formations-result from the CO_2 capture project I[M]. ELSEVIER, UK, 2005: 1-15.
[15] HUANG Bin, LIU Lianbo, XU Shisen. Electric Power, 2007, 40(3): 14-17.
[16] Ren lei- fu. 1992. Clay Mineral and Clay Salt. geological publishing house, beijing.
[17] Huang Yining, Ralph M. Paroli, Deigado Ana H., et al. An FT-Raman study of solid-state ion exchange in zeolites[J]. Spectrochimica Acta Part A. 1998, 54(10):1347-1354；

Advanced Materials Research Vols. 989-994 (2014) pp 446-449
© (2014) Trans Tech Publications, Switzerland
doi:10.4028/www.scientific.net/AMR.989-994.446

Electrochemical Behavior of the Initial Atmospheric Corrosion of 2Cr13 Steel in Guiyang City Atmosphere

Li Lunyou[1, a], Hu Yanan[2,b*]

[1]Guizhou steel rope(group) Co, Ltd,[2]School of Materials and Metallurgy, Guizhou University, Guiyang, 550025,China

[a]820005196@qq.com,[b*]980789785@qq.com(corresponding author)

Keywords: 2Cr13 Martensite Stainless Steel,City Atmosphere,Initial Atmospheric Corrosion, electrochemistry

Abstract: Used electrochemical tests and the natural atmospheric exposure experiment to study initial atmospheric corrosion of 2cr13 steel in Guiyang city . Measured impedance spectrum curves and polarization curves of experimental steel in the local rain medium.Weight method measured the corrosion rate. The results showed that the exposure period of 0 to 60 days, with longer time, the corrosion current increased firstly then decreased, and the corrosion current decreased after the firstly increased. Impedance spectra showed that passivation process was controlled by the electrochemical reaction. Measured the corrosion rate of 0.000280 ~ 0.000280 mm/a, which belongs to the corrosion level 2 - very corrosion resistance.

1.Introduction

Martensite stainless steel is a kind of steel that can be achieved by different heat treatment process to adjust its mechanical properties of stainless steel. Typical brands of martensitic stainless steel are Cr13 and Cr16 type,etc. In recent years, the martensitic stainless steel are used in the manufacture of oil well pipe under the environment of high temperature and high pressure oil fields, a lot of researches on adding alloying elements into Cr13 stainless steel to improve its CO_2 corrosion resistance. Some studies showed that the composition has the characteristics, such as containing chromium more than 12% , without nickel or containing small amounts of nickel (2.0%) , high carbon (generally more than 0.1%)[1], resulting in the weak corrosion resistance of martensitic stainless steel in chloride or sulfide medium , only suitable for mild corrosion environment, such as atmosphere and water, etc. With the development of urban industry,higher requirements of corrosion resistant performance of martensitic stainless steel are put forward. Therefore, this paper, electrochemical behavior of the initial atmospheric corrosion of 2Cr13 steel in Guiyang city atmosphere, is necessary. It will provide theoretical basis for the application of life and production .

2.Experiment Materials and Methods

2.1 Experiment Materials. Material for experiment was bought from market as Φ 100 mm stainless steel bar, chemical compositions (mass %) are shown in table 1 below:

Table 1 Chemical composition of stainless steel (wt%)

sample	C	Cr	Ni	Mn	Si	S	P
2Cr13	0.2	12.59	0.15	0.57	0.19	0.006	0.021

The samples of electrochemical experiments and atmospheric exposure test were cut by electric spark numerical control line cutting machining. Electrochemical sample were cut into 10 mm x 10 mm x 5 mm, the samples connected to conductor by soldering with tin.Seal the samples with epoxy resin and curing agent whose mass ratio is 4:1, only to set aside a 10 mm x 10 mm of working surface. Size of atmospheric exposure samples were about 50mm x 30 mm x 4 mm.

After the preparation of all samples were completed, the samples need be sanded and polished. Then dry them after cleaning with deionized water, acetone and ethanol.

2.2 Experiment Methods. This experiment adopts the electrochemical and natural environment exposure test methods [2] to study the early atmosphere corrosion.

In France Bio-Logic VSP electrochemical workstation. Polarization curves and electrochemical impedance spectroscopy curves were obtained by potentiodynamic scanning method. Polarization curves scanning were ranged -0.7V~1.9V(SCE) and simulated with Tafel fit. The frequency range of alternating current impedance was 100 KHz ~ 10 mHz, and AC excitation signal amplitude was 10 mV, then equivalent circuits were simulated with Zview fit.Corrosive medium was Guiyang local rain water. Using three electrodes system, the working electrodes were 2Cr13 stainless steels.

The samples and ground plane were 45 ° on the exposed rack. Exposure experiment was started since November 27, 2012, and the exposure periods were 15 days, 30 days, 45 days and 60 days respectively. Exposure site was on the top floor of a laboratory in Guiyang; the environment parameter of exposure scene was as follows: the average temperature of 11 ℃, the average monthly humidity of 90%, monthly rainfall for 13 days.

3.Results and discussion

3.1 the polarization curve. As shown in figure 1, the polarization curves with different test periods of the experimental steel made parallel movement at different degree.Cathode area appeared oxygen reduction limiting current platform, and anode area presented pre- passivation phenomenon. In different curves,just current density and the corrosion potential were in different sizes.

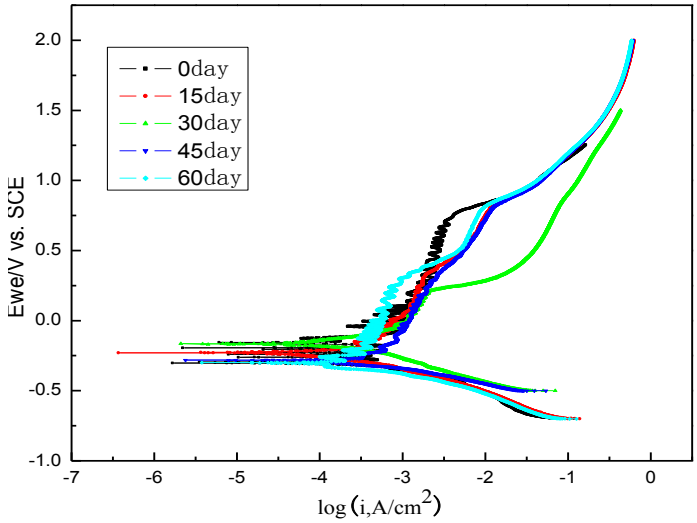

Figure 1 Polarization curves of experimental steel with different exposure periods in Guiyang city atmosphere

Fit the polarization curves by Tafel, the results shown in table 2. It showed that under different exposure period, polarization curves of experimental steel all had passivation area with a little difference. It told that in the local rain water medium, the experimental steel can be passivation. Corrosion current density *Icorr* is used to determine the electrochemical corrosion reaction speed.The greater the *Icorr* was, the faster the corrosion happened. In general, lower the nature corrosion potential *Ecorr* was , the greater the corrosion speed would be[3]. The figure 1 and table 2 showed that 15 to 45 days exposure period, with longer time, the corrosion current density increased, the easier the corrosion would be.To 60 days, *Icorr* reduced and the corrosion slowed down. Corrosion current *Icorr* was below 0.4 μA, and the corrosion potential is closed to positive.Therefore,the experimental steel in local rain medium had good corrosion resistance.

Table 2 Fitting results of stainless steel polarization curve with Tafel

Exposure period	0 day	15 day	30 day	45 day	60 day
E_{corr} (mV)	-161.561	-235.787	-167.060	-272.33	-253.890
I_{corr} (μA)	0.120	0.166	0.275	0.363	0.119

3.2 the polarization curve. The figure 2 showed that ac impedance spectrum with different test period of experiment steel in the local rain water had similar characteristics, and they were composed of high frequency single capacitive reactance arc. The greater the radius of the semicircle of the capacitive reactance were , the bigger the capacitive reactance were [4]. The characteristics of the impedance spectrum showed that passivation process was controlled by the growth and dissolution of the surface passivation membrane. The whole process was controlled by electrochemical reaction. Without the atmospheric corrosion, charge transfer resistance was the biggest. In 15-45 days, the capacitive reactance arc radius decreased; the charge transfer resistance decreased, and its corrosion resistance ability in gradually declined. But when the exposure time reached 60 days, the capacitive reactance arc radius increased again, which showed that the corrosion resistance improved.

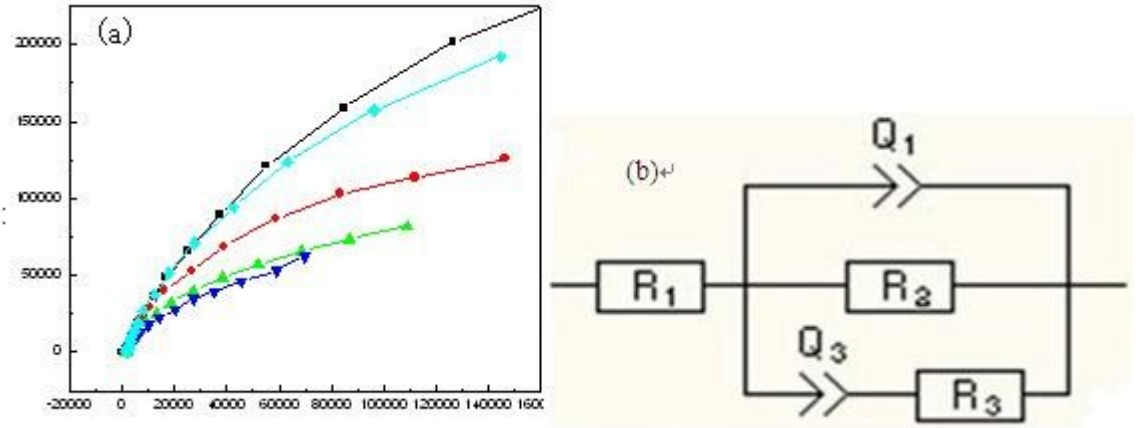

Figure 2 Impedance spectrum curves of experimental steel in different exposure period in Guiyang atmospheric environment (a) the equivalent impedance matching circuit (b)

Like table 3 the solution resistance R1 didn't change too much. Charge transfer resistance R2 of system was very big.This kind of high impedance was supposed to produce a passivation membrane [5]. In 15-45 days, as the atmospheric exposure period increased, the charge transfer resistance R2 decreased. Because samples adsorbed intermediate from the air when the exposure time be longer, and electrolyte concentration, solution conductivity increased. When exposure period reached to 60 days, the impedance resistance increased many and its corrosion resistance improved. This is because the experimental steel surface formed a protective membrane layer.

Table3 Fitting results of impedance spectrum curves of 2Cr13 in Guiyang atmospheric environment

Exposure period	0 day	15 day	30 day	45 day	60 day
R1*(0hm)*	1106	1464	1403	1514	1559
R2*(0hm)*	688597	238089	135685	94817	535576

3.3 corrosion rate of natural environment exposure test

Table 4 The corrosion rate of the experiment steel under different test period

Exposure period (day)	15	30	45	60
corrosion rate (g/㎡ h)	0.0014	0.000389	0.000286	0.000248
The average corrosion depth (mm/a)	0.00158	0.000439	0.000323	0.000280

From the table 4, with the growth of the exposure time, corrosion rate gradually reduced. Within 30 days，the corrosion rate firstly increased with exposure time increased, then corrosion rate reduced very significantly. When exposure period was more than 30 days, corrosion rate changed little,which explained that a relatively stable phase formed in the rust layer with the exposure time increasing . Based on the tenth level standard of metal corrosion resistance in the

former Soviet union [6]， when the exposure period was more than 15 days, the experimental steel was completely corrosion resistant in Guiyang atmosphere. When exposure period was 15 days, it belonged to level 2 -very corrosion resistance.

4. Conclusion

(1) When the exposure period was 0 to 60 days, with longer time, the corrosion current increased firstly then decreased. The corrosion rate is largest in 45 days.
(2) The impedance spectrum showed that passivation process was controlled by the electrochemical reaction,and the charge transfer resistance decreased firstly, then increased with the increase of exposure period.
(3) weight method measured the corrosion rate 0.000280 ~0.00158 mm/a in Guiyang atmospheric environment.It belonged to the level 2 - very corrosion resistance.

Acknowledgments

The authors are indebted to project supported by Social development project, Guizhou Province-Research and Application of Critical Equipment Material in Deep Processing of Phosphate Rock Resources (SY [2013]3072) ,the Research Award Fund for Outstanding Young Science and Technology Talents, Guizhou Province(201315) and the Contract of Science and Technology of Guiyang City(2012205 6-3).

Reference

[1] BoXinTao. Some trends on the development of stainless steel [J]. Journal of heat treatment, 2007, 22 (4) : 4 to 8.
[2] Lin Cui, Wang Fengping, Li Xiaogang. Atmospheric corrosion research method [J]. Journal of Chinese Society for Corrosion and Protection, 2004, 24 (4) : 249-256.
[3] Cao C N, Principle of corrosion electrochemistry [M]. Beijing: chemical industry press, 2008:216-218.
[4] Cao C N, Zhang J Q. Introduction of the electrochemical impedance spectroscopy [M]. Beijing: science press, 2002:45-49
[5] Wang Jun, Han Wei, Li Hongxi etc. Present situation of atmospheric corrosion electrochemical methods [J]. Journal of corrosion science and protection technology, 2002, 14 (6) : 333.
[6] Chen Changfeng Fan Chengwu, Zheng Shuqi etc. The XPS analysis of the surface of G3 nickel-based alloy in high temperature and high pressure H2S/CO2 [J]. Journal of the Chinese Journal of Nonferrous Metals, 2008.

Advanced Materials Research Vols. 989-994 (2014) pp 450-453
© (2014) Trans Tech Publications, Switzerland
doi:10.4028/www.scientific.net/AMR.989-994.450

The Difficulties of Dyeing of Flax Fiber and the Improving Method

ZHANG Qiongyin[1,a], LIU Zhaodi[2,b], ZHANG Yue[3,c],XU Lanbing[4,d*]

[1,2,3,4]Jilin University, Changchun Jilin China 130062

[a]qiongyinzhjilin@163.com,[b]751908729@qq.com,[c]2226110410@qq.com,[d*]xlb822@163.com

Keywords: flax, dyeing properties , fiber modification , improvement methods

Abstract. Flax fiber moisture, permeability, with good wearability. But the flax fiber dyeing performance is poor, light color , there will be color difference, dyeing unequal phenomenon . Through the analysis of the performance of flax fiber dyeing , tells the story of flax fiber dyeing difficulties. This paper introduces the urea, bulking agent, sodium hydroxide, ultrasonic, rare earth and other methods to improve the dyeing properties of flax fiber.

Introduction

As people 's awareness of environmental protection , natural fibers back into the spotlight . Flax fiber moisture absorption, good ventilation , high strength , abrasion resistance, and less dust , easy to clean , with good gloss , comfortable, cool, popular with the international market [1]. Compared with the ramie, hemp , Apocynum , linen fabric style of primitive simplicity, elegant, wearing more comfortable, better serviceability. But flax fibers are also inadequate , fiber toughness, rough, impurity more, in the dyeing process, the fabric color is not bright light,and poor color fastness, , and sometimes there will be color difference[2] . It has been conducting research on flax fibers modified, to solve the problem of poor performance issues flax fiber dyeing.

The difficulties of dyeing of flax fiber

The inherent factors of the difficulties of dyeing of flax fiber are that the flax fibers have a high degree of crystallinity and a high degree of orientation, with more closely structure, the inclination is small, and non-fiber ingredient is high. Flax fibers in the microstructure, the crystalline region is larger than the area of the amorphous region, the smaller the space occupied by the dyeing of the dye molecules can. Meanwhile, the high degree of orientation also hinders the penetration of dye molecule.[3]

Flax fiber contents of at least 5% lignin, lignin is very difficult to be dyed. Removal of lignin in flax roving chemical degumming processes are usually two ways: one is the low temperature chlorination, the other is a high-temperature sulfonation. Regardless of the method, the removal of lignin is less than 40 %. Therefore, after retting flax fiber net no other reason except lignin is difficult to be dyed.[4]

Hemp single fibers bonded together by pectin cross each other, is very difficult to staining. Single flax fiber is very short, only 11 ~ 25mm, cannot be directly spinning. Therefore, to ensure the spinnability and yarn strength, degumming pectin is not completely removed when carrying out the roving. Roving degummed residual pectin spun fibers together, so it is not easy to dip dyeing uniformity, prone to white core yarn and yarn color flowers. [4]

Chemical reactions of flax cellulose mostly occur in the three free hydroxyl group and an aldehyde group at the end of macromolecules. The hydroxyl group is reacted with an inorganic acid-base, and the aldehyde group’s chemical reactions are the dye was adsorbed moisture, oxidation, esterification, etherification and graft reaction. During the formation of the flax roving process to chemically degumming, strong oxidation of serious damage to this process the molecular structure of cellulose hydroxyl and aldehyde groups, thereby reducing the dye is covalently bound to the cellulose and the formation conditions.[4]

The methods of improving the dyeing of flax fiber

To solve the problem of poor dyeability of flax fiber, at home and abroad have been modified flax fiber research,to improve its dyeing properties. The so-called modified flax fiber for flax fiber

is inadequate, chemical or physical methods for its processing, to get some special properties. After modification of hemp fiber processing, improved dyeing properties of the fabric, fabric color is bright, shades affordable.The main method of hemp fiber modification are the following

The urea pretreatment

Put the linen cloth into a certain concentration of urea solution for the pretreatment before staining under the condition of high temperature, it can improve the levelness and dyeing percentage of the linen cloth, and at the same time it does not reduce the dyeing fastness. To a certain extent, it solves the problem of staining difficulties and uneven dyeing on linen cloth. Urea reacts with linen cloth, which makes fiber swell and become more rough on the surface[5].During the dyeing process, urea improves the adsorption capacity to dye of the linen cloth, and increases the chance of reaction between dye and fiber, then improves the dyeing rate and the dyeing depth. After urea modified flax fiber strength decreased slightly, but the decrease is tiny. The reason for the fiber strength decrease of flax fiber is that some fiber on the surface becomes swell and broken after urea treatment.[6].Though the fiber strength decreases slightly, the dyeing properties improves a lot.

The expanders pretreatment

After adding the liquid expanders, the surface tension of the solution will reduce ， the surface area is easy to expand, adding solid expanders, expanders are directed adsorbed on a solid surface. When the expansion agent adsorbed on solid surfaces generally, although reducing the surface tension of the solid, the surface area is difficult to expand. Flax fibers are composed of a linear polymer, the surface area is relatively large, very elongated shape than the flexibility of the molecular chain is preferred. After adsorption flax fiber bulking agents, surface tension reduction, the fiber surface becomes easy expansion, easy to stretch the length of the fabric becomes plump and fluffy。Adsorbed on the fiber surface expansive role of the stronger, more able to reduce the surface tension of the fibers, the better the effect of expansion. Expanders can use flax fiber volume expansion in the same weight, and can significantly improve the absorption characteristics of flax fiber.

Beam expanders unused surface modified flax fiber is smooth, the fibers are arranged between the fiber bundles tightly. Expansion of the role of the use of bulking agents for processing flax fiber, flax fiber bundle expands, the gap between the fiber bundles of fibers increases, the loose arrangement improves the surface roughness of flax fiber to increase its gross efficiency, this facilitates dye adsorption flax fibers in the dyeing process, help to improve the probability of occurrence of dye staining reaction with the fiber, thereby increasing the depth of staining when dyeing. [7]

Dyeing on ultrasonic environment

In the absence of ultrasonic environment, flax fiber dyeing rate is low. In the presence of ultrasonic, as the ultrasonic cavitations effect can make bubbles in the flax fiber left from fiber surface, and disappear quickly. Because ultrasound provides additional momentum to the dye molecules, it is not only can overcome the repulsive force between each other, but also advantageous to the contact between the dye and fiber, and improve the adsorption rate of the dye on the fiber surface. Ultrasound can improve the affinity of reactive dyes to flax fiber, accelerate the absorption of fiber to dye, improve the dyeing rate of dye and the amount of color of the fiber.

But when the ultrasonic frequency reaches 40 kHz, the ultrasonic cavitations effect is too big, and make the friction heat between the fibers, temperature rise, and the adsorption ability of dyeing liquid on the contrary will decline [8].In a relatively short period of time, the ultrasound dyeing is often can achieve even greater effect than that of normal dyeing. When dyeing, if extend the effect time of the ultrasonic, dyeing rate can slow increase; if Increase the frequency of ultrasonic, the ultrasonic can promote the efficiency of dyeing more obvious. The frequency is to higher , the acoustic cavitation in a relatively short period of time is more obvious. The ultrasound dyeing

technology with energy conservation and emissions reduction, shorten processing time and improve the performance of textiles, and many other advantages, it is an important way to improve the flax fiber of dyeing performance.

The alkali treatment

Alkali treatment is mainly generated by the principle of alkaline cellulose flax cellulose with high concentration sodium hydroxide solution. Because of the alkali treatment process to generate alkali cellulose is an exothermic process, so the alkali treatment were completed at normal atmospheric temperature. Flax fiber after sodium hydroxide modified, either dyeing, fabric dyeing rate are improved obviously[2].General with the increase of the concentration of sodium hydroxide, dyeing rate increases, especially vat dye, fabric dyeing rate increased significantly. Also, sodium hydroxide and flax cellulose, flax fibers swell phenomenon, The fiber elastic, with silk, improve the capillary effect and increase the permeability of fiber fiber, The hemp fiber improves elasticity and softness, so that enhance the crease resistance of flax textile. In addition, the flax fibers modified by sodium hydroxide, the crystallinity and orientation degree increases with the concentration of sodium hydroxide and basic linear decline, The polymerization degree of the fiber in alkali treatment decreased rapidly at the beginning, then tends to a constant value. The degree of fiber aggregation, crystallinity and orientation degree increases with the increasing of the concentration of sodium hydroxide and decreased. Dyeing performance of linen fibers decreased with increasing crystallinity, degree of orientation and improved.

Application of Rare Earth in flax dyeing

Rare Earth can be divided into by sulfuric acid complex salt solubility: Light rare earth, rare earth and heavy rare earths. Textile industry is generally based on rare earth chloride. This rare earth chloride ions comes into the flax fibers, then the original arrangement of the fibers is changed, reducing the degree of orientation and crystallinity of the flax fibers, increasing gap between the fibers, dye relatively easily access to fiber interior. Further, a feature of contact of rare earth ions can make the rare earth dye nitrogen, oxygen react to form an ionic organic ligand bond. But complexion ability of rare earth ions is weak. Not all fiber can be coordinated, only partially replaced. Part of the rare earth ions complex with flax fiber, on the one hand has enough acceleration effect, on the other hand combined with fiber, and become the new dye uptake of dye seat. Both in combination with the dye flax fiber and rare earth ions and improve the uptake rate of the fiber. After adding rare earth flax dyeing process, not only can improve the dyeing rate and vividness of dyes and dye to make different dyes of half time approaching. This improves compatibility linen fabric and leveling effect, rare earths used in the dyeing process flax not only improve the flax colored rate fixation rate, But also increased the vividness of linen fabric. Application of rare earth-stained, stained linen for solving difficult problems on providing new solutions for promoting the development of flax textile industry has very important significance.[4,9,10]

The new dye sodium copper chlorophyll

In recent years, there have been reports that some of the synthetic dyes dyeing textiles will cause serious harm to people's health and human living environment.，which forced some new dyes, extracted from natural plant pigment, non-toxic harmless, is the real green dye. And the extraction of plant dyes also has some health care functions. The fabrics dyed by plant pigments are natural shapes, colors, and not easy to fade; There are some natural pigment also has the insect, the role of sterilization, Some clothes such as underwear, children's clothing, the sensitivity of towels, bedding, particularly need these functions. Development of plant dyes are catering to the modern people to return to the nature of consumer psychology. Chlorophyll is a plant widely spreading in the pigment chlorophyll, but poor stability, make its application limited. However, chlorophyll derived from sodium copper chlorophyll stability is relatively high, the water solubility is very good. It is a bright green color pigment. The studies show that, in the dyeing process with sodium copper chlorophyll concentration increased, the dyeing rate is not always increased but increased at first and

decreased again in the peak. When the mass concentration of 1 g /L, dyeing rate reached its peak.[11]

Epilogue

Linen fabric heat quickly, wearing a cool , solid wear, but the poor performance of its coloring , there are many difficulties in the dyeing process of flax fibers . In order to improve the dyeing properties of flax fibers , we can use urea, expansive for flax pretreatmentwe,can also be dyed in rare earth, alkaline and ultrasonic environment,we can also use the new sodium copper chlorophyll dye dyed flax these methods can effectively improve the dye uptake flax fiber.

References

[1] GAO Shuzhen, ZHAO Amu: Research flax fiber dyeing properties [J], Journal of Qiqihar University, Vol.17 , No.1 , Mar.2001. In Chinese
[2] WU Hongling, XU Shunji, JIANG Shaojun: Research on dyeing properties of alkali modified flax fibers [J], Progress in Textile Technology, No. 2 , 2007. In Chinese
[3] GUO Yalin, ZHAO Ming, HUANG Gu, etc: Affect the structural properties of flax fiber dyeing performance [J], Journal of Dalian Institute of Light Industry, Vol. 20, No. 1, Mar. 2001. In Chinese
[4] SHI Jiaqiang, DONG Qinxia: Application flax fiber dyeing Difficulties and rare in flax roving dyeing [J], Textile Auxiliaries, Vol.14, No .2, Apr.1997. In Chinese
[5] JIANG Xiankai, SUN Hongyan, LIN Long,etc: Urea improved dyeing properties of flax fiber pad[J], Journal of Natural Science of Hei Longjiang University, Vol.22, No.11, February.2005. In Chinese
[6] SUN Hongyan, JIANG Xiankai, DAI Xuduo,etc: Improvement of flax fiber pad dyeing properties [J], Chemistry and Bonding, Vol. 27, No. 3, 2005. In Chinese
[7] JIN Zheng, JIANG Xiankai, SUN Hongyan, etc: Expanders for flax fiber pad dyeing performance improvements [J], Journal of Natural Science of Hei Longjiang University, Vo l.25, No.1. In Chinese
February.2008
[8] CUI Guixin: Study on the application of ultrasound in dyeing of linen fabric [J], Textile Auxiliaries, Vol. 29 , No.12 , Dec.2012. In Chinese
[9] DONG Qinxia, WEN Yuhua, MENG Fanjie: Application of Rare Earth in flax dyeing [J], Textile Auxiliaries,Vol.9, No.4, Dec.1992. In Chinese
[10] WEI Zengzhong: On the application of rare earth chloride in flax dyeing [J], Heilongjiang Textile, Aug. 1997. In Chinese
[11] WANG Lijuan, FENG Hao, LI Jian: Sodium copper chlorophyll flax fiber dyeing performance study [J], Chemistry and Industry of Forest Products, Vol. 27 Supplement, Oct. 2007. In Chinese

Advanced Materials Research Vols. 989-994 (2014) pp 454-457
© (2014) Trans Tech Publications, Switzerland
doi:10.4028/www.scientific.net/AMR.989-994.454

Spatial Distribution of Heavy Metal in Urban Soil of China

Xiuxia LI

School of Art and Design，Xinxiang University,Henan,China,453000

14878670@qq.com

Keywords：topsoil; heavy metal; pollution

Abstract: There are significant regional differences of the heavy metals contents in urban soils in China. The heavy metals contents in urban soils of the eastern, central and western regions are quite different, and the pollution of capital cities and prefecture -level cities are different. The study about spatial variability, time differences, pollution levels and environmental risks of heavy metals from China's urban soil show that the heavy metal contents in Chinese cities are over the soil background value in China, especially the contents of Cd and Pb , which were 91.37 times and 41.91 times to the Chinese soil background value. And the content of Ni l is only 1.59 times to the Chinese soil background value.There are also obvious differences among different functional areas the city. Meanwhile, the metal content of urban soils change with the length of time of urban development. Nemero comprehensive pollution index of China's urban soil heavy metal was 45.404, which is heavily polluted. The potential ecological risk index of China's urban soil heavy metal is 71.56, which is high potential ecological risk. Different levels of urban pollution with development degrees cause the different environmental risks.

0 Introduction

At present, urban soil heavy metal is still hot topics in the study of environmental science, urban soil is the main medium of heavy metals. As a result, the soil heavy metal research to find out the relationship between human activity and city environment which is of great significance, many scholars studies have found that the city of soil heavy metal has two sources of natural and human activity, especially the accumulation of human activities on the urban soil heavy metal has great influence. Emissions from human activity of various substances in the form of atmospheric particles gas exists in the urban environment, causing the urban environmental problems, these substances into the urban soil in the form of atmospheric dust and so on, which pose a threat to human health through different channels[1].

China is a large country, and a huge number of cities is intensive human activities, but different regions have different levels of urban development. At present the study of China's urban soil heavy metal few, this article analysis the different cities in China from different angles of soil spatial distribution characteristics of heavy metals, understand the different geographical and economic development level in different cities of China the characteristics of spatial distribution and the pollution of heavy metals in soil, thought the city social and economic development.

1. Materials and methods

Urban soil sampling and experimental materials and methods are shown in table 1, the depth of the urban soil sampling of 0 ~ 20 cm 0 ~ 10 cm. Urban soil sampling points the main layout in different functional areas of the city, such as parks, green residential areas such as roads, using mixed four points from 1 to 1.5 kg of samples, indoor after drying, sieving, grinding process such as standby experimental samples. Sample digestion method is HNO3-HCl-HClO4, HNO3 -H2SO4-H2O2, HF-HClO4-HNO3 and mixed acid digestion. Finally, digestion samples by atomic absorption method, atomic fluorescence method, X-ray fluorescence spectrometry and different methods such as plasma emission spectrometry determination of Cu, Pb, Zn Ni Hg As Cd Cr content in urban soil samples values, these methods are in accordance with relevant national soil sample treatment method[2].

2. Results and discussion

China's urban soil heavy metal content changes

China's urban elements of Cu,Pb,Zn,Cd,As, Mn, Ni ,Cr, Hg and so on which content in soil change range is13.2~112.14 mg/kg ,12.98~25 380.55 mg/kg,58.80~2386.84 mg/kg, 0.11~130 mg/kg ,3.6~39.8 mg/kg,551.47 ~620.39 mg/kg ,12.3 ~73.5 mg/kg ,29.7 ~590.1mg/kg, 0.06~0.414 mg/kg.The average content of each is40.78 mg/kg 1132.71 mg/kg 306.35 mg/kg 8.86 mg/kg18.48 mg/kg 576.17 mg/kg 35.83 mg/kg 112.81 mg/kg0.21 mg/kg，which are China's soil environmental background value of 1.80, 43.57, 4.13, 88.60, 1.65, 0.99, 1.33, 1.85, 1.33 times.Besides Hg, the rest of the standard deviation of heavy metal elements are larger, that they have larger discrete degree, especially the Pb.

China's urban the spatial variation of soil heavy metal pollution

China's urban soil heavy metal content has obvious space difference, as shown in figure 1，shows that China's urban soil heavy metal Cu and Ni, content of the wast> content of the central>content of the east. The content of Pb, Cd and Hg are the east> the central>the wast, the content of Zn and Cr are the east>the west>the central, the central of As is the central> the eastern > the western. At the same time, the Chinese provincial level city of Cu, Pb, Zn, Ni, Hg and Cr content in soil were higher than prefecture city, and the content of Cd and As is the regional cities above the provincial level.

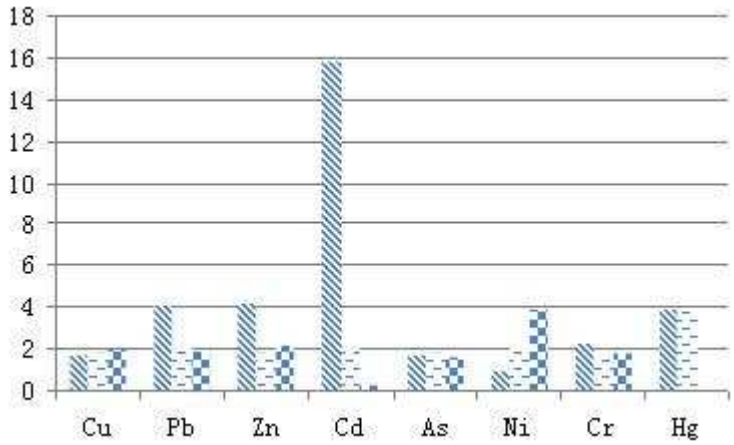

Fig 1. Metal content in different regions

the research on a single city of heavy metals in soil mainly carried out in accordance with the functional partition, city differences in soil heavy metal content in different regions[3]. characters of space distribution of soil heavy metals of guangzhou city, the study found that the soil heavy metal integrated pollution index for the size of the order isold industrial area>traffic area>the new residential area>the new development zone>business zone >the old residential areas>park. Such as Wu yongfeng study of Guiyang city soil heavy metal content differences, different functional areas of potential ecological harm degree of order is industrial park>park>traffic area>suburban farmland>residential area. Such as Yaode qingdao the results showed that the trend of the distribution of all kinds of heavy metal element content is in the southwest and south coastal is higher, central is the second, the east within the scope of the basic background value. Wang zhikun for Luoyang research has shown that the Luoyang city with the approaching of the suburbs to the city of heavy metal pollution, soil heavy mental, the initial pollution→mild contamination→middle level pollution→serious contamination→very high levels of pollution. Kang lingfen the study found that lanzhou city industrial park, the soil polluted by heavy metals is the most serious, followed by the road on both sides and residential areas, and degree of soil contaminated the lightest in the park.

China's urban soil heavy metal time difference

for China's urban soil heavy metal content of the research time is less, in different cities of soil heavy metals were as the city the increase of the formation of a certain land use type time accumulated gradually, and gradually accumulated content. Such as Li Youguo study of soil heavy metal content in nanjing city soil heavy metal with the increase of land use of our time has obvious trend of accumulation, a significant time difference. Gu Dening of Zhengzhou city soil heavy metals such as the study found that zinc content is higher in early urbanization area, the distribution of other elements and the relationship between urbanization history is less obvious. Fu Juanlin study of hangzhou city residential quarters of soil heavy metal content in residential area with the increase of the formation of the residential area time increased significantly.

2.China's urban soil heavy metal pollution assessment and risk analysis

Soil heavy metals in the overall China city, the Nemerow comprehensive pollution index is 45.40, belonging to heavy pollution Pb, zinc, Hg, Cd, Cr, the comprehensive pollution index were 13.98, 22.84, 948.65, 6.88, 4,. 55, belong to high levels of pollution.The most polluted heavy metal elements are Cu, Cd, Ni,As ,which the comprehensive pollution index were 2.35 ,2.55, 2.60, belongs to the moderate pollution, pollution is the lightest of heavy metal elements Cu.

Level every provincial capital cities in China and in the special administrative region, Hong Kong, Guangzhou, Changsha, Shanghai, Hangzhou, Nanjing belong to high levels of pollution of heavy metal pollution, basic is concentrated in the coastal city in the east. Changchun, Guiyang and Xi 'an cities such as the pollution of heavy metal pollution is moderate; Urumqi, shenyang, Hefei, Zhengzhou, Taiyuan and other mid-western cities of heavy metal pollution is light pollution. In the regional city, is located in the east or coastal, such as Xuzhou, Qingdao, Xiangtan, Zhuzhou belongs to high levels of pollution of heavy metal pollution, Baotou, Zhangzhou, Shenzhen belong to moderate pollution of heavy metal pollution, Luoyang and Wenzhou for light pollution. Taicang city for light pollution of heavy metal pollution. China city of Qingdao is the most serious soil heavy metal pollution, inside the comprehensive pollution index was 955.09, mainly due to the Qingdao's Cd pollution is very serious, its value to the Chinese soil Cd element background value of 1340.21 times; Soil heavy metal pollution in cities is the lightest taicang city at county level. Soil heavy metal pollution in cities is the lightest Taicang city at county level[4].

Research shows that China's urban soil heavy metal composite potential ecological risk index was 71.56, potential ecological risk degree is advanced. Including Cu, Pd, As, Hg comprehensive potential ecological risk index were 190.72, 357.33, 43858.45, 144.93, 924.92, and the potential ecological risk degree is advanced. Ni, Cr composite potential ecological risk index were 58.08, 52.12, potential ecological risk degree for the intermediate. Zn composite potential ecological risk index is70.63, potential ecological risk degree is higher. Potential ecological risk was highest heavy metals Cd, the lowest for Cr, In the provincial capital cities and in the special administrative region, Hong Kong, Changsha, Shanghai, Shenyang, Hangzhou, Taiyuan city soil heavy metal potential ecological risk degree is advanced. Guiyang and Hefei have higher degree of soil heavy metal potential ecological risk. Changchun, Guangzhou,Xi 'an and Nanjing city belongs to the intermediate soil heavy metal potential ecological risk degree, Urumqi and Zhengzhou city soil heavy metal potential ecological risk is low. Regional cities, Xiangtan, Zhuzhou, Luoyang, Xuzhou, Qingdao Zhangzhou, Shenzhen city soil heavy metal potential ecological risk degree is high. Baotou city soil heavy metal potential ecological risk is higher, the wenzhou city soil heavy metal potential ecological risk is low. County-level city Taicang city soil heavy metal potential ecological risk of intermediate, the highest potential ecological risks of soil heavy metals in Chinese cities are Qingdao, comprehensive potential ecological risk index is 40222.51,is mainly due to the Qingdao Cd content is higher, and Cd toxicity coefficient is higher.Zhengzhou city soil comprehensive potential ecological risk index is 21.93, the lowest potential ecological risk degree.

3.Conclusion

Soil heavy metal content in Chinese cities exceeds the soil background value, especially the Cd and Pb pollution is serious, the content of China soil background values are 91.37 times and 41.91 times, Ni pollution lighter, its content is 1.59 times of China soil background values. China's urban soil heavy metal content is obvious regional differences, the eastern, central and western regions of urban soil heavy metal content difference is bigger, have different pollution level in the provincial capital cities and regional cities, city also exists obvious difference between different functional areas.

Within the soil heavy metals in Chinese cities, the comprehensive pollution index is 45.40, belong to high levels of pollution.China's urban comprehensive soil heavy metal potential ecological risk index is 71.56, potential ecological risk degree is advanced.Different levels of urban pollution degree is differ, environmental risk is also different.

Reference

[1] Li X, Huang C. Environment impact of heavy metals on urban soils in the vicinity of industrial area of Baoji city, P.R.China[J]. Environmental Geology, 2007, 52: 1631-1637.

[2] Zhong X, Zhou S, Zhao Q. Spatial characteristics and potential ecological risk of soil heavy metals contamination inthe Yangtze River delta—a case study of Taicang city, Jiangsu Province[J]. Scienia Geographica Sinica, 2007, 27:395-400.

[3] Chen H, Zhou J, Jin Y, et al. Concentration and chemical speciation of Cu, Zn, Pb in Wenzhou urban soils[J]. Journal of Soil and Water Conservation, 2007, 21: 75-78.

[4] Xi C, Dai T, Zhang H, et al. Investigation and assessment on pollution of soil heavy metals in Xiangtan City [J].Bulletin of Soil and Water Conservation, 2008, 28: 133-137.

Advanced Materials Research Vols. 989-994 (2014) pp 458-461
© (2014) Trans Tech Publications, Switzerland
doi:10.4028/www.scientific.net/AMR.989-994.458

Research on chloride appropriate dosage for incorporated accelerated corrosion

Qixia Liu[1, a], Shulin Zhan[1,b]

[1] College of Civil Engineering and Architecture, Zhejiang University, Hangzhou 310058, China

[a]qixia@zju.edu.cn, [b]jzcl@zju.edu.cn

Keywords: Incorporated Accelerated Corrosion, Nacl, cl^-, Potential

Abstract. Mixing chlorine is one of the ways to ensure the theory and practical steel bars corrosion rate closer when mixing concrete for laboratory electrochemical accelerated corrosion and appropriate chloride dosage should guarantee the steel bars are in the critical corrosion state when we start to accelerated corrosion. By comparing the specimens' experimental compressive strength, chloride-permeation resistance, corrosion potential measured by the half-cell potential method and polarization potential curves measured by the linear polarization potential method with different Nacl dosage, we get the appropriate Nacl dosage is nearly 1.90%, namely cl^- content is about 1.15%.

Introduction

The durability of concrete is insufficient, especially premature failure of concrete structures caused by steel bars corrosion has become a big disaster [1], so it's necessary to study the steel bars corrosion in concrete. Laboratory electrochemical accelerated corrosion is a simple and effective method to get reinforced concrete corrosion specimens [2] and the key point of experiment is to ensure theory and practical steel bars corrosion rate closer so that in actual control current, stipulated time etc. condition we can get needed corrosion specimens, further to ensure the accuracy of experiment. But for electrochemical corrosion, some research has shown that the difference between theory and practical corrosion rate is bigger if we don't mix chlorine in concrete, more than 40% [3], that's because steel bars are passivated at first and have a reaction of electrolysis of water on the surface leading to part of the current loss until OH^- on the surface is reduced enough that can cause the passivation membrane damage and then the steel bars start to corroded if we don't mix chlorine. Therefore in order to ensure the theory and practical steel bars corrosion rate closer we can mix chlorine when mixing concrete. But, for the critical content of cl^- leading to steel bars corrosion, Glass etc. have a conclusion on the critical value, including 0.2%~0.7%,0.4%,1.15%, 0.4%~2.5% etc.[4], not a certain value; and chloride appropriate dosage for incorporated accelerated corrosion should make sure that steel bars are in the critical state of corrosion after 28d's standard curing. So for laboratory electrochemical corrosion, because of uncertain critical content of cl^- and the particularity of appropriate dosage, research on chloride appropriate dosage for incorporated accelerated corrosion has important significance. The content of chlorine and cl^- are a proportion of gelled material in this paper.

Experiment

Materials. (1) Cement: a company in Hebei province, P·I 42.5;(2) Fine aggregate: river sand, fineness modulus of 2.9, medium sand;(3)Coarse aggregate: grading continuously, grade 5 ~ 25;(4) High efficiency water reducing agent: a company in Jiangsu province, JM-II series;(5) Water: tap water;(6) Chloride: Nacl;(7) Steel bars: a company in Zhejiang province, · 16.

Design of Concrete. We need C30 concrete which having sand rate 40% and water cement ratio 51%. By the regulation of water reducing agent to make sure the concrete slump is 180~ 220 mm. Cooperate for finalized per cubic meter of concrete is cement C = 402 kg, water W = 188 kg, sand S = 734 kg, stone G = 1076 kg, water reducing agent A = 1.61 kg. In order to study the appropriate dosage as Nacl plays the role of chlorine, we design 7 kinds of dosage. Specific Nacl content are shown in

Table 1, especially R0 doesn't contain Nacl as a comparison.

Table 1 Different Nacl and cl^- content

No.	Dosage of Nacl（%）	cl^- content（%）
R0	0	0
C1	0.33	0.20
C2	0.66	0.40
C3	1.00	0.61
C4	1.90	1.15
C5	3.30	2.00
C6	5.00	3.04

Test Methods. Nacl is a kind of early strength agent and affects the concrete compressive strength. According to the mechanism that Nacl causes early strength, the cl^- playing the role of early strength agent is fixed in the form of compounds with minerals in cement[5], but steel bars corrosion causing by the damage of passivation membrane needs free cl^-.Therefore, in order to reduce the mixed Nacl's effect on concrete mechanics performance and ensure the exist of free cl^-, we prepare 7 groups of 100mm×100mm×100mm specimens with different Nacl content according to table1 and measure the compressive strength of 3d, 7d, 28d and electric flux of 28d after 28d's standard curing. After that, we provide the basis for determining Nacl appropriate dosage by comparing the results of 6 groups with Nacl with the reference group.

Corrosion of steel bars in concrete is an electrochemical process and electrochemical method is the direction to detection steel rebar corrosion, half-cell potential method and linear polarization potential method are two kinds of widely used methods [6].This article combines two methods to more accurately evaluate the state of steel rebar corrosion. Therefore, we make 6 100mm ×140mm× 280mm specimens with Nacl content of C1 ~ C6 shown in table 1 and place a ·16 in each specimen's central cross-section, which having 20mm protective layer thickness and extending the specimen's ends 15 mm respectively. In order to reduce the humidity effect on corrosion potential, we put the 6 specimens in outdoor for 1d after 28d's standard curing .Through the comparison of experimental steel bars corrosion potential with half-cell potential method and polarization potential with linear polarization potential method that we determine the appropriate cl^- content.

Results and Discussions

Concrete Compressive Strength and Electric Flux. The compressive strength of 3d, 7d and 28d for 7 groups of specimens is shown in figure 1 and 28d's electric flux is shown in figure 2. Figure 1 shows that compressive strength of 3d, 7d for the six groups of specimens with Nacl is higher than the specimen not has Nacl, so Nacl plays a role of early strength agent. Compared with R0 , the compressive strength of 28d for the specimens with dosage of C1 ~ C5 increases by 9.32% , 6.12%, 6.50%, 2.93% and 1.40% respectively ,but the specimen with C6 decreases10.22%, which meaning the dosage is excessive leading to the decrease of strength in case of C6 with 5.00% Nacl. As is shown in figure 2,compared with R0 the electric flux decreases by 15.10%, 11.85% and 15.10% respectively for the specimens with C1 ~ C3, while for the specimens with C4 ~ C6 electric flux increases by 37.37%, 146.93% and 202.21% respectively. That's because when we mix Nacl, in the case of content with C1 ~ C3, the compressive strength of 28d is higher than R0 leading to the increase of close-grained degree, but cl^- is fixed in the form of compounds, so just for the reason of the increase of concrete's resistance to cl^- permeability resulting in a decline in electric flux; while for C4 and C5, the compressive strength of 28d is higher than R0 leading to the increase of concrete's resistance to cl^- permeability, but for the reason of the increase of Nacl resulting in existing free cl^- and leading to the increase of migration cl^- for electrical flux experiment, so the measured electric flux increases ; in the case of content with C6, the excessive Nacl not only makes the concrete compressive strength of 28d fall, which leading to the reduce of concrete's resistance to cl^- permeability, but also causes the increase of free cl^-, so the measured electric flux increases. Considering concrete

compressive strength, C2 ~ C5 changes smaller, and in the case of C4 free cl^- starts to exist, so the Nacl's dosage should be nearly C4, namely the appropriate cl^- content is about 1.15%.

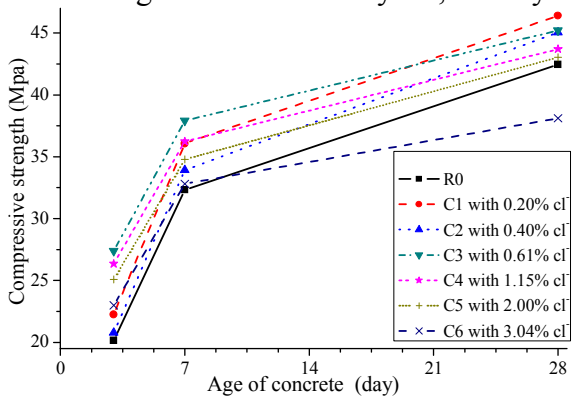

Fig. 1 Concrete compressive strength as the age changes

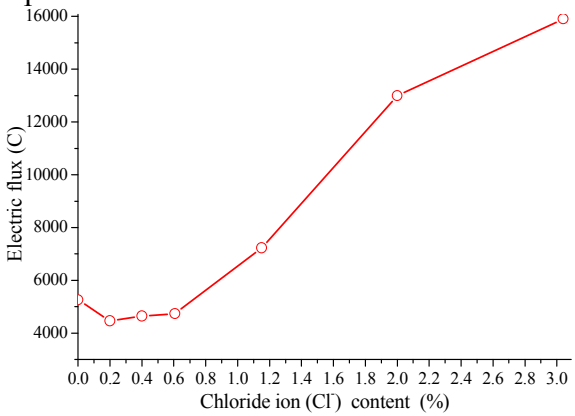

Fig. 2 Concrete coulomb electric flux as the chlorine ion changes

The Detection to Steel bars Corrosion with Half-cell Potential Method. Figure 3 shows how to detect with half-cell potential method and each specimen is divided equally into seven parts along the vertical section so that we can get six test points. The 6 specimens' steel corrosion potential curves after 28d in curing room and 1d in outdoor place is shown in figure 4.If we use half-cell potential method and under the condition of single electrode method, it is considered that the steel bars begin to corrosion when the potential is less than -400mv, but the potential is susceptible to environmental relative humidity, water cement ratio, protective layer thickness, cl^- content etc., so the steel bars corrosion state should be comprehensive evaluation by combining with other test methods [7].As is shown in figure 4, six test points' corrosion potential for the specimens with dosage of C1 ~ C3 are greater than - 400 mv, but from specimen with dosage of C4 six test points' corrosion potential are less than -400mv and specimen with C4 has a mutation compared with specimen with dosage of C3. Although the evaluation method with half-cell potential method is rough but we can still get that steel bars start to corrode from the dosage of C4, so the Nacl's dosage should be nearly 1.90%, namely the appropriate cl^- content is about 1.15% .

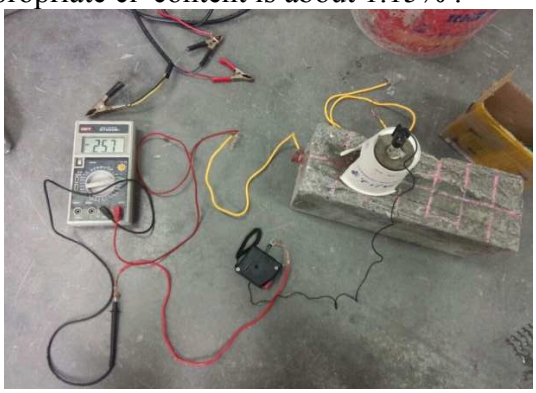

Fig. 3 The detection to steel bars corrosion in concrete with half-cell potential method

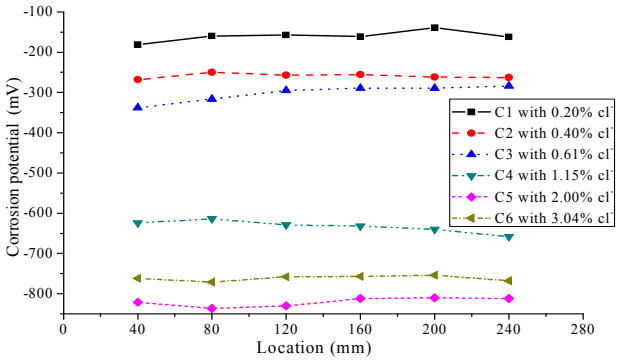

Fig. 4 Steel bars corrosion potential with half-cell potential method

The Detection to Steel bars Corrosion with Linear polarization potential method. Figure 5 shows how to detect with linear polarization potential method and both of the specimens' ends are sealed with epoxyresin. We measure the six different Nacl content specimens' potential within 60 minutes under constant current of 7.03 A, as is shown in figure 6. It can be found that the anode steel potential rapidly rises to the positive direction since power for the specimens with dosage of C1 ~ C3 and the potential value holds steady after 60 minutes' test, meaning the curves are passivated and the steel bars' surface passivation film is in good condition for that specimens. Since the dosage of C4, the anode steel potential rises to positive direction at first and gradually declines within 60 minutes for the specimens with dosage of C4 and C6, suggesting that the steel bars' surface passivation film is partially damaged and the steel bars exist damage; the anode steel potential has been negative at the

first 30 minutes and then holds a stable upright for specimen with dosage of C5, suggesting the steel bars' surface passivation film is damaged seriously than specimen with dosage of C6 and supporting the result that steel corrosion potential with half-cell potential method for specimen with dosage of C5 is minimum in figure 4, possibly caused by the reason that the steel rebar has been partial corrosion before making the specimen with dosage of C5 . Therefore, it can be concluded in the case of the specimen with dosage of C4 that the steel bars passivation film begins to appear partial damage and bars start to corrode with polarization potential method, so the Nacl's dosage should be controlled nearly the situation of C4, namely the appropriate cl^- content is about 1.15% .

Fig. 5 The detection to steel bars corrosion in concrete with linear polarization potential method

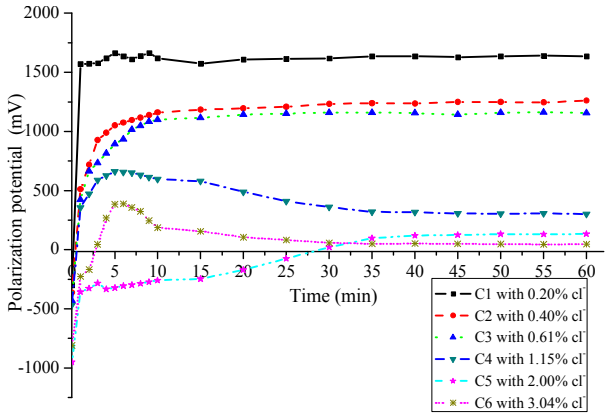

Fig. 6 Steel bars polarization potential with linear polarization potential method

Summary

According to this paper's experimental study, we find that when the mixed chloride is Nacl for incorporated accelerated corrosion, no matter in order to reduce the mixed Nacl's effect on concrete mechanics performance and ensure the exist of free cl^-, or through the comparison of steel corrosion potential with half-cell potential method and steel polarization potential with linear polarization potential method, if incorporated accelerated corrosion experiment depends on this paper's concrete mix proportion and materials , the appropriate Nacl dosage content is nearly 1.90%, namely the cl^- dosage content is about 1.15%, that can ensure the steel bars in concrete are in critical state of corrosion when we start to accelerated corrosion.

References

[1] Weiliang Jin, Ditao Niu, The state-of-the-art on durability and life-cycle design theory of engineering structures, Engineering Mechanics. 28 (2011) 31-37.
[2] Weizhong Gan, Weiliang Jin, Mingzan Gao, Applicability study on accelerated corrosion methods of steel bars in concrete structure, Journal of Building Structures. 23 (2011) 41-47.
[3] Yanhong Zeng, Xianglin Gu, Weiping Zhang, Qinghua Huang, Accelerated corrosion technique for reinforcement steel bars in concrete, Structural Engineers. 25 (2009) 101-105.
[4] GK Glass, NR Buenfeld, The presentation of the chloride threshold level for corrosion of steel in concrete, Corros. Sci. 39 (1997) 1001-1013.
[5] Zhenguo Gao, Yonghui Luo, Hao Shi, The research and exploit for concrete hardening accelerator without Na^+ and K^+, Low temperature construction technology. 3(2002) 67-68.
[6] Xiaoyong Luo, Yanghang Shi, Comment on onsite testing technology of corrosion for steel in reinforced concrete, Low temperature construction technology. 23(2008) 39-45.
[7] Weiping Zhang , Yu Zhang, Yaqin Liu, Electrochemical methods for investigation of reinforcement corrosion in concrete, Low temperature construction technology. 28(1998) 21-32.

Advanced Materials Research Vols. 989-994 (2014) pp 462-466
© (2014) Trans Tech Publications, Switzerland
doi:10.4028/www.scientific.net/AMR.989-994.462

Effects of feed rate and pH value on the physical and electrochemical properties of LiNi0.4Co0.2Mn0.4O2cathode material for lithiumion battery

Fang Du, Liangfu Peng

Southwest University for Nationalities, College of Electrical and Information Engineering, Chengdu 610000, China

duf2547@163.com

Key words: cathode material, co-precipitation method, morphology, electrochemical properties, LiNi0.4Co0.2Mn0.4O2

Abstract. The layered LiNi0.4Co0.2Mn0.4O2was synthesized by co-precipitation method using carbonate sodium as precipitant. The microscopic structural features and morphologies of as-prepared cathode materials were investigated using X-ray diffraction (XRD) and scanning electron microscopy (SEM). And then, the charge-discharge measurements were carried out to determine the electrochemical properties in a voltage range of 2.5-4.6 V. The results show that the pH value in the process of co-precipitation reaction plays a greater part on the electrochemical properties than feed rate does. The cathode materials prepared at higher pH value illustrate better electrochemical properties in the voltage range of 2.5-4.6 V, which can be attributed to a less cation mixing in the cathode material as well as the smaller primary particles and the smaller second particles.

Introduction

Lithium-ion batteries have currently become attractive for portable electronic devices because of their higher output voltage and energy density than other rechargeable systems. Since the introduction of lithium ion batteries in 1990, the layered LiCoO2 cathode has been a popular cathode material because of its ease of production and excellent electrochemical properties, such as high energy density, stable cycling performance and wonderful ratecapability1, 2.However, the relatively high cost and toxicity of cobaltas well asa lure of larger practical cyclic capacity have led to the study of other cathode materials for lithium ion batteries 3 [1-5].

LiNi1-y-zCoyMnzO2cathode materialpossessing the same structure as LiCoO2hasattracted a lot of interest because it combines lower cost with largerpractical cyclic capacity by introduction of Mn and Ni compared to LiCoO24–9. So far, LiNi1-y-zCoyMnzO2cathode materials with different electrochemical performance by adjusting the ratios of Ni, Co and MninLiNi1-y-zCoyMnzO2 have been successfully commercialized. Nevertheless, the new application of lithium ion batteries on the smart phone challenges the present commercialized cathode materials including LiNi1 y zCoyMnzO2 cathode material 10. So, the researches on the enhancement of cyclic capacity of the LiNi1-y-zCoyMnzO2cathode material still draw a great attention11 [6-10]. In general, the increase of Ni content in the LiNi1-y-zCoyMnzO2 is believed as an effective approach to the enhancement of cyclic capacity. However, a high content of Ni in the LiNi1-y-zCoyMnzO2 leads to a deterioration of safety for lithium ion battery and a difficulty for fixing lithium ion batteries in practical application. Therefore, other researches focus on the enhancement of cyclic capacity of the LiNi1-y-zCoyMnzO2 cathode material via raising the upper cut-off voltage which usually result in a poorer cyclic performance12. And, the investigations on doping or coating LiNi1-y-zCoyMnzO2 cathode material were highlighted in recent year since doping or coating was supposed as an significant modification method for many cathode materials and was greatly helpful to the cyclic performance of LiNi1-y-zCoyMnzO2 cathode material even when the upper cut-off voltage is raised to 4.6V. Nevertheless, few work concerns about the effect of the synthesis condition on the electrochemical properties of LiNi1-y-zCoyMnzO2 cathode material when the upper cut-off voltage is raised to 4.6 V [11-14].

In this paper, LiNi0.4Co0.2Mn0.4O2 was chosen as the target cathode material. And then, the effects of feet rate as well as pH value on the physical and electrochemical properties at voltage range of 2.5–4.6 V were investigated in detail.

Experimental

All samples were prepared via a conventional process including co-precipitation and calcinations. The reagent-grade NiSO4·6H2O, CoSO4·7H2O and MnSO4·H2Owere used as starting materials. Firstly, NiSO4·6H2O, CoSO4·7H2O and MnSO4·H2O were dissolved in distilled water in term of formula (Ni0.4Co0.2Mn0.4)CO3. The content of sulfate salt solution was specified as 1 mol L-1. Na2CO3 was used as precipitant and was dissolved into solution of 2 mol L-1. Meanwhile, 1 mol L-1 ammonia solution was used as additive to facilitate the morphologies of (Ni0.4Co0.2Mn0.4)CO3 particles. The sulfate salt solution, Na2CO3 solution and ammonia solution were separately fed into a tank reactor. The ammonia content in the reaction solution was maintained about 0.2 mol L-1 in the process of co-precipitation reaction. The pH values in the reaction solution were adjusted by Na2CO3 solution. And, the temperature of reaction was kept approximately 50 °C. The co-precipitate was aged 2 hours at temperature of 50 °C and then washed using distilled water. And soon afterwards, the co-precipitate was dried at 120 °C over night. The dried co-precipitate was mixed with the excess 5% amount of Li2CO3 in term of Li1.0Ni0.4Co0.2Mn0.4O2. The mixtures were fired in a furnace at 550°C for 5 h and then sintered at 900 °C for an additional 12 h. Finally the samples were cooled directly to room temperature at furnace. The samples prepared at different feed rates of 3 mlmin-1, 5 mlmin-1 and 7 mlmin-1 when the pH value was kept at 9.5 were designated as a, b and c, respectively. Additionally, the samples prepared at different pH values of 9.0, 10.0 and 10.5 when the feed rate was maintained at 7 mlmin-1 were labeled as d, e and f.

The structure for as-synthesized cathode materials were characterized by X-ray diffraction (XRD, D/max 2200/PC, Rigaku, 40kV, 20mA, Cu Kα radiation, λ=1.5406 Å), the size and morphology of the cathode materials were observed with a scanning electron microscope (SEM, Hitachi S-5200).
For the electrochemical measurements, the LiNi0.4Co0.2Mn0.4O2 materials were mixed with 10 wt% carbon black and 10wt% polytetrafluoroethylene binder. This mixture was coated on an aluminum mesh and dried under vacuum at 100°C for 12 h. The cell consisted of a cathode, lithium metal anode and Celgard 2500 separator. The electrolyte was a 1:1 (in volume) mixture of ethylene carbonate (EC) and dimethyl carbonates (DMC) containing 1 M LiPF6. The galvanostatic charge and discharge were controlled between 2.5 and 4.6 V on Arbin BT2000 instrument.

Results and discussion

Table 1 Lattice parameters and ratios of I(003)/I(104) for cathode materials (a, b, c) prepared at different feed rates and for cathode materials (c, d, e, f) prepared at different pH values

Sample	a (Å)	c (Å)	V (Å3)	c/a	I(003)/I(104)
a	2.87627	14.23316	101.97	4.948	0.78
b	2.86459	14.21553	101.02	4.963	0.79
c	2.87627	14.26473	101.91	4.959	0.91
d	2.87049	14.22815	101.53	4.957	0.75
e	2.86821	14.22428	101.34	4.959	1.09
f	2.87051	14.23717	101.59	4.960	1.55

Figure 1 shows XRD patterns for cathode materials (a, b, c) prepared at different feed rates and for cathode materials (c, d, e, f) prepared at different pH values. The positions of peaks in all XRD patterns are almost the same.And, the XRD patterns can be indexed based on α-NaFeO2 structure with R $\bar{3}$ m space group.No impurity phase was detected in all patterns.

In earlier report 13,14, the c/a ratio was used to determine the hexagonallity of a layered material. And it is believed that the material possesses layered characteristics when the c/a ratio is more than 4.899.Moreover, it is generally supposed that the cations ordering of the α-NaFeO2 structure can be indicated from the I(003)/I(104) peak intensity ratio 15,16. So, the lattice parameter values as well as the ratios of I(003)/I(104)are calculated and given in table 1. The lattice constants of a and c for

different sample are slightly different and there is no obvious regularity. Furthermore, the c/a ratios for all samples are very close and more than 4.899, which indicate the as-prepared cathode materials possess layered characteristics. And, there is no obvious regularity, as well. Nevertheless, there are distinct difference among the I(003)/I(104) ratios for different cathode materials. The I(003)/I(104) ratios of cathode materials are lower than 1.2 when the pH value is less than 10.0 in the process of co-precipitation reaction. Moreover, the I(003)/I(104) ratios of cathode materials rise when the pH values increase and the I(003)/I(104) ratio reaches to 1.55 when the pH value is 10.5 in the process of co-precipitation reaction, which indicate that the cations mixing can be alleviated by raising the pH value in the process of co-precipitation reaction. The reason can be attributed to a more homogeneity of transition metal ions in the co-precipitant when the pH value rises in the process of co-precipitation reaction. The complexation of aqueous ammonia is unfavorable to co-precipitation reaction for different transition metal ions though aqueous ammonia is greatly helpful to the formation of spherical particles. The complexation of aqueous ammonia becomes weaker when the pH value rises in the process of co-precipitation reaction. So, a more homogeneity of transition metal ions in the co-precipitant can be achieved when the pH value rises.

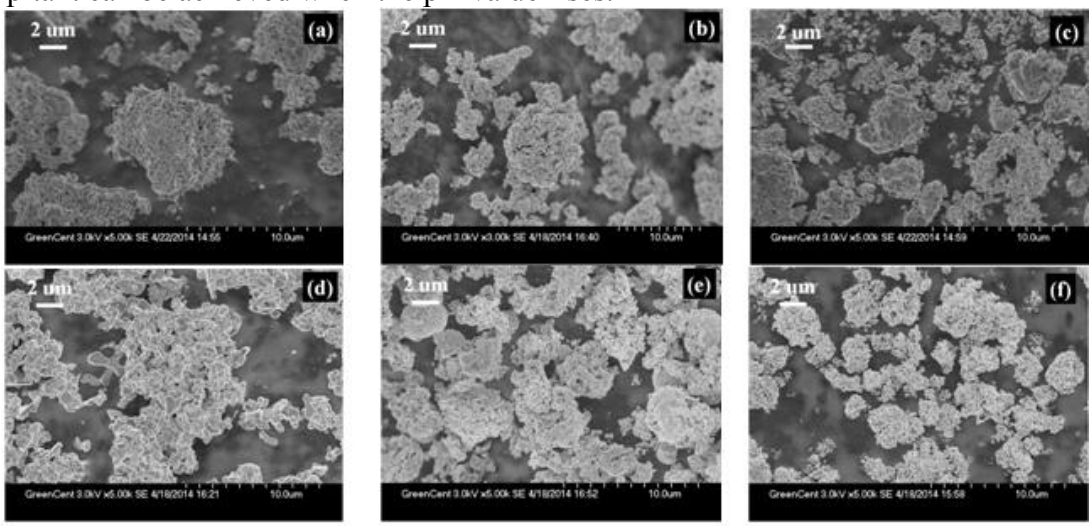

Fig. 2. SEM images for cathode materials(a, b, c) prepared at different feed rates and for cathode materials (c, d, e, f) prepared at different pH values

Figure 2 shows the SEM images for cathode materials(a, b, c) prepared at different feed rates and for cathode materials (c, d, e, f) at different pH values. The morphologies of cathode materials prepared at different feet rates are similar, which indicates that the feet rates of 3 mlmin-1, 5 mlmin-1 and 7 mlmin-1 have few influence on the morphologies of cathode materials. The second particles with a diameter about 5 um are agglomerated from the primary particles with a diameter about 200 nm. Nevertheless, the morphologies of cathode materials prepared at different pH values are thoroughly different though the second particles are still composited of the primary particles. The diameters of the primary particles reduce when the pH value rises in the process of co-precipitation reaction. What is more, the second particles become smaller when the pH value rises. The reason can be explained as follows. In general, the morphologies of cathode materials follow the morphologies of co-precipitates. The co-precipitation reaction include two steps of nucleation and nuclei growth. The nucleation and the nuclei growth are associated with the complexation of aqueous ammonia. The lower pH value is, the stronger complexation is when the aqueous ammonia is specified. A stronger complexation is in favor of the lower nucleation rate and the higher speed of nuclei growth. So, the lowest pH value of 9.0 leads to the biggest primary particles and the relative larger second particles due to a looser agglomeration. Vise verse, the highest pH value of 10.5 results in the smallest primary particles and the relative smaller second particles because of a tighter agglomeration.

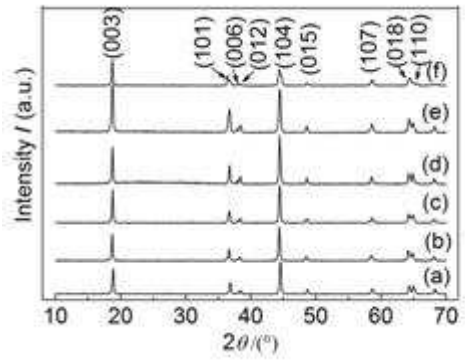

Fig. 1.XRD patterns for cathode materials(a, b, c) prepared at different feed rates and for cathode materials (c, d, e, f) prepared at different pH values

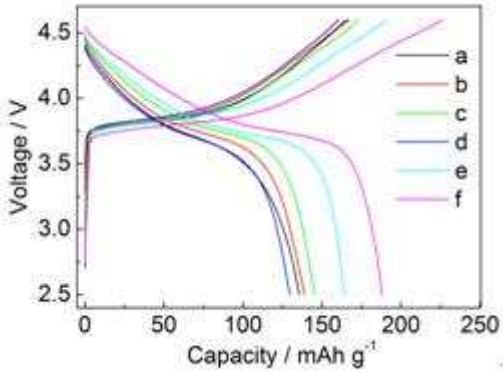

Fig. 3. The initial charge-discharge curves for cathode materials(a, b, c) prepared at different feed rates and for cathode materials (c, d, e, f) prepared at different pH values

Figure 3 shows the initial charge-discharge curves for cathode materials(a, b, c) prepared at different feed rates and for cathode materials (c, d, e, f) prepared at different pH values in the voltage range of 2.5–4.6 V and at 0.1 C. The first discharge capacities for cathode materials prepared at different feed rates of 3, 5 and 7 mlmin-1 are close. The first discharge capacities of sample a, b, c are 135.7 mAh g-1, 139.2 mAh g-1 and 145.5 mAh g-1, respectively.In contrast, the first discharge capacities for cathode materials prepared at different pH values of 9.0, 9.5,10.0, 10.5 are obviously different. The first discharge capacities of sample d, c, e, f are 130.7 mAh g-1, 145.5 mAh g-1, 164.6 mAh g-1 and 188.1 mAh g-1, respectively. Those results are consistent with that the less cation mixing was detected by XRD patterns and the smaller primary was observed in the SEM images when the pH values rise.

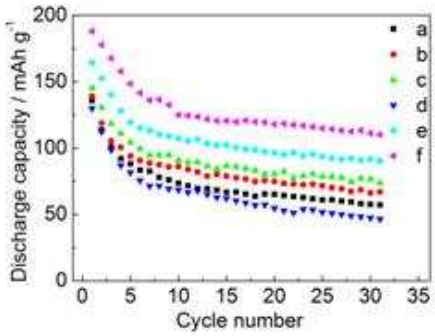

Fig. 4. The cyclic performance for cathode materials(a, b, c) prepared at different feed rates and for cathode materials (c, d, e, f) prepared at different pH values

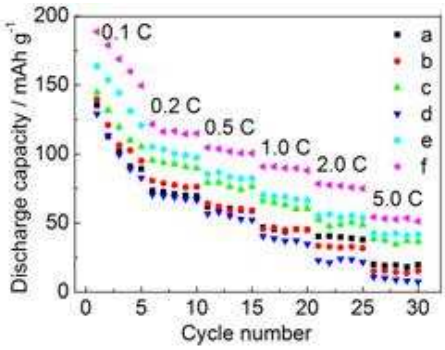

Fig. 5. The rate capabilties for cathode materials(a, b, c) prepared at different feed rates and for cathode materials (c, d, e, f) prepared at different pH values

Figure 4 demonstrates the cyclic performance of 0.1 C for cathode materials (a, b, c) prepared at different feed rates and for cathode materials (c, d, e, f) prepared at different pH values in the voltage range of 2.5–4.6 V. The discharge capacity retentions for sample a, b, c are 42.3%, 48.3% and 50.7%, respectively. And, the discharge capacity retentions for sample d, c, e, fare 36.0%, 50.7%, 54.9% and 58.5%, respectively. It is apparent that the higher pH values in the process of co-precipitation reaction are, the better cyclic performances are for the cathode materials prepared at different pH values.

Fig. 5 shows the rate capabilities for cathode materials(a, b, c) prepared at different feed rates and for cathode materials (c, d, e, f) prepared at different pH values in the voltage range of 2.5–4.6 V. All samples deliver undesirable rate capabilities. The discharge capacity of sample f are 116.2 mAh g-1 at 0.2 C , 101.8 mAh g-1at 0.5 C, 89.5 mAh g-1 at 1.0 C, 76.0 mAh g-1 at 2.0 C and 53.2 mAh g-1 at 5.0 C though it displays the highest discharge capacity of 188.1 mAh g-1 at 0.1 C.

Conclusions

The layered LiNi0.4Co0.2Mn0.4O2 cathode materials have been successfully via co-precipitation method using carbonate sodium as precipitant. The feed rate in the co-precipitation reaction has few influence on the structures, morphologies and electrochemical properties of as-prepared cathode materials when the feed rates altered among 3 mlmin-1, 5 mlmin-1 and 7 mlmin-1. However, pH values in the co-precipitation reaction play a important role on the structures, morphologies and electrochemical properties of as-prepared cathode materials. The less cation mixing was detected in the cathode material prepared at a higher pH value. Moreover, the smaller second particles agglomerated from the smaller primary particles were observed in the cathode material prepared at a higher pH value. So, the cathode materials prepared at higher pH value display better electrochemical properties in the voltage range of 2.5–4.6 V.

Acknowledgements

The authors appreciate the financial support from Science & Technology Department of Sichuan Province (2013GZX0145-3) and CAEP (2013A0302014). We are indebted to Jiahui Lin and Yong Jin for their kind help and fruitful discussions.

References

[1] J.Dahn , E.Fuller , M.Obrovac ,et al. Thermal stability of LixCoO2, LixNiO2 and λ-MnO2 and consequences for the safety of Li-ion cells.Solid State Ionics1994; 69(3): 265.
[2] Fan J and Fedkiw PS. Electrochemical impedance spectra of full cells: Relation to capacity and capacity-rate of rechargeable Li cells using LiCoO2, LiMn2O4, and LiNiO2 cathodes.JPower Sources1998;72(2): 165.
[3] Lu Z, Macneil D and Dahn J. Layered Li [NPCol-, MndO2 cathode mater ia ls for lithium—ion batter ies.J Electrochem Soc2002; 149(10): A1332.
[4] Lu Z, MacNeil D and Dahn J. Layered cathode materials Li [NixLi (1/3− 2x/3) Mn (2/3− x/3)] O2 for lithium-ion batteries. Electrochem Solid-State Lett2001; 4(11): A191.
[5] Yabuuchi N and Ohzuku T. Novel lithium insertion material of LiCo1/3Ni1/3Mn1/3O 2 for advanced lithium-ion batteries.J Power Sources 2003; 119: 171.
[6] Belharouak I, Sun YK, Liu J,et al. Li (Ni1/3Co1/3Mn)O2 as a suitable cathode for high power applications.J Power Sources2003;123(2): 247.
[7] Zhang S, Deng C, Yang S, et al. An improved carbonate co-precipitation method for the preparation of spherical Li [Ni1/3Co1/3Mn1/3] O2 cathode material.J Alloys Compd2009; 484(1-2): 519.
[8] Deng C, Zhang S, Fu B, et al. Characterization of Li2MnSiO4and Li2FeSiO4cathode materials synthesized via a citric acid assisted sol–gel method.Mater Chem Phys2010;120(1): 14.
[9] Lu CH and Shen BJ. Electrochemical characteristics of LiNi1/3Co1/3Mn1/3O2 powders prepared from microwave-hydrothermally derived precursors.J Alloys Compd2010; 497(1-2): 159.
[10] JeonHJ ,MonimSA ,KangCS, et al.Synthesis of Lix[Ni0.225Co0.125Mn0.65]O2as a positive electrode forlithium-ion batteries by optimizing its synthesis conditionsvia a hydroxide co-precipitation method.J Phys Chem Solid2013;74: 1185-1195.
[11] HU CY, Zheng L, Guo J, et al.Synthesis and electrochemical properties of Li[NixCoyMn1−x−y]O2(x, y=2/8, 3/8) cathode materials for lithium ion batteries.Rare Met2009;28(1): 43.
[12] ShiSJ,TuJP,Tang YY,et al. Preparation and characterization of macroporousLi1.2Mn0.54Ni0.13Co0.13O2cathode material for lithium-ion batteriesvia aerogel template.J Power Sources2013; 240: 2313.
[13] Gao Y ,Yakovleva MV,Ebner WB.Novel LiNi1−xTix/2Mgx/2O2 compounds as cathode materials for safer lithium-ion batteries.ElectrochemSolid-State Lett1998; 1(3): 117-119.
[14] ReimersJN,RossenE ,Jones CD,et al. Structure and electrochemistry of LixFeyNi1-yO2.Solid State Ionics1993;61(4): 335-344.

Advanced Materials Research Vols. 989-994 (2014) pp 467-470
© (2014) Trans Tech Publications, Switzerland
doi:10.4028/www.scientific.net/AMR.989-994.467

Optical Absorption Study of Ar^+ Implanted $SrTiO_3$ Single Crystals

Yanshan Wang[1], Meiju Zhang[1], Yunduan Gao[1], Defeng Liu[1], Yawen Chen[2], Pengfei Wang[2, a, *]

[1]AVIC Beijing Chang Cheng Aeronautical Measurement and Control Technology Research Institute, Beijing 100176, China

[2]Shandong Jiaotong University, Jinan 250357, China

[a]pfwang0213@126.com

Keywords: absorption spectrum, argon ion implantation, strontium titanate

Abstract. The UV-Visible absorption spectroscopy was performed to study the SrTiO3 (STO) single crystals implanted with the fluences of 1.5×10^{15} and 1.875×10^{16} Ar^+/cm^2. The two absorption peaks at 425 and 742 nm were recorded for the low-fluence implanted samples, while the additional peak at 520 nm was measured only for the high-fluence implanted samples. Through the evolution of the absorption peak with the annealing temperature, the 425, 520, and 742 nm peaks are attributed to the isolated oxygen vacancies, oxygen bivacancies, and oxygen interstitials, respectively. The thermal evolution of absorption spectra reveals that the STO lattice defects have poor thermal stability and disappear completely after 400°C annealing treatment.

Introduction

Safe and effective management of radioactive wastes concerns human health and environmental safety and has become an important research subject. The solidification of radioactive wastes is recognized as the most reasonable approach. Currently, the main solidification approaches for radioactive wastes are cement solidification, asphalt solidification, plastic solidification, glass curing, and artificial rock curing. The artificial rock curing is regarded widely as the second generation of solidification body [1, 2]. Strontium titanate possesses the good thermal conductivity, high density, and strong irradiation stability and has very promising prospect for the application of solidifying radioactive wastes [3, 4]. Strontium titanate material will suffer from high-energy particle irradiation during service. Lattice defects lead to the significant degradation of intrinsic performance. Therefore, an understanding of the microstructure, formation mechanism, and evolution of lattice defects is necessary for predicting the reliability and safety of strontium titanate solidification body. There have been various methods to study lattice defects, such as rutherford back scattering/channel analysis, transmission electron microscopy and positron annihilation spectroscopy [5, 6]. Now, we will use the optical absorption spectroscopy to research the strontium titanate lattice defects.

Experiment

The samples are bulk $5\times5\times0.5$ mm^3 STO single crystals and were implanted by 30keV argon ions with the fluences of 1.5×10^{15} and 1.875×10^{16} Ar^+/cm^2. The implantation temperature is room temperature. After the argon ion implantation treatment, the samples were annealed isochronally up to the temperature of 200, 250, 300, 350, and 400 ºC for 30 min. A UV3101-PC UV-VIS-NIR spectrophotometer was used to invesgated the implantation defects.

Results and Discussion

Fig. 1 shows the STO crystals before and after ion implantation. It can be seen that the virgin sample is colorless and transparent. This is because that the STO single crystal has a band gap of 3.3 eV and does not absorb the visible light. After ion implantation treatment, the generation of the lattice defects

results in the striking change. The sample impanted with the fluence of 1.5×10^{15} Ar^{+}/cm^{2} becomes pale blue colour. The sample implanted with the fluence of 1.875×10^{16} Ar^{+}/cm^{2} presents dark blue colour. The change in sample colour stems essentially from the implantation-induced defects which can be measured by optical absorption spectroscopy.

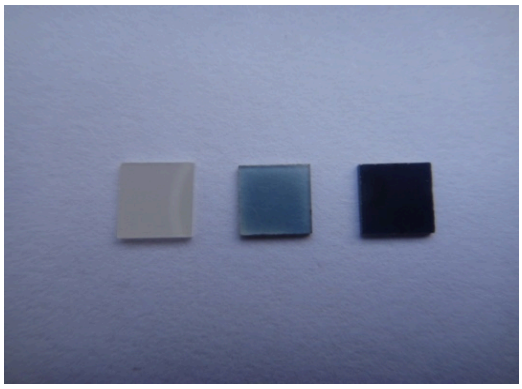

Fig. 1 The photograph of the STO samples implanted with different fluences. virgin (left), 1.5×10^{15} (middle) , and 1.875×10^{16} (right)

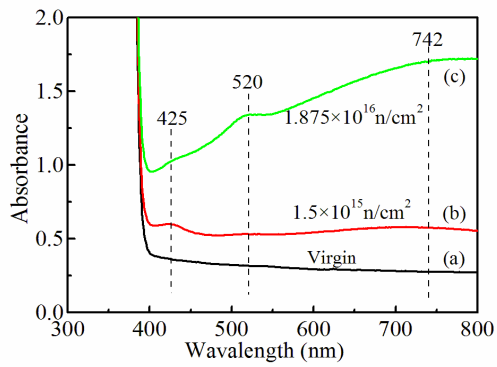

Fig. 2 The optical absorption spectra of the STO samples implanted with different fluences. virgin (a), 1.5×10^{15} (b) , and 1.875×10^{16} (c)

Fig. 2 shows the absorption spectra of the samples implanted with different fluences. As can be seen from Fig. 2(a), the spectrum of the vrigin STO sample presents no absorption peak in the visible light region and has a good visible light transmittance. In addition, less than 375 nm wavelength in the region has The strong light absorption in the region less than 375 nm originates form the electron transition from the top of valence band to the bottom of conduction band, namely the intrinsic absorption band. During the implantation process, the interaction of argon ions with STO lattice atoms leads to the production of a large number of lattice defects. Some defects can introduce the intermediate level between the conduction band and valence band. These new defect levels can be revealed by the absorption spectrum, as shown in figure 2(b) and 2(c). Figure 2(b) show the absorption spectrum of the sample impanted with the fluence of 1.5×10^{15} Ar^{+}/cm^{2}. Tt can be seen obviously changes have taken place in absorption spectra. In addition to the obvious increase of absorption intensity in entire visible light region, the most obvious change is the presence of the two absorption peaks at 425 and 742 nm. When the implantation fluence increases to 1.875×10^{16} Ar^{+}/cm^{2}, as shown in fig. 2(c), the absorption intensities of 425 and 742 nm peaks increase obviously because the the increase of defect concentrations with increase of implantation fluence. It is worth noting that there is 520 nm absorption peak which is absent in low fluence implanted sample and can only appear in high fluence implanted sample. This result demonstrates that the defects corresponding to 520nm peak is not produced directly by ion implantation but can be produced by the gradual defect accumulatation. Hence, the 520 nm peak is likely to come from complex defects. The previous finding shows that the 742 nm peak has nothing to do with impurity and originates from the crystal defects [8]. There exists disagreement with respect to the origination of 425 nm peak. C. Lee supports

that the 425 nm peak comes from iron or nickel impurity defects [9]. K.W. Blazey supports that the 425 nm peak originates froms the complex defects which consist of transition element and oxygen vacancy [8,10]. C.M. Liu discovers that the peak is related to nitrogen impurities [11]. D. Kan and T. Sun believe that oxygen vacancies can introduce shallow acceptor level near the top of valence band the [12,13]. Therefore, the 425 and 520 nm peaks are related to oxygen vacancies and should originate from the electron transitions from acceptor level of oxygen vacancies to conduction band.

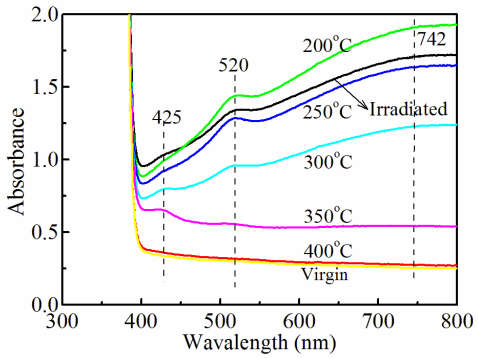

Fig. 3 The absorption spectra of the STO sample implanted with the fluence of 1.875×10^{16} after the annealing treatment with the temperature of 200-400 ºC

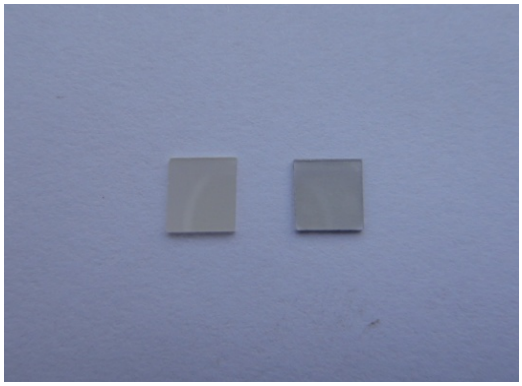

Fig. 4 The photographs of virgin STO sample (left) and the STO sample post-implantation annealed up to the temperature of 400 ºC (right).

In order to determine the assignation of the three absorption peaks, the subsequent annealing treatment was carried out for the STO sample implanted with the fluence of 1.875×10^{16} Ar^{+}/cm^{2}. The post-annealing measured absorption spectra are presented in Fig. 3. After 200 ºC annealing treatment, the intensity of 425 nm peak absorption peak decreases, however the intensity of 520 nm absorption peak increases. Namely, the absorption peak intensity of the 425 and 520 nm peaks have an opposite tendency. This implies that the 425 nm peak corresponding defects can migrate and aggregate into 520 nm peak corresponding defects. The used STO samples are undoped single crystals and donot contain impurities such as iron, nickel, and nitrogen. Therefore the 425 and 520 nm should come from crystal defects. Isolated oxygen vacancy can aggregate into oxygen bivacancy but has a little possibility of aggregation into more complex oxygen clusters. It can be concluded that the 425 nm and 520 nm absorption peaks are very likely originate from isolated oxygen vacancy and oxygen bivacancy, respectively. When the temperature rises to 350 ºC, the 520 nm absorption peak intensity reduced obviously but the 425nm absorption peak intensity is reduced slightly. This is because that oxygen bivacancy can dissociate into isolated oxygen vacancy during annealing treatment. The dissociation of oxygen divacancy into isolated oxygen vacancy partly compensates for the reducation of the intrinsic isolated oxygen vacancy concentration. After the higher annealing temperatures, the 425, 520, and 742 nm absorption peaks are all gradually reduce. when the temperature rises to 400 ºC, the absorption spectrum is similar the spectrum of the vrigin sample. It is noted that the 425 nm and

742 nm absorption peaks disappear at the same time. This shows that 742 nm absorption peak come likely from oxygen interstitials. Fig.4 shows the photographs of the vrigin sample and the sample annealed up to the temperature of 400 ºC. The sample annealed up to the temperature of 400 ºC is very similar to the virgin sample. Both of them appear colorless and transparent. It is demonstrated that the implantation-induced lattice defects has poor thermal stability and can be removed after the annealing treatment up to the temperature of 400 ºC.

Conclusions

We performed UV-Visible absorption spectroscopy to study the implantation defects of STO single crystals. The three absorption peaks at 425, 520, and 742 nm were measured. Through the evolution of the absorption peak with the annealing temperature, they are ascribed respectively to the isolated oxygen vacancies, oxygen bivacancies, and oxygen interstitials. The implatation defects of STO single crystal have poor thermal stability and can removed after the 400°C annealing treatment.

References

[1] Chunxia Che, Yangcheng Teng, and Qiang Gui, Research and application status of radioactive waste solidification, Materials Review, Vol. 20, 2006 (2), P. 94-97
[2] Jingxuan Jia, Rongjun Wu, Jiaoya Wang, et al, Research of alarm threshold value of noble gas monitoring channel in containment for PWR nuclear power plant, Radiation Protection, Vol. 33, 2013(2), P. 91-101
[3] Ruizhu Zhang, Jie Yang, Dakao Yan, et al, Consolidation of high-level radioactive wastes into strontium by CS method, Materials Science Forum, Vol.704-705 (2012), P. 625-630
[4] Ruizhu Zhang, Yongwei Gao, Jiansheng Wang, et al, Leaching properties of immobilization of HLW into SrTiO3 ceramics, Advanced Materials Research Vol. 332-334 (2011), P. 1807-1811
[5] Y. Zhang, C. M. Wang, M. H. Engelhard, et al, Irradiation behavior of SrTiO3 at temperatures close to the critical temperature for amorphization, Journal of Applied Physics 100, 113533 (2006)
[6] M. Song, X. Guo, N. Ishikawa, et al, Formation of defect clusters in SrTiO3 crystal implanted with xenon ions, Materials Science Forum, Vol. 561-565 (2007), P.1757-1760
[7] D. J. Keeble, R. A. Mackie, W. Egger, et al, Identification of vacancy defects in a thin film perovskite oxide, Physical Review B 81, 064102 (2010)
[8] Shosuke Mochizuki, Fumito Fujishiro, Kenichiro Ishiwata, et al, Defect-induced optical absorption and photoluminescence of verneuil-grown SrTiO3 crystal, Physica B, 376-377 (2006), P. 813,819
[9] C. Lee, J. Destry, and J. L. Brebner, Optical absorption and transport in semiconducting SrTiO3, Physical Review B 11, 6(1975), P. 2299-2310
[10] K. W. Blazey and H. Weibel, Optical absorption spectra of reduced transition-metal ion-doped SrTiO3, J. Phys. Chem. Solids Vol. 45, 8/9 (1984), P. 917-922
[11] C. M. Liu, Z.L. Yuan, Y.F. Ju, et al, Optical properties and microstructure of nitrogen-doped SrTiO3, Can. J. Phys. 86, 1345-1348 (2008)
[12] Caisuke Kan, Takahito Terashima, Pyoko Kanda, et al, Blue-light emission at room temperature Ar-irradiated SrTiO3, Nature Materials, Vol. 4, 2005,P. 816-819
[13] Tao Sun and Ming Lu, Band-structure modulation of SrTiO3 by hydrogenation for enhanced photoactivity, Appl. Phys. A (2012) 108: 171-175

Advanced Materials Research Vols. 989-994 (2014) pp 471-474
© (2014) Trans Tech Publications, Switzerland
doi:10.4028/www.scientific.net/AMR.989-994.471

Au Nanoparticles Prepared by Microwave Irradiation

Yan Qiao[1, a], A Ning Jiang[2, b]

[1]Testing Technology School, Baotou Light Industry Vocational Technical College, Baotou, Inner Mongolia, 014035, China;

[2]Testing Technology School, Baotou Light Industry Vocational Technical College, Baotou, Inner Mongolia, 014035, China;

[a] 761472825@qq.com, [b] 279888963@qq.com

Keywords: microwave irradiation, Au nanoparticles, 3.5 G PAMAM.

Abstract: Using 3.5 G PAMAM as a stabilizing agent, Au nanoparticles have been prepared by reducing $HAuCl_4$ with microwave irradiation. The influence of microwave irradiation at the same ratio of 3.5 G PAMAM to $HAuCl_4$ for the different time and at the different ratio of 3.5 G PAMAM to $HAuCl_4$ for the same time on Au nanoparticles´size and shape has been studied. Au nanoparticles were characterized by UV-vis spectra and TEM. At the same ratio of 3.5 G PAMAM to $HAuCl_4$, the microwave irradiation time has a little influence on the Au nanoparticles´size and shape, meanwhile more dispersed Au nanoparticles were obtained with the appropriate increase of reactive time. At the same irradiation time, bigger and more aggregative Au nanoparticles were acquired as the ratio of 3.5 G PAMAM to $HAuCl_4$ was decreased.

Introduction

Metal nanoparticles have attracted many researchers' attention because of its special stability, electromagnetic properties and optical properties. Especially, gold nanoparticles have aroused great interest in the past decades [1-4]. Methods for preparing nanoparticles include the general chemical method, physical method and comprehensive method. Comprehensive method combines the advantages of chemical and physical preparation of nanoparticles, such as microwave method, laser deposition method. The microwave method is rapid, simple, uniform, and energy saving, but also more uniform nanoparticles can be obtained in the formation of nanoparticles in the reaction.

People have been successfully synthesized Pt, Ag, Pd, Cu and other metal nanoparticles by microwave method, which have small particle size, narrow distribution and good catalytic performance [5-6]. Using 3.5 G PAMAM as a stabilizing agent, Au nanoparticles have been prepared by reducing HAuCl4 with microwave irradiation. The influence of microwave irradiation at the same ratio of 3.5 G PAMAM to HAuCl4 for the different time and at the different ratio of 3.5 G PAMAM to HAuCl4 for the same time on Au nanoparticles´size and shape has been studied.

Organization of the Text

1 The Experimental Part

1.1 Reagents

Ethylenediamine, Methanol: Analysis of pure, Sinopharm Chemical Reagent Co., Ltd; Methacrylate: Chemical pure, Sinopharm Chemical Reagent Co., Ltd; Chloroauric acid: Purity of more than 96%, Shanghai No.3 Reagent Factory; redistilled water.

1.2 The synthesis of 4.5 G PAMAM dendrimer

Methyl acrylate reacted first in methanol by Michael addition reaction with ethylenediamine as core according to the method of Literature[7]. PAMAM dendrimers (generations) were obtained with amine terminated by Ester aminolysis reaction of the product (half generation) by vacuum distillation purification and large excess of ethylenediamine. Methyl acrylate reacted in methanol by Michael addition reaction with the product (generation) by vacuum distillation and purification, 3.5 G

PAMAM dendrimers are prepared by repeating the above process. Its molecular structure is shown in figure 1. The products were identified by IR, characterization of 1H NMR and elemental analysis, the results are consistent with the literature.

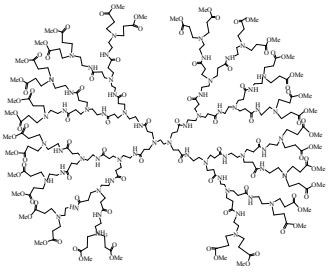

Fig 1 3.5 G PAMAM molecular structure

1.3 Synthesis of the colloidal gold

After 5 min of the ultrasonic oscillation of the mixed solution of 20 mL in the conical flask with a 100 mL 0.88 mL 3.5 G PAMAM aqueous solution (5.54 mmol/L), 8.62 mL water, 10 mL of anhydrous ethanol and 0.5 mL $HAuCl_4$ aqueous solution (9.706 mmol/L) (n (3.5G PAMAM): n ($HAuCl_4$) =1:1), 700 W output power of microwave irradiation were 10 s, 20 s, 30 s, 40 s, 50 s at 2450 MHz after microwave modification and electric stirring. The color of the solution quickly changed from light yellow to purple red at the microwave irradiation; After irradiation and being removed the conical flask, the solution were continued stirring for 30 min to prepare stable gold nanoparticles at room temperature. The colloidal gold that the 3.5 G PAMAM and $HAuCl_4$ molar ratio was 1 were prepared for the different time 10 s, 20 s, 30 s, 40 s, 50 s .The same method can be used for proper exposure time of 30 s, the colloidal gold were prepared at the different ratio of 3.5 G PAMAM to $HAuCl_4$ 3.5 G PAMAM and $HAuCl_4$ molar ratio of 5, 2, 1, 1/2, 1/5. the colloidal gold is stable because the color has not changed and there is no precipitate after being stored at room temperature for several months.

1.4 Sample characterization

Using TU-1810SPC made by Beijing Purkinje General Instrument Co., Ltd. ultraviolet visible (UV-Vis) absorption spectrum analyzer test specimens of UV-vis; The Hitachi H-600 transmission electron microscope (TEM) morphology of the specimens were observed, a voltage of 100 kV, the metal sol drops in the previously covered Formvar film copper net, natural drying electron microscope specimen; RIGAKU DMAX-3C Rigaku X - ray diffraction, a voltage of 30 KV, current of 25 mV, the metal sol at 40 ℃ vacuum rotary evaporation into thick sol, then vacuum drying to get solid samples.

2 Results and Discussions

2.1 Absorption spectra of UV-Vis

Figure 2 is uv-vis spectra after microwave irradiation with different time at the same ratio of n（3.5 G PAMAM）：n（$HAuCl_4$）= 1. As can be seen from the diagram, the absorption peak of 3.5 G PAMAM dendrimers are 288.5 nm and 228 nm; The absorption peak around 530 nm is the surface plasmon resonance absorption peak of gold nanoparticles; Gold nanoparticles' size and shape have effect of the surface plasmon resonance absorption peak position; on the contrary, surface plasma resonance absorption peak position also reflects the gold nanoparticles in the size and shape. The surface plasma resonance absorption peak which change red shift increases from 520 nm to 530 nm when the irradiation time increased from 10 s to 20 s. The resonance absorption peak position has a little mobile as the exposure time has been extended. The further increase of the irradiation time don't lead to obviously change in surface plasmon resonance absorption peak of gold nanoparticles.

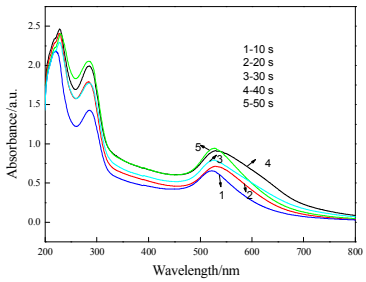

Fig 2 UV-vis spectra of Au nanoparticles prepared by microwave irradiation at the different time

Figure 3 is uv-vis spectra of gold nanoparticles at the different ratio of 3.5 G PAMAM to $HAuCl_4$ for the same time of 50 s. As can be seen from the diagram, surface plasmon resonance absorption peak position increases gradually from the beginning of the 517 nm to 552 nm, the resonance absorption peak change red shift and gradually widen. Which shows that, Au nanoparticles' size become larger and have a tendency to cluster.

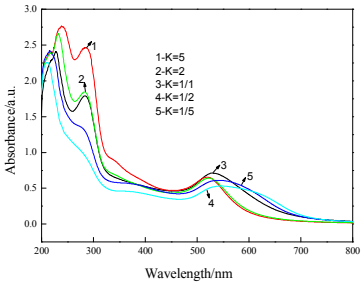

Fig 3 UV-vis spectra of Au nanoparticles prepared by microwave irradiation at the different ratio of reactants for 50s
（$K=n_{(3.5\ GPAMAM)}/n_{(HAuCl4)}$）

2.2 TEM Characterization Results

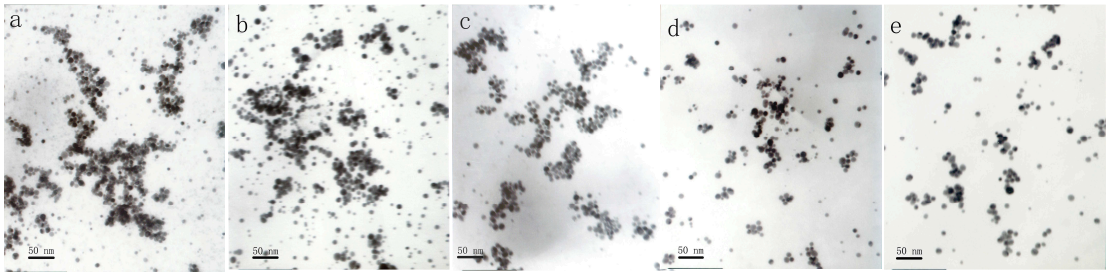

Fig 4 TEM Photographs and particles size distribution histograms of Au nanoparticles prepared by microwave irradiation at the different time
a: t=10 s; b:t=20 s; c:t=30 s; d:t=40 s; e:t=50 s

Figure 4 is TEM picture of gold nanoparticles prepared by using microwave irradiation for the different time at the same ratio of n（3.5 G PAMAM）：n（$HAuCl_4$）= 1. As can be seen from the diagram, Au nanoparticles´size and shape had no obvious change for the different time, which is consistent with the result of ultraviolet visible spectrum measured above. Furthermore that can be seen from figure 4, gold nanoparticles have better dispersion as irradiation time may be extended appropriately. Gold nanoparticles disperse best when irradiation time was 50 s.

Figure 5 is TEM picture of gold nanoparticles at the different ratio of 3.5 G PAMAM to $HAuCl_4$ for the same time of 50 s. As is showed in figure 5 of a, gold nanoparticles size was the smallest and the most homogeneous distribution. Bigger and more aggregative Au nanoparticles were acquired as the ratio of 4.5 G PAMAM to $HAuCl_4$ was decreased, which is consistent with the result of ultraviolet visible spectrum measured above.

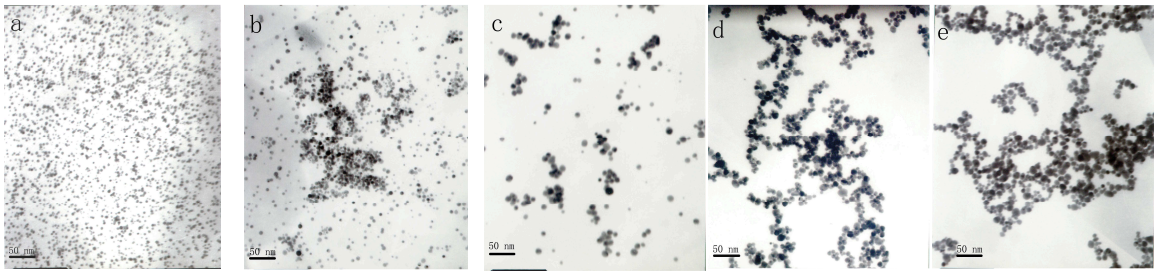

Fig 5 TEM Photographs and particles size distribution histograms of Au nanoparticles prepared by microwave irradiation at the different ratio of reactants for 50s
a:K=5; b :K=2; c:K=1; d:K=1/2; e:K=1/5
（$K=n_{(3.5\ GPAMAM)}/n_{(HAuCl4)}$）

Summary

Using 3.5 G PAMAM as a stabilizing agent, Au nanoparticles have been prepared by reducing $HAuCl_4$ with microwave irradiation. At the same ratio of 3.5 G PAMAM to $HAuCl_4$, the microwave irradiation time has a little influence on the Au nanoparticles´size and shape. At the same irradiation time, bigger and more aggregative Au nanoparticles were acquired as the ratio of 3.5 G PAMAM to $HAuCl_4$ was decreased. In short, at the same irradiation time of 50 s and at ratio of 3.5 G PAMAM to $HAuCl_4$ of 5, the smallest nanoparticles has been obtained and distribution is the most uniform.

References

[1] Toshima N, Teranishi T, Asaauma H, et al. Platinum cluster catalysts supported on porous chelate resin-metal complexes: Effect of resin porosity on catalytic activity[J]. J. Phys. Chem., 1992, 96: 3796-3799.
[2] Du Y K, Xu J Z, Yang P, et al. Influence of 1-butanethiol and metal ions on hydrogenation of trans, trans-2,4-hexadienal at platinum nanocatalysts[J]. Colloids and Surfaces A., 2005, 257-258: 75-78.
[3] Du Y K, Xu J Z, Shen M, et al. Alkanethiol-stabilized decahedron of gold nanoparticles[J]. Colloids and Surfaces A., 2005, 257-258: 535-537.
[4] Fu X Y, Wang Y, Wu N Z, et al. Shape-selective preparation and properties of oxalate-stabilized Pt colloid[J]. Langmuir., 2002, 18: 4619-4624.
[5] Yang L P, Tu W X. Studies on Au colloidal nanoparticles synthesized by microwave irradidtion[J]. *Acta Phys-Chim Sin*. ,2006, 22(4): 513-516.
[6] Boxall D L, Lukehart C M. Rapid synthesis of Pt or Pd/carbon nanocomposites using microwave irradiation[J]. Chem. Mater ., 2001, 13: 806-810.
[7] Tomalia D A, Baker H, Dewald J, et al. Dendritic macromolecules: Synthesis of starburst dendrimers[J]. Macromolecules., 1986, 19(9): 2466-2468.

Advanced Materials Research Vols. 989-994 (2014) pp 475-479
© (2014) Trans Tech Publications, Switzerland
doi:10.4028/www.scientific.net/AMR.989-994.475

Test and Research on Controlled cooling technology for high Carbon High silicon wire rod of S87B

Lei Zhang[1,a], Jianlin Sun[1,a,*], Yan Li[1], Juan Cui[2], Fang Zhang[2]

[1]School of Material Science and Engineering, University of Science and Technology Beijing, Beijing 100083, China

[2]Xingtai Iron and Steel Company Limited, Xingtai 054027, China.

[a]sjl@ustb.edu.cn

Keywords: Thermal physical simulation, high-carbon steel, controlled cooling, phase transformation of pearlite

Abstract. In this paper, critical temperature of phase transformation and continuous cooling transformation (CCT) curve of S87B were determined by hot uniaxial compression tests. At several of cooling speed, the microstructures were studied. The results indicate that the critical temperature of phase transformation become lower with cooling speed increasing, the min interlamellar spacing of pearlite was 0.125μm when the cooling speed was 4℃/s, the best cooling speed of phase transformation area was during (3-4)℃/s..

Introduction

With the span of large span cable-stayed bridge and suspension bridge becoming more and more widely, the higher workable performance of bridge cable was put forward. The bridge over akashi channel in Japan used 1770 MPa grade of φ5 mm galvanized steel wire [1], Sutong bridge (1088 m) first adopted 1770 Mpa grade of 7 mm galvanized steel wire [2]. With the span of bridge increase to 2000 m or more, such as the mainspan of the Italian messina bridge reach 3300 m. So it is necessary to develop the galvanized steel wire for bridge cable of 1860 Mpa and higher strength level.

Through appropriate sorbite and alloying technology to improve the tensile strength of wire rod is basis of getting high strength galvanizing steel wire for bridge cable [3-5]. High tensile strength and well plasticity index of hot rolled wire were accepted by reasonable technology of controlling cool process. In this paper, critical temperature of phase transformation and continuous cooling transformation (CCT) curve of S87B were determined by hot uniaxial compression tests, which provided the basis for the establishment of controlled cooling process.

Determination of the critical point of phase transition temperature

Table1. Chemical compositions of test samples /wt%

Chemical element	C	Si	Mn	P	S	Cu	Ni	Cr
Percentage	0.88	0.94	0.74	0.006	0.004	0.01	0.02	0.03

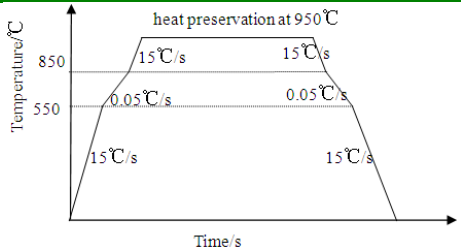

Fig.1 The critical transition temperature measuring process schematic diagram

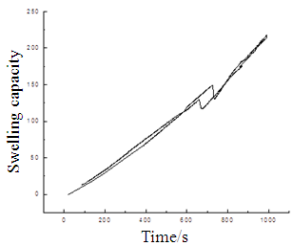

Fig.2 Critical point of phase transition temperature

Experimental samples and method. The selected sample for thermal simulation of cylindrical specimens, Specifications for Φ 6 × 15mm, its chemical composition as shown in Table 1.The critical

point of phase transition temperature of steel is measured by YB/T5127-93. Heating and cooling rate is less than 20℃ /s. First, according to the production process and documentation, we are finding phase transition temperature of Similar Steel. Then, set a reasonable range, see Fig.1.

Experimental results and analysis. Relationship curve of Temperature-Swelling capacity is given, see Fig.2. Take advantage of tangents method; find Ac1, Accm, Ar1, Arcm. The determination results see Table 2, the critical point of phase transition temperature, see Fig.3.

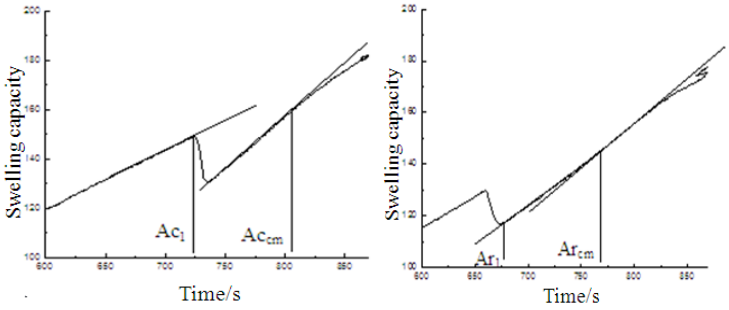

Fig. 3 Sketch Map of Ac_1, Ac_{cm}, Ar_1, Ar_{cm}

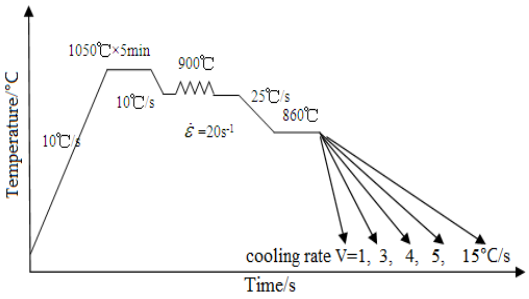

Fig. 4 Test technology of CCT curve for S87B

Table 2. Temperature of A_{c1},A_{ccm},A_{r1},A_{rcm}/℃

Ac_1	Ac_{cm}	Ar_1	Ar_{cm}
735	815	660	765

S87B CCT curve and its application

S87B structure depends not only on component, but also closely related to Controlled rolling and Control cooling [6-7]. If Controlled rolling and controlled cooling parameters is unsuitable, may appear fragile tissue like martensite or bainite, not conducive to deep processing. So, we should make reasonable controlled rolling and controlled cooling process. The best method for determining CCT curve is basic experimental methods.

Experimental samples and method. Laboratory sample is cylindrical specimens, specifications for Φ6×15mm, Chemical composition, see Table 1. The experimental program is developed, see Fig.4. The experimental steel sample is heated to 1050℃ at 10℃/s velocity, heating 5 minutes, and then cooled to 900℃. The experiment has simulated the deformation process of finish rolling. Deformation is 35%, the rate of deformation is 20s-1,then cooled to 860℃,last cooled to room temperature continuously at different cooling rates(1, 3, 4, 5, 15℃/s).

Experimental results and analysis. Under different cooling rate metallography and phase transformation point of S87B is as shown in Fig.5 and Table 3. CCT curve of S87B see Fig.6.

when cooling rate is 5℃/s, metallurgical structure started a small amount of martensite, the content of pearlite and lamellar spacing became narrowing, with the cooling speed increasing. when cooling speed is 15℃/s, the content of the martensite is 50%. The interlamellar Spacing, pellet size of Pearlite and the strength, toughness of steel are closely related; the smaller of the interlamellar Spacing, pellet size of Pearlite, the higher of the strength, toughness of steel. The main reason is because of ferrite and cementite thin slices, increase of the phase interfaces, Under the action of external force, the Deforming resistance will increase, but Increasing martensite content will greatly reduce the plasticity and toughness of steel, so sorbite which have good plasticity and toughness is the most ideal initiation structure. With the cooling speed increasing, transformation temperature of Pearlite decreasing, Phase transformation zone temperature reached the maximum when the cooling speed is during 3~4℃/s. when Cementite appeared, the temperature is during 645~625℃, the temperature of pearlite transformation is during 580-560℃. So, the best cooling speed of phase transformation area was during three and 4℃ per second.

3 The influence of controlled cooling process after rolling on Phase transformation and the microstructure and properties of S87B

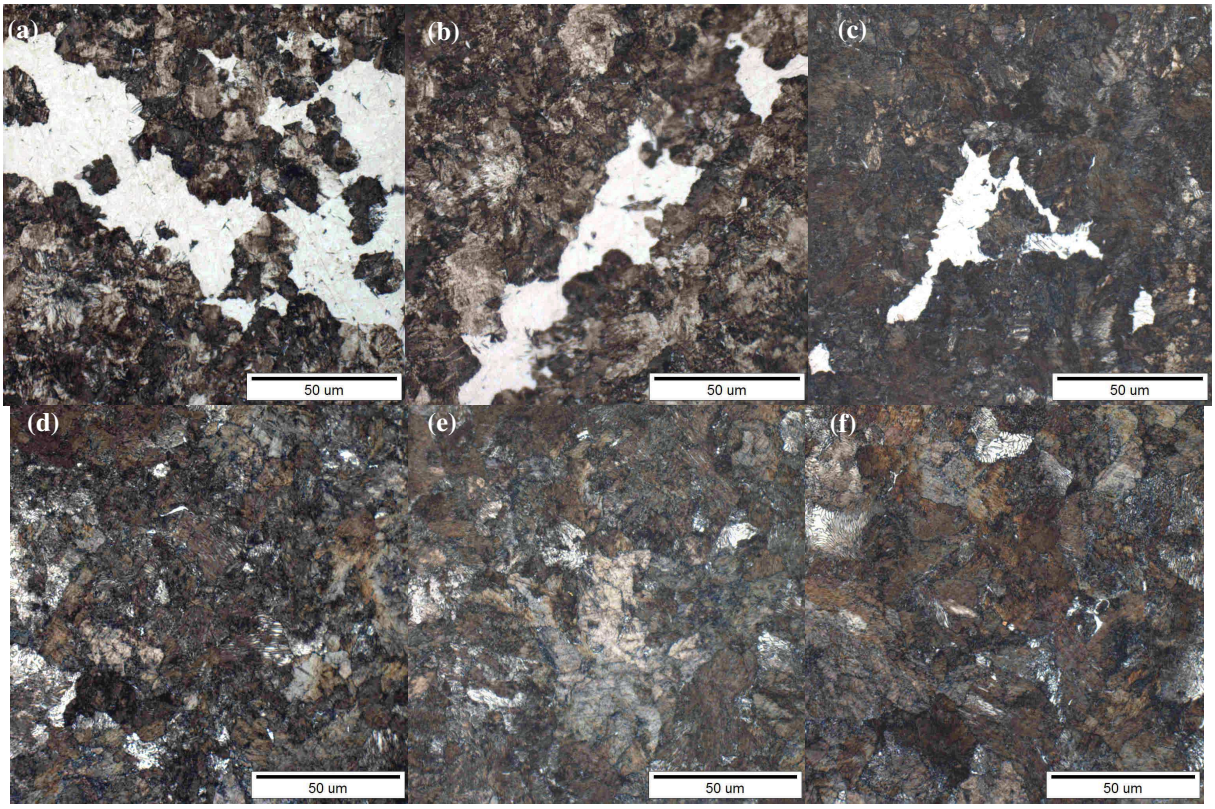

((a) 15℃/s,(b) 10℃/s,(c) 5℃/s,(d) 4℃/s,(e) 3℃/s,(f) 1℃/s)

Fig.5. Metallographic photos of S87B at different cooling speed

Table3. The temperature of phase transformation point and volume fraction under different cooling rates for S87B

No.	cooling velocity/℃·s^{-1}	metallurgical structure	P phase-transition temperature/℃		M phase-transition temperature /℃	volume fraction /%
			P_s	P_f		
f	1	Thin like or massive cementite ＋Pearlite ＋Sorbite	700	645	-	Fe3C(4),P(10),S
e	3	Thin like or massive cementite ＋Pearlite ＋Sorbite	645	580	-	Fe3C(2),P(8),S
d	4	Thin like or massive cementite ＋Pearlite ＋Sorbite	625	565	-	Fe3C(1),P(7),S
c	5	Pearlite＋Sorbite+ Martensite	620	550	180	P(6),S(85),M
b	10	Sorbite+ Martensite	590	535	190	S(70),M
a	15	Sorbite+ Martensite	585	530	190	S(50),M

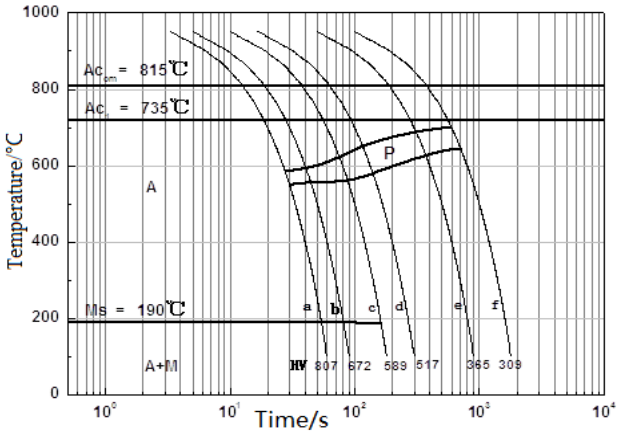

Fig.6 CCT of S87B

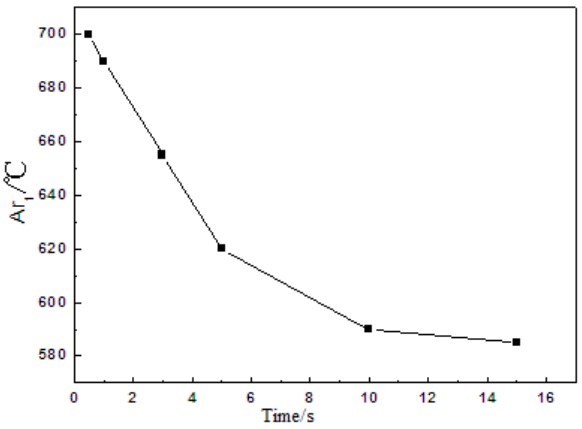

Fig.7.The influence of phase transition temperature of Ar1 on different cooling speed of S87B

Because deformation of wire is done in the pass system, so, in production, Deformation cannot be adjusted widely. Therefore, it is necessary to control the final rolling temperature. In this chapter, it discusses about the influence of cooling velocity on phase transformation and metallurgical structure.

The influence of cooling velocity on Phase transformation rules. During 1 and 5℃/s, temperatures of Ar_1 fell by 60℃. See Fig.7.

The influence of cooling velocity on metallurgical structure. Experimental method. Experimental materials such as shown in Table 1.By scanning electronic microscope, it was observed that metallurgical structure and the pearlite interlamellar spacing at under different cooling speed, then, by Image Tool it was measured that the tissue content and the pearlite interlamellar. The specimen which is using mechanical property test according to experimental scheme of Fig.8 make the Thermal Simulation Experiment of Compress Deformation, then as shown in Fig.9 the Deformation region of the specimen reprocessed into cylinder , measuring their mechanical properties.

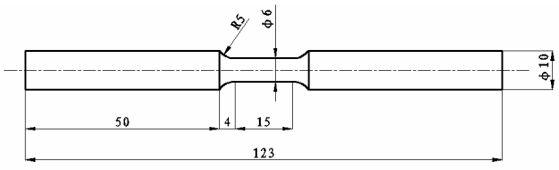

Fig.8 Thermal simulation processing map of the sample

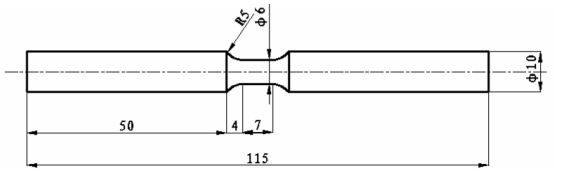

Fig.9 Tensile specimen processing map

Experimental results and analysis. When the cooling rate was 4℃/s, Cementite, pearlite and sorbite appear, sorbite content increases with the increasing of cooling rate. When the cooling rate of 4℃ /s, sorbite content reached the maximum, about 90%; When the cooling rate of 5℃/s, martensite appear, and sorbite content have shown a sharp decline; When the cooling rate of 15℃/s, sorbite content supplies only a small proportion of structure, martensite is about 50%. Pearlite photos see Fig.10, pearlite interlamella and Mechanical properties see Table 4.

The diameter of pearlitic colony will depend crucially on the original austenite grains, and interlamellar Spacing of Pearlite will depend crucially on formation temperature of Pearlite, It decreases with the decrease of formation temperature of Pearlite [10-11] (or the increase of supercooling degree).When the cooling rate was 4℃/s, grain size and pearlite interlamellar achieved the minimum. When the cooling rate was less than 5℃/s, grain size diminishes with increasing of cooling rate, when the cooling rate was 4℃ /s, the min interlamellar spacing of pearlite was 0.125μm. When the cooling rate of more than 4℃/s, with increasing of cooling rate, martensite content increase sharply, Pearlite nucleation sites reduce, pearlite interlamellar is increasing.

When the pearlite interlamellar spacing decreases, ferrite and cementite becomes thinner, under the action of external force it can slip and produce plastic deformation, and can also be bent, so that the capability of plastic deformation of the steel increased。Reduce the pearlite colony diameter, increasing grain orientation tends of unit volume of pearlite interlamellar , It makes the possibility of stress concentration decreases caused by large amount of plastic deformation occurs in the partial,

thus decreasing the diameter of pearlitic colony and interlamellar Spacing of Pearlite can improve the strength and toughness [10].

So, the best cooling speed of phase transformation area was during (3-4)℃/s.

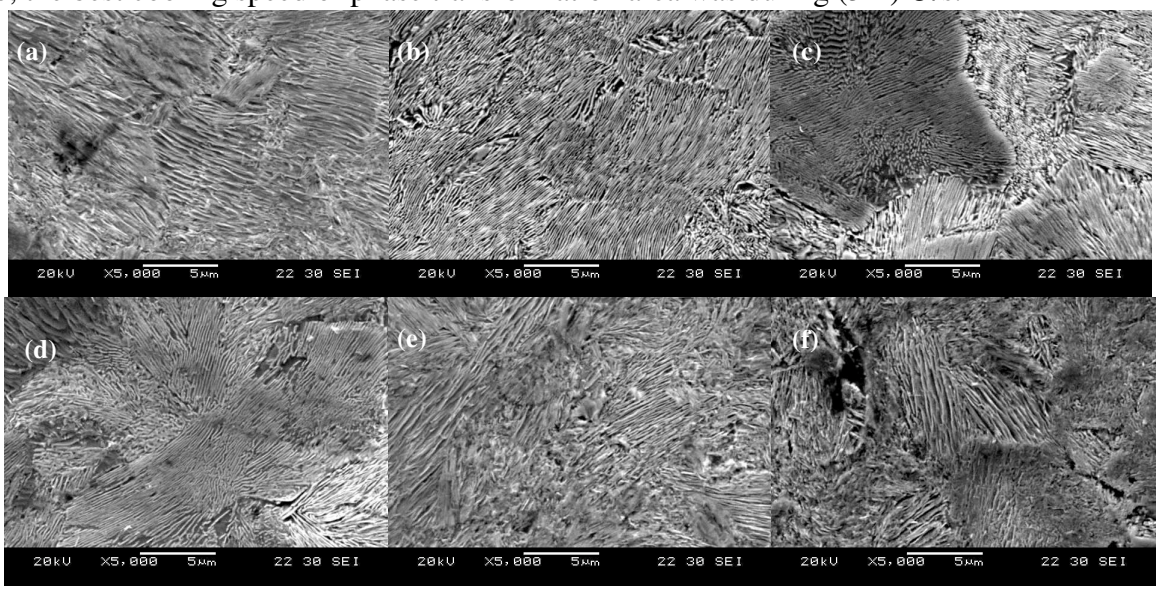

(a)15℃/s,(b) 10℃/s,(c) 5℃/s,(d) 4℃/s,(e) 3℃/s,(f) 1℃/s

Fig.10. pearlite photos of S87B under different cooling rate

Table4. Grain size and pearlite interlamellar spacing of S87B

Cooling rate /℃·s^{-1}	pearlite interlamellar /μm	Mechanical properties		
		Rm/MPa	A/%	Z/%
1	0.1734	1210	10	36
3	0.1598	1235	12	35
4	0.1250	1250	11	38
5	0.1460			
10	0.1300			

Conclusions

(1) Critical temperature of phase transformation of S87B: Ac_{cm}＝815℃; Ac_1＝735℃; Ar_{cm}＝765℃; Ar_1＝660℃; Ms＝190℃.

(2)When the cooling rate was 4℃/s, metallurgical structure is Fe_3C and P; When the cooling rate was 5℃/s, metallurgical structure is Fe_3C+P+M.

(3)When the cooling rate was 4℃/s, the min interlamellar spacing of pearlite was 0.125μm.

(4)The best cooling speed of phase transformation area was during three and 4℃ per second.

References

[1] T. Taru, N. Matuyama, T. Eguch et al: Structural Engineering International, 2002(3): 209-213
[2] Sang Chunming, Zhou Daiyi, Bai Bingdong. Steel Wire products, 2008(2):11-15.
[3] XU Wenlei', NING Shiwei. Steel Wire Products, 2010(2):27-30.
[4] Luan baifeng, Zhang da, Guo ning. Transaction of Materials and Heat treatment.2011 (7):78-82.
[5] Zhang Weijun, Sun Jinmao. Steel Wire products, 2005, 31(3):1-3.
[6] M. Kazeminezhad, A. Karimi Taheri. Materials & Design, 2003, 24(6): 415-421.
[7]N. Guo, B.F. Luan, Z. Zhou. Transaction of Materials and Heat treatment, 2012(4):44-49.
[8] K.K. Ray, D. Mondal. Acta Metallurgica et Materialia, 1991, 39(10): 2201-2208.
[9] A.M. Elwazri, P. Wanjarab, S. Yue. Materials Characterization, 2005, 54(4-5): 473-478.
[10] F.B.Pickering, B.Garbarz. Scripta Metallurgica,1987, 21, 249-253.
[11] N. Ridley. Metallurgical and Materials Transactions A, 1984, 16A, 1019-1036.

Advanced Materials Research Vols. 989-994 (2014) pp 480-483
© (2014) Trans Tech Publications, Switzerland
doi:10.4028/www.scientific.net/AMR.989-994.480

Simultaneous determination of ruthenium, zinc and zirconium in waste zirconium dioxide loaded ruthenium-zinc catalysts using inductively coupled plasma optical emission spectrometry

Xiao Juan Wei[1, a], Jian Ming Pan[2, b]

[1]Zhejiang Province Key Laboratory of Nobel Metal Catalytic Materials and Technology, China

[2]Zhejiang Metallurgical Research Institute, Hangzhou, Zhejiang, China

[a]jan1088@163.com, [b]pjm111999@163.com

Keywords: Ruthenium, Zinc, Zirconium, Waste zirconium dioxide loaded ruthenium-zinc catalysts, ICP-OES, KOH-KNO_3 fusion

Abstract: A technique for simultaneous determination of Ru, Zn and Zr in waste Ru-Zn/ZrO_2 catalysts using ICP-OES after sample digestion by high temperature fusion with KOH-KNO_3 mixture was described. Such experiment conditions were investigated as the influence of sample digestion methods, fusion time, fusion temperature, the dosage of KOH-KNO_3 mixture and interfering ions on the determination. Under the optimized conditions, the limits of detection (LODs) of Ru, Zn and Zr for tested solutions were 11, 8 and 5 ng mL^{-1}, respectively. The relative standard deviations (RSDs) for Ru, Zn and Zr were 2.01, 2.55 and 1.92 % ($C_{Ru, Zn, Zr}$ = 1 mg L^{-1}, n = 7), respectively. The linear ranges of calibration graphs for Ru, Zn and Zr were 0 ~ 100.00 mg L^{-1}, 0 ~ 50.00 mg L^{-1} and 0~60.00 mg L^{-1}, respectively. The proposed method was applied to determine the practical samples with good recoveries and satisfactory results.

Introduction

In 1989, the Asahi Chemical Industry Co. industrialized the process for producing cyclohexene from the selective hydrogenation of benzene based on Ru-Zn/ZrO_2 catalysts, and a cyclohexene selectivity of 80% as well as a benzene conversion of 40% were obtained, which set off research upsurge of catalysts for hydrogenation of benzene to cyclohexene [1, 2].Every year waste Ru-Zn/ZrO_2 catalysts to come into being were considerable. Quantitative determination of Ru, Zn and Zr in waste Ru-Zn/ZrO_2 catalyst samples not only could calculate the attrition rate of ruthenium in the catalytic reaction, but also had a great significance to recycle Ru, Zn and Zr. Hence, a reliable and efficient analytical technique was required for determining Ru, Zn and Zr in waste catalyst samples.

Several analytical techniques were applied for the determination of ruthenium in various samples, such as neutron activation analysis (NAA) [3, 4], atomic absorption spectrometry (AAS) [5-7] and inductively coupled plasma atomic emission spectrometry (ICP-OES) [8], NAA could hardly be considered a routine approach due to the complexity and cost of the required instrumentation. Atomic absorption spectrometry (AAS) could also be applied for ruthenium determinations in various samples. However, such method suffered from severe matrix effects and simultaneous multielement determination was very difficult. ICP-OES was considered one of the most suitable instrumental techniques for determination of Ru, Zn and Zr in different samples owing to its excellent analytical performance, such as multielement capability, wide linear dynamic range, low detection limit and good precision.

Another crucial step in the analysis of PGEs was sample digestion. It was well known that (metallic) Ru was very resistant to chemical attack [9]. Another problem encountered in Ru analytics was that oxidative conditions during the digestion stage might lead to Ru losses due to formation of volatile RuO_4. For this reason the use of a lower amount of nitric acid compared to the aqua regia composition (3:1 (v/v) HCl–HNO_3) in Ru digestions had been recommended [10]. Digestions in closed vessels with different acid mixtures also had been applied in determinations of low concentrations of Ru and other platinum group elements, e.g. in geological and environmental

materials [11, 12]. In addition, a fusion method with KOH-KNO_3 mixture had been applied for the determination of Ru only in carbon-supported catalysts [13]. As far as we know, there was no report on simultaneous determination of Ru, Zn and Zr in waste Ru-Zn/ZrO_2 catalyst samples by fusion method with KOH-KNO_3 mixture in the literature. Zn and ZrO_2 were very easy to digest by acid or alkali in the high temperature. The aim of this study was to achieve a complete Ru digestion with no losses. The Ru, Zn and Zr contents in the digested samples were determined with the ICP-OES technique. A fusion method with KOH-KNO_3 mixture and a Teflon pressure vessel digestion method were applied for the digestions of Ru, Zn and Zr in waste Ru-Zn/ZrO_2 catalyst materials. The factors affecting experiment conditions were investigated such as the influence of sample digestion methods, fusion time, fusion temperature, the dosage of KOH-KNO_3 mixture and interfering ions on the determination. The practical application of this method to the determination of Ru, Zn and Zr in waste Ru-Zn/ZrO_2 catalyst samples was performed.

Experimental

Instrumentation. A Perkinelmer Optima 7000DV ICP-OES (Perkinelmer, America) was used in this work. The used instrument operating conditions and wavelength were given in Table 1. The instrumental parameters were adjusted according to the manufacturer's recommendations. A muffle furnace WT-221GC (Shanghai Shiyan Electric Furnace, China) was used for sample digestions with the fusion method.

Table 1 ICP-OES operating conditions for determination of Ru, Zn and Zr

Instrument parameter	
Wavelength [nm]	Ru 240.272; Zn 206.200; Zr 343.823
Incident power [kW]	1.4
Cooling gas [L min^{-1}]	15
Auxiliary gas [L min^{-1}]	0.2
Nebulizer gas [L min^{-1}]	0.8
Pump rate [L min^{-1}]	1.5
Nebulizer pressure [kPa]	108

Reagents and Sample Solutions. All reagents used were suprapure grade. Doubly distilled water was used throughout the experiment. Acidic standard 1000mg L^{-1} solutions of ruthenium (III), zinc (II) and zirconium (Ⅳ) (Sigma-Aldrich, Germany) were used. The mixed stock standard solution was prepared by mixing ruthenium (III), zinc (II) and zirconium (Ⅳ) standard solutions, and working standard solutions were obtained by appropriate stepwise dilution of the mixed stock standard solutions. The other reagents were as follows: KNO_3 (Sinopharm), KOH (Sinopharm), HCl (30%, Sinopharm), HNO_3 (65%, Sinopharm).

Digestion by a fusion method. 50-100 mg of the waste catalyst samples were weighed to porcelain crucibles, where the mixture of 1 g KNO_3 and 1g KOH was added to the crucibles and mixed with the samples. The crucibles were covered by lids and inserted into a cold muffle furnace. The furnace was heated to 600 °C and held 1 hour. After cooling down overnight (approximately to 30 °C), the melts were dissolved with 100 mL hot 10% HCl (v/v) solution. To convert Ru to a stable chloro-complex ($RuCl_6^{2-}$), the solutions were transferred into 250ml volumetric flasks and filled to the mark with 10% HCl (v/v) solution. The solutions were diluted and their HCl concentration was adjusted to a minimum of 4% (v/v), depending on the calibration used, prior to the ICP-OES determination. A suitable amount of the reagent blank solution, obtained by fusion, was added to the calibration standards.

Teflon pressure vessel digestion. Waste catalyst samples of 50-100 mg were carefully weighed into the teflon pressure digestion vessel. Digestions were carried out using 6:1 HCl-HNO_3 mixtures for reducing Ru losses due to formation of volatile RuO_4. For the digestions, 20 mL 6:1 HCl-HNO_3 mixtures were added to the digestion vessels. The vessels were closed and the samples were digested in the drying oven with for 6 hour at 180°C. The solutions were carefully allowed to cool to

room temperature prior to opening the vessels. The solutions were heated to dryness and 10 mL of conc. HCl was added. The heating step was repeated three times. After that, the solutions were transferred into 250ml volumetric flasks and filled to the mark with 10% HCl (v/v) solution. The samples were further diluted and their HCl concentration was adjusted to 4% (v/v) prior to the ICP-OES determination.

Results and Discussion

Selection of Digestion Methods. The same waste Ru-Zn/ZrO_2 catalysts sample with Ru, Zn and Zr content of 10.35%, 2.32% and 50.67% was pretreated by the fusion method with KOH-KNO_3 mixture and the teflon pressure vessel digestion method according to the recommended procedure, and then determined by ICP-OES. The results were given in Table 2. As could be seen, the result by the fusion method was in good agreement with the certified values, but the teflon pressure vessel digestion method cause the result of Ru and Zr content on the low side. In waste Ru-Zn/ZrO_2 catalysts sample a part of ruthenium was existed in the form of oxided ruthenium, which was difficult to digest with acid. In additional, $ZrO_2$was not easy to digest with wet method. In this work, fusion method was selected to pretreat samples.

Table 2 Comparison of the two digestion methods

Method	Found [%]
Fusion method	Ru 10.23; Zn 2.25; Zr 50.35
Teflon pressure vessel digestion method	Ru 8.12; Zn 2.26; Zr 20.15

Effect of Fusion Time. Fusion time was an important parameter that influences the digestion of sample. A fusion time in the range of 0.5-2 hour at 600 $^{\circ}$C was investigated. A very short fusion time cannot insure completely dissolution of sample. Therefore, 1 hour was chosen as optimum.

Effect of Fusion Temperature. Fusion temperature was also an important parameter that influences the digestion of sample. A fusion temperature in the range of 400-800 $^{\circ}$C for 1 hour was investigated. A very low fusion temperature cannot insure completely dissolution sample. Therefore, 600 $^{\circ}$C was chosen as optimum

Effect of the dosage of KOH-KNO_3 mixture. 100 mg waste catalyst samples were weighed, the dosage of KOH-KNO_3 mixture (mass ratio 1:1) in the range of 1-4 g was investigated. The result indicated that a very low dosage of KOH-KNO_3 cannot insure completely dissolution sample. Therefore, 2 g KOH-KNO_3 mixture (mass ratio 1:1) was chosen as optimum dosage.

Interferences. The influence of Ca, Mg, Al, Fe, Co, Ni, Bi and Ag, which were the most impurity elements in waste Ru-Zn/ZrO_2 catalyst samples for hydrogenation of benzene to cyclohexene on the determination of Ru, Zn and Zr was investigated. The solutions of 1 mg L^{-1} ruthenium (III), 1 mg L^{-1}zinc (II) and 1 mg L^{-1} zirconium (Ⅳ)containing the corresponding interfering ions were prepared and operated according to the recommended procedure. The results showed that the content of Ca, Mg, Al, Fe, Co, Ni, Bi and Ag up to 5 times more Ru, Zn and Zr had no significant effect on the determination. The content of Ca, Mg, Al, Fe, Co, Ni, Bi and Ag were less than 0.01% in waste Ru-Zn/ZrO_2 catalyst samples by the emission spectrum analysis. In addition, a mass of potassium were brought into the matrix in the fusion process. The influence of potassium on the determination of Ru, Zn and Zr also was investigated. The results showed that the content of potassium up to 120 times more Ru, Zn and Zr had no significant effect on the determination. So the developed method was not affected by the potential interferences from the major matrix elements and potassium.

Analytical Performance. With the use of established experimental parameters as shown in Table 1, the analytical performance of the method was evaluated. The limits of detection were calculated as three times the standard deviation of the reagent blank signal (n=7), in accordance with IUPAC recommendations. The limits of detection (LODs) and the relative standard deviations

(RSDs) of the proposed method were listed in Table 3. Experiment indicated Ru, Zn and Zr concentration within the range of 0 ~ 100.00 mg L^{-1}, 0 ~ 50.00 mg L^{-1} and 0 ~ 60.00 mg L^{-1} had a linear relation with emission intensity, respectively.

Table 3 Limits of detection and precision (RSDs)

Element	Wavelenght [nm]	RSD[a] [%]	Detection limit [ng mL^{-1}]
Ru	240.272	2.01	11.00
Zn	206.200	2.55	8.00
Zr	343.823	1.92	5.00

[a] Ru, Zn and Zr, 1.00 mg L^{-1}, n = 7.

Sample analysis. The practical waste Ru-Zn/ZrO_2 catalyst samples were determined by ICP-OES, with the use of established experimental parameters. Repeat 6 times, the results of found and method recovery were given in Table 4. The recoveries of Ru, Zn and Zr were 93.30% ~ 99.57%, 95.51% ~ 100.51% and 95.41% ~ 99.24%, respectively. The developed method is an ideal kind of method for simultaneous determination Ru, Zn and Zr in waste Ru-Zn/ZrO_2 catalysts.

Table 4 Found results and average recovery

Element	Average Found [%]	Average Recovery [%]
Ru	11.35	97.59
Zn	3.25	102.12
Zr	46.56	96.57

Conclusions

The method with first using KOH-KNO_3 mixture (mass ratio 1:1) as fusion reagents to simultaneously determine Ru, Zn and Zr in waste Ru-Zn/ZrO_2 catalysts for hydrogenation of benzene to cyclohexene by ICP-OES was established, which was simple, quick, high precision. A satisfactory result was obtained when applying it in the practical sample.

Acknowledgements

This work was financially supported by Zhejiang Province Key Laboratory of Noble Metal Catalytic Materials and Technology construction (2013F10008).

References

[1] H. Nagahara, M. Ono, M. Konishi and Y. Fukuoka: Appl. Surf. Sci Vol. 121 (1997), p. 448
[2] J.M. Wu, Y.F. Yan and J.L. Chen: Chem. Ind. Eng. Prog Vol. 22 (2003), p. 295
[3] D.K. Essumang: Bull. Environ. Contam. Toxicol Vol. 84 (2010), p. 720
[4] M. Takeda, H. Minowa and M. Ebihara: J. Radioanal. Nucl. Chem Vol. 272 (2007), p. 363
[5] S. Scaccia and B. Goszczynska: Talanta Vol. 63 (2004), p. 791
[6] M. Taddia and P. Sternini: Ann. Chim Vol. 91 (2001), p. 239
[7] J.L. Fabec: At. Spectrosc Vol. 4 (1983), p. 46
[8] J.L. Fabec and M.L.Ruschak: Anal. Chem Vol. 55 (1983), p. 2241
[9] M. Balcerzak: Crit. Rev. Anal. Chem Vol. 32 (2002), p. 181
[10] M.Balcerzak: Anal. Sci Vol. 18 (2002), p. 737
[11] D. Savard, S.J. Barnes and T.Meisel: Geostand. Geoanal. Res Vol. 34 (2010), p. 281
[12] L. Qi, J. Gao, X. Huang, J. Hu, M.F. Zhou and H. Zhong: J. Anal. At. Spectrom Vol. 26 (2011), p. 1900
[13] M. Balcerzak, E. Święcicka and E.Balukiewicz: Talanta Vol. 48 (1999), p. 39

Advanced Materials Research Vols. 989-994 (2014) pp 484-489
© (2014) Trans Tech Publications, Switzerland
doi:10.4028/www.scientific.net/AMR.989-994.484

Propagation Characteristics of Seismic Waves Taking Stratigraphic Composition into Consideration

Binbin Xu[1, a], Kentaro Nakai[2, b] and Toshihiro Noda[2, c]

[1]Tianjin Port Engineering Institution Ltd. of CCCC.; Key Lab. of Geotechnical Engineering of Tianjin; Key Lab. of Geotechnical Engineering, Ministry of Communication, Tianjin 300222, China;

[2]Department of Civil Engineering, Nagoya University, Nagoya 464-8601, Japan.

[a]xubinbin@tpei.com.cn, [b]nakai@i.soil.civil.nagoya-u.ac.jp, [c]noda@i.soil.civil.nagoya-u.ac.jp

Keywords: propagation characteristic, seismic wave, stratigraphic composition, soil-water coupled.

Abstract. In this paper, soil-water coupled dynamic analyses are carried out to investigate the influence of stratigraphic composition on the propagation properties of the seismic waves. SYS Cam-clay model is used as the constitutive model which can describe the different state of clayey and sandy soils. Two cases are considered for the composition of ground: one is the sandy ground with diluvial sand, alluvial sand and reclaimed sand; the other one is the clayey layer at the ground surface. It is found that for the sandy ground even though there is certain amplification of the input acceleration wave during the dense sand layer the subsequent seismic waves through the loose sand layers are attenuated significantly due to the occurrence of the liquefaction. While for the clayey ground, even though there is no risk of liquefaction damages at the ground surface the acceleration amplitude is greatly amplified and there is a risk that the structure itself would fail in the strength.

Introduction

Every year there are significant damages caused by the earthquake all over the world, especially the liquefaction damages during the earthquake, which would result in the decrease of bearing capacity, uneven settlement of the ground etc. Many researchers have devoted their efforts to predict the seismic responses of the upper structures [1, 2, 3, 4]. However, those analyses paid attention on the dynamic responses of the structures with given seismic waves observed at the ground surface and there is nearly no glimpse about the propagation of seismic waves from underground engineering bedrock to the ground surface. On the other hand, the forecast of liquefaction is usually considered by an approximate methods based on a microtopography classification in simple, or the FL/PL methods which are explained in Specifications for Highway Bridges [5], but it is proved to be an inaccuracy method by the practical engineering. It is attributed to that neither the influence of the fine fraction content of a liquefiable layer nor the difference in the stratigraphic composition of the depths direction is strictly taken into consideration.

In this paper, a soil-water coupled dynamic finite deformation analysis code called *GEOASIA* [6] is employed to investigate the propagation of seismic waves through the ground taking the stratigraphic into consideration. The research background is introduced in section 1. In section 2, the calculation conditions including the mesh partition, the soil parameters and the input seismic wave are demonstrated. The calculation results are presented in section 3 in detail and the conclusions are shown in section 4.

Calculation Conditions

Mesh Partition. The finite element mesh and the ground composition are shown in Fig. 1. The ground is assumed to be saturated and the plane strain condition is used. The width and the depth of the ground are 76.1m and 30m respectively. There are two kinds of ground type named Case 1 and Case 2. The detailed components of Case 1 are mudstone, diluvial sand, alluvial sand and reclaimed sand from the bottom to the surface, while in Case 2 there are mudstone, diluvial sand and alluvial clay. As for the boundary conditions, the nodes at the bottom are fixed in both horizontal and vertical

directions and the nodes at two side surfaces are only fixed horizontally. The undrained condition is applied at the two side surfaces and the bottom and the atmosphere condition is used at the ground surface. Also, to provide cyclic boundaries as constraint conditions, an equal displacement condition is applied to all components of all nodes at the same height on the two side surfaces [7, 8].

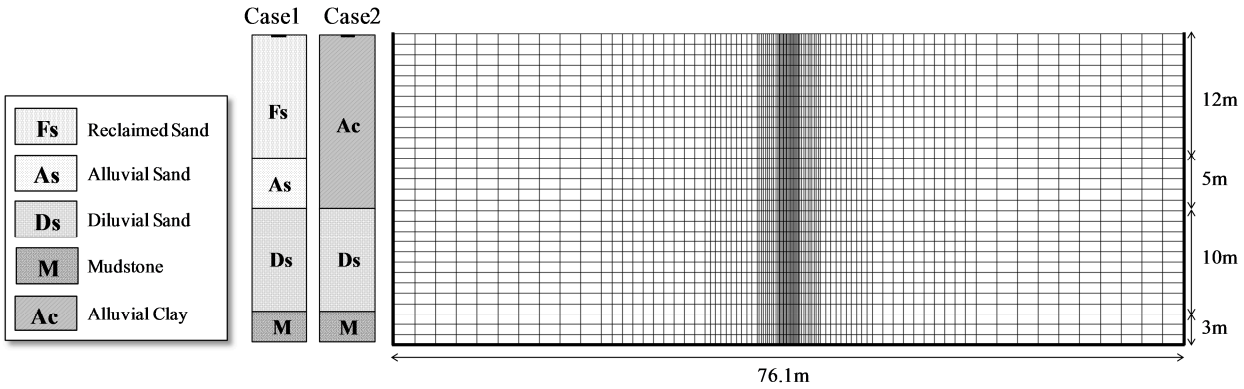

Fig. 1 Finite element mesh and ground compositions

Soil Parameters. The elasto-plastic properties used for analysis are determined by reproducing the mechanical behaviors of the undisturbed specimen sampled from the original ground by the SYS Cam-clay model [9]. A serial of undrained triaxial compression tests and one-dimensional compression tests are carried out on the remolded and undisturbed samples and the numerical calculation based on the constitutive model are also carried out. Through the curve fitting of the experimental and numerical results the soil parameters including elasto-plastic parameters and evolutional parameters can be determined, as shown in Table 1. As can be seen in Table 1, the soil parameters of diluvial sand, alluvial sand and reclaimed sand are exactly same, which is one of the most important contribution of the SYS Cam-clay model, that is only one group of material constant is employed to describe the same soil with different initial states from loose state to dense state.

Table 1 Elasto-plastic parameters and evolutional parameters

	Mudstone	Diluvial sand	Alluvial sand	Reclaimed sand	Alluvial clay
Elasto-plastic parameters					
Critical state index M	0.60	1.10	1.10	1.10	1.60
NCL intercept N	2.10	1.989	1.989	1.989	2.51
Compression index $\tilde{\lambda}$	0.17	0.05	0.05	0.05	0.21
Swelling index $\tilde{\kappa}$	0.003	0.0002	0.0002	0.0002	0.02
Poisson's ratio ν	0.3	0.3	0.3	0.3	0.3
Evolution parameters					
Degradation index of structure a	0.01	5.0	5.0	5.0	0.6
Degradation index of overconsolidation m	10.0	0.12	0.12	0.12	5.0
Rotational hardening index b_r	0.001	3.0	3.0	3.0	0.001
Limitation of rotational hardening m_b	1.0	0.9	0.9	0.9	1.0
Soil density ρ (g/cm^3)	2.707	2.675	2.675	2.675	2.754
Permeability k (cm/s)	1.0×10^{-7}	4.0×10^{-3}	4.0×10^{-3}	4.0×10^{-3}	1.0×10^{-6}

Input Seismic Wave. Fig. 2 shows the acceleration time history and Fourier amplitude spectrum of the input seismic wave in the analysis. This seismic wave is based on the Tokai-Tonankai-Nankai triple segment type earthquake. The maximum acceleration is 300 gal, and the predominant periods are in the range of 0.2 to 0.4s, with a long continuation time of the principal motion, at approximately 100 seconds. The acceleration is input equally in the horizontal direction to all nodes on the bottom

surface of the ground corresponding to engineering bedrock. A viscous boundary [10, 11] is set on the bottom surface corresponding to Vs=570 m/sec.

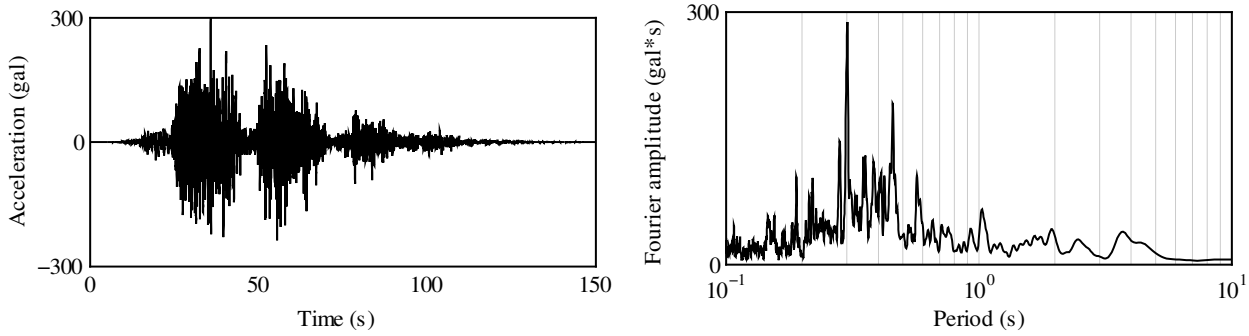

(a) Acceleration time history (b) Fourier amplitude spectrum

Fig. 2 Acceleration time history and the Fourier amplitude spectrum of the input seismic wave

Calculation Results

The calculation is not just for the duration of the earthquake but will continue after the termination of the seismic motions until the excess pore water pressure dissipates and the consolidation settlement completely converges. During the calculations, the corresponding acceleration waves at two different layers are observed and the Fourier amplitude spectrum analysis is also carried out for the observed acceleration waves. Figs 3-6 illustrate the acceleration response and the Fourier amplitude spectrum at the boundary of two different layers from the bottom to the ground surface in Case 1. In the diluvial sand layer (Fig. 4), the measured acceleration amplifies specially in the long-period wave around 0.3s. On the other hand in the reclaimed and the alluvial sand layers (Figs 5-6), the acceleration is amplified during the early stage of the earthquake, but after the stage of maximum acceleration, the observed acceleration attenuates specially in the short-period wave which is known as the characteristic behavior when the liquefaction takes place. Therefore, the emphasis of the seismic analysis should be put on the liquefaction risk when the surface layer is loose sandy soils, although the amplitude of the acceleration is attenuated due to the liquefaction.

Meanwhile we should note the contradiction in the liquefaction analysis: the liquefaction of the sandy ground would result in the losing of bearing capacity and cause the inclination of structure or uneven settlement of the ground; on the other hand the input seismic wave of the structure at the ground surface would be attenuated significantly due to the possible liquefaction, which, to some extent, would reduce the seismic response of the structure and increase the seismic instability of the structure.

Moreover, in SYS Cam-clay model, the non-linear isotropic Hooke's law is assumed for the elastic deformation of soil skeleton, and the bulk modulus $\tilde{K}$ and shear modulus $\tilde{G}$ are acquired from the following equation:

$$\tilde{K} = \frac{J(1+\mathrm{e}_0)}{\tilde{\kappa}} p' \ , \ \tilde{G} = \frac{3(1-2\nu)}{2(1+\nu)} \tilde{K} \ . \tag{1}$$

where e_0, p' and ν are the initial void ratio, mean effective stress and Poisson's ratio respectively; and $J = (1+\mathrm{e})/(1+\mathrm{e}_0)$, where e is the void ratio at current time. As shown in Eq. 1, since the rigidity of the ground falls with reduction of p', the natural period of the ground increases gradually, and the own natural periods of the reclaimed and alluvial sand layers become dominant at greater than that before the occurrence of the earthquake.

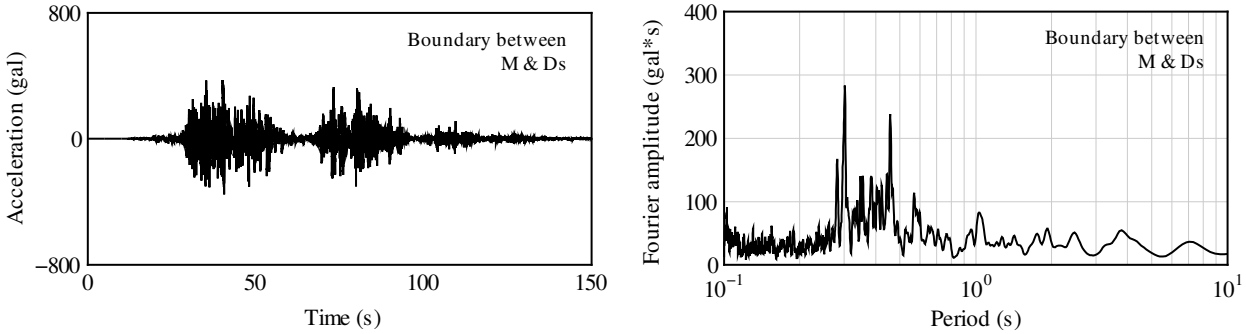

(a) Acceleration time history (b) Fourier amplitude spectrum

Fig. 3 Acceleration response and the Fourier amplitude spectrum at M and Ds boundary for Case 1

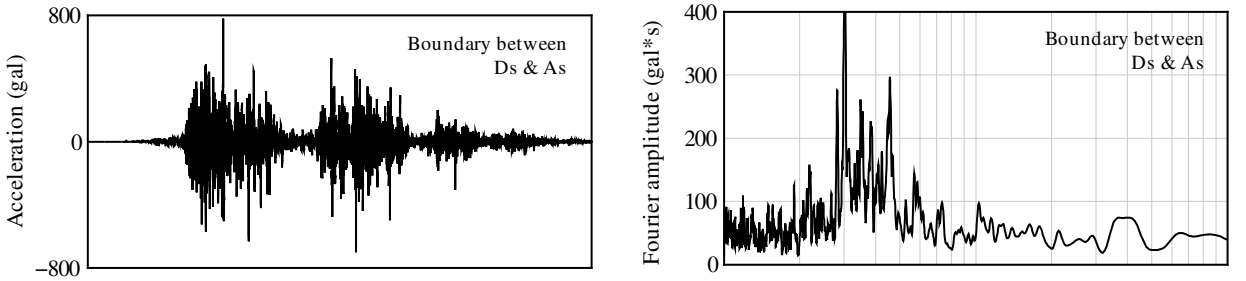

(a) Acceleration time history (b) Fourier amplitude spectrum

Fig. 4 Acceleration response and the Fourier amplitude spectrum at Ds and As boundary for Case 1

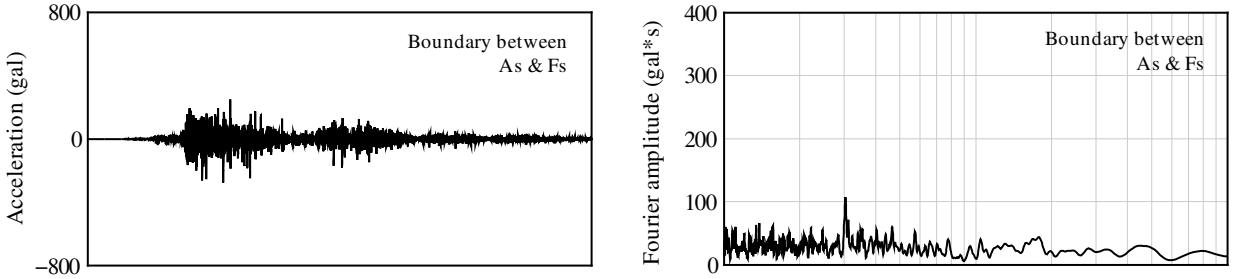

(a) Acceleration time history (b) Fourier amplitude spectrum

Fig. 5 Acceleration response and the Fourier amplitude spectrum at As and Fs boundary for Case 1

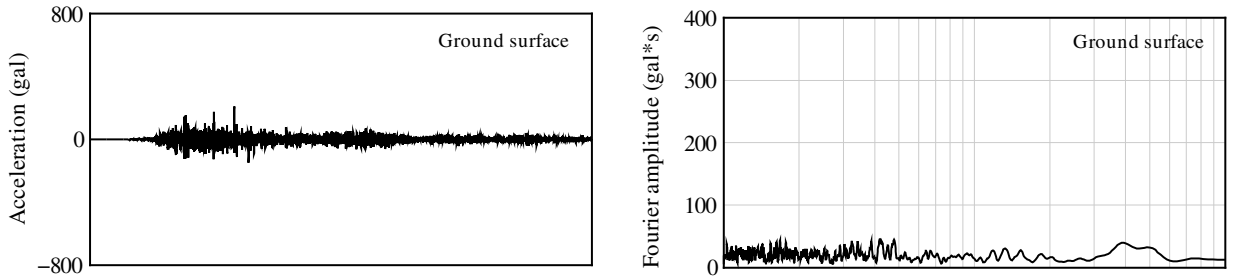

(a) Acceleration time history (b) Fourier amplitude spectrum

Fig. 6 Acceleration response and the Fourier amplitude spectrum at ground surface for Case 1

Figs. 7-9 depict the acceleration response and the Fourier amplitude spectrum at each layer boundary from the bottom to the ground surface in Case 2. For the subsurface clay soil, the decrease in the effective stress is much smaller compared with the subsurface sandy soil in Case 1, as there is no liquefaction in the clayey layer. Therefore, acceleration is greatly amplified in the alluvial clay layer. Paying attention to the Fourier amplitude spectrum, the oscillation at the subsurface layer is predominant at long period component around 0.6 to 1.0s in Fig. 9. From Eq. 1, a smaller shear modulus can be observed in clay, due to a larger swelling index $\tilde{\kappa}$, to clarify the longer period of clayey ground in Case 2.

Comparing Figs 6 and 9, there are significant differences in the acceleration time history and Fourier amplitude spectrum due to the different stratigraphic compositions. Note that in this analysis there are no upper structures. If there are upper structures, the stiffness of the system would changes a lot and the soil-structure interaction should be taken into consideration in order to obtain a precise seismic response.

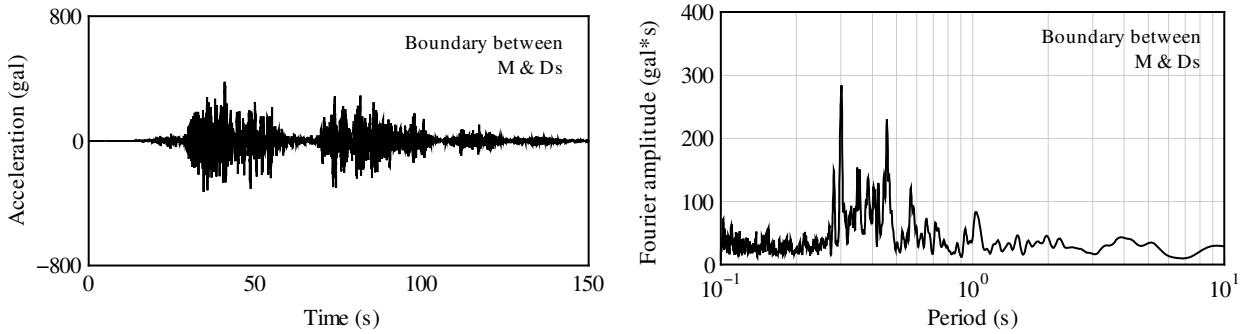

(a) Acceleration time history (b) Fourier amplitude spectrum

Fig. 7 Acceleration response and the Fourier amplitude spectrum at M and Ds boundary for Case 2

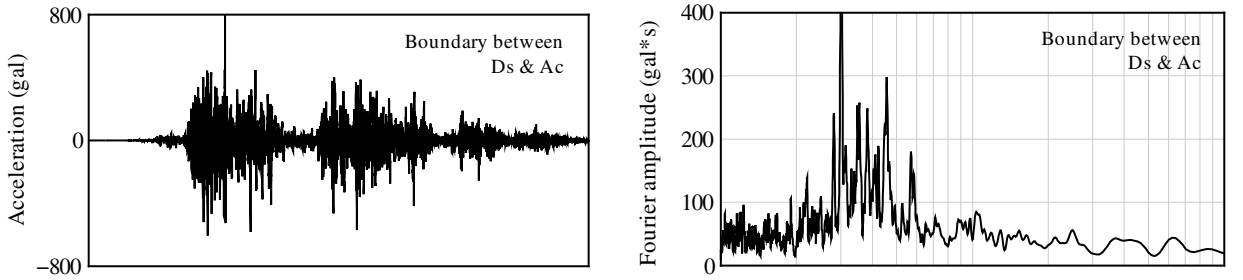

(a) Acceleration time history (b) Fourier amplitude spectrum

Fig. 8 Acceleration response and the Fourier amplitude spectrum at Ds and Ac boundary for Case 2

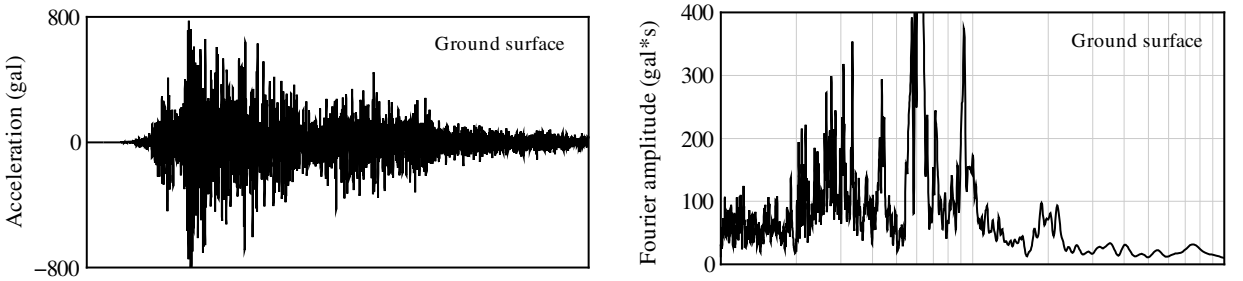

(a) Acceleration time history (b) Fourier amplitude spectrum

Fig. 9 Acceleration response and the Fourier amplitude spectrum at ground surface for Case 2

Conclusions

In this paper, soil-water coupled dynamic analyses taking the stratigraphic composition into consideration are carried out to investigate the influence on the propagation of seismic waves and the acceleration waves at the boundary of each two layers with their Fourier amplitude spectrum are measured and demonstrated sequentially. The conclusions are as follows:

(1) When the composition of the ground is sandy soil, although the acceleration waves are amplified significantly in the dense sand layer next there would be considerable attenuation in the amplitude of the acceleration due to the liquefaction in the loose sand layer. Also as the rigidity of the ground reduces due to the liquefaction, the natural period of the ground gradually increases.

(2) When there is a clay layer at the ground surface, the accelerations are amplified significantly in long-period components in the clay layer. Even though there is no risk of liquefaction in the surface

clay layer, the stability of the structure is considerably reduced due to the amplification of the acceleration and the bending strength of the structure itself should be verified specially.

(3) It should be pointed out that the influence of the difference in the stratigraphic composition along the depth is rarely taken into consideration in the conventional seismic analyses. Therefore, it is necessary to consider the influence of stratigraphic composition exactly for the high accuracy liquefaction judgment and seismic responses.

References

[1] T.D. Stark, M.H. Beaty, P.M. Byrne, G. Castro, F.C. Walberg, V.G. Perlea, P.J. Axtell, J.C. Dillon, W.B. Empson and D.L. Mathewsh, Seismic deformation analysis of Tuttle Creek Dam, Canadian Geotechnical Journal, 49(3) (2012) 323-343.

[2] J. Zhao, Y. Zheng and G. Wang, The foundation liquefaction and permanent deformation analysis of diversion dike for nuclear power plant, Applied Mechanics and Materials, 90-93 (2011) 1865-1869.

[3] R. Uzuoka, N. Sento and K. Kazama, Seepage and inertia effect on rate-dependent reaction of a pile in liquefied soil, Soils and Foundations, 48(1) (2008) 15-26.

[4] A. Tateishi, F. Oka, Y. Kotani and R. Asai, Numerical analysis of uplift behavior of an underground structure due to liquefaction using an effective stress analysis method, Proc. of International Symposium on Performance-Based Design in Earthquake Geotechnical Engineering, (2009) 1071-1079.

[5] Japan Road Association. Specifications for Highway Bridges, Part V Seismic Design (English edition) 2000.

[6] A. Asaoka and T. Noda, All soils all states all round geo-analysis integration, International Workshop on Constitutive Modelling - Development, Implementation, Evaluation, and Application, (2007) 11-27.

[7] A. Asaoka, T. Noda and K. Kaneda, Displacement/traction boundary conditions represented by constraint conditions on velocity field of soil, Soils and Foundations, 38(4) (1998) l73-181.

[8] T. Noda, H. Takeuchi, K. Nakai and A. Asaoka, Co-seismic and post-seismic behavior of an alternately layered sand-clay ground and embankment system accompanied by soil disturbance, Soils and Foundations, 49(5) (2009) 739-756.

[9] A. Asaoka, T. Noda, E. Yamada, K. Kaneda and M. Nakano, An elasto-plastic description of two distinct volume change mechanisms of soils, Soils and Foundations, 42(5) (2002) 47-57.

[10] J. Lysmer and R.L. Kuhlemeyer, Finite dynamic model for infinite media, ASCE, 95(4) (1969) 59-877.

[11] T. Noda, A. Asaoka and M. Nakano, Soil-water coupled finite deformation analysis based on a rate-type equation of motion incorporating the SYS Cam-clay model, Soils and Foundations, 48(6) (2008) 771-790.

Advanced Materials Research Vols. 989-994 (2014) pp 490-493
© (2014) Trans Tech Publications, Switzerland
doi:10.4028/www.scientific.net/AMR.989-994.490

Effect of SO_2 on Mn-Mg-O_x catalyst treated by non-thermal plasma for NO catalytic oxidation

Ruiyun Lai[1] , Xiaolong Tang[2,1,a], Honghong Yi[2, 1], Kai Li[1], Ying Xiang[1], Xin Sun[1]

[1] Faulty of Environmental Science and Engineering, Kunming University of Science and Technology, Kunming 650500, China

[2] Civil and Environmental Engineering School, University of Science and Technology Beijing, Beijing 100083, China

[a]txiaolong@126.com

Keywords: Mn-Mg-O_x catalysts, non-thermal plasma, NO,catalytic oxidation

Abstract: The effect of MgO addition on SO_2 tolerance of MnO_x for the NO catalytic oxidation was investigated in this work. MgO addition significantly promotes the SO_2 resistance of MnO_x at low temperature range of 50–250℃. The slight decrease in catalytic activity over Mn-Mg-O_x exposure to SO_2 is attributed to the partially deactivation of the catalytic active site poisoned by SO_2. Through XRD and FT-IR characterization, MgO may effectively inhibit the competitive adsorption between NO_x and SO_2 in manganese site, and enhance SO_2 adsorption on the magnesia surface.

Introduction

At present, selective catalytic reduction (SCR) with NH_3 has been proven to be one of the most efficient methods to elimination of the NO_x [1] . However, this process has several problems[2]. Selective catalytic oxidation (SCO) is an ideal potential technology for simultaneous removal of NO_x and SO_2 from flue gas.

Researches have been reported that some transition metal oxides exhibited high catalytic activity for NO oxidation, Mn/TiO_2 [3], CeO_2-ZrO_2 [4] , $Co/KxTi_2O_5$ [5], are proving to be very effective in the oxidation reaction process. Previous work of our team had proved that MnO_x catalysts have good catalytic activity and wide activity temperature window [2, 6-8]. However, the NO conversion of these catalysts was pronounced deactivation with the presence of SO_2.In this work, the Mn-Mg-O_x catalysts were synthesized by low temperature solid phase reaction method (SP) and modified by the non-thermal plasma, then used for NO catalytic oxidation at low temperature. In particular the effect of SO_2 on the NO conversion was investigated.

Experimental

Catalyst preparation. Mn-Mg-O_x catalysts were prepared by the low temperature solid phase reaction method (SP). Firstly, the manganese acetate, potassium permanganate and magnesium nitrate were mixed and ground fully for 30 minutes. The manganese acetate/ potassium permanganate mole ratio was 2:3, and Mn/Mg was 5:1, 3:1, and 1:1.The mixture was placed in the baking oven at 70℃ for 48 h. The product was filtered and washed with de-ionized water (3~4 times) and absolute ethanol (2~3 times), then dried at 100℃over night. Finally, the catalyst precursor treated by non-thermal plasma (NTP) for 1 h used dielectric barrier discharge (DBD).

Catalytic activity. Catalytic activity measurements for oxidation were performed at 50℃~250℃ in a Pyrex tube fixed-bed flow reactor of 10 mm internal diameter with a gas hourly space velocity of 30000h^{-1} . The reaction gas mixture contained 500ppm NO, 5%O_2, 100ppm SO_2 (when used) diluted in N_2. The sample weight, flow rate were 0.3g, 200mL/min, respectively. The reactions and reactive products of NO, NO_2, SO_2 were measured by Flue Gas Analyzer (KM9106). The NO conversion is defined as $X\,(\%) = (NO_{inlet} - NO_{outlet})/NO_{inlet} \times 100\%$.

Catalytic characterization. X-ray diffraction (D/MAX-2200) patterns were recorded with a Rigaku diffractometer operated at 36 kV and 30 mA by using Ni-filtered Cu Kα radiation (λ=0.15406 nm) at a rate of 5 (°) /min from 2θ=20° to 80°. Fourier transform infrared spectroscopy (FT-IR) of Varian 640-IR was used to determine sulfur-containing species on the catalyst surface. The FT-IR spectra were recorded using the KBr pellet technique on a Thermo spectrometer in the 4400-390cm^{-1} wavenumber range. Before analysis, the sample was ground, and made into pellets with KBr. The analysis temperature was at ambient temperature, and the analyses done ex-situ.

Results and discussion

Catalytic performance of NTP treated catalysts. Fig.1 summarize the results of the catalytic oxidation activities of conventional catalysts compared with catalysts modified by NTP. From Fig.1, the NO conversion of all the plasma treated samples rose by 5%-10%, compared with the conventional catalysts. The results indicated that the NO catalytic oxidation activity of these catalysts treated by NTP were significantly improved.

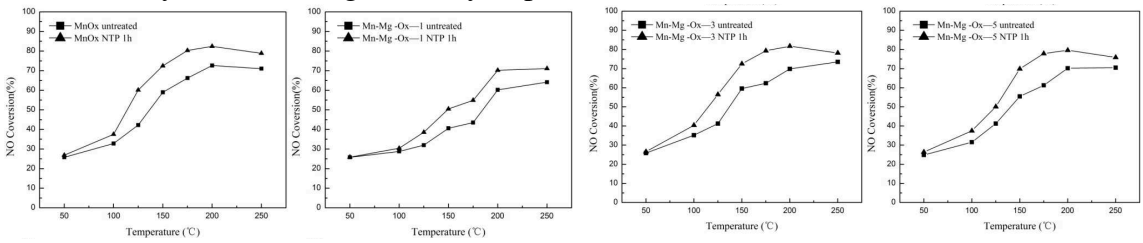

Fig.1. Catalytic performance of NTP treated MnOx and Mn-Mg-Ox-X at 200℃

Catalytic performance of MnO_x compared with Mn-Mg-O_x in the absence of SO_2. Fig.2 shows the catalyst performance for NO oxidation during 50℃~250℃ over MnOx, Mn-Mg-Ox-X, where X represents the molar ratio of Mn to Mg, e.g. Mn-Mg-Ox-(1, 3, 5). In the initial phase, the rate of chemical reactions is increasing with the rise of temperature. Then, NO conversion will decrease at high temperature (250℃),duo to the thermodynamic stability of NO–NO_2,when temperatures above 200℃ the dissociation of NO_2 becomes evident. The NO catalytic oxidation activity was MnO_x≈Mn-Mg-O_x-3>Mn-Mg-O_x-5>Mn-Mg-O_x-1. The NO conversion over the Mn-Mg-Ox-3 was about 82% at 200℃, even at 175℃ and 250℃ it achieved 80% and 79% respectively. However, the catalytic activity of MnOx was close to Mn-Mg-Ox-3.

Effect of SO_2 on MnOx and Mn-Mg-Ox-3. As shown in Table 1, Mn-Mg-Ox-3 catalyst，which treated with N_2 plasma for 60 min, showed high catalytic activity compared with the other samples when SO_2 added. From the above catalytic activity tests showed that MnO_x and Mn-Mg-O_x-3 show a good performence.

Table.1 The NO conversion of over different samples when absence of SO_2 and presence of SO_2.

Sample	NO conversion (absence of SO_2)	NO conversion (presence of SO_2)
Mn-Mg-O_x-1	70.5%	65.4%
Mn-Mg-O_x-3	82%	79%
Mn-Mg-O_x-5	79.7%	70.8%

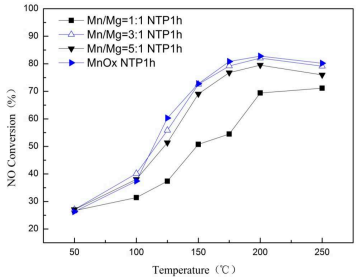

Fig.2 The NO catalytic oxidation activities of MnOx, Mn-Mg-Ox-1, Mn-Mg-Ox-3, Mn-Mg-Ox-5 catalysts

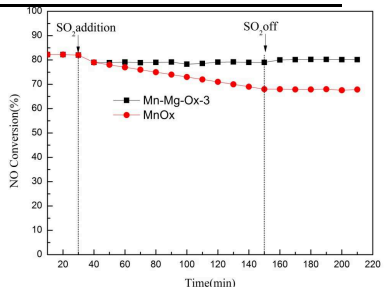

Fig.3. Effect of SO_2 on MnOx and Mn-Mg-Ox-3 at 200℃

In Fig.3, the effect of 100ppm SO_2 addition on the catalytic activity of MnO_x and Mn-Mg-O_x-3 at 200℃ is shown.After the measurement of steady-state conversions in SO_2 absence condition, 100ppm SO_2 was introduced to the reaction gas mixture and NO conversion was measured as a function of time. Over the MnOx catalyst, the NO conversion was gradually reduced with the reaction continuing when 100ppm SO_2 was added into the feed gas mixture. On the other hand, the NO conversion over Mn-Mg-O_x-3 only slightly decreases and was leveling off at 78-79% for a long time. This phenomenon could be explained that a small amount of SO_2 still adsorbed on the Mn-Mg-O_x-3 surface after removing SO_2 from feed gas lead to the activity decreased slightly,but not restored to its previous state. The activity tests results showed that SO_2 has notable negative effect on the MnO_x catalyst, but totally different to the Mn-Mg-O_x-3 catalyst. Also, these results imply that the addition of MgO may be an effective method to avoid the process of sulfation of the MnO_x catalyst surface.

Catalyst characterization. The XRD patterns of the fresh and aged Mn-Mg-Ox-3 (exposed to feed containing 100ppm SO_2) are revealed in Fig.4. For comparison, the XRD patterns of the fresh and aged MnOx are also shown. No magnesium oxides peaks were detected in all samples, mainly due to the low Mg loading. As shown in Fig.4, the peaks of the XRD profile of these are weak, it can be identified most of the weak peaks belong to Mn_3O_4. From the Fig.4 other diffraction peaks of MnO_2 (2θ=12.8°, 18.2°, 28.8°, 37.5°, 49.9°), and Mn_3O_4 (2θ=23.9°, 32.9°, 38.2°) could be observed. Li Hua et al [9], observed that the the catalysts co-existence of MnO_2-Mn_2O_3 might account for the increased oxidation of NO. This was concordant with our experimental result. Furthermore, no new peaks (magnesium- sulfur compounds such as MgS, $MgSO_3$, and $MgSO_4$) ware observed in the spectra of all the aged catalysts.

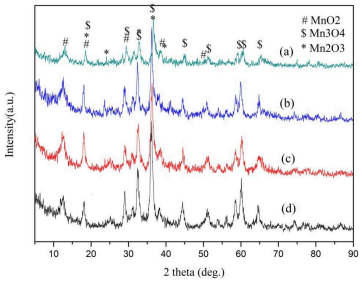

Fig.4. XRD patterns of fresh and aged MnOx and Mn-Mg-Ox-3 exposed to 100 ppm SO_2: (a) aged MnOx, (b) fresh MnOx, (c) aged Mn-Mg-Ox-3, (d) fresh Mn-Mg-Ox-3.

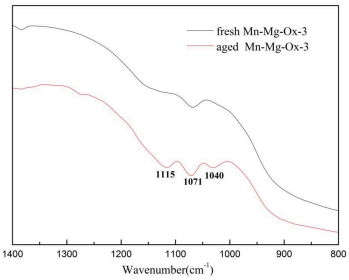

Fig.5. Comparison of FT-IR between fresh and aged Mn-Mg-Ox-3catalyst exposed to 100 ppm SO_2.

Fig.5 exhibits the FT-IR spectra obtained over the fresh and aged Mn-Mg-O_x-3 exposed to 100ppm SO_2. Absorption bands assigned to sulfite species were observed in the aged Mn-Mg-Ox-3. Schneider et al [10], researched infrared absorption properties of SO_2 adsorbed on MgO. The spectrum clearly shows absorption broads in the region 950-1400cm^{-1} are attributed to sulfate and sulfide SO_3^{2-} groups. Wang et al [11], also have found that the band at 1040 cm^{-1} was attributed to the S-O stretching vibration of sulfite-like species produced by the strong chemisorbed SO_2 on the surface reacting with the oxygen lattice of $MgAl_2O_4$, and found that the band at 1395 cm^{-1} and 1070 cm^{-1} were characteristic of the surface sulfate species. Hence, the peaks of 1115 cm^{-1}, 1074 cm^{-1} and 1040cm^{-1} over aged Mn-Mg-Ox-3 could be characterized to the formation of surface sulfur species.

The high stability of the Mn-Mg-O_x-3 catalyst after 2h of reaction on stream in the presence of SO_2 shows that the active sites of catalysts have little effect when addition of SO_2. The phenomenon can be explained that the sulphate or sulphate cannot be adsordates which are stable under reaction condition inhibit further the adsorption of SO_2 or SO_3 from the gas phase [12]. However, NO molecule which significantly smaller compared to SO_2 or SO_3 can be chemisorbed on the unoccupied cations of the catalyst to form active bidentate nitrate species. A similar explanation was also reported by Costa and Efstathiou for the SO_2 stability of Pt/ MgO-CeO_2 during H_2-SCR of NO reaction [13]. The results presented here further show that MgO addition may effectively inhibit the competitive adsorption between NO_x and SO_2.

Conclusions

Mn-Mg-O_x-3 with high resistance to sulphur poisoning for the SCO was demonstrated in this work. Mn-Mg-O_x-3 catalyst presents stability of industrial importance since no stable catalysts in the reaction SCO in the presence of particularly SO_2 have been reported so far. The slight decrease in catalytic activity over Mn-Mg-O_x-3 could be attributed to the partially deactivation of Mn sites poisoned by SO_2. Through XRD and FT-IR characterization, the high SO_2 tolerance of Mn-Mg-O_x-3 at low temperature could be attributed to the effective inhibition of the competitive adsorption between NO_x and SO_2 on catalytic active site and the enhancement of SO_2 adsorption on the magnesia surface with MgO addition.

Acknowledgements

This work was supported by National Natural Science Foundation of China (20907018, 21177051) and Program for New Century Excellent Talents in University (NCET-12-0776)

References

[1] PranitS. Metkar, Michael P. Harold, Vemuri Balakotaiah. Selective catalytic reduction of NOx on combined Fe- and Cu-zeolite monolithic catalysts: Sequential and dual layer configurations, Appl. Catal. B-Environ., 111–112 (2012): 67-80

[2] Li K., Tang X.L., Yi H.H., et al. Low-temperature catalytic oxidation of NO over Mn–Co–Ce–O_x catalyst, Chem. Eng. J., 192 (2012): 99-104

[3] E. Park, S. Chin, J. Jeong, et al. Low-temperature NO oxidation over Mn/TiO_2 nanocomposite synthesized by chemical vapor condensation: Effects of Mn precursor on the surface Mn species, Micropor. Mesopor. Mat., 163 (2012): 96-101

[4] Idriss A., Noelia G.-H., Agustín B.-L., et al. Influence of the physico-chemical properties of CeO_2–ZrO_2 mixed oxides on the catalytic oxidation of NO to NO_2, Appl. Surf. Sci., 256 (2010): 7706–7712

[5] Qiang Wang, So Ye Park, Linhai Duan,et al. Activity, stability and characterization of NO oxidation catalyst Co/K$x$$Ti_2O_5$, Appl. Catal. B-Environ., 85 (2008): 10–16

[6] X.L. Tang, K. Li, H.H. Yi, et al. MnOx Catalysts Modified By Nonthermal Plasma for NO Catalytic Oxidation, J. Phys. Chem. C, 116 (2012): 10017−10028

[7] K. Li, X.L. Tang, H.H. Yi, et al. Non-thermal Plasma Assisted Catalytic Oxidation NO over Mn-Ni-O_x Catalysts at Low-Temperature, Chem. Eng. J., 383-390 (2012): 3092-3098

[8] K. Li, X.L. Tang, H.H. Yi, et al. Research on manganese oxide catalysts surface pretreated with non-thermal plasma for NO catalytic oxidation capacity enhancement, Appl. Surf. Sci., 264 (2013): 557-562

[9] Li H., Tang X.L., Yi H.H., et al. Low-temperature catalytic oxidation of NO over Mn-Ce-O_x catalyst, J. Rare Earth, 28 (2010): 64-68

[10] William F. Schneider, John Li, Kenneth C. Hass. Combined Computational and Experimental Investigation of SO_x Adsorption on MgO, J. Phys. Chem. B, 105 (2001): 6972-6979

[11] J. Wang, C.L. Li. SO_2 adsorption and thermal stability and reducibility of sulfates formed on the magnesium–aluminate spinel sulfur-transfer catalyst, Appl. Surf. Sci., 161 (2000): 406–416

[12] J.P. Breena, R. Burcha, C. Hardacrea, et al. An investigation of the thermal stability and sulphur tolerance of Ag/γ-Al_2O_3 catalysts for the SCR of NO_x with hydrocarbons and hydrogen, Catal. Today, 70 (2007): 36–44

[13] Costas N. Costa, Petros G. Savva, et al. Industrial H_2-SCR of NO on a novel Pt/MgO–CeO_2catalyst, Appl. Catal. B-Environ., 75 (2007):147–156

Advanced Materials Research Vols. 989-994 (2014) pp 494-497
© (2014) Trans Tech Publications, Switzerland
doi:10.4028/www.scientific.net/AMR.989-994.494

Synthesis and characterisation of a novel thermoresponsive dendronized monomer bearing azobenzene moiety

Chang-An Yang[1,a], WenJun Xiao*[2,b], EnXiang Liang[1], Ying Lu[1], GangYong Li[1]

[1]Department of Chemistry and Chemical Engineering, Hunan Institute of Science and Technology, Yueyang 414006, Hunan Province, PR China

[2]Key Laboratory of Organosilicon Chemistry and Material Technology of Ministry of Education, Hangzhou Normal University, Hangzhou 311121, PR China

[a]Chang_anyang@163.com, Corresponding Author: [b]xiaowj2008@126.com

Keywords: Thermoresponsive, Dendronized monomer, Azobenzene moiety, Lower critical solution temperature (LCST), Phase transition behavior

Abstract. Novel thermoresponsive dendronized monomer bearing azobenzene moiety, 4-(4′-(3, 4, 5-tris (2-(2-methoxyethoxy) ethoxy) benzyloxy) phenylazo) benzyl methacrylate, has been successfully synthesized. The chemical structures of intermediate compounds and dendronized monomer were confirmed by FTIR and ^{1}H NMR. The phase transition behaviors of these intermediate compounds and dendronized monomer were investigated. These intermediate compound and dendronized monomer showed remarkably reversible thermoresponsive phase transition behaviors.

Introduction

Stimuli-responsive polymers, often referred to as "smart or intelligent" polymer systems, which exhibit reversible property changes in response to changes in environmental factors such as temperature, pH or light, have attracted considerable research interest due to their promising potential [1-3]. Recently, thermo- and light-responsive polymers have been reported. Most of these polymers were synthesized by copolymerization of thermo-responsive monomer and light-responsive monomer [4-7]. However, few works have been done on the synthesis of thermo- and light-responsive dendronzied polymer based on dendronized monomer with thermo- and light-responsive moieties.

In this paper, a novel thermoresponsive dendronized monomer bearing azobenzene moiety, 4-(4′-(3, 4, 5-tris (2-(2-methoxyethoxy) ethoxy) benzyloxy) phenylazo) benzyl methacrylate, has been successfully synthesized (Fig. 1). The chemical structures of intermediate compounds and dendronized monomer were confirmed by FTIR and ^{1}H NMR. The phase transition behaviors of these intermediate compounds and dendronized monomer were investigated. The synthesis and characterisation of thermo- and light-responsive dendronized polymer based on the dendronized monomer will be reported in the near future.

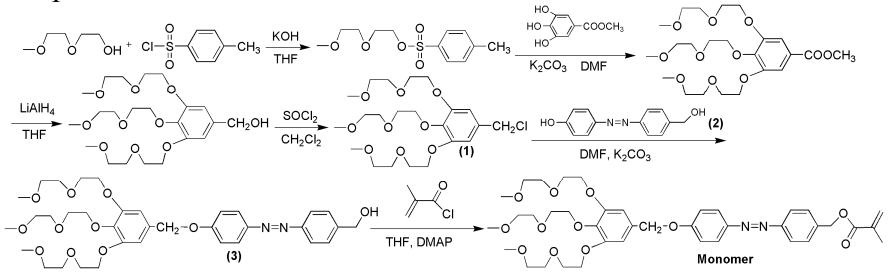

Fig. 1 Synthetic route of the dendronized monomer

Experimental Section

The preparation of the thermoresponsive dendronized monomer bearing azobenzene moiety, 4-(4′-(3, 4, 5-tris (2-(2-methoxyethoxy) ethoxy) benzyloxy) phenylazo) benzyl methacrylate, is described as follows. Firstly, 2-(2-methoxyethoxy) ethyl 4-methylbenzenesulfonate was prepared by esterification of 2-(2-methoxyethoxy) ethanol and *p*-toluenesulfonyl chloride. Secondly, methyl 3, 4,

5-tris (2-(2-methoxyethoxy) ethoxy) benzoate was synthesized by etherification of methyl 3, 4, 5-trihydroxybenzoate with 2-(2-methoxyethoxy) ethyl 4-methylbenzenesulfonate. Thirdly, 3, 4, 5-tris (2-(2-methoxyethoxy) ethoxy) benzyl alcohol was synthesized by reduction of methyl 3, 4, 5-tris (2-(2-methoxyethoxy) ethoxy) benzoate with $LiAlH_4$. Fourthly, 3, 4, 5-tris (2-(2-methoxyethoxy) ethoxy) benzyl chloride was obtained by the chlorination of 3, 4, 5-tris (2-(2-methoxyethoxy) ethoxy) benzyl alcohol with $SOCl_2$. Fifthly, 4-(4′-(3, 4, 5-tris (2-(2-methoxyethoxy) ethoxy) benzyloxy) phenylazo) benzyl alcohol was prepared by the etherification of 3, 4, 5-tris (2-(2-methoxyethoxy) ethoxy) benzyl chloride and 4-((4′-Hydroxy) phenylazo) benzyl alcohol. Finally, the dendronized monomer, 4-(4′-(3, 4, 5-tris (2-(2-methoxyethoxy) ethoxy) benzyloxy) phenylazo) benzyl methacrylate, was obtained by esterification of methacryloyl chloride and 4-(4′-(3, 4, 5-tris (2-(2-methoxyethoxy) ethoxy) benzyloxy) phenylazo) benzyl alcohol. The rude product was purified by column chromatography to obtain the dendronized monomer. The chemical structures of intermediate compounds and dendronized monomer were confirmed by ^{1}H NMR and FTIR.

Results and Discussion

Characterisation of the intermediate compounds and dendronized monomer

The intermediate compounds methyl 3, 4, 5-tris (2-(2-methoxyethoxy) ethoxy) benzoate and 3, 4, 5-tris (2-(2-methoxyethoxy) ethoxy) benzyl alcohol were prepared and characterized in the literature [8]. 3, 4, 5-tris (2-(2-methoxyethoxy) ethoxy) benzyl chloride (**Compound 1**) was obtained by the chlorination of 3, 4, 5-tris (2-(2-methoxyethoxy) ethoxy) benzyl alcohol with $SOCl_2$, colorless liquid, yield: 92%. Fig. 2 shows the ^{1}H NMR spectra of 3, 4, 5-tris (2-(2-methoxyethoxy) ethoxy) benzyl chloride. The chemical shifts are illustrated as follows: ^{1}H NMR (δ, ppm, $CDCl_3$): 6.69-6.64 (m, 2H, Ar-H), 4.50 (s, 2H, -CH_2Cl), 4.29-4.20 (t, 6H, -OCH_2-), 3.89-3.76 (t, 6H, -OCH_2-), 3.76-3.62 (t, 6H, -OCH_2-), 3.62-3.50 (t, 6H, -OCH_2-), 3.45 (s, 9H, -CH_3).

4-((4′-Hydroxy) phenylazo) benzyl alcohol (**Compound 2**) was synthesized by reduction of 4-((4′-Hydroxy) phenylazo) benzoate with $LiAlH_4$, orange solid, yield: 84%. Fig. 3 shows the ^{1}H NMR spectra of 4-((4′-Hydroxy) phenylazo) benzyl alcohol. The chemical shifts are illustrated as follows: ^{1}H NMR (δ, ppm, DMSO): 7.73-7.70 (m, 4H, Ar-H), 7.45-7.43 (m, 2H, Ar-H), 6.78-6.80 (m, 2H, Ar-H), 4.55 (s, 2H, -CH_2O-).

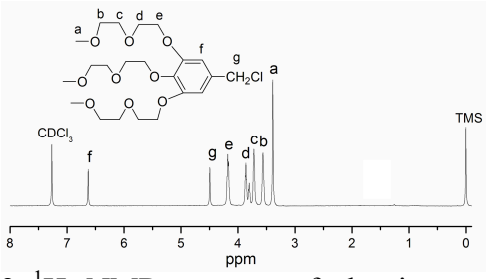

Fig. 2 ^{1}H NMR spectra of the intermediate compound, 3, 4, 5-tris (2-(2-methoxyethoxy) ethoxy) benzyl chloride, in $CDCl_3$-*d*.

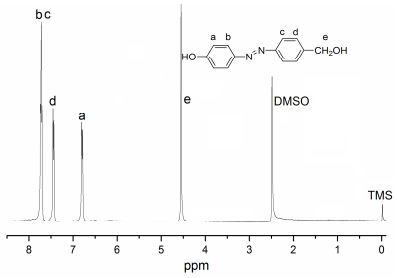

Fig. 3 ^{1}H NMR spectra of the intermediate compound, 3, 4, 5-tris (2-(2-methoxyethoxy) ethoxy) benzyl chloride, in DMSO-*d*.

4-(4′-(3, 4, 5-tris (2-(2-methoxyethoxy) ethoxy) benzyloxy) phenylazo) benzyl alcohol (**Compound 3**) was prepared by the etherification of 3, 4, 5-tris (2-(2-methoxyethoxy) ethoxy) benzyl chloride and 4-((4′-Hydroxy) phenylazo) benzyl alcohol, orange liquid, yield: 88%. In the FTIR spectra Fig. 4a, a strong adsorption band appeared at 3340 cm^{-1}, which is attributed to the -OH stretching vibration. Fig. 4b shows the ^{1}H NMR spectra of 4-(4′-(3, 4, 5-tris (2-(2-methoxyethoxy) ethoxy) benzyloxy) phenylazo) benzyl alcohol. The chemical shifts are illustrated as follows: ^{1}H NMR (δ, ppm, $CDCl_3$): 7.93-7.81 (m, 4H, Ar-H), 7.51-7.49 (m, 2H, Ar-H), 7.08-7.06 (m, 2H, Ar-H), 6.69 (s, 2H, Ar-H), 5.30 (s, 2H, -CH_2O-), 5.03 (s, 2H, -CH_2O-), 4.19-4.18 (t, 6H, -OCH_2-), 3.87-3.81 (t, 6H, -CH_2O-), 3.72-3.67 (t, 6H, -OCH_2-), 3.56-3.54 (t, 6H, -CH_2O-), 3.38-3.36 (s, 9H, -OCH_3), 1.68 (s, 1H, -OH). The peak area ratio of methylene peak g (peak g. Fig. 4b) and methylene peak l (peak l. Fig. 4b) is 1 : 1 and no impure peak is observed, indicating the pure **compound 3** is obtained.

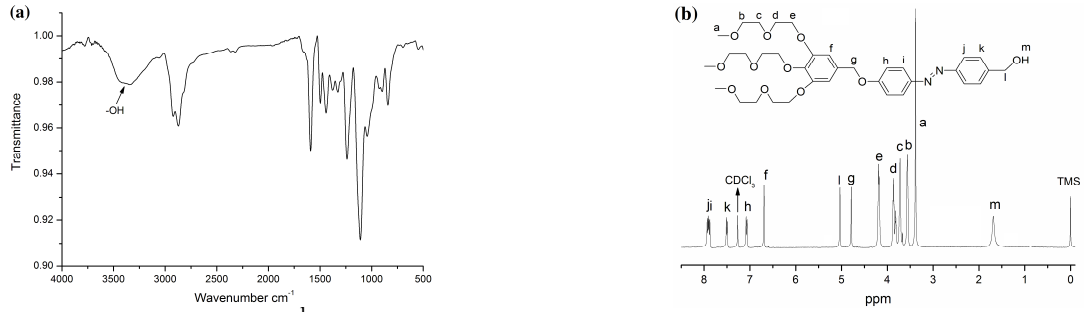

Fig. 4 FTIR spectrum (a) and ^{1}H NMR spectra (b) of the intermediate compound, 4-(4′-(3, 4, 5-tris (2-(2-methoxy ethoxy) ethoxy) benzyloxy) phenylazo) benzyl alcohol.

The dendronized monomer, 4-(4′-(3, 4, 5-tris (2-(2-methoxyethoxy) ethoxy) benzyloxy) phenylazo) benzyl methacrylate, was obtained by esterification of methacryloyl chloride and 4-(4′-(3, 4, 5-tris (2-(2-methoxyethoxy) ethoxy) benzyloxy) phenylazo) benzyl alcohol, orange liquid yield: 85%. In the FTIR spectra Fig. 5a, the –OH stretching vibration band at 3340 cm^{-1} wasn't observed. A strong C=O stretching band appeared at 1718 cm^{-1}, which is attributed to the ester bond. The adsorption band at 1636 cm^{-1} is attributed to the C=C stretching vibration, which confirms the formation of 4-(4′-(3, 4, 5-tris (2-(2-methoxyethoxy) ethoxy) benzyloxy) phenylazo) benzyl methacrylate. Fig. 5b shows the ^{1}H NMR spectra of 4-(4′-(3, 4, 5-tris (2-(2-methoxyethoxy) ethoxy) benzyloxy) phenylazo) benzyl methacrylate. The chemical shifts are illustrated as follows: ^{1}H NMR (δ, ppm, $CDCl_3$): 7.93-7.87 (m, 4H, Ar-H), 7.52-7.50 (m, 2H, Ar-H), 7.08-7.06 (m, 2H, Ar-H), 6.69 (s, 2H, Ar-H), 6.19 (s, 1H, =CH-), 5.62 (s, 1H, =CH-), 5.27 (s, 2H, -CH_2O-), 5.04 (s, 2H, -CH_2O-), 4.19-4.18 (t, 6H, -OCH_2-), 3.87-3.81 (t, 6H, -CH_2O-), 3.72-3.67 (t, 6H, -OCH_2-), 3.56-3.54 (t, 6H, -CH_2O-), 3.38-3.36 (s, 9H, -OCH_3), 1.99 (s, 3H, -CH_3). The peak area ratio of vinyl peak m (peak m. Fig. 5b) and methylene peak l (peak l. Fig. 5b) is 1 : 2 and no impure peak is observed, indicating the pure dendronized monomer is obtained.

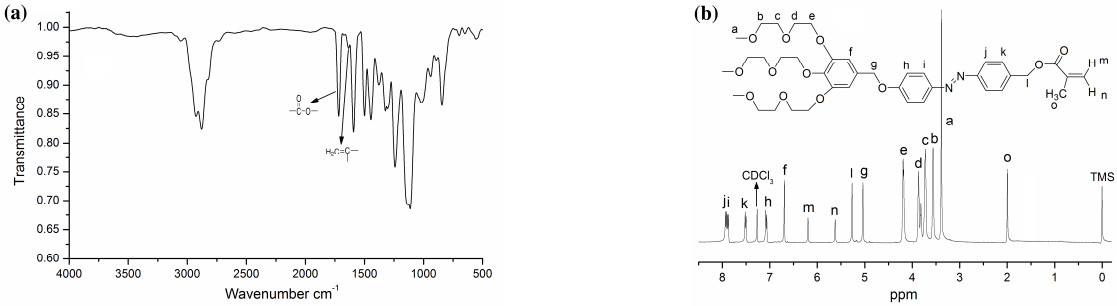

Fig. 5 FTIR spectrum (a) and ^{1}H NMR spectra (b) of the dendronized monomer, 4-(4′-(3, 4, 5-tris (2-(2-methoxyethoxy) ethoxy) benzyloxy) phenylazo) benzyl methacrylate.

Phase transition behaviors

Fig. 6 shows the DSC traces of intermediate compound 3 and dendronized monomer. From Fig. 6, it will be seen that each of the compounds has only a phase transition, which attributes to the glass transition. Melting point and LC phase transition are not observed during the heating and cooling process.

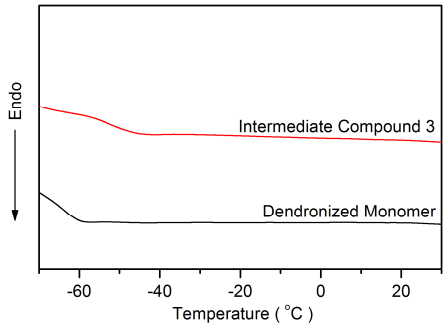

Fig. 6 DSC curves of intermediate compound 3 and dendronized monomer during the second heating at a rate of 10 °C min^{-1}.

The lower critical solution temperatures (LCSTs) of intermediate compound 3 and dendronized monomer in deionized water were measured by visual method. Fig. 7 illustrates the appearance changes of 5.0 mg ml^{-1} intermediate compound 3 and dendronized monomer in deionized water during phase separation. When intermediate compound 3 was dissolved in pure deionized water at the concentration of 5.0 mg ml^{-1} at room temperature, it was turbid; however, when the temperature was decreased to 15 °C (LCST), it became a transparent solution, meaning the occurrence of phase transition (Fig. 7a). Just as expected, dendronized monomer aqueous solution at the concentration of 5.0 mg ml^{-1} did also exhibit a sharp and rapid phase transition around 11 °C (LCST) (Fig. 7b).

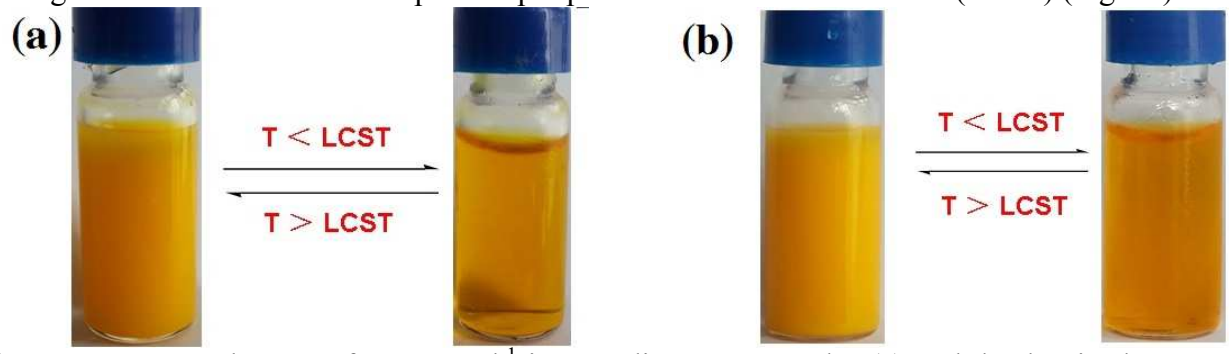

Fig.7 Appearance changes of 5.0 mg ml^{-1} intermediate compound 3 (a) and dendronized monomer (b) in deionized water during phase separation.

Summary

A novel thermoresponsive dendronized monomer bearing azobenzene moiety, 4-(4′-(3, 4, 5-tris (2-(2-methoxyethoxy) ethoxy) benzyloxy) phenylazo) benzyl methacrylate, has been successfully synthesized. The chemical structures of intermediate compounds and dendronized monomer were confirmed by FTIR and ^{1}H NMR. The phase transition behaviors of these intermediate compounds and dendronized monomer were investigated. The intermediate compound 3 and dendronized monomer both showed remarkably reversible thermoresponsive phase transition behaviors.

Acknowledgment

This work is supported by the National Natural Science Foundation of China (NNSFC Grants: 21106037, 21303035), the Scientific Research Fund of the Hunan Provincial Education Department (No: 11A040), and Hunan Provincial Natural Science Foundation of China (No: 12JJ4015).

References

[1] E. S. Gil, S. M. Hudson, Prog. Polym. Sci. 29 (2004) 1173-1222.
[2]J. Zou, B. Guan, X. J Liao, M. Jiang, F. G. Tao, Macromolecules. 42 (2009) 7465-7473.
[3]D. Roy, J. N. Cambre, B. S. Sumerlin, Chem. Commun. (2009) 2106-2108.
[4] F. D. Jochum, P. Theato, Chem. Commun. 46 (2010) 6717-6119.
[5] X. D. Tao, Z. G. Gao, T. Satoh, Y. Cui, T. Kakuchi, Q. Duan, Polym. Chem. 2 (2011) 2068-2073.
[6] T. Yoshida, S. Kanaoka, S. Aoshima, J. Polym. Sci. Part A: Polym. Chem. 43 (2005) 5337-5342.
[7] L. X. Liu, W. Li, K, Liu, J. T Yan, G. X. Hu, A. F. Zhang, Macromolecules. 44 (2011) 8614-8624.
[8] W. Li, A. F Zhang, A. D. Schlüter, Chem. Commun. (2008) 5523-5525.

Advanced Materials Research Vols. 989-994 (2014) pp 498-501
© (2014) Trans Tech Publications, Switzerland
doi:10.4028/www.scientific.net/AMR.989-994.498

Temperature controlled dispersion of multi-walled carbon nanotubes in water with poly[(N-isopropylacrylamide)-co-(ionic liquid)]

WenJun Xiao[1,a], Chang-An Yang*[,2,b], JiaJian Peng[1], JiaYun Li[1], Ying Bai[1]

[1]Key Laboratory of Organosilicon Chemistry and Material Technology of Ministry of Education, Hangzhou Normal University, Hangzhou 311121, PR China

[2]Department of Chemistry and Chemical Engineering, Hunan Institute of Science and Technology, Yueyang 414006, Hunan Province, PR China

[a]xiaowj2008@126.com, Corresponding Author: [b]Chang_anyang@163.com

Keywords: Temperature controlled, Ionic liquid, Multi-walled carbon nanotubes (MWCNT)

Abstract. We synthesized a novel polymeric functional ionic liquid (IL), i.e. poly[(N-isopropylacrylamide)-co-(ionic liquid)] (P(NIPAAm-co-IL)), which can make multi–walled carbon nanotubes (MWCNTs) well dispersed in water. This method is a noncovalent technique, and the resulting solution was sensitive with temperature.

Introduction

Carbon nanotubes (CNTs) have attracted much attention due to their superior chemical, mechanical, thermal and electrical characteristics [1,2]. The application of CNTs require them to be firstly dispersed in solvents in many case [3]. But the dispersion of CNTs in solvent, especially in water, is still a challenge work because CNTs are prone to aggregate. It is well known that water is the cheapest solvent. But CNTs is difficult to be dispersed stably in water due to mutual poor compatibility. Both covalent [4,5] and noncovalent [6,7] techniques can solve this problem. With covalent technique, concentrated nitric acid is usually used to treat CNTs, and the conjugated structure of CNTs are destroyed, consequently impairs some of their important properties[4,5]. Compared with the covalent technique, noncovalent technique is a milder route. Generally, some agents such as surfactants are used in this route [8,9], but only moderate effects were obtained in the filed hybrid materials.

Recently, ionic liquids (ILs) have been studied extensively due to their potential applications as green solvents, reusable catalysts, separation and extraction media, electrolytes, heat-transfer fluids and so on [10,11]. ILs have strong solubility of organic and inorganic materials including CNTs. Fukushima firstly reported that pristine single-walled (SWCNTs) could be dispersed in imidazolium ion-based ILs through a possible cation-Π interaction [12]. Later Chen et al. confined 1-butyl-3-methylimidazolium hexafluorophosphate [bmim][PF_6] in multi-walled CNTs (MWCNTs) [13]. It is worth noting that the dispersion of CNTs in ILs is a noncovalent technique, and the inherent properties of CNTs suffer no change by this method. However, at present, ILs are expensive. Thus it is important to decrease the amounts of ILs to disperse CNTs.

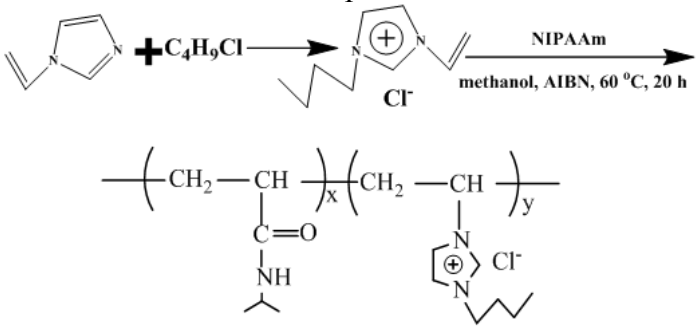

Fig. 1 The procedure for the synthesis of P(NIPAAm-co-IL)

Zhou et al. found that MWCNTs can be dispersed stably in water with the aid of a very small amount of amido-functionalized ILs. But the recycling of ILs and MWCNTs was not mentioned in their route [14]. Marcilla et al. proved a reversible phase-transfer method for dispersion of CNTs in

water with the aid of special polymeric ILs. In their system ILs and MWCNTs could be recycled effectively. But the reversible phase-transfer process was controlled by the salt additives, which increased the cost and introduced impurity. In this work, we synthesized a novel temperature-responsive polymeric functional ionic liquid poly[(N-isopropylacrylamide)-co-(ionic liquid)] (P(NIPAAm-co-IL)) to disperse MWCNTs in water.

Experimental Section

The synthesis of the polymeric functional IL is illustrated in Fig. 1. Firstly, ionic liquid momomer (ILM) 1-vinyl-3-butylimidazolium chloride was prepared from the N-alkylation of 1-vinylimidazole with 1-chlorobutane. Then the P(NIPAAm-co-IL) was synthesized by the free radical copolymerization of the ILM and isopropylacrylamide (NIPAAm) using azobisisobutyronitrile (AIBN) as the initiator in methanol at 60 ºC for 20 h, the structure of P(NIPAAm-co-IL) was characterized by NMR (Fig. 2) .

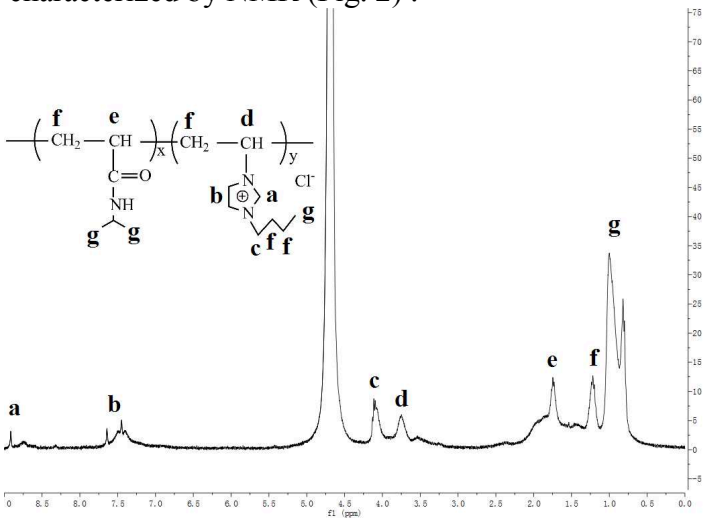

Fig. 2 ^{1}H-NMR Spectra of P(NIPAAm-co-IL) (solvent: D_2O, n_N/n_I = 2:1)

Results and Discussion

The temperature-responsive property of P(NIPAAm-co-IL) aqueous solution (mass percent: 5%) with different mole ratio of NIPAAm to ILM (n_N/n_I) is shown in Fig. 3. No temperature-responsive phenomenon was observed when the n_N/n_I = 2:1. As n_N/n_I = 8:1, the temperature-responsive property can be observed. While n_N/n_I was increased to 10:1 or higher, the temperature-responsive property of the solution gets obviously. Moreover, the critical solution temperature (LCST) of P(NIPAAm-co-IL) is 32 ºC in our system.

At room temperature, P(NIPAAm-co-IL) aqueous solution (mass percent: 5%, n_N/n_I = 10:1) can disperse a certain quantity of MWCNTs (mass ratio of MWCNTs/P(NIPAAm-co-IL) = 1:5), and the resulting solution can exist stably more than six month. It has been accepted that the imidazolium ions possibly interact with the Π-electron network of the CNTs by the way of a "cation-Π" interaction [12,14]. When the mass ratio of MWCNTs/P(NIPAAm-co-IL) = 1:5 or lower, enough imidazolium ions stabilize MWCNTs. Likewise, the P(NIPAAm-co-IL)/MWCNTs suspensions shows temperature responsive property. When the temperature is 32 ºC or higher, the solution become greyish white, and some MWCNTs gradually precipitate (Fig.3).

In order to further understand the temperature response of P(NIPAAm-co-IL) in the presence of MWCNTs, the UV-vis absorbance of P(NIPAAm-co-IL) aqueous solution were carried out (Fig. 4). It can be seen that there is a significant increase in absorbance of the P(NIPAAm-co-IL) aqueous solution about 30 ºC due to the coil-globule transition of poly(N-isopropylacrylamide) (PNIPAAm).

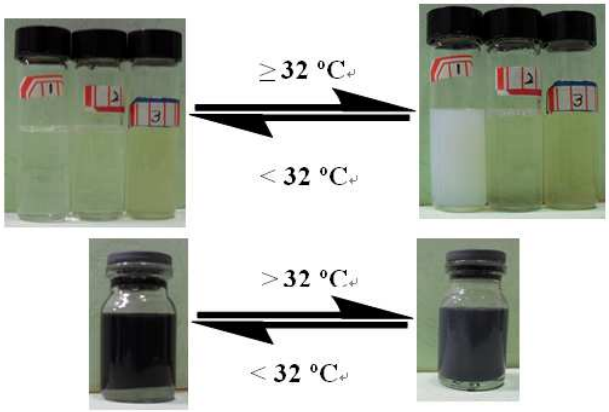

Fig. 3 The temperature-responsive property of P(NIPAAm-co-IL) with different n_N/n_I: 10:1 (1), 8:1 (2), 2:1 (3); and the temperature-responsive property of P(NIPAAm-co-IL)/MWCNTs aqueous solution.

The aqueous P(NIPAAm-co-IL)/MWCNTs suspensions also show a small but significant increase at 30 ºC, which corresponds to the LCST of P(NIPAAm-co-IL). Therefore, the temperature-responsive characteristics of P(NIPAAm-co-IL) are still retained in the presence of MWCNTs.

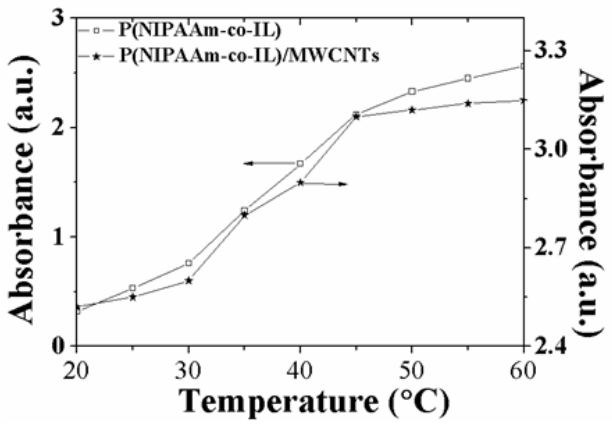

Fig. 4 Absorbance at 200 nm for the aqueous P(NIPAAm-co-IL)/MWCNTs suspension and the aqueous P(NIPAAm-co-IL) solution.

Furthermore, the aqueous P(NIPAAm-co-IL)/MWCNTs suspension were dried at temperatures below and above LCST (i.e., 20 and 60 ºC, respectively) to form thin composite films. The morphologies of the composite films show a high degree of aggregation in the films dried at 60 ºC (Fig. 5). Meanwhile the electrical conductivity of these composites were high for films dried at 60 ºC at all the concentrations studied (i.e., 10 and 20 wt % MWCNTs) (Table 1). High electrical conductivity of the film dried at 60 ºC is due to better nanotube-nanotube contacts resulting from

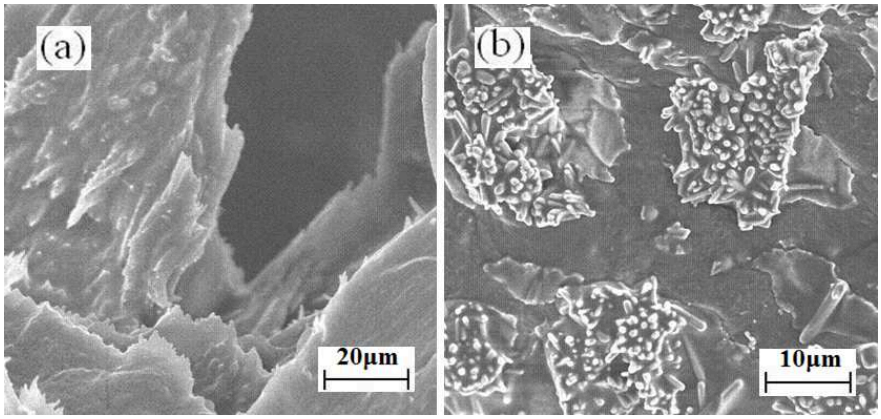

Fig.5 SEM micrographs of P(NIPAAm-co-IL)/MWCNTs composites dried at: (a) 20 ºC and (b) 60 ºC. (mass ratio of MWCNTs/P(NIPAAm-co-IL) = 1:5)

Weaker polymer-nanotube interaction. It leads to a more aggregated and heavily networked microstructure, which is much like the case in the liquid suspension. While the film dried at 20 ºC, the close association between polymer and MWCNT restricts the electron flow by creating an insulating layer and reducing the contact points between MWCNT.

Table 1. Electrical conductivity of P(NIPAAm-co-IL)/MWCNTs composites

wt% MWCNTs	Drying Temp (ºC)	Electrical Conductivity (S m^{-1})
10%	20	0.24
10%	60	0.43
20%	20	1.25
20%	60	3.68

Conclusion

In conclusion, we synthesized a polymeric functional IL P(NIPAAm-co-IL), which can make MWCNTs well dispersed in water. The resulting solution was sensitive with temperature. This system would have potential applications in polymer nanocomposite preparation.

Acknowledgment

This work is supported by the National Natural Science Foundation of China (NNSFC Grants: 21303035, 21106037) , the Scientific Research Fund of the Hunan Provincial Education Department (No: 11A040), and Hunan Provincial Natural Science Foundation of China (No: 12JJ4015).

References

[1] M. F. Yu, O. Lourie, M. J. Dyer, K. Moloni, T. F. Kelly and R. S. Ruoff: Science, Vol. 287 (2000), p. 637.
[2] S. Berber, Y. K. Kwon and D. Tomanek: Phys. Rev. Lett., Vol. 84 (2000), p. 4613.
[3] V. A. Sinani, M. K. Gheith, A. A. Yaroslavov, A. A. Rakhnyanskaya, K. Sun, A. A. Mamedov, J. P. Wicksted and N. A. Kotov: J. Am. Chem. Soc., Vol. 127 (2005), p. 3463.
[4] Y. B. Wang, Z. Iqbal and S. Mitra: J. Am. Chem. Soc., Vol. 128 (2006), p. 95.
[5] P. M. Ajayan and J. M. Tour: Nature, Vol. 447 (2007), p. 1066.
[6] P. J. Boul, D. G. Cho, G. M. A. Rahman, M. Marquez, Z. Qu, K. M. Kadish, D. M. Guldi and J. L. Sessler: J. Am. Chem. Soc., Vol. 129 (2007), p. 5683.
[7] K. Yurekli, C. A. Mitchell and R. Krishnamoorti: J. Am. Chem. Soc., Vol. 126 (2004), p. 9902.
[8] X. Gong, J. Liu, S. Baskaran, R. D. Voise and J. S.Young: Chem. Mater., Vol. 12 (2000), p. 1049.
[9] X. Zhang, T. Liu, T. V. Sreekumar, S. Kumar, V. C. Moore, R. H. Hauge and R. E. Smalley: Nano Lett., Vol. 3 (2003), p. 1285.
[10] V. I. Parvulescu and C. Hardacre: Chem. Rev., Vol. 107 (2007), p. 2615.
[11] T. Welton: Chem. Rev., Vol. 99 (1999), p. 2071.
[12] T. Fukushima, A. Kosaka, Y. Ishimura, T. Yamamoto, T. Takigawa, N. Ishii and T. Aida: Science, Vol. 300 (2003), p. 2072.
[13] S. Chen, G. Wu, M. Sha and S. Huang: J. Am. Chem. Soc., Vol. 129 (2007), p. 2416.
[14] X. Zhou, T. Wu, K. Ding, B. Hu, M. Hou and B. Han: Chem. Commun., (2009), p. 1897.

Advanced Materials Research Vols. 989-994 (2014) pp 502-505
© (2014) Trans Tech Publications, Switzerland
doi:10.4028/www.scientific.net/AMR.989-994.502

Rapid Repair of Titanium Aero Structure with Cracks

Yinsai Guo[1, a], Yi Zhang[2, b]

[1]Department of graduate, Xijing University, Xi'an710123, China;

[a]guoysxj@163.com, [b]zhangyijd@163.com

Keywords: Titanium alloy, laser rapid repair, crack, scratch, cladding.

Abstract. Titanium alloy structure is an indispensable structure in aviation industry. It has high sensitivities for gap, scratch and other surface defects. Therefore, it is easy to produce various damages, such as crack, scratch and break. This paper describes a new laser rapid repair system which solves the technical problem that modern aviation titanium alloy components can not be repaired by conventional repair techniques. The rapid repair for titanium alloy components can be achieved by means of it. Meanwhile, the repair quality of aviation titanium alloy structure can be improved.

Introduction

On account of low density, high specific strength, corrosion resistance and other characteristics, titanium alloy is an excellent structural material in the aviation industry. It has many disadvantages, including poor processing property and difficult machining in cold working, easy absorption impurities (such as carbon, hydrogen and nitrogen) in hot working, poor abrasion resistance and complex production process [1]. Therefore, it is easy to produce various damages such as crack and fracture, and so on. Limitations of repair techniques on traditional machining exist in aviation industry. For instance, large deformation, 50% performance loss and serious fatigue damage can be generated after repair on account of the large heat input of welding process in traditional TIG welding [2]. Therefore, it is very urgent to develop an advanced repair technology.

Disadvantages of Traditional Process

Welded Structure. Titanium has low thermal conductivity and excellent welding performance. However, heat-affected zone of matrix generated by argon arc welding, which makes it form overheated structure, takes shape brittle precipitate phase and decreases the strength of the joint [3]. For differences of operator proficiency in argon arc, welding joint can be formed in different welding height and width, which can result in different degrees of stress concentration in welding. Uneven grain structure, broad heat-affected zone, and inevitable porosity defect exist in welding. For instance, porosity is one of the most common welding defects in titanium alloy welding process. The formation of porosity can be caused by O, N, H, CO and HO. These defects lead to different plasticity and mechanic performance of static and dynamic in weld joint, heat affected zone and base substrate, which decreases the bearing capacity of part and affects the service life of part [4].

Riveted Structure. On account of the stress concentration existing in the riveted structure, and the aging of engineering structure, fatigue crack will present near the rivet, and sudden destruction structure will be occur with the crack propagation to a certain degree, which leads to disastrous consequences. Traditional methods of repair process can be adopted, including the supplement method and patching method. The repair process of the supplement method includes first hitting the

stop-crack hole, then restoring the original stiffness and strength of the base plate riveted by the lining board with the same thickness and material. The repair process of patching method includes cutting the part surrounding crack, filling the cutting part with a board, and connecting the board with the original structure by a lining board, which is shown in Fig. 1. It can be seen that structure strength is weakened by the rivet hole in traditional titanium alloy riveting process. It is difficult for titanium connecting rivets to form the pier head at the room temperature directly. Titanium alloy rivet is made to enter into the superplastic temperature zone by heating so as to deform [5].

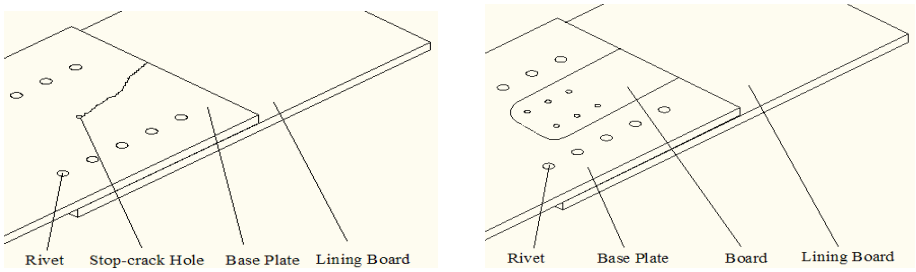

Supplement method Patching method

Fig. 1 Riveting repair of titanium alloy structure

New System and Process of Rapid Repair for Titanium Aero Structure

A System of Rapid Repair for Titanium Aero Structure. Laser rapid repair is an advanced manufacturing technology based on laser cladding and laser rapid prototyping. It has the unique advantages including controllable energy, no mold, near net forming and high degree of flexible, which offers a new repair method to complex and expensive parts. It utilizes molten pool that is formed by the laser irradiation to combine cladding material and undone repair substrate in the process [6]. The key of laser processing technology quickly repairing titanium aircraft components is to design a laser repair system meeting the repair demand. The system has the advantages including good appearance of weld, small heat affected zone and deformation zone, simple operation and high efficiency, high energy density and welding, which is especially suitable for high melting point and high reflectivity titanium alloy structure repair.

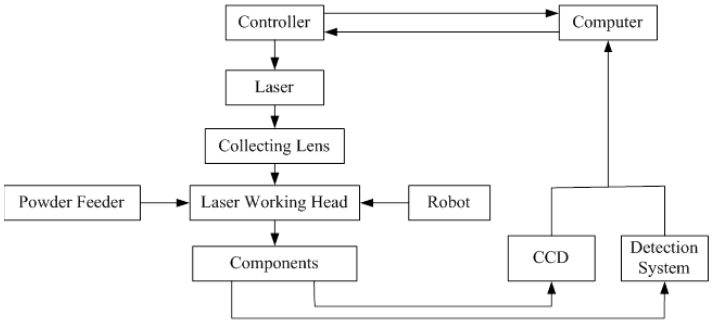

Fig. 2 A system of rapid repair for titanium aero structure

The working principle of laser system is shown in Fig. 2. It consists of controller, PC machine, laser device, collecting lens, robot, laser working head, powder feeding system, CCD, detection system, etc. Laser emitted by laser device enters into the working head through collecting lens, as a heat source for welding. According to the shape and size of the structural damage, the laser working head in a three-dimensional robot motion control system moves automatically. Powder grains under the action of the carrier gas are sent out from the feeding device. Under the constraint of the spray powder feed channel, they are jetted out in accordance with a certain track, falling into the molten pool formed by the laser irradiation. Meanwhile, the signals, such as flow, temperature, pressure, sound, displacement and speed sensed by the detection system and welding surface topography

conversed by CCD are displayed on a PC. The laser working head and feeding device are automatically adjusted by the controller so as to achieve the dynamic response of the control of conveying speed and throughput accurately and timely.

Process of Repair Technology

Aviation titanium component is repaired by the system.
Process is shown as follows:
(1) Testing the scope and trend of the crack by the non-destructive flaw detection technique and measuring tools, and evaluating the damage. The basic method of repair is determined according to the detection result.
(2) A programming of scanning line for laser working head.
(3) Cleaning up welding parts, removing oil, water, sewage and surface oxide.
(4) According to the programs and sensor signals, the working system consisting of the laser working head, powder feeder and robot breaks holes and welds automatically.
(5) Checking the welding and effects through the CCD, trimming the surfaces by re-programming.
(6) Non-destructive detection after welding.

Laser Rapid Repair for Titanium Piece

Laser Welding Repair of Crack. $CWCO_2$ laser can repair penetrating crack of thin-walled titanium parts. The process is shown in Fig. 3.

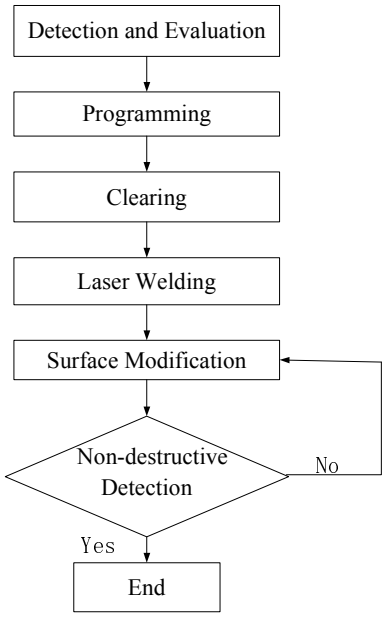

Fig. 3 Process of welding

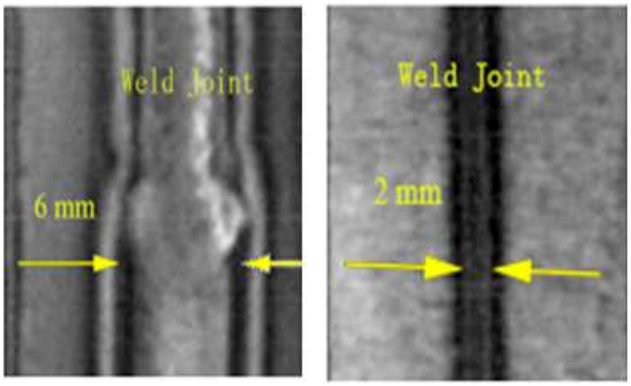

(a) Manual arc welding; (b) $CWCO_2$ laser welding

Fig. 4 Two kinds of welding

The comparative morphology of the two kinds of seam welding is shown in Fig. 4. It includes (a) manual arc welding and (b) $CWCO_2$ laser welding (power 800 W, velocity 90 mm / min, spot 1.8 mm, argon gas protection). It can be seen that the weld joint width of $CWCO_2$ laser welding is about 60 percent less than that of manual arc welding. Laser welding has many advantages including smooth surface, stable quality, minimal deformation, pulsed laser welding narrower and the almost indiscernible weld heat-affected zone. Experiments show that laser welding is the ideal means of the repair of titanium alloy sheet crack [7].

Laser Cladding Repair of Crack. Based on the discrete/accumulation principle of rapid prototyping, laser cladding repair is that the metal powder is melted by a laser beam and then piled up one by one on the damage structure under the control of programs. Based on this, the full metal components can be formed. The essence of laser cladding repair technique is a three-dimensional laser cladding accumulation under computer control. A non-penetrating crack usually occurs in non-thin-walled parts, the depth of which cannot be measured directly. According to the shape of the defect, the crack will be gradually removed by polishing, then repair model is established hierarchically in the groove after grinding by the laser cladding. The process is shown in Fig. 5. Eventually, the damaged structure is rebuilt and the performance of the structure is restored to meet the requirements of size, shape and roughness.

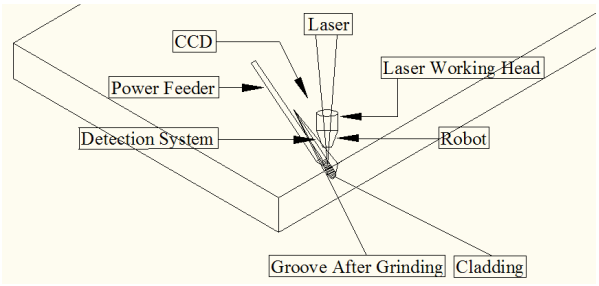

Fig. 5 Method of laser cladding repair for crack

Conclusions

A new laser-based rapid repair system is designed in this paper, which solves the problem that the damaged aviation titanium alloy components cannot be rapidly repaired by conventional repair technique. The penetrating cracks of thin-walled titanium parts can be rapidly repaired by laser welding and the non-penetrating cracks of no-thin-walled titanium parts can be rapidly repaired by laser cladding repair. This provides a guarantee for titanium alloy components damage rapid repair.

Acknowledgements

This study was supported by Graduate Student Innovation Fund of Xijing University.

References

[1] Jie Zheng, Study on aviation composite structure repair technology, J. technological innovation. 2013, (12) 100-101. "In Chinese".

[2] Richter K H, Laser material processing in the aero engine industry. Proceedings of the 3rdPacific International Conference on Application of Lasers and Optics. 2008, 1005-1010.

[3] Li R F, Li Z G, Zhua Y Y, et al, A comparative study of laser beam welding and laser-MIG hybrid welding of Ti-Al-Zr-Fe titanium alloy, J. Materials Science and Engineering A. 2011, 528:1138-1142.

[4] Lu W, Shi Y W, Lei Y P, et al, Effect of electron beam welding on the microstructures and mechanical properties of thick TC4-DT alloy, J. Materials and Design. 2012, 34:509-515.

[5] Cao Z Q, Cardew Hall M, Interference fit riveting technique in fiber composites lam inate, J. Aerospace Science and Technology. 2006, 10(4):327-330.

[6] Xinzhi Sheng, Shuqin Lou, Principles of Laser, [M]. Tsinghua University Press. 2010."In Chinese".

[7] Lei Xue, et al, Laser Rapid Repair of the Aircraft Components of Titanium Alloy, J. Rare Metal Materials and Engineering. 2006, (11):1818-1820. "In Chinese".

Advanced Materials Research Vols. 989-994 (2014) pp 506-510
© (2014) Trans Tech Publications, Switzerland
doi:10.4028/www.scientific.net/AMR.989-994.506

Determination of novel Brominated Flame Retardants in Flexible Polyurethane Foam by GC-MS

Chen Yingjie[a], Dai Peigang[b], Liuzhi Peng[c] ,
Du Chao[d], Liang Shangjin[e]

Guangdong Testing Institute of Product Quality Supervision, Guangzhou 510000, China;

[a]jietchen@163.com, [b]dipye@163.com, [c]fm@gqi.org.cn,

[d]yyhdc@163.com, [e]Lsj19842008@163.com

Keywords: Brominated Flame Retardants, Supercritical Carbon Dioxide Fluid Extraction, GC-MS.

Abstract. A method of supercritical CO_2 fluid extraction gas chromatography-mass spectrometry(GC-MS)was developed for the determination of 2 novel brominated flame retardants(BB-153 and TBECH)) in flexible polyurethane foam. The optimum conditions as follows: extraction temperature: 60℃, pressure:30Mpa, CO_2 mass flow rate: 8g/min ,flow rate of methanol entrainer: 3mL/min and extraction time: 60min. The calibration curves were linear in the range of 0.1 ～50μg/mL with correlation coefficient of 0.9995～0.9999 and detection limits (S/N=20) of 0.05μg/mL. The average recoveries of the target compounds in sample were in the range of 97.3%～98.8%(BB-153), 99.2%～105.8% (TBECH)respectively. The results showed that this method was sensitive, reliable and environmental for the determination of 2 novel brominated flame retardants(BB-153 and TBECH)) in flexible polyurethane foam.

Introduction

Fire retardant properties (BFRs) of building material is the necessary measure to control the risk of fire. Brominated flame retardants has excellent flame retardant performance, widely used in electronic products, textiles, plastic products. The most common BFRs are Polybrominated diphenyl ethers (PBDEs), Hexabromocyclododecane(HBCD) and tetrabromobisphenol A (TBBPA) [1].It is estimated that the annul demand of BFRs is 7.0×10^7kg-8.7×10^7kg in China, with an increasing rate of 7%-8% [2-3]. The abuse of BFRs leads them widely exist in various environmental media (air, soil, rivers and lakes) and organisms[1,4]. Studies show that certain BFRs have a greater harm on the human nervous system, endocrine system and reproductive system [5]. The Stockholm convention has put Hexabromobiphenyl, Tetrabromodiphenyl ether and pentabromodiphenyl ether (commercial pentabromodiphenyl ether) [6].Some new halogenated flame retardant, such as 1,2-bis(2,4,6-tribromophenoxy)ethane (BTBPE) was used instead of disabling the brominated flame retardants, novel halogenated flame retardant increases steadly [7].

Detection of BFRs mainly concentrated in the electronics, textiles, plastics. Soft furniture flame retardant polyurethane foam for brominated flame retardants in detection has been not reported. On the sample pre-treatment, Textiles are usually through ultrasonic extraction , electronic products are usually through Soxhlet extraction. Then all the samples arer detected by GC-MS. CO_2 has excellent liquid dissolved and gaseous diffusion in supercritical state [8]. Supercritical CO_2 fluid extraction is not only used for the extraction of volatile oil, but also gradually increased in the flame retardants. The supercritical CO_2 fluid extraction technology was first introduced into plastic brominated flame retardants[9-10]. Abdel mnim Altwaiq [11] develped the research on the extraction separation of DecaBDE from HIPS .Some researches such as extraction of TPP from electronic printed circuit board by supercritical carbon dioxide and removal of polybrominated diphenyl ethers from plastic solution by supercritical carbon dioxide were also reported in China[12-13]. The representative brominated flame retardants (BB-153 and TBECH) were studied, through one step foaming, in combination with GC-MS detection. Compared with traditional Soxhlet extraction, this method

results are reliable, can be used for detecting the brominated flame flexible flame retardants in polyurethane foam.

1Test

1.1 Materials

Polyether glycol (PPG-5623, hydroxyl value of 28.0 KOH mg/g with a degree of functionality of 3, CSPC); polyether polyol (POP CHF-628, hydroxyl value of 28.0 KOH mg/g with a degree of functionality of 3, Jiangsu Changhua Polyurethane Science & Technology Co., Ltd); toluene diisocyanate (TDI 80/20, degree of functionality of 3, Shanghai Basf Coating Co., Ltd); dibutyltin dilaurate (PUCAT L-33, Foshan City Puhui New Material Co., Ltd); stannous octoate (YOKE T-9, Jiangsu Yoke Technology Co., Ltd.); niax silicone L-540/STL DR; 2,2',4',4',5,5-hexabromodiphenyl ether (BB-153); 1,1,2-dibromo-4-(1,2-dibromoethyl)-cyclohexane (TBECH, J&K Scientific Ltd); triazine triamine phosphate (MPOP, Hefei Fine Collection Institute of Chemical Industry); and deionized water (self-made).

1.2 Appratus

GC-MS（7890A 5975C， Agilent ）, Supercritical CO2 Fluid Extraction（Meichen High Separation Technology Company）, Rotary Evaporator（RE-52AA Shanghai Yarong Biochemical Instrument Factory）, Ultrasonic extraction instrument.

1.3 Preparation

According to the formula [4], the PPG, POP and deionized water were all combined in a 1000 ml plastic beaker. Dibutyltin dilaurate, niax silicone, stannous octoate and the corresponding flame retardant were then added and stirred with a mechanical mixer for 2 h with the material temperature kept at 25 °C. Finally, TDI 80/20 was added, and the mixture was stirred at high speed for 4 to 5 s and then immediately poured into the natural foaming moldwith the temperature maintained at 25 °C for 24 h. The densities of the prepared materials were controlled to be 50 ± 2 kg/m3.

1.4 Sample pretreatment

1.4.1 Supercritical fluid extraction：The samples were broken with scissors, weigh accurately 1.0g, Wrapped with thin non-woven fabric, then put sample in the extraction pool. Optimize the extraction conditions with different temperature, pressure and entrainer. The flame retardant was extacted from the treated polymer sample by dissolving it in 100mL on a suitable solvent for 1min and filtering it through a membrane disk filter (0.2μm).External standard quantification was used for the procession.

1.4.2 Soxhlet extraction：The samples were broken with scissors, weigh accurately 1.0g, the sample was extracted with 70mL toluene in the soxhlet extraction for 4h ， keeping the reflux times at 5-6 times per hour. After cooling to room temperature, condensed the solution into 10mL by Rotary Evaporator .the extraction solution was filtered through a membrane disk filter ((0.2μm). The solution was analized by GC-MS. External standard quantification was used for the procession.

1.4.3 Ultrasonic extraction：The 1.0g sample into 20mL toluene, ultrasonic 30min. Collection of extraction solution. Constant volume to 20mL, GC-MS analysis from the 1mL to the sample bottle.

1.5 GC-MS Analysis：HP-5 Trace Analysis 5% Phenyl colum（30 m x 250 μm x 0.25 μm），Temperature programmed：Initial oven temperature of 100℃,holding 1min，then ramped at 30℃/min to 300℃, and hold for 2min.Thecarrier gas, UHP helium,was set at constant flow, 3mL/min. The mass analysis was performed in the electron impact ionization(EI) mode. Ionization energy：70eV，Ion source temperature：230℃，The maximum value：270℃，Quadrupole temperature：150℃，The maximum value：200℃.

2 Results

2.1 Optimization of pretreatment conditions

2.1.1 Time

Temperature and pressure are the key parameters of supercritical fluid extraction. At certain temperature, Elevated temperature increased volatility and the rate of diffusion of solute, improves

the extraction efficiency, Meanwhile, Elevated temperature also reduces the density and the solvent power of the supercritical fluid. Typically, higher extraction temperature is better for larger molecular weight and polar compounds. Brominated flame retardants have larger molecular weight. TBECH belongs to weak polar molecule. Figure 1 shows the efficiency of extraction BB-153 and TBECH with condition as follows: pressure 30MPa, CO_2 volume flow rate: 8g/min, entrainer: methanol (flow rate 3mL/min), extraction time: 60min. The results show that, The extraction efficiency of two compounds increased gradually With the increase of temperature between 20℃～60℃. The extraction efficiency was highest at 60 ℃.

2.1.2 Pressure

In critical state，Density of material is sensitive to the change of pressure. Small change of pressure will cause the larger change in fluid density. While the increase of the density will also lead to improve solubility. So separation can be achieved through adjusting the solubility. But higher pressure will cause adverse effect to apparatus. Extraction was proceed as follows: temperature at 60℃, CO_2 volume flow rate: 8g/min, entrainer: methanol (flow rate 3mL/min), extraction time: 60min. The extraction efficiency as shown in Figure 2 increased with the increase of extraction pressure. But when the extraction pressure exceeds 30MPa, the extraction efficiency close to steady state, and more high boiling point compounds was extracted.

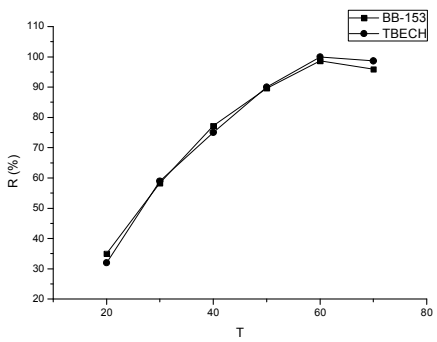

Figure 1 Effect of temperature on brominated retardants in supercritical CO_2 fluid extraction

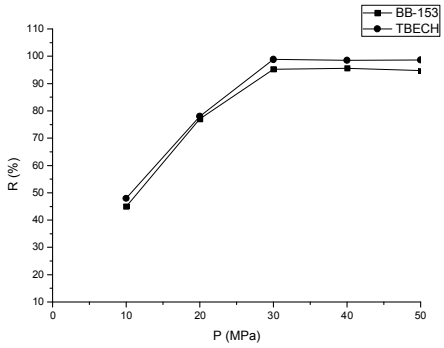

Figure 2 Effect of pressure on brominated flame flame retardants in supercritical CO_2 fluid extraction

2.1.3 Entrainer

Supercritical CO_2 extraction is very suitable for non-polar and polar compounds. For the polar compounds, the extraction can be achieved by adding entrainer .Without any entrainer, the efficiency of BB-153 and TBECH reached only 32.8% and 32.5% respectively. Because of the weak polar, we extracted the sample using different entrainer such as methanol, toluene, and 1-propanol.The result showed highest efficiency with methanol. Due to the small polar, toluene and CO_2 dissolve each other.

So the optimum condition as follows: xtraction temperature: 60℃, pressure:30Mpa, CO_2 mass flow rate: 8g/min ,flow rate of methanol entrainer: 3mL/min and extraction time: 60min.

2.2 Qualitative and quantitative

Blank samples were injected onto GC-MS. The Mass spectra showed in Figure 3-4. For BB-153 and TBECH, the most abundant was used for quantitation (m/z 627.5 for BB-153 and m/z 267.0 for TBECH). Total ion current chromatogram of two compounds showed in Figure 5. Total BB-153 and TBECH can be analyzed using GS-MS, but 4 isomers(α, β, γ, δ) of TBECH has to be done by LC-MS-MS, however, studies t determine the degree of interconversion between isomers have not been completed [8,15].

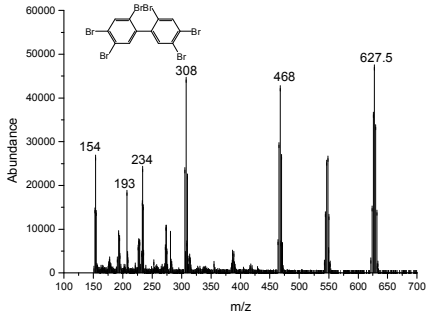

Figure 3 Full scan mass spectra of BB-153

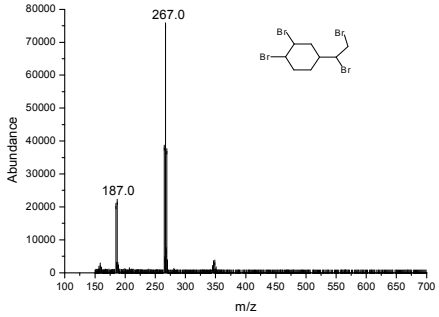

Figure 4 Full scan mass spectra of TBECH

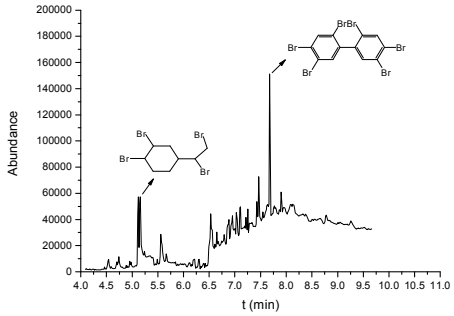

Figure 5 Total ion current chromatogram of BB-153 and TBECH

2.3 Relevant parameters

Toluene as solvent, two compounds were arranged in 0.1, 0.5, 2, 5, 10, 20, 50 μ g/mL standard solution. Accurate draw 1mL standard solution to the sample bottle, draw the standard curve in the chromatographic conditions, The linear correlation coefficient was 0.9995～0.9999， Table 2 showed the results.

Table 2 Relevant parameters of BB-153 and TBECH

No.	compound	CAS No.	Linear range μg/mL	*r*	Detection limit μg/mL
1	BB-153	59080-40-9	0.1-50	0.9995	0.05
2	TBECH	3322-93-8	0.1-50	0.9999	0.05

2.4 Precision and Recovery

After ultrasonic extraction, Soxhlet extraction, and super critical CO_2 extraction, precision and recovery were obtained. The details were showed in Table 3.

Table 3 Precision and Recovery

Project	Recovery（%）		RSD（%）（n=5）	
	BB-153	TBECH	BB-153	TBECH
Ultrasonic extraction	83.8-85.6	85.4-87.5	5.0	4.2
Soxhlet extraction	91.2-92.3	92.5-93.6	3.0	2.8
super critical CO2 extraction	32.8-33.8	32.5-33.2	4.8	3.6
super critical CO2 extraction（methanol as entrainer）	97.3-98.8	99.2-105.8	3.2	8.0

2.5 Detection of real sample

The retardant flexible polyurethane foam buying from market was detected with this method. Both BB-153 and TBECH were not found.

3 Conclusion

In this work, we set a method of super critical CO2 extraction/GC-MS to detect the content of brominted flame retardant , using flexible retardant polyurethane foam as target. The results showed that this method was sensitive, reliable and environmental for the determination of 2 novel brominated flame retardants(BB-153 and TBECH)) in flexible polyurethane foam.References

References

[1] Cynthia A. de Wit. An overview of brominated flame retardants in the environment. [J]. Chemosphere 46 (2002) 583–624.
[2] Jiang Y Q. Current situation and development of bromine retardant worldwide. [J].Chemical Techno-Economics 2006 24(9):14–19.
[3] Mai B X, Chen S J, Luo X J, Chen L G, Yang Q S, Sheng G Y et al., Distribution of polybrominated diphenyl ethers in sediments of the Pearl River Delta and adjacent South China Sea.[J].Environmental Science and Technology. 2005. 39(10):3521-3527.
[4] Jiangping Wu, Ying Zhang, Xiaojun Luo, Yazhe She et al., A review of polybrominated diphenyl ethers and alternative brominated flame retardants in wildlife from China: Levels, trends, and bioaccumulation characteristics.[J]. Journal of Environmental Sciences 2012, 24(2) 183–194.
[5] Per Ola Darnerud. Toxic effects of brominated flame retardants in man and in wildlife. [J]. Environment International 29 (2003) 841– 853.
[6] http://chm.pops.int/Implementation/NewPOPs/The9newPOPs/tabid/672.
[7] Hoh E，Zhu L Y，Hites R A. Environ. Sci. Techno., 2005,39(8) : 2472 - 2477.
[8] R. Marr, T. Gamse. Use of supercritical fluids for different processes including new developments-a review. [J]. Chemical Engineering and Processing 39 (2000) 19-28.
[9] Gamse T，Steinkellner F，Marr R， et al． Solubility studies of organic flame retardants in supercritical CO_2.[J]. Ind Eng Chem Res, 2000, 39(12) : 4888 -4891.
[10] Gamse T，Marr R． Removal of flame retardants from electronic waste materials using supercritical CO_2-extraction.[J]. Chemie IngenieurTechnik， 2001，73(6) : 590 – 593.
[11] Abedl mnim Altwaiq，Marion Wolf，Rudi van Eldik． Extraction of brominated flame retardant from polymeric waste material using different solvent and supercritical carbon dioxide.[J].Analytica Chemica Acta, 2003, 491(1) : 111 -123．
[12] WANG Jing，WANG Hong-tao, Li Jun .Study of Extraction of Flame Retardants from Electronic Printed Circuit Board by Supercritical Carbon Dioxide[J]. Journal of Xiamen University (Nature Science) 2008, 47(4) : 547- 551.
[13] PENG Shao-hong, LIANG Sha, ZHAO Xiang-yang,YU Mei.Study on removal of polybrominated diphenyl ethers from plastic solution by supercritical carbon dioxide.[J].Modern Chemical Industry, 2012, 32(10):50-53.
[14] Liu Yi-jun. Polyurethane Resin and Its Application. [M]. Beijing：Chemical Industry Press, 2012:122-138.
[15]Terry M. Kolic. The Analysis of Halogenated Flame Retardants by GC–HRMS in Environmental Samples.[J]. Journal of Chromatographic Science, 2009,47(1):83-91.

Advanced Materials Research Vols. 989-994 (2014) pp 511-514
© (2014) Trans Tech Publications, Switzerland
doi:10.4028/www.scientific.net/AMR.989-994.511

Affect of Brominted Flame Retardant on The Flexible Polyurethane Foam

Chen Yingjie[a], Liuzhi Peng[b] ,Dai Peigang[c],
Li Danlin[d], Wu Lijie[e]

Guangdong Testing Institute of Product Quality Supervision, Guangzhou 510000, China;

[a]jietchen@163.com, [b] fm@gqi.org.cn, [c]dipye@163.com,

[d]745826558@qq.com, [e] 82673229@qq.com

Keywords: FPUF，Brominated Flame Retardants，Combustion Performance.

Abstract. Different flexible polyurethane foams (FPUF) were prepared with one step method. Combustion performance of them were tested throughout oxygen index (OI), cone calorimeter (Cone). The results showed that flame performance prepared by 10% wt brominated flame retardants, and 10% wt MPOP was better. In irradiance 30kW/m^2, sample thickness 50mm conditions, heat release rate peak seprarately decreased to 284.0 kW /m^2 and 270.8 kW /m^2. In the coordination of N and P, the FPUF adding MPOP showed ideal flame retardancy .It is worth noting that when the content of MPOP exceeds 10%, the physical performance decreased rapidly with the increases of brittleness and hardness.

Introduction

Due to accelerated indurstrialization and urbanization, building materials have obtained dramatic growth in china. Polyurethane (PU) has special structure and excellent performance, so It has been used in great demand.Since as product of Polyhydric alcohol (R-OH) and isocyanates (RN = C = O), the combustion process of polyurethane (PU) releases large amounts of toxic gases, sothat PU is highly fire risking materials [1].The flexible polyurethane foam (FPUF) is type of polyurethane molding material with porous structure which is the most flammable polyurethane material.

the flammability of the FPUF limits its application in many fields, and therefore, enhancing urgency of the flame retardancy research of FPUF [2] . Flame retardants of FPUF include reactive flame retardant and additive flame retardant according to the effect between flame retardants. and the base materials. The reactive flame retardant effects persistently with more thermal stability，but difficult to apply in industrial production；In contrast, the additive flame retardant which is the earliest used with simple production process，is widely used until now [3]. In this paper, Flexible polyurethane foams (FPUF) were prepared with one step method by choosing different additive flame retardants foam. Then combustion performance of FPUF were tested throughout oxygen index (OI), cone calorimeter (Cone) and smoke toxicity .The result will provide reference for proper selection of flame retardants.

1Test

1.1 Materials

Polyether glycol (PPG-5623, hydroxyl value of 28.0 KOH mg/g with a degree of functionality of 3, CSPC); polyether polyol (POP CHF-628, hydroxyl value of 28.0 KOH mg/g with a degree of functionality of 3, Jiangsu Changhua Polyurethane Science & Technology Co., Ltd); toluene diisocyanate (TDI 80/20, degree of functionality of 3, Shanghai Basf Coating Co., Ltd); dibutyltin dilaurate (PUCAT L-33, Foshan City Puhui New Material Co., Ltd); stannous octoate (YOKE T-9, Jiangsu Yoke Technology Co., Ltd.); niax silicone L-540/STL DR; 2,2’,4’,4’,5,5-hexabromodiphenyl ether (HBB); 1,2-dibromo-4-(1,2-dibromoethyl)-cyclohexane (TBECH, J&K Scientific Ltd); triazine triamine phosphate (MPOP, Hefei Fine Collection Institute of Chemical Industry); and deionized water (self-made).

1.2 Appratus

Oxygen index measuring instrument（Fire Testing Technology, FTT）,Cone Calorimeter（Fire Testing Technology, FTT）, Mechanical Agitator.

1.3 Preparation of FPUF

According to the formula of Table1，The PPG, POP and deionized water were added into 1000ml plastic beaker, Then Dibutyltin dilaurate, Niax silicone, stannous octoate and corresponding flame retardant were added,the reaction mixture was stirred by mechanical mixer for 2hs under the temperatureof 25 ℃.Finally , TDI 80/20 was added then stirred with high speedfor 4 to 5s, immediately poured into the natural foaming mould[4], keep the temperature 25 ℃ for 24hs. The density of products were controlled at 50±2kg/m^3.

Table 1 Formalation of FPUF

Material	Ingredient/g
PPG	75-90
POP	10-25
TDI 80/20	31.5-40
Stannous octoate	0.2-1.5
Dibutyltin dilaurate	0.1-0.5
Niax silicone	0.6-1.0
Flame retardants	2.0-15.0
Deionized water	1.8-2.0

1.4 Test Method

1.4.1 Oxygen Index tested According to ISO 4589-2:1996, with test temperature （23±2）℃, humidity at (50%～55)% and sample size 100mm×10mm×10mm.

1.4.2 Heat release rate tested according to ISO 5660-1:2002，with irradiance setting at 30kW/m^2 and sample size 100mm×100mm×50mm.

2 Results

2.1 Oxygen Index(OI)

Because of The flame retardancy of POP itself, the oxygen index of blank FPUF still reached 21.6% without addition of flame retardant . The oxygen index of FPUF adding RDT-9 (10%) is higher than that adding MA(10%). Since the phosphorus flame retardant effected by building the main barrier of air and combustion products,and Chlorine flame retardant is by radical dilution of oxygen in the air. So the cooperative effect can achieve better than only use of MA. In the halogen flame retardant, brominated flame retardants is particularly prominent. The oxygen index reached 24.6% through adding HBB(5%) and TBECH(5%)， In contrast, The oxygen index adding MPOP(10%) is best，reaching 25.2%，which attributed to the cooperation of N- P. Charring of solid phase and isolation of air phase improve flame retardant effect.

2.2 Heat Release Rate(HRR)

Heat release rate refers to the thermal radiation intensity of presupposition, the rate of heat release on per unit area after ignition, with unit kW/m^2. Heat release rate can be divided into average heat release rate and peak heat release rate (pHRR). The average heat release rate has practical function on the early evaluation of the contribution of the material itself, early flame retardant and fire safety design[5] . The peak heat release rate(pHRR) is one of the most important fire characteristic parameters of materials.The irradiance 30kW/m^2 is closest to the actual fire conditions. So 30kW/m^2 was determined in the cone calorimeter test. Figure 1 shows the heat release rate curve of the four specimen in the irradiance of 30kW/m^2.Among them, the heat release rate of blank FPUF is the highest. pHRR of FPUF adding RDT-9 and MA is reduced but still high, both excceeding

500kW/m^2. Meanwhile FPUF adding HBB(5%)and TBECH(5%) reduced to 284kW/m^2. pHRR of FPUF adding MPOP(10%) becomes the lowest, which indicate 5% lower than the brominated flame retardant.

2.3 Total Heat Release（THR）

The total heat release of cone calorimeter test refers to the total heat release per unit area of the sample after complete combustion with unit MJ/m^2. Total heat release is an important parameter for thermal hazard evaluation of actual material. The more total heat material release, the more potentially fire dangerous the material is. From Figure 2, THR of Blank FPUF is far greater than the other four kinds of prepared FPUF with additive flame retardant. In the combustion process of FPUF adding MPOP, Is obviously to observe the surface expansion phenomenon. The isolation of charring increase the effect of the flame retardant, which leads to the minimum total heat release.

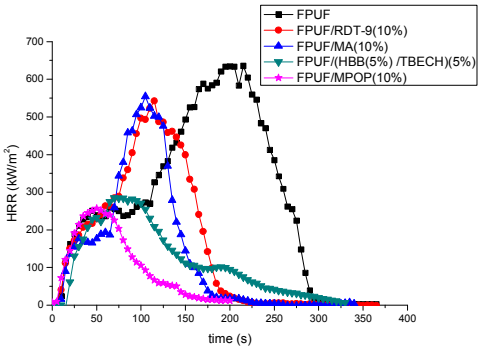

Figure 1 The heat release rate curve

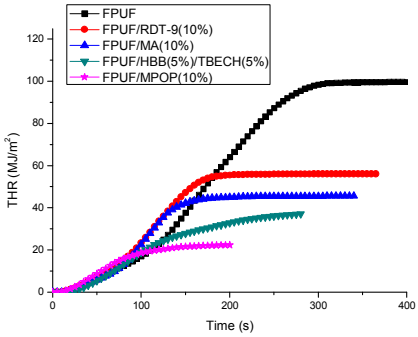

Figure 2 The total heat release curve

2.4 Mass loss rate（MLR）

The weight sensor supportting sample pool in the cone calorimeter records automatically. the mass loss rate, using five point finite - difference method. This parameter is closely related to the heat release rate, ratio of extinction area, and the formation rate of CO. The material burns more violent. With lager mass loss rate Figure 3 shows the mass loss rate curve of different of FPUF adding different flame retardants with the mass fraction 10%. Among of them, the one adding MPOP(10%) shows the least mass loss rate, the burning slow relatively. Through the observation of the combustion process, All the specimen were ignited within 5s. Furthermore all of the surface participate combustion, With rapidly shrinking. Carbonization quality after combustion residues from 3% to 5%. Adding flame retardant changes the mass loss rate relatively, but in the high irradiance, surplus quality shows less difference. The charring rate of FPUF adding MPOP is the highest.

2.5 Specific Extinction Area（SEA）

Specific extinction area refers to smoke produced capacity per unit mass after decomposition evaporation of combustible sample, with unit m^2 /kg. From Figure 4, FPUF adding HBB and TBECH demonstrate strong smoke producing ability, with following incomplete combustion phenomenon. This proves the smoke hazards of the brominated flame retardants, which pose high health risks to humans[6]. FPUF adding MPOP produce least smoke, which show ideal flame retardancy.

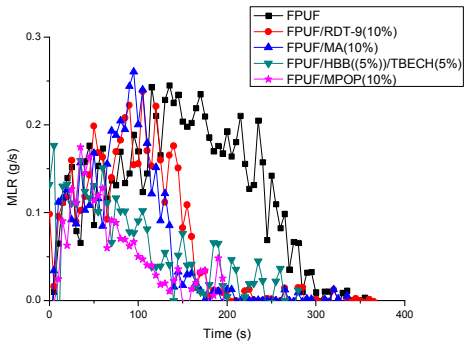

Figure 3 The mass loss rate curve of different FPUF

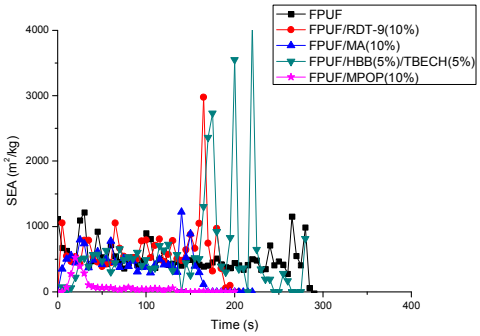

Figure 4 SEA curve of different FPUF

3 Conclusion

Flexible polyurethane foams (FPUF) were prepared with one step method by choosing different additive flame retardants foam. Combustion performance of FPUF were tested throughout oxygen index (OI), cone calorimeter (Cone) and smoke toxicity. The results showed that flame performance prepared by 10% wt brominated flame retardants, and 10% wt MPOP were better. In the coordination of N and P, the FPUF adding MPOP showed ideal flame retardancy .It is worth noting that when the content of MPOP exceeds 10%, the physical performance decreased rapidly with the increases of brittleness and hardness.

Halogenated flame retardant has high smoke risk, which has been gradually phased out. Effect of Nonhalogen, and coordinative flame retardant is prominent, which has become the future development direction of flame retardant products. For preparation FPUF composite material with excellent comprehensive performance, Developing coordination and functional research of organic, inorganic additive type , intumescent flame retardant and reactive halogen free flame retardant research will represent the general trend.

References

[1] Usta N. Investigation of fire behavior of rigid polyurethane foams containing fly ash and intumescent flame retardant by using a cone Calorimeter. [J]. Journal of Applied Polymer Science, 2012, 124(4):3372-3382.

[2] Ravey M, Pearce E. M. [J].Journal of Applied Polymer Science, 1997, 63: 47-74.

[3] Zhang Xiaoguang，Wang Lieping. [J]. CHEMICAL INDUSTRY AND ENGINEERING PROGRESS，2012.31.(7):1521-1527.

[4] Liu Yijun. The Synthesis and Application of Polyurethane .[M]. Beijing：Chemical Industry Press, 2012:122-138.

[5] Shu Zhongjun，Xu Xiaonan，Li Xiang. Fire Performance Evaluation of Polymer Material [M]. Beijing：Chemical Industry Press, 2007: 61-62.

[6] Tian Shi,She-Jun Chen. [J]. Chemosphere.74(2009): 910-916.

Advanced Materials Research Vols. 989-994 (2014) pp 515-518
© (2014) Trans Tech Publications, Switzerland
doi:10.4028/www.scientific.net/AMR.989-994.515

Effect of reinforcement addition on microstructure and mechanical properties of Al matrix composites

Guojun Ma[1,2,a], Yutian Ding[1,b], Peipeng Jin[2,c]

[1] State Key Laboratory of Gansu Advanced Non-ferrous Metal Materials, Lanzhou University of Technology, Lanzhou 730050, China.

[2] College of Mechanical Engineering, Qinghai University, Xining 810016, China.

[a]mgj2150@126.com, [b]dingyutian@126.com, [c]jinpeipeng@hotmail.com

Keywords: Al matrix composites, Whisker, Hot extrusion, Mechanical properties, Microstructure

Abstract. The study investigates the influence of different fraction of Mg_2B_2O5 whiskers (5, 10, 15 and 20vol.%) on the microstructure of the hot extruded composite as well as on the mechanical properties in the same condition. The results indicate that the process is available for producing the composite, image analysis shows the whisker tends to cluster together with increasing content of reinforcement. When the content of the reinforcement is 10%, the composites exhibit the best mechanical properties, meanwhile, it demonstrate cluster is unfavorable to the improvement of properties of materials. The ductile failure of 6061Al matrix, the reinforcement fracture and the whisker-matrix interface debonding acted as the main mechanism of fracture nucleation.

Introduction

Magnesium borate whisker reinforced aluminum matrix composites have attracted much attention [1], because of its low cost and good properties such as high specific strength and modulus, low coefficient of thermal expansion, and so on. It is considered to be a potential candidate in many fields, for example, aerospace, relaxation and automobile.

Powder metallurgy (PM) processed composites with good mechanical properties can be produced when the reinforcements are homogeneously distributed in the matrix [2]. However, clustering is difficult to avoid in the case of a large reinforcement concentration or a large particle size ratio of matrix powders to reinforcement powders [3]. Many investigations demonstrated that the clustering could degrade the tensile properties of the composites [4]. However, mechanism responsible for the degradation of tensile properties is still not well understood.

The principal objective of this current investigation as to determine how the microstructural parameters, such as the whisker volume fraction and extent of clustering affect the tensile properties and fracture roughness of $Mg_2B_2O_5w$/6061 Al matrix composite.

Experimental procedure

The atomized 6061Al powders with average diameter of 48 μm and composition in mass%: 0.8~.12 Mg, 0.4~0.8 Si, 0.15~0.4 Cu, balance Al, were used as a matrix, and $Mg_2B_2O_5$ whiskers with average diameter of 0.5~1.5 μm and length of 10~80 μm were added as the reinforcement. The SEM images of them are shown in Fig. 1. It can be seen that the Al particles are in general rounded with relatively uniform particle size, and the whiskers are commonly long cylinders with smooth superficial aspect.

The material used was 6061 aluminum alloy reinforced with 5, 10, 15, and 20 vol.% of $Mg_2B_2O_5$ whisker. The composites were prepared by a PM route which involves blending, cold compaction and extrusion (at the extrusion ratio of 25:1 and 530℃). In this manner, extruded bars, 8mm in diameter and ≈1000mm in length, were obtained. Die wall lubrication was applied by brushing a thin layer of zinc stearate lubricant. Fig. 2 shows schematically the geometry of the extrusion press and the extrusion die and a powder blend compact ready for extrusion.

The microstructures and tensile fractographs of the powders and extruded composites were observed using scanning electron microscopy (SEM, JSM-6700F). The density of each of the samples

was measured using Archimedean principle. The measured density was compared to the value obtained using rule-of-mixtures so as to determine the volume fraction of porosity. Tensile testes were performed at room temperature and an initial strain rate of $1\times10^{-3}s^{-1}$ on an Instron1195 tensile tester. Tensile specimens with a gauge diameter of 5 mm and a gauge length of 25 mm were machined from the extruded samples along the axis direction, in accordance with the Chinese National Standard GB6397-86.

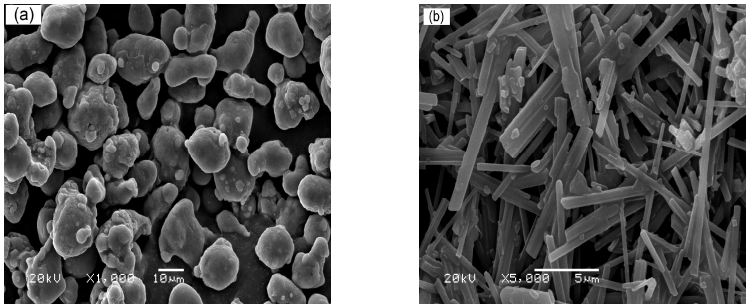

Fig. 1 SEM images of 6061 powders and $Mg_2B_2O_5$ whiskers (a) 6061Al powders; (b) $Mg_2B_2O_5$ whiskers

Results

Microstructure. The $Mg_2B_2O_5$w distributions in various composites are shown in Fig. 2. Compared with the original state of whiskers, its aspect ratio has been relatively reduced. For the composites with a volume fraction of 5~10 vol.%, the $Mg_2B_2O_5$w were homogeneously distributed (Fig. 2a~b). For the composites with higher reinforcement contents (15 vol.%), although the distributions of the whiker were still relatively homogeneous, clusters began to appear (Fig. 2c). When the content of reinforcement reached 20 vol.%, a large amount of whiskers came into contact with each other, as shown in Fig. 2d, some pores induced by cluster could be seen in the whisker clusters.

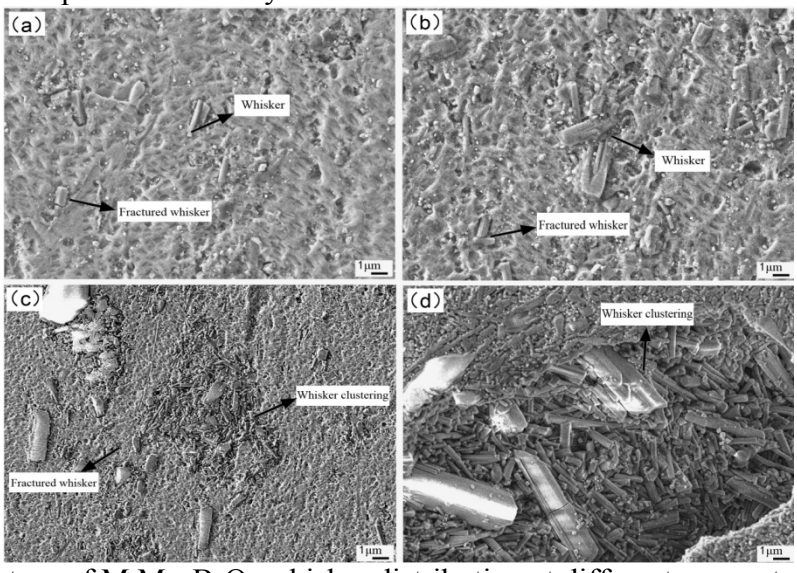

Fig. 2 Microstructure of M $Mg_2B_2O_5$ whisker distribution at different concentrations (a)5vol.%, (b)10vol.%, (c)15vol.%, (d)20vol.%.

Fig. 3 shows the theoretical and measured density of the composites with different reinforcement concentrations. The measured density deviated from the theoretical one when the reinforcement concentration was larger than 10 vol.% due to the porosity formation in the clusters. And the deviation was especially obvious at the content of 20 vol.% due to increased porosity formation, which was in accordance with SEM observations (Fig. 2d).

Mechanical properties and fractographs. Fig. 4 shows the variation of ultimate tensile strength (σ_b), 0.2% offset strength ($\sigma_{0.2}$) and elongation (δ) with the vol.% of whisker. In comparison with the unreinforced alloy, the $Mg_2B_2O_5$w/6061 composites present significantly higher strength for the whole content range. Meanwhile, the volume fraction of the $Mg_2B_2O_5$ whisker was found to have a

significant effect on the tensile properties of the composites, both σ_b and $\sigma_{0.2}$ started to decrease beyond about 10 vol.% of $Mg_2B_2O_5w$. Elongation of the composites always decreased with increasing reinforcement content. This figure clearly shows that the amount of the reinforcement plays a significant role in controlling the tensile properties of the composites. It is also important to note that the whisker clustering also have a significant effect on the tensile properties of the composites. As shown in Fig. 4, the yield strength and ultimate tensile strength started to decrease at a higher whisker contents, mostly due to the increased amount of clustering. This seems to be especially true for the composite containing 20 vol.% of whisker when the strength is expected to be much higher than at lower whisker levels. But, it is lower due to the increased amount of clustering.

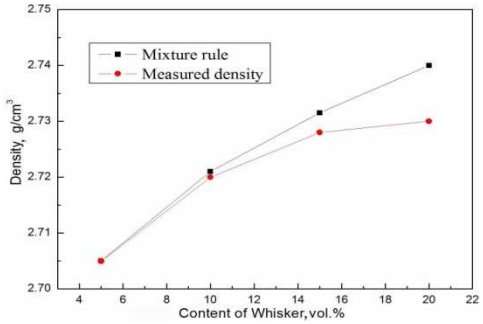

Fig. 3 Density at different $Mg_2B_2O_5$ whisker reinforcement concentrations

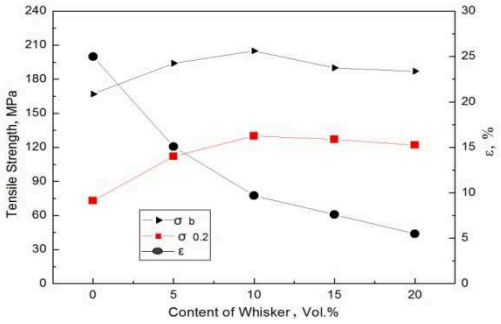

Fig. 4 The effect of content of whisker on the mechanical properties of the composites

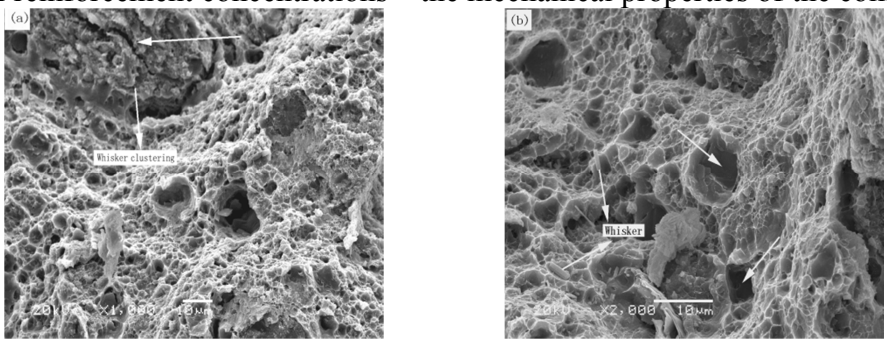

Fig.5 Fracture surface morphologies of $Mg_2B_2O_5w$/6061Al matrix composites

Even though the composites did not exhibit much ductility on a macroscopic scale, SEM fractographs indicated that the fracture occurred by a locally ductile mechanism. Fig. 5 shows the morphologies of the tensile fracture surfaces of the 10 vol.% composite.

Discussion

Fracture. As it can be easily observed form the fractographs (see Fig. 5(a)), some clustered regions, $Mg_2B_2O_5$ whiskers in the composites, cracked in a direction perpendicular to the fracture surface. The high magnification view of the fracture surface shows some whiskers pulled out from aluminum matrix and lots of small dimples (see Fig. 5(b)). So the regions nearby the reinforcement act as points of weakness in the material and probable position for the initiation of tensile failure.

It is considered that the difference of thermal expansion coefficients between whisker and Al alloy matrix leads to the large residual stress of joints and high density dislocation in the extruded composites, and all of these go against the plastic deformation of the matrix [5,6]. Under an applied load, the matrix is placed under great constraint with an inability for strain relaxation to take place. This cause the onset of void nucleation and propagation, which take place at a lower far field applied strain. So the regions nearby the reinforcement act as points of weakness in the material and probable position for the initiation of tensile failure.

Since the reinforcement is less restricted to plastic deformation for the matrix, the composites with lower reinforcement content are good at the elongation, as shown in Fig. 4. For the composite with 15 vol.% $Mg_2B_2O_5$ whisker, it present relatively low elongation, and its fractograph showed some large pits due to the whisker clusters, which indicated that the whisker clusters were an important reason for the composite failure. Otherwise, decohesion at the matrix/whisker interface and ductile fracture

in the matrix were also the fracture mode of the composites. In general, the performance of the composites depend on the specific fracture mode.

Strength. The mechanical properties of Al matrix composites are mainly attributed to the interface bonding state and distribution of whiskers in the matrix [7,8]. First of all, with excellent interface bonding strength, the load could transfer from the weaker matrix, across the matrix/reinforcement interface, to the typically higher stiffness reinforcement. In this manner, strengthening could take place by the reinforcement "carrying" much of the applied load. The interfacial bonding strength of the composites is improved effectively according to the improvement of the extrusion ratio (25:1) in the previous study. As shown in fig. 3b, the whisker distribution in the matrix is homogeneous for the 10 vol.% $Mg_2B_2O_{5w}$/Al matrix composite, and the ultimate tensile strength (σ_b), 0.2% offset strength ($\sigma_{0.2}$) increased by 19% and 44%, separately, compared with extruded 6061 Al alloy; However, the strength of the materials started to decrease beyond about 10 vol.% of $Mg_2B_2O_5w$.

That is because there are other factors that affect the strength of the composites, including the clustering and lower aspect ratio of the whisker. As shown in fig.2(c~d), when the whisker content is more than 10 vol.%, clustering in the matrix is more obvious and serious, otherwise, some pores induced by cluster, demonstrated by density test, could be seen in the whisker clusters for the 20 vol.% $Mg_2B_2O_5w$/Al matrix composite. Decreased plasticity and fracture toughness are attributed to the stress concentrations in the matrix at the poles of the reinforcement and/or at the regions of reinforcement clusters [9]. Furthermore, when the load was transferred from the matrix to the clusters, the clusters firstly cracked because of internal defect and the load at other region increased abruptly, therefore, the strength of the composites inevitably decreased [10].

Conclusions

(1). Processing methods that produce microstructures with a more uniform distribution of reinforcements could potentially result in composites with improved mechanical properties.

(2). The strength of the composites was not always increased with increasing volume fraction of the reinforcements, among other factors, to the presence of clustered whisker, especially for an whisker concentration higher than 10 vol.%.

(3). During the tensile deformation, the whisker clustering produced great effects on the mechanical response of the matrix and the whiskers.

(4). 4The whisker clustering region would promote early the interface debonding and void formation in the ductile matrix.

References

[1] J.Z. Fan, L.K. Shi, Aerospace Materials & Technology, vol. 42 (2012) no. 1, p. 1-7.
[2] CORROCHANO J, CERECEDO C, VALCÁRCEL V, LIEBLICH M, Materials Letters, vol. 62 (2008) no. 1, p. 103-105.
[3] Z.Y. Liu, Q.Z. Wang, B.L. Xiao, Z.Y. Ma, Composites: Part A, vol. 41 (2010) no. 2, p. 1686-1692.
[4] Corbin SF, Wilkinson DS, Acta Metal Mater, vol. 42 (1994) no. 4, p. 1311-1318.
[5] H.Q. Gao, W.D. Fei, Materials Letters, vol. 59 (2005) no. 3, p. 3756 -3760.
[6] D.Y. Ding, D.Z. Wang, W.L. Zhang, Materials Letters, vol. 45 (2000) no. 3, p. 6-11.
[7] M. Vedani, F.D Errico, E. Gariboldi, Composites Science and Technology, vol. 66 (2006) no. 2, p. 343-349.
[8] Z.W. Wang, S. Min, Materials and Engineering A, vol. 528 (2011) no. 12, p. 1131-1137.
[9] S.V. Kamat, J. P. Hirth, R. Mehrabian, Acta Metall, vol. 37 (1989) no. 9, p. 2395-2401.
[10] Slipenyuk A, Kuprin V, Milman Y, Acta Mater, vol. 54 (2006) no. 1, p. 157-166.

Advanced Materials Research Vols. 989-994 (2014) pp 519-522
© (2014) Trans Tech Publications, Switzerland
doi:10.4028/www.scientific.net/AMR.989-994.519

Preparation and properties of complex antioxidants LDPE antioxidant film

Hui Yang[a], Li Li[b], Fuxin Yang[c*], Yingyue Zhou[d], Lijuan OU[e], Shuaifeng Hu[f]

College of Food Science and Technology，Shanghai Ocean University，Shanghai 201306，China
[a]18817771246@163.com, [b]l-li@shou.edu.cn, [c]fxyang@shou.edu.cn, [d]yyzhou@shou.edu.cn,
[e]379626988@qq.com, [f]314911709@qq.com

Key words: BHA; BHT; TA; LDPE; antioxidant

Abstract. Low density polyethylene (LDPE) films contains BHA, BHT or BHA, BHT, TA were successfully produced by extrusion. Three types of antioxidant films that were L(LDPE), LBB(LDPE+0.5%BHA+0.5%BHT), and LBBT(LDPE+0.5%BHA+0.5%BHT+0.5%TA) was designed. The Mechanics, moisture permeability, scanning electron microscopy (SEM) and antioxidant activity of the film were detected. The results showed that antioxidant consisting of BHA, BHT and TA has a better compatibility with LDPE film. The antioxidant film has a better performance on mechanical strength and the rate of DPPH radical scavenging ability, but poor to water vapor transmission rate.

Introduction

In recent years, with the food security problems which caused by the abuse of food additives gradually become the focus, and the vacuum or modified atmosphere packaging cost too much in practical application, the domestic and foreign scholars have put research emphasis on the antioxidant packaging materials, a novel alternative that is being researched is the incorporation of antioxidants into polymers with the aim of being transmitted to oxygen-sensitive food, improving its chemical stability[1].

BHA is a fat-soluble antioxidants that stabilize to heat and suitable for fatty foods or fat-rich foods. BHT can act as antioxidants by high stability, great antioxidant activity and heat resistance, and it has also been developed as a excellent source to be used as additives in film to protect them from oxidation during polymer manufacturing/processing[2]. Tartaric acid (TA) is kind of antioxidant that can increase the effectiveness of preservation by chelating metals[3].The objectives of the present work was to develop an active antioxidant film to improve food preservation by the addition of two types of antioxidants that are 0.5%BHA+0.5%BHT and 0.5%BHA+0.5%BHT+0.5%TA in LDPE, by blending and flat extrusion. The new polymer developed was characterized by the analysis of its barrier properties, optical, mechanical properties, scanning electron microscopy (SEM), thermal, and its antioxidant efficiency.

1 MATERIALS AND EQUIPMENT S

1.1 Materials and Reagents

The Low Density Polyethylene(LDPE) was kindly provided by China Petrochemical (Shanghai, China). Food grade absolute 2(3)-tert-Butyl-4-methoxyphenol (BHA), 2,6-di-tert-butyl-4- methyl phenol (BHT), 2,3-Dihydroxybutanedioic acid (TA) were purchased from Biotechnology Co., Ltd., Zhengzhou days (Zhengzhou, China). 2,2-Diphenyl-1-(2,4,6-trinitrophenyl)hydrazyl (DPPH) was supplied by Biochemical Technology Co., Ltd. Shanghai Jing Pure (Shanghai, China). Ethanol (95% purity) was acquired from Sinopharm Group Reagents (Shanghai, China).

1.2 Film Preparation

Three kinds of antioxidant film were designed in this study: L(LDPE), LBB(LDPE+0.5%BHA+0.5%BHT), LBBT(LDPE+0.5%BHA+0.5%BHT+0.5%TA), in which 0.5% was mass fraction and the remainder was LDPE. The process of film preparation was as follows: LDPE+Antioxidants⟶Twin Screw Extruder⟶Blending⟶Flat Extrusion⟶Preservative Film.

2 MEASUREMENT INDICATORS

2.1 Water vapor Permeability

The water vapor permeability (WVP)of the films were determined at 100% RH and 37.8℃ using an PERMATRAN-W1/5 (Mocon, Germany) in accordance with the method of ASTME398[4].

2.2 Mechanical Properties

The mechanical properties of films including elongation at break (EB) and tensile strength (Ts) were carried out at 25℃ and 50%RH. Experiments were performed using a Tensile Testing Machine DCP-KZ30 (Chengdu, China) according to the method of ASTM-09[5].

2.3 Scanning Electron Microscopy (SEM)

S3400N (Hitachi) scanning electron microscope was used to research the morphology of films. The samples were mounted on the specimen holder with aluminum tape and then sputtered with gold in sputter coater for 30s at 20mA[6]. All samples were determined using an accelerating beam at a voltage of 20.0 kV.

2.4 Thermal Analysis

Thermogravimetric analyses were performed using a NETZSCH TG209/F3 thermal analyzer (German). The samples (ca. 5mg) were heated in 100μL ceramic crucible from 35℃ to 900℃ under a nitrogen atmosphere at 15℃/min to measure and record any volatilization of volatile compounds, as well as the degradation temperatures of the films developed[7].

2.5 Antioxidant Efficiency

Antioxidant activities of the films containing antioxidants were determined by the DPPH method. The tests were carried out as follows: a 12 cm^2 piece of each sample and 100ml of 95% ethanol (area-to-volume around 6dm^2/L) were placed in tubes which covered with aluminium foil to protect the contents from light to undergoing the process of extraction, and then the tubes were conserved at 65℃ for 3h[8]. The DPPH scavenging activities of extraction solutions was measured according to the method of Zheng lin[9].

3 RESULTS AND DISCUSSION

3.1 Mechanical Properties And Water Vapor Permeability

Table.1 Test results of mechanical properties and water vapor permeability of the film

Group	Thickness (mm)	Ts (Mpa)	EB (%)	WVP ($\times10^{-15}g\cdot m^{-1}\cdot s^{-1}\cdot pa^{-1}$)
L（control）	0.018	12.76	56.4	7.679
LBB	0.032	13.23	51.7	6.869
LBBT	0.024	17.25	42.2	6.564

Mechanical properties and water vapor permeability test results are shown in Table.1. Ts of LBB and LBBT increased from 12.76 to 13.23(3.7%) and from 12.76 to17.25(35.2%)Mpa compared to L(control), respectively, after addition of BHA, BHT and BHA, BHT, TA. Conversely, EB of LBB and LBBT decreased from 56.4% to 51.7% and from 56.4% to 42.2%. Based on these results, it can be concluded that the incorporation of antioxidants improved its rigidity and reduced the effectiveness of its flexibility. The reason for this phenomenon may be owing to crosslinking of the molecular chain of LDPE resin under the condition of high temperature during the process of modified granulation and flat extrusion. Thus, it is very difficult for the occurrence of slip between the molecular chain, reducing EB and increasing Ts of the films .Table.1 also sets out the water vapor permeability (WVP) of the films. All the films containing antioxidants had lower WVP values than the pure LDPE film. TA incorporation caused the decrease in WVP. Presumably because the active agents enhance the molecular interactions of LDPE that make the film more uniform compact, thus preventing water molecules through effectively.

3.2 Scanning Electron Microscopy(SEM)

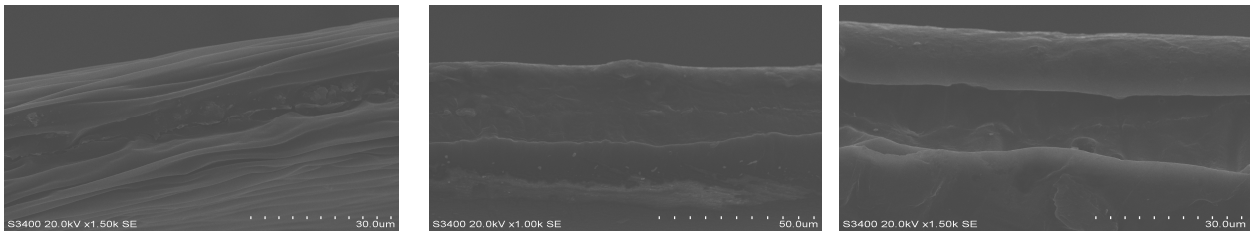

L **LBB** **LBBT**

Fig.1. SEM micrographs of cross-section of films

SEM micrographs representative of all films are presented in Fig.1. The pure LDPE film showed a smooth, compact and continuous microstructure with no irregularities compared to antioxidants-containing films. The film adding antioxidants images displayed that antioxidants distributed evenly in the resin base material, no bubbles, and there are no stress concentration caused by antioxidants gather. These phenomenon concluded that antioxidants have a preferable compatibility with film under high temperature.

3.3 Thermal Characterization

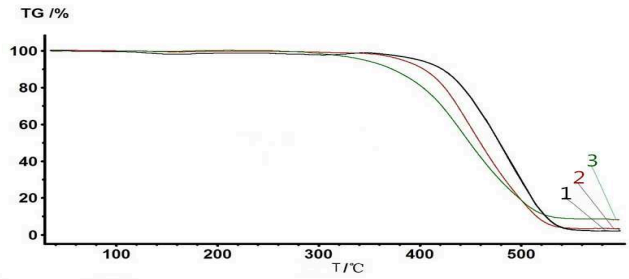

Fig.2 TGA curves of film

The results are shown as Fig.2, the drastic mass loss of pure LDPE materials occurred in a main step at a temperature between 400℃ and 500℃. The highest temperature of the experiment is set to 600℃, control film almost degraded completely, no residue, while the experimental groups were part of residues at the end of the experiment. The thermal decomposition process of LDPE is a chain reaction triggered by free radicals, the polymer chain will fracture into carbon free radicals randomly during the process of reaction, and the carbon free radicals react to generate low molecular weight hydrocarbons further[10], the antioxidants that were added into the films will have the effect of scavenging free radicals, leads to the weaken of free radical reactions, thus the thermal decomposition of the film is inhibited. From the change trend of the entire thermograms, the whole films have a lesser mass loss under the condition of 320℃, relatively stable, are suitable for the preservation of normal usage.

3.4 Antioxidant Efficiency DPPH radical has been extensively used to measure the ability of compounds as free radical scavengers. This method is based on the inhibition of the DPPH radical that is a stable free radical by antioxidants, and consequently decolorize in the present of antioxidants resulting in a decline in absorbance values. The antioxidant activity of different films is shown in Fig.3. The control film exhibited radical scavenging activity of 2.30% on DPPH. Films with antioxidants showed a higher level of radical scavenging activity with values of 20.79 and 18.63% for LBB and LBBT, respectively. The results demonstrated that the DPPH scavenging activity of the film increased significantly with the incorporation of antioxidants. The film that contained TA(LBBT) was found less effective against quenching DPPH radical in comparison with LBB may be due to the addition of TA that made the connections between LDPE polymer chains more dense so that the release of antioxidants sustained certain restrictions.

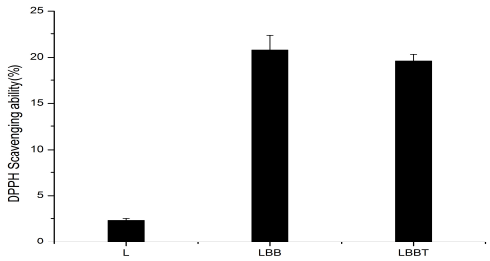

Fig.3 Figures of DPPH radical scavenging ability of film

4 Conclusions

The study results revealed that the LDPE film incorporated with BHA, BHT and TA in concentration of 0.5% has a perfect potential for application as a antioxidant film. LDPE film showed some antioxidant activity, which was remarkably improved by the addition of antioxidants. This incorporation made the film uniform density, increased the film tensile strength, reduced the water vapor transmittance coefficient and improved the heat resistance, which demonstrated that the film containing BHA, BHT and TA could be used as a kind of food packaging material.

References

[1] SONG Huan, LI Xiao-mei. Determineation of Antioxidant Contents in Commercial Food Packages by Ultra Performance Liquid Chromatography[J]. Food Science, 2008, 29(9) : 448-450.

[2] Sun Ying-ying. Studies On the Detection of Antioxidants of BHA And BHT by Surface-Enhanced Raman Scattering[D]. Jiang Nan University 2012.

[3] DU Lei, ZHOU Guang-hong. Research of the Artificial Beef Marbling[J]. Modern Food Science and Technology, 2008, 24(8): 851-855.

[4] ASTM,E398,Standard Test Method for Water Vapor Transmission Rate of Sheet Materials Using Dynamic Relative Humidity Measurement [S]. 2003.

[5] ASTM,D882-09, Standard Test Method for Tensile Properties of Thin Plastic Sheeting[S]. 2009.

[6] Ghasemlou M, Khodaiyan F, Oromiehie A. Physical, mechanical, barrier, and thermal properties of polyol-plasticized biodegradable edible film made from kefiran[J]. Carbohydrate Polymers, 2011, 84(1): 477-483.

[7] Mu C, Guo J, Li X, et al. Preparation and properties of dialdehyde carboxymethyl cellulose crosslinked gelatin edible films[J]. Food Hydrocolloids, 2012, 27(1): 22-29.

[8] Lopez de Dicastillo C, Nerin C, Alfaro P, et al. Development of new antioxidant active packaging films based on ethylene vinyl alcohol copolymer (EVOH) and green tea extract[J]. Journal of agricultural and food chemistry, 2011, 59(14): 7832-7840.

[9] ZHENG Lin，LIN Song-yi，LIU Jing-bo. Study on DPPH Free Radical Scavenging Activity of Egg White Protein Hydrolysates[J]. Food Industry, 2009 (3): 1-3.

[10] LIANG Xing-quan, LIU Ju, LIN Bao-feng. Study on Thermal Decomposition Kinetics of LDPE in the Presence of Ferriferous Oxide[J]. Applied Chemical Industry, 2012, 41(6): 1010-1014.

Advanced Materials Research Vols. 989-994 (2014) pp 523-526
© (2014) Trans Tech Publications, Switzerland
doi:10.4028/www.scientific.net/AMR.989-994.523

Photo-switchable Binding between a Photochromic Calix[4]arene Derivative and Lanthanum Ions

Zhilian Liu [a *], Xiaohui Li [b] and Zhenning Yu [1c]

School of Chemistry and Chemical Engineering, University of Jinan, Jinan 250022, China

[a]chm_liuzl@ujn.edu.cn, [b]1607805736@qq.com, [c] 827275389@qq.com

Keywords: Photoswitches; Lanthanum nitrates; calix[4]arene derivatives; photochromic spiropyrans

Abstract. The spectroscopic behavior of a photochromic compound 5, 11, 17, 23-tetra-*tert*-but yl-25, 27-bis(1',3',3'-trimethyl-6-nitrospiro-[2-H-1-benzopyran-2,2'-indoline]-8-methoxycarbonylmethox y)-26,28-dihydroxycalix[4]arene (**1**) and its complex with lanthanum nitrate was described. Compound **1** has typical photochromic properties for its two spirobenzopyran groups. The complexation spectroscopic behavior has been investigated in anhydrous acetonitrile by UV-vis, fluorescence spectra and ESR spectra. The results obtained proved the formation of complexes and indicated that the spectroscopic behavior of the supramolecular system could be regulated by light. The system might be used as *on-off* switches.

Introduction

Photochromism was firstly brought forward in the fifties of the twentieth century by Fischer and Hirshberg [1, 2]. In the past fifty years, people have developed many potential applications as photochromic materials, optical storage, optical memories and optical switches. Spiropyran system is one of the earliest and the most extensive systems. Under the irradiation of ultraviolet light (or in dark conditions), the closed, colorless, neutral spiropyran (SP) forms are isomerized to their open, colored, zwitter-ionic merocyanine forms (MC). Meanwhile, the s-p hybridization of a single C atom changes to p-conjugation over the whole molecule. The characteristics indicate its potential applications in photoswitchable molecular devices [3-8]. Calixarenes, with three-dimensional cavities, which are regarded as the third supramolecular receptor, are popular building blocks in supramolecular chemistry [9, 10]. Their derivatives can selectively bind a variety of molecules and ions. Therefore, we chose calix[4]arenes as host frames and spirobenzopyrans as light responsible groups to establish a receptor which not only might bind guests but also spectroscopic behavior of the supramolecular system might be regulated by light. This kind of design idea would be useful in photoswitchable devices.

Results and discussion

Compound **1** carries two spirobenzopyran groups so it should have typical photochromic properties. Therefore, we measured UV-vis spectra of compound **1** under three different conditions (under dark conditions, upon ultraviolet light irradiation and visible light irradiation). As expected, the acetonitrile solution of compound **1** (0.05 mM) had no absorption above 400 nm upon visible light irradiation because the spirobenzopyran groups of compound **1** were in closed, colorless forms (Calix-2SP) under this condition. Then, the solution was kept in the dark for 16 minutes. It turned to purple and had maximum absorption at 555 nm in the visible region which caused by part conversion of closed forms to open, colorful forms (Calix-2MC). After the solution was irradiated by ultraviolet light for 20 minutes, the absorbance at 555 nm was increased by about two folds for further conversion from closed forms to open forms. Visible light irradiation could almost make the absorbance decrease to zero again. This reversible photochromic processes were described in Figure 1.

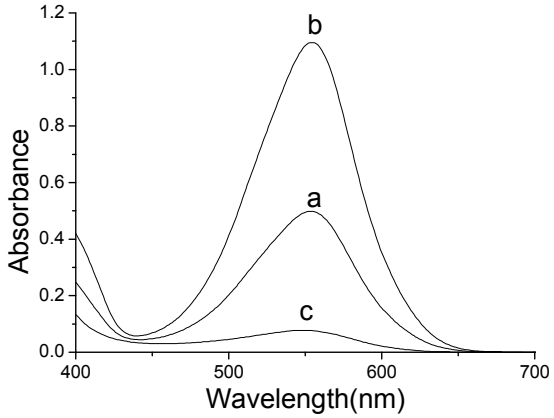

Fig. 1 Photochromism of compound **1** in acetonitrile in the dark 16 min (a); upon UV irradiation 20 min (b); and then upon visible light irradiation 10 min (c).

As mentioned above, our interest is to develop a light responsible supramolecular system whose spectroscopic behavior could be regulated by light stimuli. Our above results have proved that the synthetic receptor **1** possessed good photochomic properties as well as binding ability with lanthanum ions. Next, we would like to investigate whether its spectroscopic behavior could be regulated by light. The mixed solution of compound **1** (0.05 mM) and an equivalent lanthanum nitrates was kept in the dark. Eleven hours later, the absorbance at 487 nm increased by more than two folds (Curve a, Figure 2). Then, the above solution was irradiated by visible light. Just as expected, a remarkable decrease was observed as shown in Figure 2 (Curve b). UV irradiation caused the absorbance increase again (Curve c, Figure 2). What's more, its spectrum almost returned to its initial absorbance after it was kept under dark conditions for 11 hours again (Curve d, Figure 2). For low energy of the mercury lamp (15 W), curve c is under curve d. These results demonstrate that light can modulate spectroscopic behavior of **1**-La^{3+} supramolecular system. Proposed photoswitching processes are described in Scheme 1.

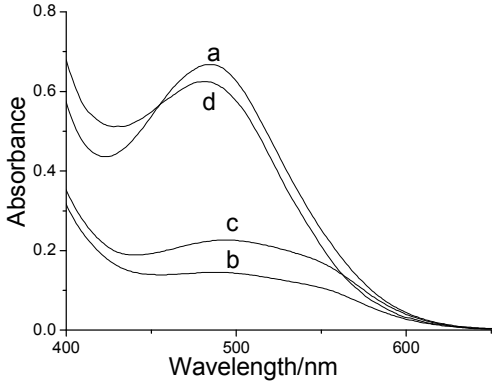

Fig. 2 UV-vis absorption spectra of the mixture of compound **1** (50 μM) and 1 *equiv.* lanthanum nitrates in the dark 11h (a); upon visible light irradiation 5 min (b); and then upon UV irradiation 25 min (c); finally in the dark 11h (d).

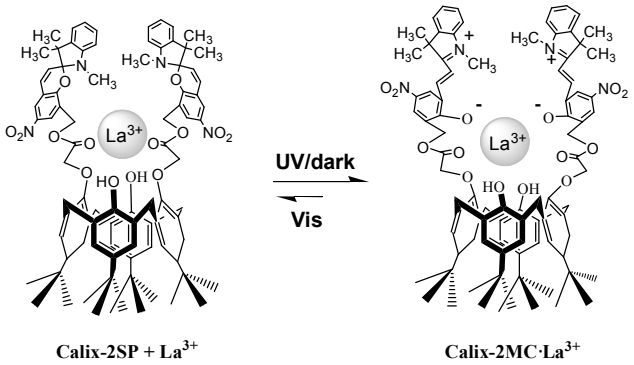

Scheme 1. Proposed photoswitchable binding processes of compound **1** and lanthanum ions.

Emission spectra studies provided consistent results with those of absorption spectra. It was reported that closed forms of spiropyran derivatives have no emission while open forms can emit weak light at about 635 nm [11]. The open forms of compound **1** can emit light at 635 nm (Curve a, Figure 3). After the addition of lanthanum nitrates, a remarkable hypsochromic shift (about 40 nm) occurred in the emission spectra companied with intensity increase (Curve b, Figure 3). The shift just accords with the blue shift in the absorption spectra. Then, the mixture of compound **1** and La^{3+} was irradiated by visible light and a significant decrease of emission intensity was observed (Curve c, Figure 3). This result is corresponding to the curve b in Figure 3. The open forms of compound **1** (Calix-2MC•La^{3+}) were isomerized to its closed forms (Calix-2SP) which have no emission.

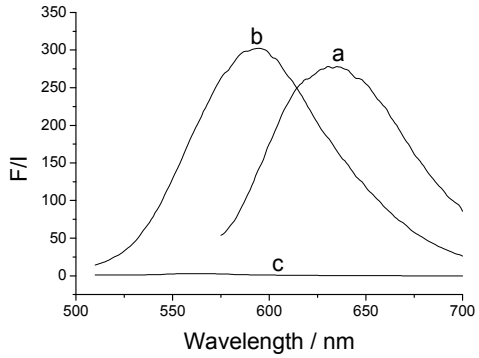

Fig. 3 Emission spectra of compound **1** (20 μM) before (a); and after the addition of 20 μM $La(NO_3)_3$ in acetonitrile after 48h in dark (b); then irradiated by visible light for 15 min (c).

Another interesting experimental result was obtained by studies on ESR (Electron Spin Resonance). After the addition of lanthanum nitrates to the acetonitrile solution of compound **1**, the mixture was irradiated by 355 nm and then 532 nm light. Quite different signals were detected as shown in Figure 5. There were no detectable signals in control experiments of compound **1**'s solution and lanthanum nitrates' solution under the same conditions. These results might be due to the binding interaction between the open forms of compound **1** and La^{3+}, which could attributed to the energy level splitting of the unpaired electron in lanthanum atomic orbits induced by magnetic field. After the irradiation of visible light, the interaction disappeared so the mixture was just like two independent system of compound **1** and lanthanum nitrates which both have no ESR signals at this condition. Weak signals (right, Figure 4) were due to the incomplete conversion of open forms to closed forms upon visible light irradiation. Further studies on photoswitch mechanism is under way.

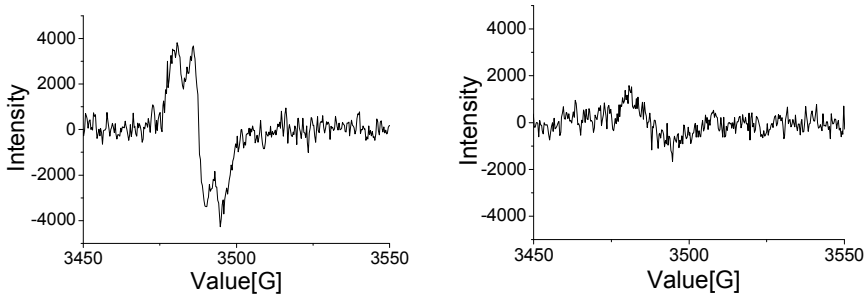

Fig. 4 ESR spectra of the mixture of compound 1 (0.01 M) and lanthanum nitrates (0.1 M) irradiated by 355 nm UV light (left) and then by 532 nm visible light (right).

Conclusion

In conclusion, the spectroscopic behavior of the supramolecular system containing photochromic calixarene derivatives and lanthanum ions can be regulated by light with remarkable changes in absorption spectra , emission spectra and ESR spectra. These photoswitchable changes may be as *on-off* switches in optical sensors and switches.

Acknowledgement

We are grateful to the support of the Shandong excellent Young Scientist Research Award Fund (Project No. BS2011CL007) and National Undergraduates' Training Programs for Innovation and Entrepreneurship of University of Jinan (No. 201310427014).

References

[1] E. Fischer, Y. Hirshberg, *J. Chem. Soc,*. (1952), p. 4522.
[2] Y. Hirshberg, E. Fischer, *J. Chem. Phys.,* Vol.21 (1953) 1619.
[3] F. M. Raymo and S. Giordani, *J. Am. Chem. Soc.,* Vol.123 (2001), p. 4651.
[4] F. M. Raymo and S. Giordani, *Org. Lett.,* Vol.3 (2001), p. 1833.
[5] F. M. Raymo, R. J. Alvarado, S. Giordani, M. A. Cejas, *J. Am. Chem. Soc.,* Vol.125 (2003), p. 2361.
[6] X. F. Guo, D. Q. Zhang, Y. C. Zhou, D. B. Zhu, *Chem. Phys. Lett.,* Vol.375 (2003), p. 484.
[7] X. F. Guo, D. Q. Zhang, Y. C. Zhou, D. B. Zhu, *J. Org. Chem.,* Vol.68 (2003), p. 5681.
[8] Z. L. Liu, L. Jiang, Z. Liang, Y. H. Gao, *Tetra. Lett.,* Vol.46 (2005), p. 885.
[9] C.D. Gutsche, Calixarenes: RSC Monographs in Supramolecular Chemistry, vol. 1, Royal Society of Chemistry, Cambridge (1989).
[10] J. Vicens, V. Böhmer (Eds.), Calixarenes: A Versatile Class of Macrocyclil Compounds, Kluwer Academic Publishers, Dordrecht (1991).
[11] Horie, K.; Hirao, K.; Mita, I., *Chem. Phys. Lett.*, Vol.119 (1985), p. 499.

Advanced Materials Research Vols. 989-994 (2014) pp 527-530
© (2014) Trans Tech Publications, Switzerland
doi:10.4028/www.scientific.net/AMR.989-994.527

Highly efficient photodegradation of MO dye by TiO_2 nanoparticles

Xinzuo Fang[1,a] and Lisheng Gao[2,b]

[1]School of Chemistry and Materials Science, University of Science and Technology of China, Hefei 230026, China;

[2]Institute of Intelligent Machines, Chinese Academy of Sciences, Hefei 230031, China

[a]fangxz@mail.ustc.edu.cn, [b]lsgao@iim.ac.cn

Keywords: photodegradation, MO, solar irradiation, TiO_2

Abstract: use the sol-thermal method to synthesis nanoparticle TiO2 which is well developed, small diameter and good dispersion. XRD and BET methods were used to analyze the crystal structure and specific surface area. Under nature solar light, the photodegradation activity of TiO_2 is tested. The results show that the TiO_2 sample displayed better photodegradation activity than P25 under solar irradiation.

Introduction

Water pollution is one of the most urgent questions in our daily life [1]. Azo dyes which contain nitrogen to nitrogen double bonds (-N=N-) and carbon to carbon double bonds (-C=C-)) constitutes a significant portion that are widely used in industries today [2]. From last decade, there are many methods under research to solve this problem, such as chemical method, physical method, adsorption and biological methods [3-5]. But all the methods did not work as well as people expected. Since 1972, Fujishima and Honda [6] found TiO_2 can split water into H_2 and O_2 in their research, the TiO_2 semiconductor has attracted extensive attention. As we all known, TiO_2 is very stable, easy to obtain, non-toxic and high photocatalytic[7-10], so TiO_2 semiconductor is considered as the most promising photocatalyst in the future, and its application is wider as the researches are being done. Photodegradation of dyes with solar light can make it an economically viable process since solar energy is an abundant natural energy source. So taken the reality, the solar light is a good choice.

In this work, we choose methyl orange (MO) as pollutant. MO is an orange-colored anionic dye with λ max at 464 nm. MO has various harmful effects on human beings: it may cause eye or skin irritation, or inhalation, it may cause gastrointestinal irritation with nausea, vomiting, and diarrhea[11]. We use nanoparticle TiO_2 synthesized by sol-hydrothermal method as photocatalyst to decompose MO with solar light. And the catalyst exhibit high photocatalytic activity than P25.

2. Experiment

2.1. Sample preparation

A given quantity of ethylene glycol (EG) and citric acid (CA) was dissolved under vigorous stirring at 80℃. Then about 1.5mL $Ti(OC_4H_9)_4$ solution and 25mL water was added dropwise under a vigorous stirring to the solution. Stired until a transparent solution was obtained. Then the transparent solution was directly loaded in an autoclave for hydrothermal reaction and kept at 200℃ for 10h. After the hydrothermal treatment, the precipitates were separated from the solution by centrifugation, washed with distilled water and anhydrous alcohol, and then dried in an oven at 60℃.

All the chemical materials are analytically pure grade and used without further purification

The obtained samples were analyzed with an X' Pert Pro MPD diffractometer using Cu (Kα1/Kα2) radiation. The XRD patterns were recorded in a diffraction angle range from 20° to 80°.

The specific surface area was determined by nitrogen adsorption method (Ommishop 100CX, BECKMAN COULTER).

2.2. Photocatalytic degradation of MO

The experiments of photodegradation were carried out outdoors under direct solar light. In a typical experiment [12-13], before irradiation, the glass vessels containing 30ml MO and some quantity as prepared samples were put in the dark 30 minutes to obtain the absorption-desorption equilibrium between the dye and photocatalyst. After that, those reactors were put outdoors (GPS coordinates=31.9, E=117.2) to react.

3. Results and discussion

3.1. Crystalline structure and morphological characterization

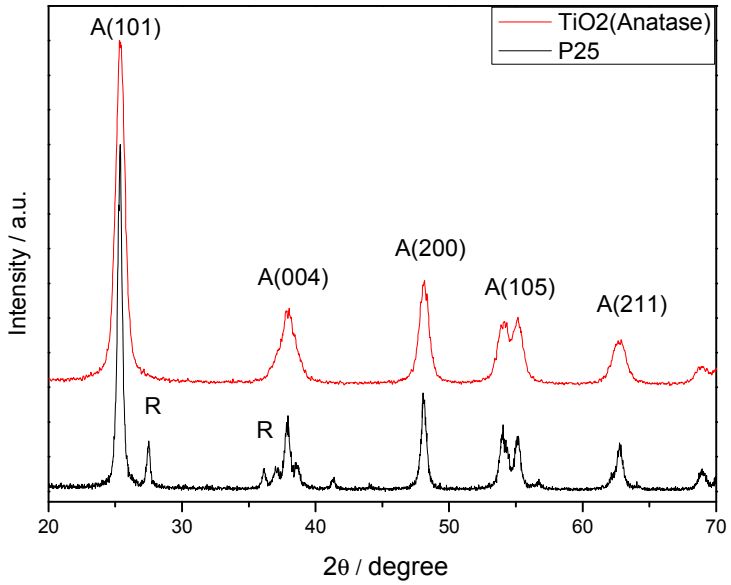

Fig 1: X-ray diffraction patterns of TiO_2 sample and TiO2 P25

As shown in figure 1, TiO_2 samples synthesized by the sol-hydrothermal method is highly crystallized and all the X-ray diffraction peaks correspond to characteristic peak of crystal plane of anatase which shows that the TiO2 sample is pure anatase phase. The peaks of 27.6 and 36.2 show that the commercial TiO2 is composed by anatase phase and rutile phase.

After BET analysis we get the specific surface area (S_{BET}) of TiO_2 sample and P25 are 225.2 and 41.7m^2/g. The S_{BET} of TiO_2 sample is more than 5 times larger than that of commercial P25.

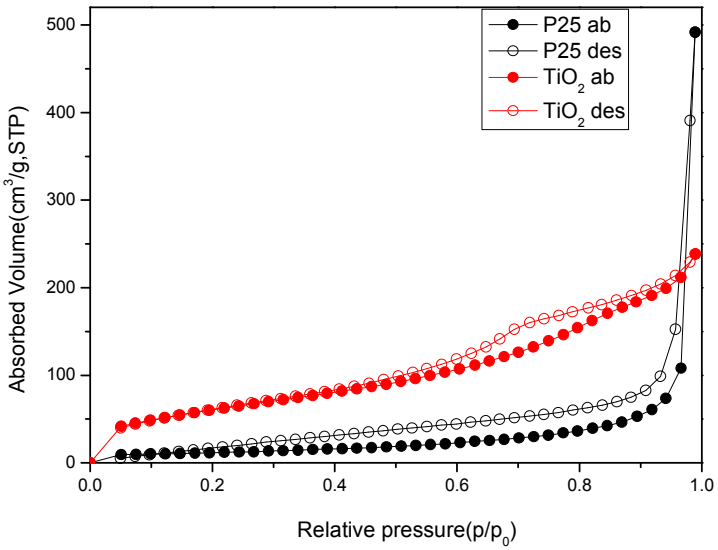

Fig 2: Nitrogen adsorption and desorption isotherms of TiO_2 samples and P25

3.2. photodegradation of MO

The photodegradation efficiency of MO was evaluated according to the percentage

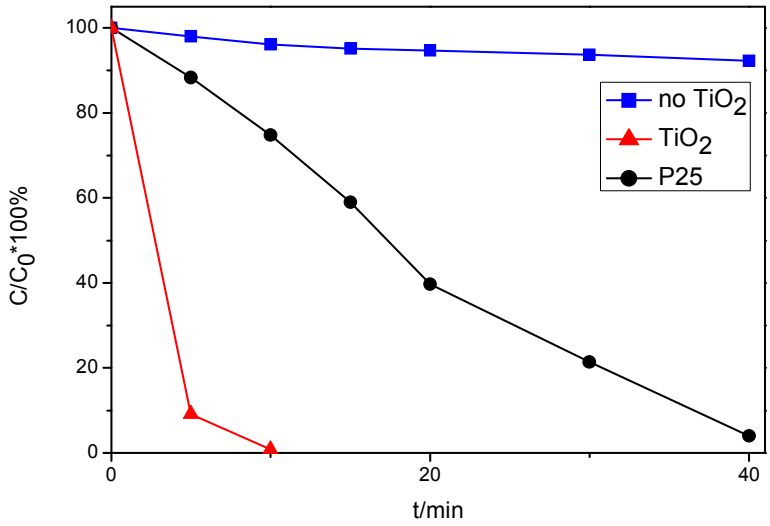

Fig3: The photodegradation of MO by no sample, TiO_2 sample and P25 (C_0=24mg/L,C_{P25}=1.4g/L,C_{TiO2}=1.4g/L）

degradation of MO solution. Figure 3 show the photodegradation of MO using different catalyst. When no catalyst is added, after 40 min irradiation under solar light the decomposition of MO is very little and can be negligible. However, about 99% is decomposed with the TiO_2 catalyst in ten minutes under sunlight. Compared to TiO_2 sample, the commercial P25 can only photo decompose 95% by a long time irradiatio.

4. Conclusion

In this work, we successfully photodegradated MO through a high efficient photocatalyst TiO_2 synthesized by sol-hydrothermal method. Through XRD and BET analysis, the photocatalyst is pure anatase phase, about 10nm and has a very high specific surface area 225.2m^2/g. Under solar light irradiation, TiO_2 can completely photo decompose MO in ten minutes, about five times higher than that of P25. In conclusion, the TiO_2 sample is a high effective photocatalyst that can be used for future industrial pollution applications.

References

[1] T. Robinson, G. McMullan, R. Marchant, et al: Bioresource Technology, vol. 77 (2001), no. 3, p. 247-255
[2] Y. M. Slokar, A. M. Marechal: Dyes and Pigments, vol. 37(1998) no. 4, p.335-356
[3] T. Soltani, M.H. Entezari: Ultrasonics Sonochemistry, vol. 20 (2013) no. 5, p. 1245–1253
[4] S. Mozia, M. Tomaszewska, A. W. Morawski: Dyes and Pigments, vol. 75 (2007) no.1 p. 60-66
[5] O. Turgay, G. Ersoz, S. Atalay, et al: Separation and Purification Technology, vol. 79 (2011) no. 1, p. 26 – 33
[6] A. Fujishima and K. Honda: Nature, vol. 238(1972), p. 37-38
[7] M.W. Xu, S.J. Bao, X.G. Zhang: Materials Letters, vol.59 (2005) no.17, p. 2194–2198
[8] A.B.Prevot, C.Baiocchi, M.C.Brussino, et al: Environmental Science & Technology, vol.35 (2001) no. 5, p. 971– 976
[9] O. Y. Ke, S. Xie and X. O. Ma: Ceramics International, vol. 39(2013) no. 7, p. 7531–7536
[10] S. Al-Quadawi and S. R. Salman: Journal of Photochemistry and Photobiology A: Chemistry, vol. 148(2002) no. 1, p. 161-168
[11] A. M. Lotito, U. Fratino, G. Bergna, et al: Chemical Engineering Journal, vol.195(2012) no. 1, p. 261-269
[12] M. Hirano, H. Dozono, T. Kono: Materials Research Bulletin, vol. 46 (2011) no. 9, p.1384 – 1390
[13] M. Muruganandham, M. Swaminathan: Solar Energy Materials & Solar Cells, 81 (2004) no.4, p. 439 – 457

Advanced Materials Research Vols. 989-994 (2014) pp 531-535
© (2014) Trans Tech Publications, Switzerland
doi:10.4028/www.scientific.net/AMR.989-994.531

Preparation of visible-light active Mn-doped TiO_2 photocatalyst and its photodegradation of methylene blue from solution

Yin Chen [a], Xiaojun Ma [b]

Tianjin University of Science & Technology, Tianjin 300222, China

[a]chenyin880828@163.com, [b] mxj75@tust.edu.cn

Keywords: Mn-doped TiO_2, sol-gel method, methylene blue, photodegradation.

Abstract. Mn-doped TiO_2 nanocrystal photocatalysts were prepared by the sol-gel method using $MnSO_4 \cdot H_2O$ as manganese source. The catalysts were characterized by XRD, SEM, EPR, UV-Vis, their photocatalytic activity for methylene blue (MB) degradation was investigated. The results showed that Mn was doped into the crystal lattice of TiO_2, and had no influence on TiO_2 crystal structure; the size of TiO_2 nanoparticle gradually decreased with Mn doping concentration increasing. The Mn-doped TiO_2 catalysts have enhanced absorption in the visible light region, and its visible light absorptivity increased with Mn doping concentration increasing. The UV-Vis showed the Mn-doped TiO_2 showed higher photocatalytic activity than the undoped TiO_2 for methylene blue degradation under visible light irradiation. It is also found that the MB photodegradation rate of Mn-doped TiO_2 improved by 46% than that of the undoped TiO_2.

Introduction

Since the 1970s when Fujishima, a Japanese scholar, discovered that TiO_2 electric light can be used in water catalytic decomposition, the nanometer TiO_2 has been widely applied in air purification and sewage disposal owing to its strong photocatalytic activity, stable chemical property, thorough degradation of organic matter, no secondary pollution and non-toxicity [1-3]. However, TiO_2 has relatively wide band gap (anatase 3.2eV, rutile 3.0eV) and narrow absorption spectrum, thus only ultraviolet light with the wave length less than 387.5nm can be absorbed. The visible light which accounts for more than 90% of the sunshine fails to excite its photocatalytic activity, thus limiting the further generalization of TiO_2 photocatalyst [4, 5]. Therefore, it is necessary to place great emphasis on the improving the absorbency of visible light of TiO_2.

To improve the photocatalytic efficiency of TiO_2, researchers have adopted different means to modify nanometer TiO_2 in recent years, such as precious metal deposition, ion doping, compound semiconductor and surface sensitization, among which ion doping of transition metal is an effective method [6]. Esparza et al [7] prepared doping photocatalyst of nanometer Co-TiO_2, Fe-TiO_2, and Mn-TiO_2 through hydrothermal method, and the results show that doping photocatalyst absorbs more light than TiO_2 Degussa P25 and nanometer TiO_2 in visible light region. Abdelaal et al [8] prepared Pd/TiO_2-CS photocatalyst by sol-gel method, which could degrade methylene blue solution effectively in visible light region with the degradation rate up to 99.5%. Khan et al[9] found that TiO_2 doped with V could reduce the band gap of TiO_2 and enlarge the specific surface area, leading to the red shift of TiO_2 spectral absorption threshold. Besides, it could also reduce the recombination velocity of electrons and holes with the methylene blue degrading effectiveness of 5 times higher than that of pure TiO_2.

Therefore, Mn-doped TiO_2 nanocrystal photocatalysts were prepared by the sol-gel method using $MnSO_4 \cdot H_2O$ as manganese source. The catalysts were characterized by using scanning electron microscope (SEM), X-ray diffraction (XRD), ultraviolet–visible-light reflectance (UV-vis) spectroscopy, and electron paramagnetic resonance spectrometer (EPR), their photocatalytic activity for methylene blue (MB) degradation was also investigated under visible light irradiation.

Materials and Methods

Preparation of Samples. Gradually and successively blend $Ti(OC_4H_9)_4$ and $MnSO_4 \cdot H_2O$ (molar ratios of Titanium and Manganese are respectively 1:0, 500:1, 400:1, 300:1, 200:1 and 100:1) of certain quantities into a beaker filled with 90ml of anhydrous ethanol in stirring state, and keep one hour of fast stirring on a magnetic stirring apparatus to get the mixed solution A. According to the ratio that $n(H_2O)$: $n(Mn+Ti)$ =4:1, the mixed solution B can be acquired by dissolving distilled water in 60ml of anhydrous ethanol. Blend solution B slowly into solution A in stirring state and then put it into a water bath kettle of 40°C for a certain time of mechanical stirring. Wash the powder with distilled water and dry the powder in 105°C for one hour. After grinding, put the powder in a vacuum tube furnace and in a heating rate of 5°C/min for three hours and calcine for 3 hours when heat reached to a temperature of 450□. Samples can be acquired after natural cooling. According to molar ratios of Titanium and Manganese, samples are labeled as Ti, Mn/500Ti, Mn/400Ti, Mn/300Ti, Mn/200Ti, Mn/100Ti respectively.

Characterization of Samples. Observe the morphology of photocatalyst samples by FEI NANOSEM 430 scanning electron microscope of thermal field emission. Determine the XRD spectrum of samples by Rigaku D/max2500 powder X-ray diffractometer. With the use of Cu Kα ray, λ=1.5405Å, 40kV of tube voltage, 100mA of tube current, 20-80° of scanning angle 2θ, 8°•min-1 of scanning speed, the average diameter D(nm) of photocatalyst samples can be calculated through Scherrer formula $D=K1\lambda/(\beta 1/2 \cos\theta)$, in which K1 is the crystal shape factor with the value of 0.89, β1/2 is the peak width at half height (rad), and θ is the diffraction angle (°). Use Varian Cary 5000 ultraviolet and visible spectrophotometer made in US to determine the UV-vis spectrum of samples and use Bruker A300 electron paramagnetic resonance spectrometer made in Germany to determine the EPR spectrum of samples, of which the operating frequency is 9.64GHz and the power is 63nW.

Photocatalytic Property Determination of Samples. Dissolve 0.05g of photocatalyst into a certain concentration of methylene blue solution of 100ml, and put it into a homemade photocatalytic reactor away from light for magnetic stirring of 0.5 hour, reaching the adsorption equilibrium for the solution. Expose the solution covered with an optical filter (400-800nm of wavelength) under an energy-saving lamp of 65W with a fixed height. Observe the absorbency of methylene blue solution at maximum absorption peak λ=665nm every two hours. Calculate the decolourization ratio D by formula $D=(A_0-A)/A_0\times100\%$, in which A_0 stands for the initial absorbency and A stands for the absorbency after a certain time of reaction.

Results and Discussion

SEM. With the increase of Mn doping concentration, the sample color changes from white to yellow and deepens gradually. Figure 1 showed the scanning electron microscope of all samples. All samples in the figure are nanometer circular particles. Pure TiO_2 dispersed more evenly with identical particle size and smooth surface and large particle size. With the increase of Mn doping concentration, there were slight coacervations for TiO_2 samples with rough surface and small particle size. It can be inferred that Mn was helpful in reducing TiO_2 particle size, enlarging specific surface area, and providing better adsorption conditions for photocatalytic degradation.

XRD. Figure 2 showed the spectrum of nanometer TiO_2 of different Mn doping concentration. It can be seen from Figure 2 that all samples showed characteristic diffraction peak of anatase crystal face TiO_2 (101), (004), (200), (105), (211), (204), (220), (215)[10] with no rutile, proving that a small amount of Mn will not change the crystal structure of samples. With the increase of Mn doping concentration, the diffraction peak when 2θ=25.3° decreased, showing the deterioration of crystal quality. When the diffraction peak gradually became widen, it showed that grain sizes of the catalyst became smaller, which was in line with test results of scanning electron microscope. This could be due to the fact that Mn mixing into the crystal lattice of TiO_2 and the ionic radius of Mn 0.46Å was smaller than that of Ti. Because of the small doping amount of Mn and equal distribution, diffraction peak of Mn cannot be found beyond the detection peak in this figure.

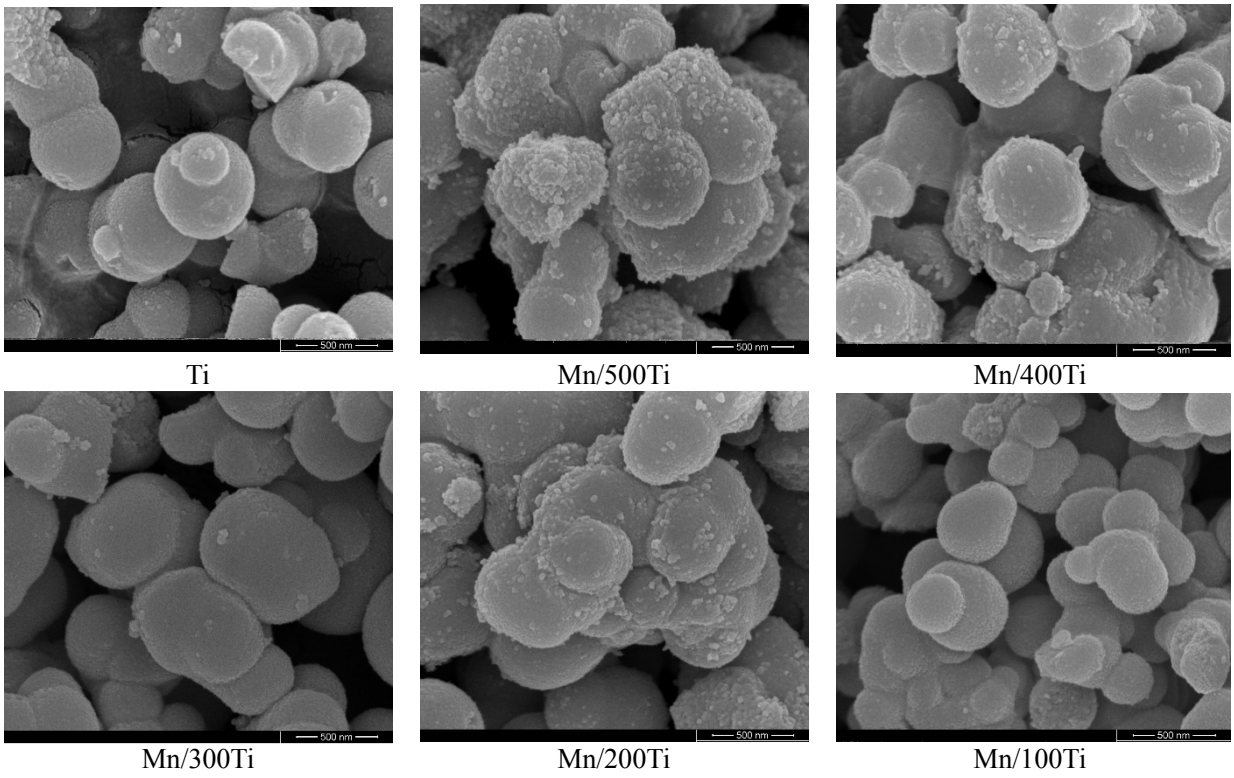

Fig. 1 SEM images of Mn/TiO_2

Table 1 showed average particle sizes of samples calculated by formula Scherrer. The sizes in the table were measured in nanometer. With the increase of Mn doping concentration, particle size decreased, showing that the size of TiO_2 sample could be suppressed by doping Mn.

Table 1. Average sizes of Mn/TiO_2 nanoparticle

Samples	Ti	Mn/500Ti	Mn/400Ti	Mn/300Ti	Mn/200Ti	Mn/100Ti
Average sizes ($D_{(101)}$)/nm	30.20	25.42	23.86	23.13	20.46	19.06

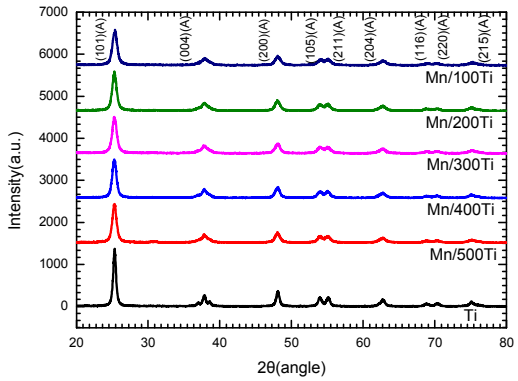

Fig. 2 The XRD spectrum of nanometer TiO_2 of different Mn doping concentration

UV-vis. Figure 3 showed the UV-vis spectral absorption curve of nanometer TiO_2 with different Mn doping concentration. It can be seen that Pure TiO_2 mainly absorbed UV-light with wavelength less than 390nm, the absorption capacity of visible light was relatively poor. This was due to the fact that forbidden band length of anatase type TiO_2 was 3.2eV and visible light energy was not enough to inspire electron hole pairs of photoproduction. The absorption spectrum of TiO_2 samples doped with Mn in visible light region was enlarged, of which the wave band of 390nm-650nm was enlarged the most. This was mainly because Mn^{2+} produced impurity level in forbidden band of TiO_2, reducing the energy electron transition from valence band (VB) to conduction band (CB).

With the increase of Mn doping concentration, the absorption amounts of samples in visible light region were also increased. Absorption spectrums of Mn/400Ti and Mn/300Ti were close to each other due to Mn doping amounts. The content of Mn in samples was quite low and the dispersibility was good, so there was no oxide absorption peak found in this figure.

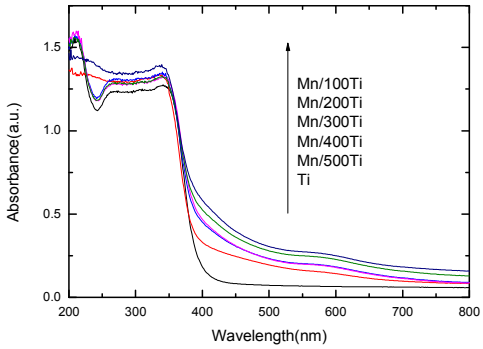

Fig. 3 The UV-vis spectral absorption curve of TiO_2 with different Mn doping concentration

EPR. Nano-powder of TiO_2 doped with Mn is a good diluted magnetic semiconductor, so EPR can be used to analyze the dosage concentration of Mn. In EPR spectrum, Mn has six hyperfine splitting structures, which means that Mn^{2+} replaces Ti^{4+} in crystal lattice, existing on the surface of lattice or forming a cluster of Mn [11]. Figure 4 showed the EPR spectrum of TiO_2 with different Mn doping concentrations. It can be seen that samples of TiO_2 doped with Mn had six hyperfine splitting spectrums, while pure TiO_2 samples had no such phenomenon. Thus, it can be inferred that Mn had successfully blend into the crystal lattice of TiO_2. With the increase of Mn doping concentration, six hyperfine structures became flat due to excess amount of Mn that clustering on crystal surface.

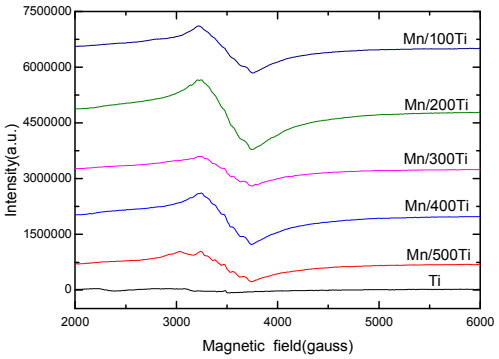

Fig. 4 EPR spectrum of Mn TiO_2

Photodegradation of methylene blue. Figure 5 showed the curve of TiO_2 doped with Mn degrading methylene blue under visible light. Degrading effects of all samples of TiO_2 doped with Mn precede that of pure TiO_2. Compared to pure TiO_2, decolorization rates of samples, including Mn/500Ti, Mn/400Ti, Mn/300Ti, Mn/200Ti and Mn/100Ti increase by 31%, 18%, 15%, 46% and 18% respectively. The decolorization rate of Mn/500Ti is apparently higher than those of Mn/400Ti and Mn/300Ti, because a small amount of Mn can be evenly dispersed in the TiO_2 crystal lattice more easily while a large amount of Mn caused clustering. Decolorization rates of Mn/400Ti and Mn/300Ti were significantly lower than that of Mn/200Ti, which suggested that a moderate amount of Mn improved the visible-light catalytic activity of TiO_2 more easily. This was because Mn could fully fill TiO_2 crystal lattice when its content was increased to a certain extent, making all excited electrons could easily transit to the impurity level provided by Mn. However, the decolorization rate of methylene blue started to decrease when the molar ratio of Mn and Ti reached 1:100, because the accumulation of Mn provided a recombination center for electron hole pairs.

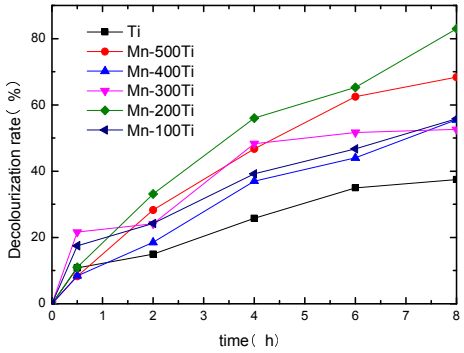

Fig. 5 The curve of TiO_2 doped with Mn degrading methylene blue under visible light

Conclusion

Mn was doped into the crystal lattice of TiO2, and had no influence on TiO2 crystal structure. The growth of particle size of TiO_2 powder was suppressed by doping Mn, and the depressor effect enhanced with the increase of Mn doping concentration. The particle size of TiO_2 ranged from 19nm to 25nm after Mn-doped.

TiO_2 possesses relatively strong absorbency and photocatalytic activity after the doping of Mn. The sample of Mn/200Ti had the best degradation effect of methylene blue under visible light, which is 64% higher than that of unmodified TiO_2.

Acknowledgements

Fund Project: the National Natural Science Foundation of PR China (No. 31270607).

References

[1] A.S. Fujishima and K. Honda: Nature, Vol. 238 (1972) No.7, p.37-38.
[2] J.H. Carey, J. Lawrence and H.M. Tosine: Bull of Environ Contam Toxical, Vol. 16 (1976) No.6, p.697-701.
[3] S.N. Frank and A.J. Bard: Journal of the American Chemical Society, Vol. 99 (1977) No.1, p. 303-304.
[4] M.R. Hoffmann, S.T. Martin, W. Choi and et al: Chemical Reviews, Vol. 95 (1995) No. 1, p.70-96.
[5] S.T. Chen, L. Chen, S. Gao and G.Y. Cao: Power Technology, Vol. 160 (2005) No.3, p.198-202.
[6] P.R. Sambrano, G.F. Nobrega, C.A. Taft and et al: Surface Science, Vol. 580 (2005) No.4, p.71-79.
[7] P. Esparza, T. Hernández, M.E. Borges and et al: Catalysis Today, Vol. 210 (2013) No.7, p. 135-141.
[8] M.Y. Abdelaal and R.M. Mohamed: Journal of Alloys and Compounds, Vol. 576 (2013) No.4, p.201-207.
[9] H. Khan and D. Berk: Journal of Sol-Gel Science and Technology, Vol. 68 (2013) No.2, p.180-192.
[10] R. Chauhan, A. Kumar and R.P. Chaudhary: Spectrochimica Acta Part A Molecular and Biomolecular Spectroscopy, Vol. 98 (2012) No.8, p.256–264.
[11] H.J. Zhou, D.M. Hofmann, A. Hofstaetter and et al: Journal of Applied Physics, Vol. 94 (2003) No.3, p.1965-1968.

Advanced Materials Research Vols. 989-994 (2014) pp 536-539
© (2014) Trans Tech Publications, Switzerland
doi:10.4028/www.scientific.net/AMR.989-994.536

Adsorption and inhibitive properties of 1-phenylaminomethyl -benzimidazole on corrosion of mild steel in Hydrochloric acid

Tiejun Su [1, a, *], Kehua Li [2,b]

[1]Yangtze University College of Technology and Engineering, Jingzhou 434020, China

[2] Yangtze University Colleges of Chemistry and Environmental Engineering, Jingzhou 434023, China

[a]sutj@qq.com

Keywords: Mild steel ;Weight loss; Polarization; Acid inhibition.

Abstract. The corrosion inhibition of mild steel in 5.0 M HCl by 1–phenylaminomethyl-benzimidazo -le(PMB) was studied by gravimetric and potentiodynamic polarization methods. Inhibition efficiency of PMB increased with increase in the concentration of inhibitor and decreased with the increase in temperature. PMB acts as anodic-type inhibitor for mild steel. The adsorption of PMB on mild steel surface obeys the Langmuir adsorption isotherm.

Introduction

Hydrochloric acid are widely used in various industrial processes such as acid pickling and acidic cleaning , the petrochemical processes, oil well acidification,which generally leads to serious metallic corrosion[1,2]. As the most effective and economic method, inhibitors are applied in the acid solution to control the metal dissolution[3]. Benzimidazole and its derivatives have received considerable attention on their inhibition properties for metallic corrosion over the past years [4,5].

In this paper, the corrosion inhibition performance of 1-phenylaminomethyl-benzimidazole (PMB, Fig. 1) for mild steel in hydrochloric acid solutions was investigated by weight loss and electrochemical techniques.

Experimental details

Materials. Mild steel was used for weight-loss and electrochemical tests. For weight loss tests, the rectangular coupons with the size of 4.0×1.3×0.2 cm were used. The acid solutions used in the work were prepared from analytical grade HCl and deionised water. The concentration of inhibitors was ranged from 0.1 to 2.0 mM.

PMB was synthesized according to the procedure described elsewhere[6]. Reaction equation is shown in figure 1.

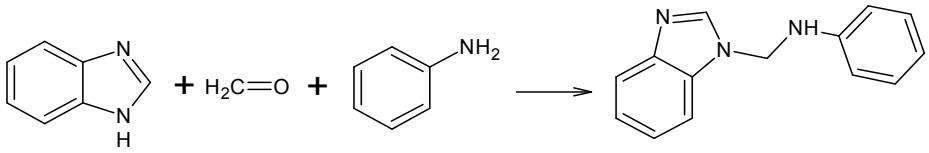

Fig.1. Reaction equation on the inhibitor(PMB)

Weight loss measurements. Weight loss measurements were carried out under total immersion using 250mL capacity beakers containing 200mL test solution without and with different concentrations of inhibitor in 5.0M HCl solutions . The temperature of the solutions was held at 303-333K by a thermostat water bath. After 4 h of immersion in the acid solutions in air without bubbling, the samples were taken out and carefully washed with deionised water and ethanol, and then dried and weighed.

The corrosion rate(v) in g m^{-2} h^{-1} was calculated from the following equation:

$$v = \frac{W_0 - W}{St}$$

where W_0 and W are blank and inhibited mass loss, respectively, S is the area of specimen, and t is the corrosion time.

With the calculated corrosion rate, the inhibition efficiency (η) was calculated as follows:

$$\eta = \frac{v_0 - v}{v_0} \times 100\%$$

where v_0 and v are the corrosion rates of the mild steel coupons in the absence and presence of inhibitor, respectively.

Electrochemical measurements. The classical three-electrode system was used for electrochemical measurements. A platinum electrode and a saturated calomel electrode (SCE) with a Luggin capillary served as counter electrode and reference electrode, respectively. After an hour immersed in the non-de-aerated solutions under unstirred conditions, electrochemical measurements were carried out by CHI660E electrochemical workstation. Potentiodynamic polarization curves were recorded at a sweeping rate of 0.5 mV s^{-1}. The inhibition efficiency, (η), was calculated from the following equation:

$$\eta = \frac{i_{corr} - i_{corr(inh)}}{i_{corr}} \times 100$$

where i_{corr} and $i_{corr(inh)}$ are the corrosion current densities obtained in uninhibited and inhibited solutions, respectively.

Results and discussion

Weight loss measurements. The result of weight loss method was used to evaluate the inhibitive effects of PMB on the corrosion of mild steel. Fig.2 and Fig.3 show the values of corrosion rate and inhibition efficiency in the absence and presence of different PMB concentrations ,respectively.

It is evident from Fig.2 that the corrosion rate of mild steel in 5.0 M HCl increases with temperature but decreases in the presence of PMB. Furthermore, the inhibition efficiency increases with increase in PMB concentration. The inspection of the table further reveals a decreasing trend in inhibition efficiency with increasing experimental temperatures for all the system studied.

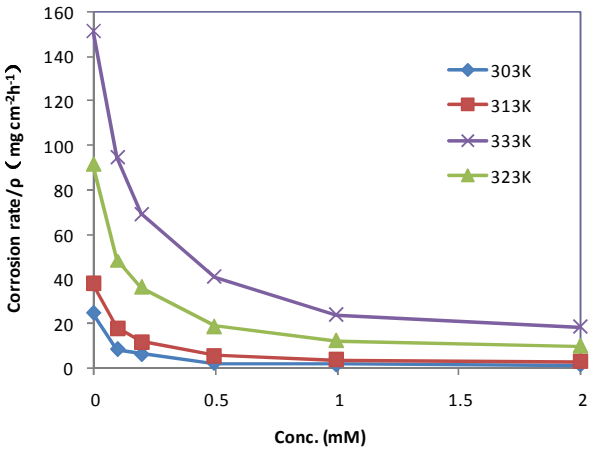

Fig.2 The relationship between corrosion rate and concentration at different temperatures

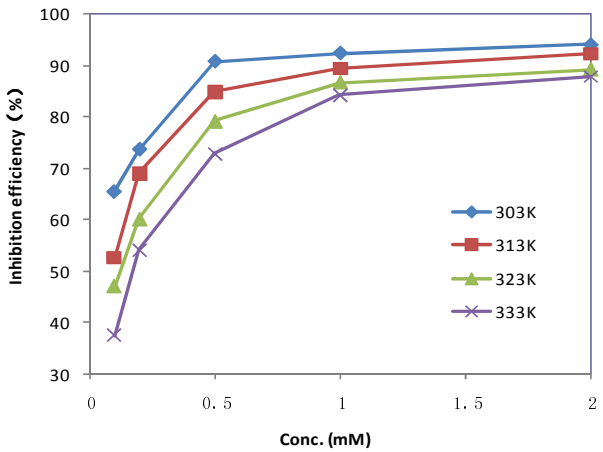

Fig.3 The relationship between inhibition efficiency and concentration at different temperature.

Adsorption and thermodynamic considerations. Since the mechanism of the interaction between inhibitor and the metal surface can explained using adsorption isotherms, a direct relationship between inhibition efficiency (η) and the degree of surface coverage ($\theta = \eta/100$) can be assumed for different concentrations of the inhibitor. Data obtained from weight loss measurements were tested graphically by fitting various adsorption isotherms and kinetic-thermodynamic models including Langmuir, Freundlich, Hill de Boer, Parsons, Frumkin,Temkin, etc. By far, the experimental data for PMB, best fitted the Langmuir isotherm (Fig. 4), with a clarified relationship between C_{inh}/θ *and* C_{inh}. The correlation coefficient R^2 was used to determine the fitting of the

experimental data to this unique isotherm. The isotherm is characterized by the mathematical model given below:

$$\frac{C_{inh}}{\theta} = C_{inh} + \frac{1}{K_{ads}}$$

where K_{ads} denotes the equilibrium constant for the adsorption process.

Fig. 4 shows the plots of C_{inh}/θ versus C_{inh} and the expected linear relationship is obtained for PMB. The strong correlations ($R^2 \geqslant 0.9997$) confirm the validity of this approach. The slopes of the straight lines are 1.0377,1.0438,1.0647,1.0573 at the experimental temperatures(303-333K), suggesting that adsorbed inhibitor molecules form monolayer on the mild steel surface and there is no interaction among the adsorbed inhibitor molecules.

The adsorption parameters derived from the plot are listed in Table 1. The equilibrium constant of adsorption K_{ads} is related to the standard free energy of adsorption ΔG_{ads}, with the following equation:

$$K_{ads} = \frac{1}{55.5}\exp\left(\frac{-\Delta G^{\theta}_{ads}}{RT}\right)$$

The heat of adsorption was evaluated according using the Van't Hoff equation:

$$\ln K_{ads} = -\frac{\Delta H^{\theta}_{ads}}{RT} + \text{constant}$$

where ΔH^{θ}_{ads} and K^{θ}_{ads} are the heat of adsorption and equilibrium constant of adsorption, respectively.

Again another thermodynamic parameter (ΔS^{θ}_{ads}) was calculated by the use of the basic thermodynamic equation:

$$\Delta G_{ads} = \Delta H_{ads} - T\Delta S_{ads}$$

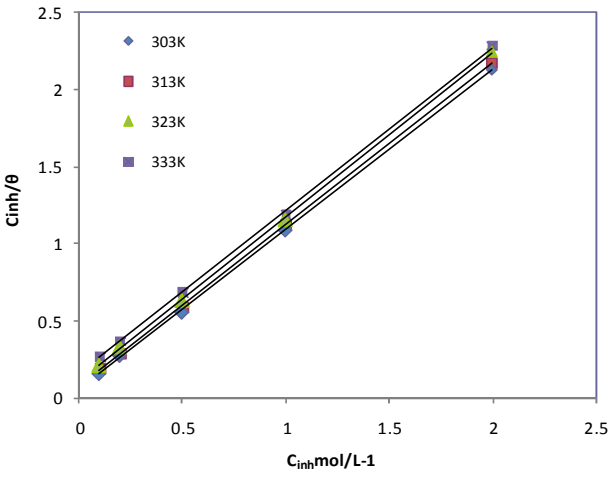

Fig.4 The relationship between C_{inh}/θ and C_{inh} for PMB at different temperatures.

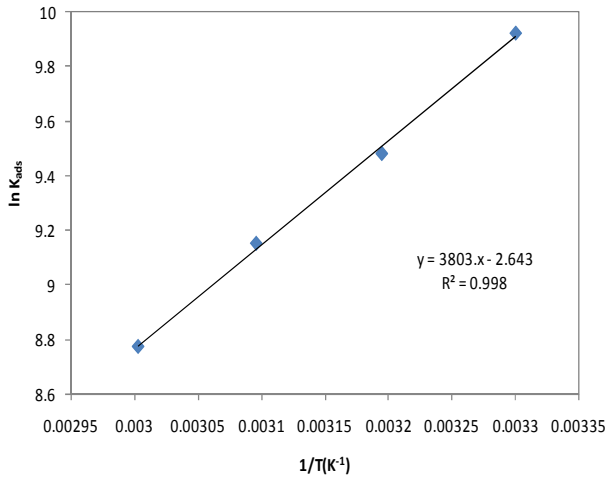

Fig. 5 The relationship between ln Kads and 1/T for PMB

The values of K_{ads} (Table 1) indicate that the binding power of the inhibitor to the metal surface decreases with increasing temperature. Such behavior can be interpreted on the basis that an increase in temperature results in the desorption of some molecules of the PMB from the metal surface. The values of the ΔG_{ads} in all the cases are negative. The negative values signify a spontaneous adsorption of the inhibitor molecules and stability of the adsorption layer. Fig. 5 shows the relationship between $\ln K^{\theta}_{ads}$ and 1/T for PMB and the absorptive heat (ΔH^{θ}_{ads}) was approximated from the slope of the graph under the experimental conditions and presented in Table 1. The negative value of ΔH^{θ}_{ads} (-31.63 kJ mol^{-1}) at all the temperature studies reflect the exothermic nature of the adsorption process of the inhibitor molecules on steel surface. ΔS^{θ}_{ads} values of 11.20 – 11.53 kJ mol^{-1} (Table 1) were obtained by substitution of corresponding values of other thermodynamic values at 303 – 333 K. The positive sign of ΔS^{θ}_{ads} arises from substitutional process, which can be attributed to the increase in the solvent entropy and more positive water desorption entropy. This leads to an increase in disorder due

to the fact that more water molecules can be desorbed from the metal surface by one inhibitor molecule.

Table 1 Thermodynamic parameters of adsorption of PMB on the mild steel surface at different temperatures.

T(K)	K^{θ}_{ads}(M^{-1})	R^2	ΔG^{θ}_{ads}(kJ mol^{-1})	ΔH^{θ}_{ads}(kJ mol^{-1})	ΔS^{θ}_{ads}(kJ mol^{-1})
303	20358.31	0.9997	-35.11	-31.63	11.53
313	13107.88	0.9998	-35.13	-31.63	11.20
323	9434.85	0.9999	-35.37	-31.63	11.59
333	6469.56	0.9997	-35.42	-31.63	11.38

Potentiodynamic polarization measurements. Table 2 shows the electrochemical corrosion parameters such as corrosion potential (E_{corr} versus SCE), corrosion current density (i_{corr}), cathodic and anodic Tafel slopes (ba, bc). From Table 2,when the concentrations of PMB are increased, the values of corrosion current density decrease sharply associated with the increase in the inhibition efficiency, which indicates that the presence of inhibitor lowers the corrosion rate considerably.In adition, the presence of PMB in the acidic solution results in a slight shift of corrosion potential towards more negative in comparison to that in its absence, therefore PMB can be considered basically as an cathodic inhibitor.

Table 2 Potentiodynamic polarization parameters for the corrosion of mild steel in 5.0M HCl without and with different concentrations of PMB at 308K.

Conc.	E_{corr}(mv)	i_{corr}(μA/cm^2)	b_a(mV/dec)	bc(mV/dec)	η/%
blank	-383	713.40	20.24	-11.93	-
0.2mM	-395	160.90	58.56	-32.47	77.4
1.0mM	-388	83.93	89.57	-58.72	88.2
2.0mM	-388	70.30	102.91	-65.59	90.1

Conclusion

Based on the results of investigation, the following conclusions are drawn:

1. PMB acts as a good inhibitor for the corrosion of steel in 5.0M HCl. The inhibition efficiency increases with the increase in inhibitor concentration but decreases with the increase in temperature.
2. The adsorption of PMB obeys the Langmuir adsorption isotherm.
3. Values of standard enthalpy of adsorption and standard free energy of adsorption indicate that the adsorption of PMB on the surface of mild steel involves both physical and chemical processes.
4. PMB acts as cathodic inhibitor by inhibiting the cathodic reactions.

Acknowledgements

Fund Project: the Science Research Creative Funds for Yangtze university college of technology and engineering (13J0603)

References

[1] S.A.A. El-Maksoud, A.S. Fouda, Mater. Chem. Phys. 93 (2005) 84.
[2] H. Keles, M. Keles, I. Dehri, O. Serindag, Mater. Chem. Phys. 112 (2008) 173.
[3]M. Abdallah, Corros. Sci. 45 (2003) 2705.
[4] K.F. Khaled,, Electrochim. Acta 48 (2003) 2493.
[5] X. Wang, H. Yang, F. Wang, Corros. Sci. 53 (2011) 113.
[6]S.Bahadur,A,K.Goel,R.S.Varma,J.Indian Chem.Soc.53, (1976) 1163

Advanced Materials Research Vols. 989-994 (2014) pp 540-543
© (2014) Trans Tech Publications, Switzerland
doi:10.4028/www.scientific.net/AMR.989-994.540

Progress in Preparation of Nano-sized Magnesium Hydroxide from Concentrated Seawater and Brine

Haihong Wu [a], Chunjuan Gao [b], Bijun Luo [c], Dan Wu [d], ShaoYan Lu [e] and Xiping Huang [f*]

Institute of Tianjin Seawater Desalination and Multipurpose Utilization,

State Oceanic Administration, Tianjin 300192, China

[a]email: hongwhh@163.com, [b]email: gcj326@163.com, [c]email: luobj0222@163.com, [d]email: wudan_jay@126.com, [e]email: y4771558@163.com, [f]email: Xipinghuang@163.com

Keywords: Nano-sized magnesium hydroxide; Concentrated seawater; Brine; Preparation

Abstract: The nano-sized magnesium hydroxide is a valuable intermediate for chemical industry materials. This review covers the preparation methods of nano-sized magnesium hydroxide using concentrated seawater or brine as raw material, including alkaline method, calcium method, ammonia method and other new methods. Additionally, the development trend of preparing nano-sized magnesium hydroxide from concentrated seawater or brine was analyzed.

1 Introduction

Nano-sized magnesium hydroxide is one of the important chemical materials and intermediates, which can be used as waste water neutralization agent, flue gas desulfurization agent, food preservation additives, etc [1]. In particular, it appears to have a special flame retardant properties when filled into polymer materials such as rubber, plastic and resin. In the use and disposal process, it is an extremely promising environment-friendly green flame retardant without any harmful substances emissions [2-3].

Magnesium resources is rich in China, in addition to the salt lake brine, brine wells mine, underground brine and other natural liquids mineral resources, seawater desalination, sea salt production, salt lake potassium and other industries also produce thousands of tons seawater and brine a year, which contain rich magnesium ions[4]. The development of magnesium resources in China mainly concentrated in the low value-added products such as magnesium sulfur, magnesium chloride, magnesium fertilizer, or in the form of ore direct export, which caused great waste of resources. Developed nano-sized magnesium hydroxide products with high added value is in the more and more important position [5-6].

2 Technology experimental study

The magnesium hydroxide can be prepared by variours routes. Typically by mixing concentrated seawater or brine with basic compounds such as sodium hydroxide, calcium hydroxide or ammonia. And the nano-sized magnesium hydroxide products can be obtained by controlling the reaction time, temperature, magnesium ion concentration as well as the pH value, etc. There are three kinds of methods commonly used: alkaline method, calcium method and ammonia method.

2.1 Alkaline method

Alkaline method uses sodium hydroxide as precipitation agent, the purity of sodium hydroxide is higher, so it is not easy to introduce impurities and the morphology, particle size distribution and crystal structure of the products are easy to control, which is suitable for the preparation of high purity product [7]. Wu et al. [8] used Zhanjiang coastal waters as raw material, sodium hydroxide as a precipitating agent, by adding glycol in water thermal system, and controlling the reaction

temperature at 170 ℃, reaction time with 4 h, received a good dispersion, crystalline regular, high purity magnesium hydroxide nanoparticles. Ma et al. [9] used concentrated seawater after desalination as raw material, after calcium removal, precipitation, ceramic membrane separation washing, centrifugal filtration and vacuum drying processes, the high purity nano-sized magnesium hydroxide was obtained. The product quality was better than chemical industrial standard (magnesia content is 67.9% , calcium oxide content is 0.2%) and the average diameter was below 100 nm. Ren et al. [10] used Tianjin Hangu potassium salt preparation mother liquor as raw materia to prepare nano-sized magnesium hydroxide. Different hydrothermal treatment methods, including hydrothermal treatment at low temperature, at high temperature, in magnesium hydroxide solution and hydrothermal treatment after seeding as well, were used to treat the magnesium hydroxide powder. The studies showed that the method of hydrothermal treatment after seeding could easily be used into industry production.

2.2 Calcium method

Calcium method uses calcium hydroxide (usually in the style of limestone or dolomite) as precipitation agent. The advantage of calcium method is the low cost of raw material, but the complex process and large energy consumption cannot ignore in calcination and digestion. Moreover the insoluble impurities in raw materials and impurities produced from the reaction are difficult to be removed, which has a bad effect on the product purity[11]. Han et al. [12] taked the natural brine from salt lakes as raw material, lime milk as precipitator, controlled the temperature at 40～90 ℃ and adopted special calcium-removing technique to obtain magnesium hydroxide with the mean particle size about 80 nm. The quality of the product reaches the national standard, the $Mg(OH)_2$ content of the product was more than 98% , the CaO content was less than 0.2%. In addition, Zhao et al.[13] introduced PLC automatic control system for controlling the reaction time, temperature, the magnesium ion initial concentration in the solution, alkaline solution dropping speed as well as the pH value to the nano-sized magnesium hydroxide preparation, and discussed the considerable economic benefits of using concentrated seawater after desalination to prepare nano-sized magnesium hydroxide.

2.3 Ammonia method

Ammonia method uses ammonia as precipitation agent, the magnesium hydroxide crystallization performance used ammonia method is normally better than calcium method and alkaline method. As ammonia is a weak base, the pH is about 10 and the solution has a buffer action after the reaction completion. In addition, the mother liquor can be reused at the same time: the compound fertilizer containing N, P, K, Mg and B can concentrated prepared, in the other way, the ammonia can collected and reused when adding lime milk into[14]. Zheng et al. [15] studied the pH value, magnesium ion concentration, ammonia dropping rate, temperature, the amount of dispersant and other factors on the preparation of nano-sized magnesium hydroxide on the basis of ammonia method, and proposed optimum prepared conditions: the pH of ammonia is 14; the concentration of $MgCl_2$ is 0.5 mol/L; the rate of adding ammonia is 2.0 ml /min; the reaction temperature is 50℃-60℃ and the reaction time is 60 min. It was also found, along with ammonia added in the system, the pH value was gradually increased, first appeared translucent gel precipitated, and finally formed a stable gel precipitation, the longer the gel suspension time, the slower sedimentation rate is. When the solvent containing ethanol, the formation of precipitation sedimentation is fast, the right amount of alcohol can inhibit the precipitation cementation and crystal growth in one direction, which can also overcome the reunion of powders. Wang et al. [16] used Jilantai Salt Lake Brine as magnesium source, took the optimum conditions to prepare a polygonal sheet nano-sized magnesium hydroxide powder, the product was with good dispersion and the average particle size is 89.5 nm. The preparation process is divided into four steps：the magnesium cement preparation, acid leaching of magnesium, acid extract purification and powder preparation. Studies show that the most suitable acid infusion pH is 7.0-7.5, while small

amount of ethanol can promote the precipitation of calcium sulfate, at the same time facilitate magnesium hydroxide dispersion, and PEG200 dispersant can effectively prevent agglomeration of the magnesium hydroxide particles.

2.4 Other methods

Using the traditional methods of preparing nano-sized magnesium hydroxide, the main question is difficult to remove impurity ions, and the product size distribution was wide and the dispersion was poor. Many scholars try to adopt new method to prepare nano-sized magnesium hydroxide. Feng et al. [17] used a strong base anion resin in the experiment, prepared nano-sized magnesium hydroxide by ion exchange method. The product is with hexagonal sheet structure and with good dispersion, the particles average size is about 100 nm. The impurity ions can be replacement to the resin using this method, successfully solved the impurity ion elution difficult problem. Lu et al. [18] used the "sulfur hydride - hydrothermal method" to prepare nano-sized magnesium hydroxide, and the product was with larger particle size and better filtration performance. But its irregular morphology and significantly aggregation can not be ignored, and the reaction process was with poisonous gas H_2S released, when futher reclaimed the tail gas, the cost corresponding increased together. According to this method, Jin et al. [19] studied the effects of particle morphology on product properties. The result was that the faster the heating rate and the lower the $MgCl_2$ initial concentration, the smaller magnesium hydroxide particles formed, the easier it is hydrothermal modification, which is good for forming rule morphology and good dispersion nano-sized magnesium hydroxide.

3 Development trend

The concentrated seawater and brine resources is rich in China, only the Saline Lake brine magnesium salt reserves amounted to 48.16 tons. But this resources utilization rate is not high. Extracting magnesium salt from concentrated seawater or brine, especially those with high value-added nano-sized magnesium hydroxide is of great significance. According to the gap with developed countries in the product quality and also manufacturing scale, to strengthen the production and application study of nano-sized magnesium hydroxide is imminent:

1. To improve nano-sized magnesium hydroxide morphology control, especially in special morphology and particle size distribution. High quality nano-sized magnesium hydroxide products is significative to improve the international competitiveness.
2. To suppress aggregation of nano-sized magnesium hydroxide in the production process. To speed up the study of surface modification, recognizing modification mechanism, constantly trying new modification methods, especially to develop the nano-sized magnesium hydroxide exclusive modifier, is the focus of nano-sized magnesium hydroxide material in application.
3. To make the full use of concentrated seawater or brine to prepare nano-sized magnesium hydroxide . The low cost and high concentration make it a good raw material, which could reduce the production cost, meanwhile, the reuse of concentrated seawater and brine is meaningful for the environment.

Acknowledgment

This work was supported by the public science and technology research funds projects of ocean (201405008), The Central Nonprofit Research Institutes Special Funds Project (K- JBYWF- 2013-T3).

References

[1] C. Henrista, J.P. Mathieu and C. Vogels, et al., Morphological study of magnesium hydroxide nanoparticles precipitated in dilute aqueous solution, Journal of Crystal Growth. 249 (2003) 321-330.
[2] J. Lv, L. Qiu and B. Qu, Controlled synthesis of magnesium hydroxide nanoparticles with different morphological structures and related properties in flame retardant ethylene-vinyl acetate blends, Nanotechnology. 15 (2004) 1576-1581.
[3] M. Sain, S.H. Park and F. Suhara, Flame retardant and mechanical properties of natural fibre-PP composites containing magnesium hydroxide, Polymer Degradation and Stability. 83 (2004) 363-367.
[4] Z.L. Dong, Y.S. Zhang and X.P. Huang, et al., Progress in Preparation of Magnesium Hydroxide Powder from Concentrated Seawater and Brine, Chemical Industry and Engineering. 28 (2011) 71-75.
[5] X.P. Huang, L.C. Wang and Y.Q. Wang et al., Development and Utilization of Magnesium Series Products Prepared by Seawater and Brine, Chemical Industry and Engineering. 27 (2010) 530-536.
[6] X.P. Huang, Q. Zang and S.Y. Guo, et al., The Present State and Future Outlook of the Exploitation & Utilization of Magnesium Resource in Sea Water and Brine about Our Country, Journal of Salt and Chemical Industry. 33 (2004) 1-6.
[7] S.P. Liu, W.X. Zhang and M. Wei et al., Progress in Research and Surface Modification of Nano-sized Magnesium Hydroxide, Hebei Chemical Industry. 33 (2010) 3-6.
[8] J.S. Wu, J.Y. Guo and J.E. Feng, et al., Characterization and Preparation of Nanometer Magnesium Hydroxide with Seawater in Zhanjiang, Jounral of Salt and Chemical Industry. 37 (2008) 35-37.
[9] J.H. Ma, J. Zhou and B.H. Sun et al., Technology of Manufacturing Nano-Sized Magnesium Hydroxide from Concentrated Seawater After Desalination, Chemical Industry and Engineering. 24 (2007) 428-432.
[10] P.F. Ren, J.M. Chen and Y.H. Song, et al., Study on the Preparation of Ultra fine Magnesium Hydroxide Flame Retardant in Different Hydrothermal Treatment Methods, Chemical Industry and Engineering Progress, 24 (2005) 186-189.
[11] C.J. Gao, Y.S. Zhang and X.P. Huang, et al., Study on Producing Magnesium Hydroxide by Concentrated Seawater-calcium Method, Journal of Salt and Chemical Industry. 40 (2011) 5-7.
[12] H.B. Han, H. Zhao and Y.J. Liu et al., Study on new preparation technology of nano-sized magnesium hydroxide by lime - brine method, Inorganic Chemicals Industry. 40 (2008) 31-33.
[13] B.C. Zhao, H.M. Shi and S.R. Wang, et al., Discussion on Preparation of Nanometer Magnesium Hydroxide with Concentrated Seawater from Seawater Desalination, Information of China Construction. 3 (2011) 55-62.
[14] L. Liu, Research of preparation of magnesium hydroxide flame retardants from brine, Chemial Technology Market. 33 (2010) 14-16.
[15] J. Zheng, K.W. Chen and G.X. Sun et al., Preparation of NanometerMagnesium Hydroxide with Brine and Ammonia, Chemical Industry and Engineering. 27 (2010) 34-37.
[16] S.Q. Wang, C.H. Li and J.R. Liu et al., Preparation for High-Purity and Uhrafine Magnesium Hydroxide with Salt Lake Brine, Jounral of Salt and Chemical Industry. 37 (2008) 1-5.
[17] C. Feng, M. Yang amd Y.S. Li, et al., Preparation of high purity and ultrafine magnesium hydroxide by Ion exchange resin method, Nanoscience & Nanotechnology. 6 (2009) 26-29.
[18] Y.R. Liu, Prepare hydrogen sulfide and magnesium hydroxide used magnesium and alcali sulphide concentration brine as raw materia. C.N. Patent 1145575. (1997).
[19] Y.C. Jin, L. Xiang and Y. Jin, Synthesis of $Mg(OH)_2$ Particles via Decomposition of Hydrosulfide Compound and Hydrothermal Treatment, Sea-Lake Salt and Chemical Industry. 32 (2002) l-3.

Advanced Materials Research Vols. 989-994 (2014) pp 544-547
© (2014) Trans Tech Publications, Switzerland
doi:10.4028/www.scientific.net/AMR.989-994.544

The Network Prediction of Hot Temperature Flow Stress and Dynamic Recrystallization of AZ61 Alloy

Quan Li[1,a], Wenjun Liu[1,2], Renju Cheng[1], Cheng Li[1],Shan Jiang[1], Suqin Luo[1],Xianquan Jiang[1], Fusheng Pan[1,2]

[1]Chongqing Academy of Science and Technology, Chongqing 401123, China

[2]College of Materials Science & Engineering, Chongqing University, Chongqing 400030, China

[a]156723583@qq.com

Keywords: Magnesium alloy, Flow stress, Network, Prediction

Abstract : In this paper, the Back-Propagation neural network (BP network) and the establishment of the AZ61 magnesium alloy high temperature constitutive model and test data obtained for training the neural network, after training the neural network to become a knowledge-based constitutive model formed AZ61 magnesium alloy flow stress and dynamic recrystallization of the neural network model tested by the neural network model with traditional regression methods predict contrast, results showed that the higher the accuracy of the neural network model for dealing with a large number of test data to establish the constitutive relations of materials with high stress and promotion of value.

1 **Introduction**

Magnesium alloy for its lightweight characteristics, in recent years in the automotive, aerospace, electronics industry gained rapid development, showing broad application prospects. Because the crystal structure of the magnesium alloy is hexagonal, plastic forming ability, the development and application of wrought magnesium alloys in order to keep its hot forming process, in order to improve the yield and product performance, you need to master the system wrought magnesium alloys during hot deformation the flow behavior and organizational evolution. Physical modeling and numerical simulation is now usually magnesium alloy used SPSS regression analysis, the model created by the accuracy of the method is not high, the error is larger, the need to search for more accurate mathematical model of high-temperature flow stress. In this paper, Back-Propagation neural network (referred to as the BP network) to establish AZ61 magnesium alloy high temperature constitutive model, using experimental data obtained for neural network training, after training the neural network will become a knowledge-based relationship model through the neural network model to predict the test compared with the traditional SPSS regression analysis to verify its feasibility.

2 Test

From the diameter of 200 mm semi-continuous casting made of magnesium alloy taken the same position as the sample size number Φ10mm × 15 mm, the nominal chemical composition of the material is: 6% Al, 1% Zn, 0.3% Mn, the balance being Mg and trace impurities. After 400 ℃ × 12 h homogenization treatment, performed on Gleebl-1500D thermal simulation test machine direction isothermal heat constant speed uniaxial compression tests, before deformation heating heating rate of 2 ℃ / s, thermal insulation 2min. Compression technology for the 16 combinations of temperature and strain rate deformation: the deformation temperature was 300 ℃, 350 ℃, 400 ℃ and 450 ℃, strain rates were 0.01s-1, 0.1s-1, 1s-1 and 5s-1.

3 neural network model

3.1 Sample Data Organization

Magnesium alloys in high temperature deformation, deformation strain hardening is balanced by dynamic softening process, so we had a large degree of deformation in the flow stress remained stable phenomenon. Due to the impact of dynamic softening process, the relationship between the

flow stress and dynamic material recrystallized grain size and deformation temperature, strain rate and extent of deformation of a complex nonlinear. In this paper, the artificial neural network approach to build its high-temperature flow stress and dynamic recrystallization mathematical model size, the deformation temperature and strain rate is set to enter the amount of the network, the flow stress and recrystallized grain size to the network output amount, before training network, the first group of 16 test samples obtained data were normalized so that all data between the property of a 0-1, and the network output value by anti-normalization after that obtain the original data of physical space. Normalization method derived from Formula 1[1]:

$$d = \frac{d - d_{\min}}{d_{\max} - d_{\min}} \quad (1)$$

In the formula, $d_{\min}$ and $d_{\max}$ are respectively the minimum and maximum values for the sample data.

3.2 neural network structure determination

Number of neurons in the hidden layer of BP network training accuracy and convergence speed of neural network training process has a great impact, you need to be determined by trial and error. As used herein, the neural network back-propagation network (BP network), the network consists of three layers: an input layer, middle, layer (hidden layer) and output layer. The input layer has two nodes, respectively, deformation temperature and strain rate, the output layer also has two nodes, representing the recrystallized grain size and flow stress.

Literature[2] indicates that, the geometric mean can be used to select the processing unit the number of rules to the intermediate layer. For the three networks, where the number of nerve cells between the hidden layer is selected by the following formula:

$$h = \sqrt{m \cdot n} + \alpha \quad (2)$$

$$h \geq \frac{N \cdot m}{n + m} \quad (3)$$

In the formula, h is the number of units in the hidden layer, m is the number of units of the input layer, n is the output layer unit, N is the learning capacity of the sample, α is a constant. Among α may be equal to 0[3], that constant can take between 0-10[4].

From the middle layer of the test cell count less paper h_0 = 6, select the appropriate criteria to detect and evaluate training, network; If the network reaches a predetermined performance requirements, you can determine the number of units in the middle layer, an intermediate layer unit otherwise increase number is $h_{i+1} = h_i + 1$,Then use the same criteria to detect and evaluate training , network. In this paper, the middle layer to find the optimal number of cells in the process, using BP network training algorithm ordained decline, according to the literature shows that α=0.6~0.95，η=0.45~0.90[5-6]，Getting the optimal number of units after the middle layer, Changing the learning rate of the system X and Momentum coefficient Y to determine their optimal values. $\eta = 0.45, 0.50, 0.55, 0.60,$ and $\alpha = 0.60, 0.65, 0.70, 0.75, 0.80, 0.85, 0.90, 0.95,$ Training, examine and evaluate network, In order to get the best learning rate η and momentum coefficient α.

4 neural network test results

In the middle layer of cells to find the optimal number of training, when the intermediate layer unit is 7 or more, the network oscillations in the initial stages of training, and with the increase in the number of units of the oscillation and intensified, but the number of units in the middle layer of when 7-9, the initial training as training progresses oscillations gradually stabilize and eventually converge to a small error. After the increase in the number of cells in the middle layer, network with fewer steps training can converge to a certain error range. As the network prediction performance

than training time, mainly on the middle layer after several different units, predict the performance of the network to determine the optimal number of cells in the middle layer. According to the results of the training, the number of units when the intermediate layer 11, the network showed a more excellent performance, so the establishment of BP neural network model 2-11-2. The algorithm selection of additional momentum method, the key parameters back-propagation algorithm is a constant learning rate and momentum coefficient. Under the pilot program parameters considered, network performance can get better training, network training error that little difference. Compared to predict the effect of training and its effect in terms of a bit weak, but overall, the results are good. And when momentum coefficient increases when training oscillations occur in the initial stages and has exacerbated the phenomenon, but in training to 100 steps up 200 steps, the network will be stabilized. Occasionally, the network is slow decrease, but in most cases, the network decreased rapidly. Figure 1 is the flow stress and the prediction error image training error. Figure 2 is the recrystallized grain size and the prediction error image training error.

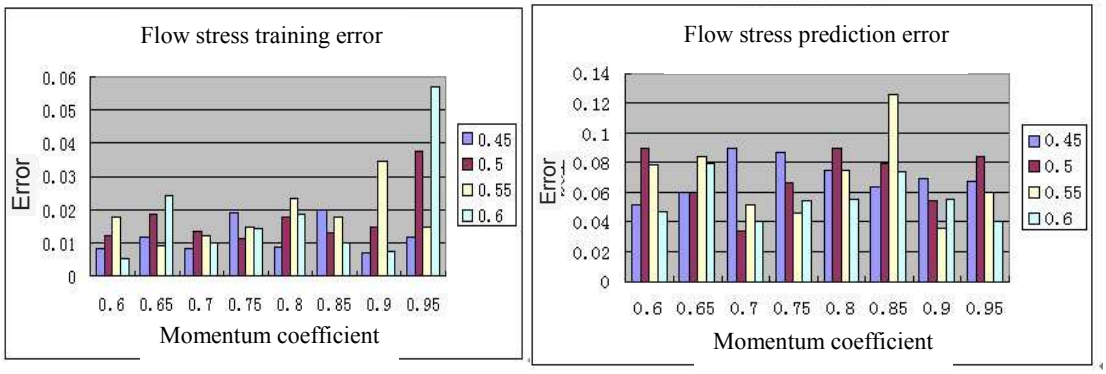

Fig1 The flow stress of the training error and prediction error map

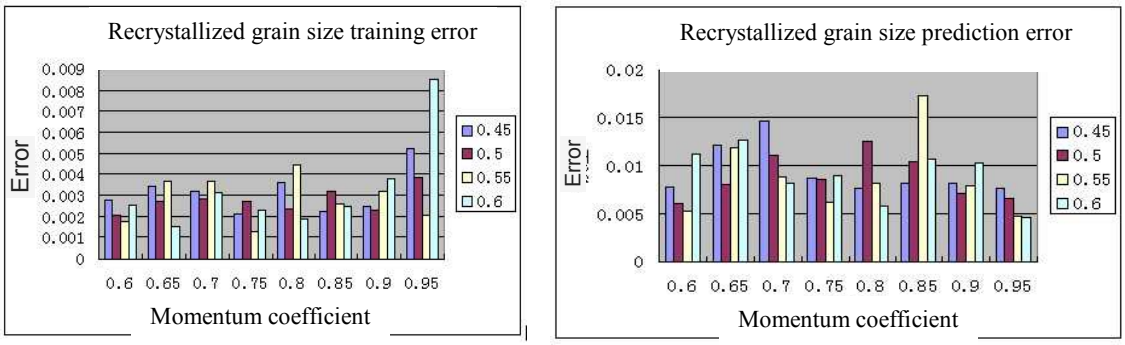

Fig2 Recrystallized grain size of the training error and prediction error in Figure

Comprehensive analysis of the above data can be obtained: flow stress optimal neural network model is the momentum coefficient of 0.7, the learning rate of 0.5 model. You can get the training error is less than 1.5%, forecast error is less than 3.5%; recrystallized grain size of the optimal neural network model is the momentum coefficient of 0.95, learning rate of 0.55 model. You can get the training error is less than 0.2%, forecast error is less than 0.5%.

5 Conclusions

In this paper, Back-Propagation neural network (referred to as the BP network) to establish a high-temperature constitutive model AZ61 magnesium alloy, and use the data obtained in the test for neural network training, after training the neural network to become a knowledge-based constitutive relational model, the formation of AZ61 magnesium alloy flow stress and dynamic recrystallization neural network model, compared with the traditional test to predict regression method by which the neural network model, the results show that the neural network model can accurately predict the AZ61 magnesium alloy Flow stress and dynamic recrystallization grain size changes with deformation temperature and strain rate. The predicted and measured results agree

higher accuracy than the traditional regression methods. Showed its ability to partially replace the test with. This not only greatly reduces the required tests to characterize the flow behavior of the material, but also to avoid the experience of many of the constitutive model constants to determine the problem. The model for processing large amounts of test data to establish the material constitutive relationship with high stress and promotional value.

Acknowledgement

This work is supported by the Chongqing High-level Overseas Talent Base Construction Projects; International Science and Technology Cooperation Project (2013DFA71070); Chongqing International Science and Technology Cooperation Base Project (cstc2011gjhz50001)

References

[1] NIU JI-tai, SUM LEI-Jian, LI HAI-tao. research micro-alloy hot-rolled austenitic grain size model based on artificial neural networks, Materials Science and Technology, 1997,7 (1) 12-16.

[2] XIA SHAN-mu, Li DA-yong. the mechanical properties of cast iron for fast prediction of artificial neural networks, Applied Sciences, 2002,20 (3) :309-312.

[3] DAI QI-Xun, DAI XI-Min. Journal of Neural Network in austenitic steel design Steel Research, 1997,9 (6) :37-40.

[4] LIU XUE-feng, WANG LING-yun, artificial neural network model aluminum-lithium alloyhigh temperature deformation flow stress of Chongqing University (Natural Science Edition), 2001,24 (2).

[5] P.D.Hodgson, D.Mcfarlane,R.K.Gibbs. The Mathematical Modeling of Hot Rolling. Journal of Japan society for Technology of Plasticity,1987,(28):195－197.

[6] Oh.Si, Wu WT, Tang J P, et al., Capabilities and Applications of FEM Code Deform . Journal of Materials Processing Technology, 1991,27:25－42.

Advanced Materials Research Vols. 989-994 (2014) pp 548-551
© (2014) Trans Tech Publications, Switzerland
doi:10.4028/www.scientific.net/AMR.989-994.548

The Finite Element Simulation of Thermal Deformation and Microstructure Evolution Forecast of AZ61 Alloy

Quan Li[1,a], Wenjun Liu[1,2], Renju Cheng[1], Cheng Li[1],Shan Jiang[1], Suqin Luo[1],Xianquan Jiang[1], Fusheng Pan[1,2]

[1]Chongqing Academy of Science and Technology, Chongqing 401123, China
[2]College of Materials Science & Engineering, Chongqing University, Chongqing 400030, China

[a]156723583@qq.com

Keywords: Magnesium alloy, Finite element, Simulation, Forecast

Abstract: In this paper, rigid-plastic finite element simulation software Marc / Auto-forge reflect compression AZ61B magnesium alloy case. Simulation results show that the stress, strain and temperature distribution within the sample is uneven, uneven distribution affect the organization, and with the changes in the deformation process and calculation results with the experimental data exactly. The finite element method can be used in the actual production forecast after tissue deformation components, optimization of process parameters to control the quality of the finished piece.

1 Introduction

Metal temperature of various parts of the work piece and tooling, different stress during hot deformation, and microstructural evolution during deformation is closely associated with these factors. Based on the basic theory of rigid-plastic finite element, finite element simulation software Marc / Auto-forge, AZ61 magnesium alloy thermal compression process further simulation and analysis, analysis of thermal deformation of AZ61 magnesium alloy, and the evolution of the microstructure results were forecasts.

2 Sample finite element model

Cylindrical sample is Φ15 × 20mm, and to reduce the computation time, the symmetry of the sample, take half as analog objects. Take a four-node quadrilateral element model of division 48 units and 65 nodes. Analysis method using an updated Lagrange method described thermal coupling large deformation rigid-plastic finite element method, the use of the material yield criterion Von Mises criterion.

Boundary conditions:

(1) boundary conditions: all nodes cylindrical symmetry axis of the sample in the x-direction displacement is zero, ux = 0.

(2) friction conditions: between deformation tools and rolling contact surfaces follow Coulomb friction coefficient between the die and the sample taken 0.2.

(3) heat transfer boundary conditions[1]: the presence of the free surface of the sample and the cycle of convective and radiative heat transfer environment. There is no contact between the sample heat when in contact with the mold. The first two boundary conditions referred to in the third boundary condition in heat transfer. Can be written as a unified formula:

$$q = -\lambda\left[\frac{\partial t}{\partial n}\right] = \alpha\left(t - t_{\infty}\right)$$

In the formula, t is the surface temperature, t_{∞} is the ambient temperature, α is the heat transfer coefficient.

Convective heat transfer coefficient environment take 0.17KW/m2 • K according to test conditions. And radiation heat transfer coefficient between the environment in accordance with the laws of the radiation is converted into other small radiation heat transfer coefficient can be expressed by the following formula based on radiation law[2-3].

$$h_r = \sigma\varepsilon\left(t + t_\infty\right)\left(t^2 + t_\infty{}^2\right)$$

In the formula, σ is the Boltzmann constant, σ = 5.67 × 10-11KW/m2K4, ε thermal emissivity material, 0.15[4].

Thermal contact between the sample and mold simplified contact heat conduction problems with the contact between the two solid thermal conductivity, paper = 20 KW/m2 • K. Ambient temperature and mold temperature, and were taken 20 ℃ 350 ℃. The thermal deformation of metal deformation, thermal power conversion factor of 0.9. Further, the sample contacting surface and the mold will produce frictional heat, the heat is distributed evenly to the parts of the specimen and the mold[5-6].

3 Simulation results and analysis

3.1 Equivalent strain distribution

Figure 1 is a sample of AZ61 magnesium alloy at different deformation temperature equivalent strain distribution. Be seen, the equivalent strain of the sample is very uneven in the top of the sample, due to friction, the minimum strain, and the sample portion and the corner portion of a sample core greatly deformed. Other parts of the deformation distribution be between the maximum and minimum by the Ministry to the top of the heart, the center to the edge showed a decreasing trend. Can also be seen from Figure 1, as the temperature increases, the deformation easily throughout the strain increases at a lower temperature (300 ℃ to 400 ℃) increase in the amount of more instructions corresponding to the temperature variables influenced; but at around 450 ℃, 400 ℃ to reduce the amount of increase, indicating less affected by temperature corresponding variables.

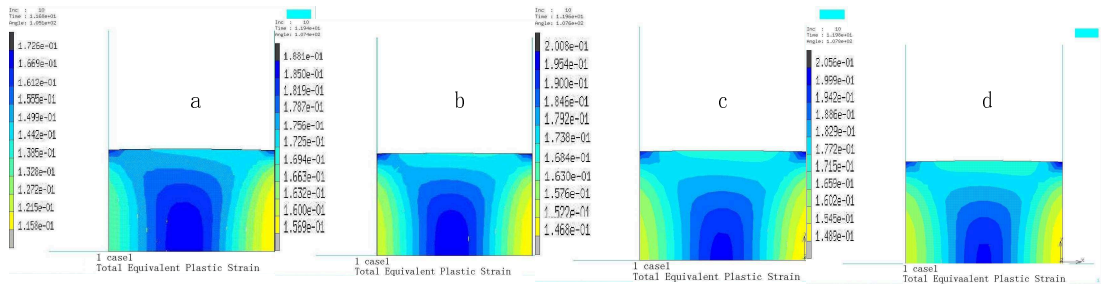

Fig.1 Equivalent strain distribution during the deformation step 10
(a: deformation temperature 300 ℃, strain rate of 0.01s^{-1}; b: deformation temperature 350 ℃, strain rate of 0.01s^{-1}; c: deformation temperature 400 ℃, strain rate 0.01s^{-1}; d: deformation temperature 450 ℃, strain rate 0.01s^{-1})

3.2 Equivalent stress distribution

Figure 2 is the effective stress variation with temperature distribution seen from the figure, the force effect of the sample and a very uniform, the top of the sample, due to friction, the minimum strain, and the sample and the sample angle core section deformed great. Other parts of the distribution between the maximum and minimum distortion between the central portion by the top edge portion to the central portion showed a decreasing trend with increasing temperature, easily deformed, the entire stress increases, but the increase in the amount of not more than , indicating little effect of temperature on the strain.

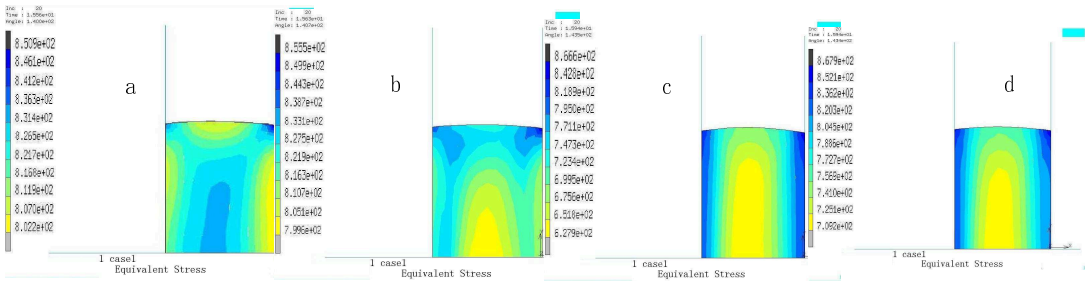

Fig.2 Mises stress distribution of deformation at Step 20

(a: deformation temperature 300 ℃, strain rate of 0.01s^{-1}; b: deformation temperature 350 ℃, strain rate of 0.01s^{-1}; c: deformation temperature 400 ℃, strain rate 0.01s^{-1}; d: deformation temperature 450 ℃, strain rate 0.01s^{-1})

3.3 Temperature distribution

Figure 3 shows the temperature distribution at different strain rates throughout the sample. Since the thermal conductivity of the sample surface exists between the presence of convection and radiation heat, top of the sample and mold, so the temperature decreases from the inside and outside. At low strain rate, prolonged heat and thermal conductivity, high temperature deformation rate when compared to low. Further, the deformation rate increases, an increase in the plastic work, the conversion of heat also increased, thereby increasing the temperature of the sample. Deformation rate of 0.01s-1, the internal temperature of the sample is less than the deformation temperature, when the strain rate 0.1s-1, the temperature of the sample over the central portion deformation temperature. In another modification of the same condition, the amount of deformation increases, the time required to deform at low extension, thus lower the sample temperature.

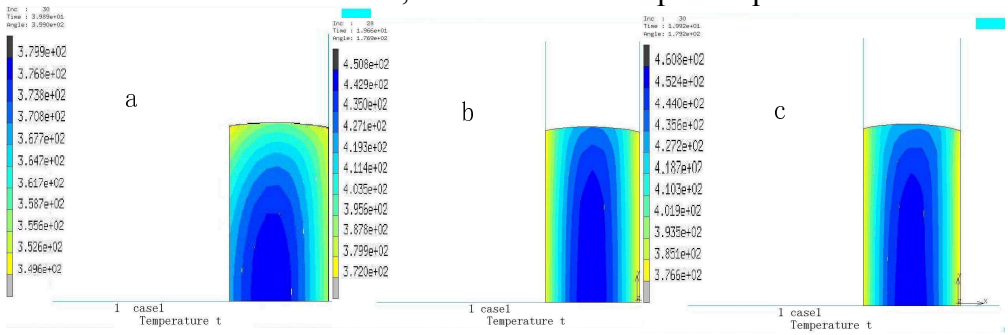

Fig.3 Deformation temperature distribution at step 30

(a: deformation temperature 350 ℃, strain rate of 0.01s^{-1}; b: deformation temperature 350 ℃, strain rate of 0.1s^{-1}; c: deformation temperature 350 ℃, strain rate 1s^{-1})

3.4 Tissue distribution of dynamic recrystallization

Figure 4 is a dynamic recrystallization grain size distribution, in each case, the uneven distribution of the grain sample. Heart large specimen deformed grains relatively small; while reducing the amount of deformation from the inside out, recrystallized grain size also increases. Deformation temperature, the grain size becomes large accordingly, and the strain rate increases, the grain size becomes smaller.

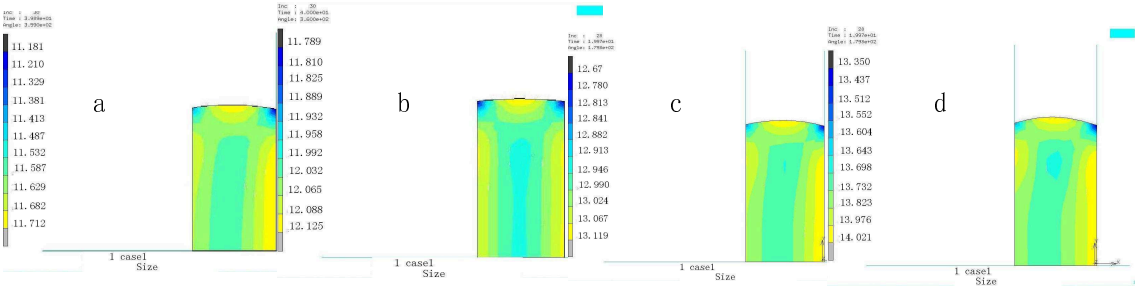

Fig.4 Grain size distribution at Step 20

(a: deformation temperature 300 ℃, strain rate of 0.01s^{-1}; b: deformation temperature 350 ℃, strain rate of 0.01s^{-1}; c: deformation temperature 400 ℃, strain rate 0.01s^{-1}; d: deformation temperature 450 ℃, strain rate 0.01s^{-1})

4 Conclusions

In this paper, the rigid-plastic finite element simulation software Marc / Auto-forge consider the coupling of heat transfer and deformation, and can reflect more fully the compression deformation of AZ61B magnesium alloy. Simulation results show that the stress, strain, temperature inside the uneven distribution of the sample, with a corresponding impact on tissue distribution is not uniform and varies with the deformation process, comparing the calculation results with the experimental data prove the finite element method used herein have higher accuracy in reference to the actual production can predict the deformation member, optimize the process parameters to control the quality of the finished piece.

Acknowledgement

This work is supported by the Chongqing High-level Overseas Talent Base Construction Projects; International Science and Technology Cooperation Project (2013DFA71070); Chongqing International Science and Technology Cooperation Base Project (cstc2011gjhz50001)

References

[1] S.F.Wong, P.D.Hodgson, C.J.Chong, P.F.Thomson. Physical Modeling with Application to Metal Working, especially to Hot Rolling. J.Mater.Process.technol.1996,62:260－274.

[2] P.R.Ding, D.Y.Ju, S.Imatani, T.Inoue. Numerical Simulation of Coupled Thermo－Mechanical Behavior of a Cylinder Billet During Hot-forging Process. Journal of Shanghai Jiaotong University. 2000, 5(1):263－269.

[3] NIU JI-tai, SUM LEI-Jian, LI HAI-tao. research micro-alloy hot-rolled austenitic grain size model based on artificial neural networks, Materials Science and Technology, 1997,7 (1) 12-16.

[4] XIA SHAN-mu, Li DA-yong. the mechanical properties of cast iron for fast prediction of artificial neural networks, Applied Sciences, 2002,20 (3) :309-312.

[5] DAI QI-Xun, DAI XI-Min. Journal of Neural Network in austenitic steel design Steel Research, 1997,9 (6) :37-40.

[6] LIU XUE-feng, WANG LING-yun, artificial neural network model aluminum-lithium alloy high temperature deformation flow stress of Chongqing University (Natural Science Edition), 2001,24 (2).

Advanced Materials Research Vols. 989-994 (2014) pp 552-555
© (2014) Trans Tech Publications, Switzerland
doi:10.4028/www.scientific.net/AMR.989-994.552

Research progress of tungsten nanorods and nanoplatelets

Ai-min Jiang[1, a], Xian-quan Jiang[2, b], Jin Yang[3, c*],Rong-jie Yang[4, d],Rong-Yu[5, e]

[1, 2,3,4,5]Chongqing Academy of Science &Technology, China

[a, c,d,e]44290159@qq.com,[b]jsq89@sina.com

Keywords: tungsten carbide nanorods; synthesis method; growth mechanism; application

Abstract. Because of the characteristics of both one dimensional nanostructure and excellent physical and chemical properties, the kinds of novel nanomaterials -tungsten carbide nanowires, have important academic significance and practical meaning. The research development of one-dimensional nano- structured tungsten carbide is reviewed. The production methods of one-dimensional nanostructured tungsten carbide, such as nanotubes, nanorods, nanowires and nanoneedles by thermal decomposition technique, vapour deposition technique, magnetron sputtering technique, Eruptive heating technique and template technique respectively are systematically introduced. This paper summarizes the growth mechanisms and the problems involved in the existing synthesis methods. The research tendency is also forecasted.

1. Introduction

Transition metal carbides in general, tungsten carbide in particular, find potential applications due to their special properties, such as high melting point, superior hardness, low friction coefficient, high oxidation resistance, and good electrical conductivity[1-2].WC nanonneedle was shown to have platinum-like behaviour for the chemisorption of hydrogen and oxygen, its applicability as an alternative electrocatalyst of Pt in1970s, the study on production and application of WC nanoneedle has already attracted extensive attention. The early studies showed that this combination of an early transition metal with carbon yielded materials with attractive catalytic activity, stability, selectivity and resistance to poisoning[3-6]. WC nanoneedle has excellent electron emission performance as field emission [7], at the same time it has a very high resolution and good oxidation resistance [8], so tungsten carbide probe was widely used for scanning tunneling microscope (STM) probe and field emission electric device. In addition, tungsten carbide nanowires can be used to intensifying cemented carbide, making PCB carbide micro-drill [9]. The rapid intrinsic growth characteristic of nanometer WC grain during sintering process lead nano-grained cemented carbides with excellent mechanical performances is not acquired [10]. Because of its small size, one-dimensional nano-structured has good dimensional stability of thermodynamics[11]. Preparation of nano-materials is a key issue to control their pore to get a good compactness of nano-particles; it could be settled by adding some nanowires.

In recent years, Several methods are used in preparation of tungsten nanorods and nanoplatelets, which include thermal decomposition method[12,13], vapour deposition[14], magnetron sputtering[7,15], Eruptive heating technique[16] and template[17,18].Therefore, it is of both academic and realistic value to study the preparation methods of one-dimensional nanostructures tungsten carbide and its growth mechanism.

2. Synthesis ofone-dimensional nanostructures tungsten carbide

As one of the perfect one-dimensional nano-materials, tungsten carbide has high strength performance with high surface area and energy, which shows broad applications and is worthy of development.

2.1. Thermal decomposition

Thermal decomposition generally proceeds as a two-step process. First, precursor is formed in a surfactant liquid. The precursor is then resolved at high temperatures in argon atmosphere to obtain one-dimensional nanostructures materials. This method is without template and the simple way.

Aangaraju[12] have reported thermal pyrolysis of the composite hybrid to produce Tungsten carbide nanorods and nanoplatelets. The composite hybrid which is $[C_{21.95}H_{41.19}N_{1.33}]_3PW_{12}O_{40}$was synthesized by dissolving hexadecyltrimethylammounium bromide (CTAB) in distilled water and this solution was added slowly to the 12phosphotungstic acid $(H_3PW_{12}O_{40})_{11}$.And then, pyrolyzed the hybrid in a horizontal tube reactor at the 1000℃.The product was a mixture of WC naorods and nanoplatelets. The diameters of the WC rods are 30-50 nm with varying lengths of 600-1000 nm, and thesizes of the platelets are around 55 nm, see Fig. 1 (a).

Swati etal[13].have also reported a direct pyrolysis to produce of WC Nanotubes at the 1000℃.And the process of researching is: 0.82g $W(CO)_6$ and 0.41g Magnesium powder was introduced into stainless steel cell ,and then put the cell into tube reactor at room temperature under atmospheric conditions，the temperature was raised at a heating rate of 20℃/min, the cell was heated at 900℃ for 3h,the reaction took place at a flowing nitrogen atmosphere, the cell was slowly cooled to room temperature, and 0.842 g black powder was obtained. Energy dispersive X-ray analysis of the sample showed that four phases of MgO, WC, C and α-W_2C in it. The final black product was treated with HCl 35%, used ethanol extract and dried for 12h, what remains is 0.49 g WC Nanotubes. From the Fig. 1 (b), it can be seen that the diameter of WC Nanotubes is 30-70nm, the length is 1-10μm and with several morphology.

2.2. Vapour Deposition

Chemical vapor deposition is the main method among the methods of fabricating nanowires. An implement specific substrates are usually required to ensure nanowires grew. Takayuki Arie etal[14].Synthesized carbide needles on a tungsten tip using a catalytic chemical vapour deposition method and have applied the needle as a STM tip. The tungsten tip was prepared from a tungsten wire with a diameter of 0.3 mm by electrochemical etching in KOH solution. A 50 nm thick Ni film as a catalyst was evaporated onto the tungsten tip. The Ni coated tungsten tip was set in a reactor tube and placed with the point toward the gas flow. The Ni-coated tip was then heated at 750 ℃under a pressure of 17.33Pa in Helium atmosphere for 2 h in order to form round Ni particles. Immediately after the heat treatment, thermal CVD was performed without breaking the vacuum. Benzene was fed as the starting material with a carrier gas of Helium. The carbide needles were synthesized on a tungsten tip by 1 h deposition at the pressure of10Pa. Fig. 1(c) shows the SEM image of the products on a tungsten tip by catalytic CVD，The needles are fabricated on the point of the tungsten tip and have sizes of typically 1μm in length and about 100 nm in diameter.

2.3. Magnetron Sputtering

Wang etal[7].Synthesized tungsten carbide nanowires by the magnetron sputtering, in them reports , WC_x films with thickness in the range of15–60 nm were sputter-deposited on n-type Si(100), 10Vcm substrates. A dc magnetron sputtering system using awater-cooled WC targets (50:50 wt %) with 99.5% purity was used. The deposition was carried out under an argon flow rate of 24 sccm, a dc power of 200 W, and a pressure of 1 Pa at room temperature. The typical deposition rate was measured to be around 0.36 Å/ s. The as-deposited samples were subsequently subjected to thermal annealing in quartz tube furnace with a temperature ranging from 600 to850°C in N_2 ambient for 30 min. the nanowires are all with a straight body. Fig.1 (d) shows the typical SEM image for the 700°C-annealed sample, the typical diameter and length of the nanowires are of 13–15 nm and 0.2–0.3 mm.

2.4 Eruptive heating

Eruptive heating is a special way of synthesizing nano structure materials by controlling the heating rate of reactants in a very short time .Oliveira etal[16] have prepared nano-sized tungsten carbide whisker by using eruptive heating by mixing graphite powder with tungsten powder ,then heat at a ultrafast heating rate of the starting material from the ambient temperature to the target

temperature T=1600℃within fractions of a second. The test piece was held at the target temperature for 30 minit was cooled down naturally to ambienttemperature.Fig.1 (e) show magnified appearances of the nanometer scale WC whiskers grown from the surface have sizes of typically length of several tens of nanometers and about several hundred nanometers in diameter.

2.5Template technique

Nicolas etal[17] present a study of preparation of one-dimensional nanostructures of tungsten carbide by taking the multi-wall carbon nanotubes as a template. The CNTs were added to the precursor aqueous salt solution ($(NH_4)_{10}W_{12}O_{41}\cdot 5H_2O$) and stirred vigorously at 80 °C for 20 min, before the slow evaporation of the solvent at room temperature. The resulting material was further dried overnight at 120 °C and finally calcinated at 350 °C for 2 h. The carburization of WO3 by the CNTs was expected to occur under dynamic vacuum at temperatures ranging between 1000 and 1300°C. Fig.1(f) shows SEM images of the materials synthesized at 1200 °C starting from a mechanical mixture of WO3 and CNTs.

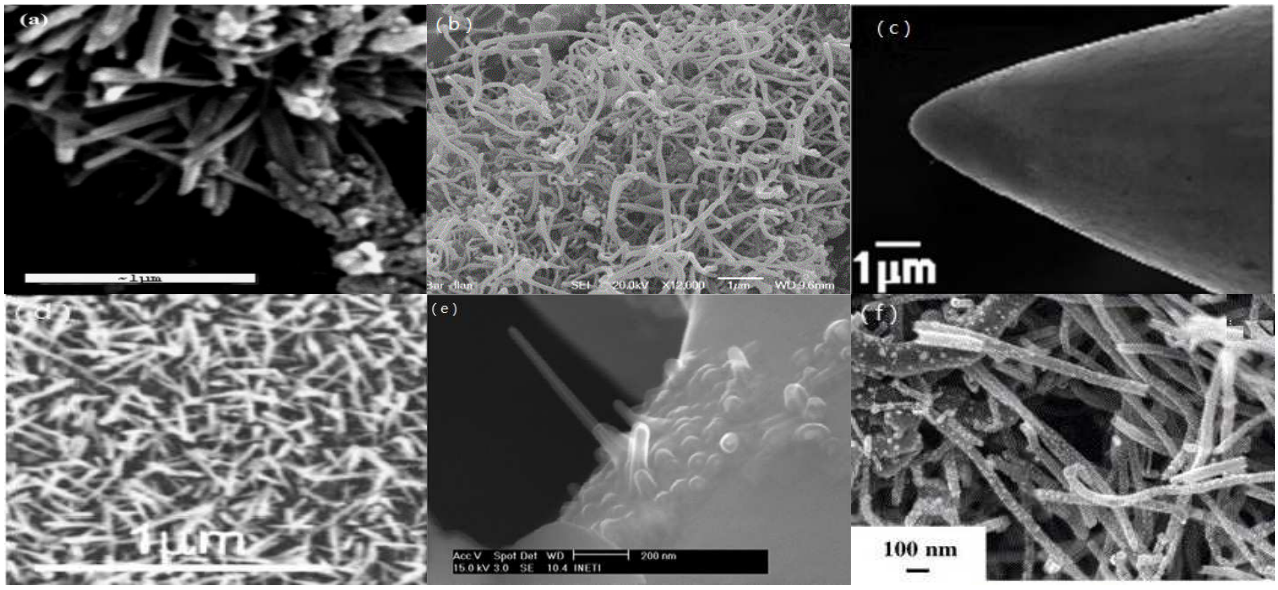

Fig.1 SEM micrographs of the one-dimensionalnano structures

3 The growth mechanisms

Nowadays, theories on VLS [19], VS [20] are often borrowed to explain the growth of one-dimensional nano materials. However, it difficult explain the mechanism of the growth of WC using the traditional growth theory, for example, the detailed mechanism of the VS synthesis of the WC nanowires is unclear. So it is necessary to analyze and summarize on the mechanism of growth of WC nanowires. Meanwhile, in order to provide a universal and controlled reform to guide the preparation of the nanowires.

Takayuki etal[14] believed that nickel play a crucial role in the growth process of WC nanometer needle, but the mechanism is not clear yet. The needles are not grown on a flat substrate but only on a substrate with a curvature, so the curve radius of the substrate is a key factor that affects the nucleation of the WC needle.

Using XRD, Wang etal[7] analyzed the WC_x films. the result to show: the growth of dense nanowires at 700°C, and the disappearance of nanowires at 750–800°C,carbon plays an important role in the growth and collapse of nanowires on annealed WC_x films, the self-catalytic growth of W_2C nanowires should be attributed to the formation of α-W_2C structures caused by carbon depletion in the WC_x films during thermal annealing, in addition, the collapse of W_2C nanowires in samples annealed at temperatures 700°C is due to the nanowires experiencing a structure transformation from α-W_2C(002)phase into grains of β-W phase.

4 Concluding remarks

In recent years, as a one-dimensional material, nanostructure WC have become the focus of attention, with its good physical and chemical properties, WC will surely have broad applying prospects in the new nano-material field. The preparation method was extremely rich and diversified, each with distinct features of its own, but there are disadvantages such as complicated technology, great investment of equipment and strict conditions. Therefore, a feasible and economical ways should be searched, and this will be one of the important technological problems to be solved in a quite long time at present and even in the future.

5 Acknowledgements

The authors are grateful to Chongqing Academy of Science &Technology for supplying of materials and testing of samples .the research work in this paper was Supported by Natural Science Foundation Project of CQ CSTC(NO.CSTC2012jjA50030), Chongqing science and technology key Projects Fund (No. CSTC 2012ggB50001).

References

[1]Kosolapva.T.Ya. Carbides Properties, Production, and Application., Plenum Press: New York, 1971.
[2] Schwartzkopf, P.; Kieffier, R. Refractory Hard metals Borides, Carbides, Nitrides, Silicides. The MacMillan Company: New York, 1953.
[3] Levy, R.; Boudardt, M. Science 1973, 181, 547.
[4] Xiao. T, Hanif. A, York. E. P. A, Sloan. J, Green.H. L.M. Phys Chem. Chem. Phys. 2002, 4, 3522.
[5] Bendelt, L. H. Cuthill, J. R. Mealister, N. Erickson, N. E. Science 1974, 184, 563.
[6] Noston, J. E, Laramore. G. E, Park, R. L. Science 1974, 185,285.
[7] Wang S J , Chen C H , Chang S C , et al. Appl Phys Lett , 2004 , 85 (12) :2358-2360.
[8] Arie T, Akita A, Nakayama Y. J Phys D: Appl Phys, 1998 , 31 : 49 -51.
[9] li ZHANG,
[10]Sadangi R K, McCandlish L E, Kear B H. International Journal of Powder Metallurgy, 1999, 35(1):27- 33.
[11] Wang G W, Zhao Y P, Yang G T. Materials & Design, 2004, 25(6):453- 457.
[12] Sangaraju S, David S, Aharon G. J Physical Chemistry B, 2005, 109(41): 19056- 19059.
[13] Swati V P, Vilas G P, Aharon G. Advancsd Materials, 2006,18(15):2023- 2027.
[14]Takayuki A,Seiji A,Yoshikazu N. J.Phys.D:Appl Phys, 1998,31(14): 49- 51
[15]Zheng H J,Ma C A,WangW, et al. Electrochemistry Communications, 2006,8(6):977- 981.
[16] Oliveira F A C,Granier B, Badid J M, etal. International Journal of Refractory Metals &Hard Materials, 2007,25(4):351- 357
[17] Nicolas K, Barbara P, Valerie K. Materials Letters, 2006，60 (13/14):1774- 1777.
[18] Shi X L,Yang H, Sun P, etal. Carbon, 2007, 45(9):1735- 1742.
[19] Wu Y Y, Yang P D. J Am Chem Soc, 2001, 123 (13): 3165 3166.
[20] Pan Z W, Dai Z R, Wang Z L. Science, 2001 (291): 19471949.

Advanced Materials Research Vols. 989-994 (2014) pp 556-559
© (2014) Trans Tech Publications, Switzerland
doi:10.4028/www.scientific.net/AMR.989-994.556

A Method for Scale-up of Grooved Nanofibers via Flat Off-centered Core-shell Structure Spinneret

Huihui Wu[1,a], Xiaohua Meng[1,b], and Yongchun Zeng[1,c]

[1]College of textiles, Donghua University, Shanghai, 201620, China
[a]1129019@mail.dhu.edu.cn, [b]xiaohua_meng@126.com, [c]yongchun@dhu.edu.cn

Keywords: Electrospinning, Composite polymers, Grooved nanofibers

Abstract. An approach to the scale-up of grooved nanofibers via a flat off-centered core-shell structure spinneret has been developed in this study. The spinneret with a flat surface involves shell-holes and off-centered core-needles. The position of the core-needle in the hole and the electrospinning process do influence the formation and structure of the grooved nanofibers. The production rate of the core-shell nanofibers can be enhanced by increasing the hole and needle number of the spinneret. This novel design is expected to provide a promising method towards the massive production of grooved nanofibers.

Introduction

In recent years, many researchers have attempted to enhance the production rate of electrospinning process in more sophisticated ways, such as increasing the number of spinning sites. The previously reported approaches can be generally classified based on the feed method at the spinning site: either a confined or unconfined fluid-volume feed[1]. Our previous work[2] developed a multihole system with a flat spinneret to scale up the productivity of electrospun nanofibers. It was reported that grooved and micro-textured surfaces could provide directional cues for the morphogenesis of cells with a preferred direction[3]. However, scaling up the productivity with conventional needle co-electrospinning system may lead to a complicated device. In this study, the flat off-centered core-shell structure spinneret is developed to enhance the productivity and to improve the fiber morphology of the electrospun grooved nanofibers. Experimental work is carried out to compare the spinning process and fiber morphology of this new design and the conventional needle co-elelctrospinning system.

Experimental

Material Preparation. Polystyrene (PS) (Mw=350 000 g/mol, Aldrich); Elastane PU2180A10 (Mw=70 000~150 000 g/mol^{-1}, BASF); N,N-dimethylformamide (DMF) (Shanghai Chemical Reagents Co., Ltd, China); All of these were used without further purification. Homogeneous PS solution and PU solution with the concentrations of 20 wt% and 7 wt% respectively were prepared by dissolving the corresponding pellets in DMF. The solution was prepared by gently stirring for 5 h with an electric mixer (AM200, Shanghai Only, Inc., China) at the ambient temperature.

Experimental Setup. The scheme of the designed multihole co-electrospinning system is shown in Fig. 1. The novel spinneret consists of an aluminum electrode and a plastic plate made of polytetrafluoroethylene (PTFE). The electrode is a cylinder with 50-mm diameter and 20-mm height. A 2-mm-outer-diameter tube was inserted into the electrode to provide shell solution feeding. The plastic plate with 2-mm thickness was used for creating the electrospinning jet. A solution chamber was formed between the electrode and the plastic plate. Holes with 1.5-mm diameter were drilled in the plastic plate to eject shell solution. Blunt-type needles with 0.8-mm outer-diameter and 0.5-mm inner-diameter were inserted through the electrode and off-centered into the holes to eject core solution. The polymer solutions were forced from syringes via syringe pumps (KDS 220, KD Scientific, Inc. USA) to the spinneret. A voltage power supply (ES-60P 10W/DDPM, Gamma High Voltage Research, USA) was applied to the spinneret and the aluminum foil-grounded collector.

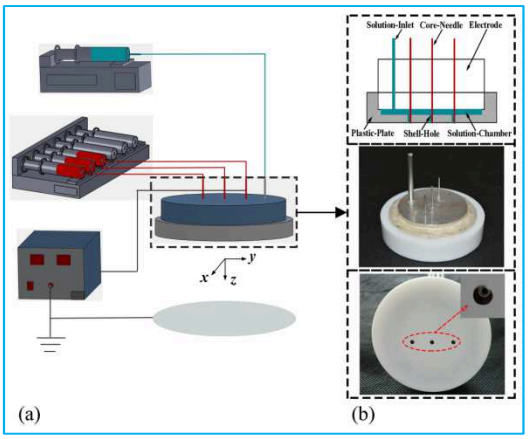

Figure. 1 Schematic of the multihole co-electrospinning system: (a) experimental setup (b) off-centered core-shell structure spinneret.

Characterization. The morphology of the resultant core-shell fibers were observed under a Scanning Electron Microscope (SEM) (JS M- 560 0LV, Japan) after gold coating (coating time is 60 s). A Transmission Electron Microscope (TEM) (JEM-2100, JEOL, Japan) was used to study the internal morphology of the core-shell fibers. The average fiber diameter was calculated from the SEM images using Photoshop Cs 6 (Adobe System Inc., San Jose, CA, USA) software from a collection of 500 fibers.

Results and discussion

Nanofibers with special structures, such as porous nanofibers, grooved nanofibers and nanosprings (or self-crimping nanofibers) have found various applications[4, 5]. In this study, by adjusting the position of the core-needle in the shell-hole (the core-needles is off-centered) and regulating the parameters of the electrospinning process, nanofibers with grooved structures are obtained in a simple way. Fig. 2a shows the SEM image of the grooved nanofibers in the fiber mat produced with the modified flat core-shell spinneret. The inserted SEM and TEM images (Fig. 2b) show the detail structure of the grooved nanofibers. As can be noted, the fibers have remarkable grooves on their surfaces along the fiber axial both in width and depth. The typical fiber morphology of these fibers may be ascribed to the off-centered configuration and the shrinkage of core component. The same solvent of the core and shell component make it easy to dissolve the thin side of shell layer near the central needle.

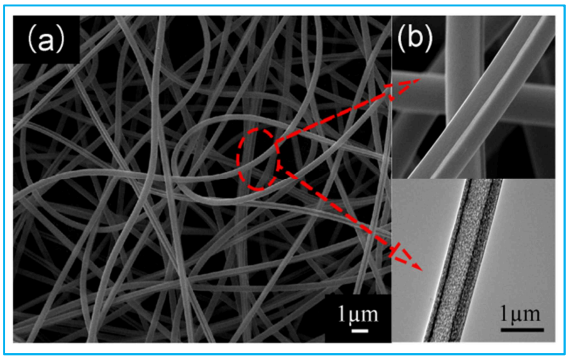

Figure. 2 Special structure fibers: (a) SEM image of the produced grooved fibers (b) Inserted SEM and TEM images of the detail structure of the grooved nanofibers. The working distance is 20cm and the applied voltage is 20kV. The flow rates of the core-needle is 0.5 ml/h and the shell- hole is1.5 ml/h, respectively.

Here, we define the rate of the core as $\boldsymbol{R_c}$, and of the shell as $\boldsymbol{R_s}$, while the parameter $\boldsymbol{p}$ means proportion of $\boldsymbol{R_s}$ to $\boldsymbol{R_c}$. And to illustrate the structure of the grooves on surface of the nanofibers, a parameter f is defined to describe the grooves width accounted for the proportion of the fiber diameter, which can be regulated by adjusting the electrospinning process. It is calculated as $\boldsymbol{f} = \frac{D_g}{D_f} \times 100\%$, where D_g is the width of the grooves and D_f is the diameter of the nanofibers. Fig. 3 further illustrates the proportion of the shell and core rate, the total flow rate and the various voltages effect on the grooves of the nanofibers. Fig. 3a illustrates the changes of f along with the proportion of the shell and core rate ($\boldsymbol{p}$). As we can see that, with the increasing proportion of the shell component, f decreases from 59% to 35% gradually. Fig. 3b shows the changes of f along with the total flow rate $\boldsymbol{R}$ ($\boldsymbol{R}$=$\boldsymbol{Rs}$ + $\boldsymbol{Rc}$) under the proportion of the core and shell rate ($\boldsymbol{p}$) is 4. It shows that $\boldsymbol{f}$ firstly increases from 41% to 45%, then reduces to 35% rapidly.Fig. 3c illustrates the changes of $\boldsymbol{f}$ along with various voltages. As the same trend of R, $\boldsymbol{f}$ grows from 25% sharply, and then down to 35%. By regulating the special grooved structure, the off-centered core-shell nanofibers can be have more applications on the organization applications and molecular templates.

Scale-Up Analysis

Under the same conditions, the productivity of the co-electrospinning setup is determined by the number of the jets. For the three-hole flat core-shell spinneret, the productivity is about 3 times of the conventional setup, which is about 1.5ml/h for the core-needles and 4.5 ml/h for the shell-holes. The production rate of core-shell fibers can be scaled up by increasing the hole and needle numbers.

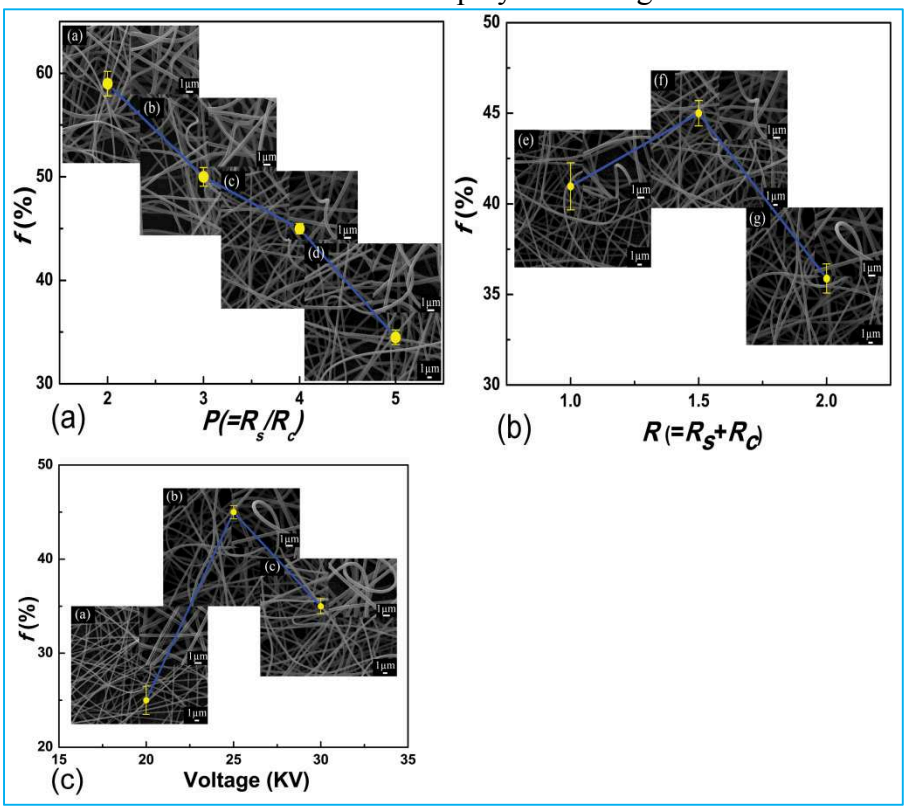

Figure. 3 The effect of f along with (a) the proportion of shell rate Rs to core rate Rc (Rs + Rc =1.5ml/h) (b) the flow rate of R=Rs+ Rc (p=4:1) (c) various voltages.(The working distance keeps 20cm.)

Conclusion

A co-electrospinning setup for the scale-up of the grooved nanofibers has been developed. We compared fiber morphology under different electrospinning process produced by the new designed flat off-centered core-shell structure spinneret. This method provides a promising method towards the massive production of core-shell nanofibers.

Acknowledgment

This work was financially supported by the National Natural Science Foundation of China (11272088), the Fundamental Research Funds for the Central Universities.

Literature References

[1] N.M.Thoppey, J.R.Bochinski, L.I.Clarke, R.E.Gorga, Polymer, Vol. 51, (2010), p.4928.
[2] Y. Zheng, X. Liu, Y. Zeng, Journal of Applied Polymer Science, Vol. 130, (2013), p.3221.
[3] Haibao, C.Binrui, Z.Zipeng, A.A.Laxmi, L.Dong, L.Shaorong, M.Chuanbin, Biomaterials, Vol. 32, (2011), p.4744.
[4] S. Chen, H. Hou, P. Hu, J.H. Wendorff, A. Greiner, S. Agarwal, Macromolecular Materials and Engineering, Vol. 294, (2009), p.265.
[5] N.M.S. Bettahalli, I.T.M. Arkesteijn, M.Wessling, A.A.Poot, D.Stamatialis, Acta Biomaterialia, Vol. 9, (2013), p.6928.

Advanced Materials Research Vols. 989-994 (2014) pp 560-563
© (2014) Trans Tech Publications, Switzerland
doi:10.4028/www.scientific.net/AMR.989-994.560

The preparation and characterization of polybenzoxazole copolymerized with multiwalled carbon nanotube via direct Friedel-Crafts acylation

Yong Chen [a], Jun Qian [b], Qixin Zhuang [c] and Zhewen Han [d]

Key Laboratory for Ultrafine Material of Education, School of Materials Science and Engineering, East China University of Science and Technology, Shanghai 200237, China;

[a]chenyong178@163.com, [b]qianjun@ecust.edu.cn, [c]qxzhuang@ecust.edu.cn, [d]zhwhan@ecust.edu.cn

Correspondence to: Jun Qian (E-mail: qianjun@ecust.edu.cn)

or Zhewen Han (E-mail: zhwhan@ecust.edu.cn)

Keywords: Poly (p-phenylene benzobisoxazole) (PBO), Multiwalled carbon nanotube, Copolymerization.

Abstract. Multiwalled carbon nanotube (MWCNT) was subjected a copolymerization reaction with 4, 6-diaminoresorcinol salt (DAR•2HCl) and terephthalic acid (TA) in polyphosphoric acid (PPA) by Friedel-Crafts acylation reaction without any acid treatment or modification. The structure and morphology of the as-prepared poly (p-phenylene benzobisoxazole) (PBO)/MWCNT nanocomposites were characterized by X-ray diffraction (XRD) and scanning electronic microscope (SEM). The SEM images indicated that MWCNTs can disperse in PBO matrix uniformly without agglomeration and MWCNTs have been introduced into PBO matrix by covalent bonding via Friedel-Crafts acylation between MWCNTs and TA.

Introduction

Polybenzobisoxazole(PBO), possessing high tensile strength, high temperature resistance and excellent chemical resistance [1, 2], shows a widely application in aviation, spaceflight, and other special fields. However, only about 15% of the theoretical tensile strength has been achieved in the momericialized PBO fibers attributed to the low-molecular length (about 200 nm for fiber spinning) and defects [3]. To fully exploit the mechanical properties of PBO, several studies have been made on PBO/CNT composites to take advantage of longer length of CNTs compared with that of PBO molecular chain [4, 5]. And all the synthetic routes of PBO/CNT nanocomposite reported before had need to acid treatment on CNT to introduce carboxyl group into CNT (CNT-COOH). In this study, we prepared PBO/MWCNT nanocomposite via a one pot reaction of 4, 6-diaminoresorcinol salt (DAR•2HCl) and terephthalic acid (TA) with MWCNTs in polyphosphoric acid (PPA) by Friedel-Crafts (F-C) acylation [6, 7]. Unlike other synthetic routes reported before [5, 8, 9], the synthetic route for PBO/CNT nanocomposties does not need any acid treatment or modification on CNT. Moreover, the structure and morphology of PBO/MWCNT nanocomposites have been investigated in this study.

Experiment

Materials

4,6-diaminoresorcinol dihydrochloride (DAR• 2HCl) was obtained from commercial sources and dried under vacuum at 40℃ for 24 h, terephthalic acid (TA) was purchased from Shanghai Lingfeng Chemical, the reaction medium, poly(phosphoric acid) (PPA) with 80.8% phosphorus pentoxide (P_2O_5), was freshly prepared using as-received phosphoric acid and P_2O_5 (Shanghai first Chemical

Co., Shanghai). MWCNT with an average diameter of 40～60 nm was provided from Nanotech Port Company, Shenzhen, China. All reagents were used without further purification.

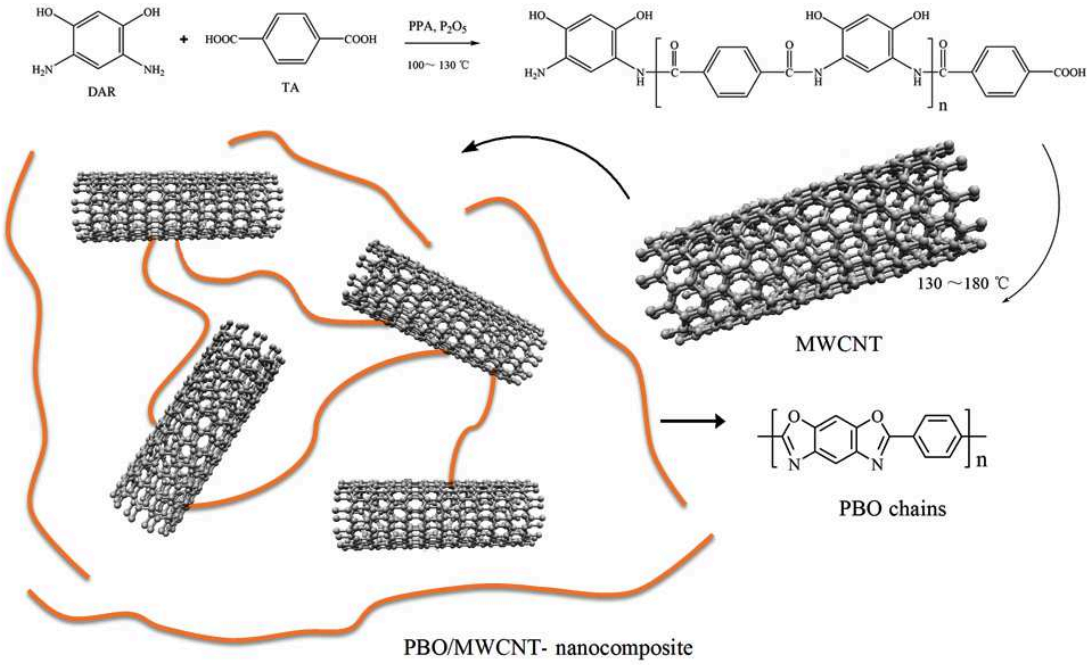

Scheme 1 Schematic illustration of preparation of PBO/MWCNT nanocomposite

The preparation of PBO/MWCNT nanocomposites

The PBO/MWCNT nanocomposites were synthesized by a one-step procedure from DAR•2HCl, TA and MWCNT with PPA as the condensing medium. In a typical synthesis of PBO/MWCNT nanocomposite with MWCNT composition of 2 wt. %, 2 g DAR•2HCl, 1.56 g TA and 0.04 g MWCNT were mixed together with 7.51 g P_2O_5 and 11.62 g PPA in a three-necked separable flask equipped with a mechanical stirrer in the presence of nitrogen atmosphere. The reaction mixture was stirred for 1 h at the room temperature to ensure full mixing of the monomers. The reaction temperature was raised to 90℃ and held for 6 h in vacuum, then to 100℃ and held for 6 h, and to 110℃ and held for 6 h. After the hydrogen chloride in DAR• 2HCl was fully removed, the reaction temperature was raised to 120℃ for 12 h in nitrogen, then to 130℃ for 12 h, and then to 180℃ for 12 h. The highly viscous polymerization dope (dark green in color) in PPA was precipitated in water and purified by extraction of the PPA with water for 1 day. The composite was desiccated at 80℃ in a vacuum oven.

Results and discusstions

To investigate the effect of MWCNTs on the ordered structures of PBO matrix, XRD patterns of PBO/MWCNT nanocomposites were measured and shown in Fig. 1. Two typical diffraction peaks at 2θ=15° and 26° for polybenzazole can be observed in the spectrum of PBO. Diffraction peaks for MWCNTs are not detectable in spectra and all the diffraction peaks can be assigned to the ordered structure of PBO in PBO/MWCNT nanocomposites. This indicates that the ordered structure of PBO matrix largely remains after introducing MWCNT, consistent with earlier reports for PBO/CNT composites [10].

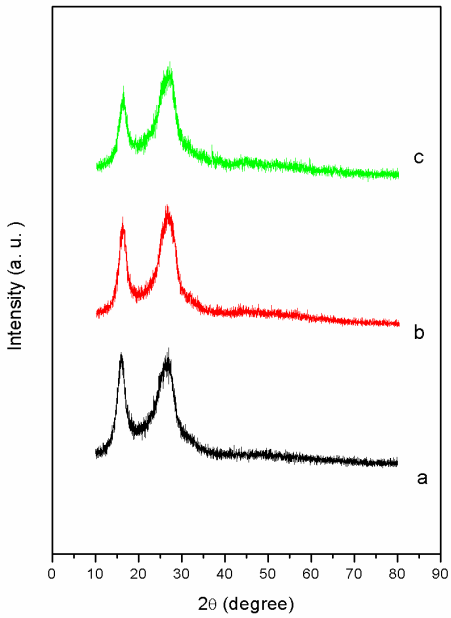

Figure 1 The Wide-angle X-ray diffraction patterns of PBO/MWCNT nanocomposites with MWCNT compositions of (a) 0 wt%, (b) 2 wt% and (c) 4 wt%

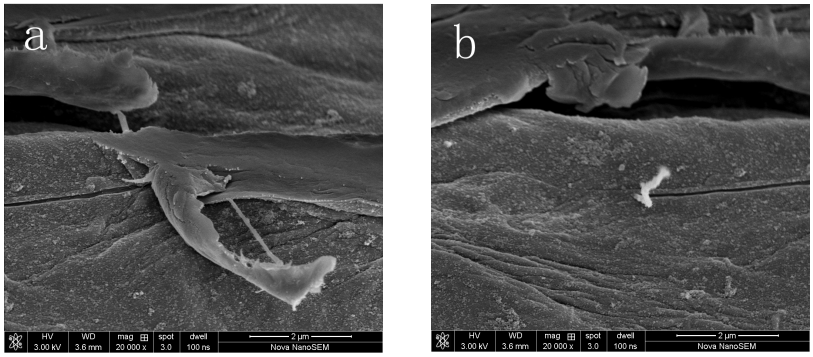

Figure 2 SEM images of PBO/MWCNT nanocomposites of the cross-section, the scalebar of both a and b is 2 μm

Homogeneous dispersion of MWCNTs in PBO matrix is one of the most important necessities in fully taking advantage of the excellent physical property of MWCNTs. The morphology of resulting products was characterized by SEM, as shown in Fig. 2. SEM images in Figs. 2a and 2b show that MWCNTs uniformly disperse in PBO matrix without agglomeration. Moreover, these images also demonstrate the MWCNTs have been introduced into PBO matrix by covalent bonding via Friedel-Crafts acylation between MWCNTs and TA.

The thermal behavior of PBO and PBO/MWCNT nanocomposites is studied by TG (Fig. 3). In the TG curves of all the samples, only one degradation step at about 660℃ owing to the decomposition of the PBO molecular chains is observed. The results in Fig. 3 indicate that PBO/MWCNT nanocomposites still mantain PBO's outstanding thermostability without appreciable weight loss up to 680℃. Remarkably, the thermal stabilities of all the PBO/MWCNT nanocomposites are better than that of PBO when it is below 650℃ with higher on-set thermal degradation temperature T_d. Moreover, with increasing the amount of MWCNT, the larger residual weight of PBO/MWCNT nanocomposites. It can be concluded that the MWCNTs homogeneously dispersed in PBO matrix and the covalent bonding at the MWCNT/PBO interface are expected to improve the thermal stability of PBO/MWCNT nanocomposites.

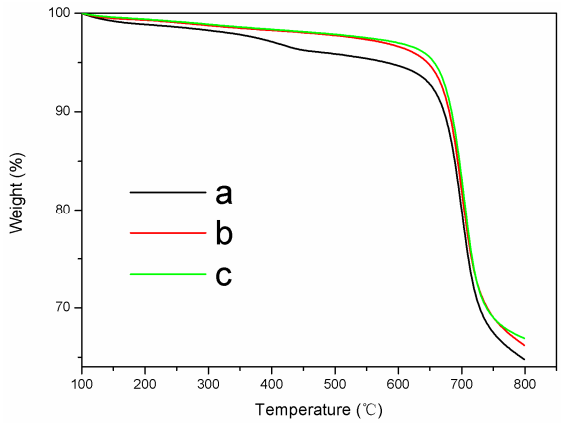

Figure 3 The thermal behavior of PBO/MWCNT nanocomposites with MWCNT compositions of (a) 0 wt%, (b) 2 wt% and (c) 4 wt%

Conclusion

In this study, a series of PBO/MWCNT composites with different MWCNT contents are synthesized through in-situ polymerization via Friedel-Crafts acylation reaction. The structure and morphology of the obtained PBO/MWCNT composites have been investigated. The results show that MWCNTs uniformly disperse in PBO matrix without agglomeration and MWCNTs have been introduced into PBO matrix by covalent bonding via Friedel-Crafts acylation between MWCNTs and TA.

References

[1] J. F. Wolfe, B. H. Loo, F. E. Arnold, Macromolecules. 14 (1981) 915-920.

[2] J. F. Wolfe, F. E. Arnold, Macromolecules. 14 (1981) 909-915.

[3] Chae H. G, Kumar S, Journal of Applied Polymer Science. 100 (2006) 791-795.

[4] C. Zhou, S. Wang, Q. Zhuang, Z. Han, Carbon. 46 (2008) 1232-1240.

[5] Z. Xie, Q. Zhuang, Q. Wang, X. Liu, Y. Chen, Z. Han, Polymer. 52 (2011) 5271-5276.

[6] H. J. Lee, S. W. Han, Y. D. Kwon, L. S. Tan, J. B. Baek, Carbon. 46 (2008) 1850-1859.

[7] J. B. Baek, C. B. Lyons, L.S. Tan, Macromolecules. 37 (2004) 8278-8285.

[8] Z. Hu, J. Li, P. Tang, D. Li, Y. Song, Y. Li, L. Zhao, C. Li, Y. Huang, Journal of Materials Chemistry. 22 (2012) 19863-19871.

[9] C. Zhou, X. Qiu, Q. Zhuang, Z. Han and Q. Wu, Journal of Applied Polymer Science. 124 (2012) 4740-4746.

[10] S. Kumar, T. D. Dang, F. E. Arnold, A. R. Bhattacharyya, B. G. Min, X. Zhang, R. A. Vaia, C. Park, W. W. Adams, R. H. Hauge, R. E. Smalley, S. Ramesh, P. A. Willis, Macromolecules. 35(2002) 9039-9043.

Advanced Materials Research Vols. 989-994 (2014) pp 564-567
© (2014) Trans Tech Publications, Switzerland
doi:10.4028/www.scientific.net/AMR.989-994.564

Different chemical oxidant of benzene series pollution site repair effect

Dinglong Li[1,a], Xinlei Fang[1,b], Minda Yu[1,c], Hao Lv[1,d] and Yan Yang[1,e,*]

[1]School of Environmental & Safety Engineering, Changzhou University, Changzhou 213164, China
[a]hjaq@cczu. edu. cn,fxllmd@163. com,[a]ymdy165@163. com,[c]blackth2009@163. com,
[e]yy129129@163. com

Keywords: contaminated sites, Chlorobenzene,O-dichlorobenzene,Oxidant,Site remediation.

Abstract. this study intends to compare through the experiment research of potassium permanganate, Fenton reagent, sodium persulfate, hydrogen peroxide, four kinds of commonly used oxidant chlorobenzene in contaminated soil, the removal effect of O-O-dichlorobenzene;, selected a typical ground soil bioremediation is the best antioxidant effect. Research under the condition of different on the dose, 4 kinds of oxidants to chlorobenzene and O-O-dichlorobenzene; removal effect. Combined pollution ground soil properties screen of chlorobenzene in contaminated soil, the highest removal rate of dichlorobenzene oxidant and best delivery dosage, to apply typical ground soil bioremediation, the results show that the effect is the best Kmno4.

With the adjustment of industrial structure and layout of the city,facing a lot of old chemical plant relocation or closure of the situation,some of the original factory land into a green city,commercial and even residential areas. In the process,these companies left in the original area of contamination to the environment and the health of residents around poses a serious threat. Therefore,in view of the characteristics of contaminated sites and repair needs,using the appropriate repair techniques for contaminated sites for efficient,fast and safe repair is necessary.

Relocation site for the chemical industry where the typical contaminated sites,mainly from the production process of organic pollutants and sewage process. Chemical companies in the relocation of contaminated sites,and chlorobenzene substances is a common legacy pollutants. Since chlorobenzene substances chemically more stable,but also has toxicity,it is difficult to be natural microbial degradation,likely to cause pollution of the environment of persistent and dichlorobenzene has a strong stimulating effect,long-term exposure harmful to human skin,conjunctiva and respiratory organ irritation,and cause acute or chronic neurological disorders[1,2]. Therefore,the study of chlorobenzene substances contaminated soil remediation technology has important practical significance.

At present,for contaminated soil organic matter oxidation reagents major repair hydrogen peroxide,Potassium permanganate,Fenton reagent and Activated persulfate,these types of oxidants have their optimum reaction conditions and the type of contaminants. Fenton reagent and potassium permanganate on the removal of soil organic matter,there have been a number of related studies[3,5]. Couttenye use of electron spin resonance, etc. (EPR) detects the acidic and neutral (pH=2~7)· SO-4 in the presence condition,the presence of an alkaline (pH>12) under the conditions of· OH. Therefore, the use of activated persulfate itself and generated·SO-4 and·OH radical degradation activity of organic pollutants in wastewater,groundwater and soil organic matter management have potential applications,recently to study abroad focus [6].

Materials and methods

Selected soil

Puts the soil 100. 0 g of the sieve after removing impurity in the beaker, says apply adequate amount of Chlorobenzene and O-dichlorobenzene; soluble in acetone solution, then mixed with 1000. 0 g original soil, configured to concentration of 100 mg/kg 1000. 0 g of contaminated soil. To place it in the fume hood avoid light preservation, acetone volatile backup with completely, the soil aging one week after measuring the concentration of Chlorobenzene and O-dichlorobenzene;.

The preparation of oxidant solution

Respectively according to take the right amount of potassium permanganate, sodium persulfate, preparation of 0. 4mol/L, 0. 4mol/L the oxidant liquid reserves of 1000 mL, avoid light preservation. Fenton reagent preparation: the concentration of 30%H2O2 and 0. 4 mol/LFeSO4 five to one preparation by the molar concentration of 1000 ml. Hydrogen peroxide concentration of 30% H2O2.

The experiment design

1. 31 Determination of the original soil water content,contaminants and simulate pollution soil samples after aging contaminants.

In the early stage of the experiment,the physical and chemical properties of soil were determined,the main physical and chemical properties of the soil including soil texture, moisture content,soil organic contaminants,and so on.

The original soil soil samples of chlorobenzene and dichlorobenzene detection Soil sample pretreatment by ultrasonic extraction,contaminants using gas chromatography tes

This experiment chooses four kinds of oxidant,each antioxidant soil water ratio of five to one for processing the pollution of soil,and set up three groups. Oxidant concentration in the same experiment,but choose different delivery dosage (1ml,2ml,3ml,4ml,5ml) and oxidant in the process of the experiment of spraying manner, antioxidants on the dose see (table 1).

Table 1: The moisture content of 20% to simulate pollution soil (soil water ratio 5:1)oxidation treatment

oxidant	reagent	concentration	dose
Potassium permanganate	KMnO4	0. 4mol/L	1ml, 2ml, 3ml, 4ml, 5ml
Sodium persulfate	Na2S2O8	0. 4mol/L	1ml, 2ml, 3ml, 4ml, 5ml
Hydrogen peroxide,	H2O2	0. 4mol/L	1ml, 2ml, 3ml, 4ml, 5ml
Fenton reagen	H2O2 FeSO4	30% 0. 4mol/L	1ml, 2ml, 3ml, 4ml, 5ml

Will response after the soil samples of natural air drying and air drying after the soil samples using ultrasonic extraction method to extract,gas chromatography to determine the content of chlorobenzene and dichlorobenzene.

Sample analysis

Determination of the concentration in the soil

Extraction method

Soil samples:after antioxidant treatment of soil,after natural drying. Add 25mL of hexane solution points three times after ultrasonic extraction 1. 5h,collect extract with right amount after 500℃ muffle furnace burning after 4 hours of Na2SO4 to remove moisture,impurities in the solvent is overmuch,can be over 0. 45um microporous membrane filter in removing impurity.

The chromatographic conditions

Chromatography is set according to the national standard method of determination of chlorobenzene

In the recovery liquid concentration determination

In the recovery liquid concentration determination:take inlet chromatography for determination of directly.

Results analysis and discussion:

Infected aging after two weeks of chlorobenzene content in the contaminated soil samples is 18. 5 mg/kg, O-dichlorobenzene content is 39. 0 mg/kg. Oxidant mixture concentration is 0. 1mol/L.

After four antioxidant treatment measure the contaminants and removal rate as shown in the figure below:

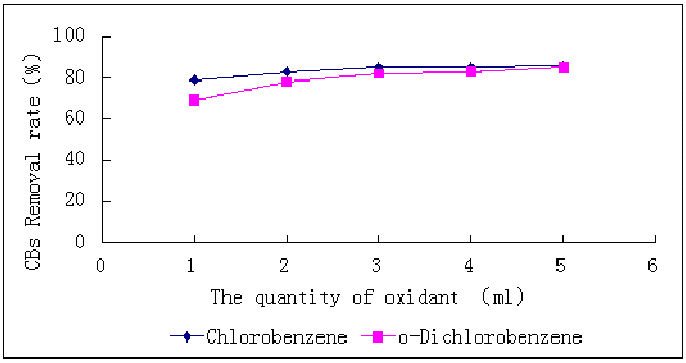

Figure 1: Kmno4 for two kinds of pollutants removal rate

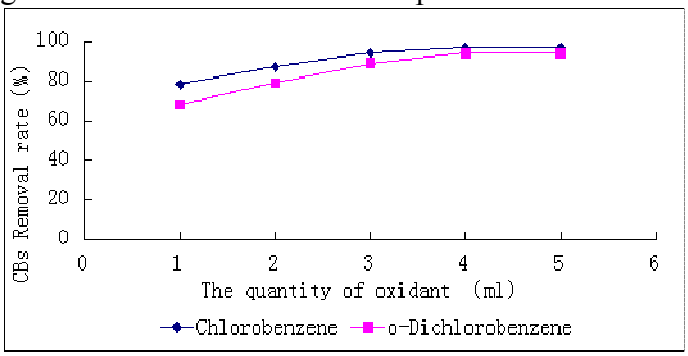

Figure 2: Na2S2O8 for two kinds of pollutants removal rate

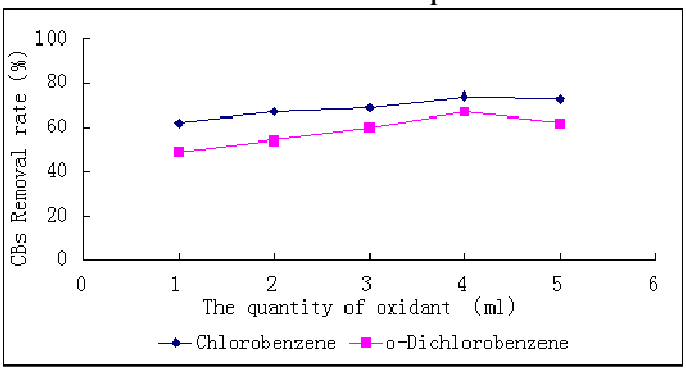

Figure 3: H2O2 for two kinds of pollutants removal rate

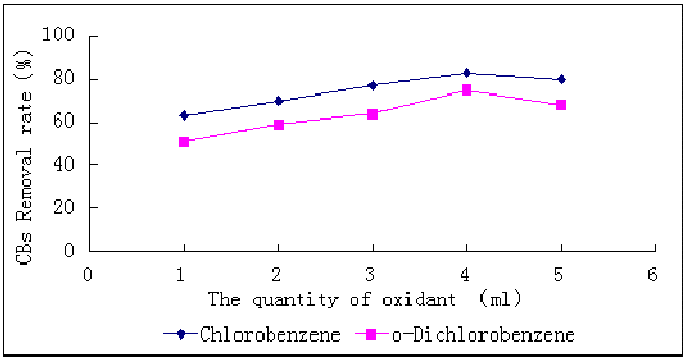

Figure 4: Fenton reagent for two kinds of pollutants removal rate

1 From the above four graphs, the same type of oxidizer in the oxidation effect of different concentrations, generally within a certain range, the oxidizing agent is measured with increased oxidative better, up to 97%.

2 Seen from the above diagram,the simulation polluted soil after three different oxidizing agent significantly reduce pollutants,oxidizing agents,in the removal of the same dose of sodium persulfate is best, followed by high potassium permanganate.

3 Through the above chart shows that under the condition of considering economic benefit and effect of removing, oxidant dosage for 4ml effect.

Acknowledgements

This work was financially supported by Jiangsu Province environmental protection scientific research project (2012038).

References

[1] A. M. Mastral , M. S. Callén:A review on polycyclic aromatic hydrocarbon (PAH) emissions from energy generation［J］. Environmental Science & Technology，Vol. 34(2000)No. 15,p. 3051-3057.

[2] Y. Feng,Y. L. Lv,W. T. Jiao,et al. Beijing Coking Plant a different workshops abandoned land Polycyclic aromatic hydrocarbons in soil(PAHs) Distribution and Risk Assessment[J]. Journal of Ecotoxicology,Vol. 4(2009)No. 3,p. 399-407.

[3] H. W. Sun,Q. S. Yan:Influence of pyrene combination state in soils on its treatment efficiency by Fentonoxidation[J]. Journal of Environmental Management, Vol. 88(2008)No. 3,p. 556-563.

[4] G. S. Brown,L. L. Barton:Thomson B M. Permanganate oxidation of sorbed polycyclic aromatic hydrocarbons[J]. Waste Management，2003，Vol. 23(2003)No. 8,p. 737-740.

[5] Y. J. Cui,S. Y. Yang,P. Wang,et al. Organically polluted soil and groundwater remediation by in situ Fenton oxidation[J]. Progress in Chemistry,Vol. 20(2008)No. 8,p. 1196-1201.

[6] S . Y. Yang ,X. Yang，P. Wang，et al. Advances in persulfate oxidation activation methods of persulfate oxidation[J]. Modern Chemical Industry，Vol. 29(2009)No. 4,p. 13-19.

Advanced Materials Research Vols. 989-994 (2014) pp 568-571
© (2014) Trans Tech Publications, Switzerland
doi:10.4028/www.scientific.net/AMR.989-994.568

Design, Synthesis and Anticancer Activity of 4-Morpholinothieno[3,2-*d*]-pyrimidine Derivatives Bearing Chromone Moiety

Chengyu Sun [a], Chen Chen [b], Chunjiang Wu[c], Pengwu Zheng*[d] and Wufu Zhu*[e]

School of Pharmacy, Jiangxi Science & Technology Normal University, Nanchang 330013, China

[a]sunchengyu0902@126.com,[b] chen5950677@163.com,[c]wuchunjiang999@126.com
*[d]zhengpw@126.com, *[e]zhuwufu-1122@163.com

Keywords: PI3K/mTOR Inhibitors; 4-Morpholinothieno[3,2-*d*]pyrimidine; Chromone; Anticancer activity

Abstract. A series of 4-morpholinothieno[3,2-*d*]pyrimidine derivatives containing chromone moiety (**5a-5e**) were synthesized and their structures were confirmed by ^{1}H NMR and MS spectrum. The synthesized compounds were evaluated for their cytotoxicity against three cancer cell lines (PC-3, H460, SGC-7901). Two of them exhibited moderate cytotoxicity and high-selectivity against one or more cell lines. At 10μM levels, the inhibition rate of compound **5c** against SGC-7901 cell lines was 58.9%, and that of compound **5d** against PC-3 cell lines was 56.4%.

Introduction

Cancer is one of the major diseases that threaten human health. The incidence of cancer is the second only to cardiovascular and cerebrovascular diseases, and it's mortality rate is the highest among all diseases [1]. Currently, there are three main methods for treating the cancer: surgical resection, chemotherapy, and radiation therapy. However, with the advancement of science, the limitations of these three treatments are also increasingly prominent. Therefore, searching for highly efficient and safe chemotherapeutic agents for treating cancer remains desirable.

Recent studies have found that the phosphatidylinositol 3-kinase(PI3K) and its downstream protein kinase B(Akt/ PKB), mammalian target of rapamycin (mTOR) consisting of PI3K-Akt-mTOR signaling pathway controls many important biological processes in the development process of tumorigenesis[2-3]. Therefore, inhibition of this pathway had become a hot topic in cancer prevention and targeted therapy.

After years' effort of the researchers, many small molecule inhibitors of this pathway were entered the clinic study [4-6]. Among these compounds, thienopyrimidines are the most important of all types, as well as the earliest in this pathway. The most representative compound is GDC-0941 (Fig. 1), which is a selective PI3K inhibitor currently undergoing Phase I clinical trials[4]. The structure–activity relationships (SARs) studies indicated that the 4-morpholinothieno[3,2-*d*] pyrimidine scaffold played a key role in their antitumor activity[4,7].

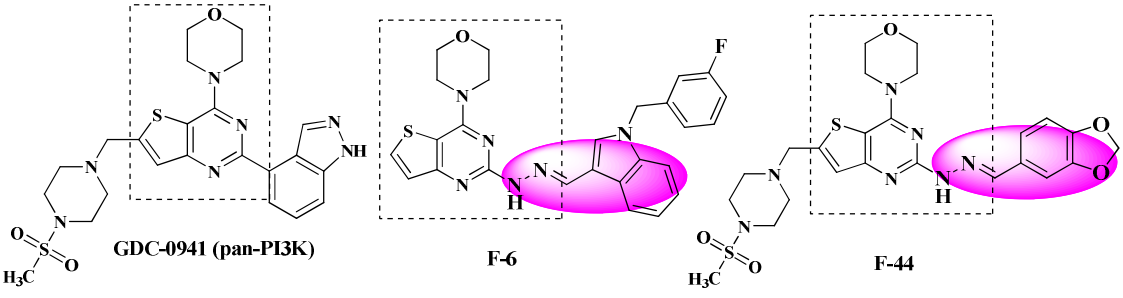

Fig. 1 Structures of GDC-0941 and the representative compounds in our previous study

In our previous study [8,9], with GDC-0941 as a lead compound, we designed and synthesized a series 4-morpholinothieno[3,2-*d*] pyrimidine derivatives with an arylmethylene hydrazine moiety at

C-2 position(Fig.1). Among these compounds, most of them showed excellent anti-tumor activity. The 3D-QSAR study found that the introduction of arylmethylene hydrazine at C-2 position significantly enhanced the anti-tumor activity and selectivity.

In this study, replacing the aryl group with the active pharmacophore chromone, a series of 4-morpholinothieno[3,2-*d*]pyrimidines (**5a~5e**) which had not been reported yet were designed and synthesized. All the target compounds were evaluated for their cytotoxicity against three cancer cell lines (PC-3, H460, SGC-7901).

Materials and methods

All melting points were obtained on a Büchi Melting Point B-540 apparatus (Büchi Labortechnik, Flawil, Switzerland) and were uncorrected. 1H-NMR spectra were performed using Bruker 300/400 MHz spectrometers (Bruker Bioscience, Billerica, MA, U.S.A.) with TMS as an internal standard. Mass spectra (MS) were taken in electrospray ionization (ESI) mode on Agilent 1100 LC-MS (Agilent, Palo Alto, CA, U.S.A.). All the materials were obtained from commercial suppliers and used without purification, unless otherwise specified. Yields were not optimized. TLC analysis was carried out on silica gel plates GF254 (Qindao Haiyang Chemical,China).

Synthesis of compounds

Substituted chromone aldehyde derivatives (D1-D5).

The synthesis of substituted chromone aldehyde derivatives was according to the procedures in our previous research[10].

4-(2-hydrazinylthieno[3,2-*d*]pyrimidin-4-yl)morpholine (4)

The synthesis of 4-(2-hydrazinylthieno[3,2-*d*]pyrimidin-4-yl)morpholine(**4**) was according to the procedures in our previous researches[8,9].

General Procedure for Preparation of Compounds 5a-5e.

A mixture of 4-(2-hydrazinylthieno[3,2-*d*]pyrimidin-4-yl)morpholine (0.1 g, 0.40 mmol), substituted aldehyde (**D1-D5**, 0.42 mmol) and a drop of glacial acetic acid in absolute ethanol (8 mL) was refluxed for 2–5 h. The mixture was cooled, separated by filtration and washed with EtOH to give off a yellow solid. The crude product was recrystallized from ethanol or purified by chromatography on silica gel using MeOH/CH_2Cl_2 to afford yellow solids **5a-5e** respectively.

(*E*)-6-isopropyl-2-((2-(4-morpholinothieno[3,2-*d*]pyrimidin-2-yl)hydrazono)methyl)-4*H*-chromen-4-one (5a)

Yellow powder. Yield 49%. mp 163-165°C. ESI-MS m/z: 450.1 $(M+H)^+$,448.2 $(M-H)^-$. ^{1}H NMR (400 MHz, DMSO) δ 10.98 (s, 1H), 8.75 (s, 1H), 8.26 (s, 1H), 8.13 (d, *J* = 5.6 Hz, 1H), 7.98 (s, 1H), 7.80 (d, *J* = 8.8 Hz, 1H), 7.70 (s, 1H), 7.27 (d, *J* = 5.4 Hz, 1H), 3.94 (s, 4H), 3.80 (s, 4H), 3.13 (d, *J* = 7.5 Hz, 1H), 1.30 (d, *J* = 7.0 Hz, 6H).

(*E*)-6-fluoro-2-((2-(4-morpholinothieno[3,2-*d*]pyrimidin-2-yl)hydrazono)methyl)-4*H*-chromen-4-one (5b)

Yellow powder. Yield 58%.mp 228-231°C. ESI-MS m/z: 426.1 $(M+H)^+$.

(*E*)-6-bromo-2-((2-(4-morpholinothieno[3,2-*d*]pyrimidin-2-yl)hydrazono)methyl)-4*H*-chromen-4-one (5c)

Yellow powder. Yield 62%.mp 267-269°C. ESI-MS m/z: 486.0, 488.0 $(M+H)^+$.

(*E*)-6-methyl-2-((2-(4-morpholinothieno[3,2-d]pyrimidin-2-yl)hydrazono)methyl)-4H-chromen-4-one (5d)

Yellow powder. Yield 55%.mp 223-225°C. ESI-MS m/z: 422.2 (M+H)+

(*E*)-2-((2-(4-morpholinothieno[3,2-*d*]pyrimidin-2-yl)hydrazono)methyl)-4-oxo-4*H*-chromene-6-carboxylic acid (5e)

Yellow powder. Yield 69%.mp 280-282°C. ESI-MS m/z: 452.1 $(M+H)^+$,450.1 $(M-H)^-$.

Biological Evaluation

The cytotoxic activities of compounds were evaluated with human lung cancer (H460), human prostate cancer (PC-3) and human Gastric cancer (SGC-7901) cell lines by the standard MTT assay *in*

vitro, with GDC-0941 as the positive controls. The cancer cell lines were cultured in minimum essential medium (MEM) supplement with 10% fetal bovine serum (FBS).Approximately 4×10^3 cells, suspended in MEM medium, were plated onto each well of a 96-well plate and incubated in 5% CO_2 at 37°C for 24 h. The test compounds at indicated final concentrations were added to the culture medium and the cell cultures were continued for 72 h. Fresh MTT was added to each well at a terminal concentration of 5 μg/mL and incubated with cells at 37°C for 4 h. The formazan crystals were dissolved in 100 μL DMSO each well, and the absorbency at 492 nm (for absorbance of MTT formazan) and 630 nm (for the reference wavelength) was measured with the ELISA reader. All of the compounds were tested three times in each of the cell lines.

Results

Chemistry

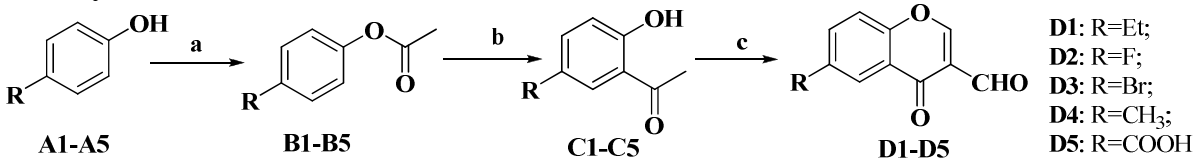

Fig. 2 Synthetic route of chromone aldehyde derivatives(**D1-D5**)

Reagents and conditions: (a) Ac_2O(1.05eq) ,conc. H_2SO_4,0°C, 1h; (b) anhydro $AlCl_3$, 120°C,6-7h; (c) DMF,$POCl_3$, r.t,12h.

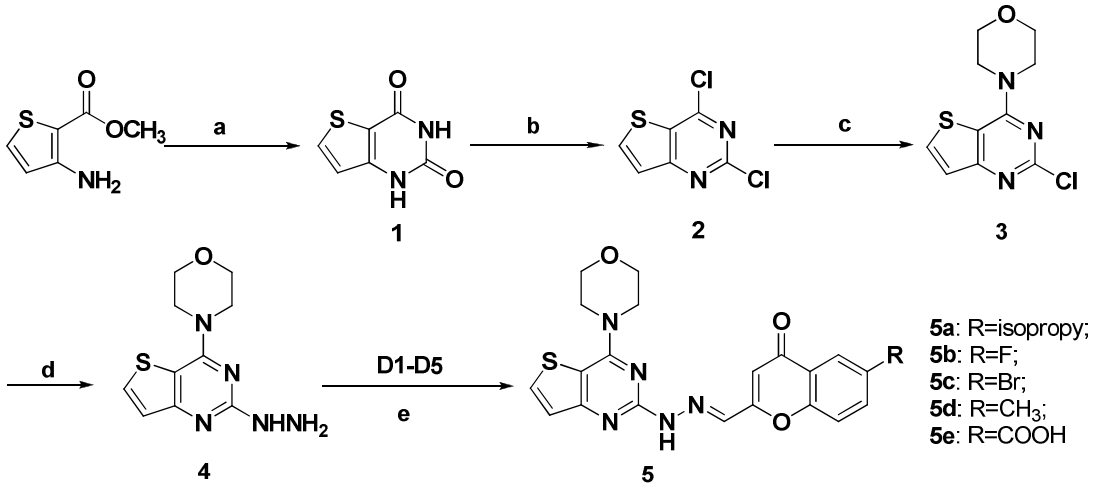

Fig. 3 Synthetic route of 4-morpholinothieno[3,2-d]-pyrimidine derivatives(**5a-5e**)

Reagents and conditions: (a) 5 eq urea, 190°C, 2.5 h; (b) $POCl_3$, DMF (cat.), reflux, 8 h; (c) 2.1 eq morpholine, MeOH, 0°C, 30 min, r.t., 1–2 h; (d) 80% $NH_2NH_2\cdot H_2O$,reflux, 8–10 h;(e) EtOH, reflux, 2–4h.

Biological assay

The in vitro anticancer activities of above synthesized compounds were studied on the PC-3, H460 and SGC-7901 cell. The test results of compounds **5a-5e** were listed in Table 1.

Table 1.The inhibition rate of PC-3, H460 and SGC-7901 cell by **5a-5e** at 10μM levels

Compound	Inhibition rate at 10μM (%)		
	PC-3	**H460**	**SGC-7901**
5a	32.7	12.3	33.3
5b	24.7	5.7	34.9
5c	39.6	30.6	58.9
5d	56.4	22.2	20.7
5e	ND	ND	ND
GDC-0941	74.1	58.7	70.4

ND：Not determined

From Table 1, we could see that some of the target compounds showed moderate activity against the tested cancer cell lines and most of them showed more activity against SGC-7901, PC-3 cancer cell lines than H460 cell line. The substituents of chromone aldehyde at C-6 position played a key role to the activity, especially the bromine atom (**5c**) and methyl group (**5d**).

At 10μM levels, the inhibition rate of compound **5c** against SGC-7901 cell line was 58.9%, and the inhibition rate of compound **5d** against PC-3 cell line was 56.4%. Although their inhibition rate is lower than GDC-0941, it still showed that the introduction of chromone moiety is essential to this kind of compounds. This result suggested that 4-morpholinothieno[3,2-*d*]-pyrimidine derivatives bearing chromone moiety is worthy to study further.

Conclusions

In conclusion, a series of 4-morpholinothieno[3,2-*d*]-pyrimidine derivatives bearing chromone moiety were designed, synthesized and evaluated for their activity against the cancer cell lines. The pharmacological results indicated that some of them exhibited moderate cytotoxicity and high-selectivity against one or more cell lines. And compounds **5c**, **5d** demonstrated better anticancer activity than other compounds. Further modification and SAR studies based on 4-morpholino thienopyrimidine are ongoing in our group.

Acknowledgments

We gratefully acknowledge the generous support provided by Science and Technology Project Founded by the Education Department of Jiangxi Province (No. GJJ13578) and Project Program of Key Laboratory of Drug Design and Optimization, Jiangxi Science & Technology Normal University.

References

[1] Heron M. Leading causes for 2006. National Vital Statistics Reports, 2010, 58 (14): 1-100

[2] Rodon J, Dienstmann R, Serra V, *et al*. Development of PI3K inhibitors: lessons learned from early clinical trials. Nature Reviews Clinical Oncology, 2013, 10(3): 143-153.

[3] Vanhaesebroeck B, Stephens L, Hawkins P. PI3K signalling: the path to discovery and understanding. Nature Reviews Molecular Cell Biology, 2012, 13(3):195-203.

[4] Folkes AJ, Ahmadi K, Alderton W.K, *et al*. The identification of 2-(1H-indazol-4-yl)-6-(4-methanesulfonyl-piperazin-1-ylmethyl)-4-morpholin-4-yl-thieno[3,2-d] pyrimidine (GDC-0941) as a potent,selective, orally bioavailable inhibitor of class I PI3 kinase for the treatment of cancer. J. Med. Chem., 2008, 51(18): 5522-5532.

[5] Heffron TP, Berry M, Castanedo G, *et al*. Identification of GNE-477, a potent and efficacious dual PI3K/ mTOR inhibitor. Bioorg. Med. Chem. Lett., 2010, 20(8): 2408–2411.

[6] Daniel P, Sampath D, Berry M, *et al*. Discovery of (thienopyrimidin-2-yl) aminopyrimidines as potent, selective, and orally available pan-PI3-kinase and dual pan-PI3-kinase/mTOR inhibitors for the treatment of cancer. J. Med. Chem., 2010, 53(3): 1086–1097.

[7] Junttila T. T., Akita R. W., Parsons K, *et al*. Ligand-Independent HER2/HER3/PI3K Complex Is Disrupted by Trastuzumab and Is Effectively Inhibited by the PI3K Inhibitor GDC-0941. Cancer Cell,15, 429–440 (2009).

[8] Wu Fu Zhu, Xin Zhai, Sai Li, *et al*. Synthesis and cytotoxic activity of novel 2,6-disubstituted-4-morpholinothieno[3,2-d]pyrimidines as potent anti-tumor agents. Chin. Chem. Lett., 2012, 23(6): 703-706.

[9] Wufu Zhu, Xin Zhai, Qiangqiang Fu, *et al*. Design, synthesis and anticancer activity of 4-morpholinothieno[3,2-d]pyrimidine derivatives bearing arylmethylene hydrazine moiety. Chem. Pharm. Bull., 2012, 60(8): 1037-1045.

[10] Q.-D. Tu, D. Li, Y., *et al*. Design and Syntheses of novel N'-((4-Oxo-4*H*-Chromen-3-Yl)Methylene)Benzohydr-azide as Inhibitors of cyanobacterial Fructose-1,6-/Sedoheptulose-1,7-Bisphosphatase. Bioorg. Med. Chem., 2013, 21 (11): 2826-2831.

Advanced Materials Research Vols. 989-994 (2014) pp 572-575
© (2014) Trans Tech Publications, Switzerland
doi:10.4028/www.scientific.net/AMR.989-994.572

Vertical Flow Constructed Wetland Spherical Lightceramsite Substrate Nitrogen Factor Research

Yang Yu[1,a] , Haijiao Yu[2,b],Tao Jiang [2,c]

[1]Hainan Highway Survey and Design Institute,Haikou570206,China;
[2]School of Municipal and Environmental Engineering,Shenyang Jianzhu University,Shenyang110168, China.
[a] 11185038@qq.com,[b] yuhaijiao.love@qq.com,[c] jiangtao0801@126.com

Keywords: vertical flow constructed wetland; ceramsite; canna; adsorption; nitrification and denitrification

Abstract. Haydite as filler, selecting canna as wetland plant denitrification effect of vertical flow constructed wetland research. In terms of the mechanism of denitrification, in view of the ceramsite adsorption, microbiological nitrification and denitrification reaction, plants absorb test in three aspects and to study the effect of various factors. Adsorption experiment, ceramsite to NH_4^+–N adsorption reached the maximum at 4 h, adsorption intensity is 0.0045 mg/g, device of NH_4^+–N in the running 92 days maximum theory is 1296 g. Microbial average intensity of nitration was 0.750 $mg.h^{-1}.kg^{-1}$. The denitrifying intensity of 1.090 $mg.h^{-1}.kg^{-1}$. Canna root, stem and leaf nitrogen content were increased by 7.73%, 7.73% and 9.92% per plant cannas average of 1.189 g, nitrogen absorption during the running period of 10 plants absorb about 11.89 g. Vertical flow constructed wetland, the choice of spherical light ceramsite substrate adsorption strength, suitable for packing of wetland. Canna better effect on the absorption of nitrogen, of the three microbes plays a main role for denitrification.

Introduction

In recent years, with the rapid development of economy, the water environment deteriorating, 50% more than 80% of the lakes and river in China by different levels of pollution, eutrophication of lakes in severe cases nationwide.Nitrogen is the key to cause the pollution index, thus control the eutrophication of water bodies must focus on nitrogen removal. Artificial wetland is sewage flows through kinds of plant medium, the filtration, sedimentation, adsorption, such as physics, chemistry, and pollutants and microorganism various kinds of biochemical reaction to remove the pollutant treatment process [1], because of its low energy consumption, easy management, has the advantages of landscape effect is widely used. Artificial wetland according to different structures can be divided into the surface flow, undercurrent and vertical flow three types [2], the vertical flow constructed wetland in three denitrification effect is relatively outstanding. Packing is the carrier of artificial wetland plants, microorganisms, to purify the pollutants in wastewater has important role. For a long time, with zeolite, gravel, fly ash as the research of artificial wetland packing is more, such as such as Zhang Yingying [3], etc., but with ceramsite packing research is less. The value of the spherical light ceramsite as artificial wetland packing were studied The main mechanism of nitrogen removal in constructed wetland system is a microbial nitrification and denitrification reaction. In terms of the choice of wetland plant, studies have shown that ecological wetland in canna on nitrogen uptake is larger, the highest can reach more than 80%. Therefore ceramsite as matrix of wetland plants, canna for vertical flow constructed wetland research on the treatment effect of the low concentration contaminated water is more worthy of promotion.

Nitrogen Removal Factor Test

1.1Research of Ceramic Matrix of NH_4^+-N and NO_3^--N Isothermal Adsorption Effect

Table 1 Performance indexes of spherical light ceramsite filler physics [4]

Particle size	Packing density	Density	porosity	Non-uniform coefficient	Specific surface area
mm	g/cm^3	g/cm^3	%	-	cm^2/g
0.5-32	0.7-1.2	1.2-2.6	55-58	K_m=1.80	2×10^4-1.5×10^5

Materials: spherical light ceramsite, $(NH_4)_2SO4$, Nessler's reagent, sodium potassium tartrate and other reagents were analytically pure.

Test Method: With NH_4^+-N =100mg/L, PH=7.3. 100g ceramic drying at 105℃, after sterilization in an Erlenmeyer flask, the 200ml solution, and the absorbent cotton stuffed bottle. Oscillation in constant temperature oscillation box 25 ℃, 150r/min, in 1, 2, 3, 11, 12... The sampling, 24 hours two times, 10ml each time, every time after sampling with culture medium supplement. The supernatant of NH_4^+-N concentration in solution, two times the average. The saturated adsorption capacity by variation of NH_4^+-N reaction in solution to represent. In addition, the test of ceramsite saturated adsorption capacity of NO_3^--N method for the same.

Method: NH_4^+-N : Nessler's reagent colorimetric method; NO_3^--N: UV Spectrophotometry

Formula:M= (C-c) V/ (1000W)

M:the adsorption strength, ceramic mg/g; C, c:concentration, ammonia nitrogen adsorption and solution of mg/ L; V:the solution volume, taken as the test of mL; W:ceramic mass, g.

1.2 Study on Strength of Microbial Nitrification and Denitrification

The optimum temperature range of nitrification in soil is 30-40℃, while in pure cultures of 25-35℃, 6.6-8.0 is the best pH range. 6-8 is a denitrification the optimum pH, optimum temperature range is 20-30℃. In the test set constant temperature is 25℃, pH=7.3.

Material: $(NH_4)_2SO_4$(0.05mol/L), K_2HPO_4(0.2mol/L),KH_2PO_4(0.2mol/L), according to the volume ratio of 30:7:3 preparation, C/N is about 3:1. and pH=7.3.

Test Method： Two copies of the 100 g ceramic matrix in two of 250 mL glass flask, adding 100 concentration of mL was NH_4^+-N containing 100 mg/L medium, grade 1 (sample 2 (adsorption), microbial uptake of sample), all wrapped with cotton gauze plugging. Sterilization of 30min 1 bottles in the autoclave, removal and 2 bottles placed in the constant temperature box oscillation oscillation 48h, temperature 25℃, rotate speed is 150 r/min, every 6 hours for two water samples of supernatants of 10mL, 0.45μm membrane, the analysis of NO_3^--N content in filtrate, the results averaged. Each water sample with medium supplement. When the concentration of stable NO_3^--N in cultured supernatant, stop test.

Method: Ultraviolet Spectrophotometry **Formula**: $W1= (C_2-C_1) \times (V_1-V_2) \times k/ (t*m)$

W_1:NO_3^--N concentration, unit mass of filler in unit time of $mg.kg^{-1}.h^{-1}$; C_2 ,C_1: represent the mass concentration;NO_3^--N:6h mg/L ;V_1:the volume of culture medium, V_2:water volume packed samples, L; k: water coefficient; m :sample mass, g; t:time, h.

1.2.2 The Denitrification Reaction Test

Material:proportion of glucose ($C_6H_{12}O_6$) (0.02mol/L), KNO3 (0.03mol/L), K_2HPO_4 (0.2mol/L), KH_2PO_4 (0.2mol/L), according to the volume ratio of 10:30:7:3 preparation, C/N is about 3:1. and PH=7.3.

Test Method： Similar to the nitrification reaction test, the difference is the No.1 and No.2 bottle after bottle sterilization and sterilization of rubber stopper tightly and sealed bag, Placed in temperature is 25℃ constant temperature box in the oscillations of the 48 h .The remaining steps above.

Method: Ultraviolet Spectrophotometry **Formula**: $W_1= (C_1-C_2) \times (V_1+V_2) \times k/ (t * m)$

W_1:NO_3^--N concentration, consumption in the denitrification reaction unit in unit time and mass of $mg.kg^{-1}.h^{-1}$; the rest of the symbolic meaning.

1.3 The Amount of Nitrogen Absorption Plant

Material:Artificial wetland in the optimal operation parameters for 84 days, the influent from raw water, the following indexes of water mass.

Table 2 Experimental wastewater mass index

Wastewater quality indicators	pH	NH_4^+-N （mg/L）	TN （mg/L）	TP （mg/L）	DTP （mg/L）
Parameter	6.85-7.43	3.76	3.84	0.34	0.21

Test tank size: 0.8mx0.6mx0.6m;Canna:10 strains (2*5);In order to facilitate drainage, bottom along the direction of flow of 5 ‰ slope.

Test Method

Trial begins to choose has trained plant close to the size of the 3 plants, canna, washed with distilled water, dry, place each canna were divided into three parts for the stem, leaf, root, weighing record, and then placed in the filming for the 105 ℃ oven for 30 minutes, temperature to 60 ℃, 72 hours drying, and then weighing record, the three parts of canna separately after cut up by two grinding, through 80 mesh sieve, stay for chemical analysis. End of the test, randomly selected from the above three strains of canna in artificial wetland plant processing.

Method: TN: potassium persulfate oxidation ultraviolet spectrophotometry; Water and mass: electronic balance weighing method

Formula:P= (M2 * K2 * W2 M1 * K1 * W1)

P:all parts of Canna in growth running total absorption of nitrogen; M1, M2 test before and after the Canna mass; K1, K2 test before and after water coefficient. W1, W2 as the nitrogen content of Canna in vivo test before and after the.

Results and Discussion

2.1 Analysis of Ceramsite Isothermal Adsorption Test

Initial concentration of NH_4^+-N solution is 100mg/L, the concentration of NH_4^+-N decreased at first and then slowly increased.4h NH_4^+-N concentrations reached the lowest at NH_4^+-N , haydite on the maximum adsorption capacity, adsorption capacity of 0.032mg/g. After the start of the desorption occurs, 6h, analytic rate was 11.35%; 12h, analytical rate was 19.50%; 24h, 23.75%. 3H NO_3^--Nresolution for the lowest concentration, the ceramsite on NO_3^--N maximum adsorption capacity, adsorption capacity of 0.024mg/g.

2.2Nitrification and Denitrification Strength Test Analysis

2.2.1 Nitration Strength Test: Denitrification intensity on the use of NH_4^+-N variation before and after culture to approximate representation. In this experiment, the nitrification intensity can directly reflect the wetland system for NH_4^+-N removal capacity.Along with the extension of time, the filler adsorption desorption equilibrium system. 6h, microbial nitrification intensity of 1.354mg.h-1.kg-1; 12h, the nitrification intensity of 0.722mg.h-1.kg-1; 24h, the nitrification intensity of 0.633mg.h-1.kg-1. The nitrification intensity of 0.750mg.h-1.kg-1. Because of the influence of nitrification by dissolved oxygen is larger, with increasing filler depth, dissolved oxygen reduction, nitrification intensity will decline.

2.2.2 The Denitrification Reaction Strength Test: Denitrification intensity on the use of NO_3^--N variation before and after culture to approximate representation. In this experiment, the TN of the influent is NH_4^+-Nand the concentration of NO_3^--N and test, and denitrification intensity to a certain extent, reflect the ability of nitrogen removal and wetland system.Along with the extension of time, the filler adsorption desorption equilibrium system. 6h, microbial denitrification intensity of 0.930mg.h-1.kg-1; 12h, denitrification intensity of 1.030mg.h-1.kg-1; 24h, denitrification intensity of 1.210mg.h-1.kg-1. The average denitrification intensity of 1.090mg.h-1.kg-1. Because of the influence of denitrification intensity by the dissolved oxygen is larger, with increasing filler depth, dissolved oxygen reduction, denitrification intensity increased.

2.3 Analysis of Plant Nitrogen Absorption Test

Before and after the test of Canna physiological characteristics all have a change within a certain range, after the test of Canna plant weight is 2.85 times before the test, and studies have shown that plants absorb changes in plant growth depends to a great extent, the mass of unit plant nitrogen content with plant growth changes very little, Canna in the growth process in the water in which was a slight increase. Therefore be Canna Roots, stems, leaves the average nitrogen content respectively increase 7.73%, 12.4%, 9.92%.

Summary

1.Spherical light ceramsite absorption of NH_4^+-N solution of 100mg/L reached the maximum at 4h, the saturated adsorption amount was 0.032mg/g, equilibrium desorption rate as 34.5%. Spherical light ceramsite absorption of NO_3^--N solution of 100mg/L reached the maximum at 3h, the saturated

adsorption capacity is 0.024mg/g, desorption rate of 37.3%. Equilibrium adsorption strength increased first then decreased and finally tends to the balance trend. Spherical light ceramsite as adsorption intensity, microbial adhesion, equilibrium analytical rate is low, therefore suitable as filler of artificial wetland system.

2.In vertical flow constructed wetland, spherical light ceramsite as filler, the average nitrification strength microorganism was $0.75mg.h^{-1}.kg^{-1}$, average denitrification intensity of $1.09mg.h^{-1}.kg^{-1}$. During the operation the condition, total nitrogen about 2079.41g.

3. Artificial wetland plant cannas unit weight of root, stem and leaf nitrogen content were increased by 7.73%, 7.73% and 9.92% per plant cannas average of 1.189 g, nitrogen absorption during the running period of 10 plants absorb about 11.89 g. Canna on nitrogen absorption effect is better .

Reference

[1] Hatano K Trettin C C, House C H. Microbial populations and decomposition aetivity inthine subsurface flow constructed wedanda[J].In:Constructed wetland for water qualitv improvement. Gerald A M. Florida: Lewis Publishers.1993.540-547

[2] Nie Zhidan, years Yuegang, gold Xiangcan, comparative study of [J]. environmental science,3 type artificial wetland treatment in eutrophic water, 2007,28 (8): 1675-1680

[3] Zhang Yingying, Ding Weimin, Chen Xiujuan, et al. The nitrogen removal mechanism and influencing factors of composite vertical flow analysis [J]. environmental engineering, 2009, 27 (5): 36-39

[4] Jiang Yue, Dong Yan, Wen Hui, et al.3 floating bed plant growth characteristics and allocation of nitrogen, phosphorus Chinese [J]. environmental science, 2011, 31 (5): 774-780

Advanced Materials Research Vols. 989-994 (2014) pp 576-580
© (2014) Trans Tech Publications, Switzerland
doi:10.4028/www.scientific.net/AMR.989-994.576

Effect of Post-weld Heat Treatment on Carbide Precipitation and Impact Properties of Coarse-grained Heat-affected Zone of Q690 Steel

Zhenshun Li[1,2,a], Shengli Li[1,2,b], Lei Tian[1,2], Xianghai Zhang[2] and Jizhi Liu[2]

[1]School of Materials Science and Engineering, Shandong University, Jinan 250061, China;

[2]Engineering Research Center of Large Size Alloy Structural Steel Bars of Shandong Province, China.

[a]lzsh276003@163.com, [b]lishengli@sdu.edu.cn, (Corresponding Author)

Keywords: post-weld heat treatment, CGHAZ, fracture, temper embrittlement, intergranular fracture.

Abstract. The effect of post-weld heat treatment (PWHT) on carbide precipitation and impact properties of coarse-grained heat-affected zone (CGHAZ) of Q690 Steel was studied in this paper. Carbide particles precipitated primarily at prior austenite grain boundaries and martensitic lath boundaries. When the PWHT temperature is 520–570 °C, temper embrittlement occurs. This temperature range is also where the number of carbide particles per unit area at grain boundaries reaches its maximum. The high number of particles per unit area increases the rate of crack initiation at grain boundaries under rapid loading; linking of microcracks along grain boundaries which are already weakened by impurity segregation results in TE and intergranular fracture.

1. Introduction

The heat-affected zone (HAZ) of high-strength low-alloy steels develops poor mechanical properties owing to the thermal cycling experienced during welding; the CGHAZ, whose microstructure typically consists of martensite or bainite (when the heat input is high) is generally considered to be the weakest section [1,2]. Post-weld heat treatment (PWHT) can improve the microstructure and mechanical properties of the CGHAZ; this happens through several processes, including tempering of martensite, decomposition of martensite-austenite (M-A) constituent and elimination of residual stresses [3,4]. Although there have been many industry standards and fabrication codes which attempt to provide PWHT parameters such as duration and temperature, the main purpose of these codes are to eliminate residual stresses; the recommended parameters usually cover a wide range, and must be tailored for a specific steel.

Generally, precipitation of carbide lowers the toughness of high-strength steel, depending on the morphology, distribution and size of the precipitates [5,6]. The loss in toughness caused by carbide is associated with its effect on initiation of fracture[7,8]. To reduce or eliminate welding residual stresses and avoid thermal stresses induced by uneven temperature distribution during cooling, PWHT is often conducted under conditions of high temperature and slow cooling. However, temper embrittlement (TE) usually occurs when as-quenched martensite is slowly cooled through or isothermally heated in the temperature range of 400–600 °C [9]. It is now well established that TE is caused mainly by the segregation and build-up of residual impurity elements (e.g. S, P, Sb, Sn) at grain boundaries [10]. The effect of carbide on TE and the accompanying intergranular fracture mode still needs to be identified; Morozov et al. reported that the temper embrittlement of Cr-Mo-V steel during tempering is affected mainly by carbide formation [11]. The temper embrittlement and intergranular fracture of high carbon carburized steel is also found to be related to cementite formation at austenite grain boundaries during quenching [12]. Details of the mechanisms are not yet understood. The purpose of this paper is to clarify in detail the effect of carbide on TE, and to propose a reasonable PWHT process.

2. Material and experiments

Commercial Q690 steel of 808 MPa yield strength was used. The compositions are given in Table 1. The welding tests were conducted using a YD-500 arc welding machine and carried out by means of multi-layer and multi-pass welding. The welding parameters were: welding current, 230 A, arc voltage, 24.5 V, welding speed, 1.75 mm·s-1. The PWHT included tempering samples at different temperatures (420, 470, 520, 570 or 620 °C) for 1.5 h, followed by cooling in the furnace to 200°C. Microstructures were etched using 3% nital or LePera etchant (50 ml of 1% $Na_2S_2O_5$ aqueous solution+50 ml picric acid 4% in ethanol) and examined by optical microscopy and SEM. Charpy specimens (10×10×55 mm) were etched prior to notching to facilitate accurate placement of the V notch tip within the CGHAZ. Charpy impact tests were performed on a Charpy impact tester (Model: JB30B, Jinan, China) at a temperature of −20 °C. The fracture surfaces of the Charpy specimens were also observed by SEM.

Table 1 Chemical composition of experimental steel (mass fraction, %)

C	Si	Mn	P	S	Cr	Ni	Mo	Nb+V+Ti	B	Alt	Fe
0.07	0.32	1.63	0.008	0.004	0.23	0.13	0.13	＜0.2	0.0014	0.034	Bal.

3. Experimental results

Microstructures of the CGHAZ, as-welded and after PWHT, are shown in Fig. 1. The CGHAZ consists primarily of lath martensite with a small amount of carbides situated at prior austenite grain boundaries and martensitic lath boundaries (Fig. 1a); this is related to the effect of auto-tempering since the carbon content of the steel is low. No significant changes were observed in the morphology of martensitic laths after PWHT at any temperature (Fig. 1b–d). Fig. 1c shows numerous small carbide particles, which have reprecipitated along grain and lath boundaries at 520 °C; the number of these particles per unit area is greatest for this tempering temperature. At 620 °C, particle coarsening occurs and there are fewer particles (Fig. 1d).

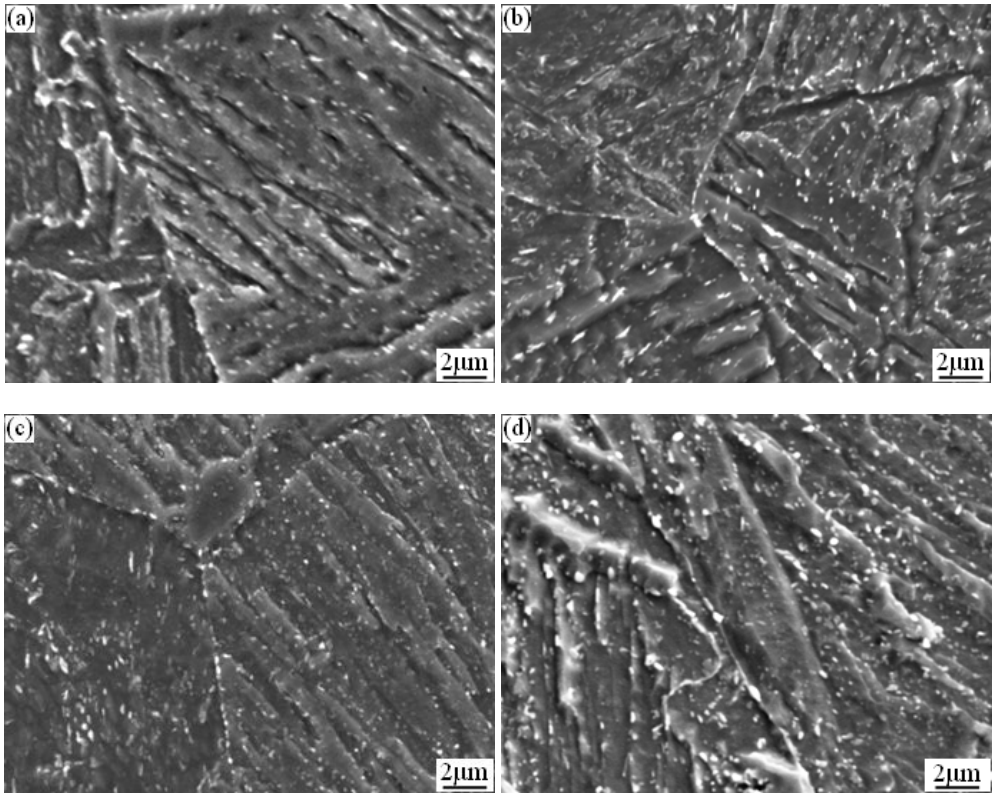

Fig. 1 SEM micrographs of CGHAZ tempered at different temperatures: (a) as-welded, (b) 420 °C,(c) 520 °C, (d) 620 °C

During multipass welding, the CGHAZ formed by the first heating cycle is modified by the subsequent thermal cycles, which form localized and discontinuous zones. It is often found that the intercritically reheated coarse-grained heat-affected zone (IC CGHAZ) displays the lowest toughness [13]. Despite its small size the IC CGHAZ may have an effect on toughness, so the microstructure evolution after PWHT was observed (Fig. 2). As can be seen from Fig. 1a and Fig. 2a, the main difference between the CGHAZ and IC CGHAZ is the presence of a “necklace” structure of blocky particles located at prior austenite grain boundaries. According to the interpretation of the formation mechanism of MA constituent (high-carbon martensite with some retained austenite) by Biss [14], these blocky particles are a mixture of MA constituent and a small amount of bainite. When etched with LePera etchant, the MA constituent (white color) can be distinguished [15] (Fig. 2b). Fig.2b–d shows that the MA constituent decomposes gradually with increasing temperature; by 520 °C it has decomposed completely.

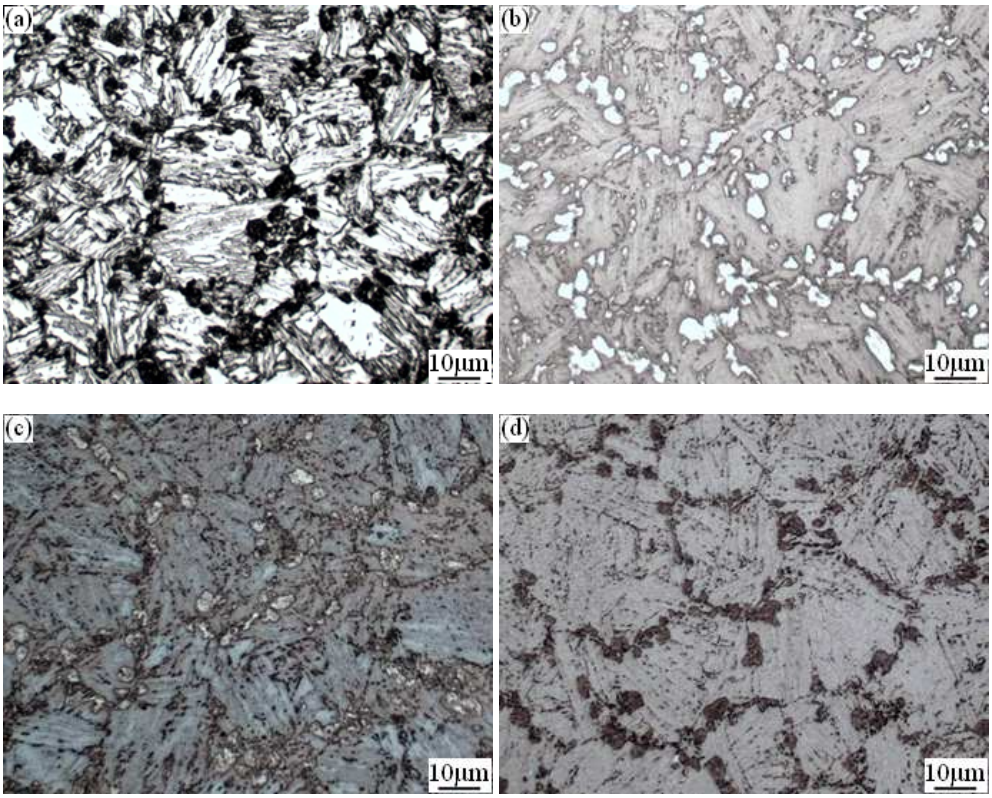

Fig. 2 Optical micrographs of IC CGHAZ tempered at different temperatures: (a, b) as-welded, (c) 420 °C, (d) 520 °C

Table 2 shows the the testing results of Charpy impact energy at different tempering temperature. Tempering the steels at 420°C and 470°C increased the impact energy. However, an abrupt decrease in impact energy was seen at 520 °C and 570 °C, before another increase at 620 °C. The minimum energy at 520 °C to 570 °C

Table 2 The Charpy impact energy of CGHAZ at different tempering temperature.

Temperature/ °C	—	420	470	520	570	620
Charpy impact energy/ J	92.1	143.2	158.1	69.0	55.1	162.5

Fig. 3 shows the fracture surfaces of the CGHAZ, as-welded and after PWHT. The fracture appearance of the as-welded CGHAZ was mostly quasi-cleavage, with many ridges (Fig. 3a). Tempering the specimen at 420 °C changed the fracture surface to show predominately ductile microvoid coalescence, indicating a ductile fracture mechanism. The fracture surface of the sample tempered at 520 °C contains many smooth intergranular facets; this is because the fracture mode has begun to change to brittle intergranular fracture. As the tempering temperature increases to 620 °C, the fracture surface again shows similar features to those observed at 420 °C.

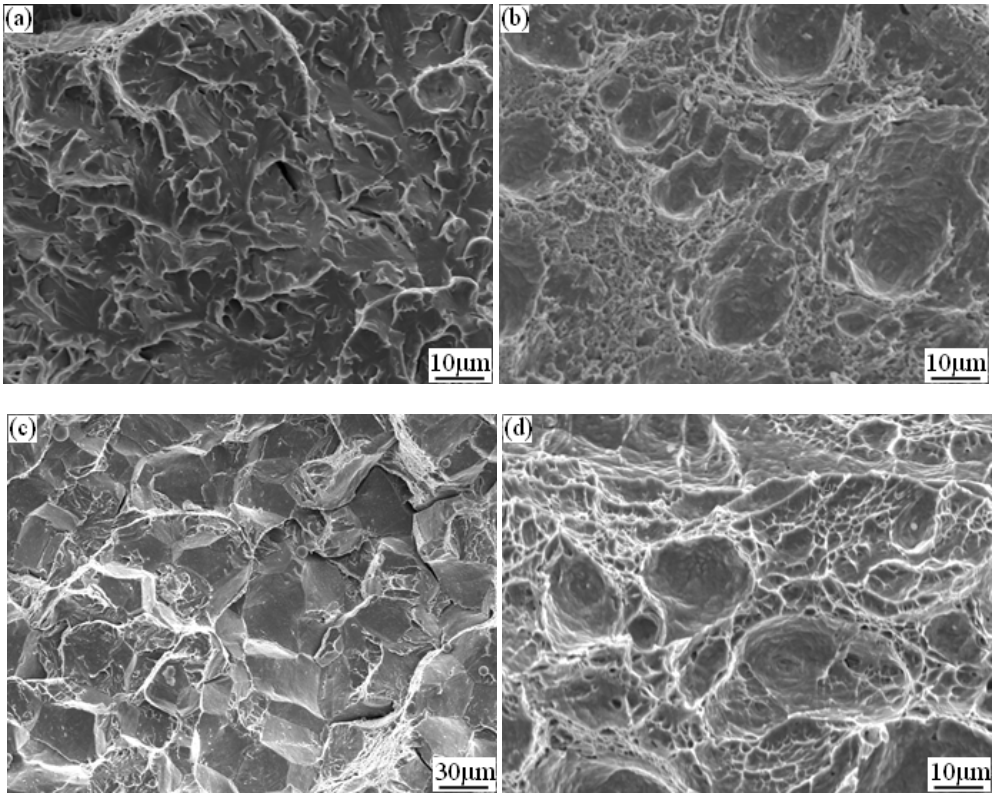

Fig. 3 Fracture surface appearances (SEM) of CGHAZ tempered at different temperatures: (a) as-welded, (b) 420 °C, (c) 520 °C, (d) 620 °C

4. Discussion

The IC CGHAZ is often described as a local brittle zone caused by the presence of MA constituents containing mainly high carbon martensite, which has a twin structure and a hard, brittle nature [16]. On loading, the coarse MA particles readily crack or debond from the matrix, and act as the principal crack-initiation sites because of stress concentration at the MA/matrix interface [17, 18]. The cracks propagate initially within the IC CCHAZ, and further propagation of cracks into the surrounding matrix results in quasi-cleavage (see Fig. 3a). Meanwhile, the initiation and propagation of cracks will be accelerated because of the overlap of applied stresses and residual welding stresses caused by nonuniform thermal expansions and solidifications during the welding processes. After tempering, decomposition of MA constituent and reduction or elimination of residual stresses enhance the impact toughness. The fracture mode changes to ductile microvoid coalescence (see Fig. 3b, d).

Carbides at grain boundaries usually lower toughness, because cracks are initiated when piled-up groups of dislocations meet carbides. When TM and intergranular fracture occur, the amount of carbides is expected to play a role. Previous studies pointed out that, in addition to microstructures, the decrease in impact toughness and onset of intergranular fracture are affected by external conditions such as test temperature (which influences the toughness of the matrix) and loading rate [19]. Research by Ronald showed that no embrittlement-associated fall in toughness was observed using samples tested in slow bending [20]. Under impact loading conditions, to relieve the substantial potential energies gained rapidly, more dislocations form inside a grain, and glide on multiple slip planes in more activated slip systems. Since there are more carbide particles at grain boundaries in the temperature range where TE occurs, massive microcracks emerge at the very beginning of loading. The high number of particles means that there are many microcracks, and these microcracks can become linked during further loading along the grain boundaries, which are already weakened by the impurity segregation. As a result, a sudden decrease in impact energy occurs, accompanied by the change in fracture mechanism to intergranular fracture.

5. Conclusions

(1) When the PWHT is performed at 420 °C, 470 °C, or 620 °C, the impact toughness of CGHAZ can be improved, mostly as a result of the decomposition of MA constituents. At 520 °C and 570 °C, temper embrittlement and intergranular fracture occur, which appear to be associated with the combined effects of precipitation of carbides and the prior segregation of impurities at grain boundaries. Therefore PWHT around 520–570 °C should be avoided.

(2) The carbides nucleate primarily at prior austenite grain boundaries and martensitic lath boundaries. In the temperature range where temper embrittlement occurs, the number of carbide particles per unit area reaches a maximum.

(3) Carbides at grain boundaries are associated with massive microcracks under rapid loading in the temperature range of temper embrittlement; the linking of microcracks along grain boundaries already weakened by impurity segregation results in temper embrittlement and intergranular fracture.

6. References

[1] J.A. Gianetto, J.E.M. Braid, J.T. Bowker, W.R. Tyson, J. Offshore Mech. Arct. Eng. 119(1997) 134-144.

[2] E. Bonnevie, G. Ferrière, A. Ikhlef, D. Kaplan, J.M. Orain, Mater. Sci. Eng., A. 385(2004) 352-358.

[3] Sangho Kim, Sunghak Lee, Young-Roc Im, et al, Metall. Mater. Trans. A. 32(2001) 903-911.

[4] Fukuhisa MATSUDA, Kenji IKEUCHI, Yasuto FUKADA, et al, Trans. JWRI. 24(1995) 1-24.

[5] I. de S. Bott, J. C. G. Teixeira, J. Mater. Eng. Perform. 8(1999) 683-692.

[6] K.S. Kweon, J.H. Kim, J.H. Hong, C.H. Lee, Sci. Technol. Weld. Joining. 5(2000) 161-167.

[7] Gareth Thomas, Metall. Trans. A. 9(1978) 439-450.

[8] N.Bandyopadhyay, C. J. McMahon, Metall. Trans. A. 14(1983) 1313-1325.

[9] V. V. Zabil'skii, Met. Sci. Heat Treat. 29(1987) 32-42.

[10] H. Ohtani, H. C. Feng, C. J. McMahon, Metall. Trans. 5(1974) 516-518.

[11] A. M. Morozov, V. A. Nikolaev, A. M. Parshin, V. V. Rybin, Met. Sci. Heat Treat. 19(1977) 461-465.

[12] Henry K. Obermeyer, George Krauss, J. Heat Treat. 1(1980) 31-39.

[13] Sunghak Lee, Byung Chun Kim, Dongil Kwon, Metall. Trans. A. 24(1993) 1133-1141.

[14] V. Biss, R. L. Cryderman, Metall. Mater. Trans. B. 2(1971) 2267-2276.

[15] R.M. Alé , J.M.A. Rebello , J. Charlier , Mater. Charact. 37(1996) 89-93.

[16] K.S.Kweon, J.H.Kim, J.H.Hong, et al, Sci. Technol. Weld. Joining. 5(2000) 161-167.

[17] Ivan Hrivnak, Fukuhisa Matsuda, Zhonglin Li, et al, Trans. JWRI. 21(1992) 241-250.

[18] C.L. Davis, J.E. King, Metall. Mater. Trans. A. 25(1994) 563-573.

[19] H. Kwon, C. H. Kim, J. Mater. Sci.18(1983) 3671-3678.

[20] T. M. F. Ronald, Metall. Trans.1(1970) 2583-2592.

Advanced Materials Research Vols. 989-994 (2014) pp 581-586
© (2014) Trans Tech Publications, Switzerland
doi:10.4028/www.scientific.net/AMR.989-994.581

Preparation of Polypropylene/Sisal Fiber Composites and Study on the Fiber Orientation

Rongyuan Chen[a], Zan Huang[b], Wei Zou[c], Haichen Zhang[d], Jinping Qu[e]*

National Engineering Research Center of Novel Equipment for Polymer Processing, Key Laboratory of Polymer Processing Engineering of Ministry of Education，South China University of Technology, Guangzhou 510640，China.

[a]rychen2011@163.com, [b]huangzan_80@aliyun.com, [c]zw55624@163.com,

[d]hczhang_2012@163.com, [e]jpqu@scut.edu.cn

Keywords: Twin screw extruder, vane extruder, polypropylene, sisal fiber, orientation.

Abstract. The polypropylene/sisal fiber composites were prepared by twin screw extruder and vane extruder, respectively. The tensile test specimens perpendicular to the extrusion direction and parallel to the extrusion direction were prepared from the extruded composites, respectively. SEM observation showed that fiber orientation of sisal fiber in the composites was not obvious when the content of sisal fiber not more than 15wt%. When the content of sisal fiber was 15wt%, the ability to orientate of sisal fiber in the composite prepared by vane extruder was better than that of in the composite prepared by twin screw extruder, which the fiber orientation of sisal fiber was obvious along the extrusion direction in the composite. Tensile tests showed that the tensile properties of the composite parallel to the extrusion direction with 15wt% sisal fiber prepared by vane extruder were the best compared with other composites in this work. The results illustrated that the orientation of sisal fiber in the composites was beneficial to the improvement of the tensile properties of the composites.

Introduction

In recent years, the research and application of adding natural fibers to plastics as filling material to prepare for fiber reinforced composites have received extensive concern [1-4]. Sisal fiber (SF) as one kind of various fibers with high break strength has been widely used for reinforcing material [5-7]. Polypropylene (PP) is one of the most being in common use polymer materials with good physicochemical properties. Using sisal fiber to reinforce polypropylene not only reduces the cost, but also combines the advantages of the two materials, which has been studied extensively [8-10].

In the present, melt blending method was usually used to prepare for natural fiber/polymer composite, which is mainly carried out by the screw extruder based on shear force field. During the process, fibers are easy to degrade or suffer some damages because of the strong shear force of screws and the strong friction between the screw and the barrel [11]. Different from shear force field, in elongation force field, velocity gradient has the same direction with materials flow direction, which is helpful for the orientation and dispersion of fibers. Some methods realized local applications of elongational deformation flow field in polymer processing with high efficiency but low consumption [12-16]. Qu J.P. et al. invented a vane extruder based on elongational deformation, which is helpful for the orientation and dispersion of fibers in the composites [11,11-19].

In this study, the PP/SF composites were prepared by twin screw extruder and vane extruder respectively. The tensile test specimens perpendicular to the extrusion direction and parallel to the extrusion direction were prepared from the extruded composites, respectively. Tensile tests and SEM morphological observation of the specimens were carried out. The orientation of SF in the composites prepared by the two extruders was characterized. The tensile properties and the relationship between the orientation of SF and tensile properties were also investigated in this work.

Experimental

Materials and Equipment. Polypropylene (N-Z30S) with a density of 0.9 g/cm^3 and MFI (190°C, 2.16kg) 25 g/10 min was supplied by China Petroleum & Chemical Co., China; Sisal fiber was supplied by Dongfang Sisal Co., China.

The vane extruder (VE) used in this work is self-designed. Figure 1 shows the schematic diagram of the vane extruder. The vane extruder is novel equipment for polymer processing, which comprised of several vane plasticating and conveying unit. The vane extruder extrusion completes a plasticating and positive displacement conveying process based on elongational rheology in a short thermo-mechanical history [20]. The temperature profile from hopper to die of VE was determined by 170-180-185-180°C. The twin screw extruder (TSE) used in this work is a traditional extruder, the screw diameter is 50, the length to diameter ratio is 38. The temperature profile from hopper to die of TSE was determined by 170-175-180-180-185-185-180-180°C.

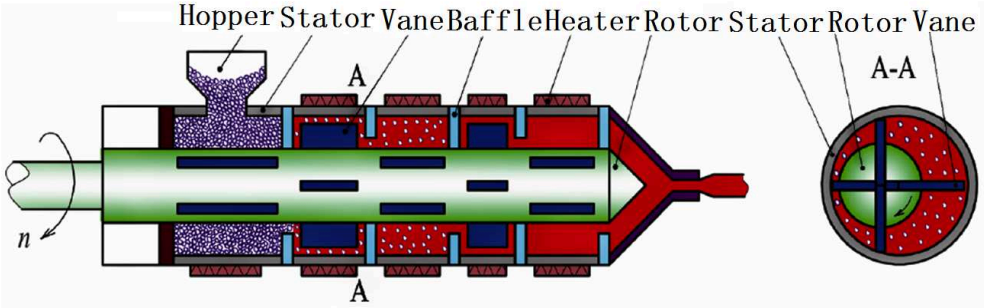

Fig.1 The schematic diagram of vane extruder

Preparation and Characterization. The dried SF was cut to about 10mm and blended with PP according to the mass ratios (PP/SF, 95/5, 90/10, 85/15) in a mixing machine. The mixtures of PP/SF were then fed into the VE and TSE for extrusion processing with a rotation speed of 60r/min. Subsequently, the dried composite strips were compressed into composite sheets with the thickness of 1mm according to the extrusion direction orderly in the mould. The composites were kept in the mould under 190°C, 10MPa for 6min and then cooled to room temperature. The composites sheets were then cut perpendicular to the extrusion direction and parallel to the extrusion direction to prepare for the tensile specimens.

The tensile tests of the composites were carried out using an Instron Universal Testing Machine (model 5566, USA) with a crosshead speed of 2 mm/min. All of the data are the average from six determinations. The brittle fractured surface and the tensile test fractured surface of the PP/SF composites were coated with Au for SEM (S-3700N, Hitachi, Japan) observation.

Results and Discussion

Figure 2 shows the brittle fractured surface of PP/SF composites (with 15% SF) prepared by TSE and VE. In Fig. 2, TSE (a) and VE (a) show the fractured surface perpendicular to the extrusion direction, TSE (b) and VE (b) show the fractured surface parallel to the extrusion direction. It can be seen from TSE (a) and TSE (b) that there is no remarkable SF orientation in PP/SF composite. On the surface in TSE (a), there are fibers and grooves parallel to the surface, and there are also fibers and holes perpendicular to the surface. In TSE (b), the morphology is similar to TSE (a). The result indicates that the SF in the PP/SF composites prepared by TSE in our experiment oriented along the extrusion direction was not obvious and the ability of orientation of SF was weak. For the PP/SF composites prepared by VE, it can be seen from VE (a) and VE (b) that the orientation of SF in the composite was obvious. In VE (a), there are fibers and holes perpendicular to the fractured surface. In VE (b), there are fibers and grooves parallel to the fractured surface. The result indicates that the SF in the PP/SF composites prepared by VE in our experiment oriented along the extrusion direction was obvious and the ability of orientation of SF was strong.

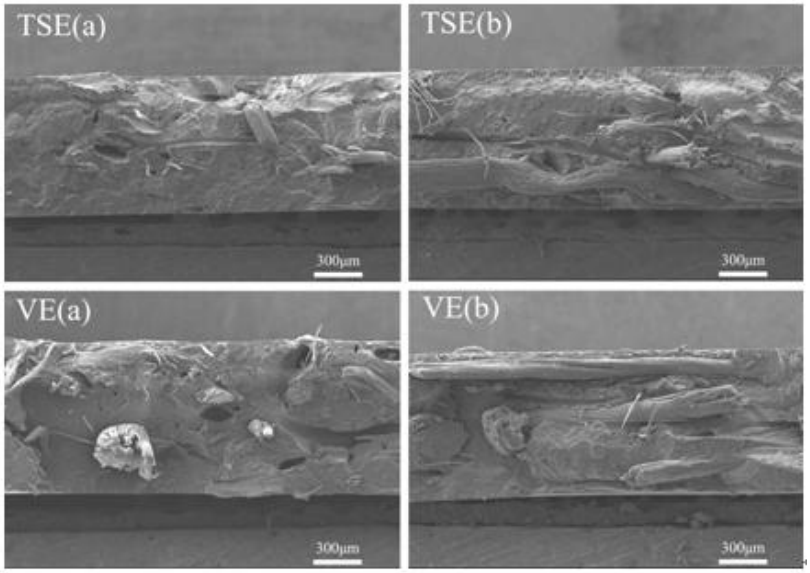

Fig.2 SEM of brittle fractured surface of PP/SF composites (with 15% SF) prepared by TSE and VE (a- perpendicular to the extrusion direction, b- parallel to the extrusion direction)

The tensile test fractured surface of PP/SF composites (with 15% SF) prepared by TSE and VE was observed by SEM in Fig. 3. In Fig. 3, TSE (c) and VE (c) show the fractured surface perpendicular to the extrusion direction, TSE (d) and VE (d) show the fractured surface parallel to the extrusion direction. In our tests, the tensile tests direction was the same with extrusion direction. It is similar to the observation in Fig. 2. In Fig. 3, on the tensile fractured surface of PP/SF composite prepared by TSE, there are fibers and grooves parallel to the surface, and there are also fibers and holes perpendicular to the surface (See TSE (c) and (d)). For the composite prepared by VE, it can be seen from VE (c) and VE (d) that along the extrusion direction, the SF in the composite oriented obviously (See VE(c) and (d)). Combined with the fiber orientation character in Fig. 2 and Fig. 3, the results indicate that the VE processing of the PP/SF composite is more conducive to improve the SF orientation along the extrusion direction compared with the TSE processing in our experiment condition.

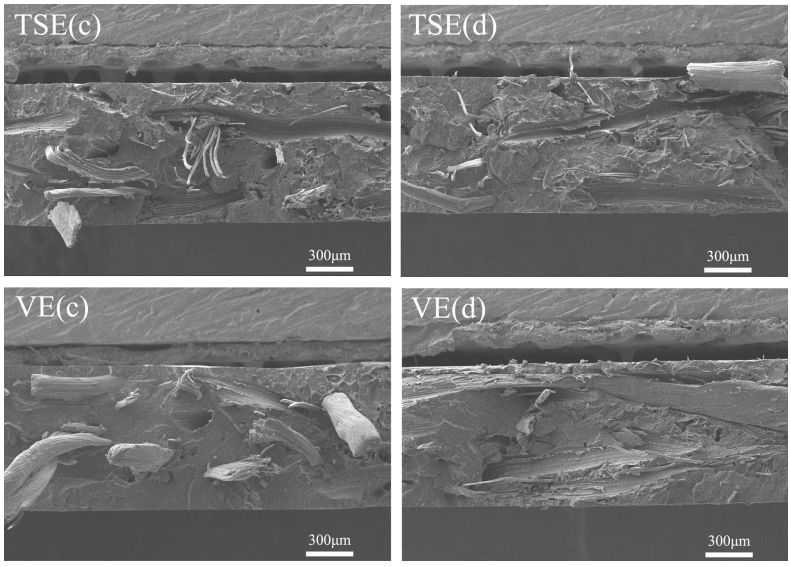

Fig.3 SEM of tensile test fractured surface of PP/SF composites (with 15% SF) prepared by TSE and VE (a- perpendicular to the extrusion direction, b- parallel to the extrusion direction)

In order to investigate the interfacial properties of SF and PP matrix in the PP/SF composites, SEM of enlarged scale of tensile test fractured surface of PP/SF composites (with 15% SF) prepared by TSE and VE were observed in Fig. 4. It can be seen that the interfacial compatibility between PP matrix and SF was bad. Not only processing by TSE but also by VE, there is obvious gap between PP matrix and SF. Moreover, it can be seen from Fig. 4 that there are grooves formed from the fiber

pull-out from PP matrix during the tensile test process. Compared with TSE processing, the grooves in the composite prepared by VE was much coarser. The result indicates that VE processing has a better squeezing action than TSE processing on the PP/SF composites, which is beneficial to improve the interfacial properties and mechanical properties of the composites.

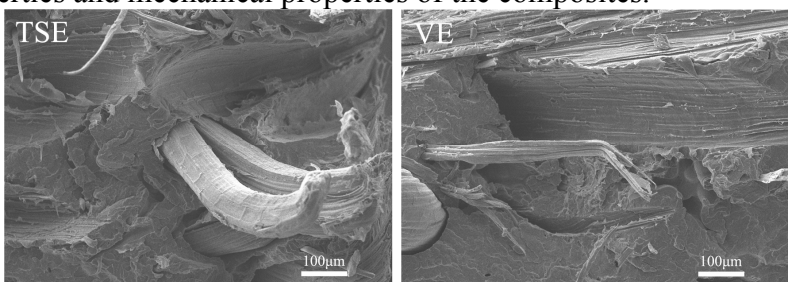

Fig.4 SEM with enlarged scale of tensile test fractured surface of PP/SF composites (with 15% SF) prepared by TSE and VE

The tensile properties of PP/SF composites prepared by TSE were shown in Table 1. It can be seen that both perpendicular to the extrusion direction and parallel to the extrusion direction, the tensile strength, tensile modulus and elongation at break of PP/SF composites with different SF content decreased significantly compared with pure PP. This mainly because that there are a lot of polar hydroxyl groups in SF, while polypropylene chains are nonpolar, the interfacial compatibility between PP matrix and SF is poor [21]. The weak interface interaction between SF and PP matrix cannot transfer stress and energy effectively under tensile stress. The tensile property of the composites then decreased. When the SF content was 5wt%, the tensile strength and elongation at break of the composite perpendicular to the extrusion direction and parallel to the extrusion direction were similar, but the tensile modulus was very different. When the SF content was 10wt%, the difference of tensile strength of the composite between perpendicular to the extrusion direction and parallel to the extrusion direction was increased, while the differences of tensile modulus and elongation at break were little. When the SF content was 15wt%, the differences of tensile strength, tensile modulus and elongation at break of the composite between perpendicular to the extrusion direction and parallel to the extrusion direction were little. For the three composites with different SF content, the tensile properties of the composites perpendicular to the extrusion direction and parallel to the extrusion direction have little change. As the TSE processing is based on shear force flow, the orientation of SF in the composite prepared by TSE was poor.

Table1 Tensile properties of PP/SF composites prepared by TSE

Tensile property	PP	PP/5wt% SF		PP/10wt% SF		PP/15wt% SF	
		PL[d]	PD[e]	PL	PD	PL	PD
TS[a] (MPa)	31.66	24.88	24.50	27.86	24.31	23.19	21.97
TM[b] (MPa)	261.11	209.50	229.90	205.08	211.39	217.90	205.11
EAB[c] (%)	15.48	11.36	11.17	10.88	11.12	12.48	11.71

Table2 Tensile properties of PP/SF composites prepared by VE

Tensile property	PP	PP/5wt% SF		PP/10wt% SF		PP/15wt% SF	
		PL[d]	PD[e]	PL	PD	PL	PD
TS[a] (MPa)	33.33	27.04	26.72	26.28	23.42	28.71	19.20
TM[b] (MPa)	275.74	211.08	209.69	213.90	190.51	259.71	193.26
EAB[c] (%)	16.29	12.67	12.31	11.43	10.36	13.2	10.22

[a] TS refers to tensile strength, [b] TM refers to tensile modulus, [c] EAB refers to elongation at break, [d] PL refers to perpendicular to the extrusion direction, [e] PD refers to parallel to the extrusion direction

Table 2 shows the tensile properties of PP/SF composites prepared by VE. Similar to the composites processed by TSE, the tensile properties of PP/SF composites prepared by VE was decreased significantly compared with pure PP. It is due to the poor interfacial compatibility between PP matrix and SF. When the SF content was 5wt%, the tensile strength, tensile modulus and elongation at break of the composites perpendicular to the extrusion direction and parallel to the

extrusion direction were closed to each other. This indicates that in our experiment, the SF orientation in the composite with low SF content was poor. With the SF content increase, the difference of tensile strength, tensile modulus and elongation at break of the composites perpendicular to the extrusion direction and parallel to the extrusion direction became obvious. Compared with the composite with 5wt% SF and 10wt% SF, the tensile strength, tensile modulus and elongation at break of the composite parallel to the extrusion direction were increased when the SF content was 15wt%. For the composite perpendicular to the extrusion direction, the tensile properties were decreased compared with the composite with 5wt% SF and 10wt% SF. This may due to that with the increasing content of SF, the orientation of SF in the composite was easier and obvious, which increased the tensile properties of the composite parallel to the extrusion direction but decreased the tensile properties of the composite perpendicular to the extrusion direction. When the SF content was 15wt%, as the VE processing is based on elongation force field, the SF in the composite along the extrusion direction was easy to orient under elongation force. The orientation of SF in the composite with 15wt% SF can be seen in Fig. 2 and Fig. 3. As a result, the tensile properties of the composite parallel to the extrusion direction were the best.

Compared the TSE processing and VE processing, the comprehensive tensile properties of the composite parallel to the extrusion direction prepared by VE were better than that by TSE. On the one hand, the thermo-mechanical history of VE processing is short; the materials are not easy to degrade. For the TSE processing, the materials are easy to degrade. In our experiment, the color of the composite prepared by TSE was yellow and darker. It is due to the degradation of SF in the composite. On the other hand, the orientation of SF in the composite prepared by VE was much easier than that by TSE. Especially, when the SF content was 15wt%, the tensile strength of the composite parallel to the extrusion direction prepared by VE was greater than that by TSE. The result indicates that VE offers advantages than TSE on processing fiber reinforced polymer composites.

Summary

The PP/SF composites (SF content, 5wt%-15wt%) were prepared by TSE and VE, respectively. The orientation of SF in the composite prepared by VE was much easier than that prepared by TSE. When the SF content was 15wt%, the orientation of SF in the composite prepared by VE was obvious. The tensile properties of the PP/SF composites with 15wt% SF parallel to the extrusion direction prepared by VE were the best of all the composites in this work. The orientation of SF in the composites was beneficial to improve the tensile properties of the composites in the orientation direction.

Acknowledgment

The authors wish to acknowledge National Natural Science Foundation of China-Guangdong Joint Fundation Project (U1201242), 973 Program (2012CB025902), The National Research Foundation for the Doctoral Program of Higher Education of China (20120172130004), New Century Excellent Talents in University (NCET-11-0152), Pearl River Talent Fund for Young Sci-Tech Researchers of Guangzhou City (2011J2200058).

References

[1] Ratna Prasad A V, Mohana Rao K. Mechanical properties of natural fibre reinforced polyester composites: Jowar, sisal and bamboo. Materials & Design, 2011, 32(8): 4658-4663.

[2] George J, Sreekala M S, Thomas S. A review on interface modification and characterization of natural fiber reinforced plastic composites. Polymer Engineering & Science, 2001, 41(9): 1471-1485.

[3] Shalwan A, Yousif B F. In state of art: mechanical and tribological behaviour of polymeric composites based on natural fibres. Materials & Design, 2013, 48: 14-24.

[4] Faruk O, Bledzki A K, Fink H P, et al. Biocomposites reinforced with natural fibers: 2000–2010. Progress in Polymer Science, 2012, 37(11): 1552-1596.
[5] Lu S R, Ling R H, Luo C X, et al. Sisal fibre/polypropylene composites modified with carboxyl terminated hyperbranched polymer. Plastics, Rubber and Composites, 2013, 42(9): 361-366.
[6] Megiatto Jr J D, Silva C G, Ramires E C, et al. Thermoset matrix reinforced with sisal fibers: effect of the cure cycle on the properties of the biobased composite. Polymer Testing, 2009, 28(8): 793-800.
[7] Jeencham R, Suppakarn N, Jarukumjorn K. Effect of flame retardants on flame retardant, mechanical, and thermal properties of sisal fiber/polypropylene composites. Composites Part B: Engineering, 2014, 56: 249-253.
[8] Lu S R, Ling R H, Luo C X, et al. Sisal fibre/polypropylene composites modified with carboxyl terminated hyperbranched polymer. Plastics, Rubber and Composites, 2013, 42(9): 361-366.
[9] Kaewkuk S, Sutapun W, Jarukumjorn K. Effects of interfacial modification and fiber content on physical properties of sisal fiber/polypropylene composites. Composites Part B: Engineering, 2013, 45(1): 544-549.
[10] Han S, Ren K, Geng C, et al. Enhanced interfacial adhesion via interfacial crystallization between sisal fiber and isotactic polypropylene: direct evidence from single – fiber fragmentation testing. Polymer International, 2014, 63(4):646-651.
[11] Jin – Ping Q, Li – Ming L, Bin T, et al. Effect of dynamical converging channels on fiber organization and damage during vane extrusion of sisal fiber – reinforced polypropylene composites. Polymer Composites, 2012, 33(2): 185-191.
[12] Rauwendaal C, Osswald T, Gramann P, et al. Design of dispersive mixing devices. International Polymer Processing, 1999, 14(1): 28-34.
[13] Folgar F, Tucker C L. Orientation behavior of fibers in concentrated suspensions. Journal of Reinforced Plastics and Composites, 1984, 3(2): 98-119.
[14] Chiba K, Nakamura K. Numerical solution of fiber suspension flow through a complex channel. Journal of non-newtonian fluid mechanics, 1998, 78(2): 167-185.
[15] Advani S G, Tucker III C L. The use of tensors to describe and predict fiber orientation in short fiber composites. Journal of Rheology, 1987, 31(8): 751-784.
[16] Yang Z, Chen R, Zhao Y, et al. Preparation and mechanical properties of pithecellobium clypearia benth fibre/polypropylene composites processed by vane extruder. Journal of Reinforced Plastics and Composites, 2014, 33(2): 150-165.
[17] Qu, J. P. Can. Pat.CN200810026054X, 2009.
[18] Qu J P, Yang Z T, Yin X C, et al. Characteristics study of polymer melt conveying capacity in vane plasticization extruder. Polymer-Plastics Technology and Engineering, 2009, 48(12): 1269-1274.
[19] Qu J P, Chen H Z, Liu S R, et al. Morphology study of immiscible polymer blends in a vane extruder. Journal of Applied Polymer Science, 2013, 128(6): 3576-3585.
[20] Qu J P, Zhang G Z, Chen H Z, et al. Solid conveying in vane extruder for polymer processing: effects on pressure establishment. Polymer Engineering & Science, 2012, 52(10): 2147-2156.
[21] Wu C, Jia S, Chen R, et al. Composites of sisal fiber/polypropylene based on novel vane extruder: Effect of interface and damage on mechanical properties. Journal of Reinforced Plastics and Composites, 2013, 32(24): 1907-1915.

Advanced Materials Research Vols. 989-994 (2014) pp 587-590
© (2014) Trans Tech Publications, Switzerland
doi:10.4028/www.scientific.net/AMR.989-994.587

Mechanical Properties of Chopped Carbon Fiber Reinforced PBS/CF Composites

Wei Li[1, a], Jin-Ping Qu[2, b]

[1]National Engineering Research Center of Novel Equipment for Polymer Processing, Key Laboratory of Polymer Processing Engineering of the Ministry of Education, South China University of Technology, Guangzhou 510640, China

[a]liweigdut2007@163.com, [b]jpqu@scut.edu.cn

Correspondence to: Jin-ping Qu (Email: jpqu@scut.edu.cn)

Keywords: PBS; Carbon fiber; Mechanical properties.

Abstract. Chopped carbon fiber (CF) reinforced PBS/CF composites were prepared by twin-screw extrusion processing. The effect of adding a certain quantity of CF in composites on the tensile, flexural and impact properties have been investigated. The results indicated that the tensile properties, flexural properties and impact properties of the PBS/CF composites were first improved and then decreased with the increase of the content of CF.

1. Introduction

Composites enhanced with short fiber have been receiving great attention in recent years [1]. PBS is a kind of completely biodegradable plastics, possesses good melt processability, biocompatibility, good thermal stability and high toughness related to its low glass transition, which is widely used in packaging materials, hygienic products, agricultural film and other fields [2, 3]. In order to widen its applications, the physical properties of PBS need to be improved by addition of fibers. Nowadays, the reinforcing materials in polymer composites are typically carbon fibers (CF). Carbon fiber (CF) is a kind of non-metallic materials. Carbon fibers have become very important as a kind of reinforcement for polymeric composites over the last 40 years because of their high strength, high modulus, good electrical conductivity, low density, strong ability to adapt environment and good corrosion resistance to chemicals [4, 5]. The objectives of this study are to fabricate PBS/CF composites and to investigate the effects of the carbon fiber content on the mechanical properties of the composites. In this paper, the performance of the composites are discussed in terms of the tensile, flexural and impact properties.

2. Experimental

2.1 Materials

Poly (butylene succinate) (PBS) with a density of 0.91 $g.cm^{-3}$ and MI of 4.5g/10 min (130°C, BIONOLLE 1903MD) was provided by Showa Co. Ltd, Japan. The melting temperature of the PBS was about 120°C. Its tensile strength was 40MPa, with impact strength 6KJ/m^{-2}.

The carbon fiber (HTS-50PAN) used was also a commercial product (TOHO Products Co. Ltd, Japan) with an average diameter of 7um and an average length of 2～12mm. Its density was approximately 1.76 $g.cm^{-3}$. Its tensile strength was 3.7GPa, tensile modulus is 230GPa.

2.2 Composites preparation

The pure PBS was dried in an oven at 50°C for 8 hours. Then the carbon fibers were put in the chamber of a stove for 10 min and oxidized at 450°C. The carbon fibers mass fraction were 1%, 2%, 3%, 4%, 5%. Then the carbon fibers were directly mixed with the PBS in a high-speed mixer for around 15 min to prepare PBS/CF composites. For the purpose of comparison, pure PBS was also

melt blended under similar processing conditions in the mixer. In the first step the PBS/CF composites were homogenized in the twin-screw extruder. The mixture was cooled to room temperature and cut to the granules again. Then the samples were hot pressed at 130°C under 10 MPa for more than 6 min using a flat-plate sulfide machine to obtain composite sheets (4 mm thickness).

2.3 Characterization

The tensile properties of the PBS/CF composites were measured according to GB/T 1040—2006 using an Instron universal testing machine (model 5569) with the tensile speed 2 mm/min and the distance of 50 mm. The flexural testing was performed according to GB/T 1446—2006 standard at a cross-head speed of 2 mm/min. The impact strength according to GB/T 1843-2008. The average values of strength and modulus of each composites were obtained from five specimens. All the tests were performed at the room temperature, 50% relative humidity.

3. Results and discussion

3.1 Tensile property

Tensile properties of the PBS/CF composites reinforced by CF with different fiber content are represented in Figure 1. When the CF content reaches 2 wt%, the tensile strength and modulus reach

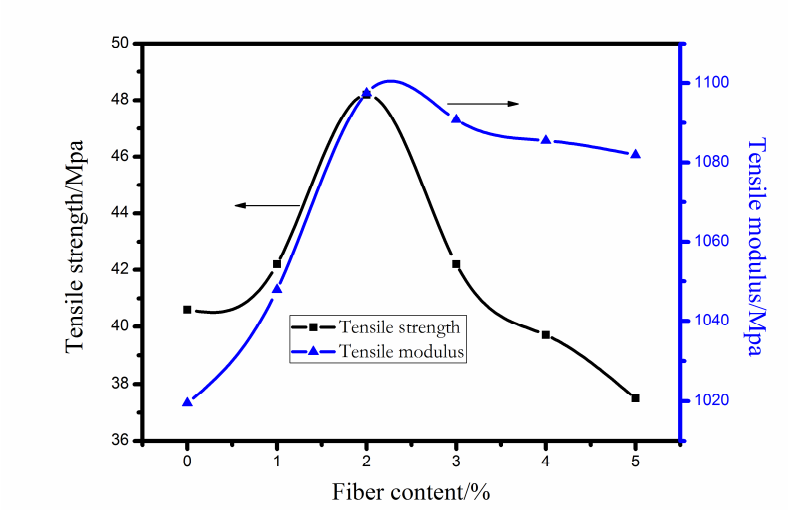

Fig. 1 The relationship of the tensile strength/modulus of composites and the content of carbon fiber

its maximum (48.1 MPa and 1097.5MPa), which is about 18.7% and 7.7% higher than that of pure PBS. The increase in tensile strength and modulus of PBS/CF is primarily attributed to the presence of carbon fiber, which allows a uniform stress distribution from continuous PBS matrix to dispersed fiber phase [6,7]. Tensile strength of composites subsequently decreases sharply along with the increase of fiber content. Tensile modulus then decreases slightly. The decrease in tensile strength and modulus may be due to the presence of so many fibers that cause more possibility of crack initiation, composite failure and fiber agglomeration within PBS/CF composites, leading to stress concentration and become a source of fracture, which have a negative impact on the tensile properties of the composites [2].

3.2 Flexural properties

It is observed that with the increase of fiber content from 0 to 3wt%, the flexural strength gradually increased, When the CF content reaches 3wt%, the flexural strength reaches its maximum (29.7MPa), which is about 9.14% higher than that of pure PBS. It is due to that the carbon fibers are coated effectively by the PBS, making carbon fiber evenly distributed in PBS. When the carbon fiber content increases continuously, the flexural strength of composites decreases. It is because it's easy to form fiber agglomeration, carbon fibers are not coated effectively by the PBS.

The flexural modulus goes up almost linearly with increasing fiber loading between 0 and 1wt %. When the fiber content is less than 4wt%, flexural modulus nearly remains constant. When the fiber content is greater than 4wt%, flexural modulus increases greatly. The modulus of the PBS/CF composites increases by 104.1% than the pure PBS with the fiber mass fraction reaches to 5%.

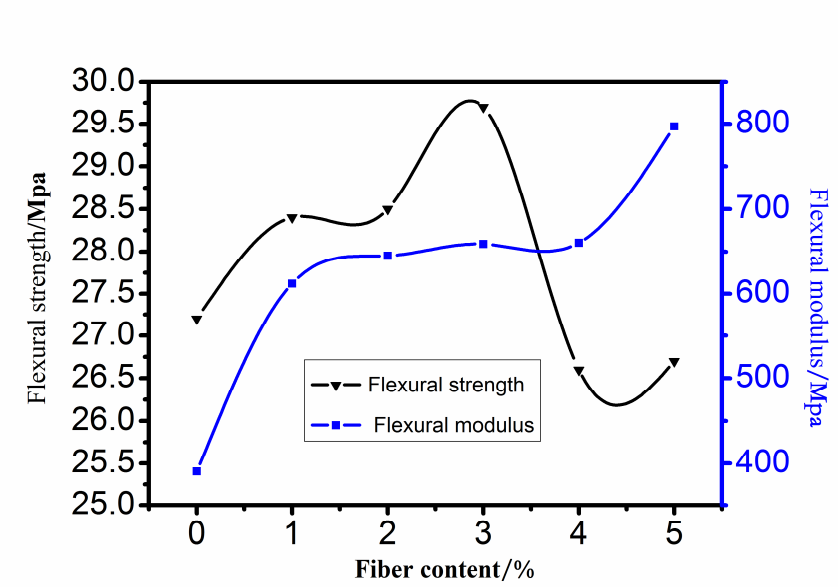

Fig.2 The relationship of the flexual strength/modulus of composites and the content of carbon fiber

3.3 Impact properties

The results of impact test on the PBS/CF composites are shown in Figure 3. The incorporation of

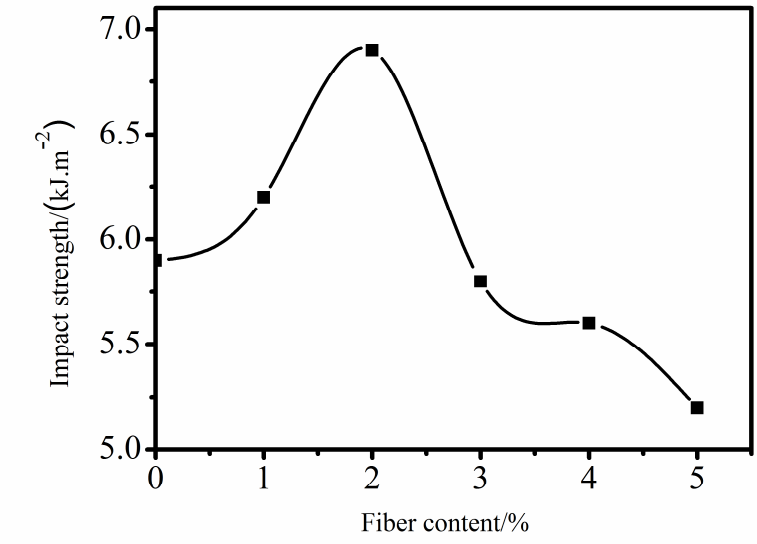

Fig.3 The relationship of the impact strength of composites and the content of carbon fiber

CF enhances impact strength of pure PBS. When the CF content reaches 2wt%, the impact strength reaches its maximum. The highest impact strength of the composites is 6.9kJ /m^{-2}, about 17% higher than that of the pure PBS. It is because PBS has good flexibility, which can deliver stress to make material not damaged under the external force. When the fiber content increases, low ductility of the fiber makes PBS constrainted, which decreases the impact strength.

4. Conclusion

In this study, the importance of carbon fibers in PBS/CF composites has been highlighted. It is observed that with the increase of fiber content from 0 to 2wt%, the tensile and impact strength are all gradually increased, and over 2wt% fiber content they are decreased or nearly remain constant. When the CF content reaches 3wt%, the flexural strength reaches its maximum (29.7MPa), which is about 9.14% higher than that of pure PBS. When the carbon fiber content increases, the flexural strength of composites decreases. The experimental results show that the mechanical strength or modulus of composites exits an optimum value at certain fiber content, which is 2wt% in this study.

Acknowledgements

The authors wish to acknowledge National Natural Science Foundation of China-Guangdong Joint Fundation Project (U1201242), 973 Program (2012CB025902), The National Research Foundation for the Doctoral Program of Higher Education of China（20120172130004）, New Century Excellent Talents in University (NCET-11-0152), Pearl River Talent Fund for Young Sci-Tech Researchers of Guangzhou City (2011J2200058).

References

[1] Wambua P, Ivens J, Verpoest I. Natural fibers: can they replace glass in fiber reinforced plastics? Compos Sci Technol 2003; 63: 1259–64.

[2] Fujimaki T. Processability and Properties of Aliphatic Polyesters, 'BIONOLLE', Synthesized by Polycondensation Reaction [J]. Polym Degrad Stabil, 1998, 59 (1/3): 209-214.

[3] Weng Yunxuan, Niu Lijie, Xu Guozhi, Production Situation and Development Trend of Biodegradable Plastics in the World [J]. China Plastics, 2008, 22(12):1-5.

[4] Xiaoming Zhang, Xiongya Liu. Fiber reinforced thermoplastic composites and its application [M]. Beijing：Chemical industry press，2007.

[5] Yanxia Zhang．The research of carbon fiber reinforced nylon composites [D]．ShangHai：Donghua university master's degree thesis，2010．

[6] Colom X, Carrasco F, Pages P, Canavate J. Effects of different treatments on the interface of HDPE/lignocellulosic fiber composites. Compos Sci Technol 2003; 63:161–9.

[7] Mohanty S, Verma SK, Nayak SK. Dynamic mechanical and thermal properties of MAPE treated jute/HDPE composites. Compos Sci Technol 2006; 66: 538–47.

[8] Li Li, Changlin Cao. Effect of Carbon fiber content on mechanical properties of short carbon fiber reinforced PE composite[J]. Foundry Technology, 2012(1)：26-28．

[10] Xin Gao, Yanjiang Song, Xiaodong Wang. Mechanical properties of carbon fiber reinforced polyimide composites [J]. Journal of composite materials, 2009，26(3)：50-54．

[11] Xiaojun Lv, Qi Zhang, Zhaoqing Ma. Wet and heat aging on the mechanical properties impact of carbon fiber/epoxy resin composites [J]. Materials engineering, 2005(11)：50-57．

[12] Liu Lifang, Yu Jianyong, Cheng Longdi, et al. Mechanical Properties of Poly Biocom-posites Reinforced with Surface Modified Jute Fibre [J].Compos Part A, 2009, 40(5)：669-674.

Advanced Materials Research Vols. 989-994 (2014) pp 591-594
© (2014) Trans Tech Publications, Switzerland
doi:10.4028/www.scientific.net/AMR.989-994.591

Study on Optimization of degradation of landfill leachate by electrochemical oxidation process with Response Surface Methodology

Yang Yu[1,a],HaiJiao Yu[2,3,b],Yinping Zhao[2,c]
[1]Hainan Highway Survey and Design Institute, Haikou, Hainan, 570206,China
[2]School of Municipal and Environmental Engineering in Shenyang Jianzhu University, Liaoning, Shenyang, 110168, China
[3]Institute of Applied Ecology. Chinese Academy of Sciences, Liaoning, Shenyang, 110164, China
[a]11185038@qq.com, [b]yuhaijiao.love@qq.com, [c]825670047@qq.com

Keywords: Optimization, landfill leachate, electrochemical oxidation process, surface methodology

Abstract. This experiment used the response surface methodology to optimize the treatment effect of electrochemical oxidation degradation of landfill leachate. The relationship between current intensity, aeration and pH value was studied by the response surface methodology. The analysis of quadratic polynomial regression and response surface was studied by Design expert7.0 software, and the model was optimized.

Introduction

Response surface method (RSM) is a comprehensive experimental design and mathematical modeling optimization method that evaluates the factors, which affects electrochemical degradation process and their interactions by establishing a continuous variable surface model, and determines the best level scope. It can decrease the time of test, finally achieve the goal of optimizing this response[1], and provide technical support for the electrochemical treatment of landfill leachate.

1 The experimental materials and methods

1.1 Waste water sources and water quality

This experiment adopts the landfill leachate collected from a landfill site of Shenyang. The main ingredients of the landfill leachate are shown in Table 1.

Table 1 .The main ingredients of the garbage leachate

main ingredients	units	contents
COD	mg/L	5000~20000
NH_3	mg/L	1000~1300
Cl^-	mg/L	500~4000
pH	1	7.5~8.5

1.2 Test equipment and methods

Instruments: WFJ2100 visible spectrophotometer; HI98127 written pH meter; FA1004N electronic balance; GSP-77-03 air compressor; WYJ - 302 B_2 DC regulated power supply.

Test method: COD fast airtight catalytic decomposition method (including photometry).

2The results and discussion

2.1 Box - Benhnken Design (BBD) Design of experiment

Selecting Box - Benhnken Design (BBD) experimental design methods, current intensity(X_1), aeration(X_2) and pH value(X_3) as the independent variables, COD removal rate as response variables(Y).By using the Design expert7.0 software to fit a quadratic polynomial regression and analyze the response surface. Factors coding table as shown in table 2.

Table 2 .Box - Benhnken Design coding table

Variable Coding value X_i	X_1	X_2	X_3
1	1.0	0.05	6.0
0	1.5	0.10	8.0
-1	2.0	0.15	10.0

Quadratic polynomial experience model: $Y=\beta_0+\sum_{i=1}^{3}\beta_i X_i+\sum_{i=1}^{j-1}\sum_{j=1}^{3}\beta_{ij}X_iX_j+\sum_{i=1}^{3}\beta_{ii}X_i^2$

In the formula: Y is predict response value; β_0, β_i, β_{ii} is offset, linear and second-order displacement coefficient; β_{ij} is interaction coefficient; X_i is independent coding value.

Through the Box - Benhnken Design (BBD), 12 IBFact point and 5 center point were concluded. According to the experiment scheme, the experimental result was achieved. The result is shown by table 3.

Table 3 .The RSM design and experimental result table

Std	Type	X_1(A)	X_2(m^3/h)	X_3	Y %
1	IBFact	1.00	0.05	8.00	29.13
2	IBFact	2.00	0.05	8.00	48.1
3	IBFact	1.00	0.15	8.00	24.73
4	IBFact	2.00	0.15	8.00	50.96
5	IBFact	1.00	0.10	6.00	33.32
6	IBFact	2.00	0.10	6.00	52.13
7	IBFact	1.00	0.10	10.00	30.24
8	IBFact	2.00	0.10	10.00	51.07
9	IBFact	1.50	0.05	6.00	33.7
10	IBFact	1.50	0.15	6.00	31.09
11	IBFact	1.50	0.05	10.00	33.21
12	IBFact	1.50	0.15	10.00	30.92
13	Center	1.50	0.10	8.00	49.48
14	Center	1.50	0.10	8.00	48.92
15	Center	1.50	0.10	8.00	49.01
16	Center	1.50	0.10	8.00	49.20
17	Center	1.50	0.10	8.00	49.53

2.2 The result of the experiment and analysis

Fitting the experimental results by the Design expert7.0 software, the fitting model of the relationship between COD removal rate and the factors was shown as the quadratic polynomial:$Y=49.23+10.61X_1-0.80X_2-0.60X_3+1.81X_1X_2+0.51X_1X_3+0.080X_2X_3-0.77X_1^2-10.23X_2^2-6.77X_3^2$

The variance analysis of quadratic polynomial is shown by table 4.

Table 4 .The response surface quadratic polynomial model of variance analysis table

Sourse	Sum of Squares	df	Mean Square	F Value	p-value
Model	1600.46	9	177.83	175.64	<0.0001
X_1	899.73	1	899.73	888.67	<0.0001
X_2	5.18	1	5.18	5.12	0.0581
X_3	2.88	1	2.88	2.84	0.1355
X_1X_2	13.18	1	13.18	13.01	0.0087
X_1X_3	1.02	1	1.02	1.01	0.3489
X_2X_3	0.026	1	0.026	0.025	0.8781
X_1^2	2.49	1	2.49	2.46	0.1608
X_2^2	440.56	1	440.56	435.14	<0.0001
X_3^2	192.92	1	192.92	190.55	<0.0001
Residual	7.09	7	1.01		
Lack of fit	6.79	3	2.26	30.39	0.0033
Cor total	1607.55	16			

Statistical significance of quadratic polynomial model was expressed by F value, F shows that the more the value is, the more significant the model is. At the same time, when the P value is lower than 0.0500, it shows a significant model factors. When the P value is greater than 0.100, it shows no significance of the model factors. The F value of this experimental model is 175.64, which is more than 1. P value is less than 0.0001, which shows that the regression is significant. R^2 (decision coefficient of the model) is used to further test the effectiveness of the model. When R^2 value is between 0 and 1, closer to 1 indicates that the model can effectively reflect the experimental data, R^2 = 0.9956 means that 99.56% of changes of response surface can be predicted by this model. Adj - R^2 = 0.9899 (model adjust decision coefficient) showed that 98.99% of the response values change can be explained by the model, and there was a high model fitting and a little experiment error. As a result, this quadratic polynomial model can suitable real curved surface properly. The affection of various factors on COD removal rate can be ranged as: current intensity>aeration>pH value.

2.3 Analysis of two factor interaction effect

Dimension reduction analysis with the date in the table 3. To observe the interaction of current intensity, aeration rate and pH value on the removal rate of COD, analyzed by Design expert 7.0 software, the response surface and contour plots was showed from fig.2-7.

Fig.2 and fig.3 show that when the pH-value is 8, the effects between current intensity and aeration rate on COD removal rate. From Fig.2, the interaction between current intensity and aeration is obvious; the current intensity's effect on the removal rate of COD was significant. Because the aeration rate can accelerate the mass transfer rate of reaction, reduce the concentration polarization effects of the electrochemical reaction. Oxygen can produce strong oxidizing activity material such as: H_2O_2,·OH, OCl^- and so on. If aeration rate is excessive high, it's not conducive to pollutants adsorbed on the particle surface, causeing the COD removal rate decreased. The removal rate of COD increases rapidly, with increasing current intensity. However, If the current is too intensive, there will be no conducive to pollutant removal rate. The higher current intensity leads to the side reaction increase[2] . While the electrochemical energy consumption increases, the rate of current decreases. Under the condition of 0.1 m^3/h aeration and 2.0A current intensity, the removal rate of COD is favorable, about 59%.

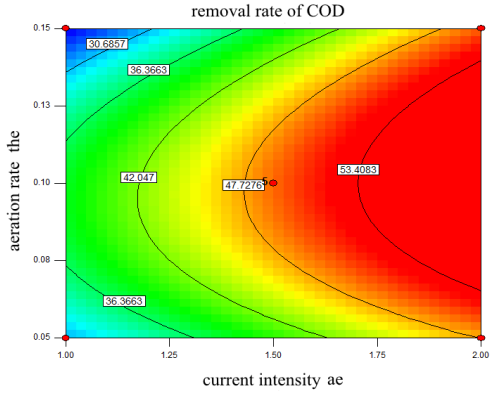

Fig.2.The current intensity - air contour map

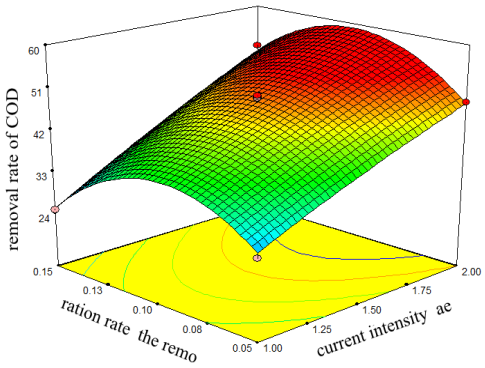

Fig.3.Current intensity - air three-dimensional stereogram

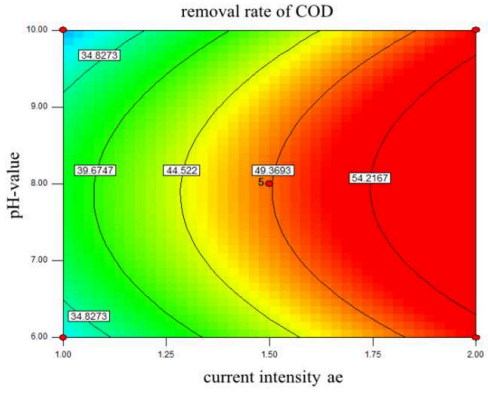

Fig. 4.The current intensity - pH contour map

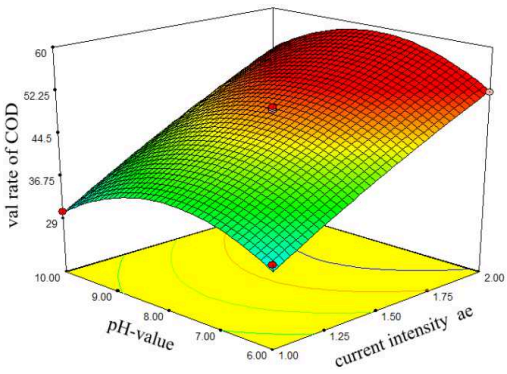

Fig. 5.Current intensity - pH 3 d stereogram

Fig.4 and fig.5 show that when the aeration rate is 0.1m^3/h, the effect between current intensity and pH value on the removal rate of COD. From Fig.4, the interaction of current intensity and the pH value is not obvious. When the pH value is certain, the removal rate of COD changes with the current. When the current is certain, the removal rate of COD increased and then decreased with the increasing pH value. When pH value is too low, the hydrogen evolution side reaction can occurred, the current efficiency was reduced, and part of organic matter may exist in flocculation morphology. It's insoluble in water and difficult to electrolysis[3]. When the pH value is too high, the final product may exist in the formation of carbonate and bicarbonate which are consumption of •OH[4].While the amount of OCl^- under weakly alkaline conditions better formed more , it causes decrease in COD removal. When the current is 2.0A, the pH value is 8, the removal rate of COD reached best value.

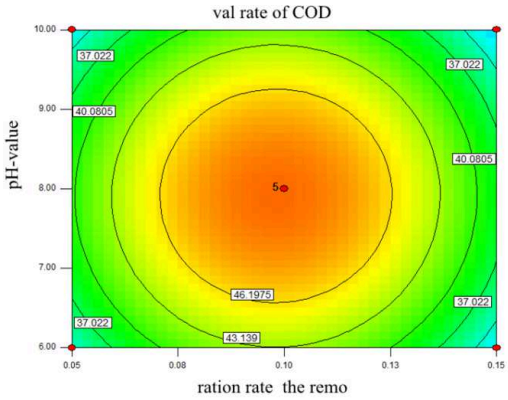

Fig. 6.Air - pH contour map

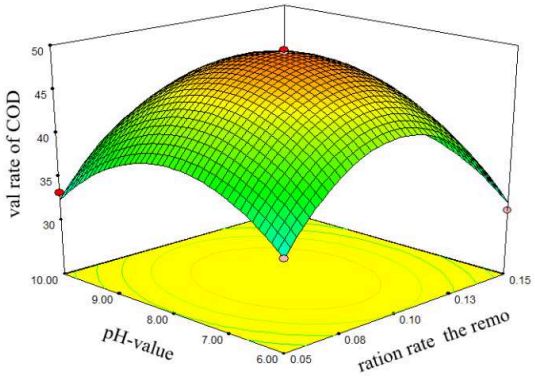

Fig. 7.Air - pH 3 d stereogram

Fig.6 and Fig.7 shows that the current intensity is 1.5A, the effect between aeration rate and pH value on the removal rate of COD. The removal rate of COD increased and then decreased with increasing aeration rate. However, with the change of pH value change is not obvious. When the aeration rate reaches 0.1m^3/h and pH value is about 8, the removal rate of COD is best, about 49%.Aeration rate and pH value have no significant interaction.

The interaction among the factors affects sequence with removal rate of COD is that the current - aeration > current -pH value > Aeration rate -pH value. The current intensity had significant influence on COD removal rate. Aeration and pH value had no significant effect on the properties.

3 Summary

The model shows that highest COD removal rate when the best current intensity, air and pH value were 1.94 A, 0.10 m^3/h and 8.35. Through The analysis of quadratic polynomial regression and response surface was showed, that the regression model to reach significance level, better fitting in study area, the precision, reliability and accuracy of the model are in the feasible range. The higher degree of agreement with the experimental results. Finally, we verified the parameters with the experiment, under the optimal conditions that the removal rate of COD was 57.69%, The relative error between the experimental values and the relative values is 0.1%. The model has guiding significance to the optimization of electrochemical oxidation process to landfill leachate with operation parameters and the effect of treatment.

References

[1] Deniz B. Isal H. B. Modeling and optimization I: Usabili-ty of response surface methodology. Journal of Food Engi-neering,2007,78(1) : 836-845.

[2] Li G, Liu S,Song S,et al. Electrochemical oxidation pretreatment of waste leachate study [J]. Journal of applied chemical industry.2009(03): 382-385.

[3] Mariam T, Duc Nghiem L. Landfill leachate treatment using hybrid coagulation-nanofiltration processes[J]. Desalination. 2010, 250(2): 677-681.

[4] Wang J . Study on the degradation of landfill leachate simulated wastewater by catalytic wet air oxidation [D]. Jilin university, 2008.

Advanced Materials Research Vols. 989-994 (2014) pp 595-598
© (2014) Trans Tech Publications, Switzerland
doi:10.4028/www.scientific.net/AMR.989-994.595

Experimental Research on Silicon-based Composite Resistance Characteristic under Thermal Load

Zhaoheng Du[1,a], Xiaofeng Hu[1,b], Ming Wei[1,c] and Lei Wang[1,d], Bofeng Ren[2,e]

[1]Research Institute of Electrostatic and Electromagnetic Protection, Mechanical Engineering College, Shijiazhuang 050003, China;
[2]Luoyang Electronic Equipment Test Center of China, Luoyang 471003, China;

[a]duzhaoheng188@163.com, [b]snowfox2270@163.com, [c]weiming1968@sohu.com, [d]wl810603@sina.com, [e]renbofengrbf@sina.com

Keywords: Silicon-based composite; hyperthermia resistance; resistance change; thermal load

Abstract. In order to research the resistance characteristic of silicon-based composite tiles under high temperature thermal load on aircraft during its reentry into the earth's atmosphere, the ordinary resistance measurements were comparatively discussed according to the operational environment of composite, two parallel electrodes probe test method was proposed, and the resistance test platform under high temperature thermal load was developed, by which the resistance characteristic of silicon-based composite tiles was continuous monitored under different thermal load. The result shows that: If the temperature is not higher than 600℃, the resistance will increase with the decrease of temperature until it reached the resistance value at room temperature; If the temperature is higher than 700℃, the resistance characteristic will be changed everlastingly; If the temperature is higher than 800℃, the resistance will be less than 1kΩ and will not change any more.

Introduction

Aircraft in its mission process will go through complicated meteorological environment such as the troposphere, the stratosphere and the thermosphere, among which the surface material will experience highly significant changes about speed, altitude and temperature[1]. In this process air containing with lots of atmosphere dust, ice and other friction particles will collide with aircraft and deposit electrostatic charge on the surface of the aircraft[2,3]. Especially in aircraft's reentry process, the surface of the material will collide with the particle heavily forming high temperature gas sheath called "blackout range". So triboelectrification situation is more complex and severe[4]. When the amount of aircraft's charge is so large that the aircraft electric field strength continues to increase to the threshold of air breakdown in the tip of wing or nose, strong electrostatic discharge will occur which radiate strong electromagnetic field[5,6], interrupting communication systems, navigation systems and other sensitive equipment[7]. It will pose a serious threat to flight safety.

To prevent damage to the aircraft caused by high temperature, thermal insulating material is used. But it may reduce the performance of communication systems, navigation systems and other sensitive equipment. For a long time, researchers tend to focus on materials insulating characteristics, but they concerns little about its electrical characteristics such as resistance characteristic[8]. Therefore, this paper proposed a series of experimental to research the typical insulating material's resistance characteristic under different thermal load.

Resistance characteristics test method

To evaluate the resistance characteristic of silicon-based composite, the ratio of the voltage U and the surface leakage current is called the surface resistance R_s, generally, and the ratio of the voltage U and the volume leakage current Iv is called the volume resistivity Rv. When silicon-based composite conducts current, surface resistivity and volume resistivity operate simultaneously. The two are connected in parallel relationship. Testing the surface resistance require excluding the influence of

volume resistivity. Testing the volume resistivity require excluding the influence of surface resistance at the same time. Using a three-electrode system testing can solve this problem.

However, the methods has a severely requirement on the material surface flatness. So it is essential to make a standard sample to test, leading time-consuming and laborious. At the same time the material can't be measured non-destructive testing. In the other hand, silicon-based composite used in the installation is not the shape of a standard sample and can't be modified. So using standard sample test can't represent the use of the actual situation. Electrostatic charge is leaked though surface resistance as well as volume resistivity. Thus, using a three-electrode system which can't support elevated temperature is improper and a new test method is required.

For this reason, an elevated temperature two-electrode resistance properties test system is developed which is proposed in Fig.1. This test system uses two parallel electrodes, greatly reduces the contact area, and ensures the full contact and stability of the contact partner. The electrode length is L. The distance between the two electrodes is d. The general requirement is L=(3~7)d. As measured by a high resistance meter, the resistivity of the sample is as follows:

$$\rho_s = R_s L / d$$

This test system is in line with the EOS/ESD-S11.11-1993 standard. This method can not only measure the resistance of homogeneous material, but also is suitable for multi-layer composite material measurement. The unit of the test result is Ω/□. To ensure the accuracy of the test, when the measured resistivity value is greater than 10^6Ω/□, the measured voltage is 100V. When the resistivity value is less than 10^6Ω/□, the measured voltage is 10V.

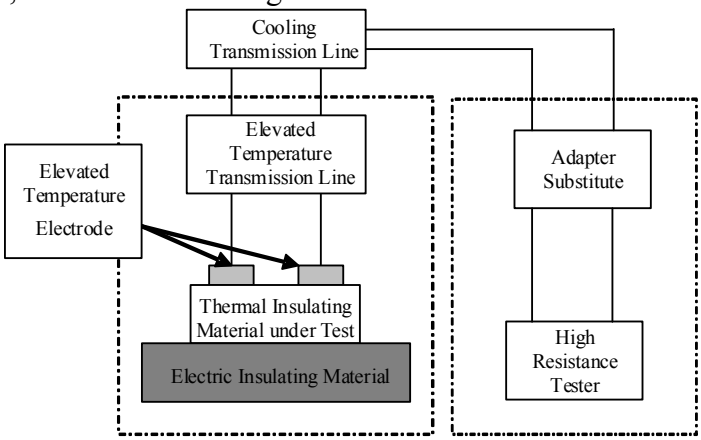

Fig.1 Elevated temperature two-electrode resistivity properties test system

Silicon-based composite materials resistance testing at room temperature

The original silicon-based composite sample and the sample after reentry environment of high temperature ablation are placed in special chamber to assimilate with the environmental temperature and humidity for 48 hours. The internal environment of the chamber maintains 23±2℃,, relative humidity (12±3)%. The test results are shown in Table 1.

As shown in Table 1, the resistivity of original silicon-based composite sample has little difference at different positions, the resistivity are all greater than 10^{10}Ω/□, and the results of several tests appear greater than 10^{12}Ω/□. It indicates that original silicon-based composite material has a very high resistivity at room temperature, it doesn't have electrostatic discharge capability, and anti-static performance is poor. The resistivity of silicon-based composite sample after reentry environment is less than 10^8Ω/□, and most of them are between (10^3~10^4)Ω/□ and even less than 1kΩ/□ at some test direction. It indicates that silicon-based composite sample after reentry environment has a good anti-static properties. But resistivity of the un-burned face of the silicon-based composite sample after reentry environment is very greater than the burned face. The resistivity of the un-burned face is greater than 10^{11}Ω/□, which suggests that this face isn't affected by the reentry environment's elevated temperature. That is because that although the silicon composites changed a lot after

atmospheric ablation, the great thermal insulating capacity help the material to be affected by high temperature and remain a huge resistivity which is almost the same as the original silicon-based composite material.

Table.1 Silicon-based composite materials resistance testing at room temperature

Materials under test	Face under test	Resistivity（Ω/□）
Original composite sample	Frontage	5.25×10^{10} 1.99×10^{10} 3.58×10^{10} 6.33×10^{10} 1.12×10^{11} $>10^{12}$ 4.27×10^{11} $>10^{12}$ 2.30×10^{10} $>10^{12}$ 7.93×10^{10} 4.46×10^{11} 8.30×10^{11} 5.36×10^{11} 7.78×10^{11} $>10^{12}$
	Reverse side	8.66×10^{11} 9.86×10^{10} $>10^{12}$ 6.99×10^{11} $>10^{12}$ $>10^{12}$ 7.06×10^{11} 9.67×10^{10} 1.85×10^{12} 1.96×10^{12} 7.23×10^{11} $>10^{12}$ 1.17×10^{12} 1.95×10^{12} 8.23×10^{11} 1.77×10^{12}
Sample after reentry	Burned Face	2.21×10^{3} 1.61×10^{3} 1.78×10^{3} 2.56×10^{3} 5.35×10^{4} 6.21×10^{4} 5.20×10^{4} 4.32×10^{4} <1k <1k <1k <1k 3.07×10^{8} 4.25×10^{8} 6.23×10^{8} 2.56×10^{7}
	Un-Burned Face	2.68×10^{11} 3.61×10^{11} 3.72×10^{11} 4.96×10^{11} $>10^{12}$ $>10^{12}$ $>10^{12}$ 1.11×10^{12} 1.92×10^{12} 1.02×10^{12} 9.09×10^{11} 8.96×10^{11} 2.22×10^{11} 4.52×10^{11} 8.16×10^{11} 6.77×10^{11}

Silicon-based composite materials resistance testing at elevated temperature

As shown in Fig.1, the platform consists of high-temperature heating systems, cooling systems and the conduction resistance testing system. We use the high temperature furnace in the range of 50 ~ 1000 ℃. Resistance tester is US-made ACL800 resistance tester in the range of $(10^3\sim10^{12})\Omega/\square$. Silicon-based composite material is heated to 300 ℃, 600 ℃ and 700 ℃ individually. The resistance variation with temperature in the cooling process in air naturally is shown in Fig.2, Fig.3 and Fig.4

As shown in Fig.2, Fig.3 and Fig.4, the resistivity will have irreversible change if heated to 700℃ instead of 300℃ and 400℃. The resistivity will decrease will the increase of temperature. From the test results above, it can be found that the resistivity of silicon-based composite materials increases with decreasing temperature. If the thermal load temperature reaches a certain level, the material resistance irreversible changes will take place. In this case, the resistivity will be less than 1kΩ/□ at any temperature. The material which doesn't have irreversible changes, the resistivity changes with temperature can be described with a theoretical model as follow:

$$R = R_0 e^{-BT}$$

Where $R_0 = 7.58\times10^{18}$, B= 0.0142. So, material resistivity increases exponentially with temperature. The higher of the temperature thermal load, the smaller of the parameter R_0 will be.

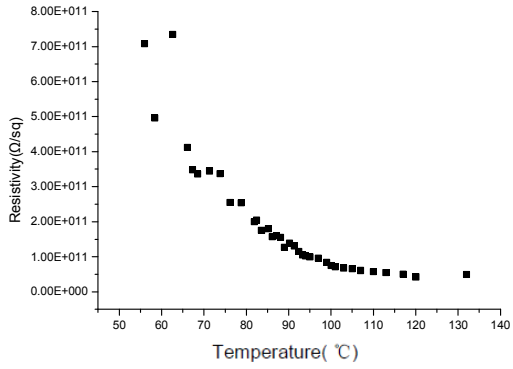

Fig.2 Resistivity changes after heated at 5min 300 ℃

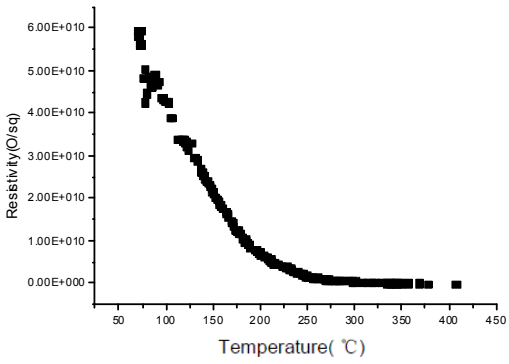

Fig.3 Resistivity changes after heated at 15min 600 ℃

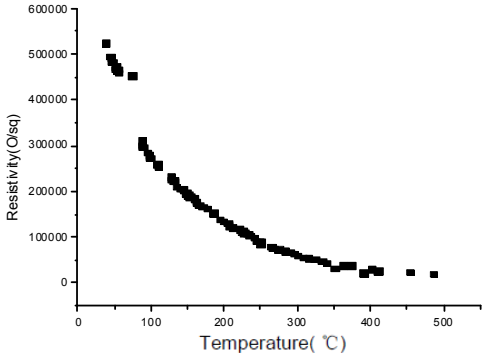

Fig.4 Resistivity changes after heated at 10min 700 ℃

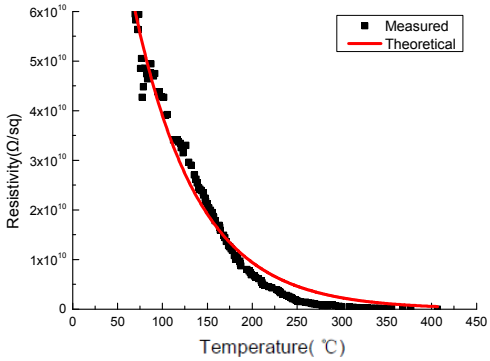

Fig.5 Resistivity changes of measurement and theory

Conclusion

In this paper, elevated temperature two-electrode resistivity properties test system is used to study the resistivity characteristic with temperature. We would come to the conclusion:

(1) The resistivity of silicon-based composite materials at room temperature is maintained at $10^{10}\Omega/\square$ above, and the material has a poor electrostatic discharge capability.

(2) The resistivity of silicon-based composite materials could recover to normal condition if the normal condition is not greater than 600℃.

(3) When the temperature of the heat load is greater than 700℃, the material resistance irreversible changes will take place, and the resistivity can't recover to normal condition

References

[1] Temnikov A.G., Chernenskii, L .L., Technical Physics Letters, vol.37(2011)n0.10,p. 907-910
[2] Haverkamp, H., Wilhelm, S., and Sorokin, A., Atmospheric Environment. vol. 38 (2004)no.18,p. 2879-2884
[3] Beard, Kenneth V., Ochs III, Harry T., Geophysical research letters. vol 31(2004)no.14,p.L14111
[4] Vatazhin, A B, Starik, A M, Kholshchevnikova, E K, Fluid Dynamics. vol.39(2004)no.3, p.384-392
[5] Hughes, J F., Physical Science, Measurement and Instrumentation, Management and Education - Reviews, IEE Proceedings A. vol.128(1981)no.4,p.244-256
[6] Hucke, HERBERT M., Proceedings of the IRE. vol.27(1939)no.5,p.301-316
[7] Fedorov, V A., Cosmic Research. vol.49(2011)no.4,p.374-381
[8] Temnikov, A G, Gilyazov, M Z, Matveev, D A., Technical Physics Letters. vol.37(2011)no.9,p. 845-848

Advanced Materials Research Vols. 989-994 (2014) pp 599-602
© (2014) Trans Tech Publications, Switzerland
doi:10.4028/www.scientific.net/AMR.989-994.599

Electrical Simulation Experiment and the Analysis of Thermal Conductivity of Materials

Li Wenbo[1,2],Jin Yingai[1,2] ,Yin Shuang[3],Chen Peiyan[1,2]

[1.] College of Automotive Engineering, Jilin University, Changchun 130025, China
[2.] State Key Laboratory of Automotive Simulation and Control, Jilin University, Changchun 130025, China
[3.] College of Communication Engineering, Jilin University, Changchun 130025, China

Keywords: Electrical Simulation ； unsteady heat conduction； boundary; innovation experiment

Abstracts: Jilin university innovation experiment Electrical Simulation Experiment and the Analysis of Thermal Conductivity of Materials aims to solve the problem of thermocouple measuring tenderness in error. Thermocouple is used to measure temperature when measuring unsteady heat conduction in laboratory. The improved measuring method of unsteady heat conduction puts the breakthrough on the electric simulation method. The text bench is constructed by different shapes of conductive plate which is made of the graphite conductive paint, and voltmeter is refitted by diodes and controlled transformer. Through the test bench, we finished the simulation of unsteady heat conduction under the similar thermal conductive boundary conditions. Finally, the error analysis of experiment and the advantages of electric simulation method are given in this paper.

0. Introduction

The method of students measuring unsteady heat conduction is based on the single plate gas heating. Heat transfers from the heating surface to the non-heating surface. When the plate reaches the heat through, students will take thermocouples to measure the temperature, then draw the curve of heating temperature and time, and compare the curve to the theoretical curve. However, in non-steady state conditions, thermocouple measurement has errors. Considering the errors, we improve experiment device by using the method of electro-thermal stimulation.

Electro-thermal simulation takes mathematical model. It takes potential distribution to simulate the temperature distribution, electrical resistance to simulate the thermal resistance and electrical current to simulate the thermal current. We ensure the similar geometry and boundary in electrical conduction and the actual heat conductor and determine the temperature distribution of actual heat conductor through measuring the potential distribution of conductor, and then conclude the heat flux intensity.

1. The experiment content

1.1 Experimental apparatus

The experimental device consists of a modified voltage meter, transformer, and different shapes of the self-made modified graphite conductive plates, guide, slick and multi-voltage DC power supply. During the experiment, add the DC power to the ends of the measured material. In order to ensure the safety of circuit, we connect the circuit with a sliding rheostat in series, and then put the refitted voltmeter to one side of the circuit and the probe in parallel. After lapping the circuit, close the switch, and then start the measurement when stable. Adjust the sliding rheostat to the zero potential of the probe, and then make the probe move slowly along the metal guide trail from one side to the other side. Then record the moving distance of X, observe the number of light emitting diodes of converted voltage meter and write down the data (The light emitting diodes use silicon tube and the turn-on voltage is 0.7V). Disposal the data and circulate the potential of each position. Then draw the potential line and determine the isotherm according to the geometric proportion. The experimental device improves the circuit part. We use probe measure the changes of voltage in different positions, and take light emitting diode to display the size of voltage. Based on the

simulation of the temperature field experiment, we study the changes of voltage in different positions of different material by changing the sheet material and shape. Then infer the curve of temperature variation with time in one dimensional unsteady heat conduction and compare the curve with the theoretical curve, and then get the most suitable material.

1.2 Experimental procedures

1. Turn on the power supply. Adjust the range of DC power supply and make the power output 15V DC voltage.
2. When the output voltage of DC power is stable, put the probe on different locations to measure different voltages on different position.
3. Record the number of light emitting diode and each value when the probe is on different position of material.
4. Statistic the data and draw the diagram.

2. Experimental Innovations

2.1 Use electric simulation method

The device gets a temperature distribution of heat conduction indirectly by measuring the electric quantity. Using simple designed test bench can complete the measurement of different materials, and the circuit board which displays the electrical quantity can make the change more intuitive.

2.2 Modified voltage meter, graphite conductive paint and wood made of graphite conductive plate

Conversion voltage meter is composed of a plurality of light emitting diode. Because of the difference of the number of each row of the diode, the voltage of each row of light-emitting diodes are also different, so as to achieve the purpose of reacting the difference of pressure. We use graphite conductive paint and wood to make the graphite conductive plate.Our graphite electrically conductive spray paint on plastic sheeting and get 1.5KΩ per square centimeter of conductive graphite plates, and the test requirement was roughly in line with, and wood cutting, where you can change the shape of the material, you can achieve the purpose of measuring different shaped plate potential.

2.3 Aluminum Strip Posted on graphite electrically conductive plates on each side

In order to make the thermal conductive boundary condition the same, we need to make conductive plates on both sides form equipotential surface, so as to achieve the purpose of modeling two isothermal heat transfer plate surface. Our team decided to affix two aluminum sheets on both sides of graphite conductive plates, and due to the electrical resistance of aluminum graphite is much less than the electrical resistance of graphite conductive paint, this method reaches the purpose of equipotential surface of conductive plate on both sides.

3. Analysis and comparison of experimental results of thermal conductivity

3.1 Electrical simulation method of experimental data and results

Put the plate on a rectangular coordinate system, and the low voltage on the ordinate is the “1 ‘’side, the high voltage on the ordinate is the “6 ‘’ side.

Table1 Below is to measure the material responds to different locations

Abscissa / Voltage /V / Ordinate	1	2	3	4	5
1	9.71	9.70	9.72	9.78	9.86
2	12.41	12.45	12.24	12.31	12.40
3	14.35	14.28	14.31	14.50	14.18
4	16.18	16.19	16.34	16.44	16.28
5	18.21	18.33	18.09	18.12	18.16
6	20.20	20.10	20.08	20.66	20.84

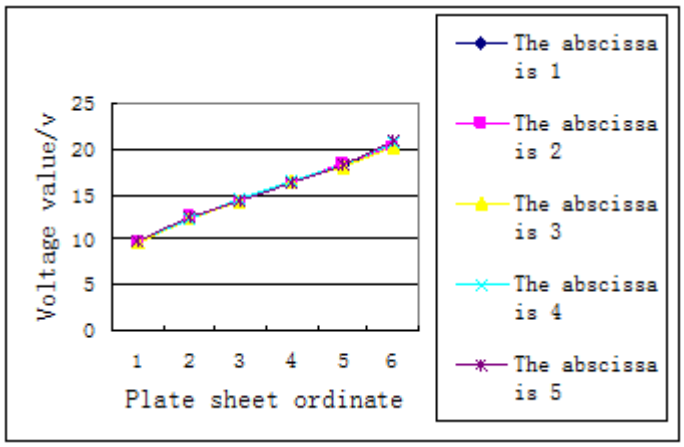

Fig.1 Plate voltage distribution curve

3.2 Direct measurement of thermal conductivity of experimental data and results

Table 2 Thermal conductivity of experimental data and results

Voltage/V	Temperature/$^{\circ}C$				
10	17.9	22.2	23.3	26.1	30.4
15	19.7	24.4	25.6	28.7	34.8
20	21.0	25.8	27.2	30.8	38.1
25	22.9	27.7	29.3	33.2	42.3
30	21.5	27.8	29.6	33.7	43.1

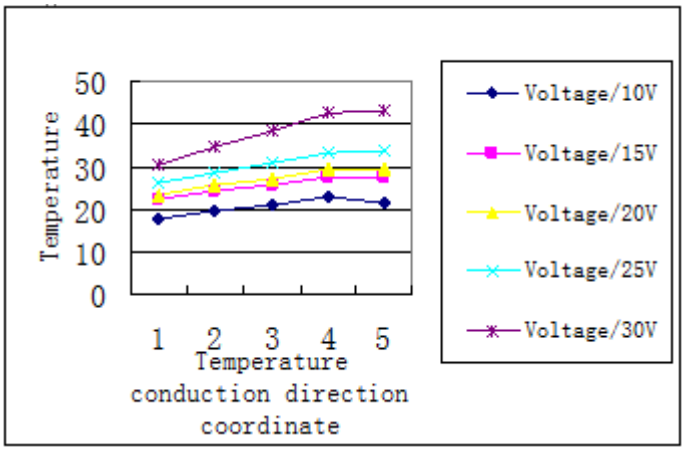

Fig.2 Plate sheet temperature

3.3 **Experimental comparison**

It's not difficult to find direct measurement and simulation of plate temperature distribution simulation of temperature distribution in roughly the same when using the electrical simulation method to analog the distribution of electric potential of materials, and changes of uniform. And electrical simulation method line trend is obvious, and the precision is higher.

4 Error analyses

4.1 Plate ends cannot guarantee form two equipotential surface

This experiment puts two pieces of aluminum sheet on both sides, resistance aluminum strip is much less than the graphite conductive plate, so that the voltage across the board evenly. But because the aluminum strip can not fully contact with graphite conductive plate, there is a certain amount of the contact resistance.

4.2 Other errors

Other errors include uneven distribution of electrical resistance of conductive graphite plates, laboratory temperature influence on electrical resistance of conductive graphite plates, artificial measurement readings.

5. Conclusions

Innovation is the key to national unremitting self-improvement. Students will obtain the ability of innovation in practice after learning and thinking in the class. In this experiment, we combined the electrical knowledge and heat transfer theory, and put it in the experiment. During the process of test bench building and measuring, we also met many problems, but through positive thinking and discussing in team, we got through them. The innovative experimental experience plays a significant role in our life.

6. References

[1] YangShiming. TaoWenquan. Heat transfer.HIGHER EDUCATION PRESS, 2006.
[2] Chen Guitang. Wang Yongzhen. Engineering Thermodynamics [m]. Beijing: Beijing Institute of technology press, 2008.
[3] Yu Junmin. electrical measurement technology. China electric power press, 2007
[4] Yao Wenxuan, Teng Zhao Sheng. applying experimental plan of college students ' innovative thinking and practice of cultivating creative ability of China [j]. higher education research journal, 2010,33 (2)

Advanced Materials Research Vols. 989-994 (2014) pp 603-606
© (2014) Trans Tech Publications, Switzerland
doi:10.4028/www.scientific.net/AMR.989-994.603

Study on the impact of DO and organic matter on aerobic granular sludge treating municipal sewage

Yang Yu[1, a], Haijiao Yu[2,3, b] and Chenci Ma[2, c]

[1]Hainan Highway Survey and Design Institute, Haikou, Hainan, 570206S,China
[2]School of Municipal and Environmental Engineering in Shenyang Jianzhu University, Liaoning, Shenyang, 110168, China
[3]Institute of Applied Ecology. Chinese Academy of Sciences, Liaoning, Shenyang, 110164, China
[a]11185038@qq.com, [b]yuhaijiao.love@qq.com, [c]789654123zxcvbn@sina.com

Keywords: aerobic granular sludge, SBR, municipal sewage, denitrification and phosphorous removal, DO, organic matter.

Abstract. The experiment uses municipal sewage as the research object and runs SBR reactor in completely aerobic conditions. Through controlling different of DO concentration and COD concentration, we study spreading comparison. The results show that when DO concentration was 1mg/L, the removal effect of aerobic granular sludge process in SBR treating municipal sewage was best, the average removal rate of COD, ammonia nitrogen, total nitrogen and phosphorous was 90.12%,98.95%,87.65% and 83.74% respectively. When COD concentration of influent was about 400mg/L, the treatment effects of aerobic granular sludge for COD, ammonia nitrogen, total nitrogen and phosphorous were all better, the average removal rate was up to 92.33%,98.83%,88.17% and 80.25% respectively.

INTRODUCTION

Aerobic granular sludge process has been proposed as a promising approach to control water contamination in recent years [1, 2].Due to the its own characteristic of structure,simultaneous removal of nitrogen and phosphorous was achieved successfully in a one-reactor system,the system had the distinctive advantages of high activity of microorganisms,good performance of solid-liquid separation,high resistance to organic impact load and long biological chain.Because of all the advantages of AGS system,it had broad development prospect [3].In this study,we compared the influence of dissolved oxygen and organic compound on the municipal wastewater removal performance of aerobic granular sludge process by dynamic tests.The aim of the study was to provide technical support and theoretical basis for the stable operation of aerobic granular sludge process and practical engineering application.

Materials and Methods

The municipal wastewater was used for the experiments. CH_3COONa,NH_4Cl,KH_2PO_4,$NaHCO_3$,$MgSO_4$,$CaCl_2$ and tap water was added into the municipal wastewater in order to achieve the water quality for the test(Table 1).The nutrient solution (Table 2)was combined with the synthetic wastewater with the ratio of 1mL/L.The AGS system was seeded with activated sludge which is mainly flocculent sludge from the secondary sedimentation tank of A^2/O process of the north wastewater treatment plant,Shenyang,China.

Table 1 Water quality for the test

COD/($mg \cdot L^{-1}$)	NH_4^+-N/($mg \cdot L^{-1}$)	PO_4^{3-}-P/($mg \cdot L^{-1}$)	pH
350~400	25~30	6~10	7.0~8.0

Table 2 Composition and concentration of nutrient solution

Contents	Concentration/(mg·L^{-1})	Contents	Concentration/(mg·L^{-1})
$FeCl3·6H_2O$	1300	$CuSO4·5H_2O$	300
$ZnSO4·7H_2O$	120	$CoCl2·6H_2O$	150
$MnCl2·2H_2O$	120	KI	180

A sequencing batch reactor (SBR) with working volume of 7L was used in this study.The temperature of the reactor was controlled by water bath heating system in constant temperature(28℃).The reactor was operated in cycles of five phases,including fill instant(5min),aerobic phases(6h),sludge settling(5min),effluent discharge(5min) and idle phases(345min).In this study,all the indexes were determined according to the standard methods described in w*ater and waste water monitoring and analysis method*（*forth edition*）which was drafted by State Environmental Protection Agency.

Results and Methods

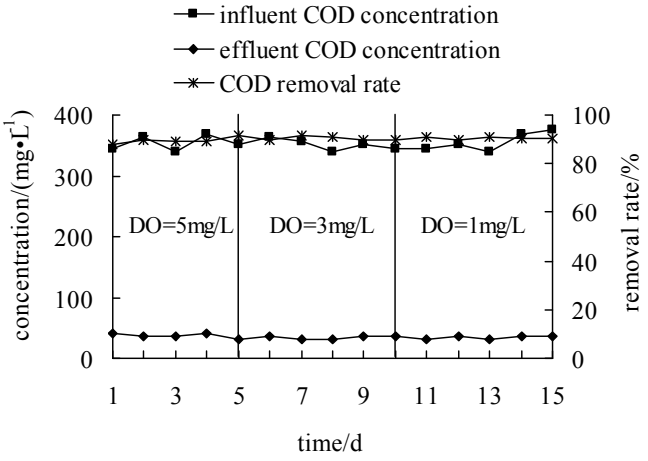

Fig. 1. Removal effect of COD

As shown in Fig.1,when DO was 5mg/L,3mg/L and 1mg/L,the decreased specific DO concentration did not lead to obvious change on the removal efficiency of COD by aerobic granular sludge,the average removal rate of COD was 90.12%.Therefore,when DO concentration was under 1mg/L,it had little effect on the removal efficiency of COD,aerobic granular sludge had good degradation effect of COD.

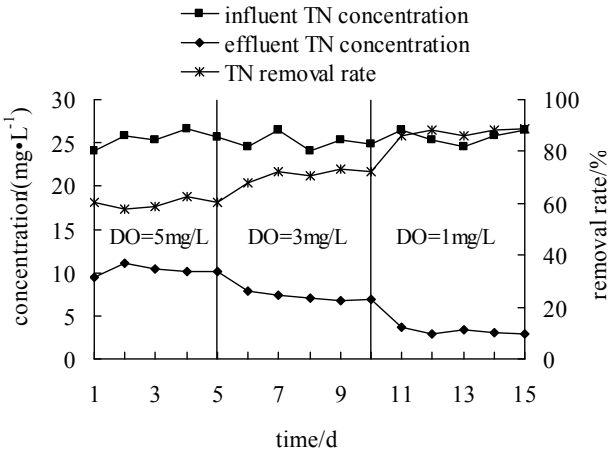

Fig. 2. Removal effect of total nitrogen

As shown in Fig.2,the degradation effect of total nitrogen increased as DO concentration decreased in the reactor,the average removal efficiency of total nitrogen was very low as 59.96%.When DO concentration was 3mg/L,the effluent total nitrogen concentration was still around 7mg/L,it not

achieve a good removal effect.When DO concentration was 1mg/L,the effluent total nitrogen concentration decreased to 3.5mg/L,the average removal rate of total nitrogen increased to 87.65%.

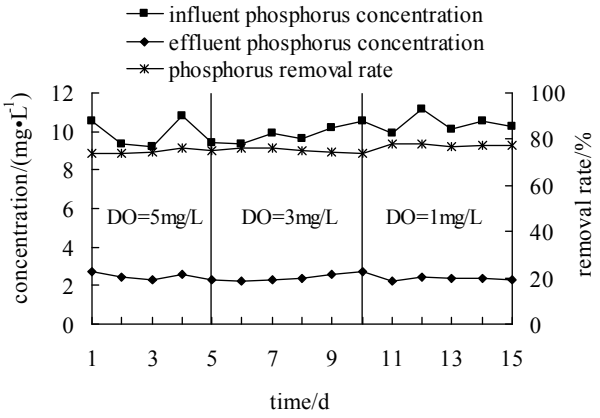

Fig. 3. Removal effect of phosphorus

As shown in Fig.3,when time of aeration is enough,DO concentration had little influence on the effluent PO_4^{3-}-P concentration.The effluent PO_4^{3-}-P concentration was maintained at about 3mg/L.

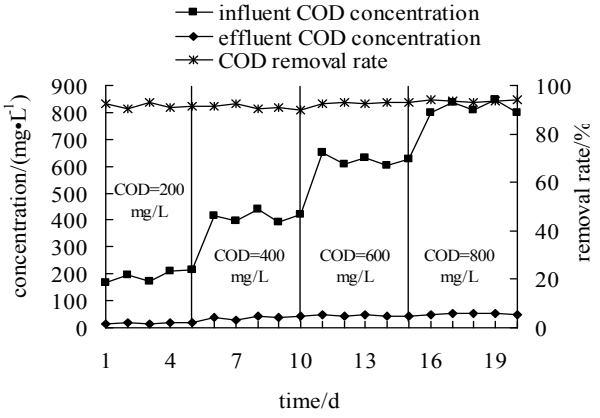

Fig. 4. Removal effect of COD

As shown in Fig.4,aerobic granular sludge could achieve good degradation effect as the influent COD concentration increased.The effluent COD concentration was maintained under 50mg/L,achieved the A in first grade discharge standard.It suggested that aerobic granular sludge had strong shock resistance to influent COD loading rate.

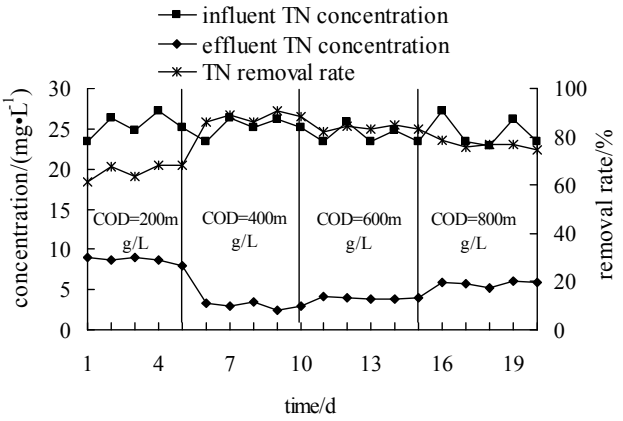

Fig. 5. Removal effect of total nitrogen

As shown in Fig.5,when COD concentration was 200mg/L,the average removal efficiency of TN was only 65.75%.When COD concentration increased up to 400mg/L,the efficiency of denitrification increased steadily and the removal efficiency of total nitrogen increased

considerably.With the further increase of COD concentration,the removal efficiency of total nitrogen started to decrease gradually.

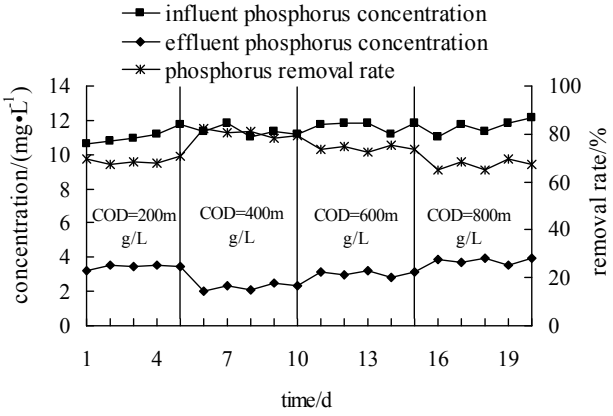

Fig. 6. Removal effect of phosphorus

As shown in Fig.6,when the influent COD concentration was 200mg/L,the average removal efficiency of phosphorous was very low as 68.72%.When COD concentration was 400mg/L,the organic carbon resources in the reactor was sufficient,the activity of microorganisms increased gradually and the average removal efficiency of phosphorous increased 11.53%.With the further increase of COD concentration,the removal efficiency of phosphorous started to decrease.

Conclusions

(1) When DO concentration was controlled at 1mg/L in the SBR reactor,aerobic granular sludge process had the best removal efficiency of nitrogen and phosphorous.

(2) When the influent COD concentration of the SBR reactor was controlled at 400mg/L,aerobic granular sludge system had optimal removal efficiency on COD,total nitrogen and phosphorous.

References

[1] F. Jang, L. Dong, H.X. Feng, et al. Study on the Influential Factors and Formation Mechanism of Aerobic Granular Sludge. Chemistry & Bioengineering, Vol. 26 (2009) No.1, p.15.

[2] S.G. Liu, Z.K. Mei, W.M. Xie, et al. Cultivation and Granulation Process of Aerobic Granular Sludge Applied to Treat Municipal Wastewater. Research of Environmental Sciences, Vol. 23 (2010) No.7, p.918.

[3] C.S. Zhang, W.J. Zhang, Q. Fang, et al. Effect of DO on nitrogen removal process by granular sludge in shortened simultaneous nitrification and denitrification. Chinese Journal of Environmental Engineering, Vol. 3 (2009) No., p.413.

Advanced Materials Research Vols. 989-994 (2014) pp 607-610
© (2014) Trans Tech Publications, Switzerland
doi:10.4028/www.scientific.net/AMR.989-994.607

Flame retardancy finishing on wool fabric via sol-gel method

Zhang Wei, Zhang Qiang-hua, Chen Guo-qiang, Xing Tie-ling*

National Engineering Laboratory for Modern Silk, College of Textile and Engineering,

Soochow University, Suzhou, China

Email: xingtieling@suda.edu.cn

Keywords: flame retardancy; wool; sol-gel; silica/phosphorus

Abstract. In this paper, silica sols were prepared through sol-gel method and applied onto wool fabric flame resistant finishing. In order to gain good flame retardance of wool fabric, the parameters of preparing pure silica sol and the concentration of doped phosphorus (ammonium biphosphate) in silica sol were optimized taking the LOI values of the treated wool as evaluation index.

Introduction

Sol-gel method, a chemical synthesis method initially used for the preparation of inorganic materials such as glasses and ceramics, was generally based on two steps: hydrolysis of metal alkoxides to produce hydroxyl groups, followed by polycondensation of the hydroxyl groups and residual alkoxyl groups to form a three-dimensional network [1]. With a high degree of homogeneity at molecular level, the sol-gel reaction was proved to be an effective way to provide unique capability and novel materials in many fields [2]. As to textiles, sol-gel approach had been successfully applied to functional finishing such as water-repellency [3], antibacterial finish [4] and so on. However，there are little reports on the flame retartancy finishing on wool fabric through sol-gel method. Indeed, flame retartancy finishing on wool, which was one of the most important raw materials in textile industry, was necessary to improve the safety performance as fires occurred frequently. In this work, process parameters of preparation of sols were fully discussed taking the LOI value of the treated wool as index.

Experimental

Material. Wool fabrics (GB/T7568.1-2002) were purchased from Shanghai Textile Industry Institute of Technical Supervision. Tetraethoxysilane(TEOS) was purchased from Sinopharm Chemical Reagent Co.,Ltd. Ethanol(EtOH), hydrochloric acid(HCl) and ammonium biphosphate were purchased from China Sun Specialty Products Co.,Ltd.

Preparation of flame retandancy sols. The silica sol was prepared using tetraethoxysilane as precursor, ethanol as cosolvent, and hydrochloric acid as catalyst. More specifically, tetraethoxysilane was mixed with some ethanol, and then dropped distilled water for pure silica sol or ammonium biphosphate solution for phosphorus doped silica sol while stirring continuously at room temperature. The pH value of both pure and phosphorus doped silica sols were adjusted by hydrochloric acid. Then the whole system was kept stirring at a suitable temperature.

Application of the flame retandancy sols to wool fabric. The wool fabric was treated with the prepared sols at the reacting temperature for an hour on constant temperature vibrator, and then the wool fabric was cured at 160℃ for 6 min, and finally the wool fabric was dried in the air.

Measurements. The limiting oxygen index (LOI) was measured by LCK-09 automatic oxygen index tester according to GB/T 5454-1997.

Results and Discussion

Effect of dosage of water on LOI value of wool treated with pure silica sol preparation

As shown in Figure 1, water dosage affected LOI value of treated wool fabric complicatedly. When the mole ratio of water and tetraethoxysilane (n[H_2O]:n[TEOS]) was lower than 4:1, the LOI value

of the fabric decreased first and then increased with the increase of water dosage. On the other hand, the LOI value of the fabric decreased continuously when the ratio was greater than 4:1. This was because that the hydrolysis was not complete when the mole ratio was smaller than 4 according to Equation 1. The silica particles kept growing until the water dosage was enough to complete the reaction. That was to say, at the very beginning, the silica particles were fairly small that they could penetrate into the fabric well and then adhere to it tightly because of the small size effect, achieving 26.6% of LOI value when n[H_2O]:n[TEOS]=1:1. With the water dosage increasing, on one hand, the size of silica particles became bigger which weaken the small size effect; on the other hand, the number of the silica particles became more which enhanced the effective component of the flame retardant. However, when n[H_2O]:n[TEOS]>4, the hydrolysis reaction was complete and the number of silica particles did not increase with the water increasing. This dilution of the flame retardant system led to the decrease of the LOI of the treated wool fabric. What was more, it was remarkable that small dosage of water could cause the instability of doped silica sols especially when the additive had poor solubility. From the above, n[H_2O]:n[TEOS]=1:1 was chosen to prepare pure silica sol while n[H_2O]:n[TEOS]=20:1 to prepare phosphorus doped silica sols.

$$\text{Hydrolysis : } Si(OEt)_4+4H_2O \leftrightharpoons Si(OH)_4+4EtOH \quad (1)$$

$$\text{Condensation : } \text{-Si-OH+HO-Si-} \rightarrow \text{-Si-O-Si-+ } H_2O \quad (2)$$

$$\text{-Si-OH+EtO-Si-} \rightarrow \text{-Si-O-Si-+EtOH} \quad (3)$$

Effect of dosage of HCl on LOI value of wool treated with pure silica sol preparation

The reactivity of silicon alkoxide was low so that catalyst either acid or base was needed. Therefore, the structure and the morphology of the resulting network strongly depended on the use of catalyst. As to silica alkoxides, acidic environment accelerated the hydrolysis resulting in the formation of high-density and low fractal dimension structures; while base catalyst promoted the condensation leading to dense and colloidal particulate structures [1]. In this paper, acid catalyst was chosen to prepare silica sols because this kind of sols performed well when applied on fabrics. Figure 2 shows the effect of the HCl dosage on LOI value of the treated fabric. It could be seen from Figure 2 that the LOI value increased from 25.4% to 26.6% with the increase of n[HCl]:n[TEOS] from 0.048 to 0.108. However, the pH of the system dropped much below 1 when the ratio reached 0.108 causing a great loss of mechanical strength of the treated fabric. In conclusion, n[HCl]:n[TEOS]=0.096 was chosen to prepare silica sol which applied in wool fabric treatment.

Effect of dosage of EtOH on LOI value of wool treated with pure silica sol preparation

Ethanol, acting as cosolvent in the preparation of silica sols, was also one of the products of condensation according to Equation 3. It could promote the reaction on molecular level at a small amount but could be an inhibiter or a diluent when the dosage reached the limit. This was proved by Figure 3, LOI value increased gradually with the dosage of EtOH increasing to n[EtOH]:n[TEOS]=3 and then decreased rapidly. As a result, the suggested ratio of EtOH and TEOS was 3 when the LOI value was the highest as 26.7%.

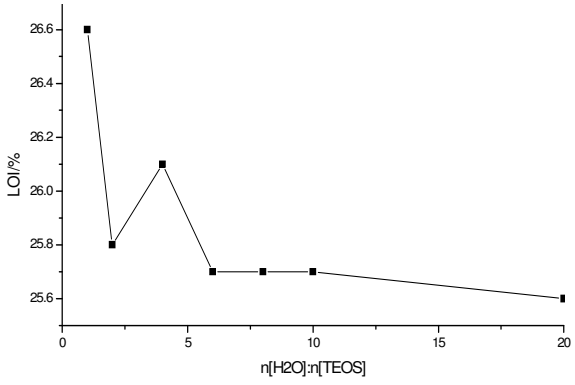

Fig.1 Effect of water dosage on LOI value

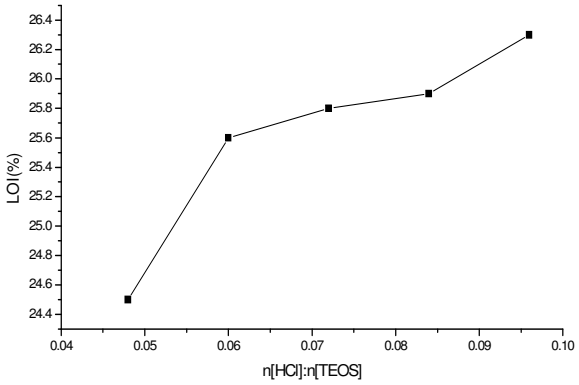

Fig.2 Effect of HCl dosage on LOI value

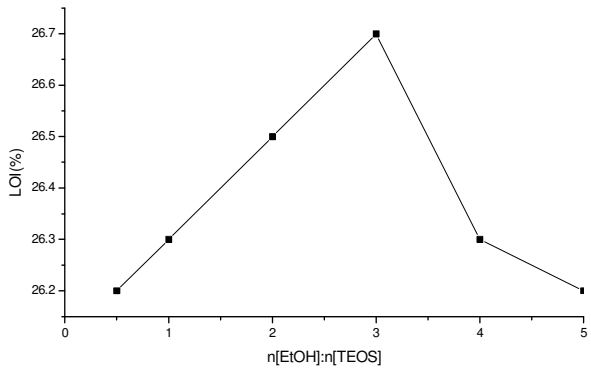

Fig.3 Effect of EtOH dosage on LOI value

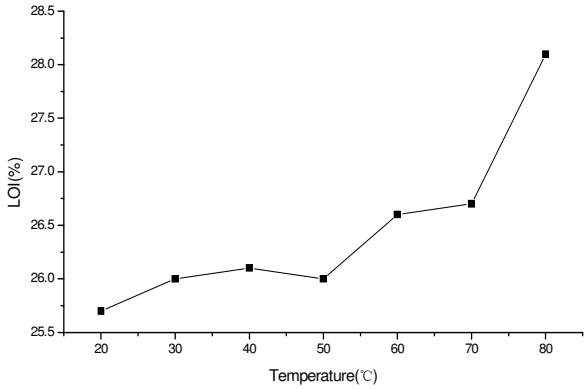

Fig.4 Effect of reaction temperature on LOI value

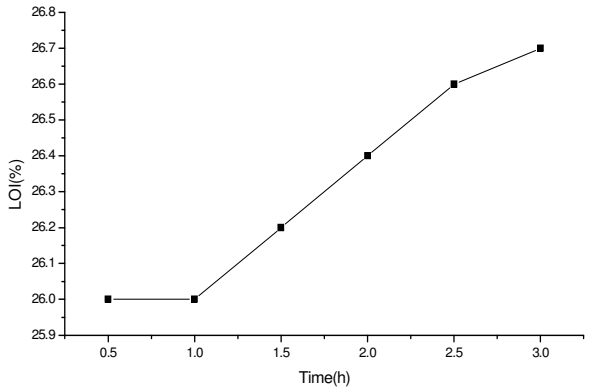

Fig.5 Effect of reaction time on LOI value

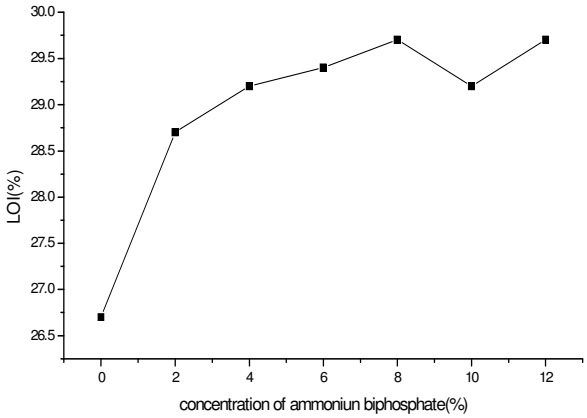

Fig.6 Effect of ammonium biphosphate on LOI value

Effect of reaction temperature and reaction time on LOI value of wool treated with pure silica sol preparation

The effects of reaction temperature and reaction time on LOI value of the treated wool were showed in Figure 4 and Figure 5, respectively. It can be seen that with the temperature or time increasing, the LOI value of the treated wool trended to increase as well. That was due to the less reactive silica alkoxides whose reaction needed enough energy to complete. For reaction temperature, although the LOI value gained the highest as 28.1% at 80℃, the better choice was 26.7% at 70℃ considering the yellowing and the mechanical strength of treated fabric. As to reaction time, the LOI value didn't change much at the first hour, and the LOI value of the treated fabric tended to increase gradually and reached the highest as 26.7% when the reaction lasted for 3 hours. Thus the optimal reaction condition was chosen as 3 hours at 70 ℃.

Effect of ammonium biphosphate concentration on LOI value of wool treated with phosphorus doped silica sol

Ammonium biphosphate, as a flame retardant additive, was doped into the pure silica sol to improve the flame retardance of the treated wool. Considering the poor solubility of ammonium biphosphate, n[H2O]:n[TEOS]=20:1 was chosen while other parameters were the same with the process in preparing pure silica sol. Figure 6 showed the LOI values of different concentration from 2% to 12% of ammonium biphosphate doped in silica sol. From that a significant improvement of LOI value of the wool treated with phosphorus doped silica sol was observed even at a small concentration (28.7%at 2%) comparing with the wool treated with pure silica sol (26.7%). For the wool treated with phosphorus doped silica sol, the LOI value increased with the increasing of ammonium biphosphate concentration before 8% which was explained by the flame retardance based on phosphorus. But this growth was not linear which was due to the synergistic effect based on silica and phosphorus. After 8% there was a decline on LOI value and then continued to rise. This was because the effect of flame retardant based on phosphorus alone was beyond the synergistic effect based on silica and phosphorus. However the concentration of phosphorus was

limited because the sol was too unstable to apply on fabric when the concentration was beyond 12%. From the above, concentration on 8% of ammonium biphosphate was a better choice for preparing phosphorus doped silica sol.

Summary

Through the experiment, the optimal process of preparing pure silica sol was as follows: n[TEOS]:n[H_2O]:n[EtOH]:n[HCl]=1:1:3:0.096, T=70℃,t=3h. As to phosphorus doped silica sol, concentration of ammonium biphosphate at 8% presented a better synergistic effect based on silica and phosphorus when treated with wool fabric. The flame retardance of the treated wool was improved with a LOI value for 26.7% for pure silica sol treated and 29.7% for phosphorus doped silica sol treated compared with 25.2% for raw wool.

Acknowledgment

The work is supported by PAPD, National Natural Science Foundation of China (No 51203107), Industry-academic Joint Technological Innovations Fund Project of Jiangsu Province (No. BY2012120).

Reference

[1] J. Wen, G. L. Wilkes. Organic/inorganic hybrid network materials by the sol-gel approach, Chem. Mater. 8(1996)1667-1681.
[2] J. Alongi, G. Malucelli. State of the art and perspectives on sol-gel derived hybrid architectures for flame retardancy of textiles, J. Mater. Chem. 22(2012)21805-21809.
[3] B. Mahltig, H. Bottcher. Modified silica sol coatings for water-repellent textiles, J. Sol-Gel Sci. Technol. 27(2003)43-52.
[4] S. Tarimala, N. Kothari, N. Abidi. New approach to antibacterial treatment of cotton fabric with silver nanoparticle–doped silica using sol-gel process, J. Appl. Polym. Sci. 101(2006)2938-2943.

Advanced Materials Research Vols. 989-994 (2014) pp 611-614
© (2014) Trans Tech Publications, Switzerland
doi:10.4028/www.scientific.net/AMR.989-994.611

Minimum Particle Diameter of the Vanadium/ Iron Co-doped Nano-TiO_2 Transparent Hydrosol at Room Temperature

Ling Li [1, a*], Wenming Zhang [1, b], Huayan Zhang[1, c], ZiHao Xu[1], Sen Wang[1], Xiaowei Li[1*] and Guoyi Dong[1]

[1] Heibei Key Laboratory of Optic-electronic Information Materials, College of Physics Science and Technology, Heibei Unversity, Baoding 071002, China

[a]lilinghbu@163.com, [b]wmzhanghbu@126.com, [c]zhanghy4321@163.com

Keywords: nano-TiO_2 transparent hydrosol, V/Fe co-doped, minimum particle diameter, photocatalysis

Abstract. Vanadium/iron co-doped nano TiO_2 transparent hydrosol with an average particle size of 3.8 nm was synthesized by a novel complexation-controlled hydrolysis method at room temperature and atmospheric pressure by using $TiCl_4$, ferric nitrate, ammonium metavanadate, etc. as raw materials. The composition, phase structure, particle size, absorbance spectrum, and photocatalytic performance of samples were characterized by XRD, EDS, nano laser particle size analyzer, and UV-Vis spectrophotometer. The photocatalytic properties of V/Fe doped TiO_2 were studied through degrading acid 3R dye, and the results show that when the content of V/Fe was 0.5%, the degradation rate reached more than 96% under irridation for 60 min.

Introduction

TiO_2 is an important semiconductor of photo-catalytic material due to its chemical stability, nontoxicity and chemical and photochemical anticorruption, which plays an important role in wastewater treatment and air decontamination [1,2]. However, it is also flawed. First, its band gap is relatively so wide that it can use solar energy accounts for only 3%-5%. Second, Photo-generated electrons and holes is very easy to composite. A effective approach through doping transitional metal ions towards nano TiO_2 has been theoretically, or experimentally researched to lead to mid-band gap[4,5]. A series of studies found that iron doping can make effective separation of photo-generated electrons and holes, induce defects in the lattice and have a red shift band edge [6,7], meanwhile, Vanaduim doping is extremely promising due to its long carrier lifetime [8,9]. Compared to single metal ion doping, multiple ion doping can synergy effect according to the different influence metal ions on the TiO_2 crystal lattice to enhance modified TiO_2 photocatalytic properties. For instance, Estrellan et al. [10] synthesized the iron and niobium co-doped titanium dioxide by sol-gel method, and the results showed a highest activity compared to the undoped TiO_2 and the commercially available TiO_2. Zhang et al. [11] prepared a cooper(II) and iron(III) co-modified TiO_2 by sol-gel process, and the capability of the codoped catalyst was higher than that of pure TiO_2. The traditional preparation method of metal doping TiO_2 nanoparticles includes the sol-gel process, hydrothermal methods [12], emulsion precipitation [13], and so on.

In this paper, a series of mesoporous nano-TiO_2 material co-doped with V/Fe were synthesized by a novel complexation-controlled hydrolysis method at room temperature synthesis, using $TiCl_4$, $Fe(NO_3)_3 \cdot 9H_2O$, and NH_4VO_3 as raw materials, their photocatalytic properties were also studied.

Experimental Section

Sample Preparation. The synthesis process of nano-TiO_2 mesoporous material doped with V/Fe by complexation-controlled hydrolysis method was described as follows: 11mL of $TiCl_4$ solution slowly dropped into doubled- distilled water with a speed of 1d/s, and then let it stand until clarification. Some proper $Fe(NO_3)_3 \cdot 9H_2O$, and NH_4VO_3 were added to the solution untill completely dissolved, and then filtered it. A white viscous paste was synthesized by using ammonia

to adjust the solution pH=7~8. The clear and transparent solution was obtained after filtered, washed, and added appropriate complexing agent. The V/Fe co-doped TiO_2 dioxide photocatalyst transparent latex was synthesized after adjusting it pH=5~6, controlling its hydrolysis.

Characterization. The particle size of doped TiO_2 emulsion and its distribution was measured by The Zeta potential of nano particle size analyzer. The phase analysis experiment was conducted by D8 Advance X-ray diffractometer(Cu Kα radiation, $\lambda = 1.5406$ Å). The UV-Vis absorption of the product was determined by UV-1810 spectrophoto-meter. The efficiency of degradation was calculated from

$$B\%=[(A_0-A)/A_0]\times 100\% \quad (1)$$

A_0 and A were the initial absorbance and final absorbance at the maximum absorption peak, respectively.

Results and Discussion

Sample size analysis. Nano particle and Zeta potential analyzer analysis of TEM analysis of the synthetic samples showed that the sample particle size distribution was relatively narrow, the particle size was uniform, the average particle diameter was 3.8 nm (see Figure 1(a)). Figure 1(b) shows the pictures of pure TiO_2 and V/Fe doped TiO_2 transparent hydrosol, and the right one is V/Fe doped TiO_2 shows green colour while the pure TiO_2 shows no colour, it indicated that the V/Fe doped TiO_2 sample had longer absorbance length which consistent to the UV-Vis absorption spectra.

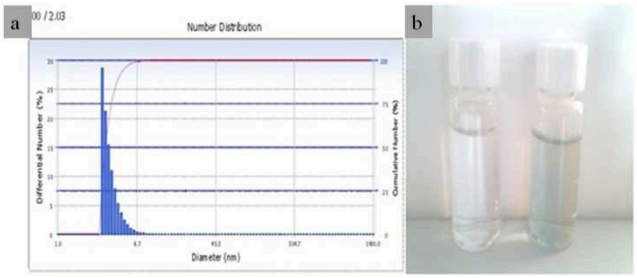

Fig. 1 (a) Particle diameter scatter diagram of sample;
(b)Pictures of pure TiO_2 and V/Fe doped TiO_2 transparent hydrosol

XRD analysis. XRD patterns showed that the pure TiO_2 was of anatase phase. After drying at room temperature, calcining at 400℃ for two hours (see Figure 2), the sample coped by V/Fe showed the characteristic peaks of anatase TiO_2, and the crystallinity was very good. It can be concluded that the nano-structures of V/Fe co-doped TiO_2 was not changed.

UV-Vis analysis. The UV-Vis results were shown in Figure 3, curve a was the UV-Vis absorption spectra of pure nano-TiO_2 hydrosol; curve b was the UV-Vis absorption spectra of V/Fe doped TiO_2 hydrosol. In the spectra it could be clearly seen that the absorption edge of curve b compared with curve a moved to the visible region nearly about 50nm. It could be concluded that the TiO_2 doped V/Fe broadened the spectral response of it, and then it improved their effective utilization of the sunlight.

EDS spectrum of the V/Fe doped TiO_2 sample. The EDS analysis of the the V/Fe doped TiO_2 sample was shown in Figure 4, which conducted with a scanning electron microscope. EDS spectrum are collected from different catalyst particles, and similar spectrum are obtained. The similar spectrum indicates the catalyst composition is homogeneous, it also demonstrates the presence of Ti, O, V, Fe.

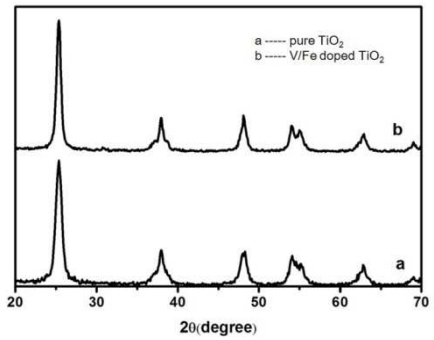

Fig. 2 XRD spectra of the samples
(a) Pure TiO_2; (b) 0.5% V/Fe doped TiO_2

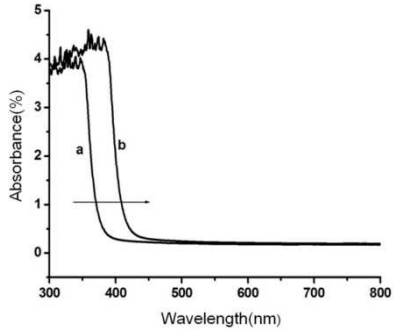

Fig.3 The UV-Vis absorption spectra
(a) Pure TiO_2; (b) 0.5% V/Fe doped TiO_2

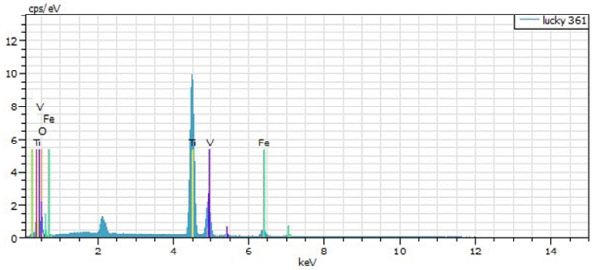

Fig. 4 SEM-EDS analysis of V/Fe doped TiO_2 sample

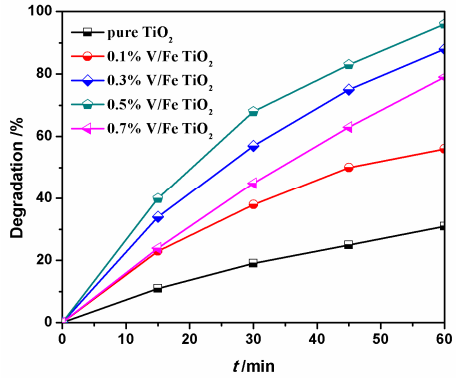

Fig. 5 Influence of different proportion of V/Fe on degradation rate

The property of photocatalysis. The effect of V/Fe content in the final product on its photocatalysis was investigated. When V/Fe content was 0.5%, maximum absorbance value (Amax) reached the maximum. As was shown in Figure 6, the Amax value for 0.5% content was the largest among all products with different V/Fe content, and its efficiency for degrading navy blue dye was almost 100%. This phenomenon might occur for the following reasons: When doping ions got into the crystal lattice, a series of doping levels would be formed, and increased doping level resulted in the increase of the electronic transition probability in a certain degree.

Conclusions

In this paper, V/Fe-doped nano TiO_2 transparent hydrosol was synthesized by a novel complexation-controlled hydrolysis method at room temperature. By this method, nano-TiO_2 prepared was anatase structure, and its crystallinity was better. Furthermore, the nano-TiO_2 transparent latex by this method had a narrow particle size distribution, had a uniform particle size of 3.8nm. The photocatalytic activity of V/Fe-codoped TiO_2 was significantly improved, and the starting position of the sample's absorbance had obviously red shift. Its influence sphere had extended to the visible spectral region area, and it had greatly improved the utilization of sunlight. When the content of V/Fe was 0.5%, the degradation rate on the concentration of 50 mg/L of Acid Red 3R dye solution was 96% or more under solar irridation for 60 min.

Acknowledgements

We gratefully acknowledge the financial support from the following sources: National Natural Science Foundation of China (NSFC) (Grants 21201053), Specialized Research Fund for the Doctoral Program of Higher Education (20121301120005), Outstanding Youth Fund in Hebei Province Department of Education (YQ2013009), Fund in Hebei Province Natural Science (F2014201078), China Postdoctoral Science Foundation Funded Project (2013M540213), and Hebei University Talent Introduction Fund (2012-233).

References

[1] A. Fujishima, A. Honda, Electrochemical photolysis of water at a semiconductor electrode, Nature 238 (1972) 37-40.
[2] Z.Y. Liu, X. Quan, H.B. Fu, X.Y. Li, K. Yang, Effect of embedded-silica on microstructure and photocatalytic activity of titania prepared by ultrasound-assisted hydrolysis, Appl. Catal. B: Environ. 52 (2004) 33-40.
[4] S. Liu, E. Guo, L.W. Yin, Tailored visible-light driven anatase TiO_2 photocatalysta based on controllable metal ion doping and ordered mesoporous structure, J. Mater. Chem. 22 (2012) 5031-5041.
[5] Y.H. Ni, Y. Zhu, X. Ma, A simple solution combustion route for the preparation of metal-doped TiO_2 nanoparticles and their photocatalytic degradation properties, Dalton Trans. 40 (2011) 3689-3694.
[6] K. Zhang, W.C. Oh, The Photocatalytic Decomposition of Different Organic Dyes under UV Irradiation with and without H_2O_2 on Fe-ACF/TiO_2 Photocatalysts, J. Kor. Ceram. Soc. 46 (2009) 561-567.
[7] P. Pongwan, B. Inceesungvorn, K. Wetchakun, S. Phanichphant, N. Wetchakun, Highly Efficient Visible-Light-Induced Photocatalytic Activity of Fe-doped TiO_2 Nanoparticles, Engineering Journal 16 (2012) 143-151.
[8] K. Bhattacharyya, S. Varma, A.K. Tripathi, S.R. Bharadwaj, A.K. Tyagi, Effect of Vanadia Doping and Its Oxidation State on the Photocatalytic Activity of TiO for Gas-Phase Oxidation of Ethene, J. Phys. Chem. C 112 (2008) 19102-19112.
[9] W.F. Zhou, Q.J. Liu, Z.Q. Zhu, J. Zhang, Preparation and properties of vanadium-doped TiO_2 photocatalysts[J]. J. Phys. D: Appl. Phys.43 (2010) 035301(6pp).
[10] C. R. Estrellan, C. Salim, H. Hinode, Photocatalytic decomposition of perfluorooctanoic acid by iron and niobium co-doped titanium dioxide, J. Hazard. Mater. 179 (2010) 79-83.
[11] D.F. Zhang, Enhanced photocatalytic activity for titanium dioxide by co-modification with copper and iron, Transtion Metal Chemistry 35 (2010) 933-938.
[12] Q.H. Zhang, L. Gao, Preparation of Oxide Nanocrystals with Tunable Morphologies by the Moderate Hydrothermal Method: Insights from Rutile TiO_2, Langmuir 19 (2003) 967-971.
[13] P.D. Cozzoli, A. Kornowski, H. Weller. Low-Temperature Synthesis of Soluble and Processable Organic-Capped Anatase TiO_2 Nanorods, J. Am. Chem. Soc. 125 (2003) 14539-14548.

Advanced Materials Research Vols. 989-994 (2014) pp 615-618
© (2014) Trans Tech Publications, Switzerland
doi:10.4028/www.scientific.net/AMR.989-994.615

Design of the Portable Detector for Formaldehyde

Fu Li[1, a], Fu Xiuwei [1, b]

[1] College of Information & Control Engineering, Jilin Institute of Chemical Technology, Jilin 132022, China;

[a]fuli247012412@126.com, [b] fxw7720268@163.com

Keywords: Electrochemistry Transducer, MCU, Formaldehyde.

Abstract. The design of the portable formaldehyde detector based electrochemical sensors with microcontroller is introduced in the paper .In conducting the test, the formaldehyde-containing gas diffusion to the sensor internal to react with the internal electrolyte and generates a weak current signal, the current signal through the working circuit is converted to a voltage signal, the voltage signal via the signal processing circuit, and it is collected and processed by MCU after input to the A/D. the signal is communicated with operator through the buttons and LCD.

Introduction

Formaldehyde[1,2] is a poison of virgin pulp which can be combined with proteins. The respiratory would be subject to severe irritation after people inhale high concentrations of formaldehyde, and body would be felt eye edema, stabbing pain and headache. Perhaps bronchial asthma can also occur. In recent years, due to the improvement of people's living standards, Buying a new house decorated rooms become the first choice after an affluent life. A lot of synthetic boards are used in house decoration, which contain formaldehyde. The formaldehyde of synthetic board play glued and antiseptic role on it, at the same time, the formaldehyde of residues and uninvolved in the reaction would be gradually released into the surrounding environment, which induce large amount of formaldehyde continued to stay in air of indoors. In the background of greatly increased of all kinds of illnesses are caused by formaldehyde, a portable, cost-effective and low-power characteristics of formaldehyde detector is designed in this paper. Portable formaldehyde detector is designed based on principles of microcontroller and electrochemical sensors. Meanwhile, it combines the existing detection methods and device on the market.

Implementation of formaldehyde detection in the air

The choice of detection method. At present, there are so many different kinds of formaldehyde detectors on the market. One of the more common is to use test paper photoelectric photometry[3]. When the formaldehyde gas blow to the soaked hair color agent dipstick and the soaked hair color agent TAB combination will change color due to chemical reaction. The reflected light quantity of Suffered light can be reflected by the degree of discoloration. The amount of reflected light intensity change rate can be used as the formaldehyde content of the response value of the measured gas. Pre-set test line, the density of formaldehyde gas can be measured by measuring response rate. In terms of gas gathering some use automatic suction (built-in micro-pump), some use diffusion.

For test paper photoelectric photometric method to analyze the concentration of formaldehyde, it has the advantage of high sensitivity, easy operation, fast measurement speed. And this method that is based on the analysis of the formaldehyde concentration often uses is visual colorimetric method, its disadvantage is that: As many colored solution is not stable enough, can not survive long, often need to in the determination of mixed solution at the same time, more time-consuming and cumbersome; Visual colorimetric accuracy is low, generally a relative error of $\pm$ 5 ~ 20%.

This design uses a sensor detection method, and sensor type used in this design is electrochemical sensors. The concentration of formaldehyde gas can be converted to weak current signal. A weak

current signal will be converted to a stable voltage measurement signal by the current voltage conversion circuit and enhance the stability of the electrical signals.

Electrochemical formaldehyde sensor working principle and model selection. Electrochemical sensors we used are constant potential electrolysis sensor. Sensors can be equivalent by a number of internal capacitance, resistance, the equivalent capacitance and resistance are random variation. The basic principle of controlled potential electrolysis type sensor is controlled by external circuit that controls the potential of the test substance that occur in the oxidation-reduction reaction on the working electrode, reaction produces electric current is directly proportional to the concentration of the analyte in a sample.

After the analysis of the design requirements and several types of electrochemical sensors which be provided on the market, this design using the Swiss Membrappr company CH2O sensor was finally determined.

Formaldehyde detector design

The overall design of formaldehyde detector. The signal of overall design comes from SCM[4] and can be displayed by digital tube. reference value would be set by used of button. According to the results of compared to acquisition value and reference value, implementation of control is completed. The overall system block diagram is shown in Fig. 1.

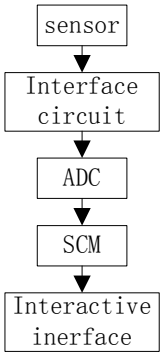

Fig. 1 The overall structure of the system

Sensor Interface Design. The output signal of the sensor is a weak current signal level μA, if handled improperly, the interference signal can easily sneak in and it will affect the stability and accuracy of the system. In order to prevent the weak signal in the process of transmission and the interference signal disturbance, the sensor interface circuit should contain constant electric displacement and the reference voltage circuit. An electrochemical sensor interface circuitry is shown in Fig. 2.

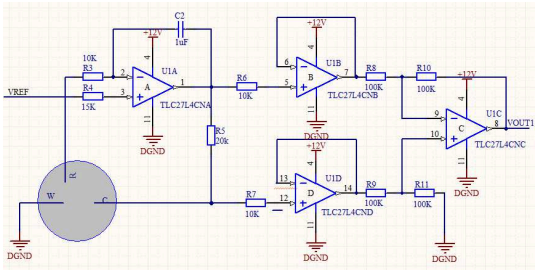

Fig. 2 Electrochemical sensor interface circuitry

As shown in figure 3,it is a reference voltage supply circuit and the reference voltage value is produced by LM385-1.2, the reference voltage VREF = 1.235 V.

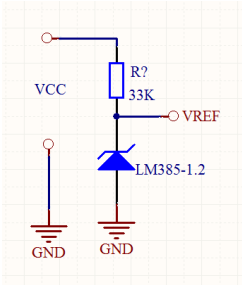

Fig. 3 Reference voltage circuit

The signal processing circuit. By the interface circuit of the sensor output voltage signal, first, because is small, need further amplification. Secondly, as a result of electrochemical sensor there is a certain temperature drift, the output value of the signal is not very stable. To compensate for this, it can be adjusted from the aspects of hardware. As shown in figure 4.

In this design, a hardware circuit design can adjust work zero and magnification of the circuit, Amplified output signal Vout2 into the A / D to achieve analog-digital conversion, digital signal output to the microcontroller STC89C51, implemented by software functionality. The design of the MCU adopts STC89C51RD +, A/D conversion module using TLC1549 10. The specific circuit is shown in Figure 5.

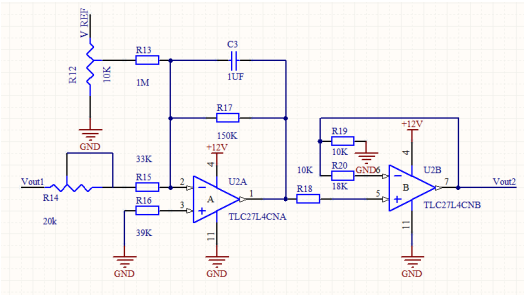

Fig. 4 The signal processing circuit

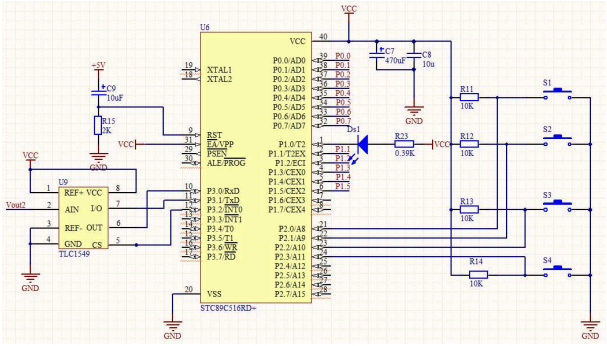

Fig. 5 MCU peripheral circuits

Design of the overall system software. The first step of system boot is initialization, after initialization is completed, sensor would be detected and the results are displayed on digital tubes. Corresponding alarm would happen when the wrong report is detected. Detection value can be set by buttons to normal. Flowchart of the overall system is shown in figure 6.

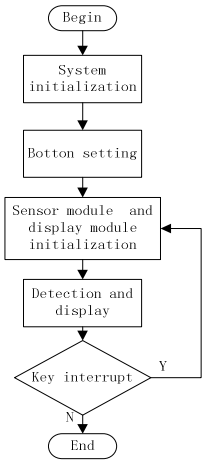

Fig. 6 Overall flow chart

Conclusion

The unique design in this article has the simple hardware circuit to reduce the number of the using chips most efficiently in terms of power consumption, and the MCU chip FLASH application is greatly combined to reduce system power consumption. First of all, an electrochemical sensor is used in the design, with high sensitivity and accuracy, but also has the advantages of small size and is very suitable for portable products.

References

[1] ZHU Li-Fang: Methods of determination of formaldehyde in the air (Environmental Pollution and Control), Vol. 13 (1991) No. 3, p.33-36. (In Chinese)

[2] DU Juan: *The Design of the Portable Field Formaldehyde Detector* (MS., Zhengzhou University, China 2010), p.28-32.

[3] Allen, J. Bard, R. Larry, Faulkner, SHAO Yuan-hua etc: *Electrochemical Method Principle and Application* (Chemical Industry Press, Beijing 2005).

[4] HE Li-min: *MCS51 MCU Application System Design* (Beihang University Press, Beijing 1990).

Advanced Materials Research Vols. 989-994 (2014) pp 619-622
© (2014) Trans Tech Publications, Switzerland
doi:10.4028/www.scientific.net/AMR.989-994.619

Numerical simulation of the nanofluid phase separation by lattice Boltzmann method

Shouguang YAO[1], Xinwang JIA[1a],Changjiang ZHOU[1], Yuhong Nie[1]

[1] Jiangsu University of Science and Technology, Zhenjiang, 212003, China
[a]email: justhxs@163.com

Keywords： nanofluid, lattice Boltzmann method, phase separation

Abstract. Using shan-chen model of lattice Boltzmann method,considering the interaction between nanoparticles and base fluid, by modifying the nanofluids single-component multiphase model, established the nanofluid multi-component heterogeneous lattice Boltzmann model. The model was used to simulate square cavity phase separation of nanofluids, get the Nanofluid separation phase diagram, compared it with pure water phase separation diagram, the results show that, nanofluid in gas-liquid two phase separation process, the addition of nanoparticles is beneficial to produce bubbles, meanwhile the addition of nanoparticles caused a micro convection inside the base fluid, improved the performance of the spread of the base fluid, leaded to the transmission effect, hindered the coalescence of bubbles.

Introduction

Lattice Boltzmann method is a fluid dynamics simulation method developed from mesoscopic recently with the characteristics of simple code, easy to deal with complex boundaries, and suitable for large-scale parallel computing. It has attracted more and more attentions [1]. Currently, the method is used to simulate single-phase fluid quite successfully, but seldom used to simulate the phase change problem.

Nanofluid is a two-phase medium with the existence of a complex interaction between nanoparticles and base fluid. There is velocity difference between nanoparticles and base fluid resulting in the presence of drag force, Brown force, the force caused by the potential energy, as well as gravity and buoyancy [2].

In this paper, a phase separation model for nanofluids was established by the use of pseudo-potential model on the base of considering the force between nanoparticles and the base fluid. And then the model was used to simulate the phase separation process of pure water and nanofluids.

Lattice Boltzmann model for nanofluids

Lattice-Boltzmann equation (LBE) for nanofluids can be expressed as [3]:

$$f_i^\sigma\left(\boldsymbol{x}+\boldsymbol{e}_i\Delta t,t+\Delta t\right)-f_i^\sigma\left(\boldsymbol{x},t\right)=-\frac{1}{\tau^\sigma}\left[f_i^\sigma\left(\boldsymbol{x},t\right)-f_i^{\sigma eq}\left(\boldsymbol{x},t\right)\right]+\frac{2\tau^\sigma-1}{2\tau^\sigma}\frac{F_\alpha^\sigma De_i}{B_i c^2},\ \mathrm{i}=0,1\ldots8 \tag{1}$$

The function $f_i^\sigma\left(\boldsymbol{x},t\right)$ is the particle distribution function of $\sigma=1,2$ components with lattice velocity vectors e_i, B_i is the adjustable coefficient, D is the dimension, F^σ is applied force, τ^σ is the dimensionless relax time.

the equilibrium distribution function $f_i^{\sigma eq}\left(\boldsymbol{x},t\right)$ can be defined as：

$$f_i^{eq}=\rho^\sigma w_i\left[1+\frac{\boldsymbol{e}_i\cdot\boldsymbol{u}^\sigma}{c_s^2}+\frac{\left(\boldsymbol{e}_i\cdot\boldsymbol{u}^\sigma\right)^2}{2c_s^4}-\frac{u^{\sigma 2}}{2c_s^2}\right] \tag{2}$$

Where w_i is the lattice weighting factor.

The mean viscosity of the nanofluid can be written as

$$\nu=\frac{2\sum_\sigma c_\sigma\tau^\sigma-1}{6}\frac{(\Delta x)^2}{\Delta t} \tag{3}$$

Where c_σ is the concentration of different components.

Coupling Forces

The main problem for the usage of two-phase lattice Boltzmann model in nanofluids is to determine the force acting on each phase [4-6]

Assume F_σ is the sum of internal and external forces. For nanoparticles, F_σ includes gravity F_G, drag force F_D, brown forces F_B. For the base fluid, F_σ just includes brown force and drag force.

$$F_G = -\frac{4}{3}\pi r_p^3 g\Delta\rho \tag{4}$$

Where, $\Delta\rho$ is the density difference between the base fluid and nanoparticles, r_p is the nanoparticle radius.

$$F_D = -6\pi\mu d_p \Delta u \tag{5}$$

Where, Δu is the speed difference between the base fluid and nanoparticles, μ is Fluid dynamic viscosity.

$$F_B = \zeta\sqrt{\frac{6d_p\mu k_B T}{\Delta t}} \tag{6}$$

Where ζ is a Gaussian random number, Δt is a time step of Gaussian particle motion, k_B is Boltzmann constant.

Phase separation model for nanofluids

For the gas-liquid, surface tension should be introduced to promote two-phase separation. According to the interaction potential, the force of σ fluid particles can be obtained as [7]:

$$\boldsymbol{F}_\sigma(\boldsymbol{x}) = -\psi_\sigma(\boldsymbol{x})\sum_{\bar{\sigma}}\xi_{\sigma\bar{\sigma}}\sum_i \psi_{\bar{\sigma}}(\boldsymbol{x}+\boldsymbol{e}_i\delta_t)\boldsymbol{e}_i \tag{7}$$

In order to reflect the impact of the surface tension, the equilibrium velocity was changed to a new velocity:

$$\rho_\sigma \boldsymbol{u}_\sigma^{eq} = \rho_\sigma \boldsymbol{u} + \tau_\sigma F_\sigma \tag{8}$$

Where $\boldsymbol{u}$ is the velocity of the mixed fluid:

$$\rho\boldsymbol{u} = \sum_\sigma \rho_\sigma \boldsymbol{u}_\sigma = \sum_\sigma\sum_i \boldsymbol{e}_i f_{\sigma i} \tag{9}$$

ρ is the density of mixed fluid：

$$\rho = \sum_\sigma \rho_\sigma \tag{10}$$

Numerical simulation and analysis

The nanofluids were simulated by the model established above. The grids were 500*500, and all the physical property parameters were the dimensionless, value of relaxation time τ was 1.0. The particle size of Al_2O_3 is 30nm. The density of Al_2O_3, water and gas is 3970kg/m3,998.2kg/m3, and 0.55kg/m3 respectively.

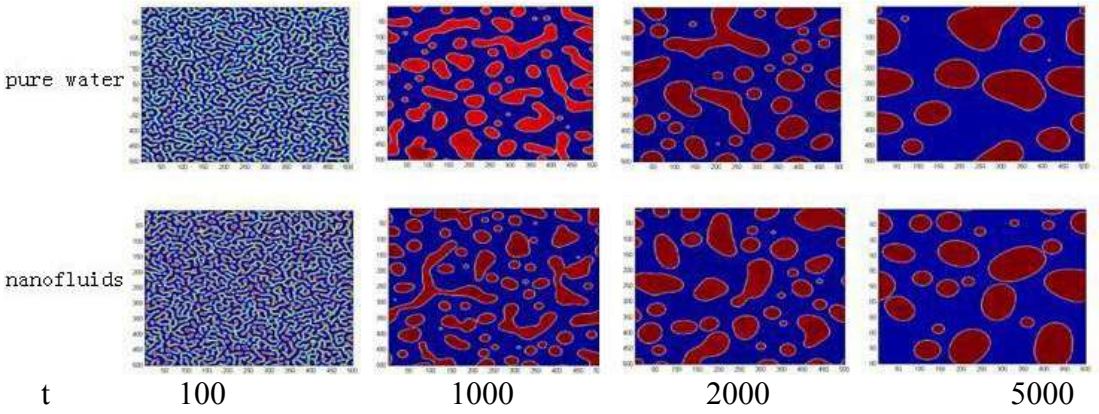

Fig.1 Gas-liquid separation contrast figure of the Al2O3 - H2O compared with pure water

Figure1 shows the separation process from a uniform phase to two-phase, in which the red means gas phase and the blue is liquid phase. It can be seen from the figures that the phase separation can be divided into two stages. The first stage is that the density of whole flow field gradually changes from the initial uniform to gas-liquid. The second stage is the two phases after separation will go on evolution by the surface tension. It can be seen from the figure that the gas phase fluid eventually evolved into the sphere until it reaches a steady state dynamics.

The fluid separations of Al_2O_3-H_2O nanoparticles at volume concentration 0.1% and water were also compared in Figure1. It can be seen that the phase separation processes of water and nanofluids at the beginning ($100<t<1000$) are substantially the same.But with the separation process, the bubbles in nanofluids have been distributed uniformly in steps from 2000 to 5000, and the number of bubbles will be more, and gradually reaches a steady state. On the contrary, the separation of water is still continuing, the distribution of the bubbles is not uniform and the number of bubbles is less that that in the nanofluids. This indicates the existence of nanoparticles is beneficial to the generation of bubbles, and the separation process is easier than water.This can be explained as follows: the internal micro-convection in the base fluid produced by the involvement of nanoparticles can improves the diffusion properties of the base fluid, causing the transmission effects and hinder the coalescence of bubbles. The result is consistent with the literature [8].

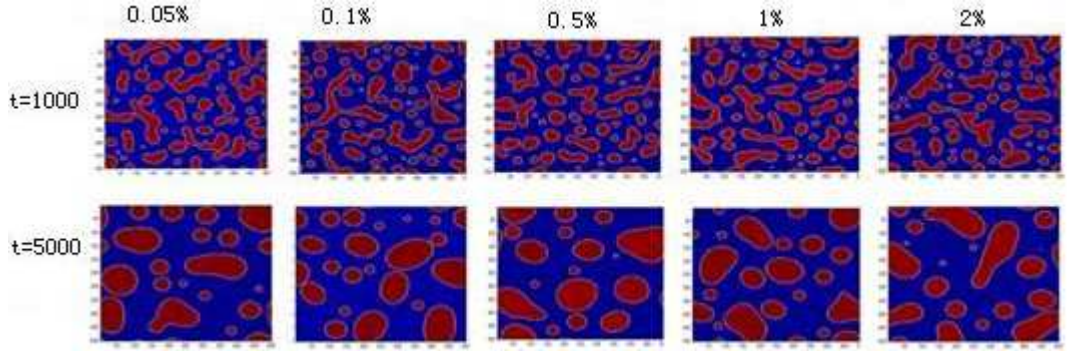

Fig.2 Gas-liquid separation of the different concentrations

To study the effect of different concentrations of nanoparticles on the separation process, different concentrations of nanofluids were simulated, and the separation process were shown in Figure 2. It can be seen from the figure that the separation efficiency is not strengthened with the increase of the concentrations of nanoparticles. Increasing the concentration may promote liquid separation or weak the separation. It is the interaction result of the rate of new active nucleations formed on the surface of the nanoparticle and the reduction caused by particle deposition. It is in good agreement with the experimental results in [9].

Conclusion

A new Lattice Boltzmann model was established to simulate the phase separation of water and nanofluids. By analyzing the separation progress, some results can be obtained:

(1) The phase separation of pure water is basically similar with nanofluids. But the existence of nanoparticles is beneficial to the generation of bubbles, and the separation process is easier.

(2) The separation efficiency is not monotonously strengthened with the increase of the concentrations of nanoparticles.

Acknowledgement

In this paper, the research was sponsored by the National Natural Science Foundation of China (Grant No. 51176069)

References

[1]Yanling He, Yong Wang, Qing Li. Lattice Boltzmann Method. Theory and Application Beijing: Science Press, 2011.

[2]Qi Cong, Yan Shengnan, Tian Yurong.Rectangular cavity nano fluid two-phase lattice Boltzmann simulation of natural convection. Dalia: Chinese Society of Engineering Thermophysics, 2012.

[3] Barrios G, Rechtman R, Rojas J, et al: Fluid Mech, 2005, 522: 91-100.

[4] Nemati H, FarhadiM, Sedighi K, et al: Heat Mass Transfer, 2010, 37:1528-1534

[5]Cui Tengfei,Xuan Yimin,Li Qiang: CIESC Journal, 2012, 5 (63):41-46.

[6]Guo Yangli, Xu Hehan, Shen Shengqiang: CIESC Journal, 2012, 10 (63):3057-3061.

[7]Li Longjian, Zeng Jianbang, Huanjie. Flow boiling simulation lattice Boltzmann method. Dalian: Chinese Society of Engineering Thermophysics, 2012

[8]Zhang Shuyang. Nanofluids strengthen gas-liquid mass transfer research. Tianjin: Tianjin University, 2010.

[9]Shuai Meiqin, Shi Mingheng: Journal of Engineering Thermophysics, 2008,29(12): 2101-2103.

Advanced Materials Research Vols. 989-994 (2014) pp 623-625
© (2014) Trans Tech Publications, Switzerland
doi:10.4028/www.scientific.net/AMR.989-994.623

The Emission Property of Phosphors LEDs Based on ZnCuInS/ZnSe/ZnS Quantum Dots

BI Ke[1a], LIU Wen-yan[2], XU Tian-yue[1b], ZHANG Tie-qiang[1], ZHANG Yu[1,2]

[1]State Key Laboratory of Superhard Materials, College of Physics, Jilin University, Changchun 130012, China

[2]State Key Laboratory of Integrated Optoelectronics, College of Electronic Science and Engineering, Jilin University, Changchun 130012, China

[a] email: bk823546780@sina.com. [b] email: xutianyue1989@163.com

Keywords: ZnCuInS/ZnSe/ZnS Quantum Dots; GaNLED; Photoluminescence; Phosphors

Abstract. In this research, ZnCuInS/ZnSe/ZnS quantum dots(QDs) have been studied as an excellent red emitting source for blue GaN LED because of its non-toxic deep red emmission, and large Stokes shift properties. In the paper ZnCuInS/ZnSe/ZnS core/shell quantum dots were prepared with the particle size of 4.5nm. According to the measurement of photoluminescence spectrum emitted by ZnCuInS/ZnSe/ZnS core/shell quantum dots, the emitting peak of 700 nm and the full was achieved as red emitter.It was found that absorption edge and photoluminescence peak shifted to shorter wavelength with decreasing the nanocrystal size due to quantum size effect.Meanwhile, we were prepared ZnCuInS/ZnSe/ZnS core/shell quantum dot light emitting diodes and their photoluminescence properties were studied. After the suitable bias was applied on the films, increasing the ZnCuInS/ZnSe/ZnS QDs concentration in the blue GaN chips, red emission increased with decreasing LED’s blue light.

Introduction

In the past few years, most people using colloidal synthesis method to synthesize two yuan and one yuan-type semiconductor nanocrystals, which has a high colloidal stability, but it has a good single-particle dispersion. These properties and their resistance to photo-bleaching make QDs attractive for applications such as biomedical tags[1][2][3], hybrid light-emitting diodes[4][5], solar cells[6], photo-refractive devices[7], and potential laser development[8]. Recently the I-III-VI QDs have been gaining increased attention. ZnCuInS/ZnSe/ZnS quantum dot Ⅰ-Ⅱ-Ⅵ compound semiconductor material has many advantages: band gap ZnCuInS/ZnSe/ZnS is 1.6eV, the band gap is very close to the top of the solar cell material.

Experimental Section

Indium (III) iodide (InI3, 99.99%) and selenium powder (Se, 100 mesh) were purchased from Alfa Aesar. Copper (I) iodide (CuI, 98%), dichlorodiphenyltrichloroethane (DDT, 98%), tributyl phosphine (TBP, 95%), diethyl dithiocar bamic acid zinc (DECZn, 98%), oleyl amine (OAm, 80-90%) and zinc oxide (ZnO, 99.99%) were obtained from Aladdin. Acetone, methanol, hexane, toluene were purchased from Aldrich. All chemicals were used directly without further treatment.

Synthesis of ZnCuInS/ZnSe/ZnS QDs

In the typical procedure of 3.3 nm ZnCuInS/ZnSe/ZnS QDs, 20 mL ODE was loaded into 100 mL three-necked flask, and was degassed under N2 for 10 min. 2mL CuI/OAm (45mM), 2 mL InI3/OAm, and 6 mL DECZn/TBP/ODE were loaded into the flask under N2. The mixture was heated to 343K for 30 min and then was heated to 483K for 50 min. The color of solution varied from colorless to red which meant the formation and growth of ZnCuInS core. Then, 2 mL Se/TBP and 2 mL ZnO/OA/ODE solution were added drop by drop into the solution of ZnCuInS core to grow a ZnSe shell. 10 min later, 3 mL DECZn/TBP/ODE were added into the flask for the growth of a ZnS shell.

Preparation ZnCuInS/ZnSe/ZnS quantum dot phosphor LED's

In the preparation of ZnCuInS/ZnSe/ZnS quantum dot light emitting diode device, the ratio ZnCuInS/ZnSe/ZnS quantum dots associated with the reagent will directly affect the amount of its quantum dot light-emitting devices.When the coating layer is simultaneously dropwise, evaporated to dryness and the dispensing temperature is controlled to some extent determines the uniformity of the film thickness and the film surface. In this paper, 0.06ml, 0.16ml, 0.26ml, 0.36ml four different quantum dot solution dispensing volume of the test sample.First with a small pipette to extract soluble in hexane solution ZnCuInS/ZnSe/ZnS quantum dot solution, in order to dispense GaNLED chip surface was uniform quantum dots.

ZnCuInS/ZnSe/ZnS quantum dots based on sulfur vacancies-vacancies luminous copper-based.With the increase of the thickness of the shell, in which the surface of the sulfur vacancy will gradually decrease, thus the conduction band electrons and copper vacancy recombination luminescence occurs as a major way, and the emission peak blue shift.As shown, the absorption peak wavelength ZnCuInS/ZnSe/ZnS quantum dots, respectively, and an emission peak wavelength of 600nm, 700nm. PL emission peak wavelength of 700nm.

PL luminescence mechanism ZnCuInS/ZnSe/ZnS quantum dots is a donor - acceptor pair (donor-acceptor pair, DAP) recombination.References about DAP recombination theory, therefore, the weak size dependency of DAP recombination comes from the change in the Coulomb interaction with changing DAP separation, according to the equation.the binding energy of the quantum dot DAP following expression:

$$E_{DAP} = E_g - E_D - E_A + \frac{e^2}{4\pi\varepsilon r}$$

Where E_{DAP} DAP and Eg are the binding energy of the band gap materials; E_D and E_A are the donor and acceptor ionization energy.

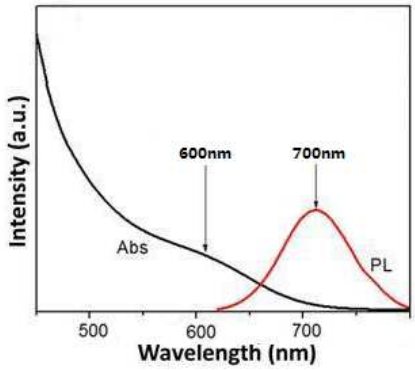

Fig.1 (a) Absorption and PL spectra of ZnCuInS/ZnS QDs,

Figure2 (a) of ZnCuInS/ZnSe/ZnS quantum dot light emitting diode emission spectra at different voltages.Respectively, 10v, 15v, 20v compare with the gradual increase in the voltage at both ends of the light emitting diode, lead to a high electric field spectral redshift.Figure2 (b) is the device voltage - current density characteristic curve. As the voltage increases the current density will be increased accordingly, light-emitting diodes in the 12V current density 250mA/cm^2. Figure2 (c) the voltage of the device -. Luminance characteristic curve, the figure shows, the brightness of the device at 10V 80cd/m^2, when the brightness of 8V 40cd/m^2. (C) comparing apparent from Fig2 (b) the reason for the low efficiency of the device is ZnCuInS/ZnSe/ZnS core-shell quantum dot surface not handle light emitting layer resulting in poor film formation.

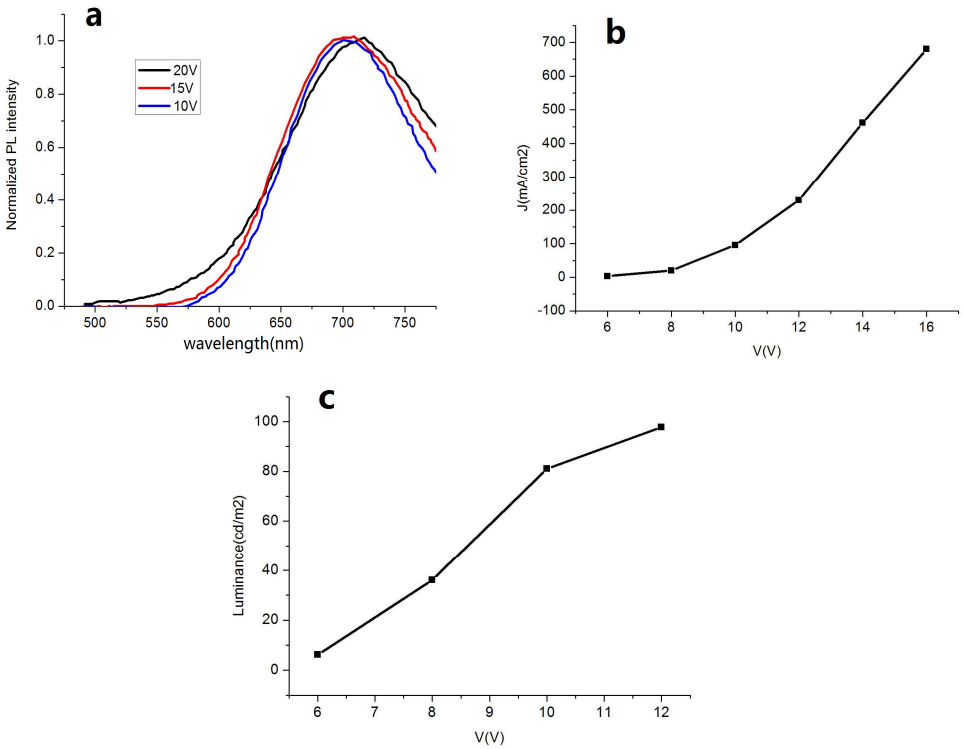

Fig. 2 (a) luminescence spectra, (b) voltage-current,
(c) voltage-luminance curves of ZnCuInS/ZnS core-shell Quantum dot light-emitting diodes.

Conclusion

For 4.5nm size ZnCuInS/ZnSe/ZnS quantum dot can produce a peak wavelength of 700nm.Compared with the organic light-emitting materials, quantum dot phosphors are the main advantages of LED low power consumption and long service life.we have studied the size- and temperature-dependent spectra of ZnCuInS/ZnSe/ZnS core/shell/shell QDs. The PL spectra were recorded for several ZnCuInS/ZnSe/ZnS QDs with different diameters. The Stokes shift obtained by taking the difference between the positions of the absorption and emission peaks was found to increase with the increased QD size. The energy band gap of QDs with different diameters was investigated as a function of temperature in the range 50-373 K and fitted with two empirical expressions, from which the Huang-Rhys factor and the average phonon energy were achieved. The electron-phonon coupling was found to be stronger for QDs with smaller diameters.Stokes shift is measured by the difference between the absorption and emission peaks between the obtained position deviation 378meV, PL indicates the electron transport zone and on the defect level, and increases with dot size increases. Successfully fabricated article ZnCuInS/ZnSe/ZnS quantum dot phosphor LED light emitting diode device, and the obtained peak value of 700nm red light, according to the calculation method of the CIE color coordinates are (0.632,0.252).

References

[1] Bruchez M, Moronne M, Gin P, et al. Science, 1998, 281: 2013.
[2] Yu W W, Chang E, Falkner J C, et al. J. Am. Chem. Soc, 2007, 129: 2871.
[3] Yu W W. Expert Opin. Biol. Ther, 2008, 8: 1571.
[4] Tessler N, Medvedev V, Kazes M, et al. Science, 2002, 295: 1506.
[5] Zhang Y, Xie C, Su H P, et al. Nano Lett, 2011, 11: 329.
[6] Huynh W U, Dittmer J J. Science, 2002, 295: 2425.
[7] Winiarz J G, Zhang L, Lal M, et al. J. Am. Chem. Soc, 1999, 121: 5287.
[8] Klimov V I, Mikhailovsky A A, Xu S, et al. Science, 2000, 290: 314.

Advanced Materials Research Vols. 989-994 (2014) pp 626-628
© (2014) Trans Tech Publications, Switzerland
doi:10.4028/www.scientific.net/AMR.989-994.626

The Synthesis of Ionic Liquid Crystal Polymer and the Study of as Chromatographic Stationary Phase

Shuang FU[1, a], Jie ZHANG[1, a]

[1]College of Pharmacy, Qiqihar Medical University, Qiqihar, 161006, China

[a]email: fsjt1980@163.com

Keywords: Ionic Liquid Crystal Polymer; Synthetic; Chromatographic Stationary Phase

Abstract. This paper was about the synthesized of ionic liquid crystal polymer of benzoic acid type of the tree, and had some tests about the structure characterization and performance, studied the performance of the liquid crystal, let it as the chromatographic stationary phase, preliminary surveying the separation of benzene and homologues. The studies have shown that ionic liquid crystal polymer as chromatographic stationary phase has certain development space and research value.

Introduction

Ionic liquid crystal polymer is composed of ionic liquid monomer polymer polymerization with characteristics of liquid crystal compounds, and it composite properties of ionic liquid and liquid crystal polymer. Liquid crystal unified it's order and the liquid's liquidity at the molecular level, ionic liquid crystal polymer has low steam, thermal stability and chemical stability of higher unique physical and chemical properties[1], in many fields of application and interests had attracted much attention[2][3].This type of amphiphilic ion salt not only has the surface activity, but also has the characteristics of ionic liquids and thermotropic liquid crystal[4][5]. So the synthesis of different types and function of ionic liquid crystal polymer is one of the researcher's keen topic[6][7].

The commonly used GC stationary liquid is mainly high molecular compound, a small number of liquid crystal polymer, and ionic liquids as the candidate also presents a certain of use prospects[8][9].The highly branched structure of tree molecular and it's unique monodispersity, presents a good film[10],conform to the requirements and characteristics of chromatographic stationary phase[11], it's possible to be used for chromatographic stationary phase.

In this article we try to through ionic liquid crystal polymer synthesis of benzoic acid type of the tree, regulate the temperature of the liquid crystal phase, make it as a fixed liquid chromatography, within the scope of the liquid crystal phase separation of the boiling point and polarity , position isomer and some chiral compounds such as difficult separation material, and show their role in the chromatographic separation and functions, their has not been reported that the ionic liquid crystal polymer as chromatographic stationary phase.

Polymer synthesis and performance testing

(1)The preparation of the Polyamide-Amine(PAMAM) tree macromolecular polymer

The synthesis of PAMAM: With ethylenediamine and acrylic acid methyl ester as raw materials by Michael addition reaction ,producing a four yuan ester, then with excessive ethylenediamine ammonolysis reaction, generate four amide compounds. Repeat Michael and ammonolysis reaction steps, and get different type algebra of PAMAM macromolecular compounds.

(2)The preparation of 3, 4, 5-three place of alkoxy benzoic acid

To 3,4,5-hydroxy benzoic acid methyl ester and bromine 3 generation of n-alkane as raw materials, in Tetrahydrofuran solvent though reaction can get 3,4,5-three replace alkoxy benzoic

acid methyl ester, and in potassium hydroxide alcohol solution hydrolysis again get 3,4,5-three replace alkoxy benzoic acid.

(3)The synthesis of alkoxy replace benzoic acid-polyamide-amine salt

Take PAMAM which with the group-NH_2 and 3,4,5-three replace alkoxy benzoic acid ,reaction in the solution of tetrahydrofuran, in the system the proportion of -NH_2 and -COOH is 1:1,so we can get the alkoxy replace benzoic acid polyamide-amine salt ion liquid crystal.

(4)Benzoic acid type ionic liquid crystal polymer's performance test

To characterization of the synthesis of ionic liquid crystal on the physical and chemical properties, which includes: solubility, heat stability, liquid crystal state and temperature range.

(5)Chromatographic separation performance test and application test

Prepared for capillary column and packed column, and after aging of the columns to separate respectively of benzene homologues, alcohol homologue, fat hydrocarbon homologue and so on, then we should determinate of column efficiency and relative polarity, separating degree, studying the effect of aging temperature on column performance.

Test results

According to the DSC heating curves of ionic liquid crystal polymer, we can see the temperature of the liquid crystal phase is 130-180℃.Using the hot stage polarized microscopy to observe, the liquid crystal polymer belongs to nematic liquid crystal.

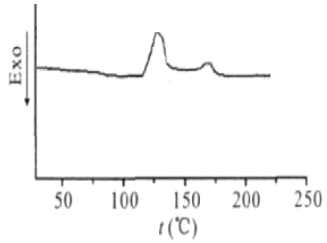

Fig.1 DSC heating curves

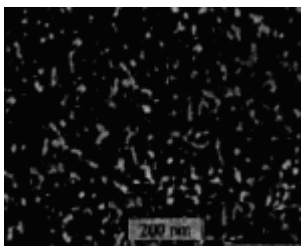

Fig.2 Ionic liquid crystal polymer POM images

Coating single white 101 with ionic liquid crystal polymer preliminary, and use that as the chromatographic stationary phase of GC to the prepare for packed column and to test the separation performance of benzene and homologues. Test results show that the ionic liquid crystal as chromatographic stationary liquid method is feasible and needs to be further research.

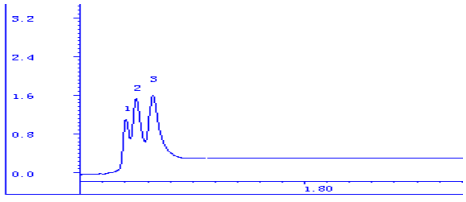

Fig.3. GC - separation of benzene homologue

（No. 1 peak: benzene; No. 2 peak : methylbenzene; No. 3 peak: meta-xylene）

Conclusion

Using the ionic liquid crystal polymer as chromatographic stationary phase is a new research direction and which shows a good application prospect. This experimental research contents include organic synthesis, analytical test, chromatographic analysis and chemical and physical comprehensive knowledge and technology and has strong theoretical research value and a higher level of science and technology. In the meantime, the research has a broad market space, and the production, sales and application can generate economic and social benefits.

Acknowledgement

In this paper, the research was sponsored by the Science and Technology Research Project of Heilongjiang Province Education Department (Project No. 12541932).

References

[1] Han X, Armstrong D W. Ionic Liquids in Separations[J]. Accounts Chem Res, 2007, 40(11): 1079-1086.

[2] Jean-Moise Suisse, Ste´phane Bellemin-Laponnaz, Laurent Douce. A new liquid crystal compound based on an ionic imidazolium salt[J]. Tetrahedron Letters, 2005, 46: 4303-4305.

[3] Rogers R D, Seddon K R. ACS Symposium Series 856: Ionic Liquids as Green Solvents[J]. American Chemical Society: Washington, DC, 2003.

[4] A. Kulbickas, J. Tamuliene, L. Rasteniene, et al. Optical study and structure modelling of PPI liquid crystalline dendrimer derivatives[J]. Photonics and Nanostructures-Fundamentals And Applications, 2007, 5: 178-179.

[5] Tomalia D A, Esfand R. Poly (amidoamine) dendrimers: from biomimicry to drug delivery and biomedical applications[J]. Drug Discovery Today, 2001, 6: 427-436.

[6] Qixian Zhang. Synthesis and characterization of novel azobenzene ionic liquid crystals[D]. Northeast Normal University 2011.

[7] Minyang Zheng. lonic liquid crystals of long alkyl iminazole salts andtheir liquid crystalline properties[J]. New Chemical Materials. 2012, 40(9), 27-30.

[8] Wei Gao. Applications of ionic liquids in chromatographic analysis and determination of ionic liquids by chromatography[J]. Chinese Journal of Chromatography, 2010, 28(1), 14-22.

[9] Ruo-nong FU. Recent development of room temperature ionic liquids as stationary phases in gas chromatography[J]. Chemical Regent, 2013, 35(6):481-490.

[10] Shi-an ZHONG. Terminal Modification of Polyamidoamine and the Synthesis of Dendritic Azobenzene Side-Chain Liquid Crystalline Copolymers[J]. Polymer Materials Science and Engineering, 2009, 25(8): 8-11.

[11] Shen Shuchang, Zhang Weibing, Fu Shuang. Preparation Phenylethylene-Butyl Acrylate Viny ltriethoxy Siloxane Terpolymer for Solid Phase M icroextraction Coating[J]. Chinese Journal of Analytical Chemistry, 2007, 6:865-868.

Advanced Materials Research Vols. 989-994 (2014) pp 629-633
© (2014) Trans Tech Publications, Switzerland
doi:10.4028/www.scientific.net/AMR.989-994.629

Research on Properties of CB/EVA Semiconductive Shielding Composites

Baozhong HAN[a], Chunyang LI, Chengcheng ZHANG, Changming LI

[1]Key Laboratory of Engineering Dielectrics and Its Application, Ministry of Education, Harbin University of Science and Technology, Harbin, 150080, China

[a]email:hbzhlj@163.com

Keywords: Carbon black; Ethylene/vinyl acetate copolymer; Semiconductive shielding composites; Volume resistivity; Rheological property

Abstract. In order to select suitable carbon black (CB) for manufacturing semiconductive shielding materials of XLPE insulated high voltage cable, the composites were prepared with the melt blending method by adding CB with different properties into ethylene/vinyl acetate copolymer (EVA). The volume resistivity, mechanical property and rheological property of the composites were measured. The effects of the properties and content of CB on the various properties of the composites were investigated and their mechanism was analyzed. The research results show that both structure and specific surface area of CB have great effects on the volume resistivity and rheological property of the composites. Because high structure CB usually has high specific surface area, the high structure CB/EVA composites have low percolation threshold and low rheological property. The EVA composites containing low structure CB with larger specific surface area exhibit low conductivity and high melt viscosity. When the mass fraction of CB with low structure and small specific surface area reaches 35%, the volume resistivity of the composites is approximately 100 Ω·cm and the rheological property of the composites is obviously superior to the composites filled with high structure CB. The CB with small specific surface area and low structure as conductive filler is beneficial for good conductivity and extrusion processability of the semiconductive shielding materials.

Introduction

With the acceleration of urbanization in our country, the construction and development of large pumped storage power station, and the intensive development of large coal, large hydropower, large nuclear power and large renewable energy base, the demand for XLPE insulated high voltage cable continue increasing in recent years. According to the statistics, the consumption of the XLPE insulated cables above 110 kV in our country has exceeded 12000 km in consecutive three years. The consumption of the cross-linking semiconductive shielding materials used for producing high voltage cables is about 12000 tons. After long-term efforts of the domestic researchers in China, the domestication problems of the cross-linking semiconductive shielding materials used for the cables of 35 kV and below 35 kV of voltage level were solved during the period of "11th Five-Year Plan". However, the semiconductive shielding materials for XLPE insulated cables above 110 kV always relay on the imports, and the major suppliers are a handful of multinational companies such as Nordic Chemical Company, DOW Chemical Company of the United States and so on [1]. The main reason to restrict the domestication of the semiconductive shielding materials for our high voltage cables is the lack of the high performance resin with a special grade and that the production technology for the ultra-pure materials is not mature enough. Electric field intensity in the high voltage cable insulation is large and any defects on the surface of the semiconductive shielding could cause serious distortion of the electric field, which would be the hidden danger to initiate the electrical tree. Therefore, the semiconductive shielding materials for high voltage cables are required to have smooth extrusion performance [2-4]. However, in order to ensure that the semiconductive shielding materials for XLPE insulated cables have good conductivity, a large quantity of carbon black (CB) is added into the polymer matrix. This would usually lead to the poor processing performance for semiconductive shielding materials and the rough extruded surface. To

solve the above problems, the ethylene copolymer is usually used as the resin for the semiconductive shielding materials [5-8]. In this paper, the semiconductive composites were prepared through the melting blending method by using CB and ethylene/vinyl acetate copolymer (EVA). The main performance of the materials was measured and compared with the semiconductive shielding materials of high voltage cables from Dow Chemical Company. The goal of this paper is to provide theoretical guidance for selecting CB for subsequent development of semiconductive shielding materials used in the domestic XLPE insulated high voltage cables.

Experimental Methods

CB and EVA were blended evenly to prepare the semiconductive composites by using the internal mixer at a temperature of 110 °C. The semiconductive composite specimens were molded through hot compression by using flat vulcanizing machine under a pressure of 15 MPa at 110 °C, and then cooled to below 40 °C at the speed of 10 °C/min and placed in the dry environment for 24 h at room temperature for testing.

Specimens with 2.0 mm in thickness, 110 mm in length and 50 mm in width were prepared for testing conductivity. Volume resistivity was measured by four electrode system according to the national standard GB/T 3048.3 2007 with the current electrode gap of 100 mm and the potential electrode gap of 20 mm.

For the rheological properties test, the four heating zones of torque rheometer at 90, 110, 115 and 115 °C were set, respectively. The semiconductive composites were extruded through the capillary mould with the aspect ratio of 20:1 at a rotation speed of 10r/min, 20r/min, 30r/min, 40r/min and 50r/min, respectively. The extrusion pressure was recorded and the extrusion quality at every minute was measured. The curves of the shear rate and shear viscosity to the shear stress were plotted using the analysis software of the torque rheometer.

Results and Discussions

Volume resistivity of composites

The composites with different CB contents were prepared using six kinds of CB with different specific surface areas and EVA containing 28% VA. The main performance parameters of the CB were listed in Table 1.

Table 1 Basic performance parameters of CB

Property	Parameter Values					
	CB1	CB2	CB3	CB4	CB5	CB6
Iodine absorption value (mg/g)	1200	1125	830	100	74	280
DBP absorption value (ml/100g)	430	420	280	155	148	80

Iodine absorption method is a common method for measuring the specific surface area of CB. The greater value showed CB had larger specific surface area. The structure of CB mainly depends on the shape and size of the aggregate, and the agglomeration degree between aggregate. Dibutyl phthalate (DBP) absorption method was used to characterize the structure of CB through the needed minimum amount of DBP for infiltrating the gap filled with CB chain branches or fiber structure and the surface. The higher the structure of CB, the larger the DBP value.

The relationship between the content of all kinds of CB and the conductivity of the CB/EVA composites measured in the experiment is shown in Figure 1. As shown in Figure 1, the percolation threshold of the CB1/EVA and CB2/EVA composites is lower. When the mass fraction of CB is 8.5%, volume resistivity is less than 1000 Ω·cm. However, when the mass fraction of CB reaches 20%, volume resistivity is close to 1 Ω·cm. This is because CB1 and CB2 as high structure carbon black are easy to form conductive path in the matrix resin. Therefore, the composites have good electrical conductivity. CB4, CB5 and CB6 are low structure CB, so the percolation threshold of CB4/EVA, CB5/EVA and CB6/EVA composites are high. Although the specific surface area of CB6

is larger than that of CB4 and CB5, the composites containing CB6 have the largest volume resistivity due to the lowest structure. This suggested that the structure of CB has greater effect on the electrical conductivity of the composites against the specific surface area.

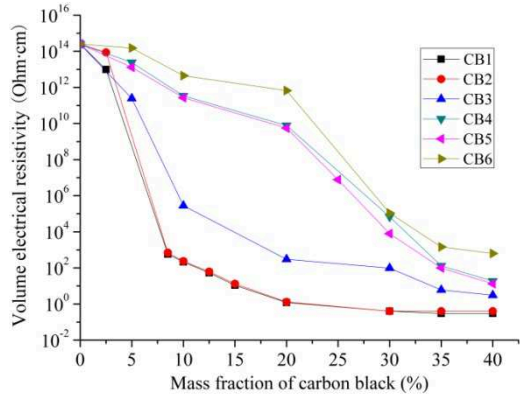

Fig. 1 Relationship between volume resistivity of EVA/CB composites and CB content

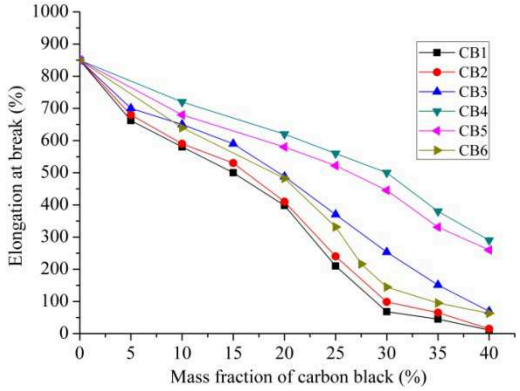

Fig. 2 Elongation at break of CB/EVA composites

Mechanical properties of composites

The blunt dumbbell specimens with 2.0 mm in thickness were prepared. The mechanical properties of the composites filled with CB were measured according to the national standard GB/T 1040.2-2006 with the tensile rate of 250 mm/min. The results were presented in Figures 2 and 3.

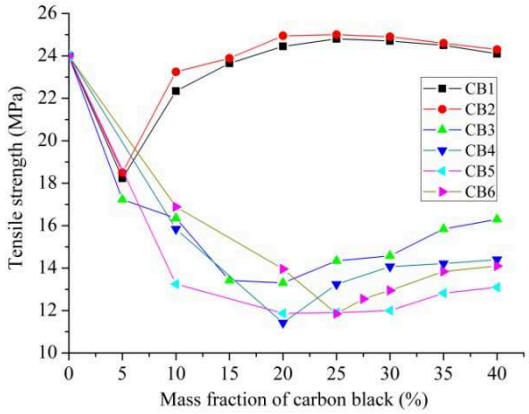

Fig. 3 Tensile strength of CB/EVA composites

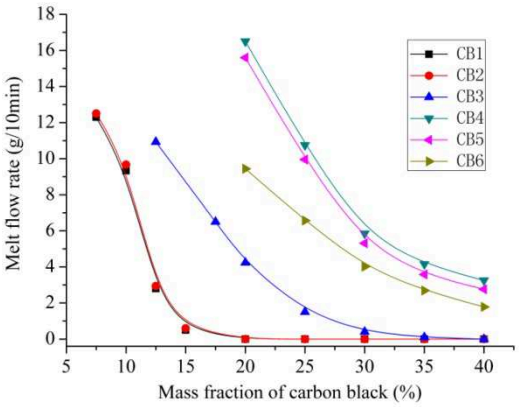

Fig 4 Relationship between MFR of EVA/CB composites and content of CB

As shown in Figure 2, with the increase of CB content, the elongation at break of CB/EVA composites gradually decreases. CB1/EVA, CB2/EVA and CB6/EVA show the biggest change of the elongation at break in turn. It can be seen from Figure 3 that with the increase of CB content, the tensile strength of the composites filled with CB3, CB4, CB5 and CB6 firstly reduces rapidly and then has a slow increasing trend. However, when the CB content increases, the tensile strength of CB1/EVA and CB2/EVA composites decreases firstly and then increases, finally it is nearly equal to pure EVA. The above results show that the addition of CB restricts the migration of EVA molecular chain segments. Commonly, the greater the effect, the larger the specific surface area of CB. However, the change is slightly abnormal for CB6/EVA, which may be related to the content of impurity and the surface state. In addition, after adding CB the intermolecular forces of matrix resin significantly reduces. This leads to that the tensile strength of the composites decreases. Because CB1 and CB2 are high structure CB, they would play a role similar to the reinforcing in rubber. When the addition amount reaches a certain value, the bound node between EVA molecular increases. This leads to that the tensile strength of the composites increases. When the addition amount of the other four types of CB is high, the tensile strength of the composites increases slightly through increasing the physical crosslinking points.

Melt flow rate of the composites

The extruded temperature for semiconductive shielding of XLPE insulated high voltage cables would not exceed 120 °C, otherwise the pre-crossinked process may occur and cause the surface defects. Therefore, the melt flow rate of the composites was measured at 120 °C. The mobility obviously drops due to the addition of more CB in the composites. The weights of 21.6 kg and capillary with inner diameter in 2.095±0.005 mm were used for the experiment. The experimental results are shown in Figure 4.

It can be seen from Figure 4 that the properties and the amount of CB had a significant impact on the mobility of the composites. When the mass fraction of CB1 and CB2 with high structure and large specific surface area reaches 15%, the melt flow of the composites is difficult. When the CB content is the same, the melt flow rate of CB4/EVA composites is the biggest and the mobility of CB5/EVA is also good and close to that of CB4/EVA. The melt flow rate of CB6/EVA and CB3/EVA was larger than that of CB5/EVA in turn. The results indicate that the melt viscosity of the composites was greatly affected by the specific surface area of CB, and the addition of high structure CB is hard to prepare the composites with good mobility.

Under the same experimental conditions, the melt flow rate of semiconductive shielding materials for XLPE insulated high voltage cables produced by Dow Chemical Company is 2.89, which is nearly equal to the CB4/EVA and CB5/EVA composites containing 40 wt. % of CB.

Rheological properties of composites

Figures 1, 2 and 4 show that when the content of CB6 having low structure and large specific surface area reaches 40 wt. %, the volume resistivity of EVA composites is still greater than 600 Ω·cm. It is far greater than the maximum volume resistivity (100 Ω·cm) of the semiconductive shielding for high voltage cables specified by the standard. The elongation at break and melt flow rate is small. Therefore, CB6 with low structure and large specific surface area is not applicable to prepare the semiconductive shielding materials for XLPE insulated high voltage cables. As shown in Figures 1 and 4, when the volume resistivity of high structure CB/EVA composites does not exceed 100 Ω·cm, the content of CB has a significant effect on the melt viscosity. Therefore, CB1 and CB2 with high structure and large specific surface area are also suitable as conductive fillers for semiconductive shielding materials of XLPE insulated high voltage cables. Based on the above analysis, in the follow-up study of the rheological properties of the composites CB3/EVA, CB4/EVA and CB5/EVA are selected for comparison with the semiconductive shielding materials produced by DOW Chemical Company. The experimental results are shown in Figure 5.

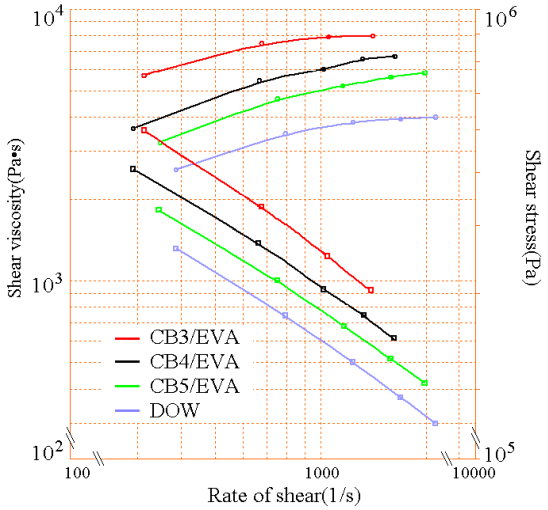

Fig 5 Rheological property of semi-conductive shielding materials

As shown in Figure 5, the shear stress and shear viscosity of CB5/EVA composites are the lowest in the three types of CB/EVA composites and the rheological curve is close to that of the products of DOW Chemical Company. The rheological properties of CB3/EVA are the worst and that of CB4/EVA is the second worst. Based on the above results, it indicates that CB4 and CB5 can

be used to prepare the semiconductive shielding materials of XLPE insulated high voltage cables and the CB5 is comparatively better.

Conclusion

(1) EVA composites containing CB with high structure and large specific surface area have low percolation threshold and good electrical conductivity, but their melt viscosity is high and their rheological property is poor. This type of CB is not suitable for producing the semiconductive shielding materials of XLPE insulated high voltage cables.

(2) Volume resistivity of EVA composites containing CB with low structure and large specific surface area is small and difficult to achieve the standard requirement of semiconductive shielding materials for high voltage cables. The composites have high melt viscosity and small elongation at break.

(3) CB with lower structure and small specific surface area is appropriate to produce the semiconductive shielding materials for XLPE insulated high voltage cables and the comprehensive performances of the composites are outstanding.

Acknowledgement

The authors thank National Basic Research Program of China (973 Program) (grant No. 2012CB723308) and Research Funds for Science and Technology Innovation Talents of Harbin City (Excellent Academic Leader) (grant No. 2012RFXXG079) for their financial supports.

References

[1] Yan Wei, Zhen Jian, Xue Zhigang. Development situations of semiconducting XLPE cable shielding material. China Synthetic Resin and Plastics, 2012, 29(4):75-79

[2] Ma Shuyan. Analysis on the defect of the conductor screen for cross-linked power cable. .Electric Wire & Cable, 1999, (6):20-21

[3] Jin Jinyuan. XLPE Cable Inner and Outer Semiconductive Shielding Layer Quality Defects and the Improvement. Optical Fiber & Electric Cable and Their Applications, 2013, (6):32-34

[4] Lee Wei-Kuo. A Study of Electric Stress Enhancement.Part 1. Implication in Power Cable Design[J]. Dielectrics and Electrical Insulation,2004,11(6):976-982

[5] Fang Ye, Zha Junwei, Zhao Hang, et al. Preparation and Electrical Properties Study of Ethylene-vinyl Acetate Copolymer (EVA)/Carbon Black (CB)-Multi-walled Carbon Nanotubes (MWNTs) Semiconductive. Insulating Materials, 2012, 45(6):20-23

[6] Su Chaohua, Niu Zheng. Development of Semi-conductive Shielding Material of Thermoplastic EVA. Plastics Science and Technology, 2009, 37(5):67-70

[7] Niu Zheng, Pei Haiyan. Study on Semi-conductive Insulation Shielding Material of Strippable Crosslinked EVA. China Plastics Industry, 2009, 37(5):46-49

[8] Chen Zhe, Huang Xingyi, Jiang Pingkai. Study of the LLDPE/POE/CB Semiconductive Composites with High Flowablity. Electric Wire & Cable, 2009, (2):28-32

Advanced Materials Research Vols. 989-994 (2014) pp 634-637
© (2014) Trans Tech Publications, Switzerland
doi:10.4028/www.scientific.net/AMR.989-994.634

Hygrothermal Ageing Modeling and Numerical Testing of Unidirectional Polymeric Composites

Bhatti Imran Shaban[1,a], Yan Zhao[1]

[1] School of Materials Science & Engineering, Beihang University, China

[a]imran_shaban@hotmail.com

Keywords: Hygrothermal Ageing, Unidirectional Polymeric Composites, Finite Element Modeling.

Abstract. Moisture severely affects aerospace structures and offshore platforms during their service life span. It deteriorates the mechanical performance of polymeric composites through long term and cyclic hygrothermal ageing. This reduction in mechanical performance must be considered during product design to ensure long-term structure endurance. In order to decide the long-term moisture effects on composite components, they are exposed to a rapid moisture conditioning. Presently the available qualified methodologies allowing only simple geometry and an assumption that diffusivity rates are independent of the flow path or direction. Therefore a more advanced finite element method is required. In this research work the finite-element analysis was performed to study the moisture diffusion in unidirectional composites. The final goal for this study was to determine the exposure time for rapid moisture conditioning that produces the most accurate moisture distribution in composite laminates.

Introduction

Polymer matrix based Composites are widely used in aerospace structures, automotive industry and for offshore platforms because of their high strength-to-weight ratio [1]. These composite materials in service conditions are exposed to harsh conditions involving a wide range of temperature and humidities. The absorbed moisture has many destructive effects on the composite performances. Therefore understanding the mechanism of moisture diffusion and moisture induced damage is very essential to improve the long-term stability of advanced composites [2]. Composite materials allow moisture to be absorbed through the environment, which severely affect the structural integrity of structures [3,4]. During moisture absorption, physical changes such as micro-cracks proliferation and swelling, as well as chemical changes such as hydrolysis and chemical scission increase, this caused damage to material [5,6]. The reduction in mechanical properties is often due to degradation at matrix/fiber interface [7,8].

Moisture diffusion through unidirectional carbon fiber based polymeric composites is widely studied in literature [9,10]. In this research moisture diffusion dynamics of a Polymeric composite 5228/CF303 has been studied experimentally and analyzed numerically. The final goal was to determine the desired exposure time using Abaqus to precisely measure moisture diffusion.

Materials and Experimental Procedure

Materials Carbon fiber polymeric based composite material 5228/CF303 was provided by Beijing Aeronautical Manufacturing Technology Research Institute, China used in this study.

Hygrothermal Aging Specimens were prepared for hygrothermal aging test having dimensions 60 x 60 x 2 mm^3. All these samples were then put into absorption chamber contained distilled water and hygrothermally tested at 71^{o}C. During test all specimens were periodically taken out, wiped out and then carefully weight. After moisture absorption for 28 days, specimens were dried and weighted. The specimens were again put into humidity chamber and tested hygrothermally (both absorption /desorption) for 56, and 112 days respectively. The moisture content $\boldsymbol{M_t}$, the moisture at any time in the sample can be defined as [11]

$$M_t = \frac{W - W_d}{W_d} \qquad (1)$$

where W is the weight of the soaked material and W_d is the weight of dry material.

Background and Theory

Classical Moisture Diffusion Theory Moisture absorption in composite panel is modeled as *1D* diffusion. Fick's second law is used to model to model absorption [12]

$$\frac{\partial c}{dt} = D_z \frac{\partial^2 c}{dz^2} \qquad (2)$$

where c is the moisture concentration, D_z is the diffusion coefficient, t is the time and z is the coordinate representing width of the specimen. The analytical solution of the model described in Eq. (2) is given by [13]

$$G = \frac{m - m_i}{m_m - m_i} = 1 - \frac{8}{\pi^2} \sum_{j=1}^{\infty} \frac{\exp[-(2j+1)^2 \pi^2 (\frac{D_z t}{h^2})]}{(2j+1)^2} \qquad (3)$$

where m_i is the initial weight of the moisture, m_m is the weight of moisture in the material when it is fully saturated, in equilibrium with the environment, D_z is the diffusion coefficient and h is the plate thickness. The diffusion coefficient can be calculated from eq(4) using Figure 1

$$D = \pi \left(\frac{h}{4m_m}\right)^2 \left(\frac{m_2 - m_1}{\sqrt{t_2} - \sqrt{t_1}}\right)^2 \qquad (4)$$

Finite Element Formulation and Modelling A heat and mass transfer analogy was implemented to enable the analysis to be run on a general purpose finite element code. The moisture diffusion dynamics generally present in finite element code is based on Fick's law. The commercial Finite Element Method (FEM) software Abaqus was used to model the mass diffusion process in this research. The basic solution variable is the normalized concentration [14]

$$\varphi = {}^{c}/_{S} \qquad (7)$$

where c is the mass concentration of the diffusing material and s is the solubility in the base material. Automatic time incrimination is used for transient analysis.

Results and Analysis

Water Absorption After hygrothermal aging test, the moisture absorption behavior of 5228/CF303 is shown in Figure 1 drawn using Eq (1).

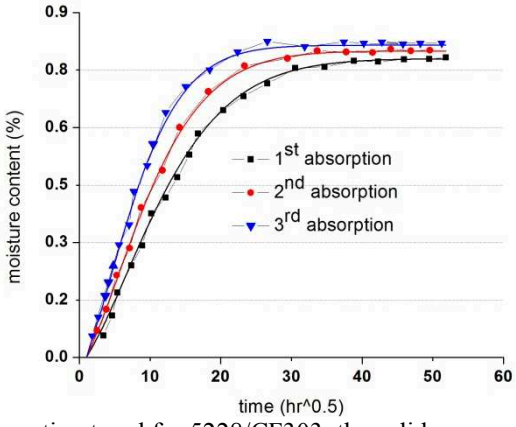

Figure 1. Moisture absorption trend for 5228/CF303, the solid curves are plotted using Eq (3)

Eq. (4) was used to calculate the value of moisture diffusion coefficient *D*. Values required in Eq. (4) were obtained from Figure 1 for all three different absorption curves. Table 1 listed all the values of Diffusion coefficient.

Numerical Simulation of Moisture Absorption using Abaqus/FEA. The modelling procedure consists of finding the temporal and spatial distribution of moisture within the composite layers and modeling the mechanical-diffusion interaction. The experimental data was used to carry out the coupled mechanical-diffusion analysis. 2D and 3D models were developed in Abaqus to simulate moisture diffusion from any surface and varying moisture/ temperature conditions. The varying moisture/ temperature condition for this study be defined as *rapid conditions* will typically refer to 71.1°C, 95% RH, while *service conditions* will refer to 26.7°C, 82% RH. Various sets of analysis were performed in this study, first to establish the accuracy of the Abaqus models. The 2D model is geometrically in two dimensions but it effectively characterizing in 1D only. After confirming the accuracy, modified diffusion coefficient with edge effect was used to a 3D model incorporating moisture diffusion along edges.

Table 1 Moisture Diffusion Kinetics Parameters

Absorption	m_m	D(mm^2/hr)
First	0.782	1.8E-04
Second	0.804	2.4E-04
Third	0.815	3.7E-04

Table 2 Parameters used in Simulation

Diffusion coefficient	3.7E-04
Moisture Equilibrium	1.438% at 95% RH
Thickness	5 mm
Length	15 mm
Width	5 mm
Initial moisture content	0.0%
Edge correction factor	1.698e-3
Diffusion coefficient after edge correction factor	4.3873
Fiber volume fraction	68%

Comparison of Simulation Results With Experimental Data Experimental tests were performed using 5228 /CF303 thin composite specimens exposed to following conditions: 71.1°C at 95% RH for 28, 56 and 112 days respectively. For comparison purposes test results of 112 days were used. Test results were compared with a 2D Abaqus model shown in Figure 2 in which diffusion was deliberately set along depth, for comparison with classical 1D Fick's diffusion model. Similarly for 3D model absorption behaviour is shown in Figure 3, which is in close agreement with simulation results and with the experimental data.

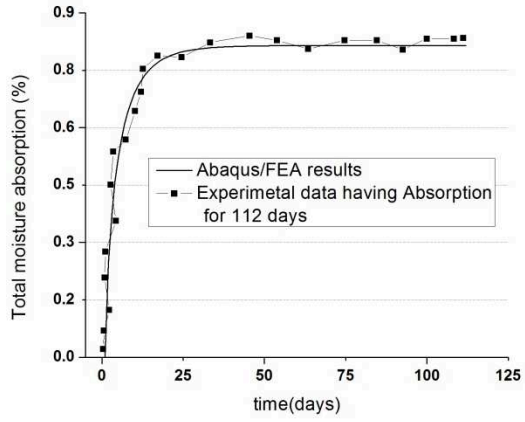

Figure 2 Comparison of 2D Abaqus model with Experimental data having absorption for 112 days

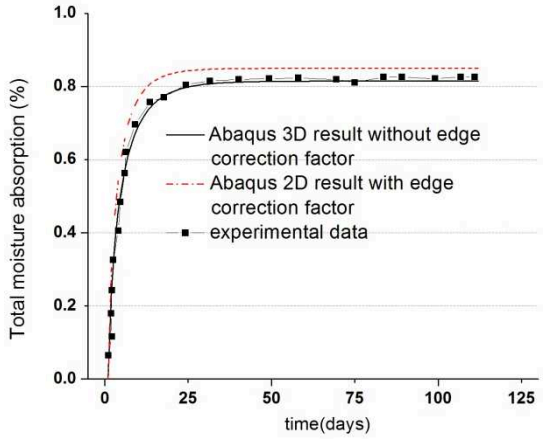

Figure 3 Comparison of 2D and 3D Abaqus model with

In Figure 4 2D moisture diffusion across depth of specimen is deliberately calculated and shown to compare with classical Fickian diffusion. The assumption behind was that for a plate whose thickness is adequately thin compared to its length and width or in case if the edges are insulated. Figure 5 is showing that moisture was absorbed through all the surfaces. The Abaqus analysis was set up with the assumption that the 3D model was made of a homogenous material. Various runs were tested and showed the same results as in Figure 3.

Specimens were placed in rapid moisture conditions for 112 days at 71.1°C and 95% RH, while service conditions were calculated to be soaked for 10 years to reach the required exposure concentrations. Using Abaqus 3D analysis the average moisture content through the part after 10 years of service at 26.7°C and 82% RH was calculated to be 3889 ppm.

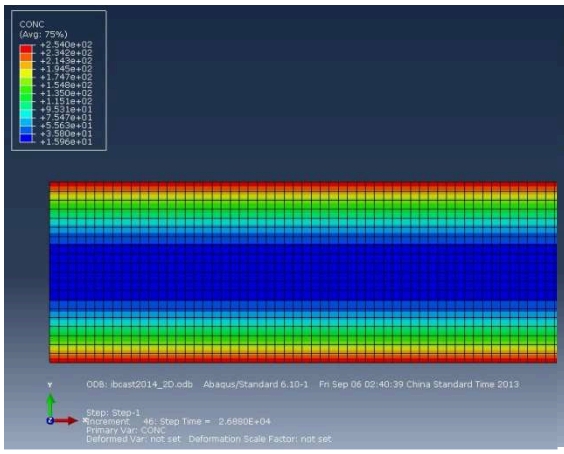

Figure 4 2D model with moisture absorption applied across depth of the specimen

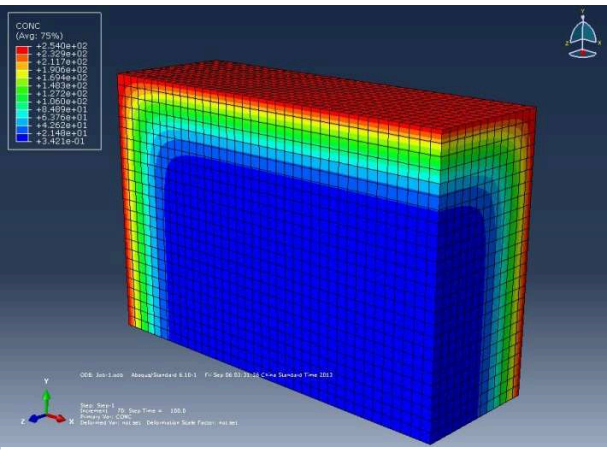

Figure 5 3D model with moisture diffusion applied across all surfaces

Conclusion

In this study hygrothermally ageing of polymeric composites was performed. 2D and 3D model were developed in Abaqus to simulate moisture diffusion. 2D Abaqus model was compared with experimental data having absorption of 112 days and found in close agreement. In the final part study determine the average moisture content of composite material for service conditions. So in sum we study a carbon fiber based polymeric composite material 5228/CF303 experimentally and analyzed by numerical modeling for its potential applications in offshore platforms and aerospace structures.

References

[1] L.A. Pilato, M.J. Michno, Advanced composite materials, Springer, 1994.
[2] X. Jiang, H. Kolstein, F.S.K. Bijlaard, Moisture diffusion in glass–fiber-reinforced polymer composite bridge under hot/wet environment, Compos. Part B Eng. 45 (2013) 407–416.
[3] C.-H. Shen, G.S. Springer, Effects of Moisture and Temperature on the Tensile Strength of Composite Materials, J. Compos. Mater. 11 (1977) 2–16.
[4] F. Pierron, Y. Poirette, A. Vautrin, A Novel Procedure for Identification of 3D Moisture Diffusion Parameters on Thick Composites: Theory, Validation and Experimental Results, J. Compos. Mater. 36 (2002) 2219–2243.
[5] C.J. Tsenoglou, S. Pavlidou, C.D. Papaspyrides, Evaluation of interfacial relaxation due to water absorption in fiber–polymer composites, Compos. Sci. Technol. 66 (2006) 2855–2864.
[6] Y. Wang, T.H. Hahn, AFM characterization of the interfacial properties of carbon fiber reinforced polymer composites subjected to hygrothermal treatments, Compos. Sci. Technol. 67 (2007) 92–101.
[7] X. Lv, R. Wang, W. Liu, L. Jiang, Surface and interface properties of carbon fiber composites under cyclical aging, Appl. Surf. Sci. 257 (2011) 10459–10464.
[8] A. Boubakri, K. Elleuch, N. Guermazi, H.F. Ayedi, Investigations on hygrothermal aging of thermoplastic polyurethane material, Mater. Des. 30 (2009) 3958–3965.
[9] E. Barjasteh, S.R. Nutt, Moisture absorption of unidirectional hybrid composites, Compos. Part A. 43 (2012) 158–164.
[10] I.S. Bhatti, Z. Yan, Moisture Diffusion Characterization of Carbon Fiber Based Polymeric Composites Under Recurrent Hygrothermal Ageing, Appl. Mech. Mater. 390 (2013) 531–536.
[11] Y. Joliff, L. Belec, M.B. Heman, J.F. Chailan, Experimental, analytical and numerical study of water diffusion in unidirectional composite materials – Interphase impact, Comput. Mater. Sci. 64 (2012) 141–145.
[12] A. Fick, Ueber diffusion, Ann. Phys. 170 (1855) 59–86.
[13] W. Jost, Diffusion in Solids, Liquids and Gases, Academic Press, 1960.
[14] Abaqus, Abaqus Analysis User's Manual; Mass Diffusion Analysis, (2010).

Advanced Materials Research Vols. 989-994 (2014) pp 638-643
© (2014) Trans Tech Publications, Switzerland
doi:10.4028/www.scientific.net/AMR.989-994.638

Attenuation characteristics of ultrasonic velocity and acoustic-based TC4 alloy uniformity Nondestructive Evaluation

Wu guanhua[1,a], Lu yifan[2,b], Huang yingxia[3,c], Wu wei[3,c]

[1,2,3]Detection Technology, Ministry of Education Key Laboratory of Nondestructive Nanchang Aeronautical University(330063)

[a]5615651@qq.com, [b]woluyifan@163.com, [c]545064996@qq.com, [c]18418990@qq.com

Keywords: grain α-phase ultrasonic nondestructive evaluation flooding longitudinal wave velocity acoustic attenuation coefficient

Abstract. ultrasound characteristics of the material microstructure nondestructive evaluation of its experimental sample TC4 titanium alloy microstructure of two-phase microstructure:. A-phase and α + β phase. Phase material microstructure and grain area ratio directly affects the material uniformity, uniformity of material differences caused by different grain characteristics which ultrasound parameters. Flooding experiments using ultrasonic method for measuring the material longitudinal wave velocity; measuring the sound attenuation coefficient, combined with the area ratio of the sample α using multiple pulse method. Associated with the sample area ratio between the speed of sound and sound attenuation analysis of α-phase titanium alloy TC4 through the material properties of ultrasound to characterize the degree of uniformity of the material microstructure, nondestructive evaluation of materials in order to achieve the purpose of the microstructure.

Introduction

TC4 alloy is a type of α+β titanium alloy, it owes comprehensive mechanical properties, high strength and good thermal processing characteristics. Besides, it can be heat strengthened. It has been successfully applied in the aerospace, petrochemical, shipbuilding, automotive, pharmaceutical and other sectors [1]. Forged TC4 alloy leads to the unevenness of forging organization due to the deformation, leading to the unevenness of the organization being heat-treated and the unevenness of properties distribution. Therefore control the uniformity of TC4 organization can control the uniformity of properties of parts to reduce post-processing deformation.

Conventional grain uniformity detection mainly rely on metallographic analysis and hardness measurement, it will result in parts damage that can caused waste. This paper explores a measurement based on ultrasonic velocity and attenuation characteristics, nondestructive evaluation on and grain size of TC4 [2], so that we can improve speed of the measurement of the uniformity of organization and reduce the cost of testing goals.

Ultrasound evaluation of the material microstructure uniformity principle

Sonic evaluation principles

Ultrasonic velocity is an important parameter for evaluation of the uniformity of the organization of materials, it has close relationship with the modulus of elasticity and density of the medium [3]. Longitudinal wave velocity through solid can be expressed as:

$$C_L = \sqrt{\frac{E}{\rho}}\sqrt{\frac{1-\sigma}{(1+\sigma)(1-2\sigma)}} \quad (1)$$

Where, E is Young's modulus of elasticity of the medium, σ is Poisson's ratio, ρ is density of the material. Seen from the above equation, the greater the elastic modulus of the medium, the smaller the density is, and the greater the speed of sound will be.

Although the elastic modulus is a mechanical property that is insensitive to the organization, however, because it is related to the interatomic forces and interatomic spacing, whereas the interatomic spacing is associated with the crystal structure, so the change in the organizational structure still has influence on the elastic modulus . Such as when α-Fe converts to β-Fe, hardening on annealed steel may cause the elastic modulus to drop [4].

Attenuation evaluation principles

Ultrasonic attenuation in the material is another important parameter evaluation of the uniformity of the organization of materials[5]. Ultrasonic attenuation includes: diffusion attenuation, absorption attenuation and scattering attenuation[6]. Diffusion attenuation is mainly related to the diameter of the probe, the sample size and the acoustic wavelength. The geometry consistency of specimen in the test is good, so on the same test conditions, diffusion attenuation is not considered[7].

Materials and methods of experiment

Materials of experiment

Materials of experiment is a heterosexual ring forging made by some manufacture of Forge, its main components are shown in Table 1.1. Taking a rectangular sample from the cross-section of the base material, and then wire cut 8 size of 21 * Ø10 cylindrical specimens from the rectangular sample.

Table 1.1 Ingot chemical composition of the TC4 sample(w%)

element	Al	V	C	N	H	O	Fe	Ti
proportion	6.2	4.1	<0.1	0.02	0.002	0.007	0.13	allowance

Equipment of experiment

Ultrasonic water immersion C-scan system is used for data collection, its components are: Olympus 5077 pulse emission analyzer, PC, high-speed data acquisition card, flooding ultrasound probe, mechanical scanning systems. The system can avoid some human factors, it operates smoothly, its probe positions accurately , it owes high efficiency, it achieves automatic ultrasonic testing and saves labor costs. Figure (3-1) is a diagram of ultrasonic water immersion C-scan system:

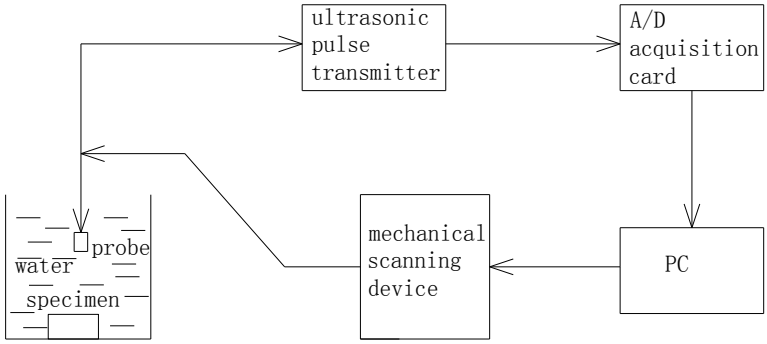

Figure 3-1 Diagram of ultrasonic water immersion C-scan system

Results and analysis of experiment

Measuring the proportion of α phase of the grain

1)Pictures of metallographic phase of the sample

8 samples are corroded in low-power corrosive liquid [8] (the proportion of the ingredients HF: HNO3: H2O = 10%: 15%: 75%) for about 2 minutes, then place them on the sandpaper whose roughness is 1500 to grind coarsely until the surface being grinded is relatively smooth, and then place them on the sandpaper whose roughness is 2000 to grind fine until the surface is smooth and there is no scratches. Put the workpiece being grinded in the high-powered corrosive liquid [8] (the ratio of its components: HF: HNO3: H2O = 7%: 10%: 83%) for corrosion around 5 seconds. Then rinse the surface of the workpiece, using hot hair dryer to dry the surface, and finally put the workpiece being dealt with on the microscope of electron microscope (400-fold) to take pictures.

Phase diagram is below as shown:

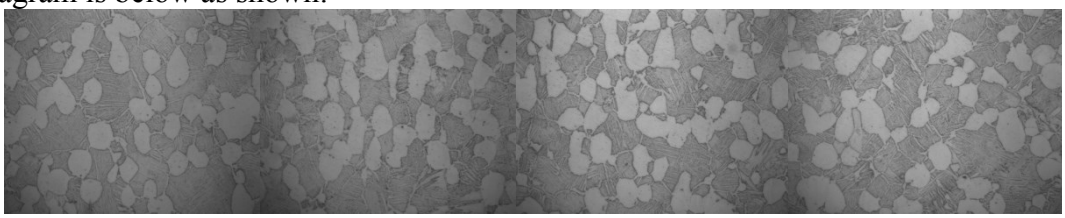

sample 1 sample 2 sample 3 sample 4

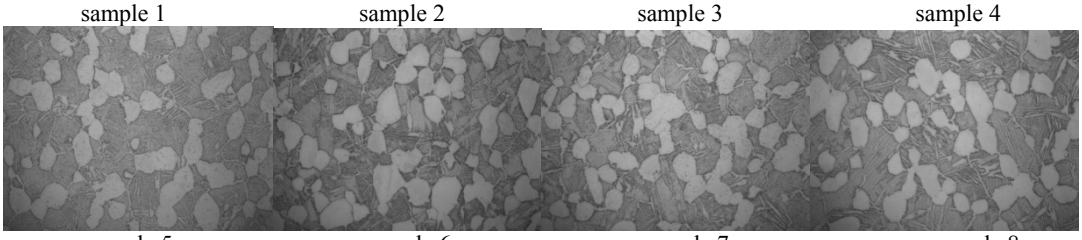

sample 5 sample 6 sample 7 sample 8

2) Measuring the average size of grain

Using Image J software to measure the α phase of the sample. First, balance the original picture illumination and enhance the de-noising, then do binaryzation, then denoise, at last, do segmentation [9], the software will calculate and identify. Figure 4-2 is a phase diagram after processed by Image J. The software is an open source software that can write different programs based on pictures of different illuminance to denoise. It is suitable for the analysis of multi-phase microstructure. The ratio of α phase of sample is shown in the Table 4-1.

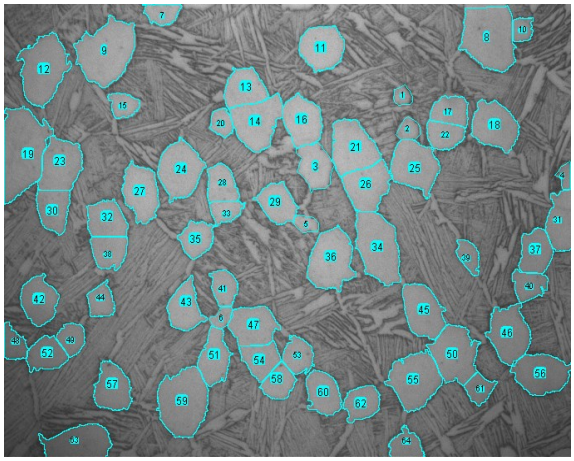

Figure 4-2 Phase diagram after processed by Image J

Table 4-1 α phase rat

Workpiece number	α phase ratio
1	0.3511
2	0.3703
3	0.3680
4	0.3663
5	0.3367
6	0.3428
7	0.3131
8	0.3370

Sound velocity measurement sample

When sound waves spread in the same medium, the speed of longitudinal wave propagation velocity is greater than any other wavelength-shaped, and it owes strong ability of penetrating, so experiment in this paper uses vertical longitudinal wave method to measure the sound speed of sample [10].Longitudinal wave velocity is calculated as:

$$CL=2T/\Delta t \quad (4\text{-}1)$$

The experiment uses immersion focusing probe, with the frequency of 10 MHz, the wafer diameter of 6 mm, focal length of 30 mm, focus mode of line focus, time domain sampling rate of 500 M, the mechanical scanning step of 0.1 mm. The measured sonic domain waveform of sample is shown in Figure 4-3, the sound speed of sample is shown in Table 4-2:

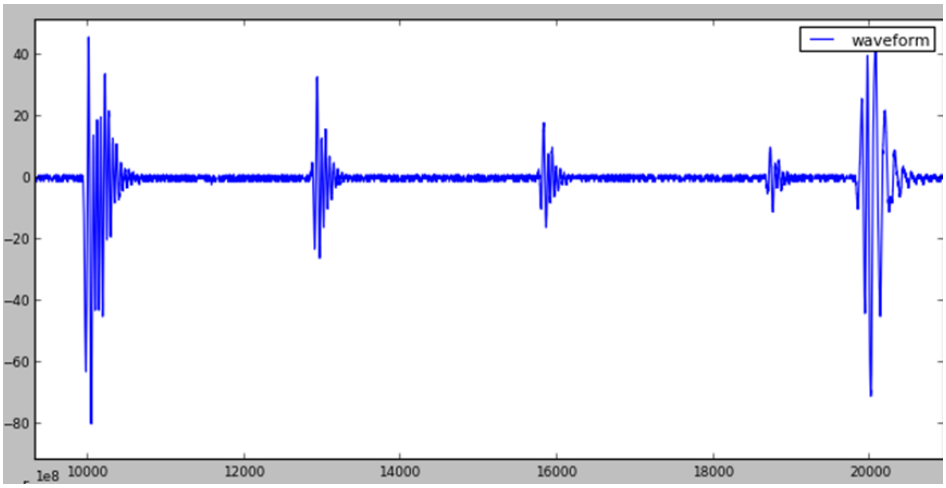

Figure 4-3 Measured sonic domain waveform of sample

Table 4-2 Sound velocity values of sample

Sample Code	1	2	3	4	5	6	7	8
CL (m/s)	6161.41	6116.64	6148.98	6157.55	6228.14	6201.32	6250.34	6217.76

measurement of attenuation coefficient of sample

The experiment uses multiple pulse method to measure of the acoustic attenuation coefficient of sample, placing the sample inside the tank of water immersion scanning system horizontally, adjusting the gain so that the bottom echo occurs repeatedly, the attenuation coefficient (dB / mm) is calculated as [11]:

$$\alpha = \frac{20\lg(B_m/B_n)-\delta}{2(n-m)T} \quad (4\text{-}2)$$

Where: m, n is the number of bottom echo emission; Bm, Bn is the m, n time height of the bottom echo; is reflection losses, each reflection loss is about (0.5-1.0) dB. T is thickness of the sample. The measured sound attenuation coefficient of sample is shown in Table 4-3.

Table 4-3 Acoustic attenuation coefficient of sample

Sample Code	1	2	3	4	5	6	7	8
attenuation coefficient (dB/mm)	0.133	0.168	0.148	0.138	0.112	0.122	0.101	0.115

Results and analysis of experiment

The relationship between the ratio of α phase of sample grain and the longitudinal wave velocity

Figure (2-2) is a variation trend of the ultrasonic velocity of TC4 titanium alloy specimens with its proportion of the α phase of the grain varies. It can be observed from FIG: ultrasonic velocity decreases as the ratio of α phase of the grain increases, the results of this have similarity with other observations reported in the literature [12]. However, because there are many factors that will affect the propagation velocity of ultrasonic waves. In addition to structure, there are stress, dislocation damping, atom relaxation and magnetic effect, etc. Its mechanism is very complicated. Thus, studying further on the changing relationship between velocity and grain size is also necessary.

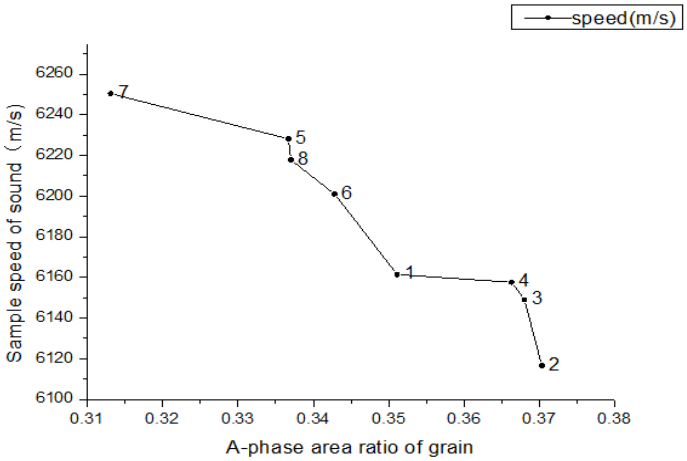

Figure 5-1 Proportion of the α phase of the sample grain and trend of the ultrasonic velocity

The relationship between the area ratio of α phase of sample and acoustic attenuation coefficient

When the acoustic wave spreads in the medium of uniform grain material, the scattering due to the grain boundaries will cause the attenuation of sound waves. By measuring attenuation coefficient when the sound wave spreads in the medium to evaluate the medium grain size [13]. The acoustic attenuation coefficient of titanium alloy TC4 sample will increase with the increase of the area ratio of α phase, it is shown in Figure 5-2. In the heat treatment process, with the α-phase single area ratio and the ratio of the number increases, the scattering when sound wave spreads in media aggravates, resulting in the increase acoustic attenuation coefficient.

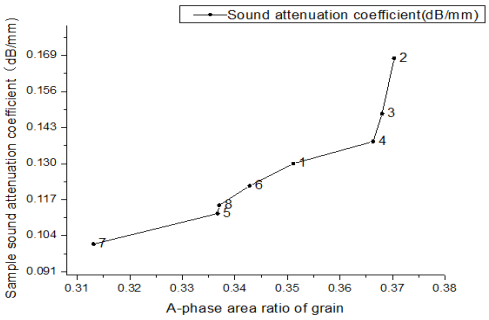

Figure 5-2 The proportion of α-phase area of grain of sample and longitudinal wave velocity trend conclusion

Conclusion

Its velocity of longitudinal wave is measured through the ultrasonic signals of TC4 specimens collected by ultrasonic flooding system; the relationship that the proportion of the sample α phase corresponding to the velocity of longitudinal wave is: ultrasonic velocity decreases as the ratio of α phase of the grain increases. With the increase of the ratio of α phase of the grain, it will lead to the variation in elastic modulus and density. Measure the acoustic attenuation coefficient by using multiple ultrasonic pulse method. The relationship between α-phase area ratio of the sample and the acoustic attenuation coefficient is as follows: the acoustic attenuation coefficient increases with the proportion of the α phase area of the grain gradually increasing.

References

[1] Yu Hong. Titanium and Its Alloys. Automotive Technology and Materials. 2004, (12):6-9

[2] Ci Naichao, Fu Mingxi, Non-ferrous Materials and Preparation [M].Beijing：Chemical Press, 2006

[3] Rhine Adams C, Pete Wells M, Titanium and Titanium Alloys [M]. Beijing：Chemical Press,2005:15

[4] Xu Zhidong, Fan Ziliang.Elastic modulus of metallic materials with temperature variation phenomenological interpretation[J].SouthWest JiaoTong University. 1993(2):87-92

[5] GB5168-85《Methods of Inspecting High and Low Times Organization of two-phase Titanium 》

[6] Yang Siqian,Liu Yanhua,Li Jinglong Programming Calculation of Sound Field of the Beam Axis of Flooding Focused Probe [TB].1999,28(2)13-17

[7] Yin Chang;Liu Xiaozhou;Gong Xiufen;Liu Jiehui; Measurement of the Speed of Sound and Acoustic Attenuation Coefficient of Steel Material [A]; Acoustic technology；2007.05

[8] Du Gonghuan,Zhu Zemin,Gong Xiufen. Basis of Acoustics〔M〕.Nanjing: Nanjing University Press,2001

[9] Abramoff,M.D,Magelhaes,P.J,Ram,S.J."ImageprocessingwithImageJ" Biophotonicsinter nation, volume11,isse7,pp.36-42,(2004)

[10] Hu Jiankai,Zhang Qianlin. Principles and Methods of Ultrasonic Testing〔M〕.Hefei: University of Science and Technology of China Press,1993

[10] Xu Yanlin, Wang Zengyong, Huang Zhenxiang．Ultrasonic Evaluation Techniques of The Average Size of the Grain of Austenitic Stainless Steel．NDT, 200l, 23(6)：246-248

[11] Zhang Lina, Summary of the Analysis Methods of the Time-frequency of Digital Signal Processing. Information technology [TP391．42], 1009-2552(2013)06－0026－03

[12] Liu Zhenqing,Chen Guang. Spectral Analysis of Ultrasonic Nondestructive Testing Technique [J].2001,23(2):85-88

[13] BOUDAAB, BENCHAALAA, LEBAII.I S．Grainsize influence onultrasonic velocities andattenuation[J]．NDT EInternational, 2003.36(1)：1-5．

Advanced Materials Research Vols. 989-994 (2014) pp 644-647
© (2014) Trans Tech Publications, Switzerland
doi:10.4028/www.scientific.net/AMR.989-994.644

Preparation and Application of Blocked & Crosslinked Waterborne Polyurethane Microemulsion as Paper Strengthening Agent

Xiao-Juan LAI[1,a], Mi-Na GONG[1,b] and Lei WANG[1,c]

[1] College of chemistry and chemical engineering, Shaanxi University of Science & Technology, Xi'an 710021, China

[a]3578466@163.com, [b]237214407@qq.com, [c]05wanglei@sust.edu.cn

Keywords: waterborne polyurethane, paper strengthening agent, blocked ratio

Abstract. By means of self-emulsifying, blocked & crosslinked cationic polyurethane(CBPU) microemulsion was prepared with isophorone diisocyanate(IPDI), polycaprolactone glycol, bisphenol A, methyldiethanolamine(MDEA) as cationic hydrophilic chain-extending agent, imidazole as blocking agent and N-[(1,1-dimethyl-2-acetyl)ethyl]-β-dihydroxyethylamino propanamide(DDP) as crosslinking agent. Effects of the CBPU blocked ratio on the physical properties of the treated paper were studied. The experimental results show structures of tertiary amine group, imidazole ring and urethane group are found in CBPU molecular structure. The morphology of the particle is uniform spheric structure and its size is related to the content of tertiary amine groups of CBPU. The paper strength, especially the wet strength can be obviously increased with the increasing of the blocked ratio of CBPU. The optimum blocked ratio of CBPU is 10%.

Introduction

Waterborne polyurethane(WPU) plays an important role in paper surface treatment because of its environmental friendly characteristics and excellent film forming ability[1]. The ketone or hydrazine are groups stable in aqueous phase and can react at ambient temperature, so the ketone-hydrazine crosslink reaction can be used for self crosslinkable waterborne polyurethane at room temperature, meanwhile, the properties of waterborne polyurethane films can be enhanced[2]. Isocyanate(-NCO) terminated polyurethane can react with hydroxyl of paper fibres, which has the bridging action among the apart fibers, combination between fibers is improved and strength properties especially the wet strength of paper products can be significantly increased. However, -NCO is sensitive to water and it can not be applied directly to wet end chemistry of papermaking[3]. Because blocked isocyanate isn't sensitive to water and it can recover its reaction activity well after deblocking, blocked isocyanate will become an important way to realize polyurethane-reinforcement of paper. The deblocking temperature of polyurethane is depended mainly by the blocking agent. When isocyanates are blocked with different blocking agent, deblocking temperatures exhibited a great difference. The deblocking temperature of polyurethane blocked with imidazole is about 110~130℃[4], which is consistent with paper drying temperature. However, synthesis of blocked & crosslinked cationic waterborne polyurethane microemulsion and its application as paper strengthening agent is rarely reported. In this paper, a sery of cationic waterborne polyurethane microemulsions(CBPU) was prepared with isophorone diisocyanate(IPDI), polycaprolactone glycol(PCL), bisphenol A(BPA) as main materials, with imidazole as blocking agent, methyldiethanolamine(MDEA) as cationic hydrophilic chain-extending agent, and N-[(1,1-dimethyl-2-acetyl)ethyl]-β-dihydroxyethylamino propanamide (DDP) as crosslinking agent. the structure of CBPU was characterized by dynamic laser light scattering(DLS) and transmission electron microscopy(TEM). The effects of blocked ratio(BR) of CBPU on paper properties were studied.

Exprimental

Materials

Isophorone diisocyanate(IPDI) and polycaprolactone polyol (PCL, Mn=1000) were obtained from Bayer, Germany. N-methyldiethanolamine(MDEA), chemically pure, Tianjin Chemical Reagent Factory; bisphenol A(BPA), industrial grades, Shanghai Xingzhi Chemical Plant; imidazole (IDZ), dibutyltin dilaurate (DBTDL), 1-methyl-2-pyrrolidone(NMP), analytically pure, Tianjin Kermel chemical reagent Co., Ltd. Adipic dihydrazide (ADH), industrial grades, was purchased from Japan Kyowa Hakko Chemical Co. Ltd. Acetic acid, analytically pure, Tianjin Tianli chemical reagent Co., Ltd. N-[(1,1-dimethyl-2-acetyl)ethyl]-β-dihydroxyethylamino propanamide (DDP), self designed[5].

Preparation of blocked & crosslinked waterborne polyurethane

According to Table 1, IPDI, PCL and DBTDL were added in a three-necked flask, then IPDI was added into flask. The reaction mixture was stirred at 70 °C for 2h. Then, the reaction mixture was cooled to 40 °C, and the quantitative MDEA, BPA and DDP were added into the mixture, the reaction was going on for 2h, and NCO-terminated polyurethane prepolymer was obtained. IDZ was added into the flask and reacted for 1h at 40℃. After cooling the reaction mixture to room temperature, acetic acid was fed into the reactor and mixed thoroughly to neutralize MDEA unit in polyurethanes. The resultant polyurethane prepolymer was then dispersed in distilled water under vigorous stirring. Finally, cationic blocked polyurethane microemulsions was obtained. ADH was added to the above waterborne polyurethane emulsion and agitate it until ADH dissolves in the emulsion. The molar ratio of DDP to ADH is 2:1, and blocked & crosslinked waterborne polyurethane (CBPU) was prepared.

The reaction activity of CBPU is determined mainly by –NCO number released by CBPU after deblocking. FH is used to express reaction activity of CBPU in this paper. FH was calculated according to the following formula: FH=m(-NCO) g/100 g CBPU. The greater the FH value, the reaction activity of CBPU after deblocking is stronger. Table 1 shows the reaction activity of CBP.

Table 1 Theoretical composition and properties of CBPU

Sample codes	BR (%)	n(IPDI) (mol)	n(PCL) (mol)	n(MDEA) (mol)	n(BPA) (mol)	n(DDP) (mol)	n(IDZ) (mol)	FH (g/g)
CBPU0	0	1.0	0.35	0.50	0.05	0.1	0	0
CBPU5	5	1.0	0.35	0.45	0.05	0.1	0.1	0.586
CBPU10	10	1.0	0.35	0.40	0.05	0.1	0.2	1.162
CBPU15	15	1.0	0.35	0.35	0.05	0.1	0.3	1.750
CBPU20	20	1.0	0.35	0.30	0.05	0.1	0.4	2.343

Application of CBPU on paper surface

The waterborne polyurethane microemulsions was coated on dry filter paper (qualitative analysis filter paper, basis weight is 78g/m^2, purchased from Hangzhou special paper Co. ,Ltd.). The coated filter paper was dried at 60℃ for 20min, and then at 130℃ for 10min, dry and wet tensile strength of paper and folding strength of paper were tested after treatment for 24h.

Particle size and morphology of polyurethane emulsions

The the particle size and particle distribution were determined by a dynamic light scattering (Namo-ZS, Malvern, Britain) at 25℃. The particle morphology was observed with transmission electron microscopy (H-600, Hitachi, Japan).

Strength test of paper

Tensile strength of paper is tested on a ZL-300A tensile tester of paper and paperboard (Changchun paper test machine Co., Ltd.). The folding strength of paper is tested on a DCP-MIT135A folding strength instrument(Sichuan Changjiang papermaking instrument Co., Ltd.).

Results and disscussion

The particle morphology and particle size of polyurethane emulsions

Correlation of blocked ratio of CBPU, hydrophilic groups content and emulsion appearance, particle size of polyurethane emulsions were shown in Table 2. The content of tertiary amine group decreased when blocked ratio of CBPU increased from 0% to 20%, particle size of polyurethane emulsions increased and colour of emulsion also changed. The content of hydrophilic chain-extending agent MDEA decreased rapidly, so the interfacial tension between polymer and water increased, leading to the increase of particle size.

Table 2 Colour, particle size and distribution of polyurethane emulsions

BR(%)	ω(MDEA)(%)	Colour of emulsion	Particle size of emulsion	
			Average particle size(d/nm)	Particle size distribution (PdI)
0	7.20	Blue	29.80	0.238
5	6.51	Blue	33.80	0.214
10	5.81	Blue	79.74	0.201
15	5.10	Opal blue	162.80	0.115
20	4.39	Milky white	296.80	0.168

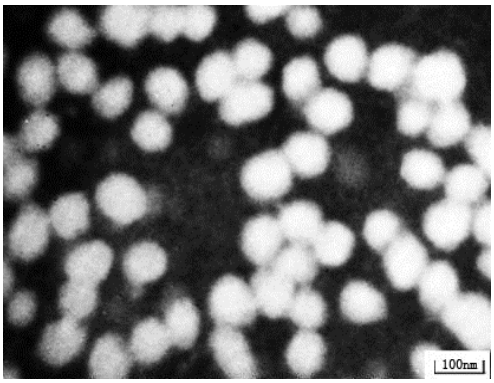

Fig.1 TEM micrograph of CBPU10(×300000)

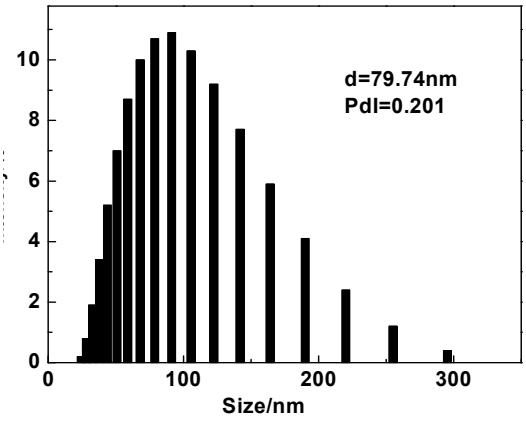

Fig.2 Particle distribution of CBPU10

Fig.1 is micrograph of CBPU10 with magnification of 300000. Fig.1 shows that the morphology of the particle of CBPU emulsion is regular spheric structure, the emulsion particles are well dispersed with uniform particle size distribution. Fig.2 shows the particle distribution of CBPU10 when the blocked ratio is 10%. As shown in Fig.2, the average particle size of CBPU10 with a concentration of 0.2 wt% is about 79.74nm and distribution coefficient (PdI) of the emulsions is 0.201.

Effects of the blocked ratio of CBPU on the physical properties of paper

Table 3 Effects of blocked ratios on paper strength

BR (%)	FH (g/g)	tensile strength of dry paper(N/1.5cm)		tensile strength of wet paper(N/1.5cm)	wet strength/dry strength(%)	folding strength(times)	
		transverse	vertical	vertical	vertical	transverse	vertical
blank sample		18.9	28.2	*	*	6	9
0	0	25.5	34.4	1.8	5.31	12	18
5	0.586	29.4	43.1	11.3	26.25	14	23
10	1.162	34.8	51.5	13.4	28.37	23	38
15	1.750	34.8	53.2	16.6	31.31	25	38
20	2.343	36.7	54.8	19.4	35.58	28	40

Notes: 1, blank sample is paper treated only with deionized water; 2, * shows the results are not in measuring range of instrument.

The blocked ratio has important effects on molecule structure of CBPU. On the one hand, it can determine the the relative content of –NCO in CBPU, on the other hand, it has influence on the relative molecular mass of CBPU. Both of the aspects have an important effect on physical properties

of paper treated by the CBPU. When the blocked ratio is higher, the relative content of –NCO is more and relative molecular mass of CBPU is smaller. Effects of blocked ratios on paper properties are shown in Table 3.

Table 3 shows that FH value increases from 0g/100g CBPU to 2.343g/100g CBPU when the blocked ratio increases, tensile strength of dry and wet paper and folding strength of treated paper can be improved. The tensile strength of dry paper (vertical) increases from 28.2N to 54.8N when the blocked ratio increases to 20%. The vertical folding strength also increases from 9 to 40 times when the blocked ratio increases from 0 to 20%. Physical strength of blank sample is provided mainly by the hydrogen bond between paper fibers which is easy to be destroyed by water, and the paper's physical strength and water resistance is poor. In paper treated with blocked waterborne polyurethane, CBPU with high blocked ratio can form –NCO groups after the deblocking happening at high temperature. –NCO groups thus react with hydroxyl of paper fibres and urethane groups were generated, so chemical crosslinking points formed between cellulose of the paper fibers. The hydrogen bond between paper fibers changed into chemical bond, chemical bond is not easy to be destroyed by water and the physical strength, especially the wet strength of paper is enhanced through this method. When the blocked ratio is higher, strength of treated paper is improved more obviously. The tensile strength of wet paper (vertical) increases from 1.8N to 19.4N, and wet strength/dry strength increases from 5.31% to 35.58% when the blocked ratio increases from 0 to 20%, while the tensile strength of wet blank sample is too weak to measure.

Strength properties of paper increase rapidly first and then slowly with increasing blocked ratio. As the blocked ratio increases from 0 to 20%, -NCO number released by CBPU after deblocking also continually increases, then strength properties of paper were enhanced. However, relative molecular mass of CBPU will decreased with increasing blocked ratio, and polyurethane hard segments content will decrease with decreasing ω (MDEA), thus the bridging action of blocked polyurethane among the paper fibers will decrease. In addition, crystal imidazole was produced after deblocking reaction, which is also disadvantageous for strength increasing of paper. Both the above effects result that the strength properties of paper increase rapidly first and then slowly with increasing blocked ratio. Considering all these factors, the optimal blocked ratio of CBPU is 10%.

Conclusions

A novel paper strengthening agent was prepared by means of self-emulsifying, with IPDI, PCL, MDEA, DDP, bisphenol A as main materials, with imidazole as blocking agent. The morphology of the particle of CBPU emulsion is regular spheric structure with uniform particle size distribution. The average particle size of CBPU10 is 79.74nm. The paper strength especially wet strength can be obviously improved by increasing blocked ratio of CBPU. The best blocked ratio is 10%.

References

[1] Denise P. Queiroz, A.M.Botelho do Rego and Maria Norberta de Pinho: Journal of Membrane Science Vol. 281 (2006), p. 239

[2] Xiaojuan Lai, Yiding Shen and Lei Wang: Journal of Polymer Research Vol. 18 (2011), p. 2425

[3] Li Ganghui, Shen Yiding and Tang Xin: China Pulp & Paper Industry Vol. 30 (2009), p. 36

[4] Li Jin, Xie Yimin and Yang Zhiyong: Paper Chemicals Vol. 18 (2006), p. 18

[5] Zhao Jing, Shen Yiding and Lai Xiaojuan: Acta Polymerica Sinica Vol. 9 (2010), p. 1122

Advanced Materials Research Vols. 989-994 (2014) pp 648-651
© (2014) Trans Tech Publications, Switzerland
doi:10.4028/www.scientific.net/AMR.989-994.648

The Fatigue Life Prediction for EB-PVD Thermal Barrier Coating

Hao Yong[1,a], Qi Hong-yu[1,2,b,*]

[1] School of Energy and Power Engineering, Beihang University, Beijing 100191, China;

[2] Collaborative Innovation Center of Advanced Aero-Engine, Beijing 100191, China;

[a] haoyongsy@gmail.com, [b] qhy@buaa.edu.cn

* Corresponding author: Qi Hong-yu, email:qhy@buaa.edu.cn

Keywords: thermal barrier coating, thermal fatigue, life prediction.

Abstract. The electron beam-physical vapor deposition (EB-PVD) coatings were selected to analyze the fatigue life. Firstly the failure mechanisms of oxidation and thermal fatigue of TBCs were considered together. The weight of thermally grown oxide (TGO) were measured during oxidation experiments and modeled. Thermal fatigue experiments were induced by thermal mismatched stress and thermal fatigue with holding time. The failure mechanism was obtained by the finite element analyses. The life prediction model was modified by the shear and normal strain range close to the interface of the top coat and TGO. Based on the experiment data, the life prediction model of thermal fatigue of TBCs was set up for EB-PVD coatings. Finally, using the life prediction model, the life of TBCs was predicted under the designed load case. The life prediction model was verified and all experiment data fall into the factor of 3 scatter band.

Introduction

The application of thermal barrier coatings (TBCs) is an effective way to protect aero-engine blades from hot gas. Currently, two methods are used for depositing TBCs on substrate, which are plasma spray (PS) and electron beam-physical vapor deposition (EB-PVD).

Combination of high temperature oxidation and thermal fatigue finally result in the failure of TBCs[1~3]. Spallation and crack are typical failure modes of TBCs. Obviously, the oxidation and thermal stress-strain play an important part in TBCs service under high temperature [4~6]. The failure mechanisms of TBCs manufactured domestically is not clear and the potential of TBCs cannot be fully used due to the lack of a reliable life prediction method.

The work reported here is arranged as follows. Using the materials data, the stress-strain at the interface was obtained by finite element method. The failure mechanism under thermal fatigue load was understood deeply. Finally, the predictive results of EB-PVD thermal barrier coating were demonstrated against existing thermal fatigue life model.

Experiments of oxidation and thermal fatigue

The oxidation of bond coat

The EB-PVD coating is reported to be more strain tolerant in direction perpendicular to the columns (in-plane coating directions) and thus more resistant to crack growth compared with the PS coatings. Another different is the morphology of the bond coat/top coat interface, mechanical adhesion for PS and chemical adhesion for EB-PVD respectively. The interface of top coat/bond coat has been modified by EB-PVD processing. According to the service temperature of aero-engine, the oxidation temperatures were chosen as 1050℃. The oxidation time was at least 100 hours.

Measurement of the gained weight: The substrate material is K3 super-alloy. It was coated with bond coating only to avoid oxidation of substrate. The thickness of bond coating is 0.08 to 0.1mm. A precision balance was used to measure the weight of specimen at different time during oxidation. Each point was measured twice and took the average value as the experiment data (Table.1).

Table 1 Gained weight data of EB-PVD under 1050℃

Time (h)	0	5	10	20	30	45	60	70	100
Weight (mg)	0.0	1.9	1.7	1.	9.9	10.7	11.1	11.3	12.3

Thermal fatigue

The EB-PVD specimens were coated with the zirconia-yttria (6%~8% Y_2O_3.ZrO_2) on a nickel-chromium-aluminum (Ni22Cr10Al1.0Y) bond coat. The metal substrate is Ni-based superalloy (DZ40M). The ceramic layer is 0.125mm thickness and the bond coat is 0.07~0.08mm thickness. The load-case consists of a 2.5min heating from room temperature to 1150℃, a holding time of 0.5min and a cooling time of 4.5min respectively.

In order to simulate service condition of turbine blade, the test was carried out with thimble and cooled internally. The thimble transformed heat into outside surface of the sample. The effective heating length is about 50mm to avoid "edge phenomenon"[7]. Two kinds of thermal fatigue test were designed according to the service conditions of TBCs. One was to take into account the influence of thermal stress induced by mismatch through heating up and cooling down. The other was through holding at elevated temperature to take into account the influence of oxidation. Some specimens had been pre-oxidation considering the influence of oxidation on life. Therefore, a typical thermal fatigue test consisted of heating up, holding at elevated temperature and cooling down on the basis of pre-oxidation. The test was designed to take into account the influence of three loading cases, which are mismatch, oxidation and the combined effect (mismatch and oxidation) on life respectively. The fundamental purpose of the specimens without pre-oxidation time is to verify the validity of life prediction model.

The TBCs under thermal cyclic load can lead to distinctly different failure modes, but it is generally acknowledged that TBCs life is governed by a sequence of crack nucleation, propagation and coalescence that occurs prior to final failure by large-scale buckling and spallation. For failure modes of the buckling and spallation, the axial stress is compressive stress and the radial stress is tensile stress

According to the analysis of some literatures, the location of the TBCs failure lies in the interface between the bond coating and top coating. The location of failure also occurs at interface in this work. In other words, the buckling and spallation is at the "peak" of the sinusoidal interface. On the other hand, the strain range in life model was taken as axial strain or normal strain in previous work. Using finite element method, the critical location was analyzed under 2um TGO. The stress distributions close to the interface were shown in Fig.1. The off-peak was selected as the critical location.

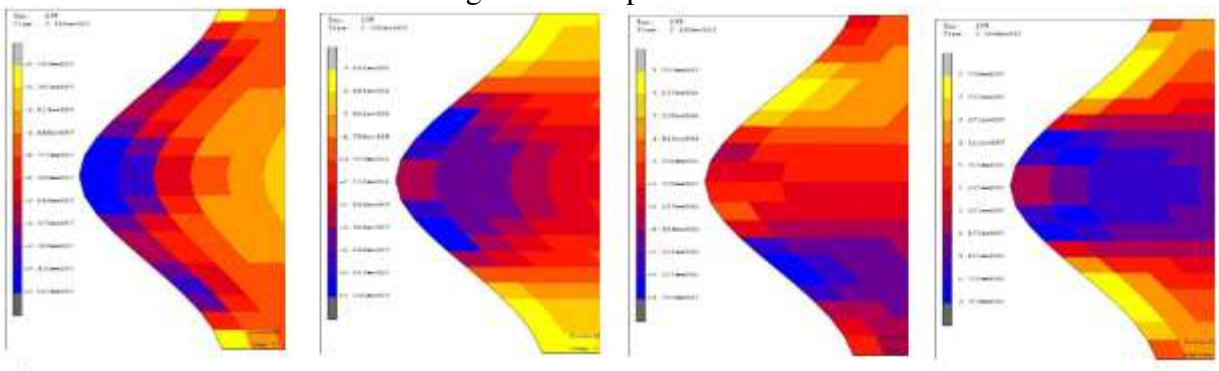

a. axial stress b. normal stress c.shear stress d.Von Mises stress

Fig.1 The stress distribution in top coat with 2 um TGO

Life prediction for TBCs

Life prediction model

Based on the Manson-Coffin model, the prediction model is as follows[8-12]:

$$N_f = (\Delta\varepsilon / \Delta\varepsilon_f)^{-b} \quad (1)$$

where N_f is cycle numbers, $\Delta\varepsilon$ is strain range at critical location, $\Delta\varepsilon_f$ is critical strain range and b is material parameter.

Since oxidation has an important influence, it will be considered in this model. So the life prediction model for TBCs is as follows:

$$N = [(\Delta\varepsilon_{f0} / \Delta\varepsilon)(1 - \frac{\delta}{\delta_c})^c + (\frac{\delta}{\delta_c})^c]^b \quad (2)$$

where δ is TGO's thickness, δ_c is critical TGO's thickness. When TBCs cracks caused by oxidation only and c is material parameter. For equation (6), the parameters except for $\Delta\varepsilon_f$ and δ_c are determined in thermal test. The oxide thickness is adopted for δ. $\Delta\varepsilon$ is obtained from finite element analysis [13-15]. In previous work, the $\Delta\varepsilon$ is a normal strain range. Now the $\Delta\varepsilon$ (in Eq.2) is modified as a couple parameter of the shear and normal strain range at critical location in present work. The modified model was as follows:

$$N = [(\Delta\varepsilon_{f0} / \sqrt{\Delta\varepsilon_{rr}^2 + \Delta\varepsilon_{ra}^2})(1 - \frac{\delta}{\delta_c})^c + (\frac{\delta}{\delta_c})^c]^b \quad (3)$$

where $\Delta\varepsilon_{ra}$ and $\Delta\varepsilon_{rr}$ are the shear and normal strain range at critial location.

Calculation of model parameters and life prediction

There are four independent parameters in life prediction model for TBCs, which are δ_c (critical thickness of TGO), $\Delta\varepsilon_f$ (failure strain without oxidation), b and c. These parameters can be obtained by correlation between test results and life prediction model. The data of the specimens of S3, S4 and S5 were used for obtaining the parameters. Then the S1 and S2 were verified the precision of the model. The modified model has better ability for life prediction. All experiment data fall into the factor of 3 scatter band.

Table 2 The experiment and prediction data.

Specimen	S1	S2	S3	S4	S5
Pre-oxidation time	-	-	10	50	100
Experiment data	621	298	512	438	382
Prediction life (previous work)	3870	210	408	170	150
Prediction life (Present work)	753	236	490	400	320

Conclusions

According to the service temperature of aero-engine, the oxidation temperatures were chosen as 1050℃. The kinetic model of oxidation was establish and the gained weight could describe well the oxidation of bond coating.

The cylindrical specimens with TBCs were manufactured. The sinusoidal interface was modeled by FEM. The stress-strain at interface of TBCs was simulated under the transient temperature load as the boundary condition. The shear and normal strain range were selected as control parameters for the mechanical damage of thermal fatigue.

Considering the influence of oxidation on life is an essentially difference between thermal fatigue test of TBCs and the metal, the oxidation damage was coupled into the fatigue model. The life prediction model of thermal fatigue of TBCs was evaluated and verified. All experiment data fall into the factor of 3 scatter band.

Acknowledgements

This project was supported by the Beijing Municipal Science & Technology Commission (D131100003113003) and the Hi-Tech Research and Development Program (863) of China (2012AA052102) and Program of International S&T Cooperation of China (2013DFA61590)

References

[1] Sheffler K: J Eng Gas Turb Power.Vol.110 (1988), p.605.

[2] Robert Eriksson, Hakan Brodin :Surf Coat Tech.Vol.205(2011),p: 5422.

[3] Qi Hongyu, Yang Xiaoguang: Comp Materi Scie. Vol.57 (2012), p: 38.

[4] Zhu D.M, Miller A: Surf Coat Tech. Vol.160 (2004), p: 293.

[5] Dae-Jin Kim, In-Hwan Shin: Surf Coat Tech. Vol.205 (2010), p: 451.

[6] Qi Hongyu, Yang Xiaoguang: Key Eng Mater. Vol.324 (2006), p: 595.

[7] M.T. Hernandez, D. Cojocaru: Comp Mater Scie. Vol.50 (2011), p: 2561.

[8] Gabe D, Green W: Comp Technol. Vol.67 (2005), p: 81.

[9] Taimas E, Mullejans S: Acta Mater. Vol.48 (2000), p: 4699.

[10] Cruse T. A.: J Eng Gas Turb Power. Vol.110 (1988), p: 110.

[11] Grecing D, Shadley J:J Therl Spr Technol. Vol.3(1995), p:371.

[12] Chang G. C, Phucharoen W,Miller R: Surf Coat Tech. Vol.132(1987),p:307.

[13] I.T. Spitsberg, D.R. Mumm, A.G. Evans:Mater Scie Eng. Vol,.394(2005), p: 176.

[14] Himanshu Bhatnagar, Somnath Ghosh: Int J Sol Str. Vol.43 (2006), p: 4384.

[15] L. Yang, Q.X. Liu, Y.C. Zhou: J Mater Scie –Tech.Vol.30 (2014), p: 371.

Advanced Materials Research Vols. 989-994 (2014) pp 652-655
© (2014) Trans Tech Publications, Switzerland
doi:10.4028/www.scientific.net/AMR.989-994.652

Research on Performance Features of Shape Memory Alloys

Guomin LIN[1,a], Yanhua LI[2,b]

[1]Postgraduate Department, Xijing University, Xi'an, China

[2]Information and Navigation Institute, Air Force Engineering University, Xi'an, China

[a]gmlin@21cn.com [b]liyanhua108@21cn.com

Keywords: Shape Memory Alloys(SMAs); Fe-based; Cu-based; Ti-Ni based

Abstract. The shape memory effect,the classification and the principle of shape memory alloys are introduced.The performance features such as melting point,density, resistivity,thermal conductivity, thermal expansion coefficient, phase-change heattensile strength fatigue limit, grain size, transition temperature,lag size,one-way shape memory, two-way shape memory of Fe-based,Cu-based and Ti-Ni based shape memory alloys are researched in detail.

Intoduction

Development and widely application of intelligent materials will result in a major revolution in materials science. The measure indicator of SMAs general used of qualitative indicator, it is measured mainly from following aspects[1]: the perception function which can detect and discriminate outside of stimulus strength; the drive function which can response outside changes; response can be selected and controled according to set of way; its reaction compared with sensitive, timely and appropriate; it can quickly to recovery to original state after external stimulus elimination. The measure indicator of SMAs should also take into account the unified between the strong function and low complexity from the use, therefore, a quantitative indicator is proposed, it called intelligent effect represented. SMAs are an important intelligent material, based on the analysis of performance features the shape memory alloys are studied in this article detailedly.

Shape memory effect

SME refers to material under conditions of temperature changes in the outside can change its shape and has a reversible change. SME divided into one way, two-way and full-way memory effect[2]. One-way memory effect is refers to shape memory alloy deformation in lower of temperature, after heating it can recover shape before deformation, this is only a shape memory phenomenon in heating process; when heating it recovery high temperature phase shape; when cooling it can recovery cryogenic phase shape of phenomenon so it called two-way memory effect; when heating it recovery high temperature phase shape, and cooling becomes the same shape and orientation instead of cryogenic phase shape of phenomenon is called full-way memory effect.

Principle of shape memory alloys

Shape memory alloy is heated to a critical temperature above for shape memory heat treatment, formed martensite phase after rush cold, then exert a deformation, SMA is heated to critical temperature above again, makes crystal phase reverse shift, make the cryogenic martensite phase inverse becomes high temperature austenitic phase (also known as parent phase) and recovery to inherent shape before deformation or return to martensite phase through internal elastic energy is released in follow-up cooling. Figure 1 as shown in schematic diagram of martensite phase change. In the process of phase-change of SMAs, rigid, resistance, friction and number of sound waves of materials are changed. At the same time because the SMA contract in heating and phase change under external field, resulting in large deformation and stress, so material can be strengthened. Using these features, shape memory material can be used as intelligent materials actuation device so

that material is not only self-diagnosis, but with ability of self-injury and self healing. SMAs are divided into Fe-based, Cu-based and Ti-Ni-base shape memory alloy.

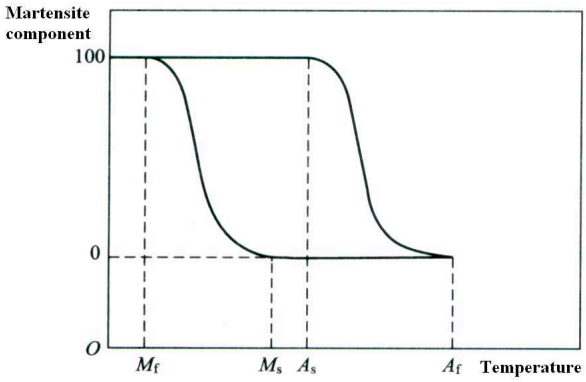

Figure1. Martensitic phase change diagram

Fe-based shape memory alloys

Fe-based SMA is divided into two categories: based on thermo elastic martensite phase change and based on non-thermo elastic reversible martensite phase change. Fe-based SMA has some features such as high strength, ease of processing etc. Structure, organization and performance of Fe-based SMA are shown in table 1.

Tab. 1 Structure, organization and performance of Fe-based shape memory alloys

alloy	composition	martensite crystal structure	characteristics of phase change	recovery rate(%)	M_s range /K
Fe-Pt	25%(1)	bct	thermal elastic	40~80	280
Fe-Pd	30%(1)	fct	thermal elastic	40~80	180~300
Fe-Ni-Co-Ti	Fe-33Ni-10Co-4Ti(2)	bct	thermal elastic	80~100	-150
Fe-Ni-C	Fe-31Ni-0.4C (2)	bct	non-thermal elastic	50~85	77~150
Fe-Cr-Ni	Fe-19Cr-10Ni (2)	hcp/bct	non-thermal elastic	25	—
Fe-Mn-Si	Fe-(28~33)Mn-(4~6)Si (2)	hcp	non-thermal elastic	30~100	200~390
Fe-Mn-Si-Cr	Fe-28Mn-6Si-5Cr(1)	hcp	non-thermal elastic	100	300
Note:(1)Original number of molecules (2)Number of molecules					

Study of martensite form, through appropriate alloy formation, iron-based alloys can be achieved in thermal elastic or non-reversible thermo elastic martensite change, which developed based on these two kinds of phase change of Fe-based SMAs. Fe-based SMA has to meet following conditions[3]: ①Parent phase has high yield strength or low elastic limit; ②Martensite phase intersect causes a small change in volume and strain; ③Martensite analogy (c/a) and favor twinning substructure; ④The less M_s favor twinning substructure and increase the yield strength of the parent phase. Fe-Mn-Si base alloy with cheap, easy to processing as a fitting has the advantage of easy install and avoid weld defects. Fe-based shape based on the alloy provides a set of fitting pipe connection technology, its advantages are anti-corrosion, good sealing, resistance to high pressure, strong connection etc.

Cu-based shape memory alloys

Cu-based SMA has some good performances such as shape memory, super elastic, high damping and good conductivity, simple production process, low cost, high performance[4]. Cu-based SMA system includes: Cu-Zn, Cu-Zn-AL, Cu-AL, Cu-Zn-Sn, Cu-Zn-Ni, Cu-Zn-Si, Cu-Zn-Ca, Cu-AL-Ni, Cu-AL-Mn, Cu-AL-Si, Cu-AL-Nb, Cu-AL-Be. Performance of Cu-based shape

memory alloys (shown as in table 2).Cu-based SMA can be used as automatic fasteners, for example, heat-shrinkable joints,using a memory alloy fitting, its inner diameter is smaller than the connection pipe outside diameter 4%, expansion of pipe diameter under the low temperature, then set on the connected pipe. When the tube temperature rises above A_s it will shrink to the original shape, so as to connect the connected pipes securely. SMA is a thermo-sensitive materials, it can select appropriate alloy to control M_s, Af and temperature change range according to environmental conditions, to control the temperature by the shape memory of SMAs.

Tab. 2 Performances of Cu-based shape memory alloy

Performance	Unit	Cu-Zn -AL	Cu-AL-Ni
Melting point	℃	950~1020	1000~1500
Density	kg/cm^2	7800~8000	7100~7200
Resistivity	μΩ·m	0.07~0.12	0.1~0.4
Thermal conductivity	W/(m·℃)	120(20℃)	75
Thermal expansion coefficient	—	$(16\sim18)\times10^{-6}$	$(16\sim18)\times10^{-6}$
Specific heat capacity	J/(kg·℃)	390	400~480
Phase change heat	J/kg	7000~9000	7000~9000
Modulus of elasticity	GPa	70~100	80~100
Yield strength	MPa	150~300	150~300
Tensile strength (Martensite)	MPa	700~800	1000~1200
Elongation (Martensite)	%	10~15	8~10
Fatigue limit	MPa	270	350
Grain size	μm	50~100	25~60
Transition temperature	℃	-200~170	-200~170
Lag size	℃	10~20	10~20
Maximum one-way shape memory	%	5	6
$N=10^2$	—	1	1.2
$N=10^5$	—	0.8	0.8
$N=10^7$	—	0.5	0.5
Maximum heating temperature(1h)	℃	160~200	300
Damping ratio SDC	%	30	10
Reply the stress	MPa	200	—
Maximum pseudo elastic strain (single crystalline)	%	10	10
Maximum pseudo elastic strain (poly crystal)	%	2	2

Ti-Ni based shape memory alloys

Ti-Ni based SMA in addition to its unique shape memory function, also has some excellent characteristics such as wear resistance, corrosion resistance, high damping and hyper-elastic. its expansion rates is above 20%, its fatigue life up to 10 million times, its damping elastic is 10 times higher than normal spring, its corrosion resistance excellent than the current best medical stainless steel, Ti-Ni based SMA can meet the demand for all kinds of engineering and medical applications. Application of Ti-Ni shape memory alloys[5].(1)Produce a radio communication antenna for shape memory. Ti-Ni shape memory intelligent magnetic material can be produced a spaceship's radio communication antenna(as shown in figure 2). First step. Ti-Ni alloy wire is heated to 65 ℃, making it is translated into the austenitic phase (as shown in figure 2 (a)), then alloy wire is cooled to below 65℃ and translated into martensite phase. Second step.At room temperature martensite alloy wire is cut into small pieces, then bent into a shape of antenna, the small pieces of cross are welded fixed in antenna (Figure 2 (b)).Third step. Press the antenna into a small group, its volume is reduced to one-tenth, so that spaceships easy to carry (Figure 2 (c)).Last step. When need to use the antenna, just heat the small group to 77℃, so that martensite translated into austenite completely, the antenna will automatically open, and restoration the original size and shape completely(Figure 2 (d)). (2)engineering fastening rivet under special circumstances[6].In difficult operating environment such as in a closed vacuum, using shape memory alloy rivets fastened to achieve allowable riveting. Operation by first memory address into the rivet tail opening, before fastening, after cooling in the

dry ice rivet tail straightened, then insert the fastener in the hole, the temperature rise shape recovery, open implementation fastening the rivet tail.(3) the TI-NI shape memory alloys are widely used in the field of medicine, such as orthodontics, plastic surgery, and so on.

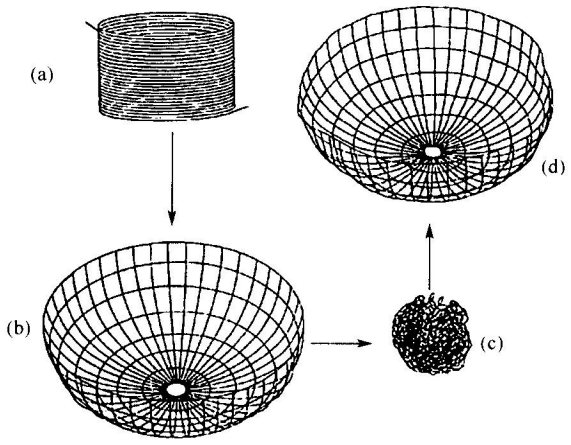

Figure2. Radio communication antenna produce process of shape memory

Summary

Shape memory alloys are a kind of intelligent material, it always applicates in many fields. In order to better use SMAs, one-way shape memory effect, two-way shape memory effect and full way memory effect are realized first. More important is to master the performance features of shape memory alloys such as Fe-based,Cu-based and Ti-Ni based shape memory alloys are researched in detail.

References

[1] LI Bing. Development Trend of Shape Memory Alloy Materials [J]. Metal World, 2005 (12): 26-29

[2] ZHANG Guanglei, DU Yanliang. Intelligent Materials and Structural Systems [M], Beijing: Beijing University Press, 2010.8

[3] MENG Liang, MENG Pinjia. Progress of Molecularly Imprinted Sensor Based on Photonic Crystal Hydrogels [J]. Materials Review; 2012 (23): 61-64

[4] LI Qingshan. Function and Intelligent Materials [M]. Beijing: National Defense Industry Press, 2006

[5] ZHANG Jinsheng. General Survey to Application of Intelligent Materials[J].Journal of Shan Dong University of Technology, 2002, 32(3):77-82

[6] ZHANG Guanglei, DU Yanliang. Intelligent Materials and Structural Systems [M], Beijing: Beijing University Press, 2010.8

Advanced Materials Research Vols. 989-994 (2014) pp 656-659
© (2014) Trans Tech Publications, Switzerland
doi:10.4028/www.scientific.net/AMR.989-994.656

Structural and optical properties of Al co-doped ZnCoO thin film

Ping Cao[1,a], Yue Bai[2,b]

[1]School of Science, Changchun Institute of Technology, Changchun, 130012, China;

[2]Changchun institute of Optics, Fine Mechanics and Physics, Chinese Academy of Sciences, Changchun,130033,China.

[a]pingshuicaio@126.com, [b]baiy@ciomp.ac.cn

Keywords: ZnCoO; co-doping; thin film

Abstract. Al co-doped ZnCoO thin film has been prepared by a sol-gel method. The structural and optical properties of the sample were investigated. X-ray diffraction and UV absorption spectroscopy analyses indicate that Al^{3+} and Co^{2+} substitute for Zn^{2+} without changing the wurtzite structure. With the Al doping, the visible emission increased and the UV emission decreased, which is attributed to the increase of O vacancies and Zn interstitials.

Introduction

Diluted magnetic materials (DMSs) have attracted a great deal of attention in recent years as enabling materials in the emerging field of ‘‘spintronics’’. The low Cure temperature (T_C) of DMSs hindered their future applications. According to the previous ab initio studies on the magnetism of diluted magnetic semiconductors, it was expected that room temperature ferromagnetic DMSs can be realized by TM ions doped ZnO [1-7]. As Co is highly soluble in ZnO, Co doped ZnO has been studied widely [8-12].

In this paper, $Zn_{0.99-x}Co_{0.01}Al_xO$ thin film has been prepared by a sol-gel method and the structural and optical properties of the sample were investigated.

Experimental

The sol was composed of $Zn(NO_3)_2 \cdot 6H_2O$, $Al(NO_3)_3 \cdot 9H_2O$, $Co(NO_3)_2 \cdot 6H_2O$ and Polyvinyl Pyrrolidone (PVP) in an ethanol solution. The total concentration of metal ions was controlled at 0.1 mol/l. The concentration of Al^{3+} was adjusted to 0.002 mol/l and the concentration of Co^{2+} was maintained at 0.001 mol/l. The films were spin-coated on Si (100) and quartz substrates at 2000 r/min. After the deposition, the substrates were first heated to 100 ℃ in air for 10 min to evaporate the solvent, then at 350 ℃ in O_2 for half an hour to eliminate the organic component in the film. This process may be repeated many times to reach the desired thickness. Then thermal annealing was performed for 1 h in an O_2 environment at 700℃ in order to crystallize the film. The thicknesses of the samples were all near 150 nm.

X-ray diffraction (XRD) measurement was taken on a Siemens D500 diffractometer using CuK_a radiation of 1.5418 Å. A UV-360 Spectrophotometer (Shimadzu) was used for the optical characterization. Photoluminescence (PL) spectra were measured using the 325 nm line of a He-Cd laser as an excitation source.

Results and Discussion

X-ray diffraction patterns of the sample are shown in Fig.1. The diffraction pattern can be identified as the wurtzite structure, which indicates that the Co and Al codoping can not disturb the structure of ZnO. No additional peaks (such as Co, CoO) are observed in the sample, which indicates no impurity exists in the films. The XRD result indicates that Al ions are doped into ZnCoO crystal lattice successfully with substituting positions of Zn ions.

Visualization of Al and Co incorporation into the ZnO lattice is realized using EDX, by which the correlation between the local microstructure and the chemical composition can be established. According to the Figure2, the Co concentration in the samples are calculated with 0.75% and the Al concentration in the sample are calculated with 1.5% And the rest is lost in the solution, not participating in the reaction.

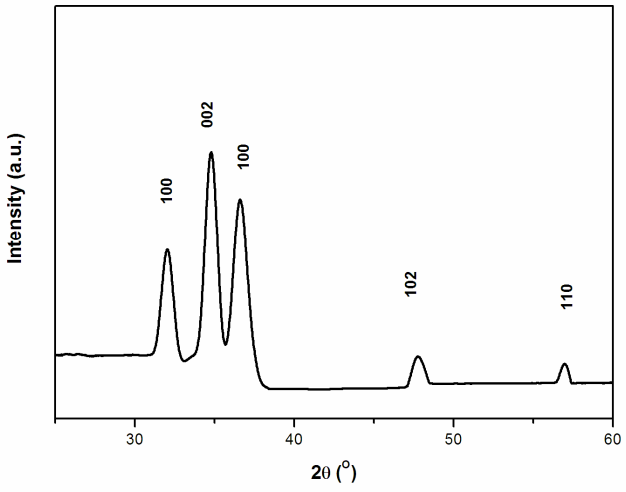

Fig.1 XRD patterns of the sample

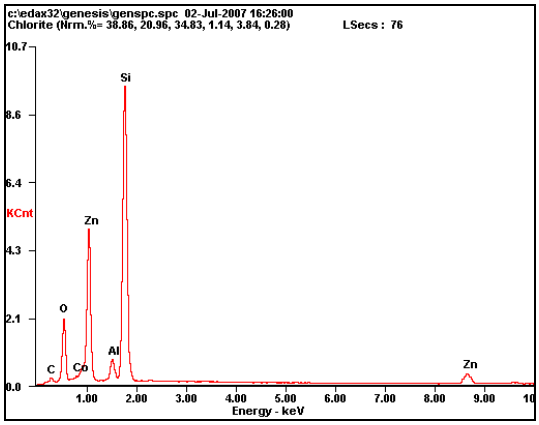

Fig.2 The EDX spectrum of the sample

Optical absorption spectrum for Al-doped ZnCoO thin film is presented in Fig.3. The blue-shift of the absorption edges can be seen with Al doping. The sample optical band gap obtained from the absorption spectra is raised to 3.7 eV, as the result of the lowest states filling in the conduction band by Al donor electrons—the Burstein-Moss effect [13]. Meanwhile, the absorption peaks at 567, 612 and 649 nm are observed which should be correlated with the *d-d* transitions of the tetrahedrally coordinated Co^{2+} ions and attributed to the ${}^4A_2(F)\rightarrow{}^2E(G)$, ${}^4A_2(F)\rightarrow{}^4T_1(P)$, and ${}^4A_2(F)\rightarrow{}^2A_1(G)$, respectively [14], indicating Co^{2+} ions are doped into the ZnO crystal lattices successfully.

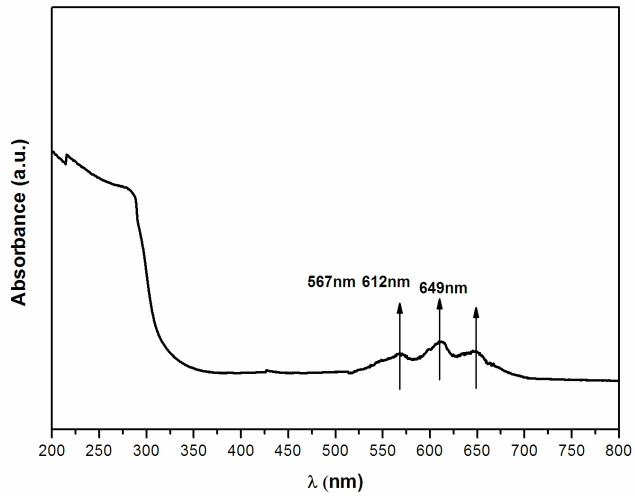

Fig.3 Room temperature optical spectra of the sample

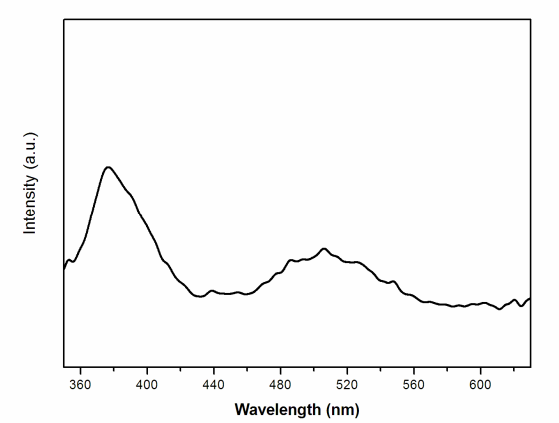

Fig.4 Room temperature PL spectra of the sample

Fig. 4 gives the room temperature PL spectrum of the sample. The UV emission corresponds to the near band edge emission, and the green emission peak is generally referred to as a deep-level or trap-state emission such as O vacancies [15], Zn vacancies and Zn interstitials [16]. With the Al doping, the visible emission increased and the UV emission decreased, which is attributed to the increase of O vacancies and Zn interstitials.

Conclusions

In conclusion, the (Al, Co) co-doped ZnO thin film has been prepared by sol-gel method. The XRD and the optical absorption spectra results indicate that Al and Co ions are doped into ZnO crystal lattice successfully with substituting positions of Zn ions. Visualization of Al and Co incorporation into the ZnO lattice is realized using EDX. With the Al doping, the visible emission increased and the UV emission decreased, which is attributed to the increase of O vacancies and Zn interstitials.

Acknowledgements

This work is supported by the National Natural Science Foundation of China under Grant No. 11104018 and No. 11372309 and education department of Jilin province under Grant No. 2012284 and No. 2014321.

References

[1] T. Dietl, H. Ohno, F. Matsukura, J. Cibert, and D. Ferrand: Science Vol. 287(2000), p.1019

[2] Said Benramache, Hachemi Ben Temam, Ali Arif, Abderrazak Guettaf, Okba Belahssen: Optik - International Journal for Light and Electron Optics, Vol.125, (2014), p. 1816

[3] Shu-yuan Zhang, Quan-xi Cao, Yin-hua Yao: Infrared Physics & Technology, Vol.61 (2013), p.1

[4] Fenglin Xian, Xiaoxiong Wang, Linhua Xu, Xiangyin Li, Wangfeng Bai :Journal of Luminescence, Vol.144(2013), p.154

[5] Qiang Li, Yuyin Wang, Lele Fan, Jiandang Liu, Wei Kong, Bangjiao Ye: Scripta Materialia, Vol.69 (2013), p. 694

[6] M.–H. Tsai, T.–Y. Jiang, C.–Y. Huang: Journal of Magnetism and Magnetic Materials, Vol. 324(2012), p.1733

[7] K.C. Barick, M. Aslam, D. Bahadur: Journal of Alloys and Compounds, Vol.587, (2014), p. 282

[8] R. Siddheswaran, R.V. Mangalaraja, Maria Elana Gómez, Ricardo E. Avila, C. Esther Jeyanthi: Journal of Alloys and Compounds, Vol. 581(2013), p. 146

[9] Ping Li, Sha Wang, Jibiao Li, Yu Wei : Journal of Luminescence, Vol 132(2012), p.220

[10] Songqing Zhao, Kunkun Yan, Qiang Liu, Limin Yang, Chun Huang, Kun Zhao, Aijun Wang: Optik - International Journal for Light and Electron Optics, Vol.124 (2013), p.1105

[11] Xiaohong Yu, Changzhen Liu, Dawei Meng, Can Lu, Jie Liu, Huixia Li, Yongqian Wang, Junxia Wang: Materials Letters, Vol.122 (2014), p. 234

[12] Yuanwen Zou, Zhongbing Huang, Yan Wang, Xiaoming Liao, Guangfu Yin, Jianwen Gu: Colloids and Surfaces B: Biointerfaces, Vol.102(2013), p. 29

[13] E. Burstein: Phys. Rev.Vol. 93(1954), p.632

[14] M. Bouloudenine, N. Viart, S. Colis, J. Kortus, and A. Dinia: Appl. Phys. Lett. Vol.87 (2005), p.052501

[15] K. Vanheusden, W.L. Warren, C.H. Seager, D.R. Tallant, J.A. Voigt: J. Appl. Phys. Vol.79 (1996), p.7983

[16] E.G. Bylander: J. Appl. Phys. Vol.49 (1978), p.1188

Advanced Materials Research Vols. 989-994 (2014) pp 660-664
© (2014) Trans Tech Publications, Switzerland
doi:10.4028/www.scientific.net/AMR.989-994.660

The most probable mechanism function of PVC thermal decomposition

Ning Xu[1, a], Guangcheng Li[1,2,b] and Rongfeng Guan[1,c]

[1]Yancheng Institute of Technology, Key Laboratory for Advanced Technology in Environmental Protection of Jiangsu, Yancheng 224051, Jiangsu Province, China

[2]School of Chemical Engineering, Anhui University of Science and Technology, Huainan 232001, Anhui Province, China

[a]xuning196402@163.com, [b]liguangcheng1912@126.com, [c]rongfengg@163.com

Keywords: non-isothermal kinetics, differentiation-integration method, most probable mechanism function

Abstract. The most probable mechanism function of non-isothermal kinetics about polyvinyl chloride thermal decomposition process was studied by the differential method (A-B-S)-integral method (C-R). The results show that the most probable mechanism function accorded with the mechanism function A1.5 when the heating rate of was 5 ^{o}C/min and the decomposition rate was 0.01-0.10.

Introduction

Thermal stability of polyvinyl chloride (PVC) has been an important research topic in the field of PVC processing and applications [1], the field of thermal analysis kinetics with many dynamic models and the corresponding calculation methods is widely used to describe the possible reaction mechanism of solid phase reaction, and has made many useful results [2-5]. In this paper, the differential method (Achar-Brindly-Sharp, referred to as A-B-S) and integral method (Coats-Redfern, referred to as C-R) to calculate the most probable mechanism function of PVC thermal decomposition provided a new way for the study of the PVC thermal stability.

Experimental section

PVC, SG-5, industrial grade, Sinopec Qilu Petrochemical Co., Ltd.; Methyl tin mercaptide, industrial, Ed Nantong Chemical Co.; bis (2-ethylhexyl) phthalate (DOP), AR, Sinopharm Chemical reagent Co., Ltd.; two-roll mill, model SK-160B, Shanghai rubber Machinery Factory.

100 parts of PVC powder, 30 parts of DOP, 1.5 parts of methyl mercaptan were mixed, masticated at 160 ^{o}Cfor 5min with a two-roll mill, and tableted.

Thermal gravimetric analysis (TGA) experiments were performed on an American Perkin-Elmer TGA7 analyzer at the heating rate of 5, 10, 20, 30 ^{o}C/min and temperature range of 25-600 ^{o}C in a N_2 atmosphere.

Results and Discussion

The thermogravimetric (TG) curves and the corresponding differential thermogravimetry (DTG) curves of PVC thermal pyrolysis were shown in Fig. 1 and 2, respectively. It can be seen that the PVC thermal decomposition temperature increased with the increase of the heating rate. Table 1 listed the decomposition rate (α, less than 0.25) and temperature basic data of PVC thermal decomposition process at the different heating rates.

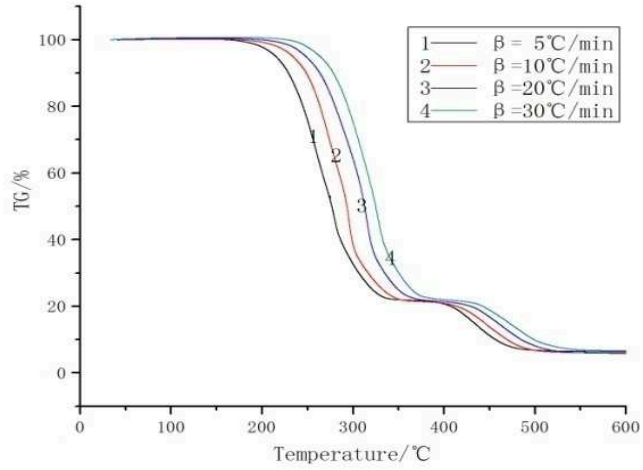

Fig. 1. TG curves of PVC at different heating rates.

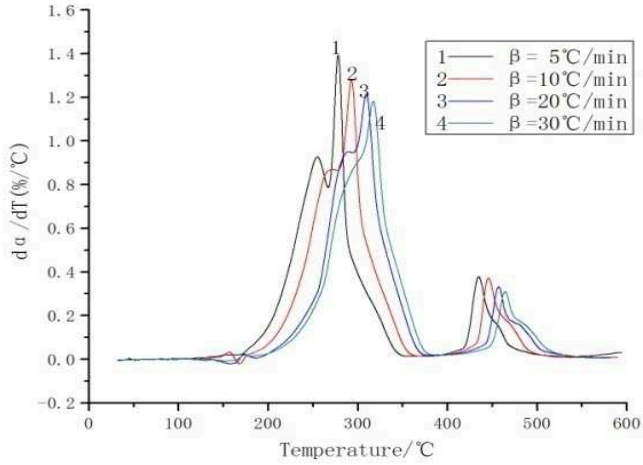

Fig. 2. DTG curves of PVC at different heating rates.

Table 1 Data of PVC thermal decomposition at different heating rates.

α	T（°C）				$d\alpha/dT\times10^{-3}$（%/°C）			
	β (°C/min)							
	5	10	20	30	5	10	20	30
0.01	187.13	204.17	221.69	241.32	0.82	0.86	0.92	1.63
0.02	198.30	216.08	232.61	248.66	1.38	1.56	1.46	2.14
0.03	205.42	223.73	238.89	254.47	1.91	2.22	1.84	2.63
0.04	210.73	229.36	243.77	259.37	2.48	2.81	2.17	3.10
0.05	215.00	233.63	248.02	263.61	2.98	3.33	2.48	3.65
0.06	218.61	237.37	251.79	267.37	3.49	3.82	2.79	4.45
0.07	221.76	240.76	255.21	270.72	3.96	4.33	3.08	5.30
0.08	224.51	243.79	258.31	273.70	4.38	4.85	3.55	6.01
0.09	226.92	246.49	261.14	276.23	4.76	5.37	4.18	6.53
0.1	229.12	248.74	263.58	278.47	5.17	5.84	4.82	6.93
0.11	231.11	250.77	265.77	280.51	5.55	6.26	5.39	7.25
0.12	232.97	252.62	267.78	282.41	5.92	6.64	5.93	7.52
0.13	234.72	254.33	269.66	284.19	6.26	6.97	6.49	7.74
0.14	236.40	255.92	271.42	285.88	6.56	7.29	6.99	7.93
0.15	237.99	257.42	273.09	287.47	6.86	7.56	7.46	8.07

0.16	239.53	258.83	274.68	289.00	7.12	7.81	7.85	8.21
0.17	241.01	260.18	276.20	290.45	7.39	8.03	8.20	8.35
0.18	242.43	261.45	277.66	291.84	7.62	8.21	8.49	8.48
0.19	243.79	262.68	279.08	293.18	7.86	8.37	8.73	8.59
0.2	245.10	263.55	280.47	294.47	8.08	8.48	8.92	8.70
0.21	246.37	264.97	281.84	295.72	8.28	8.55	9.08	8.79
0.22	247.59	266.06	283.19	296.95	8.49	8.61	9.21	8.87
0.23	248.77	267.12	284.53	298.15	8.68	8.64	9.32	8.95
0.24	249.92	268.16	285.85	299.33	8.86	8.67	9.41	9.01
0.25	251.03	269.19	287.14	300.48	9.02	8.68	9.47	9.07

TG-DTG data in Table 1 were treated with multiple scanning method Flynn-Wall-Ozawa (F-W-O) [6], the linear regression between reciprocal temperature 1/T and lgβ under the same conversion rate α and the corresponding four different heating rates β was done by minimal square method, the activation energy E was calculated from the slope, and the pre-exponential factor A was obtained from the intercept. F-W-O method is shown in eq. (1):

$$\lg\beta = \lg\left[\mathrm{AE}/\left(\mathrm{G}(\alpha)\mathrm{R}\right)\right] - 2.313 - 0.4567\mathrm{E}/(\mathrm{RT}) \quad (1)$$

Where, β is a linear heating rate, R is the universal gas constant, A is the pre-exponential factor, E is the activation energy, α is the decomposition rate.

The data in Table 1 were substituted into equation 1, lgβ on 1/T was done by the minimal square method, the resulting activation energy E can be calculated from the slope, the resulting data were shown in Table 2.

Table 2 Data calculated by F-W-O method.

α	r	SD	Slope (k)	intercept	E（KJ/mol）
0.01	-0.99304	0.04941	-3463.42	8.24718	63.05
0.02	-0.99721	0.03130	-3879.93	8.93615	70.64
0.03	-0.99673	0.03389	-4106.46	9.28127	74.76
0.04	-0.99599	0.03755	-4236.44	9.45345	77.13
0.05	-0.99597	0.03764	-4310.70	9.52900	78.48
0.06	-0.99600	0.03750	-4359.56	9.56303	79.37
0.07	-0.99606	0.03719	-4396.49	9.58005	80.04
0.08	-0.99618	0.03661	-4423.26	9.58333	80.53
0.09	-0.99646	0.03529	-4450.72	9.59346	81.03
0.10	-0.99676	0.03376	-4480.77	9.61375	81.58
0.11	-0.99698	0.03256	-4507.16	9.63052	82.06
0.12	-0.99719	0.03140	-4532.48	9.64764	82.52
0.13	-0.99741	0.03017	-4556.65	9.66449	82.96
0.14	-0.99762	0.02893	-4581.51	9.68413	83.41
0.15	-0.99782	0.02766	-4605.52	9.70352	83.85
0.16	-0.99803	0.02635	-4629.47	9.72381	84.28
0.17	-0.99821	0.02507	-4654.05	9.74622	84.73
0.18	-0.99840	0.02369	-4677.17	9.76687	85.15
0.19	-0.99858	0.02233	-4698.25	9.78440	85.53
0.20	-0.99877	0.02077	-4717.60	9.79944	85.89
0.21	-0.99897	0.01902	-4735.33	9.81203	86.21
0.22	-0.99915	0.01728	-4749.30	9.81817	86.46
0.23	-0.99932	0.01543	-4760.95	9.82047	86.68
0.24	-0.99947	0.01363	-4771.02	9.82026	86.86
0.25	-0.99959	0.01198	-4779.85	9.81823	87.02

A-B-S equation was solved with the most probable mechanism function, shown in the following [7]:

$$\ln[(\mathrm{d}\alpha/\mathrm{dT})/\mathrm{f}(\alpha)] = \ln(\mathrm{A}/\beta) - \mathrm{E}/(\mathrm{RT}) \quad (2)$$

C-R equation was shown in the following [8]:

$$\ln[\mathrm{g}(\alpha)/\mathrm{T}^2] = \ln[(\mathrm{AR}/\beta\mathrm{E})] - \mathrm{E}/(\mathrm{RT}) \quad (3)$$

The TG-DTG resulting experimental data α, β, T, dα/dT were substituted into the differential eq. (2) and the integral eq. (3), among the 19 mechanism functions, its f (α) and G (α) is the most probable mechanism function when the activation energy E is closest calculated by two calculated methods with better linear correlation coefficient and small standard deviation.

The eq. (4) was obtained by multiplying eq. (2) and (3):

$$Z(\alpha) = f(\alpha)\mathrm{G}(\alpha) = (\mathrm{RT}^2/\mathrm{E}) \times (\mathrm{d}\alpha/\mathrm{dT}) \quad (4)$$

The dα/dT data in Table 1 and the activation energy E in Table 2 were substituted into the above obtained equation, the experimental curve Z (α) was obtained. The f (α) and G (α) in the 19 mechanism function equations (Table 3) were substituted into equation (4), a standard curve Z '(α) = f (α) G (α) was obtained.

$Z(\alpha)/Z'(\alpha)$-α curve was done, if the experimental curve $Z(\alpha)$ with the standard curve $Z'(\alpha)$ overlaped in a certain one or several curves at certain decomposition stage, it is the most probable mechanism function at this stage and heating rates. By comparison it is found that when β=5 °C/min, α=0.01-0.10, it accorded with the mechanism function $G(\alpha)=[-\ln(1-\alpha)]^{2/3}$, that was the mechanism function A1.5, seen form Fig. 3.

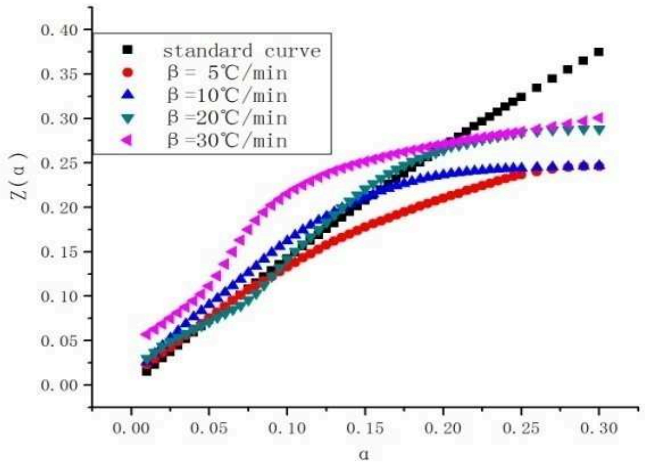

Fig. 3 $Z(\alpha)$-α curves at different heating rates.

Table 3 Common mechanism functions

Function	Mechanism	f（α）	G（α）
Power law	P_4	$4\alpha^{0.75}$	$\alpha^{0.25}$
Power law	P_3	$3\alpha^{2/3}$	$\alpha^{1/3}$
Power law	P_2	$2\alpha^{0.5}$	$\alpha^{0.5}$
Power law	P_1	1	α
One-dimensional diffusion	D_1	0.5α	α^2
Two-dimensional diffusion	D_2	$[-\ln(1-\alpha)]^{-1}$	$\alpha+[(1-\alpha)\ln(1-\alpha)]$
Ginstling-Brounshtein	D_4	$1.5[(1-\alpha)^{-1/3}-1]^{-1}$	$(1-2/3\alpha)-(1-\alpha)^{2/3}$

Avrami-Erofeev	A_2	$2(1-\alpha)[-\ln(1-\alpha)]^{0.5}$	$[-\ln(1-\alpha)]^{0.5}$
Avrami-Erofeev	A_3	$3(1-\alpha)[-\ln(1-\alpha)]^{2/3}$	$[-\ln(1-\alpha)]^{1/3}$
Avrami-Erofeev	A_4	$4(1-\alpha)[-\ln(1-\alpha)]^{0.75}$	$[-\ln(1-\alpha)]^{0.25}$
Contracting area	R_2	$2(1-\alpha)^{0.5}$	$1-(1-\alpha)^{0.5}$
Contracting volume	R_3	$3(1-\alpha)^{2/3}$	$1-(1-\alpha)^{1/3}$
First-order reation	F_1	$1-\alpha$	$[-\ln(1-\alpha)]$
3/2-order reation	$F_{1.5}$	$(1-\alpha)^{1.5}$	$2[(1-\alpha)^{-0.5}-1]$
Z-L-T funtion	D_3	$1.5(1-\alpha)^{0.75}[(1-\alpha)^{-1/3}-1]^{-1}$	$[(1-\alpha)^{-1/3}-1]^2$
	$P_{2/3}$	$2/3\alpha^{-0.5}$	$\alpha^{1.5}$
	$A_{1.5}$	$1.5(1-\alpha)[-\ln(1-\alpha)]^{1/3}$	$[-\ln(1-\alpha)]^{2/3}$
	F_2	$(1-\alpha)^2$	$(1-\alpha)^{-1}-1$
	F_3	$0.5(1-\alpha)^3$	$(1-\alpha)^{-2}-1$

Differential-integral method results showed that: there is a certain interaction between the function and activation mechanism. The linear correlation coefficient r was calculated in Table 4. The table shows that r is close to -1, indicating that the differential-integral method to calculate the result is better, and the obtained data had high reliability.

Table 4 Linear correlation coefficient calculated by Differential, integral method.

T/K	linear correlation coefficient/r
522.05	-0.99932
536.65	-0.99877
552.05	-0.99858

Summary

There is a certain interaction between the function and activation mechanism calculated by differential-integral method, a good linear relationship was obtained by differential-integral method, the obtained data had high reliability, which provides a new way to scientifically and rationally describe the most likely reaction mechanism in the solid-phase reaction.

Acknowledgements

This work was financially supported by the National Key Technology R&D Program of China (2013BAC13B01) and the National Natural Science Foundation (21276220).

References

[1] Bacaloglu R, Fisch M, Ploym. Degr. Stab.,1994, 45 (3): 301.

[2] Lynn J H, Thermochim Acta, 1992, 203: 519.

[3] Chen H W，Wang W W，Huang X Z，Zhao Z H, J. China Power Eng., 2011, 31 (9): 709.

[4] Xiao Z B, Guo M M, Guo R K, China Nat. Prod. Res.Dev., 2013, 25: 1325.

[5] Zhou C, Zhang S F, Wen L Y, Bai C G, Lv X W, Wang Kun, J. China Coal Soc., 2011, 36 (8): 1370.

[6] Flynn J H, Wall L A, Ploym. Lett., 1966, (4): 323.

[7] Achar B N N, Bridley G W, Sharp J H, Proc. Int. Llay. Conf., 1966, (1): 167.

[8] Coats A W, Redfern J P, Nature, 1964, 201: 68.

Advanced Materials Research Vols. 989-994 (2014) pp 665-670
© (2014) Trans Tech Publications, Switzerland
doi:10.4028/www.scientific.net/AMR.989-994.665

Preparation of Polyacrylic Acid/Rice Straw Composite Superabsorbent and the Loading and Release Properties for Urea

Feng Zhang[1,a], Gui Tang[1,b], Songtao Yu[2,c], Guihua Hou[1,d] and Ning Xu[1,e]

[1]Key Laboratory for Advanced Technology in Environmental Protection of Jiangsu Province, Yancheng Institute of Technology, Yancheng 224051, China

[2]Shanghai Research Institute of Chemical Industry, Shanghai 200062, China

[a]zhangfeng@ycit.cn, [b]601295580@qq.com, [c]5115804@qq.com, [d]houguihua@ycit.cn, [e]xuning196402@163.com

Keywords: Superabsorbent; Rice straw; Composite; Slow release; Urea

Abstract. A novel polyacrylic acid/rice straw (PAA/RS) composite superabsorbent was prepared. The factors that can influence the water absorption of the composite were investigated, including the concentration and neutralization degree of AA, the weight ratios of N, N'-methylenebisacrylamide (MBA) to AA and RS to AA. The results show that gel effect plays a key role in the preparation of PAA/RS composite. The addition of an appropriate amount of rice straw to the composite can significantly improve the water absorption. Under the optimized condition, the water absorption of the prepared PAA/RS composite was 285.4 g/g. The composite exhibits good loading and slow-release properties for urea and is promising in agricultural and horticultural applications.

Introduction

Superabsorbents have been widely applied in hygienic products [1], agriculture [2], horticulture [3], wastewater treatment [4] and drug-delivery systems [5] owing to their excellent water-absorbing capacity and water retention performance. Straw is a naturally biodegradable and renewable resource. The main components of straw are cellulose, hemicellulose, and lignin [6]. There are various functional groups on these components, such as hydroxyl, carboxyl, ether, and amino groups [7]. The existence of these functional groups is a good reason for straw to be employed in the preparation of composite superabsorbents.

Although much progress has been made in the preparation of straw-based composite superabsorbents, most researches are focused on wheat straw [8,9]. The researches on composite superabsorbents based on rice straw are few. Rice is one of the main staple food crops in the world and is widely grown. As by-product of rice cultivation, rice straw offers several advantages such as low cost, renewability and biodegradability. However, rice straw has not been properly used except for limited utilization as pulp, feed and other purposes. A large amount of rice straw is directly burned or discarded without any disposal. It is a huge waste of natural resource. Besides, the open field burning of rice straw causes serious environmental pollution [10]. Therefore, it is essential to explore effective ways to utilize rice straw.

In this paper, a novel polyacrylic acid/rice straw (PAA/RS) composite superabsorbent was prepared. The factors that can influence the water absorption of the composite were investigated systematically. The loading and release properties for urea of the composite superabsorbent were also studied.

Experimental

Materials. Rice straw (RS) was obtained from the suburb of Yancheng, Jiangsu Province of China. Acrylic acid (AA) was purchased from Sinopharm Chemical Reagent Co., Ltd. and distilled under reduced pressure prior to use. *N, N'*-Methylenebisacrylamide (MBA), sodium hydroxide (NaOH), urea, potassium persulfate (KPS), *p*-dimethylaminobenzaldehyde were purchased from

Sinopharm Chemical Reagent Co., Ltd. and used as received. Deionized water was used in all experiments.

Preparation of PAA/RS composite superabsorbent. Rice straw was cut short, milled in an electromagnetic mill and sifted through a 100-mesh sieve. A series of composite superabsorbents were prepared. In a typical process, 0.83 g of rice straw powder and 25 mg of MBA were added into a 100 mL three-necked flask equipped with a nitrogen inlet, a stirrer and a condenser. Then, 24.3 mL of NaOH solution (2 mol/L) and 3.7 mL of water were added. Subsequently, 5.0 g of AA was added. The mixture was stirred at 300 rpm and purged with nitrogen for 30 min. After the mixture was heated to 70 ^{o}C, 0.10 g of KPS dissolved in 2 mL of water was injected to initiate the polymerization. The reaction was performed for 4 h. The obtained wet gel was dried at 70 ^{o}C to a constant weight.

Characterization. The morphology of the prepared PAA/RS composite was observed on a Quanta 200 scanning electron microscope. A Lambda 35 UV-Vis spectrophotometer was used to determine the absorbance and trace the concentration change of urea in water during the release process.

Measurement of Equilibrium Water Absorption. A weighed quantity of superabsorbent was soaked in excessive water at room temperature for 12 h to reach swelling equilibrium. The swollen sample was separated by filtration through a 100-mesh sieve and weighed. The equilibrium water absorption (WA) was calculated by Equation 1:

$$WA = \frac{m_2 - m_1}{m_1} \tag{1}$$

where m_1 and m_2 are the weights of the dry sample and the swollen sample, respectively. The WA value was calculated as grams of water per gram of dry sample.

Loading of Urea. Pre-weighed dry PAA/RS composite samples were immersed in excessive aqueous solutions of urea with different concentrations for 12 h to reach swelling equilibrium. The swollen gels were filtered and weighed. The equilibrium swelling degree was calculated according to Equation 1. Then, the swollen gels were vacuum dried at 40 ^{o}C. The loading percentages of urea were calculated by Equation 2:

$$loading(\%) = \frac{M_1 - M_0}{M_1} \times 100 \tag{2}$$

where M_1 and M_0 are the weights of the loaded and unloaded dry samples, respectively.

Release of Urea from PAA/RS Composite in Water. About 1.5 g of swollen PAA/RS composite gel loaded with aqueous solution of urea or 50 mg of dried PAA/RS composite loaded with urea was placed in a beaker containing 100 mL of water with slight stirring. At various time intervals, 2 mL of solution was drawn out from the medium and the amount of released urea was determined by a spectrophotometric method [11]. After each sampling, 2 mL of water was added to the release medium to keep the volume constant.

Results and discussion

In order to sift out the optimum condition to prepare PAA/RS composite superabsorbent, various factors that can influence the water absorption of the composite were investigated, including the concentration of AA, the neutralization degree of AA, the weight ratios of MBA to AA and RS to AA.

PAA/RS composite superabsorbent was prepared through solution polymerization. Rice straw was uniformly dispersed in the aqueous solution of AA and crosslinking agent MBA. With the polymerization of AA and MBA, the viscosity of the reaction mixture increased gradually and gelation took place suddenly. The concentration and neutralization degree of AA are important for the preparation of PAA/RS composite. As the amount of AA was 3.0 g and the neutralization degree was 0 (the total amount of water was 30.0 mL and the ratio of MBA to AA was 0.5 wt%), PAA/RS composite gel could be obtained. If the neutralization degree of AA was increased to 30 mol%, gelation did not happen and viscous flowable product was generated. When the amount of AA was

increased to 3.75 g, gel could be produced if the neutralization degree of AA was not more than 50 mol%. However, when the neutralization degree of AA was increased to 70 mol%, gel could not be obtained. If the amount of AA was 5.0 g, gel could be produced even if the neutralization degree of AA was up to 70 mol%. The experimental phenomena indicate that gel effect plays a key role in the preparation of PAA/RS composite superabsorbent. It is well known that the polymerization rate is proportional to the concentration of monomer. As the concentration of AA was low, the initial polymerization rate was slow. In addition, partial neutralization of AA could also slow down the reaction rate. The low viscosity of the reaction medium could not cause gel effect and accelerate the polymerization reaction. Meanwhile, most crosslinking agent MBA was consumed through homopolymerization or copolymerization with AA in the earlier stage of the reaction. Owing to the lack of crosslinking agent in the later stage of the reaction, gel could not be generated.

Table 1 Effects of preparation factors on water absorption of PAA/RS composite (the amount of AA and water was 5.0 g and 30.0 mL, respectively; the ratio of KPS to AA was 2 wt%)

Sample	Neutralization degree of AA (mol%)	Weight ratio of MBA to AA (wt%)	Weight ratio of RS to AA	Water absorption (g/g)
1-1	0	0.5	1:6	12.0
1-2	30	0.5	1:6	195.5
1-3	50	0.5	1:6	205.7
1-4	70	0.5	1:6	123.3
1-5	100	0.5	1:6	---
2-1	70	0.05	1:6	---
2-2	70	0.1	1:6	115.3
2-3	70	0.25	1:6	179.1
2-4	70	0.5	1:6	123.3
2-5	70	1	1:6	105.5
2-6	70	2	1:6	71.4
3-1	70	0.5	0	81.1
3-2	70	0.5	1:10	104.9
3-3	70	0.5	1:6	123.3
3-4	70	0.5	1:3	117.1
3-5	70	0.5	1:2	109.4

The effects of the neutralization degree of AA, the weight ratios of MBA to AA and rice straw to AA on the water absorption of the PAA/RS composite are shown in Table 1. It can be observed that the neutralization degree of AA and the weight ratio of MBA to AA greatly influence the water absorption of the PAA/RS composite. As the neutralization degree of AA was 0, the water absorption of the prepared PAA/RS composite was only 12.0 g/g. With the increase of the neutralization degree of AA, the water absorption increased and reached the maximum when the neutralization degree was 50 mol%. Then, the water absorption decreased with the further increase of the neutralization degree of AA. As the neutralization degree of AA was 100 mol%, gel was not formed. The water absorption of the PAA/RS composite increased with the decrease of the ratio of MBA to AA until to 0.25 wt% and then showed a downward trend. When the ratio of MBA to AA was decreased to 0.05 wt%, gel could not be generated due to the excessively low crosslinking degree. The effects of the neutralization degree of AA and the weight ratio of MBA to AA on the water absorption of the PAA/RS composite can be explained by the Flory's swelling theory. The relationship between swelling ratio and network structure parameters given by Flory is expressed as Equation 3 [12]:

$$q_m^{5/3} \cong \frac{\left(\frac{i}{2v_u S^{1/2}}\right)^2 + \left(\frac{1}{2} - \chi_1\right) \Big/ v_1}{v_e / V_0} \tag{3}$$

where q_m is the swelling ratio; i/v_u is the concentration of the fixed charges of the network; S is the ionic strength of the solution; $(1/2-\chi_1)/v_1$ is the network-medium affinity; v_e/V_0 is the crosslinking density.

According to Equation 3, with the increase of the neutralization degree of AA, the concentration of the fixed charges of the network increases, resulting in the increase of the water absorption of the PAA/RS composite. However, as the neutralization degree of AA is too high, the excessive Na^+ ions will reduce the electrostatic repulsion by screening the negative charges of $–COO^-$ groups, thus resulting in the decrease of water absorption. Similarly, in accordance with Equation 3, the water absorption increases with the decrease of the ratio of MBA to AA. However, excessively low concentration of crosslinking agent leads to weak strength of gel and even it is hard for network structure to be formed, resulting in low water absorption.

From Table 1, another interesting result can be obtained that the addition of an appropriate amount of rice straw can significantly improve the water absorption of the composite. However, the water absorption of rice straw is very low (about 2.0 g/g). The water absorption of the superabsorbent prepared without rice straw was 81.1 g/g. The addition of rice straw increased the water absorption. When the weight ratio of RS to AA increased from 1:10 to 1:2, the water absorption increased to 123.3 g/g and then decreased. The optimum weight ratio of RS to AA was 1:6. Even if the weight ratio of RS to AA was 1:2, the water absorption of the PAA/RS composite was still higher than the superabsorbent prepared without rice straw. It is meaningful for the reduction of production costs of superabsorbent. The reason that the introduction of rice straw improves the water absorption of the PAA/RS composite may be that rice straw contains a lot of functional groups and can chemically bond with and improve the polymer network during the polymerization process [6]. However, with the increase of the content of rice straw, the hydrphilic polymer content in the composite decreases, which goes against water absorption. Therefore, as the weight ratio of RS to AA is higher than the optimum one, the water absorption of the composite decreases.

Based on the above discussion, the optimum conditions to prepare the PAA/RS composite superabsorbent are as follows: the neutralization degree of AA, 50 mol%; the weight ratio of MBA to AA, 0.25 wt%; and the weight ratio of RS to AA, 1:6. Under the optimized condition, the PAA/RS composite superabsorbent was prepared and the water absorption was determined to be 285.4 g/g. Figure 1 shows the SEM image of the PAA/RS composite superabsorbent prepared under the optimized condition. It can be observed that rice straw is uniformly embedded in the polymer substrate, exhibiting good compatibility between rice straw and polymer substrate.

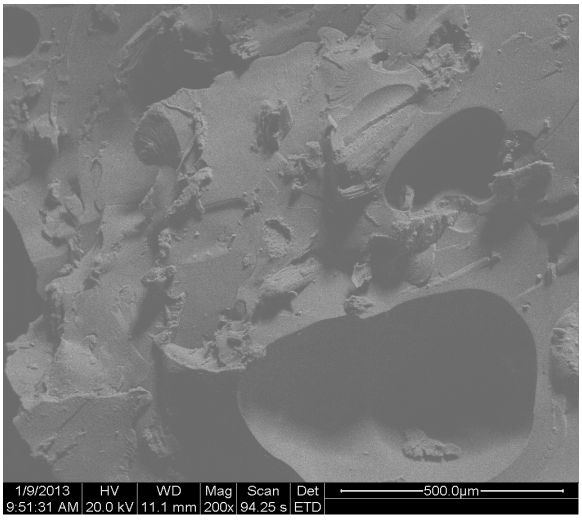

Fig. 1 SEM image of the PAA/RS composite superabsorbent prepared under the optimized condition

The applications of superabsorbents in agriculture and horticulture have shown encouraging results, which can help reduce irrigation water consumption, lower the death rate of plants, and improve fertilizer retention [13,14]. The combination of superabsorbent and fertilizer can improve nutrition of plants and mitigate the environmental impact from water-soluble fertilizer. The loading and release properties for urea of the prepared PAA/RS composite superabsorbent were investigated. Figure 2 shows the swelling degree of the PAA/RS composite superabsorbent (prepared under the optimized condition) and the loading percentages of urea under different concentrations of urea. It can be observed that the concentration of urea has no obvious influence on the swelling degree of the PAA/RS composite. The reason is that urea is not ionized in water and does not influence the ionic strength of the solution. Even if the concentration of urea was 50 g/L, the swelling degree was still up to 258.2 g/g. From Figure 2, it can also be observed that the loading percentage of urea increases with the increase of the concentration of urea. As the concentration of urea increased from 0.5 g/L to 50 g/L, the loading percentage of urea increased from 12.4% to 92.5%. Besides, the loading percentages of urea obtained from experiment are nearly equal to those calculated from the corresponding swelling degree and the concentration of urea, indicating that urea in the solution is not specially absorbed by the PAA/RS composite superabsorbent.

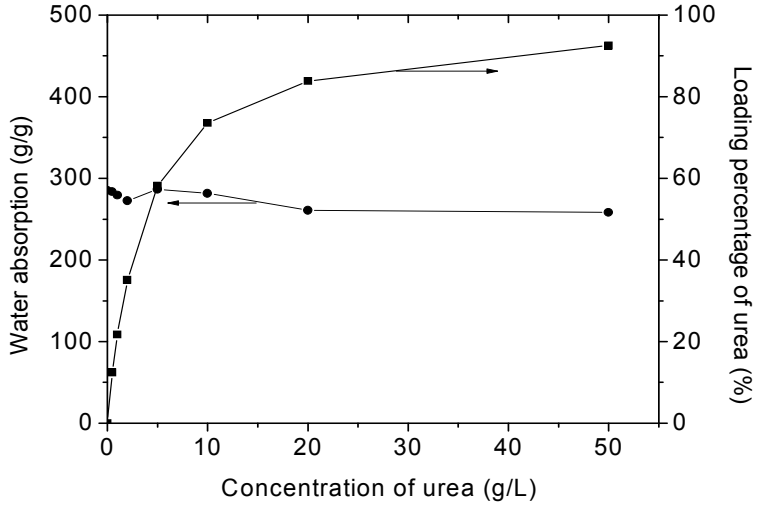

Fig. 2 Swelling degree of the PAA/RS composite superabsorbent (prepared under the optimized condition) and loading percentages of urea under different concentrations of urea.

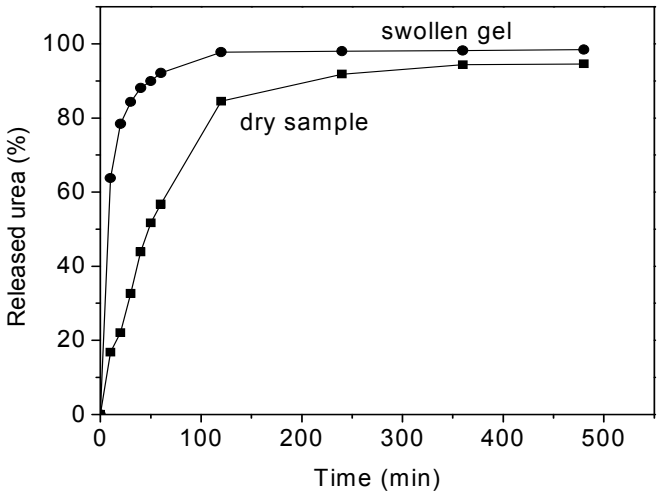

Fig. 3 Release of urea from swollen gel (swollen in the solution with the urea concentration of 20 g/L) and dry sample (with the urea loading of 58.2%) in water.

Figure 3 shows the release behavior of urea from the swollen gel (swollen in the solution with the urea concentration of 20 g/L) and the dry sample (with the urea loading of 58.2%) in water. It is well known that urea is easily dissolved in water. Once urea is added into water, it will be quickly

dissolved. Compared with the untreated urea, the release rate of the urea loaded in the PAA/RS composite decreases greatly. For the swollen gel, it needed about 50 min to release 90% urea contained in it. In the case of the dry sample, to release 90% urea, it needed more than 2 hours. It indicates that the release of urea into water from the PAA/RS composite is physically retarded by the crosslinked network. The results imply that the PAA/RS composite superabsorbent has a good slow-release property for urea.

Summary

In conclusion, a novel PAA/RS composite superabsorbent was prepared. The optimized conditions to prepare the composite superabsorbent are as follows: the neutralization degree of AA, 50 mol%; the ratio of MBA to AA, 0.25 wt%; and the weight ratio of RS to AA, 1:6. The method provides an effective route to utilize rice straw, which is meaningful for the environmental protection and the reduction of product costs of superabsorbent. The loading and release properties for urea show that the prepared PAA/RS composite superabsorbent is promising in agricultural and horticultural applications.

Acknowledgments

This work was supported by the National Key Technology R&D Program of China (No. 2013BAC13B01); National Nature Science Foundation of China (No. 11204266, 21276220); Nature Science Foundation of Jiangsu Province (No. BK2012676); Practice Inovation Training Program for Jiangsu College Students.

References

[1] H.A. Abd El-Rehim: Radiat. Phys. Chem. Vol. 74 (2005), p. 111.

[2] L.H. Xie, S.Y. Lv, M.Z. Liu, C.M. Gao, X.G. Wang and L. Wu: J. Agri. Food Chem. Vol. 61 (2013), p. 3382.

[3] B.L. Ni, M.Z. Liu and S.Y. Lv: Chem. Eng. J. Vol. 155 (2009), p. 892.

[4] Y.J. Tang, X. Wang and L.H. Zhu: Polym. Bull. Vol. 70 (2013), p. 905.

[5] M. Sadeghi and H.J. Hosseinzadeh: J. Bioact. Compat. Pol. Vol. 23 (2008), p. 381.

[6] L.H. Xie, M.Z. Liu, B.L. Ni and Y.F. Wang: Ind. Eng. Chem. Res. Vol. 51 (2012), p. 3855.

[7] S. Ibrahim, W.Z. Shuy, H.M. Ang and S.B. Wang: Asia-Pac. J. Chem. Eng. Vol. 5 (2010), p. 563.

[8] J. Liu, Y. Su, Q. Li, Q.Y. Yue and B.Y. Gao: Bioresour. Technol. Vol. 143 (2013), p. 32.

[9] Q. Li, Z.H. Ma, Q.Y. Yue, B.Y. Gao, W.H. Li and X. Xu: Bioresour. Technol. Vol. 118 (2012), p. 204.

[10] B. Gadde, S. Bonnet, C. Menke and S. Garivait: Environ. Pollut.Vol. 157 (2009), p. 1554.

[11] W.W. George and D.C. Joseph: Anal. Chem. Vol. 26 (1954), p. 452.

[12] A. Pourjavadi and M.S. Amini-Fazl: Polym. Int. Vol. 56 (2007), p. 283.

[13] S.P. Jin, G.R. Yue, L. Feng, Y. Han, X.H. Yu and Z.H. Zhang: J. Agric. Food Chem. Vol. 59 (2011), p. 322.

[14] J. Abedi-Koupai, F. Sohrab and G. Swarbrick: J. Plant Nutr. Vol. 31 (2008), p. 317.

Advanced Materials Research Vols. 989-994 (2014) pp 671-675
© (2014) Trans Tech Publications, Switzerland
doi:10.4028/www.scientific.net/AMR.989-994.671

Low-temperature catalytic combustion of VOCs over MnO_x –ZnO mixed oxides supported on cordierite ceramic

Qiong Huang[1,a,*], Yingwen Chen[2,b], Shubao Shen[2,c], Mindong Chen[1,d]

[1] School of Environmental Science and Engineering, Jiangsu Key Laboratory of Atmospheric Environment Monitoring and Pollution Control, Nanjing University of Information Science & Technology, Nanjing 210044, China

[2] College of Biotechnology and Pharmaceutical Engineering, Nanjing University of Technology, Nanjing 211816, China

[a]hqhaixia@163.com,[b]yw_chen@126.com, [c]zsbshen@gmail.com, [d]chenmdnuist@163.com

Keywords: Cordierite; MnO_x–ZnO/Cord catalyst; Catalytic combustion; VOCs

Abstract. Catalytic combustion of VOCs was investigated over Mn–Zn mixed oxides supported on cordierite ceramic (Cord) and over the promoted Mn-Zn oxides with γ–Al_2O_3 coating. The properties and performance were characterized by using the XRD, SEM, BET, and TPD techniques. Mn-Zn oxides catalysts with different kinds of γ–Al_2O_3 sol coating were found to possess a high activity, and the Mn–Zn/γ–Al_2O_3/Cord (Mn/Zn=2) was identified as the most active that the temperature of complete combustion of toluene was 250°C. Effects of variation of preparation conditions, including molar ratio of Mn and Zn, loading, calcination temperature and different kinds of γ–Al_2O_3 dipping were investigated.

Introduction

Volatile organic compounds (VOCs) include a wide range of organic compounds that exit in the gaseous state in ambient air. Offensive odors and toxic air emissions as well as the formation of ground–level ozone and petrochemical are environmental problems [1]. Catalytic combustion has been regarded as one of the most promising technologies to eliminate VOCs emissions. The major advantage of catalytic combustion is that it can efficiently treat very dilute pollutants at concentrations of less than 1%, which cannot be thermally combusted without additional fuel [2-3]. Catalysts with noble metals or transition metal oxides are active for VOCs abatement [4], but the noble metal are expensive. Therefore, many different transition metal oxides are substituted to catalytic combustion of VOCs, e.g., CuO [5], Mn_2O_3 [6], and Fe_2O_3 [7]. These oxides can be deposited on supports to increase their dispersion and activity.

Therefore, the Mn-Zn mixed oxides supported on cordierite ceramics were investigated in this manuscript. The changes in the physicochemical states of the catalysts were also examined by using the XRD, SEM, and TPD. The activities of catalytic combustion of toluene were discussed, along with the effect of the type of support, Mn-Zn oxides loading amount, loading ratio and calcination temperature. Moreover, the Mn–Zn/γ–Al_2O_3/Cord catalysts with the sol-dipping method were reported in this manuscript.

Experimental

Preparation of Mn–Zn/Cord or Mn–Zn/γ–Al_2O_3/Cord catalyst

A series of Mn–Zn precursors were synthesized by the wet impregnation method. A solution was prepared and contained 5.3g $Mn(NO_3)_2$ solution (50wt%), 4.3g $Zn(NO_3)_2 \cdot 6H_2O$ and 19.7g H_2O. And then, 5.0g of cord were immersed in the solution for 6 h without stirring. After dried at 80°C for 2 h, they were calcined in air up to 450°C for 2 h with the heating rate of 5°C/min. For comparison, catalysts with the different molar ratio of Mn–Zn, the loading of metal oxides, calcination temperature and sol-dipping were prepared using a similar procedure.

Catalytic oxidation measurement

Catalytic combustion of toluene was carried out in a conventional fixed–bed reactor under atmospheric pressure. About 2.7 g of catalysts were loaded in a quartz reactor with quartz beads packed at both ends of the catalyst bed. The temperature of catalyst bed was measured with a thermocouple in the range of 150–300°C for Mn–Zn oxides catalysts, at a toluene concentration of 1000 ppm and the GHSV of 10,000 h^{-1}. The inlet and outlet gas composition were analyzed after stepwise changes in the reaction temperature by on–line gas chromatograph equipped with the FID detector [8].

Results and discussion

Fig 1 shows the XRD analysis of the Mn–Zn/Cord catalysts after calcination at 300, 450, 600, 700 and 900°C. Some significant diffraction peaks of cordierite ceramics with 2θ at 12.0°, 25.2°, 30.6°, 33.0° and 34.2° appeared, which indicated a higher stable structure of cordierite. It was also observed that below 600°C, the catalyst was amorphous or nano-crystallite due to their crystal sizes below the detection limit of the X-ray technique. When heating the sample at 600°C, the XRD pattern of the catalyst showed the characteristic peak of $ZnMn_2O_4$ at 34.2°, 38.3° and 42.9°, indicating the growth of the crystal sizes of the $ZnMn_2O_4$.

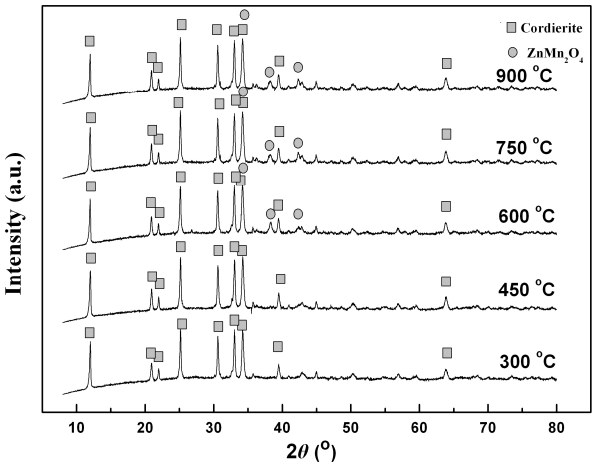

Fig. 1. XRD patterns of the Mn–Zn/Cord calcined.

The morphological properties of the catalysts are investigated by SEM as shown in Fig 2. From the SEM images in Figure 2(a), it could be seen that the cordierite featured a smooth surface without any spherical particle. However, the catalyst with 10 wt% loading of Mn–Zn oxides showed the morphological structures like the spherical particles with a diameter around 0.3μm, and most of the particles appeared as uniform particle size on the surface of cordierite. The results also implied that the highly dispersed particles of Mn-Zn oxides supported on cordierite were responsible for the high activity of the combustion reaction [9]. The morphological structures of Mn–Zn/γ–Al_2O_3/Cord samples with different kinds of γ–Al_2O_3 sol coating (A, B, C and D) are shown in Fig 3. As can be seen in Figure 3(a), a compact film of γ–Al_2O_3 could be found on the surface of cordierite, but some parts were not. It was attributed to the incomplete γ–Al_2O_3 coating or abscission from the surface of cordierite. Figure 3(b) shows a uniform and well-proportioned morphological structure, composed of a number of spherical particles with a large degree of porosity. The size of these particles was about 0.3 μm and it was the same as Mn-Zn/Cord catalyst. The uniform mixture of Mn-Zn oxides and higher surface area could be the reason responsible for a higher activity of toluene combustion on the samples prepared by sol-dipping method. The difference of these Figure c and Figure d was that the agglomeration was caused easily in the process of preparation, and hence affected the redox properties.

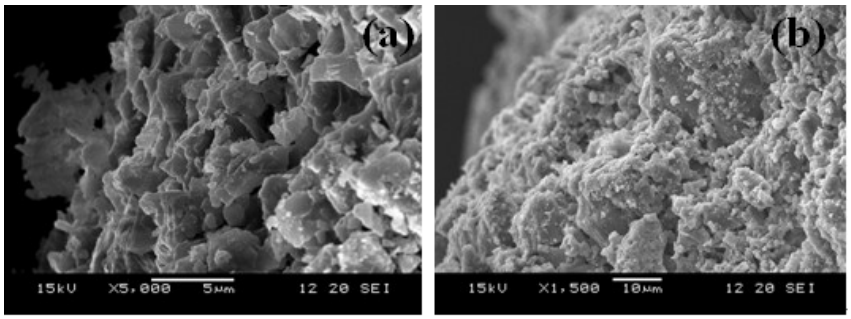

Fig. 2. SEM images of cordierite ceramics (a) and Mn–Zn/Cord (b).

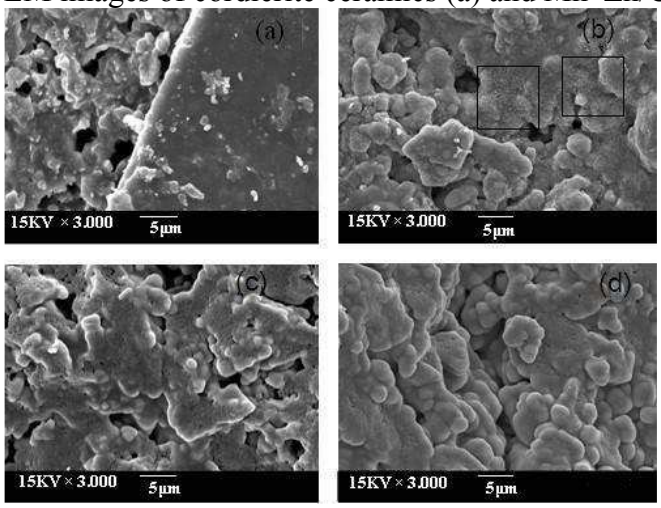

Fig. 3. SEM images of Mn–Zn/γ–Al_2O_3/Cord with different γ–Al_2O_3 sol.

NH_3–TPD profiles of the Mn–Zn/γ–Al_2O_3/Cord catalysts are presented in Fig 4 and two peaks can be identified at low and high temperatures. The adsorption peaks were locked at around at 250°C and 500°C. They affirmed as weak and strong acidity sites. The low temperature peak could be attributed to ammonia weakly held or physically adsorbed on the catalysts, whereas the high temperature peak could be assigned to the chemisorbed ammonia. Hence, the γ–Al_2O_3 dipping decreases the amount of weak acidity and increases the strong acidity for these catalysts.

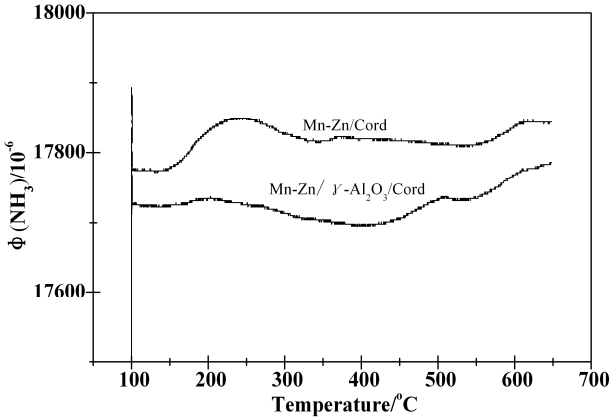

Fig. 4. NH_3–TPD profiles of the Mn–Zn/Cord or Mn–Zn/γ–Al_2O_3/Cord

The conversion curves of toluene over Mn-Zn/Cord catalysts with different molar ratio of metal oxides, loading ratios, calcination temperatures and different kinds of γ–Al_2O_3 dipping versus reaction temperatures are shown in Fig 5. The Mn-Zn mixed oxides supported on cordierite could show a good activity. In a blank experiment, the cordierite ceramics showed only 20% toluene conversion at 300°C. Among these mixed metal oxides, the catalyst with the Mn-Zn molar ratio of 2, which showed 8.0 m^2/g surface areas, was found to have the highest activity for toluene conversion. The conversion of the toluene oxidation reached 90% at about 300°C. Moreover, it could be found that MnO_x was confirmed to have a higher activity than ZnO and the conversion of MnOx/Cord and ZnO/Cord are 82% and 65% at 300°C, respectively. The samples with a kind of Mn-Zn molar ratio were attributed to a well interaction of removing lattice of oxygen [7].

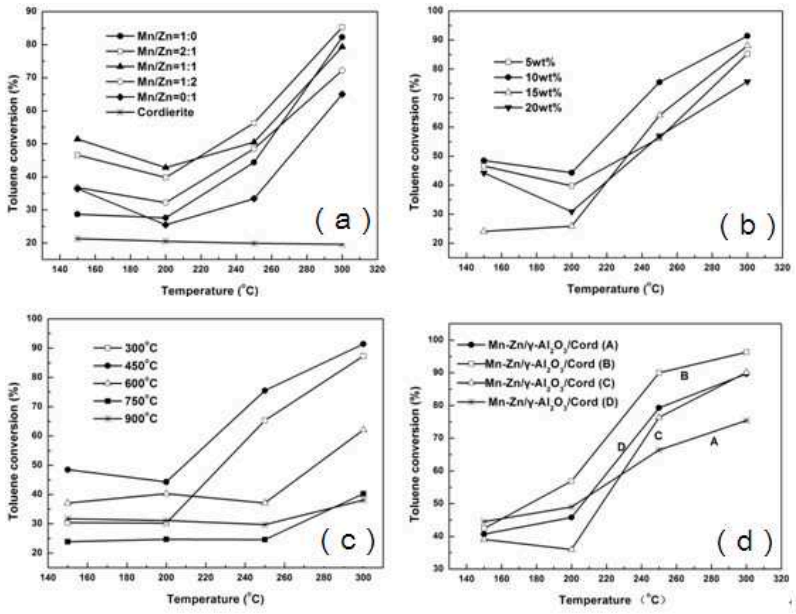

Fig. 5 Toluene conversion vs. reaction temperature over different molar ratios, loading ratio, calcination temperatures and sol-dipping.

To make further investigation, a series of cordierite supported Mn–Zn oxides catalysts are prepared with different Mn-Zn oxides loading. The activities are shown in Fig 5(a) as a function of the reaction temperature. When the Mn–Zn loading was 10 wt%, the total conversion temperature was lowered to 300°C. It exhibited the higher activity due to a higher dispersed of Mn-Zn oxides. The activities of the Mn–Zn/Cord catalysts calcined at different temperatures are investigated in Fig 5(c). Among all of these samples, the activity of Mn–Zn/Cord catalyst with 450°C of calcination temperature showed the highest activity for catalytic combustion of toluene. Meanwhile, due to the formation of $ZnMn_2O_4$ at 600 °C, the activity decreased gradually with increasing calcination temperature, not like $CoFe_2O_4$ [10].

It was well documented that the activities of these samples with γ–Al_2O_3 coating could be affected greatly through the surface area, acidity properties and distribution of active components [11-12]. The activities of Mn-Zn/γ–Al_2O_3/Cord with different kinds of γ–Al_2O_3 sol are shown in Fig 5(d). Among of these Mn-Zn/γ–Al_2O_3/Cord, the catalyst of Mn-Zn/γ–Al_2O_3(B)/Cord exhibited the best activity and the conversion of the toluene oxidation reached 90% at 250°C. The result also showed that the higher distribution of the activity species showed higher the catalytic activity. Meanwhile, a decrease in the amount of weak acid sites would result in enhanced catalytic activity [13], because it was disadvantageous for increasing the amount of toluene chemisorbed.

Conclusion

The catalytic combustion of toluene over Mn-Zn oxides supported on cordierite or γ–Al_2O_3/Cord was examined. The results indicated that $ZnMn_2O_4$ formed by calcination at the temperature higher than 600ºC was a not suitable phase for catalytic oxidation. The uniform mixture of Mn-Zn oxides and higher surface areas can be the reason responsible for a higher activity of toluene combustion on the samples prepared by sol-dipping method. Due to the active sites and surface property, the catalysts with the weak acidity and γ–Al_2O_3 dipping showed higher activity.

Acknowledgements

This work is financially supported by the Natural Science Foundation of China (51172107). We also thank the Project Funded by the Priority Academic Programme Development of Jiangsu Higher Education Institutions (PAPD).

References

[1] T. Garcia, B. Solsona, D. Cazorla–Amoros et al: Appl Catal B: Environ Vol 62 (2006), p. 66

[2] A. Kadkhodayan, A. Brenner: J. Catal Vol 117 (1989), p.311

[3] S. Scire, S. Minic, C. Crisafulli, et al: Appl. Catal. B: Environ Vol 40 (2003), p.43

[4] S. Lambert, C. Cellier, E.M. Gaigneaux, et al: Catal. Commun Vol 8 (2007), p.1244

[5] J.S. Yang, W.Y. Jung, G.D. Lee, et al: J. Ind. Eng. Chem Vol 14 (2008), p.779

[6] L.M. Gandía, A. Gil, S.A. Korili: Appl. Catal. B: Environ Vol 33 (2001), p.1

[7] F.G. Duran, B.P. Barbero, L.E. Cadus, et al: Appl. Catal. B: Environ Vol 92 (2009), p.194

[8] M. Chen, X.M. Zheng:J. Mol. Catal A: Chem Vol 221 (2004), p.77

[9] W.B. Li, W.B. Chu, M. Zhuang, et al: Catal. Today Vol 93 (2004), p.205

[10] J.H. Tong, L.L. Bo, Z. Li, et al: J Mol CatalA: Chem Vol 307 (2009), p.58

[11] S.C. Kim. W.G. Shim: Appl Catal B: Environ Vol 92 (2009), p. 429

[12] Z.M. Liu, J.L. Wang, J.B. Zhong, et al: J. Hazard. Mater Vol 149 (2007), p.742

[13] B. Rivas, J.I. Gutierrez–Ortiz, et al: Appl. Catal. A: Gen Vol 314 (2006), p.54

Advanced Materials Research Vols. 989-994 (2014) pp 676-679
© (2014) Trans Tech Publications, Switzerland
doi:10.4028/www.scientific.net/AMR.989-994.676

Lonic Liquid [Bmim]OH Grafted Catalyst for Cycloaddition of Carbon Dioxide

Xuelan Zhang[1, a], Dengfeng Wang[1,b]

[1]College of Chemistry, Chemical Engineering and Materials Science, Zaozhuang University, Zaozhuang, 277160, P.R. China

[a]mhszxl@163.com, [b]bitwdf@163.com

Keywords: Graft, Ionic Liquid, Cycloaddition, Carbon dioxide.

Abstract. An ionic liquid 1-butyl-3-methylimidazolium hydroxide ([Bmim]OH) was grafted on silica gel by post-grafting method. Such grafted ionic liquids (GILs) which were verified by means of FTIR, element analysis N_2 adsorption-desorption and TG could be used as highly effective heterogeneous catalysts toward propylene carbonate synthesis through cycloaddition of carbon dioxide with propylene oxide under solventless and mild conditions.

Introduction

In recent times room temperature ionic liquids have attracted increasing interest in the area of green chemistry [1]. Although ionic liquid was initially introduced as an alternative green reaction medium [2], today it has marched far beyond showing its significant role in controlling the reaction as catalyst [3]. So far, a variety of RTILs have been successfully applied in many important chemical reactions such as Friedel-Crafts acylation, Michael addition, and conjugate addition [4]. The cycloaddition of CO_2 has been reported over "green" ionic liquids such as 1-butyl-3-imidazolium tetrafluoroborate [5], 1-octyl-3-methylimidazolium tetrafluoroborate [6] and pyridinium or ammonium salt [7, 8]. High catalytic performance was achieved over these catalysts. Unfortunately, the reaction was carried out in homogeneous catalytic systems with the drawbacks of poor catalyst recovery and product separation. Hence, there was a crucial need to exploit more highly efficient heterogeneous catalysts.

Grafted ionic liquids (GILs), which were prepared by fixing ionic liquids onto solid supports, kept important physical and chemical features of ionic liquids. Therefore, they were considered as promising catalysts in many catalytic reactions. For the cycloaddition of CO_2, some GILs exhibited high catalytic performance [9]. However, there are few reports focusing on non-metal GILs and their application. Moreover, since non-metal basic ionic liquid 1-butyl-3-methylimidazolium hydroxide ([bmim]OH) was regarded as an effective catalyst in Michael addition, Markovnikov addition, aldol condensation and three-component condensation with advantages of good nucleophilicity and stability, it had aroused great academic interest [10-14]. Thus, in the present work, grafted ionic liquids were prepared from non-metal ionic liquid [bmim]OH and used as catalysts for the cycloaddition of PO with CO_2.

Experimental

Catalysts preparation. Chromatography silica gel was purchased from Qingdao Haiyang Chemical Co. Ltd. Other solvents and reagents were commercial analytic reagents without further purification. The ionic liquid hydroxide [Bmim]OH was synthesized from 1-butyl-3-methylimidazolium chloride ([Bmim]Cl) [2, 15, 16]. The ionic liquid [Bmim]BF_4 was synthesized from [Bmim]Cl [17]. Grafted ionic liquids (GILs) were prepared using the method proposed by the literature [18]. The method of [Bmim]BF_4/SiO_2 synthesis was similar to that of [Bmim]OH/SiO_2.

Catalyst characterization. Elemental analysis was performed by using a Vario EL analyzer. The Fourier transform infrared (FTIR) spectroscopy results of the samples were recorded using

self-supported wafers on a NICOLET NEXUS 470FT-IR spectrophotometer with 4cm^{-1} resolution. Nitrogen adsorption/desorption isotherms were obtained at liquid nitrogen temperature on a Micromeritics ASAP-2000 instrument (Norcross, GA), using static adsorption procedures. Surface area (S_{BET}) was measured using the BET method. Thermogravimetric analysis (TGA) was carried out on a Setaram TGA-92 thermal analyzer apparatus connected to a PC via a TAC7/DX thermal controller. The samples were heated from 303 K to 1073 K at 10 K/min in nitrogen environment.

Catalytic test. The cycloaddition of CO_2 with epoxide was carried out in an 80 mL stainless steel autoclave equipped with a magnetic stirrer. In a typical reaction process, the PO and catalyst were poured into the reactor. Then CO_2 was added to the mixture of PO and the catalyst ([Bmim]OH/SiO_2) in an autoclave. Then, the reactor was heated to 393 K and kept for 4 h. After the reaction, the autoclave was cooled to room temperature and the excess of carbon dioxide was vented slowly. The liquid product was separated by centrifugation from the reaction mixture and was analyzed using a GC–950 gas chromatograph with a thermal conductivity detector and a packed column (GDX-203).

Results and discussion

Structural characterization. FTIR spectra of hydroxyl ionic liquid [Bmim]OH/SiO_2 was showed in Fig.1. The absorbance in the region 3000~2700 cm^{-1} was due to aliphatic C-H stretching vibration [19, 20, 21], and the bands of imidazolium ring symmetrical stretching vibration could be found at 1570 cm^{-1}. Besides, the absorbance at 1398 and 1468cm^{-1} could be assigned to methylic C-H bending vibration [20, 21]. All these results suggested the existence of ILs on the surface of silica gel.

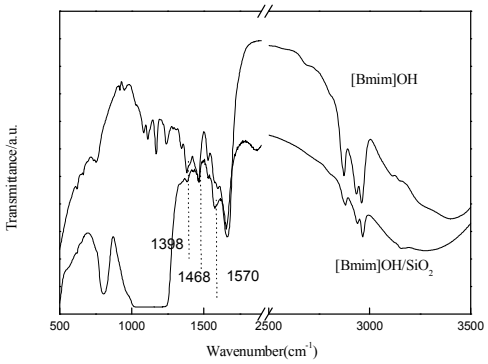

Fig.1 FTIR spectra of the sample.

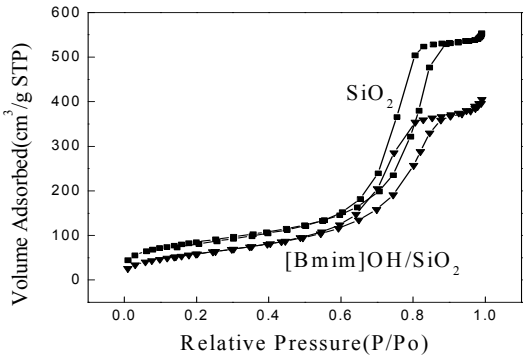

Fig. 2 Nitrogen adsorption-desorption isotherms of sample

The content of element nitrogen, carbon, and hydrogen in samples was listed in Table 1. Obviously, no N and C element was found in the silica gel, and then the two elements in grafted samples only came from ionic liquids, the weight percent of [Bmim]OH could be obtained according to that of N. Thus, C/N molar ratios could be regarded as a standard whether the homogeneous complex was successfully grafted on the support [22]. In theory, when the C/N molar ratios of GILs [Bmim]OH/SiO_2 reached 3, equimolar ionic liquids interacted with silanol group of silica gel. Thus, the FTIR spectra and elemental analysis results undoubtedly indicated that the active component [Bmim]OH was successfully grafted on the support of silica gel.

Table 1 Results of element analysis

Sample	Element analysis (wt %)			n_C:n_N	Norg (mmol·g^{-1})
	N	C	H		
Silica gel	-	-	0.73		
[Bmim]OH/SiO_2	1.96	5.83	1.14	2.97	1.4

N_2 adsorption/desorption isotherms of samples displayed type IV isotherms with clear hysteresis loops associated with capillary condensation (Fig 2). This indicated that the materials remained mesoporous before and after the graft, but the BET surface area and pore volume decreased due to the presence of grafted groups (Table 2).

Table 2 Texture of the samples

Sample	BET surface area/($m^2 \cdot g^{-1}$)	Pore volume/($cm^3 \cdot g^{-1}$)	Pore diameter/(nm)
silica gel	310.88	0.86	11.38
[Bmim]BF_4/SiO_2	254.46	0.81	11.31
[Bmim]OH/SiO_2	240.82	0.67	10.70

In order to investigate the thermal stability of the grafted basic ionic liquids, typical TG-DTA curve was illustrated in Fig 3. The first was associated with the elimination of outer layer water; the second was due to the decomposition of [Bmim]OH /SiO_2; and the last one could be assigned to condensation of silanol group. The samples showed thermal stability under 543 K.

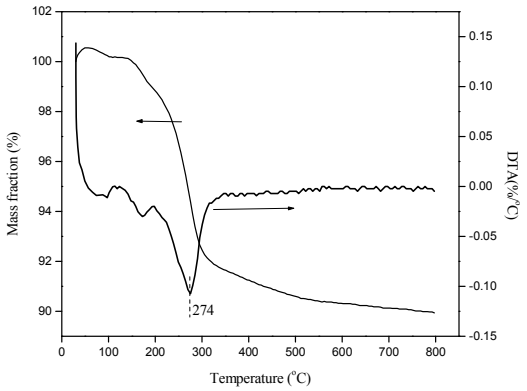

Fig. 3 TG-DTA curve of [Bmim]OH/SiO_2 in N_2 atmosphere

Catalytic performance. D The cycloaddition reaction of carbon dioxide with propylene oxide was carried out without any solvents. The typical results of the different catalysts were listed in Table 3. Pure silica gel was inactive (entry 1) and all other catalysts presented 100% selectivity towards PC. It was found that [Bmim]OH displayed high activity for PC synthesis (entry 3). Notably, [Bmim]OH /SiO_2 showed the same high catalytic activity as [Bmim]OH (entries 4). More important, [Bmim][OH]/SiO_2 exhibited better performance than [Bmim]BF_4/SiO_2 in the present work (entry 6). It was consider that the role of OH^- might be as that of fluorine anions reported elsewhere, in which, the latter could activate PO via nucleophilic attack its β-carbon atom [7, 9]. And the OH^- might have a stronger nucleophilicity compared to fluorine anions.

Table 3 Activity of different catalysts in cycloaddition of carbon dioxide[a]

Catalysts	Conversion of propylene oxide (%)
Silica gel	—
[Bmim]Cl	98.8
[Bmim]OH	100
[Bmim]OH/SiO_2	99.1
[Bmim]BF_4	94.9
[Bmim]BF_4/SiO_2	93.2
[Bmim]OH/SiO_2[b]	89.0

[a] Reaction conditions: catalyst 0.00126mol, PO 0.07mol, $p(CO_2)$ 2MPa, 10h，120°C; [b] After using four times.

Furthermore, [Bmim]OH /SiO_2 could be used four times with little loss of activity (entry 7). FTIR spectra of [Bmim]OH /SiO_2 after using four times was similar to that of fresh. Thus, it could be included that this catalyst did not change after it was used five times and the catalytic reaction was heterogeneous. Under the optimal conditions, the PO conversion could reach 99%.

Conclusions

The grafted ionic liquids [Bmim]OH/SiO_2 were synthesized by the covalent bond of [Bmim]OH with silica gel. Such grafted ionic liquids possessed good thermal stability and mesoporous structure. In addition, the GILs exhibited high catalytic performance for cycladdition of CO_2 under mild conditions without any additional solvent.

Acknowledgements

This work was financially supported by the Shandong Province Natural Science Foundation (ZR2012BL07), Zaozhuang science and technology development plan project (201342) and the Ph.D. Scientific Research Fund Program of Zaozhuang University(307070808).

References

[1] A. Kumar and S. S. Pawar: J. Org. Chem Vol. 69 (2004), p. 1419

[2] J. Q. Wang, X. D. Yue, F. Cai and L. N. He: Catal. Commun Vol. 8 (2007), p. 167

[3] B. C. Ranu and R. Jana: J. Org. Chem. Vol. 70 (2005), p. 8621

[4] H. Sun, D. G, Zhang, F. Wang, C. B. Liu: J. Phys. Chem. A Vol. 111 (2007), p. 4535

[5] J. J. Peng and Y. Q. Deng: New J. Chem. Vol. 25 (2001), p. 639

[6] H. Kawanami, A. Sasaki, K. Matsui and Y. Ikushima: Chem. Commun. (2003), p. 896

[7] Y. J. Kim and R. S. Varma: J. Org. Chem. Vol. 70 (2005), p. 7882

[8] J. M Sun, S. I. Fujita and M. Arai: J. Organomet. Chem Vol. 690 (2005), p. 3490

[9] L.F. Xiao, F. W. Li, J. J.. Peng and C. G..Xia: J. Mol. Catal. A: Chem. Vol. 253 (2006), p. 265

[10] C. R. Brindaban and B. Subhash: Org. Lett. Vol. 7 (2005), p. 3049

[11] J. M. Xu, B. K. Liu, W. B. Wu, C. Qian, Q. Wu and X. F. Lin: J. Org. Chem. Vol. 71 (2006), p. 3991

[12] H. Sun, D. J. Zhang, F. Wang and C. B. Liu: J. Phys. Chem. A Vol. 111 (2007), p. 4535

[13] S. Abelló, F. Medina, X. Rodríguez, Y. Cesteros, P. Salagre, J. E. Sueiras, D. Tichit and B. Coq: Chem. Commun. (2004), p. 1096

[14] B. C. Ranu, R. Jana and S. Sowmiah: J. Org. Chem. Vol. 72 (2007), p. 3152

[15] C. P. Mehnert, N. C. Dispenziere and R. A. Cook: Chem. Commun. (2002), p. 1610

[16] J. J. Yin, Y. H. Huang, J. J. Peng, P. Q. Zhao, C. G. Xia: J. Lanzhou University Technolog Vol. 32 (2006), p. 72

[17] J. G. Huddleston, A. E. Visser, W. M. Reichert, H. D. Willauer, G. A. Broker and R. D. Rogers: Green Chem. Vol. 3 (2001), p. 156

[18] M. H. Valkenberg, C. deCastro and W. F. Hölderich: Green Chemistry Vol. 4 (2002), p. 88

[19] S. R. Rubero and S. Baldelli: J. Phys. Chem. B Vol. 110 (2006), p. 4756

[20] P. Naumov, G. Jovanovski and A. Todorovska: Spectrochimica. Acta. A Vol. 58 (2002), p. 1903

[21] S. Tait and R. A. Osteryoung: Inorg. Chem. Vol. 23 (1984), p. 4352

[22] D. Brunel: Micropor. Mesopor. Mat. Vol. 27 (1999), p. 329

Advanced Materials Research Vols. 989-994 (2014) pp 680-683
© (2014) Trans Tech Publications, Switzerland
doi:10.4028/www.scientific.net/AMR.989-994.680

The Molecular Orientation in Monomolecular Layer of Phthalocyanine and Porphyrin Derivatives

Chun-Peng Zhang[1], Hui-Miao Guo[1], Hai-Ning Cui[1,a,*], Hai-Shui Wang[2], Shi-Quan Xi [3]

[1]Department of Optical Information Science and Technology, College of Physics and College of Zhaoqing (526061) , Jilin University, Changchun(130012), P. R. China

[2]School of Chemistry and Chemical Engineering, South China University of Technology(510641), Guangzhou, P. R. China

[3]Changchun Institute of Applied Chemistry, Chinese Academy of Sciences, Changchun (130022) P. R. China

[a]cuihaining2009@126.com

Keywords: Copper phthalocyanine film, porphyrin film, monomolecular layer, structural characterization.

Abstract. Systematic research on monomolecular layer of copper (Ⅱ) phthalocyanine (CuPc) and porphyrin derivatives bas been done. In this paper an attention is focused upon the molecular orientation in monomolecular layer of some symmetrically substituted porphyrin and asymmetrically substituted CuPc derivatives by means of the surface pressure-area (π-A) isotherm method, polarized UV-visible spectra.

Introduction

Phthalocyanine (Pc) and Porphyrin (Por) derivatives, as highly conjugated and symmetric disk-shaped molecules, exhibit a wide variety of physical, chemical and electrical properties. The monolayer and nanometer assembly films of these macrocycle derivatives by means of Langmuir-Blogdett (LB) technique allow functional molecules to be arranged in a highly ordered structure and offer the possibility of application in many aspects[1-3]. In this paper，of particular interests are determination of the molecular orientation in the film. Structural studies of Pc and Por films have fallen far behind to the studies of their physical properties. Therefore, based on the traditional methods and improve technique we have further started the investigations of the key problems of structural characterization of nanomolecular layer films by use of surface pressure-area (π-A) isotherms and polarized UV-vis spectra which are very powerful nondestructive techniques for exploring molecular aggregation, orientation, and molecular structure in films.

Experiments

For improving the film forming properties the Pc and Por derivatives synthesized were as following. (1) Symmetrically substituted macrocycles: 5,10,15,20-tetra-(p-iso-pentyloxy carbonyl-benzene) porphine [TPIAPP]. (2) Asymmetrically substituted macrocycles: mono-(p-carbonyl-penoxy)-tri-(2, 4-di-tert-pentyl penoxy) phthalocyanine copper (II) {CuPc-cp[dtpp]$_3$} , as shown in Table 1. They were prepared according to the procedures reported by Snow et al [4-7]. Details of the preparation and characterization were described elsewhere[5-6]. KSV-5000 Langmuir trough (Finland) with a Wilhelmy balance and domestic LB trough were employed for the surface pressure-area (π-A) isotherm measurements and the LB films fabrication. The monolayer was deposited when the substrate was moving downwards for X type film; upwards and downwards for Y type film. Polarized spectra of films were observed using a UV-VIS spectrophotometer (Shimadzu UV-3000).

Table 1. Schematic structure of the copper phthalocyanine and Porphyrin derivatives

CuPc (-O- -C_5H_{11})$_3$ (-O- -COOH) ⟶	CuPc-cp[dtpp]$_3$
5, 10, 15, 20-tetra-(p-iso-pentyloxy -carbonyl-benzene) porphine ⟶	TPIATPP

Determination studies of the molecular orientation

Since the orientation of molecule in the ordered layer determines the functional feature of the films, in order to study it the plane dichroism of Pc and Por film was characterized by polarized UV-Vis absorption spectra. The macrocycle is considered as a flat circular plate on which π-π* transition dipole is uniformly distributed according to Yoneyama[8]. The experimental data and calculation results are listed in Table 2. In the calculate equations and Table 2, $A_{\parallel}$ and $A_{\perp}$ are the absorbance of the film for polarized light with electric vectors both parallel (∥) and perpendicular (⊥) to the dipping direction, respectively. The dichroic ratio D can be expressed as $A_{\parallel}/A_{\perp}$. The coordinates (x, y, z) and incidence angles in the optical geometry are given as Fig.1 and following: y-axis is dipping direction of the film, z-axis is a normal line of the substrate of the film; the orientational angles θ is between z-axis and a normal line of Pc and Por macrocycles; ϕ is between x-axis and XY plane projection of the normal line of macrocycles;β' is incidence angles for direction of polarized incident light on the substrate of the film; the refraction angle $= \sin^{-1}(n^{-1}\sin^{-1}\beta')$ and refraction index in the film n = 1.39; $A_{\parallel}$ and $A_{\perp}$ can be obtained from polarized UV-VIS spectra.

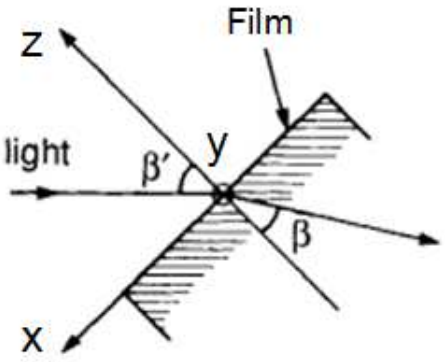

Fig. 3 Direction of polarized incident light on the film and expressing the macrocycle orientation, y-axis: dipping direction, z-axis: a normal line of the substrate of the film and centre axis represented by the circular plane.

Table.2 Polarized UV-vis experimental data and orientation calculations of macrocycle in ordered films of CuPc-cp[dtpp]$_3$ and TPIAPP.

		CuPc-cp[dtpp]$_3$	TPIAPP
Number of layers		35	9
Type of the film		X	Y
$\beta'=0^0$	$A_{\parallel}$	0.301	0.454
	$A_{\perp}$	0.308	0.441
	D_{β}	0.977	1.029
$\beta'=30^0$	$A_{\parallel}$	0.349	0.477
	$A_{\perp}$	0.323	0.422
	D_{β}	1.080	1.130
	$\langle\cos^2\theta\rangle$	0.770	0.743
	$\langle\theta\rangle$	28.7^0	30.5^0

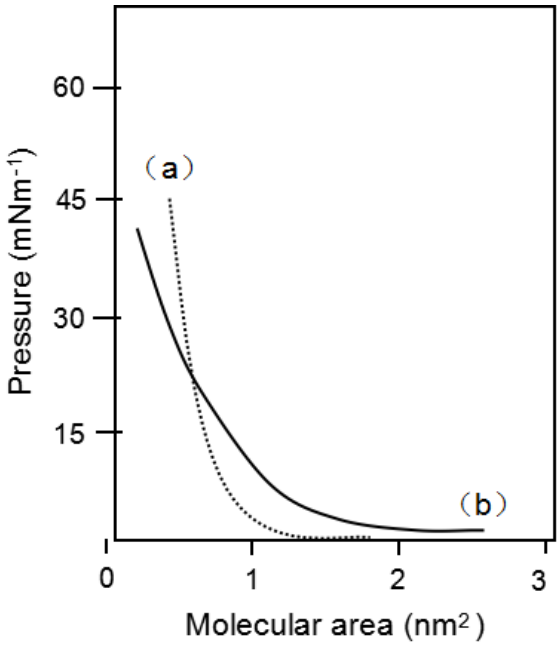

Fig. 2 A normal surface pressure-area (π-A) isotherm of Pc and Por; (a) CuPc-cp[dtpp]$_3$; (b) TPIATPP.

As we know, as the minimum plane area occupied by macrocycle of molecule would be 1.6 nm^2 and the surface area of the edge is 0.4-0.8 nm^2. According to Table 2, XY plane (substrate surface) projection area of the 'tilted' molecule on the substrate is about 1.60 nm^2 × cos28.7^0≅ 1.40 nm^2 for x type LB film of CuPc- cp[dtpp]$_3$; XY plane projection area of the 'tilted' molecule on the substrate is about 1.60 nm^2 × cos30.5^0≅ 1.38 nm^2 for TPIAPP.

The molecular orientation of various Pc and Por macrocycle plane in ordered films has systemically been studied by the information of area per molecule from Pi-A isotherm. Among these Pi-A isotherms representative isotherm of CuPc-cp[dtpp]$_3$ and TPIATPP are shown in Fig. 2. The collapse pressure of molecules and the area per molecule obtained by extrapolating the Pi-A curve (or the limiting area at zero pressure) show in Fig. 2 too.

According to the area per molecule found in our study, the monomolecular ring area for Pc and Por in film are less than that of real macrocyle area. If we compare experimental area (approximately 0.96 nm^2 and 1.23 nm^2 for CuPc-cp[dtpp]$_3$ and TPIATPP respectively) per molecule obtained on the water surface with the cross-sectional area of the 'tilted' molecule on the substrate which is about 1.40 and 1.38 nm^2 , there is a difference in area of 1.40 nm^2 - 0.96 nm^2=0.44 nm^2 for former and 1.38 nm^2 - 1.23 nm^2= 0.15 nm^2 for latter. We conclude that the orientation in the film on water is not preserved in the deposited film on the substrate, owing to the interactions between the molecules and the substrate during the deposition process, especially it maybe caused by surface flowing of the monolayer during the transfer process in the vertical dipping and up motion.

Further the measured CuPc and TPIATPP area of 0.45-0.85 nm^2 at transfer process in Fig.2 is incompatible with an arrangement of the macrocycle plane parallel to the water surface in which area value is near 1.6 nm^2 . The measured spectra data and plus calculation of molecule area in the film for polarized UV-VIS method is 1.40 and 1.38 nm^2 is also incompatible with an arrangement of the macrocycle parallel to the water surface (or substrate surface) in which area value should be near 1.6 nm^2. In the same reason the rings are not perpendicular to the surface either. Thess indicate a tilted of the planes of macrocycle with respect to one another for both CuPc-cp[dtpp]$_3$ and TPIAPP .

Acknowledgements

Authors would like to thank Prof. W. Q. Chen (Changchun Institute of Applied Chemistry, China) for his support and Dr. Y. Wang for his partial experiment data.We acknowledge partial financial supports from Jointly Funded Project (No. 61179055) of Chinese Civil Aviation Authority and National Natural Science Foundation of China, Talent Grant (2013-ZQXY-05） of Educational Commission of Guangdong Province, China.

References

[1] K. P. Gentry, G. Thomas: (2009) Phys. Rev. B , 80:174118

[2] A. Capobianchi, A. M. Paoletti, G. Rossi, G. Zanotti, G. Pennesi: (2009) Sensors and Actuators B: Chemical 142 (1): 159.

[3] S. Baker; M. C. Petty; G. G. Roberts and M. V.Twigg: Thin Solid Films, 1982, 99, 53

[4] A. W. Snow and N. L. Jarvis: J. Am. Chem. Soc., 1984, 106, 4706

[5] H-N Cui; W. Y.Wang; E. L.Zhou: Thin Solid Films, 1992, 214, 238~242

[6] Y. Zang; W. Q. Chen and Q. Shen: Chem. J.of Chinese Universities, 1993, 11, 1483 and 1995, 11, 547

[7] Hai-shui Wang, Ms. Thesis of Changchun Institut of Applied Chemistry,China, 1992

[8] Yoneyama,M.; Sugi , M. J. Appl. Phys., 1986, 25, 961

Advanced Materials Research Vols. 989-994 (2014) pp 684-687
© (2014) Trans Tech Publications, Switzerland
doi:10.4028/www.scientific.net/AMR.989-994.684

Research on grinding Ti6Al4V alloy with inner-lubricating wheel

Huo Wenguo, Zhang Xiangyu, Dong Qingyun, Cai lanrong and Shao Juan[a]

Tianjin Key Laboratory of High Speed Cutting & Precision Machining; Tianjin University of Technology and Education; Tianjin 300222; China

[a]wghuo@163.com

Keywords: Ti6Al4V alloy; Green grinding; Inner-lubricating wheel

Abstract. The new wheel could reduce grinding friction and prevent of chip adhesion by lubrication between wheel and workpiece surface. Investigation of the simulation dry grinding Ti6Al4V alloy with monolayer brazed CBN (cubic boron nitride)and diamond grinding wheels, and systematically studies the effect of process parameters on the microstructure of specimen. the cutting properties generated during grinding with internal lubricating wheel. Grinding simulation was carried out with this internal lubricating wheel. The machining properties were assessed in terms of grinding temperature. The results indicate that graphite significantly improve machinability during dry grinding of Ti6Al4V alloy.

Introduction

Ti6Al4V alloy have been widely used in aerospace because of its excellent combination performance of high specific strength at elevated temperature, their fracture resistant characteristics, and their exceptional resistance to corrosion[1-3]. But the unique physical and chemical properties that make Ti6Al4V alloy suitable for many applications also result into the difficulty to ground. Ti6Al4V alloy has the low thermal conductivity and high chemical reactivity with many wheel materials. Its low thermal conductivity increases the temperature at the grinding zone[4,5]. Hence, the wheel wear off very rapidly due to high grinding temperature and strong adhesion between wheel and workpiece. Additionally, the low elasticity modulus of Ti6Al4V alloy and its high strength at elevated temperature further impair its machinability.

A great deal of methods have been tried to improve the Ti6Al4V integrity on grinding[6]. Taking into account the current development towards ecological friendly coolant strategies, it has been reported[7] that the use of liquid nitrogen as a coolant can produce superior surface integrity, with compressive surface residual stresses and without surface oxidation. Due to the inert nature of the liquid nitrogen, the grinding process becomes environmentally conscious.

One attractive alternative is the minimum quantity lubrication grinding or use of solid lubricants. Dry grinding is not an option because it results in workpiece damage, poor surface integrity and accelerated wheel wear due to insufficient chip removal. That substantially enhances cutting performance in terms of increasing wheel life and improving the quality of the ground parts[8].

Solid lubricants for grinding should satisfy the following requirements: be able to sustain the high temperatures present in the grinding process, be nontoxic, ease in application and be cost effective[9].

The above mentioned studies indicate the great potential of using solid lubricants for low cost and environmental friendly grinding under the condition that the proper material and application method are identified. This study focuses on investigating the effect of graphite in solid lubrication grinding and aims at developing an application method that eliminates the use of any oils or toxic organic lubricants.

Design of the internal lubricating wheel matrix

Internal cooling of the cutting tool, by introducing a solid internally through the tool to remove heat generated during cutting processes, is very promising. The internally cooled grinding wheel is characterized by the internal insert hole and the solid graphite powder. The micro-holes located at

the wheel shell face as the output for the graphite powder. This simple reconfigurable internal lubricated cutting wheel enables low cost and easy use of the wheel in production.

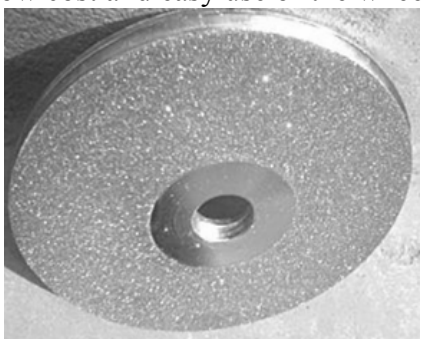

Fig.1 Monolayer brazed wheel

Single abrasive Analysis of monolayer brazed wheel

It is well established that the heat generation occurs in three zones in the cutting domain, primary deformation zone (shear plane), secondary deformation and frictional zone along the tool–chip interface, and frictional zone at tool-workpiece interface[1]. The heat generation in the cutting process using a single micro-graphite internal lubricating wheel is shown in Fig. 2.

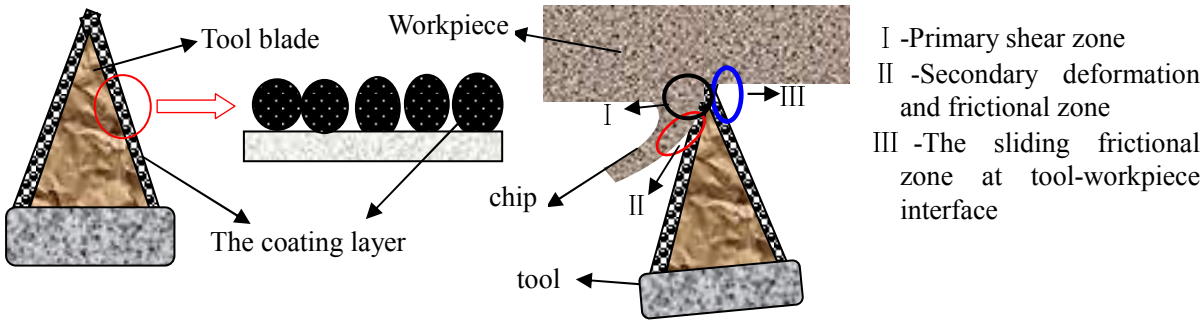

Fig.2 Lubricating schematic of the micro-graphite internal tool

A two-dimensional finite element model is shown in Fig.3, constructed with the grinding parameters and the mechanical properties of the workpiece as input variables.

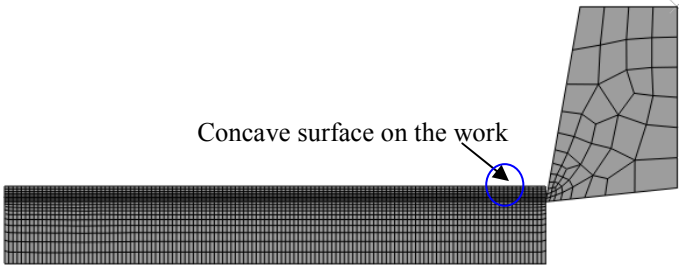

Fig.3 Initial chip formation analysis of single abrasive

The size of the geometric model is several times larger than the size of the cutting zone, using approximately 5200 rectangular solid elements with a finer mesh in the cutting zone and with fixed remote boundaries. The loading in the cutting zone is imposed by displacement vectors proportional to the local undeformed chip thickness, which is a function of turning parameters. For a given set of inputs, the model predicts the temperature generated by the internal micro-graphite self-lubricating tool, as well.

The Simulation Process of single abrasive grinding. Simulation procedure begins by computing the cutting zone as depicted can be determined. The initial condition of the whole model is the room temperature 20℃. The loading process is the motive cutting tool, so the second condition is motive. And the process is controlled by the time variable t, and the last result is considered as the next

initial condition. At last, certain position of the two dimensional map of the temperature distribution has been gotten shown in Fig.4.

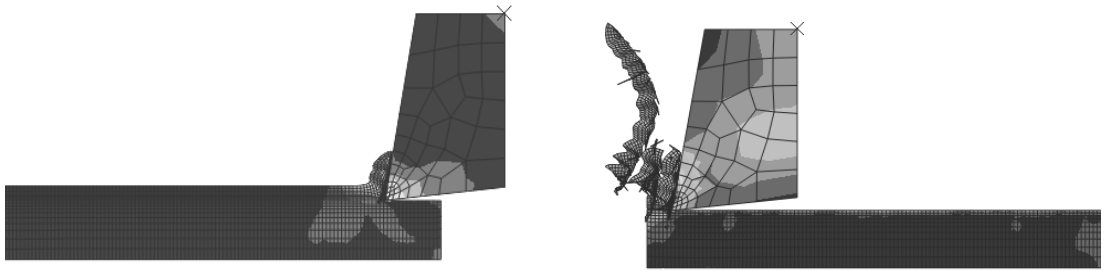

t =0.8ms t = 3.2ms

Fig.4 Temperature distribution of steady-state chip formation analysis step

To find the cooling efficiency of the internal lubricating structure, surface temperature of workpiece was lower compare with general grinding wheel without internal cooling structure.

Metallographic structure. The plastic deformation layer and the surrounding materials were contrasted under the optical microscope to differentiate microstructure changes in the machined layer. Fig.4 displays morphological features of the ground Ti6Al4V surfaces produced by monolayer brazed wheel. There have a thiner plastic deformation layer were found on the workpiece surface after monolayer brazed wheel grinding in dry conditions.

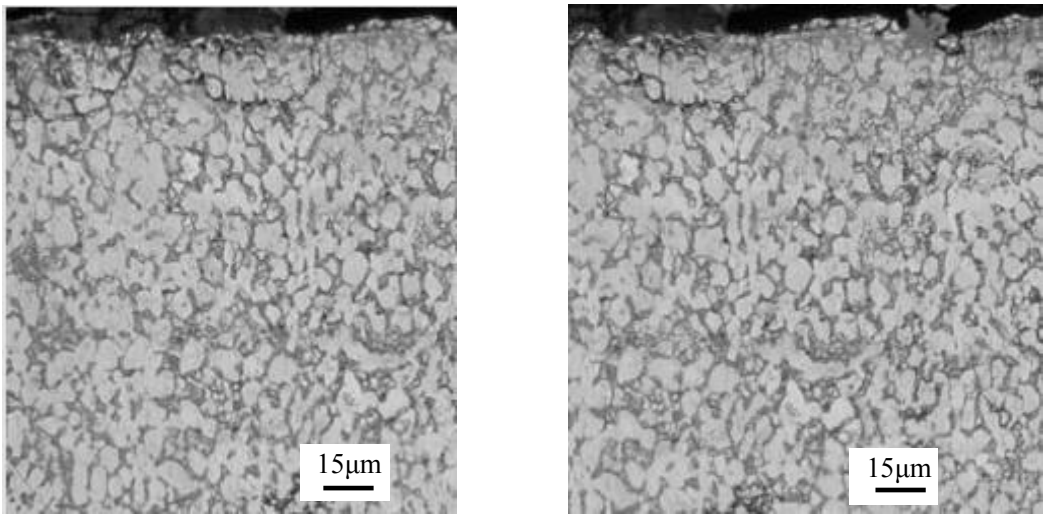

（a）Grinding by monolayer diamond brazed wheel （b）Grinding by monolayer brazed CBN wheel

Fig.4 Microstructure of workpiece surface by (×1400)（v_s=15m/s，v_w=2m/min，a_p=0.025mm）

Cross-section Metallographic structure images of CBN wheel grinding surface are shown in Fig.4a, about 15μm heat affected zone can be observed on the cross-section of ground surface, however, due to the brought high grinding zone temperature by diamond wheel grinding, about 35μm, in Fig.4b. This proves that CBN wheel grinding with optimum grinding parameter does not generate enough heat to produce distinctness plastic deformation layers even in dry conditions. Apart from the plastic deformation layer that appeared after the belt grinding in dry conditions, no other microstructural changes were found beneath the monolayer brazed wheels grinding surfaces.

Conclusions

Severe tearing and plastic deformation of the ground surface were not observed when machining Ti6Al4V alloy with monolayer brazed wheel by the Simulation Process of single abrasive grinding and grinding test, especially after prolonged machining under dry cutting conditions. At the initial stages of grinding the plastic flow of microstructure was not detected almost. At the end of grinding, slight plastic flow, tearing and deformation of the microstructure was detected. This caused the formation of a white layer of hardened material on top of the machined surface, the thickness of which was less than 0.01 mm.

Acknowledgments

This project is supported by the National Natural Science Foundation of China (Grant No. 51305301) and Tianjin Research Program of Application Foundation and Advanced Technology (Grant No. 14JCQNJC05100).

References

[1] R.R. Boyer, An overview on the use of titanium in the aerospace industry, Materials Science and Engineering, 1996, A213:103-114.

[2] A.R. Machado and J. Wallbank, Machining of titanium and its alloys-a review, Proceedings of the Institution of Mechanical Engineers 1990, 204:53-60.

[3] X. Yang and C.R. Liu, Machining titanium and its alloys, Machining Science and Technology. 1999,3 (1) :107-139.

[4] S.A. Bentley, N.P. Goh, D.K. Aspinwall, Reciprocating surface grinding of a gamma titanium-aluminize intermetallic alloy, Journal of Materials Processing Technology, 2001, 118:22-28.

[5] R. Hood, D.K. Aspinwall, W. Voice. Creep feed grinding of a gamma titanium aluminized intermetallic alloy using SiC abrasives, Journal of Materials Processing Technology.2007, 191: 210-214.

[6] S. Paul and A.B. Chattopadhyay, Determination and control of grinding zone temperature under cryogenic cooling, International Journal of Machine Tools and Manufacture .1996, 36 (4):491-501.

[7] T. Nguyen, I. Zarudi and L.C. Zhang. Grinding-hardening with liquid nitrogen: Mechanisms and technology. International Journal of Machine Tools and Manufacture, 2007, 47(1): 97-106.

[8] T.Tawakoi, M. J. Hadad and M. H. Sadeghi. Influence of oil mist parameters on minimum quantity lubrication-MQL grinding process, International Journal of Machine Tools and Manufacture, 2010, 50（6）: 521-531.

[9] S. Shaji and V. Radhakrishnan, Investigations on the application of solid lubricants in grinding. Proceedings of the Institution of Mechanical Engineers. Part B J. Engineers Manufacture. 2002, 216: 1325-1343.

[10] Z. B. Yang, J H. Xu, A J. Liu, Numerical simulation of transient evolvement of molten pool in laser deep penetration welding, Transactions of the China Welding Institution, 2012,31(10):9-13

Advanced Materials Research Vols. 989-994 (2014) pp 688-693
© (2014) Trans Tech Publications, Switzerland
doi:10.4028/www.scientific.net/AMR.989-994.688

The studies of ScB_2 (0001) surfaces from the first-principles

Zhao Hui[1,a], Han Qian[1,b]

[1]Department of Physics, Anshan Normal University, Anshan 114005, China

[a]hzhao@aliyun.com [b]chem_qianhan@126.com

Keywords: Density functional theory, ScB_2 (0001) Surfaces, Stability

Abstract. We conduct first-principles total-energy density functional calculations to study the ScB_2 (0001) surfaces. The optimized surface structures and electronic properties are obtained. The results show that Sc-terminated surface is thermodynamically more favorable in most of range μ_B. The relaxations indicate that it is mainly localized within top three layers and it is less relaxation for Sc-terminated surface. The surface induced features in DOS disappear slowly for the B-terminated surface but vanish rapidly for the Sc-terminated surface. For the Sc-terminated surface, it shows strong metallic property. Simultaneously, both termination surfaces are found charge accumulation relative to the idea surface. Sc-B bonds are strengthened result in the outermost interface spacing are all contracted.

Introduction

In the past year, the *ab initio* approaches have been widely used to explore a lot of metal borides with various *M*/B content such as semi-(M_2B), mono-(*M*B), di-(MB_2). Especially, the discovery of superconductivity at T_c=39K in MgB_2 [1] has attracted interest in studying the physical properties of transition metal diborides with hexagonal AlB_2-type structure, which have a stacking of intercalated graphite like boron sheets and hexagonal layers of metals[2]. Moreover, diborides also play an important role in materials for new heat corrosion and wear resistant alloys and coating [3,4,5,6,7].

In addition to many studies of bulk properties of MB_2, comparable interests in their surface have been generated. The MB_2 (0001) surface is terminated by either the metal layer or the boron layer, namely a polar surface. Experimentally, the structural and electronic properties of ZrB_2 (0001) [8], NbB_2 (0001) [8], HfB_2 [9, 10], TaB_2 (0001) [11,12,13,14] and MgB_2 (0001) surfaces have been investigated. Meanwhile, first principles calculations of TiB_2 (0001) [15], ZrB_2 (0001) [16], HfB_2 (0001) [17], TaB_2 (0001) [8, 12, 17], NbB_2 (0001) [18] and MgB_2 (0001) [19] surfaces have been performed. In these papers, it is found that (Ti, Zr, Hf)B_2 (0001) and MgB_2 (0001) surfaces are stable with metal terminations, while (Nb, Ta)B_2 (0001) surface with B-terminated are likely to be more stable. The surface termination is different between group Ⅳ(Ti, Zr, Hf) and group Ⅴ(Nb, Ta). In our previous work, we have studied the group Ⅵ diborides CrB_2 and MoB_2 (0001) surfaces. Though many calculations about metal diborides surfaces have been performed in the recent year, the understanding of ScB_2 (0001) surfaces behavior is still lacking. To our knowledge, no first-principles total energy calculation has been reported for ScB_2 (0001) surfaces. Therefore, it is necessary to understand many properties of ScB_2 (0001) surfaces and to compare the stability of diborides' surfaces which can be useful for molecules adsorption or reactivity on the surface, composite interface.

Computational details

For this study we employ density functional theory (DFT) as implemented in CASTEP [20]. CASTEP uses a plane-wave basis set for expanded wave functions and ultrasoft pseudopotentials[21] to describe the computationally expensive electron-ion interaction. The generalized gradient approximation (GGA) with the Perdew-Burke-Ernzerhof (PBE) scheme[22] is adopted for the exchange correlation potential. The plane-wave basis set cutoff is 400eV for all

cases, which is sufficient in leading to good convergence for total energy and forces acting on the atoms. The special points sampling integration over the Brillouin Zone is employed by the Monkhorst-Pack method [23] with 6×6×4 for bulk and 10×10×1 for surface calculations.

The crystal structure of AlB_2-type metal diboride is designated as C_{32} with the space group symmetry 191, P6/mmm. For the ScB_2 bulk, the lattice parameters are a = 3.140 Å, c = 3.506 Å, which agrees with other theoretical and experimental results [24,25,26]. In the present surface calculations, symmetric slabs are used for eliminating the spurious dipole effects. We have performed the convergence tests, nine (1 × 1) layers are investigated in our paper, which are plus at least 15 Å of vacuum layer to model the ScB_2 (0001) surfaces as shown in Fig.1. In the calculations, all atomic coordinates in the surface structures are relaxed until the forces on each of them are less than 0.01 eV/Å.

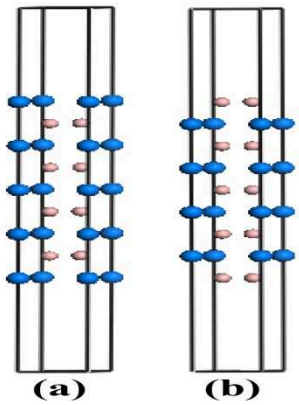

Fig. 1. The structure models of Sc-terminated (a) and B-terminated (b) ScB_2 (0001) surfaces. The big blue and small red balls represent metal and B atoms, respectively.

Results and discussions

Surface energy

The smaller the surface energy is, the more stable the structure is. For the sake of comparing the relative stability of the Sc- and B-terminated surface, we calculate their surface energy at first. The surface energies for different terminated (0001) surfaces as a function of chemical potential of B ($\mu_B - \mu_B^{bulk}$) are shown in the Fig. 2. The surface energies (γ) of ScB_2 (0001) surfaces can be defined as [17, 19, 27, 28]:

$$\gamma = \frac{1}{2S_0}(E_{slab} - N_M\mu_M - N_B\mu_B + PV - TS) \quad (1)$$

where S_0 is the surface area. E_{slab} is the total energy of the slab. N_M is the number of each type of atom in the cell. μ_M is the chemical potential of the various species. P, V, T and S denote the pressure, volume, temperature and entropy of the system. The terms PV and TS can be neglected at 0 K and typical pressures. If we assume that the ScB_2 (0001) surface is in equilibrium with bulk ScB_2 ($\mu_{ScB_2}^{bulk} = \mu_{Sc} + 2\mu_B$), thus, their surface energies (γ) can be rewritten as

$$\gamma = \frac{1}{2S_0}[E_{slab} - N_{Sc}\mu_{ScB_2}^{bulk} + (2N_{Sc} - N_B)\mu_B] \quad (2)$$

The chemical potential of bulk ScB_2 ($\mu_{ScB_2}^{bulk}$) is related to its 0 K heat of formation (ΔH_f^0), which express as:

$$\mu_{MB_2}^{bulk} = \mu_M^{bulk} + 2\mu_B^{bulk} + \Delta H_f^{MB_2}$$

The above inequality is determined by constrains: $\mu_M \le \mu_M^{bulk}$ and $\mu_B \le \mu_B^{bulk}$. Therefore, the chemical potential of B is restricted within the range: $\frac{1}{2}\Delta H_f^{ScB_2} \le \mu_B - \mu_B^{bulk} \le 0$.

Our calculated heats of formation of ScB_2, ΔH_f^0 is -2.72eV. Fig. 2 shows surface energy of B-terminated is raised with increasing the chemical potential of B, while the Sc-terminated surface energy is reduced with increasing the chemical potential of B. Furthermore, the surface energy of

ScB_2 (0001) surface with Sc-terminated is lower than B-terminated surface at the low chemical potential of B. Simultaneity, the Sc-terminated surface is more stable than B-terminated surface over wide range of allowed chemical potential of B. Therefore, Sc-terminated surface is thermodynamically more favorable than B-terminated surface. From above analysis, we can conclude that Sc-terminated surface can be easily achieved for ScB_2 (0001) surfaces. The formation of Sc-terminated surface is preferred to B-terminated surface.

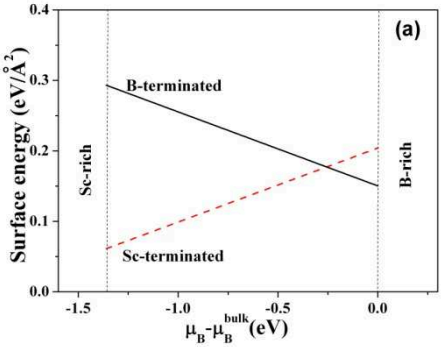

Fig. 2. Surface energies of (a) ScB_2 (0001) surfaces as a function of the chemical potential of Boron.

Structural relaxations

A ratio of the change of interlayer spacing Δ_{ij} is defined as follows: $\Delta_{ij} = (d_{ij} - d_0)/d_0$, which d_{ij} is the distance between the *i*th and *j*th planes of the surface. d_0 is the interlayer distance in the corresponding bulk. Table 1 shows the results of the surface relaxations of the Sc-terminated and the B-terminated ScB_2 (0001) surfaces.

From Table 1, one can see that the effects of relaxation are mainly localized within the top three atomic layers. When the slab thickness, *n*, is more than seven, the atomic interlayer relaxations are converged. For the ScB_2 (0001) surface, the outermost interlayer spacing of Sc-terminated and B-terminated surfaces are contracted by 2.5% and 9.9%, respectively. The second interlayer spacing is correspondingly expanded by 1.6% with Sc-terminated surface and B-terminated of ScB_2 (0001) surface is expanded by 4%. From above introduction, we can see that the outmost interlayer relaxation of ScB_2 (0001) surface with Sc-terminated is smaller relative to that of B-terminated surface. Thus, Sc-terminated ScB_2 (0001) surface is likely to be stable without introducing large relaxation. Therefore, the formation of Sc-terminated surface prior to B-terminated surface could be judged not only from surface energy but also from the degree of relaxation. The Sc-terminated surface is likely to be stable without introducing large relaxation, which is consistent with the calculated results of TiB_2 [15], ZrB_2 [29], and HfB_2 [17]. However, it is different from TaB_2 [12, 17] and NbB_2 [18].

Table1. Surface relaxations Δ_{ij} ($\Delta_{ij} = (d_{ij} - d_0)/d_0$) of ScB_2 (0001) surfaces.

Termination	Interlayer	Slab thickness				
		3	5	7	9	11
Sc	Δ_{12}	3.5	-2.5	-2.6	-2.5	-2.5
	Δ_{23}		1.2	1.5	1.6	1.5
	Δ_{34}			7	-0.024	0.21
	Δ_{45}					0.17
	Δ_{56}					0.5
B	Δ_{12}	4.1	-7.1	-8.5	-9.9	-10
	Δ_{23}		5.3	4.9	4	4.4
	Δ_{34}			1	0.4	-0.6
	Δ_{45}				1	1.2
	Δ_{56}					0.5

Density of states

Fig. 3 shows the total density of states (DOS) and layer resolved projected DOS for the ScB_2 surfaces together with those for the bulk. At the lower energy region, the total DOS curves of surfaces are quite similar with the bulk. However, the curves of the surface layers near the Fermi energy (E_F) are enhanced with respect to those of the bulk layers. Furthermore, the ‘‘pseudo-gap”

existing in bulk disappears after the cleavage of (0001) surfaces, which can be seen in Fig. 3a. In the layer resolved projected DOS, there are obvious differences between Sc-terminated surface and B-terminated surface. For the Sc-terminated (0001) surface, electron state energies of $3d^1$ and $4s^1$ are enhanced. Because the electrons are shared, which fill the surface state that makes the Fermi energy ~~is~~ enhanced. So the metallic property of surface is strengthened, that is to say, the activity and the adsorption of the surface are also strengthened. Nevertheless, for the B-terminated surface that can be shown B-B covalent bond is strong. Consequently, B-terminated surface does not have strong metallic property and activity.

From the Fig. 3b, for the Sc-terminated surface it shows that excess electrons take the orbitals near E_F and those features are mainly localized in the top two surface layers. Furthermore, the DOS of the third layer is already virtually identical to those of the bulk. For the B-terminated surface, the strong hybridization between Sc orbitals and B orbitals enhances the DOS just at E_F. Talking into all the above factors, the surface induced features in DOS disappear slowly for the B-terminated surface but vanish rapidly for the Sc-terminated surface.

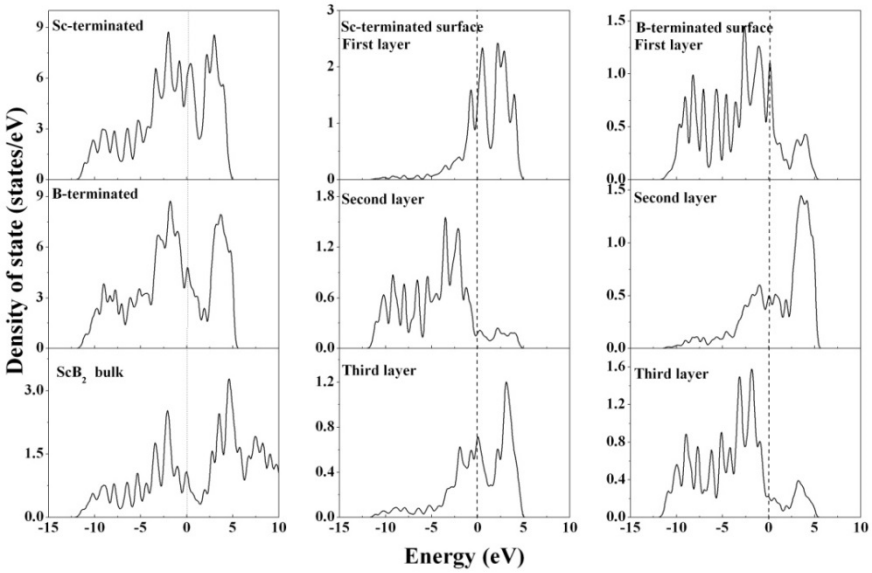

Fig. 3. Total density of states of ScB_2 surfaces and bulk (a); the layer resolved projected DOS of the first, second, and third layers from the top surface of Sc-terminated (b) and B-terminated (c) surfaces, respectively.

Electronic structure

To further understand the electronic of structure of the ScB_2 (0001) surfaces, we study the distributions of valence charge density of relaxed surfaces and differences between the charge densities relative to the isolated atoms on the $(11\bar{2}0)$ plane are shown in the Fig. 4. It can be observed from the both termination surfaces that strong covalent B–B bonds exist between B atoms in the same layer and that Sc–B bonds are formed between the neighboring layers. However, they are not well localized at the B sites but distributed over the whole crystal. ScB_2 is actually metallic Sc held together by covalent B–B and ionic Sc–B bonding. As shown in Fig. 3a and 3b, it is obvious for both termination surfaces that charge accumulates in the interlayer region between the first and second layers while the regions of charge depletion extend up to the vacuum. As a result, the interlayer Sc–B chemical bonds are reinforced and the outermost interlayer distances are largely reduced. For the B-terminated surface, both in plane (sp_xp_y) and out-of-plane (p_z) electrons of the surface B layer are slightly redistributed due to lack of one nearest-neighbor Sc layer. At the Sc-terminated surface, the second surface B layer has two nearest-neighbor Sc layers as in the bulk, and only its out-of-plane (p_z) electrons are perturbed by the electron redistribution of the surface Sc layer. The difference of electrons redistribution results in the charge accumulation in the interlayer region between the first and the second layers for the B-terminated surface is more than that for Sc-terminated after full relaxation.

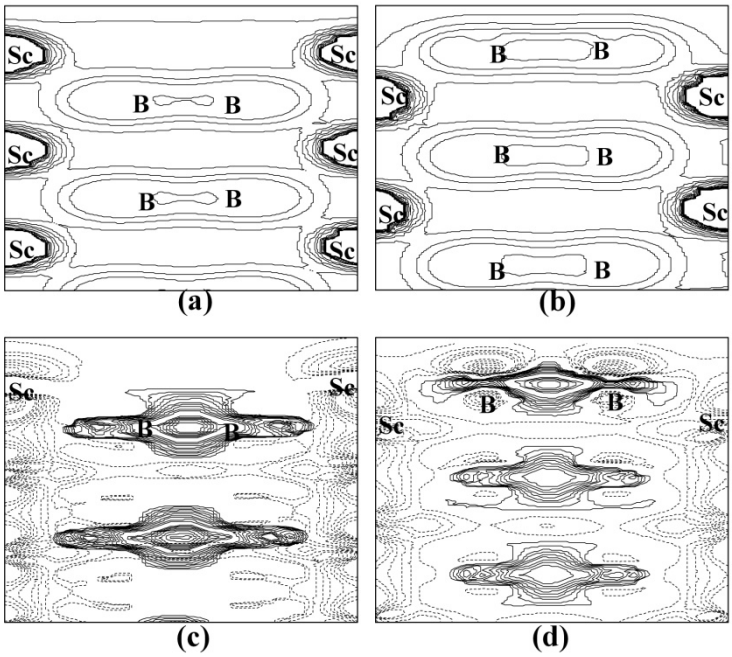

Fig.4. Charge density contour maps (a, b) and difference in charge density (c, d) on the $(11\bar{2}0)$ plane for Sc-terminated and B-terminated ScB_2 (0001) surfaces after full relaxation, respectively. Solid and dotted lines indicate positive negative values, respectively.

The calculations for TiB_2 [15] and MgB_2 [19] surfaces have similar tendency about the interlayer relaxation but the different electrons redistribution of metal atoms brings about the different interlayer relaxation. We also investigated the difference charge density for the ScB_2 (0001) surface relative to the isolated atoms in order to gain some insight into the origin of the inward relaxation of the ScB_2 (0001) surfaces. From Fig. 3c, the difference charge density plots indicate the charge accumulation of B layers and the formation of Sc-B bonds. Furthermore, the charge of B and Sc atoms are accumulated and the accumulated charge will strengthen the chemical bonds of Sc-B. As a result, the bonds between the first and the second layers are strengthened and the first interlayer spacing is contracted. The second interlayer spacing is expanded due to the third layer's nearest-neighbor two B layers. So Sc-B bonds of the first interlayer are more strengthened than that of outermost interlayer. In Fig. 3d, for the B-terminated surface, it is also results in the contraction of the first interlayer spacing. However, the charge accumulation in the interlayer region between the first and the second layers for the B-terminated surface is more than that for Sc-terminated. Consequently, the B-terminated surface has lager relaxation than Sc-terminated surface as shown in Table 1.

Conclusions

In summary, we have studied the metal-terminated and boron-terminated ScB_2 (0001) surfaces using first principles total energy plane-wave pseudopotential method based on density functional theory. The surface energies of ScB_2 (0001) surfaces with different surface terminations as the functions of the chemical potential of B are calculated, which demonstrates that Sc-terminated surface is energetically more favorable than graphitic-boron-terminated surface. The effects of relaxation are mainly localized within the top three atomic layers for both termination surfaces and the outermost interlayer relaxations for metal-terminated surfaces are smaller than those for B-terminated surfaces. From the electronic structure, B-terminated surface does not have strong metallic property and activity. On the other hand, the charge accumulation in the interlayer region between the first and the second layers for the B-terminated surface is more than that for Sc-terminated surface. Finally, it is likely that Sc-terminated surface is more stable than B-terminated surface.

References

[1] J. Nagamatsu, N. Nakagawa, T. Muranaka, Y. Zenitani, J. Akimitsu, Nature 63 (2001) 410.
[2] R.W.G. Wyckoff, *Crystal Structures* (Intenscience, New York, 1965).
[3] M.I. Matkvich, G.V. Samsonov, P. Hagenmuller, T. Lundstrom, *Boron and Refractory Borides*, (Springer, Berlin, 1977).
[4] G.V. Samsonov, I.M. Vinitskii, *Handbook of Refractory Compounds*, (Metallurgiya, Moscow, 1976).
[5] T.I. Serebryakova, V.A. Neronov, P.D. Peshev, *Vysokotemperaturnye Boridy* (Metallurgiya, Moscow, 1991).
[6] R.B. Kaner, J.J. Gilman, S.H. Tolbert, Mater. Sci. 308 (2005) 1268.
[7] W. Zhou, H. Wu, T. Yildirim, Phys. Rev. B 76 (2007) 184113.
[8] T. Aizawa, S. Suehara, S. Hishita, M. Arai, Phys. Rev. B 71 (2005) 165405.
[9] W. Hayami, R. Souda, T. Aizawa, T. Tanaka, Surf. Sci. 415 (1998) 433.
[10] Y. Yang, J.R. Abelson, J. Crys. Growth 310 (2008) 3197.
[11] H. Kawanowa , R. Souda , S. Otani , Y. Gotoh, Phys. Rev. Lett 81 (1998) 2264.
[12] H. Kawanowa, R. Souda, K. Yamamoto, S.Otani, Y. Gotoh, Phys. Revs. B 60 (1999) 2855.
[13] C.L. Perkins, R. Singh, M. Trenary, T. Tanaka , Y. Padermo , Surf. Sci. 470 (2001) 215.
[14] E. Deligoz, K. Colakoglu, Y.O. Ciftci, Solid State Commun. 150 (2010) 405.
[15] Y.F. Han, Y.B. Dai, D. Shu, J. Wang, B.D. Sun, J. Phys.:Codens. Matter 18 (2006) 4197.
[16] W. Hayami, T. Aizawa, T. Tanaka, S. Otain, J. Phys. Chem. B 108 (2004) 15233.
[17] K. Yamamoto, K. Kobayashi, H. Kawanowa, R. Souda, Phys. Rev. B 60 (1999) 15617.
[18] S. Suehara, T. Aizawa, T. Sasaki, Phys.Rev.B 81 (2010) 085423.
[19] Z.Y. Li, J.L. Yang, J.G. Hou, Q.S. Zhu, Phys. Rev. B 65 (2002) 100507.
[20] M.D. Segall, P.L.D. Linadan, M.J. Probert, C.J. Pickard, P.J. Hasnip, S.J. Clark, M.C. payne, J. Phys.:Condens. Matter 14 (2002) 2717.
[21] D. Vanderbilt, Phys. Rev. B 41 (1990) 7892.
[22] J.P. Perdew, K. Burke, M. Ernzerhof, Phys. Rev. Lett. 77 (1996) 3865.
[23] H.J. Monkhorst, J.D. Pack, Phys. Rev. B 13 (1976) 5188.
[24] I.R Shein, A.L. Ivanovskii, J. Phys.: Condens. Matter 20 (2008) 415218.
[25] T. Oguchi, J. Phys. Soc. Japan 71 (2002) 1495.
[26] P. Vajeeston, P. Ravindran, C. Ravi, R. Asokamani, Phys. Rev. B 63 (2001) 045115.
[27] K. Rapcewicz, B. Chen, B. Yakobson, J. Bernhole, Phys. Rev. B 57 (1998) 7281.
[28] I. Batyrev, A. Alavi, M.W.Finnis, Faraday Discuss.114 (2000) 33.
[29] H. Ihara, M. Hirabayashi, H. Nakagawa, Phys. Rev. B 16 (1977) 726.

Advanced Materials Research Vols. 989-994 (2014) pp 694-696
© (2014) Trans Tech Publications, Switzerland
doi:10.4028/www.scientific.net/AMR.989-994.694

Synthesis and fluorescnce study of Cobalt(II) deuteroporphyrin dimethyl ester

Chuan-ming Yu[a], Bing-cheng Hu[b]

School of Chemical Engineering, Nanjing University of Science & Technology, Nanjing, Jiangsu, China

[a]yuchuanming31@163.com, [b]hubingcheng210094@163.com

Keywords: Hemin; porphyrin; metal-porphyrin

Abstract. A series of metal-*DPDME (metal deuteroporphyrin dimethyl ester)* complex were synthesized through dehydrogenation, deferrization, esterification, metal-complexation using hemin as raw materials. Found red shift at Soret band and blue shift at Q band in UV-Vis spectrum which is different from tetraphenylporphyrin, and different excitation and emission peaks in fluorescence spectrum between *DPDME* and *Co(II)-DPDME.*

Introduction

Porphyrins and porphyrin-like compounds (termed below as porphyrins) are necessary for the functioning of many biological system. Porphyrins often exist in a number of natural molecules, especially the metal-porphyrins always have some special physiological activity[1,2]. Such as Myoglobin, hemoglobin, chlorophyll, magnesium porphyrin), hemoglobin (iron porphyrins), etc.

Porphyrins with special structure make them functional diversity. Therefore, through the design of functional molecule base on porphyrin can change its redox activity, obtain unique optical, electrical, magnetic and other properties. thus make it can be applied to optical information storage, molecular recognition and bionic catalysis, etc.[3~6]. Hemin is a kind of porphyrins, and exists in creaturely blood. Its properties is very close to tetraphenylporphyrin but there are some differences. In this title, we synthesized a series of metal deuteroporphyrin dimethyl ester based on hemin and studied its UV-Vis Absorption and fluorescence.

Experimental

Experimental equipment

The 1H NMR spectra were recorded on Bruker AVANCE III 500 MHz spectrometer with DMSO-d_6 as the solvent and TMS as the internal standard. Chemical shifts are reported in δ(parts per million) values. High-resolution mass spectra were recorded under on TSQ Quantum-HPLC/MS/MS (Thermo, USA). Analytical thin-layer chromatography (TLC) was carried out on silica gel plates (60F254), and spots were visualized with ultraviolet (UV) light. The UV-Vis spectra were measured by Shimadzu UV-1800 spectrophotometer. The fluorescence spectra were recorded on Horiba Jobin Yvon FluoroLog-3 spectrometer.

General procedure for the preparation of metal-DPDME

Porphyrins were prepared according to the synthetic route described in Scheme 1 and detailed procedures are according to literatures, which summarized as follows: Deuterohemin was obtained starting from hemin, which was dissolved in resorcinol Under nitrogen atmosphere, followed by deferrization with iron powder in acetic oxide, and methyl esterification with methanol in chloroform. Treatment deuteroporphyrin dimethyl ester*(DPDME)* with metal salt in DMF afforded target compounds.

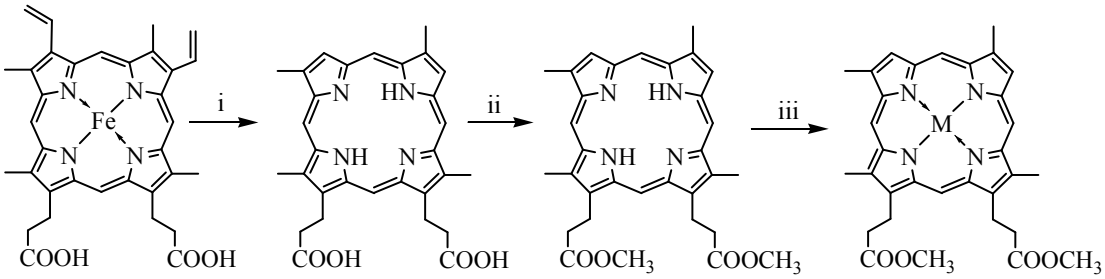

Scheme 1. Reagents: (i) resorcinol, ether, acetic anhydride, HCl, $FeSO_4$, N_2 86%; (ii) CH_3OH, H_2SO_4, ultrasound, 99%; (iii) metal salt, CH_3OH, $CHCl_3$, 92%

Results and discussion

Fig. 1 shows the UV-Vis spectrum of *DPDME* and *Co(II)-DPDME* complexes. Compared to *DPDME*, the Soret band of *Co(II)-DPDME* shows an obviously lager red shift (11 nm) due to significantly affect by substituent-induced, meanwhile a relatively lager blue shift (12 nm and 15 nm, respectively) due to the increased symmetry by metal complexing effect. At the Q band, *DPDME* and *Co(II)-DPDME* have only two absorption peaks, it's different from tetraphenyl porphyrin (TPP) which has 4 absorption peaks at Q band. That due to the $-CH_2CH_2COOCH_3$ substituted at 13, 17 position.

Tabe 1 shows the fluorescence excitation and emission wavelength of *DPDME* and *Co(II)-DPDME*. The excitation wavelength number reduces from 5 to 1 when *DPDME* was substituted with metal *Co(II)* in its circle. While the emission peak shows a little blue shift (2 nm) due to the same effect.

Table 1. Fluorescence excitation and emission wavelength of DPDME and Co(II)-DPDME

	Ex	Em
DPDME	371, 415, 495, 533, 570	577, 630
Co(II)-DPDME	396	575, 628

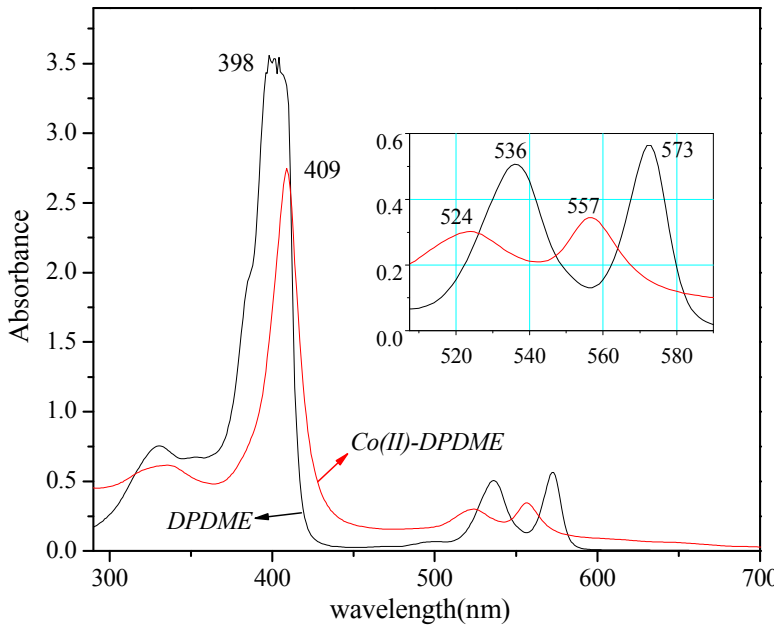

Fig. 1 UV-Vis absorption spectrum of DPDME and Co(II)-DPDME in CH_3OH ($5\cdot10^{-5}$ M)

To investigate the influence of metalsubstitution effect on UV-Vis absorption, fluorescence excitation and emission, we synthesized a series of metal substituted *DPDME*, such as

Fe(II)-DPDME, Fe(III)Cl-DPDME, Sn(II)-DPDME, Ni(II)-DPDME, Zn(II)-DPDME, Mn(II)-DPDME, They all show different levels of red shift at Soret band, and also only one excitation peak in fluorescence spectrum. We consider that porphyrin structure with metal can increase its density of electron cloud because the metal extranuclear electrons can bring better conjugative effect at porphyrin ring. Thereby, the excitation energy decreases, and shows red shift in UV-Vis spectrum. Different groups on porphyrin ring may affect the fluorescence excitation, but the metal complexing effect can reduce greatly the impact from these groups, thus only one peak found in the fluorescence excitation spectrum.

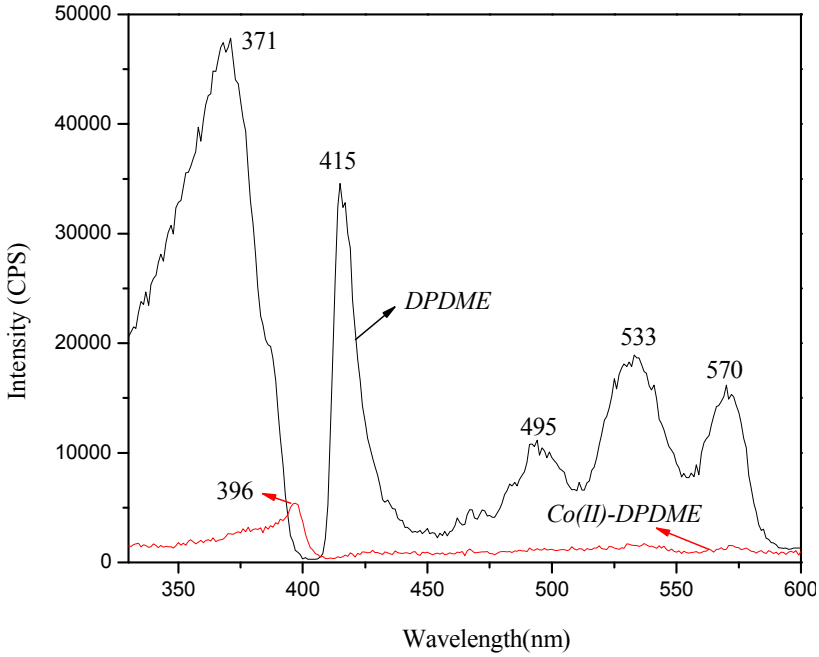

Fig.2 Fluorescence excitation spectrum of DPDME and Co(II)-DPDME in CH_3OH ($5 \cdot 10^{-5}$ M)

Summary

We synthesized a series of metal-*DPDME* compounds based on hemin which is different from tetraphenylporphyrin. Found that there are only 2 peaks at Q band while 4 in tetraphenylporphyrin, and the metal complex shows obviously red shift at Soret band and blue shift at Q band. Compared to *DPDME*, in the excitation spectrum, metal-*DPDME* there is only one peak, and show little blue shift (2 nm) due to the metal complexing effect.

Acknowledgements

The project was financially supported by Jiangsu Natural Science Foundation (No. BK2009386), Science and Technology Development Foundation of Nanjing University of Science and Technology (No. 2010GJPY043).

References

[1] R.K. Dinello and C.K. Chang. in: D. Dolphin (Ed.), The Porphyrins, vol. I (Academic Press, New York 1978), p. 295

[2] I. Sylvaina, R. Zerrouki and R. Granet: Bioorg. Med. Chem. Vol. 10 (2002), p. 57

[3] B. C. Hu, W. Y. Zhou and D. S. Ma: Catal. Commun. Vol. 10 (2008), p. 83

[4] C. M. Drain, A. Varotto and I. Radivojevic. Chem. Rev. Vol 109 (2009), p. 1630

[5] Q. Liu, and C.C. Guo: Sci. China, Ser. B Chem. Vol. 55 (2012), p. 2036

Advanced Materials Research Vols. 989-994 (2014) pp 697-700
© (2014) Trans Tech Publications, Switzerland
doi:10.4028/www.scientific.net/AMR.989-994.697

A Study of the Effect of Starch in Polymer Blends of Carboxymethyl Cellulose and Chitosan

Noppawat Keungputpong[a], Nuanjan Matchariyakul[b]
and Sunan Tiptipakorn[c]

Department of Chemistry, Faculty of Liberal Arts and Science, Kasetsart University, Kamphaengsaen, NakhonPathom 73140, Thailand

[a]nop_13010@hotmail.com, [b]faasnjm@ku.ac.th, [c]faassntk@ku.ac.th

Keywords: Chitosan, Carboxymethyl cellulose, Glutaraldehyde, Starch, Crosslinking.

Abstract. This research is divided into 2 parts. In part I, the optimal ratio of polymer blends between chitosan (CS) with carboxymethyl cellulose (CMC) by using glutaraldehyde (GL) as crosslinked agent. In part II, the effect of starch on the properties of polymer blends was determined. The chemical interaction of the blends was studied with Fourier Transform Infrared Spectroscope (FT-IR). The thermal properties of polymer blends were also determined with differential scanning calorimeter (DSC) and thermogravimetric analyzer (TGA). Moreover, the study of physical property was performed with a Swelling Test method. From test results in part I, the optimal ratio between CS (0.8%w/v) and CMC (0.8%w/v) was 3:2 by volume. Furthermore, the FT-IR spectra reveals the chemical interaction (C=N). In part II, the blend which was added with 50 percent by weight of starch show the highest glass transition temperature. The maximum rate of decomposition temperature and the percentage of swelling were increased with the increase of starch.

Introduction

There are many studies about the blends of carboxymethyl cellulose with chitosan, because these kinds of the blends can be used as hydrogel [1-4]. However, it has been reported that thermal and swelling properties of the blend are lower than those of CMC and CS.

Chitosan (CS) is bio-polymer, which has safety, because it is naturallydegraded. The CS has a capability of absorption of cholesterol and fatty acid. The limitations are low thermal decomposition and non-dissolve in water (pH = 6.8-7.2) [5].

Carboxymethyl cellulose (CMC) is hydrocolloid and hydrophilic-polymer [6]. It can be use viscosityimprover and stabilizer. Furthermore, it dissolves in water. The low value of thermal decomposition could limit the use of CMC [7].

Glutaraldehyde (GL) is aldehyde compounds, which is used as crosslinking agent. The crosslinking has an effect of the increase of strength and thermal properties. Moreover, the stability of acid-base is increased by the use of GL [8].

Starch is polysaccharide that composes of amylose and amylopectin. The different in the amount of amylose and amylopectinleads to the difference in thermal, mechanical and swelling properties [9].

The main objectives of this study are to prepare and study the properties of crosslinked CMC/CS by using GL as crosslinking agent and compare the properties of crosslinked CMC/CS with and without starch.

Experimental

Materials. Chitosan (CS) powder ($\bar{M}_n$ = 8.2x10^4, $\bar{M}_w$ = 4.4x10^5) and carboxymethyl cellulose (CMC) powder ($\bar{M}_n$ = 1.3x10^5, $\bar{M}_w$ = 8.1x10^5) were purchased from Sigma-Aldrich Co. LLC., USA. Glutaraldehyde (GA) solution (25wt%, M_w = 100.11, b.p. = 106^{o}C) under trade name of UNILAB

was obtained from AjexFinechem, New Zealand. Starch soluble powder (M_w = 100.11, b.p. = 667.9°C). The percentage of amylose in the use starch 36%

Preparation of CS/CMC by using GL as crosslinked agent. CS was dissolved in 0.8% (w/v) acetic acid aqueous solution to make a 0.8% (w/v) CS solution and NaCMC was dissolved in deionized water to make a 0.8% NaCMC(w/v) aqueous solution. The volume ratios of CS and CMC are 1:0, 0:1, 1:1, 1:2, 2:1, 2:3 and 3:2. In the meantime, GL (0.1% mole of the amino groups on CS) was added into the solution in order to cross-link the CS. GL waschosen as the cross-linking agent. The complete mixing at room temperature for 2 h was obtained. Finally, the blends were eliminated solvent at 60°C for 10 h.

Preparation of CS/CMC/starch by using GL as crosslinked agent. The volume ratio of CS and CMC is 3:2 that is added starches (0.0, 5.0, 15.0, 25.0, 33.3, 50.0, 60.0, 66.7, 71.4, 75.0, 85.0 and 100 wt%). After that, GL (0.1% mole of the amino groups on CS) was added into the solution in order to cross-link the CS. After the complete mixing at room temperature for 2 h, the blends were eliminated solvent at 60°C for 10 h.

Characteristics of the blends. FT-IR spectra were recorded with a Perkin Elmer spectrometer at 4 cm^{-1} resolution using 64 scans in the range of 2000 – 750 cm^{-1}.The thermo gravimetric analysis of the blends was carried out using the Mettler Toledo, SDTA851^e thermal gravimetric analyzer. The temperature was increased in the range of 30 – 800°C with heat flow rate 20°C/min under N_2 atmosphere. The glass transition temperatures of the polymer blends were carried out with the Mettler Toledo, DSC822^{e}differential scanning calorimeter (Mettler Toledo, SDTA851^e) in the nitrogenatmosphere at a heating rate of 10°C/min in the range of 25 – 210°C.

Swelling of the blends. The blends were dried in an oven at 60°C to constant weight and then immersed in water. After the excess solution on the blend surface had been removed with filter paper, the weight of swollen samples wasimmediately measured. The swelling ratio was determined as follows Eq.1:

$$\% \text{ swelling} = (W_s - W_d)/W_d \times 100 \quad (1)$$

where W_s and W_d are the weights of the samples in swollen and drystates, respectively.

Results and Discussion

FT-IR Analysis. Fig. 1 shows that the crosslinked bonds (C=N) between amino group of chitosan and carboxyl group of carboxymethyl cellulose were found at 1581 cm^{-1}. Fig. 2 shows that the crosslinked bonds of the blends were increased with the increase of starch. However, at the starch content of 50wt%, the crosslinked bonds are the most among other blends. The values of crosslinked bonds are decreased due to gelatinization of starch [9].

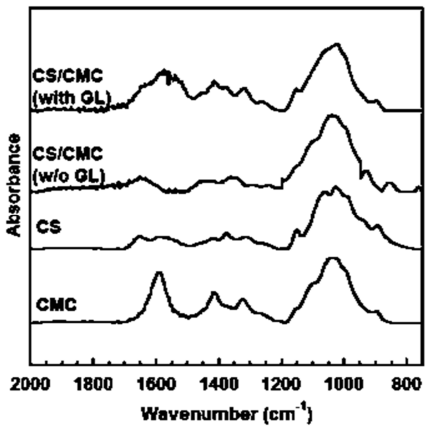

Figure1.FT-IR spectra of polymer blends between CSwith CMC(3:2)by using GL as crosslinking agent.

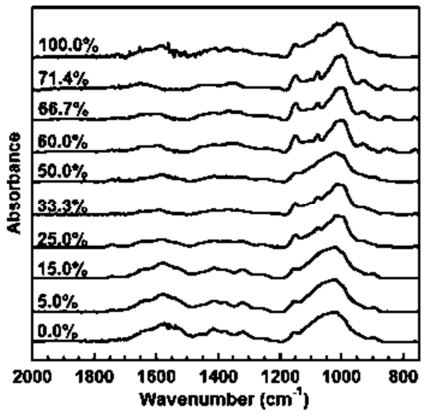

Figure2.FT-IR spectra ofpolymer blends with added starch (0.0, 5.0, 15.0, 25.0, 33.3, 50.0, 60.0, 66.7, 71.4, 75.0, 85.0 and 100 wt%).

Thermal properties

Thermo gravimetric analysis. Fig. 3 shows that the maximum rate of decomposition temperature in polymer blends (CS:CMC= 3:2) is 272°C. It is because the most stable structure or the most crosslinked bonds is the ratio of 3:2. Crosslinked bonds depend on the amount of amino group in CS. Fig. 4 shows that at the starch content of 0 – 71.4 wt%, the maximum rates of decomposition temperature of the blends were increased due to thermal stability of starch.

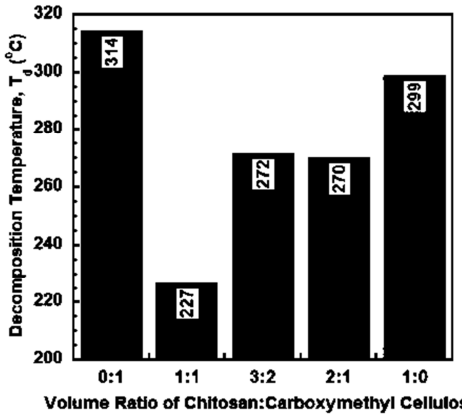

Figure 3.Maxinum rates of decomposition temperature of polymer blends between CS with CMC (0:1, 1:1, 3:2, 2:1 and 1:0 by volume).

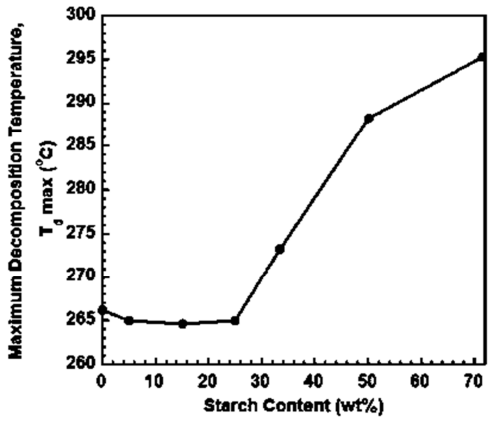

Figure 4.Maxinum rates of decomposition temperature of polymer blends between CS with CMC (3:2 by volume) with added starch.

Differential Scanning Calorimetry. Fig. 5 shows thatthe glass transition temperatures of the blends were increased with starch content (0 - 50 wt%). Beyond 50 wt%, the values were decreased with starch content . According to the result of Fig. 2, at the starch content of 50 wt%, the crosslinked bonds are the highestamount other blends. Therefore, the glass transition temperature at this content is the greatest.

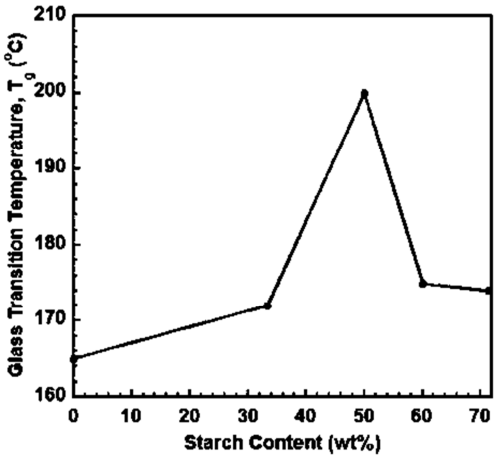

Figure5.Glass transition temperature of polymer blends between CS with CMC (3:2 by volume)with added starch

Swelling analysis. Fig. 6 shows that the swelling percentage of the blend was increased with starch content (0 – 71.4 wt%). It is attributed that the main property of starch has higher ability to absorb moist than CS and CMC.

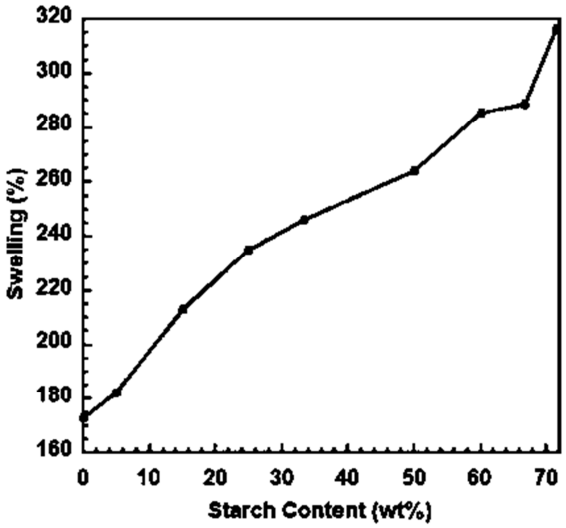

Figure 6.Swelling of polymer blends between CS with CMC (3:2 by volume)were added starch.

Summary

The stability of structure and thermal properties were increasedby adding GL in polymer blends. In part I, the optimal ratio of CS and CMC in the blends was 3:2. In part II, The stability of structure, thermal and swelling properties were increased and crosslinking was decreased with adding starch. In addition, maximum crosslinking and maximum glass transition temperature were found at 50 percent by weight of starch.

Acknowledgements

This research receives financial supports from Thailand Research Fund (MRG5680029) and Kasetsart University Research and Development Institute.

References

[1] R.Carmen, M. L. Popaa, G. Lisaa and G.C.Chitanu: Carbohydrate Polymers. Vol. 62 (2005), p. 35–41.

[2] O.Hannes, I. Filpponen, L. S. Johansson and O. J. Rojas:Biomacromolecules. Vol. 12 (2011), p. 4311–4318.

[3] S. J.Kim, S. R.Shin, S. M.Lee, I. Y.Kim and S. I.Kim:Struct. Vol. 13 (2004), p. 1036–1039.

[4] T. Shiga:Advances in Polymer Science. Vol. 134 (1997), p. 131–163.

[5] Information on http://www.greenclinic.in.th/chitosan.html.

[6] Information on http://eu.lib.kmutt.ac.th/elearning/Courseware/BCT611/chapter4.html.

[7] Information on http://edtech.ipst.ac.th/index.php/2011-07-29-04-02-00/18-2011-08-09-06-29-06/3722012-07-09-02-32-53

[8] J. S. M. S.Carla, F. Sousa, G. Gübitz and A. C. Paulo:Food Technology and Biotechnology. Vol. 42(2004),p. 51–56.

[9] K. Jiraporn, T. Boonprasop and C. Vudjung:Abstracts of NESTC. (2012), p. 33-44.

Advanced Materials Research Vols. 989-994 (2014) pp 701-704
© (2014) Trans Tech Publications, Switzerland
doi:10.4028/www.scientific.net/AMR.989-994.701

A new type aluminum alloy Backup Frame of FAST Project

Zhao Baoqing[1, a], Wang Qiming[1, b], Zhao Qing[1, c], Gu Xuedong[1,d], Hu Jinwen[1,e]

[1]National Astronomical Observatories, Chinese Academy of Sciences, China

[a]E-mail: bqzhao@bao.ac.cn,[b]E-mail: qmwang@bao.ac.cn,[c]E-mail: qzhao@bao.ac.cn,
[d]E-mail:xdgu@bao.ac.cn, [e]E-mail:jwhu@bao.ac.cn

Keywords: FAST project; aluminum alloy truss; backup frame; precision; strength

Abstract. Distinct from conventional truss, FAST project reflector elements require light weight, high accuracy backup structure. A new type of aluminum alloy frame backup element is designed and simulated. According to which, an aluminum alloy backup element prototype is manufactured and assembled at the under-construction site. And with a serial of measure experiments, the prototype data meets the requirements. Thus the design and experiments verify the efficiency of the structure.

Introduction

Five-hundred-meter Aperture Spherical radio Telescope (FAST) project will become the largest single aperture spherical radio telescope in the world [1]. One of the three out- standing features of FAST is the active main reflector which is divided into about 4300 elements located on the cable net structure [2]. Reflector elements require high precision, light weight, lasting corrosion resistance, each of which consists of a backup frame unit and a panel unit. [3]. Backup frame unit is of importance to the element stiffness and precision by supporting panel unit.

Steel grid structure or space truss structure is conventional in buildings industry, which cannot meet the requirements of FAST reflector. Reflector's density is asked less than 8.5kg/m^2, the surface precision is no more than RMS 2.5mm, and corrosion issue, etc (as shown in Table 1). In this paper, aluminum alloy is adopted on space truss structure backup frame for its light weight (about 1/2.8 of density ratio between aluminum and steel) and anticorrosion after surface anodized.

Table 1 The original backup frames performance contrasts

Backup types	Reflector unit surface density (kg/m^2)	Maximum displacement (mm)	RMS (mm)	Characteristics
Monolayer steel structure	10.1	12.64	2.94	higher dead weight; larger displacement and RMS; easier corrosion to welded joints
String prestressed steel structure	8.21	17.52	3.89	higher dead weight; larger displacement and RMS; hard to control the prestressed force of steel rod； easier corrosion to welded joints
Steel truss structure	8.04	19.44	3.56	higher dead weight; larger displacement and RMS; easier corrosion to welded joints
Steel space truss structure	9.64	3.67	1.84	higher dead weight; larger displacement and RMS; easier corrosion to welded joints

Where, $RMS = \sqrt{(\sum (d_i - \bar{d})^2) / n}$, d_i-the displacement of nodes, $\bar{d}$-the average displacement of the all nodes, n-the number of nodes.

Material of the backup frame

Pipe material Besides the common feature of aluminum alloy: anti-corrosion, greater strength and stiffness, light weight, the tensile strength is the main factor to choose the pipe material. Aluminum alloy 6061-T6 is of the tensile strength 265MPa, more than Q235 steel, which satisfied the FAST brace rod strength requirements. In addition it has even good anti-corrosion performance [4]. So we choose aluminum alloy 6061-T6 as the backup frame material.

Materials of sealing plate, the sleeve and the bolt ball FAST project requires reflector element with high precision. The backup frame as supporting structure of the reflector element must have high strength and rigidity. And the nodes should have higher technical specs than the pipe. That is, bolt should be damaged preceding the rod in the destructive test. The heat affected zone of welded aluminum alloy has lower hardness than the rest of the region [5]. In the development process, the combination connector referenced the connection method of a construction project [6][7], as shown in figure 1. We selected 2A12-T4 as the materials of sealing plate and sleeve, and chose the high strength aluminum alloy as material of bolt ball.

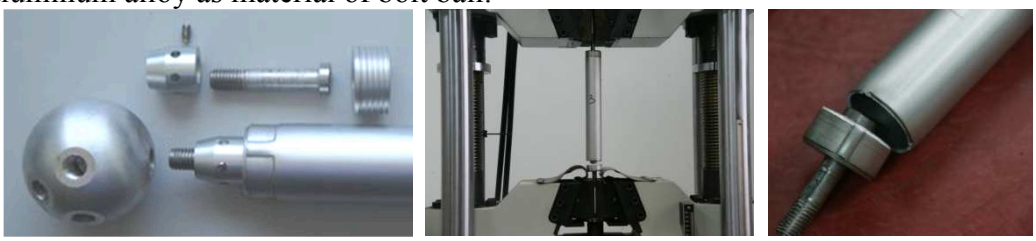

Figure 1 The connector of rod and the destructive test

Materials of bolt and the connecting ear plate Annual average humidity at FAST project site is more than 80%, under this environment steel is easy to corrode, so the connecting bolts are made of stainless steel, connecting ear plates are made of 304 stainless steel.

Simulation studies

This paper uses a length of 11.93m, 11.78m, and 12.24m triangular element as the simulation model. The diameter of aluminum alloy pipes is 37mm, the thickness is 1.8mm, and the height of backup frame is 1000mm.

The open porosity of panel unit which installs on the backup frame unit is 50%. Due to the maximum wind speed is 14m/s at the FAST project site, wind load is 0.06kN/m2. Using MIDAS software to calculate, the three corners are respectively released 0, 1, 2 direction constraint. Under the interaction of various conditions, displacements of backup frame nodes are shown in figure 2.

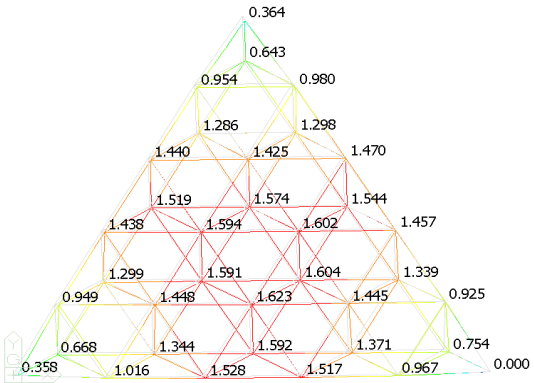

Figure 2 The simulation results

The simulation results are shown in Table 2. After loading the weight of upper panel unit and wind, the maximum displacement of backup frame nodes is 5.97mm, and the RMS is 1.98mm.That meet the reflector surface accuracy requirements of FAST project.

Table 2 Calculation results of displacements

Load type	Maximum displacement (mm)	RMS（mm）
Dead weight	1.61	0.53
Wind load	3.82	1.27
Panel weight & dead weight	3.29	1.09
Dead weight, wind load, panel weight	5.97	1.98

Fabricate and measure

On the basis of design and simulation, we fabricated and assembled the new aluminum alloy reflector element in Da Wodang, Pingtang County of Guizhou Province in 2011, as shown in figure 3.

We used a total station instrument to measure the new reflector's surface shape as the element was assembled. However, the measurement data results（by the software MATLAB） show that the RMS is 4.01mm. It cannot meet the accuracy requirement of FAST reflector, as shown in figure 4.

(a) The backup frame unit installation (b) The panel unit installation

Figure 3 The installation of the reflector unit

In order to meet the surface shape accuracy requirement of FAST project, the adjustment joint which displacement is larger than 4mm is regulated. After that, measured again as shown in Figure 5.The RMS is 2.29mm, meet the requirement.

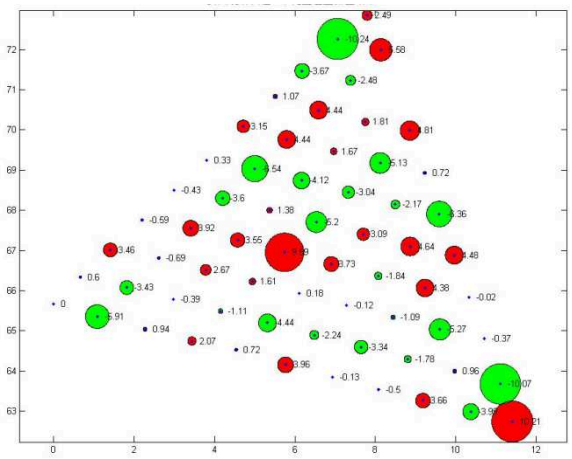

Figure 4 Displacements before adjustment

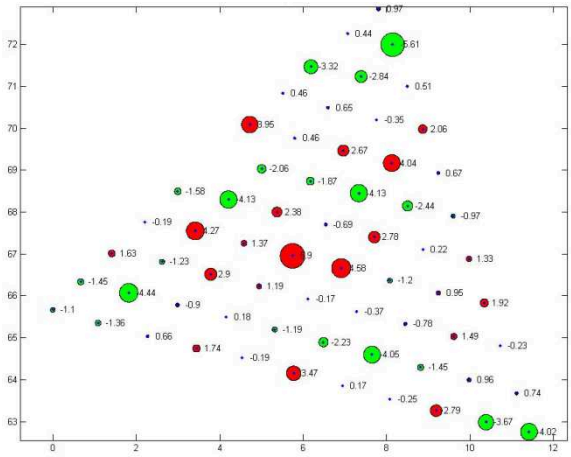

Figure5 Displacements after adjustment

To verify the shape preserving ability of the new aluminum reflector unit, we remeasured it in 2013. Reflector surface displacement of nodes as shown in Figure 6, and RMS=2.42mm. It still met the surface precision requirements of FAST project.

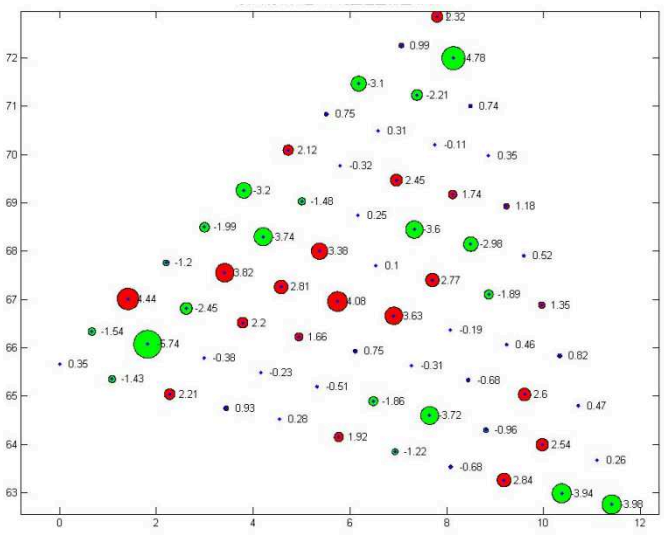

Figure 6 Displacements after three years

Summary

1) The new type aluminum alloy backup frame developed by space grid structure, meets the reflector requirements of FAST. Its stiffness, strength, local stability can be guaranteed;

2) The aluminum alloy backup frame's surface density is only 3.90kg/m^2. Also, the density of whole reflector element including the upper part panel unit is 7.69kg/m^2. That can meet the light weight, easily to manufacture requirements of FAST project.

3) In the past 3 years, the reflector unit can still meet the requirements of precision. The ability of shape preserving and anticorrosive can meet the requirements of FAST project.

References

[1] Nan Rendong. Five hundred meter aperture spherical radio telescope (FAST) [J]. Science in China: SeriesGPhysics, Mechanics & Astronomy,2006,Vol.49, No.2: 129-148.

[2] Nan Rendong, Ren Gexue, Zhu Wenbai, et al. Adaptive cable mesh reflector for the FAST [J]. Acta Astronomica Sinica, 2003, 44: 13-18.

[3] RENDONG NAN, DI LI, CHENGJIN JIN, et al. The five-hundred-meter aperture spherical radio telescope (FAST) project [J]. International Journal of Modern Physics D,Vol.20, No.6(2011)989-1024.

[4] Ministry of Construction of the People's Republic of China. Code for design of aluminum alloy structures (GB50429-2007), 2008.

[5] J.BACKLUND et al., Proc. NALCO-7, Cambridge, 16th April, 1998, pp. 171-181.

[6] Hao Chengxin, Qian Jihong, Song Tao, Zhao Pengfei, Zhao Jida. Research and application of aluminum truss structure [J]. Journal of building structures, Vol.24 No.4, 2003.8.

[7] Qian Jihong, Hong Yong, Hao Chengxin. Aluminum alloy pipe and head assembly, connection method and device.CN 1271798 A [P], 2000.

Advanced Materials Research Vols. 989-994 (2014) pp 705-709
© (2014) Trans Tech Publications, Switzerland
doi:10.4028/www.scientific.net/AMR.989-994.705

Changes in water adsorption desorption isotherms of cement mortars caused by carbonation coupled with humidification-drying cycles

Son Tung Pham

Laboratory of Civil Engineering and Mechanical Engineering, National Institute of Applied Sciences, 35000 Rennes, France

E-mail: spham@insa-rennes.fr

Keywords: Water adsorption; Carbonation; Pore size distribution; Humidification drying cycles

Abstract. The objective of this work was to examine the influence of carbonation on the water vapor adsorption desorption isotherms of cement materials. Two types of Portland mortars, which were CEM I and CEM II, were carbonated at 20°C, 65% relative humidity and 20% of CO_2 concentration. The pore size distributions were determined from the water adsorption method. We also studied the coupling effect between carbonation and humidification-drying cycles. The results showed a reduction in microporosity and a small increase in the mesoporosity. The pores clogging due to formation of calcium carbonate was highlighted by the reduction of the quantity of adsorbed water and the decrease in the hysteresis isotherms. The results of this study also indicated that the humidification-drying cycles coincide only from the second cycle because of a difficult evacuation of water during desorption, even at low humidity.

Introduction

The carbonation is a natural aging process for all cement materials. It corresponds to the progressive transformation of principal constituents of cementitious matrix, the portlandite $Ca(OH)_2$ and the calcium silicate hydrate C-S-H into calcite $CaCO_3$, in contact with the carbon dioxide in the air and in the presence of water in the pores. This transformation is accompanied by a decrease in pH. The principle reactions are:

$$CO_2 + Ca(OH)_2 \rightarrow CaCO_3 + H_2O \quad (1)$$

$$C_xS_yH_z + xH_2CO_3 \rightarrow xCaCO_3 + ySiO_2.tH_2O + (x-t+z)H_2O \quad (2)$$

The progress of these carbonation reactions causes a change in the microstructure, which is highlighted by various parameters such as variations in water content. The carbonation reactions of portlandite and C-S-H indicate that the process releases part of the water of hydrate structures. Therefore, the carbonation at first induces a local accumulation of moisture in the pores. [1] observed an increase in the quantity of evaporable water content in carbonated materials by drying at 105°C. This released water can certainly participate in the composition of the interstitial solution and contribute to the transport of corrosive agents.

This excess water will be discharged after a certain time and the material is in equilibrium with environmental moisture. Houst [2] and Johannesson and Utgenannt [3] observed that, at a given relative humidity, the carbonated mortar contains less water than the non-carbonated one. This decrease in water content is probably due to the reduction in porosity as a result of carbonation. Thus, Meyer [4] found that carbonated concretes dried faster than non-carbonated ones.

Some authors present the water activity by the saturation level and they also find that, for a relative humidity equal to 65%, the saturation ratio of non-carbonated material is higher than that of the carbonated material, which is coherent with the reduction of porosity after carbonation [5], [6].

However, the concrete structures in-situ is also subjected to humidification-drying cycles, which results in a much more complicated water activity. This has motivated us to perform this work in order to approach the laboratory results to in-situ results. In this work, the water activity of non-carbonated and well-carbonated cement mortars were firstly studied using water vapor adsorption. Then we examined effects of humidification-drying cycles on the water activity. The pore size distributions were also calculated from water vapor adsorption desorption isotherms in order to study the microstructural changes caused by carbonation.

Materials and methods

Mortar

The cements used in this study were:

- CEM I 52.5 N PM-ES-CP2
- CEM II / B-M (LL-V) 32.5 R

These cements were fabricated by Lafarge company in accordance with European norm EN 197-1 “Cement – Part 1: Composition, specifications and conformity criteria for common cements”.

The CEM I and CEM II mortars were prepared by mixing respectively the cements CEM I and CEM II with French normalised sand certified in accordance with norm EN 196-1 and ISO 679:2009. The water/cement and sand/cement ratios were 0.5 and 3, respectively. At the end of the mixing, the mortar was placed in cylindrical moulds (Ø = 40 mm, h = 60 mm) and stored in a humid chamber in order to avoid precocious desiccation in the vicinity of the surface exposed to drying. The samples were demoulded after 24 hours and then cured in water for 90 days in a humid chamber (20°C, 100% relative humidity). The cure in water prevents the natural carbonation during storage.

Bier et al. [7] observed the creation of macroporosity after carbonation of a mortar, which was not rich in portlandite and contained fly ash. The CEM II is poor in portlandite in comparison with CEM I, and therefore the CEM II was also chosen for this study because we want to ensure significant changes not only in the micro porosity but also in the domains of meso and macro pores.

Pre-treatment

We employed a method of pre-treatment basing on the work of Thierry [8] and Parrot [9]. The specimens are dried at 105°C until constant weight. Finally, the specimens are placed for 7 days in a climatic chamber at 65% relative humidity. The advantages of this method are to homogenise the internal humidity in the samples and to prevent the natural carbonation during the pre-treatment process.

Carbonation test

To implement the test, the specimens were subjected to CO_2 in an environmentally controlled chamber at 20°C, 65% relative humidity and 20% CO_2 concentration for 32 days to ensure a complete carbonation. The carbonation device consists of a climatic chamber Vötsch VP1300 connected to a CO_2 tank (Figure 1). The concentration of CO_2 in the chamber is controlled by an automatic CO_2 regulator.

Samples collected in carbonated and non-carbonated specimens were then grinded into powders to 80 μm using a mortar – pestle and a sieve, and subsequently used for water adsorption.

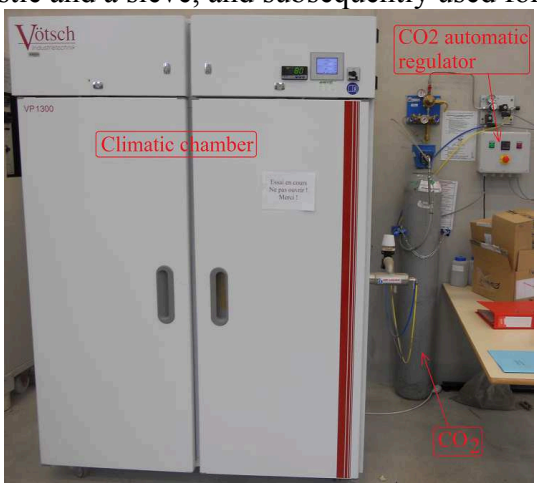

Figure 1. Accelerated carbonation test device

Water adsorption

It is well known that cement paste has a multiscale structure that spreads from the nano- and microstructure to the mesoscopic scale and then to the macroscopic scale, which is visible to the

naked eye. The nano- and microscopic scales consist of sheets of C-S-H. These sheets associated with packets are called grains and constitute a second level of the observation, which is the mesoscopic scale.

We examined the water vapor adsorption on grinding powders originating from the test samples to study the microscopic scale. For this test, we used a humidification regulator connected to the microbalance of the thermal analysis Mettler Toledo machine. The regulator controlled automatically the temperature at 20°C and changed the relative humidity every one hour (Figure 2). The highest relative humidity which can be generated in this device is 95%. Change in mass of the sample was automatically followed by the microbalance. This method is also known as the dynamic adsorption.

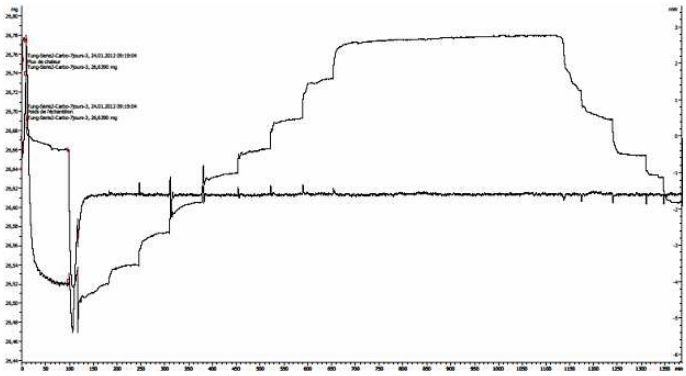

Figure 2. Example of a dynamic sorption test

Results and discussion

The tests were carried out on the powders obtained by grinding samples to 80 μm. In this case, the macroporosity is virtually eliminated and the adsorption takes place essentially in the micropores and mesopores. To study the influence of humidification-drying cycles on the isotherms, we stop the desorption at 10% relative humidity and then proceed the second sorption cycle. The results are presented in Figure 3 for CEM I mortar and in Figure 4 for CEM II mortar. Firstly, we note that the sorption branch of the second cycle is different from that of the first cycle. Secondly, the desorption of the second cycle coincides with the desorption of the first cycle. From this moment, for any cycle, the adsorption branches are coincident with the desorption branches.

As the material was dried at 105°C to constant weight before testing, water molecules in inter layers of C-S-H were indeed evacuated during this deep drying. Then, during the first adsorption cycle, the water molecules returned to the internal structure of the C-S-H. Desorption at 10% relative humidity could not exclude these internal water molecules of C-S-H. This explains why the cycles coincide only from the second adsorption.

Changes in isotherms curves are similar for both types of mortar and can be summarized as follows:

- On the curve of the non-carbonated sample, water is continuously adsorbed until 90% relative humidity. On the contrary, this water is desorbed with difficulty during the desorption step. Only at relative humidity below 20% that much of the water is desorbed. This results in a significant hysteresis of the isotherms.

- On the curve relative to the carbonated sample, a hysteresis is also observed but less marked than that of the non-carbonated sample. This is because the carbonation develops from the inner wall of the pores and eventually tends to homogenize the pore radius whose initial morphology is ink-bottle type (Figure 5).

- Comparing the two types of sample (carbonated and non-carbonated), we note that the isotherms of carbonated samples are generally below the isotherms corresponding to the non-carbonated samples. Thus, at the same relative humidity, the carbonated mortars adsorbed less water than the non-carbonated ones. This is explained by the gradual clogging of the pores by the products of carbonation ($CaCO_3$).

We present in Figure 6 the evolutions of the pore size distributions curves recorded from the reference samples (non-carbonated) and those obtained after carbonation. We observe for both types of mortar a reduction in the microporosity (r <2 nm) and a small variation in the mesoporosity between 2 and 4 nm. The relative changes in porous volume are almost zero beyond 5 nm. The water vapor adsorption desorption isotherms seem therefore poorly adapted to effectively characterize the pores size distribution beyond 5 nm. This is because the steam condensation occurs rapidly in these mesopores.

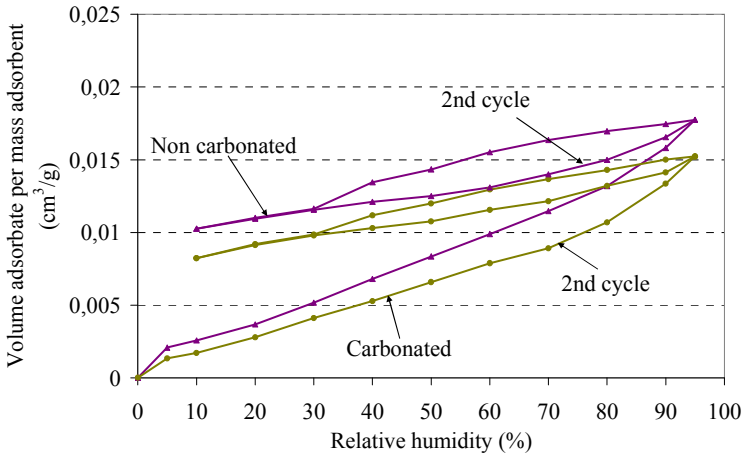

Figure 3. Cycles of water adsorption desorption isotherms of CEM I mortars

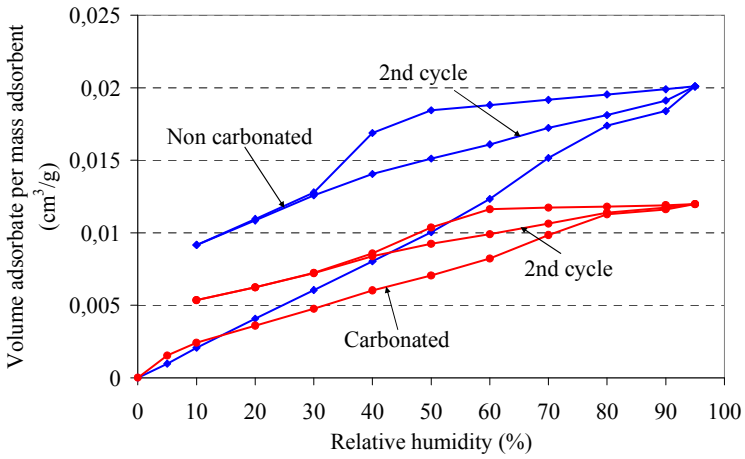

Figure 4. Cycles of water adsorption desorption isotherms of CEM II mortars

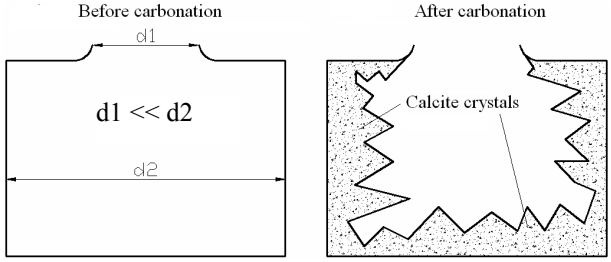

Figure 5. Schematic of ink-bottle pores before and after carbonation.

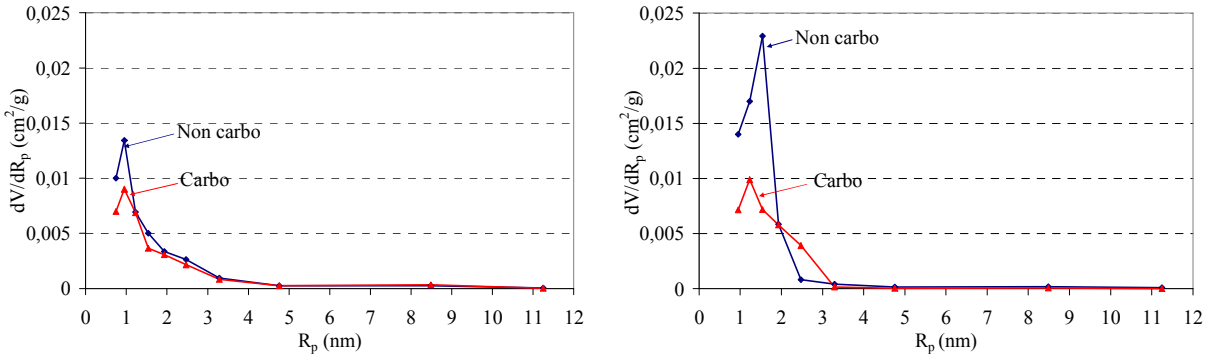

Figure 6. Pores size distribution of CEM I (left) and CEM II mortar (right).

Conclusions

This work was devoted to the study of changes in water adsorption desorption isotherms and in pores size distribution caused by carbonation of Portland cement mortars. The water adsorption results indicated that:

- Firstly, there is a decrease in the volume of micropores with radius smaller than 2 nm, which is due to the shrinkage in the C-S-H structure.
- Secondly, there is a small increase in the volume of mesopores with radius over 2 nm, which highlighted the cracks caused by the carbonation shrinkage.
- Thirdly, carbonated mortars adsorb less water than non-carbonated ones because of pores clogging due to calcium carbonate crystals formed during carbonation. This also induced a homogenization in internal radius of ink-bottle pores, which was highlighted by the reduction in the hysteresis of the isotherms.
- Finally, the results indicated that the water molecules evacuated during drying at 105°C return into the C-S-H microstructure during adsorption and can not be desorbed afterward at low relative humidity even under 10%. This explains why the humidification-drying cycles coincide only from the second cycle.

References

[1] S.E. Pihlajavaara, 1968, Some results of the effect of carbonation on the porosity and pore size distribution of cement past, Materials and Structures, Vol 1, Issue 6, pp. 521-526.
[2] Houst Y.F., The role of moisture in the carbonation of cementitious materials, International journal for restoration buildings monuments, Vol 2, 1996, pp. 49-66.
[3] B. Johannesson, P. Utgenannt, Microstructurals changes caused by carbonation of cement mortar, Cement and concret research, Vol 31, 2001, pp. 925-931.
[4] A. Meyer, 1968, Investigations on the carbonation of concrete, In 5th International Symposium on Cement Chemistry, The Cement Association of Japan, pp. 394-401.
[5] N. Hyvert, Application de l'approche probabiliste à la durabilité des produits préfabriqués en béton, PhD thesis, Université Paul Sabatier – Toulouse III, 2009.
[6] H. Ranaivomanana, Transfers dans les milieux poreux réactifs non saturés : application à la cicatrisation de fissure dans les matériaux cimentaires par carbonatation, PhD thesis, Université Toulouse III – Paul Sabatier, 2010.
[7] T.A. Bier, J. Kropp, H.K. Hilsdorf, The formation of silica gel during carbonation of cementitious systems containing slag cements, Proc. 3rd CANMET/ACI Conf on the Use of Fly ash, Silica Fume, Slag and Natural Pozzolans in Concrete, Trondheim, Norway, Vol 2, 1989, pp. 1413–1428.
[8] M. Thiery, Modelling of atmospheric carbonation of cement based materials considering the kinetic effects and modifications of the microstructure, PhD thesis, L'école nationale des ponts et chausses, 2005.
[9] L.J. Parrott, A review of carbonation in reinforced concrete, Cement and Concrete Association, 1987, 41 pages.

Advanced Materials Research Vols. 989-994 (2014) pp 710-714
© (2014) Trans Tech Publications, Switzerland
doi:10.4028/www.scientific.net/AMR.989-994.710

Research Progress of Sintered Wall Material Products Synchronous Cutting Machine

Hongmei Liu[1, a], Chengqun Wu[2,b], Xin Zhang[3,c] and Yuanbin Xu[2,d]

[1]Engineering Training Center, Nantong University, Nantong, Jiangsu, 226019, China

[2]College of Mechanical Engineering, Nantong University, Nantong, Jiangsu, 226019, China

[3]Office of Nantong Wall Material Innovation, Nantong, Jiangsu, 226001, China

[a]liu.hm@ntu.edu.cn, [b]qywn2013@163.com, [c]ntqgjn@163.com, [d]13100028@yjs.ntu.edu.cn

Corresponding Author: Chengqun Wu. Tel: +86 13962985797. E-mail:qywn2013@163.com.

Keywords: sintered wall material products, synchronous cutting machine, forming quality.

Abstract. By means of raw performance analysis of silt sintered porous brick, the importance of synchronous cutting machine in the molding process was revealed. On basis of the analysis of the present situation of research and application of synchronous cutting machine at home and abroad, according to the forming characteristics of silt sintered porous brick, technical parameters of synchronous cutting machine was explained and the development trend of the synchronous cutting machine was expected.

Introduction

With the implementation of national relevant policies about environmental protection and waste use, building energy saving and so on, some small and medium brick-making enterprises will be faced with shut down because of their backward production facilities, low yield and high energy consumption. This will inevitably cause that a large number of brick-making equipments will be abandoned, directly affect the enterprises which use the rivers and lakes silt as a raw material for the production of sintered wall materials products. There is an urgent need to improve the qualified rate of products and achieve upgrading of enterprises' capacity by optimizing forming process, transforming production equipment, combining enterprises' status and the cost[1]. After a lot of research, it was found that automation degree of brick auxiliary equipments, represented by cutting machine, are not high and ought to be enhanced. They can be regarded as a pilot of small and medium wall material enterprises' automation transformation and ought to get the attention of industry management departments.

Materials performance analysis of of silt sintered porous brick

Silt sintered porous brick take rivers and lakes mud or sludge as the main raw material, pass through scientific and rational hole structure design, appropriately supplemented by rice husk, wood chips as pore-forming when molding, drying and roasting. It is mainly used in non-load-bearing parts of the building wall. It has good characteristics of light weight, energy conservation, thermal insulation and has great application prospect. Using Rivers and lakes silt instead of the traditional clay to produce silt sintered porous brick not only protect farmland, but also make full use of dredged sludge. Silt's physical and chemical properties is basically the same as clay's. Its plasticity index basically reached the requested range of sintered porous brick. But its sticky particles content, water-retaining property and accepted control range of molding moisture content are inferior to clay's, and this increases the difficulty of controlling the production of molded body. Therefore, there is an urgent need to improve the performance of molding equipment[2-4].

A issued revised standard of China GB13544-2012 Sintered Porous Brick and Block, has been implemented at April 1, 2012. The new standard provides that all products are used rectangular hole or rectangular bar hole. Holes rate is increased from $\geq 25\%$ to $\geq 28\%$, the density level indicators are

enhanced and the decision criteria of intensity level, size of the deviation and weathering performance get increased. This will definitely make it more difficult to produce and ask higher requests on cutting machine.

Domestic Situation

In recent years, with the rapid development of brick machinery equipment in china, development of synchronous cutting machine has made enormous progress, brick enterprise basically gets rid of manual cutting mode of production. Manual cut makes use of manpower to push and pull wire frame which forms a right angle with article billet, and it can cut a article billet by pushing or pulling every time. Because the article billet is continuously extruded from the host machine, the manual cut can't achieve the synchronization with the article billet in the pushing and pulling progress, which billet constantly keep moving forward. In the pushing or pulling progress, wire is cut to the left or the right, leading beginning billet side to be short, and the end side to be long. According to the walking speed and cutting length of the article billet, of which cutting surface becomes the angle slope, it does not come true to ensure that the section is a right angle. China has issued a revised standard JC/T-2011 Building Industrial Automatic Cutting Machine, which has been implemented in July 1, 2012. New standard adds the unlabeled shape and position tolerance and load test time requirements on the pattern when automatic cutting machine installs, which puts forward higher requirements for development of automatic cutting machine. There are two common types of automatic cutting machine in the domestic market and brick company. They are rotary wire synchronous cutting machine and synchronous vertical cutting machine.

Rotary wire synchronous cutting machine. Rotary synchronous cutting machine relies on friction produced from billet and roll strip on the bracket, promotes the main roller of maximum diameter to turn, drives the cutting bow to do rotary motion under the action of sprockets and gears, and finishes cutting billet off.

This typological cutting machine has advantages of manual work saving, stable billet's length, convenient operation, low investment cost and power savings, which is widely used in the domestic small and medium-sized brick enterprises. But when rotary wire synchronous cutting machine is used to cut, cutting section is arcuate instead of flat, so in the next process that is the progress of cutting billet, it will have waste by reason of more cost of both ends of premium billet. In addition, the dynamic movement of rotary wire and cutting bow comes from friction produced by billet and active roll tightly in the forward process, because its friction is limited, when billet's moisture content has less that is hard billet, under the satiation that the cutting bow operation has great resistance, cutting is easy to cause lateral deformation and destroy section size and smoothness of wet slab, even having a phenomenon of cutting difficultly.

In view of these above issues, researchers have made improvements. To change the running line of cutting bow obtain a vertical and flat cutting sections and greatly reduce the waste of a billet's head during cutting of the wire running routes [5], to increase the sending device composed of electric motors, rollers, gear wheels and belts quickly send billet to the cutting table and reduce manual work consumption. But disadvantages of limited cutting force and poor stability can't be solved, costs have been raised.

Synchronous vertical cutting machine. Synchronous vertical cutting machine is mainly composed of cutting device, control device and clay device. Its cutting device can slide back and forth on the track, and can be synchronized car which realizes synchronized movement with clay bar. When length of clay bar reaches the set value, synchronized car and mud sport moves forward, and complete the action of cutting clay. After the clay cutting is finished, synchronous control mechanism releases clay bar and quickly start motor to take the clay to cutting table, clay cutting device returns to the initial position and prepare for the next cutting action under the action of returning device. Clay cutting device commonly consists of fixing drive of cutting clay wire and driving power that realizes cutting movement. Driving power usually is provided for cylinder [6].

Some advanced brick and building material enterprises devote themselves to research and application of synchronous vertical cutting machine in the domestic state. This cutting length of

typological synchronous cutting machine can be set continuously, cutting speed can reach to 1.25m/s, power is in the 1.5kW, entire working process is controlled by the PLC automation, cutting efficiency and section quality have been significantly improved. SQT500x300-Nai vertical cutting machine produced by Shandong Mining Machinery Maike Building Materials Machinery Limited Company is mainly used for cutting vertically clay bar extruded from vacuum extruder, and same length clay bars accelerate delivery to a blank conveying machine. The cutting steel wire of cutting machine have pneumatic tension, wire tension can be adjusted for different products, wire has sharp cutting, long service life, and flat brick section. Its working process is controlled by the PLC automation, the driven shaft of a blank conveying machine is equipped with sensors before cutting, which can take speed of clay to feedback accurately to the control center. The drives cutting frame and clay to do synchronous motion, making clay section and the bottom surface perpendicular, which reduces greatly clay's waste[7].

Present situation of overseas

After decades of development, synchronous cutting machine used for the production of sintered wall materials has a variety of types such as the products of United States Steele, France Ceric, Italy Cosmec and Bedeschl, Germany Keller and Lingl and Netherlands Debao. Synchronous cutting machine control technology continues to improve, in order to achieve structural optimization, and ultimately improve cut quality and brick yield[8]. In addition, the forming process of brick such as extrusion, transmission, billet cutter and setting are integrated so that a high degree of intelligence and automation is gain, the cycle time is further shortened and processing efficiency is improved.

Overseas equipment companies always take parameters such as maximum cutting width (TB), maximum cutting length (TS) and maximum cutting height (TH) to measure the performance of cutting machine. They provide more than one cutting table to meet the production requirements of different size products and the performance of each table is instructed detailedly. Their cutting machine are equipped with automatic wire cleaning, expanding and feeding device. This can improve wire's service life drastically. The universal cutting machine produced by Keller, a German company, can cut different sizes of strips by using different cutting platform. Its rack is welded by steel structure and the speed of the strips is measured by means of measuring roller/measuring belt with pulser. The high cutting accuracy is achieved by electronic control and maximum cutting frequencies up to 60 times per minute. It is fitted with wire cleaning and tightening devices. The machine has compact structure, high working efficiency and universality.

Most wall material enterprises just take cutting speeds, equipped with power and overall dimensions as the technical parameters of cutting machine. They have no detailed instructions about product specifications and their cutting machine are not equipped with automatic wire cleaning, expanding and feeding device. Wire's working life is short and it is usually changed a time between 15-30 minute, which cause greet loss. Therefore, optimizing the cutting machine of the whole structure, improving working life of wire and cutting machine's commonality can improve their efficiency. This should become the focus of the study.

Core technical parameters discussion

According to molding characteristics of silt sintered porous brick and application status of cutting machine, several requests about designing and manufacturing synchronous cutting machine are made as follow.

Rack and cutter. Rack designment requires full consideration of their structure reasonability on the basis of ensuring stability. Simplifying Frame structure as far as possible and reducing its quality can reduce the manufacturing cost of synchronous cutting machine.

Cutting machine tool is usually a thin wire or strip blades, wire is widely used. High quality durable tool is the precondition of improving the quality of cut surface and ensuring cutting machine work continuously. The main methods of increasing tool working life are shown as follow: (1) Using high quality steel or taking rust prevention, cold treatment and copper plating on steel wire surface.

Steel carbon spring steel wire (like 65 and 70 wire), set of spring wires (65Mn), strings of steel wire are commonly used, of which the latter's quality is better. (2) Using tension spring as the tool's compression spring so that major telescopic allowance is left when wire contact with hard objects. (3) Increasing the steel angle appropriately, reducing the cutting force and adjusting wire position. (4) Achieving wire's auto-feed. The cutting wire produced by Wienerberger, the world's largest brick and tile manufacturing enterprise, is continuous. Cutting 70 times, wire auto-feed a time. It ensures the uninterrupted production of extruders, significantly reduces wire breakage or replacement wire downtime caused by loss and increases production efficiency[9].

Control system. Cutting machine control systems, PLC, with its superior performance, is gradually replacing the traditional manual control and relay control. Traditional manual control has disadvantages of complex mechanical structure, poor reliability and low production efficiency. Relay's automation degree is increased, but the difficulties of debugging and fault diagnosis limit its further development. Compared to these two forms above, it has outstanding advantages of flexibility, high reliability and strong anti-interference capacity. At present, PLC programmable controller is used as most synchronous cutting machine control system and its advanced technology was mainstream direction. But relay-contact control circuit is still in use. Its technology is lower. Maintenance electrician level is not high when using this kind system so that there is a certain market and this control will be phased out[10-12].

Drive. Precise adjustable drive unit is the key to improve the efficiency of cutting machine, is a prerequisite for achieving cutting machine trouble-free production. For synchronous cutting machine, regardless of hydraulic drive device, pneumatic drive device, electric drive device, or composite form, all of the intended action can be controlled accurately, the appropriate feedback can be made and high quality efficient process can be gain if suitable matching relationship between drive and control system is established[13].

Conclusion and prospect

Synchronous cutting machine's performance is an important factor affecting silt sintered porous brick molding quality. On the basis of the existing advanced manufacturing and control technology, taking green and environmental protection as the idea, taking efficiency and low-cost as the target, increasingly requests are made to synchronous cutting machine in terms of structure optimization, control precision, stability, intelligentization and so on. Combining with enterprise's status, on the premise of without a significant increase in business costs, improving automation degree of brick machine auxiliary production represented by synchronous cutting machine can enhance products' qualified rate, realize enterprise capacity upgrades, promote structural adjustment and upgrading of the brick and tile industry and new wall material enterprises.

Acknowledgements
This research was supported by grant 2013-742-2 from the Economic and Information Commission of JiangSu Province of China.

First Author

Name: Hongmei Liu. Tel:+86 13706293646. E-mail address: liu.hm@ntu.edu.cn.

References

[1] F.Su: Enterprise Economy Vol. 07 (2011), p. 124-126.

[2] H.M.Liu, X.Y.Lu, A.D.Zhu, et al: New Building Material Vol. 09 (2011), p. 42-44.

[3] Hongtao He, Qinyan Yue, Yuan Su, et al. Preparation and mechanism of the sintered bricks produced from Yellow River silt and red mud[J]. Journal of Hazardous Materials, 2012 (203–204):53-61.

[4] X.Zhang, X.H.Zhu, A.D.Zhu, et al: Wall materials innovation and building energy conservation Vol. 12 (2012), p. 18-26.

[5] L.J.Li: machinery Vol. 05 (1990), p. 23-26.

[6] Z.Y.Hao: Brick and Tile Vol. 08 (2007), p. 45-46.

[7]L.Xiao,S.W.Zhao:Wall materials innovation and building energy conservation,01,pp.60-61,2008.

[8] B.J.Cui: Brick and Tiles Vol. 11 (2011), p. 82-86.

[9] Xiaoli Li, Alexandar Djordjevich, and Patri K. Venuvinod. Current-sensor-based feed cutting force intelligent estimation and tool wear condition monitoring[J]. Industrial Electronics, 2000, 47(2):697-702.

[10] Defu Zhang, Mingjian Huang, Cuicui Xu, et al. The Principle of PLC and Application in Construction Materials Industry[C].In: 2009 International Workshop on Information Security and Application (IWISA 2009). China, QingDao, 2009.

[11] D.F.Zhang: Jinan University, 2010.

[12] Machado C, Fonseca J, and Mendes J. Automatic velocity control in cutting-off machines[J]. Industrial Technology,2003,2(10):1046-1051.

[13] C.Liu, S.D.Zhao: Mechanical Science and Technology Vol. 06 (2013), p. 796-800.

Advanced Materials Research Vols. 989-994 (2014) pp 715-718
© (2014) Trans Tech Publications, Switzerland
doi:10.4028/www.scientific.net/AMR.989-994.715

The Higher Order Crack Tip Fields for Anti-plane Crack in Linear Functionally Graded Piezoelectric Materials

Dai Yao[1, a], Chong Xiao[1, b], Li Shimin[2,b]

[1]The Academy of Armored force Engineering, Beijing, 100072

[2]Beijing Special Vehicle Institute, Beijing, 100072

[a]dai_yao@sina.com, [b]chongxiao2005@163.com

Keywords: higher order fields, linear FGPMs, eigen-expansion method, anti-plane crack

Abstract. The crack tip field in functionally graded piezoelectric materials (FGPMs) under mechanical and electrical loadings is studied. Different from previous analyses, all material properties of the functionally graded piezoelectric materials are assumed to be linear function of *y* perpendicular to the crack. The crack surfaces are supposed to be insulated electrically. Similar to the Williams' solution of homogeneous elastic materials, the higher order crack tip fields of FGPMs are obtained by the eigen-expansion method.

Introduction

Functionally graded piezoelectric materials (FGPMs) are composites with continuously varying properties that have significant advantages over discretely layered materials. Such a gradient can be obtained from a resistivity non-uniformity introduced into the PZT ceramic, it can be done by doping it with small amounts of various additives, or by stacking piezoelectric composites of different compositions on the top of each other [1]. Therefore, it is of great importance to study the fracture behavior of FGPMs. Ma et al. [2] investigated the electro-elastic behavior of a Griffith's crack in a functionally graded piezoelectric strip. Ou [3] studied the internal crack problem located within one functionally graded piezoelectric strip. The crack is normal to the edge of the strip and the material properties vary along the direction of crack length. Hsu [4] investigated the fracture behavior of an arbitrarily oriented crack in a functionally graded piezoelectric material subjected to anti-plane mechanical and in-plane electric loads. To make the analysis tractable, in all of the above mentioned references the material properties are assumed to be an exponential function. To our knowledge, none of the literature has reported the analysis for fracture mechanics of linear FGPMs. In this paper, we attempt to obtain the higher order mechanical and electric crack tip fields by eigen- expansion method.

Basic equations

It is assumed that there is a crack of length $2L$ in functionally graded piezoelectric material planes, as shown in Fig.1. The FGPM is poled in the *z* direction and isotropic in the *xoy* plane. It is loaded by anti-plane shear tractions and in-plane electric displacements, the crack is electrically impermeable and the crack surfaces are traction free. The present work employs the following linear functions to describe the continuous variations of material properties,

$$c_{44} = c_{440}(1+\beta y), \quad e_{15} = e_{150}(1+\beta y), \quad \varepsilon_{11} = \varepsilon_{110}(1+\beta y) \tag{1}$$

where c_{44} is the shear modulus, e_{150} is the piezoelectric coefficient, ε_{110} is the dielectric parameter at $y = 0$.

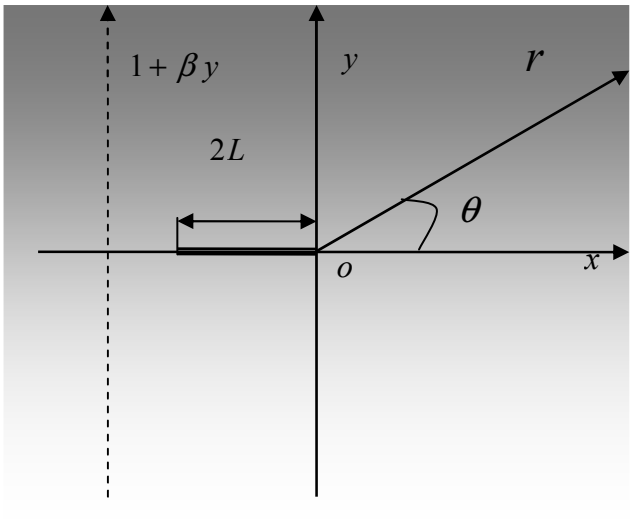

Fig.1Anti-plane crack in FGPMs

The governing equations can be written as

$$\begin{aligned}\nabla^2 w+\frac{\beta}{1+\beta r\sin\theta}(\sin\theta\frac{\partial w}{\partial r}+\frac{1}{r}\cos\theta\frac{\partial w}{\partial\theta})=0\\ \nabla^2\phi+\frac{\beta}{1+\beta r\sin\theta}(\sin\theta\frac{\partial\phi}{\partial r}+\frac{1}{r}\cos\theta\frac{\partial\phi}{\partial\theta})=0\end{aligned}\tag{2}$$

where $\nabla^2=\frac{\partial^2}{\partial r^2}+\frac{1}{r}\frac{\partial}{\partial r}+\frac{1}{r^2}\frac{\partial^2}{\partial\theta^2}$ is the two-dimensional Laplace operator.

The higher order crack-tip field

The displacement component w and the electric potential ϕ can be expanded as follows

$$w=\sum_{i=1}^{\infty}r^{\frac{i}{2}}w_i(\theta),\qquad \phi=\sum_{i=1}^{\infty}r^{\frac{i}{2}}\phi_i(\theta)\tag{3}$$

where, $w_i(\theta)$ and $\phi_i(\theta)$ are eigen-functions.

Substitute Eq. (3) into Eq.(2). According to the linear independence of $r^{-3/2}$, r^{-1}, $r^{-1/2}$,…, $r^{i/2-2}$,…, the system of ordinary differential equations are obtained.

$$\begin{cases}\frac{1}{4}\mathbf{w}_1(\theta)+\frac{\partial^2\mathbf{w}_1}{\partial\theta^2}=0\\ \mathbf{w}_2(\theta)+\frac{\partial^2\mathbf{w}_2}{\partial\theta^2}=0\\ \cdots\\ \frac{i^2}{4}\mathbf{w}_i+\frac{\partial^2\mathbf{w}_i}{\partial\theta^2}+\beta[\frac{i(i-2)}{4}\sin\theta\mathbf{w}_{i-2}+\cos\theta\frac{\partial\mathbf{w}_{i-2}}{\partial\theta}+\sin\theta\frac{\partial^2\mathbf{w}_{i-2}}{\partial\theta^2}]=0\\ \cdots\end{cases}\tag{4}$$

where $\mathbf{w}=\begin{bmatrix}w\\ \phi\end{bmatrix}$.

In the case of electrically impermeable crack, the crack surfaces are free of electric charges and the electric displacement inside the crack is zero. As the crack surface is free, the boundary conditions are

$$\sigma_{zy}\big|_{\theta=\pm\pi}=0,\ \ D_y\big|_{\theta=\pm\pi}=0 \tag{5}$$

Further, they can be expressed as

$$w_i'(\pm\pi)=0 \qquad \phi_i'(\pm\pi)=0 \tag{6}$$

Solving the system of ordinary differential equations, we can obtain the results

$$\begin{cases} w_1(\theta)=A_{11}\sin\dfrac{\theta}{2} \\ w_2(\theta)=A_{21}\cos\theta \\ w_3(\theta)=A_{31}\sin\dfrac{3\theta}{2}-\dfrac{1}{12}\beta A_{11}\cos\dfrac{3\theta}{2}-\dfrac{1}{4}\beta A_{11}\cos\dfrac{\theta}{2} \\ w_4(\theta)=A_{41}\cos 2\theta \\ w_5(\theta)=A_{51}\sin\dfrac{5\theta}{2}+\dfrac{1}{20}\beta A_{31}\cos\dfrac{5\theta}{2}+\dfrac{3}{32}A_{11}\beta^2\sin\dfrac{3\theta}{2}+\dfrac{1}{16}\beta^2 A_{11}\sin\dfrac{\theta}{2}-\dfrac{1}{4}\beta A_{31}\cos\dfrac{\theta}{2} \\ w_6(\theta)=A_{61}\cos 3\theta-\dfrac{1}{12}\beta A_{41}\sin 3\theta+\dfrac{1}{4}\beta A_{41}\sin\theta \\ \cdots\cdots \end{cases} \tag{7}$$

$$\begin{cases} \phi_1(\theta)=B_{11}\sin\dfrac{\theta}{2} \\ \phi_2(\theta)=B_{21}\cos\theta \\ \phi_3(\theta)=B_{31}\sin\dfrac{3\theta}{2}-\dfrac{1}{12}\beta B_{11}\cos\dfrac{3\theta}{2}-\dfrac{1}{4}\beta B_{11}\cos\dfrac{\theta}{2} \\ \phi_4(\theta)=B_{41}\cos 2\theta \\ \phi_5(\theta)=B_{51}\sin\dfrac{5\theta}{2}+\dfrac{1}{20}\beta B_{31}\cos\dfrac{5\theta}{2}+\dfrac{3}{32}B_{11}\beta^2\sin\dfrac{3\theta}{2}+\dfrac{1}{16}\beta^2 B_{11}\sin\dfrac{\theta}{2}-\dfrac{1}{4}\beta B_{31}\cos\dfrac{\theta}{2} \\ \phi_6(\theta)=B_{61}\cos 3\theta-\dfrac{1}{12}\beta B_{41}\sin 3\theta+\dfrac{1}{4}\beta B_{41}\sin\theta \\ \cdots\cdots \end{cases} \tag{8}$$

where: A_{ij} and B_{ij} are the undetermined coefficients.

Substituting Eq. (7) and (8) into Eq.(3),the displacement component w and the electric potential ϕ are obtained.

$$\begin{aligned} w=&r^{\frac{1}{2}}A_{11}\sin\frac{\theta}{2}+rA_{21}\cos\theta+r^{\frac{3}{2}}(A_{31}\sin\frac{3\theta}{2}-\frac{1}{12}\beta A_{11}\cos\frac{3\theta}{2}-\frac{1}{4}\beta A_{11}\cos\frac{\theta}{2})+r^2A_{41}\cos 2\theta \\ &+r^{\frac{5}{2}}(A_{51}\sin\frac{5\theta}{2}+\frac{1}{20}\beta A_{31}\cos\frac{5\theta}{2}+\frac{3}{32}A_{11}\beta^2\sin\frac{3\theta}{2}+\frac{1}{16}\beta^2A_{11}\sin\frac{\theta}{2}-\frac{1}{4}\beta A_{31}\cos\frac{\theta}{2})+ \\ &r^3(A_{61}\cos 3\theta-\frac{1}{12}\beta A_{41}\sin 3\theta+\frac{1}{4}\beta A_{41}\sin\theta)+\cdots \\ \phi=&r^{\frac{1}{2}}B_{11}\sin\frac{\theta}{2}+rB_{21}\cos\theta+r^{\frac{3}{2}}(B_{31}\sin\frac{3\theta}{2}-\frac{1}{12}\beta B_{11}\cos\frac{3\theta}{2}-\frac{1}{4}\beta B_{11}\cos\frac{\theta}{2})+r^2B_{41}\cos 2\theta \\ &+r^{\frac{5}{2}}(B_{51}\sin\frac{5\theta}{2}+\frac{1}{20}\beta B_{31}\cos\frac{5\theta}{2}+\frac{3}{32}B_{11}\beta^2\sin\frac{3\theta}{2}+\frac{1}{16}\beta^2B_{11}\sin\frac{\theta}{2}-\frac{1}{4}\beta B_{31}\cos\frac{\theta}{2})+ \\ &r^3(B_{61}\cos 3\theta-\frac{1}{12}\beta B_{41}\sin 3\theta+\frac{1}{4}\beta B_{41}\sin\theta)+\cdots \end{aligned} \tag{9}$$

Then,the stress and the electric displacement components can be obtained

$$\begin{aligned} &\tau_{xz} = c_{44} w_{,x} + e_{15} \phi_{,x}, \ \tau_{yz} = c_{44} w_{,y} + e_{15} \phi_{,y} \\ &D_x = e_{15} w_{,x} - \varepsilon_{11} \phi_{,x}, \ D_y = e_{15} w_{,y} - \varepsilon_{11} \phi_{,y} \end{aligned} \tag{10}$$

Further,the stress and the electric displacement components can be obtained. The mode III stress intensity factor (SIF) and electric displacement intensity factor (EDIF) of the crack tip are defined as

$$\begin{cases} K^T = \lim\limits_{r \to 0} \sqrt{2\pi r} \sigma_{yz}(r,0) = \dfrac{\sqrt{2\pi}}{2} (c_{440} A_{11} - e_{150} B_{11}) \\ K^D = \lim\limits_{r \to 0} \sqrt{2\pi r} D_y(r,0) = \dfrac{\sqrt{2\pi}}{2} (e_{150} A_{11} + \varepsilon_{110} B_{11}) \end{cases} \tag{11}$$

Conclusion

The higher order crack-tip mechanical and electric fields for linear FGPMs are obtained by the methods of eigen-expansion in this paper. The first two items of crack-tip higher order asymptotic fields of FGPMs have the same mathematical form as ones of homogeneous piezoelectric material. The non-homogeneous material parameter β first appeared in the third order asymptotic field and β^2 items in the fifth order one. The stronger effect of non-homogeneity reflects in the higher order items. The explicit expression of stress intensity factor and electric displacement intensity factor are presented. The coupling effect between mechanical and electrical quantities at the crack tip can be recognized from the expression.

Acknowledgements

The research is supported by the National Natural Science Foundation of China (No11172332.)

References

[1] S.M. Kwon: Acta Mechanica. Vol.167 (2004), p. 73

[2] L. Ma, L.-Z. Wu, Z.-G. Zhou, L.-C. Guo: Composite Structures. Vol.69 (2005), p. 294

[3] Y.-L. Ou, C.-H. Chue: International Journal of Solids and Structures. Vol.43 (2006), p. 6148

[4] W.-H. Hsu, C.-H. Chue: Journal of the Chinese Institute of Engineers. Vol.32 (2009), p. 383

Advanced Materials Research Vols. 989-994 (2014) pp 719-722
© (2014) Trans Tech Publications, Switzerland
doi:10.4028/www.scientific.net/AMR.989-994.719

The Crack Tip Fields for Anti-plane Interfacial Crack Between Functionally Graded and Homogeneous Piezoelectric Materials

Dai Yao[1, a], Chong Xiao[1, 2,b]

[1]The Academy of Armored Force Engineering, Beijing, 100072

[2]Changping Sergeant School, Academy of Equipment, Beijing, 102200

[a]dai_yao@sina.com, [b]chongxiao2005@163.com

Keywords: crack tip fields, piezoelectric materials, interfacial crack, weak-discontinuity

Abstract. The problem of an anti-plane crack situated in the interface of functionally graded piezoelectric materials (FGPMs) and homogeneous piezoelectric materials (HPMs) is considered under the impermeable assumption of crack surfaces. The mechanical and electrical properties of the FGPMs are assumed to be exponential functions of y perpendicular to the crack. The higher order crack tip stress and electric displacement fields for FGPMs and HPMs are obtained by the eigen-expansion method. The stress intensity factor and electric displacement intensity factor are obtained explicitly.

Introduction

Due to their brittleness, the fracture problems of a cracked body in piezoelectric materials have been investigated in recent years. In particular, they have been attracted extensive attention in order to meet the demand of high strength and high temperature applications. However, for the interfacial crack problem of piezoelectric materials, some results have been reported. Li and Lee [1] solved anti-plane fracture for the weak-discontinuous interface in a non-homogeneous piezoelectric bi-material structure. Li et al. [2] investigated the problem of a penny-shaped interfacial crack between a functionally graded piezoelectric layer and a homogeneous piezoelectric layer. Furthermore, Zhang et al. [3] studied the dynamic interaction of two collinear interfacial cracks between two dissimilar functionally graded piezoelectric/piezomagnetic material strips subjected to the anti-plane shear harmonic stress waves. Ing and Chen [4] investigated the transient response of an interfacial crack between two functionally graded piezoelectric strips. It is worth noting that these literatures on interfacial crack of piezoelectric materials are focused on the singular part of crack tip fields. The fracture behavior of an interfacial crack between FGPMs and HPMs has not been studied by using the eigen-expansion method. The purpose of this paper is to present the higher order fields and explicit expression of intensity factors.

Basic equations

Fig. 1 shows the configuration of FGPMs bonded to HPMs denoted as materials 1 and 2, respectively. Consider an impermeable crack of length $2L$ located at the interface subjected to anti-plane shear loads and the in-plane electric displacements. The material properties of the FGPM are assumed as the following exponential forms

$$c_{44}^{(1)} = c_{44}^{(2)} e^{\beta y}, \quad e_{15}^{(1)} = e_{15}^{(2)} e^{\beta y}, \quad \varepsilon_{11}^{(1)} = \varepsilon_{11}^{(2)} e^{\beta y} \tag{1}$$

where $c_{44}^{(2)}$ is the shear modulus, $e_{15}^{(2)}$ is the piezoelectric coefficient, $\varepsilon_{11}^{(2)}$ is the dielectric parameter of the HPM.

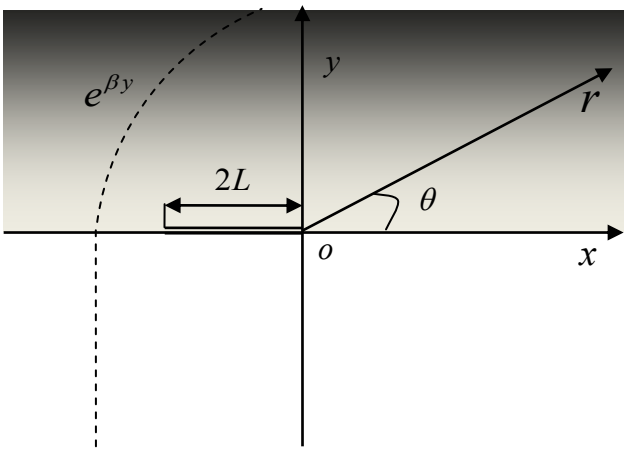

Fig.1Anti-plane interface crack

Since the poling directions of piezoelectric materials are orientated along z -axis, the anti-plane mechanical field and in-plane electrical field are coupled. The governing equations can be written as

$$\nabla^2 \mathbf{w}^{(k)} + \delta_{1k}\beta[\sin\theta \frac{\partial \mathbf{w}^{(k)}}{\partial r} + \frac{1}{r}\cos\theta \frac{\partial \mathbf{w}^{(k)}}{\partial \theta}] = 0 \ k = 1,2 \tag{2}$$

where $\mathbf{w}^{(k)} = \begin{bmatrix} w^{(k)} \\ \phi^{(k)} \end{bmatrix}$, $\nabla^2 = \frac{\partial^2}{\partial r^2} + \frac{1}{r}\frac{\partial}{\partial r} + \frac{1}{r^2}\frac{\partial^2}{\partial \theta^2}$ is the two-dimensional Laplace operator and δ_{1k} is the Kronecker delta.

The higher order crack-tip fields

The displacement component w and the electric potential ϕ can be expanded as follows

$$w^{(k)} = \sum_{i=1}^{\infty} r^{\frac{i}{2}} w_i^{(k)}(\theta), \qquad \phi^{(k)} = \sum_{i=1}^{\infty} r^{\frac{i}{2}} \phi_i^{(k)}(\theta) \tag{3}$$

where, $w_i^{(k)}(\theta)$ and $\phi_i^{(k)}(\theta)$ are eigen-functions.

Substitute Eq. (3) into Eq.(2). According to the linear independence of $r^{-3/2}$, r^{-1}, $r^{-1/2}$,…, $r^{i/2-2}$,…, we obtained the system of ordinary differential equations

$$\begin{cases} \frac{1}{4}\mathbf{w}_1^{(k)}(\theta) + \frac{\partial^2 \mathbf{w}_i^{(k)}}{\partial \theta^2} = 0 \\ \mathbf{w}_2^{(k)}(\theta) + \frac{\partial^2 \mathbf{w}_2^{(k)}}{\partial \theta^2} = 0 \\ \cdots \\ \frac{i^2}{4}\mathbf{w}_i^{(k)} + \frac{\partial^2 \mathbf{w}_i^{(k)}}{\partial \theta^2} + \delta_{1k}\beta[\frac{i-2}{2}\sin\theta \mathbf{w}_{i-2}^{(k)} + \cos\theta \frac{\partial \mathbf{w}_{i-2}^{(k)}}{\partial \theta}] = 0 \\ \cdots \end{cases} \tag{4}$$

In the case of electrically impermeable crack, the crack surfaces are free of electric charges and the electric displacement inside the crack is zero. As the crack surface is free, the boundary conditions are

$$\sigma_{zy}^{(1)}\Big|_{\theta=\pi} = 0, \ D_y^{(1)}\Big|_{\theta=\pi} = 0, \ \sigma_{zy}^{(2)}\Big|_{\theta=-\pi} = 0, \ D_y^{(2)}\Big|_{\theta=-\pi} = 0 \tag{5}$$

Further, they can be expressed as

$$\frac{\partial \mathbf{w}_i^{(1)}}{\partial \theta}(\pi) = 0, \quad \frac{\partial \mathbf{w}_i^{(2)}}{\partial \theta}(-\pi) = 0 \tag{6}$$

Solving the system of ordinary differential equations, we can obtain the results

$$\begin{cases} \mathbf{w}_1^{(1)}(\theta) = \mathbf{A}_{11}\sin\dfrac{\theta}{2} \\ \mathbf{w}_2^{(1)}(\theta) = \mathbf{A}_{21}\cos\theta \\ \mathbf{w}_3^{(1)}(\theta) = \mathbf{A}_{31}\sin\dfrac{3\theta}{2} - \dfrac{1}{12}\beta\mathbf{A}_{11}\cos\dfrac{3\theta}{2} - \dfrac{1}{4}\beta\mathbf{A}_{11}\cos\dfrac{\theta}{2} \\ \mathbf{w}_4^{(1)}(\theta) = \mathbf{A}_{41}\cos 2\theta \\ \mathbf{w}_5^{(1)}(\theta) = \mathbf{A}_{51}\sin\dfrac{5\theta}{2} + \dfrac{1}{20}\beta\mathbf{A}_{31}\cos\dfrac{5\theta}{2} + \dfrac{1}{32}\mathbf{A}_{11}\beta^2\sin\dfrac{3\theta}{2} + \dfrac{1}{48}\beta^2\mathbf{A}_{11}\sin\dfrac{\theta}{2} - \dfrac{1}{4}\beta\mathbf{A}_{31}\cos\dfrac{\theta}{2} \\ \mathbf{w}_6^{(1)}(\theta) = \mathbf{A}_{61}\cos 3\theta - \dfrac{1}{12}\beta\mathbf{A}_{41}\sin 3\theta + \dfrac{1}{4}\beta\mathbf{A}_{41}\sin\theta \\ \ldots\ldots \end{cases} \tag{7}$$

$$\begin{cases} \mathbf{w}_1^{(2)}(\theta) = \mathbf{C}_{11}\sin\dfrac{\theta}{2} \\ \mathbf{w}_2^{(2)}(\theta) = \mathbf{C}_{21}\cos\theta \\ \mathbf{w}_3^{(2)}(\theta) = \mathbf{C}_{31}\sin\dfrac{3\theta}{2} \\ \mathbf{w}_4^{(2)}(\theta) = \mathbf{C}_{41}\cos 2\theta \\ \mathbf{w}_5^{(2)}(\theta) = \mathbf{C}_{51}\sin\dfrac{5\theta}{2} \\ \mathbf{w}_6^{(2)}(\theta) = \mathbf{C}_{61}\cos 3\theta \\ \ldots\ldots \end{cases} \tag{8}$$

where $\mathbf{A}_{ij} = \begin{bmatrix} A_{ij} \\ B_{ij} \end{bmatrix}$, $\mathbf{C}_{ij} = \begin{bmatrix} C_{ij} \\ D_{ij} \end{bmatrix}$ are the undetermined coefficients.

Substituting Eq. (7) and (8) into Eq.(3), the displacement component and the electric potential for the FGPM and HPM regions are obtained. Then the stress and electric displacement fields will be obtained based on constitutive relations as

$$\begin{aligned} &\tau_{xz}^{(k)} = c_{44}^{(k)} w_{,x}^{(k)} + e_{15}^{(k)} \phi_{,x}^{(k)}, \ \tau_{yz}^{(k)} = c_{44}^{(k)} w_{,y}^{(k)} + e_{15}^{(k)} \phi_{,y}^{(k)} \\ &D_x^{(k)} = e_{15}^{(k)} w_{,x}^{(k)} - \varepsilon_{11}^{(k)} \phi_{,x}^{(k)}, \ D_y^{(k)} = e_{15}^{(k)} w_{,y}^{(k)} - \varepsilon_{11}^{(k)} \phi_{,y}^{(k)} \end{aligned} \tag{9}$$

The mechanical and electric conditions must satisfy the following continuity conditions along the interface

$$\tau_{yz}^{(1)}|_{\theta=0} = \tau_{yz}^{(2)}|_{\theta=0}, \quad D_y^{(1)}|_{\theta=0} = D_y^{(2)}|_{\theta=0} \tag{10}$$

Substituting Eq. (9) into Eq.(10), the relations between $\mathbf{A}_{ij}$ and $\mathbf{C}_{ij}$ can be obtained

$$\begin{aligned}\mathbf{C}_{11} &= \mathbf{A}_{11}\\ \mathbf{C}_{31} &= \mathbf{A}_{31}\\ \mathbf{C}_{51} &= \mathbf{A}_{51} + \frac{11}{480}\beta^2\mathbf{A}_{11}\end{aligned} \tag{11}$$

Substituting Eq.(7), (8) and (11) into Eq.(3), the displacement component and the electric potential for the FGPM and HPM regions are obtained. The higher order stress and electric displacement fields will be given based on Eq. (9) finally. Then we obtain the stress intensity factor (SIF) and electric displacement intensity factor (EDIF) as

$$\begin{cases} K^T = \lim\limits_{r\to 0}\sqrt{2\pi r}\,\sigma_{yz}^{(1)}(r,0) = \dfrac{\sqrt{2\pi}}{2}(c_{44\ 44}^{(2)}A_{11} - e_{15}^{(2)}B_{11}) \\ K^D = \lim\limits_{r\to 0}\sqrt{2\pi r}\,D_{y}^{(1)}(r,0) = \dfrac{\sqrt{2\pi}}{2}(e_{15}^{(2)}A_{11} + \varepsilon_{11}^{(2)}B_{11}) \end{cases} \tag{12}$$

Conclusion

The higher order fields of an interfacial crack between FGPMs and HPMs under the impermeable electrical boundary condition of crack surfaces are presented. The first order displacement and electric potential fields of FGPMs are identical to the ones of HPMs. The second order displacement and electric potential fields of them have the same mathematical form; however, the magnitudes of them depend on the undetermined coefficients. The fields are the theoretical basis for determining stress intensity factor and carrying out the experimental analysis. Therefore, the study is of obvious universal theoretical significance and engineering value to various physical weak-discontinuous problems of piezoelectric materials.

Acknowledgements

The research is supported by the National Natural Science Foundation of China (No11172332.)

References

[1] Y.-D. Li, K.Y. Lee: European Journal of Mechanics - A/Solids. Vol.28 (2009), p. 241

[2] Y.S. Li, W.J. Feng, Z.H. Xu: Meccanica. Vol.44 (2009), p. 377

[3] P.-w. Zhang, Z.-g. Zhou, B. Wang: Applied Mathematics and Mechanics-English Edition. Vol.28 (2007), p. 615

[4] Y.S. Ing, J.H. Chen: Theoretical and Applied Fracture Mechanics. Vol.63–64 (2013), p. 40

Advanced Materials Research Vols. 989-994 (2014) pp 723-726
© (2014) Trans Tech Publications, Switzerland
doi:10.4028/www.scientific.net/AMR.989-994.723

The Preparation and Detection of Quality Standard about Houttuynia Spray

Ting Xia[1,a], Qidan Chen[2,b], Jiankang Wang[3,c], Jing Zeng[4,d] and Jingyan Guo[5,e]

[1,2,3,4,5] Zhuhai College of Jilin University,Guangdong,China

[1,3]Tianjin university of science and technology,Tianjin, China

[a]email: xiatingsyu@foxmail.com, [b]email:5349970@qq.com, [c]email:8242245@qq.com,

Keywords: Houttuynia spray, Preparation, Quality Standard, Detection

Abstract. To explore of houttuyniae cordata quercetin best extraction solution and detection of quality standard about houttuynia spray. The study extracted quercetin from houttuyniae cordata using alcohol water extraction, ultrasonic extraction and supercritical CO2 extraction respectively, and then choosed the best solution to prepare sprays of houttuynia cordata. To conform the state pharmaceutical quality standards, quality standards were detected from four aspects in spray volume of each press, particle size, injection experiment and installation. The method of oultrasonic extraction was the best extraction method, and the concentrations of 70% ethanol was the most efficient extraction of quercetin.The technology of spray preparation is fast and feasible, and the method of content detection is reliable.These results showed houttuyniae cordata could develop spray and conform the state pharmaceutical quality standards.

Introduction

Houttuynia is one of the commonly used Chinese herbal medicine as the genus of the saururaceae plants. Its stems and leaves can be used as a medicine, and these are fishy smell when crushed. It has some pharmacological effect of antibacterial, anti-inflammatory, preventing allergy and relieving cough. These are often used to treat in the treatment of respiratory diseases [1-2]. Some studies have shown that the effective components in the flavonoids and volatile matter of herba houttuyniae. Quercetin is the main flavonoid components, and it has the effect of reinforcement the blood vessels used to treat on chronic bronchitis.

In recent years, a lot of new technology on traditional Chinese medicine extraction, various chromatography and combined technology was applied to the quantitative analysis of traditional Chinese medicine (TCM) flavonoids[3]. There was research reported that the method of ultrasonic extraction in the flavonoids from Houttuynia cordata could accelerate dissolution of active ingredients of plants, in addition, the secondary effects of ultrasonic extracts could accelerated the release,spread and thoroughly mixed with the solvent. so the method of ultrasonic extraction is a common and effective extraction because it has a high rate of extraction, fast, easy to operate in the low temperature[4].

This topic used the technology of ultrasonic extraction, supercritical CO2 extraction and the traditional water extraction of alcohol distillation to extract the quercetin in houttuyniae cordata, and choosed the optimal extraction approach to prepare spray of houttuyniae cordata. According to the Chinese pharmacopoeia 2010 regulations, the four aspects of injection volume of each press, particle size, injection experiment and installation were used to measure the quality standards of spray [5-6]. These woud lay a solid theoretical basis for its sprays on the market as soon as possible and better adapt to industrialization.

Methods

Equipment and materials. AsT240AD ultrasonic cleaning, magnetic stirring heating jacket (Co., Ltd. of Xianglong Electronics,China), HA221-50-06 supercritical CO2 extraction equipment (Co.,

Ltd. of Jiangsu Hua scientific equipment,China), Agilent 1200 Semi-preparative HPLC(Agilent, United States),vacuum filtration pumps . 90%, 80% and 70% ethanol , Houttuynia.

Methods.

1) ultrasonic extraction. Houttuynia cordata was weight 10.0g and added to the concentration of 90%,

80 % and 70 % ethanol 100ml. These bottles were placed in an ultrasonic cleaning vessel for 40min and 20min respectly. Filtrate was recovered by vacuum filtration.

2) Chromatography. Silica gel HPLC plates were cleaned twice by mobile phase development before use. Studies on individual reaction solutions were carried out using acetonitrile-0.4% phosphoric acid (45:55) as the mobile phase. The chromatographic column was ODS 4.6mm×150mm.The injection volume was 20μl and the flow rate was 1.0ml min-1 for initial studies. The detection wavelength was 280 nm. The plates were developed at room temperature. Theoretical plate number is based on the peak of quercetin, and the content of determination should not be lower than 1500, the separation of tinidazole and internal standard substance should be beyond 2.0.

3) Supercritical CO2 extraction. Houttuynia cordata was weight 200.0g and extracted for 3h and 105 ℃ in supercritical CO2 extraction equipment.Extrat was weighed.

4) alcohol-water distillation extraction. Houttuynia cordata was weight 10.0g and distilled at 40℃ in 90% ethanol according to the proportion of 1:20, and then extracted for 10min to obtain Houttuynia cordata from ethanol. Filtrate was recovered by vacuum filtration.

Results

1) The optimal solution. In this study, Compared with two other methods, the method of alcohol-water distillation is unstable, and temperature is difficult to control. The extract in the method of supercritical CO2 extraction is solid and less at room temperature. For these reasons, the method of supercritical CO2 extraction is not suitable for further detecting content and be adopted. However the method of ultrasonic extraction is easy to operate, and efficient. materials were extracted in a confined environment. This method is good reproducibility and can reduce errors by setting different parameters to obtain the optimum ultrasonic liquid ratio. So In this study, the method of ultrasonic extraction is the optimal solution.

2) The standard curve. Standard quercetin was placed in 100mL volumetric flask, and ethanol was added to the mark to make the concentration of 12,24,36,48 ug/ml. Bubbles were dislodged by ultrasonic equipment. The peak height and peak area of quercetin were measured by HPLC at 280nm , and its concentration and area were shown in Fig. 1 and Fig. 2. The regression equation was calculated, y=33725x+1.1E+5, and obtained the correlation coefficient (γ= 0.996).

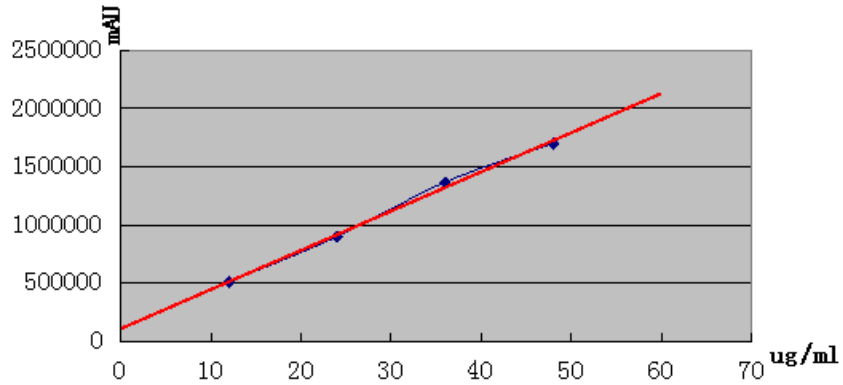

Fig. 1 The standard curve between the concentration of quercetin and peak area

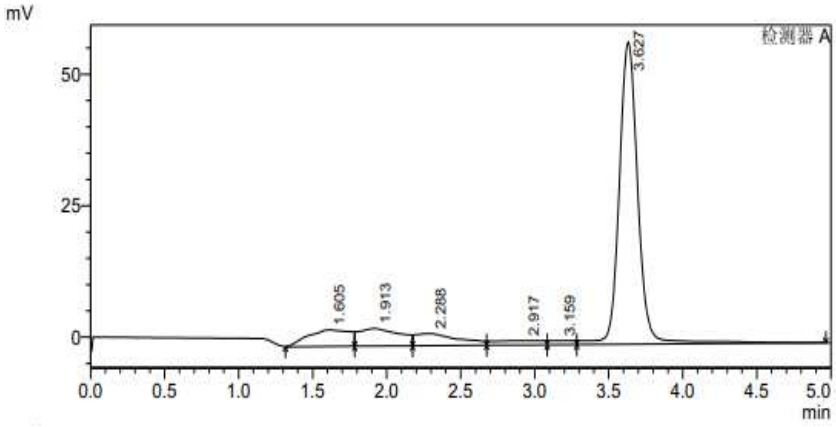

Fig. 2 The standard chromatogram of quercetin

3) Sample determination. Measuring 10ml extract from 70%, 80% and 90% ethanol respectively, ethanol was adding 100ml in every volumetric flask. Each sample peak area was obtained by the standard curve. Each sample was analysised five times to reduce the experimental error. The chromatogram of each sample was contrasted with standard chromatogram of quercetin, and The content of quercetin in the sample solution was obtained according to the standard curve of quercetin. Measurement results are shown in Table 1. The results showed that the content of quercetin from houttuynia cordata in the 70% ethanol solution was highest.

Table 1 Peak area of quercetin in the sample solution

sample solution	mean remaining time	mean peak area
70% ethanol extract	3.557	21356
80% ethanol extract	3.554	12002
90% ethanol extract	3.598	5413

4) Detection of Quality Standard about Houttuynia Spray. The extract of houttuynia was prepared by ultrasonic method, and filled in spray bottles after filtering. Based on the total dose (10ml) and the amount of each drug, the total spray times require more than 100 times. taking four bottles to test, getting off the cap and pressing pressure valve continuously in the beaker until the jet was over. The number of injections was calculated. The mean number of jet was 105 in the four bottles.

Taking four bottles and getting off the cap, every bottle was weighed after spraying several times. Pressing pressure valve injector once, and then the bottle was accurately weighed. Weight difference between once and twice was a spray volume. The operation was repeated three times and obtained three spray volumes. Pressure valve was pressed continuously 10 times excluding the weight, and three spray volumes were measured according to the above. Then pressure valve was pressed continuously 10 times excluding the weight, and four spray volumes were measured according to the above. The average volume in every bottle was calculated and was 80% to 120% of the labeled amount of spray unless otherwise specified. The result showed that per spray volume in the samples was 0.7931g. Taking four bottles and getting off the cap, every bottle was accurately weighed after spraying five times. The operation was repeated three times and calculated press volume of each spray bottle. The result showed that each press volume in every bottle was 0.1143g, 0.1253g, 0.1148g and 0.1189g respectively.

Particle size of houttuynia extract was observed under the common microscope. The morphology was commenced corners umbrella type as shown in Fig. 3. These results showed that the extract of houttuynia sprays was clarify and yellow transparent liquid. Injection rate, total injection volume and particle size conformed to the 2010 edition of Chinese Pharmacopoeia.

Fig. 3 Quercetin in houttuynia spray under microscope

Discussion

Compared with the conventional dosage forms, the spray was made with extract of houttuynia can make up for the deficiencies that drugs are difficult to reach the throat and tonsils. Meanwhile the pharmaceutical spray has the advantages of fast absorption, easy to use, low production cost and so on. Therefore, this study selected spray for delivery dosage. Quercetin has good effects of expectorant cough, prevention of asthma and depressurization [7-8]. Quercetin was made for spray which can be used as treatment of respiratory system diseases, and improve main ingredients and efficacy.

The content of quercetin in houttuynia extract was measured by HPLC using ultrasonic method. The results showed that 70% alcohol can extract quercetin from houttuynia cordata more efficiently. According to t the 2010 edition of Chinese Pharmacopoeia, the results showed that the formulations conformed to requirements and quality standards. This study explored the optimal method and condition by preparation of houttuynia spray and detection of quality standard. These laid a theoretical foundation for the further industry research and has important research prospects.

Acknowledgements

This study was financially supported by the foundation about Major Discipline of Zhuhai College of Jilin University.

References

[1] Kumar M, Prasad SK, Krishnamurthy S and Hemalatha S: submitted to Journal of Adv Pharmacol Sci(2014).

[2] Jiang Y, Lu Y, Zhang YY and Chen DF: submitted to Journal of Nat Prod Res (2014).

[3] He B, Liu Y, Tian J, Li CH and Yang SY: submitted to Journal of Zhongguo Zhong Yao Za Zhi (2013).

[4] 2010 edition of China pharmacopoeia appendix I department plans to increase changes: a mist aerosol, powder, spray.

[5] Zhu ZF: submitted to Journal of chemical industry and engineering (2010).

[6] Dong XY, Yao HF, Ren FZ and Jing H: submitted to Journal of Guang Pu Xue Yu Guang Pu Fen Xi. (2014).

[7] Lu S: submitted to Journal of Gene (2014).

[8] Surapaneni KM, Jainu M: submitted to Journal of Pharmacognosy Res(2014).

Advanced Materials Research Vols. 989-994 (2014) pp 727-730
© (2014) Trans Tech Publications, Switzerland
doi:10.4028/www.scientific.net/AMR.989-994.727

Ethylene Oligomerization by Ni(II) Complex Based on Peptide

BAI Wei[1], CAO Chen-Gang[1,a*], PEI Haixiang, HU Kaihui[1], ZHOU Hui[1], PENG Min[1], JIANG Tao[1,b*], Dong Jin-Yong[2]

[1]College of Material Science and Chemical Engineering, Tianjin University of Science and Technology, Tianjin, China

[2]Beijing National Laboratory for Molecular Sciences, Beijing, China

*Corresponding author: [a]chengangcao@tust.edu.cn, [b]jiangtao@tust.edu.cn

Keywords: Ethylene, oligomerization, Ni(II) complex, peptide.

Abstract. A kind of peptide based Ni(II) complexes (general formula $[ZN{=}C(An){-}C(An){=}NZ](NiBr_2)_2$, $Z{=}(4\text{-}NHR\text{-}3,5\text{-}C_6H_2(CH_3)_2)_2CH(4\text{-}C_6H_5)$, R=dipeptide, An=acenaphthenequinone) has been synthesized. Ethylene oligomerizations were carried out by using those complexes in combination with ethyl aluminium sesquichloride (EAS) and produced olefin . The effects of important parameters such as temperature and EAS concentration. on the catalytic activity and the distribution of resulting oligomer were investigated. under the conditions of employing toluene as solvent, a reaction temperature of 50℃ and an ethylene pressure of 1.0 MPa..

Introduction

Ethylene oligomerization presents one of the major industrial processes for the production of linear α-olefins. Such linear oligomers are used primarily as comonomers for the production of linear low-density polyethylene, plasticizers and synthetic lubricants[1]. In the past decades, nickel complexes based on coordination models of ligands such as bidentate N∧N and tridentate N∧N∧N have attracted great attention in both academic and industrial researches of catalytic chemistry [2-4], since which show good catalytic activities towards ethylene oligomerization.

Poly(amino acids) have attracted considerable attention in recent years due to their non-toxicity, biocompatibility, nutritional function and pharmacological efficacy as a drug carrier. But almost no peptide was used as ligands for nickel(II) complexes. Considering these previous findings, we were interested in exploring and synthesizing some new ligands in order to develop new nickle(II) complexes for ethylene oligomerization catalysis. Here, We report the synthesis of novel nickel complexes based petide ligands, resulting in highly active catalysts for the oligomerization of ethylene. The catalytic activities for ethylene oligomerization and distribution of oligomer have been investigated at various oligomerization conditions.

Experimental

All manipulations for air- or/and moisture-sensitive compounds were carried out under a nitrogen atmosphereusing standard Schlenk techniques.. All other chemicals were obtained commerciallyand were used without further purification unless statedotherwise.

Synthesis of Ni(II) complex based on peptide

The nickel(II) complex based on peptide ligands were synthesyzed according to the reference[5,6]and previous work in our group.[6] The synthetic procedure is generally shown in Scheme 1. 1H-NMR, 13C-NMR spectra of ligand were recorded on a Varian Gemimi-2000 (300 MHz) spectrometer The complexes obtained were fully characterized by IR and ICP-MS.

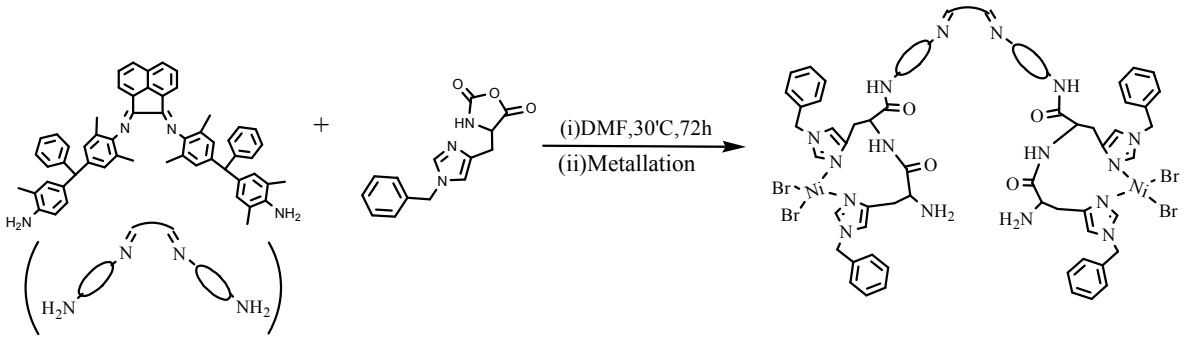

Scheme 1. Synthesis of ligands and catalyst precursors

Procedure for ethylene oligomerization

Ethylene oligomerizations were performed in a common procedure with the conditions following: a 250-mL round-bottom flask equipped with a magnetic stirrer and a thermometer outside, 80 ml of toluene, 30 min runs, atmospheric pressure of Ethylene, ethyl aluminium sesquichloride (EAS) as cocatalyst. The product was cold to lower temperature in ice-bath and terminated by silica gel, then analyzed quickly by gas chromatography (GC) for determining the composition and mass distribution of oligomers.

Results and discussion

To probe the effects of reaction parameters on catalytic activity, oligomerization behavior was investigated by changing the ammount of catalyst, the ratios of EAS and the reaction temperature.The results are summarized in Tables 1.

Table 1 Ethylene oligomerization Results Carried Out at Atmospheric Pressure of Ethylene

run	Ni(II) complex (μmol)	Al/Ni (mole)	T (℃)	Acivity (10^6g/(molNi.bar.h))	distribution of oligomer (%)			
					C_{10}	C_{12}	C_{14}	C_{16}
1	2.86	150	30	1.62	3.58	70.89	14.59	2.66
2	1.74	150	30	1.88	3.08	68.16	11.64	2.04
3	0.84	150	30	1.95	1.39	62.18	7.77	3.74
4	0.84	300	30	2.31	4.09	72.57	9.04	1.77
5	0.84	600	30	3.33	4.89	75.99	10.40	0.88
6	0.84	900	30	3.22	9.55	77.62	7.60	0.00
7	0.84	300	0	1.05	0.00	73.68	8.51	1.56
8	0.84	300	60	0.77	13.61	74.54	5.57	1.80

Remarkably high activities are observed when using EAS as a co-catalyst and Toluene as the solvent.The reaction parameters significantly affected their catalytic activities. With Al/Ni molar ratios in the range of 150–900 the catalytic system demonstrated increasing activities up to an Al/Ni ratio of 600, then slightly decreasing activities with higher Al/Ni ratios. Which might result from chain transfers to aluminium with the consequence of ceasing oligomer chain propagation. Also, the reaction temperature reasonably affected catalytic activity. The highest oligomerization activity was observed at the temperature of 30℃ with an activity of 3.33g/(μmolNi·bar·h).

The effect of amount of catalyst on distribution of oligomer was shown in Fig. 1, while effects of different MAO/Ni molar ratios and temperatures on distribution of oligomer were shown in Fig. 2 and Fig. 3.

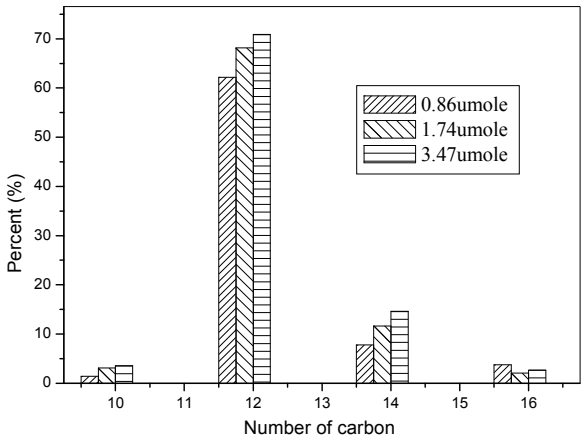

Fig. 1 The effect of amount of catalyst on distribution of oligomer

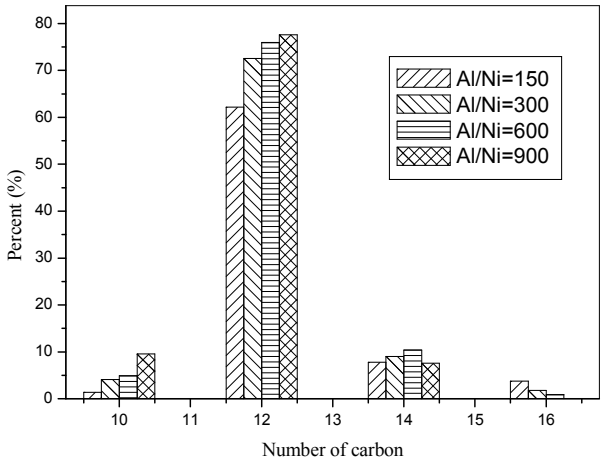

Fig. 2 The effect ofthe molar ratio of Al/Ni on distribution of oligomer

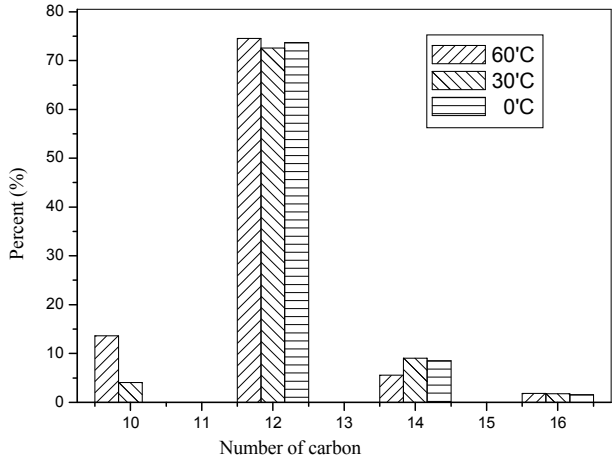

Fig. 3 The effect of temperature on distribution of oligomer

This kind of nickel complexe show a high tendency towards the formation of C_{12}-C_{14} fraction products. In a general, The selectivities of C_{12} olefins were obviously increased when increasingthe ratio of Al/Ni and the amount of Ni(II) complex. lower olefins were produced at higher oligomerization temperature.

Summary

A kind of novel peptide based neutral nickel(II) complexe, [ZN=C(An)-C(An)=NZ]$(NiBr_2)_2$, Z=(4-NHR-3,5-$C_6H_2(CH_3)_2)_2CH(4$-C_6H_5), An=acenaphthenequinone, R=dipeptide) was synthesized. Activated by EAS, this complex exhibited higt catalytic activities for ethylene oligomerization, with a high tendency towards the formation of C_{12}-C_{14} olefins fraction products.

Acknowledgements

This work was financially supported by the Science Foundation of Tianjin University of Science Technology, Natural & Science Foundation of China (U1162114, 51203115), PetroChina Innovation Foundation (2013D-5006-0501), Beijing National Laboratory for Molecular Sciences and Training Programs of Innovation for Undergraduates

References

[1] F.Speiser, P.Braunstein, and L.Saussine.Acc. Chem. Res., Vol.38 (2005), p.784–793

[2] L.K. Ittel, S.D Johnson,, M. Brookhart,, Chem. Rev., Vol. 100(2000), p. 1169–1203

[3] V.C. Gibson, S.K Spitzmesser,, Chem. Rev., Vol. 103 (2003), p. 283–315

[4] V. C.Gibson, C Redshaw. and G. A. Solan, Chem. Rev., Vol. 107 (2007), p. 1745.

[5] B K Bahuleyan, G W Son, D W Park, C S Ha and I Kim, J Polym Sci: Part A: Polym Chem, Vol. 46(2008), p. 1066–1082

[6] G M Kim, Y H Bae, W H Jo, Macromol. Biosci. Vol. 5 (2005), p. 1118–1124

Advanced Materials Research Vols. 989-994 (2014) pp 731-734
© (2014) Trans Tech Publications, Switzerland
doi:10.4028/www.scientific.net/AMR.989-994.731

Synthesis of Nickel(II) Complexes and its Application to Ethylene Oligomerization

KOU Jianbo[2,4], ZHAO Shuna[3], CAO Chen-Gang[1,a*], ZHOU Hui [1], HU Kaihui[1], PENG Min[1], SU Guosui [4], JIANG Tao[1,b*], Dong Jin-Yong[5]

[1]College of Material Science and Chemical Engineering, Tianjin University of Science and Technology, Tianjin, 300457 China

[2]Hebei University of Science and Technology, Shijiazhuang, 050018 China

[3] Shijiazhuang Zhongtian Biotechnology Co. Ltd., Shijiazhuang 052165 China

[4]Technology Center,China Tobacco Hebei Industrial Co.,Ltd.,Shijiazhuang 050051 China

[5]Beijing National Laboratory for Molecular Sciences, Beijing,100080 China

*corresponding author, [a]chengangcao@tust.edu.cn, [b]jiangtao@tust.edu.cn

Keywords: Ethylene, oligomerization, Ni(II) complex. Diimine, Synthesis

Abstract. A kind of N-((3-chloro-1H-indol-2-yl) methylene)-2,6-diisopropylbenzenamin Ni(II) complex has been synthesized. Ethylene oligomerizations were carried out by using those complexes in combination with methyl aluminoxane (MAO) and produced olefin. The effects of important parameters such as temperature and MAO concentration. on the catalytic activity and the distribution of resulting oligomer were investigated.

Introduction

Olefin oligomerization catalyzed by transition metal complexes have attracted great attention in both academic and industrial research, since such linear oligomers are used primarily as comonomers for the production of linear low-density polyethylene, plasticizers and synthetic lubricants[1-3]. In the past decades there has been growing interest in late transition metal catalysts. Various Schiff base ligands have been reported especially due to their easy preparation and promising catalytic properties of their late transition metal complexes.[4-8]

Following this new trend we would like to report the synthesis and ethylene oligomerization behavior of nickel complex based on coordination models of ligands such as bidentate NΛN α-diimine ligands. The catalysts showed moderate activity towards ethylene oligomerization in combination with methyl aluminoxane (MAO). The oligomerizations were carried out under various conditions.

Experimental

All manipulations for air- or/and moisture-sensitive compounds were carried out under a nitrogen atmosphereusing standard Schlenk techniques.. All other chemicals were obtained commerciallyand were used without further purification unless statedotherwise.

Synthesis of Ni(II) complex

The nickel(II) complex based on peptide ligands were synthesyzed following the route shown in fig.1

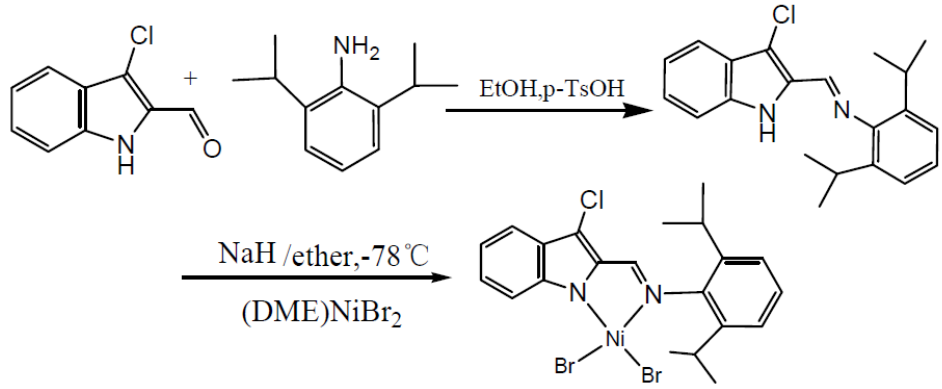

Fig.1 The synthetic procedure of nickel(II) complex.

Procedure for ethylene oligomerization

Ethylene oligomerizations were performed in a common procedure with the conditions following: a 250-mL round-bottom flask equipped with a magnetic stirrer and a thermometer outside, toluene as solvent, 30 min runs at various pressure of ethylene, MAO as cocatalyst. The product was cold to lower temperature in ice-bath and terminated by silica gel, then analyzed quickly by gas chromatography (GC) for determining the composition and mass distribution of oligomers.

Results and discussion

Synthesis and characterization of diimine based Ni-complex

3-chloro-1H-indole-2-carboxaldehyde (3.00 mmol) and 2,6-diisopropylbenzenamine (3.10 mmol) (excess) were dissolved in 50 ml of C_2H_5OH in a round-bottom flask. Five drops of p-TsOH were added, and the sealed solution was stirred at 50°C overnight. After filtration, the yellow solid was recrystalyzed with ethanol and dried to givewhite needle crystal in 65% yield. The ligand was charactized with ^{1}H-NMR(shown in Fig.2)

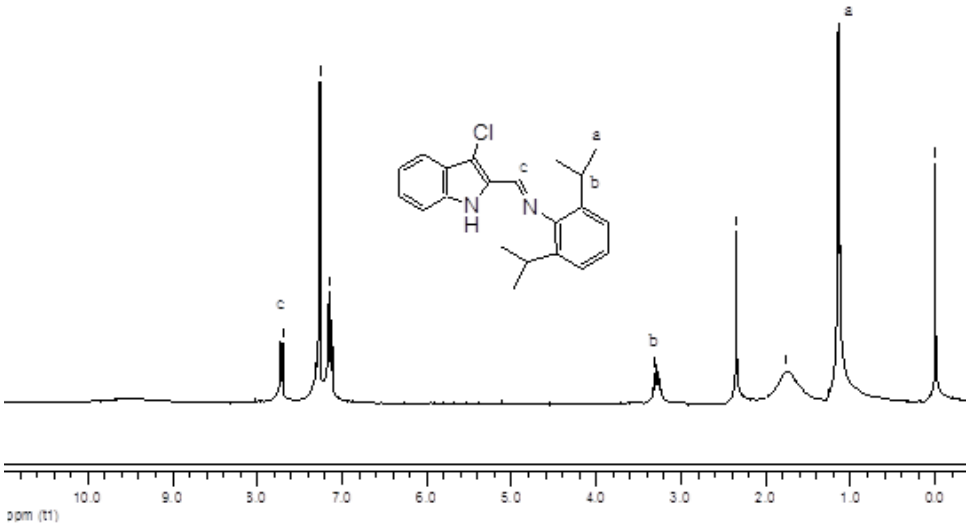

Fig.2 ^{1}H-NMR of N-((3-chloro-1H-indol-2-yl) methylene)-2,6-diisopropylbenzenamine

To a stirred solution of N-((3-chloro-1H-indol-2-yl) methylene)-2,6-diisopropylbenzenamine (3.00 mmol) in dried diethyl ether (30 mL) at-78°C, NaH (3.00 mmol) was added. The mixture was allowed to warm to room temperature and stirred for additional 2 h. The resultant solution was dried in vacuum to give ligand as yellow powder. A 1.1 equiv. of the ligand and (DME)$NiBr_2$ (DME = 1,2-dimethoxyethane) were added together with CH_2Cl_2 as sovent in a Schlenk flask under nitrogen. Stirring was begun and continued overnight. Diethylether was added to the reaction to precipitate the complex, and the resultant solids were filtered, washed with ether, and dried in vacuo. Yield: 90.1%.

Since Ni-complex could not be characterized by ^{1}H-NMR, we characterize the compound by FTIR spectroscopy(shown in Fig.3). In the case of bidentate (N,N) complexes, absorptions band at 404 cm^{-1} - 421 cm^{-1} is assigned to υ(Ni - N) in figure 3.

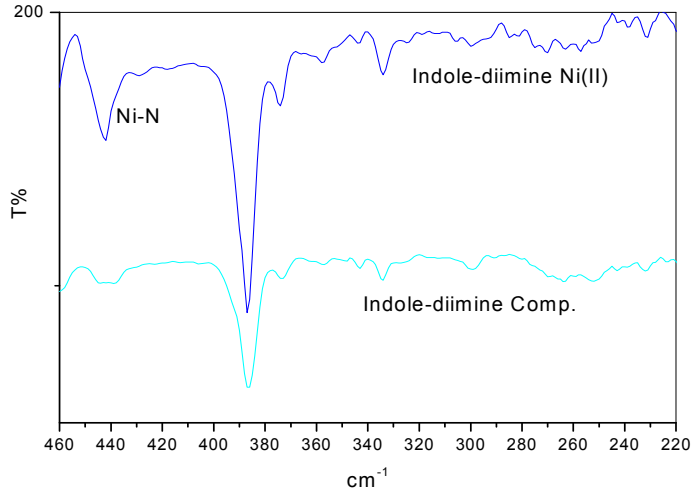

Fig.3 FTIR spectroscopy of nickel diimine complex

Ethylene oligomerization results with Nickel(II) Complexes

We carried out ethylene polymerizations by using complex in the presence of MAO. The catalytic activities for ethylene oligomerization and distribution of oligomer have been investigated at various oligomerization conditions.The results are summarized in Tables 1.

Table 1 Summary of ethylene oligomerization results with Nickel(II) Complexes [a]

				Distribution of Olefins(%)[c]					
RUN	Al/Ni	Tp(℃)	R_p[b]X 10^{-4}	1-Butene	Trans-2 -butene	Cis-2- butene	1-Hexene	Trans-2- Hexene	Cis-2- Hexene
1	300	30	2.2	23.3	8.2	12.0	16.9	24.3	15.2
2	500	30	6.0	18.4	7.7	12.8	17.6	26.3	17.2
3	700	30	5.6	16.9	9.0	14.1	15.1	27.8	17.1
4	1200	30	6.3	17.2	8.3	14.6	14.2	26.9	18.6
5	2000	30	7.2	16.1	8.7	13.8	15.2	28.1	18.1
6	700	10	3.6	62.2	0.0	6.6	14.0	10.7	6.5
7	700	20	7.6	40.6	4.2	7.8	14.5	24.4	8.5
8	700	50	1.3	51.8	0.0	7.8	17.8	15.5	7.1

(a) Conditions: catalyst = 30 μmol, toluene 80mL, P_{C2H4} = 1 atm, and time = 30 min (b) Average rate of propagation as g-product/mol-Ni atm h. (c) Determined by GC

All the catalysts showed good activity towards ethylene oligomerization when activated with MAO.The reaction parameters significantly affected their catalytic activities. With Al/Ni molar ratios in the range of 300–2000 the catalytic system demonstrated increasing activities with higher Al/Ni ratios. Also, the reaction temperature reasonably affected catalytic activity. The highest oligomerization activity was observed at the temperature of 20°C.The effect of eaction parameters on distribution of oligomer was shown in table 1, This kind of nickel complexe show a high tendency towards the formation of C_4-C_6 fraction products.

Summary

A kind of novel N-((3-chloro-1H-indol-2-yl) methylene)-2,6-diisopropylbenzenamine nickel(II) complexe was synthesized. Activated by MAO, this complex exhibited higt catalytic activities for ethylene oligomerization, with a high tendency towards the formation of C_4-C_6 olefins fraction products.

Acknowledgements

This work was financially supported by the Science Foundation of Tianjin University of Science and Technology, Natural & Science Foundation of China (U1162114, 51203115), PetroChina Innovation Foundation (2013D-5006-0501), Beijing National Laboratory for Molecular Sciences and Training Programs of Innovation for Undergraduates.

References

[1] G. J.P. Britovsek, V. C. Gibson, D. F. Wass, *Angew. Chem. Int. Ed. Engl.,* vol. 38 (1999), p.428

[2] B. L. Small, M. Brookhart and A. M. A. Bennett, *J. Am. Chem. Soc.*, vol.**120**(1998), p.4049

[3] L.K. Ittel, S.D Johnson,, M. Brookhart,, Chem. Rev., Vol. 100(2000), p.1169

[4] K. Rappe, W. M. Skiff, C. J. Casewit, *Chem. Rev*., vol.100(2000), p.1435,

[5] F.Speiser, P.Braunstein, and L.Saussine.Acc. Chem. Res., vol.38 (2005), p.784

[6] V.C. Gibson, S.K Spitzmesser,, Chem. Rev., Vol. 103 (2003), p.283–315

[7] V. C.Gibson, C Redshaw. and G. A. Solan, Chem. Rev., Vol. 107 (2007), p.1745.

[8] B K Bahuleyan, G W Son, D W Park, C S Ha and I Kim, J Polym Sci: Part A: Polym Chem, Vol. 46(2008), p.1066

Advanced Materials Research Vols. 989-994 (2014) pp 735-738
© (2014) Trans Tech Publications, Switzerland
doi:10.4028/www.scientific.net/AMR.989-994.735

In Situ Formation ofInsect Repellent Delivery System

Derong LIN[1,a], Lijiang HU[2,b]

[1]School of Food Science, Sichuan Agricultural University, Ya'an, 625014, China

[2]Department of Chemistry, Harbin Institute of Technology, Box 713, Harbin,150001, China

[a]email:youngsumass@126.com,[b]email:hulijiang2008@126.com

Keywords: Silsesquioxane; Insect repellant (Citral); Polymerization; Polymer delivery system

Abstract. Conventional pesticide applications repeatedly failed to adequately control mosquito and sandflypopulations in desert areas, due to effects of either intense heat, blowing sand, ultraviolet light and/or combinations of them under severe environmental conditions. Application of citral oil to the skin provides temporary relief from pests only until the volatile terpene evaporates or is photodegraded by light. It would be advantageous to encapsulate the citral into a solid or waxy polymer that would slowly release a constant stream of citral from reservoir of the naturally occuring pesticide dissolved in the solid polymer. Polysilsesquioxanes have already proven to block UVB and are known to be oxidatively robust. In this study, a solid polysilsesquioxane pesticide delivery system was prepared free radical polymerization of an oligovinylsilsesquioxane in the presence of citral.The molecular consequences of the free radical polymerization were analyzed by MALDITOF spectrometry and the UV absorption properties of the resulting polymer-citral solution were measured by scanning spectrophotometry (SSP).

Introduction

Mosquitoes are important vectors of arthropod-borne viruses such as yellow, dengue and chikungunya fevers, causing worldwide outbreaks of severe epidemic diseases every year.Naturally occurring terpene oils have been found to be less hazardous substitutes for synthetic pesticides. One common constituent of these oils is Citral, which has shown promise as both insect repellent and insecticide [1]. In recent years, the growing interest inpolyhedral oligomeric silsesquioxane or polysilsesquioxaneis evidenced by the increased number of studiespublished and from both experimentaland theoretical investigations due to the unique physical and chemical properties of silsesquioxanes [2]. One of the important advantages of these silsesquioxane nanostructured hybrids is that they are toolarge to have appreciable vapor pressures and hence do not add to air pollution as a volatile organic vapor[3]. Another important advantage of silsesquioxane hybrids is that they can have a high sun protection factor (SPF) for protection from UV radiation and the prevention of skin damage[4]. As mentioned above, silsesquioxane area good candidate as chemical delivery system to provide constant and longer protection against insect vectors of diseases and simultaneously prevent UV radiation skin damageundersevere environmental conditions.

Objective

Place the file in any of the directories where MS Word looks for templates. These directories are defined within MS Word under Tools/Options/File Locations. In this study, the objective was to create a silsesquioxane delivery system for citral. The method chosen to accomplish this is to prepare a vinyl substituted silsesquioxane oil (VS) that is miscible with citral. Then the vinyl groups would be reacted with radicals to link some of the oligomers together such that a solid solution of citral in the free radical modified vinyl SSO (citral/VS) can form (Scheme 1).

Vinylsilsesquioxanes and even VMS are known to react under free radical conditions[5]. While generally monomers such as VMS are better copolymerized with more reactive organic vinyl monomers[6], the polyvinylsilsesquioxanes have sufficient vinyl groups to allow permit the oligomeric materials to be covalently linked together and even crosslinked. We originally had been

interested in whether or not the citral would react under free radical conditions to covalently link the citral with the VS. We used mass spectrometry to structurally characterize the VS-citral and UV-Visible spectroscopy to evaluate the transparency of the materials.

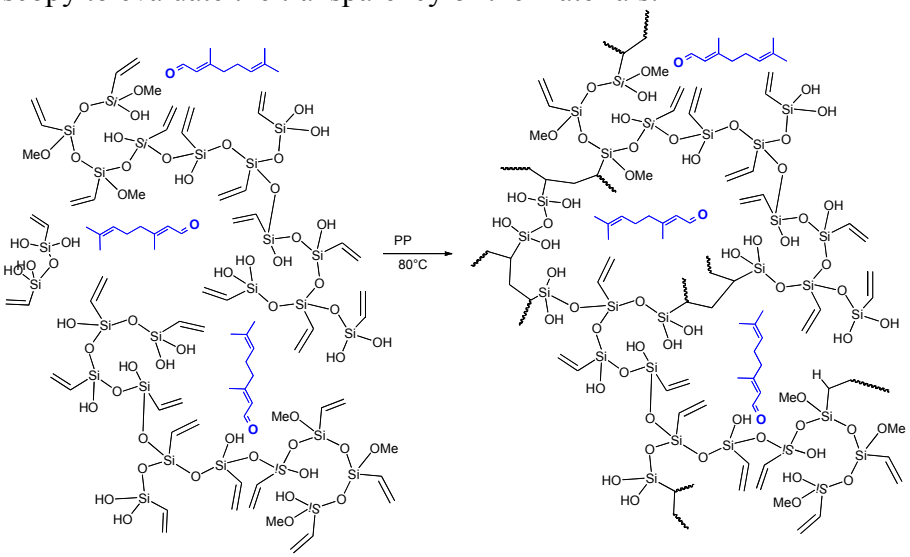

Scheme 1. Free radical polymerization of oligosilsesquioxane around citral molecules.

Methods

For the hydrolytic condensation reaction, vinyltrimethoxysilane (VMS, 96.0~97.0%, Sigmas Aldrich, St. Louis MO) wasplaced in beaker. Ethanol wasadded to give a3:1molar ratio with respect to VMS. The corresponding molar ratio of water to Si was 1:1. The polymerization was catalyzed with formic acid, added in a 0.5:1 molar ratio with respect to VMS. The beaker was sealed with a plastic film and left for a day at 35 ºC. Then needle–sized holes were made in the plastic film and the reaction was continued for another day at35 °C. Finally, the plastic film was removed and the reaction continued for one more day at 65 ºC. The reaction products,polyvinyl-silsesquioxane (VS),were homogeneous, viscous liquids that were soluble in THF and ethanol.

To a 250 mL two-neck round bottom flask, VS (1 g), citral(Alfa Aesar, 95%) (8 g), and 140 mL of distilled water were added and stirred continuously for 4 h. Then, sodium dodecyl sulfate (4.0 g) and potassium persulfate (0.05g) were added into the flask and the emulsion was stirred at 80 °C for 1 h. Next, potassium persulfate (0.08g) and 5% NaOH solution were added dropwise into the solution and mixed at 80 °C. The solution was allowed to cool to 40 °C where it was stirred continuously for additional 12 h. The reaction was filtered to remove insoluble residues and the THF solution was added dropwise into a beaker of methanol to precipitate the product. Finally, the solid and waxy resulting product was collected and dried in a vacuum oven at room temperature for 24 h to remove the methanol.

Results

The citral would also react to form covalent linkages with the VS[7], which would prevent its release as an insecticide or repellent. This was discounted as a serious possibility by the known propensity of citral and related terpenes to undergo free radical cyclization [8] instead of polymerization and with our mass spectrometric and thermal gravimetric analyses below.

FTIR spectroscopy shows that the citral is still present in the VS-citral material (Fig. 1A). The FTIR spectrum of the citral where typical bands at 1669.95, 2753.61 and 1627.90 cm^{-1} are primarily ascribed to the stretching of C=O, H-C and C=C groups, respectively. The FTIR spectrum of VS exhibits the typical band at 3423 cm^{-1}due to hydrogen bonding Si–OH groups. The obvious bands at 1120~1129 $cm^{-1}$are from Si–O–Si anti-symmetric stretches, and 1602 cm^{-1} is ascribed to the stretching of the C=C group. The FTIR spectrum of the VS-citral has all of the citral and VS bands.

Measured in the range of the ultraviolet-B (UV-B) region (280–320 nm) (Fig. 1B),the average transparency value of the VS-citraloligomer in the range of the UV-B spectrum (280–320 nm) causing the risk of skin cancer are only about 13%[9], indicating that this hybrid has a better light absorption and can provide a physical barrier for blocking the UV-B radiation absorbed by the skin.

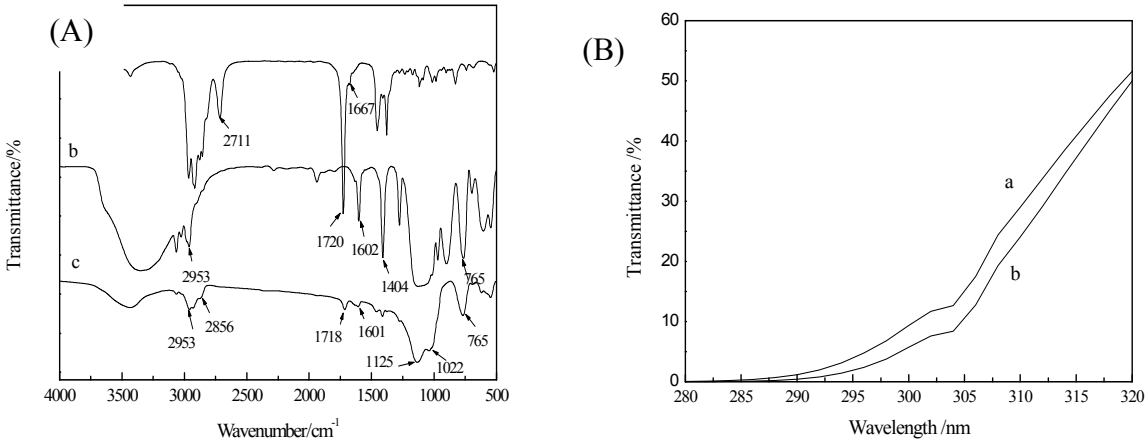

Fig. 1. (A) FTIR spectra of (a) citral, (b) VS and (c) VS-citral;(B) The transparency of citral (a) and VS-citral (b) measured in the range of the UV-B region (280–320 nm).

Mass spectrometry shows that the only peaks above monomer molecular weights are those of oligovinylsilsesquioxanes. Fig. 2 shows MALDI-TOF mass spectra in the m/z = 925.2-1200. This range correspond to VS oligomers, and the proposed structural formulas corresponding to the peaks data were assigned with the generic formula $(RSiO_{1.5})_n$ (n = even number≥6; complete cage structure) or $[RSiO_{1.5-(x+y)/2n}]_n(OH)_x(OCH_3)_y$ (n = 4, 5, 6...; x, y = 1, 2, 3...; incomplete cage, ladder and branchedlinear structures)(as seen inTable 1)[10].These peaks data have excellent compliance between the experimental measurement value (m/z) and the calculated molecular weight according to ion adducts $(M + H^+)$ [11].

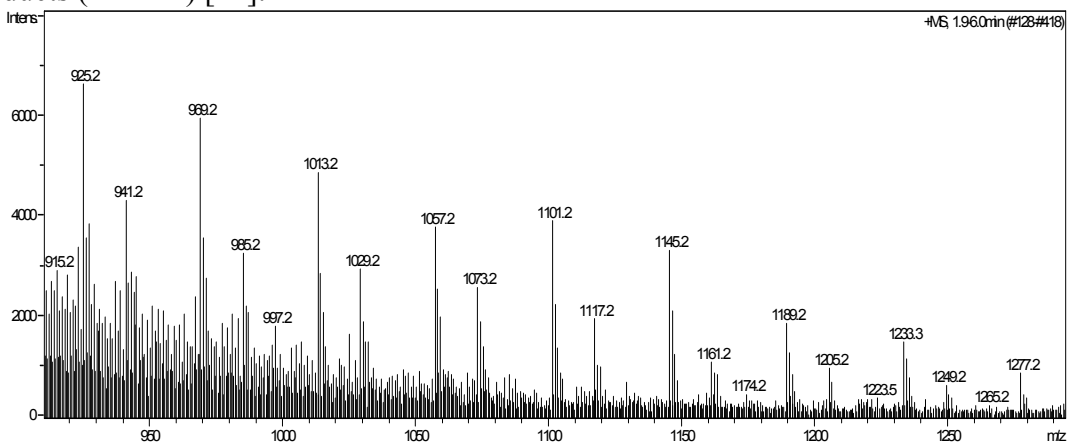

Fig. 2 MALDI-TOF mass spectra in the m/z = 925.2-1277.2 Da range correspond to the VS-citral oligomers.

Table 1 VS-citral oligomers assigned by MS in the m/z = 925.2-1200 Da

M/Z (exp.)	Assigned structure	M/Z (pre.)
915.2	$T_{10}(OH)(OCH_3)_5H^+$	915.0
969.2	$T_{10}(OH)_7(OMe)_5H^+$	970.5
985.2	$T_{10}(OH)_6(OMe)_6H^+$	983.1
1013.2	$T_{11}(OH)_{11}(OMe)_2H^+$	1014.2
1029.2	$T_{11}(OH)_{10}(OMe)_3H^+$	1029.0
1073.2	$T_{12}(OH)(OMe)_5H^+$	1073.0
1101.2	$T_{12}(OH)_{11}(OMe)_2H^+$	1103.0
1117.2	$T_{12}(OH)_8(OMe)_3H^+$	1117.0
1145.2	$T_{12}(OH)_8(OMe)_5H^+$	1145.1
1161.2	$T_{12}(OH)_7(OMe)_6H^+$	1159.1
1189.2	$T_{12}(OH)_5(OMe)_8H^+$	1187.1

Conclusions

We have successfully prepared a silsesquioxane-based delivery system for citral that contains more than 15wt% citral for slow release to provide long term protection against insect pests. The material is easy to prepare from commercially available VMS, a common coupling agent, and citral, a common terpene, essential oil. This insect repellent/pesticide should provide a cost effective alternative to synthetic chemical based systems.

Acknowledgement

Financial supports are acknowledged the Aerospace supported Fund, China, under the contract number of2012-HT-HGD-11.

References

[1] P. Kumar, S Mishra, A Malik and S Satya: Parasitol Res Vol.112 (2013), p. 69

[2] K. Kanamoriand K Nakanishi: Chem Soc Rev Vol. 40 (2011), p.754

[3] W.L. Hergenrother, C.J. Lin, A.S. Hilton, T.E. Hogan and D.R. Brumbaugh:J Appl Polym Sci Vol. 115 (2010), p.79

[4] X.D. Chen, D Wang, X.D. Li, Y Liu and L.J. Hu: Mater Sci Forum Vol. 610-613, (2009), p.1039

[5] T. Sato: Setchaku Vol. 50 (2006), p.215

[6] Z.M. Rzaev, L.V. Bryksina, S.K. Kyazimov and S.I. Sadykh-Zade: Vysokomolekulyarnye Soedineniya, Seriya A Vol. 14 (1972), p.259

[7] D. Wang, Z.Y. Cao and Q. Wang:Adv Mater Res Vol. 391-392 (2012), p.1498

[8] B. Wang, A.P. Ramirez, J.J. Slade and J.P. Morken: J Am Chem Soc Vol. 132 (2010), p.16380

[9] P. Chen, T Liu, D Wang, Q Zhang and L.J. Hu:Ferroelectrics Vol. 411 (2011), p.36

[10] I.E. dell' Erba, D.P. Fasce, R.J.J. Williams, R Erra-Balsells, Y. Fukuyama and H. Nonami:J Organometal ChemVol. 686 (2003), p.42

[11] D. Wang, H. You and L.J. Hu: Rapid Commun. Mass Spectrom. Vol. 25 (2011), p.1652

Advanced Materials Research Vols. 989-994 (2014) pp 739-742
© (2014) Trans Tech Publications, Switzerland
doi:10.4028/www.scientific.net/AMR.989-994.739

Structure of bridged silsesquioxane material bearing a pendant dodecylamine

Derong LIN[1,a], Lijiang HU[2,b]

[1]School of Food Science, Sichuan Agricultural University, Ya'an, 625014, China

[2]Department of Chemistry, Harbin Institute of Technology, Harbin,150001, China

[a]email:youngsumass@126.com, [b]email:hulijiang2008@126.com

Keywords: Bridging polysilsesquioxane; Hydrophobic property; Atomic force microscopy(AFM)

Abstract. In this study, the optimum reaction conditions of preparing bridged monomer by dodecylamine (DDA) and of γ-(2,3-epoxypropyl) trimethoxysilane (GPMS) were obtained at 60℃ water bath for 36h. The synthesized materials were characterized by infrared spectroscopy(IR), atomic force microscopy(AFM), Scanning Electron Microscopy (SEM) and water contact angle (CA). The result of FTIR indicates the formation of the DDA and GPMS bonded reactions during the synthesis of monomer, and preparation of the skeleton structure. Characterization of AFM on the structure of the surface morphology of the acid-catalyzed materials indicates the formation of layered structure. The acid-catalyzed materials were characterized by SEM indicates the rough structure of micron-level, which was conducive to the hydrophobic properties of the material.

Introduction

The organic bridging groups, varied in composition, length, rigidity, and functionalization, can exhibit self-assembling properties which may direct the formation of a tridimensional hybrid network by a self-organization process in the course of the hydrolysis and polycondensation of the trifunctional silyl groups [1-3]. Since the organic group remains an integral component of the material, this variability provides an opportunity to modulate bulk properties such as porosity, thermal stability, refractive index, optical clarity, chemical resistance, hydrophobicity, and dielectric constant [4] .

In this research, the same self-assembly hybrid material, containing a pendant hydrophobic chain in the organic bridge, was generated by the same reaction, the polycondensation was produced with the same catalyst, formic acid, but the basic ordered structures of hybrid organic-inorganic multilayers were characterized by AFM techniques.

Separated by hydrophobic regions with a thickness equal to the length of a tail-to-tail association of dodecylamine (DDA) chains in all-trans conformations. Strong hydrogen bonds as those formed among urea groups present in organic bridges, alone or combined with aromatic-stacking or hydrophobic interactions, produce a variety of self-assembled structures[5,6] . On the other hand, the use of organic surfactant templates has been extensively used to synthesize silica-based materials with well-ordered mesoporous structures [7].

Methods

The hydrolysis and condensation of the precursor were performed in the same glass tubes employed in the synthesis, using an aqueous solution of in the following molar ratios: HCOOH/Si = 3, H_2O/Si = 1.05. (In a typical synthesis 1.77 mL of the 88 wt % formic acid solution was added to the precursor synthesized using 3 mL of Glycidoxypropyl(trimethoxysilane) (GPMS, Dow Corning Z-6930) and 1.251 g of dodecylamine (DDA, Fluka, 98%).) The reaction was carried out either in mass or using THF as solvents. (In a typical synthesis 5 mL of solvent was added to the precursor synthesized using 3 mL of GPMS and 1.251 g of DDA.) The tubes were left open and placed in a thermostat at 50 °C for 24 h. Solvents and volatile products were evaporated continuously during the reaction. The product was milled, placed in a Petri dish, and heated in an oven at 110 °C for 3 h. The GSSO was formed.

Results

For dodecyl chains (n = 12) the distance between inorganic domains (d) in the bilayer structure was reported as 3.4 nm[8], observed by Small-angle X-ray scattering (SAXS) and that calculated by the software ACD Labs/3D Viewer, in close agreement with X-ray diffraction (XRD) pattern of the product (n = 18) shows the peak (d = ca. 5.3 nm) with higher-order reflections[9].

However, the distance equals to 2.17 nm characterized by an atom force microscope (AFM) in this study. Fig. 1 shows 3 images of AFM measurements: (a) 3-dimantion scanning of AFM from which (b) and (c) Materials and membranes for GSSO carried out atomic force microscopy. GSSO shown in Figure 2 is an AFM scan three-dimensional map material, particle size analysis and the cross-sectional analysis through analysis of three-dimensional map and the particle size, can be clearly seen that the resulting layered material has a regular structure. This is because the monomer during the reaction between lauryl chain intermolecular force guided self-assembly reaction, the formation of an orderly layered structure. Profiles can be calculated through the layer spacing, 50nm distance, a total of 23 layers, so the average interlayer spacing of 2.17nm.

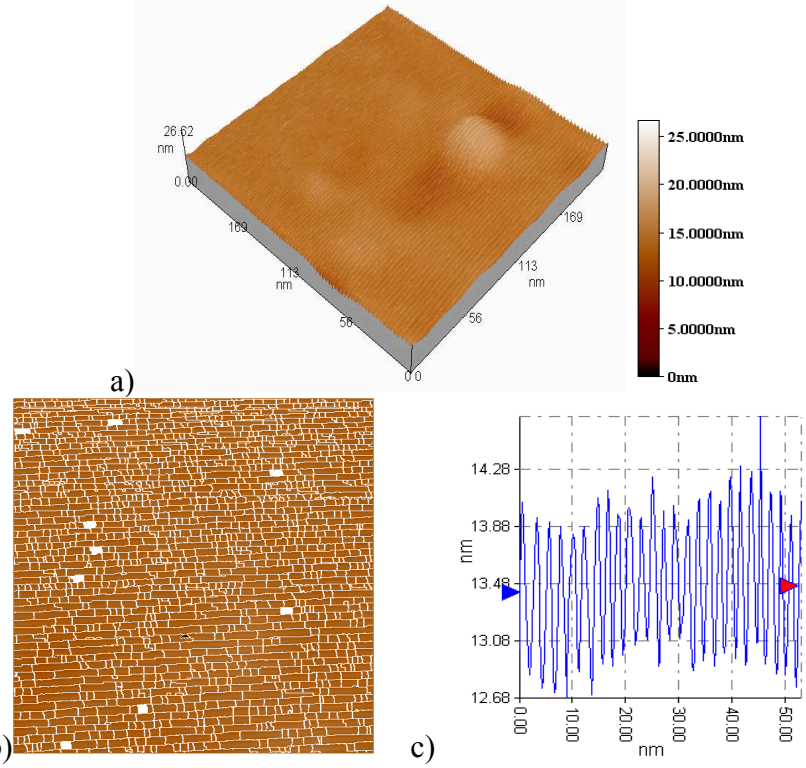

Fig. 1 GSSO materials: (a) AFM scan three-dimensional map (b)particle size analysis(c)the cross-sectional analysis

Figure 2 shows the FTIR spectrum of the bridged silsesquioxane. The presence of two bands at 1040 and 1118 cm^{-1} evidences the presence of ladder structures formed by Si-O-Si bonds. The broad band centered at about 3400 cm^{-1} corresponds to the C-OH groups and includes a small fraction of unreacted Si-OH groups. Two small bands at 1350 and 1590 cm^{-1} evidence the presence of a small residual fraction of formic acid as HCOO- anions (possibly forming salts with tertiary amine groups) [10].Another evidence of the presence of a self-structuring process was obtained from SEM micrographs (Figure 3). Some ordered regions are observed consisting of a self-assembly of semicy- lindrical shells. There seems to be a relationship between the curved structures observed in SEM images and the concentric semicylindrical shells observed at a lower magnification.

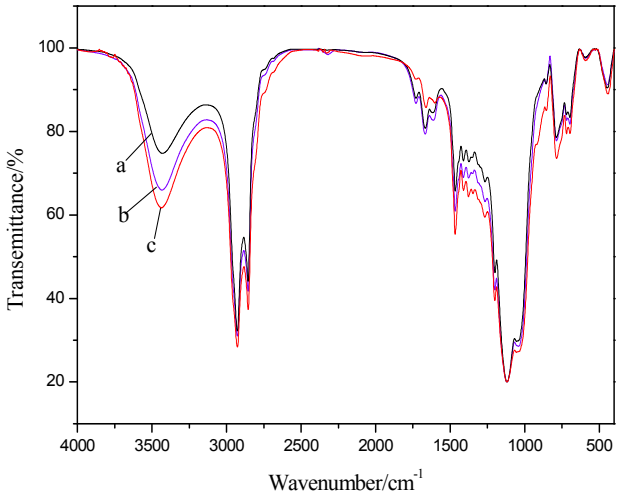

Fig.2 The FTIR of the GSSO(a)，GSSO(b) and GSSO(c) materials

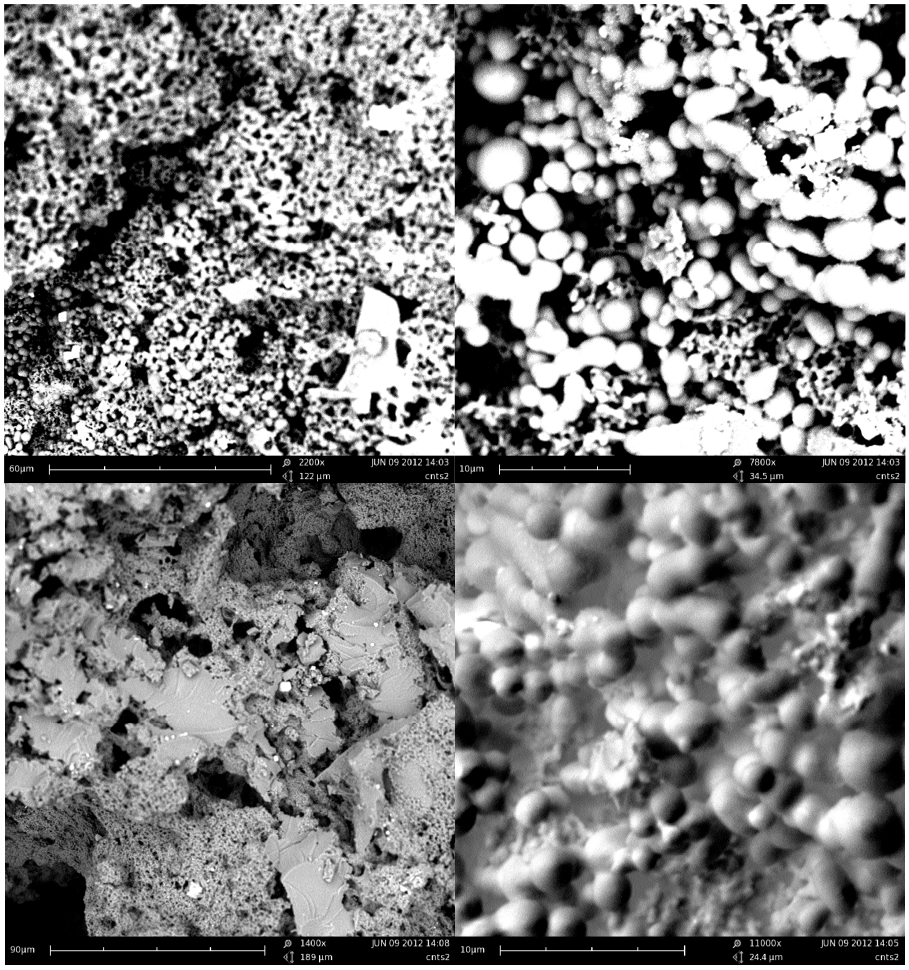

Fig.3 The SEM of the GSSO materials

Figure 4 shows a water contact angle of the material GSSO test results, the contact angles are: 102.51° (a) and 113.40° (b) for GSSO materials. The structure of the material reflects the configuration of the hydrophobic structural importance roughness.

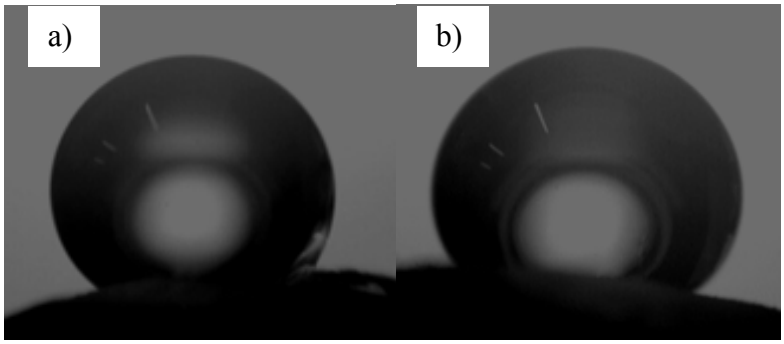

Figure 4 Contact angles: surface of the GSSO (a); inside of the GSSO (b)

Conclusions

A precursor of a bridged silsesquioxane bearing a hydrophobic pendant chain in the organic bridge was synthesized by the stoichiometric reaction of GPMS with DDA. Its hydrolytic condensation led to a bridged silsesquioxane characterized by the presence of both ordered and disordered domains. Experimental evidence obtained from AFM, FTIR, SEM techniques suggested that the basic structure of ordered domains consisted of a multilayer structure separated by hydrophobic regions with a thickness equal to the length of the tail-to-tail association of DDA chains in all-trans conformations. To our knowledge, this is the first example of the presence of this kind of structure in a cross-linked hybrid material. A hierarchical organization of ordered domains into semicylindrical shells was observed on a microscopic scale.

Acknowledgement

Financial supports are acknowledged the Aerospace supported Fund, China, under the contract number of2012-HT-HGD-11.

References

[1] D. R. Lin, L.J. Hu, H You and R.J.J. Williams: Eur. Polym. J Vol.47 (2011), p 1526

[2] D. R. Lin, Q. Zhao, L.J. Hu and B.S. Xing: Chemosphere Vol.103 (2014), p 188

[3] D. R. Lin, L.J. Hu, Z. Li and D.A. Loy: J. Porous.Mat Vol.21 (2014), p 39

[4] E. Chomski and G. A. Ozin: Adv. Mater Vol.12 (2000), p 1071

[5] J.J.E. Moreau, L Vellutini, M. Wong Chi Man and C. Bied: Chem. Eur. J Vol.9 (2003), p 1594

[6] J.J.E. Moreau, B.P. Pichon, M. Wong Chi Man, C. Bied, H. Pritzkow, J.L. Bantignies, P. Diedonne and J.L. Sauvajol: Angew. Chem Vol.43 (2004), p 203

[7] S. Inagaki, S. Guan, Y. Fukushima, T. Ohsuna and O. Terasaki: J. Am. Chem. Soc Vol.121 (1999), p 9611

[8] J.J.E. Moreau, B.P. Pichon, G. Arrachart, M. Wong Chi Man, C Bied: New J. Chem Vol.29 (2005), p 653

[9] A. Shimojima and K. Kuroda: Chem. Rec Vol.6 (2006), p 53

[10] N. B. Colthup, L. H. Daly and S. E. Wiberley in: *Introduction to Infrared and Raman Spectroscopy*; Academic Press: New York, 1975.

Advanced Materials Research Vols. 989-994 (2014) pp 743-746
© (2014) Trans Tech Publications, Switzerland
doi:10.4028/www.scientific.net/AMR.989-994.743

Hedgehog buckyball: high-symmetry complete polyhedral oligomeric silsesquioxanes (POSSs) characterized by UV-MALDI-TOF mass spectrometry

Derong LIN[1,a], Lijiang HU[2,b]

[1]School of Food Science, Sichuan Agricultural University, Ya'an, 625014, China

[2]Department of Chemistry, Harbin Institute of Technology, Harbin,150001, China

[a]email:youngsumass@126.com, [b]email:hulijiang2008@126.com

Keywords: Hedgehog Buckyball (HBB); POSSs; UV-MALDI-TOF

Abstract. In this study, we report the first example of a fullerene-like cage, a stable hedgehog buckyball (HBB). The HBB preparation can be performed using a normal hydrolytic condensation which we previously produced based on [(3-methacryloxy)propyl]trimethoxysilane (MPMS). MPMS was also used as a precursor for this study, but a longer condensation time was employed to produce more viscous products with a larger molecular weight (denoted MPOSS or MSSO).A high-symmetry complete POSS formulated as $R_{60}Si_{60}O_{90}$ or T_{60} ($T=RSiO_{1.5}$). The MSSO characterization can be determined by FTIR and GPC and NMR and is assigned from the peaks of UV-MALDI-TOF MS.

Introduction

The buckyball, C_{60}, was named "Molecule of the Year" for 1991 by Science[1]. Since the discovery of the C_{60} buckyball (FBB), fullerene science has continued to accelerate, investigating both the basic science and its potential applications[2]. One investigation involves a major focus on its analogue, the Si_{60} cluster[3]. For Si_{60} clusters, the cages should not be very stable due to the use of three $3sp^3$ orbitals to bond to other Si atoms. Thus the cages need some other atoms for the fourth bond whereas the C_{60} fullerene uses the second period sp^2 orbitals along with a pi bond to bond exclusively with other C atoms. Most investigations focus on endohedral Si_{60} isomers (using the fourth bond of the $3sp^3$ orbital) which are unstable[4]. To produce a stable Si_{60} configuration, Wang and Yang investigated (by ab initio calculations based on density functional theory) a Si-60 fullerene-like cage passivated using F or Cl atoms[5]; however, this research is limited by a complex experimental synthesis.

Theoretically, four $3sp^3$ hybrid orbitals (each containing an unpaired electron) of a Si atom are generated before the bond formation. These orbitals then bond to other four-atom electrons using the four generated hybrid orbitals which produces a stable configuration. A significant difference between FBB and HBB is the four-bond (from three $2sp^2$ hybrid orbits and one original 2p orbital) connection of each C atom on the FBB surface and the three-bond (from three of four $3sp^3$ hybrid orbits) connection of each Si atom (bridged three O atoms) on the HBB surface. For the remaining connections, one bond (from one of four $3sp^3$ hybrid orbitals) connects an organic group in a vertical direction outside the HBB surface. These organic groups exhibit much more functionality, activity and selectivity and are easier to assemble than the double bonds in the FBB surface, which facilitates the synthesis of hybrid materials possessing unique properties and the ability to set up applications[6].

Methods

The hydrolytic condensation of [(3-methacryloxy)propyl]trimethoxysilane (MPMS, Sigma G 1535, USA) was carried out in beakers placed in a water bath using C_2H_5OH and HCOOH (The First Factory of Chemical Agents at Tianjin, China) in a molar ratio of OH/Si = 3 and HCOOH/Si = 3～6 with stirring. The reaction process was performed in three steps: (1) plastic films were used to

seal the beakers for 7 days; (2) then several small needle-sized holes were made on the films for another 2 days; (3) finally the beaker was opened for several days until viscoelasticity was obtained; i.e., MSSO was formed. The temperature was held below 50 ℃ for all steps.

Results

^{29}Si NMR spectroscopy could be used to quantitatively measure the degree of condensation (extent of reaction) by the relative abundance of the T^3 silicon nuclei, Si–(O–Si)$_3$[7]:–65.681 ppm is characteristic of the T^3 species, and –56.577 ppm can be assigned to T^2 structures, Si–(O–Si)$_2$(OH) [8]. No T^0 or T^1 structures were present in the ^{29}Si NMR spectrum, indicating sufficient viscous sol to contain HBB T_{60}(Fig 1A).

The typical FTIR MSSO spectrum band at ~3423 cm^{-1} is primarily ascribed to stretching of the OH in Si–OH groups that are plausibly hydrogen bonded to other Si–OH groups and from water hydrogen bonded to itself and to the Si–OH groups. The obvious bands at about 1120–1129 cm^{-1} derive from Si–O–Si antisymmetric stretches. A decrease in the intensity of the Si–O–CH_3 group band at 2840 cm^{-1} was also evidenced(Fig 1B).

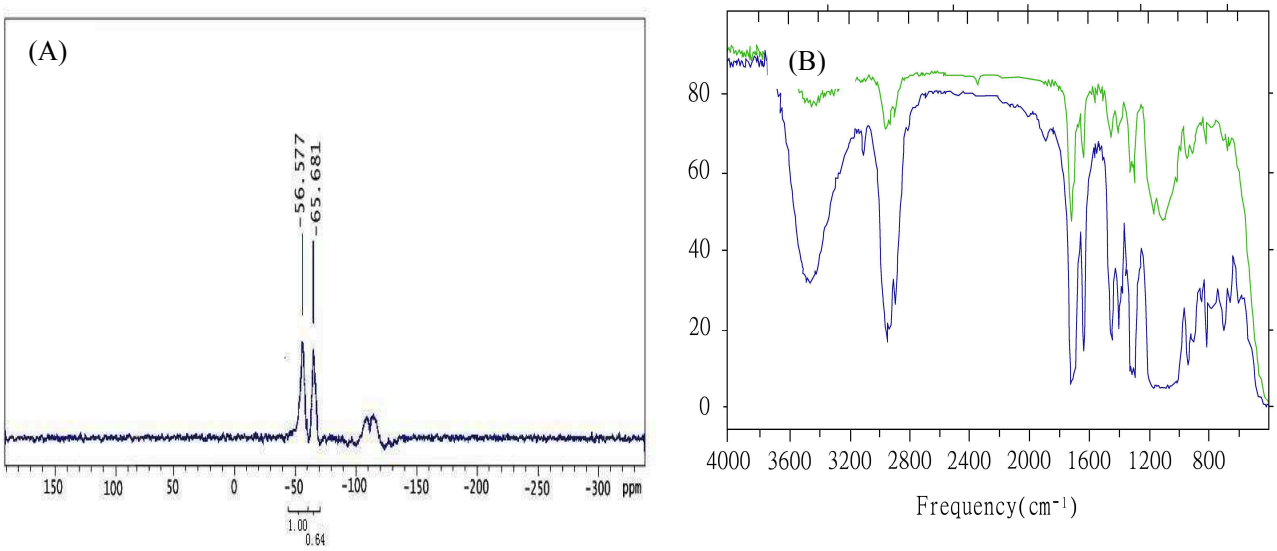

Figure 1. (A)^{29}Si NMR spectrum of MSSO;(B) FTIR spectrum of MSSO

Fig. 2A, 2B and 2C show the UV-MALDI-TOF MS in the m/z = 0–11000 Da range corresponding to MSSO oligomers. Three high-symmetry complete MSSOs, T8, T20 and T60 (see Fig. 3), were assigned (see Table 1).These predicted structures have a compliance between the experimental measurement value and the calculated molecular weight according to ion adducts ($M+H^+$ or $M+Na^+$ or $M+K^+$)[9]. T_{60}, one of three high-symmetry complete MSSOs, is a fullerene-like HBB and is denoted as MP-HBB as shown in Fig. 3c. The difference between HBB and FBB (as mentioned above) provides an ideal vehicle for exciting research which will be timely, rapidly evolving, multidisciplinary and even appealing on an aesthetic level.

Fig. 2D shows the mass distribution of the MSSOs measured by a gel permeation chromatography (GPC) device which provides refractive index data. The distribution profiles indicate that the oligomers are formed in three successive groups with average molecular weights of 1413.8, 4538.8 and 16260.0 (see Fig. 2D (b) 3, 2 and 1, respectively) corresponding to T_{60}, T_{20} and T_8 respective locations. Further investigation will be conducted on this MP-HBB to separate it from multiple MSSO structures using a gel permeation column[10]. The intensity of the MP-HBB present can be determined by GPC[11] or size exclusion chromatography (SEC) [12], and the mass of the eluant is again measured by a mass spectrometer.

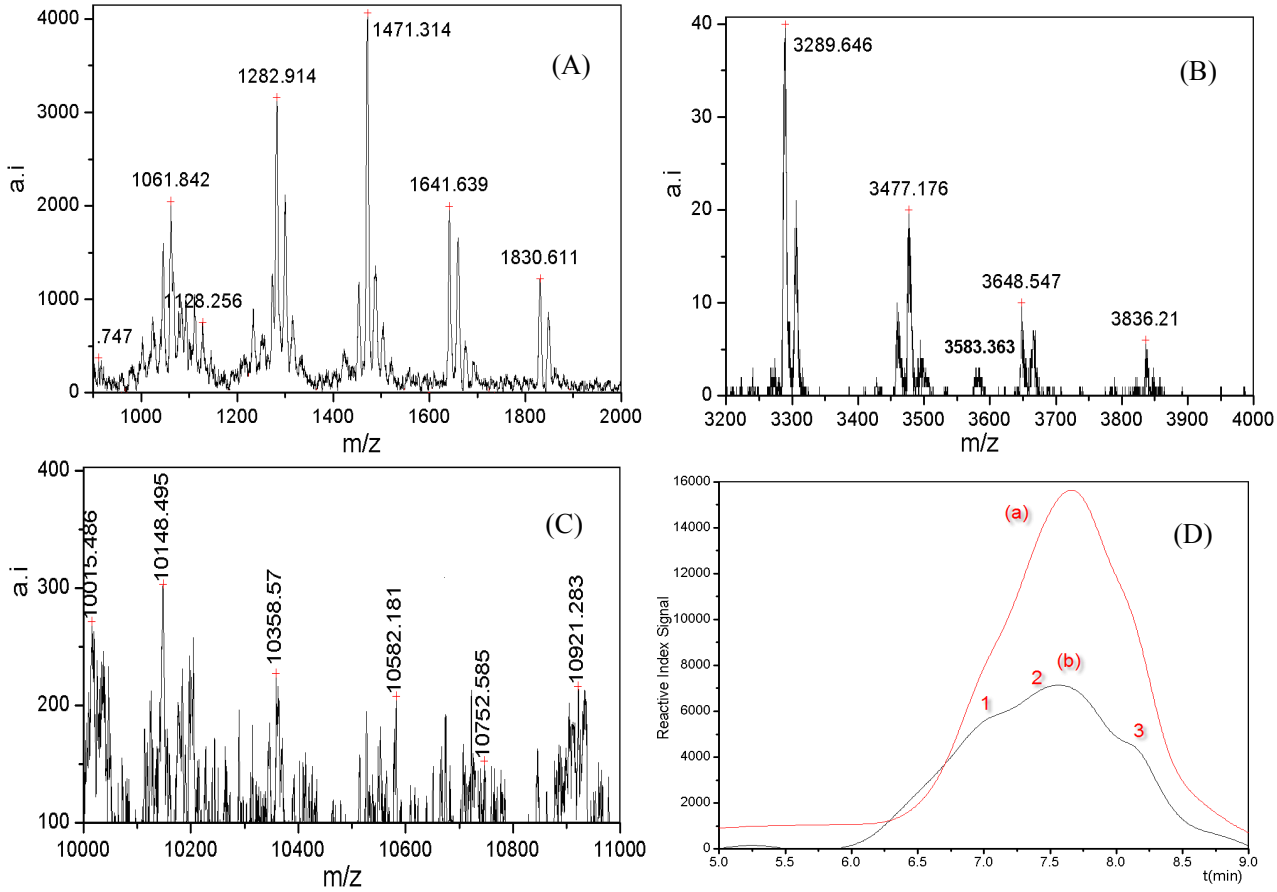

Figure 2. The UV-MALDI-TOF MS of MSSO oligomers:(A) m/z =0–2000 Da;(B) m/z = 3200–4000 Da;(C). m/z = 10000–11000 Da;(D) The GPC of MSSO oligomers

Table 1. MSSO assigned by the UV-MALDI-TOF mass spectrum (m/z =0–11000 Da)

Exp. m/z	Assigned structure	Calc. m/z ($+Na^+$, H^+, K^+)	Sym.
1 471.31	$R_8Si_8O_{12}$ ($+K^+$)	1 472.98	O_h
3 583.36	$R_{20}Si_{20}O_{30}$ ($+H^+$)	3 585.96	I_d
10 752.59	$R_{60}Si_{60}O_{90}$ ($+H^+$)	10 755.88	I_h

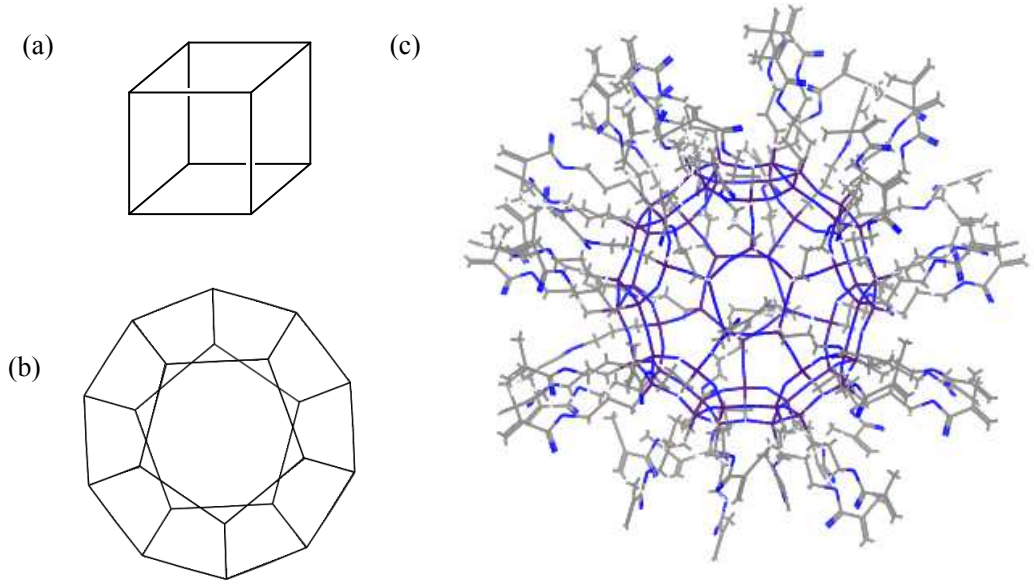

Figure 3. Structures of three high-symmetry complete MSSOs: (a) T_8, (b) T_{20} and (c) T_{60}. The organic groups (R) are bonded to the Si atom, R = $–CH_2CH_2CH_2OC(O)C(CH_3)=CH_2$.

Conclusions

We report the first example of a fullerene-like cage, a stable hedgehog buckyball (HBB): a high-symmetry complete POSS formulated as R_{60}-$Si_{60}O_{90}$ or T_{60} and characterized with a UV-MALDI-TOF MS. The organic groups in a vertical direction outside the HBB surface exhibit much more functionality, activity and selectivity and are easier to assemble.

Acknowledgement

Financial supports are acknowledged the Aerospace supported Fund, China, under the contract number of2012-HT-HGD-11.

References

[1] D. E. Koshland: Science Vol.254 (1991), p. 1705

[2] D. A. Loy and R. A. Assink: J. Am. Chem. Soc Vol.114 (1992), p.3977

[3] S. Yoo, J Zhao, J Wang and X.C. Zeng: J. Am. Chem. Soc Vol.126 (2004), p13845

[4] B. X. Li, P Cao and X Zhou: Phys. Lett. A Vol.288 (2001), p 41

[5] L. Wang and D. R. Yang: Mol. Simul Vol.36 (2010), p 493

[6] D. A. Loy and K. J. Shea, Chem. Rev Vol.95 (1995), p 1431

[7] D. R. Lin, L.J. Hu, H You and R.J.J. Williams: Eur. Polym. J Vol.47 (2011), p 1526

[8] F. J. Feher, D Soulivong and F. Nguyen: Chem. Commun (1998), p 1279

[9] R. Bakhtiar and F. J. Feher: Rapid Commun. Mass Spectrom Vol.13 (1999), p 687

[10] C. X. Zhang and R. M. Laine: J. Am. Chem. Soc Vol.122 (2000), p 6979

[11] M. Z. Asuncion and R. M. Laine: J. Am. Chem. Soc Vol.132 (2010), p 3723

[12] M. J. Abad, L Barral, D.P. Fasce and R.J.J. Williams: Macromolecules Vol.36 (2003), p 3128

Advanced Materials Research Vols. 989-994 (2014) pp 747-750
© (2014) Trans Tech Publications, Switzerland
doi:10.4028/www.scientific.net/AMR.989-994.747

Effect of temperature on the growth and biochemical composition of *Sargassum muticum*

Chunying Yuan[a], Shuo Yang[b], Yue Wang[c], Qingman Cui[d]

Tianjin Key Laboratory for Marine Chemistry and Resource, College of Marine Science & Engineering, Tianjin University of Science and Technology, Tianjin 300457

[a]email: cqm80@163.com, [b]email: yangshuo@tust.edu.cn, [c]email:wangyue@tust.edu.cn, [d]email:cqm80@tust.edu.cn

Keywords: Temperature, *Sargassum muticum*, growth, biochemical composition.

Abstract. Under the laboratory conditions, the effect of temperature (10, 15, 20, 25, 30℃) on growth and biochemical composition of *Sargassum muticum* was studied, the results showed that: the optimum growth temperature of *S. muticum* was 15 ℃ in the range of 10-30 ℃; the contents of chlorophyll a, carotenoid, soluble protein, soluble sugar and brown algae polyphenols were the highest at the temperature of 25 ℃, it was speculated that these components appeared compensatory increase duo to the high temperature stress. The contents of these biochemical components were the lowest at 30 ℃.

Introduction

Sargassum muticum belongs to the Sargassaceae, *Sargassum*, is a common species along the Yellow and Bohai coast. *S. muticum* is an important industrial raw material for its high algin content (30%). Shuqing Cao et al[1] studied indoor artificial breeding technology of *S. muticum*; Xiulian Chang et al[2] reported the adsorption effect of *S. muticum* on cadmium ion. In addition, some scholars have studied the active substances from *S. muticum* and their anti-tumor, antibacteria activities[3-5]. In this research, the effect of temperature on the growth and biochemical composition of *S. muticum* was studied by the indoor experiment, in order to provide theoretical basis for the artificial cultivation of *S. muticum*.

Materials and Methods

Experimental Materials

Biological Materials. *S. muticum* was collected from Qinhuangdao coastal area.

Main Instruments. TGL-16LM high-speed refrigerated centrifuge, Hunan Xingke Scientific Instrument Co., Ltd.; T6 Ultraviolet visible spectrophotometer, Beijing Purkinje General Instrument Co., Ltd.; 250C Digital light incubator, Jintan Xinnuo Experimental Instrument Factory.

Experimental Methods

Experimental Design. The experiment was designed five temperature gradients (10, 15, 20, 25, 30 ℃), with 3 replicates per treatment.

Seaweed Farming. The robust algae tips were selected and cutted into 3-5 cm long fragments, placed in 250 ml erlenmeyer flask respectively. The relative mass of algae was 1.56±0.12 g. Natural seawater from Tianjin sea was used for experiment. Experimental conditions: pH was 8, the salinity was 33, light intensity was 25 μmol/m^2 • s. The air was passed into erlenmeyer flask during the experiment. Cultivation water was replaced once a day. The experiment lasted for 15 days.

Determination of Indices

The Specific Growth Rate(*SGR*). The fresh weight was measured every 5 d. *SGR* was calculated as the following formula:

$$SGR=(\ln Wt-\ln W_0)/t\times 100\%$$

W_0: initial fresh weight of algae (g), *Wt*: fresh weight of algae at the end of the experiment, *t*: the experimental time.

Biochemical Components. The chlorophyll a and carotenoid contents were determined according to the method of Wellburn[6]. Soluble sugar and soluble protein contents were measured using Anthrone sulfuric acid method and Kaumas brilliant blue method[7]. Brown algae polyphenols was determined according to Folin phenol colorimetry[8].

Statistical Analysis

SPSS17.0 software was used in statistical treatment. The experimental results were expressed as the mean + SD.

Results and Discussions

The Effect of Temperature on Specific Growth Rate of *S. Muticum*. The result was shown in Figure 1, the specific growth rate of *S. Muticum* increased with the increase of temperature, when the temperature reached 15 ℃, SGR reached the maximum, when the temperature reached 30 ℃, the growth of *S. Muticum* was negative. It indicated that *S. Muticum* had a poor adaptation to high temperature. The optimum temperature for growth was 15 ℃ in the temperature range of 10-30 ℃.

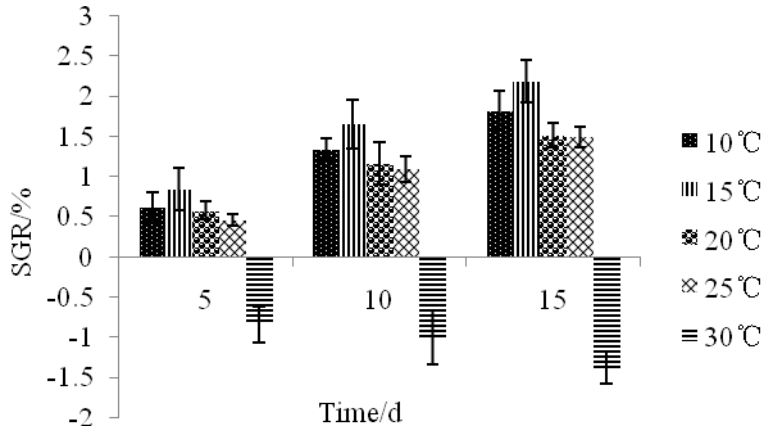

Fig.1 The effect of temperature on specific growth rate of *S. Muticum*

The Effect of Temperature on Chlorophyll a and Carotenoid Content of *S. Muticum*. The experimental result was shown in Figure 2, the chlorophyll a and carotenoid contents of *S. Muticum* increased gradually with the increase of temperature, when the temperature reached 25 ℃, the chlorophyll a and carotenoid content was the highest, when the temperature reached 30 ℃, chlorophyll a and carotenoid content was the lowest. According to observation, *S. Muticum* appeared bleaching phenomenon at 30 ℃. Lewey et al[9] found that the faster growth, the lower pigment content by studying pigment composition and photosynthesis of *S. Muticum* every month, thought it might be that generation speed of pigment was more lower than algae growth speed, resulting in pigment reduction because of dilution.

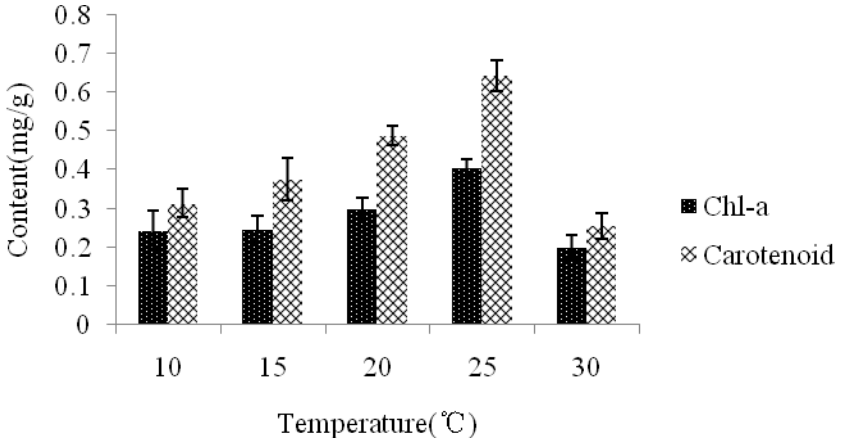

Fig.2 The effect of temperature on chlorophyll a and carotenoid content of *S. Muticum*

The Effect of Temperature on Soluble Protein and Sugar Content of *S. Muticum*. Most soluble proteins in plants are enzymes involving in various metabolism, determination of its content is an important index for understanding total metabolism. The result showed that the soluble protein content was thehighest at 25 ℃, and that was lowest at 30 ℃(Figure 3). It might be that algae growth was inhibited, and the enzyme levels of algae increased compensatorily in the low light, thereby improving the effective utilization of algae to light energy, which was a positive physiological adaption to nature, had the important ecological significance[10]. Our study also found that the soluble sugar content in *S. Muticum* showed little difference before 25 ℃, but decreased dramatically when the temperature reached 30 ℃(Figure 3).

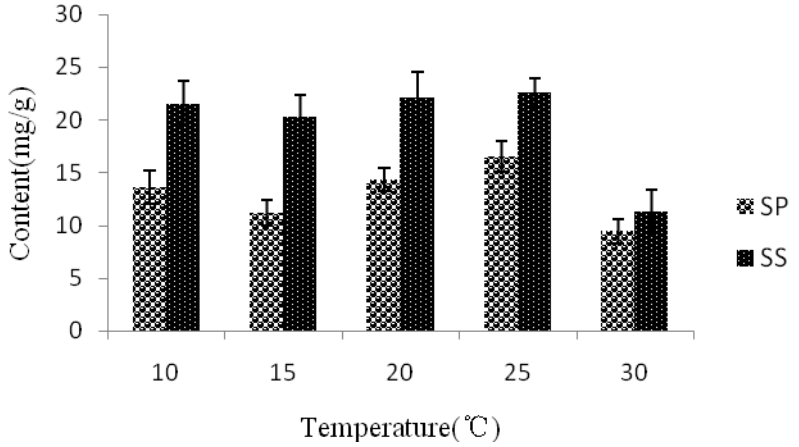

Fig.3 The effect of temperature on soluble protein and sugar content of *S. Muticum*

Effect of Temperature on Brown Algae Polyphenols Content in *S. Muticum*. Brown algae polyphenols is a large class of chemical substances against herbivores, is the most common secondary metabolites and the unique molecular defense substance in plants[11]. In this study, brown algae polyphenols content was the highest at 25 ℃, it might be that high temperature started defense function of *S. Muticum*, which was a stress response of *S. Muticum*. Brown algae polyphenols content was the lowest at 30 ℃, it might be caused by the death of partial algae.

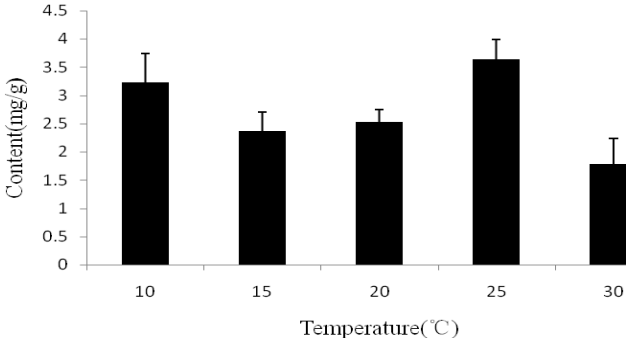

Fig.4 Effect of temperature on brown algae polyphenols content of *S. Muticum*

Conclusions

Effect of temperature on the growth of *S. Muticum* was significant, the most suitable growth temperature was the range of 10-30 ℃; the chlorophyll a, carotenoid, soluble protein, soluble sugar and brown algae polyphenols contents of *S. Muticum* were the highest at 25 ℃, and these biochemical components were the lowest at 30℃.

Acknowledgements

This work was financially supported by the Science Foundation of Tanggu District (Project No.2010XN08-05).

References

[1] CAOShuqing,ZHANG Zeyu, WANG Guoshu, et al. Indoor artificial seeding of seaweed *Sargassum muticum*. Journal of Dalian Fisheries University, 2008,23(5):359-363.

[2] CHANG Xiulian，WANG Wenhua，FENG Yongmei，et al. Investigation of cadmium (Ⅱ) biosorption on *Sargassum kjellmanum*. Marine Science Bulletin, 2003, 22(4): 26-31.

[3] SUN Haofen,YANG Luofei, MENG Lu,et al. Research of steroids from *Sagassum muticum*. Journal of Qingdao Technological University, 2012, 33(4): 68-71.

[4] MA Weiwei, LI Li，ZHOU Gefei. *in vitro* Immunoregulatory and antitumor activity of sulfated polysaccharides from *Sargassum muticum*. Food Science, 2013, 34(7): 270-274.

[5] LI Li, QU Yan, CAO Wubo，et al. Antibacterial and immune activity of petroleum ether extract phase from the *Sargassum muticum*. Food Science and Technology, 2012, 37(8): 220-224.

[6] Wellburn A R. The spectral determination of chlorophyllsa and b，as well as total carotenoids, using various solvents with spectrophotometers of different resolution. Plant Physiology, 1994, 144(3): 307-313.

[7] CHEN Yuquan. 2002. Biochemistry Experiment Method and Technology. Beijing: Science Press, 95-97.

[8] HUANG Shuping,TAN Taiming, XU Changcheng, et al. Studies on polyphenol content determination of luffa by Folin-Ciocalteu colorimetry**.** China Vegetables, 2010, 1(4): 47-52.

[9] Lewey S, Gorham J. Pigment composition and photosynthesis in *Sargassum muticum*. Marine Biology,1984, 80: 109-115.

[10] JIANG Hongbo, TIAN Xiangli, DONG Shuanglin, et al. Effects of temperature and light intensity on the growth and biochemica l composition of *Sargassum thunbergii*, Chinese Journal of Applied Ecology, 2009, 20(1): 185-189.

[11] YANG Huicheng, DONG Shiyuan, LIU Zunying, et al. Advances in chemical composition and biological activity of algae polyphenols. Chinese Journal of Marine Drugs, 2007, 26(5): 53-59.

Advanced Materials Research Vols. 989-994 (2014) pp 751-754
© (2014) Trans Tech Publications, Switzerland
doi:10.4028/www.scientific.net/AMR.989-994.751

Numerical Simulation of Cr12MoV Steel During Quenching Process

Zhang Wei[1,a], Qu Zhoude[2,b], Deng Xiaohu[1,c,*], Duan Xing-wang[3]

[1]Key Laboratory of High Speed Cutting and Precision Machining, Tianjin University of Technology and Education, Tianjin, 300222, China

[2]Tianjin Engineering Center of Digital Manufacturing Die & Mould, Tianjin University of Technology and Education, Tianjin, 300222, China

[3]School of Materials Science and Engineering, Taiyuan University of Science and Technology, Taiyuan, 030024, China

[a]zhangweius@163.com, [b]tshjqu@163.com, [c]dengxh@tute.edu.cn

*Author for correspondence: Deng Xiaohu (1984-), dengxh@tute.edu.cn

Keywords: Quenching. Numerical simulation. Temperature field. Microstructure field. Stress field

Abstract. The excessive residual stress induced by quenching in steels will easily result in distortion and failure of parts. In order to obtain the more suitable quenchant, quenching process of Cr12MoV steel with different mediums involving water and oil are simulated, respectively. In present paper, the influence of nonlinear surface heat transfer coefficient, thermodynamic parameters and latent heat are considered comprehensively. The distribution of temperature, microstructure, hardness and residual stress after quenching for Cr12MoV steel are simulated by DEFORM finite element software. According to the results mentioned above, the variations of each field of the steel are analyzed.

Introduction

Mould is the basis of industrial development, which is indispensable forming tool for achieving mass production and new product research and development. In the past few decades, the mould industry is developing rapidly. Demands of the mould have been growing around 15% per year, especially in recent years. The mould industry has fairly high requirements for the specification, performance, quantity and quality of the model steels. Cr12MoV steel is the most widely used cold work model steel, and it is widely applied to extruding mould, cold drawing mould, forming mould and so on. Cr12MoV steel has a higher demand for heat treatment technology because of the limit of its mechanical property, if unreasonable method is adopted, it will easily give rise to the failure of mould [1]. The heat treatment is a traditional hot working method, which is frequently applied to improve the comprehensive mechanical properties of steels [2]. It is a complex couple process involving temperature, transformation, stress and strain. It is difficult for traditional heat treatment to control the internal quality by empirical methods. With the development of algorithms of numerical simulation and computer technology, researchers turn to the study of the process by numerical simulation technology [3-5]. In present paper, the coupling problem is solved by DEFORM and conduct numerical analysis. The results obtained by numerical simulation method have an important guiding significant for the formulation of actual heat treatment process.

Numerical Thermal of Heat Treatment Process

Material Selection. The material of workpiece is Cr12MoV steel. The chemical compositions of Cr12MoV steel are listed in Table 1.

Analysis of Model. Cylindrical sample with diameter of 20 mm and height to diameter ratio of 2.5 : 1. Based on the symmetry, 1/2 of the cross section of cylindrical specimen is chose for meshing. The finite element model of Cr12MoV steel is presented in Fig. 1.

Quenching Process. In this paper, oil and water are simulated as cooling medium, respectively. The quenching process of Cr12MoV steel consisted of heating up to 1025℃ and quenching for 1h before cooling to room temperature.

Table 1: Chemical composition of Cr12Mov steel (wt,%)

C	Cr	Mo	V	Mn	Si	S	P
1.50	12.00	0.81	0.21	0.42	0.31	0.001	0.025

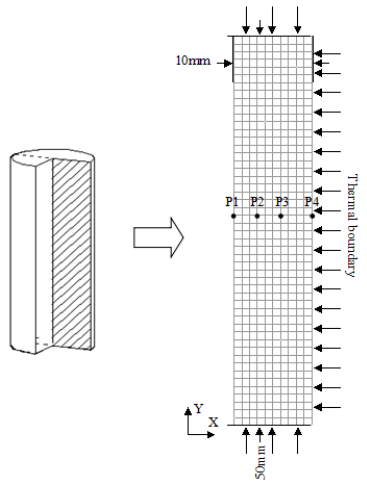

Fig. 1 2-D Finite Element Mesh of a Cylinder

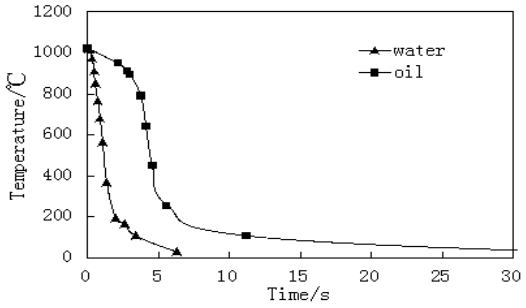

Fig. 2 The Temperature Distribution of Specimen

Results and Discussion

Simulation Results of Temperature Field. As is shown in figure 1, outer (point P4) of the model is chose as tracing point. Fig. 2 illustrates the temperature variations with time during quenching process. Based on the result of figure 2, it is obvious that the temperature of water cooling specimen drops quickly. When quenching for about 7s, temperature of the specimen outer (point P4) has dropped to 30℃. As for oil cooling, it presents a small temperature difference between the inner and outer of oil cooling specimen at the initial stage. With the increase of cooling time, the temperature difference continues to grow. When quenching for about 50s, the temperature of the whole sample gradually drops to the room temperature.

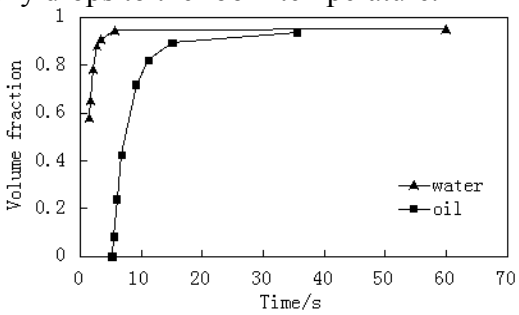

Fig. 3 Volume Fraction of Martensite

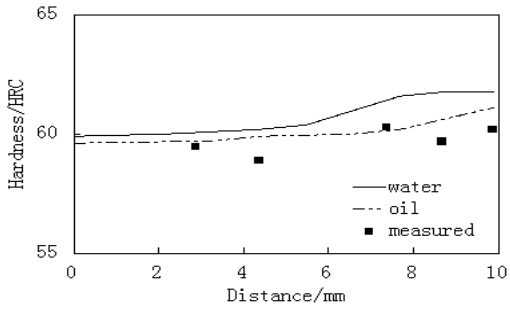

Fig. 4 The Hardness Distribution of Specimen

Simulation Results of Microstructure Field. As is shown in figure 1, outer (point P4) of the model is chose as tracing point. Fig. 3 shows the distribution curves of martensite after quenching. When quenching for about 1s, the outer (point P4) of specimen begins to produce martensite during water cooling process. The martensite volume fraction grows quickly and the maximum reaches 95% until the end of the quenching. For the oil cooling process, when quenching for about 5s, the outer (point P4) of specimen begins to produce martensite and the maximum reaches 93.5%.

Fig. 4 shows the hardness distribution at different distance after quenching. The distance from the center of axisymmetric specimen to surface is chose as transverse axis in figure 4. Based on the result of figure 4, it can observe that the results of hardness agree well with the measure values.

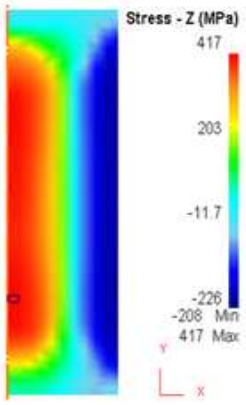

(a) Stress Field of Water Cooling Specimen

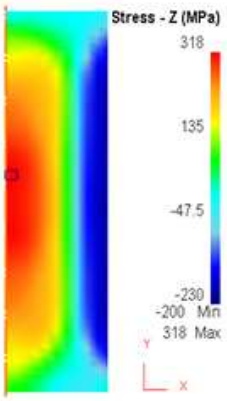

(b) Stress Field of Oil Cooling Specimen

Fig. 5 Stress Induced by Temperature

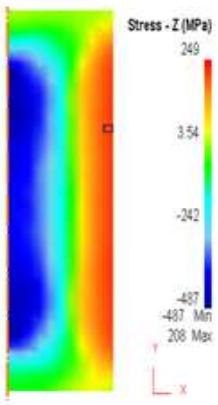

(a) Stress Field of Water Cooling Specimen

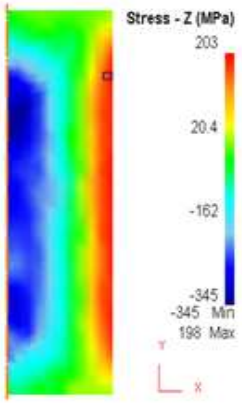

(b) Stress Field of Oil Cooling Specimen

Fig. 6 Stress Induced by Phase Transformation

Simulation Results of Stress Field. Based on the complexity of internal stress distribution, the stresses induced by temperature change and phase transformation are simulated, respectively. At the initial stage of quenching, martensite transformation does not occur, the thermal stress of quenching specimen is mainly caused by temperature change. Stress field of the Cr12MoV steel after quenching is shown in Fig. 5. Figure 5(a) shows that the maximum tensile stress reaches 417MPa in the center after water cooling. While the maximum compressive stress reaches -208MPa on the surface. Fig. 5(b) shows that the maximum tensile stress and compressive stress are 318MPa and -200MPa in oil cooling process, respectively. The results show that the residual stress of water cooling specimen is fairly large.

When quenching for a while, the outside of specimen begins to produce martensite. The stress of specimen is mainly induced by phase transformation. Stress field of the Cr12MoV steel after quenching is shown in Fig. 6. Figure 6 shows that the influence the phase transformation on residual stress is different from the temperature. Figure 6(a) shows that the maximum tensile and compressive stress of specimen reaches 208MPa and -487MPa after water cooling, respectively. Compared with the result of figure 6(a), the oil cooling specimen obtains a relatively low residual stress.

In order to get a clearer change of residual stress, as is shown in figure 1, the four points of model are selected as tracing points. Fig. 7(a) shows the stress curves of the oil cooling specimen caused by temperature change. Stress curves of the oil cooling specimen caused by phase transformation are shown in Fig. 7(b). The results show that temperature and phase transformation have an important effect on residual stress after quenching. The stress change curves of the water cooling specimen are omitted. The residual stress of specimen after water specimen is too large to satisfy the actual requirement.

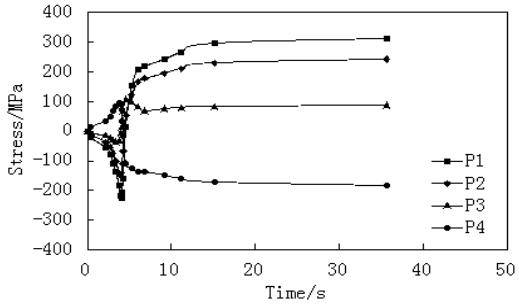

(a) Stress Induced by Temperature

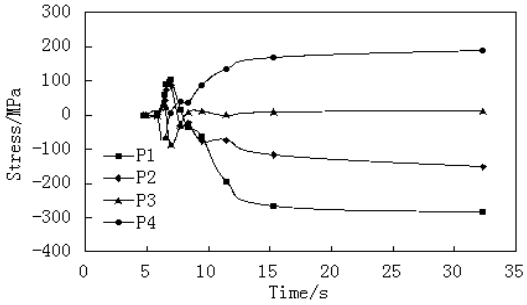

(b) Stress Induced by Phase Transformation

Fig. 7 Stress Distribution Curves of Oil Cooling Specimen

Conclusion

On the basis of these results, the following conclusions are obtained.

1) The changes of the temperature, microstructure, hardness and stress in quenching process for Cr12MoV steel are simulated by DEFORM finite element software.

2) The volume fraction of iron-carbon phases are rely on temperature history and carbon content. Water cooling can obtain more martensite than oil cooling. The results of hardness of water cooling and oil quenching specimen obtained by simulation agree well with the experimental results.

3) The results show that the temperature and phase transformation, which are very important factors during quenching process, exert highly influence on the residual of quenching specimen. Oil cooling can reduce residual stress of quenching specimen. Therefore, oil cooling is more suitable quenching medium for Cr12MoV steel.

Acknowledgements

In this paper, the research is supported by Natural Science Foundation of Tianjin (13JCYBJC38900); Scientific Research Starting Foundation of Tianjin University of Technology and Education (KYQD12008).

References

[1] Wu Xiao-feng, Ma Kun, Xu Na, etc. Main problems and research development in application of Cr12MoV die steel[J]. Die & Mould Industry, 2009, 35(9): 55-62.

[2] Sanguk Jin, Sangshik Kim, Youngseon Lee, et al. Effect of Various Heat and Surface Treatment Conditions on the Fatigue Behavior of SKD11 Steel[J]. Met. Mater. Int, 2009, 15(6): 917-923.

[3] Ju Dong-ying, Deng Xiao-hu. Modeling and Simulation of Iron-Carbon Phase Transformation During Tempering of Steel[J]. Rare Metal Materials and Engineering, 2012, 41(S1): 006-012.

[4] Arimoto K, Yamanaka S, Michiharu N, et al. Explanation of the origin of quench distortion and residual stress in specimens using computer simulation[J]. Microstructure and Materials Properties, 2009, 4(2): 168-186.

[5] Xu Wencai. Research on the cushion property of corrugated board [J]. Packaging Engineering, 1997, 18(2): 78-79.

Advanced Materials Research Vols. 989-994 (2014) pp 755-758
© (2014) Trans Tech Publications, Switzerland
doi:10.4028/www.scientific.net/AMR.989-994.755

Effect of NH4Cl Flux on Structural and Luminescent Properties of CaS: Eu^{2+} Phosphors

Zhang Yunjie[1], Zhao Jie[1,2,a]*, Wang Dajian[1,2,b], Ma Jian[1]

[1]School of Materials Sci. & Eng., Tianjin University of Technology, Tianjin 300384, China

[2]Tianjin Key Lab for Photoelectric Materials and Devices, Tianjin 300384, China

[a]vzhaoj @ tjut.edu.cn, [b]djwang @ tjut.edu.cn

[*]Author for correspondence: Zhao Jie. Email: vzhaoj @ tjut.edu.cn

Keywords: Two steps. Microstructure. Diffusion. Photoluminescence. Phosphor

Abstract. CaS:Eu^{2+} phosphors were prepared by two steps method at a relatively low temperature (1050°C) using NH_4Cl as a flux. The influences of NH_4Cl flux concentrations on the crystal structure, morphology and photoluminescent properties of CaS:Eu^{2+} phosphors were investigated by X-ray diffraction (XRD), scanning electron microscope (SEM), photoluminescence (PL), respectively. XRD analysis shows that when the raw materials added with the NH_4Cl flux, the crystal structure was not changed .The SEM images indicate that increase of the NH_4Cl flux enlarged the grain size of the phosphor particles. The luminescence intensity of CaS:Eu^{2+} was enhanced with adding NH_4Cl flux and up to the maximum emission intensity when the addition of NH_4Cl flux is 1wt%.

Introduction

With the energy crisis and environmental pollution, people are more and more concerned about the energy saving and environmental friendliness. White light-emitting diodes (LEDs) , the so-called next generation solid-state lighting, have attracted closely attention due to their potential application in many fields, such as device indicators, backlights, automobile headlights, general illumination, etc[1–3]. Besides, they also have many advantages over the existing incandescent and halogen lamps in reliability, energy saving, maintenance and safety. As the two methods available for creating white light LED, One is to use an ultraviolet InGaN chip with RGB (red, green, and blue) multiphase phosphors produce a white light. The other is to use a blue light GaN (gallium nitride) LED chip loaded with a yellow phosphor YAG ($(Y_{1-a}Gd_a)_3(Al_{1-b}Ga_b)_5O_{12}:Ce^{3+}$) to obtain a white light, which is the most common way to generate white light[4–5]. However, this white emitting color changes with input power and it has a low color rendering index due to the absence of red emission from the phosphorYAG:Ce^{3+}. Therefore, it is extremely essential to seek for appropriate and effective red-emitting phosphors for SSL.

As we all known, CaS:Eu^{2+} phosphors as a member of alkaline earth sulfide families, which possesses potential applications in photo-, electro-, cathode ray, field emission displays and luminescence paint, has been widely studied since 1971[6]. Many studies have suggested that CaS:Eu^{2+} phosphors show a wide range of excitation wavelengths and have a similar refractive index by comparison with LED windows , so that it's able to increase the escape cone and gain a higher light extraction for SSL devices.

Eu^{2+}-activated CaS phosphors are usually prepared by flux assisted solid state reaction method ,which Significantly lower sintering temperature and holding time, and to obtain phosphor powders with desirable phases and properties. It has been reported that the flux acted an essential role in manipulating the grain size, particle distribution and shape of phosphors, thus affecting the PL intensity. For these reasons, the samples of our paper were synthesized by two steps method at a relatively low temperature 1050°C using NH_4Cl as a flux. The effects of different NH_4Cl flux concentrations on the crystal structure, morphology, and photoluminescent performance was investigated. Meanwhile, the amount of NH_4Cl flux was optimized to get the maximum emission intensity of CaS:Eu^{2+} phosphors.

Experimental procedure

Sample preparation. $CaS:Eu^{2+}$ phosphors samples were prepared from raw materials containing High purity Eu_2O_3 (>99.99%, the others are analytical grade except C), $CaSO_4$, S, C, NH_4Cl powders. The molar ratio of $CaSO_4$ and S was from1:3 to 1:4,the concentration of Eu was 0.1% to 0.2% mole per mol of CaS and different amount(0 wt%, 1 wt%, 2 wt%, 3 wt%, and 4 wt%) of NH_4Cl were added as a flux, respectively. The starting components were mixed in anhydrous alcohol as solvent and grinded by an agate mortar and pestle. Then , the mixed powders were dried in vacuum oven at 70℃。After drying, the mixture were placed into a small alumina crucible, which was put into another crucible of larger diameter filled with C powders, The large crucible with its contents was placed in a muff furnace under ordinary atmospheres and heated to 1050℃ for 40-50 min. The samples were cooled to room temperature and grinded again by an agate mortar and pestle. Next, the as-obtained powders was fired under N_2 92–H_2 8 vol% atmosphere for 1h at 1000℃ for the finally products.

Sample characterization. The crystal structure of the products was identified by XRD with a diffractometer (Rigaku D/max-2500/pc, Japan). A morphology study of $CaS:Eu^{2+}$ phosphors was performed on field emission-scanning microscopy (FE-SEM; Model S-4800, Hitachi Japan). Excitation and emission spectra of the samples are measured by a fluorescence spectrometer equipped with a xenon light source (Hitachi F-4600, Japan). All measurements were carried out at room temperature.

Results and discussion

Excitation and emission spectra of $CaS:Eu^{2+}$ with different amounts of NH_4Cl flux are shown in Figure 1. The excitation spectrum of $CaS:Eu^{2+}$ phosphor has a very broad bands in the rang of 200-600 nm, which are attributed to $4f^7(^8S_{7/2}) \rightarrow 4f^65d(t_{2g})$ transition of Eu^{2+} ion[3].The phosphors have strong absorption from 400-600 nm, so that it can be well excited by blue light for white LEDs application. All the phosphor powders were excited by 476 nm blue light, the emission wavelengths were all in the red region, at around 654nm, which results from the transition from the lowest field splitting component of the $4f^65d^1$ excited state to its $4f^7$ ground state[3]. As can be seen in Fig 1, the addition of NH_4Cl flux can enhance the excitation and luminescen-ce intensity of $CaS:Eu^{2+}$ phosphor. Intensity of emission spectrum reached the maximum When the amount of NH_4Cl flux was 1 wt%. As the content of NH_4Cl flux above 1 wt%, the photoluminescence intensity of the samples decreases, the possible reason of the effect of NH_4Cl flux concentrations on the PL intensity was discussed in detail as follows.

According to CaS reaction mechanism, The reaction kinetics of CaS is guided by a single reaction controlled by a three -dimensional diffusion Reaction mechanism. In the formation of CaS, NH_4Cl firstly lowers the decomposition temperature of sulfates and then act as a role in the reaction process to accelerate the kinetics of the phase formation and make the morphology changes by enhancing diffusion coefficient [7].

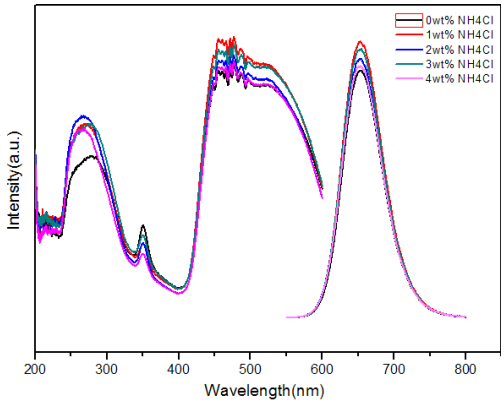

Fig. 1 Excitation (Monitoring wavelength: (λem = 653 nm) and emission (Excitation wavelength prepared: λex = 476 nm) spectra of $CaS:Eu^{2+}$ with different amounts of NH_4Cl.

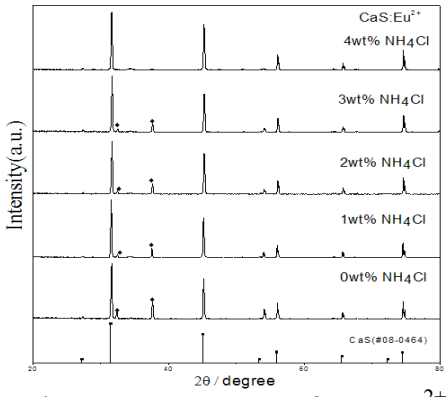

Fig. 2 XRD patterns of $CaS:Eu^{2+}$ Phosphors with different NH4Cl flux concentrations by two steps.

In general, the luminescence intensity is bound up with the crystallinity and phase purity of powders. The existed impurity would enhance the defect concentration in major lattice and break the energy transfer from the host to the activator, and then greatly decrease the PL intensity. It is clearly observed that with the addition of NH_4Cl flux, the impurity phase CaO gradually decreased up to disappear and the sample powders had stronger crystallinity than that without NH_4Cl flux in Fig2. This fits well with the enhancing of the PL intensity. Also, the morphology of particles are crucial for the PL intensity. A bigger particle size and narrower size distribution are beneficial to reduce light scattering and promote light absorption for phosphors. As shown in Fig 3, the particles size of the phosphor with adding the NH_4Cl flux are much uniform , smooth and bigger than without adding the NH_4Cl flux, which suggest that the increase of the PL intensity is likely due to the enlarged grain size. However, There are obvious agglomeration appearance between the particles of the samples With gradually increasing the NH_4Cl flux in Fig 3, the different of grain size are co-exsit, which results in the amount of NH4Cl flux over 1 wt%, the photoluminescence intensity of the samples decreases. Above all, the increase of the PL intensity is consistent with the changes of phase composition of all samples and their morphologies.

Fig. 2 shows the XRD patterns of $CaS:Eu^{2+}$ with various amounts of NH_4Cl flux. The main phase is matched well with the standard card No.08-0464 CaS as reference, and the XRD peaks correspond to face-centered cubic structure. The concentrations of flux have a huge impact on the phases of the samples. Without NH_4Cl flux, the phases of samples include CaS phase and CaO phase. As the addition of NH_4Cl flux, the peak intensities of main phase CaS increase but the intensities of impurity phase CaO gradually decrease up to disappear when the amount of NH_4Cl is 4 wt%. Besides, we found that $CaS:Eu^{2+}$ phosphor with NH_4Cl flux had stronger crystallinity .

The photoluminescent properties of phosphors is in close contact with their morphology, such as grain size, grain shape, size distribution and so on . Figure 3 displays the SEM image of CaS: Eu^{2+} powders synthesized by two steps with various amounts of NH_4Cl. There are dramatic changes in the samples' morphology. The particles Without NH_4Cl flux were inhomogeneous, rough and agglomeration , but with adding the NH4Cl flux, the particle sizes of the phosphors are enlarged and It exhibits smooth, uniform and nearly spherical-like morphology，which is due to NH4Cl flux accelerates the kinetics of the formation of $CaS:Eu^{2+}$ powders by enhancing diffusion coefficient resulting in the Eu^{2+} could enter into the lattice site of Ca^{2+} easily. However, with gradually increasing the NH4Cl flux, An agglomeration appearance between the particles of the samples.

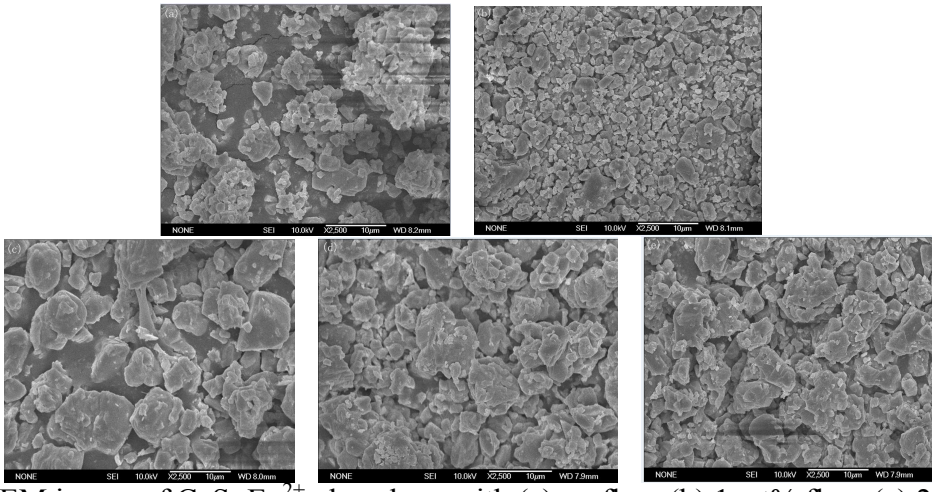

Fig. 3 SEM image of CaS: Eu^{2+} phosphors with (a) no flux, (b) 1 wt% flux, (c) 2 wt% flux, (d) 3 wt% flux, and (e) 4 wt% flux.

Conclusion

$CaS:Eu^{2+}$ phosphors were prepared by two steps method at a relatively low temperature 1050°C using NH_4Cl as a flux. The influences of NH_4Cl flux concentrations on the crystal structure, morphology and photoluminescent properties of $CaS:Eu^{2+}$ phosphors was investigated. The report

showed that with the addition of the NH_4Cl flux, $CaS:Eu^{2+}$ phosphors had a stronger crystallinity and grains sizes were enlarged. Compared with that of phosphor without NH_4Cl flux, excitation and emission intensity of samples with the addition of the NH_4Cl flux are obviously enhanced, and this improvement of luminescence was analyzed in details. When the content of NH_4Cl is 1wt%, the photoluminescence intensity up to maximum.

Acknowledgments

This work was financially supported by the National Natural Science Foundation of China under Grant nos. 21076161, 50802062, and 50872091 and Tianjin Key Discipline of Materials Physics and Chemistry under Grant no. 10SYSYJC28100.

References

[1] Fred Schubert E, Kim JK： Science 308 (2005):1274

[2] Chen, Huang-Yu, et al. *Materials Research Bulletin* 47.6 (2012): 1412-1416.

[3] Xu X-R, Su M-Z . Luminescence and luminescent materials. Beijing: Chemical Industry Press, 2004 (in Chinese).

[4] J.K. Park, M.A. Lim, C.H. Kim, H.D. Park, J.T. Park, S.Y. Choi, Appl. Phys. Lett. 82 (5) (2003) 683–685.

[5] A. Mills, Adv. Semicond. Mag. 8 (2005) 9–23.

[6] Lehmann W, Ryan F M. Journal of The Electrochemical Society, 1971, 118(3): 477-482.

[7] Zhang, Le, et al. *Journal of the American Ceramic Society* 95.12 (2012): 3871-3877.

Advanced Materials Research Vols. 989-994 (2014) pp 759-762
© (2014) Trans Tech Publications, Switzerland
doi:10.4028/www.scientific.net/AMR.989-994.759

Preparation and Properties of Multi-elements Doped Perovskite-Type Mixed Conductors for IT-SOFC Cathodes

Fu Jiang[1], Zhao Jie[1,2,a]*, Fu Yong[1], Li Rongrong[1]

[1]School of Materials Sci. & Eng., Tianjin University of Technology, Tianjin 300384, China

[2]Tianjin Key Lab for Photoelectric Materials and Devices, Tianjin 300384, China

[a]vzhaoj @ tjut.edu.cn

*Author for correspondence: Zhao Jie. Email: vzhaoj @ tjut.edu.cn

Keywords: LSCCF cathode. Multi-elements doping. Mixed conductor. Thermal stability

Abstract. Multi-elements doped $LaCoO_3$-based mixed conductors $La_{0.7}Sr_{0.1}Ca_{0.1}Co_{0.8}Fe_{0.2}O_{2.9}$ (LSCCF-112) and $La_{0.7}Sr_{0.2}Ca_{0.1}Co_{0.7}Fe_{0.3}O_{2.85}$ (LSCCF-213) were synthesized by conventional solid state reaction (CSSR). The forming process, microstructure and crystal structure of the prepared samples were analyzed by TG/DTA, SEM and XRD. The mixed conductivities of the samples were measured using DC four-terminal method in 150-950 ℃. Thermal expansion coefficients (TEC) of the samples were tested in 20-950℃. LSCCF-112 and LSCCF-213 exhibit pure perovskite phase and porous structure after sintered at 1200 ℃. The average TECs of LSCCF-112 and LSCCF-213 are 18.17×10^{-6} K^{-1} and 17.52×10^{-6} K^{-1} respectively. The mixed conductivity of the samples shows semiconducting behavior up to 700-750℃ and then decreases as the temperature is further raised. At intermediate temperature (IT), the conductivity values of the samples are both much higher than 100 S/cm.

Introduction

Solid oxide fuel cell (SOFC) as an energy conversion device has attracted people's great attention recently. The reason for the interest in SOFC lies in its high efficiency, low-pollutant emission and fuel versatility, etc. [1-2]. Nevertheless, the operating temperature of SOFC is about 1000 ℃. Such high temperature causes some problems including electrode sintering, interfacial reaction and thermal mismatch between the electrode and the electrolyte, and high cost, which limits the practical application of SOFC technology [3-4]. One possible way to overcome these problems is to reduce the operating temperature of SOFC. Toward achieving IT-SOFC goal, considerable effort has been done. Lowering operating temperature to IT (600-800 ℃), however, leads to a significant decrease in cathode catalytic activity [4]. Although $La_{1-x}Sr_xMnO_{3-d}$ (LSM) is commonly used as a cathode in high temperature SOFC, it cannot be used at temperature below 800 °C as the polarization of LSM increases considerably [5]. Perovskite-type oxides containing Co ions in their B sites are known to be promising cathode materials for use in IT-SOFC due to high mixed conductivity and catalytic activity in 600-800 ℃. However, TECs of the oxides are much larger ($20.0\text{-}23.0\times10^{-6}$ K^{-1}) than those of commonly used electrolytes ($10.8\text{-}12.5\times10^{-6}$ K^{-1}), which causes mismatch between the cathode and electrolyte. This mismatch degrades the long-term stability and durability for thermal cycling in SOFC systems [6]. They are also limited in the application. Therefore, it is important to develop high performance cathode materials for IT-SOFC technology. The aim of this paper is to study the preparation and properties of Sr, Ca and Fe co-doped $LaCoO_3$-based mixed conductors as cathode materials in IT-SOFC.

Experimental

Sr, Ca and Fe co-doped cathode materials $La_{1-x-y}Sr_xCa_yCo_{1-z}Fe_zO_{3-\delta}$ (x=0.1, 0.2; y=0.1; z=0.2, 0.3) were prepared by the CSSR method. Analytically pure La_2O_3, $CaCO_3$, $SrCO_3$, Fe_2O_3 and Co_2O_3 as raw materials were used. In order to remove moisture and impurity, the powders were initially pretreated in the air atmosphere. La_2O_3 powders was heated to 900℃ for 90 min, other powders to

300℃ for 120 min. Required amounts of the raw materials were mixed and ground thoroughly using an agate mortar and pestle. The mixed powders were calcined at 1000℃ for 120 min using DC-B10/16 intelligent high temperature furnace, then the powder was ground for 60 min. 10% (mass percent) polyvinyl alcohol as agglomerant were added to the calcined powders, sieved using a 100-mesh sieve after grinding, then pressed into samples with size of 25 mm×8 mm×4 mm using DY-60 electric tablet machine. The samples were sintered at 1200 ℃ using above-mentioned furnace. The samples were first heated to 350 ℃ at 3 ℃/min for 10 min, then at 4 ℃/min to 650 ℃ for 60 min, finally at 5 ℃/min to 1200 ℃ for 360 min, cooled with furnace subsequently. Sintered samples were black. Volume shrinkage rates were about 14%-15%.

Thermo-gravimetry and differential thermal analysis (TG-DTA) in 20-1200 ℃ was carried out using EXSTAR6300 differential thermal analyzer in argon at a heating rate of 10 ℃/min for determining the formation process and sintering temperature of LFCCF. Phase structures of the sintered samples were demonstrated by D/Max-2500 X-ray diffraction (XRD) instrument with CuKα radiation, operating at 40 kV and 150 mA. XRD patterns were collected with a scanning speed of 8 °/min over the angular range 10-80 °. All the XRD patterns were analyzed using Jade software and compared with the standards from JCPDS database. JEOL JSM-6700F scanning electron microscope (SEM) was employed to examine the microstructures and porous of the sintered samples. The mixed conductivity of the sintered samples was measured in air by DC four-terminal method in 150-950 ℃. Thermal expansion curves from 20 ℃ to 950 ℃ were tested at heating rate of 5 °/min using TMA/SS6300 device, Al_2O_3 as a reference.

Results and Discussions

TG-DTA curve of LSCCF-112 precursor is shown in Fig.1.

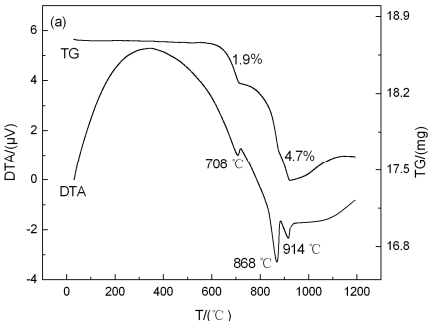

Fig. 1 TG-DTA curves of LSCCF-213 precursor

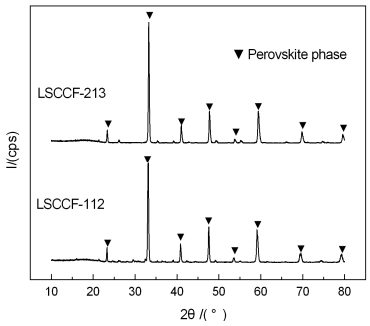

Fig. 2 XRD patterns of the LSCCF samples

The first mass loss (1.9%) takes place in 600-700 ℃ with a weak endothermic peak at 708 ℃. This may be associated with the release of the lattice oxygen originating from the reduction of Co^{4+}+/ Fe^{4+}. The TG curve reveals the second mass loss (4.7%) in 750-930 ℃ accompanied by two endothermic peaks in DTA curve. The obvious peak at 868 ℃ was caused by releasing large amounts of CO_2 owing to the decomposition of $CaCO_3$ and $SrCO_3$. The peak at 941 ℃ may correspond to the formation of perovskite structure [7]. Therefore, the calcining temperature should be above 1000 ℃ to obtain a single perovskite phase.

The XRD patterns of the samples sintered are shown in Fig.2. The impurity peaks are not found in LSCCF-112 and LSCCF-213 samples. Single perovskite structure has been obtained after sintered at 1200 ℃ for 360 min, comparing the data from XRD with normal feature diffraction lines of pure $LaCoO_3$. The cell volumes of LSCCF-112 and LSCCF-213 are bigger than that of pure $LaCoO_3$ with the same structure, which may be owing to the partial substitution of La^{3+} by bigger Sr^{2+} and Co^{3+} by bigger Fe^{3+}. ABO_3 perovskite-type structure has a strong ability to tolerate the ionic radius changes of A site and B site.

Fig.3 (a) and (b) show the SEM micrographs of the cross-sections of LSCCF-112 and LSCCF-213 samples after sintered at 1200 ℃-360 min.

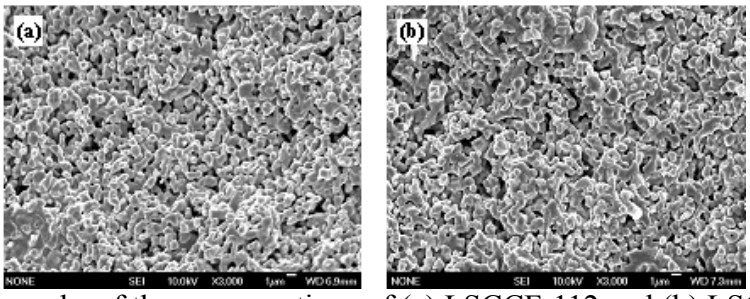

Fig. 3 SEM micrographs of the cross-sections of (a) LSCCF-112 and (b) LSCCF-213 samples

As shown in Fig.3（a & b）, LSCCF-112 and LSCCF-213 samples appear to have uniform microstructure. The particle size is in the range of 0.5-1μm. In addition, many homogeneous distributed pores can be observed from the inner of sintered samples. Due to the decomposition or volatilization of organic-additive during sintering process, pores will be leaved in composite oxide. Suitable porosity and homogeneous grain size are benefit for the conductivity of samples.

Fig. 4 shows the mixed conductivities of LSCCF-112 and LSCCF-213 samples measured in air from 150 to 950 ℃. As shown in Fig. 4, The mixed conductivity of LSCCF-112 and LSCCF-213 samples shows semiconducting behavior up to 700-750℃ and then the decrease may be observed as the temperature is further raised.

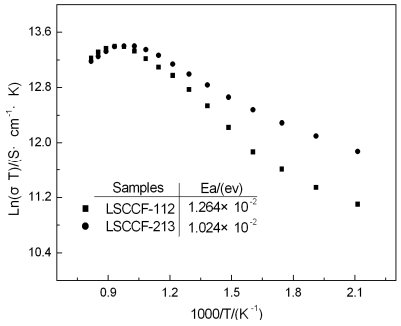

Fig. 4 Arrhenius plots of LSCCF samples

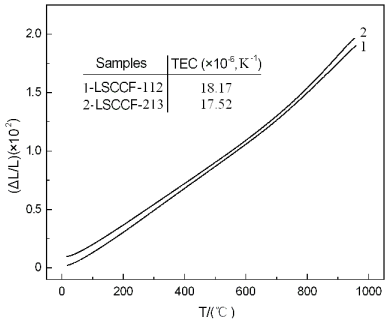

Fig. 5 Thermal expansion curves of LSCCF samples

At any given temperature, mixed conductivity values of LSCCF-213 are higher than that of LSCCF-112 , which may be ascribed to increasing Co^{4+}/ Fe^{4+} content and the charge carrier concentration with doping-Sr increasing. The mixed conductivity values of LSCCF-112 and LSCCF-213 are both much larger than 100 $S \cdot cm^{-1}$ at 600-800℃, which meet the needs of IT-SOFC cathodes. The highest conductivity values were observed for LSCCF-112 (643 $S \cdot cm^{-1}$ at 750 ℃) and for LSCCF-213 (676 $S \cdot cm^{-1}$ at 700 ℃). At lower temperatures (150-500 ℃), $ln(\sigma T)$ versus T^{-1} shows linear relationship, and the small polaron hopping is regarded as the main conduction mechanism. At higher temperatures (>500 ℃), A significant decrease in conductivity may be ascribed to the creation of oxygen vacancies for charge balance [8]. The oxygen vacancies may act as scattering centers, or as traps for electrons, which reduce carrier mobility. The activation energies (*Ea*) can obtain from the slopes of the linear part of Arrhenius plots. *Ea* values of LSCCF-112 and LSCCF-213 are 0.01264 eV and 0.01024 eV respectively.

The Thermal expansion curves of LSCCF samples sintered at 1200 ℃for 360 min are shown in Fig. 5. Their thermal expansion curves are approximately linear from 20 to 950 ℃. The TECs of the samples exhibit a reducing tendency with increasing amount of doped Fe^{3+}. The average TECs of LSCCF-112 and LSCCF-213 are 18.17×10^{-6} K^{-1} and 17.52×10^{-6} K^{-1} respectively. Although the TECs of samples still are mismatch with extensively used electrolytes, it is obvious that TECs decrease compared with only Sr^{2+} doped oxides (TEC, $20\text{-}23\times10^{-6}$ K^{-1}). This is owing to Ca can stabilize the lattice for Ca-O bond stronger than the Sr-O bond, and electronic charge compensation occurs preferentially by the formation of $Fe^{3+}\rightarrow Fe^{4+}$ compared to $Co^{3+}\rightarrow Co^{4+}$ [9]. Ca^{2+} and Fe^{3+} Substituting have effects on lattice and thermal stability. The Thermal expansion is one of the important factors to evaluate the cathode.

Conclusions

Perovskite-type $La_{1-x-y}Sr_xCa_yCo_{1-z}Fe_zO_{3-\delta}$ (x=0.1, 0.2; y=0.1; z=0.2, 0.3) have been prepared by CSSR method. XRD analysis show that the LSCCF-112 and LSCCF-213 both exhibit a single phase with perovskite structure after sintered at 1200 ℃ for 360 min. At 600-800 ℃, the mixed conductivities of LSCCF samples are both much higher than 100 S/cm. LSCCF-112 and LSCCF-213 have the highest conductivity of 653 $S \cdot cm^{-1}$ at 750 ℃ and 686 $S \cdot cm^{-1}$ at 700 ℃ respectively, which can meet the electrical performance needs of IT-SOFC cathodes. Compared with only Sr^{2+} doped oxides, the TECs of Sr, Ca and Fe co-doped oxides reduce obviously. Therefore, Sr, Ca and Fe co-doped LCCCF is a promising cathode material system for IT-SOFC. Much effort should be spent on reducing the TEC of LSCCF cathode materials in the future in order to accelerate the practical application of the SOFC technology.

Acknowledgments

This research was supported by the National Undergraduate Innovation Training Programs (Grant No. 201210060012).

References

[1] K Wang, D Hissel, M.C Pera: International Journal of Hydrogen Energy, Vol. 36(2011), p. 7212

[2] W.T. Hong, T.H. Yen, T.D. Chung, et al: Appl. Energy, Vol. 88(2011), p. 3990

[3] S. Yoo, T.H. Lim, J. Shin, et al: Journal of Power Sources, Vol. 226(2013), p. 1

[4] C. Sun, R. Hui, J. Roller: Journal of Solid State Electrochemistry, Vol. 14(2010), p. 1125

[5] S.P. Jiang, J. Mater: Sci., Vol. 43(2008), p. 6799

[6] R. Li, L. Gao, L. Ge, et al: Journal of Power Sources, Vol. 106(2011), p. 9939

[7] J. Zhao, Y.C. Ma, C.Li, et al: Materials Science & Technology, Vol. 18 (2010), p. 56

[8] J. M. Porras-Vazquez, P. R. Slater: Fuel Cells, Vol. 12(2012), p. 1056

[9] J. G. Jiang, C. Cui: Materials Science & Technology, Vol. 15 (2007), p. 575

Advanced Materials Research Vols. 989-994 (2014) pp 763-766
© (2014) Trans Tech Publications, Switzerland
doi:10.4028/www.scientific.net/AMR.989-994.763

Research on Microstructure and Properties of Plasma Powder Spray Welding Layer Based on 3D Printing

Meheretu Embabo[1,2,a], Wang Zhongmin[1, b], Han Haichuan[1, c]

[1]Colledge of Mechanical Engineering, Tianjin University of Technology and Education, Tianjin, 300222, China

[2]Adama University of Technology and Science, Adama, Ethiopia

[a]mercy84j@yahoo.com, [b]wzmin86@126.com, [c]haoxiaohuo777@gmail.com

Keywords: Plasma powder spray welding, Process parameters, Microstructure, Properties

Abstract. Plasma powder spray welding method is used for depositing successive layers of metal, which forms a 3-Demensional (3D) solid component. Fe45 alloy powder is chosen to spray welding on Q235 steel. Welding process parameters of plasma powder spray welding are studied, which affected the performance of carbon steel weld layer. Then changes of alloy powder spray welding and influences of weld microstructure after spray welding are analyzed. Experiments results show that in the case of only changing transferred arc current, the microstructure and mechanical properties of the weld is obviously better, grain size distributes uniformity, and hardness is moderate.

Introduction

The plasma powder spray welding, which is combined with 3D printing to make products from design to manufacture is a kind of advanced welding technology now, and products being made from design to manufacture are realized easily [1]. 3D printing technology is called 'the third industrial revolution' in the field of manufacturing industries, through this technology products will be turned into personalization [2]. Plasma spray welding technology has the advantages of low alloy material consumption, powder easy preparation, low cost, etc. It can get the density of low dilution rate of surfacing welding layer, high efficiency, and it is easy to realize automation [3]. A metallic 3 D printers are developed by a research team at Michigan, but it uses plastic as raw materials to make products. To reduce the time of production and it has been stated there was a need to automate the production and testing method [4][5].

In this paper the component is formed by melting and depositing the metal using plasma powder spray welding method. A welding robot is used and programmed in relation to the shape of the component to realize plasma powder spray welding. The welding parameters are generated as the requirement for the material. The test material is also used according to the specification of the material.

Materials and 3D Printing Process

The whole welding system includes plasma powder spray welding machine, an industrial robots, and a working table, etc. And the welding machine is controlled by a color touching screen, whose interface is simple and practical. Load of the robot is small and flexible, its effective working range is 1500 mm, it has six degrees of freedom (DOF) which makes it move freely in 3D space.

In this paper, Q235 steel is used for the base material, Fe45 steel powder is used for producing the 3D printed component, and the chemical compositions of base metal and spraying powder are shown in Table 1. The melting temperature of the powder is about 1100°C to 1200°C, the powder particle size range from 60-120 (mesh).

Table 1 Q235 steel and Fe45 powder composition (wt. /%)

Composition / Metal	C	Si	Mn	S	P	B	Cr	Ni
Q235	0.12 ~0.2	0.3~0.7	0.3	0.045	0.04			
Fe45	0.5~0.6	3 ~4		16~18		3~4	16~18	12~14

Main process parameters include welding current, welding speed, powder feed rate, plasma gas flow, torch oscillation (amplitude and frequency), and arc length, etc. In order to check the quality of the 3D printed layer, two groups experiments are conducted, one group is performed with varied welding currents and fixed powder speeding rate, another group is conducted with varied powder speeding rates and the fixed welding current. Experimental parameters are shown in Table 2.

Table 2 Two groups experiment parameters

Powder Type	No. of Experiments	Powder Feed Rate(%)	Current(A)
Fe45	B1	15	60
	B2	15	80
	B3	15	100
	B4	15	120
	B5	15	140
	B6	15	160
	B7	5	70
	B8	10	70
	B9	15	70
	B10	20	70
	B11	25	70
	B12	30	70

Result and Discussion

3D Component-Printed

The 3D component is printed by plasma powder spraying welding method being shown in Fig.1.

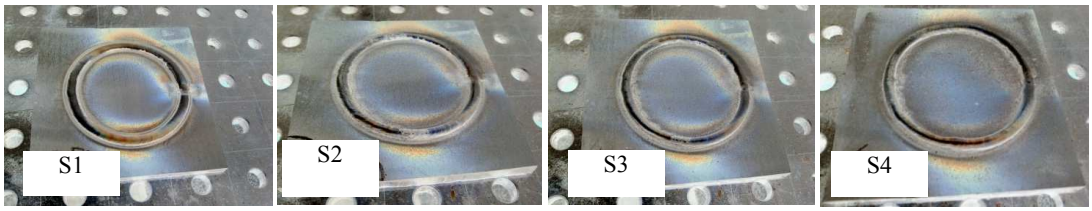

Fig. 1 Macroscopic samples of Fe45 powder sprays

Analysis and Discussion

1) Microstructure of 3D printed layer with varied current

Fig.2 shows the change in welding line under common microscope which is used to observe the current nearby the spray and also in experiments from B1 to B6 in Table 2, the amount of powder feed rate is constant 15% and the amount of arc current is vary from 60A to 160A. Both the shieling gas and plasma gas is used with purity of 99.99% argon. The rate of shielding gas and protective gas supply is 2.7L/min and welding speed is 2mm/s.

Within the range of 60A to 160A arc current it affects the following parameters. The electric current is small, plasma arc energy is also small, width of the ion beam is relatively small and narrow, and the formation of internal welding formation is irregular, and it has some cracks.

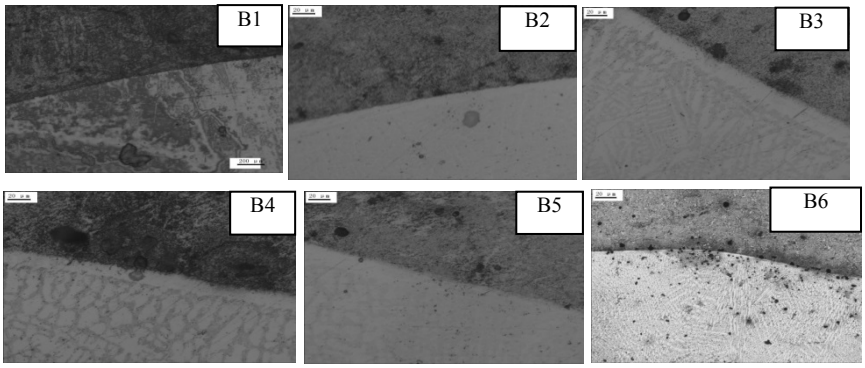

Fig.2 Microstructure of Fe45 alloy powder spray welding layer

2) Microstructure of the 3D printed layer with varied powder feed rate

As impact it clearly discusses about change in arc current, impact tow will focus on the variation of powder feed rate. In Fig.3 powder feed rate from B7 to B12 in Table 2 vary from 5 % to 35% and all the other parameter is constant including arc current.

Microstructure of the weld fusion line is shown in Fig.3, when the powder feed rate is 5%, spray layer and weld fusion zone organization distributed more evenly. When the amount of feed powder rate reaches 10%, the grain size and distribution of tissue more are evenly distributed. When the powder feed rate reaches 15-35 %, we can see a excessive welds occur, due to the excessive powder.

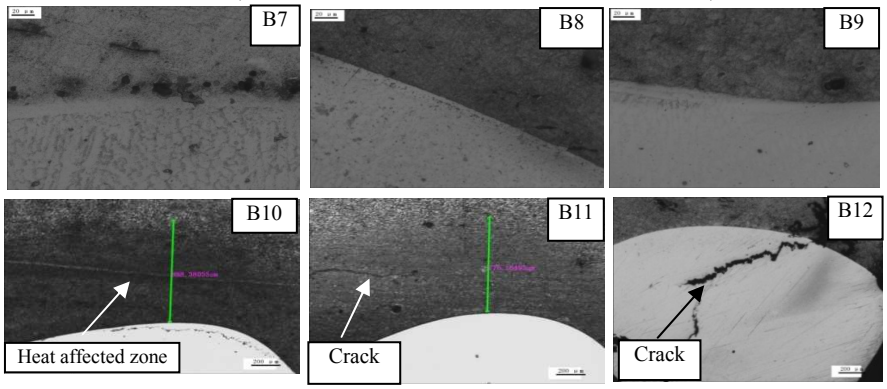

Fig.3 Microstructure of the layer with powder feed rate increasing

3) Properties of 3D printed layer near the fusion line

Hardness is one of the majors that determine the quality of the product because it directly affects service life and resistance to fatigue. We use orthogonal experiment method to check the hardness near the fusion line this experiment carried for variation in arc current and all other parameters are constant. Fig.4 shows the hardness of spray near the fusion line. According to Fig.4, as the amount of arc current increasing by 20A with constant powder feed rate, the hardness and spray layer are fluctuating.

4) Properties of spray layer with varied spraying powder feed rate

Fig.5 shows when the amount of powder feed rate increases by 5%, as the increasing or decreasing of powder feed rate, the performance of welding nearby fusion line and in the spray layer itself also varies.

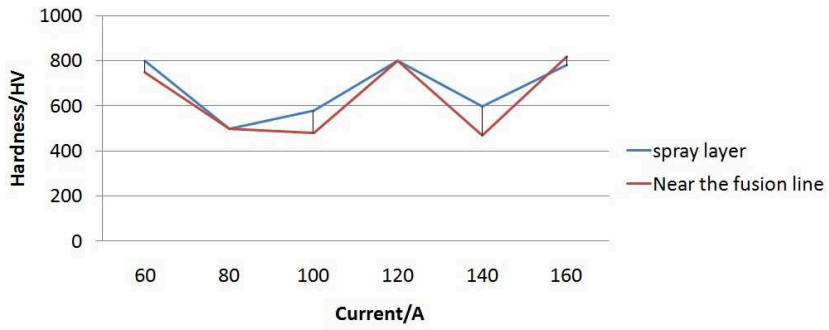

Fig.4 Hardiness of spray layer with arc current increasing

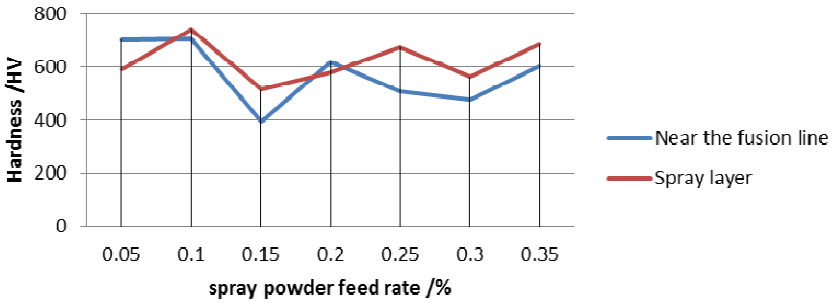

Fig.5 Hardness of spray layer with feed rate increasing

Conclusion

3D printing technology is discussed and plasma powder spray welding based on 3D printing is studied, the microstructure of spray layer is analyzed, also. In this paper Fe45 steel powder is used as the main material of the process and Q235 steel plat as a base metal. Experiments are carried out in two ways: one is that the amount of powder feed rate is constant and the amount of arc current is varying, the other is that the arc current is constant and feed rate being varied. Through orthogonal experiments with different process parameters, they describe the impacts of transfer amount of arc current and amount of feed rate on the properties of the seam near the fusion line and in spray layer.

References

[1] H.G. Liu, Q.Yang, G.F. Liu: Information Analysis of 3D-Printing Rapid Prototyping Technology at Home and Abroad. Journal of Intelligence, 2013, p.40-46

[2] X. Y. Wang: 3D Printing Technology and the Development of Industry and Prospect Analysis. China High-tech Enterprises, 2012, 26, p.3-5

[3] Y.Z. He, S.H. Si, X.M. Yuan: Experimental Study on the Property and Microstructure of the Alloy Overlay of Plasma Spray Welding. Journal of Materials for Mechanical Engineering, 2002, p.18-20

[4] Y. Yu, S.K. Huang, G.Y. Zeng, etc: Research on the Application of High Wear-resistance Fe-based Coating Deposited by Plasma Spraying. Metal materials and metallurgical engineering, 2011, 05, p.7-9

[5] Information on http://tech.huanqiu.com/digi/2013-12/4632230.html

Advanced Materials Research Vols. 989-994 (2014) pp 767-770
© (2014) Trans Tech Publications, Switzerland
doi:10.4028/www.scientific.net/AMR.989-994.767

The Bioactivity of Gradient Composite Bioceramic Coating with Two Kinds of Rare Earth Oxide Fabricated by Wide Band Laser Cladding

Peize Jiang[1,a], Qibin Liu[1,2,b], Lingyan Zhang[1,c], Haibin Jiang[1,d], Zheng Zhang[1,e]

[1]College of Materials and Metallurgy, Guizhou University, Guiyang550003, China

[2]Guizhou Key Laboratory for Microstructure and Strength of Materials, Guiyang550003, China

[a,]306054877@qq.com [b,]qbliu2@263.net [c,] 381429875@qq.com [d,]466493199@qq.com [e,]1127181159@qq.com

Corresponding author: Qibin Liu. Email: qbliu2@263.net

Keywords: Laser cladding; Bioceramic coating; Rare earth oxide La_2O_3 and CeO_2

Abstract. To improve bioactivity of gradient bioceramic coating, the coating with two kinds of rare earth oxide was produced by wide band laser cladding technique. As the experimental results, whichadded0.6wt.% La_2O_3 fixedly, and increased the addition amount of the CeO_2, when the addition of CeO_2fulfill 0.4wt.%, the amount of HA-β-TCP is the largest in this experiment. Soaking the specimens in SBF for 14 days, the coating blended 0.6wt% La_2O_3 and 0.4wt% CeO_2, then a great quantity of Ca-P white particles can be found on coating, which confirmation this bioceramic coating is of best bioactivity.

Introduction

Hydroxyapatite(HA), a kind of bioactive materials, which is widely used in the repairing and replacing of bones. However, HA is too brittle to be used in replacement of bones, which must be enough strength to resist impact force. Titanium alloy has high strength and toughness, but bad compatibility and bioactivity[1]. So the combination of HA coating with Ti alloy [2] is a good way to solve this problem.

At present, the technological method to solve the problem mentioned-above is plasma spraying and laser cladding. However, the bond strength between bioceramic coating [3] fabricated by plasma spraying and Ti alloy is low. Laser cladding technology can improve bond strength. Q.B Liu et al [4] found that when the addition of rare earth oxide La_2O_3 is 0.6wt.% or $CeO_2$is 0.4wt.%, The bioactivity phase can be obtained in coating. However, these previous experiments are only involved in single rare earth oxide, which improve the microstructure and bioactivity of coating.

In this paper, the influence of mixed rare earth oxide (La_2O_3+CeO_2) on bioactivity of bioceramic coating is searched.

Experimentals

Experimental material

The substrate material is medical titanium alloy Ti-6Al-4V (TC4). The cladding materials are $CaHPO_4 \cdot 2H_2O$, $CaCO_3$, La_2O_3, $CeO_2$and 45-50μm Ti powder.

Experimental procedures

The powder mixture of 78%$CaHPO_4$•$2H_2O$+22%$CaCO_3$, which is represented as M was sintered to generate HA. To improve the crystallinity of HA, $La_2O_3$and $CeO_2$are added into coating materials. The additions of La_2O_3 is fixed to 0.6wt.% , the addition of CeO_2 into coating was 0.0wt.%, 0.2wt.%, 0.4wt.%, 0.6wt.%, 0.8wt.%, respectively. To decrease thermal stress between coating and substrate during laser cladding, gradient design of three-layer was adopted. Using X stood for rare earth oxide. X was added into M powder. The M+X mixture was mixed with various amount of Ti powder, as listed in Table 1, and these three kinds of gradient powders was clad onto Ti alloy byTJ-HL-T5000 CO_2 laser system equipped with integral mirror and processing lathe.

Table 1 Composition of the gradient coating

Composition	The first gradient layer	The second gradient layer	The third gradient layer
M+X (wt.%)	30	70	100
Ti (wt.%)	70	30	0

The parameters of the wide band laser cladding process are as follows. The output power P is 2.1 kW, scanning speed V is 180 mm/min, and dot size D is 12 mm×2 mm.

In order to analyze the bioactivity of bioceramic coating, the specimens were soaked in simulation body fluids (SBF) for 14 days. The SBF was the same as the one developed by Kokubo ea al [5]. After 14 days, the morphology and composition of coating were observed or tested with metallographic microscopes, X-ray diffraction and scanning electron microscopy.

Results and discussions

X-ray diffraction of the bioceramic coatings

The XRD result of the bioceramic coating with rare earth oxide of CeO_2 and La_2O_3 after soaked in SBF for 14 days is showed in Fig.1.

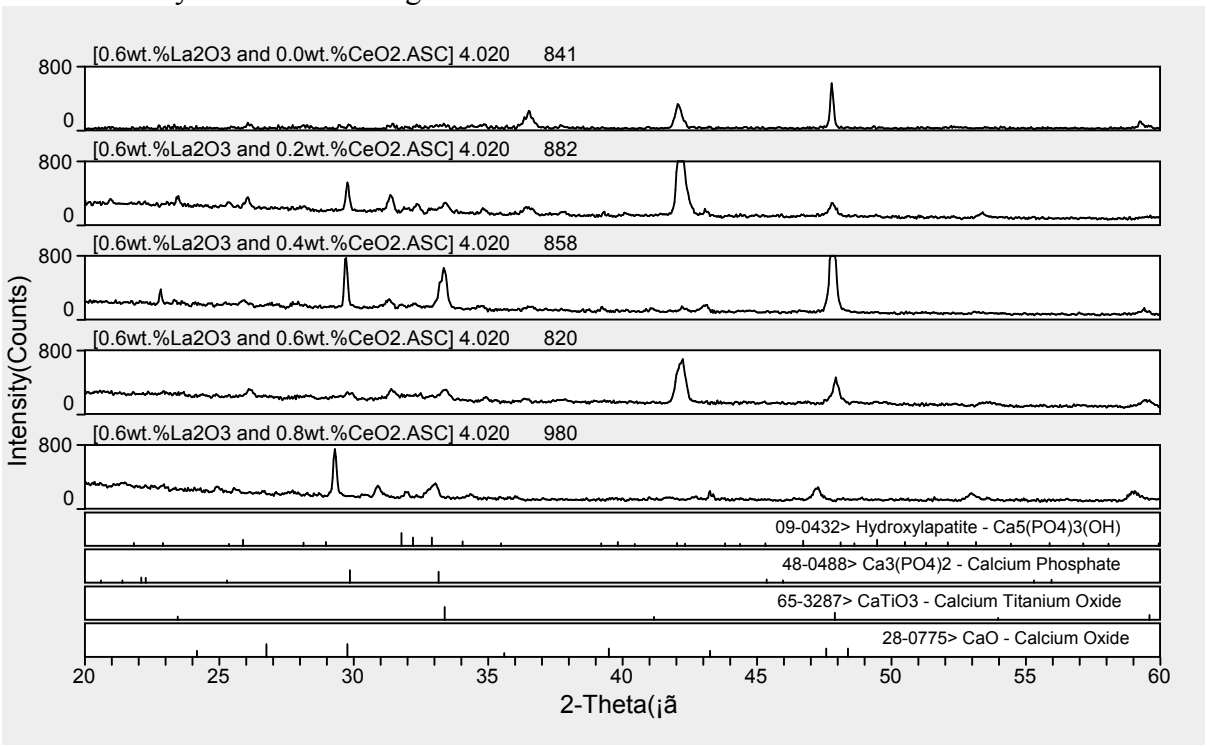

Fig.1. The XRD result of the bioceramic coating with different content of CeO2 and La_2O_3 after soaked in SBF for 14 days

The addition of La_2O_3 is fixed to 0.6wt.%.It is seen that when the addition of CeO_2 is 0.0wt.%, the diffraction peak of HA and β-TCP near 2θ equal 32° is not obvious. When the addition of CeO_2 is 0.2wt.% some diffraction peaks of HA and β-TCP appeared. When the addition of CeO2 is 0.4wt.%, the characteristic peak of HA and β-TCP become most obvious. However, when the addition of CeO_2 ranged from 0.6wt.% to 0.8wt.%, the peak of HA and β-TCP is low.

2 SEM and EDS analysis

When the addition of La_2O_3 is fixed to 0.6wt.%, the SEM and EDS results of the bioceramic coating with 0.0wt.%, 0.2wt.%, 0.4wt.%, 0.6wt.%, 0.8wt.% CeO_2 after soaked in SBF for 14 days is showed in Fig.2a-e.

It is seen that when the addition of the La_2O_3 is 0.6wt.% and CeO_2 is 0.0wt.%, there are only a few of Ca-P white spherical particles can be observed on coating, and the coating is not completely covered. When the addition of the La_2O_3 is 0.6wt.% and CeO_2 is 0.2wt.%, the coating is completely covered, and the contents of Ca and P are higher. When the addition of the La_2O_3 is 0.6wt.% and

CeO_2 is 0.4wt.%, a great quantity of Ca-P white particles can be found on coating，and it shows that the specimen has the highest contents of Ca and P. But when the addition of the CeO_2 increase 0.6wt.% or 0.8wt.%, some parts of the coating were broken, and the composition of P becomes high, but the composition of Ca is also low.

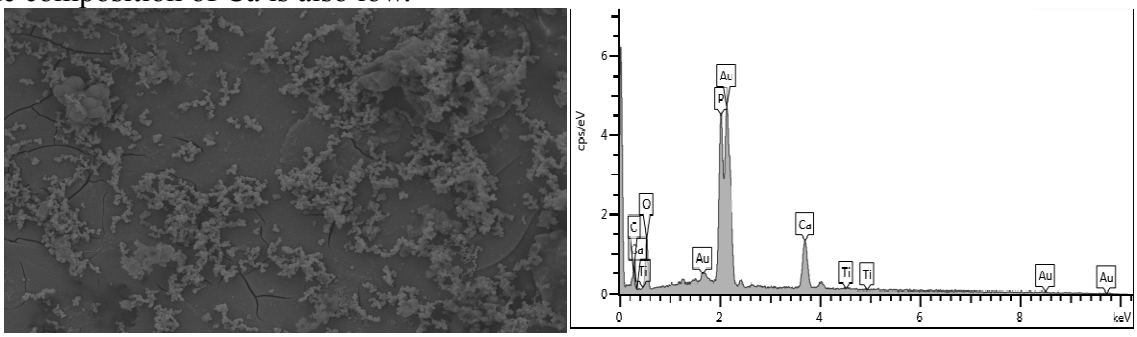

Fig.2a. The SEM and EDS result of 0.0wt.% CeO_2 for 14 days

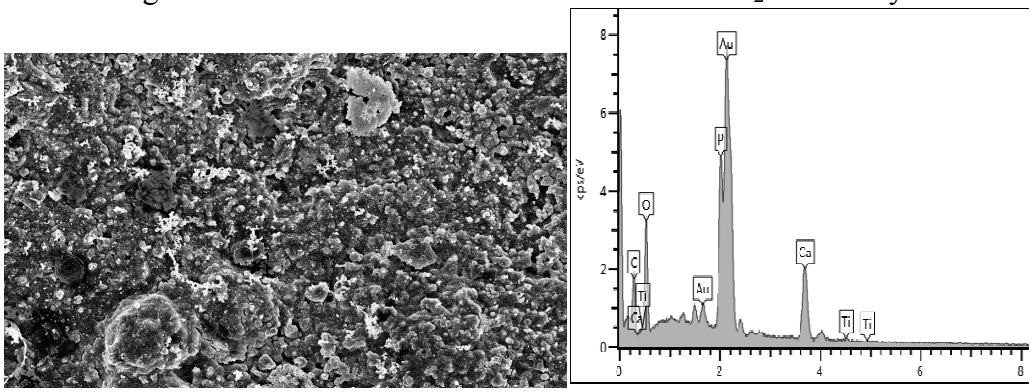

Fig.2b. The SEM and EDS result of 0.2wt.% CeO_2 for 14 days

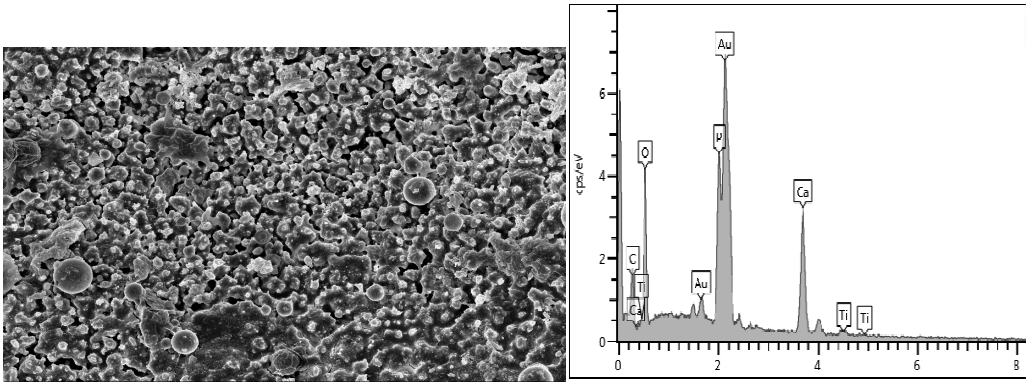

Fig.2c. The SEM and EDS result of 0.4wt.% CeO_2 for 14 days

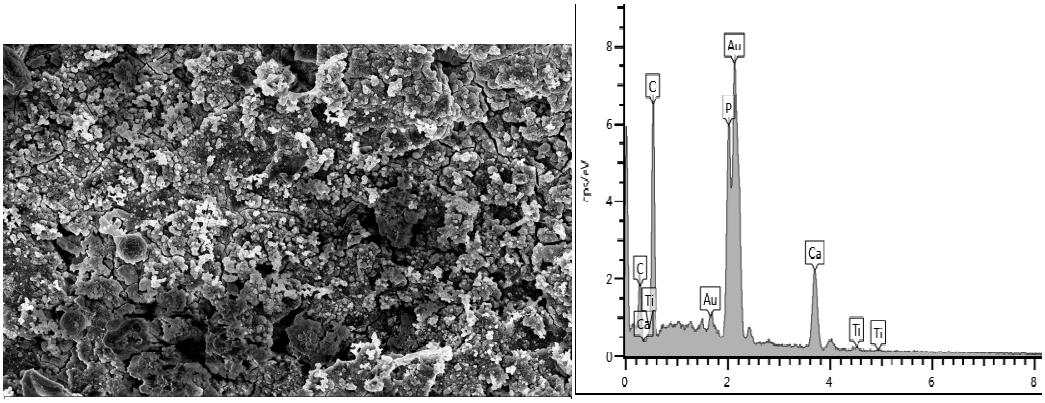

Fig.2d. The SEM and EDS result of 0.6wt.% CeO_2 for 14 days

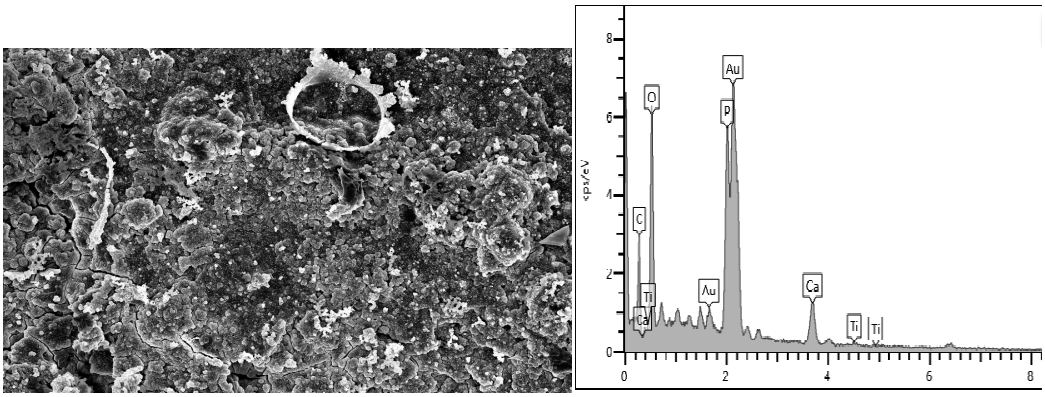

Fig.2e. The SEM and EDS result of 0.8wt.% CeO_2 for 14 days

Conclusion

When add two kinds of rare earth oxide into bioceramic coating, it can be found that the bioactivity of coating is improved. As the addition of La_2O_3 is 0.6wt.% and CeO_2 is 0.4wt.%, the diffraction peak of HA and β-TCP is highest, and a great quantity of Ca-P white particles can be found on coating, and the contents of Ca and P are most.

Acknowledgment

The authors gratefully acknowledge the foundation, the bioactivity of gradient composite bioceramic coating with mixed rare earth oxide fabricated by wide band laser Cladding (2013128), which is supported by Student Research Training (SRT).

References

[1] Lingyan Zhang, Q.B.Liu, The Bioactivity of Gradient Composite Bioceramic Coating with Different Contents of Multiple Rare Earth Deoxide Fabricated by Wide Band Laser Cladding, Advanced Materials Research Vols. 706-708 (2013) pp 318-322

[2] Q.B.Liu, Bangcheng Yang, Mechanical Properties on Gradient Bioceramic Composite Coating Produced by Wide-Band Laser Cladding, C. Key Engineering Materials. 342-343 (2007) 681-484

[3] Zhang Yaping, Gao Jiacheng, Wen Jing(1999) Metal Heat Treatment(In Chinese), 10:9-11.

[4] Q.B.Liu, J.L. Zou, M.Zheng,et al,Effect of Y_2O_3 Content on Microstructure of Gradient Biocera Composite Coating Produced by Wide-Band laser Cladding, J.Journal of Rare Earths. 23(2005) 446-450

[5] TADASHIK, HIROAKIT, How useful is SBF in predieting in vivo bone bioactivity, J. Journal of Biomaterials. 27(2005) 2907-2915

Advanced Materials Research Vols. 989-994 (2014) pp 771-774
© (2014) Trans Tech Publications, Switzerland
doi:10.4028/www.scientific.net/AMR.989-994.771

Discussions on the pretreatment of the air-conditioning /cotton blended fiber

-------the application of tea saponin

Yongjiu ZHANG, Yiyan ZHANG

School of Textil&Garments,Hebei University of Science and Technology,Shijiazhuang,050018 China

Email:kdzhangyiyan123@126.com

Keywords: air conditioning fiber; pretreatment; the optimal process; tea saponin

Abstract. The air-conditioning/cotton blended fiber was pretreatment to investigate the effects of the sodium hydroxide, hydrogen peroxide, scouring agent, tea saponin, oil removing agent, the processing temperature and the processing time on the fabric. The values of capillary, strength, whiteness were got after single factor tests. The results showed that the best pretreatment process was at 90℃, tea saponin 4g/L，oil removing agent 3g/L and the processing time 30min.Through this process, the strength of the fiber was 165cN, the whiteness was 71.2% and the capillary is 10cm.Tea saponin is a main factor only second to temperature.

Introduction

The appling of air conditioning fiber originated in the America, which was used for the astronaut clothing and the protection of space tests for the precision instruments[1]. When the outside temperature is high, air conditioning fiber can absorb heat, reducing body temperature; while the temperature is reduced ,the air conditioning fiber can emit heat, increasing body temperature [2][3]. The air conditioning fiber belongs to functional viscose fiber, whose function greatly induce after the pretreatment and the dyeing processes. There remians many problems to be solved in actual[4][5].

Tea saponin (bu-gong tea saponin), the natural tea saponin as the main raw material, supplemented by nano TiO_2, chitosan and bleaching composition (POD) as the raw materials, is a new, efficient, environmental, safety one of pretreatment auxiliaries [6-8], the application has been reported in relevant fields [9][10][11].

This experiment adding Bu Gong tea saponin as one of various factors, through single factor tests of air conditioning fiber/cotton blended yarns, get the optimization process.

Materials and instruments

Air conditioning fiber / cotton blended yarns

Caustic soda, scouring agent, hydrogen peroxide, hydrogen peroxide stabilizer (WL-7220), Bo-Gong tea saponin, oil removing agent (PISCEAN LIP 200), HH-4 constant temperature water bath pot, electronic balance , capillary effect tester, whiteness tester (WSB- II), yarn strength tester (YG0208)

Test methods

Indexes are shown as in the Fig1-5 after the singel tests about the temperature,the amount of tea saponin,the amount of scouring agent,the amount of degreasing agent and the time.

As can be seen from Fig1 in different processing temperatures, the strength of yarns increased from 159cN to 162cN, which change is small, but with the increase of temperature, the white of yarns improve from 67.9% to 72.6%, and the value of capillary significantly change and improve from 8.5cm to 10cm. So, in the preproces, the best processing temperature is chosen as 90℃.

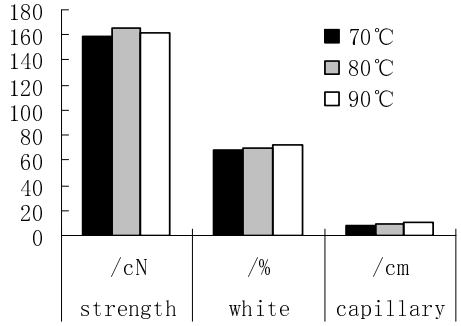

Fig1.The effect of temperature

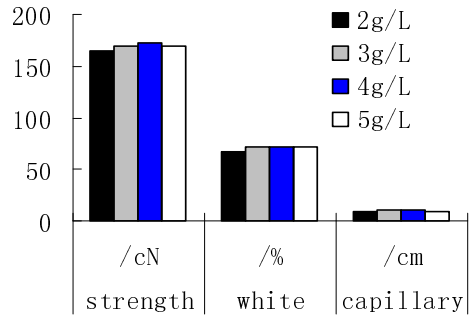

Fig2.The effect of the amount of tea saponin

From Fig 2 we can know that the yarns after different content of tea saponin,the change of strength is not obvious ,while the white and the capillary of the yarns increased in a certain range. When the content reachs 4g/L,the value no longer increase.So in the preprocessing step,the amount of sea saponin was selected for 4g/L.

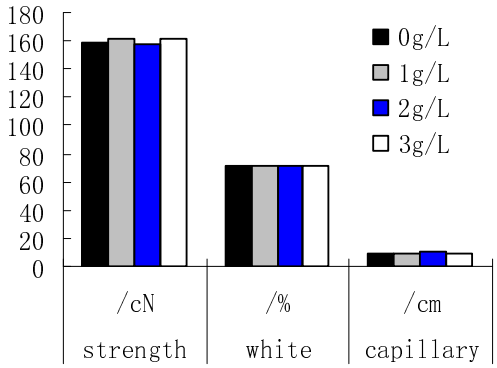

Fig3.The effect of the amount of scouring agent

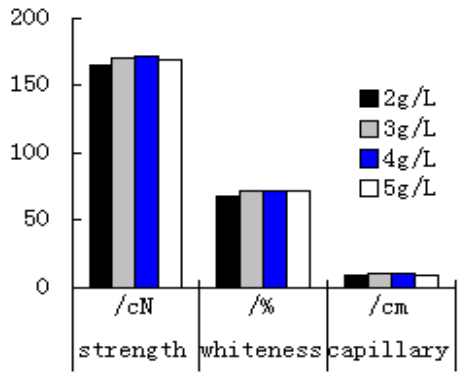

Fig4.The effect of the amount of degreasing agent

The amount of scouring agent's effect can be see from Fig 3.The difference of the maximum value and the minimum of the strength is 3 cN, for the white is 1.1%,and for the capillary the difference is 1.5cm.Overall,the difference is not large. The strength, whiteness and the capillary are

of no obvious change with the increase of the scouring agent.So in this pretreatment, the scouring agent be ignored.

The effect of degreasing agent displays in the Fig 4.The impact of the processing time for capillary is small for the difference of the maximum and the minmum is 0.5cm.So we can ignore the influence for calillary.Considering effects for both of the strength and the capillary as the followings.We can be see from the Fig 4,after dosage of degreasing agent reachs the amounts of 4g/L,the strength is weaker.while the white have no insignicant change. When the amout of degreasing agent reachs 3g/L,the whiteness and the capillary reach the maximum.If the amount continue,the strength increase 2cN,corresponding the white decrease 0.5%,the capillary remain unchanged. So the optimum amount is 3g/L.

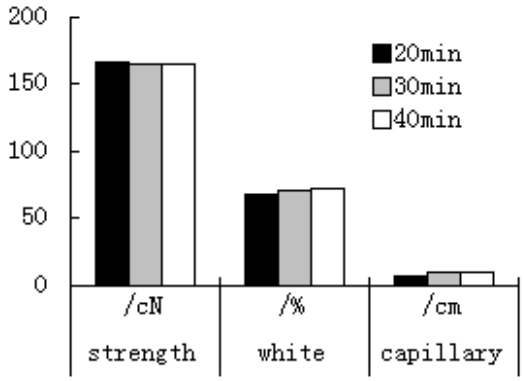

Fig5 The effect of processing time

Form the Fig 5,we can know in different time, the strength of the yarn did not change significantly, but the whiteness and capillary increase with the increase of treatment time. When the processing time reaches 30min, the whiteness and capillary of the yarn no longer increase with time.Form the point of savieng energy and economic benfits, the shorter time the better if the quality of product is guaranteed. Therefore, the optimum processing time is selected for 30min.

Conclusion

(1) the effects on the test results: temperature > tea saponin> sodium hydroxide> scouring agent> hydrogen peroxide > time, the content of tea saponin was a factor only second to the temperature.

(2) Through single factor experiments,take the whiteness, strength and capillary effect as indexes, the optimum pretreatment process of air conditioning fiber / cotton blended yarns is obtained: 90℃, tea saponin dosage 4 g/L, oil removing agent dosage 3g/L, the processing time 30min.

(3) after the optimum pretreatment,,the air conditioning fiber / cotton blended yarns strength is 165cN, the brightness can reach 71.2%, the capillary is 10cm.

Reference

[1] Song Zhaotang. Thermoregulation fiber and textile[J] printing and dyeing auxiliary., 2004, 21 (3): 1-4

[2] Wei Lina, Zhang Yongjiu, Li Ya. The dyeing properties of Intelligent temperature adjusting viscose / cotton blended fabric [J]. Hebei textile.2009 (2): 79-87

[3] Shi Haifeng, Zhang Xingxiang. Application of microcapsule technology in the thermoregulated textiles [J]. industry in textile, 2001,19 (12) 1-5

[4] Chen Liang, Shi Jiangyang, Chu Yongmei.the The study on the measurement of dyeing for the outlast air conditioning fiber[J]spinning technology, 2010 (2): 38-42

[5] Zhang Linlin The refined of the air conditioning fiber/cotton knitted fabric[J]dyeing and finishing technology.2010 (7): 32-7

[6] Wang Gaofu, bu Zhuqi. Bu Gong The overview of tea saponin [J]. dyeing and finishing technology, 2011, 33 (11): 41-42

[7] Liu Zhaoxue, Chen Guangjie, Ho Yili. Pretreatment of cotton fabric with tea saponin,[J] dyeing ,2009, 35 (17): 17-21

[8] Cao Jiliang, Meng Chunli. The one bath of dyeing scouring bleaching process for modified cotton fabric with tea saponin [J].dyeing, 2010, 36 (6): 19-21

[9] Liu Ruining, Liu Yang, Cui Shuling. The pretreatment of cotton with the tea saponin composites[J]. dyeing 2011, 37 (5): 16-17

[10] Xu Xianhua.The hazy printing of hemp and cotton blended fabric [J]. dyeing, 2013 (7): 24-26

[11] Miu Qinhua, Ding Jian, Xu Shanru.The pretreatment of Rayon / linen blended fabric with tea saponin [J]Dyeing 2012, 38 (1): 17-21

Advanced Materials Research Vols. 989-994 (2014) pp 775-778
© (2014) Trans Tech Publications, Switzerland
doi:10.4028/www.scientific.net/AMR.989-994.775

Effect of Mixed Multiple Rare Earth Oxide on the Microstructure of Bioceramic Coating Prepared by Wide Band Laser Cladding

Zheng Zhang[1.a], Qibin Liu[1.2.b], Lingyan Zhang[1.c], Hangbin Jiang[1.d], Peize Jiang[1.e]

[1.] College of Materials and Metallurgy, Guizhou University, Guiyang 550003 China

[2.] Guizhou Key Laboratory for Microstructure and Strength of Materials, Guiyang 550003, China

[a.]1127181159@qq.com [b.]qbliu2@263.net [c.] 381429875@qq.com [d.] 466493199 @qq.com [e.] 306054877@126.com

Corresponding author: Qibin Liu. Email: qbliu2@263.net

Keywords: Bioceramic; Rare earth; Microstructure; Laser cladding.

Abstract. In order to researching the microstructure of bioceramic coating on the surface medical titanium alloy (Ti–6Al–4V), the gradient bioceramic coatings are fabricated by wide-band laser cladding. The influence of multiple rare earths oxide La_2O_3 and CeO_2 on microstructure of bioceramic coating were studied. The experimental results demonstrated that mixed La_2O_3 and CeO_2 have an effect on forming-ability of HA\β-TCP in bioceramic coating and also refined the grain of bioceramic coatings. The largest amount of HA\β-TCP is presented among all the groups when the contents of La_2O_3 and CeO_2 are 0.6wt.%, 0.4 wt.%, respectively.

Introduction

Hydroxyapatite（HA）, β-tricalcium phosphate（β-TCP）, kinds of bioceramic materials, used widely in the human hard tissue replacement and repair in clinic[1-2]. Nevertheless, HA and β-TCP cannot used in human directly because man-made HA-β-TCP not strength enough as well as real bones. Furthermore, this materials have deficiency to resist the corrosion from human body fluid [3,4] .Therefore ,researchers devote themselves to developing a HA\β-TCP scaffold with high compressive strength and acceptable biocompatibility. Due to their biocompatibility and excellent mechanical performance, Qibin Liu et al[5,6] fabricated bioceramic coating deposition on the surface of Ti-6Al-4V with different contents rare earth oxide in raw material powder before, finding the rare earth oxide have positive effect on the composition gradient coating. Kokubo et al [7] think about that if the bonelike apatite will be implanted in the living human body, it is that bonelike materials whether coordinate with our living body that like real living bone firstly. Therefore, the conjugated apatite formation should be checked by soaking in a solution called simulated body fluid (SBF) in vitro for14 days.

Materials and methods

Here, experimental materials and methods are presented.

Materials

The medical titanium alloy (Ti-6Al-4V) as substrate and raw coating materials include titanium powder (Ti), calcium hydrogen phosphate ($CaHPO_4 \cdot 2H_2O$), Calcium carbonate ($CaCO_3$), and a trace of La_2O_3 and CeO_2. The composition gradient coating was shown in Table 1.In both, M stand for the mixed powder which contain $CaHPO_4 \cdot 2H_2O$, $CaCO_3$ and La_2O_3\$CeO_2$,"T"correspond to another powder. Here, the "M" above $CaHPO_4 \cdot 2H_2O$ 78%, $CaCO_3$ 22%. Addition of rare earth oxide CeO_2\$La_2O_3$ into M are CeO_2 0wt.% La_2O_3 0.6wt.%, CeO_2 0.2wt.% La_2O_3 0.6wt.%, CeO_2 0.4wt.% La_2O_3 0.6wt.%, CeO_2 0.6wt.% La_2O_3 0.6wt.% and CeO_2 0.8wt.% La_2O_3 0.6wt.%, respectively.

Methods

To enhance the bonding strength between coating and substrate, a gradient coating with three layers was designed. Meanwhile, added in a few different contents mixed La_2O_3\CeO_2 individually.

The laser cladding instrument is TJ-HL-5000 Type 5kW CO2 laser and processing lathe. Processing parameters in our study are laser output power 1.7 kW, scanning speed 80mm/min and beam size14mm×2mm.and then soaked some of them in simulation body fluid (SBF) in vitro for 14 days, some for 7days, and one sample soaked in distilled water, updating the SBF and distilled water once time per day. The microstructure on the surface was analyzed by Scanning Electron Microscope (SEM), and the bioceramic coating was investigated by X-ray diffraction (XRD).

Table 1 Composition design of gradient coating

Layer number	raw placed materials	
	M（weight percent）	T（weight percent）
1st coating	30	70
2nd coating	70	30
3rd coating	100	0

Experiment result and discussion

The surface of bioceramic coating was researched by XRD and SEM.

XRD analysis of gradient bioceramic coating.

The XRD result of the bioceramic coating with different contents CeO_2 and La_2O_3 0.6wt.% after soaked in SBF for 14 days is showed in Fig.1.

It is showed that gradient bioceramic coatings with five multiple mixed rare earth oxide of La_2O_3 and CeO_2, and apatite phases (HA/ β -TCP) will be finded at the range of 30◦ to 35◦. The diffraction peak of HA/ β -TCP near2 θ equal to 32◦ presented most obviously when the La_2O_3 and CeO_2 are 0.6wt.%, 0.4wt.%, respectively. When the addition of CeO_2 is not 0.4wt.% , the diffraction peaks of HA / β -TCP not obvious as the groups of CeO_2 followed 0.4wt.%.

So, it is obviously that the optimal contents multiple mixed rare earth oxide of $La_2O_3$0.4wt.%, $CeO_2$0.6wt.% promoted the forming-ability of HA/ β -TCP more than any of other contents in our five group samples.

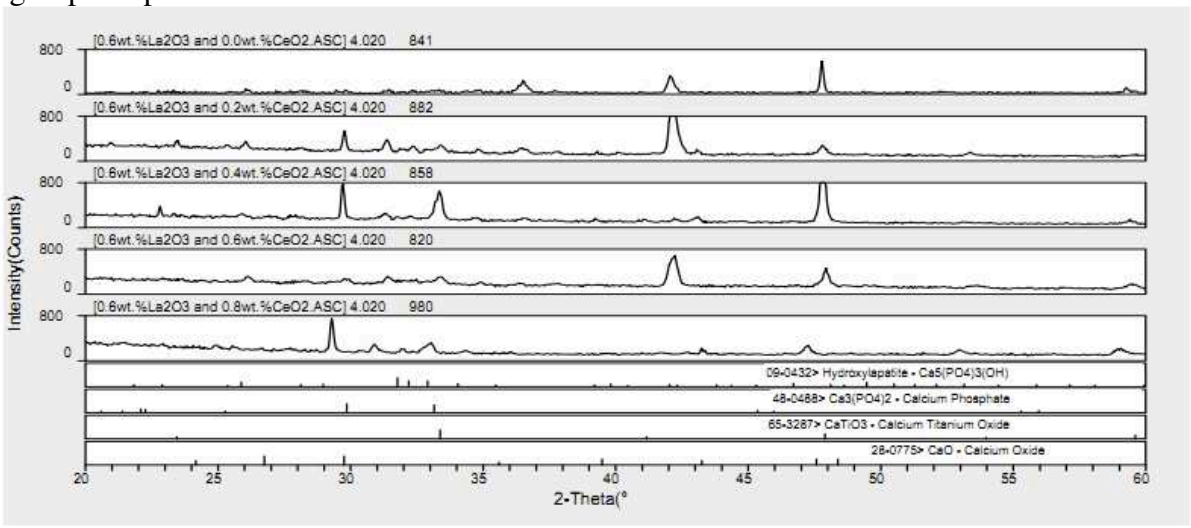

Fig.1 The XRD result of the bioceramic coating with different contents CeO_2 and La_2O_3 0.6wt.% after soaked in SBF for 14 days

SEM analysis of gradient bioceramic coating

Experimental results of the bioceramic coating with 0.0wt.%, 0.2wt.%, 0.4wt.%, 0.6wt.%, 0.8wt.% CeO_2 and 0.6wt.% La_2O_3 and then soaked in SBF for 14 days is showed in Fig.2a-e. The SEM results implied that the ratio of La_2O_3 and CeO_2 added in various, which have an effect on morphology of bioceramic phases during laser cladding.

The Fig.2a showed when the addition was followed La_2O_3 0.6 wt.%, CeO_2 0.0wt.%, there are just some of amorphous particles and a little white spherical particles with cracks. As the amount of CeO_2 increasing, the more globular white particles are presented and such particles change to finer, and the cracks are covered by some spherical particles partly (Fig.2b). The best morphology are fined when the ratio of La_2O_3 0.6wt.% and $CeO_2$0.4wt.% added, on the surface of samples are covered by spherical particles completely and there is no cracks appear(Fig.2c).

However, when the ratio of CeO_2 added in more than 0.4wt.%, the microstructure of biocermic coating diverged from the best apatite morphology (Fig.2d, Fig.2e).

So, bioceramic coating of HA / β -TCP indicated that apatite phases formed on substrates. Evidently, therefore, the bioceramic coating fabricated by wide band laser-cladding soaked in SBF with the ratio of La_2O_3 0.6wt.% and CeO_2 0.8wt.% has the optimal effect for the bioceramic microstructure.

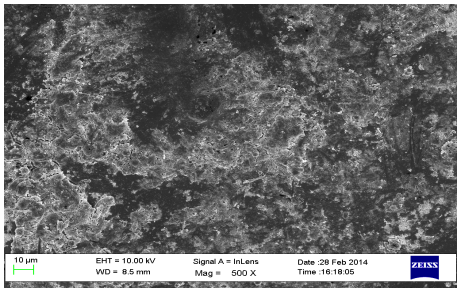

Fig.2a SEM with La_2O_3 0.6 wt%, CeO_2 0.0wt % soaked in SBF for 14 days

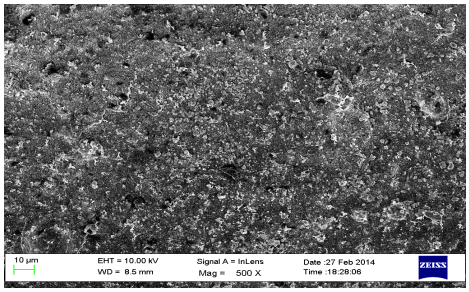

Fig.2b SEM with La_2O_3 0.6 wt%, CeO_2 0.2wt % soaked in SBF for 14 days

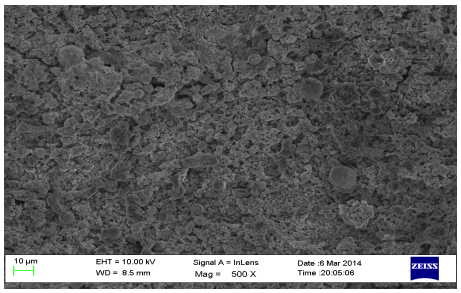

Fig.2c SEM with La_2O_3 0.6 wt%, CeO_2 0.4wt % soaked in SBF for 14 days

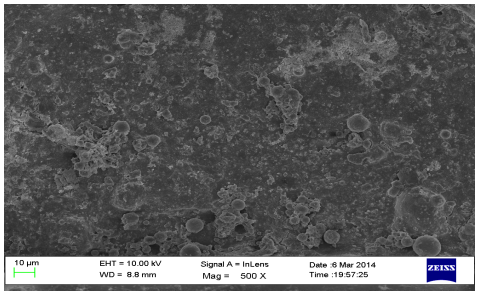

Fig.2d SEM with La_2O_3 0.6 wt%, CeO_2 0.6wt % soaked in SBF for 14 days

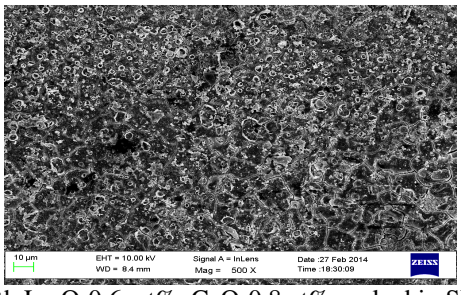

Fig.2e SEM with $La_2O_3$0.6 wt%, $CeO_2$0.8wt% soaked in SBF for 14 days.

Conclusion

HA and β-TCP was fabricated by wide band laser-cladding on the surface of medical titanium alloy (Ti–6Al–4V), which were added in different contents of La_2O_3 and CeO_2 and then soaked in SBF for 14 days. The best combination of La_2O_3 and CeO_2, which promoted more HA and β-TCP was fabricated by wide band laser and made the morphology of bioceremic better than others are $La_2O_3$0.6wt.% and $CeO_2$0.4wt.%.

Acknowledgement

The authors gratefully acknowledge the foundation, effect of mixed multiple rare earth oxide on the microstructure and performance of bioceramic coating prepared by wide band laser cladding, which is supported by The National Student Innovation Training Program.

References

[1] Yu Yaoting,Zhang Xingdong.Biomaterials[M].Tianjin University Press,2000.

[2] K.D. Groot, Biomaterials 1 (1980) 47–50

[3] Liu YX, Kim JH, Young D, Kim SW, Nishimoto SK, Yang YZ. Noveltemplate-casting technique for fabricating b-tricalcium phosphatescaffolds with high interconnectivity and mechanical strength andin vitro cell responses. J Biomed Mater Res 2010;9 2 A:997–1006

[4] C.R.F. Azevedo, Eng. Failure Anal. 10 (2003) 153–164.

[5] Liu Qibin, Zheng Min, Zhu Weidong, et al(2005) Journal of Functional Materials(In Chinese) 36: 50-53.

[6] Min Zheng, Ding Fan, Xiu-kun Li, Jian-bin Zhang Qi-bin Liu Microstructure and in vitro bioactivity of laser-cladded bioceramic coating on titanium alloy in a simulated body fluid Journal of Alloys and Compounds489 (2010) 211–214

[7] T. Kokubo, H. Takadama, Biomaterials 27 (2006) 2907–291

Advanced Materials Research Vols. 989-994 (2014) pp 779-782
© (2014) Trans Tech Publications, Switzerland
doi:10.4028/www.scientific.net/AMR.989-994.779

The chemistry model of ion-ion interaction energy of full ionized hydrogen plasma

Lishuai GUO[1, a], Xingrong ZHENG[1, b], Zhirong WU[1, c]

[1] Department of Physics, Long-Dong University, Qingyang, 745000, Gansu, China

[a]email: zcbz@163.com, [b]email: zhengxingrong2006@163.com, [c]email: 756280302@.com,

Keywords: The Chemistry model; Ion-ion Interaction Energy; Hydrogen Plasma

Abstract. The ion-ion interaction contribution to the Helmholtz free energy is one of thermodynamic properties which discribing full ionized hydrogen plasma. Based quantum statistical theory and its simulation results to construct the free energy model of statistical mechanics, it is great significant to understand the properties of full ionized hydrogen plasma under high temperatures and pressures. Using Fortran program, we calculated the isotherms with some sensitive parameters, making comparison between our results and the formers. We find that former formula proposed by Chabrier appears variation at ultra-high temperatures($> 10^7$K), implying a prominent limit of low temperature, while we developed a more reasonable formula of the ion-ion interaction contribution to the Helmholtz free energy. Analyses on isotherm curves indicate that the thermodynamic properties of the ion-ion interaction contribution to the Helmholtz free energy described by our approximant is very stable at all temperatures and pressures without any unphysical effects at low temperatures.

Introduction

Hydrogen is diatomic molecules at room temperature and atmospheric pressure, but the ionization reaction of hydrogen atom was occurred and form plasma at high temperatures and high pressures. The study of hydrogen plasma is great significant, which understand the properties of hydrogen under high temperatures and pressures. In addition, hydrogen plasma is the normal state of the matter and a good conductor of electricity, it is great importance for the development of condensed matter physics, materials science, a planetary physics and weapons physics [1][2]. In recent years, with the deeper research about the hydrogen plasmas, many researchers, as W.Stolzmann [3][4][5][6], Gilles Chabrier [7][8][9] and Setsue Ichimaru [10][11], have studied the interaction of the charged particles at any electron degeneracy, Coulomb coupling and arbitrary chemical mixtures. ie. the interaction between the ion and ion, electronic and electronic, ion and electronic. Their formulas have good agreement with the experimental result, but in some small region, their results appear a small variation.

In this paper, the chemistry model of ion-ion interaction energy of full ionized hydrogen plasma is described and compared with former theoretical results. We carried on the detailed calculation for all ion-ion contribution to the Helmholtz free energy, and obtained all variable computational results in a broad range of temperatures and densities, including computational results of ionic correlation contribution to the Helmholtz free energy f_{ii} (dimensionless parameter) vs. the mean distance between the electrons r_s ($r_s = r_i$), density $\log\rho$, the degeneracy parameter Θ and the Coulomb coupling parameter Γ_i are further discussed in a broad range of temperature.

Theoretical analysis

The Helmholtz free energy F of a fully ionized plasmas consisting of electrons and ions is given by

$$F(T,V,N_{i,e}) = F^{id} + F^{coul} \tag{1}$$

where the Helmholtz free energy F is function of species $N_{i,e}$, volume V, and temperature T. F^{id} denotes the ideal free energy of ions and electrons, F^{coul} represents the Coulomb interaction contributions to the free energy, and it is expressed by

$$F^{coul} = F_{ee} + F_{ii} + F_{ie}. \tag{2}$$

For the ion-ion interaction contribution to the Helmholtz free energy f_{ii} (dimensionless parameter), we adopted the Pade formula [12] which is given by

$$f_{ii} = \frac{F_{ii}}{N_i k_B T} = -\frac{b_0 \Gamma_i^{3/2} + b_2 \Gamma_i^{9/2} \varepsilon_{ii}}{1 + b_1 \Gamma_i^{3/2} + b_2 \Gamma_i^{9/2}} \tag{3}$$

The weak coupling limit($\Gamma_i \ll 1$)is determined by the Debye-Huckel OCP law. ε_{ii} is the free energy in the strong coupling limit [5]. The coefficients b_k are given by

$$b_0 = \frac{1}{\sqrt{3}} \frac{\langle Z^2 \rangle^{3/2}}{\langle Z \rangle^{1/2} \langle Z^{5/3} \rangle^{3/2}}, b_2 = 1000 \left(\frac{3}{4\pi} \right)^{3/2},$$

$$b_1 = \frac{3}{4\pi} \frac{\sqrt{\tau}}{b_0 \langle Z \rangle \langle Z^{5/3} \rangle^3} \left[\frac{\pi^{3/2}}{8} \sum_{ij} \varsigma_i \varsigma_j Z_i^2 Z_j^2 (\gamma_i + \gamma_j)^{1/2} - 2\pi\tau \sum_i \varsigma_i^2 \frac{(-1)^{2s_i}}{2s_i + 1} \left(\frac{\gamma_i}{2} \right)^{3/2} E_2 \left(-Z_i^2 \sqrt{\frac{2}{\tau \gamma_i}} \right) \right].$$

Where γ_k gives the ratio of the electron mass with respect to the ion mass of k^{th} species: $\gamma_k = m_e / m_k$. In addition, the ion-ion interaction contribution to the Helmholtz free energy f_{ii} of Gilles Chabrier [7] is expressed by

$$\begin{aligned} f_{ii}(\Gamma_i) = {} & A_1 [\sqrt{\Gamma_i (A_2 + \Gamma_i)} - A_2 \ln(\sqrt{\Gamma_i / A_2} + \sqrt{1 + \Gamma_i / A_2})] \\ & + 2A_3 [\sqrt{\Gamma_i} - \arctan(\sqrt{\Gamma_i})] \end{aligned} \tag{4}$$

At $\Gamma_i \geq 1$, this formula gives f_{ii}, which differs from the HNC calculations and the fit of DWSC[13] by no more than 0.8%. This difference approximately coincides with that between the MC and HNC results for u_{ii}. Therefore, it should be attributed to the lack of the bridge functions in the HNC approximation. On the other hand, Eq. (4) recovers the DH-Abe free energy with an error smaller than 0.6% at $\Gamma_i < 1$.

However, the revised formula of the ion-ion correlation contribution to the Helmholtz free energy f_{ii} of Gilles Chabrier[8] is expressed

$$\begin{aligned} f_{ii}(\Gamma_i) = {} & A_1 [\sqrt{\Gamma_i (A_2 + \Gamma_i)} - A_2 \ln(\sqrt{\Gamma_i / A_2} + \sqrt{1 + \Gamma_i / A_2})] \\ & + 2A_3 [\sqrt{\Gamma_i} - \arctan(\sqrt{\Gamma_i})] + B_1 [\Gamma_i - B_2 \ln(1 + \frac{\Gamma_i}{B_1})] + \frac{B_3}{2} \ln(1 + \frac{\Gamma^2}{B_4}) \end{aligned} \tag{5}$$

The above analytic expansion is not applicable for $\Gamma_i \geq 1$. The most accurate up to date numerical results for the internal energy of the liquid OCP at $1 \leq \Gamma_i \leq 200$ have been obtained by MC simulations by DeWitt and Slattery [14] and by Caillol [15]. These authors have also constructed analytic fits to their data with the standard deviations comparable to the numerical MC noise. Unfortunately, these fits cannot be extended to small Γ_i, which hampers obtaining the free energy. On the other hand, the hypernetted-chain(HNC) result for F_{ii} at $\Gamma_i = 1$ is slightly inaccurate because the HNC approximation neglects the so-called bridge functions in the diagrammatic representation of the interactions. To circumvent the difficulty, DeWitt and Slattery[16] used small differences between HNC and MC at $\Gamma_i = 0.8$ and 0.6 to get the corrected value of $f_{ii}(\Gamma_i = 1)$=-0.4368.

Comparision and discussion

In this section, we present a systematic comparison of the chemistry model of the ion-ion interaction contribution to the Helmholtz free energy of the fully ionized hydrogen plasmas for different temperatures from $T=5000K$ to $T=10^8K$, and mainly provided isotherms of the Helmholtz free energy f_{ii} (dimensionless parameter) vs. the mean distance between the ions r_i and the Coulomb coupling parameter Γ_i, particle density $\log\rho$, the degeneracy parameter Θ.

In Fig.1, we mainly introduced four isotherms with some sensitive parameters like the ion-electron interaction contribution to the Helmholtz free energy f_{ii}, the Coulomb coupling parameter Γ_i, particle density $\log\rho$, the degeneracy parameter Θ, the volume V etc., are further discussed at $T=10^4K$.

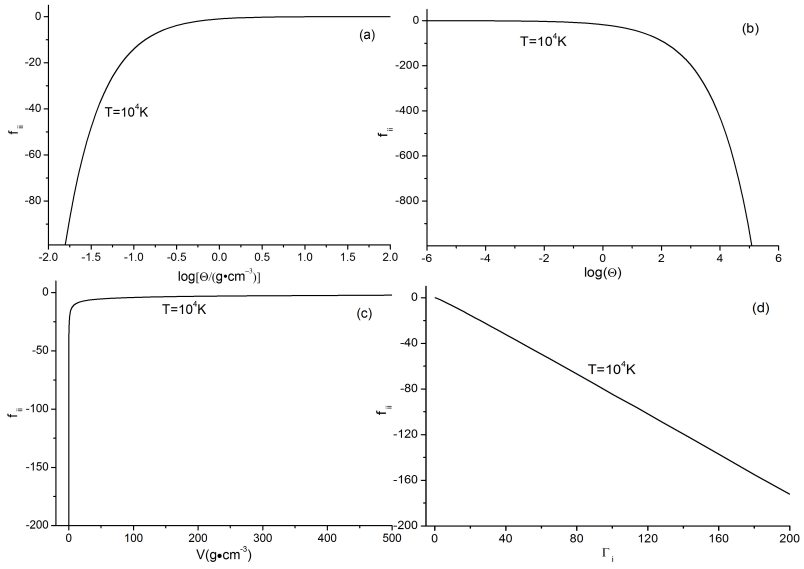

Fig.1 The Helmholtz free energy f_{ii} vs. the Coulomb coupling parameter Γ_i, particle density $\log\rho$, the degeneracy parameter Θ and the volume V at $T=10^4K$.

As shown in Fig.1, we obtained four isotherms that the values of temperature is $T=10^4K$ are smooth . In picture (a)(c), we see that the values of the ion-ion interaction contribution to the Helmholtz free energy f_{ii} get big with the value of Θ and V increases, while the ion-electron interaction contribution to the Helmholtz free energy f_{ii} get small with the value of $\log\rho$ and Γ_i increases, as shown in picture (b)(d).

In Fig.2, we mainly introduced several isotherms about the ion-ion interaction contribution to the Helmholtz free energy, and made comparsion between the formers and our result.

We give comparsion for f_{ii} between Gilles Chabrier's results[7,8]and our results. As shown in Fig.2, our results and the results of Gilles Chabrier's first articles[8] have very good conformance, but our results and the results of Gilles Chabrier's second articles[7] have very big difference in bigger region of r_s. In addition, Fig.2 show the Helmholtz free energy f_{ii} vs. the mean distance between the ions r_i by with the datas given by Gilles Chabrier's theoretical analysis for different temperatures from $T=5000K$ to $T=10^8K$. As shown in picture(d), f_{ii} which come from the table 1 of Ref.[7] appears variation when temperature reached 10^6K, especially, the temperature reached 10^7K and 10^8K, and the range of this variation get very big, as shown in picture (e),(f), while f_{ii} which come from the table 1 of Ref.[8] don't appear variation in all the temperature range.

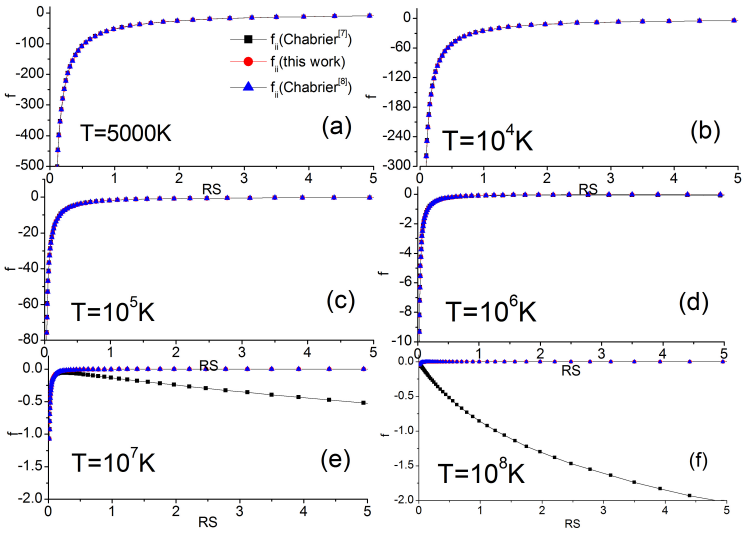

Fig.2 The comparsion of the Helmholtz free energy f_{ii} for different temperatures.

Conclusion

From the above results of several chemistry model of the ion-ion interaction contribution to the Helmholtz free energy, we can see that former theoretical formulas have unreasonable fields ultra-high temperatures, their theoretical formulas has its own advantages and disadvantages. Therefore, we obtained an approximant making up their own shortcomings. Analyses on isotherm curves indicate that the thermodynamic properties of the ion-ion interaction contribution to the Helmholtz free energy described by our approximant is very stable at all temperatures and pressures.

Acknowledgement

In this paper, the research was sponsored by the Nature Science Foundation of Qingyang City, Gansu Province (Project No. 2012KZ76).

References

[1] Nellis W J, Ross M, Holmes N C, SCHience, 269（1995）1249.
[2] Ebeling W, Forster A, Fortov V E and Grynaznov V K, Thermophysical properties of hot dense plasmas, ed. B. G. Teuber VerlagsgesellSCHhaft Stuttgart Leipzig 1991 p7.
[3] Stolzmann W and Blöcker T , Physics Letters A，221 (1996) 99-103.
[4] Stolzmann W and Blöcker T , Astron.Astrophys.，361 (2000) 1152.
[5] Stolzmann W and Blöcker T , Astron.Astrophys.，314 (1996) 1024-1040.
[6] Stolzmann W and Ebeling W , Physics Letters A，248 (1998) 242-246.
[7] G.Chabrier and A.Y.Potekhin,Phys.Rev.E 58 (1998) 4941-4949.
[8] G.Chabrier and A.Y.Potekhin,Phys.Rev.E 62 (2000) 8554-8563.
[9] G.Chabrier and J.,Phys.(Pairs) 51 (1990) 1607.
[10] Ichimaru.S, Iyetomi.H, Tanaka.S,Phys.Rep 149(1987) 91-205.
[11] Ichimaru.S,.Rev. Mod.Phys. 54(1982) 1017.
[12] W.Ebeling and W.Richert Phys.stat.sol.(b),128 (1990) 467.
[13] H. DeWitt, W. Slattery, and G. Chabrier, Physica B 228(1996), 158.
[14] H. E. DeWitt and W. Slattery, Contrib. Plasma Phys. 39(1999) 97.
[15] J. M. Caillol, J. Chem. Phys. 111(1999) 6538.

Advanced Materials Research Vols. 989-994 (2014) pp 783-788
© (2014) Trans Tech Publications, Switzerland
doi:10.4028/www.scientific.net/AMR.989-994.783

Study on Catalyst for Catalytic Ozonation to Leachate and Catalytic Process

Baojun JIANG[1, 2, a], Zhujun TIAN[1, b], Jinming JIANG[3, c]

[1]Songliao Institute of Water Environmental Science, Changchun 130021, China

[2]Dpartment of Environment and Resources, Jilin University, Changchun 130021, China

[3]Dpartment of Municipal and Environmental Engineering, Jilin Jianzhu University, Changchun 130118, China

[a]email: jiangbaojun.happy@163.com, [b]email: tzj@slwr.gov.cn, [b]email: jjmwolf@outlook.com.

Keywords: leachate; catalytic ozonation; mO_3/mCOD; mCatalyst/mCOD

Abstract. Five kinds of catalyst were prepared with Chromium, cadmium, cobalt, copper, nickel loading on the γ–Al_2O_3. Catalyst loading rate, effects to the ozone suction rates and water quality change situation of catalytic ozonation to leachate were studied. It can be found that when the mO_3/mCOD equaled 0.11, 0.15 and 0.26 separately, and mCatalyst/mCOD fixed at 5, the cobalt has the highest loading rate, the cadmium catalyst could improve the ozone absorption rate, the chromium catalyst makes against the ozone absorption rate, the copper catalyst can increase the COD removal rate and the nickel catalyst has advantages for the NH_3–N removal rate. Results indicate that: the leachate COD removal rate increased by 20.2 percent by the copper catalyst adding and the NH_3–N removal rate rise 20.7 percent with the nickel catalyst; the best dosage of the ozone in catalytic ozonation is mO_3/mCOD at 0.12 to 0.13; the degree of oxidation is exited.

Introduction

Because rainwater and surface water sank into landfill site, plus the degradation of trash by biological chemistry and chemical action, a kind of liquid is produced with high concentrated organic and inorganic matter. It named landfill leachate, also called infiltration liquid [1]. Their characteristics are that they have very high color index, show dark brown, dust and black appearance, the index could reach 2 000 to 40 000 times (dilution times); high COD concentration (100–90 000 mg/L); high NH_3–N concentration (6–10 000 mg/L); heavy metal content is always low with the landfill leachate produced by general garbage, but when industrial refuse and household garbage are missed landfill, the dissolution number of heavy metal is markedly increased[2]. Presently, the landfill leachate are treated by the oxidation of ozone or hydrogen peroxide process, photochemical catalytic oxidation process, biological flocculation process and new biological reactors[3]. There are related reports about the process of heterogeneous metal–catalyzed oxidation to treat the landfill leachate, however, the study of direct catalytic oxidation to deal with the landfill leachate with different carrier loaded different heavy metal are lack. The purposes of this research are that the influence of heterogeneous metal catalyzed oxidation to the landfill leachate COD concentration, NH_3–N concentration and color index and so on, to seek the optional supported metal catalyst, in the hope of removing the leachate color index effetely, reducing the COD and NH_3–N concentration hardly, increasing the biodegradability and improving follow–up biological reaction.

Material and Methods

Sources and Characteristics of the Landfill Leachate

The experiment landfill leachate was collected from the simulative reactor of landfill, there were five of them, and they were cylindrical Plexiglas's column with 0.15 meters inside diameter and 1.75 meters altitude. The supplementary rubbish taken from Changchun some landfill site, the

compacted density was 850kg/m^3 in the reactors for trash, Fig.1 is shown one of them. Each time 550mL leachate was produced by one averagely. The landfill leachate was mixed uniformly for the catalytic reaction, water quality features is show in table 1.

Table 1 Water quality of leachate

Water–quality index	pH	COD/(mg·L^{-1})	NH_3–N/(mg·L^{-1})	BOD_5/(mg·L^{-1})	Color index
Indication range	7.20–8.02	699.83–2424.05	144.45–455.82	142.2–557.07	150–450

Test Apparatus

The landfill leachate had the catalytic oxidation reaction in a steel reactor (80mm inside diameter and 350mm altitude), the model number of ozonater was 3S–A3, the ozone volume was measured by wet gas flow meter (LML–2), it was charged through micoporous aeration head in the reactor, the off gas was absorbed by potassium iodide solution. The test apparatus and its flow chart are shown in Fig.2.

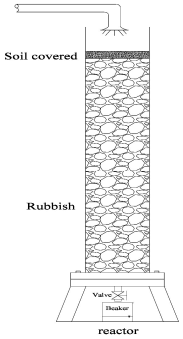

Fig.1 The reactor for landfill leachate production

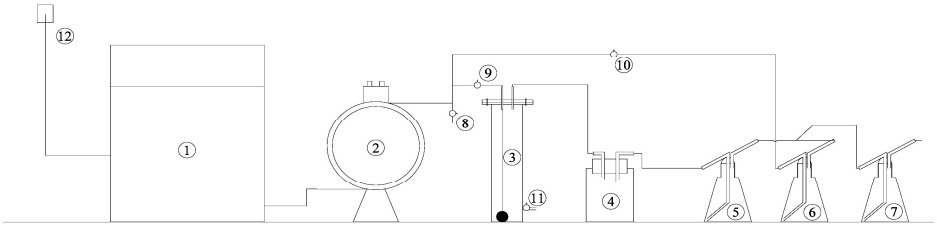

1 ozone generator; 2 gas flow meter; 3 reaction column; 4 Bottle Protection;
5 6 7 Ozone absorption bottle; 8 9 10 11 valve; 12 power supply

Fig.2 System set up for catalytic ozonation processes

Test Method

The catalytic oxidation reactions were happened in the above reactor with five different catalysts added, the carrier of catalysts were activated aluminum oxide (γ–Al_2O_3), when the ozonator adjusting knob was fixed at 90 percent, the average ozone concentration was 1.345mg/L in whole gas volume, the average time concentration was 16.6mg/min, when the ozone was passing through the steal reactor, because of the liquid blocking, and the per minute volume was compressed, so the concentration per unit time was used. The first test: the leachate volume was 400mL at every experiment; 4 min ozone, with no catalyst for parallel, the dosage of the catalyst was five times of the COD gross (mCOD), there was one hours stop time after the action, the COD concentration, NH_3–N concentration and chromaticity color was measured. The second test: the leachate volume was 1000mL at every time, the time of charging into ozone were 2 min, 4 min, 6 min, 8 min, 10 min; the dosage of the catalyst was equaled five times of COD gross too, one hour stop time, the index were determined as the first test.

Analytical Methods

All COD concentration was performed by potassium dichromate method, dilution inoculates method for BOD, NH_3–N concentration was analyzed by Nessler's reagent colorimetric method, color index was measured by Dilution method, pH was analyzed by portable tester.

Catalyst Preparation

Five kinds heavy metal were used they were Chromium, cadmium, cobalt, copper, nickel, their chloride were dissolved separately with the concentration of 0.1 mol/L, when the supported metal

catalyst is being prepared, coarse metal grains could easily get with high concentration for dipping, and there is a narrow size distribution with catalytic metal grains, in order to conquer those defect, the low concentration maceration extract are commonly used for repeatedly dipping [4]). Three times super saturation impregnation to 5 copies activated aluminum oxide whit the weight of 40g, impregnating solution was poured out carefully after every impregnation; 2 hours drying at 180℃ in oven after that; then they were roast at 600℃ with 3 hours in electric muffle furnace; They were taken out for evaporation in desiccators' whit cooling at the end.

Results and Discussion

Catalyst Load

The moore load rate about the heavy metal of chromium, cadmium, cobalt, copper, nickel is shown in Fig.3, the mole load rate means that it is a mole ratio between the mole of the heavy metal and the mole of activated aluminum oxide, when catalyst weight was calculated, the carrier mass change should be considered by roasting, the mass change ratio of this research is 7.19 percent. The all catalyst load rate are minor as their showing, and the numerical order from big to small is cobalt catalyst, cadmium catalyst, chromium catalyst, copper catalyst, nickel catalyst,. The main part of the supported catalysts is the active ingredient [5], which loaded on the carrier surface, if the load rate is better, and they have a strong function to ozone and contaminant, so the best working should be found, while there is low load rate, such as the copper catalyst and the nickel catalyst, if they have efficient organic catalysis, so the volume of using could be decreased to save natural resources.

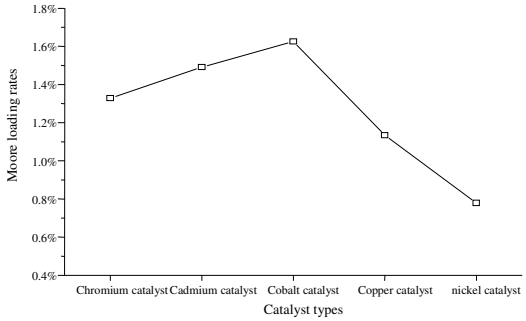

Fig.3 The mole loading rate of Chromium, Cadmium, Cobalt, Copper, nickel catalyst

Catalytic Ozonation

The catalytic ozonation could bring about large quantity of high oxidative radicals at reaction process for oxidative decomposition to organic matter to water purification the same as other advanced oxidation process, such as O_3/H_2O_2, O_3/UV, H_2O_2/UV, $O_3/UV/H_2O_2$, TiO_2/UV and CWAO [6]. Legube and others pointed out that there are two directions at the heterogeneous catalytic ozonation, one is that the organic matter could turn into chelate ring complex for catalyst adsorption, and greater nucleophilic sites were formed, so the capability of ozone could be improved, the desorption happened after the next oxidation to the organic matter, the new adsorptive site started up; the other is that the catalyst could absorb the ozone, and cause them to disintegration at the surface, the high oxidative radicals produced too, which could oxidize the hard small molecule organic material that the ozone could not done [7–8].

1) The Effects of Catalyst to the Ozone Suction Rates

When mCatalyst/mCOD was fixed at 5, the ozone abortive power to different the landfill leachate by five kinds of the loaded catalyst and no catalyst added is shown in Fig.4, it can be seem that the all ozone ratio of absorption is the high lever at $mO_3/mCOD=0.11$, when $mO_3/mCOD$ ratios is equaled 0.15, the rates is in the middle lever; and when $mO_3/mCOD=0.26$, they have the low lever; that is to say there is greatest value for the landfill leachate absorbing the ozone with an increase in dosage, however, it can be learn that it is distinct the effects of catalyst to the ozone suction rates by the five kinds and no catalyst added at the same time $mO_3/mCOD$, it could be considered that the ozone dosage is in non–saturation for the leachate at $mO_3/mCOD=0.11$ and in excessive dosage at $mO_3/mCOD=0.26$, so the effects id catalyst to the ozone suction rates maybe

distinguished at mO_3/mCOD=0.15, the result is the cadmium catalyst, consider from the advanced oxidation, the kind of catalyst many more help for the conformation of free radical to the ozone, but to the chromium catalyst and the nickel catalyst, they get the negative absorption rate compared with no catalyst addition, so if the dosage of ozone is steady. Although there are the lower ozone suction rates, the higher lever for the pollutant removal. The ozone dosage could be saved, and the charge of sewage disposal be decreased too.

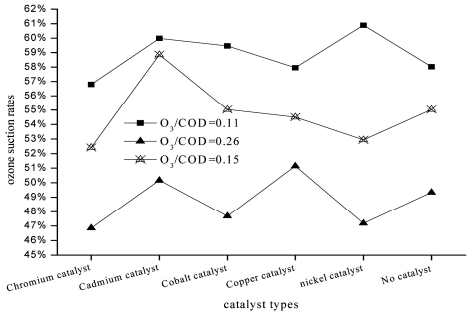

Fig.4 The effects of catalyst to the ozone suction rates

2) The Ozone Dosage and mCatalyst/mCOD were Fixed to the COD and NH_3–N Removal Rates of Difference Landfill Leachate

Fig.5 and Fig.6 are separately showing that when the ozone dosage and mCatalyst/mCOD were fixed to the COD and NH_3–N removal rates of difference landfill leachate by five kinds of catalyst and no catalyst addition, the landfill leachate came from the simulation reactor with the timely collection at bottom in this research, the most of trash for the landfill leachate were kitchen waste, they were at the end stage of the landfill, so the COD concentration and NH_3–N concentration were lower than the actual landfill in the leachate, when the anaerobic microbial degradation was at the first phase, the most of matter were macromolecular in the leachate. It can be seem from the Fig.5, the COD removal rates are rinsing with the mO_3/mCOD ratios increasing, when the ratio exceeds a certain value, the COD removal rates have fallen; on the contrary, the NH_3–N removal rates are rising without stopping (Fig.6). From the same point of the advanced oxidation, the overall oxidation capacity was enlarge by the dosage of ozone adding in, so the large dosage of ozone is one of ways to produce the .OH. The leachate COD removal amount is numerous by this route. While the reason for the decline removal rates, it maybe that a large number of small molecules are produced at the end, they could be easily oxidized by potassium dichromate, thus the test of the COD are larger; the ammonia nitrogen were made from the route of macromolecular oxidize to the micromolecule; the oxidation–reduction potential of •OH is 2.8V higher than 1.33V for the potassium dichromate [9–10], the ammonia nitrogen removal rate is increased, this proved that the ammonia nitrogen could be oxidized by .OH, when the five kinds of catalyst are compared each other. The COD removal effect could be inspected at mO_3/mCOD=0.15 showing in Fig.5, it can be seem that the ability of ozone to dislodge the COD is improved assuredly, the copper catalyst has the best effect of 55.8 percent,20.2 percent enhanced to the no catalyst added in; and followed by the cobalt catalyst, is illustrate that the copper catalyst is the best with the ozone to treat the leachate; because it is need the high mO_3/mCOD ratio to the ammonia nitrogen treatment, the mO_3/mCOD=0.26 is used to the parallel comparison, Fig.6 shows that the cobalt catalyst is the best one with 40.3 percent, so it can increase the ammonia nitrogen removal rate about 20.7 percent.

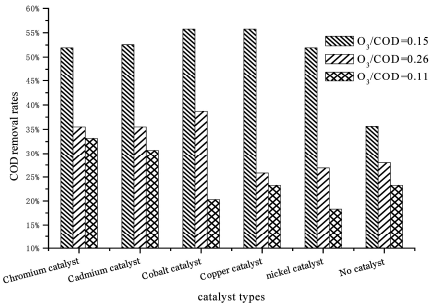

Fig.5 Ozone dosage and mCatalyst/mCOD were fixed to the COD removal rates

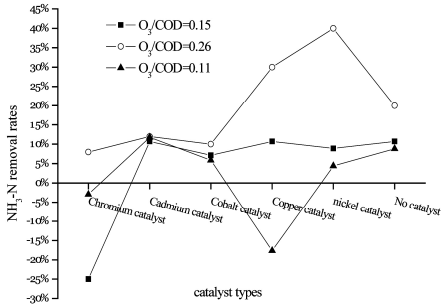

Fig.6 Ozone dosage and mCatalyst/mCOD were fixed to the NH_3–N removal rates

3) The Effect of Different Ozone Dosing and Fixed mCatalyst/mCOD Ratio to the Same Landfill Leachate

The Fig.7 and Fig .8 are showing the results of the catalyst added and no catalyst separately, they are the counter–tests which are shown in Fig.5 and Fig.6 means that the effects of different ozone dosing and fixed mCatalyst/mCOD ratio to the same landfill leachate. Because there is better results to the nickel catalyst combining with the ozone for the ammonia nitrogen removal, and the superfluous ozone dosage, the nickel catalyst was chosen for this part, it can be seem that whatever the catalyst added or not, the highest removal rate of the COD all came out at the mO_3/mCOD being in 0.12 to 0.13, but the treatment coursed of the ammonia nitrogen are very different, when the COD removal rate is at the highest point, the removal rate of the ammonia nitrogen is at the negative peak shown in Fig.7, combined with the analysis of Fig.5 and Fig.6, the passivity of .OH oxidation to the ammonia nitrogen further confirmed and the ammonia nitrogen could not be oxidized by the potassium dichromate easily, a lot of ammonia nitrogen appeared at the beginning of this section is shown in Fig.8, this phenomenon is related with the low COD removal rates, that means the ammonia nitrogen could be liable formed by the nickel catalyst combining with the ozone, as shown in Fig.7 and Fig.8, the leachate removal rate is decreasing at the later period of the experiment, the same as in Fig.5 and Fig.6. The color of the leachate could be dislodged simply by the ozone.

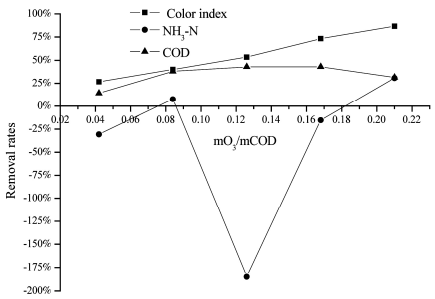

Fig.7 Different ozone dosing to the same landfill leachate

According to all results been analyzed, the process of catalytic ozonation to the landfill leachate conformed the two routes of heterogeneous catalytic, the routes advanced by Lebube and the others, and the non–preference of hydroxyl radical is considered at oxidation, but the difficulty level of matters are disaccord, so there maybe three stages for catalytic ozonation to the landfill leachate: firstly, the stage of deamination oxidation, organic material could been taken off amino group by the catalyst combing with the ozone easily, the ammonia nitrogen formed; secondly, the stage of comprehensive oxidation, any matters could be oxidized sufficiently before the highest COD removal rate; the end is excess oxidation, the catalyst maybe out of use and the oxidation ability of the hydroxyl radical are weaken or staying to the hard matters.

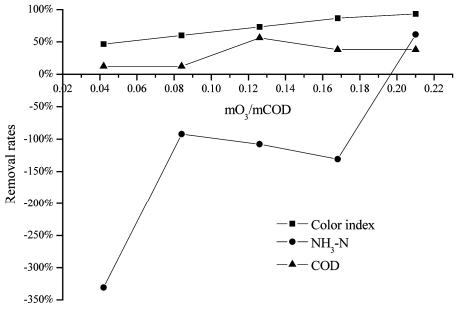

Fig.8 Different ozone dosing and fixed mCatalyst/mCOD ratio to the same landfill leachate

Conclusions

(1)Under the mO_3/mCOD equaled 0.11, 0.15 and 0.26 separately, and mCatalyst/mCOD fixed at 5 circumstances, the cobalt has the highest loading rate, the cadmium catalyst could improve the ozone absorption rate, the chromium catalyst makes against the ozone absorption rate, the copper catalyst can increase the COD removal rate and the nickel catalyst has advantages for the NH_3–N removal rate.

(2)The copper catalyst and the nickel catalyst are the best catalyst with comprehensive survey, the leachate COD removal rate increased by 20.2 percent by the copper catalyst adding, and the NH_3–N removal rate rise 20.7 percent with the nickel catalyst.

(3)When the mCatalyst/mCOD is 5, the best dosage of the ozone in catalytic ozonation is mO_3/mCOD at 0.12 to 0.13.

References

[1] SHEN Dong-sheng, HE Ruo and LIU Hong-yuan.Biological Treatment Technology for Landfill [M]. Chemical Industry Press,Beijing, 2003:45–46.

[2] WANG Bao-zhen, WANG Lin. Municipal Solid Waste Leachate Treatment and Disposal [M] .Chemical Industry Press,Beijing. 2005:78–79.

[3] SHEN Xiao-xing, CHEN Zhe-ming and FANG Shi. Treatment of stabilized landfill leachate by coagulation–catalytic ozonation processes[J]. Journal of Zhejiang university (Agric. &Life Sci), 2006, 32(4):49–454.

[4] ZHANG Ji-guang. Catalyst preparation process technology[M]. China Petroleum and Chemistry Press,Beijing 2004:101–102.

[5] Preparation of Ag A l_2O_3 selective catalytic reduction monolithic catalyst[J]. J T singhua U n iv(Sci&T ech), 2008,48(6):1004–1007.

[6] MA Jun, ZHANG Tao and CHEN Zhong-lin. Path way of Aqueous Ferric Hydroxide Catalyzed Ozone Decom positionand Ozona–tion of Trace NitrObenzene[J]. Environmental Scinece, 2005, 26(2):78–82.

[7] Legube B, Karpel N, Vel Leitner. Catalytic ozonation: a promising advanced oxidation technology for water tratment[J]. Catalysis Today, 1999, 53:61–72.

[8] LI Yu and ZHANG Rong. Co / B i catalyst for catalytic wet air oxidation of ammonia–nitrogen degradation of landfill leachate[J]. Chemical Journal of Chinese Universities, 2005, 26(3):430–435.

[9] LI Jing and LIU Guo-rong. Application ofAdvanced Oxidation Technologieswith O_3toWastewater Treatmen[J]. Pollution Control Technology, 2007, 20(6):55–58.

[10] LIU Wei-hua, JI Min and ZHANG Xin. study on catalyzing ozone oxidation elimination trash infiltration fluid difficult to degrade the organic matter[J]. Environmental Chemistry, 2007, 26(1):58–61.

Advanced Materials Research Vols. 989-994 (2014) pp 789-792
© (2014) Trans Tech Publications, Switzerland
doi:10.4028/www.scientific.net/AMR.989-994.789

Carbon nanotubes-assisted Fabrication of TiO_2 Nanocomposite Film for Optimum Electrochromic Application

Shuping LIU[1, a], Wei WANG[2, b], Linlin CUI[3, c], Huanan GUAN[4,d]

[1]College of Tourism and Cusine, Harbin University of Commerce, Harbin 150076, China

[2]College of Food Engineering, Harbin University of Commerce, Harbin 150076, China

[3]College of Food Engineering, Harbin University of Commerce, Harbin 150076, China

[4]College of Food Engineering, Harbin University of Commerce, Harbin 150076, China

[a]email: liusp201@163.com, [b]email: yueyingliuguang@aliyun.com.cn; [c]email: cuilinlin82@126.com; [d]guanhuanan3@163.com

Keywords: Electrochromic; TiO_2; Carbon nanotubes; Layer-by-Layer

Abstract. Electrochromic composite film consisting of TiO_2, chitosan (CS) and carbon nanotubes (CNTs) were fabricated on quartz and FTO substrates by the layer-by-layer self-assembly method (LbL). The multilayer film was characterized by UV-vis spectrum, scanning electron microscopy (SEM), cyclic voltammetry (CV) and chronoamperometric (CA) and in situ spectral electrochemicalmeasurements. The composite material shows high electrochromic performance, with the optical contrast of 11.5% and coloration efficiency of 21.7 cm^2/C at 800 nm. The results indicate great promise for the TiO_2-based film as a potential material in electrochromic devices.

Introduction

Electrochromic materials can change the optical properties through reversible color changes when an electrical voltage is applied [1]. These materials are particularly suited to smart windows, optical displays and rear-view mirrors [2]. The widely studied transition metal oxides can be divided into tungsten, titanium, vanadium, nickel oxides and molybdenum.

Among the electrochromic materials, titanium oxide (TiO_2) was extentively studied as active material in electrochromic devices due to its peculiar properties such as chemical stability, low cost and environmentally friendly [3]. To improve the performance of electrochromic materials, several methods have been developed to prepare TiO_2 films, including sol-gel, anodization, hydrothermal and electrolytic deposition method [4]. Schmuki et al. prepared the TiO_2 mesoporous structures by anodizationn of a thin Ti film, which are superior to nanopaticles or nanotubes for high contrast electrochromic applications [5]. Lin et al. fabricated TiO_2 nanowires through one-step hydrothermal process, which displays enhanced optical transparency and fast color-switching time [6]. However, all above techniques have some disadvantages which limit the practical application such as toxic reagents, high energetic and rigorous equipments. The layer-by-layer (LbL) method which can control the structure, thickness and composition of the films, is promising for the fabrication of TiO_2 films [7].

In this paper, we successfully present a composite film containing TiO_2, chitosan (CS) and carbon nanotubes (CNTs) by LbL assembly method. CNTs were used to fabricate TiO_2-based composite film. Chitosan was chosen as cationic polyelectrolyte for dispersing CNTs to from a stable CS-CNTs composite, which was assembled with anionic TiO_2 sol. The composite film displays high electrochromic performance with high optical contrast, fast switching times and high coloration efficiency. These results can be helpful for exploring applications in electrochromic devices.

Experimental details

CNTs (diameter: 8-15 nm, length: 50 μm) were purchased from Beijing DK nano technology Co. LTD. Chitosan was purchased from Amresco. CS-CNTs composite was prepared according to the procedure of Xu et al. [8].

Layer-by-layer films were assembled onto FTO-coated glass and quartz substrates. First, the substrates were immersed into CS solution (1 g/L) for 2 h. Then the CS–supported substrates were alternately dipped into the TiO_2 sol for 10 min, CS-CNTs solution for 10 min. After deposition of each layer, the substrates were rinsed with deionized water. Repeat the above process until the desired number of $[TiO_2/CS\text{-}CNTs]_n$ was obtained.

All the electrochemical experiments were performed on the CHI 605C electrochemical workstation (Shanghai Chenhua Instrument Factory, China). The electrolyte was 1 M $LiClO_4$ in propylene carbonate (PC). UV-vis absorption spectra were recorded on a UV-5100B (Shanghai metash instruments Co. LTD). Scanning electron micrographs (SEM) were obtained with a Hitachi S-4800 instrument.

Results and discussion

UV-visible spectroscopy was used to monitor the procedure of the $[TiO_2/CS\text{-}CNTs]_n$ film. As shown in Fig. 1, the films of $[TiO_2/CS\text{-}CNTs]_n$ (n = 0-10) exhibit the characteristic absorption with the bands at 203 nm and 242 nm in the UV region. The former results from an overlap of TiO_2 (at 202 nm) and CS (at 210 nm) bands, and the latter is due to the characteristic absorption of TiO_2 (242 nm), as compared to that of TiO_2 and CS solution. In addition, the inset of Fig. 1 displays suggesting that TiO_2 and CS-CNTs were constantly deposited in the composite films.

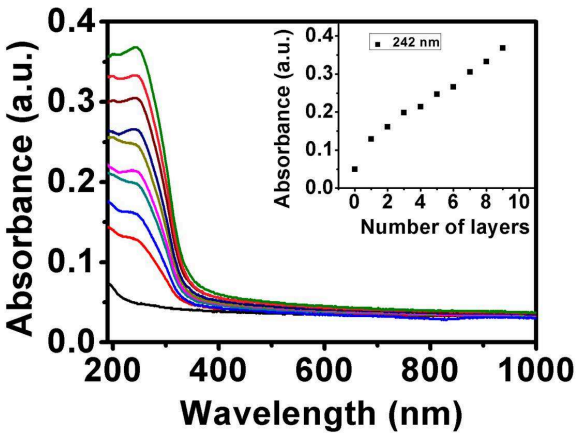

Fig. 1 UV-vis absorption spectra of $[TiO_2/CS\text{-}CNTs]_n$ film (with n = 1-10) film. Inset: plots pf the absorbance values for quartz supported $[TiO_2/CS\text{-}CNTs]_n$ composite films at 242 nm.

Scanning electron microscopy (SEM) can be used to provide the detailed information concerning the surface morphology and the thickness of the composite film. As shown in Fig. 2a, the surface of the $[TiO_2/CS\text{-}CNTs]_{20}$ film surface is rough and consists of a multitude of small domains having round shapes with diameters along the horizontal axis of about 20-30 nm. This perhaps arises from

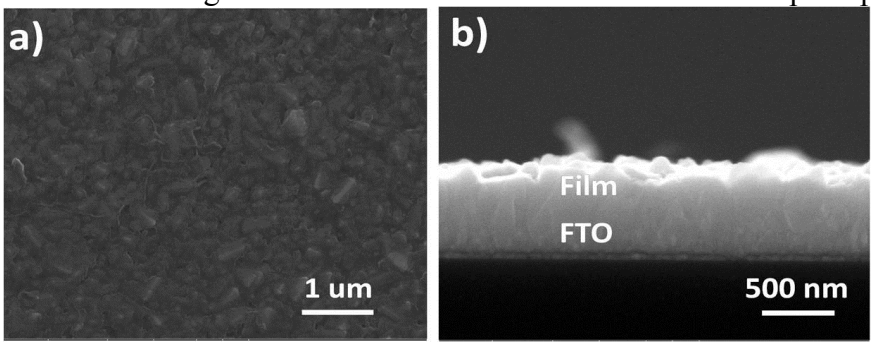

Fig. 2 Top-view (a) and cross-sectional SEM (b) images of $[TiO_2/CS\text{-}CNTs]_{20}$ films on a FTO glass.

the absorption of bi- and multilayer aggregates of the TiO_2 and/or the CS chains. Furthermore, the nanowires are also observed by SEM images, which are evidences for the presence of CNTs. Fig. 2b shows the cross-section observation, the thickness of the composite film is about 240 nm.

Cyclic voltammetry (CV) was used to elucidate the general electrochrmical behavior of the film. As shown in Fig. 3, the redox chemistry of the $[TiO_2/CS\text{-}CNTs]_{20}$ film was examined by switching the potential from -1.0 to 0 V. One couple of peaks was observed with a negative anodic peaks potential of -0.82 V. This can be ascribed to Li ion insertion into and extraction from TiO_2 framework as followed:

$$TiO_2 + xLi^+ + xe^- \longleftrightarrow Li_xTiO_2$$

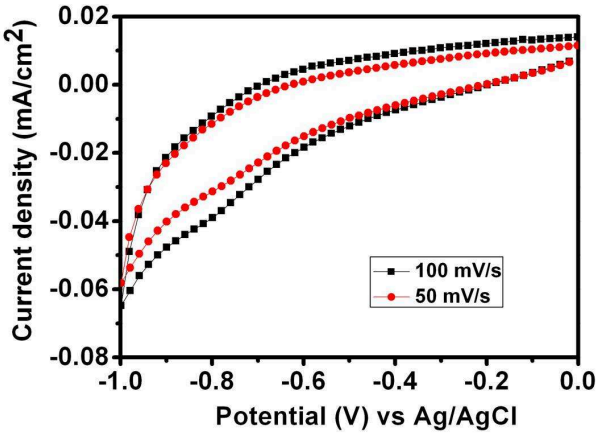

Fig. 3 Cycle voltammograms of $[TiO_2/CS\text{-}CNTs]_{20}$ film in 1 M $LiClO_4$ PC solution at different scan rates.

Fig. 4 displays the potential, current, transmittance change and coloration efficiency under a square wave potential of -2.0 and +2.0 V. As shown in Fig. 4c, the optical contrast of $[TiO_2/CS\text{-}CNTs]_{20}$ film is 11.5%. Then response time is defined as the requirement for 90% of the total absorbance change to be reached. In our experiments, the coloration and bleaching time is 7.2 s and 0.6 s, respectively. The bleaching process is faster than the coloring process, which is in accordance with the time needed for the oxidation and reduction of the TiO_2. The coloration efficiency (CE) represents the change in the optical contrast (ΔOD) for the charge consumed per unit of electrode area.

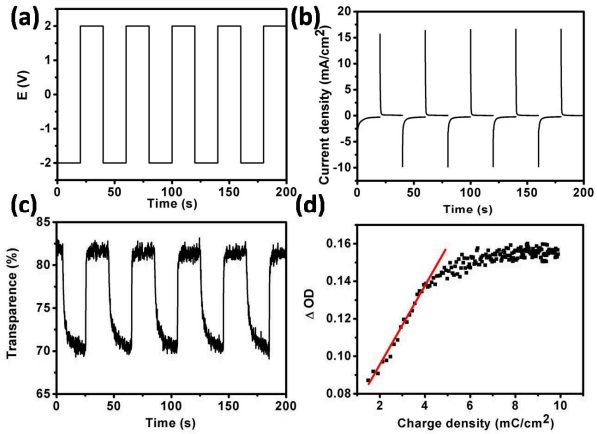

Fig. 4 (a) Potential, (b) chronoamperometry curves, (c) optical transmittance change and (d) coloration efficiency at 800 nm of $[TiO_2/CS\text{-}CNTs]_{20}$ film during subsequent double-potential steps (–2.0 V and +2.0 V).

$$CE\ (\eta) = \Delta OD/(q/S) = \Delta A/(q/S) = \log(T_b/T_c)/\ (q/S)$$

Where ΔOD is the optical contrast at a given wavelength wavelength λ, q is injected/ejected electronic charge, S is the electrode area, ΔA is the absorbance change, T_b and T_c is the transmittances in the bleached and colored states respectively. The CE was extracted as the slope of the line fitted to the linear region of the curve. Fig. 4d displays the plots of ΔOD versus the

extracted charge density. The CE value of the $[TiO_2/CS\text{-}CNTs]_{20}$ composite film is 21.7 cm^2/C at 800 nm, which lies in a typical range of 20-50 cm^2/C.

Conclusion

The nanocomposite material composed of TiO_2, CS and CNTs was successfully fabricated using LbL assembly method. The film material is synthesized by forming a stable CS-CNTs composite, followed by deposition of anionic TiO_2 sol. The composite film showed electrochromism with high optical contrast, fast switching times and high coloration efficiency. Furthermore, the stable film was obtained by incorporation of CNTs into the multilayer film. Therefore, the TiO_2-based composite film may become a promising candidate for application in electrochromic devices.

Acknowledgement

The authors are thankful for the financial support from the Natural Science Foundation of China (Grant No. 21301041 and No. 31201376).

References

[1] Nguyen Minh Vuong, Dojin Kim, Hyojin Kim. Electrochromic properties of porous WO_3-TiO_2 core-shell nanowires [J]. Journal of Materials Chemistry C. 2013 (1) 3399-3407.

[2] Feng Lin, Jifang Cheng, Chaiwat Engtrakul, Anne C. Dillon, Dennis Nordlund, Rob G. Moore, Tsu-Chien Weng, S. K. R. Willians, Ryan M. Richards. In situ crystallization of high performing WO_3-based electrochromic materials and the importance for durability and switching kinctics [J]. Journal of Materials Chemistry. 2012 (22) 16817-16823.

[3] Min-Han Yang, Ting-Ting Chen, Yu-Shiuan Wang, Hsin-Tien Chiu,Chi-Young Lee. Electrochromism of rutile nanowires, vertically aligned along the [001] direction, due to alkali metal ion intercalation [J]. Journal of Materials Chemistry. 2011 (21) 18738-18743.

[4] Yan-Yan Song, Zhi-Da Gao, Jian-Hua Wang, Xing-Hua Xia, Robert Lynch. Multistage Coloring Electrochromic Device Based on TiO_2 Nanotube Arrays Modified with WO_3 Nanoparticles [J]. Advanced Functional Materials, 2011 (21) 1941-1946.

[5] Kiyoung Lee, Doohun Kim, Steffen Berger, Robin Kirchgeorg, Patrik Schmuki. Anodically formed transparent mesoporous TiO_2 electrodes for high electrochromic contrast [J]. Journal of Materials Chemistry. 2012 (22) 9821-9825.

[6] Jing-Zhi Chen, Wen-Yin Ko, Yin-Cheng Yen, Po-Hung Chen, Kuan-Jiuh Lin. Hydrothermally Processed TiO_2 nanowire electrodes with antireflective and electrochromic properties [J]. ACS Nano. 2012 (8) 6633-6639.

[7] Fritz Huguenin, Valtencir Zucolotto, Antonio J. F. Carvalho, Ernesto R. Gonzalez, Osvaldo N. Oliveira, Jr. Layer-by-Layer Hybrid Films Incorporating WO_3, TiO_2, and Chitosan [J]. Chemistry Material. 2005 (17) 6739-6745.

[8] Shuping Liu, Lin Xu*, Guanggang Gao, Bingbing Xu,Weihua Guo. Electrochromic multilayer films with enhanced stability based on polyoxometalate and TiO2 [J]. Materials Chemistry and Physics. 2009 (116) 88-93.

Advanced Materials Research Vols. 989-994 (2014) pp 793-796
© (2014) Trans Tech Publications, Switzerland
doi:10.4028/www.scientific.net/AMR.989-994.793

Evaluation the effect of anti-oxidation of chondroitin sulfate

Liping XU[a], Xin WANG[b]

Key Laboratory of Food Science and Engineering, School of Food Engineering, Harbin University of Commerce, Harbin, 150076, China

[a]email: xuliping@126.com, [b]email:wangxinfood@163.com

Keywords: Chicken cartilage; CS; Anti-oxidation

Abstract. Study of the antioxidant activity of chondroitin sulfate extracted from chicken cartilage. The total antioxidant capacity, inhibition the capacity of anti-superoxide anion, hydroxyl radical, anti-liposome and Alkyl radical was determined, respectively; the effect of the anti-oxidation of chondroitin sulfate was observed. The result indicated that chondroitin sulfate had the strong elimination ability to the five free radicals. The ability of total antioxidant the values of scavenging activities of the maximum inhibition rate to anti-superoxide anion, hydroxyl radical, anti-liposome and alkyl radical was 30.56 U/mL, 97.74%, 80.69% ,48.05% and 78.57%, respectively.

Introduction

Chondroitin Sulfate (Chondroitin Sulfate, CS) as a kind of acid mucopolysaccharide is widely existed in connective tissue of animal. The content of CS accounts for 20-40% of cartilage after drying，The type and content of CS is different, because of the species, age, part and so on [1].

CS has good role of anti-oxidation and inhibition free radicals as the main acid mucopolysaccharide in cartilage of mammals [2]. CS has the effect of antioxidant by improving pancreatic cells, relieving edema, and restoring the endogenous antioxidant, inhibiting of lipid per-oxidation, reducing activation of the neutrophilic granulocyte according Campo et al reported [3-4]. CS has the activity of anti-fibrosis and the role in scavenging radicals and slowing the aging process and improving the inflammation of the fat by reducing the content of the total cholesterol, Triglycerides and malondialdehyde [5-6].

CS also has many physiological functions as special sugar glycosaminoglycans in animal cartilage, such as anti-arthritis, regulate lipid, adhesion and moisture in animals, anticoagulant, antioxidant, and enhance immunity, antitumor, antiviral, anti-inflammatory, etc [7]. CS has been reported more patents in food applications，and made from shark capsule that has sell in the market already a long time as a senior health foods in the United States, Australia, Japan and other countries. Cartilage as a good nourishing and strong agent and soup has good effect of curative for treating the joint disease, because that contains rich glycosaminoglycan and collagen [8]. The research reported that CS has a good inhibition on the aorta and coronary atherosclerosis. It is considered to be the effective drugs for preventing and treating cardiovascular diseases [9].

Materials and Apparatus

Standard CS (sigma), CS (self-prepared), linoleic acid (Harbin ZhongJia Reagent co., LTD), Absolute Ethyl Alcohol (Tianjin Tianli Chemical Reagent co., LTD), Pyrogallol (Tianjin Hua Ke Mi Ou Chemical Reagent co., LTD), $FeSO_4$ (Tianjin Shuang Chuan Chemical Reagent co., LTD), Lecithin(Beijing bio-engineering high-tech Companies), TBA, TCA, Vc, HCl, NaOH (Chinese medicine in Shanghai Chemical Reagent co., LTD), H_2O_2(Tianjin Zhiyuan Chemical Reagent co., LTD), $FeCl_3$(Shanghai Jinshan Chemical Factory), Na_2HPO_4, NaH_2PO_4(Tianjin TianxinChemical industry development center), etc are all AR level.

R-205 Rotary evaporators Shanghai ShenSheng biological technology co., LTD, H198/28 pH meter Beijing Haixing Shunda Distribution Company, TU-1900 UV-Vis Spectrophotometer Shanghai precision scientific instrument co., LTD, Ultrasound KQ-500VDE type KunShan Ultrasonic Instrument Co., Ltd...

Method

Determination of total antioxidant ability

Total antioxidant ability was determined strictly according to the kit specification. Absorbance of reaction system increase 0.01 as a unit of total antioxidant ability in per milliliter of sample in every minute at 37℃. The ability of total antioxidant was calculated according to the following equation.

$$\text{Total antioxidant ability(U/mL)} = \frac{As - Aj}{0.01} \div t \times N \times n$$

In the paper, As stands for absorbance of the determination tube, Aj is absorbance of the contrast tube, t is 30(min), n is the dilution ratio of sample, N is the dilution ratio of reaction system.

Determination of inhibition of Hydroxyl free radical ability

The concentration of CS were prepared 0.1, 0.2, 0.3, 0.4, 0.5, 0.6 (mg/mL) with distilled water, respectively. The solution of $FeSO_4$, CS, H_2O_2 (6mmol/L) was pipetted 2mL, respectively, and then added salicylic acid (6mmol/L) 2mL after standing 10min. The solution was diluted to 25 mL with distilled water and determined absorbency after standing for about 10 min at 520nm after heating 60 min by water-bath at 37℃. CS was replaced with distilled water as contrast tube, and then determined based on the method of the determination tube. The inhibition of hydroxyl free radical ability of CS was compared with the same concentration of Vc as the standard. The inhibition of Hydroxyl free radical ability was calculated according to the following equation.

$$\text{Inhibition ratio}(\%) = \frac{Ac - As}{Ac} \times 100$$

In the paper, As is absorbance of the determination tube, Ac is absorbance of the contrast tube

Determination of inhibition of Super oxygen anion free radical ability

The concentration of CS were prepared 0.1, 0.2, 0.3, 0.4, 0.5, 0.6 (mg/mL) with distilled water, respectively. The solution of Phosphate buffer（0.05 mol/L, pH=8）4.5mL was pipetted to heating 20 min by water-bath at 37℃,and then added 1mL sample and 0.4mL pyrogallol (25mmol/L), The solution react 5 min by water-bath at 37℃ after mixing fully. The solution was added to 1mL HCl (80mmol/L) and determined absorbency at 520nm after shaking up about 5min. CS was replaced with distilled water as contrast tube, and then determined based on the method of the determination tube. A dynamic unit was the inhibition of the super oxygen free radicals of per liter sample was be equivalent to 1mg Vc react 40min at 37℃. The inhibition of hydroxyl free radical ability of CS was compared with the same concentration of Vc as the standard. The inhibition of Hydroxyl free radical ability was calculated according to the following equation.

$$\text{Inhibition ratio}(\%) = (1 - \frac{A_1 - A_2}{A_3}) \times 100\%$$

In the paper, A_1 is the solution of Phosphate buffer（0.05 mol/L, pH=8）4.5mL and sample (1mL) and pyrogallol (25mmol/L) 0.4 mL and 1mL HCl (80mmol/L), A_2 is the solution of Phosphate buffer（0.05 mol/L, pH=8）4.5mL and sample (1mL) and 1mL HCl (80mmol/L), A_3 is the solution of Phosphate buffer（0.05 mol/L, pH=8）4.5mL and ethanol (1mL) and pyrogallol (25mmol/L) 0.4 mL and 1mL HCl (80mmol/L),

Determination of inhibition of Alkyl free radical ability

The concentration of CS were prepared 0.1, 0.2, 0.3, 0.4, 0.5, 0.6 (mg/mL) with distilled water, respectively. 2mL sample was mixed with 0.1mL linoleic, the 5mL ethanol and 5mL phosphate buffer (0.1mol/L pH=8) was added into the solution, and then irradiated 120min with 10W UV lamp. The solution was added 4mL TCA (20%) and 1mL TBA (3%) before heating 90 min by water-bath at 95℃. The supernate was determined absorbency at 532nm after centrifuging about 10 min (4000r/min). CS was replaced with distilled water as contrast tube, and then determined based on the method of the determination tube. The inhibition of hydroxyl free radical ability of CS was compared with the same concentration of Vc as the standard. The inhibition of Alkyl free radical ability was calculated according to the equation of determination of inhibition of Hydroxyl free radical ability.

Determination of the Resistance of liposome per-oxidation ability

The Disperse system of PBS was prepared with 300mg lecithin dissolve in the solution of 30mL PBS (10mmol/L，pH=7.4) and treated for a few minutes by ultrasonic, 15gTCA, 0.375gTBA, 2.1mLHCl was dissolved into 100mL distilled water.1mL LLS, 1mL400μmol/L $FeCl_3$, 1mL 400μmol/L Vc and 1mL samples of different concentrations of CS was added to the sample tube in turn, and then added 2mL TCA–TBA–HCl mixture after avoiding light and heating 100min in 100℃ water bath. The supernate was determined absorbency at 532nm after and heating 60min in 37℃ water bath centrifuging about 10 min (4000r/min). CS was replaced with distilled water as contrast tube, and then determined based on the method of the determination tube. The inhibition of hydroxyl free radical ability of CS was compared with the same concentration of Vc as the standard. The Resistance of liposome per-oxidation ability was calculated according to the equation of determination of inhibition of Hydroxyl free radical ability.

Test results

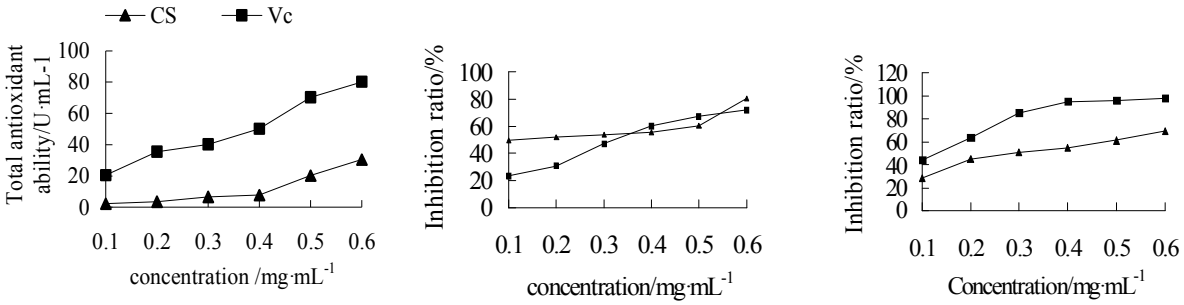

(a)Total antioxidant ability(b)Hydroxyl free radical ability(c)Super oxygen anion free radical ability

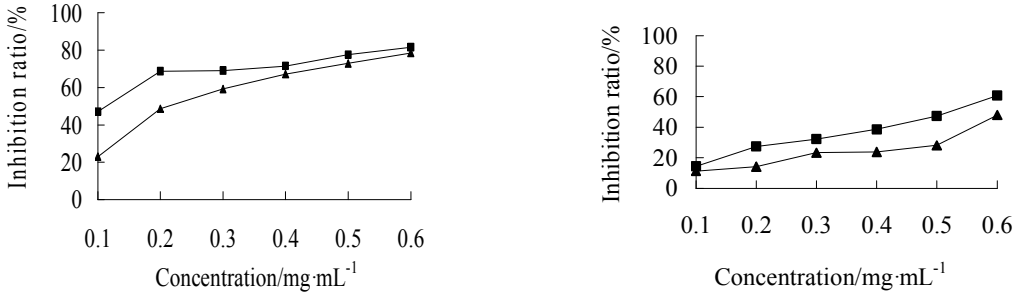

(d) Alkyl free radical ability (e) Resistance of liposome per-oxidation ability

Fig.1 The experimental result

The result implied that CS has the antioxidant ability and enhanced with the increase of concentration of CS as seen in Figure (a), the antioxidant ability of CS compared with the Vc is lower than Vc. The total antioxidant ability of CS is up to 30.56 U/mL when the concentration is 0.6 mg/mL.

The inhibition of Hydroxyl free radical ability of CS tended to smooth and steady with the increase of the concentration from 0.1 to 0.4 mg/mL as seen in Figure (b). The result implied that the inhibition of Hydroxyl free radical ability of CS increased with the increasing concentration. The antioxidant ability of CS compared with the Vc is higher than Vc with the increase of the concentration from 0.1 to 0.4 mg/mL and lower than Vc with the increase of the concentration from 0.4 to 0.5 mg/mL that due to CS occur self-oxidation. Hydroxyl free radical inhibition rate is up to the highest peak when the concentration is 0.6 mg/mL. The inhibition rate of CS and Vc is 80.69% and 72.36% respectively.

CS has the inhibition of Super oxygen anion free radical ability and enhanced with the increase of concentration of CS as seen in Figure (c), the antioxidant ability of CS compared with the Vc is higher than Vc. The inhibition of Super oxygen anion free radical ability of CS is up to 97.74% when the concentration is 0.6 mg/mL.

The inhibition of Alkyl free radical ability of CS is higher than Vc when the concentration is lower 0.4 mg/mL and then is very close. CS has the inhibition of Alkyl free radical ability and enhanced with the increase of concentration of CS as seen in Figure (d).

CS has the resistance of liposome per-oxidation ability and enhanced with the increase of concentration of CS as seen in Figure (e), the antioxidant ability of CS compared with the Vc is lower than Vc. The resistance of liposome per-oxidation ability of CS is up to 48.05% when the concentration is 0.6 mg/mL.

Conclusion

Chondroitin sulfate has the inhibition for five kinds of free radicals in chicken cartilage. The total antioxidant capacity, inhibition the capacity of anti-superoxide anion, hydroxyl radical, anti-liposome and Alkyl radical was determined, respectively. The result indicated that chondroitin sulfate had the strong elimination ability to the five free radicals. The ability of total antioxidant the values of scavenging activities of the maximum inhibition rate to anti-superoxide anion，hydroxyl radical, anti-liposome and alkyl radical was 30.56 U/mL, 97.74%, 80.69% ,48.05% and 78.57%, respectively.

Acknowledgement

In this paper, the research was sponsored by the Education project of Heilongjiang Province (Project No.12541194)

References

[1] Chen Hong-li, Yang Yong-feng, Yu Jian-jun. Extraction chondroitin sulfate with pepsin. [J]. Applied chemical industry, 2009, 38(12):1766-1768.

[2] Lu Jing-guang, Ji Sheng-li, Zhang Zun-jian. Research the progress of chondroitin sulfate and derivatives. [J]. Chinese Journal of Marine Drugs, 2006, 25(1): 59-63.

[3] Xiong Shuang-li, Jin Zheng-yu. Research the properties of Chondroitin sulfate and copper ion complexion. [J]. Food science, 2008, 29(4):54~57.

[4] Campo G M, Avenoso A, Campo S, et al. Administration of hyaluronic acid andchondroitin-4-sulfate limits endogenous antioxidant depletion and reduces cell damage in experimental acut epancreatitis[J]. Pancreas, 2004, 28:45-53.

[5] Song Guang-yi, Huang Bo, Dong Yao, et al. of. The effect of per-oxidation of high homocysteine levels of Chondroitin sulfate. [J]. China Public Health.2008, 24(5):603.

[6] Wu Yan-yan, Tong Qiao-xia, Luo Rui-de. The effects on rat model of alcoholic fatty liver of Chondroitin sulfate. [J]. Gastroenterology and liver disease, 2006, 15(4):387-389.

[7] Takanishi GC, Borst CA. Glucosamine and chondroitin in the treatment of osteoarthritis [J]. Women's Health Primary Care, 2001, 4(1):61

[8] Yang Pei-rong. The application of Chitosan and its hydrolysate in food industry.[J]. Jiangsu Food and Fermentation. 2001, 4: 26-27

[9] Shan Jing-shan, Zhang Shu-lin, Zhao Ke-xin. The current research of anti-atherosclerotic drugs.[J]. Theory and practice of medicine.2005,18(4):410-412.

Advanced Materials Research Vols. 989-994 (2014) pp 797-802
© (2014) Trans Tech Publications, Switzerland
doi:10.4028/www.scientific.net/AMR.989-994.797

On Pretreatment Experimental Study of High Strength Gypsum by Yunnan Phosphorus Gypsum

Sicheng QUAN[1,a], Zhiman ZHAO[1,b], Rui TIAN[2,c], Song HAN[1,d]

[1]Faculty of Civil Engineering of Kunming University of Science and Technology, Kunming, 650500,China

[2]Yunnan Yuntianhua Int'l Chemical Sanhuan Branch Company, Kunming,650500,China

[a]e-mail: quansichen@aliyun.cn, [b]e-mail: lzd2005@126.com
[c]e-mail:lx-tair@ynkg.com,[d]e-mail: 365189012@qq.com
※Corresponding author: Zhao Zhiman, provide phone: 86-13529317921; Fax:86-0871-63864560

Keywords: Phosphogypsum; Preprocessing; Lavation; High Strength Gypsum

Abstract. This thesis mainly studies the preprocessing of making high strength gypsum powder by using phosphogypsum. And bring out the new preprocessing of phosphogypsum from the traditional methods. And the new method improved the traditional 3 kinds of processing methods. After processing of phosphogypsum, strength and crystal morphology were compared to shown the better one.

Introduction

Phosphogypsum is solid waste of the production of phosphate fertilizer and phosphate acid. The production of 1t phosphoric acid produce about 4.5-5t phosphogypsum(According to production of phosphoric acid by wet process , and 100% phosphate acid) [1]. Phosphogypsum includes dehydrate gypsum ($CaSO_4 \cdot 2H_2O$)and hemihydrate gypsum ($CaSO_4 \cdot 1/2H_2O$)， The dehydrate gypsum ($CaSO_4 \cdot 2H_2O$) is the majority. The situation of Phosphogypsum utilization is unsatisfactory all the world around. Generally, the way they dispose the phosphogypsum is direct emissions or threw away.

By the end of 2011, China has accumulated more than 300 million tons of phosphogypsum. Yunnan Yuntianhua Int'l Chemical Sanhuan Branch Company produced the phosphoric acid about 3 million tons to 4 million tons each year and by-product phosphogypsum about 15 million tons to 20 million tons but there are no effective treatment method except stacking. As early as in 2006, the state environmental protection administration stipulated the phosphogypsum of two phosphate fertilizer companies' by-product as hazardous waste. So it is necessary to seek the rational use of phosphogypsum way in order to realize the sustainable development of phosphate fertilizer industry and high utilization of phosphogypsum.

Phosphogypsum is containing phosphorus, fluorine, organic matter, silica, iron, aluminum and other impurities. Phosphorus, fluorine impurities formed into calcium-phosphate and calcium-fluoride in process of gypsum conversion reaction which is dissolvable and covered the surface of crystal, and severely hampered the development of gypsum crystal and made the mechanical properties of high-strength gypsum deeply affected. But phosphogypsum and chalk can be separation by wet screening and washing sieve, in order to reduce the impurity to acceptable range[2].So the preprocessing can eliminate harmful impurities, make the phosphogypsum could be use. The traditional methods of phosphogypsum preprocessing are water-washing, lime neutralization and floatation. In addition there are other methods can get the Solid calcium sulfate and ammonium chloride after the treatment and the filter [3]. This paper focuses on 3 kinds of traditional methods of phosphogypsum preprocessing and the new method of phosphogypsum preprocessing which were put forward in this paper, to reflect the optimal method of phosphogypsum preprocessing.

The Experiment

Material

(1)Phosphogypsum：Sallow, attached water content of 0.745%, Add 50% water, PH value measurement was about 6.Taken from the Yunnan Yuntianhua Int'l Chemical Sanhuan Branch Company. With the testing entrust to the Yunnan nonferrous geological testing center and the laboratory of the academy of chemical industry, the result showed the main ingredients was $CaSO_4 \cdot 2H_2O$, and its content was 86.49%. The main mineral composition was as shown in table 1. By the experiment of high temperature drying after drying the phosphogypsum crystallization morphology as shown in Figure 1 and Figure 2. It was not hard to find there are plenty of flocculent attachments around the phosphogypsum and the floc was the impurities. The XRD spectra analysis diagram was as shown in Figure 3.

Table 1 Mineral composition of Phosphogypsum (%)

Test material	Form	SiO_2	Al_2O_3	Fe_2O_3	MnO	MgO	CaO	K_2O	P_2O_5	SO_3	Cl^-	Organics
Phosphogypsum	Powder	14.52	1.66	0.15	0.005	0.17	31.94	0.22	0.94	45.38	0.027	0.25

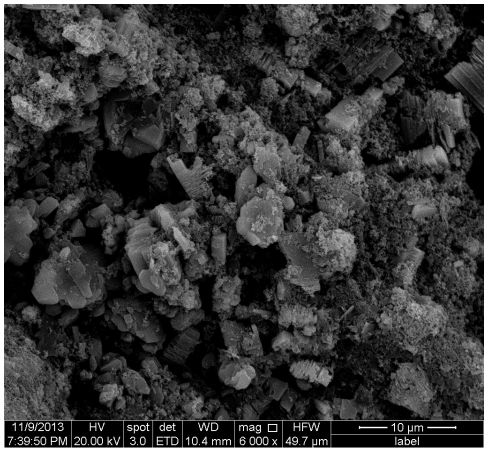

Fig1.SEM photo of phosphogypsum

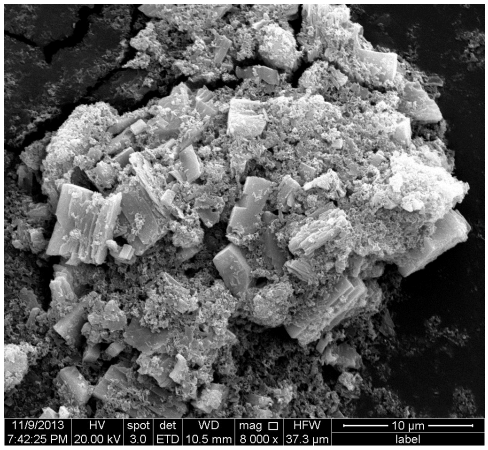

Fig2.SEM photo of phosphogypsum

(2)Quicklime：Quicklime(CaO) used for experiment which bought from market.

The Method of Preprocessing

No matter what kind of preprocessing method is, It is necessary to grinding phosphogypsum at first to make the phosphogypsum cake crushing and fine grinding(300mesh), thus it will make the phosphogypsum well reacted in the process of preprocessing.

1) Traditional Methods of Preprocessing：

(1) Lime Neutralization:

500ml water was added into 1000g phosphogypsum and then the slurry was poured into a blender to stirring for 10min. At last some hydrated lime ($Ca(OH)_2$, about 0.5g to1.5g) were added into the slurry till the PH value measurement was about 7.

(2) Water-Washing:

4000ml water was added into 1000g phosphogypsum and then the slurry were poured into a blender to stirring for 10min, Set aside for 30min. Next, the upper liquid were poured out, the PH value of the slurry left was measured. And next, 4000ml water was added into the slurry. The operation above was repeat till the PH value measurement of slurry was about 7.

(3)Floatation:

4000ml water was added into 1000g phosphogypsum and then the slurry were poured into a blender to stirring for 10min, Set aside for 30min. And then the upper oily suspension was scraped off. The operation above was repeat till no oily suspension appeared.

2) New Method of Preprocessing (Hereinafter referred to method of Lavation)

750ml water was added into 1000g phosphogypsum and then the slurry was poured into a blender to stirring for 30min. Next the upper liquid was poured out, then some hydrated lime ($Ca(OH)_2$,about 0.3g to1.3g),were added into the slurry till the PH value measurement was about 7.

Method of Preparation Phosphogypsum Building Powder

The phosphogypsum which has been processed were put into the autoclave kettle. The Autoclave temperature was turned to140 ℃, pressure to 0.55 MPa, and last for 6h. After the autoclave, the phosphogypsum was put into the bellows, and it was drying to oven dry in 40 ℃. Get it out and grinding fine, the material we get is phosphogypsum building powder.

Test Method and Steps.

The size of the mold is 160 mm x 40 mm x 40 mm, ratio of gypsum and water is 20%. Then cast it into form, Natural curing 2h and then demoulding, put it into the bellows, and drying it to oven dry in 40 ℃. Test the compressive strength and rupture strength of it. The result is as shown in table 3 and Figure 5.

Experimental Results and Discussion

Table 2 Impurity content of phosphogypsum before and after the preprocessing (%)

Impurities types	Before Preprocessing	Lime Neutralization	Water-Washing	Floatation	Lavation
t-P_2O_5	0.85	0.29	0.15	0.84	0.17
w-F	0.38	0.13	0.02	0.37	0.08
Organics	0.23	0.23	0.01	0.02	0.06

(Notice: ”t” short for “total” ,”w” short for “water-soluble”)

Lime Neutralization：The process of Lime Neutralization is the most complicated of the traditional methods of preprocessing. The effect of impurities eradication is worse than the Water-Washing, in the 3 kinds of traditional preprocessing methods. As shown in Table2 and Figure 4. In addition, the phosphogypsum remaining was the most of the traditional methods. And the cost of the time and the water was the fewest, and the Lime Neutralization was the most efficient of the traditional methods. Most of the research considered that synthesizes each kind of factors; the Lime Neutralization is the best of the traditional methods [4]. If the commercial process should be considered the Lime Neutralization was the most suitable of the traditional methods. And the Crystal form picture of phosphogypsum was as shown in Figure 6. The crystal of phosphogypsum was bulky near column, but there were still some impurities around. The reaction principle was as follows: As most of the soluble impurities were phosphorus and fluorine. So add the lime into the phosphogypsum, it will react as follow in the free water [5].

$$P_2O_5 + 3Ca(OH)_2 \text{ — } Ca_3(PO_4)_2 + 3H_2O \quad (1)$$

$$2F^- + Ca(OH)_2 \text{ — } CaF_2 + 2OH^- \quad (2)$$

Water-Washing： The process of Water-Washing was less complicated than the Lime Neutralization. The effect of impurities eradication was the best of the traditional preprocessing methods. As shown in Table2 and Figure 4. But the phosphogypsum remaining was the fewest of the traditional methods, because it will lose a lot of phosphogypsum when pour the upper liquid out again and again. And the Water-Washing cost a lot of the time and the water, both of the cost was the most of the traditional methods. To deal with1000g phosphogypsum will cost more than 10000ml water in total, nearly 10 times of the phosphogypsum. So the Comprehensive processing efficiency of the Water-Washing was less than the Lime Neutralization. The principle of the Water-Washing was clean up most of the soluble impurities which would affect the quality of the phosphorus gypsum in the phosphogypsum by adding water in and pout it out again and again. Clean up the impurities such as free phosphoric acid ($P_2O_4^{2+}$), free fluorine (F^-), soluble phosphate (P_2O_5), alkali metal salt and organics which are undissolved and floating on the surface of the liquid. [6] The crystal form picture of phosphogypsum was as shown in Figure 7, there were still some impurities around the crystal of phosphogypsum, but the content of the impurities was low and the form of crystal was near column.

Floatation: The process of Floatation was the most simple of the traditional methods of preprocessing. But the effect of impurities eradication was the worst of the traditional methods of

preprocessing. As shown in Table2 and Figure 4. The phosphogypsum remaining was a little bit more than the Water-Washing of the traditional methods. And the energy cost was less than the Lime Neutralization. So the Comprehensive processing efficiency of the Water-Washing was the lowest of the traditional methods. The principle of the Floatation was clean up the undissolved impurities which are floating on the surface of the liquid by scraping the upper oily suspension off. But this method could hardly clean up the impurities which was soluble. And the soluble impurities usually have important influence on the quality of the phosphorus gypsum [7]. The crystal form picture of phosphogypsum was as shown in Figure 8.

Lavation: The process of Lavation was more complicated than the Lime Neutralization, The effect of impurities eradication was nearly catching up with the Water-Washing. As shown in Table2 and Figure 4. And the phosphogypsum remaining was just a little bit less than the Lime Neutralization of the traditional methods and the cost of the water were a little more than Lime Neutralization. So synthesizes each kind of factors, the processing efficiency of Lavation is better than the all kinds of traditional methods. The principle of the Lavation was clean up some organics and the soluble impurities at first, and then clean up the remain acid soluble impurities with the lime. The crystal form picture of phosphogypsum was as shown in Figure 9.

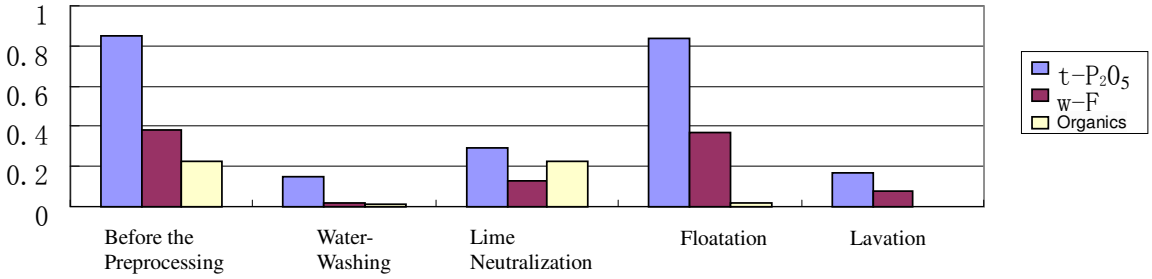

Fig4. The content of impurities before the preprocessing and use the different methods of preprocessing

Table 2 Compressive strength and rupture strength of gypsum in 2h by use different methods of preprocessing

	Lime Neutralization	Water-Washing	Floatation	Lavation
rupture strength (MPa)	1.9	2.1	1.7	2.1
compressive strength (MPa)	2.6	2.9	2.1	2.8

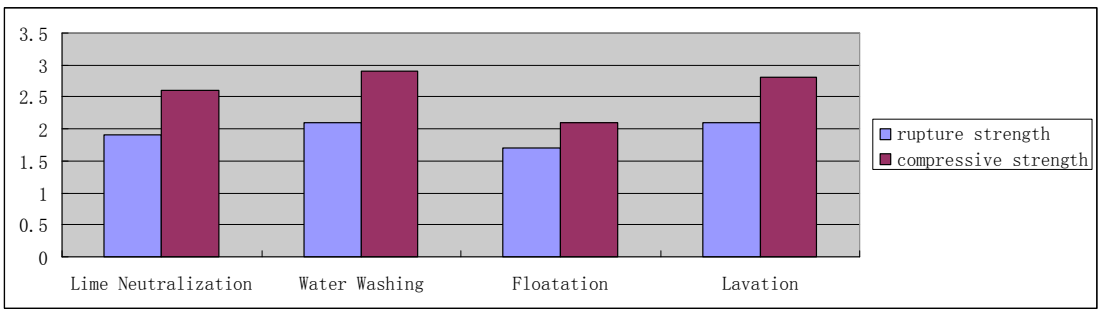

Fig5. Histogram of the compressive strength and rupture strength of gypsum

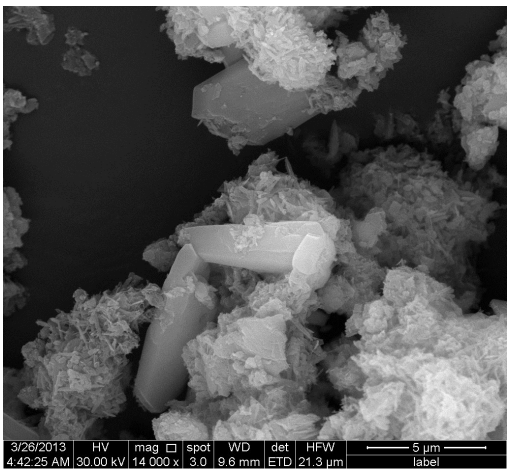

Fig 6. The SEM photo of Crystal form by the method of lime neutralization.

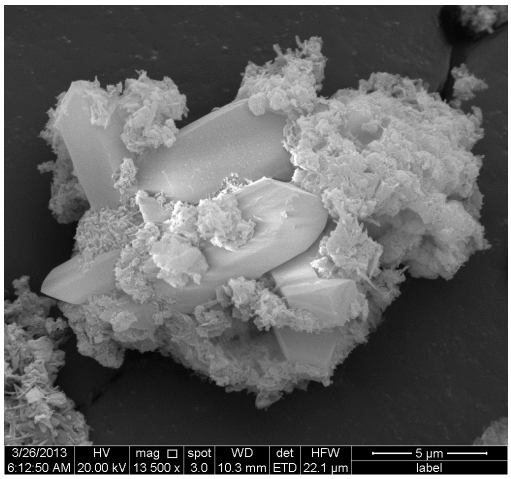

Fig 7. The SEM photo of Crystal form by the method of water-washing.

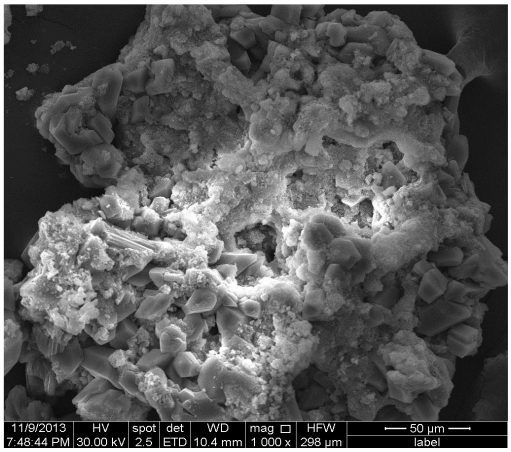

Fig 8. The SEM photo of Crystal form by the method of floatation.

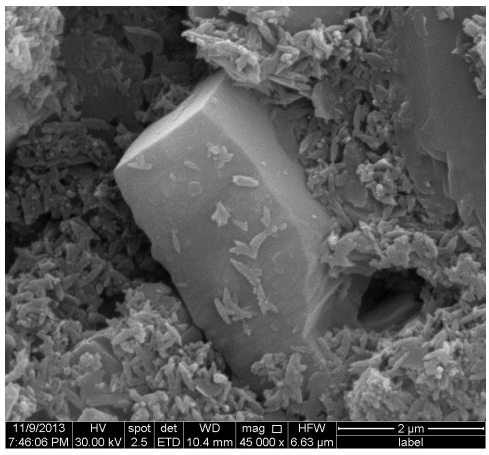

Fig 9. The SEM photo of Crystal form by the method of lavation.

Conclusion

The result showed: Effect of the lavation was just less than water-washing, but have a high efficiency. The phosphogypsum remaining was just less than lime neutralization. Otherwise the cost of the time was the shortest. Synthesizes each kind of factors, the lavation was better than the traditional methods. Although there are some impurities around the crystal but the form of the crystal was near column which was good for developing of strength. 3 kinds of traditional preprocessing methods can partly meet the requirements of the use of phosphogypsum as building materials. The lime neutralization effect is good; The process of water-washing is simple, and the effect of impurities eradication is the best of the traditional preprocessing methods but have a large energy consumption. Process of the floatation is the most simple and low energy consumption but the effect of impurities eradication is not good. The effect of impurities eradication of new preprocessing method is really good and has low energy consumption, overall consideration , the new method is better than the 3 kinds of traditional preprocessing methods.

Acknowledgements

In this paper, the research was supported by the National Natural Science Foundation (Project No.51264017).

※Corresponding author: Zhao Zhiman, provide phone: 86-13529317921; Fax:86-0871-63864560

Reference

[1] Wan Bangjiang, WuHong HU. Pretreatment and Utilization of Phosphogypsum. Science and Technology of West China [J] , 2011,10(25):5-7

[2] Mridul Garg. Environment hazard mitigation of waste gypsum and chalk: Use in construction materials, Construction and Building Materials [J].2011, 25:944-949

[3] Yang Ronghua ， Song Xigao. Research on purification of phosphogypsum and preparation of calcium sulfate whisker. Inorganic Chemicals Industry [J] ,2012,4:31-34

[4] Zhou Jie，Yang Cheng-Jun，XU Jian，Shi Bin，Yang Min. Study on the Pretreatment Technology of High—strength Gypsum with Phosphogypsum. Guangzhou Chemical Industry [J], 2011, 39:75-77

[5] Zeng Ming，Ruian Yan，Chen Jing，Wang Chong—Ying，Zhang Bing，Zhou Zi —chen. Effects Comparison of Different Pretreatment Methods to Phosphogypsum. The World of Building Materials [J], 2011, 32(2):18-21

[6] Ru Xiaohong，Ma Baoguo，Huang Yun. Research progress of a—hemihydrate gypsum prepared by phosphogypsum. New Building Materials [J] .2011, 11:15-18

[7] E.M. El Afifi, M.A. Hilal, M.F. Attallah, S.A. EL-Reefy. Characterization of phosphogypsum wastes associated with phosphoric acid and fertilizers production. Journal of Environmental Radioactivity [J].2009(100):407-412

Advanced Materials Research Vols. 989-994 (2014) pp 803-808
© (2014) Trans Tech Publications, Switzerland
doi:10.4028/www.scientific.net/AMR.989-994.803

Research on the treatment of the Yellow River micro-polluted water in Shanxi by ozone-activated carbon process

Xiaobin TANG[1], Jianfeng ZOU[1], Kaifan HE[1], Jian LIU[1], Jianjun ZHOU[2], Fujin WANG[2], Yixing YUAN[1],Junguo HE[1, a]

[1]School of Municipal and Environmental Engineering, Harbin Institute of Technology, 73 Huanghe Road, Harbin, China.

[2]Yellow River Water Supply Ltd.

[a] junguohe@263.net.

Keywords: ozone, activated carbon, petroleum substances, volatile phenol

Abstract. In this study, the micro-polluted water of a reservoir filled with Yellow River water in Shanxi was used as the raw water. The removals of chemical oxygen demand (COD_{Mn}), ammonia nitrogen, petroleum substances, and volatile phenol were investigated by ozone-activated carbon process. Results showed that ozone-activated carbon process had a good removal of the pollutants mentioned above. The optimum dosage of ozone for each pollutant was 2.0 mg/L, 2.5 mg/L, 3.0 mg/L, 3.0mg/L, with the corresponding removal efficiency of 59.36 %, 88.01%, 79.31%, and 88.16%, respectively. The treated water quality could meet the standards for Drinking Water Quality (GB5749-2006) in China.

Introduction

The raw water of Shanxi located in the middle and lower reaches of the Yellow River is polluted by the wastewater of upstream industrial and mining enterprises. The conventional treatment process is difficult to guarantee the water quality because of the high concentrations of organic matter, ammonia nitrogen, petroleum substances, and volatile phenol in raw water. The organic matter in raw water can lead to the formation of disinfection by-products (DBPs) [1]. High concentrations of ammonia nitrogen can induce hematin prion disease (especially for infants), and produce nitrosamines which are thought to be carcinogens [2]. In addition, petroleum substances and volatile phenol have the risk of carcinogenesis, malformation, mutagenicity [3,4]. Ozone-activated carbon process, which contains a series of sub-process such as ozonation, activated carbon absorption, microbial adsorption and microbial biodegradation [5], is widely used in micro-polluted water treatment. Recently, organic matter and ammonia nitrogen have been studied by a large number of researchers. However, there is a visible difference in operation conditions and removal efficiencies to treat different raw water. Meanwhile, the removal of petroleum substances and volatile phenol by ozone-activated carbon process in drinking water treatment is very scarce. Therefore, the research on the treatment of the Yellow River micro-polluted water in Shanxi by ozone-activated carbon process is necessary and of practical significance.

Material and Method

Raw Water Quality

The raw water investigated in this study was collected from the reservoir filled with Yellow River water in Shanxi, and the water quality was shown in Fig. 1. The concentration range of COD_{Mn}, ammonia nitrogen, petroleum substances, and volatile phenol was 3.16-4.69mg/L, 0.75-1.16mg/L, 0.066-0.178mg/L, 0.005-0.015mg/L, respectively. This result indicated that the raw water was with characters of micro-pollution.

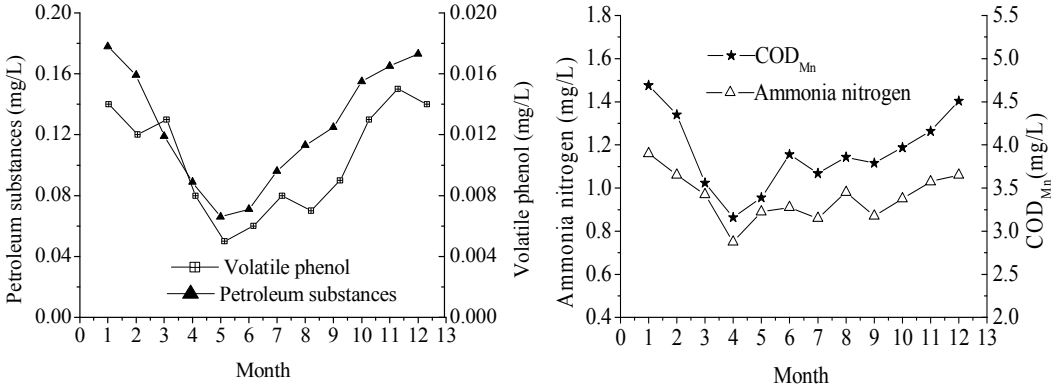

(a). petroleum substances and volatile phenol (b) COD_{Mn} and ammonia nitrogen

Fig. 1 The quality of the raw water

Experimental Device

The experimental flow chart was shown in Fig. 2.

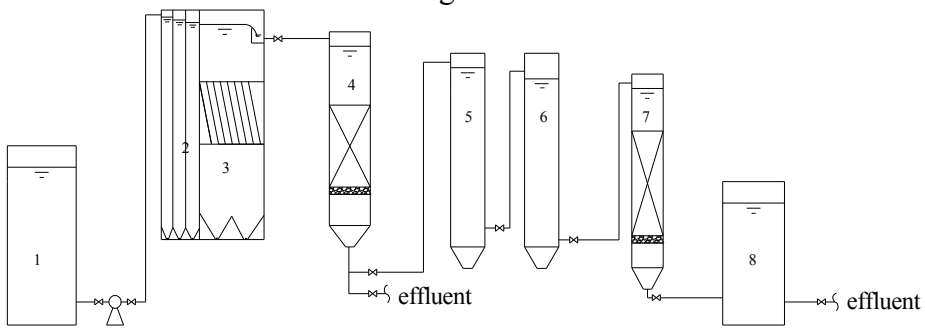

Fig. 2 Experimental flow chart (1: water tank; 2: flocculation reactor; 3: sedimentation tank; 4: filter chamber; 5: the first ozonation contact reactor; 6: the second ozonation contact reactor; 7: activated carbon filter; 8: disinfecting tank.).

Analytical Methods

Detecting indicators and methods in the test were shown in Table 1.

Table 1 Water quality indicators and analytical methods

Water quality indicators	Analytical methods
COD_{Mn}(mg/L)	Acidic potassium permanganate titration
Ammonia nitrogen(mg/L)	Nessler reagent spectrophotometric
Petroleum materials(mg/L)	UV spectrophotometry
Volatile phenols(mg/L)	4- amino antipyrine chloroform extraction spectrophotometry

Results and Discussion

The removal efficiency of COD_{Mn}

Fig. 3 showed the variation of the COD_{Mn} removal efficiency with the ozone dosage ranging from 0.5 mg/L to 5mg/L. With the increase of ozone dosage, the COD_{Mn} removal rate after ozonation varied little,and the highest removal rate was 9.01%. The micromolecular organic was easy to be oxidized by ozone, while macromolecular organic was difficult to be removed completely [6]. The COD_{Mn} concentration of the activated carbon filter effluent decreased first and then increased with the increase of ozone dosage. The removal rate of COD_{Mn} ranged from 33.09% to 59.36% when the ozone dosage in the range of 0~2.0 mg/L. Ozonation could make complex macromolecular organic matter disconnect, break long-chain organic into small shorter chains. Moreover, the adsorptivity and biodegradability of organic matter was improved when the types of organic functional groups were modified by ozonation [7]. When the ozone dosage was more than 2mg/L, the COD_{Mn} removal of carbon filter was decrease form59.36% to 38.69%. High concentrations of ozone could partially mineralize the assimilable organic carbon (AOC). In

addition, the microbial activity could be affected by high concentration of ozone. Therefore, the optimum ozone dosage for COD_{Mn} removal was 2.0mg/L.

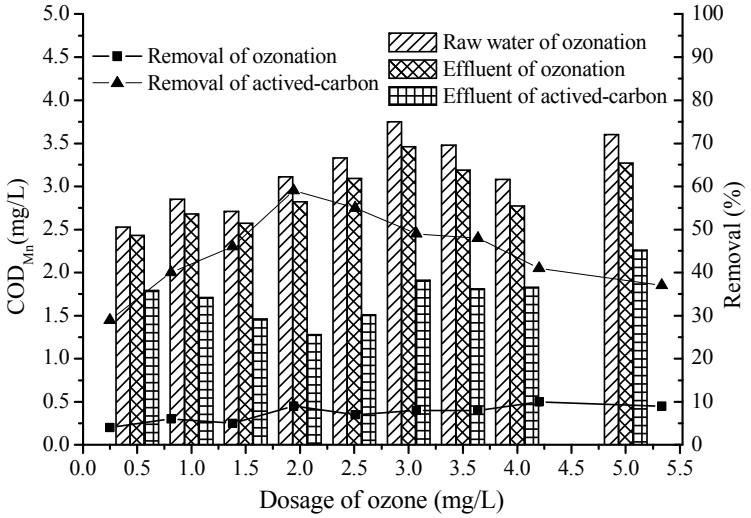

Fig. 3 The removal of COD_{Mn} by ozone-activated carbon process

The removal efficiency of ammonia nitrogen

Fig. 4 showed that the ammonia nitrogen concentration of ozone contact reactor effluent increased from 0.63mg/L to 0.98mg/L when the dosage of ozone was in the range of 0-2.5mg/L. This result indicated that the nitrogen-containing compounds were oxidized into ammonia nitrogen by ozone. Ammonia nitrogen concentration of the ozone contact reactor effluent was slightly increased when the ozone dosage was more than 2.5mg/L, which was restricted by the total nitrogen-containing compounds of the inflow . Carbon filter had high ability to remove ammonia nitrogen, and the removal efficiency was increased from 36.08% to 88.01% when the ozone dosage was in the range of 0-2.5mg/L. With the increase of ozone dosage, the concentration of dissolved oxygen (DO) in water, and the activities of the nitrite bacteria and nitrifying bacteria were increased [8]. Consequently, the ammonia nitrogen was oxidized to nitrate rapidly. When the ozone dosage was continued increasing, the activity of nitrifying bacteria was suppressed ,leading to a decrease of ammonia nitrogen removal rate. Therefore, the optimum ozone dosage for ammonia nitrogen removal was 2.5mg/L.

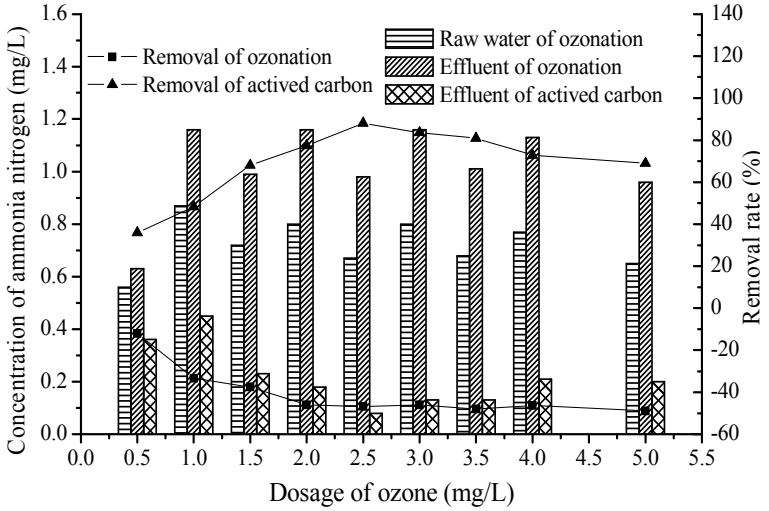

Fig. 4 The removal of ammonia nitrogen by ozone-activated carbon process

The removal efficiency of petroleum substances

The removal efficiency of petroleum substances was shown in Fig. 5. With the increasing ozone doses the petroleum substances removal rate after ozonation had an upward trend first , then followed by a stable trend. At a lower dosage (<1.0 mg/L), the removal efficiency increased slightly from 9.36% to 13.48 %, which may be because of the competitive reaction of the petroleum substances, organic matters and other reducible compounds [9]. When the ozone dosage ranged

from 1.0 mg/L to 3.0mg/L, the petroleum substances removal rapidly increased from 13.48% to 47.76%. The organic matters and reducible compounds were mostly oxidized causing a decrease of the competitive reaction; therefore, the petroleum substances removal was increased. When the ozone dosage was increased above 3.0mg/L, the petroleum substances removal efficiency tended to be stabilized.

At the ozone dosage of 0.5mg/L, the petroleum substances concentration of the actived-carbon filter effluent decreased to 0.069mg/L, and the removal rate was 32.75%. This result indicated that carbon filter had a good ability to remove petroleum substances. At the ozone dosage ranging of 0.5-3.0mg/L, the effluent concentration of petroleum substances decreased from 0.071 mg/L to 0.025 mg/L with the removal rate increasing from 32.75% to 79.31%. The reason was that the adsorption and biodegradability of petroleum substances were improved after ozonation [10]. At a higher ozone dosage (>3mg/L), the petroleum substances concentration of actived carbon filter effluent gradually increased. The adsorption and decomposition of microorganism were affected by the high concentrations of ozone and mineralization of organic matters [11]. When the ozone dosage was 3.0mg/L, the petroleum substances concentration of activated carbon filter effluent was less than 0.05mg/L, meeting the drinking water standards.

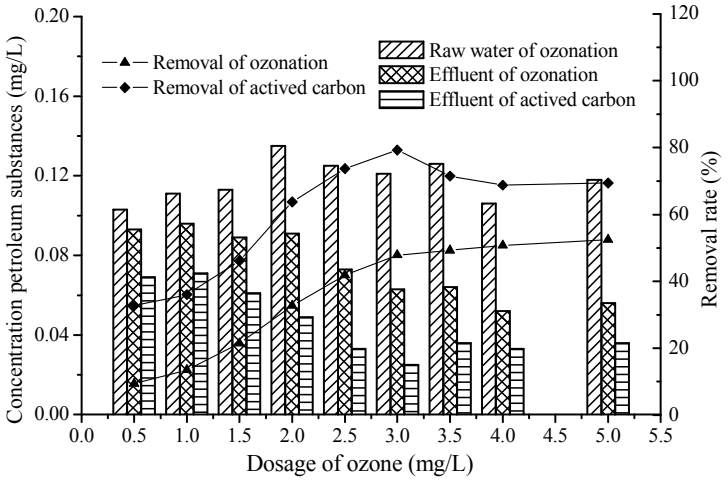

Fig. 5 The removal of petroleum substances by ozone-activated carbon process

The removal efficiency of volatile phenol

The variation of volatile phenol removal with different ozone dosage was investigated, and the results were demonstrated in Fig. 6. When the dosage of ozone increased from 0.5 mg/L to 3.5mg/L, the concentration of volatile phenol of the ozonation contact reactor effluent significantly decreased,and the removal rate increased from 18.37% to 52.38%. When the ozone dosage was higher than 3.5mg/L, the volatile phenol removal rate after ozonation increased slightly. Because the electrophilic reaction of ozone and volatile phenol were conducted, and ozone trended to attack the para-hydroxy or ortho-hydroxy of volatile phenol. As a result, the volatile phenol was oxidized into quinones firstly, and then oxidized into carbonyl and carboxyl-containing organics fatty acid [12]. After ozonation, the volatile phenol concentration of effluent was in the range of 0.004-0.006mg/L. Because of some intermediate and final products may have better adsorption and biodegradation, the volatile phenol removal rate of actived carbon filter effluent rapidly increased when the ozone dosage ranged from 0.5mg/L to 3.0mg/L. At the ozone dosage of 3.0mg/L, the volatile phenol removal rate reached a maximum of 88.16%, and the volatile phenol concentration was less than 0.002mg/L. Increasing the dosage of ozone further, the concentration of volatile phenol kept stable. It was due to that the residual concentration of volatile phenol was too low in the system, which would affect the mass transfer process, add the solid-liquid interface mass transfer resistance when activated carbon adsorbed volatile phenol [13]. Besides, the residual concentration of volatile phenol was lower than the detection limit of the instrument. Therefore, the ozone optimum dosage should be higher than 3.0mg/L to guarantee the removal efficiency of volatile phenol.

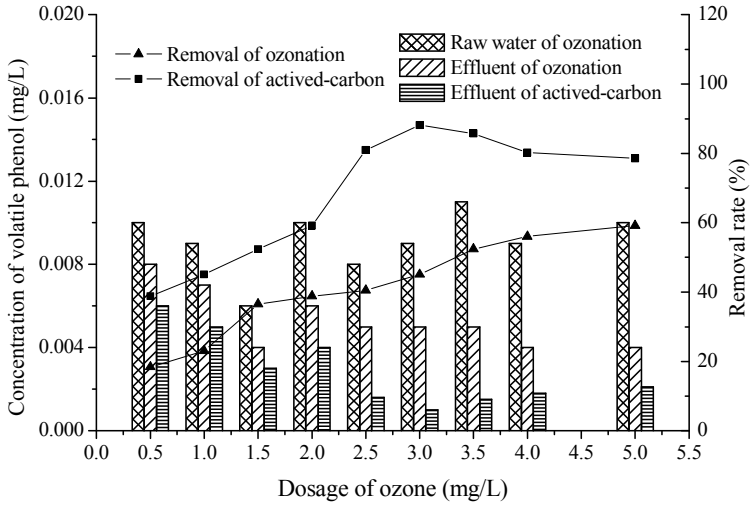

Fig. 6 The removal of volatile phenol by ozone-activated carbon process

Conclusion

In this paper, the micro-polluted water of a reservoir filled with Yellow River water in Shanxi was investigated by ozone-activated carbon process. The following conclusions can be made from this study:

(1) The optimum ozone dosage of ozone-activated carbon process to remove COD_{Mn}, ammonia, petroleum substances, and volatile phenol were 2.0 mg/L, 2.5 mg/L, 3.0 mg/L, 3.0mg/L, with the removal rate of 59.36 %, 88.01%, 79.31%, and 88.16%, respectively. The concentrations of various pollutants after treatment were 0.82 mg/L, <0.1 mg/L, 0.025 mg/L, <0.002 mg/L, respectively.

(2) Ozone-activated carbon process was useful to remove COD_{Mn}, ammonia nitrogen, petroleum substances, and volatile phenol. By optimizing the ozone dosage, the concentration of various pollutants could meet the standards for Drinking Water Quality (GB5749-2006) in China.

References

[1] Hui Li, Yanfeng Liu, Ming Guo, Rui Zhang, Jing Du. Research on Yellow River Water Purification Using the Combined Process Containing Hydrogen Peroxide Catalyzed Ozone-Activated Carbon-Sand Filtration Treatment. Advanced Materials Research, 2011, (374-377): 995-999.

[2] Weifang Ma, Guowei Chen, Dongmei Han, Hao Guo. Application of Combined Process of Ozone/Activated Carbon and UF in Bean Sprouts Spray Water Reuse Project. China Water and Wastewater, 2011, 27(2): 71-76. (in chinese)

[3] Randy N. Roth, Barry J. Simpson, Mark J. Nicolich, F. Jay Murray, Thomas M. Gray. The relationship between repeat-dose toxicity and aromatic-ring class profile of high-boiling petroleum substances. Regulatory Toxicology and Pharmacology, 2013, 67: 530-545.

[4] Meysam Eisapour, Farzaneh Shemirani, Behrooz Majidi, Majid Baghdadi. Ultrasound assisted cold-induced aggregation: an improved method for trace determination of volatile phenol. Microchim Acta, 2012, 177: 349-355.

[5] Wanbo Yu. Application of an Advanced Technology For Ozone - Biological Activated Carbon In Drinking Water Treatment With Micr -Organic Pollutants. Environment Technology, 2003, (2): 11-15. (in chinese)

[6] Shaoming Lu, Jincui Liu, Shaowen Li, Elizabeth Biney. Analysis of up-flow aerated biological activatedcarbon filter technology in drinking water treatment. Environment Technology, 2013, 34(16): 2345-2351.

[7] Hongjing Chen, Yougan Xiao, Gongluo Huang, Hui Wang. Combined Process of Ozonation and Biological Activated Carbon for Treatment of Micro-polluted Source Water. China Water and Wastewater, 2011, 27(17): 18-21. (in chinese)

[8] Arwa Lagha, Abdelmottaleb Ouederni. Treatment of dissolved sulfides in water by combined process using ozone and activated carbon. Desalination and Water Treatment, 2014: 1-8.

[9] Eman A. Emam. Effect of ozonation combined with heterogeneous catalysts and ultraviolet radiation on recycling of gas-station wastewater. Egyptian Journal of Petroleum, 2012, 21: 55-60.

[10] Claudio Di Iaconi. Biological treatment and ozone oxidation: Integration or coupling. Bioresource Technology, 2012, 106:63-68

[11] Yong Yu, Tianqiang Xie, Yanxiang Lin, Wanmin Bao. Study on ozone oxidation technique for the treatment of oil-polluted ground water. Industrial water and wastewater, 2001, 32(2): 14-15.

[12] T. Charinpanitkul, P. Limsuwan, C. Chalotorn, N. Sano, T. Yamamoto, P. Tongpram, P. Wongsarivej, A. Soottitantawat, W. Tanthapanichakoon. Synergetic removal of aqueous phenol by ozone and activated carbon within three-phase fluidized-bed reactor. Journal of Industrial and Engineering Chemistry, 2010, 16: 91-95.

[13] Guangzhou Qu, Dongli Liang, Dong Qu, Yimei Huang, Ting Liu, Hui Mao, Puhui Ji, Donglin Huang. Simultaneous removal of cadmium ions and phenol from water solution by pulsed corona discharge plasma combined with activated carbon. Chemical Engineering Journal, 2013, 228: 28-35.

Advanced Materials Research Vols. 989-994 (2014) pp 809-813
© (2014) Trans Tech Publications, Switzerland
doi:10.4028/www.scientific.net/AMR.989-994.809

Dye Adsorbent Prepared by Crosslinking of Poly (γ-glutamic acid) and Gelatin

Wei WANG[1, a], Shuping LIU[1,b], Huanan GUAN[1], Jinzhong LIANG[1], Chong TAN[2]

[1]School of Food Engineering, Harbin University of Commerce, Harbin, 150076, China

[2]Research Center on Life Sciences and Environmental Sciences, Harbin University of Commerce, Harbin, 150076, China

[a]email: yueyingliuguang@aliyun.com.cn, [b]email: Liusp 201@163.com

Keywords: γ-PGA; gelatin; adsorbent; Rhodamine B

Abstract. The present paper describes the preparation of novel biodegradable adsorbent based on cross-linking of poly (γ-glutamic acid) (γ-PGA) and gelatin and characterization of its Rhodamine B dye adsorption capability. Cross-linking effect was measured with the effect of adsorbent adsorbing ionic dyes Rhodamine B. In the experiment, the various factors which had influence on the adsorption effect, including preparationtemperature, preparation pH value, concentrations of cross-linking agent, cross-linking time were analyzed. The results showed that the adsorbent had good adsorption performance after cross-linking. The adsorbent was characterized by fourier transform infrared spectrum (FTIR), revealing that there were amide bonds between gelatin and poly (γ-glutamic acid) by cross-linking reaction.

Introduction

Dyes are widely used in various industries including textile, leather, paper, coating and plastics [1], but dyes in effluents has raised global concerns over their harmful impact on the environment and organisms. The presence of dyes in water consumes oxygen and elevates biochemical oxygen demand destroying the aquatic life [2]. Furthermore, some dyes and their degradation products, such as aromatic amines, possess high carcinogenicity [3]. Additionally, due to its high water-solubility, it is estimated that 10-20% of reactive dye remains in wastewater during production and nearly 50% of reactive dyes may be lost to the effluents during dyeing process [4] [5]. Variety of dye treatment technologies have been used for the removal of dyes from the wastewater, such as chemical coagulation-flocculation, oxidation, biological process, membrane-based separation processes [6-10]. Of the various methods of dye wastewater treatment, adsorption is a classical technique which can quickly decrease the concentration of dissolved dyes in effluents. However, high cost and low adsorption capacity makes the process impossible for industrial applications. Therefore, there is a need to develop alternative novel adsorbents which will make the process economically feasible and high adsorption capacity.

Poly-γ-glutamic acid is an anionic polypeptide synthesized by *Bacillus* species through a fermentation process and consists of numerous repetitive glutamic acid units connected by amide linkages between α-amino and γ-carboxylic acid functional groups [11] [12]. The γ-PGA is water-soluble, biodegradable, edible and nontoxic finds application in various fields including cosmetics, food, medicine, agriculture and wastewater treatment [13-15]. In several previous studies, γ-PGA has been shown to be an effective adsorbent for removal of various dyes and metals [16] [17]. However, γ-PGA is water-soluble, its application as an adsorbent for dye removal still remains to be explored. Therefore, the objectives of this study were to find a suitable carrier which can make γ-PGA not swept along with the water, and keep its adsorption properties on dyes. In this paper adsorbent was prepared by cross-linking reaction between γ-PGA and gelatin with glutaraldehyde as cross-linking agent, and its dye removal capability was evaluated in a batch mode adsorption process with Rhodamine B as a test dye.

Methods

Materials

The analytical-grade chemicals reagent gelatin and glutaraldehyde were purchased from Tianjin Chemical Reagent Factory and Tianjin Bodi Chemical Co. ltd. The test dye Rhodamine B was purchased from Tianjin Chemical Reagent Factory.

Poly (γ-glutamic acid) was prepared in our laboratory using the biosynthetic methods [18]. Briefly, γ-PGA was produced from *Bacillus subtilis* B-1, which was maintained on beef extract peptone medium slant to produce in appropriate cultivation conditions. γ-PGA was precipitated by the addition of absolute ethyl alcohol and filtered. The γ-PGA was redissolved in distilled water, dialyzed against distilled water, and freeze-dried for further experiments.

Preparation of adsorbent

50 g of gelatin and 15 g glycerol were mixed in 1L of distilled water and vigorously stirred until mixing well. The mixture was then evenly spread on slides and was dried at 60 ℃ to obtain gelatin film and used for further experiments.

γ-PGA was dispersed in glutaraldehyde solution and vigorously stirred until mixing well, and gelatin film (γ-PGA: gelatin film=1:1) was added to obtain the adsorbent. The effects of all factors on the preparation of adsorbent were studied by experiments following single factor (different preparation temperatures, different preparation pH values, different concentration of crosslinking agent, and different times). After cross-linking reaction, the adsorbent was washed several times with distilled water for characterization and adsorption experiments.

Adsorption experiments

For all the batch adsorption experiments, 20 mL of Rhodamine B dye solution at 3 mg/L in glass vials was used for further adsorption experiments. Then, 0.050 g of adsorbent was added to the dye solution and shaken at room temperature by magnetic stirrer for 1h. After 10 min, the supernatant for Rhodamine B dye solution at 552 nm was measured by using a spectrophotometer (721E, Shanghai Spectrum Instruments Co., Ltd, China). A quantitative determination of dye concentration was achieved by using the linear regression equation, y=0.2157x+0.0309（R^2=0.9995）, obtained from the calibration curve prepared with a range of Rhodamine B dye concentration (1-5 mg/L). Each sample was measured three times, and average serial data were calculated.

The amount of dye adsorbed C_e (mg/g) was calculated from the following equation:

$$C_e = \frac{(\rho_0 - \rho_e)V}{m} \tag{1}$$

Where, ρ_0 (mg/L) is the initial dye concentration, ρ_e (mg/L) is the dye concentration after adsorbed, V (L) is the volume of dye solution, m (g) is the mass of adsorbent.

Characterization of adsorbent

Fourier transform infrared spectrum (FTIR)

FTIR spectra of gelatin film, pure γ-PGA and adsorbent were recorded in a FTIR spectrophotometer (model FTIR 6700, Thermo Fisher Scientific Nicolet, USA) by homogenizing a small amount of each sample separately with KBr crystals, recording the spectra in the wavelength range from 4000-400 cm^{-1}.

Results and discussion

Adsorption experiments

1) Effect of preparation temperature on adsorption

The effect of preparation temperature on adsorption capacity was investigated and the results can be seen Fig.1. The results show that the adsorption capacity of the adsorbent increases with increasing the preparation temperature from 20 to 60 ℃, and the maximal value is 0.4024 mg/g. The phenomenon showed that higher temperature favored the preparation of the adsorbent and the adsorption of Rhodamine B. It could be due to the fact that increasing the preparation temperature may make the molecular activity stronger.

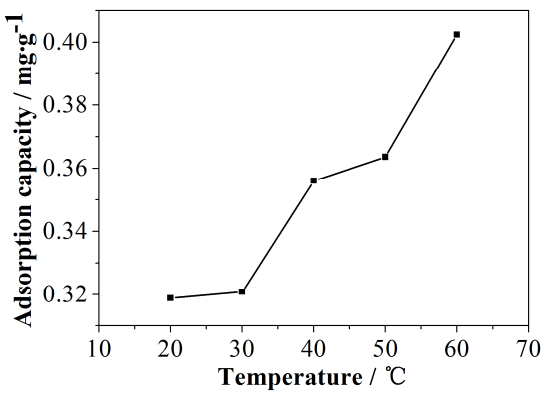

Fig.1. Effect of preparation temperature on adsorption (Rhodamine B dye solution: 3 mg/L 20 mL, pH: nature, amount of adsorbent: 0.5 g, crosslinking agent's concentration: 0.15 %, preparation time: 1 h)

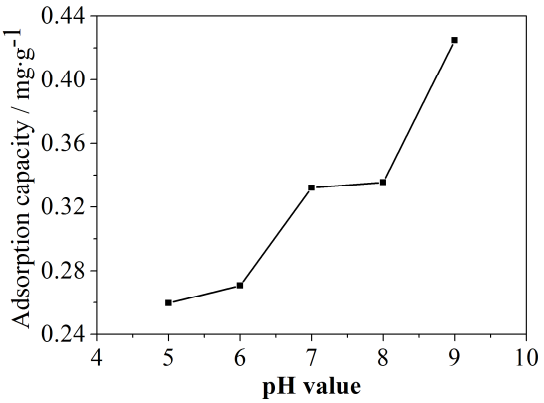

Fig.2. Effect of preparation pH value on adsorption (Rhodamine B dye solution: 3 mg/L 20 mL, temperature: 60 ℃, amount of adsorbent: 0.5 g, crosslinking agent's concentration: 0.15 %, preparation time: 1 h)

2) Effect of preparation pH value on adsorption

Fig.2 shows the relationship between the preparation pH value and the adsorption capacity of the adsorbent. The results show that when the pH value of preparation system raised from 5 to 9, the adsorption capacity increases from 0.2596 to 0.4248 mg/g. The phenomenon showed that higher pH value favored the preparation of the adsorbent and the adsorption of Rhodamine B. It may be attributed to the fact that, at higher pH value, more carboxyl group dissociated and got involved in adsorption of Rhodamine B.

3) Effect of crosslinking agent's concentration on adsorption

The effect of crosslinking agent's concentration on adsorption capacity was investigated and the results can be seen Fig.3. The results show that the adsorption capacity of the adsorbent increase with increasing drastically the crosslinking agent's concentration from 0.05 to 0.15 %, and the maximal value is 0.4228 mg/g. When the crosslinking agent's concentration from 0.20 to 0.25 %, the adsorption capacity decreased from 0.4132 to 0.3112 mg/g. This change can be explained that 0.15 % crosslinking agent's favored of the adsorbent and the adsorption of Rhodamine B.

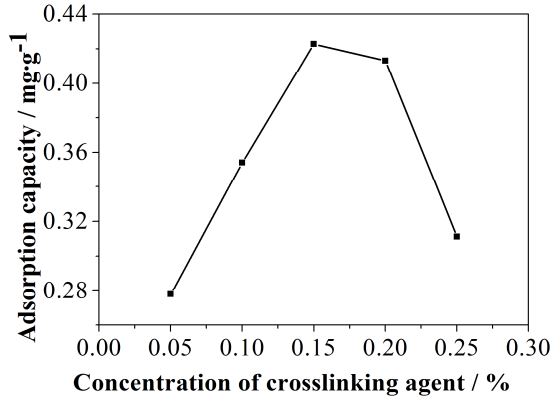

Fig.3. Effect of crosslinking agent's concentration on adsorption (Rhodamine B dye solution: 3 mg/L 20 mL, temperature: 60 ℃, pH: 9, amount of adsorbent: 0.5 g, preparation time: 1 h)

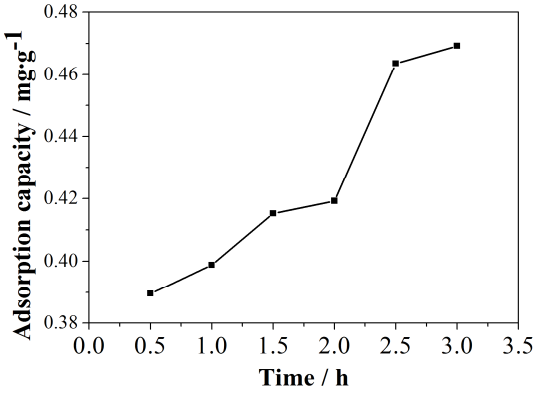

Fig.4. Effect of preparation time on adsorption (Rhodamine B dye solution: 3 mg/L 20 mL, temperature: 60 ℃, pH: 9, crosslinking agent's concentration: 0.15 %, amount of adsorbent: 0.5 g)

4) Effect of preparation time on adsorption

Fig.4 shows the relationship between the preparation time and the adsorption capacity of the adsorbent. In the range of preparation time 0.5-3 h, the adsorption capacity of the adsorbent

increases, and the maximal value is 0.4692 mg/g. As the extension of preparation time, crosslinking reaction was carried out completely.

Characterization of adsorbent

FTIR spectra of gelatin film (a), pure γ-PGA (b) and adsorbent (c) are shown in Fig.5. Compared with the FTIR spectra of gelatin film (a), pure γ-PGA (b) and adsorbent (c), the adsorption bond at 1627cm^{-1}, corresponding to -C= stretching vibration, disappears on the spectra of the adsorbent (c), and corresponds to -C=O stretching vibration (Amide absorption bands I). The absorption band at 1580cm^{-1}, assigned to NH bending and C-N stretching vibration (Amide absorption bands Ⅱ), shifted obviously. In addition, the absorption bonds at 3260cm^{-1}, attributed to N-H and O-H stretching vibration weakened. It can be concluded from the information of FTIR that γ-PGA react with gelatin through crosslinking reaction.

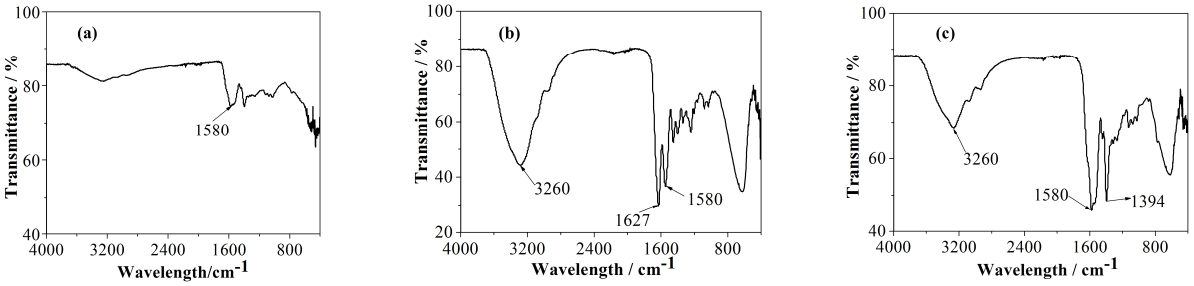

Fig.5. FTIR spectra of gelatin film (a), pure γ-PGA (b) and adsorbent (c)

Conclusion

In this work, we have successfully prepared the adsorbent based on cross-linking of poly (γ-glutamic acid) and gelatin, which could rapidly remove ionic dyes Rhodamine B from aqueous solution. The adsorption capacity was 0.4692 mg/g in given preparation conditions (temperature: 60 ℃, pH: 9, crosslinking agent's concentration: 0.15 %, preparation time: 3.5 h). The adsorbent was characterized by FTIR, revealing that there were amide bonds between gelatin and poly (γ-glutamic acid) by cross-linking reaction. Thus, these results suggest that the adsorbent could be considered a potential adsorbent for removal of dyes from wastewater.

Acknowledgement

This work was financially supported by the National Natural Science Foundation of China (Grant No.31201376), Harbin University of Commerce Doctor Start-up Fund Research (No.12DL018), the Scientific Research Fund of Heilongjiang Provincial Education Department (No. 12531152), China Postdoctoral Science Foundation (No. 2013M531009), Heilongjiang Postdoctoral Fund (LBH-Z13002) and the Fundamental Research Funds for the Central Universities (No. DL09BB15).

References

[1] K Ravikumar, B Deebika, K Balu. Decolourization of Aqueous Dye Solutions by a Novel Adsorbent: Application of Statistical Designs and Surface Plots for the Optimization and Regression Analysis [J]. J. Hazard. Mater., 2005, 122(1-2): 75-83.

[2] Inbaraj B.S., Chien J.T., Ho G.H., Yang J., Chen B.H.. Equilibrium and kinetic studies on sorption of basic dyes by a natural biopolymer poly (γ-glutamic acid). Biochem. Eng., 2006a, 31, 204-215.

[3] Inbaraj B.S., Chiu C.P., Ho G.H., Yang J., Chen B.H.. Removal of cationic dyes from aqueous solution using an anionic poly-γ-glutamic acid-based adsorbent. J. Hazard. Mater., 2006b, 137, 226-234.

[4] P V Messina, P C Schulz. Adsorption of Reactive Dyes on Titania-Silica Mesoporous [J]. J. Colloids Interf. Sci., 2006, 299(1): 305-320.
[5] S Netpradit, P Thiravetyan, S Towprayoon. Evaluation of Metal Hydroxide Sludge for Reactive Dye Adsorption in a Fixed-Bed Column System [J]. Water Res., 2004, 38(1): 71-78.
[6] S Sadri Moghaddama, M R Alavi Moghaddama, M Aramib. Coagulation/Flocculation Process for Dye Removal Using Sludge from Water Treatment Plant: Optimization through Response Surface Methodology [J]. J. Hazard. Mater., 2010, 175(1-3): 651-657.
[7] M S Lucas, J A Peres. Decolorization of the Azo Dye Reactive Black 5 by Fenton and Photo-Fenton Oxidation [J]. Dyes Pigments, 2006, 71(3): 236-244.
[8] S Ledakowicz, M Solecka, R Zylla. Biodegradation, Decolourisation and Detoxification of Textile Wastewater Enhanced by Advanced Oxidation Processes [J]. J. Biotechnol., 2001, 89(2-3): 175-184.
[9] S Chakraborty, M K Purkait, S DasGupta. Nanofiltration of Textile Plant Effluent for Color Removal and Reduction in COD[J]. Sep. Purif. Technol., 2003, 31(2): 141-151.
[10] M K Purkait, S DasGupta, S De. Micellar Enhanced Ultrafiltration of Eosin Dye Using Hexadecyl Pyridinium Chloride [J]. J. Hazard. Mater., 2006, 136(3): 972-977.
[11] Inbaraj B.S., Chiu C.P., Ho G.H., Yang J., Chen B.H.. Effects of temperature and pHon adsorption of basic brown by the bacterial biopolymer poly (γ-glutamic acid). Bioresour. Technol., 2008, 99, 1026-1035.
[12] Inbaraj B.S., Wang J.S., Lu J.F., Siao F.Y., Chen B.H.. Adsorption of toxic mercury (Ⅱ) by an extracellular biopolymer poly (γ-glutamic acid). Bioresour. Technol., 2009, 100, 200-207.
[13] Shih I.L., Van Y.T.. The production of poly (γ-glutamic acid) from microorganisms and its various application . Bioresour. Technol., 2001, 79, 207-225.
[14] Ho G.H., Ho T.I., Hsieh K.H., Su Y.C., Lin P.Y., Yang J., Yang K.H., Yang S.C.. γ-Polyglutamic acid produced by *Bacillus subtilis* (natto): structural characteristics, chemical properties and biological functionalities. Chin. Chem. Soc., 2006, 53, 1363-1384.
[15] Bajaj I., Singhal R.. Poly(glutamic acid) - an emerging biopolymer of commercial interest. Bioresour. Technol., 2011, 102, 5551-5561.
[16] Wang T.L., Kao T.H., Inbaraj, B.S., Su Y.T., Chen B.H.. Inhibition effect of poly (γ-glutamic acid) on lead-induced toxicity in mice. Agric. Food Chem., 2010, 57, 12562-12567.
[17] Wang C.H., Lin Y.T., Yeh C.L., Sharma Y.C.. Magnetic Fe_3O_4 nanoparticles for adsorptive removal of acid dye (new coccine) from aqueous solutions. Water Sci. Technol., 2010, 62, 844-851.
[18] Wang Fengqing. Researched on *Bacillus subtilis* Producing Poly γ-glutamic acid With Fermentation, Dissertation for the Degree of Master, Harbin University of Commerce, 2011.

Advanced Materials Research Vols. 989-994 (2014) pp 814-819
© (2014) Trans Tech Publications, Switzerland
doi:10.4028/www.scientific.net/AMR.989-994.814

Study on the Growth Model of Expandable Graphite

Fei YE[1,a], Chenguang ZHU[1,b], Zihao ZHANG[2]

[1]School of Chemical Engineering, Nanjing University of Science & Technology, Nanjing, Jiangsu 210094,China

[2]Science & Technology on Electro-optical Information Security Control Laboratory, Sanhe, 065201, China

[a]email:nust_leavesfly@163.com, [b]email:zhuchenguang_67@sohu.com

Keywords: Expandable graphite; Expanded graphite; Mechanism; Expansion model

Abstract. The expansion mechanism of expandable graphite (*EG*) was studied systematically in this paper. Based on the feature of the structure and the linear expansion of expandable graphite, a simple expansion model was established by the energy balance and mass balance equation. And the model was modified by setting of the boundary conditions. The result showed that a good agreement is confirmed by comparing the test data and model, especially the two inflection points of the growth rate. The study may provide theory support for improving using condition and expand application fields of the expandable graphite.

Introduction

Expanded graphite has broad range of applications because of its specific properties[1] .In recent years, the researchers have done a lot of research about the expandable graphite, and the research focused mainly on the preparation and application, for instance, low-temperature and sulfur-free expandable graphite[2]. Many hypotheses are presented on the expansion mechanism of expandable graphite, like Martin proposed the "bubble" theory about the expansion of bromine-graphite[3], and Koichi thought that bromine in *EG* was chemically bonded to the graphite layers rather than existing as gas bubbles[4]. But both of them suggested that gaseous bromine bubbles within the lamellar structure of the graphite crystal are considered to be analogous to Griffith cracks, and Olsen proposed that bisulfate compounds existed as "pockets" at grain boundaries, with much of the graphite remaining unaffected in a study[5]. Dowell suggested that the defects in natural graphite may be the origin of the "gas-filled cell"[6], and Chung assumed that the precursor of bubbles are intercalated filled penny-shaped cracks distributed within a graphite crystal[7]. These researches achieve two consensus by analysis: First, expansion of expandable graphite is due to the defects among the graphite crystal layers. The second, expansion mechanism is analogous to Griffiths cracks theory.

The principal factor for the expansion of the *EG* is the defect within the graphite crystal [8]. The source of penny-shaped cracks is defects either preexisting in the graphite or caused by the intercalating conditions.

Under the high temperature, the generated gas from the intercalae species decomposition will diffuse into the defects and form a relatively closed system. And then the defects will grow into "bubbles", and pull the graphite layers along the c axis direction with the temperature increasing. The defects will extend the entire plane of the graphene sheets or part. Subsequently the intercalate species penetrate into the graphite matrix, and diffuse out of the particle through the interconnected network which caused by the defects. It changes the height of the graphite particles in *c* direction, and then the expandable graphite turns into worm-like.

As a new carbon material, the expanded graphite has wide application in many industries. Although there are many studies, most of them are just qualitative studies which involving a large number of experiments, and the quantitative analysis is inadequate. As the expansion volume is a major parameter to measure expansion properties, it draws more attention. Because the expansion of *EG* is a linear growth along the *c*-axis, we utilise the height changes along the c axis instead of the expansion volume to simplify the complex relationship during the expansion. A simple mathematical model is therefore proposed to describe the inherent law in this article.

Expansion Model of EG

As showed by Inagaki[9], the cavity in expanded graphite looks like a body of rotation whose form closely resembles an ellipsoid. Through the research on the mechanism of expansion, the expansion process of *EG* is considered to be similar to Griffiths cracks. According to Griffith strength theory, the internal stress of cracks between graphite layers must satisfy[10-11]:

$$P_0 = \sqrt{\frac{\pi ET}{2c(1-\sigma^2)}}$$

Here E is Young's modulus, T is the surface tension, σ is the Poisson ratio, c is the size of crack.

When the internal stress of crack $P_G=P_0$, the crack between the graphite layers will grow up to form the macrodefect. Since all the formation of macrodefect is conducted under pressure P_G, the expansion process for a single particle is almost isobaric and momentary. Therefore, we can assume that the entire expansion process is approximately isobaric.

According to the request ,we proposed the model assume:

（1）The graphite particle has the form of a cylinder with radius r and height h;

（2）The gas in the cavity obeys the ideal gas law;

（3）The expansion process is nearly isobaric;

（4）The boundary conditions for the expansion are the initial height and the height of the particle after expansion.

The equations involved during the expansion process are as follows.

Energy balance equation

The radiation energy flux,which is absorbed by the cylindrical particle surface at a unit time, is spent on particle heating and evaporation of the intercalate:

$$2\pi rh\sigma T_r^4 = mC_p \frac{dT}{dt} + H_1 I_1 \tag{1}$$

Here m , C_p , T are the mass, thermal capacity, temperature of *EG*; t is time; h is the current height of particle; T_r is radiation temperature; σ is the Stefan–Boltzmann constant; and I_1 is the rate of the phase transformation in macrodefect; H_1 is phase transition heat.

Mass balance equation

The number of moles of gas between the graphite layers with the number of interlayer diffusion of the gas into the environment should be equal to the number of of gas generated by the phase transition:

$$\pi r^2 n \frac{dh}{dt} + Q = I_1 \tag{2}$$

Here n is the mole density of gas in the graphite matrix and Q is the gas flow from the grain boundary phase into the environment

$$Q = \chi \frac{\Delta P}{r} S, mol/s \tag{3}$$

Where $\Delta P=P_G-P_E$, P_E is the environmental pressure; χ is the filtration coefficient; S is the filtration area, $S=2\pi rh$.

The solution of the equations

For simplicity equation, we neglect the particle heating $mC_p \frac{dT}{dt}$.Because it is small enough by comparing with the phase transition heat of intercalate, then the equation (1) simplifies to:

$$I_1 = 2\pi rh \frac{\sigma T_r^4}{H_1}, mol/s \tag{4}$$

Consolidated the above equation (2), (3), (4) , the equation (5) is derived:

$$\frac{dh}{dt} = \beta f(r)h, \quad m/s \tag{5}$$

Here

$$\beta = 2\chi RT_G \frac{\Delta P}{P_G}, m^2/s \tag{6}$$

$$f(r) = \frac{r\alpha - 1}{r^2}, m^{-2} \tag{7}$$

$$\alpha = \frac{\sigma T_r^4}{H_1 \chi \Delta P}, m^{-1} \tag{8}$$

The solution of equation (5):

$$h = h_0 \exp[\beta f(r)t] \tag{9}$$

Then the accuracy of the model is verified by the 300μm-diameter sulfuric graphite. According to the literature, the height of *EG* is nearly 1/10 of its diameter, so the initial height of *EG* h_0=3×10^{-5}m.

Assuming that H_1=45KJ/mol, χ=1.6×10^{-10}mol/(s.Pa.m)[12], P_G=P_0=1Mpa[13], T_r=1000K, T_G=500K, R=8.31J/(mol.K), P_E=0.1MPa, σ=5.67×10^{-8}J/(s.m^2.K).Then through the equation (6),(7),8),(9), the equation (10) is obtained:

$$h = h_0 \exp(21.6t) \tag{10}$$

The Fig 1 shows a relation that the growth of expandable graphite versus with time in the c direction.

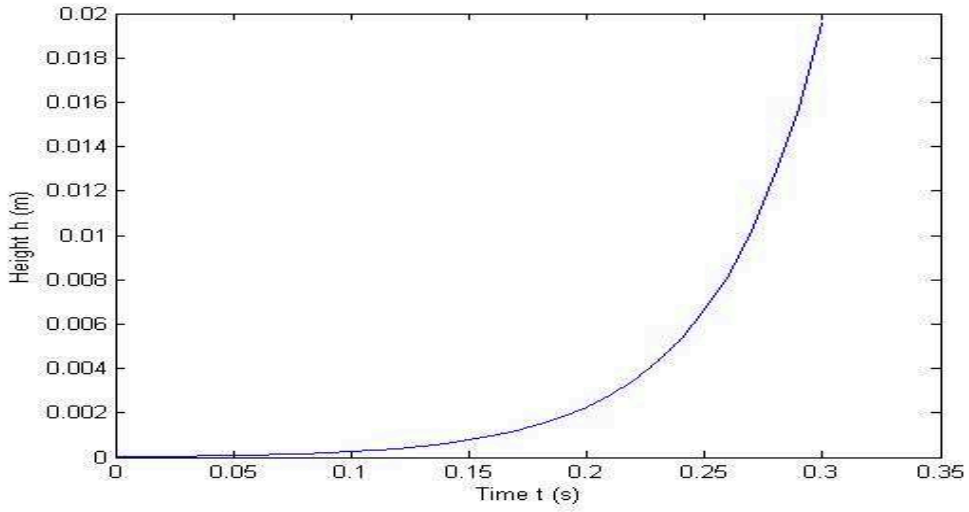

Fig 1 Relation between height change (h) of EG and time (t)

As showed in Fig 1, the height change of the particle in the c-axis direction is monotonic growth. And the change over time tends to infinity, which is clearly inconsistent with the facts. Therefore, the equation (9) needs modification. Supposing that the maximum expansion ratio of sulfuric graphite is 110 times, the height of particles is approximately 3.3mm at this time, and the rate of expansion is 0.

Setting $\beta f(r) = \nu$, then equation (5) translating into:

$$\frac{dh}{dt} = \nu h \tag{11}$$

Here v is the height growth rate per unit time of *EG*. As we assume that the expansion process is isobaric, but the pressure is actually changing with the height of particles, so v is also changing with the height of particles, then the equation (11) translating into:

$$\frac{dh}{dt} = v(h)h \tag{12}$$

And $h(0) = h_0$, when $P_G = P_0$, the $v(h)$ is a reduced function of h. Then we assume that $v(h)$ is a linear function of the h:

$$v(h) = v - \Delta h \tag{13}$$

To determine the coefficient Δ, we introduce the maximum height h_m that the EG can expand. From the equation (13), $\Delta = v/h_m$, then

$$v(h) = v(1 - \frac{h}{h_m}) \tag{14}$$

Combining Equation (11),(14):

$$\frac{dh}{dt} = vh(1 - \frac{h}{h_m}), h(0) = h_0 \tag{15}$$

Equation (16) is obtained by the method of separation of variables:

$$h(t) = \frac{h_m}{1 + (\frac{h_m}{h_0} - 1)e^{-vt}} \tag{16}$$

The Fig 2 shows a relation that the growth of expandable graphite versus with time in the c direction.

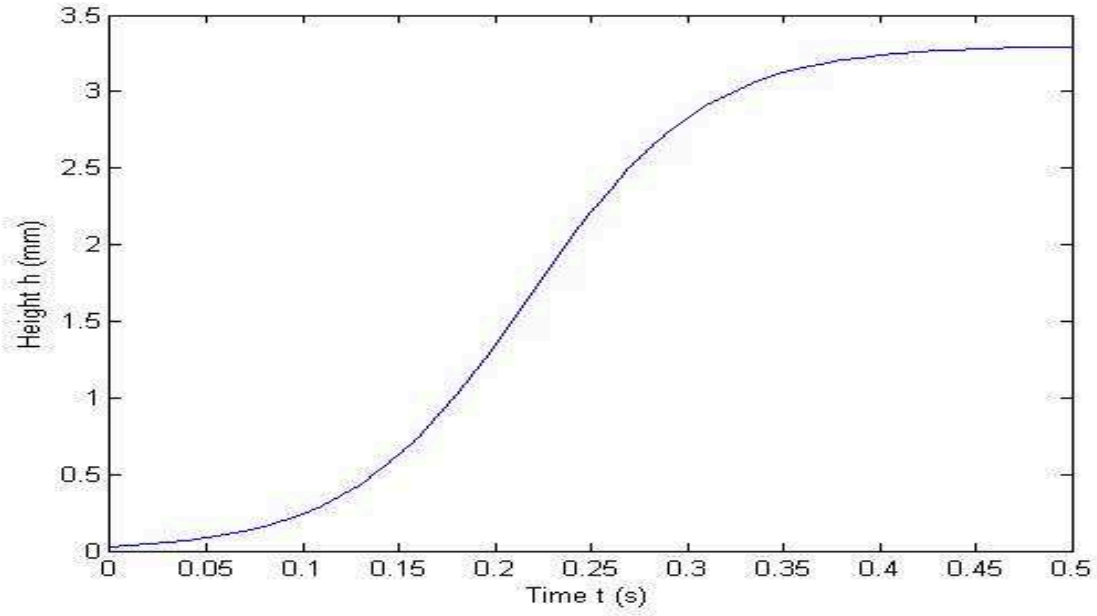

Fig 2 Relation between height change (h) of EG and time (t)

The real-time thermal expansion process of *EG* was successfully observed by using a high-speed digital camera[14], and the height change of *EG* with time is shown in Fig 3.

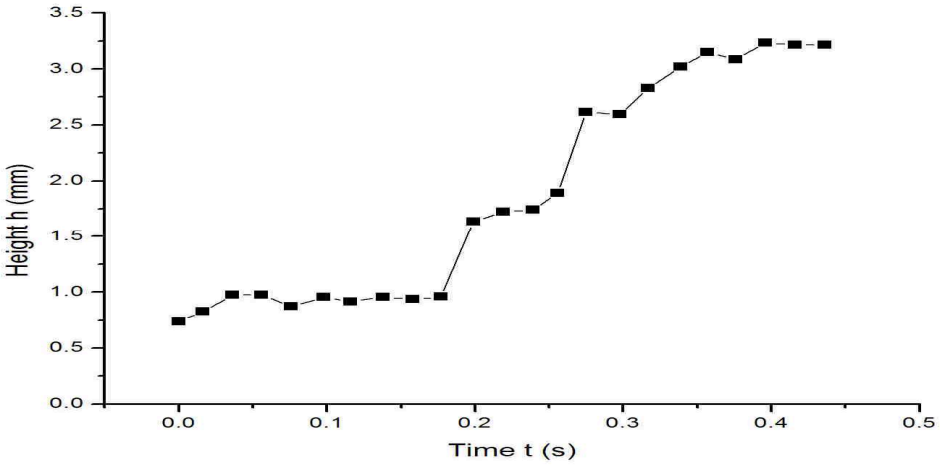

Fig 3 Relation between height change (h) of sulfuric graphite and time (t)

Judging from Fig 2 and Fig 3, it is obvious that the experimental data curve and the model curve have better consistency.

Conclusion

Based on the linear growth law along the *c*-axis direction of the expandable graphite and the energy balance, mass balance equation, we proposed a simple mathematical model in this paper, and the model is confirmed by the test result. The research shows that there are two inflection points during the growth of expandable graphite. One is where the rate increases rapidly, and the other is where the rate decreases rapidly. Results of the proposed model were compared with the experimental data as showed in Fig 2 and Fig 3, and they agreed well.

Acknowledgement

In this paper, the research was sponsored by National Natural Science Foun-dation of China (Project No.51076066) and Science and Technology on Electro-optical Information Security Control Laboratory of China(Project No. 9140C150308130C1570).

References

[1] Chen Zhigang, Zhang Yong, Yang juan, Preparations, structures and applications of exfoliated graphite[J]. Journal of Jiangsu University, 2005, 26(3) :248-252.

[2] Lin Xue-mei,Pan Gong-pei. Advances in the application of expandable graphite[J]. Jiangsu Chemical Industry, 2005, 33(6) :13-17.

[3] Martin W H, Brocklehurst J E. The thermal expansion behavior of pyrolytic graphite-bromine residue compounds [J]. Carbon, 1964(1):133-141.

[4] Koichi Aoki, Toshio Hirai, Seishi Yajima. Preparation and thermal expansion of pyrolytic graphite-bromine residual compounds [J]. Journal of Materials Science, 1971(6) :140-149.

[5] Olesen L C, Seeman S E,Scott H W. Expanded pyrolytic graphite: Structural and transport properties[J]. Carbon, 1970(8):85-93.

[6] Dowell M B. Exfoliation of intercalated graphite. Part 1. Effect of graphite cristallinity[C]. Extended Abstracts of 12th Biannual Conf. on Carbon, 1975:31-35.

[7] Anderson S H, Chung D D L. Exfoliation of intercalated graphite[J]. Carbon, 1984, 22(3):253-163.

[8] Chung D D L. Review exfoliation of graphite [J]. Journal of Materials Science, 1987(22) :4190-4198.

[9] Inagaki M, Suwa T. Pore structure analysis of exfoliated graphite using image processing of scanning electron micrographs[J]. Carbon, 2001(39):915-920.

[10] Mysyk R D, Whyman G E, Yaroshenko A P, Savoskin M V. Theoretical model and experimental study of pore growth during thermal expansion of graphite intercalation of compounds [J]. Journal of Thermal Analysis and Calorimetry, 2005(79) :515-519.

[11] Inagaki M, Suwa T. Pore structure analysis of exfoliated graphite using image processing of scanning electron micrographs[J]. Carbon, 2001(39):915-920.

[12] Emel'yanov K B, Zelenko V L, Kheifets L I. Macrokinetics and mathematical simulation of intercalated graphite particle expansion under fast heating[J]. Theoretical Foundations of Chemical Engineering, 2010, 44(4) :407-412.

[13] Chung D D L, Wong L W. Measurement of thermal stress in graphite intercalated with bromine [J]. International Journal of Thermophysics, 1988, 9(2): 279-282.

[14] Longo A, De Nicola S, Carotenuto G. Thermal expansion of graphite intercalation compounds[C]. Italy: tntconf,2008.

Advanced Materials Research Vols. 989-994 (2014) pp 820-822
© (2014) Trans Tech Publications, Switzerland
doi:10.4028/www.scientific.net/AMR.989-994.820

Coupled hydrogen and oxygen isotope analyses for the mainstream of Poyanghu Lake (Jiangxi Province) and their environmental implications

Dongrong LAI [1,a] , Andong Wang [1,b], Congguan LI [2], Yiping Chen[1], Zhaobin Yan[1], Jianjun Wan [1]

[1] State Key Laboratory Breeding Base of Nuclear Resources and Environment (Ministry of Education), College of Earth Sciences, East China Institute of Technology, Nanchang 330013, China

[2] Eastern China Institute of Measurement and Testing Technology, Nanchang 330029, China

Email addresses: [1,a] drlai@ecit.cn (Dongrong Lai); [1,b] adw008@mail.ustc.edu.cn (Andong Wang)

Keywords: Poyanghu Lake, hydrogen isotope, oxygen isotope, meteoric water

Abstract. Poyanghu Lake located in the northern Jiangxi Province is the largest freshwater lake and also the second largest lake in China. In the present contribution, several water samples have been collected and carried out for hydrogen and oxygen isotope analyses. The results suggest that they have relatively higher hydrogen and oxygen isotopic ratios than those of meteoric water. Combined with previous data, we propose that the Poyanghu Lake water display higher stable isotopic compositions due to the strong evaporation and water-rock interaction.

Introduction

Hydrogen and oxygen isotopic determinations for various waters from river, lake, sea, glacier and the like are of importance and have been widely carried out in the fields of hydrology, meteorology and environment sciences[1][2][3]. It is easy to identify the water resources via hydrogen and oxygen isotopes due to the notable isotopic composition differences between various waters[1][4]. Additionally, the stable isotopic compositions of waters could also be influenced by isotopic fractionation, evaporation and diffusion effect to some degree [2][5]. In this regard, we can trace water cycle and the mixing between two or more water bodies through hydrogen and oxygen isotope ratios. In the past decades, a large number of hydrogen and oxygen isotopic investigations have undertaken for atmospheric precipitation and various waters from China, and great achievements have been obtained.

Poyanghu Lake located in the northern Jiangxi Province close to the middle reaches of the Yangtze River, is the largest freshwater lake and also the second largest lake in China. It covers an area of 4125 square kilometers and has a total reservoir storage of 27.6 billion cubic meters, which are vital for economic and social development and environmental protection for the whole Jiangxi province[6]. In the past few years, voluminous studies involving hydrology, meteorology and ecology have been conducted. In the previous study, we have analyzed DIC (Dissolved Inorganic Carbon) contents and carbon isotopic compositions of the waters from Poyanghu Lake[7]. In the present study, we determine the hydrogen and oxygen isotope compositions of the waters from Poyanghu Lake, which provide new insights on the water resources and recycle.

Samples and analytical methods

Thirty-two water samples have been collected in the time of later April and later October of year 2011 from different locations of Poyanghu Lake, of which eighteen samples have been conducted for hydrogen and oxygen isotope analyses in this study. The sample pretreatment and isotopic determinations were done in the Key Laboratory of Nuclear Resources and Environment (ECIT), Ministry of Education. The hydrogen and oxygen isotopes were determined by using methods of TC/EA-MAT253 and CO_2 equilibrium-MAT253, respectively. Detailed analytical processes were presented by Tao et al. (2006) and Yuan et al. (2013) [3][8]. The precision ranges for δD and $\delta^{18}O$ are $\leq 2‰$ and $\leq 0.2‰$, respectively.

Results and discussion

The δD values for 18 water samples range from -26.40‰ to -37.73‰ with a weighted mean value of -32.65‰, and the $\delta^{18}O$ for samples have a range from -3.59‰ to -5.44‰ with a weighted mean value of -4.79‰. The deuterium excess parameters defined by Dansgarrd (1964) of the determined samples have a range of -1.57 to 9.86‰, which are lower than that of global meteoric water [9]. Our new δD and $\delta^{18}O$ data are in good agreement with the published data of Chen et al. (2011), which are plotted in the right side of the global meteoric water line (GMWL) [1]. It is noted here that both δD and $\delta^{18}O$ values are systematically higher than those of Yangtze River. Linear simulation result shows that the equation is $\delta D = 4.66\delta^{18}O - 10.32$.

In the past few years, voluminous investigations involving chemistry, biology, hydrology, geology and environmental sciences have been conducted for Poyanghu Lake, and many great achievements have been made[1][2][7][10]. The new analytical results indicate that the hydrogen and oxygen isotopic trend is consistent with the previous report of Ding et al. (2013) [2]. As above presented, we sampled the waters at the time of later April and later October, which are the dry seasons of Poyanghu Late. It implies that the evaporation is larger than water supply, thus the δD and $\delta^{18}O$ values are relatively higher than those from rainy seasons. The deuterium excess parameters also confirm this conclusion.

Ion chemistry analyses for waters from Poyanghu Lake suggest that they are strongly influenced by rock decay and water-rock interaction in the dry season, in combination with evaporation, which can make the waters from Poyanghu Lake have higher δD and $\delta^{18}O$ values[1][3][5][11][12].

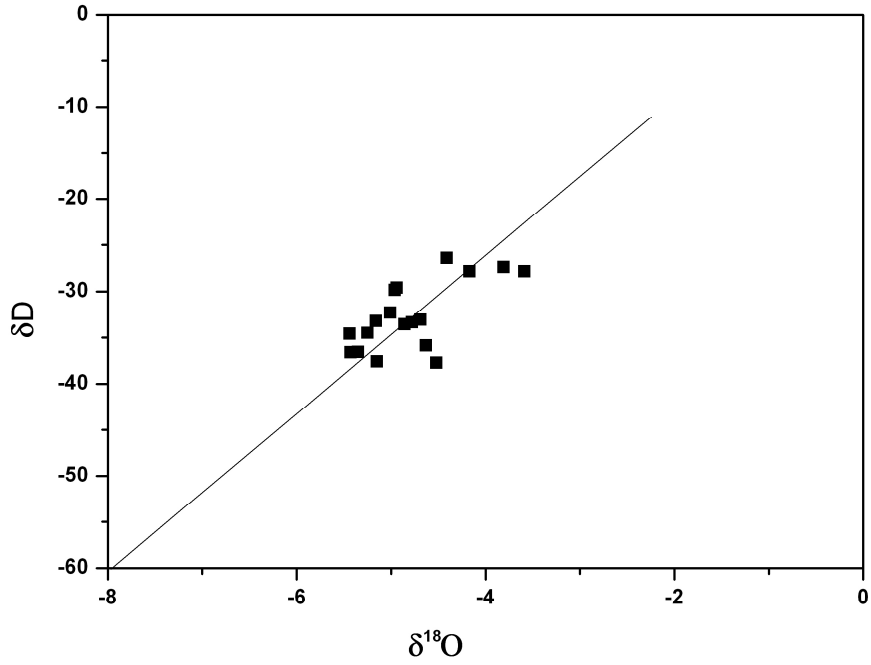

Figure 1 The diagram showing the linear features of δD vs. $\delta^{18}O$ for the analytical samples

Conclusion

Coupled hydrogen and oxygen isotope analyses for water samples from Poyanghu Lake indicate that they have relatively higher δD and $\delta^{18}O$ values than those of meteoric water, which are plotted in the right region of global meteoric water line. The deuterium excess parameters display a wide range, which are lower than that of global meteoric water. In combination with previous data, we propose that the analytical samples have relatively higher δD and $\delta^{18}O$ values due to the evaporation and water-rock interaction.

Acknowledgement

This study was financially supported by grants from Department of Education of Zhejiang Province (NO. 11722) and the Natural Science Foundation of Jiangxi Province (NO. 20122BAB203026).

References

[1] Chen X M, Gan Y Q, Liu Y D, et al. Spatial Distribution Characteristics of Hydrogen and Oxygen Isotopes in the Mainstream of Yangtze River [J]. Geological Science and Technology Information, 2011, 30(5): 110-114.

[2] Ding T P, Gao J F, Shi G Y, et al. Spacial and Temporal Variations of H and O Isotope Compositions of the Yangtze River Water and Their Environmental Implication [J]. Acta Geologica Sinica, 2013, 87(5): 661-676.

[3] Yuan H Z, Zhang L P, Geng M M, et al. Comparison of Methods for Hydrogen and Oxygen Isotopes Analysis of Water Samples by Flash HT and GasBench Ⅱ-IRMS System [J]. Journal of Chinese Mass Spectrometry Society, 2013, 34(6): 347-352.

[4] Tan Z C, Lu B H, Wang J Y, et al. Isotope Hydrology: Progress and Prospects [J]. Journal of Hehai University (Natural Sciences), 2009, 37(1): 16-22 (in Chinese).

[5] Shi H, Liu S R, Zhao X G. Application of Stable Hydrogen and Oxygen Isotope in Water Circulation [J]. Journal of Soil Water Conservation, 2003, 17(2): 163-166 (in Chinese).

[6] Hu C L, Zhou W B, Xia S Q. Characteristics of Major Ions and the Influence Factors in Poyang Lake Catchment [J]. Environmental Chemistry, 2011, 30(9): 1620-1626.

[7] Lai D R, Yan Z B, Chen Y P, et al. Dissolved inorganic carbon isotopes characteristics and their influencing factors of lakes in Nanchang [J]. Journal of East China Institute of Technology (Natural Science), 2012, 35(2): 143-148.

[8] Tao C, Zhang M Z, Yang H M, et al. The Research and Application of Gasbench- IRMS $H_2/H_2O(l)$ Equilibrium H/D Isotope Analysis [J]. Journal of Chinese Mass Spectrometry Society, 2006, 27(4): 215-220.

[9] Dansgaard W. Stable isotopes in precipitation [M]. Tellus, 1964, 16: 438-468.

[10] Wang Y P, Wang L, Xu C X, et al. Hydro-geochemistry and genesis of major ions in the Yangtze River, China [J]. Geological Bulletin of China, 2010, 29(2/3): 446-456.

[11] Lu B H, Sun T T, Xu B H, et al. Isotopic synchronous monitoring of runoff of main stem of Yangtze River [J]. Journal of Hehai University (Natural Sciences), 2009, 37(4): 378-381.

[12] Wu J L, Lin L, Zeng H A, et al. Characteristics of Oxygen Isotopic Composition of the Lakes Along the Mid-lower Reaches of the Yangtze River [J]. Marine Geology and Quaternary Geology, 2006, 26(3): 53-56.

Advanced Materials Research Vols. 989-994 (2014) pp 823-826
© (2014) Trans Tech Publications, Switzerland
doi:10.4028/www.scientific.net/AMR.989-994.823

Experimental Study the affection of the Dust Emission on Sand Stockpile by the Height of Windbreak Wall and Wind Speed

Zeqin LIU[1, a], Liying MA[1, b], Xinyu ZHAO[1, c]

[1]Key Laboratory of Tianjin Refrigeration Technology, Tianjin University of Commerce, Tianjin, 300134, China

[a]email:liuzq@tjcu.edu.cn, [b]email:549081682@qq.com, [c]email:295858566@qq.com

Keywords: Windbreak Wall; Wind Speed; Bulk Stockpile; Dust Emission

Abstract. Based on the perspective of saving investment and reducing dust emission, the method of experimental study and the working principle of windbreak wall were adopted in this paper to explore the affection of the dust emission on sand stockpile by the height of windbreak wall and natural wind speed. According to the experimental testing, the data processing and analysis by the origin software, the studied results indicated that, the dust emission of the same particle size of powder (sand) increased with increasing the wind speed, the dust emission of the same particle size and the same wind speed of powder reduced with increasing the height of the windbreak wall., When the height of windbreak wall is 5/6 times of the height of the stockpile for a certain height of the bulk stockpile, the dual purposes of the minimum dust emission of bulk stockpile and saving investment could be gained. In the practical engineering application, the height of the windbreak wall should be chosen according to the actual situation (the density of the stockpile, particle size as well as the local wind speed).

Introduction

With the rapid development of urbanization in the country, the quantities of outdoor bulk stockpiles were increasing with the rapid growth of industry and the population (such as coal pile, garbage, construction, municipal, sand stockpile of demolition construction site, engineering mound, etc). The environmental pollution (such as the recent fog and haze-ridden) caused partly by the dust from bulk stockpiles was also seriously. Therefore, it is not only the requirement of the "People's Republic of China Air Pollution Prevention Law" to suppress the bulk material pile dust, to improve air quality and to save energy, but also is the general public problem demanding prompt solution currently. At present, there are many methods of suppressing dust suppression, such as covering on the surface of bulk stockpile, spraying dust inhibitor on the bulk stockpile, setting windbreak wall or dust screen on the direction of wind. This paper mainly carried out an experimental study to explore the best control fugitive dust-stopping effected by the fitting height of the windbreak wall and the wind speed to a certain height of bulk stockpile from the investigation of influences of different heights of windbreak wall, different wind speeds and bulk material sizes to the amount of dust emission on bulk stockpile.

The working principle of windbreak wall

When the wind sped reaches a critical value, the scattering particle on the surface of the stockpile may be obtained the sufficient momentum to overcome the gravity itself and other forces of impeding particles' migration, then the particle can be broken away from the stationary state; the critical wind speed makes the particle to break away from the stationary state is called threshold wind speed. According to the study of dust diffusion law, the relationship between the dust quantity from the bulk stockpile and the wind speed can be written as following:

$$Q = a(V - V_0)^n \quad (1)$$

Where, Q is the dust emission of bulk stockpile; V is wind speed; V_0 is threshold wind speed; α is the correlation coefficient; n is the index (n> 1.5).

From the Equation (1), it can be seen that the amount of dust emission is in proportion to the high power of the difference between the wind speed and threshold wind speed, that is, the dust phenomenon occurs when the speed of wind speed is greater than the threshold wind speed. Therefore, in order to reduce the amount of dust emission, the difference between the wind speed and the threshold wind speed should be reduced. To gain the purpose of reducing the dust emission from the bulk stockpile, the windbreak wall is precisely based on aerodynamics to reduce the wind speed, to loss the maximum kinetic energy of wind speed and to decrease the elimination of the vortex of the wind speed.

Experimental Apparatus

This experiment is based on a given height (0.07m) of bulk stockpile, the analysis was carried out to obtain the most appropriate wind speed and the height of the windbreak wall by measuring the amount of dust emission from the bulk stockpile under different wind speeds, different heights of windbreak wall and different bulk material sizes. The equipment used in the testing included air flow test bench, EYETech laser particle size grain shape analyzer, electronic balance, etc.

The air volume needed in the experiment was provided by the air flow test bench, the bench was composed of the axial fan, hemispherical dome of the adjustable tube, two damping screens, two visual sealed doors, take pressure ring chamber and the test section, The size of the air volume system was: 2500 (mm) x1000 (mm) x1000 (mm) (L x W x H), wind outlet section dimensions 400 (mm) x 400 (mm), as shown in the Fig1. The ranges of the air flow provided by the air flow test bench were from 14 m^3/h to 6300 m^3/h, the air temperature between -5 ℃ and 50 ℃; and the accuracy class repeatability was I class, the meter accuracy was 0.5 class.

Fig.1. Air flow test bench

In this experiment, the amount of dust was measured by the electronic balance with the measuring range of 0-500g, 0.1g precision, its diagram was shown in the Fig2. Particle size was measured by the EYE-Tech laser particle size particle shape analyzer, which is more advanced with a dual-channel option, and the laser lens are detachable, as shown in the Fig3.

Fig.2. Electronic balance

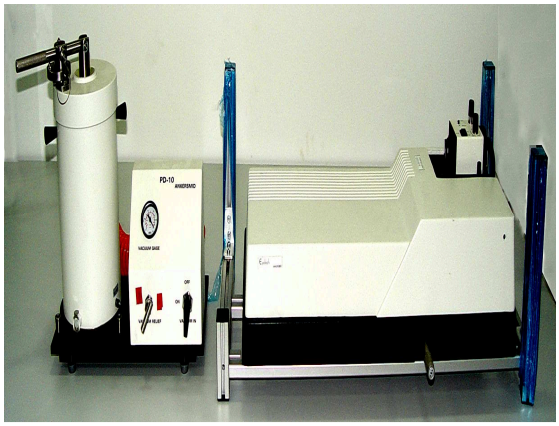

Fig.3. Particle and shape analyzer of EYETech

Experimental results, analysis and discussion

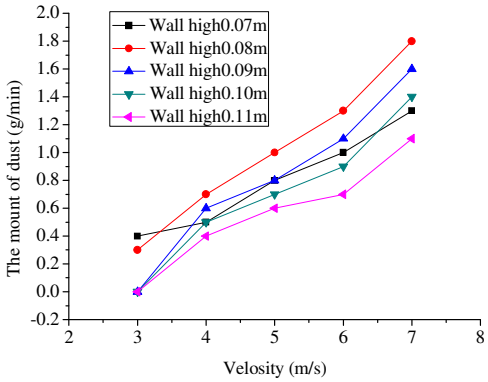

Fig.4. The amount of dust emission of sand pile with particle size 163.74μm changes with wind speed

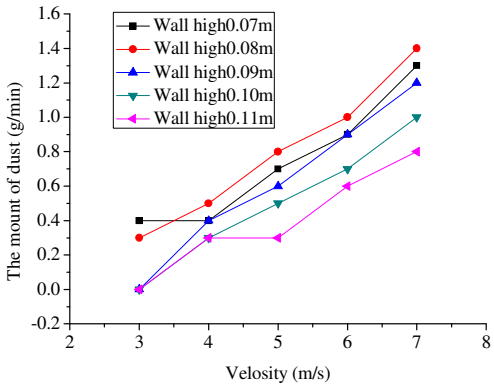

Fig.5. The amount of dust emission of sand pile with particle size 188.38μm changes with wind speed

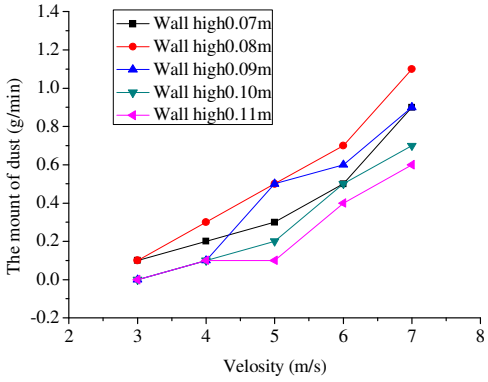

Fig.6. The amount of dust emission of sand pile with particle size 331.35μm changes with wind speed

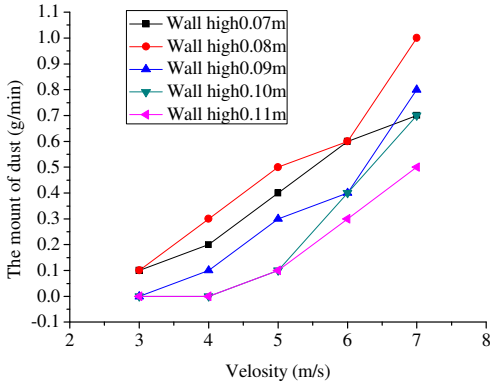

Fig.7. The amount of dust emission of sand pile with particle size 372.81μm changes with wind speed

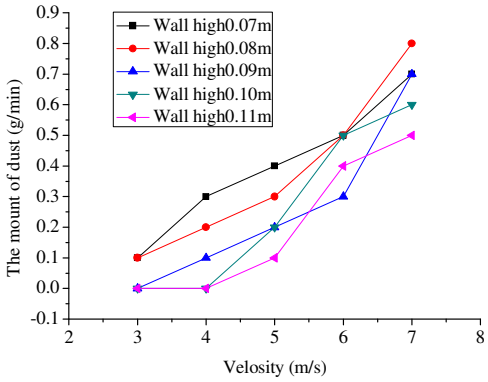

Fig.8. The amount of dust emission of sand pile with particle size 398.63μm changes with wind speed

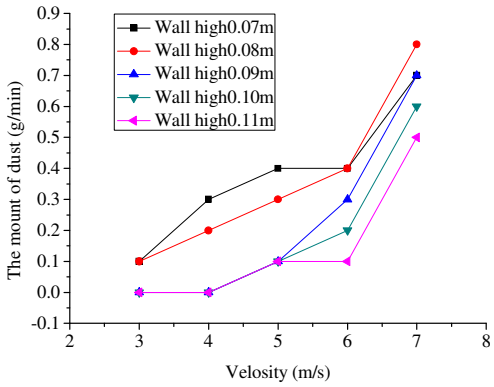

Fig.9. The amount of dust emission of sand pile with particle size 535.19μm changes with wind speed

Fig4 to Fig9 are six schematic diagrams: the amount of dust emission from the sand bulk stockpile with different sizes changed with changing the different wind speeds and different heights of windbreak wall. As can be seen from the Fig4 to the Fig9, the amount of dust emission of the same particle size (sand) increased with increasing of the wind speed; under the same particle size and wind speed, the amount of dust emission reduced with increasing of the height of windbreak wall. Simultaneously, it can also be seen from the figure, sand particle size was between 163.74μm and 331.35μm, when the wind speed was 3m/s and the height of windbreak wall was equal to or

greater than 0.9m, the dust emission phenomenon hardly occurred. For the bulk material whose size was between 372.81μm and 535.19μm, when the wind speed was from 3m / s to 4m / s, as well as the height of windbreak wall was equal to or greater than 0.9m, the dust emission phenomenon hardly occurred. This result was due to the height of bulk stockpile was 0.075m, and when the height of windbreak wall was above 0.09m, the kinetic energy of wind speed was rapidly cut down by windbreak wall, the high-speed area from flowing around was away form the top of the stockpile, wind speed at the windward reduced in the role of windbreak wall, the scattering particle on the surface of the stockpile can not be obtained enough momentum to overcome the gravity itself and other forces of impeding particles' migration, so the particles would remain stationary without phenomenon of dust emission.

Conclusion

The experiment was conducted to separately study the affections of different bulk material particle sizes, different wind speeds and heights of windbreak wall to the amount of dust emission on bulk stockpile. By analysis and clearing up to the data, the result was that the amount of dust emission of the same particle size increased with increasing the wind speed. Under the same particle size and wind speed, the amount of dust emission reduced with increasing the height of windbreak wall. It can also be draw that for sand particle whose size was between 163.74μm and 331.35μm and the wind speed was 3m/s; as well as particle size was between 372.81μm and 535.19μm and the wind speed was between 3m/s to 4m/s, when ratio of the height of windbreak wall and height of bulk stockpile was less than 6/5, the amount of dust emission will rapidly reduce with increasing the height of windbreak wall. When the ratio of the height of windbreak wall and the height of stockpile was greater than 6/5, the amount of dust emission will increase slowly with increasing the height of windbreak wall. Therefore, in practical engineering, for the bulk stockpile with a certain height, the height of windbreak wall should be set to 6/5 times of the height of bulk stockpile, and the dual purposes of the minimum dust emission of bulk stockpile and saving investment could be gained.

Acknowledgement

The study was supported by the fund Program of the Development of Science and Technology of Tianjin under the contract No. 043114411.

References

[1] Dong Jipeng. Simulation and Research of Windbreak Shelter Effect on Material piles under Intense Wind [D]. Qingdao University of Science and Technology Master Thesis, 2009.

[2] Cong Xioachun, Zhang Xu. Experimental Research on the Threshold Velocity of Raw Ore Particles [J]. China Mining Magazine 2003,12(9):32-34.

[3] Li Hongjian. A Numerical Study on Shelter Effect on Coal Pile of Porous Fences [D]. Zhejiang University Master Thesis, 2007.

[4] Li Lixin, Zhang Yongbing. Prevention and Control of Dust with Wind-Shade Wall [J]. Environmental Protection 2005.5:37-71.

[5] Cong Xiaochun, Chen Zhilong, Zhan Shuifen. Experimental Study of Static Dust Emission from a Coal Pile in the Open Air Yard [J]. Journal of China University of Mining & Technology, 2010,39(6):849-853.

[6] Zhao Xinyu. Research on the relationship between dust suppression effect of windbreak wall and bulk material properties [D]. Tianjin University of Commerce Master Thesis, 2012.

Advanced Materials Research Vols. 989-994 (2014) pp 827-830
© (2014) Trans Tech Publications, Switzerland
doi:10.4028/www.scientific.net/AMR.989-994.827

Adsorption removal of Phosphorus from wastewater by Steel slag filter material

Juanting WANG[1, a], Yanzhen YU[1, b], Longlong GAO[1,c]

[1] School of Civil Engineering and Architecture, University of Jinan, Jinan 250022, China

[a]email: wjt0305@163.com, [b]email: cea_yuyz@ujn.edu.cn, [c]email: cea_yuyzujn@163.com

*Corresponding Author: Yanzhen Yu

Keywords: Steel slag filter material; adsorption; phosphorus; kinetic model

Abstract. Spherical steel slag filter material with high porosity, large specific surface area was made by using steel slag as the main raw material, adding binder and pore forming agent. The influences of PH, phosphorus concentration and adsorption time on the adsorption effect of steel slag filter material were investigated. The adsorption characteristics of steel slag filter on phosphorus were studied based on adsorption isotherm model and adsorption kinetics model. Adsorption results were used to fit Langmuir and Freundlish formula. The correlation of Freundlish model was significant and the correlation coefficient was 0.92907.

Introduction

Eutrophication is a water pollution problem known as the "ecological cancer" [1]. The occurrence of eutrophication caused the deterioration of water quality, increasing the difficulty and cost of water treatment, reducing the dissolved oxygen in the water, threatening the survival of aquatic organisms and reducing the water body function, restricting the people's survival and development. Therefore, eutrophication has been paid attention worldwide. The occurrence of eutrophication is caused by excessive emissions of nitrogen, phosphorus and other nutrients, and the amount of which beyond the self-purification capacity of water body. Currently, the main methods to eliminate the phosphorus are biological method and chemical method. The cost of biological phosphorus removal is low, but phosphorus removal efficiency is not good. As a result, the biological method is often adopted along with chemical method, improving the effect of phosphorus removal. Chemical phosphorus removal methods mainly include chemical precipitation, ion exchange method, crystallization, adsorption method. Adsorption of phosphorus removal method has been paid much more attention for its advantages, such as simple operation and good effect[2-3]. Developing new cheap adsorbent has become a hot point of the multitudinous scholars.

Steel slag is produced in the process of steelmaking. The stacking and landfill of steel slag takes up a lot of land and polluting the surrounding environment. Therefore, realizing the recycling utilization of steel slag becomes a correct way for the sustainable development of iron and steel industry. [4-5]The researchers found that steel slag has good adsorption properties for printing and dyeing wastewater and heavy metal wastewater, especially for phosphorus-containing wastewater. Steel slag has been used as the main raw material, adding a certain pore forming agent, to prepare steel slag filter material by sintering, which was the filler of aeration biological filter to realizing synchronous implementation of denitrification and phosphorus removal. The adsorption of phosphorus removal effect and adsorption characteristics of steel slag filter material were investigated to provide the theoretical support for simultaneous nitrogen and phosphorus of aeration biological filter with steel slag filtration material.

The test materials and methods

Test materials

Steel slag in the experiment was taken from some steel mills in Shandong. Steel slag was smashed into the powder and passed through the 60 mesh screen after drying. adding a certain

amount of pore forming agent and bonding agent, the mixture was formed into 3-5 mm balls. These raw balls were roasted in the muffle furnace, receiving steel slag filter material.Different concentration of phosphorus solution in the experiment was formed by the analysis of pure KH2PO4 which was dried for two hours under 105℃.Testing equipment: PH meter, electric drum wind drying oven, constant temperature oscillator, 721 spectrophotometer.

Test method

The solution of phosphorus of "total phosphorus" was measured by ammonium molybdate tetrahydrate spectrophotometry.

Adsorption isotherm model

Langmuir model and Freundlich model was used to analysis the phosphorus adsorption properties of steel slag filter material.

The results and discussion

The influence of various PH on the phosphorus adsorption of steel slag filter material

Take 5.0 g filter material respectively in 250 ml plug taper bottle, which contain 100 ml solution of 15.0 mg/L (P). The PH value was adjusted with sodium hydroxide solution and hydrochloric acid respectively to 2.25, 2.57, 2.92, 6.09, 11.06, 12.02. And then, plug taper bottles were rested on the thermostatic oscillator for oscillating adsorption 24 h. The concentration of residual phosphorus in the solution was measured after filtering at last.

Figure 1 shows that under the condition of various PH, the adsorption capacity of steel slag filter material for phosphorus:

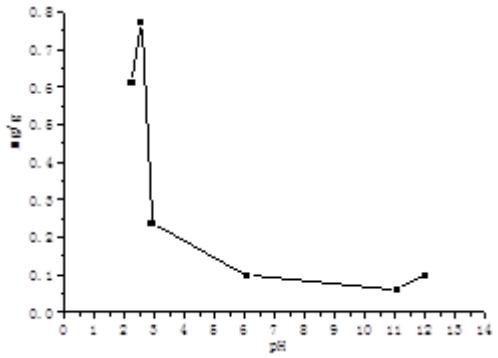

Figure.1 Adsorption quantity at different pH values

The figure 1 shows that the influence of pH on the adsorption capacity is wide. Under the condition of various pH, the steel slag filter material shows different adsorption characteristics. At the pH of 2.5, the maximum adsorption capacity reached 0.77 mg/g, but during common sewage pH range, the adsorption capacity turned out to decrease from 0.1 mg/g to 0.055 mg/g. Along with the increase of pH, the adsorption capacity of steel slag filter material for phosphorus has a tendency to reduce, but steel slag filter material is still a good adsorbent for phosphorus.

The influence of various concentration of phosphorus solution on the phosphorus adsorption of steel slag filter material

Take 5.0 g filter material respectively in 250 ml plug taper bottle, which contain 100 ml solution of various concentration of phosphorus (5 mg/L, 10 mg/L, 25 mg/L, 20 mg/L, 25 mg/L, 30 mg/L, with P). And then, plug taper bottles were rested on the thermostatic oscillator for oscillating adsorption 24 h. The concentration of residual phosphorus in the solution was measured after filtering at last.

Figure 2 shows that the adsorption capacity of steel slag filter material for phosphorus increased with the increasing of phosphorus concentration in the solution and the maximum adsorption capacity reached 1.125 mg/g. Initial phosphate concentration in the solution has great influence on the adsorption, when the initial concentration in the solution increased from 4.71 mg/L to 29.4 mg/L, the saturated adsorption capacity increased from 0.315 mg/g to 1.12 mg/g. When the phosphorus concentration in the solution is less than 15 mg/L, adsorption quantity increases slowly, when more than 15 mg/L, filter material for phosphorus adsorption capacity increased significantly. The initial

mass concentration of phosphorus in the solution is the main factor affecting the adsorption. The higher the phosphorus concentration in the solution, the greater the amount of phosphorus is available to steel slag filter material. Large concentrations difference of phosphorus between the surface of filter material and the solution is advantageous to the phosphorus migration to the surface of the filter material.

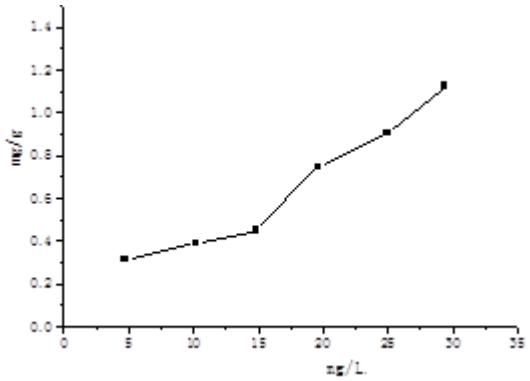

Figure.2 Adsorption quantity under different concentrations of phosphorus

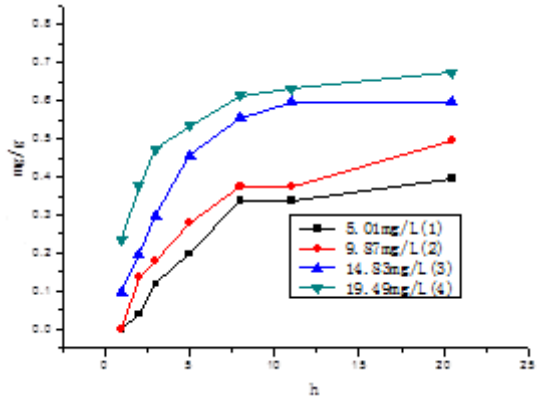

Figure.3 Adsorption quantity under different times

The influence of adsorption time on phosphorus removal effect in various concentration phosphorus solutions

Take 5.0 g filter material respectively in 250 ml plug taper bottle, which contain 100 ml solution of various concentration of phosphorus (5 mg/L, 10 mg/L, 25 mg/L, 20 mg/L, 25 mg/L, 30 mg/L, with P). oscillation adsorption was carried under 25 ℃ in thermostat oscillator respectively for 1 h, 2 h, 3 h, 5 h, 8 h, 11 h, 20.5 h. The concentration of residual phosphorus in the solution was measured after filtering at last.

Under the condition of different initial concentration of phosphorus (5.01 mg/L, 9.87 mg/L, 14.83 mg/L, 19.49 mg/L), the characteristics of the filter material on the adsorption of phosphorus in the solution was shown in figure 4.2. The initial concentration of phosphorus in the solution ranges from 5.01 mg/L to 9.87 mg/L, 14.83 mg/L, 19.49 mg/L, the filter material for the adsorption of phosphorus in the solution are 0.396 mg/g, 0.495 mg/g, 0.595 mg/g and 0.672 mg/g, respectively. Adsorption is mainly finished in the first 10 h, and adsorption rate gradually reduce with time, tending to be stable after 10 h.

The adsorption isotherm

At particular temperature, solid adsorption phenomena in the solution can be analyzed by use of the Langmuir equation and the Freundlich equation 1. The performance of the steel slag phosphorus adsorption in solution is also can be described by the above equation, and the corresponding expression 2, respectively

The Freundlich equation:

$$\ln q_e = \ln k_F + \left(1/n\right)\ln C_e \quad (1)$$

Langmuir equation:

$$C_e = q_m C_e / q_e + K_L \quad (2)$$

Ce: the equilibrium concentration of phosphorus, mg/L, qe: the equilibrium adsorption of adsorbent, mg/g; n and kF are parameters in the Freundlich equation, qm and KL are parameters in the Langmuir equation; qm: the saturated adsorption of per volumetric absorbent, mg/g. According to the experimental results of phosphorus steel slag, draw the adsorption isotherm. Adsorption experiment data was fitted to Langmuir equation and the Freundlich equation respectively.

According to the type (1), the adsorption capacity of the filter material under different concentrations and the Langmuir and Freundlish related parameters were calculated and showed in the table 1.

Table. 1 Filter material adsorption capacity for phosphorus

	1	2	3	4	5	6
C_0(mg/L)	4.713	10.169	14.831	19.592	24.948	29.413
C_e(mg/L)	3.126	8.185	12.351	15.823	20.386	23.759
M(g)	5.033	5.061	5.079	5.053	5.057	5.260
q_e(mg/g)	0.315	0.392	0.488	0.746	0.902	1.125
C_e/q_e	9.913	20.881	25.294	21.211	22.593	21.119
Log(C_e)	0.495	0.913	1.091	1.199	1.309	1.376
Log(q_e)	-0.501	-0.407	-0.311	-0.127	-0.045	0.051

The experimental data in table 1, was respectively fitted to Langmuir and Freundlish model and phosphorus adsorption equation of Langmuir and Freundlish, respectively:

Langmuir type: $\ln q_e = 0.62285 \ln C_e - 2.0403$, correlation coefficient R2 = 0.61931.

Freundlish type: $\ln q_e = 0.62285 \ln C_e - 2.0403$, correlation coefficient R2 = 0.92907.

The result showed that the steel slag filter material adsorption conforms to the model of Freundlish, showing that filter material for the adsorption of phosphorus is closer to the multilayer adsorption mode. The physical adsorption effect is superior to the chemical adsorption in the process.

Conclusion

(1) Under the condition of different initial concentration of phosphorus, adsorption is mainly finished in the first 10 h, and adsorption rate gradually reduce with time, tending to be stable after 10 h.

(2) The initial mass concentration of phosphorus in the solution is the main factor affecting the adsorption. The adsorption capacity of steel slag filter material for phosphorus increased with the increasing of phosphorus concentration in the solution

(3) The steel slag filter material adsorption fits the Freundlish model more precisely, showing that filter material for the adsorption of phosphorus is closer to the multilayer adsorption model. The physical adsorption effect is superior to the chemical adsorption in the process.

Acknowledgement

This work was funded by the National Scientific Foundation China (NSFC51178207), Shandong Provincial National Science Foundation (ZR2011EEM003), the Natural Science Foundation of Shandong Province (ZR2012EEL21).

References

[1] Wang Rongbin, Li Jun, Zhang Ning. Development of Biological Phosphorus Removal in WastewaterTreatment Process[J]. Environmental Engineering, 2007, 25 (1):84-88.

[2] Drizo A, Forget C, Chapuis R P, et al. Phosphorus Removal by Electric Arc Furnace Steel Slag and Serpentinite[J]. Water Research, 2006, 40(8): 1547-1554.

[3] Chen Yizhong, Wang Liping, Du Erdeng et al. Adsorption Removal of Phosphorus from Wastewater by Dewatered Alum Sludge from Wasterworks[J]. CHINA WATER & WASTEWATER, 2012, 7(23):88-91.

[4] Wang Shuai, Xie Li, Zhou Qi. Adsorption Properties and Kinetics of Chromium from Aqueous Solution by Steel Slag[J]. CHINA WATER & WASTEWATER, 2007, 35(11): 1510-1514.

[5] Hanwen Liang,Junxin Liu,Yuansong Wei, et al. Evaluation of phosphorusremoval from wastewater by soils in rural areas in China[J].Journal of Environmental Sciences,2011,22(1):15-22.

Advanced Materials Research Vols. 989-994 (2014) pp 831-836
© (2014) Trans Tech Publications, Switzerland
doi:10.4028/www.scientific.net/AMR.989-994.831

Simulation of vapor absorption of aqueous LiBr solution on alternate heat and mass transfer surfaces of corrugated plates and mesh pecking

Ruibing Cao [a], Yaping Chen [b] and Jiafeng Wu [c]

Key Laboratory of Energy Thermal Conversion and Control of Ministry of Education
School of Energy and Environment, Southeast University, Nanjing 210096, China

[a]crbde@163.com, [b]ypgchen@sina.com, [c]wujiafeng@seu.edu.cn

Keywords: aqueous LiBr absorption; falling film; alternate heat and mass transfer; corrugated plates; mesh pecking; solar chillers

Abstract. The traditional tube-shell absorber is relatively too bulky to be used in a small absorption chiller for solar air conditioning. As the outer-surface of solution film on the traditional absorber surface is easier to be saturated, several alternate heat and mass transfer absorber schemes have been proposed. However, the film-inversion absorber uses only half surfaces while the dual-side film-inversion absorber scheme is of good performance but too complicated to fulfill. The scheme using stainless steel mesh packing as the film guider is much easier and more uniform in distributing film, and it can also act as the framework for exposing dual-side film to the vapor for adiabatic mass transfer. The alternate heat and mass transfer configurations with plate surfaces and mesh packing are of promising performance for small chiller absorbers.

Introduction

Using solar energy resources for air conditioning refrigeration is from the demand side to broaden electric power capacity bottleneck in summer, it conforms to the green energy and sustainable environment development requests. For solar energy air conditioning refrigeration, the LiBr absorption chiller is the first choice. Because of the construction features, the traditional tube-shell heat exchangers have relatively large size, uneven distribution on discrete tube banks, and the driving force of absorption is liable to getting weak due to the saturation of the free surface layer of the film, thus the heat and mass transfer efficiency is low. Absorption process has direct impact on the performance of evaporation as well as the entire LiBr absorption chiller, and absorber is also the biggest heat exchanger of a LiBr absorption chiller. Therefore extensive attentions have been drawn by domestic and foreign experts on heat and mass transfer enhancement of the absorption process. For small chillers used in solar driven air-conditioning, the compact type heat exchangers, such as plate heat exchangers, plate-fin heat exchangers and plate-shell heat exchangers provide good alternatives. Grogori et al. [1] and Kyeong et al.[2] studied absorption heat and mass transfer on wavy falling film and micro-scale surface treatment. Andreas, et al. [3] and Reay [4] analyzed the characteristics of compact heat exchanger for absorption heat transformers, heat pumps and refrigeration systems respectively. Wang, et al. [5] studied the heat and mass transfer separate absorber scheme, the rich solution is first cooled in a heat exchanger and then enters an adiabatic absorber to absorb steam vapor. Because the transmitting heat in absorption process is mainly the latent condensation heat of coolant vapor, while the equivalent heat should be carried off by pre-cooling the rich solution with the sensible heat, it needs to increase the solution circulation flow rate to avoid crystallizing. In this way the rich solution is diluted to moderate solution, and its mass transfer driving force is therefore weakened. Nevertheless, if alternative cooling and adiabatic absorption is divided into several steps, it may avoid crystallizing.

Chen, et al. [6,7] developed a novel lithium bromide absorption chiller based on plate-shell heat exchanger with dual-scale cross-corrugated plate bundle. Each plate has large vertical corrugations and small horizontal ones. The diamond-shaped outer channels are formed by large corrugations of adjacent plates, so that the vapor with large specific volume at very high vacuum could enter in. The falling film distribution is promoted and the heat and mass transfer is augmented with small horizontal corrugations. Meanwhile on the other side of plates, the cooling water convection heat transfer coefficient is also enhanced by zigzag path channels, and sufficient flow area for adequate

resistance requirement is also met. The experiment results [7] showed that the overall heat and mass transfer coefficients of the dual-scale cross-corrugated plate bundles could reach almost twice higher than those of the plane one, shown in Fig. 2. A modification has been made recently to use the trapezoidal corrugations instead of the triangle corrugations, to enhance structural strength by increasing the contacting area between the neighboring corrugations.

Previous research results indicate that along the lithium bromide solution falling film flow, as the vapor absorption process continues, the temperature increases and the concentration of solution decreases at the liquid film layer near the liquid and vapor interface. It indicates that the absorption driving force is getting weak, even though the temperature is low and the solution is rich at inner layer of the film. Islam, et al. [8] designed two film inversion schemes for plates and tubes. By inverting the liquid film and exposing the cooler and richer LiBr solution film layer to the vapor periodically, the heat and mass transfer coefficients could be enhanced.

The aforementioned film-inversion schemes have the common drawback that only half of the heat transfer area is used to form liquid film distribution and inversion configurations, thus its gain in efficiency may not compensate to the loss in the overall area. To this point, Chen, et al. [9,10] present a dual-side film-inversion absorber scheme, which consists of upper and lower plate bundles and film-inverting guiders, leading film from both sides of each plate couple of the upper plate bundle to opposite sides of the lower one, as shown in Fig. 1. When the film is inverted, the rich solution near the wall with lower temperature turns into the interface, thus it makes the vapor absorption enhanced. However, the structure of dual-side inverse film scheme is quite complex.

In view of the difficulty in manufacture and installation of dual-side inversion guiders, Chen, et al. [11] presented a modified scheme with corrugated mesh packing inserts to substitute film guiders between the upper and lower plate bundles. The corrugated mesh packing will lead the fluid from the upper plate bundle to the lower one with uniformed distribution, and both inside and outside of fluid film with different temperature and concentration will mix and redistribute at the entrance edges of the lower plate bundle. On the other hand, because mesh packing itself, with knitting latitude and longitude metal threads, forms innumerable capillaries and coarse surface to increase perturbation, and forms two-side exposition surfaces in each grid center for the fluid film, with sufficient vapor channels in the corrugated mesh packing layers. Thus the mesh packing is also a perfect adiabatic mass transfer surface. The scheme with mesh packing inserts between the plate bundles is a compound enhancement approach which carries alternately on cooling absorption and adiabatic absorption.

Mathematical models

Along with the rapid expanding of CFD commercial software, numerical simulation speeds up for more vivid comprehension of the mechanism. Since the falling film absorption process is complicated by combining the heat and mass transfer, its mechanism has not been fully understood. This paper presents the numerical simulation of the heat and mass transfer absorption process with both film-inversion and film-mixing between two dual-scale cross-corrugated plates. Some assumptions and simplified conditions are listed as follows:

1) The gas in the absorber is pure steam vapor which is homogeneous and isobaric;

2) All the solution can be uniformly sprinkled over the upper frame of the plate surface, and the falling film covers over the heat transfer surface without any splash loss; consider only the vapor absorption of the falling film that covers the heat-transfer surface;

3) The absorption process is in the steady state, and the flow of liquid film is laminar;

4) Within the film, the liquid convection and the diffusion along the flow direction can be neglected.

The continuity equation, momentum equation, energy equation and mass equation are listed as follows:

$$\begin{cases} \dfrac{\partial(\rho u)}{\partial x}+\dfrac{\partial(\rho v)}{\partial y}=0; & \dfrac{\partial(\rho u^2)}{\partial x}+\dfrac{\partial(\rho uv)}{\partial y}=\dfrac{\partial}{\partial y}\left(\mu\dfrac{\partial u}{\partial y}\right)+\rho g \\ C_p\dfrac{\partial(\rho ut)}{\partial x}+C_p\dfrac{\partial(\rho vt)}{\partial y}=\dfrac{\partial}{\partial y}\left(\lambda\dfrac{\partial t}{\partial y}\right); & \dfrac{\partial(u\xi)}{\partial x}+\dfrac{\partial(v\xi)}{\partial y}=\dfrac{\partial}{\partial y}\left(D_m\dfrac{\partial \xi}{\partial y}\right) \end{cases} \tag{1}$$

The boundary equations are:

$$\begin{cases} x=0: \quad u_0=\Gamma/(\rho\delta_1);\ v=0;\ t=t_1;\ \xi=\xi_1 \\ y=0(\text{before}) \text{ or } y=\delta(\text{after inversion}): u=0;\ v=0;\ \partial\xi/\partial y=0;\ t=t_w \\ y=\delta(\text{before}) \text{ or } y=0(\text{after inversion}): \dfrac{\partial u}{\partial y}=0;\ \lambda\dfrac{\partial T}{\partial y}=-\Delta h\dfrac{\rho D_m}{\xi}\dfrac{\partial \xi}{\partial y};\ \ \mathrm{f}(p,t,\xi)=0 \end{cases} \tag{2}$$

The thickness of the film is calculated by following equation:

$$\delta=1.35\left(\frac{3\Gamma\mu}{\rho^2 g}\right)^{1/3} \tag{3}$$

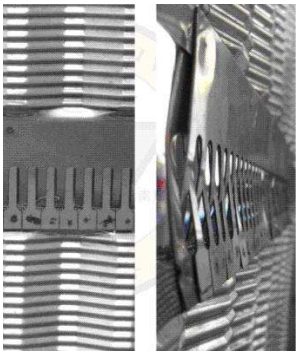

Figure 1 Dual-side film-inversion plates

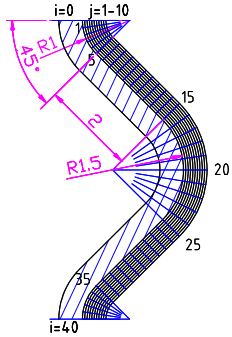

Figure 2 Grids of film on one corrugation

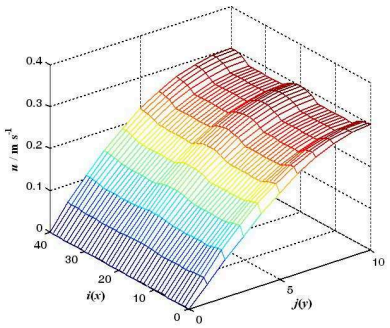

Figure 3 Distributions of velocity of solution film on first corrugation

Simulation results

Falling film-inversion on dual-scale corrugated plates. The mathematical model of the inversed falling film absorption process was established by using Matlab 6.5 software. The velocity field, temperature field, and concentration field are respectively built up in the Matlab programming environment. Calculation subprograms of numerical simulations on the density, film thickness, isobaric specific heat capacity and viscosity are conducted. The basic data used in the calculation are shown in Table 1. Fig. 2 shows the grids of film on one corrugation of the corrugated plate.

Table 1 Basic parameters

item	value	item	value
inlet temperature of rich solution t_1 [ºC]	52	absorption pressure p [kPa]	1.2
inlet concentration of rich solution ξ_1 [kg kg^{-1}]	60%	total number of corrugations per plate	10
solution spray rate Γ [kg m^{-1} s^{-1}]	0.04	wall temperature t_w [ºC]	38

As the value of component velocity normal to the plate surface v is very small, the solution velocity is mainly determined by the component velocity along solution flow u. Fig. 3 shows that the profile of velocity u is a parabolic curve; and its value at the interface is related to the film thickness δ, which is determined by the spray density of solution Γ plus the absorbed vapor.

Fig. 4(a) shows that after inversion the film layers at the interface and at the wall surface exchange their positions. When the former interface contacts with wall surface, its velocity reduces to zero; while the velocity of the film layer at the former wall surface increases quickly from zero to a high

value and then levels off. Fig. 4(b) shows that the temperature profile of the solution film convexes slightly; and after inversion when the former interface contacts with wall surface, its temperature reduces to the wall temperature; while the temperature of the film layer at the former wall surface increases to the saturation temperature very quickly. Because of the poor conductivity of the liquid film, the latent vapor heat absorbed by the interface undergoes a big thermal resistance when it is transferred to the wall surface through the film. Consequently, the temperature at the interface remains high. Fig. 4(c) shows that after film-inversion, the former near the wall film layer now exposes to the vapor, and forms a fresh interface with rich concentration and lower temperature; after absorbing a lot of vapor, its concentration decreases first sharply, then gradually. The concentration of the film at the interface reduces quickly and reaches the saturated condition after absorbing vapor along flow direction; while the concentration of the film near the wall surface has little change due to low diffusivity.

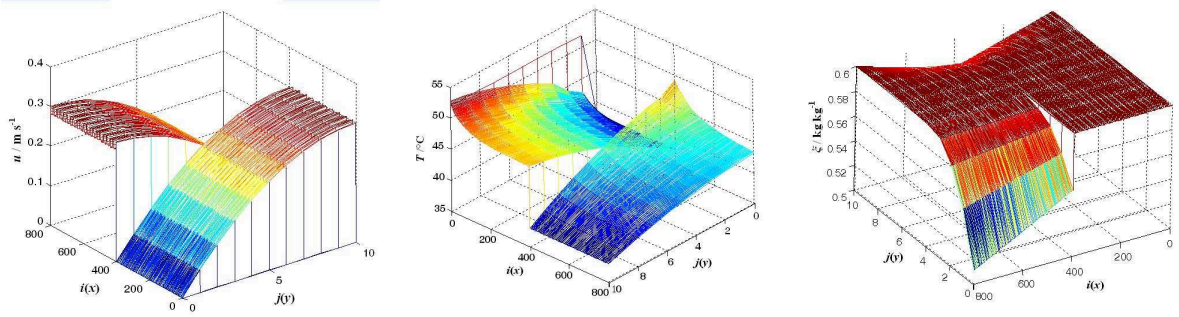

(a) velocity (b) temperature (c) concentration

Figure 4 Distribution of velocity, temperature and concentration of inverse film

Film-mixing with mesh packing. To simplify the computation, the pure uniform mixing model is adopted, namely the parameters of the film at the inlet edge of the lower plate are equal to the average value of film at the outlet edge of the upper plate, while the mass transfer in the mesh packing is neglected. Fig. 5(a) and Fig. 5(b) show the distributions of temperature and concentration of the films before and after film uniform mixing. Fig. 5(c) shows the ratio of the concentration of once film-inverse scheme over those of the once uniform mixing scheme at the lower plate. It shows that the average concentration of once film-inverse scheme is about 2% lower than those of the once mixing scheme. Considering the adiabatic mass transfer on the mesh packing, the heat and mass transfer coefficients of the scheme with mesh packing inserts between dual-scale cross-corrugated plate bundles are certainly higher than those of the film inversion scheme. From the Fig. 5(b) it can be seen that at the end of the process the mean value of concentration is still much higher than that at the free interface, which is near the saturation value, thus there is still plenty room for promotion with exposing the inside body of the film with multi- mixing.

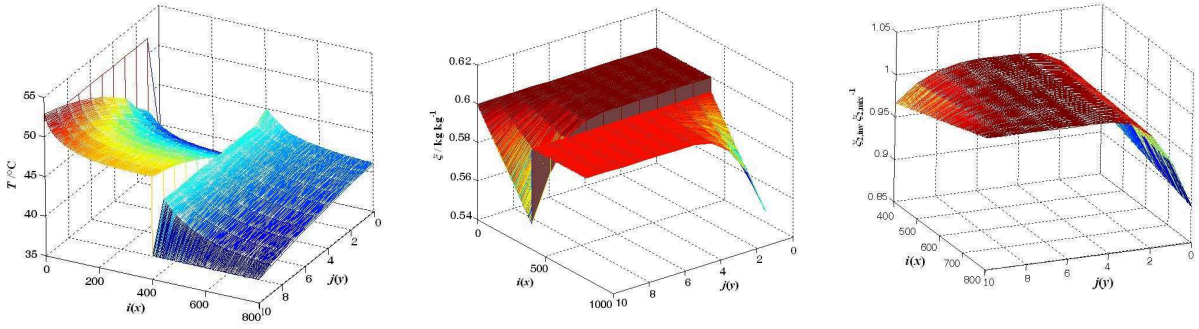

(a) temperature (b) concentration (c) concentration ratio

Figure 5 Distribution of temperature and concentration of film homogeneous

Summary

As the guiders in film-inversion scheme is too complicated to manufacture and install, a mesh packing scheme is suggested to substitute the dual-side inversion guiders between the plate bundles. The corrugated mesh packing block not only leads the fluid to the lower plate bundle with uniformed distribution, but also provides perfect adiabatic mass transfer surface, with big enough vapor channels though in. And also it is very easy to be installed between the plate bundles.

Mathematic models were established and solved numerically of the falling film heat and mass transfer absorption on dual-scale cross-corrugated plates with either film-inversion or mixing of aqueous Li-Br solution. The distributions of velocity, temperature and concentration in the film before and after the film-inversion or mixing provide better understanding of the mechanism of heat and mass transfer in these absorption processes. The simulation results predict that the average concentration of once film-inverse scheme is slightly lower than that of the once mixing uniform scheme. However, considering the adiabatic mass transfer on the mesh packing, the heat and mass transfer coefficients of the mesh packing insert scheme are certainly higher than those of the other schemes including traditional tube bundle or plane-plate heat exchanger schemes.

Acknowledgment

This work is supported by the National Nature Science Foundation Programs of China (No. 51276035 and No.51206022) and Provincial science and technology innovation and transformation of achievements of special fund project of Jiangsu Province (BY2011155).

Nomenclature

C_p	specific heat content, J kg^{-1} K^{-1}	Greek letters	
D	mass diffuse coefficient, m^2 s^{-1}	β	mass transfer coefficient, m s^{-1}
h_m	heat transfer coefficient, W m^{-2} K^{-1}	Γ	spray density of solution, kg m^{-1} s^{-1}
i	grid node number in x direction	δ	thickness of film, m or mm
j	grid node number in y direction	λ	conductivity, W m^{-1} K^{-1}
K	overall heat transfer coefficient, W m^{-2} K^{-1}	μ	dynamic viscosity, kg m^{-1} s^{-1}
m	vapor mass flux of vapor, kg m^{-2} s^{-1}	ξ	concentration, kg kg^{-1}
p	pressure, Pa	ρ	density, kg m^{-3}
t	temperature, K or °C	subscripts	
u	component velocity in x direction, m s^{-1}	0	initial
v	component velocity in y direction, m s^{-1}	1	inlet
x	flow direction along the plate	2	outlet
y	normal to the plate surface direction	w	wall

References

[1] M. S. Grogori, K. M. Omar and J. L. Chiristophor: Absorption of gas into a wavy falling film. *Chemical Engineering Science*, Vol. 60 (3), (2005), p. 827-838.

[2] K. J. Kyeong, P. C. Woo and K. Y. Tae. The effect of micro-scale surface treatment on heat and mass transfer performance for a falling film H2O/LiBr absorber. *Int. J. Refrigeration*, Vol. 26, (2003), p. 575-585.

[3] G Andreas and S. Karl. Analysis of the process characteristics of an absorption heat transformer with compact heat exchangers and YFE-E181. *Int. J. thermal science*, 39, (2000), p. 30-38.

[4] D. A. Reay. Compact heat exchangers, enhancement and heat pump. *Int. J. Refrigeration*, Vol. 25, (2002), p. 460-470.

[5] L. Wang, G.M. Chen and Q. Wang, et al. Thermodynamic performance analysis of gas-fired air-cooled adiabatic absorption refrigeration systems, *Applied Thermal Engineering*, Vol. 27 (8-9), (2007), p. 1642-1652.

[6] Y. P. Chen, Y. B. Li and M. H. Shi. Numerical Simulation of Characteristics of Falling Film Absorption on Vertical Corrugation Plates for Aqueous Li-Br Solution. In: Wang B. X., ed. *Proc. of the 6th Int. Symposium on Heat Transfer*, (China Sciences Multi-Media Electronic Publishing House, Beijing, China, 2004), p.630-634.

[7] Y. P. Chen, Y. B. Li and K. Y. Wang, et al. Experimental study on falling film absorption with aqueous Li-Br solution on two-scale corrugation plate surfaces. In: Hua B., Guo Z. Y. eds. *Proc. of 3rd ISHTEEC*, (South China University of Technology Press. Guangzhou, China, 2004), p. 335-339.

[8] MR Islam, N. Wijeysundera and J. C. Ho. Performance study of falling-film absorber with film-inverting configuration. *Int. J. Refrigeration*, Vol. 26, (2003), p. 909-917.

[9] Y. P. Chen, C. J. Shi and M. H. Shi. Heat and mass transfer enhancement during absorption process with double-side film-inverting configuration. *J. Chemical Industry and Engineering*, Vol. 59(1), (2008), p. 19-24. (in Chinese)

[10] Y. P. Chen, C. J. Shi and M. H. Shi, et al. Numerical simulation of heat and mass transfer enhancement in absorption process with double-side film-inversion. *Proceedings of the Sixth International ASME Conference on Nanochannels, Microchannels and Minichannels.* ICNMM2008, (Darmstadt, Germany, 2008).

[11] Y. P. Chen, F. Liu, R. B. Cao, et al. Study on alternate heat and mass transfer Absorption Process of Aqueous LiBr Solution for Solar Chillers. *Proceedings of the Second International Conference on Building Energy and Environment*, T08-17, (Boulder, Colorado, USA. 2012).

Advanced Materials Research Vols. 989-994 (2014) pp 837-840
© (2014) Trans Tech Publications, Switzerland
doi:10.4028/www.scientific.net/AMR.989-994.837

A Novel Multilayer Structure With Frequency Selected Surface for Electromagnetic Compatibility

Jie Li [1, a], Donglai Xu [2,b]

[1] School of Electrical and Electronic Engineering, Wuhan Polytechnic University, Wuhan, China

[2] School of Science and Engineering, Teesside University, Middlesbrough, TS1 3BA, UK

[a] lijie_whpu@foxmail.com, [b] D.Xu@tees.ac.uk

Keywords: Electromagnetic Compatibility; Multilayer Structure; Frequency Selected Surface.

Abstract. Electromagnetic wave absorbers can be widely used in Electromagnetic Compatibility (EMC). We proposed a novel multilayer structure of metal alloy-ferrite-plastic composites. A new structure with Frequency Selected Surface (FSS), which has filter characteristic, embedded in the composites was fabricated to improve the absorption performance. In bandwidth of 8.04GHz, the reflectivity was smaller than -8dB and the thickness was only 2.6mm. The reflectivity was measured using a standard NRL Arch technique in a frequency range of 3-18 GHz. The experimental results indicate that it is possible to make a desirable thin, broadband EMW absorber by the incorporation of an FSS into the magnetic absorbing materials.

Introduction

Electromagnetic wave (EMW) absorbers play a key role in solving electromagnetic compatibility and interference problems in radar and wireless communication systems. To this end, the EMW absorbers not only need to exhibit a low reflectivity over a wide frequency range, but also need to be thin and lightweight. Among various EMW absorbing materials, magnetic absorbing materials made by dispersing magnetic fillers in an insulating matrix continue to play a leading role in the investigation and application of thin broadband absorbers. One advantage of magnetic absorbing materials is that they have both magnetic and dielectric losses. Spherical ferrite and carbonyl iron particles are among the most conventional magnetic fillers for absorption applications [1-3]. Other promising magnetic fillers include flaky iron particles [4] and magnetic metal fibers [5-6]. It is established that a multilayer structure design could significantly improve the performance of the absorbers [7]. However, low thickness and ease of implementation considerations require the absorbers to have a small number of layers.

Frequency-selective surfaces (FSS), which are planar periodic arrays of conducting patches or aperture elements, have been widely used for many years in antenna applications, such as beam multiplexers, microwave and optical filters [8]. In recent years, however, it has been reported that the FSS could also be used as a part of the EMW absorbers to significantly modify and improve the absorption performance of the absorbers [9-12]. In Ref. [9], an FSS was deposited on a metal-backed dielectric absorbing layer. The absorption band of the dielectric layer was found to be either shifted or broadened due to the presence of the FSS. In Ref. [10] and [11], the FSS screens were embedded in carbon fiber absorbing materials. It was found that both the FSS pattern and its location in the composite were critical for the absorption properties of the materials. In addition, an optimized design of an EMW absorber utilizing FSS screens embedded in multilayer dielectric absorbing materials was also implemented [12].

This work is concerned with the incorporation of FSS into magnetic absorbing materials, which is previously unreported. Some metal-backed double-layered magnetic absorbers were prepared, with an FSS sheet either on the top or embedded between the layers. The effects of the presence and location of the FSS sheet on the absorption performance were examined experimentally. The data

demonstrate that the incorporation of FSS into magnetic absorbing materials provides an effective solution to thin broadband EMW absorbers.

Experiment details

Hexagonal ferrite and Fe-Co alloy particles were prepared by a conventional ceramic process and a mechanical alloy method, respectively. Both types of particles are in the range of a few micrometers and exhibit a narrow size distribution and a low degree of agglomeration. The ferrite-plastic and alloy-plastic sheets were prepared by dispersing the ferrite and alloy particles separately in plastic, refining, and vulcanizing. In these sheets, the plastic is self-made neoprene, and the volume fraction of the particles is about 50%. The thicknesses of the ferrite-plastic and alloy-plastic sheets are 1.7 mm and 0.8 mm, respectively. The FSS sheet was fabricated by printing a two-dimensional array of metallic patterns on a dielectric substrate. The thickness of the FSS sheet is about 0.1 mm. The metallic patterns and dimensions of frequency-selective surface FSS1 are given in Fig. 1.

The absorber samples for measurements were prepared by superposing the ferrite-plastic sheet, the alloy-plastic sheet, and/or the FSS sheet, in a special sequence on a metal substrate. The size of these absorber samples was 18cm×18cm. Five measurement samples were prepared. The sheet sequences in these samples are given in Table 1. For convenience, ferrite, alloy, and metal are used to label the ferrite-plastic sheet, the alloy-plastic sheet, and the metal substrate, respectively, in Table 1 and the following discussions.

Table 1 Structures of absorber samples for reflectivity measurements

Layer	Sample 1	Sample 2	Sample 3	Sample 4	Sample 5
L1	ferrite	alloy	FSS1	ferrite	ferrite
L2	alloy	ferrite	ferrite	FSS1	alloy
L3	metal	metal	alloy	alloy	FSS1
L4			metal	metal	metal

The reflectivity of the absorbers is generally used to specify their absorption performance. In this work, the reflectivity of the absorber samples was measured by using a standard NRL arch method. The NRL arch method is a near-field, nondestructive, and contactless method, originally developed by Naval Research Laboratory. This method uses a transmitting antenna and a receiving antenna that are mounted on a circular arch that is in a plane perpendicular to the absorber surface. The reflectivity of the sample is measured and compared with that from a plane metallic plate. In our experiments, the antennas were wideband horns and were connected to an S-parameter test set of an HP8722ES network analyzer system. The measurements were carried out with normal incident over a frequency range from 3 to 18 GHz. In order to eliminate microwave energy that travels around the sample, some pyramidal absorbers were placed behind the sample.

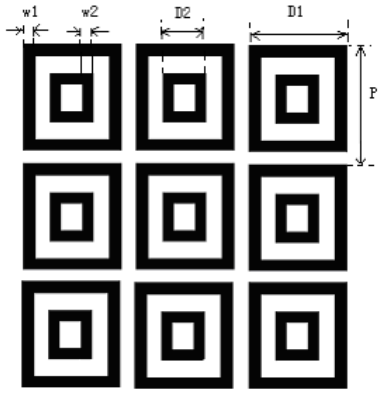

Fig. 1 Schematic diagram of frequency-selective surface FSS1.
P=16.5mm, D1=15mm, D2=6mm, w1=w2=1.5mm

Results and Discussion

Fig. 2 shows the measured reflectivity as a function of frequency for the absorber samples without using the FSS sheet. In sample 1, the first and second layers are the ferrite and alloy sheets, respectively. In sample 2, the first layer is the alloy sheet and the second layer is the ferrite sheet. Note that the two samples have the same thickness.

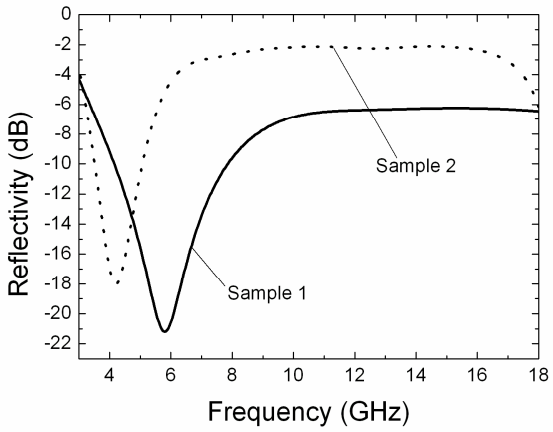

Fig. 2 Reflectivity versus frequency for the absorbers without FSS

The data in Fig. 2 indicate that the absorption performance of sample 1 is evidently better than that of sample 2. For example, the bandwidth at –8 dB for sample 1 and sample 2 are 5.02 GHz and 1.92 GHz, respectively. The reason for this difference in absorption response lies on different impedance match conditions. According to the electromagnetic parameter measurements, the permeability of the ferrite-plastic composite is of the same order of magnitude as that of the alloy-plastic composite, while the permittivity of the ferrite-plastic composite is lower than that of the alloy-plastic composite. As a result, the impedance match condition between sample 1 and the free space is better than that between sample 2 and the free space. A desirable match condition can be achieved by optimal selection of the materials in each layer and the thickness of each layer.

Fig. 3 shows the measured reflectivity versus frequency for sample 3, sample 4, and sample 5. The alloy sheets in all of these three samples are between the ferrite sheets and the metal substrate, as in sample 1. The FSS1 sheet in sample 3 is on the top of the ferrite sheet. In sample 4, the FSS1 sheet is embedded between the ferrite and alloy sheets. In sample 5, the FSS1 is embedded between the alloy sheet and the metal substrate.

Table 2 Thickness and absorption bandwidth of sample 1 and sample 4

	Sample 1	Sample 4
Thickness	2.5 mm	2.6 mm
Bandwidth at –8 dB	5.02 GHz	8.12 GHz
Bandwidth at –10 dB	3.72 GHz	5.94GHz
Bandwidth at –12 dB	2.8 GHz	4.42 GHz
Minimum reflectivity (frequency)	-21.2dB(5.8GHz)	-14.69dB(6.84GHz)

Three important results are evident in Fig. 3. (1) When the FSS1 is embedded between the ferrite and alloy sheets, the absorption band is evidently broadened as well as shifted to a higher frequency range in comparison to the sample without the FSS1. Table 2 lists some bandwidths, the minimum reflectivity, and the thicknesses of sample 1 and sample 4. Note that the thicknesses in Table 2 are the total thicknesses of all of the sheets. (2) When the FSS1 is positioned adjacent to the metal substrate, the absorption response closely resembles that of the absorber without the FSS1. (3) In the case of the FSS1 positioned on top of the absorber, the absorption band is shifted to a higher frequency range with a significant reduction in the absorption.

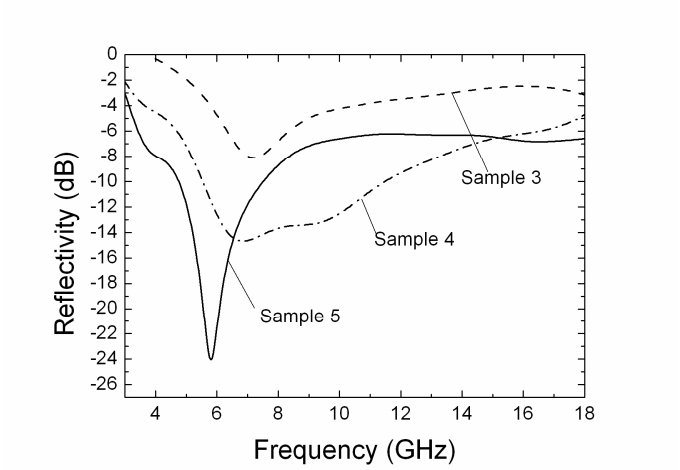

Fig. 3 Reflectivity versus frequency for the absorber samples with FSS1

Conclusions

The effects of the presence, position, and metallic patterns of an FSS sheet in a double-layered magnetic absorber on the absorption performance have been studied experimentally. The absorption of a magnetic absorber with an FSS embedded strongly depends on the position of the FSS within the absorber and the metallic patterns of the FSS sheets. When the FSS is embedded between the two magnetic layers, the absorption band can be significantly broadened. The absorption bandwidth and peak can be changed through the selection of the FSS pattern. The results indicate that, with optimal design, it is possible to make a desirable thin broadband EMW absorber by the incorporation of FSS into magnetic absorbing materials.

References

[1] VIAU G, RAVEL F, ACHER O,FIEVET F: Journal of Magnetism and Magnetic Materials Vol. 140–144 (1995), p. 377–378.

[2] OLMEDO L, CHATEAU G, DELEUZE C and FORVEILLE J L: Journal of Applied Physics Vol. 73 (1993), p. 6992–6994.

[3] SHIN J Y, OH J H: IEEE Transactions on Magnetics Vol. 29 (1993), p. 3437-3439.

[4] MATSUMOTO M and MIYATA Y: IEEE Transactions on Magnetics Vol. 33 (1997), p. 4459–4464.

[5] M.Z. Wu, H. H. He, Z. S. Zhao and X. Yao: J Phys D: Appl Phys Vol. 33 (2000), p. 2398-2401.

[6] M.Z. Wu, H. H. He, Z. S. Zhao and X. Yao: J Phys D: Appl Phys Vol. 33 (2000), p. 2927-2930.

[7] J.J. Pesque, D.P. Bouche, R. Mittr:IEEE Trans MTT Vol. 40 (1992), p. 1789-1796.

[8] T.K. Wu and S.W. Lee: IEEE Trans Antennas Propagat Vol. 42 (1994), p. 1484-1490.

[9] F. Terracher and G. Berginc: Proc IEEE AP-S Int Symp,U.S. (2000), p. 846-849.

[10] Yanan Sha, K.A. Jose, C.P. Neo: Microwave and optical technology letters Vol. 32 (2002), p. 245-249.

[11] K.A. Jose, Yanan Sha, V.K. Varadan and C.P. Neo: IEEE Antennas and Propagation Society International Symposium Vol. 16-21 (2002), p. 576 – 579.

[12] S. Chakravarty, R. Mittra, N.R. Williams: IEEE Trans MTT Vol. 49 (2001), p. 1050-1059.

Advanced Materials Research Vols. 989-994 (2014) pp 841-844
© (2014) Trans Tech Publications, Switzerland
doi:10.4028/www.scientific.net/AMR.989-994.841

Study on processing technology of brewer's grains on acid dye brilliant cresyl blue wastewater

Yihua Jiang[1, a,*], Xinlong Jiang[2,b] and Chenggang Cai[2,c]

[1]Zhejiang Shuren University, Hangzhou, China

[2]Institute of Food and Fermentation Engineering,Zhejiang Shuren University, Hangzhou, China

[a]email:hzjyih828@163.com, [b]email:jxinl2003@163.com, [c]email:ccg0516@sina.com

Keywords: brilliant cresyl blue; brewer's grains; Adsorption Conditions; Orthogonal experiment.

Abstract. Orthogonal experiment optimization of adsorption conditions with the factors of pH value, adsorption time, adsorbent amount of brilliant cresyl blue wastewater by brewer's grains were studied. The results showed that optimum adsorption conditions were as follows: 100 mL brilliant cresyl blue dye solution of 150 mg·L^{-1},adding 5.0 g·L^{-1}brewer's grains of 60~80 mesh and adsorbed for 2.0 h,extraction temperature 30℃,pH 5.0. Under the optimal conditions, the maximal absorption rate got 95.12%.The brewer's grains is a promising, cheap, efficient, new biological materials of adsorption for brilliant cresyl blue in wastewater.

Introduction

With the development of acrylic manufacturing technology and increasing amount of dyeing wastewater emissions, the waster water had been the main pollution sources in China. The traditional dye wastewater treatment method had not been widely applied for the high cost or low efficiency. Biological adsorption method had been concerned for the advantages of simple operation, low cost and non-secondary pollution, etc [1-3].Brewer's grains is the main by-product of beer industry. It is produced in large quantities yet lacks effective utilization, which results in significant environmental pollution.As a typical representative of cationic dye used in acrylic material, adsorption conditions of the brilliant cresyl blue was studied by brewer's grains, so as to utilize the brewer's grains as the low cost material for cationic dye wastewater purification and the brewer's grains reutilization, then the results would be the theoretical basis for the comprehensive utilization of the material.

Material and Methods

Preparation of absorbent

The brewer's grains was from the bee laboratory in our school, washed with tap water, and dried at 50 °C to constant weight. Then the brewer's grains biosorbent were crushed using a universal grinder and sieved (60–80 mesh), and the resulting particles were stored in a desiccator until use.

Preparation of dye solution

The brilliant cresyl blue used in the experiment was a kind a cationic dye, with the molecular weight of 332.87 and molecular formula of $C_{17}H_{20}N_4O{\cdot}HCl$, the maximal adsorption wavelength λ_{max} was of 630 nm. The dye were dried at 80 °C to a constant weight and prepared for 500 mg·L^{-1} and diluted to suitable concentrations for utilization.

Adsorption rate Determination

A series of 100 mL brilliant cresyl blue dye solution were placed in 250 mL conical flask and adjusted the pH to scheduled value with 0.1 mol·L^{-1} L HCl or NaOH, then added the brewer's grains, the bottles were settled in constant warm water shaker and shaken for a scheduled time, then the grains and solution were separated by a filter, the solution were centrifuged at 5000 r·min^{-1} to separated the particles, then the supernatant adsorption were measured at 630 nm with 7220 spectrometer. The concentration were calculated by a standard curve equation. The adsorption rate (P/%) were calculated by the following equation:

$$P = (C_0 - C_e) / C_0 . \quad (1)$$

In which, the C_0 was the initial dye concentration ($mg \cdot L^{-1}$); the C_e was the dye concentration ($mg \cdot L^{-1}$) at equivalent state.

Orthogonal experiment optimization of adsorption conditions

The orthogonal test design has been widely applied in many research fields of medical, industrial production etc with less test times, high efficiency, simple calculation and other advantages[4-5].Adsorption experiment optimization including adsorption time,adsorption temperature, adsorbent quantity, initial concentration, pH value choice, for which several factors are parallel single factor experiment, study their influence on adsorption.

100 mL of the brilliant cresyl blue solution were shaken at 150 $r \cdot min^{-1}$ in 250 mL conical flask, single factors experiments of different particles (20-40, 40-60, 60-80, 80-100 and over 100 meshes), pH value (1, 2, 3, 4, 5, 6, 7), adsorption time (0.25, 0.5, 0.75, 1.0, 1.5, 2.0,2.5 h) ,adsorbent quantity (1, 2, 3, 4, 5,6 $g \cdot L^{-1}$),temperature (30, 35, 40, 45, 50 °C), initial concentration(25, 50,100, 150, 200, 250,300 mg/L) were carried out. The results showed that with the decrease of the adsorbent particles, the adsorption rate increased till the particles of 60-80 meshes, the adsorption rate reached nearly the maximal value. And the 60-80 meshes of brewer's grains were selected in further experiments. With the increasing of adsorbent temperature from 30 to 50 °C, the adsorption rate of brilliant cresyl blue changed little and the optimal dye temperature was of 30 °C, then 30 °C adsorbent temperature were selected in the following experiments. The single factor test results were shown in Fig 1.According to Fig 1,we designed the $L_9(3^4)$ program of orthogonal test in Table 1.Results were disposed by the intuitive analysis and variance analysis, significant test of brilliant cresyl blue adsorption factor by Duncan [6].

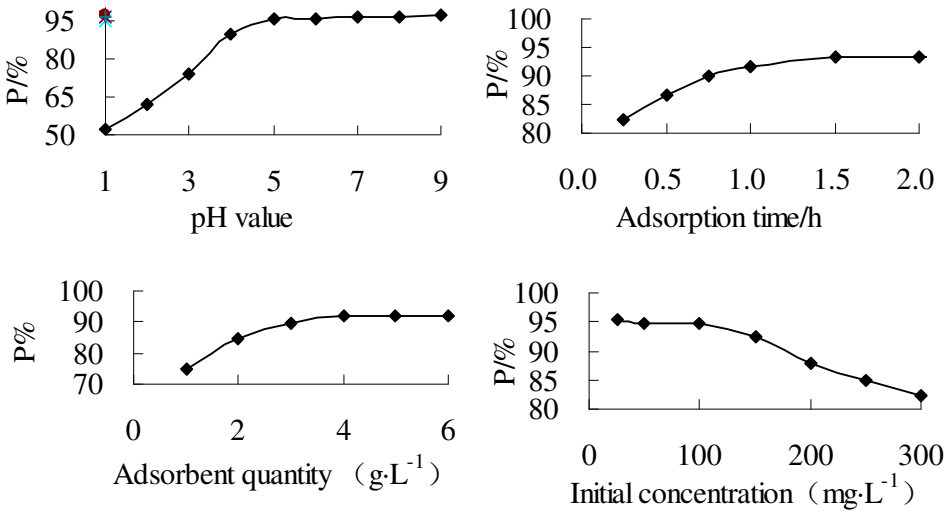

Fig.1 Effects of different factors on brilliant cresyl blue adsorption rate

Table 1 Levels and factors of orthogonal experiment design

Level	A pH value	B adsorption time /min	C adsorbent quantity/$g \cdot L^{-1}$	D initial concentration/$mg \cdot L^{-1}$
1	4	60	3	50
2	5	90	4	100
3	6	120	5	150

Result and analysis

The test results of orthogonal experiment

Based on the results of single factors experiments, the adsorption experiments were carried out by orthogonal experiment design according to Table 2.

The intuitive analysis

From Table 2 can be seen, the effect of the adsorbent quantity on the rate of adsorption was the maximum.The range of data R was visible, the effect order of various factors on the adsorption: adsorbent quantity > pH value >adsorption time > initial concentration, the optimum adsorption conditions were: $A_2B_3C_3D_2$, namely pH value was 5, adsorption time was 120 min, adsorbent quantity was 5 $g \cdot L^{1}$, initial concentration was 100 $mg \cdot L^{-1}$. The result of orthogonal experiment is consistent with the single factor experiment.

Table 2 Orthogonal experimental program and results of adsorption (n = 3)

No.	A	B	C	D	P/%
1	1	1	1	1	82.35
2	1	2	2	2	87.39
3	1	3	3	3	93.88
4	2	1	2	3	91.04
5	2	2	3	1	93.92
6	2	3	1	2	92.75
7	3	1	3	2	94.97
8	3	2	1	3	87.34
9	3	3	2	1	95.01
K_1	87.87	89.45	87.48	90.43	
K_2	92.57	89.55	91.15	91.70	
K_3	92.44	93.88	94.26	90.75	
R	4.70	4.43	6.78	1.28	

The analysis of variance

We can see from Table 3, the adsorbent quantity was significant influencing factor.The other factor is not significant factor.It could consider to determine, as determined by the Duncan method after checking back.

Table 3 Analysis of variance

source of variation	SS	df	MS	F	significance
A	42.9300	2	21.4650	16.2670	
B	38.3536	2	19.1768	14.5329	
C	69.0398	2	34.5199	26.1605	*
D	2.6391	2	1.3195	1.0000	
SS_T	152.9625	8			

Note: $F_{0.05}(2, 2)=19.00$; "*"represents a significant influencing factors.

The Duncan analysis[6]

First were found between the level of various factors $r_{0.05}$,$r_{0.05}$ ($r_{0.05}$=6.09,$r_{0.01}$=14), then calculate the value of R_k (standard error is 0.562, the R_k= standard error *r). According to the calculation results,it was compared for each factor level significantly.From Table 4 can be seen, in addition to initial concentration,other factors had significant differences.The adsorbent quantity was significantly each other,the adsorption time of 90 min and the pH value 4.0 were significantly to the other, respective. Considering the use of energy and resources, comprehensive analysis to determine the optimal adsorption conditions of brilliant cresyl blue was $A_2B_3C_3D_3$.

Tables 4 Compare significant difference in four levels of factors

1（A）				2（B）				3（C）				4（D）			
Level	P	$P_{0.05}$	$P_{0.01}$	Level	P	$P_{0.05}$	$P_{0.01}$	Level	P	$P_{0.05}$	$P_{0.01}$	Level	P	$P_{0.05}$	$P_{0.01}$
2	92.57	a	A	3	93.88	a	A	3	94.26	a	A	2	91.70	a	A
3	92.44	a	A	2	89.55	b	A	2	91.15	b	AB	3	90.75	a	A
1	87.87	b	A	1	89.45	b	A	1	87.48	c	B	1	90.43	a	A

The optimal process validation

Under the optimal adsorption conditions, repeated for 3 times,the adsorption rate were: 95.13%,95.18%,95.05%, the average of adsorption rate was 95.12%, RSD=1.75% (n=3). It was the same basically to result of orthogonal experiment.

Conclusion

The results of orthogonal experiment showed that the adsorbent quantity was significant influencing factor on brilliant cresyl blue adsorption rate. The optimal processing conditions were as follows: pH value 5.0, adsorption time 2.0 h, adsorbent quantity 5.0 $g \cdot L^{-1}$, initial concentration of 150 $mg \cdot L^{-1}$,adsorbent temperature 30 °C,shaker rotation of 150 $r \cdot min^{-1}$,the particles of 60-80 meshes. Under the optimal conditions, the average of adsorption rate was 95.12%. The brewer's grains is a promising, cheap, efficient, new biological materials of adsorption for brilliant cresyl blue in wastewater.

Acknowledgments

This work was supported by Zhejiang province department of education research project(No.Y201329873),the key discipline of Zhejiang province in Colleges and Universities, China (No.YH2013S08) .

References

[1] L.S. Feng, C.H. Li, H.Y. Liu, H. Wang, Journal of Anhui Agricultural Sciences, vol. 24, 2010, pp. 13325–13328, 13357.(In Chinese)

[2] Y.Z. Sun, R.M. Gong, X.P. Zhang, H.J. Liu, C. Yang, China Environmental Science, Sl , 2005, pp. 61–64.(In Chinese)

[3] W.H. Zou, K. Li, H.J. Bai, X. Zhao, R.P. Han,Journal of Zhengzhou University (Engineering Science), vol. 6, 2010, pp. 87–90.(In Chinese)

[4] G. Taguchi,System of experimental design:engineering methods to optimize quality and minimize costs. In White Plains:unipub:1987;Vol.1.

[5] C.X.Ma, K.T.Fang, Erkki Liski. A new approach in constructing orthogonal and nearly orthogonal arrays[J]. Metrika,2000,50(3):255-268.

[6] R.Qian,Biostatistics [M]. Beijing: Higher Education Press, 1999.126- 129. (in Chinese)

Advanced Materials Research Vols. 989-994 (2014) pp 845-848
© (2014) Trans Tech Publications, Switzerland
doi:10.4028/www.scientific.net/AMR.989-994.845

A new harmless disposal method of aluminium phosphide residue

Xiangcheng Wang ‡[1, a], Dan Li ‡[2, b], Shengliang Duan[3, c], Debing Li[4, d], Xiuli Qi[5, e]

[1] Institute of Chemical Defense, Beijing 102205, China

[2] Institute of Chemical Defense, Beijing 102205, China

[3] Institute of Chemical Defense, Beijing 102205, China

[4] Institute of Chemical Defense, Beijing 102205, China

[5] Institute of Chemical Defense, Beijing 102205, China

[a]lwjwhr@sina.com, [b]912317454@qq.com, [c]shengliang@126.com, [d]debin@126.com, [e]qixiulilily@163.com

‡Both authors contributed equally.

Keywords: Aluminium phosphide, harmless diposal, poly aluminium chloride (PAC)

Abstract. Treatment phosphine gas with absorption oxidation, let gas went through the oxidant solution. Use concentration of sodium hypochlorite 1%-8% (w/w) as oxygenate, the absorption rate of phosphine [φ] was various form 41% to 61%. Compared with the other phases, such as hydrogen peroxide, potassium permanganate, iron trichloride, sodium hypochlorite is better as oxidation agent in the process of phosphine gas absorption oxidation.

Introduction

56% Aluminium phosphide fumigant is used extensively at home and abroad, it has already been applied to the pest control range of other food outside the industry, and has achieved very good results. Aluminium phosphide absorbed moisture in the air to produce phosphine in process of decomposition. Phosphine is colorless and tasteless, low boiling point, and the diffusion is speedly, slightly heavier than the air, insoluble in water, slightly soluble in water, soluble in alcohol and ether. Aluminium phosphide fumigant decomposes to produce a large amount of residue after fumigating treatment. Aluminium phosphide residue containing phosphine 3% above has not been volatiled[1], decomposed and utilized. So, we have always attached great importance to deal with aluminium phosphide residue. Treatment of aluminium phosphide residue generally adopts two ways, one is chemical treatment, and the other is buried in a deep pit far away from the water source region. How to do better on the proposal of aluminium phosphide residue in a non-toxic, harmless treatment, safety, environmental protection way, had been explored in the topic of us.

Residue processing for a completely reaction residue, another is incompletely reacted residue. Complete reaction residue, which is the main component of some impurities (Paraffin) and alumina, there is no toxic and harmful substances. Safe transport to the far away from water and animal living area of at least 50 meters place, can dig deep and bury. The incompletely reacted residue must be specially treatment.

56%Aluminium phosphide tablets in the ingredients are mainly aluminium phosphide, ammonium carbamate and talcum powder. Aluminium phosphide (tablet, pill, powder) reacted with acid /water to release phosphine, carbon dioxide, ammonia and other gases. The following related chemical reaction such as:

$$2AlP + 6H_2O \rightarrow 2Al(OH)_3 + 2PH_3 \uparrow \quad (1)$$

$$H_2NCOONH_4 \rightarrow CO_2 \uparrow + 2NH_3 \quad (2)$$

$$H_2NCOONH_4 + H_2O \rightarrow (NH_4)_2CO_3 \quad (3)$$

$$5PH_3 + 8KMnO_4 + 12H_2SO_4 \rightarrow 5H_3PO_4 + 8MnSO_4 + 4K_2SO_4 + 12H_2O \quad (4)$$

$$2NH_3 + H_2SO_4 \rightarrow (NH_4)_2SO_4 \quad (5)$$

Aluminium phosphide residue decomposed is offwhite appearance, mainly ingredients were aluminium hydroxide, ammonium carbonate and eupholite or talcum powder and so on, individual are taupe or celadon because of containing impurities.

Our research method is adopting hydrolysis and oxidation to treat aluminium phosphide residue. First, Aluminium phosphide residue is hydrolyzed to phosphine and aluminum hydroxide, then phosphine was oxidized to phosphate, such as phosphoric acid, sodium phosphate and so on. And aluminum hydroxide was further converted to poly aluminium chloride (PAC). The PAC is one kind of important water treatment medicinal drug. Harmless treatment complete, in accordance with the requirements of environmental friendly chemical industry.

$$2AlP + 3H_2O \rightarrow 2Al(OH)_3 + 2PH_3\uparrow \quad (1)$$

$$PH_3 + 2NaClO \rightarrow H_3PO_2 + 2NaCl \quad (6)$$

$$Al(OH)_3 + HCl \rightarrow (AlCl_3)n + H_2O \quad (7)$$

Experiment

Measurement. Detection method of phosphine gas be measured through GB/T16037-1995. Phosphine absorped in potassium permanganate solution was oxidized to phosphate, and then reacted with ammonium molybdate into ammonium molybdophosphate, ammonium molybdophosphate is reduced with p-benzenediol to phosphomolybdate blue, Shades of blue is proportional to the phosphine content, so the content of phosphine can be determined by colorimetry. The chemical reaction involved as following:

$$5PH_3 + 8KMnO_4 + 12H_2SO_4 \rightarrow 5H_3PO_4 + 8MnSO_4 + 4K_2SO_4 + 12H_2O \quad (4)$$

$$2H_3PO_4 + 24(NH_4)2MoO_4 + 21H_2SO_4 \rightarrow 2(NH_4)3PO_4 \cdot 12MoO_3 + 21(NH_4)2SO_4 + 24H_2O \quad (8)$$

$$2(NH_4)3PO_4 \cdot 12MoO_3 + 4\,C_6H_4(OH)_2 + 3H_2SO_4 \rightarrow$$

$$2H_7[P(Mo_2O_7)_5Mo_2O_5] + 4C_6H_4O_2 + 3(NH_4)_2SO_4 \quad (9)$$

Oxidation absorption liquid consists of oxidant dissolved in aqueous solution[2]. When the phosphine gas flow through the absorption liquid, it was oxidation and absorption. The absorption rate of phosphine[φ] was calculated based on the original concentration of phosphine gas(C_0) and final concentration (C) as follows:

$$\varphi = \frac{C_0 - C}{C_0} \times 100\% \quad (10)$$

According to the literature[3], determine alumina and basicity in the aluminium polychloride (PAC).

Use Ion Chromatography to determination content of sodium hypophosphite in solution.

Process of Aluminium phosphide hydrolysis(P1). *Preparation of phosphine* Put 56% Aluminium phosphide tablets 60g into 250ml four necked flask with thermometer, nitrogen inlet protection, stirring, 100ml water was dripping slowly, the gas of phosphine generated by absorption

into the solution which containing an oxidizing agent to turn into hypophosphorous acid or hypophosphite.

Keep the temperature not more than 25℃ . The tail gas discharged outdoors.

Process of poly aluminium chloride(PAC). *Preparation of PAC* -- In the former four necked flask, the residual was transfer to another 500ml reactor, added 150ml 20% hydrochloric acid and 12ml 20% sulfuric acid, stirring, keep the temperature between 95℃ to 110℃ after 4h-5h reaction. When the temperature reduced to 50℃，the solid particles were filtered from the solution, then adjust pH = 3.5-4 with aqueous ammonia. Cooling, solution of PAC was gained. Appearance was yellowish transparent liquid; specific gravity was not less than 1.19.

Results and discussion

Different absorption rate vs different concentration of sodium hypochlorite. Studies show that, in the process of preparation of phosphine, the absorption rate of phosphine [φ] was different with the different concentration of sodium hypochlorite[C]. Under the condition of pH=10, the concentration of effective chlorine was from 1% to 8%, absorption time was 30 minute, comparative study of the effect of oxidation. Result was shown in Fig. 1.

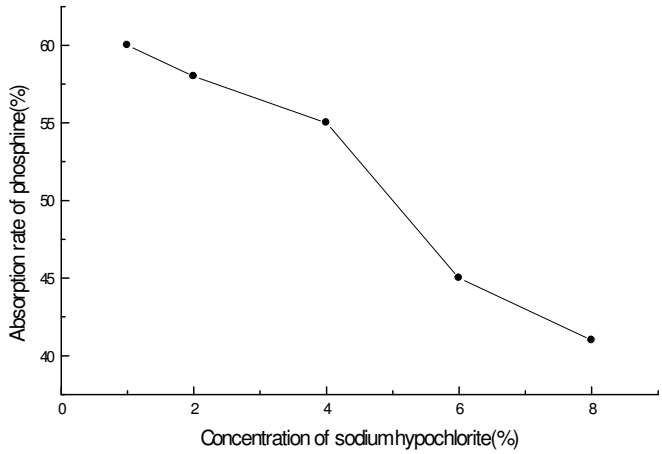

Fig. 1 Effect of absorption vs the different concentration of sodium hypochlorite

The data in Fig.1 indicated that the absorption oxidation effect of low concentration liquid was better than high concentration, but in order to keep the speed of response necessary, need to add sodium hypochlorite constantly, and need to add potassium hydroxide or sodium hydroxide to maintain basic.

Effect of different oxygenate on phosphine gas

In the same condition of 10% (w/w) by absorption into the oxygenate solution, flow the phosphine gas as the process P1. Researches the absorption oxidation rate was different from oxygenant. Result was shown in Fig. 2.

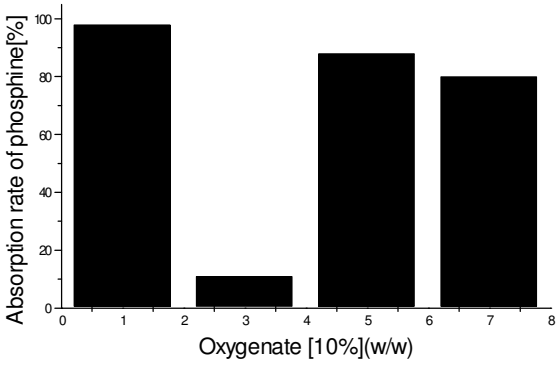

1-sodium hypochlorite, 3- hydrogen peroxide, 5- potassium permanganate, 7- iron trichloride

Fig. 2 Effect of different oxygenate

The data in Fig.2 indicated that compared with the other phases, such as hydrogen peroxide, potassium permanganate, iron trichloride, sodium hypochlorite is better as oxidation agent.

According to research, whether the acidic, alkaline or neutral conditions, always gained hypophosphite.

Conclusions

The concentration of sodium hypochlorite effect oxidation evidently. Low concentration sodium hypochlorite liquid was better than high concentration. In the process of absorption oxidation, the phosphine gas was completely converted to hypophosphite.

Acknowledgements

The authors want to thank Dr. Liu Yong-jing and Dr. Zhang Hong-peng of Institute of Chemical Defense for him to providing study conditions. We sincerely appreciate all of them for their help.

References

[1] Kyowa Kako KK. Method for removing arsine and/or phosphine [P]. JP:1266836,24.10.1989.

[2] CHENG Jianzhong etal. Study on the treatment of PH3 in the process of making sodium hypophosphine [J]. Acta Scientiarum Naturalium Universitatis Nankaiensis, 2001, 34(2):31-34

[3] GB/T 22627-2008

Advanced Materials Research Vols. 989-994 (2014) pp 849-852
© (2014) Trans Tech Publications, Switzerland
doi:10.4028/www.scientific.net/AMR.989-994.849

Experimental Study on Sewage Treatment by Vortex-grid Flocculation Technology

Fengping Hu[1, a], Huanhuan Li[1, b], Linyuan Wang[1, c], Zhengong Tong[1, d], Qi Zhang[1, e] and Hongling Dai[1, f]

[1]School of Civil Engineering and Architecture, East China Jiao Tong University, No.808 Shuanggang east street, Nanchang city, Jiangxi province, China 330013

[a]hufengping1968@126.com, [b]huan7029@126.com, [c]wlywly@ecjtu.jx.cn, [d]zzggtt@ecjtu.jx.cn, [e]zhangqi1970@163.com, [f]tmxydhl@126.com

Keywords: Vortex-grid flocculation tank, Inclined tube sedimentation tank, Vortex-grid flocculation reactor, Enhanced coagulation, Sewage

Abstract. The aim of this test is to study the effect of treating COD_{Cr}, NH_3-N, TP and turbidity of sewage with addition of coagulant PAC by using technology of combining vortex-grid flocculation tank with inclined tube sedimentation tank. The results show that the removal rate of devices treating COD_{Cr}, NH_3-N, TP and turbidity are 68.36%, 22.22%, 82.60% and 80.90% respectively after the stability of the device operation on the condition that the dosage is 25 mg/L and the optimum flocculation time is 17 min.

Introduction

Enhanced Coagulation is a treatment process, which developed on the basis of conventional coagulation treatment. By adding an excess of coagulant, new coagulant, auxiliary coagulant aid or other agents, and adjusting the pH simultaneously, the effect of coagulation is enhanced and the removal rate of conventional treatment process treating pollutants is improved [1]. This means that the particles and the turbidity are removed maximally, the remaining coagulant content and sludge production are reduced, the quality of water is improved, and the cost of making water is minimized [2]. In recent years, researches related to enhanced coagulation process field have made great achievements [3-6], and is faced with the progress of breakthrough [7]. This present work mainly investigates the effect of the process of combined vortex-grid flocculation tank with inclined tube sedimentation tank removing COD_{Cr}, NH_3-N, TP and turbidity in sewage through pilot scale test.

Test Materials and Methods

Raw Water Quality. Sewage of East China Jiaotong University as a test of raw water, because of the sewage through precipitation after flowing into the Kongmu Lake, SS and turbidity of raw water was low. Test raw water quality is shown in table 1.

Tab.1 Test of raw water quality

Water quality index	Range	Average
pH	6.65~7.86	7.25
Water temperature/℃	6~28	18
COD_{Cr}/mg/L	138.62~190.36	167.01
NH_3-N/mg/L	17.78~26.78	19.85
TP/mg/L	1.98~3.49	2.60
Turbidity/NTU	12.47~18.58	16.08

Test Device. The internal structure of vortex-grid flocculation tank is shown in Fig.1. Vortex-grid flocculation tank design treatment capacity 5 m^3/h, 1000 mm × 750 mm of tank size, height of 2.3 m, divided into 12 lattices. Design a single lattice for square, each lattice side length of 0.25 m. Hole size of the paragraphs holes in all 200 mm × 130 mm. 1 to 9th shafts placed 22 vortex-grid flocculation reactors, 10~12th shafts placed 16 vortex-grid flocculation reactors. The Vortex-grid flocculation reactor structure chart is shown in Fig.3. The reactor dimensions are Φ150 mm,

opening rate of 70%. Set DN 65 mm perforated sludge discharge pipe at the bottom of each reaction.

Vortex-grid flocculation reactor is independent property rights of the patent product (patent number: CN 200920141662.5). It integrated vortex theory and the small grid flocculation technology. The water flow can produce greater friction to form hydraulic condition better vortex. In wastewater treatment process, not only can improve the flocculation reaction efficiency, improve water quality, but also saving energy, optimizing water treatment process.

Inclined tube of inclined tube sedimentation tank with inclined pipe diameter 30 mm, installation angle is 60°, length is 900 mm, and inclined tube placed can greatly improved the sludge-water separation effect. Settling tank dimensions is length × width × height of 1.75 m × 1.0 m × 2.3 m. The profile of inclined tube sedimentation tank is shown in Fig.2. The two tanks are connected by DN 150 mm pipe, transition section built together with settling tank.

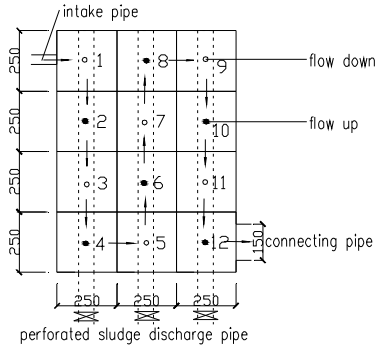

Fig.1 The internal structure of the vortex-grid flocculation tank

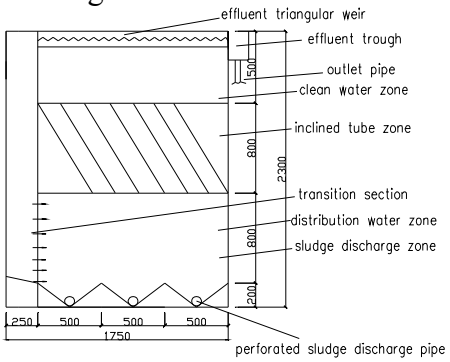

Fig.2 The sectional view of inclined tube sedimentation tank

Raw water pressurized by the pump through the inlet pipe into vortex-grid Flocculation tank. In the inlet pipe, coagulant dosed into the pipes by the metering pump, and raw water fully mixed with coagulant flows into each shaft. After completion of coagulation, water flows into the transition section and then into the inclined tube area, floc formation of micro-vortex flocculation process due to gravity and inclined tube sedimentation sink to the sludge thickening zone, solid-liquid separation was conducted. Solid-liquid separation of water overflow from the water zone into the annular groove, finally outflow of the pool. Sludge after separation is collected by the perforated sludge discharge pipe of sludge concentration zone.

Analysis. Analysis indicators of the test include pH, temperature, COD_{Cr}, NH_3-N, TP and turbidity. Analysis methods adopt the fourth edition of Monitoring and Analyzing Methods of Water and Wastewater of national standard test method [8].

Test Method. Test adopts continuous influent by submersible pumps. After the device run stable, influent flow and coagulant dosage were regulated into vortex-grid flocculation tank. To take a water sample and take six times a day in a row. Then each water sample COD_{Cr}, NH_3-N, TP and turbidity were measured, and take its average. The test is analysis removal efficiency of sewage by the combined process.

Test Results and Analysis

Determination of PAC Dosage. The influent flow was 5 m^3/h, the turbidity of the raw water around 15.87~16.98 NTU. Under different PAC dosage, combined vortex-grid flocculation tank and inclined tube sedimentation tank process for raw water turbidity removal rate is shown in Fig.4.

As is shown in Fig.4, when the influent flow was 5 m^3/h and the PAC dosage from 5 mg/L gradually increased to 35 mg/L, combined process for turbidity removal first increased and then decreased. When PAC dosage was increased to 25 mg/L, the effluent turbidity of the inclined tube sedimentation tank was 3.21 NTU; the turbidity removal rate reached a maximum value of 80.9%, and continues to increase the dosage, the turbidity removal rate decreased. In this experiment, the effluent turbidity control below 5 NTU, the dosage used in this test was 25 mg/L.

Fig.3 The vortex-grid flocculation reactor structure chart

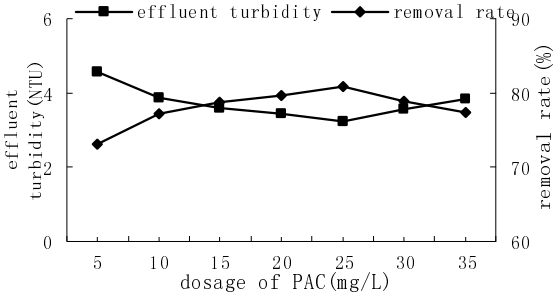

Fig.4 Effluent turbidity and removal rate of different dosage

Removal Rate of COD_{Cr}. As is shown in Fig.5, the dosage was 25 mg/L, influent COD_{Cr} in the range of 151.2~184.56 mg/L, under various flow the effluent COD_{Cr} in the range of 50.36~70.72 mg/L, removal rate of COD_{Cr} around 62%. When the optimum flocculation time is 17 min (5 m^3/h of the influent flow), effluent COD_{Cr} reduced to 50.36 mg/L; COD_{Cr} removal rate reached 68.37%.

Through vortex-grid flocculation process, removal of organics is mainly water easily precipitates suspended organics, tiny suspended and colloidal organics. While the removal of dissolved organic matter in a more limited.

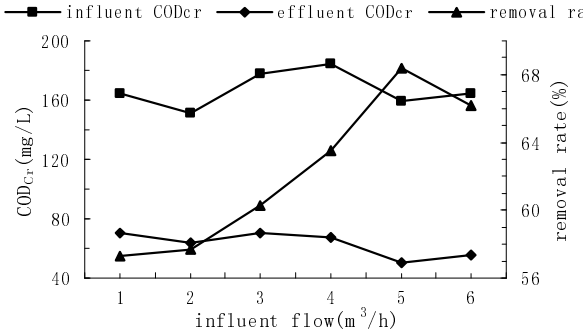

Fig.5 Removal rate of COD_{Cr}

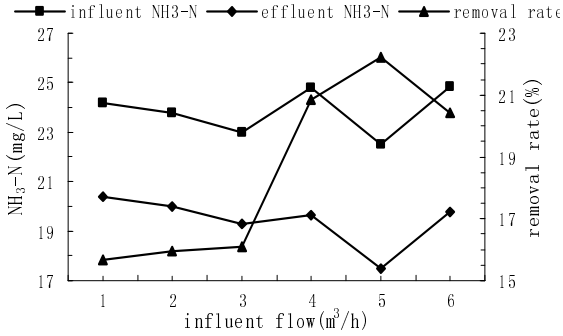

Fig.6 Removal rate of NH_3-N

Removal Rate of NH_3-N. As is shown in Fig.6, the dosage was 25 mg/L, influent NH_3-N in the range of 22.5~24.8 mg/L, under various influent flows, the effluent NH_3-N was between 17.50~20.39 mg/L, the removal rate of NH_3-N is about 18.4%. The optimum flocculation time is 17 min, the effluent NH_3-N to a minimum was 17.50 mg/L, removal rate of NH_3-N was 22.22%.

Vortex-grid flocculation for removal rate of NH_3-N of domestic sewage was relatively low, which is because the domestic sewage of the NH_3-N exists mainly in dissolved form. In the experiment, removing some of the smaller parts of NH_3-N is due to some particles adsorbed NH_3-N and suspended solid particles of colloidal particle surface removed by coagulation.

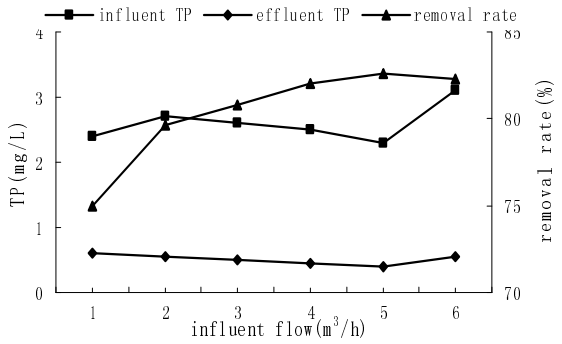

Fig.7 Removal rate of TP

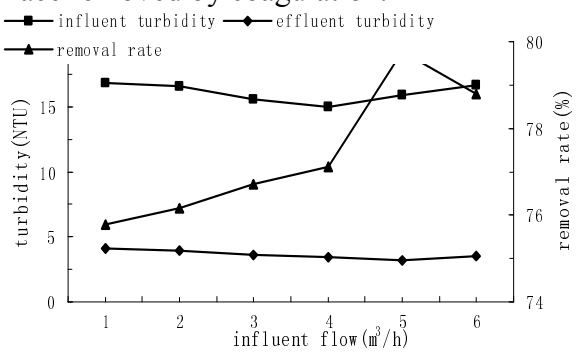

Fig.8 Removal rate of turbidity

Removal Rate of TP. As is shown in Fig.7, the addition of coagulant was 25 mg/L, influent TP was between 2.30~3.10 mg/L, the effluent TP is below 0.50 mg/L, the removal rate of TP is about 80.4%. The optimum flocculation time is 17 min, the effluent TP reached the lowest of 0.40 mg/L, TP removal reached 82.61%.

Vortex-grid flocculation mainly uses the PAC chemical phosphorus removal. Phosphorus of the sewage mostly in the form of phosphate existence, its removal mainly relies on metal complexation

reaction to phosphate, and thus precipitated. At the same time, during precipitation process these phosphate precipitates can also absorb organic phosphorus and polyphosphate. Therefore, enhanced coagulation on the various forms of phosphorus has certain removal effect [9].

Removal Rate of Turbidity. As is shown in Fig.8, the dosage was 25 mg/L, water turbidity in the range of 15.98~16.84 NTU, under various flow the effluent turbidity changed in the range of 3.21~4.08 NTU, removal rate of turbidity around 77%. The optimum flocculation time is 17 min, the effluent turbidity to a minimum of 3.21 NTU, the turbidity removal rate reached 79.77%.

Conclusion

When process of combining vortex-grid flocculation tank with inclined tube sedimentation tank treats sewage, optimum coagulant dosage is 25 mg/L on the condition that the influent flow is 5 m^3/h and the optimum flocculation time is 17 min;

Under the condition of 25 mg/L of coagulant dosage and 17 min of optimum flocculation time (corresponding to the influent flow is 5 m^3/h), effluent COD_{Cr}, NH_3-N, TP and turbidity were 50.36 mg/L, 17.50 mg/L, 0.40 mg/L and 3.21 NTU respectively, and the removal rates were 68.36%, 22.22%, 82.60% and 80.90% respectively.

Acknowledgement

This work was financially supported by the National Natural Science Foundation (61272197) and (51268012), Landing Plan of Scientific and Technological Project of Jiangxi Provincial Colleges and Universities (KJLD2013037), Science and Technology Project of Jiangxi Provincial Department of Water Resources (2012021) and Cultivation Plan of Leadership for Excellence Jiangxi Province and Poyang Lake 555 Engineering.

References

[1] Wang Zheng. Research progress in the treatment processes of micro-polluted source water in China [J]. Industrial Water Treatment, 2012,32(10):1-3.

[2] Kimbedy B A, Morteza A. Conventional and optimized coagulation for nom removal [J]. J.AWWA, 2000,92(10):44-58.

[3] Wu C D, Xu X J, Liang J L, et al. Enhanced coagulation for treating slightly polluted algae-containing surface water combining polyaluminum chloride (PAC) with diatomite [J]. Desalination, 2011,279(1-3):140-145.

[4] Walsh ME, Zhao N, Gora SL, et al. Effect of coagulation and flocculation conditions on water quality in an immersed ultrafiltration process [J]. Environmental Technology, 2009,30(9):927-938.

[5] Lu Jing-fang and so on. Improvement and development trend of wastewater reuse technology [J]. Environment Science & technology, 2010,33(3):76-79.

[6] Shuang Xue and so on. Effect of enhanced coagulation on the characteristics of dissolved organic matter in secondary treated effluents [J]. Acta Scientiae Circumstantiae, 2013,33(8):2199-2208.

[7] Wang Dong-sheng. Treatment of micro-polluted water source by enhanced coagulation technology [M]. Beijing：Science Publications, 2009:4.

[8] Monitoring and Analyzing Methods of Water and Wastewater [M]. 4th ed. Beijing：China Environment Science Publications, 2002.

[9] Yuzhe Liu and so on. Pilot scale study on treatment of domestic wastewater by enhanced coagulation technology [J]. Environmental Science & Technology, 2011,34(6):132-136.

Advanced Materials Research Vols. 989-994 (2014) pp 853-858
© (2014) Trans Tech Publications, Switzerland
doi:10.4028/www.scientific.net/AMR.989-994.853

Study on Removing Atrazine and Chlorothalonil in Raw Water in Reservoirs in North China by PAC Adsorption and Enhanced Coagulation

Jianfeng ZOU[1, a], Xiaobin TANG[1], Miao YU[1], Jianjun ZHOU[2], Fujin Wang[2], Junguo HE[1], Yixing YUAN[1]

[1]Department of Municipal & Environmental Engineering, Harbin Institute of Technology, Harbin, 150090, China

[2]Yellow River Water Supply Ltd, Taiyuan, 030000, China

[a]email: z-maplemelody@163.com

Keywords: PAC adsorption; enhanced coagulation; Atrazine; Chlorothalonil

Abstract. By the coagulation-flocculation jar test, the PAC adsorption property and coagulation removal property of Atrazine and Chlorothalonil, and influence on removal effect of Atrazine and Chlorothalonil by PAC Adsorption and Enhanced Coagulation in combination have been acknowledged, with different doses of PAC or polyaluminium chloride. The results of test showed that PAC can absorb Atrazine and Chlorothalonil effectively, and that the removal effect of the enhanced coagulation for Atrazine and Chlorothalonil is affected by coagulation effect. Enhanced coagulation cannot remove Atrazine effectively, while it can remove 75% of Chlorothalonil. PAC adsorption and enhanced coagulation in combination can remove Atrazine and Chlorothalonil effectively. For the initial concentration of 0.1 mg/L of Atrazine, dosage of 60mg/L of PAC and 20mg/L polyaluminium chloride can reach more than 98% removal efficiency, and make treated water standard. For the initial concentration of 0.1 mg/L of Chlorothalonil, dosage of 20mg/L of PAC and 20mg/L polyaluminium chloride can reach more than 90% removal efficiency and make treated water up to standard.

Introduction

Water is the most widely distributed natural resource in the world, is also one of the most fundamental and essential resources of human life and economic production [1]. The problem of the lack of water in North China is severe. With the increase in the population and land subsidence by the over-exploitation of groundwater, surface water resource is gradually replacing groundwater resource in North China. However, surface water resource is more easily contaminated by sudden water pollution than groundwater resource.

Researches at home and abroad show that, common technology including coagulation, deposition, filtration, etc. can only remove 20-30% of the organic matter in raw water contaminated [2,3,4,5]. But by means of increasing the dosage of coagulant and changing in pH, the removal effect of organic matter can be improved [6]. At the same time, the increasing dosage will raise the production cost of water and make the concentration of metal ion like Al, Fe, Mn, etc. increase, which are detrimental to health.

PAC addition is one of the most effective methods removing organic matter in raw water [7]. With the combination of PAC adsorption and common technology, not only can common technology be more perfect, but also the removal efficiency of organic pollutant can be improved, which is an ideal method to solving sudden water pollution problem [8]. H. Jiang's study shows that common technology can't remove EDCs effectively unless it is combined with PAC adsorption [9]. Maria's research shows that PAC Adsorption and Enhanced Coagulation are complementary to each other in improving the removal effects of Humic Acid and Phenol [10]. N. Gao and B. Chen's study shows that PAC adsorption is effective against Atrazine [11].

In this experiment, the PAC adsorption property and coagulation removal property of Atrazine and Chlorothalonil, and the influence on removal effect of Atrazine and Chlorothalonil by PAC Adsorption and Enhanced Coagulation in combination have been acknowledged.

Experimental methods

Experimental Water Sample

Experimental water is taken from raw water of a reservoir in North China. The characteristics of the raw water are summarized in Table 1.

Tab. 1 Experimental water sample

turbidity	pH	temperature	COD_{Mn}	ammonia nitrogen
1.5-2.5NTU	7.5-8.0	18-22℃	1.0-1.5mg/L	0.05-0.2mg/L

Experimental procedures

1) PAC isothermal adsorption experiment

Compound the experimental water with 0.1mg/L of Atrazine/Chlorothalonil and take 1000mL mixed water in a 2000mL beaker. Add PAC to the water, the concentration of which is 20mg/L, 40mg/L, 60mg/L, 80mg/L, 100mg/L. The adsorption time is 100min. After filtering water with 0.45 μm filter membrane, detect the residual concentration of Atrazine/Chlorothalonil.

2) PAC adsorption characteristic experiment

① Compound the experimental water with 0.1mg/L of Atrazine/Chlorothalonil and take 800mL mixed water in a 1000mL beaker. Add some PAC to the water. Put beakers on the six-up agitator. Mix respectively in 10min, 20min, 30min, 40min, 50min, 60min (80r/min). After filtering water with 0.45 μm filter membrane, detect the residual concentration of Atrazine/Chlorothalonil.

② Compound the experimental water with 0.1mg/L of Atrazine/Chlorothalonil and take 800mL mixed water in a 1000mL beaker. Add PAC to the water, the concentration of which is 20mg/L, 40mg/L, 60mg/L, 80mg/L, 100mg/L. Put beakers on the six-up agitator. Mix in 40min (80r/min), after filtering water with 0.45 μm filter membrane, detect the residual concentration of Atrazine /Chlorothalonil.

3) Coagulation removal characteristic experiment

Compound the experimental water with 0.1mg/L of Atrazine/Chlorothalonil and take 800mL mixed water in a 1000mL beaker. Add polyaluminium chloride to the water, the concentration of which is 0mg/L, 10mg/L, 20mg/L, 30mg/L, 40mg/L, 50mg/L. Put beakers on the six-up agitator. Mix at high speed in 0.5min (350r/min), mix at low speed in 5min (120r/min) and 10min (80r/min). After 20 minutes' standing, take supernatant fluid and detect turbidity and the residual concentration of Atrazine/Chlorothalonil.

4) PAC adsorption and enhanced coagulation in combination Removing Atrazine and Chlorothalonil experiment

Compound the experimental water with 0.1mg/L of Atrazine/Chlorothalonil and take 800mL mixed water in a 1000mL beaker. Add PAC to the water, the concentration of which is 20mg/L, 40mg/L, 60mg/L, 80mg/L, 100mg/L. Put beakers on the six-up agitator. Mix in 40min (80r/min). Add polyaluminium chloride to the water, the concentration of which is 20mg/L. Mix at high speed in 0.5min (350r/min), mix at low speed in 5min (120r/min) and 10min (80r/min). After 20 minutes' standing, take supernatant fluid and detect the turbidity and the residual concentration of Atrazine/ Chlorothalonil.

Detecting methods

Turbidity: the turbidimetric apparatus of HACH 2100AN;

Atrazine: after the liquid-liquid extraction, detect Atrazine using high performance liquid chromatography;

Chlorothalonil: after the liquid-liquid extraction, detect Chlorothalonil using gas chromatography.

Results and discussion

PAC isothermal adsorption experiment

Figure.1 and Figure.2 are Freundlich adsorption isotherm of Atrazine and Chlorothalonil respectively. Both of their R2 are greater than 0.9, which are fitting well. Adsorption isotherm of Atrazine is $qe=0.9768\times Ce^{0.4555}$. When the initial concentration is 100μg/L and the residual concentration is 2μg/L, it is needed to add 73.16mg/L of PAC. Adsorption isotherm of Chlorothalonil is $qe=0.6701\times Ce^{0.7624}$. When the initial concentration is 100μg/L and the residual concentration is 10μg/L, it is needed to add 23.21mg/L of PAC.

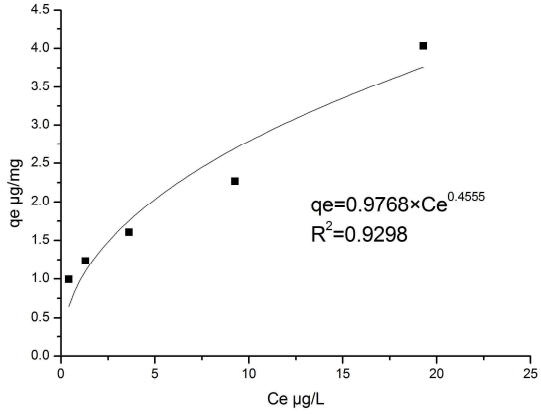

Fig. 1 Adsorption isotherm of Atrazine

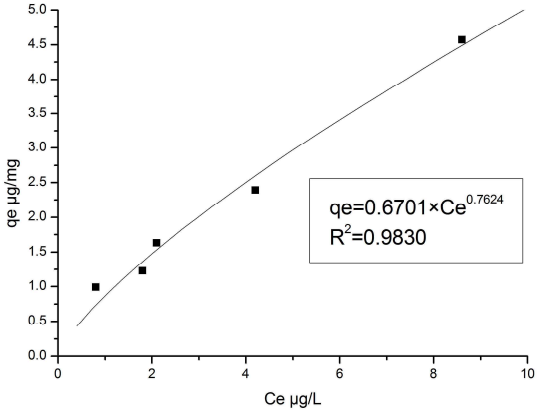

Fig. 2 Adsorption isotherm of Chlorothalonil

PAC adsorption characteristic experiment

Figure.3 indicates that most of the adsorption of PAC for Atrazine and Chlorothalonil occurs within the first 10min. Atrazine reaching adsorption equilibrium needs 50min to 60min and Chlorothalonil needs about 40min. It's obvious that the adsorption of PAC for Chlorothalonil is higher than that of Atrazine.

Figure.4 shows that the removal rate of Atrazine and Chlorothalonil grows as the dosages of PAC are added more. In this process, the removal rate of Chlorothalonil is always higher than Atrazine, but the gap is diminishing. When the dosages of PAC reaches 80mg/L, the removal rate of Atrazine and Chlorothalonil is reaching 99%, which is almost completely removed. In this experiment, both of the initial concentration of Atrazine and Chlorothalonil are 0.1mg/L. Dosage of 80mg/L of PAC can reach more than 98% removal efficiency of Atrazine, which makes the treated water up to standard. Dosage of 30mg/L of PAC can reach more than 90% removal efficiency of Chlorothalonil, and make treated water up to standard.

The adsorption property of Chlorothalonil is better than Atrazine, which is decided by the size of the molecular weight and the degree of hydrophobicity. Apertures of PAC include micropores, mesopores and macropores. Macropores are channels of solute reaching the inside of PAC. Mesopores are both channels and adsorption sites. Micropores are the most important adsorption sites of PAC adsorbing pollutant. Both Atrazine and Chlorothalonil are low molecular weight organic matters, which can reach the effective adsorption sites of PAC through channels of mesopores and macropores. Consequently, the molecular weight size isn't the reason that their adsorption properties are different.

Some studies approved that hydrophobic organic compound is far more easily adsorbed by PAC than hydropholic and semi-hydropholic organic compound. According to the physical properties of Atrazine and Chlorothalonil, both of their dissolvabilities are quite low. Atrazine's dissolvability is 33mg/L and Chlorothalonil is 0.6mg/L. Compared with Atrazine, Chlorothalonil dissolves harder in water. Based on the viewpoint of molecular structure, Atrazine contains 2 hydrogen bond donors and 5 hydrogen bond receptors, while Chlorothalonil only has 2 hydrogen bond receptors. This indicates that the hydrogen bond force of Chlorothalonil is less than Atrazine, because of which

Chlorothalonil is more easily separated from water. Therefore, the difference between the hydrophobic properties of Atrazine and Chlorothalonil is an important influence factor for the adsorption property of PAC.

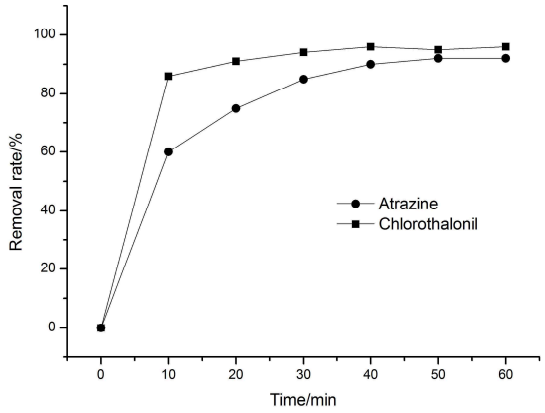

Fig. 3 The influence of different adsorption time for the removal of Atrazine and Chlorothalonil

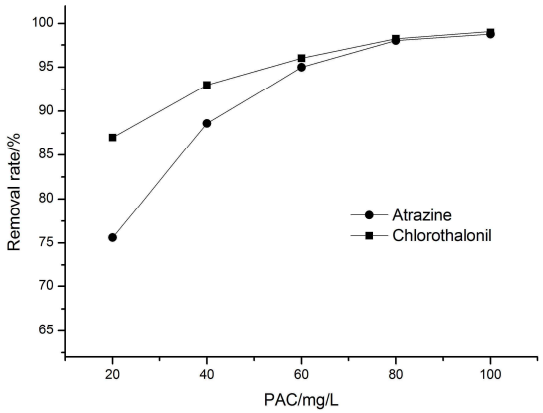

Fig. 4 The influence of different PAC dosages for the removal of Atrazine and Chlorothalonil

Coagulation removal characteristic experiment

Figure.5 shows that the removal rate of Atrazine first raises and then drops with increasing of coagulant dosage. When coagulant dosage is 20mg/L, the removal rate of Atrazine can reach the maximum value of 16.2%. Figure.6 shows that when coagulant dosage is more than 20mg/L, the removal rate of Chlorothalonil is up to above 75%. The removal rates of turbidity and Atrazine /Chlorothalonil are relevant. It is indicated that the removal efficiency of Atrazine and Chlorothalonil is affected by caugulation.

Coagulant improves water quality through four ways, which are compressed electric double layer, adsorption and bridging, aggregation function and adsorption and electrical neutralization respectively. Polyaluminium chloride used in the experiment is inorganic polymeric coagulant. Because of Hydroxyl ions' bridging and polyvalent anions' polymerization, polyaluminium chloride can provide a large number of polyvalent polymeric cations. In this experiment, adsorption and bridging and adsorption and electrical neutralization play major roles. The increase in coagulant dosage can enhance the number of hydroxide which hydrolysis produces and improve the positive charge density, which can enhance coagulation for organic matters.

In this experiment, the molecular weight of Atrazine and Chlorothalonil are 215.72 and 265.91, the dissolvability of Atrazine and Chlorothalonil are 33mg/L and 0.6mg/L respectively. Both of them are low molecular weight organic matters and difficult to dissolve in water, but there is a big gap for removal rate between them in coagulation process. It is chiefly because the benzene ring of Chlorothalonil has 4 chlorine atoms, which makes the showing of the stronger electronegativity of Chlorothalonil be more easily adsorbed by coagulant.

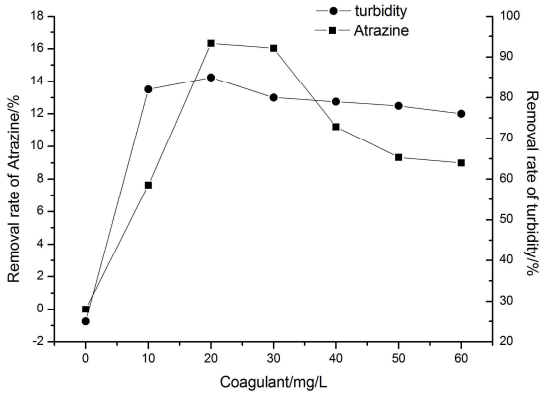

Fig. 5 The influence of different coagulant dose for the removal of Atrazine and turbidity

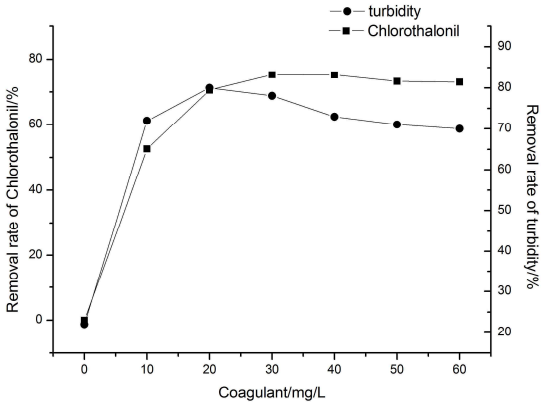

Fig. 6 The influence of different coagulant dose for the removal of Chlorothalonil and turbidity

PAC adsorption and enhanced coagulation in combination Removing Atrazine and Chlorothalonil experiment

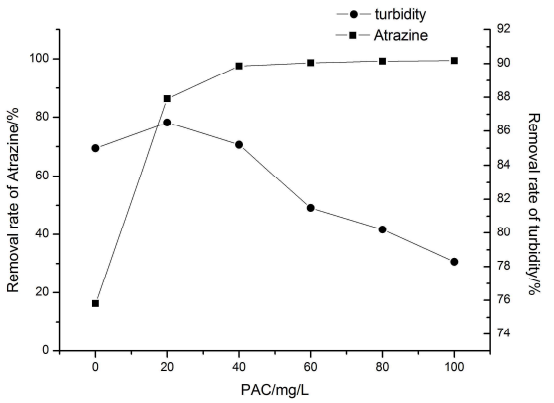

Fig. 7 The influence of PAC Adsorption and Enhanced Coagulation in combination for the removal of Atrazine and turbidity

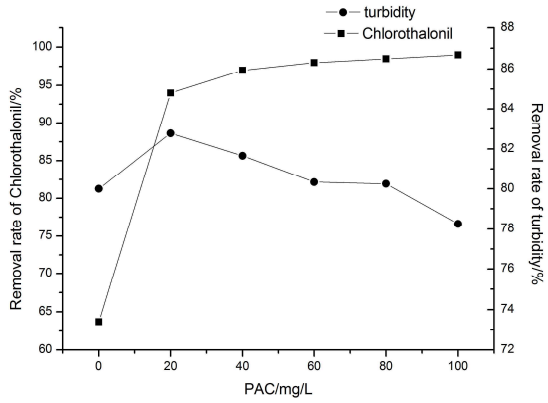

Fig. 8 The influence of PAC Adsorption and Enhanced Coagulation in combination for the removal of Chlorothalonil and turbidity

According to Figure.7 and Figure.8, the removal rate of Atrazine and Chlorothalonil are increasing as PAC dosages increase. Compared with coagulation alone, the removal rates of Atrazine and Chlorothalonil increase by 70% and 30% respectively. At the same time, it is observed that PAC dosage has an effect on coagulation. When PAC dosage is below 20mg/L, PAC is conducive to coagulation. Then with the increase of PAC dosage, the removal rate of turbidity starts falling. But in the whole experiment process, the turbidity of treated water is below 1NTU.

Compared with PAC adsorption alone, PAC dosages are less than 20mg/L, which makes treated water standard. Dosage of 60mg/L of PAC can reach 98.71% removal efficiency which makes treated water up to standard. Dosage of 20mg/L of PAC can reach more than 95% removal efficiency which makes treated water up to standard. It is because that coagulation enhances precipitation process and adsorbs a part of organic matters.

Conclusion

① Freundlich adsorption isotherm is an appropriate description for PAC adsorption property. PAC can adsorb Atrazine and Chlorothalonil effectively, and the adsorption rate and removal rate of Chlorothalonil are better than Atrazine.

② Enhanced coagulation cannot remove Atrazine effectively, but can remove 75% of Chlorothalonil. For the initial concentration of 0.1 mg/L of Atrazine and Chlorothalonil, enhanced coagulation cannot make treated water up to standard.

③ For the initial concentration of 0.1 mg/L of Atrazine, dosage of 60mg/L of PAC and 20mg/L polyaluminium chloride can reach more than 98% removal efficiency, and make treated water standard. For the initial concentration of 0.1 mg/L of Chlorothalonil, dosage of 20mg/L of PAC and 20mg/L polyaluminium chloride can reach more than 90% removal efficiency, and make treated water up to standard.

References

[1] Wenjie HE, Weiguang LI, Xiaojian ZHANG, Tinglin HUANG. Technology for Safeguarding Safe Drinking Water [M]. China Building Industry Press, 2006: 25-26.

[2] Jiuhui QU, etc. Technology Principle for Safeguarding Safe Drinking Water [M]. Science Press, 2007: 88~89.

[3] Xinglin LV. Study on Emergency Treatment Process for Chlorothalonil Pollution in Raw Water by PAC Adsorption and Enhanced Coagulation [D]. Harbin Institute of Technology, 2010: 5~10.

[4] Beibei CHEN. Study on Emergency Treatment Process for Sudden Organic Pollution of Souce Water in Zhenjiang [D]. Tongji University, 2008: 10~11.

[5] Shuang LI, Xiaojian ZHANG, Xiaojun FAN. Distribution and Control Countermeasures for Different Molecular Weight Range of Organic Matter in Raw Water [J]. Acta Scientiae Circumstantiae, 2003, 23(3): 327~331.

[6] W. Krasner. Jar-test Evaluations of Enhanced Coagulation [J]. Jour. AWWA, 1995 (10): 93~107.

[7] Jinchu FAN. Research on PAC Used in Water Treatment [J]. China Water & Wastewater, 1997, 13(2):7~9.

[8] Yi HOU, Naiyun GAO, Nan ZHANG. Research Status at Home and Abroad on PAC Enhancing Micro-polluted Water Treatment [J]. Urban Water Supply, 2008(6): 37-39.

[9] H. Jiang, C. Adams. Treatability of Chloro-s-triazines by Conventional Dranking Water Treatment Technologies [J]. Water Research, 40(2006): 1657~1667.

[10] Maria Tomaszewska, Sylwia Mozia. Removal of Organic Matter by Coagulation Enhanced with Adsorption on PAC [J]. Desalination, 2004, 161(1): 79-87.

[11] Beibei CHEN, Naiyun GAO, Cheng LIU. Research on Removing Atrazine Sudden Pollution of Raw Water by PAC [J]. Water Supply and Drainage, 2007, 33(7):9~13.

Advanced Materials Research Vols. 989-994 (2014) pp 859-862
© (2014) Trans Tech Publications, Switzerland
doi:10.4028/www.scientific.net/AMR.989-994.859

Modified reduced graphene oxide with enhanced solubility and conductivity and its application

Zeng Xiaopeng

School of Chemistry and Biological Engineering, University of Science and Technology Beijing, Beijing 100083, China.
zengxiaopeng2005@sina.com

Keywords: Graphene, modified, solubility, conductivity

Abstract. Graphene oxide was modified with phenyl isocyanate first, and then reduced by a two step method- reduction with hydrazine hydrate first and an additional reduction in H_2/Ar. The reduction with hydrazine hydrate in the first step can effectively remove the epoxy groups on the graphene, and the disposure of reduced graphene oxide (RGO) with H_2 will change the residual amides and carbamate esters into conjugated C=N-ph structure. The introduced phenyl isocyanate not only acts as a functionalized group to prevent the aggregation of graphene but also will increase the electron concentration because of additional benzene. The resulted functionalized graphene can well dispersed in DMF, and the electrical conductivity of the functionalized graphene can reach 3.42×10^4S/m， which is far high than the method only reduce with the chemical reductant or H_2/Ar. The prepared functionalized graphene is beneficial for the fabrication of graphene-based polymer nanocomposites. The conductivity of resulted modified graphene/PMMA composite with 5wt% filler content is 3.2S/m.

Introduction

Graphene as a two-dimensional nano-material have attracted a lot of attention because of its unique properties [1]. The potential application of graphene is to introduce it into polymer to fabricate polymer-based composites [2]. For preparation properties enhanced graphene/polymer composites the graphene must be well dispersed in polymer matrix. By reducing the precursor of graphene oxide to obtain reduced graphene oxide (RGO) is a method for low-cost and large-scale production of graphene [3, 4]. However, loss of oxygen-containing groups on the basic plane of graphene by chemical reduction will lead to the poor dispersibility in various solvents. Modification to RGO will improve the dispersion of RGO in solvent but usually result into a graphene with low conductivity [5].

In our work we modified the graphene oxide with phenyl isocyanate, then reduced the modified graphene oxide with a two step method- hydrazine hydrate first and an additional disposure in H_2/Ar at 500^{o}C for 2h. The resulted graphene show both good solubility in DMF and high conductivity.

Experimental section

Preparation of graphene

The detailed preparation procedures of graphite oxide (GO) were described in our previous work.[6] Then the as-synthesized GO (200mg) was dispersed in 20mL DMF. The mixture was sonicated for 2h. Then phenyl isocyanate was put into the graphene oxide suspension and the mixture was stirred for 24 h at room temperature. After that, hydrazine monohydrate (15μL per 12mg of GO) was subsequently added into the suspension, which was placed in an 80^{o}C water bath for 2h with continuous stirring. After filtering and washing, the obtained black product finally dried in a vacuum oven at 60^{o}C for 12h, and the resulted sample was designated as f-RGO. For comparison, the product without adding phenyl isocyanate in the same process was designated as RGO.

Then the as-prepared f-RGO (GO: phenyl isocyanate (w/w) = 1:4) was heated for 2h in a tube furnace under a mixture of hydrogen and argon at 500^{o}C. The flow was controlled by a mass flow controller and the ratio of H_2/Ar was 1:1. The resulted sample was marked as f-RGO-500. The

graphene obtained from phenyl isocyanate modified graphene oxide (GO: phenyl isocyanate (w/w) = 1:4) directly reduced by H_2/Ar in the same condition was designated as H-RGO.

Preparation of RGO/PMMA composites

The f-RGO-500/PMMA nanocomposite was prepared by a solution based intercalation method similar to our previous work [7].

Characterization

The crystal structures of the samples were characterized by powder X-ray diffraction (XRD) on a Philips X'Pert Pro X-ray polycrystalline diffractometer with Cu Kα radiation. The UV-Vis spectrum was used to characterize the solubility of graphene dispersion on a TU-1901 spectrophotometer. Samples were also characterized by Raman spectroscopy with excitation wavelength at 532 nm (Nicolet Almega XR). The electrical properties were measured by using a HL 55WIN Hall System by Vander Paw method. Before measurement, the prepared f-RGO-500/PMMA particles were firstly ground into powder using an agate mortar, and then were pressed into thin pieces using a tablet press under a pressure of 20MPa.

Results and discussion

In this work, the absorbance of RGO/DMF dispersion with a concentration of 0.08 mg/mL is only 0.002 at 550nm after one day. This indicates that the RGO dispersion without modification has a poor dispersion in DMF. The conductivity of RGO is 1130 S/m, also far lower than that reported [8]. Fig. 1 (a) indicates that after modified with phenyl isocyanate the solubility of f-RGO is improved, and with the increase of phenyl isocyanate addition the resulted absorbance of f-RGO increase. The absorbance of f-RGO dispersion with a concentration of 0.08 mg/mL at 550nm after one day was 0.360, 0.572, 0.578 and 1.087, respectively. Because the absorbance is corresponding to the solubility, the results show modification with phenyl isocyanate can well improve the solubility of RGO in DMF. However, it has been found that the modified agent at the graphene sheets will decrease the conductivity of graphene [5, 9]. From Fig. 1 (b) we could know that when GO: phenyl isocyanate (w/w) is 1:4, the conductivity of the sample with a highest solubility is only 759S/m. The decrease of conductivity maybe attribute to the reaction between phenyl isocyanate and GO. The generated amides and carbamate esters can not be reduced by hydrazine hydrate. The low conductivity of graphene is harmful for preparing high conductive graphene based composites.

In order to improve the conductivity of phenyl isocyanate modified RGO but without decrease its solubility, we further reduced the f-RGO with H_2/Ar atmosphere. The disposure with H_2/Ar is not only beneficial for the remove of the residual oxygen groups on RGO surface, but also can change the generated amides and carbamate esters into conjugated C=N-ph structure. In a word there is a significant enhancement in electrical conductivity of graphene. Fig. 2 shows the electrical conductivity of RGO, f-RGO (GO: phenyl isocyanate (w/w) = 1:4), H-RGO and f-RGO-500. The conductivity of f-RGO-500 is 2.78×10^4S/m, which is 25 times higher than RGO. And also far higher than that directed reduced by H_2/Ar from phenyl isocyanate modified graphene oxide.

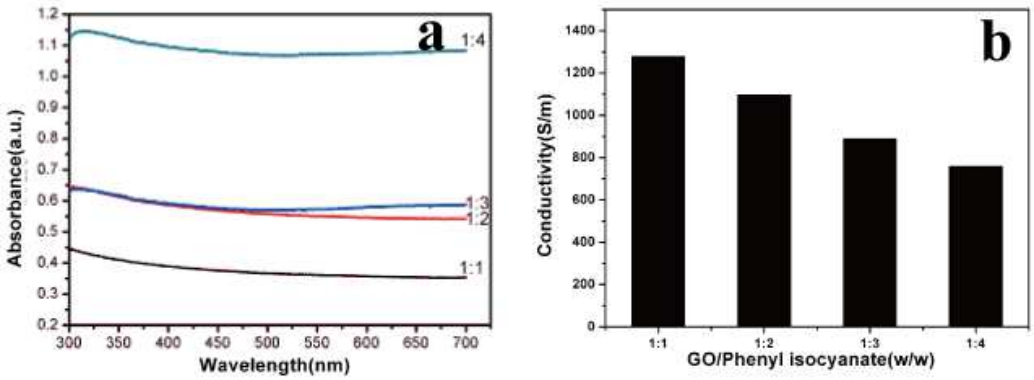

Fig. 1 The properties of phenyl isocyanate modified RGO with different phenyl isocyanate addition. (a) UV-Vis spectrum of phenyl isocyanate modified RGO solution with a concentration of 0.08mg/mL after one day. (b) electrical conductivity of phenyl isocyanate modified RGO

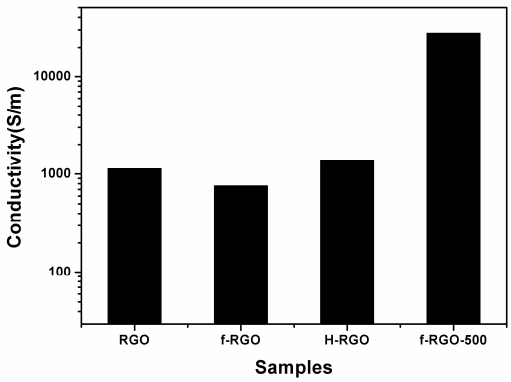

Fig. 2 Electrical conductivity of RGO, f-RGO (GO: phenyl isocyanate (w/w) = 1:4), H-RGO and f-RGO-500

The X-ray diffraction patterns of GO, RGO, f-RGO (GO: phenyl isocyanate (w/w) = 1:4) and f-RGO-500 are shown in Fig. 3. From Fig. 3 we could know that f-RGO-500 only have a characteristic peak at 26.0°, similar to RGO but more sharp. Which indicates that the sample of f-RGO-500 have a better crystal structure. There are two peaks in f-RGO. The (001) characteristic peak is attributed to GO. The results mean that the f-RGO is not well reduced, which is consistent with its low conductivity. The better crystal structure of f-RGO-500 is further confirmed by Raman spectrum. The D peak, located at about 1350cm^{-1}, is due to first-order zone boundary phonons of graphene. And the G peak located at about 1580cm^{-1} is caused by the in-plane optical vibration. The intensity ratio of the D and G peak of graphene has been used as a metric of disorder in graphene. From Table. 1 we could know that the ratio of I_D/I_G decreases by degrees from GO to f-RGO-500. The better crystal structure of f-RGO-500 is helpful for the transmission of charge carrier. So f-RGO-500 has a better conductivity.

It must be noted that the f-RGO-500 not only exhibit high electrical conductivity but also an improved solubility in DMF. Fig. 3 shows that after 6 days the absorbance of f-RGO (GO: phenyl isocyanate (w/w) = 1:4) is only 0.42 at 550nm, but the corresponding absorbance of f-RGO-500 is 0.82. The reason is that the resulted conjugated C=N-ph structure of f-RGO-500 will help to inhibit the reaggregation of graphene sheets.

The good dispersion and high conductivity of f-RGO-500 is helpful for preparation of high conductive graphene based composites. And the electrical conductivity of resulted 5wt% f-RGO-500/PMMA composites is 3.2S/m. The value is similar to the graphene/PMMA with the same filler addition reported by Jang et al [10].

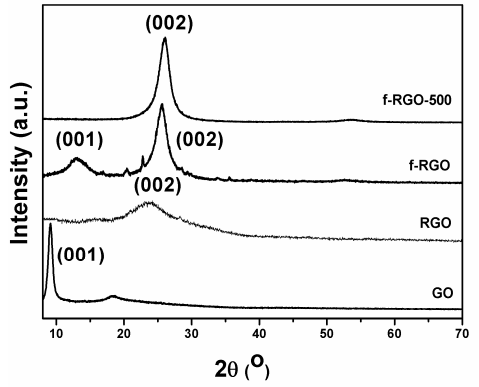

Fig. 3 X-ray diffraction patterns of GO, RGO, f-RGO (GO: phenyl isocyanate (w/w) = 1:4) and f-RGO-500

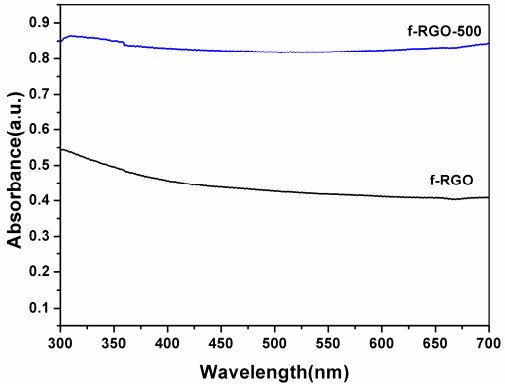

Fig. 4 UV-Vis spectrum of f-RGO-500 and f-RGO (GO: phenyl isocyanate (w/w) = 1:4) solution with a concentration of 0.08 mg/mL after 6days.

Table. 1 I_D/I_G of GO, RGO, f-RGO-500 from Raman spectrum

Samples	GO	RGO	f-RGO-500
I_D/I_G	1.36	1.25	1.18

Conclusions

Phenyl isocyanate modified reduced graphene oxide with significant improved solubility and conductivity was prepared with a two step route of reduction. The solubility in DMF and conductivity (2.78×10^4S/m) of f-RGO-500 are both far superior to f-RGO and RGO. The high conductivity and solubility of f-RGO-500 make it have potential application in preparing high conductive graphene/polymer composites.

References

[1] Y. Zhu, S. Murali, W. Cai, et al.: Advanced Materials, vol. 22 (2011) no. 35, p. 3906-3924.
[2] S. Stankovich, D.A. Dikin, G.H.B. Dommett, et al.: Nature, vol. 442 (2006) no. 7100, p. 282-286.
[3] M.J. Fernandez-Merino, L. Guardia, J.I. Paredes, et al.: The Journal of Physical Chemistry C, vol. 114 (2010) no. 14, p. 6426-6432.
[4] C. Zhu, S. Guo, Y. Fang, et al.: ACS nano, vol. 4 (2010) no. 4, p. 2429-2437.
[5] Y.F. Fan, Y.S. Liu, Q. Cai, et al.: Synthetic Metals, vol. 162 (2012) no. 21, p. 1815-1821.
[6] X.P. Zeng, J.J. Yang, W.X. Yuan: European polymer journal, vol. 48 (2012) no. p. 1674-1682.
[7] X. Zeng, J. Yang, L. Zhang, et al.: Powder Diffraction, vol. (2014) no. p. 1-7.
[8] S.F. Pei, J.P. Zhao, J.H. Du, et al.: Carbon, vol. 48 (2010) no. 15, p. 4466-4474.
[9] M.E. Uddin, T. Kuila, G.C. Nayak, et al.: Journal of Alloys and Compounds, vol. 562 (2013) no. p. 134-142.
[10] J.Y. Jang, H.M. Jeong, B.K. Kim: Macromolecular Research, vol. 17 (2009) no. 8, p. 626-629.

Advanced Materials Research Vols. 989-994 (2014) pp 863-866
© (2014) Trans Tech Publications, Switzerland
doi:10.4028/www.scientific.net/AMR.989-994.863

Aero-optical Effects of Mc=0.5 Supersonic Mixing Layer

TIAN Lifeng[1], YI Shihe[2], ZHU Yangzhu[2,a], ZHAO Yuxin[2] and HE Lin[2]

[1]Air Defense Forces Academy, Zheng Zhou 450052, China

[2]College of Aerospace Science and Engineering, National University of Defense Technology, Chang Sha 410073, China

[a]email: zyzhb123@139.com

Keywords: Mixing layer, NPLS-WT, Aero-optics

Abstract. Supersonic turbulent mixing layer requires high spatiotemporal resolution of measuring techniques to study its aero-optical effects. However, the spatiotemporal resolution of existing techniques is not high enough. NPLS-WT (NPLS based wavefront technique) is a new aero-optics measuring technique developed in 2010. Its time resolution is 6ns, and spatial resolution and time correction resolution can reach up to micrometers and 200ns respectively. NPLS-WT was used in this paper to study aero-optical effects induced by Mc=0.5 supersonic mixing layer. The fine wavefront aberration information is revealed by the OPD of high resolution. The results show that the wavefront in near field is not sensitive to the resolution, and large-scale structures play a dominant role on the wavefront in near field. The cumulative effects analysis show us that the density difference between large-scale structures and free stream is the main reason to wavefront aberration, and the larger the vortex is, the more obvious the effect to wavefront aberration is.

Introduction

Aero-optical effect of supersonic mixing layer is vital in many fields, for example, missiles with optical seekers [1] and air-borne laser weapon systems[2]. Mechanism study about it not only helps us understand the relationship between flow structures and the corresponding aero-optical aberrations, but also supplies important theoretical basis for aero-optics control to improve its aero-optical performance. For high speed and existence of vortices of different scales in supersonic mixing layer, the aero-optical measurement techniques must have high spatiotemporal resolution.

Nowadays, there are many techniques to measure aero-optical aberration, for example, Shack-Hartmann wavefront sensor (SHWS)[3-5], small-aperture beam technique (SABT)[6-7], interferometer[8], and so on. The resolution of SHWS is related to the size and spacing of small lens, and can reach up to 100-500μm[4]. Its temporal response frequency is related to the sampling frequency of camera, and is generally not higher than 2500Hz[5]. The frequency of SABT is up to 100 kHz, but its spatial resolution is lower than that of SHWS by one or two orders[7]. The temporal response frequency of interferometry is related to the sampling frequency of camera, which is generally not higher than 2500Hz, and its spatial resolution can reach up to micrometers[8]. According above stated, resolutions of these techniques are not high enough, and they are affected by the integral effects, environmental influences and boundary layer of wind tunnel inevitably. So, they are not so suitable to study aero-optical effects induced by supersonic mixing layer[9].

As a new aero-optics measuring technique, NPLS-WT can study the transient wavefront aberration induced by a cross-section of supersonic flow field at high spatiotemporal resolution[9]. This advantage makes it a powerful tool to study the aero-optical effects of supersonic mixing layer. Using NPLS-WT, the aero-optical effect of supersonic mixing layer was studied in this paper to find out the relationship between aero-optical aberrations and flow structures of supersonic mixing layer.

NPLS_WT

NPLS is a new flow visualization technique developed by the authors in 2005[10]. It can visualize the transient structure of a cross-section in supersonic flow field at high spatiotemporal resolution.

The spatial resolution of NPLS can reach up to micro dimension, and its temporal resolution is 6ns, and its temporal correlation resolution can reach up to 200ns. If tracer particles are seeded uniformly into supersonic free stream, NPLS images can reveal density distribution of the flow field qualitatively. Based on this character of NPLS, Tian L F, et al proposed NPLS-DT (NPLS-based Density Technique) to study density field in supersonic flow[11].

Integrating NPLS-DT and ray tracing method, Yi S H, et al developed a new wavefront measurement technique, NPLS-WT[9]. In NPLS-WT, the refractive index is computed from density field using Gladstone-Dale relationship[9]. The incidence location, incidence direction, and arrival location of ray are set artificially, and then Ray tracing method is performed to get optical information. So, NPLS-WT has obvious advantages[9]: (1). High spatiotemporal resolution; its time resolution is 6ns, and spatial resolution and time correction resolution can reach up to micrometers and 200ns respectively. (2). It can avoid the integral effects and study the wavefront aberration induced by the flow field of interest locally; (3). It can also avoid the influence from the test section boundary layers and environmental disturbances.

Aero-optical effects of supersonic mixing layer

The transmission of a collimated light beam through supersonic mixing layer with index-of-refraction variation leads to aero-optical aberration, as shown in Fig.1. The Mach numbers of the two free streams are 1.4 and 3.5 respectively, and they are pressure-matched at the end of the splitter plate. The total pressure of the lower stream is 101kPa.

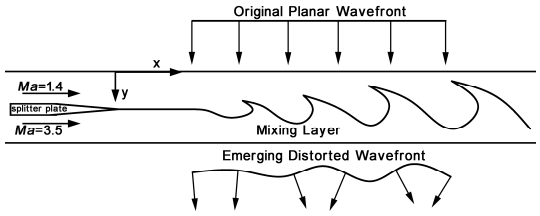

Fig.1. Planar optical wavefront distorted by supersonic mixing layer

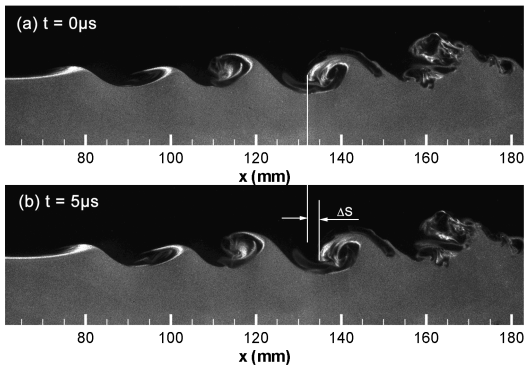

Fig.2. NPLS images of supersonic mixing layer

The NPLS images of the supersonic mixing layer with time interval of 5μs are shown in Fig.2, and the corresponding density fields measured using NPLS-DT are shown in Fig.3. The flow region is from x=61mm to x=183mm, and the spatial resolution of Fig.2 and Fig.3 is 120.6μm/pixel. The transition of the mixing layer is shown in Fig.2 and Fig.3 obviously, and the vortices become bigger as flowing downstream. The figures revealed vortices of different scales, so we can study their different effects on aero-optical aberration. From Fig.2, we can find that in 5μs, the motion of vortex of large scale is mainly the translation downstream, and the deformation is not obvious.

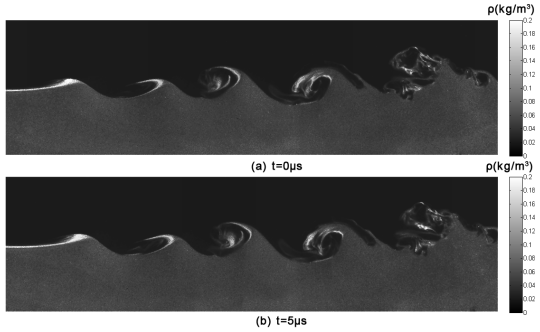

Fig.3. Corresponding density fields of Fig.2

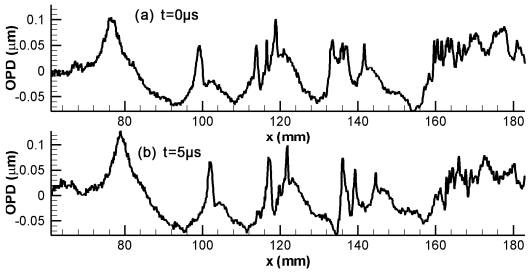

Fig.4. Optical path difference induced by supersonic mixing layer

As shown in Fig.4, are distorted wavefronts induced by the supersonic mixing layer shown in Fig.2. From Fig.4 and Fig.2, we can find that the OPD curve shape and the vortices in supersonic

mixing layer are matched spatially. Similar to the temporal evolution of large-scale vortex in supersonic mixing layer, the change of corresponding OPD curves is mainly the translation downstream, and the deformation is not obvious.

Multi-resolution analysis

In order to study the influence of large-scale structure on aero-optical aberration, OPDs induced by the same flow field of different resolution were studied by multi-resolution analysis. The upper images in Fig.5 are density field at different resolution of the same flow region. From (a) to (d), the resolution becomes lower. The lower images in Fig.5 are corresponding OPD curves. Comparing the curves in Fig.5, it could be found that a higher resolution results in a more detailed OPD curve, and a lower resolution results in a smoother OPD curve, in which less information in embodied. Therefore, high resolution is a major advantage of NPLS-WT, compared with other methods. From the OPD curves in Fig.5, we can easily conclude that the wavefront aberration is not sensitive to resolution, and the large scale flow behavior is aero-optically dominant.

Cumulative aero-optical interactions

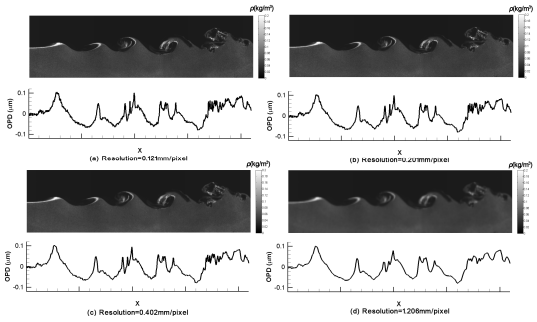

Fig.5. Density fields of different resolution and corresponding OPD

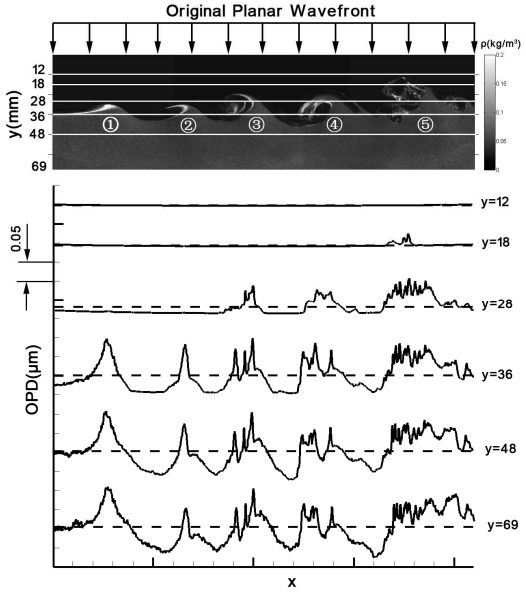

Fig.6. Density field and corresponding OPD at different location

One of the advantages of NPLS-WT is that the incidence location, incidence angle, and arrival location of the ray can be set artificially. Therefore, NPLS-WT can study the interested flow field locally and study the effects of different flow structures to aero-optical aberration. Using NPLS-WT, the OPDs at different locations during the transmission of the ray in supersonic mixing layer were measured, as shown in Fig.6. The dotted lines indicate OPD=0, and the distance between minor ticks is 0.05μm. Within the region y=0 to 12mm, the flow field with uniform density does not affect the OPD curve obviously. From y=12 to 18mm, the difference in density between vortex ⑤ and free stream of upper layer results in obvious changes of OPD curve at corresponding location. To y=28mm, composite effects from vortices ③, ④, and ⑤ lead to changes of OPD curve at corresponding locations, and the effect from vortex ⑤ becomes more obvious. To y=36mm, all of the five vortices affects the OPD curve, and there are local changes of OPD curve at the locations of the vortices. From y=36 to 48mm, although the effects of all the vortices exist, the density difference of vortices and free stream is small in this region, so the corresponding effect on OPD curve is not obvious. From y=48 to 69mm, the density field of free stream is uniform, so the OPD curve almost does not change.

Conclusions

Using NPLS-WT, the transient distorted wavefronts were measured at high spatiotemporal resolution. The results revealed that the changes of OPD curve and the large-scale vortices of supersonic mixing layer matched spatially. In 5μs, the change of OPD curve is mainly translation downstream, and its deformation is not obvious. The results of multi-resolution analysis revealed that the wavefront in near field is not sensitive to the resolution, and large-scale structures play a dominant role on the wavefront in near field. So, avoiding the emergence of large-scale flow structures in supersonic mixing layer can help improve aero-optical performance. The cumulative effects analysis show us that the density difference between large-scale structures and free stream is the main reason to wavefront aberration, and the larger the vortex is, the more obvious the effect to wavefront aberration is.

Acknowledgement

The authors are grateful for various contributions of Innovation Fund Program for Standout Graduate Students of NUDT (Grant NO. B130103), Hunan Provincial Innovation Foundation for Postgraduate (Grant NO. CX2013B002) and the National Natural Science Foundation of China (Grant NO. 11172326 and 11302256).

References

[1] Chew L. Coherent structures effects on shear layer optics [C]. AIAA Paper, 1990, 90-0185.

[2] Yi S H, Hou Z X, Zhao Y X. Supersonic free-vortex aerowindow and its optical quality [M]. Changsha: Press of NUDT, 2005.

[3] Neal D R, Copland J, Neal D. Shack-Hartmann wavefront sensor precision and accuracy [J]. Proc. of SPIE, 4779: 148-160.

[4] Trolinger J, L'Esperance D. Optical diagnostics for quantifying flow control effects on aero optical wavefront degradation [C]. AIAA Paper, 2005, 2005-4658.

[5] Tyson R K. Introduction. In: Tyson R K, editor. Adaptive-optics engineering handbook, Optical engineering series, vol. 67. New York: Marcel Dekker, 2000.

[6] Jumper E J, Hugo R J. Optical phase distortion due to turbulent-fluid density fields: quantification using the small-aperture beam technique [C]. AIAA Paper, 1992, 92-3020.

[7] Jumper E J, Fitzgerald E J. Recent advances in aero-optics [J]. Progress in Aerospace Phenomena, 1982, (37): 299-339.

[8] Welsh B M, Ellerbroek B L, Roggemann M C, et al. Fundamental performance comparison of a Hartmann and a shearing interferometer wave-front sensor [J]. Applied Optics, 1995, 34(21): 4186-4195.

[9] Yi S H, Tian L F, Zhao Y X, et al. Aero-optical aberration measuring method based on NPLS and its application [J]. Chinese Sci Bull, 2010, 55(31): 3545-3549.

[10] Zhao Y X, Yi S H, Tian L F, et al. Supersonic flow imaging via nanoparticles [J]. Sci China Ser E, 2009, 52(12): 3640-3648.

[11] Tian L F, Yi S H, Zhao Y X, et al. Study of density field measurement based on NPLS technique in supersonic flow [J]. Sci China Ser G, 2009, 52(9): 1357-1363.

Advanced Materials Research Vols. 989-994 (2014) pp 867-870
© (2014) Trans Tech Publications, Switzerland
doi:10.4028/www.scientific.net/AMR.989-994.867

Simulation Realization of Frequency-Variable and Speed-Adjustable System Based on Vector Control

SHE Yan

Shunde Polytechnic, Foshan 528300, China

Shelley186@sohu.com

Keywords: AC Motor; SVPWM; FOC; Simulation

Abstract. To provide the necessary design parameters for the actual motor control system, The paper introduces the modeling course of voltage space vector pulse wide modulation (SVPWM) arithmetic and AC motor under MATLAB/SIMULINK environment, discuss founding dynamic model of frequency-variable speed-adjustable system based on vector control, according to the principle of SVPWM. The paper presents the new detailed method of realizing simulation, key problems and results of the simulation were analyzed in detail. The experimental simulation results show that this system has smaller fluctuations of voltage and torque, quicker response speed, and all of the indicators accord with the performance of the actual motor. the simulation arithmetic have value to realize controlling motor with digital signals processing.

Introduction

The simulation technique is a method for experimental study by computer based on the mathematical model, is a very effective tool for the analysis of complex systems. In a sense, numerical simulation can be comparable with the real system as long as constructing of a sufficiently accurate mathematical model. In the general computer simulation software of control system, Math Works's MATLAB SIMULINK is a very excellent simulation software. Only draw the control system diagram of required analysis and design on the graphics window, the model system can be linearized and simulated by the software itself.

In the electric drive system, Through apply the simulation technology, build the simulation model of the motor and the transmission, without programming and under the artificial environment or conditions, simulate model on computer to replace the real operation of the motor in the working field experiment. In this way, the researchers not only can obtain reliable data, and saves the time and cost. With intuitive oscilloscope window, real-time motion curve of the motor's parameters(such as speed, torque, etc.) can be displayed. More important is to modify the system parameters until the desired characteristics. Practice has proved, the application of the simulation system in the research of asynchronous motor vector control system, can realize the optimization design, has a certain application value and practical significance to the high performance of the variable frequency and speed system.

SIMULINK asynchronous motor

In order to understand more clearly internal model of motor and reflect accurately the transition process of the simulation, motor modules inside SIMULINK is not used during the simulation, but the dynamic model is modeled and encapsulated according to the asynchronous motor. It can reflect the physical characteristics of asynchronous motor, and is convenient for simulation calculation. According to the mathematical model of induction motor in the literature [1] and [2], the simulation model is obtained in the two phase static αβ coordinate system[3], and is encapsulated in the front of the module by 3S/2S transformation. Set the following parameters: rated power 2kW, rated voltage 220V, rated current 4.1A, rated speed 1400r/min, number of pole-pairs Pn=2, Ls=0.165H, Lr=0.162H, Lm=0.149H, Rs=4.5Ω, Rr=5.4Ω, moment of inertia J= 0.00095kgm^2.

SIMULINK implementation of SVPWM algorithm[4][5]

SVPWM control technology starts from the angle of motor, focus on the circular magnetic field in motor with constant amplitude, i.e. sinusoidal magnetic flux. It is the ideal circular flux trajectory by the three-phase symmetrical sine wave voltage as the reference, uses the actual magnetic flux generated by three-phase inverter different switch mode to approximate the reference flux circle, the flux trajectory is obtained by the addition of voltage space vector control, so as to achieve higher energy. The three-phase inverter bridge circuit is designed according to certain rules to control transistor of the three bridge arm on-off, can output three-phase sinusoidal voltage by the DC voltage. Therefore, bridge arm's on-off state of the three-phase bridge circuit is eight. The definition of these 8 switches combined into 8 basic specific space vector, are labeled as V4 (100), V6 (110), V2 (010), V3 (011), V1 (001), V5 (101) and 2 zero vector V0 (000), V7 (111). The first is specific, can form a regular hexagon, respectively in the theta = ω t =0 °, 60 °, 120 °…, and the 6 vector size is determined by the DC power supply voltage Ud and can not control, the 360° area is divided into six 60 degree sector, but not directly obtain arbitrary phase angle and the vector V of the absolute value controlled. By using a linear combination of these 8 kinds of voltage vector can obtain more reference vector different from specific basic space vectors of phases, according to calculated relevant state time, control the switch turn-on and turn off. Generally divided into four steps:

(1) Determine located region of the reference vector. (2) Calculate two adjacent switching voltage vector's action time. (3) Calculate a, b, c three-phase corresponding comparator switch point. (4) Produces the three-phase voltage Ua, Ub, Uc.

Determine the vector sector. The located sector of voltage vector is calculated by two dimensional static coordinate α axis and β axis's component u_α and u_β (the circle is divided into 6 sectors, sector number is indicated by N). If $u_\beta > 0$, then A=1, or A=0; if $\sqrt{3}u_\alpha - u_\beta > 0$, then B=1, or B=0; if $-\sqrt{3}u_\alpha - u_\beta > 0$, then C=1, or C=0. Sector N=A+2B+4C.

Calculate the boundary vector time T_x, T_y. Define $X = \sqrt{3}u_\beta \times Ts/Ud = \sqrt{3}\sin\theta \cdot Ts \cdot u_s / Ud$, $Y = \frac{1}{2}(\sqrt{3}u_\beta + 3u_\alpha) \times Ts/Ud = \sqrt{3}\sin(\theta + 60^0) \cdot Ts \cdot u_s / Ud$, $Z = \frac{1}{2}(\sqrt{3}u_\beta - 3u_\alpha) \times Ts/Ud = \sqrt{3}\sin(\theta - 60^0) \cdot Ts \cdot u_s / Ud$.

According to different sectors of the voltage vector calculate 2 adjacent vector's action time T_x, T_y, the values as shown in the following table 1. The multiplexer can constitute a model graph. When $T_x + T_y > T_s$, $T_{x1} = T_x \frac{T_s}{T_x + T_y}$, $T_{y2} = T_y \frac{T_s}{T_x + T_y}$.

Find out the 3 vector switching points T1, T2, T3. Define $T_a = \frac{T_s - T_x - T_y}{4}$, $T_b = T_a + T_x/2$,

Table 1 The boundary vector time assignment table in different sectors:

N	1	2	3	4	5	6
Tx	Z	Y	-Z	-X	X	-Y
Ty	Y	-X	X	Z	-Y	-Z

Table 2 Three compare register assignment table in different sectors:

N	1	2	3	4	5	6
T1	Tb	Ta	Ta	Tc	Tc	Tb
T2	Ta	Tc	Tb	Tb	Ta	Tc
T3	Tc	Tb	Tc	Ta	Tb	Ta

$T_c = T_b + T_y/2$.The last step is to value the above three parameters in table 2 according to the different sectors. The multiplexer can constitute a model graph.

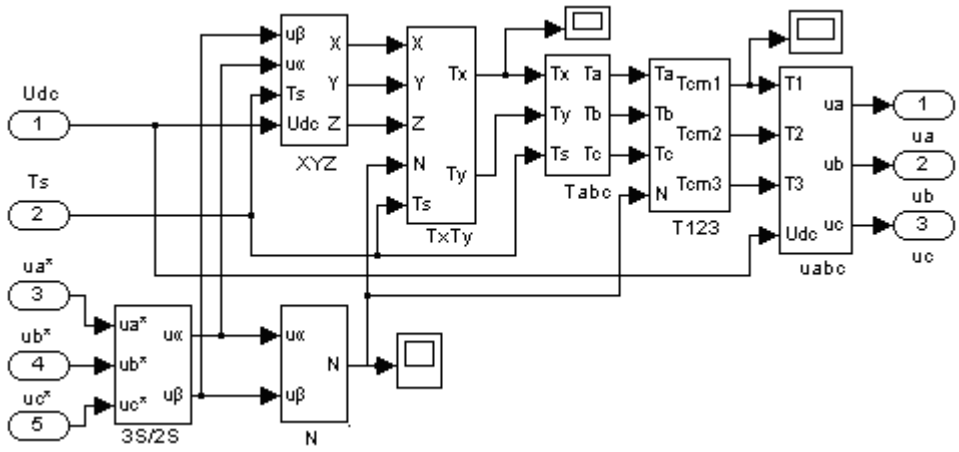

Fig. 1 SVPWM simulation model

Generation of PWM waveform and realization of inverter.SVPWM is using the equivalent time's triangular wave of constant frequency and amplitude to modulate 3 input time T1,T2,T3,the triangular wave compared with space vector switching point Tx, once Tx and the triangular wave are equal, just change PWM wave state. Switch set determines period and amplitude of the triangle wave[2]. At the same time switching device in the abstract, the switch device of upper and lower bridge arm is equivalent to 1 ideal switch.

SVPWM simulation model. Above each model diagram separately are packaged to connect, SVPWM simulation model is shown in Figure 1. Assume switching frequency is 2.4KHz when f_S =50Hz, Udc=600V.

Flux Model SIMULINK[6]

According to the rotor flux observation model of M-T coordinates, obtained the simulation model.

Simulation of Vector Control Inverter

The above simulation models are encapsulated to form the simulation model diagram of closed-loop variable-frequency and speed control system as shown in figure 2.Through simulation, the SVPWM output voltage waveform, speed and torque diagram and is consistent with the actual output of the graph, these have certain reference value[7][8]. The simulation results of SVPWM model output waveform is figure 3.

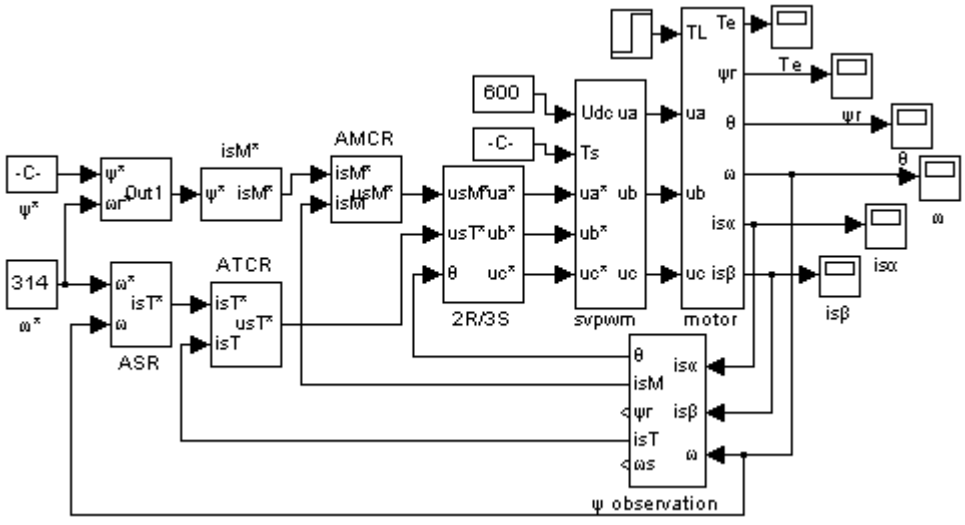

Fig. 2 Simulation model diagram of variable-frequency and speed control system

Conclusion

Simulation is an important tool of product design. Using MATLAB SIMULINK is convenient for simulation easily to the asynchronous motor and variable-frequency and regulative-speed system, the model is intuitive without the need of programming, easy to understand and use. The simulation results show, the output voltage waveform and current is sinusoidal, that validate the space vector modulation. Show that the vector control system with SVPWM has good dynamic, static performance; Compared to the traditional modulation, has Smaller fluctuation of torque and current in this way, higher utilization ratio of DC voltage. Realizes the decoupling between flux and torque control, asynchronous motor got same transient response characteristics with DC motor, effectively improve the control effect and system performance. Simulation results of the flux, speed and torque are basically consistent with the requirements of the actual motor control. The control algorithm can be used for digital signal processor, to realize the digital motor controlled, providing theoretical basis and necessary system parameters for further research and design of AC drive system.

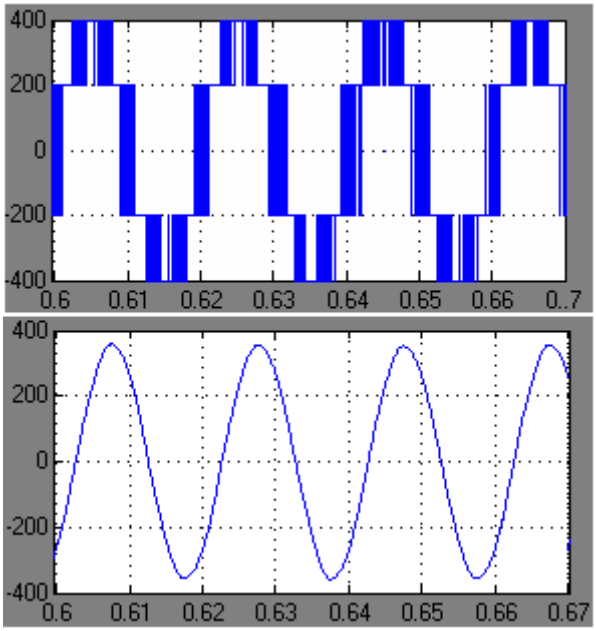

Fig. 3 SVPWM output voltage waveform and simulation results after filtering（50Hz）

Reference

[1] LI Huade. AC Adjustable Speed Control System[M]. Beijing:Electronics Industry Press,2003.3.
[2] CHEN Jian. Power electronics[M] . Beijing: Higher Education Press,2002.
[3] PAN Xiaosheng, HAO Shiyou. 50 cases of MATLAB motor simulation essence[M]. Beijing: Electronics Industry Press,2007.8.
[4] WANG Chenyuan, LI Haodong, XIA Jiakuan. Study of Intelligent Vector Control System Based on TMS320F240[J]. Applied Power Electronics Conference and Exposition,2001,2（5）:550-553.
[5] ZHOU Yuanshen. AC& DC Adjustable speed system and MATLAB simulation[M]. Beijing: Chinese Power Press, 2004.
[6] LI Yong, HUANG Lipei, LI Fahai, All Digital Space Vector PWM Induction Motor Drive Based on Flux Control[J]. IEEE TENCON,2003,3（8）:598-601.
[7] SHE Yan, LI Ling. Simulation of Variable Frequency System Based on SVPWM Vector Control [J].Electric Machines & Control Application, 2009, 36 (7) : 63-66.
[8] GONG Yunfei, FU Lixin. Simulation of PMSM Vector Control System based on Matlab [J]. Micro motor, 2007, 40 (2):33-36.

Advanced Materials Research Vols. 989-994 (2014) pp 871-875
© (2014) Trans Tech Publications, Switzerland
doi:10.4028/www.scientific.net/AMR.989-994.871

Research Status and Application Prospect of Deep Cryogenic Treatment Technology on Cemented Carbide

Tuhua Guan[1, a], Hongmei Liu*[1, b], Yuanbin Xu[2, c], Chengqun Wu[2, d], Lv Yi[2, e]

[1]Engineering Training Center, Nantong University, Nantong, Jiangsu, 226019, China

[2]College of Mechanical Engineering, Nantong University, Nantong, Jiangsu, 226019, China

[a]tygth@ntu.edu.cn, [b]liu.hm@ntu.edu.cn, [c]1203904927@qq.com, [d]qywn2013@163.com, [e]260443169@qq.com

Corresponding Author:Hongmei Liu. Tel: +86 13706293646. E-mail address: liu.hm@ntu.edu.cn.

Keywords: cryogenic treatment, cemented carbide, action mechanism, progress parameters.

Abstract. Cryogenic treatment as an effective non-destructive modification of material, has been widely applied. Equipments and technologies of cryogenic treatment were described, the current research status of cryogenic treatment technology on cemented carbide was reviewed, the action mechanism of cemented carbide cryogenic treatment was analyzed. Finally, in this paper some views and outlooks of cryogenic treatment technology in industrial applications were put forward.

Introduction

Cemented carbide is mainly made of a hard carbide phase (WC,TiC) powder and a binder of cobalt(Co), nickel (Ni) or molybdenum (Mo), sintered by powder metallurgy technique. Cemented carbide with high hardness, high toughness and wear resistance and a series of advantages, widely used in cutting tools, molds, measuring tools, wear parts, and other areas of the industrial production. With the rapid development of domestic precision manufacturing, the requirements of quantity and quality of carbide also increase quickly, the current production of cemented carbide has been unable to meet production requirements. Therefore, research of new techniques and new methods to improve the performance of ordinary cemented carbide is in dire need to solve the problem.

Cryogenic treatment as a treatment process of material is researched by scholars both at home and abroad, and constantly applied in the real production. Cryogenic treatment [1] is that the materials are placed in a specific device which can control the temperature, usually the temperature is below -130℃, it can change the material microstructure and phase structure. This change in macro performance for hardness, wear resistance, toughness and dimensional stability of materials are improved and enhanced, so as to achieve the purpose of improving and strengthening the material properties.

Cryogenic treatment applied in iron and steel material is relatively mature, reached a consensus on its action mechanism. The general mechanism can be summarized as [2-4]: 1) Cryogenic treatment can be retained austenite into martensite, thereby enhancing the strength and hardness of the material. 2) Cryogenic treatment can precipitate fine carbides, improving the wear resistance of material. 3) Grain refinement of the internal organization of the material, to improve the toughness of the material. But the action mechanism of cemented carbide cryogenic treatment is still in the research stage, there is a big controversy. The current research status of cemented carbide cryogenic treatment was reviewed in this paper, in order to playing a certain reference value for further research on carbide cryogenic treatment.

Cryogenic treatment process

Heating and cooling rate. There are different views about cryogenic process heating and cooling rate. One point is that it should strictly control the heating and cooling rate, they think too fast heating and cooling rate can cause internal stress within the material, so that the material deformation cracks occur. Another point is that it should use rapid cryogenic cooling method and rapid thermal method,

they think it can make easier for transformation of austenite to martensite, thereby strengthening the material properties.

Cryogenic processing time. Cryogenic treatment of the holding time is determined by the material. Some materials can achieve the anticipated effect in a short period of time, thereby reducing costs. But most scholars believe that prolonging the time of cryogenic insulation fully retain austenite to martensite, and more conducive to separate out carbide particles.

Number of cryogenic treatment. For the number of cryogenic treatment, forming a more unified point of view. Studies have shown that repeat treatment can increase the cryogenic effect, and that twice cryogenic effect is best, because the second cryogenic treatment can continue to repeat the first change, but after several times of cryogenic treatment, material has been in a stable state, so there is no need to deal with again.

Combination of heat treatment and cryogenic treatment. The process sequence arrangement of cryogenic, quenching and tempering has been hotly debated, which has not formed a unified point of view, from the current research result, different performance requirements of material should be taken to different process order. Cryogenic treatment before tempering is suitable for flexible, bearing large impact load of the mold, cryogenic treatment after tempering is suitable for high hardness requirements, smaller dynamic load of the mold.

Cemented carbide cryogenic treatment of domestic and foreign research status

Cemented carbide cryogenic treatment of foreign research status. In 1965, the United States put cryogenic treatment into practical application in the first place. Since then, the scholars of the United States, Britain, Russia, Japan and other countries in the world have launched a more in-depth and extensive research. Cryogenic treatment as a way to improve the service life of the carbide cutting tools have been widely used.

Thankur D, etc. [5-6] studied the effects of cryogenic treatment to improve the mechanical properties of carbide cutting tools, the study found that cryogenic treatment can improve carbide hardness, wear resistance, bending strength, impact toughness and magnetic coercive force, However, it will decrease the permeability. Cryogenic treatment changes the physical properties of the Co phase, densified Co binder phase can be more strongly fixed WC particles.

TV SreeramaReddy, etc [7] studied the P30 coated carbide cutting tools for cryogenic treatment at -176℃, which composition is WC-17.23% Co-1.42%. And then machine C45 steel workpiece through the use of untreated and cryogenic treatment of cemented carbide tools P30. The results have shown that: in the process of machining, after cryogenic treatment of cemented carbide cutting tools flank wear and cutting force is lower than the untreated carbide cutting tools, and the smoothness of workpiece surface is better. They believe this is due to the cryogenic treatment Carbide Co binder phase in contraction, thereby firmly bonding WC hard phase, making it more uniform.

Simranpreet singh Gill, etc [8] studied the effect of cryogenic treatment on carbide coating bond strength. The TiAIN coated carbide tools were subjected to cryogenic treatment at two levels -110℃ and -196℃ of temperature independently. The experimental results showed that: better wear resistance and processing properties after the coated carbide tools at -110℃ cryogenic treatment conditions than lower temperature cryogenic treatment and untreated.

Vadivel, K, etc [9] studied the various performances of cryogenically treated and untreated coated carbide tools in turning of nodular cast iron. From the results, carbide tools after cryogenic treatment exhibit better performance in the surface roughness of the workpieces, and flank wear than the untreated one. This is due to cryogenic treatment makes carbide distribution of η phase is more subtle.

Cemented carbide cryogenic treatment of domestic research status. The research on the cryogenic treatment technology in China began from the 1980s, although the research started late, but also made some encouraging results. Chen Zhenhua, etc [l0] researched the mechanical properties of two WC-Co cemented carbide YG8 and YG25 after cryogenic treatment different time. The results showed that: cryogenic treatment can effectively improve the hardness, strength, wear resistance and fatigue life of these two carbide. Cryogenic processing time is the main process parameters, optimum process time of YG8 alloy is 2h, while YG25 for 8h. The main reason for the performance change is

that cryogenic treatment can improve the carbide surface residual compressive stress and promote the martensitic phase transformation in the binding phase Co. Deng Ya, etc [11] studied the effects of cryogenic treatment on the structural properties of TiN coated carbide composite system, the thickness of 2μm TiN coating deposited in YW2 cemented carbide substrate, the TiN/YW2 system was cryogenic treatment respectively 10h, 20h, 30h and 40h at -196℃. The results showed that: the optimum comprehensive mechanical properties of TiN/YW2 were cryogenic treatment in 30h, after cryogenic treatment stress induced grain reverse in the coating caused TiN preferred orientation, so the hardness of the system was improved. After the cryogenic treatment, diffuse distribution of granular ϒ phase significantly reduce or disappear, pore clusters get close, organizations become more compact, reduce the crack, improve the fracture toughness and bonding strength of TiN/YW2 system. Liu Xiaohu, etc [12] researched the effect of cryogenic treatment on the carbide phase structure through XRD analysis and performance testing. The results showed that: cryogenic treatment can make cemented carbide alloy phase atomic migration and rearrangement and tend to be uniformity, so as to improve high cobalt carbide phase composition, while can make the solid solution of W and C more uniform distribution, improving solid solution strengthening effects, thus significantly improve the bending strength of low cobalt magnetic carbide. Yuan, YG, etc [13] studied the effects of cryogenic treatment on WC-Co cemented carbide grinding residual stress. The results showed that: cryogenic treatment can reduce the residual stress on the surface of the cemented carbide. Residual stress depends on the cryogenic treatment process parameters, such as cryogenic temperatures, cooling and heating speed, residual stress change with soaking temperature, but does not obviously change with immersion time. Jiang Y, etc [14] studied the mechanical properties and magnetic energy of the WC8wt%-Co cemented carbide, which is insulated at -196℃ for 72h. The results showed that: After cryogenic treatment, the hardness, compressive strength, abrasion resistance and fatigue resistance of the cemented carbide significantly enhanced, while the bending strength and toughness did not change significantly. Magnetic properties show that with the increase of the coercive force, the saturation magnetization decreases. Changes in the mechanical properties depend largely on soaking time, which maybe the cryogenic treatment changed the residual stress and martensite.

The domestic application of cemented carbide cryogenic treatment has also carried on the related research. He Huibo, etc [15]studied the performance of the TiAIN coated carbide inserts (YT15), which is cryogenic treatment at -196℃ for 30h. The study found that after cryogenic treatment of coated carbide inserts, the cutting force and temperature dropped significantly, especially at higher cutting speed, the flank wear is also significantly smaller, and improved the cutting smoothness on the surface of the workpiece. Niu Qinlin, etc [16] studied cryogenic treatment on the influence of different Co content carbide reamer. The experimental results showed that cryogenic treatment can improve the hardness of carbide reamer, and the higher Co content, the more obvious effect. Yan, HJ, etc [17] studied YT30 cemented carbide inserts cryogenic treatment process using orthogonal experimental method. the orthogonal experimental results showed that cryogenic temperature is the first influence factor, followed by the cooling rate, then the tempering temperature, finally the cryogenic heat preservation time. Cryogenic treatment can promote the occurrence of carbide Co binding phase by α-Co converted to ε-Co phase, thereby improving the hardness and wear resistance of the tool.

Carbide industrial popularization and application of cryogenic treatment technology and development trend

Research the action mechanism of cryogenic treatment is the foundation of the cryogenic technology industry promotion. Cryogenic treatment technology compared with heat treatment technology is a relatively new technology, the current research on the action mechanism of cemented carbide cryogenic treatment is less. If there is no in-depth analysis of the mechanism, there is no way to grasp the real law of the cryogenic treatment on the impact of material properties.

Cryogenic treatment process is the key to the industrial promotion of the cryogenic treatment technology. Cryogenic treatment process determines the effect of treatment, cryogenic treatment is not a separate process, it is an extension of the cold treatment and heat treatment, so we need to cooperate with other process, form relatively perfect process route. At the same time, the setting of process parameters also determine the effect of cryogenic treatment, such as cooling rate, holding time, soaking temperature, processing times and quenching or tempering parameters such as temperature, time. Cryogenic treatment process route and process parameters selection will eventually lead to different treatment effect.

Cryogenic treatment equipments are the guarantee of the technology applied. Cryogenic treatment device should be temperature controlled, controlled cooling rate and high temperature uniformity characteristics in order to meet the requirements of industrial production. In addition, we must reduce the cost of production, to meet the increasing performance demands of carbide. Application of cryogenic treatment technology will produce great economic and social benefits, for which the following several aspects can strengthen China's cemented carbide cryogenic treatment technology into a large scale industrial application.

1) Strengthen the action mechanism research of carbide cryogenic treatment. The application and development of carbide cryogenic treatment technology are based on the theory of its action mechanism, the current research on the mechanism of carbide cryogenic treatment has not been able to reach a consensus. Through the research of the mechanism of cryogenic treatment, it can provide a theoretical guidance for the development of high performance carbide and the promotion of cryogenic treatment technology.

2) Due to the type and composition ratio of cemented carbide are diverse and complex, from the present study is difficult to form a unified process method, which is one of the bottlenecks restricting the technology into industrial applications. It must determine the critical evaluation of factors, explore the relationship between the primary and secondary effects of various factors, and the optimization of process parameters on this basis, given the optimum process, which will promote the popularization and application of cemented carbide cryogenic treatment.

3) The lag of industrial cryogenic equipment hindered the application of cryogenic treatment technology promotion, the technology of liquid nitrogen cooling, temperature control, thermal insulation and liquid nitrogen dispersion need to be improved, to develop safe and reliable performance, high efficiency and energy saving, simple operation, and can meet the demand of industrial mass production equipment.

Summary

It is no doubt that cryogenic treatment technology can change the performance of cemented carbide, for carbide cryogenic treatment technology to form the industrial application, it must deeply analyze the action mechanism, select the appropriate treatment process, develop advanced cryogenic equipment. This will improve the technical level and comprehensive competitiveness of manufacturing. Because domestic research started late and restricted by technology, the research of carbide cryogenic treatment is still in the preliminary stage. But whether it is from the perspective of the demand of cemented carbide, or from improving its mechanical properties, reducing production costs, using cryogenic treatment technology to further improve the performance of carbide is an inevitable choice. In the future, with the continued research by domestic and foreign scholars, cryogenic treatment technology will gradually mature, carbide will also get more extensive application.

Acknowledgements

This research was supported by grant 2013-742-1, 2013-742-2 from the Economic and Information Commission of JiangSu Province of China.

References

[1] Jiang Yong. Understanding the fatigue behavior of WC-Co based cemented carbide and stress analysis method[D].Hunan university,2013.

[2] Gu Kaixuan, Zhang Hong, Wang Junjie, etc. Effect of cryogenic treatment on microstructure and properties of 40CrNiMoA steel[J]. Hot Working Technology, 2012,41(18):189-191.

[3] Chen Gang, Wang Qiongshuang, Han Jichu, etc. Study of the microstructure and properties of deep cryogenic treatment and tempering on M42 high-speed steel[J]. Journal of Hunan university (Natural Sciences), 2012,39(4):53-58.

[4] Liu Yong, Yu Wenping, Zhang Jindong, etc. Effect of deep cryogenic treatment on microstructure and mechanical properties of T8A steel[J].Transactions of Materials and Heat Treatment. 2010, 31(10):48-52.

[5] Thankur D, Ramamoorthy B, Vijayaraghavan L.Influence of different post treatments on tungsten carbide-cobalt inserts[J]. Materials Letters,2008,62(28):4403-4406.

[6] Sreerama Reddy T V, Sornakumar T, Venkatarama Reddy M,et al. Machinability of C45 steel with deep cryogenic treated tungsten carbide cutting tool inserts[J].Int. J. Refract. Met Hard. Mater. 2009, 27 :181-185.

[7] T.V. SreeramaReddy, T.Sornakumar, M.VenkataramaReddy, etc. Machinability of C45 steel with deep cryogenic treated tungsten carbide cutting tool inserts[J]. Refractory Metals and Hard Materials. 2009,27(1):181-185

[8] Simranpreet singh Gill, Jagdev singh, Harpreet singh, etc.Investigation on wear behaviour of cryogenically treated TiAlN coated tungsten carbide inserts in turning[J].Machine Tools and Manufacture.2011,51(1):25-33

[9] K. Vadivel,R.Rudramoorthy.Performance analysis of cryogenically treated coated carbide inserts[J].Advanced Manufacturing Technology.2009,42(3-4):222-232

[10] Chen Zhenhua, Jiang Yong, Fan Lian, etc.Influence of cryogenic treatment on microstructure and properties of WC-Co cemented carbides[J].Transactions of Materials and Heat treatment,2011,32(7):26-30

[11] Deng Ya, Nie Chaoying, Ding Ying, etc.Effect of cryogenic treatment on mechanical properties of TiN coated cemented carbide[J].Transactions of Materials and Heat treatment,2012, 33(9): 106-111

[12] Liu Xiaohu, Shi Kaihua, Liu Zhi, etc.Effect of deep cryogenic treatment on phase structure and properties of cemented carbides[J].Rare Metals and Cemented Carbides,2013,41(6):42-45

[13] Yuan, YG;Xu, CH.Influence of cryogenic treatment on grinding residual stress of WC-Co cemented carbides[C].Advanced Materials Research,2012:1746-1750

[14] Yong, J;Ding,C.Effect of cryogenic treatment on WC-Co cemented carbides[J].Material Science and Engineering.2011,528(3):1735-1739

[15] Hui-Bo He, Wen-Qiang Han, et al.Effect of deep cryogenic treatment on machinability and wear mechanism of TiAlN coated tools during dry turning[J].Precision Engineering and Manufacturing. 2014,15(4):655-660

[16] Qiulin Niu, et al.Analysis on the Microstructure of Carbide Reamers after the Cryogenic Treatment[J].Advanced Materials Research.2011,188:26-31

[17] Yan, HJ; Xu, HH; Li, XM.Experimental research on deep cryogenic treatment process of YT30 cemented carbide inserts[C].Advanced Materials Research,2011:702-705

CHAPTER 2:

Applied Mechanics, Construction and Testing Technologies

Advanced Materials Research Vols. 989-994 (2014) pp 879-882
© (2014) Trans Tech Publications, Switzerland
doi:10.4028/www.scientific.net/AMR.989-994.879

The fatigue performance evaluation of pressure vessel steel using modified staircase method

Huan Xue[1,a], Rongfeng Li[1], Lixin Wu[1], Wenjie Peng[1], JingQin Hu[2]

[1]Research and Development Center of Wuhan Iron and Steel (Group) Corp., Wuhan, 430080, China

[2]Quality Inspection Center of Wuhan Iron and Steel group Corp., Wuhan, 430080, China

[a]stonemechanics@163.com

Keywords: Modified Staircase Method, Fatigue Limit, Pressure Vessel Steel.

Abstract. Increasing attention has been paid on fatigue performance evaluation in the recent years. More efficient fatigue testing methods are imperatively needed to accomplish the test requirement. The modified staircase theory is introduced in this paper. Traditional staircase method and modified staircase method are respectively used to evaluate the fatigue performance of pressure vessel steel Q345R. Results show the fatigue limits are 194MPa and 193MPa respectively, which indicates the modified staircase method can enhance the testing efficiency about 50% and keep the test veracity.

Introduction

Cyclic loading lower than the material yield strength often appears on the most of metallic components that popular used in mechanical engineering. The fatigue phenomenon happens after the cyclic loading runs a long time, which is the main failure mode of metallic component. About 80% of failure of metal products caused by fatigue according to statistics, most of which is suddenly broken, the loss is often more serious. The pressure vessel steel is the typical one, whose fatigue crack problem leads disastrous loss. Therefore, the fatigue performance evaluation of these high risk steel are necessary [1].

The fatigue design is set up based on lots of experiment data, thus the simple and low cost standard testing samples are usually used in fatigue test with the considerations of cost and operability. So the standard fatigue test occupies a pivotal position in the study of fatigue design and performance evaluation [2-3]. Traditional staircase is the main testing method to determinate fatigue limit of materials. Many researches have been done on this field in the recent years. Chen et al. [4] adopt the method of computer imitation, and through studying over a dozen materials-draw the conclusion：when using staircase method to determine the fatigue limit of material, the stress increment is selected at range from 2% to 6% of the fatigue limit, and the disperse has important influence on the precision of fatigue limit. Song et al. [5] carried out the fatigue tests on butt and angle welded joints of high strength steel with one point experiment and the minimum of specimen experiment. The effects of butt and angle welded joints on the fatigue life were analyzed with mathematical statistics. Yin et al. [4] describes the method of mathematical statistics related to fatigue. The method can make the fatigue test result with great dispersion be processed reasonably, so as to provide correct test data for appraisal of material fatigue and estimation of fatigue life.

However, along with the increasing demand for the security considerations of high-strength drive shaft product, the relevant assessment of fatigue properties of metallic materials attracts more and more attention. More efficient fatigue testing methods are imperatively needed to accomplish the test requirement. The modified staircase method is one of the best candidates to solve the problem, which is introduced in the second section of this paper. Traditional staircase method and modified staircase method are respectively implemented to evaluate the fatigue performance of pressure vessel steel Q345R in the third section. Results are compared and analyzed in the last section.

Modified staircase method

Some data can not be directly measured, such as fatigue strength, the critical pressure of explosion, armor-piercing distance of bullet et al. These kinds of data can only be measured by sensitivity tests. The staircase method is actually one of the most effective sensitivity tests until now. However, the traditional staircase method only focuses on the current data, and can not use the accumulated data tested before. Large number of samples and corresponding test fees are needed to ensure the predictive precision. In order to solve the problem, new methods are developed to estimate percentiles and percentages of sensitivity variables by combining previous experimental data and current test data. The modified staircase method is one of the most effective one which is already brought into Chinese National Standard [8].

For the same group of products or the same type of steel with different specifications can use the previous experimental data as the base of next fatigue test. Before the test, two important parameters, the average fatigue strength and deviation, of previous data should be founded. For several group of data, the average data can be adopted to be the reference value.

$$\bar{\sigma}_{\mathrm{y}}=\frac{1}{n}\sum_{i=1}^{n}\sigma_i \qquad \bar{\mu}_{\mathrm{y}}=\frac{1}{n}\sum_{i=1}^{n}\mu_i \tag{1}$$

The initial stress in the traditional staircase method has not been clearly regulated, which is often 20% to 30% of the tensile strength. Whereas, a wide initial stress will greatly increase the testing time. In another aspect, the stress step is often set to be 5% of the fatigue limit, which is also with indeterminacy [8]. But in the modified staircase method fatigue test the initial stress and the stress increment should be the average fatigue strength $\bar{\mu}_{\mathrm{y}}$ and deviation of the reference data $\bar{\sigma}_{\mathrm{y}}$ respectively.

Rearrange the test data in order to count the frequencies of failure and non failure of the specimens tested at different stress levels. Use statistical analysis only for the events 'failure' and 'non-failure'. Use the analysis for the group with the least number of observations. Denote the stress levels arranged in ascending order by $S_0<S_1<\ldots\ldots S_l$ where l is the number of stress levels, denote the number of events by f_i, and denote the stress step by d. Estimate the parameters for the statistical distribution of the fatigue strength, Equation (2), from:

$$\hat{\mu}_y=\mathrm{S}_0+d\left(\frac{A}{C}\pm\frac{1}{2}\right) \qquad \hat{\sigma}_y=1.62\mathrm{d}(\mathrm{D}+0.029) \tag{2}$$

Where $\mathrm{A}=\sum_{i=1}^{l}if_i$, $B=\sum_{i=1}^{l}i^2f_i$, $C=\sum_{i=1}^{l}f_i$, $D=\frac{BC-A^2}{C^2}$. In Equation (2), take the value of ±1/2 as: -1/2 when the event analyzed is failure; +1/2 when the event analyzed is non-failure. This condition is generally satisfied when $\mathrm{d}/\sigma_{\mathrm{y}}$ is selected properly within the range 0.5 to 2. Estimate the lower limit of the fatigue strength at a probability of failure P for the population at a confidence level of 1-α, if the assumption of a normal distribution of the fatigue strength is correct, from the equation:

$$\hat{y}_{(p,1-\alpha)}=\hat{\mu}_y-k_{(p,1-\alpha,\nu)}\hat{\sigma}_y \tag{3}$$

Where the coefficient $k(\mathrm{P},1\text{-}\alpha,\nu)$ is the one-sided tolerance limit for a normal distribution. Take as the number of degrees of freedom, ν, the number which was used in estimating the standard deviation.

Traditional staircase fatigue test of Q345R

The fatigue performance evaluation of pressure vessel steel Q345r using traditional staircase method has been carried out. The initial stress is set to be 200Mpa, and the stress step is set to be 20Mpa, which is 5% of the tensile strength of Q345r. Figure 1 shows the stress up and down sequence of staircase. 14 effective samples with 7 effective stress pairs are selected.

The degree of freedom of this test is 6. For a 10% probability of failure, at a confidence level of 95%, A=10.0, B=16.0, C=7.0, D=0.245, and the standard deviation is 8.9Mpa. The average fatigue strength $\hat{\mu}_y$ is calculated to be 218.6Mpa, and the lower limit of the fatigue life $\hat{y}_{(p,1-\alpha)}$ is estimated to be 194Mpa.

S	Test Sequence														
(MPa)	1	2	3	4	5	6	7	8	9	10	11	12	13	14	15
300															
280															
260															
240							*				*		*		
220		*		*		o		*		o		o		*	
200	o		o		o				o						

Fig. 1 Traditional staircase test result of Q345r

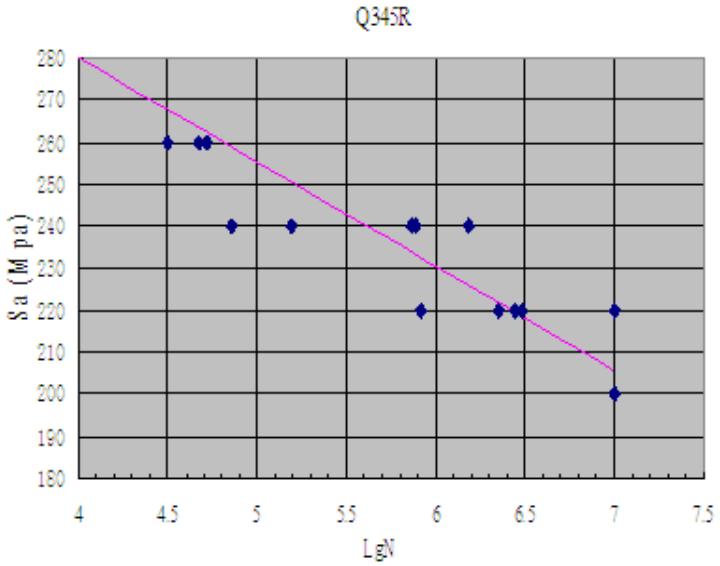

Fig. 2 S-N curve of Q345r

The Figure 2 shows the S-N curve result of Q345r, the curve fitting equation is LogN=15.3233-0.0404×S, the coefficient of association r=-0.90. For a 50% probability of failure, the fatigue strength at 1.0×10^7 cycle is 206Mpa.

Modified staircase fatigue test of Q345R

The test result by traditional staircase method is chosen to be the reference data, in which the average fatigue strength is 218.6Mpa and the deviation is 8.9Mpa. According to the test rule of modified staircase method, the initial stress and the stress step are set to be 220Mpa and 10Mpa respectively. 8 effective samples with 4 effective stress pairs are selected. The test result of modified staircase method is shown in Figure 3.

S	Test Sequence										
(MPa)	1	2	3	4	5	6	7	8	9	10	11
260											
250											
240											
230						*					
220	*		*		o		*				
210		o		o				o			
200											

Fig. 3 Modified staircase result with 8 samples

S	Test Sequence						
(MPa)	1	2	3	4	5	6	7
260							
250							
240							
230						*	
220	*		*		o		
210		o		o			
200							

Fig. 4 Modified staircase result with 6 samples

The average fatigue strength $\hat{\mu}_y$ is calculated to be 217.5Mpa, and the lower limit of the fatigue life $\hat{y}_{(p,1-\alpha)}$ is estimated to be 193Mpa. In the traditional method test, 16samples have been tested and 14 effective samples with 7 effective stress pairs are selected, however only about half of the samples have been used in the modified staircase test. The difference of the lower limit of the fatigue life between two methods is very small, the relative error is below 1%.

The test result, when only 6 effective samples with 3 effective stress pairs are selected, is shown in Figure 4. The average fatigue strength $\hat{\mu}_y$ is calculated to be 218.3Mpa, and the lower limit of the fatigue life $\hat{y}_{(p,1-\alpha)}$ is estimated to be 194Mpa. The result comparison between traditional staircase and modified staircase method test is shown in Table 1. It indicates that the lower limits of the fatigue life are very close of the two methods. The experiment result approves that modified staircase method can greatly enhance the testing efficiency and keep the test veracity.

Table 1 Comparison between traditional staircase and modified staircase method

Test Method	Materials	Sample Number	Fatigue Limit （Mpa）	Relative Error
Traditional staircase	Q345r	16	194	/
Modified staircase	Q345r	8	193	1%
Modified staircase	Q345r	6	194	1%

Conclusions

1. The initial stress and stress step should be the average fatigue strength and deviation of reference data respectively in the modified staircase method fatigue test.

2. Traditional staircase method and modified staircase method are respectively used to evaluate the fatigue performance of pressure vessel steel Q345R.

3. The test results show the modified staircase method can enhance the testing efficiency about 50% and keep the test veracity.

References

[1] Z. T. Gao, X. T. Jiang, J. J. Xiong: Fatigue performance experimental design and data processing (Press of Beijing University of Aeronautics and Astronautics)

[2] C. R. Chen: Fatigue and fracture, Press of Huazhong university of science and technology, 2002

[3] Lin S K, Lee Y L, Lu M W. International Journal of Fatigue, 2001, 23(1), 75~83

[4] L. Chen， Y. H. Guo, J. Zhou. Journal of Tianjin Institute of Technology, 1999, 15(3), 55-58

[5] X. D. Song, P. M. Lv. Journal of Chang'an University, 2004, 24(2), 91-93

[6] W. K. Yin, F. R. Zhu, W. Y. Peng, Z. L.Liao. Hong Du Science and Technology, 1995, 8, 33-42

[7] Chinese National Standard: Metallic materials Fatigue testing- Axial force controlled method, GB/T3075-2008.

[8] Chinese National Standard: Metallic materials Fatigue testing Statistical planning and analysis of data, GB/T24176-2009.

Advanced Materials Research Vols. 989-994 (2014) pp 883-886
© (2014) Trans Tech Publications, Switzerland
doi:10.4028/www.scientific.net/AMR.989-994.883

The Welding Residual Stress Analysis on High Performance Bridge Steel with Different Testing Method

Huan Xue[1,a], Rongfeng Li[1], Li Yu[1], Dong Liu[1], Wenjie Peng[1]

[1]Research and Development Center of Wuhan Iron and Steel group Corp., Wuhan, 430080, China

[a]stonemechanics@163.com

Keywords: Bridge Steel, Welding Residual Stress, X-ray Method, Hole-drilling Method, Indentation.

Abstract. The residual stress on X groove welding plate of high performance bridge steel 4MnNbq is analyzed. The X-ray diffraction method, hole drilling method and indentation method are respectively used to test the residual stress on welding line, heat-affected zone and base metal. The longitudinal and transversal residual stress are analyzed and compared. The results show that the stress along welding line direction is far larger than the transversal one and the stress on base metal are comparatively smaller than the welding line. The testing results of three methods match well, while the results of X-ray method and hole drilling method are much closer, the relative error of indentation method is comparatively larger.

Introduction

The bridge steels are often used in the structure with large span and load, so that the plate thickness, mass and constrain degree are high. The welding performance of bridge steel is one of the most important one in all of the assess index. The uneven welding heat source for heating and cooling components and the resulting uneven plastic flow will make inharmonic strain or initial strain distribution, resulting in welding residual stress and deformation. The residual stress not only affects the performance of corrosion, cracking and fatigue strength, but also has a huge impact on the physical and mechanical properties of materials, which can greatly break the strength of the structure. Thus, the welding residual stress distribution test plays an important role on product life judging. Currently, the welding residual stress measurement methods can be divided into mechanical and physical method [1]. Mechanical methods contain stress releasing and stress superposing methods. The typical representative methods of each are hole-drilling and indentation method. Non-destructive measurement method includes X-ray, magnetic, ultrasonic method, in which the X-ray method is the most accurate and widely used one [2-4].

Resentlly, researchers do a mount of work to investigate the residual stress distributing condition in welding structures. C. Ding et al. [5] studied the effects of relieving residual welding stress with different heat treatment methods, and Rodrigues et al. [6] analyzed the welding residual stress on X60 UOE pipe line by hole-drilling method. The residual stress condition of build welding pipe line were studied by Z. W. Zhang et al. [7], the result shows the stress on the in and outside surface of the pipe line were tensile stress. Although many methods were used to test the welding residual stress in these researches, few of them use different methods on the same sample, and do the comparison between the methods. In order to investigate the difference of welding residual stress using different testing method, the X-ray diffraction method, hole drilling method and indentation method are respectively used to test the residual stress on welding line, heat-affected zone and base metal of X groove welding plate of high performance bridge steel 4MnNbq in this paper. The longitudinal and transversal residual stress are analyzed and compared.

Experiment materials

The testing material is 14MnNbq, of which the yield strength is 380Mpa and the tensile strength is 520Mpa. The sample size is 650×300×24mm. WQ-1 soldering wire and +SJ101 soldering flux is used in the welding process. The input welding power is 36KJ/cm [8]. The mechanical property of

deposited metal is with R_{el}=470MPa. The double X type groove hidden arc welding is used in the test with 60° groove angle and 6mm truncated edge. The testing plates are butted in transversal direction. The baking process of soldering flux is 350˚C×1 h with (150±10)˚C interlamination temperature.

Experiment Methods and Results Analysis

X-ray method. XRD techniques are used to determine the distance between crystallographic planes, i.e. the d-spacing, and thus its application is limited to crystalline, polycrystalline and semi-crystalline materials. When a material is in tension, the d-spacing increases and when a material is in compression the d-spacing decreases. The presence of residual stresses in a material produces a shift in the x-ray diffraction peak angular position that is directly measured by the detector. For a known x-ray wavelength λ and n equal to unity, the diffraction angle 2θ is measured experimentally and the d-spacing is then calculated using Bragg's law[4], and the residual stress can be calculated by:

$$\sigma = -\frac{E}{2(1+\nu)} \cdot \frac{\pi}{180} \cdot \cot\theta_0 \cdot \frac{\partial 2\theta}{\partial \sin^2 \psi} \tag{1}$$

Where σ is the surface residual stress, E is elastic modulus, ν is Poisson's ratio, θ_0 is the diffraction angle on stress free condition, Ψ is the separation angle between surface normal line and selected crystal plane normal line, θ is the diffraction angle. Then

$$M = \frac{\partial 2\theta}{\partial \sin^2 \psi}, \quad K = -\frac{E}{2(1+\nu)} \cdot \frac{\pi}{180} \cdot \cot\theta_0 \tag{2}$$

While $\sigma = K \cdot M$, M is the slope of 2θ-$Sin^2\Psi$ curve, and K is the stress constant.

IXRD X-ray residual stress tester made by Proto is used to do validate test along length direction. The residual stress test process using X-ray method is according to national laboratory standards GB/T7704-2008 [9]. In this experiment, the round φ2mm collimator is employed. As the sheet pile is ferritic steels, CγKα radiation and vanadium foil filters is used. Diffraction crystal face is (211) with the stress constant K =-318MPa / (°). The stress testing field is shown in Figure 1.

Figure 2 shows the test result of welding residual stress using X-ray method. X axis is the distance between test position and the welding line. Y axis is the residual stress value. Inside the 30mm away from the welding line zone, the longitudinal stress is tensile stress, which reaches 200Mpa. And the transversal stress is compressive one, which is about 0~-50Mpa. It is found that the stress along welding line direction is far larger than the transversal one. The stress on the base metal, which is far away from the welding line, is around -50~-100Mpa. At 40mm distance from the weld line, the longitudinal stress changes from tensile stress to compressive one.

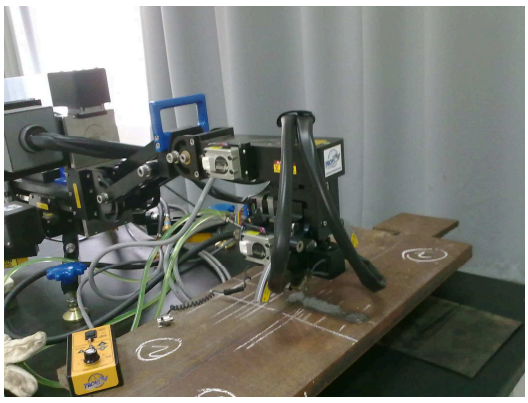

Fig. 1 Stress testing field using X-ray method

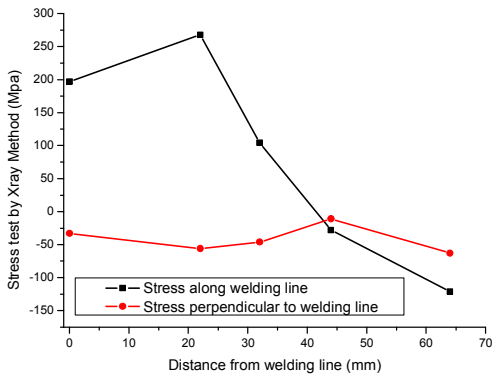

Fig. 2 Welding residual stress test by X-ray method

Hole drilling method. Due to the small size of workpiece invasive, high accuracy, less expensive equipment and easy to field operations, the hole drilling method is often used on surface residual stress measurement of engineering project 5. The hole drilling method is firstly proposed by Mather. J in 1932 6, and makes a great development in the recent years. The main features of the development of the system is inclined to drill small diameter blind hole, i.e. hole diameter becomes smaller and

smaller. The basic idea of the hole drilling method is to drill a small hole on the uniform stress field of a balanced component, the stress around the hole will be released which generates strain. The released strain can be measured by the attached resistance strain gauge around the hole (moderate distance away from the holes). According to elastic mechanics, the relationship between the released strain and stress can be set up. Then the magnitude and direction of two principal stress can be calculated. Paste the resistance strain gauge 0 °, 45 °, 90 ° respectively on a two-dimensional stress state infinite plate as shown in Figure 2. Drill a hole at the center of stain rosette, the hole depth is equal to or slightly greater than the hole diameter. When the hole depth reaches 1.2 times of the hole diameter, the strain nearly complete releases. As the hole depth is far smaller than the plate thickness, the theoretical solution of hole drilling method can be used as approximate solution on blind hole method.

In this test, the two sides of weld line are tested by hole-drilling method. The residual stress is nearly with symmetrical distribution on two sides, as shown in Figure 3. It can be also found that the longitudinal stress is far larger than the transversal one and the stress on base metal are comparatively smaller than the welding line zone. It should be noted that the residual stress only decrease tested by hole-drilling method when the separation from welding line increase, which is different from the result tested by X-ray method.

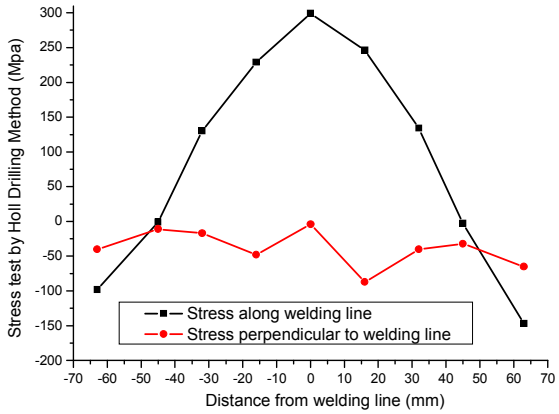

Fig. 3 Welding stress test by hole-drilling method

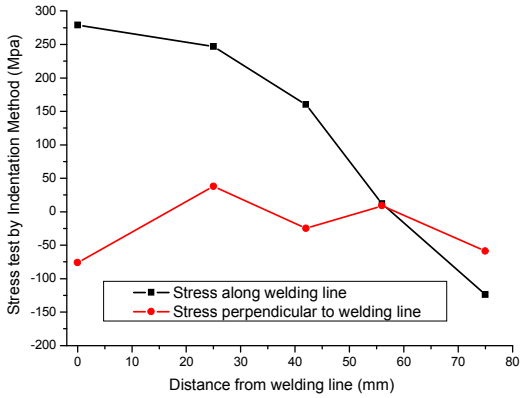

Fig. 4 Welding stress test by indentation method

Indentation method. The basic idea of the indentation method is shown in Figure 5 12. Put a hard steel ball with small diameter at the center of the testing point of component. Apply an impact energy W or static pressure P to generate a spherical-shaped indentation on the surface of component. The surrounding stress field is only corresponding to the ball's diameter D, the static pressure P or the impact energy W, and the distance from the force applying center R. The introduction of stress field F1 will affect the stress field in the original one F0, causing the stress redistribution. The stresses will be superposed in the elastic region to generate the stress field F2, along with a certain strain increment, which is closely related with the initial stress state. Therefore, the relationship of the initial stress field F0 and the strain increment can be established. Then the residual stress can be determined by measuring the strain increment in the indentation formatting process. The mechanical and mathematical model of this method can be established, which has strict scientific basis in theory. The absolute value of the indentation strain increment increases with tensile stress and strain increases. On the contrary, the compression stress makes the strain increment decreases. The linear relationship between residual stress and strain increment relates with the steel material, surface condition, ball diameter, the strain gage size, distance between strain gage and ball center, impact energy, static pressure and other factors.

Before the indentation test, the calibration experimentation should be done on 14MnNbq material. The calibrating plate should full anneal to erase the internal stress, and the material property change should be avoided in this process. A plate with 300mm long and 20mm thick is used in the calibration to get different stain increment at different load level. Figure 4 shows the result tested by indentation method. The stress at welding line reaches 250Mpa, and decreases when the distance between the test point and the weld line increases. The Transversal stress is nearly compressive stress.

Comparison and alalysis.

The comparison of the welding residual stress on two directions is shown in Figure 5 and Figure 6. Generally, the testing results of three methods match well, while the results of X-ray method and hole drilling method are much closer, the relative error of indentation method is comparatively larger. The X-ray method is non-destructive way with high accuracy, however its equipment is expensive and hard to move. The indentation method is with easier operation but with lower accuracy. And some details in the indentation testing which need to be pay attention are concluded: a. the accuracy of the calibration testing will effect the system error of residual stress measurement a lot; b. when the stress gradient is large, the testing position will influence the testing result; c. the strain gage paste and the indentation alignment is important to the experiment accuracy; d. the testing point should be not less than three, the mean value method can be used to cancel the dispersity of the test.

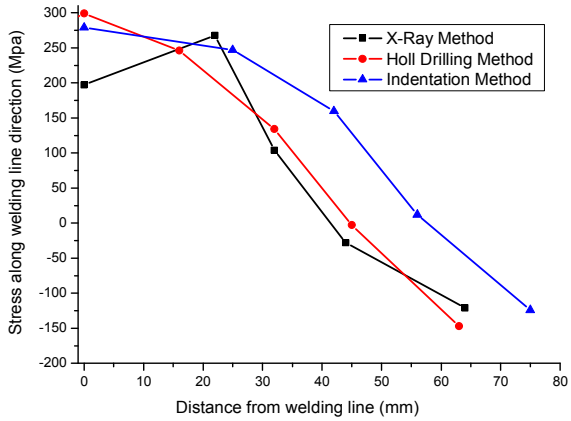

Fig. 5 The longitudinal welding stress comparison

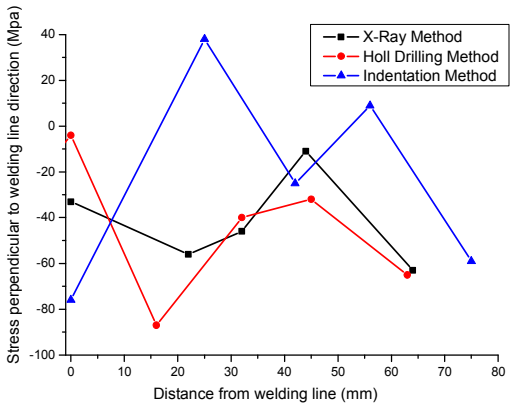

Fig. 6 The transversal welding stress comparison

Conclusions

1. The residual stress testing principle of X-ray, hole-drilling and indentation method are introduced.

2. The X-ray diffraction method, hole drilling method and indentation method are respectively used to test the residual stress on X groove welding plate of high performance bridge steel 4MnNbq.

3. The results show that the stress along welding line direction is far larger than the transversal one and the stress on base metal are comparatively smaller than the welding line.

4. The testing results of three methods match well, while the results of X-ray method and hole drilling method are much closer, the relative error of indentation method is comparatively larger.

References

[1] G. Jiang, M. H. Tan, W. M. Wang, W. He: Machine Tool & Hydraulics, Vol. 35, No. 6 (2007), p. 213

[2] Z. C. Zhang: Journal of Jilin Institute of Chemical Technology, 2001, 18(4): 73-75.

[3] J. W. He, K. B. Xu, J. B. Li: International Academic Developments, No. 4 (1998), p. 75

[4] C. Ding, B. G. Tang, S. B. Wang, X. M. Yue, W. R. LI, P. P. Wang: Journal of Zhengzhou Unibersity of Light Industry. 2005, 20(4): 68-70

[5] Rodrigues L D，Freire J L F，Vieira R D: Experimental Techniques，2008，32(1)：58-63．

[6] S. W. Zhang, Q. L. Zhang, G. D. Zhang: Journal of Vibration,Measurement & Diagnosis, 2007, 27(1): 77-79

[7] K.Miao, J. B. Liu, H. X. Dong, F. M. Li, W. G. Mu. Research on Iron& Steel, 2008, 36(6): 37-39.

[8] Chinese National Standard: Non-destructive testing- Practice for residual stress measurement by X-ray, GB/T 7704-2008.

Advanced Materials Research Vols. 989-994 (2014) pp 887-890
© (2014) Trans Tech Publications, Switzerland
doi:10.4028/www.scientific.net/AMR.989-994.887

A Study on the Sample Overheat Phenomenon of Fatigue Test

Huan Xue[1,a], Jia He[1], JingQin Hu[2], Lanxiang Kuang[1], Wenjie Peng[1]

[1]Research and Development Center of Wuhan Iron and Steel group Corp., Wuhan, 430080, China

[2]Quality Inspection Center of Wuhan Iron and Steel group Corp., Wuhan, 430080, China

[a]thomas8110@163.com

Keywords: Fatigue Test, Overheat Phenomenon, Frequency Adjustment, Sample Design.

Abstract. The overheat phenomenon often appears in the fatigue test of some high strength materials. It leads the deconcentration of test data and low efficiency of experiment process, or even failure of the whole test. The frequency adjusting method (FAM) and sample shape design technology are developed to solve this problem. Experiment result shows that the FAM can moderately ameliorate the overheat phenomenon. The resistivity of overheat phenomenon of the funnel type sample is far stronger than the straight bar type one.

Introduction

According to statistics, about 80% of failure of metal products caused by fatigue, most of which is suddenly broken, the loss is often more serious. Therefore, the study of metal fatigue and fatigue design promotion is with great significance to improve the machinery reliability and service life of metal products [1-2]. The up-and-down method is the most famous method to determine the fatigue life of samples, which is firstly proposed for sensitivity testing by W. J. Dixon and A. M. Mood, and developed by many other experts [3]. However, the estimates for variance are not exact and the previous data can not be effectively used in the traditional up-and-down method which leads low test efficiency. Along with the rapid development of the rail, automobile and other new steel products, the fatigue test requirement in many laboratory increases rapidly. In order to solve the contradiction, many researchers try to develop new fatigue testing method with higher efficiency [4, 5].

J. Y. Zhang et al. [6] developed a new up and down procedure for two details in series. The fatigue strength of these two details were independent with each other, failure of one detail did not influence the other one, and the fatigue life test of existing detail could be continued after the other detail failed. Their results indicated that the present procedure can reduce experiment time significantly. H. M. Fu et al. [7-9] established a two dimensional up and down method, which was applicable for small samples and could be used for estimating percentiles and percentages of sensitivity variables by combining previous experimental data and current test data. The information that could be used in the two-dimensional up-and-down method was much more than that in the traditional methods. Because this method could make full use of the current test data and the previous data, while the traditional methods could only use current test data. Fewer specimens were required in the two dimensional up and down method and the result was more accurate for the same number of specimens. Chen et al. [10] adopt the method of computer imitation, and through studying over a dozen materials-draw the conclusion: when using staircase method to determine the fatigue limit of material, the stress increment is selected at range from 2% to 6% of the fatigue limit, and the disperse has important influence on the precision of fatigue limit.

However, the overheat phenomenon became popular in some of the high strength metal materials. In some cases, the generated heat even made the surface of the sample bluing, as shown in Figure1. This kind of overheat phenomenon will bring larger error into the experiment, or even change the testing result. For most of the cases, this phenomenon at least reduces the testing efficiency and enlarges the dispersity of the result data. This paper investigates the influence on the sample overheat phenomenon of fatigue test. In the Third Section, the frequency adjusting method (FAM) is introduced to control the overheat factor. In the Fourth Section, samples with 4 different shapes are designed and used to do the fatigue test respectively, and results are compared and concluded.

The overheat influence on fatigue test

The fatigue strength of materials is often tested by up and down method. The accuracy of up and down method is decided by the consistency of every sample in the same group. If some of the samples get fever, or even bluing, the credence of the testing result will greatly decrease. In some cases, the overheat phenomenon will directly stop the test as the high load experiment can not be performed. According to the principle of conservation of energy, the energies in the fatigue test should satisfy the equation below:

$$W_{Work}+W_{Heat}+W_{Loss}=W_P \quad (1)$$

Where W_P is the total output power of the testing equipment, W_{Work} is the driving power of the sample working, W_{Loss} is the normal energy loss in the fatigue test and W_{Heat} is the abnormal overheat energy on the testing sample. Usually, in the fatigue test, variation of W_{Loss} is little. When WP is fixed, W_{Work} decreases if W_{Heat} increases. When W_{Heat} is too larger, the W_{Work} will be very small, which means even the working current reach the superior limit, the load is lower than the target value. In another aspect, W_{Heat} of most of materials in real application is very low as they are used in low frequency condition. However, the overheat appeared in the lab high frequency test is far away from the real working condition, thus their material fatigue limit is also inaccuracy. Therefore, the overheat phenomenon should be avoid in the fatigue test, which is of great importance.

Fig. 1 The overheat phenomenon of fatigue test sample

The frequency adjusting method

According to the thermodynamic principles, as internal loss always exists, materials generate heat when they vibrate, and heat goes larger when frequency is higher. While, in the fatigue test process, the sample is vibrate in certain frequency which is corresponding to the natural frequency of the whole testing system. The overheat or even bluing phenomenon are effected by working frequency. Theoretically, decreasing the testing frequency can reduce the total formability of sample in unit time, which leads less generated heat. For harmonic oscillating type fatigue testing machine, decreasing the natural frequency of the testing system can reach this aim, based on the resonating principle.

Specificlly, two counter blocks are set on two sides of original body frame of testing machine, which increase the deadweight of the system, shown in figure 2. Different counter blocks with different weight can be selected according to the overheat level of the sample. The experiment results shows that this frequency adjusting method can lighten the overheat problem for some of materials.

Fig. 2 Tesing machine with and without counter weight blocks

The sample shape design technology

Although FAM can treat the overheat problem for some of materials, the frequency can be only adjusted in a small range, therefore FAM is helpless for the materials with large internal loss and strong heat generation. In the national standard of fatigue test GB/T3075-2008 and GB/T24176-2009 [11-12], the sample shape is not regulated detailedly. The sample shape can be designed with choice. Thus the sample shape design can be considered to solve the overheat problem. In this work, the pressure vessel steel Q345r is used to do the fatigue contrast test with four groups of different type of shape designed samples. Sample of type 1 is a common standard one with Φ 5 straight column shape waist and M12 diameter of screw terminal end, which is the reference type. Sample of type 2 is with Φ 5 funnel shape waist and also M12 end, which is used to investigate the influence of heat generation of funnel shape waist sample. In order to enlarge the apparent force of the sample, each terminal end is increased with 27mm in type 3 compared to type 2. The minimal diameter on funnel shape waist is reduced to Φ 4 in the sample of type 4, which can be used to check the diameter size influence on overheat phenomenon. The testing material is Q345r with 550Mpa tensile strength and 350Mpa yield strength. The stress step is set to be 20Mpa which is 3%~5% of the tensile strength.

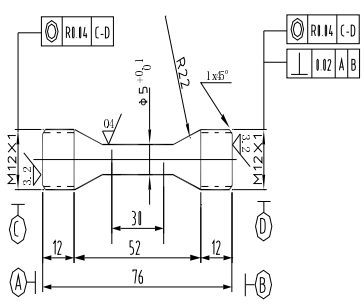

(a) Type 1: Straight type with M12－Φ 5

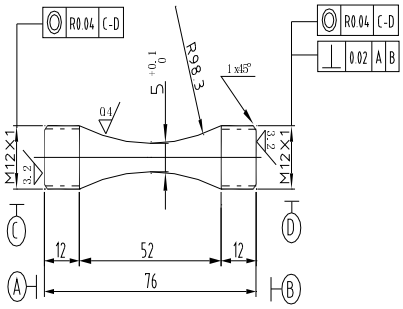

(b) Type 2: Funnel type with M12－Φ 5

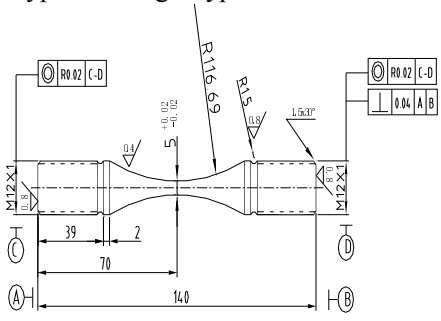

(c) Type 3: Funnel type with M12－Φ 5 and long end

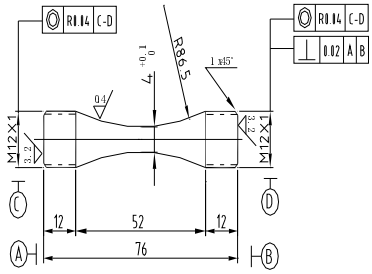

(d) Type 4: Funnel type with M12－Φ 4

Fig. 3 (a)-(d) Design map of four types of samples

Results and analysis

Up and down method is used to determine the testing stress level: 200Mpa, 220Mpa, 240Mpa, 260Mpa, 280 Mpa. The results are shown in Table 1. Fatigue sample of type 1 works well at 200Mpa, 220Mpa stress load level. Heat generates and gets fever on the sample surface at 240Mpa level. The test can not be continued at 260Mpa, as the overhear phenomenon appears and the driving load can not reach the target value even when the working current reach the maximum rating. For type 2 samples, they perform better than type 1. The Heat generates at 260Mpa level, but the test is still forced to be ended at 280Mpa. The performance of samples of type 3 with long terminal end is similar to type 2. The overhear phenomenon stops the test at 280Mpa. Samples of type 4 works well at all of the stress levels include high loading one, which means the resistivity of overheat phenomenon of the funnel type sample with thin waist is the strongest of the four types. The complete up and down test is done by type 4 samples. For a 10% probability of failure, at a confidence level of 95%, the standard deviation is 8.9Mpa. The average fatigue strength $\hat{\mu}_y$ is calculated to be 218.6Mpa, and the lower limit of the fatigue life $\hat{y}_{(p,1-\alpha)}$ is estimated to be 194Mpa.

Table1 Fatigue test comparison between different type of samples

Sample type	Sample Shape	Low Load 220Mpa	Middle Load 240Mpa	Medium-high Load 260Mpa	High Load 280Mpa
Type 1	M12- ϕ 5 Straight waist	Regular Test No heat	Regular Test Medium Heat	Can not Test Overheat	Can not Test Overheat
Type 2	M12- ϕ 5 Funnel waist	Regular Test No heat	Regular Test Low Heat	Regular Test Medium Heat	Can not Test Overheat
Type 3	M12- ϕ 5 Long end	Regular Test No heat	Regular Test Low Heat	Regular Test Medium Heat	Can not Test Overheat
Type 4	M12- ϕ 4 Funnel waist	Regular Test No heat	Regular Test No heat	Regular Test No heat	Regular Test Low Heat

Conclusions

1) The influence on the sample overheat phenomenon of fatigue test is introduced.

2) The frequency adjusting method (FAM) and sample shape design technology are developed to solve this problem. Experiment result shows that the FAM can moderately ameliorate the overheat phenomenon. The resistivity of overheat phenomenon of the funnel type sample with thin waist is the strongest of the four types.

References

[1] Z. T. Gao, X. T. Jiang, J. J. Xiong: Fatigue performance experimental design and data processing (Press of Beijing University of Aeronautics and Astronautics)

[2] C. R. Chen: Fatigue and fracture, Press of Huazhong university of science and technology, 2002

[3] W. J. Dixon, A. M. Mood. A Method for obtaining and analyzing sensitivity data. J Amer Statistical Assoc, 1928, 43, 109-126

[4] J. Y. Zhang, D. L. Wang. Up and down method for fatigue strength with two details in series. Journal of Experimental Mechanics, 2006, 21(5), 579-583

[5] Lin S K, Lee Y L, Lu M W. Evaluation of the staircase and the accelerated test methods for fatigue limit distributions[J]. International Journal of Fatigue, 2001, 23(1), 75~83

[6] J. Y. Zhang, D. L. Wang. Up and down method for fatigue strength with two details in series. Journal of Experimental Mechanics, 2006, 21(5), 579-583

[7] H. M. Fu, G. Yin, Two-dimensional up-and-down method. Acta Aeronautica Et Astronautica Sinica 1998, 19 (6), 748-753

[8] H. M. Fu, G. Yin, A method for determining fatigue limits with small samples. Journal of Mechanical Strength, 1999, 21(2), 115-117

[9] H. M. Fu, Formulas for tolerance limits and confidence limits of nomal population percentiles and percentages. Acta Aeronautica Et Astronautica Sinica 1994, 15 (1), 94-101

[10] L. Chen, Y. H. Guo, J. Zhou. Journal of Tianjin Institute of Technology, 1999, 15(3), 55-58

[11] Chinese National Strandard: Metallic materials Fatigue testing- Axial force controlled method, GB/T3075-2008.

[12] Chinese National Strandard: Metallic materials Fatigue testing Statistical planning and analysis of data, GB/T24176-2009.

Advanced Materials Research Vols. 989-994 (2014) pp 891-897
© (2014) Trans Tech Publications, Switzerland
doi:10.4028/www.scientific.net/AMR.989-994.891

Numerical Simulation Study of Stress-Magnetization Effect on Different Notch Steel Specimens

Xiaowen Xi[1, a], Shangkun Ren[1, b], Yin Huang[1, c]

[1] Key Laboratory of Nondestructive Testing of Ministry of Education, Nanchang Hangkong University, Nanchang, 330063, China

[a]email: xixiaowen_nchk@163.com, [b]email: renshangkun@yeah.net, [b]email: 870654391@qq.com

Keywords: stress-magnetization effect; finite element analysis; metal magnetic memory

Abstract. To study the mechanism of metal magnetic memory(MMM) testing technology, the stress-magnetization effect on 20 steel specimens with different notch angles under exercise of the geomagnetic field and tensile load is simulated by using the finite element analysis(FEA) software ANSYS. With the stimulation, the stress and magnetic flux leakage distribution of the specimens is given. The results showed that internal stress distribution of different notch specimens under external tensile effects is different; The curves of relationship between damage degree of stress concentration and the distribution of magnetic flux leakage is also related to the defect shape and structure; Magnetization decreases with increases of stress at first and then increases with continuing increase of stress, which is called stress magnetization reversal. It provides an important reference for the quantitative research of metal magnetic memory technology.

Introduction

Metal magnetic memory testing method is a new type of magnetic nondestructive testing method, which has incomparable advantages to traditional magnetic testing method. It has great significance on early prevention of fracture failure of ferromagnetic materials and major malignant accidents[1-2]. The method, based on the principle of stress-magnetization effect on ferromagnetic components, that is, under the action of working load and geomagnetic field, the magnetic domain organization will orientate in a irreversible way, thus forming leakage magnetic field in stress concentration zone, is used to locate early injured parts with the main characteristics of stress concentration on the surface and near surface of the ferromagnetic components by examining the leakage magnetic field[3]. The essence of stress magnetization effect law is the magnetization law of component caused by stress. It mainly studies the leakage magnetic field distribution caused by the tensile stress under the action of magnetic field[4-5]. At present, the technology research mainly focuses on the basic experiments of testing mechanism. However, little is explored on the numerical simulation study of the testing mechanism.

Based on the principle of stress-magnetization effect of ferromagnetic components, attribute is assigned to ferromagnetic material with different prefabricated defects by using the finite element simulation software(ANSYS)[6]. With force-magnetic coupling finite element analysis of the 20# steel under external stress and ground magnetic field conditions, the distribution law of magnetic memory signals and specimen stress of the surface air layer of different notch specimen is given and analyzed with testing mechanism, providing a reference value for the quantitative study of metal magnetic memory technology.

Coupled field principles

Coupled field analysis considers interaction and coupling of two or more disciplines(physics) in the process of the finite element analysis[7]. For example, piezoelectric analysis considers the interaction between the piezoelectric structure and the electric field, which solves the problem of the distribution of the piezoelectricity caused by load displacement, and vice versa.

Sequential coupling method consists of two or more analysis carried out by a certain sequence, every kind of analysis carried out in different physical environments. By applying the previous

results as the load to the following analysis, the coupling of two different physical fields is realized. Sequentially coupled field analysis data flow 1 is as follows:

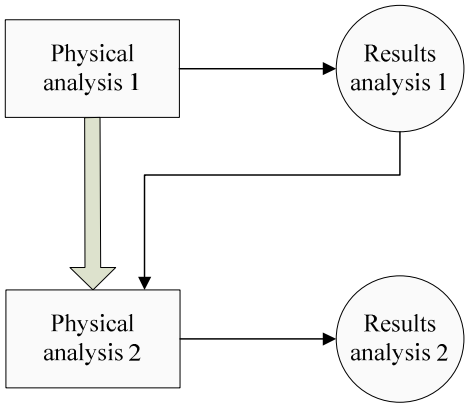

Fig. 1 Sequential coupling analysis data flow diagram

Numerical simulation analysis metal magnetic memory testing technology mainly considers the influence of stress on leakage magnetic field of ferromagnetic component, while the magnetic field effect on the stress is very small, even negligible. So the ANSYS simulation analysis adopts sequential coupling numerical simulation analysis that combines structure static analysis and static magnetic analysis.

Numerical simulation of stress-magnetization effect

Same-size 20# steel specimen with different gap prefabricated defects are chosen as the research object; Leakage magnetic field above A, B, C, respectively from the notch tip of 0mm, 3mm, 6mm, is extracted; Measurement point M is on path A, 11mm from the notch tip. Specimen size and main technical parameters are as shown in Figure 2, where the specimen is 2mm thick.

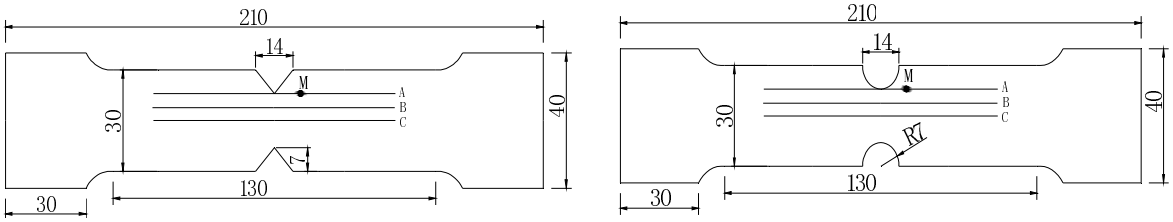

（a）V-notch specimen （b）Semi-circular notch specimen

Fig. 2 Sample sizes of different notch specimens

Table 1 Main technical parameters of 20 # steel

Parameter	E(GPa)	Poisson's ratio	σ_S(MPa)	μt
Value	203	0.28	235	285

2.1 Finite element model and mesh

Given the sample is symmetrical, in order to save computing time, computer hardware resources and to ensure the accuracy of the condition, a 1/2 modeling under test conditions is adopted[8]. To extract the data of leakage magnetic field of the external air layer of the sample, a model of air layer around the sample area is built, as shown in figure 3, where the inner is the sample model, the outer is air model.

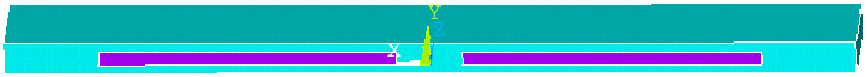

（a）whole mode

（b）V-notch specimen （c）Semi-circular notch specimen

Fig. 3 Solid models of different notch specimens

When dividing grid unit, method of manual control unit size and freedom divide is adopted, making the grid of ferromagnetic material area and the air layer area near prefabricated defects relatively dense and grid away from the prefabricated defects relatively sparse. Grid distribution of the specimen is as shown in figure 4.

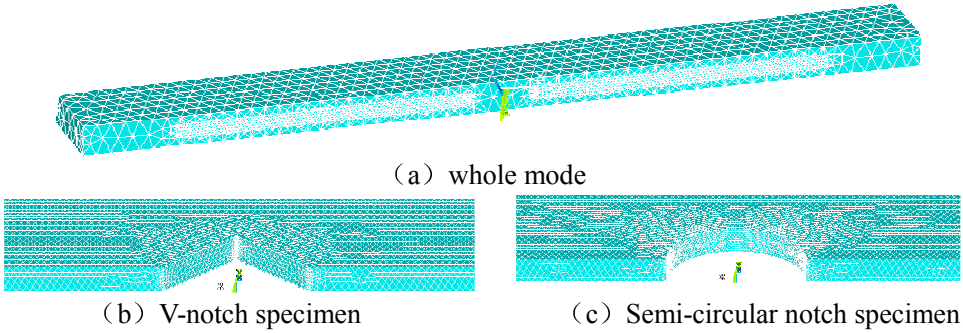

（a）whole mode

（b）V-notch specimen （c）Semi-circular notch specimen

Fig. 4 Finite element models of different notch specimens

2.2 Load and Solve

The simulation analysis is divided into static analysis and static magnetic analysis. With nonlinear static analysis, internal unit stress distribution of tensile samples is given; With the result of nonlinear static analysis, the magnetic properties of ferromagnetic unit material is assigned; With magnetism analysis, the leakage magnetic field values of the surface of model under the function of exterior stress and earth magnetic field.

In static analysis, displacement constraints and tensile load are respectively imposed on symmetric plane and about face of the model. These two different tensile loads are then written to load step, making it possible to carry out nonlinear static analysis under the condition close to real experiment. In static magnetic analysis, by applying a 39.8 A/m size of external environment magnetic field, the size of the earth's magnetic field on average, the leakage magnetic field values of the path A, B and C, 1mm from the notch tip, is extracted by using APDL parametric program of ANSYS.

2.3 Results and Discussions

2.3.1 Stress distribution

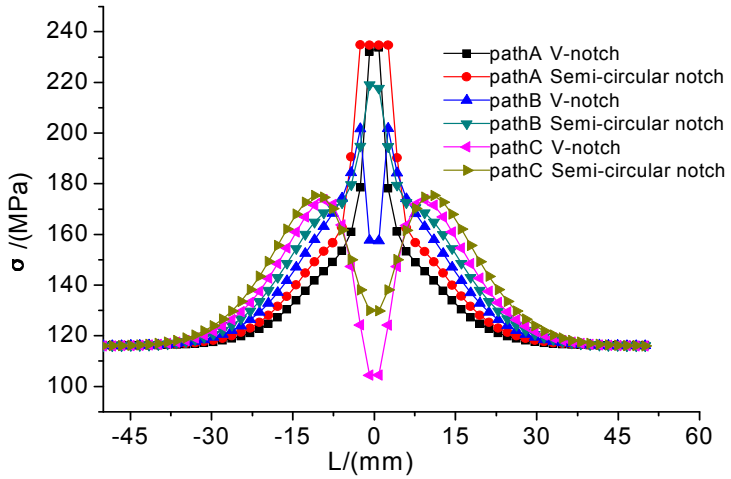

Fig. 5 Specimen equivalent stress distribution curve under 130MPa tensile load

In post-processing phase of ANSYS, equivalent stress distribution data of the path A, B and C of two samples were extracted respectively by using APDL of ANSYS, as shown in figure 5. The simulation results show: At the center of gap of the path A, stress concentration degree and the width of the semi-circular notch specimen are slightly larger than those of the v-notch specimen; Near the gap of the path B, stress concentration degree of the semi-circular notch specimen are

significantly greater than that of the v-notch specimen and the stress concentration distribution of the v-notch is bimodal; Near the gap of the path C, the degree of stress concentration of the two shapes gap are roughly similar, stress distribution is both bimodal. Hence, the semi-circular notch specimen is more prone to fracture and is with greater potential danger.

2.3.2 Surface leakage magnetic field distribution

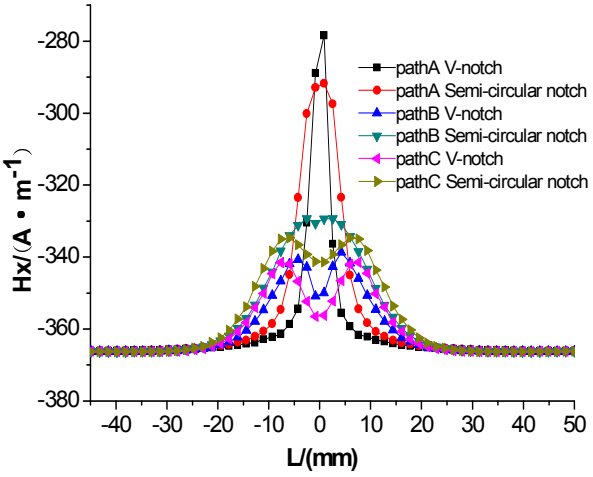

（a）Tangential component

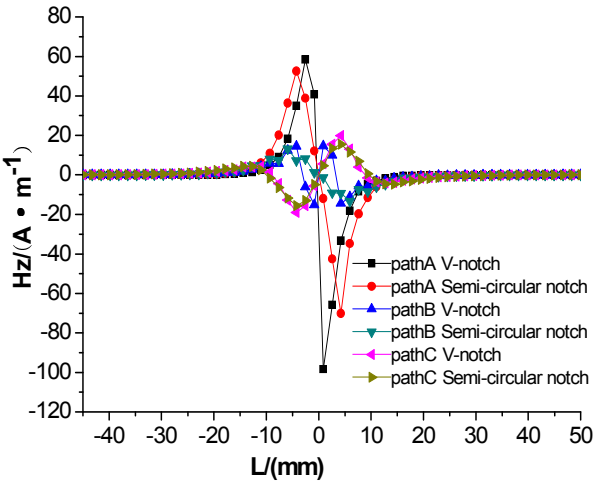

（b）Normal component

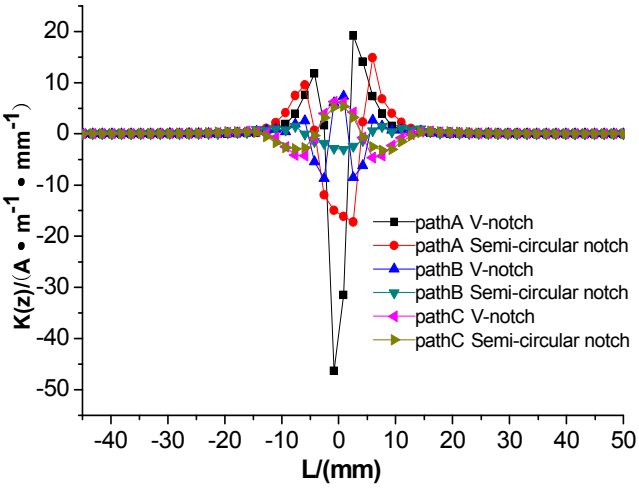

（c）Gradient(K) of normal component

Fig. 6 Magnetic flux intensity distribution curves under 130MPa tensile load

To analysis surface leakage magnetic field distribution of different notch specimens, we respectively extract tangential component H_X and normal component H_Z, leakage magnetic flux intensity of V-notch and semi-circular notch specimens in the path A, B and C, under the 130MPa constant tension load, as shown in figure 6(a) and (b). The gradient(K) is given by using the normal component of leakage magnetic flux intensity, as shown in figure 6(c). The figure 6 shows: under the same tension level, V-notch specimens has a higher peak value, while the semi-circular notch specimen has a wider horizontal width; Conclusion from the tangential component H_X: it's a bimodal curve in the path B of v-notch specimen, but the semi-circular notch specimen is unimodal curve; Conclusion from the normal component H_Z and the gradient (K): with the change of path, the change law of leakage magnetic flux intensity is basically the same. But in path B, v-notch specimens has double peaks and troughs, which shows the stress distribution is intermittent; while semi-circular gap only has single peak and trough and the stress distribution is in a row. This is due to the fact that internal stress distribution of the semi-circular notch specimen is symmetrical oval, while the V-notch specimen is butterfly distribution.

The simulation results show that relation curve between the degree of damage of stress concentration and the distribution of magnetic flux leakage is also related to the defect shape

structure. In this case, the semi-circular notch specimen is more prone to fracture, providing an important reference for the quantitative research of metal magnetic memory technology.

2.3.3 Stress magnetization relationship

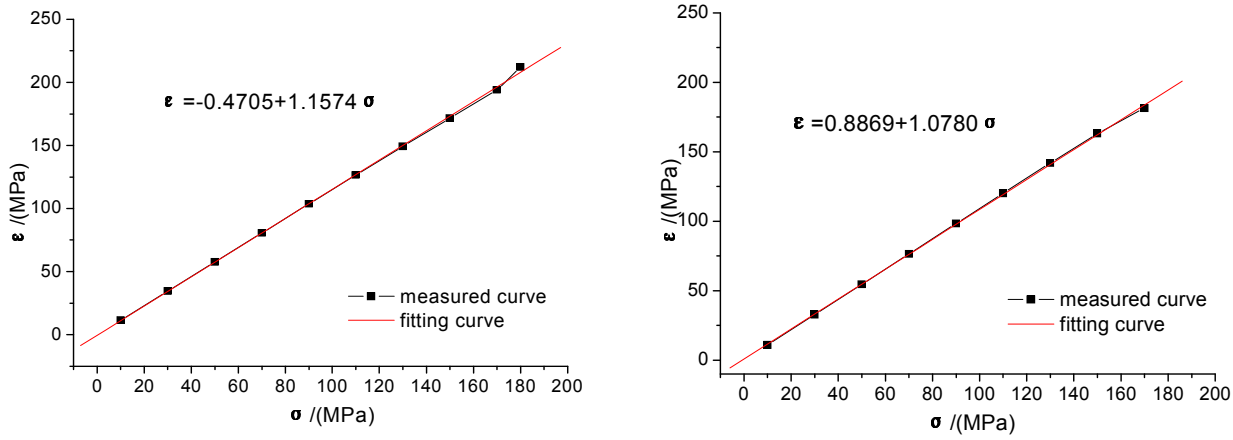

（a）Semi-circular notch specimen （b）V-notch specimen

Fig. 7 Relationship between stress and tension of different notch specimens at point M

Figure 7 shows change curve of stress(ε) of the sure points M at the V-notch and semi-circular notch specimens along with the change of external loads tensile(σ). Seen from figure 7(a) and (b), the internal stress at sure points M and external tension is a linear relationship (Other point of the specimens also can come to this conclusion). From their fitting curve, the slope of the semi-circular notch specimen is bigger, namely with the increase of external tension, stress value of the sure points M on the semi-circular notch specimen increases more rapidly. The results show that the semi-circular notch specimen is more prone to fracture.

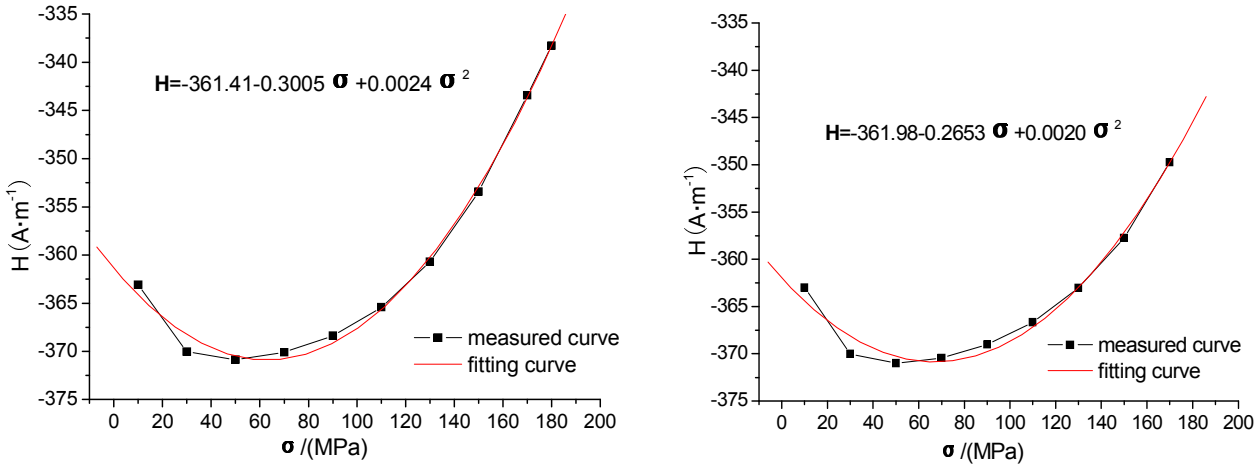

（a）Semi-circular notch specimen （b）V-notch specimen

Figure 8 Relationship between magnetic flux intensity and tension of different notch specimens

Figure 8 shows change curve of the leakage magnetic flux intensity of the sure points M at the V-notch and semi-circular notch specimens along with the change of external loads tension(σ). From figure 8(a), for the semi-circular notch specimen, as external loads tension increases from the initial state to the 70MPa, leakage magnetic flux intensity decreases gradually with the increase of tension; when the external loads tension is over 70MPa, the leakage magnetic flux intensity increases as the tension increases. The relationship curves between the leakage magnetic flux intensity and the tension shows the magnetization reversal effect of stress, where the fitting curve is $H=-361.41-0.3005\sigma+0.0024\sigma^2$; Also, figure 8(b) shows the same stress magnetization reversal effect (Reverse position tension value is about 70MPa, about 40% of the maximum tension value), where the fitting curve is $H=-361.98-0.2653\sigma+0.0020\sigma^2$.

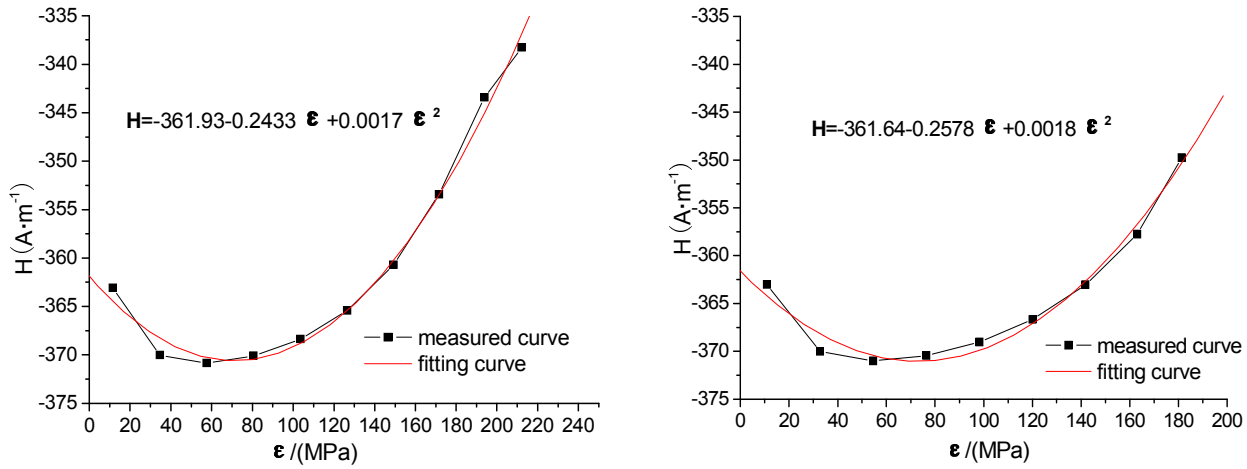

（a）Semi-circular notch specimen （b）V-notch specimen

Fig. 9 Relationship between magnetic flux intensity and stress of different notch specimens

Through static analysis of the specimens, stress values of different units are given by extracting the stress path values of path A, B and C; And through the static magnetic analysis, magnetic field values of different units are given by extracting surface leakage magnetic field values of the specimens. Through analysis of the obtained data, we can obtain relationship curve between leakage magnetic field values and the internal stress(ε) of the sure points M at the V-notch and semi-circular notch specimens, as shown in figure 10. From figure 9(a) and (b), it can be concluded that different notch specimens show the same stress magnetization reversal effect at 70MPa.

The results show that as external loads tension and internal stress increase from the initial state to 70MPa, leakage magnetic flux intensity decreases gradually with the increase of stress; when the external loads tension and internal stress is more than 70MPa, the leakage magnetic flux intensity increases as the stress increases. The relationship curve between the leakage magnetic flux intensity and the stress shows the magnetization reversal effect of stress. Magnetic effect of stress has dual function relations, namely, one magnetization state has double magnetization characteristics. The simulation results laid a certain theoretical basis for segmented quantitative evaluation for magnetic memory testing technology.

Conclusions

The subject of numerical simulation research is 20# steel specimens with V-notch and semi-circular notch. APDL parametric program is used to extract the leakage magnetic field value of surface air layer above ferromagnetic specimen. Different notch flat specimens are used to analyze the stress distribution, surface leakage magnetic field distribution and the stress magnetization relationship distribution. Under the joint action of the geomagnetic field and external stress, different notch specimens has different stress concentration coefficient, resulting in different internal stress distribution and distribution width of the specimen, which generates different permeability. Generally speaking, the stress changes the state of magnetization of the specimens, making different notch specimens have the different magnetic memory signals distribution law and different characteristics of the stress magnetization reversal phenomenon. The simulation results show that:

(1) Through study the law of surface leakage magnetic field of different notch specimens, the internal stress distribution and width distribution can be obtained by analyzing tangential component H_X, normal component H_Z and the gradient(K), leakage magnetic flux intensity of different notch specimens. The semi-circular notch specimen internal stress distribution is symmetrical oval, while the V-notch specimen is butterfly distribution.

(2) The relation curve between degree of damage of stress concentration and the distribution of magnetic flux leakage is related to the defect shape structure. In this case, the semi-circular notch specimen is more prone to fracture, providing an important reference for the quantitative research of metal magnetic memory technology.

(3) Through study the law of stress-magnetic effect of different notch specimens, the results show that as external loads tension and internal stress increases from the initial state to 70MPa, leakage magnetic flux intensity decreases gradually with the increase of stress; when the external loads tension and internal stress is over 70MPa, the leakage magnetic flux intensity increases as the stress increases. The relationship curves between the leakage magnetic flux intensity and the stress shows the magnetization reversal effect of stress. The simulation results laid a certain theoretical basis for segmented quantitative evaluation of magnetic memory testing technology.

Acknowledgement

In this paper, the research was sponsored by the Nature Science Foundation of China (Project No. 51261023).

References

[1] A.A. Dubov. Proc of CHSNDT 7th Conference on NDT and International Research Symposium. Shantou China: 1999, 181-187.

[2] A.A. Dubov. Chemical and Petroleum Engineering, 2012, 12(47): 867-839.

[3] Jilin Ren, Junming Lin. Beijing: China Electric Power Press, 2000.

[4] Shangkun Ren, Li Zhou, et al. Journal of iron and steel research, 2010, 22(12): 48-52.

[5] Lihong Dong, Binshi Xu, et al. NDT & E International, 2008, 41(3): 184-189.

[6] Weimin Zhang, Junjie Yuan. China Mechanical Engineering, 2009, 10(1): 34-37.

[7] Hongjun Hu, Weijiu Huang. Beijing: China Machine Press, 2012.

[8] Shangkun Ren, Xinlei Li, et al. Journal of Nanchang Hangkong University, 2008, 22(2): 11.

Advanced Materials Research Vols. 989-994 (2014) pp 898-902
© (2014) Trans Tech Publications, Switzerland
doi:10.4028/www.scientific.net/AMR.989-994.898

Study on Factors of Axial Crushing of Thin-walled High-strength Steel Sections Used in Passenger Car

Guifan Zhao[1,a], Yaowei Hu[1,b*], Xiao Cheng[1,c] and Ke Xiao[2,d]

[1]School of Automobile Engineering, Harbin Institute of Technology, Weihai, Shandong, China

[2]Department of Quality, Jiangxi Changhe Automobile Co., Ltd., Jingdezhen, China

[a]zgf7071@163.com, [b]*huyaoweiwhhit@163.com, [c]15069426785@163.com, [d]xiaoke@changhe-suzuki.com

Keywords: Thin-walled Rectangular beam, Crashworthiness, Orthogonal Test, Simulation Analysis

Abstract. This paper firstly studied the structure of front longitudinal, then reviewing comprehensive literature draw the similarity of collision of the thin-walled tube and front longitudinal,finally ensure the study of collision of the thin-walled tube. And establishing three kinds of thin-walled welded rectangular beam finite element model of spot welding, seam welding and laser welding, arrive a more superior technology through researching and analyzing the model.

Introduction

The request for lighter and more efficient energy absorbing components for various

Transportation systems have led to an increased interest in thin-walled high-strength steel sections. The energy absorption capabilities of such components are very important in improving the vehicle crashworthiness without increasing the body weight[1,2]. As a result, it is necessary to design across-section which minimizes the amount of forces transferred to occupants. Effort has been spent in experimental research and in developing safe design criteria using plastic hinge analysis. The motivation for this research is the desire to design a cross-section that deforms in a regular controlled manner[3-6], but also the desire for cost-to-weight effectiveness.

This study first established the finite element model of laser welding ,then chosen material, thickness and welding position as three influencing factors designed three factors and three levels orthogonal test which could reduce 27 sets to 9 groups of simulation analysis. Analysis of thin-walled rectangular beam of energy absorption as the test results as evidence of its axial compression, use orthogonal visual analysis to interpret the test results, and ultimately come to material, thickness and welding position resistant thin-walled tube collision resistance of trends and tests designed to find the optimal values within the range.

Design of Experiment

In this paper, the orthogonal experiment $L_9(3^4)$ was carried out, analyzing the effect of the front side plate material, thickness, welding position. Orthogonal table show in the table 2. Data in accordance with the table front side front and rear to fill the order, both before and after the text relative to the vehicle's direction is. The selected material properties as shown in Table 3.

Table 1.Factors and levels

Factor	1	2	3
Material	MAT24-saph400	MAT24-B340/590	MAT24-b180h1
	MAT24-saph400	MAT24-saph440	MAT24-586
Thickness	2mm	1.8mm	1.6mm
	2mm	2.2mm	2.4mm
Welding position	250:250	200:300	300:200

Table 2.Orthogonal table

Number	A	B	C
1	1	1	1
2	1	2	2
3	1	3	3
4	2	1	2
5	2	2	3
6	2	3	1
7	3	1	3
8	3	2	1
9	3	3	2

Table 3. Material properties

Material	density [kg/mm^3]	E [MPa]	EU	SIGY [MPa]
saph400	7.8e-9	210	0.24	261.49
b180h1	7.8e-9	210	0.27	221.73
B340/590	7.8e-9	210	0.30	414.00
saph440	7.8e-9	210	0.24	360.00
586	7.8e-9	210	0.30	586.00

Numerical simulations

FE modeling

The explicit non-linear finite element code LS-DYNA was used to predict the response of the thin-walled sections subjected to axial crushing[7]. The finite element model was created by the mesh generator program True Grid. Even if the cross sections can be modeled using one or two (square) symmetry planes, the full sections were modeled using the quadrilateral Belytschko-Tsay shell element with four nodes. Stiffness-type hourglass control was used to eliminate the zero energy modes, and five integration points were used throughout the thickness in order to capture the local element bending accurately. The load was applied at the upper end of the specimen using a rigid block modeled with brick elements. The length of both sections was410mm and the sheet thickness was 1.2 mm. At the lower 100mm of the model, all degrees of freedom were constrained except the longitudinal translation degree of freedom in order to allowed formation in axial direction. The lower end of the specimen was fixed by constraining all six degrees of freedom, while at the upper end the rotational degrees of freedom were fixed to avoid unrealistic deformation modes and thus numerical problems[8].

The contact between the rigid block and the specimen was modeled using a ‘nodes impacting surface’ with a friction coefficient of 0.3in order to allow sliding movement[9,10]. To account for the contact between the lobes during deformation, a single surface contact algorithm without friction was used. Several simulations were carried out to determine the proper mesh density and an element size of 3mm*3mm was found sufficient, giving a total of 11,120 shell elements for the square tube.

Simulation results

Experimental program in this section is showed in Table 1, the test results can be obtained as Fig.1through the different models crash simulation tests. Figs.2 show, respectively, the axial deformation behavior for the square tube analyzed at a velocity 15 m/s. The energy absorption curve of 9 experimental groups showed in Fig.3.

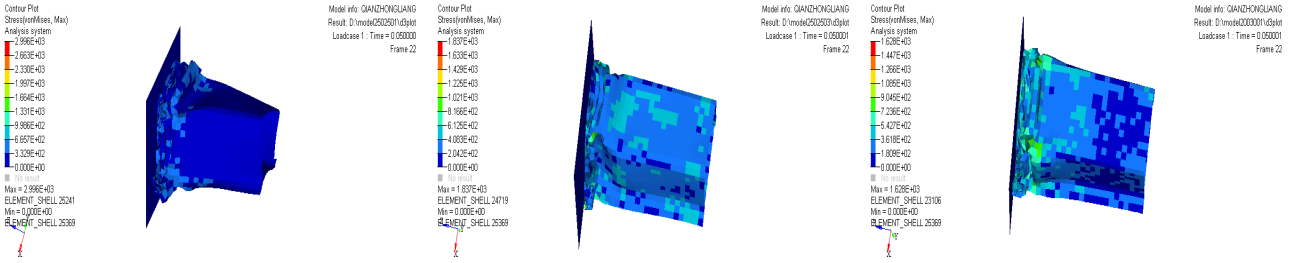

(a) (b) (c)

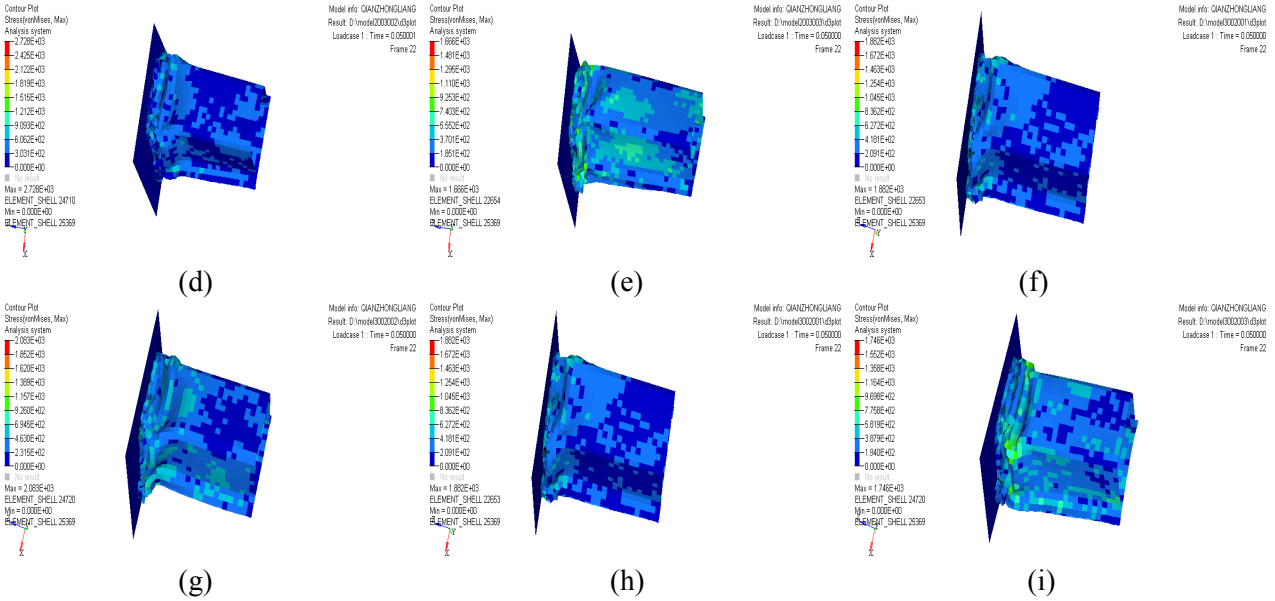

(d) (e) (f)

(g) (h) (i)

Fig.1 Axial crushing of 9 experimental groups

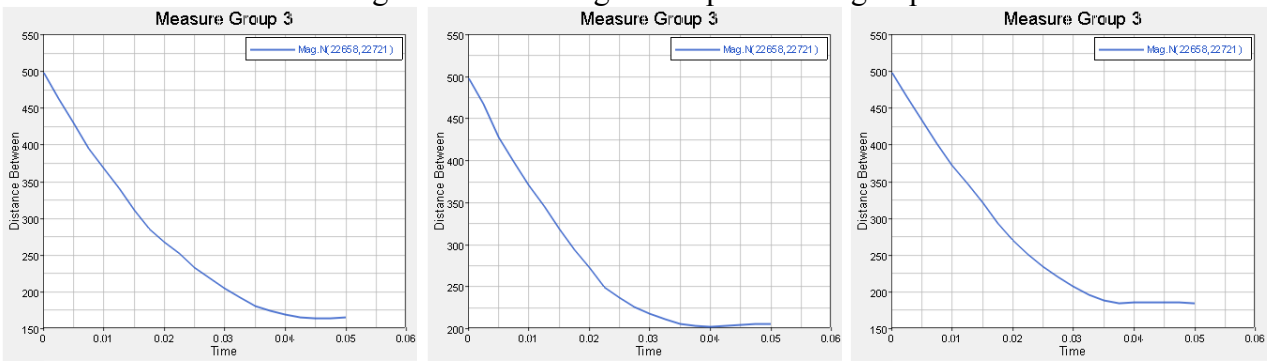

(a) (b) (c)

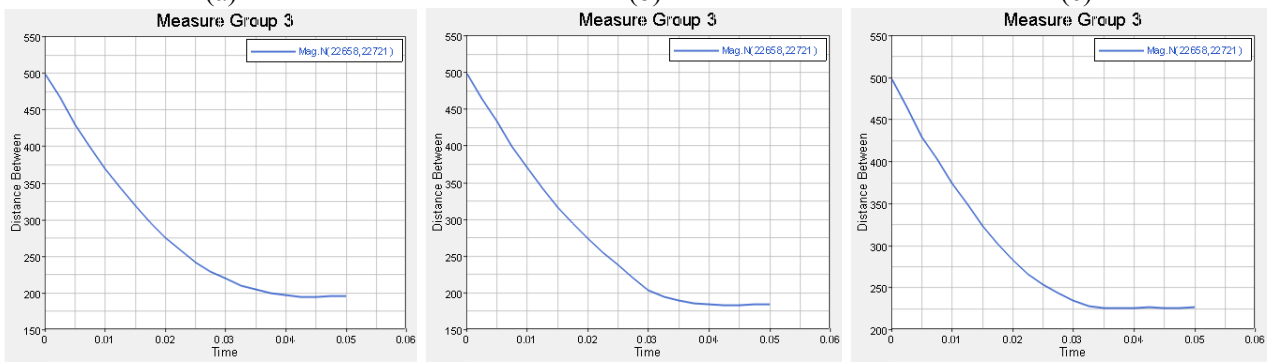

(d) (e) (f)

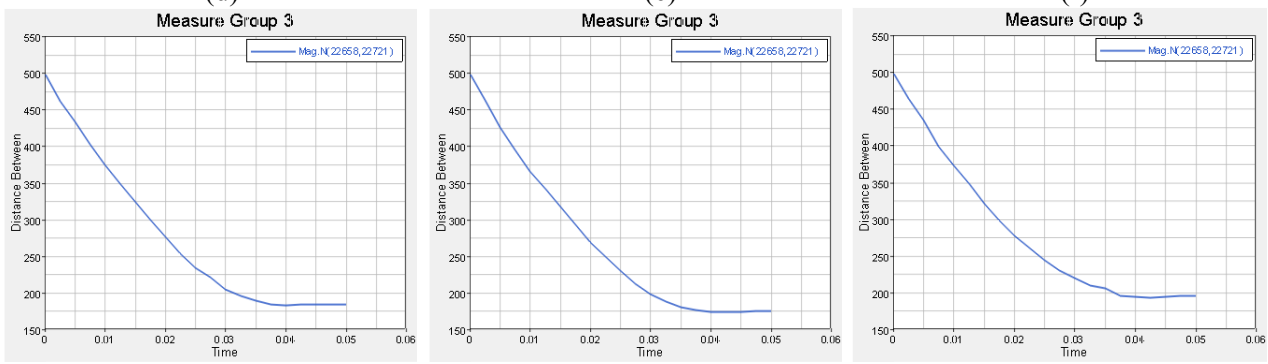

(g) (h) (i)

Fig.2 Displacement of 9 experimental groups

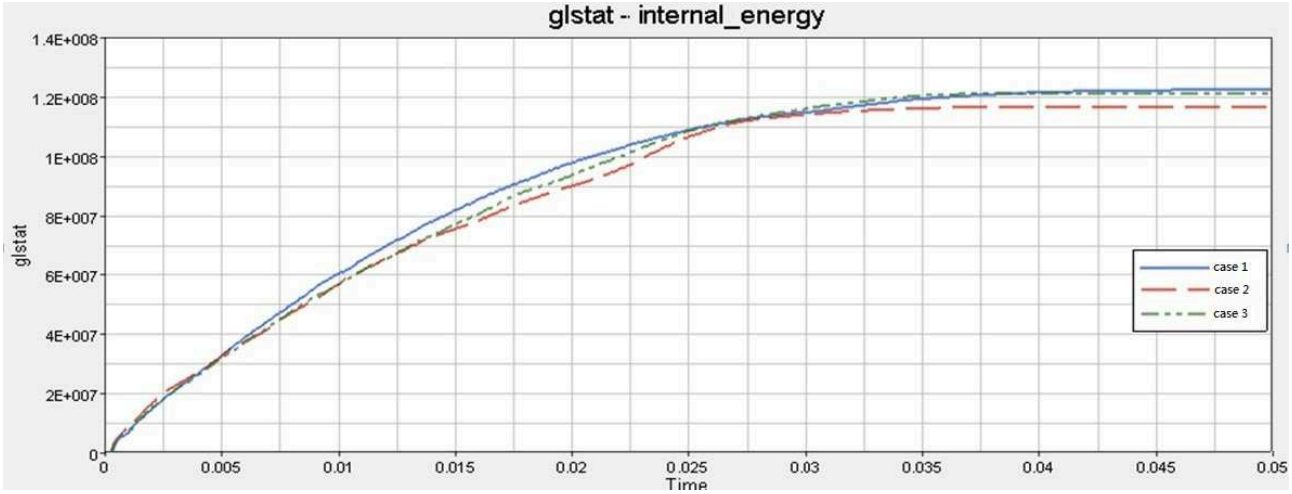

(1)The energy absorption curve of Group 1-3

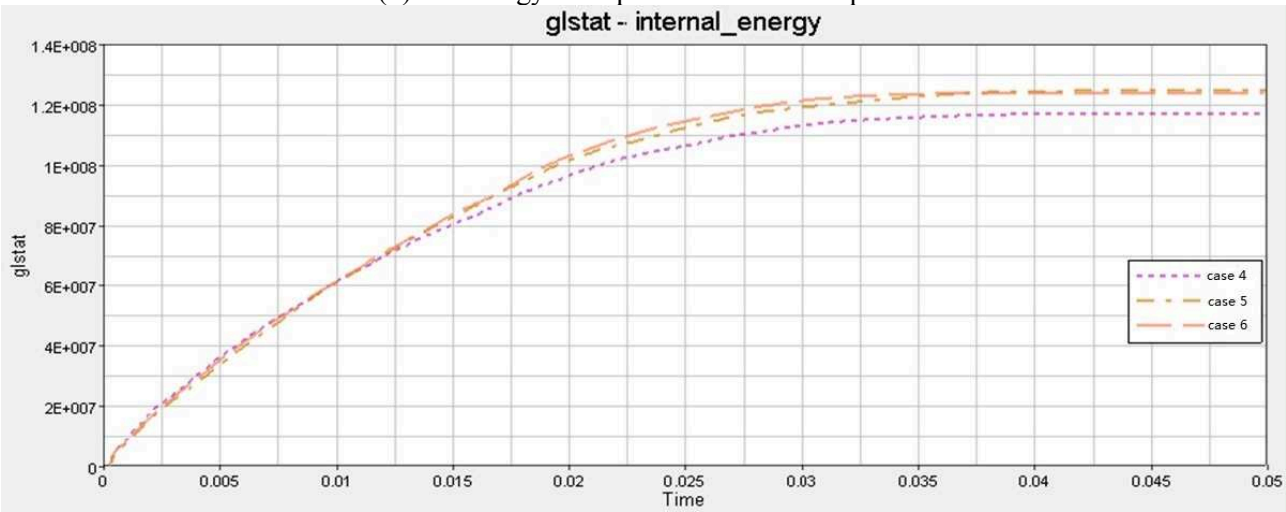

(2)The energy absorption curve of Group 4-6

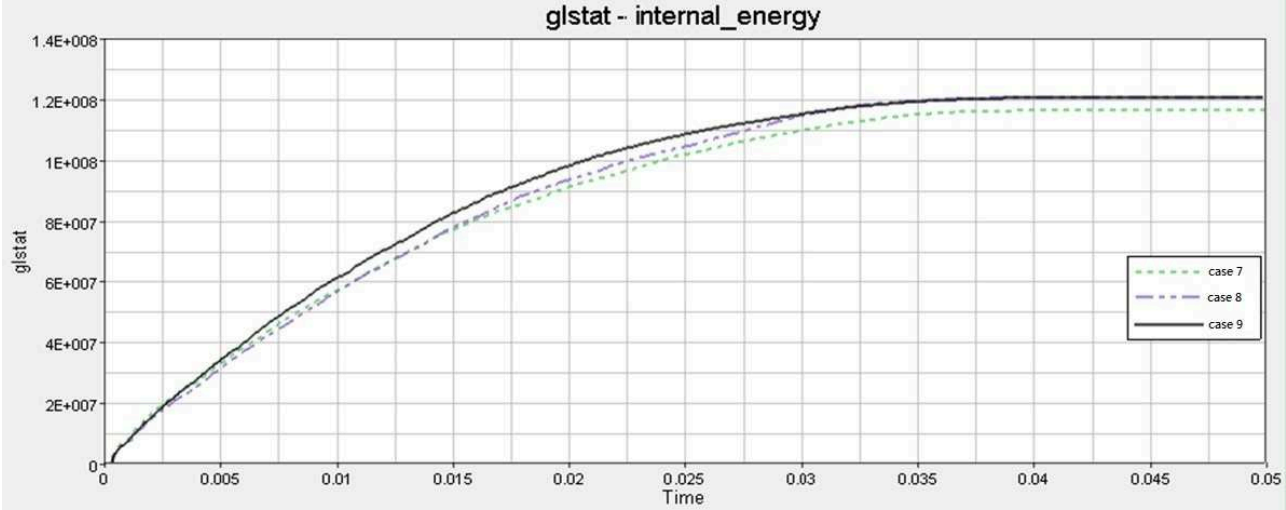

(3)The energy absorption curve of Group 7-9

Analysis

As show in frg.2, there are differences among those groups. The axial compression of Group 6 is the smallest of the nine solutions which uses in a front and a welding tip material MAT24-saph400, a thickness of 1.6mm, the end material MAT24-B340/590, a thickness of 2.4mm through graphical comparison of the curve above. As can be seen from the table orthogonal visual analysis, thickness is the biggest influence on the structure crashworthiness among the three factors .As increasing the thickness of the front and rear plate board, thin-walled tube suction energy increases. The followed

one is materials. The higher material yield strength is, the higher structural strength, the better the energy absorption effect. Welding position has less effect. It can be seen from Figure 4-5, the welding position changes from 2/3 to 3/2, the effect of absorption decreases, which indicates energy absorbing is better when the position of the welding is closer to the rigid wall. Seen from the visual analysis of orthogonal experiment table, in the existing scenario, the combination of A (3) B (1) C (2).has the best effect of energy absorbing.

Conclusion

The main objective of this paper is to study the crashworthiness of thin-walled rectangular beam welding in different ways. And finally obtain thin-walled beam structure crashworthiness optimal range through analysis accompanied by a summary of results between the plate thickness, different materials and welding positions.

There are a lot of inadequacies which can be seen as follows:

(1) In future work, welding components can be used to analyze the actual calculation to verify results of this paper.

(2)This article finds that the crashworthiness of thin-walled structure heavily depends on materials splicing, thickness and welding positions. In the next step, these three factors can be optimized multidisciplinary targeted structural for better crashworthiness of thin-walled rectangular beam.

Reference

[1] ZHANG RUI .Finte Element Analysis Based on Pro-E, HyperMesh and Ansys. 2008 International Conference on Computer Science and Software Engineering.2008.

[2] JIANG Xue-wu, WU Xin-yue, and ZHU Shi-jian, Comprehensive application of UG, HyperMesh and MSCMarc in finite element analysis, Computer Aided Engineering, 2007,16:11-14

[3] Zafer Kazancı, Klaus-Jürgen Bathe. Crushing and crashing of tubes with implicit time integration. J. Impact Engineering (2012),40.

[4] Scott D.R. On modeling of the weld in finite element analyses of tailor-welded blank forming operations. Queen's University, Canada, 2004,172-186.

[5] NagelG M, Thambiratnam D P. Dynamic Simulation and Energy Absorption of Tapered Thin-walled Tubes Under Oblique Impact Loading.

[6] AbramowiczW,JonesN. Dynamic Axial Crushing of Circular Tubes[J]. J. Impact Engineering, 2000,2.

[7] Shakeri H.R., Buste A., Worswick M.J., et al. Study of damage initiation and fracture in aluminum tailor welded blanks made via different welding techniques. J. Light Metals. 2002, 2.

[8] Pallett R J, Lark R J. The use of tailored blanks in the manufacture of construction components. J. Materials Processing Technology, 117 (1-2): 249-254, 2001.

[9] Zhang Meng, Xu Min. Research on Seam Edge Detection Method for Tailored Blanks Laser Welding with Same Thickness. International Conference on Engineering and Business Management, 2010.

[10] Tarigopula V, Langseth M, H opperstad.O.S, et al. Axial crushing of thin-walled high strength steel sections. J. Impact Engineering, 2006.

Advanced Materials Research Vols. 989-994 (2014) pp 903-907
© (2014) Trans Tech Publications, Switzerland
doi:10.4028/www.scientific.net/AMR.989-994.903

Study on the borehole stability in Liulin coal reservoirs

Liyang Song[1, a],Lijia Xiao[1, a],Jiwei Wang[2, a],Jin Zhang[1,a],Tianlin Zhuang[2,a]

[1]China University of Petroleum in Beijing,100000, China

[2]Northest Petroleum University,Daqing, 163318, China

[a]wangjiwei2008@163.com

Keyword: borehole stability; core reservoirs; under-balanced drilling

Abstract. This paper studied the borehole stability in Liulin bituminous core reservoirs during under-balanced drilling. The equivalent depth method was applied to study the formation pore pressure. The floor drain test method was applied to study the ground stress. Core strength experiments combined with logging data were used in the establishment of core strength predicting model. Mechanics analysis model was founded to study the borehole stability in the core reservoir. According to the studying and analyzing results, the under-balance drilling in Liulin coal reservoirs enjoys good borehole stability.

Introduction

To study the borehole stability in coal reservoirs, plenty of information and data should be collected, which include geological, logging, drilling data. The logging data, including acoustic time difference data, formation density, gamma, caliper logging data are significantly important to the study of the formation pore pressure, ground stress, core strength, and borehole stability. After collecting enough data, the borehole stability can be analyzed by applying acoustic time difference method, equivalent depth method, and floor drain test method. According to the logging and calculating results, the transverse distribution of reservoir strength profile can be founded. After establishing the mechanics analysis model, the relationship among collapse pressure, well track and ground stress orientation of the bituminous core reservoir can be founded, so that the characteristic of the borehole stability in Liulin core reservoirs during under-balanced drilling can be described.

Formation pore pressure research

The acoustic time difference method was applied to study the compaction degree and porosity of the reservoir. The formula is shown as follows:

$$\Delta t = \Delta t_0 e^{cH} \tag{1}$$

Transform this formula as:

$$log\Delta t = AH + B \tag{2}$$

The equivalent depth method was used to calculate the formation pressure. The formula is shown as follows:

$$P_A = \frac{1}{10^3} \times g \times (\rho_{bw} H_A - \frac{\rho_{bw} - \rho_w}{C} \ln \frac{\Delta t}{\Delta t_0}) \tag{3}$$

According to the pressure test in Liulin core reservoir, the pore pressure data of the wells are shown in figure 1:

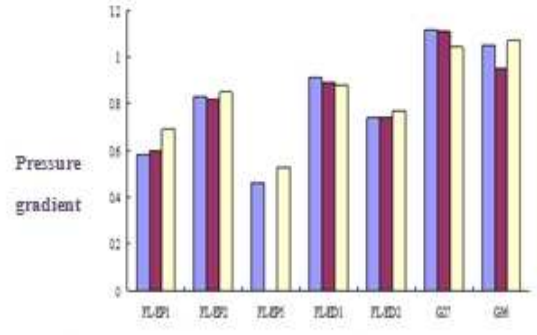

Figure 1 Pore pressure of the wells in Liulin core reservoir

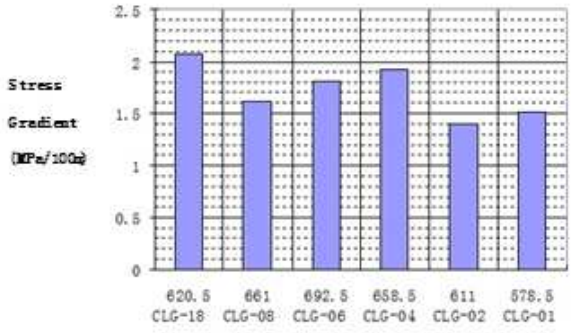

Figure 2: Level minimum stress gradient of different wells

Then, we can calculate the formation pressure and formation pressure gradient of each wells. According to figure 1 and the calculation result, the average formation pressure is 5.60MPa, and the formation pressure gradient is 0.46～1.12MPa/100m.

Ground stress research

Floor drain test method was applied to determinate the ground stress. The formula is shown as follows:

$$\sigma_H = \left(\frac{\mu}{1-\mu} + A\right)(\sigma_v - \beta \cdot P_o) + \beta \cdot P_o$$
$$\sigma_h = \left(\frac{\mu}{1-\mu} + B\right)(\sigma_v - \beta \cdot P_o) + \beta \cdot P_o \quad (4)$$

A and B are two factors that reflect the horizontal tectonic stress. A and B are different at different region.

To get A and B, the practical σh and σH should be calculated, the calculating process is shown as follows:

$$\sigma_h = P_s + 10^{-6} \times \rho_m g H_w \quad (5)$$
$$\sigma_H = 3\sigma_h - P_f - \beta \cdot P_o + |\sigma_t| \quad (6)$$
$$|\sigma_t| = P_f - P_r \quad (7)$$

Then, the expression of A and B can be gotten:

$$A = \frac{\sigma_H - \beta \cdot P_o}{\sigma_v - \beta \cdot P_o} - \frac{\mu}{1-\mu}$$
$$B = \frac{\sigma_h - \beta \cdot P_o}{\sigma_v - \beta \cdot P_o} - \frac{\mu}{1-\mu} \quad (8)$$

The critical fracture stress can be expressed as:

$$P_{fc} = 3\sigma_h - \sigma_H - \beta \cdot P_o + |\sigma_t| \quad (9)$$

The formation fracture pressure and level minimum principal stress can be determined by floor drain experiment method, so that the level maximum principal stress can be determined. This is the major method to determine the field ground stress.

The testing and calculating results are shown in figure 2. This project deduced the tectonic stress coefficient according to the calculating formula of the fracture pressure. According to figure 2, level maximum principal stress gradient >=overlaying stress gradient>minimum stress gradient. The maximum stress gradient is about 2.4, the overlying stress gradient is about 2.38, and the minimum principal stress gradient is about 1.52. The difference between the maximum principal stress gradient and the overlying stress gradient is small, while the difference between maximum and minimum principal stress gradient is big, so that the stability of the horizontal borehole is sensitive to the borehole trajectory.

Formation strength research

To study the formation strength of the bituminous coal reservoir, the core strength experiments and logging data were needed. The strength model is shown as follows:

$$UCS = A(1-\mu_d)\left(\frac{1-2\mu_d}{1+\mu_D}\right)^2 \rho^2 \cdot V_p^4\left(1+0.87V_{cl}\right) \tag{10}$$

The strength model coefficient can be determined by core strength experiments. According to the logging data and core strength experimental results, the transverse strength distribution of this region is shown in figure 3 and figure 4:

According to figure 3, the strength distribution difference of each well block is big. CLY-23 and CLY-36 well blocks, which are in the red contour region, have the axial compressive strength of above 16MPa. CLY-10 well block, which is in the yellow contour region, has the axial compressive strength of above 10MPa. The range of the axial compressive strength in CLY-24 well block is about 6～10MPa, which is in the blue contour region. The green contour region stands for the CLY-02 well block, which has the axial compressive strength less than 5MPa.

According to figure 4, the strength distribution different of different well blocks in Number 8 reservoir is also very significant. CLY-10 well block, which is in the red contour region, has the compressive strength of above 22MPa. The range of compressive strength of CLY-32 well block, which is in the yellow contour region, is 12～20MPa. The axial compressive strength in the blue and green contour region is lower than 10MPa.

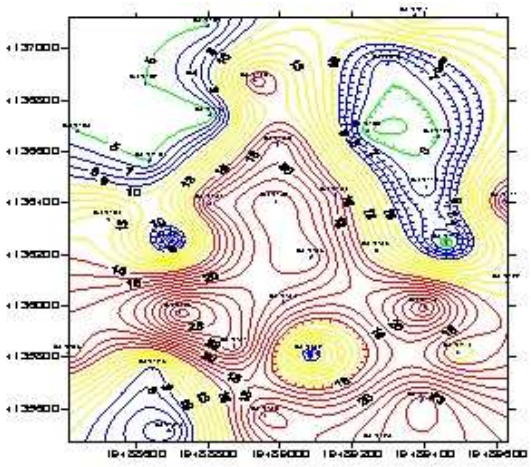

Figure 3: transverse formation strength distribution of Number 3+4 reservoir

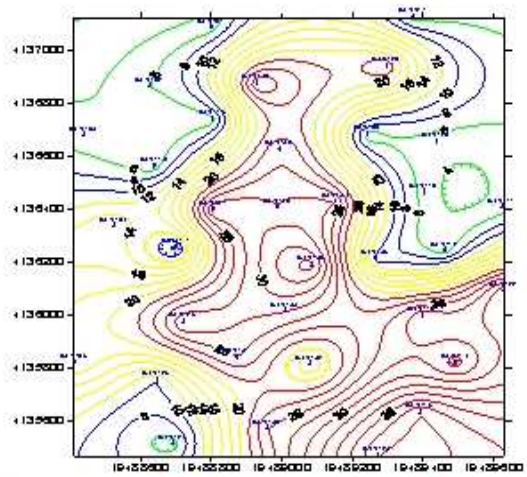

Figure 4: transverse formation strength distribution of Number 8 reservoir

In this case, the stability of the horizontal wells should be studied.

Borehole stability research

The mechanic model of the vertical well is:

$$\tau = C + \sigma n \times \tan(\varphi) \tag{11}$$

$$\sigma_1' = [1+\sin(\varphi)]/[1-\sin(\varphi)] \times \sigma_3' + C_0 \tag{12}$$

The minimum principal stress can be expressed as:

$$\sigma r' = Pw - Pp \tag{13}$$

At $\theta = 0°$ and $\theta = 90°$, we have:

$$\sigma_{\theta=0}' = 3\sigma'H,min - 3\sigma'H,max - Pw + Pp \tag{14}$$

$$\sigma_{\theta=90}' = 3\sigma'H,max - 3\sigma'H,min - Pw + Pp \tag{15}$$

The callapse pressure can be expressed as:

$$P_{collapse} = (\sigma_{\theta=90}' - C0)/[1 + (1+\sin(\varphi))/(1-\sin(\varphi))] + Pp \tag{16}$$

The fracture pressure can be expressed as:

$$P_{fracture} = \sigma_{\theta=0}' + T + Pp \tag{17}$$

The borehole stability of the CLH03&04 wells were studied in this project. According to the formation pore pressure, formation stress, and formation strength data, the overlying stress gradient of 3-4 wells is 2.38MPa/100m, the level maximum stress gradient is 2.40MPa/100m, the level minimum stress gradient is 1.45MPa/100m, and the pore pressure coefficient is 0.46.The well track of CLH03&04 wells are shown in figure 5 and figure 6:

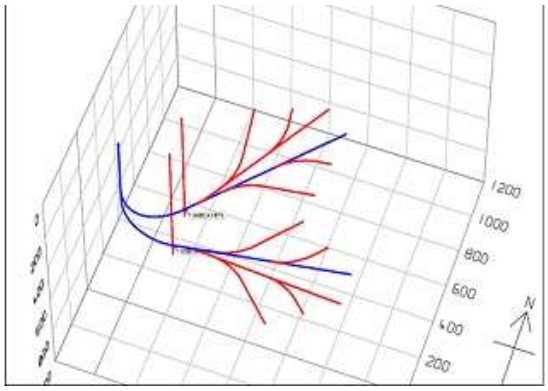

Figure 5 Well track of CLH03

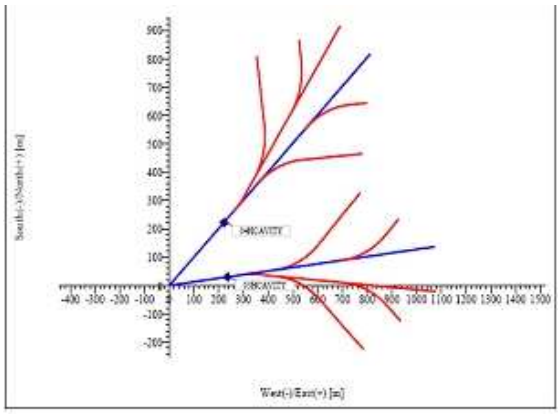

Figure 6 Well track of CLH04

The horizontal maximum principal stress orientation is 45°north by east. Calculate the collapse pressure according to the data given. The horizontal collapse pressure of CLH03 about 0.88MPa, and the horizontal collapse pressure of CLH04 is about 0.83MPa.

The relationship between collapse pressure, well track and formation stress orientation are shown in figure 7:

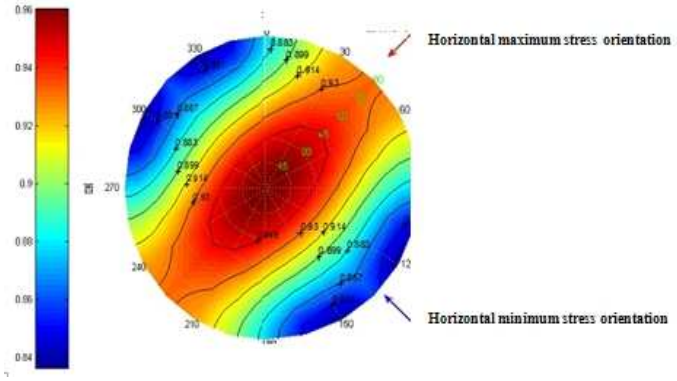

Figure 7 Relationship between collapse pressure, well track and formation stress orientation

In general, the two wells possess good construction conditions, and the borehole stability is well.

Conclusion

● According to the formation pore pressure research results, the average Liulin coal reservoir pressure is 5.60MPa, and the range of the pressure gradient is 0.46～1.12MPa/100m.

● According to the ground stress research results, the difference between the maximum and minimum principal stress is significant, so that the stability of the horizontal borehole is sensitive to the borehole trajectory.

● According to the formation strength research results, the transverse strength difference within Linlin coal formation is significant, so that the stability of the horizontal well should be studied.

● According to the borehole stability research, the stability of CLH03&04 is well, which provides good condition for the under-balanced drilling.

Reference

[1] Z.Chen.N.Khaja.Formation Damage Induced by Fracture Fluids in Coalbed Methane Reserviors.SPE 101127, 2006.
[2] Kevin E.Nick,Michael W.Conway.The Relation of Diagenetic Clays and Sulfates to the Treatment of Coalbed Methane Reservoirs. SPE 30736, 1995.
[3] Ian Palmer,Hans Vaziri.Completions and Stimulations for Coalbed Methane Wells. SPE 30012,1995.
[4] Wong, R. C. K, & Yeung, K. C. (2002, January 1). Borehole Stability in Oil Sands Under Drilling. Petroleum Society of Canada.
[5] Morita, N. (2004, January 1). Well Orientation Effect on Borehole Stability. Society of Petroleum Engineers.
[6] McLellan, P., & Hawkes, C. (1999, January 1). Borehole Stability Analysis For Underbalanced Drilling. Petroleum Society of Canada.

Advanced Materials Research Vols. 989-994 (2014) pp 908-912
© (2014) Trans Tech Publications, Switzerland
doi:10.4028/www.scientific.net/AMR.989-994.908

An improved CEM with regard to the crack-tip

Yongsheng LIN [1, a]

[1] State Key Laboratory of Water Resources and Hydropower Engineering Science, Wuhan University, Wuhan, Hubei 430072，China

[a]email: lys3689@163.com

Keywords: Composite Element Method (CEM); Discontinuous; Local Enrichment; Asymptotic Crack-tip Displacement Fields

Abstract. This paper expounds the basic principles of composite element method (CEM).In order to model the discontinuity of the displacement, the asymptotic crack tip displacement fields are added to the CEM approximation for the local enrichment by using the framework of partition of unity. Thus, the crack tip can be inserted into anywhere within the element. The crack-tip displacement mode is given, and some formulas are derived and established in a CEM program. The evaluation of stress intensity is discussed. Numerical simulations illustrate that the proposed algorithm has similar accuracy compared to the FEM, and it has advantage of convenient of pre-process.

Introduction

Numerical simulation of discontinuities is always a hot and difficult problem in engineering and receives much concern since it has important realistic meaning. In the past four decades, many numerical analysis theories and methods have been proposed and developed to simulate the discontinuities, among them the finite element method (FEM), the distinct element method(DEM)[1] and discontinuous deformation analysis method(DDA)[2]. The recently developed element-free Galerkin method [3], manifold method [4], extended finite element method (XFEM) [5], composite element method (CEM) [6][7][8][9][10] are also more and more popular because of their special merits.

The concept of CEM was first proposed to simulate hollow bolt in rock masses [11].Now, it has been developed to model the discontinuities. The basic idea of CEM is that the complicated pre-process to mesh generation is converted into complex calculation by using composite elements. Using CEM can simplify the pre-process greatly. The large-scale discontinuities will not be necessarily modeled by special regular elements, and so the mesh generation work can be concentrated on the other important aspects—such as the structure configuration, the stress gradient, etc. The most significant advantage of CEM is that each composite element can contain a lot of discontinuities. The main disadvantage of CEM is that discontinuities must extend to the element boundaries, so the mesh generation is limited.

In this paper, the CEM is improved by adding the asymptotic crack-tip displacement fields which based on the framework of partition of unity. Thus, the crack-tip can be inserted into anywhere within the element, and the pre-process to mesh generation is much easier than ever. Numerical simulations illustrate the improved composite element method (ICEM) has similar accuracy compared to the FEM.

The basic principle of CEM

Suppose an inhomogeneous domain shown in Fig.1 which is divided into four sub-domains by four discontinuity segments. The whole domain is defined as a composite element, and the four sub-domains are termed as sub-elements. The displacement $\{\Delta u\}_{rl}$ in sub-element is interpolated from the nodal displacement $\{\Delta\delta\}_{rl}$ assigned to the composite element as(Fig.2)：

$$\{\Delta u\}_{rl} = [N]\{\Delta\delta\}_{rl} \quad \text{within the sub-element rl}$$
$$l = 1, 2, \cdots, n \tag{1}$$

in which $[N]$ is the shape function matrix of the conventional FEM. Note that Eq. (1) is valid only in each of the sub-elements respectively. The loads of each sub-element are converted to the respective nodal loads of the composite element. According to the principle of virtual work, the equilibrium equation can be established. The displacements, strains as well as the tresses of each sub-element can be calculated with the solved nodal displacements of composite element.

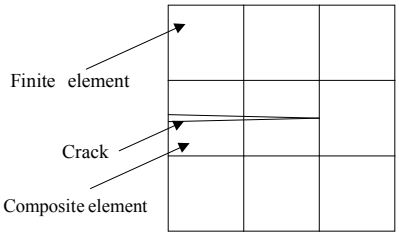

Fig.3. CEM model containing a crack

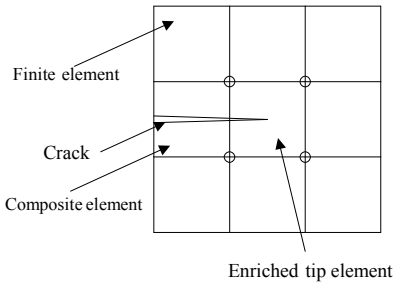

Fig.4. ICEM model containing a crack

Improved CEM

The CEM model containing a crack is shown in the Fig 3, in which the crack tip must be at the edge of an element. In order to make the crack tip inserted into anywhere within an element, the asymptotic crack tip displacement fields proposed in XFEM [5] are added to the CEM approximation for the local enrichment, which is shown in Figure 4. Four sets of virtual nodes are added to the crack tip element nodes with a circle mark shown in Figure 4. The displacements in the tip element can be interpolated from the interpolation formula as

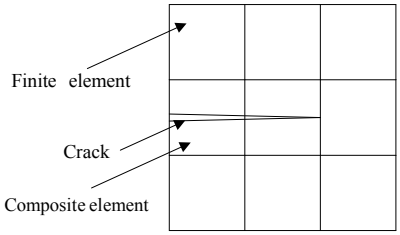

Fig.3. CEM model containing a crack

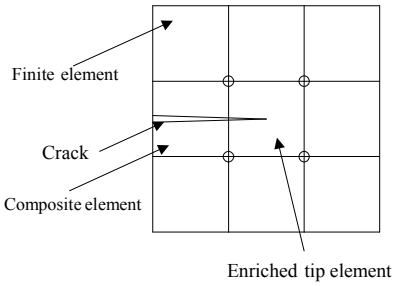

Fig.4. ICEM model containing a crack

$$u = \sum_{I \in \Omega_\Lambda} N_I(x)\left[u_I + \sum_{j=1}^{4} \phi_j(x) b_I^j\right] \tag{2}$$

in which u_I is the displacement of node i and b_I^j is the set of displacement at node i. The functions $\phi_j(x)$ are defined as

$$\phi_j(x) = \left\{\sqrt{r}\sin(\frac{\theta}{2}), \sqrt{r}\cos(\frac{\theta}{2}), \sqrt{r}\sin(\theta)\sin(\frac{\theta}{2}), \sqrt{r}\sin(\theta)\cos(\frac{\theta}{2})\right\} \tag{3}$$

Where (r,θ) are the local polar co-ordinates at the crack tip (Fig 5). It should be pointed out that the first function in (3), $\sqrt{r}\sin(\theta/2)$, is discontinuous across the crack faces whereas the last three functions are continuous.

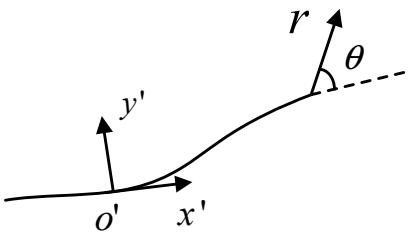

Fig.5. Local coordinate system

By the virtual work principle the equilibrium equation of the crack tip element can be deduced as follows

$$K^e \delta^e = R^e \tag{4}$$

where R^e is called the element loads matrix formed by r_i^e

$$r_i^e = \left\{ r_i^u, r_i^{b1}, r_i^{b2}, r_i^{b3}, r_i^{b4} \right\} \tag{5}$$

and K^e is called the element stiffness matrix formed by k_{ij}^e

$$k_{ij}^e = \begin{bmatrix} k_{ij}^{uu} & k_{ij}^{ub} \\ k_{ij}^{bu} & k_{ij}^{bb} \end{bmatrix} \tag{6}$$

$$k_{ij}^{rs} = \int_{\Omega^e} \left(B_i^r \right)^T D B_j^s d\Omega \quad (r,s = u,b) \tag{7}$$

$$B_i^u = \begin{bmatrix} \dfrac{\partial N_i}{\partial x} & 0 & \dfrac{\partial N_i}{\partial y} \\ 0 & \dfrac{\partial N_i}{\partial y} & \dfrac{\partial N_i}{\partial x} \end{bmatrix} \tag{8}$$

$$B_i^b = \begin{bmatrix} B_i^{b1} & B_i^{b2} & B_i^{b3} & B_i^{b4} \end{bmatrix} \tag{9}$$

$$B_i^{bn} = \begin{bmatrix} \dfrac{\partial (N_i \phi_n)}{\partial x} & 0 & \dfrac{\partial (N_i \phi_n)}{\partial y} \\ 0 & \dfrac{\partial (N_i \phi_n)}{\partial y} & \dfrac{\partial (N_i \phi_n)}{\partial x} \end{bmatrix}^T \quad (n = 1,2,3,4) \tag{10}$$

The above formulas are established in an ICEM program.

Evaluation of stress intensity factor

The paper [12] suggests that the precision of stress intensity factor using J-integral is high. Stress intensity factor take the following form:

$$\begin{cases} K_1 = \dfrac{2}{E^*} I_1 \\ K_2 = \dfrac{2}{E^*} I_2 \end{cases} \tag{11}$$

where E^* is defined in terms of material parameters E (Young's modulus) and ν (poisson's ratio) as

$$E^* = \begin{cases} E & (\text{plane stress}) \\ \dfrac{E}{1-\nu^2} & (\text{plane strain}) \end{cases} \tag{12}$$

The interaction integral is

$$I = -\int_A (\sigma_{ik}\varepsilon_{ik}^{aux}\delta_{1j} - \sigma_{ij}u_{i,1}^{aux} - \sigma_{ij}^{qux}u_{i,1})q_{,j}dA \quad (13)$$

where (aux) mark is the auxiliary field.

Numerical example

Consider the geometry shown in Fig 6: a plate of width $a = 7m$ and height $b = 16m$ with an edge crack of length $a = 3.5m$. The plate is subjected to a tensile load of $\sigma = 1.0Pa$ .The material properties are assumed to be that of plate with young's modulus 1000 Pa , and poisson ratio 0.3.

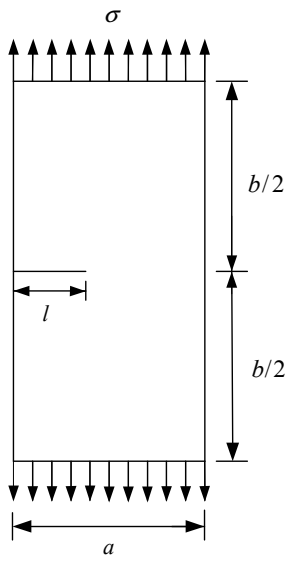

Fig.6. Plate problem with an edge crack

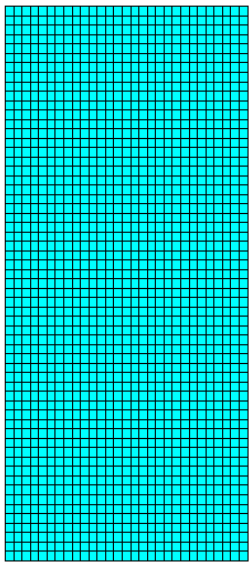

Fig.7. FEM mesh

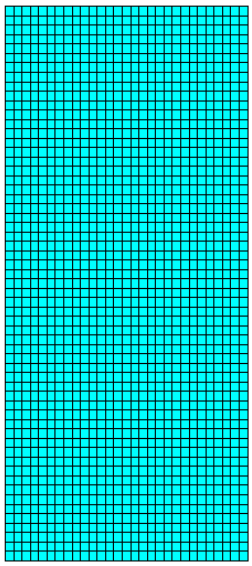

Fig.8. ICEM mesh

The exact solution for this problem is given by [13]

$$K_1 = \sigma\sqrt{\pi l}(1.12 - 0.231\left(\frac{l}{b}\right) + 10.55\left(\frac{l}{b}\right)^2 - 21.72\left(\frac{l}{b}\right)^3 + 30.39\left(\frac{l}{b}\right)^4) \quad (14)$$

Table I SIF for a plat with an edge crack

Exact K_1	Method	Numerical K_1	Relative errors
9.3738	FEM	8.9795	-4.2%
	ICEM	9.8918	5.2%

Both FEM and ICEM are used in the simulation. The ANSYS software is used in the FEM simulation. The FEM mesh is shown in Fig.6 and ICEM mesh is shown in Fig.7.The numerical results and the exact solution are shown in Table I. The value calculated by the ICEM is greater than the exact value, whereas the value calculated by the FEM is less than the exact value. The results are excellent in terms of overall accuracy.

Conclusion

In this study, the CEM is improved by adding the asymptotic crack tip displacement fields to the CEM approximation. The near-tip asymptotic fields are used near the crack tip. Its use represents the main improvement of this technique over that presented in [6]. The crack-tip displacement mode is given, and some formulas are derived. In addition, a method of the stress intensity factors can be computed accurately with relatively coarse meshes is given.

In contrast to the CEM [6], the crack-tip can be inserted into anywhere within the element. The addition of the near-tip asymptotic fields allow for the entire crack geometry to be modeled independently of the mesh. Thus, the ICEM can simplify the pre-process greatly.

The example shows the feasibility of the ICEM. The problem of crack growth needs further study.

References

[1] Cundall P A. A computer model for simulating progressive，large-scale movement in blocky rock system [A]. In：Rock Fracture，Proc. Symp. Int. Soc. Rock Mech.[C]. Nancy：[s. n.], 1971, 129～136

[2] Shi G H. Discontinuous deformation analysis：a new numerical model for the statics and dynamics of deformable block structures[J]. Engineering Computations，1992，9(2)：157～168

[3] Belytschko T，Lu Y Y，Gu L. Element-free Galerkin methods[J]. Int. J. for Num. Methods in Engng.，1994，37(2)：229～256

[4] Shi G H. Manifold method [A]. In：Proc. of the First Int. Forum on DDA and Simulation of Discontinuous Media[C]. Berkeley，California，USA：[s. n.]，1996，52～204

[5] Moes N,Dolbow J,Belytschko T.A finite element method for crack growth without remeshing[J]. International Journal for Numerical Methods in Engineering，1999, 46: 131–150.

[6] Chen S H，Qiang S. Composite element model for discontinuous rock masses[J]. Int. J. Rock Mech. Min. Sci.，2004，41(5)：865–870.

[7] Chen S H，He Z G，Egger P. Study of hollow friction bolts in rock by a three-dimensional composite element method[A]. In：Proceedings of the 10th Congress of the ISRM-Technology Roadmap for Rock Mechanics[C]. South Africa：A. A. Balkema，2003. 203–206.

[8] Chen S H，Xu Q，Hu J. Composite element method for seepage analysis of geo-technical structures with drainage hole array[J].

Journal of Hydrodynamics(Ser. B)，2004，16(3)：260–266.

[9] CHEN S H, FENG X M, SHAHROUR I. Numerical estimation of REV and permeability tensor for fractured rock masses by composite element method[J]. Int J Numer Anal

[10] CHEN Sheng-hong, FENG Xue-min. COMPOSITE ELEMENT MODEL FOR ROCK MASS SEEPAGE FLOW [J]. Journal of Hydrodynamics, 2006，18(2)：219–224.

[11] Chen S H，Egger P，Migliazza R, et al. Three-dimensional composite element modeling of hollow bolt in rock masses[A]. In：Proceedings of the ISRM International Symposium on Rock Engineering for Mountainous Regions-Eurock′2002. 25–28.

[12]ToshioN,YouheiO,ShuichiStressintensityfactoranalysisofinterfacecracksusingXFEM[J],International Journal for Numerical Methods in Engineering ,2003,56:1151—1173.

[13] Ewalds H, Wanhill R. Fracture Mechanics. Edward Arnold: New York; 1989.

Advanced Materials Research Vols. 989-994 (2014) pp 913-917
© (2014) Trans Tech Publications, Switzerland
doi:10.4028/www.scientific.net/AMR.989-994.913

Efficiency Prediction of Limestone-gypsum Wet Desulphurization Based on Support Vector Machine

Jianmeng Yang [1,a], Boshuo Sun [1,b], Nianzhe Qi [1]

[1]School of Energy, Power and Mechanical Engineering, North China Electric Power University, Baoding 071003, China

[a]yjm8123445@126.com, [b]sunboshuo@126.com

Keywords: wet desulfurization efficiency, support vector machine regression, grid method parameter optimization, prediction model.

Abstract. This paper studies the prediction of power plant desulfurization efficiency, based on support vector machine through the meshing method for parameter optimization, establish a prediction model, with the running of the actual data to predict the results: mean square error (MSE) is 0.00259324, the correlation coefficient (R) is 0.979927%, the largest error is less than 1.5%, the results show that the established forecast model based on support vector machine (SVM) with high accuracy to predict the desulfurization efficiency, and can satisfy the engineering need of flue gas desulfurization efficiency prediction.

Introduction

Nowadays air quality in the world continues to deteriorate, and main pollution gas is SO_2. The SO_2 emissions has already increased to 25.49 million tons in China [1], and China has become the largest SO_2 emissions country in the world. The 12th Five-Year Plan clearly pointed out that the total SO_2 emission will below to 20.864 million tons in 2015 and reduced by 8 percent than 2010. At present, the power stations, one of largest SO_2 emissions industries, is facing a huge problem. Therefore efficiency prediction of desulphurization is particularly important to power station. There are many factors impact the efficiency prediction of wet desulphurization, the factors have a high degree of relevance, so it is not easy to predict the efficiency of wet desulphurization. This paper based on support vector machine through the meshing method for parameter optimization, established prediction model and predicted the efficiency of desulphurization. Support Vector Machine（SVM）was based on statistical theory, which first raised by Vapnik [2], it based on statistical theory. The SVM initial development is to solve classification problems, and later extended to solve the problem nonlinear regression forecast.

The Meshing Method for SVM Parameter Optimization

In order to keeping prediction accuracy, we not only need to choose reasonable kernel function, but also choose kernel function parameter g and penalty parameter c. Generally radial basis function (exp ($g\times|xi-xj|^2$)) was chosen as a kernel function[3 4], choose a reasonable parameter can get a better regression prediction accuracy. We can get an optimal parameter by CV（Cross Validation）, it can avoid effectively under and over learning state, and finally the test set was predicted and can get an optimal accuracy.

Cross Validation. Cross Validation is a statistical analysis method which verify the model performance, its basic thought is classify original data in some sense. A part as train set, and others as validation set. At first classifier was train by train set, then utilize verify set test the model which was trained. Prediction accuracy we got as a performance index of building a model.

Example shows that the parameters which were chosen by cross validation were more effectively than those parameters which were selected randomly. Justify related parameters (kernel function parameter g and penalty parameter c) to get optimal prediction accuracy when we predict by SVM.

This paper used K—fold Cross Validation(K—CV)method to get parameter c and gas optimal parameter.

Search optimal parameter by the meshing method. Optimal parameter c and g are searched by meshing method, we can search the highest model prediction accuracy by CV method, namely the globally optimal solution. In a given range of exponent which are meshed, to search parameter c and parameter g, at first we also can search roughly in a bigger range, and then based on result from searched roughly, the range to search optimal parameter c and parameter g can be reduced. In search process maybe have many groups of parameter c and parameter g correspond to the optimal prediction value, considering the high parameter c will result in over learning state, namely train set classification accuracy is too high while test set classification accuracy is too low, so in all parameters c and parameters g which satisfy condition, we choose the minimum penalty parameter c as the optimal selection.

Build up the Forecast Model

The influencing factors of efficiency prediction of limestone - gypsum wet desulphurization. Wet flue gas desulfurization process involves a series of chemical and physical factors, the efficiency of desulphurization depend on many factors. In design aspect of desulphurization system: Liquid-gas ratio, flue gas velocity, the oxidation air amount etc. In flue gas inlet aspect of desulphurization system: Gas volume, gas temperature, dust contained in the flue gas, concentration of sulfur dioxide in inlet etc. In operational control parameters aspect of desulphurization system: slurry pH of absorption tower, concentration of absorption tower slurry, calcium-sulfur ratio etc. On the basis of document [5], [6], [7], [8], author select Liquid-gas ratio, flue gas velocity, the oxidation air amount, gas temperature, dust contained in the flue gas, concentration of sulfur dioxide in inlet, slurry pH of absorption tower, concentration of absorption tower slurry, calcium-sulfur ratio as independent variable and efficiency of desulphurization as dependent variable.

Build model and regression prediction. This paper select radial basis function (exp ($g\times|xi-xj|^2$)) as kernel function, after selecting kernel function, we will search optimal parameter about g and c. On the basis of method 2.2, parameter c and parameter g are searched in a given and meshed range of exponent 2, firstly the range can be set $2^{(-8)}\sim2^{(8)}$, step size of parameter c and parameter g can be set 1, get a probable result. Then we can reduce the range to $2^{(-4)}\sim2^{(4)}$ and set step size 0.5, through above method, the optimal parameter c and parameter g which can be searched from Fig.1 and Fig.2 respectively are 1 and 0.17678.

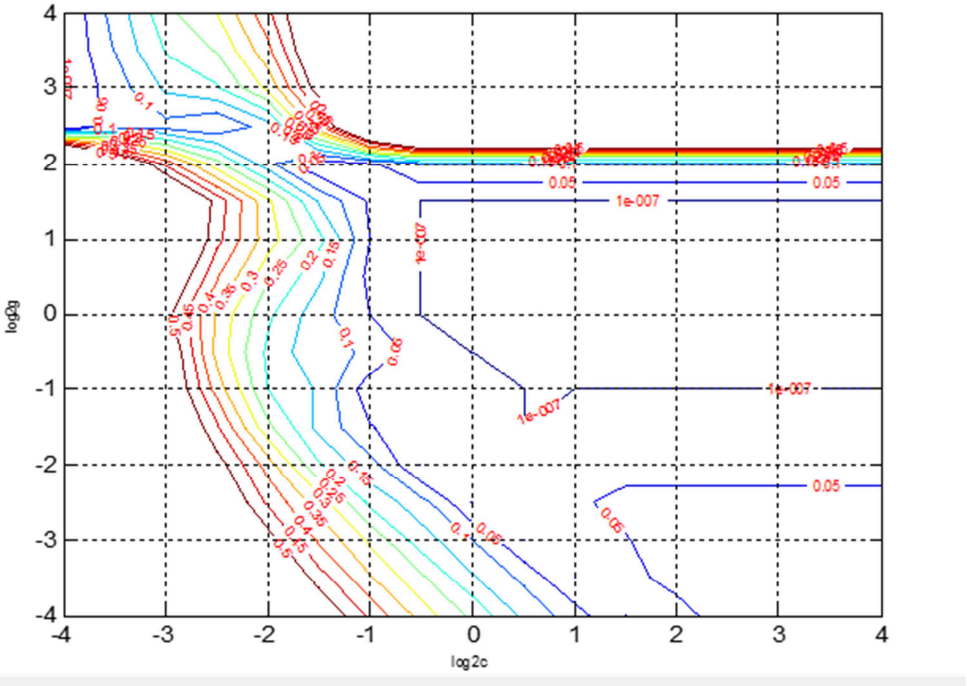

Fig.1. The contour map of parameter fine select

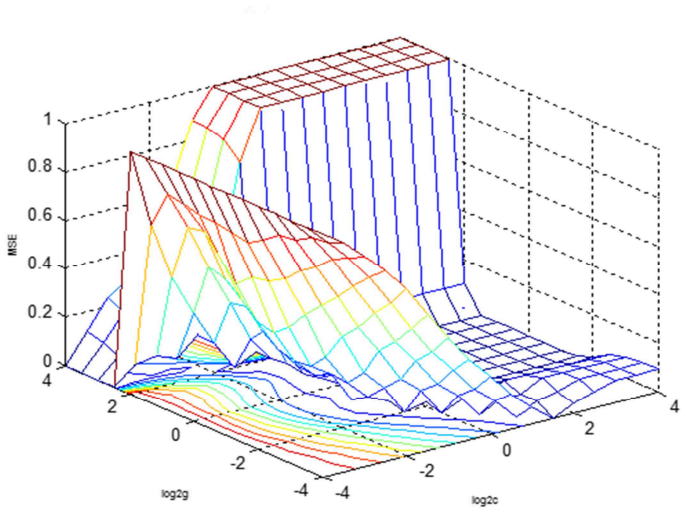

Fig.2. The 3 d figure of parameters fine select

The Predicted Result and Error Analysis

The final regression prediction results as shown in Fig. 3, From Fig. 3 we can found predicted data has the high degree to match the original data, at the turning point of curve two points almost coinciding. The result illustrates the prediction based on model of SVM have high degree of accuracy and this method can better predict the desulfurization efficiency.

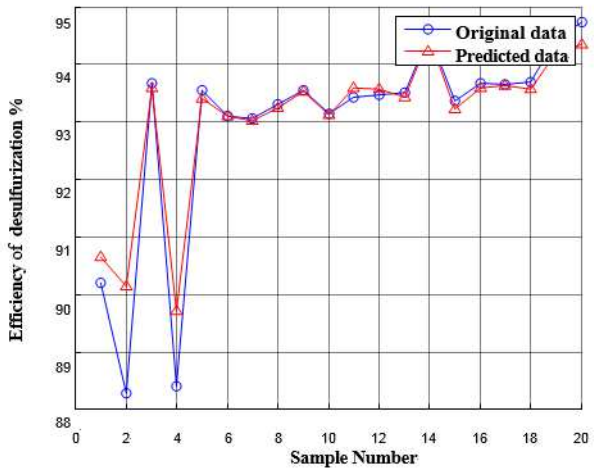

Fig.3. Comparison of desulfurization efficiency between predicted results and actual measurements

For analyzing degree of accuracy we listed SVM model prediction data, original data of desulfurization efficiency and relative error in Tab. 1. As Tab.1 shown, we can find the maximum relative error not over 1.5%，majority relative error between -1.0% and 1.0%，through analysing relative error, we can find different operating parameter have different effect on desulfurization efficiency in limestone-gypsum wet desulphurization process.

Tab.1. Relative errors between actual measurement and predicted values results %

Sample Number	Actual Value	Predicted Value	Relative Error
1	90.2042	90.6526	-0..69
2	88.2792	90.1388	-0..92
3	93.6708	93.5950	-0.48
4	88.4000	89.7058	-0.73
5	93.5542	93.4114	-0.49
6	93.1042	93.1008	-1.35
7	93.0667	93.0332	-0.0065
8	93.2083	93.2583	0.17
9	93.5500	93.5344	0
10	93.1500	93.1227	0.15
11	93.4333	93.6022	1.33
12	93.4833	93.5774	1.5
13	93.5250	93.4383	0.09
14	94.5292	94.4847	0.32
15	93.3708	93.2251	1.2
16	93.6708	93.5974	-0.37
17	93.6667	93.6465	0.21
18	93.7000	93.5846	-0.41
19	94.4625	94.2043	-0.70
20	94.7542	94.3623	0.27

Conclusion

The power plant of unit limestone-gypsum wet desulphurization efficiency is related to a number of factors, which are interrelated and interact with each other, these factors put forward higher requirements to forecasts for the accuracy of the desulfurization efficiency. This paper try to use SVM method to predict desulfurization efficiency and get the optimal penalty parameter c and kernel function parameter g through meshing method; establish model based on operational data from power

station, illustrate the model built by SVM have a high degree of accuracy to predict the desulfurization efficiency through comparing actual values and predicted values, the method can satisfy the engineering need of flue gas desulfurization efficiency prediction and contribute to environment.

References

[1] The rescue group of China sustainable development, China Sustainable Development Report, Science Press, Beijing, 2012.

[2] Vapnik V. The nature of statistical learning theory, Springer, New York, 1995.

[3] Chunlin Wang *et al*. Support vector machine modeling on the unburned carbon in fly ash, Proceedings of the CSEE. 2005, 25(20)72-76.

[4] Lei Wang *et al*. Regression forecast and abnormal data detection based on support vector regression, Proceedings of the CSEE. 2009, 29, (8)94-98.

[5] Dongming Guo. The technology and equipment of desulphurization, Chemistry Industry Press,Beijing,2011, p.38-51.

[6] Zhiqiang He *et al*. Optimum operation of limestone-gypsum wet flue gas desulfurization, China Electric Power Press, Beijing,2011, p.40-50.

[7] Yi Zhong *et al.* Factors influencing desulfurization efficiency of wet flue gas desulfurization system, Zhejiang University Engineering Science. 2008, 42, (5)172-176.

[8] Zhixuan Wang. Thermal power plant desulfurization equipment operation and maintenance training materials, China Electric Power Press, Beijing,2011, p.22-30.

Advanced Materials Research Vols. 989-994 (2014) pp 918-922
© (2014) Trans Tech Publications, Switzerland
doi:10.4028/www.scientific.net/AMR.989-994.918

Research on failure mechanism consistency in accelerated wear test of metal materials

Ma Xiaobing[1,2,a], Cheng Bo[1,b]

[1]School of Reliability and Systems Engineering, Beihang University , Beijing, China

[2]Science & Technology Laboratory on Reliability & Environmental Engineering, Beijing, China

[a]maxiaobing@buaa.edu.cn, [b]buaachengbo@gmail.com

Keywords: wear, accelerated test, failure mechanism consistency, normal load, relative speed

Abstract. The accelerated wear test of metal materials is researched, and the boundary conditions which required by failure mechanism consistency receive a meaningful exploration. This work presents a physical model about the boundary of accelerated stress to support accelerated test design. According to the material properties, the accelerated stress is restricted by three boundaries which are the boundary of the normal load, the boundary of relative speed and the boundary of their product. This research shows that failure mechanism consistency in accelerated wear test manifests as consistency of parameters in statistics, yet in physics, it depends on the three boundaries.

Introduction

As one of the main reasons for property degradation and failure of mechanical products, wear and wear life prediction are conspicuous important in material and machinery science. Because of various factors in complicated wear process and the long-life of wearing parts, it is obviously difficult to obtain failure data at a normal stress level. Therefore, in order to assess the product life, the importance of accelerated wear test is becoming ever more prominent.

The premise of accelerated test is failure mechanism consistency. Existing consistency judgment method is based on the statistical characteristic of failure data. However, for the accelerated wear test, the physical influence of stress range to failure mechanism should be further considered.

To research the physical influence of stress boundaries to failure mechanism consistency, three aspects would be considered to limit the stress level. A stress boundary model based on failure mechanism consistency offers advice to the accelerated test.

1. Mechanism of accelerated wear test

For a sliding contact, the wear of friction pair is difficult to estimate because of the mixed conditions. Fortunately, the Archard's equation [1] can calculate the wear volume appropriately.

$$V = K\frac{Wx}{H} \tag{1}$$

Where V is the wear volume, W is the normal load, x is the sliding distance, H is the material hardness, and K is a non-dimensional wear coefficient. From the Archard's equation, a new form can be deduced, Eq. 2, where K and H which the material and condition influence only are grouped in a new parameter k.

$$\frac{d(V)}{d(t)} = kWv \tag{2}$$

The left part of the equation called volume abrasion rate, which determines the wear life of products. According to Eq. 2, it is showed that the crucial factor of wear life is Wv, the product of normal load and relative speed. Therefore, Wv is an appropriate choice to be the accelerated stress.

Yet in some cases, as the special form of the Wv accelerated wear test, normal load or relative speed may act as the accelerated stress. Acceleration coefficient could be derived from Eq. 2

$$K_J = \frac{t'}{t} = \frac{W \cdot v}{W' \cdot v'} \tag{3}$$

Eq. 3 is used to calculate the approximate acceleration coefficient beforehand. However, the lifetime t should not be regarded as the reliability live.

2. Statistic judgment of failure mechanism consistency

Weibull distribution [2] is widely used to describe the lifetime of products where wear is the main failure mode.

$$F(t)=1-\exp\{-(\frac{t}{\eta})^m\} \quad t>0 \tag{4}$$

For the accelerated wear test, lifetime under each accelerated stress level S_i still obeys weibull distribution: $t_i \sim W(\eta_i, m_i)$. Failure mechanism consistency is equals to the shape parameter consistency in the statistical sense.

$$m_1 = m_2 = \cdots = m_k \tag{5}$$

A new equation is obtained from the logarithm of Eq. 4

$$\ln[-\ln(1-F_i(t))] = m_i \ln t - m_i \ln \eta_i \tag{6}$$

According to Eqs. 5 and 6, straight lines which are parallel to each other should be fitted for logarithmic test data, and the slope is m_i.

3. Physical boundaries of accelerated stress

The consistency of statistical characteristic is the necessary but not sufficient condition for that of failure mechanism. Before the accelerated wear test, it is necessary to limit the accelerated stress Wv, which contains the boundaries of normal load, relative speed, and the product of the two.

3.1 Boundary of the product

In accelerated wear test, Wv is regarded as accelerated stress. Considering the Amonton's friction equation, the power used to overcome the frictional force can be deduce.

$$P_f = F_f v = (W\mu) \cdot v = \mu \cdot Wv \tag{7}$$

Eq. 7 shows that the input power contains two factors, the constant μ and the accelerated stress Wv which is the key factor to the input power. In general, the power is divided into two parts: the bigger one is wasted as heat, and the other one is used to let the material wear off. In fact, the accelerated stress Wv is always regarded as frictional heating factor whose increase leads to the rapidly rising of the contact temperature. However, for the wear of metals, the high temperature is the cause of gluing which will trigger sharp abrasion, a different failure mechanism. In order to guarantee the consistency of failure mechanism, the contact temperature should be lower than θ_c, the critical temperature of gluing.

$$\theta_b + \theta_u < \theta_c \tag{8}$$

Where θ_b is the environment temperature, θ_u is the temperature rise. Formula 8 could be described by an empirical equation of frictional heating factor.

$$Wv < c_1 \tag{9}$$

In formula 9, c_1 is a constant which could be confirmed by table lookups or test.

3.2 Boundary of the normal load

As depicted in Fig. 1, the friction pair contact with each other by a lot of protrusions with small radius of principal curvature.

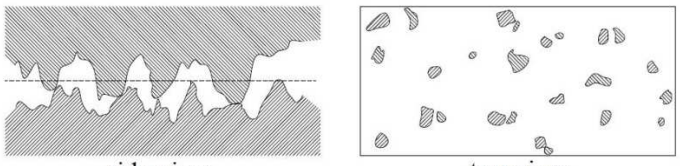

Fig.1. Micrograph of friction contact surface

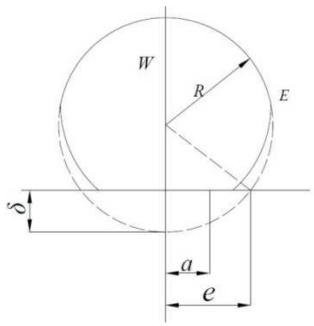

Fig. 2. Elastic deformation in point contacts

Researches show that in the friction process, most of these protrusions deform elastically. The extra high normal load would lead to plastic deformation which causes changes of material property and unreasonable quick-wearing. In order to guarantee failure mechanism consistency in the test, normal load should be limited by a clear ceiling. Fig. 1 is a sketch map of deformation and stress in an ideal situation of point contacts [3].

Based on elastic mechanics, the relations of the physical quantity in Fig. 2 can be derived.

$$\delta = \sqrt[3]{\frac{9W^2}{16E^2R}} \quad , \quad a = \sqrt[3]{\frac{3WR}{4E}} \quad , \quad W = \frac{4}{3}E\sqrt{R\delta^3} \tag{10}$$

Where δ is the displacement, W is normal load, E is the elastic modulus, R is the mean radius of contact points. Apparent contact area A and average pressure P are easily derived.

$$A = \pi R\delta \quad , \quad P = \frac{W}{A} = \frac{4E}{3\pi}\sqrt{\frac{\delta}{R}} \tag{11}$$

If the average pressure is extra-high, plastic deformation will appear in contact points. The critical condition of elastic deformation is related to BH (Brinell Hardness), formula 12.

$$P < \frac{H}{3} \tag{12}$$

In the accelerated wear test, failure mechanism consistency asks for the ceiling of normal load, and it can be derived from formulas 11 and 12.

$$W < \frac{\pi^3 R^2 H^3}{48E^2} = c_2 \tag{13}$$

3.3 Boundary of the relative speed

Tests show that even though the normal load and the product are relatively low, the high speed is also a challenge to the failure mechanism consistency. In the friction process, the real contact area is

much smaller than the apparent contact area. As is illustrated in Fig. 1, real contact area is only the top of some protrusions. The change of normal load will only influence the number of actual contact points, instead of contact pressure.

The high speed leads to the change of friction heat and the material property. This kind of wear can't be used in the accelerated wear test because of different failure mechanisms. In the test design stage, the friction heat restriction must be considered, and the relative speed should be restricted.

$$v < c_3 \tag{14}$$

Where c_3 is a constant which is influenced by material and working condition, and can be obtained by test or from design handbook.

3.4 Boundaries of accelerate stress

In conclusion, the accelerate stress Wv should be restricted in the test. Formulas 9, 13 and 14 have provided the boundaries, formula 15.

$$Wv < c_1, \quad W < c_2, \quad v < c_3 \tag{15}$$

It can be expressed in another way, formula. 16.

$$\ln W + \ln v < \ln c_1, \quad \ln W < \ln c_2, \quad \ln v < \ln c_3 \tag{16}$$

In the accelerated wear test, failure mechanism consistency requires the restrictions on accelerate stress, and they are represented in Fig.3 and formula 16. The three boundaries explain failure mechanism consistency in physics.

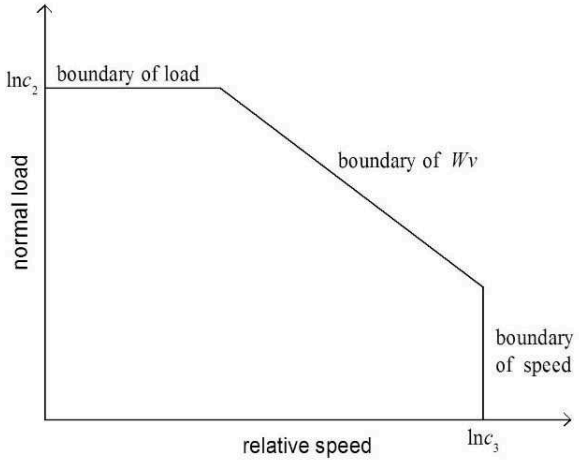

Fig. 3. Boundaries of accelerate stress.

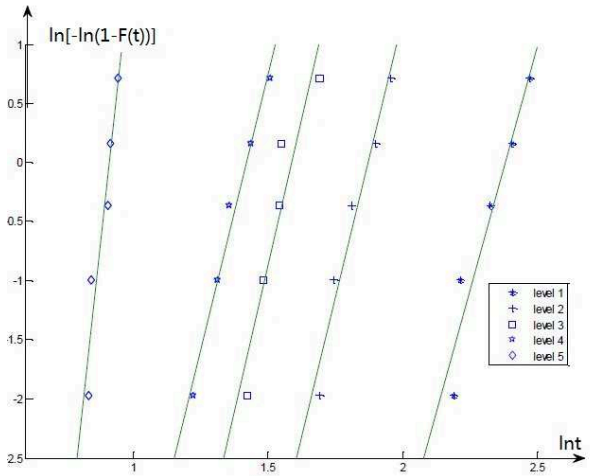

Fig.4. Weibull probability graph.

4. Case study

In this section, the normal load will be used as accelerate stress. This case makes a presentation about the relation between load ceiling and failure mechanism consistency.

In this case, copper pin and steel pin rub against each other on the pin and disk test rig [4]. The copper pin with hardness of 80 has a diameter of 3 mm, and the disk turns at a constant speed of 40rpm. Wear mass loss of the copper pin is detected, and it is regarded as failure criterion. In the test, normal load is set at 5 levels, $W_1 = 100\text{N}$, $W_2 = 110\text{N}$, $W_3 = 140\text{N}$, $W_4 = 160\text{N}$, $W_5 = 190\text{N}$.

4.1 Statistic analysis of failure mechanism consistency

As is illustrated in Eq. 6, five straight lines appear in the Weibull probability graph, Fig.4. With statistical methods, the shape parameter on each accelerated stress level can be solved.

$$m_1 = 8.5 \quad m_2 = 9.4 \quad m_3 = 9.8 \quad m_4 = 9.3 \quad m_5 = 20.7 \tag{17}$$

It shows that the shape parameter of the fifth level is very different from the others. When test takes that level, the failure mechanism consistency has already changed.

4.2 Physical analysis of failure mechanism consistency

The contact area of the pin and disk is 7.07mm^2, so the pressure of five levels can be solved. Using formula 15, the critical pressure of plastic deformation could be obtained [5], Table 1.

Table 1 Load and pressure of five levels

Level	1	2	3	4	5
Load[N]	100	110	140	160	190
Pressure[N/mm^2]	14.1	15.6	19.8	22.6	26.9
critical pressure[N/mm^2]	26.7				

When the load is on the fifth level, for the copper pin, plastic deformation has occurred. For failure mechanism consistency, the contact pressure should be restricted to less than 26.7N/mm^2.

This case explains that in accelerated test, normal load has a ceiling. In fact, failure mechanism consistency requires the boundaries of normal load, relative speed, and the product of them.

5. Summary

Based on the physical characteristics of failure mechanism consistency in wear accelerated test, a new method is proposed, which could be used to find the boundary of accelerated stress. In this method, normal load, relative speed, and their product are considered to restrict the accelerated stress. This method also fits the wear tests under lubrication condition [6].

This study suggests that, for saving time and cost, the range of the accelerated stress should be determined before the test, and this presetting is based on the failure mechanism consistency.

Acknowledgements

This work was financially supported by the National Natural Science Foundation of China (No. 61104133).

References

[1] M. B. Peterson and Ward O. Winer, in: *Wear control handbook*, edited by American Society of Mechanical Engineers (1980).

[2] Zhao Yu, Yang Jun and Ma Xiaobing, in: Data analysis of reliability, edited by National Defense Industry Press, Beijing (2011).

[3] Wen Shizhu and Huang Ping, in: Principle of tribology, edited by Tsinghua University Press, Beijing (2002).

[4] Rajkumar K, Kundu K and Aravindan S: Accelerated wear testing for evaluating the life characteristics of copper–graphite tribological composite. Materials & Design, 2011, 32(5): 3029-3035.

[5] Ramalho A: A reliability model for friction and wear experimental data. Wear, 2010, 269(3): 213-223.

[6] Kovalchenko A, Ajayi O and Erdemir A: Friction and wear behavior of laser textured surface under lubricated initial point contact. Wear, 2011, 271(9): 1719-1725.

Advanced Materials Research Vols. 989-994 (2014) pp 923-926
© (2014) Trans Tech Publications, Switzerland
doi:10.4028/www.scientific.net/AMR.989-994.923

Stability Analysis of Single-pier Variable Cross-section Box-girder Continuous Bridge

Yin Guansheng[1, a], Bai Jie[2,b],Feng Junjie[3,c]

[1]School of Science, Chang'an University, Xi'an, Shanxi,China

[2]School of Science, Chang'an University, Xi'an, Shanxi,China

[3]School of Science, Chang'an University, Xi'an, Shanxi,China

[a]yings@chd.edu.cn, [b]563709075@qq.com, [c] 505341446 @qq.com

Key words: single variable cross-section,box-girder; stability,torsion, ANSYS software

Abstract. On the basis of Umansky box-girder torsion theory, the software of ANSYS is applied to simulate related engineering model. In considering a variety of live load conditions, the lateral stability of multi-span single-pier variable cross-section box-girder under torsion eccentric load is analyzed. Analysis results reveal that under different working conditions, the factors affecting the transverse stability of the bridge and the proportion of the value on each, such as gravity, the span ratio and the distance between support are different; When the overload ratio is 2 times larger, the bridge stability safety coefficient decreases along the curve and changes rapidly. In the future design of this kind of bridge, the overall lateral stability should be paid much more attention. Some methods and suggestions about how to prevent the emergence of security and stability problems are put forward in the end.

Introduction

With the rapid development of urban expressway and the long-span bridges, considering the heavy traffic and economic factors, such as high-speed ramp or ramp bridge often took the form of multi-span variable cross-section box girder bridge. bridge deck are usually wide, the lower construction using single column pier design. The design of the structure not only increases the headroom under the bridge pavement, and improve the automobile traffic and the driver's field of vision, but also more economical and beautiful. But as the middle of bridge pier is usually single pier and single support or consolidation, the effective support is not formed in bridge deck torsion, the overall stability of the bridge is poor, easily happened accident caused by overload.On August 24, 2012, Harbin 3rd ring bridge approach Yang Ming beach bridge on Honghu road ramp bridge suddenly parted. 130 meters of a bridge collapse and 4 big trucks Falling from the bridge, the accident has caused 3 people death and 5 people injured, resulting in a larger social impact, as shown in figure 1.

Fig.1 The collapse of Yang Ming beach bridge

There are many similar accidents to this accident, we can find that the accident partly because of eccentric overload. But understanding is not in place for the deformation of variable cross-section

box beam bridge under different loads; the designer thoughtless about the design consideration, tends to focus on the longitudinal analysis, but not on the "space", "whole" of the bridge analysis. The structure design is unreasonable would have an impact on the stability of the bridge, it is a matter requiring our serious attention.

Evaluation the Stability of Bridge Lateral

The Current Specification Requirements and Insufficients. The current code for design of high way reinforced concrete and prestressed concrete bridges and culvers (JTG D60-2004) 3.5.8 for wide bridge seat require that it should be ensure the upper and lower surface smooth with beam bottom and the top pier-pad, the force should be uniform and the rubber bearing should no outrunning [1]. But the standard does not state which type of the pier bearing and the specific arrangement explicitly.Lack of provision for the lateral stability of bridge and the possibility of overturning stability coefficient. This caused the specification blank in the lateral stability of design and construction of the bridge, influence of structural security.

The classification of single-pier box bridge. according to the mechanical character and failure forms, The single-pier box bridge generally can be divided into 3 types[2]: ①Intermediate single-pier and girder are consolidated of supporting ,we called "PGC" for short. ②Intermediate single-pier and girder are hinged of supporting , we called "PGH" for short. ③The bridge is curved bridge and Intermediate single-pier and girder are supported with supports connection,we called "CPGH" for short.

Because of the above three kinds of single-pier bridge has different arrangement types,so there are different characteristics when the bridge in the event of instability failure. The "PGC" due to it consolidation, which increased the box girder section of transverse stability stiffness, let the parts of Piers join into the lateral stability of the bridge.When the "PGH" and "CPGH" set single fulcrum,it would test the cantilever weight and Eccentric loads. If the torsional stiffness is not enough, the bridge will be happened girder torsion, then the single pier and single support would easily sideslip. At the end of the fulcrum, the support will produce outrunning phenomenon, finally the overturning of bridge structured.

The Restrained Torsion Theory of Thin-walled Box Girder

Thin-walled rods restraint torsion theory. The mechanism of thin-walled box girder in the eccentric loads is more complicated when it influenced by environment, terrain and design. Such as curved bridge, even without considering the live load, only under the counterweight, it also exist the torque. This makes the box girder torsion research more complex.

Combinate the thin-walled box girder theory, this paper will discussing the constrained torsion of box section beam**.**

According to Umansky closed section thin-walled bar theory [3],the figure 2 below show a simple diagram of Thin-walled beam torsion under the eccentric load.

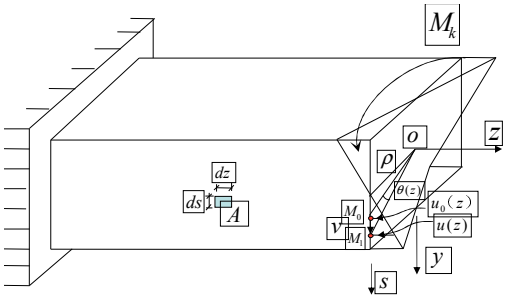

Fig.2 Thin-walled beam torsion under the eccentric load

The axial displacement of Closed-section constraint torsion :

$$u(z,s)=u_0(z,0)\text{-}\overline{\omega}(s)\ \beta'(z) \tag{1}$$

where $\beta'(z)$ means that the degree of warping section is a certain relationship with the torsion angle.

According to plane stress - strain problem and warping stress balance, we finally get an expression restrained torsion warping stress

$$\sigma_\omega = \frac{B_\omega \overline{\omega}(s)}{I_\omega} \tag{2}$$

The differential unit of tank wall point A in figure 2 is analyzed. Since the distribution of the warping normal stress in each box girder cross-section curves is not equal, beam section generate shear flow to be equilibrium [4]. Unit A shows in Fig.3.

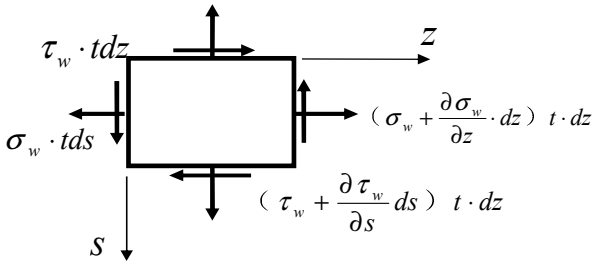

Fig. 3 Differential unit of point A on the Box wall

From figure 3, $\sum F = 0$, we can get the differential relationship of shear τ and σ_x:

$$\frac{\partial \sigma_x}{\partial z} + \frac{\partial \tau}{\partial s} = 0 \tag{3}$$

Then By cross section s integration and consolidation, we can eventually be:

$$\tau = \frac{T}{\Omega t} - E\frac{\beta'''(z)}{t}\overline{S}_{\overline{\omega}} \tag{4}$$

From equation (4), shear stress of restrained torsion on the cross section is two shear stress values , the first one is free torsion shear stress; the second is the shear stress due to the change of constraint stress. we will focus on the effect of second item on thin-walled box girder.

Analyses an engineering example

this paper will introduce an overpass bridge gate, in which is a three-span prestressed concrete continuous variable cross-section of thin-walled box girder bridge, The bridge part is 30 + 50 + 30 metres. The total width of the bridge is 9 meters, which has 8 meters effective width, the middle bridge single-pier support and side pier are two supports. Diaphragms of box girder in the bridge pier and abutment play shear effect. The paper building models by The solid element SOLID65, using 0.5 meters as a unit grid division, and load groups loading onto the corresponding node. Fig.4 is Simplified uniform section model within the scope of variable cross-section box girder and fig. 5 is Schematic diagram of the bridge superstructure model.

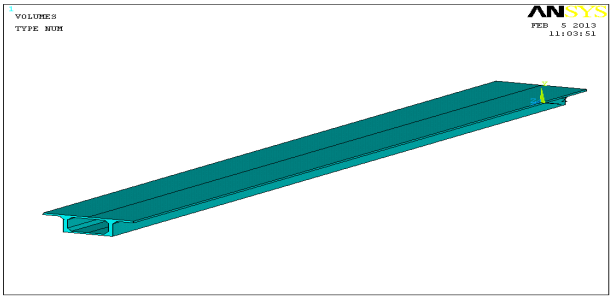

Fig.4 Simplified uniform section model within the scope of variable cross-section box girder

Fig.5 Upper structure model of the engineering example bridge

In this paper, according to the most unfavorable load single row layout. Considering the maximum eccentric, only the most lateral of bridge can be load between the single column piers. In accordance with The code for design of highway reinforced concrete and prestressed concrete bridges and culvers,we introduce three kinds of load.(1) Highway level I load,(2) two times of

Highway level I load, (3) three times of Highway level I load.Use ANSYS software calculate three kinds of conditions on the simplified model. We can get bridge deformation graph under these load, especially under different conditions the torsional pattern. Figure 6 and 7 shown the deformation of the box bridge in condition(1).

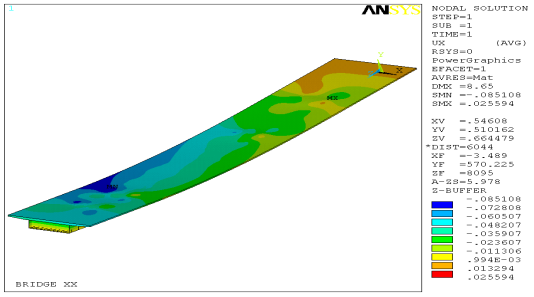

Fig.6 Deformation displacement diagram of the box bridge under working condition 1(horizontal)

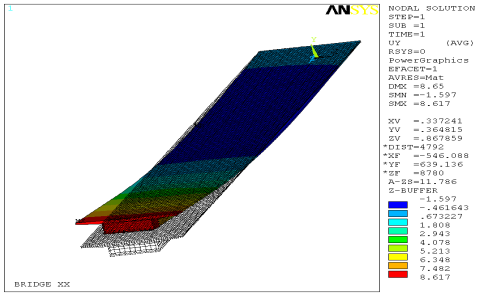

Fig.7 Deformation displacement diagram of the box bridge under working condition 1(vertical)

The horizontal and vertical displacement diagram shows that the degree of restraint torsion warping effect will continue to increase if the box girder with the load increasing, the value of shear stress will also increasing [5]. Wheather the stress is fully consistent with the corresponding analytical solutions of the theory needs further perfection and enrichment

Conclution

From the result in different load conditions,we know factors such as weight, proportional spacing degree and the proportion of each supports can influence the lateral stability of this kind of bridge not identical in value. It should pay more attention to the impact of various factors.

When the overload ratio is 2 times larger, the bridge stability safety coefficient decreases along the curve and changes rapidly.Must cause engineers and technical personnel enough attention to this phenomenon.

Acknowledgements

This work was financially supported by the Ministry of Transport of The Western Traffic Construction Project(2009 318 812 063), The Transportation Technology Projects of Shanxi Province(09-10K).

References

[1] Code for design of highway reinforced concrete and prestressed concrete bridges and culvers.S

[2] Li Pandao, Zhang Jing, Wang Mei:*Study ofchecking method for overturning stability of beam bridge supported by single-column pie*.World Bridge, 2012,40(6) p52-56

[3] He Shuanhai:Bridge structure theory and calculation method. Beijing: China communications Press.2003

[4] You Jinlan.D: *Research of the curve prestressed concrete box girder torsion*.Xi'an.Chang'an University.2008

[5] Qian Xiaoming.J. *The research of sinngle column pier ramp bridge performance against overturning*.Value Engineering.2010.15 p78-82

Advanced Materials Research Vols. 989-994 (2014) pp 927-930
© (2014) Trans Tech Publications, Switzerland
doi:10.4028/www.scientific.net/AMR.989-994.927

Effect of convex platform on stress distribution in nickel-based superalloy plate produced by Vacuum Countergravity Casting

Chunming Zou[1, a], Shanqiang Su[1,b], Hongwei Wang[1,c] and Zunjie Wei[1,d]

[1] National Key Laboratory for Precision Hot Processing of Metals, Harbin Institute of Technology, Harbin, 150001, China

[a]zouchunming1977@163.com, [b]qingkongsu@163.com, [c]wanghw@hit.edu.cn, [d]weizj@hit.edu.cn

Keywords: Nickel-based Superalloy, Vacuum Countergravity Casting, Stress-affected Zone, Wall Thickness Differences.

Abstract. The effect of convex platform shape on stress distribution in nickel-based superalloy thin plate produced by Vacuum Countergravity Casting (VCC) has been studied by numerical simulation. The result shows that convex platform significantly changes the stress distribution in its adjacent area. The stress-affected zone (SAZ) of both types of convex platform appears uneven. SAZ is significantly greater in the diagonal direction than that in the horizontal direction. The angle effect contribution rate (AECR) is defined. When S1=1mm and S=6, AECR has the larger values in both convex platform shapes, and AECR of square convex platform is even up to 7.589. When S1 is larger than 2mm, the relationship between angle effect and S1 or S is not obvious for square convex platform.

Introduction

Nickel based superalloy investment castings have been applied widely in the aviation engine and rocket engine [1,2]. However, the near-net shape large thin-walled nickel based superalloy castings are easy to appear misrun, oxide or shrinkage. Casting processes for large thin-walled superalloy castings are always the focus of research [3,4]. In one of countergravity casting processes, vacuum countergravity casting process combines the advantages of vacuum refining and countergravity process, with high quality of casting alloy melt and the strong forming ability, which is expected to solve the misrun, oxide or shrinkage problem of the large thin-walled casting as well as enhance the filling ablilty.

Another problem in forming the large thin-walled nickel based superalloy castings is stress problem. Stress distribution in casting directly affects casting dimension accuracy and subsequent heat treatment process. The effect of wall thickness difference rate on stress distribution in the plate casting has been reported[5]. In recent study, it was found that stress distribution of the large thin-walled casting was affected not only by wall thickness difference of castings but also by the shape of convex platform [6]. This paper focuses on the effect of convex platform shape on stress distribution of the casting.

Selection of process parameters

In order to accurately study the effect of convex platform on the surrounding thin plate, the plate structure as shown in Fig. 1 was designed. The plate casting has a size of 400mmx350mm. The plate has a convex platform with different shapes (circular convex platform and square convex platform). Circular convex platform has a diameter of 30 mm and the square convex platform has a square cross shape with the diagonal length equal to the diameter of the circular convex platform. Metal fills into the cavity through the slot gating system by the plate edge.

S1 is wall thickness and S2 is the height of convex platform. The thickness difference rate is defined as S = S2/S1. The greater the value of S is, the greater the changing in wall thickness is. Wall thickness is taken 1 mm, 2 mm and 4 mm. Each thickness has four S values (S = 2, 4, 6 and 8 respectively).

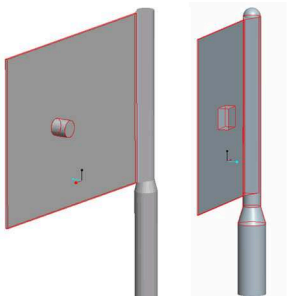

Fig. 1 Sketch of convex platform with a different shape on the thin plate

In order to illustrate the effect of S and shape of convex platform, the stress influence area is divided into N parts along the center of convex platform to periphery by using the relative proportion line method. The zone that stress value is larger than 93.33% of the maximum value is defined as the stress-affected zone (SAZ). Using K4169 superalloy as the research object, the pouring temperature selects 1773K. Interfacial heat transfer coefficient between the ceramic shell mold and melt is 700 w/(mK). The ceramic shell mold preheats at 1173K. The filling speed is 200mm/s, and forming pressure is 150KPa. Required alloy thermal parameters for filling and solidification simulation are shown in Table1.

Table 1 Required alloy thermal parameters for filling and solidification simulation

Density [Kg/m^3]	Liquidus temperature [K]	Solidus temperature [K]	Latent heat [J/Kg]	Thermal expansion coefficient [/K]	Dynamic viscosity [cp]	Thermal conductivity [w/(mK)]	Specific heat [J/(kgK)]
8220	1632	1516	293902	2E-5	3.53	29.44	57.70

Results and discussion

Fig. 2 shows that convex platform significantly changes the stress distribution in its adjacent area. Plate without the convex platform only has an affected zone produced by gating system, while the plate with a convex platform has more than one affected zone. SAZ (red area around the convex platform) near both types of convex platform appears uneven. SAZ is significantly greater in diagonal direction than that in horizontal direction. Comparing stress distribution in the plate (S1=1mm) with a square convex platform and in a plate with circular convex platform, the impact of convex platform shape on the stress distribution is obvious. When S1=1mm, stress distribution is very complicated. The stress value along diagonal direction of the plate is significantly larger than that along the other direction, especially, in the plate with a square convex platform, shown as Fig. 3g) and h). This phenomenon called “angle effect” has appeared on the each condition of S1. The larger S1 is, the weaker the phenomenon appears. When S1 is more than 2mm, the influence of convex platform shape is weakening obviously (see Fig. 4 and Fig.5).

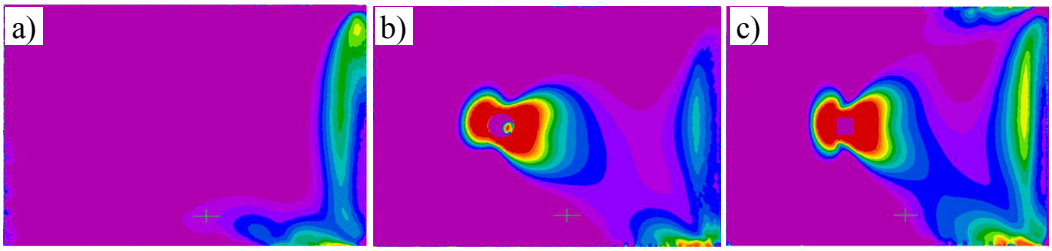

Fig. 2 Stress distribution in the plate a) without convex platform, b) with a circular convex platform and c) with a square convex platform

In order to quantify the effect of convex platform in the plate, SAZ has been measured and calculated, the result is shown in Table 2. When wall thickness is relatively thin (S1=1), with the increase of S, SAZ of convex platform increases first and then decreases, reaching a maximum value

at S=6. SAZs of both circular convex platform and square convex platform have the same changing trend. The difference between the two shapes is that SAZ value of a square convex platform along diagonal direction is generally larger than that of circular convex platform.

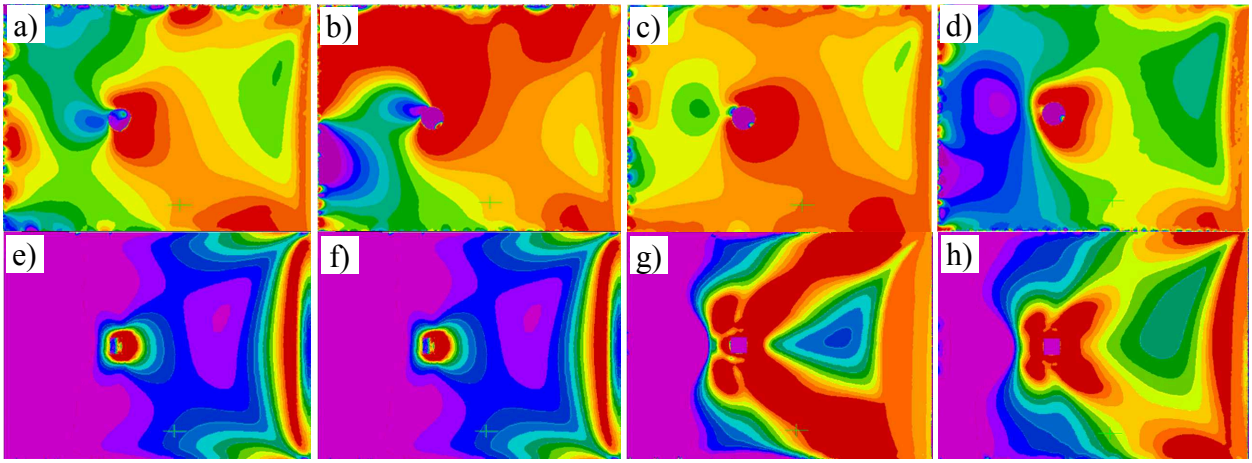

Fig. 3 Stress distribution in the plate with a circular convex platform a) S1=1mm and S=2, b) S1=1mm and S=4, c) S1=1mm and S=6, d) S1=1mm and S=8, and in the plate with a square convex platform e) S1=1mm and S=2, f) S1=1mm and S=4, g) S1=1mm and S=6, h) S1=1mm and S=8.

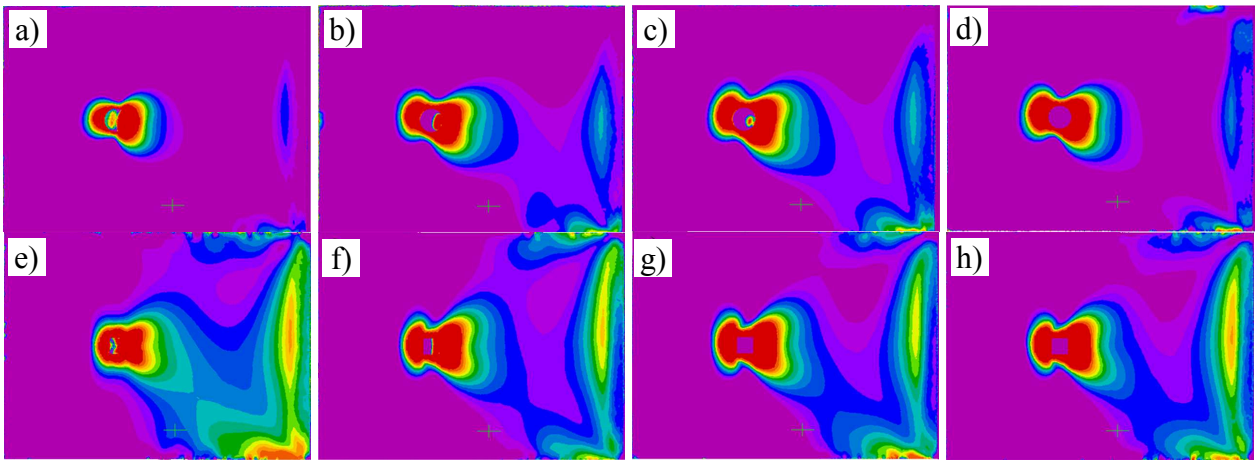

Fig. 4 Stress distribution in the plate with a circular convex platform a) S1=2mm and S=2, b) S1=2mm and S=4, c) S1=2mm and S=6, d) S1=2mm and S=8, and in the plate with a square convex platform e) S1=2mm and S=2, f) S1=2mm and S=4, g) S1=2mm and S=6, h) S1=2mm and S=8.

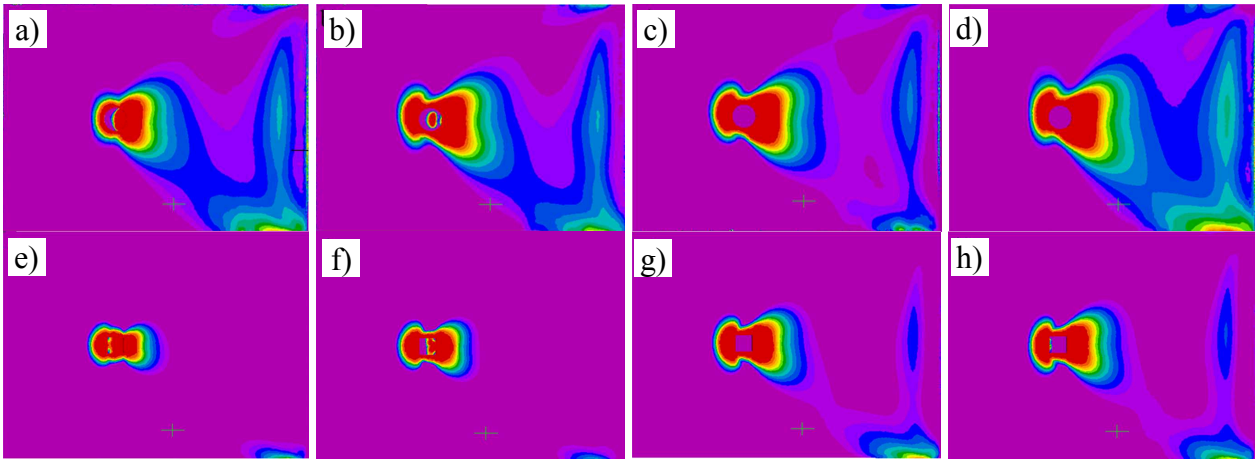

Fig. 5 Stress distribution in the plate with a circular convex platform a) S1=4mm and S=2, b) S1=4mm and S=4, c) S1=4mm and S=6, d) S1=4mm and S=8, and in the plate with a square convex platform e) S1=4mm and S=2, f) S1=4mm and S=4, g) S1=4mm and S=6, h) S1=4mm and S=8.

To visualize the angle effect on the shape of convex platform, the angle effect contribution rate (AECR) is defined as $J=D_d/D_f$. D_d is the length of SAZ along diagonal direction, and D_f is the SAZ length along horizontal direction. The greater the value of J is, the more significant the angle effect is. Table 3 shows AECR of convex platform with different shape. When S1=1mm and S=6, AECR has the larger value in both convex platform shapes, and AECR of square convex platform is even up to 7.589. When S1 is larger than 2mm, the relationship between angle effect and S1 or S is not obvious for square convex platform.

Table 2 SAZ of convex platform with different shape

Wall thickness S1 [mm]	Circular convex platform				Square convex platform			
	S=2	S=4	S=6	S=8	S=2	S=4	S=6	S=8
1	46.6	49.8	52.2	40.9	51.2	58.7	83.1	65.1
2	29.5	36.6	36.6	40.9	33.5	41.8	44.7	50.1
4	23.2	34.7	36.6	29.5	26.9	40.3	43.7	34.2

Table 3 AECR of convex platform with different shape

Wall thickness S1 [mm]	Circular convex platform				Square convex platform			
	S=2	S=4	S=6	S=8	S=2	S=4	S=6	S=8
1	1.215	-	1.392	1.418	1.097	1.178	7.589	2.591
2	1.105	1.109	1.351	1.024	1.132	1.142	1.224	1.223
4	1.278	1.267	1.194	1.212	1.154	1.158	1.194	1.155

Conclusions

1. Convex platform significantly changes the stress distribution in its adjacent area. The stress-affected zone (SAZ) of both types of convex platform appears uneven.

2. SAZ length is significantly greater in the diagonal direction than that in the horizontal direction. The angle effect contribution rate (AECR) is defined. When S1=1mm and S=6, AECR has the larger value in both convex platform shapes, and AECR of square convex platform is even up to 7.589. When S1 is larger than 2mm, the relationship between angle effect and S1 or S is not obvious for square convex platform.

Acknowledgements

This work is supported by the National Natural Science Foundation of China (51001041) and Foundation of National Key Laboratory for Precision Hot Processing of Metals.

References

[1] Arun K. Sehra, Woodrow Whitlow Jr. Progress in Aerospace Sciences Vol. 40 (2004), p.199.

[2] Yiwei Dong, Kun Bu, Yangqing Dou, Dinghua Zhang. Journal of Materials Processing Technology Vol. 211 (2011), p. 2123.

[3] Zhiwen Yu, Faguo Li, Jiao Zhang, Anping Dong, Baode Sun. Special Casting & Nonferrous Alloys Vol. 32 (2012),p.1103. In Chinese.

[4] Hitchiner Manufacturing Co., Inc. Reactive Alloy Casting Processes. (2008), p.1

[5] Chunming Zou, Yongju Li, Shanqiang Su, Hongwei Wang, Zunjie Wei. China Foundry Week 2013, Jinan, China (2013), p. 105. In Chinese.

[6] Shanqiang Su. Study on Mold Filling and Solidification Process of Superalloy Castings with Mutations in Wall Thickness. Harbin Institute of Technology Dissertation (2013). In Chinese.

Advanced Materials Research Vols. 989-994 (2014) pp 931-934
© (2014) Trans Tech Publications, Switzerland
doi:10.4028/www.scientific.net/AMR.989-994.931

Calculation about Stress Concentration Coefficient of Welded Cruciform Joints of Magnesium Alloy Based on FEM

Bolin HE[1, a], Yingxia YU[1, b], Xiaodong ZHANG[2, C], Songsong XIA[1,d]

[1]School of Mechanical & Electronic Engineering, East China Jiaotong University, Nanchang 330013, China

[2]Pu Zhen Carriage Works, CSR Corporation Limited, Nanjing, 210032, China

[a]yyxhbl@163.com, [b]hebolin@163.com, [c]nanchang156312@163.com, [d]807564262@qq.com

Keywords: Stress Concentration Coefficient; Welded Cruciform Joints; Tangent Line Angle; FEM

Abstract. Geometrical parameters of welded joint affect the stress concentration coefficient seriously. In order to increase the fatigue property of welded structure, it has great significance to reduce stress concentration coefficient of welded structures by researching and improving the geometry of welded joints. In this paper, the effects of weld tangent line angle θ on the stress concentration coefficient of welded cruciform joints of magnesium alloy were analyzed by using ABAQUS finite element program, and the change rule of stress concentration coefficient with the variation of the parameter was also researched. The calculation results indicate that reducing the weld tangent line angle θ can effectively decrease the stress concentration coefficient of welded cruciform joints, so as to improve the fatigue property of welded structures. In order to have high reliability and safety of welded structures of magnesium alloy, the true weld tangent line angle θ should be controlled less than 25°.

Introduction

Welding, as an advanced industrial manufacturing technology, plays a pivotal role in national economic and industrial production. The welding technology has a widely applications in metal structure manufacturing. Due to the particularity of welding technology, the welded structures have great safety concerns. According to information statistics [1], about 80% to 90% failure of welded structure is belonged to fatigue fracture. The stress concentration sensitivity of structural materials is primarily determined by their properties, theoretical stress concentration factor, the size of the objects under investigation, loading conditions [2]. There are a lot of factors influencing fatigue strength of welded structures, but stress concentration is the most important one. Effectively controlling stress concentration of welded joints has an important meaning for improving the fatigue strength of welded structures.

The main reasons for causing stress concentration of welded joints have following aspects. (1)The weld defects existing in the welding process: due to the complexity of the welding process, some defects often occur in the welds, such as porosity, and lack of fusion, slag inclusions and undercut beads etc, and they will cause stress concentration, but the cracks and lack of fusion cause the most serious stress concentration; (2) Unreasonable weld appearance: too large weld reinforcement of welded cruciform joints and convex fillet welds can form a larger stress concentration. (3)Unreasonable welded joint design: abrupt change of cross-section and plus cover plate of welded joints may cause big stress concentration coefficient. Unreasonable weld layout, such as the T-shaped unilateral weld joints, also can cause stress concentration [3]. Magnesium alloys are very attractive materials in order to achieve high performance and energy saving of machines and structures, because of their advantages such as light weight, high strength-to-weight ratio and high specific stiffness at both ambient and elevated temperatures. [4]. In this paper, main geometry parameters of welded cruciform joints of magnesium alloy were analyzed by using ABAQUS finite element program, including the weld tangent line angle and weld leg size which is determined as a constant factor. The change rule of stress concentration coefficient with the variation of the parameter was also researched. It provides theoretical foundation for reasonably controlling the stress concentration of welded joints of magnesium alloy.

Calculation Model of Stress Concentration Coefficient

An exhaustive finite element analysis of the effects of weld tangent line angle θ on the stress concentration coefficient of welded cruciform joints were studied by using the finite element software ABAQUS. In the past, some researchers studied the effect of geometry parameters on the stress concentration coefficient of welded joints [5-10]. But some of the finite element calculations adopted plane strain model, a simplified model of low precision. The paper adopts three-dimensional entity elements, which has higher precision and real data closer to the stress state of real structures. There are many factors which has the effect on stress concentration phenomenon of welded cruciform joints, including weld tangent line angle θ, weld leg size and so on, as shown in Fig. 1.

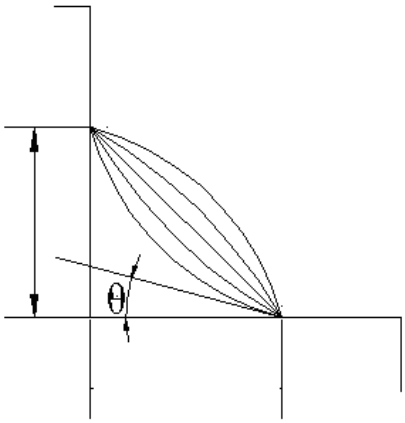

Fig.1. The influence factor on stress concentration phenomenon of welded cruciform joint

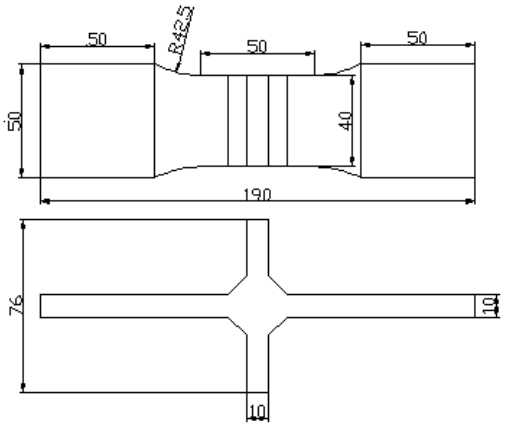

Fig.2 The specimen's shape and size

This paper focuses on the weld tangent line angle θ. The specimen's shape and size is shown in Fig. 2.

During stress concentration coefficient of welded cruciform joint, fully integral tetrahedron entity unit C3D10 is adopted. Dense mesh in stress concentration areas and relatively sparse mesh in other areas are used. It can not only improve the calculation accuracy, but also save calculation time and costs. Due to the symmetry of calculation model, the paper take one-eighth of the welded cruciform joint is used during the finite element numerical analysis [11]. Stress concentration coefficient is defined as a ratio of the maximum principal stress to the average stress of the section in welded joints. The calculation formula of stress concentration coefficient is showed in Eq.1. The tensile load is 100MPa. The finite element model is showed in Fig. 3. The material used for calculation is MB8 magnesium alloy.

$$k_t = \frac{\sigma_{\max}}{\sigma_m} \tag{1}$$

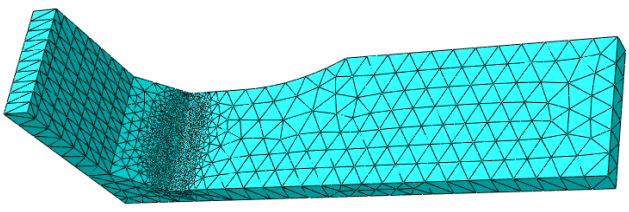

Fig.3. The finite element model and mesh partition

Calculation Results and Analysis

During examining the influence of tangent line angle θ on the stress concentration coefficient of welded cruciform joints, weld leg size K is selected as 8mm, the weld tangent line angle θ is changed from 0 to 90 degrees. Calculation results are shown in Table 1 and Fig. 4 and Fig. 5.

Table 1 Effect of r, θ on the stress concentration coefficient (w=6mm)

θ /°	0	10	20	30	45	60	70	80	90
Kt	1.390	1.902	2.516	3.428	4.032	4.927	5.297	5.499	5.703

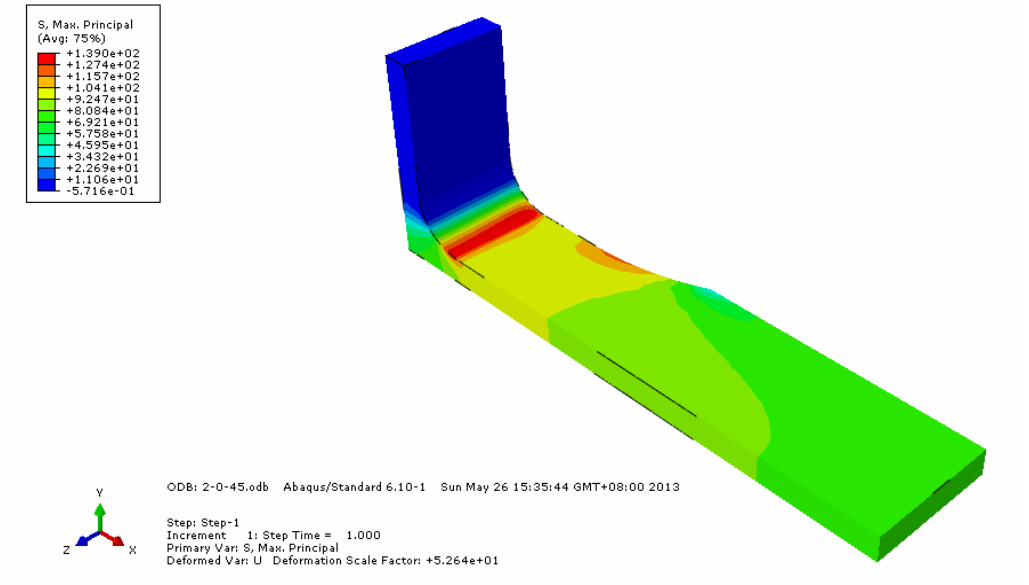

Fig.4 Max principal stress distribution

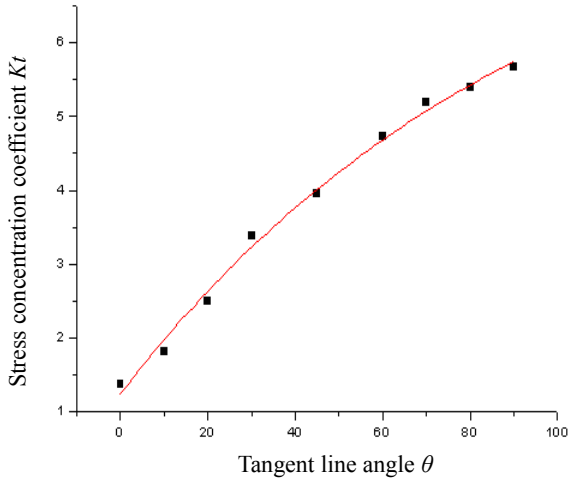

Fig. 5 Effect of θ on stress concentration coefficient

From Fig. 4 and Table 1 it can be seen that the stress concentration coefficient is very big at the weld toe of welded cruciform joints.

From Table 1 and Fig. 5 it can also be seen that weld tangent line angle θ has great effect on the stress concentration coefficient of welded cruciform joints of magnesium alloy. For the same weld leg size, with increasing of weld tangent line angle θ, the stress concentration coefficient increases gradually. When the weld tangent line angle θ is changed from 0°to 30°, the stress concentration coefficient is increased from 1.390 to 3.428, the growth rate is 146.42%.

From the calculation results it can be seen that the weld tangent line angle θ has great effect on the stress concentration coefficient stress of welded cruciform joints of magnesium alloy. The reason is that when increasing of the weld tangent line angle θ, it will lead to great sudden change in cross section of weld toe, and leads to great change for the stress concentration coefficient. To make the weld in an inward curving form will lead to low stress concentration coefficient. In order to

obtain high strength of welded cruciform joints, the best way is to grinding the weld to obtain an inward curving form. For the safe use of welded structures, the true tangent line angle θ should be smaller than 25^o.

Conclusion

(1) Weld tangent line angle θ has great effect on the stress concentration coefficient of welded cruciform joints of magnesium alloy. When the weld tangent line angle θ is changed from 0° to 30^o, the stress concentration coefficient is increased from 1.390 to 3.428, and the growth rate is 146.42%.

(2). In order to obtain high strength of welded cruciform joints of magnesium alloy, the best way is to grind the weld to obtain an inward curving form. For the safe use of welded structures, the stress concentration coefficient should be controlled less than 3, and the true tangent line angle θ should be smaller than 25^o.

Acknowledgement

The research was sponsored by the National Nature Science Foundation (No.51265013), Natural Science Foundation of Jiangxi Province (No.20114BAB206020), Science Foundation of education office of Jiangxi Province (GJJ12302) and visiting scholar plan of universities in Jiangxi province.

References

[1]H Y Fang.The Learning of Welded Structures [M]. China machine press, Beijing 2008 (in Chinese).

[2]A. D. Pogrebnyak, M. N. Regul'skii, and A. V. Zheldubovskii. Assessment of the effect of stress concentration on the fatigue resistance of structural materials under asymmetrical loading[J]. Strength of Materials, 2013, 45(1):82-92

[3]Y H Zhang.The Design and Application of Welded Structures[M]. Chemical Industry Press, Beijing 2009) (in Chinese).

[4]K. Tokaji, M. Kamakura, Y. Ishiizumi, N. Hasegawa. Fatigue behavior and fracture mechanism of a rolled AZ31[J]. International Journal of Fatigue, 26 (2004) 1217-1224.

[5]T R Gurney. Finite element analyses of some joints with the welds transverse to the direction of stress[J]. Welding Research International, 1976, 6 (1):40-52.

[6]Y B Shao. Geometrical effect on the stress distribution along weld toe for tubular T and K joints under axial loading[J]. Journal of Constructional Steel Research, 2007, 63(10):1351-1360.

[7]A Ndiaye, S Hariri, G Pluvinage. Stress concentration factor analysis for notched welded tubular T joints[J]. International Journal of Fatigue, 2007, 29 (12):1554-1570.

[8]D C Li, L J Cao. Finite element analysis of stress concentration factor of butt-welded joint[J]. Journal of Xi An Petroleum Institute, 1997, 12 (1)30-32(in Chinese).

[9]F R Mashiri, X L Zhao, P Grundy. Stress concentration factors and fatigue behaviour of welded thin walled CHS-SHS T-joints under in-plane bending[J]. Engineering Structures, 26(2004) 1861-1875

[10]Y P Shi, Y R Zhou. Detailed Examples for ABAQUS Finite Element Analysis[M]. China Maching Press, Beijing 2006) (in Chinese).

[11] B L He, X D Zhang. Finite element calculation about stress concentration coefficient of welded butt joints based on the ABAQUS[J]. Applied Mechanics and Materials, 2011 (80-81): 807-811

Advanced Materials Research Vols. 989-994 (2014) pp 935-938
© (2014) Trans Tech Publications, Switzerland
doi:10.4028/www.scientific.net/AMR.989-994.935

Finite element calculation about stress concentration coefficient of welded butt joints of Magnesium Alloy

Yingxia YU[1, a], Bolin HE[1, b], Xiaodong ZHANG[2, C], Siyong LEI[1,d]

[1]School of Mechanical & Electronic Engineering, East China Jiaotong University, Nanchang 330013, China

[2]Pu Zhen Carriage Works, CSR Corporation Limited, Nanjing, 210032, China

[a]yyxhbl@163.com, [b]hebolin@163.com, [c]nanchang156312@163.com, [d]siyonglei1@163.com

Keywords: Stress Concentration Coefficient; Welded Butt Joints; Weld Toe Inclination Angle; Weld Edge Transition Arc Radius

Abstract. Geometrical parameters of welded joint affect the stress concentration coefficient seriously. In order to increase the fatigue property of welded structure, it has great significance to reduce stress concentration coefficient of welded structures by researching and improving the geometry of welded joints. In this paper, the effects of weld toe inclination angle θ and weld edge transition arc radius r on the stress concentration coefficient of welded butt joints of magnesium alloy were analyzed by using ABAQUS finite element program, and the change rule of stress concentration coefficient with the variation of the two parameters was also researched. The calculation results indicate that reducing weld toe inclination angle or increasing transition arc radius can effectively decrease the stress concentration coefficient of welded butt joints, so as to improve the fatigue property of welded structures. For the safe use of welded structures, the true weld edge transition arc radius r should be greater than 3mm, and weld toe inclination angle θ should be smaller than 30°.

Introduction

Welding, as an advanced industrial manufacturing technology, plays a pivotal role in national economic and industrial production. The welding technology has a widely applications in metal structure manufacturing. Due to the particularity of welding technology, the welded structures have great safety concerns. According to information statistics [1], about 80% to 90% failure of welded structure is belonged to fatigue fracture. The stress concentration sensitivity of structural materials is primarily determined by their properties, theoretical stress concentration factor, the size of the objects under investigation, loading conditions [2]. There are a lot of factors influencing fatigue strength of welded structures, but stress concentration is the most important one. Effectively controlling stress concentration of welded joints has an important meaning for improving the fatigue strength of welded structures.

The main reasons for causing stress concentration of welded joints have following aspects. (1)The weld defects existing in the welding process: due to the complexity of the welding process, some defects often occur in the welds, such as porosity, and lack of fusion, slag inclusions and undercut beads etc, and they will cause stress concentration, but the cracks and lack of fusion cause the most serious stress concentration; (2) Unreasonable weld appearance: too large weld reinforcement of welded butt joints and convex fillet welds can form a larger stress concentration. (3)Unreasonable welded joint design: abrupt change of cross-section and plus cover plate of welded butt joints may cause big stress concentration coefficient. Unreasonable weld layout, such as the T-shaped unilateral weld joints, also can cause stress concentration [3]. Magnesium is the lightest structural metal available. It has a density of 1.74 g/cm 3, which is 35.6% lower than that of aluminum and 61.3% lighter than titanium [4]. Among the three contenders, alloys of magnesium are attractive due to the conjoint influence of light weight, high strength-to-weight ratio and high specific stiffness at both ambient and elevated temperatures. In this paper, main geometry parameters of butt-welded joints of magnesium alloy were analyzed by using ABAQUS finite

element program, including weld toe inclination angle and weld edge transition arc radius which are two key factors. The change rule of stress concentration coefficient with the variation of the two parameters was also researched. It provides theoretical foundation for reasonably controlling the stress concentration of welded joints.

Calculation Model of Stress Concentration Coefficient

An exhaustive finite element analysis of the effects of weld toe inclination angle and weld edge transition arc radius on the stress concentration coefficient of welded butt joints were studied by using the finite element software ABAQUS. In the past, some researchers studied the effect of geometry parameters on the stress concentration coefficient of welded joints [5-8]. But some of the finite element calculations adopted plane strain model, a simplified model of low precision. The paper adopts three-dimensional entity elements, which has higher precision and real data closer to the stress state of real structures. There are many factors which has the effect on stress concentration phenomenon of welded butt joints, including weld toe inclination angle θ, weld edge transition arc radius r, the thickness of weld t , reinforcement weld metal h, weld width w and so on, as shown in Fig. 1.

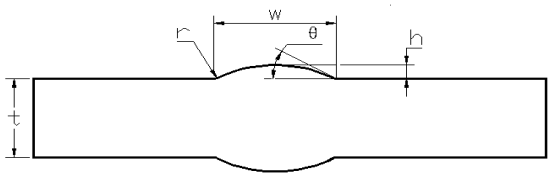

Fig.1. The influence factors on stress concentration of welded butt joint

This paper focuses on the main factors, including weld toe inclination angle θ and weld edge transition arc radius r. The specimen's size is shown in Fig. 2.

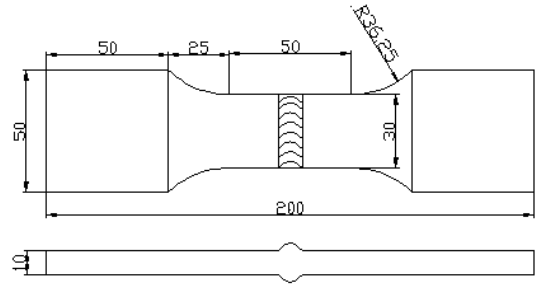

Fig.2 The specimen's shape and size

During stress concentration coefficient of welded butt joint, fully integral tetrahedron entity unit C3D10 is adopted. Dense mesh in stress concentration areas and relatively sparse mesh in other areas are used. It can not only improve the calculation accuracy, but also save calculation time and costs. Due to the symmetry of calculation model, the paper take one-eighth of the welded butt joint is used during the finite element numerical analysis [9]. Stress concentration coefficient is defined as a ratio of the maximum principal stress to the average stress of the section in welded butt joints. The calculation formula of stress concentration coefficient is showed in Eq.1. The tensile load is 100MPa. The finite element model is showed in Fig. 3.

$$k_t = \frac{\sigma_{\max}}{\sigma_m} \tag{1}$$

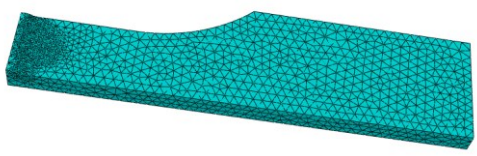

Fig.3. The finite element model and mesh partition

Calculation Results and Analysis

During examining the influence of weld toe inclination angle θ and weld edge transition arc radius r on the stress concentration coefficient of welded butt joints, weld width w is selected as 6mm, weld toe inclination angle θ is changed from 10 to 60 degrees, weld edge transition arc radius r changes from 0.2 mm to 8mm. Calculation results are shown in Table 1 and Fig. 4.

Table 1 Effect of r, θ on the stress concentration coefficient (w=6mm)

r(mm) \ θ(Degree)	10	20	30	40	50	60
0.2	1.590	2.108	2.467	2.641	2.793	2.831
0.5	1.451	1.766	2.094	2.227	2.301	2.356
1	1.370	1.619	1.803	1.885	1.959	2.003
2	1.317	1.455	1.556	1.619	1.658	1.689
3	1.266	1.381	1.441	1.487	1.519	1.545
4	1.231	1.333	1.377	1.412	1.440	1.459
5	1.211	1.285	1.343	1.365	1.390	1.412
6	1.184	1.262	1.302	1.328	1.353	1.362
7	1.176	1.240	1.279	1.297	1.320	1.336
8	1.169	1.223	1.251	1.278	1.294	1.311

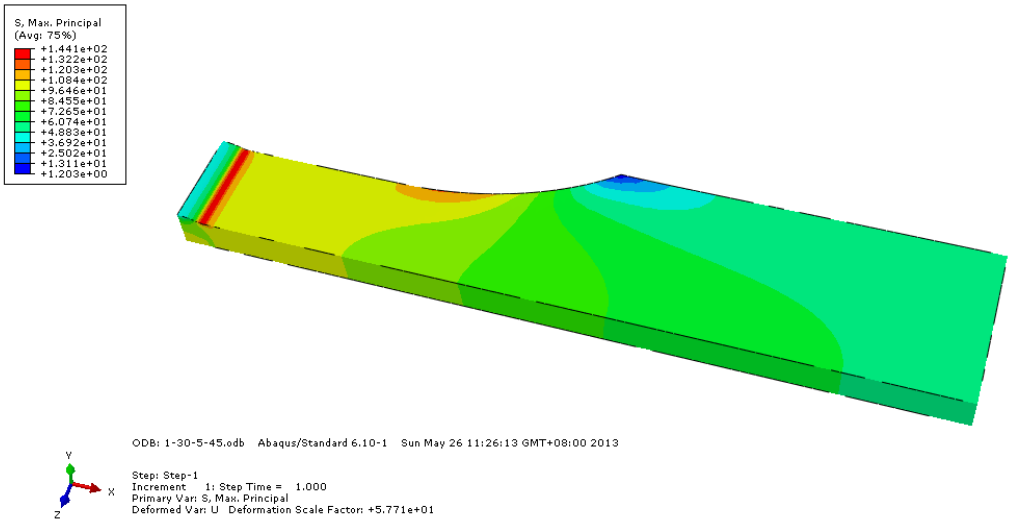

Fig.4 Max principal stress distribution

From Fig. 4 it can be seen that the stress concentration coefficient is very big at the weld toe of welded butt joints. From Table 1 it can also be seen that weld edge transition arc radius r has great effect on the stress concentration coefficient of welded butt joints. For the same weld edge inclination angle, with increasing of transition arc radius r, the stress concentration coefficient decreases gradually.

From Table 1 it can be seen that when the weld edge transition arc radius r is in the smaller value range, a small change of r will cause greatly decreasing of the stress concentration coefficient. On the contrary, when the weld edge transition arc radius r is in the bigger value range, a small change of r will cause very small decreasing of the stress concentration coefficient. When the weld edge transition arc radius r is changed from 0.2mm to 3mm, the stress concentration coefficient is reduced from 2.467 to 1.441, the rate of descend is 41.58%. When the weld edge transition arc radius r is changed from 3mm to 8mm, the stress concentration coefficient is reduced from 1.441 to 1.251, the rate of descend is 13.19%.

From Table 1 it can be seen that the weld toe inclination angle θ has great effect on the stress concentration coefficient of welded butt joints. For different transition radius r, the stress concentration coefficient Kt is increasing as the inclination angle θ increases.

When weld edge transition arc radius r is equal to 0.5mm, with the increase of weld toe inclination angle θ from 10°to 60°, the stress concentration coefficient is increased from 1.451 to 2.356, the growth rate is 62.37%.

Conclusion

(1) Weld edge transition arc radius r has great effect of on the stress concentration coefficient of welded butt joints of magnesium alloy. When weld toe angle is equal to 30°, with increasing of transition arc radius r from 0.2mm to 3mm, the stress concentration coefficient is reduced from 2.467 to 1.441, the rate of descend is 41.58%. With increasing of transition arc radius r from 3mm to 8mm, the stress concentration coefficient is reduced from 1.441 to 1.251, the rate of descend is 13.19%.

(2) Weld toe inclination angle θ has also great effect of on the stress concentration coefficient of welded butt joints. When weld edge transition arc radius is equal to 0.5mm, with the increase of weld toe inclination angle θ from 10° to 60°, the stress concentration coefficient is increased from 1.451 to 2.356, the growth rate is 62.37%. When weld edge transition arc radius is equal to 8 mm, with the same increase of weld toe inclination angle θ, the stress concentration coefficient is increased from 1.169 to 1.311, the growth rate is 12.15%.

(3) For the safe use of welded structures, the true weld edge transition arc radius r of welded butt joints of magnesium alloy should be greater than 3mm, and weld toe inclination angle θ should be smaller than 30°.

Acknowledgement

The research was sponsored by the National Nature Science Foundation (No.51265013), Natural Science Foundation of Jiangxi Province (No.20114BAB206020), Science Foundation of education office of Jiangxi Province (GJJ12302) and visiting scholar plan of universities in Jiangxi province.

References

[1]H Y Fang.The Learning of Welded Structures [M]. China machine press, Beijing 2008 (in Chinese).

[2]A. D. Pogrebnyak, M. N. Regul'skii, and A. V. Zheldubovskii. Assessment of the effect of stress concentration on the fatigue resistance of structural materials under asymmetrical loading[J].Strength of Materials, 2013, 45(1):82-92

[3] Y H Zhang.The Design and Application of Welded Structures[M]. Chemical Industry Press, Beijing 2009) (in Chinese).

[4] K. Tokaji, M. Kamakura, Y. Ishiizumi, N. Hasegawa. Fatigue behavior and fracture mechanism of a rolled AZ31[J]. International Journal of Fatigue, 26 (2004) 1217-1224.

[5] T R Gurney. Finite element analyses of some joints with the welds transverse to the direction of stress[J].Welding Research International, 1976, 6 (1):40-43.

[6] Y B Shao. Geometrical effect on the stress distribution along weld toe for tubular T and K joints under axial loading[J].Journal of Constructional Steel Research, 2007, 63(10):1351-1355.

[7] A Ndiaye, S Hariri, G Pluvinage. Stress concentration factor analysis for notched welded tubular T joints[J]. International Journal of Fatigue, 2007, 29 (12):1554-1570.

[8]F R Mashiri, X L Zhao. Stress concentration factors and fatigue behaviour of welded thin walled CHS-SHS T-joints under in-plane bending[J]. Engineering Structures, 26(2004) 1861-1875.

[9] Y P Shi, Y R Zhou. Detailed Examples for ABAQUS Finite Element Analysis[M]. China Maching Press, Beijing 2006) (in Chinese).

Advanced Materials Research Vols. 989-994 (2014) pp 939-942
© (2014) Trans Tech Publications, Switzerland
doi:10.4028/www.scientific.net/AMR.989-994.939

Effect study of water on the mechanical behavior of gangue in Chongqing Tongliang mine

Zang Yajun [1, a]

[1]School of Tourism and Land resources , Chongqing Technology and Business University, Chongqing 400067. China

[a]zyjcdut@163.com

Keywords: Water, Gangue, Mechanical behavior, Mine

Abstract: This paper first analyzes the strength and deformation characteristics of gangue dispersion, Subsequent analysis of the effect of water on the strength, deformation characteristics. And discusses the permeability characteristics of gangue dispersion and dispersion of particle size, pore characteristics and the dumping years effect on its permeability.

Introduction

Coal gangue is one of the most important coal mine industrial waste, different from other continuous solid material, the shear strength and deformation character has its own characteristic, such as low strength, easy to break, the water stability is bad[1-3]. With the increasing of water content, gangue dispersion cohesion, internal friction angle and matric suction decreases, which reduces the shear strength of dispersion on the whole. This paper studies the mechanics characteristics of gangue dispersion, in order to obtain the gangue hill stability control significance of the conclusion.

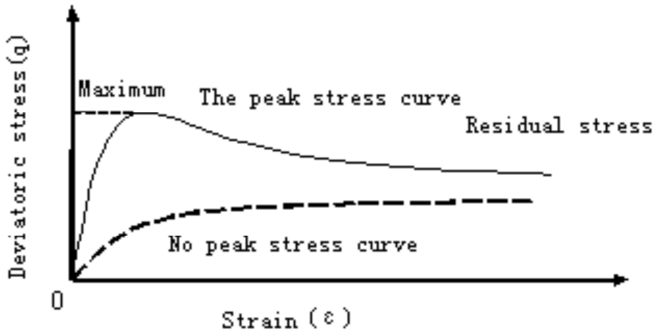

Fig 1 Typical stress-strain curve of rockfill

1. Strength properties of gangue dispersion and effect of water on its strength

Gangue dispersion on shear strength of coal gangue slope stability, safety is significant. It is an important mechanical index determines its stability, and water is an important factor affecting the strength.

(1) Gangue dispersion shear strength

Different from the traditional materials, when the gangue shear failure, the shear strength did not disappear, but according to the compaction degree different, still maintain the original or slightly lower. As shown in Figure 1. In addition, the shear strength is not only related with the characteristic of the granular own gangue dispersion, but also causes and external load on the shear slip plane normal stress on.

Research shows that: gangue granular strength increases with the particle dispersion, c decrease, φ rise[4]. As shown in Figure 2; In addition, the same water condition, gangue internal friction angle φ increases with the density increasing, the strength envelope slope increased, while cohesion c is basically unchanged[5]. As shown in Figure 3.

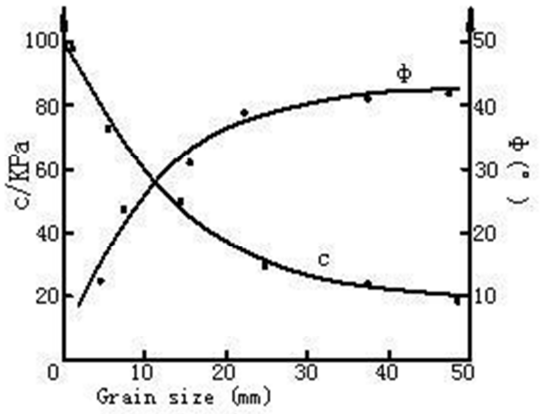

Fig 2 The relationship between shear strength of waste pile materials and grain size

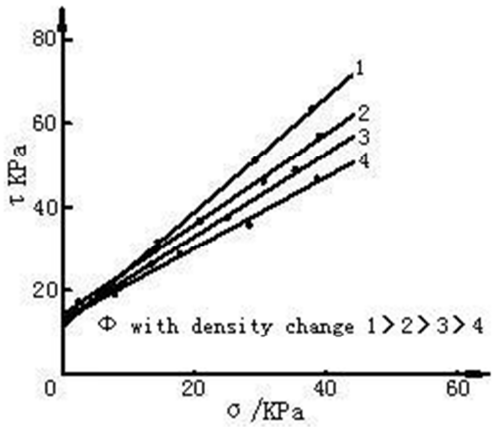

Fig 3 Tested curves of σ-τ simulating shearing in laboratory

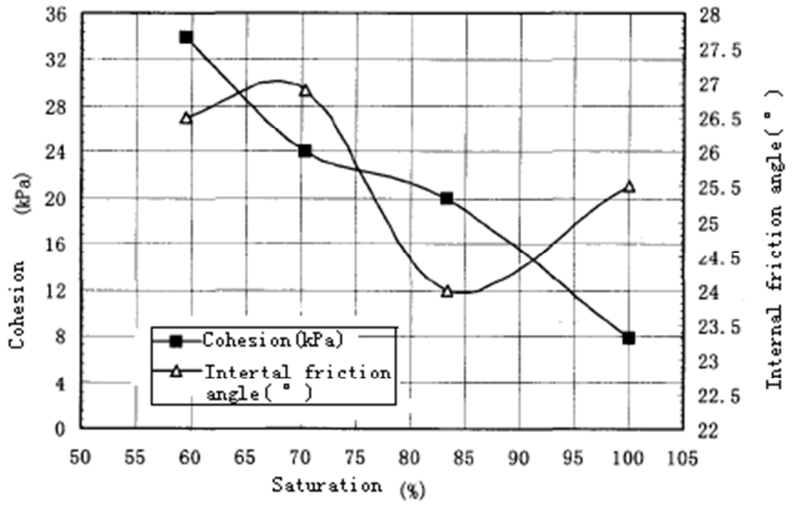

Fig 4 Relation of cohesion and internal friction angle versus saturation of waste pile materials

According to the constitution, gangue accumulation height and accumulation time, performance of gangue granular Chongqing area for inviscid, less viscous, high viscosity or mud three basic characters, different characters of gangue dispersion force, deformation characteristics are different, the shear strength characteristics of the different.

(2) Effect of water on the gangue strength

With the increasing of water content, gangue dispersion cohesion, internal friction angle and matric suction decreases, which reduces the shear strength of dispersion on the whole. Experiments show that: with the increase of the bulk saturation, cohesive strength decreased, but the decline gradually flatten. The variation of cohesion saturation there exists a critical value. In addition, as the saturation increases, basically does not change the friction angle of dispersion, as shown in figure 4.

2. Deformation characteristics of gangue dispersion and water effect on it

(1) Compression deformation characteristic of dispersion

Gangue in situ observation settlement curve shows that the compression deformation is divided into the instantaneous deformation and creep deformation, they follow the deformation law of different. Gangue instantaneous deformation is mainly due to the particle displacement, pore volume caused by the decrease of; and there are two main reasons for creep[6]：One is gangue particles in some corner or edge contact local soft interface is plastic deformation of crushed under the action of external force; two is the grain refinement, slip filling pore, which is the main cause of creep.

(2) Effect of water on gangue dispersion deformation

Waste water stability is poor, long-term immersion occur chemical weathering in the water, on one hand the gangue softening, and broken, the slip; On the other hand, lead to some soluble matter is dissolved and gangue in ground water and away, the total volume of waste reduction, resulting in compression deformation. Figure 5 shows the ability to resist deformation of gangue dispersion on the change of water content showed strong sensitivity.

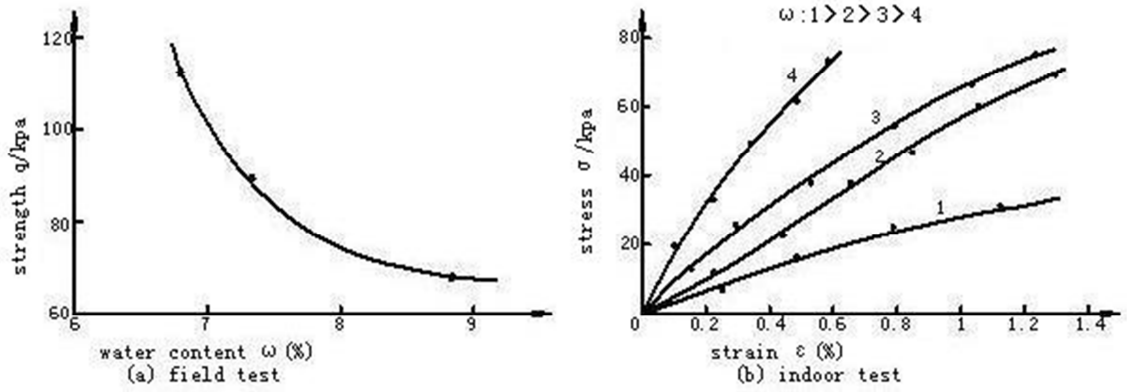

Fig 5 Effect of moisture content on mechanical property of coal mining wastes

For the same kind of gangue granular, compression deformation is mainly controlled by the saturation of the dispersion, in the same load, the greater the water content is, the pore is bigger than lower, deformation of greater; in addition, the compression curves of dispersion is not linear, but similar to a hyperbolic relationship.

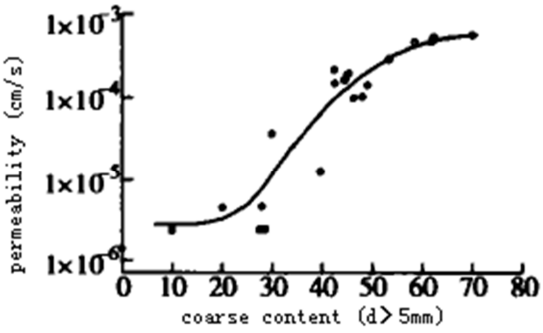

Fig.6 Relation between coefficient of permeability and coarse grain content

3. Permeability characteristics of gangue dispersion

(1) Effect of gangue dispersion particle size and pore characteristics and its effect on permeability

Gangue dispersion is a typical porous medium, natural accumulation conditions, good permeability, permeability coefficient is generally greater than 10^{-2}cm/s orders of magnitude, is a strong permeable material. Experiments show that: the permeability coefficient of coal gangue with pore ratio is gradually increasing trend, there is obvious relation between index. At the same time, the permeability of gangue dispersion varies with the thickness of asphalt content, and compaction characteristics of particle crushing, see Figure 6.

(2) Influence of dumping years on permeability

Infiltration rates were measured on the same slope to different dumping years coal gangue, seen from Figure 7, the dumping years has a certain effect on the gangue infiltration rate. The longer the dumping years, gangue penetration rate, high porosity of coal gangue gangue 30 years above the soil initial infiltration rate is high. Different area gangue dumping years different degrees of differentiation, the differentiation caused by different particle size, initial infiltration rate of different height.

In addition, in different slope coal gangue to vegetation coverage than sunny slope, shady slope vegetation coverage, plant litter leaves covering the ground, the protective layer is formed in the process of decay, which in the differentiation, porosity can improve the gangue soil, is beneficial to the dispersion and infiltration flow. Therefore, the same dumping years gangue hill slope soil infiltration rate is generally higher than that in sunny slope soil infiltration rate.

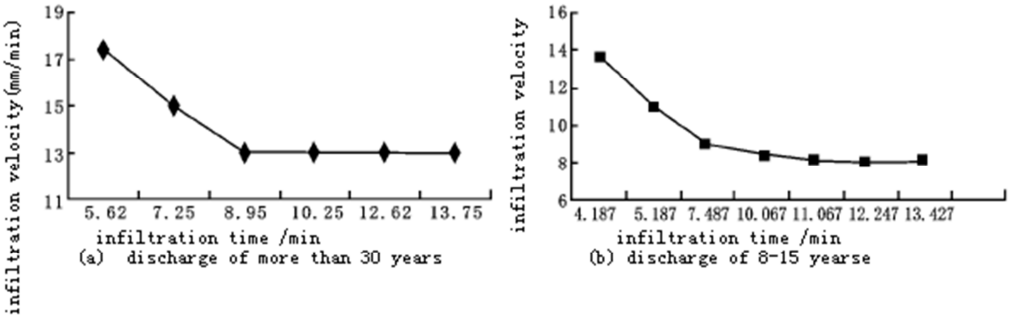

Fig 7 Infiltration process of various letting time of coal wastes

Summary

As for gangue particle structure of the accumulation body, different from other continuous solid material, the shear strength and deformation characteristics also have their own characteristics, the main conclusions are as follows:

(1) Shear strength and material dispersion is different from traditional gangue. Mainly displays in: when the shear failure, the shear strength does not disappear, the compacting degree different, still maintain the original or slightly lower; In addition, the shear strength is not only related with the characteristic of the granular its dispersion, but also causes and external load on the shear slip plane normal stress on;

(2) Along with the increase of gangue dispersion saturation, cohesive strength decreased, but the decline tends to be smooth, so the variation of cohesion saturation there exists a critical value;

(3) Into the instantaneous deformation and creep deformation of gangue compression deformation, they follow the deformation law of different;

(4) The coefficient of permeability and porosity of coal gangue has an exponential relationship between the apparent ratio, and permeability dispersion and particle breakage characteristics related to compaction;

(5) The longer the dumping years, gangue penetration rate is larger; gangue granular infiltration rate and the cumulative infiltration time inverse correlation.

References

[1] SKARZYNSKA K M, ZAWISZA E. The study of saturated coal mining wastes under the influence of long-term loading[C]// Rainbow AKM. 2nd International Symposium on the Reclamation, Treatment and Utilization of Coal Mining Waste. London: British Coal Corporation, 1987: 295–302.

[2] MICHALSKI P, SKARZYNSKA K M. Compact ability of coalmining wastes as a fill material[C]// Treatment and Utilization of Coal Mining Wastes, Symposium on the Reclamation. Durham: British Coal Corporation, 1984.

[3] (ZHANG Jun-ying. Change law of foundation reverse force under fully mechanized caving condition[J]. Coal Science and Technology, 1996, 24(11): 28–31.

[4] HUANG Le-ting, TANG Zhi-xin. Compression test of water immersed coal gangue foundation in mining area[J]. Journal of Coal Science &Engineering, 2000, 21(5): 468–472.

[5] MA Ping, SHI Dong-lai. Study on expansive character of coal wastes[J]. University of Science and Technology Changchun Journal, 2006, 29(3): 52–58.

[6] LI Shu-zhi, LIU Jin-hui,WANG Hua-guo. Foundation bearing capacity of coal wastes[J]. Coal Science and Technology, 2000, 28(3): 13–14.

Advanced Materials Research Vols. 989-994 (2014) pp 943-946
© (2014) Trans Tech Publications, Switzerland
doi:10.4028/www.scientific.net/AMR.989-994.943

Experimental Research on Tensile Strength of Out-of-Plane Composite Joints for Integrated Composite Cabins

Donghua Zhang [1, a], Xiaohong Zhou [1, b], Longwei Zhou [2, c]

[1] Beijing Electro-mechanical Engineering Institute, Beijing, 100074, China

[2] School of Astronautics, Beihang University, Beijing, 100191, China

[a]email: jane117@163.com, [b]email:hebeisongwei@163.com, [c]email:rayzhow@aliyun.com

Keywords: Composite; Static test; Strength; Adhesive-Bonded; Bolt; Joint

Abstract. An experimental study of tensile failure behaviors of L-shaped adhesive-bonded and bolted hybrid composite joints, which are designed to connect composite cabins, is performed. A set of rigid jigs was designed to fix the specimens and ensure to apply an axial tensile load. The damage processes, failure loads and ultimate failure patterns of the joints are obtained from the tests. Some indentation around the fastener hole and remarkable discontinuity departure between the top and bottom L-shaped laminates which leads to the catastrophic failure can be observed on the specimens. It follows that the discontinuity is the weak spot and required to be strengthened.

Introduction

In this paper a new optimal design of soccer robot control system which is based on mechanical analyses and calculations on the pressure and transmutation states of chip kick mechanics, this new control system with high precision for speed control and high dynamic quality.

Due to high strength and stiffness ratios and excellent integrated fabrication abilities for complex configurations of composite materials, increasing applications have been widely used in aerospace industry. The integrated composite structure technique, which means large, complex composite structures can fabricated in one step, attracts widespread attention since it can bring remarkable benefits in structural safety, low cost and light weight [1-3]. Out-of-plane adhesive-bonded joints, such as T-, L- and π-shaped joints, which are typical connectors of integrated composite structures, are focused on recently. At the same time, it is noticed that composite bolted joints can endure great loads and be removed without destroying composite structures as well as easy to maintain. Thus, taking the advantages of both bolted joints and bonded joints, an out-of-plane L-shaped adhesive-bonded and bolted hybrid composite joint is proposed to join cabins in current work.

Out-of-plane joints are load conjunction in the integrated structures, which not only play important roles in load carrying and transferring but also show obvious weakness, and thus require to be understood deeply. Aiming to the T-, L- and π-shaped joints, systematic studies have been studied by Shenoi et al. [4-7], Feih et al. [8,9] and Zhao et al. [1-3,10-14]. The finite element models and progressive damage analyses have been carried out and verified by experiments [1-3,7-10]. The mechanical behaviors of the joints under tensile or/and flexible loading have been clarified and the failure mechanisms have been explored [2,3,7,9,12]. Also the influences of geometries, configuration and materials on the mechanical behaviors of the joints have been provided [3,4,11].

An experimental study on the failure behavior of the hybrid composite joint is presented. Some basic information for the load carrying and transferring capacity of the joint can be provided.

Specimen and set-ups

The sketch map and geometric dimensions of the joint are shown in Fig.1. The L-shaped joint mainly consists of four parts: bottom L-shaped laminates (in green), top L-shaped laminates (in blue), middle strengthened-laminates (in brown) and double upstanding stiffened laminates (in yellow), all the laminates are made of unidirectional carbon/epoxy composites with T700 grade

fibers. The stacking sequences of the four laminates are as follows: The bottom L-shaped laminates: $[45/0/-45/90]_{3s}$ with thickness 3mm; The middle strengthened-laminates: $[45/0/-45/90]_{3s}$ with thickness 3mm; The top L-shaped laminates: $[45/0/-45/90]_{2s}$ with thickness 2mm; The double upstanding stiffened laminates: $[45/0/-45/90]_{4s}$ with thickness 4mm. All the four laminates were put into a prepared mold together and then the joint was obtained using RTM process.

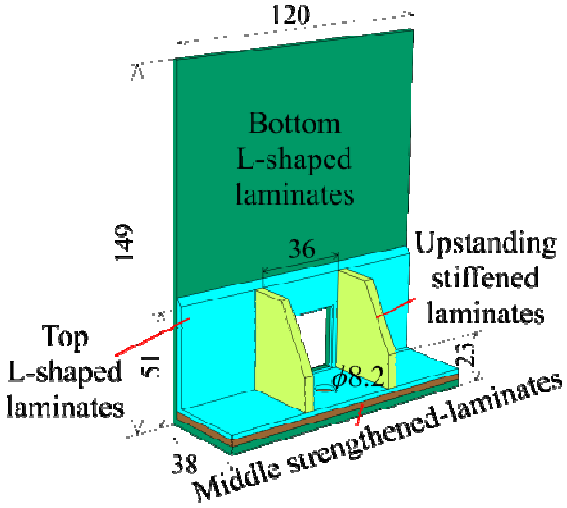

Fig 1 Sketch map of a typical L-shaped joint (Unit:mm)

To obtain tensile mechanical behaviors of the specimens, a set of rigid jigs was designed to fix specimens and ensure the axial tensile load, as shown in Fig 2. The upper jig is fixed with the bottom L-shaped laminates with several bolts, while the lower part is fastened with the specimen using an 8mm-diameter bolt with 10N·m tightening torque. Both ends of the jigs were clamped by the test machine grips. In order to ensure the joint be subjected to axial tensile load, the middle plane of the jig's gripped end, the axis of bolt and the loading plane of test machine are located at one same plane, as shown in the side view of Fig. 2.

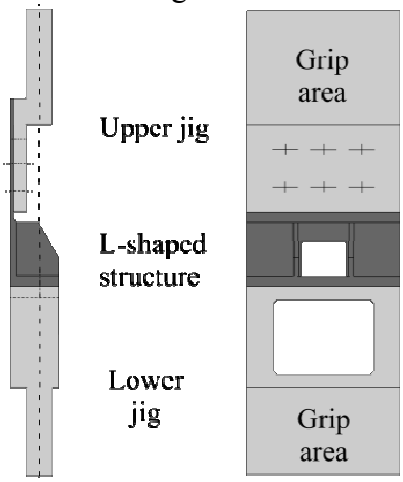

Fig 2 Jigs and assembly (a) side view (b) front view

Experimental procedures

Static tensile tests of the joints were implemented in a 250kN servo hydraulic test machine (Instron 8803). Two specimens were tested. Before the test starts, the specimens were assembled with steel jigs, a 10N·m tightening torque was applied to the 8mm-diameter bolt using a torque wrench. Then the assembly body was placed in the grips of the testing machine, taking care to align the long axis of the gripped specimen with the test direction. The constant loading rate of the cross head was 1mm/min until the ultimate failure of the specimens occurred. Continuous records of load-displacement data were obtained by a digital data acquisition system, in which the peak value of the load-displacement curve was deemed as the ultimate failure load. Failure sequences and locations of the specimens were recorded by videos and photographs.

Results and discussion

The mechanical behaviors of the joints are obtained by the static tensile tests, including failure procedure, failure load and ultimate failure pattern. Table 1 gives the final failure loads of both specimens which are defined as the peak value in load-displacement curves. During the loading procedure some noise emitted while there was no notable cracks or other kind of damage in the specimens. The load continued to increase and some visible damage was first occurred at the corner of the discontinuity denoted point 1 as show in Fig 3. Then the damage propagated from both edges to the middle along the marked wave line 2. After the cracks ran through the whole adhesive interface, the top L-shaped laminates departed from bottom L-shaped laminates along direction 3 shown in Fig.3, which led to the catastrophic failure of the joint.

Table 1 Static test results for L-shaped composite joint

No.	Final Failure Load/kN	Failure Locations
Specimens 1	9.88	Discontinuity departure between
Specimens 2	10.95	two L-shaped laminates
Average failure load/kN	10.42	-

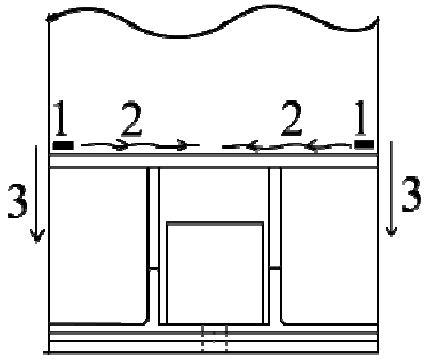

Fig 3 Schematic crack growth path

The typical ultimate failure pattern of specimens in tests is shown in Fig 4, from which a notable departure can be observed. In addition, after the specimens were disassembled from the jigs, a clear indentation can be found around the fastener hole caused by the bolt.

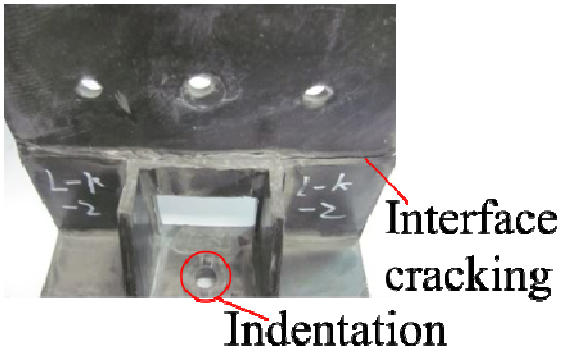

Fig 4 Ultimate failure pattern

Conclusion

A kind of L-shaped adhesive-bonded and bolted hybrid composite joint consisting of bottom L-shaped laminates, top L-shaped laminates, middle strengthened-laminates and double upstanding stiffened laminates was designed. Tensile experiments of two specimens were carried out to explore their mechanical behaviors. The average failure load is 10.42kN, which satisfies the requirement of designers. With the increasing tensile load, the damage onset occurs at the corner of the discontinuity between the bottom and top L-shaped laminates, which runs through the whole adhesive interface and then leads to the departure of the two L-shaped laminates. At the same time, a small amount of local indentation can be observed around the fastener hole. Thus the discontinuity

part between two L-shaped laminates is the weak spot that it should be strengthened to improve the load carrying and transferring capability of the L-shaped adhesive-bonded and bolted hybrid composite joints.

References

[1] Libin Zhao, Tianliang Qin, Yuli Chen, etc. Three Dimensional Progressive Damage Models for Cohesively Bonded Composite Π Joint [J]. Journal of Composite Materials, 2014 48 (6) 707-721.

[2] Libin Zhao, Tianliang Qin, RA Shenoi, etc. Strength Prediction of Composite Π Joint under Tensile Load [J]. Journal of Composite Materials, 2010 44 (23) 2759-2778.

[3] Yue Fu, Jianyu Zhang, Libin Zhao. Strength Prediction of Composite Π Joint under Bending Load and Study of Geometric and Material Variations Effects [J]. Journal of Composite Materials, 2013 47 (8) 1029-38.

[4] Shenoi R. A., Hawkins G. L. Influence of Material and Geometry Variations on the Behaviour of Bonded Tee Connections in FRP Ships [J]. Composites, 1992 23(5) 335-345.

[5] Phillips H.J., Shenoi R. A., Moss C.E. Damage Mechanics of Top-hat Stiffeners Used in FRP Ship Construction [J]. Marine Structure, 1999 (12) 1-19.

[6] Phillips H.J., Shenoi R. A. Damage Tolerance of Laminated Tee Joints in FRP Structures [J]. Composite part A, 1998 29 (A) 465-478.

[7] Blake J. I. R., Shenoi R. A., House J., et al. Progressive Damage Analysis of Tee-joints with Viscoelastic Inserts [J]. Composites: Part A, 2001 (32) 641-653.

[8] Feih S, Shercliff H.R. Composite Failure Prediction of Single-L Joint Structures Under Bending [J]. Composites Part A-Applied Science and Manufacturing, 2005 (36) 381-395.

[9] Feih S, Shercliff H.R. Adhesive and Composite Failure Prediction of Single-L Joint Structures Under Tensile Loading [J]. International Journal of Adhesion & Adhesives, 2005 (25) 47-59.

[10] Libin Zhao, Tianliang Qin, Hai Huang, etc. Model Investigation on Composite Failure Prediction of Π Joint Structures [J]. Rare mental materials and engineering, 2009 38 (3) 105-108.

[11] Jianyu Zhang, Libin Zhao, Tianliang Qin, etc. Influence of Π Overlaminates on the Mechanical Behavior of All-composite Adhesively Bonded Π Joints [J]. Journal of Reinforced Plastics and Composites, 2014 (33) 923-934.

[12] Libin Zhao, Xiaoxiao Zhang, Jianyu Zhang, H Huang, XZ Liang. Failure Analysis of Woven Composite Π Joint under Bending Load [J]. Advanced Science Letters, 2011 4 (8-10) 2752-2758.

[13] Jianyu Zhang, Lei Peng, Libin Zhao, Binjun Fei. Fatigue Delamination Growth Rates and Thresholds of Composite Laminates under Mixed Mode Loading [J]. International Journal of Fatigue, 2012 (40) 7-15.

[14] Lei Peng, Jianyu Zhang, Libin Zhao, Rui Bao, Hongqin Yang, Binjun Fei. Mode I Delamination Growth of Multidirectional Composite Laminates under Fatigue Loading [J]. Journal of Composite Materials, 2011 45 (10) 1077-90.

Advanced Materials Research Vols. 989-994 (2014) pp 947-950
© (2014) Trans Tech Publications, Switzerland
doi:10.4028/www.scientific.net/AMR.989-994.947

Modeling and simulation analysis on building temperature and toughness

Zhang Qian

Si Chuan College Of Architectural Technology, Deyang, 618000, China

Keywords: high-rise buildings;, collapse risk; multi-level fuzzy probability;

Abstract: There are many links between temperature and toughness of the building. To quantify the association between them, a model of temperature and toughness is proposed to analyze toughness relationship at different temperatures of the building. Collapse warning is performed by difference of security risks in temperature grades of buildings to obtain model relationship of temperature and toughness, so as to achieve an accurate assessment of the risk of collapse for high-rise building under different fire rating. The experimental results show that, proposed method at different building fire levels on accession of efficiency, time and accuracy of building collapse risk are better than traditional methods, which is capable of efficiently assessing the risk of high-rise buildings collapse in exceptional temperature.

1 Introduction

With the continuous development of economic level and building technology more and more high-rise buildings are built, fire disaster is prone to an upward trend and brings huge losses to people's lives and property. Evaluation of the building temperature and toughness is an effective and important initiative in preventing and controlling building fire accident. The evaluation of temperature and toughness of the high-rise buildings need not only take into account the non-occurrence of fires or less, but also evacuation and spread prevention on the occurrence of fire fighting. Collapse evaluation of high-rise buildings involves multiple factors, whose attributes are divided into different categories and levels, and are difficult to be quantified with great fuzziness and randomness[1,2]. High-rise building temperature becomes anomalies when a fire occurs and takes security threats to building, so collapse prevention becomes focus tissue of scholars' analysis. Relationship model between building temperature and toughness is the focus research in the field of construction safety[3-5].

2 evaluation model based on multi-level fuzzy comprehensive probability

On assessment of temperature and collapse risk factor of buildings, collapse risk factors $U_i(i=1,2,...,n)$ can be evaluated by one-level fuzzy probability assessment, the process as:

Single factor of toughness fuzzy as U_{ij} weights (fuzzy numbers) $\pi_{ij}(j=1,2,...,m_i)$, that is taking weights as fuzzy numbers: π_{ij} = 'Close to $\lambda_{ij,0}$ '=

$$\frac{\beta_{ij,1}}{\lambda_{ij,1}}+...+\frac{\beta_{ij,p}}{\lambda_{ij,p}}+\frac{1}{\lambda_{ij,0}}+\frac{\beta_{ij,p+1}}{\lambda_{ij,p+1}}+...+\frac{\beta_{ij,2p}}{\lambda_{ij,2p}} \quad (1)$$

Where $\lambda_{ij,0}$ indicates the relative weights, as can given by an expert assessment or fuzzy analysis, $\sum_{j=1}^{m_j}\lambda_{ij,0}=1$ so as to meet the operational requirements of fuzzy probability; $\beta_{ij,m}(m=1,2,...,2p)$ can be selected based on the actual situation, by the fuzzy theory as any of 0.5,0.6,0.7,0.8,0.8; $\lambda_{ij,m}$ is determined by the value $\lambda_{ij,0}$. The fuzzy probability formula:

$$
\begin{aligned}
&(a_{i1}\pi_{i1}+a_{i2}\pi_{i2}+...+a_{im_i\pi_{im_i}})(P)\triangleq \\
&\vee_{a_{i1pi1}+...+a_{mi}p_{imi}=p}(\pi_{i1}(p_{i1})\wedge...\wedge\pi_{im}(P_{im})) \\
&P_i(V_k)=v_{i1,k}\pi_{i1}+v_{i2,k}\pi_{i2}+...+v_{im_i,k}\pi_{im_i}
\end{aligned}
\tag{2}
$$

In fact, formula (2) can be seen fuzzy weight π_{ij} as on a fuzzy subset of domain $\{\lambda_{ij,1},...,\lambda_{ij,p},\lambda_{ij,0},\lambda_{ij,p+1},...,\lambda_{ij,2p}\}$, corresponding to $\{\beta_{ij,1},...,\beta_{ij,p},1,\beta_{ij,p+1},...,\beta_{ij,2p}\}$, where π_{ij} is fuzzy weight of toughness evaluation factors U_{ij}, p_{ij} is any of corresponding field $\{\beta_{ij,1},...,\beta_{ij,p},1,\beta_{ij,p+1},...,\beta_{ij,2p}\}$, $\pi_{ij}(p_{ij})$ is corresponding membership, a_{ij} means elements of jth row for fuzzy matrix v_i, for specific subset of toughness assessment V_k, a_{ij} is jth row kth column element $v_{ij,k}$.

Further to obtain one–level toughness of evaluation matrix by probability of fuzzy $R=(\bar{\sigma}_{ik})_{n\times 5}$.

To get assessment matrix R of different temperature grades by fuzzy probability, toughness of risk fuzzy probability can be assessed. Setting fuzzy weight $\pi_i(i=1,2,...,n)$ of different temperature grades for toughness evaluation factors U_i, as formula (1), replacing π_{ij} by π_i, fuzzy probability assessment matrix R instead of the corresponding fuzzy matrix v_i, repeating operation process above, in standard information sheet $\bar{\sigma}_k$ of risk fuzzy probability assessment for toughness, standard information vector set is eventually obtained at different temperature rating.

$$\bar{\sigma}=(\bar{\sigma}_1,\bar{\sigma}_2,\bar{\sigma}_3,\bar{\sigma}_4,\bar{\sigma}_5) \tag{3}$$

Then concentrating by the maximum value of the standard information the toughness assessment levels is determined:

$$\bar{\sigma}_N=\max_k[\bar{\sigma}_k] \tag{4}$$

The assessment to determine the level of building toughness is Nth level. Assessment model of toughness fuzzy probability for third level or above building can be followed by analogy. The above process can be achieved through computer programming, and ultimately obtain accurate assessment of the risk of high-rise buildings toughness under different temperature levels.

3 Experimental analysis of material stress after fire

Simulation experiments are proposed to the relationship between fire and force. The reinforcement material size is fixed. To observe properties after the fire, model observation points A is chosen as junction point of the surface layer and the below layer on vertical center axis. From Figure1 to Figure5, it can be seen that longitudinal normal stress, vertical stress, transverse normal stress, longitudinal and transverse shear stress are increased by time.

Longitudinal normal stress of 0.7 MPa as tensile stress of 0.37 MPa increases to 1.5 MPa as 0.80MPa, an increase of 116.2%, compressive stress of 0.7 MPa as 1.5 MPa increases to 0.62MPa as 1.32MPa, an increase of 113.0%. Vertical stress of 0.7 MPa as 1.5 MPa increase to 0.12MPa as 0.25MPa, an increase of 108.3%. Transverse normal stress of 0.7 MPa as tensile stress of 0.66 MPa increases to 1.5 MPa as 1.42MPa, an increase of 115.2%, compressive stress of 0.7 MPa as 1.5 MPa increases to 0.24MPa as 0.53MPa, an increase of 120.3%. Longitudinal shear stress of 0.7 MPa as 1.5 MPa increases to 0.10MPa as 0.21MPa, an increase of 110.0%. Transverse shear stress of 0.7 MPa as 1.5 MPa increases to 0.06MPa as 0.13MPa, an increase of 116.7%. Above on, as time increases, the dynamic response of the pavement surface layer varies, which is important factor for structural damage.

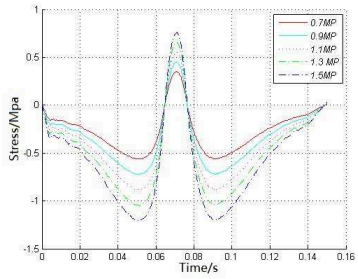

Figure1 Longitudinal normal stress variation

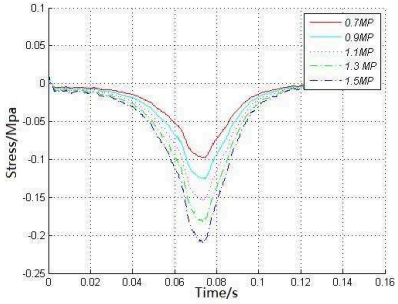

Figure2 Vertical stress variation

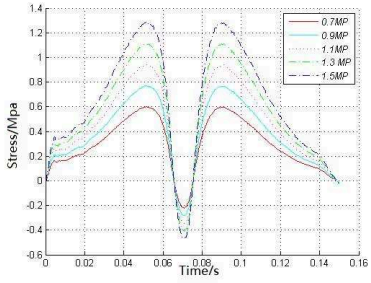

Figure3 Load variation of transverse normal stress

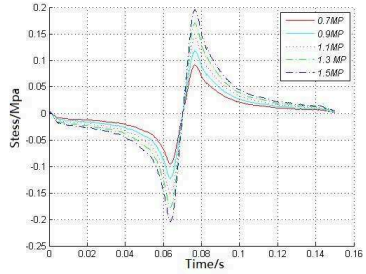

Figure 4 Load variation of longitudinal shear stress

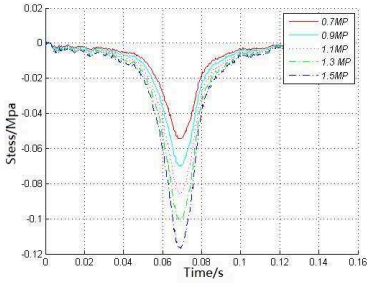

Figure 5 Load variation of transverse shear stress

4 Conclusions

This paper proposes a model between temperature and toughness, through which analyzes toughness relationship at different temperatures and perform collapse warning based on different

temperature grades. Obtaining the relationship model between temperature and the toughness of the buildings, and an accurate assessment of risk of collapse for the high-rise building under different fire rating is achieved. The experimental results show that, proposed method at different building fire levels on accession of efficiency, time and accuracy of building collapse risk are better than traditional methods, which is capable of efficiently assessing the risk of high-rise buildings collapse in exceptional temperature.

References

[1] Liu Guoguang, Wu Zhiwei, Xu Youhua. Study on pedestrian wind environment of a super high rise building by wind tunnel test[J]. Bulletin of Science and Technology. 2013,9:81-85.
[2] Du Hongbing, Zhou Xinquan, Zhang Jinzong. Fuzzy synthetic evaluation for fire safety of high-rise building[J]. Journal of China University of Ming & Technology. 2002,31(3):242- 24**5.**
[3]Hu Baoqing, Lu Zhaoming, Liu Min. Fuzzy optimal cluster model and its application in fire safety evaluation for high-rise buildings[J]. Fuzzy Systems and Mathematics. 2004, 18(4): 77-85.
[4] Wu Zuopeng, Wu Liqiong. Strength loss of reinforced concrete construction in fire. Fire Science and Technology，1995（3）：2～4.
[5] Hu xiao. The design of the building collapse and fire-resistant building. Fire Science and Technology.2004，23（5）：453～454.

Advanced Materials Research Vols. 989-994 (2014) pp 951-953
© (2014) Trans Tech Publications, Switzerland
doi:10.4028/www.scientific.net/AMR.989-994.951

Relationship modeling between tensile strength of steel building and temperature

Zhang Qian

Si Chuan College Of Architectural Technology, Deyang, 618000, China

Keywords: steel-reinforced concrete structure; ultrasonic frequency spectrum; strength properties;

Abstract: In certain high temperatures conditions, tensile strength of steel concrete varies due to changes in ambient temperature environments, which greatly influences structural characteristics and material properties. For this reason, relational model between reinforced tensile strength of building and temperature is proposed. Information of reinforced concrete structure collecting by ultrasonic sensors is processed to be anti-inference and build relationships employing PSO algorithm. Experimental results show that this model can be a good measure of property relationships between temperature and tensile strength of reinforced concrete structure.

1 Introduction

Tensile strength of reinforced concrete varies with ambient temperature, providing reinforced concrete in high temperature environment results in reducing tensile strength, which affecting safety performance of buildings [1]. Fire as a common form of disaster, is kind of a high-temperature environment and will bring great security risk to architectures of reinforced concrete structure [2]. To measure tensile strength properties of steel-reinforced concrete after high temperature could judge safety performance of constructions in a high temperature environment [3]. Therefore, measurements of tensile strength of steel-reinforced concrete in high temperature environment has become a hot issue in construction field and gained many scholars' attention [4-5].

2 Relationship modeling of tensile strength and temperature

2.1 tensile strength measurement theory of steel-reinforced concrete

In high ambient temperature conditions, ultrasonic pulse signal is employed to calculate spectral characteristics of ultrasonic deformation parameters, so as to obtain tensile strength of steel-reinforced concrete. The steps are as follows:

Set ultrasonic pulse propagation velocity as V, area of concrete as S, duration of fire as t, average temperature during the fire as T, data set of ultrasonic pulse signal as $\{a_1, a_2, \cdots, a_n\}$, number of ultrasonic pulse signals as n, spectral deformation parameters of ultrasonic characteristic can be calculated by following equation:

$$\varepsilon = \frac{V \times \sqrt{S^2 - t^2} \times \sum_{i=1}^{n} a_n}{T \times n} \tag{1}$$

According to above equation, spectral characteristics parameter of ultrasonic deformation is calculate to describe deformation degree. Using the following formula tensile strength coefficient of steel-reinforced concrete can be calculated:

$$\delta = \frac{\varepsilon \cdot a_i^2}{\left| a_j + a_i \right| - (T-1)^2} \tag{2}$$

According to formula, it is possible to obtain tensile strength coefficient of steel-reinforced concrete, so as to describe tensile strength properties.

Employing the following formula, residual factor of tensile strength of reinforced concrete can be calculated:

$$\eta = \frac{V^2 - t^2 - 1}{\delta \times a_i^2} \tag{3}$$

Residual factor of tensile strength is obtain to present errors in measurement process.

2.2 model of measure establishing

By PSO algorithm neural network is optimized to improve efficiency of weights and thresholds in the model. Specific optimization process of PSO algorithm is: first set $E_i = (e_{i1}, e_{i2}, \cdots, e_{iC})$ as *i*th particles, then optimal solution of tensile reinforcement vulnerability information at high temperature by an iterative method is presented. In each iteration, particles adjust its position by individual extreme (Q_{win}) and global minimum (f_{win}). Particle velocity is indicated as $S_i = (s_{i1}, s_{i2}, \cdots, s_{iC})$. Particle velocity and position are updated as in formula (4) as follows.

$$\begin{gathered} s_{id}^{i+1} = \lambda \times s_{id}^{i} + b_1 \times stoch() \times (Q_{win} - e_{id}^{i}) \\ b2 \times stoch() \times (f_{win} - e_{id}^{i}) \\ e_{id}^{i+1} = e_{id}^{i} + s_{id}^{i+1} \\ \lambda = \lambda_{\max} - (\lambda_{\max} - \lambda_{\min}) M / M_{\max} \end{gathered} \tag{4}$$

Wherein λ is inertia weight; s_{id}^{i} is current speed of particle, s_{id}^{i+1} means adjusted speed of particles; b_1 and b_2 are learning factors, $stonch()$ means random numbers in (0,1) domain; e_{id}^{i} is current position of particle indicates, e_{id}^{i+1} is adjusted position of particle; $\lambda_{\max}$ means maximum of inertia weight, $\lambda_{\min}$ means minimum of inertia weight; M indicates number of current iteration, while $M_{\max}$ means maximum number of iterations. PSO algorithm ensures that mean square error of the neural network is minimized, achieving the optimization of neural networks. Therefore, mean square error of the desired output and the actual output of the network is employed as fitness function of neural network optimization PSO, there are:

$$F = \frac{1}{M} \sum_{i=1}^{M} [\sum_{r=1}^{L} (y_{rc} - y_r)^2] \tag{5}$$

Where M is used to describe number of training samples; L means output dimension; y_{rc} represents output value of the model, y_r means actual output value. PSO optimization method can obtain the optimal positioning information to ensure the search to find minimum of construction area, and thus be able to get tensile steel vulnerabilities accurately.

3Analysis of experiment results

In order to verify effectiveness of the proposed method, experiments are needed. Different methods are carried out to measure performance of tensile strength of steel-reinforced concrete in high temperature environment. The average temperature in the case of fire is 500 centigrade, while different algorithms are used for performance measurement of tensile strength of steel-reinforced concrete; results analyzed are shown in Figure 1:

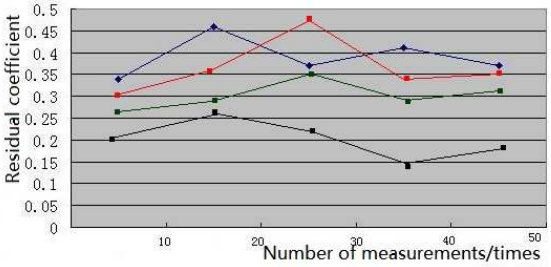

Figure 1 Experiment results in average temperature 500 centigrade of fire

According to the above diagram, it is said that by the proposed model for tensile strength properties of steel-reinforced concrete measurement results are acquired and error is minimized. Relevant experimental data are analyzed in the following Table1:

Table1 Experimental data set of tensile strength

Algorithm	Measure times	Actual strength	Measured strength
Algorithm by Ultrasonic characteristics	23	0.76	0.57
Deformation difference algorithm of image pixels	35	0.75	0.63
Infrared signals	46	0.76	0.58
Proposed algorithm	37	0.74	0.72

According to Table 1, using proposed model of steel-reinforced concrete under high temperature, performance measurement of tensile strength is measured and results are accurate.

4 Conclusions

Relationship model between temperature and tensile strength of steel buildings is presented. Employing ultrasonic sensors to collect information of steel-reinforced concrete structure, anti-jamming in processing, using PSO algorithm, relationships are built. Experimental results show that this model can be a good measure of property relationships between temperature and tensile strength of steel-reinforced concrete structure.

References

[1] Wang Fujun. Matlab- Based Simulation of Ultrasonic Motors [J].Computer simulation,2012.4: 405-408.

[2] Li Changqi,Qu Shiru. Vehicle Identification Based on Ultrasonic Ranging and BP Neural Network [J]. Computer Measurement & Control,2009.9.

[3] Yu Wei,Chen Yihua,Feng Weizhong,et al. Design of wireless ultrasonic level measurement system [J]. Industry and Mine Automation,2012.2.

[4] Li Qing,Jia Jingpu. Design and Study of Ultrasonic Flow meter for High-temperature Flow Measurement [J]. Coal Technology,2012.1.

[5] Cai Zhongxing.Design of transceiver circuit and flow totalizer display module of Ultrasonic gas flow meter[D]. University of Electronic Science and Technology of China,2009.

Advanced Materials Research Vols. 989-994 (2014) pp 954-957
© (2014) Trans Tech Publications, Switzerland
doi:10.4028/www.scientific.net/AMR.989-994.954

Study on the Affects of Partition of the Parallel and Cross Tunnel Adjacent Construction

Wei Zheng[1,a], Lin Gao[1,b]

[1]Hunan Urban Construction College, Xiangtan, Hunan Province 411101, P.R. China

[a]46233318@qq.com, [b]249537800 @qq.com

Keywords: Adjacent construction; Affects of partition; Vertical spacing; Level spacing

Abstract: This paper was based on the parallel and cross section on the east coast of Xiangjiang river crossing tunnel on Yingpan road in Changsha City, and studied on the affects of partition of it adjacent construction. The conclusions were drawn as followings: When the vertical spacing is larger than 4D, it didn't need to consider the influence of vertical spacing on parallel interchange tunnels close construction, can be considered as two parallel tunnels. And when the level spacing is larger than 4D, it didn't need to consider the influence of level spacing on parallel interchange tunnels close construction, can be considered as two intersecting tunnels.

Introduction

For the two tunnels near construction, Japan made a lot of research, for example, the railway system, the power system and the highway system promulgated The Guide of Railway Tunnel Adjacent Construction, The Guide of Adjacent Construction and The Guide of Highway Tunnel Adjacent Construction respectively in 1998, 1999, and 2000, and some other research results[1-2]. The Guides gave a systematic discussion on the problem of approaching excavation, put forward some concepts such as adjacent degree and affects of partition and pointed out that the interaction of new tunnel and existing tunnel mainly depended on those: (1) the spacing of the tunnels, (2) the relative positional relationship of the tunnel facades, (3) the scale of new tunnel, (4) the construction method of new tunnel, (5) topographic and geological conditions, (6) the construction quality of existing tunnel lining. The adjacent degree classifications of parallel tunnel and cross tunnel on the guide [3] were shown in table 1 and table 2(based on The Guide of Railway Tunnel Adjacent Construction). According to the relative positional relationship of tunnels, the guide divided the adjacent degree into three ranges such as unconditional range, important range and limits.

Table 1. Approximation degree division of parallel tunnel

Two tunnel position	Spacing	Adjacent degree classification
New tunnel is higher	＜1D	Limits
	1～2.5D	Important range
	＞2.5D	Unconditional range
New tunnel is lower	＜1.5D	Limits
	1.5～2.5D	Important range
	＞2.5D	Unconditional range

Note: D is the tunnel diameter, and the same below.

There were many literatures and regulation studied on the affects of tunnel adjacent construction, but most of the literature only consider the two-hole or three-hole tunnel, for example, based on the structure stress principle and earth surface displacement principle, the literature[4] studied on the mechanical behavior of approaching construction of two parallel shield tunnels, got the affects of partition of it adjacent construction, and then protracted the partition graphs, the literature[5] studied on interrelationship of three parallel shield tunnels, and put forward the expression of adjacent influence subzone and partition graphs, the literature[6] studied on the affects of partition of adjacent construction of two cross shield or mining method tunnels, and got some achievements.

Table 2. Approximation degree division of cross tunnel

Two tunnel position	Spacing	Adjacent degree classification
New tunnel is higher	＜1.5D	Limits
	1.5～3.0D	Important range
	＞3.0D	Unconditional range
New tunnel is lower	＜2.0D	Limits
	2.0～3.5D	Important range
	＞3.5D	Unconditional range

The above showed that, the studying on the affects of partition of adjacent construction of parallel or cross tunnels more limited on the level of interrelationship of two-hole or three-hole tunnel and only considered a single case(parallel or cross), two cases were considered at the same time was little. It would encounter multiple tunnels be paralleled and crossed underground, when vigorously developing the underground traffic. It would bring some problems, for example, how to determine the affects of partition of adjacent construction of parallel-cross tunnels, and then determined the construction technology of it. For that reason, this paper was based on the parallel and crossed section on the east coast of Xiangjiang river crossing tunnel on Yingpan road in Changsha City, studied on the affects of partition of it adjacent construction, and provided an important reference for building underground highway in the future.

The Calculation Model

It can be obtained from the project that the north and south mainline tunnels were located under the C and D ramps, and they crossed each other at 90 degrees. The average depth of the two ramps is 11.5 m. So the crossing angle of up and down tunnels was fixed at 90 degrees and the depth of C and D ramps was fixed at 11.5 m in the model. Firstly, the up parallel tunnels was excavated, secondly, the down parallel tunnels was excavated. Based on the earth surface displacement principle and structure stress principle, this paper focused on studying the affects of partition of the down tunnels when the up tunnels was excavated, and the selection of threshold value was according to table 3 and table 4.

Table 3. Standard of adjacent influence subzone based on the displacement criterion(mm)

Affects of partition	Surface settlement	Classification standard
Strongly affected zone A	$U \geqslant 10$ or $U \leqslant -30$	$I \geqslant 2$
Weakly affected zone B	$5 \leqslant U < 10$ or $-30 < U \leqslant -10$	$1 \leqslant I < 2$
No affected zone C	$-10 < U < 5$	$0 < I < 1$

Note: U represents surface settlement and I represents conventional degree of influence.

Table 4. Standard of adjacent influence subzone based on the structure strength criterion (MPa)

Affects of partition	Structural additional stress	Classification standard
Strongly affected zone A	$F \geqslant 1.1$ or $F \leqslant -5.5$	$I \geqslant 2$
Weakly affected zone B	$-5.5 < F \leqslant -3$ or $0.6 \leqslant F < 1.1$	$1 \leqslant I < 2$
No affected zone C	$-3 < F < 0.6$	$0 < I < 1$

Note: F represents structural additional stress and I represents conventional degree of influence.

This paper had established a total of 24 models under different pitch conditions. The details of the program were shown in Table 5.

Table 5. The condition of different spacing tunnel

Level spacing	Vertical spacing	Program	Level spacing	Vertical spacing	Program
0.5D	0.2D	0.5D-0.2D	2D	0.2D	2D-0.2D
	0.4D	0.5D-0.4D		0.4D	2D-0.4D
	0.6D	0.5D-0.6D		0.6D	2D-0.6D
	1.2D	0.5D-1.2D		1.2D	2D-1.2D
	2.5D	0.5D-2.5D		2.5D	2D-2.5D
	4D	0.5D-4D		4D	2D-4D
1D	0.2D	1D-0.2D	4D	0.2D	4D-0.2D
	0.4D	1D-0.4D		0.4D	4D-0.4D
	0.6D	1D-0.6D		0.6D	4D-0.6D
	1.2D	1D-1.2D		1.2D	4D-1.2D
	2.5D	1D-2.5D		2.5D	4D-2.5D
	4D	1D-4D		4D	4D-4D

Effects of Partition Determine

Based on the Earth Surface Displacement Principle. After calculating the 24 conditions, this paper counted and analyzed the maximum displacement value of lining of each condition, then acquired two diagrams, fig.1 and fig. 2 The former showed that the additional vertical displacement value of vault of built tunnel was changed by vertical spacing and the latter showed that the additional vertical displacement value of vault of built tunnel was changed by level spacing.

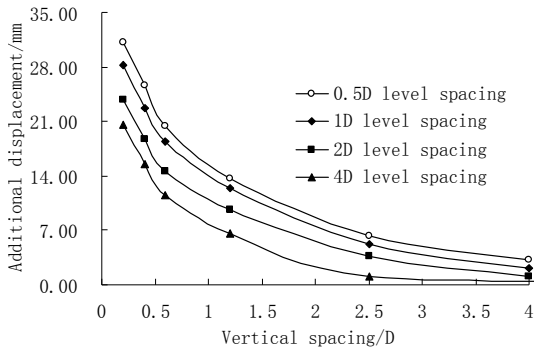

Fig.1 Additional vertical displacement value of vault of built tunnel is changed by vertical spacing

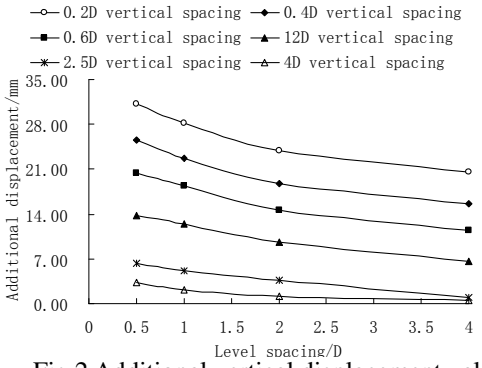

Fig.2 Additional vertical displacement value of vault of built tunnel is changed by level spacing

The fig.2 showed that: When the vertical spacing was greater than 4D，it was small that the construction of the upper tunnel caused the displacement increase of the lower existing tunnel(the value of 1D vertical spacing was 3.24mm, the 2D vertical spacing was 2.12mm, the 3D was 1.12mm, the 4D was 1.00mm, and all were less than the threshold 5mm). Therefore, it can be thought that the construction of the upper tunnel influence on the displacement of the lower existing tunnel can be ignored.

Based on the Structure Stress Principle. After calculating the 24 conditions, this paper counted and analyzed the maximum tensile stress value of lining of each condition, then acquired two diagrams, fig.3 and fig. 4 The former showed that the additional tensile stress value of primary support of built tunnel was changed by vertical spacing and the latter showed that the Additional tensile stress value of primary support of built tunnel was changed by level spacing.

The fig.4 showed that: hen the vertical spacing was greater than 4D，it was small that the construction of the upper tunnel caused the additional tensile stress increase of the lower existing tunnel(the value of 1D vertical spacing was 0.60MPa, the 2D vertical spacing was 0.43MPa, the 3D was 0.28MPa, the 4D was 0.14MPa, and all were less than the threshold 0.6MPa). Therefore, it can be thought that the construction of the upper tunnel influence on the tensile stress of the lining of the lower existing tunnel can be ignored. It was consistent with the displacement criterion.

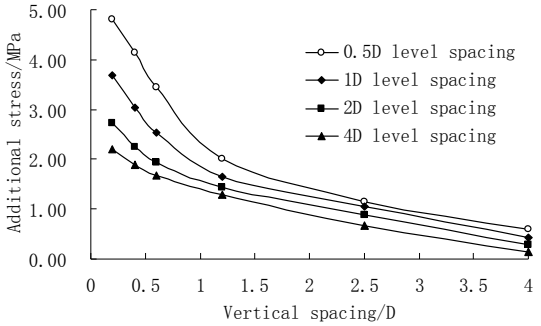

Fig.3 Additional tensile stress value of primary support of built tunnel is changed by vertical spacing

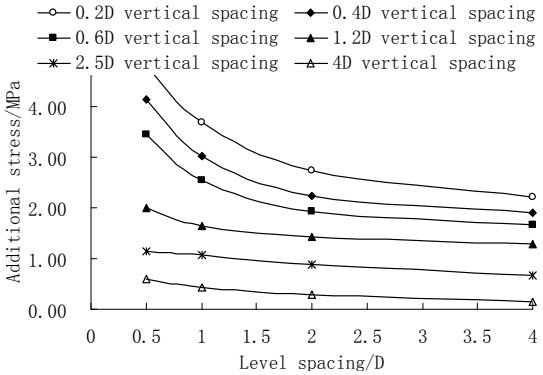

Fig.4 Additional tensile stress value of primary support of built tunnel is changed by level spacing

Conclusions

Based on the earth surface displacement principle and structure stress principle, this paper studied on the affects of partition of tunnel that was located on Yingpan road in Changsha City and crossed Xiangjiang River, and got the following results:

(1) When the vertical spacing between upper and lower tunnel is less than 4D, it must to consider the influence of vertical spacing on parallel interchange tunnel close construction; When the vertical spacing between upper and lower tunnel is larger than 4D, it didn't need to consider the influence of vertical spacing on parallel interchange tunnels close construction, can be considered as two parallel tunnels.

(2) When the level spacing between parallel tunnel is less than 4D, it must to consider the influence of level spacing on parallel interchange tunnel close construction and the influence was less and less obvious with the increase of level spacing; When the vertical spacing between parallel tunnel is larger than 4D, it didn't need to consider the influence of level spacing on parallel interchange tunnels close construction, can be considered as two intersecting tunnels, and the adjacent degree classifications are same to that in table 2.

References

[1] Compiled by Japan Society of Civil Engineers, translation by Zhu Wei. Tunnel standards (Shield articles) and Commentary. Beijing: China architecture & building press，2001.

[2] QIU Wenge. The Study on mechanics principle and countermeasure of approaching excavation in underground works[D]. Chendu：Southwest Jiaotong University，2003.

[3] Takeshi Asano，Mototsugu Ishihara，Yasuaki Kiyota. An observational excavation control method for adjacent mountain tunnels. Tunnelling and Underground SPaee Technology. 2003，18：291-301.

[4] WEN Yumin. The mechanics behavior analysis in approaching construction of two parallel shield tunnels[D]. Chendu：Southwest Jiaotong University，2005.

[5] ZHENG Yuchao. Study on the influence degree of adjacent construction of three parallel shield tunnels[D]. Chendu：Southwest Jiaotong University，2006.

[6] YUAN Zhu. A study on influence zoning of railway settlement durying tunnel construction underpassing by conventional method[D]. Chendu：Southwest Jiaotong University，2010.

Advanced Materials Research Vols. 989-994 (2014) pp 958-960
© (2014) Trans Tech Publications, Switzerland
doi:10.4028/www.scientific.net/AMR.989-994.958

The Application of MASW Method on the Studying of the Vibrations in Civil Engineering

Kun LUO[1, a]

[1] East China Jiaotong University, Nanchang 330013, China

[a]LK360111@163.com,

Keywords: Surface wave; vibration; Shear wave; MASW; Inverse problems;

Abstract. Surface-wave dispersion analysis is widely used in civil engineering to infer a shear wave velocity model of the subsoil for a wide variety of applications. Combining with a example, multi-channel analysis of surface waves method (MASW) was discussed in this paper. The entire MASW's procedure of three steps: acquiring ground roll data in the field, processing the data to determine dispersion curve, and back calculation of the geologic parameters for different depths. Based upon all the research results by far, MASW method is an efficient methods because of its high accuracy that is achieved by both special field technique and data processing technique.

Introduction

Waves that propagate in a medium can be roughly divided into two main categories: body waves(P and S) and surface waves(e.g., Rayleigh, Love, etc.). Body waves propagate through the whole body of the earth, whereas surface waves along (or near) the surface of the earth. Surface waves are generated only at a free boundary and can be essentially of two types: Love waves and Rayleigh waves. Rayleigh waves are always generated when a free surface exists in a continuous body. In a vertically heterogenous medium the phase velocity of the Rayleigh wave is a function of frequency and this dependence is strictly related to the mechanical parameters of the medium. Hence, if we can determine the dispersion curve (Le., phase velocity VS. frequency), it is possible in principle to calculate the mechanical parameters of the medium.

At present, China's railway network topped 100,000 km, and more than 10,463 km high-speed railway line has been placed into commercial, another 12,060 km are currently under construction. While all the people enjoy the advantages of the railway, however, the buildings along the railway line will be influenced by the vibration caused by the railway, and the key point to solve the vibrations in civil engineering is to investigate the geologic parameters of the building foundation along the depth. In this paper, the application of MASW method was used to solve this problem in the studying of the vibrations in civil engineering.

2 The entire procedure of MASW method

The entire procedure of generating V_s profile consists of three steps, shown in

- The first step, acquiring ground roll data in the field. In MASW method, multiple number (usually twelve or more) of receivers with so-many-channel seismograph are used .
- The second step, processing the data to determine dispersion curve (a plot of frequency *VS*. phase velocity). If the dispersion curve is estimated on the basis of experimental data, it is then possible to solve the inverse problem, i.e., the model parameters are identified on the basis of the experimental data collected on the boundary of the medium. This is the essence of surface wave methods
- The third step, inversion. Back calculation of the V_s for different depths.

4 The application of MASW method

The great wall of China, it starts at the Jiayuguan Pass of Gansu Province in the west and ends at the Shanhaiguan Pass of Hebei province in the east. As the one of the Eight Wonders in the world, the Great Wall of China has become the symbol of the Chinese nation and its culture. However, the Great Wall was undercrossed several times by the Beijing-Zhangjiakou High Speed Railway. In order to safeguard the safety of the Great Wall, its dynamic response caused by the High Speed railway need to be simulated by super computer, and the parameters of the soil are one of the key points for the accurately calculation. In this paper, the multi-channel analysis of surface waves method will be used to solve this dynamic problem.

The measurement site is on the top of the junction of the railway line and the Great Wall, and the testing apparatus for the instant surface wave exploration consists of a trigger connector, hammer, seismometers, computer, power and etc.

The raw data collected by surface wave exploration is the waveform data of the surface wave vibration along the surface, and its can be used only after analysis, calculation and interpretation of the raw data. In this project, the surface wave analysis software was used. Firstly, processing the data to determine dispersion curve. Secondly, back calculation of the V_s for different depths, and then the stratigraphic parameters can be got by analysis. The results of inversion calculation on every site are shown in Tab.1, and the detail results shown in Fig.1-2.

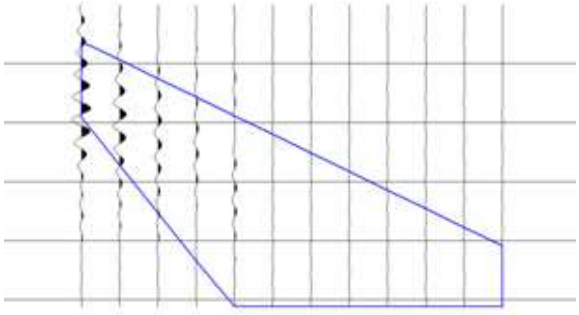

Fig.1. The record of Rayleigh wave signal

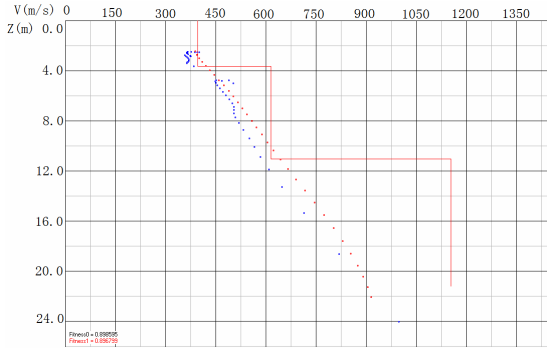

Fig.2. Depth-shear wave velocity inversion curve

Tab.1 The results of inversion calculations

Layer	Depth/m	Vs/m/s	Poisson's ratio	Elastic modulus/GPa
1	0~3.8	392.05	0.25	0.96
2	3.8~7.5	615.3	0.25	2.37
3	>7.5	1154.2	0.25	8.33

5 CONCLUSIONS

Based upon all the research results by far, followings are concluded on MASW method, MASW is an efficient method of investigating elastic property of near-surface materials. It is efficient because of its

high accuracy that is achieved by both special field technique and data processing technique. It is efficient because of its fast speed of accomplishing necessary results. MASW makes it possible to produce not only quantitative display of near-surface elastic property in the form of vs profile but also qualitative display of the image of near-surface heterogeneity. MASW is a method that can be fully automated to investigate elastic property of near-surface materials for the usage in various engineering fields.

ACKNOWLEDGEMENT

The authors wish to acknowledge the support and motivation provided by the National Natural Science Foundation (No.51268015), and Jiangxi natural science foundation (No.2013BAB216006), and Science Foundation of The Education Department of Jiangxi Province (GJJ11445).

REFERENCES

[1] Rix, G. J., and Leipski, E. A., 1991, Accuracy and resolution of surface wave inversion[A], American Society of Civil Engineers: 17-32.
[2] Choon B. Park Richard, D. Miller, 1997 Multi-Channel Analysis of Surface Waves [A], Kansas Geological Survey:1-24
[3] Haskell, N. A., 1953, The dispersion of surface waves on multilayered media[J], SSA Bull., 43: 17-34.
[4] Heisey, J. S., Stokoe II, K. H., and Meyer, A. H., 1982, Moduli of pavement systems from spectral analysis of surface waves[J], Transportation Research Record, 852: 22-31
[5] Park, C. B., Miller, R. D., and Xia, J., 1996a, Multi-channel analysis of surface waves using Vibroseis, Presented at the 66th Ann. Mtg. of SEG, 68-71.

Advanced Materials Research Vols. 989-994 (2014) pp 961-965
© (2014) Trans Tech Publications, Switzerland
doi:10.4028/www.scientific.net/AMR.989-994.961

Experiment Research on Mechanical Properties and Penetration Performance of UHMWPE Fiber Concrete

Yuwu Zhang, Luhui Yan, Lin Zhu, Sheng Zhang, Lingfeng Li

Basic Education School of Commanding Officer, National University of Defence Technology, Changsha 410073, China
zyw_86@126.com

Keyword: UHMWPE fiber, concrete, mechanical properties, penetration performance, experiment

Abstract. The basic mechanical properties and penetration performance of a new type of fiber concrete reinforced by UHMWPE fiber were experimental investigated. The strengths of the cube compression, splitting tensile and beam bending of this FRC with four kinds of fiber volume fraction (FVF) was researched firstly. Then, the penetration tests for the FRC with FVF of 0.8% were then conducted. The results show that the UHMWPE fiber is of excellent effects to improve the tension strength and toughness of concrete. The penetration depth and cratering area of the FRC by bullet penetration are decreased obviously compared with plain concrete which testifies the remarkable effect of this kind of fiber on enhancing penetration resistance of concrete. Last but not least, the application prospect and field of UFRC were discussed.

Introduction

Concrete is extensively used in protection engineering. People have carried on abundance experiments and theoretical researches on penetration and perforation of concrete [1, 2]. Ordinary concrete has low tension strength and bad toughness so that it is easily to be broken up and collapsed under blast and impact which affects its protective capacity. Nowadays, the rapid development of new penetration weapons and applications in wars, it claims a higher requirement to performance of concrete against impact and penetration [3]. A practicably way to enhance the resistant-penetration capacity of concrete is fiber reinforced to concrete (FRC) that can certainly improve the strength, toughness and crack-resistance of concrete [4]. At present, almost all studies on the anti-penetration of FRC are mainly concentrated on the steel fiber concrete (SFRC). The influences of fiber addition, forms at fiber ends, fiber dimensions and other factors on anti-penetration performance and mechanism of the SFRC are investigated [5-7]. And some empirical formulas for penetration depth are suggested [8]. However, some problems of construction work and durability in application which are possibly led by the characteristics of the steel fiber, such as huge density, high stiffness, easily rust and so on, are still needed to be further researched and resolved.

Ultra high molecular weight polyethylene (UHMWPE) is a new kind of ballistic fiber [9] which has excellent properties of impact-resistance. UHMWPE fiber not only has similar strength and modulus as high-stiffness fibers (e.g. steel fiber), but has similar fineness and density as flexible fibers (e.g. polypropylene fiber). When the fiber is applied to cement-base composite, this kind of fiber reinforced cement-base composite (FRCC) represents more outstanding tensile strength and toughness than that of FRCC reinforced by steel fiber [10]. Up to now, the research report about FRC reinforced by UHMWPE fiber (UFRC) which based on concrete with coarse aggregate is not still seen, not to mention the penetration studies of the UFRC.

In the present study, four kinds of UFRC with different fiber volume fraction (FVF) were produced based on C70 high strength concrete, and their basic mechanical behaviors were studied through a detailed experimental program. In addition, the experiments of UFRC targets with 0.8% of FVF against 12.7 mm Armor Piercing ammunition were conducted with different projectile velocities. On the base of the experiment results analyses the application prospect of the UFRC is discussed.

Mechanical Properties

Primary materials and Mix design of concrete. Primary materials：Ordinary P.O42.5 cement is used throughout the program. Coarse aggregate is size of 3~10 mm aggregate. River sand is with 2.8 fineness modulus. FDN-5 water reducer which can reduce water 15% and silica ash were also used. The UHMWPE fiber is the ZTX99-1200D supplied by Hunan ZhongTai Special Equipment Co, Ltd, China. The performance parameters of the UHMWPE fiber are illustrated in Table 1.

Table 1 Mechanical properties of UHMWPE fiber

Diameter /μm	Length /mm	Density /g•m^{-3}	Tensile strength /MPa	Elastic modulus /GPa	Limit elongation /%
20~50	30	0.97	3000	100	2.5~4.0

Plain concrete(PC) and four kinds of UFRC with FVF of 0.1%(U1), 0.3%(U3), 0.5%(U5) and 0.8%(U8) are respectively produced based on C70 high strength concrete. The max design of the concrete is projected with the water-binder ratio of 0.3, the sand rate of 42%, the silica ash content of 10% and the water reducer content of 2.5%.

Strength. The experiments of cubic uniaxial compressive, splitting tension and beam bending at four-point were performed according to the Chinese national standard. The failure patterns and the strength results of plain concrete (PC) and UFRC at compressive, tension and bending were respectively shown in Fig. 1~Fig. 3 and Table 2. In Table 2, f_c, f_t and f_b respectively stands for strength of compressive, tension and bending, ζ_c, ζ_t and ζ_b is the correspondent strength enhancement rate (SER) of UFRC comparative to the PC.

It is concluded from Fig.1~Fig.3 that the UHMWPE fiber possesses very well effects on crack-resistant to concrete. When compressed, the UFRC cube is basically preserved integral only with failure of crack and spalled on the surfaces of the cube compare with collapse failure of the PC cube. Under tension, PC cube rapidly split in half, but splitting failure time of UFRC cube is delayed and the cube may not be separated as the FVF exceed to 0.3%. While bending, the failure of UFRC shows such a process that many small cracks are firstly initiated at the bottom of beam, then the main crack is formed, broadened and extended to the top of beam at limit load, and the craze place of the main crack is moved from center of beam outward to supports with the FVF increase. Relatively, the instantly fracture happened one craze for the PC beam.

We can also find from Table 2 that compare with PC, the compressive strength improvement of UFRC is unobvious, whereas the tensile strength and bending strength have a great enhancement. The SER of tension is more than 25% when FVF of 0.3%~0.5%, and SER of bending can be exceed to 18% if FVF of 0.3%~0.8%.

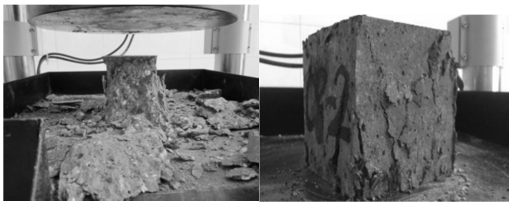

(a) PC (b)U3

Fig. 1 Compressive failure forms

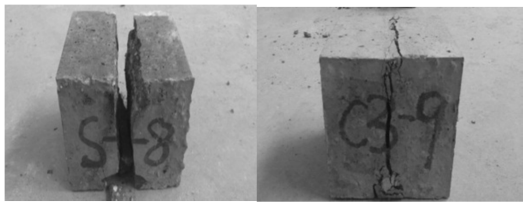

(a)PC (b)U3

Fig. 2 Splitting tensive failure forms

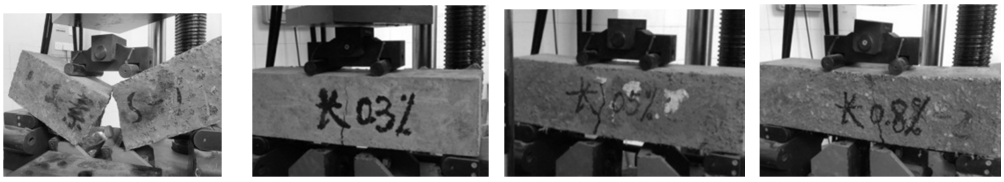

(a)PC (b)U3 (c)U5 (d)U8

Fig.3 Bending failure forms

Table 2 Strengths of compression, tension and bending

Code	f_c/MPa	ζ_c /%	f_t/MPa	ζ_t /%	f_b/MPa	ζ_b /%
PC	72.2	0	5.30	0	6.30	0
U1	78.5	8.73	6.10	15.09	6.71	6.51
U3	74.1	2.63	6.68	26.04	7.46	18.41
U5	71.1	-1.52	6.66	25.09	7.77	23.33
U8	70.1	-2.91	6.21	17.17	7.44	18.10

Bending toughness. Fig. 4 gives the change rules of deflection with loads at test concretes bending. A set of toughness indices can be used to evaluate the bending toughness of FRC. Like shown in Table 3, BT_5, BT_{10} and BT_{20} are the bending toughness indices which are respectively defined as the ratio of area included by deflection curve when deflection equal to 3.0 times, 5.5 times and10.5 times first deflection at craze to area of that at craze, and $RS_{5,10}$ and $RS_{10,20}$ are residual strength indices, where $RS_{5,10}=20(BT_{10}-BT_5)$ and $RS_{10,20}=10(BT_{20}-BT_{10})$. Based on Fig.3, the corresponding toughness indices of UFRC and PC are calculated and given in Table 3.

Table 3 Indices of bending toughness

Code	BT_5	BT_{10}	BT_{20}	$RT_{5,10}$	$RT_{10,20}$
PC	1	1	1	0	0
U1	1	1	1	0	0
U3	3.87	6.40	10.97	50.6	45.7
U5	4.02	6.47	10.62	49.0	41.5
U8	4.15	7.19	11.46	60.8	42.7

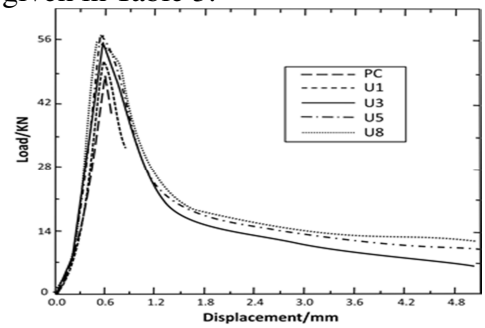

Fig.4 Curves of deflection with load at bending

We can find from Fig.3 and Table 3 that UHMWPE fiber has favorable virtue to increase the concrete toughness. If FVF exceeds to 0.1%, toughening effect of fibers on concrete is especially obvious, and the trend of toughness increase seems increase with the growth of fiber content. However, this trend becomes slow after the FVF is over 0.3%.

Penetration experiment

Introduction. PC targets and UFRC targets with 0.8% of FVF were investigated. The shape of targets is cylinder with diameter 315 mm and thickness of 250 mm. 6 PC targets (PP1~PP6) and 6 UFRC targets (UP1~UP6) were performed under three classes of velocities impacted by projectile which are respectively referred to the low-speed (about 540m/s), medium-speed (about 700m/s) and high-speed (about 840m/s). The projectile applied in the test is diameter of 12.7 mm, length of 63 mm and the weight of 48 g which is shot by the ordinary ballistic gun. The input velocities are measured by two light screen targets (LST) and an electronic instrument (ES).

Results and analysis. The damage forms on the front face of targets are shown in Fig. 5. The results including input velocity (v_0), penetration depth (H) and crater diameter (D) are presented in Table 4.

(a)UP1 (b)UP3 (c)UP5 (d)PP1 (e)PP3 (f)PP5

Fig.5 Damage forms on the front face of targets

As shown in Fig.5 and Table 4, it can be found:

(1)Both the two types of targets generated funnel pits when impacted by projectile, and the dimensions of the funnel pits increase with the increase of input velocity. Compared to PC targets,

UFRC targets had smaller crater dimension, furthermore, average crater diameter and depth decreased 20%~35% and 10%~15% at the same class velocity, respectively.

(2) Both the two types of targets generated radial cracks, the number and width increased with the increase of input velocity. The UFRC targets produced 4~8main cracks which were less and smaller than that of PC targets which had 6~9 main cracks. Furthermore, the front parts of PC targets scattered entirely when the confined steel hoop of target released at high class velocity after penetration. Though the UFRC targets had some cracks at the end of penetration, they were unconnected. Therefore, the UFRC targets can keep good integrity.

(3) The penetration depth of the targets increased with the increase of input velocity. And the penetration depth of projectile to UFRC targets decreased obviously compared with that of PC targets. The reduction rate was 19%~23% that seems the input velocity had no significant effect.

Table 4 Penetration depth, dimensions of funnel crater

Code	v_0/ms^{-1}	H/cm	D/cm	Code	v_0/ms^{-1}	H/cm	D/cm
PP1	540	7.0	14.5	UP1	540	6.5	7.5
PP2	537	9.1	15.0	UP2	543	6.0	11.6
PP3	706	10.9	20.4	UP3	705	9.0	12.2
PP4	697	11.2	16.4	UP4	705	8.9	13.1
PP5	837	13.4	19.9	UP5	844	10.8	15.9
PP6	840	13.4	18.8	UP6	828	9.7	14.9

Combined with the results of mechanical properties experiment, it is can be included that though UHMWPE fiber had no significant effect on the compressive strength of concrete, the great improvement on tension property of the UFRC plays a significant role in resistant -penetration of the material. In addition, the enhancement of anti-penetration capacity of the UFRC also results in the blocking effect of fiber on the generation and development of cracks that can keep targets in good integrity when impacted to some extent.

3. Discussion

According to the experiment results, it certified that the UFRC performed better properties in tensile strength, toughness and anti-penetration than PC. The UFRC as a more excellent material not only enriches the type of construction material, but can be applied in every field of civil engineering. Particularly, as a result of its outstanding performance against blast and impact, UFRC is expected to be a significant approach to resolve the existing problems in protection engineering. In addition, the density of UHMWPE fiber is lower than steel fiber and UFRC has more workable and durability than SFRC. Overall, UFRC has spacious application prospect in civil engineering especially in protection engineering, and it worth to be researched further.

4. Conclusions

The experiments results presented in this paper lead to the following conclusions:

(1) Adding four different UHMWPE fiber contents, obvious improvement on the compressive strength of concrete is not observed, whereas a great boost to tensile strength, bending strength and toughness of concrete is evident.

(2)The crater volumes, damage extents and penetration depths of the UFRC targets with 0.8% of fiber decreased greatly compared with PC targets impacted by projectile. All the observations verified that UFRC had excellent protection capacity.

(3)UFRC has spacious application prospect in protection engineering. This paper provides important reference on further research and actual application.

References

[1]X.J. Li: *Damage Effects of Conventional Weapons and Engineering Protection Techniques* (The Third Military Engineering Research Institute of the Chief Staff Headquarter, China 2001).
[2]M.J. Forrestal, D.Y. Tzou: International Journal of solids and structure, Vol. 34 (1997), p.4127.
[3]F.N. Jin: *Penetration weapon and calculation* (People's Liberation Army Publishing House, China 2006).
[4]Y.N. *Zhang. Study on performance and application of high strength high performance fiber reinforced concrete* (Ph.D., Tongji University, China 2010). p.27.
[5] X.Z. Hu, Y.S. Liu, X.J. Wang and X.G. Gu: Journal of Ballistics, Vol. 20(2008) No.2, p.5.
[6] Z.D. Rong, W. Sun, Y.S. Zhang, W. She, W.H. Zhang: Journal of Ballistics, Vol. 22(2010) No. 3, p.63.
[7] X.N. Zhao, Y. He, X.F. Zhang, N.S. Zhang, Y.X. Wang: Journal of Experimental Mechanics, Vol. 26(2011) No. 2, p.216
[8] B. Wang, F.N. Jin, H.Z. Xu: Explosion and Shock Waves, Vol. 24(2004) No. 4, p.376.
[9] X.Q. Wang, X. Zhu, Z.Y. Mei, X. Chen: Explosion and Shock Waves, Vol. 29(2009) No. 1, p.29.
[10] G. Fisher: *Deformation behavior of reinforced ECC flexural members under reversed cyclic loading conditions* (Ph.D., University of Michigan, America 2001). P.30.

Advanced Materials Research Vols. 989-994 (2014) pp 966-969
© (2014) Trans Tech Publications, Switzerland
doi:10.4028/www.scientific.net/AMR.989-994.966

Treatment of Simulated Acid Mine Drainage by Permeable Reactive Barrier: Column Study

Changfeng Cai[a], Fuzhang Qi[b], Xiaoliang Lin[c] and Lin Jiang[d]

School of Chemical and Biological Engineering, Anhui Polytechnic University, Anhui 241000 CHINA

[a]ccf2005@ahpu.edu.cn, [b]qfzcom@sina.com,[c]princeplace@163.com,[d]linda3227@126.com

Keywords: acid mine drainage, column study, metal ions, sulfate

Abstract. Three polyvinyl chloride (PVC) columns filled with different ratios of reactive media, ceramsite and corncob, were conducted to assess the treatment performance of simulated acid mine drainage (AMD). The results indicated that the columns could effectively remove sulfate and metal ions from AMD with the removal efficiency of 57.7% and 96.5% respectively. The removal efficiency decreased with the increasing inlet velocity and at the same sample ports the sulfate and metal ions concentrations at the velocity of 1 ml/min were lower than that at the velocity of 2ml/min and 3ml/min.

Introduction

Acid mine drainage (AMD) is a serious environmental problem that causes adverse effects on the quality of groundwater and surface water and is generated from the exposure of pyrites and other metal-bearing sulphate minerals to moisture and air, which results in chemical and biological oxidation processes[1,2]. Due to its adverse effects, lots of measures are taken [3,4]. One of the most promising of these innovative solutions is the use of permeable reactive barriers (PRBs) filled with reactive material to intercept and decontaminate plumes in the subsurface [5,6]. PRBs are an in situ passive alternative technique compared to traditional systems such as effluent neutralizing using limestone [7,8].

Adding sulfate reducing bacteria (SRB) to PRB is an alternative technique for the treatment of AMD [9]. With SRB, sulfate and metal ions can easily be removed. However the elements in AMD may not be sufficient for the growth and reproduction of SRB and the elements needed must be added. Considering all, corncob is chosen because it is easy-obtained and inexpensive. Corncob is a by-product during the harvest of corn and it is a good choice that corncob can be used in the treatment of AMD.

Various reactive media were tested for the treatment of AMD and the results were satisfying [10,11,12]. However some reactive media are not easy obtained and it is financially reasonable to use local reactive media [13]. Herein ceramsite is chosen for the reactive medium of the column study.

In this study column experiments are used to assess the effects of ceramsite and corncob on the removal efficiency of AMD and evaluate their application future in wastewater remediation. The other objectives are to select the best ratio of reactive medium for the treatment of AMD by PRB.

Materials and Methods

Experimental setup

Three PVC columns (160 mm in inner diameter and 500mm in length) were packed with ceramsite (2-3mm and 4-6mm in diameter) and corncob (2-4 mess in size). The ratios of ceramsite of 1-3 mm in diameter, ceramsite of 3-5 mm in diameter and corncob of 2-4 mess in the columns, namely column 1#, column 2# and column 3#, were 1:1:1, 2:2:1, and 3:3:1. 300 ml activated sludge and 180 ml SRB were added into the column.

The ceramsite was purchased from Tianjiangshi Wuqing Tongshang Co.,LtD, the activated sludge was collected from Zhu Jiaqiao wastewater treatment plant, Wuhu, Anhui province, China and SRB was collected from Anhui University of Technology, Hefei, Anhui province, China. The columns were allowed to activate for 6 d, which was favorable to the formation of SRB biofilms. AMD used in the experiment was synthesized with the initial pH of 5 and the components of simulated AMD were as follows (units are in mg/L of water): NH_4Cl, 191, K_2HPO_4, 75, Na_2SO_4,

2215, $MgSO_4 \cdot 7H_20$, 3844, $CuCl_2 \cdot 2H_2O$, 79.7, $FeSO_4 \cdot 7H_2O$, 149, $Pb(NO_3)_2$, 47.9, $ZnCl_2$, 62.8, $Cd(NO_3)_2 \cdot 4H_20$, 82.5. The HCl solution was used to adjust the pH.

AMD was pumped in at the bottom of the column by a peristaltic pump in order to better simulate lower flowrates. Four sampling ports were installed on each column at distances of 10, 20, 30 and 40 cm above the inlet and sealed to the column wall and the sampling ports were numbered 1~4 from the bottom to top of this column; a glass syringe was inserted to each port to allow sampling.

Analytical methods

All reagents were of analytical grade and were purchased from Shanghai Chemical Reagent Factory (Shanghai, China). Sulfate measurements were carried out using the standard analysis methods. The pH value was measured with a model of PHB-5, purchased from Shanghai Leici Analysis Equipment Plant (China). Metal ions were measured using TASS 990 atomic absorption spectrophotometer, purchased from Beijing Purkinje General Instrument Co., Ltd.

Results and Discussions

Effects of the ratios of reactive medium on the column performance

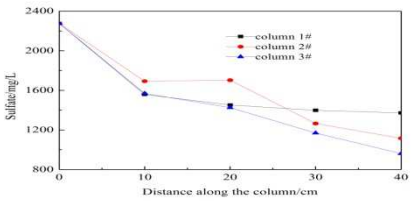

Fig.1 Change in sulfate values at four sample ports of columns

Fig.1 presents the variation of sulfate values at four sample ports. The sulfate values decreased with the increasing distance, varying from 2200 mg/L to 960 mg/L with the maximum removal efficiency of some 57.7%. It can be seen that the removal efficiency of column 3# was better than column 1# and column 2# because the porosity of column 3# was smaller that the other two and the feeding water passed slower in the column. With more contact time with SRB and activated sludge the sulfate was removed faster. The removal efficiency will be higher with the increasing residence time. The results indicated that the columns could effectively removal sulfate and with the increasing sample ports the removal efficiency will be higher and reached the goal needed.

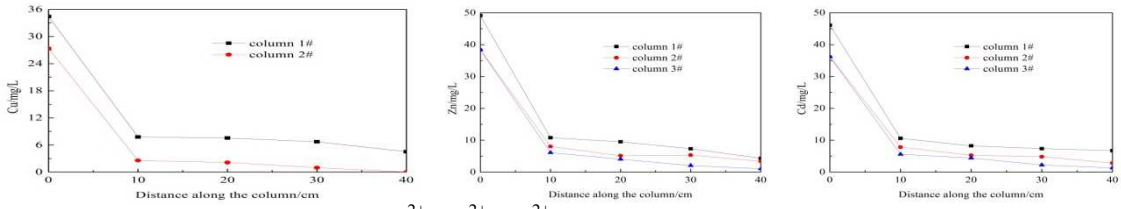

Fig.2 Variation of Cu^{2+}, Zn^{2+}, Cd^{2+} at four sample ports of columns

The variation of Cu^{2+}, Zn^{2+}, Cd^{2+} at four sample ports of columns are shown in Fig.2. Due to some mistakes the data of column 3# lacked. The data obtained showed that the metal ions decreased with the increasing distance and the removal efficiency of column 3# was higher than column 2# and 3#. The results revealed that the ratio of reactive medium in the column was an important factor in treating AMD.

Effects of inlet velocity on the column performance

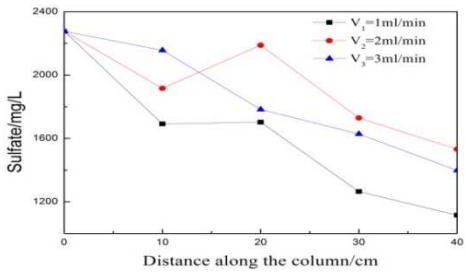

Fig.3 Variation of sulfate at four sample ports at different inlet velocity in column 2#

The variations of sulfate concentration in the column at four sample ports and inlet were presented in Fig. 3. At the same sample ports the sulfate concentrations at the velocity of 1 ml/min were lower than that at the velocity of 2ml/min and 3ml/min. The results suggested that the sulfate concentrations decreased from the inlet to the NO.4 sample ports. Apparently the sulfate was degraded by the column and the removal efficiency decreased with the increasing inlet velocity because with the increasing inlet velocity the residence time of feeding water in the column decreased and the contact time between the feeding water and SRB became shorter.

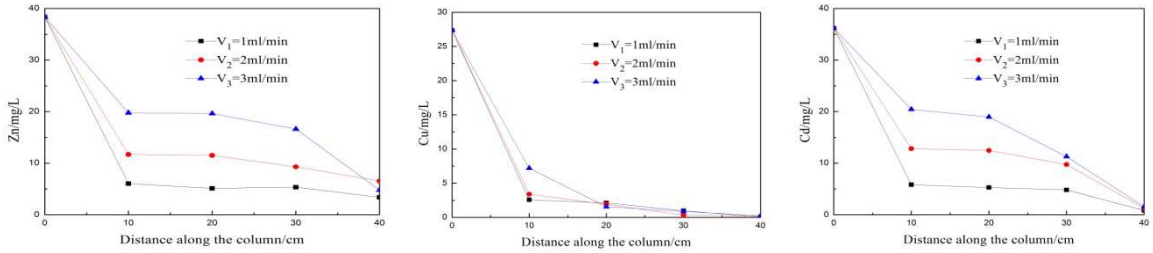

Fig.4 Variation of Zn^{2+}, Cu^{2+} and Cd^{2+} at four sample ports in column 2#

The changes in Zn^{2+}, Cu^{2+} and Cd^{2+} concentration in column 2# at four sample ports and inlet were presented in Fig. 4. The results demonstrated that with the increasing inlet velocity the removal efficiency decreased and at the velocity of 1 ml/min, the removal efficiency reached the maximum, above 99%. The metal ions concentrations at the velocity of 1ml/min at the sample ports were lower than that at the velocity of 2ml/min and 3ml/min. Removing the metal ions by SRB needed time and the lower inlet velocity means the longer residence time in the column.

Summary

Columns experiments were used to assess the effects of ceramsite and corncob on the performance of PRB and the results indicated that the columns filled with ceramsite and corncob can effectively remove sulfate and metal ions. The sulfate concentrations decreased from the inlet to the NO.4 sample ports with the removal efficiency of 57.7% and the removal efficiency of the metal ions reached over 96.5%. The sulfate concentrations and metal ions at the velocity of 1ml/min at the sample ports were lower than that at the velocity of 2ml/min and 3ml/min. Above all the best ratio of ceramsite of 1-3 mm in diameter, ceramsite of 3-5 mm in diameter and corncob of 2-4 mess in this study was 3:3:1.

Acknowledgements

This work was financially supported by the National Natural Science Foundation of China (51274001) and the Opening Project of State Key Laboratory of Coal Recourses and Safe Mining (SKLCRSM10KFA05).

References

[1] C.M. Neculita, G.J. Zagury, B. Bussière, Passive treatment of acid mine drainage in bioreactors using sulphate-reducing bacteria: critical review and research needs, J. Environ. Qual. 36 (2007) 1–16.

[2] I.S. Chang, P.K. Shin, and B.H. Kim, Biological treatment of acid mine drainage under sulphate-reducing conditions with solid waste materials as substrate, Water Res. 34 (2000), pp. 1269–1277.

[3] Sheoran, A. S, Sheoran, V, Choudhary, R. P, Bioremediation of acid-rock drainage by sulphate-reducing prokaryotes: A review, Miner. Eng. 2010, 23 (14), 1073-1100.

[4] Lefebvre, O, Neculita, C. M, Yue, X, Ng, H. Y, Bioelectrochemical treatment of acid mine drainage dominated with iron, J. Hazard. Mater. 2012, 241–242 (0), 411-417.

[5] Jarvis, A. P, Moustafa, M, Orme, P. H. A, Younger, P. L, Effective remediation of grossly polluted acidic, and metal-rich, spoil heap drainage using a novel, low-cost, permeable reactive barrier in Northumberland, UK, Environmental Pollution 2006, 143 (2), 261-268.
[6] Gibert, O, Rötting, T, Cortina, J. L, de Pablo, J, Ayora, C, Carrera, J, Bolzicco, J, In-situ remediation of acid mine drainage using a permeable reactive barrier in Aznalcóllar (Sw Spain), J. Hazard. Mater. 2011, 191 (1–3), 287-295.
[7] Liendo, M. A, Navarro Hidalgo, G. E, Sampaio, C. H, Heck, N. C, Synthesis of ZVI Particles for Acid Mine Drainage Reactive Barriers: Experimental and Theoretical Evaluation, Journal of Materials Research and Technology 2012, 1 (2), 75-79.
[8] Pruden, A, Messner, N, Pereyra, L, Hanson, R. E, Hiibel, S. R, Reardon, K. F, The effect of inoculum on the performance of sulfate-reducing columns treating heavy metal contaminated water, Water Research 2007, 41 (4), 904-914.
[9] Yi, Z.-J, Tan, K.-X, Tan, A.-L, Yu, Z.-X, Wang, S.-Q, Influence of environmental factors on reductive bioprecipitation of uranium by sulfate reducing bacteria, International Biodeterioration & Biodegradation 2007, 60 (4), 258-266.
[10] Miller, M. L, Bhadha, J. H, O Connor G. A, Jawitz, J. W, Mitchell, J, Aluminum water treatment residuals as permeable reactive barrier sorbents to reduce phosphorus losses, Chemosphere 2011, 83 (7), 978-983.
[11] Öztürk, Z, Tansel, B, Katsenovich, Y, Sukop, M, Laha, S, Highly organic natural media as permeable reactive barriers: TCE partitioning and anaerobic degradation profile in eucalyptus mulch and compost, Chemosphere 2012, 89 (6), 665-671.
[12] Zhang, J, Xu, Y, Li, W, Zhou, J, Zhao, J, Qian, G, Xu, Z. P, Enhanced remediation of Cr(VI)-contaminated soil by incorporating a calcined-hydrotalcite-based permeable reactive barrier with electrokinetics, J. Hazard. Mater. 2012, 239–240 (0), 128-134.
[13] Lapointe, F, Fytas, K, McConchie, D, Efficiency of Bauxsol™ in Permeable Reactive Barriers to Treat Acid Rock Drainage, Mine Water and the Environment 2006, 25 (1), 37-44.

Advanced Materials Research Vols. 989-994 (2014) pp 970-974
© (2014) Trans Tech Publications, Switzerland
doi:10.4028/www.scientific.net/AMR.989-994.970

New Method to Predict the Bearing Capacity and End-Bearing Ratio of Friction-type Long Pile

Zheng QIAN[1, a] and Kui-Hua WANG[1]

[1] Research Center of Coastal and Urban Geotechnical Engineering, Zhejiang University, Hangzhou 310012, China;

[a]johnchain@126.com

Keywords: Finite-Element-Method; Friction-type long pile; Bearing capacity; End-bearing ratio.

Abstract. The purpose of this paper was to predict piles' bearing capacities and end-bearing ratios. Finite-Element-Method was derived to establish the simulation models. The studying processes were firstly to set some unified pile top settlements and then to vary pile diameters to obtain the results, thus the performance of pile could be observed. It was found that closing to ultimate state, loads under the unified settlements were approximately linear to pile diameters, and equivalent unit side-friction forces were nearly constant, and the end-bearing ratios were piecewise linear to pile diameters. Based on these findings, predictive formulas were established. Following the formulas, while piles' bearing capacities of two certain diameters and one end-bearing ratio of them were known, the bearing capacities, side-friction forces and end resistances of other concerned diameters could be predicted.

Introduction

To predict pile's bearing capacities is always a challenge because of the complexities of soil. But there are still many researchers making unremitted efforts and thus various predictive methods have been created, such as Hyperbola Method [1,2], Grey Theory[3,4], Least Squares[5,6], etc. But these methods were generally used to predict the ultimate bearing capacities of which piles were non-destructive by static load tests, and they could not distinguish the side-friction forces and end resistances. Furthermore, these methods were only suitable for one certain section and were useless while pile's section size was changed. This paper found some regularity phenomena while studying measured piles with the help of Finite-Element-Method. These findings could help to predict piles' bearing capacities, side-friction forces and end resistances of different diameters under the unified settlement conditions. Based on the findings, a new predictive method was put forward.

In this method, two conditions must be known at the beginning. The first was piles' bearing capacities of two diameters under a unified settlement, and the second was any one end-bearing ratio of them. Based on the known conditions, piles' bearing capacities of other concerned diameters could be calculated directly, and then end resistances could be obtained through the end-bearing ratios, and side-friction forces could be obtained finally.

Method of Prediction

Pre-studies

Finite-Element-Method is a good tool for studying because of the lower cost, flexible parameters changing and various operating modes. The study, of which the most concerned objects were the relations between pile diameter and forces, was based on FEM simulation. Thus the pile diameter was varied with values of 0.5m, 0.6m, 0.75m, 0.8m, 1.2m, 1.4m, and 1.5m, and then each calculated result of them was recorded. (Note: Pile diameters did not fully meet the conventional values in the study.) Pile top settlements were set as 26mm, 30mm, 36mm, and 40mm. The achieved pile's bearing capacities were shown in Fig 1.

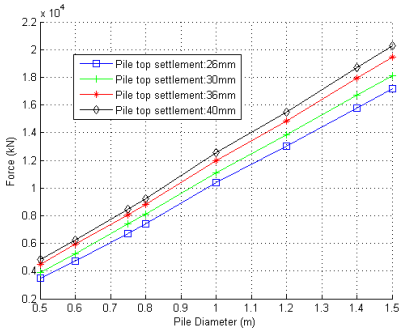

Fig 1. Pile's Bearing Capacities in Different Diameters

Fig 1 illustrated that pile's bearing capacities were linear to the diameters under each unified settlement. After that, other parameters in simulation, such as pile's elastic modulus, friction coefficients between pile and soil, soil's effective unit weights, were varied in the latter analyses. The regularity was unchanged. Namely the phenomenon of that pile's bearing capacities were linear to the diameters under the unified settlement could be seen in each single calculation. Lack of space forbids, these diagrams were no longer listed in the article.

According to the usual expression, pile's bearing capacity could be written as

$$Q = Q_s + Q_p = \pi D \cdot \Sigma q_{si} \cdot l_i + \frac{\pi}{4} D^2 \cdot q_p \tag{1}$$

Assumed that pile diameter D was the only variable in Equation (1), the Q was a quadratic parabola. But Fig 1 showed that Q was a diagonal line, so it could be determined that D was not the only variable in Equation (1), and the unit side-friction force q_{si} and unit end resistance q_p were all probable variables. For convenience sake, the unit side-friction force was substituted by equivalent unit side-friction force $q_{seq} = \frac{\Sigma q_{si} \cdot l_i}{\Sigma l_i} = \frac{\Sigma q_{si} \cdot l_i}{L}$, ($L$ was pile length). The q_{seq} and the q_p of each pile diameter under each unified settlement were shown in Fig 2 and Fig 3.

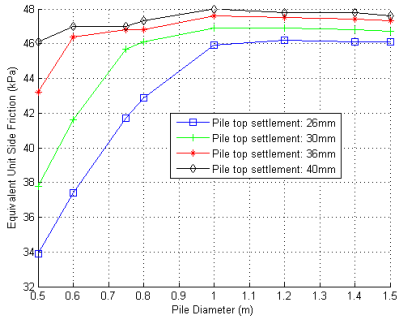

Fig 2. q_{seq} of Different Pile Diameters

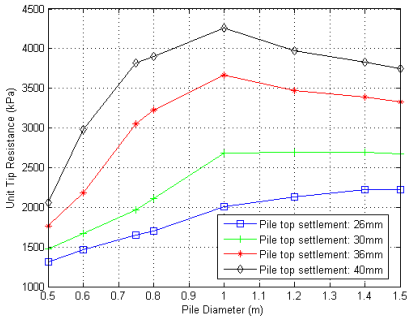

Fig 3. q_p of Different Pile Diameters

Fig 2 illustrated that under each unified settlement, q_{seq} of $D \geqslant 1$m kept nearly unchanged and could be regarded as constant. Under the settlements of 36mm and 40mm, q_{seq} of D between 0.6m and 1m had the similar regularity with $D \geqslant 1$m. Under the settlements of less than 36mm, q_{seq} slipped mightily. Considering that pile's bearing capacity was closer to ultimate when the settlement was greater, meanwhile the conventional bored pile's diameters were larger than 0.6m, the q_{seq} of different diameters could be simplified as constant at the state of ultimate.

Fig 3 showed q_p had no clear regularities. It was understandable. The progresses of pile capacity's development were firstly side-friction forces and secondly end resistance, so diversely, while under a unified pile top settlement the side-friction forces of different diameters reached ultimate, the end resistances were in distinct situations, some might had been far from ultimate, some might had closed to, and some might had reached. Interestingly, the end-bearing ratio, another evaluation criterion of end resistance, showed different features. Fig 4 recorded the calculated results of the end-bearing ratios of each diameter under each unified settlement. From the diagram, it could be seen that end-bearing ratios presented piecewise linear characteristics and the piecewise point was at D=1m.

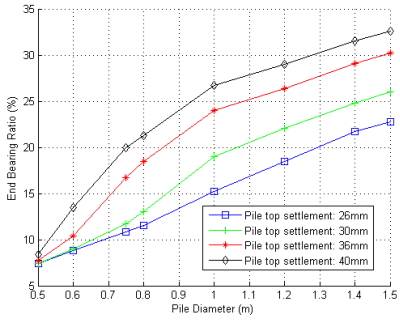

Fig 4. End-Bearing Ratios of Different Pile Diameters

Assumed conditions and Formulas Derivations

Three assumed conditions were set up based on the understanding of Fig 1, 2, and 4:

1. Closing to the ultimate state, pile's bearing capacities under unified settlements were linear to diameters.
2. Were pile's bearing capacities closing to the ultimate state, the equivalent unit side-friction force was constant.
3. Closing to the ultimate state, pile's end-bearing ratios under unified settlements were piecewise linear to diameters.

With the three assumptions, if pile's bearing capacities of any two certain diameters under certain unified settlements and one end-bearing ratio of them were known, then pile's bearing capacities and end-bearing ratios of other concerned diameters could be inferred, also the side-friction forces and end resistances could be obtained consequently.

Changing Equation (1) into the functions of pile diameter D:

$$Q(D)=\pi D\cdot q_{seq}\cdot L+\gamma(D)\cdot Q(D)=a\cdot D+b \tag{2}$$

$$\gamma(D)=c\cdot D+e \tag{3}$$

$\gamma(D)$ was end-bearing ratio; a, b, c, e were factors, a and b were determined by pile's bearing capacities of two diameters, c and e were determined by subsequent calculations. Changing Equation (2) into:

$$\pi D\cdot q_{seq}\cdot L+(c\cdot D+e)\cdot(a\cdot D+b)=a\cdot D+b \tag{4}$$

Expanding and transposing Equation (4) to:

$$a\cdot c\cdot D^2+(\pi\cdot q_{seq}\cdot L+a\cdot e+b\cdot c-a)\cdot D=b\cdot(1-e) \tag{5}$$

Substituting $n\cdot D$ to D in Equation (5):

$$a\cdot c\cdot n^2\cdot D^2+(\pi\cdot q_{seq}\cdot L+a\cdot e+b\cdot c-a)\cdot n\cdot D=b\cdot(1-e) \tag{6}$$

Then (5)×n−(6):

$$a\cdot c\cdot n\cdot(1-n)\cdot D^2=b\cdot(1-e)\cdot(n-1) \tag{7}$$

Rearranging Equation (7) into

$$\frac{c}{e-1}=\frac{b}{a\cdot n\cdot D^2} \tag{8}$$

The factors of c and e could be determined by solving Equations (3) and (8), so the end-bearing ratio of another pile diameter could be determined as well. Putting the values of a, b, c and e into Equation (3) and (2), end resistances and side-friction forces could be obtained subsequently.

Calculations and Verifications

Example 1: There were two pile diameters, the one 1m and the other 1.5m. The known conditions were under the pile top settlement 30mm, $Q(1.0)$=11097kN , $Q(1.5)$=18139kN, and $\gamma(1.0)$=19%. Because two values of Q could determine one straight line, so the factors of a and b were: a=14084,b=-2987, and the Q was expressed as $Q(D)$=14084D-2987. Putting the above conditions into Equations (3) and (8), the factors of c and d could be obtained, which were c=0.1334 and e=0.0566. Then the end-bearing ratio of D=1.5m could be obtained according to Equation (3), which was $\gamma(1.5)$=0.1334×1.5+0.0566=25.7%. The $\gamma(1.5)$ obtained by ABAQUS was 26%. The

two results showed they were fit well. The followed-up processes of solving end resistance and side-friction force were omitted.

Example 2: Were the known conditions of Example 1 unchanged, how to predict pile's bearing capacity and end-bearing ratio of diameter D=1.2m under the pile top settlement 30mm? Since the factors of a, b, c and d were calculated, pile's bearing capacity Q and end-bearing ratio γ could be calculated directly, which were $Q(1.2)=14084\times 1.2-2987=13914kN$, and $\gamma(1.2)=0.1334\times 1.2+0.0566=21.7\%$. The $Q(1.2)$ obtained by ABAQUS was 13823kN, and the $\gamma(1.2)$ was 22.1%. The results showed they were fit well, so the prediction was correct.

Example 3: Were the known conditions of Example 1 unchanged, how to predict pile's bearing capacity and end-bearing ratio of diameter D=0.8m under the pile top settlement 30mm? Similarly with what Example 2 had done, $Q(0.8)=14084\times 0.8-2987=8280kN$, and $\gamma(0.8)=0.1334\times 0.8+0.0566=16.3\%$. The $Q(0.8)$ obtained by ABAQUS was 8123kN, and the $\gamma(0.8)$ was 13%. The two bearing capacities were fit, but the end-bearing ratios were not. The results illustrated that the linear characteristics of bearing capacities were stable and end-bearing ratios were not. The characteristics of end-bearing ratios were piecewise linear. So while calculating end-bearing ratios, always following one formula was a bad way. The recommended way was to calculate the ratio of adjacent diameter of target one at first, and then to calculate the target one. Now did Example 3 again. The adjacent diameter of 0.8m was 1.0m, so recalculating end-bearing ratio of D=0.8m based on the ratio of D=1.0m,

$$c+e=0.19$$

$$\frac{c}{e-1}=\frac{-2987}{14084\times 0.8\times 1^2}$$

Obtained c=0.2922, e=-0.1022, and $\gamma(0.8)=0.2922\times 0.8-0.1022=13.2\%$. Now the γ was fit well with the result of ABAQUS.

The processes of calculating the results under the settlements of 36mm and 40mm were similar with above examples, so in this article they were not repeated. Under the settlement of 26mm, the gaps between predictions and ABAQUS results became greater. The reason was that under the situation of settlement 26mm, piles with different diameters were in different working stages, some had been ultimate and some had been not, even some had been far from ultimate, so the assumption of q_{seq}=constant was no longer stood.

Summary

Based on the Finite-Element-Method simulations and analyses of friction-type long piles, some conclusions were put forward: If working conditions (such as soil layers, pile length, concrete's elastic modulus, etc.) were unified, then

1. Closing to the ultimate state, pile's bearing capacities under unified settlements were linear to diameters.
2. Closing to the ultimate state, the equivalent unit side-friction forces under unified settlements were nearly constant.
3. Closing to the ultimate state, the unit end resistances of different diameters under unified settlements changed irregularly, but the end-bearing ratios kept piecewise linear to diameters and could be regarded as linear especially while the intervals between pile diameters were small.
4. Known Q-S curves of two pile diameters and any one end-bearing ratio of them, the predictions for concerned diameters could be made, which included bearing capacities and end-bearing ratios. Subsequently, the end resistances and side-friction forces could be obtained.

References

[1] GAO Xiao-Juan, ZHU Xiang-Rong. Forecasting Ultimate Bearing Capacity of Single Squeezed Branch Pile by Hyperbola Method. Rock and Soil Mechanics, Vol.27(2006), No.9, 1596-1600.

[2] HU Huan-Xiao, LIU Jing, ZHU Shi-Ping. Prediction of Single Ultimate Bearing Capacity of Screwed Casting Pile. J. Cent. South Univ. (Science and Technology), Vol.38(2007), No.6, 1239-1245.

[3] REN Lian-Wei, LIU Han-Long, ZHANG Hua-Dong, ZHENG Hao. Application of Gray System Theory on Prediction of Ultimate Bearing Capacity of Jet Grouting Soil-Cement-Pile Strengthened Pile. Journal of Disaster Prevention and Mitigation Engineering. Vol.29(2009), No.2,193-200.

[4] WANG Cheng-Hua，ZHANG Mei-Na. The Improved Prediction Method of Load-Settlement Curves of Bored Piles by Grey Theory. Journal of Shenyang Jianzhu University (Natural Science), Vol.29(2013), No.2, 270-276.

[5] DONG Qing-Hua. Calculation and Prediction of Ultimate Pile Load. Rock and Soil Mechanics, Vol.22(2001), No.4, 463-466.

[6] ZHENG Da-Ye, QIAN De-Ling. Prediction of The Ultimate Bearing Capacity of The Integrate Pile by Using The Partial Least-Squares Regression Method. Journal of Hefei University of Technology, Vol.26(2003), No.6, 1248-1252.

Advanced Materials Research Vols. 989-994 (2014) pp 975-977
© (2014) Trans Tech Publications, Switzerland
doi:10.4028/www.scientific.net/AMR.989-994.975

Research on the succession of *Artemisia ordosica* community in Mu Us sandy land

Junhong Zhang[1, a]

[1]Chongqing Water Resources and Electric Engineering College（Chongqing Institute of Water Resources and Science）Chongqing, China 402160
[a]zhangjunhong2001@163.com

Keywords: *Artemisia ordosica* community; biological soil crust; Mu Us sandy land

Abstract. Mu Us sandy land is an important ecological barrier in Northern China. *Artemisia ordosica* is the dominant species in Mu Us sandy land, the development of biological soil crust in *Artemisia ordosica* community seriously impediment precipitations, which result in the deterioration of soil water within 40cm, where most of *Artemisia ordosica* roots distribution. That led to the recession of *Artemisia ordosica* in the fixed sand dunes in a long time.

Introduction

Mu Us sandy land is an important ecological barrier in Northern China. *Artemisia ordosica* is the dominant species in Mu Us sandy land, which covers about 32% of the total area[1]. With tolerance to drought, sand buried, resistance to barren and wind erosion, and easy breeding, *A. ordosica* plays an important role in maintaining the local ecosystem stability. The succession of *A. ordosica* community in Mu Us sandy land experiences the following stages: pioneer stage in shifting sand dunes -- sparse stage in semi-fixed sand dunes -- build phase in fixed sand dunes -- degradation stage in old fixed sand dunes -- shifting sand dunes[2]. Previous studies considered that soil moisture was an important factor which driving the cycle succession of *A. ordosica* community. However, at present, most of the researches on soil moisture in Mu Us sandy land were timing, fixed-point sampling, the dates were little and lack of continuity, which couldn't reflect the dynamic of soil moisture. In this paper we analyzed the soil moisture of *A. ordosica* community of pioneer stage in shifting sand dunes, sparse stage in semi-fixed sand dunes and build stage in fixed sand dunes with a long-term continuous monitoring, analyzed the characteristics of soil moisture of different succession stages of *A.ordosica* community, supplied conditions of precipitation to soil moisture and the redistribution of biological soil crust (BSC) to precipitation; in order to better understand the role of soil moisture in the succession process of *A. ordosica* community in Mu Us sandy land, which could provide a scientific and reasonable way for local government to rebuild vegetation in Mu Us sandy land.

1. Soil water characteristic of *Artemisia ordosica* community

There were horizontal and vertical difference of soil moisture with all of the three kinds of samples(Fig. 1). Soil moisture at 10 cm deep is affected by precipitation most obvious, soil moisture content can reach 15% quickly after large precipitation enents (> 10 mm rainfall), and then gradually decline to 5%. During growth period, mean soil moisture content at 10 cm deep of fixed, semi-fixed and flow sand were 6.98±0.22%, 6.63±0.31%, and 11.16±0.11%. Soil moisture content of flow sand is significantly greater than the fixed and semi-fixed sand, while there were no significant difference betweent fixed and semi-fixed sand.

During growth period, mean soil moisture content at 20 cm deep of fixed, semi-fixed and flow sand were 3.58±0.17%, 7.71±0.23%, and 8.35±0.17%. Soil moisture content of flow sand is significantly greater than the fixed and semi-fixed sand, while soil moisture content of fixed sand is significantly lower than semi-fixed and flow sand.

There were large fluctuations of soil moisture at 30 cm. The mean soil moisture content at 30 cm deep of fixed, semi-fixed and flow sand were 7.14±0.17%, 7.80±0.16%, and 12.44±0.11%. Soil moisture content of flow sand is significantly greater than the fixed and semi-fixed sand, while soil moisture content of fixed sand is significantly lower than semi-fixed and flow sand.

During growth period, mean soil moisture content at 40 cm deep of fixed, semi-fixed and flow sand were7.86±0.13%, 7.31±0.23%, and 8.82±0.27%. Soil moisture content of flow sand is significantly greater than the fixed and semi-fixed sand, while soil moisture content of fixed sand is significantly lower than semi-fixed and flow sand.

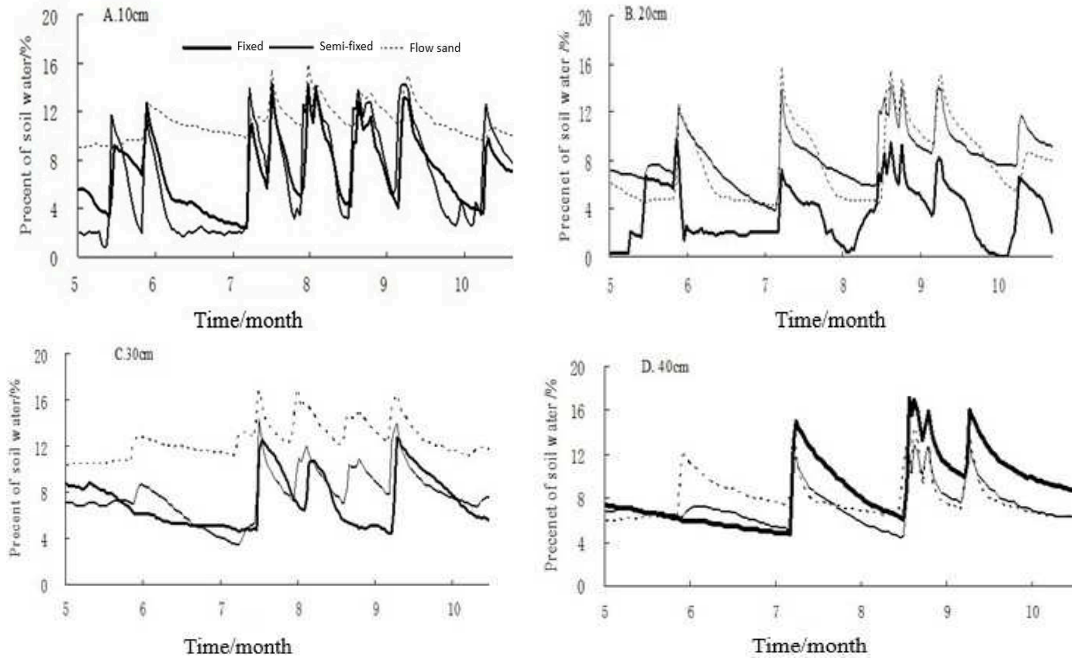

Fig. 1 Soil moisture dynamic of the three kinds of samples in different depth

2. Roots distribuction characteristic of *Artemisia ordosica*

Roots are the important organs for plant to uptake soil moisture. In the three kinds of sand-dunes, the most *A. ordosica* roots were all coarse roots, followed by medium-coarse roots and fine roots, and the three kinds of roots biomass were all exponential-like decreased with the increase of soil depth. The proportion of fine roots range of 0~40 cm in the fixed, semi-fixed and drifting sand-dunes were 79.11%, 74.71% and 53.23%, respectively[3]. *A.ordosica* in the fixed, semi-fixed sand-dunes mainly uses the 0~40 cm soil moisture while *A. ordosica* in the drifting sand-dunes could use more soil moisture below 40cm.

3. Biological soil crusts characteristic in *Artemisia ordosica* community

Biological soil crusts are assemblages of bryophytes, lichens, algae, cyanobacteria and fungi that exist at thesoil surface and are a prominent feature of arid and semi-arid ecosystems worldwide[4]. Research has demonstrated that conservation of soil crusts is fundamental to maintaining core ecosystem processes. Soil crusts are known to stabilise soils, regulate the balance between water infiltration and run-off, fix nitrogen and carbon, and influence the germination, survival, and nutritional status of vascular plants. Mechanical disturbances such as stock trampling and vehicle traffic cause changes in crust cover and composition, with severe or repeated disturbance resulting in complete crust removal. Knowledge of where crusts occur in the landscape and where they are most susceptible to disturbance would enhance prioritisation of conservation and restoration activities, particularly in landscapes where degrading processes are unevenly distributed within and among patches of remnant vegetation[5,6].

The BSC coverage was 83.74% on average in fixed sand dunes, and in semi-fixed sand dunes the BSC cover was 23.54% on average. The distribution proportion of mosses, lichens and alga dominated BSC were 28%, 21% and 51% in fixed sand dunes, and 6.3%, 2.5% and 91.2% in semi-fixed sand dunes, respectively[2]. Most of the BSC in semi-fixed sand dunes was alga crust which belongs to the initial developmental stage. The development of BSC in *A.ordosica* communities could significantly improve the soil physicochemical properties and affect the

redistribution process of precipitation. Regardless of precipitation size, the response times of BSC were significantly greater than NBSC at the same depth, the initial infiltration coefficient and the mean infiltration coefficient of BSC were all significantly lower than NBSC at the same precipitation, which means the presence of BSC hindered the infiltration of precipitation, this situation was more obviously in small precipitations; most of the absorbing roots of *A. ordosica* were within the 40cm soil, primarily take advantage of soil water in this level, but the development of biological soil crust seriously impediment the less than 20mm precipitations, which is the most common precipitation events, that would resulting in the deterioration of soil moisture within 40cm, and led to the recession of *A.ordosica* in the fixed sand dunes in a long time; at the same time, the change of precipitation pattern could have an important impact on soil moisture and vegetation succession.

Summary

Regardless of precipitation size, the response times of BSC were significantly greater than NBSC at the same depth, the initial infiltration coefficient and the mean infiltration coefficient of BSC were all significantly lower than NBSC at the same precipitation, which means the presence of biological soil crust hindered the infiltration of precipitation, this situation was more obviously in small precipitations; most of the absorbing roots of *Artemisia ordosica* were within the 40cm soil, primarily to take advantage of soil water in this level, but the development of biological soil crust seriously impediment the less than 20mm precipitations, which is the most common precipitation events, that would resulting in the deterioration of soil water within 40cm, and led to the recession of *Artemisia ordosica* in the fixed sand dunes in a long time; at the same time, the change of precipitation patterns would have an important impact on soil water and vegetation succession.

Acknowledgements

Funding was provided by talent introduction of scientific research project of Chongqing Water Resources and Electric Engineering College < Vegetation pattern of and their ecological effects on soil and water conservation > (KRC201305); The Major projects of Chongqing Water Bureau< Research and extension conservancy of water resources and water ecological restoration plants applied in water conservancy projects > (Yu Shui Ke 201306).

References

[1] S.L. Li, M.J.A. Werger, P.A. Zuidema, F.H. Yu, M. Dong: Seedlings of the semi-shrub *Artemisia ordosica* are resistant to moderate wind denudation and sand burial in Mu Us sandland, China. Trees, Vol. 24 (2012), p. 515-521.

[2] J.H. Zhang, B. Wu, Y.H. Li, W.B. Yang, Y.K. Lei, H.Y. Han, J. He: Biological soil crust distribution in *Artemisia ordosica* communities along a grazing pressure gradient in Mu Us sandy land, northern China. Journal of Arid Land, Vol. 5 (2013) No.2, p. 172-179.

[3] J.H. Zhang, H.Y. Han, Y.K. Lei, Y.H. Li, W.B. Yang, D.F. Yang, X.B. Zhao: Correlations between distribution characteristics of *Artemisia ordosica* root system and soil moisture under different fixation stage of sand dunes. Journal of southeast forestry university, Vol. 32 (2012) No.6, p.1-5.

[4] D.J. Eldridge, R.S.B. Greene: Microbiotic soil crusts: A view of their rolesin soil and ecological processes in the rangelands of Australia. Australian Journal of Soil Research, Vol. 32(1994), p.389-415.

[5] Y.G. Su, X.R. Li, Y.W. Cheng, H.J.Tan, R.L. Jia: Effects of biological soil crusts on emergence of desert vascular plants in North China. Plant Ecology, Vol. 191(2007), p.191:11-19.

[6] S.B. Lan, L. Wu, D.L. Zhang, C.X. Hu: Successional stages of biological soil crusts and their microstructure variability in Shapotou region (China). Environmental Earth Sciences, Vol. 65(2012), p.77-88.

Advanced Materials Research Vols. 989-994 (2014) pp 978-981
© (2014) Trans Tech Publications, Switzerland
doi:10.4028/www.scientific.net/AMR.989-994.978

Research on performance of coupled heat pump system with different backfill material

JIE LIU

School of Energy and Power Engineering, Jiangsu University, 212013, Zhenjiang

E-mail: lj3539@126.com

Keywords: ground-coupled heat pump; ground heat exchanger; backfill material

Abstract. Combined the problems during the promotion of ground-coupled heat pump technology with the growing of power peak load, and considering the advantages of underground storage, this paper proposes a multi-source building air conditioning system based on heat storage capacity of the soil.On the basis of energy balance, established a mathematical model of the ground heat exchanger storaging, releasing cold and stopping running. Through simulation, analysis the effects of different types of backfill material to system operation.

Introduction

Ground-coupled heat pump technology and underground storage technology are two hot research topics in the field of air conditioning currently. The former is known to be one of the most promising air conditioning technologies in the 21st century, because of its use of renewable geothermal energy [1-2]. The latter will enable the transfer of air conditioning peak electricity load so as to ease the tension in electricity supply, but also can be effectively utilize a lot of industrial waste heat and waste heat and solar energy to reduce CO_2, NO_X, SO_X and CFC emissions in partial areas [3]. Multi-source building air conditioning systems based on heat storage capacity of the soil will both combine their respective merits and complement its short.

The system makes full use of the advantages of energy storage technologies and ground-coupled heat pump technology, transfers the energy storage device to the underground heat exchanger system of ground-coupled heat pump and rolls the heat exchanger and storage devices into one, which can reduce the area of energy storage devices effectively [4].Combined soil storage technology with ground-coupled heat pump system can regulate and control the soil temperature artificially by running through different programs, resolve the problems of ground-coupled heat pump system that the soil temperature field can not effectively restore because of the long-running. At low power time, turn on the unit and store a lot of cool or heat to underground for used at peak time, which play a load shifting and reduce the power system peak difference.

The ground heat exchanger use of vertical U-tube, in the soil, with the same thermal properties of soil and pipe, the same initial soil temperature and same pitch of heat exchanger manifold, so as to summer conditions for example, conducting unsteady numerical for underground heat exchanger by FLUENT software in the case of different backfill materials, thereby analysis operating characteristics of the system.

Mathematical model of soil storage and release cold process

The heat exchanger disposed in a vertical drilling and sealed by backfilling backfill material to form a whole with the surrounding soil, the fluid exchange heat by flowing with the tube wall, backfill material and soil in the heat exchanger [5]. Physical model shown in Figure 1.

In order to make the mathematical model can accurately describe the heat transfer process in the soil, and to facilitate the theoretical analysis and problem solving, as in the establishment mathematical model of soil storage and release cold process follows similar assumptions:(1)soil is isotropic and homogeneous rigid porous media body, and the moisture content is consistent and uniform;(2)it pass calorie in the form of pure thermal between the coil and soil, ignore the effects of soil moisture migration;(3)ignore the thermal contact resistance between U-tube wall and backfill material, between backfill material and soil, and the pipe and backfill material, backfill material and the hole wall are closed contact;(4)the initial temperature of soil, backfill material and U-tube are

consistent;(5)ignoring the radiation heat transfer between surface of the soil and the surrounding environment;(6)consider the soil and backfill is uniform, and its thermal properties do not change with temperature change;(7)ignore the heat transfer of U-tube bottom.

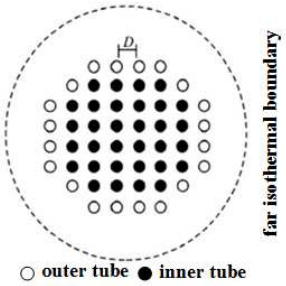

Fig.1. Underground pipe Heat Exchanger floor plan

The mathematical model is mainly based on the following several equations.

1. Tube fluid energy balance equation:

$$\frac{\partial t_f}{\partial \tau} = -u\frac{\partial t_f}{\partial \tau} + \alpha_f\left(\frac{\partial^2 t_f}{\partial x^2} + \frac{\partial^2 t_f}{\partial y^2} + \frac{\partial^2 t_f}{\partial z^2}\right) \tag{1}$$

2. Wall energy balance equation:

$$\frac{\partial t_p}{\partial \tau} = \alpha_p\left(\frac{\partial^2 t_p}{\partial x^2} + \frac{\partial^2 t_p}{\partial y^2} + \frac{\partial^2 t_p}{\partial z^2}\right) \tag{2}$$

3. Energy balance equation of backfill material region:

$$\frac{\partial t_b}{\partial \tau} = \alpha_b\left(\frac{\partial^2 t_b}{\partial x^2} + \frac{\partial^2 t_b}{\partial y^2} + \frac{\partial^2 t_b}{\partial z^2}\right) \tag{3}$$

4. Energy balance equation of soil area

$$\frac{\partial t_s}{\partial \tau} = \alpha_s\left(\frac{\partial^2 t_s}{\partial x^2} + \frac{\partial^2 t_s}{\partial y^2} + \frac{\partial^2 t_s}{\partial z^2}\right) \tag{4}$$

5. Initial conditions:

$$t_f = t_p = t_b = t_s = t_0(\tau = 0) \tag{5}$$

Subscripts above formulas, f represents the fluid, p represents the coil, b represents the backfill material, s represents the soil, u is the fluid Flow rate, m / s; t is the temperature,℃; τ is the run time, s; α represents the thermal diffusivity, m^2 / s. The flow of exports is fully developed; the wall of pipe in contact with backfill material, backfill material in contact with the soil is coupled; soil surface and the bottom of it are adiabatic boundary conditions; soil remote is thermostatic boundary conditions; boundary of k-ε equation use wall function. The system is running, it is considered the soil heat exchanger, soil and backfill material are in equilibrium, the initial temperature is 288K.

Numerical Simulation and Analysis

Based on the above model, remain the backfill material other parameters unchanged, the main changes are thermal conductivity of backfill materials, selected three types of backfill material, their thermal conductivity are 1.5W / (m.℃), 2.0 W / (m.℃)and2.5 W / (m.℃) , simulated calculations when the system is in storage and release cold conditions. The system conducts three days pre-storage, and then releases cold 8 hours, storages 8 hours, outages 8 hours, the cycle of process is 20 hours, the whole process run for 30 days. The parameters used in the calculation of the simulation are shown in Table 1.

Table 1 The simulation conditions of different backfill material

Parameter	Value	Unit
coil inside/outside diameter	20/24	mm
depth of well	80	m
inside diameter of drilling	100	mm
initial temperature of the soil	15	℃
inlet temperature of storage / release cold	2/20	℃
tube fluid velocity	0.5	m/s
pin pitch	40	mm
soil thermal conductivity	2.5	W/(m.K)
thermal conductivity of pipe(HDPE)	0.517	W/(m.K)
drilling spacing	0.6	m

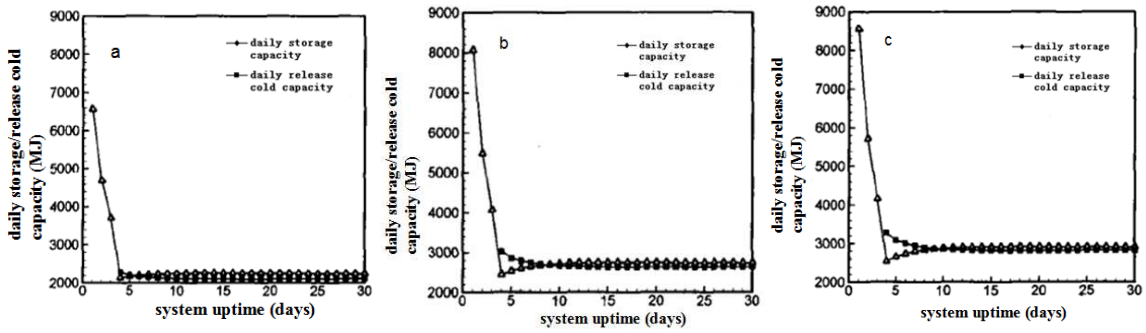

(a)PVC; (b) PB; (c) HDPE

Fig.1. The daily storage and release cold capacity of outer tube

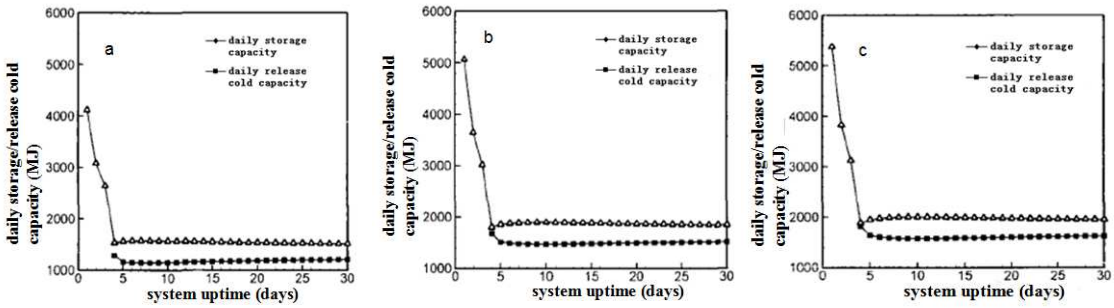

(a)PVC; (b) PB; (c) HDPE

Fig.2. The daily storage and release cold capacity of inner tube

The figures show that after the system during the three days of pre-storage start running into the normal cyclical, inner tube due to the early pre-storage effect, after running into the normal cyclical, daily release cold capacity is greater than the storage capacity, then the daily storage capacity increases day by day, daily release cold capacity reduced until daily storage capacity is greater than daily release cold capacity and the difference between them have reached a constant, then the system enters the steady state.

After the system reaches steady state, the daily storage capacity of inner tube were 2821.61MJ, 2917.73MJ, 2968.28MJ, daily release cold capacity were 2724.14MJ, 2821.11MJ, 2885.25MJ, daily release cold rates were 96.93%, 96.95%, 97.00%; the daily storage capacity of outer tube were 1889.11MJ, 1958.58MJ, 1998.86MJ, daily release cold capacity were 1569.12MJ, 1623.64MJ, 1662.98MJ, 2885.25MJ, daily release cold rates were 82.92%, 83.13%, 83.30%.

Figures 3 and 4 respectively are the change curve fig of the average outlet temperature of the inner and outer tube when the system at steady state operation.

The figure shows that the system is in the initial process of steady state operation, the outlet water temperature of the inner and outer tube changes are large, with the progresses of storage and release cold, the outlet water temperature changes gradually stabilized. In a stable operation period, for the three types of backfill materials, the outlet temperature of inner tube followed from 11.34℃, 11.23℃ and 11.15℃ changes to 16.22℃, 16.09℃ and 15.99℃. The inlet temperature of inner tube followed from 11.93 ℃, 11.82 ℃, and 11.74 ℃ changes to 16.54 ℃, 16.41 ℃, and 16.32 ℃.

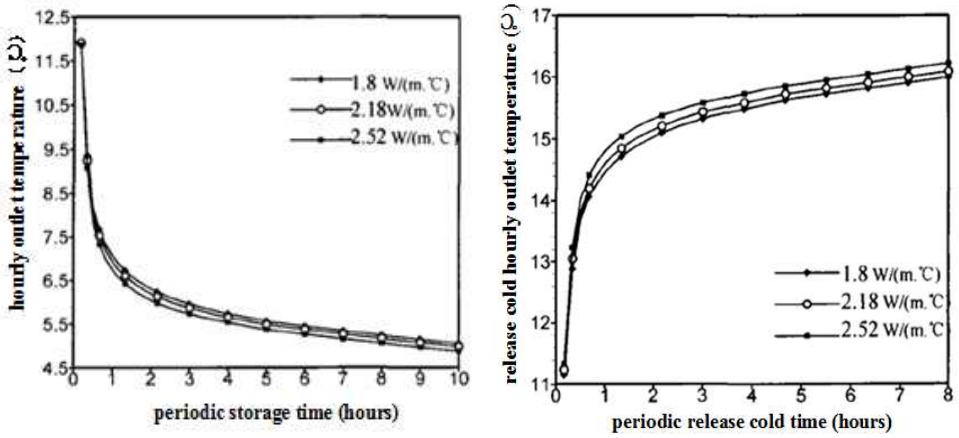

Fig.3. Import and export temperature change of inner tube

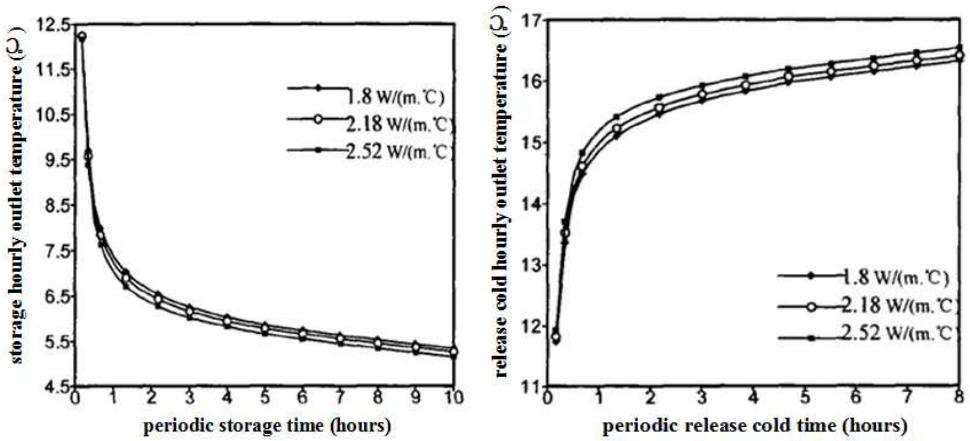

Fig.4. Import and export temperature change of outer tube

Conclusion

(1) The thermal conductivity of the backfill material is more preferably, the system to reach steady-state operation takes longer time; while under the same conditions of the pipe, the outer coil to reach steady state in a short time, but the inner coil will require a longer time to become stable.

(2) Preferable thermal conductivity of backfill material can enhance heat transfer between U-shaped pipe and its surrounding soil, improve release efficiency and release cold, and improve the quality of cooling capacity.

(3) Select the preferable thermal conductivity of backfill material, and make it reasonable match to the heat transfer capacity of soil can help to improve running characteristics, to maximize the effectiveness of soil storage.

References

[1] Olof Andersson, Leif Rydell, Tom Algotsson. Industrial Energy Conservation with UTES A Cass Study from ITT Flygt Emmaboda in Sweden[C].9th International Conference on Thermal Energy Storage, Warsaw in Poland,2003,1:359—366.

[2] Ping Yin. Ground source heat pump in China. Beijing: China Building Industry Press,2001.1-8

[3] Dwayne S.Breger, James E.Hubbell, Hamid El Hasnaoui. Thermal energy storage in the ground Comparative analysis of heat transfer modeling using U-tubes and boreholes [J].Solar Energy, 1996, 56(6):493—503.

[4] Yang Yao, Zuiliang Ma, Yanshun Yu. Study of soil storage and ground-coupled heat pump integrated system [J]. Fluid Mechanics, 2004, 32 (6):48-51.

[5] Suyu Luo. Numerical simulation of soil heat storage with ground source heat pump integrated system. Energy saving .2007, 6:9-12.

Advanced Materials Research Vols. 989-994 (2014) pp 982-985
© (2014) Trans Tech Publications, Switzerland
doi:10.4028/www.scientific.net/AMR.989-994.982

Numerical Simulation of the Kinetic Energy Projectile Oblique Penetration into the Concrete

Jun CHEN[1,a], Xiaojun YE[2,b]

[1]New Star Institute of Applied Technology, Hefei, 230031, China

[2]Nanchang Military Academy, Jiangxi, 310103, China

[a]email:358759332@qq.com, [b]email:tykfye@163.com

Keywords: the kinetic energy projectile; oblique penetration; concrete targets; trajectory

Abstract. ANSYS-LS/DYNA 3D finite element software projectile penetrating concrete target three-dimensional numerical simulation , has been the target characteristics and destroy ballistic missile trajectory , velocity and acceleration and analyze penetration and the time between relationship , compared with the test results , the phenomenon is consistent with the simulation results. The results show that : the destruction process finite element software can better demonstrate concrete tests revealed the phenomenon can not be observed , estimated penetration depth and direction of the oblique penetration missile deflection .

Introduction

Concrete is widely used in military field , has been an important object penetration studies. In practical applications , due to the impact of air resistance and gravity during the flight by such factors as the projectile at launch , tend to produce yaw phenomenon , that is the practical application of projectile penetrating the vast majority with dip angle of attack and penetration . And the inclination angle of attack will lead to the presence of penetrating ballistic deflection , seriously affecting the penetration depth and overload law elastomers and elastomer has the potential to withstand the high lateral loads and damage even ricochet phenomenon [1] . Ricochet serious impact on the penetration depth and overload law elastomers , leading role in missile power far below the design range [2] . Projectile Penetrating Concrete is a complex mechanical process transient . A very short time because of the penetration process , the experimental study of the penetration process is difficult to carry out comprehensive and accurate analysis and numerical simulation of high accuracy and reliability of the technology , which can serve as a basis for the analysis of practical problems [3] . Therefore, the text -based ANSYS-LS/DYNA 3D finite element software, the projectile penetrating concrete target process oblique three-dimensional numerical simulation and finite element analysis.

A simplified finite element model of the experimental projectile material is high strength steel, the head shape is oval, the aspect ratio of 6, diameter of 57mm. Concrete target for the semi-infinite rectangular, length 2m, width 2m, height of 3m. In modeling, the projectile using a local coordinate system to model . To reduce the amount of calculation , taking half shells and the model for modeling the target plate . Projectile at a speed of 500m / s and 15 ° inclination Penetrating Concrete Target . A simplified model for the physical structure of the original core role of the target missile target , shown in Figure 1 .

Fig.1 Projectile simplified finite element model of the target

Material models and parameters

Concrete material models and parameters

Concrete Target using Johnson-Holmquist-Concrete damage accumulation model [4] , the HJC model considers the high-pressure , high strain rate and large deformation , material of equivalent strength concrete pressure , strain rate , and functions injury ; while pressure is volumetric strain of functions, including the permanent fragmentation effects ; damage is a function of the equivalent plastic strain and plastic volumetric strain and stress. With the accumulation of damage , reduce the cohesive strength of the material . Model parameter determination portion HJC methods found in [3] , the material parameters : Unconfined compressive strength fc = 35.0MPa, the elastic modulus Ec = 27GPa, Poisson's ratio v = 0.2, the density ρ = 2.4g/cm3, anti- tensile strength ft = 3.4MPa.

Projectile material models and parameters

Elastomers using Johnson-Cook [2] material model , a typical application of this model include projectile penetration, explosive metal forming and impact . Because this involves the material behavior simulation under high pressure conditions , so the use of Gruneisen equation. LS-DYNA calculation parameters , see User Manual [3] .Specific parameters in Table 1.

Table1 Parameters of materials

material	ρ/(g.cm^{-3})	E/GPa	μ	G/GPa	K/GPa
steel	7.85	210	0.29	77	

Note: ρ is mass density; E is Young's Modulus; μ is Poisson's ratio; G is shear Modulus; K is bulk modulus.

Failure criterion

High compressive strength of concrete , tensile compressive strength of only about 1/10 [6] , in practical engineering application mainly under compressive loads. HJC material model for concrete compressive damage constitutive equation , considering only the material compression failure , the unit will produce distortion and no concrete failure , serious discrepancies with the actual phenomenon . Tensile failure due to lack of standards, did not produce concrete targets through the expansion of micro-cracks due to the formation of pits , caving phenomenon . Using compression and tensile failure strain of concrete materials to determine whether the failure of the joint , can simulate destruction of concrete materials . By adding * MAT _ ADD _ EROSION [5] material model , which set the size of the tensile strength , when more than the set value , the unit fails unit tensile stress strain . Therefore, the actual properties of tensile compressive strength of concrete is not in numerical simulation of projectile impact on concrete targets on tensile failure must be properly considered in order to obtain results with the actual match .

Model

Concrete with plastic , crushing many complex mechanical behavior , such as cracking , projectile and concrete are used eight-node hexahedral solid elements (SOLID164), with a single point of integration LAGLANGE algorithm. When meshing , cracks must be part of the target plate model for a more dense mesh to avoid a large number of unit failure on the results lead to considerable error , improve accuracy and efficiency. Define the contact between the projectile and target plate surface and surface erosion of the contact (* CONTACT_ERODING_SURFACE_TO_SURFACE), symmetry boundary conditions imposed on the projectile and target plate plane of symmetry and non-reflective boundary conditions imposed on the target plate boundary. In order to avoid a single point of integration hourglass phenomenon brought zero energy modes , adding options to control the hourglass (* CONTROL_HOURGLASS) in keywords to control . Numerical model uses cm-g-μs units.

Projectiles Oblique numerical simulation analysis

By numerical simulation LS-DYNA, was shot at a speed of 500m / s and 15 ° inclination impacting target of destruction and ballistic trajectory , and analyzes the impact angle of penetration depth and speed.

Figure 2 shows the projectile and target oblique penetration response process . Since the angle is too large , exceeding the elastic limit of the body tilt , projectile ricochet finally happened .

3 combined stress cloud analysis shows throughout the penetration process by Target affect the free surface effect , severe concrete damage. Due to the inclination exists projectile by the large lateral loads and overturning moment . Elastomer surrounding concrete surface subjected to tensile breaking waves separated approximate unconstrained state. The simulation results show that the process of oblique penetration Concrete Target elastomers can be divided into three stages: the axial penetration, lateral movement and rotation. Press trajectory can be divided into sections and slip segments crater , ballistics section .

1) crater segment. Combined stress cloud 2 analysis shows that in the early penetration, due to the projectile head just touch the target plate , surface contact area is small , penetration resistance is small, the head of a small missile force until the projectile force symmetry , playing the body posture remains unchanged. At this stage, concrete target destruction mainly tensile wave damage. Since the target after the missile body , mainly to overcome the resistance of the target plate , while reflecting tensile wave asymmetry, uneven concrete suffered the same resistance , so the head of the upper and lower surface of the elastomer in the concrete material damage inconsistent. So in the early penetration, projectile against lateral loads and torques , projectile penetration force and a positive force similar situation , so projectile motion attitude and direction of motion are not changed, ballistic crater segment is approximately linear .

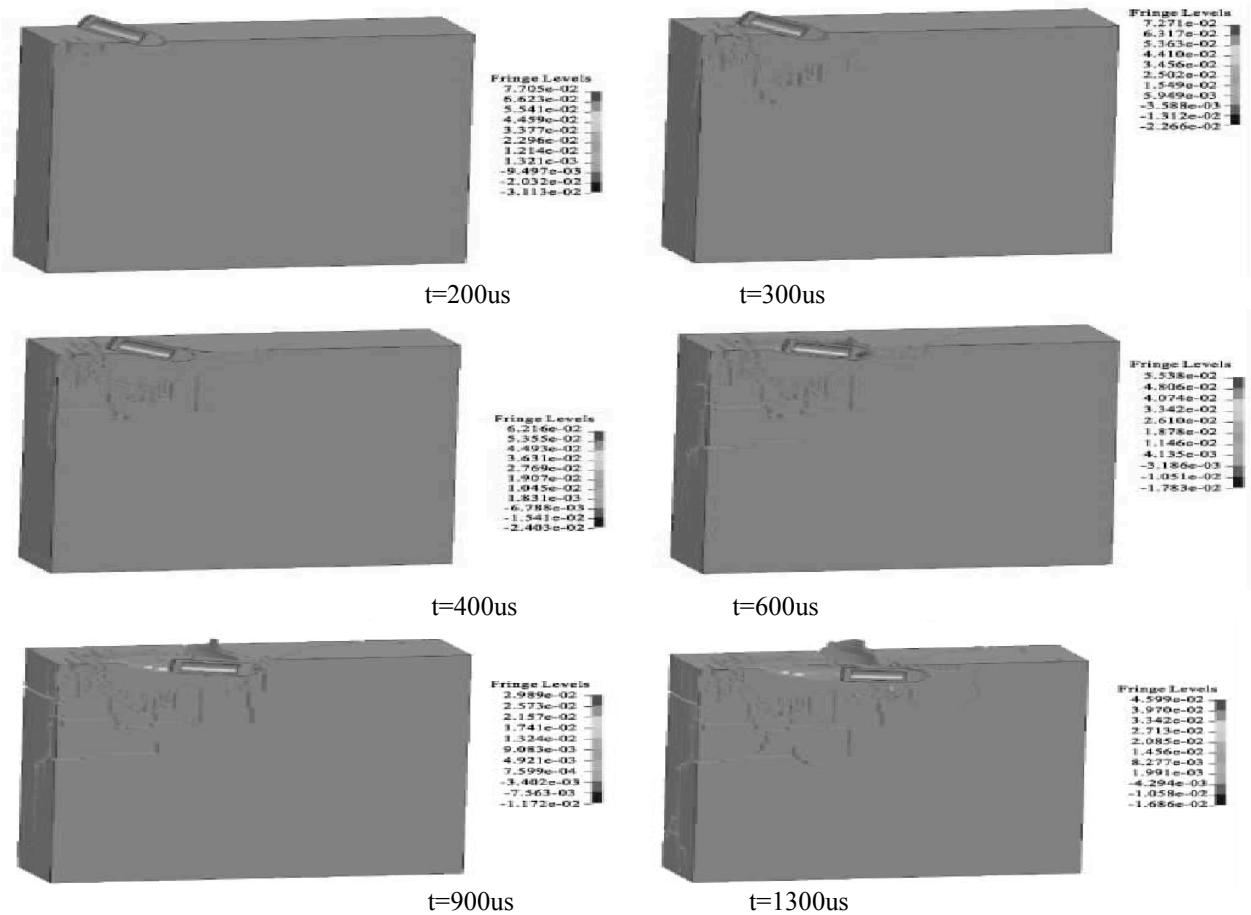

Fig.2 Projectile penetration process

2) slip segment. As can be seen from the stress cloud , after the projectile penetrating into the slip section , projectile axial resistance , but also to withstand lateral forces and overturning moment

action , projectile motion attitude change. Due to the presence of dip , the reflected wave asymmetric stretching around the concrete material damage elastomers are also asymmetrical . With the lower surface missile force area increases, along with increased resistance ; due to reflection on the surface of the tensile elastic waves generated damage accumulation , the formation of cracks. This asymmetry is no obvious damage by impact cratering stage missile force direction and moment . However , after the end of a pit , with increasing penetration depth , the intensity of the reflected wave stretching down on the surface of the surrounding concrete warheads continue peeling , and the lower surface of the concrete material is no longer around warhead easily peel off , causing the upper and lower surface of the warhead force area asymmetry. Under warhead surface to withstand greater pressure to squeeze and produce torque , so that the missile body to produce lateral slippage and rotation. Stress can also be seen from the cloud , under the stress elastomer surface is much larger than on the surface , projectile motion attitude changed to a lateral translational and rotational . Throughout the stage , playing the body posture and has been in the direction of the force change .

3) trajectory segments. As the penetration process , increasing penetration depth , axial velocity decreases, the resistance axis projectile close to balance , projectile penetration continues to squeeze Target, penetration capabilities so that the front of the concrete missile damage occurred while playing Because of the inertia of the body and tail of the downward movement , the formation trajectory. Projectile motion, because the angle is too large , the last wave under the combined effects of tensile and compression waves peeling concrete , concrete target missile fly will eventually happen ricochet .

Conclusions

Because oblique penetration test is difficult, less domestic oblique penetration test data, so when doing concrete ramp penetration studies in this regard , numerical simulation can provide a good basis for the tests and theoretical studies . This paper uses a large dynamic finite element software LS-DYNA projectile penetrating into concrete target to be a three-dimensional numerical simulation, and analysis of the experimental results agree . Obtained from the following conclusions:

1) Numerical simulation of projectile penetrating into concrete targets, using HJC damage material model can more accurately simulate concrete target into the pit , and is accompanied by a significant crack propagation . When impacting target tilt angle is too large, ricochet may occur.

2) trajectory and change with changing angle . Beyond a certain inclination range (30 ° left and right) trajectory deflected concave trend began to emerge .

3) In the projectile penetrating into concrete targets during the initial penetration, speed versus time is linear. With the increasing penetration depth , the axial velocity decreases, projectile velocity is almost a linear relationship changes over time . Meanwhile, the different penetration acceleration variation.

References

[1] Brown S J. Energy release protection for pressurized sys-tems Part Ⅱ: Review of studies into impact / Terminal ballis-tics[J]. Applied Mechanics Reviews, 1986, 39 (2) : 177－ 202.

[2] Holmquist T J, Johnson G R, Cook W H. A computation alconstitutive model for concrete subjected to large strains, high strain rates, and high pressure［C］/ / The 14th Inter-national Symposium on Ballistics, 1993: 519 － 600.

[3] LSTC. LS-DYNA keyword user‘s manual［M］. California :LSTC, 2003.

[4] J Glucklich. Fracture of plain concrete［J］. Journal of the Engineering Mechanics Division, ASCE 1963, 89 (6) : 127－ 138.

[5] Dai Qb, Yan L-h. Analysis on the Plugging Model of Concrete Targets struck by Rigid Projectiles, J. Journal of Ballistics. 19(2007)51-54.

Advanced Materials Research Vols. 989-994 (2014) pp 986-989
© (2014) Trans Tech Publications, Switzerland
doi:10.4028/www.scientific.net/AMR.989-994.986

Analysis on Aerostatic Stability for Jianghai Direct Ship Channel Bridge in Finished Stage

Yu Li[1,a], Wang Sen[1], Che Yanyang[1], Zhao Guohui[1]

[1] Key Laboratory of Ministry of Communications for Bridge Detection & Reinforcement Technology, School of Highway, Chang'an University, Xi'an, 710064, China

[a]liyu@chd.edu.cn

Keywords: cable-stay bridge; aerostatic response; finite element; nonlinear analysis; aerostatic stability

Abstract. Based on the wind tunnel experiment for aerostatic force of section model of Jianghai direct ship channel bridge of Hongkong-zhuhai-macau great bridge in its finished stage, one calculation program considering the geometric nonlinearity and aerostatic nonlinearity is prepared by using ANSYS parametric design language in order to calculate the nonlinear aerostatic response for long-span cable-stay bridges. Then, the FEA model of Jianghai direct ship channel bridge of Hongkong-zhuhai-macau great bridge in its finished stage is established to analyze the three-dimensional nonlinear aerostatic stability. And the aerostatic response with different position of bridge is also calculated. The research result indicates that the aerostatic instability can not occur in Jianghai direct ship channel bridge of Hongkong-zhuhai-macau great bridge in its finished stage. And, the max torsion deformation, transverse and vertical displacements of finished stage occur in the mid-span of each span and decrease gradually near to both sides.

Introduction

As shown in Fig.1, Jianghai direct ship channel bridge of Hongkong-zhuhai-macau great bridge is a three-tower cable-stayed bridge with the span arrangement of 129+258+258+129 m. This bridge adopts steel tower scheme with 109.8 m middle tower and 108.50 m edge tower. The main girder is a steel box beam with the width of 39.75 m. The height of bridge centerline is 4.58 m.

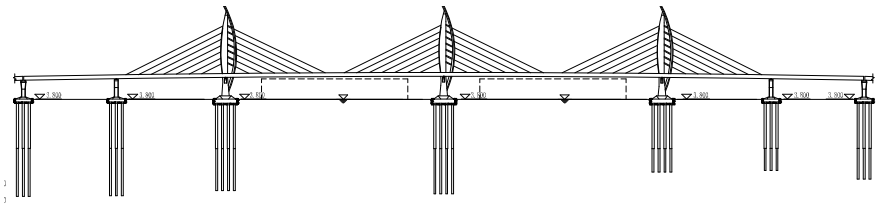

Fig. 1: Jianghai direct ship channel bridge

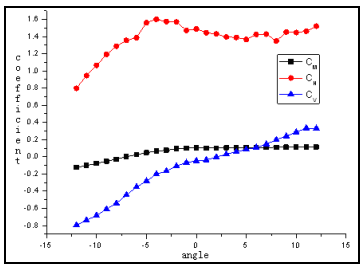

Fig. 2: Three component factors (15 m/s)

Analysis on Aerostatic Stability

Combined wind tunnel test with ANSYS program[1-5], nonlinear aerostatic response and stability are carried on according to the finished stage of Jianghai direct ship channel bridge of Hongkong-zhuhai-macau great bridge. So, torsion divergence mechanism is obtained according to the aerostatic force, displacement and torsion affected by wind speed. As shown in Fig.2, three component factors of 15m/s wind speed in finished stage are applied in the nonlinear aerostatic and stability analysis.

As shown in Fig.3, aerostatic force is applied in bridge FEA modal. Then, the nonlinear aerostatic response is computed. So, it can be known that this bridge is aerostatic instable when the wind speed of girder is 301 m/s. This conclusion can also be known from Fig.4~Fig.6 which calculate the torsion, horizontal and vertical displacement. These figures show that the slope of the curve, which reflects the change of torsion deformation affected by wind speed, increases greatly when this bridge is close to instable in the finished stage.

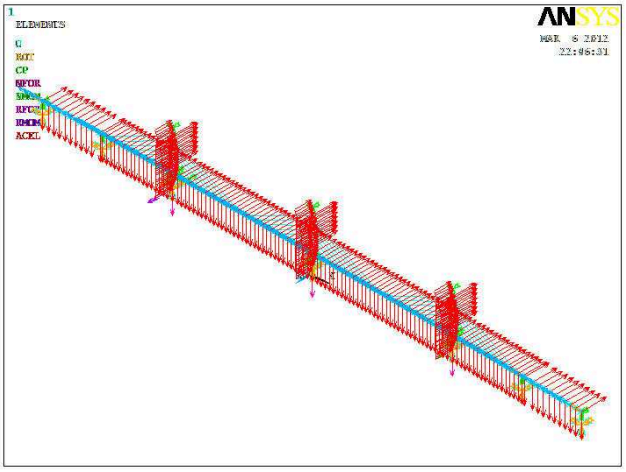

Fig. 3: Aerostatic force applied in bridge

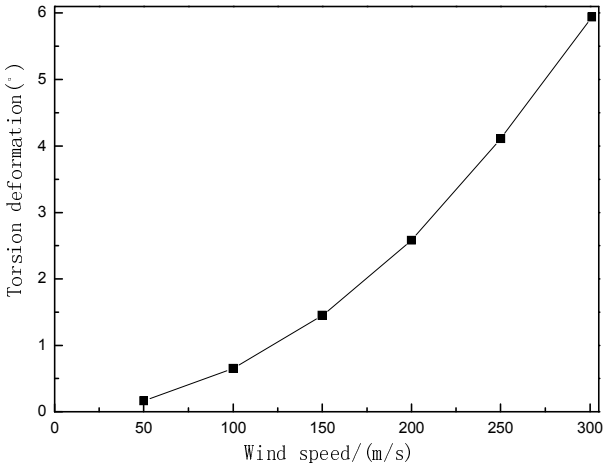

Fig. 4: Effect of wind speed on torsion

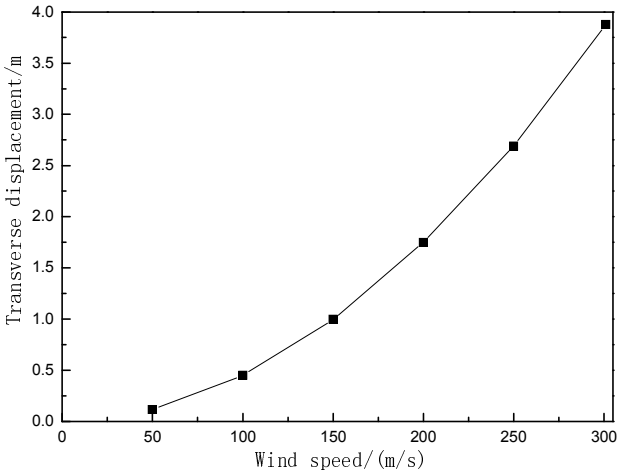

Fig. 5: Effect of wind speed on transverse displacement

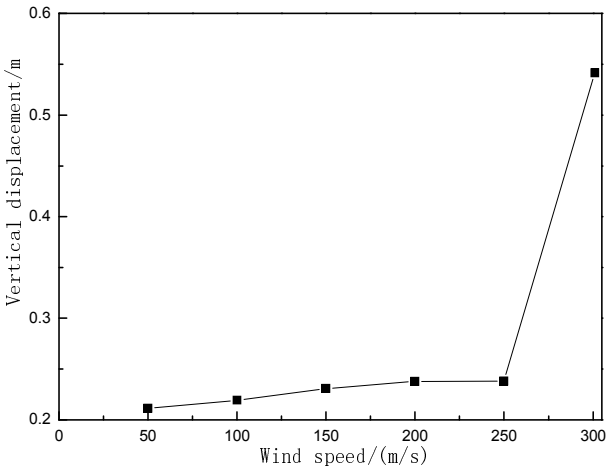

Fig. 6: Effect of wind speed on vertical displacement

Analysis on Aerostatic Response

Fig.7 shows the aerostatic torsion, transverse and vertical displacement of the girder of Jianghai direct ship channel bridge of Hongkong-zhuhai-macau great bridge in finished stage under different wind speed.

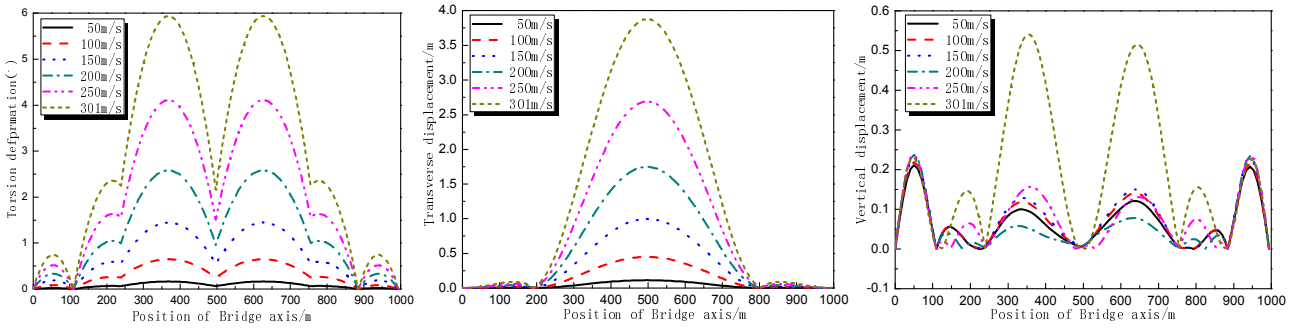

(a) torsion deformation (b) transverse displacement (c) vertical displacement

Fig. 7: Displacement of girder under different wind speed

(1) As shown in Fig.7(a), the torsions of girder in the same bridge position increases greatly with the increase of wind speed. Under the same wind speed, the max torsion deformation of finished stage occurs in the mid-span of each span and decreases gradually to both sides. In addition, when the wind speed is near to the aerostatic instable wind speed, great torsion deformation can be produced by the small wind speed increment.

(2) As shown in Fig.7(b), the transverse displacement of girder in the same bridge position increases greatly with the increase of wind speed. Under the same wind speed, the max transverse

displacement of finished stage occurs in the mid-span of each span and decreases gradually to both sides.

(3) As shown in Fig.7(c), the vertical displacement of girder in the same bridge position increases greatly with the increase of wind speed. Under the same wind speed, the max transverse displacement of finished stage occurs to in the mid-span of each span and decreases gradually to both sides.

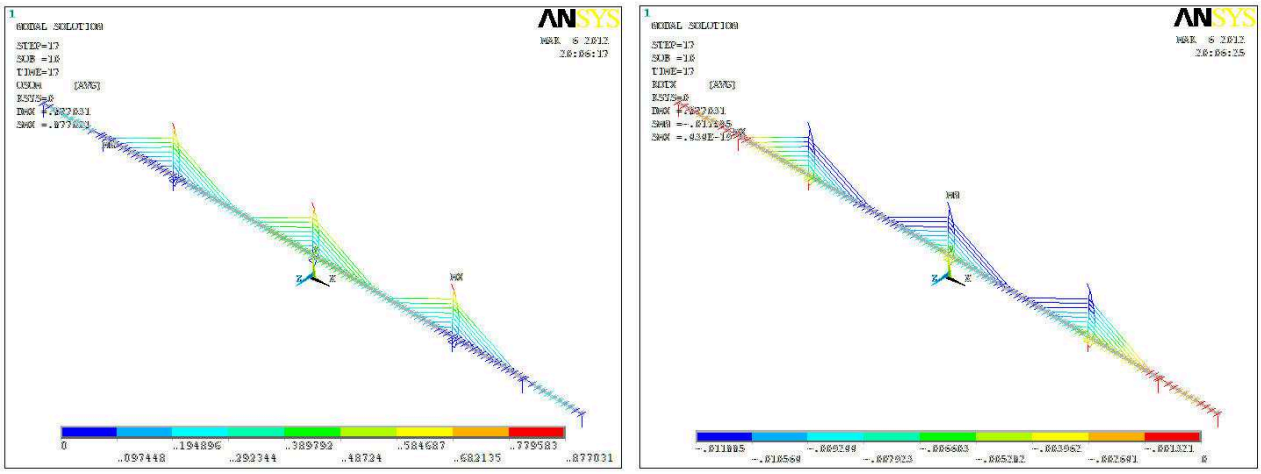

(a) displacement deformation (b) torsion deformation of bridge

Fig. 8: Aerostatic displacement in construction stage (U=100 m/s)

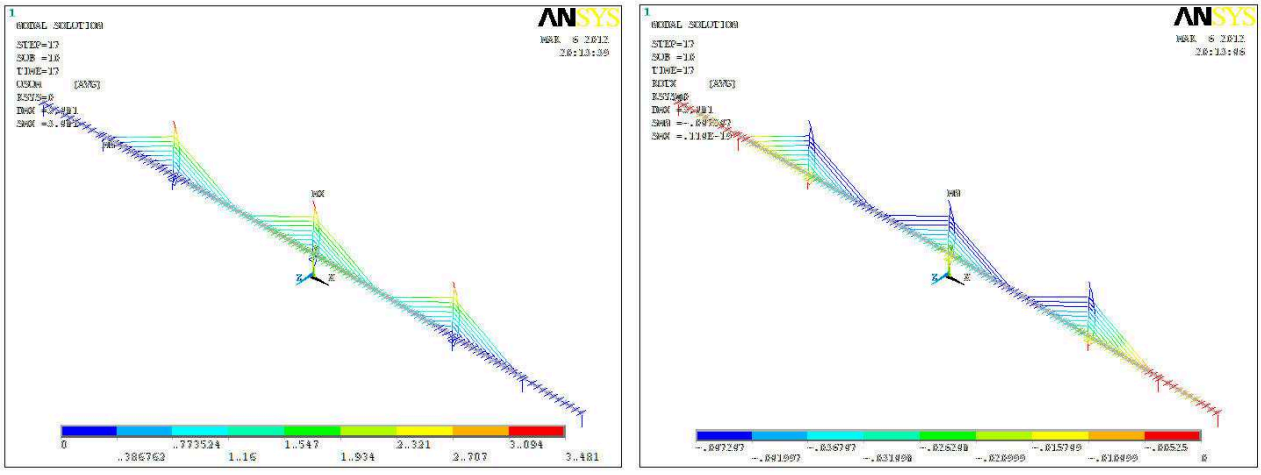

(a) displacement deformation (b) torsion deformation of bridge

Fig. 9: Aerostatic displacement in construction stage (U=200 m/s)

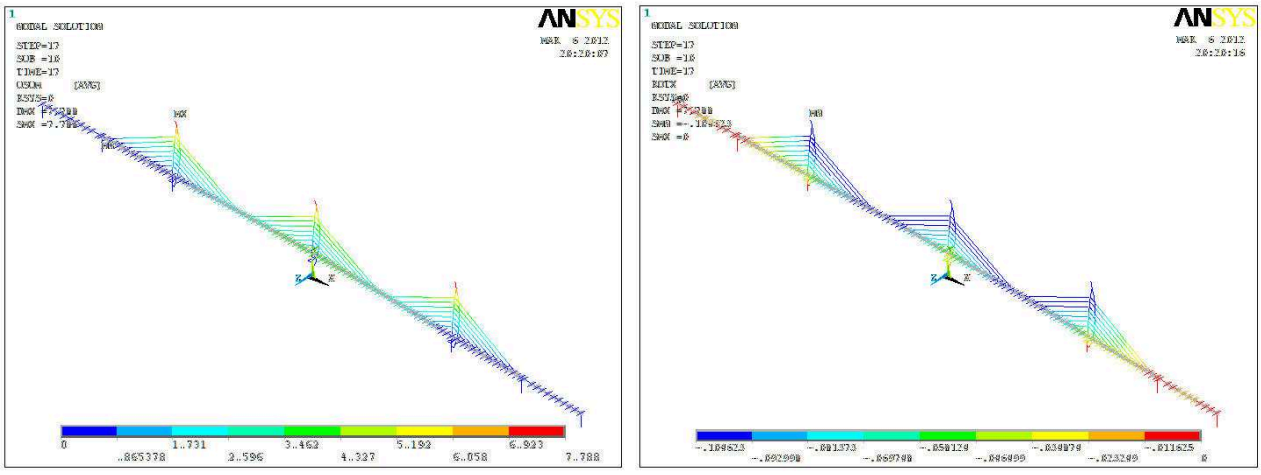

(a) displacement deformation (b) torsion deformation of bridge

Fig. 10: Aerostatic displacement in construction stage before instability (U=300 m/s)

Fig.8~Fig.10 show the aerostatic torsion and displacement figures of the girder of Jianghai direct ship channel bridge of Hongkong-zhuhai-macau great bridge in finished stage under different wind speed. The followings are the result.

(1) When the wind speed is equal to 100 m/s, the max torsion and displacement are respectively 0.63 degree and 0.877 m.

(2) When the wind speed is equal to 200 m/s, the max torsion and displacement are respectively 2.71 degree and 3.481 m.

(3) When the wind speed is equal to 300 m/s which close to the aerostatic instable wind speed, the max torsion and displacement are respectively 5.99 degree and 7.788 m.

Conclusion

(1) The aerostatic instable wind speed of finished stage is 301 m/s which is two times greater than the checking wind speed from *Wind Design Code for Highway Bridge*. So, the aerostatic instability can not occur in Jianghai direct ship channel bridge of Hongkong-zhuhai-macau great bridge in its finished stage.

(2) The max torsion deformation, transverse and vertical displacements of finished stage occur in the mid-span of each span and decrease gradually near to both sides.

Acknowledgements

This work was financially supported by the Fundamental Research Funds for the Central Universities (2013G1211006) and natural science foundation of Shaanxi Province (2014JQ7253).

References

[1] ZHANG Xinjun. Influence of Some Factors on the Aerodynamic Behavior of Long-Span Suspension Bridges[J]. Journal of Wind Engineering and Industrial Aerodynamics, 2007, 95: 149-164.

[2] CHENG Jin, JIANG Jianjing, XIAO Rucheng, eta1. Nontinear Aerostatic Stability Ana1ysis of Jiang Yin Suspension Bridge[J]. Engineering Structures, 2002, 24: 773-781.

[3] VIROTE B, YINGSAK L, PANITAN L. Nonlinear Aerostatic Stability Analysis of Suspension Bridges[J]. Engineering Structures, 2006, 28: 793-803.

[4] Boonyapinyo V, Yamada H, Miyata T. Wind-induced nonlinear lateral-torsional buckling of cable-stayed bridges [J]. Journal of Structural Engineering, ASCE, 1994, 120(2): 486-506.

[5] Virote B, Yingsak L, Panitan L. Nonlinear aerostatic stability analysis of suspension bridges [J]. Engineering Structures, 2006, 28: 793-803.

CHAPTER 3:

Bio- and Medicine Research

Advanced Materials Research Vols. 989-994 (2014) pp 993-996
© (2014) Trans Tech Publications, Switzerland
doi:10.4028/www.scientific.net/AMR.989-994.993

Spectrophotometric method for the assay of norfloxacin lactate

Yanhong Lei

College of chemistry, Jiujiang University, Jiangxi,Jiujian,332005,china

lei_4300@163.com

Keywords: UV-spectrophotometry; norfloxacin lactate;drug analysis.

Abstract. A selective method was developed for the determination of norfloxacin lactate by Spectrophotometric method. The method was simple with high sensitivity and selectivity.It was shown that recovery of the method by standard addition method was respectively valued 102.05% for norfloxacin lactate

1 Introduction

Since the fluoroquinolone drugs emerged, their antimicrobial activity was very popular. Because of norfloxacin is fat-soluble and almost insoluble in water, absorption was poor in the animal body, low bioavailability, so its lactic acid, nicotinic acid salt, hydrochloride salt etc. were commonly used., these salts were soluble in water .Frequently-used norfloxacin agents are: norfloxacin lactate injection, norfloxacin lactate soluble powder, etc. Different dosage forms and application combined with other drugs could affect its effectiveness.Norfloxacin lactate was the third generation quinolone synthetic antimicrobials, chemical structure, as shown in figure 1.[1]

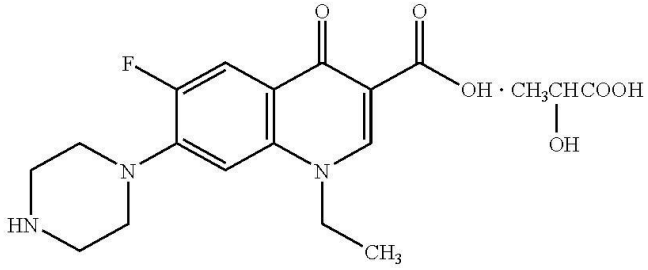

Fig 1 Chemica l structure o f norfloxacin lactate

Because this drugcould strengthen to penetrated cells, tissues, the drug was widely distributed in the body after making preparations to absorb. The drug was not affected by plasmid conduction resistance, and with no cross resistance between many antibiotics, medicinal stable aqueous solution, the treatment was significantly lower than poisoning dose, and tdischarge quickly (96 h all from the eduction in urine). This product had the advantages of wide antimicrobial spectrum, strong antibacterial activity. For example: the gram-negative bacilli, especially enterobacteriaceae, dysentery bacillus coli, pseudomonas aeruginosa, deformation, etc. The drug had strong antibacterial activity.For some gram positive cocci (such as staphylococcus aureus), chlamydia, mycoplasma .Suitable for sensitive bacteria caused by the respiratory tract, urinary tract, gastrointestinal tract infection, such as acute bronchitis acute, chronic bronchitis, pneumonia, acute and chronic pyelonephritis, typhoid fever, etc.

A quantitative analysis of norfloxacin lactate were capillary electrophoresis,high performance liquid chromatography, polarography , fluorescence spectrophotometry, etc[2-3]. This article used the ultraviolet spectrophotometry.The method was simple, rapid, economical and practical.

2 Experimental

2.1 Instruments and reagents

Spectral data were obtained from measurements on a TU-1901 UV-visible spectrophotometer (Beijing Purkinje General Insrument Co., Ltd). ultra pure water machine (Ai Ke ,Taiwan), electronic analytical balance (sartorius ,Germany),

2.2 The preparation of the solution[5]

Norfloxacin lactate reference substance dried to constant weigh in 105 ℃

Volumes of the analyte- norfloxacin lactate was selected .The preparation was weighed - norfloxacin lactate 0.1250 g, and then made it dissolved in anhydrous methanol. After that, transfer the solution into a 250-ML volumetric flask to make a constant volume so as to prepare the relevant stock solution. The contents was mixed thoroughly.As 500.0μg • mL-1 reserves of the fluid .All solutions were prepared with analytical grade reagent and doubly distilled water was used throughout.

3 Results and discussion

3.1 Absorption spectrum

Select the right amount of norfloxacin lactate .This solution was transferred to a 10 mL volumetric flask and diluted to the anhydrous methanol. Volumes of each analyte were micropipetted directly into the cuvette as required by an auto-controlled microstirrer. A blank of reagent was used as reference.The spectrophotometric data were measured and collected from 190 to 340 nm every 1 nm. The absorption curve was shown in figure 2,By the appended drawings, norfloxacin lactate had the biggest absorption in the 276 nm wavelength(figure 2), 276 nm was choosed for measuring wavelength[4].

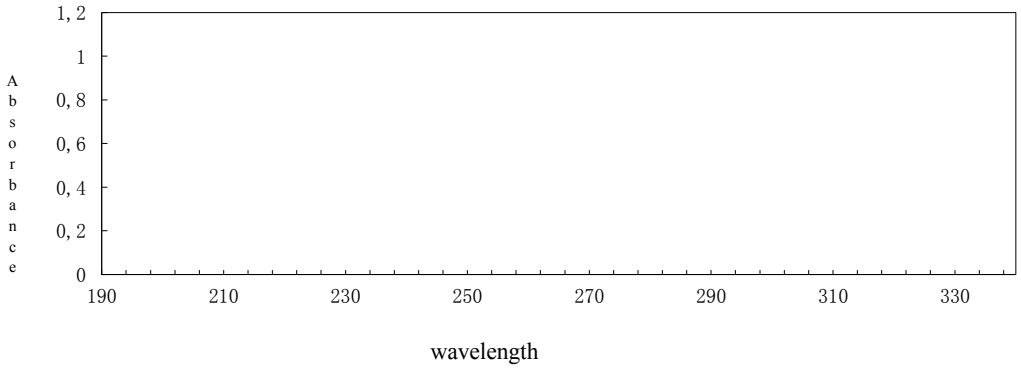

Figure 2 Fig 1 UV-spectra of norfloxacin lactate

3.2 Calibration of single components

The response absorbance of the component with concentrations was measured . With the use of the selected optimum experimental conditions, the data for norfloxacin lactate were recorded at 190-340 nm ,Linear behaviour of the analytes was established in the concentration ranges:2.0μg • mL-1 to20.0 μg • mL-1 (Fig. 3).

The regression models for the analytes was:

norfloxacin lactate A=0.0784C-0.0085 (n=10), R^2 =0.9998.

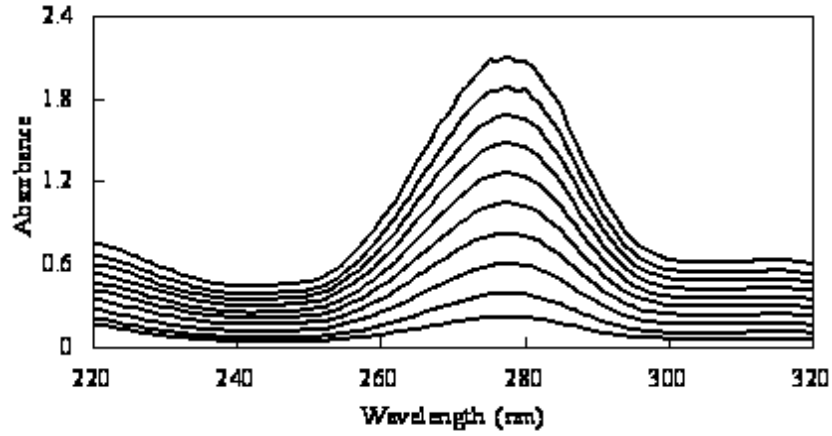

Fig 3 UV-spectra of norfloxacin lactate 2. 0μg • mL^{-1} to20.0 μg • mL^{-1}

3.3 The influence of pH

This study examined the pH in 1. 81-9.15, (figure 4), The change of PH was not obvious to effect norfloxacin lactate

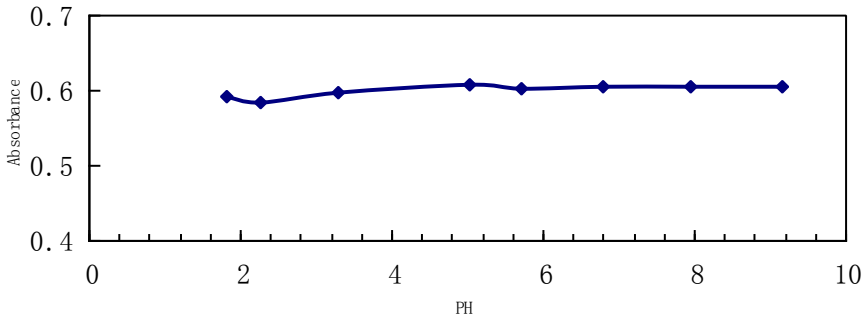

Fig 4 The pH of norfloxacin lactate (1. 81-9.15)

3.4 The stability of the drug at room temperature

Preparation of different concentration of norfloxacin lactate placed 48 h at room temperature interval sampling, analysis and determination of absorbance， measured results were shown in table 1 ,place the length of time didnot affect the solution's absorbance values .

Table 1 Norfloxacin lactate absorbance stability

Concentration	time					RSD(%)
	0 h	1h	12h	24h	48h	
6.325μg• mL^{-1}	0.4866	0.4891	0.4889	0.4827	0.4892	0.57
12.63μg• mL^{-1}	1.0024	1.0011	0.9893	0.9893	0.9938	0.63
18.98μg• mL^{-1}	1.4614	1.4571	1.4568	1.4489	1.4539	0.32

Note: the above values were determined at 276 nm absorption wavelength

3.5 Samples analysis and conclusion

The Serum samples were placed into centrifuge tube, adding 0.5 mL 0.50mol•L -1HCl and vortexing 1 min ,then adding 5.00 mL isopropyl alcohol and vortexing 5min. After turbulence mixing, centrifuged at 4000 r/min for 20 min, then the supernatant solution was analyzed following the follow mentioned procedure . nitrogen dried with constant temperature heating device, ultrapure

water dissolved residue, moved to 25 mL volumetric flask volumetric. Use the standard addition method for recycling test. The results in table 2.

Table 2 The analysis results of determination of practical samples

Samples	Concentration/($mg \cdot L^{-1}$)			Recovery/%
	Measuredvalue	Added	Found	
norfloxacin lactate	5.201	2.000	7.308	102.05

4 Conclusion

Ultraviolet spectrophotometric method determinated norfloxacin lactate with the features of easy operation, fast, the characteristics of high accuracy, and is suitable for the application at the local level

Reference

[1] Xing Ge,Juan Zheng, Xiaohong Bai.Journal of Shanxi Medical University,2009,p.612-616

[2]Genhe Guo, Wei Pan,Desen Su.chromatography,Vol.23(2005),p. 401-403

[3]Jie Ling, Zeping Rao,Yuzheng He.Chinese journal of hospital pharmacy.Vol.20(2000),p. 141-142

[4]Chunqing Wang,Shuyuan Xu,Jianhua Wang. Spectrum instrument and analysis. 2000,p .45–46

[5] Yanhong Lei,Shucai Liang,Shan Ye.etc.Chinese Journal of Modern Drug Application, Vol.2(2008),p.32-33

Advanced Materials Research Vols. 989-994 (2014) pp 997-1002
© (2014) Trans Tech Publications, Switzerland
doi:10.4028/www.scientific.net/AMR.989-994.997

Co-expression of threonine dehydratase and acetolactate synthase in Escherichia coli for L-isoleucine production

Jian WANG [1,a], Jia-kai SUN [2,b], Qing-yang XU [2,c]

[1]College of Biological and Agricultural Engineering, Jilin University,

Changchun, 130022, China.

[2]Key Laboratory of Industrial Microbiology, Ministry of Education, School of Bioengineering, Tianjin University of Science and Technology, Tianjin, 300457, China

[a]email: wangjian99@jlu.edu.cn, [b]email: sunjkai2013@163.com, [c]email: xuqingyangqyx@163.com

Keywords: threonine dehydratasegene (*ilv*A)； acetolactate synthase (*ilv*BN)； L-isoleucine; *E. coli*

Abstract. Metabolic engineering of *Corynebacterium glutamicum* has sought to divert carbon into L-isoleucine. However, the fermentation period of this strain is long. The *C. glutamicum* YILW strain (Leu^L, AHV^r, SG^r, Leu-ME^r) was previously derived by repeated compound mutagenesis which could accumulate 20.2 g/L L-isoleucine in a 5-L jar fermentor. Overexpression of the threonine dehydratase gene (*ilv*A) from *Corynebacterium glutamicum* YILW and coexpression of threonine dehydratase and acetolactate synthase (*ilv*BN) from it were employed to divert carbon flux toward L-isoleucine. The strain *E. coli* TRFC with the expression of *ilv*A could accumulate L-isoleucine of 6.8 g/L without accumulation of any L-threonine by fed-batch fermentation in a 5-L jar fermentor. However, the production of L-isoleucine by the strain *E. coli* TRFC with the co-expression of *ilv*A and *ilv*BN was decreased by 19.1%, and the production of L-valine was increased by 40% compared with that of *E. coli* TRFC with the expression of *ilv*A.

Introduction

L-isoleucine belongs to the aspartate-derived family of amino acids, which can not be synthesized by mammals and is therefore of commercial interest as pharmaceuticals, food and feed additive. There is also a great demand for L-isoleucine as cosmetics. Currently, the most economic route toward L-isoleucine production is via microbial synthesis, predominantly using *Corynebacterium glutamicum* achieved by random mutagenesis. However, the industrial production of L-isoleucine by random mutagenesis strain has not been yet well developed, primarily because rational construction is complex, since four common enzymes are involved in the biosynthesis of all branched-chain amino acids (valine, isoleucine and leucine)[1,2]. Moreover, many byproducts produced by rational construction strain increase the difficulty of separation. Furthermore, the fermentation period of *C. glutamicum* is long [3,4].

Escherichia coli has been widely used for amino acid production due to its ease of genetic manipulation, fast growth rate and low-cost cultural requirements. The biosynthetic pathway of L-isoleucine and its regulation have been well studied in *E. coli* [5]. L-isoleucine biosynthetic pathway from L- threonine consists of 5 steps catalyzed by threonine dehydratase (TD), acetohydroxy acid synthase (AHAS), acetohydroxy acid isomeroreductase, dihydroxy acid dehydratase and transferase. It has been discovered that the limiting steps in L-isoleucine biosynthesis involve threonine dehydratase (*ilv*A) and acetohydroxy acid synthase (*ilv*BN). It was reported that an L- isoleucine over-producing strain was constructed, when the genes for a threonine deaminase that is resistant to feedback inhibition by L-isoleucine and for an active acetohydroxy acid synthase II from *E. coli* were introduced into a L-threonine-producing recombinant strain of *E. coli* K-12 [6]. In another report, a L-threonine-producing strain of *E. coli* was further engineered to construct an L-isoleucine producing strain by amplifing the *thrABC*, *ilv*A, *ilv*IH, and *yga*ZH genes, and *ilv*CED and *lrp* genes by chromosomal promoter replacement [7].

An *C. glutamicum* YILW strain (Leu^L, AHV^r, SG^r, $Leu\text{-}ME^r$) was previously derived by repeated compound mutagenesis, which could accumulate 20.2 g/L L-isoleucine at the end of fermetation (60 hours) in a 5-L jar fermentor [3]. In this paper, the *ilv*A gene from *C. glutamicum* YILW was overexpressed and *ilv*A and *ilv*BN genes from it were co-expressed in a threonine-producing strain *E. coli* TRFC. The effects of *ilv*A gene expression and *ilv*A- *ilv*BN genes co-expression on L-isoleucine fermentation were compared.

Materials and methods

Bacterial strains and plasmids

The strains and plasmids used in this study are listed in Table 1.

Tab. 1 Strains and plasmids used in this study

Strain/Plasmid	Relevant characteristics	Reference/Source
Strains		
C. glutamicum YILW	The L-isoleucine producing strain, Leu^L, AHV^r, SG^r, $Leu\text{-}ME^r$	[3]
E. coli TRFC	The L-threonine producing strain, Ile^L, AHV^r, carrying a pTHR101 plasmid containing a threonine operon	[8]
E. coli DH5α		TAKARA
Plasmids		
pXMJ19	*C.glutamicum*/*E.coli* shuttle vector, 6.6 kb, *ptac*, $lacI^q$, Cm^r	TAKARA
pXMJ10	pXMJ19 derivative carrying *ilv*A	this study
pXMJ102	pXMJ19 derivative carrying *ilv*A *&ilv*BN	this study

Media and culture conditions

Luria broth (LB) medium supplemented with the appropriate antibiotics was used in the strain construction experiments. The seed medium contained (in g/L) the following: sucrose, 40; yeast extract, 2; KH_2PO_4, 1.5; $(NH_4)_2SO_4$, 10; $MgSO_4 \cdot 7H_2O$, 0.5. The medium for L-isoleucine fermentation contained (in g/L) the following: sucrose, 70; yeast extract, 3; KH_2PO_4, 3; $(NH_4)_2SO_4$, 2; $MgSO_4 \cdot 7H_2O$, 0.5; $FeSO_4 \cdot 7H_2O$, 0.1; $MnSO_4 \cdot 7H_2O$, 0.1. The initial pH values of both seed and fermentation medium were adjusted to 7.0 with 4 M NaOH.

The *E. coli* seed culture was grown overnight in 500 mL baffled flasks containing 30 mL of seed medium at 36 °C and 200 r/min and was added aseptically into a 5 L fermenter (Biotech-2002 Bioprecess controller, Baoxing, Shanghai, China) containing 3 L fermentation medium to give 10% v/v inoculum size. The temperature was maintained at 36°C and the pH was adjusted to 7.0 with 25% (v/v) ammonia. The DO level was maintained at approximately 20% saturation by adjusting the agitation and aeration rates. When the initial carbon source was depleted, 800 g/L glucose solution was fed into the fermenter.

Construction of pXMJ10 and pXMJ102

The plasmid pXMJ19 was digested with BamH Ⅰ and Hind Ⅲ for the integration of *ilv*A gene from *C. glutamicum* YILW to form pXMJ10. The primers of P_1 and P_2 (Tab. 2) were used for the PCR of *ilv*A. The *ilv*BN gene of *C. glutamicum* YILW was cloned into the plasmid pXMJ10 to yield pXMJ102. The primers of P_3 and P_4 (Tab.2) were used for PCR of *ilv*BN. *E. coli* DH5α transformed with the pXMJ102 was verified by PCR with primers of P_5 and P_6, and then used as templates to determine the DNA sequences of *ilv*A and *ilv*BN. Then, *E. coli* TRFC was transformed with the plasmids pXMJ10 and pXMJ102, respectively.

Tab. 2 Primers used in this study

Name	Primer（5'→3'）[a]
P_1	GGCAAGCTTCTATGCCAAAGTAGGTGC
P_2	TATGGATCCGATCCTGACCCGAAACTAG
P_3	TAGCTAGGATCCTTGGACGGGTCCTGTGAAAAT
P_4	GCGCTAGAATTCCTACCACACACATGTAATTAGACGG
P_5	GACAATTAATCATCGGCTCG
P_6	CAGGCTGAAAATCTTCTCTC

a: The restriction sites are underlined.

Analytical methods

Biomass was calculated as described before [9]. Specific growth rate (μ) was calculated according to Cheng et al.[10].

The concentration of L-isoleucine, L-threonine and L-valine in the broth were were analyzed as 2, 4-fluoro-dinitrobenzene derivatives by high-performance liquid chromatography (Agilent Technologies, Santa Clara, CA, USA). Concentration of acetic acid was measured by a Bioprofile 300A biochemical analyzer (Nova Biomedical, Waltham, MA). The TD and AHAS were analyzed by sodium dodecyl sulphate-polyacrylamide gel electrophoresis (SDS-PAGE), and protein concentration was determined by Bradford method [11].

Results

Expression of *ilv*A and *ilv*BN

In order to evaluate the expression of TD and AHAS in *E. coli* TRFC, cell lysates of *E. coli* TRFC (pXMJ10) and *E. coli* TRFC (pXMJ102) were analyzed by SDS-PAGE using *E. coli* TRFC as the control (Fig.1). Strong protein bands around 46 kDa consistent with the molecular mass of TD were observed in cell lysates of *E. coli* TRFC (pXMJ10) and *E. coli* TRFC (pXMJ102) as compared with the control strain. Two strong protein bands around 67 and 18.7 kDa consistent with the molecular masses of the two subunits of AHAS were also observed in cell lysates of *E. coli* TRFC (pXMJ102). These data indicate that both TD and AHAS could be well expressed in *E. coli* TRFC.

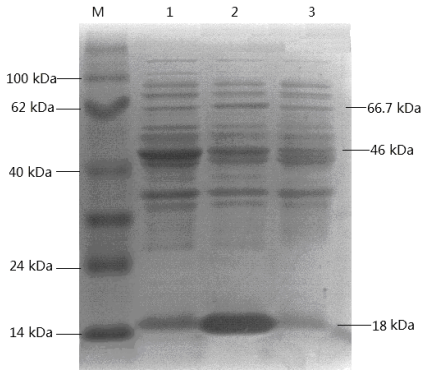

Fig.1 SDS-PAGE analysis of *E. coli* TRFC, *E. coli* TRFC (pXMJ10) and *E. coli* TRFC (pXMJ102)
M—Marker；1—*E. coli* TRFC (pXMJ10)；2—*E. coli* TRFC (pXMJ102)；3—*E. coli* TRFC

Effects of over-expression of *ilv*A and *ilv*BN on cell growth

To investigate the effects of over-expression of *ilvA* and *ilvBN* on cell growth, strains of *E. coli* TRFC, *E. coli* TRFC (pXMJ10) and *E. coli* TRFC (pXMJ102) were cultivated in a 5 L fermenter. As shown in Fig.2, *E. coli* TRFC grew exponentially with a maximum specific growth rate of 0.29 h^{-1} at 8 h and achieved a biomass of 33.6 g/L at the end of fermentation. The growth of both *E. coli* TRFC (pXMJ10) and *E. coli* TRFC (pXMJ102) was delayed. Biomass of *E. coli* TRFC (pXMJ10) and *E. coli* TRFC (pXMJ102) were 15.2% and 24.4% lower than that of *E. coli* TRFC, respectively. The maximum specific growth rate of *E. coli* TRFC (pXMJ10) was 0.27 $h^{-1}$and that of *E. coli* TRFC (pXMJ102) was 0.23 h^{-1}. Cell growth was retarded to some extent due to metabolic burden caused by the plasmid replication and expression of the exogenous genes, especially for the co-expression of *ilv*A and *ilv*BN.

Effects of over-expression of *ilv*A and *ilv*BN on acetic acid accumulation

One common concern in conducting high cell density fermentations is the formation of acetic acid in *E. coli* cultures, which retards growth and inhibits product formation [12~14]. Although acetic acid was accumulated during L-isoleucine fermentation process and acetic acid accumulation rates were increased quickly during the exponential growth with all the three strains, the concentrations

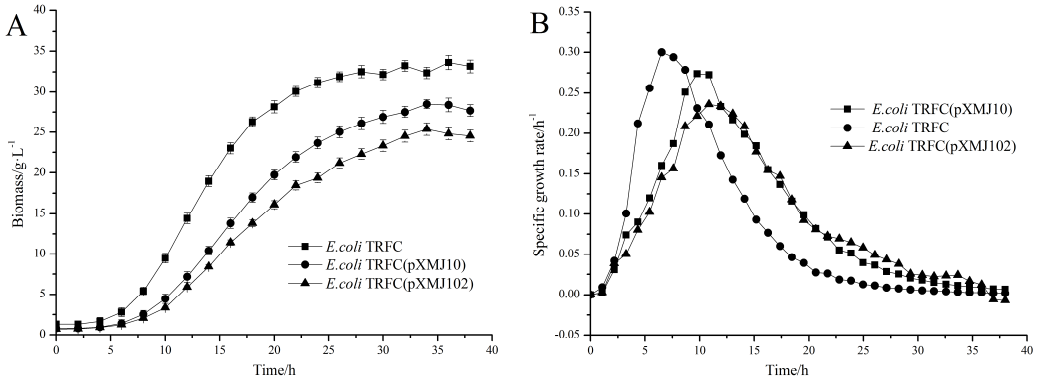

Fig.2 Growth Curve (A) and specific growth rates (B) in L-isoleucine fermentation by *E. coli* TRFC, *E. coli* TRFC (pXMJ10) and *E. coli* TRFC (pXMJ102)

of them were different (Fig.3). The maximal acetic acid concentrations of *E. coli* TRFC (pXMJ10) and *E. coli* TRFC (pXMJ102) achieved 145.5 mM and 167.2 mM, which were 11.9% and 28.6% higher than that of *E. coli* TRFC (130 mM) respectively. Obviously, the co-expression of *ilv*A and *ilvBN* increased the accumulation of acetic acid.

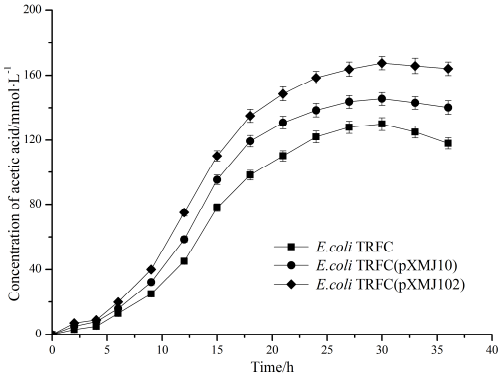

Fig.3 Concentrations of acetic acid in L-isoleucine fermentation by *E. coli* TRFC, *E. coli* TRFC(pXMJ10) and *E. coli* TRFC (pXMJ102)

Effects of over-expression of *ilv*A and *ilv*BN on L-isoleucine production

To investigate the effects of over-expression of *ilv*A and *ilv*BN on L-isoleucine production, glucose consumption rate, concentrations of L –isoleucine, L-threonine and L-valine in the broth of *E. coli* TRFC, *E. coli* TRFC (pXMJ10) and *E. coli* TRFC (pXMJ102) were determined or calculated. As shown in Fig.4, the glucose consumption rate of *E. coli* TRFC achieved a maximum of 9.8 $g \cdot L^{-1} \cdot h^{-1}$ and was kept at a high level until the end of fermentation. The glucose consumption rates of *E. coli* TRFC (pXMJ10) and *E. coli* TRFC (pXMJ102) were 5.5 $g \cdot L^{-1} \cdot h^{-1}$ and 5.9 $g \cdot L^{-1} \cdot h^{-1}$ respectively, which were 43.9% and 39.8% lower than that of *E. coli* TRFC. As shown in Fig.5, 85 g/L L-threonine was accumulated in the broth of *E. coli* TRFC, but no L- threonine was accumulated in the broth of *E. coli* TRFC (pXMJ10) or *E. coli* TRFC (pXMJ102). Furthermore, no L-isoleucine was accumulated in the broth of *E. coli* TRFC, but 6.8 g/L and 5.5 g/L L-isoleucine were accumulated in the broth of *E. coli* TRFC (pXMJ10) and *E. coli* TRFC (pXMJ102), respectively. These data suggest that the flux of carbon can be diverted from threonine pathway to L-isoleucine pathway by the expression of *ilv*A. The concentration of L-isoleucine in the broth of *E. coli* TRFC (pXMJ102) was 19.1% lower than that of *E. coli* TRFC (pXMJ10), which suggest that coexpression of *ilv*A and *ilv*BN does not enhance L -isoleucine synthesis in *E. coli*. The concentration of L-valine in the broth of *E. coli* TRFC (pXMJ102) was increased by 40% as compared with that of *E. coli* TRFC (pXMJ10).

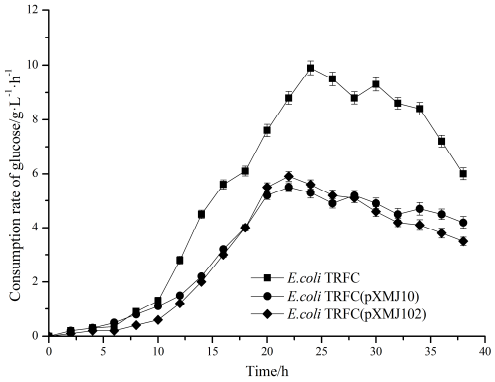

Fig.4 Glucose consumption rates in L-isoleucine fermentation by *E. coli* TRFC, *E. coli* TRFC (pXMJ10) and *E. coli* TRFC (pXMJ102)

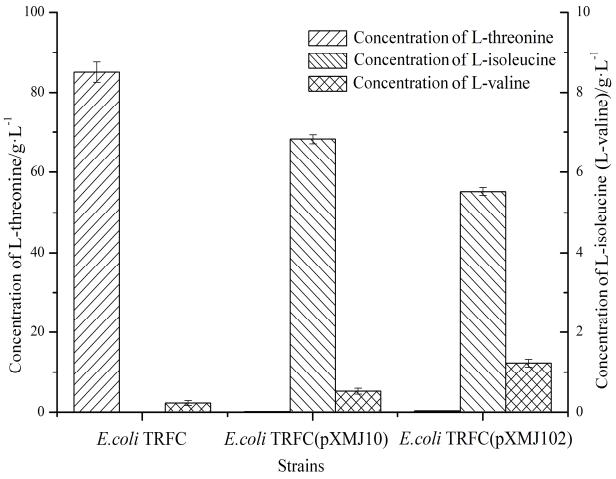

Fig.5 L-threonine, L-isoleucine and L-valine produced by *E. coli* TRFC, *E. coli* TRFC (pXMJ10) and *E. coli* TRFC (pXMJ102)

Conclusions

Metabolic engineering of *C. glutamicum* has sought to divert carbon into L-isoleucine [4,15~18]. However, the fermentation period of this strain is long. In this study, the flux of carbon was diverted from threonine pathway to the production of L-isoleucine by the expression of *ilv*A of *C. glutamicum*. Co-expression of *ilv*A and *ilv*BN decreased the production of L-isoleucine by 19.1%, but increased the production of L-valine by 40% as compared with expression of *ilv*A only.

In this study, the co-expression of *ilv*A and *ilv*BN increased the accumulation of acetic acid which maybe can explain why the production of L-isoleucine is low. In that case, production of L –isoleucine will be further improved by cutting off the flow of carbon to acetic acid or directing it to a benign product [20].

Acknowledgement

In this paper, the research was sponsored by the Key Project of Tianjin Science and Technology Supporting Program (12ZCZDSY01900).

References

[1] Holátko J., Elisáková V., Prouza M., Sobotka M., Nesvera J., Pátek M. [J]. J Biotechnol, 2009, 139(3): 203–210.

[2] Denina I., Paegle L., Prouza M., Holátko J., Pátek M., Nenvera J., Ruklisha M., [J]. J Ind Microbiol Biotechnol, 2010, 37(7): 689–699.

[3] Xie X.X., Xu L.L., Shi J.M., Xu Q.Y., Chen N. [J]. J Ind Microbiol Biotechnol, 2012, 39(10):1549–1556.

[4] Yin L.H., Hu X.Q., Xu D.Q., Ning J.F., Chen J., Wang X.Y., [J]. Metab Eng, 2012, 14: 542-550

[5] Chen J.W., Bennett D.C. and Umbarger H.E., [J]. J Bacteiol , 1991,173(10): 2328-2340.

[6] Hashiguchi K., Takesada H., Suzuki E., and Matsui H., [J]. Biosci Biotechnol Biochem, 1999, 63: 672-679

[7] Park J.H., Oh J.E., Lee K.H., Kim J.Y., Lee S.Y., [J]. ACS Synth Biol, 2012, 1(11): 532-540.

[8] Chen N., Huang J., Feng Z., Yu L., Xu Q.Y., Wen T.Y., [J]. Appl Biochem Biotechnol, 2009, 158(3): 595–604.

[9] Wang J., Huang J., Shi J.M., Xu Q.Y., Xie X.X., Chen N., [J]. Ann Microbiol, 2013, 63(4): 1219–1224.

[10] Cheng L.K., Wang J., Xu Q.Y., Xie X.X., Zhang Y.J., Zhao C.G., Chen N., [J]. Ann Microbiol, 2012, 62: 1625–1634.

[11] Bradford, M., [J]. Anal. Biochem. 1976, 72, 248-254.

[12] Doelle H.W., Ewing K.N., Hollywood N.W., [J]. Adv Biochem Eng, 1982, 23: 1-35.

[13] Han K., Lim H.C., Hong J., [J]. Biotechnol Bioeng, 1992, 39(6): 663-771.

[14] Nahku R., Valgepea K., Lahtvee P.J., Erm S., Abner K., Adamberg K., Vilu R., [J]. J Biotechnol, 2010, 145(1): 60-65.

[15] Colón G.E., Nguyen T.T., Jetten M.S., Sinskey A.J., Stephanopoulos G., [J]. Appl Microbiol Biotechnol, 1995, 43(3): 482-488

[16] Morbach S., Sahm H.,and Eggeling L., [J]. Appl Environ Microbiol, 1995, 61(12): 4315-4320.

[17] Morbach S., Sahm H., AND Eggeling L. [J]. Appl Environ Microbiol, 1996a, 62(12): 4345–4351.

[18] Morbach S., Kelle R., Winkels S., Sahm H., Eggeling L. [J]. Appl Biochem Biotechnol, 1996b, 45(5): 612–620.

[19] Barak, Z., Chipman, D. M., and Gollop, N. [J]. J Bacteriol, 1987, 169, 3750−3756.

[20] Eiteman M.A., Altman E., [J]. Trends Biotechnol, 2006, 24(11): 530-536.

Advanced Materials Research Vols. 989-994 (2014) pp 1003-1006
© (2014) Trans Tech Publications, Switzerland
doi:10.4028/www.scientific.net/AMR.989-994.1003

Developing a sensitive reporter system for monitoring of pancreatic and duodenal homeobox gene 1 (Pdx1) and neurogenin 3 (Ngn3)-mediated transdifferentiation from human hepatic cells into insulin-producing beta-like cells

Chao Xie[1, 2, b], William Donelan[2, c], Shun Lu[2,d] , Li-Jun Yang[1, 2, a]

[1]Key Laboratory of Industrial Microbiology, Ministry of Education and Tianjin City, College of Biotechnology, Tianjin University of Science and Technology, Tianjin, 300457, China

[2]Department of Pathology, Immunology, and Laboratory Medicine, University of Florida College of Medicine, Gainesville, Florida 32610，USA

[a]email:yanglj@pathology.ufl.edu, [b]email:xiechao@ufl.edu, [c]email:wdonelan@pathology.ufl.edu, [d]email:lushun@ufl.edu

Keywords: Pdx1; transdifferentiation; Ngn3; Insulin

Abstract. It is well known that cellular differentiation is not a terminal process. Transdifferentiation is the conversion of one differentiated cell type to another. There are many examples of induced transdifferentiation between cell types by expression of ectopic transcription factors. Here we show that combined lentiviral expression of Pdx1 or Pdx1-VP16 fusion protein and Ngn3 can direct the transdifferentiation of hepatic cells into insulin producing cells. We showed that the Pdx1 or Pdx1-VP16 fusion protein and Ngn3 together synergistically increased transactivation for the insulin gene. This provides a useful model to study the transdifferentiation process.

Introduction

The wide variety of differentiated tissues that arise in a developing organism are due to selective expression and suppression of transcription factors that regulate the downstream gene expression in a given cell type [1][2][3]. Several transcription factors have been discovered that act as “master switch genes” and their expression has been demonstrated to direct differentiation of various cell types and tissues. More recently, it has been found that manipulation of such master gene switches can lead to the transdifferentiation of cells by shifting their gene expression and phenotype from one differentiated cell type to another [4] [5]. Pancreas tissue is composed of several cell types and requires specific transcriptional factors to direct the differentiation of each. Developmental differentiation of pancreatic endocrine cells requires the coexpression of Neurogenin 3 (Ngn3) with Pdx1 [6]. This study we specifically study the role of Pdx1 over expression in Huh7 human hepatocarcinoma cells on the activation of endocrine insulin and provides a useful model to study the transdifferentiation process and understanding the molecular and cellular events in cell type transformations.

Methods

Cell Lines and Cell Culture. Huh7 human hepatocarcinoma cells were cultured in DMEM supplemented with 10% FBS, 1% Penicillin/Streptomycin, and 1% Kanamycin in a 37° incubator with 100% humidity and 5% CO2.

Construction of Plasmids. The human Pdx1 expression plasmid (pCMV6-XL5) was purchased from Origene. The mouse Pdx1 expression plasmid was constructed by insertion of mouse Pdx1 cDNA into BamH1and Xba1 site of pCDNA3 vector (Invitrogen). The truncated mouse Pdx1 expression vectors were constructed by introduction of the stop codon at the amino acid position of 121, 161 and 2001, respectively, using the stander site-directed mutagenesis method. The Rat Insulin I Promoter (RIP) luciferase reporter was constructed by removing the TK promoter from the pRL-TK plasmid and cloning the RIP promoter into this site using the BglII and HindIII restriction sites.

Lentiviral Vector Preparation, Titration, and Transduction. The RIP-GFP reporter was constructed as previously published [7]. The lentiviral vector containing the mouse Pdx1-VP16 fusion gene was constructed as previously published [7] [8]. The lentiviral vectors containing rhGFP and mouse Pdx1 were constructed as previously published [9]. The lentiviral vector containing mouse Ngn3 was constructed by inserting the cDNA of mouse Ngn3 into the pTYF vector cassette under the control of elongation factor-1 alpha (eEF-1α) promoter. Lentiviral vector were generated and titrated by Dr. Lung-Ji Chang at the University of Florida as previously described [10]. For lentiviral transduction, Huh7 cells were transduced with different genes as indicated at a multiplicity of infection (MOI) of 10 in the presence of 10μg/ml polybrene for 24 hours. The transduction efficiency was monitored by transducing Huh7 cells with lentiviral vector encoding rhGFP. The insulin promoter activities in Huh7 cells were detected by observing RIP-GFP expression under fluorescence microscopy.

Transfections and Luciferase Assay. Cells were cultured as previously indicated and transfected with 0.1-1.0μg DNA (as indicated) using Lipofectamine 2000 Reagent (Invitrogen) according to manufacturer's protocol. 0.02μg TK-Luc plasmid was used as a transfection control in all experiments. Cell lysates were harvested and measured 24 hours post transfection using the Dual Luciferase Reporter Kit (Promega) according to manufacturer's protocol except that only 50ul of each substrate reagent was used (as optimized by our lab) to read samples using a Lumat LB 9507 Luminometer (Berthold Technologies). All luciferase assays were done in triplicate.

RT-PCR Analysis. Total RNA was extracted from Huh7 cells transduced with different combinations of transcription factors by using Trizol according to manufacturer's protocol. Gene expression was detected by RT-PCR. The forward and reverse PCR primers were designed (IDT Technologies) to be located in different exons. The reaction was first incubated at 94°C for 3 min in a GeneAmp PCR System 2700 (Applied Biosystems). Amplification was performed for 35 cycles at 94°C for 30s, 56°C for 30s, and 72°C for 30s and followed by 72°C for 7 min. The PCR products were separated in 2% agarose gels by electrophoresis in TAE buffer. Digital images were captured and analyzed with a Quantity One Imager (BioRad).

Results

Pdx1-VP16 and Ngn3 together strongly induced insulin promoter activity. In order to monitor the activation of the insulin gene during the reprogramming of hepatic cells into insulin producing cells, we constructed a lentiviral vector with the rat insulin I promoter driving the green fluorescence protein (RIP-GFP) as a monitor signal. The transduction efficiency of Huh7 cells was determined by lentiviral vector expressing humanized GFP (rhGFP) driven by elongation factor 1 alpha promoter (EF1α), which is active without cell specificity. We observed more than 99% of transduced Huh7 cell expressing GFP at day 2 (data not shown). RIP-GFP was transduced into Huh7 cells with combinations of Pdx1/Ngn3 or Pdx1-VP16 /Ngn3 as indicated. We consecutively observed GFP expression at 48, 72, and 96 hours after Huh7 cells were transduced with Pdx1/Ngn3, or Pdx1-VP16/Ngn3 (Fig. 1). The results show that Pdx1-VP16 is much more effective than Pdx1 to activate RIP-GFP. Green fluorescence was observed in 50% of Huh7 cells transduced with Pdx1-VP16/Ngn3 at day 2 compared with only 2% of cells treated with Pdx1/Ngn3.

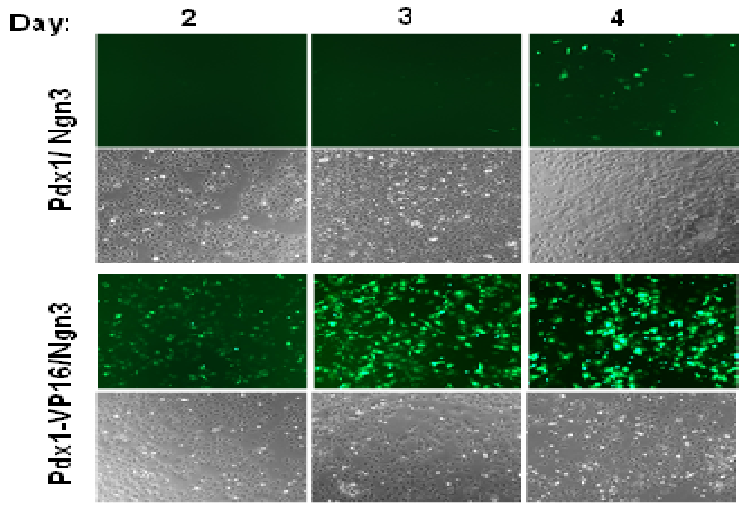

Figure 1 Pdx1-VP16 and Ngn3 together induced insulin promoter activity time related.

Quantitative analysis of the promoter activity of insulin induced by Pdx1 or Pdx1-VP16. By using the luciferase assay we quantitatively analyzed the promoter activity of transcription factors in the transdifferentiated Huh7 cells for several pancreatic transcription factors. Huh7 cells were treated with lentivirus carrying Pdx1, Pdx1-VP16, Ngn3, Pdx1/Ngn3 or Pdx1-VP16/Ng3 for 72 hours and then transfected separately with luciferase reporter genes RIP. The relative luciferase activities are shown in Fig. 2.Ngn3 alone can directly activate RIP promoters.Ngn3 combined with Pdx1 or Pdx1-VP16 further increase RIP activation, indicating Pdx1 and Pdx1-VP16 both have synergistic effect on the activation of insulin genes.

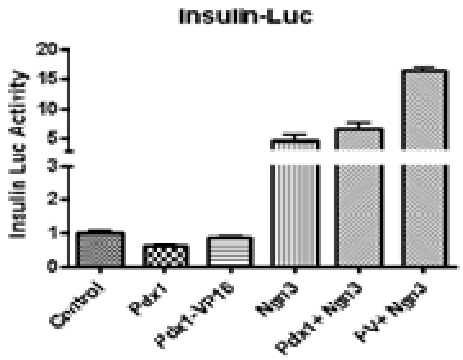

Figure 2 Pdx1-VP16 and Ngn3 together enhance the transcriptional activity of insulin.

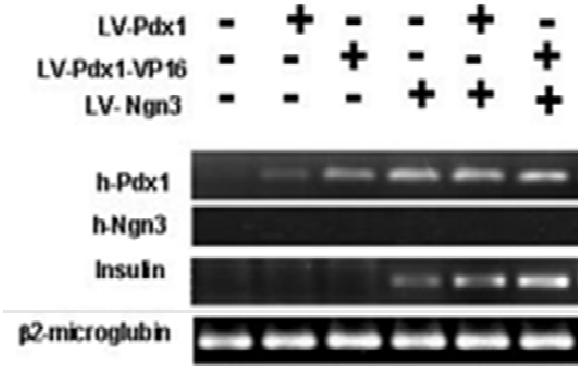

Figure 3 Pdx1-VP16 and Ngn3 together enhance the expression of insulin.

Pdx1 and Ngn3 induced insulin gene expression. To investigate the gene expression profile of Huh7 cells with different treatment after 96 hours, cellular RNA samples were collected and RT-PCR analysis was performed (Fig. 3). β2 –microglubin served as control. We found insulin endogenous expression couldn't be activated by Pdx1 or Pdx1-VP16 alone. Ngn3, Pdx1/Ngn3, and Pdx1-VP16/Ngn3 activated Isl1, which are involved in endocrine pancreas development.

Conclusion

The liver is largely composed of hepatocytes, which occupy 78% of parenchymal liver volume in the rat [11] [12]. Hepatocytes carry out the primary functions of the liver such as metabolism, detoxification, and protein synthesis of several essential compounds including serum albumin,

fibrinogen, and transferrin. The dominant mechanism for controlling the expression of hepatocyte specific genes is at the transcriptional level [13]. The molecular mechanism by which Pdx1 regulates the expression of these hepatic genes has not previously been defined.

In this study, we have established an effective model by lentiviral expression of Pdx1-VP16/Ngn3 into Huh7 cells in which to study the process of hepatic transdifferentiation into insulin producing cells. We have demonstrated that coexpression of Ngn3 with Pdx1 is important for the activation of insulin. Our research will provide a model to screen insight for the mechanism of transdifferentiation of hepatic cells into insulin producing cell by Pdx1.

References

[1] Slack,J.M. & Tosh,D. Transdifferentiation and metaplasia--switching cell types. Curr. Opin. Genet. Dev. 11, 581-586 (2001).
[2] Eguchi,G. & Kodama,R. Transdifferentiation. Curr. Opin. Cell Biol. 5, 1023-1028 (1993).
[3] Li,W.C., Yu,W.Y., Quinlan,J.M., Burke,Z.D. & Tosh,D. The molecular basis of transdifferentiation. J. Cell Mol. Med. 9, 569-582 (2005).
[4] Weintraub,H. et al. Activation of muscle-specific genes in pigment, nerve, fat, liver, and fibroblast cell lines by forced expression of MyoD. Proc. Natl. Acad. Sci. U. S. A 86, 5434-5438 (1989).
[5] Horb,M.E., Shen,C.N., Tosh,D. & Slack,J.M. Experimental conversion of liver to pancreas. Curr. Biol. 13, 105-115 (2003).
[6] Watada,H. Neurogenin 3 is a key transcription factor for differentiation of the endocrine pancreas. Endocr. J. 51, 255-264 (2004).
[7] Cao,L.Z., Tang,D.Q., Horb,M.E., Li,S.W. & Yang,L.J. High glucose is necessary for complete maturation of Pdx1-VP16-expressing hepatic cells into functional insulin-producing cells. Diabetes 53, 3168-3178 (2004).
[8] Tang,D.Q. et al. In vivo and in vitro characterization of insulin-producing cells obtained from murine bone marrow. Diabetes 53, 1721-1732 (2004).
[9] Tang,D.Q. et al. Reprogramming liver-stem WB cells into functional insulin-producing cells by persistent expression of Pdx1- and Pdx1-VP16 mediated by lentiviral vectors. Lab Invest 86, 83-93 (2006).
[10] Chang,L.J. & Zaiss,A.K. Lentiviral vectors. Preparation and use. Methods Mol. Med. 69, 303-318 (2002).
[11] Blouin,A., Bolender,R.P. & Weibel,E.R. Distribution of organelles and membranes between hepatocytes and nonhepatocytes in the rat liver parenchyma. A stereological study. J. Cell Biol. 72, 441-455 (1977).
[12] Zhao,R. & Duncan,S.A. Embryonic development of the liver. Hepatology 41, 956-967 (2005).
[13] Derman,E. et al. Transcriptional control in the production of liver-specific mRNAs. Cell 23, 731-739 (1981).

Advanced Materials Research Vols. 989-994 (2014) pp 1007-1010
© (2014) Trans Tech Publications, Switzerland
doi:10.4028/www.scientific.net/AMR.989-994.1007

A method for the determination of atropine in pharmaceutical preparation using CE-ECL

Qian XIANG, Xiaodong YANG[a*], Ying GAO [b*]

Changchun Institute of Technology, Changchun 130021, China

[a]email: y86908051@126.com, [b]email:gaoy5680@163.com

Keywords: capillary electrophoresis-electrochemiluminescence (CE-ECL); tris(2,2'-bipyridyl) ruthenium ; atropine

Abstract. In this paper, a sensitive determination method for atropine based on end-column electrochemiluminescence of tris(2,2'-bipyridyl) ruthenium (Ⅱ) detection is described. The conditions affecting separation and detection were investigated. Favorable ECL intensity of atropine was achieved in a solution consisting 5 mmol/L $Ru(bpy)_3^{2+}$ and 50 mmol/L phosphate at applied voltage of 1.20V. The standard curve was linear between 1 and 20 μmol/L for atropine. The calibration equation and regression coefficients were: $y = 128.38x-36.76$ and $R = 0.998$ in terms of peak height response as a function of analyte concentration. A detection limit of 5×10^{-8} mol/L (S/N= 3) was achieved. The proposed method was applied satisfactorily to the determination of atropine in three pharmaceutical preparations.

Introduction

Atropine is an anticholinergic drug, which produces many effects in the body, including relief from spasms of the gastrointestinal tract, the bladder and the biliary tract. This is helpful in controlling conditions such as colitis, spastic bladder, diverticulitis, renal and biliary colic, peptic ulcer and irritable bowel syndrome. At present, several analytical methods including chemiluminescence μTAS [1], reversed micellar mediated chemiluminescence technology [2] and HPLC [3] have been reported for the analysis of atropine in pharmaceutical preparation.

The CE–ECL is a sensitive analytical technology for the determination of analytes containing tertiary amine group because the tertiary amine has high enhancement effect on the $Ru(bpy)_3^{2+}$ ECL. The development of ECL detection for CE and applications of tris(2,2'-bipyridyl)ruthenium(II) in electrochemiluminescence have been critically reviewed [4]. In this paper, a end-column ECL method based on $Ru(bpy)_3^{2+}$ system has been developed for the determination of atropine in pharmaceutical preparation. Electrochemiluminescence (ECL) reagent $Ru(bpy)^{2+}$ was put in the cell positioned at the capillary outlet, by applying a proper potential, the atropine can react with $Ru(bpy)^{2+}$ and emit photons simultaneously. By measuring the intensity of the emitted light, we can get the corresponding concentration of atropine. This method could be used in sensitive and highly selective monitoring atropine in small volume of pharmaceutical preparation, indicating that it was practical and valuable in clinical and biochemical laboratories for pharmaceuticals analysis and quality control.

Experimental

Tris(2,2'-bipyridyl) ruthenium (Ⅱ) chloride hexahydrate was purchased from Aldrich Chemical Co.(Milwaukee, WI, USA). Atropine sulfate were obtained from Sigma (St. Louis, MO, USA). All reagents used in the analysis were of analytical purity and were from Beijing Chemical Reagent Factory (Beijing, China). The double-distilled water was prepared using Mili-Q ultra-high purity water system (Millipore, Bedford, MA, USA). All solutions were made up using double-distilled water and filtered through a 0.45 μm membrane before use. Atropine Sulfate Injection, Compound Diphenoxylate Tablets and Atropine Sulfate Tablets were obtained from local pharmacy (Jilin, China).

At the beginning of experiment each day, in order to maintain an active and reproducible inner surface, the capillary was activated with 0.1 mol/L NaOH for 5 min, followed by double-distilled water for 5 min and running buffer for 5 min. Sample separation was performed in a 50 cm long fused-sillica capillary (Yongnian Optical Fabric Factory Hebei, China) with a 25 μm internal diameter. Electrokinetic injections were performed at 10 kV for 7 s. Electrophoresis separation voltage was set at 15 kV. Every run was repeated at least three times.

Separation and detection experiments were carried out with a CE–ECL instrument (Xi'an Remax Electronics Co., Xi'an, China), consisting of a high-voltage power supplier for separation and injection, a potential control system, a chemiluminescence detection system, and a data processor. A solution of 5 mmol/L $Ru(bpy)_3^{2+}$ and 50 mmol/L at pH 7.0 was added to the ECL detection reservoir. A three-electrode configuration was employed in the detection cell consisting of a 500 μm Pt disk as a working electrode, Ag/AgCl as a reference electrode and Pt wire as a counter electrode. A voltage of 800 V was supplied at photomultiplier tube for collecting the ECL signal.

A 0.2 g amount of pulverized Compound Diphenoxylate Tablets or Atropine Sulfate Tablets was weighted accurately, fragmented in an ultrasonic bath at 40 °C with 1 ml water as the solvent for 10 min. The extracts were filtered through a 0.45 μm membrane before use and stored this at 4°C in a refrigerator.

Results and discussion

The cyclic voltamogram of $Ru(bpy)_3^{2+}$ solution was obtained. As is shown in Fig. 1, the oxidation current of $Ru(bpy)_3^{2+}$ increased to a peak at about 1.15 V (dotted line). However, for the system consisting of atropine and $Ru(bpy)_3^{2+}$, the rise both in the anodic current and in the cathodal current were observed as the potentials were scanned to +1.15 and −1.13V (solid line), respectively. It indicated that atropine can react with the ruthenium species.

The hydrodynamic voltammogram for the atropine was investigated for assessing the influence of the detection potential on the ECL responses in a potential range of 1.0 ~ 1.3 V (Fig.2). At lower voltage, a very weak ECL response was observed. Until at 1.1 V, the increase of ECL intensity starts to be visible. Finally, the ECL intensity of atropine reached a plateau at 1.2 V. Thus applied voltage 1.2 V was chosen for further experiment.

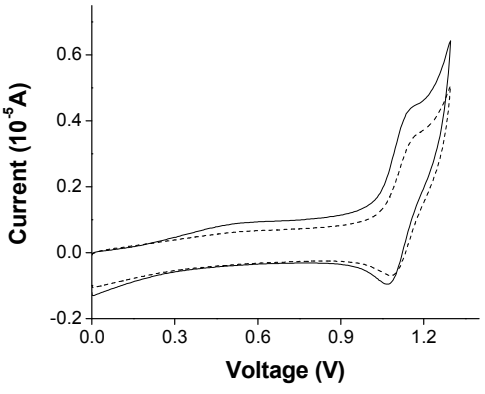

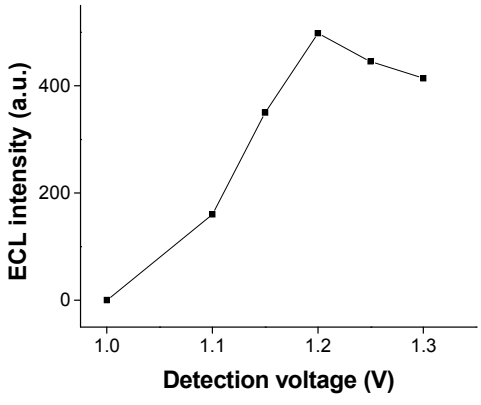

Fig.1. Cyclic voltammogram of atropine and $Ru(bpy)_3^{2+}$ Fig.2. Effect of detection voltage on ECL intensity of atropine

The detection buffer pH value has a significant effect on the ECL response of the analyte in detection cell. The previous work indicated that $Ru(bpy)_3^{2+}$ has a good ECL efficiency in a weak basic solution due to the deprotonation of the amine species to form a reducing free radical intermediate for the ECL coreaction [5-9]. Fig. 3 gave the effect of buffer pH on the ECL response of atropine. Similar to the amines ECL reaction, with increasing pH of buffer, the ECL intensity of atropine increased remarkably. The optimized ECL intensity of the drug is obtainable at phosphate buffer at pH 7.0.

The separation voltages from 11 to 18 kV were studied. When the separation voltage increases, the electroosmosis flow increases, and more analytes reached the working electrode within a given time. Consequently, ECL intensity increases and migration time shortens at high separation voltage. In this study, a separation voltage of 15 kV was chosen considering the detection sensitivity, separation performance, and migration time.

Under the optimal conditions, namely ECL detection at 1.2 V, electrophoresis separation voltage at 15 kV, 5mmol/L $Ru(bpy)_3^{2+}$ and 50mmol/L phosphate buffer at pH 7.0 in the detection reservoir, the calibration graph of atropine concentration versus ECL ntensity was linear in the range from 1 to 20 μmol/L. The egression equation could be expressed as: $y = 128.38x-36.76$ with a correlation coefficient of 0.998. Detection limit of 5×10^{-8} mol/L for atropine was obtained (S/N= 3).

The precision of the proposed method was determined by reduplicate injections (n =7) of 1×10^{-5} mol/L atropine standard solution. The relative standard deviations of migration time and ECL intensity were 0.17％ and 5.16％, respectively.

The developed CE–ECL method was employed for the determination of atropine in three drugs under the optimized conditions. Identification of the analyte was confirmed by comparing the electropherograms of the drug solution with that of the drug solution spiked with atropine, where the increase of peak height at certain migration time was directly proportional to the amount spiked with atropine.

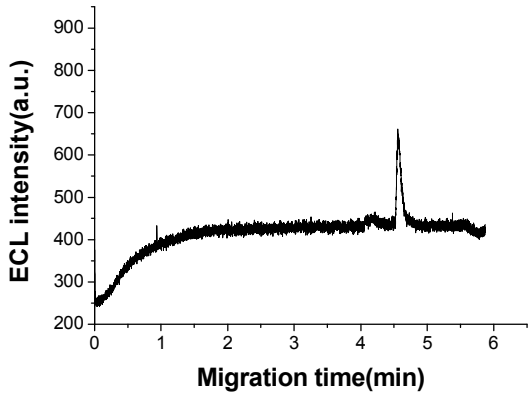

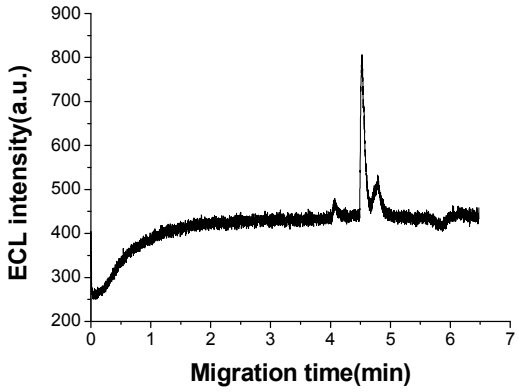

Fig. 3 Electropherogram of diluent Atropine Sulphate Injection. Fig. 4 Electropherogram of Compound Diphenoxylate Tablets

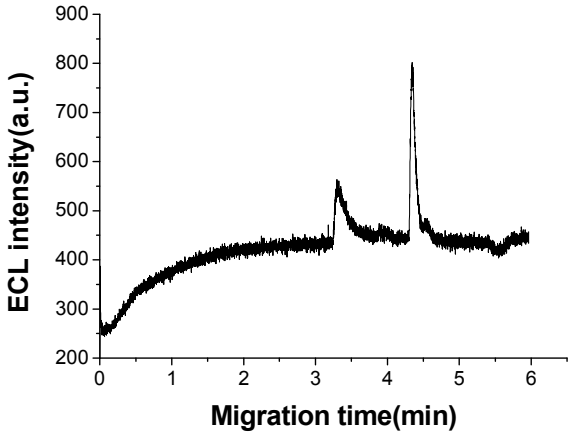

Fig.5. Electropherogram of Atropine Sulfate Tablets

Three drugs included Atropine Sulphate Injection, Compound Diphenoxylate Tablets and Atropine Sulfate Tablets. Fig.3, Fig.4 and Fig.5 show typical electropherograms of the three drugs with the optimized conditions. The analytes are visible as neat electrophoretic peaks without interference.

Concluding remarks

CE-ECL method was studied for determination of atropine in pharmaceutic preparations. The developed method was found not only a good alternative for the rapid determination of atropine with good selectivity, wide linearity and reliable stability, but also an efficient supplementary technique for the preliminary investigation of other alkaloids in pharmaceutic preparation.

Acknowledgements

This project was supported by National Natural Science Foundation of China (No. 51275055), the Scientific and Technological Developing Scheme of Jilin Province (No.201205042), the Natural Science Foundation of Jilin Province, China (No. 20140101153JC).

References

[1] Paul A. Greenwood, Carolyn Merrin, Tom McCreedy, Gillian M. Greenway. Chemiluminescence μTAS for the determination of atropine and pethidine [J]. Talanta, 2002 56 539-545.

[2] Terufumi Fujiwara, Imdad U Mohammadzai, Katsumi Murayama, and Takahiro Kumamaru. Solvent extraction coupled on-line to a reversed micellar mediated chemiluminescence detection dystem for trace-level determination of atropine [J]. Anal. Chem. 2000 72 1715-1719.

[3] Yan Ping, Wei Jun, Ni Zhen-Yu, Xie Jian-Wei. Simultaneous determination of pyraloxime methylchloride, atropine sulfate, benactyzine hydrochloride in Jielin Injection by ion pair-HPLC [J]. Chinese Journal of Spectroscopy Laboratory. 2003 20 419-423.

[4] Li Jing, Wang, Erkang. Applications of tris(2,2'-bipyridyl)ruthenium(II) in electrochemiluminescence [J]. Chemical Record. 2012 12(1) 177-187.

[5] Ying Gao, Yuanhong Xu, Bingyan Han, Jing Li, Qian Xiang, Sensitive determination of verticine and verticinone in Bulbus Fritillariae by ionic liquid assisted capillary electrophoresis–electrochemiluminescence system [J]. Talanta 2009 80 448–453.

[6] Qian Xiang, Hao Wang, Yuanhong Xu, Liang Sun, Ying Gao. Detection of galanthamine in Bulbus lycoridis radiatae by capillary electrophoresis with an end-column electrochemiluminescence of tris(2,2'-bipyridyl)ruthenium(II) [J]. Asian Journal of Chemistry 2011 23(4) 1553-1556.

[7] Hanwen Sun, Liqing Li, Ming Su. Simultaneous determination of lidocaine, proline and lomefloxacin in human urine by CE with electrochemiluminescence detection [J]. Chromatographia, 2008 67 399–405.

[8] Liu Yan-Ming, Cao Jun-Tao, Tian Wei, Zheng Yan-Li. Determination of levofloxacin and norfloxacin by capillary electrophoresis with electrochemiluminescence detection and applications in human urine [J]. Electrophoresis 2008 29 3207-3212.

[9] Zhifeng Fu, Lin Wang, Yonghong Wang. Capillary electrophoresis–lectrochemiluminescent detection of N,N-dimethyl ethanolamine and its application in impurity profiling and stability investigation of meclophenoxate[J]. Analytica Chimica Acta 2009 638 220–224.

Advanced Materials Research Vols. 989-994 (2014) pp 1011-1014
© (2014) Trans Tech Publications, Switzerland
doi:10.4028/www.scientific.net/AMR.989-994.1011

Effect of natural clarifying agents ZTC1+1 Ⅱ on purification of *Angelica* polysaccharides

ChunLei Li[1,a], Yun Men [1,b], Lin Yang[1,c], AiMei Yang[1,d],Qi Shang[1,e]

[1]School of Life Science and Engineering, Lanzhou University of Technology, Lanzhou, 730050, People's Republic of China, fax number: 86-931-2973924

[a]E-mail: licl@lut.cn, [b]E-mail:menyun19@163.com, [c]E-mail:yanglin-401@163.com,

[d]E-mail: aimeiyang@163.com, [e]E-mail: sq490580778@qq.com,

Keywords: natural clarifying agentsZTC1+1Ⅱ; purification, *Angelica*; Polysaccharide;

Abstract. Apply the univariate and orthogonal experiments, the purity of polysaccharide as index, to optimize the best purification conditions of natural clarifying agents ZTC1+1Ⅱon Angelica polysaccharides. To determine the optimal temperature, the amount of clarifying agent, the concentration of the extracting solution of *Angelica*, flocculation time, to select stable and feasible polysaccharide purification process.

Introduction

Angelica (*Angelica* sinensis) is a common traditional Chinese herb, used the roots as medicine, which has been used for promoting blood circulation, relieving pain, laxative,etc. *Angelica* polysaccharides has wide bioactivities, such as gastrointestinal protection[1-3], anti-ulcer[4], antitumor[5], anti-hepatic, injury[6], and radioprotecti-ve action[7]. The natural clarifying agents has a lot of species on the market, such as the 101 juice clarifying agents, chitosan, ZTC1+1 natural clarifying agentsⅡ, Ⅲ. References indicates natural clarifying agents ZTC1+1 Ⅱhas the better effect and economic benefits [8-10], natural clarifying agents ZTC1+1 Ⅱ is a new type of pharmaceutical adjuvant, safe and non-toxic, the clarifying agents consists of two parts, one part of the main flocculation (A), another part of the auxiliary flocculation (B), they can removed the starch, tannin, mucus, proteins and other macromolecules impurities in the extracting solution and preserve the main ingredient [11-12]. We report herein the effect of natural clarifying agents ZTC1+1 Ⅱ on the purification of Angelica polysaccharides.

Investigations, results and discussion

To measure the polysaccharide content by the phenol - sulfuric acid method[15] , take the glucose content (mg) as abscissa, absorbance for ordinate, get a regression equation: $y=0.0562x+0.009$($R^2 = 0.9994$). According to the above method, take the treated and untreated solutions, measure the polysaccharide content and calculate the amount of purity.

Results

Univariate test data was listed as Table. 2, and Orthogonal test datas were listed as Table. 3, 4

Table 2 Univariate test data

Group	Polysaccharide purity					
concentration	blank0.1	blank0.2	blank0.5	0.1	0.2	0.5
	65.95%	65.76%	66.84%	67.28%	68.26%	67.27%
dosage	blank	2% B+1% A	4% B+2% A	6% B+3% A	8% B+4% A	
	62.86%	66.34%	62.58 %	60.78%	67.96%	
temperature	blank	20℃	40℃	60℃	80℃	
	61.03%	61.10%	63.56%	63.08%	61.09%	
time	blank	2h	6h	10h	12h	
	62.17%	62.74%	61.69%	63.74%	62.26%	

Table 3 Orthogonal test data

Number	A	B	C	D	Polysaccharide purity
1	1	1	1	1	61.95
2	1	2	2	2	66.06
3	1	3	3	3	64.47
4	2	1	2	3	65.37
5	2	2	3	1	59.97
6	2	3	1	2	60.54
7	3	1	3	2	59.64
8	3	2	1	3	58.62
9	3	3	2	1	61.95
k1	64.160	62.320	60.370	61.290	
K2	61.960	61.550	64.460	62.080	
k3	60.070	62.320	61.360	62.820	
range	4.090	0.770	4.090	1.530	

Table 4 Orthogonal test data Analysis

Factors	DEVSQ	DOF	F	Sig
A	124.695	2	15.375	0.000
B	6.187	2	0.763	0.481
C	40.259	2	4.946	0.019
D	34.481	2	4.251	0.031
Deviation	72.994	18		

Discussion

In the univariate test, the purity of polysaccharide is highest, when the conditions are: 0.2g / ml, 8% B +4% A, 40 ℃, elected the best purification conditions of *Angelica* polysaccharides by natural clarifying agents ZTC 1+1 Ⅱ. In the Orthogonal test, according to the F, the degree of influence on the purity of *Angelica* polysaccharide is clarifying agents dosage, temperature, concentration; and indicate that $P<0.05$ in amount, temperature, concentration from Sig, so the 3 factors were significant, but $P>0.05$ in flocculation time, not significant.

Experimental

Equipment

Visible spectrophotometer (Precision and Scientific Equipment Co. Ltd. in Shanghai), Analytical balance, Digital thermostat water bath(H-SS, Medical Equipment factory in Jiangsu province), Rotary evaporator(RE-5000, Bilang Equipment Co. Ltd. in Shanghai), Incubators (HH-B11, Yuejin medical Equipment Co., Ltd. in Shanghai), Low-speed desktop centrifuge (TDL-5-A, Shanghai

Anting scientific Equipment Factory), natural clarifying agents ZTC1+1Ⅱ (Zheng tian cheng Technology Co., Ltd. In Tianjin).

Materials

Angelica, Phenol, Sulfuric acid, Ethanol (95%), Glucose.

Methods of test

Preparation of the extracting solution of *Angelica*

The dried powder of *Angelica* was extracted by distilled water twice (the extract condition: 1:8 and 1:6 of solid-liquid ratio, 2h of extraction time, 95°C for extraction temperature) .The extract was concentrated to 0.1g/ml.

Univariate test

Prepare the natural clarifying agents ZTC1+1Ⅱsolution: A and B form the solution of 1% with distilled water and 1% acetic acid solution respectively, after swelling 24h and reserve [13]. Here, set a blank test for each group, the supernatant after clarifying was concentrated to 1g/ml, and measured the polysaccharide purity.

The concentration of the extracting solution influence on clarifying agents effect. Set three concentrations: 0.1g/ml, 0.2g/ml, 0.5 g/ml. Under certain temperature and flocculation time, added 8%B +4%A by volume fraction, then centrifuged 10min (5000r/min) and concentrated the supernatant to 1g/ml, repeated the test twice.

The dosage of clarifying agents. Set four dosage: 2% B +1% A, 4% B +2% A, 6% B +3% A, 8% B +4% A (the sequence of natural clarifying agents was clarifier B before clarifier A, 2h intervals, stirred it every 30min) [14]. Keep the same temperature and time, place overnight (12h), then centrifuged 10min (5000r/min) and concentrated the supernatant to 1g/ml, repeated the test twice.

The flocculation temperature of clarifying agents. Set four temperature: 20℃, 40℃, 60℃,80℃. Added 8%B and 4%A after heated 15min in each temperature, (2h intervals ,stirred it every 30min), place overnight (12h), then centrifuged 10min (5000r/min) and concentrated the supernatant to 1g/ml, repeated the test twice.

The flocculation time of clarifying agents. Set four time: 2h, 6h, 10h, 12h. Added 8%B and 4%A (2h intervals ,stirred it every 30min), stand 2h, 6h, 10h, 12h respectively, then centrifuged 10min (5000r/min) and concentrated the supernatant to 1g/ml, repeated the test twice.

Orthogonal test

To take the amount of clarifying agent (A), flocculation time (B), flocculation temperature (C) and solution concentration (D) as factors, each factor were set 3 levels, as Table.1.

Table 1 Level of form factors

levels	A (ml/100ml)	B(h)	C(℃)	**D(g/ml)**
1	4% B+2% A	4	40	0.1
2	6% B+3% A	8	60	0.2
3	8% B+4% A	12	80	0.5

Acknowledgment

The author Aimei Yang was the corresponding author.

References

[1] C. H. Cho, Q. B. Mei, P. Shang, S. S. Lee, H. L. So, X. Guo, and Y. Li, *Planta Med*.,2000, 66, 348.

[2] Y. N. Ye, E. S. L. Liu, V. Y. Shin, M. W. L. Koo, Y. Li, E. Q. Wei, H. Matsui, and C.H.Cho,*Biochem.Pharmacol*.,2001, 61, 1439.

[3] Y. N. Ye, W. L. M. Koo, Y. Li, H. Matsui, and C. H. Cho, *Life Sci.*, 2001, 68, 961.

[4] Y. N. Ye, H. L. So, E. S. L. Liu, V. Y. Shin , and C. H. Cho, *Life Sci.*,2003, 72, 925

[5] P. Shang, A. R. Qian, T. H. Yang, M. Jia, Q. B. Mei, C. H. Cho, and Z. N. Chen, *World J. Gastroenterol.*,2003, 9, 1963.

[6] Y. N. Ye. E. S. L. Liu, Y. Li, H. L. So, C. C. M. Cho, H. P. Sheng, S. S. Lee, and C. H. Cho, *Life Sci*.,2002.69.673.

[7] Q. B. Mei, J. Y. Tao, H. D. Zhang, Z. X. Duan, and Y. Z. Chen, *Acta Pharmacol*. *Sin.*, 1988,9,279.

[8] Z. Cheng, B. Y. Wang, Y. Yu, *Journal of Hebei Traditional Chinese Medicine and Pharmacology* [in Chinese], 2003,18(2):27.

[9] H. Yan, *Guiding Journal of Traditional Chinese Medicine and Pharmacy* [in chinese], 2005,11(1):80.

[10] G. B. Guo, H. B. Ning, *Chinese Herbal Medicines* [in Chinese], 2011, 18(4):58.

[11] H. N. Wang, Y. Z. Xie, F. Y. Fan, *China Pharmacy* [in Chinese], 2008, 19(21):1625-1628.

[12] Z. X. Zhu, Q. W. Liang, W. L. Cheng, *Journal of Pharmaceutical Practice* [in Chinese], 2009, 27 (4):274-278.

[13] N. Zhu, Y. Y. Zhang, Y. N. Gao, *Chinese Traditional Patent Medicine* [in Chinese], 2008,30(10):1439-1443.

[14] Z. H. Guo, Q. Liang, X. Liu, S. X. Jiang, *Lishizhen Medicine and Materia Medica Research* [in Chinese], 2005,16(9):876-877.

[15] L. L. Wang, L. M. Zhang, Journal of TianJin University of Science and Technology, 2006, 12 (4):29-32.

Advanced Materials Research Vols. 989-994 (2014) pp 1015-1019
© (2014) Trans Tech Publications, Switzerland
doi:10.4028/www.scientific.net/AMR.989-994.1015

Effect of Ginkgo Biloba Extract on Contractility Enhancement of diaphragm of Rats with Type 2 Diabetes

Xusheng LI [1, a], Renyan Wu [2, b], Ye Hu [1, c]

[1]Medical college, Jinhua Polytechnic, Jinhua City, Zhejiang, 321017, China
[2]Department of educational supervision, Jinhua Polytechnic, Jinhua City, Zhejiang, 321017, China

[a]email: jhclxs@hotmail.com, [b]email: wurenyan@163.com, [c]email: huye8254@vip.sina.com

Keywords: Diabetes Mellitus; Ginkgo Biloba Extract; Diaphragm; Contraction Capacity

Abstract. To investigate the effects of Ginkgo biloba extract (GbE) on the activities of energy metabolism enzymes and contraction capacity of diaphragm from type 2 diabetic rats. Forty SD mile rats were randomly divided into normal control group (n=10) and model group (n=30). Type 2 diabetes models were induced by feeding with high-sucrose-high-fat diet and intraperitoneal injecting 25mg/kg streptozotocin. 20 successful models were rearranged to two groups: diabetic group and GbE treatment group, 10 rats in each. Then the saline and $8mg \cdot kg^{-1} \cdot d^{-1}$ of GbE were respectively intraperitoneal injected, once a day continuously for 8 weeks. Then diaphragm contractility was assessed using Peak twitch tension (Pt), Maximum tetanic tension (P0) and fatigue index (FI) in vitro diaphragm strip preparations. Cytochrome oxidase (CCO), lactate dehydrogenase (LDH) and succinate dehydrogenase (SDH) in diaphragm were detected and the varieties of diaphragm ultrastructure were observed. Compared with control group, Pt, P0 and FI in diabetic group decreased significantly ($P < 0.01$); the activity of CCO, LDH and SDH in the tissues was obviously reduced than those in control group ($P < 0.01$). The ultrastructure in diabetic group under electron microscope indicated that diaphragm mitochondrions swelled and degenerated. The above changes were inhibited by GbE. GbE can enhance contraction capacity of diaphragm from type 2 diabetic rats by increasing the aerobic oxidation capacity, glycolytic capacity and the function of respiratory chain.

Introduction

As a principal part of glucose consumption under insulin stimulation, skeletal muscles are main target sites of diabetes. As an important respiratory muscle, diaphragm has a characteristic of lifetime sustained contractility, and plays a crucial role in maintaining pulmonary function of organisms [1]. Previous study showed that ginkgo biloba extract (GbE) could reduce diaphragm injury caused by free radical and excessive nitric oxide on rats with type 1 diabetes [2]. This study is intended to explore the impact of GbE on diaphragm contractility of rats with type 2 diabetes and on enzyme activity of energy metabolism.

Materials and Methods

Experimental Drug and Reagent. The GbE was purchased from Beijing Double-Crane Natural Pharmaceutical Co., Ltd. (Shuxuening Injection, batch number: 319163.0606) with each strip containing 5 ml and equated to 17.5 mg of GbE (containing 4.2 mg of total flavonoid glycosides and 0.70 mg of Ginkgolide). The streptozontocin (STZ) was bought from Sigma and was used to be dissolved in 0.1 mmol/L citric acid buffer before application, pH=4.0. Test kits for cytochrome oxidase (CCO), succinate dehydrogenase (SDH) and lactate dehydrogenase (LDH) determination were purchased from Nanjing Jiancheng Bioengineering Institute.

Experimental Animals and Schemes. 40 clean male SD rats with weight of 180-250g were provided by Laboratory Animal Center of Wenzhou Medical University, 10 of which were for control group and 30 of which were for model group according to the random number table. The control group was fed with common fodder and the model group was fed with high-sugar and

high-lipid fodder (composition: 10.0% lard, 20.0% sucrose, 2.5% cholesterol, 1.0% cholate and 66.5% routine fodder), and the two groups were free to eat and drink during the experiment. 4 weeks later, rats of the model group were intraperitoneally injected with STZ as per 25mg/kg after 16h of fasting, and rats of the control group were intraperitoneally injected with equivalent volume of citric acid buffer. After 72h, for blood sampling at caudal vein, a glucometer (one Touch Ⅱ type, JNJ China) was used to measure caudal vein blood glucose, and results ≥13.8mmol/L was considered as modeling success. 20 successfully established rats were randomly selected to be divided into two groups: the diabetic group and GbE treatment group. Rats of the GbE treatment group were intraperitoneally injected with GbE with dosage of $8mg \cdot kg^{-1} \cdot d^{-1}$ and rats of the control group and diabetic group were intraperitoneally injected with equivalent volume of normal saline, once per day for 8 weeks.

Diaphragm Contractility Measurement. Under anesthesia of pentobarbital intraperitoneal injection, the abdominal cavity was rapidly cut. Diaphragm of the left costal region (including the central tendon and portion of ribs) was taken and stored in plate with Krebs solution. Mixed gas of 95% O_2 and 5% CO_2 was continuously induced. The diaphragm was cut into muscle strips with width of about 0.8 cm in the direction of muscle fiber for use. By referring to test methods of Coombes and Xingping Shen et al. [3, 4], muscle strips were vertically suspended in Maclntyre bath tube filled with 37℃ Krebs solution (95% O_2, 5% CO_2). The rib end was fixed at bottom of the tube and the central tendon was connected to a tension convertor (Speck Instrument Co., Ltd.). The muscle was adjusted to the optimum initial length (L0) and stabilized for 20 min. Two platinum electrodes were placed at both ends of the muscle strip and the diaphragm muscle was stimulated by electronic stimulator with voltage exceeding the limit (about 20V). Output signals of the tension convertor were recorded by a smart eight-channel physiological recorder. Parameters measured are shown as follows:

(1) Single contractile tension (Pt): Pt at L0 of each muscle strip was measured for two times, the interval of stimulations (strength 20.00V, waviness width 2 ms) was 2 min. The average value of two times was considered as measured value and was corrected with cross-sectional area (CSA) of the muscle (unit: kg/cm_2) [4].

(2) Maximum tetanic tension (P0): kept for 10 min after single contraction stimulation, stimulation of 100 Hz, 20.00V, 2 ms waviness width and 400 ms string length was applied on the muscle strip to measure P0. The value was corrected with CSA (unit: kg/cm_2).

(3) Fatigue index (FI): applied stimulation on the muscle strip with 20.00V, 2 ms waviness width, 30 strings per minute, 5 for each string, 5Hz per wave, the interval of strings was 1s and the total simulation duration was 10 min to reach diaphragmatic fatigue. 2 minutes later, measured the tension after fatigue and took the average value of two times as measured value. The FI value was the ratio of the measured value and Pt.

Enzyme Activity Assay of Diaphragmatic Energy Metabolism. Prepared muscle strips and took portion of diaphragm to weigh and cut it into pieces. Normal saline was added with proportion of 1:10 (mass ratio) to make homogenate. Centrifuged for 10 min at 400×g and took 200 μl of supernatant to dilute to 5 times volume concentration and then assayed the enzyme activity. Protein levels were assayed respectively by Coomassie brilliant blue method. The operation was in strict accordance with the kit instruction.

Diaphragm Ultra Microstructure Observation. Took the diaphragm tissues and prepared into 1 mm 3 clips. Fixed the clips in 2.5% glutaral solution and rinsed by PBS generally. Dehydrated with graded acetone and embedded by Epon812. Sliced with LKB ultra microtome and then observed under Hitachi H600A transmission electron microscope.

Data Statistics. The data was represented as mean±standard deviation ($\bar{x} \pm s$). Statistical analysis was conducted with SPSS 10.0. For multi-group comparison, one-way analysis of variance was used; for comparison of two groups, *t*-test was used.

Test results

Diaphragmatic Contractility Comparison of Rats Groups. Compared with the control group, Pt, P0 and FI of diaphragms of rats in the diabetic group were obviously reduced ($P < 0.01$); Pt, P0 and FI of diaphragms of rats in the GbE treatment group were significantly higher than that of rats in the diabetic group ($P < 0.05$, Table 1).

Table 1. Comparison of contraction capacity in diaphragm of the three groups ($\bar{x} \pm s$)

Group	n	P_t (kg/cm^2)	P_0 (kg/cm^{-2})	FI
Control	10	0.73±0.11	1.96±0.17	0.46±0.10
Diabetic	9	0.37±0.12 [b]	1.09±0.33 [b]	0.29±0.04 [b]
GbE treatment	10	0.52±0.16 [b c]	1.56±0.50 [a c]	0.40±0.13 [c]

[a] $P<0.05$, [b] $P<0.01$ *vs* control; [c] $P<0.05$ *vs* diabetic

Diaphragmatic Energy Metabolism Enzyme Comparison of Rats Groups. Compared with the control group, CCO, LDH and SDH activities of rats in the diabetic group were obviously reduced ($P < 0.01$); CCO, LDH and SDH activities of rats in the GbE treatment group were significantly higher than that of rats in the diabetic group ($P < 0.01$, $P < 0.05$, Table 2).

Table 2. Comparison of the activities of energy metabolism enzymes in diaphragm of the three groups ($\bar{x} \pm s$)

Group	n	CCO (U/mg pro)	LDH (U/g pro)	SDH (U/mg pro)
Control	10	32.44±5.67	1.62±0.27	15.57±1.16
Diabetic	9	21.65±7.41 [b]	1.34±0.32 [b]	10.32±1.80 [b]
GbE treatment	10	28.91±6.46 [c]	1.48±0.39 [c]	13.34±2.08 [d]

[b] $P<0.01$ *vs* control; [c] $P<0.05$, [d] $P<0.01$ *vs* diabetic

Diaphragm Ultra Microstructure Observation. Regarding to rats in the normal control group, mitochondria of the diaphragm were in the shape of a round or ellipse with complete membrane and no swelling. The mitochondrial cristae were closely and regularly arranged in concentric circles or longitudinal rows. The muscle fibers were aligned and closely arranged with clear sarcomere bands (Figure 1A). Concerning rats in the diabetic group, diaphragm mitochondrial swelling existed and the membrane was obscure with portion ruptured. Cristae were disorganized with amount reduced or cristae even disappeared and vacuoles formed. The muscle fibers organization was in a mass (Figure 1B). For rats in the GbE treatment group, ultra microstructure of the diaphragmatic mitochondria was obviously better than that of rats in the diabetic group. Most mitochondrial cristae were regularly arranged and minority of them were swelling, obscure and ruptured or with vacuoles. The muscle fibers were regularly arranged with clear bands (Figure 1C).

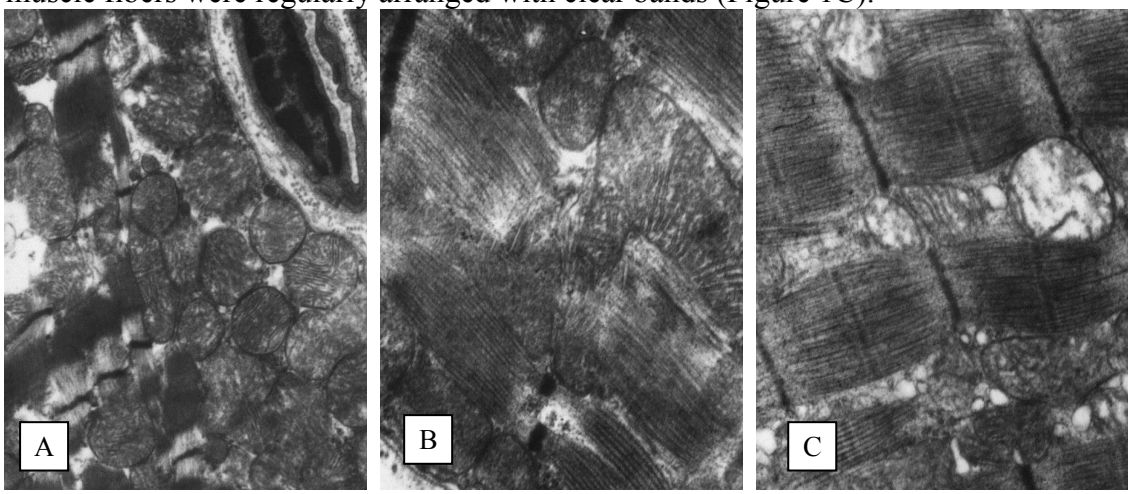

Fig.1. Ultrastructure of diaphragm from three groups

A：Control group（×10 k）; B：Diabetic group (×20 k)；C：GbE treatment group（×20 k）

Conclusion

The hyperglycemic state of diabetes generally had toxic effect and skeletal muscles were main part of diabetic damages. Damages of diabetes to diaphragmatic structure and functions were different from that to other skeletal muscles [5]. Besides general biochemical, physiological and structural functions of skeletal muscles, diaphragm had a characteristic of lifetime sustained contractility, which was crucial for maintaining normal pulmonary function. For rats fed with high-sugar and high-lipid fodder as well as low-dose STZ, the fasting blood glucose and insulin level were significantly increased with hyperlipidemia accompanied. Characteristics of type 2 diabetes emerged in these rats [6]. Results of this experiment showed that diaphragmatic contractility (Pt and P0) and fatigue index (FI) of the rat models were reduced, which was similar to previous study results [4]. Diaphragmatic damages of rats with type 2 diabetes were verified through electron microscope inspection.

Enzyme was an essential substance for metabolic activities of organism. In respiratory muscles, regular activities of enzymes (including CCO and SDH) were vital foundation for keeping respiratory movement. Located at inner mitochondrial membrane, CCO, which was the last electron transferrer in the respiratory chain, could directly transfer electron to oxygen to stimulate it into oxygen ions. As CCO was the terminal of respiratory chain, the intensity of its activity had direct impact on the electron transferring efficiency of the respiratory chain and was significant for cellular energy production. LDH was the key enzyme in glycolytic metabolism and reflected the anaerobic metabolic level of muscles. SDH was bound with inner mitochondrial membrane and was the only enzyme bound with inner membrane in tricarboxylic acid cycle, the activity of which marked the rate of tricarboxylic acid cycle progress and reflected the impact on aerobic metabolic capacity. Results of this experiment showed that activities of diaphragmatic CCO, LDH and SDH of rats in the diabetic group declined, which probably revealed electron transfer barriers in diaphragmatic respiratory chain of rats with type 2 diabetes during the 8th week and showed glycolysis and aerobic oxidation metabolic capability reduction. This indicated that energy metabolic barriers existed in diaphragm with diabetes. It was further verified by mitochondria dilation, cristae shortening and vacuolization in diaphragm of rats with diabetes under electron microscope. However, it was reported by Xingping Shen et al. [7] that the diaphragmatic SDH activities of rats with type 1 diabetes were enhanced during the 4th week. It was considered that, to adapt metabolic changes in the organism, aerobic oxidative metabolism provided energy for muscle contraction in the diaphragm during incipient diabetes. As the diabetic course extended, mitochondrial damages were intensified and eventually resulted in SDH activity decline.

GbE, main effective ingredients of which are Flavonoid Glycosides and Terpene Lactones, is the extractive separated and purified from leaves of gingko belonging to ginkgoaceae and has functions of oxidation resistance, anti-inflammatory effect, hypoglycemic and hypolipidemic effects as well as insulin resistance improvement [8]. Researches showed that contractility of skeletal muscle could be greatly enhanced and fatigue could be delayed with GbE [9]. Our preliminary studies confirmed that GbE could not only protect organs of rats with diabetes but also reduce diaphragmatic mitochondria damages and free radical injuries of myocardium as well as inhibit NO production [2, 10]. Results of this study indicated that GbE could enhance the aerobic oxidative metabolism and glycolysis capability of the diaphragm of rats with type 2 diabetes, improve the function of mitochondrial respiratory chain and strengthen diaphragmatic energy supply, and accordingly improve contractility of the diaphragm.

Based on the analysis of the mechanical theory as the foundation, designed the soccer robot pick the ball institutions optimal design process, found aim function, select design variables and the corresponding optimization algorithm to optimize a complete set of institutions. At last through the test to get the final performance parameters of the institution. Experiments show that the system has higher accuracy and stability, the new optimize pick the ball have design basic requirements, and achieved good ideal control effect.

References

[1] McGuire M, MacDermott M. The influence of streptozotocin-induced diabetes and the antihyperglycaemic agent metformin on the contractile characteristics and the membrane potential of the rat diaphragm [J]. Exp Physiol, 1998, 83 (4): 481-487.

[2] LI Xusheng, CHEN Guorong, MAO Sunzhong, et al. Protective effects of extract of Ginkgo biloba on diaphragm of diabetic rats [J]. Chinese Journal of Pathophysiology, 2004, 20 (7): 1234-1237.

[3] Coombes JS, Powers SK, Rowell B, et al. Effects of vitamin E and α-lipoic on skeletal muscle contraction properties [J]. Appl Physiol, 2001, 90 (4): 1424-1430.

[4] SHEN Xingping, SHU Changda, HE Jun. Changes of diaphragmatic function and morphologic features in diabetic rats [J]. Chinese Journal of Pathophysiology, 2002, 18 (8): 970-973.

[5] Merino-Ramirez MA, Juan G, Ramon M, et al. Electrophysiologic evaluation of phrenic nerve and diaphragm function after coronary bypass surgery: prospective study of diabetes and other risk factors [J]. J Thorac Cardiovasc Surg, 2006, 132 (3): 530-536.

[6] Zhou Zhen, Jiang Tiankang, Chen Haiqing, et al. Effect of Ginkgo biloba extract on hypohepatia of Type 2 diabetic rats [J]. Pharmacology and Clinics of Chinese Materia Medica, 2008, 24 (4): 44-46.

[7] SHEN Xingping, SHU Changda, LI Qiongying, et al. An enzyme histochemical study of diaphragm in diabetic rats [J]. Chinese Journal of Pathophysiology, 2002, 18 (10): 1276-1279.

[8] Kudolo GB, Delaney D, Blodgett J. Short-term oral ingestion of Ginkgo biloba extract (EGb 761) reduces malondialdehyde levels in washed platelets of type 2 diabetic subjects [J]. Diabetes Res Clin Pract, 2005, 68 (1):29-38.

[9] Xie Wei, Yang Yongliang, Liang Li, et al. Anti-effect of extract ginkgobiloba on fatigue in skeletal muscle [J]. Chinese Journal of Clinical Rehabilitation, 2006, 10 (32): 98-100.

[10] LI Xusheng, CHEN Guorong, LI Jianming, et al. The beneficial effect of Gingko biloba extract on myocardial impairment in diabetic rats [J]. Chinese Journal of Pathophysiology, 2005, 21 (2): 176-178.

Advanced Materials Research Vols. 989-994 (2014) pp 1020-1024
© (2014) Trans Tech Publications, Switzerland
doi:10.4028/www.scientific.net/AMR.989-994.1020

Study on Degradation of Radix Isatidis Polypeptide in Artificial Gastrointestinal Environment

Nan Nan[1,a], Xijing Liu[2,b]

[1]Library, HEBEI UNITED UNIVERSITY, Tangshan, 063009, China
[2]School of Applied Chemistry and Biological Technology, Shenzhen Polytechnic, Shenzhen, 518055, China

[a]email:nn_6050207@163.com, [b]email:43135672@qq.com

Keywords: Radix Isatidis; Degradation; Artificial Gastric Juice; Artificial Intestinal Juice

Abstract. Radix Isatidis is a traditional Chinese medicine for treatment of influenza and inflammation in China. In this paper, in order to study the degradation situation of Radix Isatidis polypeptide in artificial gastrointestinal environment, the SDS-PAGE (Sodium dodecyl sulfate-polyacrylamide gel electrophoresis) method was used to detect the degradation of Radix Isatidis polypeptide in artificial intestinal juice and gastric juice, and it showed that Radix Isatidis peptides could be degradated to different degrees. HPLC (High Performance Liquid Chromatography) was used to determine the change of peptides degradation, and it indicated that free amino acid levels did not change significantly. The result after degradation was also detected by BCA method, and it showed that there were still a large number of polypeptides in the liquid. From this experiment we can come to this conclusion that Radix Isatidis polypeptides in artificial gastrointestinal juice mostly degraded into a series of different molecular weight peptides.

Introduction

Radix Isatidis is the dried root of plants *Isatis indigotica* Fort., with properties of relieving internal heat or fever, relieving sore throat and detoxifcation [1]. Pharmacological studies prove that Radix Isatidis has functions of antibiosis, antivirus, anti-inflammatory, anti-endotoxin, anti-tumor and immunomodulation [2].

There are a large number of reports about the material basis of clearing away heat and toxic material of Radix Isatidis, e.g. Chen considerd the total amino acids and total alkaloids were the effective parts of anti-inflammatory [3]. Liwei He deemed that polysaccharide may be one of the active components of Radix Isatidis [4].

Some scholars considered organic acid as one of effective constituents of Radix Isatidis [5], while Xu pointed out that water extract, total alkaloid and epigoitrin had strong antiviral effect. The nucleotide composition such as guanosine, adenosine and uridine in Radix Isatidis were deemed by someone the main active ingredients [6].

The degradation situation of Radix Isatidis polypeptide in artificial gastrointestinal environment was studied in this article, and it provided experimental base for further research in antiviral active ingredients and pharmacological effect of Radix Isatidis.

Medicine and Reagents

Radix Isatidis (locality of growth: Gansu Province); Pepsin, Trypsin, Sodium Dodecyl Sulfate (SDS), Bis-acrylamide, Acrylamide and Ammonium Sulfate (AP) (Sigma products); TEMED (Aldrich); SDS-PAGE Protein Marker (Pharmacia, low molecular weight protein standard); 4×Sample Buffer (Fermentas); Coomassie Brilliant Blue R-250 (Amresco repacking); Silver Nitrate (Chengdu Chemical Reagent Factory); Ammonium Sulfate (Yueyang Baoqing chemical); 10kD Centrifuge Tube (Millipore); BCA Kit (Beyotime Institute of Biotechnology); Methanol and Acetonitrile (Merck, chromatographic pure), Ethanol (Tianjin Chemical Reagent, AR); Disodium Hydrogen Phosphate, Sodium Dihydrogen Phosphate, Sodium Bicarbonate, Hydrochloric Acid, and Glacial Acetic Acid (Tianjin Nankai Chemical, AR); DNFB (Josiah Reagent); Tris (Serva).

Instrument

Multiskan MK3 Automatic Enzyme Mark Instrument (Thermo); Agilent 1100 High Performance Liquid Chromatography; Eclipse XDB C_{18} Reverse Phase Chromatography Column (250 mm×4.6 mm, 5μm); DZKW-D-2 Electric-heated Tthermostatic Water Bath (Zhengzhou North South Instrument Equipment Co. Ltd); KY-IA-Constant Temperature Shaker; Avanti J30I Large Capacity Refrigerated Centrifuge; ALPLTA 1-2 freeze Dryer (CHRIST); Milli-Q Ultrapure Water Machine (Milipore); Transferpettor (Eppendorf); Miniprotein Electrophoresis System (Bio-Rad); 170-8170 Gel Imaging Analyzer (Bio-rad).

Method and Results

Preparation of Radix Isatidis Total Peptide: Accurate amount of medicinal herbs was pulverized and then sifted by NO.2 screen mesh. After 24 hours of extraction by 10 times amount of ultrapure water, centrifuged the samples 15 mins at 6000rpm and decanted the supernatant fluid into a beaker. Added $(NH_4)_2SO_4$ powder slowly into the beaker to 80%, overnight aging. Then centrifuged the suspension to obtain the sediment, which namely the Radix Isatidis total polypeptide after freeze drying. It should be compounded to polypeptide solution of 0.25g/L by distilled water when used.

Degradation of Radix Isatidis Polypeptide in Artificial Gastrointestinal Environment: 100μL artificial gastric juice or intestinal juice was put in 7 centrifuge tubes of 1.5ml respectively. Put these tubes in constant temperature bath (37ºC), and added polypeptide solution (pre-heated at 37 ºC) into each tube, then digested the solution in 37°C. The samples were taken at 0, 1, 5, 15, 30, 90, 180 mins respectively, and appropriate amount of 0.168 mol/L Na_2CO_3 solution was added in the tubes, adjusting PH to terminate the enzyme reaction. The samples were centrifuged and supernatante was obtained. The protein concentration was detected by BCA method, and the degradation of Radix Isatidis polypeptide was detected by SDS-PAGE method. The sample results were contrasted with the control test (0 min).

SDS-PAGE Method: The SDS-PAGE result of Radix Isatidis polypeptide after degradation of artificial Gastric juice was shown in Figure 1. From this image, it can be found that the molecular weight rang of Radix Isatidis polypeptides was about 26-100kD, of which the main content band was near 26kD, the second was near 34kD, while the polypeptide abundance of other molecular weight was relatively low. The pepsin band was near 36kD. There was no obvious difference happened in digestion product contrasted with the control test within 5 minutes. As time goes on, the band near 26kD obviously became pale, but no significant change occured near 34kD, and no new band appeared.

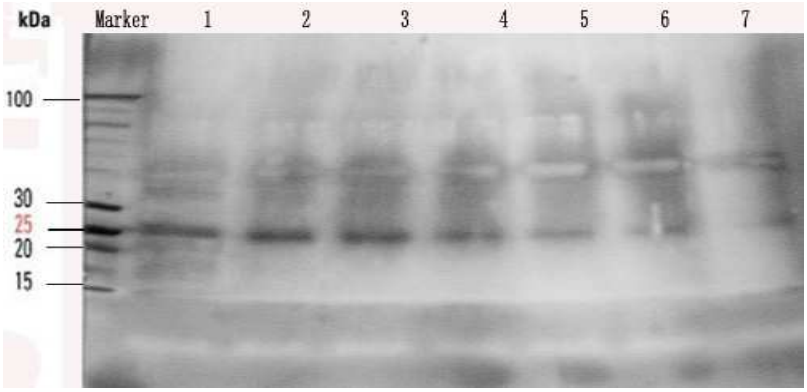

Figure 1. The SDS-PAGE electrophoretic image of Radix Isatidis polypeptide after degradation of artificial Gastric juice

The SDS-PAGE result after degradation of artificial intestinal juice was shown in Figure 2. The pepsin band was near 24kD. As time goes on, the band near 34kD turned pale gradually, and there was no obvious change near 26kD.

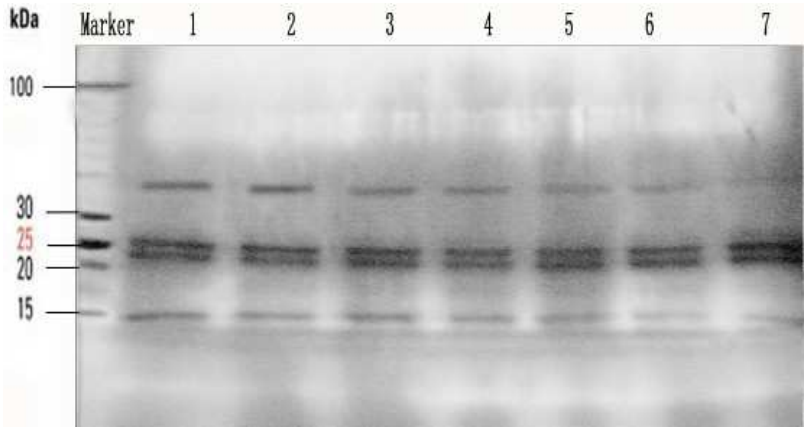

Figure 2. SDS-PAGE electrophoretic image of Radix Isatidis polypeptide after degradation of artificial intestinal juice

Content Determination of Radix Isatidis Peptide by BCA: The content of Radix Isatidis peptide digested by artificial gastric juice decreased within 1 minute, then increased significantly, and reached a maximum at 15 minutes, at last the content decreased slowly and became stable after 90 mins. The content of Radix Isatidis polypeptides digested by artificial gastric juice decreased within 1 minute, and then increased significantly. It reached a maximum at 45 mins, then the content curve declined slowly and became stable after 180 mins (Figure 3).

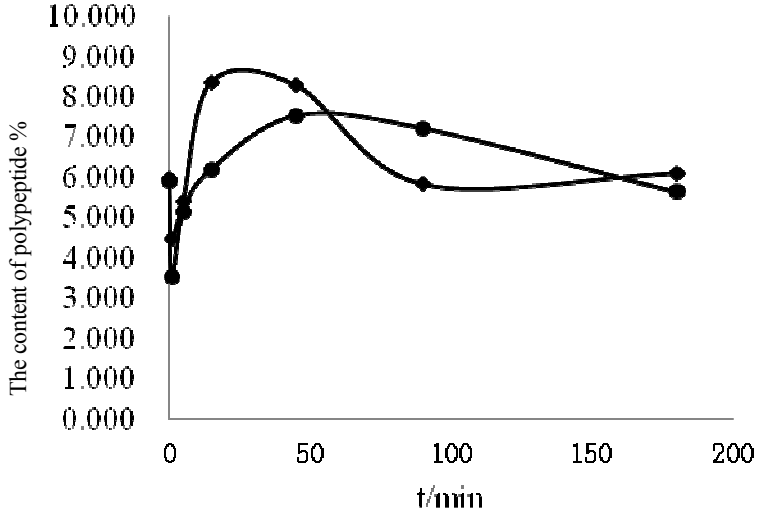

Figure 3. The curve of peptides concentration changes after digestion
●artificial gastric juice ◆artificial intestinal juice

Amino Acids Content Determination by HPLC: Determination of free amino acids content in the samples based on HPLC profile involving pre-column derivatization with 2,4-dinitro-fluorobenzene (DNFB) [7].

Sample Preparation: 5g of Radix Isatidis powder was weighed accurately, and sifted by NO.2 screen mesh. After 24 hours of extraction (4ºC) by 10 times amount of ultrapure water, the samples were centrifuged 15 mins at 6000rpm and transferred the solution to coors porcelain porcelain dish. After the volume of the liquid was evaporated to about 50mL, transferred it to a 100mL volumetric flask and maked up to volume with ultrapure water. The samples were detected according to the method above. Sample size: 10 μL.

Standard Curve: The linear equations and relevant linear range of threonine, proline, arginine and valine were shown below:

A = 8262C + 45.299 (threonine, 0.0117~1.17μg)
A = 4629.3C + 1306.1 (proline, 0.067~6.7μg)
A = 604.02C + 255.37 (arginine, 0.2954~29.54μg)
A = 8703.5C - 4.3392 (valine, 0.0044~0.44 μg)

Chromatographic Conditions: Agilent ODS C_{18} chromatographic column (5μm, 250mm × 4.6mm); A solution: 0.014mol/L phosphate buffer solution (adjusted pH to 8.2 with sodium dihydrogen

phosphate), B solution: acetonitrile water solution (acetonitrile: water 1:1); elution gradient: 0-5min, 20~35%B; 5-10min, 35~50%B; 10-20min, 50~80%B. Column temperature: 30°C. Detection wavelength: 0-8.2 min, 360 nm; 8.2-10.0 min, 398 nm; 10-20 min, 360 nm; Step length: 4 nm.

The results (TABLE 1) showed that after degradation by artificial gastrointestinal juice, arginine content increased to a certain degree, while the others had no obvious changes.

TABLE 1. THE AMINO ACIDS CHANGES AFTER DEGRADATION

time	artificial gastric juice				artificial intestinal juice			
（min）	threonine	proline	arginine	valine	threonine	proline	arginine	valine
0	0.065	2.199	1.604	0.089	0.065	2.173	1.636	0.089
5	0.064	2.199	1.605	0.087	0.068	2.168	1.777	0.087
15	0.068	2.185	1.604	0.087	0.065	2.196	1.789	0.087
30	0.067	2.174	1.604	0.088	0.064	2.182	1.807	0.088
90	0.064	2.199	1.608	0.088	0.068	2.170	1.829	0.087
180	0.067	2.187	1.607	0.089	0.066	2.193	1.827	0.087

Discussion

According to the experiment results, the molecular weigh of Radix Isatidis polypeptides was about 26-100kD, and the main content bands were near 26kD and 34kD. After digestion by artificial gastric juice, the band near 26kD faded, while there was no obvious change near 34kD. After digestion by artificial intestinal juice, the band near 34kD faded, and there was no obvious change near 26KD. It indicated that the Radix Isatidis polypeptides were digested by gastrointestinal juice.

In order to ensure the determination accuracy, four dominant amino acids (threonine, proline, arginine and valine) of the Radix Isatidis were chosen to measure their content. The determination results by HPLC showed that the arginine content had a small amount of increase, while the rests had no obvious changes. The determination results by BCA method showed that there were still a lot of polypeptides in the solution after digestion.

It was considered traditionally that the protein or macromolecuar peptides can only be absorbed by human body after being hydrolyzed completely to amino acid. But modern research had shown that the degradation products of protein in alimentary canal were mostly low molecular peptides, which were absorbed into circulatory system in complete form and used by organism. Low molecular weigh peptide has decided advantages in quick absorption, low energy consumption and high absorptivity comparing to free amino acid during the absorption process. After preliminary pharmacological experiments, it showed that Radix Isatidis polypeptide had anti-influenza virus activity, and it was one of the effective medicinal parts of Radix Isatidis, which accorded with the reports.

Conclusion

In this paper, according to the experiment, there was molecular weight change of Radix Isatidis polypeptides existed during the degradation progress, while no significant change in amino acid content. The result indicated that, without further decomposion, Radix Isatidis polypeptides were degraded into low molecular weigh polypeptides. The conclusion was also confirmed through determination results by BCA method. Thus we can deduce it is the small molecule peptides instead of the free amino acids that are absorbed into the human body circulatory system in complete form and used by organization. Due to the diversity of polypeptide pharmacological activity, it is necessary to pay much attention to plant polypeptide, rather than eliminate it during the production traditionally.

Acknowledgement

This research is sponsored by Natural Science foundation of Guangdong Province of China (S2011010004460).

References

[1] Sun Dong-dong, HE Li-wei and Chen Jian-wei et al. Optimization of extraction technology o Banlangen Radix isadix Isatidis based on multi-index comprehensive determination. Journal of Beijing University of traditional Chinese Medicine.36(3):183-187. 2013.

[2] Yang Feng-yun, Fu Ting-ming and Guo Li-wei, et al. Degradation of earthworm extracts prepared by wet superfine grinding in artificial gastrointestinal environment. Acta Pharmaceutica Sinica, 47(1):110-115. 2012.

[3] Chen Kai, Dou Yue, Meng fan-gang et al. preliminary screening of anti-inflammatory fraction of isatidis radix[J]. Chinese Journal of Experimental Traditional Medieal formaulae. 18(6): 200-203. 2012.

[4] Zhu Ting, Yin Ruwen. Extract technology of total polysaccharides and active components effect from root of Isatis indigotica. Chinese Journal of New Drugs.22(12):1390-1395. 2013.

[5] Tang Jie, Wan Jin, Ma Yong-gui, et al. Research on the isolation and purification of organic acids from Radix Isatidis with macroporous adsorptive resin. Chin Hosp Pharm, 3(18):1504. 2011.

[6] Xiao Hui, Lu Qing-fei, Wang Yi-ming. et al. Studies on extraction process of nucleosides for Radix Isatidis. Chinese Journal of New Drugs, 18(4):353-356. 2009.

[7] Liu bo, Han xiaodong, Zhang Minting. Application AQC as a pre-column derivatization reagent for HPLC determination of free amino acids in borojo sorbilis cuter. ACTA scientiarum naturalium universtatis sunyatseni. 52(4):100-104. 2013.

Advanced Materials Research Vols. 989-994 (2014) pp 1025-1028
© (2014) Trans Tech Publications, Switzerland
doi:10.4028/www.scientific.net/AMR.989-994.1025

Repetitive-element PCR technology for identification of mulberry pathogens

Gang LI[1], Hongzhi SONG[1], Jun WANG[1, 2], Fu-an WU[1, 2, a]

[1]School of Biotechnology, Jiangsu University of Science and technology, Zhenjiang 212018, P.R. China

[2]Sericultural Research Institute, Chinese Academy of Agricultural Sciences, Zhenjiang 212018, P.R. China

[a] email: fuword@163.com

Key words: Identification; Repetitive-element PCR; *Pseudomonas syringae*

Abstract: The coronatine is a new-type and high-efficient biogenic chlorosis-inducing phytotoxin. It's also a new potential chemical regulator. Plants can get higher stress and disease resistance with spraying coronatine at a low concentration, which has broad application prospects. It's an effective way to ferment coronatine industrially using *Pseudomonas syringae*. The REP universal primers were used to establish the repetitive sequence PCR technology. Clustering analysis and classification were used to screen the wild strains producing coronatine from Jiangsu and Zhejiang area. The results showed that 29 strains were divided into five groups with similarity coefficient of 0.65. The cluster analysis showed the highest diversity of *P. syringae* pv. *mori* appeared in mulberry organization form Chun-An, which is relevant with the regional water conditions. It provides a new thought to screen the wild strains producing coronatine.

Introduction

Recent years, Mulberry bacterial blight is a major and serious disease that does harm to the leaves and twigs of mulberry, and is widespread in sericultural areas of our country[1]. It damages the sericulturists's benefit and the development of sericulture seriously in our country. The appropriate classification on pathogenic bacteria is the key issue to determine the outbreak and prevalence of mulberry disease and to take timely measures to prevent and control it. The pathogens of this disease is the *Pseudomonas syringae* pv. *mori* (*Psm*). However, gene tic cluster analysis of *Psm* has not been done before.

Bacteria repetitive-element PCR technology is convenient, sensitive and high repeatable[2]. It can realize efficient classification research on bacteria and occupy a main position in the field of classification identification on pathogenic bacteria[3]. Martín-Sanz[4] used repetitive-element PCR and multiple-locus sequence typing to classify *P. syringae* isolated from pea, and he also found that pathogens were isolated successfully from 88 strains with repetitive-element PCR. It was a great significance to diagnose pathogens and the breeding of resistant strains[5]. However, the use of repetitive-element PCR in classification of *P. syringae* had not been reported.

Therefore, this report used repetitive-element PCR to explore classification of *P. syringae* and analyze mulberry pathogens preliminarily. This method provided technical guidance to screen a superior *P. syringae*.

Extraction of total genomic DNA

29 samples were screened from mulberries in Jiangsu and Zhejiang province. Bacterium solutions were sucked into King's B culture medium and strains were incubated at 32 °C for 12 hours. Single colony was picked into liquid medium and cultured to logarithmic phase. The Biospin bacterial genomic DNA extraction kit of BioFlux Company was used for extraction of genomic DNA of strains.

REP-PCR amplification

The primers sequences are: 5'-III ICG ICG ICA TCI GGC-3' (Rep1-R) and 5'-ICG ICT TAT CIG GCC TAC-3' (Rep2-I)[6].

25 μL reaction mixtures contained 2.5 μL 10 × reaction buffers, 2.0 μL DNA template, 1.5 μL Mg^{2+}, 1.0 μL dNTP, 0.5 μL rTaq enzyme and 0.5 μL of each primer. Add double-distilled water to 25 μL.

PCR amplification reactions were performed with a Thermal Cycler (Applied Biosystems, Singapore). The process was as follows: Initial degeneration at 95 °C for 6 min; 30 cycles including degeneration at 94 °C for 1 min; an anneal at 44 °C for 1 min; extension at 65 °C for 8 min; and a final extension at 65 °C for 16 min before cooling at 4 °C.

The PCR products were separated by the 1% agarose gel electrophoresis for 20-30 min at 5 V/cm.

Make statistics of stripe information on agarose gel. Clear and repetitive stripes were recorded as "1", while the same location without stripe recorded as "0" in the electrophoretogram. The original matrix was clustered by unweighted pair-group method with arithmetic means (UPGMA) using the NTSYSpc software. The evolutionary tree of *P. syringae* strains was got.

Results

Genomic DNA extracted from the 29 strains was tested by 1.0% agarose gel electrophoresis.

Figure 1 shows the electrophoresis results of genomic DNA of strains 1-29. The results showed that genomic DNA of the strains had no RNA and degraded DNA contamination. It can meet the requirements of the following study. According to the optimized PCR conditions by our previous experiments, the DNA of 29 strains was amplified by REP-PCR. In addition, the amplified products were subjected to 1.0% agarose gel electrophoresis and were analyzed by gel imaging and analysis system. Figure 2 shows the electrophoresis results of PCR of strains 1-29.The results showed that the bands of amplification were distinctive and could be used to achieve the goal of genotyping smoothly.

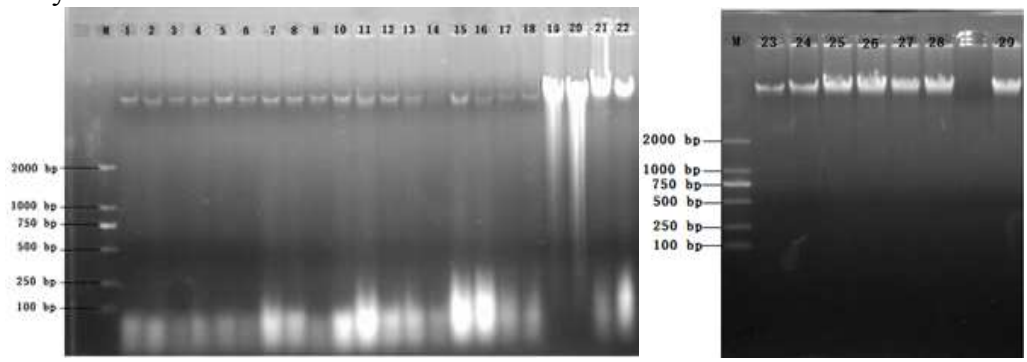

(a) Strains of 1-22 (b) Strains of 23-29

Fig.1 The electrophoresis results of genomic DNA

The original sequence matrixes of 29 strains were inputted in NTSYSpc 2.11a software to produce phylogenetic tree (Figure 3). The results showed that most of the 29 *Pseudomonas* can be distinguished. It indicated that Bacterial REP-PCR typing techniques can put *P. syringae* of different regions into gathers types accurately.

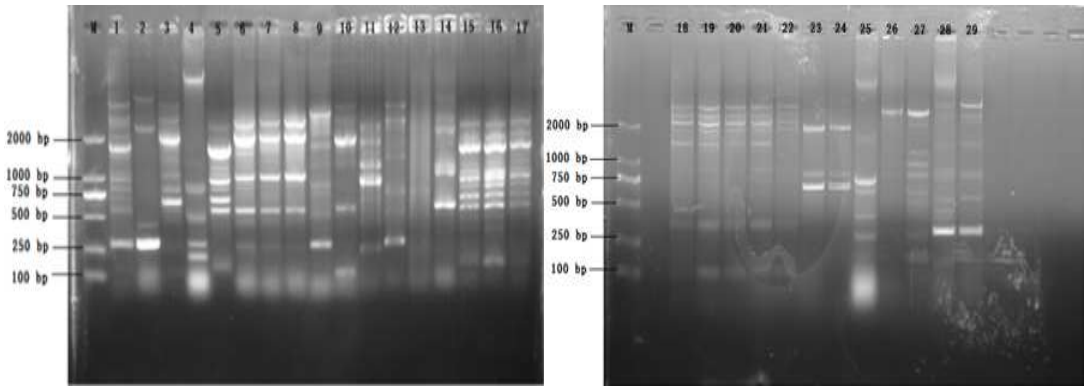

(a) Strains of 1-17 (b) strains 18-29

Fig. 2 The electrophoresis results of PCR

The 29 strains were divided into five subgroups with the genetic coefficient of 0.65.

The first subgroup contained the strain 1; the second subgroup contained the strain 3, 15, 16, and17; the third subgroup contained the strain 5 only; the fourth subgroup contained the strain 2, 13, 9, 11, 18, 21, 19, 20, 22, 6, 7, 8, 23, 24, 10, 12, 26, 14, 27; the fifth subgroup contained the strain 4, 28, 29, 25.

As the results showed, strains isolated from Zhejiang Chun-An could be found in five genetic subgroups; strains isolated from Jiangsu Rugao and Sheyang were divided into two subgroups; strains screened from Jiangsu Hai-An and Zhenjiang were in the same subgroups. Mulberry field of Jiangsu Chun-An was located at Qiandao Lake the 1600 mm isohyet nearby, that is rich in moisture. Complex and diverse groups of *P. syringae* could be founded in this area.

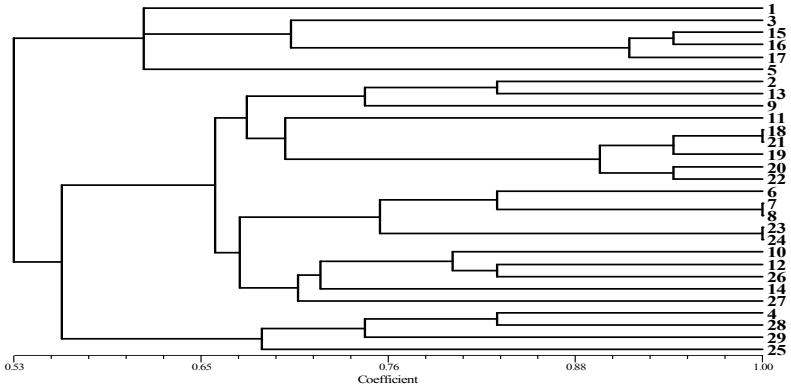

Fig. 3 REP-PCR cluster results of 29 strains

Conclusion

The 29 strains screened from Jiangsu and Zhejiang was clustered successfully. Sequence information was imported into the NTSYSpc 2.11a software to generate the evolutionary tree. Figure showed most of 29 *P. syringae* can be distinguished, which proved the REP-PCR genotyping was accurate relatively. The repetitive-element PCR system of *P. syringae* was established successfully, which provides the reference information for screening wild strains producing high-yield coronatine.

Acknowledgement

This work was financially supported by the Jiangsu Province Science and Technology Support Program, China (BE2012365) and Postgraduate Innovation Project of Jiangsu Province, China (CXLX13_700).

References

[1] X Ji, G Lu, Y Gai, et al. Biological control against bacterial wilt and colonization of mulberry by an endophytic *Bacillus subtilis* strain[J]. Fems Microbiol Ecol, 2008, 65(3):565-573.

[2] B R Mohapatra, A Mazumder. Comparative efficacy of five different rep-PCR methods to discriminate *Escherichia coli* populations in aquatic environments.[J]. Water Science & Technology, 2008, 58(3).

[3] J D Taylor, D J Doyle, P J Blackall, et al. Use of REP-PCR and 16S rRNA gene sequencing for comparison of *Mannheimia haemolytica* isolates obtained from fatal cases of bovine respiratory disease in the USA and Australia[J]. Aust Vet J, 2014, 92(1-2):15-23.

[4] A Martín-Sanz, M P de la Vega, J Murillo, et al. Strains of *Pseudomonas syringae* pv. *syringae* from Pea Are Phylogenetically and Pathogenically Diverse[J]. Phytopathology, 2013, 103(7):673-681.

[5] N R Bhardwaj, J S Srivastava, V Upadhyay, et al. Genetic variability among isolates of *Xanthomonas citri* subsp. citri based on rep-PCR[J]. Applied Biological Research, 2014, 16 (1): 1-6.

[6] J Versalovic, F J de Bruijn, J R Lupski. Repetitive sequence-based PCR (rep-PCR) DNA fingerprinting of bacterial genomes[J]. 1998:437-454.

Advanced Materials Research Vols. 989-994 (2014) pp 1029-1032
© (2014) Trans Tech Publications, Switzerland
doi:10.4028/www.scientific.net/AMR.989-994.1029

Optimum Process for Extraction of Total Flavonoids from Castor leaves by orthogonal test

Yihua Jiang[1, a,*], Xinlong Jiang[2,b] and Chenggang Cai[1,c]

[1]Zhejiang Shuren University, Hangzhou, China

[2]Institute of Food and Fermentation Engineering,Zhejiang Shuren University, Hangzhou, China

[a]email:hzjyih828@163.com, [b]email:jxinl2003@163.com, [c]email:ccg0516@sina.com

Keywords: Castor leaves;Total Flavonoid; Extraction; orthogonal test.

Abstract: Optimization of total flavonoid extraction from Castor leaves using orthogonal test methodology with the factors of ethanol concentration, extraction temperature,extraction time,solid/liquid ratio on the yield of total flavonoids were investigated.The results showed that optimum extracting conditions of total flavonoids from castor leaves were as follows: adding 1:40 $g \cdot mL^{-1}$ of 30% alcohol and extracting for 30 min,extraction temperature 70℃. Under the optimal conditions, the maximal yield of flavonoids was of 1.81%.

Introduction

Castor (Ricunus communis L.) is euphorbiaceae ricinus annual or perennial.At present, castor seed and castor oil is as the main use of castor[1],castor contained ricinine and ricin for some agricultural pests also show different degrees effect of contact, stomach toxicity, antifeedant[2].Castor leaves is rich in flavone,which is the main component of rutin and quercetin[3],rarely to be comprehensive utilization.Flavonoid compounds are known to be responsible for antioxidant,anticancer,anti-inflammatory,and antibacterial activity.It is causing a great waste of resources. Therefore, extraction of castor leaf flavone have important realistic to enhance the value of castor plant resources and obtain higher economic benefit.

In this paper,using ethanol as solvent, the extraction process such as extractant,extraction temperature, the ratio of solvents to materials, and extraction time were optimized by orthogonal test from castor leaves,with the yield of flavonoids(Y/%) as the index. Then the results would be the theoretical basis for the comprehensive utilization of the material.

Material and Methods

Material

Fresh castor leaves were collected from our campus in November, 2012.It dried at 40 ℃ to constant weight and were crushed using a universal grinder and sieved (60–80 mesh), and the resulting particles were stored in a desiccator until use. All reagents were of analytical grade.Rutin standard sample was purchased from chinese medicine group shanghai chemical reagent company.

Experimental Methods

Extraction process

Accurate weighing dry castor leaves powder →adding a certain amount of ethanol solution→ Extraction solvent extraction→ filtering→collected the supernatant→constant volume,extracting liquid was obtained→measuring.

Product analysis

Content of flavonoids in the extract was determined by spectrophotometric method, using rutin as standard sample. According to the reported method in the article[4],the regression equation C (mg)=0.6503A+0.01032 between concentration of flavonoids and absorbance was established,the linear range was 0 ~ 1.0mg,the correlation coefficient r was 0.999 7.

Orthogonal test optimization of extraction process

Extraction experiment optimization including ethanol concentration, extraction temperature, solid-liquid ratio, extraction times choice, for which several factors are parallel single factor experiment, study their influence on extraction.Single factors near the optimal value should be firstly found before the orthogonal test so as to found the most approximately real situation.

Dry samples of 0.5000 g were weighed into 250 mL cone flask with plug,respectively, and added amount of extractant,extraction under certain conditions, the filtrate volume was to 50mL with the corresponding extraction agent.For different ethanol concentration (20,30,40,50, 60, 70%), extraction temperature (40, 50, 60, 70,80,90℃), extraction time (0.25,0.5,1.0,1.5,2.0,2.5h), the ratio of material to liquid (1:10,1:20,1:30,1:40,1:50,1:60 $g \cdot mL^{-1}$)and other conditions to do parallel single factor experiments.The single factor test results were shown in Fig 1.According to Fig 1,we designed the $L_9(3^4)$ program of orthogonal test,the factors and levels were listed in Table 1.Results were disposed by the intuitive analysis and variance analysis, significant test of flavonoids extraction factor by Duncan [5].

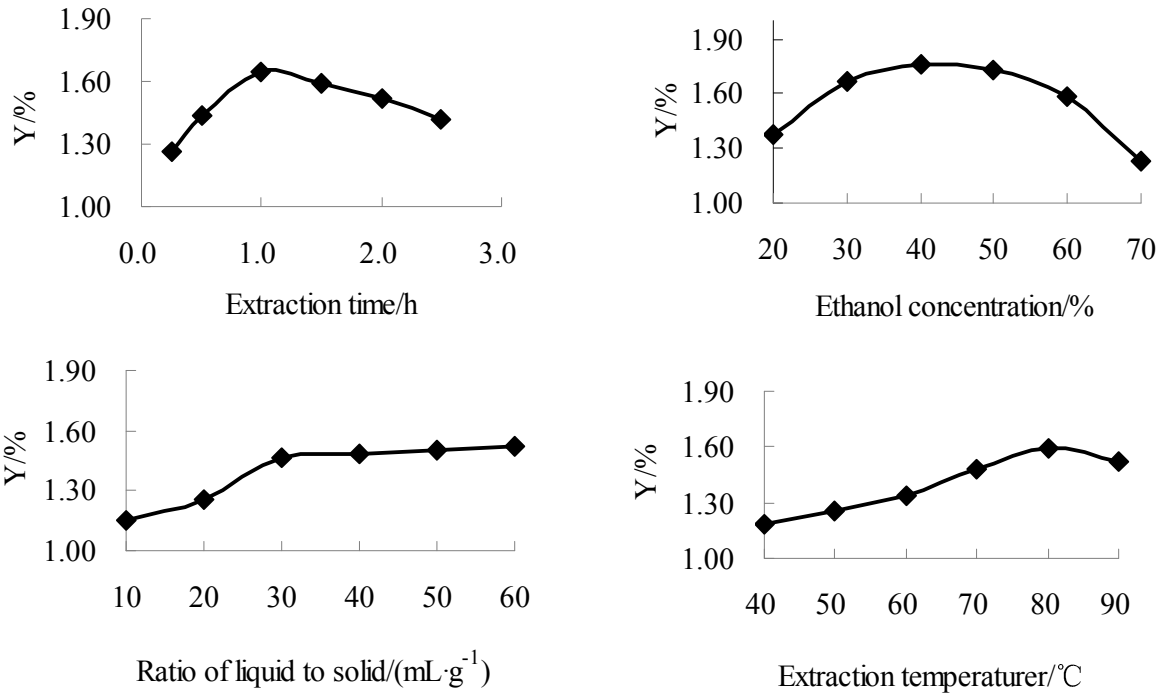

Fig.1 Effects of different factors on extraction yield

Table 1 Levels and factors of orthogonal experiment design

Level	A Extraction time (h)	B Ethanol concentration (%)	C The ratio of liquid to solid ($mL \cdot g^{-1}$)	D Extraction temperature (℃)
1	0.5	30	20	70
2	1.0	40	30	80
3	1.5	50	40	90

The verification experiment and recovery rate experiment

Verification experiments were conducted in accordance with the optimum extraction conditions, were determined for 3 times, calculating the average content of flavonoids.At the same time ,the recovery experiment were conducted by adding standard solution.

Result and analysis

The test results of orthogonal test

Based on the results of single factors experiments, the extraction experiments were carried out by orthogonal test design according to Table 2.

The intuitive analysis

From Table 2 can be seen, the effect of the ratio of liquid to solid on the rate of extraction was the maximum.The range of data R was visible, the effect order of various factors on the extraction: the ratio of liquid to solid > extraction temperature > ethanol concentration > extraction time, the optimum extraction conditions were: $A_2B_2C_3D_3$, namely ethanol concentration was 40%, extraction time was 1 h, ratio of solid to liquid was 1:40 $g \cdot ml^{-1}$, extraction temperature was 90℃. The results of orthogonal test about extraction temperature on the flavonoids had differences to the single factor experiment , which may be the interaction between various factors effect.

Table 2 Orthogonal experimental program and results of extraction (n = 3)

No.	A	B	C	D	the yield of flavonoids (Y/%)
1	1	1	1	1	1.66
2	1	2	2	2	1.71
3	1	3	3	3	1.81
4	2	1	2	3	1.74
5	2	2	3	1	1.82
6	2	3	1	2	1.69
7	3	1	3	2	1.79
8	3	2	1	3	1.74
9	3	3	2	1	1.70
K_1	1.73	1.73	1.70	1.73	
K_2	1.75	1.76	1.72	1.73	
K_3	1.74	1.73	1.81	1.76	
R	0.02	0.03	0.11	0.04	

The analysis of variance

We can see from Table 3, the ratio of liquid to solid (C) was a significant influencing factor only.It could consider to determine, as determined by the Duncan method after checking back.

Table 3 Analysis of variance

source of variation	SS	df	MS	F	significance
A	0.0009	2	0.0004	1.0000	
B	0.0013	2	0.0006	1.4615	
C	0.0206	2	0.0103	23.7692	*
D	0.0025	2	0.0012	2.8462	
SS_T	0.0594	8			

Note:$F_{0.05}$ (2, 2) =19.00; "*" represents a significant influencing factors.

The Duncan analysis[10]

First were found between the level of various factors $r_{0.01}$, $r_{0.05}$ ($r_{0.01}$=14, $r_{0.05}$=6.09), then calculate the value of R_k (standard error is 0.016, the R_k= standard error *r), then according to the calculation results,it was compared for each factor level significantly.From Table 4 can be seen, the ratio of liquid to solid has significant differences only.The ratio of material to liquid 1:20 $g \cdot ml^{-1}$ and 1:30 $g \cdot ml^{-1}$ have no significant difference, but significant difference with 1:40 $g \cdot ml^{-1}$. Considering the use of energy and resources, comprehensive analysis to determine the optimal extraction conditions of total flavonoids of castor leaves was $A_1B_1C_3D_1$, which was extracted by 30% alcohol solution, extraction time 30 min,solid-liquid ratio 1:40 $g \cdot ml^{-1}$, extraction temperature 70℃.

Tables 4 Compare significant difference in four levels of factors

1（A）				2（B）				3（C）				4（D）			
Level	Y	$P_{0.05}$	$P_{0.01}$	Level	Y	$P_{0.05}$	$P_{0.01}$	Level	Y	$P_{0.05}$	$P_{0.01}$	Level	Y	$P_{0.05}$	$P_{0.01}$
2	1.75	a	A	2	1.76	a	A	3	1.81	a	A	3	1.76	a	A
3	1.74	a	A	3	1.73	a	A	2	1.72	b	A	2	1.73	a	A
1	1.73	a	A	1	1.73	a	A	1	1.70	b	A	1	1.73	a	A

The verification experiment

Under the optimum extraction conditions, Repeated for 3 times,the measured flavonoids were: 1.8071%, 1.8205%, 1.8132%, the average content of flavone was 1.8136%, RSD=0.37% (n=3). It was the same basically to variance analysis.

The Recovery rate experiment

It were added to 0.2mg/ml rutin solution 1, 2, 3, 4, 5.00ml in the extract of known flavonoids respectively, determination of the content of flavonoids, calculated the recovery rate. The average recovery of measured castor leaf total flavonoids was 100.1%, RSD=1.22% (n=5).

Conclusion

The results of orthogonal test showed that ratio of liquid to solid was significant factors influencing on extraction total flavonoids from castor leaves. The optimal processing conditions were as follows: ethanol concentration 30%,the ratio of solvents to materials 40 $ml \cdot g^{-1}$, extraction temperature 70℃, and extraction 30 min , under the optimal conditions, the maximal yield of flavonoids was of 1.81%.

References

[1] Y.H.Chen,L.J.Chen,Q.F.Shi,Analysis of chemical compositions of the essential oil in the leaf of Ricinus communis[J].Journal of Xinyang Agricultural College,2012.22(3) :117-119.(in Chinese)
[2] Y.M.Wen, Y.F.Feng , M.Z.Zheng,Extraction and Content of the Ricinine for Different Parts oof Ricinus communis[J]. Agrochemicals, 2008.47 (8): 584-585.(in Chinese)
[3] X.L.Jiang,Extracting and determination of the total flavones from leaves and flowers of Castor [J].China Brewing, 2010, 1: 129-131. (in Chinese)
[4] L.J.Zhang,W.H.Zhang,H.J.Zhang,Determination of the total content of flavones in QianshanSemen Cassiacs. Food Sci,2003, 24:101-103.(in Chinese)
[5] R. Qian,Biostatistics [M]. Beijing: Higher Education Press, 1999.126-129. (in Chinese)

Advanced Materials Research Vols. 989-994 (2014) pp 1033-1036
© (2014) Trans Tech Publications, Switzerland
doi:10.4028/www.scientific.net/AMR.989-994.1033

Comparative bioenergetics of diploid and triploid Pacific oysters *Crassostreas gigas* at different temperatures

XiaoYan Li [1, a], ZhiMin Zhou[2, b]

[1]College of Life Science and Technology of Dalian University, Liaoning,Dalian,116622,China,
[2]Science and Technology on Underwater Test and Control Laboratory, Dalian, 116013, China
[a]112731815@qq.com; [b]zzm@dlut.edu.cn

Keywords: Triploids; Diploids; *Crassostrea gigas*; Energy budget; Temperature.

Abstract. The energy budgets, assimilation and conversion efficiency of 1-year-old-triploid Pacific oysters *Crassostrea gigas*, were compared with those of sibling diploids to clarify the mechanism of energy metabolism. No significant difference was found between diploids and triploids in oxygen consumption. The net growth efficiencies of triploids and diploids were 37.4% and 33.9% respectively, and the gross growth efficiencies of them were 28.8% and 22.7%. The influence of ploidy and temperature on K_1 was significant, but the variation of K_2 may be attributable to ambient temperature. The ratio of gonad dry weight and dry tissue of triploids was 5％on average, and diploids about 25.6%. Our results showed that triploids, which do not reproduce and only have limited gonadal development, spend more energy for growth and more efficient in using energy than diploids do.

Induction

Pacific oysters, *Crassostrea gigas*, are one of the most important commercial mollusks in the world. The biological characters of them are suitable for mariculture[1]. Triploid Pacific oysters *Crassostrea gigas* were induced, cultivated and cultured in the middle of 1980s in the USA[7].Study on shellfish-triploid industrialization has developed rapidly and formed production scale in China rapidly. At Present, the dilemmas of shellfish culture are the decline of germplasm resources, decrease of resistance, aquaculture waters of self-pollution and ecological environment of aging, etc. Research on triploid shellfish started lately, but advanced rapidly in recent years, most of the study focused on viability[4-5], growth traits[3], gonadal development[12], disease resistance[5], and biochemical comparison of soft tissues[7][11], etc. The influence of multiple lows heterozygosity on the physiological energetics of growth in the coot clam. Comparison of glycogen utilization during starvation in diploid and triploid Pacific oysters has already reported[8].Scientists[2][4] found the difference of survival, growth, death and productive potential between triploid Sydney rock oyster, *Saccostrea commercialis* and diploid. Muki S[9]studied the effects on growth, gametogenesis, physiology, and biochemical composition in diploid and triploid Pacific oysters *Crassostrea gigas* by elevated temperature.

1 Materials and Methods:

1.1 Materials

1-year-old Pacific oysters *Crassostrea gigas*, used in the experiment were induced from farm in Dalian. They were domesticated for 20d, they were fed *Cholovella spp* four times a day during the period , so that the concentration of *Cholovella spp* was 6×10^4/ml.

1.2 Method :

Ploidy identification: Ploidy was identified by PARTES-Ⅲ flow cytometry.

Experimental design: Five temperature levels was designed for 5℃,10℃,15℃,20℃,25℃, according to ploidy each level had two groups with 15 oysters respectively. Temperature acclimation heated or cooled 0.5℃per day respectively for 2 weeks before experiment which started from the natural water temperature, the former with a temperature controller (WMZK2- 01) while the latter was put in Environmental incubator (MFD-233) until reached the required temperature.

Oxygen consumption rate and ammonia excretion rate : As the experiments were controlled in a 5.5L jar, the Oxygen consumption rate and ammonia excretion rate were determined by Winkler and Nessler’s reagent respectively.

Feeding rate: The experiments were carried out at different temperatures and weight within 8 hours. Food concentration was determined by flow cytometry for per 2 hours in order to maintain the concentration stable at 6×104/ml.

Assimilation efficiency: Food and feces were collected by glass fiber filtration membranes, burnt at 500 ℃ in muffle furnace (SX-4-10)for 6h. 0.5M ammonium of salt was washed away formate under the same condition, food and feces were weighed after dried at 65℃ for 48h, which was burnt to ash. Assimilation efficiency was determined according to the ash weight ratio, which was calculated from the equation:

$$Ab = 1 - (F_{ash} / F_{organ}) / (E_{ash} / E_{organ}) . \quad (1)$$

Ab is the assimilation efficiency , F_{ash}/F_{organ} is the ratio of ash-content and organ-content of food, and E_{ash}/E_{organ} is the ratio of ash-content and organ-content of feces.

Scope of growth and energy conversion efficiency: The energy of feeding(C), assimilation(A), respiration(R), excretion(U) and scope of growth(P) was calculated according to food consumption, oxygen consumption, excretion and assimilation efficiency. K_1=P/C×100%, K_2=P/A×100%

2 Results

2.1 Growth budget and other energytic components of triploid Pacific oysters and sibling diploid

Table 1 The feeding energy and scope of growth for triploid and diploid oysters at different temperature and weight

Temperature(℃)	ploidy	Food onsumption(KJ/individual)	Assimilation (KJ/individual)	oxygen consumption (KJ/individual)	Scope of growth(KJ/individual)	excretion(KJ/individual)
5	2n	100.3±16.3	45.2±7.3	37.9±6.3	1.8±0.6	5.4±1.1
	3n	117.8±28.0	60.4±15.1	37.39±4.3	13.1±3.8	9.8±7.0
10	2n	238.7±21.6	119.3±10.8	49.14±3.4	66.5±5.1	3.9±2.1
	3n	251.2±38.4	149.5±27.6	52.7±7.6	85.2±13.0	11.6±7.1
15	2n	236.9±28.4	139.8±16.8	61.5±2.6	72.2±9.9	6.0±4.4
	3n	251.0±24.3	170.7±16.5	64.7±6.1	87.6±5.6	18.3±4.9
20	2n	267.2±52.2	190.9±18.6	103.1±28.4	92.0±7.8	8.0±4.9
	3n	281.5±146.0	236.5±38.6	104.9±19.7	110.9±14.3	20.6±5.4
25	2n	301.6±47.3	241.2±37.9	143.65±22.7	84.5±7.0	13.1±8.8
	3n	321.0±44.5	285.7±39.6	146.8±24.1	113.5±10.6	25.4±6.1
30	2n	290.5±57.3	229.0±48.8	202.73±58.9	10.3±21.2	16.0±11.2
	3n	303.0±56.6	267.5±48.0	211.21±39.0	26.9±3.9	29.4±5.5
average	2n	239.2±76.5	160.9±73.5	99.7±64.6	54.6±37.5	8.7±7.0
	3n	253.2±78.2	195.0±84.5	102.95±64.6	72.9±41.0	19.2±8.8

2n:dry weight is 52.5± 19.17mg；3n:dry weight is 60.2± 26.3mg；

Temperature had a significant effect on food consumption (Ftem=101.57, p<0.001), there were no significance by ploidy. The pacific oysters growth of scope, triploid and diploid *Crassostrea gigas* increased in temperature. It was affected significantly by weight covariates test (F=6.32, P<0.019); the analysis of covariate model showed that the scope of growth was affected significantly by ploidy and temperature (Ftem=119.12,p<0.001; Fploidy=29.29,p<0.001) at the same weight, so the assimilation energy take effect(Ftem=126.5,p<0.001; Fploidy=18.41,p<0.001).

There were no significant difference between diploids and triploids on oxygen consumption, although any differences were detected between them. At temperature of 10-30℃,P/A（the ratio of growth energy and assimilation energy）decreased with an increase in temperature, while R/A(the ratio of respiration energy and assimilation energy) increased ,the relationship between them was expressed as :

$$3n: R/A = 10.1 + 2.3t (R2 = 0.82, F = 13.4, P < 0.05) . \quad (2)$$

$$P/A = 231.9 - 6.9t (R2 = 0.958, F = 68.2, P < 0.05) . \quad (3)$$

$$2n: R/A = 9.7 + 2.5t (R2 = 0.87, F = 21.5, P < 0.05) . \quad (4)$$

$$P/A = 218.8 - 7.0t (R2 = 0.953, F = 61.4, P < 0.05) . \quad (5)$$

From the above equations, each unit increase in temperature, *R/A* increasing and decreasing amplitude of Pacific oysters, *Crassostrea gigas* diploid was higher than triploid.Temperature and

ploidy had a significant effect on ammonia excretion (Ftem=40.6,p<0.001; Fploidy=79.5 ,p<0.001), ammonia excretion of triploids was about as 2.1times as diploids.

Table 2 Comparion of energy distribution and net growth efficiency for triploid with diploid at different temperatures

Temperature(℃)	ploidy	Assimilation efficiency%	Net growth efficiency%	Gross growth efficiency%	R/A%	P/A%
5	2n	45.0	4.0	1.8	87.7	1.27
	3n	54.0	21.8	11.8	60.5	38.2
10	2n	50.0	55.7	27.9	39.6	147
	3n	59.5	57.0	33.9	31.0	201
15	2n	59.0	51.7	30.5	45.4	109
	3n	68.0	51.4	34.9	38.4	132
20	2n	71.4	48.2	34.4	54.5	85.8
	3n	84.0	46.9	39.4	44.7	104
25	2n	80.0	35.0	28.0	60.0	57.6
	3n	89.0	39.7	35.4	51.5	76.6
30	2n	78.8	4.5	3.5	87.6	5.8
	3n	88.3	10.1	8.9	78.8	12.9
average	2n	67.3	33.9	22.8		
	3n	77.0	37.4	28.8		

3 Conclusion

There was an obvious difference in scope of growth comparison of energy budget between triploid pacific oysters and *Crassostrea gigas* with diploid, which was consistent with the investigation results of growth characteristics in a culture cycle. Many studies showed that the weight of 1-year-old triploid Pacific oysters was as 1.2 -1.5 times as diploids ones, while the highest was 1.7 times. The growth advantage in other species also showed obvious, such as the average weight of triploid Sydney rock oyster *Saccostrea commercialis* which were as 1.3-1.4 times as diploids.

The ratio of gonad dry weight and dry tissue of triploids was 5％on average, while diploids was about 25.6%. The results showed that triploids, which do not reproduce and have limited gonadal development, spend more energy for growth and use energy more efficient than diploids do. In addition, the high energy conversion efficiency of triploids can reduce the effect of Culture Environment arising from the populations of biological settlement. It can alleviate the current culture of self-pollution to some extent .

Acknowledgement

The study was supported by the National Natural Science Foundation of China (Grant No. 51349005 and 51375074).

References

[1] C. Chambon, A. Legeay, G. Durrieu, P. Gonzalez and P. Ciret, et al. Influence of the parasite worm Polydora sp. on the behaviour of the oyster Crassostrea gigas : a study of the respiratory impact and associated oxidative stress[J]. Marine Biology. 2007(152):329-338.

[2] A. Kesarcodi-Watsona, J. S. Lucasa and D. W. Klumpp. Comparative feeding and physiological energetics of diploid and triploid Sydney rock oysters, Saccostrea commercialis: I. Effects of oyster size[J] .Aquaculture. 2001(203): 177-193.

[3] I. Laing.Oysters – Shellfish Farming[J]. Encyclopedia of Ocean Sciences (Second Edition)2009: 274-286.

[4] Koehn R K, Shumway S E. A genetic/physiological explanation for differential growth rate among individuals of the American oyster *Carssostrea virginica* (Gmelin) [J].Mar Biol Lett,1982(3):35-42.

[5] Muki S, Brace B, Roger M. Effects of elevated temperature on growth, gametogenesis, physiology, and biochemical composition in diploid and triploid Pacific oysters Crassostrea gigas Mtunbetg[J].J Fxp Mar Biol Ecol, 1992(161):15-25.
[6] Ilie S. Racotta ,Elena Palacios, Ana M.Ibarra. Comparative biochemical composition of ploidy groups of the lion-pawscallop(Nodipecten subnodosus Sowerby)supports the physiological hypothesis for the lack of advantage in triploid mollusc's growth in food-rich environments. [J].Mar Biol,2008(153):1245-1256.
[7] P.J. C. Honkoop Physiological costs of reproduction in the Sydney rock oyster *Saccostrea glomerata* how expensive is reproduction.Oecologia,2003(135):176–183.
[8] J.-C.Amiard, et al.Influence of Ploidy and Metal–MetalInteractions on the Accumulation of Ag, Cd and Cuin Oysters *Crassostrea Gigas* Thunberg. Arch.Environ. Contam. Toxicol., 2005(48): 68–74.
[9] W.J. Diehl and R. K. Koehn.Multiple-locus heterozygosity, mortality, and growth in a cohort of Mytilus edulis[J].Mar Biol,1985(88):263-271.
[10] Katherine Costil.Juliette Roye.Michel Ropert, et al. Spatio-temporal variations in biological performances and summer mortality of the Pacific oyster *Crassostrea gigas* in Normandy(France). Helgol Mar Res,2005(59):286–300.
[11] John A. Nell, Elizabeth Cox,Ian R. Smith and Greg B. Maguire. Studies on triploid oysters in Australia: farming potential of all-triploid Pacific oysters, Crassostrea gigas (Thunberg)[J]. Aquaculture 1994(126): 243-255.
[12] Tabarini**,**et al. Induced triploidy in the bay scallop, *Argopecten irradians*, and its effects on growth and gametogenesis. Aquaculture,1984(42):151-160.

Advanced Materials Research Vols. 989-994 (2014) pp 1037-1040
© (2014) Trans Tech Publications, Switzerland
doi:10.4028/www.scientific.net/AMR.989-994.1037

Prognostic Significance of Glycoprotein 96 in Human Hepatocellular Carcinoma

Xiaoping WANG[1,*], Huanping LIN[1], Bing XU[1], Kepei ZHANG[1], Jinggang FANG[1] and Yixin YANG[2]

[1]Key Laboratory of Molecular Biology and Pathology, Shaanxi University of Chinese Medicine, Xianyang, Shaanxi 712046, PR China

[2]Department of Biological Sciences, Emporia State University, Emporia 66801, Kansas USA

[*]wxpphd72@yahoo.com

Keywords: Glycoprotein 96(gp96); Hepatocellular Carcinoma; Prognosis

Abstract. Glycoprotein 96(gp96) is highly expressed in cancer tissues. Recent studies indicate the possible roles of gp96 in the development and progression of hepatocellular carcinomas but detailed information is still ambiguous. The aim of the study is to investigate the correlation between clinicopathology and immunolocalization of gp96 in human hepatocellular carcinoma. Immunohistochemistry demonstrated that gp96 expression in hepatocellular carcinomas with metastasis was significantly higher than those with non-metastasis. Gp96 expression was significantly associated with the presence of tumor infiltration, lymph node and remote metastasis.

Introduction

The Heat shock proteins (HSPs) have been reported to be overexpressed in a wide range of human tumors including breast, endometrial, ovarian, colon, lung and prostate [1,2]. Studies have also shown that HSPs expression have a close relationship with carcinoma prognosis [3,4]. They may combine with oncogene products to form complexes and transport them into intracellular special sites and promote cancer cell proliferation and heterogeneous differentiation [5,6]. Recent studies have also shown that gp96 is highly expressed in cancer tissues and have been used as prognostic markers in some tumors [7,8].

Study indicates the possible roles of gp96 in the development and progression of hepatocellular carcinomas but detailed information is still ambiguous [8]. Primary hepatocellular carcinoma is one of the most malignant cancers, and there may be a correlation between the progression of hepatocellular carcinoma and over-expression of gp96. The present study aimed to evaluate the association between the extent of expression of gp96 and various clinicopathological parameters, tumor proliferative capacity. The results showed that there exists a significant correlation between the expression of gp96 and the progression in primary hepatocellular carcinoma.

Material and Methods

Immunochemistry Reagents. Mouse anti-human gp96 monoclonal antibody was obtained from StressGen Biotechnologies (Victoria, British Columbia, Canada). EnVisionTM kits were purchased from Dako Corp (Carpinteria, CA, USA).

Tissue Samples. This investigation was approved by the Ethics Committee on Human Study at Shaanxi University of Chinese Medicine (2004-4B). Paraffin specimens of primary hepatocellular carcinoma from 80 patients undergoing hepatocellular resection were collected from the affiliated Hospital, Shaanxi University of Chinese Medicine, Xianyang, China from 2000 to 2012. None of the patients received any kind of anti-cancer treatment or other therapies prior to surgery. The patients consisted of 56 males and 24 females, with a mean age of 54.2 ± 3.5 years, ranging from 35 to 76 years. Routine pathological diagnosis showed that all cases were primary hepatocellular carcinoma. Among the cases, 36 cases had regional lymph node metastases, and 18 cases had remote metastases. The specimens were fixed in 10% buffered formalin and embedded in paraffin. Serial sections, 5-μm-thick, were cut and placed on poly-lysine coated glass slides.

Immunohistochemical Staining Methods. All sections were deparaffinized and rehydrated with graded alcohols. Endogenous peroxidase was then blocked with 3 mL/L H_2O_2 diluted in methanol for 30 min at room temperature. Antigen retrieval was performed by treating the slides in citrate buffer in a microwave for 10 min. The slides were incubated in a moist chamber with gp96 mouse monoclonal antibody (1:100) at 4℃ overnight. After a complete wash in phosphate buffered saline (PBS), the slides were incubated with horseradish peroxidase labeled goat anti-mouse antibody (1:100) for 45 min at 37℃. After a complete wash in PBS, the slides were developed in 0.5g/L freshly prepared 3,3'-diaminobenzedine solution (DAB, Sigma Co, St.Louis, Mo, USA) for 8 min, and then counterstained with hematoxylin, dehydrated, air dried, and mounted. Normal mouse IgG was used to substitute for the primary antibody as a negative control. Only distinctive intranuclear or intra-cytoplasm immunoreactivity was considered positive.

Statistical Analysis. gp96 expression differences between hepatocellular carcinomas and tissues adjacent to cancer were analyzed statistically using u test. The relationship between expression of gp96 in primary carcinoma tissue with or without metastasis was analyzed statistically using χ^2 test. $P < 0.05$ was considered statistically significant.

Results

Immunolocalization of gp96 in Primary hepatocellular Carcinomas and Adjacent Tissues to Cancer. The results of immunohistochemistry of gp96 were summarized in Table 1. gp96 immunoreactivities were detected in 65 of 80 primary tumors (81.3%) and in 15 of 80 mucous membranes adjacent to cancers (18.7%). Gp96 was mainly stained in the cytoplasm of cancer cells. gp96 positive rates in hepatocellular carcinoma group were significantly higher than that in adjacent tissues to cancer ($P < 0.05$, Table 1).

Relationship between Clinicopathology and Expression of gp96 in Primary hepatocellular Carcinomas. Results showed that gp96 expressed higher in low differentiation of hepatocellular carcinomas than that in tissues adjacent to cancers ($P < 0.05$). There were significant differences of gp96 expression between metastasis groups and non-metastasis groups ($P < 0.05$). To assess if gp96 bear a pronounced prognostic effect in patient subgroups, we conducted an extensive analysis of gp96 protein expressions. We stratified by nodal status (absence vs presence of lymph node metastases) and presence of organ metastases. In cross-tables, gp96 expression was significantly associated with the presence of organ metastases and lymph node positivity (Table 1).

Table 1 Relationship between clinicopathology and immunoreactivity of gp96 in primary hepatocellular carcinomas

Pathologic types	gp96		
	n	- (%)	+ (%)
Tissues adjacent to cancers	80	65 (81.3)	15 (18.7)
hepatocellular carcinomas[a]	80	5(6.3)	75 (93.7)
Lymph node metastasis[b]			
yes	32	0 (0)	32 (100)
no	48	5(10.4)	43 (89.6)
Remote metastasis[c]			
yes	16	0 (0)	16 (100)
no	64	5(7.8)	59(92.2)

[a]$P < 0.05$, vs tissues adjacent to cancers; [b]$P < 0.05$, [c]$P < 0.05$, vs non-metastasis groups.

Discussion

In this study we examined the expressions of gp96 in 80 hepatocellular carcinoma samples by immunohistochemistry. The results showed that almost all of the detected hepatocellular carcinomas

expressed gp96, which had significant differences compared with that in tissues adjacent to cancers. By way of immunohistochemistry, we found that there was a definite correlation between expression of gp96 and development of hepatocellular carcinomas.

The Heat shock protein (HSP) family is group of highly conserved proteins synthesized after heat induction or other stressors [1,2]. During the growth and development of normal cells, gp96 is constitutively expressed at low levels but the expression was dramatically enhanced by stressful conditions [2]. In non-transformed cells at normal conditions, gp96 is expressed at very low levels. It is, however, present at elevated levels in the major fraction of tumors and in many transformed cell lines. It is commonly assumed that in tumor cells the expression of gp96 at elevated levels is the consequence of oncogenic transformation and enhanced expression of gp96 has a close relationship with epithelial carcinoma cells growth [3,4]. Recent studies have shown that gp96 is highly expressed in cancer tissues and have been used as prognostic markers in some tumors, such as gastric cancers, colonic tumors, breast cancers, lung cancers and so on, which have also been verified to be associated with the development and progression of the above-mentioned carcinomas [3-7]. In this experiment, we found that gp96 was highly expressed when hepatocellular carcinomas progressed, but their roles in hepatocellular carcinoma are not clear. It is reasonable to propose that gp96 up-regulation in these tumor cells are closely related with tumor cell survival and proliferation. It is believed that tumor cells are a group of highly proliferative heterogeneous cells which progress gradually through mutant oncogene products [9-11]. Continuous expression of HSP in tumor cells may be required to serve as molecular chaperones in regulating and stabilizing these products during tumor growth process. At the same time, the existence of mutant or oncogene products may stimulate HSP synthesis.

The present study further supports the clinical significance of gp96 expression in the progression of hepatocellular carcinoma. In the study, gp96 expression was found to be associated with important clinicopathological characteristics for patients' management. Our results showed that not only the expression of both gp96 in hepatocellular carcinoma was higher than that in tissues adjacent to cancer, but also the expression of gp96 in hepatocellular carcinomas with metastasis was definitely higher than that of hepatocellular carcinomas without metastasis. The results indicate that up-regulation of gp96 is likely to have some relationship with progression, invasion and metastasis of hepatocellular carcinomas.

Study revealed that considerable expression of HSPs was found in tumor cells, showing that HSPs may be induced by other stresses and participate in broader array of defenses during cell growth and cell differentiation of tumors [10,11]. Thus, it may be presumed that under various stimuli and stressful conditions, in order to avoid the damage caused by deleterious factors such as nitrosamines, 3,4-benzopyrene-oncogenesis evocator, bronchopulmonary epithelial cells have to transcribe and translate high levels of HSPs in order to sustain normal metabolism and functions of cells. Under these conditions, bronchopulmonary epithelial cells should synthesize HSPs rapidly to exert a protective role for themselves. The progression of hepatocellular carcinoma is a gradual process under the long-term influence of various stimuli. During the process, inducible HSP synthesis increases gradually. This viewpoint was confirmed by our results, in that gp96 was expressed at a higher level in hepatocellular carcinoma than that in tissues adjacent to cancer. The expression levels of gp96 may be useful prognostic markers for hepatocellular carcinoma.

Conclusion

In this study, we examined the expressions of gp96 in primary hepatocellular carcinoma samples by way of immunohistochemistry. Human hepatocellular carcinomas existed with high level of expression of gp96. Gp96 expression was significantly associated with the presence of tumor lymph node and remote metastasis. There is a close correlation between the overexpression of gp96 and progression of hepatocellular carcinomas. The expression characters of gp96 in hepatocellular carcinoma may be useful to study the pathogenesis and progression of hepatocellular carcinoma.

Acknowledgements

This work is supported by Scientific Research Program Funded by Shaanxi Provincial Education Department (No.2007JK233, 2010JK484), the Key Project of Ministry of Education of China (No.205002) and the National Natural Science Foundation of China (No.81172135, 81310108008).

References

[1] Morimoto RI. Cells in stress: transcriptional activation of heat shock genes [J]. Science, 1993 259 (5100) 1409-1410.

[2] Ciocca DR, Calderwood SK. Heat shock proteins in cancers: diagnostic, prognostic, predictive, and treatment implications [J]. Cell Stress Chaperones, 2005 10 (2) 86-103.

[3] Lebret T, Watson RW, Molinie V, O'neill A, Gabriel C, Fitzpatrick JM, Botto H. Heat shock proteins HSP27, HSP60, HSP70, and HSP90: expression in bladder carcinoma [J]. Cancer, 2003 98 (5) 970-977.

[4] Lee AS. The glucose-regulated proteins: stress induction and clinical applications [J]. Trends. Biochem. Sci. 2001 26 (8) 504-510.

[5] Wang XP, Zhou YX, Ying XP, Guo LS, Zhao YH, Fang Y. Interaction between heat shock protein 72 and alpha-fetoprotein in human hepatocellular carcinoma [J]. Clinica Chimica Acta, 2007 379 (1) 158-162.

[6] Wang XP, Chen W, Li X, Lin HP, Wang QX. Heat shock protein 72 associated with CD44v6 in human colonic adenocarcinoma [J]. Cell Biology International, 2008 32 (7) 860-864.

[7] Wang Q, An L, Chen Y, Yue S. Expression of endoplasmic reticulum molecular chaperon GRP96 in human lung cancer tissues and its clinical significance [J]. Chin. Med. J. 2002 115 (11) 1615-1619.

[8] Wang XP, Wang QX, Ying XP. Correlation between Clinicopathology and Expression of Heat Shock Protein 72 and Glycoprotein 96 in Human Gastric Adenocarcinoma [J]. The Tohoku Journal of Experimental Medicine, 2007 212 (5) 35-41.

[9] Wang XP, Wang QX, Guo LS, Ying XP, Zhao YH. Immunolocalization of Heat Shock Protein 72 and Glycoprotein 96 in Human Colonic Adenocarcinoma [J]. Acta Histochemica, 2008 110 (2) 117-123.

[10] Fisher DL, Mandart E, Doree M. Hsp90 is required for c-Mos activation and biphasic MAP kinase activation in Xenopus oocytes [J]. EMBO J. 2000 19 (7) 1516-1524.

[11] Wang XP, Lin HP, Wang QX, Li SZ, Sun LJ, Yang YX. HSP72 and gp96 in gastroenterological cancers [J]. Clinica Chmica Acta, 2013 417 (1) 73-79.

Advanced Materials Research Vols. 989-994 (2014) pp 1041-1043
© (2014) Trans Tech Publications, Switzerland
doi:10.4028/www.scientific.net/AMR.989-994.1041

An Evaluation of the Potential for Pharmacokinetic Interaction Between Tramadol and Cytochrome P450 2D6 Inhibitor Promethazine

LIU Ping[1,a], SUN Liang[1], ZHANG Jian[1], GUO Rui-chen[2]

[1]Shandong Provincial Hospital affiliated to Shandong University, Jinan, China, 250021

[2]Institute of Clinical Pharmacology, Qilu Hospital of Shandong University, Jinan, China, 250012

[a]e-mail:grc7636@126.com

Keywords: Tramadol; Promethazine; CYP2D6; Drug Interaction

Abstract. In this single-center, randomized, open-label, 3-way crossover study, subjects received each of the following: a single dose of Tramadol Hydrochloride Injection (THI) 35 mg, a single dose of Promethazine Hydrochloride Injection (PHI) 45 mg, and single dose of Compound Tramadol Hydrochloride Injection (CTHI) 80mg. Blood was collected and plasma was analyzed for the pharmacokinetic parameters (maximum plasma concentration [Cmax], time to Cmax [Tmax], area under the plasma concentration-time curve, plasma elimination half-life, clearance, and apparent volume of distribution) of Tramadol and Promethazine. In general, several pharmacokinetic interactions were observed between Tramadol and Promethazine in the present study.

Introduction

Tramadol is a synthetic, centrally acting analgesic that has been widely used for chronic pain management. Its analgesic effect results from two different pharmacologic actions. Tramadol displays a weak agonistic effect at the μ- and δ-opioid receptors and a weaker affinity for κ-opioid receptors[1]. This weak, specific, opioid effect of tramadol is mediated by an active metabolite, (+)-M1 (O-desmethyltramadol). This metabolite is formed via the genetically polymorphic P450 CYP2D6 iso-enzyme system. The biological activity of this system is variable, and individuals may be classified as extensive or poor metabolisers of tramadol. Tramadol has an affinity for opioid receptors that is about 6000 times weaker than morphine, but the (+)-M1 metabolite has an affinity about 200 times greater than tramadol[2]. It was[3] reported much higher concentrations of the (+)-M1 metabolite and greater analgesic efficacy of tramadol in extensive metabolisers compared to poor metabolisers. Promethazine (PMZ) is a histamine antagonist (H1 antagonist) which is widely used in human and veterinary medicine. The drug is often given in conjunction with an opiate analgesic such as pethidine, particularly in obstetrics. Researchers found that it was the principal P450 related to CYP2D6 responsible for the metabolism of promethazine in human liver microsomes[4]. Further studies in humans confirm that Promethazine is substrate and inhibitor of the polymorphic cytochrome P450 (CYP) isozyme CYP2D6[5].

This novel compound injection -- Compound Tramadol Hydrochloride Injection(CTHI)（35mg/2ml Tramadol Hydrochloride, 45mgl/2ml Promethazine Hydrochloride）has first been developed by Fatai Pharmaceutical Company(China) and approved for phase I clinical trial by State Food and Drug Administration (SFDA) of China.The objective of this study was to assess the potential pharmacokinetic interaction of Tramadol and Promethazine after administration of CTHI of each in healthy young subjects.

Methods

Chemicals and reagents

The Compound Tramadol Hydrochloride Injection (35mg Tramadol Hydrochloride/45mg Promethazine Hydrochloride)(CTHI) was provided by Huatai Pharmaceutical Company (Beijing, China). The internal standard, Donepezil and Tinidazole were commercially obtained from Chengchuang and Fangming Pharmaceutical Company (Shandong, China), respectively. Methanol,

acetoacetate of chromatographic grade were purchased from J. T. Baker(USA), and pure water was prepared by Wahaha water (Wahaha Company, China).

Study Design

Subjects were randomized to a dosing sequence in which they received each of the following: a single dose of THI 35mg, a single dose of PHI 45mg, and single doses of CTHI. The treatment phases were separated by 14-day washout periods.

Blood Sampling

Blood samples were obtained by venipuncture from the antecubital vein and collected before dosing and at 0.5，0.75，1，1.5，2，2.5，3，4，6，8，12 , 24 , 36, 48 and 60 h after administration. Plasma was separated, decanted, frozen and stored at -80 ℃ for analysis.

Instrumentation

LC–MS analysis was conducted using an Agilent (Agilent Technologies, Palo Alto, CA) 1100 series HPLC system consisting of a G1311A Quat pump, a G1379A degasser, and an ALS G1313A autosampler interfaced to an Agilent 1100 series G1946D mass spectrometer equipped with an electrospray ionization (ESI) interface. Selected ion monitoring (SIM) chromatograms were acquired using Agilent Chemstation version 10.02.

Statistical Analysis

Analysis of variance was used for statistical comparisons of pharmacokinetic parameters between groups. A general linear model containing fixed effects for sequence, period, treatment, and subjects was used as the basis for analysis. All statistical tests were 2-sided, with a 5% significance level. Statistical analyses were performed using SPSS version 12.0 (SPSS Institute Inc., USA).

Results

The pharmacokinetic parameters (mean ± SD) for Tramadol without and with Promethazine are summarized in Table 1. Coadministration of Promethazine resulted in significant alterations in Cmax, AUC, Cl/F and Vz/F of Tramadol. The AUC of Tramadol were decreased more than 30% by coadministration of Promethazine ($P < 0.001$); The Cl/F was increased about 50% by coadministration of Promethazine ($P < 0.001$); The Vz/F was increased more than 27% by coadministration of Promethazine ($P< 0.01$). However, Coadministration of Promethazine produced no significant alterations in the Tmax and $t_{1/2}$($P > 0.05$).

The pharmacokinetic parameters (mean ± SD) of Promethazine without and with Tramadol are summarized in Table 2. Coadministration with Tramadol produced significant changes in the pharmacokinetic parameters of Promethazine, which were found to be similar to those obtained in previous studies.

Table 1. Pharmacokinetic parameters for Tramadol after administration of CTHI 80mg and THI 35mg (mean±SD)

	CTHI group (with Promethazine) n=18	THI group (without Promethazine) n=18
C_{max} (μ g / L)	131.9±36.1	182.6±50.8*
T_{max} (h)	1.0±0.1	1.1±0.2
AUC_{0-t}(μg·L/h)	1055.1±195.8	1600.7±470.2**
$AUC_{0-\infty}$(μg·L/h)	1076.3±199.9	1650.0±501.7**
$t_{1/2}$ (h)	6.2±1.1	6.7±1.2
CL/F (L/h)	33.6±6.4	23.3±7.5**
V_z/F (L)	301.9±76.1	219.2±57.8**

C_{max} maximum plasma concentration; T_{max} = time to Cmax; AUC_{0-t} = area under the plasma concentration-time curve from time zero to the last measurable concentration; $AUC_{0-\infty}$ = AUC from time zero to infinity; $t_{1/2}$ = plasma elimination half-life; Cl/F = oral clearance; F=bioavailability; Vz/F = apparent volume of distribution. *$P < 0.05$, **$P<0.01$

Table 2. Pharmacokinetic parameters for Promethazine after administration of CTHI 80mg and PHI 45mg (mean±SD)

	CTHI group (with Tramadol) n=18	PHI group (without Tramadol) n=18
C_{max} (μ g / L)	31.2±9.6	26.8±11.6*
T_{max} (h)	1.8±0.9	1.8±1.0
AUC_{0-t}(μg·L/h)	606.8±116.5	598.8±176.7**
$AUC_{0-\infty}$(μg·L/h)	659.8±117.7	651.1±181.8**
$t_{1/2}$ (h)	16.2±3.7	15.9±4.1
CL/F (L/h)	71.5±13.1	74.5±21.2*
V_z/F (L)	1659.4±493.0	1731.3±751.0**

C_{max} maximum plasma concentration; T_{max} = time to Cmax; AUC $_{0-t}$ = area under the plasma concentration-time curve from time zero to the last measurable concentration; $AUC_{0-\infty}$ = AUC from time zero to infinity; $t_{1/2}$ = plasma elimination half-life; Cl/F = oral clearance; F=bioavailability; Vz/F = apparent volume of distribution. *P < 0.05, **P<0.01

Discussion

The CYP2D6 isozyme is believed to play a role in the metabolism of several other antihistamines in addition to Promethazine, including diphenhydramine and chlorpheniramine[6]. Thus, it is largely responsible for opioid receptor mediated analgesia, whereas (+)-tramadol and (-)-tramadol inhibit re-uptake of neurotransmitters serotonin and noradrenaline. O-Desmethylation to M1 requires CYP2D6 for its formation. Promethazine is a potent inhibitor of the CYP2D6 isozyme. A previous study has shown that several CYP isozymes, including CYP3A4, CYP2B6 and CYP2D6, are involved in the metabolism of Tramadol. The results of the present study suggest that there is sufficient enzymatic capacity to metabolize Tramadol in the environment of CYP2D6 inhibition produced by a single dose of Promethazine.

In this study in healthy subjects, coadministration of with the Tramadol protease inhibitor Promethazine generally had significant effects on the pharmacokinetic profile of either drug. Specifically, there were statistically significant differences in the Cmax, AUC, C1/F and Vz/F of Tramadol with or without coadministration of Promethazine.

Conclusion

In this study, a single dose of the CYP2D6 inhibitor Promethazine had a clinically relevant effect on the pharmacokinetic profile of Tramadol.

Acknowledgement

This research was supported by grants from the National Natural Science Foundation of China (No.81300964), the China Postdoctoral Science Foundation (No.2013M531611) and the Scientific and Technological Programme for Traditional Chinese Medicine of Shandong province (No.2013-190).

References

[1] PING LIU, SUN LIANG,et al.,(2009): EUROPEAN JOURNAL OF DRUG METABOLISM AND PHARMACOKINETICS., 34, 193-200.
[2] Zahari Z, Ismail R.,(2013):Drug Metab Pharmacokinet., Jun 11.
[3] Coller JK,Michalakas JR,et al., (2012):Br J Clin Pharmacol.,74(5):835-841.
[4] Nakamura K,Yokoi T,et al.,(1996):Pharmacogenetics., 6(5):449-457.
[5] He N, Zhang WQ,et al.,(2002):Eur J Clin Pharmacol., 57(12):847-851.
[6] Foster A, Mobley E, et al.,(2007):Pain Pract.,7(4):352-356.

Advanced Materials Research Vols. 989-994 (2014) pp 1044-1047
© (2014) Trans Tech Publications, Switzerland
doi:10.4028/www.scientific.net/AMR.989-994.1044

Effect of crude polysaccharides from *Discorea bulbifera* L. on the liver in the mice bearing U14 cervical carcinoma

Hongxia Cui[1, 2, a]

[1]College of Environmental and Chemical Engineering, Yanshan University, Qinhuangdao, Hebei 066004, China; [2]Hebei Province Key Laboratory of Applied Chemistry, Qinhuangdao, Hebei 066004, China; [a]hxcui@ysu.edu.cn

Keywords: Dioscorea bubifera L., liver, cervical carcinoma, GPT, SOD.

Abstract. To explore the effect of crude polysaccharides of *Dioscorea bulbifera* L. (DBLP) on liver organs in mice bearing cervical cancer, the effects of DBLP on the liver weight in vivo, sections of liver were examined. Glutamate pyruvate transaminase(GPT) and Glutamic oxalo acetic Transaminase(GOT) activites of blood serum in tumor-bearing mice were detected by the colorimetric method. Superoxide dismutase(SOD) and Glutathione reductase(GR) of hepatic tissues were also determined by means of colorimetric method. Our results showed that the liver index, GPT and GOT activities of blood serum, SOD and GR activities of hepatic tissues of DBLP groups were almost the same as that of negative groups. however, the liver index, GPT and GOT activities of blood serum were decreased in DBLP groups compared to CTX groups. And the SOD and GR activities of hepatic tissues of DBLP groups were higher than that of CTX groups. These results demonstrated that DBLP had no effect on liver organs in mice bearing cervical cancer. These data would be a foundation for the appication of DBLP in antitumor, which indicated that DBLP would be a potential antitumor drug. And the further studies, such as antioxidant, should be developed.

Introduction

Cervical cancer is the second leading cause of cancer death among women worldwide, with an estimated 510000 newly diagnosed cervical cancer cases and 288000 deaths[1]. In developing countries, cervical cancer is often the most common cancer in women. It is now clear that persistent infection with human papillomavirus (HPV) is required for the development and maintenance of cervical cancer[2]. Although the efficacy of chemotherapy for the majority of cancer types has improved over the last three decades, high toxic effects of chemotherapeutic drugs causing a severe reduction in quality of life are still formidable problems in clinical medicine[3]. Medicinal plant-based traditional system of medicine commonly known as Ayurvedic medicine in India and traditional Chinese medicine have been the primary source of medication for centuries in the Asian subcontinent[4, 5]. The bulbs of Dioscorea bulbifera have been long used in African traditional medicine for the treatment of leprosy, tumours, pig cysticercosis, sore throat, cuts and sores, dysentery, syphilis, ulcers, pain and inflammation[6, 7].

In previous studies, crude polysaccharides from *Discorea bulbifera* L.(DBLP) was also be found to have antitumor effect on the mice bearing U14 cervical carcinoma[8]. The present work was then undertaken to evaluate the liver impact of the DBLP on tumor models of the mice with U14 cervical carcinoma.

Materials and methods

A. Chemical and reagents

Dioscorea bulbifera L. was purchased from Tangren Drugstore of Qinhuangdao in China. Cyclophosphamide (CTX) was obtained from Shanxi Powerdone Pharmaceutics Co., LTD. in China (the Lot number was 1008421), and diluted to a concentration of 25mg/ml by distilled water before using. Glutamate pyruvate transaminase(GPT) kit, Glutamic oxalo acetic Transaminase(GOT) kit,

Superoxide dismutase(SOD) kit, and Glutathione reductase(GR) kit were provided by Nanjing Jiancheng Biology Engineering Institute. All other chemicals used were of analytical reagent grade.

B. Cell lines

Mouse U14 cervical cancer cell line was purchased from Peking Cancer Hospital Cell Bank of Chinese Academy Medical Sciences, and passaged in Kun Ming mice abdomen.

C. Animals

Female Kun Ming mice of SPF (Specific pathogen free, 6 weeks old, 18 to 22 g) were provided by the Experimental Animal Center of Chinese Military Academy of Medical Sciences, the lot Number was SCXK-(Army) 2007-004. Mice were kept in a clean room with appropriate temperature (20±1℃) and humidity, and provided 8 to 10 h illumination every day. They were fed with a standard pellet diet and water *ad libitum*. The animals were treated according to the National Institute of Health Guide for the Care and Use of Laboratory Animals and their experimental purpose was approved by the animal Ethics Committee of the University.

D. Extraction of the rude polysaccharides

The rude polysaccharides of *Dioscorea bulbifera* L. was extracted by the method according to reference[8]. The total sugar in crude polysaccharides of *Dioscorea bulbifera* L.(DBLP) samples was determined using a phenol-sulphuric acid method as described by Dubois *et al*[9]. The concentration of the total sugar was 43.8 %.

E. Experimental design

U14 cervical cancer cells were passaged in abdomen for increasing. On the 7th day, ascites was extracted, and cell concentration was adjusted to 1×10^7 cells/ml. 0.2ml cancer cell suspension was injected into the left axilla s.c. of each mouse. The mice were starved for 12 h before the establishment of tumor model. The successful rate of vaccination was 100%. Mice were randomly divided into 4 groups (10 mice /group). The 4 groups were designated as control (tumor), CTX control, DBLP low and high dose. Another 10 natural mice were blank control. After 24 h of tumor inoculation, DBLP was given orally at a dose of 100 and 150 mg/kg respectively. The group administered with vehicle alone (sterile distilled water, p.o.) was taken as control and the group treated with CTX (25 mg/kg, i.p.) was considered as the standard reference drug. All groups were continuously treated 15 d. On the day 16th, all animals were havested for analysis of liver index and the activity of GPT, GOT, SOD, and GR.

F. Effect of rude polysaccharides on liver

By the end of the experiment on day 16, the livers were collected for examination immediately after the mice were killed. Liver index was expressed as mg/g of body weight(remove the tumor weight). The liver of treated and control mice were excised and fixed in 4% formalin, embedded in paraffin, and cut in 4 μm sections for histology study.

G. Analysis the activity of GPT and GOT of blood serum in mice bearing U14 cervical carcinoma

Blood samples were collected for stewing 1 h and centrifuged at 3500 rpm for 15 min to obtain serum. The levels of serum activity of GPT and GOT were determined by colorimetric method using commercially available kits according to manufacture's instructions.

H. Analysis the activity of SOD and GR of hepatic tissue in mice bearing U14 cervical carcinoma

By the end of the experiment on day 16, the livers were collected for examination immediately after the mice were killed. The livers were prepared to homogenate by adding 99% normal saline(NS)(liver:NS=1:99, g:v). The liver homogenates were then centrifuged at 2500 rpm for 10 min to obtain liquid supernatant. The levels of liver SOD and GR activities were determined by colorimetric method using commercially available kits according to manufacture's instructions. One unit of enzyme activity of SOD was defined as the amount of protein needed to decrease the reference rate to 50% of maximum inhibition. One unit of enzyme activity of GR was defined as the amount of enzyme needed to transform 1mM NADPH.

I. Statistical analysis

All the results were expressed as the mean±S.D. An one-way ANOVA using SPSS 13.0 software was used to conduct a statistical comparison of differences among the groups and a value of $p<0.05$ was considered as significant.

Results

A. Effect of rude polysaccharides on liver

To determine if DBLP has any side effect on liver, we conducted the liver index and pathological examination of hepatic tissues. The results of liver index was shown in Table 1. As shown in Table 1, liver index of blank control, negative control, CTX(25mg/kg), low dose of DBLP(100mg/kg), and high dose of DBLP(150mg/kg) treated group was 4.25±0.64, 5.43±0.73, 6.96±0.32, 5.68±0.94, and 5.96±0.68, respectively. There was no obviously pathological change in hepatic tissues between DBLP treated mice and control. The sections of liver showed that central vein and hepatic lobule were distinct, hepatocellular disposed compact and orderly (data not shown).

Table 1 The effect of DBLP on liver organs

Groups	Treatment(mg/kg)	Liver index(mg/g)
Blank control	Vehicle	4.25±0.64
Negative control	Vehicle	5.43±0.73
CTX	25	6.96±0.32
Low dose of DBLP	100	5.68±0.94
High dose of DBLP	150	5.96±0.68

Results were expressed as mean±S.D., n=10. All the results have no significant differences.

B. Analysis the activity of GPT and GOT of blood serum in mice bearing U14 cervical carcinoma

The GPT and GOT activities of blood serum were also determined and the data were showed in Table 2. The GPT and GOT activities of blood serum of Blank control were 24.69±4.62IU/L and 39.39±3.18IU/L, respectively. However, The GPT and GOT activities of Negative control were increased to 34.34±3.92IU/L and 48.19±3.18IU/L, respectively. The GPT and GOT activities of CTX were also increased to 55.45±6.52IU/L and 66.01±2.14IU/L, respectively. And the The GPT and GOT activities of DBLP groups were decreased compared with CTX groups.

Table 2 The GPT an GOT activities of blood serum in mice

Groups	Treatment(mg/kg)	GPT(IU/L)	GOT(IU/L)
Blank control	Vehicle	24.69±4.62	39.39±3.18
Negative control	Vehicle	34.34±3.92	48.19±2.21
CTX	25	55.45±6.52	66.01±2.14
Low dose of DBLP	100	35.28±3.84	50.02±1.51
High dose of DBLP	150	37.34±3.76	52.37±8.32

Results were expressed as mean±S.D., n=10. All the results have no significant differences.

C. Analysis the activity of SOD and GR of hepatic tissue in mice bearing U14 cervical carcinoma

Table 3 The SOD and GR activities of hepatic tissue in mice

Groups	Treatment(mg/kg)	SOD(U/mg prot)	GR(U/g prot)
Blank control	Vehicle	258.42±24.43	13.44±1.62
Negative control	Vehicle	223.57±36.83	11.69±2.48
CTX	25	156.76±38.76	8.98±1.58
Low dose of DBLP	100	221.59±20.08	11.34±1.21
High dose of DBLP	150	215.33±27.96	10.86±0.98

Results were expressed as mean±S.D., n=10. All the results have no significant differences.

As shown in Table 3, the SOD and GR activities of hepatic tissue were detected and the results of blank control were 258.42±24.43U/mg and 13.44±1.62U/mg, respectively. The SOD activities of negative control was decreased to 223.57±36.83U/mg and that of CTX was decreased to 156.76±38.76U/mg. And the SOD activities was increased in hepatic tissue of mice with cervical cancer (DBLP group) compared to CTX ($p<0.05$). In addition, as shown in Table 3, levels of GR activities was also higher in hepatic tissue of mice with cervical cancer (DBLP groups) compared to the CTX. There was almost no differencese about GR activities between DBLP groups and negative control.

Discussions

Chinese medicinal herbs preparations have been increasingly used for cancer therapy in Asian countries in an attempt to assist in killing tumor cells and reducing the toxicity of chemotherapy[10, 11]. DBLP had been found to be antitumor ractivity before.

In order to find the effect of DBLP on liver organ in mice bearing tumor. We promoted the present investigation. The liver index of DBLP groups were differences compared to negative control groups and decreased compared to CTX groups. This indicated that the DBLP didn't have effect on the liver organ of mice. The activities of GPT and GOT of blood serum in mice bearing cervical cancer (DBLT) were also no differences according to negative control groups and reduced compared to CTX. And the activities of SOD and GR of hepatic tissues in mice bearing cervical cancer(DBLT) were no differences according to negative control groups and increased compared to CTX.These results demonstrated further that DBLP didn't have effect on mice liver organ.

Summary

The rude polysaccharides of *Dioscorea bulbifera* L. in China exhibited the no effect on the liver organ in mice bearing cervical cancer. But DBLP had the protection potent on liver organs compared with CTX. Further studies about the antioxidant of DBLP are needed to be investigated, which is of potential research and development value in the field of pharmaceutical.

References

[1] D. Saslow, P.E. Castle, J.T. Cox, D.D. Davey, M.H. Einstein, D.G. Ferris, S.J. Goldie, D.M. Harper, W. Kinney, A.B. Moscicki, K.L. Noller, C.M. Wheeler, T. Ades, K.S. Andrews, M.K. Doroshenk, K.G. Kahn, C. Schmidt, O. Shafey, R.A. Smith, E.E. Partridge, Gynecologic cancer advisory group, F. Garcia, American caner Society Guideline for human papillomavirus (HPV) vaccine use to prevent cervical cancer and its precursors, CA Cancer J. Clin. 57(2007) 7-28.

[2] N. Munoz, F.X. Bosch, S. de Sanjose, R. Herrero, X. Castellsague, K.V. Shah, P.J. Snijders, C.J. Meijer, Epidemiologic classification of human papillomavirus types associated with cervical cancer, N. Engl. J. Med. 348(2003) 518-527.

[3] D.T. Rein, C.M. Kurbacher, The role of chemotherapy in invasive cancer of the cervix uteri: current standards and future prospects, Anticancer Drugs 12(2001) 787-795.

[4] M.J. Balunas, A.D. Kinghorn, Drug discovery from medicinal plants, Life Sci. 78(2005) 431-441.

[5] S. Lukman, Y. He, S. Hui, Computational methods for Traditional Chinese Medicine: a survey, Comput. Meth. Prog. Bio. 88(2007) 283-294.

[6] Cogne, Phytochemical investigation of plants used in African medicine: Dioscorea sylvatica (Dioscoreaceae), Urginea altissima (Liliaceae), Jamesbrittenia fodina and Jamesbrittenia elegantissima (Scrophulariaceae), Doctorat Theses, University of Lausanne, Lausnne 2002.

[7] T.B. Nguelefack, R.C. Dutra, A.F. Paszcuk, E.L. Andrade, L.A. Tapondjou, J.B. Calixto, Antinociceptive activities of the methanol extract of the bulbs of *Dioscorea bulbifera* L. var sativa in mice is dependent of NO-cGMP-ATP-sensitive-K^+ channel activation, J. Ethnopharmacol. 128(2010) 567-574.

[8] Hongxia Cui. Antitumor activity and possible mechanism of crude polysaccarides from Discorea bulbifera L. on the mice bearing U14 cervical carcinoma. Advanced Materials Research, 2012, 560-561: 374-379

[9] M. Dubois, K.A. Gilles, J.K. Hamilton, P.A. Rebers, and F. Smith, Colorimetric method for determination of sugars and related substances, Anal. Chem. 28(1956) 350-356.

[10] G.B. Zhou, S. J. Chen, Z. Y. Wang, and Z.Chen, Back to the future of oridonin: again, compound from medicinal herb shows potent antileukemia efficacies in vitro and in vivo, Cell. Res. 17(2007) 274-276.

[11] Y. Gao, H. Gao, and E. Chan, Antitumor activity and underlying mechanisms of Ganopoly, the refined polysaccharides extracted from Ganoderma Lucidum, in mice, Immunol. Invest. 34(2005) 171-98.

Advanced Materials Research Vols. 989-994 (2014) pp 1048-1051
© (2014) Trans Tech Publications, Switzerland
doi:10.4028/www.scientific.net/AMR.989-994.1048

Design, Synthesis, and Biological Evaluation of Sorafenib Analogs Bearing a Sulfonylurea Unit as Novel VEGFR2 Kinase Inhibitors

Wufu Zhu[1, a*], Chunjiang Wu[1] , Shan Xu[1], Wei Li[2]， Haihong Fang[1], Zhichao Chen[1]， , Xuhuang Tu[1], and Pengwu Zheng[1, b*]

[1]School of Pharmacy, Jiangxi Science & Technology Normal University, Nanchang 330013, China;

[2]Key Laboratory of Jiangxi Province Natural Active Pharmaceutical Ingredients, College of Chemistry and Biology Engineering, Yichun University, Yichun 336000, China

[*a]zhuwufu-1122@163.com@163.com, [*b]zhengpw@126.com

Keywords: VEGFR2 Kinase inhibitors; Sorafenib; Sulfonylurea; Anticancer activity

Abstract. Two sorafenib analogs (9a，9b) containing sulfonylurea unit were synthesized and their chemical structures were confirmed by 1H NMR and MS spectrum. The synthesized compounds were evaluated for the inhibition rate against VEGFR2 kinase at 10 μ M level. The inhibition rates of compound 9a and 9b against VEGFR2 kinase were 61.0±11.1% and 22.6±2.6%, respectively. The results showed that the introduction of sulfonylurea unit is favorable for the activity, and further study is being carried out.

Introduction

Cancer is a global killer, taking the lives of over 7 million people a year. Although a range of antitumor drugs and therapies are available, drug resistance and adverse side effects are still serious problems. Therefore, the search for highly efficient and safe chemotherapeutic agents for treating cancer remains desirable[1].

Sorafenib, a novel oral multiple-targeted antitumor drug with a diarylurea skeleton, has been approved by the FDA for the treatment of primary renal carcinoma and primary liver cancer [2], and research on potent sorafenib analogs has been the focus of many studies [3-4]. Interestingly, recent optimizations of the diarylurea framework of sorafenib led to discovery of sulfonylurea-based sorafenib analogs with excellent antitumor activity, and the N-methyl-4-phenoxypicolinamide motif was retained in the target compounds, while the urea unit was replaced by sulfonylurea unit. The structures and design of the target compounds was shown in Fig.1.

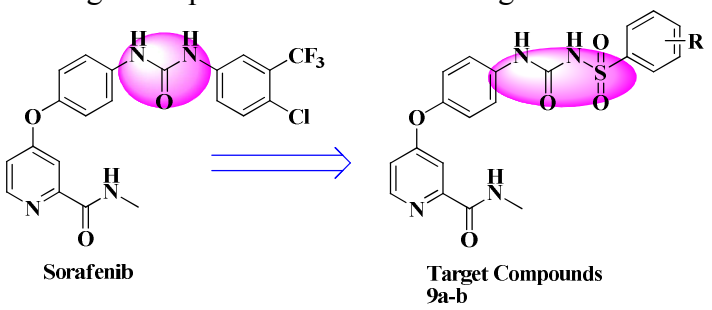

Fig. 1 Structures of sorafenib and the target compounds

The synthetic routes for target compounds were illustrated as outlined in Scheme 1. Chlorination of the commercially available picolinic acid in thionyl chloride in the present of NaBr afforded **2**, which was subsequently reacted with 30% methylamine to give the corresponding compound **3** as pale-yellow crystals.

Etherification of **3** with 4-aminophenol in the presence of potassium *tert*-butoxide led to the formation of intermediate **4**. Compound **8** was prepared from commercially available **5** *via* sulfonylation, ammonlysis and acylation reactions. Condensation of **4** and **8a-b** in toluene furnished the target compounds **9a–b** in good yield.

Materials and methods

All melting points were obtained on a Büchi Melting Point B-540 apparatus (Büchi Labortechnik, Flawil, Switzerland) and were uncorrected. The IR spectra were recorded by means of the KBr pellet technique on a Bruker FTS 135 spectrometer. NMR spectra were performed using Bruker 400 MHz spectrometers (Bruker Bioscience, Billerica, MA, USA) with TMS as an internal standard. Mass spectra (MS) were taken in ESI mode on Agilent 1100 LC–MS (Agilent, Palo Alto, CA, USA). Elemental analysis was determined on a Carlo-Erba 1106 Elemental analysis instrument (Carlo Erba, Milan, Italy). All the materials were obtained from commercial suppliers and used without purification, unless otherwise specified. Yields were not optimized. TLC analysis was carried out on silica gel plates GF254 (Qindao Haiyang Chemical,China).

Synthesis of compounds[5]

4-Chloropicolinoyl chloride (2)

2-Picolinic acid (10g,0.081mol) and sodium bromide (1.3g,0.013mol) are suspended in chlorobenzene (13mL). After heating to 50℃, thionyl chloride (24mL) is added to such a degree. The reaction mixture is subsequently heated to 85℃ and stirred for 20 h. After cooling to room temperature, the majority of the chlorobenzene and excess thionyl chloride are removed by distillation under reduced pressure. Toluene(15mL) is added and the distillation under reduced pressure is repeated , in order to remove residual thionyl chloride and the majority of the toluene. After toluene has been added again(50mL),this solution was used directly in the next stage.

4-Chloro-*N*-methylpicolinamide (3)

Methylamine as a 33% aqueous solution is added to the reaction vessel. The solution is cooled to 0℃.The toluene solution with the crude 4-chloropyridine-2-carbonyl chloride hydrochloride is added to such a degree that the temperature of the reaction mixture does not exceed 20℃. After stirring further at 20℃ for 6h, the reaction solution is suction filtered. The filtrate toluene layer is washed three times with water (60mL), the aqueous layer is washed twice with toluene (20mL), then the solvent is evaporated to dryness under reduced pressure to give a brown oily liquid. The crude 4-chloro-*N*-methylpyridine-2-carboxamide is thus obtained. 37% Hydrochloric acid (25mL) is added with stirring to a solution of the crude 4-chloro-*N*-methylpyridine-2-carboxamide in THF (60mL) to such a degree that the temperature of the reaction mixture does not exceed 20℃.After cooling to 0℃, stirring is continued for 1 h. The product is filtered off, wash with THF (10mL) and dried under reduced pressure. The solid was dissolved in water (80mL), The solution is adjusted to pH 7 using a 20 percent NaOH solution and keep the temperature at 0℃, stirring is continued for 1 h. The product is filtered off, wash with water and dried under reduced pressure to afford 9.8g 4-chloro-*N*-methyl-pyridine-2-carboxamide as light yellow solid (**3**).Yield: 70%, ^{1}H -NMR (400 MHz, DMSO) δ 8.85 (s, 1H), 8.63 (d, J= 5.2 Hz, 1H), 8.03 (s, 1H), 7.76 (d, J= 5.2 Hz, 1H), 2.84 (d, J= 4.8 Hz, 3H).

4-(4-aminophenoxy)-N-methylpicolinamide (4)

A mixture of 4-chloro-*N*-methyl-pyridine-carboxamide (5g, 0.029mol), parahydroxyaniline (4.1g, 0.038mol) is dissolved in DMF(50mL), and the mixture is stirred at room temperature for 1 h, then a solution of **3** (5.0g, 0.029mol) in DMF (15mL) and NaI are added respectively.The mixture is heated to 85-90℃ for 5 h. After cooling to 15℃, 37% hydrochloric acid (10mL) is added to such a degree that the temperature of the reaction mixture does not exceed 30℃.After stirring further for 1 h, the precipitated product is filtered off and washed with dichloromethane.After the still-moist product has been dissolved in water, the pH of the mixture is adjusted to from pH 3 to 3.5 at 20℃ by adding 10% sodium hydroxide solution . The mixture is seeded with the title compound and subsequently stirred for 30 min. Afterward, addition of further 10% sodium hydroxide solution at 20℃within 1 h establishes a pH of from 6 to 7 and the mixture is stirred for a further 30 min. The suspension is filtered, the solid is washed with distilled water and dried at approx. 60℃ under reduced pressure. In this way, 4.2g of the title compound are obtained as light brown crystals.^{1}H-NMR(400 MHz, DMSO) δ 8.77 (d, J= 4.5 Hz, 1H), 8.46 (d, J= 5.5 Hz, 1H), 7.34 (s, 1H), 7.18-7.02 (m, 1H), 6.87 (d, J= 7.9 Hz, 2H), 6.65 (d, J= 7.9 Hz, 2H), 5.21 (s, 2H), 3.37 (s, 1H), 2.78 (d, *J*= 4.4 Hz, 3H).

General Procedure for Preparation of Compounds 8a-b

Compounds **8a-8b** were synthesized from **5a-5b** according to the reported procedures [6-7].

General Procedure for Preparation of Compounds 9a-b

4-(4-aminophenoxy)-N-methyl-pyridine carboxamide(0.41mmol) and 4-chloro phenyl sulfonamido ethyl(0.41mmol) was added to the toluene(5mL).Refluxed for about 6 hours to precipitate a brown solid, filtration and dried to give the title compounds (**9a-b**).

4-(4-(3-(4-Chlorophenylsulfonyl)ureido)phenoxy)-N-methylpicolinamide （9a）

Yield：43.2%. ESI-MS [M+H] m/z: 459.1;m.p.:118-122℃;^{1}H NMR (400 MHz, DMSO) δ 9.11 (s, 1H), 8.77 (s, 1H), 8.48 (d, *J* = 5.5 Hz, 1H), 7.97 (d, *J* = 8.5 Hz, 2H), 7.71 (d, *J* = 8.5 Hz, 2H), 7.46 (d, *J* = 8.9 Hz, 3H), 7.33 (s, 1H), 7.17 – 7.05 (m, 4H), 2.77 (d, *J* = 4.7 Hz, 3H).

4-(4-(3-(2,4-Difluorophenylsulfonyl)ureido)phenoxy)-N-methylpicolinamide（9b）

Yield：45.8%. ESI-MS [M+H] m/z: 462.1;m.p.:236-237℃; ^{1}H NMR (400 MHz, DMSO) δ 8.90 (s, 1H), 8.80 (d, *J* = 4.6 Hz, 1H), 8.51 (d, *J* = 5.5 Hz, 1H), 7.60 (d, *J* = 8.8 Hz, 2H), 7.38 (d, *J* = 2.2 Hz, 1H), 7.16 (dd, *J* = 11.3, 5.7 Hz, 3H), 2.79 (d, *J* = 4.7 Hz, 3H)

Biological Evaluation

The kinase activity of VEGFR2 was measured by the mobility shift assay. All kinase assays were performed in 384-well plates in a 50 μL reaction volume. The kinase base buffer contains 50 mM HEPES, pH 7.5, 10 mM $MgCl_2$, 0.0015% Brij-35 and 2 mM DTT. The stop buffer contains 100mM HEPES, pH 7.5, 0.015% Brij-35, 0.2% Coating Reagent #3 and 50 mM EDTA. Dilute the compounds to 500 μM by 100% DMSO, then transfer 10 μL of compound to a new 96-well plate as the intermediate plate, add 90 μL kinase buffer to each well. Transfer 5 μL of each well of the intermediate plate to 384-well plates. The following amounts of enzyme and substrate were used per well: kinase base buffer, FAM-labeled peptide, ATP and enzyme solution. Wells containing the substrate, enzyme , DMSO without compound were used as DMSO control. Wells containing just the substrate without enzyme were used as low control. Incubate at room temper-ature for 10 min. Add 10 μL peptide solution to each well. Incubate at 28℃ for specified period of time and stop reaction by 25 μL stop buffer. At last collect data on Caliper program and convert conversion values to inhibition values. Percent inhibition = (max-conversion)/(max-min)*100. “max” stands for DMSO control; “min” stands for low control.

Results

chemistry

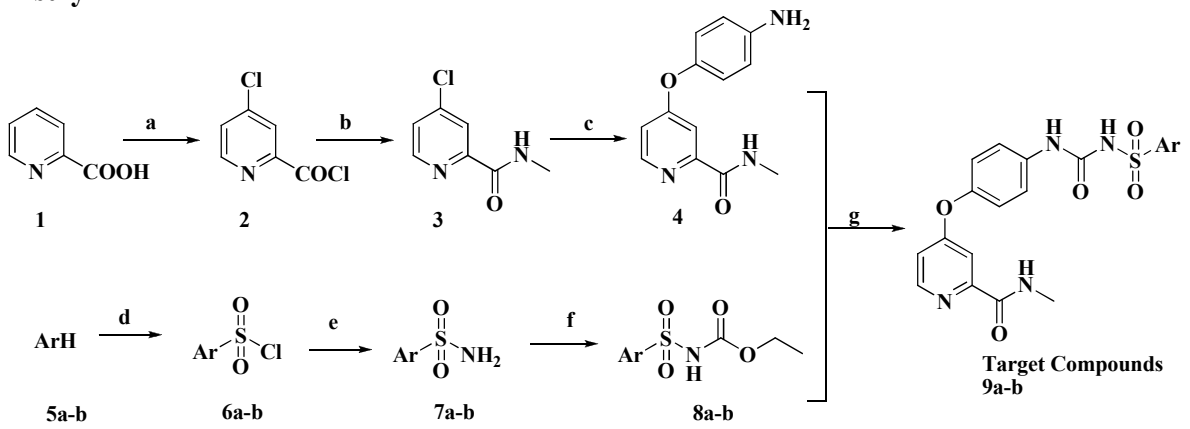

Scheme 1. Synthetic route of target compounds 9a-b

Reagents and conditions: (a) $SOCl_2$,NaBr, chlorobenzene,85°C, 20h; (b) 30% $MeNH_2$, toluene, 20℃, 6 h; (c) *t*-BuOK, NaI, DMF; (d) Chlorosulfonic acid, CH_2Cl_2 r.t., 12h; (e) Aqueous ammonia, CH_2Cl_2 r.t., 2h; (f) K_2CO_3, acetone, reflux,15h;(g) Toluene, reflux, 6h.

Biological assay

The *in vitro* anticancer activities of above synthesized compounds **9a** and **9b** were studied on the VEGFR2 kinase. The test results of compounds **9a-b** were listed in Table 1.

Table 1 Structures and inhibition rate of target compounds 9a, 9b against VEGFR2 kinase at 10μM

Compounds No.	Ar	VEGFR2 (10μM inhibitory %)
9a	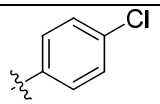	61.0±11.1
9b	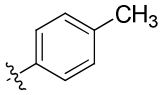	22.6±2.6
Sorafenib	-	94.9±1.1

From Table 1, we could see that the two target compounds showed moderate activity against the tested kinase, especially compound **9a** with the inhibition rate of 61.0±11.1% at 10μM. Although their inhibition rate is lower than GDC-0941, it still showed that the replacement of urea with sulfonylurea unit is benefit to this kind of compounds. This result suggested that sulfonylurea sorafenib analogs worthy to study further, and more compounds will be designed, synthesized and evaluated in future.

Conclusions

Two sorafenib analogs containing sulfonylurea unit were synthesized and their chemical structures were confirmed. Compound **9a** was more active than **9b**, and the inhibition rates of compound **9a** against VEGFR2 kinase at 10μM was 61.0±11.1%. The results showed that the introduction of sulfonylurea unit is favorable for the activity.

Acknowledgments

We gratefully acknowledge the generous support provided by Science and Technology Project Founded by the Education Department of Jiangxi Province (No. GJJ13578, GJJ13580) and Project Program of Key Laboratory of Drug Design and Optimization, Jiangxi Science & Technology Normal University.

References

[1] Zhu W, Liu Y, Zhai X, et al. Design, synthesis and 3D-QSAR analysis of novel 2-hydrazinyl-4-morpholinothieno [3, 2-d] pyrimidine derivatives as potential antitumor agents, Euro. J. Med. Chem. 57(2012) 162-175.

[2] Guida T, Anaganti S, Provitera L, et al. Sorafenib inhibits imatinib-resistant KIT and platelet-derived growth factor receptor β gatekeeper mutants. Clin. Cancer Res.13(2007) 3363-3369.

[3] Barbosa M L C, Lima L M, Tesch R, et al. Novel 2-chloro-4-anilino-quinazoline derivatives as EGFR and VEGFR-2 dual inhibitors[J]. Euro. J. Med. Chem. 71(2014) 1-14.

[4] Yao J, He Z, Chen J, et al. Design, synthesis and biological activities of sorafenib derivatives as antitumor agents[J]. Bioorg. Med. Chem. Lett. 22(2012) 6549-6553.

[5] M Logers, R Gehring, O Kuhn and M Matthaus, WO. Patent 2006034796. (2006)

[6] Scarborough, M Robert. WO. Patent 2007056219A1. (2007)

[7] Tsai,Henry J. D-420720, a novel orally active sulfonamide compound dipeptidylpeptidase inhibitor:structure and activity relationship of arylsulfonamide to dipeptidylpeptidase inhibitor[J].Drug Develop. Res. 69(2008) 514-519.

Advanced Materials Research Vols. 989-994 (2014) pp 1052-1055
© (2014) Trans Tech Publications, Switzerland
doi:10.4028/www.scientific.net/AMR.989-994.1052

The Effects of the Film Made by Citral β-Cyclodextrin Inclusion Complex Combined with Chitosan on Fresh Beef

Haijun Chen, Fuxin Yang, Lijuan Ou, Dongxiang Zhou, Li Li *

Shanghai Engineering Research Center of Aquatic-Product Processing & Preservation, College of Food Science and Technology, Shanghai Ocean University, Shanghai 201306, China
navy0510@gmail.com, fxyang@shou.edu.cn, 379626988@qq.com, dxzhou@shou.edu.cn, l-li@shou.edu.cn
* Correspondence should be addressed to Li Li (L-li@shou.edu.cn)

Keywords: Chitosan; Citral; β-CD; Antimicrobial-film; Beef; Preservation

Abstract: Films of chitosan (Ch), Ch+0.5%(v/v) the citral(CI), Ch+2.5%(w/v) the citral β-cyclodextrin inclusion complex (β-CD-CI) and the physics mixture CI and β-CD-CI were prepared on the quality of fresh beef during refrigerated storage at 4±1℃ were investigated, and verified the preservation effect of wrap fresh beef. The control and the treated beef samples were analyzed periodically for the total volatile basic nitrogen (TVBN), aerobic bacterial count (ABC), the sensory evaluation, and pH. The results indicate that all treatments retarded the decay of the beef samples. The chitosan film with the β-CD-CI exhibited superior to the preservation ability compared with control pure chitosan film treatment in maintaining the quality of fresh beef samples and significantly extended the shelf life by approximately 5 days.

Introduction

Currently, there are mainly two approaches for fresh-keeping packaging technology of beef: one is based on packaging techniques, such as modified atmosphere packaging; the other is based on packaging materials, such as finding suitable materials with antibacterial properties [1].

Beef is a highly perishable food commodity with a rather short shelf life due to microbial activity which is by far the most important cause of spoilage and may be manifested as visible growth, textural changes or off-odors and off-flavors [2]. This situation causes significant economic losses for the beef industry and as consequence the meat industry is looking for effective, natural, preservation methods that provide meat products with extensive shelf life.

Citral (CI) is the main component of lemon grass oil. It is a naturally occurring isoprenoid with two isomers, reportedly exerts anti-fungal activity against some citrus postharvest pathogens such as P. italicum and Penicillium digitatum, which demonstrated the citral have anti-bacterial propriety [3]. The β-CD cavity provides stabilization to protect the guest molecules and prevention of evaporation, degradation and oxidation; therefore, β-CD has been widely applied in the fields of chemical segregation analysis, medicine, food, and pesticides.

Cyclodextrin inclusion complexation is very effective for the stabilization and controlled release of functional additives [4]. It is suitable for the packaging structure design and food preservation [5]. However, there are few reports on the β-cyclodextrin inclusion complex of CI in the scientific literature. This study provides a theoretical basis for preservation, processing, and storage of beef.

Materials and Methods

Materials

Chitosan (Ch) (40-100 mesh, food grade), Ethanol anhydrous (purity≥99.5%), Tween-20, Nutrient agar, and Sodium chloride (purity≥99%) were purchased from Sangon Biotech (Shanghai) Co., Ltd. (Shanghai, China); Citral (CI) (purity≥97.0%, food grade), β-Cyclodextrin (β-CD), Glycerol (Gly), Acetic acid, Biolog-90mm, and Sterilized homogenization bags were purchased from Sinopharm Chemical Reagent Co., Ltd. (Shanghai, China); Fresh beef was purchased from Shanghai meat Co., Ltd. (Shanghai, China);

Electric mixing water bath (JB 90-S, specimen model factory, Shanghai, China); Kjeltec™ 2300 Analyzer Unit (FOSS Tecator AB, Sweden); PH meter10 (Sanxin Co., Ltd., Guangxi, China);

Cleanbench (STIK (shanghai) instrument equipment Co., Ltd. China); Bag Mixer, French Interscience Co., Ltd.

Preparation of the Film

The compound of citral and β-CD was prepared by using a co-precipitation method described by J. Lia et al [6] and the proportion of component about prepared film referenced by Y.X. et al with minor modification. Explanation: preparing other films was similar to the B4 films.

B1: the control (the sterilized deionized water);

B2: Ch 1.5%(w/v) +Tween-20 0.4 %(v/v) +Gly 25%(v/w) +A-acid 1%(v/v);

B3: Ch 1.5% (w/v) +CI 0.5 %(v/v) +Tween-20 0.4 %(v/v) + Gly 25%(w/v) + A-acid 1%(v/v);

B4: Ch 1.5%(w/v) +β-CD-CI 2.5% +Tween-10 0.4%(v/v) + Gly 25%(w/v) +A-acid 1%(v/v);

The film of B4 was prepared according to the following steps.

Chitosan solutions (1.5%, w/v) were prepared by dispersing chitosan in an aqueous solution of lactic acid (1%, v/v) and stirred with a magnetic stirrer at 50℃ [7].After the chitosan was dissolved completely, Glycerol 1%(v/v)as a plasticizer and Tween-20 0.4%(v/v) as a surface-active agents were added into the solution and stirred for 30 min. Lastly, adding β-CD-CI 2.5% (w/v) dissolved and stirred for about 1h till homogeneous. The final antibacterial chitosan compound film solution was prepared. The 60ml film solution was poured into the rectangular mold with 20*15*5cm, and then drying at 45℃ for 3-4 hrs come out with the films.

The Preliminary Verification of the Film's Antibacterial Property

The different films were paste it in agar plates of four zones, replicated three times, and the chitosan film as control group. Keeping the constant temperature at 37±1 ℃ and incubated for 24 hrs. Observed at each patch, the size of transparent circle represents its ability of inhibiting bacterial, and record the diameter. From the Fig.1 shows that the different compound chitosan films have certain antibacterial effect.

Figure.1 Compound chitosan films inhibit capability

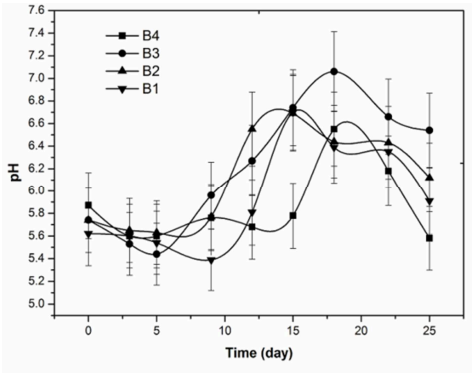

Figure2. Changes in ph of beef samples

Methods

Treatment of Beef Samples. The samples were selected from the fresh beef shank. Beef fillets (25g) were preserved under 4±1℃ conditions. The samples were wrapped with different films. Then the samples were airproof in PE bags. Each sample must be labeled and sealed, in accordance with the films of B1, B2, B3, and B4. The wrapped beef samples were stored in the lab refrigerator at 4±1 ℃ and the relative humidity maintained 80%~95% for 30 days. The pH values, sensory characteristics, microbial and TVBN of the beef samples were detected on the storage day of 0, 3rd, 7th, 11th, 14th, 17th, 20th, 24th and 27th.

Measurements of the pH. The beef samples were sampled periodically and homogenized in distilled water (1:10; w/v), and the homogenate was used for pH determination after allowing to stand for 30 min.

Measurements of the Sensory Evaluation. The samples were evaluated by 6 members experienced. Panelists were asked to evaluate the viscosity, color, flavor, and texture, using a 10-point hedonic scale (10=like extremely and 1=dislike extremely). A score of 6 was defined as the lowest limit of consumer's acceptability.

Microbiological Analysis. The each sample was transferred into sterile homogeneous bags with 225mL of 0.85% NaCl solution and subsequently homogenized in a Stomacher lab blender. Serial dilutions (10-1–10-8) were spread on Plate Count Agar. From this dilution, other decimal dilutions were prepared and appropriate gradient were selected to determine the aerobic bacterial counts by

the pour plate method. The inoculated plates were incubated for 24hrs at 37 ℃ for total viable counts. Bacterial counts were expressed as log10 colony forming units (CFU)/g sample.

Measurements of the Total Volatile Basic Nitrogen (TVBN). Total volatile basic nitrogen (TVBN) is recommended to be used in the integrated assessment of meat quality as it is important parameters of its freshness. It was determined by distillation after the addition of MgO to homogenized beef sample. The distillate was collected in a flask containing 3% aqueous solution of boric acid and a mixed indicator of methyl red and methylene blue. Finally, the boric acid solution was titrated with 0.1 N HCl. The quantity of TVBN in mg/100g was calculated from the volume (V) of HCl added.

Statistical Analysis. A statistical analysis of data was performed using SPASS and all measurements were performed in triplicate. Data were subjected to analysis of variance to compare the effects of different treatments. The least significant difference procedure was used to test for differences between means ($P \leq 0.05$).

Results and Discussion

The pH Analysis. When the PH value increase to the 6.4, at the time defined the beef meat is corrupted and not edible. Beef normally reaches its lowest pH value of 5.4 to 5.6 at 3 to 4 days after slaughter. After the lowest pH level is reached, the pH started to rise again slowly and steadily. The pH values for the treatments during storage were presented in Fig.2. During the storage, the pH value of control sample (B1) significantly increased from 5.62 on first day to 6.4 on Day 13. The B2 and B3 group came to 6.4 on Day 13 and Day 12, while the B4 group was corrupted on Day 18 which prolonged the shelf life for about 5 days compared with B1group.

Sensory Evaluation. This test parameter is not as an assess criterion of food quality or within effective shelf-life period, but as representation of people subjective perception of beef meat appearance. The results of the sensory assessment of samples were given in Table 1. During the storage, the sensory evaluation of control group was increased. The B1 group was lower than 6 scores after 15 days; the B4 samples kept fresh in 20 days which prolonged shelf life about 5 days.

Table 1. Change in sensory evaluation of beef samples

time(days)	0	1	3	6	9	12	15	17	20	23	25	27
B_1	10	10	8	8	7	7	6	6	6	2	2	2
B_2	10	10	9	8	7	8	8	8	7	6	5	3
B_3	10	10	9	8	8	7	7	7	7	6	4	3
B_4	10	10	9	8	8	7	7	7	6	6	6	4

Microbiological Analysis. Many studies have regarded 10^6CFU/g (6 Log10 CFU/g) as the acceptable limit of meat [8]. Measured changes in ABC during the storage period were shown in Fig3. The initial ABC of fresh beef B3 samples was 1.08 Log10 CFU/g, rapidly increased to 3.89 and 6.08 Log10 CFU/g on Day 11 and Day 24 respectively. B1 samples were most quickly corrupted on Day 21. While the ABC value of samples wrapped with B4 film was lower than other treatments during the storage. The B4 film was better effective in inhibit the microbial compared with the other treatments and prolong the shelf-life about 5 days than the control. B4-film with better preservation ability was potentially attributed to β-CD-CI.

The Total Volatile Basic Nitrogen (TVBN). The Fig.4 shows that the changes in TVBN values of the beef samples during storage. The initial TVBN value of the control was 6.05mg N/100 g. The values of all treatments increased on various degrees during storage. TVBN values increased ($p < 0.05$) with storage time; With the limitation of 20 mg N/100 g, samples wrapped with B4 reached a significantly ($p < 0.05$) lower TVBN value of 15.45 in comparison with the samples wrapped with B2, B3 or B1 controls, which attained higher levels of 18.67, 17.23 and 21.77, respectively. (Fig.4) The addition of citral deterred further reduction in TVBN values. Generally, 20 mg TVBN/100g of beef is considered as the acceptable limit. The shelf-life of control was only about 12days, while samples wrapped with B4 film reached limit value at 16 days of storage and prolonged the shelf life about 4 days.

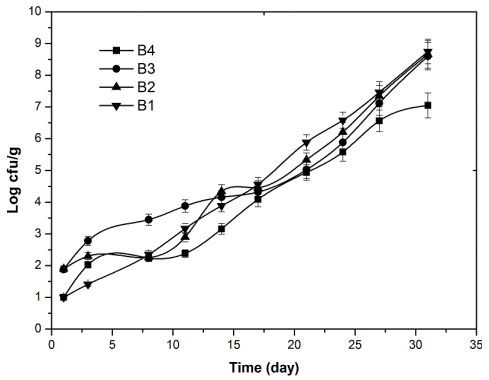

Figure.3 Changes in aerobic bacterial count

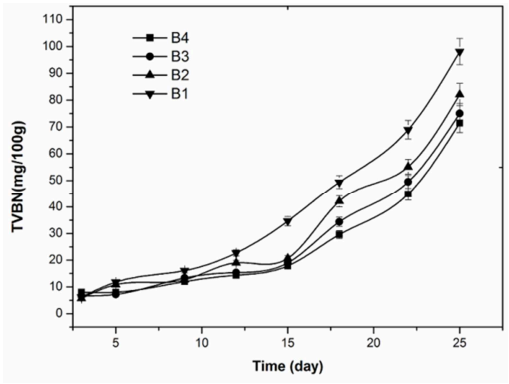

Figure.4 Changes in TVBN

Conclusions

The pH value of control sample significantly increased from 5.62 on first day to 6.4 on Day 13, while the B4 group was corrupted on Day 18 which prolonged the shelf life for about 5 days. The control samples exceeded the acceptable limit of TVBN on the Day 12th, while samples wrapped with the chitosan film containing β-CD-CI reached TVBN limit on the Days 16th. Chitosan combined with β-CD-CI was the most effective of the four compared groups in maintain the quality of the beef, it also prolonged the storage period about 4 days. In conclusion, using film of Chitosan combined with β-CD-CI would prolong the beef's shelf-life for about 5days than normal storage in 4±1℃.

Acknowledgments

This work was supported by the Innovation Program of Shanghai Municipal Education Commission (14YZ120), the National High Technology Research and Development Program of China (863 Program, 2012AA092301) and the Shanghai Engineering Research Center of Aquatic-Product Processing & Preservation (11DZ2280300).

References

[1] Shahidi F, Arachchij Kv, Jeon Y J, Food applications of chitin and chitosans. Trends in Food Science & Technology 1999; 10 (2), 37-51.

[2] Nychas, G.J.E., Skandamis, P.N., Tassou, C.C., Koutsoumanis, K., 2008. Meat spoilage during distribution. Meat Science 78, 77–89.

[3] Caccioni, D. R. L., Guizzardi, M., Biondi, D. M., Renda, A., & Ruberto, G. (1998). Relationship between volatile components of citrus fruit essential oils and antimicrobial action on Penicillium digitatum and Penicillium italicum. International Journal of Food Microbiology, 43(1e2), 73e79.

[4] Wang J, Cao Y, Sun B, Wang C. Physicochemical and release characterisation of garlic oil-β-cyclodextrin inclusion complexes. Food Chemistry 2011; 127 (4), 1680-1685

[5] Darmadji P, Izumimoto M. Effect of chitosan in meat preservation. Meat Science 1994; 38 (2), 243-254.

[6] Li J, Zivanovic S, Davidson P, Kit K. Characterization and comparison of chitosan/PVP and chitosan/PEO blend films. Carbohydrate Polymers 2010; 79 (3), 786-791.

[7] Siripatrawan, U., & Harte, B.R. (2010). Physical properties and antioxidant activity of an active film from chitosan incorporated with green tea extract. Food Hydrocolloids, 24, 770-775.[18]

[8] Duan J, Jiang Y, Cherian G, Zhao Y. Effect of combined chitosan-krill oil coating and modified atmosphere packaging on the storability of cold-stored lingcod fillets. *Food Chemistry* **2010**; 122 (4), 1035-1042.

Advanced Materials Research Vols. 989-994 (2014) pp 1056-1059
© (2014) Trans Tech Publications, Switzerland
doi:10.4028/www.scientific.net/AMR.989-994.1056

Polysaccharide from Eucheuma gelatinae enhance immunocompetence against murine H22 tumor in vivo

Juan Tang[1,2,a], Zhen Kong[1,b], Dongyue Liu[3,c] and Anjun Liu[1,d,*]

[1]Key Laboratory of Food Nutrition and Safety, Ministry of Education, Tianjin University of Science and Technology, Tianjin, China, 300457

[2]Qingdao Agricultural University, Qingdao, China, 266109

[3]Tianjin Hi-tech Transformation Center, Tianjin, China, 300203

[a]email:dtangjuan@163.com, [b]email:kz19880309@163.com, [c]email: dongyueliu@hotmail.com, [d]email: laj@tust.edu.cn

Keywords: polysaccharide, Eucheuma gelatinae, immunocompetence, H22 tumor cells.

Abstract. New antitumor strategies are underway and play important roles in clinical trials for combating cancer in future. Eucheuma gelatinae contains a certain amount of polysaccharides, which has various biological activities. In this study, the antitumor effect of Eucheuma gelatinae polysaccharide on murine H22 tumor bearing mice has been investigated. Histological stain, flow cytometry and other methods are applied to evaluate the effects of Eucheuma gelatinae polysaccharide on immunocompetence in vivo. The data indicates that Eucheuma gelatinae polysaccharide has antitumor effect in vivo by enhancing immunocompetence of the tumor bearers.

Introduction

Polysaccharide has been highly concerned on antivirus[1], antioxidant[2] and antitumor effects in these years[3], which is consisted in mushroom, cartilage, and many other kinds of natural product[4]. Eucheuma gelatinae, commercially known as "cottonii" and "spinosum", contains a certain amount of polysaccharide as food reserves[5]. In order to take full advantage of Eucheuma gelatinae, alkaline extraction of acidic polysaccharide from Eucheuma gelatinae has been designed in our previous work. It has been report that polysaccharide from Eucheuma suppresses breast tumor via hormone modulation and apoptosis induction[6], however, the effects of Eucheuma gelatinae polysaccharide on other kinds of tumor need to be further elucidated.

Hepatocellular carcinoma is one of the deadliest cancers in the world. This dreaded disease is hard to be cured by traditional methods such as surgery, chemotherapy, and radiation[7]. To provide new method for cancer therapy, the antitumor effect of Eucheuma gelatinae polysaccharide (EGP) on murine H22 tumor bearing mice has been investigated in the present study. Histological stain was used to illustrate the protective effect on spleen and thymus of H22 tumor bearers with EGP treatment. $CD3^+$, $CD4^+$, $CD8^+$ and $CD19^+$ cells in peripheral blood lymphocyte were analyzed by flow cytometry (FCM). The levels of interleukin 2 (IL-2), IFN-γ and TNF-α in peripheral blood were also determined.

Materials and Methods

Chemicals. 3-(4,5-Dimethylthiazol-2-yl)-2,5-diphenyltetrazolium bromide (MTT), concanavalin A (ConA) and lipopolysaccharide (LPS) were provided by Sigma Chemical Co. Fetal calf serum (FCS) was from Hangzhou Sijiqing Co. The RMPI-1640 medium was purchased from HyClone, Thermo Scientific Inc. All other reagents were of reagent grade.

EGP preparation. Eucheuma gelatinae was purchased from Hainan local market. Fresh Eucheuma gelatinae was smashed into small pieces and treated with 0.5 mol/L NaOH at room temperature for 12 h. The filtrate was collected and centrifuged at 3000 rpm for 20 min to get the supernatant. The value of pH was adjusted to 3.0 with 0.1 mol/L HCl, then centrifuged at 3000 rpm for 20 min to remove the

precipitation. The supernatant was deposited by 80% (v/v) ethanol and left overnight at 4 °C to obtain the crude polysaccharides by centrifugation at 5000 rpm for 20 min. The precipitation was redissolved in dehydrated alcohol for three times, and lyophilized to yield Eucheuma gelatinae polysaccharide.

Animal experiment. Sixty eight-week-old Balb/c mice with an average body weight of 20.0 ± 2.0 g were divided into four groups with fifty mice each group, which were blank group, model group, low-EGP group and high-EGP group. Blank group and model groups were both applied saline solution orally throughout the experimental period. Low-EGP group was given EGP with 300 mg/kg per day, while the high-EGP group was given EGP with 600 mg/kg per day in the same period. On day 14, the mice from model group, low-EGP group and high-EGP group were transplanted with murine H22 cells in the right thigh of the lower limb with 0.2 ml of 5 ×106 cells. All groups received the oral administration for 4 weeks.

Histological staining by H-E. Thymuses and spleens were carefully dissected from the mouse and placed in a petri dish containing sterile normal saline. Then the organs were placed in a petri dish with 10% neutral-buffered formalin for more than 3 h, and dipped in running water overnight, and gradually dehydrated in ethanol of different strengths, dimethylbenzene, and embedded in paraffin, and processed for histological examination after staining with hematoxylin-eosin.

Lymphocyte subsets analysis in peripheral blood. A small amount of blood was collected from the mice alive, and lymphocytes were obtained via removal of the erythrocytes. 1×106 cells were incubated with either isotypic control or monoclonal antibodies (mAb) against $CD3^+$, $CD4^+$, $CD8^+$ and $CD19^+$ for 30 min on ice in the dark. After incubation, antigen expression was measured by flow cytometry (BD FACSCalibur, USA), and analyzed by CellQuest Pro. software.

Evaluation of interleukin 2 (IL-2), IFN-γ and TNF-α in peripheral blood. After the mice sacrificed, the serum of each mouse was prepared for IL-2, IFN-γ and TNF-α assessment using ELISA kits (Dakewe Biotech. Co., Shenzhen, China). Under the manufacturer's instruction, the plate was read at 450 nm on a BD Microplate Reader.

Statistical analysis. Experiments were performed at least three times with similar results. Results were presented as the mean ± standard deviation (S.D.) for all treatments. Student's t-test and ANOVA were performed for their statistic significance of difference with controls. The data was considered statistically different from controls at $p < 0.05$.

Results and Discussions

Histological analyses of thymuses and spleens from H22 tumor bearing mice with EGP treatment. As shown in Figure 1, the histological analyses of thymuses from normal mice manifested a clear border between cortex and medulla, whereas the thymuses from H22 tumor bearing mice showed a shrunken medullar area and an indistinct medullar boundary. Meanwhile, Figure 2 showed obvious areas between splenic red pulp and white pulp in blank group, however, this structure was wrecked in H22 tumor bearers. After EGP treatment, thymuses and spleens illustrated a normalized structure, which meant EGP had protective effects on the immune organs against tumor.

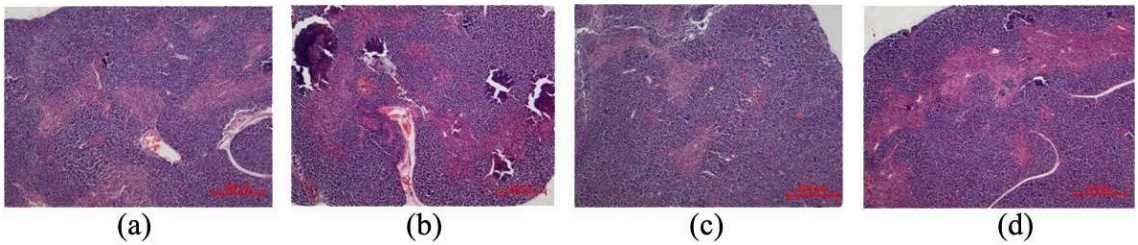

Fig. 1 HE staining of thymus (magnification ×4). (a) blank control group, (b) model group, (c) low-EGP group, (d) high-EGP group.

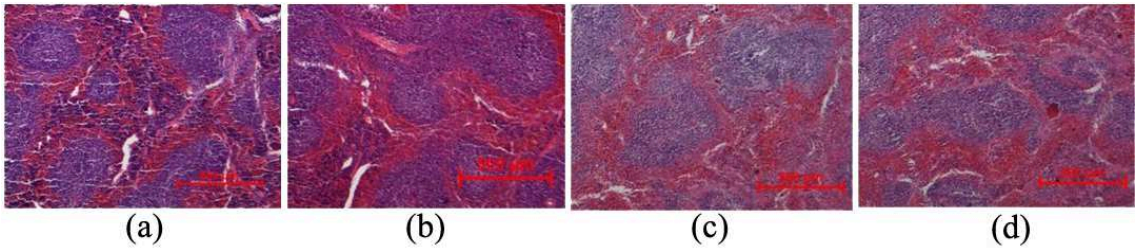

Fig. 2 HE staining of spleen (magnification ×4). (a) blank control group, (b) model group, (c) low-EGP group, (d) high-EGP group.

Effect of EGP on lymphocyte subsets in H22 tumor bearers. The different proportions of lymphocyte subsets in mice peripheral blood were shown in Figure 3 and Table 1. According to the results, the percentage of $CD3^+$, $CD19^+$ and $CD8^+$ cells in model group was notably descended as compared to the blank group. After high level of EGP treatment, the percentage of $CD3^+$, $CD19^+$, $CD4^+$ and $CD8^+$ cells were partial restored to the blank group.

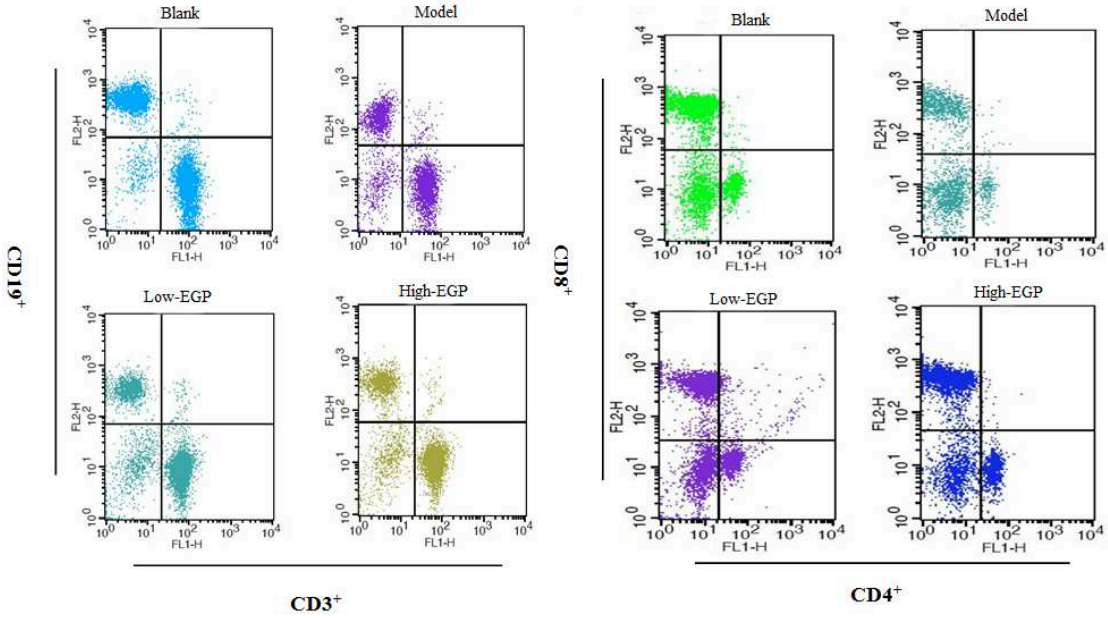

Fig. 3 Effect of EGP on lymphocyte subsets in peripheralblood of different groups

Table 1 Distribution of lymphocyte subsets in peripheral blood of different groups

Groups	$CD3^+$ cells [%]	$CD19^+$ cells [%]	$CD4^+$ cells [%]	$CD8^+$ cells [%]	$CD4^+$ / $CD8^+$
Blank	66.23±1.59	24.78±2.03	58.25±6.04	12.45±1.98	4.73±0.25
Model	46.63±0.84a	15.67±1.98a	45.98±6.60	5.28±1.26a	8.92±0.88
Low-EGP	45.04±0.56	17.54 ±1.02	37.88±5.67	11.34±5.72	4.14±1.59
High-EGP	69.51±0.64b	19.88±0.98	54.86±4.89	19.29±2.08b	2.85±0.05

[a]$p < 0.05$ compared to blank group, [b]$p < 0.05$ compared to model group.

Effect of EGP on IL-2, IFN-γ and TNF-α levels in serum of H22 bearing mice. The concentration of IL-2, IFN-γ and TNF-α levels in serum was analyzed to assess the immune function of EGP. As shown in Figure 4, the amounts of IL-2, IFN-γ and TNF-α in EGP groups were significantly higher than the model group, which indicated EGP could enhance immunocompetence in H22 tumor bearing mice.

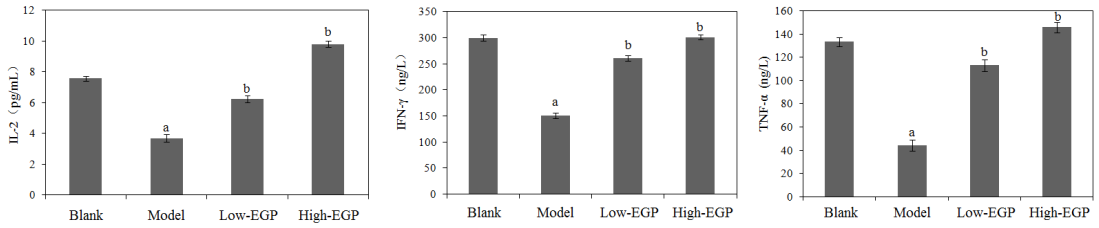

Fig. 4 Effects of EGP on IL-2, IFN-γ and TNF-α levels in different groups. ap<0.05 vs. blank group, bp<0.05 vs. model group.

Conclusions

In this study, EGP showed significant protective effect on immune organs in H22 tumor bearing mice. Treated with EGP could up-regulate the levels of IL-2, IFN-γ, TNF-α and enhance T lymphocyte subsets in blood of H22 tumor bearing mice, which indicated that EGP could improve the anti-tumor immune response in tumor bearers.

Acknowledgements

Financial support was kindly supplied by grants from the Foundation of National 863 Plan (No.2013AA102204).

References

[1] Gao Y, Li C, Yin J, Shen J, Wang H, Wu Y, Jin H, Fucoidan, a sulfated polysaccharide from brown algae, improves cognitive impairment induced by infusion of A β peptide in rats. Environmental Toxicology and Pharmacology. 33 (2012) 304-311.
[2] Chattopadhyay N, Ghosh T, Sinha S, Chattopadhyay K, Karmakar P, Ray B, Polysaccharides from Turbinaria conoides: Structural features and antioxidant capacity. Food Chemistry. 118 (2010) 823-829.
[3] Alekseyenko TV, Zhanayeva SY, Venediktova AA, Zvyagintseva TN, Kuznetsova TA, Besednova NN, Korolenko TA, Antitumor and antimetastatic activity of fucoidan, a sulfated polysaccharide isolated from the Okhotsk Sea Fucus evanescens brown alga. Bull Exp Biol Med. 143 (2007) 730-732.
[4] Mišurcová L, Škrovánková S, Samek D, Ambrožová J, Machů L, Health benefits of algal polysaccharides in human nutrition. Adv Food Nutr Res. 66 (2012) 75-145.
[5] Bixler HJ, Porse H, A decade of change in the seaweed hydrocolloids industry. Journal of Applied Phycology. 23 (2010). 321-335.
[6] Namvar F, Mohamed S, Fard SG, Behravan J, Mustapha NM, Alitheen NBM, Othman F, Mohamed S, Polyphenol-rich seaweed (Eucheuma cottonii) extract suppresses breast tumour via hormone modulation and apoptosis induction. Food Chemistry. 130 (2012). 376-382.
[7] Liu A, Liu D, Zhao S, Zheng J, Cao D, Zhang H, Up regulation of annexin A2 on murine H22 hepatocarcinoma cells induced by cartilage polysaccharide. Cancer Epidemiology. 35 (2011) 490-496.
[8] Huang H, Cieh S, Tso TK, Chien T, Lin H, Tsai Y, Orally administered mycelial culture of Phellinus linteus exhibits antitumor effects in hepatoma cellbearing mice. Journal of Ethnopharmacology. 133 (2011). 460-466.
[9] Zhao L, Dong Y, Chen G, Hu Q, Extraction, purification, characterization and antitumor activity of polysaccharides from Ganoderma lucidum. Carbohydrate Polymers. 80 (2010). 783-789.

Advanced Materials Research Vols. 989-994 (2014) pp 1060-1063
© (2014) Trans Tech Publications, Switzerland
doi:10.4028/www.scientific.net/AMR.989-994.1060

Analysis of paclitaxel in pharmaceutical injection by ultra performance convergence chromatography

Xiao GONG[1,a], Xiaobing HUANG[1,b], Yonghua WEI[2,c], Ningli QI[1,d], Lijing LIN[1,e*], Yangyang LIU[1, f]

[1]Agricultural Product Processing Research Institute, Chinese Academy of Tropical Agricultural Sciences, Zhanjiang, 524001, China

[2]School of Biological Sciences and Engineering, Shannxi University of Technology, Hanzhong 723001, China

[a]email: yiyesuifeng@126.com, [d]email: huang5102@126.com, [c]email: weiyonghua1983@126.com, [d]email: qiqi120518@163.com, [e]email: 49031788@qq.com, [f]email: hws082319@163.com

Keywords: Paclitaxel; Ultra-performance Convergence Chromatography; Diode Array Detector

Abstract. A simple and sensitive ultra-performance convergence chromatography system coupled with a diode array detector for analysis of paclitaxel, 10-deacetyl-7-epipaclitaxel and cephalomannine in paclitaxel injection was developed. The analyses were carried out on a Waters Acquity UPC^2 BEH 2-EP using the mobile phase of mixture of supercritical CO_2 and methanol with a linear gradient elution from 92:8 to 82:18 at 50 °C. The method offers good linearity, higher resolution, and good repeatability. LOD and LOQ were 0.45 and 1.32 ng, respectively.

Introduction

Paclitaxel is a natural hydrophobic diterpenoid extraction originally isolated from the bark of the Pacific yew tree, Taxus brevifolia in the 1960s. Later it was discovered that endophytic fungi in the bark synthesize paclitaxel [1]. As a mitotic inhibitor used in cancer chemotherapy, paclitaxel can stabilize and protect microtubules from disassembly, and then interfere with the normal breakdown of microtubules during cell proliferation. Being one of the most widely used anticancer drugs today, the commercial formulation of paclitaxel has been made into injection and was approved by Food and Drug Administration (FDA) for the clinic treatment of various tumors, including ovarian, breast, non-small cell lung, and prostate tumors, etc [2][3][4]. However, paclitaxel is very similar to many related compounds in taxane family in chemical structure and polarity, such as 10-deacetyl-7-epipaclitaxel and cephalomannine. So a rapid, efficient, economical and practical separation and analysis method is particularly necessary.

A number of papers have reported methods for the determination of paclitaxel in biological fluids, including capillary electrophoresis (CE) high performance liquid chromatography (HPLC) and ultra-performance liquid chromatography (UPLC) [5][6][7][8]. However, these methods still have several disadvantages including tedious operation, poor resolution and long analytical period. As a new generation of SFC, the ultra-performance convergence chromatography (UPC^2) was brought to market in 2012. The analysis time and usage of organic solvent while improving resolution were drastically reduced, which makes its application in routine analysis more attractive [9][10]. To date, UPC^2 has not been used for separation and determination of paclitaxel and impurities in the study of commercial injection formulations.

According to the general acceptance criterion of paclitaxel and/or paclitaxel injection developed by The United States Pharmacopeia (USP), the resolutions of R1 (between 10-deacetyl-7-epipaclitaxel and cephalomannine) and R2 (between cephalomannine and paclitaxel) in system suitability tests are not less than 1.0 and 1.2, respectively [11]. A rapid and sensitive method is indispensable for Quality Control Departments, as paclitaxel does not exist in any official pharmacopoeia monograph. The objective of this study was to develop a UPC^2 method for separation and determination of paclitaxel and two major types of pharmaceutical impurities, namely 10-deacetyl-7-epipaclitaxel and cephalomannine.

Design of the Experiments

The standards of paclitaxel (≥99.6%), 10-deacetyl-7-epipaclitaxel (A) and cephalomannine (B) were obtained from National Institute for Food and Drug Control (Beijing, China). Paclitaxel injection was purchased from Youcare Pharmaceutical Group Co., Ltd. HPLC grade methanol was obtained from Fisher Scientific Co. (Pittsburgh, PA). Other chemicals were of analytical reagent quality.

The standard solutions of paclitaxel was prepared at a concentration around 0.2 mg/ml in methanol, and stored at -4 °C. A calibration curve was constructed using five increasing concentrations of working solution ranged from 0.6 to 200 μg/ml. A mixed standard solution of known concentrations of paclitaxel and related compounds A and B were obtained by dissolving in methanol. 5.0 ml of the resulting solution was transfer to a 50 ml volumetric flask and bringing to volume with methanol.

The qualitative analysis was performed at 50 °C using an Acquity UPC^2 BEH 2-EP column (3.0 mm × 100 mm, 1.7 μm). Chromatographic separation was carried out using a gradient elution of (A) CO_2 (99.999%) and (B) methanol (100%) as follows: 0-0.2 min, A 92%, B 8.0%, 0.2-2.5 min, A 92-82%, B 8-18%, 2.5-4.0 min, A 82%, B 18%. Linear concentration change was performed in all cases. The back pressure was set at 2200 psi. The flow rate was kept at 2.2 ml/min, the injection volume was 2.0 μl, detection wavelength at 227 nm. Identification and quantification of paclitaxel was performed by comparison of retention time and peak areas obtained for standard solution and samples. The measurement was performed in triplicate to test the repeatability.

The linearity obtained on the previously optimized chromatographic conditions from the injections of five increasing concentrations of the standard solutions was evaluated on the calibration curve of the peak area (y) versus the concentration of paclitaxel (x). The correlation coefficient (r) obtained was used to assess linearity. The limit of detection (LOD) and quantification (LOQ) was determined considering a signal to baseline noise ratio of three and ten with reference to the background noise obtained from blank sample. The precision was analyzed by conducting six consecutive replicate injections of the standard and sample solutions. Method accuracy was evaluated by the recovery within the proposed limits (100 ± 2%).

Test results

Optimization of chromatographic conditions

The chromatographic conditions were optimized to separate each individual standard with good resolution within a reasonable analysis time. Different chromatographic columns were tested including Waters Acquity UPC^2 BEH (3.0 mm × 100 mm, 2.1 μm), BEH 2-EP (3.0 mm × 100 mm, 1.7 μm), CSH fluoro-phenyl (3.0 mm × 150 mm, 1.7 μm) and HSS C_{18} SB (3.0 mm × 150 mm, 1.8 μm) column, and the UPC^2 BEH 2-EP column resulted in a better resolution. In order to improve separation of paclitaxel and related compounds A and B commonly coexisting impurities in the synthesis process of paclitaxel, different cosolvent B including methanol, n-hexane, and acetonitrile were investigated. The best result was obtained when using solvent of mixture CO_2/methanol with a linear gradient elution mode. The back pressure directly influences the elutive power of supercritical fluid by changing the density of supercritical CO_2. In this work, an optimal back pressure of 2200 psi was selected for UPC^2 analysis. The most suitable flow rate and temperature were chosen as 50 °C and 2.2 ml/min, respectively.

Separation of paclitaxel and related compounds

Paclitaxel and related compounds A and B were separated under the present UPC^2 conditions, and the elution orders on UPC^2 were determined by C-10 alkoxy (OAC) and C-13 side chain. The compound with a smaller aromatic chain was eluted earlier as shown in Figure 1. UPC^2 is a rapid analysis method with a good baseline separation between adjacent peaks before 4.0 min compared with HPLC method (45-70 min) and had an excellent peak resolution by comparison with the separation behavior of reverse phase HPLC. Which could be partly explained by a perfect solubility of paclitaxel in supercritical CO_2 leading to a good peak shape and resolution. Paclitaxel and related

compounds A and B were eluted according to the size of side chain, and related compound A with less double bond was eluted earlier, follow by related compound B with the difference in a C-10 OAC. The results suggested that the mode of UPC^2 separation of paclitaxel and related compounds was more similar to gas chromatography than liquid chromatography.

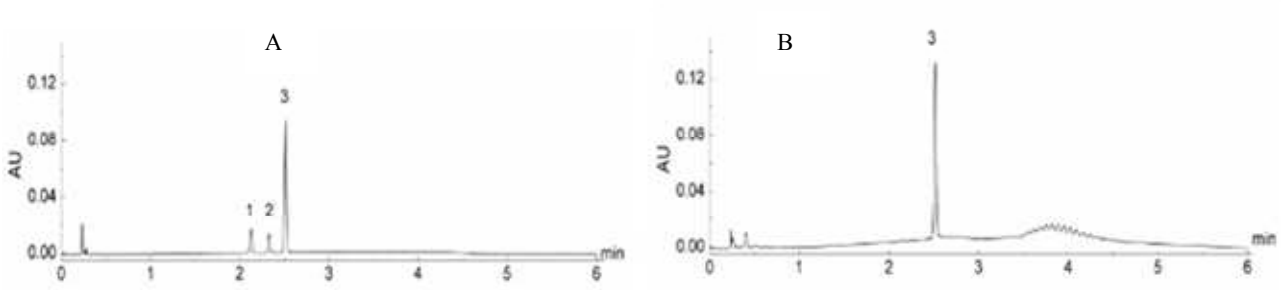

Fig. 1. Chromatograms of mix standard (A) and paclitaxel injection (B)
(Peak numbering: 1-cephalomannine, 2-10-deacetyl-7-epipaclitaxel, 3-paclitaxel)

Validation of the method

The relative retention with reference to paclitaxel (retention time of 2.53 min) are about 0.84 and 0.93 for related compound A and B, respectively. The resolutions of R1 and R2 are 4.7 and 4.0, respectively, which are stipulated in USP. The RSD of six replicate injections is 0.04% for retention time, and 0.22% for peak area, suggesting a good advantage of resolution and repeatability.

The equation of linear regression obtained for five increasing concentrations in the range of 0.6 and 196 μg/ml was: $y = 994.74 x + 404.67$ and the correlation coefficient (r) is 0.9999, suggesting the method allows the acquisition of reliable data for injection with low and/or high contents of paclitaxel, when using the conditions optimized in this study.

The LOD and LOQ were approximately 0.45 and 1.32 ng, respectively. It can be noticed from the values obtained that LOD and LOQ were low, suggesting that the UPC^2 method allows the detection of small quantities of paclitaxel, especially for the quality control in the paclitaxel injection production.

The result of recovery tests showed that the percent recoveries of paclitaxel in the paclitaxel injection ranged from 98.92 to 101.31%, with a RSD within the proposed limits (100 ± 2%) varied from 0.99 to 1.19 (Table 1). In general, good recovery percentages and accuracy were achieved for paclitaxel when using the optimized method.

Table 1. Recoveries of paclitaxel form samples (n = 6)

Sample	Fortification level	Recovery (%)	RSD (%)
1	80%	98.92	0.99
2	100%	99.39	0.89
3	120%	101.31	1.19

Conclusion

A simple method using UPC^2/DAD for the determination of paclitaxel and two major types of related compounds A (10-deacetyl-7-epipaclitaxel) and B (cephalomannine) was developed for the first time, allowing a rapid, sensitive, and high reproducible separation and quantification. The results are acceptable and this method permitted the isolation of paclitaxel from the other two commonly coexisting impurities in the paclitaxel synthesis process, with an excellent resolution ($R > 4.0$) compared with that ($R = 1.8$) of previously reported using HPLC methods [11]. Furthermore, the considerably reduced organic solvent in the analysis suggested that UPC^2 was a much more environmentally friendly method, and might provide a prospective future for quality control in the production process of paclitaxel injection.

Acknowledgement

This work was supported by the Scientific and Technologic Funds of Key Laboratory of Tropical Crop Products Processing (Grant No. KLTCPP-201402) and the Special Fund for Agro-scientific Research in the Public Interest (Grant No. 201303077). The authors are grateful to the technical help from Yongwei Xu (Waters Co., Ltd).

References

[1] Wani MC, Taylor HL, Wall ME, Coggon P, et al. Plant antitumor agents. VI. Isolation and structure of taxol, a novel antileukemic and antitumor agent from Taxus brevifolia [J]. Journal of the American Chemical Society, 1971, 93(9): 2325-2327.

[2] Bharadwaj R, Yu HT. The spindle checkpoint, aneuploidy, and cancer [J]. Oncogene, 2004, 23(11): 2016-2027.

[3] Jordan MA, Wilson L. Microtubules as a target for anticancer drugs [J]. Nature Reviews Cancer, 2004, 4(4): 253-265.

[4] Ganguly A, Yang HL, Cabral F. Paclitaxel-dependent cell lines reveal a novel drug activity [J]. Molecular Cancer Therapeutics, 2010, 9(11): 2914-2923.

[5] Hempel G, Lehmkuhl D, Krümpelmann S, Blaschke G, et al. Determination of paclitaxel in biological fluids by micellar electrokinetic chromatography [J]. Journal of Chromatography A, 1996, 745(1-2): 173-179.

[6] Kim SC, Yu J, Lee JW, Park ES, et al. Sensitive HPLC method for quantitation of paclitaxel (Genexol®) in biological samples with application to preclinical pharmacokinetics and biodistribution [J]. Journal of Pharmaceutical and Biomedical Analysis, 2005, 39(1-2): 170-176.

[7] Sun P, Wang X, Alquier L, Maryanoff CA. Determination of relative response factors of impurities in paclitaxel with high performance liquid chromatography equipped with ultraviolet and charged aerosol detectors [J]. Journal of Chromatography A, 2008, 1177(1): 87-91.

[8] Zhang SQ, Chen GH. Determination of paclitaxel in human plasma by UPLC-MS-MS [J]. Journal of Chromatographic Science, 2008, 46(3): 220-224.

[9] Heaton DM, Bartle KD, Rayner CM, Clifford AA. Application of supercritical fluid extraction and supercritical fluid chromatography to the production of taxanes as anti-cancer drugs [J]. Hrc-Journal of High Resolution Chromatography, 1993, 16(11): 666-670.

[10] Zhou Q, Gao BY, Zhang X, Xu YW, et al. Chemical profiling of triacylglycerols and diacylglycerols in cow milk fat by ultra-performance convergence chromatography combined with a quadrupole time-of-flight mass spectrometry [J]. Food Chemistry, 2014, 143(0): 199-204.

[11] United States Pharmacopeial Convention. Paclitaxel and paclitaxel injection [M]. USP35-NF30. 35th ed., New York, 2012.

Advanced Materials Research Vols. 989-994 (2014) pp 1064-1067
© (2014) Trans Tech Publications, Switzerland
doi:10.4028/www.scientific.net/AMR.989-994.1064

Study on the genotoxicity of organic extracts of the water from a reservoir by using comet assay

Juanting WANG[1, a], Yanzhen YU[1, b], Xuan LI[1,c]

[1] School of Civil Engineering and Architecture, University of Jinan, Jinan 250022, China

[a]email: wjt0305@163.com, [b]email: cea_yuyz@ujn.edu.cn, [c]email: cea_yuyzujn@163.com

*Corresponding Author: Yanzhen Yu

Keywords: organic extracts; comet assay; DNA damages; genotoxicity

Abstract. In the experiment, a systematic study on the genotoxicity of organic extracts of the water in a reservoir at wet season and dry season. And the study was done by using comet assay. The study was to appraise the waters qualities after every treatment step from the view of the DNA damages on the mouse spleen lymphocytes. The results of the experiment can provide reliable basis for adjusting the treatment reasonably to purify raw water of different qualities.

Introduction

With the rapid development of industry and agriculture, discharged industrial wastewater didn't reached the standards，most of the household wastewater discharged without treatment, and Irrational and massive use of chemical substances such as mechanical fertilizers and pesticides in country area, causing serious non-point source pollution, a large number of synthetic organics entering water environment[1]. These organic compounds are not easy to be degraded. And the organic matters enter the human body through the food chains. Some studies showed that many kinds of organic compounds entering water cause directly or indirectly or acute or chronic poisoning action. Some can accumulated within the organization, change the DNA, leading the organization to cancerous [2-6]. In recent years, potential hazards of organic compounds within water and the removal efficiency of organic pollutants in drinking water have captured widespread concerns [7].

In this experiment, simulation experiments were carried out in accordance with the domestic conventional water treatment process. In this experiment, simulation experiments were carried out in accordance with the domestic conventional water treatment processes, respectively in dry season and the wet season set water, heavy water, filtered water and tap water of 4 water samples were tested, study of conventional water treatment process for organic pollutant removal efficiency, compared to wet period, dry season water quality and the effluent quality, timely find the weak link of processing technology for water quality, according to timely adjust the process combination to provide a reliable reference. For further reflect the hazards of organic pollutants in drinking water on the human body, the comet assay [8] was used to study the damage of spleen lymphocytes of DNA [9-10]. Lymphocyte is an important class of immune cells, is the early signal of canceration.

Experimental Materials and Methods

In the experiment, the water treatment process is accordant to international common technique for water treatment. Collected 4 water samples: source water (A), settled water after the addition of coagulant (B), filtered water after sand filter (C), finished water disinfected with Cl2, (D). The water sample is divided into two phases, the dry season (January), the wet period (August). The organic enrichment was conducted. And the compositions of organic extractive of each water sample was analyzed by use of GC/MS. Re-dissolved the inrichment of substances and configured these solution into high concentration, medium concentration and low concentration to feed female mice. Continued the experiment for 5 days, then killed the mice, and got lymphocytes of the mice to do the comet assay.

Results and Discussions

The composition of organic extracts analyzed by GC/MS

Table 1 The contents of Organic Extraction Solution at dry season

Water samples	fat hydrocarbon	halogenated hydrocarbon	monocyclic aromatic	polycyclic aromatic	esters	phenol	ketone	alcohol	Heteroc-yclic	other	total
inflow	3	0	24	7	4	0	2	0	2	0	42
Settled	5	0	17	3	3	0	1	0	1	0	30
filtered	5	0	20	7	4	1	1	1	1	1	41
effluent	6	2	15	5	3	0	1	0	1	0	33

Table 2 The contents of Organic Extraction Solution at wet season

Water samples	fat hydrocarbon	halogenated hydrocarbon	Halogenated benzene	monocyclic aromatic	polycyclic aromatic	ether	ester	acid	phenol	ketone	alcohol	Hetero-cyclic	other	total
inflow	3	0	1	18	12	0	4	0	1	1	0	2	2	44
Settled	7	0	1	14	7	0	8	0	1	2	1	1	1	43
filtered	6	0	1	24	13	1	7	0	1	3	2	3	1	61
effluent	6	2	1	23	10	0	5	2	1	2	2	2	1	57

The table 1 and 2 analyze the compositions of organic extractive of the water at dry season and wet season respectively with GC/MS. Ten and thirteen kinds of organic matters were identified respectively in the water at dry season and wet season. 42 and 44 kinds of organic matters are detected separately in inflow water at dry season and wet season. Whether at the dry season and the wet season, the number of monocyclic aromatic hydrocarbons and polycyclic aromatic hydrocarbons is in the first place. Through comparison, the numbers and types of the organic compounds of the wet season are more than the dry season. The rainy climate of the city which the reservoir located plays an important role for some organic ingredients of the chemical fertilizers and pesticides to enter into the drinking water sources following the surface run off.

The results of the comet assay on the mice spleen lymphocyte are presented in Figure 1 and Figure 2.

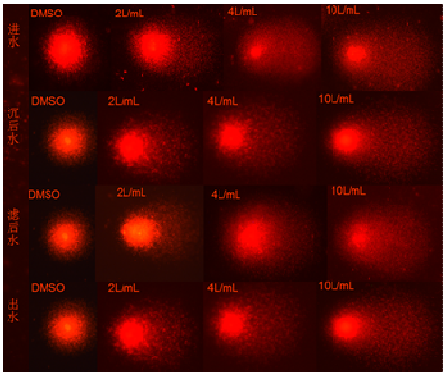

Fig 1 The DNA damages induced by the organic extraction solution of the dry season

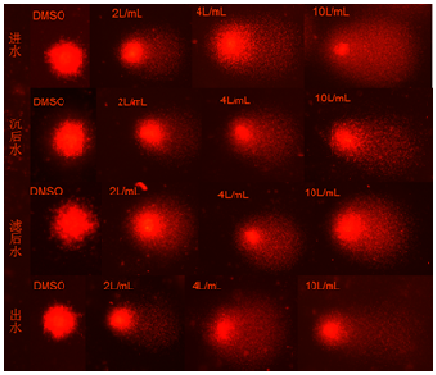

Fig 2 The DNA damages induced by the Organic extraction solution of the wet season

The results of lymphocyte DNA damage

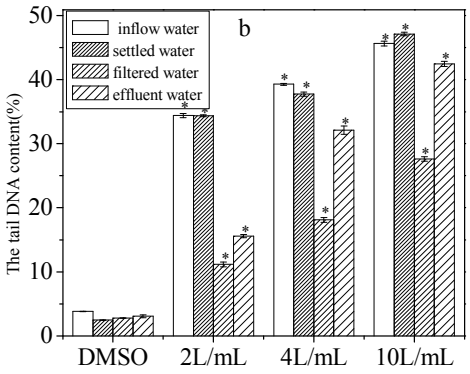

Fig 3 The results of the tail DNA content comets subjected to different concentration OESs of four water samples collected at dry season

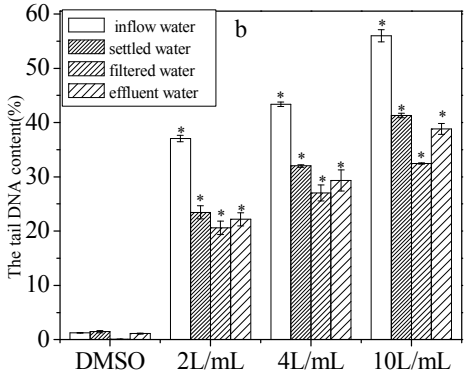

Fig 4 The results of the tail DNA content comets subjected to different concentration OESs of four water samples collected at wet season

Figure 3 and Figure 4 show that, whether it is wet or dry water, the organic extracts from raw water, Precipitation water, filtered water and the factory water are all harmful to mice spleen lymphocytes. And with the increase of concentration of organic compounds, the content of tail DNA Increases, namely DNA damage degree increases. The untreated water damage of DNA is the highest, and the damage of filtered water is the lowest. Disinfected water is higher than the filtered water, which is mainly because the chlorine disinfection produces disinfection by-products.

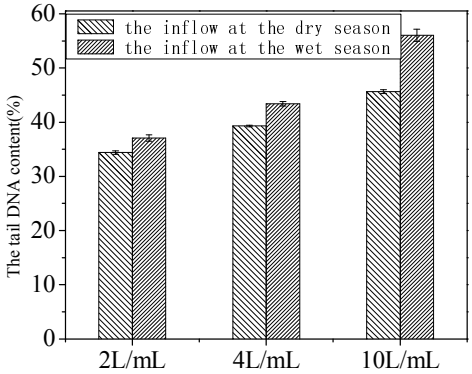

Fig.5 The comparison between dry season and abundant season, the results of the tail DNA content of the comets subjected to different concentration OESs of the influent water samples.

Figure 5 shows that inlet water organic extracts of the different concentration during the mutagenicity and the plentiful periods have the influence on the comet tail DNA content, the response valves in the plentiful period are much higher than that in the mutagenicity period, and the difference is getting more obvious with the increase of the concentration of the extracts. There is the big relationship between the difference and the rainy seasons during the plentiful periods and the chemical fertilizer and pesticide on the fields, most of these chemical fertilizer and pesticide component enters into the drinking water as the rain water flushing and the surface runoff.

Conclusion

The pollution of the drinking water comes up with the new challenges for the water treatment process. Although the water quality convensional phsical and chemical monitoring of the reservoir during the mutagenicity and the plentiful periods is not exceeding the standard, but the kinds and quantities of the organic matter in the organic extracting in the water sample during the plentiful period is much higher than that during the mutagenicity period, and the damage degree on the DNA of the mice lymphocyte is higher than the latter. So the proper adjustment or adding the necessary

pre-treatment according to the inlet water quality is performed in the water treatment process, and also need to adapt to the changing of the raw water quality, ensure the good drinking water quality. For example, use the granulometric active carbon to replace the quick sand filter, decrease the disinfection by-products prosoma; develop and apply the new type disinfectant, and prevent the formation of the disinfection by-products.

Acknowledgement

This work was funded by the National Scientific Foundation China (NSFC51178207), Shandong Provincial National Science Foundation (ZR2011EEM003), the Natural Science Foundation of Shandong Province (ZR2012EEL21).

References

[1] Zhuang Ying. Potential Impairments of Organic Pollutants in Water on Human Health and Its Prevention Measures [J].Environment and Health，2001,18(3):187-189

[2] Xu Kefeng,Li Zhong, Zhao Yuechun et al. Health Hazard of Persistent Organic Pollutants (POPs) and Its Progress in Treatment Technologies [J]. Sichuan Environment, 2003, 22 (4) : 29-34

[3] SI YANYTSYA V, KOC HKODAN V, GONCHARUK V. Natural organic matter removal from water by complexation- ultrafiltration [J]. Desalination, 2008, 223(1/3): 91- 96.

[4] ZUL AR I SAM AW, I SMA I L A F, Razman Salmi. Behaviours of natural organic matter in membrane filtration for surf ace water treatment a review [J]. Desalination, 2006, 194(1/3): 211-231.

[5] Cui Yuchuan, Fu Tao. Harm of Water Pollution and Organic Pollutants in Drinking Water Resources in China[J]. URBAN ENVIRONMENT & URBAN ECOLOGY, 1998, 11(3): 23 - 25.

[6] Liu Zhengtao, Environmental Behavior Characteristics and Research Progress of Persistent Organic PollutantsJ], Research of Environmental Sciences, 2005,3(18):93-101.

[7] Li Zhaoli, LI Yiqiang，Evaluation of Genotoxic Effects Induced by Organic Pollutants in the Yangtze River in Nanjing Section [J]. Research of Environmental Sciences 2006, 19 (3):105-108.

[8] Chen Ying, Wang Lei, Wang Zijian. Development and Application of Comet Assay for Detecting Genotoxic Substances in Environmental Samples [J]. Acta Pedologica Sinica, 2005, 27(2): 148- 150.

[9] Zhu Huigang, Comprehensive Evaluation index of organic Mutagens in Water [J], Shanghai Environmental Sciences, 1995, 10(14): 44-49.

[10] CLAIRTA, KRAMERJR, SYDORM, et al. Concentration of aquatic dissolved organic matter by reverse osmosis [J]. Water Res, 1991, 25(9): 1033 - 1037.

Advanced Materials Research Vols. 989-994 (2014) pp 1068-1072
© (2014) Trans Tech Publications, Switzerland
doi:10.4028/www.scientific.net/AMR.989-994.1068

Wireless power transmission system of radio-telemetry system for physiological parameters detection

Jia Zhiwei[1,a], Ren Heran[2] ,Yan Guozheng[3]

[1] College of Electrical and Information Engineering, Changsha University of Science and Technology, Changsha, 410004, China

[2] Beijing Electro-mechanical Engineering Institute, Beijing, 100074, China

[3] 820 Institute, School of Electronic Information and Electrical Engineering, Shanghai Jiao Tong University, Shanghai, 200240, China

[1]email: jiayege@hotmail.com

Keywords: Wireless power transmission; Telemetry system; Transmission stability; Biology safety

Abstract. To deal with the power shortage of the implantable radio-telemetry system for animal physiological parameters dictation, a wireless power transmission system based on electromagnetic induction is proposed. The parameters of the couple coils are optimized considering the safety and stability of this power transmission, transmitting coil of rectangle section solenoid and three-dimensional receiving coil are selected. Experiments show that at least 150mW power could pick up on the load in a volume of Φ10.5 mm×11 mm with a transmission efficiency of 2.56%. Vivisection experiments verified the feasibility of the integrated radio-telemetry system based on this power supply technology.

Introduction

Implantable biological parameters telemetry technique, which could obtain the information of animals directly, could also monitor the organism physiological and biochemical parameters of animals in free in real time and long time. Many improvements have made in the detection technology for physiological parameters [1-2], and these parameters were detected in radio-telemetry way. Unfortunately, owing to the battery mode, these devices could not keep monitoring in long time. Implantable ECG (Electrocardiograph) telemetry system from Young-Ho YOON et.al[3] adopted the transcutaneous energy transmission technology(TET). However, the transmitting coil has to be fixing on the animal body, and it is impossible to keep the animal in free. wireless power transmission technology based on electromagnetic induction becomes a feasible way to solve energy problems of this radio-telemetry system.

The transmission stability and biology safety in electromagnetic field are the main problem in this application. Many institutions and researchers have done fruitful work in the resolution of the problem of transmission stability. The main index to evaluation the biology safety is the value of specific absorption rate (SAR), the approximate value of the whole body average SAR can be acquired utilizing the incremental impedance of the primary coil [4,5]. These existing methods paved the way for the optimal design of wireless power transmission system, and the optimization model for wireless power transmission system working in gastrointestinal (GI) tract has developed and verified through in vivo experiments [6,7].

Unfortunately, the primary coil of animal physiological parameters telemetry system should expand the spatial extent to release the constraint on the active range of animal. Thus, the corresponding restraints from stability and safety are entirely different with the one in GI tract. To optimal the design of wireless power transmission module for implanted physiological parameters telemetry system, the transmission efficiency stability and biology safety are analyzed, and the system is optimized refer to existing model.

System overview

As shown in figure 1, Physiological parameters telemetry system consists of four parts: wireless energy supply modules, implantable micro-electronic capsule, wireless data recorder in vitro and the PC data processing software.

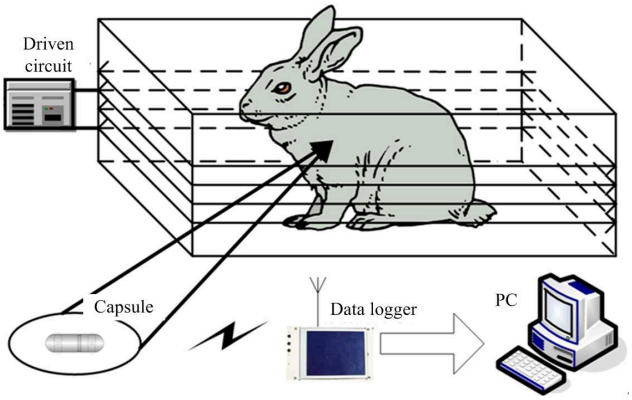

Fig.1. System overview

The function modules focus on the head of this implantable microelectronic capsule, where integrates sensors for collection of animals ECG, body temperature and blood pressure signal. These physiological parameters were converted into electrical signals and sent to in vitro in the way of wireless communication after process. They were received by data logger, displayed in real-time, saved into multimedia card and process in PC.

Wireless energy supply module consists of two parts: a transmitting coil generates an alternating magnetic field by the driven of an alternating current. The receiving sets induced electromotive force and power the telemetry system after rectification and regulation. The animal posture and position are changing relative to the transmitting coil, which lead the unstable of power transmission. Uniform magnetic field and three dimension receiving sets are proposed to resolve this problem. Considering the size of the animal, the transmitting coil is a solenoid with rectangular cross-section, similar to an animal cage. To induce a time-vary magnetic field, an inverter is used to change the DC power to AC power in the transmitting coil circuit, and a full-bridge form of class D inverter is adopted because of the flexibility and the deformation. The implanted capsule is cylinder with a size of Φ10.5 mm×11 mm.

Optimization model based on stability and security

The position and orientation of experimental animals in unconstrained state are continuously changing. For one thing, the relative position and orientation of transmitting coil and the implanted receiving coil are changing, which leads to the unstable of power transmission. For the other thing, these changing will drift the natural frequency of the transmitting coil.

The construct of uniform magnetic field proposed a solution for the problem of position stability [4-7]. The uniformity of magnetic field related with the stability of receiving power, thus, magnetic field uniformity is introduced to evaluate the resolution of this problem. Orientation change would vary the projected area of the receiving coil on the magnetic field direction, and affects the induction electromotive force and transmission efficiency. Thus, the projected area could evaluate the influence of orientation change on transfer efficiency. The three dimension receiving sets are wildly used since it could decrease the power fluctuation leading by the orientation change. The moving of experimental animal inside the transmitting coil would drift the natural frequency of transmitting circuit. Since the drift would rise impendence and decrease the driven current, the degree of frequency drift could indicate by the decrease of driven current in the same driven voltage. The stability of power supply could achieve through the analysis of position, orientation and frequency. For a series resonant circuit, the power on load was deduced in [7].

The most important international standards on safety in electromagnetic field comes from the ICNIRP (International Commission on Non-Ionizing Radiation Protection)(1998), when the

frequency is between 100 KHz and 10 MHz, electromagnetic influences on biological tissue mainly depend on the specific absorption rate (SAR, W/kg). Whole body average SAR (SARWA) describes the electromagnetic power absorbed by the organism, could measure using impedance incremental method. According to the guide line of ICNIRP, the safety threshold is SARWA ≤0.4 W/kg.

Measuring the impedance increment ΔZ of the transmitting coil before and after putting inside an experimental animal with a mass of M kg using LCR meter, when the animal is in safe, there is:

$$\mathrm{SAR}_{\mathrm{WA}} = \Delta Z \cdot I_m^2 \cdot M^{-1} \Rightarrow I_m \le \sqrt{0.4M / \Delta Z} \tag{1}$$

To conclude, for given space and power demands, the three elements of the mathematical programming problem can be confirmed as follows: the objective function is $Max(\eta_{\min})$, the variables are different kinds of transmitting coils and receiving coils, and the constraint conditions are power needed and the value of SARWA. The limitation of size is contained in the design of receiving coil. Finally, the problem can be expressed as follows:

$$Max(\eta_{\min}) \tag{2}$$

Subject to

$$\begin{cases} P_{\min} \ge P_0 \\ I_m \le \sqrt{0.4M / \Delta Z} \end{cases}$$

Where I_m is the driven current, and P_0 is the power demanded.

Experiments and Results

The power requirement of the telemetry system is providing not less than 150 mW of power in a volume of Φ10.5 mm × 11 mm for any position and orientation in the work region. According to this power requirement, a wireless power transmission module consists of rectangular solenoid transmitting coil and 3-D receiving coil is proposed (figure 2). The size of transmitting coil is 450 mm×350 mm×150 mm, and constructed with 180 strands of AWG 38 enamelled copper wire. The three coils are geometrically orthogonal to one another and wound on a common ferrite core. Core should be the high permeability MnZn ferrite R10K to increase the magnetic flux, and the winding wire should be Litz wire AWG44 to reduce the skin effect and proximity effect losses in coils.

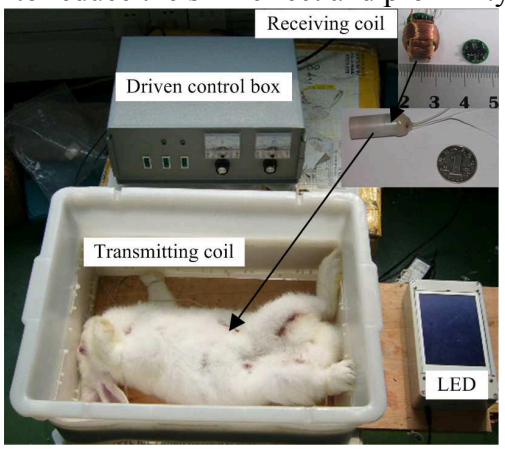

Fig.2. Wireless power transmission module

The experimental is a New Zealand rabbit with a mass of 4.2kg. To optimize the structure of the transmitter coil, the turns of transmitter coil varies from 16 to 36 with step of 2. The stability parameters and impedance increment are measured. Then the corresponding current constraint and power transmission efficiency are acquired and illustrated in figure 3. When the turns of transmitting coil rises, the transmission efficiency increases as well, inversely, the current lower limit constrained by power requirement and current upper limit constrained by biology safety in electromagnetic field decrease. When there exists intersection between the upper limit and lower limit of the current, the corresponding system meet all the conditions, and comply with the design requirements. Instead, if there were no intersection existed, the corresponding system is in unsafe. Obviously, systems of transmitting coils with turns of 20 to 34 are feasible, and the highest

efficiency is the one with 34 turns. However, the intersection of 34 turns is tiny, and it is hard to apply in practice, thus, the transmitting coil with 32 turns is adopted. The corresponding efficiency is 2.86%.

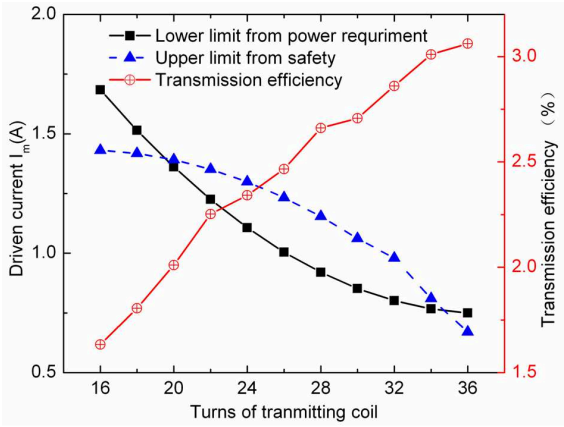

Fig.3. Inductive current feasible region and power transmission efficiency

To test the position stability and orientation stability of this transmission system, the receiving coil is put in the middle of the roof of the transmitting coil (where the magnetic flux density is the minimum) and in the worst frequency drift condition. Figure 4 shows the variations in the receiving power when pivoting angles θ_1, θ_2 change from 0 to 360 degrees by step of 10. The trough of the receiving power is approximately 150mW, and the corresponding efficiency is 2.64%. Therefore, the wireless power transmission module is capable to providing energy for less than 150mW to meet the energy requirements of the system in any state. Especially， owing to the machining errors of the receiving sets, the enclosed area of the three coils are unequal, and the practical efficiency is less than the theoretical value.

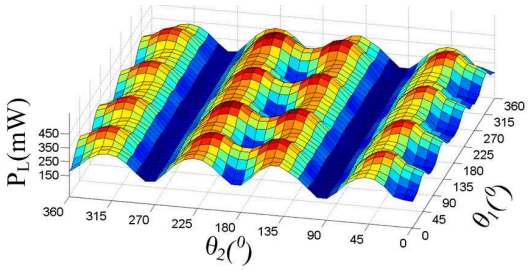

Fig.4. Receiving power in different orientations

The receiving sets are integrated into the telemetry system and implanted it into the body of anesthetized rabbit. Putting the rabbit in the transmitting coil and powering the system, the physiological parameter signals of ECG, body temperature and pressure were monitored. The body temperature turns to be 37.2~37.3 °C with a resolution of 0.1 °C. The pressure is 74~83 mmHg with Systolic blood pressure standard deviation of 1.47 mmHg and diastolic one of 0.90 mmHg. Compared with the practical signal, the measurement error is within the allowable range and the system meets the design requirements.

Conclusions

According to the energy demand characteristics of animal physiological parameters implantable telemetry system, the power transmission stability and safety in the application of wireless power transmission technology are analyzed, and a wireless power transmission system consists of rectangular solenoid transmitting coil and three dimensions receiving coil are proposed. The transmission performance is described by optimization model and optimal parameters are calculated. Experiments show that this energy supply module could supply power not less than 155mW continuously under a driven current of 0.9A, which satisfied the biology safety in electromagnetic field. Experiments in vitro demonstrate that the telemetry system based on wireless

power could monitor the physiological parameters of experimental animal properly, which verify the feasibility of the design of the wireless power transmission module.

Acknowledgement

In this paper, the research was sponsored by the National Natural Science Foundation of China (No. 60875061), the Shanghai Science Committee Foundation (No.09DZ1907400), and the Natural Science Foundation of Hunan Province, China (No.13JJ4055).

References

[1] Kiourti A, Nikita K S. A review of implantable patch antennas for biomedical telemetry: Challenges and solutions [wireless corner][J]. Antennas and Propagation Magazine, IEEE, 2012, 54(3): 210-228.

[2] Liu Dasheng Yan Guozheng. Design of an ECG radio-telemetry system using single supply[J]. Electronic Measurement Technology, 2012, 35(8): 107-111(in Chinese)

[3] Yoon Y-H, Jung E-S, Kang H-K, et al. Design of implantable wireless biomedical signals telemetry system[C]//Industrial Electronics Society, 2004. IECON 2004. 30th Annual Conference of IEEE. 2004, 3: 2982-2986.

[4] Lenaerts B, Puers R. Omnidirectional Inductive Powering for Biomedical Implants[M]. Springer Netherlands, 2009.

[5] Carta R, Thoné J, Puers R. A wireless power supply system for robotic capsular endoscopes[J]. Sensors and Actuators A: Physical, 2010, 162(2): 177-183.

[6] Jia Z, Yan G, Liu H, et al. The optimization of wireless power transmission: design and realization[J]. The International Journal of Medical Robotics and Computer Assisted Surgery, 2012, 8(3): 337-347.

[7] Jia Zhiwei, Yan Guozheng, Jiang Pingping, et al. Efficiency optimization of wireless power transmission systems for active capsule endoscopes[J]. *Physiological Measurement*, 2011, 32(10): 1561-1573

[8] International Commission on Non-ionizing Radiation Protection (ICNIRP). Guidelines for Limiting Exposure to Time-varying Electric, Magnetic, and Electromagnetic Fields (up to 300GHz). ICNRP: Oberschleissheim, 1997.

Advanced Materials Research Vols. 989-994 (2014) pp 1073-1076
© (2014) Trans Tech Publications, Switzerland
doi:10.4028/www.scientific.net/AMR.989-994.1073

Study on degradation of traditional Chinese Medicine wastewater with Cu/Cu_2O composite photocatalyst

Chunhua YUAN

College of Chemistry and Chemical Engineering, Inner Mongolia University of Science & Technology, Baotou 014010 china

email: yuanchunhua79@126.com

Keywords: Cu/Cu_2O; photocatalyst; composite material; catalytic performance

Abstracts. This paper uses alcohol thermal method, takes the mixed solution of N,N-two DMF and ethanol as solvent, in particular concentration of copper nitrate, prepares composite photocatalyst Cu/Cu_2O by control of temperature, then investigates the composite with XRD. The experimental results show that, the catalyst prepared has good dispersing, its average particle size is 7.96nm, and Cu comes into the Cu_2O lattice conducted the corresponding lattice distortions. In the 40W tungsten lamp irradiation, the photocatalyst can achieve effective degradation of traditional Chinese medicine wastewater, whose degradation rate can reach 97.3% and the COD removal rate can reach 95.6%.

Introduction

Photocatalysis almost will not have secondary pollution, and has advantages of high efficiency and high removal rate. Semiconductor Photocatalysts Cu_2O of band gap energy 2.0～2.2 eV is a typical narrow bandgap p-type semiconductor[1], which can be excited photocatalytic reaction by$400 \leq \lambda \leq 600$ nm visible light, so it can make full use of solar energy. If Cu_2O semiconductor is a photocatalyst, we need to consider how to improve the quantum efficiency of photocatalytic reaction. Supported noble metals (such as Au, Ag, and Cu) can quickly transfer the photogenerated electrons; effectively prevent the recombination of electron hole pairs, so as to improve the quantum efficiency of semiconductor [2].

In this paper, N,N-two DMF and ethanol mixed solution as solvent, copper nitrate as raw materials, we assemble and synthetize Cu/Cu_2O composite materials[3], and use it to degrade Chinese traditional wastewater under visible light[4].

Materials and methods

Experimental instrument and chemical reagent

Instruments: electronic analytical balance (FA1004 Shanghai Hengping Scientific Instrument Co., Ltd), hydrothermal reaction kettle (120mL Dalian Equipment Factory), electric thermostatic drying oven (101 Beijing ever-bright medical instrument factory), X ray diffraction (Rigaku-12KW Japan), tungsten (40W Lianhua Lighting Co., Ltd.) 722s visible spectrophotometer (Shanghai precision scientific instrument Co., Ltd.).

Reagent: copper nitrate, N,N-two dimethyl formamide, hydrogen peroxide (30%), anhydrous ethanol. All are analytically pure agent.

Preparation of Cu/Cu_2O composite

100mL $Cu(NO_3)_2$ solution of concentration 0.07M was prepared by adding1.691g $Cu(NO_3)_2 \cdot 3H_2O$ into the volume ratio of 1:2 DMF and ethanol mixed solvent. 100mL 0.07M Cu(NO3)2 solution was added into the hot water kettle of volume 120mL, the hot water kettle was placed into the electrothermal blowing dry box, first at 180℃ for 6 h, then the reaction temperature up to 200℃ to 2 h reaction, after the reaction, hot water kettle in the oven to slow below 150 ℃, then removing to chill under the water. A precipitate filtered was washed by anhydrous ethanol, and then was baked under temperature 60℃ for 3 h in the drying oven. Then the brown Cu/Cu_2O composite powder was got.

Characterization of Cu/Cu_2O materials

The samples were characterized by suing XRD phase analysis with D/Max-3c X-ray powder diffraction. Test conditions: Cu target k_a line, Ni filter, voltage 40kV, current 40mA, the scanning range of 20°～80°（2θ）, scanning speed of 2°/min with X ray diffractometer.

Source of wastewater

The example waste water came from a Chinese medicine pharmaceutical factory of Inner Mongolia. The waste water was brown, with a pungent smell of rancid, CODcr(2289.04mg/L). Before the photocatalytic degradation experiments was performed, the waste water was first filtered and diluted with medium speed filter paper.

Photocatalytic degradation of wastewater

The visible light[5] source came from a tungsten filament lamp of 40W , and the lamp spacing was 10 cm.The photocatalytic reaction process included: (1) A certain amount of Cu2O/Cu powder was added into the traditional Chinese Medicine Wastewater; (2) First, in the absence of light, Ultrasonic dispersing for 13min, and then the magnetic stirring for 120 min, so that the organic molecules could reach adsorption / desorption equilibrium on the catalyst surface, then turning on the light; (3) Beginning with the light point, every 20 min, the 5mL suspension samples was removed, centrifuged for 10 min, and then the upper liquid learned. The absorbance A of photocatalytic solution was measured by using 722S spectrophotometer in the 465nm. Its degradation rate and COD removal rate were calculated according to the following formula: Degradation rate（η）=（A_0-A_1）/A_0×100%.

Results and discussion

XRD analysis of the complex catalyst Cu/Cu_2O

Through comparing the XRD spectra of the samples with Cu_2O, and contrasting with the standard card of JCPDS , fingerprint peaks can be respectively regarded as Cu_2O (space group Pn3m; a0=0.4252 nm. JCPDS 05-0667) and Cu (space group Fm3m; a0=0.3613 nm. JCPDS 04-0836). Calculating average grain size according to half width of diffraction peak of the sample Cu (111) and Cu_2O (111) , using the Scherrer formula （Scherrer）：$d=K\lambda/(\beta\cos\theta)$, the product's average particle size is about 7.96nm. By contrast XRD chart of pure Cu_2O, we found that Cu/Cu_2O(111） peak intensity decreased and the half peak width became large. This showed that the crystallinity of the catalyst reduced, which was a universal feature of nanoparticles. Their specific surface area s was calculated by the formula of S＝6×103 /（ρd）. In this formula, ρrepresents the theoretical density of the grain, specific surface area reaches 133.55m2/g.

Degradation of traditional Chinese Medicine Wastewater by Cu/Cu_2O

1) Relationship between the rate and amount of degradation

The 0.020g, 0.040g, 0.060 g, 0.080g, 0.100g and 0g (not) Cu/Cu_2O powders were respectively added to seven 100mL traditional Chinese medicine wastewater whose initial absorbance was 0.811. As shown in Figure 2, in the pure light conditions, the organic matter in wastewater was almost no decomposition or decomposition speed was very slow, but it could be degraded more than 70% with light 20min ,if it was added the catalyst.

2) Effect of traditional Chinese medicine wastewater initial concentration on the degradation rate

0.006g catalyst samples was taken to treat 10mL traditional Chinese medicine wastewater solution of different dilution, after ultrasound 13min in natural light, its absorbance value was measured and its degradation rate was calculated, then the variation diagram of degradation rate with different dilution ratio was made, as shown in figure 3. As you can see from figure 3, with the increase of wastewater dilution , the contact probability of organic pollutants molecules and catalyst will increase, and the degradation rate also increase; when the dilution ratio reaches 25 times, the contact of the catalyst surface and organic pollutant molecules will saturate; further dilution of organic matter, too low concentration will lead to other measurement errors, catalytic degradation rate will become lower on the contrary. Therefore, when the traditional Chinese medicine wastewater is diluted to 25 times ,the treatment effect is the best.

3) Recycling rate experiment

For the study of repeated utilization ratio of catalyst in the process, the catalyst samples was repeated for processing experiment of traditional Chinese medicine wastewater. Figure 9 gives the catalytic activity of the catalyst for three times recycle. After calculating the degradation rate, the variation diagram of degradation rate changing with time under different frequency of use, as shown in figure 4. In the industrialization process, the recycle reactivation of the catalyst will cause the processing cost greatly increased, so there is no catalyst used for drying and reactivation in experimental process. The experimental results show that, each time use will largely reduce the catalytic activity of the catalyst. There are two possible reasons: First, in the process, a part of catalyst losses; second, the surface of the catalyst is adhered by organic matters to decrease the degradation rate.

Conclusions

(1) Taking the mixed solution of N, N- two DMF and ethanol as solvent, using alcohol thermal method in particular copper nitrate concentration, by controlling the temperature and time, the better dispersed composite photocatalyst Cu/Cu_2O is synthesized; this particles are investigated by XRD and SEM, which results showed that the Cu comes into the Cu_2O lattice which happens certain distortion of crystal lattice.

(2) Under simulated sunlight irradiation, using composite photocatalyst Cu/Cu_2O to degraded wastewater from traditional Chinese medicine, the best catalytic conditions are: traditional Chinese medicine wastewater is diluted 25 times, the amount of catalyst is 0.6g/L, ultrasonic dispersion time is 13min, then magnetic force stirred the wastewater for 2h under the condition of no light, finally irradiating it with 40W tungsten lamp, the degradation rate can reach 97.3%, and the COD removal rate is measured to reach 95.6%.

Acknowledgments

It is a project supported by the Creative Foundation of Inner Mongolia University of Science & Technology (No. 2010NC025), and the Science and Technology Bureau of Baotou (No. 2010Z1002)

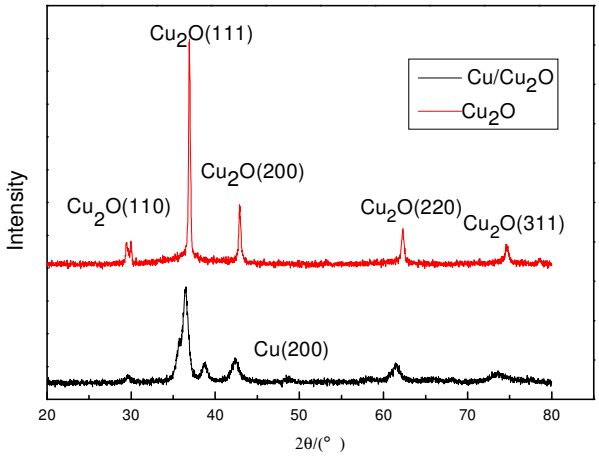

Fig.1. XRD diagram of Nano composite Cu/Cu_2O

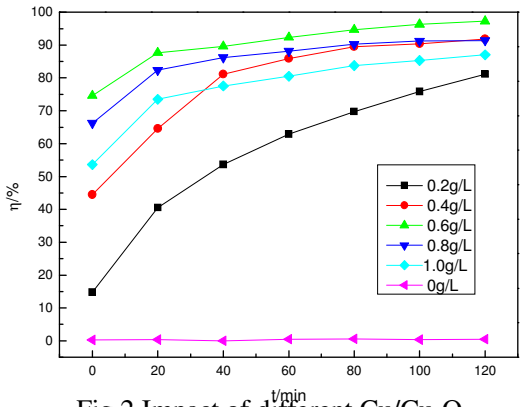

Fig.2 Impact of different Cu/Cu_2O concentrations on degradation rate

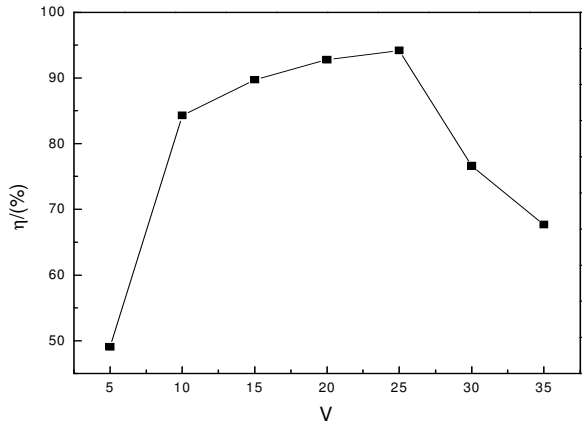

Fig 3 Impact of initial methyl concentration on degradation rate

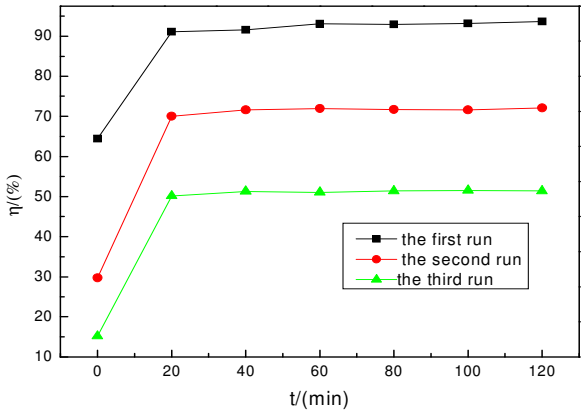

Fig 4 Results of photodegradation of methyl orange with catalyst for three times

References

[1]Yoshitaka Nakano, Shu Saeki, Takeshi Morikawa. OpticalBandgap Widening of p-Type Cu_2O Films by Nitrogen Dop-ing[J], Appl Phys Lett,2009,94:022111.

[2] Yanlong Tian, Binbin Chang, JieFu etc. Graphitic carbon nitride/Cu_2O heterojunctions: Preparation,characterization, and enhanced photocatalytic activity undervisible light[J]. Journal of Solid State Chemistry 212(2014):1–6.

[3]Zhou Bo,Liu Zhiguo,Yang Yanqiang,and Su Wenhui.Experimental Study on Photoc-atalytic Activity of Cu(2)O/Cu Nanocomposites under Visible Light[J], Catalysis Letters, 2009,132(1-2): 75-80.

[4] Zhonghua Li, Jiawen Liu, Dongjun Wang, Yuan Gao, Jun Shen ,Cu_2O/Cu/TiO_2 nanotube Ohmic heterojunction arrays with enhanced photocatalytic hydrogen production activity[J], International Journal o f Hydrogen Energy, 37 (2012): 6431-6437.

[5] Nian JN, Hu CC, Teng H. Electrodeposited p-type Cu_2O for H_2 evolution from photoelectrolysis of water undervisible light illumination[J], Hydrogen Energ 2008, 33:897-903.

Advanced Materials Research Vols. 989-994 (2014) pp 1077-1081
© (2014) Trans Tech Publications, Switzerland
doi:10.4028/www.scientific.net/AMR.989-994.1077

Design Consideration of a Health-Information-Technology-Supported Intelligent Urinalysis System

Tao Dong

Department of Micro and Nano Systems Technology (IMST), Faculty of Technology and Maritime Sciences (TekMar), Buskerud and Vestfold University College (HBV), Tønsberg, N3103, Norway;

E-mail: Tao.Dong@hbv.no

Keywords: information automation; health information technology; biomedical automation; intelligent toilet;

Abstract. Urinalysis is not only widely employed in medical diagnosis but also suitable for household daily monitoring of personal health conditions. However, current urinalysis methods and instruments require more professional knowledge, while the sampling and treatment of urine samples are manual and inconvenient. In this work, a new-concept automatic urinalysis system is proposed to provide personal urinalysis services for home users. The system forms an eco-friendly intelligent toilet, which is of great significances in the future healthcare network. The basic strategy is to design a fixed supporting platform and various disposable urinalysis lab-on-chips with great expansibility and high flexibility. The intelligent device has multiple functions of automatic urine sampling, rapid on-chip detecting, auto-decontaminating and personalized health information technology (HIT) supporting, thus to provide a low-cost solution of automatic urinalysis services for both inpatients in hospitals and home-users. The structure of the urinalysis system logically resembles the frame with fixed smart cellphones and various mobile application programs. Besides, a biological lighting module is also designed to harvest the energy in wasted urine by continuous culturing vibrio fischeri, a luminescent bacterium. The integrated urinalysis system could create the possibility of remote medical services for home users, and meanwhile generates a new branch in the field of microsystem, which is entitled as 'HIT-oriented lab-on-chips'.

Introduction

Urine is an abundant bio-fluid that can be readily obtained by convenient means [1]. Urinalysis methods are also mainly used in labs and hospitals nowadays, which mostly include physical urinalysis tests, microscopic tests and chemical ones [2]. The advantages of urinalysis mainly focus on its non-invasiveness and high sensitivity. The results of urinalysis could be employed to detect personal health changes at early stage [3]. Compared with sampling processes of blood, the sampling of urine is much easier and can be repeatable in a single day. Medical studies have been carried out to prove the correlation between urinary components and respective human diseases, such as diabetes, kidney diseases etc. [2] Besides, urine metabolomics is a sunrise method for diagnosis, especially appropriate for kidney cancers and chronic inflammatory diseases.[4,5] The results of urine tests can also reflect some toxicological or metabolic responses of human bodies [6,7].

The routine methods of urinalysis have been studied for more than 100 years and could provide credible diagnostic information, [8]. Consequently, urinalysis is generally adopted by hospitals, and actually, it is also suitable for monitoring of daily health conditions for home users. However, current urinalysis tests in hospitals still require complex procedures, and the manual sampling of urine is rather inconvenient. Being more intelligent and automatic, urinalysis tests more and more rely on automatic instruments. Some automatic urinary analyzers have been developed after a long history of biomedical engineering on automatic urinalysis [9,10]. Nowadays, the automatic instruments can bring more convenience to the operators in the labs. The main challenge of urinalysis still lies in the sampling procedure, because urine samples, unlike tissue samples, must be collected and handled in a uniform manner to ensure consistency; but there is no consensus standard for urine collection and preservation [11].

For home users, the researchers in University of Illinois (USA) firstly developed a bio-sensing application programs (APPs) for iPhones that can read the results of commercial urinalysis strips [12], by which multiple items in urine samples could be analysed [4]. Moreover, the group of researchers also developed another iPhone APP that turns iPhones into a spectrophotometer for detecting pathogens in water [13]. These bio-sensing APPs for iPhones provide good examples for household urinalysis systems, but the above programs only solve the problems of detection. TOTO®, the Japanese company developed an intelligent toilet as a systematic solution for household urinalysis. The intelligent toilet of TOTO® can automatically take and test human urine samples. However, only a couple of items in urine samples could be monitored by the TOTO® intelligent toilet system, and its cost is too high so that the brilliant product might be difficult to become a household appliance. Furthermore, a fixed urinalysis device was integrated inside that intelligent toilet; so it was difficult to expand its functions without re-designing of the system. In this work, an intelligent urinalysis system (IUS) with automated sampling, rapid on-chip detecting, auto-decontaminating and personalized health-information-technology (HIT) supporting is proposed as a new strategy.

Strategy and Design

The basic design is a new-concept intelligent toilet with great expansibility and high flexibility in the detection capability. With the practical cost taken into consideration, it would inevitably increase the total cost dramatically by integrating all the test laboratory of urine together with the assay reagents into the intelligent toilet system, reducing the possibility of widespread popularity. The current smart cell phone prompts an alternative structure for Intelligent Urinalysis System (IUS). The hardware of the smart cell phone can be designed as universal module under a certain criteria, which make it more popularizing. Diversity of cell-phone users could have various demands, which can be fulfilled through cheap application programs downloaded from internet. Of course, there should be a standard operation system that connects APPs and the hardware. Similarly, a universal module for intelligent toilet can be adopted in the design of IUS, which make it be easily fabricated like the hardware of smart cell-phone (Fig. 1). The corresponding operation system of IUS is the public healthcare information system (HIS). Moreover, the various demands from different users for IUS can be realized by use of disposable urinalysis Lab-on-chips (LOC), similar to APPs in the smart cell-phone system [14,15]. These LOCs can be low-cost, with standard I/O port, and convenient for the running and data reading on IUS, which makes the maintain cost of IUS much lower than previous design.

Challenges and feasible solutions

The IUS is complicated with lots of challenges, but there is no real difficulty for every technique link. (Fig. 2) Firstly, in the sampling module, the sampling probe has dual functions: cleaning the skin before sampling, and collecting the urine automatically. As led into the sample preparation module, the collected urine is filtrated and the big particles are separated [16,17]. With the help of pump and valves module, the pre-processed sample is transferred into the disposable LOCs. Various disposable LOCs have different function of urinalysis, which is based on the optical detection and has uniform specification and I/O interface. And the optical signal from the LOCs can be read in the chip readers and submitted to the HIS through the internet [18].

The advanced HIS is indispensable for the intelligent toilet system. It is not only the type of IUS chip from the user, but also the user oneself that should be recognized by the HIT. The type of IUS chip can be labeled by barcode. Particularly, the HIS not only can transfer the medical information, but also play a key role in the running of IUS. For example, the identification of IUS chip type decides the corresponding driving program. The sample preparation module, pump and valve module and the chip reader operate synergistically under certain program. Without HIS, the whole IUS will be disabled.

Figure 1 The strategy and concept design of IUS. The system will be integrated by three parts, which resembles the system of smart cell phone. Disposable urinalysis LOCs and their driver programs equal to the APPs on smart cellphones; The intelligent close tool with urine sampling module, sample preparation module, valves and pumps module and detection module, logically resembles the hardware of a smart cellphone; HIT System, such as human-machine interface, databases, patients' identification programs, is like the Android operation system.

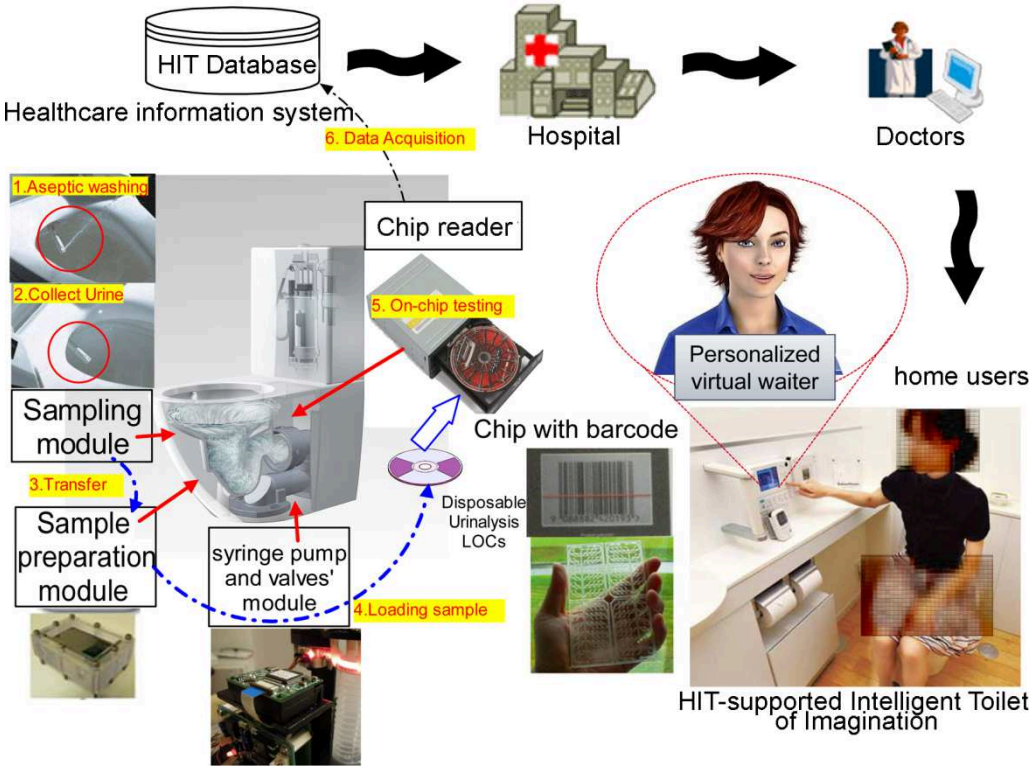

Figure 2 The configuration and components of IUS. The system is composed of disposable urinalysis lab-on-chips, driver programs, and the intelligent close stool which has urine sampling module, sample preparation module, valves and pumps detection module and the chip reader. The HIT system will support the function of devices and linked to doctors in hospitals.

Biological lighting device using energy from urine

The urine sample contains plenty of organic substances, which can be detected in IUS. Besides, the urine sample is also a waste biological power source. However, it is not economic to harvest energy from the urine. In the back-process of the IUS, a low-cost energy harvesting module is added, which is actually a biological reactor using the nutrient materials in the urine to cultivate a non-pathogenic bacteria, *Vibrio Fischeri*. (Fig. 3) *Vibrio Fischeri* is a natural bioluminescent bacterium in sea water. This robust bacterium can survive in urine and convert the bioenergy into the optical energy with the wavelength of 490nm. With the bioreactor module made of transparent material, the optical energy can be used as part of the lighting in the lavatory. This bioreactor operates very simple: the urine and oxygen is passively fed from the upper stream; the constant temperature in the lavatory provide a required temperature for bacteria growth; and the waste medium can be flushed away through the sanitary sewer. Therefore, as a module of IUS, this biological energy device can provide free lighting based on the toilet system.

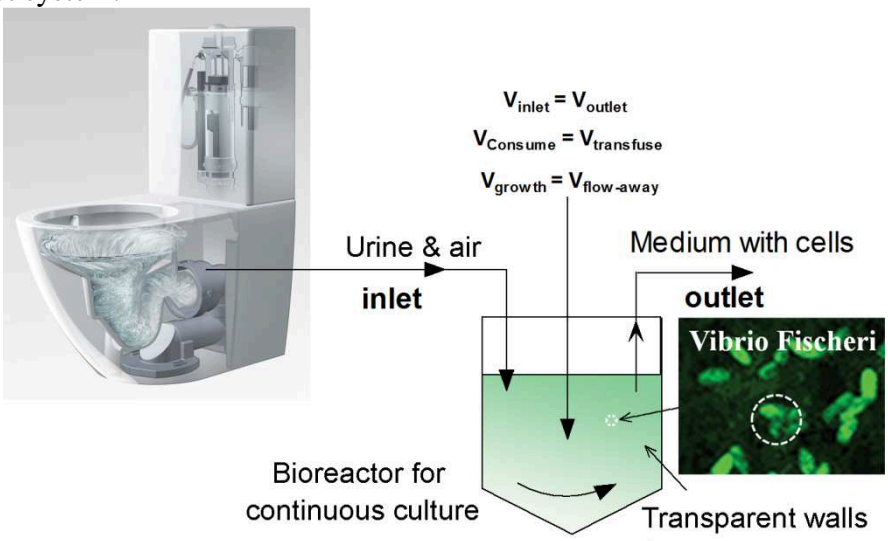

Figure 3 A passive bioreactor for continuous culturing of bioluminescent bacteria is proposed to provide long-term illumination using the energy in urine.

Summary and future work

The intelligent system is a very creative design to update the current toilet to a multi-functional and low-cost urinalysis with the integration of automated sampling, rapid on-chip detecting, auto-decontaminating and personalized HIT supporting. This system can be used as people's daily monitoring platform, bringing convenience to the doctor and the patients. Besides, the information collected by the HIT can be used to build a medical database with filtering the private personal information. This IUS plan is feasible in both technique and applications. Besides, IUS creates the possibility of remote personal medical services, and could generate a promising branch in the field of microsystem, entitled as 'HIT-oriented LOC'. The HIT-oriented LOC is being developed toward the popular trend, where the whole LOC measurement system is disintegrated into cheap disposable chips and the external equipment that can be repeatedly used. With this trend, the LOC is designed to be as simple as possible using expensive drives, photoelectric sensors, and so on integrated into the external equipment for repeated service. Such a design will significantly reduce the cost for the chip test to become affordable for common users.

Acknowledgements

The author would like to specially acknowledge Xinyan Zhao and Shilun Feng of Sensovann AS (Norway) for his constructive opinions. This work is supported by Norsk regional kvalifiseringsstøtte fra Oslofjorfondet (Touchsensor for urinprøvetaking og analyse, Prosjekt nr: 234972), Norsk regional kvalifiseringsstøtte fra Oslofjorfondet (High-throughput photo-detector array, Prosjekt nr: 229857)

and Norwegian long term support from NorFab (Living-Cell-based LOC project). The Research Council of Norway is acknowledged for the support to the Norwegian Micro- and Nano-Fabrication Facility, NorFab (197411/V30). The research activities are also sustained by Trilobite Microsystems AS (Norway), Sensovann AS (Norway), Institute of Hydrobiology (Chinese Academy of Sciences) and Xiamen University (China). In particular, the authors would like to acknowledge PhD Zhaochu Yang for providing technical contributions and drawing the diagrams of IUS. The master students, Shilun Feng, Carlos Honrado and Cátia Barbosa are also acknowledged for their contributions of information retrieval.

References

[1] S. Ganti and R. H. Weiss, Urol Oncol, Vol. 29 (2011), p. 551-557.

[2] X. Wu, Crit Care Nurs Clin North Am, Vol. 22 (2010), p. 121-128.

[3] C. A. Schinstock, M. H. Semret, S. J. Wagner, T. M. Borland, S. C. Bryant, K. B. Kashani, T. S. Larson, and J. C. Lieske, Nephrology Dialysis Transplantation, Vol. 28 (2013), p. 1175-1185.

[4] K. Kim, P. Aronov, S. O. Zakharkin, D. Anderson, B. Perroud, I. M. Thompson, and R. H. Weiss, Mol Cell Proteomics, Vol. 8 (2009), p. 558-570.

[5] A. S. Taha, V. Grant, and R. W. Kelly, Postgrad Med J, Vol. 79 (2003), p. 159-163.

[6] A. Stopforth, B. V. Burger, A. M. Crouch, and P. Sandra, Journal of Chromatography B-Analytical Technologies in the Biomedical and Life Sciences, Vol. 834 (2006), p. 134-140.

[7] C. Brauer, A. Tipold, H. Desel, and V. M. Stein, J Small Anim Pract, Vol. 50 (2009), p. 423-425.

[8] J. A. Armstrong, Kidney Int, Vol. 71 (2007), p. 384-387.

[9] S. Uesugi, Rinsho Byori, Vol. 41 (1993), p. 1-7.

[10] N.N.M.M Pires and T. Dong, Journal of Biomedical Optics, Vol. 18 (2013), 097001.

[11] M. A. M. A. Roelofs-Thijssen, M. F. Schreuder, M. Hogeveen, and A. E. van Herwaarden, Clinical Biochemistry, Vol. 46 (2013), p. 1252-1256.

[12] R. Abraham and M. Erwig, Journal of Visual Languages and Computing, Vol. 18 (2007), p. 71-95.

[13] D. Gallegos, K. D. Long, H. J. Yu, P. P. Clark, Y. X. Lin, S. George, P. Nath, and B. T. Cunningham, Lab on a Chip, Vol. 13 (2013), p. 2124-2132.

[14] X. Zhao, Z. Yang, N. Pires, N. Hoivik, et al., Lab on a Chip, Vol. 12 (2012), p. 602-612.

[15] X. Zhao and T. Dong, Anal Chem, Vol. 84 (2012), p. 8541-8548.

[16] T. Dong, Z. C. Yang, Q. H. Su, M. T. Nhut, E. B. Egeland, F. Karlsen, Y. L. Zhang, M. J. Kapiris, and H. Jakobsen, Microfluidics and Nanofluidics, Vol. 10 (2011), p. 855-865.

[17] N. Tran-Minh, Q. H. Su, Z. C. Yang, H. Jakobsen, F. Karlsen, et al., Biomedical Microdevices, Vol. 13 (2011), p. 179-190.

[18] L. Zhang and T. Dong, Journal of Micromechanics and Microengineering, Vol. 23 (2013), 045011.

Advanced Materials Research Vols. 989-994 (2014) pp 1082-1087
© (2014) Trans Tech Publications, Switzerland
doi:10.4028/www.scientific.net/AMR.989-994.1082

An Improved Medical Image Fusion Method Based on Nonsubsampled Contourlet Transform

Yanchun YANG [1, a], Jianwu DANG[1, b],Yangping WANG[1, c]

[1] School of Electronic & Information Engineering,Lanzhou Jiaotong University,730070,Lanzhou,China

[a]email: yangyanchun102@sina.com, [b]email: dangjw@mail.lzjtu.cn

[c]e-mail: wangyangping@mail.lzjtu.cn

Keywords: Nonsubsampled Contourlet Transform(NSCT); Pulse Coupled Neural Network (PCNN);Region Spatial Frequency; Sum-modified Laplacian; Medical Image Fusion

Abstract. In order to further improve the quality of medical image fusion,an improved medical image fusion method, based on nonsubsampled contourlet transform(NSCT),is proposed in the paper. A fusion rule based on the improved pulse coupled neural network (PCNN) is adopted in low frequency sub-band coefficient. Because human visual is more sensitive to all local region pixels instead of single pixel,it is more reasonable that the region information stimulates PCNN instead of single pixel. Each neuron of PCNN model is stimulated by the region spatial frequency of low frequency sub-band coefficient .Low frequency sub-band coefficient is determined by the times of firing. When choosing the bandpass directional sub-band coefficients, the directional characteristics of NSCT has been made best use of in the paper.A fusion rule based on sum-modified Laplacian is presented in bandpass directional sub-band cosfficients.The experiment results show that the proposed method can greatly improve the quality of fusion image compared with traditional fusion methods.

Introduction

With the development of medical imaging technology, the multi-modality imaging technology has been widely used in clinical diagnosis and treatment. Different medical imaging can provide different medical information for doctors.For example ,computed tomography (CT) image has high spatial resolution ,which clearly shows structures of bone.It can provide a good reference for the location of lesions.The image of magnetic resource imaging (MRI) can be used to obtain information among tissues,which is helpful for determining the range of lesions.The images of PET and SPECT can provide functional and metabolism information of the human body.Hence,one can easily conclude that none of these modalities is able to carry all relevant information in a single image. Therefore, multi-modality medical image fusion is required to obtain all possible relevant information in a single composite image. Medical image fusion combines the advantages of various modalities and complementary information to provide more effective information for medical diagnosis and treatment[1].

During the last decade,many image fusion methods have been proposed. Wavelet transform has been widely used in virtue of localization and direction[2]. However, it has serious limitations in dealing with high dimensional signal like images. To overcome the limiations of wavelet transform. Do and Vetterli developed a true two-dimensional (2-D) sparse image representation method,namely,the contourlet transform(CT)[3],which has the characteristics of localization,multi-direction and anisotropy. However, the contourlet transform lacks of shift-invariance and results in pseudo-Gibbs phenomena along the edges to some extend. Relative to the contourlet transform, nonsubsampled contourlet transform(NSCT)[4] inherits the perfect properties of the contourlet transform,and meanwhile possesses the shift-invariance. When the NSCT is introduced into the image fusion field,more information for fusion can be obtained and the impacts of misregistration on the fused results can also be reduced effectively.So,the NSCT is more suitable for image fusion.

Pulse coupled neural network(PCNN) is derived from the synchronous neuronal burst phenomena in the cat visual cortex . PCNN with bionics background, is a new neural network which is different from traditional artificial neural network and has great potential for applications in image fusion research field[5].In the paper,an improved medical image fusion method based on NSCT is proposed.The source images are decomposed by using NSCT. A fusion rule based on improved pulse coupled neural network (PCNN) is adopted in low frequency sub-band coefficient. Each neuron of PCNN model is stimulated by the region spatial frequency of low frequency sub-band coefficients. A fusion rule based on sum-modified Laplacian is presented in bandpass directional sub-band cosfficients. The fused image is reconstructed by performing the inverse NSCT .The effectiveness of the proposed method is demonstrated with the experiments.Better fusion qualities are achieved in terms of both visual quality and objective evaluation.

Meterials and Methods

In this section, we will briefly review the theory of the NSCT,which will be used to decompose the source images in the paper.

The NSCT is a shift-invariant version of the contourlet transform. To get rid of the frequency aliasing of the contourlet transform and to achieve shift-invariance, Cunha, Zhou, and Do proposed NSCT based on nonsubsampled pyramid decomposition and nonsubsampled filter banks (NSFB). Fig. 1 shows the decomposition framework of NSCT. The nonsubsampled pyramid provides multi-scale decomposion and the nonsubsampled filter banks provide directional decomposion.A nonsubsampled pyramid split the input into a lowpass subband and a highpass subband.Then a nonsubsampled DFB decomposes the highpass subband into several directional subbands.The scheme is iterated repeatedly on the lowpass subband.

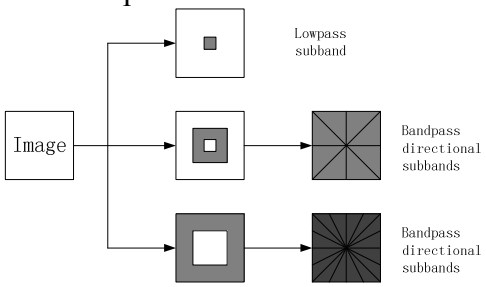

Fig.1Nonsubsampled Contourlet transform

A PCNN model [6]neuron consists of three parts:the receptive field,modulation field and pulse generator. There are many PCNN parameters to be selected in the medical image fusion, it is difficult to control and use.So an improved PCNN simplied model is adopted in the paper .The model is shown in Fig. 2. Its mathematical model is given in formula(1)～(5):

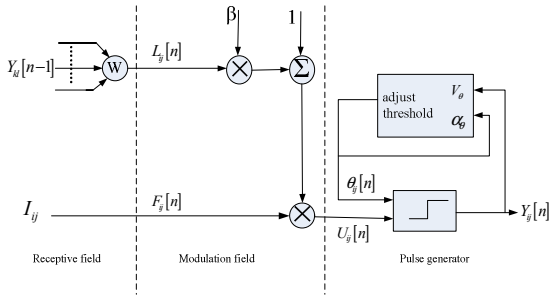

Fig.2 Improved PCNN simplied model

$$F_{ij}[n] = I_{ij} \tag{1}$$

$$L_{ij}[n] = V_L \sum_{k,l} W_{ijkl} Y_{kl}[n-1] \tag{2}$$

$$U_{ij}[n] = F_{ij}[n]\left(1+\beta L_{ij}[n]\right) \tag{3}$$

$$\theta_{ij}[n] = \exp\left(-\alpha_\theta\right)\theta_{ij}[n-1] + V_\theta Y_{ij}[n-1] \tag{4}$$

$$Y_{ij}[n]=\begin{cases}1, & U_{ij}[n]>\theta_{ij}[n]\\ 0, & U_{ij}[n]\le\theta_{ij}[n]\end{cases} \quad (5)$$

In the expressions, n denotes the current iteration (discrete time step). Here n varies from 1 to N (N is the total number of iterations). The indexes i and j refer to the pixel location in the image, Y_{ij} is output of the neuron, U_{ij} is the interior modulation result . There are two parts in Branch trees, eg. Feed input F_{ij} and link input L_{ij} . β is the linking strength, W_{ijkl} is the synaptic gain strenghs, α_θ is the time constant of the threshold adjuster. V_L and V_θ are the amplitude gain.

The Proposed Fusion Method

A .*The* fusion rule of the low frequency sub-band coefficient

As the coefficients in the coarsest scale subband represents the approximation component of the source image,the simplest way is to use the conventional averaging method to produce the composite coefficients.However,this method will reduce the fused image contrast,and cannot obtain fused approximation of high quality for medical image. Here PCNN model derives from the research on cat visual cortex.Its mode of information processing is much closer to the mode of human visual processing.And then PCNN has the flexible structure which can be changed according to different tasks. In the existing medical image fusion methods based on PCNN model,the coefficient of multiscale decomposition usually stimulates a neuron.There is one-to-one correspondence between pixels and neurons.Because human visual is more sensitive to edges and direction features instead of single pixel.According to human visual system,human eyes is not sensitive to the gray value of a single pixel.Image definition is embodied by all local region pixels.Therefore it is more reasonable that the regional information stimulates PCNN instead of single pixel[7].

SF (Spatial frequency) [8] reflects the overall image space activity. The larger the spatial frequency is, the richer the details of the image are, and the more clear the image is . SF is defined as follows:

$$SF=\sqrt{RF^2+CF^2} \quad (6)$$

Where RF and CF are row frequency and column frequency respectively. the $F(i,j)$ is the gray value of pixel at position (i,j) .The window is usually a $M\times N$ square neighborhood.The window size is usually 3×3 .

$$RF=\sqrt{\frac{1}{MN}\sum_{i=1}^{M}\sum_{j=2}^{N}(F(i,j)-F(i,j-1))^2} \quad (7)$$

$$CF=\sqrt{\frac{1}{MN}\sum_{j=1}^{N}\sum_{i=2}^{M}(F(i,j)-F(i-1,j))^2} \quad (8)$$

In order to sufficiently reflect the edge and details information of source image. In the paper, each neuron of PCNN model is stimulated by the region spatial frequency of low frequency sub-band coefficients.It can fully get the edge and details information of image and improve the quality of image fusion.The implementation is described as follows:

Step1:Low frequency sub-band coefficients of image A and image B are $C_{i0}^{A}(m,n)$ and $C_{i0}^{B}(m,n)$ respectively. Region spatial frequency of each low frequency subband coefficients are calculated by SF_A and SF_B . SF_A and SF_B are normalized between 0 and 1,which can be taken them separately as the feeding input $F_{ij,A}$ and $F_{ij,B}$ to stimulate a corresponding PCNN.

Step2:Initialize parameters, $L_{ij}[0]=U_{ij}[0]=0$, $\theta_{ij}[0]=0$,and $M_{ij}[0]=Y_{ij}[0]=0$.

Step3:Calculate each intermediate results according to the formula(1)～(5).

Step4:Let $M_{ij}[n]=M_{ij}[n-1]+Y_{ij}[n]$.

Step5:If $n<N_{\max}$,turn to Step3～Step4,until $n=N_{\max}$,then iteration stops. $M_{ij,A}[N_{\max}]$ and $M_{ij,B}[N_{\max}]$ are separately the firing times at the location (i,j) for $C_{i0}^{A}(m,n)$ and $C_{i0}^{B}(m,n)$.So the fused coefficients can be selected as follow:

$$C_{i0}^{F}(m,n)=\begin{cases}C_{i0}^{A}(m,n) & if: M_{ij,A}[N_{\max}]\geq M_{ij,B}[N_{\max}]\\ C_{i0}^{B}(m,n) & else\end{cases}$$

B. The fusion rule of the bandpass directional sub-band coefficients

The coefficients in the bandpass directional sub-band represent the details component of the source image. Fusion rule in the bandpass directional subband is the key part of medical image fusion. Due to the particularity of medical image ,it is required that the fused image should be suitable for eye resolution, it can show the image texture and rich details. For the bandpass directional subband coefficients,a fusion rule based on sum-modified Laplacian[9] is presented. The complete expression of ML(modified-Laplacian) and SML(sum-modified Laplacian) are shown in Equation (9) and Equation (10):

$$\begin{aligned}ML_{i,k}(m,n)=&\left|2C_{i,k}(m,n)-C_{i,k}(m-step,n)-C_{i,k}(m+step,n)\right|\\&+\left|2C_{i,k}(m,n)-C_{i,k}(m,n-step)-C_{i,k}(m,n+step)\right|\end{aligned}\tag{9}$$

$$SML_{i,k}(m,n)=\sum_{p}\sum_{q}W_{i,k}(p,q)\left[ML_{i,k}(m+p,n+q)\right]^{2}\tag{10}$$

Where ‘step’ is the variable spacing between the pixels,in the paper ‘step’ always equals 1. $C_{i,k}(m,n)$ is the coefficient in the bandpass directional sub-band at position (m,n).Where $W_{i,k}(p,q)$ is the corresponding window function.A weighted template is used to highlight the center pixel of the window.The template size is 3×3, The $W_{i,k}(p,q)$ is given as:

$$W_{i,k}(p,q)=\frac{1}{16}\begin{bmatrix}1&2&1\\2&4&2\\1&2&1\end{bmatrix}.$$

So the fused coefficients can be selected as follow:

$$C_{i,k}^{F}(m,n)=\begin{cases}C_{i,k}^{A}(m,n) & if: SML_{i,k}^{A}(m,n)>SML_{i,k}^{B}(m,n)\\ C_{i,k}^{B}(m,n) & else\end{cases}$$

Where $C_{i,k}^{A}(m,n)$ and $C_{i,k}^{B}(m,n)$ are separately the bandpass directional sub-band coefficients at the ith scale, kth direction. $SML_{i,k}^{A}(m,n)$ and $SML_{i,k}^{B}(m,n)$ are separately the sum-modified Laplacian of the bandpass directional sub-band at the location (m,n) for image A and image B.

Experimental Results and Analysis

To evaluate the performance of the proposed image fusion method,we use a pair of CT and MRI images for human brain with perfect registration in Fig.3,all images have the same size of 256×256 pixel with 256-level grayscale.A CT image shows structures of bone,an MRI image shows areas of soft tissue.However,in clinical applications,doctors need to see the position of bone and tissue to determine pathology and aid in diagnosis.So the fused image is usually needed in practice,which includes as much of the information in CT image and MRI image as possible. Fig.3 (a) illustrates the original CT image for patients. Fig.3 (b) illustrates the original MRI image for patients. Fig.3 (c) shows fused image based on discrete wavelet transform(DWT)[10]. Fig.3 (d) shows fused image based on NSCT[11].Fig.3 (e) shows fused image based on Guo’s method in reference[12]. Fig.3 (f) shows fused image attained by our proposed method. In order to verify the superiority of this method,parameters of our proposed method are set as $V_L=1$, $V_\theta=20$, $\beta=3$, $\alpha_\theta=0.8$, $\alpha_L=1$,

$N_{\max}=200$, $W=\begin{bmatrix}0.707 & 1 & 0.707\\ 1 & 0 & 1\\ 0.707 & 1 & 0.707\end{bmatrix}$. Experimental results showed that the parameters can get good fusion effect.

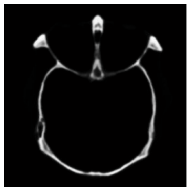
(a) CT image

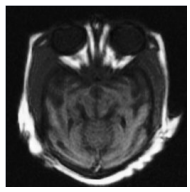
(b) MRI image

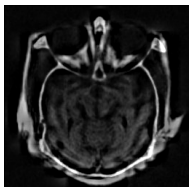
(c) result based on DWT

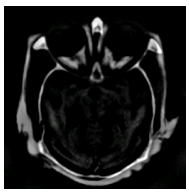
(d) result based on NSCT

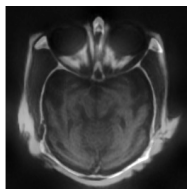
(e) Guo's method

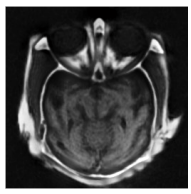
(f) our method

Fig.3 Experimental results

Fused results in Fig.3 can obviously find the fused images of Fig.3 (c) and Fig.3 (d) introduce many 'artifacts' around edges.Soft tissue information is weakened in Fig.3 (e).In Fig.3 (f) is much richer than other fused images .The image contents like tissues are clearly enhanced.Other useful information like brain boundaries and shape are almost perfectly preserved.

In addition to visual analysis,we conduct quantitative analysis on the above experimental results by different fusion algorithms.The selected quantitative criterions are entropy(IE),mutual information (MI)and $Q^{AB/F}$ proposed by Xydeas and Petovic[13]. IE represents the information content of the fused image.High entropy value images provide more information than lower entropy value images. MI is a metric defined as the sum of mutual information between each input image and the fused image. The larger the value is,the better the fusion result is. $Q^{AB/F}$ considers the amount of edge information transferred from the input images to the fused image. The larger the value is,the better the fusion result is.

Tab.1 Performance of different fusion methods in Fig.3

	DWT method	NSCT method	Guo's method	Proposed method
IE	6.1326	3.8510	6.9786	6.8436
MI	2.1010	1.5407	2.2789	2.8333
$Q^{AB/F}$	0.6167	0.5482	0.4166	0.7054

Table 1 gives the quantitative results of Fig. 3.From Table 1 ,it can be concluded that quantifying indicators of our proposed method outperform other fusion methods. Hence visual and quantitative analysis demonstrate that the fusion results of our proposed method contain more details and edges information than those of other fusion methods being compared while the information distortion is very small.

Conclusion

Medical image fusion technique can be applied to a wide variety of medical fields such as clinic diagnosis and therapy , computer assistant diagnosis , long-distance medical treatment , radiation therapy and surgery plan design , etc.In order to better meet the needs of clinical diagnosis and treatment, an improved medical image fusion method based on nonsubsampled contourlet transform is proposed in the paper. The proposed method enhances the fusion medical image information, effectively retains the source image details and edges information to achieve good fusion results.

Acknowledgement

The paper is jointly supported by the National Natural Science Foundation of China(No. 60962004, No. 61162016, No.31360291). Science and Technology Support Program Projects of Gansu province (1104FKCA102, 1104GKCA057) .The Youth Science Foundation of Lanzhou JiaoTong University(2014001).

References

[1] Bhatnagar G,Wu Q. M. J,Liu Zheng. Human visual system inspired multi-modal medical image fusion framework [J]. Expert Systems With Applications, 2013,40(5):1708-1720.

[2] HillP R, BullD R, C N. Canagarajah. Image fusion using a new framework for complexwavelet transforms[A]. In: Proceedings IEEE Interational Con- ference on Image Processing[C], Genova, Italy 2005, 2: 1338-1341.

[3] L.Yang,B.L.Guo,W.Ni.Multimodality medical image fusion based on multiscale geometric analysis of contourlet transform[J].Neurocomputing,2008,72(8):203-211.

[4] Da Cunha A L, Zhou J P, Do M N. The nonsubsampled contourlet transform：theory, design, and applications[J]. IEEE Transactions on Image Processing(S1057-7149), 2006, 15(10)： 3089-3101.

[5]Wei Huang,Zhong Liang-jing. Multi-focus image fusion using pulse coupled neural network [J]. Patter Recognition Letters, 2007, 28(9)：1123-1132.

[6] Chen Hao.Study on multi-source image fusion based on multi-scale transform[D]. [Doctoral dissertation],Changchun:Chinese Academy of Science,2010.

[7] Xia Jia-xing,Duan Xian-hua,Wei Shi-chao. Application of adaptive PCNN based on neighborhood to medical image fusion[J]. Application Research of Computers,2011,28(10): 3929-3933.

[8]Kong Jun, Zheng Kai-yuan, Zhang Jing-bo, et al. Multi-focus image fusion using spatial frequency and genetic algorithm [J]. International Journal of Computer Science and Network Security,2008, 8(2) : 220-224.

[9] Wei Huang,Zhong Liang-jing. Evaluation of focus measures in multi-focus image fusion[J]. Pattern Recognition Letters(S0167-8655), 2007, 28(4)：493-500.

[10]Pajares G, Cruzm. A wavelet-based image fusion tutorial[J]. Pattern Recognition, 2004, 37 (9) : 1855-1872.

[11] Jia Jian, Jiao Li-chen, Sun Qiang. The Nonsubsampled Contourlet Transform in Multisensor Images Fusion[J]. ACTA ELECTRONICA SINICA, 2007 ,35(10):1934-1938.

[12] Guo Chuan-qi,Wang Wen-ge,Chu Bin-bin. Improved image fusion algorithm based on PCNN[J]. Computer Engineering and Applications,2011,47(19): 176-178.

[13] Xydeas C S,Petrovic V.Objective image fusion performance measure. Electronics Letters, 2000, 36(4): 308-309.

Advanced Materials Research Vols. 989-994 (2014) pp 1088-1092
© (2014) Trans Tech Publications, Switzerland
doi:10.4028/www.scientific.net/AMR.989-994.1088

Interactive medical image segmentation method with only positive label examples

Chenguang Zhang[1, a], Yan Zhang[2,b*] and Xiahuan Zhang[1, c]

[1] College of information and technology, Hainan University, Haikou, China

[a]lzhang_chenguang@sina.com, [b]zhangyanouc@sina.com, [c]zhanggongzi@emails.bjut.edu.cn

Keywords: Interactive image segmentation; graph based learning; smoothness constraint

Abstract. In this paper, a novel interactive medical image segmentation method called SMOPL is proposed. This method only needs marking some pixels on foreground region for segmentation. To do this, SMOPL characterize the inherent correlations among foreground and background pixels as Hilbert-Schmidt independence. By maximizing the independence and minimizing the smoothness of labels on instance neighbor graph simultaneously, SMOPL gets the sufficiently smooth confidences of both positive and negative classes in absence of negative training examples. Then a image segmentation can be obtained by assigning each pixel to the label for which the greatest confidence is calculated. Experiments on real-world medical images show that SMOPL is robust to get a high-quality segmentation with only positive label examples.

Introduction

The underlying objective of medical image segmentation is to partition it into different anatomical structures, thereby extracting the components of interest, such as blood vessels and liver tumors, from their background for further medical diagnosis or surgical treatment. Many researchers in computer vision or machine learning have concentrated on achieving fully automated medical image segmentation[1,2,3]. However, fully automated segmentation often fails to detect the target boundary, due to the lack of the global knowledge on the objects. Moreover, when the image itself is noisy or contains many objects of complex shape, the exact target boundaries are very hard to identify automatically[4,5]. In very complex segmentation situations, manual segmentation may be a possible way, but it's subject to operator variability, often tedious and time-consuming[1].

To alleviate the problem, a number of interactive segmentation methods[6, 7, 8] were proposed. These methods , as combination of human experts and machine intelligence, can usually provide improved segmentation accuracy and efficiency with minimal user intervention than automated and manual methods. Despite the obvious advantage and the popularity of interactive methods, most of them require users to mark out a small number of pixels in foreground and background as positive and negative training examples. How to get a exact segmentation with only a small number of positive pixels is a meaningful and practical issue, and is also the objective that the paper is going to address. However, As far as we know, the related work is still few. Some literatures, that claim their methods can get good segmentation performance even in the absence of negative examples, in fact utilize the negative class information labeled by users in other images and can be seemed as automated category of segmentation methods.

In this paper, we put forward a novel interactive medical image segmentation method, called SMOPL. SMOPL explores the consistency on instance level and category level simultaneously. For instance level, SMOPL think the confidences of positive or negative class should be smooth, i.e., not vary too much on nearby pixels. By minimizing the smoothness of confidence on predefined graph, where nodes represent instances and edges reflect similarity between instances, the confidence information spreads from labeled pixels to unlabeled pixels. However, if there is no labeled background pixels as negative training examples, no confidence information of negative class would be spread out. As a sequence, all pixels would be classified simply as foreground. For the reason stated above, this paper introduced category regular terms. For category level, SMOPL quantifies the

inherent correlations among different classes by Hilbert-Schmidt independence criterion(HSIC)[9]. By maximizing the independence, the confidence flow from positive class to negative class. Finally, SMOPL combines the two aspects into a quadratic optimization problem. And by resolving the problem, SMOPL is expected to derive the confidence of positive and negative classes on all pixels in absence of negative training examples. Then a image segmentation can be obtained by assigning each pixel to the label for which the greatest confidence is calculated. Experiments on real-world medical images show that SMOPL is robust to achieve promising classification performance and high-quality segmentation even only with positive label examples.

The Model: Learning with Only Positive Examples

Notions. First introduce the notions that will be used throughout this paper. Let $V=\{(x_i,y_i)\in\mathcal{X}\times\mathcal{Y}\,|\,i=1,..,v\}$ be positive pixels set with label $y_j(j=1,...,v)$ and $U=\{(x_j,y_j)\in\mathcal{X}\times\mathcal{Y}\,|\,j=v+1,..,v+u\}$ be the unlabeled pixels set with label $y_j(j=v+1,...,u)$ unknown. Here, $\mathcal{X}$ and $\mathcal{Y}$ represent spaces of pixels and labels respectively. Moreover, let

$$X=[x_1,x_2,...,x_{v+u}],\quad Y=[y_1,y_2,...,y_{v+u}]\ . \tag{1}$$

represent feature matrix and label matrix respectively, where each $y_i=(y_{i1},y_{i2})^{\mathrm{T}}$ is a 2-dimensional real vector, with $y_{il}(1\le l\le 2)$ representing the confidence of x_i being associated with label *l*. Define a $2\times(v+u)$ matrix $Y_0=[y_1^0,y_2^0,...,y_v^0,0,...,0]$, called initial label matrix, with $y_i^0(1\le i\le v)$ is predefined as:

$$y_{il}^0=\begin{cases}1 & x_i \text{ is associated with label } l\\ 0 & \text{otherwise}\end{cases}\ . \tag{2}$$

Learning Framework. SMOPL is designed to derive the optimal assignment $y_j(j=v+1,...,u)$ to unlabeled pixels, such that the vector-valued confidence function *Y* satisfies the following two constraints: 1) it should be sufficiently smooth with respect to instance(pixel) graph, where each node represent one instance and each edge weight reflect the similarity between corresponding pair wise instances; 2) *Y* should be consistent with the inherent correlation of different classes. According to the constraints, the learning framework of proposed SMOPL can be formulized as

$$E(Y)=\mu_1E_{loss}(Y)+\mu_2E_s(Y)+\mu_3E_c(Y)\ . \tag{3}$$

$E_{loss}(Y)$ is fitting constraint which means a good confidence function should not change too much from the initial label assignment. $E_s(Y)$ measures the label smoothness, which have been addressed as manifold regularization in existing graph-based methods. The second item $E_c(Y)$ reflects the intrinsic correlation between positive label and negative label, which is novel and the key contribution of this paper. The trade-off among these three constraints is captured by a group positive parameter μ_1, μ_2 and μ_3.

Fitting constraint and Smoothness Constraint. Fitting constraint penalize the deviation from initial label matrix. It can be simply defined as:

$$E_l(F)=\sum_k\sum_{1\le i\le v}(f_{ik}-y_{ik})^2=\mathrm{Tr}\left[(Y-Y_0)(Y-Y_0)^{\mathrm{T}}\right]\ . \tag{4}$$

For smoothness item $E_S(Y)$, it needs to construct a weighted neighborhood graph $G=(V,E)$ on both labeled and unlabeled instances, where each vertex corresponds to an instance, and the weigh of edge is defined as:

$$w_{ij}=\begin{cases}\exp\left(\dfrac{-\|x_i-x_j\|^2}{2\sigma^2}\right) & i\ne j, i\in N_k(j) \text{ or } j\in N_k(i)\\ 0 & \text{otherwise}\end{cases}\ . \tag{5}$$

Where $N_k(i)$ is the k-nearest neighbors of x_i, $\|\cdot\|$ refers to the 2-norm and parameter σ is empirically estimated as the average distance between all instances. Then label smoothness on the graph can be defined as:

$$E_S(Y) = \frac{1}{2}\sum_k \sum_{i,j} w_{ij}(f_{ik} - f_{jk})^2 = \mathrm{Tr}[YLY^{\mathrm{T}}] \ . \tag{6}$$

In above equation, L is unnormalized graph Laplacian matrix, which is defined as

$$L = D - W \ . \tag{7}$$

W is the adjacent matrix of graph G and D is a diagonal matrix with its (i,i)-element equal to the sum of the ith row sum of W. Tr[A] refers to the trace of matrix A. Minimizing the smoothness function can impel label information spreading out from labeled pixels to unlabeled pixels and derive a sufficient smooth confidence vector.

Class Consistency constraint. For the second item $E_c(Y)$, we address it by Hilbert-Schmidt independence criterion. Given Gram matrix G with respect to Y [10]

$$\mathrm{G} = Y^{\mathrm{T}}\Pi Y \ . \tag{8}$$

where Π is the category structure matrix, it can be simply set as all ones 2×2 matrix. Also it can be estimated in a iteration process. When Y_{t-1} have been estimated in the last iteration t-1, Π could be set as:

$$\Pi = Y_{t-1}Y_{t-1}^{\mathrm{T}} \ . \tag{9}$$

Also given the Gram matrix K with respect to X. Then the dependence of X and Y can be formulized as[9]

$$E_c(Y) = \mathrm{Tr}[\mathrm{HKHG}] = \mathrm{Tr}[\mathrm{HKH}Y^{\mathrm{T}}\Pi Y] \ . \tag{10}$$

Maximizing the dependence would derive an optimal Y, which is consistent with the category structure Π, and spur positive confidence information flowing to negative class.

Solution. Incorporate loss function (4) and the two regularization terms (5) and (9) into Eq. (3), we get the cost function of SMOPL:

$$\mathcal{Q}(Y) = \mu_1 \mathrm{Tr}\left[(Y - Y_0)(Y - Y_0)^{\mathrm{T}}\right] + \mu_2 \mathrm{Tr}[YLY^{\mathrm{T}}] - \mu_3 \mathrm{Tr}[Y\mathrm{HKH}Y^{\mathrm{T}}\Pi] \ . \tag{11}$$

Then the final confidence function can be calculated by

$$Y^* = \underset{F}{\mathrm{argmin}}\, \mathcal{Q}(Y) \ . \tag{12}$$

To solve the above optimization problem, differentiate $\mathcal{Q}(Y)$ with respect to Y and let it be zero, we have

$$\frac{\partial \mathcal{Q}(Y)}{\partial Y^{\mathrm{T}}} = 2\mu_1(Y - Y_0)^{\mathrm{T}} + 2\mu_2 LY^{\mathrm{T}} - 2\mu_3 \mathrm{HKH}Y^{\mathrm{T}}\Pi = 0 \ . \tag{13}$$

$$(\mu_1 I + \mu_2 L)Y^{\mathrm{T}} - \mu_3 \mathrm{HKH}Y^{\mathrm{T}}\Pi = \mu_1 Y_0^{\mathrm{T}} \ . \tag{14}$$

$$(\mathrm{HKH})^{-1}(\mu_1 I + \mu_2 L)Y^{\mathrm{T}} - \mu_3 Y^{\mathrm{T}}\Pi = \mu_1 (\mathrm{HKH})^{-1} Y_0^{\mathrm{T}} \ . \tag{15}$$

Let $A = (\mathrm{HKH})^{-1}(\mu_1 I + \mu_2 L)$, $B = \mu_3 \Pi$ and $C = \mu_1 (\mathrm{HKH})^{-1} Y_0^{\mathrm{T}}$, then Eq. (15) can be seen as

$$AY^{\mathrm{T}} - Y^{\mathrm{T}}B = C \ . \tag{16}$$

This is a Sylvester Equation, which have many mature solutions. By solving this equation , we get the optimal solution Y^* of Eq.(12) and the each instance will be assigned to the label for which the greatest confidence is calculated.

Parameter setting. In this section, we would show the performance of SMOPL on both synthetic and real-word datasets. The parameters used in SMOPL are all fixed as const in the following experiments. First, SMOPL needs to construct a k-nearest neighbor graph. Number of nearest neighbor was set to be 8. And the three trade-off parameters μ_1, μ_2 and μ_3 were set to be 0.001, 0.998, 0.0010 respectively. Gram matrix K is taken with the same value with adjacent matrix W,

except that W is zeros on diagonal, and K is ones. Finally, for reducing calculated amount, category structure matrix Π is simply set to be 2×2 matrix with all elements are ones.

Experiments

Whole segmentation process can be summarized as the following steps: 1) Demand user labeling a few pixels on interested regions to indicate the foreground that need to be separated; 2)Use unlabeled pixels and labeled pixels to form testing data set and training data set respectively; 3)Construct neighbor graph of all pixels, including labeled and unlabeled pixels. Each pixel is associated with a three-tuple (R,G,B) feature, and the neighborhood of a pixel is spatially defined to be a 5×5 patch with the pixel as the center; 4)Solve Eq.(12) to obtain the potentials that unlabeled pixels belong to positive and negative categories. 5)Obtain a final segmentation by assigning to each pixel the label corresponding with maximum confidence.

The experiments and performance evaluation were carried on medical images from different modalities, including contrast enhanced ultrasound, CT scan of tumors and MRI slices etc. Results are shown in Fig.1, where (a) is the raw images, (b) is the images with manual scribbles to indicate the foreground, and (c) is the segmentation results of SMOPL. From Fig.1, it can be seen that though user only labels positive pixels and there is no any negative category information used for training or recognition in SMOPL, SMOPL can still get a high quality segmentation.

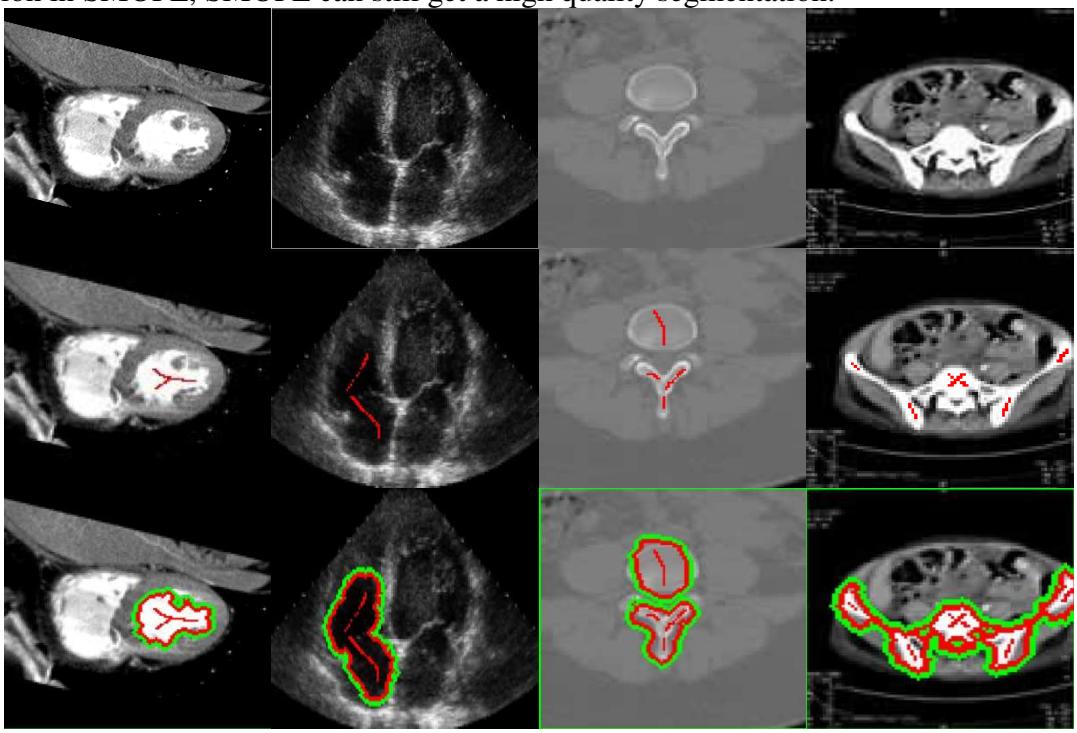

Fig.2 Medical images segmentation results of SMOPL. The first row are the original images. The second row are the partially labeled images with red pixels representing foreground. The third row are the segmentation results.

Summary

In this paper, a novel interactive medical image segmentation method is proposed by us. This method only needs user to label positive instances to complete segmentation, which is the main different between ours with others, as other interactive segmentation methods must have labeled positive and negative instances simultaneously. The idea behind the algorithm is the conformity of pixels and categories. By minimizing the smoothness of label information of pixels, the label information spreads from labeled pixels to unlabeled pixels, and by maximizing the intrinsic correlation of categories the label information flows from positive class to negative class. Then all the pixels get the

confidence value of all categories and each pixel can be assigned to the label with maximum confidence. Experiment results on synthetic datasets and real-world medical images show that SMOPL is robust to achieve promising classification performance and high-quality segmentation even only with positive label examples.

Acknowledgments

This work was supported by the College Scientific Research Program of Hainan Province for contract No.Hjkj2012-01(Research on graph-based semi-supervised learning method in semantic image retrieve).The corresponding author is Yan Zhang, Email: zhangyanouc@sina.com

References

[1] B.N. Li, et al. Computers in Biology and Medicine. Vol. 41(2011), p.1-10.

[2] C. MCINTOSH, et al. Medical Imaging, IEEE Transactions on. Vol. 31(2012), p.33-50.

[3] A.A.Qazi, V.Pekar, et al. Medical physics. Vol. 38(11)(2011), p.6160-6170.

[4] H. W.Kang, S.Y.Shin. Graphical Models. Vol.64(5)(2002), p.282-303.

[5] F. Zhao, X.H Xie. Annals of the BMVA. Vol.7(2013), p.1-22.

[6] L.Grady. IEEE Transactions on Pattern Analysis and Machine Intelligence. Vol.28(11)(2006), p. 1768-1783.

[7] S.Andrews, G. Hamarneh，A.Saad, in: *Proceedings of the 13th International Conference on Medical Image Computing and Computer assisted Intervention: Part III*, edited by T.Z. Jiang, et al. Publications/ Springer Verlag, Berlin, German(2010), p. 9-16.

[8] Y. Li, J. Sun，et al. ACM Transactions on Graphics. Vol. 23(3)(2004)，p.303-308.

[9] A.Gretton, B.Bousquet, et al, In: *16th International Conference on Algorithmic Learning Theory*. Edited by S. Jian Publications/Springer Verlag, Berlin (2005), p. 63-77.

[10] L.Song, A.Smola, et al. In: *Proceedings of the 24th international conference on Machine learning*, edited by Zoubin Publication/ACM, USA(2007), p. 815-822.

[11] B. Schölkopf, R. C. Williamson, et al, in: *Advances in Neural Information Processing Systems* 12, Edited by S.A. Solla, T.K. Leen and K.R. MüllerDenver, Public*ation*/Cambridge MA, USA(1999), p.582-588.

[12] W.K. Li, Q.H. Guo. Geoscience and Remote Sensing, IEEE Transactions on. Vol.49(2)(2011),p. 717-725.

Advanced Materials Research Vols. 989-994 (2014) pp 1093-1096
© (2014) Trans Tech Publications, Switzerland
doi:10.4028/www.scientific.net/AMR.989-994.1093

The Influence of Perceptual Load on Inhibition of Return

Xingjuan LIU[1], Zhihao FAN[2], Jianzhong ZHOU[3]

Department of Psychology,College of Humanities Jilin Agriculture University Changchun,130118, China

[1]email: xingzi1980@126.com, [3]email: xyzjz@163.com

Keywords: Inhibition of return (IOR), Flanker interference, Perceptual load.

Abstract. Inhibition of return (IOR) refers to a slower response to a target which appears at a previously attended location. We investigated whether perceptual load effects onset time of IOR in detection tasks. The results showed that the onset time of IOR was complex in different level of perceptual load. IOR effect was significant when perceptual load was low at 350ms, but the facilitation effect was significant at 850ms and 1350ms when perceptual load was high. The results indicated the onset time of IOR was influenced by perceptual load, indicating that perceptual load hinder the spatiotemporal correspondence between the cue and target integration.

Introduction

The efficiency of selection is a major question toward understanding selective attention. It is considered that the conflict between early and late selection models was resolved by perceptual load theory[1].According to this theory, to what extent the task-irrelevant stimuli are processed is determined by whether there are spare attentional resources left when they are used to process the task-relevant stimuli. If the current task has high perceptual load fill attentional capacity, irrelevant stimuli will be excluded before they interfere with task performance, but if perceptual load is lower the spare capacity will be directed automatically to the irrelevant information, which will then interfere with task performance [2]. Wei &Zhou（2005）reviewed studies that investigate the impact of perceptual load on selective attention, and studies that examine the interaction between the distribution of attentional resources and other cognitive processes or factors, such as working memory load[3].

Inhibition of return (IOR) proposed by Posner and Cohen (1984) demonstrated that When attention is summoned by an uninformative exogenous cue that precedes the presentation of a target by more than 300 msec SOA (stimulus-onset asynchrony), response times (RTs) to stimuli that appear at that location are usually slower than RTs to stimuli that appear at uncued locations [4]. Liu, Zhang and Zhou(2013) investigated whether the effect of distractors in IOR in discrimination tasks was changed by the location and number. The results showed that the trend of the general IOR effect was approximately the opposite in the two experiments. Different manner of cue target integration was adopted by participants when location and number of distractors were taken into account[5].

In present experiment, perceptual load and flanker task and the IOR procedure combination was made in our experiment, participants responded to a letter (M) present in the peripheral box, which appeared simultaneously with high or low perceptual load and with the peripheral distractor stimulus outside the peripheral box. We measure the inter effect of IOR and perceptual load and flanker interference.

Experiment

Participants

Eighteen participants (14 females) participated in the present experiment (age19~22). All the participants had normal or corrected-to-normal vision. They were naïve to the purpose of the experiment and were paid after the experiment.

Apparatus and Stimuli

Stimuli were presented on a monitor (VGA) of a Dell/PC-compatible computer, and responses were recorded via the computer keyboard using E-prime software, which controlled the presentation of stimuli, timing operations and data collection. The target on each trial appeared in the central of one of four boxes, displayed to the upper or the down or the left or the right of fixation point (a plus sign "+"), which remained on the central of screen throughout the whole trial and only disappeared between trials. Each white box subtended 1.8° of visual angle and the fixation point was subtended 0.9°of visual angle in the horizontal and vertical directions. The distance between the center fixation and one of the peripheral boxes was 5.5° of visual angle.

Procedure

Fig 1 depicted the sequence of events on each trial. A fixation point was displayed together with the four boxes for 500ms, and then the cue appeared for 100ms, participants were required to gaze at the fixation point and not scan. One of the boxes became white for 100ms as a cue. Following the cue, the fixation point was displayed together with the four boxes for 50ms. Then the empty boxes remained on the screen for 250 or 750 or 1250ms. The target was displayed at any of peripheral position for 2000ms or until response. If no response was obtained within 2,000 ms after target offset, then the next trial began.

Design

The experiment had a 2×3×2×2 within-subjects variables, cue validity (valid, invalid), SOA (350ms and 850ms and 1350ms) and distractor identities (compatible, incompatible), perceptual load(low, high). We used those SOAs to determine the temporal window at which the effect of attentional orienting is maximal.

When distractor was present, there are two distractor identities (compatible, incompatible). A distractor letter was presented besides the target position and was equiprobably compatible (e.g., an M when the target was an M), incompatible (e.g., an N when the target was an M).

A total of 64 practice trials were run before the 528 experimental trials. There were 1/3 of trials for each SOA condition. There were half of trials for each compatible condition. Participants sit about 50cm from the screen in a dimly lit, quiet room.

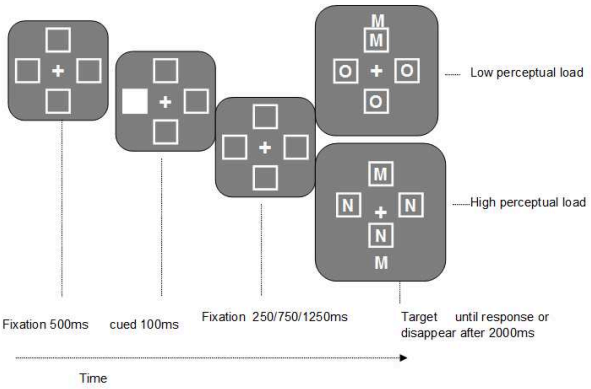

Fig.1 Illustration of Sequence and timing of a trial in Experiment

Results

Trials with RTs smaller than 100ms (anticipations) or larger than 1056ms (misses) outliers were defined as the saccade latencies. Fig. 2 and Fig. 3 illustrate the results of experiment.

RT of correct trials was submitted into a repeated variance analysis (ANOVA). The main effect of cue validity was significant, $F(1, 17) = 3.58$, $p<0.05$, RT was faster to targets at the valid location (623ms) than at the invalid location (634ms), which was the typical facilitation effect. The main effect of SOA was significant, $F(2, 34) = 10.02$, $p<0.001$, RT was faster to targets at 350ms than at 1350ms. The main effect of distractor was not significant, $F(1, 17) = 1.33$, $p>0.05$.The main effect of perceptual load was significant, $F(1, 17) = 11.20$, $p<0.01$, RT was faster to targets when

perceptual load was high than when distractor was low. The interaction between cue validity and perceptual load was significant, F (1, 17) =6.767, p<0.001. The interaction was significant between cue validity and distractor, F (1, 17) = 3.071, p<0.01, showing that the trend of IOR at two distractor conditions was different.

When perceptual load was low, RT of correct trials was submitted into a 2×2×3 repeated variance analysis (ANOVA). The main effect of cue validity was significant, F (1, 17) = 2.60, p>0.05, the main effect of SOA was not significant, F (1, 17) = 1.09, p>0.05. The main effect of distractor identities was not significant, F (1, 17) = 1.33, p>0.05. The interaction between cue validity and SOA was significant, F (1, 17) =3.767, p<0.05. The interaction between cue validity and distractor identities was not significant, F (1, 17) =2.007, p>0.05. The three interaction among SOA and distractor identities and cue validity was significant, F (1, 17) =3.217, p<0.05. Results of simple effect showed that IOR was significant at 350ms in spite of distractor identities was compatible or incompatible. There were significant facilitation when SOA was 850ms and 1350ms.

When perceptual load was high, the main effect of cue validity was significant, F (1, 17) = 8.60, p<0.01, the main effect of SOA was significant, F (2, 34) = 6.19, p<0.01. The main effect of distractor identities was not significant, F (1, 17) = 1.33, p>0.05. There had no significant interaction. Results of simple effect showed there were significant facilitation when SOA was 850ms and 1350ms.

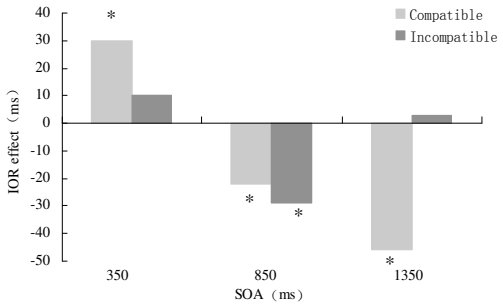

Fig. 2 IOR effect in the peripheral target detection task as a function of cue validity, distractor identities, SOA in the condition of low perceptual load.

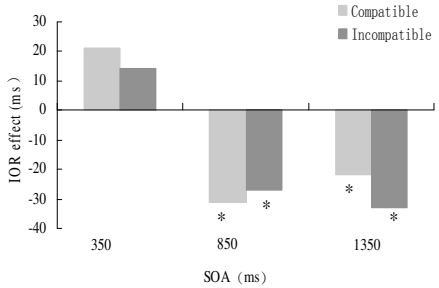

Fig. 3 IOR effect in the peripheral target detection task as a function of cue validity, distractor identities, SOA in the condition of high perceptual load

Discussion

The results showed that the onset time of IOR was approximately with previous research when perceptual load was low (only 350ms), but it disappeared (850ms and 1350ms) when perceptual load was high, those results were not coincident with the results of Lupiáñez, et al [6]. However, facilitation was significant when perceptual load was high. IOR magnitude was different with previous research when an interference letter was present together with the target. Liu, Tang and Zhou (2013) investigated whether flanker interference effects onset time of IOR in discrimination tasks. The results showed that the onset time of IOR was the opposite in incompatible and compatible condition. IOR effect was significant when distractor identities were compatible at

950ms, but the facilitation effect was significant at 950ms when distractor identities were incompatible [7].

In present experiment, the earlier onset of IOR when perceptual load was low indicated that an attentional set favoring encoding of new event representations, on the other hand, would delay the response to the target. In present experiment, the perceptual load is critical for onset of IOR, an advanced onset of IOR when perceptual load was low. Different tasks may propose different attention sets. Participants tend to create a new object file for the target in the experiment and tend to integrate the target with the cue (i.e. updating the existing file created by the cue) when perceptual load is low. But when perceptual load is high, the current task has no spare attentional resources, other stimuli will be excluded before they interfere with task performance, IOR effect disappeared [8].

The results from the present study indicated earlier onset time of IOR when perceptual load was low, indicating that low perceptual load and distractors compatible makes the spatiotemporal correspondence between the cue and target integration. When perceptual load was low at 1350ms, exactly the opposite result occurred, indicating that inhibitory tagging was applied to stimuli falling. Another prediction that can be drawn from Lupiáñez et al.'s view is that in our experiment, cue and target integration was more harmful than in the common cuing tasks where adding perceptual load and when perceptual load was high. This suggestion would surely predict later onset of IOR in those experiment conditions.

Acknowledgement

The research reported here was supported by general planning project of Ministry of Education Humanities and Social Sciences (12YJAZH211) and the innovative undertaking training program of University Students in Jilin Agriculture University (The Construction of Beyond Curriculum) and Humanities and Social Sciences in the Twelfth Five-Year Plan project of Education Office in Jilin Province (201226). We thank Jing Li and Jin Dan for help with data acquisition.

References

[1] Lavie, N. Perceptual load as a necessary condition for selective attention [J]. Journal of Experimental Psychology, 1995,21(3), 451-468

[2]Lavie, N., Hirst, A., Fockert, J. W. et al. Load theory of selective attention and cognitive contro[J]l. Journal of Experimental Psychology, 2004,133(3), 339-354

[3]Wei P, & Zhou X, L. The Perceptual Load Theory and Selective Attention[J]. Advances in Psychological Science, 2005,13（4）：413-420

[4] Posner, M. I., & Cohen, Y. Components of visual orienting. In H Bouma, D Bouwhuis (Eds.). Attention and performance X. Erlbaum Associates .Ltd, 1984, 1531–556.

[5] Liu, X.J., Zhang, M., Zhou, J.Z. Distractors Processing Modulate the Onset of Inhibition of Return in Discrimination tasks. ICME International Confenence on Complex Medial Engineering ,2013

[6] Lupiáñez, J., Milliken, B., Solano, C., Weaver, B., Tipper, S. P. (2001). On the strategic modulation of the time course of facilitation and inhibition of return [J].The Quarterly Journal of Experimental Psychology, 54A(3),753-773

[7]Liu, X.J., Tang, X., Zhou, J.Z. The Influence of Flanker Interference on Inhibition of Return. IEEE. International Confenence on Mechatronics and Automation, 2013.

[8] Liu, X.J., Zhang,Y., Wang, H.Y., Zhang, M. Three Factors Theory of the Time Course of Inhibition of Return and Its Development[J]. Journal of Psychological Science, 2014,37（01）,31-36

Advanced Materials Research Vols. 989-994 (2014) pp 1097-1102
© (2014) Trans Tech Publications, Switzerland
doi:10.4028/www.scientific.net/AMR.989-994.1097

The design and application of the information management platform for the prevention and control of AIDS on the basis of the residents' health records

Songhe Shi[1, 2, a], Shengwu Xiong[3, b]

[1]School of Computer Science & Technology, Wuhan University of Technology, Wuhan, China

[2] Department of Computer Science and Biostatistics, College of Public Health, Zhengzhou University Zhengzhou, China

[3]School of Computer Science &Technology, Wuhan University of Technology, Wuhan, China

[a]zzussh@126.com, [b]xiongsw@whut.edu.cn

Keywords: Design and application, information management platform, control of AIDS, residents' health records

Abstract. Relying on the Acquired Immune Deficiency Syndrome(AIDS) prevention and control system of project areas and existing health information network, according to the requirements of prevention and treatment of AIDS, and the "National Norms of Basic Public Health Services" as well as the "Community Comprehensive Prevention and Control of Major Contagious Diseases Programs and Procedures" and other regulatory requirements, this project, based on the residents' health records, using B/Sstructure, SSHframe, MVCmodel, ORACLE 10.0 database, is to develop residents' health records information management platform for the comprehensive prevention and control of AIDS, and make the existing AIDS epidemic system, the hospital information management system, residents' health records and health information system interconnected. It contributes to the participation of the administrative department of health, centers for disease control and prevention, hospital and community, and easily promotes organizations to provide technical support for the prevention and control system of AIDS. The platform has been successfully run in five project regions in Henan province, and has established 2, 365, 802 residents' health records about HIV/AIDS prevention and control, produced a good social and economic benefits. Its outlook is promising.

Introduction

The latest twenty years has witnessed the widespread of HIV/AIDS, making it a public health and social issue which is a serious threat to human survival and development [1,2]. The ways of transmission of HIV/AIDS in Chinahave changedsignificantly .Nowadays the AIDS epidemic situation bears two main characteristics: the first isthatthe number of people affected is still on the rise, with an increase by 10% annually. The second is thatthe number of sexual transmission rises obviously. From January to September of 2013 in Henan Province, the reported casesaccounted for 93.37 percent of that year (the entire country reported cases 89.9%), increased by 37.44%compared with the same period last year ,which turned out to be the dominantpathway of transmission. It is more obvious that the spread of HIV/AIDS tends to transmit from high-risk groups to the general population. The situation of HIV/AIDS prevention and control is at stake. From this point of view, it is critically important to set up a special information platform for the prevention and control of AIDS based on residents' health records, with the existing residents' health records, new farm cooperation, medical information system and the realization of AIDS for system information connectivity, so as to form a whole crowd of AIDS prevention and control of information, data, automatic analysis of network dynamic information analysis platform, reduce the new HIV infections and AIDS case fatality rate, and improve the life quality of HIV/AIDS patients[3].

The system design

A.The overall planning. According to the "prevention and control of AIDS in henan province scale field epidemiologicaland intervention studiessub-topic ofbuilding a new type of electronic health records and information resource center, relying on the project area of HIV/AIDS prevention and control system of network, network medical treatment system, combined with AIDS comprehensive prevention and control work in Henan province, using B/S structure, MVC pattern, ORACLE database 10.0, based on data mining technology, the application of national and international related technical standards and specifications, design and establish the residents' health records information management platform for the prevention and control of AIDS. HIV/AIDS prevention and control of information data, is to collect data for statistical analysis, make connectivity with the existing system, establish the portal website, publish the relevant information of HIV/AIDS prevention and control

B. The analysis of system demands. Design the information management system of AIDS comprehensive prevention and control about residents' health records, realize the compre-hensive management of permanent residents in AIDS prevention and control, including the management of basic information, medical information, residents follow-up information, intervention (tertiary prevention) information, evaluation of information; AIDS patients medical information, including the outpatient service, the hospital information management; Free AIDS antiviral drug bidding and purchasing and inventory information and issuing information management, etc.

1) Function demands. This system is divided into four parts, information collection, and statistical analysis information publishing and information maintenance. Information collection, including Basic information, medical information, residents special file information, medical information management.Statistical analysis is mainly according to the specification requirements in AIDS prevention and control of data for statistical analysis. Information release publish policies and regulations, such as HIV/AIDS knowledge in the form of web site. System maintenance mainly includes system management and data maintenance. System management includes user management, organization management and role management, data maintenance, including data backup and data maintenance, data dictionary initialized, etc.Medical tube combined with prevention system in network management. Through information network, making the system for the prevention and control of AIDS easy to organize and promote, which include the administrative department of public health, disease control center, hospital, community participation.

2) Organization information management. Organization information management is used to build new subordinate institutions, such as henan team build ShangCai, QueShan, Shen Qiu institutions at the county level, and the lower agency users to build institutions at a lower level (township, village, group, etc.)

3) User management. To realize the user rights allocation, which is divides into administrator users and ordinary users. User management is responsible for the allocation of user management institutions. Users can have multiple user at the same level, the superior users will be able to manage (add, modify, and delete) users at a lower level. For example, the distribution of Henan team project department is five project counties user information (user name, password), other can be assigned by the user at the county level, in order to reduce the superior user management work.

4) Role management. Role management is responsible for the assigned user rolessuch as input, query, modify permissions. Distribution project director, audit or an administer for information collection table, etc (Fig. 1).

5) Data maintance. It includes the data dictionary maintenance, data backup, initialization, etc.

C. Information collection. According to the implementation scheme and operation procedures for major communicable diseases community comprehensive prevention and control, it is used to collect the basic information, including basic information, medical information, special archives information, drug bidding procurement inventory issue information, and hospital and clinic medical information.

1) Statistical Analysis. To combine the needs of HIV/AIDS and HIV/AIDS epidemic statistical rules and reporting standards "with other related regulations, conducting statistical analysis, data mining for AIDS prevention and control of information. Including HIV/AIDS epidemic trend analysis, such as regional, urban and rural areas, age, gender, culture, occupation, marital status; and marching Comprehensive evaluation of individual and group for AIDS situation and analyzing HIV/AIDS epidemic tendency in horizontal and vertical analysis project.

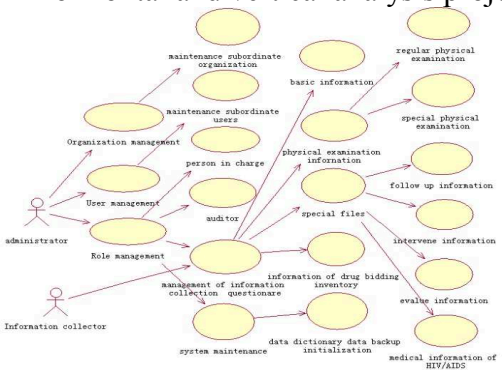

Fig. 1 The analysis of system demands

2) Community residents. A special file by inputting rate of AIDS prevention and control ,AIDS knowledge awareness, people health education people and education, HIV/AIDS transmission, AIDS prevalence rates and new infections. HIV infection rates, new HIV infections, etc.

3) Patients with HIV/AIDS. HIV/AIDS case fatality rate, rate of mother-to-child transmission of HIV/AIDS, HIV/AIDS patients receive ARV treatment, people living with HIV treatment in hospital, clinic, all expenses of outpatient, times of hospitalization expenses and AIDS patients living quality analysis, etc.

4) Information publish. Develop HIV/AIDS education scientific research sites, release crowd AIDS prevention knowledge.

D. Performance Requirement

1) System usability. The direct user of this system is mainly some basic grassroots health workers whose computer skills are low, so System usability should be taken in to consideration, starting from the business scenario, close to the actual business , fully consider the person in charge of the operation habit, business degree of familiarity and understanding of information system, design the easy operation interface, reduce its doubt in the process of using , improve the efficiency of the organization of business .System also should have reliability, security, openness and scalability, sophistication and maturity, usability and maintainability.

2) The system standards. All system hardware, software interface use the international general standard and are compatible.Conform to the AIDS epidemic information specification (trial) (the centers for disease control and prevention[2005] no. 56) for disease control and prevention,implementation scheme and operation procedures for the major communicable diseases community comprehensive prevention and control , the national basic public health service specification (2011 edition) requirements.

Overall design of system

A. Network architecture. System based on the provincial, city and county (district), villages and towns (street), village five network operations, has now completed the construction of medical information network and Internet infrastructure and provides the foundation for the system [4]. System aim to buildin the backbone network as the center at the provincial level, through VPN to the village, form a safe and reliable network architecture, thus improve the organization internal information sharing, promote business collaboration ability, improve supervision organization of business level and efficiency.

Work adopts VPN and other security technology access to the Internet,has realizedthe connection among system data and residents' health records, hospital information system and new agricultural

data and the ministry of health data platform, network cover the pilot and fixed medical institutions[5] .

Project implement areas should make full use of existing resources, establish provincial data center in the data center. The subordinate management departments at different levels directly have access to the provincial data center through the Internet, and march the work of information collection, query and summary and analysis.

B. System frame structure. System based on J2EE architecture; adopt the idea of service oriented. Data access method .adopt data mapping mechanism make the business logic componentization form a good system architecture. Through demand research, in view of the index system of business doing analysis and study, take system parametric design idea, implement the feature to address business needs, monitor and extensible , so as to realize zero maintenance specially, rapid deployment and requirements. System use the MVC pattern design technology architecture, and carry on the design layer ,part the interface display, logic control and logic realization, norm the format of data packet at all levels , make the data interaction in the entire framework with a standard format .

The system uses JAVAEE technology, innovative MVC framework. The view layer completely use static HTML pages. This part can be write by the system administrator, according to the need to increase or decrease in form and content, establishing a database automatically by the special program, is not restricted by traditional design method of database. The advantages is fast response, maximum reduce the burden of server and later maintenance costs. Model layer adopt the idea of generic programming, the system modules can be used. The increase in all kinds of health declaration in late time, only need to write a pure HTML page for each table in the system under the specified directory can have all of the functions add and delete, export data, and complete .Optimizing the system background program, making the server resource consumption to reduce as far as possible, coupled with the Oracle database excellent performance, so the system can response quickly and easily carrying huge amounts of data. System uses the WEB 2.0 client technology at the front desk, make the front desk display more human. When input the id number, for example, can realize the id check, etc.

C. Database design. The overall mission of system development is to implement HIV/AIDS prevention and control of systematization, standardization and automation. Design database system should fully understand the requirements of various aspects, including the current and future may expand demand situation, thus the database structure should fully satisfy all kinds of information input and output.

1)According to the characteristics of the system, respectively carrying on the detailed investigation and analysis for the basic information management, user management, examination management, information management, follow-up intervention evaluation management, medical information management, user management, category management, system log management and administrator management, summed up the demand information, the function module is mainly for the function of corresponding modules to add, delete, check, and change.

2)According to the requirements of system function analysis and summary, taking into account the future increase in the number of users and function extension, the system design of the data table is basic information table, the health checkup table, AIDS special archive table, AIDS drugs (free anti-viral drugs, and other basic drugs) management table, the outpatient service table, the hospital medical information management table, dictionary management table, the system administrator category table and system administrators table.

3)Data table consists of a data item, combined with the practical application of this system, the database of each table contains the following data items: the users table to store the user information, including the user name, real name, id number, contact information, etc..

E. The realization of system main function. The window after login shows as figure 2, in which the medical information of the region and the status of HIV/AIDS epidemic can be seen.

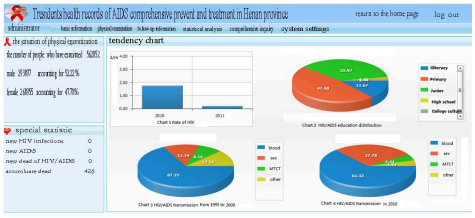

Fig. 2 Login interface

The age statistics of new HIV infection about Caidu town Shangcai county of Zhumadian city in Henan province

year	Total	0~		12~		18~		45~		60~		Total	
		infection	ratio(%)	infection	ratio(%)	infection	ratio(%)	infection	ratio(%)	infection	ratio(%)	infection	ratio(%)
2006	79	37	46.84	0	0.00	0	0.00	0	0.00	0	0.00	37	46.84
2007	89	48	53.93	0	0.00	0	0.00	0	0.00	0	0.00	48	53.93
2008	192	88	45.83	0	0.00	0	0.00	0	0.00	0	0.00	88	45.83
2009	109	59	54.13	0	0.00	0	0.00	0	0.00	0	0.00	59	54.13
2010	140	2	100.00	0	0.00	24	48.98	36	40.45	0	0.00	62	44.29
Total	609	234	49.68	0	0.00	24	48.98	36	40.45	0	0.00	294	48.28

Fig. 3 Statistical analysis

1) Information acquisition and examination. It includes basic information (family archives, personal file), medical information (regular physical examination, special physical examination) information, evaluation information， follow-up intervention information and medicine information acquisition.

2) Statistical analysis. According to region, age, gender, culture, occupation, type analysis new infections, HIV/AIDS route of transmission, mother to child transmission rate and fatality rate in spouse transmission rates, HIV infection status of family, etc., are allshown in figure 3 to 18, 3-19.

3) Data mining. Output data to SPSS system, export data to make use of Clementine 11.0 after using decision tree, neural network and so on, mining technology to analyze data, and achieved good results.

4) Health information management.

(1)Outpatient clinic information input. Patients to the rural clinic, the doctor record main symptom, diagnosis and medical information, and subscribe electronic prescriptions issued. The supervision department supervise the prescription usage; make more reasonable use of antiviral drugs.

(2)Drug inventory information query. Query pharmacy warehouses of drug usage, timely warning for the lacking medicines, reduce inventory, reduce the drug circulation time.

(3) Control effect evaluation. Patient management, the evaluation table staff management design control effects, from meetings to attend, report forms, patient management, financial management and evaluation of control effects.

5) Hospital medical information collection**.** Make the hospital information system of medical institutions, new farming data to achieve docking, data can be automaticallytransmitted to the database platform.

6) Information distribution. To open HIV/AIDS education scientific research sites,and release crowd AIDS prevention knowledge.

F. System implementation and application

The platform, with a good application prospect, has been successfully run in five regions of Henan probince, and hasestablished a

2, 365, 802 residents' health records (including 560000 HIV screening examination data), produced a good social and economic benefits.

Original county AIDS prevention and control of information collection work is mainly the superior department requirements, accomplished by the county center for disease control and the township medical institutions.The information acquisition of other systems are usually performed by the method of manual entry, prevention and control of information at the grass-roots level statistics is done by hand.Through the information platform which can realize permanent residents online data entry and realize information sharing with other information system , the information management will be available to healthy people, can save manpower by more than 20%.Through the platform can also realize the management of HIV/AIDS patients' health information, making AIDS free antiretroviral treatment and opportunistic infections and drug resistance to extend from the original manual operation to drug distribution and medical information operation, due to the grass-roots network software and hardware is perfect,can realize the management of AIDS grassroots medical information, dynamic supervision and management of the doctor medical behavior,without any increase in construction costs, Originally the HIV/AIDS patients in medical institutions after hospital subscribe the hospitalization cost information to the aiFangBan or jointly,easy to waste medical

resources, and make real-time control difficult[6,7].Through the system dynamically regulated hospital information, control the unreasonable expenses, make the medical expense unreasonable growth fell by 15%, according to ShangCaiXian outpatient hospital compensation in total 2012 21123497.44 yuan, 37980252.61 yuan in 2013, a total of 2 years to save cost 8865562.51 yuan, has obvious economic benefits.

Discuss

1. System innovation. Information of Residents' health records at home and abroad related to HIV/AIDS prevention and controlisrare, while HIV/AIDS patients is the main object of information acquisition of HIV/AIDS prevention and control system.Few information iscollected about the permanent residents in prevention, therefore could not get information about the crowd new HIV infections, unable to understand the development of AIDS natural history, cannot evaluate the crowd control effects.What's more, all kinds of network system are independent, which cannot make information shared, or increase the workload of grass-roots staff information recorded.

2. Platform uses general. Generation system design survey report and print report. System uses J2EE technology and MVC framework, the view layer fully implemented with static HTML pages, fast response speed, maximum limit reduce the burden of server and later maintenance costs. Users can according to the specified requirements designed questionnaire page format, and make connection with the background database .Model layer adopt the idea of generic programming, once written, the system modules can be called. System uses the WEB 2.0 client technology at the front desk, make the front desk display more human. System has a variety of information acquisition interface, by adopting the technology of data extraction, realize the sharing among residents' health records, new farming information platform, information platform , hospital information management system and the data of AIDS resources, realize import and export about correlate data and data mining and analysis to the system data.

3. The whole crowd management. Platform establish AIDS prevention and control of health records for all the residents, which can be used for HIV/AIDS and also for the non- patients. The platform can directly get new HIV infections, HIV/AIDS case fatality rate, the mother-to-child transmission rate, etc.

4. Information management platform. Combined with tertiary prevention strategy of AIDS, the platform can realize the information management of HIV drug purchase inventory for opportunistic infections, patients with HIV/AIDS clinic and hospital medical information management, and can control unreasonable medical expenses and also provide technical support for convenient medical environment of patients

References

[1] Chinese Communist Party Central Committee, State Council. Views on deepening medical and health system reform (2009), 3-17.
[2] State Council. "Twelve Five" during the deepening medical and health system planning cum embodiment (2012), 3-14.
[3] Health Department. Health management information platform construction Guide. The Guardian do comprehensive letter (2011) 350, 2011.4.
[4] Hu Xin-ping, Zhang Zhi-mei, Dong Jian-cheng. Medical Informatization Based on Cloud Computing Concepts and Techniques. Medical Informatics.2010,31(3):6-9.
[5] Yu Lei, Lu Yang, Zhu Xiao-ling, Feng Lin. Research advances on technology of Internet of things in medical domain. Applications Research of Computer, 2012, 29(1):1-6.
[6] Health Department. Views on the strengthening of health statistics and information technology personnel building. Health Office ZongFa (2012)43.2012-4-10.
[7] Yongyan Yang. Talent to become the driving force behind the development of foreign medical informatics. Chinese information industry (e-Healthcare).2011,(7):46-47.

Advanced Materials Research Vols. 989-994 (2014) pp 1103-1106
© (2014) Trans Tech Publications, Switzerland
doi:10.4028/www.scientific.net/AMR.989-994.1103

Mobile Nurse Information System with Efficient Physiological Monitoring for Patient

Wu Fei[1, a], Wang Hong[1, b]

[1]Department of Information, The 309th Hospital of PLA, Beijing, 100091, China

[a]email: wufei81@126.com, [b]email: wang_hong@yahoo.com

Keywords: Mobile Nurse Information System; Physiological Monitoring; SOA; iPad;

Abstract. Current traditional physiological monitoring is accomplished by individual cardiogram monitor device attached to each patient's bed. A nurse will have to frequently monitor the vital signs at patient's bedside, which is inefficient and time consuming. Although some hospitals have deployed the central monitoring system, it still has space limit to the nurses and high cost. Our research work is to develop a mobile nurse information system with efficient physiological monitoring for patient based on iPad. Patient's real-time physiological signals captured by the physiological monitoring system are integrated to the mobile nurse information system. Nurses could get just-in-time access to the data of the physiological monitoring system at anywhere through the clinical use of the mobile nurse information system. Trial version in our hospital showed that the system is feasible and efficient enough to apply in clinical settings.

Introduction

Continuous monitoring of the vital signs of patients is one of the major problems faced by the medicalcare nowadays. Monitoring should be accurate, precise and carried out in real time [1].Current physiological monitoring systems consist of single patient monitoring systems, where sensors are hardwired to a cardiogram monitor device next to bed [2]. In case of a large hospital where multiple patients need to be monitored simultaneously, a nurse will have to frequently monitor the patient's physiological parameters at each patient's bedside because human intervention is needed frequently. This is inefficient and time consuming. Although some hospitals use the central monitoring system, it still has space limit to the nurses and high cost.

As we have designed and implemented an iPad mobile nurse information system which supports real-time data communications for nurse during clinical works. It allows the nurse to enter and retrieve parts of the clinical information relevant for her tasks anytime and anywhere, which can improve efficiency and quality of medical care in the clinical setting[3]. So we continue our research to integrate patient's real-time physiological parameters delivered by the physiological monitoring system to the exsisting mobile nurse information system, which would allow the nurse to monitor many patients simultaneously at anywhere when needed. Meanwhile, an alert mechanism has been included for automatic emergency alerts after automatically recognizing emergency messages.

To provide more freedom to patients when monitoring their physiological signals, it is important to integrate wireless communication technology for modern healthcare monitor systems [4]–[10].But for the inpatient, it is more useful that nurse can monitor the their real-time physiological signals when needed without space limit. So this paper presents a mobile nurse information system with efficient physiological monitoring, emphasizing on patient's real-time physiological signals wireless transmission and graphical presentation to the nurse's mobile device. The proposed system makes use of wireless local area network (WLAN) and SOA Infrastructure together with web service technology to integrate the distributed and fragmented medical data across heterogeneous sources especially real-time physiological parameters delivered by the cardiogram monitor device. It is thus possible to integrate several cardiogram monitor devices to extract patients' various physiological parameters[such as blood pressure, pulse, saturation of haemoglobin (SpO2), and electrocardiogram (ECG)], and to monitor multiple physiological signals without space limit using wireless communication capability.

System Architecture

This innovative concept of "Mobile Nurse Information System with Efficient Physiological Monitoring for Patient" is primarily established on the integration of four major concepts. The mobile nurse information system, physiological monitoring system, medical data integration and the wireless communication set the foundation of the proposed system. Figure 1, provides the proposed architecture of the prototype, which is designed to improve efficiency and save life in a clinical setting scenario.

Mobile nurse information system, which is running on an IPad that can be carried by nurse during the clinical work, works in WLAN environment, can invoke the web services provided by the web service server to access the clinical information from hospital database servers which are the database of Hospital Information System (HIS), Lab Information System (LIS) and Electronic Medical Record (EMR). Furthermore, multiple physiological signals provided by the cardiogram monitor devices at bedside are collected by the Monitor center server, then uploaded to the physiological signals database if preservation is needed. These physiological signals are provided by the web service server to the end users, so a presentation of graphical physiological data can be displayed on the nurse's IPad when needed. As shown in Fig.1.

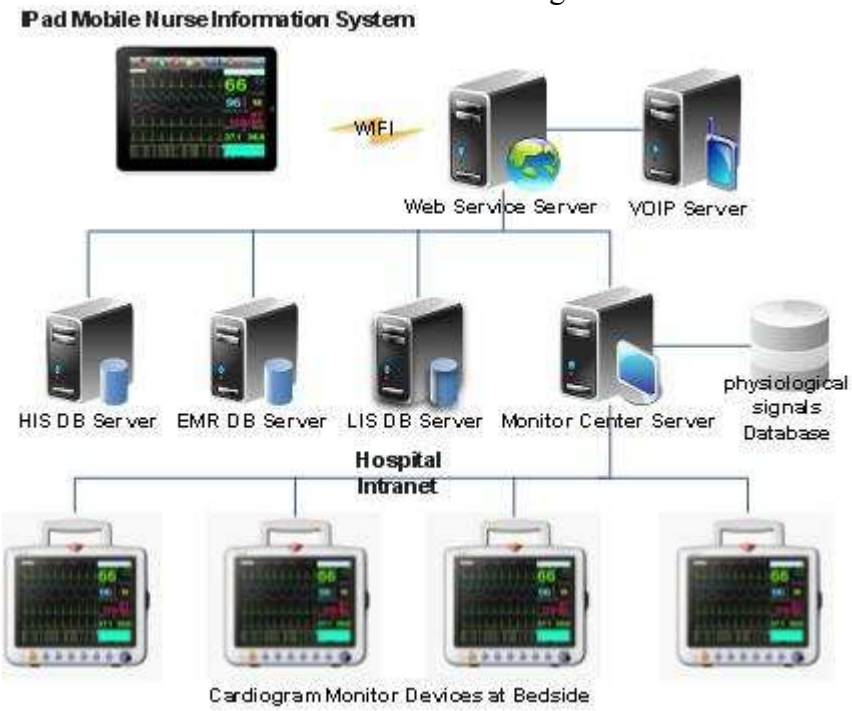

Fig.1. Overall system hardware architecture

System Software Designs

The software modules in mobile nurse information system is analyzed and designed with an service-oriented method, and represented by using unified modeling language (UML) [11]. The design phases are as follows: requirement analysis, object model design, code implementation for software model, simulator execution, and upload to real iPad for final test.

The system architecture deployment diagram of our proposed mobile nurse information system is as shown in Fig. 2. The whole system architecture mainly consists of nurse mobile device, Voice over Internet Protocol (VOIP) server,Monitor center server and Web Service Server. While for the Web Service Server and Monitor Center Server, Microsoft Visual Studio 2008 software is used to develop web services andf window application programs. And for mobile nurse information system, Xcode5 is used to develop ios application programs. Open Database Connectivity (ODBC) components are used to access oracle database, VoIP is integrated for communication between nurses and other medical staffs. The function and design of each software module is introduced as follows.

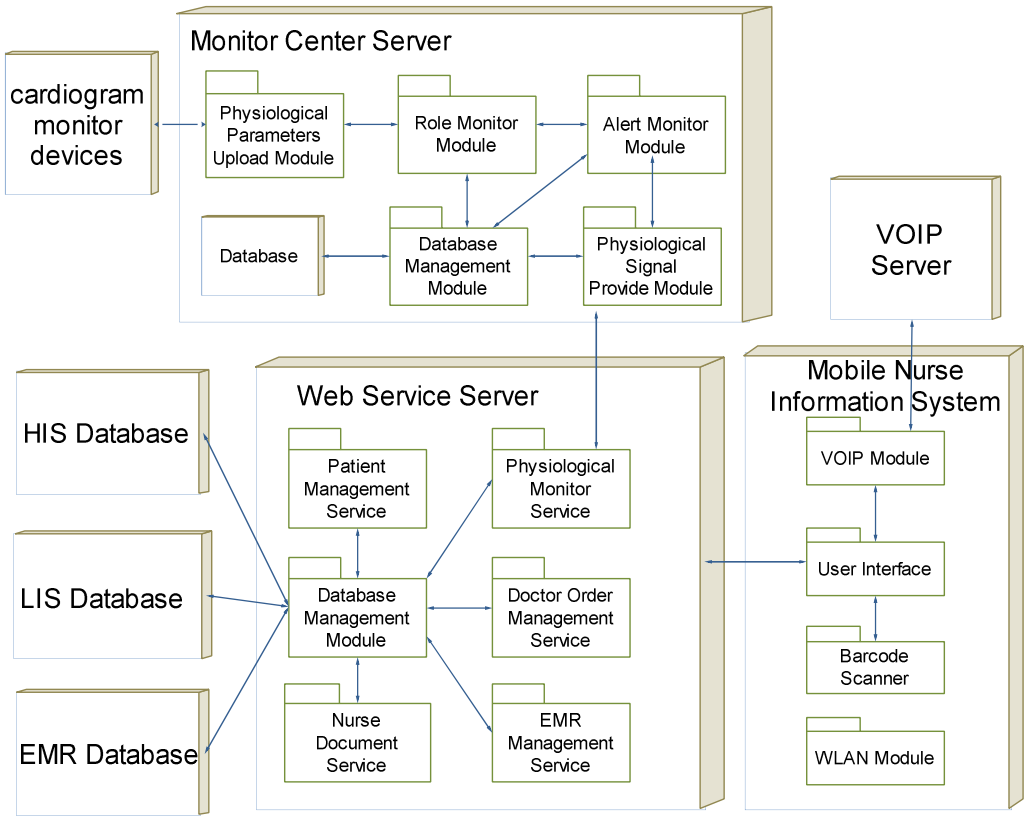

Fig.2. System architecture deployment diagram.

1) Mobile nurse information system

The mobile nurse information system is an ios application running on an iPad. Camera of the IPad is used for barcode scanner that can scan patient identification wristband to identify patients, this would improve the accurate of medical care which is directly related to the patient's health. This system allows the nurse to input and retrieve parts of the clinical information relevant for her tasks by invoking the web services deployed in the web service server. The function of mobile nurse information system is described as follows:

a) Identify patients by scan the wristband of patient. Manage patient such as admission, discharge and laboratory request.

b) Electric nursing record documentation module provides nurses with required fields for the input of important and necessary patient information.

c) Doctor order management module provides nurses with medical order check, execution time record and reminding.

d) Display real-time physiological parameters data in graphical form, when the patient's health condition becomes abnormal, the proposed system can automatically inform the nurse with alert.

2) Web service server

Web service server provides the web services to access the clinical information from hospital database servers. It supports real-time data communications between heterogeneous meidcal systems (EMR system,LIS system, physiological monitoring system etc.) and provides web-based data accesses by invoking the web services using mobile devices.

3) Monitor center server

The monitor center server provides following functions:alert mechanism setting, role and alert monitoring, physiological parameter uploading and provide physiological parameter to the web service server. Role monitoring and alert monitoring functions are the core of the monitor center server software[7]. We design four levels of priority urgency alert when cardiogram monitor device are sending the alert. These alert are classified as Normal, Urgent, Critical, Very critical[12][13]. An alert is send to the nurse's iPad by monitor center server when the patient's physiological parameter

becomes abnormal[14]. Meanwhile, the abnormal physiological information are upload to database for storage and analysis or transmit the information to physicians and nurse for further processing.

Conclusion

The described system is a prototype that is deployed in our hospital. By now, nurses in our hospital are using this system for clinical works, they can monitor many patients simultaneously at anywhere when needed. It is proved that the system can optimize the work flow of nurse, reduce medical errors, improve efficiency and quality of medical care, especially save life in a clinical setting. Most of nurses agreed that this system is more helpful and convenient than tradition clinical information systems.

References

[1] Wang P. “The real-time monitoring system for in-patient based on Zigbee”.Proceedings of the 2008 Second International Symposium on Intelligent Information Technology Application-Volume 01. IEEE Computer Society, 2008: 587-590.

[2] Belardinelli, A., Franchi, D., Bedini, R., Ripoli, A., & Palagi, G.. “Ward informative system: hospital application of telemedicine”. IEEE In Computers in Cardiology, pp. 413-416,1999.

[3] Wu, Fei, and Hong Wang. "Mobile Clinical Information System for Hospital Ward Rounds." Applied Mechanics and Materials 513 (2014): 2502-2505.

[4] U. Anliker, J. A. Ward, P. Lukowicz, G. Tr¨oster, F. Dolveck, M. Baer,F. Keita, E. B. Schenker, F. Catarsi, L. Coluccini, A. Belardinelli,D. Shklarski, M. Alon, E. Hirt, R. Schmid, and M. Vuskovic, “AMON:a wearable multiparameter medical monitoring and alert system,” IEEE Trans. Inf. Technol. Biomed., vol. 8, no. 4, pp. 415–427, Dec. 2004.

[5] M. F. A. Rasid and B. Woodward, “Bluetooth telemedicine processor for multichannel biomedical signal transmission via mobile cellular networks,”IEEE Trans. Inf. Technol. Biomed., vol. 9, no. 1, pp. 35–43, Mar.2005.

[6] E. Kafeza, D. K.W. Chiu, S. C. Cheung, andM. Kafeza, “Alerts in mobile healthcare applications: requirements and pilot study,” IEEE Trans. Inf.Technol. Biomed., vol. 8, no. 2, pp. 173–181, Jun. 2004.

[7] Y.-H. Lin, I.-C. Jan, P. C.-I. Ko, Y.-Y. Chen, J.-M.Wong, and G.-J. Jan, “A wireless PDA-based physiological monitoring system for patient transport,” IEEE Trans. Inf. Technol. Biomed., vol. 8, no. 4, pp. 439–447, Dec.2004.

[8] R.-G. Lee, C.-C. Hsiao, K.-C. Chen, and M.-H. Liu, “An intelligent diabetes mobile care system with alert mechanism,” Biomed. Eng. Appl.,Basis Commun., vol. 17, no. 4, pp. 186–192, Aug. 2005.

[9] R.-G. Lee, C.-C. Lai, S.-S. Chiang, H.-S. Liu, C.-C.Chen, and G.-Y. Hsieh,“Design and implementation of a mobile-care system over wireless sensor network for home healthcare applications,” in Proc. 28th Annu. Int. Conf.IEEE-EMBS, New York, Aug. 30–Sep. 3, 2006, pp. 6004–6007.

[10] R.-G. Lee, C.-C.Hsiao,C.-C. Chen, and M.-H. Liu, “Amobile-care system integrated with Bluetooth blood pressure and pulse monitor, and cellular phone,” IEICE Trans. Inform. Syst., vol. E89-D, no. 5, pp. 1702–1711, May 2006.

[11] Unified Modeling Language (UML) Specification 1.5, Object Management Group. (2003, Mar.), [Online]. Available: http://www.omg.org/cgibin/doc?formal/03-03-01

[12]Lee, R. G., Chen, Y. C., Hsiao, C. C., & Tseng, C. L. (2007). A mobile care system with alert mechanism. Information Technology in Biomedicine, IEEE Transactions on, 11(5), 507-517.

[13] Lee, Ren-Guey, et al. "An intelligent diabetes mobile care system with alert mechanism." Biomedical Engineering: Applications, Basis and Communications 17.04 (2005): 186-192.

[14] R.-G. Lee, I.-C. Chou, C.-C. Lai, M.-H. Liu, and M.-J. Chiu, “A novel QRS detection algorithm applied to the analysis for heart rate variability of patients with sleep apnea,” Biomed. Eng. Appl., Basis Commun., vol. 17,no. 5, pp. 258–262, Oct. 2005.

Advanced Materials Research Vols. 989-994 (2014) pp 1107-1110
© (2014) Trans Tech Publications, Switzerland
doi:10.4028/www.scientific.net/AMR.989-994.1107

College Female Students' Physical Health Evaluation Index Correlation Research Based on the PDCA Cycle Model

SHOU Jie

Changshu Polytechnic University, Changshu, 215500

shoujie112@sohu.com

Keywords: College female students, Physical health evaluation, PDCA cycle model

Abstract. With internet and computer abundantly available, most of college female students become "indoor woman", immerse into network environment and ignore outdoor activities as well as physical exercise. The above phenomenon is the main factors that cause college female student's physique drop. College female student self good health is education department main control aspect .In order to get clear understanding of college female students group physical conditions, college would carry out physical health test to students every year. Based on learning some related quality management theory and the PDCA management model, this paper makes use of the principle component analysis to conduct discussion on China's college female students' physique health test management mechanism design so as to further perfect current procedure of China's college female students' physique health test work, improve the quality of management work, improve the college female students' physique and truly reach the target for the college female students' overall development.

1. Introduction

From recently years' college students' physical health data, it can be known that their physique is in the drop tendency. Chinese college physical investigation indicates that national physique monitoring result in 2010 has been reduced around 10% in lung capacity by comparing with that in 1985, college female student 800meters running and male students 1000 meters running have been respectively reduced 10.3% and 10.9% as well as other aspects indicator have remarkable droppings. This paper makes research on college students' physical health test data in one college feedback to education department in order to explore college students' physical conditions through analysis process.

For the research on college students physical health data, many people has made efforts, it provides directional reference for college students' physical improvement through research result. Among them, Ye Chao-Zhong Based on college students' physical health situation testing and evaluation, make research on their sports fitness habits, consciousness and other relative problems, with an aim to explore the root cause of students' physical health drop [1]; Tang Qing-Hu Gathering health management relative theory and method, explore college students' physical health follow-up service management mode so as to change current situation of only testing not interference [2]; Li Yang etc. Analyze recent 3 years 1895 national minority college students' physical health factors from silence university in Gansu province, get relationships among factors, main influence factors and each nationality college physical situations [3-5].

2. PDCA Cycle Model of the College Students' Physique Health Test

2.1 Closed-loop Management Theory

The closed-loop management is a management method based on the comprehensive closed-loop system, closed-ended management, management control and information system and other principles. The closed-loop management mechanism is a kind of management system based on the closed-loop management principle. It regards the management process as a closed-loop system, and takes each link, work management as the closed-ended sub-system, and make the management inside the system and sub-system constitute a continuous close loop, and make the system movement maintain in a

balance point; On the other way, faced with constant changing of the subjective environment, the system can conduct flexible, rapid, and right information feedback and conduct corresponding reformation according to the reflected information, and make the contradiction and question be solved in time, at the same time, it can constantly achieve its own improvement by applying the repeat cycle of "decision-making, control, feedback, decision-re-making, re-control, conduct feedback again…".

2.2 PDCA Deming Cycle Theory

The PDCA cycle (see Fig.1) is also called as Deming Cycle, which is the acronym of the English words of Plan, Do, Check and Act. Firstly, it was proposed by the American quality management expert PHD Deming. Currently, it is universally acknowledged as the scientific procedure that shall be observed by the overall quality management. The whole process of the overall quality management is the process of the quality plan making and the organization achievement. And this process ceaseless operates according to the PDCA cycle. To summarize, it is namely to develop in rolling.

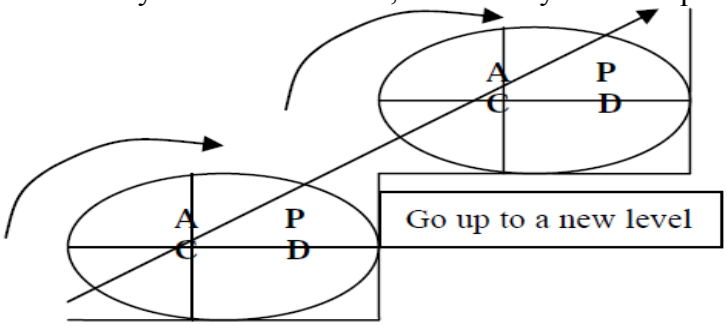

Fig.1 PDCA cycle

2.3 Principle Component Analysis

The principle component analysis is a kind of statistic analysis that transforms many variables to a few principle components by applying the data dimensionality reduction technology. In the standard, it selects the height (1 X), weight (2 X), vital-capacity (3 X), stamina (4 X), strength (5 X) and speed (6 X) the six variables. It makes use of the linear combination method, and transforms many indexes into some typical comprehensive indexes based on losing fewer data information. In these comprehensive indexes, they are independent to each other and the information doesn't overlap. Through the principle component, it can not only decline the dimensions, but also can keep most of the original data information.

1.The Basic principle of the principle component analysis

Presume that there are n geography samples, and in every sample, there are P variables which constitutes a $n \mathrm{r}\ p$ -order of geography data matrix

$$X = \begin{bmatrix} X_{11} & X_{12} & \cdots & X_{1P} \\ X_{21} & X_{22} & \cdots & X_{2P} \\ \vdots & \vdots & \vdots & \vdots \\ X_{n1} & X_{n2} & \cdots & X_{np} \end{bmatrix} \tag{1}$$

When the P is larger, it will be troublesome to inspect in the p dimension space. In order to overcome this difficulty, it need conducting dimension reduction process, namely makes use of fewer comprehensive indexes to substitute the original more variable indexes. And it will make these fewer comprehensive indexes reflect more information reflected by the original more variable indexes. At the same time, they are mutually independent to each other.

2. Calculation Steps

(1)Calculate the related coefficient matrix

$$R = \begin{bmatrix} r_{11} & r_{12} & \cdots & r_{1P} \\ r_{21} & r_{22} & \cdots & r_{2P} \\ \vdots & \vdots & \vdots & \vdots \\ r_{p1} & r_{p2} & \cdots & r_{pp} \end{bmatrix} \tag{2}$$

$r_{ij}\left(i,j=1,2,\cdots,p\right)$ is the related coefficient of the original variable X_i and X_j, $r_{ij}=r_{ji}$ its calculation formulation is:

$$r_{ij}=\sum_{k=1}^{n}\left(X_{ki}-\bar{X}_i\right)\Big/\sqrt{\sum_{k=1}^{n}\left(X_{ki}-\bar{X}_i\right)^2\sum_{k=1}^{n}\left(X_{kj}-\bar{X}_j\right)^2} \tag{3}$$

(2)Calculate eigenvalue and eigenvector

Solve the characteristic equation, it often applies the Jacobi to work out the eigenvalue, and conduct sorting by their value

$$\lambda_1\geq\lambda_2\geq\cdots,\geq\lambda_p\geq 0 \tag{4}$$

work out the corresponding eigenvector $e_i\left(i=1,2,\cdots,p\right)$ of the eigenvalue l_i respectively, require $\|e_i\|=1$, namely $\overset{p}{\underset{j=1}{\text{e}}}e_{ij}^2=1$.

Calculate the principle component contribution rate and the accumulative contribution rate.

Contribution rate:

$$l_i\Big/\overset{p}{\underset{k=1}{\text{e}}}l_k\left(i=1,2,\cdots,p\right) \tag{5}$$

Accumulative contribution rate:

$$\sum_{k=1}^{i}\lambda_k\Big/\sum_{k=1}^{p}\lambda_k\left(i=1,2,\cdots,p\right) \tag{6}$$

Calculate the loading of the principle component:

$$I_{ij}=p\left(z_i,x_j\right)=\sqrt{l_i}e_{ij}\left(i,j=1,2,\cdots,p\right) \tag{7}$$

Scores of each principle component:

$$Z=\begin{bmatrix}z_{11} & z_{12} & \cdots & z_{1m}\\ z_{21} & z_{22} & \cdots & z_{2m}\\ \vdots & \vdots & \vdots & \vdots\\ z_{n1} & z_{n2} & \cdots & z_{nm}\end{bmatrix} \tag{8}$$

3.Empirical analysis

Physique health conditions empirical analysis based on weight test data Sampling 10357(boys 5552;girls 4805) students' physical health test data standardization conditions is as Table 1 shows.

Table 1: Partial sample data standardization result table

Sample No.	Height ratio	Weight ratio	Lung ratio	Sprint	Long jump ratio	Grip and body forward flexion	800m	Situp
1	1.00000	1.00000	1.00000	1.00000	1.00000	1.00000	1.00000	1.00000
2	1.08791	1.08682	1.08900	1.09009	1.07595	1.08900	0.98108	1.09118
3	0.99972	0.99872	1.00072	1.00172	0.98873	1.00072	0.90155	1.00272
4	1.04567	1.04462	1.04672	1.04776	1.03418	1.04671	0.94299	1.04881
5	1.02357	1.02255	1.02459	1.02562	1.01232	1.02459	0.92306	1.02664
…	…	…	…	…	…	…	…	…
4801	1.03421	1.03318	1.03524	1.03628	1.02284	1.03524	0.93265	1.03731
4802	1.09001	1.08892	1.09110	1.09219	1.07803	1.09110	0.98297	1.09328
4803	0.92314	0.92222	0.92406	0.92499	0.91299	0.92406	0.83249	0.92591
4804	0.92798	0.92705	0.92891	0.92984	0.91778	0.92891	0.83685	0.93077
4805	1.05423	1.05318	1.05528	1.05634	1.04264	1.05528	0.95070	1.05739
Sample 1 is reference vector								

From Table 1 data, it can be known that $D^*_{min}=0$, $D^*_{max}=1.0241$, use statistics software can get normal P-P figure and K-S single sample test result as Figure 1 shows.

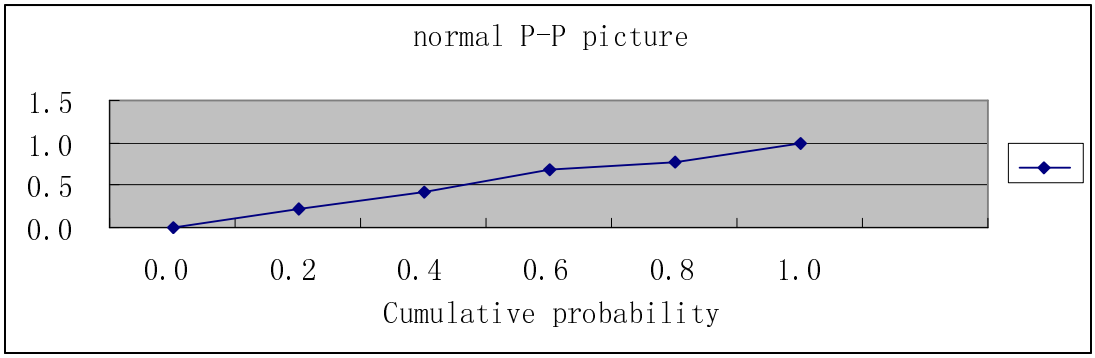

Figure 1: Female students physical health test comprehensive evaluation correlation degree result

From Figure 1, it can be known that students' comprehensive test correlation degree is approximately a straight line, and the straight line basic coincides with diagonal line, bilateral test result is $p=0.058>0.05$, it can judge that female students' comprehensive test correlation degree conforms to normal distribution.

Summary

This paper carried out research on college female students physical health feedback data to education department, focused analysis on weight and physical health other indicators correlation degree conditions and test value deviation judgments, studied different sources student physical health data differences. This research provided theoretical basis for physical health test data analysis so as to make contribution for improving college female students' physique.

Acknowledgements

This work was financially supported by the Teaching Reform Project of Changshu Polytechnic University "Discussion on the reform of College Students' physical research and teaching content of our university".

References

[1] YE Chao-zhong. Zhejiang Sport Science, 35(1), 77-79(2013)

[2] Du Xiao-an,Zhu Bin. Journal of Chengdu Physical Education Institute, 36(8),(2010)

[3] LI Yang,LIU Wan-wu,Yang Li-ran. Sichuan Sports Science, (1), 38-42,(2013)

[4] Cheng Long,Huang Sen,Zeng Li-ping. Journal of Guangzhou Physical Education Institute, 29(1),(2009)

[5] YIN Mai-man,Zhang Fan-rong,YU Zhu-xian. Journal of Shenyang Sport University, 2006, 25(3), 76-77,(2006)

Advanced Materials Research Vols. 989-994 (2014) pp 1111-1114
© (2014) Trans Tech Publications, Switzerland
doi:10.4028/www.scientific.net/AMR.989-994.1111

The risk factors for pediatric care and preventive measures

Libing Liu

Xijing University, Henan, China
E-Mail:zshazhu@163.com

Keyword: Pediatric care; Risk factors; Preventive measures

Abstract: In pediatric care, self-awareness of care object whose cooperation degree of care is not high is weak, exacerbated by the drugs used, testing equipment and technical level of nurses, professional ethics and many other factors, the risk factors for pediatric care throughout the children are always admitted. Thus, it is necessary to strengthen understanding of the risk factors for pediatric care and take effective preventive measures. This article analyzes the major risk factors focused on pediatric care and presents preventive measures accordance with different types of risk factors, in order to control and eliminate the risk factors and avoid the risk of incidents, ensure the safety of children, and provide reference for maintenance hospitals and medical staff image.

1 Introduction

With the intensified health system reform, public expectations for medical care services are increasing. However, due to the complexity of the risk and high-risk, uncertainties and other factors in the healthcare industry, nursing is frequently exposed to risk factors, which is widespreadly concerned in society. Whether or not nursing practices, proper treatment, medical devices using properly, will directly affect the emergence and expansion of risk factors. Thus, nurses in pediatric care must strengthen the understanding and analysis of risk factors, and through effective preventive measures, ensure that children can get accurate and timely treatment and care, reduce and avoid the risk of events fundamentally.

2 Major risk factors in the pediatric care

In pediatric care, due to small age, weak cognitive ability, poor cooperation, the children and their families should communicate with nurses, which have an important impact on good nurse care and harmonious relationship with nurses. In practice , because of the children themselves impact, the quality of nursing staff levels, parents' expectations and drugs, equipment and other factors, risk factors for pediatric care are more complex. By randomly investigating Children's Hospital nurses and parents, the risk factors of child care are shown as Figure1.

Small age	64%
Difficult to cooperation	46%
Weak cognitive ability	47%

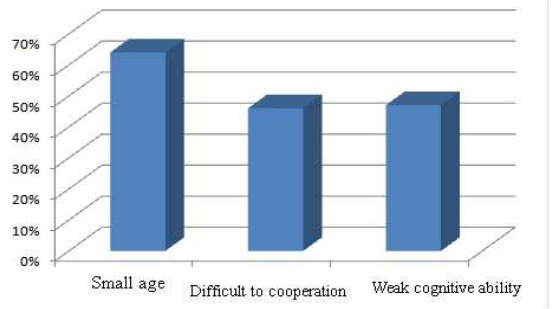

Figure 1 The risk factors of child care

2.1 Self-awareness and coordination of care objects

In pediatric care, for nursing younger objects, their awareness of the disease and ability to properly express are weak, and there is a deviation between the actual description of the disease and their own feelings, which results in not promptly informing their parents and caregivers when the occurrence of certain children adverse reactions, which can delay the optimal duration of treatment and have bad impact on the therapeutic effects.

Meanwhile, the low age of nursing objects, mostly good move, have different degrees of fear, resistance and contradiction for transfusion, injections and medication, and are often not cooperative with nursing care, which is not only to increase the difficulty of the work of nurses and difficult to guarantee nursing results, but also bring back the risk factors.

2.2 Nurses skill level and professional ethics

Pediatric care is difficult, arduous tasks, facing the objects who have a natural resistance and psychological conflict for normal care in a good moving age. In order to successfully complete the task of nursing, nurses not only need to have a strong technical level , but also have a high degree of professional morality , good work to appease children, and ensure that children can calm emotions with nursing care.

2.3 Expectations of parents

Now the children are mostly the only children, and have the meticulous care and spoiled love by parents and elders. Once a child's body appears some discomfort, parents are often anxious and manifest the anxious mood in the course of medical treatment, and have extremely high expectations of the hospital and health care of staff.

In practical nursing work, now generally higher quality of life for children, excess nutrients phenomenon is more obvious, which makes it difficult to identify some of the blood vessels in children. Although it is sometimes objective affecting factors of children intravenous, but some parents have the dissatisfaction for nurse care, and place anxiety and resentment upon nurses, causing nurse-patient relationship tensions.

2.4 The detection of drugs and medical equipment

In nursing accident, accidents caused by defective drugs and medical equipment to detect faults occupy a higher proportion. Especially in pediatric care, due to children's little age, weak expression for condition of physical discomfort, when because of drug and medical monitoring equipment, etc, causing the body discomfort, the children is often difficult to express it, leading to a significant risk. The reason is that some of the hospital's nursing staff have not well done" three investigations and the seven detection" institution for the detection of drugs and medical devices, neglect cryogenic storage of drugs, avoid direct sunlight and other requirements, have inadequate understanding of especially those likely to bring children the risk of drug whose use is not strict, did not fully comply with the requirements of the attending physician and the medication prescribed. At the same time, it is existent that deficiencies for the periodic inspection and maintenance of medical monitoring equipment, some equipment of aging components are still in use, which is extremely large risk for the pediatric care.

In summary, in pediatric care, the cooperation degree of children, nursing skill level and professional ethics, understanding and support of parents, drug safety regulations and medical testing equipment are important factors affecting the safety of pediatric care, once these factors have the problems which will bring unpredictable danger to pediatric care.

3 Pediatric nursing hazard precautions

Pediatric nursing is a very stringent work which requires technical level, comprehensive occupation quality, particularity starting from the actual situation of children make care object feel a

pediatric care, grasps its physical condition and psychological changes, in a strict system and under standard operating minimizes the risk factors, and effectively protects the safety of children, to promote the harmonious sound for nurse-patient relationship.

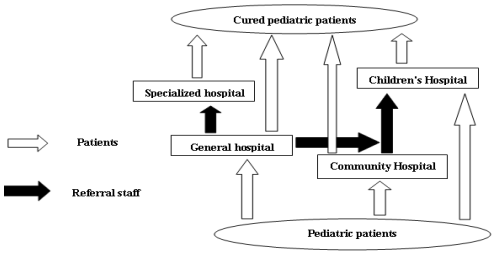

Figure 2 Child care treatment process

The main aspects of child care should be noted by investigating:

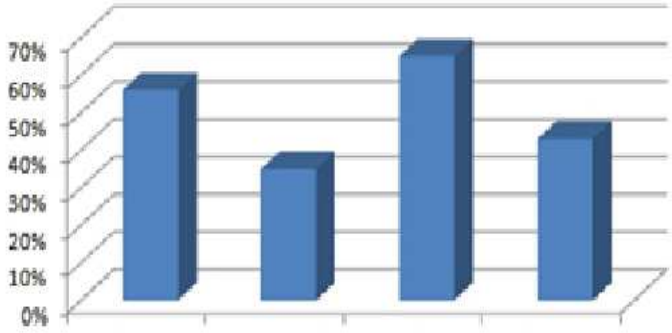

Figure 3 Measures to strengthen child care

3.1 Strict implementation of the care system, compliance with the operating norms

Nurses should strictly carry out the relevant systems in their daily work as specified operational guidelines, continue to strengthen awareness of the importance of pediatric care, within a strict framework of the system to standardize operation and reduce the chance of mistakes care to ensure that normal treatment of children. In this regard, it should strengthen the hospital pediatric care supervision and management, when they are contrary to the work of the system, and the lack of a sense of responsibility resulted in a threat to the normal treatment of children, nurses should be punished according to the relevant provisions, to ensure the system while increasing the majesty of pediatric care in nurses work seriously.

3.2 Strengthen the quality of training for nursing services

In pediatric care, nursing expertise and personal ethics to avoid risk factors, resolve conflicts and disputes between nurses and patients have an important impact. Thus, we must improve nursing care skill levels and professional ethics to guard against the risk.

On the one hand, strengthening the pediatric nurses professional training, organizational learning of common related knowledge of pediatric diseases enable them to master the common diseases and even a special focus on diseases features of children, which will be flexibly applied to nursing practice; On the other hand, strengthening the various pediatric nursing care skills training operations, such as scalp vein puncture, so that they can skillfully and accurately carry out nursing. Meanwhile, it is necessary to strengthen ethics education for nurses, cultivate their good work attitude and high moral character, promote their well-treated in the pediatric care of children, and they should try to meet the legitimate needs of the parents and maintain a good nurse-patient relationship.

3.3 Strengthen nurse-patient communication, expand positive reports

Parents of children in terms of their child's condition are extremely for anxiety and anxiety which is easy to be passed on nurses, resulting that the normal care is affected. To solve this problem, nurses should strengthen communication with children, patiently guide them to make the right description of the disease, and strengthen communication with parents, inform parents the disease promptly and related care conditions of children, patiently answer the doubts of parents and achieve peace communication with parents.

At the same time, media-related medical disputes, disputes between nurses and patients are reported more frequently, which brings a series of negative effects to the image of the majority of medical workers. For this, the medical staffs at the same time try to avoid mistakes, which maybe make the media proper guidance, expand health care coverage in the front, so that the community understands high-risk and high stress of the health care at work, giving them more encouragement and understanding.

3.4 Strengthen drug management, standardize equipment use

Sound management system is at source to control the risk, especially a high priority in pediatric care medication management. In terms of drug use, nurses must strictly follow the doctor's prescription, to avoid trespassing for ideas. At the same time, nurses need to standardize equipment use to strengthen knowledge and understanding of the instruments, not only to learn how to use the instrument, but also understand the appropriate principles to avoid the blind operation of the instrument and the harm to the children.

In summary, the importance of pediatric care decides that nurses must follow the relevant systems and regulations, compliance with the operating norms, and continuously improve the overall quality of care, using the rigorous attitude and the scientific way to improve the quality of nursing care and ensure the safety of children.

4 Conclusion

In pediatric care, dangerous accidents are from many factors, both subjective and objective. In order to effectively protect the safety of children, nurses must correctly recognize potentially a variety of dangerous factors, through feasible precautions to minimize the risk of occurrence, thus ensure the quality of care at the same time to get the trust of parents and the community, and establish good image of nurses, maintain a harmonious relationship between nurses and patients.

References

[1] Yangyun. Nurse-patient communication in pediatric nursing[J]. Nursing practice and research, 2011, 22(3): 18-21.

[2] Su Xiaomei. The risks and preventive measures in pediatric care[J]. China health care nutrition, 2012, 4(11): 23-27

[3] Wang Xueli, Sunping, Huang Xiangzhu, Chenyan, Cai Aiai. Nursing care risk and management strategies[J]. Journal of Yangtze University(Natural Science Edition), 2011, 9(8): 121-124

[4] Li Hongwei, Wei Qishan, Xu Sujuan. Pediatric nursing disputes and preventive measures[J]. Gansu Science and Technology, 2010, 13(10): 221-226

[5] Zhouli. Outpatient infusion in children with risk factors and related nursing strategy[J]. Chinese Journal of Clinical Rational Drug Use, 2012, 32(9): 76-79

Advanced Materials Research Vols. 989-994 (2014) pp 1115-1119
© (2014) Trans Tech Publications, Switzerland
doi:10.4028/www.scientific.net/AMR.989-994.1115

Design and Evaluation of the Primers for Rift Valley Fever（RVF）Virus RT- PCR Detection

Yang Zexiao[1,a], Wang Bo[1], Xu Qiumei[2], Yao Xueping[1], Zhu Ling[1], Xu Zhiwen[1], Wang Kaiyu[1], Li Guili[1], Peng Shanzhen[1], Wang Yin[1,b]

[1]College of Veterinary Medicine, Sichuan Agricultural University, Yaan Sichuan 625014, China;
[2]College of Basic Sciences, Sichuan Agricultural University, Yaan Sichuan 625014, China;

[a] email:yzxyang2003@126.com, [b] email:704029604 @qq.com

Keywords: Rift Valley Fever Virus, RT-PCR, overlap extension PCR, detection

Abstract. Rift Valley Fever (RVF) is a notifiable multiple species diseases in the OIE list, and causes human and agricultural losses in endemic regions. To develop the rapid method for detecting of RVF, 2 specific primers for reverse transcriptase polymerase chain reaction (RT-PCR) and 7 overlapping oligo primers were designed according to the nucleotide sequence information of RVFV published in GenBank, and a DNA fragment about 318 bp of the segment S was synthesized in vitro by overlap extension PCR to construct the recombinant plasmid pMD19-T-RVFVS. Then, the 2 specific primers were evaluated via a serial of tests, including reaction temperature optimization test, sensitivity and specificity tests. The results showed that the 2 designed primers are suitable for RVFV RT-PCR detection which is a rapid method with good specificity and sensitivity, the detection limit was approximately 85 copies of the cloned viral genomic fragments (pMD19-T- RVFVS) as well as resulted in no cross-reaction for peste des petits ruminants virus(PPRV), Epidemic encephalitis B virus, *E.coli* , *Salmonella* and *Pasteurella multocida* etc common pathogens isolated from ruminants detection.

Introduction

Rift Valley Fever (RVF) is a globally-relevant, acute disease in domestic and wild ruminants and humans in Africa and the Middle East which causes human morbidity and mortality as well as economic damage to the livestock industry in endemic regions caused by the Rift Valley Fever Virus(RVFV)[1]. Infection of RVFV is characterized by resorption or abortions of the fetus in pregnant domestic ruminants, a approaching 100% mortality ratio in newborn lambs, and human infections may result in chills, headache, limb pains and so on influenza-like symptoms, and severe retinitis, encephalitis, hemorrhagic fever and even death although most patients are benign [2,3,4,5]. Rift valley fever virus, a mosquito-borne Bunyavirus, is an enveloped RNA segmented virus with a tri-segmented single-stranded RNA genome of negative or ambisense polarity (S, M and L) belonging to the genus Phlebovirus of family Bunyaviridae[6]. Cattle, goats and sheep etc. domesticated ruminants and wild ruminant species, especially sheep, are the most susceptible to RVFV. Mosquitoes bites, contact with sick animals bodily fluids, consumption of contaminated animal carcasses, and Aerosol exposure all play a major role in the transmission cycle of RVFV [5,7]. In addition, there are currently no high-performance therapeutics or approved vaccines for preventing or treating RVFV infection for humans or ruminants. RVFV is thus considered a potential bioterrorism threat and adopted in OIE-listed notifiable diseases. Since RVFV was first recorded at a farm in the Rift Valley of Kenya in 1930, it has caused recurrent outbreaks among humans and animals in the African continent and led to millions of dollars of losses in the affected areas[1]. RVFV has been isolated from over 30 mosquito species of which several have a global distribution [5], according to the widespread range of the insect vectors, RVFV maybe have the potential to spread to Europe and the Americas [1,8], thus the potential introduction of RVFV into non-endemic countries has become the agricultural and public health concerns in the world. Rapid and reliable diagnostic tools for RVFV detecting are very important in veterinary and public health, and the RT-PCR assay has been showed useful for many pathogens detection. Because there are no RVFV in China and few studies about RVF, in this paper we designed 2 specific primers for RVFV

RT-PCR and evaluated its reliability after a 318 bp DNA fragment of the segment S was synthesized in vitro by overlapping PCR.

Materials and Methods

Reagents and Samples.

DNA Maker DL2000, pMD19-T Vector kitand dNTPs were provided by the TaKaRa Biotechnology(Dalian) Co.,Ltd.DH5α competent cells,2×Taq PCR MasterMix(KT201), Pfu DNA polymerase, TIANprep Mini Plasmid Kit（DP103）, and TIANgel Midi Purification Kit（DP209) were provided by the TIANgen Biotech(Beijing) Co., Ltd, Peste des petits ruminants virus(PPRV) vaccine, Epidemic encephalitis B accine, *E.coli* , *Salmonella* and *Pasteurella multocida* isolated from ruminants were provided by Sichuan Agricultural University animal quarantine lab.

Primer Preparation.

2 specific primers and 7 overlapping oligo primers (listed in table 1) were carefully designed using DNAStar according to the sequence data of the RVFV segment S published in GenBank (accession no:HE687307). All of these primers were prepared by the TaKaRa Biotechnology (Dalian) Co., Ltd.

Table 1. Primers used for RVFV RT-PCR detection

Primer name	Sequence (5′–3′)	Products size(bp)
P1	ATGCACCATCGTCCTAGTCAC	318
P2	GCAGCTCCTCATTGCTAGAGT	
F1	CACCATCGTCCTAGTCACGAGGTTCGCTTGCGATTTTCTGATTTCTACAATGTCGGAGA	
F2	TTGCATCAAACGTTGCACCTCCACCAGCAAAGCCTTTCCAGAGACTTATTGATCTAATA	
F3	GTTCCCCAATCTAAAAGAAGCCATATCCTGGCCTCTTGGAGAACCCTCACTAGCTTTCT	
F4	AATGATGACATTAGAAGGGATCAGATTGCTACTCTAGCAATGAGGAGCT	
R1	CAACGTTTGATGCAAAGTCTCCAAGTCCGACTCGGTATGGGAATTCTCCGACATTGTAG	
R2	TTTAGATTGGGGAACCTTGTGAAATCACTAAGAGTCATATGGCCTATTAGATCAATAAG	
R3	TCTAATGTCATCATTCCTGTGCACTCTAGTAGAGCTTAGGTCAAAGAAAGCTAGTGAGG	

Synthesis of target segment S fragment

The conserved segment S sequence fragment of RVFV was synthesized *in vitro* using an overlap extension PCR method as described in reported literature [9].

Overlap extension reaction

For the primary extension procedure, a 25 μL reaction volume containing 2.5μL 10×Pfu DNA polymerase buffer,6 μL of dNTPs (2.5 mmol/L), 1μL (10μmol/L) of each of the overlapping oligo primers (F1/R1, F2/R2, F3/R3, or F4/R3),1μL of Pfu DNA polymerase, and 13.5 μL ddH_2O was used. The reaction conditions were 94℃ for 30s and 72℃ for 15min. Then, the secondary extension reactions were carried out until the full-length target DNA fragment production had been synthesized in the 50 μL volume reaction including 1μL 10×Pfu DNA polymerase buffer, 8 μL of dNTPs (2.5mmol/L), 1μL of Pfu DNA polymerase, and 20 μL of each of the two overlap previous extension reaction products. The reaction conditions were kept the same as the above-mentioned primary extension procedure.

Amplification and identification of target fragments

The full-length target DNA fragments were amplified by PCR using the primers P1 and P2 in a 50 μL reaction volume containing 25μL of 2×Taq PCR MasterMix, 1μL (10μmol/L) of each of the primers (P1/P2), 5μL of the products of last secondary extension reaction. The PCR was conducted as follows: denaturing at 95 ℃ for 5 min; followed by 35 cycles at 94 ℃ for 40 s, 57 ℃ for 30 s, and 72 ℃ for 30 s; and then terminated by an elongation at 72 ℃ for 8 min. 5μL of PCR products were analyzed in a 1.0% agarose in TAE Buffer gel containing 0.5 mg/mL GreenView through electrophoresis, which was then photographed under a UV imaging system (Bio-Rad).

The PCR products were subsequently separated and purified according to the TIANgel Midi Purification Kit（DP209）instructions and were then directly cloned into the pMD19-T Vector

followed by a transformation into the DH5α competent cells. Then, the recombinant plasmids constructed were extracted using a TIANprep Mini Plasmid Kit and were subsequently identified by PCRs (using P1/P2 and RV-M/M13-47 as primers, respectively) and by sequencing analysis [10].

Optimization of reaction temperature

The optimum reaction conditions for specific primers P1 and P2 was determined by a PCR assay which used the recombinant plasmids contained the overlap extension PCR products as the templates. The reaction volume and conditions are same as the PCR above but different from a gradient of annealing degree from 56℃ to 62 ℃ for 30 s. In all, 5μL of PCR products were analyzed.

Specificity and Sensitivity tests

The specificity of RVFV RT-PCR with the 2 specific primers was assessed through comparing the recombinant plasmids contained the target RVFV fragment to the Peste des petits ruminants virus(PPRV) vaccine, Epidemic encephalitis B Vaccine, *E.coli* , *Salmonella* and *Pasteurella multocida* isolated from ruminants and to a blood sample of sheep. RNA and DNA (cDNA) templates were prepared using a commonly reported method from literature [10].To assess the sensitivity, the recombinant plasmids constructed above were estimated by a ND-1000 ultraviolet spectrophotometer (Nano Drop Co.,Ltd,USA) and were then amplified in a 10-fold serial dilution[9] by RT-PCR using the optimum reaction system and conditions as determined above.

Results

Synthesis of the target RVFV Fragment

To evaluate the characteristics of 2 designed specific primers for RVFV RT-PCR detection, a 318 bp-length conserved target DNA fragment of RVFV segment S was synthesized *in vitro* by an overlapping PCR (see Fig. 1 lane1), and the target fragment was cloned into a pMD19-T vector to construct the recombinant plasmid as described above, Then, the recombinant plasmid was identified by two types of PCR methods and sequencing analysis (see Fig.1 lane2,3,4). The PCR products of the recombinant plasmid from the pMD19-T vector usual primers were about 456 bp, which were 138 bp longer than the PCR products from the special primers (P1/P2). And the Blast analysis of the sequencing result of the recombinant plasmid of RVFV (see Fig.2) revealed that it had a 100% homology with the reference sequences (HE687307) that are published in GenBank. This is highly indicative that the target RVFV DNA fragment was successfully synthesized and its recombinant plasmid was constructed, and then named the plasmid as pMD19-T-RVFVS.

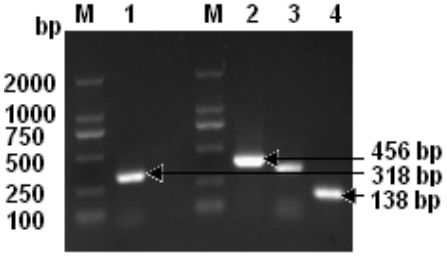

Fig.1. Synthesis result of target DNA fragments and its identification. M: DNA marker DL2000,1: target DNA fragments,2: PCR(RV-M/M13-47 as primers) products of pMD19-T-RVFVS, 3: PCR(primer P1/P2) products of pMD19-T-RVFVS,4:PCR(primer RV-M/M13-47) products of pMD19-T vectors

ATGCACCATCGTCCTAGTCACGAGGTTCGCTTGCGATTTTCTGATTTCTACAATGTCGGAGAATTCCC
ATACCGAGTCGGACTTGGAGACTTTGCATCAAACGTTGCACCTCCACCAGCAAAGCCTTTCCAGAGA
CTTATTGATCTAATAGGCCATATGACTCTTAGTGATTTCACAAGGTTCCCCAATCTAAAAGAAGCCAT
ATCCTGGCCTCTTGGAGAACCCTCACTAGCTTTCTTTGACCTAAGCTCTACTAGAGTGCACAGGAATG
ATGACATTAGAAGGGATCAGATTGCTACTCTAGCAATGAGGAGCTGC

Fig.2. Sequencing results of synthesized target DNA fragments of RVFV

Optimization of reaction temperature.

To optimize the annealing temperature of designed specific primers, pMD19-T-RVFVS were used as template for RT-PCR. The results (as shown in Fig.3) show that the PCR products present in lane 4 (59℃) are present in a greater quantity, which indicates that the optimum conditions for creating a high specificity and amplification efficiency are 59℃ as the ideal annealing degree for amplification cycles.

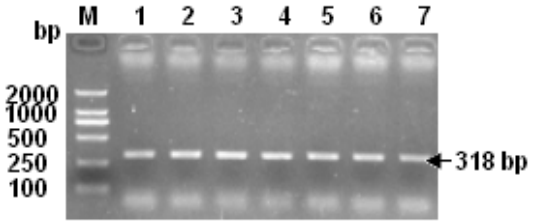

Fig.3.The optimization results of annealing degree determination.M: DNA marker DL2000,1:56℃, 2:57℃,3:58℃, 4:59℃, 5:60℃, 6:61℃, 7:62℃

Specificity and sensitivity of RVFV RT-PCR

The specificity and sensitivity of the RVFV RT-PCR with designed primers were assessed in the tests that were previously described in the methods section. There was a clear electrophoresis band located at about 318 bp that was only observed for the pMD19-T-RVFVS detection (lane8), and no specific amplification for the detection of the Peste des petits ruminants virus(PPRV), Epidemic encephalitis B virus, *E.coli*, *Salmonella* and *Pasteurella multocida* isolated from ruminants, nor was there from the normal blood sample of sheep (as shown in Fig.4). For the sensitivity, the expected PCR products could be observed (lane 4) when almost 85 copies target fragments (pMD19-T-RVFVS) were detected (as shown in Fig.5).

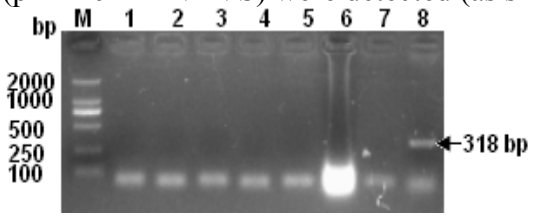

Fig. 4.The specificity test results of RVFV RT-PCR. M: DNA marker DL2000, 1: PPRV, 2: Epidemic encephalitis B virus, 3: *E.coli*, 4: *Salmonella*, 5. *Pasteurella multocida* 6: healthy sheep blood sample, 7: ddH_2O, 8: pMD19-T-RVFVS

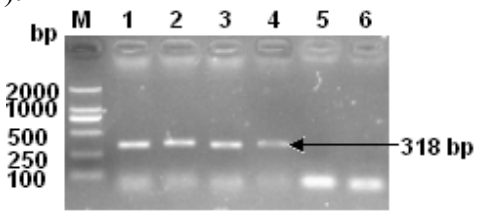

Fig. 5. The sensitivity test results of RVFV RT-PCR M: DNA marker DL2000, 1:8.5×10^4 copies, 2:8.5×10^3 copies,3. 850 copies, 4: 85 copies, 5. 8.5 copies, 6: Negative control

Conclusion and Discussion

RVFwas first occurred in African continent in 1930 and reported outside Africa in the Arabian Peninsula in 2000and RVFV has caused devastating effects on livestock and human health in the endemic areas[11]. As a zoonotic-arbovirus, many studies indicate RVFV has the capacity to emerge in new regions of other parts of the world. Together with the intensification of world trade and communication, the risk of RVFV spreading from Africa to non-endemic regions is increasing[12].Rapid diagnostic tools for RVFVdetection are highlighted need for controlling the spreed of RVF, and the detection of RVFV in non-endemic countries may have important socio-economic and public health implications. To our knowledge, many available techniques such as RT-PCR, real-time RT-PCR[3,4] and ELISA[2,12] have been developed for RVFV detection in the endemic areas, but there was few studies on RVFV including the RVFV detectin methods in China and some other non-endemic countries because RVF have not happened in the boundary regions and there is no RVFV strains used for reseaches in China.Here, according to the nucleotide sequence information of RVFVs published in GenBank, and a segment S fragment about 318 bp of RVFV the was synthesized in vitro by overlap extension PCR and cloned into pMD19-T vector to construct the recombinant plasmid. Meanwhile, based on the synthesis of RVFV segment S fragment in vitro, 2 designed specific primers for RT-PCR were evaluated and proved to be suitable for the detection of RVFV, and the RT-PCR with the 2 primers has good specificity and sensitivity, the detection limit was about 85 copies of the cloned viral genomic fragments,and no cross-reaction for peste des petits ruminants virus(PPRV), Epidemic encephalitis B virus, E.coli , Salmonella and Pasteurella multocida etc common pathogens isolated from ruminants detection. In conclusion,the designed primers and the RT-PCR described this paper supplied important mateirals and a rapid useful technological reserve for RVFV detction and set basis for the studies about RVFV detction in China.

Acknowledgements

This study was supported by Grants from the planning subject of 'the twelfth five-year-plan' in national science and technology for the rural development in China(2013BAD12B04), and “211-Projects” Shuangzhi Plan in Sichuan Agricultural University. Wang Bo,Li Guili, Xu qiumei Yao Xueping ,and Wang Kaiyu should also be considered as first authors. Corresponding author: Wang Yin, Yang Zexiao

References

[1] Caroline AL, Powell DS, Bethel LM, Oury TD, Reed DS, Hartman AL.Broad spectrum antiviral activity of favipiravir (T-705): protection from highly lethal inhalational rift valley Fever[J]. PLoS Negl Trop Dis. 2014, 8(4):e2790.

[2]Shuetsu Fukushi, Mina Nakauchi, Tetsuya Mizutani, Masayuki Saijo, Ichiro Kurane, ShigeruMorikawa.Antigen-capture ELISA for the detection of Rift Valley fever virus nucleoprotein using new monoclonal antibodies[J]. Journal of Virological Methods,2012, 180:68–74.

[3]William C.Wilsona, Marco Romito, Dane C. Jasperson, Hana Weingartl, Yatinder S.Binepal, MoabiR.Maluleke, David B.Wallace, Petrus Jansenvan Vuren, Janusz T. Paweska. Development of a Rift Valley fever real-time RT-PCR assay that can detect all three genome segments[J]. Journal of Virological Methods,2014, 193:426–431.

[4] Marianne Maquart, Sarah Temmamc, Jean-Michel Héraud, Isabelle Leparc-Goffart, Catherine Ctre-Sossah, Koussay Dellagi, Eric Cardinale, Hervé Pascalis.Development of real-time RT-PCR for the detection of low concentrations of Rift Valley fever virus[J]. Journal of Virological Methods,2014, 195:92–99

[5]Jeroen Kortekaas.One Health approach to Rift Valley fever vaccine development[J]. Antiviral Research,2014,106:24–32

[6]Turell, M.J., Linthicum, K.J., Patrican, L.A., Davies, F.G., Kairo, A., Bailey,C.L. Vector competence of selected African mosquito(Diptera:Culicidae) species for Rift Valley fever virus[J]. J. Med. Entomol. 2008. 45:102–108.

[7] Gerdes, G.H.. Rift Valley fever[J]. Rev. Sci. Tech. 2004, 23:613–623.

[8]Turell MJ, Britch SC, Aldridge RL, Kline DL, Boohene C, Linthicum KJ. Potential for mosquitoes (Diptera: Culicidae) from Florida to transmit Rift valley fever virus[J]. Journal of Medical Entomology,2013,50: 1111–1117.

[9] Z. Yang, L. Li, Y. Wang, X.Yao, X.Hai, Z.Yang, B Zhou, K.Wang and Y. Zhang. Development of a RT-PCR for the Detection of European brown hare syndrome virus.Advanced Materials Research , 2011,271-273,:410-416

[10] Z. Yang, G. Pang, Y. Wang, X.Yao, Y. Zhang,Z.Yang, K.Wang, X.Dai.Development of the Multiplex PCR for Porcine Circovirus Detection.Acta Agriculturae Boreali-occidentalis Sinica, 2010,19:8-12.

[11]Balkhy, H.H., Memish, Z.A.. Rift Valley fever: an uninvited zoonosis in the Arabian peninsula[J]. Int. J. Antimicrob. Agents, 2003 21:153–157.

[12] S. Jäckel , M. Eiden , A. Balkema-Buschmann , M. Ziller , P. Jansen van Vuren , J.T. Paweska,M.H. Groschup.A novel indirect ELISA based on glycoprotein Gn for the detection of IgG antibodies against Rift Valley fever virus in small ruminants[J]. Research in Veterinary Science ,2013,95:725–730

Advanced Materials Research Vols. 989-994 (2014) pp 1120-1124
© (2014) Trans Tech Publications, Switzerland
doi:10.4028/www.scientific.net/AMR.989-994.1120

Detection on the Pulse Signal of Human Body Based on Piezoelectric Impedance Technique

Zhang Jun[1, a], Guo Bangzeng[1,b], Tang Hongmei[1,c]

[1]Mechanical Engineering School, Anhui University of Science and Technology, Huainan Anhui 232001, China

[a]zhj63@163.com, [b]624413359@qq.com, [c]tanghongmeiemail@126.com

Keywords: Pulse wave; Piezoelectric effect; Piezoelectric impedance sensor; Pressure index; Physical sign

Abstract. Pulse wave is one of important physiological characters of human body. Detection on pulse sign is helpful for health care and treatment of disease. In order to detect the change of pulse signal of human body, the work principle of detection based on the piezoelectric impedance technique was presented and a new piezoelectric impedance sensor was designed. With an experiment platform set up, detection experiments of pulse signal were created. Two methods were used to deal with the experimental data. Results from a series of experiments intuitively show that with pressure applied to human body bigger and bigger, the pressure index increases gradually. It illustrates that the change of pulse signal is bigger and bigger. The result indicates that this method has good sensitivity and provides a new detection method. The experiment shows that the piezoelectric impedance technique is feasible to detect the change of pulse sign.

Introduction

With the development of economy and progress of the society, people's living standard has been improved. However, followed by bad living habits and unreasonable diet structure, the incidence and death rate of cardiovascular disease are rising year by year, which has seriously damaged people's health[1]. The statistic shows that cardiovascular disease has become the number one killer in disease[2]. Characteristic of pulse wave is closely related to cardiovascular disease. Chinese traditional pulse-taking is based on a variety of pulse conditions, such as the pulse strength and pulse rate, to diagnose whether a person is sick and what kind of disease[3].

Physical signs are important parameters to diagnose physical function and disease status[4]. In recent years, the acquisition and processing on physical signs has been hot in the field of medical instruments. Traditional pulse condition can only artificially diagnose. Along with the development of medical equipment, physical therapy of pulse condition through the electronic equipment has a profound significance [5].Modern signal processing method is applied to the experimental research of pulse condition which opens up a new research method of objective pulse-taking. With the development of computer and modern signal processing technology, the intelligent test has become the trend of the pulse signal detection[6]. This paper design the experiment scheme application of piezoelectric impedance technology, different pressure added to the human body simulates the change of human physiological information. The impedance values measured by the piezoelectric materials were analyzed, and the relationship between human physiological information and impedance values was determine. That detection of pulse can be come true.

Piezoelectric effect

Piezoelectric effect. Piezoelectric effect[7]is composed of positive piezoelectric effect and inverse piezoelectric effect. Piezoelectric effect reflects the relationship between elastic property and dielectric property of crystal.

The piezoelectric material occur deformation under the effect of external force and produces polarization phenomenon inside. At the same time, the surface creates opposite charge. When the external force is removed, it restores to electrically neutral state. This effect is called positive piezoelectric effect or piezoelectric effect.

Polarization. The so-called polarization refers to apply a strong electric field to make "electric domain" regular. Then the piezoelectric ceramic chip shows piezoelectric property. When the polarization electric field is removed, the electric domain basically remains same, but the piezoelectric material still holds strong rested polarization[8], as shown in Fig .1.

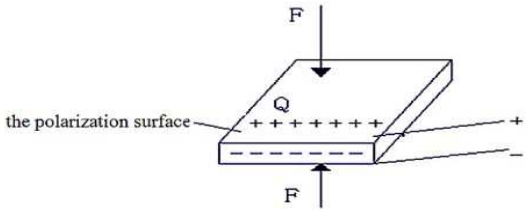

Figure 1. Principle of polarization

On the contrary, when an electric field is applied along the polarization direction, positive and negative ions produce relative displacement under the action of coulomb force, which leads internal stress and generates macroscopic deformation. This phenomenon is called inverse piezoelectric effect.

Design of piezoelectric impedance sensor

The principle of piezoelectric impedance sensor is piezoelectric and converse piezoelectric effect of piezoelectric ceramic chip. In the experiment, the sensor was fixed on arm of human body. Through an impedance analyzer, piezoelectric impedance sensor was excited by a sweep frequency excitation signal. The signal had a certain frequency range. Under the action, PZT transmitted the impedance value to impedance analyzer, as shown in Fig .2. Namely the PZT played a role of sensor. Therefore by measuring impedance value, detection was achieved. According to the laboratory existing conditions, aluminium chip was chosen as the base. PZT chip was pasted by horizontal way. The size of the base: 30×25×2 mm, the size of piezoelectric ceramic chip: 24×4×0.35 mm.

Figure 2. British WK6500B series impedance analyzer

In the experiment, piezoelectric ceramic chip was installed on the aluminum base by pasting way. Conductive silver glue of A2 / HA2 type was used to paste. A2 was used as paste glue and HA2 was used as conductive silver glue, as shown in Fig .3. The both were mixed according to the ratio of 1.5 :1 in application. The sticking steps were as follows:

(1) Aluminium base was polished to ensure the electrical conductivity;

(2) The PZT-4 ceramic chip was pasted on the aluminium base. At the same time, the surface of aluminium base was wiped by cotton swab dipped acetone. Thus grinding debris was eliminated;

(3) The mixed conductive silver glue was daubed on the cathode of piezoelectric ceramic chip by a toothpick. The glue at the middle of piezoelectric ceramic chip was thicker than that on both sides;

(4) The edge of piezoelectric ceramic chip was overlapped the line on aluminium base by a toothpick. The piezoelectric ceramic chip was pressed by a toothpick to guarantee some overflowing colloid;

(5) Until the conductive silver glue was completely solidified, the excess glue was scraped off by a knife. The piezoelectric ceramic chip was wiped around by a swab dipped acetone to ensure the positive pole and negative pole in off state.

(6) The resistance between anode and aluminium base was measured by a multimeter. If the resistance was infinite, it meant normal.

Wiring way: Since the top and the bottom of PZT piezoelectric ceramics chip both had a layer of silver, PZT was directly used as electrode. One end of wire was welded on piezoelectric ceramic chip, and the other end was welded on aluminium base, as shown in Fig .4.

Figure 3. Conductive silver glue of A2 / HA2 type

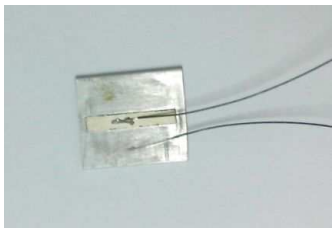

Figure 4. Piezoelectric impedance sensor

The experiment of physical signs based on piezoelectric impedance technique

Purpose of the experiment. Piezoelectric impedance technique is used to detect the change of pulse signal. Its basic idea is to diagnose the change through detection of impedance, because human body impedance changes differently under different conditions. The electrical impedance of PZT is closely related to human body impedance .And it is affected by different degree when the body is affected by outside. By measuring the change of PZT electrical impedance, the body's pulse signal is judged. The purpose of experiment is to design a plan verified that piezoelectric impedance technique is feasible to detect the change of pulse signal.

In the experiment, piezoelectric sensor was fixed above elbow by 8 cm ~ 9 cm with telescopic belt. Namely it was located in brachial artery. Under different pressure from 100 kHz to 120 kHz frequency, impedance curves were measured by impedance analyzer. Impedance analyzer was set to measure impedance's real part and imaginary part. Scanning point was set for1600 and frequency sweep's speed was set for MAX. In order to minimize artificial error, five groups of data were continuously measured.

Processing methods of experimental data. Image processing method: Image processing method is intuitive and simple. The abscissa was kept unchanged from 100 kHz to 120 kHz frequency, the five group data of impedance's real part displayed on a spectrum curve at the same time. By comparing the peak value and the tendency of the curve, conclusion was drawn.

Mathematical processing method: So far, the present data processing methods are various, such as impedance difference between average method, impedance differential mean value method, impedance root mean square difference method, impedance covariance method. In the four processing methods, impedance root mean square difference method and impedance covariance method are intuitive, convenient and also have strong treatment effect, good reliability. Therefore the two methods are selected to analyze experimental data. By comparing both methods, the best method is determined.

Analysis of the result. With a turgoscope, the pressure applied to arm was increased by 20 mmHg each time, as shown in TABLE I.

TABLE I. Pressure Table Applied To Arm

Number	Pressure（mmHg）
1	0
2	20
3	40
4	60
5	80

The analysis of experimental data. Under different pressure, the corresponding impedance values were integrated together. Diagram of impedance real part (X axis) and frequency was obtained, as shown in Fig .5.

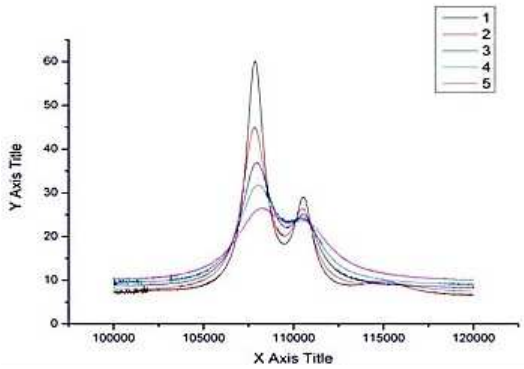

Figure 5. The real part of impedance

The image processing method. By observing figure 5, it is concluded that the spectrum curve changes obviously under different pressure. Impedance decreases gradually with the increase of pressure. Due to the increase of pressure, human pulse signal change, such as blood flow, velocity, which lead the change of impedance. It proves that piezoelectric impedance technique is feasible to detect human pulse sign.

The mathematical processing method. By mathematical processing method, the influence index on impedance was defined as the pressure level (Pressure Index). Root mean square deviation method (RMSD) and covariance method (COV) were selected to analyze experimental data[9]. Due to the spectrum curve ranging from 100 kHz to 120 kHz was stable, so this part was used as processing object. The results were shown in Fig .6 and Fig .7.

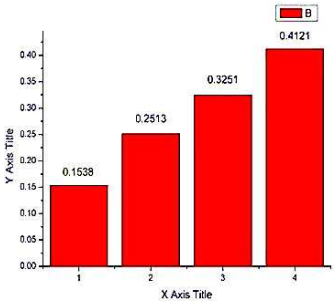

Figure 6. Root mean square deviation method

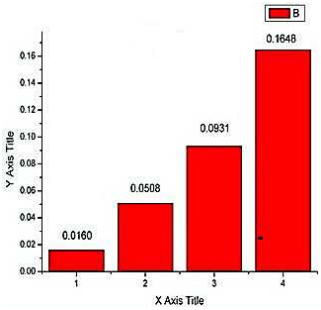

Figure 7. Covariance method

By observing the figures, it is concluded that the results are coincident with theory. As the pressure is bigger and bigger, the pressure index increases gradually. It illustrates that the physical signs change more and more obviously. For the two methods, covariance method is better, because it changes more obviously and has more accurate result.

Conclusion

In this paper, in order to detect and recognize pulse condition, a new piezoelectric impedance sensor was designed. An experiment platform was set up. A series of experiments of pulse signal based on piezoelectric impedance technique were created. With two methods to deal with the experimental data, the result intuitively shows that with pressure applied to human body bigger and bigger, the pressure index increases gradually. It illustrates that the change of pulse signal is bigger and bigger. This relationship between piezoelectric impedance and pulse signal powerfully proves that piezoelectric impedance technique is feasible to detect physical signs. At the same time, a new detection method of pulse signal is provided.

References

[1] Xu Tao. Research on extraction and recognition method of the human pulse condition [D]. Shandong University of Science and Technology, 2008

[2] Yu Lu. Research and Application of Pulse Signal Processing Methods Based on Virtual Instrument [D]. China Medical University, 2009.

[3] Ren Chengcheng. Design of the pulse sensor based on the PVDF piezoelectric film [D]. Dalian university of technology, 2011.

[4] Cheng Chao. A Development of the Simultaneous Acquisition System of ECG Signal and Pulse Wave. College of Bioengineering, South-Central University for Nationalities. 2011.

[5] Ren Kai. Analysis on Chinese medicine pulse signal based on the LabVIEW [D]. Changchun University of Science and Technology, 2012.

[6] Wang Guoli. Research on intelligent pulse signal testing system [D]. Shandong University, 2005.

[7] Chen Jie, Huang Hong. Sensor and detecting technology [M]. Higher education press, 2002.

[8] Tao Juan. The study of structure health diagnosis based on the EMI and the ANN technology. Anhui University of Science and Technology.2013.

[9] Gao Qin. The Research of Piezoelectric Impedance Technology Applying to the Dynamic Signal Beam. Anhui University of Science and Technology. 2012.

CHAPTER 4:

Resource, Energy and Electronic Development, Environmental Engineering

Advanced Materials Research Vols. 989-994 (2014) pp 1127-1130
© (2014) Trans Tech Publications, Switzerland
doi:10.4028/www.scientific.net/AMR.989-994.1127

The Making of Mathematical Models for Ecological Cities

XU Ying [1, a]

[1]Yunnan University, Kunming City 650091, China

[a]xuying2013@yeah.net

Keywords: Ecological city; mathematical models; index mechanism

Abstract. Ecological city, in a broad sense, is a new cultural notion based on mankind's profound understanding of the relationship between human and nature, new-type social relationship in accord with ecological rules which coordinate society, economy and nature, and also a sustainable lifestyle. In a narrow sense, ecological city is a highly effective, harmonious and healthy environment where people gather.

This passage will clarify the definition ecological city and comprehensively depict the systematic model and index system in current ecological cities. A new mathematical model, related theories and calculation as well as its significance are to be mentioned.

Conception of ecological city.

The conception of ecological city is put forward with the constant development of mankind civilization based on deeper understanding of relationship between human and nature. As the most thorough habitat which has been constructed by human, city is the real indication of values and will in the process of human transforming nature in different historic phases. Ecological city not only expresses people's wishes to seek self-development, but also demonstrates a deep understanding of abundant laws which indicate the relationship between people and nature.

Theory of ecological city has developed from the original ecological principles applied in cities to a comprehensive ecological city theory involving natural ecological idea, economic ecological idea, social ecological idea and compound ecological idea.

From different angles, it is easy to find out ecological city's special essence. To look on the side of ecological philosophy, ecological city is essentially symbolizes harmony between human and nature as well as value orientation of ecological city. It can be realized only if people's socialization and cultural awareness reach a special level. To look on the side of ecological economics, green energy including solar energy, hydropower and wind power will be the major energies. Besides, intelligence will be the developing direction of resources and non-renewable natural resources will be effectively preserved and used in a recyclable way. To look on the side of ecological sociology, education, technology, culture, moral and law will be "ecologically", advocating ecological values and ethics.

As a renowned scientist has concluded, the essence of ecological city is to comprehensively research society, economy and nature, applying ecological engineering, social engineering and system engineering to develop a sustainable environment where people live a satisfactory and effective life.

System model of ecological city in our country.

As a matter of fact, city is a compound ecological system which consists of society, economy and nature. In recent years, with the rapid development of modernization, the coordination between downtown areas and uptown areas is becoming a prominent problem. Although society, economy and nature are three systems with their own characters, structures, functions as well as developing principles, their existence and development are limited by structures and functions of the other systems. Below is a figure indicating a compound ecological system of society, economy and nature.

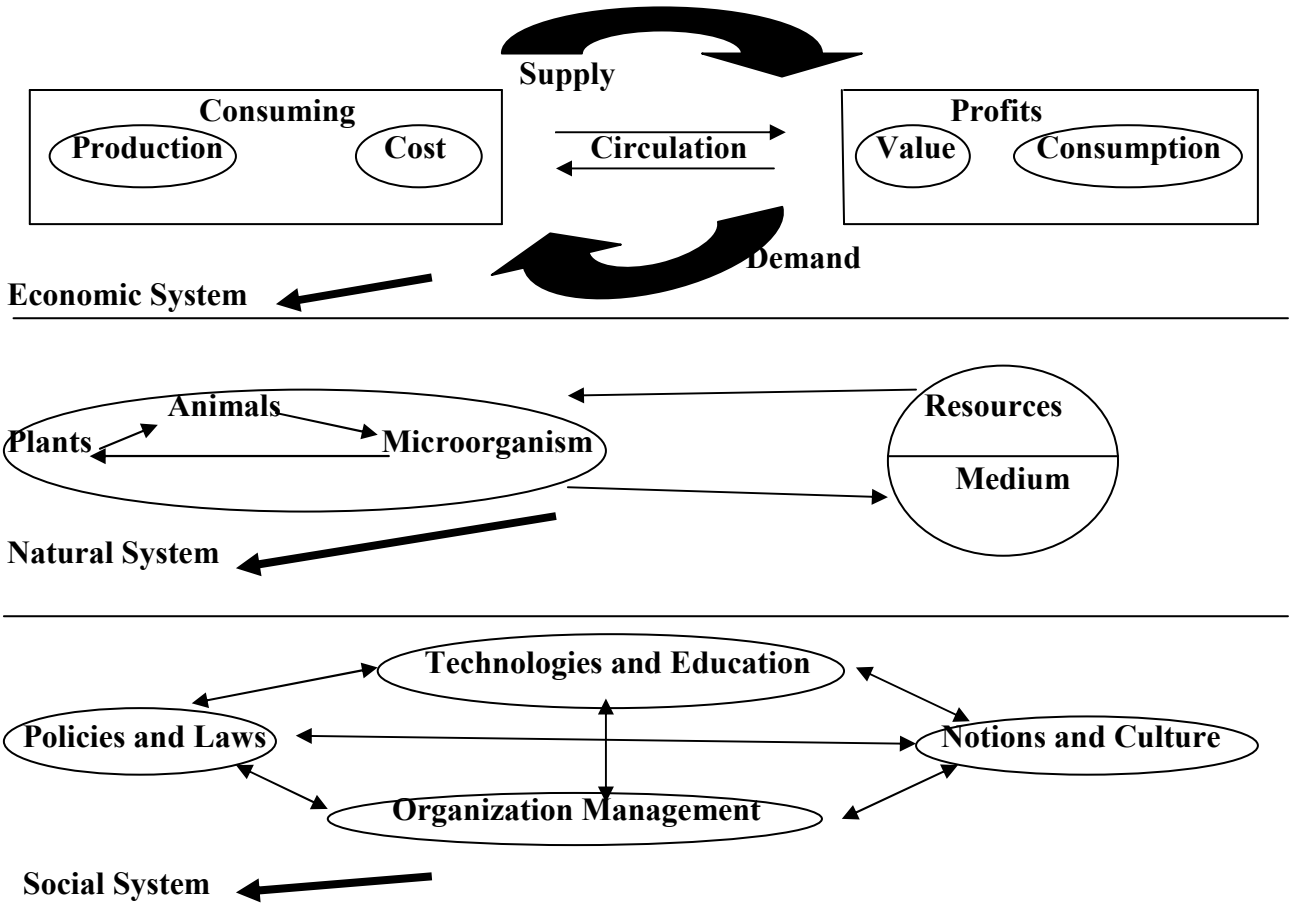

Figure 1. Compound ecological system of society, economy and nature

In order to describe, assess and predict the trend of a ecological system, a body of index systems must be put forward. What's more, as compound ecological system is made up of society, economy and nature, the index system ought to be divided into three aspects

When we make a index system of ecological city, the fact that the ecological system of a city is a enormous system which contains countless factors should be focused. Therefore, it is impossible to analyze each factor of them. In this circumstance, it is essential to select some comprehensive, symbolic and reasonable factors to research.

Scholars from both abroad and home have researched and investigated a lot about index systems and mathematical models of ecological cities. However, none of them have ever quantified the relationship between society, economy and nature in the ecological compound system, failing to indicate the mobile balance between them.

Mathematical models of ecological city.

According to Figure 2, X,Y,Z respectively expresses a city's social benefit, economic benefit and natural benefit. As known to us, the total sum of three coordinate figures of point P_2 is $x_2 + y_2 + z_2$, which is bigger than that of P_0. And the product of P_0's three coordinate figures is bigger than that of P_2.Thus, it can be concluded that P_0's ecological comprehensive benefit is bigger than that of P_2.Therefore, it is not advisable to simply add all figures in every son system, but set up a steadily developing theory.

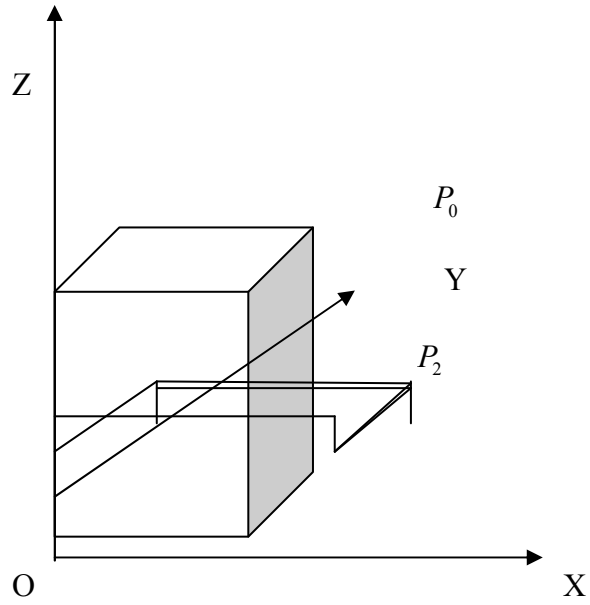

Figure 2. The model of a city's ecological system

A city is a compound ecological system which includes society, economy and nature. Although they have totally different structures, functions and developing laws, their existence and development are restricted and influenced by structures and functions of the other systems. Therefore, the complicated relationship between the three system ought to be taken into consideration. A city is unable to infinitely develop social benefits, economic benefits and natural benefits in a known condition instead of pursuing the coordination and stability of three systems to make a ideal state. If we regard social benefit X, economic benefit Y and natural benefit Z as variable quantities, a function f(X, Y, Z)=0 will be created. To suppose G=X*Y*Z, a ecological city should be in pursuit of the maximum of G.

Establishment of index system of the mathematical model

First-class index	Second-class index	Third-class index	Index value	Present value	Standard value	Weight
G	Social System Index **X**	Mortality rate	Q_{x1}	X_1	X_{s1}	V_{x1}
		Health Status	Q_{x2}	X_2	X_{s2}	V_{x2}
		Education Popularity	Q_{x3}	X_3	X_{s3}	V_{x3}
	Economic System Index **Y**	National Revenue	Q_{y1}	Y_1	Y_{s1}	V_{y1}
		Financial Expenditure	Q_{y2}	Y_2	Y_{s2}	V_{y2}
		Agricultural Production	Q_{y3}	Y_3	Y_{s3}	V_{y3}
	Natural System **Z**	Green Coverage	Q_{z1}	Z_1	Z_{s1}	V_{z1}

Chart 1. Index system of a city's ecological system.

Chart 1 shows a general status of the index system of a city's ecological system. In this chart , G expresses the comprehensive index figure of a ecological system.

In all of the index figures, third-class index Q is the basis of the entire ecological model, and the calculation formulas are as below:

$$Q_{xi}=1-\frac{x_{si}-x_i}{x_{si}-Min[x_i]}\ (1)\quad Q_{yi}=1-\frac{y_{si}-y_i}{y_{si}-Min[y_i]}\ (2)\quad Q_{zi}=1-\frac{z_{si}-z_i}{z_{si}-Min[z_i]}\qquad (3)$$

Second-class index respectively expresses social system, economic system and natural system, and the formulas are as follows:

$$X=\sum_{i=1}^{n} v_{xi}*Q_{xi}\qquad (4)\qquad Y=\sum_{i=1}^{n} v_{yi}*Q_{yi}\qquad (5)\qquad Z=\sum_{i=1}^{n} v_{zi}*Q_{zi}\qquad (6)$$

$$G=X*Y*Z\qquad (7)$$

Summary

The making of a city's ecological system is able to help provide references and suggestions for a special city and assess the ecological level of a city.

Undoubtedly, discussion from the angles of the establishment of index system and mathematical model will lead a city to a promising future.

References

[1] Zhu Xingping, Cao Ronglin, Study of a Mathematical Model for Ecological Cities, 2004.

[2] Zhang Caihong, DongYan, Construction of Ecological Sustainable Chinese Cities[J],2002.

[3] Huang Guangyu, Chen Yong, On City Ecology and Ecological Cities[J], 1997.

[4] Zhang Kunmin, Wen Zongguo, The Progress of Ecological Sustainable Development Index of Cities[J], 2001.

Advanced Materials Research Vols. 989-994 (2014) pp 1131-1134
© (2014) Trans Tech Publications, Switzerland
doi:10.4028/www.scientific.net/AMR.989-994.1131

Multilayer Architecture on Urban Public Crisis Decision Support System

Yongchang Ren

College of Information Science and Technology, Bohai University, Jinzhou, P.R. China

1213552916@qq.com

Keywords: urban management; public crisis; decision support system; DSS; architecture

Abstract. Traditional urban public crisis management and emergency management, ancillary support role of information technology is obviously insufficient, and it impacts crises disposition effect, this paper proposes using decision support system ancillary support, studies multilayer architecture on urban public crisis DSS. Firstly, it studies universal DSS system architecture composed of human man-machine interaction, database, model base, knowledge base, method base and so on five parts; Then, based on the general structure, for the characteristics and functional requirements of urban public crisis decision, it studies multilayer architecture consists of support layer, application layer, integration layer, management layer and user layer, etc.; Finally, to describe the layers of multilayer architecture. The content of this paper is the foundation for the development of urban public crisis DSS.

Introduction

With the accelerated pace of the urban construction, urban construction process, various contradictions and problems in the urban construction process are also increasingly apparent, various crisis is inevitable manifestation of these contradictions and problems. Urban government faced crisis are increasingly diverse, losses caused by the crisis are great, the crisis has uncertainties, knock-on effect, amplification and other characteristics. The ability of urban government to deal with public crisis is facing a severe test. Therefore, crisis management has become an important function of the modern urban government, Strengthening the construction of urban public crisis management system and improving the capacity of the urban government to deal with crisis is a major issue that the current urban government at all levels is facing.

Using traditional urban public crisis management and emergency management, ancillary support role of information technology is obviously insufficient, informatization construction is relatively weak, policymakers can not get timely and comprehensive information about the event, and it impacts crises disposition effect. Decision Support System (DSS), using data mining techniques to provide decision makers with analysis of the problem, establish model to simulate decision processes and programs environment, call various information resources and analytical tools to make decisions, intelligent decisions are the future development direction [1,2]. This paper studies multilayer architecture on urban public crisis decision support system, addresses the critical issues of DSS development, improve decision level of the disposal of urban public crisis, reduce accident losses, and reduce decision risk.

General System Structure

In the late 1970s to the early 1980s developed the DSS has five main components: man-machine interaction, database, model base, knowledge base and method base. Later, on the basis of the five components also develops their own management system, that man-machine interactive system, database management system, model base management system, method base management system and knowledge base management system. DSS provides four functions, namely information service, scientific computing, decision consultation, artificial intelligence. Universal information system structure is shown in Fig. 1 [3,4].

Five components are described as follows: (1) Man-machine interactive system, it is man-machine interface of decision support system for receiving and testing user requests, call the

internal functional software of the system for decision service, so that the model runs, data calls, and knowledge reasoning achieve organic unity, effectively solve decision problems. (2) Database management system, is a basic component of DSS for the establishing, using and maintaining the database, the database unified management and control to ensure the security and integrity of the database. (3) Model base management system, the main functions are: To provide users with characteristic information about the model attribute, to guide user to quickly and accurately find relevant models, to provide relevant information to the user to add the source code of model and execute code modify and model changes. (4) Method base management system, Methods base management system (MBS) is primarily a software system, together with the programs and data, a new generation of MBS should have a scalable application components, new components can be added at any time, can be connected to multiple databases, and apply relational control system. (5) Knowledge base management system, when the DSS direct to intelligent to develop, the research of knowledge and reasoning become increasingly important. When developing the knowledge base should consider the following issues: for natural language understanding to create semantic and pragmatic environment, for modeling and numerical calculation to provide the necessary analysis basis, add and extend the thinking skills of decision-makers.

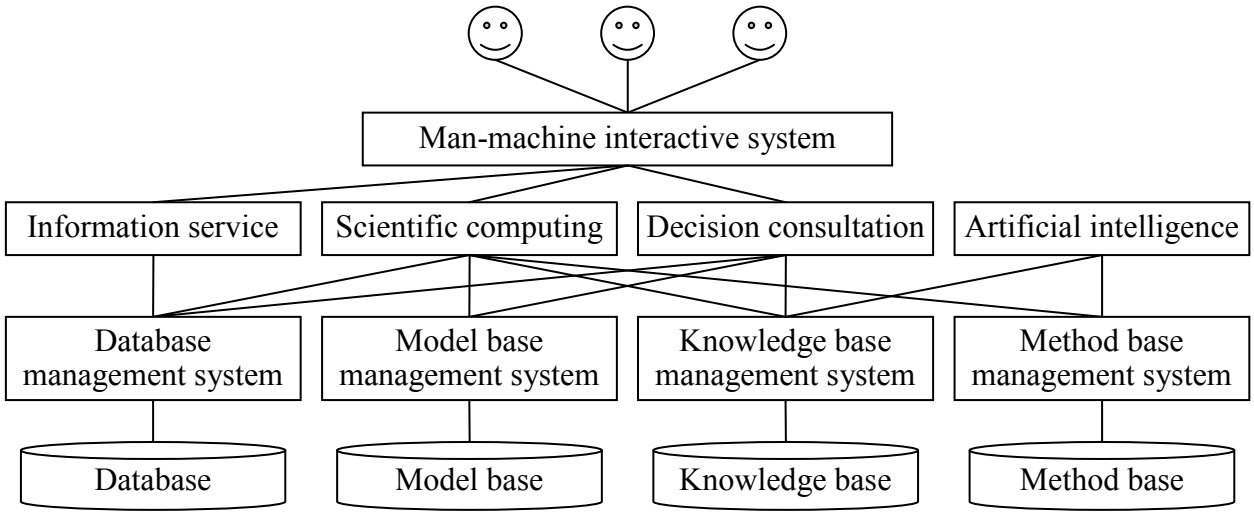

Fig. 1. Structure of decision support system

Multilayer Architecture

As information systems have been expanding, increasing the complexity, the impact of information systems architecture model on the performance of information systems is great, information systems with different functions for architecture patterns have different requirements, a variety of information systems architecture patterns in development and application process has great differences. Select and design rational architectural pattern is even more important than ratio algorithm design and data structure design.

Multilayer architecture divided system function and components into different levels, in general, only the top-level components and functions can be accessed by a user outside the system, only adjacent layers can have the function to call. Advantages of multilayer architecture is the development and design of the system can gradually layered conduct, from bottom simple functions gradually establish high-level complex and abstract functions; flexibility and scalability, as between adjacent levels interact through a clear interface, so a particular level can be replaced and enhanced, and even add a new level. Disadvantages multilayer architecture is that not all systems can be decomposed into a clear hierarchy; divided clear, logically consistent level is very difficult; strict hierarchical call structure will reduce the performance of the system.

According to the characteristics of urban public crisis decision support systems, and the implementation requires of emergency treatment, the paper design architecture consisting of support

layer, application layer, integration layer, management layer and user layer, etc. five layers, shown in Fig. 2 [5-7].

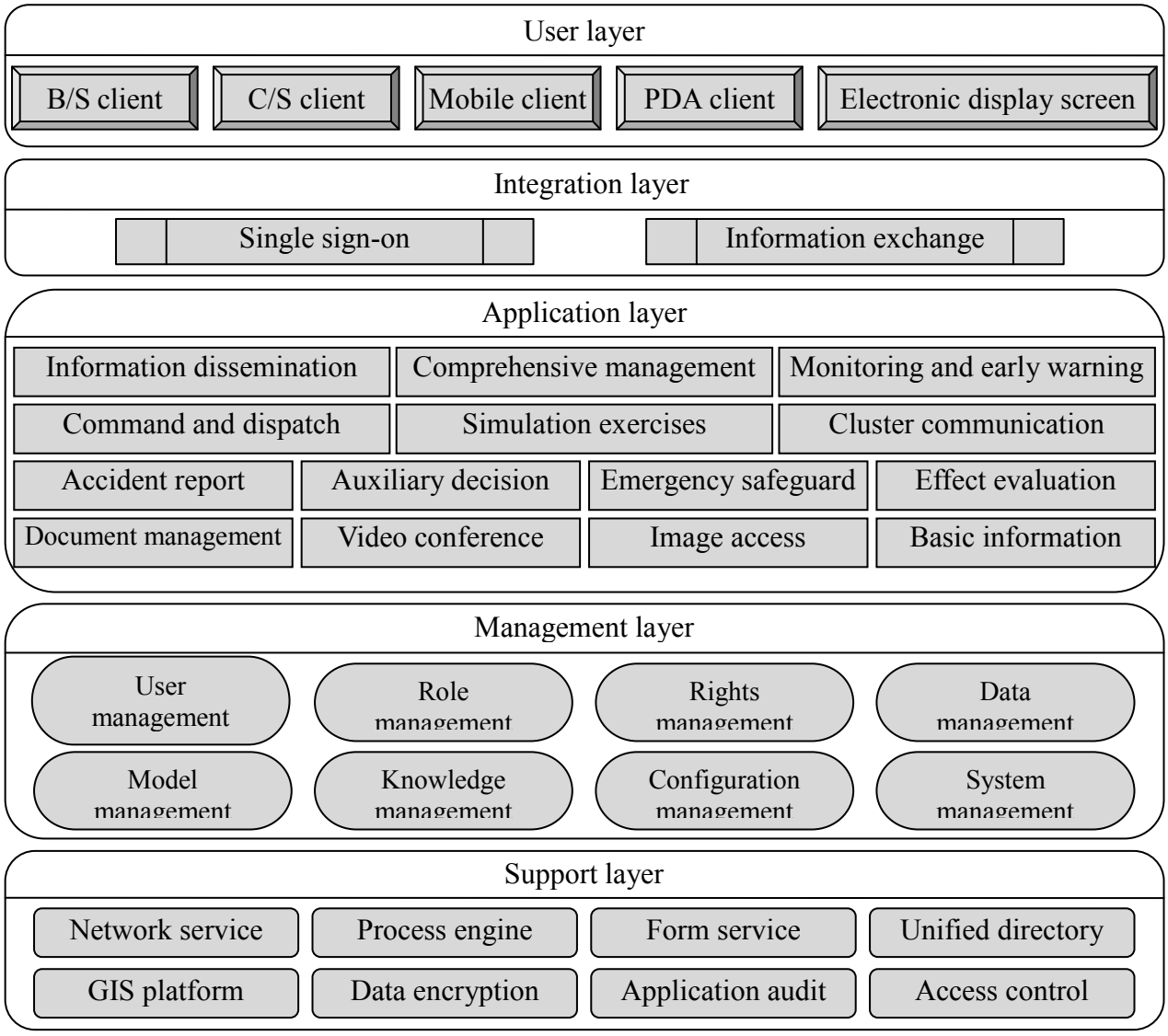

Fig. 2. Multilayer architecture on urban public crisis decision support system

Describe the Multilayer Architecture

The multilayer architecture shown in Fig. 2 is described as follows:

(1) Support layer. It is the support platform of public crisis decision support system, is the foundation of system operation, providing support services for system operation. Mainly includes network services, workflow engine, unified directory, GIS platform, data encryption, application auditing, and access control and so on.

(2) Application layer. The main function is to all aspects of emergency manage business processes to provide information technology support. In daily work, using information technology to simplify the work of handling procedures, improve work efficiency. When a crisis event occurs, through the integration of various systems analysis resources, to provide comprehensive and detailed information and data for the leaders and experts, play a supporting role in crisis emergency decision.

(3) Integration layer. It mainly includes single sign-on and information exchange two functions. Among them, the single sign-on, is one of the more popular systems integration solutions, when users access to multiple applications system, simply log in once, namely accessed through a single

sign-on system, without re-login; data exchange, system data is stored in multiple databases, data exchange for the entire system to provide a unified data exchange standards, among the various systems, heterogeneous databases and different networks systems to provide integrated method.

(4) Management layer. Conduct systematic management, is a necessary means to keep the system running properly sustained, using systematic view to implement systematic management for system, namely follow system ideas, using systems thinking method to conduct a full range and whole process of management on management objects. Main function includes: user management, role management, rights management, data management, model management, knowledge management, configuration management, system maintenance.

(5) User layer. To provide users with the channel of information exchange between systems, unified and integrated the various applications, the relevant data resources, and other relevant information of system, when user uses the system, you can use different personalized application interface according to their use and role. It includes B / S client, C / S client, mobile client, PDA client, electronic displays and other in various ways.

Conclusion

Urban public crisis management is government management functions, aimed at reducing the risk of vulnerability and improving the ability to respond to disasters [8]. For a long time, the emergency management of government for urban public crisis emphasizes "prevention", when the event occurs, it seem helpless, real or imagined. The reason is the theory and approach of urban public crisis management is imperfect, decision process depends on the person's subjective experience of thinking, the lack of effective decision support. This study according to the characteristics of urban public crisis, proposed using DSS assist government departments urban public crisis management decisions, research on multilayer architecture on urban public crisis decision support system to provide support for the development of DSS.

Acknowledgment

This work is supported by social science fund project of Liaoning province (L12BZZ009).

References

[1] Behnam Malakooti, "Systematic decision process for intelligent decision making," Journal of Intelligent Manufacturing, vol. 121, no. 5, pp. 1342-1355, 2009.

[2] X. S. Han, "Decision-making models and operational Mechanisms of Government on Urban Emergency Management," Doctor’s degree of Harbin Institute of Technology, 2009.

[3] Y. C. Ren, P. Zhu, "DSS Models and Its Representation of Government on Urban Emergency Management," Computer Technology and Development, vol. 23, no. 2, pp. 177-180, 2013.

[4] H. S. Gao, "Decision Support System: Theory, Method and Case," Tsinghua University press, 2000.

[5] C. B. Yang, "Analysis and design of the provincial emergency management information system," Master’s degree of Shandong University, 2009.

[6] Neil Mather and Samia Oussena, "Atlas of karst area based on Web GIS technology," Environmental Geology, vol. 54, no. 5, pp. 1029-1036, 2008.

[7] X. Peng, Y. C. Ren, "Basic Architecture of Government on Urban Emergency Management System," Computer Technology and Development, vol. 23, no. 2, pp. 207-210, 2013.

[8] Tomáš Ludík and Jaroslav Ráček, "Process Methodology for Emergency Management," IFIP Advances in Information and Communication Technology, vol. 35, no. 9, pp. 302-309, 2011.

Advanced Materials Research Vols. 989-994 (2014) pp 1135-1140
© (2014) Trans Tech Publications, Switzerland
doi:10.4028/www.scientific.net/AMR.989-994.1135

Accurate Calculation Receiving Power of the Electromagnetic Wave Scattering between Two Stations on Sea Surface

Xianmao LI[1, 2, a], Tianlin DONG[1, b], Gaoming HUANG[2, c]

[1]Department of Electronics and Information Engineering, Huazhong University of Science and Technology, Wuhan, 430074, China

[2]School of Electronics Engineering, Naval Engineering University, Wuhan , 430033 China

[a]email: xianmao916@163.com, [b]email: dtlHust@hust.edu, [c]email: hgaom@126.com

Keywords: Sea Surface Scattering; Double Stations; Beaming Area; Receiving Power; Electronic Reconnaissance

Abstract. This paper studies receiving power of electromagnetic wave scattering on sea surface transmitted by directional antenna. Analyzes different overlapping conditions of transmitter beaming and receiver beaming on the sea surface, deduces the calculation formulae, and calculation of the receiving power of scattering wave in case of different across angle between radiator and receiver beams on sea surface. The result shows that the across angle is a important factor of receiver to receive electromagnetic wave scattering power on sea surface, and it gives an accurately calculating method by receiver to receive electromagnetic wave scattering power from sea surface. The method can apply to the condition that radar or jammer transmitters beam to sea surface and reconnaissance or radar receiving the scattering power from sea surface at another position, etc..

Introduction

The electromagnetic wave scattering on sea surface of double station is very important for electronic reconnaissance receiver, electronic warfare jamming and bistatic radar etc., the key to solve this conundrum is calculation of the receiving power of the receiver[1].The power received by the receiver of scattering electromagnetic wave lies on transmitting power, beam direction, antenna beam shape, sea surface scattering coefficient, frequency of electromagnetic wave, radiator transmitting direction, relative position, antennae beams alignment relation, etc.[2-7]. When the transmitting and receiving equipments are in different positions, the receiving area of transmitter is not exactly the same as the area that transmitting the sea, especially when the beams of receiver and transmitter both are strongly directional as like Fig.1, the beaming area on the sea are different between receiver and transmitter, we can also say the acreage of the overlapping area is very important to the receivering power. The Fig.2 gave the shape and acreage of the overlapping area. This paper will analyses and calculates some typical receiving area of double stations electromagnetic wave scattering, provide calculation method of receiving power in a typical case.

Calculation receiving power of scattering wave

Take the condition of air base equipment transmitter & air base equipment receiver as a typical case, we anzlyse as following.

When the transmitting and receiving equipment are all air based, the antennae beams overlapping area is the main scattering area, and is overlapping by two ellipse, the max acreage of the overlapping area is shown like Fig2, the center of ellipses are the same, but their long axis directions are different. The particular case is inclusion relation, the area of small ellipse stand for the area of overlapping area, the situation when ellipses are not included is shown like Fig.2. Because of strong directional of receiver and transmitter, the power densities are different from the middle of antenna beaming area and the edge of antenna beaming area, so, the power density of electromagnetic wave is different in different cell on sea. For receiver, it's also directional of antenna beaming, so, the receive gain is different in different cell of overlapping area on the sea.

For the scattering coefficients of sea surface, it's relative to transmitter beaming direction to the sea and receiver's direction to the sea, when the transmitter and the receiver's antenna beaming direction are all strong enough, in the lapping area, there is little difference between the radiation beaming direction and the receiver's direction, when calculating the engineering sense the scattering coefficients of sea surface can be took for same in the lapping area. When get the scattering coefficients of sea surface bewteen transmitter and the receiver, we can calculate the receiver's receiving power of scattering wave by integral method.

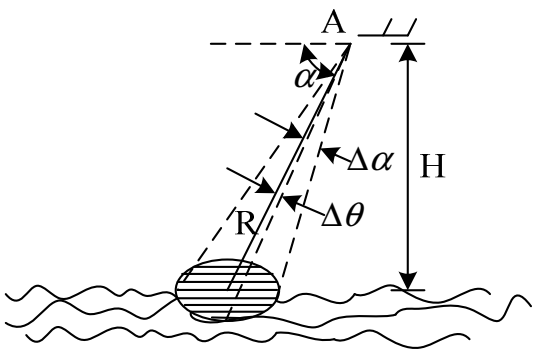

Fig.1. Beaming area of air base transmitter quipment & air base receiver equipment on sea surface

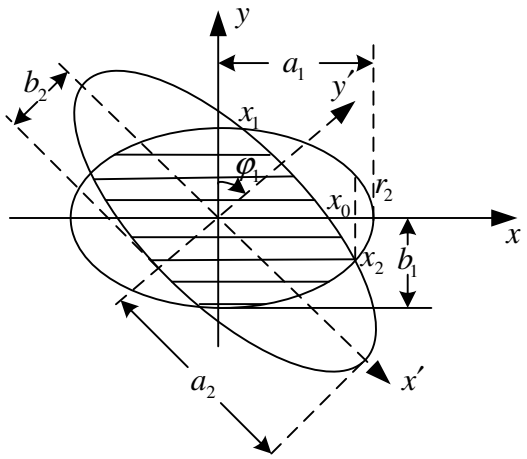

Fig.2. Overlapping area of air base transmitter quipment ra & air base receiver equipment

Use the integral method to calculate the receiving power as following. First, we can get the formula as below when antena beams beaming sea surface as like Fig.1：

$$R=\frac{H}{\sin\alpha},\quad a=\frac{2R\Delta\alpha}{\sin\alpha},\quad b=2R\Delta\theta .$$

Suppose (x, y) is the point of intersection of two ellipses, using coordinate transformation, (x, y) in ellipse2 corresponding to the second coordinate system is (x', y') so can get formula as below[8]:

$$x'=x\cos\varphi_1-y\sin\varphi_1 \tag{1}$$

$$y'=x\sin\varphi_1+y\cos\varphi_1 \tag{2}$$

$$\frac{x^2}{a_1^2}+\frac{y^2}{b_1^2}=1 \tag{3}$$

$$\frac{x'^2}{a_2^2}+\frac{y'^2}{b_2^2}=1 \tag{4}$$

Simultaneous equation(1)-(4),can get：

$$\begin{cases} V_1x^2\pm V_2x\sqrt{1-x^2/a_1^2}=A_1 \\ y=\pm b_1\sqrt{1-x^2/a_1^2} \end{cases} \tag{5}$$

Thereinto:

$$V_1=\cos^2\varphi_1\left(1-\frac{b_1^2a_2^2}{a_1^2b_2^2}\right)+\sin^2\varphi_1\left(\frac{a_2^2}{b_2^2}-\frac{b_1^2}{a_1^2}\right),\qquad V_2=2b_1\sin\varphi_1\cos\varphi_1\left(\frac{a_2^2}{b_2^2}-1\right),$$

$$A_1=a_2^2-b_1^2\cos\varphi_1\left(\sin^2\varphi_1+\frac{a_2^2}{b_2^2}\cos^2\varphi_1\right).$$

For formula(5) upper line, to use the computer approximation method, we can calculate four x values, and according formula(5) down line, we can get four y values. so it can form four (x, y).

According to the Fig.2, we can get the intersection point of ellipse and X-axis $(x_0,0)$, it between x_1 and x_2, from the formula below

$$\frac{x_0^2\cos^2\varphi_1}{a_2^2}+\frac{x_0^2\sin^2\varphi_1}{b_2^2}=1 \tag{6}$$

Can get :

$$x_0=\frac{1}{\sqrt{\cos^2\varphi_1/a_2^2+\sin^2\varphi_1/b_2^2}}.$$

According to the shape symmetry of ellipse and the symmetry of antenna gain distribution, can calculate the Y-axis's right side of receiving power, then the full power of receiver is double it. According to the graphic character, use the Descartes coordinate, in common condition divided the integral into 0 to x_1, x_1 to x_0, x_0 to x_2, we can establish the formula as below:

$$P_r=\frac{2\rho P_t\lambda^2}{(4\pi)^3 R_t^2\bullet R_r^2}\bullet\left[\int_0^{x_1}\int_{-b_1\sqrt{1-\frac{x^2}{a_1^2}}}^{b_1\sqrt{1-\frac{x^2}{a_1^2}}}G_t(\theta_t,\alpha_t)\bullet G_r(\theta_r,\alpha_r)dydx+\int_{x_1}^{x_0}\int_{-b_1\sqrt{1-\frac{x^2}{a_1^2}}}^{M_+(x)}G_t(\theta_t,\alpha_t)\bullet G_r(\theta_r,\alpha_r)dydx\right.$$
$$\left.+\int_{x_0}^{x_2}\int_{-b_1\sqrt{1-\frac{x^2}{a_1^2}}}^{M_-(x)}G_t(\theta_t,\alpha_t)\bullet G_r(\theta_r,\alpha_r)dydx\right] \tag{7}$$

ρ —specifies direction of average scattering coefficient for double stations

R_t —distance between transmitter to the center of scattering area on sea surface

R_r —distance between receiver and the center of scattering area on sea surface

P_t —transmitting power

$G_t(\theta,\alpha)$ —the gain of transmitter antenna[9,10]

$G_r(\theta,\alpha)$ —the gain of receiver antenna

$$M_\pm(x)=-\frac{m_2}{2m_1}x\pm\frac{1}{2m_1}\sqrt{(m_2^2-4m_1m_3)x^2+4m_1a_2^2}$$

Thereinto:

$$m_1=\sin^2\varphi_1+\frac{a_2^2}{b_2^2}\cos^2\varphi_1,\quad m_2=2\sin\varphi_1\cos\varphi_1\left(\frac{a_2^2}{b_2^2}-1\right),\quad m_3=\cos^2\varphi_1+\frac{a_2^2}{b_2^2}\sin^2\varphi_1.$$

$$G_t(\theta,\alpha)=G_{t0}\bullet\frac{\sin\left(2.78\frac{\theta-\theta_{01}}{\theta_{1,0.5}}\right)\sin\left(2.78\frac{\alpha-\alpha_{01}}{\alpha_{1,0.5}}\right)}{\left(2.78\frac{\theta-\theta_{01}}{\theta_{1,0.5}}\right)\left(2.78\frac{\alpha-\alpha_{01}}{\alpha_{1,0.5}}\right)} \tag{8}$$

$$G_r(\theta,\alpha)=G_{r0}\bullet\frac{\sin\left(2.78\frac{\theta-\theta_{02}}{\theta_{2,0.5}}\right)\sin\left(2.78\frac{\alpha-\alpha_{02}}{\alpha_{2,0.5}}\right)}{\left(2.78\frac{\theta-\theta_{02}}{\theta_{2,0.5}}\right)\left(2.78\frac{\alpha-\alpha_{02}}{\alpha_{2,0.5}}\right)} \tag{9}$$

$G_t(\theta,\alpha)$ is the pattern function of receiver antenna, we must put transform x, y to θ,α for $G_r(\theta,\alpha)$, so we can get the receiver gain on sea surface.

For get θ,α, set the center of scattering area as the origin, set (x, y) as sea surface, establish the Cartesian coordinate system. Set the position of receiver is (x_r, y_r, z_r), the current integral position is $(x_1, y_1, 0)$ as Fig.3 showing.

Triangle ΔOBC have three sides R_r, r and l.

$$R_r = \sqrt{x_r^2 + y_r^2 + z_r^2}$$

$$r = \sqrt{x^2 + y^2}$$

$$l = \sqrt{(x - x_r)^2 + (y - y_r)^2 + z_r^2}$$

set[11,12] $p = \frac{1}{2}(R_r + r + l)$

Because of

$s = \frac{1}{2} R_r l \sin\theta_r = \sqrt{p(p-R_r)(p-r)(p-l)}$,

So can get:

$$\theta_r = \arcsin\left(\frac{2}{R_r l}\sqrt{p(p-R_r)(p-r)(p-l)}\right) \tag{10}$$

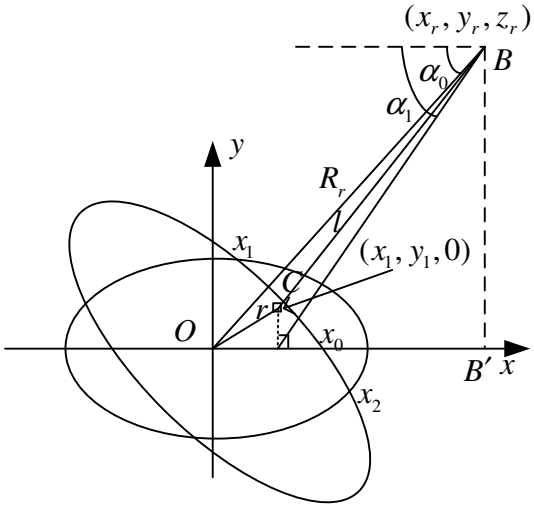

Fig. 3. Integral calculation diagram of overlapping ellipses scattering area

Because the long axis direction of ellipse and X-axis direction are the same, and the antenna directivity diagram symmetric longitudinal is the same with the long axis direction of ellipse, so, the point B' (the projection of point B) must lay on X-axis, the projection of point C on X-axis is $(x\ ,0)$.

$$\alpha_r = (\alpha_1 - \alpha_0) = \arcsin\left(\frac{z_r}{\sqrt{(x - x_r)^2 + z_r^2}}\right) - \arcsin\left(\frac{z_r}{R_r}\right) \tag{11}$$

By formula（8）~（11）and $G_r(\theta,\alpha)$, $G_r(\theta,\alpha)$, we can get $G_r(x, y)$, and get $G_t(x, y)$ in same method. Put $G_r(x, y)$, $G_t(x, y)$ to formula（8）, use the Descartes coordinate integral to x, y, so the receiving power P_r can be got.Considering the curvature of earth, we can calculate α_{02}, R_r or α_{01}, R_t, as Fig.4 showing.

Supposing R_r, H_r is known, and R_E is known.

$$\frac{\sin\alpha_E}{R_E}=\frac{\sin(\alpha_z+\pi/2)}{R_E+H_r}$$

$$\alpha_z=\arcsin\left(\frac{R_E+H_r}{R_E}\sin\alpha_E\right)-\frac{\pi}{2} \tag{12}$$

$$\alpha_r=\frac{\pi}{2}-\alpha_z-\alpha_E \tag{13}$$

$$R_r=\frac{R_E\sin\alpha_r}{\sin\alpha_E} \tag{14}$$

Take formula (12)~(14) as simultaneous equations, can get $\alpha_r, \alpha_z, \alpha_E$.

$$z_r=R_r\sin\alpha_z$$
$$\alpha_0=\pi/2-\alpha_z$$

Simulation

Take the condition air base equipment transmitter & air base equipment receiver as a typical case, we can calculate receiving power as following.

Suppose point A is radar, point B is electronic reconnaissance. The height of point A is H_1, The height of point B is H_2. The azimuth angle of point A is φ_1, the azimuth angle of point B is 0º. The antenna of radar A is unilateralism sinc, the antenna of receiver B is unilateralism sinc too.

(1)Set $\rho=0.1$, $\lambda=0.03m$, $P_t=100kw$, Set $H_1=24000m$, $\alpha_{01}=70°$,by formula (8) we can know in the far area, $\Delta\alpha_1=6°$, $\Delta\theta_1=6°$;Set $H_2=7200m$, $\alpha_2=60°$, by formula(9) we can know in the far area, $\Delta\alpha_2=15°$, $\Delta\theta_2=20°$. Set $\varphi_1=60°$, then we can calculate Pr=-50.13dBw （0.0097mw） by formula(8).

(2) Let $\varphi_1=-90°\sim 90°$,and set other parameter same as conditon(1). By different across angle of two ellipse, we get different Pr values, and plot a figure as Fig.5.

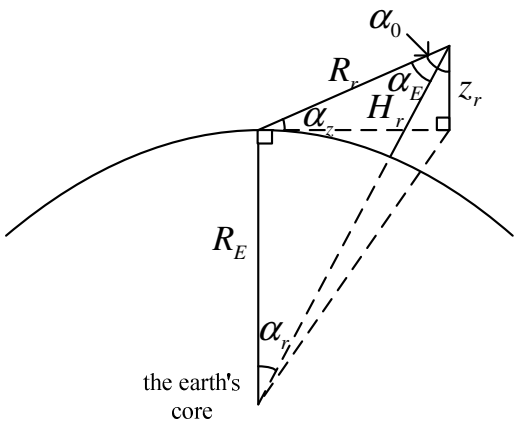

Fig. 4. The diagram of conversion of parameters on the sea considering the curvature of earth

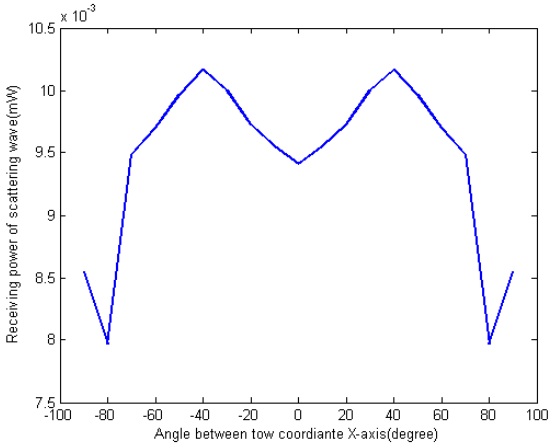

Fig. 5. Receiving power of scattering wave by different across angle of two ellipse.

Conclusion

This paper can get the receiving power by analysis and calculation on typical condition base on directional transmitter antenna and directional receiver antenna. It's very important for study the sea electronic countermeasure reconnaissance, multi-path effect of active jamming electronic warfare, the phenomenon of adding target batch quantitative analysis, and also, it have important reference value for working effectiveness analysis for bistatic radar on sea.

Acknowledgement

In this paper, the research was sponsored by the Nature Science Foundation of China (Project No. 61372165) and 863 Project of China (Project No. 2012AA7014061).

References

[1] Smith, J.R., Jr.; Burkholder, R.J. Channeling phenomenon in electromagnetic forward scattering at low grazing [J].Geoscience and Remote Sensing, IEEE Transactions on, 2004 (8) 1731 - 1738.

[2] Soriano G., Guerin C., Saillard M.. Microwave ocean scattering at low-grazing angles with the GmoM[C]. Proceedings of the 7th European Radar Conference, 2010 5-8

[3] Jerry R. Smith, Jr. Robert J. Burkholder . Channeling Phenomenon in Electromagnetic Forward Scattering at Low Grazing. Geoscience and Remote Sensing, IEEE Transactions on,2004 (8) 1731-1738.

[4] Smith, J.R. ; Russell, S.J. ; Brown, B.E. etc.. Electromagnetic forward-scattering measurements over a known, controlled sea surface at grazing. Geoscience and Remote Sensing, IEEE Transactions on, 2006 (42) 1197-1207

[5] Xuguang YAN, Fuyuan PENG, Guohua XU , Xutao LI. Ana lysis of tempora l and frequency character istics of fore2sca ttered la ser in ocean channel. Laser Technology 2005 (3) 266-269

[6] Tao ZHANG, Qun ZHANG, Binfeng LUO, Shouhong ZHANG. Shadow Imaging for Bistatic Radar Ba sed on Forward Scattering by Joint Time Frequency Analysis. ACTA ELECTRONICA SINICA, 2001 (6) 726-729

[7] Rongrong WANG, Fang LIU. Study on the Backsca tter ing Enhancement of 22D Sea Surface with the Sta tionary Pha seMethod. Journal of Xinyang Normal University: Natural Science Edition.2010 (6) 219-226

[8] LIU Da1, HAN Xiao bing, FANG Long. The Research and Implementation of 3-Dimensional Cartesian Coordinate System Direct Conversion Algorithm[J]. Geomatics & Spatial Information Technology, 2012 (5) 175-182.

[9] Guoyu Wang, Lian-dong Wang,etc. *Digital Simulation And Evaluation of Radar EW System* [M]. Beijing: National Defence Industry Press, pp.85-86, 2004.

[10] Wanhai Yang. *Modeling and Simulation of Radar System* [M]. Sian: Xidian University Press, 2007 157.

[11] Qixiao Ye, *Yonghuan Shen. Applied Math Manual* (Second Press) [M]. Beijing: Science Press, 2006 65-70.

[12] Math Manual Compile Group. *Math Manual* [M]. Beijing: Higher EducationPress, 1979 349-354.

Advanced Materials Research Vols. 989-994 (2014) pp 1141-1145
© (2014) Trans Tech Publications, Switzerland
doi:10.4028/www.scientific.net/AMR.989-994.1141

Simulation and Analysis for Damage of certain Electrical Power Equipment in Battlefield

YANG Xin-yu[1,2,a], MA Qi-shuang[1], CHENG Pei-yuan[2],
ZHANG Qiang[2], ZHANG Lin[2]

[1]School of Automation Science and Electrical Engineering, Beijing University of Aeronautics and Astronautics, Beijing, 100191, China;

[2]School of Air and Missile Defense, Air Force Engineering University, Xi'an, 710051, China

[a]email: yangxinyu_2004@163.com

Keywords: Electrical Power Equipment; Battlefield Damage; Treat Mechanisms; Simulation

Abstract. For the need of simulation research of technical support and obtain basic rush repair data of certain ground-to-air electrical equipment in battlefield condition, this paper studies on the simulation for damage of certain electrical power equipment in battlefield. It analyzes threat mechanisms and basic damage theories of power unit and compiles simulation procedure adopting Monte Carlo method. By simulation, it can analyze vulnerability and distributing of damage parts for electrical power equipment. All this provides reference for rush repair and instruct to defend in battlefield condition.

Introduction

Equipment battlefield damage means the affair that effect the equipment's completing tasks on the battlefield, including combat damage and non combat damage. The combat damage show differences in damage patterns, characteristics and rules with the usual equipment fault, and it is an important problem to equipment survivability and sustained combat capability. The electrical power equipment of surface-to-air missile weapon plays an irreplaceable task in the air defense of the future war, and its prominent position and role will become the focus of the enemy attack, so the battle damage repair is facing severe challenges. But we are unable to establish effective repair database at present, so we can only use the existing simulation methods to establish the Surface-to-air Missile Battle Damage Simulation System, providing more efficient, powerful decision-making information for equipment repairment. This paper is on the battlefield damage simulation.

The Battle Damage Simulation is a simulation of the equipment damage that using military expert knowledge, logical mathematical model, computer deduction and pre-designed rules, data and procedures depicting actual or assumed operational process.

Damage Analysis

2.1 Threat mechanism analysis

Threat mechanism refers to all the possible conditions of the damage of weapon system due to hostile action in the battlefield environment. It is the fundamental cause of the damage of weapons and equipments. In the analysis of threat mechanism, we need to consider three factors: the enemy attack, the launcher itself, the natural environment. The main factors causing the damage of the launcher in the battlefield environment is the enemy's attack, and it is the key research content of this article.

The failure mechanism of general shells, bombs and missiles on the equipment is basically the same. The explosion of the bomb will form a fragment field and has a certain strength of the shock wave, the fragments and blast wave (mainly is the fragment) damage to the equipment. The following is specific analysis of its damage to the equipment.

2.2 The destruction of fragments

The quantity and quality of entirely prefabricated fragment generally have a loss after explosion. In the synthesis of various factors, in order to obtain high speed fragment (greater than 2000 m/s), the loss of the quality of broken piece is ofen 10~20%.

1. Quality of fragment

The average quality of fragments is calculated according to the formula of Magis, i.e.

$$\mu = C_f \frac{td^{1/3}}{1+2C/M} \bullet f_1 T_S \tag{1}$$

In the formula, t is the average wall thickness of the body(mm); d is the average diameter of projectile(mm); M is the quality of the metal shell of projectile(kg); C is the quality of explosive(kg); C is experimental coefficient, C_f =0.132804.

2. The initial velocity of fragment

Gurney formulas is widely used in the calculation of initial velocity of fragment, and to the cylindrical shell, gurney formula for the initial velocity of fragment is as follows:

$$v_0 = \sqrt{2E}\sqrt{\frac{\beta}{1+\beta/2}} \tag{2}$$

In the formula, $\sqrt{2E}$ is Gurney Constant, or called gurney velocity(m/s); β is the explosion load coefficient of ammunition, $\beta = \frac{m_c}{m_s}$.

3. The attenuation of initial velocity of fragment.

The velocity of fragment decays gradully because of air resistance. The fragment flys out at a speed of v_0, and after a distance of S, the velocity of fragment is:

$$v = v_0 \exp(-\frac{C_D \rho A}{2q} S) \tag{3}$$

In the formula, A is the windward area of fragment(m^2); q is the quality of the single fragment(kg); ρ is the air density at the hight of fragment(kg/m^3); C_D is the air resistance coefficient of the fragment.

4. Effective range of fragment

Assume that the necessary energy for a single fragment to hit the target is $E_{\min}$, the blow velocity of fragment is v_f (m/s),then the effective distance of fragment R(m) is:

$$R = \begin{cases} \dfrac{\ln(\frac{v_f}{\sqrt{2gE_{\min}/q}})}{0.5C_D \rho g \Phi_a / q^{1/3}}, & v_f \geq \sqrt{2gE_{\min}/q} \\ 0, & v_f < \sqrt{2gE_{\min}/q} \end{cases} \tag{4}$$

Probability model of equipment damage

For the equipment of ground to air missile weapon system in planar distribution, calculate the damage probability respectively according to the distribution of the equipment, the site location, size and vulnerability of the key parts, after identifing the parameters of position, size and vulnerability of different vital parts. In order to effectively calculate the damage probability, we make the following assumptions: Considering only the performance of warhead, the instantaneous posture of the missile, the instantaneous velocity of the warhead and the location of the critical point; Hit is wounded.

3.1 The establishment of the coordinate system

For the convenience of discussion, establish the following Cartesian coordinates referencing the parameters of ground coordinate system used in ground to air missile tactics:

- O, origin of coordinates, the geometry center of launching vehicle;
- OX axle (OS axle), in the level which include in origin, parallel and opposite with the horizontal projection of enemy's missile;

- OZ axle (OH axle), perpendicular to level and include in origin;
- OY axle (OP axle), include in origin, perpendicular to OX axle and OZ axle.

Then according to the definition of ground parameters coordinate system, coordinates of the warhead explosion point can be determined as (x_0, y_0, z_0)， the coordinates of the center of the each equipment as (x_i, y_i, z_i)， $i = 1,2,...,n$ are codes for each vehicle. The length, width and height of the equipment **i** are (l_i, b_i, h_i)， the area equipment damage may occur are as follows:

$$\{(x,y,z)\,|\,(x_0-x)^2+(y_0-y)^2+(z_0-z)^2 \le R_0^2, (x-x_i)^2 \le \frac{l_i^2}{4}, (y-y_i)^2 \le \frac{b_i^2}{4}, (z-z_i)^2 \le \frac{h_i^2}{4}\}$$

3.2 The criteria determining the equipment into the kill zone of warhead

Because the dynamic kill zone of missile is a hollow cone, cannot be judged by the above conditions, it must be further refined. The judgment of equipment **i** into the dynamic damage zones are: (1)Conditions of angle($\phi_1 \le \theta \le \phi_2$); (2)Conditions of distance($R_i \le R_0$).

The largest and least angle of missile's vertical axis with missile debris are ϕ_1 and ϕ_2, when the missile debris attract, the below must be followed. $\phi_1 \le \theta \le \phi_2$

$O_i\ (x_i, y_i, z_i)$ is the geometry center of i th launching vehicle, the distance with $B_m(x_0, y_0, z_0)$ can be recorded with follow.

$$R_i = \sqrt{(x_0-x_i)^2+(y_0-y_i)^2+(z_0-z_i)^2} \quad (i = 1,2,...,n)$$

Effective kill radius is R_0, $R_i \le R_0$

3.3 Calculation of the percentage of the number of hitting equipment fragment among total number of pieces.

The calculation is relatively simple when the range is spherical scattering area, so this paper deals only with hollow cone condition:

1. Calculation of the parameters of dynamic killing zone

$$\phi_1 = \arctan\frac{v_{fm}\sin(\phi-\frac{\Omega}{2})}{v_m + v_{fm}\cos(\phi-\frac{\Omega}{2})} \tag{5}$$

$$\phi_1 = \arctan\frac{v_{fm}\sin(\phi-\frac{\Omega}{2})}{v_m + v_{fm}\cos(\phi+\frac{\Omega}{2})}$$

ϕ, the flying direction angle of static. Ω, the flying angle of static. v_m, missile speed. β, the angle of missile vertical axis and level. v_{fm}, the average velocity of missile warheads.

2. Method for determining the equipment into missile dynamic damage area

According to the definition of preformed fragment warhead kill zone, some equipment to fall into the effective range must both meet the angle and distance conditions, and the effective range is as shown below.

When the equipment lies into the hollow cone damage area, percentage of effective fragment causing equipment damage is determined by the following formula:

$$P_1 = \frac{\alpha}{360}\int_{\varphi_1'}^{\varphi_2'} \Phi(\varphi)d\varphi$$

$\Phi(\varphi)$, distribution density of missile warheads.

3.4 The damage probability of equipment

The equipment is simplified as equivalent fragile body, which consists of six aspects, and detriment of each face may cause equipment damage. But the facing-missile area, vulnerable area and bullet proof strength of each surface are not identical, so probability of equipment damage is:

$$p = 1 - \prod_{i=1}^{6}(1-p_i^f) \tag{6}$$

In the formula, p_i^f is the probability that the surface **i** of components is destroyed.

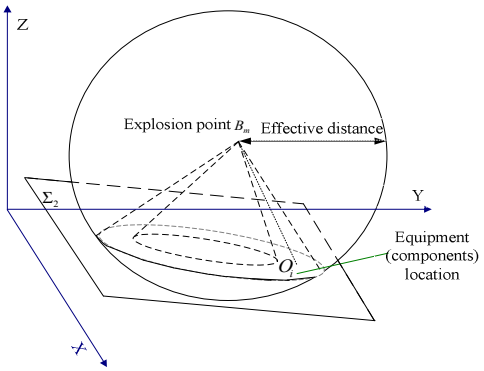

Fig. 1 The effective range of hollow cone scattering warhead

The probability of equipment damage under the premise that a single effective fragment hits a surface of the equipment is:

$$p_s = \frac{S_v}{S} = A_v$$

In the formula, p_s is the damage probability of this surface of the component under the condition that a single effective fragment hits the target; S_v is the key area of components (Vulnerable area); S is the total facing-missile area of a component; A_v is the vulnerable coefficient of the surface of components.

The damage probability of single effective fragment is p_s, with no account of damage accumulation, and considering that each effective fragment damage to the components are independent and hitted by **i** fragments, the damage probability is:

$$p(i) = 1-(1-p_s)^i$$

Then the probability of damage to surface is:

$$p^f = \sum_{i=1}^{N} g(i)p(i) = \sum_{i=1}^{n} \frac{n_e^i}{i!} e^{-n_e}[1-(1-p_s)^i]$$

$$= e^{-n_e}[\sum_{i=1}^{n} \frac{n_e^i}{i!} - \sum_{i=1}^{N} \frac{n_e^i}{i!}(1-p_s)^i]$$

When **N** is large, it can be simplified as:

$$p^f = e^{-n_e}[\sum_{i=1}^{n} \frac{n_e^i}{i!} - \sum_{i=1}^{N} \frac{n_e^i}{i!}(1-p_s)^i]$$

$$= e^{-n_e}(e^{n_e} - 1 - e^{n_e(1-p_s)} + 1) \tag{7}$$

$$= 1 - e^{-n_e p_s}$$

Through (7) and (8) can get the damage probability of equipment.

Simulation examples of electric equipment damage

According to the above principle, simulate the damage probability of equipment. Using the Monte Carlo method. The simulation process is as Fig.2.

According to the process and the algorithm described in the former section, program and simulate with VC++6.0. Set attack missile velocity: 650m/s, the number of the fragments: 15000, initial velocity of fragment:1500m/s, static scattering range: 0.52, static flying direction angle: 0.34, the quality of the fragments: 2g, the required minimum kinetic:1040J, missile coordinates: (25m,2m,15m), the volume of equipment: 12000×3000×3150mm.

It can simulate that the number of positive effective fragment accounts for 47.8% of the total number of equipment, the top 47.8%, the right side 4.4%. Combined with other factors, we can finally obtain the damage probability of power equipments.

Conclusion

This method of using damage ray to describe fragment has characteristic of simple calculation principle, It is suitable for the research of battle damage of the equipment whose metric shape is regular. Because there are many projects of equipments' important function, the computation of this method is very large. With the help of the computer simulating equipment damage, this disadvantage will be overcome. Through a large number of simulation results, we can analysis the fragility and damage surface of main equipments, and it has great reference value for the repairment of ground to air missile in wartime, guidance equipment protection, and reducing the probability of battle damage.

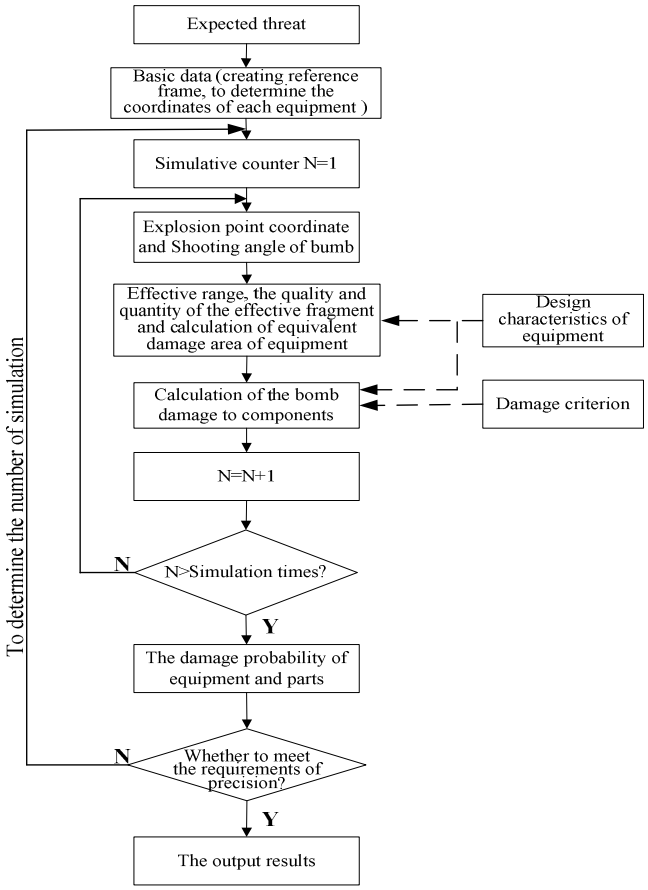

Fig. 2 The process of battle damage simulation

References

[1] HE Jian-bin, SU Qun-xing. The Metod of Ray Analysis in Battle Damage Simulation of Equipment[J]. Computer Simulation, 2005.09

[2] Shao Gang, Jiang Hua. Research of Ocean Battlefield Simulation System Based on GPU[J]. Computer Science and Application, 2012, Vol.02 (04), pp.178-183

[3] WANG Guang-yan,HU Qi-wei. Research of battlefield damage analysis based on computer simulation[J].Systems Engineering and Electronics, 2006.11

[4] Tan D M, Qu W L. The Finite Element Mode Updating of Stucture Based on Wavelet Packe Analysis an Support Vector Machine[J]. Huazhong Univ. of Sci. &Tech,2009,37(9):105-120

[5] WANG Dong, YANG Jiang-ping. Simulation Modeling on the Battle Damage of Phased-array Radar Antenna and Its Evaluation[J]. Journal of Air Force Radar Academy,2009.10, vol.23(5)

[6] WU Hong-bin, SHENG Ji-guang. Mathematical Model and its Application of Relaying Protection Device Reliability Assessment[J]. Power System Protection and Control, 2009,37 (9): 65-68

Advanced Materials Research Vols. 989-994 (2014) pp 1146-1149
© (2014) Trans Tech Publications, Switzerland
doi:10.4028/www.scientific.net/AMR.989-994.1146

Application Research on Technique of Re-entry Old Wells in Sulige Area

Xue Yafei[1,2] , Zhu Zhiying[3,a], Li Da[1,2]

[1]PetroChina Changqing Oilfield Company Sulige Research Centre, Xian, 710018, China

[2]National Engineering Laboratory of Exploration and Development in Low Permeability Oil and Gas Field, Xian, 710018, China

[3]China University of Petroleum Institute of Petroleum Engineering, Beijing, 102249, China

[a]email:zhiying_2008@hotmail.com

Keywords: Re-entry; Increasing Yield, Sulige Gas Field

Abstract. To the gas field had been developed for a long term, the yield is hard to keep a high value. How to improve the daily production is a key problem. Fracturing again in old wells can be an effective method to solve the problem. In this paper, we introduce this technique. We choose well and layer firstly, and then decide a suitable fracturing measure. Finally, fracturing evaluation shows the method can improve the yield effectively. This experience can be popularized.

Geologic aspects

Sulige gas field is located in the Ordos basin in the west of YiShan slope, is a Large lithologic trap gas reservoir develop from Carboniferous - Permian coal measures. The main gas-bearing section is dyas sandstone reservoir of Shihezi formation He8 section and Shanxi formation Shan1 section [1].

The reservoir porosity of He8 section ranges from 4.0% to 13.0%, and mean value is 8.9%; permeability is $(0.03\sim2.0)\times10^{-3}$ μm^2, and mean value is 0.5425×10^{-3} μm^2. The reservoir porosity of Shan1 section ranges from 4.0% to 13.0%, and mean value is 8.5314%; permeability is $(0.04\sim1.0)\times10^{-3}$ μm^2, and mean value is 0.3566×10^{-3} μm^2. It can be viewed as low porosity low permeability sandstone reservoir [2].

Since 1999, large-scale exploration began in Sulige gas field. And 2003, the development of gas field started. In 2013, 1473 wells' capacity was lower than 3000m3/d by investing, which occupied 31%. And by the development of gas field, the number will be more and more. It will be very hard to keep a stable capacity. In order to improve the capacity of old wells, we introduce fracturing to exploit potentialities in old wells [3].

Oil production technique for re-entry in old wells

The main points on fracturing are decided which well and which layer should be fractured.

The principle of choosing well is as follow [4]:

1) In the well bore, the production string structure is simple. Packer and hydraulic anchor can deblock the gas well.
2) Wellbore configuration and casing setting depth are suitable. And casing pressure resistance is strong.
3) Well cementation is good.
4) In original gas-producing zone, the content of H2S is low. String corrosion is light.

The principle of choosing layer in the well is as follow[5]:

1) Reservoir's geological conditions: to alternate layer, logging data, physical property, effective thickness should be considered.
2) Gas productivity: the production of adjacent well with the same layer to alternate layer should be higher.
3) We give up fracture at the beginning of design because of high water ratio. In the late age of production, geological evaluation shows it changes into unhydrous layer probably.

4) Choose the layer which initial evaluation is low capacity, but by geological evaluation and development of production technique become better, the well has the development potential.

Based on these principles, research on each step, and form the technology which is suitable for Sulige gas field. Find the well which is expected to increase production, and then gas field practice is followed.

Application and Effect Evaluation

We choose 31 wells to fracturing again, and achieved a certain effect to increase production. Now take SuDong 62-69 as an example to description the process.

Reservoir's geological evaluation on SuDong 62-69

As shown in Table 1, He5 section, Shan1 section, and Mawu2 section is gas-bearing layer, have the development potential, and can implement the transfer layer fracturing.

Table 1 Logging data and explanation on SuDong 62-69

Layer	well section (m)	thickness (m)	resistivity (Ωm)	AC (μs/ m)	densisty (g/cm^3)	VSH (%)	POR (%)	PER ($10^{-3}\mu m^2$)	SG (%)	conclusion
He_8^U	2938.9-2944.8	5.9	94.26	224.73	2.56	7.33	7.97	0.242	62.10	Gas-bearing layer
He_8^D	2991.5-2997.5	6.0	48.25	237.80	2.50	11.90	10.14	0.385	68.70	Gas reservoir
$Shan_1$	3028.9-3032.5	3.6	62.83	230.48	2.53	14.01	8.84	0.206	64.90	Gas-bearing layer
$MaWu_1^4$	3152.6-3154.0	1.4	227.32	163.44	2.67	2.46	5.73	0.161	65.30	Gas-bearing layer
$MaWu_1^4$	3154.0-3156.0	2.0	173.35	169.68	2.70	4.30	7.85	0.602	79.78	Gas reservoir
$MaWu_2^2$	3164.0-3166.0	2.0	265.54	163.78	2.65	1.33	3.08	0.096	50.60	Gas-bearing layer
$MaWu_4^1$	3192.63-3195.25	2.62	229.15	167.59	2.68	1.64	7.14	0.330	61.50	Gas-bearing layer

Production dynamic analysis on SuDong 62-69

In Figure 1, daily gas production before shutting in well is 0.478×104m3/d, oil/casing pressure is 1.8/8.9MPa, cumulative gas is 610.91×104m3 . Casing pressure falls flat, daily gas production fluctuates slightly and water content is low.From Table 2, we can see that such as SuDong 62-66 and Tong 18, have a good performance, production and cumulative gas are not bad. He2 layer and Shan1 layer are better potential productivity. Till now, we know that SuDong 62-69 has the ability of yield increase, and can be transfer layer construction.

Wellbore conditions evaluation on SuDong 62-69

Completion tool structure: distance between tubing and bushing 4.58m+ tubing hanger 0.45m+27/8 " + 324 tubing 3126.29m+ AJ-110 safety joint 0.55m+KDB-114 hydraulic anchor 0.37m+ K344-108 packer 0.38m+27/8 " 3 tubing 28.97m+KHT-100 sliding sleeve sand jet 0.64m+K344-112 packer0.38m+27/8 " 2tubing 19.32m+sandbeasting tee 0.22m. Steel grade of tubing in this well is N80, 80S. In target perforated zone, cementing quality is excellent, H2S content is lower, and wellbore conditions meet requirements of reconstruction.

Fracturing design

From logging data, we know that gas bearing interval is 2.0m, reservoir thickness is 6.6m in MaWu22 section. In MaWu14 section gas bearing interval is 1.4m, reservoir thickness is 3.4m. Because the distance between MaWu22 and MaWu14 is short, two sections are carried out acid fracturing together. For these two sections, initial fracturing used gelled acid and drag-reducing acid. Production is lower at the production tail. Reconstruction use clean steering acid fracturing fluid to improve the fracturing effect.

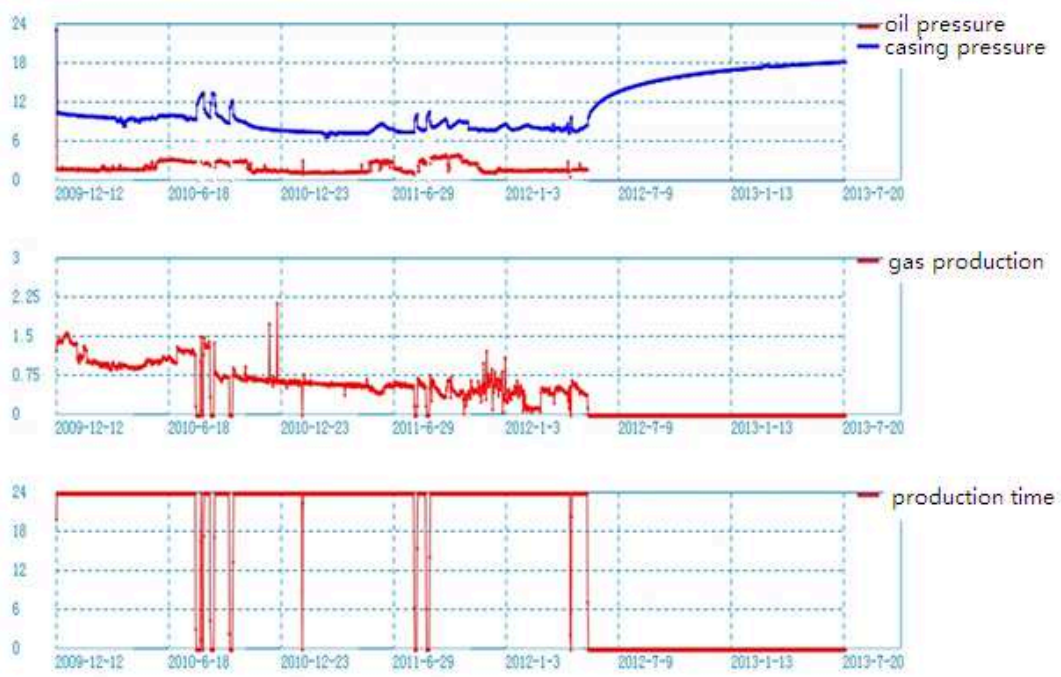

Figure 1 Production curve before fracturing again on SuDong 62-69

Table 2 Production situation of adjacent wells

Well number	Developed layer	Effective thickness (m)	SOP Time	Casing pressure (MPa)	Daily gas producton ($10^4m^3/d$)	cumulative gas (10^4m^3)
SuDong 62-66	He_{8U}, $Shan_1$, $Shan_2$	30.2	2008.12.22	10.4	1.372	2386.3
Tong 18	He_8, $Shan_2$	18.6	2009.4.7	7.5	1.657	2266.61

Logging data shows that in Shan1 section, gas bearing interval is 3.6m, reservoir thickness is 3.6m. He_8^D section and He_8^U section gas bearing interval is 6.0m and 5.9m respectively, and reservoir thickness is 6.0m and 9.3m. In these three sections, gas bearing formations are with developing potential, should implement hole fracturing, and should control the scale.And to $Shan_1$, He_8^D, He_8^U sections, use low concentrations of guanidine gum fracturing fluid, develop effective long cracks, and improve fracturing effect.

Table 3 Fracturing construction parameter list

layer	Perforated interval (m)	The amount of proppant(acid) (m^3)	The average sand ratio (%)	Fluid recovery (m^3/min)	Nitrogen dosage (m^3)
$MaWu_2^2$ +$MaWu_1^4$	3164.0-3167.0 3152.6-3156.0	Drag-reducing acid 115 Steering acid 120		3.0-4.0	
$Shan_1$	3029.0-3032.0	20	22	2.6-2.8	8.1
He_8^D	2993.0-2996.0	30	24	2.8-3.0	9.7
He_8^U	2940.0-2943.0	30	23	2.6-2.8	10.5

Fracturing construction and effect analysis

Detailed fracturing construction parameters are shown in Table 3. By reconstruction, get a better result. As shown in Table 4, drainage cycle is short, flowback rate is high. And in Figure 2, it shows that daily production after reconstruction is 1.2117×104m3/d, raise the yield which is 0.7337×104m^3/d.

Table 4 Gas testing result list on SuDong 62-69

Drainage cycle (d)	Flowback ratio (%)	Shut-in recovery time (d)	Shut-in recovery oil pressure (MPa)	Shut-in recovery casing pressure (MPa)	Static pressure (MPa)	Flowing pressure (MPa)	Daily gas production ($10^4m^3/d$)	Open-flow production ($10^4m^3/d$)
7	82.5	3	19.2	19.2	24.83	19.11	8.8108	15.3625

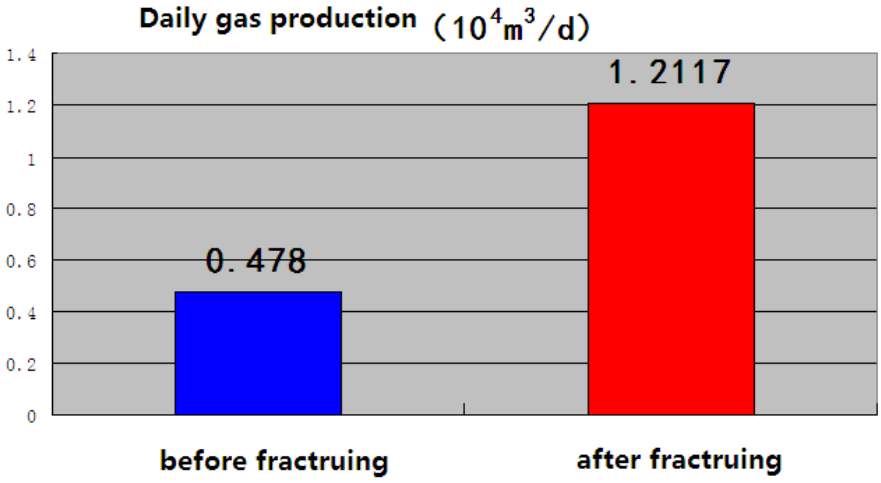

Figure 2 Capacity comparison before and after fracturing on SuDong 62-69

Conclusion

Fracturing again for old wells is an effective method to improve the yield. It is a complex process. Sulige gas field had been developed for a long term. The yield decreased and it is hard to find replaced layer. So, it is necessary to pay attention to old wells. According to research experience about fracturing again at home and abroad, we should choose well and layer firstly, and then decide a suitable processing measure. Finally, this reconstruction can improve the yield.

By the principles of choosing well and layer, decide the well and layers. We should choose the one continuity of sand is better, adjacent well productivity is better in target layer. And then evaluate wellbore technology, decide it is suitable to fracture or not. When the answer is yes, we can implement fracturing. Using low damage kill fluid and fracturing fluid to reduce the damage to the reservoir. By analyzing SuDong 62-69, we know that fracturing again for old well can improve the yield, and this experience can be popularized.

References

[1]Kang Yili, Luo Pingya. Present Situation and Prospect on China Tight Sandstone Gas Reservoir Exploration and Development Key Engineering Technology [J]. Petroleum Exploration and Development, 2007, 34(2): 239-245. (in chinese)

[2]Zhuang Hua. Research on Gas Productivity Prediction Based on Logs for Post-frac Tight Sandstone Reservoirs in Sulige Area. Master thesis, Jilin University, 2013. (in chinese)

[3]Wang Qiang, Sun Wanli, Zhang Zhentao. Application of Re-entry Old Well in Compact Clasolite Gas Reservoir in West Sichuan. Drilling and Production Technology, 2005, 289(3):55-57.(in chinese)

[4]Deng Wenlong. Research on Re-entry Old Well Choosing Well's Direction in ChuanXi. Western China Exploration Engineering, 2009, 7:73-75. (in chinese)

[5]Zhang Ruifen. Application of Fracture Technology to Multiple Layers in Deep Reservoir of Bawu Gas Field. Well Testing, 2004, 4:54-55. (in chinese)

Advanced Materials Research Vols. 989-994 (2014) pp 1150-1156
© (2014) Trans Tech Publications, Switzerland
doi:10.4028/www.scientific.net/AMR.989-994.1150

Unsteady Heat Transfer Analysis: Saving-Energy and the Regionalism Design on Air-Conditioning System for Car

Li OUYANG[1, a], Die LI[1, a]

[1]School of Automobile Engineering, Wuhan University Technology, Wuhan, 430070, China

[a]email: ouyangli-002@163.com

Keywords: Unsteady Heat Transfer Analysis; Regionalism Design; Car; Air-conditioning Load; Saving-energy

Abstract. In this paper, based on unsteady heat transfer calculation method, the results of the heat transfer through the enclosure of car compartment are given, in order to analyze dynamic energy-saving effect of the regionalism design on air-conditioning system for car. The result demonstrates that the regionalism design on the air-conditioning system has important saving-energy effect.

Introduction

The solar radiation is an important source of air-conditioning load [1]. The solar radiation distribution of the same car driving in different cities is different because of the different date change of temperature curve, sunlight duration curve, and illumination intensity curve in the different areas [2][3][4]. In addition, there is also data informed us that the heat through the enclosure of car compartment is calculated by using unsteady heat transfer calculation method, which is higher than that by steady heat transfer calculation method under the same calculation condition [5]. In this paper, based on the geographical and meteorological data of four cities with typical weather conditions [6], including Wuhan, Kunming, Haerbin and Huhehaote, the unsteady heat transfer calculation method is adopted to calculate air-conditioning load of the same car, which is assumed to be driven in four cities. Analysis on the solar radiation influence on car air-conditioning load using unsteady calculation method can provide more accurate date for studying on the saving-energy effect of the regionalism design on air-conditioning system of the car. We also conclude the regionalism design on air conditioning system for car is available for saving energy.

Air Conditioning Load Unsteady-State Heat Transfer Calculation

Heat Transfer through the Car Envelope and Roof The per-hour value of summer outdoor air temperature is given by

$$T_{out}(t) = \overline{T}_{out} + (T_{out,\max} - T_{out})\cos(15t - 225) \quad (1)$$

where $T_{out}(t)$ is the per-hour value of outdoor air temperature, ℃. T_{out} is the per-hour value of summer outdoor air dry-bulb temperature, ℃. $\overline{T}_{out}$ is the value of a calculation day's summer average outdoor air temperature, ℃. $T_{out,\max}$ is the maximum value of summer outdoor air temperature, ℃, we have

Wuhan: $T_{out}(t) = 31.9 + 6.3\cos(15t - 225)$ (2)

Kunming: $T_{out}(t) = 22.2 + 6.9\cos(15t - 225)$ (3)

Haerbin: $T_{out}(t) = 26.0 + 8.3\cos(15t - 225)$ (4)

Huhehaote: $T_{out}(t) = 25.0 + 9.4\cos(15t - 225)$ (5)

The following Table 1 lists the summer outdoor air temperature in four cities.

Direct Normal Irradiance The direct normal irradiance through the atmosphere is given by

$$I_{dh} = I_0 P \csc\beta \quad (6)$$

where the solar irradiance I_0 is 1353W/m^2. P is the atmospheric transmissivity, 0.65 ~ 0.75, and β is the zenith angle.

The solar direct radiation intensity on vertical plane with the east direction angle ε can be given by

$$I_{dv} = I_{dh} \cos\beta \cos(\alpha - \varepsilon) \tag{7}$$

where α is the solar azimuth.

When the car is driven to east direction, the angle between the east and the normal of the north side surface is 270°, the angle between the east and the normal of the front side is 0°, the angle between the east and the normal of the south side is 90°, and the angle between the east and the back side is 180°.

The solar direct radiation intensity on the slope of φ is given by

$$I_{\varphi} = I_{dh}(\sin\beta\cos\varphi + \cos\beta\cos\alpha\sin\varphi) \tag{8}$$

In this paper, with regard to the car windows, the angle between the side and the horizontal plane is 90°, except the angle between the front window and the horizontal plane is 60°. Table 2 gives the solar zenith and azimuth in four cities.

Table 1 Summer outdoor air temperature in four cities

	Wuhan	Kunming	Haerbin	Huhehaote
T_{out} (℃)	35.2	25.8	30.3	29.9
$\overline{T}_{out}$ (℃)	31.9	22.2	26.0	25.0
$T_{out,\max} - T_{out}$ (℃)	6.3	6.9	8.3	9.4

Table 2 Solar zenith and azimuth in four cities

Solar Time	Solar zenith (°)				Solar azimuth (°)			
	Wuhan	Kunming	Haerbin	Huhehaote	Wuhan	Kunming	Haerbin	Huhehaote
6	10	8	14	13	108	109	105	106
7	23	22	25	24	101	103	95	97
8	35	35	35	36	95	98	84	87
9	48	48	46	47	87	93	71	76
10	61	62	55	58	77	86	55	61
11	73	75	62	66	58	74	32	37
12	80	85	65	70	0	0	0	0

Diffuse Solar Radiation Intensity The diffuse solar radiation intensity on the horizontal plane can be calculated in according with the following formula.

$$I_{sh} = 0.5 I_0 \sin\beta \frac{1 - P^{CSC\beta}}{1 - 1.4\ln P} \tag{9}$$

The diffuse solar radiation intensity on the inclined plane is given by

$$I_{s\varphi} = \cos^2\frac{\varphi}{2} I_{ah} \tag{10}$$

Then, the total solar radiation intensity on the east side of the car body in summer is

$$J(t) = I_{dv} + I_{\varphi} + I_{ah} + I_{s\varphi} \tag{11}$$

The following Table 3 gives the summer total solar radiation intensity on the east lateral wall of the car body at various moments in four cities.

Table 3 Summer total solar radiation intensity on the east lateral wall of the car body (W)

Time	6	7	8	9	10	11	12	13	14	15	16	17	18
Wuhan	360	602	662	663	548	373	161	160	149	134	105	76	59
Kunming	201	412	432	456	464	368	159	157	145	138	112	82	78
Haerbin	368	547	625	672	576	402	186	181	153	146	116	97	91
Huhehaote	374	569	674	680	583	408	190	185	151	148	119	99	95

J(t) can be sorted out the following formula:

$$J(t)=\sum_{n=1}^{m} B_n \cos(\omega_n' t-\phi_n')+B_0 \tag{12}$$

where B_n is the nth fluctuation of solar radiation intensity.B_0 is the 0th external disturbance, that is to say the average daily solar radiation intensity of certain latitude and orientation, W/m^2.ϕ_n' is the initial phase of the nth variation of solar radiation intensity, rad. ω_n', 2π/T[(rad/h)], is the nth frequency of the variation of solar radiation intensity.

Only the first is taken account for the calculation of the total solar radiation intensity on the east side of the car body in summer, then

Wuhan: $J(t)=514\cos(0.26t-2.05)+171$ (13)

Kunming: $J(t)=319\cos(0.26t-2.19)+168$ (14)

Haerbin: $J(t)=519\cos(0.26t-2.07)+174$ (15)

Huhehaote: $J(t)=529\cos(0.26t-2.06)+174$ (16)

It is easy to obtain the outdoor sol-air temperature curves from the following formula

$$T_e(t)=T_{out}(t)+\rho J(t)/\alpha_{out} \tag{17}$$

where $T_{out}(t)$ is the hourly calculation value of outdoor temperature, ℃. ρ is the solar radiation absorptivity of the outer surface of the car body, for the dark car, ρ=0.9. J(t) is instantaneous value of solar radiation, W/m^2, α_{out} is convective heat transfer coefficient of the outer surface of the car body, W/(m$^2\cdot$℃). Then,

$$T_e(t)=T_{out}(t)+0.9J(t)/50 \tag{18}$$

On account of the hourly values, $T_e(t)$, which can be fitted wave function, as follows:

Wuhan: $T_e(t)=34.98+3.4\cos(18t-278)$ (19)

Kunming: $T_e(t)=25.22+2.3\cos(18t-286)$ (20)

Haerbin: $T_e(t)=29.13+4.8\cos(18t-297)$ (21)

Huhehaote: $T_e(t)=28.13+5.2\cos(18t-280)$ (22)

Temperature Difference Heat Transfer Air-Conditioning Load On the base of the harmonic response method, the unsteady heat transfer gain at the t moment may be evaluated from

$$Q_t=KF\theta \quad \text{W} \tag{23}$$

where we define the equivalent temperature deference θ as

$$\theta=\overline{T_e}-T_{in}+\frac{\alpha_{in}}{K}\sum_{n=1}^{m}\frac{c_n}{\nu_{e,n}}\cos(\omega_{e,n}t-\phi_{e,n}-\varepsilon_{e,n}) \tag{24}$$

The heat transfer attenuation, $\nu_{e,n}$, is given by

$$\nu_{e,n}=e^{\sum_{i=1}^{n_1}R_iS_i/\sqrt{2}} \tag{25}$$

And the heat transfer delay time: $\varepsilon_{e,n}=\frac{1}{2}\sqrt{\frac{z}{\pi}}\Sigma_{i=1}^{n_1}\frac{x_i}{\sqrt{a_i}}$ (26)

The symbol, R denotes the thermal resistance of each layer materials, (m$^2\cdot$℃) / W, and S is the heat storage coefficient, W/ (m$^2\cdot$℃).The equivalent temperature deferences, θ, in the four cities can be calculated, and obtain

Wuhan: $$\theta = 34.98 - 25 + \frac{4}{3.83} \times \frac{3.4}{1.62} \times \cos(18t - 278 - 0.5 \times 18) = 9.98 + 2.19\cos(18t - 269) \quad (27)$$

Kunming: $$\theta = 25.22 - 25 + \frac{4}{3.83} \times \frac{2.3}{1.62} \times \cos(18t - 286 - 0.5 \times 18) = 0.22 + 1.48\cos(18t - 277) \quad (28)$$

Haerbin: $$\theta = 29.13 - 25 + \frac{4}{3.83} \times \frac{4.8}{1.62} \times \cos(18t - 297 - 0.5 \times 18) = 4.13 + 3.09\cos(18t - 288) \quad (29)$$

Huhehaote: $$\theta = 34.98 - 25 + \frac{4}{3.83} \times \frac{5.2}{1.62} \times \cos(18t - 280 - 0.5 \times 18) = 9.98 + 3.35\cos(18t - 291) \quad (30)$$

Table 4 Unsteady temperature difference heat transfer air-conditioning load of car body-wall in four cities (W)

Time	Wuhan	Kunming	Haerbin	Huhehaote
6	12.17	2.49	2.28	14.04
7	11.44	2.68	4.77	13.26
8	9.72	2.20	6.82	12.54
9	8.17	1.37	7.05	12.35
10	7.86	0.77	5.29	12.83
11	8.98	0.80	2.75	13.65
12	10.78	1.44	1.14	14.25
13	12.04	2.25	1.56	14.22
14	11.89	2.69	3.73	13.59
15	10.45	2.45	6.17	12.78
16	8.68	1.70	7.22	12.34
17	7.79	0.95	6.17	12.57
18	8.39	0.70	3.73	13.31

Air-Conditioning Load from Solar Radiation through Glass Window

The air-conditioning load from heat gain through glass window is given by

$$q_f = \beta_b J_t(t) \text{ W/m}^2 \quad (31)$$

where the conversion coefficient β_b is 0.3~0.7. And the transient total solar radiation intensity is $J_t(t)=\beta_t\beta_r J(t)$, W/m^2, in which β_t and β_r denote, respectively, the absorptivity and the deposition. Table 5 gives the transmissivity, absorptivity, deposition of the car window with different incidence angles.

Table 5 Transmissivity, absorptivity, deposition of the car window with different incidence angles

Incidence angle	0^o	15^o	30^o	45^o	60^o	70^o	80^o	90^o
Transmissivity	0.811	0.809	0.802	0.781	0.713	0.595	0.354	0
Absorptivity	0.117	0.119	0.124	0.131	0.139	0.143	0.139	0
Deposition	0.848	0.847	0.842	0.823	0.757	0.641	0.398	0

We note that the conversion coefficient β_b, can be given around 0.3 to 0.7, and the larger the space occupied by the car facilities, or the more distinctive thermal storage capacity, the smaller the value of β_b is. For example, β_b can be given smaller value for cars. So this paper assign the smaller

value to β_b. In addition, after 14 o 'clock, the air-conditioning load from solar radiation through the east of the car window is not equal to zero, but which can be approximated at zero because of giving priority to heat dissipation, for simplicity. Table 6 gives the air-conditioning load from solar radiation through the east of the car window.

Fresh Air Load Calculation

The fresh air load calculation can be evaluated according to the relation ,which is listed below:

$$Q_{fresh-air} = l_o n\rho(h_o - h_i) \quad \text{W} \tag{32}$$

where n is passenger quantity (n=4). l_o is fresh air volume per man-hour. In this paper, l_o=11m^3 per man-hour, and the minimum fresh air requirement is at least 10m^3 per man-hour. ρ is the density of the air, and ρ =1.146kg/m^3. h_o is the outdoor air enthapy, in kJ/kg , which is obtained from psychrometric chart. But h_i denotes the indoor air design enthapy, and which can also be obtained via psychrometric chart. Locating the point on the psychrometric chart where the air dry temperature is 25℃, and the relative humidity is 55%, the corresponding value for h_i is about 52.5kJ/kg. The fresh air load calculation results for four typical cities are given in Table 7.

Table 6 Air-conditioning load from solar radiation through the westward window of the car (W)

Time	Wuhan	Kunming	Haerbin	Huhehaote
6	126.72	70.752	129.536	131.648
7	207.088	141.728	188.168	195.736
8	226.404	147.744	213.75	230.508
9	224.094	154.128	227.136	229.84
10	175.908	148.944	184.896	187.143
11	100.71	99.36	108.54	110.16
12	30.59	30.21	35.34	36.1
13	11.2	10.99	12.67	12.95
14	0	0	0	0
15	0	0	0	0
16	0	0	0	0
17	0	0	0	0
18	0	0	0	0

Table 7 Fresh air load calculation results for four typical regions

City		Wuhan	Kunming	Haerbin	Fuhehaoe
Outdoor air dry temperature	(℃)	35.2	25.8	30.3	29.9
Outdoor air relative humidity	(%)	60	60	60	60
Outdoor air enthapy	(kJ/kg)	91	58	73	70
Fresh air load	(W)	1941.3	277.3	1033.7	882.4

Permeation Load from the Door and Window Slits of the Car Calculation

The permeation load from the door and window slits of the car can be written as

$$Q_{permeation} = Ll_c\rho(t_{out} - t_{in}) \quad \text{W} \tag{33}$$

where t_{out} is the outdoor air temperature, in ℃. The air density ρ=1.14kg/m^3.The symbol l_c represents the silts length of the door and window of the car (about 12m for the door silts, and 8.5m for window silts).The infiltration rate per meter opening joint in door and window L, m^3/h, varies with the air velocity, which can be given in accord with the data used in civil building. In this paper, L=4.0m^3/h for single steal window silts per meter, and L=10.0m^3/h for door silts per meter, when

the air velocity is 3m/s. The permeation load from the door and window slits of the car calculation is obtained using above data, and the calculation results for the four cities are also tabulated as

Table 8 Pereation load from the door and window silts of the car in the four cities

City		Wuhan	Kunming	Haerbin	Fuhehaote
Outdoor air dry temperature	(℃)	35.2	25.8	30.3	29.9
$Q_{pereation}$	(W)	1800.3	141.2	935.5	864.9

Heat Gain from Human Bodies

The heat gain from human bodies can be calculated from

$$Q_{human-body} = Q_s + qnn' \quad \text{W} \tag{34}$$

where Q_s is the heat gain from the driver(about 170W). n is the number of people (n=3). n' is clustering coefficient ($n' = 0.89$), and q is heat gain per hour from one people (q=108W).Thus the heat gain from human bodies $Q_{human\text{-}body}$ is about 458.4W.

Heat Load from Equipment and Illumination Calculation

The heat load from equipment and illumination is

$$Q_{equipment} = (0.6 \sim 0.75)Q_1 \quad \text{W} \tag{35}$$

Thus, $Q_{equipment}$ is about 60W,when Q_1=100W from experience point.

Unsteady-State Total Air Conditioning Load Calculation

At unsteady state, the total air conditioning load of the car can be computed from

$$Q_{total-load} = Q_{envelope} + Q_{solar-radition} + Q_{flesh-air} + Q_{permeation} + Q_{human-body} + Q_{equipment} \quad \text{W} \tag{36}$$

And the calculation results for the four cities are also presented in Table 9

Table 9 Unsteady-state total air conditioning load of the car in four cities (W)

Time	Wuhan	Kunming	Fuhehaote	Haerbin
6	4398.89	1010.142	2619.416	2411.388
7	4478.528	1081.308	2680.538	2474.696
8	4496.124	1086.844	2708.17	2508.748
9	4492.264	1092.398	2721.786	2507.89
10	4443.768	1086.614	2677.786	2465.673
11	4369.69	1037.06	2598.89	2389.51
12	4301.37	968.55	2524.08	2316.05
13	4283.24	950.14	2501.83	2292.87
14	4271.89	939.59	2491.33	2279.29
15	4270.45	939.35	2493.77	2278.48
16	4268.68	938.6	2494.82	2278.04
17	4267.79	937.85	2493.77	2278.27
18	4268.39	937.6	2491.33	2279.01

Analysis on the Energy-Saving

Comparison of the air-conditioning load of the same car travelling in Wuhan and Kunming, by use the following expression as

$$\frac{Q_{Wuhan} - Q_{Kunming}}{Q_{Wuhan}} \quad \% \tag{37}$$

Assigning the air-conditioning load calculation values of 12:00 noon to Q_{Wuhan} and $Q_{Kunming}$, respectively, and obtain

South: $\frac{4301.37 - 968.55}{4301.37} = 77.48\%$ (38)

Based on above calculation result, the transient value of the decrease percentage of air conditioning load is approximately 77.48%.

Conclusion

The transient value of the decrease percentage of air conditioning load is also up to 77.48%. The results show that the regionalism design on the air-conditioning system of car has outstanding energy-saving effect.

Acknowledgement

In this paper, the research was sponsored by the Fundamental Research Funds for the Central Universities (Project No. 2011-IV-123).

References

[1] Ling Tong, Yongjun Zhou. Numerical and Experimental Study of the Solar Radiant Energy Distribution in the Air-Conditioned Car [J]. HV&AC, 2000, 2: 9-11.
[2] Jiali Wang, Renhe Zhang, Yingchun Wang. Features of the Surface Air Temperature in Different Areas of Beijing and the Representativeness of Beijing Observatory [J]. Climatic and Environmental Research, 2012, 17(5): 563-573.
[3] Chengbo Su, Xinyan Zhang, Jinrui Lu. The Analysis of Solar Radiation Intensity in Urumqi [J]. Journal of Electric Power, 2013, 28(5): 391-395.
[4] Huiqun Li, Zuntao Fu, Xinyu Wen, and Jianbin Huang. Characteristic Analysis of Sunshine Duration Change in China During the Last 50 Years [J]. Climatic and Environmental Research, 2013, 18(2): 203-209.
[5] Shuang Wu, Contrast and Analysis on the Calculation Methods of Air Conditioning Load in Automobile [J]. Refrigeration and Air-Conditioning, 2002, 2(6): 20-23.
[6] Aiping Zheng. Air Conditioning Engineering (2nd Edition) [M]. Beijing: Science Press, 2008.

Advanced Materials Research Vols. 989-994 (2014) pp 1157-1160
© (2014) Trans Tech Publications, Switzerland
doi:10.4028/www.scientific.net/AMR.989-994.1157

Constructing of Low Carbon Ecological Index System for Planning: Liaobin New Town as An Instance

Jingcheng Yuan, Shi Chen, Muzi Huang, Lei Fang

#9, Hunnan donglu Road, Shenyang, Liaobing, PRC

#9, Hunnan donglu Road, Shenyang, Liaobing, PRC

#9, Hunnan donglu Road, Shenyang, Liaobing, PRC

#9, Hunnan donglu Road, Shenyang, Liaobing, PRC

fanglei2002@126.com, artest2007@126.com,

Keywords: Liaobin New Town, Low carbon ecology, Indicator system, Construction method

Abstract. The paper takes Liaobin New Town Low-carbon Ecological Plan as the research object, and explores the constructing process of Liaobin New Town Low-carbon Ecological Planning Indicator System(LCEPIS), mentions construction principles and methods; Secondly by analyzing regional condition, it assures the main paradox of regional development and the core of low-carbon ecological plan; Thirdly it mentions construction methods of the research object, sets up indicator system upon the procedure of frame assembling, indicator picking, indicator quantifying and indicator weighted value confirming; thirdly it introduces the specific calculating method as the indicator system is assessed and applied; finally we obtain the main outcome: Liaobin LCEPIS, meantime gain sub-conclusions such as initial picking library, chosen indicator and weight of indicator, etc. The research method could guide how to construct a regional plan indicator system, and obtained result could be referenced for similar plan indicator system.

Introduction

Low-Carbon Ecology is a key word currently, therefore we need to set up more divers criteria systems to appraise urban planning so that the function of cities will be more sustainable. Low carbon ecological indicator planning system(LCEIPS) can be an efficient tool for assessing and regulating urban planning. All the same not so many people are researching indicator system which employed to a specific city, and can be extant to the whole planning system. So we still have to work hard to deal with how we employ low-carbon ecological plan indicator system to a plan organization of a very city.

Low Carbon Ecological planning Indicator System

2.1 The Purpose and Significance of System Building

LCEPIS is set up exclusively for the whole city planning process and comprises of various ecological planning indicators which face city design. LCEPIS is an efficient tool for consolidating low carbon idea, and will have an outstanding influence to the new districts planning of China.

Constructing LCEPIS mainly has five influences, firstly it is a request of planning law; Secondly it can fulfill the idea of low carbon city; Thirdly it supplies a standard for evaluating plan, to define pros and cons and advise; Fourthly, it conceives proper law involves low carbon policy for city management and development; Lastly, it can solve city's real problems and improve indicator system's adaptability and operability, shows local scenery and city sight.

2.2 The concept and structure

LCEPIS comprise various indicator systems, each one can guide plan drafting, assess and approve plans on the next level. Consider indicator systems' inherence up to down when we filter and choose indicators to assure low carbon plan idea to operate and achieve throughout.

2.3 The principles of LCEPIS

The first principle is *Adapting the Localities*, that is treating LCEPIS as an assessing and regulating tool which fits local situation; The second is *Science and Usefulness*, that is satisfying basic principle of indicator system construction to ensure operating process for getting exact result; The third is *Implementing by Law*, that is establishing rules we need to obey so that LCEPIS can enactive the planning and management, then the law may be mended if there is any conflict between law and LCEPIS.

Local feature of Liaobing New Town

3.1 Geography

Liaobin New Town is at the north of Liaodong Bay, in the delta of Daliaohe River besides Panjin, it has coastal pattern. Present land area is 198.7 km^2, while built-up area is 34.4 km^2. Liaobin New Town has a hot summer continental climate means its four seasons are distinctive, be moister in summer while be dry in winter. Liaobin New Town should alter heating method and improve build energy conservation to improve energy consuming efficiency.

3.2 Waterfront City

Although Liaobin New City besides sea, its water supply is redundant, and chlorine content is high. Liaobin Port is an important cargo port and secondary port for containers freight. We need to face profits and challenges of seafront, especially in natural and ecological aspects, and we also need to harmonize the relationship among port, downtown and industrial area.

3.3 Leading by Manufacture

Because of both abundant resource and developed public works, Liaobin New Town can be set up to a manufacture-lead city, in that case we can build an petrol equipment and ship producing base as well as developing green foods and marine travel services in the future. For sustainable development, we need to promote recycling, energy conserving and reducing remit.

3.4 New Town Construction

Liaobin New Town is the only new city which obeys coastal middle city standard of the Liaoning coastal strategy, its construction will effect ecology system inevitably. Liaobin has vulnerable ecosystem and is a bub of bird migration, so that we must protect and preserve its resource, local species and birds habitat, and reduce huma activities as much as possible, to balance development and conservation. Liaobin New Town strategy plan began in 2008, and has been mature after researching and modifying for years. Liaobin New Town can be built to a resource-saving, friendly-to-environment and ecological coastal new town, and there a marine apparatus base of world class could be built alongside the river and coast line.

LCEPIS Constructing Process

LCEPIS Constructing Process includes 4 steps, they are listed below:

4.1 Frame setting up

LCEPIS has 3 levels from top to bottom: *Targe-level, category-level and indicator-level*. Choosing Liaobin New Town indicator system can display local feature through relying on local perspective. Liaobin New Town LCEPIS need to be classified according to plan organization structure to adapt present planning system. There are 7 categories, Industries & Economy, Resource and Energy, Land using, Transportation, Environment & Ecology, Municipal affairs & Security, Architecture & Landscape, they are all cover any part of planning system and have the same process.

4.2 Indicator filtering

In the beginning, we need to build *initial indicator filter library* which can supply data for indicators. Initial library can categorize and label collected indicators, meanwhile collect and analyze LCEPIS information when synchronizing content. Initial library of Liaobin indicator system. Initial library of Liaobin indicator system comprises 204 indicators which involves all 7 categories.

The second phase is *filtering indicators*. Picking indicators from initial library, testing it by paper surveying and interview, then analyzing collected information and getting result. The test paper

survey consists three parts, the first part tells about Liaobin New Town, the second part collects information, the third part *categorizes and labels 204 LCEPIS indicators* by the content of category level, and sets up "chosen" and "deleted" the two options, then puts simple illustration. The objective of test survey mainly are people whose work is concern with planning, architecture or similarity, then we pick out people randomly what can show its profession and participation. After test papers were being handed in, we go through them and analyze collected data to obtain the selected indicators.

4.3 Indicator quantification

The procedure of indicator quantifying is *conversing selected indicator to quantifiable indicator*, by calculating methods and range of threshold. There are 3 indicator Quantifying Calculating Methods, *Data gauging, Statistical inference and Calculation result of quantification and statistics derived from other indicators*. After deciding the calculating method, we need to set up the standard which could be expressed by threshold, then the range of threshold could be limited by maximum and minimum, and could be exemplified precisely by open interval and closed interval. When maximum equals to minimum, the standard is determined, and its threshold is the only value.

There are 5 kinds of methods to decide the range of standard threshold: (1)*Standard referring*, includes laws, ordinances, guidances and international standards; (2)*Experience summary*, means by studying and collecting experience which foreign countries have, to decide the range; (3)*Surveying and contrasting*, by researching current condition to watch the difference in various segments, get referable indicator data and compare it with plan target, for determining proper regulatory indicators; (4)*Estimating volume reversely*, by assessing carrying capacity according to basic regional development information to deduce various indicators; (5)*Layout simulation*, means we can analyze and mimic plan by simulation software, for getting proper standards. All above we need to think the relationships among indicators and employ in many ways to get proper quantified indicators.

4.4 Weighted value confirmation

There are two types of weight confirmation methods: One type is subjective weighting method which includes Delphi Method, Analytic Hierarchy Process(AHP), etc. Another type is objective weighing method, which includes Principle Component Analysis(PCA), Factor Analysis, etc. For solving problems, it is not enough only confirm weight of indicator according to the carbon remit indicator, but also we should analyze via subjective opinions.

The weight confirmation process is: (1)According to the 7 categories of indicator system to determine the target weight value; (2)Assuring the the weight value of every category; (3)After assessing indicator system, we could multiply indicator weight by category weight to get each indicator's weight value for the total target. We can employ Delphi Method to collect, arrange and evaluate data, then line them by Scaling Method into matrix, next we input formed weight matrix to Yaahp to get result of weight of each category, finally we can gain weight value and indicators.

Design of assessing indicator system method

After finishing up building indicator system, we determine how to operate it during assessing plan, it includes *Indicator Normalization*(IN) and *Quantified Result Checking*(QRC) two steps. IN is through positive converting and nondimensionalization, we can convert all actual indicator values to a very form has same unit, dimension; QRC means weighted calculating the standardized indicator assessing value to obtain final assessing result. The research employs two methods.

5.1 Indicator normalization method

LCEPIS could be categorized to 44 positive indicators, 7 reversed indicators, 4 decent indicators and 1 valued indicators. There are four normalization mode we can implement: (1)Positive indicator normalization equation prescribes that once actual value reaches threshold's lower limit it will get scores, reaches upper limit it will get full scores, overrides upper limit it still gets full scores, while it can not get any score if its value do not reaches indicator's lower limit; (2)Reversed indicator normalization equation assumes: As actual value goes down to the threshold upper limit that it starts to gain score, gets on the lower limit it scores full mark, be lower than the lower limit it still scores full mark, and goes above the upper limit it marks zero; (3)Proper indicator normalization equation assumes when actual value of indicator equals the median value of threshold the score is full, when

the value is smaller than the lower limit or bigger than the upper limit, the scores are both 0; (4)Value indicator normalization, there is only the indicator what is non-harmful treatment of residential waste is value indicator, its qualified value is 100. When actual value is 100, its nondimensionalization is 1, if actual value is not 100, its nondimensionalization will be 0.

5.2 Assessing checking

The indicator system could obtain the conclusion through weighted calculation, while its process is: (1)We normalize the two last results to gain value p; (2)We sum up all values of p to gain value D according to indicator weight; (3) We weighted calculate all value D according to the value's weight, and sum up them to get the aim result Q.

Conclusion

The research guide by low carbon idea, sets up the LCEPIS of Liaobin For actual condition, apply an comprehensive frame of system construction, principle and approach, an obtain plenty of sub-conclusions, includes basic frame of system, indicator library, etc. All conclusion will be apply to researching Liaobin plan and LCEPIS, also can consolidate the principles and request that indicator system needs to adapt area condition, and support low carbon building. The research can improve city plan's function and influence to low carbon ecological cities. However, there are still some limitation, we will go on researching and discussing tin future.

Low carbon ecological city construction will be still a major subject of city construction for a long time in future, meantime building a sustainable residential environment of city will be livelong aim for human's living and development. As the involved researches get progressed, the LCEPIS will develop and get better for a long time, and be adopted by country's plan and development law system, for helping city development and construction.

References

[1] Bert J.M de Vries, in: *Conceptualizing Sustainable Development-An Assessment Methodology Connecting Values, Knowledge, Worldviews and Scenarios*, submitted to Ecological Economics, 68, 1006-1019. (2009)

[2] Chinese society for Urban Studies(CSUS): *Chinese low carbon ecological city plan development report 2012* , China Architecture & Building Press, Beijing. (2012)

[3] Chen Fei, Zhu Dajian, in: *Research on the Content, Models and Strategies of Low Carbon Cities,* submitted to Urban planning forum, 182(4), 7-13. (2009)

[4] Goodall. C, in: *How to live a low-carbon live: The individual's guide to stopping climate change*, Sterling, London. (2007), in press.

[5] Qiu Baoxing, in: *The holistic development idea of Chinese low-carbon eco city*, submitted to Construction science and technology, 15, 12-17. (2009)

[6] Tan Zhenfeng, in: *Method and practice of continuous indicator system construction*, submitted to Plan innovation: Chinese urban plan conference 2010.

[7] Topic Group, Ministry of Housing and Urban-Rural Development: *Research about improving Plan Indicator System*, China Architecture & Building Press, Beijing.(2007), in press

[8] Zhou Lan, Zhang Jingxiang, in: *Eco-City Planning and Construction in Low-carbon Era*, China Architecture & Building press, Beijing.(2010), in press

Advanced Materials Research Vols. 989-994 (2014) pp 1161-1164
© (2014) Trans Tech Publications, Switzerland
doi:10.4028/www.scientific.net/AMR.989-994.1161

Ballast Water Discharge and the Influence of Seawater Environment

Xiaoyan Li [1, a], Sha Liu[2, b], ZhiMin Zhou[2, b]

[1]College of Life Science and Technology of Dalian University, Liaoning,Dalian,116622,China,
[2]Science and Technology on Underwater Test and Control Laboratory, Dalian, 116013, China.
[a]112731815@qq.com；[b]zzm@dlut.edu.cn

Keywords: Ballast water discharge, seawater environment,global response

Abstract. Ships have carried solid ballast for thousands of years in the form of rocks, sand or metal. In modern times, ships use water as ballast. It is more easier to load on and off a ship and more efficient and economical than solid ones. Ship fills with ballast water when it is empty of cargo, and the ballast water is discharged when it loads cargo. In ballast water ,there are hundreds of organisms carried that cause problematic ecological effects outside of their natural range. Preventing the transfer of invasive species and coordinating a timely and effective response to invasions require cooperation and collaboration between governments. Considerable efforts had already made to formulate appropriate standards for ballast water management during the convention development process.

Overview

Seawater has been used as ballast to stabilize vessels at sea since the introduction of steel hulled vessels around 120 years ago. Ballast water is pumped-in to maintain safe operating conditions throughout a voyage[1]. This practice reduces stress on the hull, provides transverse stability, improves propulsion and manoeuvrability, and compensates for weight lost due to fuel and water consumption. Ballast water is needed to provide stability and manoeuvrability during a voyage when ships are not carrying cargo or carrying not enough heavy cargo to keep more stability in the rough seas[2,3]. It is estimated that 3000-4000 million tons of untreated ballast water are discharged from ships every year in ports, vessels deballast to reduce their draft and enter ports when cargoes are loaded in coastal regions [4]. Furthermore, it is estimated that more than 10.000 marine species transported across the oceans in ballast water of cargo ships and introduced into a non-native environment everyday. Ships by take up and discharge transfer ballast water from one area or sea, to another,will seriously disturb or alter the ecosystem by introducing "invasive" micro-organisms which establish themselves in the local environment.

As early as 1995, Hyde Marine came to aware that the ballast water in ships was carrying thousands of species of aquatic animals and plants. The invasive organisms carried out the problems of marine environment and human health in and around the Great Lakes area, threatening the healthy aquatic ecosystems economies.

The invasive organisms include bacteria, microbes, small invertebrates, eggs, cysts and larvae of various species. The transferred species may survive to establish a reproductive population in the host environment and turn to invasive, out-competing native species and multiplying into pest proportions. Ballast water exchange is usually costly, time consuming and limited in effectiveness. Ballast water exchange may result in increased hull stresses and stability problems either.

With carried in ballast water, there are hundreds of organisms that cause problematic ecological effects outside their natural range. The International Maritime Organization list the ten most unwanted species in the ballast water[5]:

- Cholera Vibrio cholerae (various strains)
- Cladoceran Water Flea Cercopagis pengoi
- Mitten Crab Eriocheir sinensis
- Toxic algae (red/brown/green tides) (various species)
- Round Goby Neogobius melanostomus
- North American Comb Jelly Mnemiopsis leidyi
- North Pacific Seastar Asterias amurensis
- Zebra Mussel Dreissena polymorpha
- Asian Kelp Undaria pinnatifida
- European Green Crab Carcinus maenas

With the expansion of volume and density of international shipping ,the transfer of harmful aquatic species in ships' ballast water tanks has become one of the most significant pathways by unintentional introductions of invasive alien species into marine ecosystems. As ballast water has the character of fresh, brackish or saline which make most the coastal environment, estuaries and navigable inland waters at risk. The costs of economic, social, recreational and ecological losses are difficult to assess for such invasive species, while the losses of native species and environment restoration to pre-invasion quality are more difficult to determine and quantify.

Apart from affecting ecosystems and contributing to the extinction of native species and representing a significant threat to biodiversity therefore, invasive alien species may also cause major socio-economic damage. Reported about effects on human health deriving from alien invasive species include changes to the native food web and contaminated seafood for human consumption.

Global response

Preventing the transfer of invasive species and coordinating a timely and effective response to invasions require the cooperation and collaboration among governments, economic sectors, non-governmental organizations and international treaty organizations .The UN Convention on the law of the sea provides global framework by requiring states to work for“to prevent, reduce and control pollution caused by human of the marine environment, including the intentional or accidental introduction of harmful alien species to a particular part of the marine environment.”

In 2004, IMO adopted the International Convention for control and management of ships’ ballast water and sediments. The Convention will enter into force for 12 months after it has been ratified by 30 states representing which including 35 percent of the world’s merchant shipping tonnage. The Convention are engaged in international voyages and apply to all kinds of ships and offshore structures which carry ballast water [6-8].

The Ballast Water Management (BWM) Convention requires:

- A ship-specific Ballast Water Management Plan approved by the Administration on board
- A Ballast Water Record Book on board
- Ballast water exchange (Regulation D-1)
- An approved ballast water treatment system (Regulation D-2)
- An International Ballast Water Management Certificate.

The Convention stipulates two standards for discharged ballast water. The D-1 standard covers ballast water exchange while the D-2 standard covers ballast water treatment. The Convention requires either D-1 or D-2 standard after entry into force. If from 1st of January 2016 bagan entry into force, the Convention will require compliance with the D-2 according to the schedule in the table:

Table 1: The Convention will require compliance with D-2 according to the schedule

Constructed year		BW Capacity (m^3)	New schedule
Before 2009		Between 1500 and 5000	1st IOPP renewal survey after entry into force of the Convention
		Less than 1500 or greater than 5000	1st IOPP renewal survey after the anniversary date of delivery of ship in 2016
2009 or after		Less than 5000	1st IOPP renewal survey after entry into force of the Convention
	Between 2009 and 2011	5000 or more	1st IOPP renewal survey after the anniversary date of delivery of ship in 2016
	After 2011	5000 or more	1st IOPP renewal survey after entry into force of the Convention

If the Convention does not enter into force before 2016, the applicable date of compliance with D-2 standard will renewal survey for all ships firstly. Ships built will be required to have a treatment system after entry into force installed before delivery.

Approval of ballast water management systems[9-10]

During the Convention development process, considerable efforts had made to formulate appropriate standards for ballast water management, which are the ballast water exchange standard and the ballast water performance standard. Ships performing ballast water exchange need do with an efficiency of 95 percent volumetric exchange of ballast water and using a ballast water management system (BWMS) need to meet a performance standard based on agreed numbers of organisms per unit of volume.

Regulation D-3 of the BWM Convention requires ballast water management systems used to comply with the Convention must be approved by the Administration taking into account the Guidelines for approval of ballast water management systems (G8).

Regulation D-3 also requires that ballast water management systems which make use of Active Substances to comply with the Convention shall be approved by IMO in accordance with the 'Procedure for approval of ballast water management systems that make use of Active Substances (G9)'. Procedure (G9) consists of a two-tier process – Basic and Final Approval - to ensure that the ballast water management system does not pose unreasonable risk to the environment, human health, property or resources.

A technical group of experts has been established under the auspices of GESAMP to review the proposals submitted for approval of ballast water management systems that make use of Active Substances. The GESAMP Ballast Water Working Group (GESAMP-BWWG) reports to the Organization on whether such a proposal presents unreasonable risks in accordance with the criteria specified in the Procedure for approval of ballast water management systems that make use of Active Substances.

Summary

Ballast water treatment technology to the development of shipping industry and the enormous impact of environmental protection, along with the international convention for the effective date

draws near, ballast water treatment system shipment application has a foregone conclusion, up to now, the world has 15 research and development of ballast water treatment system by IMO's final approval.For shipyard, how to safe, effective, space, cost, operation, certification and hull damage, the respect such as secondary hazard analysis, choose the most suitable for our factory manufacture of ship ballast water treatment system, has become a pressing problem.

How to complete treatment of ballast water and solved the seawater problems fundamentally, will meet challenge of hard to imagine. The ballast water problem, is not only a technical one, but also a problem of international collaboration. The strict law enforcement to severely only by relevant countries and organizations unified action.

Acknowledgement

The study was supported by the National Natural Science Foundation of China (Grant No. 51349005 and 51375074).

References

[1] Else M. Fykse, Trine Nilsen, Agnete Dessen Nielsen, Ingun Tryland, Stephanie Delacroix, JanetM. Blatny. Real-time PCR and NASBA for rapid and sensitive detection of Vibrio cholerae in ballast water[J]. Marine Pollution Bulletin, 2012.2, 64(2): 200–206.

[2] SH Baek, SW Jung, MC Jang, B Hyun & K Shin. Survival potential of autotrophic phytoplankton species collected from ballast water in international commercial ships[J]. New Zealand Journal of Marine and Freshwater Research, 2012,46(1):125-136.

[3] Gulsen Altug, Sevan Gurun, Mine Cardak, Pelin S. Ciftci, Samet Kalkan. The occurrence of pathogenic bacteria in some ships' ballast water incoming from various marine regions to the Sea of Marmara, Turkey[J]. Marine Environmental Research, 2012.10, 81:35–42.

[4] Mindong Bai, Zhitao Zhang , Nahui Zhang, Yiping Tian. Treatment of 250 t-h Ballast Water in Oceanic Ships Using •OH Radicals Based on Strong Electric-Field Discharge – Springer[J].Plasma Chemistry and Plasma Processing Science and Business Media,2012.4.

[5] MEPC, 2011. List of ballast water management systems that make use of Active Substances which received Basic and Final Approval. Ballast Water Management, 9 August 2011.

[6] MEPC, 2012. Report of the Marine Environment Protection Committee on Its Sixty-third Session. Marine Environment Protection Committee, 2 March 2012.

[7] OECD, 2006. OECD guidelines for the testing of chemicals: Freshwater alga and cyan bacteria, growth inhibition test.

[8] IMO: International Maritime Organization-BWMConvention.[EB/OL].[2012-03-02]. http://www.imo.org/ Our- Work/Environment/Ballast Water Management/Pages/BWMConvention.aspx

[9] IMO International Convention for the Control and Management of Ships' Ballast Water and Sediments International Maritime Organization, London (2004).

[10] K.G. Nadeeshani Nanayakkaraa, Yu-Ming Zhenga, A.K.M. Khorshed Alamb, Shuaiwen Zoua, J. Paul Chen.Electrochemical disinfection for ballast water management: Technology development and risk assessment[J]. Marine Pollution Bulletin, 2011,63(5): 119-123.

Advanced Materials Research Vols. 989-994 (2014) pp 1165-1168
© (2014) Trans Tech Publications, Switzerland
doi:10.4028/www.scientific.net/AMR.989-994.1165

A High-order CMOS Bandgap Voltage Reference

Qianneng Zhou[1, a], Yunsong Li[1], Jinzhao Lin[1], Hongjuan Li[2], Chen Li[1], Yu pang[1], Guoquan Li[3], Xuemei Cai[1] and Qi Li[1]

[1]College of Electronic Engineering, Chongqing University of Posts and Telecommunications, Chongqing 400065, China

[2]College of Computer and Technology, Chongqing University of Posts and Telecommunications, Chongqing 400065, China

[3]College of Telecommunication and Information Engineering, Chongqing University of Posts and Telecommunications, Chongqing 400065, China

[a]zhouqn@cqupt.edu.cn

Keywords: Bandgap voltage reference, power supply rejection ratio, temperature coefficient

Abstract. A high-order bandgap voltage reference (BGR) is designed by adopting a current which is proportional to absolute temperature $T^{1.5}$. The high-order BGR is analyzed and simulated in SMIC 0.18μm CMOS process. Simulation results show that the designed high-order BGR achieves temperature coefficient of 2.54ppm/°C when temperature ranging from -55°C to 125°C. The high-order BGR at 10Hz, 100Hz, 1kHz, 10kHz and 100kHz achieves, respectively, the power supply rejection ratio of -64.01dB, -64.01dB, -64dB, -63.5dB and -53.2dB. When power supply voltage changes from 1.7V to 2.5V, the output voltage deviation of BGR is only 617.6μV.

Introduction

Voltage references are important blocks in many analogue and mixed signal electronic systems such as data converters and power management systems. The temperature dependence of voltage reference is undoubtedly one of the most important issues, since it directly affects the performance of such circuits. In fact, the bandgap voltage reference (BGR) is one of the most popular voltage references widely used in analogue and mixed signal electronic systems. And, the basic idea of BGR is a weighted sum of the base-emitter voltage V_{BE} of NPN BJTs and the thermal voltage V_T. Due to the nonlinearity of V_{BE}, first-order BGR has relatively high temperature coefficient (TC) in the whole temperature range, and it is not suited for the requirements of high precision circuits.

In the recent years, many temperature compensation techniques of BGR have been reported to overcome the TC limitation of first-order BGR [1-5]. Recently, demands for low-voltage BGR circuits have increased enormously because they are widely used in portable electronic applications. So, the temperature compensation technique of BGR should still be discussed to further improve TC of BGR.

In this paper, a sub-1V low TC BGR is designed by adopting a current which is proportional to $T^{1.5}$, here T is the absolute temperature. By adopting the current which is proportional to $T^{1.5}$, the designed BGR achieves well low TC in the whole temperature range. The analysis and discussion of the designed low TC BGR will be given in the following section.

Analysis and Design of Higher-Order BGR

Fig.1 shows the designed high-order BGR, which consists of a core circuits of BGR and a start-up circuit. The core circuits of BGR have two possible equilibrium points, so a start up circuit is necessary. As shown in Fig.1 (b), the start up circuit consists of MOS transistors M_{S1}~M_{S6}. The core circuit of high-order BGR, which adopts a current that is proportional to $T^{1.5}$ to improve the TC, is made up of M_1~M_{19}, resistors R_1~R_5, PNP transistors Q_1~Q_2 and amplifiers A_1~A_2. In this paper, all MOS transistors adopt the long channel device so that the channel-length modulation effect is negligibly small.

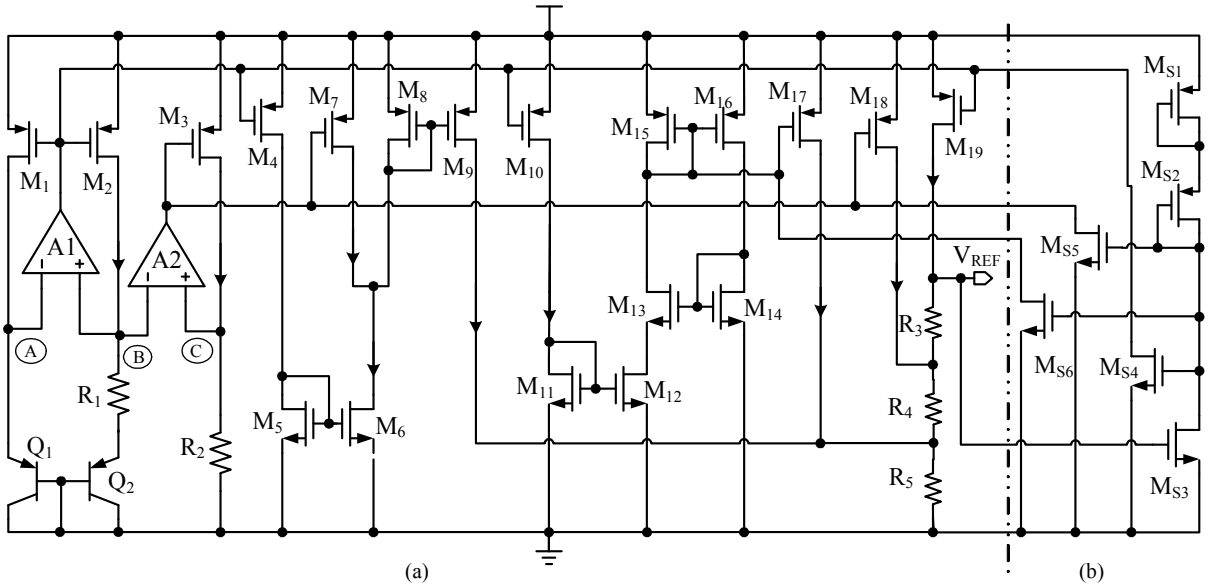

Fig. 1 Circuit of high-order BGR (a) Core circuit of BGR (b) start-up circuit

For convenience, it is assumed that I_j is the drain current of MOS transistor M_j, here j=1, 2…19. As shown in Fig.1, amplifiers A_1 and A_2 are entirely the same, and their dc-gain A_d has that A_d>>1. PNP transistor Q_2 has an emitter area that is m times that of PNP transistor Q_1, and transistors M_1 and M_2 are entirely the same. Amplifier A_1 forces voltage V_A of node A and voltage V_B of node B be equal, and amplifier A_2 forces voltage V_C of node C and voltage V_B of node B be equal voltage , i.e. V_A=V_B= V_C=V_{EB1}. Here, V_{EB1} is the emitter-base voltage of PNP transistor Q_1. So,

$$I_2 = \left(V_T \ln m\right)/R_1 \tag{1}$$

$$I_3 = V_{EB1}/R_2 \tag{2}$$

$$V_T = kT/q \tag{3}$$

where, k is Boltzmann's constant, q is electronic charge, and T is absolute temperature. Transistors M_2 and M_4 are entirely the same, and the aspect ratio of transistor M_6 is K_1 times that of transistor M_5. And, the aspect ratio of transistor M_7 is K_2 times that of transistor M_3. So, I_6=K_1I_2 and I_7=K_2I_3. By optimizing the parameters of K_1 and K_2, it is concluded that I_6=I_7 under the temperature T_{r1}. And the aspect ratio of transistor M_9 is K_3 times that of transistor M_8. So

$$I_9 = \begin{cases} 0 & when \quad T \le T_{r1} \\ \dfrac{K_3 K_1 V_T}{R_1} \ln m - K_3 K_2 \dfrac{V_{EB1}}{R_2} & when \quad T > T_{r1} \end{cases} \tag{4}$$

The aspect ratio of transistor M_{10} is K_4 times that of transistor M_2, so I_{10}=K_4I_2. Transistor M_{11} operates in the saturation region, and the gate-source voltage V_{GS1} of transistor M_{11} can be derived as

$$V_{GS11} = \sqrt{\frac{2K_4(\ln m)V_T / R_1}{\mu_n C_{OX}(W/L)_{11}}} + V_{TH} \tag{6}$$

where, μ_n is the mobility of an electron, C_{ox} is the gate oxide capacitance per unit area, and $(W/L)_{11}$ is the width-length ratio of transistor M_{11}. Transistor M_{12} operates in deep triode region, and $(W/L)_{12}$ is the width-length ratio of transistor M_{12} respectively. So, the channel resistor r_{ds12} of transistor M_{12} can be derived as

$$r_{ds} = \frac{\sqrt{(W/L)_{11} R_1}}{\sqrt{2\mu_n C_{ox} K_4 V_T (W/L)_{12} \ln m}} \tag{7}$$

Transistors M_{15} and M_{16} are entirely the same and they operate in the saturation region. Transistors M_{13} and M_{14} operate in sub-threshold region, and the aspect ratio of transistor M_{13} is α times that of transistor M_{14}. In fact, the drain current I_D of MOS transistor operating in the sub-threshold region can be modeled as

$$I_D \approx \frac{W}{L} I_{D0} \exp\left(\frac{V_{GS}}{nkT/q}\right) \tag{8}$$

where, n is the sub-threshold slop factor, I_{D0} is the process-dependent parameter, W/L is the channel width-length ratio of MOS transistor, and V_{GS} is the gate-source voltage of MOS transistor. So, the drain current I_{15} of MOS transistor M_{15} can be derived as

$$I_{15} = n(\ln\alpha)\left(\frac{W}{L}\right)_{12} \frac{\sqrt{2\mu_n C_{ox} K_4 (\ln m)}}{\sqrt{R_1 (W/L)_{11}}} \frac{k^{1.5}}{q^{1.5}} \times T^{1.5} \tag{9}$$

At the same time, the aspect ratio of transistor M_{17} is K_5 times that transistor M_{15} and $I_{17}=K_5 I_{15}$. The aspect ratio of transistor M_{19} is K_6 times that of transistor M_2, and the aspect ratio of transistor M_{18} is K_7 times that of transistor M_3. According to Eq.1-Eq.9 and the circuit shown in Fig.1, the output voltage V_{REF} of BGR can be written as

$$V_{REF} = I_{19}(R_3 + R_4 + R_5) + I_{18}(R_4 + R_5) + I_{17}R_5 + I_9 R_5 = V_{PTAT} + V_{CTAT} + V_{NL} + V_{PTAT^{1.5}} \tag{10}$$

where,

$$V_{PTAT} = \left[K_6 \times (R_3 + R_4 + R_5) V_T \ln m\right] / R_1 \tag{11}$$

$$V_{CTAT} = \left[K_7 \times (R_4 + R_5) V_{EB1}\right] / R_2 \tag{12}$$

$$V_{NL} = \begin{cases} 0 & when \quad T \le T_{r1} \\ \dfrac{K_3 K_1 R_5 V_T}{R_1} \ln m - \dfrac{K_3 K_2 R_5 V_{EB1}}{R_2} & when \quad T > T_{r1} \end{cases} \tag{13}$$

$$V_{PTAT^{1.5}} = nK_5 R_5 (\ln\alpha)\left(\frac{W}{L}\right)_{12} \frac{k^{1.5}}{q^{1.5}} \frac{\sqrt{2\mu_n C_{ox} K_4 (\ln m)}}{\sqrt{R_1 (W/L)_{11}}} T^{1.5} \tag{14}$$

According to the above analysis, V_{PTAT} and V_{CTAT} are a voltage with positive- and negative- TC respectively, V_{NL} is a voltage with piecewise-linear temperature characteristic, and $V_{PTAT}^{1.5}$ is proportional to $T^{1.5}$. Therefore, $(\partial V_{ref}/\partial T)_{T=Tr}=0$ can be achieved by optimizing the appropriate values of R_1~R_5, K_1~K_7, m and the width-length of transistors M_{11}~M_{12} in theory.

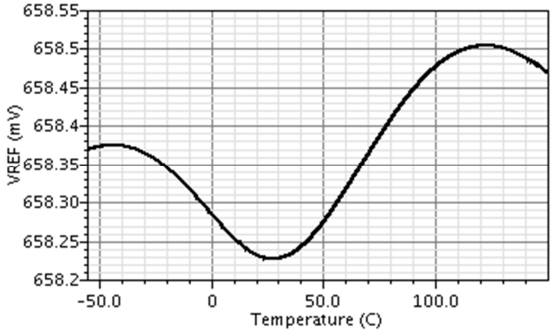

Fig. 2 Simulation result of BGR output voltage V_{REF} as a function of temperature

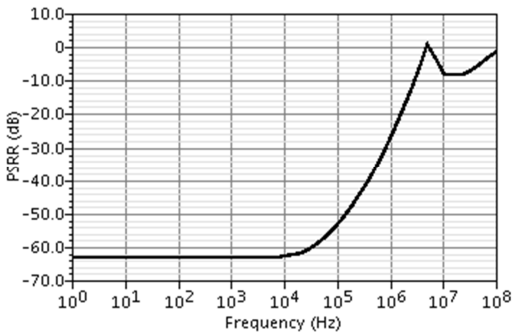

Fig. 3 Simulated PSRR of BGR output voltage V_{REF}

Simulation Results

To verify the circuit shown in Fig.1, the high-order BGR is designed and simulated in SMIC 0.18μm CMOS process with a 1.8-V power supply voltage. Fig.2 shows the simulated temperature property of high-order BGR. Simulation results show that the high-order BGR achieves a TC of 2.54ppm/°C when temperature ranging from -55°C to 125°C. The simulated PSRR of high-order BGR is shown in Fig.3. Simulation results show that the high-order BGR at 10Hz, 100Hz, 1kHz, 10kHz, 100kHz and 1MHz achieves, respectively, the PSRR of -64.01dB, -64.01dB, -64dB, -63.5dB, -53.2dB and -27.3dB. Fig.4 shows the simulated line-regulation of high-order BGR. When power supply voltage V_{dd} changing from 1.7V to 2.5V, the output voltage V_{REF} of high-order BGR has only

a deviation of about 617.6μV. Finally, performances of the designed high-order BGR are summarized in Table 1.

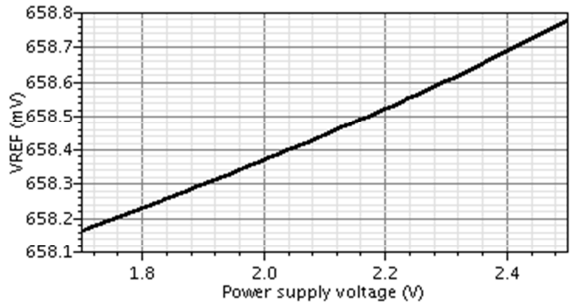

Fig. 4 Simulation results of BGR output voltage V_{REF} as a function of power supply voltage

Table 1 Performances of high-order BGR

Process		0.18μm CMOS
Supply Voltage (V)		1.8
Temperature coefficient (ppm/°C)		2.54
PSRR@25°C(dB)	10Hz	-64.01
	100Hz	-64.01
	1kHz	-64
	10kHz	-63.5
	100kHz	-53.2
	1MHz	-27.3

Conclusion

A low temperature coefficient high-order BGR is designed by adopting a current which is proportional to $T^{1.5}$ in this paper. Simulation results show that the high-order BGR provides an output voltage with excellent stability and a low TC performance. It is well suited for analogue and mixed signal systems.

Acknowledgment

This work was supported in part by National Science Foundation of China (Grant No. 61102075, and 61301124), Natural Science Foundation Project of CQ CSTC (Grant No. cstcjjA40011, cstc2011jjA1380), 121 Project of CQ CSTC (Grant No. cstc2014jcsfglyjs0012, cstc2014zktjccxyyB0008), Scientific and Technological Research Program of Chongqing Municipal Education Commission (Grant No. KJ120503, KJ120507, and KJ120533), 2013 Program for Innovation Team Building at Institutions of Higher Education in Chongqing (Grant No. G2013-46), Special Project of Internet of Things from Ministry of Industry and Information Technology, and Chongqing Development Plan of Innovative Young Talents (Grant No. cstc2013kjrc-qnrc0126).

References

[1] Z. K. Zhou, Y. Shi, Z. Huang, P. S. Zhu, Y. Q. Ma, Y. C. Wang, Z. Chen, X. Ming, and B. Zhang: A 1.6-V 25-mA 5-ppm/°C curvature-compensated bandgap reference. IEEE Transactions on Circuits and Systems-I: Regular Papers, Vol.59 (2012), p.677-684.

[2] C. M. Andreou, S. Koudounas, and J. Georgiou: A novel wide-temperature-range, 3.9ppm/ºC CMOS bandgap reference circuit. IEEE Journal of Solid-State Circuits, Vol.47 (2012), p.574-581.

[3] M. D. Ker, J. S. Chen: New Curvature-compensation Technique for CMOS Bandgap Reference with Sub-1-V Operation. IEEE Transactions on Circuits and Systems-II: Express Briefs, Vol.53 (2006), p.667-676.

[4] Y. H. Lam, W. H. Ki: CMOS Bandgap References with Self-Biased Symmetrically Matched Current-Voltage Mirror and Extension of Sub-1-V Design. IEEE Transactions on Very Large Scale Integration Systems, Vol. 18 (2010), p.857-865.

[5] D. C. W. Ng, D. K. K. Kwong, N. Wong: A Sub-1V, 26Mw, Low-Output-Impedance CMOS Bandgap Reference with a Low Dropout or Source Follower Mode. IEEE Transactions on Very Large Scale Integration Systems, Vol.19 (2011), p.1305-1309.

Advanced Materials Research Vols. 989-994 (2014) pp 1169-1172
© (2014) Trans Tech Publications, Switzerland
doi:10.4028/www.scientific.net/AMR.989-994.1169

Multistage Amplifier Using Dual-Miller with Nulling-Resistor and Dual-Feedforward Structure

Qianneng Zhou[1, a], Qi Li[1], Jinzhao Lin[1], Hongjuan Li[2], Chen Li[1], Yu Pang[1], Guoquan Li[3], Xuemei Cai[1] and Yunsong Li[1]

[1]College of Electronic Engineering, Chongqing University of Posts and Telecommunications, Chongqing 400065, China

[2]College of Computer and Technology, Chongqing University of Posts and Telecommunications, Chongqing 400065, China

[3] College of Telecommunication and Information Engineering, Chongqing University of Posts and Telecommunications, Chongqing 400065, China

[a]zhouqn@cqupt.edu.cn

Keywords: Dual-miller compensation with nulling-resistor, dual-feedforward compensation, three-stage amplifier.

Abstract. This paper designs a high-gain wide-bandwidth multistage amplifier by employing the dual-miller compensation with nulling-resistor and dual-feedforward compensation (DMCNR-DFC) in 0.35μm BCD process. The designed DMCNR-DFC multistage amplifier achieves well performance including gain-bandwidth product (GBW) and slew rate (SR). Simulation results show that the DMCNR-DFC multistage amplifier achieves a dc gain of about 121.1dB and GBW of about 6.1MHz with 52^o phase margin.

Introduction

Operational amplifiers are important building blocks in the analog integrated systems and mixed-signal systems because their behavior dominates the performance of these function blocks. However, with the channel lengths and supply voltage of MOSFET transistor scaling down in the modern CMOS process, the classical single-stage cascode amplifier is no longer suitable for obtaining high dc-gain and large output swing simultaneously. Under low supply voltage condition, multistage operational amplifiers are increasingly utilized by analog designers to provide high gain and large output voltage swing simultaneously [1-5]. In fact, three-stage amplifier is a good trade-off between gain and complexity [1-5]. Nonetheless, three-stage amplifier is a multiple-pole system, and which suffers from the closed-loop stability problem. The stability is a well important design constraint in implementing a three-stage amplifier. Therefore, a three-stage amplifier must be properly compensated in frequency.

In this paper, based on the classical nested miller compensation (NMC) technique [1], a three-stage amplifier, which adopts dual-miller compensation with nulling-resistor and dual-feedforward compensation (DMCNR-DFC), is designed and analyzed.

Analysis and Design of DMCNR-DFC Three-Stage Amplifier

The topology of DMCNR-DFC three-stage amplifier is shown in Fig.1. A_{v1}, A_{v2} and A_{v3} form the basic three-stage amplifier. A_{v1} is a high-gain first-stage, A_{v2} is a high-gain and wide output-swing second-stage, and A_{v3} is the last stage with wide output-swing. A_{va} and A_{vf} form two feedforward stages. R_{m1}-C_{m1} and R_{m2}-C_{m2} form miller compensation with nulling-resistor. A_{va} and A_{v2} form the push-pull second-stage of three-stage amplifier, and A_{vf} and A_{v3} form the push-pull output stage of three-stage amplifier. Therefore, the DMCNR-DFC three-stage amplifier has an improvement transient response.

Transconductances of gain stage A_{vj} are expressed as g_{mj}, here j=1, 2, 3. $r_{o(1,2)}$ and $C_{o(1,2)}$ are the equivalent output resistances and lumped parasitic capacitance of gain stages respectively, and R_L

and C_L are the loading-resistor and loading-capacitor respectively. g_{ma} and g_{mf} are the equivalent transconducatances of A_{va} and A_{vf} respectively. To simplify the analysis, it is assumed that $C_L>>C_{m1}=C_{m2}>>C_{o(1,2)}$, $g_{m(1,2)}r_{o(1,2)}>>1$, $g_{m3}R_L>>1$, $R_L>>R_{m(1,2)}$ and $g_{m3}=g_{mf}$. Based on those assumptions, the open-loop small-signal transfer function of DMCNR-DFC three-stage amplifier can be derived as

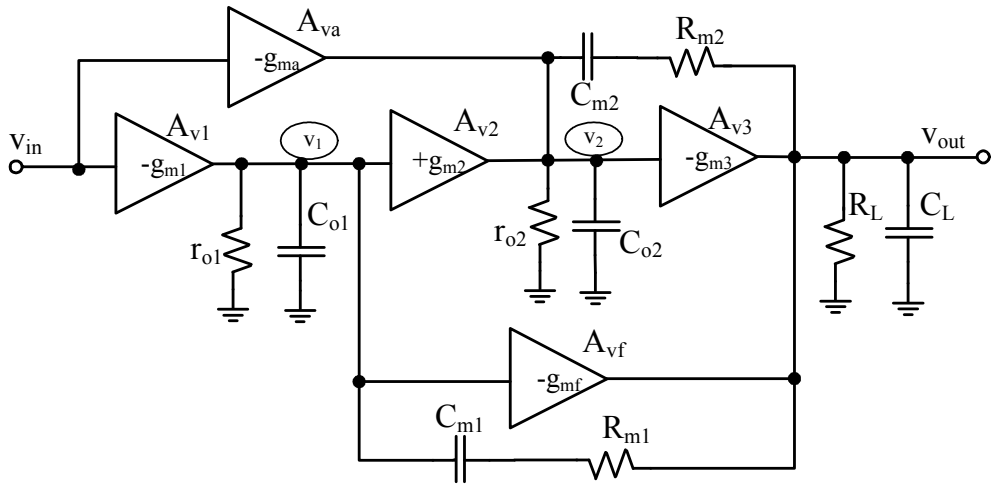

Fig. 1 Topology of DCMCNR-DFC three-stage amplifier

$$A_v(s) \approx \frac{g_{m1}g_{m2}g_{m3}r_{o1}r_{o2}R_L(1+s/z_1)(1+s/z_1)(1+s/z_1)}{(1+s/p_1)(1+s/p_2)(1+s/p_3)(1+s/p_4)(1+s/p_5)} \tag{1}$$

where,

$$z_1 = \frac{1}{C_{m2}\left[(R_{m2}+R_{m1})-1/g_{m3}\right]} \tag{2}$$

$$z_2 = \frac{g_{m3}(R_{m2}+R_{m1})-1}{R_{m1}C_{m1}(g_{m3}R_{m2}-1)} \tag{3}$$

$$z_3 = \frac{g_{m1}g_{m2}(R_{m2}-1/g_{m3})}{R_{m2}(g_{ma}C_{o1}+g_{m1}C_{o2})} \tag{4}$$

$$p_1 = \frac{1}{g_{m2}g_{m3}r_{o2}r_{o1}R_LC_{m1}} \tag{5}$$

$$p_2 = \frac{1}{R_{m2}C_{m2}} \tag{6}$$

$$p_3 = \frac{g_{m2}R_{m2}}{(R_{m2}C_{o2}+R_{m1}C_{o1})} \tag{7}$$

$$p_4 = \frac{g_{m3}}{C_L} \tag{8}$$

$$p_5 = \frac{1}{(R_{m1}C_{o1})//(R_{m2}C_{o2})} \tag{9}$$

Based on the above assumptions, zero z_2 can cancel pole p_3, and zero z_3 and pole p_5 can be pushed to a higher frequency than unity-gain frequency. By selecting $R_{m1}>>1/g_{m3}$, it is conclude that zero z_1 can cancel pole p_2. Therefore, the DMCNR-DFC three-stage amplifier can be approximated to a system with two poles, whose open-loop transfer function can also be written as

$$A_v(s) \approx \frac{g_{m1}g_{m2}g_{m3}r_{o1}r_{o2}R_L}{(1+s/p_1)(1+s/p_4)} \tag{10}$$

To ensure the stability of a unity-gain feedback system, pole p_4 should be larger than gain bandwidth produce (GBW), so it is concluded that GWB=$g_{m1}/C_{m1} \leq p_4 = g_{m3}/C_L$. Based on the above analysis, the designed DMCR-DFC three-stage amplifier achieves wider GBW than the conventional NMC three-stage amplifier for a given C_L.

Fig.2 shows the transistor-level circuit of DMCNR-DFC three-stage amplifier. Transistors M_1~M_9 form gain-stage A_{v1}, and gain-stage A_{v2} consists of transistors M_{10}~M_{13}. Gain-stage A_{v3} is made up of transistor M_{14}. M_{15} forms A_{vf}, and A_{va} is made up of transistors M_1~M_9 and M_{13}. R_{m1}-C_{m1} and R_{m2}-C_{m2} form the compensation network respectively.

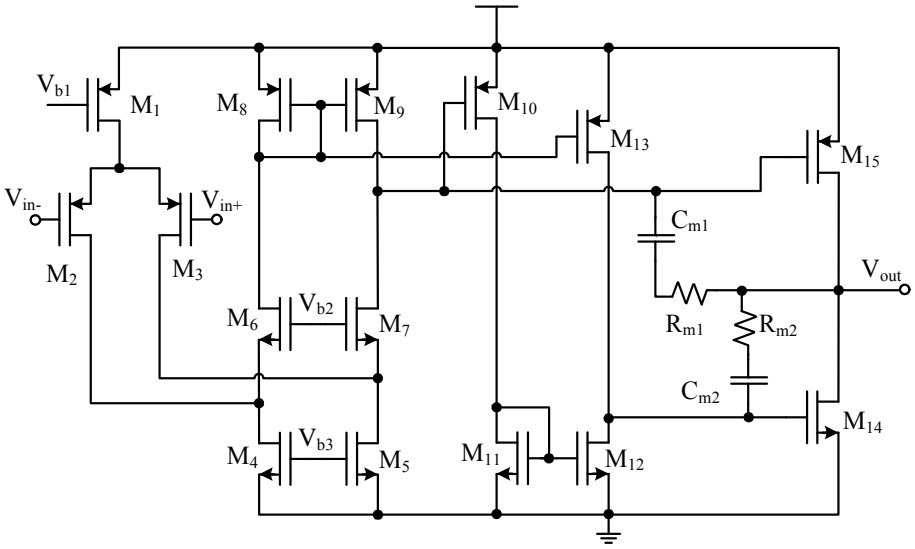

Fig. 2 Transistor-level circuit of DMCNR-DFC three-stage amplifier

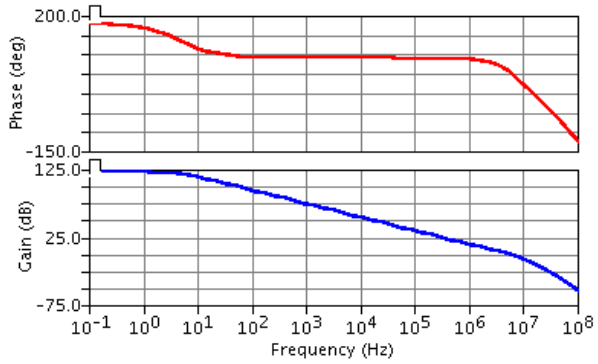

Fig. 3 Open-loop frequency response of DMCNR-DFC three-stage amplifier

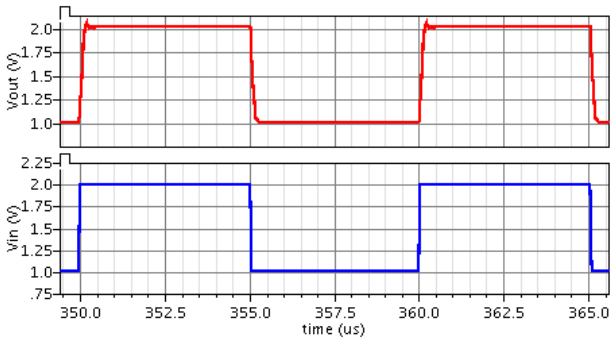

Fig. 4 Transient response of DMCNR-DFC three-stage amplifier

Simulation Results

The DMCNR-DFC three-stage amplifier is designed and simulated in 0.35μm BCD process with a 5-V power supply voltage. Fig.3 shows the simulated open-loop frequency response of the DMCNR-DFC three-stage amplifier under 100-pF load capacitor and 25-kΩ load resistor. The DMCNR-DFC three-stage amplifier achieves a dc gain of 121.2dB, phase margin of 52° and GBW of about 6.1MHz.

Fig.4 shows the simulated transient response of the DMCNR-DFC three-stage amplifier in a unity-gain negative feedback configuration to a 125-kHz 1-Vpp pulsing input signal. Simulation results show that the DMCNR-DFC three-stage amplifier achieves positive slew rate (SR^+) of 6.3V/μs and negative slew rate (SR^-) of 6.32V/μs. Finally, performance summary of three-stage amplifier are given in Table 1. From Table 1, the DMCNR-DFC three-stage amplifier achieves a well performance.

Table 1 Performances of three-stage amplifier

	Ref. [2]	Ref. [3]	This paper
Process	0.18μm CMOS	0.35μm CMOS	0.35μm BCD
Supply Voltage (V)	1.5	1.5	5
Load Capacitive (pF)	250	150	100
I_{dd} (mA)	0.023	0.02	0.2
A_{dc} (dB)	~100	110	121.2
GBW (MHz)	4.4	4.4	6.1
Phase margin	73°	57°	52°
Average SR (V/μS)	1.8	1.8	6.31

Conclusion

A DMCNR-DFC three-stage amplifier, which adopts dual-miller compensation with nulling-resistor and dual-feedforward technique, has been designed and analyzed in this paper. By adopting the dual-miller compensation with nulling-resistor and dual-feedforward technique, the RHP zero can be removed, and the designed DMCNR-DFC three-stage amplifier achieves well small-signal performance and large-signal performance.

Acknowledgment

This work was supported in part by National Science Foundation of China (Grant No. 61102075, and 61301124), Natural Science Foundation Project of CQ CSTC (Grant No. cstcjjA40011, cstc2011jjA1380), 121 Project of CQ CSTC (Grant No. cstc2014jcsfglyjs0012, cstc2014zktjccxyyB0008), Scientific and Technological Research Program of Chongqing Municipal Education Commission (Grant No. KJ120503, KJ120507, and KJ120533), 2013 Program for Innovation Team Building at Institutions of Higher Education in Chongqing (Grant No. G2013-46), Special Project of Internet of Things from Ministry of Industry and Information Technology, and Chongqing Development Plan of Innovative Young Talents (Grant No. cstc2013kjrc-qnrc0126).

References

[1] R. G. H. Eschauzier, L. P. Kerklaan , J. H. Huijsing: A 100-MHz 100-dB operational amplifier with multipath nested Miller compensation structure. IEEE Journal of Solid-State Circuits, Vol.27 (1992), p.1709-1717.

[2] L. Zhang, Z. Chang, Y. Wang, Z. Yu: Current-reuse single miller feedforward compensation for multi-stage amplifiers. Electronics Letters, Vol.49 (2012), p.94-96.

[3] P. Xiao, W. Sansen, L. G. Hou, J. H. Wang, W. C. Wu: Impedance adapting compensation for low-power multistage amplifiers. IEEE Journal of Solid-State Circuits, Vol.46 (2011), p.445-451.

[4] S.A. Aamir, P. Harikumar, J. J. Wikner: Frequency compensation of high-speed, low-voltage CMOS multistage amplifiers. 2013 IEEE International Symposium on Circuits and Systems, Beijing, p.381-384.

[5] S. Guo, H. Lee: Dual active-capacitive- feedback compensation for low power large-capacitive-load three-stage amplifiers. IEEE Journal of Solid-State Circuits, Vol.46 (2011), p.452-464.

Advanced Materials Research Vols. 989-994 (2014) pp 1173-1176
© (2014) Trans Tech Publications, Switzerland
doi:10.4028/www.scientific.net/AMR.989-994.1173

Photovoltaic Inverter Output Current Research of Adaptive Active Harmonic Compensation Device

Chang fengjun[1,a] Ma hongquan[1,b] Cui chang[2,c] Zhang jing[1,d]

[1] School of Electronics and Information Engineering, University of Science and Technology Liaoning, Anshan, Liaoning 114044

[2] Electronic information engineering college, Southwest university Chongqing 800715

[a] cc.cfj@163.com [b] 1294534437@qq.com [c] ascuichang@163.com [d] 1027748417@qq.com

Keywords: Photovoltaic inverter The adaptive In-place Active compensation

Abstract: With the continuous improvement of photovoltaic power generation technology, people has higher requirement on the performance of the photovoltaic inverter. Currently, PV Inverter Grid process of the home and abroad, because the inverter put DC power into AC power frequency electric use the inverter principle and PWM control technology inevitably produce harmonics problems at the sine wave inverter formed. According to this kind of harmonic interference problem, the adaptive in-place active harmonic compensation technology were proposed, this effectively suppress the harmonic pollution to power network, solved the PV inverter output harmonic and reactive power problems, effective purification of power grid, filled the domestic and foreign photovoltaic inverter without output current harmonic compensation gap.

Introduction

Because of the traditional non-renewable energy reducing increasingly, more and more people demand for renewable energy. In renewable energy, solar energy is the most valuable, and photovoltaic power generation is the main form of solar energy utilization. Photovoltaic inverter can make the photovoltaic panels will direct current (DC) can convert into grid AC power, is one of the important equipment of photovoltaic power station. When the photovoltaic inverter output alternating current, the inevitable problems is harmonic interference, and photovoltaic inverter currently on the market in the design process, this problem have not considered, so the inverter output current have harmonic, and power grid was polluted.

After the experiment, we found that for the same grid photovoltaic inverter, regardless of the size of the input current, its output current harmonic are exist in, when the input current in DC side is about 100 A, output current waveform is shown in figure 1, the sinusoidal current waveform contains a lot of harmonic.

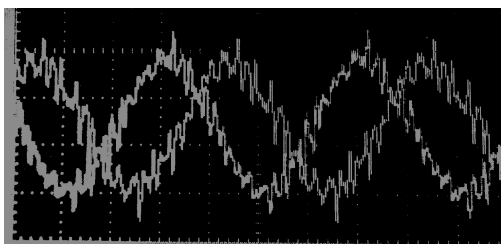

Figure 1: When the input current is 104 A, output current waveform

In view of the grid inverter output current harmonic problems, this paper puts forward added a tracking in the inverter harmonic compensation device, according to the size of the inverter output current and harmonic content, this article use the adaptive compensation on-spot, measures the size can fundamentally solve the problem of photovoltaic inverter output current harmonic.

Principle of active filter

In grid photovoltaic inverter, we use CT inverter output current signal, and then the CT take the signal collected into the instruction current arithmetic circuit, the current in the circuit real-time monitoring by instruction current arithmetic circuit, and converts analog current signal to digital signal, A/D conversion circuit, namely into the inverter in the high speed digital signal processor (DSP) for digital signal processing, and the harmonic wave will be separated, and in the form of A pulse width modulation (PWM) signal to the compensation current generating circuit sends out the drive pulse, drive IGBT power modules, the generation and power grid harmonic current amplitude is equal and opposite polarity compensation current injection inverter circuit, the harmonic current compensation or offset, the active power harmonic elimination inverter output.

Harmonic active power compensator system block diagram as shown in figure 2,

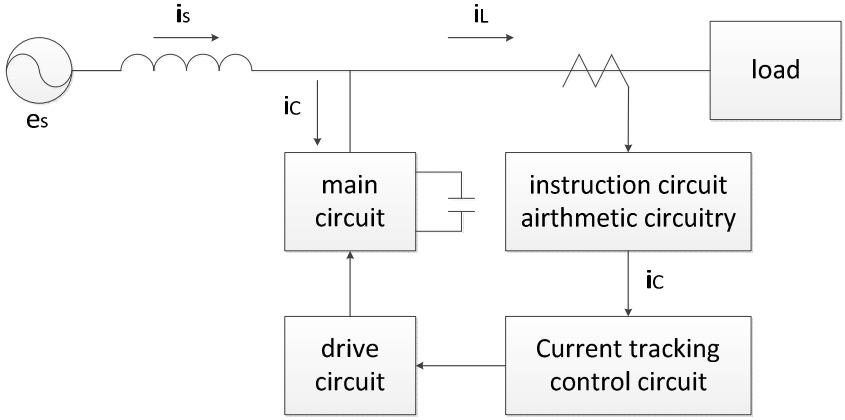

Figure 2: Harmonic compensator system diagram

Note: I_L -- the load current; I_C --output current for the harmonic compensator; I_S -- grid current.

The load current according to the Fourier series expansion:

$$I_L = \sum_{n=1}^{\infty} I_n \sin\left(n\omega t + \theta_n\right) = I_1 \cos\theta_1 \sin\omega t + I_1 \sin\theta_1 \cos\omega t + \sum_{n=2}^{\infty} I_n \sin\left(n\omega t + \theta_n\right) \quad (1)$$

Among them, I_{1p}: the fundamental active current, $I_{1p} = I_1 \cos\theta_1 \sin\omega t$ (2)

I_{1q}: the fundamental wave reactive current, $I_{1q} = I_1 \sin\theta_1 \cos\omega t$ (3)

I_n: the higher harmonic current, $I_n = \sum_{n=2}^{\infty} I_n \sin\left(n\omega t + \theta_n\right)$ (4)

If the control of output current, harmonic compensator is made, by the higher harmonic current can be effectively offset, inhibition, thus can reach the effect of filtering harmonics.

Grid inverter adaptive active compensation device design

Most of the interconnection of photovoltaic inverter in the market now is to control the operation of the DSP chip as the control center, by monitoring the unit, the monitoring data through the electrical signal feedback to the control center. The design of the inverter in the DSP as the core, to make full use of DSP high speed operation ability, through the inverter, the output current transformer to detect harmonic and reads the harmonic information sent to the DSP control center, adopt the side of DC of inverter DC power supply input for the compensator, according to a harmonic signal received, DSP control the drive circuit, through the IGBT inverter, generated the equal and opposite polarity compensation current, so as to realize harmonic compensation on-spot function. Because the inverter harmonic compensation device design in the internal of inverter, reduce the hardware cost, and basically do not increase the inverter volume.

Harmonic compensator and the network topology structure of the inverter as shown in figure 3, add the harmonic compensator inverter to the output current, there would be a perfect combination of harmonic compensator to the inverter circuit, achieve the function of inverter and harmonic compensator work at the same time, make the inverter output current waveform is perfect without harmonic, power grid without pollution.

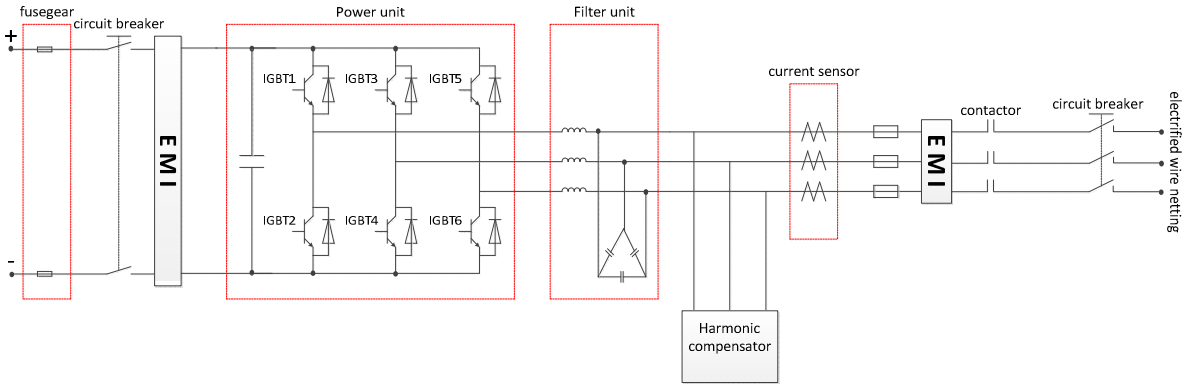

Figure 3: With harmonic in situ compensator of the photovoltaic inverter main circuit network topology

Modeling and simulation

Application of matlab in simulink simulation experiments, Simulink provides an integrated environment for modeling, simulation and synthesis analysis. Figure 4 shows a graphical simulation in simulink.

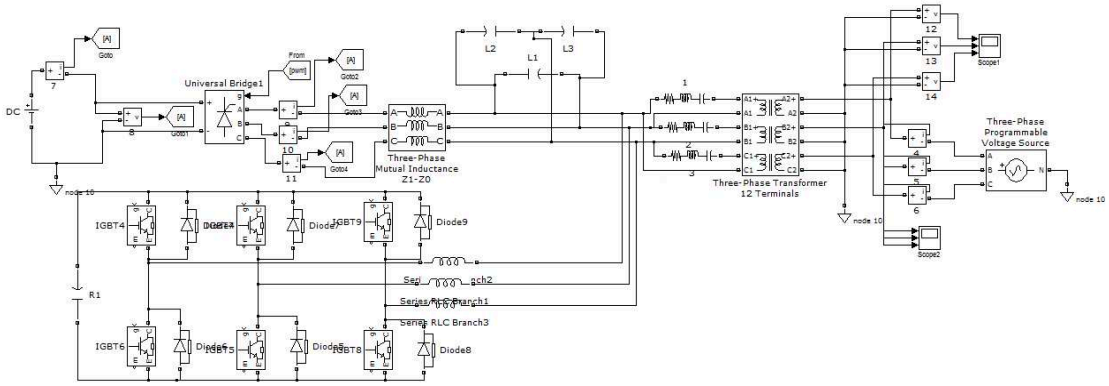

Figure 4: Graphical simulation modeling of the compensator

Without adding compensator of the inverter output waveform as shown in figure5,

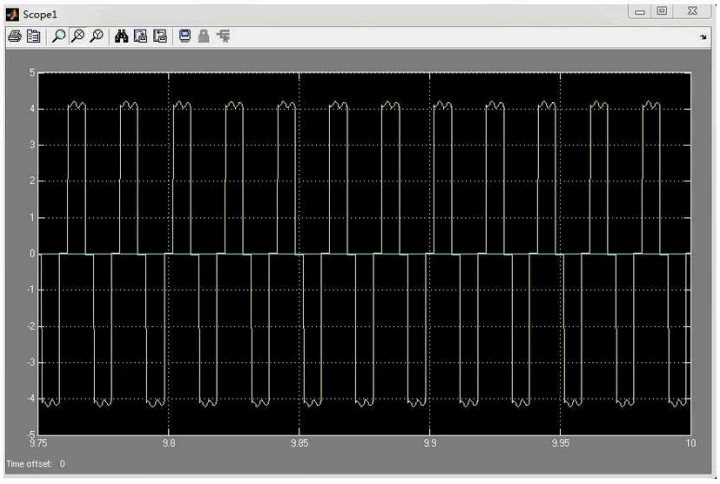

Figure 5: No compensator waveform

After adding harmonic compensator, output current waveform have markedly improved, as shown in figure 6,

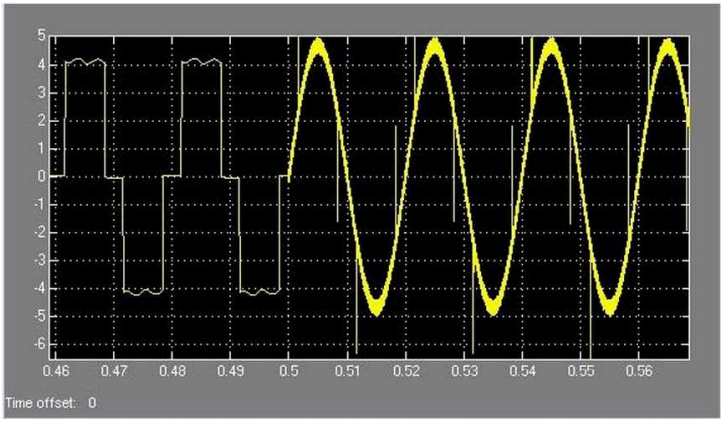

Figure 6: After joining compensator output waveform

Summary

Experimental results show that the new design of the PV inverter output current harmonic compensation device has good harmonic compensation effect, in future photovoltaic inverter design and applications; we can increase this harmonic compensation device, to avoid the inverter output current harmonic pollution the grid.

Reference

[1] Cao taiqiang. Research on photovoltaic generation system and its control technologies[D]. Southwest Jiaotong University. (2011)

[2] Zhu qiliang. Reasearch on harmonic current elimination method for photovoltage grid-connected inverter[M]. Central south university. (2013)

[3] Wang ping, Sun yugeng, Xu huijun, Zhang ke, Song liangyu. Harmonic analysis and active compensation for the DC-link of inverter[J]. Proceedings of the Csee. (2005), 25(14) : 52-56

[4] Wang ping. A study on intelligent detection and control approaches of distortion currents for active power filters[D]. Tianjin university. (2005)

[5] Zhang qiang, Liu jianzheng, Li guojie. Instantaneous current detection and compensation of single-phase photovoltaic grid-connected inverter[J]. Automation of Electric Power Systems. (2007), 31(10) : 50-54

Advanced Materials Research Vols. 989-994 (2014) pp 1177-1180
© (2014) Trans Tech Publications, Switzerland
doi:10.4028/www.scientific.net/AMR.989-994.1177

A New Optimal Method For Load Transfer in Power Distribution Network

Qun WANG[1, a], Li YAO[1, b], Zhanlong ZHANG[1, c]

[1]Department of Electrical Engineering and Automation, Tianjin University, Tianjin, 300072, China

[a]email: wangqunsnake@sina.com, [b]email:yaoli@tju.edu.cn, [c]email:langshena@126.com

Keywords: Load Transfer; Power Distribution Network; Optimal Method; System Reconfiguration

Abstract. According to the problem that when power failure occurs in distribution systems, load transfer is to recover the load downstream failures without any violation as fast as possible. This target is reached by switch operations and load cut. Using the stochastic optimization method to the solution of the problem, we can improve the efficiency of solution for the operation personnel to provide the reference scheme of load transfer. Test results of a 33 bus sample network have shown that the new method for load recovery can significantly reduce the losses caused by the failures and improve system reliability.

Introduction

With the deepening of the distribution automation technology, load transfer technology has gradually gained more power companies and researchers attentions. Load transfer for distribution network is that after the failures in network have been isolated to recover the load downstream failure without any violation as fast as possible. The actual distribution network service restoration scheme is always decided not only by a dispatcher alone, it is necessary for the distribution network restoration method based on group decision making, to satisfy the demand of the future development for smart distribution grid. Because of its advantage, load transfer is becoming one of the most important core functions of distribution automation system.

According to the loss of power information, we can use one or more tie switches to completely restore all load in failure area based on switches, electrical distance, transfer capacity and other information [1]. If the loss can not be recovered, we will cut less important loads in the security. Considering the load change on the impact of load transfer for different time, load transfer schemes are given based on the different load value and time [2]. From the above literature can be seen, this kind of method has a prominent advantage is fast scheme; but it can not get an optimal plan [3].

In literature [4], genetic algorithm is succeeded in the application of the fault restoration in distribution network and has achieved good results. To get fast calculation, the control variables [5] of the method are only the state of switches without considering the load in failure zone, so the result is relatively simple. In Literature [6, 7] the non- dominated sorting genetic algorithm is used in multi-objective and multi- constraint restoration of distribution network to get the optimal solution. The model is relatively complete except that it may have a long calculation time.

This paper proposes a load transfer based on the combination heuristic algorithm with particle swarm optimization. The strategy is first use heuristic method to find a feasible solution and optimize it using the particle swarm algorithm to obtain a better solution.

The mathematical Model Of Load Transfer

The objection of recovering the downstream load is to minimize switching operation and restore more important loads in conditions of meeting the system security constrains. So the control variables correspond to switches in line and load to cut in loss area. In order to realize the objectives of distribution network service restoration, this paper mainly uses the following indices to measure service restoration schemes.

The load transfer is formulated as an optimization problem which minimizes loss in failure areas and switching numbers.

$$p = \sum_{j=1}^{n} d_j P_{j,cut} + \sum_{l=1}^{m} | \alpha_{l0} - \alpha_l | \tag{1}$$

The quantities of restored load is sum of current, which the service restoration schemes restore the power supply for the outage areas by transferring the load to other feeders.

$$\min(\sum_{j=1}^{n} d_j P_{j,cut}) \tag{2}$$

In the type (2): n stands for the number of nodes, d_j stands for the weight coefficient of load, $P_{j,cut}$ stands for the load to cut.

The evaluation index is defined as the number of switches operated during the process of service restoration, which represents the cost from switching operations.

$$\min(\sum_{l=1}^{m} | \alpha_{l0} - \alpha_l |) \tag{3}$$

In the type (3): m stands for the branch numbers, α_{j0} stands for the state of branch j, α_l stands for the state of branch j when after load transfer.

The power flow equation constrains is that when the grid operates in stable state, the power flow calculation can be finally convergence.

$$\begin{aligned} P_i &= U_i \sum_{j \in i} \alpha_l U_j \left(G_{ij} \cos\theta_{ij} + B_{ij} \sin\theta_{ij} \right) \\ Q_i &= U_i \sum_{j \in i} \alpha_l U_j \left(G_{ij} \sin\theta_{ij} - B_{ij} \cos\theta_{ij} \right) \\ & \left(i = 1, 2, \cdots, n \right) \end{aligned} \tag{4}$$

Other constrains are that radial network structure must be retained always, bus voltage magnitude should be strictly between upper and lower limits and the load to cut can not exceed the maximum load in the failure areas.

For the above model, the method proposed in this paper use a method combined heuristic algorithm with particle swarm optimization, so as to realize the complementary advantages of heuristic algorithm and random optimization method. We can get the optimal solution and improve the calculation speed simultaneously.

The Optimization Process Of Load Transfer

The strategy uses heuristic search to get a fast solution, namely through one or more tie switches to restore the failure power areas. If the surplus capacity of the tie switches is insufficient to completely restore all the lost loads, we will find a group of combination switches and disconnect them to remove the downstream loads of these switches to get an initial transfer solution satisfying security constrains. After that, the method uses the particle swarm algorithm to optimize load cutting area to get a possible small load shedding solution. In this way, the method realizes a good combination of heuristic algorithm and random algorithm. The method can improves the speed of computation and avoid the whole network optimization stochastic algorithm to obtain a best solution using the optimization ability of random algorithm.

The specific steps are as follows:

Step 1. Conduct a breadth first search from the whole network to get the work area, the fault areas. which have been isolated and the electricity loss region.

Step 2. Calculate the maximum spare capacity of the candidate tie switches.

Step 3. Close a tie switch to restore the failure areas.

Step 4.Cut partial loads if the failure areas can not be restored to get the initial recovery plan.

Step 5. Optimize the cut load on the base of initial plan to get the best solution.

Test results

The following example system from the actual distribution system, the original network consists of 465 physical nodes, 36 tie switches. The figure1 below shows the structure diagram of the fault part and the area network to transfer, which assumes the fault branch occurs between node 110 and node 162, the branches to isolate fault are the two between node 1 and 110 and node 161 and 162, the areas in node 161 downstream are the area to be recovery.

Table.1 Zone loads

Node list	Active load	Reactive load	load state	Load controllability
101	**0.0722**	**0.0001**	**2**	**1**
102	**0.0778**	**0.0001**	**1**	**1**
103	**0.0333**	**0.009**	**3**	**1**
104	**0**	**0.000112**	**3**	**3**
154	**0**	**0.000112**	**3**	**2**
161	**0.05**	**0.01**	**3**	**3**

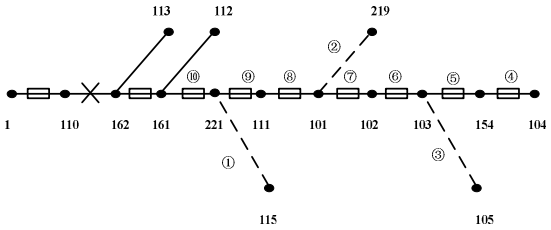

Figure.1 The part distribution system

According to the network analysis, the load nodes in failure area in are node 101, 102, 103, 104, 154,161, the remaining nodes have no load. The area is directly connected with three tie switch which are the dotted line branches. The total demand of each zone is listed in Table 1. The loading capacity of each feeder is 100 MVA.

Because the results depend on the maximum spare capacity index of tie switches, so we set different branch current limit value to test the algorithm. Firstly we have the initial network flow calculation, then give each branch current rating: $I_{rating}=I_{now}+\triangle I$, I_{now} stands for the branch current value, $\triangle I$ stands for the spare capacity of each branch.

When $\triangle I=1.0$, we can restore the power loss zone by the heuristic procedure because that the tie switches have enough capacity to restore all loads. The switch to close is the tie switch between node 101 and 219.

When $\triangle I=0.2$,we will recover the loss zone by operating switches since that the failure zone can not be restored by closing a tie switch. The switch to close is the tie switches between node 115 and 221 and node 105 and 103. The switch to disconnect is the switch between node 111 and 221.

When $\triangle I=0.08$, we will cut the loads in failure zone because that a feasible solution can not be found by the heuristic searching without enough spare capacity of tie branches. The switches to close are the switches between node 105 and 103 and node 115 and 221. The switches to disconnect are the ones between node 101 and 102 and node 102 and 103 and node 161 and 221. Table 2 is the loads of different nodes in failure zone. The results in table 3 use the method in literature [8].

Table.2 Load after restoration

Node list	Initial active load	End active load
101	**0.0722**	**0.0722**
102	**0.0778**	**0.0778**
103	**0.0333**	**0.0006693**
104	**0**	**0**
154	**0**	**0**
161	**0.05**	**0**

Table.3 Load of two methods

	Algorithm in literature	Our algorithm
Active load	**0.2233**	**0.2233**
Important active load	**0.0722**	**0.0722**
Less important active load	**0.05**	**0.12847**

From the above comparison, it shows that our algorithm can recover more load than the heuristic algorithm.

As a comparison with the traditional PSO algorithm, we select 3 test examples, which have 3,10 and 17 tie switches connecting with failure zone. When $\triangle I=0.2$, the load currents in failure zone are 0.2342, 0.383 and 1.3473. The simply networks are as shown in the figure 2,3 and 4, node 0 is the virtual power point.

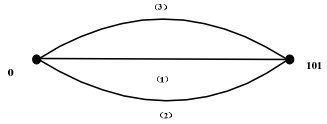

Fig.2 3 tie switches network

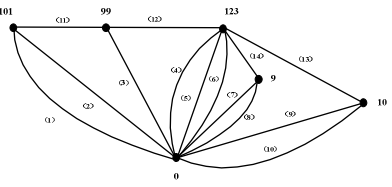

Fig.3 10 tie switches network

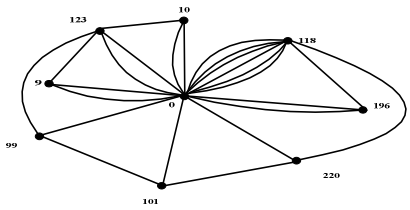

Fig.4 17 tie switches network

According to the three examples, the result is shown in the Table 4.

Table.4 The result of 3 examples

	3 tie distribution system			10 tie distribution system			17 tie distribution system		
	The active load to cut	The switches to disconnect	Time (s)	The active load to cut	The switches to disconnect	Time (s)	The active load to cut	The switches to disconnect	Time (s)
Traditional pso algorithm	0	218,219	31.062	0.0375	2,3,4,5,6, 8,9,13,14	34.722	0.50229	8,22,34,3559,101,107,120,137, 148,166,175,187,215,221,234	38.785
Our algorithm	0	218,219	31.024	0	1,5,6,7,8, 9,11,13	32.816	0.52087	11,13,15,17,19,21,22,24,34,35 136,175,190,215,219,231	32.916

From the above comparison, computing results of two algorithms are basically same, but with the increase of tie switches, the calculation of our method is faster than the traditional method due to that the generation of traditional random solution does not necessarily satisfy the topological constraints which leads to a large number of infeasible solutions. If the system scale increases, more tie switches can be used, our system have a large advantage than the traditional algorithms.

Conclusion

This paper uses the method combining heuristic algorithm and random algorithm to study load transfer in distribution network. According to the model structure and practical problems, we use a new encoding method in stochastic optimization process to meet the radial topology constraint. Because of without needing to verify the topology, it can reduce the time of calculation and get a better solution.

References

[1] Karen Nan Miu, Hsiao-Dong Chiang, Gary Daring. Fast Service Restoration for Large-scale Distribution Systems with Priority Customers and Constraints. [J], 1997.

[2] Karen Nan Miu, Hsiao-Dong Chiang, Service Restoration For Unbalanced Radial Distribution Systems with Varying Loads: Solution Algorithm [J], 1999.

[3] Michael R. Kleinberg. Improving Service Restoration of Power Distribution Systems Through Load Curtailment of In-Service Customers [J]. Trans on power system, 2011,26(3):251-254.

[4] K. Miu, H.-D, Multi-tier service restoration through network reconfiguration and capacitor control for large scale radial distribution systems[J], Trans on power system 2000:15(3):1001-1007.

[5] K. N. Miu and H.-D. Chiang, Electric distribution system load capability: Problem formulation, solution algorithm, and numerical results[J].Trans on power system,2000, 15(1):436-442.

[6] Michael Kleinberg, Kar en Miu. Service Restoration of Power Distribution Systems Incorporating Load Curtailment. 2009.

[7] Lu Zhigang and so on. Distribution System Restoration Based on Improved Binary Particle Swarm Optimization[J]. Automation of electric power system .2006:30 (24):39-42.

[8] Yan Ping and so on A fast efficient service restoration method for distribution network [J]. Automation of electric power system .2000:24 (4):52-56.

Advanced Materials Research Vols. 989-994 (2014) pp 1181-1184
© (2014) Trans Tech Publications, Switzerland
doi:10.4028/www.scientific.net/AMR.989-994.1181

Reliability Evaluation for Distribution System Including Protection System Failures

Zhanlong ZHANG[1, a], Li YAO[1, b] ,Qun WANG[1, c]

[1]Department of Electrical Engineering and Automation, Tianjin University, Tianjin, 300072, China.

[a]email: langshena@126.com, [b]email: yaoli@tju.com.cn, [c]email: wangqunsnake@sina.com

Keywords: Distribution System; Reliability; Component groups; Protection failures

Abstract. A new model and method for incorporating the effect of protection system failures into distribution system reliability evaluation are developed this paper. Firstly, the distribution system is partitioned into zones with the auto (or non-auto) switch being the boundary; through the network equivalent approach, for each load point, three component groups are respectively formed by two types of zone-elements. Then two types of protection failures and their impacts on reliability modeling are discussed. Finally, the reliability Markov model of load point with protection failures has been developed. The test results of the samples demonstrate the practicability and validness of the method.

Introduction

Distribution network is the key intermediate links between the system power facilities and consumers. Utility statistics show that distribution-system failures account for approximately 80% of the average customer interruptions [1]. Therefore, with accurate and effective distribution network reliability analysis, outage duration and losses can be reduced and the quality of power supply is improved, which has important theoretical and practical significance.

The current principal methods for distribution network reliability analysis are analytical method, simulation method [2] and the combination method [3]. Analytic method is most widely applied in the above three methods, and its basic method is FMEA (Failure Mode and Effects Analysis). Nevertheless, formulation of the failure effect table will be very complicated while the system is complex. In order to simplify the analytical process, a lot of research has been made by domestic and foreign scholars. A variety of effective algorithm, such as the network equivalent method [4], the minimal path method [5] and fault-spreading-method [6] are spawned according to different simplification methods of the network topology.

Based on the zone element equivalent and Markov state space method, a new reliability evaluation method for distribution system with the protection fault is proposed in this paper.

Equivalent Network Model

The one-line diagram of the distribution system can be partitioned into two types of zones with the auto (or non-auto) switch being the boundary [5]. The zone partition of a distribution system is shown as Fig.1 (a).

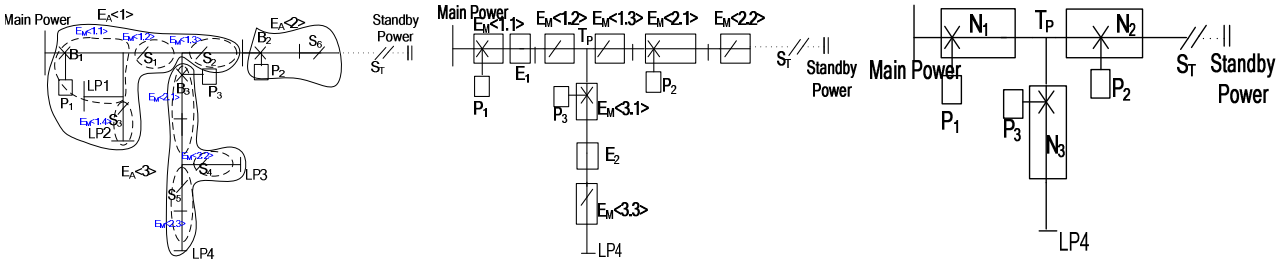

(a) Zone partition of network (b) Equivalent to the minimal path (c) The final equivalent model

Fig.1. Reliability-network equivalent

In the Fig.1, P_1, P_2 and P_3 are protection devices, LP_1 - LP_4 are load points, S_1 - S_6 are isolation switches, S_T is contact switch; B_1, B_2 and B_3 are circuit breakers; E_A<1>, E_A<2> , E_A<3>are three A-type zones; E_M<1.1>–E_M<1.4> are four M-type zones inside E_A<1>.

According to the related definition of Ref. [5], the transferring node, A-type minimal path, M-type minimal path, backup minimal path, and common pathway can be calculated for each load point. The failures of M-type and A-type zone elements in anti-minimal path will also affect the load point, and these zone elements can be replaced by the equivalent component in the minimal path according to the network equivalent thought. Further, after the preliminary process of network equivalent, the zone elements in the minimal path and the backup minimum path can be equivalent into three regional groups based on its location in the system (the location includes: between the main power supply and transferring node; between the contact switch and the transferring node; between the loading point and the transferring node). As shown in Fig.1 (b) and (c).

Analysis of Reliability Parameters

Generally, the devices in E_M have the same failure impact on a given load point. So the M-type zone elements are treated as the basic analysis unit for reliability evaluation. On the calculation of equivalent repair rate, the frequency balance approach can be used here, and the equivalent failure rate and repair rate can be obtained as following:

$$\lambda_{\mathrm{ZoneM}} = \sum_{i=1}^{n} \lambda_i \tag{1}$$

$$\mu_{\mathrm{ZoneM}} = \frac{\prod_{i=1}^{n} \mu_i * \sum_{i=1}^{n} \lambda_i}{\prod_{i=1}^{n} (\lambda_i + \mu_i) - \prod_{i=1}^{n} \mu_i} \tag{2}$$

In which, λ_i and μ_i are respectively the average failure rate and the average repair rate of the devices (including the switch) of E_M; λ_{ZoneM} is the failure rate of E_M; μ_{ZoneM} is the average repair rate of E_M; and N is the number of devices(including the switch) in the E_M.

The zone elements in the anti-minimal path considered in this paper contain two types: one is the A-type zone element connecting to the directly $P_A(L_i)$ (Note E_{Aj}); the other one is the M-type zones elements at $P_A(L_i)$ but not $P_M(L_i)$.In order to analyze the fault influence of zone elements mentioned above, the network equivalent method will be used here, i.e., they will be replaced by the equivalent component in the minimal path, as component E_i in Fig.2-(a). Corresponding to the two types of zone elements above, the reliability parameters of the equivalent components can be obtained using the formula (1) and the following equation:

$$\lambda_{EA} = \lambda_{AS} + (1-p)(\sum_{j=1}^{N_S} \lambda_{ZoneMj} - \lambda_{AS}) \tag{3}$$

In which, λ_{EM} and λ_{EA} are respectively the equivalent failure rate of the M and A-type zone element that in the anti-minimal path; P and λ_{AS} are respectively the reliable action rate and the average failure rate of the automatic switch of E_{Aj}; λ_{ZoneMj} calculated by formula (1) is the average failure rate of the EM in E_{Aj}; NS is the number of the switches in E_{Aj}.

And the equivalent repair rate of zone element can be calculated with the following formula

$$\mu_{\mathrm{EM}} = \mu_{\mathrm{EA}} = \frac{1}{T_S} \tag{4}$$

In which, T_S is the time of fault isolation [5].

For any load point, its minimal path system can be simplified to the network structure shown in Fig.1 (c).In order to use the Markov method to calculate the reliability indices of the load point in the next section, it is necessary to calculate reliability parameters of the three component groups.

Combined with the reliability parameters of the M-type zone element in the minimal path and the equivalent element of the anti-minimal path, we can get the equivalent failure rate and repair rate of the three component groups by applying the formula (1) and (2).

Reliability Evaluation Including Protection System Failures

There are two significant failure modes of the protection system. The fail-to-operate protection failures and the fail-to-operate protection failures have different effects on the system reliability as the fail-to-trip failures of circuit breakers. Therefore, the two failure modes are taken into account in an integrated manner. While the undesired-tripping protection failures will be considered separately.

Based on the equivalent model and the reliability parameters of three component groups, in this paper, the Markov state space method is used to calculate the load point reliability index. The Markov model for load point reliability analysis is shown in Fig.2.

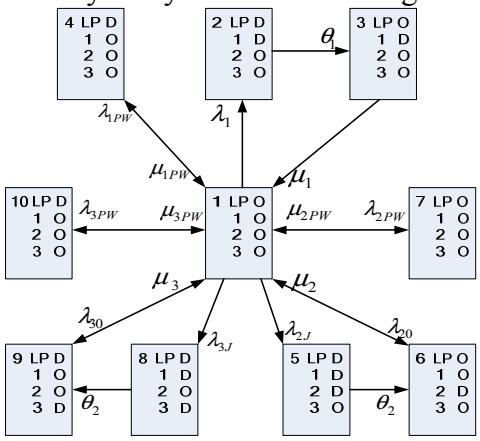

Fig.2. The Markov model for load point reliability analysis

The following abbreviations have been used in the model:

LP is the load point to be evaluated, 1-3 are the three component groups $N_1 - N_3$; O represents that load point/component group is in good condition, and D represents the outage state. λ_i / μ_i are failure and repair rates of the three component groups, $\lambda_{iPW} / \mu_{iPW}$ are failure and repair rates of protection associated with undesired-tripping failure mode. Besides, $\lambda_{2J} / \lambda_{3J}$ is the failure rate of N_2 / N_3 associated with fail-to-operate protection failures, and $\lambda_{20} / \lambda_{30}$ is the failure rate of N_2 / N_3 associated with the protection is normal. θ_1 is the reciprocal of the time that for fault isolation and switch shifting, θ_2 is the reciprocal of the time that for fault isolation.

The states of the proposed Markov model are explained as follows:

State 1 represents the normal operating condition. When a fault is occurred on N_1, the model transfers to state 2, and followed by the process of switch shifting, then the model goes to state 3.In state 3, the faulted component group is repaired and the model returns to state 1. When the fault occurs on N_2, the model transfers from state 1 to 5 with the fail-to-operate protection failures in N_2,causing its adjacent healthy component(N_1)tripped by backup protection. In state 5, both LP and N_1 are under outage condition, and then they return to the normal state after the fault isolation in state 6.As the protection in N_2 is normal, the model transmits from state 1 to 6 directly. The system transfers from state 6 to state 1 by repairing N_2.The model states have the similar transfer process when the fault occurs on N_3. Finally, we use a two-state process to model the effect of the undesired-tripping failure mode, as state 4/7/10 in Fig.2, respectively.

The probabilities associated with the different states of the Markov model in Fig.2 can be calculated using the Markov state space method. The outage probability of load point is defined as the probability of having LP in the D state, and this performance index can be calculated using the following equation:

$$P_{L_i} = P_2 + P_4 + P_5 + P_8 + P_9 + P_{10} \quad (5)$$

The average year outage time U_L, average outage rate λ_L, and average outage time of the load point γ_L can be calculated with the following formula (6)-(8).

$$U_{L_i} = P_{L_i} * 8760(h) \quad (6)$$

$$\lambda_{L_i} = \lambda_1 + \lambda_{1PW} + \lambda_{20} + \lambda_{2J} + \lambda_{30} + \lambda_{3J} + \lambda_{3PW} \quad (7)$$

$$\gamma_{L_i} = \frac{U_{L_i}}{\lambda_{L_i}} \quad (8)$$

Test results

This article uses the feeder F4 of the IEEE RBT Bus6 distribution system to verify the validity and the correctness of the method. The parameters of the equipment and the network configuration can be found in the Ref. [7]. Since protection data for components of RTS are currently unavailable, we assume that the probability of the fail-to-operate mode protection failure is 0.003, take the value of 0.0089/year for the undesired-tripping mode protection failures, the average time to repair the protection device is 8h. The result of the case above is shown at table1.

Table1 System reliability induces including protection failures

SAIFI	SAIDI	CAIDI	ASAI
1.708	6.237	3.653	99.929%

Comparing the calculation results in Ref. [7], the failure of the protection will have effect on the reliability of the system. We can see that these indices all show an increase over those of the perfect protection model in Ref. [7]. Thus, with considering the failure of protection, the reliability calculations can reflect the actual reliability of the system better.

Conclusion

For the purpose of application in the power system reliability evaluation including protection failures, a new method based on the network equivalent thought and the Markov state space method is proposed for the reliability evaluation of distribution system. With the component groups and the analysis of the effect of the two types of protection failures, a new reliability Markov model of load point with protection failures are developed to calculate the reliability index. The results of the numerical case proved the validity of the algorithm and the necessity of the consideration of protection failures.

References

[1] BILLINTON R, BILLINTON J. Distribution system reliability indices [J].Power Delivery, IEEE Transactions on, 1989, 4(1):561-568.

[2] LIU Yang, ZHOU Jiaqi, et al. The parallel Monte-Carlo simulation of bulk power system reliability evaluation based on Beowulf cluster [J]. Proceedings of the CSEE, 2006, 26(20): 9-14.

[3] Wan Guocheng, Ren Zhen, et al. Hybrid method for the reliability evaluation of the complex distribution system [J]. Proceedings of the CSEE，2004, 24(9):92-98.

[4] BILLINTON. R. Reliability Network Equivalent Approach to Distribution System Reliability Evaluation. IEE Proceedings of Generation, Transmission and Distribution, 1998, 145(2): 149-153.

[5] Xu-dong W, Jikeng L, et al. Reliability evaluation for distribution system with the switch fault[C]// SUPERGEN'09. International Conference on. IEEE, 2009: 1-6.

[6] Xie Kaigui, Zhou Ping, et al. Reliability evaluation algorithm for complex medium voltage radial distribution networks based on fault-spreading-method [J]. Automation of Electrical Power, 2001, 25(4): 45-48.

[7] CHEN Can, WU Wenchuan et al. Reliability Evaluation for Large-Scale Distribution Network Based on Component Groups [J]. Power System Technology, 2012, 36(008): 81-86.

Advanced Materials Research Vols. 989-994 (2014) pp 1185-1188
© (2014) Trans Tech Publications, Switzerland
doi:10.4028/www.scientific.net/AMR.989-994.1185

The New Technology of PV Power Generation System based on Extremum Seeking Control

SHI Jiying[1,a],ZHANG Kai[1,b],ZHANG Yongge[1,c]

[1]Key Laboratory of Smart Grid(Tianjin University),Ministry of Education,Tianjin 300072,China

[a]eesjy@163.com,[b]zksnail@126.com, [c]loodycheung@163.com

Keyword: maximum PV energy tracking ; **SM-ESC**; adaptive parameters adjustment;RTDS

Abstract: A novel is based on a simplified two-diode model of photovoltaic (PV) module,which can more accurately predict the output characteristic of the solar cells I-U curve. On this basis, Aiming at promptness and stability tracking the maximum power point of the photovoltaic cells under the conditions of the constant temperature and light intensity, a novel control strategy based on sliding mode based extremum seeking control (**SM-ESC**) system for optimally tracking the maximum power point of the photovoltaic cells is proposed.To achieve higher control quality, an adaptive adjustment method is further presented on the basic of stabilizing conditions of **SM-ESC** system, avoiding complicated manually parameter adjustment.Thus photovoltaic system can quickly stabilize at the maximum power point, less volatile when tracking the optimum output curve. Simulation results show the effectiveness and validity of the control strategy and adjustment method proposed .

0 Introduction

Due to Japan's recent nuclear crisis and petroleum price hikes, the search for renewable energy sources has become an issue of immediate concern. A promising candidate attracting much global attention is solar energy, as it is green and also inexhaustible. A maximum power point tracking (MPPT) controller is employed in such a way that the output power provided by a photovoltaic (PV) system is boosted to its maximum level.

A number of currently employed MPPT approaches [1–5] can be described as follows. Approach 1, Constant voltage tracking method is simple, easy to control, but poor adaptability and can't be adjusted immediately when the external environment voltage value changes;Approach 2, the perturbation and observation method (P&O), is a method perturbing the cell load so as to vary the operating point toward the MPP. A resulting disadvantage is the oscillation in the vicinity of MPP, resulting in a power loss and a degraded solar energy conversion efficiency. Approach 3, the incremental conductance method, is a method that intends to locate the maximum power operating point such that the condition $dP/dV = 0$ is satisfied. A major drawback in practical applications is that an error while locating the MPP is inevitably encountered as a consequence of the low precision sensors used. Therefore, sliding mode based extremum seeking control (**SM-ESC**) system for optimally tracking the maximum power point method is used in this paper.

1 PV cells equivalent model

In general engineering applications, solar photovoltaic cells is mainly a single diode model, but the accuracy of the equivalent circuit is low, especially in low light conditions, compared with the two-diode model can not accurately represent the characteristics of photovoltaic cells[6]

Therefore, this paper is based on the two-diode model, the equivalent circuit diagram shown in Fig.2 .The output characteristics of its simplified equation for PV cells:

$$I_{PV} = I_L - I_o\left\{\exp\left[\frac{(\mathrm{U}_{PV}+\mathrm{I}_{PV}\mathrm{R}_s)}{U_T}\right]-1\right\} - I_o\left\{\exp\left[\frac{(\mathrm{U}_{PV}+\mathrm{I}_{PV}\mathrm{R}_s)}{(p-1)U_T}\right]-1\right\} - \frac{U_{PV}+I_{PV}R_s}{R_{sh}} \tag{1}$$

Where, I_{PV} is the output current of the PV array, U_{PV} is the output voltage of the PV array, I_L is the current generated by the incidence of light, I_o is the reverse saturation current

Generally,manufacturers provide the maximum power point voltage U_{mref} and current I_{mref} of PV cells under the conditions of standard test conditions. When the light intensity and temperature changes, by introducing compensation coefficients, the voltage U_m and current I_m of the maximum power point can be obtained.

$$I_{\mathrm{m}} = I_{mref}\frac{S}{S_{ref}}(1+\alpha\triangle T) \tag{2}$$

$$U_{\mathrm{m}} = U_{mref}\ln(e+b\triangle S)(1-c\triangle T) \tag{3}$$

The optimal output power of the photovoltaic cell reference:

$$P_{max}\approx U_m\times I_m \tag{4}$$

Where, $S = 1000W/m$ intensity of solar radiation as the reference; $T = 25\ ℃$ temperature of cells as the reference; $\triangle S$ is the actual light intensity difference between the reference light intensity;$\triangle T$ is the actual temperature difference between the reference cell temperature; e is the base of natural logarithms, and its value is about *2.718 28*; compensation coefficients *a, b, c* are constants. According to a large number of experimental data, it is typically recommended as $a = 0.002\ 5\ /\ ℃$, $b = 0.000\ 5\ /\ (W/m^2)$, $c = 0.002\ 88\ /\ ℃$.

2 Maximum power point tracking photovoltaic systems

The output of the PV array is affected by temperature and light intensity. As we all know, in the same light intensity and temperature conditions, there exist only unique voltage to make the output power of the PV cell maximum. Accordingly, the maximum power point tracking may be converted to an optimum value of the voltage U^* to track such maximum power output P_s:

$$U^*=ArgmaxP_s(U) \tag{5}$$

Extremum Seeking Control belongs adaptive control areas, it does not require the detailed model of system, just need some feedbacks to achieve the optimal output of the system. This paper uses sliding mode based extremum seeking control[7,8] to achieve maximum power point tracking.

When SM-ESC used in photovoltaic power generation system MPPT, the input is the power output of the PV system, the output is reference voltage DC side of the PV system. Control structure diagram shown in Fig.1.

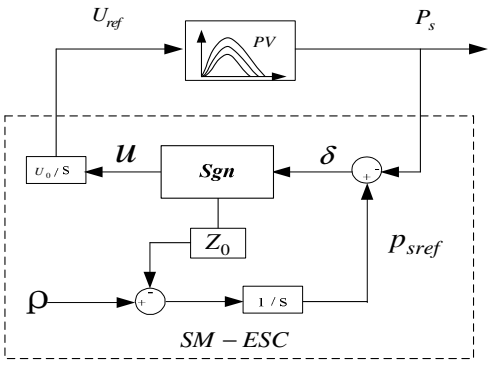

Fig. 1 The controlling block diagram **SM-ESC**

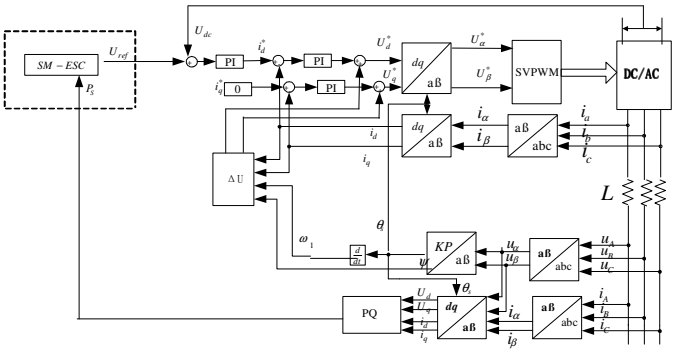

Fig. 2 The controlling block diagram of the the converter based on **SM-ESC**

In Fig.1,P_s is the active power of PV system; P_{sref} is an increasing function (intermediate variables); U_{ref} is the reference voltage of the DC capacitor of the inverter side; $Sgn(\delta)$ is the sign function.

2.1 The maximum power tracking based on SM-ESC

The control strategy is double loop control as shown in Fig. 2,the outer-loop is control of DC voltage constant, the inner loop is the current loop . By setting the reference current value of the q-axis component $q=0$ to achieve a power factor of 1, and then get through the SVPWM modulation inverter drive signal, in order to achieve capacitor voltage constant and decoupling PQ control.

When $P_s < P_{ref}$,U_{ref} is at the left of U^*, $Sgn(\delta) = 1$, U_{ref} increases, and P_s tends to increase to reach the maximum value. When $P_s > P_{ref}$, U_{ref} is in the right side of U^*, $Sgn(\delta) = 1$,U_{ref} decreases, the corresponding P_s tends to increase to reach the maximum value. when P_s reach its maximum value, the output voltage of the photovoltaic cell is the optimal value U^*.

In this Paper the control system is relatively simple, the input is only the active power of the PV cell output, after determining the appropriate parameters ρ, U_0, Z_0 ,the control system can be quickly stabilized.

2.2 Adaptively adjusting the SM-ESC parameters

Because the parameter ρ, U_0, Z_0 values will determine the effect of the control method of controlling, Parameters can only guarantee the control system is stable, but may not be the optimal parameters. To overcome this drawback, we propose a parameter adaptive control strategy.

So the relative rate of change between P_s and P_{max} can be a factor to adjust the parameters, so that when P_s tracking P_{max} process, the relative rate of change as equal as possible, the curve is relatively small shocks

Define parameters adjustment coefficient:

$$\gamma = \frac{\left| p_{\max}(t) - p_{\max}(t-\Delta t) \right|}{\left| p_s(t) - p_s(t-\Delta t) \right|} \tag{6}$$

Where, $P_s(t)$ is the output power of the PV power system at t time; $P_{max}(t)$ is the maximum output power calculated by formula (4) at t time under the given conditions; $\triangle t$ is sampling period.

In power tracking process, the adjustment rules of the parameters Z_0 and U_0 are:

$$Z_0 = Z_0 \times \gamma, U_0 = U_0 \times \gamma \tag{7}$$

When $P_s(t)$ changes faster than $P_{max}(t)$,$\delta<1$, then from the formula(7), U_0 , Z_0 will decrease, the change rate of $P_s(t)$ will decrease correspondingly; when $P_s(t)$ changes slower than $P_{max}(t)$, $\delta>1$, then from the formula(7),U_0 ,Z_0 will decrease, the change rate of $P_s(t)$ will decrease correspondingly; when the change rate of $P_s(t)$ and $P_{max}(t)$ is same, $\delta=1$, parameters remain unchanged.

3 Simulation and Conclusions

Tab.1 The parameters of the solar cells

parameters	I_{mref}/A	U_{mref}/V	R_{sh}	R_s
KC200GT	7.61	26.3	0.22	180.5

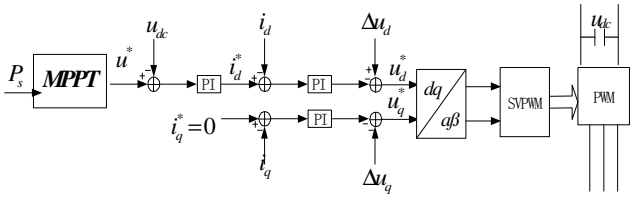

Fig. 3 The controlling block diagram of **SM-ESC**

In this paper, built the PV power system in RTDS, The solar cells parameters are shown in the table 1. Initial parameters ρ, U_0, Z_0 are: 0.014, 1.124, 0.076; $\triangle t$ is 0.1s. The system's control schematic diagram shown in Fig.3.

The solid curve in Fig.4 is the waveforms that adopt above-mentioned adaptive parameter adjustment, $\triangle t$ is 0.1s, as can be seen, the power curve of the adjusted parameters and optimal power curve fitting is very good, compared with no parameters adjustment, the control performance is improved obvious. This proves that this paper proposed adaptive parameters adjustment method is effective.

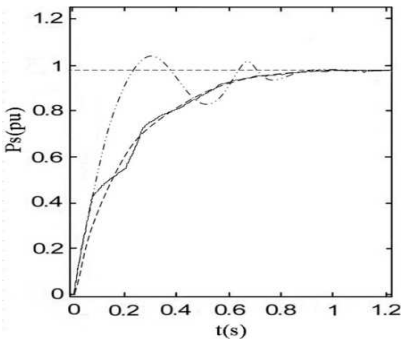

Fig.4 The comparison of optimal power output curves

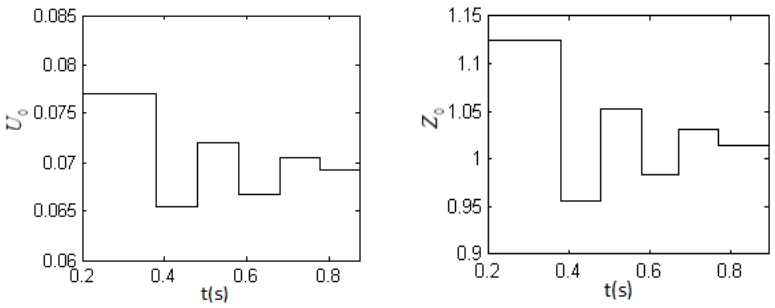

Fig.5 The process of the adaptive parameters adjustment

Fig.5 two curves are the adjustment process of the Z_0, U_0 two parameters adaptive adjustment .Through the parameters adaptive adjustment, Z_0, U_0 turn to 1.023 and 0.069 from the initial value 1.124, 0.076.

This paper proposed a new method that considering the adaptively adjusting the **SM-ESC** parameters to achieve the maximum power tracking of PV system based on the two-diode model of photovoltaic (PV) module. The simulation on the RTDS results show the effectiveness of the proposed method, this method's theory is relatively solid and simply to implement, it has a certain application prospect.

References

[1] Kuo,Y.C.; Liang, T.J. Novel maximum-power-point-tracking controller for photovoltaic energy conversion system. IEEE Trans. Ind. Electron. 2002, 48, 594–601.

[2] Liu, F.; Duan, S.F.; Liu, B.; Kang, Y. A variable step size INC MPPT method for PV systems. IEEE Trans. Ind. Electron. 2008, 55, 2622–2628.

[3] Cesare, G.D.; Caputo, D.; Nascetti, A. Maximum power point tracker for portable photovoltaic systems with resistive-like load. Sol. Energy 2006, 80, 982–988.

[4] Wen, F.; Diao, Z.; Chao, Y.; Mo, R. The Design and Implementation of Photovoltaic Grid-connected Simulating Device Based on FPGA. In Proceedings of the IEEE Power and Energy Engineering Conference, Chengdu, China, 28–31 March 2010.

[5] Benmessaoud, M.T.; Zerhouni, F.Z.; Zegrar, M.; Stambuli, A.B.; Tioursi, M. New approach modeling and a maximum power point tracking method for solar cells. Comput. Math. Appl. 2010, 60, 1124–1134.

[6] KUROBE K , MATSUNAMI H.New two-diode model for detailed analysis of multicrystalline silicon solar Cells [J] . Appl Phys,2005(44) : 8314-8321.

[7] KARTIK B. ARIYUR, MIROSLAV KRSTIC´, Real-Time Optimization by Extremum-Seeking Control[M] , Canada,2003

[8] Yaodong Pan ,Ümit Özgüner, Tankut Acarman . Stability and performance improvement of extremum seeking control with sliding mode[J]. International Journal of Control,2003, VOL. 76, NOS 9/10, 968–985

Advanced Materials Research Vols. 989-994 (2014) pp 1189-1191
© (2014) Trans Tech Publications, Switzerland
doi:10.4028/www.scientific.net/AMR.989-994.1189

Evaluation of the Yangtze River Littoral Wetland Soil with Total Organic Carbon

Zhiwen Luo[1, 2, a], Xing Wang[1]

[1.] Material and Chemical Engineering college, Sichuan University of Sciences & Engineering, Zigong 643000, China

[2.] College of Resources and Environmental Science, Chongqing University, Chongqing 400044, China

[a]email: luoyanlizw@sina.com

Key words: Yangtze River; littoral wetland; total organic carbon; soil;

Abstract. The Three Gorges Reservoir as an important hydraulic project of Yangtze River, the environmental issues attracts worldwide attention, and the environmental problems of littoral wetlands of the Three Gorges Reservoir are more important aspect. Total organic carbon(TOC) content by potassium dichromate oxidation spectrophotometry of downstream the Three Gorges Reservoir in Fengjie, Kaixian, Wushan, Fengdu, Daning estuary in the five regions in soil were determined. Then the organic carbon content of the soil classification comparison, analysis of the causes of soil organic carbon content of the various main reasons for differences, soil classification: the same region, same altitude, different species; the same area, the same species, different altitudes. Finally, by calculating the content of these five regions of the average total organic carbon is about 10.43g/kg.

Introduction

Gorges Reservoir is a special land resource, how to protect and take advantage of this special fluctuating zone of wetland resources, the Gorges Reservoir wetland ecological fragile zone into a stable eco-system, with the Three Gorges Reservoir urgent protection and construction.

By potassium dichromate oxidation-spectrophotometric determination of the five areas of the Three Gorges Reservoir River that Fengjie, Wushan, Fengdu, Wushan, Kaixian, different types of soil organic carbon content [1-3]. Then through the soil organic carbon content of these comparison and analysis, can be more accurate understanding of local environmental conditions and recognize the impact of the construction of the Three Gorges Reservoir on the local environment.

Materials and Methods

Experimental program

Take six dry and clean 100mL glass tube with stopper digestion , glucose standard solution were added 0.00,0.50,1.00,2.00,4.00,6.00 ml, which corresponds to the quality of organic carbon were 0.00,2.00,4.00,8.00,16.0 and 24.0mg . Digestion with a plug to each tube in about 50 ml of water was slowly added, with continued cooling to room temperature. Constant volume with water to 100 ml engraved lines, stopper and shake well. At a wavelength of 585 nm at, with 10mm cuvette with water as a reference, were measured absorbances. To zero concentration corrected absorbance of the vertical axis to the corresponding organic carbon mass (mg) as abscissa, a calibration curve.

Sampling and analytical methods

Accurately weighed amount of sample was carefully added to 100 ml glass tube with stopper digestion, Avoid contact with the wall. The constant volume test solution after standing 1h, the supernatant to take about 80ml centrifuge tubes to 2000 r / min centrifugation 10 min, then put it aside to clarify; digestion or standing in a stoppered glass tube directly to the clarification. Finally, the supernatant absorbance was measured.

The absorbance of the sample against a standard curve of the organic carbon content of seeking its concentration by the following equation (1), obtained in soil organic carbon content (dry weight, mass fraction,%).

$$\omega_{oc} = \frac{(A - A_0 - a)}{b \times m \times 1000} \times 100 \quad (1)$$

m -- the specimen sample volume, g;
ω_{oc} - soil organic carbon content in the sample (dry weight, mass fraction),%;
A --absorbance of the sample digestion solution;
A_0 -- absorbance of the blank test;
a -- the intercept of the calibration curve;
b -- the slope of the calibration curve.

Results

The average organic carbon content Wushan, Kaixian, Fengjie different altitudes intervals are shown in Figure 2.

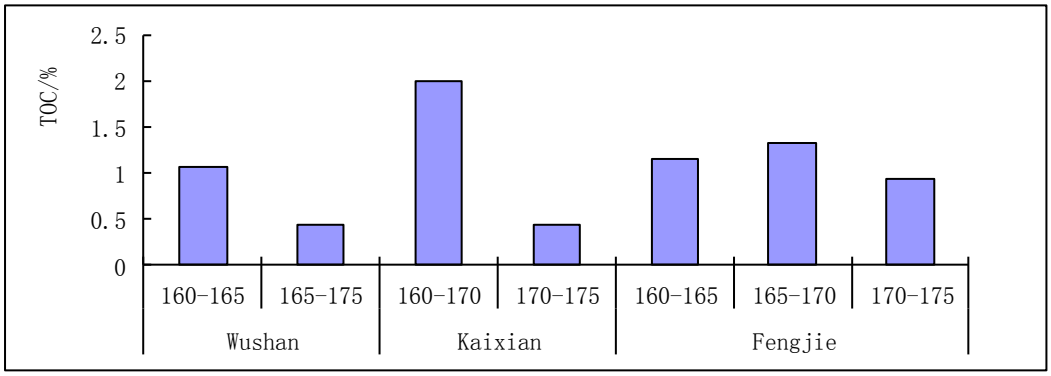

Fig.1 The average TOC of different elevation of sites

ANOVA analysis of variance by the average organic carbon content different altitudes range of Wushan, F value = 12608.90403, P value = 3.77196E-8 <0.05, illustrate the average organic carbon content of soil plants at different altitudes that are distinctly different.

ANOVA analysis of variance by the average organic carbon content at different altitudes range of Kaixian, F value = 177637.85295, P value = 1.90136E-10 <0.05, illustrate the average organic carbon content of soil plants at different altitudes that are distinctly different.

ANOVA analysis of variance by the average organic carbon content at different altitudes range of Fengjie, F value = 13240.98621, P value = 1.16227E-11 <0.05, illustrate the average organic carbon content of soil plants at different altitudes that are distinctly different.

Discussion

Through the average organic carbon content of soil plants at different altitudes range Wushan, Kaixian, Fengjie three regions made ANOVA analysis of variance, we can find that they have a significant difference in the average organic carbon content of different altitudes. There are many reasons for this is: (1) different soil elevation plants were flooded at different times, but not more time, the more longer flooded soil organic carbon accumulation, this may be because of the long time waterlogged soil moisture is saturated , the lack of oxygen, forming anaerobic environment, in such extreme conditions, the organic matter is reduced CH_4 generated causing loss of soil organic carbon; (2) the ability of different waterlogging plants at different altitudes, making the soil organic carbon content of plants exist differences; different (3) the extent of different plants root system, plants absorb organic adsorption capacity and ability is not the same, resulting in differences in

plants and organic carbon content in rhizosphere soil; (4) anti-erosion ability of soil at different altitudes type, organic carbon content of such differences.

Conclusions

A: at low altitude range of plant rhizosphere soil in its time period and the proportion of submerged outcropping above the higher elevations of the range, and the plant soil organic carbon content less than the higher altitude range, because at low altitude range Plants flooded soil moisture is saturated long time, the lack of oxygen, the formation of an anaerobic environment, under such extreme conditions, the organic matter is reduced CH_4 generated caused a loss of soil organic carbon, resulting in an elevation range of different plants on soil There are significant differences in organic carbon content.

II: rhizosphere soil organic carbon content was significantly different to its plant soil in the Three Gorges reservoir area Fengjie, Kaixian, Wushan region, the dominant species in different regions of the adsorption capacity of organic carbon differ, wetland plants while repairing instructions, Choose a different plant species should be selected depending on the adsorption capacity of the plant, to get the best of environmental benefits.

Three: at low altitude and high altitude range of organic carbon content of the soil itself a significant difference in Fengjie 160-165m above sea level in the interval between the submerged due outcropping on stage and in the soil constantly in water and air, causing the soil organic carbon content higher than the low altitude and high altitude range; while Daning River mouth due to its long been scouring the river,170-175m elevation range of soil organic carbon content is less than the low altitude and high altitude range.

Four: adsorption capacity of different plants differ organic carbon, which plants can learn by comparing the adsorption of organic carbon is better, and choose the soil and its impact on the surrounding environment better for plants. Organic carbon so the Three Gorges Reservoir wetland soils in Three Gorges Reservoir with the restoration, protection can play a key role in the Three Gorges reservoir area planted vegetation, vegetation restoration guiding role.

Acknowledgements

This research was supported by the Sichuan Province Education Department natural science research projects (11ZB251).

References

[1]Post W.M,Emanuel W R,Zinke P J, et al. Nature,1982,(298):156-159.
[2]Ouse WR,Lafleur P M,Griffis T J. Physical Geography,2000,21(4):345-367
[3]Gill P.A. Symposium,1999,43
[4]Jones M.B, Mulhuri F.M. Kenya. Journal of Tropical Ecology, 1997,13(3):347-356.
[5]Brix H,Sorrel B K,Lorenzen B. Aquatic Botany,2001,69:313-324.
[6]Beare M H, Gregorich E G,St-Georges P. Soil Biology and Biochemistry, 2009,41:611-621.

Advanced Materials Research Vols. 989-994 (2014) pp 1192-1195
© (2014) Trans Tech Publications, Switzerland
doi:10.4028/www.scientific.net/AMR.989-994.1192

Public Greenbelt Layout Optimization for Ecological Civilization City Construction

Chunguang CHANG[a], Minghao QI[a], Wan LI[b], Kai YIN[b]

School of Management, Shenyang Jianzhu University, Shenyang, 110168, China

[a]email: ccg7788@sohu.com, [b]email:ccg777@sohu.com

Keywords: Ecological Civilization; City Construction; Public Greenbelt; Layout Optimization

Abstract. For boosting public greenbelt (PG) construction level, hastening urban ecological civilization construction velocity, the optimization model and its algorithm for urban PG layout is studied. The layout optimization presupposition of urban PG is described. The bi-objective optimization model for urban PG layout is established. The optimization objectives consist of maximum consistency between PG distribution and population distribution, maximum PG area in certain region. In model constraints, budget capital investment sum for PG construction, distance tolerance threshold from each citizen's habitation to nearest PG, sum of PG needed to be upgraded and reconstructed from grade two to grade one, minimum oxygen supply capacity from given greenbelt, maximum potential supply area of PG. Genetic algorithm (GA) is employed to solve above model, the main cycles of GA for above model are designed. Above greenbelt layout optimization model and its algorithm are validated.

Introduction

How to realize optimal layout of city public greenbelt (PG) is an unavoidable detail difficult problem in ecological civilization construction. Issues relating to PG layout or ecological city must be studied. In this regard, several studies link sustainability to the PG layout or ecological city. i.e., Gómez, F. et al. summarize a very extensive study conducted in the city of Valencia, Spain, on the role of green areas in the comfort of the city [1]. Oh, Kyushik et al. suggest efficient methods to manage the greenbelt through the adoption of a landscape ecological value assessment [2]. green space system planning and ecological adjustment measures is studied in [3]. Landscape structure in the greenbelt zone around the Seoul is studied in [4]. Capability to oxygen release of urban green space is studied in [5]. A successful practice of Vitoria-Gasteiz for sustainable urban planning is analyzed in [6]. The status of canal waterfront greening and plant landscape is studied in [7].

Much valuable, profound research on ecological civilization construction, PG layout appears. However, research on PG layout optimization for ecological civilization city construction from quantitative aspect still needs to be performed more profoundly.

Problem Description of City PG Layout Optimization

When performing city PG layout optimization for given region, relation between PG distribution and population distribution; investment capital limit; maximum tolerance degree for distance from each citizen to the nearest PG; detail upgrade and reconstruction requirement for current city PG proposed from the whole city planning; oxygen supply capability requirement of varied plots for PG; potential constructive or reconstructive PG area limit from land usage type and usage type modification should be considered. In addition, some more detail suppose conditions are considered as follows:(1) The given region can be divided several plots according to the longitude and latitude values. (2) There are already several pubic greenbelts in given region, such as park, large greenbelt, and so on. The current pubic greenbelts are secondary grade ones, and they can be upgrade to the first ones by upgrade and reconstruction. (3) When calculating pubic greenbelt area, the secondary grade pubic greenbelt area is taken as the basic unit. If the plot of secondary grade pubic greenbelt is upgraded and reconstructed, the whole plot will be upgraded and reconstructed. (4) Certain plots

of secondary grade pubic greenbelt is claimed to be upgraded and reconstructed to the first grade one. (5) There existent many potential plots which can be reconstructed into pubic greenbelt. (6) The capital invested into the pubic greenbelt construction in given region is limited. (7) The demand degree for pubic greenbelt on varied plots in given region are different. (8) Oxygen supply capability of the first pubic greenbelt is twice that of the secondary pubic greenbelt. (9) Investment capitals per unit area on varied plots are different. However, the investment capitals per unit area on upgrade or reconstruct the secondary grade pubic greenbelt into the first one is same. (10) In the same plot, the investment capitals per unit area on upgrade or reconstruct the secondary grade pubic greenbelt into the first grade one is higher than that construct the secondary grade one.

Model Establishment of City PG Layout Optimization

Variables are set as follows, latitude value i and longitude value j of plot; population sum p_{ij} on plot (i, j); area x_{ij}, 0-1 variable y_{ij}, required budget capital Δc per unit area and minimum number threshold h of the secondary grade PG needed to be constructed on plot (i, j); area s_{ij} of the initial secondary grade PG on plot (i, j); threshold u_{ij} of maximum area may be constructed into the secondary grade PG on plot (i, j); required budget c_{ij} capital per unit area to construct secondary grade PG on plot (i, j); total sum C of budget capital for construct PG within certain region; demand parameter γ of PG per person. The optimization model is established as follows.

$$\text{Min } f_1 = \sum_{i=1}^{n}\sum_{j=1}^{n}\{p_{ij} / [(s_{ij} + x_{ij})(1 + y_{ij})] - \sum_{i=1}^{n}\sum_{j=1}^{n} p_{ij} / \sum_{i=1}^{n}\sum_{j=1}^{n}[(s_{ij} + x_{ij})(1 + y_{ij})]\}^2 \tag{1}$$

$$\text{Max } f_2 = \sum_{i=1}^{n}\sum_{j=1}^{n}(s_{ij} + x_{ij})(1 + y_{ij}) \tag{2}$$

s.t.

$$\sum_{i=1}^{n}\sum_{j=1}^{n} x_{ij}(c_{ij} + \Delta c y_{ij}) \le C \tag{3}$$

$$s_{ij} + x_{ij} \ne 0 \quad i, j = 1, 2..., n \tag{4}$$

$$\sum_{i=1}^{n}\sum_{j=1}^{n} y_{ij} \ge h \tag{5}$$

$$\sum_{j=1}^{n}(s_{ij} + x_{ij})(1 + y_{ij}) \ge \gamma p_{ij} \qquad i, j = 1, 2..., n \tag{6}$$

$$\sum_{i=1}^{n}(s_{ij} + x_{ij})(1 + y_{ij}) \ge \gamma p_{ij} \qquad i, j = 1, 2..., n \tag{7}$$

$$x_{ij} \le u_{ij} \qquad i, j = 1, 2..., n \tag{8}$$

$$x_{ij} \ge 0 \qquad i, j = 1, 2..., n \tag{9}$$

$$y_{ij} \in \{0,1\} \qquad i, j = 1, 2..., n \tag{10}$$

Formula (1) denotes to maximize the structure consistency between PG layout and population distribution within certain region. Formula (2) denotes to maximize the PG area. Formula (3) denotes that for certain region, the capital investment sum should not be exceeded the total sum of budget capital for construct PG. Formula (4) denotes that the distance between each citizen's inhabitancy and PG should not exceed certain threshold. Formula (5) denotes that the number of upgrading the secondary grade PG into the first grade one is larger than h. Formula (6) and formula (7) respectively denotes that oxygen supply capability of pubic greenbelt on the plot from each latitude and each longitude direction should meet the minimum demand of population on the plot. Formula (8) denotes the maximum potential PG supplying area on the plot. Formula (9) and formula (10) respectively denotes the range of variable x_{ij} and variable y_{ij}.

Model Solving of City PG Layout Optimization

Above model is a bi-objective model, here, considering the important degree and dimension relation of the two objective functions, the weighting coefficients of the two objective functions are set as ξ_1 and ξ_2, then, above two objective functions can be integrated into as follows:

$$\text{Min } f = \xi_1 \sum_{i=1}^{n}\sum_{j=1}^{n}\left[\frac{p_{ij}}{(s_{ij}+x_{ij})(1+y_{ij})} - \frac{\sum_{i=1}^{n}\sum_{j=1}^{n} p_{ij}}{\sum_{i=1}^{n}\sum_{j=1}^{n}(s_{ij}+x_{ij})(1+y_{ij})}\right]^2 - \xi_2 \sum_{i=1}^{n}\sum_{j=1}^{n}(s_{ij}+x_{ij})(1+y_{ij}) \tag{11}$$

GA is employed to solve above problem. The chromosome encoding is a matrix composed of x_{ij} and y_{ij}. Basic cycles of GA are designed as follows.

Step1: Initiate. Set up the highest evolution generation T, population M, crossover rate and mutation rate Pc, Pm.

Step2: Generate M individuals randomly as the initial population $P(0)$;

Step3: Judge whether the individual is feasible by formulas from (3) to (8), if not, go step 2;

Step4: Evaluate fitness and judge whether the individual is better or not by formula (11);

Step5: Slection. According to the individual fitness, use proportional model to choose individual.

Step6: Crossover. One-point crossover is adopted according to the Pc;

Step7: Judge whether the individual is feasible by formulas from (3) to (8), if not, go step 6;

Step8: Mutation. Choose the gene of individual according to Pm;

Step9: Judge whether the individual is feasible by formulas from (3) to (8), if not, go step 8;

Step10: Judge the termination. If $t \le T$, $t \to t+1$ turn to step2, else $t > T$ stop.

Applying Instance Analysis

To validate the validity of above city PG layout optimization and algorithm, the applying instance from practical work is abstracted. γ=12 m^2/ person, Δc = 6 hundred ¥/ m^2; C =6 hundred million¥; h=5; p_{ij}, s_{ij}, u_{ij}, c_{ij} is respectively listed in table 1, table 2, table 3 and table 4.

Table 1 p_{ij} (Unit: 1000 persons)

i \ j	1	2	3	4	5	6	7
1	5	3	4	7	8	6	5
2	8	2	3	6	7	8	6
3	8	6	5	4	5	7	7
4	7	4	6	5	6	6	5
5	7	5	3	3	4	5	4
6	6	4	4	5	6	3	3
7	4	5	2	3	4	4	5

Table 2 s_{ij} (Unit: 10 thousand m^2)

i \ j	1	2	3	4	5	6	7
1	4	6	4	4	5	3	0
2	2	7	5	5	6	0	5
3	4	3	0	3	4	4	3
4	9	5	3	5	5	8	5
5	0	4	6	4	0	8	6
6	2	3	4	5	4	7	4
7	3	2	7	6	6	7	8

Table 3 u_{ij} (Unit: 10 thousand m^2)

i \ j	1	2	3	4	5	6	7
1	9	6	7	12	13	10	9
2	10	4	6	10	12	13	10
3	13	10	9	7	9	12	8
4	12	7	10	9	10	10	12
5	12	9	6	6	7	9	7
6	10	7	7	9	10	6	6
7	7	9	4	6	7	7	9

Table 4 c_{ij} (Unit: hundred ¥/ m^2)

i \ j	1	2	3	4	5	6	7
1	4	5	4	3	4	4	5
2	3	4	3	4	4	5	4
3	4	3	4	3	4	4	5
4	5	4	5	4	5	4	3
5	4	5	4	4	4	3	4
6	3	4	3	4	4	5	4
7	4	5	4	3	4	3	3

By above model and algorithm, satisfactory feasible solutions is obtained, limited by paper's length, only one satisfactory feasible solution is listed in table 5. Of course, many satisfactory feasible solutions can be obtained, in practical layout work, many more factories are considered, then the satisfactory feasible solution for the practical problem is generated finally.

Conclusion

Table 5 Area of PG on plot (i, j) after optimization (Unit: 10 thousand m^2)

i \ j	1	2	3	4	5	6	7
1	6	3.6	4.8×2	9.8	9.6	7.2	4
2	10	2.4	3.6	7.2	9	8	8
3	9.6	9.8	6	4.8×2	6	8.4	6
4	8.4	4.8	5	6	6	7.2	12
5	9	4	3.6	3.6	4.8×2	6	4.8
6	10	4.8×2	6	5	6	3.6	3.6
7	4.8×2	5	2.4	3.6	4.8	4.8	6

PG construction level is significant symbol for evaluating city ecological civilization construction level. How to implement layout optimization of PG is a complex system engineering. Focusing on layout optimization problem of pubic greenbelt during ecological civilization city construction, the optimization model and its algorithm of PG layout will provide quantitative solution scheme for this domain. They will provide satisfactory feasible scheme for practical PG layout optimization work, improve quantitative optimization precision of PG layout. With more profound development of town, the significance of PG layout optimization problem will become more and more obvious. On the basis of town layout theory, based on system theory, employing novel intelligent modeling technique in system engineering domain to study pubic greenbelt layout optimization is one of the important future research trend in this domain.

Acknowledgement

The research was sponsored by the Shenyang Scientific and Technological Planning (Project No. F13-317-5-12; F12-276-5-04), the National Soft Science Research Program (Project No. 2013GXS4D109) , the Natural Science Foundation of Liaoning Province (Project No. 201202181), Program for Liaoning Excellent Talents in University (Project No. WJQ2011011) and Science Research Foundation of Shenyang Jianzhu University (Project No. 2013108).

References

[1] Gómez, F, Jabaloyes, J, Montero, L, De Vicente, V, and Valcuende, M. Green areas, the most significant indicator of the sustainability of cities: research on their utility for urban planning[J]. Journal of Urban Planning and Development, 2011,137(3), 311–328.

[2] Oh Kyushik, Park Jihye, et al. An assessment of landscape ecological value of greenbelt areas in the seoul metropolitan area [J]. Journal of Environmental Impact Assessment, 2011, 20(6): 867-878.

[3] Shi Tiemao, Yuan Wei, Zhao Yanbo. Research on the Green Space System Planning and Ecological Ajustment Measures in Shenzhang New City [J]. Journal of Shenyang Jianzhu University (Social Science), 2013, 15(1): 1-4.

[4]Lee Chang-Seok, Hong Sun-Kee, et al. Landscape structure in the greenbelt zone around the seoul, the metropolis of Korea [J]. The Korean Journal of Ecology, 2001, 24(6): 385-394.

[5] Shi Tiemao, Pan Xuwe, et al. Study on the Capability to Oxygen Release of Urban Green Space[J]. Journal of Shenyang Jianzhu University (Natural Science), 2013, 29(2): 349-353.

[6] Itziar Aguado, José M Barrutia, Carmen Echebarria. The green belt of Vitoria-Gasteiz. A successful practice for sustainable urban planning [J]. Boletín de la Asociación de Geógrafos Españoles, 2013, (61):181-193.

[7] Li Ke，Wang Jun，Shi Lu，Yin Hang. Research on the Status of Southern Canal Waterfront Greening and Plant Landscape in Shenyang [J]. Journal of Shenyang Jianzhu University (Social Science), 2013, 15(2): 153-158.

Advanced Materials Research Vols. 989-994 (2014) pp 1196-1199
© (2014) Trans Tech Publications, Switzerland
doi:10.4028/www.scientific.net/AMR.989-994.1196

Design, Simulation and Experiment of Polarization transformers based on twisted chiral metamaterials

Zhuo Yang[1,a], Zhisheng Jing[1,b], Qiangyong Su[1,c],
Guowei Qin[1,d],Zelong Zhou[1,e]

[1]Department of Air Defense Fire Control,Wuhan Mechanical College, Wuhan 430075, China

[a]email: student.yz@163.com,[b]email: alpjzs@icloud.com,[c]email: suxiangyong@163.com,
[d]email: xiaoguo66@sohu.com,[e]email: zhouzelong2005@163.com

Keywords: Polarization; Chirality; Microwave

Abstract. In this paper, we proposed a metamaterial polarization transformer which exhibits linear dichroism and linear conversion dichroism simultaneously. Through simulation and experiment studies in the microwave regime, it was found that only cross-polarization transmissions of x-polarized waves and co-polarization transmissions of y-polarized waves are allowed in the designed structures. As a result, the proposed metamaterials can transform any polarizations into y-polarizations with signal-to-noise ratios over 20 dB and transmissions over 0.6.

Introduction

Manipulating the polarizations of electromagnetic waves is at the heart of many applications such as liquid crystal display [1], wireless communications [2] and optical data storage [3]. Over the past decade years, metamaterials turned out to be a strong candidate for controlling the polarizations [4-8]. Generally, there are two methods to achieve certain polarized electromagnetic waves using metamaterials. One mechanism is linear or circular dichroism [9], to suppress one polarized wave and just to transmit its orthogonal polarized wave. Another one is linear or circular conversion dichroism, to transform one polarized wave into its orthogonal polarized wave [10, 11]. Based on latter phenomena, linear polarization transformers have been proposed in many works [12-13]. These works can achieve a relatively high conversion from x-linear polarized wave to y-linear polarized wave or the opposite one. But small amounts of co-polarization transmissions of x-polarized or y-polarized waves still exist in the transmitted waves, which will reduce the "purity" of the transmitted waves.

In this letter, we proposed a kind of linear polarization transformer based on chiral metamaterials (CMMs). The proposed structure consists of two layer chiral split ring resonators (SRRs), which can exhibit both linear dichroism and linear conversion dichroism. The structure can transform any polarized incidences into y-polarized waves with a high transmission. Moreover, the transmitted wave has a high signal-to-noise (S/N) ratio, which is defined as $|t_{yi}|^2 / |t_{xi}|^2$, in which i denotes any incidence polarization, *x*, *y* denote the x-polarizations and y-polarizations of the transmitted waves, respectively. As a result, the suggested CMMs can be used to transform any polarized waves into linear polarizations with high transmissions and S/N ratios.

Design of the chiral metamaterials

Figure 1(a) shows the schematic diagram of the CMM unit cell used in the simulations and experiments. The square SRRs placed on both sides of an FR-4 board with a relative permittivity of 4.2 and a dielectric loss tangent of 0.025. Copper with a thickness of 30 μm is used for the metallic parts. The structure parameters of the CMMs are as following: a = 12 mm, b = 8 mm, c = 0.5 mm, d = 1.5 mm and w = 2 mm. Figure 1(b) shows the photographs of the experimental samples with an overall size of 220 × 220 mm2. It is notable that the single layer SRR has chirality due to the structural symmetry breaking.

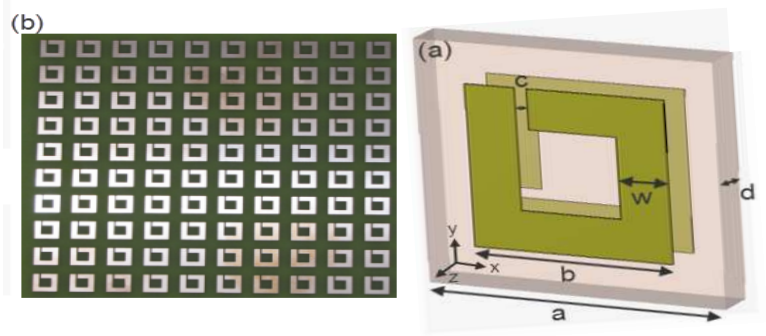

(a) Schematic diagram of the CMM unit cell. (b) Photograph of the fabricated sample slab.

Fig. 1. Polarization transformers based on twisted chiral metamaterials

Simulation, Experiment and Analysis

We used Finite-Difference Time-Domain (FDTD) to simulate the transmissions of the CMMs. The periodic boundary conditions were applied to the x and y directions, and the PML boundary conditions were applied to the z direction. The metal copper was regarded as Perfect Electric Conductor (PEC) in the microwave regime. For the experiments, we measured the transmission coefficients in an anechoic chamber.

Figure 2 shows the simulated and experimental results of the transmission coefficients for propagation along the – *z* directions. It's clear that the simulations and experiments deliver consistent results. In the experiment, the transmission coefficients at 9.36 GHz are: t_{xx} = 0.06, t_{yy} = 0.63, t_{xy} = 0.14, t_{yx} = 0.62. Compared to the previous studies, the transmission coefficient t_{xx} is extremely low, leading to a high S/N ratio of 20.3 dB. Hence, this structure can achieve a high "purity" of transformation from x-polarization to *y*-polarization.

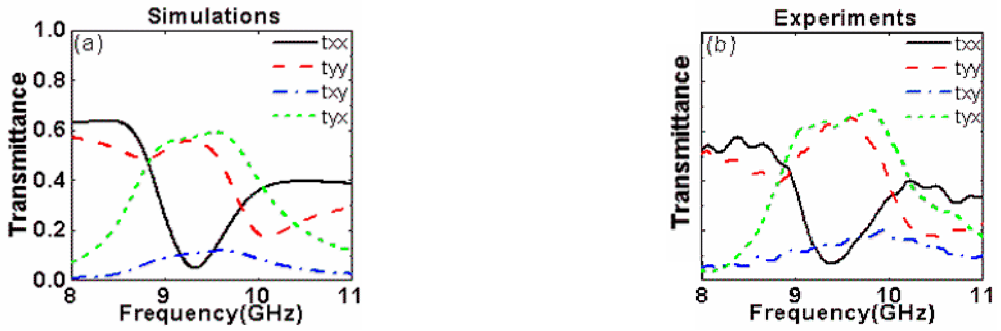

(a) Simulated

(b) experimental results for the circular transformation coefficients.

Fig. 2. Results of simulations and experiments

By using the transformation matrix in Ref. 14, we can calculate transmission coefficients of elliptical polarization incidences with different axial ratios. The axial ratio of the elliptical polarization is defined as the ratio of the amplitude of electric field in the x-axis to that in the y-axis. Figure 3 shows the S/N ratios of different elliptically polarized incidences, in which the numbers denote the axial ratios, the + and – denote right-handedness and left-handedness.

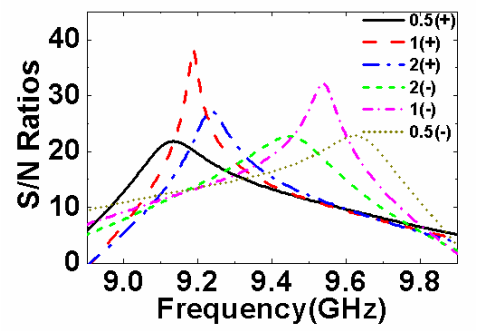

Fig. 3. The S/N Ratios of the elliptically polarized incident waves with different handedness and axial ratios.

From Fig. 3, all the elliptically and circularly polarized incident waves can be transformed into *y*-polarized waves with S/N ratios over 20 dB. However, their peak values lie at different frequencies.

Compared with the previous studies on metamaterial linear polarization transformers, the peculiarity of the proposed CMMs are the simultaneous presences of linear dichroism and linear conversion dichroism. The linear dichroism is due to the two-dimensional chirality of the single SRR layer. The employed square SRR is a kind of planar CMMs, which will exhibit circular conversion dichroism and linear dichroism. The arrangement of two layers of such SRRs with a twisting will keep these properties. By contrast, if stacking two layers of these SRRs which are mirror images of each other with respect to the *yz*-plane, these properties will be canceled. The linear conversion dichroism is due to the couplings between the two layers [14]. The *x*-polarized incidences can excite magnetic resonance mode which will couple electromagnetic waves into the slab, where polarization is rotated by 90° .

Conclusion

To summarize, we have designed a thin CMM structure based on twisted chiral SRRs. From the simulated and experimental results, the CMMs can transform incident waves into y-polarized waves by exhibiting both linear dichroism and linear conversion dichroism. It was found that all the polarizations can be transformed into y-polarizations with S/N ratios over 20 dB and transmissions over 60%. The proposed CMM polarization transformers have thin structures and can be used to manipulate the polarizations in the microwave regime.

References

[1] J. Lub, P. van de Witte, C. Doornkamp , et al. Stable Photopatterned Cholesteric Layers Made by Photoisomerization and Subsequent Photopolymerization for Use as Color Filters in Liquid-Crystal Displays[J] .Adv. Mater. 2003,15 (17)1420-1425.

[2] M. R. Andrews, P. P. Mitra, R. de Carvalho, et al. Tripling the capacity of wireless communications using electromagnetic polarization[J] .Nature, 2001,409, 316-318.

[3] B. Yao, M. Lei, L. Ren et al. Polarization multiplexed write-once-read-many optical data storage in bacteriorhodopsin films[J]. Opt. Lett. 2005,30(22) 3060 -3062.

[4] J. Hao, Y. Yuan, L. Ran, et al. Manipulating Electromagnetic Wave Polarizations by Anisotropic Metamaterials[J].Phys. Rev. Lett. 2007,99, 063908.

[5] J. Y. Chin, M. Lu, T. J. Cui, Metamaterial polarizers by electric-field-coupled resonators[J]. Phys. Lett. 2008, 93, 251903 .

[6] M. Mutlu, A. E. Akosman, A. E. Serebryannikov, et al, Asymmetric chiral metamaterial circular polarizer based on four U-shaped split ring resonators[J]. Opt. Lett. 2011,36, 1653 .

[7]W. Sun, Q. He, J. Hao et al., A transparent metamaterial to manipulate electromagnetic wave polarizations[J]. Opt. Lett. 2011,36, 927.

[8]Mehmet Mutlu, Ahmet E. Akosman, Andriy E. Serebryannikov et al. Diodelike Asymmetric Transmission of Linearly Polarized Waves Using Magnetoelectric Coupling and Electromagnetic Wave Tunneling [J]. Appl. Phys. Lett. 2012,100, 051909.

[9]J. K. Gansel, M. Thiel, M. S. Rill, et al, Gold Helix Photonic Metamaterial as Broadband Circular Polarizer[J], Science,2009,325, 1513.

[10]V. A. Fedotov, P. L. Mladyonov, S. L. Prosvirnin, et al., Asymmetric Propagation of Electromagnetic Waves through a Planar Chiral Structure[J].Phys. Rev. Lett.2006,97, 16,7401.

[11]C. Menzel, C. Helgert, C. Rockstuhl, et al. Asymmetric Transmission of Linearly Polarized Light at Optical Metamaterials[J]. Phys. Rev. Lett. 2010,104, 253902 .

[12]J. Han, H. Li, Y. Fan, et al. An ultrathin twist-structure polarization transformer based on fish-scale metallic wires[J]. Appl. Phys. Lett. 2011,98, 151908.

[13]C. Huang, Y. Feng, J. Zhao et al., Asymmetric electromagnetic wave transmission of linear polarization via polarization conversion through chiral metamaterial structures[J]. Phys. Rev. B, 2012,85, 195131.

[14]C. Menzel, C. Rockstuhl, F. Lederer et al., Advanced Jones calculus for the classification of periodic metamaterials[J]. Phys. Rev. A ,2010,82, 053811.

Advanced Materials Research Vols. 989-994 (2014) pp 1200-1203
© (2014) Trans Tech Publications, Switzerland
doi:10.4028/www.scientific.net/AMR.989-994.1200

The Research of Atmospheric Pressure Cold Plasma Jet Generated by Auto-excited-Pulsed DC Discharge

Yelin HU[1], Qiu WANG[1, a] and Zhaoquan CHEN[2, b]

[1]College of Electrical & Information Engineering, Anhui University of Science and Technology, Huainan, Anhui 232001, China

[2] Faculty of Physics, St. Petersburg State University, St. Petersburg, 198504, Russia

[a]email:1643493602@qq.com, [b]email: zqchen@aust.edu.cn

Keywords: Cold plasma jet; atmospheric pressure; high-voltage DC power supply; periodically pulsed discharge

Abstract. In order to obtain stable cold plasma jet under atmospheric pressure condition, we designed a high-voltage DC power supply based on the principle of multilayer piezoelectric ceramic transformer (MPT). At the same time, we developed a cold plasma jet device that its shape is similar to the gun structure. The total weight of device, including the power supply and the generator, is less than 500 g. In the experiments of argon plasma under atmospheric pressure, current–voltage measurements show that the discharge actually appears periodically pulsed with a frequency of about 30 kHz. The discharge current has a pulse-width that is about 100 ns, while its peak value reaches about 32 mA. The maximum length of the plasma is about 3 cm. The further study showed that the discharge current pulse frequency is determined by the ion drift mechanism.

Introduction

In recent years, atmospheric pressure cold plasmas are widely used for various applications, such as surface and materials processing, Ozone synthesis, gas treatment, and biomedical applications [1]-[6]. Among the applications, the biomedical applications of the plasma, such as sterilization, are attracting significant attention. Plasma jet devices have obvious advantages over the traditional dielectric barrier discharge devices in the biomedical applications, since the plasma jet is produced in open space [4]. Furthermore, for the applications of plasma medicine, such as wound treatment, it has strict requirements for the safety of the plasma devices. There must be having no any harm when the plasmas are touched by human bodies [7]. Fortunately, various plasma jet devices have been recently reported. However, due to diverse applications, plasma jet devices, particularly those reduce equipment costs, making simple, easy to carry devices are still urgent needed.

In this paper, we designed a high-voltage DC power based on the principle of MPT. It can output of 7kV to 11kV high-voltage dc voltage by using 9V battery to drive a MPT that link ten times voltage rectifier circuit. The volume of the high voltage dc power supply is about 10cm x 5cm x 5cm (L, W, H). Meanwhile, we developed a cold plasma jet generator that its shape is similar to the gun structure. The device can be hand held, and the plasma can be touched by a human body without any electrical shock. The total weight of the device, including the power supply, is less than 500g. In order to better describe the device, in this article the electrical characteristics of plasma are analyzed in detail.

Experimental setup

The device is driven by a homemade dc power supply. Fig.1 shown the photograph of the device .Fig. 2 showed the schematic of the plasma jet device. In the 8mm diameter quartz glass tube, the output of the power supply is connected to a stainless steel needle electrode through a resistor R of 10MΩ. The tip of the stainless steel needle has a radius of about 60μm. Needle tip is placed inside the conical nozzle, 2mm from the conical nozzle, but only for 1cm steel needle tip bare inside the conical nozzle, the rest of the steel needle is inserted within the insulation sleeve, which is in order to make 10mm bare steel needle tip contact with argon gas. And the insulating sleeve is inserted in

the insulating plug, the plug is placed away from the conical nozzle at 3cm , and its purpose is to block one side of the quartz glass tube while only allow the gas flow out of conical nozzle. On the left side of the insulating plug, where there is a vertical opening that let gas flow into the quartz glass tube, particularly, the diameter of opening is 4mm. When the argon gas input into the inlet of the quartz glass tube and turn on the power supply, the plasma generated by this device has no risk of glow-to-arc transition, as shown in Fig.3. A P6015 Tektronix HV probe is used to measure the voltage on the needle, and an A6302 Tektronix current probe is used to measure the discharge current.

Fig.1 Photograph of the device

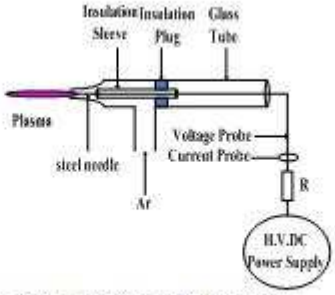

Fig.2 Schematic of the device

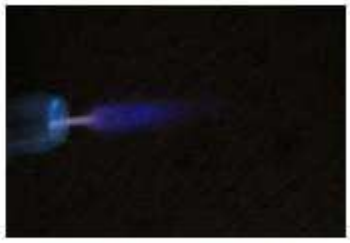

Fig.3 Photograph of the plasma jet

Experimental results and discussion

When the applied voltage is 10kV, the injection of about 30mm plasma jet in front of conical tube mouth, Figure 3 is a non-equilibrium plasma jet photo taken by the Canon A3300. It is worth emphasizing that there is no transient spark mode. This is due to two facts. Firstly, the series-connected ballast resistor R used in our device is 10MΩ. Secondly, the stray capacitance is very small, which is only about 5pF, and the value of the stray capacitance will study detail later [1], [8]. On the other hand, the current–voltage characteristics of the plasma will be studied. It is interesting to notice that the discharge is actually pulsed with a frequency in a kilohertz range.

In order to study the I-V characteristic of the plasma jet in detail. In this paper, we operate the current–voltage measurement shows the discharge current waveforms for applied voltages of 10kV. It clearly shows that the discharge currents appear actually appears periodically with a frequency about tens of kilohertz, and the discharge current has a pulse-width that is about 100ns, as shown in Fig.4 (a) and (b). Although the time between two pulses and the peak value of the current pulses are always changeable, while the mean values of them are approximately 33μs and about 30mA, respectively.

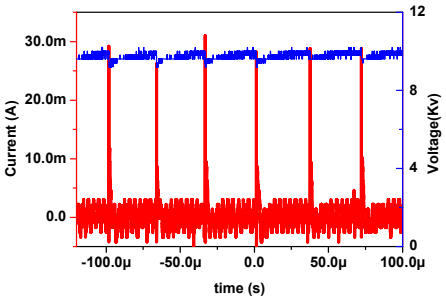

(a)

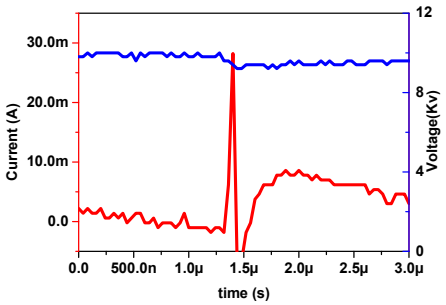

(b)

Fig.4 (a) Typical *I–V* characteristics of the plasma, (b) Close look on the *I–V* characteristics of a typical single pulse

To further study the characteristics of the pulsed discharges, we will estimate the pulsed periods as following. Generally speaking, the ion drift mobility is in formula of [9]

$$\mu_i = \frac{2.7\times10^4\sqrt{(1+M/M_i)}}{p[\mathrm{Torr}]\sqrt{(\alpha/\alpha_0^3)A}}\ \frac{\mathrm{cm}^2}{\mathrm{V}\cdot\mathrm{s}}$$

Where p is the gas pressure in the unit of Torr, α / α_0^3 is about from 10 to 12 for argon, nitrogen and oxygen plasma [9], A is the molecular weight of the gas, M is the mass of the gas molecule, and Mi is the mass of the ion. For argon plasma, its main ion is Ar^+, so M / M_i is equal to 1, A is equal to 40, In addition, the electric field along the bare needle is treat as uniform, and E=10kV/1cm=10kV/cm is acquired. Here, when we deal with α / α_0^3=10, $\mu_i = 2.51 \mathrm{cm}^2/(\mathrm{v} \cdot \mathrm{s})$ is acquired. Hence, the ion drift velocity is $v_i = \mu_i E = 2.51 \times 10^4 \mathrm{cm/s}$. Thus, the time it takes ions from the electrode into the atmosphere about 40 μs. This is very similar with our actual measured pulse period for 33μs.

It should be mentioned that the stray capacitor plays a very important role during the discharge. After each pulse, the stray capacitor is recharged until it reaches the breakdown voltage. Then, the following discharge pulse appears. The stray capacitance is estimated according to the voltage drops on the needle and the total charge for a single current pulse [8]. When the applied voltage is 10kV, the total charge Q for a single current pulse is about 3×10-9C. The voltage drop ΔV on the needle is about 600V. Therefore, according to C = Q/ΔV, the stray capacitor can be estimated to be about 5pF. Because the stray capacitor is small and the ballast resistor is big, the discharge current pulse only lasts for a very short time. Thus, the gas temperature of the plasma remains at room temperature [10]. What's more, although the discharge current peak value is quite high, the pulse-width of the current is only about 100ns, as shown in Fig. 3(b). These two characteristics result in the plasma being able to be touched by a human body without any feeling of warmth or electric shock.

Conclusion

In this paper, we reported a room-temperature atmospheric pressure plasma plume is generated by a plasma jet device, the device include a high voltage dc power supply that based on the principle of MPT, and designed a plasma jet device is similar like type of gun at the same time, the entire unit weight is about 500g. Experiments show that the equipment is safe and reliable and can be hand-held.

Acknowledgment

The authors are grateful to the financial support from Natural Science Foundation of China (Grant No. 11105002), Natural Science Foundation in Anhui Province of China (Grant No. 1408085QA16, 1408085ME101), and Open-end Fund of State Key Laboratory of Advanced Electromagnetic Engineering and Technology (HUST).

References

[1] Zhaoquan Chen, Guangqing Xia, Ping Li, et al. Production of 30-mm wide DC-driven brush-shaped cold plasmas and simulation on its discharge process [J]. IEEE Transactions on Plasma Science. 2013, 41(6): 1658-1663

[2] Ge Ziliang, Wu Yuren. Study on technological improvement of industrial ozone generator[J]. High Voltage Engineering, 1999, 25(3): 66-67.

[3] Lu Xinpei. Plasma jets and their biomedical application[J]. High Voltage Engineering, 2011, 37(6): 1416-1425.

[4] Mounir Laroussi and Xinpei Lu, Room-temperature atmospheric pressure plasma plume for biomedical applications[J]. Apply Physical Letter. 2005, 87(11):113902-1–113902-3

[5] Laroussi, Mounir. Low-Temperature Plasmas for Medicine?[J]. IEEE Transactions on Plasma Science. 2009,37(6): 714-725.

[6]Xinpei Lu, M. Laroussi, and V. Puech. On atmospheric-pressure non-equilibrium plasma jets and plasma bullets[J]. Plasma Sources Science and technology. 2012,21(3):034005-1–034005-17.

[7] Ping Li, Zhaoquan Chen, Guangqin Xia, et al. Study on DC-driven air cold plasma brushes generated without airflow supplement[J]. IEEE Transactions on Plasma Science. 2013,41(3):513-517

[8] Shunqun Wu, Xinpei Lu, et al. A touchable pulsed air plasma plume driven by DC power supply[J]. IEEE Transactions on Plasma Science. 2010,38(12):3404–3408.

[9] Y. P. Raizer, Gas Discharge Physics. New York, USA: Springer-Verlag,1991.

[10] Shunqun Wu, Zhan Wang, Quanjun Huang, et al. Study on a room- temperature air plasma for biomedical application[J]. IEEE Transactions on Plasma Science. 2011,39(6):1489–1495.

Advanced Materials Research Vols. 989-994 (2014) pp 1204-1207
© (2014) Trans Tech Publications, Switzerland
doi:10.4028/www.scientific.net/AMR.989-994.1204

The Research of Hybrid Genetic – Particle Swarm Optimization Algorithm Based Reconfiguration of The Electric Distribution Network

Xin-nan Zhou[1,a], De-ping Ke[1],Yuan-zhang Sun[1],Lu-yang Xu[2,b]

[1]School of Electrical Engineering School of Electrical and Electronic Engineering, Wuhan University,China [2]University of Manchester

[a]jiayouzhouzhou@126.com [b]23990298@qq.com

Keywords: electric distribution network, fault-diagnosis, recovery strategy, hybrid genetic – particle swarm optimization algorithm, practical example

Abstract: The fault-diagnosis and recovery strategy of the electric distribution network were discussed. The procedure of the hybrid genetic – particle swarm optimization algorithm, together with a practical example, was also introduced.

Introduction

The failure recovery is a kind of reconfiguration, depending on the structure of the distribution network itself. On the premise of keeping the radial network topology and other safety regulations, the topology of the electric distribution network can be optimized. A hybrid genetic – particle swarm optimization algorithm is used for the solution of the fault-recovery and the optimal reconfiguration of the electric distribution network. In this method, the binary particle swarm algorithm is modified by combining crossover technology and mutation technology, which are from the genetic algorithm. This modification is able to make the iteration converge to the optimal solution and give a high probability to work out the local optimal solution.

The fault diagnosis of the electric distribution network and the fault recovery strategy fitness function

With information of protection status and breakers status, the fault diagnosis can be done. The fitness function (objective function) is

$$E(S)=\sum_{k=1}^{n_r}\left|r_k-r_k^*(S)\right|+\sum_{j=1}^{n_c}\left|c_j-c_j^*(S,R)\right| \tag{1}$$

In this function, n_r is the total number of protection devices, n_c is the total number of breakers. R refers to the actual protection status， r_k is the actual status of the k-th protection device in R set R^*（S）refers to the demanded status of n_r protection devices, $r^*(S)$ is the demanded status of the k-th protection in R^*（S）set, c refers to n_c breaker statuses， c_j is the actual status of the j-th breaker in c set, $c^*(S,R)$ refers to n_c demanded statues of breakers, $c_j^*(S,R)$ is the j-th demanded status of the breaker. In this case, the minimum value of E(S) is the solution of this optimization problem.

The strategy of the fault recovery

The objective function is based on the principle of load balance, which is

$$\min f_4(x)=\sum_{i=1}^{N}(s_i/s_{i,\max}^2) \tag{2}$$

In this function, s_i is the actual load, $s_{i,max}$is the maximum load tolerance, N is the total number of components. In this research, the choice of the objective function is based on the principle of minimizing the transmission loss of the distribution network, along with the constraint condition of the fault recovery.

The process of the Hybrid Genetic – Particle Swarm Optimization Algorithm

Under the system fault condition, the fault component firstly should be located by applying the binary particle swarm algorithm. Once the fault component is found, the vector that referring to the fault branch will be reset to null. If the network is a radial network, the power flow calculation will start , otherwise the network will be rebuilt. The power flow result, such as the transmission loss and the minimum node voltage, will be set as the objective of the optimization and the network will be optimized by applying the binary particle swarm algorithm. When the initial particle swarm is found, the power flow calculation gives its fitness evaluation, the personal best solution (pbest) and the global best solution (gbest). In addition, the particle speed and position is updated. After the update, the algorithm checks the radial status. If the radial status requirement is matched the algorithm will start the crossover and mutation operation, otherwise the algorithm will update the particle speed and position again.

For the particle crossover operation, the speed update functions are

$$\begin{cases} child1(v) = p \times parent1(v) + (1-p) \times parent2(v) \\ child2(v) = p \times parent2(v) + (1-p) \times paremt1(v) \end{cases} \tag{3}$$

The whole algorithm is an iteration process. After the crossover and mutation operation, the power flow process can give the current fitness value of the particle. If the current fitness value is larger than pbest, the pbest will be updated to the corresponding position. Meanwhile, if the pbest is better than the gbest, the gbest value will be changed to the pbest value. When the the number of iterations hits the maximum limit, or the result is not optimized after a certain number of iterations, the iteration loop will stop and output the final result.

The analysis of a practical example

A typical IEEE 33-node electric distribution network is taken as an example of the network reconfiguration. Based on constraint conditions, an objective function of the network active power loss is developed. This objective function will be solved by applying the binary particle swarm optimization method.

Figure 1 shows the IEEE 33-node electric distribution network, including 32 transmission paths, 5 coupling switches, the base voltage of 12.66kV and the total load of 5084.26+j2547.32 kVA.

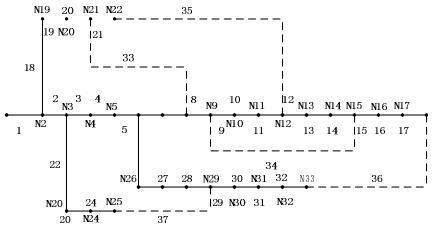

Fig.1. IEEE 33-node electric distribution network

For a fault-free network, the 33th, 34th, 35th, 36th and 37th branch are disconnected before the network reconfiguration. From power flow calculation the active power loss of the network is 202.68kW and the minimum node voltage is 0.91309p.u.

In the binary particle swarm optimization algorithm, all algorithm settings are stated as follows:1）The total number of the particle swarm is 50；2）c_1=c_2=2；3)The maximum number of the interation is 100;4)the maximum tolerance number of continuous no optimization iterations is 30;5)w=1;6)p_c=0.6;7)The value of p_m is from equation (4)

$$p_m = \begin{cases} 0.2 + (p_{m,\max} - p_{m,\min}) \times Iterations / 20, Iterations < 20 \\ 0.8, Iterations \geq 20 \end{cases} \tag{4}$$

In this equation, p_{max}=0.8,p_{min}=0.2.

After the network reconfiguration, the active power loss is reduced by 31.15% and the minimum value of the node voltage is increased by 0.02473p.u. Hence, it is concluded that the network reconfiguration is able to reduce the active power loss and increase the load node voltage.

Figure 2 shows the optimal solution and the suboptimal solution of the network reconfiguration optimization iteration problem.

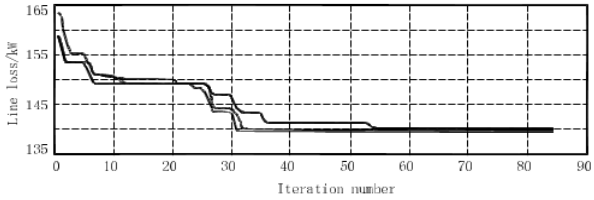

Fig.2. The reconfiguration optimization iteration of IEEE 33-node distribution network

For the fault network analysis, it is assumed that the fault is on the 8th branch. Once the fault is detected, the 8th branch will be cut out. It is necessary to determine the segment switches control to recover the fault as much as possible. Table.1 shows the recovery strategies and Fig.3 shows the relationship between the number of iterations and line power loss when the optimal solution and suboptimal solution are applied respectively.

Table 1 The recovery result of IEEE 33-node electric distribution network

	No.of opened interconnection switch	Active loss/kW	Minimum node voltage/ (p.u.)
optimal solution	7,8,12,34,37	146.19	0.93505
	7,8,32,34,37	146.47	0.93542
	7,8,14,28,32	146.62	0.93505
suboptimal solution	6,8,14,32,37	146.71	0.93075
	7,8,28,32,34	146.90	0.93542
	7,8,14,28,36	147.04	0.93779

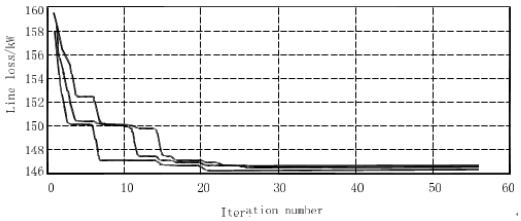

Fig.3. The fault-recovery optimization iteration of IEEE 33-node distribution network

The comparison of algorithms

For the comparison of PSO, GA and G-PSO algorithm, the previous IEEE network 33-node example applies these three algorithms independently and respectively. The number of particle swam is set to 30, the maximum number of iteration steps is 100 and the maximum tolerance number of continuous no optimization iterations is 20. Fig.4 shows the performance of all three algorithms.

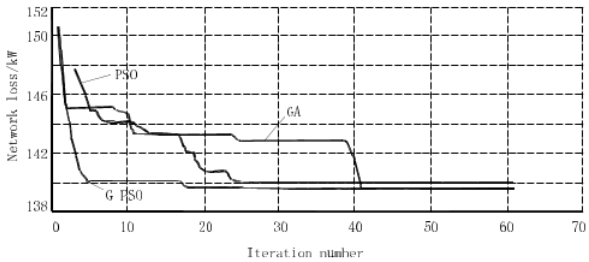

Fig.4. The performance of all three algorithms of IEEE 33-node distribution network

According to the fig.4, the G-PSO algorithm gives the best convergence characteristic since it converges after only 18 steps. The PSO algorithm converges after around 29 steps. The slowest is the GA algorithm which converges after more than 40 steps and it is found that the iteration is not so easy to converge

In conclusion, the G-PSO has not only the powerful global search performance but also the good local search ability. It gives a high probability to obtain the optimal solution with a small number of iterations and swarms.

Conclusion

The reconfiguration and fault-recovery of the electric distribution network both are nonlinear combinatorial optimization problem. This paper discussed the application of hybrid genetic – particle swarm optimization algorithm in the electric distribution network fault-recovery and reconfiguration. The test results proved the availability of this method. Based on the electric distribution network characteristics, this paper also developed and modified the application of crossover mechanism and mutation mechanism in the binary particle swarm algorithm. Finally, this paper analyzed key parameters of the hybrid algorithms and tested their effects on the convergence.

References

[1] Shu Hong-chun,Sun Xiang-fei.A study of Fault in Distribution Line Based on Rough Set Theory[J]. Proceedings of the Chinese Society for Electrical Engineering, 2001，21(10)：73～82

[2] Li Xiong-gang，Li Li.Using Petri Nets for Diagnosis of Power System Faults[J]. Guangdong Electric Power，2004，17(3)：9～13

[3] Sun Ya-ming,Lv hang. A New Approach of Fault Section Locating for Distribution Systems Based on Petri Nets in Combination with Redundant Correcting Technique[J]. Proceedings of the Chinese Society for Electrical Engineering, 2004，24(10)：61～67

[4] He Xun-yu. Research of Rough Set—RBF Neural Network Fault Diagnosis Method about Distribution Network[J]. Machinery and Electronics，2008(8)：67～70

[5] Zhao Zhi, Wang Yan-song. Fault Type Identification in Distribution Network Based on Wavelet Neural Network[J]. Proceedings of the CSU—EPSA, 2007，19(6)：93～96

Advanced Materials Research Vols. 989-994 (2014) pp 1208-1211
© (2014) Trans Tech Publications, Switzerland
doi:10.4028/www.scientific.net/AMR.989-994.1208

Effects of geomembrance on the contaminant transport in compacted clay liner system

Fan Jingjing[1, a *]

[1.] Changsha Environmental Protection Vocational College, Jing Gui Rd, Changsha, Hunan, 410004, China

[a] fjj-07@163.com

Keywords: Geomembrance, Migration, Heavy metal, Liner system

Abstract. An analytical model is established to predict the seepage performance of the liner system composed of a compacted clay liner (CCL) covered by a geomembrane (GM). The contaminant of Pb^{2+} diffusing through the geomembrane is assumed to be a steady-state process. The liner systems with low leakage performance are usually utilized in the municipal solid waste landfills to prevent the contaminants of the leachate from polluting the groundwater and soil beneath the landfill. To investigate the seepage rate of the Pb^{2+} in the liner systems of the landfill considering the effects of the geomembrance, the influence of the geomembrance on the seepage performance of the liner system is studied. Parametric analyses are conducted to study the effects of the thickness of GM and the number of defects in the GM on the leakage performance of the liner system. In conclusion, some suggestions for the design of the municipal solid waste landfills are proposed based on the analyses results.

Introduction

Protection of the groundwater and the sub-soil beneath the landfill is a major goal of environmental engineering. The composite liners composed of a compacted clay liner (CCL) covered by a geomembrane (GM) are key parts of most barrier systems designed to protect the groundwater and the sub-soil [1, 2]. To delay the pollution of the sub-soil and the under groundwater away from the toxic leachate water produced from the landfill, we use the liner system to separate the toxic leachate water from the near environment. The liner system consisting of a compact clay layer (CCL) covered by a high-density polyethylene (HDPE) geomembrance (GM) is adopted because it has the good things of great capacity, easy technique, and economy [3,4].

A number of countries have issued technique standards of the composite liner system in accordance to their scientific study and practical experience. Rowe [5] made comparative study with 3 types of the composite liner system, including GM+CCL, GM+CCL+AL and the double-layered lined system. The barrier designs lead to numerous influences because of the clogging of the leachate system. Xie [6] investigated 4 kinds of liner systems in the Chinese standard. They concluded that the degradation of organic contaminants can have a significant effects on their diffusion through composite liners. For a GM/CCL, the 100-year base concentration of benzene for the contaminant half-life of 10 years can be 1.1 orders of magnitude less than that assuming no degradation.

Previous reports mainly studied the seepage performance of the composite liner systems according to various kings of structures. The influence of the geomembrance on the seepage performance of the liner system is rarely studied. To study the influence of the geomembrance on the seepage performance of the liner system, we conduct parametric analysis on the seepage performance of the liner system with various thickness of the geomembrance and the number of defects on the geomenbrance of the compact clay layer.

Landfill design in China

Chinese standard - Technical code for liner system of municipal solid waste landfill- CJJ113-2007 [7] proposed a composite liner system. The high-density polyethylene geomembrance and the

compact clay layer liner system is composed of a compact clay layer with a thickness of 0.75m covered by the high-density polyethylene geomembrance with a thickness of 1.5 mm. The coefficient of hydraulic conductivity of the CCL should be less than 1×10^{-9}m/s.

The landfill analyzed has a length of 100 m in the oritation of the flow of the groundwater. The pollutant of Pb^{2+} is included. The Pb^{2+}, which is a very common kind of contaminant, stands for the heavy metal in the leachate water. The beginning concentration for Pb^{2+} is 2 mg/L [8]. Baed on the US standards of drinking water, the maximum contaminant level (MCL) for Pb^{2+} is 0.01 mg/L. Then the relative critical concentration for Pb^{2+} is 0.005. The contaminant characteristics are calculated based on Rowe [9-10]. The diffusion coefficient of GM is 7.2×10^{-15} m^2/s. The diffusion coefficient of CCL is 1.79×10^{-10} m^2/s. The adsorption coefficient of CCL K_d is 0.42 mL/g.

Results and discussion

The curves of concentration at the bottom of the CCL versus time are shown in Fig 1. This picture tells us that the concentration of the Pb^{2+} at the bottom of the CCL increases with the increase of time. The concentration grows rapidly before year 50. After year 50, the curve goes flat because the concentration attains its critical value, which shows clearly the transportation of the contaminant is fast in the early stage of the establishment of the municipal waste landfill.

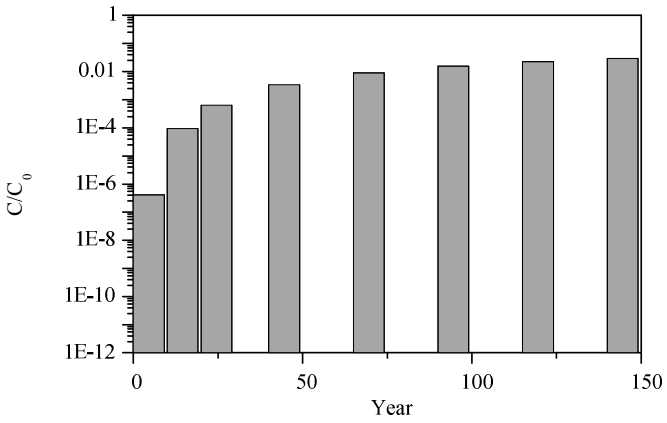

Fig 1 The concentration-time curves of Pb^{2+}

The curves of concentration versus thickness of GM are shown in Fig 2. The concentration of Pb^{2+} decreases rapidly with the increase of the depth of the liner system. The concentration of Pb^{2+} at the top of CCL is almost unchanged by the increase of the GM thickness. This suggested that the GM thickness in the common use has small influences on the concentration of Pb^{2+} at the top of the CCL. The concentration at the CCL bottom reduces slightly with the increase of the GM thickness. The concentraion of Pb^{2+} increases with the time. At year 10, the relative concentration of Pb^{2+} at the bottom of the CCL is near 0.03, while the relative concentration of Pb^{2+} at the bottom of CCL is about 0.1 at year 100.

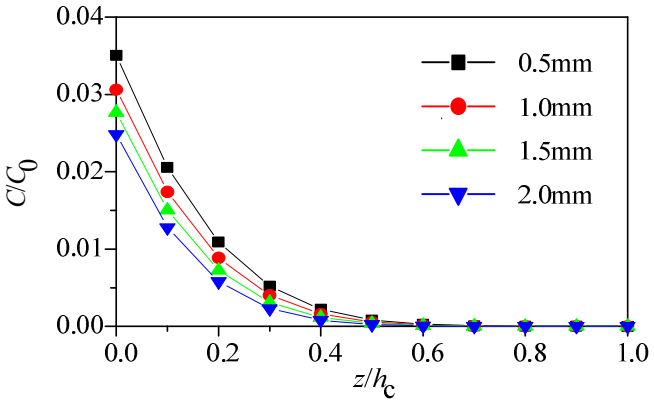

（a）10 year

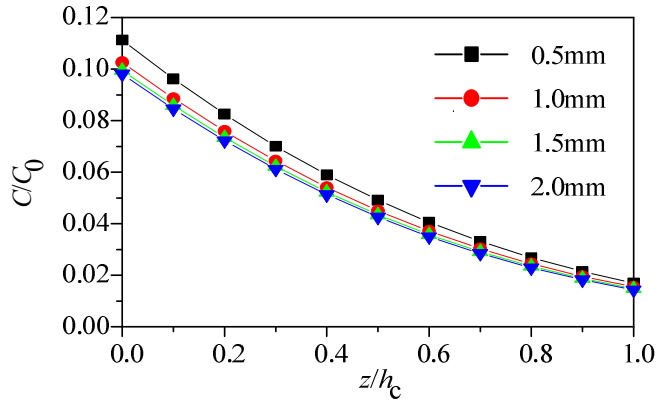

（b）100 year

Fig 2 The concentration-depth curves for different GM thickness

The influences of the number of defects in GM on the leakage performance of the liner system are shown in Fig 3. The concentration of Pb^{2+} increased remarkably with the increase of the number of defects. The relative concentration of Pb2+ at the top of CCL is 0.15 when the defects number of the GM is 2 and reduces to 0.015 when the number of defects number of the GM is 200.which indicates clearly that the migration of the Pb^{2+} through the GM is mainly by the leakage, while not by diffusion. At year 10, the concentration of the Pb^{2+} at the bottom of the CCL is almost 0, which shows that the CCL can stop most of the contaminant in a shot period. At year 100, the concentration of Pb^{2+}at the bottom of the CCL increase remarkably with the increase of the number of defects in GM, which indicates that the reduction of the number defects will help the liner system to stop the migration of the contaminant to the groudwater in a long period.

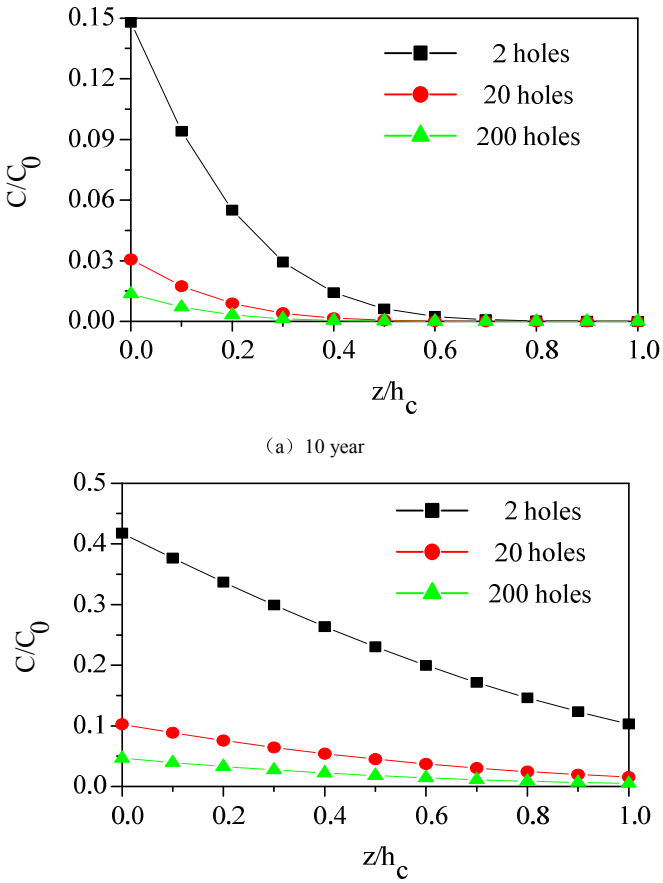

（a）10 year

（b）100 year

Fig 3 The concentration-depth curves for different number of defects

Conclusion

The effects of the GM on the seepage behavior of the composite liner system is analyzed. Parametric analysis on the thickness of the GM and the number of defects of GM are studied. The conclusions are as follows. 1) Then concentration of Pb^{2+} increases with the increase of time. The concentration grow rapidly before year 50. After year 50, the curve goes flat because the concentration attains its critical value. 2). The concentration of Pb^{2+} at the top of CCL is almost unchanged by the increase of the GM thickness. This suggested that the GM thickness has small influence on the top concentration of the CCL. The concentration at the CCL bottom reduces slightly with the increase of the GM thickness. 3) The concentration of Pb^{2+} increased remarkably with the increase of the number of defects, which indicates that the migration of the Pb^{2+} through the GM is mainly by the leakage, while not by diffusion..

References

[1]. Kandris, K. and M. Pantazidou, Landfill Base Liners: Assessment of Material Equivalency and Impact to Groundwater. Geotechnical and Geological Engineering, 2012. 30(1): p. 27-44.
[2]. Fan, J. The revelation of Kitakyushu city's experience on environmental education. in Advanced material research. 2012.
[3]. Fan, J. Vocational education on environmental protection in China: A case study of Changsha Environmental Protection Vocational College. in Advanced material research. 2012.
[4]. Dickinson S, Brachman RWI: Assessment of alternative protection layers for a geomembrane - geosynthetic clay liner (GM-GCL) composite liner. Canadian Geotechnical Journal 2008, 45(11):1594-1610.
[5]. Rowe RK, Nadarajah P: An analytical method for predicting the velocity field beneath landfills. Canadian Geotechnical Journal 1997, 34(2):264-282.
[6]. Xie HJ, Lou ZH, Chen YM, Jin AM, Zhan TL, Tang XW: An analytical solution to organic contaminant diffusion through composite liners considering the effect of degradation. Geotextiles and Geomembranes 2013, 36:10-18.
[7]. Technical code for liner system of municipal solid waste landfill, 2007, China Architecture & Building Press: Beijing.
[8].Chen, Y., et al., An analytical solution for one-dimensional contaminant diffusion through multi-layered system and its applications. Environmental Geology, 2009. 58(5): p. 1083-1094.
[9]. Rowe, R., R. Quigley, and R. Brachman, Barrier Systems for Waste Disposal Facilities. 2004, London and New York: Spon Press.
[10]. Liu CL, Zhang FE, Zhang Y, etc. Experimental and numerical study of pollution process in an aquifer in relation to a garbage dump field. Environmental Geology 2005, 48(8):1107-1115.

Advanced Materials Research Vols. 989-994 (2014) pp 1212-1215
© (2014) Trans Tech Publications, Switzerland
doi:10.4028/www.scientific.net/AMR.989-994.1212

The Higher Order Crack-Tip Fields for Anti-plane Crack in Exponential Functionally Graded Piezoelectric Materials

Dai Yao[1, a], Chong Xiao[1, b], Li Shimin[2,b]

[1]The Academy of Armored Force Engineering, Beijing, 100072
[2]Beijing Special Vehicle Institute, Beijing, 100072
[a]dai_yao@sina.com, [b]chongxiao2005@163.com)

Keywords: crack tip fields, FGPMs, eigen-expansion method, anti-plane crack

Abstract The near-tip fields of an anti-plane crack in functionally graded piezoelectric materials (FGPMs) are investigated. To make the analysis tractable as usual, the elastic stiffness, piezoelectric parameter, and dielectric permittivity of FGPMs are assumed to be exponential functions of x parallel to the crack. The boundary conditions on crack surfaces are assumed to be the stress free and electrically impermeable. The high order crack tip stress and electric displacement fields are obtained by the eigen-expansion method. This study possesses fundamental significance as Williams' solution to homogeneous materials.

Introduction

To get rid of the possible interfacial failure, the functionally graded piezoelectric materials have been introduced to reduce the stress concentration at the interface. In order to make FGPMs to have high strength, high reliability and long lifetime, the behaviors of cracks in brittle piezoelectric materials have to be analyzed. Therefore, the fracture mechanics problems of FGPMs have received much attention in recent decades. Wang and Noda [1] firstly studied the thermo- piezoelectric fracture problem of a functionally graded piezoelectric layer bonded to a metal. Li and Weng [2,3] considered the static anti-plane problem of a finite crack in a functionally graded piezoelectric material strip. It is found that the singular behaviors of both stress and electric displacement are the same as those in a homogeneous piezoelectric material. Shin [3] examined the singular stresses and electric fields in a functionally graded piezoelectric ceramic strip containing an eccentric crack off the center line under anti-plane shear loading with the theory of linear piezoelectricity. Mousavi [4] investigated the fracture behavior of a cracked functionally graded piezoelectric strip under anti-plane mechanical and in-plane electrical loading. It should be mentioned that most existing studies in fracture analysis of FGPMs are focused on the singular part of crack tip fields. No attempts have been made in giving the high order crack tip fields for FGPMs. In this paper, we extend the Williams' solution to fracture problem of FGPMs and the stress and electric displacement high order fields are obtained.

Basic equations

Consider a crack in a functionally graded piezoelectric materials under anti-plane shear tractions and in-plane electric displacements, as shown in Fig.1. The FGPM is poled in the z direction and isotropic in the xoy plane. The present work employs exponential function to describe the continuous variations of material properties,

$$c_{44} = c_{440}e^{\alpha x}, \quad e_{15} = e_{150}e^{\alpha x}, \quad \varepsilon_{11} = \varepsilon_{110}e^{\alpha x} \tag{1}$$

where c_{440} is the shear modulus, e_{150} is the piezoelectric coefficient, ε_{110} is the dielectric parameter at $x = 0$.

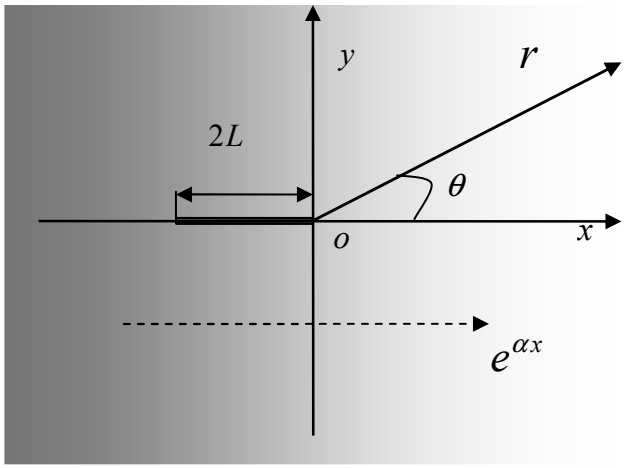

Fig.1Anti-plane crack in FGPMs

The governing equations can be written as

$$\begin{aligned}\nabla^2 w+\alpha(\cos\theta\frac{\partial w}{\partial r}-\frac{1}{r}\sin\theta\frac{\partial w}{\partial\theta})=0\\ \nabla^2\phi+\alpha(\cos\theta\frac{\partial\phi}{\partial r}-\frac{1}{r}\sin\theta\frac{\partial\phi}{\partial\theta})=0\end{aligned}\tag{2}$$

where $\nabla^2=\frac{\partial^2}{\partial r^2}+\frac{1}{r}\frac{\partial}{\partial r}+\frac{1}{r^2}\frac{\partial^2}{\partial\theta^2}$ is the two-dimensional Laplace operator.

The higher order crack-tip field

The displacement component w and the electric potential ϕ can be expanded as follows

$$w=\sum_{i=1}^{\infty}r^{\frac{i}{2}}w_i(\theta),\qquad \phi=\sum_{i=1}^{\infty}r^{\frac{i}{2}}\phi_i(\theta)\tag{3}$$

where, $w_i(\theta)$ and $\phi_i(\theta)$ are eigen-functions.

Substitute Eq. (3) into Eq.(2). According to the linear independence of $r^{-3/2}$, r^{-1}, $r^{-1/2}$,…, $r^{i/2-2}$,…, the system of ordinary differential equations are obtained.

$$\begin{cases}\frac{1}{4}\mathbf{w}_1(\theta)+\mathbf{w}_1^{(2)}(\theta)=0\\ \mathbf{w}_2(\theta)+\mathbf{w}_2^{(2)}(\theta)=0\\ \frac{9}{4}\mathbf{w}_3(\theta)+w_3^{(2)}(\theta)+\frac{1}{2}\alpha\cos\theta\mathbf{w}_1(\theta)-\alpha\sin\theta\mathbf{w}_1'(\theta)=0\\ 4\mathbf{w}_4(\theta)+\mathbf{w}_4^{(2)}(\theta)+\alpha\cos\theta\mathbf{w}_2(\theta)-\alpha\sin\theta\mathbf{w}_2'(\theta)=0\\ \frac{25}{4}\mathbf{w}_5(\theta)+\mathbf{w}_5^{(2)}(\theta)+\frac{3}{2}\alpha\cos\theta\mathbf{w}_3(\theta)-\alpha\sin\theta\mathbf{w}_3'(\theta)=0\\ 9\mathbf{w}_6(\theta)+\mathbf{w}_6^{(2)}(\theta)+2\alpha\cos\theta\mathbf{w}_4(\theta)-\alpha\sin\theta\mathbf{w}_4'(\theta)=0\\ .....\end{cases}\tag{4}$$

where $\mathbf{w}=\begin{bmatrix}w\\ \phi\end{bmatrix}$, $\mathbf{w}'=\frac{\mathrm{d}\mathbf{w}}{\mathrm{d}\theta}$ and $\mathbf{w}^{(2)}=\frac{\mathrm{d}^2\mathbf{w}}{\mathrm{d}\theta^2}$.

In the case of electrically impermeable crack, the crack surfaces are free of electric charges and the electric displacement inside the crack is zero. As the crack surface is free, the boundary conditions are

$$\sigma_{zy}\big|_{\theta=\pm\pi}=0,\ \ D_y\big|_{\theta=\pm\pi}=0 \tag{5}$$

Further, they can be expressed as

$$w_i'(\pm\pi)=0 \qquad \phi_i'(\pm\pi)=0 \tag{6}$$

Solving the system of ordinary differential equations, we can obtain the results

$$\begin{cases}\mathbf{w}_1(\theta)=\mathbf{A}_{11}\sin\dfrac{\theta}{2}\\ \mathbf{w}_2(\theta)=\mathbf{A}_{21}\cos\theta\\ \mathbf{w}_3(\theta)=\mathbf{A}_{31}\sin\dfrac{3\theta}{2}+\dfrac{1}{4}\alpha\mathbf{A}_{11}\sin\dfrac{\theta}{2}\\ \mathbf{w}_4(\theta)=\mathbf{A}_{41}\cos 2\theta-\dfrac{1}{4}\alpha\mathbf{A}_{21}\\ \mathbf{w}_5(\theta)=\mathbf{A}_{51}\sin\dfrac{5\theta}{2}+\dfrac{1}{24}(\alpha^2\mathbf{A}_{11}-6\alpha\mathbf{A}_{31})\sin\dfrac{\theta}{2}-\dfrac{1}{32}\alpha^2\mathbf{A}_{11}\sin\dfrac{3\theta}{2}\\ \mathbf{w}_6(\theta)=\mathbf{A}_{61}\cos 3\theta+\dfrac{1}{16}(\alpha^2\mathbf{A}_{21}-4\alpha\mathbf{A}_{41})\cos\theta\\ \cdots\cdots\end{cases} \tag{7}$$

where $\mathbf{A}_{ij}=\begin{bmatrix}A_{ij}\\ B_{ij}\end{bmatrix}$ are the undetermined coefficients.

Substituting Eq. (7) into Eq.(3), the displacement component w and the electric potential ϕ are obtained.

$$\begin{aligned}w=&r^{\frac{1}{2}}A_{11}\sin\frac{\theta}{2}+rA_{21}\cos\theta+r^{\frac{3}{2}}(A_{31}\sin\frac{3\theta}{2}+\frac{1}{4}\alpha A_{11}\sin\frac{\theta}{2})+r^2(A_{41}\cos 2\theta-\frac{1}{4}\alpha A_{21})\\ &+r^{\frac{5}{2}}[A_{51}\sin\frac{5\theta}{2}-\frac{1}{32}A_{11}\alpha^2\sin\frac{3\theta}{2}+\frac{1}{24}(-6\alpha A_{31}+\alpha^2A_{11})\sin\frac{\theta}{2}]+r^3[A_{61}\cos 3\theta+\\ &\frac{1}{16}(\alpha^2A_{21}-4\alpha A_{41})\cos\theta]+\cdots\end{aligned} \tag{8}$$

$$\begin{aligned}\phi=&r^{\frac{1}{2}}B_{11}\sin\frac{\theta}{2}+rB_{21}\cos\theta+r^{\frac{3}{2}}(B_{31}\sin\frac{3\theta}{2}+\frac{1}{4}\alpha B_{11}\sin\frac{\theta}{2})+r^2(B_{41}\cos 2\theta-\frac{1}{4}\alpha B_{21})\\ &+r^{\frac{5}{2}}[B_{51}\sin\frac{5\theta}{2}-\frac{1}{32}B_{11}\alpha^2\sin\frac{3\theta}{2}+\frac{1}{24}(-6\alpha B_{31}+\alpha^2B_{11})\sin\frac{\theta}{2}]+r^3[B_{61}\cos 3\theta+\\ &\frac{1}{16}(\alpha^2B_{21}-4\alpha B_{41})\cos\theta]+\cdots\end{aligned} \tag{9}$$

Then，the stress and the electric displacement components can be obtained

$$\begin{aligned}&\tau_{xz}=c_{44}w_{,x}+e_{15}\phi_{,x},\ \ \tau_{yz}=c_{44}w_{,y}+e_{15}\phi_{,y}\\ &D_x=e_{15}w_{,x}-\varepsilon_{11}\phi_{,x},\ \ D_y=e_{15}w_{,y}-\varepsilon_{11}\phi_{,y}\end{aligned} \tag{10}$$

The mode III stress intensity factor (SIF) and electric displacement intensity factor (EDIF) of the crack tip are defined as

$$\begin{cases} K^T = \lim\limits_{r\to 0}\sqrt{2\pi r}\sigma_{yz}(r,0) = \dfrac{\sqrt{2\pi}}{2}(c_{440}A_{11} - e_{150}B_{11}) \\ K^D = \lim\limits_{r\to 0}\sqrt{2\pi r}D_y(r,0) = \dfrac{\sqrt{2\pi}}{2}(e_{150}A_{11} + \varepsilon_{110}B_{11}) \end{cases} \tag{11}$$

Conclusion

The higher order displacement, electric potential, stress and electric displacement fields for exponential FGPMs are obtained in this paper. The effect of non-homogeneity reflects only in the higher order items. Due to coupling effect of piezoelectric material, the stress intensity factor and electric displacement intensity factor are depending on both displacement component and the electric potential. It is obvious that the crack tip fields and intensity factors obtained herein provide basic solutions to fracture problems of FGPMs in experimental analysis and engineering practice.

Acknowledgements

The research is supported by the National Natural Science Foundation of China (No11172332.)

References

[1] B.L. Wang and N. Noda: Theoretical and Applied Fracture Mechanics. Vol.35 (2001), p. 93

[2] C. Li and G.J. Weng: Journal of Applied Mechanics-Transactions of the Asme. Vol.69 (2002), p. 481

[3] C. Li and G.J. Weng: Acta Mechanica. Vol.149 (2001), p.1

[4] J.W. Shin and T.U. Kim: Ksme International Journal. Vol.17 (2003), p. 854

[5] S.M. Mousavi and J. Paavola: International Journal of Solids and Structures. Vol.50 (2013), p. 2449

Advanced Materials Research Vols. 989-994 (2014) pp 1216-1219
© (2014) Trans Tech Publications, Switzerland
doi:10.4028/www.scientific.net/AMR.989-994.1216

The Effects and Countermeasures of Low-carbon Economy on China's International Competitiveness of Industries

Hu Jian-bo

Guizhou University of Finance and Economics, Guiyang 550025, China

hjbbo@126.com

Keywords: Low-carbon economy; International competitiveness of industries; Trade barriers

Abstract. Contradiction between the environment and economic development have become increasingly prominent, high-carbon development model of the world economy is more difficult to maintain, low-carbon development has becomea strategic objective of all countries. Countries hold low-carbon technologies, the establishment of a green trade barriers, lack of core technology and our industry, lack of international competitiveness of exports facing enormous challenges. For this reason, the paper deeply analyzes the impact of a low-carbon economy on the international competitiveness of the industry and made a reasonable suggestions and strategies from both countries and companies on how to enhance the international competitiveness of industry.

Introduction

While human activities in the creation of wealth, promoting social progress, but also to humanity itself brought great disaster. With the increasing conflict between energy, environment and economic development, ecological imbalance, environmental degradation, human survival and development is faced with an unprecedented threat. High-carbon development model of the world economy is increasingly difficult to maintain, to become the inevitable choice of low-carbon world economy. Therefore, in order to reduce the negative impact of human activities on climate and economic environment of the countries in the world are trying to change through technological innovation and the development of energy use patterns, to minimize the consumption of high-carbon energy, reduce greenhouse gas emissions and achieve human survival economic, social and ecological sustainable development, the development of low-emission, low-pollution, low energy consumption is characterized by a low-carbon economy has become a global consensus.

Connotation of low-carbon economy

In 2003 the UK government's energy white paper firstly proposed the concept of low-carbon economy, it is the low-carbon development, generic low-carbon industry, low-carbon technologies, low-carbon living and other economic activities in resource and environmental constraints under double , with low power consumption, low emissions, low pollution characteristics, in order to reduce the negative impact of economic activity on the climate, through technical innovation and institutional reforms to reduce carbon energy consumption, reduce greenhouse gas emissions and achieve sustainable economic development and the environment. Data show that in 2012, global carbon emissions mainly from coal (43%), oil (33%), natural gas (18%) and cement (5.3 percent), shown in Fig.1.Low-carbon economy is the green economy is efficient economy, a new model is the survival and development of humanity must be chosen.

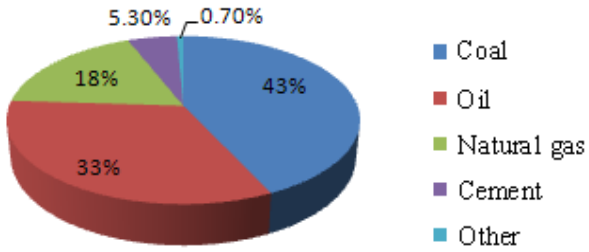

Fig.1 The main source of carbon emissions in 2012

Global Carbon Project latest data shows that in 2013, global carbon dioxide emissions reached a record 360 million tons, with the rapid economic development, China's total carbon emissions will further widen the gap with the United States, the world's first sit tight position. While per capita emissions with the United States and other countries there is a gap, but because China's economy is still in the "high-carbon" development model, per capita carbon emissions will rise. Figure 2 shows several major national per capita carbon emissions curve.

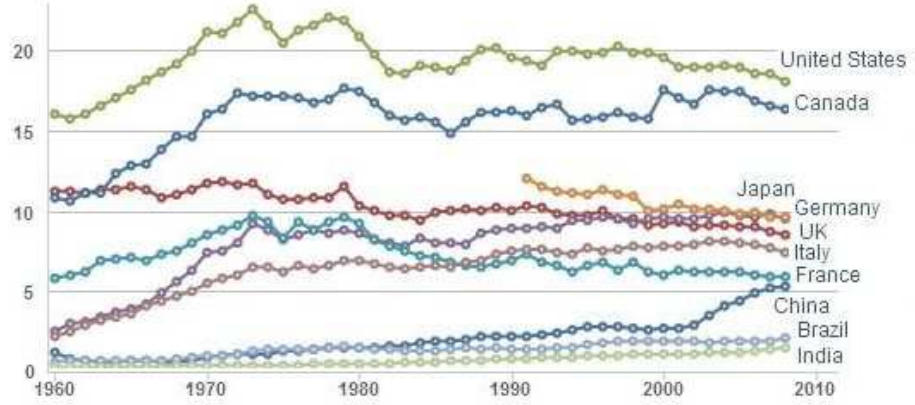

Fig.2 Countries in the world per capita carbon emissions

The impact of low-carbon economy of China's industrial competitiveness

The challenge of low-carbon economy.

1) Trade barriers to change the pattern of international competitiveness.

Starting point for a low-carbon economy in order to protect the ecological, climate and the environment, and it will result in a significant adjustment of international trade rules. Must gradually reduce the high energy consumption , high pollution products share , gradually increase energy consumption, the proportion of new energy products and thus shift to low-carbon development , the country has a low-carbon technologies or companies , which in the pattern of world trade position will become more favorable. Low-carbon economy for a number of countries made an excellent " policy tool" , especially the developed countries , because they have great technical and institutional strengths, trying to develop "low carbon economy" to create new competitive advantages, thereby those developing countries that is still going on "carbon economy" development thrown far behind , especially in China will face enormous pressure .

2) Lack of low-carbon core technology, behind its own brand

Technology is the key to low carbon economy, many developed countries have to develop core technology as the core strategy development. China's overall technological level of enterprises lag, the biggest constraint to the most high-carbon low-carbon industrial transformation of the industry. Although in recent years China has begun to attach importance to investment in related technologies, but there is still a big gap in the aspects of R&D capabilities and other restrictions on many indicators with the developed countries. Based on the current status and content of science

and technology R & D related to our country, to become a true technological innovation a big country, but also go a long way.

The opportunities of low-carbon economy.

1) Fight the initiative from international competition. With the advent of the era of low-carbon economy, the world actively "low-carbon" developed from "high-carbon", hoping to achieve the greatest voice in the transformation process, thereby seeking the most favorable policies for domestic industries. China as an emerging developing countries position in the world more and more attention, countries hope to become a partner and China, with China to jointly promote the power of the revolution. In this transformation process, our concept of sustainable development should, while rules of the international community in the fight to tackle climate change initiative, seek common interests in international negotiations to develop a fair and reasonable international policy for China low-carbon industry seek to develop space for development, laying the foundation.

2) Get support from national policies. In recent years, the state has increased the proportion of investment in low-carbon industries and support efforts to put sustainable development of energy, economy and the environment as long-term development goals, to promote industrial development shift to a low-carbon economic development model. In the automobile industry as an example: Since entered the WTO, the number of China's auto exports increased year by year, but lower prices, with well-known international car companies have a larger gap. The low-end market, low prices, low profits, is still the main way of exports of automotive products, the lack of sufficient competitive in the international arena.

Environment to improve the international competitiveness of industry recommendations of low-carbon economic

Government should strengthen supervision, the gradual transformation of economic development mode. Firstly, countries should make full use of fiscal policy to support the development of low-carbon industries, increase macro-control efforts to increase the proportion of investment in low-carbon industries, good government guiding role; Meanwhile, the government on how to deal with climate change as an environmental development planning the long-term strategic objectives, to promote economic development model to an efficient, low pollution and economic development paradigm shift. In the automobile industry, for example, the government can provide some subsidies for economic development of new energy automobile enterprises, preferential policy.

Secondly, increase government intervention, changes in tax policies, and constantly adjust the national industrial structure. Carbon tax on high-carbon industries and implement carbon trading policy interventions are effective, this policy in some foreign countries have successfully implemented and achieved some results. But a carbon tax on domestic companies, will result in increased production costs, product price increases, thereby reducing the competitiveness of domestic exports to economic growth caused some damages. Therefore, the state should reduce the corporate income tax rate. Without increasing the cost of doing business, raising the international competitiveness of the industry is impossible.

Enterprises should strengthen research and development capabilities, changing Development Mechanism. Firstly, in terms of trade policy, the enterprise should change the traditional trade patterns should not be in pursuit of high commodity export trade should be a low-carbon as a new growth point of export, should make trade-offs in terms of environmental and trade interests, out of mutual benefit win a sustainable development path. In the automobile industry, for example, China's automobile exports have been taking the low, low road, not really occupy competitiveness in the world market, the arrival of low-carbon economy era has brought us opportunities for future development of the automobile industry will weigh the benefits of the interests of both the environment and the development of national car companies once again stood

on the starting line. Although China's auto industry started late, there is a certain gap with the developed countries, but as long as we can seize the opportunities of low-carbon, low-carbon enterprises attach importance to the development of the field, to seize the initiative in the future carbon trading market is inevitable.

Secondly, continuous innovate and breakthroughs in core technologies. Core and key issues of technological innovation is the development of a low carbon economy. In our country there is a big gap with the developed countries, low-carbon technologies, like in a short time transition to a low carbon economy, the best way is the introduction of technology - digestion - the process of innovation. Therefore, China's low-carbon technologies must now rely on independent innovation, which means not only to achieve a low-carbon economy, increase costs, but also to extend the time. But the successful experience of developed countries, the development of low-carbon technologies can learn. From the experience of developed countries in recent years, the first combination of conditions to develop low-carbon development strategy firstly, then the policy needs to be based on the implementation of supporting additional investment in constant, while focusing on international cooperation.

Conclusion

China ranks first in the world of carbon dioxide emissions and withstand greater pressure to reduce emissions. Under Resources, environment and coordinated economic development background, extensive economic development model of traditional high pollution, high energy consumption has been unable to meet the demands of the times, low energy consumption, intensive model of economic development of new energy sources is imperative. In order to further improve the international competitiveness of our industry, while steady economic growth, we need to constantly change the economic growth pattern; while strengthening international exchanges and cooperation, promote the introduction of low-carbon technologies and innovations, from high-carbon economy to accelerate the transition to a low carbon economy .

Acknowledgments

We thank Project Supported by MOE (Ministry of Education in China) Project of Humanities and Social Sciences (Grant No.13YJC790045) , National Statistical Science Project of National Bureau of Statistics in China (Grant No.2013LY104), Project of Science & Technology Department of Guizhou Provice(Grant No. QiankeheJ[2013]2090), Education Department of Guizhou Provice Project of Humanities and Social Sciences (Grant No.12QN035).

References

[1] Hu Zhi-wei, Liu Yong. Provincial Competition Study from the Perspective of Low-carbon Economy[J].China Industrial Economics.2010,265(4):69-78

[2] Hu Tao, Tian Chun-xiu, Li Li-ping. Influence of Co-benefit on Policy in China[J]. Environmental Protection. 2004,(9):56-58.

[3] Fu Jia-feng, Zhuang Gui-yang, Gao Qing-xian. Conceptual Identification and Evaluation Index System for Low Carbon Economy[J].China Population, Resources and Environment. 2010,20(8):38-43

[4] Zhang Kunmin, Pan Jiahua, Cui Dapeng. Overview on Low-Carbon Economy[M]. Beijing: China Environmental Science Press.2008

[5] Zhuang Guiyang. Low-Carbon Economy: Development Road of Climate Change in China [M]. Beijing: Meteorological Press.2007

Advanced Materials Research Vols. 989-994 (2014) pp 1220-1223
© (2014) Trans Tech Publications, Switzerland
doi:10.4028/www.scientific.net/AMR.989-994.1220

The application of transformer protection in 220KV substation

Wenliang Peng[1,2, a], Wanglong Bian[3, b] , and Meng wang[1, c]

[1]Wuhan of University Technology, Wuhan 430070, China;

[2]Beijing Institute of Technology,Zhuhai, Zhuhai 519088, China;

[3]Department of Aviation Ammunition ,Air Force College of Service,Xuzhou,221003, China.

[a]sanmao332@126.com, [b]44973901@qq.com, [c]651601954@qq.com

Keywords: Monitoring, Network transmission power controller, transformer.

Abstract. This paper studies the application of the transformer protection in 220KV substation, proposed the use of the digital transformer protection device to protect the transformer. Through long-term experiments, the system is stable and high-reliability, and it can achieve effective by real-time monitoring and protect the transformer, so that the operating environment has improved radically.

1.Introduction

The transformer is widely used in power system and play an important role in the power transmission station of 220KV, using the principle of electromagnetic induction to transform and transmit the electric power.

With the development of technology, the protection device of transformer changes from mechanical to digital and use software to realize various functions. With the increasingly fierce market competition, enterprises use domestic products to reduce the costs .The system uses the transformer protection device of CSC-325ED/EE[1].

2. PRINCIPLE OF SYSTEM

The system uses the ratio of the differential to determine the inrush current and TA disconnection. With the different of the TA performance in each side of transformer and the ratio and the winding connections, there is unbalance current of the different circuit[2]. With using the Three-Fold Features, the system can ensure that it will does not occur when there is fault unbalance current in outside, and it can guarantee the sensitivity of resection in area fault. According to the overall analysis, the flow chat is shown in Figure 1.

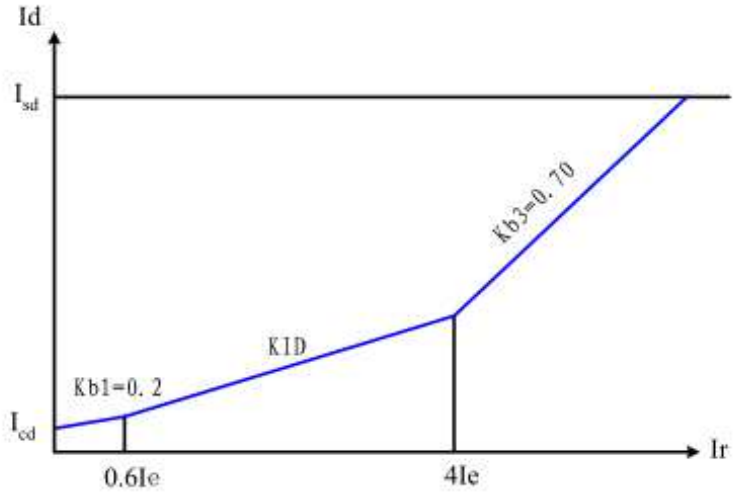

Fig1. The curve of ratio restraint

1. $I_d \geq (0.2I_r + I_{cd}), I_d \leq 0.6I_e$
2. $I_d \succ [K(I_r - 0.6I_e) + 0.2I_e + I_{cd}], 0.6I_e \leq I_r \leq 4I_e$
3. $I_d \succ [0.7(I_r - 4I_e) + K*3.4I_e + I_{cd} + 0.12I_e], I_r \succ 4I_e$
4. $I_d = \left| \frac{1}{2} \sum_{i=1}^{m} I_i \right|$

Normally the value of K is 5.

When the differential current of any phase is more than current of Instantaneous differential setting value, the differential protection will act immediately. The criterion of differential quick break protection is $I_d > I_{st}$.

3. DESIGN OF HARDWARE

There are four main transformers of 180MVA, six outlets of 220KV, twelve outlets of 110KV and thirty outlets of 10KV in the substation of 220KV[3].

According to the requirements of the system design, the protection devices of new digital transformer were used in this project and meet the requirements. The protection device provides a kind of all functional units modularization and standardization, in the form of a plug-in integration on the box body. The protective device is a functional unit with integrating all modularization and standardization[4].The device of transformer is composed of differential protection, backup protection and main protection.

Experimental results show that this system meets high-speed, high precision and high reliability. The system uses the transformer protection device of CSC-325ED/EE.

Fig.2 The diagram of CSC-326

4. DESIGN OF SOFTWARE

The design of software uses modular design. The software uses the Y/Δ to adjust the current phase of TA in the each side of the transformer, so that each side of the transformer TA can be connected to the grid by the star way[5]. The system can be improved the braking capability by using the Three-Fold Features, when the TA is saturated because of the large current of the external fault[6].

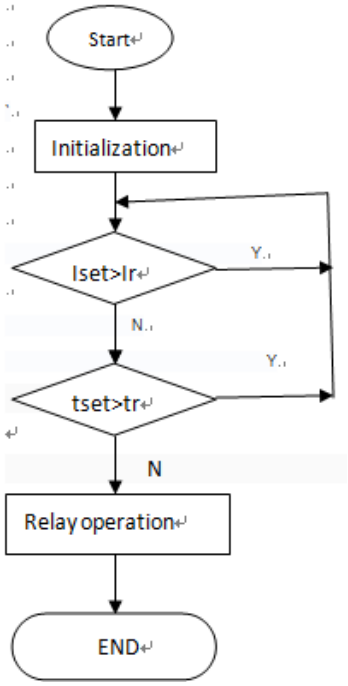

Fig.3 The diagram of Flow

First, We should set the value of the action current("I_{set}") and measure the actual current("I_r") of the protection device. IF $I_{set} > I_r$, it shows that the value of action current is greater than the value of actual current, it shows that the current of the system is normal or the fault is outside the region. IF Iset< Ir, the value of actual current is greater than the value of action current, it shows that the current of the system is abnormal and the fault is in the area and the relay is ready for action.

Second, we should set the delay time(tset) and measure the failure time(tr). IF $t_{set} > t_r$, it show that the delay time is greater than the failure time and the fault has been eliminated in the specified time and the relay will not act. IF $t_{set} < t_r$, it show that the failure time is greater than the delay time and the fault has not been eliminated in the specified time and the relay will act immediately.

In a word, the system uses the monitoring equipment to monitor the operation state of transformer, including the running state of isolating switch and circuit breaker. When the system fails, there will be alarm, and administrator only need to monitor the devices in the control room without having to go outside to inspect.

Fig.4 The diagram of transformer

5. Results & Conclusions

The paper has reviewed the author's patent on the system and method for the transformer protection in 220KV substation, and presented a novel technique to improve the efficiency of the system. The data is showed that in the last three months the system meets the requirements and it run normally and the sensitivity has been greatly improved. The system can accurately protect the transformer.

References

[1] Zhang Zhi-bao. The principle and application of transformer [M]. Chemical Industry Press. 2009：15-30

[2] Zhang Rui-mian. Relay protection of power system [M]. Beijing science and Technology Press.1994 :42-44

[3] He Jia-li,Song Cong-ju. The principle and application of transformer[M]. China Electric Power Press. 2009：41-45

[4] Xu Jian-an,Wang Feng-hua,The setting calculation of power system relay protection [M]. China Water Conservancy and Hydropower Press.2009:10-12, 22

[5] Kang Hai-zhen,Zhang Hong-qi. Transformer setting calculation and setting value management system design and development[J]. Inner Mongolia science and technology and economy. 2003（11）

[6] Zhang Yi-bin,Jin Xin-yu. Networked digital video monitoring system based on mpeg-4 [J].TV technology, 2004（05）:76-77

Advanced Materials Research Vols. 989-994 (2014) pp 1224-1227
© (2014) Trans Tech Publications, Switzerland
doi:10.4028/www.scientific.net/AMR.989-994.1224

Analysis of Data Center Power System

Hui Song[1, a], Zhitan Wang[2, b]

[1]Jilin Technology College of Electronic Information, Jilin 132021, China

[2]Jilin Data Center of Petrochina, Jilin 132000, China

[a]songhay@sohu.com, [b]36910008@qq.com

Keywords: The power system Data Center diesel generator UPS SVG

Abstract: Data center presented in this paper, has a high requirement on the power supply system, that needs emergency power supply, SVG compensation device, large diesel generator set, two lines of mains large capacity UPS and other electric equipments. And there are some differences between data center and conventional power system in many aspects,such as in the nature, quantity, the load requirements, the related electrical equipment configuration, load, power supply mode, connection,and so on.

Introduction

In data center construction, the construction of electric power system is its top priority, the various business, all kinds of server stability work, cannot leave the stable, reliable, uninterrupted power supply, if the load interruption, data center and related business department will face huge losses, so the effective power supply must ensure that all the time, the load capacity is easy, convenient maintenance.

Data center power supply system of large and complex, it is made of high voltage distribution system, the standby diesel generator unit, low-voltage distribution system, UPS system, dc system, lighting system, monitoring, management system and so on more than ten subsystems, hundreds and hundreds of thousands of devices. The following are introduced:

High Voltage Distribution System:

High voltage distribution system in the data center, in the two way grid at the same time under the premise of introduction, added two lines of emergency power supply (high pressure diesel generator set), which requires in relay protection setting, to consider its wirings, two lines of mains and two way of emergency power supply for cooperation.

Relay protection basic logic relationship consider the following: since the launch of diesel generator signal provided by the mains supply into line of voltage transformer, group both road 10 kv mains supply after losing electricity to start the diesel generator set.

In order to prevent the mains power and diesel generator power between parallel, two mains into line in the two bus switch are disconnected, closed to emergency power supply into line switch; On the contrary, only two lines of emergency power supply into line switch are disconnected, can close switch mains supply into line.

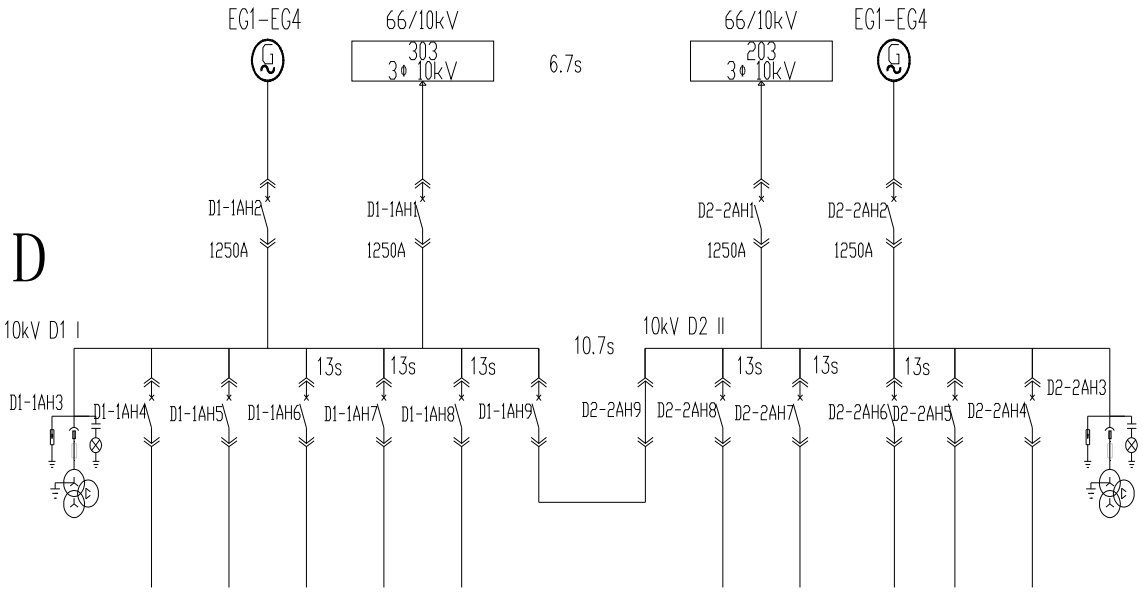

Fig.1 A Data Center High Voltage Distribution System Single Line Diagram

Table 1 Two Mains into Line Switch, Two Road Generator in Line Switch, Bus Coupler Switch Closure Relational Tables

power	Mains power supply1	Emergency power supply1	bus tie switch	Emergency power supply2	Mains power supply2
normal	●	○	○	○	●
I Period of power failure	○	○	●	○	●
II Period of power failure	●	○	●	○	○
Two Periods of power both failures	○	●	○	●	○
● switch on		○ switch off			

Diesel Generator System

Data center: standby diesel generator set is equivalent to "the third power", namely after the mains disappear, in UPS stick to 15 minutes to 1 hour in a short period of time, standby diesel generating sets "" most of the load must bring up the data center. Here most of the load is relative to the chemical plant in the "critical load". "Most of the load" includes: data center all the cabinets, power station can meet the all of the refrigeration unit, fire emergency lighting power supply, power supply, etc.

Considering generator capacity limitation, and site, the eia, economy, many factors such as fuel, many sets of diesel generator set is adopted grouping weaver operation mode. Because many machine run weaver, this kind of operation mode is the stability of the test unit itself, weaver success rate, and later operation maintenance.

Data center interrupt is not allowed in most of its load, especially load cabinet once interrupted, is likely to cause "terminal system", "important production data" and other key cabinet data loss, the loss is immeasurable. And huge data center generator capacity, the basic unit can take up all load data center, and the great amount of oil required, noise is bigger, need to increase the outdoor storage tanks and noise reduction device.

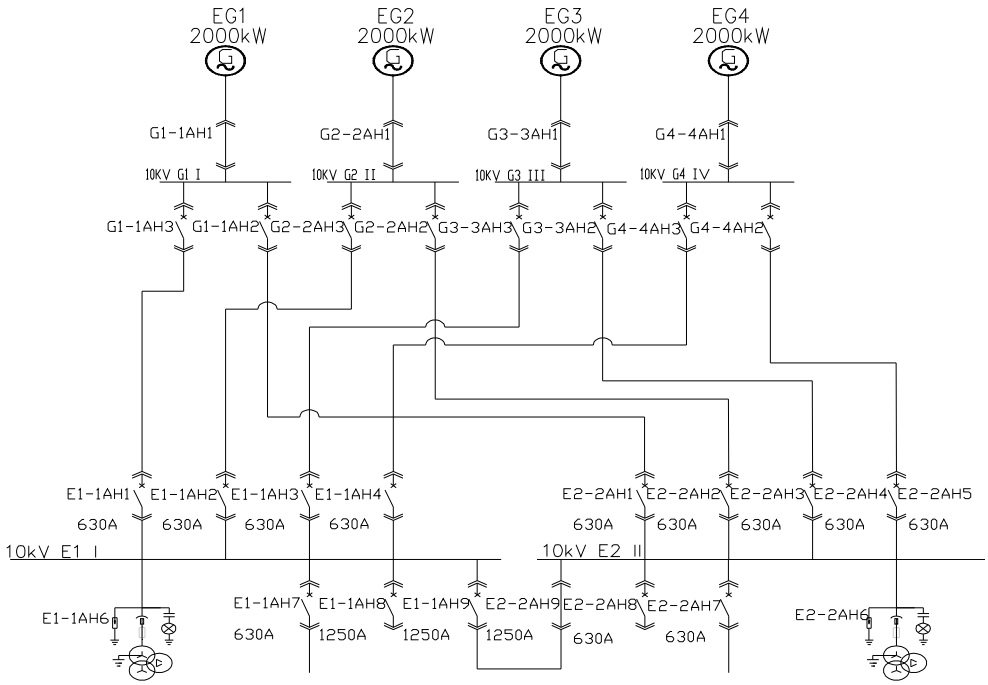

Figure 2 A Data Center Diesel Generating Sets High Local Single Line Diagram

Low-voltage Distribution System

Low-voltage distribution system in data center, can be divided into: according to the use of low pressure tank to the scene of production equipment, low voltage (UPS) to the module column header tank parts, low pressure tank to lighting, distribution box on the low voltage, low voltage to the other parts of the auxiliary facilities such as a few kinds.

Low Pressure Tank (by UPS) to Module Column Header Tank Parts. That part of the distribution. Data center computer room power distribution circuit is usually double grid access road, first advanced low ark, part to UPS, part for air conditioning and lighting, ordinary socket, UPS UPS low-voltage distribution cabinet bottom, assigned to each column header tank, after column head tank access each cabinet PDU to load.

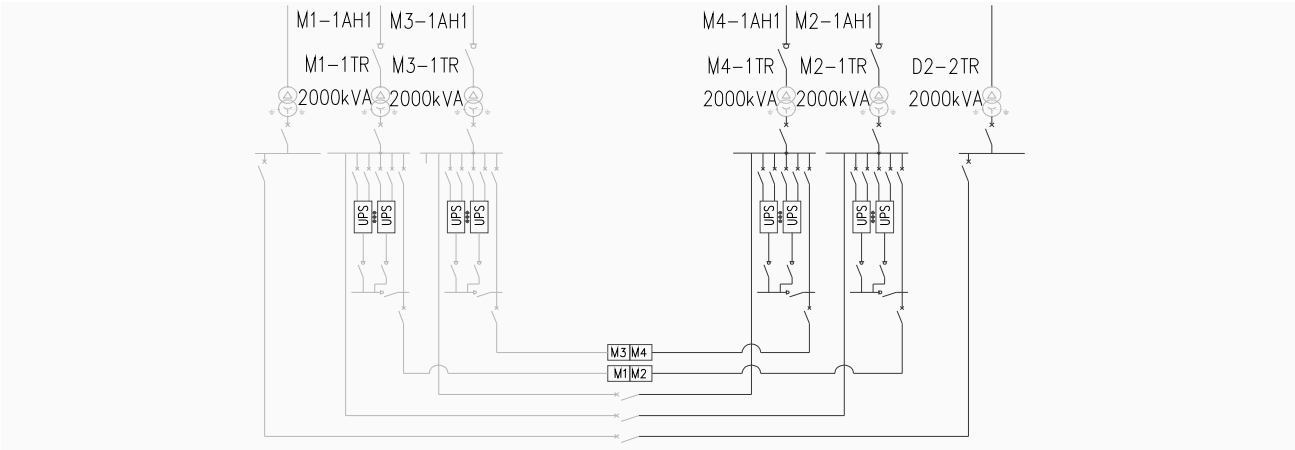

Figure3 Low Pressure Tank (by UPS) to Module Column Header Tank Part of Power Distribution Single Line Diagram

Low Pressure Tank to the Scene Production Equipment: Data center low-voltage distribution cabinets according to MNS cabinet or in the form of GGD cabinets, to meet the requirements of green data center, reduce cable usage at the same time reduce the line loss, low ark to the scene production equipment data center line is not a "one to one" form, but the site set up on-site distribution box, distribution box on the control panel, no site operation. This cable will greatly reduce the amount of, can reduce investment, reduce the line loss.

Where there is water, there is smudgy, poor environmental conditions, the protection grade of field distribution box, prevent the pollution level and the service life and so on many aspects should be specially considered, motivated the distribution box on the top should increase waterproof glen, down into the distribution box should improve channel height; For larger cable hole sealing problems should be considered, for distribution box of IP protection level put forward higher requirements; Additional protection level, because heat is no longer patency, the installation position of cooling fan, special consideration must be paid to the are thermal dissipation space has been enough.

Conclusion

Data center UPS not only as the important part of the instrument or electrical equipment to provide uninterrupted power supply support, more to take all the "cabinet", the scope of its power supply is bigger. UPS according to 2 n fault-tolerant methods and computer room IT equipment configuration, that is to say, any module UPS has a problem, can be made by another module and at the same time the UPS power supply.

"Column header tank" is "unique" data center of electrical equipment, its internal two way power from the power of the two different road section, shall be the responsibility of the static switch cabinet with two way power static switch.

Data center power at all levels are based on double power source, double the power of mutual standby transformer, power distribution equipment layout in different rooms and standby each other along a different path to the installation of power supply line, not affected by the fault at the same time. In order to ensure the data center of power supply reliability, reduce interference, set up the data center dedicated to match/substation and power supply equipment, data center substation in the post room module layout, shortening the distance between the power supply as far as possible, reduce the low voltage line loss. Although this way to reduce the investment, but this design for where there is water, also brought considerable hidden trouble of equipment, from the Angle of electrical, placing all of the power supply and control circuit, after all, in the "more" of water environment, the maintenance quantity and risk.

References:

[1] Data center design and planning of energy-saving power supply system, Jiying Wang, Beijing publishing house of electronics industry, November 2011

[2] Data center UPS power supply system design and fault handling, Zhimin Zhou,AiHua Ji Beijing Publishing house of electronics industry, January 2012

Advanced Materials Research Vols. 989-994 (2014) pp 1228-1231
© (2014) Trans Tech Publications, Switzerland
doi:10.4028/www.scientific.net/AMR.989-994.1228

Urban Ecological Environmental Quality Evaluation System Research

Xiuxia LI

School of Art and Design, Xinxiang University,Henan,China,453000

14878670@qq.com

Keywords: quality evaluation; ecological environmental quality; Zhengzhou city

Abstract：The paper extracts the urban ecological environmental quality evaluation index, based on hierarchical analysis model, the integrated use of "pressure-state-response" model, through the frequency statistics method, factor comparison method and expert evaluation method and so on to set up urban ecological environmental quality evaluation system in nearly a decade based on the related data of environment quality evaluation of Zhengzhou city. Results show that from 1998 to 1998, Zhengzhou ecological environmental quality rises year by year, the ecological environment on the basis of good for Zhengzhou city ecological security evaluation and management.

0 Introduction

City is the important carrier of human existing and developing, and the changing and variation of city development under the influence the natural environment and social environment, in which many urban problems, the most important thing is to urban ecological crisis, the urban ecological system has a high material consumption, high pollution and low reserves the unique characteristics of natural resources[1].Hence, How to understand the urban ecological environment quality and the status is the important problem in the study of the urban ecological crisis , several researchers proposed such as Cheng Chunming, Song Yongchang proposed evaluation index system of urban ecological environment quality, In this paper, we analyze and refer the methods of city ecological security evaluation in zhengzhou city, construct urban ecological environment quality evaluation index system, and through analyzing the comprehensive analysis of urban ecological environment quality, evaluate on time scales urban ecological environment quality and its trend, provide theoretical basis for city ecological security evaluation and management.

With the development of social economy, in the national regional economic layout, zhengzhou has location advantages which linking the west and the east, it has an important strategic position in the central of China development strategy object, ecological environment quality is related to economic development and can understand the ecological environment of economic development matching with the quality, can promote the economic development.

1 Urban ecological environmental quality evaluation index system

1.1 The establishment of evaluation system

There are many kinds of urban ecological environment evaluation models, a commonly used model is: hierarchical analysis model; Pressure-state-response model, "Social economic environment" three elements model, the hierarchical analysis model is used in this paper to integrated use of pressure-state-response model, urban ecological environmental quality evaluation index system can be divided into four levels:

Firstly, the goal layer, namely to urban ecological environmental quality as the general objective, comprehensive analysis and characterization of urban ecological environment quality present situation and development trend;

The second layer is the essential factor layer, taking the ecological environment pressure, urban ecological status, social and economic as three elements, evaluating from different aspects about city ecological environmental quality.

The third layer is the project, in the urban ecological environment system contains some evaluation and analysis on the basic structure for the project, will refine the second of three elements, evaluation of urban ecological environment quality from different angles

The fourth layer as an index, district respectively different urban ecological environmental indicators, in the form of a quantitative evaluation of urban ecological environment quality

1.2 The choice of evaluation index

There are many kinds of urban ecological environment, selecting in a variety of different meanings of indicators to be indicators is a systematic work, the specific choice for indexing, the frequency statistics method can be used, multiple factor comparison method and expert evaluation method, etc.

Frequency statistics method, is based on a large number of literature reading and reference for the related evaluation system, frequency statistics, for each index factor to choose those using high frequency index; Multiple factor comparison method is at the same time, many of the same element can be characterized by factor analysis, choose more representative indexes used to evaluate the system.

Expert evaluation method is preliminarily established the basis of the evaluation system, and consulting experts, to reasonably adjust the index system, to achieve the optimization purpose is accurate, reasonable and easy to operate the index factor is to build a good foundation of evaluation index system of urban ecological environment quality[2].

1.3 data sources

According to a 1998-2008 Zhengzhou city social and economic statistical yearbook, the original data is obtained arranging from many years of urban ecological environment quality evaluation index

2 Zhengzhou ecological environment quality evaluation

2.1 three-level index evaluation analysis

According to zhengzhou city from 1998 to 2008, the status of each index value, calculated by the three-level index evaluation result of each year to select the evaluation result of four years (1999, 2002, 2005, 2008)，As shown in table 2, according to the evaluation results can be seen in nearly a decade of zhengzhou city rapid economic development, social undertakings have also been a good development, it can be seen in the table, the economy, the rapid growth of the social status quo, respectively, by 0. 0005 and 0. 0059 to 0. 175 and 0. 1701,Increased by two orders of magnitude.

In economic growth at the same time, the environmental protection work is in the rapid development of social economy in the response of environmental protection index of the increase is also very quickly, This shows that the center of the government's work by economic development into environment dual economic development, improve the economic strength at the same time, and in improving quality of urban environment; The development of the city without the support of the natural resources, as can be seen from the table, produced by the lack of natural resources and ecological environment pressure increase is small, Accordingly, in zhengzhou city for nearly 10 years of development, the supply of natural resources is abundant, can basically meet the needs of urban development, to provide support for the development of city economy and social undertakings.(shown in table 1)

Tab.1 The evaluation result of the third grade index for zhengzhou

Elements	Project	1999	2002	2005	2008
Eco-environmental pressure	population structure	0.0039	0.0212	0.0473	0.0613
	Natural resources	0.0138	0.0138	0.0261	0.048
	social structure	0.0025	0.0232	0.0418	0.0958
Urban ecological status	Economic Status	0.005	0.0265	0.0531	0.175
	Environmental Status	0.0212	0.0463	0.0578	0.193
	Social Status	0.0059	0.058	0.1147	0.1701
Socio-economic response	Allocation of resources	0.0273	0.035	0.0612	0.1406
	Environmental protection	0.0018	0.0256	0.0427	0.0693

2.2 secondary index evaluation analysis

Zhengzhou ecological environment quality system secondary index is composed of the ecological environment pressure, urban ecological status and response to the three components of society and

economy.From the point of view of the ecological environment pressure, zhengzhou nearly a decade of urban ecological environment pressure rising trend, this is mainly due to a huge increase in urban population in the process of urbanization, the increase in population and increased the demand for natural resources and the social public utilities,these requirements inevitably lead to the ecological environment pressure rise;

Look from the urban ecological status, the city's economic, environmental and social conditions have improved, in the rising trend, but the present situation of urban ecological improvement and city does not conflict with the increase of the ecological environment pressure.Because of the increase of urban ecological status quo of the guideline values, this led to the improvement of urban ecological environment, the original ecological environment is not able to meet the needs of the city at present stage, which requires the urban environmental changes in the development of itself.

As a result, increased pressure on ecological environment from the aspects of demand;In social and economic response ways, social response of urban ecological environment quality has been rising in a positive state,Both in terms of resource allocation and in environmental protection, the index changes are increased, it is mainly due to the zhengzhou city for nearly a decade the steady development of economy, the gradual improvement of the people's living standard, and the continuous improvement of the urban public utilities development.(shown in table 2)

Tab.2 The evaluation result of the second grade index for zhengtzhou

Elements	**1999**	**2002**	**2005**	**2008**
Eco-environmental pressure	0.0202	0.0582	0.1152	0.2051
Urban ecological status	0.0321	0.1308	0.2256	0.5381
Socio-economic response	0.0291	0.0606	0.1039	0.2099

2.3 Zhengzhou ecological environment quality comprehensive evaluation

the city is constantly enhance its capability of sustainable development,but from 1998 to 1998 this year appear composite index to reduce the trend[3],This is mainly because in this period of time, increase the investment to the industrial production of zhengzhou city, and relatively insufficient spending on environmental governance, caused the industry to increase the influence of urban environment, urban ecological environment quality decreased After that, the environmental governance investment increase.And, based on its own rich historical culture, zhengzhou city, the city's economic development pillar industry by industry transferred to the third industry, it is reduced to some extent due to the city's economic development for the negative impact of urban environmental quality.

3 conclusion

This paper on the urban ecological environment quality evaluation is only considering the time scale, a sequence of time to study the development process of zhengzhou city, the ecological environment quality changes in only qualitative analysis, not for its ecological environmental quality to make quantitative analysis of the classification.This is mainly because of urban ecological environment quality of quantitative classification needs to give full consideration to the natural condition and social economic development situation of city, is a complicated systematic work. Although there have been some existing (condition) scale of urban ecological environment, but because of the existence of the difference of each city existing scale does not apply to every city. Therefore, establishing a classification table of applicability of urban ecological environment, is to be solved in the research of urban ecological environment problems.

Reference

[1]Siming Fan. Rigid constraint and ecological comprehensive evaluation research assessment index [M] Beijing: Science Press.1998.

[2] Fande Kong. Urban ecological environment construction and protection planning [M] .Be ijing: China Environmental Science Press.2001.

[3]Tong C. Review on environmental indicator research[J].Research On Enviromental Science, 2000.13 (4) :53.

Advanced Materials Research Vols. 989-994 (2014) pp 1232-1235
© (2014) Trans Tech Publications, Switzerland
doi:10.4028/www.scientific.net/AMR.989-994.1232

Eco-environmental construction in Zhengzhou

Xiuxia LI

School of Art and Design，Xinxiang University,Henan,China,453000
14878670@qq.com

Keywords: ecological destroy; sustainable development; Zhengzhou

Abstract: After a discussion of present problems of eco-environmental construction on municipal virescence , water environment and water ecology, and landscape as well as urban ecological system of quantity, quality and capacity in Zhengzhou, the causes of these problems are analyzed. Measures are put forward, such as knowing the meaning of municipal eco-environmental construction, increasing the environmental protect consciousness of managers and enhancing the municipal eco-systemic construction.

0 Introduction

This paper discusses the current of zhengzhou city's virescence, water environment and aquatic ecology, urban landscape and ecological construction, such as quantity, quality and capacity problems in ecological environment construction, analysis to explore the cause of the problems, and puts forward the scientific understanding of the connotation of urban ecological environment construction, raise awareness of the environment protection of city management and urban planning and technical personnel's professional quality, strengthening the construction of urban ecological engineering and urban sustainable development system of several countermeasures.

1 The current problems existing in the ecological environment construction

ecological destruction in areas surrounding the cities

At the turn of the century, zhengzhou city has carried out large-scale urban ecological environment construction and residential environment construction, urban ecological environment improved rapidly[1].During three years, 200000 big tree were transfered, the urban ecological environment construction steps onto a stage quickly, but the tree into the city to bring the negative impact of severe: Firstly,it is a large-scale ecological migration rural ecosystem seriously damage; secondly, the trunk of the greening effect is comparable to a young trees, green efficiency is not high; third is to lead to a lot of trees to injury and death.Big tree transplanting, due to habitat changes, even survival, growth is not too good, even death, big tree transplanting that year survival rate 94%, but years of survival rate is less than 90%.Fourth ecological protection is difficult.

Quantity, quality and capacity could not reach the requirements of ecological city

the number of urban green space is not enough, during 950, zhengzhou despite the afforest money surpassed the sum of the past 45 years, but in 2000 the per capita public green land area of 4.6 m^2 , and the basic requirements of the ministry of construction issued 7m^2 there is still a large gap. Forest coverage rate is 10.4%, and the global forest coverage rate is 31.7% on average, the forest coverage rate is 16.5%, Beijing forest coverage is 38.5%, forest coverage rate is 50% in Tokyo, zhengzhou is much lower than Beijing and Tokyo, and much lower than the national and global average. According to the characteristics of urban thermal field is calculated, as high heat load balanced urbanization area, zhengzhou need is greater than 2300 km^2 of forest, the forest coverage

rate is 36%[2].Based on aerobic capacity per unit area and forest carbon and oxygen balance estimation, forest area demand for 1, 900 km2, forest coverage rate is 30%.Measure according to the ecological environment quality and living demand, zhengzhou forest area will need at least 2, 200 km2, forest coverage 34%, urban ecological capacity are still inadequate.

The quality of urban green space is not high.

Urban public green space is relatively single, species is given priority to with grass, with a small amount of flowers and plants and sparse trees, low proportion of Joe, irrigation, grass not harmonious[3].This way of afforestation improving space visual effect, but low ecological benefits.In addition, the public green space distribution, large green space are mainly distributed in the central plaza and park, and a small piece of green space mostly located in the traffic circle and mainline, the green space is an island, the lack of green corridor, patch heterogeneity is poor.Because of the green space ecological effect is not high, push air flow dynamics is insufficient, the urban heat island effect will also strengthen, high frequency heat island phenomena.In recent years, zhengzhou city heat-island frequencies as high as 85.13%, heat island daily average amplitude of 0.65 degrees, the largest heat island 1.72 degrees, is relatively stable.From the annual 1999 annual heat island magnitude 1.63 degrees, has risen 0.32 degrees in 1998. Maximum heat island in the winter of 1999 was 7.17 degrees, 0.37 degrees higher than in 1984, the summer of 5.07 degrees, 0.27 degrees higher than in 1984.

Urban street trees develop to the degree of beauty and luxury.

local suitable tree species disappeared. Ginkgo, osmanthus flowers, camphor, yulan, cedar etc become urban street trees and communities select tree species, the aesthetic value of urban greening raised, the grade of the greening trees increased, but single tree species and local green features disappear, urban ecosystem is fragile.

Degeneration of biodiversity.

Due to the rapid change of the urban environment and a large number of trees being cut down, plant genetic information transmission, wild plant degradation, urban ecological self-sustaining, self-renewal, self adjusting ability. Because of the lack of "green channel", birds, amphibians, almost extinct; The center of the city environment sensitive indicator plant, the lichen plant diversity, evenness and far below the city on the edge of the forest, a significant reduction in the urban environment natural degrees.In the suburbs of sheshan, the stones for fried mountains, road building, tourism development, economic development, bamboo and other activities, logging, deforestation, removal of understory plants such as 119 species of angiosperms die or endangered [4],Fern was 16 families,28 genera and38 species, now only 15 species, frogs, snakes, rabbits and other animals almost extinct.

The ecological environment destruction

it brings species invasion. Outstanding performance to a large number of breeding of water hyacinth can cause local aquatic plants disappear, every year need to spend a lot of manpower and salvage.

2.The ecological city construction process system structure

In the ecological urban construction coordination mechanism in the process of building the system structure, always revolve around the relationship between human and nature, between people the two lines. According to the construction of ecological city as the total target, on the premise of space-time unified, affinity is symmetrical, enables each subsystem in the logical

relationship between self-consistent, orderly organization structure, adjustable on functional performance, the overall sustainable development, and be able to achieve the combination of qualitative and quantitative, to form a is the general principles of universality, finally realizes the ecological city construction to improve ability and level of synchronization.

The core of the ecological city construction, in the premise of sustainable utilization of resources and environmental protection, make a city and the regional resources, environment, economy, population and social coordination between each subsystem, such as reasonable structure, function, and thereby forms a benign circle of urban and regional and sustainable development. Therefore, construction of modern ecological city, must to structural adjustment as the main line, supported by modern science and technology, based on the bearing capacity of resources, conform to the environment of binding and BaoZhangLi, improve the economic competitiveness and support, increase of population and the control force of the society, the economic construction, ecological environment construction, social construction organically combined, relying on excellent resources environment promote the rapid and sound development of economy, society, increasingly enhanced rely on economic strength and the increasing of social civilization provide care and support for the improvement of the ecological environment.

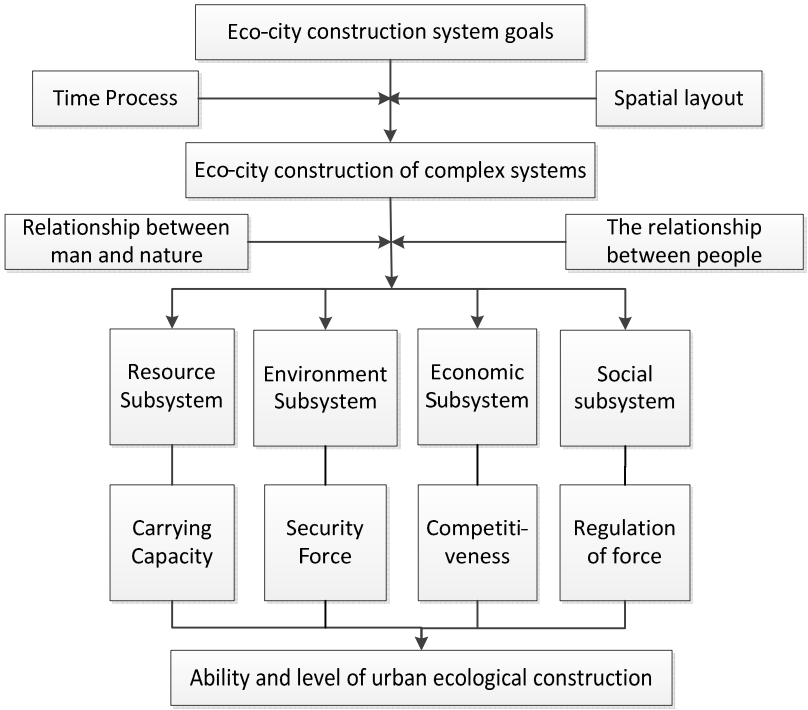

Fig 1.Flow chart of eco-city construction system

3.Several countermeasures for the construction of urban ecological environment

(1)Scientific understanding of the connotation of urban ecological environment construction, strengthen the construction of the series of urban ecological engineering

Urban construction in our country is in the midst of the fierce of ecological transition, in urgent need of urban ecological construction in the life space requirements to the quality of life, from the ecological greening requirements to ecological function requirements, from the environmental governance needs to environmental health demand, from the city beautification to urban sustainable development. Urban ecological environment construction is facing a from concept, theory, technology, engineering, materials, a profound change in the comprehensive management, require the system to learn and understand.

(2) Actively promote system reform, efforts to improve the ecological environment protection consciousness of administrators

Streamlining, separate government functions from enterprise management, the leaders from the achievements of engineering as well as the subordinate enterprise welfare projects contracting, do more investigation and study, transform government functions.Streamlining, separate government functions from enterprise management, the leaders from the achievements of engineering as well as the subordinate enterprise welfare projects contracting, do more investigation and study, transform government functions.Implementation of urban ecological environment construction bidding system, forbidden government functional departments and affiliated enterprises to participate in the bidding project, administrative justice law enforcement.Garden department should according to the urban ecological environment construction and urban construction planning, flowers, nursery stock ahead of the urban construction need, sod quantity and varieties, such as forecasts,make full use of the huge potential of market of social labor productivity, to eliminate the phenomenon of "tree city".To the government administrative personnel on a regular basis knowledge popularization education of urban ecological environment construction, improve the ecological environment of government functional departments and management staff awareness, make scientific decision and management.

(3)Restore the characteristics of "water", build the waterfront landscape, construction of ecological city

Protect the existing urban water bodies, through comprehensive environmental control to improve the water quality, and restore its coastal ecological landscape;"Water", and restore the characteristics of "water"; Dredging or restore partially fill river, in densely inhabited areas, appropriate excavation water bodies, and along the coast build large-scale green space, improve urban living environment; Make full use of the coastal tidal flats, ecological garden construction of oversize, and strive to improve the quality of ecological environment construction of zhengzhou.

Reference

[1].Lin Juan, Ji Qian.biodiversity protection[J].Shanghai environmental sciences,2000,(4): 188 ~189.

[2].Xuefeng Hu, Zhenlou Chen. The decline and fall of winter aquatic higher plants for the influence of river water quality[J]. Shanghai environmental sciences, 2001 (4): 184~187.

[3].Wei Zhuang. Pudong new area of urban ecological problems[J] Shanghai environmental s ciences.2000, (6): 251-252.

[4].Ping Liu. The ecological design method of urban human settlements environment[J]. Act a Ecologica Sinica, 2001, (6): 997-1002 .

Advanced Materials Research Vols. 989-994 (2014) pp 1236-1239
© (2014) Trans Tech Publications, Switzerland
doi:10.4028/www.scientific.net/AMR.989-994.1236

The Influence of Lanzhou Reach of Yellow River to Temperature-humidity Effect on Surrounding Lawn and Brick Underlying Surface

Guocheng Liu[1,2 a], Yu Huang[3, b] and Shangqin Gao[4, c]

[1] Key Laboratory of Ocean Environment and Ecology, Ministry of Education, Qingdao 266100, China;

[2] College of Environmental Science and Engineering, Ocean University of China, Qingdao 266100, China;

[3] Gansu Institute of Urban Planning and Design, Lanzhou 730000,China;

[4] Lanzhou Veolia Water Group, Lanzhou 730000, China.

[a]iceliugc@126.com, [b]yellowfish61@163.com, [c]93645696@qq.com

Keywords: Lanzhou reach of Yellow River, Temperature-humidity effect, Underlying surface, Distance.

Abstract. The temperature and humidity on the lawn and brick underlying surface at differnet distances from the bank of Yellow River in Lanzhou, Gansu province, China (Lanzhou reach of Yellow River) were continuously monitored from 6 a.m. to 8 p.m. for 5 days in August and September 2013, respectively. With increasing distance, the temperature gradually increased, but the humidity remarkablely declined. The influence of Lanzhou reach of Yellow River on the temperature-humidity effect on the two underlying surfaces was dependent on the distance from the bank of Yellow River. The relationship between the temperature on the lawn or brick underlying surface and the distance was a significant positive correlation, but the humidity in this thesis and the distance showed the remarkable negative correlation relationship. The maximum distance of the temperature and humidity effect from the water of Lanzhou reach of Yellow River was calculated, and their range was 236.4-317.1 m and 248.8-289.2 m, respectively,

Introduction

It is an effective means of using urban water bodies and the surrounding underlying surface to improve the ecological environment of urban [1]. Increasing the urban water and lawn area will have positive functions for the temperature-humidity effect at the surrounding region of these water bodies and lawns [2]. Yellow River is the only one overland runoff in Lanzhou, Gansu province, China (Lanzhou reach of Yellow River), which passes through the central city, and thus plays an irreplaceable and predominant role in reducing the urban heat island effect [3-4]. Therfore, the study about the influence of Lanzhou reach of Yellow River on temperature-humidity effect at its surrounding environment needs to be more in-deep. Moreover, the temperature-humidity effect on different underlying surfaces was mainly dependent on their distance to water of Lanzhou reach of Yellow River [5-6].

The objective of the present study was to determine the influence of Lanzhou reach of Yellow River on the temperature-humidity effect on the lawn and brick underlying surface. Moreover, the relationship between the temperature or humidity on the various underlying surface and the distance from these underlying surfaces to water of Lanzhou reach of Yellow River was discussed, and the maximum distance of temperature-humidity effect beside Lanzhou reach of Yellow River was also calculated. This work may provide valuable information to understand the ecological function of Lanzhou reach of Yellow River to its surrounding environment.

The distribution of monitoring point

Shanheju park and Lily park near Yellow River in Lanzhou, Gansu province, China (Lanzhou reach of Yellow River) were selected as the monitoring district, shown in Fig. 1. The temperature and humidity on two underlying surfaces (brick and lawn) were determined, respectively, and the brick and lawn underlying surface were in Shanheju and Lily park. The distance between the monitoring points was10 m.

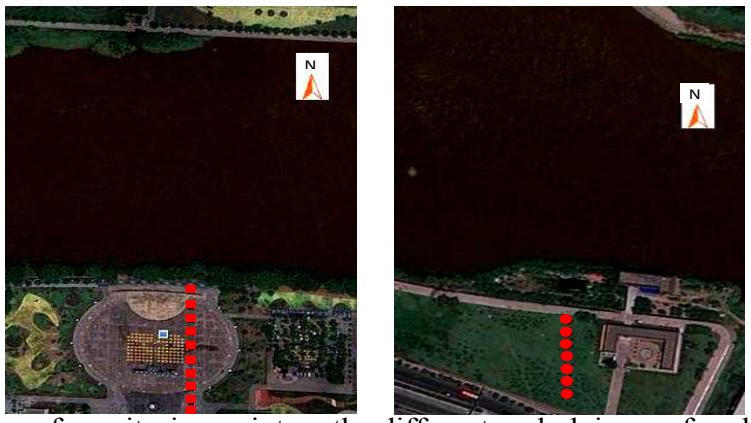

Fig. 1 The distribution of monitoring point on the different underlying surface beside Lanzhou reach of Yellow River. ■ brick underlying surface, ● lawn underlying surface.

The measure temperature and humidity

The temperature and humidity on the brick and lawn underlying surface were monitoring by temperature and humidity sensors (CN10/ML13). These sensors were placed in a distance 1.5 m from the ground of underlying surface. In order to avoid the sun, wind and other meteorological factors on the test of temperature and humidity, the sensors were placed in the protection boxes (03022, shufeng, China). The temperature and humidity of all monitoring points were recorded at every 5 min from 6 a.m. to 8 p.m. for 5 days in August and September 2013. In this study, all data of temperature and humidity were expressed as an average of the monitoring data on its respective point with standard deviation. The statistical analyses were performed through the statistical program SPSS 18.0 (SPSS Inc., Chicago, USA).

Results and discussion

The temperature and humidity on the brick and lawn underlying surface were shown in Fig. 1. It could be clearly observed the fluctuations of temperature and humidity mainly because of the changed temperature and humidity difference between day and night.

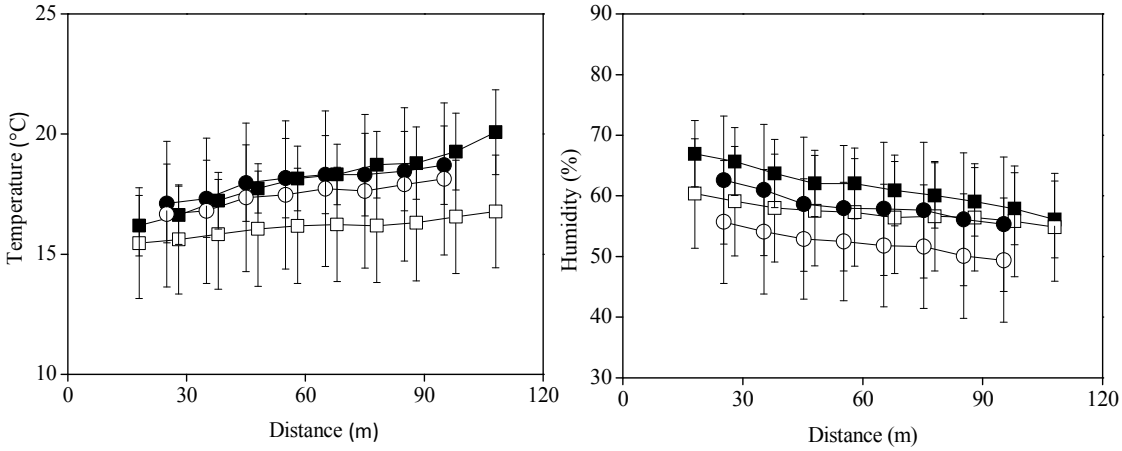

Fig. 2 The temperature and humidity of the monitoring points from different distance of Lanzhou reach of Yellow River. The solid points (■ and ●) and hollow points(□ and ○) represented the monitoring data in August and September, respectively.

With the increasing distance from the monitoring points to the water of Lanzhou reach of Yellow River, the temperature gradually increased, but the humidity declined remarkablely. For example, the temperature on the brick underlying surface in August increased from 16.2 °C to 20.1 °C as the distance lengthened in the range of 18-108 m from the side of Yellow River. However, the corresponding humidity dropped from 67.0% to 56.1%. These results implied that the temperature-humidity effect on the different underlying surfaces was significantly influenced by the distance from the Yellow River bank.

The relationship of the temperature on the lawn or brick ground in August or September and the distance from these ground location to the bank of Lanzhou reach of Yellow River was a marked positive correlation, supported by the values of the adjusted coefficient of determination (R_{adj}^2) > 0.90. But, the humidity on the two underlying surfaces in this thesis and the distance described in the above was significant negative correlation, implying that the influence of water bodies of Lanzhou reach of Yellow River on the humidity was more significant at the closer place.

Table 1 The linear relations between the temperature or humidity on the lawn and brick underlying surface and the distance from monitoring points to Lanzhou reach of Yellow River.

Underlying surface	Temperature (°C)		Humidity (%)	
	August	September	August	September
Lawn	Y=0.022X+16.8 R_{adj}^2=0.905	Y=0.020X+16.3 R_{adj}^2=0.913	Y=-0.093X+64.1 R_{adj}^2=0.900	Y=-0.082X+57.3 R_{adj}^2=0.954
Brick	Y=0.039X+15.7 R_{adj}^2=0.971	Y=0.014X+15.3 R_{adj}^2=0.937	Y=-0.111X+68.4 R_{adj}^2=0.975	Y=-0.091X+60.5 R_{adj}^2=0.908

R_{adj}^2 is the adjusted coefficient of determination and it is influenced by both the number of data points (m) and fitting parameters (p), R_{adj}^2=(1-(m-1)(1-R^2)/(m-p-1).

In this study, the temperature and humidity on the lawn and brick underlying surfaces far away from the bank of Lanzhou Reach of Yellow River (> 1000 m) were monitored. The average temperature and humidity on the lawn groud in August were 22.0 °C and 42.5%, respectively, and the monitoring data in September were 21.6 °C and 36.9%. In addition, the average temperature and humidity on the brick underlying surface in August and September were 26.1 °C/39.4% and 19.7 °C/34.1%, respectively. These data suggested that the grasses could be much helpful for cooling and humidifying to their surrounding [7].

Table 2 The maximum distance of the temperature-humidity effect of Lanzhou Reach of Yellow River on the surrounding lawn and brick underlying surface.

Underlying surface	Temperature (°C)		Humidity (%)	
	August	September	August	September
Lawn	236.4 m	265.0 m	231.9 m	248.8 m
Brick	266.2 m	317.1 m	261.2 m	289.2 m

Based on these data, the maximum distance of the temperature-humidity effect of Lanzhou Reach of Yellow River to the surrounding lawn and brick underlying surface was calculated, and the results were listed in Table 2. The maximum distance of the temperature effect was in the range of 236.4 m to 317.1 m, and the range for the humidity effect was from 248.8 m to 289.2 m. Regardless of August or September, the influence of Lanzhou Reach of Yellow River on the temperature-humidity effect of the brick ground was greater than that of the lawn underlying surface, indicating that the grasses had the buffer capacity to the influence from the water of Yellow River.

Conclusions

With the increasing distance from the underlying surface to the water of Lanzhou reach of Yellow River, the temperature gradually increased, but the humidity declined remarkablely. The temperature-humidity effect on the two underlying surfaces was significantly influenced by the distance from the bank of Yellow River. The relationship of the temperature on the lawn and brick ground and the distance was a positive correlation, but the humidity in this thesis and the distance was significant negative correlation. The maximum distance of the temperature effect from the water of Lanzhou reach of Yellow River was in the range of 236.4 m to 317.1 m, and the range for the humidity effect was from 248.8 m to 289.2 m.

Acknowledgement

This study was supported by the project from Gansu province technology hall (20605) and the project from Gansu province construction department (JK2008-20).

References

[1] F. Kimura and S. Takahashi: Atmosphere Environment, Vol. 25 (1991) No.2, p.155-164.
[2] X.J. Hu, Y.J. Song and W. Cheng: Research of Soil and Water Conservation, Vol. 13 (2006) No.6, p.87-88. Urban Water Environment of Creating Natural Ecology-A Case of Beijing Botanical Garden Water System Engineering.
[3] X.S. Hu, W. Hong, C.Z. Wu, Y.H. Zhou: Journal of Jilin Normal University (Natural Science Edition), Vol. 1 (2006) No.1, p.84-88. Advance in Study on Urban Grenning and Heat Island Effect.
[4] V.N. Nu Hoai, H.E. Farrah, G.A. Lawrance, G.L. Orr: The Science of the Total Enviornment, Vol. 214 (2006), p.221-237.
[5] N. Nishimura, T. Nomura, H. lyota, S. Kimoto: Solar Energy, Vol. 64 (1998), No. 4-6, p.197-207.
[6] W.Z. Yue and L.H. Xu: Acta Ecologica Sinica, Vol. 33 (2013), No. 6, p.1852-1859. Thermal Environment Effect of Urban Water Landscape.
[7] D. Armsona, P. Stringerb and A.R. Ennosa: Urban Forestry and Urban Greening, Vol. 11 (2012), No. 3, p.245-255.

Advanced Materials Research Vols. 989-994 (2014) pp 1240-1243
© (2014) Trans Tech Publications, Switzerland
doi:10.4028/www.scientific.net/AMR.989-994.1240

Study of morphological changes induced by man-made coastal project

XU Ting[1,2]

[1] Tianjin Research Institute for Water Transport Engineering, M.O.T, Tianjin 300456, China
[2] School of Environmental Science and Engineering, Tianjin University, Tianjin, China.

xuting1228@163.com

Keywords: EFDC, sediment, morphological, simulation, coastal project

Abstract: With rapid development of economy, the crisis of land resources is faced. Land expansion by enclosing sea in estuaries has become an important carrier for city space extension. In this paper,the large-scale marine reclamation project in the Oujiang River Estuary (ORE) of Wenzhou shoal was taken as an example.Based on the intoduction of the study area,the 3D marine numerical model (EFDC) was setup and used for simulation of sediment enviroment and morphological changes induced by the reclamation. The results indicated that the project doesn't have obvious adverse effects on its nearby sediment environment and seabed. On the contrary, it settles the problem of mouth bar of the ORE and provides some advantages to maintain and steady the deep water channel and improve the sail condition from the north mouth of Oujiang River to Huangda'ao channel.

1 Introduction

With the rapidly development of economy, and the promotion of industrialization and urbanization, the contradiction of more people and less land is becoming increasingly. The land reclamation in the estuary becomes an important carrier to extend the space of city. In recent years, many countries have tried to overcome land-based bottlenecks with the design and construction of marine reclamation projects [1-2]. Because the underwater topography and coastline shape of estuary district is complex, and the sediment environment and seabed is sensitive and fragile, the adverse effects of marine environment in maximum extent has raised wide concern while the city space extension. Therefore, the studies were performed in this paper to simulate and analyze the effects of a large-scale marine reclamation project(Fig. 1) on sediment environment and morphological changes in the Oujiang River Estuary (ORE) and its changes responding to the reclamation.

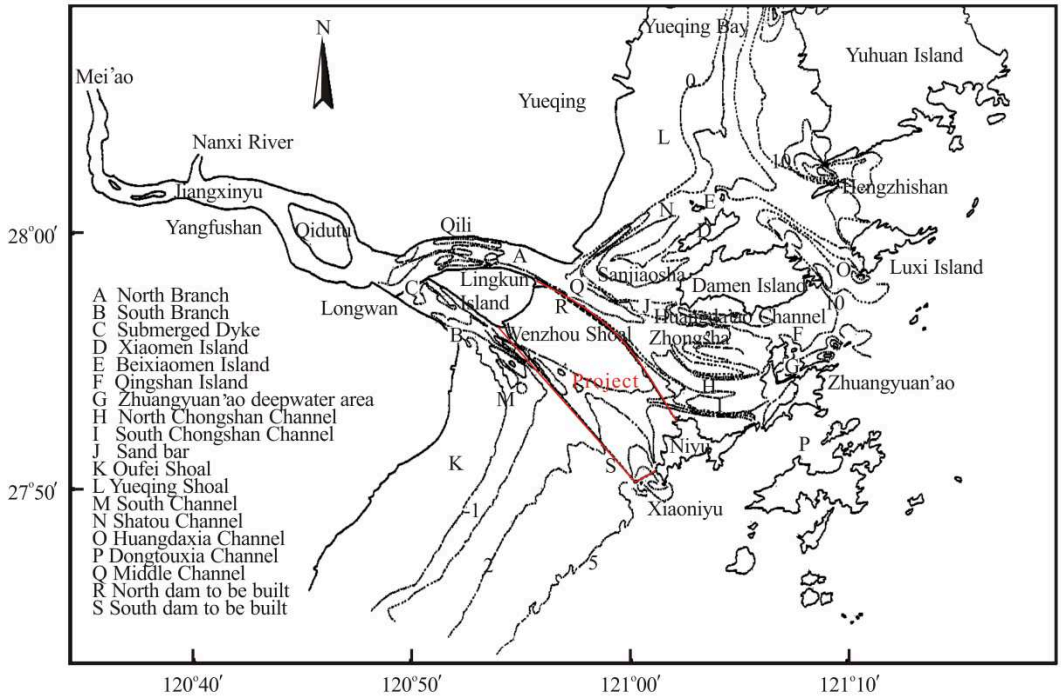

Fig.1 Sketch of the Oujiang River Estuary

2 Study area

The 388-km-long Oujiang River, which is located in the Zhejing Province of China, is the second largest river in Zhejiang Province and the fifth largest river in China. The Oujiang River is a mountain river influenced by strong tides with an average range of over 4 m. The Oujiang River Estuary(ORE) is bifurcated into the North and South Branches (Fig. 1). Outside the North and South Branches, there are numerous islands, densely covered shoals, and interlaced shoals and channels with complex topography. Wenzhou Shoal, lying between Lingkun Island and Niyu, is a large-scale, well-developed mouth bar in the ORE. It is significant to reclaim Wenzhou Shoal between the two islands (Fig. 1). First, the reclamation may create abundant land with an area of 88 km^2 to alleviate the pressure of a lack of land in Wenzhou. Second, the reclamation can exploit and utilize the deepwater coastline between Zhuangyuan'ao and Qingshan Island to promote tourism and the fishing industry on Dongtou Island. The reclamation will be a grand territory regulation project incorporating enclosing tideland for cultivation and linking islands to promote harbor industry and tourism.

3 Numerical model and setting

The Environmental Fluid Dynamics Code (EFDC) of US Environmental Protection Agency is utilized. The model solves the 3D, vertically hydrostatic, free surface, turbulent-averaged equations of motion for a variable density fluid [3]. It can be run in barotropic or baroclinic and in 2D or 3D modes. It also has the capability of simulating wetting and drying processes, and has been tested and verified in a wide range of hydrodynamic and environmental studies [4-5]. The detailed basic theory of EFDC can be seen in Hamrick(1992) and would not be given here.

The ORE is bounded by a complex shoreline, and the estuary is further complicated by its many islands and complex terrain. Based on the features of the study area, a curvilinear orthogonal grid was used to represent the complex geometry. The model grid consists of 12,161 grid cells in the horizontal direction, with grid size ranging from 10m to 1,000m. In the vertical direction, six layers are divided according to the relative water depth, i.e., the surface, 0.2H, 0.4H, 0.6H, 0.8H, and bottom layers. Throughout the computational domain, we used values of 0.01–0.025 to account for the effect of the Coriolis force and Manning's coefficients according to the distribution of medium diameters of bed materials measured in recent years. The Smagorinsky constant for the horizontal eddy viscosity coefficient assumes a typical value of 0.12. The settling velocity was set to 1.0×10^{-4} ms^{-1}; the critical shear stress for resuspension was set to 0.4 Nm^{-2}; the critical shear stress for deposition was set to 0.2 N m^{-2}; the bed sediment porosity was set to 0.5; and the bed sediment specific weight was set to 2.5.

4 Numerical simulations and results

4.1 Analysis of sediment concentration

The change of sediment concentration before and after the reclamation project was shown in Fig.2. From the suspended sediment distribution of the ORE, it was found that the distribution of the suspended sediment is similar to the underwater topography and most of high sediment concentration area is at the shallow-water zone on the two sides of the ORE shoal, Wenhzou shoal and Sanjiaosha shoal. The sediment concentration in the three sailing channels is low. Under the natural environment conditions, the sediment concentration in water has a dynamic relation with the underwater topography. Under the same dynamic conditions, the effect of stirring sand by the procedure of runoff, tidal current on shoal is larger than that on deep water area. This causes the sediment concentration in water above shoal is high and the sediment concentration in deep water is low. The muddy water of the south the ORE flows out of Koumen and then spreads to southeast. The spread range is generally within 20km and most of the sediment discharge of the north estuary goes through Huangda'ao and Chongshan water channel to the east of Dongtou islands. Meanwhile, only a small amount of sediment discharge go through Shatou channel to the south of Yueqing Bay.

On the upper part of Wenzhou shoal, the south estuary channel and its downstream of estuary and the north estuary of the downstream of Lingkun Island, the sediment concentration is mostly between 0.4kg/m^3-0.6kg/m^3. The maximum sediment concentration reaches to 0.8kg/m^3- 1.2kg/m^3. On the south of west coast in Yueqing Bay, the sediment concentration is between 0.2 kg/m^3-0.4kg/m^3. For Sanjiaosha (between the middle water channel of downstream of north estuary and the Shatou channel) and the Chongshan spit (on the west boundary of Qingshan island), the sediment concentration is usually under 0.2kg/m^3. The sediment concentration in open sea areas is low. Generally, it is lower than 0.1kg/ m^3.

Comparison of the sediment concentration field of the pre-and post reclamation construction, the basic form of the distribution of sea sediment concentration has no obvious change, only the sediment concentration near the reclamation site has experienced a little change after reclamation construction. The sediment concentration of middle water channel on the north of reclamation project is increased by about 0.03kg/m^3. The sediment concentration in south channel, Huangda'ao and Chongshan channel decreased a little by about 0.02kg/m^3. Generally, in the upstream of Qidutu and the external sea area of Oujiang River, the sediment concentration almost keeps little effects. It was concluded that there is only a little distribution change of sediment concentration in and around the ORE after the reclamation construction.

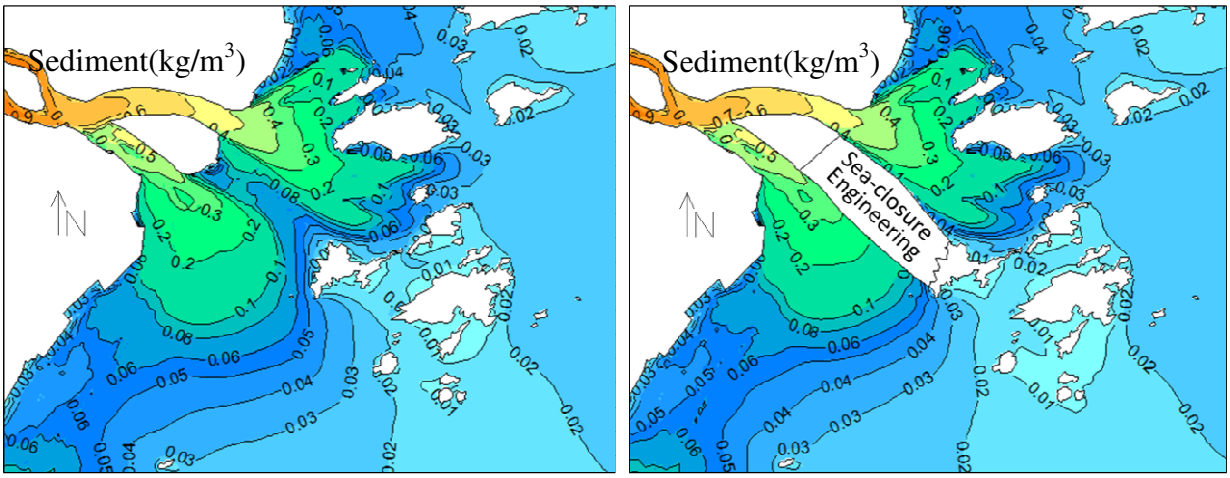

(a) before (b) after

Fig.2 Distribution of sediment concentration before and after the reclamation project

4.2 Analysis of morphological changes

The construction of reclamation project will cause the changes of hydrodynamic property of project sea area, and as a result, it will cause adjustments on the seabed topography, and then it will change the hydrodynamic environment again and lead to adjust the seabed topography. The adjustment of hydrodynamic property and seabed topography is repeated until the seabed topography reach to a relatively steady and new scour and silting balance condition to adapt the reclamation engineering. Here we do a predictive analysis on the condition which the seabed scouring and silting has been balanced after the construction of reclamation engineering.

Fig.3 showed the adjustment results of the seabed topography after reclamation construction. The simulated result showed that the fastest adjustment of the seabed topography happens in the first three years, the lag phase of the seabed adjustment is in the fourth to the sixth years, and the adjustment is mostly finished and the seabed seems to be steady in the seventh to the tenth years after the reclamation construction. The final seabed changes caused by the reclamation construction is that the ports of Longwan, north estuary and Qili and others appear to be in scour status and their scour thickness is between 0.008-0.076m.

Being affected by the sedimentation of Huangda'ao-Chongshan channel, Zhongshui channel and Lanmen sha also generates slight sedimentation, and the average sedimentation thickness is 0.058m and 0.077m, respectively. The average sedimentation thickness in Huangda'ao is 0.14m. In the deep water of Zhuangyuan'ao, the average thickness is 0.27m. In the south water way of Chongshui

channel, the sedimentation thickness is 0.34m. From the sedimentation thickness and the decrease percent of water depth, the south water way of Chongshan channel has the greatest effect from the reclamation. On the north water way of Chongshan channel and the deep water area in Zhuangyuan'ao, they receive less effect than the south water way of Chongshan channel. The south water way of Chongshan channel where the water depth decreased most is 3.4%. The north water way of Chongshan channel only decreases 1.2%, Huangda'ao channel only decreases 0.8%, the water depth of Lanmen sha decreases 1.1%, the water depth of Zhongshui channel decreases 0.7% and the water depth decreases 0.8% in the deep water area in Zhuangyuan'ao. It was found that the reclamation construction does not change the natural evolution trend of the seabed in the ORE and the seabed topography only has a slight adjustment after the reclamation construction.

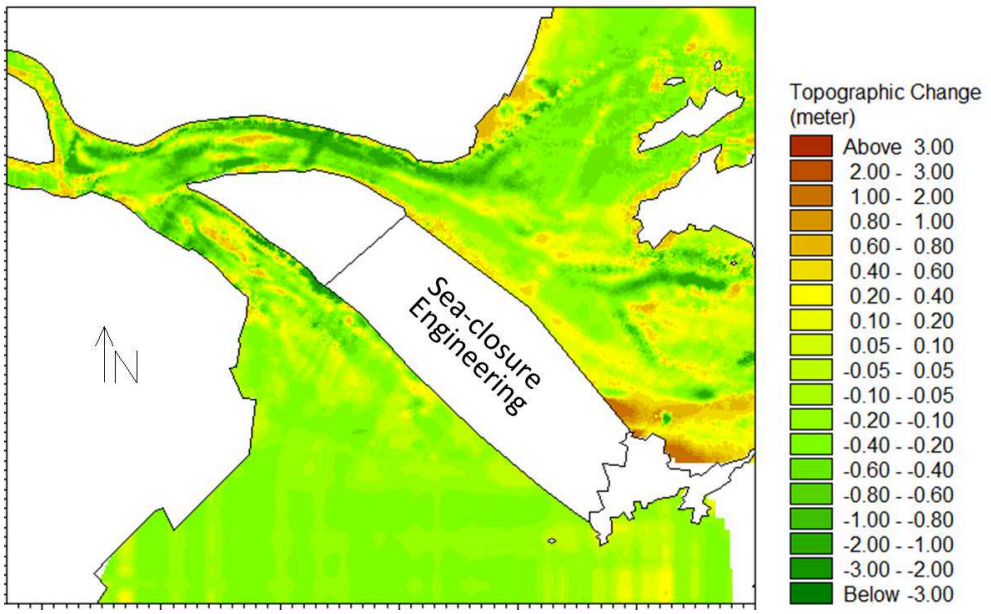

Fig.3 Erosion and deposition thickness after the completion of the project

5 Conclusions

Studying by the 3D marine numerical simulation with EFDC, the result showed that Wenzhou shoal itself has a very good condition for the reclamation. The numerical results indicated that the project doesn't have obvious adverse effects on its nearby sediment environment and seabed. On the contrary, it settles the problem of mouth bar of the ORE and provides some advantages to maintain and steady the deep water channel and improve the sail condition from the north mouth of Oujiang River to Huangda'ao channel.

References

[1] Li Meng-guo:The effect of reclamation in areas between islands in a complex tidal estuary on the hydrodynamic sediment environment. Journal of Hydrodynamics , Vol 22(2010), No 3, pp338-350.

[2] T.I. Kim , B.H. Choi , S.W. Lee: Hydrodynamics and sedimentation induced by large-scale coastal developments in the Keum River Estuary, Korea. Estuarine, Coastal and Shelf Science , Vol 11(2006), No 1, pp515-528.

[3] Hamrick JM. A three-dimensinal environmental fluid dynamics computer code: theorical and computational aspect. Special report No.317 in Applied Marine Science and Ocean Engineering 1992.

[4] Shen, J., Boon, J., Kuo, A.Y.:A numerical study of a tidal intrusion front and its impact on larval dispersion in the James River estuary. Estuary Vol 22(1999), No 1, pp681–692.

[5] Jin, K.-R., Hamrick, J.H., Tisdale, T.:Application of a three-dimensional hydrodynamic model for Lake Okeechobee. Journal of Hydraulic Engineering Vol 126(2001), No 2, pp758–771.

Advanced Materials Research Vols. 989-994 (2014) pp 1244-1247
© (2014) Trans Tech Publications, Switzerland
doi:10.4028/www.scientific.net/AMR.989-994.1244

Simulation of salinity changes induced by man-made sea embankment

XU Ting[1,2]

[1] Tianjin Research Institute for Water Transport Engineering, M.O.T, Tianjin 300456, China
[2] School of Environmental Science and Engineering, Tianjin University, Tianjin, China.

xuting1228@163.com

Keywords: EFDC, salinity changes,sea embankment; simulation.

Abstract: Understanding the salinity transport mechanism in the estuaries is of great importance for coastal engineering, disaster prevention, water security and intertidal zone aquiculture.In this paper,the large-scale sea embankment in the Oujiang River Estuary (ORE) of Wenzhou shoal was taken as an example.Based on the intoduction of the study area,the 3D marine numerical model (EFDC) was setup and used for simulation of salinity changes induced by the embankment. The results indicated that the ORE is well-mixed estuary. The Ling-Ni Embankment designed in accordance with the flow direction makes the freshwater inflow reach far away, the salinity gradient increase, and the tongue contour reach further. The salinity difference of the north and south side of the embankment sea area is increased.

1 Introduction

The salinity transport processes in estuaries are generally very complex and highly dynamic due to the presence of sinuous coastlines, islands, channels, shoals and some man-made structures [1-2]. Complexities can also arise because of the mixture of salt and fresh water as well as the synchronous impacts of runoff, tides, waves, winds and offshore currents [3-4]. The long-term stability and sustainability of the salinity environment are necessary for the continued prosperity of aquaculture. Understanding the salinity transport mechanism in the estuaries is of great importance for coastal engineering, disaster prevention, water security and intertidal zone aquiculture.

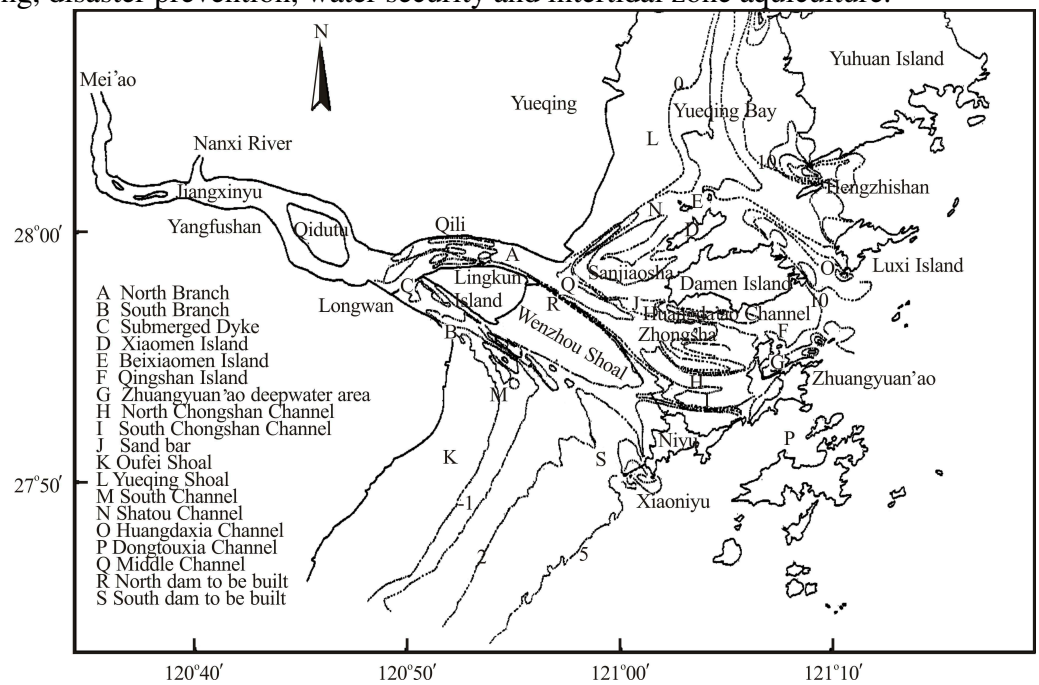

Fig. 1. Sketch of the Oujiang River Estuary

The Oujiang River Estuary (ORE) as a part of the East China Sea (ECS) is a macrotidal estuary.In order to meet booming land demands of urban expansion and deep water port construction, the construction of Ling-Ni Embankment with full length of 13km is completed in April 2005 (Fig. 1).
A three-dimensional hydrodynamic and salt transport model based on the Environmental Fluid Dynamics Code (EFDC) is developed to study the salt changes before and after the Ling-Ni

Embankment in the ORE, which contains not only the river reach inside the mouth, but also the region outside the mouth. The model is performed to comprehend the influence of the Ling-Ni Embankment on salinity distribution around the ORE.

2 Study area

The Oujiang River (OR) is a mountainous river that meanders eastwards to the East China Sea (ECS). It is the second longest river in Zhejiang Province, China with the length of 388km and has a drainage basin of 17,985 km^2.The maximum and minimum flows are 22,800 m^3/s in 1952 and 10.6 m^3/s in 1967, respectively.The Oujiang River Estuary (ORE) as a part of the East China Sea is a macrotidal estuary. The estuary, with the scales of 35 km long and 30 km wide at the mouth, is characterized by its bifurcation shape and has two outlets (north branch and south branch) into the East China Sea. The complex geometry consists of tens of staggered shoals, deep tidal creeks as well as more than 40 big and small islands, which are scattered outside mouth of the ORE. Tide in the ORE is a semidiurnal tide, with an average tidal range of 4.5 m and a maximum value over 7 m at Longwan gauge station. Freshwater meets with salt water at the mouth region with the mean salinity from 3.7 psu to 26 psu and salinity profiles are well-mixed over the water depth because of the strong tidal mixing characteristic of the ORE.

3 Numerical model and setting

The EFDC model is used to simulate the water level, current, and salinity. It solves the three dimensional equations of continuity and motions with free surface[5]. The Mellor and Yamada level 2.5 turbulence closure scheme is implemented. The model uses the stretched (or sigma) vertical coordinates and the curvilinear, orthogonal horizontal coordinates. It simulates the density and topographically induced circulation, tidal and wind-driven flows, and spatial and temporal distributions of salinity, temperature, and conservative/non-conservative tracers, including shellfish. The detailed basic theory of EFDC can be seen in Hamrick(1992) and would not be given here.

The ORE is bounded by a complex shoreline, and the estuary is further complicated by its many islands and complex terrain. Based on the features of the study area, a curvilinear orthogonal grid is used to represent the complex geometry. The model grid consists of 12,161 grid cells in the horizontal direction, with the grid size ranging from 10 to 1,000 m. In the vertical direction, six layers are divided according to the relative water depth, i.e., the surface, 0.2H, 0.4H, 0.6H, 0.8H, and bottom layers. A free-slip condition is applied to the land boundary in the north and the reclaimed zones. The time step for the circulation module is 5 min, with 1 min as sub-time step for the transport module. The mean annual flow is adopted as the upstream inflow boundary because of the lack of detailed inflow data. The upstream boundary of Mei'ao is the runoff section where the inflow is completely freshwater, and zero salinity is prescribed at this upstream boundary. The open sea salinity boundaries are interpolated from the measured distributions of salinity in a large region of the ECS.

4 Numerical simulations and results

The salinity distribution of estuarine is affected by the freshwater inflow and tidal mixing. The horizontal distribution of surface salinity field at maximum flood/ebb tides during spring tide is shown in Fig. 2. The salinity gradually declines from the open sea to the mouth until it becomes zero in the river reach and the isohalines are not smooth under the influence of irregular topography and sinuous coastlines. Horizontal gradient of the salinity in the mouth is much larger than that in the open sea because the inflow upriver freshwater and the strong mixing process of salt-fresh water. Moreover, the embankment and scattered islands constrain the spread of the river plume and it also results in the strong horizontal gradient of salinity. The salinity intrusion at maximum flood tide is less severe than that at maximum ebb tide because the current velocity reaches its maximum at the maximum flood /ebb tide, while the salinity still does not reach its maximum. That is to say, during the flood tide, the salinity intrusion has the trend to strengthen, while it becomes weaken during the

ebb tide. It is found that the salinity intrusion at the maximum flood tide is more severe than that at the ebb tide.

The average salinity is the least in the river section above Qidutu, where the average salinity is between 1 and 8psu. The isoline of 1 psu salinity is up to the west boundary of Jiangxin islet during the tidal flood and it is to the east boundary of Qidutu during the ebb tide. In the external sea area of the ORE, the isoline of salinity diffusion is ligules, which is swinging with the flood and ebb tides. The isoline of average salinity between 20 and 26 psu spreads to the middle part of Damen island. After the Ling-Ni Embankment built, the main changes of salinity distribution are concentrated near the project area. The tongue contour of freshwater reaches farther to the open sea after the project, especially on the north side of the Ling-Ni Embankment. There is no obvious effect on the surrounding areas, such as Huangda'ao channel, Zhuangyuan'ao channel, Xiaomen channely etc.

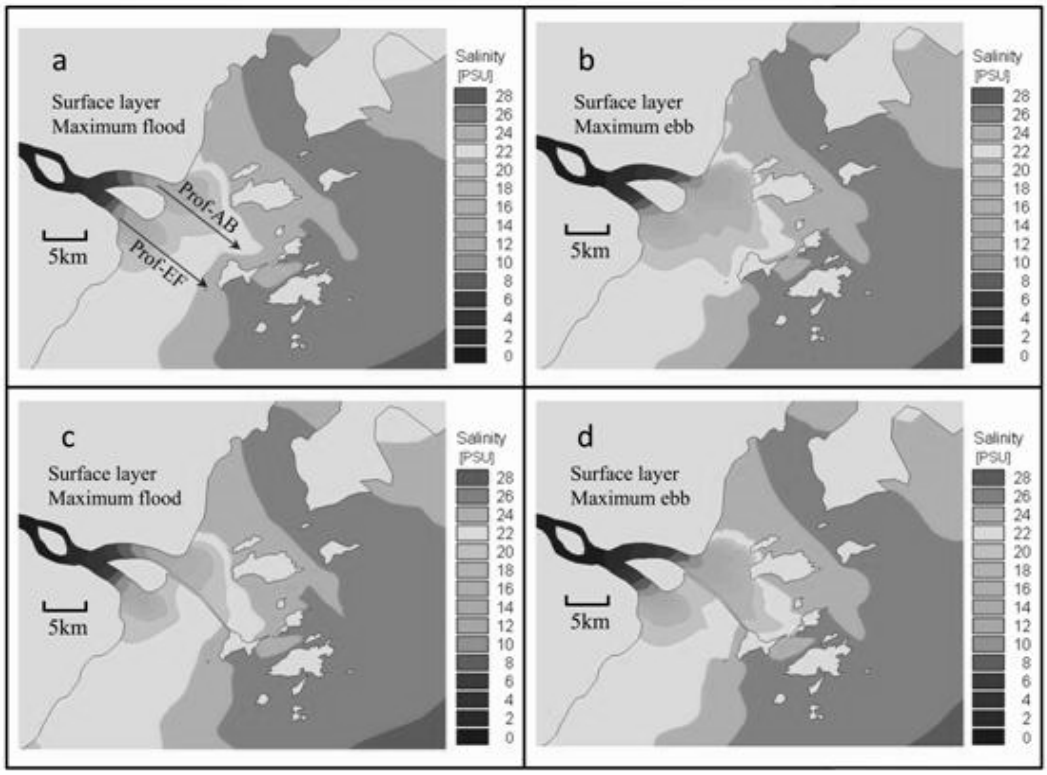

Fig.2. Distributions of surface horizontal salinity at maximum flood/ebb tide before(up, a and b) and after(down, c and d) embankment project.

It is seen from Fig. 3 that the vertical structure of salinity is almost uniform over the depth during spring tide, which demonstrates the estuary type is a well-mixed pattern. Because the ORE is amacrotidal estuary, the tidal mixing greatly exceed the river inflow, which results in a well mixed water column and the disappearance of the vertical salinity gradient. After the construction of the Ling-Ni Embankment, the salinity gradient increases because the tongue contour of freshwater reaches farther to the open sea, especially in the upper layers. For example, at the ebb slack, the isohalines of 18 reaches up to 8.4 km in Middle channel (Fig. 3(a)) under the mean annual flow before the embankment project, while it reaches up to 9.8 km (Fig.3(a)) under the mean annual flow after the embankment project. Accordingly, in South channel, the isohalines of 18 reaches up to 6.7 km at the moment of ebb slack (Fig. 3(d)) under the mean annual flow before the embankment project, while it reaches up to 7.2 km (Fig. 3(d)) under the mean annual flow after the embankment project.

5 Conclutions

Studying by the 3D marine numerical simulation with EFDC, the result showed that Wenzhou shoal itself has a very good condition for the reclamation. The numerical results indicated that the ORE is well-mixed estuary. The Ling-Ni Embankment designed in accordance with the flow

direction makes the freshwater inflow reach far away, the salinity gradient increase, and the tongue contour reach further. The salinity difference of the north and south side of the embankment sea area is increased.

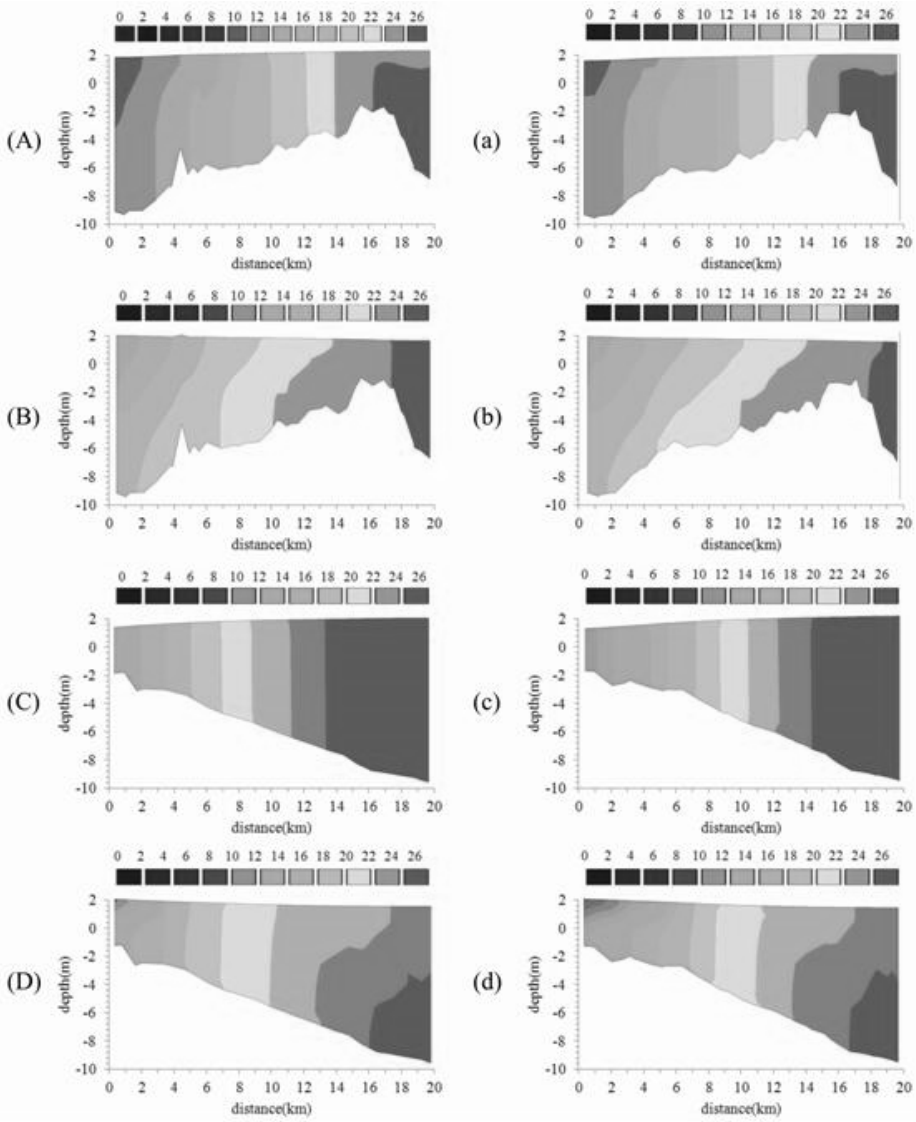

Fig.3. Transect salinity distributions along the north(A/a and B/b) and south(C/c and D/d) side branch of embankment at maximum flood(A/a and C/c)/ebb(B/b and D/d) tide before (left) and after (right) the project.

References

[1] Chen, X.: Modeling hydrodynamics and salt transport in the Alafia River estuary, Florida during May 1999–December 2001. Estuarine, Coastal and Shelf Science Vol 61(2004), No 2,pp477–490.

[2] Yang Z., Khangaonkar T. :Modeling tidal circulation and stratification in Skagit River estuary using an unstructured grid ocean model. Ocean Modelling. Vol 28(2009), No 1,pp34–49.

[3] Chen, S.-N., Sanford, L.P.: Axial wind effects on salinity structure and longitudinal salt transport in idealized, partially mixed estuaries. Journal of Physical Oceanography Vol 39(2009), pp5–20.

[4] Gong, W., Shen, J.: Response of salt intrusion to changing river flow and tidal amplitude during winter season in the Modaomen Estuary, Pearl River Delta area, China. Continental Shelf Research Vol 31(2011), pp769–788.

[5] Hamrick JM. A three-dimensinal environmental fluid dynamics computer code: theorical and computational aspect. Special report No.317 in Applied Marine Science and Ocean Engineering 1992.

Advanced Materials Research Vols. 989-994 (2014) pp 1248-1251
© (2014) Trans Tech Publications, Switzerland
doi:10.4028/www.scientific.net/AMR.989-994.1248

Forecast of Energy Consumption and Carbon Emission of Urban Traffic by Using System Dynamics

Yi Zhang[1,2], Lijuan Wan[1,2], Li Zhang[1,2] and Dongxiang Cheng[1,2]

[1]Nanjing Communications Institute of Technology, Nanjing 211188, China;

[2]Jiangsu province transportation energy saving engineering technology research center, Nanjing 211188, China.

Keywords: Carbon emission, urban traffic, energy consumption, System Dynamics.

Abstract. In the future development of city, traffic acts a very important role, which not only support the modernization of city, but also offer more travel and transportation service for the increasing city population. Therefore, it is necessary to study the urban traffic, energy consumption and carbon emission based on System Dynamics. System Dynamics not only offer quantificational references and advice about city planning for the government, but also make people understand the present status of urban traffic and possible development trend of urban traffic under the influence of different policies. In this review, the energy consumption and emission of urban traffic, the development of System Dynamics and the advantages on solving urban traffic problems based on System Dynamics are introduced.

1. Introduction

With the rapidly developing economy and the significantly rising living-standards, the traffic congestion has been increasingly serious. Reducing transportation fuel consumption would not only enhance the country's energy dependency but also help to reduce greenhouse gas emissions, improve air quality, and reduce other driving-related external costs such as traffic accident costs. At the same time, under the global background of developing low carbon economy, governments began to take into consideration how to save energy, cut emission and fully satisfy the people's travel need as much as possible.

Low carbon economy included low carbon energy, low carbon technique, low carbon industry, low carbon life and various forms base on low energy consumption, low pollution and low emission. The purpose is to promote the sustainable development of the human beings. Low carbon economy is a new change for the development route, energy consumption and human way of life. The government of the United Kingdom published the energy white paper (UK Government, 2003), which title was Our Energy Future: Creating a Low Carbon Economy. Low-carbon Economy was firstly proposed and paid wide attention in the international society [1-9].

For the complicated and dynamic huge system of urban traffic, using the theory and method of System Dynamics, the models are built for the increase of vehicles and energy consumption, which is an adventure and practice of System Dynamics used in transportation field. Furthermore, it is an attempt of solving the traffic problems by combing the System Dynamics and system engineering theory. In this review, the development history of System Dynamics was presented. Furthermore, the advantages on solving energy consumption and carbon emission of urban traffic by using System Dynamics were explained.

2. Energy Consumption and Emission of Urban Traffic.

As a very important component in the national economy, traffic acted a role of basic support and service, which is inevitable that traffic offer the service for the transportation of passengers and freight, and at the same time, traffic had a huge energy consumption and negation influence on the environment. At present, the economy of China is at a period of increasing at a high rate. With the

increase of the rate of urbanization, the ownership of private car is increasing rapidly. The service requirement for traffic is correspondingly increased. Also, the energy consumption of traffic was increased rapidly at a rate of 9.3% every year from 1971 to 2001. From the international scope, as high energy consumption trade, especially the primary oil energy, traffic was paid attention by the community. Many researchers developed very fruitful discovery about the traffic energy consumption and sustainable urban development. From the above study, the forecast of energy consumption of urban traffic in the future is very necessary. For the forecast of energy consumption of urban traffic, the forecast of traffic demand should be combined, which method was mainly dummy variable method and etc. Then, the traffic structure was modulated on the basis of forecast to make the traffic structure more adapt to the sustainable development of city. On the way of the forecast of urban traffic energy requirement, the scene methodology could be used to analyze the energy requirement and the emission of the local traffic trade by setting up different scenes. Furthermore, the relationship between traffic turnover volume and GDP per capita by using economy measurement models, and the results could be calculated by long-term energy planning substitute model. Finally, the relation between traffic turnover volume and energy requirement of traffic trade of the local city could be obtained.

It was also proposed that the relevant analytic methods on traffic energy consumption, environmental effect analysis method of traffic system and atmosphere environment effect analysis method of traffic system. And from the three ways, the sustainable development of the urban traffic energy consumption and transportation system was studied. Other researchers also proposed the strategies of reducing the urban traffic energy consumption from the view of traffic management, traffic structures, rode traffic planning, urban land use and etc. Some researchers had introduced the concept of traffic volume, mode energy consumption and environmental volume and proposed a series of thinking and methods about reducing energy consumption through optimizing urban traffic structure. The research had also been carried on with practical example. From the rules of building ecological city, how to realize the traffic sustainable development had been studied. The development of sustainable traffic was based on land use planning. The corresponding steps of developing the sustainable traffic were proposed by analyzing the influence traffic structure on land use and the sustainable development. The relation between traffic and energy consumption was analyzed from the macroscopic and microcosmic levels. [10]

3. The Development of System Dynamics.

System Dynamics (abbreviated as SD), a method using structure, functions and history, which was first created by Prof. Forrester (Jay W. Forrester) from Massachusetts Institute of Technology (MIT) of the United States in 1956. The method was the united method of structure, function and history, which had comprehensive theory and method of control, policy decision, information and etc. The systematic analysis of non-linearity, dynamic complexity, information feedback was studied quantitatively assisted by computer simulation. The purpose of System Dynamics was to analyze and study the structure and systematic behavior of feedback loop system by using the achievements of cybernetics, decision theory and information theory assisted by computer.

From the nature, System Dynamics model is a set of first order differential equations. The non-linearity and time-varying phenomena could be conveniently handled by System Dynamics model, which could act as long-term, dynamic, strategic simulation analysis and study and was properly used to analyze the structure and dynamic behavior of the analytic system. System Dynamics model could be used to study and handle the complicated system problems of society, economy, ecology and biology. System Dynamics could used to comprehensively study the complicated, multi-leveled, multi-department, non-linear system at a large scale from the macroscopic and microcosmic levels.

In the later period of 1950s, System Dynamics had been widely applied in solving the problems in business management, study on the production and labor force fluctuation, offer, storage and production and instability of financial market. In 1960s, the application of the thought and method of

System Dynamics had been widely used in various systems and all walks of life. As a basis methodology, "Principles of Systems (1968)" and "Urban Dynamic (1969)" included various theories and application fruits for American urban problems. "World Dynamics (1971)" was mainly proposed by J. W. Forrester and et al. System Dynamics was formally proposed in 1972. The important period of the formation and development of System Dynamics was from the late 1950s to the early 1970s. At the late twentieth century, System Dynamics developed very fast and was approved to the world after three severe tests. The first test (from the early 1970s to the middle 1970s) was marked by the production of two world models (WORLDII，WORLDIII), which made System Dynamics the most famous as the club of Rome. The second test (from the middle 1970s to the middle 1980s) was marked by the System Dynamics model building and the study of the problems of western country and American Long Wave economy. The third test (in the 1990s) was marked by the five studying organization practice theory and method proposed by the student of Jay W. Forrester based on System Dynamics. [11-12]

System Dynamics has been a new system engineering methodology and practical model method through the continuous development in these years. System Dynamics has been widely used in many fields and showed the special advantages, especially in land source planning, local economy development, environmental comprehensive improvement and company strategy study and etc. Especially, System Dynamics had been more active because the study organization had been paid more attention by management researchers. At present, System Dynamics has been improved constantly and applied by using quantitative analysis and conditions.

4. Advantages on Solving Urban Traffic Problems Based on System Dynamics.

Firstly, the characteristics of urban traffic problems were analyzed. The complicated and dynamic characteristics were the two main ways for the urban traffic problems. The development of traffic system was related to the development of society and economy factors and etc. Traffic system involved the policy of macro economy, traffic planning of local government, infrastructure of urban roads, international oil prices, the consumption level of residents and etc. These all would have effects on traffic structure, energy consumption and emission system. Furthermore, the factors in the same system also had mutual influence and actions. The urban traffic system was not only complicated but also dynamic. Because the various internal factors of urban traffic system were changing and influence each other, the whole system was constantly evolving and developing, which presented the dynamic characteristics. [13-14]

In the light of the above characteristics traffic, the advantages on solving urban traffic problems based on System Dynamics were shown as followings. Based on System Dynamics, structural thinking could be used and every factor could be equilibrated. From the comprehensive perspective of System Dynamics, the specific details of the corresponding levels of the system, graphic method of complicated problems which had been handled at present could be captured, the problems of complicated system could be solved by the method of simulation and forecast, and the hypothesis of the system could be reduced to a minimum. At the same time, the actions at present and the results of carrying out the new policy could be tested by System Dynamics. Therefore, the traffic structure and vehicle energy consumption and emission system composed of complication, dynamics, feedback and long term could be studied by systemic, multi-leveled and visual method of System Dynamics. The interrelation of every factor and evolution trend of the whole system could also be analyzed.

Summary

Traffic will be very important in the future development of city, which offers more travel and transportation service and supports the modernization of city. Therefore, based on System Dynamics, it is necessary to study the urban traffic, energy consumption and emission. The theory and method of System Dynamics would be used for the increase of vehicles and energy consumption for the complicated and dynamic huge system of urban traffic, which is an adventure and practice of System

Dynamics. System Dynamics can not only offer advice and quantificational references about city planning for the government, but also make people understand under the influence of different policies, the present status and possible development trend of urban traffic. Therefore, the traffic structure and vehicle energy consumption and emission system composed of complication, dynamics and feedback could be studied by systemic, multi-leveled and visual method of System Dynamics and the interrelation of every factor, and evolution trend of the whole system could also be analyzed, which is adapted in urban traffic system with the dynamic characteristics, because the whole urban traffic system was constantly developing and evolving.

Acknowledgement

This work was supported by a grant from Transportation Scientific Research Project of Jiangsu Province, Jiangsu Provincial Communications Department (2013N02-3).

References

[1] D. Andress, T.D. Nguyen and S. Das: Energy Policy, Vol. 38 (2010) No.1, p.580
[2] R.M. Bright and A.H. Stromman: Environmental Science &Technology, Vol. 44(2010) No.7, p.2261
[3] M. Grahn, C. Azar: Biomass&Bioenergy, Vol. 31(2010) No. 11-12, p.747
[4] C. Harto, R. Meyers, Energy Policy Vol. 38 (2010) No. 9, p.4933
[5] M. Hatzopoulou and E.J. Miller: Transportation Research Part D: Transport and Environment Vol. 15 (2010) No. 6, p.315
[6] H. Machado: Climate Policy, Vol. 9 (2009) No. 5, p.495
[7] A. Schafer, J.B. Heywood: Energy, Vol. 31(2006) No. 12, p.2064
[8] M. Wang, H. Huo, L. Johnson: Projection of Chinese motor vehicle growth, oil, demand, and CO_2 emissions through 2050[EB/OL]. (2006)
[9] A. Sentence: Oxford Review of Economic Policy, Vol. 25(2009) No. 3, p.391
[10] J.W. Forrester: *Industrial Dynamics*. (Pegasus Communications, America, 1961. ISBN 1-883823-36-6)
[11] J.W. Forrester: *Urban Dynamics*. (Pegasus Communications, America, 1969, ISBN 1-883823-39-0)
[12] M.V. Johansson, T. Heldt and P. Johansson: Transportation Research Part A: Policy and Practice, Vol. 40 (2006) No. 6, p.507
[13] A.A. Amekudzi, C. J. Khisty and M. Khayesi: Transportation Research Part A: Policy and Practice, Vol. 43(2009) No. 4, p.339
[14] F. Lengin, O. Kabak, S. Onsel: European Journal of Operational Research, Vol. 200(2010) No. 3, p.844

Advanced Materials Research Vols. 989-994 (2014) pp 1252-1255
© (2014) Trans Tech Publications, Switzerland
doi:10.4028/www.scientific.net/AMR.989-994.1252

Study on Feasibility of Concentrated Activated Sludge Reflow of Biochemical Pool of Small-sized Wastewater Plant

Youcai GUO[1,a], Ying CHEN[1,b]

[1] Xingtai Polytechnic College，Xingtai 054035，China
[a]1198682793@qq.com,[b]chen-gyc@163.com

Keywords: Concentrated sludge, Reflow process, Small and medium-sized wastewater plant, Energy saving and consumption reduction

Abstract. Experimental research and engineering validation show concentrated activated sludge reflow stead of traditional reflow way still meets the national discharge standard, though the treatment efficiency of wastewater plant is slightly declined and further show concentrated activated sludge reflow process used in energy saving and consumption reduction of small-sized wastewater treatment plant is feasible.

Research background

Data reported by the Ministry of Housing and Urban-Rural Development of the People's Republic of China(MOHURD) shows that 3513 wastewater treatment plants have been put into operation in China by September 2013[1]. It is estimated daily wastewater treatment ability of China has reached about 149 million m^3, annual electricity power consumption has reached more than 13 billion *KWH* and electricity power consumption cost accounts for more than half of operation cost of wastewater treatment facilities[2]. For small-sized wastewater treatment plant, high energy consumption leads to higher cost of wastewater treatment and further operation difficulty. In order to reduce energy consumption of wastewater treatment plant, extensive researches at home and abroad are carried out. Small and medium-sized wastewater treatment plant mainly adopts the means to save energy and reduce consumption including technology upgrading, process parameters optimization, replacement of energy-saving equipment, and stagger of operation and promoting the operator's level of operation. The practice shows that the countermeasures above are effective under the condition of sufficient technical support and rich fund. Compared with large-sized wastewater treatment plant, small and medium-sized wastewater plants have many problems such as low level of technology, insufficient technical personnel and financial strain which will directly restrain the normal operation of small and medium-sized wastewater plants. As a result, small and medium-sized wastewater treatment plant with financial strain and backward technology raises fund for technical upgrade and update of energy-saving equipment, and meanwhile more urgently needs practical and applicable energy saving techniques. Literature search and on-the-spot investigation show that the study on the way of concentrated activated sludge reflow used in energy saving and consumption reduction at home and abroad is still back. Hence, the author carried out a technical study and experimental analysis around concentrated activated sludge reflow stead of traditional reflow way to reduce the consumption of small and medium-sized wastewater treatment plant. Study on concentrated activated sludge reflow used stead of secondary settling tank sludge reflow to save energy and reduce consumption

Concentrated activated sludge reflow indexes and feasibility analysis of energy saving and consumption reduction. In order to ensure the treatment effect of aeration basin, one necessary condition is that activated sludge concentration of pool should be met. In the project, appropriate activated sludge concentration (2000mg/L~3000mg/L) is maintained through secondary settling tank sludge reflow to aeration basin. Reflow sludge is the precipitation sludge of secondary settling tank, whose rate of water content is commonly 99%, even up to 99.5%. As a consequence, sludge is actually still in the state of flow, whose density is slightly different from that of water, so that corresponding power consumption is higher. If secondary settling tank sludge is first sent to concentration pool, and rate of water content of sludge is about 98% (good flow state) after concentration, sludge volume of secondary settling tank sludge is reduced by more than 70%. Thus it can be seen concentrated sludge reflow can effectively reduce sludge reflow amount and energy consumption of sludge reflow. Concentrated sludge reflow in theory can reduce the energy consumption in operation, but whether technical indicators (such as microbial activity, content of *DO*) after concentrated sludge reflow meet the operation requirement of wastewater plant still needs further validation.

Experimental study. Main content of experimental research involves operation effect test of concentrated sludge reflow stead of secondary settling tank sludge flow. Feasibility of concentrated activated sludge reflow process used in energy saving and consumption reduction of small and medium-sized wastewater treatment plant is verified through comparing water quality and technical indicators.

A. System transformation. Laboratory has two sets of AO wastewater treatment Operation systems, as shown in Figure.1. Among them, aeration basin is plug flow and aeration device is evenly distributed. Flow meter is installed in all piping systems to monitor and control flow.

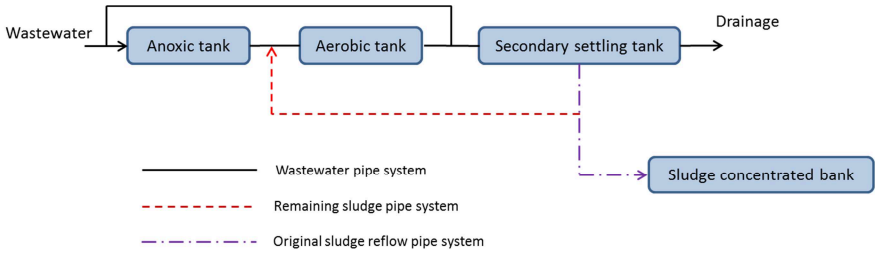

Figure.1 Sketch of original AO system

According to research need, the second set of AO system is performed with transformation, i.e., sludge reflow pipe is linked with concentrated sludge bank so that concentrated sludge is reflowed to aeration basin. The transformed pipe system is shown in Figure.2.

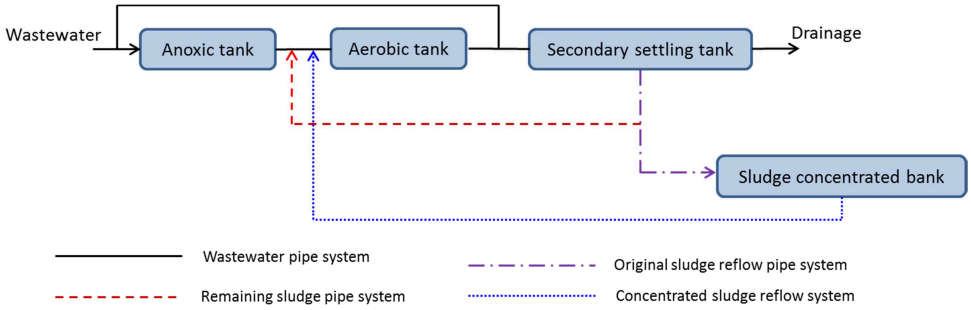

Figure.2 AO system after transformation

After transformation, the activated sludge reflow pipe of original secondary settling tank is closed. Required reflow sludge of aeration basin is supplemented by concentrated bank.

B. Experimental study and analysis. Waster used in experiment is collected from sewer of living quarter of the college. Main water quality indexes (mean) are shown in Table.1.

Table.1 Quality of experiment water

BOD_5(mg/L)	NH_3-N(mg/L)	SS(mg/L)	pH(mg/L)
80-100	30-32	200	6-9

First, after the operation is stable through debugging, the effluent quality of two sets of AO system is shown in Table. 2.

Table.2 Effluent quality

BOD_5(mg/L)	NH_3-N(mg/L)	SS(mg/L)	pH(mg/L)
20	10	30	6-9

The first AO system (without transformation) runs as usual; in the second AO system (through transformation), secondary settling tank sludge reflow pipe is closed and concentrated sludge reflow pipe is open. Besides, aeration strengthening is performed for front end of aeration basin to promote recovery of concentrated sludge as soon as possible. After continuous run for 15 days, *BOD_5* and *NH_3-N* were mainly detected. The specific operation is as shown in Figure.3.

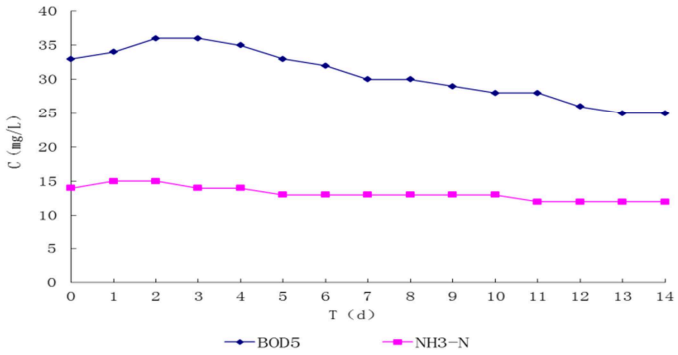

Figure.3 System operation after concentrated sludge reflow

It can be seen from Figure.3 that *BOD_5* and *NH_3-N* showed a trend of rise in early stage after concentrated sludge reflow instead of secondary settling tank sludge reflow. After 3-4 days, *BOD_5* and *NH_3-N* gradually reduced and were stable after 13 days. Compared with the first set of AO system, the treatment effect of the second set of AO system after transformation was slightly reduced. Of them, *BOD_5* and *NH_3-N* were increased by about 5 mg/L and 2mg/L, respectively. The reason for this was that activity of concentrated sludge was slightly lower than that of secondary settling tank sludge, thus, the adaptation time was longer and processing efficiency is slightly worse after sludge was into aerobic pond. But the effluent quality still meets the standard for small and medium-sized wastewater plant. In addition, it is found through inspection that the total phosphorus concentration of effluent after transformation is reduced by about 0.1 mg/L, which is because the phosphorus release amount of concentrated sludge is higher than that of secondary settling tank sludge and thus the total phosphorus amount into aerobic pond is reduced so as to better remove phosphorus of the system [3, 4]

Based on experimental research and analysis above, the treatment efficiency of the system will be slightly decreased when concentrated sludge reflow instead of secondary settling tank reflow, but the effluent quality can still meet the standard of secondary emission standard of GB18918-2002. Thus it can be concluded that the technique is feasible.

Pilot effect of concentrated sludge reflow instead of secondary settling tank reflow used in energy saving and consumption reduction

Based on laboratory study, the author selected two wastewater plants as the pilot unit. Among them, the one engages in oxidation ditch process, with average scale of processing amounting to 6, 200 tons/day, and the other engages in AO processing, with average scale of processing amounting to 200 tons/day. Both of them built with intermittent sludge concentration basin. Engineering experiment is carried out after addition of reflow pump and simple transformation of temporary reflow pipe. The data of operation for 20 days shows that effluent quality initially fluctuates significantly and tends to be stable in later period. The whole processing efficiency is reduced by 5% after transformation (meet the discharge standard) and energy consumption is reduced by 6% to 9%. Empty discharge of allowance exists in wastewater plant with scale of processing of 200 tons/day before transformation because aeration amount is significantly higher than that of required amount, so the author used aeration allowance to strengthen head end filling oxygen of oxidation pool, which will necessarily improve the activity of sludge through comparative analysis.

Summary and suggestion

A. Experimental research and pilot show that under the premise of normal operation and discharging standard of effluent quality of small and medium-sized wastewater plant, energy consumption and operation cost can be reduced by using concentrated activated sludge reflow.

B. It is suggested concentration time is controlled at about 8 h to keep the activity of sludge as much as possible. Wastewater plant with the condition can set extra regeneration basin to quickly realize quick recovery of concentrated sludge through aeration oxygenation, addition of micronutrients and humus soil[5], etc. Low activated sludge including higher inorganic component at the bottom of basin can be appropriate discharged before reflow.

C. It is suggested stripping return sludge pool instead of reflow pump is added behind sludge concentration pool in wastewater plant with aeration allowance to further reduce power consumption.

D. Small and medium-sized wastewater plant covers less area and has compact layout, which is beneficial for rope and road transformation and provides a good foundation for the application of this research result. But concentrated sludge reflow system is suggested to be added when wastewater treatment plant carries out design.

References

[1] MOHURD: Circular of the national urban sewage treatment facilities construction and operation of the fourth quarter of 2013, JAN 2014

[2] H_2o-china.com: Series Analysis Report on Chinese Urban Wastewater Treatment Marke, 2011.

[3] L. Xu, W. Liu, C. Jia, et al: Chinese Journal of Environmental Engineering, (2012) no.6, P. 3029-3034.

[4] J.F. Wang, Q.L. Zhao: Water Industry Market, (2010) no.9, p.18-23.

[5] Y. Zhu: *Preliminary Exploration of Improving Bio-regeneration of Reflow Sludge*. (MS.,Tongji University, China , 2008) , p.55-58.

Advanced Materials Research Vols. 989-994 (2014) pp 1256-1259
© (2014) Trans Tech Publications, Switzerland
doi:10.4028/www.scientific.net/AMR.989-994.1256

Analysis on fluctuation characteristics of wind power

Yang Wang[1,a]

[1] North China Electric Power University, Baoding, China;

[a]1003116521@qq.com

Keywords: fluctuation of wind power, step change, t location-scale distribution, time and spatial scale, smooth effect

Abstract. Fluctuation is an inherent property of wind power. Analyzing fluctuation of wind power has a significant meaning either for improving prediction accuracy of wind power or for overcoming disadvantages coming from wind power and power grid connection. Based on methods of statistics analysis and fitting, starting with a wind power plant, this paper analyzed the characteristics of probability distribution of wind power fluctuation. We selected wind power data from different sites and time scales, based on variation of probability distribution characteristics, this paper researched fluctuation of wind power under different spatial and time scales.This paper pointed out power fluctuation difference between single wind machine and the whole wind power plant.

Introduction

With the enlargement of capacity of wind power in power grid, people have paid more attention to effects caused by its randomness. In fact, uncertainty and variability are inherent properties of electric power system operation. Wind power aggravates uncertainty and viability of electric power system, but it does not change these two essential properties in electric power system [1].

There are two ways to describe fluctuation characteristics of wind power, one is random sequence based method, literature [2-3] builds sequence model of wind power by Markov chain Monte Carlo method and ARIMA model with amplitude limiting.The other one is probability density function based method. Available literatures performed study on wind speed [4-5], and distribution characteristics of wind power [6-7]. Based on measured data, wind power does not in line with common probability distribution.

Based on probability density function, this paper introduced step change to describe fluctuation of wind power, according to measured data, fitting probability density curve by MATLAB's fitting distribution toolbox and defining fitting offset index to depict fitting effect of different distribution further, then we recommended the best distribution here by.After that, we selected data series based on time interval of 5s and 1min respectively, analyzed power fluctuation characteristics under different time scales, and studied spatial characteristics according to wind power data from different sites. Moreover, we analyzed power fluctuation difference between single wind machine and the whole wind power plant.

All data used in this paper came from 20 wind machines in a wind power plant of Jilin City, sampling time was Sep., 2013.

1 Probability distribution of fluctuation characteristics in wind power

This paper described fluctuation of wind power by step change, we fitted frequency distribution histogram of step change of wind power on the basis of fitting toolbox provided by MATLAB, and results were shown as below:

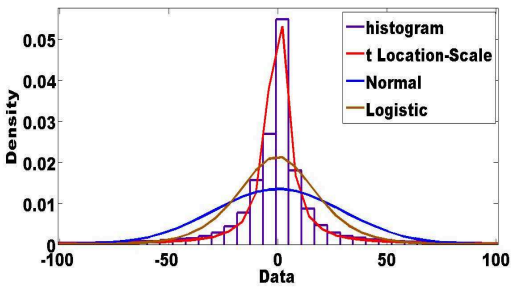

We can see directly fitting effect in t location-scale is the best.

The purpose of choosing different types of PDF is making fitting PDF close to probability distribution histogram as much as possible. For performing quantitative comparison to fitting effect of each distribution function and defining fitting offset index, we have:

$$I = \sum_{i=1}^{M} (y_i - \overline{N_i})^2, y_i = f(\overline{C_i}) \quad (1)$$

In this equation, $i = 1, 2...M$, M is the group number of probability distribution histogram, $\overline{N_i}$、$\overline{C_l}$ represents the height and central position of No. i Histogram, f is the fitting probability distribution function, y_i is the corresponding value of the fitting probability density function at the central position $\overline{C_i}$. The smaller the fitting offset I is, the more accurate the fitting is. Figure 1 is fitting index of different probability density function

Chart 1 Different fitting offset of wind machines each second

distribution pattern	index value
t location-scale	0.0276
Normal	0.0442
Logistic	0.039

We can see t location-scale has the smallest fitting offset, which means it is more appropriate to describe step change distribution.

2 Effect of different time scale towards wind power fluctuation

We calculated probability distribution parameter of wind machine based on sampling interval 5s and 1min respectively according to measured data, results were showed as below:

Chart 2 Probability distribution parameter of wind machine based on different sampling interval

Wm No.	Interval 5s				Interval 1 min			
	μ	σ	ν	95%CI /pu	μ	σ	ν	95%CI /pu
1	-0.141	4.964	0.916	0.784%	-0.374	11.682	0.702	28.19%
5	-0.148	5.260	0.910	0.846%	-0.321	12.879	0.727	27.44%
6	-0.110	4.410	0.844	0.873%	-0.171	9.000	0.632	32.64%

Remarks: 95%CI/pu means percentage of maximum step change from installed capacity will be a per unit value when confidence interval is 95%.

By analyzing figure 2, we can see that scale parameter σ appeared to be rising with the enlargement of sampling interval, maximum range of step change of wind machine's output power increased under confidence interval 95%, namely fluctuation increased.

Reasons for above situation are: wind speed has correlation with time. The shorter the time interval is, the closer the correlation with wind speeds between these two time intervals is. The change of wind speed between these two time intervals is small that is why the variation of wind power between these two time intervals is small as well. Correlation with wind speed decreased when time interval increased, so step change between these two time intervals maybe big.

We introduced average power equation in order to analyzing effect of time scale towards power fluctuation of wind machine further.

$$P_i^{av} = \frac{1}{N} \sum_{t=(i-1)N+1}^{iN} P_t \quad (2)$$

In the equation, P_i^{av} is the average power during No. i period, N is the length of time interval, P_t is the actual average power in No. t minute, L is the total amount of time interval. Below equation defined average power variation:

$$\Delta P_i^{av} = P_i^{av} - P_{i-1}^{av} \quad (3)$$

Because capacity is the integration of power and time, output capacity of wind power plant is the product of average power and time interval in each period, fluctuation of average power represents the capacity fluctuation of the wind power plant.

Figure 2 and 3 are fitting results of average power variation under time interval 5s and 1min respectively. With the enlargement of time interval, probability of average power variation increased greatly.

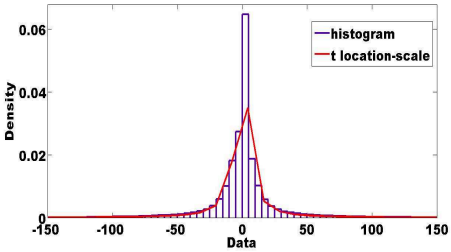

Figure 2 Variation fitting results of average power under 5s.

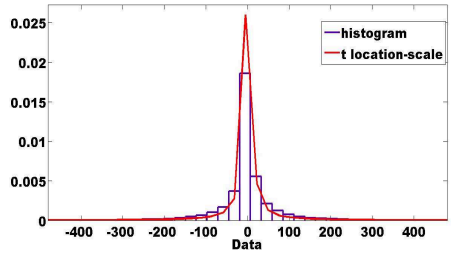

Figure 3 Variation fitting results of average power under 1min

In conclusion, when we replace $P_i^{5s}(t_k)$ with $P_i^m(t_k)$, fluctuation information between 5s to 1min will be lost. Original correlated information can not be used under this circumstance, and step change of corresponding time interval will be overestimated, in probability density distribution parameter, scale parameter will be larger, maximum range of output power from wind machine will be enlarged as well.

3 Effect of spatial scale towards wind power fluctuation

We calculated probability density distribution parameter of single wind machine and the whole wind power plant under sampling interval 1min, results were shown as below:

Chart 3 Probability distribution parameters of single wind machine and 20 wind machines

	μ	σ/*pu*	ν
single WM 1min	-0.373965	0.00779	0.702126
the whole WMs 1min	-5.0691	0.00538	1.38127

Based on chart 3, figure 4 and 5,we can see that the maximum output power of wind power plant decreased with the enlargement of spatial scale, which means more then one wind machines inhibited fluctuation of output power per minute. Fluctuation of wind power alleviated and resulted in *smooth effect*.

4 Power fluctuation comparison between single wind machine and the whole plant

Horizontal axis represented time, we chose 7 to 9 (three days in a month) as research time, main differences between power of single wind machine $P_i^m(t_k)$ and the whole wind power plant $P_\Sigma^m(t_k)$ in time sequence were shown as figure 4 and 5:

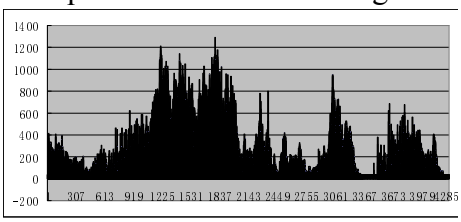

Figure 4 Output power sequence of single wind machine in 7 to 9（three days）

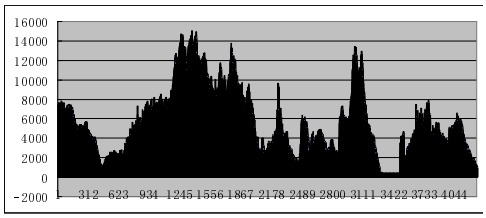

Figure 5 Output power sequence of wind machine group in 7 to 9(three days)

Curve shapes were almost the same by comparing figure 6 and 7, correlation coefficient of these two sequences was 0.906 by analyzing them based on SPSS, they were significantly correlated. Main differences between them were fluctuation of single wind machine was more obvious while wind machine group was more smooth, which meant that wind machine group had smooth effect on the fluctuation of output power, fluctuation of large scale wind power decreased while fluctuation of single machine increased in proportion.

Summary

On the basis of above analysis, t location-scale can describe fluctuation characteristics of wind power better from probability distribution. With the enlargement of time scale, fluctuation of wind power goes higher. With the enlargement of spatial scale, the maximum output power of wind power plant goes lower, then fluctuation of wind power goes smoother and smooth effect appeared. Fluctuation of single wind machine is more obvious than fluctuation of more than one wind machines, fluctuation of large scale wind power decreased while fluctuation of single machine increased in proportion.

References

[1] Reigh A. Analysis of wind generation impact on ERCOT ancillary services requirements[R]. New York: GE Energy, 2008.

[2] Papaefthymiou G, Klöckl B. MCMC for wind power simulation[J]. IEEE Trans. on Energy Conversion, 2008, 23(1): 234-240.

[3] Chen P, Pedersen T, Bak-Jensen B, et al. ARIMA-based time series model of stochastic wind power generation [J]. IEEE Trans. on Power Systems, 2010, 25 (2): 667-676.

[4] Dingming, Wu chunyi, Zhang lijun, Study on algorithm of probability distribution parameter of wind speed in wind power plant [J], proceedings of the CSEE, 2005,25(10):107-110.

[5] Carta J, Ramírez P, Velázquez S. A review of wind speed probability distributions used in wind energy analysis [J]. Renewable and Sustainable Energy Reviews, 2009, 13(5): 933-955.

[6]Zhang jietan,Cheng haozhong,Yao liangzhong etc., study on siting and sizing of distributed wind generation [J], proceedings of the CSEE, 2009, 29(16): 1-7.

[7] Villanueva D, Pazos J L, Feijóo A. Probabilistic load flow including wind power generation[J]. IEEE Trans. on Power Systems, 2011, 26(3): 1659-1667

[8]Lin weixing, Wen jinyu, Ai xiaomeng, Cheng shijie, Li weiren, probability distribution analysis on the fluctuation characteristics of wind power[J], proceedings of the CSEE, 2012,01:38-46+20.

Advanced Materials Research Vols. 989-994 (2014) pp 1260-1263
© (2014) Trans Tech Publications, Switzerland
doi:10.4028/www.scientific.net/AMR.989-994.1260

Partial Discharge Characteristics Research Based on RVM

Yueheng Meng [1, a], Huiqi Li [1, b], Yang Hu[1, c]

[1]School of Electrical and Electronic Engineering, North China Electric Power University,

Baoding, Hebei, 071000, China,

[a] 526622717@qq.com, [c]460378470@qq.com

Keywords: partial discharge; pattern recognition; feature extraction; RVM.

Abstract. In this paper, four original full typical UHF partial discharge signals are measured by using log-periodic antenna in 3-meter anechoic chamber environment. The relevance vector machine is applied for the study of partial discharge characteristics and the two relevance vector machine classifier are applied for the classification and identification of four partial discharge models. The experimental results are satisfactory. Compared with support vector machines, relevance vector machine can obtain more sparse classification model with probabilistic output value. It has a shorter test time and is more suitable for online testing. This method has a good prospect in partial discharge pattern recognition and online monitoring.

Introduction

Partial discharge is to evaluate network equipment insulation condition and to discover the main basis for a potential run risks. 80% network equipment failures are caused by its own insulation deterioration. Partial discharge is the main cause of the deterioration of the insulation and it also can be used as a reference for effectively reflect the true degree of insulation inside the equipment deterioration[1]. Experimental results show that different defect types have different partial discharge signals UHF spectrum characteristics can be detected by the UHF signal to thereby determine the characteristics of the partial discharge induced defect types[2-4]. Relevance vector machine (RVM) with low computational complexity can get a probabilistic sparse kernel-based solutions for the output, and the test time is shorter and more suitable for online testing.

This paper applies the relevance vector machine for partial discharge characteristics and conduct classification of four typical models of partial discharge through three binary RVM classifiers. The experimental results show that compared with SVM, RVM output can be obtained with a more sparse classification model values and have a shorter time and better predict generalization performance.

RVM application of partial discharge

Experimental data collection

In the 3-meter anechoic electromagnetic compatibility laboratory environment in North China Electric Power University, the dark interior of the flexible sheet broadband electromagnetic wave absorbing materials can be effectively reduced due to a variety of test results reflecting walls and ensure the impact of the multipath effect and the integrity of the original experimental data. Designed and produced a needle plate discharge, internal discharge, suspended discharge, surface discharge four typical discharge shown in Figure 1 to Figure 4.

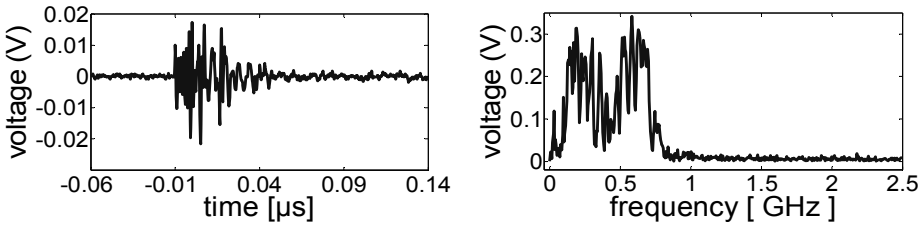

Fig. 1 Time-domain and frequency-domain figures of internal discharge model

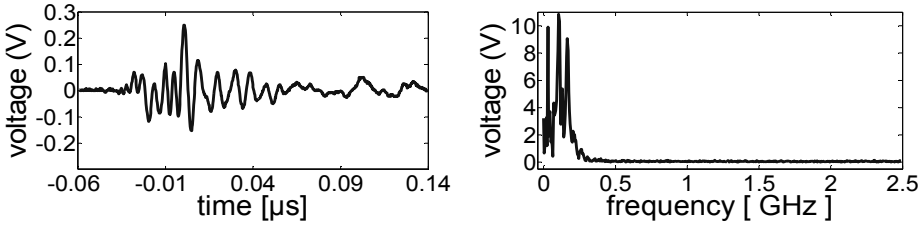

Fig. 2 Time-domain and frequency-domain figures of suspended discharge model

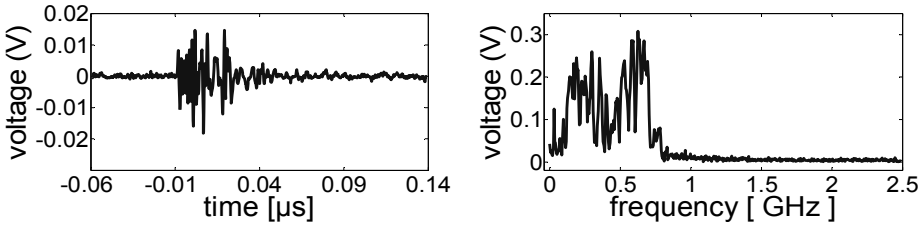

Fig. 3 Time-domain and frequency-domain figures of surface Discharge model

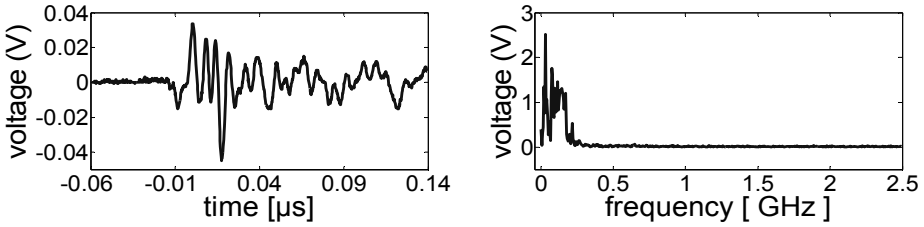

Fig, 4 Time-domain and frequency-domain figures of needle plate Discharge model

Feature amount extraction

By Figure 1 to Figure 4 analyzes available, each type has a different discharge characteristics of the distribution for each type of discharge were extracted from 120 groups discharge signal for statistical analysis, select the rise time, peak bandwidth broadband and frequency distribution. 9 kinds RVM classified as a feature quantity input. 9 kinds of feature quantities of four 10kV discharge voltage value in the model as shown in Table 1.

Tab. 1 Characteristic quantity of four partial discharge models

Rise time	Peak value	Maxima	Band Width	Frequency distribution				
10.39	0.02	0.04	0.79	0.59	0.64	0.63	0.52	0.18
29.37	0.25	0.40	0.23	0.11	0.04	0.17	0.14	0.08
10.19	0.02	0.03	0.95	0.64	0.59	0.63	0.67	0.31
2.00	0.04	0.09	0.21	0.04	0.14	0.09	0.16	0.12

Partial discharge classification based on RVM

In this paper, the four binary classification problem into law three two classification problems, the design of the three binary RVM classifier, the distribution model based on four characteristics of the discharge volume, followed by discharge to distinguish the needle plate, suspended discharge, surface discharge and internal discharge model . Classification system schematic shown in Figure 5.

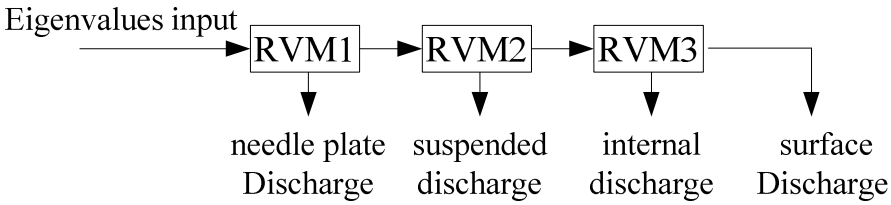

Fig. 5 Taxonomy schematic diagram

To avoid skewed data problem, 80 groups data selected randomly from 120 groups of each type experimental data as training data set and the remaining 40 groups as forecast data set. RVM is no limit on the kernel function. The common kernel functions have polynomial kernel function, sigmoid kernel function and RBF kernel function, which are defined as follows.

- Polynomial kernel function: K(xi,xj)=(γxiTxj+r)d, γ>0.
- S-type kernel function: K(xi,xj)=tanh(γxiTxj+r), γ>0.
- RBF kernel function: K(xi,xj)=exp(-γ||xi-xj||)2, γ>0.

Existing literature show that the study of partial discharge characteristics based on nu-SVC already has a higher classification accuracy. RVM and nu-SVC are applied for the classification and identification of partial discharge and are compared each other. The optimal parameters, like c=2, g=1, are obtained by cross validation of nu-SVC. The comparison of classification performance when RVM1 and SVM1 classifiers adopt different kernel functions is shown in Table 2.

Tab. 2 RVM1 and SVM1 performance based on different kernel functions

Kernel Function	Vector Number		Test Time		Identify correct rate	
Classifier	RVM1	SVM1	RVM1	SVM1	RVM1	SVM1
Polynomial kernel	23	35	0.033	0.156	92.5	95.0
S-type kernel	25	38	0.038	0.118	95.0	95.0
RBF	18	31	0.029	0.127	97.5	97.5

Through the analysis of the data in Table 2 can be seen that the use of RBF kernel function has higher final classification accuracy. The RBF kernel function is applied for three binary RVM classifier of system and the training data of the four discharge model conduct classify learning. RBF kernel function parameters are taken as 2. The classification of the four partial discharge model predicting data after the three dichotomous RVM classifier learning is shown in table 3.

Tab. 3 Four partial discharge model predictions based on RVM

Discharge Model	Associated Vector Number	Test Time	Identify correct rate
needle plate discharge	18	0.027	97.5
suspended discharge	17	0.025	97.5
internal discharge	18	0.024	92.5
surface discharge	18	0.027	87.5

As can be seen from Table 3, when classify 160 groups forecast data (40 for each type of group) classification, RVM1 and RVM2 can turn a good identification of the needle plate discharge and the suspended discharge and the classification accuracy is satisfactory. When RVM3 is used to identify the surface discharge and internal discharge, its recognition accuracy is slightly lower relative to the first two discharge model due to the similar discharge mechanism of the later two discharge model, but the effect of distinguish is relatively good .

RVM algorithm analysis

The classification and identification of partial discharge based on RVM has a high recognition rate and has the similar classification accuracy compared with the SVM. Through the calculation by the computer program, the trend of associated vector number changed along with the increasing number of iterations based on RVM1 shown in Figure 6.

As can be seen from Figure 6, when the super-parameters ultimately meet the convergence conditions after the end of learning, only 18 associated vectors play a decisive role and the decreasingly irrelative vectors greatly reduce the calculation of kernel function during the learning process of RVM. Therefore, compared with SVM, RVM has a shorter test time during data prediction and is more suitable for online testing. The set of 160 groups of prediction data under 10kV voltage into the system can be obtained the output of a specific probability value. Eight existing groups (tow group of each type) of the output results are listed below.

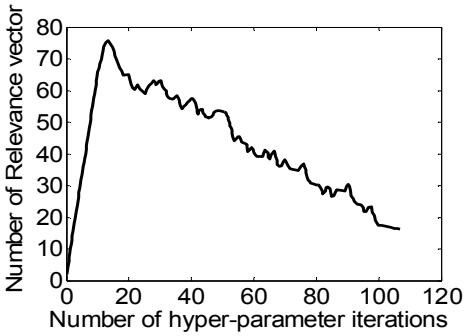

$$P = \begin{bmatrix} 0.9884 & 0.0039 & 0.0039 & 0.0039 \\ 0.9485 & 0.0172 & 0.0172 & 0.0172 \\ 0.0461 & 0.9277 & 0.0131 & 0.0131 \\ 0.0226 & 0.9428 & 0.0173 & 0.0173 \\ 0.0940 & 0.0940 & 0.4777 & 0.3343 \\ 0.2313 & 0.2313 & 0.3024 & 0.2350 \\ 0.0155 & 0.0155 & 0.1471 & 0.8219 \\ 0.0442 & 0.0442 & 0.2624 & 0.6493 \end{bmatrix}$$

Fig. 6 Associated vector machine changing trend

Conclusions

- Original full UHF signals are obtained by experiments of four discharge models and its feature values are extracted. Results can taken as references of partial discharge measurement data obtained under other conditions.
- In this paper, RVM algorithm is applied for the classification and identification of UHF signals of partial discharge. The probability output value on four models can provide effective numerical basis for the further field test.
- Compared with SVM, RVM has the equivalent classification accuracy, but has less associated vectors and lower computational complexity. So RVM has a shorter test time and is more suitable for online test.

References

[1] Jun Guo, Guangning Wu, Wen Shu. Status partial discharge detection technology and development [J]. Electro technical Society, 2005, 02 :29 -35.

[2] Xiaohui Zhao, Xuli Lu, Jinggang Yang, et. al. UHF method in transformer partial discharge detection [J]. High Voltage Engineering, 2007, 08 :111 -114.

[3] Caixin Sun, Gaofeng Xu, Ju Tang, et. al. GIS partial discharge pattern recognition method to box dimension and information dimension to identify characteristic quantities [J]. Chinese Society for Electrical Engineering, 2005, 03 :102 -106 .

[4] Zhirong Wu, Dexin Nie, Jiangbo Chen. UHV transformer partial discharge test analysis [J]. High Voltage Engineering, 2010, 01: 54 -61.

Advanced Materials Research Vols. 989-994 (2014) pp 1264-1268
© (2014) Trans Tech Publications, Switzerland
doi:10.4028/www.scientific.net/AMR.989-994.1264

Regional water resource utilization evaluation and influential factors analyses

WANG You-ying[1, a], HU Xiao-ping[1, b]

[1]SHU-UTS SILC Business School, Shanghai University, Shanghai 201800, China

[a]chenyoudy@126.com, [b]hxpjohn@163.com

Keywords: Water use efficiency, Water resources carrying capacity, Data Envelopment Analysis

Abstract: Water resource, as a kind of important economic and natural resource, plays a vital role in sustainable development of society. Currently, global water resources situation is increasingly severe, especially in China. The water resource distribution in China is uneven with low efficiency and pollution problem. Based on a full analysis of research actuality in China and abroad, this article explores water use efficiency and input redundancy of 31 provincial regions in China for the year of 2011. Reasonable indexes are chosen to evaluate the efficiency based on advanced DEA for helping establishing future policies.

1. Introduction

Water resource is the most basic natural resource for creatures, and as the organic composition of comprehensive national strength, it is also vital for manufacture activities of human beings. Water resource in China has following features. Firstly, total amount is huge while amount per capita is scanty. Secondly, its spatial distribution is uneven. Thirdly, some areas are suffering lacking in water. Furthermore, there are some problems in water utilization. Serious pollution, overuse of ground water and imperfect management all pose a threat on its sustainability. However, inefficient use of water resource is the most urgent matter, which has become the bottleneck of sustainable development in China. For this reason, this article focuses on establishing effective evaluation model for water use efficiency and conducting data analyses to figure out related influential factors. And then, reasonable solutions and advices are provided for future management policies.

2. Literature Review

Some literatures stated the utilization situation of water resource globally. William Relly, former U.S. Director of Environmental Protection, pointed out, over half of water had been wasted worldwide [1]. Firstly, how to evaluate efficiency should be researched. Liu [2] pointed out that, water use efficiency in its broadest sense contains economic, societal and ecological benefits created by water utilization; however, it simply means economic benefits in the narrow sense. Li [3] believed that, the efficiency rule of sustainable water use is to obtain maximum efficiency. In terms of assessment indicators selection, it can be conducted from various aspects (e.g., water use of different regions and different industries). Ma [4] compared water use efficiency of China with that in some developed countries and predicted the water use tendency of China. Li [5] researched and compared water use efficiency in three regions of China (i.e., the east, the middle and the west) and found that the gap of regional economic development level was the most significant factor that determined differences in regional water use efficiency and the relation between them was negative. Based on stochastic frontier approach (SFA), Zhu [6] established industrial water use calculation model and applied technical indicators to evaluate industrial water use efficiency in China from the year of 1953 to 2004, and found the tendency of steady growing. Speaking of the evaluating method, the most popular one is data envelopment analysis (DEA). These methods can be separated into two groups: single factor evaluation and total factor evaluation. The former focuses on the ratio of output and input [7-8], and the latter considers combination of total production factors [9]. However, current researches still have some limitations in distinguishing expected and unexpected output when establishing evaluation model. It is what we can do to improve.

3. Evaluation on Water Use Efficiency

3.1 Evaluation on the base of advanced DEA

Water resource production structure, consisting of inputs, production process and outputs, should be understood before assessing water use efficiency. Based on advanced DEA, This article conducts

total factor analysis, i.e., the input elements contain water use amount, labour and capital, and the output elements are GDP and wasted water. All necessary data about 31 provincial areas (decision making units) comes from Statistic Yearbook of China in 2012. Using Matlab to establish model, we calculate water use efficiency. Furthermore, according to (1), the corresponding water-saving amount is figured out. The decision-making object of the model is minimal amount of water use and wastewater simultaneously. The details are shown in Table 1.

Water-saving amount=Water use amount*(1-water use efficiency) (1)

TABLE 1 Water Resource Input, Output, Water use efficiency, and water-saving amount

city		Input			Output		Model efficiency	Amount of water conservation based on model(Million Cubic Meters)
		water use amount (Million Cubic Meters)	employment figure (ten thousand)	fixed-asset investment (hundred million)	GDP (ten thousand yuan)	Wastewater emissions (ten thousand yuan)		
Eastern region	Beijing	35.2	558.8	5578.9	16251.93	145469	1.000	0.00
	Tianjin	22.5	145.3	7067.7	11307.28	67147	1.000	0.00
	Hebei	193.7	626.2	16389.3	24515.76	278551	0.649	68.02
	Liaoning	143.7	767.0	17726.3	22226.70	232247	0.708	41.92
	Shanghai	126.3	660.7	4962.1	19195.69	214155	1.000	0.00
	Jiangsu	552.2	2125.1	26692.6	49110.27	592774	0.648	194.21
	Zhejiang	203.0	1479.5	14185.3	32318.85	420134	0.641	72.87
	Fujian	202.5	583.3	9910.9	17560.18	316178	0.431	115.20
	Shandong	222.5	1280.7	26749.7	45361.85	443331	0.784	48.03
	Guangdong	469.0	1670.8	17069.2	53210.28	785587	1.000	0.00
	Hainan	44.4	103.9	1657.2	2522.66	35725	0.516	21.45
	Total	2215.0	10001.3	147989.2	293581.5	3531298.0	0.760	561.70
Central region	Shanxi	63.8	317.9	7073.1	11237.55	116132	0.726	17.50
	Jilin	120.0	363.7	7441.7	10568.83	116162	0.660	40.84
	Heilongjiang	325.0	442.6	7475.4	12582.00	150661	0.639	117.33
	Anhui	293.1	598.5	12455.7	15300.65	243265	0.452	160.51
	Jiangxi	239.1	598.5	12455.7	15300.65	243265	0.432	136.08
	Henan	224.6	802.8	17769.0	26931.03	378785	0.527	106.28
	Hubei	288.0	779.1	12557.3	19632.26	293064	0.469	145.06
	Hunan	325.2	685.8	11880.9	19669.56	278811	0.532	152.05
	Total	1878.8	4588.9	89108.8	131222.5	1820145.0	0.560	875.65
Western region	Inner Mongolia	181.9	301.5	10365.2	14359.88	100389	1.000	0.00
	Guangxi	301.6	433.9	7990.7	11720.87	222439	0.379	187.19
	Chongqing	86.4	443.8	7473.4	10011.37	131450	0.563	37.79
	Sichuan	230.3	795.0	14222.2	21026.68	279852	0.551	103.51
	Guizhou	101.4	215.9	4235.9	5701.84	77927	0.524	48.30
	Yunnna	147.5	514.1	6191.0	8893.12	147523	0.438	82.90
	Xizang	35.2	46.0	516.3	605.83	4635	0.914	3.03
	Shanxi	83.4	388.3	9431.1	12512.30	121815	0.758	20.22
	Gansu	121.8	205.9	3965.8	5020.37	59232	0.593	49.64
	Qinghai	30.8	64.5	1435.6	1670.44	21292	0.558	13.61
	Ningxia	72.4	95.1	1644.7	2102.21	39432	0.373	45.40
	Xinjiang	535.1	171.5	4632.1	6610.05	83329	0.562	234.31
	Total	1927.8	3675.5	72104.0	100235.0	1289315.0	0.600	825.90

Table 1 shows there are huge differences in water use efficiency between 31 provincial areas. Considering the optimal water use amount and wastewater amount, five areas (i.e., Beijing, Tianjin, Shanghai, Guangdong, and Inner Mongolia) are efficient in DEA. Although not in the developed eastern region, Inner Mongolia is efficient in DEA because of its matched input and output of water and relatively perfect wastewater treatment system. Overall, the water use efficiency in eastern China is higher than that in the west and midland. As for water-saving amount, surprisingly, Gansu which suffers most severe water shortage has highest water-saving amount (49.64), presenting highest potential in saving water and highest urgency in improving current saving technology. In addition Fujian, as an eastern coastal area, has very low water use efficiency (0.431), which reflects its low-efficient wastewater treatment to some extent.

3.2 Correlation between GDP, water use amount (W) and wasted water amount (WW)

Here, GDP/W, WW/GDP and WW/W are used to analyse the correlation with water use efficiency in model. Firstly, we use (2) to standardize three ratios. And MAX and MIN represent the maximum and minimum respectively. According to table 2, GDP/W and WW/W are both positively relative with water use efficiency (Pearson correlation are 0.658 and 0.388).

$$x^*=(x-MIN)(MAX-MIN) \quad (2)$$

TABLE 2 Pearson correlations

	GDP/W	WW/GDP	WW/W	Model efficiency
GDP/W	1	-0.236	0.924**	0.325
WW/GDP	-0.236	1	0.061	-0.658**
WW/W	0.924**	0.061	1	0.146
Model efficiency	0.325	-0.658**	0.146	1

*at the level of 95% significance,
**at the level of 99% significance

4. Analysis on Influential Factors

4.1 Influential Factors Selection

It emphasizes economic, social, natural factors and water use conditions to select indicators. *Economic factors*: Resource is important to promote sustainability of economy. Per capita GDP and the proportion that investment of fixed assets accounts in GDP are selected. *Social factors*: Social factors are also closely related to water resource efficiency, such as technical factors, demographic factors and policy management, etc. Thus, regional education expense per capita is selected as social factor. *Natural factors*: Regional water resource amount is various due to differences in regional rainfall. Here, per capita water resource is selected as natural factor. *Water use conditions*: Water use patterns include domestic, industrial, agricultural and ecological water. Life water consumption per capita, agricultural use water ratio, proportion of industrial water consumption, water resources exploitation and utilization are chosen as water use conditions factors.

4.2 Influential Factors Analysis

4.2.1 Regression Analysis of Water Resource Efficiency Factors in Eastern Region

SPSS.20 is tool used to conduct analyses. The results of the regression analysis of water resources efficiency factors in eastern region are shown in table 3 and the results are processed with the independent variable backward selection method.

TABLE 3 Coefficients

Model	Unstandardized Coefficients		Standardized Coefficients	t	sig
	B	Standard error	Trial version		
constant	0.218	0.172		1.271	0.260
per capita GDP	2.060E-005	0.000	1.838	4.314	0.008
education expense per capita	0.000	0.000	-1.247	-2.814	0.037
life water consumption per capita	0.008	0.003	0.838	2.701	0.043
proportion of industrial water consumption	-1.924	0.545	-1.567	-3.530	0.017
water resources exploitation and utilization	0.120	0.054	0.808	2.229	0.076

From table 3, it is concluded that water resource efficiency has a great relevance with per capita GDP, life water consumption per capita, proportion of industrial water consumption, water resources exploitation and utilization. There is positive correlation between per capita GDP and water resource efficiency, which means that the demand of water resources increases with the economic development. The regression coefficient of life water consumption per capita (0.008) means the water is recycled and wastewater is reduced. While the regression coefficient of proportion of industrial water consumption is -1.924, it means the more use of the industrial water, the lower of the water resource efficiency.

4.2.2 Regression Analysis of Water Resources Efficiency Factors in Western and Central Regions

Similarly, the western and central regions are analysed. For the central part, the negative regression coefficient of per capita GDP means the waste water management and water circulation use are neglected. The coefficient of the proportion that fixed assets accounts in GDP (-0.586) shows that it lacks infrastructure in waste water treatment. Education expense per capita and agricultural use water ratio are positively correlated with water resource efficiency. Therefore, high level education and more agricultural water use can improve efficiency. For the western region, only per capita GDP and per capita water resource have positive correlation with water resource efficiency. It concludes that wastewater and people care wastewater and cherish usable water due to lack.

5. Conclusions and Advices

Based on previous literatures, evaluation model of regional water resource efficiency is built. The east has the highest water use efficiency while the west has the lowest one. The regression analysis is used to analyse influential factors (economic, social, natural factors and water use conditions). For the east, per capita GDP, life water consumption per capita, proportion of industrial water consumption, water resources exploitation and utilization have a significant effect on water resources efficiency. There is positive correlation between the education expenses per capita, agricultural use water ratio and water use efficiency in central region. While per capita GDP and the proportion that fixed assets accounts in GDP have a negative relation with water resources efficiency. As for western region, only per capita GDP and per capita water resource have positive correlation with water resource efficiency.

After analysing, some advice is put forward. For the east, advocacy of saving water needs to be enhanced and financial and technical support should be given to the backward area. For the central region, it should increase investment in infrastructure and strengthen the management of wastewater discharge and water recycling. Waste in agriculture should be reduced in western region. This article still has many deficiencies. Ecological water use and benefits are not studied. Furthermore, the division of regions has some problems due to uneven distribution of water resources and unbalanced economic development. More researches in this field are called for in future.

Acknowledge:
This research is financially supported by Creative Activity Plan for College Students, named “Urban water resource use efficiency evaluation and related influential factors analyses”.

References:

[1] J M. Harris, et al, "Carrying capacity in Agriculture: Globe and regional issue," *Ecological Economics*, vol. 129, no. 3, pp. 443-461, 1999.

[2] Q S. Liu, "Research on water use efficiency in Zhejiang Province," *Water Economy*, no. 3, pp. 28-30, 2010.

[3] X S. Li, "Discussion on fairness and efficiency of the sustainable use of water resource," *Ecological Economy*, no. 12, p. 13, 2001.

[4] J. Ma, T. Chen, B F. Shen, and D X. Wang, "Comparison of water use and development trends at home and abroad," *Technology Advancement of Water Resources and Hydropower*, no. 2, pp. 6-10, 2007.

[5] S X. Li, J H, Cheng, and Q S. Wu, "Analyses on regional differences of water use efficiency in China," *China Population, Resources and Environment*, vol. 18, no.31, 2008.

[6] Q R, Zhu, "An empirical study of Chinese industrial water use efficiency and water saving potential," Industrial Technology Economy, no. 9, pp. 48-61, 2007.

[7] Yong zhou, Lianshui Li, "The action of structure and efficiency on Chinese energy intensity—An empirical analysis based on AWD", Industrial Economics Research, vol 4, 2006.

[8] Dan Shi, "The effect of industrial structure change on energy consumption demand," Economic Theory and Business Management, vol 8, 2003.

[9] J.Hu, S.Wang. "Total-factor Energy Efficiency of Regions in China," Energy Policy, no. 34, pp. 3206-3217, 2006.

Advanced Materials Research Vols. 989-994 (2014) pp 1269-1272
© (2014) Trans Tech Publications, Switzerland
doi:10.4028/www.scientific.net/AMR.989-994.1269

Mineralizaton process of the bauxite in WZD area

Tao Cui

College of Resources and Environmental Engineering, Guizhou Institute of Technology, Guiyang, 550003, China

cuitao1203@163.com

Keywords: WZD area; Bauxite; Mineralizaton process

Abstract: This paper has a comprehensive analysis on mineralizaton process of the bauxite in Wuchuan -Zheng, an-Daozhen (WZD) area, northern Guizhou, China through synthesize former research. Geologic characteristic demonstrates that WZD bauxite is a typical sedimentary deposit, minerogenetic material have experienced a transporting process. Sedimentary environment of WZD bauxite is transition facies. Sedimentary environment is reduced and acidic. Accompanying frequent transgression and regression, bauxite has suffered a leaching process. In the leached period, environment is oxidized and acidic. Leaching process is the most important factor for the information of high grade bauxite. WZD bauxite has experienced several times leaching resulting in the great runoff of Fe and Si. Actually the metallogenetic process of WZD bauxite is a process that Al relative enrichment but Si and Fe runoff.

Introduction

There is abundant bauxite in WZD area. For a long time many experts and scholars have researched on rocks and minerals, chemistry, sedimentary environment, provenance, mineralization age, and mass balance calculation of the bauxite [1-15]. Though there are abundant outcomes of WZD bauxite, analysis on systematical mineralizaton process of the bauxite is poor. This study is to resume mineralizaton process of WZD bauxite according to the research on mineralogy, lithology, geochemistry and sedimentology.

Geological setting

WZD bauxite is located in Wuchuan, Zheng'an and Daozhen County, northern Guizhou, which is an important part of centre Guizhou-southern Chongqing bauxite belt [7]. The regional tectonics position of the study area is in the fold belt in northern Guizhou of the upper Yangtze Block [8]. From the oldest to the youngest, the main strata in WZD area includes Cambrian, Ordovician, Silurian, Permian, Triassic and Jurassic. Cambrian is mainly distributed in the core of anticlines, Triassic and Jurassic are mainly distributed in the core of synclines. Bauxite underlies the LiangShan formation(P2l) or Qixia formation(P2q) in the middle Permian, and overlies the HuangLong formation(C2h) of upper Carboniferous or the Hanjiadian formation of the lower Silurian(S1hj). The bauxite is stratiform and unconformable with the underlying and overlying strata. Fig.1 shows that the distribution of the bauxite is controlled by nine synclines. Thickness of the bauxite is 0.68-15.7m, and its profile can be divided into two lithology parts: the upper part and the lower part. The former is aluminous rock, dominated by high grade bauxite or half grade bauxite; the latter is low grade bauxite. According to the lithological and textural properties, the natural types of bauxite deposit can roughly be subdivided into four categories: massive bauxite, oolithic bauxite, clastic bauxite and earthy bauxite.

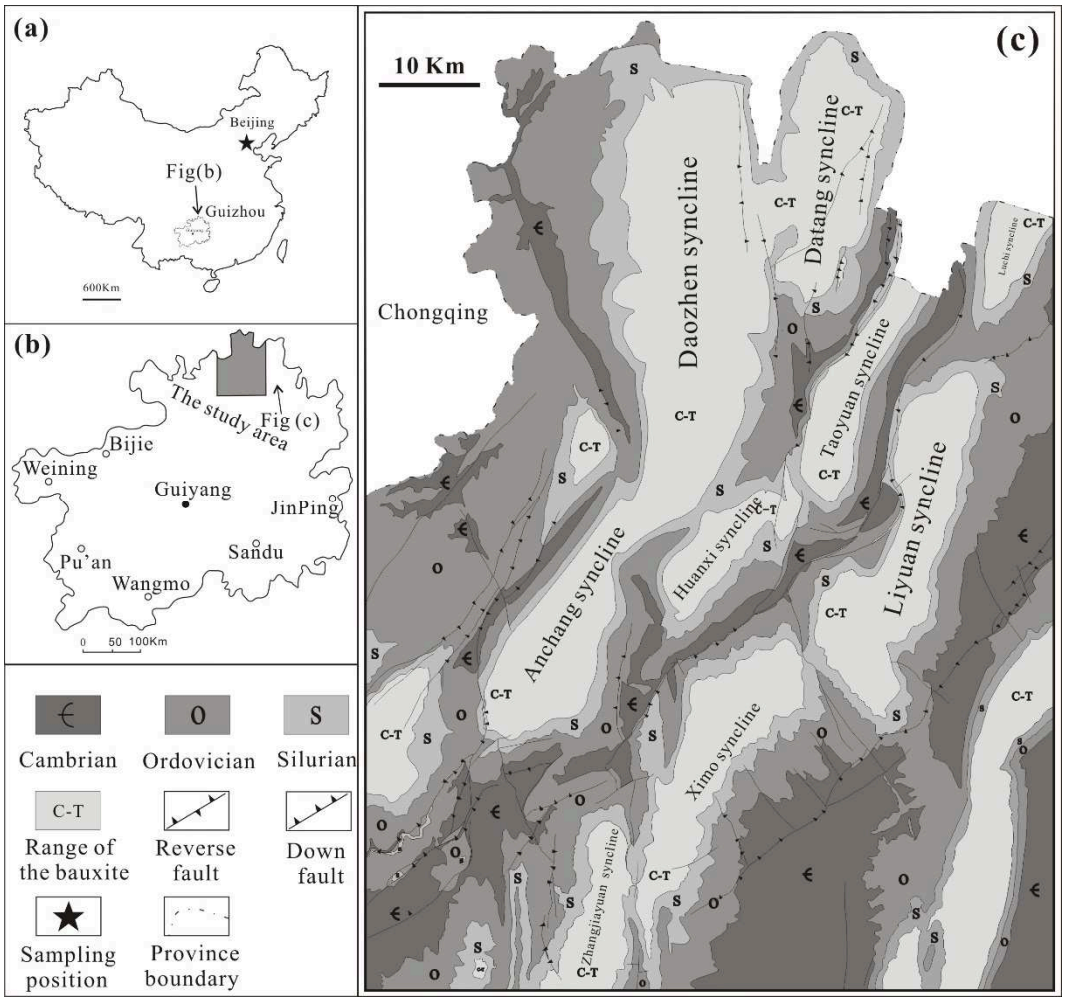

Fig. 1(a) Locality map of Guizhou, (b) The map showing the location of the study area, (c) Geology map of the WZD area in northern Guizhou

Weathering process

Weathering process is the begging of mineralization. Hanjiadian formation and Huanglong formation are the main provenances of WZD bauxite [15]. Late Silurian mud shale of Hanjiadian formation suffered weathering, and this process provided partly materials for bauxite. Lateritization in late Silurian is the earliest lateritization process. From late Silurian to late Carboniferous the study area is suffered weathering and lateritization even superficial part of Hanjiadian formation has a high content of Al relative to conventional mudstone. In late Carboniferous the study area has a high sea level, and it is covered by sea water. Limestone of Huanglong formation is formed in this period. After the formation of limestone, sea level of WZD area decreased resulting in the deposit exposed to earth surface. Rock of WZD area suffered weathering again after the exposed process. At the begging, limestone of Huanglong formation provided metallogenetic materials for WZD bauxite, as weathering process continues, mudshale of Hanjiadian formation suffered the second weathering and provided metallogenetic materials for WZD bauxite including red soil of first weathering.

Transporting process

Mode of transport of bauxite is a puzzle. Main component of WZD bauxite are clay minerals and pelitomorphic diaspore[1-15], and it shows that suspension transport is the main mode of transport of WZD bauxite. The discovery of colloidal structure indicates colloidal transport is one of mode of transport for WZD bauxite. Al is hard to transport by common water because it just can be

dissolved in strong acid or strong base, so many scholars support colloidal transport is an important mode of transport. Through systematically survey and analysis on WZD bauxite we find that mineralizaton process of WZD bauxite is not a sedimentary process of Al. In the transport process clay minerals are main component, and diaspore, boehmite and gibbsite is not the main minerals. In other words, in the transport process bauxite is not formed.

Mode of transport of WZD is complicated，several mode of transport carry metallogenetic materials together but suspension transport is the main transport.

Leaching process

Color, structure, grade and geochemistry of WZD bauxite have a vertical regularity of alternation [6, 15]. Leaching process is the key for the formation of high grade bauxite [15]. Leaching process resulting in the vertical regularity of alternation. Leaching process is happened in penecontemporaneous period. In penecontemporaneous period deposit exposed to earth surface, so in this stage, environment is oxidized and acidic. There are several leaching process in penecontemporaneous period according to the vertical regularity of alternation. Upper part and middle part of WZD bauxite have a great loss of Si and Fe, and it resulting in relative enrichment of Al. Through several leaching process, the high grade bauxite formed at last.

Conclusions

The main conclusions from this study are summarized as follows: 1) Metallogenetic process can be divided into three stages: weathering stage, transport stage and leaching stage; 2) Weathering stage is the begging of metallogenetic process, the study area has experienced two weathering process at least.

3) Suspension transport is the main mode of transport; 4) Leaching process is the last and the most important stage of metallogenetic process, in this stage WZD bauxite had a great loss of Si and Fe. Leaching process results in the vertical regularity of alternation of WZD bauxite.

Acknowledgment

This work was supported by the Guizhou Collaborative Innovation Center of Strategic Minerals Resource Development, Guizhou Institute of Technology and the project of analysis on geochemical behaviors of Platinum group elements in Emeishan basalt（XJGC20131204）, Guizhou Institute of Technology.

References

[1] G.H. Wu, Z.G. Jin, Y. Bao: J.Geology and Prospecting,Vol.44(2008),P.34 (in Chinese)
[2] Z.G. Jin, G.H. Wu, Y.Y. Zhao:J.Mineral Source and Geology,Vol.23(2009),P.139 (in Chinese)
[3] K.H. Yin: J. Acta Sedmentological Sinica, Vol.27(2009),P. 455 (in Chinese)
[4] Z.H. Han: J. Mineral Resource and Geology,Vol.22(2008),P. 430 (in Chinese)
[5] Z.Y. Lei and Y.C. Liao: J. Western Prospecting Engineering, Vol.18(2007), P. 96 (in Chinese)
[6] X.M. Wang, Y.Q. Jiao and Y.S, Du: J. Journal of Geochemical Exploration, Vol. 133(2013), P.108.
[7] P. Liu: J. Guizhou Geology,Vol.18(2004),P. 240(in Chinese)
[8] D.Q. Du, J.P. Ren and Y. Wang: J. Acta Mineralogical Sinica, Vol.23(2007), P.475 (in Chinese)
[9] G. Millot, M. Bonifas: J. Alsace Lorraine,Vol.8(1955),P.15.
[10] J.J. Middleburg, C.H. Van, J.R.W. Woittiez: J.Chen.Geol, Vol.68(1988),P.263
[11] H.W. Nesbitt, G.M. Young:J.Geol,Vol.97(1989),P.135.

[12] I.G. Hill, R.H.G. Worden, I.G. Meighan: J.Chemical Geology,Vol.166(2000),P.166.
[13] J.A. Grant: J.Economic Geology,Vol.81(1986),P.1980.
[14] W.H. Maclean: J. Mineralium Deposita,Vol.25(1990),P.46
[15] T. Cui, Y.Q Jiao, Y.S. D:J.The Chinese Journal of Nonferrous Metals,Vol.24(2013),P.6.(in Chinese)

Advanced Materials Research Vols. 989-994 (2014) pp 1273-1277
© (2014) Trans Tech Publications, Switzerland
doi:10.4028/www.scientific.net/AMR.989-994.1273

Inhibiting Effect of Nonlinear Shielding Layer on Electrical Tree Propagation inside Insulation Layer of High-Voltage Cable

Changming LI[1, a], Baozhong HAN[1, 2, b], Long ZHAO[1, c], Chunpeng YIN[1, d]

[1]Key Laboratory of Engineering Dielectrics and Its Application, Ministry of Education, Harbin University of Science and Technology, Harbin, 150080, China

[2] Far East Holding Group Co. Ltd., Yixing

[b]email:hbzhlj@163.com

Keywords: High-voltage Cable; Cross-linked Polyethylene; Nonlinear Shielding Layer; Electrical Tree

Abstract. Nonlinear insulated materials can uniform electric field distribution in non-uniform electric field. In order to inhibit the electric tree initiation and propagation inside high-voltage cross-linked polyethylene (XLPE) insulated cable, a kind of 220kV high-voltage XLPE insulated cable with new structure is designed by embedding nonlinear shielding layer into XLPE insulation layer of high-voltage cable with traditional structure in this study. Experimental and simulation results indicate that the nonlinear shielding layer can effectively inhibit electrical tree propagation inside the XLPE specimens, and obviously extend the breakdown time caused by electric tree propagation. When the electrical tree propagates into the nonlinear shielding layer sandwiched between insulation layers of cable, the electric field distribution near the tip of electrical tree is obviously improved. These findings prove the feasibility and the effectivity of inhibiting electrical tree propagation inside high-voltage cable by adding nonlinear shielding layer into the insulation layer.

Introduction

Currently, cross-linked polyethylene (XLPE) is often used as insulation in high-voltage cable of up to 220kV. Some XLPE insulation cable of 500kV also has been used in extra high-voltage line. During the application of high-voltage cable, it was found that the electrical tree aging is a leading factor to degradation and failure of XLPE insulation behavior of high-voltage cable. Therefore, the inhibition of electrical tree initiation and propagation inside the high-voltage XLPE cable has received more and more attentions in recent years.

The main causes of electrical tree initiation inside high-voltage XLPE cable include the electrical field concentration at micropore inside insulation layer and impurity/defect at surface of semiconductive shielding layer, and high-energy electrons ejected by conductor wire core [1-3]. Many factors including external electrical field strength and voltage frequency, material temperature, internal stress and assembling form have effect on electrical tree initiation and propagation[4-6]. Some researchers have weakened the effect of defects at surface of semiconductive shielding layer on the cable behavior by adding shielding layer between XLPE insulation and semiconductive layer of cables. This led to a 30% increase in AC breakdown strength of XLPE. Former Soviet Union produced 110kV XLPE insulation cable with shielding layer to prevent charge emission, thus remarkably decreasing the thickness of insulation [7]. Shenyang cable factory and Xi'an Jiaotong University added charge emission shielding layer into the 66kV XLPE insulation cable, and increased the voltage class of the cable up to 110kV in 1992. However, these technologies were not widely used because they have some shortcomings. Currently, cable companies control size and amount of defects inside the high-voltage insulation structure by using ultra-clean XLPE insulation and (ultra) smooth semiconductive shielding materials, applying three-layer co-extrusion technology of inner and outer shielding and insulation layers, using high-pressure nitrogen as heating and cooling medium, and sufficiently degassing of heated cable after extruding shielding and insulation. However, it is impossible to completely avoid the

formation of the defects inside the cable insulation structure, which are hidden troubles to the initiation of electrical tree. The decrease of life-span, even accident of insulation breakdown of high-voltage XLPE insulation cable caused by electrical tree aging happens occasionally.

The electrical conductivity γ of nonlinear dielectric varies with electrical field strength E. The relationship between γ and E can be described as $\gamma = AE^{\beta}$ (where β is a nonlinear coefficient) [8, 9]. This kind of materials has the capability to self-uniform electric field distribution under a non-uniform electric field. Therefore, it has potential to inhibit electrical tree inside high-voltage cable. The authors' research group did a lot of work on nonlinear polymer-based composites, and developed some PE-based composites with excellent nonlinear electrical conductance. Based on the results of previous researches, a high-voltage XLPE insulated cable with new structure is designed by adding nonlinear shielding layer into the conventional high-voltage XLPE insulated cable in this paper. The inhibiting effect of nonlinear shielding layer on propagation of electrical tree inside XLPE insulation of high-voltage cable is investigated through experiments and numerical simulation.

Materials and Experimental Methods

Materials and Specimen Preparation

The raw materials used include crosslinkable PE (XLPE, 4201 SC) for high-voltage cable and nonlinear crosslinkable PE-based insulation composite. When the external electrical field strength E is below 2.99×10^{6}V, the electrical conductivity γ of nonlinear insulation composite is 1.56×10^{-15}S/m. When E is higher than 2.99×10^{6}V, composite presents nonlinear electrical conductance behavior and $\gamma = 10^{-36.99} E^{3.43}$S/m.

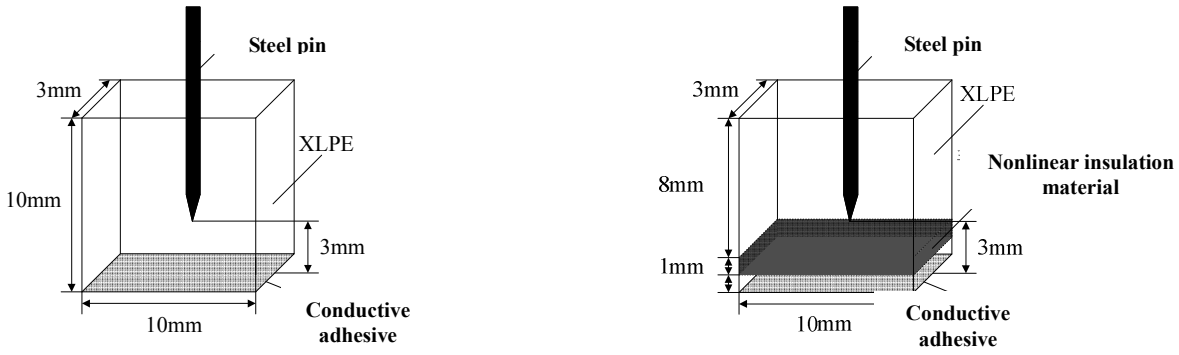

a) Plain XLPE b) XLPE with nonlinear shielding layer

Fig. 1 Test of electrical tree initiation of specimens

The preparation process for specimens of plain XLPE is as following. Step 1: press XLPE into plate specimens of 100mm×100mm×10mm by using the plate vulcanization machine and crosslink for 20 minutes at a temperature of 348K; Step 2: cool the specimens and cut them into the size as shown in Fig.1 (a); Step 3: insert steel pin into the specimens with tip top angle of 30° and curvature radius of 5μm; Step 4: put the specimens into an evacuated container and degas for 48 hours; Step 5: paint conductive adhesive at bottom of the specimens, and then put them into a drying cabinet to ensure curing of conductive adhesive; Step 6: keep the specimen at room temperature for 24 hours before the experiments on electrical tree initiation.

Test methods

Testing system for the electrical tree initiation is shown in Fig.2. The output AC voltage of the transformer used in the testing is continuously adjustable in the range from 0 to 50000V. The voltage between needle-plate electrodes is continuously raised up to its setting value at a rate of 1kV/s by adjusting the transformer. The electrical tree propagation is observed with a picture pick-up system. During the observation, the voltage is kept at its setting value.

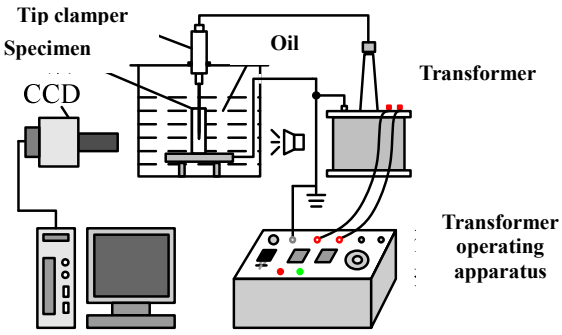

Fig. 2 Picture pick-up analysis system for electrical tree initiation

Results and Discussions

Inhibiting effect of nonlinear shielding layer on electrical tree propagation

The specimens as shown in Fig.1 a) and b) are used to perform the experiment on electrical tree initiation. Each group of specimens contains ten samples. The high voltage AC is applied to the steel pin and the grounded pole plate in the experiment to ensure initiating electrical tree quickly. The situation of electrical tree propagation for different specimens is shown in Table 1, and the typical electrical tree morphology is given in Fig.3.

Table 1 Situation of electrical tree propagation inside specimens

Voltage (kV)	Type of specimens	
	XLPE specimens	Three-layers compound specimens
20	Breakdown time in the range from 5min to 2h	No breakdown in 24h
25	Breakdown time in the range from 10s to 10min	Breakdown over at least 13h

It can be seen from Table 1 that the electrical tree in the XLPE specimens grows up very fast. It quickly expands from the pin tip to the grounded pole plate, thus causing the specimen breakdown. The breakdown time of the specimens with nonlinear shielding layer is remarkably longer than that of the plain ones. As shown in Fig.3, the nonlinear shielding layer effectively inhibits the propagation of electrical tree from the pin tip to the grounded pole plate. This is because that when the tips of electrical tree grows near the nonlinear shielding layer, especially electrical tree reach the nonlinear shielding layer, the electrical conductance of high performance nonlinear insulation materials varies with change of electrical field strength at the tip of electrical tree, which leads to homogenization and improvement of electrical field distribution at the tip of electrical tree. Here we compare the distribution of electrical field of specimens with and without electrical tree propagation through numerical simulation.

a) Plain XLPE b) XLPE with nonlinear shielding layer

Fig.3 Typical electrical tree morphology

The electrical field distribution at the pin tip of specimens is illustrated in Fig. 4 when no electrical tree propagates. As shown in this figure, the maximum electrical field strength in the two types of specimens is almost the same, and they are so high that electrical tree can be quickly initiated. In addition, the distribution of electrical field below the end of electrical tree is simulated when the end of the electrical tree with the same shape in the two types of specimens is apart 1.8mm from the bottom side of specimens. The simulation results are illustrated in Fig. 5. As shown in Fig. 5, the maximum electrical field strength at the tree tip decreases 22.5% when the electrical

tree propagates into the nonlinear shielding layer. The propagation of electrical tree is therefore inhibited.

a) Plain XLPE b) XLPE with nonlinear shielding layer

Fig. 4 Distribution of electrical field inside specimens without electrical tree propagation

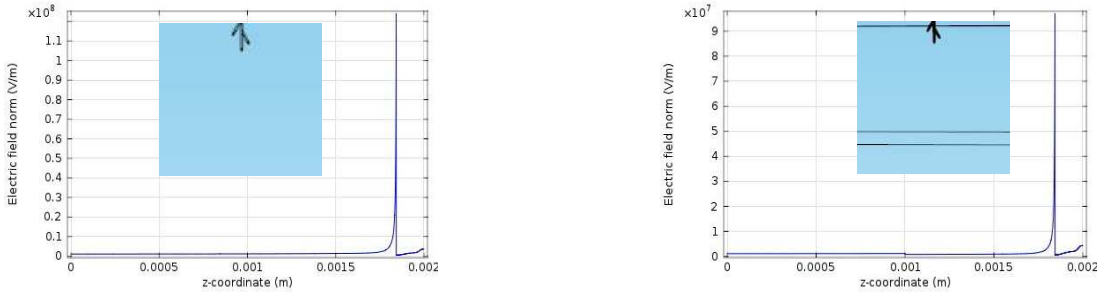

a) Plain XLPE specime b) Specimen with nonlinear shielding layer

Fig. 5 Distribution of electrical field inside specimens when electrical tree propagates into nonlinear shielding layer

Note: the bottom side of specimens is taken as coordinate base point

Simulation of electrical field distribution at electrical tree tip inside insulation of cable

The 220 kV high-voltage XLPE insulation cable with new structure is designed by using nonlinear insulation materials. The structure inside the outer semiconductive shielding layer of cable is illustrated in Fig. 6. The difference between the new-type cable and conventional cable is that the nonlinear shielding layer is used to replace the original XLPE insulation. The cable structure outside the outer semiconductive shielding layer is same as that of conventional high-voltage, composing of cushion/waterproof layer, corrugated aluminum sheath, erosion resistant coating, outer PE sheath and conductive sheath in order.

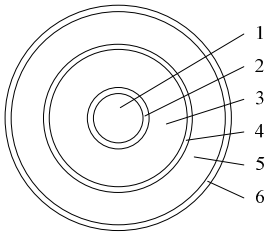

1-wire core (48.7mm in diameter)
2-inner semiconductive shielding layer (2.0mm thick)
3-inner XLPE insulation (12mm thick)
4-nonlinear shielding layer (1.0mm thick)
5-outer XLPE insulation (11mm thick)
6-outer semiconductive shielding layer (1.2mm thick)

Fig. 7 Schematic diagram of insulation structure of new-type 220 kV high-voltage XLPE insulation cable

When the electrical trees with the same shape and size generate in the 220kV high-voltage cables with new and conventional structures, and the electrical tree tip has propagated into the nonlinear shielding layer in the cable with new structure, the simulation results of electrical field distribution at the electrical tree tip in the 220kV high-voltage cables with new and conventional structures are shown in Fig. 7. It can be seen from Fig. 7 that the maximum electrical field strength at the tree tip is decreased 35.9% compared with that of cable without nonlinear shielding layer when the electrical tree tip propagates into nonlinear shielding layer of the 220 kV high-voltage XLPE insulation cable. This result is coincident with that obtained in Section 2.1. This further indicates that the addition of nonlinear shielding layer into insulation layer of high-voltage cable can improve the electrical field distribution at the tip of electrical tree, thus enhancing the resistance of cables to electrical tree.

a) high-voltage cable with conventional structure b) Specimen with nonlinear shielding layer

Fig. 7 Electrical field distribution at the tree tip inside 220 kV high-voltage XLPE insulation cable

Conclusion

Addition of nonlinear shielding layer into electrical tree initiation specimen can remarkably extend the breakdown time of specimens since the nonlinear insulation composites have the capability of homogenizing the electric field.

The presence of nonlinear shielding layer between XLPE insulation layers of high-voltage cable have obvious contribution to decreasing the maximum electrical filed strength at the tip of electrical tree, inhibiting the electrical tree propagation, extending the lifespan of high-voltage cable, and improving the stability of cable line operation.

Acknowledgement

The authors thank National Basic Research Program of China (grant No. 2012CB723308) for their financial supports.

References

[1] Y. Liu, L. Wang, L. Wang, "Necessity of reducing the insulation thickness of HVXLPE cables from the defect point of view," High Voltage Eng., vol. 32, pp. 29-32, 2006.

[2] D. Ye, "Study on the initiation characteristic and partial discharges of electrical trees, " A Thesis Submitted to Chongqing University in Partial Fulfillment of the Requirement for the Degree of Master of Engineering, pp. 2-4,2009.

[3] S.T. Li, X.Q. Zheng, "Polymer electrical treeing , " Beijing, Mechanical Industry Press, pp.1-4,2006.

[4] G. Chen, C.H. Tham, "Electrical treeing characteristics in XLPE power cable insulation in frequency range between 20 and 500 Hz , " IEEE Trans. on Dielectrics and Electrical Insulation, vol. 16, pp. 179-188,2009.

[5] J. V. Champion, S. J. Dodd, G, C. Stevens, "Analysis and modelling of electrical tree growth in synthetic resins over a wide range of stressing voltage, " J. Phys，D: Appl. Phys., vol. 27, 1020-1030,1994.

[6] R. J. Densley, "An investigation into the growth of electrical trees in XLPE cable insulation," IEEE Trans. Electrical Insulation, vol. 14, pp.148-158, 1979.

[7] D.M. Tu, X.S. Wang, X.Z. Liu, B.L. Yu, S.B. Zhang, "Development of 110kV power XLPE cable with charge emission shield, " Journal of Electrical Engine Engineering in China, vol. 13, pp. 13-18, 1993.

[8] B.Z. Han, W.M. Guo, Z.H. LI, "DC current-voltage characteristic of silicon carbide/low density polyethylene composites, " Acta Materiae Compositae Sinica, vol. 25, pp. 19-24, 2008.

[9] B.Z. Han, W.M. Guo, Z.H. LI, "Nonlinear conductivity properties of silicon carbind/silicon rubber composites," Journal of Functional Materials, vol. 39, pp. 1490-1493, 2008.

Advanced Materials Research Vols. 989-994 (2014) pp 1278-1281
© (2014) Trans Tech Publications, Switzerland
doi:10.4028/www.scientific.net/AMR.989-994.1278

The power supply area divided based on improved Voronoi diagram

Liu Li[1,a], Tang Xiao-bo[1,b], Zhao Cai-hong[1,c], Sha Zhen-ya[1,d], Chen Xin[1,e]

[1]School of Electrical & Automation Engineering, Nanjing Normal University, Nanjing 210042, China

[a]fluent.liuli@gmail.com, [b]xiaobotang@126.com,[c]61081@njnu.edu.cn,
[d]cc.cs41@gmail.com, [e]964630275@qq.com

Keywords: Power supply area, Principles of dipartition, Voronoi diagram

Abstract. This paper describes the basic principles of dipartition of the power supply area and uses Voronoi diagram on the dipartition of the power supply area. This paper put forward a model of improved Voronoi diagram based on the basic Voronoi diagram. Depending on the existing transformer substation's capacity and power supply area surrounding the spatial distribution of the load, we determine weights based on the main transformer capacity and the spatial distribution of the load. In the process of generating the power supply area, we adjust the weights depending on different regions ofthe spatial distribution of heavy load to generate the power supply area based on improved Voronoi diagram model. Then we adjust according to the basic principles of the power supply area and the result based on improved Voronoi diagram model to generate the final result. Compared to the traditional division based on artificial experience, it can reflect rationality of the power supply, improve the accuracy of the partition.

Preface

With the rapid development of China's urban power grid construction and transformation, the plan of urban network has become an important task..The necessity of the optimal partition of distribution network planning and its advantages is proposed in Paper[1].However, the methods mentioned above can not consider the fundamentals of powered partition in a comprehensive way.In paper [2],the author consider the district as the minimum load block. On the premise of the selected core blocks and the limit of the power supply radius, author incorporate and adjust a number of adjacent blocks for optimum partition which means uniform load of each partition. This paper introduces the Voronoi diagram as foundation to partition of the power supply area. It proposed to use Voronoi diagram to solve the problem of substation planning in paper[4]. However, this method is put forward in the premise of the assumption that the load capacity, new substation and the number of units are certain without considering a reasonable range of power substation load rate.This paper put forward a model of improved Voronoi diagram based on the basic Voronoi diagram. Depending on the existing transformer substation's capacity and power supply area surrounding the spatial distribution of the load, we determine weights based on the main transformer capacity and the spatial distribution of the load. In the process of generating the power supply area, we adjust the weights depending on different regions of the spatial distribution of heavy load to generate the power supply area based on improved Voronoi diagram model. Then we adjust according to the basic principles of the power supply area and the result based on improved Voronoi diagram model to generate the reasonable result.

Principles of power supply area division

1) Power supply zone should contain at least one 35KV or above substation, the distribution network should be divided into several relatively independent partition, according to substation location, Scope of supply, Load density of zone, Operation and management requirements, high-voltage substation distribution.

2) The purpose of grid partition is to sort out the power grid network structure, clear power supply range. So regional division should be on the basis of Substation Power supply radius and capacity, instead of administrative divisions.

3) Railway, freeway, administrative boundary, main roads and main rivers are important factors of Power supply Regional boundaries division.

4) Power supply Regional division should be consistent with urban development. Regional division shouldconsider thepotential of regional economic development, the prospects of regional load growth and city planning.

Weighted Voronoi diagram model

Assuming the set $S=\{p_1,p_2,...,p_n\}$ constituted of n points in the plane. We call the plane divided by the formula (1) as the basic Voronoi diagram generated by $p_i(i=1,2,...,n)$.

$$V(p_i)=\bigcap_{j\neq i}\{p\,|\,d(p,p_i)<d(p,p_j)\}(i=1,2,...,n) \quad (1)$$

Among it, $d(p,p_i)$ is the euclidean distance of p and p_i.We call $V(p_i)$ as the Voronoi diagram of p_i.Obviously, plane $V(p_i)$ is the assembly composed by all spots which distance to p_i are shorter than others in S.

Figure 1 gives the example of Voronoi diagram. Among it, black points are generating spot, broken line is the Voronoi border. The Voronoi diagram can be seen as diagram of that every vertex $p_i(i=1,2,...,n)$ expend as the same speed until encounter each other.This description has great similarity with the division of power supply area. It can reflect the substation located load centers and spatial sphere of influence, which can serve as a basis for the division of power supply area.

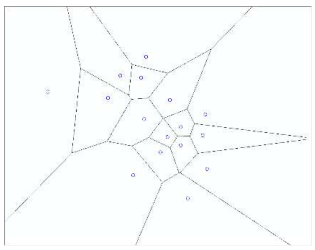

Fig.1 The basic Voronoi diagram

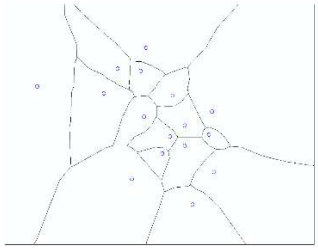

Fig.2 Weighted Voronoi diagram

The Weighted Voronoi diagram is a expanded form of the basic Voronoi diagram. Given assembly p of n points in plane, $p_i(i=1,2,...,n)$, $3\le n<\infty$, $W_i(i=1,2,...,n)$ are n given positive real number. Then:

$$V(p_i,W_i)=\bigcap_{j\neq i}\left\{x\in V(p_i,W_i)\left|\frac{d(x,p_i)}{W_i}<\frac{d(x,p_j)}{W_j},j=1,2,...,n,j\neq i\right.\right\} \quad (2)$$

It divides the plane into n parts. The Voronoi diagram which is determined by $V_n(p_i,W_i)(i=1,2,...,n)$ calls weighted Voronoi diagram. Among it, x is a random number in plane and W is the weight of p_i.The basic Voronoi diagram is a special case in the weighted Voronoi diagram of equal weight.

As the same, the weighted Voronoi diagram also can apply to space subdivision. Weighted Voronoi diagram is used in space subdivision in the circumstances of that weights of generaterd spots has heavy difference. This feature indicates that we can use weights to reflect the different impact of the uneven distribution of the load and the rated capacity of each station.

The Voronoi diagram model used in power supply area

When weighted Voronoi diagram used in spatial segmentation, different generators are correspond to diffusion velocity. But the random point x which correspond to the same generated spot $V(p_i,W_i)$ has the same diffusion velocity. We use the weighted Voronoi diagram can broadly

reflect the different substation load capacity and the load, but can not accurately reflect the specific circumstances of the generation process of the spatial distribution of the load.

Given the assembly p of n points in the plane, $p_i(i=1,2,...,n)$, $3 \le n < \infty$, W_{x_i} is the weight adjusted by the zone of x in $V(p_i,W_i)$.

$$V(p_i,W_i)=\bigcap_{j\neq i}\left\{x\in V(p_i,W_i)\left|\frac{d(x,p_i)}{W_{x_i}}<\frac{d(x,p_j)}{W_{x_j}},j=1,2,...,n,j\neq i\right.\right\} \quad (4)$$

Its weight should consider the capacity of each substation, the total load of each substation and the load density. We make power supply area reasonable by adjust the power substation range boundaries between adjacent stations.Weight is calculated as:

$$\text{weight}=\frac{\text{maximum load of substation}}{\text{the load of partition}}\times\frac{\text{the average load density of this area}}{\text{the load density of x}} \quad (5)$$

Maximum load carried by the normal operation of the substation is calculated according to capacity-load ratio 2.0. In the actual calcaulating process, we grid the power supply area, then calculate the weight of x in this area according to the average load density in the region.

Steps of power supply area partition

1) Making a general understanding to needed district, including its geographic information, administrative divisions, substations, the load distribution. Then ensuing the generated spot.

2) Importing the initial base map, generating Voronoi diagram, the initial weights take 1.Voronoi diagram can generate curved edge shapefor each substation, and each curved edge shape is formed as a power supply area which is generatedby substation.

3) Calculating the weights with the total load of initial power supply area and the load density. Generating the weighted Voronoi diagram according to the new weights. M is the number of cycles.

4) Adjusting the result based on the comprehensive analysis of the weighted Voronoi diagram addcording to the conditions of river, road, administrative divisions and so on.

Example

An example of a city's power supply area dividion. The main function of the area is living. There are four sites of residential land, commercial and financial sites, industrial sites, and administrative office space here. The total area is 52.61 square kilometers. There are currently six substations in the region. In this paper, we generate the power supply area by these six substations.As fig.3.

Fig.3 Substations distribution

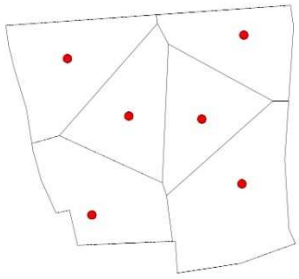

Fig.4 Basic power supply area

As fig.4,we divide entire city into 216 small district and take initial weight 1 to generate the basic Voronoi diagram. We calculate weight for each small district based on the basic Voronoi diagram. There is an example incircled area diagram 2,as fig.5.According to the cycle munber we set,we adjust each district's weight in every generating process to regenerate the weighted Voronoi diagram. The weight in every process according to formula 4 based on the last generating process. We get fig.6.

We adjust the result based on the comprehensive analysis of the weighted Voronoi diagram addcording to the congditiongs of river, road, administrative divisions and so on to get the final result. As fig.7

Fig.5 The distribution of weights

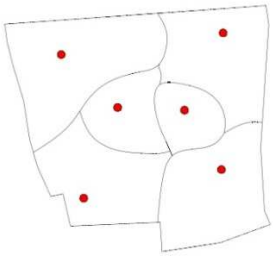

Fig.6Result on weighted Voronoi diagram

As we can see, the result of the weighted Voronoi diagram is different with the result of the basic Voronoi diagram. Compared to the basic Voronoi diagram,the weighted Voronoi diagram can reflect the urban load distribution better. Because that main function of city center area are living and commercial finance, the load density is large there. So that power supply area in there is small.However,the city is surrounded by certain industrial sites and low density living. There is so small load density that power supply area is larger. Compared to the power supply area rely on manual experience, this result based on the weighted Voronoi diagram is more reasonable to reflect Substation capacity, load distribution and regional characteristics.

Fig.7 The power supply area after be adjusted

Conclusion

In this paper, we use improved weighted Voronoi diagram model comined with the principles and the actual situation of power partitions to study the dicidion of power supply area.This paper describes the basic principles of dipartitionof the power supply area and uses Voronoi diagram on the dipartition of the power supply area. This paper put forward a model of improved Voronoi diagram based on the basic Voronoi diagram. Example shows that his result based on the weighted Voronoi diagram is more reasonable to reflect Substation capacity, load distribution and regional characteristics rather than the power supply area rely on manual experience.This method can be used as the basis of the distribution network planning.

References

[1] Li Zhi-yu. *Study and Practice about Distribution Network Planning Based on Optimal Partitioning,*Guangxi electricion,2006,4:1-4.

[2] Song meng.*Urban distribution network planing based on optimal partitioning*, Relay, 2005, 33(23):31-35.

[3] Wang Weiyuan. *Research on the Formation and Planning of Nanjing PowerGrid Partitioning*, Journalof NanjingNormal University,2009,9(4):21-24.

[4] YANG Li-xi. *Locating of Distribution Transformers and Power Supply Area Plotting Based on Voronoi Diagrams*, Journal of mapping,,2004,05:33-35.

[5] Thompson G L, Wall D L. A branch and bound model for choosing optimal substation locations[J]. Power Apparatus and Systems, IEEE Transactions on, 1981 (5): 2683-2688.

Advanced Materials Research Vols. 989-994 (2014) pp 1282-1285
© (2014) Trans Tech Publications, Switzerland
doi:10.4028/www.scientific.net/AMR.989-994.1282

Investigation on the Energy Efficiency of Innovative Hybrid Impact Hydroforming

WANG SHAOHUA[1, a], LANG LIHUI[2,b] and LIN LIJING[3,c]

[1]XueYuan Road NO.37, HaiDian District,Beijing,100191,China

[2] XueYuan Road NO.37, HaiDian District,Beijing,100191,China

[3] XueYuan Road NO.37, HaiDian District,Beijing,100191,China

[a]wangshaohua1125@sina.com, [b]lang@buaa.edu.cn, [c] linlijing0521@126.com

Keywords: Hybrid Impact Hydroforming (IHF) Technology, Pressure distribition, High energy forming, Shock wave.

Abstract. The innovative hybrid impact hydroforming (IHF) technology use high energy forming complex parts in very short time which can improving forming quality of hardforming materials like Aluminum alloy widely used in automotive and aircraft industries. The impact hydroforming technology means the most features are formed by hydroforming and the small features are rapidly reshaped by high intensity impact energy in a very short time after the traditional hydroforming. Thus, the impact energy is the most important parameter of Innovative Hybrid Impact Hydroforming. Using numerical simulation software MSC.PATRAN/DYTRAN, the whole system of hybrid impact hydroforming apparatus was analyzed. The initial gas pressure and the mass of hammer directly affect the energy efficiency. The results show greater initial gas pressure will linear increase the energy output. Moreover, the bigger mass of hammer will reduce the velocity of hammer, but it still increase the energy output. Therefore, the research is very useful for improving energy efficiency of IHFand widing its application.

Introduction

The demands on lightweight, integrity and functional components are getting higher and higher in the automotive and aerospace fields recently. Thus, to meet the harsh function requirements, the forming technology need to be improved. The impact hydroforming technology is an effective method to improve forming quality of complicate product. It includes two processes. First the shallow parts are formed by hydroforming under static liquid pressure. Second the deeper features such as table, band are reshaped by high impact energy which means the forming process is dynamic and energy density is great larger than hydroforming. The high energy can be gained from chemical energy of explosive, magnetism energy of electromagnetism, electrical energy of electric capacity, the kinetic energy of moving part. High speed cylinder is a pneumatic actuator with compressed gas which will push the hammer worked in 15 times greater than ordinary cylinder. Whereas, the diameter used also does not need to be larger. The energy output is the most important parameter of impact cylinder. Using numerical simulation software MSC.PATRAN/DYTRAN, the whole system was analyzed.

Principle of the Impact Cylinder

In order to meet the requirement of high energy output, all kinds of impact cylinder has similar principle and structure. Impact cylinder usually includes two chambers, energy storage chamber, exhaust chamber. The cylinder gets energy by the gas volume expansion work. In order to improve the output energy, the gas in exhaust chamber should rapidly reduce. In this paper, structural optimization ensured the pressure in exhaust chamber is lower enough. The impact cylinder includes control C, gas input, cylinder, hammer, exhaust hammer, gas output as Fig.1 shows.

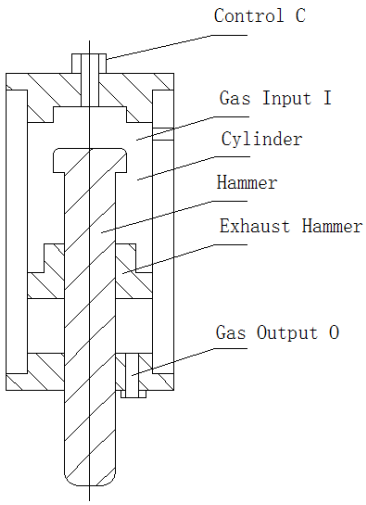

Fig. 1. The structure of impact cylinder

Firstly, reset stage. Compressed air comes into exhaust chamber of impact cylinder form vent O. The air press exhaust hammer and hammer moving upward to the top of the cylinder and sealing. Secondly, gas input stage. Compressed gas comes into energy storage chamber of impact cylinder form vent I. The air press exhaust hammer downward to the bottom of cylinder and hammer stays sealing at the top of cylinder. The original air in the cylinder exhausts by the vent O. Thirdly, ready stage. The compressed air fulfill the cylinder and the vent O is closed. Finally, work stage. The control air comes by the vent C. When the pressure is big enough, the hammer moves down, then the compressed air inflates into the whole cylinder and occupy the hammer room. So hammer gain air energy and work at a high speed. Above all, these four stages can repeat. The work process including four statues as Fig.2 shows.

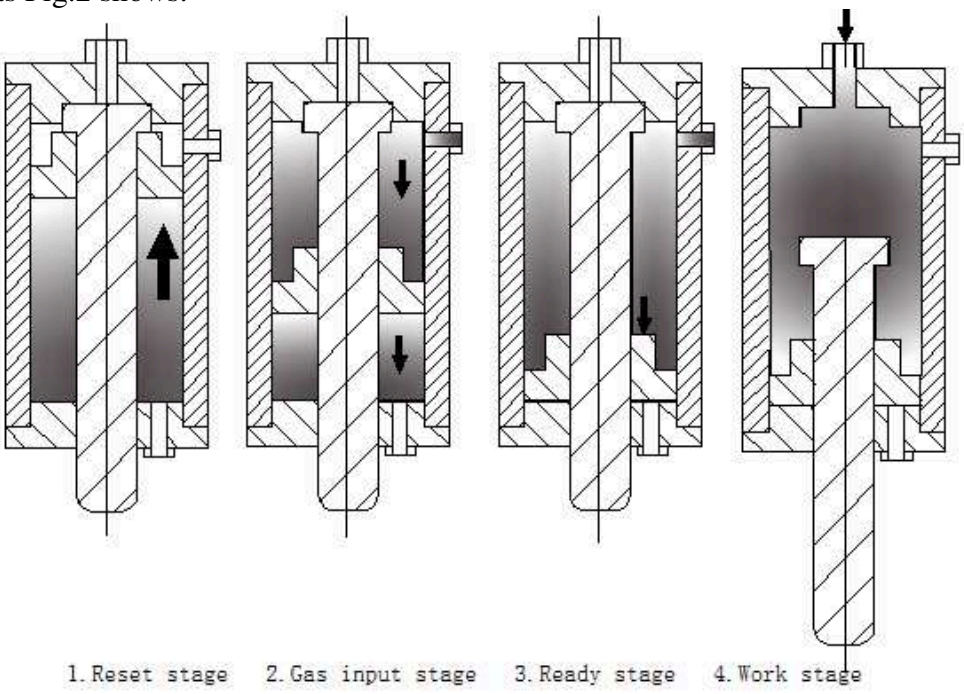

Fig.2. Four status of impact cylinder

Numerical Simulation of Impact Cylinder

The impact cylinder energy was got form the gas infalation which is a fluent dynamic problem.Choose the gas as MM/HYDRO property. The density is 1.2887kg/m^3, coefficient of heat conduction is 1.4. Gas expanding ratio is 1.2. The hammer is Lagrange hexahedral element mesh, steel material propertie which is rigid body whose movements in x and y directions were constraint.

Diametre of cylinder is 320mm, length is 500mm. The hammer is 400mm x 400mm x 100mm. The numerical simulation model of imapct cylinder.is as shown in Fig.3.

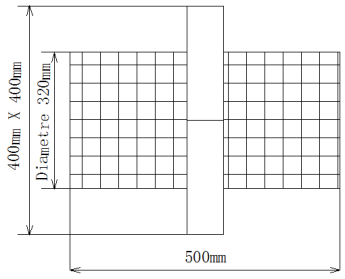

Fig. 3. The numerical simulation model of imapct cylinder.

Upper the hammer is compressed gas with 1 MPa pressure. Under the hammer is normal atmospheric gas of 0.1 MPa pressure. The internal energy of gas is 1.967 $e^5 m^2/s^2$. The botom of cylinder is gas free access interface.

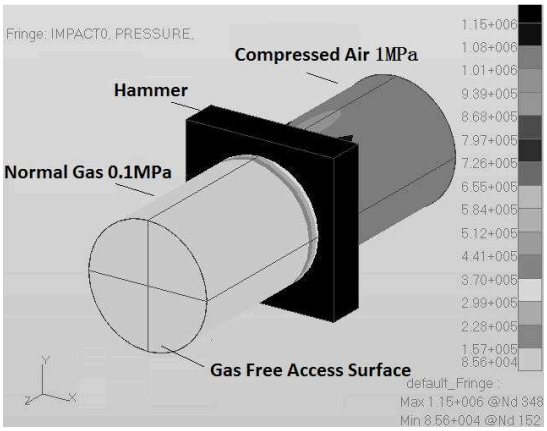

Fig. 4. The initial staus of gas and hammer

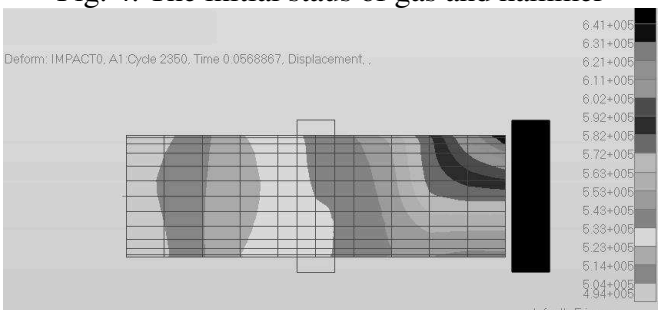

Fig. 5. The finial pressure formation of gas and the position of hammer

Fig 3.9 shows the hammer move in z direction. In addition, gas pressure distribution in space is not uniform and changes over time. So the hammer changes over time too.

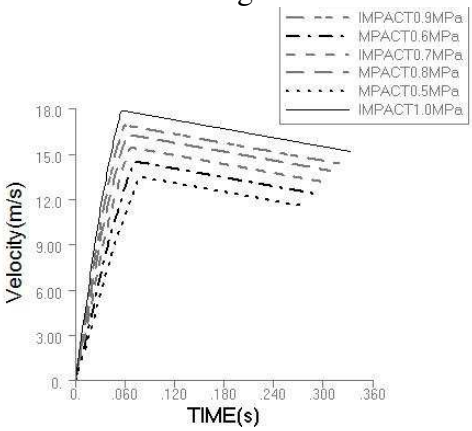

Fig. 6.Comparison of piston speed under different initial pressure

The initial pressure decide the energy output. Similate initial pressure form 0.5 MPa to 1.0 Mpa, increment is 0.1 Mpa.Cause the kinetic energy is square the velocity of hammer, So compare the velocity under varity pressure. As shown in Fig.7, the velocity increase quickly to the peak at the first time and reduces slowly later. Moreover, higher pressure, shorter time need to get the maximum. All the average work velocity is above 15m/s. The Fig 7 also proves the relationship between initial gas and velocity of hammer is linear and can be expressed by the foruma as below.

$$V_{\max} = 8.5P_0 + 9.37 \tag{1}$$

The V_{max} is the velocity of hammer, P_0 is the initial pressure of impact cylinder.

In actual working condition, when pressure and volume of gas is fixed, the gas expanding energy output is fixed. So velocity get small with the increasing of hammer mass as shown in Fig.7. When P_0 is 1.0Mpa, compare the piston velocity under hammer mass is 150KG, 200KG, 250KG, 300KG. Calculate the energy is still increse. So hammer mass lightly effect the energy output.

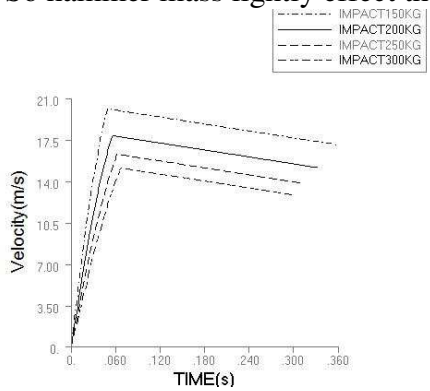

Fig. 7.Comparison of piston speed under different piston mass

Summary

As the performed FEM calculation show, the initial gas pressure linear increases the energy output and the velocity of hammer is around 15m/s under the condition of 1MPa gas pressure. Moreover the bigger mass of hammer reduces the velocity of hammer, but it still increase the energy output. The research will be great useful for the control of energy output and wide the application of impact hybrid hydroforming.

Acknowledgment

The research reported in this paper was funded by the National Natural Science Foundation of China Project under Grant NO. 51175024.

References

[1]. Yi H. K., Pavlinab E. J., van Tyne C. J.et al. Journal of Materials Processing Technology. Forum 203 (2008) , p. 532-536

[2]. Kim B. J., Van Tyne C. J., Lee M. Y.et al. Journal of Materials processing technology. Forum 187-188 (2007),p. 296-299

[3]. Abedrabbo N., Pourboghrat F., Carsley J. International Journal of Plasticity. Forum 22 (2006),p. 342-373

[4]. Li D. M., Ghosh A. K. Journal of Materials Processing Technology. Forum 145 (2004),p. 281-293

[5]. Siegert K., Jager S., Vulcan M.. CIRP Annals-Manufacturing Technology. Forum 52 Vol.140 (2003) , p. 241-244.

[6]. Novotny S., Geiger M. Journal of Materials Processing Technology. Forum 138 (2003),p. 594-599

Advanced Materials Research Vols. 989-994 (2014) pp 1286-1291
© (2014) Trans Tech Publications, Switzerland
doi:10.4028/www.scientific.net/AMR.989-994.1286

Investigation on Nutrient Loads of Lake Taihu in China

Hua WANG[1, 2, a], Kun XIA[1, 2, b], Bao LI[3, c], Yiyi ZHOU[1, 2, d]

[1]Key Laboratory of Integrated Regulation and Resource Development on Shallow Lake of Ministry of Education, College of Environment, Hohai University, Nanjing 210098, China

[2]College of Environment, Hohai University, Nanjing, Jiangsu, 210098, China

[3]Yangtze River Estuary Survey Bureau of Hydrology and Water Resource, CWRC, Ministry of Water Resources, Shanghai 200136, China

[a]wanghua543543@163.com, [b]xk19910523@163.com, [c]libao201@163.com, [d]zyy664377643@163.com

Keywords: Lake Taihu; Nutrient loads; River runoff; Atmospheric bulk deposition; Internal release.

Abstract. Based on measured data and laboratory experiments, the spatial and temporal distribution of nutrient loads of Lake Taihu from the sources of river runoff, atmospheric bulk deposition and internal release was quantitatively analyzed. Results showed that: (1) In 2011, annual river inputs of total phosphorus (TP) and total nitrogen (TN) respectively were 2382.4 tons and 50245.0 tons, and annual river outputs of TP and TN respectively were 849.1 tons and 24236.7 tons, Huxi area was the major transverse source of nutrients as a large proportion of TP(71.6%) and TN(66.2%). (2) Annual nutrient loads of Lake Taihu were 3306.6 tons TP and 48007.0 tons TN, of which the contribution of river runoff, atmospheric bulk deposition and internal release to TP accounted for 46.3%, 38.3% and 15.4%, and that to TN accounted for 54.2%, 43.7% and 2.1%, respectively. (3) Inputs of nutrients to Lake Taihu were higher in summer (June to August), of which 983.9 tons TP and 8874.9 tons TN in June, 1420.9 tons TP and 7463.3 tons TN in July, 1347.1 tons TP and 7181.3 tons TN in August. The results have great significance for eutrophication control and water environment protection in Lake Taihu.

Introduction

Lake Taihu, the second largest freshwater lake in China, plays a significant role in protecting water resources and maintaining ecological balance. In recent decades, with the rapid development of industry and agriculture, the continuous increase of population and the constant expansion of urbanization, Lake Taihu was faced with increasingly severe environmental problems, including water quality deterioration and eutrophication. In May, 2007, an estimated 4 million people in Wuxi, an industrial city located along the lake, were deprived of drinking water for nearly a week, as a carpet of algae scum or agglomerate of biological origin made local lake water unusable [1] [2]. Nutrient is the major factor leading to eutrophication, therefore, quantitative assessment of nutrient loads in Lake Taihu is of great importance for putting forward reasonable and effective eutrophication control measures. To date, many studies have been conducted on nutrient loads of Lake Taihu from a certain source, such as river runoff [3], atmospheric bulk deposition [4] and internal release [5]. These studies did gain some fruits, but few studies have simultaneously considered both transverse and vertical sources of nutrients to Lake Taihu. In this paper, we selected 2011 as a typical year to quantitatively analyze the spatial and temporal variation characteristics of nutrient loads of Lake Taihu from the sources of transverse river runoff, vertical atmospheric bulk deposition and internal release on the basis of field measurements and laboratory experiments, so as to find out the distribution of the nutrient loads of Lake Taihu. The results have great significance for eutrophication control and water environment protection in Lake Taihu.

Study Area

Lake Taihu is located in the lower Yangtze River delta between 30°56′-31°33′N and 119°53′-120°36′E. The lake is characterized by flat terrain, like a dish, which is a typical shallow lake. Lake Taihu has an area of 2338km^2 and a catchment area of 36,500 km^2, with an average depth of 1.89m. Taihu Basin belongs to subtropical monsoon climatic region, with an average temperature of 15-17 ºC, an average annual precipitation of 950-1250mm, and an average wind speed of 3.5-5 m/s. Taihu Basin has a complex and high density set of river networks. Rivers surrounding Lake Taihu flow in and out through five hydraulic areas including Huxi area, Zhexi area, Hangjiahu area, Wuchengxiyu area and Yangchengdianmao area (Figure 1).

Fig.1. Map of Lake Taihu

Transverse Nutrient Loads

TN or TP load discharged to the lake for each month was calculated by the following formula:

$$W = \sum_{i=1}^{n} C_i \cdot Q_i \quad (1)$$

Where W is nutrients of river input or onuput, t/a; C_i is water quantity concentration of hydraulic area I, mg/L, data were obtained from monitoring data of 72 inflow rivers of Lake Taihu; Qi is flow value of hydraulic area I, m^3/s, data were obtained from the Taihu Basin Authority of Ministry of Water Resources.

River inputs. Using this approach, we calculated annual inputs fluxes of 2382.4 tons TP and 50245.0 tons TN from the rivers surrounding lake draining into Lake Taihu in 2011. TP loads discharged from Huxi area, Zhexi area, Hangjiahu area, Wuchengxiyu area and Yangchengdianmao area were respectively 1706.6 tons, 285.2 tons, 50.3 tons, 317.7 tons and 22.6 tons, accounting for 71.6%, 12.0%, 2.1%, 13.3% and 0.9%. In contrast, TN loads discharged from the five areas were respectively 33283.9 tons, 4711.8 tons, 630.2 tons, 10612.2 tons and 1006.9 tons, accounting for 0.7%, 14.2%, 12.5%, 23.5% and 49.0%. Nutrients inputs from five areas in different month are shown in Figure 2.

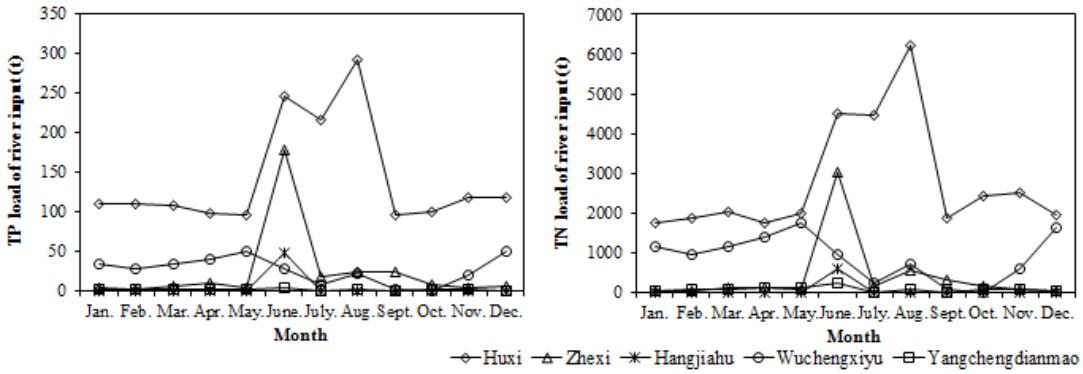

Fig.2. Distribution of river nutrients inputs in 2011

River outputs. Using this approach, we calculated annual outputs fluxes of 849.1 tons TP and 24236.7 tons TN from the rivers surrounding lake flowing out Lake Taihu in 2011. TP loads outputted from Huxi area, Zhexi area, Hangjiahu area, Wuchengxiyu area and Yangchengdianmao area were respectively 7.6 tons, 204.3 tons, 272.0 tons, 151.4 tons and 213.8 tons, accounting for 0.9%, 24.1%, 32.0%, 17.8% and 25.2%. In contrast, TN loads outputted from the five areas were respectively 171.8 tons, 3437.1 tons, 3038.2 tons, 5705.4 tons and 11884.3 tons, accounting for 0.7%, 14.2%, 12.5%, 23.5% and 49.0%. Nutrients outputs from five areas in different month are shown in Fig.3.

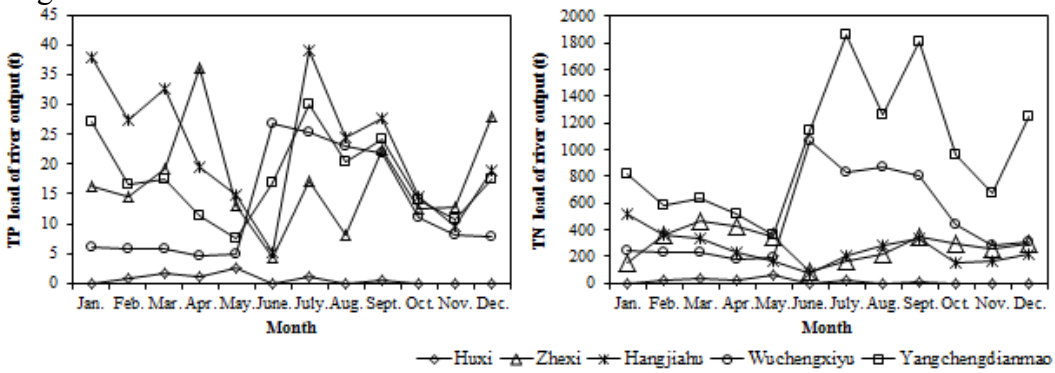

Fig.3. Distribution of river nutrients outputs in 2011

Vertical Nutrient Loads

Atmospheric bulk deposition. The surface area of Lake Taihu is large. The concentrations of TN and TP from atmospheric bulk deposition are quietly high, which may lead to a series of influences on eutrophication and water ecosystem structure. Therefore, atmospheric bulk deposition is also an important source of nutrients to Lake Taihu. The calculation formula of nutrient loads to lake from atmospheric bulk deposition is as follows:

$$Q = Q_d + Q_w = \Sigma F_{di} \times S_i \times d_i / S + \Sigma F_{wi} \times S_i / S \quad (2)$$

Where Q is the deposition fluxes of TP or TN, kg/a; Q_d, Q_w are the fluxes of dry and wet deposition, kg/a; F_{di}, F_{wi} are atmospheric deposition rate of dry and wet deposition in different sampling site, kg/(km^2·d); S_i is the area of each sampling site, km^2; d_i is the dry deposition days of each sampling site in a year, day; S is the surface area of Lake Taihu, km^2.

Based on the rainfall statistics of 2011 and the experiments of dry and wet deposition [7], we calculated the dry and wet deposition fluxes of nutrients in different seasons according to the formula (2), then estimated the deposition fluxes of each month according to the monthly rainfall, as shown in Figure 4. We found that the deposition fluxes in summer (June to August) is relatively high, which TP and TN respectively accounted for 71.9% and 44.6% of annual deposition fluxes.

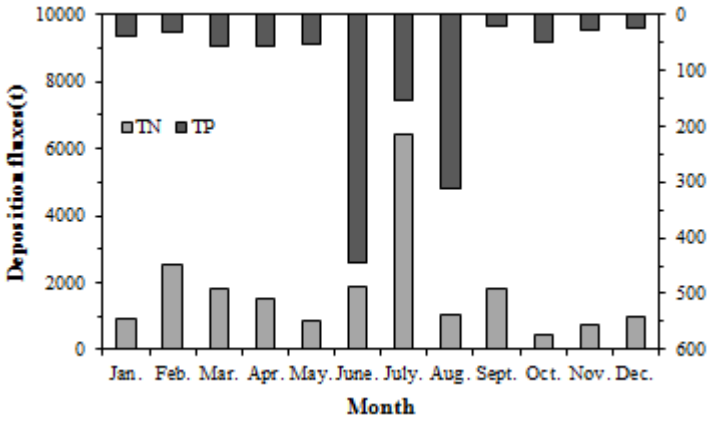

Fig.4. Distribution of nutrients from atmospheric bulk deposition in 2011

Internal release. Lake Taihu is a large shallow lake. Due to disturbance of wind waves, nutrients release and absorb along with the complex movement of sedimentation and resuspension of sediment. When the wind speed is small or the lake is calm, the resuspension flux of sediment is slight or few that it has little effect on the concentration of water quality. When the wind speed comes to the critical wind velocity of sediment resuspension, the sediment resuspension is evident, a lot of nutrients were brought into water. Nutrient loads from internal release to lake are the difference between resuspension fluxes and sedimentation fluxes, the calculation formulas of nutrient loads to lake from internal release are as follows:

$$Q = Q_r - Q_s \tag{3}$$

$$Q_r = S \cdot \sum_{i=1}^{n} (M_i \cdot T_i) \tag{4}$$

$$Q_s = S \cdot \sum_{i=1}^{n} (N_i \cdot T_i) \tag{5}$$

Where Q_r is the nutrients fluxes of resuspension, ton; Q_s is the nutrients fluxes of sedimentation, ton; S is the distribution area of sediment, m^2; M_i is the release rate of each factor under different wind speeds, $g \cdot m^{-2} \cdot d^{-1}$; Ti is the duration time of different wind speeds, day; N_i is the average sedimentation rate under different wind speeds, $g \cdot m^{-2} \cdot d^{-1}$.

The distribution area of sediment in Lake Taihu is 1632.9 km^2 [8]. The average release rate and the average sedimentation rate of nutrients under different wind speeds were obtained from sediment experiment in the laboratory [9]. Based on the above results and wind speed data of Lake Taihu in 2011 (from Taihu Basin Authority), we applied a two-dimensional mathematical model of water quantity and quality to calculate monthly nutrients fluxes to Lake Taihu from internal release (Figure 5). Results showed that: TN and TP loads from internal release were respectively 1020.6 tons and 505.3 tons in 2011, and the nutrients fluxes of internal release were larger in August, September and December.

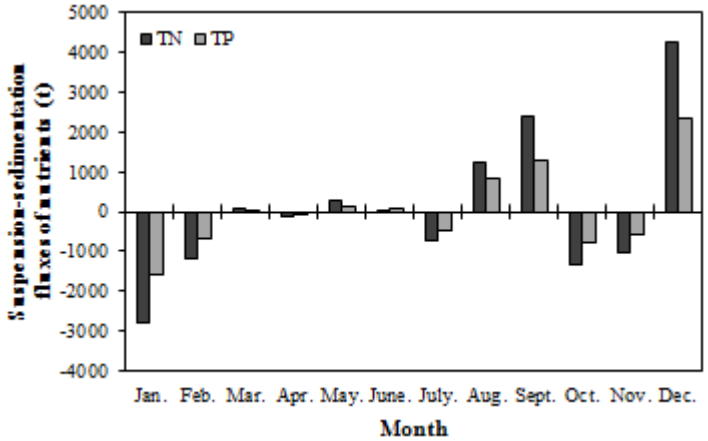

Fig.5. Distribution of nutrients from internal release in 2011

Total nutrient loads

Based on the calculation results of nutrient loads from transverse river runoff, vertical atmospheric bulk deposition and internal release, we calculated total nutrients fluxes of 3306.6 metric tons TP and 48007.0 metric tons TN from the sources to Lake Taihu in 2011.

In terms of space, TP loads from the sources of river runoff, atmospheric bulk deposition and internal release were 1533.3 tons, 1268.0 tons and 505.3 tons in 2011, accounting for 46.3%, 38.3% and 15.4% respectively; TN loads were 26008.4 tons, 20978.0 tons and 1020.6 tons, accounting for 54.2%, 43.7% and 2.1%, respectively (Figure 6). The results indicated that atmospheric bulk deposition and internal release were the major sources of nutrient loads besides river runoff, and nutrients pollution from vertical sources should also be taken into consideration and controlled. Meanwhile, Huxi area was the major source of nutrient loads for its TP and TN loads accounted for 71.6% and 66.2% respectively, so the treatment and governance of pollution sources in Huxi area should be strengthened.

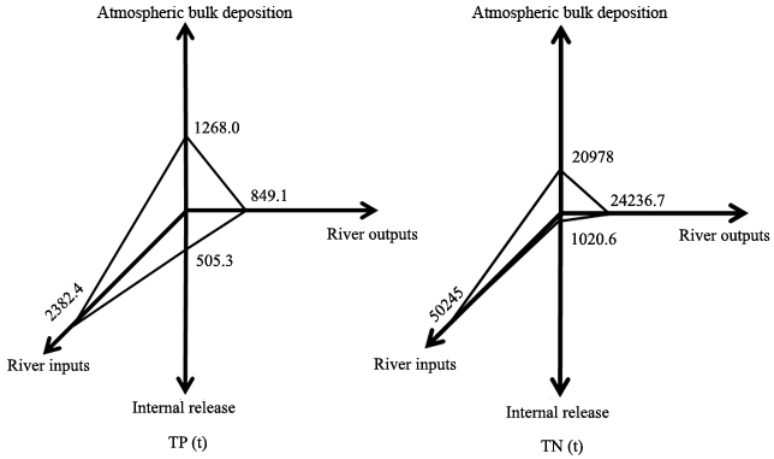

Fig.6. Spatial distribution of nutrient loads of Lake Taihu

In terms of time, nutrients loads from different sources in each month were shown in Figure 7. Nutrients loads from internal release in some months were negative as the sedimentation fluxes were larger than resuspension fluxes, and it may cause nutrient loads from all the sources to be negative, for example nutrient loads in January and October. TN loads in June, July, August and December were relatively higher which respectively were 8874.9 tons, 7463.3 tons, 7181.3 tons and 6856.9 tons, and TP loads in June, August, September and December were relative higher which respectively were 983.9 tons, 1420.9 tons, 1347.1 tons and 2448.5 tons, so nutrient loads of Lake Taihu were higher in summer (June to August), it can replenish the nutrients for the growth of algae and aquatic plants, and played a facilitating role in algae blooms.

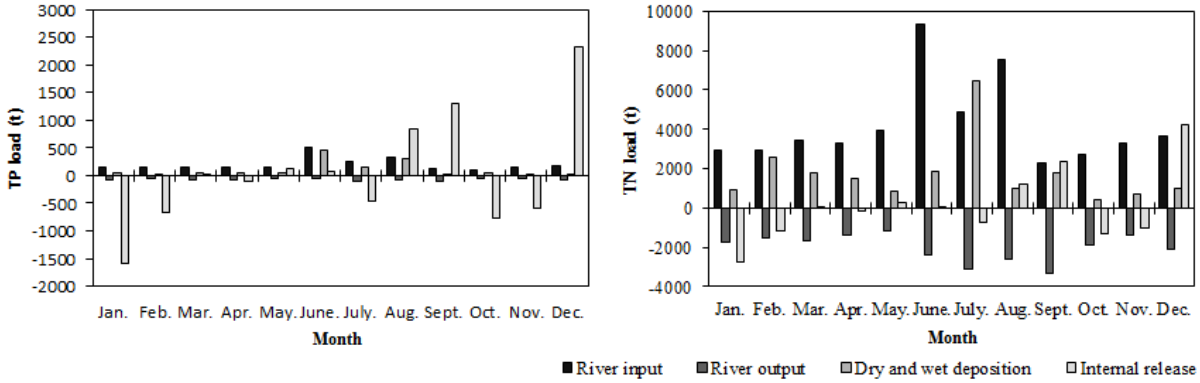

Fig.7. Temporal distribution of nutrient loads of Lake Taihu

Conclusions

In this paper, based on measured data and laboratory experiments, we quantitatively calculated nutrient loads of Lake Taihu in 2011 from the sources of transverse river runoff, vertical

atmospheric bulk deposition and internal release, and analyzed the spatial and temporal variation characteristics of nutrient loads. TP and TN loads of Lake Taihu in 2011 were 3306.6 tons and 48007.0 tons. Huxi area was the major transverse source of nutrients as a large proportion of TP (71.6%) and TN (66.2%), so the treatment and governance of pollution sources in Huxi area should be strengthened. Atmospheric bulk deposition and internal release were the major sources of nutrient loads besides river runoff as accounted for 38.3% and 15.4% of TP, and accounted for 43.7% and 2.1% of TN, respectively. Nutrient loads were higher in summer (June to August), so it can replenish the nutrients for the growth of algae and aquatic plants, and played a facilitating role in algae blooms. This paper was helpful to accurately grasp nutrient loads of Lake Taihu and propose targeted total amount control plan, so as to provide guidance for water environmental protection in Lake Taihu.

Acknowledgements

This work was supported by the Major Science and Technology Program for Water Pollution Control and Treatment of China (No.2012ZX07506-002 & No.2012ZX07101-001) and National Natural Science Foundation of China (No.51309082).

References

[1] M. Yang, J. Yu, Z. Li, Z. Guo, M. Burch, T.F. Lin [J]. Taihu Lake not to blame for Wuxi's woes. Science, 2008, 319: 158.

[2] L. Guo [J]. Doing battle with the green monster of Taihu Lake. Science, 2007, 317: 1166.

[3] S.W. Yan, H. Yu, L.L. Zhang, J. Xu, Z.P. Wang [J]. Water quantity and pollutant fluxes of inflow and outflow rivers of Lake Taihu. Journal of Lake Sciences, 2011, 23(6): 855-862.

[4] X.F. Chen, X.M. Chuai, J. Zeng, T. Liu, L.Y. Yang [J]. Nitrogenous fluxes and its self-Purification capacity in Lake Taihu. Environmental Science, 2012, 33(7): 2309-2314.

[5] L.Y. Yang, B.Q. Qin, W.P. Hu, L.C. Luo, Y.Z. Song [J]. The atmospheric deposition of nitrogen and phosphorus nutrients in Taihu Lake. Oceanologia et Lmnologia Sinica, 2007, 38(2): 104-110.

[6] H. Yu, L.L. Zhang, S. W. Yan, H. L. Li, J. Xu [J]. Atmospheric wet deposition characteristics of nitrogen and phosphorus nutrients in Taihu Lake and contributions to the lake. Research of Environmental Sciences, 2011, 24(11): 1210-1219.

[7] T. Liu, L.Y. Yang, Z.X. Hu, Y.N. Sun [J]. Spatial-temporal features of atmospheric deposition of nitrogen and phosphorus to the Lake Taihu. The Administration and Technique of Environmental Monitoring, 2012, 24(6): 20-24, 42.

[8] C.X. Fan, Y.B. Liu, H.S. Chen [J]. Approach on estimating storage sludge in Lake Taihu and its distributing characteristics. Shanghai Environmental Sciences, 2000, 19(2): 72-75.

[9] K.M. Hu, S. Wang, Y. Pang [J]. Suspension-sedimentation of sediment and release amount of internal load in Lake Taihu. Journal of Lake Science, 2014, 26(2): 191-199.

Advanced Materials Research Vols. 989-994 (2014) pp 1292-1296
© (2014) Trans Tech Publications, Switzerland
doi:10.4028/www.scientific.net/AMR.989-994.1292

The Soil Enzyme Activities with Age of Tea in Three Gorges Reservoir Area

Liping Zhang[1], Guomei Jia[1,2]*, Ying Xi[1]

[1]College of Biology and Pharmacy, China Three Gorges University, Yichang, 443002, China

[1]Department of Electrical Engineering and Automation, Luoyang Institute of Science and Technology, Luoyang, 471023, China

[2] Engineering Research Center of Eco-environment in Three Gorges Reservoir Region, Ministry of Education, China Three Gorges University, Yichang, 443002, China

* Corresponding author: Guomei Jia, Email: jjjgm@126.com

Keywords: soil invertase; Urease; Catalase; Tea garden

Abstract. Enzyme activities play key roles in the biochemical functioning of soils, including soil organic matter formation, degradation and nutrient cycling. Activities of invertase, urease, and catalase were analyzed at different age of tea garden. The results showed that urease activity only showed a significantly negative relationship with the age of tea, and a significant positive relationship with organic carbon. This indicated that soil urease acitivity could respond well to the change of soil organic carbon and is a more sensitive indicator of soil fertility than other enzyme activities. The study also found that the organic carbon was relatively low in 50yr site, compared with lower age of sites. This may be caused by the high activities of invertase and catalase per unit of organic carbon in the soil of tea which tends to help decompose and therefore decrease the organic carbon in soil

Introduction

Soil enzymes play an essential role in nutrient mineralization and the decomposition of organic matter, their activities are key drivers of nutrient suppliy to plants[1]. Soil enzymes involved in carbon, nitrogen, phosphorus transformation. They would intergrate chemical, physical and biological charateristics and are sensitive to environmental stress and respond rapidly to change in land management[2]. Soil invertase and urease have been showed to be significantly higher in tilled soils than in cultivated soil[3]. These soil enzyme acitivites are also higher in crop rotations than in monocultures[3].Therefore, there is currently great interest in the use of extracellular enzyme activites as biological indicators of soil quality.

Tea (Camellia sinensis L.) is an intensively managed perennial evergreen broad-leaved cash crop. Tea gardent area covers approximately three million hectares of the world' arable land [4]. Xue et al [5] reported the change in acid red soil enzyme activities of tea garden, However, little is known about the change in soil enzyme acitivities of other soils within tea garden with time. Better understanding of enzyme acitivities in other soil could lead to more effectways of elucidating the action of tea system in improving soil fertility. This also is vital for understanding soil quality in the sustainability of tea plantation productivity.

Materials and Methods

We conducted this study at Shazhenxi, Zigui, Yichang, Hubei Province China, approximately 30km upstream to the three Gorges Dam and Adjacent to the Three Gorges Reservoir. The site is located between latitude 30°55′04.8″N and 30°55′10.2″N; longitude is between 110°41′25.2″E and 110°41′51.2″E and altitude between 236 m and 267 m above sea level, and belongs to the humid subtropical monsoon climate zone with warm winters, early springs, hot and dry summers, and rainy, humid, foggy autumns. The rainfall in this area is abundant with an annual average 1100mm

while having an uneven temporal and spatial distribution. The soil parent material at all investigated sites are purple soil.

In the study area, three different ages of tea sites were selected (ie. 6-, 15-, and 50-year).

Table 1 Status of experimental plots

year	Water content(%)	Bulk density ($g.cm^{-3}$)	Organic C($g.kg^{-1}$)	Total N($g.kg^{-1}$)	C/N
6	31.28	1.53	4.62	0.15	30.8
15	35.26	1.61	4.03	0.16	25.19
50	25.24	1.95	2.63	0.13	20.23

Soil sampling

Soil samples (0–20 cm and 20-40cm depth) were collected in July 2008 from three random sampling quadrat (5m×5 m) at each site described above. In each quadrat the soil was collected from five points randomly, and mixed into one sample. After carefully removing the surface organic materials and fine roots, each mixed soil sample was was air-dried for the estimation of soil enzyme activities.

Invertase activity was determined after incubating the sample with 35.06mM sucrose, as substrate, for 3 h at 50℃,with 2M acetate buffer ph 5.5, the reducing sugars released were determined following the method of Schinner and von Mersi [6].

Urease activity was measured according to Kandeler and Gerber[7]. 1g DW soil was mixed with 1.75ml of 100Mm borate buffer (Ph 10.0) and 0.25ml of 820Mm urea. The mixture was then incubated at 37℃ for 1h and the reaction stopped with 6ml of acidified 2M KCl. After centrifugation (3500×g, 3min), 0.25ml of the supernatant fraction was mixed with 3.75ml of distilled water and 2ml of a reagent composed of a sodium salicylate/sodium nitroprusiate mixture(17%, w/v and 0.12%, w/v, respectively), 0.3M NaOH, and distilled water (1:1:1, v/v/v). Finally, 0.8ml of sodium dichloroisocyanurate was added to the reaction mixture. After 30min, the absorbance value of the sampled was read at 670nm.

Soil catalase was tested by the Roberge method[8], with slight modifications. Two grams sir-dried soil with 40ml distilled water and 5ml 0.3% H_2O_2, was shaken for 20min (shaking velocity was 150rpm) and filtered immediately. The filtrate was titrated with 0.1mol l^{-1} $KMnO_4$ in the presence of sulphuric acid and the results were expressed as umol $KMnO_4$ $g^{-1}h^{-1}$.

Statistical analysis

All statistical work was done using the SPSS 13.0 for Windows. One-way ANOVA was used to analyze means of age, to least significant difference at the 5% level. When significance is observed at the $p < 0.05$ level, Tukey's post hoc test was used to carry out multiple comparisons. Pearson's test was used to determine whether there was significant correlation between soil enzyme activities and soil organic matter.

Results and Discussions

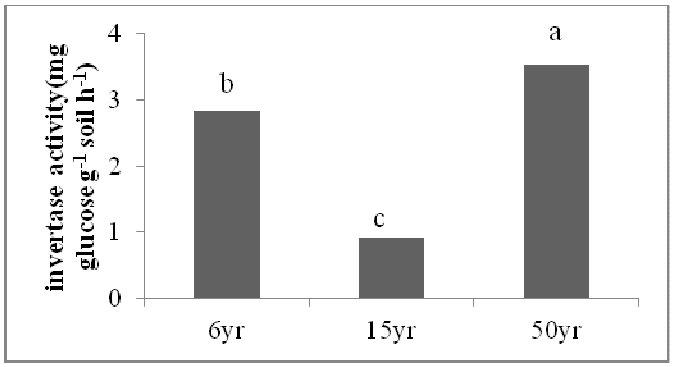

Fig.1 The change in soil invertase activity with the age of tea

For carbon cycle enzyme, invertase catalyses the hydrolysis of sucrose to D-Glucose and D-fructose. Soil invertase activity was highest under 50yr sites and lowest under 15yr site, respectively. This was consistent with Xue et al[5] which showed the 50-year-old tea orchard red soil had a comparatively higher invertase activity compared to the 8- and 90-year-old tea orchard red soil. Invertase had no significantly relationship with organic matter. This was inconsistent with Guan[9]that all kinds of enzyme activities were positively related to organic matter content.

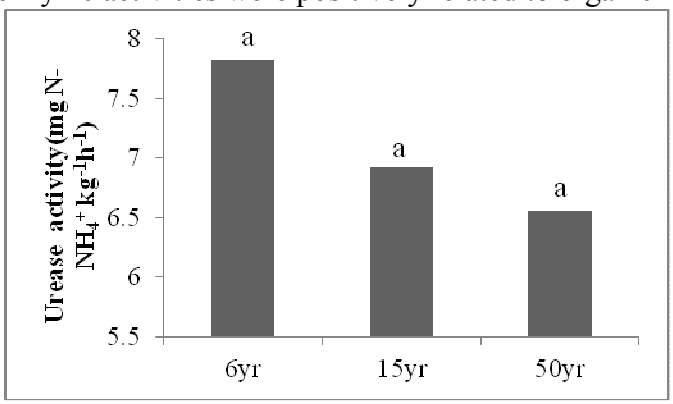

Fig. 2 The change in soil urease activity with the age of tea

For nitrogen cycle enzyme, urease is involved in the hydrolysis of urea-type substrates to CO_2 and NH_3 and its activity is crucial in the transformation of urea fertilizer. Most of the variation in urease activity among soils can be accounted for by the quantity of soil organic matter[10]. Therefore, understanding of urease activity dynamics could reveal more effective ways of managing N fertilizers [11]. In this study, although one-way ANOVA analysis showed that there was no significant difference among three sites, the age of tea had a significantly negative relationship with urease activity. Futhermore, there was a significantly positive relationship between urease activity and organic C. This was consistent with Pettit et al[12]and Rodríguez-Loinaz et al[13]. Rodríguez-Loinaz et al[13]also found that urease activity was positively correlated with organic matter content.

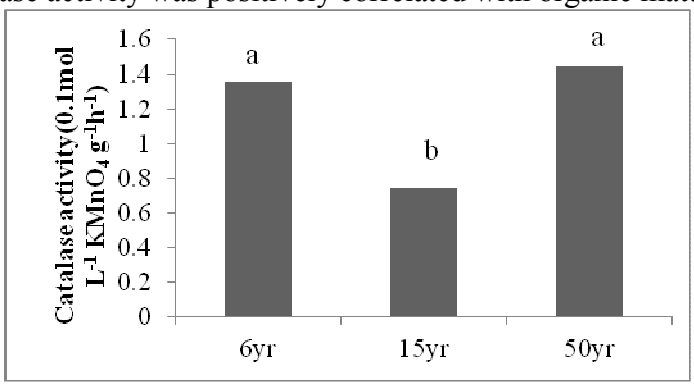

Fig. 3 The change in soil catalase activity with the age of tea

Among the oxidoreductase enzyme systems, soil catalase can also be used as a measure of biological activity. This is possible because soil catalase, although acting mainly as intracellular enzyme, remains active outside microbial cells because of an association with soil organic matter and/ or sorption on clay minerals[14,15]. Catalase splits hydrogen peroxide into molecular oxygen and water and keeps cells from damage caused by reactive oxygen species. In this study, catalase activity was similar to invertase acitivity, was highest under 50yr site and lowest under 15yr site, respectively. The increase in soil catalase activity could affect soil solution chemistry and change soil redox conditions. The change in soil solution had the potential to dissociate bonds between metals and complex organic matter and therefore alter soil storage[16]. Therefore, catalase could significantly influence on changing soil redox, chemical properites of soil dolution, and accelerating transformation of organic matte[16]. However, catalase showed no significant relationship with organic carbon and age of tea. This was inconsistent with Alef and Nannipieri[17]. Alef and Nannipieri[17] reported that catalase acitivity was very stable in soil and showed a significant correlation with the content of organic carbon. In addition, soil organic carbon was relatively low in 50yr site, compared with lower age of sites. This may be caused by the high activities of invertase

and catalase per unit of organic carbon in the soil of tea which tends to help decompose and therefore decrease the organic carbon in soil(Wang et al., 2012).

Table 2 Correlations between soil enzyme activities and organic matter, and the age of tea

	Age	OC	TN	Invertase	Urease
OC	-0.97**				
TN	-0.51	0.64			
Invertase	0.26	-0.47	-0.70		
Urease	-0.97**	0.89*	0.36	-0.01	
Catalase	0.11	-0.33	-0.64	0.99**	0.14

** Correlation is significant at the 0.01 level (2-tailed).

* Correlation is significant at the 0.05 level (2-tailed).

Conclusion

Invertase and catalase activities firstly decreased, tended to be lowest under 15yr, then they increased again, whereas urease activity showed no significant change among three sites. The correlations analysis showed that only urease and organic acarbon was positively related, and no correlation between organic carbon and invertase activity or catalase activity was observed. This suggested that soil urease acitivity could respond well to the change of soil organic carbon and is a more sensitive indicator of soil fertility than other enzyme activities measured.

Conclusion

Based on the analysis of the mechanical theory as the foundation, designed the soccer robot pick the ball institutions optimal design process, found aim function, select design variables and the corresponding optimization algorithm to optimize a complete set of institutions. At last through the test to get the final performance parameters of the institution. Experiments show that the system has higher accuracy and stability, the new optimize pick the ball have design basic requirements, and achieved good ideal control effect.

Acknowledgement

In this paper, the research was sponsored by Engineering Research Center of Eco-environment in Three Gorges Reservoir Region, Ministry of Education, China (No. KF2013-09).

References

[1] Z. Kotroczó, Z. Veres, I. Fekete, Z. Krakomperger, J.A. Tóth, K. Lajtha, B. Tóthmérész.Soil enzyme activity in response to long-term organic matter manipulation.Soil Biology and Biochemistry 2014 (70) 237-243.

[2] R.P. Dick.Soil enzyme activities as integrative indicators of soil health. In: C.E. Pankhurst, B.M. Doube, V.V.S.R. Gupta (Eds), Biological indicators of Soil Health. CAB International, Wanllingford, USA, 1997, 121-156.

[3] R.P. Dick. Influence of long-term tillage and crop rotation combinations on soil enzyme activities.J. Am. Soil Sci. Soc. Vol 48(1984), 569-574.

[4] FAO: FAOSTAT data, (2007) Http:// www.fao.org.

[5] D. Xue, H. Yao, C. Huang. Microbial Biomass, N mineralization and Nitrification, Enzyme Activities, and Microbial Community Diversity in Tea Orchard soils. Plant and Soil 2006 (288) 319-331.

[6] F. Schinner, W.Von Mersi. Xylanase-CM-cellulase- and invertase activity in soil: an improved method.Soil Biology and Biochemstry 1990 (22) 511-515.

[7] E. Kandeler, H. Gerber. Short-term assay of soil urease activity using colorimetric determination of ammonium. Biol Fertil Soils 1988 (6) 68-72.

[8] M.R. Roberge (1978) Methodology of soil enzyme measurement and extraction. Appendix in soil enzymes. In: Burns RG(ed) Soil enzymes, Academic Press, London,p 341-370.

[9] S.Y.Guan: Soil enzymes and Methodology. Agricultural Press. Beijing, 1986, 274-340(in Chinese)

[10] M.L. Zantua, L.C. Dumenil, J.M. Bremner. Relationship between soil urease activity and other soil properties.Soil Sci Soc Am J. 1977 (41) 350-352.

[11] E.L. Balota, J.C.Chaves: Rev Bras Cienc Solo 2012 (34) 1573-1583.

[12] N.M. Pettit, A.R.I. Smith, R.B. Freedman, R.O. Burns: Soil Biol Biochem 1976 (8) 479-484.

[13] G. Rodríguez-Loinaz, M. Onaindia, I. Amezaga, I. Mijangos, C. Garbisu. Relationship between vegetation diversity and soil functional diversity in native mixed-oak forests. Soil Biol Biochem 2008 (40) 49-60.

[14] P. Perucci, U. Bonciarelli, R. Santilocchi, A.A. Bianchi. Soil urease: activity, stability and kinetic properties. Biol Fert Soils 1997 (24) 311-316.

[15] Y. Tian, F. Cao, G. Wang. Soil microbiological properties and enzyme activity in Ginkgo–tea agroforestry compared with monoculture. Agroforest Syst 2013 (87) 1201-1210.

[16] B. Wang, S. Xue, G.B. Liu, G.H. Zhang, G, Li, Z.P. Ren. Changes in soil nutrient and enzyme activities under different vegetations in the Loess Plateau area, Northwest China.Catena 2012 (92) 186-195.

[17] K. Alef, P. Nannipieri: Catalase activity. In: Alef K, Nannipieri P, editors. Methods in applied soil microbiology and biochemistry. London: Academic Press, 1995, p 362-3

Advanced Materials Research Vols. 989-994 (2014) pp 1297-1300
© (2014) Trans Tech Publications, Switzerland
doi:10.4028/www.scientific.net/AMR.989-994.1297

Temperature Effect on the Hypergene Mineral Formation Process (the Case of Tailing Dumps of Komsomolsky Tin-Ore District)

Valentina Zvereva[1, 2, a], Alyona Kostina[1, 2, b], Konstantin Frolov[2, c]

[1]Far Eastern Federal University: 8, Sukhanova st., Vladivostok 690950, Russian Federation. Tel.: +7(423)2433280;

[2]Far East Geological Institute FEB RAS: 159, Prospekt 100-letiya, Vladivostok 690022, Russian Federation, Tel.: +7(423)2318750.

[a]zvereva@fegi.ru,[b]alyona5vbc@mail.ru, [c]konstantin.fk@gmail.com

Keywords: physicochemical modeling, hypergenesis, tailings, tailing dump, estimation of ecological situation, verification.

Abstract. Physicochemical modeling of drainage water in the tailing dumps of Komsomolsky tin ore district in a wide temperature range from -10 to +45 °C obtained in the article let to find Eh-pH parameters of micropore solutions from which technogenic and hypergene minerals crystallize. The modeling was made for different ratios host rock – sulfides (95:5, 90:10, 80:20 and 60:40). Qualitative and quantitative ionic composition of the solutions was determined and their impact on the surface and ground water of the area was showed.

Introduction

Long lasting and intensive development of the mining industry in the Komsomolsky district during the last 70 years led to the presence of numerous ditches, pits, tunnels and tailing dumps. It contributed to the creation of mining technogenic system with area of dozens of acres where hypergene processes are activated due to the increase of contact surface of sulfides with the weathering agents.

There are two concentrating mills and three tailings dumps (their total area is 80.8 hectares) in the district. 41.5 million tons tailings were stockpiled here. The finely-dispersed tailings mass of Komsomolsky region consists of (%): vein quartz – 37.5, tourmaline – 12.1, host sedimentary rocks – 45 and sulfides (pyrite, pyrrhotite, arsenopyrite, chalcopyrite, galena and sphalerite) – 3.8. They contain the following useful components (g/t): Sn – 0.2, Cu – 0.46, Zn – 0.094, Pb – 0.123, Ag – 1.227, Bi – 0.03, As – 0.629.

Negative impact of mining systems on the ecosphere in general and on the hydrosphere in particular is shown in many literary sources [1-3 and others].

The main purpose of this work is to assess the impact of technogenic and hypergene processes on hydrosphere in three tailing dumps of the district in a wide temperature range from -10 to +45 ° C. Climatic characteristic of the district [4] shows the annual temperature change in a range from -40 to +40 ° C. It can greatly increases under sulfides oxidation, so the upper limit was taken five degrees higher. Based on the goal the following tasks were formulated: 1. to research the process of sulfides oxidation in three tailings of the district in the temperature range from -10 to +45 ° C; 2. to determine the composition of technogenic minerals crystallized from the solutions of drainage and slime waters; 3. to find the qualitative and quantitative composition of these waters; 4. to assess their impact on the hydrosphere of the district; 5. to verify the data obtained.

Research method

Physicochemical modeling of technogenic processes occurring in the mining waste was conducted through the "Selektor" PC program. It made possible calculation of the amounts of elements carried out from the tailing dumps into the hydrosphere. The method is based on the minimization of the

Gibbs energy and estimation of the total and metastable equilibrium in multicomponent heterogeneous systems.

In our previous work the modeling was performed at the temperature of +25 ºC [5]. In this research we consider a system with a pressure of 1 atm and temperature range from -10 to +45 ºC. The water-rock ratio was taken as 10:1. The annual rainfall (400-500 kg per 1 m^2) and the selected temperature range were taken into account in the modeling. Models were opened to the atmosphere. The chemical composition of the atmosphere (10 kg) was calculated by R. Horne [6]: Ar – 3.21, C – 0.11, N – 539.48, O – 144.85. 19 independent (Al, Ar, As, B, C, Ca, Cu, Fe, K, Mg, N, Na, Pb, S, Si, Zn, H, O, e) and 452 dependent components were included in the calculations, from which 360 are dissolved particles, 18 gases and 74 hypogene and hypergene minerals.

Results and discussion

Mining wastes are presented by pyrite, pyrrhotite, galena, sphalerite, arsenopyrite, chalcopyrite, quartz, tourmaline and other minerals. Modeling of sulfides oxidation in contact with the host rock was carried out for all three tailing dumps (Table 1). The waste composition varies in its different parts, therefore simulated system for each of them were made with ratios of host rock – sulfides 95:5, 90:10, 80:20 and 60:40. Hypergene minerals crystallized from concentrated solutions of these models are shown in the Table 2.

In the simulated system of Festivalnoye deposit tailing dump – copper-tin-type of Solnechnaya concentrating mill (SCM) solutions are similar and have pH values ranging from 6.02 to 12.12 and Eh – 0.59-0.83 volts. Some of them crystallize at all ratios (g): goethite, woodwardite, kaolinite, magnesite, gypsum, hydromuscovite, others – in all ratios, except 95:5 (g): scorodite and rostite. Other minerals crystallize only at a certain ratio (g): calcite (95:5), duftite (80:20 and 60:40), alunogen (80:20 and 60:40), starkeyite (60:40) and montmorillonite (90 10).

In the simulated system of Solnechnoye deposit tailing dump – tin mineralization type of Centralnaya concentrating mill (CCM) solutions are similar and have pH values ranging from 5.98 to 12.29 and Eh – 0.58-0.84volts. In this temperature range minerals of hypergenesis zone and weathering crust crystallize from such classes as oxides, hydroxides, sulfates, carbonate, silicates, and arsenates. These are minerals of the following cations (g): Fe (goethite and scorodite), Pb and Cu (duftite) and Al (kaolinite, alunogen and rostite), Cu and Al (woodwardite), Mg (starkeyite and magnesite), Ca (gypsum and calcite), K and Al (hydromuscovite), Mg, Al and Fe (montmorillonite).

In the simulated system of the third tailing dump where ore processing waste of tin-polymetallic ore type of Perevalnoe deposit were stockpiled parameters of the solutions are similar and have pH values ranging from 6.09 to 12.06 and Eh – 0.60-0.83 volts. In these systems the same hypergene minerals crystallize as in the previous ones but are distinguished by the quantitative characteristic (Table 2).

It should be noted that the amount of crystallized minerals in all systems is low at a negative temperature, but the mineralization of these solutions is very high. For example, in the models of CCM tailings dump it is 144-284, SCM – 142-280 and the third one – 146-287 g/l. With the temperature increase from 0 up to +20 °C mineralization of the solution becomes higher (g/l): at CCM tailings dump – from 21.08 to 22.21, but then decreases to 20.55, SOF – 20.37-21.63 – to 20.37, at the third one – 21.48-22.24 – to 21.89.

At temperatures below 0 °C the model contain water in a solid form (ice), the content of which varies from 85.18 to 90.07 g and its amount decreases with the increase of host rock and decrease of sulfides in the system. Crystallization of some minerals (scorodite, starkeyite and rostite) in the models occurs at subzero temperatures in a range from 0 to -10 ° C and the other ones (calcite, alunogen, woodwardite, duftite, montmorillonite) at positive numbers from 0 to +45 °C. Other minerals (goethite, kaolinite, gypsum, magnesite) crystallize in a large range from -10 to +45 °C, but their quantity in the case of negative temperature values is much lower than for the positive ones. Thus crystallization at low temperatures is difficult.

Ionic composition of the resulting solutions is presented by the following ions of sulfide elements: As_5^+, $CuCO_3^{2-}$, Cu^{2+}, $CuCO_3^0$, CuO^0, $CuOH^+$, $CuSO_4^0$, $H_2AsO_4^-$, $H_3AsO_4^0$, $HAsO_4^{2-}$, $HCuO_2^-$, $HFeO_2^0$, FeO^+, FeO_2^-, $FeOH^{2+}$, $HPbO_2^-$, HSO_4^-, $HZnO_2^-$, $Pb(CO_3)_2^{2-}$, $Pb(SO_4)_2^{2-}$, Pb^{2+}, $PbHCO_3^+$, $PbNO_3^+$, PbO^0, $PbOH^+$, $PbSO_4^0$, $Zn(CO_3)_2^{2-}$, $Zn(SO_4)_2^{2-}$, Zn^{2+}, $ZnCO_3^0$, $ZnHCO_3^+$, ZnO^0, $ZnOH^+$, $ZnSO_4^0$, SO_4^{2-}.

Verification made with ionic and mineral composition [1] and comparison of the element contents in the modeled solutions with hydrochemical data on the mine, slime, and drainage waters [2-3] proved the validity of the obtained results.

Conclusion

Physicochemical modeling of sulfides oxidation has shown that from highly concentrated solutions hypergene minerals of Fe, Cu, Pb, Al, Mg, K and Ca crystallize, that belong to sulfates, carbonates, silicates, arsenates, oxides, and hydroxides classes. The greatest amount of ore elements (Cu, Pb, Zn, S) in the solutions is observed at negative temperatures. In the range of positive temperatures elements content in the aqueous solutions is gradually reduced by an order or two. Simulated drainage water solutions of all tailing dumps are characterized by high concentration (g/l) of S to 9.6, Pb – 66.8, Zn – 53.6, As – 46.6 and Cu – 53.9. Total mineralization of the tailings solutions is (g/l): 20 to 397 for CCM, 21-462 for SCM and 20-428 – for 3rd one. If we estimate the impact of each individual tailing dump, the maximum hydrosphere damage is caused by SCM tailing dump and the minimum – by CCM. Total removal of elements from all three tailing dumps varies from 61 to 1287 g/l.

Physicochemical modeling of the main phases of the drained tailing dumps existence in Komsomolsky tin ore district carried out by authors in the temperature range from -10 to +45 °C gives a complete picture of the drainage water formation that flows into the surface water in a dangerous, untreated form. Hydrosphere is exposed to strong anthropogenic stress with S, Zn, Cu, Pb, Fe sulfides elements and B, Mg, K, Na, Ca, Si and Al host rocks elements.

Modeling allows assessing the condition of mining technogenic system in space and time, to receive new data for the parameters of modern technogenic minerals and to show their Eh-pH existence conditions.

Acknowledgement

The research work was supported by the FEB RAS grant number 14-III-B-08-052. The authors are thankful to PhD Valeriy Bychinsky for his help in the modeling.

Table 1 – Original composition of hypogene minerals using in the models [%]

Mineral	Tailing dump		
	SCM	CCM	Third TD*
Sulfides			
Pyrite FeS_2	18	25	31
Pyrrhotite $Fe_{1-x}S_n$	27.5	25	23.5
Arsenopyrite FeAsS	25	22	11
Chalcopyrite $CuFeS_2$	25	16	9.5
Galena PbS	1.5	5	13
Sphalerite ZnS	3	7	12
Host rock			
Grossular $Ca_3Al_2[Si_3O_{12}]$	6.2	5	5.7
Albite $Na[AlSi_3O_8]$	5	6.2	5.5
Clinochlore $Si_3Al_2Mg_5H_8O_{18}$	10	10	10

Muscovite $KAl_2[AlSi_3O_{10}](OH)_2$	4.4	4.4	4.4
Biotite $NaFe_3[AlSi_3O_{10}](OH)_2$	4.4	4.4	4.4
Tourmaline $NaFe_3Al_6[BO_3]_3[Si_6O_{18}](OH)_4$	70	70	70

*Third TD – Third tailing dump

Table 2 – The composition of hypergene minerals in the results of modeling of tailings oxidation in contact with host rock [g]

Mineral	Tailing dump		
	SCM	CCM	Third TD
Ice H_2O	85.3-89.9	85.2-89.9	85.8-90.1
Goethite FeOOH	2.2-27.2	2.2-27.5	2.1-26.3
Magnesite $MgCO_3$	0.3-6.6	0.3-6.3	0.3-6.1
Calcite $CaCO_3$	0.2-1.4	0.2-1.9	0.1-1.6
Gypsum $CaSO_4 \cdot 2H_2O$	0.3-3.5	0.4-5.5	0.4-2.7
Starkeyite $Mg[SO_4] \cdot 4H_2O$	0.4-0.5	0.3-0.5	0.3
Hydromuscovite $K[Al_3Si_3O_{10}](OH)_2 \cdot 4H_2O$	0.3-3.7	0.1-3.7	0.3-3.7
Muscovite $K[Al_3Si_3O_{10}](OH)_2$	1.8-12.6	0.8-3.1	0.9-3.1
Quartz SiO_2	0.5-12.6	0.1-12.4	0.1-12.0
Caolinite $Al_2[SiO_3]_2(OH)_4$	1.4-61.6	1.3-60.7	2.76-61.6
Woodwardite $Cu_4Al_2[SO_4](OH)_{12} \cdot H_2O$	0.02-2.6	0.2-3.8	0.1-2.0
Rostite $Al[SO_4](OH) \cdot 5H_2O$	0.5-7.0	0.3-6.8	0.4-7.2
Alunogen $Al_2[SO_4]_3 \cdot 18H_2O$	2.3-55.8	14.5-54.9	0.4-55.6
Duftite $PbCu[AsO_4](OH)$	0.2-2.4	0.1-0.7	0.4-5.3
Scorodite $Fe[AsO_4] \cdot 2H_2O$	0.03-1.2	0.07-1.3	0.04-0.6
Montmorillonite $(Na.Ca)_{0.33}(Al.Mg)_2(Si_4O_{10})(OH)_2 \cdot nH_2O$	14.9-15.6	13.6	14.3

References

[1] V.P. Zvereva. Ecological subsequences of hypergene processes at tin deposits of the Far East. Dalnauka: Vladivostok, 2008.

[2] V.P. Zvereva, L.T. Krupskaya. Anthropogenic Waters in the Komsomolsk, Kavalerovskii, and Dalnegorsk Mining Areas of the Far East and Their Impact on the Hydrosphere. Russian Journal of General Chemistry, 2012, 82 (13). 2244-2252.

[3] P.V. Elpatevsky, T.N. Lutsenko. The mining complex as the factor of formation of the water chemical composition. Materials: Scientific and practical aspects of extraction of non-ferrous and precious metals. 2000 (2). 407-415.

[4] G.N. Vitvitskiy. The Far East. Physiographic characteristic. Publishing House of the USSR Academy of Sciences: Moscow, Ch. Climate, 1961. 93-115.

[5] A.M. Kostina, V.P. Zvereva, K.R. Frolov, A.D. Pyatakov, A.I. Lysenko. Impact assessment of tin ore tailing dumps of Komsomolsky district of the Far East on the hydrosphere. Chemical Technology, 2012 (5). 316-320.

[6] R. Horne. Marine chemistry. Mir: Moscow, 1972.

Advanced Materials Research Vols. 989-994 (2014) pp 1301-1304
© (2014) Trans Tech Publications, Switzerland
doi:10.4028/www.scientific.net/AMR.989-994.1301

Evaluation of technogenous processes proceeding in tailing dump of the Central Concentrating Mill of Dal'negorsk District and their effect on the hydrosphere with method of physicochemical modeling

V.P. Zvereva[1, 2, a], A.I. Lysenko[2, b], A.M. Kostina[1, 2, c]

[1]Far East Federal University, 8, Sukhanova, Vladivostok, 690091, Russian Federation

[2]Far East Geological Institute FEB RAS, 159, Prospect 100 let Vladivostoka, Vladivostok, 690022, Russian Federation

[a]zvereva@fegi.ru, [b]lion8888@inbox.ru, [c]alyona5vbc@mail.ru

Keywords: hypergenesis, physicochemical modeling, tailings, tailing dump, estimation of environmental conditions, verification.

Abstract. Modeling allowed us to show Eh-pH parameters of the technogenic mineral formation in the mining-industrial technogenic system of polymetallic ores of Dal'negorsk district, to study the process of the hypergene mineral crystallization from solutions, to consider the qualitative and quantitative ionic composition of solutions, to show the role of hypergenesis in the contamination of surface and ground waters of the area. The aim of this work is to estimate the action of the CCM tailing oxidation on the hydrosphere of the district using the method of physicochemical modeling. The results obtained testify to a significant evacuation of a wide range of elements of sulfide ores (Zn, Pb, Cu, As, S) and enclosing rocks (Si, Al, Mg, Ca, K, Na) from the CCM tailing dumps into the surface waters polluting the hydrosphere with them.

Introduction

At the present time, the problems of ecological consequences of the mining-concentrating industry are very urgent. In Dal'negorsk district this industry has been developing for more than a hundred years. More than 20 skarn and polymetal deposits are developed here by opened and closed way. In Dal'negorsk there are two Central Concentrating Mills (CCM), and at present one of them is working. It processes the sulfide polymetal ores, and its work resulted in the formation of two tailing dumps (old and new) in the Town neighborhood. The CCM old tailing dump was in operation to 1978, and then up to present a new one is being filled.

Quarries, ditches, places of stripping, adits, and tailing dumps, resulted from mining works, form the mining-industrial technogene system. Sulfides in this system become accessible for the weathering agents and are intensively oxidized producing highly concentrated micro-pore solutions, which give rise to the mining and drainage waters and from which abundant hypergene and technogene minerals are precipitated.

The aim of this work is to estimate the action of the CCM tailing oxidation on the hydrosphere of the district using the method of physicochemical modeling. To do this we posed the following tasks: elaboration of the physicochemical models of tailing oxidation and estimation of the tailing dump action on the hydrosphere using the results obtained.

Materials and methods

In our investigations we use the method of physicochemical modeling. The correspondence of the developed model with the study object is checked by verification. The model allows the objective estimation of geochemical processes proceeding in the tailing dumps, determination of the composition of the dissolved ions of chemical elements in the sulfide oxidation process, study of crystallization of hypergene and technogene minerals, and prediction of the object state in the future.

Physicochemical modeling of the technogenesis processes in the CCM tailing dumps was performed using the "Selector-Windows" program complex based on the minimization of Gibbs free energy.

In the authors' previous works [2, 3] such investigations were carried out for the thermodynamic system with 40 hypergene and technogene minerals. Later, in the literature the thermodynamic parameters were found for pyrargyrite, hisingerite, and hydrogoethite and were calculated (A.A. Tupitsin and V.A. Bychinsky, Siberian Branch of RAS) for fibroferrite and then were brought into the system. Besides, the models were added with hypogene minerals of sulfur, silver, and antimony: argentite, acanthite, and pyrargyrite, as in the wastes about 5 g/t of silver is found in the form of these sulfides. We studied the dependence of element behavior in the solution and the technogene mineral crystallization on the increase of a summary content of galena and sphalerite in the system (30 to 90 %).

The authors chose the common thermobarometric conditions for modeling – T = +25 ºC and P = 1 atm. The rain water composition: N_3^-, N_2^- NH_4^+, $NH_4N_3^0$, HNO_2^0, $NH_4NO_3^0$, NH_4OH^0, $NH_4NO_2^0$, NH_3^0, $H_2CO_3^0$, HCO_3^-, CO_3^{2-}, $C_2O_4^{2-}$, CH_4^0, O_2^0, H_2^0, N_2^0, Ar^0, He^0, Kr^0, Ne^0, OH^-, H^+, H_2O^0, NO_3^-, HNO_3^0 (pH=5.66). The models were one-reservoir and opened to the atmosphere. The chemical composition of the atmosphere was calculated after R. Horne [4]. Ten kilograms of the atmosphere includes (moles): Ar – 3.209, C – 0.1036, N – 539.478, O – 144.8472.

In modeling of the hypergene processes in the CCM new and old tailing dumps of Dal'negorsk District the calculations embraced 19 independent and 380 dependent components that included 316 dissolved particles, 18 gases, and 47 minerals and solid solutions.

Results and discussion

Modeling was carried out for the sulfide oxidation in the contact with the enclosing rocks with the change of the galena and sphalerite percent content. All models were constructed on the averaged literature data [5, 6]. As the tailing composition is variable, the modeling was done with a summary content of galena and sphalerite of 30 to 90 %, and the remainder of them (to 100 %) included other sulfide minerals (Table 1). The ratio of the enclosing rock/sulfides was: 95:5, 90:10, 80:20, and 60:40.

The results of modeling of the tailing oxidation in the CMM tailing dump with different correlation of enclosing rocks/sulfides showed that with increasing content of galena and sphalerite in them the value of the acidity-alkalinity index of the solution (pH) is changed from 6.09 to 10.94 and oxidation-reduction potential – from 0.86 to 0.57 B.

The solutions of models for all ratios of enclosing rocks/sulfides contain the following elements (mg/l): Ca – 262.8 to 348.8, Na – 31.65-836.9, Ag – 209.9-1725, As – 10.9-2231, Sb – 11-92.7, Cu – 8.3-1968, Pb – 451.3-17510, S – 902.6-4783, Zn – 349.6-13550.

Through oxidation a portion of the primary minerals remains not-destructed in all models (%): albite – 0.04 to 6.26, andradite – 7.62 to 24.50, muscovite – 1.27 to 8.83, quartz – 0.46 to 7.84. Some minerals remain in the system only at the summary content of galena and sphalerite of 90 %. These are diopside (3.32 to 6.74 %), epidote (8.88 to 23.51 %), and potassic feldspar (3.29 %) (at 70 % and ratio of 60:40).

With increasing concentration of sulfides (galena and sphalerite) the quantity of hypergene minerals, being crystallized, decreases (Table 2): goethite – from 19.78 to 0.71 % and then it disappears from the system (at the summary content of galena and sphalerite of 50 % in the system the enclosing rock/sulfides ratio is 95:5 and at 90 % – 90:10 and 80:20), gypsum – from 51.11 to 0.10 in all models, montmorillonite – from 26.20 to 16.71 (for the system of 95:5). In other systems the montmorillonite amount increases and reaches its maximum of 26.27 (galena and sphalerite sum is 70 %), then its amount falls again to 4.76 (90 %, 60:40). The following minerals are crystallized only at the enclosing rocks/sulfides ratio of 60:40: plumbojarosite – 2.75 and 6.33 % (galena and sphalerite sum is 30 %), cerussite – 0.09 (70), and adamite – 0.07 (90). Ag and Sb minerals are not precipitated, and these elements remain in full in the modeled solutions.

Table 1 – Mineral composition of the CCM tailing dumps [%]

Minerals of sulfides and enclosing rocks	Total quantity of galena and sphalerite							
	30		50		70		90	
	20-10	10-20	30-20	20-30	40-30	30-40	50-40	40-50
Sulfide minerals								
Sphalerite ZnS	20	10	30	20	40	30	50	40
Galena PbS	10	20	20	30	30	40	40	50
Pyrite FeS_2	20	20	15	15	10	10	2	2
Pyrrhotite FeS	19	19	14	14	9	9	2	2
Chalcopyrite $CuFeS_2$	14	14	8	8	3	3	0.5	0.5
Arsenopyrite FeAsS	12	12	8	8	3	3	0.5	0.5
Argentite Ag_2S	2	2	2	2	2	2	2	2
Acanthite Ag_2S	2	2	2	2	2	2	2	2
Pyrargyrite Ag_3SbS_3	1	1	1	1	1	1	1	1
Minerals of enclosing rocks								
Hedenbergite $CaFe[Si_2O_6]$	10	10	10	10	10	10	10	10
Grossular $Ca_3Al_2[SiO_4]_3$	10	10	10	10	10	10	10	10
Andradite $Ca_3Fe_2[SiO_4]_3$	11	11	11	11	11	11	11	11
Diopside $CaMg[Si_2O_6]$	8	8	8	8	8	8	8	8
Muscovite $KAl_2[AlSi_3O_{10}](OH)_2$	9	9	9	9	9	9	9	9
Epidote $Ca_2(Al,Fe)_3Si_3O_{12}[OH]$	12	12	12	12	12	12	12	12
Calcite $CaCO_3$	30	30	30	30	30	30	30	30
Albite $Na[AlSi_3O_8]$	10	10	10	10	10	10	10	10

Table 2 – The composition of hypergene minerals in the results of modeling of tailings oxidation in contact with host rock [%]

Mineral	Total quantity of galena and sphalerite							
	30		50		70		90	
	20-10	10-20	30-20	20-30	40-30	30-40	50-40	40-50
Goethite FeOOH	2.09-17.68	2.08-19.78	0.62-17.53	0.71-17.69	0.61-10.82	0.80-13.32	—	—
Gypsum $CaSO_4(H_2O)_2$	3.69-50.14	3.45-51.11	2.28-50.17	2.06-48.43	1.89-44.26	1.50-44.22	0.34-37.98	0.10-35.03
Plumbojarosite $Pb_{0.5}Fe_3(SO4)_2(OH)_6$	6.33	2.75	—	—	—	—	—	—
Cerussite $PbCO_3$	—	—	—	—	—	0.09	—	—
Adamite $Zn_2AsO_4(OH)$	—	—	—	—	—	—	0.07	—
Montmorillonite $(Na.Ca)_{0.33}(Al.Mg)_2(Si_4O_{10})(OH)_2 \cdot nH_2O$	15.21-26.20	15.51-26.21	16.97-26.74	17.14-26.73	19.36-26.26	18.70-26.27	10.45-16.24	4.76-16.71

The solution ion composition in the model variants with the summary content of galena and sphalerite of 30 to 50 % is similar and represented by: $Ag(CO_3)^-$, $Ag(CO_3)_2^{3-}$, $Ag(OH)_2^-$, Ag^+, $AgNO_3^0$, AgO^-, $AgOH^0$, $Al(OH)^{+2}$, Al^{3+}, AlO^+, AlO_2^-, AsO_4^{3-}, CO_2^0, CO_3^{2-}, $Ca(HCO_3)^+$, $CaHSiO_3^+$, Ca^{2+}, $CaCO_3^0$, $CaOH^+$, $CaSO_4^0$, $Cu(CO_3)_2^{2-}$, Cu^+, Cu^{2+}, $CuCO_3^0$, $CuHCO_3^+$, CuO^0, CuO_2^{2-}, $CuOH^+$, $CuSO_4^0$, Fe^{3+}, $Fe(OH)_2^+$, $Fe(OH)_3^0$, $Fe(OH)_4^-$, $FeSO_4^+$, $FeAsO_4^0$, FeO^+, FeO_2^-, $FeHAsO_4^+$, $FeH_2AsO_4^{2+}$, $H_2AsO_4^-$, $H_3AsO_4^0$, $HAlO_2^0$, $HAsO_4^{2-}$, HCO_3^-, $HCuO_2^-$, $HFeO_2^0$, HNO_2^0, HNO_3^0, $HPbO_2^-$, HSO_4^-, $HSiO_3^-$, $HZnO_2^-$, K^+, $KHSO_4^0$, KOH^0, KSO_4^-, $Mg(HCO_3)^+$, $MgHSiO_3^+$, Mg^{+2}, $MgCO_3^0$, N_2^0, NO_2^-, NO_3^-, Na^+, $NaAsO_4^{2-}$, $NaHSiO_3^0$, $NaOH^0$, $NaSO_4^-$, O_2^0, $Pb(OH)_2^0$, $Pb(CO_3)_2^{2-}$, $Pb(SO_4)_2^{2-}$, Pb^{2+}, $PbCO_3^0$, $PbHCO_3^+$, $PbNO_3^+$, PbO^0, $PbOH^+$, $PbSO_4^0$, SO_4^{2-}, SiO_2^0, $Zn(CO_3)_2^{2-}$, $Zn(SO_4)_2^{2-}$, Zn^{2+}, $ZnCO_3^0$, $ZnHCO_3^+$, ZnO^0, ZnO_2^{2-}, $ZnOH^+$, $ZnSO_4^0$, $HSbO_2^0$, $Sb(OH)_2^+$, $Sb(OH)_3^0$, SbO_2^-, OH^-, H^+, H_2O^0.

The ion composition of the solutions in the variants with more amount of sulfides (70 and 90 %) differs from the previous one in the absence of $Fe(OH)^{4-}$ and $FeAsO_4^0$ (at the enclosing rock/sulfides ratio of 95:5 and 90:10). In different models at 80:20 and 60:40 ratios the following ions are absent sometimes: $Ag(CO_3)_2^{3-}$, $HCuO_2^-$, $HPbO_2^-$, $HZnO_2^-$, $KHSO_4^0$, KOH^0, $MgHSiO_3^+$, $MgCO_3^0$, $Pb(CO_3)_2^{2-}$, $Pb(OH)_2^0$, $PbCO_3^0$, ZnO_2^{2-}, Cu^+, CuO_2^{2-}, Fe^{3+}, $FeH_2AsO_4^{2+}$, $FeSO_4^+$, $KHSO_4^0$, Al^{3+}, Fe^{3+}, $FeHAsO_4^+$, $FeH_2AsO_4^{2+}$, $FeOH^{2+}$, $Al(OH)^{2+}$, $Fe(OH)_2^+$, $FeAsO_4^0$, $FeSO_4^+$.

Mineralization of sulfide elements in the modeled solutions of the study variants is (g/l) from 2.85 to 17.3 (30 %), 3.56-3.61-23.3 (50 %), 4.07-28.4 (70 %); 4.82-34.7 (90 %). A total mineralization of the solutions is (g/l) 3.97-18.2 (30 %), 4.70-24.1 (50 %), 4.93-29.2 (70 %), 5.68-35.3 (90 %).

Conclusion

In conclusion it should be noted that the increasing summary content of galena and sphalerite in the system (from 30 to 90 %) makes it possible for plumbojarosite (only at 30 %) and adamite (only at 90 %) to be crystallized in the modeled systems. These minerals are precipitated at the enclosing rock/sulfides ratio equal to 60:40. In other cases Pb and Zn remain in solutions. Oxidation of Ag and Sb sulfides (argentite, acanthite and pyrargyrite) enriched the micropore solutions in these elements and increased their mineralization.

The results obtained testify to a significant evacuation of a wide range of elements of sulfide ores and enclosing rocks from the CCM tailing dumps into the surface waters polluting the hydrosphere with them. Mineralization of the solutions with the sulfide ore elements reaches 34.7 g/l, and a total mineralization is 35.3 g/l.

Acknowledgement

The authors are thankful to PhD Valeriy Bychinsky and PhD Alexey Tupitsin (A.P. Vinogradov Institute of Geochemistry SB RAS) for their help in the modeling.

References

[1] I.A. Tarasenko, A.V. Zin'kov. The environmental effects of mineralogical-geochemical transformation of the tailings of Sn-Ag-Pb-Zn ores. Vladivostok: Dalnauka, 2001. 184.

[2] V.P. Zvereva, A.I. Lysenko, A.M. Kostina. Estimation of Effect of Hypergene Processes Proceeding in the Mining-Industrial Technogene System on the Hydrosphere of Dal'negorsk District Using Physicochemical Modeling Method (Primorsky Region). Advanced Materials Research, 2013 (813) 246-249.

[3] V.P. Zvereva, A.D. Pyatakov, A.I. Lysenko, A.M. Kostina. Estimation of effect of polymetallic ore tailing dumps on hydrosphere using physicochemical modeling method (Primorsky Region). Future Energy, Environment and Materials. WIT Transactions on Engineering Sciences, 2014 (88) 493-499.

[4] R. Horne. Marine chemistry. Moscow: Mir, 1972. 398.

[5] N.V. Bulavko. Mineralogy of Skarn Deposits of the Dal'negorsk Ore Field (Primorsky Krai), Far East Publishing House. Vladivostok: Dal'nauka, 2000. 219.

[6] V.P. Zvereva. Morphology and mineralogy of hypergenesis zone of polymetal deposits of Dal'negorsk ore district (Primorye). Collection: Ore deposits of continental margins. Vladivostok: Dal'nauka, 2001. 180-190.

Advanced Materials Research Vols. 989-994 (2014) pp 1305-1308
© (2014) Trans Tech Publications, Switzerland
doi:10.4028/www.scientific.net/AMR.989-994.1305

Some Ecological Problems of Development of Mineral Raw Materials in Amurskaya Oblast'

Lyudmila Timopheevna Krupskaya[1, 2, a] , Valentina Pavlovna Zvereva[3, 4, b], Oleg Olegovich Panfilov[1, c]

[1]Pacific State University, 136, Tikhookeanskaya str, Khabarovsk, 680035, Russian Federation

[2]Far East Scientific-Research Institute of Forestry, 71, Volochaevskaya str, Khabarovsk, 680020 Russian Federation

[3]Far East Federal University, 8, Sukhanova str, Vladivostok, 690091, Russian Federation

[4]Far East Geological Institute FEB RAS, 159, Prospect 100 let Vladivostoka, Vladivostok, 690022, Russian Federation

[a]ecologiya2010@yandex.ru, [b]zvereva@fegi.ru, [c]barleon-2@mail.ru

Keywords: natural-mining industrial system, technogenic pollution, wastes, heavy metals, reclamation.

Abstract. The paper considers some ecological problems of the gold-mining enterprise in Amurskaya Oblast'. The investigations have revealed the technogenic pollution of the soil-grounds, air basin, and vegetation under the action of the processing wastes. High concentrations of heavy metals were found in the soils and vegetation in the zone of influence of the plant processing heavy concentrates at a distance of 100 and more meters. They are 2 to 90 times higher than the background values practically in all directions from the technogenic object. High TM concentrations were found also in the soils of building zone. Using the innovation approach we have elaborated the measures for decreasing the pollution negative effect on the habitat. We propose a new way of reclamation of the lands disturbed by the wastes of the mineral raw material processing with the use of the mixed bark-compost of the forest industry wastes.

Introduction

In Amurskaya Oblast' for almost 150 years they have been mining gold and have been developing the deposits of titanium-magnetite and other ores. The region possesses tremendous reserves of apatites, anorthosites, marbles, coal, and other useful minerals. Long exploitation of gold-placer deposits in Amurskaya Oblast' promoted the accumulation of great volumes of the wastes of ore processing resulted in technogene pollution of ecosphere, degradation and disappearance of the valuable species of plants and animals, intensive destruction of ecosystems, and sharp deterioration of the human habitat. Besides, the economical reorganization in Russia in 1990s didn't bring about the reconstruction of the mining enterprises. At present, the greatest threat is the emergency of many technogene systems, which year after year more and more actively undergo hypergenesis and technogenesis and contribute to the pollution of natural systems. All these cause the losses of the mining-industrial complex and threaten the people health and life. In Amurskaya Oblast', however, there so far is absent the scientifically justified system of evaluation and control of the ecological risk to provide the economical and ecological safety. In this connection the aim of our work was to reveal some ecological problems of the wastes of the gold-placer deposit processing to provide their ecological safety. So our tasks were as follows: 1. To analyze and generalize the literature data on this problem; 2. To investigate the wastes as a source of negative action on soils and vegetation and evaluate their influence on the environment state; 3. To elaborate the innovation proposals for decreasing the effect of the wastes of the mineral raw material processing on the natural systems and population of the mining settlement.

Objects and Methods of Research

The objects of investigation were the natural-mining-industrial systems. We used, as the methodological basis, the Academician V.I. Vernadsky's teaching [1] on biosphere and noosphere and the principal theses stated by B.P. Kolesnikov and N.V. Motorina in "Program and methods of study of technogene biogeocoenoses" [2].

We took the soil-ground samples according to GOST 17.4.3.01-83 and GOST 17.4.4.02-84 and the vegetation samples according to GOST 27262-87. We used, as the background index, the area, remote from the main sources of pollution, that is located at 10 km from the concentrating plant. In this case we took account of the "wind rose". Our investigations covered the area more than 12 km^2 in size. The physical-chemical, chemical, and biological methods (test-systems "Pollen sterility" and "Growth test") were used.

Results and discussion

Analysis, generalization, and systematization of the literature data and materials of the patent search testify that through the processing of mineral raw materials the environment is subjected to the intensive technogene effect [3-7 others], one of the main negative sources being the storage of the concentration wastes on the territory of the mine settlement. For their placement the productive lands, including those of the forest stock, are used. The wastes, stored as tailing dumps, contribute to the pollution of the air and water basins resulted in the deterioration of the hydrological regime of the region. Concentrations of heavy metals in the air are 37 to 43 times higher than the background characteristics and in the surface waters – 6 to 19 times. In this case the ecological value of mountain landscapes decreases, the species diversity of vegetation and animal world is reduced, the soil cover is destroyed, the erosion processes become active, and so on [3-7]. Therefore, the evaluation of the consequences of the technogene pollution of the environment by the wastes of the processing of mineral raw materials and elaboration of the nature-protection measures in the study region is an urgent problem for providing their ecological safety.

Considering the wastes as a potential source of pollution we established that their composition is represented by diverse minerals: ilmenite, magnetite, wolframite, hematite, garnet, arsenopyrite, galena, cassiterite, epidote, zircon, pyroxene, and cinnabar. The wastes are characterized by a high content of heavy metals (HM): Cu, Pb, Zn, Sn, Hg, Mn, and others. Heavy fractions are rich in not only zircon, but ilmenite also. High concentrations of Pb, Cu, and Zn were established in the northeast direction. With distance (700 m) from the concentrating plant (CP) the content of both bulk and mobile forms of HM decreases. Heavy metals migrate from the wastes not only into the soils, but into the vegetation also. The quantity of HM in the studied mobile forms in the technogene soils in the zone of the CP influence significantly exceeds the background values (2 to 92 and more times) practically in all directions from its center.

Our investigations showed that the characteristic feature of the technogene pollution of soils is the accumulation of elements in the near-surface horizon. This is governed by precipitation (with wind carrying) of dust particles onto the soil surface layer and bonding of HM with organic matters and finely dispersed particles. As a rule, within the miners' settlement the main danger for the population health is the increasing concentration of heavy metals in the air and in the upper layer of the technogene soil.

High concentrations of heavy metals (Cu, Pb, Zn, As, etc.) exceeding the background values (1.5 to 14 times) and MPC (3 to 11 times) were found also in the vegetation, in the building zone at a distance of 1.5 km from the plant processing heavy concentrates. Correlation between the content of the mobile TM in the technogene soils and cytogenetic changes in the cells of the plant-bioindicators (the "Pollen Sterility" test-system) has been revealed. A direct dependence of the pollen sterility on the degree of the technogenic pollution has been recognized.

Biological methods (test-systems, study of microflora) allowed us to estimate the ecological situation in the district as critical. When investigating the agricultural production, we found that it accumulates big amounts of heavy metals, excess being 3 to 10 LPC.

The data obtained allowed us to divide the polluted mining-industrial territory into three zones:

1) zone of critical pollution where the TM contents are 3 to 56 and more times higher than a permissible norm (territory of the concentrating plant);

2) zone of mean pollution – amount of the TM mobile forms in soils is significant, exceeding the MPC for 2 to 4 times;

3) zone of satisfactory pollution – amount of the TM mobile forms in soils don't exceed the MPC: Zn -9-13 mg/kg, Pb – 3-4 mg/kg; Cd – 0.2 mg/kg.

Imperfection of technologies used in the mining industry is one of the main factors of the negative effect on the ecosystems.

Undoubtedly, the ecological problems in the miners' settlement are caused by the technology of mining and concentrating, storage, and deposition of the wastes, as well as by the mineral composition of the processed ores and wall rocks. As a result, the process of the risk control becomes complicated, because a constantly increasing number of its parameters and factors must be taken into account. The most important group of the fundamental factors includes: technological (technogene) and organization factors and the state of the economical and social-economical situation [6]. Their action on the biosphere components should be considered in complex with regard to their mutual influence and hierarchical relations. The role of the natural factors, such as specific features of climate, landscape, relief, and others, in these processes is great. In this connection, of great importance is the estimation of the ecological tension of the study district territory. The calculations showed that the complex index of the ecological tension, which reflects the role of the geomorphogenetic, cryogenic, soil-genetic, and climatic factors in their interrelation, turned to be critical of 2300 to 7000 points, testifying the necessity of a strict regulation of the nature management in Amurskaya Oblast'.

The technogene pollution of the ecosphere in Amurskaya Oblast' contributes to the ecology-caused diseases of respiration, digestive, nerve, and other organs. We have calculated the economic damage to the population health and found that children and working people and pensioners run the danger of this action to the greatest degree.

The highest summary index of danger (HI), equal to 71, has been recognized for a group of the matters affecting the man respiration organs, and namely the suspended matters, copper, chrome, sulfur dioxide, and others.

The technogene pollution of the soil-vegetative cover makes it urgent to take the measures for decreasing the concentrations of the polluting matters and withdrawal of them beyond the soil profile, as well as the preservation and recreation of the vegetative cover to prevent the wind and water erosion and technogene pollution by means of phytoreclamation. The innovation measures are proposed for improving the habitat in the miners' settlement of Amurskaya Oblast'. We have elaborated the method of reclamation of the lands disturbed by the wastes of the mining works with the use of the mixed bark-compost of the forest-industry wastes (Figure 1), and its novelty is confirmed by the Patent of the Russian Federation (of July 10, 2013).

The original material we have obtained may be used in the study of the dynamics of development of the regional nature-mining-technical systems.

Conclusions

Our investigations made it possible to reveal some ecological problems (technogene pollution of soil-grounds, air and water basins, vegetation) arisen through the development of the mineral raw materials in Amurskaya Oblast' and to elaborate the measures for decreasing the negative action of the processing wastes on the habitat with innovation approach. We propose the way of reclamation of the lands, disturbed by the wastes of the mineral raw material processing, with the use of the mixed bark-compost of the forest-industry wastes.

Fig. 1. Reclamation of the lands disturbed with the wastes of the mining works with the use of the mixed bark-compost (Amur region)

References

[1] V.I. Vernadsky. Biosphere. Moscow: Mysl'. 1967.

[2] B.P Kolesnikov, L.V Motorina. Methods of study of biogeocoenoses in technogene landscapes, Program and methods of study of technogene biogeocoenoses. Moscow: Nauka. 1978.

[3] K.N. Troubetzkoy, Y.P. Galchenko, L.I. Bourtsev. Ecological problems of development of mineral resources in the sustainable development of nature and society. Moscow: Izd LLC "NAUCHTEKHLITIZDAT. 2003.

[4] L.T. Krupskaya, B.G. Saksin, A.M. Ivlev, et al. Evaluation of transformation of ecosystems under action of mining works in the South Far East. Khabarovsk: KSTU. 2001.

[5] L.T. Krupskaya, V.I. Oznobikhin, V.P. Zvereva, V.A. Morin, D.A. Golubev, N.G. Volobueva. Erosion Processes in Anthropogenic Systems in the South of the Russian Far East. Russian. Journal of General Chemistry, 2013 83 (13) 2686-2693.

[6] L.T. Krupskaya, V.P. Zvereva, A.V. Leonenko. Impact of Technogenic Systems on the Environment and Human Health in the Priamurye and Primorye Territories Estimation of the tin-sulfide tailing effect on hydrosphere with physicochemical modeling (Komsomolsk area). Contemporary Problems of Ecology, 2013 6 (2) 223-227.

[7] A.A. Bykov. Methodical recommendations for estimation of social-economical damage from population health disturbance caused by pollution of atmosphere air. Risk control, 1999 (3) 16-24.

Advanced Materials Research Vols. 989-994 (2014) pp 1309-1312
© (2014) Trans Tech Publications, Switzerland
doi:10.4028/www.scientific.net/AMR.989-994.1309

Study on sewage treatment process in stone production

Min Zhao[1, a], Weiwei Guo[1, a], Qiang Xiao[1, b], Jing Zhang[2, a]

[1]Traffic and Mechanical Engineering School, Shenyang Jianzhu University, Shenyang, 110168, China

[2]Institute of Scientific and Technical Information of Liaoning Province, Shenyang, 110168, China

[a]email: 15998283375@163.com, [b]email:604502338@qq.com

Keywords: Stone Processing; Wastewater Treatment; Sedimentation Tank

Abstract. In the process of stone cutting and polishing, a large amount of high turbidity water is produced, which causes the waste of water resources and the pollution of the environment. The traditional treatment process is optimized, taking problems occurred in sewage treatment process by small and medium-sized enterprises and the existing technology and method into consideration. According to the production process of stone, the amount of waste water generated every day is calculated, which provides a theoretical basis for the sedimentation tank optimization and design. The necessity of stone wastewater reuse is illustrated.

Introduction

With the development and expansion of stone processing enterprises, a large amount of water is used in stone processing. The powder from stone is mixed with water, forming a large quantity of stone wastewater. The deterioration of water quality caused by the discharge of industrial sewage is an important cause of water pollution [1]. At present, the cleaner production index has been enacted in the stone industry. Cleaner production is not only to achieve low pollution in order to guide the reasonable arrangement of process, but also to realize optimization of manufacture process. Social benefits should be achieved without affecting the economic efficiency of stone enterprises, creating a win-win situation for both the producers and the public interest [2]. Stone wastewater is recycled, which can save a lot of water effectively and reduce environmental pollution. Recycled water can be used for industrial cooling water and process water, promoting the wide extension of cleaner production.

An Overview of Stone Wastewater Treatment

In the process of cutting and grinding stone slabs, a lot of heat will be produced, which will affect service life of diamond tool. As a result, water is often used to cool the diamond tool and remove grinding powder and clean the surface of stone slabs, producing a large amount of sewage. The ingredients of stone materials are very complex, and the main component of sewage caused by them is a mixture of water, abrasive dust, slag grinding grain, marble and granite debris.

Technological Process of Stone Processing. Stone processing directly affect the sewage emissions. In processing stone slab, an amount of sewage is produced and stone procedure mainly involve block cutting, grinding, polishing, cutting, splitting, inspection, and packing. The production line diagram about stone procedure is shown in Fig.1.

When sawing block, the block stone is put on the ferry car by crane, then block is carried to block car, and block is sawed into gross slab with gang saw machine. Gross slabs are sent to the continuous grinding and polishing line for grinding and polishing by rail. When slab is polished, according to the requirements of the project, the polished slab is cut into the slabs with different sizes by bridge cutting machine.

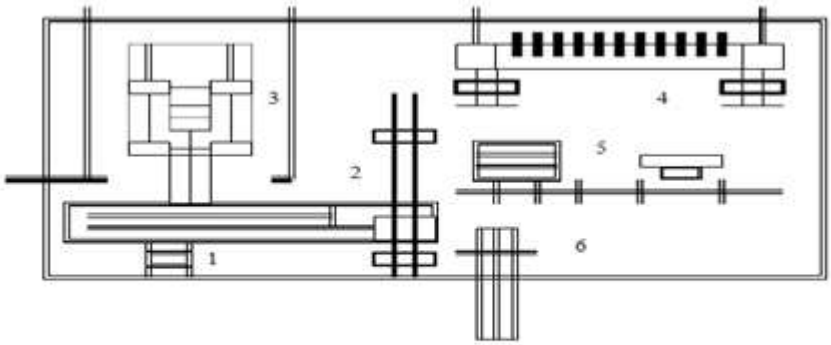

1 – Block car; 2 - Ferry car; 3 – Gang saw; 4 – Automatic grinding-polishing machine; 5 - Bridge cutting machine; 6 – Crane

Fig.1. Diagram of stone slabs production line

The Amount of Sewage Produced in Stone Processing. Equipment and operation parameters are analyzed and calculated, taking sewage treatment in processing stone slabs of middle and small-sized enterprises into consideration. Block stone with size $3250mm \times 2050mm \times 2000mm$ （$L \times B \times H$） is taken as an example. When annual working days d is300, daily working time t is 8 hours, the required equipment number is 2 block machine and a polishing line and 2 bridge cutting machine. According to the whole production process the daily water consumption amount is calculated as the following formula.

$$Q_w = (2v_s + v_m + 2v_c)t \tag{1}$$

In the formula: v_s is water consumption of block machine, which is 800L/h; v_m is water consumption of automatic grinding-polishing machine, which is 200L/min; v_c is water consumption of bridge cutting machine, which is $4m^3/h$.

Daily produced sludge is calculated as the following formula.

$$Q_m = Q_{sm} + Q_{mm} + Q_{cm} = \frac{2V_s tBHb_1 n}{L} + \frac{V_b tHb_2}{B} + 2V_c tb_3 d \tag{2}$$

In the formula: Q_{sm} is sludge produced by block machine. b_1 is sawing blade width of block machine, which is 2mm; the number of saw blade n is 8; the feed speed V_s is value range of 0 ~ 55cm/h; the saw blade spacing d is general scope for 1 ~ 2cm. Q_s is the amount of sludge generated by automatic grinding-polishing machine. According to automatic grinding-polishing machine amount grinded b_2 is 3mm; V_b is the speed of conveyor belt, which is 0 ~ 2m/min. Q_{cm} is sludge produced by the bridge cutting machine. According to the bridge cutting machine blade sawing width b_3 is 2.5mm, cutting speed V_c is 0 ~ 15m/min. On the basis of the above formula, Q_m is gotten.

Thereby the total amount of sewage generated every day is calculated as the following formula.

$$Q = Q_w + Q_m \tag{3}$$

Technology Development of Sewage Treatment of Stone

The Transformation of Traditional Processing Technology. Usually the traditional wastewater treatment technology depends on a few simple sedimentation tanks. According to the analysis of sewage treatment process, deposition velocity in sedimentation tank is slower, the purification ability is limited and a larger area of the sewage treatment sedimentation tank is required. The upper overflow water is difficult to reach the recycle standard with this method [3]. For the smaller stone enterprises, sludge is cleaned regularly at the bottom of sedimentation tank. If mud is cleaned production will be stopped. As a result, not only a lot of production time is cost, but also the enterprise's economic benefit is influenced [4].

To reform the traditional sewage treatment technology, a new type of sewage treatment technology is put forward, whose process diagram is shown in Fig.2.

Sewage from stone processing workshop flows into the sewage tank. Wastewater is sent to the primary sedimentation tank by liquid submerged sewage pump. At the same time, the suitable flocculant is put into the water to make powder particles accelerate coagulation sink and eventually the solid-liquid separation is finished. At the bottom of primary sedimentation tank the sludge is intermittently discharged into the mud pit. Because the sewage is sent to the primary sedimentation tank, the upper water is forced to overflow to the secondary sedimentation tank. Appropriate flocculant is also added to the secondary sedimentation tank. The upper clear water flows into the reservoir. The sludge is sent to the dehydration equipment for separating mud and water. After that, water which flows into the tank can be recycled, the filter mud cake is transported to another application.

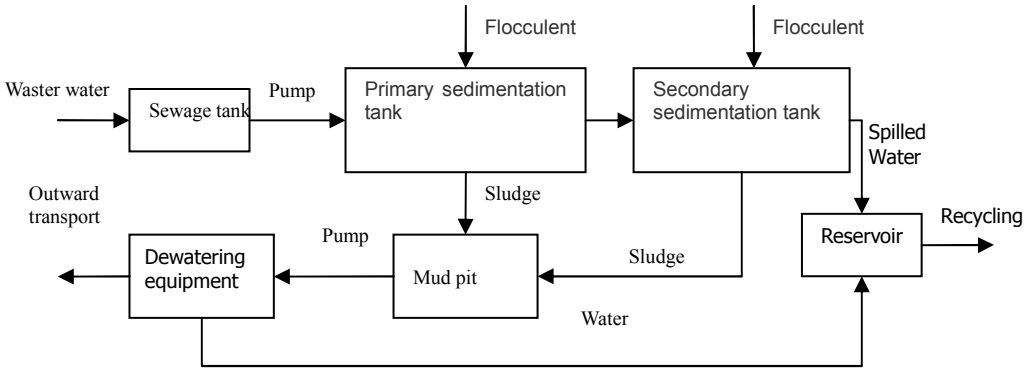

Fig.2. Flow diagram of sewage treatment process

Design of Sedimentation Tank. In the stone processing at present, sedimentation tank is commonly used in the wastewater treatment. Therefore there are four main types which involved horizontal flow, vertical flow, radial flow and inclined plate [5]. In the process of small and medium-sized enterprises construction, the economic cost and its production capacity should be taken into account. Usually only a few simple horizontal sedimentation tank is selected, but more land is occupied when using this method and the purification ability is limited. The horizontal sedimentation tank and rotating mechanism is adopted on the basis of the equipment, as shown in Fig.3. Separation effect and processing capacity of tank are improved further, the blade of inclined plate can increase the subsidence area and improve the flow state of wastewater. Compared with the general sedimentation tank, surface load and the processing ability of the sedimentation tank are largely improved.

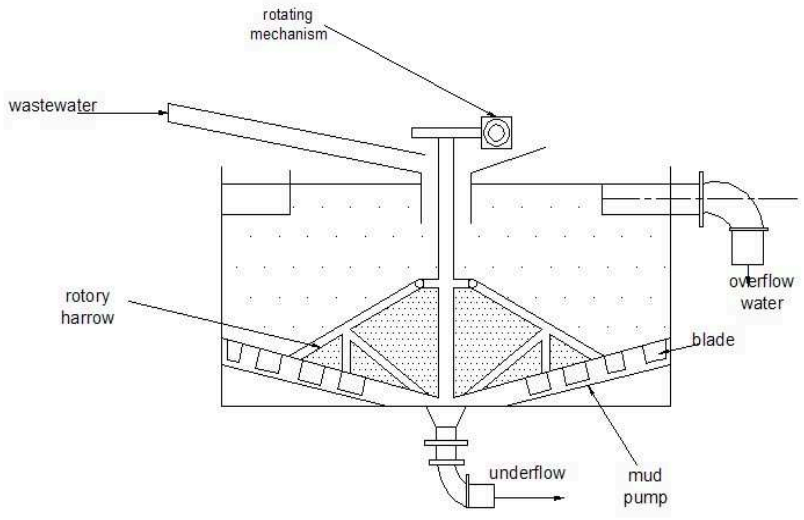

Fig.3.The new sewage sedimentation tank

In the sewage the solid particles settlement way is gravity sedimentation. Center in sedimentation tank rotary harrow revolve slowly, and the speed is $0.1 \sim 1r/\min$. The speed of primary sedimentation tank and the secondary sedimentation tank is different. Generally the speed of the secondary sedimentation tank is slightly quicker.

Conclusion

According to the production condition of small and medium-sized enterprises and the standards of wastewater treatment, the parameters of the process are designed, taking the processing of stone slabs as an example. The emissions of sewage stone processing enterprises have been calculated, taking stone processing into account. Considering the existing sewage treatment technology and method, the traditional processing technology has been transformed into interaction form which functions by the primary sedimentation tank and the secondary sedimentation tank, achieving the preliminary planning of the new sewage treatment process. In this design, rotating mechanism equipment has been adopted on the basis of horizontal sedimentation tank, improving the separation effect and processing capacity of tank.

References

[1] Qiyun Liu, Bin Mou. Environmental Protection and Comprehensive Utilization of Resources [J]. the New Century Cement Herald, 2003, (04): 42-43.

[2] V Narayanaswamy, J A Scott, J N Ness, et al. Resource Flow and Product Chain Analysis as Piratical Tools to Promote Cleaner Production Initiatives [J]. Journal of Cleaner Production. 2003. 11 (2),375—387.

[3] Xuning Wang, Xuedong Sun, Hongan Jiang, Hongzhi Zhao, Shi Li. Problems Existing in the Operation of Horizontal Flow Sedimentation Tank and Their Improving Measures [J]. China Water and Wastewater, 2006 (10): 27-30.

[4] Jianjun Li. Research on Stone Machining Sewage Treatment Process and Filter Equipment [D]. Journal of Shandong University, 2011.

[5] Yanwei Zhang. Stone Industry Comprehensive Assessment of Cleaner Production System Research and Application [D]. Shandong University, 2012.

Advanced Materials Research Vols. 989-994 (2014) pp 1313-1318
© (2014) Trans Tech Publications, Switzerland
doi:10.4028/www.scientific.net/AMR.989-994.1313

Accumulation of chromium in *Vetiveria Zizanioides* Assisted by earthworm (*Eisenia Foelide*) in contaminated soil

Ke ZHANG[1,a], Qiang CHEN[2,b], Hongbing LUO[1,c], Xiaoting LI[2,d]

[1]College of Civil Engineering, Sichuan Agricultural University, Dujiangyan, Sichuan, 611830, China

[2]College of Resource and Environment, Sichuan Agricultural University, Wenjiang, Sichuan, 611130, China

[a]Email: zhangke@sicau.edu.cn, [b]Email: cqiang@sicau.edu.cn,
[c]Email: luohongbing@sicau.edu.cn, [d]Email: s20111310@163.com

Keywords: Accumulation; *Vetiveria Zizanioides*; Earthworm; Cr Contaminated Soil

Abstract. The trial of the earthworm-assisted phytoremediation of Cr in contaminated yellow soil was made to study the performance of earthworm in Cr accumulation of Vetiver Grass (*vetiveria Zizanioides* VG). Two groups were designed, adding earth worm(marked EM) and not adding earth worm(marked NEW).The result showed *Vetiveria Zizanioides* can absorb great amounts of chromium in soil, the decline rate of Cr was up to 75% and 78% respectively in EM and NEM at 60th day. Both root and shoot can accumulate Cr from soil. As the concentration of Cr gradually increased within 0-80mg/kg，the accumulation activity of two groups presented first increase and then decrease and reached maximum 644.31mg/kg, 943.14 mg/kg in root when the Cr concentration was 80 mg/kg. It began to decrease when the Cr concentration was above 120mg/kg.*Vetiveria Zizanioides*'s accumulation ability differs in root and shoot. It presented root>shoot. With a comparative analysis, EM has higher accumulation and resistance of Cr at any designed treatments. In the analysis of relation between plants and soils, it was found that there was significant correlation in Cr contents between plants and soils ($P<0.05$). Furthermore, there was extremely significant correlation ($P<0.01$) between root and shoot in EM. There was a high retention rate of *Vetiveria Zizanioides* root to Cr. Retention rate of any treatments were all greater than 83% except 120mg/kg in EM. Plants kept much higher concentrations of Cr in roots than in their respective shoots. The biggest value was up to 96.23%. There was no obvious difference between EM and NEM in retention rate. Earthworm-assisted phytoremediation has high efficiency in Cr contaminated soil. It's an idea method to Cr contaminated soil.

Introduction

Soil contamination, a very important environmental problem, has attracted considerable public attention in recent years. Heavy metal contamination in soils is one of the world's major environmental problems. it caused great risks to human health as well as to ecosystems[1]. Toxic heavy metals can cause different health problems depending on the heavy metal concerned, its concentration and oxidation state, etc[2][3].

Chromium (Cr) is a transition element naturally occurring materials. It may exist in a series of oxidation states of which the major stable forms are the trivalent (Cr^{3+}) and the hexavalent (Cr^{6+}) [4]. In the last few years the number of Cr contaminated sites has increased and hence Cr pollution has attained considerable attention being regarded as a major area of concern worldwide.

Phytoextraction is an environmentally sound and cost-effective technology for cleaning up soils contaminated with toxic metals. This technique has repeatedly been suggested as a novel clean-up technology. It has the potential to provide cost effective, renewable alternatives to previously used remediation techniques. Vetiver grass (*Vetiveria Zizanioides*,VG) was originally produced in India and was successfully introduced to China in the 1950s. It is an ideal plant for moisture and soil conservation[5][6].

Earthworms construct a major component in soil and play an important role in soil ecosystems. They contribute to organic matter incorporation and decomposition, excavation of burrows. They play an important role in chemical element transformation[7].

But in the previous studies about animals-plants combined remediation, there's few research focused on accumulation properties of chromium in *Vetiveria Zizanioides* induced by earthworm. The goal of this study is to understand the performance of the earthworm-assisted phytoremediation of Cr contaminated yellow soil. It has an important practical significance to improve the animal-assisted phytoremediation research as well as the development of *Vetiveria Zizanioides* ecological engineering.

Materials and Methods

Soil Preparation

Uncontaminated yellow soil was collected from 0 to 20cm depth from botany garden Sichuan, China. The soil was air-dried, crushed to pass through a 2mm diameter sieve, and mixed thoroughly. 7kg soil samples were placed in plastic pots with 35cm diameter and 40cm height. There were six groups of processing and each processing set three repetitions. Chromic acid dipotassium(K_2CrO_4) was added. The final concentration of soil were 0mg/kg,10mg/kg, 20mg/kg, 40mg/kg, 80mg/kg, 120mg/kg respectively. In each processing, 15 earthworms (*Eisenia Foelide*) were taken into each plastic pot apart from control group.

Plant Materials

Vetiveria Zizanioides were obtained from Sichuan seeding company. Simple root baptism treatment was conducted before planting. 5 strains were evenly planted in each plastic pot. Keep the house temperature at 25 to 29 degrees Celsius after planting in greenhouse, watered in time.

Chromium Concentrations in Soil

Soil samples were analyzed after they had been ground in a stainless steel mill to pass through a 2mm sieve for analysis of following parameters. Soil samples were digested with HF–HNO3–HClO4 using a microwave. Concentrations of heavy metals were determined using an atomic absorption spectrophotometer(AAS- TAS-900).

Metal Concentrations in Plants

After 60 days, ground part (shoot) and underground part (root) were separately harvest. They were washed by deionized water and dried in dryer to constant weight, weighing. Both ground samples and underground samples (0.25 g) were digested in concentrated HNO3–H2O2 using a digestion block. The digested samples were brought to a constant volume (25ml) with deionized water, and the digests were analyzed for Cr using AAS.

Statistical Analysis

The data were analyzed using one-way analysis of variance (ANOVA) and Duncans Multiple Range Test in the SPSS software to compare the means of heavy metal concentrations in different treatment.

Results and Discussion

Contents of Cr in soil during experiment period

The content of Cr in soil during experiment period are presented in Fig.1 and Fig.2 The concentration of Cr in soil gradually decreased In NEW and EW groups from 10th to 60th day. In the treatment of 10mg/kg, the concentration decreased to 2.4 mg/kg, while in treatment of 120mg/kg, the concentration decreased to 54.2 mg/kg. The speed of Cr decline was slow at the concentration of 10 treatment of 10mg/kg, the concentration decreased to 2.4 mg/kg, and became faster at the concentration of 20-80t treatment of 10mg/kg, the concentration decreased to 2.4 mg/kg then dropped slightly at the concentration of 120 treatment of 10mg/kg, the concentration decreased to 2.4 mg/kg. Compared with NNW, NW has the same trend in decline of soil Cr. but at the presence of earthworm, the speed of Cr decline in soil is faster than any treatments in NEW. It indicates that earthworm play

an important role in declination of soil Cr concentration. The accumulation activity of two groups presented first increase and then decrease, and reached maximum 644.31 mg/kg, 943.14 mg/kg. Devliegher[8] explains earthworm improve plant nutrients in the soil such as Ca, Fe, Mn and the effectiveness of the metal elements such as Cr, Co from intestinal digestion and nutrient enrichment of two aspects. Deng Jifu [9] heavy metal contents in earthworms in industrial area were studied. It was found that the accumulation ability is very strong, and the enrichment of content is positively related to the content of soil.

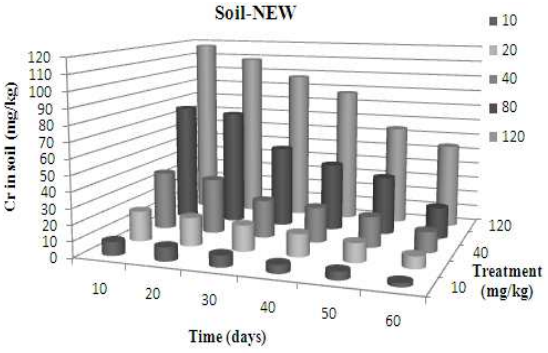

Fig.1 Changes of Cr content during the experiment period in NEW soil

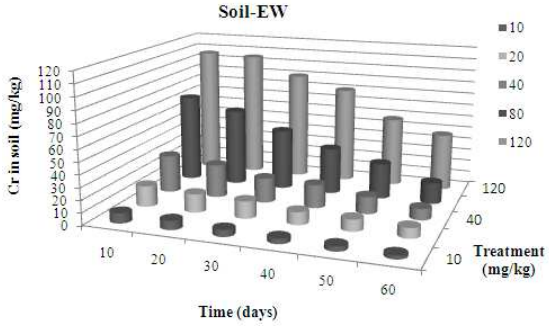

Fig.2 Changes of Cr content during the experiment period in EW soil

The degradation rate of chromium in soil is presented in Table1. In the NEW group and EW group, the degradation rate increase as time goes on. The degradation rate was 19% in the 30th day, the degradation rate was 55% at 60th day at treatment of 120mg/kg. On the contrary, in the EW group, the degradation rate in 25% 25% 30 days and 60 days, were greater than the NEW group. This suggests that earthworms play an important role in degradation of heavy metals in the soil. Earthworms play roles in many ways. Such as making holes in feeding, excreting metabolic product in the process of life activity and changing chemical behavior of heavy metals in soil, which have an impact on uptake of heavy metal direct or indirect way.

Table.1 Decline rate of soil Cr in different treatments

Cr (mg/kg)	NEW		EW	
	Decline rate within 30 days	Decline rate within 60 days	Decline rate within 30 days	Decline rate within 60 days
10	27%	76%	46%	72%
20	18%	62%	30%	59%
40	40%	67%	49%	77%
80	35%	75%	37%	78%
120	19%	55%	25%	61%
AVG	28%	67%	37%	69%

Concentration of Cr in shoot and root

The concentration of Cr in shoot and root is presented in Fig.3 and Fig.4. Different parts of the plant to heavy metal Cr accumulation to a certain extent, with increasing concentration of Cr in soil, every part of VG on the uptake of Cr is raised. The root of VG has strong accumulation ability to the heavy metal ions. It was also proved in this study. The concentration of Cr in root was up to 953.03mg/kg in treatment of 120mg/kg in NEM. While in EM, the content of Cr in all the treatment was higher than NEM except treatment of 120mg/kg. It was unexpected drop at treatment of 120mg/kg in EW, it's unusual. The reason is need to do further study.

Accumulation of heavy metals in plants in vivo distribution is related to the activity of the various metal itself, also with all kinds of plant adaptation to heavy metal tolerance mechanism. In plant adaptation mechanisms of metal, or by the root structure or certain physiological features limit the harmful heavy metal ions from the root to the aboveground part transfer, maintain the ground part of low heavy metal content, make the aerial parts of plants have higher physiological activity, Or take the

harmful heavy metal accumulation into easy to fall off part, through the parts fall off, from harmful heavy metals plant. [10][11][12]

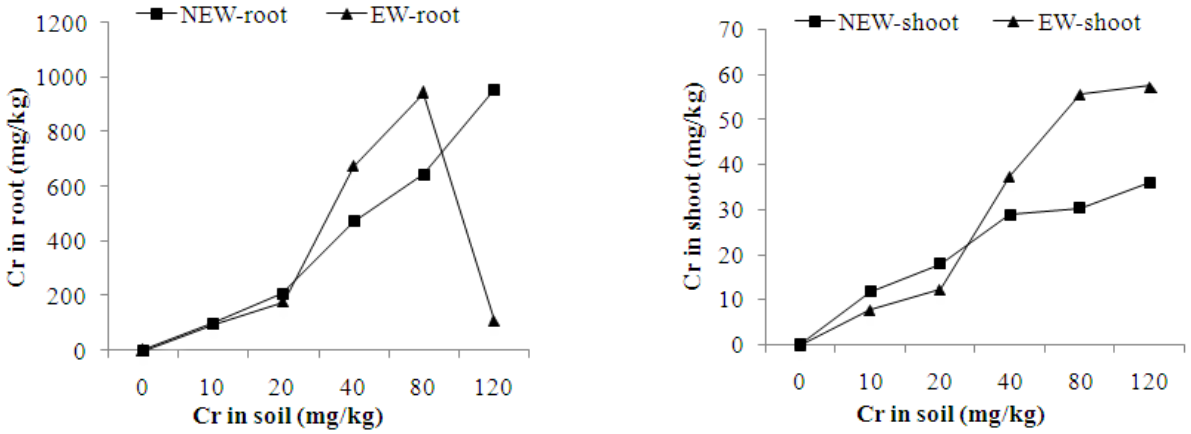

Fig.3 Fig.4 The concentration of Cr in root and shoot

VG can accumulate large amount of Cr in shoot and root. The roots can absorb more Cr than shoot. Cr content of VG from different parts of the body is characterized by underground parts > the ground, it is a common phenomenon in the plant study before. It indicates that Cr in the root rarely transport to the ground. Comparison between adding and without adding earthworm into soil for control, it was found earthworm can improve the uptake of Cr at low concentration.

Paul Truongu [13] showed that the tolerance ability of ordinary plant shoot to Cr, Ni, respectively 0.02 -0.20 mg/kg and 10-30 mg/kg. In this study the contents are significantly higher than previous studies, may caused by soil nutrient and type or some other reason, which needs further research.

Correlation Coefficient between Cr of VG and Soil

Correlation coefficient between Cr of VG and soil is presented in Table2. The results showed that Cr in shoot and root and soil Cr have good correlation. In the NEW group, the correlation of shoot and soil is significant ($P < 0.05$). In the EW group, there is significant correlation between soil and root and shoot ($P < 0.01$)

Table 2 Correlation coefficient between Cr of VG and soil

	NEW		EW	
Items	root	shoot	root	shoot
Pearson Correlation	0.987**	0.883*	0.970**	0.942**
Sig. (2-tailed)	0	0.02	0.006	0.005
N	6	6	5	6

**. Correlation is significant at the 0.01 level (2-tailed).

*. Correlation is significant at the 0.05 level (2-tailed).

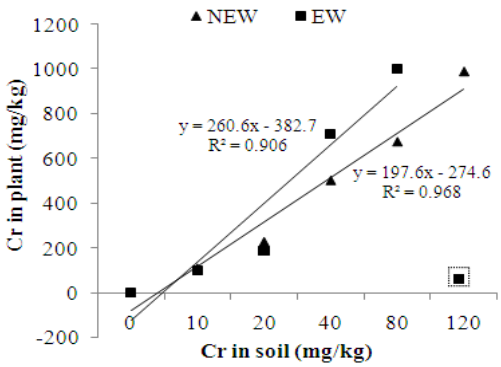

Fig.5 Linear relation between Cr content in VG plant and in soil

It was indicated from Fig.5 Increases with the concentration of Cr in soil, the concentration of VG is on the rise, It showed a linear correlation between Cr concentrations in soil and plant, correlation coefficient, r = 0.9065 and r = 0.9608. In the NEW and the EM group, the regression equation of Y=260.6x-382.7 and Y=197.6x-274.6

Accumulation Factor

Accumulation factor is presented in Table.3 Accumulation factor reflects the absorbing ability of root to heavy metal it Can be seen from table 3.VG'S s roots have very strong accumulation ability. In various concentrations, VG has the ability of chromium accumulation, which were characterized by the root is greater than the shoot. The high value in root is 16.83, in shoot in 0.12. Among which, in the NEW the largest accumulation factor is 11.83.A minimum of 7.94. In the EW group, root accumulation coefficient is 16.83, the highest value in shoot up to 0.93.

Root changes over concentration of heavy metal enrichment coefficient, when the soil heavy metal content exceeds a certain value, the accumulation factor of root is negative correlation with soil heavy metal content, this is mainly because of heavy metals to cell damage reduces the absorption of root. Root accumulation factor of Cr is quite high. Accumulation factor of shoot is very low. The result is same with previous studies. [12][14]

Table 3 Accumulation factor of VG-root and shoot to Cr

Cr (mg/kg)	NEW		EW	
	root	shoot	root	shoot
10	9.73	0.54	9.31	0.76
20	10.46	0.37	8.72	0.61
40	11.83	0.23	16.83	0.93
80	8.05	0.13	11.79	0.69
120	7.94	0.12	0.88	0.48
AVG	9.60	0.28	9.51	0.69

Table 4 Cr retention rate in VG-root

Cr (mg/kg)	NEW	EW
10	87.91%	91.84%
20	91.46%	93.00%
40	93.93%	94.47%
80	95.30%	94.12%
120	96.23%	45.62%
AVG	92.97%	83.81%

Retention Rate

Cr retention rate is presented in Table.4 Cr retention rate is all above 83% in both NEW and EW groups except treatment of 120mg/kg.Cr retention rate is Up to 96.23% in NEW group. The retention rate is up to 94.47% in EW.

Comparing the retention rates of Cr and other heavy metal to previous study [15], it can be concluded that Cr is different from other heavy metal. Content of Cr in root is much more than in shoot. And almost all Cr stranded in the root, less to stem leaves .Root retention rate of heavy metals and the soil heavy metal content and whether to join the earthworm there was no significant correlation, that is to say, for a certain heavy metals, as the change of concentration, retention is almost a constant. This conclusion is consistent to previous research[16].

Conclusion

This study shows *Vetiveria Zizanioides* has very high tolerance to Cr and could accumulate Cr in roots and shoots. Degradation rate increased after adding the earthworm. As the concentration increased, degradation rate also has a tendency to reduce. But compared to NEW, EW group is only slightly decreased at the condition of high concentration. This suggests that earthworms play an important role in soil pollution remediation.

Under the condition of earthworms significantly enhanced the uptake capacity of each part. It is only slightly decreased at the condition of high concentration. Chromium content in the soil and plant roots, shoots are extremely significant correlation in EM ($P<0.01$). The accumulation capacity of VG in shoot was significantly higher than previous study. This may be related to type of soil and *Vetiveria Zizanioides* or other reasons. It needs further research.

In terms of accumulation characteristics, *Vetiveria Zizanioides has* similar properties to other heavy metal uptake, root > shoot. But unlike other heavy metal, chromium transfer coefficient is low, high retention rate in NEW and EW, at 92.97% and 83.81% respectively. Retention rate has nothing to do with the content of chromium concentration in the soil.

Earthworm-assisted phytoremediation is an idea method to Cr contaminated soil. *Vetiveria Zizanioides* has the properties of strong resistance ability high accumulation and high biomass, etc. It can be concluded from this study .Combination of earthworm and accumulation plants (*Vetiveria Zizanioides*) have obvious effect in soil remediation of heavy metal contamination. Therefore, comprehensive bioremediation technology in the future will be the main research direction of heavy metal contaminated soil remediation.

Acknowledgement

In this paper, the research was sponsored by National Nature Science Foundation of China (Proje ct No.51278318); Science and Technology Support Project of Sichuan Institute of Science and Tech nology (Project No. 2013SZ0103) and Science and Technology Project of Sichuan Environment prot ection Bureau (Project No. 2011HB001). Special Financial Support of College (Project No. 341700 25)

References

[1] Yahua Chen, Zhenguo Shen, Xiangdong Li. The use of vetiver grass (Vetiveria zizanioides) in the phytoremediation of soils contaminated with heavy metals. Applied Geochemistry, 2004 (19) 1553-1565.
[2] Al-Khashman, Shawabkeh. Metals distribution in soils around the cement factory in southern Jordan. Environ. Pollut, 2006(140) 387-394.
[3] K.K. Chiu, Z.H. Ye, M.H Wong. Growth of Vetiveria zizanioides and Phragmities australis on Pb/Zn and Cu mine tailings amended with manure compost and sewage sludge. A greenhouse study Bioresource Technology, 2006(97) 158-170.
[4] Silvia Quaggiotti, Gianni Barcaccia, Michela Schiavon. Phytoremediation of chromium using Salix species: Cloning ESTs and candidate genes involved in the Cr response. Gene, 2007(402) 68-80.
[5] María Julieta Salazar, María Luisa Pignata. Lead accumulation in plants grown in polluted soils, Screening of native species for phytoremediation. Journal of Geochemical Exploration, 2014(137) 29-36.
[6] K.K. Chiu. Enhanced uptake of As, Zn, and Cu by Vetiveria zizanioides and Zeamays using chelating agents. Chemosphere, 2005(60) 1365-1375.
[7] Jun Dai,Thierry Becquer,James Henri Rouiller. Heavy metal accumulation by two earthworm species and its relationship to total and DTPA-extractable metals in soils. Soil Biology & Biochemistry.2004 (36): 91-98
[8] Devliegher W, Verstraete W. Lumbricus terrestris in a soil core experiment: effect of nutrient enrichment processes (NEP) associated processes (GAP) on the availability of plant nutrients and heavy metals. Soil Biol. Biochem. 1996(28) 489-496.
[9] Jifu Deng, Zhenzhong Wang, Youmei Zhang, et a1. A research on the ecological effect of the soil animals conununity by the heavy metal pollution. Chinese Journal of Environmental Science,1996(2) 1-6.
[10] Qingye Sun, Congyu Lan, Minghong Huang. Natural colonized plants on tailings of Lead/ Zinc mine. Acta Ecol Sin, 2001, 21(9) 1457-1462.
[11] Baker AJM, Proctor J. The influence of Cadmium, Copper, Lead and Zinc on the distribution and evolution of metallophytes in British Isles. Plant Syst Evol, 1990(173) 91-108.
[12] Jian Long, Changyong Huang, Ying Ten. Tolerance to heavy metals of VG and some herbages in Tiantai Lead-Zinc Mine. Chin J Appl Environ Biol, 2003, 9(3) 226-229.
[13] Troung. An overview of research on development and application of the vetiver grass system(VGS) in Queensland. The Vefiver Network, 1996, 97, 5-17.
[14] Xiezhi Yu, Jiemin Cheng. Effect of earthworm on bioavailability of Cu and Cd in soil. ACTA ECOLOGICA SINICA, 2003, 23(5) 923-928.
[15] Hanping Xia, Wensheng Shu. Resistance and uptake of heavy metals by Vetiveria zizanioides and Paspalum notatum from lead/ zinc mine tailings. Acta Ecologica Sinica 2001, 21(7) 1121-1129.
[16] Lu Han, Xiaoping Zhang, Birong Liu. VG accumulation study of several kinds of heavy metal ions in soil. JOURNAL OF BIOLOGY, 2005, 22(5) 20-23.

Advanced Materials Research Vols. 989-994 (2014) pp 1319-1323
© (2014) Trans Tech Publications, Switzerland
doi:10.4028/www.scientific.net/AMR.989-994.1319

Study on Response of *Cyperus Alternifolius* to Cr(VI) and Ni Combined Pollution

Minchao LIU[1, a], Wu ZHOU[2, b]

[1]College of Chemical and Environmental Engineering, Wuyi University, Jiangmen, 529020, China

[2]College of Chemical and Environmental Engineering, Wuyi University, Jiangmen, 529020, China

[a]email: wyuchemlmc@126.com, [b]email:wyuchemys12zw@126.com

Keywords: Cr(VI); Ni; combined exposure; Cyperus alternifolius

Abstract. In order to investigate the ability of Cyperus alternifolius in restoring water with combined heavy metal pollution, water cultured experiment was utilized to study the accumulation and the tolerance mechanism of Cr(VI) and Ni in Cyperus alternifolius under the combined Cr(VI) and Ni exposure. The results showed that under Cr(VI) and Ni combined exposure, low concentration Ni improved the enrichment and translocation ability of Cyperus alternifolius for chromium, while high concentration Ni had opposite effects. The enrichment ability of Cyperus alternifolius for chromium was stronger than for Ni. With the increasing of Cr(VI) and Ni concentrations, fresh weight increment and chlorophyll content showed upward trend firstly and then downward, MDA content showed a rising trend and increased significantly. When Ni concentration was between 0~1mg·L^{-1}, SOD and CAT activities of Cyperus alternifolius increased first and then decreased with increasing Cr(VI) concentration, and root activity increased continuously. When Ni concentration was between 10~20 mg·L^{-1}, Cr(VI) and Ni interaction decreased SOD,CAT and root activity significantly. These results show that Cyperus alternifolius had tolerance and enrichment ability to Cr(VI) and Ni, and Cyperus alternifolius can be used to restore Cr(VI) polluted water and Cr(VI)-Ni combined polluted water under low Ni concentrations.

Introduction

With the rapid development of industry, Cr and Ni flow into the water in varieties ways, which has caused a serious impact to the aquatic environment and has a serious threat to animal and human health. Obviously, it has become a major global concern environmental problem. Cr and Ni are the trace elements closely related to human health and life, however, it's toxic to the plants and animals clearly on the excess. Phytoremediation is a green remediation technology for contaminated soil. Because of its easy operation, wide adaptability and no secondary pollution, it has become a hot technology for heavy metal pollution restoration. Currently, scholars put emphasis on the remediation of single heavy metal pollution, but actually situations are that a variety of heavy metals coexists[1]. Therefore, the study of the mechanism of heavy metals in plants under the combined pollution has a double meaning in theory and practice for the remediation of heavy metals compound pollution.

Cyperus alternifolius is a fast-growing, adaptable cyperaceae perennial evergreen herbaceous plants, and has a good ability to accumulate Single Cr(VI) and Ni[2]. To explore the patience of Cyperus alternifolius, as well as the feasibility of the restoration of heavy metals compound pollution, experiments were utilized to study the accumulation and the tolerance mechanism of Cr(VI) and Ni in Cyperus alternifolius under combined Cr(VI) and Ni exposure, designing to provide a theoretical basis about the restoration of Cr(VI) and Ni complex contaminated water by Cyperus alternifolius.

Materials and Methods

Plant material

Cyperus alternifolius seedlings were selected as tested plants.

Experimental Design

Experimental design with two factors was adopted and the tested plants were cultured in Hoagland nutrient solution adding different Cr(VI) and Ni concentration. Cr(VI) and Ni in nutrient solution were added with the form of K_2CrO_4, Ni $(NO_3)_2$ respectively. Each experiment was repeated three times and the specific designs were shown in Table 1.

Table 1 Experimental design ($mg \cdot L^{-1}$)

Cr(VI)	Ni		
	1	10	20
1	treatment 1	treatment 4	treatment 7
10	treatment 2	treatment 5	treatment 8
20	treatment 3	treatment 6	treatment 9

Measurement methods

Cr(VI) and Ni: ICP (ICAP6000, Thermo Scientific). The biomass: drying weighing method[3]. Chlorophyll content: using 80% acetone extraction, spectrophotometry. SOD activity: NBT photoche- mical reduction method[3]. CAT activity: potassium permanganate titration method [3]. MDA content: thiobarbituric method[3]. Root activity: TTC method.

Results and Discussion

Fresh weight increment

As could be seen from Figure 1, Cr(VI) and Ni combined pollution had a significant impact on fresh weight increment of Cyperus alternifolius. When Ni concentration was fixed, fresh weight increment decreased with the increasing of Cr(VI) concentration. When Cr(VI) concentration was fixed, fresh weight increment showed a similar tendency. At combined pollution of Cr(VI)(1 $mg \cdot L^{-1}$) and Ni(1$mg \cdot L^{-1}$),fresh weight increment reached a maximum of 3.14 (g/plant) , and was 92.64% significantly higher than that of CK. When the dealing concentration reached up to 20 $mg \cdot L^{-1}$, fresh weight increment was lower than that of CK. This indicated that at low Cr(VI) and Ni concentrations, their interaction played a catalytic role on the growth of Cyperus alternifolius, while at high concentrations, they restrained the growth of Cyperus alternifolius and made the biomass reduce. This result was consistent with Wu's study about the effect of heavy metal Cd of Aegiceras corniculata seedlings[4].

Cr (Ⅵ) and Ni content

Studying the repair of heavy metal by plant, not only weights plants patience of heavy metals and the accumulation ability, also should consider its transfer ability of heavy metals from roots to shoots. Figure 2 indicated that when at the same Ni concentrations, the total chromium content in the upper and root of Cyperus alternifolius gradually increased with the increasing of Cr (VI) concentrations, while the cumulative amount of nickel was gradually decreasing. The upper total chromium content reached up to 1729.67 $mg \cdot kg^{-1}$ at treatment 6. Views were preliminary held that Cr (VI) had inhibitory effect on cumulative Ni of Cyperus alternifolius. When at the same Cr (VI) concentrations, the total chromium content in the upper of Cyperus alternifolius showed upward trend firstly and then downward with the increase of Ni concentrations, while the cumulative amount of Ni was gradually increasing. The upper Ni content reached a maximum of 1383.06 $mg \cdot kg^{-1}$ at treatment 7. It indicated that the enrichment ability of the Cr was greater than the Ni.

When Cr (VI) concentration was fixed, the ratio of the total chromium enrichment content in shoots and roots rose at first and went down latter with the increasing of Ni. Showing that low concentration Ni improved the enrichment and translocation ability of Cyperus alternifolius for chromium, while high concentration Ni had opposite effects. It also shows that when Cyperus alternifolius grew in the suitable Ni concentration, chromium absorption in roots was active uptake, and had a strong ability to transfer it. However, high Ni concentration had strong toxic effects on

Cyperus alternifolius, destroyed the root membranes, organelles and cytoskeleton, and declined the roots respiration and leaves transpiration. So the roots absorption of chromium couldn't be transferred to the aboveground initiatively, and resulted chromium accumulation in roots. With the chromium transport capacity weakened, chromium content in aerial part decreased , which was similar to Li's studies[5].

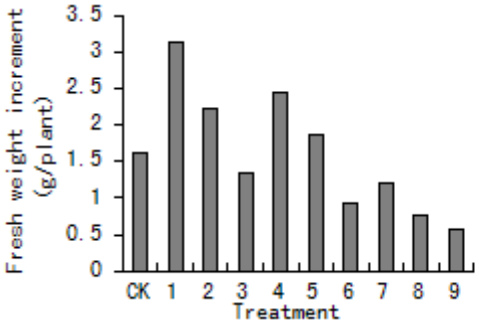

Fig.1 Effect of Cr(VI) and Ni interaction on fresh weight increment of Cyperus alternifolius

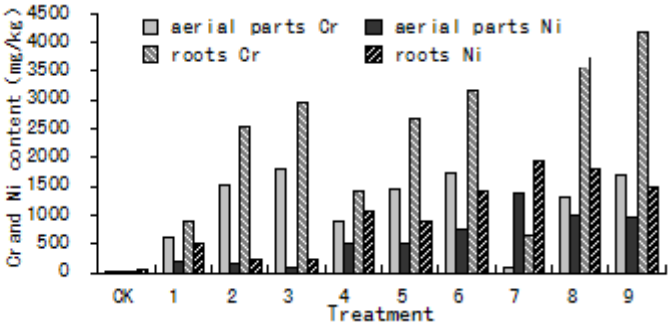

Fig.2 Cr(VI) and Ni contents in Cyperus alternifolius after combined Pb and Zn exposure

Chlorophyll content

Chlorophyll is a necessary catalyst for plants photosynthesis, and plays a important role on plants growth. Chlorophyll content is closely related to the senescence oxidation of the leaf[10]. Combined pollution can lead to the destruction and degradation of chlorophyll, which reflected the forced condition of plants. Seen from Figure 3, under the same Ni concentration, chlorophyll content of Cyperus alternifolius decreased with increasing Cr(VI) concentration. When at the same Cr(VI) concentration, chlorophyll content also showed a downgrade trend. Chlorophyll content reached a maximum of 0.42 $mg \cdot g^{-1}$ when both Cr(VI) concentration and Ni were 1 $mg \cdot L^{-1}$, and was 233.1% significantly higher than that of control. Thus, low concentration of Cr(VI) and Ni combined pollution was conducive to the synthesis of chlorophyll in leaf, showing a synergistic effect. While high concentration inhibited the synthesis of chlorophyll, producing a persecution effect on plants. For the reason, Yuan Min[6] considered that heavy metal inhibited the synthesis of the protochlorophyllide oxidoreductase and affected the synthesis of the aminolevulinic acid, thus reducing chlorophyll content. In this experiment, the decreasing of chlorophyll content may be the combination of heavy metal ions and related enzymes in plants, which changed the enzyme activity to block the synthesis of chlorophyll and affected the biosynthesis rate of chlorophyll, thus reducing chlorophyll content.

SOD and CAT activity.

Under normal growing conditions, the production of reactive oxygen in plants was in dynamic equilibrium, while under adversity stress or aging, the balance between production and elimination of reactive oxygen will be broke. Therefore, SOD and CAT activity changes in plants can characterize the degree of plant stress.

Figure 4 revealed that when Ni concentration was 1 $mg \cdot L^{-1}$, the SOD and CAT activities of Cyperus alternifolius rose at first and went down latter with increasing Cr(VI) concentration, while 10~20 $mg \cdot L^{-1}$, SOD and CAT activities downgraded as Cr(VI) concentration increased. When Cr(VI) concentration was fixed, SOD and CAT activities showed the same trend, but most were higher than under the control. SOD and CAT activities reached the maximum at treatment 4, and were significantly higher than under the control 359.37% and 212.38%, respectively. Results indicated that Cr(VI) and Ni combined stress influence of SOD activity was higher than that of CAT. SOD and CAT activities reached minimum and was lower than the control at treatment 9, showing that high concentration stress destroyed physiological metabolism in plants and inhibited SOD and CAT activities. Therefore, mild stress had a positive impact on active oxygen scavenging system in plants, as a result SOD and CAT activities increased, and they eliminated the free radicals, protected the membrane structure of plants and kept regular growth. While height stress were toxic to SOD and CAT activities, so their activities decreased, the ability of scavenging free radicals downgraded,

functional membrane and enzyme system of plants cells destroyed, physiological metabolic disordered, resulting in the decreasing of plants tolerance, finally[7].

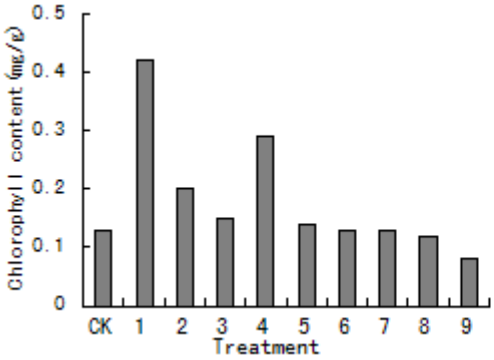

Fig.3 Effect of Cr(VI) and Ni contents on Chlorophyll content of Cyperus alternifolius

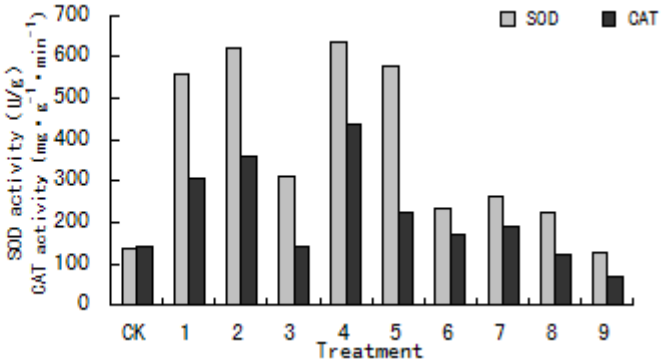

Fig.4 Effect of Cr(VI) and Ni contents on SOD and CAT activity of Cyperus alternifolius

MDA content

MDA as the final product of membrane lipid peroxidation, its accumulation can reflect the level of membrane lipid peroxidation to some extent, thus realizing the damage of plants and the degree of plants stress response. Seen from Figure 5, when Cr(VI) concentration was setted, MDA content of Cyperus alternifolius increased with the increasing of Ni concentration. When Ni concentration was setted, a similar trend was found for MDA content, and was higher than in the case of control group. MDA content had a maximum at treatment 9, it showed that the higher concentration of Cr(VI) and Ni compound pollution was, the more serious the degree of membrane lipid peroxidation had, resulting membrane system stability was lower. This was because added metals impacted the cell structure of biological, made biological membrane lipid occurred peroxidation phenomenon, and damaged the membrane structure, which causing the disorder of cell metabolism in plants and free radicals accumulation, consequently, MDA content rose sharply.

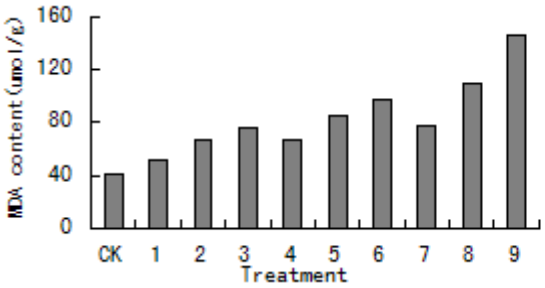

Fig.5 Effect of Cr(VI) and Ni Contents on Proline and MDA content

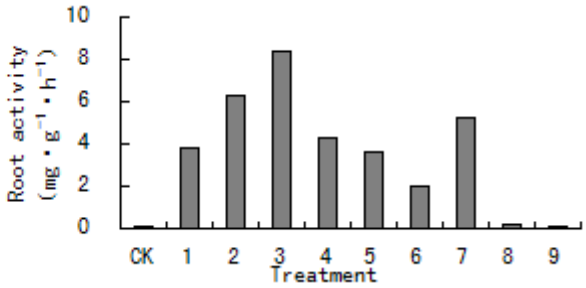

Fig.6 Effect of Cr(VI) and Ni contents on root activity

Root activity

Root is the major organs of plant to obtain nutrients, and root activity was the important physiological index to measure the growing of roots. Figure 6 shows that when Cr(VI) concentration was 1 $mg \cdot L^{-1}$, root activity of Cyperus alternifolius gradually increased with the increasing of Ni concentration, while 10~20 $mg \cdot L^{-1}$, root activity decreased as Ni concentration increased. When Ni concentration was fixed, root activity was also showing the same trend. The analysis of graph revealed that root activity increased at low concentration of Cr(VI) and Ni, having an active effect on the root growth and physiological. On the other hand, it promoted the root uptake of Cr(VI) and Ni and its transfer to the aboveground. But root activity decreased as the concentrations increased, the higher the concentration was, the greater it declined. The possible reason was that free radicals produced went beyond the scavenging abilities of the plant's own antioxidate system enzymes, and excessive free radicals damaged the succinic dehydroge- nase of root metabolism, resulting in root activity decline and the decreasing of biomass[8].

Conclusion

The experiment results show that under Cr(VI) and Ni combined exposure, low concentration Ni improved the enrichment and translocation ability of Cyperus alternifolius for chromium, while high concentration Ni had opposite effects. With increasing heavy metal concentrations, fresh weight increment and chlorophyll content rose at first and went down latter, MDA showed a rising tend and increased significantly.When Ni concentration was between 0~1mg·L^{-1}, SOD and CAT activities of Cyperus alternifolius increased first and then decreased with increasing Cr(VI) concentration, and root activity increased continuously. When Ni concentration was between 10~20mg·L^{-1}, Cr(VI) and Ni interaction decreased SOD , CAT and root activity significantly. In conclusion, Cyperus alternifolius had a strong patience and enrichment capacity to Cr(VI) and Ni, with the addition of the well-developed rhizome and huge biomass, Cyperus alternifolius can be used to restore Cr(VI) polluted water and Cr(VI)-Ni combined polluted water under low Ni concentrations.

Acknowledgements

This work was financially supported by the Innovation Project of Guangdong Education Department (Project No. 2013KJCX0186) and cleaner production engineering technology center for light chemicals of Guangdong college.

References

[1] Rodriguez L. and so on. Heavy metal distribution and chemical speciation in tailings and soils around a Pb-Zn mine in Spain[J]. Journal of Environmental Management, 2009, 90(2)1106-1116.

[2] Lingyan Gao and so on. Selection of tolerant plants of Cr(Ⅵ) and Ni and the characteristics of bioaccumulation of the plant[J]. Ecology and Environmental Sciences, 2012, 21(8) 1473-1478.

[3] Hesheng Li and so on. The experiments principle and technology of plant physiological and biochemical experiments[M]. Beijing:Higher Education Press, 2000.

[4] Guirong Wu and so on. Effect of Cd on the physiological and ecological of Aegiceras corniculatum and soil enzyme[D]. Xiamen:Xiamen University, 2007.

[5] Zhengzheng Li and so on. Effect of Pb, Zn on the chlorophyll content and antioxidant enzyme systems of Houttuynia cordata Thunb. Acta Ecologica Sinica, 2007, 27(12)5541-5546.

[6] Min Yuan and so on. Effects of Cd, Pb, Cu, Zn and As single pollution on Chlorophyll Content and Antioxidant Enzyme Systems of Eulaliopsis binata[J]. Chinese Journal of Soil Science, 2005, 36(6) 929-932.

[7] Xin Pang and so on. Effect of LA^{3+} on the activities of antioxidant enzymes in wheat seedings under lead stress[J]. Environmental Chemistry, 2002, 21(4)318-324.

[8] Aibibu Nuzhaaiti and so on. Influence of Different Zinc and Copper Levels on Cadmium Accumulation and Physiological Characterization in Vetiveria zizanioides L.[J]. Acta Scientiarum Naturalium Universitatis Neimongol, 2012, 43(5)43-550.

Advanced Materials Research Vols. 989-994 (2014) pp 1324-1327
© (2014) Trans Tech Publications, Switzerland
doi:10.4028/www.scientific.net/AMR.989-994.1324

A research of environment management policy based on the externality theory

Huichun Che[1, a], Fang Cao[2, b]

[1,2]Department of Economics, Beijing Wuzi University, Beijing, 101146, China

[a]chehuichun@126.com, [b]caofang137@126.com

Keywords: Externalities; ppp; emission Standards; pigouvian tax;

Abstract. In view of the environmental problems, the paper start with talking about the externality theory and polluter pays principle, and then introduce two kinds of environmental management policy, which are emission standard and Pigouvian Tax. By comparing them in the perspective of economic efficiency, we can learn that: Only the coordination of administrative means and economic measures, we can better solve the environmental problems.

Introduction

Externalities refers that an economic agent has brought the good (or bad) effect, yet he is not been compensated (or cost) for doing so. So we apply it to environmental issues, leading to the concept of environmental externalities. Compared with general externalities, environmental externalities have three characteristics: First, it is inevitable, everywhere and ever-present; second, its effects span a longer period of time; third, an even more important feature of environmental externalities is external diseconomy. So we must take measures to internalize it, that is, as far as possible to eliminate or reduce the environmental externalities. There are two methods to internalize the problem of environmental externalities: one is the market means, or the "invisible hand", which is the famous coase theorem; the other one is the government intervention, namely the "visible hand", which is known as environmental management policy. Environmental exists several problems such as the unclear property rights, high transaction cost, strategic behavior, and ignore the income effect, which limits coase theorem as the main method to solve the problem of environment. Therefore, When deal with environmental problems, we can more rely on government intervention to solve the problem of environmental externalities.

For governments, there are two main management means of environmental externalities, one is direct control policies, also known as administrative measures or imperative means; The other is a environmental economic policy, also known as economic means. Both direct control policies and economic stimulus are based on the theory of polluter pays principle.

Pollution Pay Principle

Environmental management is to correct the external diseconomy of environment and internalize the external costs. And the embodiment of this idea is the "polluter pays principle", which put forward by the organization for economic cooperation and development (OECD) in 1972. The definition of PPP is that the polluter shall bear the cost of controlling pollution losses determined by government to ensure that the environment is in a state of acceptable. In other words, the cost of controlling pollution losses should be included in the cost of products and services, which make pollution in the process consumption or production. The purpose of the polluter pays principle is to internalize of external diseconomy , prompting polluters actively to control pollution, otherwise, they will be suffered economic sanctions.

Environmental management policy and their comparison

Direct control policies--Emission Standards

Emission standards, also known as environmental standards, is one of the most representative methods in direct control means, which is formulated and enforced the maximum limit of each certain pollution by relevant departments. According to the rules, pollutant emission within the limits is permitted, otherwise polluters will be punished, if their pollutants exceed the limits.

As a direct control policies, The advantage of emission standard is certainty, namely to the managers directly control the behavior of polluters and can achieve the effect of environment be expected. However, this method also has great limitations: First, it reduces the economic efficiency. Relevant department needs the detailed information of MNPB and MEC (MNPB is marginal private net income, MEC is a marginal external cost) to determine the optimal drainage standard. Thus, emission standards is generally difficult to achieve the optimal pollution level in the absence of such information. If the government set up a unified emission standard for multiple pollution sources, PPP obviously can not achieve the optimal pollution level of each pollution source; Second, PPP improve the cost management. What cause thus is that many of the sources of pollution is small and scattered. So ,whether get MNPB and MEC information or understand the pollution control cost of various sources can bring expensive management costs; Third, PPP is lack of motivation to stimulate enterprise control pollution automatically. What cause this result is that enterprises don't need to pay cost within the pollutants emission standards, so that enterprises have no incentive to adopt new technology to control pollution. Hence, PPP is not conducive to enterprise's technology innovation and lower the total cost of the pollution.

Environmental economic policies--Pigouvian Taxes

Pigou, a British economist , first put forward a idea that a reasonable price about external diseconomy should be determined by the authority. So, when tax is based on the views of pigou, it was called pigouvian tax. Pigouvian tax, which is imposed on the extent of the damage to the environment, is to use tax to make up for the gap between the private cost and social cost, which make them equal.

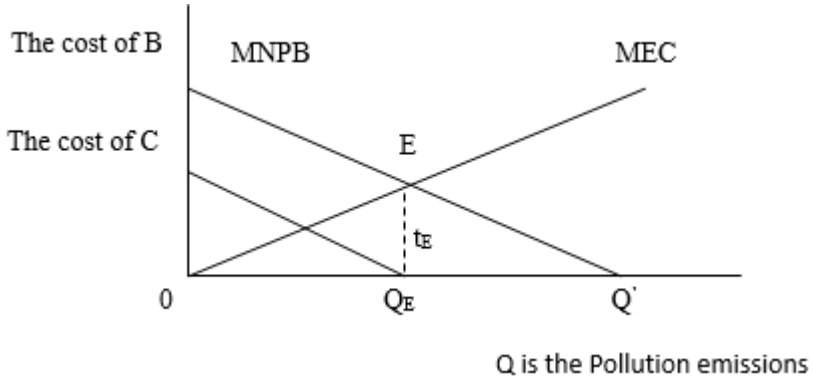

Figure1 Pigou Tax

In figure 1, MNPB is marginal private net income, MEC is a marginal external cost. Although Q_E points is the optimal production scale, the enterprise will produce untile to the point of Q' when MNPB>0. In order to limit production to Q_E, enterprises must be imposed t_E , which is equal to marginal external cost at the optimal output. In a word, imposed tax, which made enterprise's scale of production at the optimal output, is Pigou Tax.

Compare of between emission Standards and pigouvian taxes

Compared with direct control means (emission standard), pigouvian tax has greatly increased the economic efficiency. And the following are their special aspects:

Reduce the standard cost

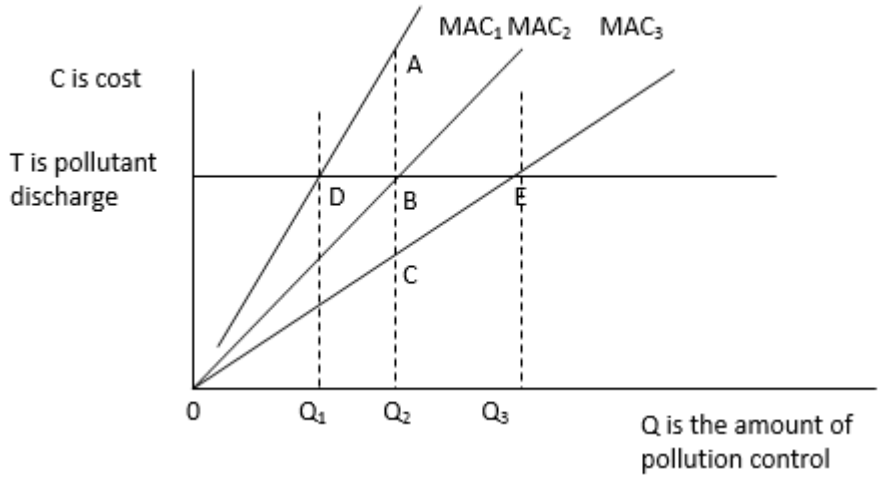

Figure2 Reducing the management cost of Pigou Tax

Assuming that there are three manufacturers in the process of production, the government's goal is to cut the emissions of pollutants to $3Q_2$, $Q_1Q_2 = Q_2Q_3$, and $Q_1 + Q_2+Q_3= 3Q_2$. And in figure 2, MAC_1, MAC_2, MAC_3 respectively said marginal governance cost . It can be learned from the figure is that the cost of factory 1 is highest, the factory 2 times, 3 factory the lowest for the same pollution reduction. If the government set up unified environmental standards and force all manufacturers controlling the emissions to Q_2, the marginal governance cost of factory 1, 2, 3 will respectively reach A, B, C. If the government set the pollutant discharge fee as t, three factories will weigh between discharge and pollution on their own according to the principle of minimizing the total cost. For example, for factory 1, if pollutant emissions is less than Q_1, pollution is much cheaper than paying taxes; if pollutant emissions is greater than Q_1, the result is opposite. In order to compare the total cost between the enforcement emission standard and the pollution charge case, we should calculate the curve under the MAC:

Total governance cost of emission standard: $OAQ_2+OBQ_2+OCQ_2$

Total governance cost of pollution charge: $ODQ_1+OBQ_2+OEQ_3$

And the difference between the two is:（$OAQ_2+OBQ_2+OCQ_2$）—（$ODQ_1+OBQ_2+OEQ_3$）$=Q_1DAQ_2—Q_2CEQ_3$

It can be learned from figure 2 is that the curve of Q_1DAQ_2 is greater than Q_2CEQ_3, so pollution charge of Pigou Tax is lower than simply implementing emission standard cost for controlling the same amount of pollution.

Reducing the costs of the government's management

For emission standard, only confirming enterprise’s pollution exceeded the standard the government can take corresponding measures. For pigouvian tax, the government must confirm that whether the enterprises will produce pollution during the economic activities. So, comparing the cost of doing this, the cost of pigouvian tax is low.

Encourage enterprises to carry out technical innovation.

For emission standards, vendors should not pay a fine if their pollution does not exceed standard, so they have no incentive to seek a low-cost technologies of control pollution.But for Pigou Tax, the pollutant discharge fee is according to the amount of pollutants. So, no matter how much enterprises have the blow down, they must also pay a certain amount of pollutant discharge fee. Therefore companies have incentive to seek a low-cost technologies of control pollution, which can reduce the pollutant discharge fee.

Conclusion

By comparing the two kinds of environmental management policy, we can learn: emission standards is conductive to the fair of environmental resources, though at the sacrifice of economic efficiency. And pigouvian tax can overcome this shortcomings. So in the real practice of

environmental management, the government usually the combine them, namely to the enterprise only pay pigouvian tax within the emission standard, otherwise they not only need to pay the pigouvian tax but also should be fined accordingly. In a word, no matter what kind of policy tools, administrative means and economic measures need to be cooperated effectively, only dong this we can better solve the environmental problems.

References

[1] Satoshi Kagami,Tomonobu Kitagawa,Koichi Nishiwaki,Tomomichi Sugihara,Masayuki Inaba, Hirochika Inoue. A Fast Dynamically Equilibrated Walking Trajectory Generation Method of Humanoid Robot [J], 2002.

[2] HIROKIK, MINORUA, YASUOK, ET al.RoboCup: a challenge problem for AI and robotics. HirokiK. RoboCup-97: Robot Soccer World Cup [C]. Berlin: Springer, 1998.38-43.

[3] Zhizhong Yin. Application of FPGA control DC motor servo system [J]. Inner Mongolia Science and Technology and Economy, 2008 177 (23) 101-103.

[4] Joerg Christian Wolf, Phil Hall, Paul Robinson, Phil Culverhouse. Bioloid based Humanoid Soccer Robot Design, 2007.

[5] Wu Chuan-yu, He Lei-ying, Design and Realization of Instructional RPPR-Robot, Research and Exploration in Laboratory.2007, 26(10)

[6] Nishiwaki K,Kagami S. High Frequency Walking Pattern Generation based on Preview Control of ZMP, IEEE International Conference on Robotics and Automation. 2006.

[7] Chen Nan and so on. For the field of industrial and highly interconnected, TI launched a new Sitara ARM9 microprocessor. [J]. Global Electronics, 2010 (5) 86-87.

[8] Vision Heading Navigation Based on Navigation Curve [A]. Proceedings 2010 International Conference on Intelligent Computing and Integrated Systems[C]. 2010.

[9] Chen Nan and so on. For the field of industrial and highly interconnected, TI launched a new Sitara ARM9 microprocessor. [J]. Global Electronics, 2010 (5) 86-87.

[10] Jonghoon ZMP Park,Youngil Youm.General ZMP Control for Bipedal Walking. IEEE International Conference on Robotics and Automation. 2007.

[11] Chunmei Xu. Mechanical servo system based on fuzzy neural network for complex control [J]. Control Engineering .2010:17 (2):146-148.

[12] Zhijun He. LM629-based motor servo control system design [J]. Mechanical design and manufacture .2009 (2) 40-42

Advanced Materials Research Vols. 989-994 (2014) pp 1328-1332
© (2014) Trans Tech Publications, Switzerland
doi:10.4028/www.scientific.net/AMR.989-994.1328

Research on the Simulation and Realization Approach of Urban Low-carbon Transport

Xiuli GAO[1, a], Tianjun HU[2, b], Peng PENG[3, c]

[1] School of Traffic and Transportation, Beijing Jiaotong University, Beijing, 100044, China

[2] School of Traffic and Transportation, Beijing Jiaotong University, Beijing, 100044, China

[3] School of Traffic and Transportation, Beijing Jiaotong University, Beijing, 100044, China

[a]email:13120952@bjtu.edu.cn, [b]email: tjh@bjtu.edu.cn, [c]email: 234172510@qq.com

Keywords: Low-carbon; Urban transport; System Dynamics; Policy Simulations

Abstract. This paper discusses the connotation of urban low-carbon transport in detail, on the basis of the analysis of low-carbon transport. Combined with the relationship among urban low-carbon transport system elements, the article establishes the system dynamics model. Finally, it simulates the development trends of low-carbon transport in Beijing in the future, and compares the simulation results of different traffic schemes. Moreover, the study puts forward the concrete policy simulations to improve urban low-carbon transport.

Introduction

Over the past centuries, the problem that greenhouse gas caused by the production and daily life leads to global warming has increasingly become the focus of global attention. The concept of "low carbon" was put forward in response to the global climate change and to reduce carbon dioxide in the process of human activities [1]. However, carbon dioxide emissions from the transport sector accounted for a large proportion [2]. Thus, urban transport sector will become one of the important departments in the low-carbon development under the background of the development of low-carbon economy. The low-carbon development path in urban transport of China is not only a crucial way to reduce global warming, but also a new choice to deal with challenges of energy security in China in the future and to achieve the sustainable development of China's urban transportation.

But in the field of low-carbon transport, low-carbon development level in China is relatively low, and research on low-carbon transport system is also less. Thus, this paper gives a correlation analysis of urban low-carbon transport system, and then on this basis, simulates the low-carbon transport trends in Beijing, and puts forward the concrete implementation ways to improve urban low-carbon transport.

Analysis of Urban Low-carbon Transport System

Urban low-carbon transport represents a neoteric development concept and behavior. Its essence is a safe, smooth, orderly and green development mode of traffic with characters of high efficiency, low energy consumption, and low emissions. It pursues dynamic development equilibrium between transportation and economy during the socio-economic development process.

Urban low-carbon transport is to improve transport structure, reduce energy consumption, and control carbon emissions from urban traffic, making per capital energy consumption or per capital carbon emissions a zero growth or even negative growth through traffic demand behavior management and improving transportation organization efficiency, under the circumstance of meeting the continuous growing traffic demand and ensuring the quality of traffic. The connotation can be explained from the following aspects.

First, low-carbon transport is a neoteric development concept. Low-carbon transport does not reduce traffic emissions unilaterally, but reduce carbon emissions or per capita carbon emissions in the transport while ensuring that the quantity and quality of traffic demand of urban residents are not affected and even increasing.

Second, low-carbon transport is a behavior. Low-carbon ways to travel not only reduce carbon emissions caused by the improper selection, also can promote the transformation between existing traffic patterns and low-carbon transport modes, and optimize the structure of traffic travel [4].

Third, low-carbon transport lays emphasis on traffic efficiency. It can not only improve the efficiency of energy use, above all, also to improve the organizational efficiency of the entire transportation system.

Fourth, low-carbon transport is closely related to innovation and application of low-carbon technologies. It can mitigate the growth rate of carbon emissions through technologies, for example, energy saving and emission reduction, development of new energy and tail gas detection and control, thereby achieving the goal of developing low-carbon transport [5].

It can be summed up from the connotation of urban low-carbon transport that urban low-carbon transport system mainly consists of the following seven parts. The interaction among sections is shown in Fig. 1-1.

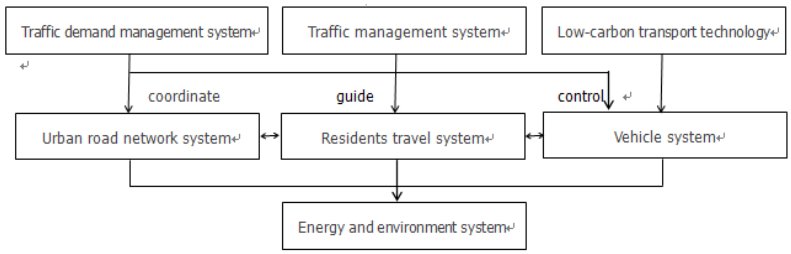

Fig. 1-1 Relation diagram of urban low-carbon transport system elements

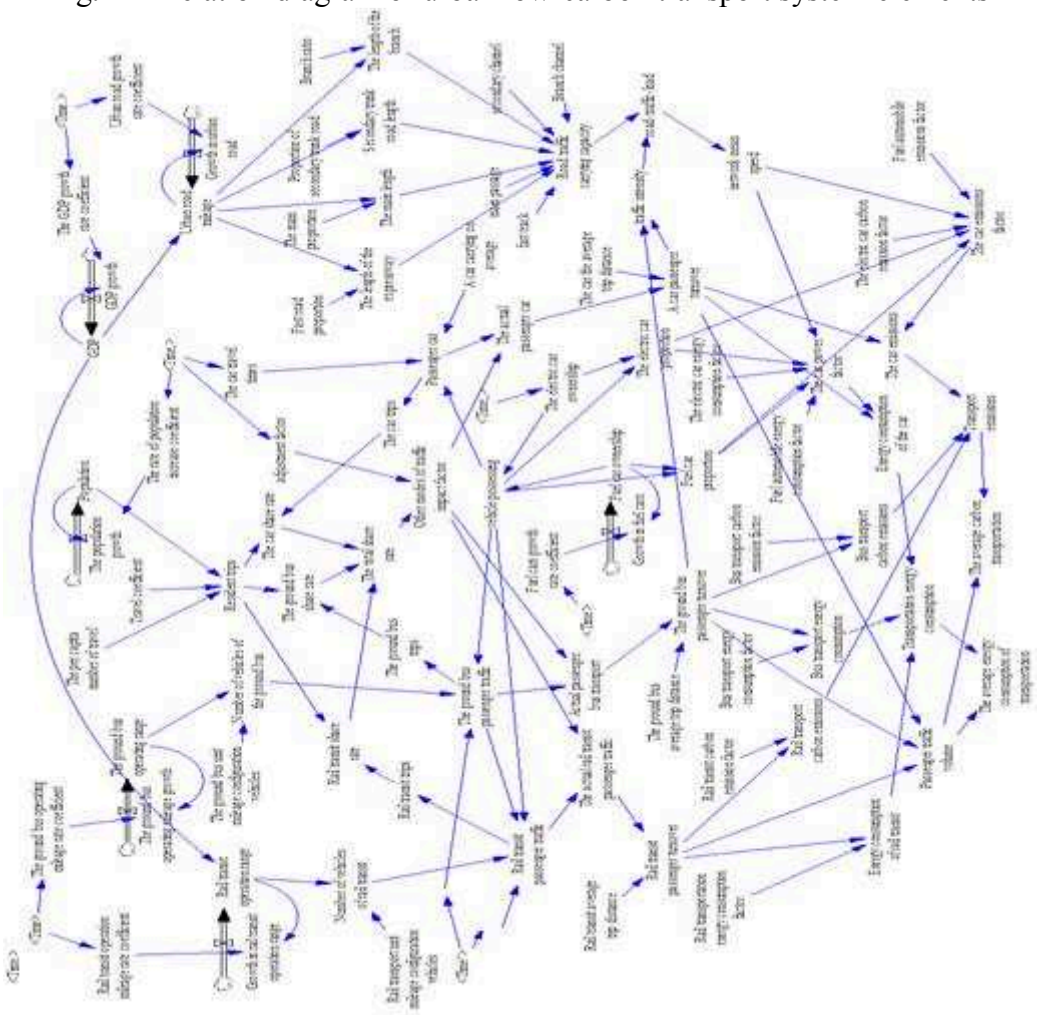

Fig.2-1 System flow chart of low-carbon transport in Beijing

Dynamics Model of Urban Low-carbon Transport System

System dynamics is a simulation calculation method to analyze complex feedback large-scale systems. It identifies the correlation and causality among the elements, according to the object, purpose and nature of systematic research, draws system flow diagram, determines the status, the rate, auxiliary variables of the system, establishes quantitative relations among key variables, and then simulates the overall behavior of the system.

The purpose of this model in the paper is to simulate scenario: change the related variables in the model and observe the effects of its implementation. For instance, the influence of the changes of transportation demands management on the realization of the low-carbon transport, thus getting the feasible suggestions on achieving system goals of low-carbon transport development.

This paper, based on the causality analysis, uses Vensim software to draw up the system flow chart to further distinguish variables' nature, with intuitive symbols depicting the relationship among system elements, and explicates system forms of feedback and control law, as shown in figure 2-1.

The system dynamics model in this paper includes the parameters of urban rail transportation, ground transportation and other aspects of the car. The analysis results of the vital parameters is gotten through the regression analysis of the statistical software SPSS, combined with the statistical yearbook data of calendar year. Some parameters can be estimated according to the transportation development trend over the years [6].

Firstly, rail traffic related parameters. They include the number of rail transit vehicles, vehicle population, ground bus passenger volume and rail transportation passenger volume. Formula is as follows.

$$y = 0.117878x_1 + 62.03115x_2 - 27.865x_3 - 39052.7$$

Where x1 stands for ground transportation passenger volume; x2 stands for rail transportation passenger volume; x3 stands for vehicle population; y stands for number of rail transit vehicles.

Secondly, the ground bus related parameters. They are the number of ground bus vehicles, vehicle population and ground bus passenger volume. The relationship is as follows.

$$y = 26.879x_1 - 123.27x_2 - 16189$$

Where x1 stands for the number of ground bus vehicles; x2 stands for vehicle population; y stands for ground bus passenger volume.

Third, the car related parameters. They are the ownership of fuel cars and electric cars. The latest statistics show that the number of vehicle in Beijing by the end of 2012 has reached 5.2 million vehicles. In order to limit the growth of car, the government in Beijing began to implement a lottery system with an average of 20000 per month on the car number since 2011.Assuming that the numbers are in a stable situation, fuel vehicle growth is about 240,000 vehicles per year in Beijing since 2011, and fuel vehicle ownership has reached to 7.1 million by 2020.

According to the electric car development planning in Beijing, the electric car ownership reached 30000 vehicles by the end of 2012, at the end of 2015 to 109000 vehicles, the growth rate of the electric car is about 0.542. Based on the planning, by the end of 2020, the electric car population has probably reached 960000 vehicles.

Select five state variables to be tested, namely: public transit passenger volume, rail transit passenger volume, bus share rate, rail transit share rate, and car share rate. As shown in Table 2-1. We can see from the table that the error values are controlled within 10%.It indicates that the simulation results are more consistent with the actual situation.

Table 2-1 State variable simulation test results

Time	Project	Actual public transit passenger volume(Thousands of people)	Actual rail transit passenger volume (Thousands of people)	Bus share rate (%)	Rail transit share rate (%)	Car share rate (%)
2005	actual value	369793	67976	24.1	5.7	29.8
	predicted value	367012	67463.2	24.2	5.8	29.9
	relative error	0.75%	0.75%	0.41%	1.75%	0.34%

2008	actual value	470863	121660	28.8	8	33.6
	predicted value	486752	125765	28.3	8.8	31.0
	relative error	3.37%	3.37%	1.74%	9.92%	7.74%
2011	actual value	503272	219280	27.7	13.2	32.7
	predicted value	514139	224014	26.9	13.6	31.6
	relative error	2.16%	2.16%	2.89%	3.03%	3.36%
	average error	2.09%	2.09%	1.68%	4.9%	3.81%

Source: Statistical Yearbook of Beijing, Beijing Traffic Development Annual Report, "Beijing Public Transportation Research Perspective of a low-carbon economy."

Simulation Program of Low-carbon Transport System in Beijing

Scheme one, adjust the car travel times. Reduce the car travel times by 2% per year. The reduced passenger volume of car is usually transferred to the ground bus and rail transport.

Scheme two, adjust the average trip distance of the car. The average trip distance is reduced from 11.49 km to 10 km.

Scheme three, limit the number of fuel cars and encourage the development of electric vehicles. To further reduce the growth rate of fuel cars, assuming that the fuel car growth will drop to 180000 vehicles per year since 2015, and further improve the electric car ownership, from the planning of 110000 vehicles in 2015 to 200000 vehicles, 2020 to 1.2 million vehicles.

Scheme four, adopt integrated program of car demand management. Integrating scheme one, two, three, we should encourage the development of electric cars.

Scheme five, increase investment in public transport and enhance the supply capacity. Operation mileage of rail traffic and bus transportation is increased on the basis of the original planning. Configuration vehicles unit mileage of rail transport are up from 8.5 vehicles/km to 9.5, and bus transportation configuration vehicles unit mileage by 1.12 / km up to 1.8 /km.

Scheme six, increase investment in urban road construction and strengthen the supply capacity.

Scheme seven, carry out comprehensive policy. The policy integrates scheme one to scheme six.

The simulations mainly focus on the influence of the change of variables on transportation energy consumption and carbon emissions. The change of transportation energy consumption and carbon emissions caused by variables' change can be achieved by modifying the relevant variables with the application of simulation model. The simulation results are as follows.

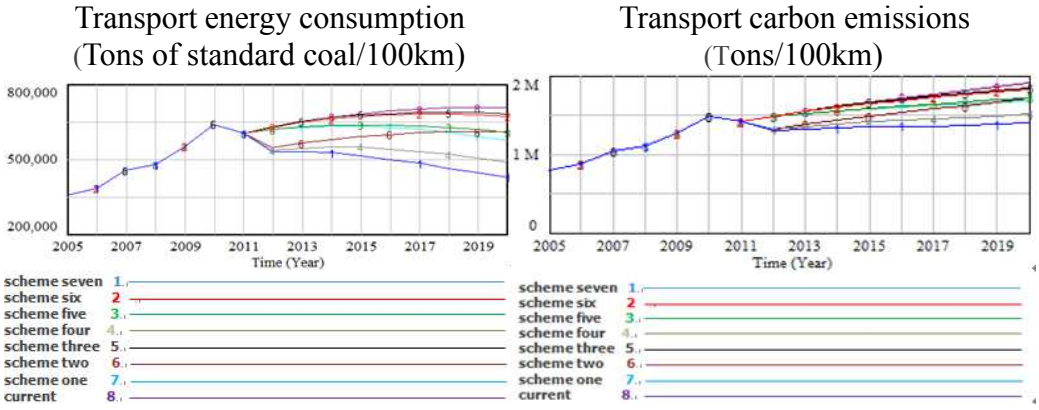

Fig. 3-1 The contrast of implementation effect on transport energy consumption（Left）

Fig. 3-2 The contrast of implementation effect on transport carbon emissions (Right)

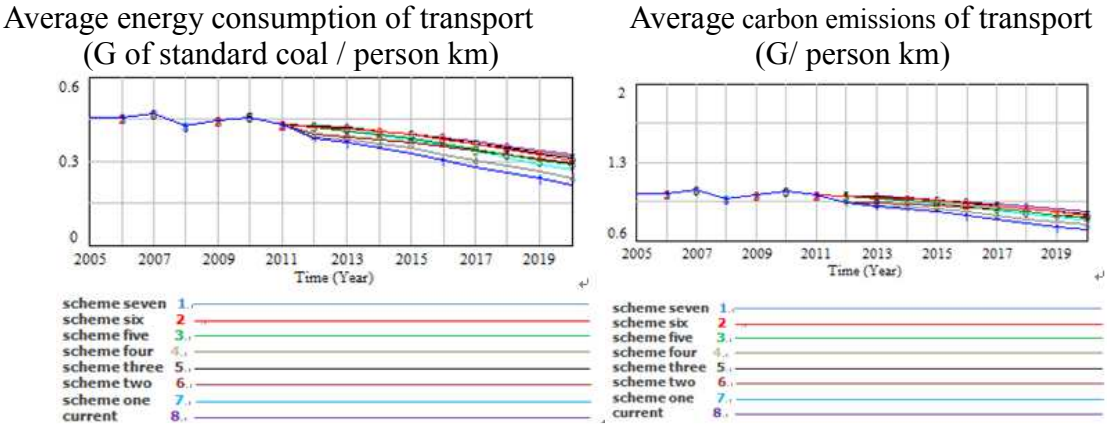

Fig. 3-3 The contrast of implementation effect on transport average energy consumption (Left)

Fig. 3-4 The contrast of implementation effect on transport average carbon emissions (Right)

In order to speed up the implementation of low-carbon transport in Beijing, combined with simulation analysis result, the future development should be focused on the following aspects:

Firstly, promote the building of public transport, and improve its supply ability, thus optimize the urban traffic structure.

Secondly, plan the road network scientifically, optimize network structure, distribute the way reasonably, and reduce the traffic load.

Third, give priority to develop new energy vehicles, such as electric vehicles, through technical innovation, to improve energy utilization efficiency and reduce carbon emissions.

Fourth, advocate low-carbon transport, encourage city residents to establish the low- carbon concept, use the way to travel with low energy consumption and low emissions, such as public transit, bicycles, and walking, provide city residents with a variety of choices to travel to lay a good foundation for low-carbon transport of the city.

Conclusions

This paper simulates the development trend of low-carbon transport in Beijing in the future, based on the related analysis on urban low-carbon transport. The simulation results conclude that the development rate of traffic carbon emissions and energy consumption in Beijing has been reduced than before and the rate of per capita carbon emissions and per capita energy consumption is declining. Those show that the development prospect of low-carbon transport in Beijing is good, and further policy guidance is needed. In addition, the article mainly studies the content about the influence of macroscopic urban traffic management policies on the development of urban low-carbon traffic, not has a further study on the impact of specific technical improvement of low-carbon traffic on system. Considering these, in the future, the traffic structure need to be further improved, and the influencing factor of transport should be considered more meticulous.

References

[1] Zhang-ping Xin, Yin-tai Zhang. Low carbon economy and low carbon city [J]. Journal of research on urban development, 2008,15 (4):98-100.

[2] IPCC. Climate Change 2007 - Synthesis Report: Contribution of Working Groups I, II and III to the Fourth Assessment Report of the Intergovernmental Panel on Climate Change[R]. Geneva: IPCC, 2007.

[3] Li-ya LIU, Low Carbon Transportation Road to Promote Urban Sustainable Development. Comprehensive Transportation, 24 (1), pp.29－32, 2010.

[4] Koji Shimada, Yoshitaka Tanaka, Kei Gomi, Yuzuru Matsuoka. Developing a Longterm Local Society Design Methodology Towards a Low-carbon Economy: An Application to Shiga Prefecture in Japan [J].Energy Policy, 2007, (35):4688-4703.

[5] Mustafa H. Babiker. Focus on low carbon technologies: The positive solution [J]. International Economics, 2005, (65): 33-49.

[6] Vuchie V R., Urban Transportation systems and Technology[M]. New York: Prentiee-Hall, Ine1981.

Advanced Materials Research Vols. 989-994 (2014) pp 1333-1337
© (2014) Trans Tech Publications, Switzerland
doi:10.4028/www.scientific.net/AMR.989-994.1333

The Spatial Effect Identification of Pollution Treatment Investment in China

Liangxiong HUANG [1, a], Min LIU[2, b]

[1]Guangdong Research Institute for International Strategies, Guangdong University of Foreign Studies, Guangzhou, 510420, China,

[2]Department of Economics, School of Economics of Ji'nan University, Guangzhou, 510632, China

[a]Email: chickyliang@126.com, [b]Email:lium33@mail.sysu.edu.cn

Keywords: pollution treatment, spatial effect, dynamic spatial panel model

Abstract. Pollution treatment investment is an important part of environment protection in terms of energy saving and emission reduction. A dynamic spatial panel model is constructed in this paper, identifying the spatial effect in pollution treatment investment of regions and discussing the mutual influences among different regions. The result shows a mutual positive influence and behavioral convergence regarding to the pollution treatment investment behavior among regions.

Introduction

Nowadays, the society has been exposed to more and more rigorous environment pollution. To solve this problem, pollution treatment investment is becoming a rising concern. On one hand, pollution treatment investment can powerfully help to mitigate the degree of loss on pollution; on the other hand, it can effectively prevent the potential emission. Besides, the externality of treatment and the local background of China: "centralized polities and decentralized economies", together cause the mutual influence on pollution treatment among different areas and form spatial effect. This paper focuses on the discussion upon the spatial effect of areal pollution treatment investment, taking the every ten thousand yuan GDP industrial pollution control project investment as the analysis object. Unit GDP pollution treatment investment reflects the strength of areal pollution treatment. Moreover, it is a qualified corresponding variable of emission quantity and energy consumption of past researches.

The spatial effect of pollution treatment investment among different areas, or mutual influence between areas, may be positive or negative. If the spatial effect is positive, it means pollution treatment investment behaviors among areas are positively correlated, the areas will converge with each other in the pollution treatment investment behavior; otherwise, they will diverge.

The empirical models and methods

In order to study the behavior characteristics of pollution treatment investment in China's provinces and analyze the spatial effect of pollution treatment investment, a spatial panel model is constructed [1]. The specific regression equation is as follows:

$$P_{it} = \theta_0 + \theta_1 P_{it-1} + \rho W * P_{it} + \psi X_{it} + \varepsilon_{it}$$

In the above equation, P represents unit GDP pollution treatment investment in the region. This paper adopts three pollution treatment investment indexes, which are industrial pollution treatment investment (*lginvt*), industrial waste gas treatment investment (*lginva*), industrial waste water investment (*lginvw*). The three indexes also respectively reflect the performance of the overall environment treatment, gas pollution treatment and water pollution treatment in the region. W represents spatial weight matrix. $W \times P_{it}$ reflects the effects of investment in other regions on the local region. The coefficient ρ represents the direction of the effects. If ρ is significant, it also indicates that the local investment has significant effects on other regions' pollution treatment. On the other hand, the pollution treatment investment of regions is always time-dependent; the investment in the past time will affect the current investment. To indicate this point, a time lag

phase is put in the regression equation. Thus, the above equation includes the lag phase of the explained variable and the spatial weights, forming a dynamic spatial panel model. The former captures time change effect, and the latter captures the spatial effect of regions.

X is controlled variable, including three categories: firstly, variables that reflect the environment factors of regions mainly including Carbon dioxide emissions per unit of GDP (*lgco2*), wastewater emissions per unit of GDP (*lgwat*) and the effective tax rate (*el*); Secondly, variables that reflect the economic structure factors, mainly including real per capita GDP and its squared term (*ly&ly2*), the proportion of Second industrial added value of GDP (*wg2*), external dependence degree (ti) and urbanization rate (*cir*). Other controlled variables, mainly average years of education (*pey*), density of population (*lpopa*).

The spatial weight matrix

Spatial weight matrix W is a $N \times N$ symmetric matrix, The diagonal elements W_{ii} set as 0. And it indicates the correlation of the region i and region j. Here three kinds of weighted matrix are used, firstly, the spatial weighted matrix based on the spatial distance, namely $W_{ij}=1/d_{ij}$. Secondly, the Rook adjacent spatial weighted matrix (*Wr*), it is $W_{ij}=1$ when two areas have a common boundary; it is $W_{ij}=0$ when two areas do not have a common boundary. Moreover, in the robustness test, the K value of the adjacent space matrix (*Wk*) is also used. Given a space unit, the weight is 1 when selecting the nearest *K* areas, otherwise zero. Generally, *K* is 4. Meanwhile, to eliminate the external influence among areas, the weighted matrix is standardized as $W_{ij}^{*} = W_{ij} / \sum_{j=1}^{N} W_{ij}$, which makes the total sum of the elements of the row equal to one.

Empirical Analysis

According to the equation (1), a dynamic spatial panel model is constructed, studying the spatial effect of pollution treatment investment of regions, and the results are presented by table 1. As in the right of the equation (1), there is endogeneity both in the time lag and the spatial weights of the explained variables. To solve the problem of endogeneity, by the method of Huang et al. [2]—the spatial systematic GMM estimators (SBB) and spatial difference GMM estimators (SAB) are used to estimate it.

The estimators that Table 1 built show that Moran'I statistics are significant, which means China's regions per unit of GDP investment environment pollution has spatial dependence. At the same time, AR (1), AR (2) and Hansen statistic result show that the selected IV in this chapter variable is reasonable.

The spatial effect coefficient ρ which reflects the pollution treatment investment is analyzed. The results show that the spatial weighted coefficients of industrial pollution treatment investment (*lginvt*), industrial waste gas treatment investment (*lginva*) and industrial waste water investment (*lginvw*) are significantly positive, indicating that the investment of unit GDP of other regions has significantly positive effect on the local region. In turn, if the spatial weighted coefficient ρ is significantly positive, the investment of unit GDP in the local region has significantly positive effect on other regions. Therefore, the investment of unit GDP among regions has mutual positive effect. The behaviors on pollution treatment investment among regions are consistent, resulting that unit GDP pollution treatment investment of close regions is adjacent to each other and spreads out. Convergence is reached finally. Similar analysis can be found in Huang et al. (2011) and Shu and Huang (2012). The former found that the pollution of the developed areas in China has "example effect" to the other areas, that is, the developed areas of sewage pose significant positive influence to the rest. The latter also found that there is positive influence among regions on each other in our country environment pollution resources loss.

Table 1 The spatial effect of pollution treatment investment

	(1)	(2)	(3)	(4)	(5)	(6)
L.lginvt	0.601***	0.370***				
	(0.025)	(0.064)				
Wlginvt	0.730***	0.684***				
	(0.032)	(0.077)				
L.lginva			0.597***	0.397***		
			(0.029)	(0.058)		
Wlginva			0.543***	0.729***		
			(0.040)	(0.100)		
L.lginvw					0.673***	0.417***
					(0.015)	(0.051)
Wlginvw					0.686***	0.778***
					(0.024)	(0.068)
Moran I	0.303***	0.303**	0.364***	0.364***	0.165***	0.165***
AR(1)	-3.456***	-3.276***	-3.747***	-3.585***	-3.767***	-3.341***
AR(2)	0.400	0.391	0.326	0.165	-0.346	-0.364
Hansen	27.122	15.983	26.040	18.114	28.185	21.175
N	330	330	330	330	330	330

Notes:①lists the variables of interest; ②L represents a first-order lag;③***,**,*respectively indicate the significance level of1%,5% and 10%;④it is standard error in the bracket;⑤AR(1)、AR(2)test residual autocorrelation;⑥Hansen tests the effectiveness of instrumental variables.

There are two reasons for the positive mutual influence of areal pollution treatment investment behavior. Firstly, since environment is public goods, there is positive externality of pollution treatment, which will benefit not only the local region, but also others. However, such mechanism makes the marginal private benefit of pollution treatment less than that of the marginal social benefit. There will be a problem of free riding. At this time, no one will actively treat the pollution, so that the level of social pollution treatment will be lower than the optimal one. In other words, if no central restriction exists or the restriction is not strong enough, pollution treatment investment behavior in different regions will converge, which means regions will reduce pollution treatment investment as much as possible. The second reason is the stronger decision power of local government on pollution treatment investment than that on emission amount. As is known to all, the reducation of emission amount depends much on technology which in short term has quite limited advancement. However, another variable affecting the pollution treatment, investment, can be easily adjusted according to governments' plans. So the local governments of regions show more strategic interaction feature on pollution treatment investment. The significantly positive ρ value also shows that strategic complementation exists among different regions, as the regions imitate each other on pollution treatment investment behavior [3].

Robustness Test

In this section, robustness test is taken, mainly replacing the spatial weighted matrix and using the matrix based on adjacent method *(Wr*), SAB estimator and MASARAR (1, 1) model used by Wang (2010). Table 2 shows the results.

Both in the SAB estimator and MASARAR (1,1) model, the spatial effect coefficient ρ which reflects the pollution treatment investment of regions is significantly positive. The pollution treatment investment behavior has mutual positive influence, going to convergence.

Table2 Robustness test: using different regression model

		SAB			MASARAR(1, 1)		
		lginvt	*lginva*	*lginvw*	*lginvt*	*lginva*	*lginvw*
Wd	ρ	0.901***	0.758***	0.856***	0.757***	0.813***	0.920***
		(0.101)	(0.139)	(0.108)	(0.181)	(0.188)	(0.190)
Wr	ρ	0.603***	0.398***	0.637***	0.532***	0.586***	0.629***
		(0.082)	(0.086)	(0.084)	(0.184)	(0.267)	(0.207)

Moreover, after the author replaces the spatial weighted matrix by using the nearest spatial weighted matrix (*Wk*) of K=4, and constructs SBB and SAB estimators and MASARAR (1, 1) model, the coefficient ρ is still significantly positive, indicating the robustness of the results.

Conclusions and policy recommendations

Pollution treatment investment is a necessary measure for environment protection and green development. In the context of Chinese political centralization and economic decentralization, regional issues are often rooted in the interactions among regions; these interactions will form the space effect. The analysis of Chinese pollution treatment investment is not an exception. This paper uses the dynamic spatial panel model, builds SBB and SAB estimators, and combines with MASARAR (1, 1) model to investigate the spatial effect of areal pollution treatment investment to explore the interactions among regions. The results show that:

Unit GDP of areal pollution treatment investment has a significant positive effect, which means regions converge on pollution treatment investment behavior. This paper argues that the conclusion is based on two points. (1) Like the pollution emissions, pollution treatment investment has externality, and the externality is positive. A regional pollution treatment investment can make other regions benefit without costs, and then it comes the regional "hitchhike" phenomenon. Because there is few restraints to this phenomenon by the central government, represented by the lack of constraint strength, provinces tend to reduce pollution treatment investment. (2) The regional competition currently is still dominated by the GDP competition and governments' passion for pollution treatment lag far behind economic growth. However, there are regional interactions of imitating each other's strategy, so regions will tend to make pollution treatment investment in the constrained standards even though the central constraints are hard.

To eradicate the externality of pollution emissions and pollution treatment and eliminate the phenomenon of market failure, government needs strong promoting policies. So the key is to arouse the enthusiasm of local governments, which can start from the current local government (officials) assessment mechanism. If the evaluation mechanism of taking GDP as the single core is not changed, there will not be enough stimulation to the local government (officials) to control pollution. And the lack of hard constraints will also lead to regional race to the bottom. The implementation of "one vote veto" system and accountability system can make hard constraints to environmental indicators, which can cause the local government's attention but let the pollution level remian in the constrained standards. This setting only guarantees the lowest level but cannot obtain a better level. So deepening the assessment mechanism and introducing the multiple target mechanism should be the future direction of development. For example, using the environment satisfaction of the local residents is conducive to form the scale effect of environmental governance, to promote energy-saving and emission reduction, and to promote environmental protection in the area. The double yardstick competition of GDP and environmental governance will promote a sound and rapid development of our country with not only faster economic growth, but also environmental improvement.

Acknowledgement

In this paper, the research was sponsored by Guangdong University of Foreign Studies Youth Project (12Q01) and the project of Canadian Studies Center of Guangdong University of Foreign Studies (B2013CCS11)

References

[1] Case, A. C., H. S. Rosen and J. R. Hines. Budget Spillovers and Fiscal Policy Interdependence: Evidence from the States[J]. Journal of Public Economics, 1993, 52:285-307.

[2] Huang Liangxiong, He Wang, Lingyun Song. The Adjustment of the Industrial Structure of Our Country is Green?[J], Economic Studies of Nankai. 2012(3):110-127.

[3] Huang Liangxiong, L. Zhang and Y. Shu. Pollution Spillover in Developed Regions in China-Based on the Analysis of the Industrial SO2 Emission[J]. Energy Procedia, 2011(5):1008-1013.

[4] Shu Yuan and Huang Liangxiong. The Loss of Environmental Pollution and Resources of China's Provinces and Their Spillover Effect[J], Journal of Audit & Economics,2012(3):86-96.

[5] Wang Meijin, Jianhao Lin, Zuangxiong Yu. China Local Government Fiscal Competition Behavior Recognition: whether "Brother Competition" and "Father and Son Dispute" Coexist?[J]. Management World. 2010(3):22-31.

Advanced Materials Research Vols. 989-994 (2014) pp 1338-1340
© (2014) Trans Tech Publications, Switzerland
doi:10.4028/www.scientific.net/AMR.989-994.1338

Characteristics of heavy atmospheric particulate pollution under Beijing fog and haze

Junxiu Liu[1,a], Peng Yang[1,b], Agudamu Liu[1,2,c], Jie Liu[1,2,d]

[1]Beijing Key Laboratory of information Service Engineering, Beijing Union University, China

[2]Civil & Environmental Engineering School, University of Science &Technology Beijing, China

[a]email:liujunxiu95@163.com,[b]email:yangpeng@buu.edu.cn,[c]email:amu_liu@163.com,
[d]email: liujie19860809@qq.com

Keywords: Beijing, $PM_{2.5}$, PM_{10}, Haze, Continued

Abstract. Three consecutive severe traffic monitoring points collected in different atmospheric particulate pollution concentrations data during February 2014 in Beijing. The results show that the hourly mean concentration of $PM_{2.5}$ often exceeded 200 ug/m^3, with a maximum concentration of 300 ug/m^3on Feb.22,2014. The hourly mean concentration of PM_{10} either exceeded 258 ug/m^3.The concentration of $PM_{2.5}$ and PM_{10} was significantly increased during haze events, especially $PM_{2.5}$ concentrations increased gradually and a slight decline in the middle, then rise.

Introduction

Atmospheric particulate matter, atmospheric aerosols dispersed systems of various particles. According to aerodynamic equivalent diameter, can be divided into total suspended particulates, repairable particulate matter and fine particulate matter. Total suspended particulate matter is the particle size <100um all particulate matter, expressed as TSP (total suspended particulate); Particulate matter refers to a particle size of <10um particle, expressed as PM_{10} (inhalable particulate matter); particle size <2.5um of particulate matter is known as fine particulate matter, expressed as $PM_{2.5}$ (fine particulate matter)[1]. Compared with coarse atmospheric particles, fine particulate matter is rich in a lot of toxic and hazardous substances and long residence time in the atmosphere, conveying distance, and thus a greater impact on human health and environmental quality.

Beijing is experiencing heavy air pollution in the past two decades, with particle matter (PM) being one of the top pollutants (Chan and Yao, 2008).PM especially fine particles often exceed the new National Ambient air Quality Standards of China ((75ug/m^3 for 24 h average) (Sun et al.2013)).Ambient air quality standard is shown in Table 1.Fine particles have a large impact on visibility. Therefore, haze events (with visibility<10 km) appear frequently in Beijing with high concentration of fine particles. [2]Paper studies during the Beijing haze, PM2.5 and PM10 concentrations and changes in variation.

Table1. Ambient air quality standard

Pollutants	Average time	Concentration limits		Unit
		one-level	second level	
SO_2	Annual	20	60	ug/m^3
	24-hour	50	150	
	1-hour	150	500	
NO_2	Annual	40	40	mg/m^3
	24-hour	80	80	
	1-hour	200	200	
CO	Annual	4	4	ug/m^3
	24-hour	10	10	
	1-hour	100	160	
Particulate matter（article size of <10um）	Annual	40	70	
	24-hour	50	150	
Particulate matter（article size of <2.5um）	Annual	15	35	
	24-hour	35	75	

Data collection and analysis

Collection point. As to 2013, Beijing has established 35 monitoring points, including 12 monitoring points urban, suburban 11 monitoring points, seven points and control points and five regional traffic pollution monitoring point. For CO, NO2, O_3, SO_2 concentration of repairable particulate matter 24-hour real-time automatic monitoring, accumulated a large amount of data, which has a very important significance for the study of air quality and characteristics of Beijing. In this paper, data from previous Gate East Avenue, South Third Ring Road, East Fourth Ring Road, three traffic pollution control points collected for the study, analysis of many types of pollutants.

Collection and analysis.

Data collection: Every evening at six to export the data, the data is updated once every hour, 24 hours a day for pollutants real-time automatic monitoring, primarily to monitor CO,NO_2, O_3, SO_2 and the concentration of repairable particulate matter, the study of $PM_{2.5}$ and PM_{10} concentrations finally study the variation of the fog and haze.

Data processing: The data collected mainly by way of text files and databases to manage things [2], and displayed in the form published on the website, to achieve the basic storage function, but the need for further post-processing. Research platform to use VB.NET to create air quality data management system, using powerful computers to achieve automatic analysis of air quality data processing, automated data management of air quality in Beijing.

Data Analysis: Take 20 to 27 February $PM_{2.5}$, the average daily PM_{10}concentrations, and compare it to study the relationship between visibility.

Results and Discussion.

The average concentration of PM2.5 and PM10 during fog and haze .Table 2 showed, $PM_{2.5}$, PM_{10} pollution is serious, three sampling points PM_{10} , $PM_{2.5}$ on February 22 average concentration (unit: ug/m^3) were 260.78ug/m^3, 267.45ug/m^3, 255.56ug/m^3 and 214.81ug/m^3, 135.3ug/m^3, 258.79ug/m^3. According to Chinese air quality environmental quality standards (GB3095-2012), the average PM_{10} concentrations three points (202.9ug/m^3) more than two standard prescribed daily average (150ug/m^3), the average $PM_{2.5}$ concentration (261.3ug/m^3) far more than two class standards prescribed daily average (75ug/m^3) [3].

Table2. Feb.22.2014 PM_{10} and $PM_{2.5}$ concentrations in Beijing

Monitoring points	PM2.5 concentrations (ug/m^3)		PM10 concentrations (ug/m^3)	
	Concentration range	Mean	Concentration range	Mean
Yongding Gate Avenue	220—306	260.78	110—375	214.81
South Ring Road	214—312	267.45	105—186	135.3
East Fourth Ring Road	199—352	255.56	154—435	258.79

Whether PM_{10} or $PM_{2.5}$ concentration monitoring points are far greater than the standard value, in fog and haze, the concentrations of $PM_{2.5}$ will continue to rise, especially under low visibility fog and haze conducive to the accumulation of particulate matter, resulting in high concentrations of aerosol pollution events [4]. Figure.1 is the trend of $PM_{2.5}$ and PM_{10} in fog and haze. As can be seen from the figure1, the value of $PM_{2.5}$ and PM_{10} uptrend in three monitoring points, with the haze of pollution increase, its value also will increase. Thus, in the fog and haze, and have the concentration increases, which also is consistent with previous studies [5].

During the haze, larger temperature difference between day and night, Beijing, and has been in the breeze among the lower wind speeds are less than three, is not conducive to the spread of pollutants. Lower ground moisture and high wind speeds and humidity often causes the rapid accumulation of growth, and a large temperature difference between day and nighttime radiation inversion makes clear that while the existence of inversion tends to inhibit the spread of pollutants, making transportation difficult at low altitude to high altitude .[6] It can be seen in the haze sustained period of time, the weather conditions are not conducive to the spread of pollutants, but is conducive, accumulation, making the fog and haze last many days, it is difficult to dissipate. In the 27th, night of rain, making the weather improved, showing that meteorological factors are the key factors of fog and haze now resolved.

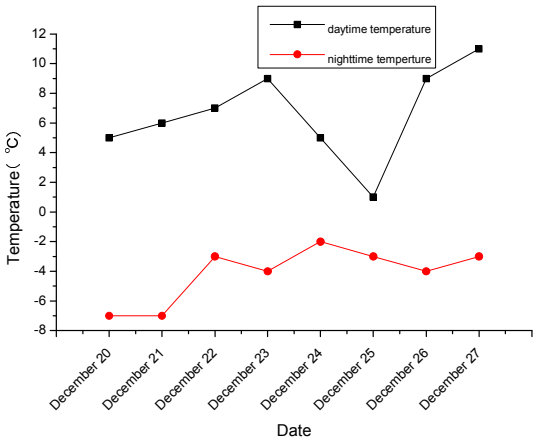

Fig.1.Changes in $PM_{2.5}$ concentration curve

Conclusion

Under fog and haze, and the concentration of $PM_{2.5}$ were 267.45 ug/m^3, 260 ug/m^3, which is higher than the national standard concentration 150 ug/m^3, the concentration is higher than the national standard 75 ug/m^3 significant, indicating that in the fog and haze have significantly increased and the concentration .Beijing meteorological factors not conducive to the spread of pollutants, making the fog and haze last longer, making it difficult to low-altitude water vapor, to form a stable boundary layer near the ground, in order to provide a better generation and accumulation of $PM_{2.5}$ add conditions.

Acknowledgement

This research is a part of the project funded by the Importation and Development of High-Caliber Talents Project of Beijing Municipal Institutions (CIT&TCD20130320), “Research on Real-time Monitoring System foe Urban Ambient Air Parameters based on Wireless Sensor Network.”

References

[1] Ning Shi, Jianhui Zhang: Beijing autumn and winter 2012-2013 Characteristics of atmospheric particulate pollution (2013).In Chinese.

[2] Jiannong Quan，Xuexi Tie. Characteristics of heavy aerosol pollution during the 2012-2013 winter in Beijing, China. Atmospheric Environment.2014.

[3] Sengcao Lai, Yeji Peng. Winter and organic carbon and elemental carbon concentration levels and distribution characteristics of Guangzhou. Process Engineering, 2004.

[4] Yue Wang, Lili Wang. Beijing heavy pollution situation and the structural analysis of the circulation period boundary (2013).In Chinese.

[5] Xing Na, XinMei Li. Aerosol optical properties of fog and haze during the Beijing. [J] .Environmental Sciences, 2012.

[6] Chanzhen Shi, Na Yu. During the aerosol optical properties of different backgrounds pollution practice. [J]. Environmental Sciences, 2013.

Advanced Materials Research Vols. 989-994 (2014) pp 1341-1347
© (2014) Trans Tech Publications, Switzerland
doi:10.4028/www.scientific.net/AMR.989-994.1341

Urban river water purification experiment by strengthening ecological engineering methods

Shuhua Yin[1,a], Yuchun Wang[1,2], Wenqi Peng[1], Yanliang Du[1], Bo Gao[1], Jijun Gao[1],Huaidong Zhou[1], Qingyi Meng[3], Qijun Li[3]

[1] China Institute of Water Resources and Hydropower Research, Beijing, 100038 China.

[2] State Key Laboratory of Simulation and Regulation of Water Cycle in River Basin, China Institute of Water Resources and Hydropower Research,Beijing,100038, China

[3] Beijin Water Science &Technology Institute ,Beijing,100048, China

[a]email: yinsh@iwhr.com

Keywords: Urban River; Enhanced Nitrogen Removal; Ecological Engineering; Water Purification

Abstract. Based on the biological purification technology combined with the engineering measures, the enhanced nitrogen purification biological experiment is implemented in Wenyu River in Beijing. The water in the river mainly is the outflow from the sewage treatment plant, in which the ammonium (NH4-N) has been effectively removed for the deeply nitrification, while treatment of the nitrate nitrogen (NO3-N) and total nitrogen (TN) is incomplete due to the denitrification. The water has low C/N value and has poor biodegradability. In this study, aiming at the water feature of low C/N and poor biodegradability, the effective way to strengthen denitrification by some enhanced techniques, such as increasing the microorganisms number and biodegradability (ie, improved nitrogen ratio), changing denitrification rates and so on, has been studied. The experimental results show that under the condition of water flow (Q) as 15 ~ 27L/hr, hydraulic detention time as (HRT) 10 ~ 18h, concentration of nitrate nitrogen (NO3-N) as 12.20 ~ 31.44mg / L, and total nitrogen (TN) as 14.50 ~ 34.71 mg / L, the removal rates of NO3-N and TN are over 30%.

Introduction

Wenyu River is the only river started from Beijing and flows in the whole year. It is a main stream for the flood control, drainage, irrigation and ecological environment protection, and it is also a river for the city sewage water. Wunyu River plays an important role for the urban socio-economic development and urban construction.

With the rapid development of the economic and the urbanization, the urban population increases dramatically, and the discharge of sewage water of industry, agriculture and domestic waste water are also increasing. Due to the lag of watershed drainage network and sewage treatment infrastructure, the river water has been polluted and water ecology has been degraded, therefore the function of the river resources, environment and ecology are lost.

In recent years, the Chinese government places great emphasis on environmental protection, and the waste water treatment rates rise constantly. The techniques of denitrify and dephosphorization cause high energy-consuming, low removal rates and the unstable running operation, therefore the outflow has high concentration of N and P, specially when the Ammonian (NH3-N) transfers to trate nitrogen passing the high Oxygen consumption area with incomplete denitrification and resulting the increasing trate nitrogen. The removal rate of total nitrogen (TN) of the waste water outflow is low, which leads to high harmfulness when the outflow is discharged to the water environment[1].

According to the current sitiation of Wenyu River, building the waste water plant to achieve the deep water purification to is impracticable because of the infrastructure investment and operating costs. The ecological projects embedded in the water courses in the river is applied to enhance the denitrification treatment process, which can also relieve the pressure on municipal infrastructure construction and sewage treatment plants, in the meantime it can beautify the natural environment,

to solve the pollution problem. an effective method of purifying water strengthening The ecological projects can be an effective method to strengthen the water purification.

Design of the Experimental Mechanics

According to the current water quality characteristics of Wenyu River, the purpose of this study is to enhanced denitrification process and to intensify the water purification of the waste plant outflow. Due to the low biodegradability of the urban river water against the denitrification process, in order to improve denitrification efficiency the experiments are designed to increase systemic biodegradability and change the denitrification way as "enhanced techniques" by increasing the number of microorganisms[2] [3] [4].

Based on the nitrate removal theory, in the experiments, the glucose is regarded as carbon source, and the elemental sulfur as an electron donor into the reaction system to promote autotrophic denitrification. The impacts of the supplement to improve the biodegradability of nitrification and changing nitrification approach on denitrification are analyzed [5] [6].

Considering the river water characteristics in the field remediation technologies in the experimental schemes, the experiments has designed "eco-reactor (channel)" (hereinafter referred to as eco- groove) as a new treatment techniques, which take advantage of natural conditions to make the river run freely to reduce energy consumption and operating costs.

The main unit in the experiments is eco-groove (ditch) with the size of 200 cm × 30 cm × 50 cm, effective depth 45 cm, and total effective volume 270L. The eco-groove is divided into two layers by the multi-stepped perforated clapboards, to form 2 spaces as aerobic and anaerobic zones, with the volumetric ratio as 1:2. The walls of eco-groove are covered with aluminum foil to prevent light in, and to simulate the working environment of the river ecological engineering. The inlet is in the aerobic zone, and the effluent outlet is in the anaerobic zone. The certain giving water discharge and level are used to control the constant flow in the experimental zone.

There are three study cases by using different hydrodynamic operation situations with the same specified eco-grooves numbered as I, II and III. The study is designed to do the comparison among those cases.

The cabinets of the eco-groove are made of plexiglass and plastic plates. The main parts of the devices include the water inlet and outlet, pumps, flow meters, and the auxiliary equipments includes water storage tank, mixing tank, access to water, water gauge, submersible pumps and so on. The devices of eco-groove are shown in Figure 1.

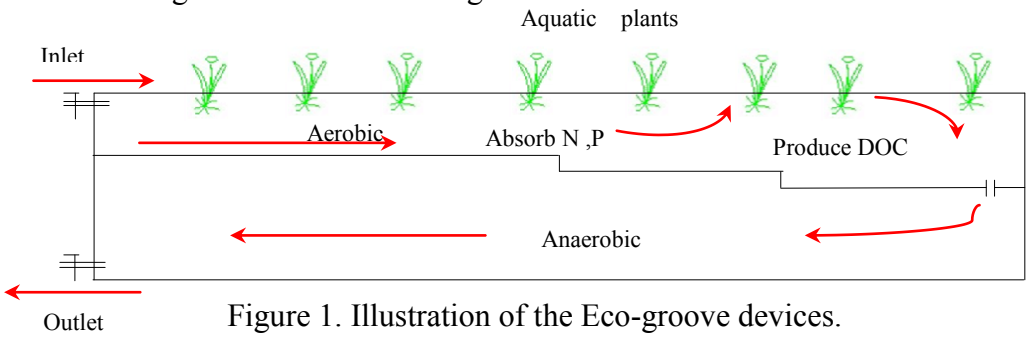

Figure 1. Illustration of the Eco-groove devices.

Water quality condition in experiments

The tests water in experiments is taken from a section of Wunyu River in a town in Beijing near. The indexes of water quality are indicated in Table 1.

Table 1. Water quality indexes in the raw ware in the experiments

Indexes	pH	COD (mg/L)	NH4-N (mg/L)	NO3-N (mg/L)	TN (mg/L)	PO4-P (mg/L)	TP (mg/L)	TOC (mg/L)
Range	6.4~8.2	10~20	0.2~4.8	12.2~31.4	14.5~34.7	0.9~4.9	1.3~5.7	0.18~0.32
Average	7.3	15	2.3	21.8	24.6	2.9	3.5	0.25

Seen from Table 1, the water has low the concentration of COD and NH4-N, and TN mainly in the form of NO3-N, and the C/N is relatively low, which means that the water has poor biodegradability.

Methods of Water Quality Analysis

To measure the different indexes, we use the spectrophotometry UV for NO3-N, the Nessler's reagent spectrophotometry for NH4-N, the potassium persulfate - UV spectrophotometry TN, the non-dispersive infrared absorption method for TOC, the temperature using rapid analyzer for DO, and the portable pH meter for pH, the potassium permanganate oxidation for COD.

Experimental operating conditions

Three experiments with different operating conditions are designed according to the real sewage treatment method. To improve the preliminary understanding of the denitrification functions of the eco-groove, we run designed three cases.

Groove I is a comparing tank without any medium, and it is used for the tests under sewage water conditions only;

Groove II is used for the ecological method, in which we supply the carbon source, increase C/N, improve water biodegradability, and promote denitrification. Some amount of aquatic grass and agave fiber are transplanted on the upper cavities of the groove. In the meanwhile, the five-week advanced pre-domesticated cultivated microorganisms in the anaerobic process in a sewage treatment plant are transferred into the test section [7].

Groove III is used for the denitrification function study of the anaerobic microbial metabolism. The spherical cavity biofilm carrier and elemental sulfur which have been domesticated and cultivated in the anaerobic process in a sewage treatment plant for 5 weeks, are added in the groove III [8].

The experiments start to operate in about 70hr's cultivation.

The inflow condition in three cases are the same. The water flow (Q) is 15~27L/hr, the hydraulic retention time (HTR) is 10~18hr, and the temperature(T) is 16-26℃.

In addition, when the cases are in the stable operation stages, the carbon sources are supplied in the ecologically tank to study the impacts on the denitrification function of increasing carbon[10].

The cases are continuously operated, and water temperature, pH, dissolved oxygen (DO), nitrate nitrogen (NO3-N and NO2-N), total nitrogen (TN), total organic carbon (TOC) etc al are monitored dynamically. The effects of enhanced denitrification and purification are analyzed through the experimental results[11][12].

Experimental results and discussion

Changes of dissolved oxygen and removal efficiency of trate nitrogen and total nitrogen

Because the inlets of the ecological groove in 3 cases are located in the upper cavities, and the same water conditions are used, the water qualities in upper cavities are used to indicate the water qualities. The evolutions of DO concentration against operating time in the 3 cases are shown in Figure 2.

As for the dissolved oxygen, it is in saturated oxidation state in upper cavities during the whole operation process. The fluctuations of DO are consistent with the daily period of sunshine and photosynthesis. The DO reduces in the below cavities. After about 72 hours, microbial environment is gradually developed till completed, and the oxygen consumption of organic matter degradation lead to anaerobic or completely anoxic states, so that DO maintains at a low level, which provides denitrification environment for the nitrate nitrogen.

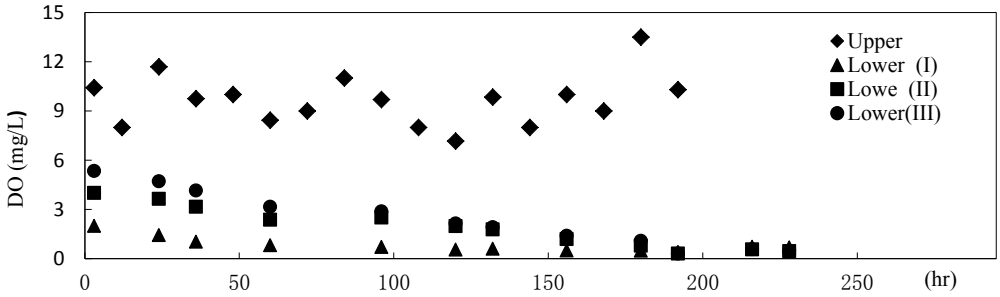

Figure 2. The evolutions of DO concentration

The saturated oxygen situation in upper cavities does not have denitrification condition. The measured results also have confirmed this point. Therefore, in this paper we only analyzes the denitrification function under anaerobic or completely anoxic environment. The removal ratios of nitrate nitrogen and total nitrogen against operating time are shown in Figure 3(a) and (b).

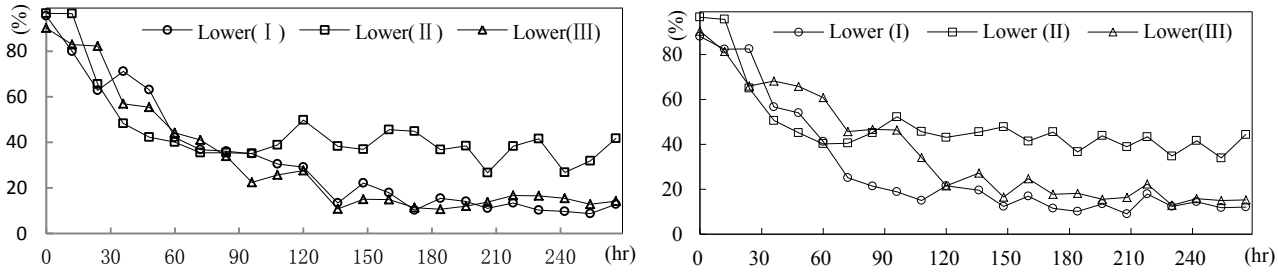

(a) The removal ratios of NO3-N (b) The removal ratios of TN

Figure 3. The evolutions of removal ratios of nitrogen

Because the experiments run after cultivation of microorganisms, anaerobic denitrification \performs strongly in the first 72 hours due to the mixing process between the influent water and original water. After 72 hours, the experiments get into the stable states, and the nitrate nitrogen denitrifications in the lower chamber are significant different among the three cases under the condition of anaerobic or completely anoxic.

The results have indicated that nitrate nitrogen and total nitrogen averaged removal ratios were 14.11% and 15.32% under operating conditions in the tank I. With the supplement of biological material and elemental sulfur were added in the tank III, the averaged removal ratios nitrate nitrogen and total nitrogen are 15.02% and 16.10%, which raised by 0.99%和 0.78% respectively comparing with those in tank I; The increase of microbial biomass is one of the factors which promotes the denitrification efficiency. The elemental sulfur, as the electron donor, improves the anaerobic metabolism of dissimilatory nutrient microbes, and change the way of denitrification. After adding the biological amterial (cultivated) and elemental sulfur in the tank III, the denitrification rates increase slightly, but have no significant improvement comparing with the tank I. It showed that for the water with poor biodegradability , the increase of microbial biomass and change of denitrification's way are not the only determining factors of denitrification. When added the biological material (cultivated) and aquatic plant in the tank II the denitrification rates improve remarkably, and the nitrate nitrogen and total nitrogen removal rate reaches 37.15% and 39.05% on average, which increased by 22.94% and 23.73% respectively comparing with the tank I. Under the conditions of anaerobic or completely anoxic, the aquatic plants are planted in the tank II, which supplys the organic carbon and increases the C/N of water, increases microbial biomass, and promotes the denitrification remarkably as a result. It shows that for the water with poor biodegradability, the addition of organic carbon and improvement of biodegradability are the key techniques to realize the denitrification under the condition of enough biomass. Additionally, the experiment results indicates that in the stable running state, the nitrate nitrogen and total nitrogen removal rates show the regular fluctuation between day and night after adding aquatic plant in the tank II, and the highest removal rate is in the midday and lowest is in the midnight, which are in accordance with the inter-diurnal variations of microbial activity.

The impact of carbon source on nitrogen removal efficiency

The experiments indicated that the supplement of the organic carbon and increasing the C/N (The C/N describes in this paper is the mass ratio of the added glucose carbon and total nitrogen in water) and improving biodegradability are the key factors to affect the nitrogen removal efficiency.

To study the relationship of organic carbon and the nitrogen removal rates and the best ratio of C/N to keep sufficient biomass, we designed another experiments the same as the tank III which add glucose and C/N in four proportion of 1, 3, 4 and 5. The nitrate nitrogen and total nitrogen removal rate curves are shown in Figure 4. The nitrate nitrogen removal rates are 47.93%、81.31%、93.21% and 91.92%, and the removal efficiency of TN was consistent with the NO3-N, shown in Figure 4. When C/N equal 4, The nitrate nitrogen and total nitrogen removal rates are the highest. While when C/N is 5, the total nitrogen removal rate was relatively low, and it might be because the carbon source is relatively superfluous, which restrains the activity of other bacteria but denitrifying bacteria in the anaerobic environment. Therefore, the nitrate nitrogen removal rate is fairly flat, and the total nitrogen removal rate is lower than that when C/N is 4.

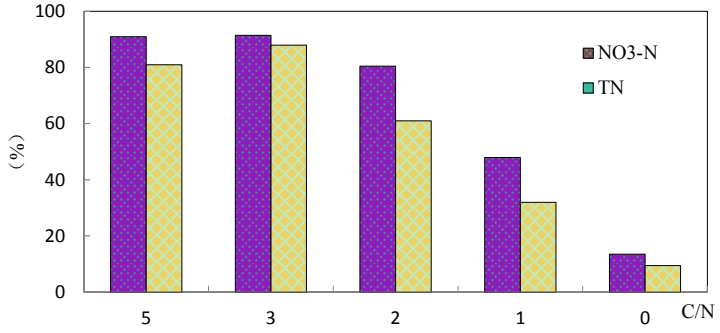

Figure 4. Denitrification efficiency under different

The above results show that the addition of carbon source could greatly enhance the denitrification of the system. When the supplementary of carbon source is none or little, the denitrification is unsatisfactory. But when the extra amount of carbon source exceeds a certain value, the denitrification rate had no significant change. According to the above experiment result, the best C/N for denitrification system of ecological slot is 4.

To enhance the denitrification efficiency, we increase the available activated carbon (glucose)and check out the efficiency of ecological slot with multiple criteria under the condition of increasing the number of microorganisms and changing the way of denitrification.

We add glucose in terms of C/N=4 in tank I, tank II and tank III, the result was shown in Figure 5(a) and (b).

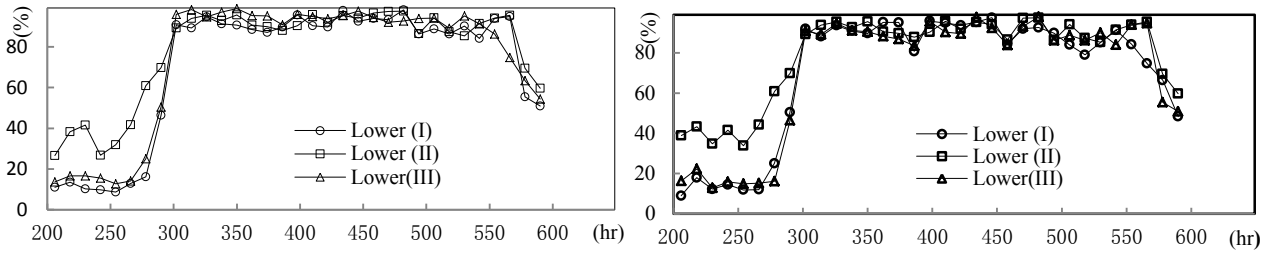

(a) The removal ratios of NO3-N (b) The removal ratios of TN

Figure 5 . Removal curves of the nitrate nitrogen and total C/N nitrogen in 600hrs

In Figure 5, the first 260 hours is the continuous operation processes of the last experiments. The denitrification rates of tank II keep in 30-40%, and that of the tank I and tank III are low. After the glucose adding, the denitrification efficiency of the three tanks enhances significantly. Through the continuous operation from 260 hours to 600 hours, the averaged nitrate nitrogen removal rateare 86.31%, 86.79% and 86.48% respectively, while the total nitrogen removal rate are 87.01%,89.89% and 87.48%.

Under the condition of enough carbon sources, the nitrate nitrogen and total nitrogen removal rate of these three tanks show no obvious difference. It showed that the supplement of carbon source is the key technique to remove the nitrate nitrogen in poor biodegradability water, and

increasing biomass and changing the way of denitrification only had no significant effect on denitrification.

Aquatic plant selection

In practical project, the supplement carbon source by adding glucose will increase the cost of project construction, and also have the shortage such as man-made factors in operations management. Breeding some aquatic plants to release TOC plentifully can not only solve carbon source problem, but also provide the good landscape value. The plants themselves can absorb some nitrogen and phosphorus nutrients through root system which is the effective way for ecological engineering to supplement carbon sources.

The organic matters secreted from aquatic plant roots are low molecular organic compounds, Polymer adhesive material, cells or tissue loss material lysate and so on, in which, the low molecular weight sugars, organic acids, amino acids and phenolic compounds in the Low molecular organic compounds, can mostly become the carbon sources for denitrification. According to the climate characteristics in Beijing, the experiment chooses four kinds of plants whose root system are well-developed called Eichhornia crassipes, Agavaceea, Isolepis cernua, and Spathiphyllum floribundum to breed suitable aquatic plant.

The aquatic plant mentioned above are cultivated in the 10L incubators respectively with a blank group, and the TOC concentrations are inspected every day. Results of the experiment indicated that the TOC secreted by Agavaceea is highest, which increaseds 1.3223mg/L comparing with the blank group; the Isolepis cernua took the second place, which increases 0.9431mg/L; the Eichhornia crassipes and Spathiphyllum floribundum are relatively weak, which Increases only 0.4940 mg/L and 0.4452 mg/L respectively, ss shown in Figure 6. Additionally, in Section 3.1,the above aquatic plants are planted in the tank II showing that the Nitrate removal efficiency improved significantly, and it proved that the Isolepis cernua and Agavaceea are the selected aquatic plants with good performance of supplementing carbon source.

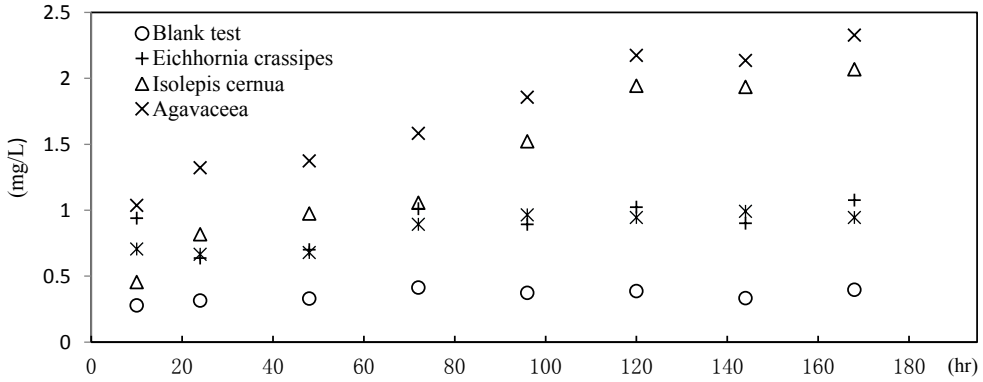

Figure 6. Curves of TOC secreted from aquatic plant roots

Conclusion

In the ecological projectas for water purification of urban rivers which are mainly discharged by sewage treatment plants, the denitrification technology of low C/N iwater is the main way to eliminate the nitrate nitrogen. The experiment shows that the denitrification in poor biodegradability water is weak, and reinforced technology can achieve the goal of further water purification. The research get the following conclusion:

The structural design of ecological groove proposed in this research can form aerobic and anaerobic reaction site which provides favorable spatial condition for denitrification.

Through the comparison of adscititious biological materials and the blank group, we find that the denitrification effects are not significant. Therefore, the microbial biomass in the blank group of the system is sufficient, and the method to cultivate the sludge taken in the experiment is effective.

The denitrification effect is optimal when adding carbon source and C/N equals 4. The removal rate of NO3-N and TN all reach more than 87%. Therefore, we can consider that the supplement of carbon sources is the key technique to strengthen denitrification in urban river.

The quantity of TOC secreted by Agavaceea and Isolepis cernua is the highest, and they are aquatic plants with good performance of supplementing carbon sources which improve the denitrification remarkably in the experiments.

According to the researches of the some experts, the process of sulfur autotrophic denitrification needs no organic carbon source. The water quality from the tank II should be better and more stable, while it is not shown obviously in those studies, and it needs further study to test environment conditions and influential factors afterwards.

Acknowledgement

This research is supported by Major Science and Technology Program for Water Pollution Control and Treatment（2012ZX07104-001）and Beijing Municipal Science & technology Commission project（D0706006040291）. The authors are grateful for the co-workers in those two projects.

References

[1] Q.J Li，R.H.Liao, Q.Y.Meng, X.L.Hu, al. BeiJing：China water conservancy and hydropower press[C]，2011, (In Chinese).

[2] W. Wang, Y.T. Lv. Enhancing Nitrogen and Phosphorus Removal Efficiency of the Municipal wastewater by step-feed, Technology of water treatment [J], Vol.37(2011), 57-9. (In Chinese).

[3]Kuba T，Smolders G，Van Loosdrecht,a1．Biological phosphorus removal from wastewater by anaerobic-anoxic sequencing batch reaet04．Water Science&Technology[J], Vol.27 (1993), 241-252．

[4] J.Zh. Luo ,W.J. Su, J. Lu,J.R. Guo, Technical modification of denitrification enhancement in T type oxidation ditches. Chinese Journal of Environmental Engineering[J], Vol.3(2009),1995-1999.

[5] G.Liu, Y.Wen, Q.Zhou,Adding Biomass for Removal of Nitrate in Horizontal Subsurface Flow Constructed Wetland. China Water & Wastewater[J], Vol.25(2009),13-16.

[6] T.Z.Osborne, P.W.Inglett, K.R.Reddy The use of senescent plant niomass to investigate relationships between potential particulate and dissolved organic matter in wetland ecosystem. Aquat Bot[J], Vol.86(2007),53-61.

[7] S.Y. Gebremariam, M.W. Beutel, Nitrate removal and DO levels in batch wetland mesocosms: Gattail (Typha spp) versus bulrush (Scirpus spp). Ecol. Eng[J],Vol.34(2008),1-6.

[8] Jacques C. Finlay, Gaston E. Small, Robert W. Sterner, Human Influences on Nitrogen Removal in Lakes, Science[J] ,Vol.342(2013).

[9] F. K. Chen, Z.B. Yu, L.W. Zhang, L. Chen, Planting Phrynium in Wavy Subsurface Flow Constructed Wetland Treating Municipal Wastewater. Journal of Henan Normal University (Natural Science Edition)[J],Vol.40(2012),118-120.

[10] Caraeo N Fl ,Cole J J,Human impact on nitrate export：An analysis using major world rivers. AMBIO，Vol. 28(2)(1999),p:167—170.

[11] Claus G，Kuntzer H J．Autotrophic denitrification by Thiobacillus denitrificans in a packed bed reactor. Applied Microbiology and Biotechnology[J], Vol.22(4)(1985),289--296．

[12] Reyes S A，Ricardo B C，Margarita S，et a1．Chemolithotrophic denitrification with elemental sulfur for groundwater treatmench[J]，Vol.4l(6)(2007),1253—1262．

Advanced Materials Research Vols. 989-994 (2014) pp 1348-1351
© (2014) Trans Tech Publications, Switzerland
doi:10.4028/www.scientific.net/AMR.989-994.1348

The Combinatorial Prediction about Chaotic Times Series of Natural Circulation Flow under Rolling Motion

Can Yuan[1, a], Qi Cai[1, a], Gang Liu[2, a], Feng Yan[1,3, a]

[1] Department of Nuclear Science and Technology, Naval University of Engineering, Wuhan 430033, China

[2] Troops of 95039, Shantou 515049,China

[3] College of marine corps, Guangzhou 510430, China

[a]email: yuancan2008@163.com

Keywords: rolling motion, chaotic series, phase space reconstruction (PSR), coupling multivariate, natural circulation (NC)

Abstract. The paper has established a combinatorial prediction model of chaotic time series based on history data and coupling data. Through the study of the flow characteristic about natural circulation under rolling motion, the single variable reconstruction and coupling multivariate reconstruction are discussed for chaotic time series based on phase space reconstruction technique, and the combinatorial prediction model has been built which bases on developing trend of history data and coupling relationship of correlative data. The paper also studied an example of coolant volume flow prediction with a relative precision of 0.9804 with the established model. The result indicated that the model with high precision and robustness could apply for natural circulation coolant volume flow prediction under rolling motion.

Introduction

Nuclear power plant may encounter additional transient outside force at any moment, for the complicated and changeful ocean condition. While the outside force cannot be ignored, the unstable status with high degree will occur in reactor systems. For instance, if the environment gives reactor system an additional swing force under the status of NC, a rolling acceleration will appear because of the small flow and outside force which cannot be neglected, which will drive or cumber the flowage of reactor coolant, affect the pressure drop distribution of systems, strengthen the coupling among the system elements, result in the fluctuation of coolant volume flow and reactor power, and lead to the emergence of obvious nonlinear characteristic phenomena[1,2] such as chaos oscillation, wave oscillation superposition. If the NC coolant volume could be forecasted by correlative data under rolling motion condition, manipulator could intervene in time and avoid accident when the flow is exceptional, and could judge the status of accident and make corresponding decision-making by the prediction result when the accident has occurred[3,5]. Therefore, prediction and analysis of corresponding parameter, which is under NC rolling condition, could make us find out the rule of unstable flow, provide a certain degree of help for judging the status of reactor systems for manipulator, and provide data support for nuclear power equipment in security.

This paper introduces the combinatorial prediction method based on history data and coupling data into predicting NC coolant volume flow, and the result indicates that this method could receive excellent effect on chaotic series prediction of NC under rolling condition.

Combinatorial prediction Model based on history data and coupling data

Chaotic time series combinatorial prediction means confirming the relationship between the past and the future on sequence axis by several methods with different principle, which is described by a series of parameters. This method could establish parameter model from the past to the future according to the existing data, and obtain the future development trend of chaotic series. The prediction principle of the method is shown in the figure 1 below:

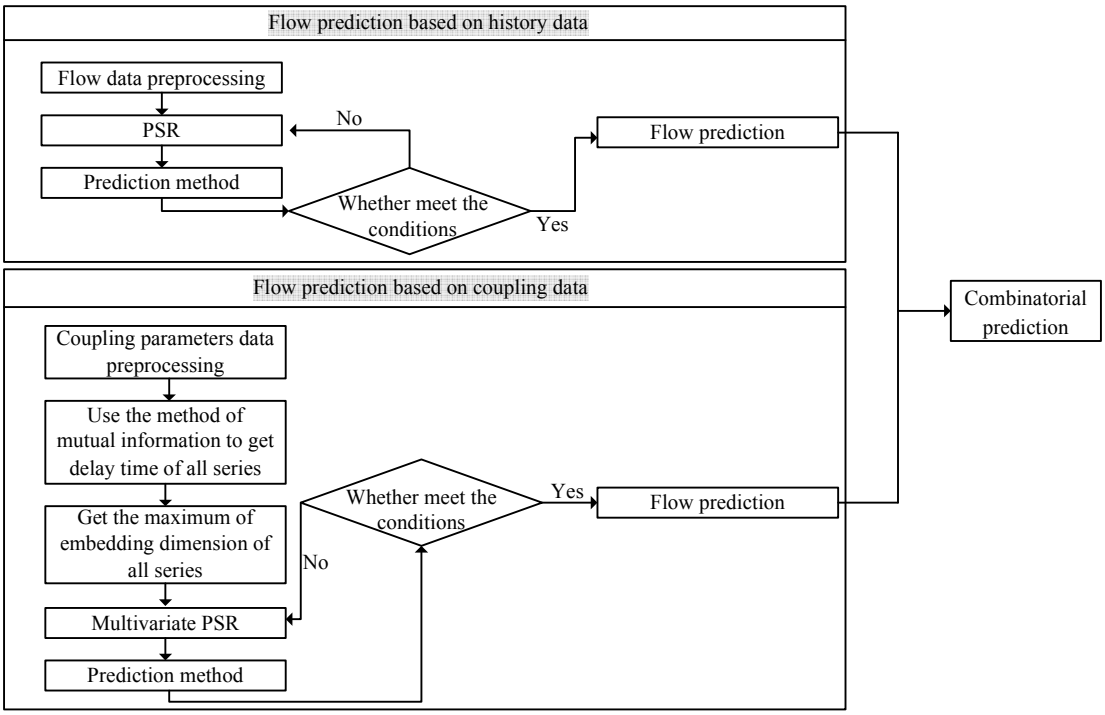

Fig. 1 Prediction principle figure of chaotic series

From the Fig. 1, no matter the single variable prediction based on history data (method 1) or multivariable prediction based on the coupling data (method 2), the key is PSR which needs to get the optimal embedding dimension and the best delay time of the corresponding variables. In the method 1, we adopt the idea of minimum prediction error for unified solution in order to get the optimal embedding dimension and delay time. However, in the actual situation, a system often shows dynamic evolution behavior and multi-level structure. So the number of coupling variable will be large. For this reason, the unified solution should not be used in method 2, otherwise the calculation could not run due to the large number of iterations. First, this paper uses the method of mutual information to get the delay time of coupling variables, and then changes embedding dimension of each series from 1 to the maximum, gets the optimal embedding dimension based on the principle of minimum prediction error.

Experiment and study

The experimental process as follows. The method 1 is described in [6].

Method 2: Step 1: set the initial condition and preprocess the data. Set the maximum of iteration to 50, decompose the coupling series with wavedec function, reduce the noise with ddencmp and wdencmp function, which could filter out the high frequency noise signal and keep low frequency information, and then normalize the data which have been reduced the noise.

Step 2: get the corresponding optimal $\tau_i (i = 1, 2, ..., K)$ using mutual information method for each of the above coupling variables, get the biggest embedding dimension $m_{\max i} (i = 1, 2, ..., K)$ by the method of false nearest neighbors, and reconstruct the phase space for these K variables.

Step 3: reconstruct the phase space based on the multivariate PSR theory, whose process is as follows:

Provided the NC flow time series expression is:

$$V = (y_1^0, y_2^0, \cdots, y_n^0) \tag{1}$$

Where the best embedding dimension and delay time are calculated by method 1, which are recorded as m_0, τ_0.

Provided the time series expression of coupling variables is Y, after reconstructing the phase space, we could get that:

$$\begin{aligned} Y_i = (&y_i^1, y_{i-\tau_1}^1, \cdots, y_{i-(m_1-1)\tau_1}^1, \\ &y_i^2, y_{i-\tau_2}^2, \cdots, y_{i-(m_2-1)\tau_2}^2, \\ &\cdots \\ &y_i^K, y_{i-\tau_K}^K, \cdots, y_{i-(m_K-1)\tau_K}^K) \end{aligned} \tag{2}$$

Where $m_j (j = 1,2,\cdots,K)$ is the value which is selected between 1 to maximal embedding dimension, $\tau_j (j = 1,2,\cdots,K)$ is the best delay time, $i = J_0, J_0+1, \cdots, N$, $J_0 = \max_{0 \le j \le K}((m_j - 1)\tau_j)$. Obtain the sample form for k-steps prediction of vector learning based on the method of Multivariate PSR:

$$\begin{aligned} Y_{train} = \begin{bmatrix} y_{J_0}^1 & y_{J_0-\tau_1}^1 & \cdots & y_{J_0-(m_1-1)\tau_1}^1 & y_{J_0}^2 & y_{J_0-\tau_2}^2 & \cdots & y_{J_0-(m_2-1)\tau_2}^2 \\ y_{J_0+1}^1 & y_{J_0+1-\tau_1}^1 & \cdots & y_{J_0+1-(m_1-1)\tau_1}^1 & y_{J_0+1}^2 & y_{J_0+1-\tau_2}^2 & \cdots & y_{J_0+1-(m_2-1)\tau_2}^2 \\ \vdots & \vdots & \vdots & \vdots & \vdots & \vdots & \vdots & \vdots \\ y_{N-k}^1 & y_{N-k-\tau_1}^1 & \cdots & y_{N-k-(m_1-1)\tau_1}^1 & y_{N-k}^2 & y_{N-k-\tau_2}^2 & \cdots & y_{N-k-(m_2-1)\tau_2}^2 \end{bmatrix} \\ \begin{bmatrix} \cdots & y_{J_0}^K & y_{J_0-\tau_K}^K & \cdots & y_{J_0-(m_K-1)\tau_K}^K \\ \cdots & y_{J_0+1}^K & y_{J_0+1-\tau_K}^K & \cdots & y_{J_0+1-(m_K-1)\tau_K}^K \\ \vdots & \vdots & \vdots & \vdots & \vdots \\ \cdots & y_{N-k}^K & y_{N-k-\tau_K}^K & \cdots & y_{N-k-(m_K-1)\tau_K}^K \end{bmatrix} \end{aligned} \tag{3}$$

$$V_{train} = \begin{bmatrix} y_{J_0+k}^0 & y_{J_0+k-\tau_0}^0 & \cdots & y_{J_0+k-(m_0-1)\tau_0}^0 \\ y_{J_0+1+k}^0 & y_{J_0+1+k-\tau_0}^0 & \cdots & y_{J_0+1+k-(m_0-1)\tau_0}^0 \\ \vdots & \vdots & \vdots & \vdots \\ y_N^0 & y_{N-\tau_0}^0 & \cdots & y_{N-(m_0-1)\tau_0}^0 \end{bmatrix}$$

Step 4: train the Elman neural network by the sample form of vector learning which has been identified in Step 3, predict the flow by the Elman neural network model, and get the mean square error between prediction values and observation values.

Step 5: judge whether iteration is completed, if completed, turn to Step 7, otherwise, turn to Step 6.

Step 6: the number of iteration add 1, and then turn to Step 3.

Step 7: calculate the minimum mean square error of all the iterations, and get the best $m_i, \tau_i (i = 1,2,\cdots,K)$.

Step 8: take out the test data, and predict the flow using the best $m_i, \tau_i (i = 1,2,\cdots,K)$ and the Elman neural network model which has been established.

Combinatorial prediction:

Step 1: Provided that the predicted time series by method 1 is Y_1, the predicted time series by method 2 is V_1, the corresponding observed time series is O, the equation is established as follows:

$$aY_1 + bV_1 = O \tag{4}$$

Eq. (4) is written in vector form:

$$(Y_1, V_1)\begin{pmatrix} a \\ b \end{pmatrix} = O \tag{5}$$

If $A = (Y_1, V_1)$, the combination coefficients $(^{a,b})$ can be calculated by the least square method:

$$\begin{pmatrix} a \\ b \end{pmatrix} = (A^T A)^{-1} A^T O \tag{6}$$

Step 2: the flow is combinatorial predicted by using m_0, τ_0 which is confirmed by method 1, $m_i, \tau_i (i = 1, 2, \cdots, K)$ which is confirmed by method 2, and the combination coefficients a, b.

The relative accuracy formula is defined as follows:

$$E = \frac{\frac{1}{n_1}\sum_{i=1}^{n_1}(y_i - \bar{y}) \times (y_i^* - \overline{y^*})}{\sigma \times \sigma^*} \tag{7}$$

Where y_i , y_i^* respectively means prediction value and observation value of i th position; $\bar{y}$, $\overline{y^*}$ respectively means the corresponding average value for y_i, y_i^*; σ, σ^* respectively means the corresponding mean square error for y_i, y_i^*. n_1 means the number of prediction value. After calculating, the relative accuracy of figure 4a is 0.9713, figure 4b is 0.9507, figure 4c is 0.9712, figure 4d is 0.9804. The result has shown that the combinatorial prediction method has higher relative precision and more perfect prediction effect.

Conclusion

For the autocorrelation, nonlinear, and high coupling of marine reactor NC under rolling condition, this paper has suggested a combinatorial prediction algorithm based on history data and coupling data, which started from the PSR theory, discussed the single variable prediction based on history data and multivariate prediction based on coupling data, and considered the special circumstances, any of them failed, and formed combinatorial algorithm which has passed through the linear weighted processing. In order to verify the effectiveness of the algorithm, this paper took the coolant volume flow as an example, and the result has shown that the model could be used for NC coolant volume flow prediction under the rolling condition, and could satisfy the actual engineering requirements with high precision, small relative error and high robustness.

References

[1] Wenchao Zhang, Sichao Tan, Puzhen Gao, et al. Nonlinear evolution characteristics of natural circulation flow instabilities under rolling motion [J]. Atomic Energy Science and Technology, 2012，6(6): 705-709.

[2] Wenchao Zhang, Sichao Tan, Puzhen Gao. Effect of rolling parameters on chaotic oscillation of a natural circulation system under rolling motion [J]. Journal of Harbin Engineering University, 2012,33(6): 798-800.

[3] Xingtang Liu, Bingcheng Liang, Li Liu, et al. The theory, method & technique for complex system modeling [M]. Beijing: science press, 2008.

[4] Deng Julong, Zhou Chaoshun. Sufficient conditions for the stability of a class of interconnected dynamic systems [J]. Systems and Control Letters，1986，5(2): 105-108.

[5] Zhenchao Wang, Yuqian Zhao, Chen Zhao. Fractal prediction algorithm of time series based on phase space reconstruction sample selection [J]. Computer Engineering and Applications, 2011，47(21): 126-130.

[6] Can Yuan, Qi Cai, Li Guo, Feng Yan. Prediction about Chaotic Times Series of Natural Circulation Flow under Rolling Motion [J]. Nuclear Power Engineering,2014, 35(1):60-63.

Advanced Materials Research Vols. 989-994 (2014) pp 1352-1355
© (2014) Trans Tech Publications, Switzerland
doi:10.4028/www.scientific.net/AMR.989-994.1352

A Rapid Determination Method of ^{40}K Concentration in the Soil

Weiwei LU[1, a], Huiguo YUE[1, b], Jin LI[1, c*], Yanxia ZHANG[1, d]

[1] Nuclear and Radiation Safety Center, MEP, Beijing, 100082, China

[a]luweiwei@chinansc.cn, [b]yuehuiguo@chinansc.cn, *[c]lijin@chinansc.cn, [d]zhangyanxia@chinansc.cn

*Corresponding author: Tel:+86-10-8220-5794; fax: +86-10-6225-9210
E-mail address: lijin@chinansc.cn

Keywords: fluorescence spectrometry; ^{40}K; radioactive concentration

Abstract. The pressed powder sample was determined by Epsilon 5 high-energy polarized energy dispersive X-ray fluorescence (EDXRF) spectrometer. The correlation coefficient of the standard curve method is 0.991 0. The precision is 2.98% and the relative deviation of the measurement standard samples is up to 6.40%, which showed that the precision and accuracy of the method were also good. Simultaneous measurement of seven soil samples with this method and γ-spectrometer were carried, the results of two analytical methods was compared using a paired t-test by SPSS program, which showed that there was no significant difference in the two sets of data. The results predicated that EDXRF could be a potential simple method for analyzing ^{40}K in soil samples.

Introduction

Radioactive concentration of ^{40}K in soil was measured usually by the gamma spectrometry. The method is accurate, but the measuring time of environmental samples by this usually takes more than 30000 s. X ray fluorescence spectrometer is X ray irradiated samples produced by the excitation light source. Emitting sample elements in different energy (discrete) X ray fluorescence characterization of these elements, by measuring the radiation energy emitted by the sample to know qualitative element, the knowledge content elements through the energy intensity, or quantitative. Previous fluorescence spectrometer was used for elemental content. Because natural radionuclides in the soil environment can be converted from corresponding, single element determination in environmental samples by X ray fluorescence spectrometer by the abundance ratio, half-life etal. Then the sample can only measure 600s enough. Therefore, in this work the X ray fluorescence spectrum measurement of K elements in soil will be converted into radioactive concentration of ^{40}K, and the spectrum comparison of measurement results with high purity germanium gamma ray, the reliability of X ray fluorescence spectrum measuring element content in soil samples.

The experimental part

The main instrument and device. Epsilon 5 high-energy polarized EDXRF spectroscopy: equipped with the highest excitation voltage of 100 kV, the maximum power of 600 W side beryllium window (thickness of 300 μ m) gadolinium anode X ray tube, PAN-32 germanium detector, active area of crystal is 300mm^2, thickness of 5 mm, the energy resolution ≤ 140 eV (2000cps Mn K_α), effective energy detection range of 0.7 ~ 100 keV, the maximum count rate can reach 2 × 10^5/s; 15 of two target (Mg, Al, Si, Ti, CaF_2, Fe, Zn, Br, Zr, Mo, Ag, CsI, CeO_2, Ge and Al_2O_3) ； 5 filters (Mo 250 μm , Zr 125 μ m, Cu 100 μ m, Al 500 μ m, Al 100 μ m): a family company: original Philips analysis instrument

Sample preparation. Take 6 g soil samples, soil samples were collected in Beijing surrounding natural soil samples or soil standard samples (GSS-1, GSS-2, GSS-3, GSS-4, GSS-5, GSS-6, GSS-7, GSS-8, GSS-9, GSS-10, GSS-11, GSS-12, GSS-13, GSS-14, GSS-15, GSD09, GSD10, GSD12, GSD 13, GSD14, GSD 01A standards) bought from China Exploration Institute of Geological

Sciences of geophysical and geochemical,then add 7 g of boracic acid as the lining, pressure of 35 t, of 10 s, the preparation of a outside diameter of 40 mm, the 33 mm in inside diameter[1].

Measurement method. Soil tablet in the EDXRF spectrometer, using CaF_2 to do the two target. Tube voltage was 25 kV. Tube current was 24 mA, 250 s measurements[2-4].

Correction of matrix effect and spectral overlap interference. Correction of matrix effect in this method using empirical coefficient and Compton scattering method, at the same time, particle size and mineralogical effect also made some correction, the mathematical formula [2 ~ 5]:

$$C_i = D_i - \sum L_{im} Z_m + E_i R_i \left(1 + \sum_{i=1}^{n} \alpha_{ij} Z_j \right) \quad (1)$$

In formula (1): Ci for unknown sample analysis of the content of element I; Di analysis calibration curve intercept of I; L_{im} interference element M on line analysis of elements I overlap interference correction factor; Z_m interference elements m content or count rate; E_i for the oblique rate analysis element I calibration curve the R_i analysis of elements; count rate of I (intensity ratio or with the internal standard); Z_j coexisting elements J content or the counting rate; n is the number of coexisting elements; alpha for matrix effect correction factor; I, J and m were analyzed for elements, coexisting elements and interference elements.

This method uses a plurality of calibration sample by equation (1) regression for the matrix effect and spectral overlap interference correction[6].

Results and discussion

Method detection limit. The detection limit is related to the substrate of the sample. Different samples because of its components and the content, scattering background intensity, spectral overlap interference degree and analysis of elements of different sensitivity, detection limits are changed. And the detection limit of each component in the sample is different, usually according to the formula (2) for calculating the detection limit.

$$L_D = \frac{3}{S} \sqrt{\frac{R_b}{t_b}} \quad (2)$$

In foumula (2): S for the analysis of elements in the sensitivity of [s^{-1} • Mg^{-1} • kg]; R_b as the background count rate; t_b for measuring the time background (s).

The method was used to measure the 50 soil samples. According to equation (2) the detection limit of elements K concentration were calculated. The average value is 10.7 mg/kg, which converted into radioactive concentration detection limit was 0.33 Bq/kg.

K (oxide) standard curve. The measuring results of the 21 standards are listed in table 1. Table 1 data of the regression analysis, K (oxide) measurement standard curve, the result is shown in figure 1. Fig. 1 the correlation coefficient of standard curve is 0.9910, a good linear relationship.

Table 1 Soil standard samples of K (oxide) concentration measurement results

Sample Name	Measured Value/%(n=10)	Sample Name	Measured Value/%(n=10)
GSS-1	2.65±0.04	GSS-12	2.628±0.03
GSS-2	2.504±0.03	GSS-13	2.307±0.02
GSS-3	2.903±0.03	GSS-14	2.612±0.03
GSS-4	1.158±0.04	GSS-15	2.442±0.02
GSS-5	1.671±0.04	GSD-9	2.052±0.03
GSS-6	1.865±0.03	GSD-10	0.125±0.03
GSS-7	0.108±0.04	GSD-1a	2.747±0.02
GSS-8	2.468±0.02	GSD-12	2.815±0.03
GSS-9	2.009±0.03	GSD-13	3.78±0.02
GSS-10	2.602±0.02	GSD-14	2.377±0.02
GSS-11	2.602±0.03		

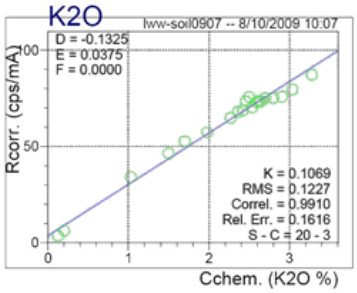

Fig.1. The standard curve of K_2O

Note: C_{chem} (K_2O%) as a percentage o, R_{corr} fluorescence intensity of potassium oxide.

Precision. 10 samples of GSD-11 soil standard samples was measured by X ray fluorescence spectrum (oxide) content. Measurement values are: 3.01%, 3.22%, 3.05%, 3.14%, 3.08%, 3.02%, 3.11%, 3.03%, 3.29% and 3.05%, and the average value is 3.10%. The standard deviation is 0.09%, The relative standard deviation is 2.98%. $\bar{x} \pm s = 3.10 \pm 0.09\%$,. The method is accurate.

Accuracy. The 2 standard GSS-16, GSD-11 are tested. The measurement results are given in table 2. As can be seen from table2, the maximum relative deviation from the reference values is 6.4%.The accuracy of the method is better.

Table 2 Standard sample measurement results and comparison reference value

Sample name	Measured Value /%	Reference valve/%	Relative deviation/%
GSS-16	2.66	2.50	6.4
GSD-11	3.11	3.28	5.2

Comparison of measurement results of energy dispersive fluorescence spectrometer and gamma spectra. By Formula (3) K_2O concentration in the sample will be converted into ^{40}K radioactive concentration[10]. $C_{K\text{-}40}$ (Bq/kg) for sample ^{40}K radioactive concentration (Bq/kg); C_{K_2O} (%) as the concentration of sample K_2O (%); 0.71 for the content of K in K_2O; 31.2 according to ^{40}K abundance, half-life calculated from the quality (g) converted into activity (Bq) coefficient.

$$C_{K-40}(Bq/kg) = C_{K_2O}(\%) \times 0.71 \times 10 \times 31.2 \quad (3)$$

Using this method and gamma spectrometer measurement of 7 soil samples. The results are listed in table 3.

Table 3 comparison of 7 soil samples from energy dispersive fluorescence spectrometer and gamma spectrometer measurement results

Sample number	^{40}K radioactive concentration /(Bq·kg^{-1})	
	Fluorescence spectrometer	Gamma spectrometer
201004S039	652	674
201004S002	568	477
201004S004	665	546
201004S007	671	702
201004S008	708	574
201004S011	668	671
201004S010	655	562

To compare in table 3 the 7 soil samples from energy dispersive fluorescence spectrometer and gamma spectrometer measurement results , paired t test was used . Probability of P calculated by SPSS program is 0.087, more than 0.05 significant level, showing that there was no significant difference between two groups of data, and the measurements are consistent. That is ,the ^{40}K content in soil can be measured by energy dispersive fluorescence spectrometer.

The measurement results correction. Cd is the main interference causing to K determination. But the content of Cd in soil is low, 4 orders of magnitude lower than the potassium content, so the Cd on the K content has less interference. K content determination process mainly uses empirical coefficient method for correction of matrix effect.

Conclusion

Sample preparation with pressed powder pellet, X ray fluorescence spectrometer analysis method was used for concentration of ^{40}K radioactivity in soil. The accuracy and precision of this method are better. So it can be used for the analysis of environmental samples with ^{40}K radioactive concentration.

References

[1] Liu Shanghua, Tao Guangyi, Ji ang. Pressed powder sample preparation method [J]. spectroscopy laboratory of X ray fluorescence analysis, 1998,6:1-2

[2] Fan Shouzhong, Zhang Qin, Li Guohui, etal. The polarized energy dispersive X- ray fluorescence spectrometric method for the determination of stream sediment and soil samples of various component [J]. metallurgical analysis, 2006, 29 (6): 29

[3] Zhang Qin, Li Guohui, Ji ang, etc. Epsilon 5 high-energy polarized energy dispersive X- ray fluorescence spectrometry determination test chamber, harmful elements [J]. Analysis in waste incineration ash 2010, 29 (4): 108

[4] Zhang Qin, Fan Shouzhong, Pan Yanshan, et al. Determination of geochemical samples in the main, secondary and trace [J]. physical and chemical examination of X - ray fluorescence spectrometry: Chemistry, 2005, 41 (8): 550

[5] Zhang Qin, Fan Shouzhong, pan Yanshan. Determination of minor and trace group multi target geochemical survey in a sample of [J]. Rock and mineral X ray fluorescence spectrometry, 2004,23 (1): 21

[6] Ji ang, Tao Guangyi, Zhuo Shangjun, et al. X ray fluorescence analysis [M]. Beijing: Science Press, 2003:112-132

[7] Zhang Biao determination of. in iron ore metallurgical analysis[J], each fly. X ray fluorescence spectrometry 2003, 23 (3), 53-54

[8] Li Dan, Xu Yingjun. quality control method of X fluorescence analysis [J]. Gansu metallurgy, 2009, 31 (1): 59-60

[9] Chen Sulan, Chen Bo, Zhang Yong. Application of X fluorescence spectrometry in soil investigation[J]. Chinese environmental monitoring, 2007, 23 (1): 19-21

[10] Qian Weicheng, Zhu Zhennan, Wu Qinghua. The analysis method of Potassium in water. GB11338-1989 [S]. Beijing: MEP, 1989

Advanced Materials Research Vols. 989-994 (2014) pp 1356-1358
© (2014) Trans Tech Publications, Switzerland
doi:10.4028/www.scientific.net/AMR.989-994.1356

Effect of Hg in Jiaozhou Bay waters-settling process

Dongfang Yang[1, 2, 3, a], Fengyou Wang[1, 2], Huazhong He[1, 2], Youfu Wu[1, 2] and Sixi Zhu[1, 2]

[1]Research Center for Karst Wetland Ecology, Guizhou Minzu University, Guiyang 550025, China;

[2]College of Chemistry and Environmental Science, Guizhou Minzu University, Guiyang 550025, China;

[3]North China Sea Environmental Monitoring Center, SOA, Qingdao 266033, China

[a]dfyang@shou.edu.cn

Keywords: Mercury (Hg), Content, Settling process, Jiaozhou bay.

Abstract. Being a close bay, vertical settling was the dominant transfer process of Hg Jiaozhou Bay. Based on the investigation data of mercury (Hg) in bottom waters in Jiaozhou bay in 1979 to 1985 (in absence of 1984), this paper tried to analysis both of the settling processes and settling mechanisms of Hg. Results showed that that Hg in Jiaozhou Bay was settling continually over year, therefore a continued accumulation of Hg contents in bottom waters appeared, especially in spring and summer. Sediments in sea bottom could be both of source and sink of pollutants, especially for persistence pollutants such as Hg. Based on the both of the settling processes and settling mechanisms, the improve of recycle rate and the emission reduction of Hg should be the major pollution control strategies in Jiaozhou Bay.

Introduction

Jiaozhou Bay is close bay located in south of Shandong Peninsula. Being surrounded by economic developed cities such as Qingdao, Jiaozhou and Jiaonan etc., this bay has long been suffering from various pollutants such as benzene hexachloride, petroleum hydrocarbon, and heavy metals, all of whose pollution levels had reach certain degrees [1-11]. Hg is one of the most critical environmental pollutants, with characteristics of high toxicity, bioaccumulation, and persistence, and has been widely used in chloral-alkaline industry, plastic industry, electronic industry, metallurgical industry etc. [12-13]. Previous studies showed that both of surface and bottom waters in Jiaozhou Bay were polluted by Hg [5, 8, 10].

Having in mind that water mass exchange capacity in such close bay is limited, and the pollution reduction should be more difficult once has been polluted, it is essential to understand the major transfer process of Hg. Based on the investigation data of mercury (Hg) in bottom waters in Jiaozhou bay in 1979 to 1985 (in absence of 1984), this paper tried to analysis the both of the settling processes and settling mechanisms of Hg, and to provide basis for pollution control of Hg.

Material and method

Study area. Jiaozhou Bay is located in the south of Shandong province (35°55′-36°18′ N, 120°04′-120°23′ E), with total area, average water depth and the width of bay mouth of 390 km^2, 7 m and 3 km, respectively (Fig. 1). The main rivers are Haibo Rriver, Licun Rriver, Baisha Rriver, Dagu Rriver, Yanghe Rriver, and Loushan Rriver, all of wich have seasonal hydrological features, and are transfer canals for pollutants into the bay [1- 3]. This bay is typically a closed bay, and is surrounded by economic developed cities such as Qingdao, Jiaozhou and Jiaonan etc.

Data source. The data was provided by North China Sea Environmental Monitoring Center. The measurement methods of Hg in water samples was follow by The Chinese National Specification for Marine Monitoring (1991) [14]. The survey as conducted in May, August and November 1979, July, August and October 1980, April, August and November 1981, April, June, July and October 1982, May, September and October 1983, and April, July and October 1985,

respectively. We defined April, May and June as spring, July, August and September as summer, and October, November and December as autumn, respectively.

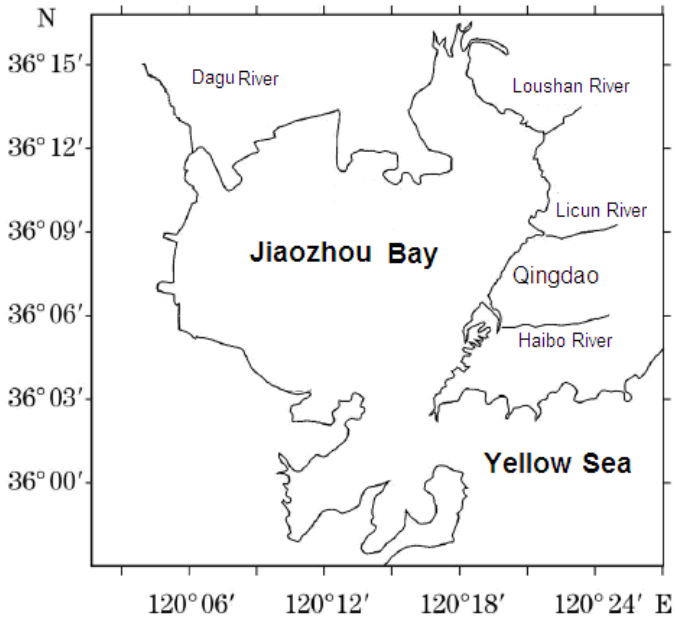

Fig. 1 Geographical location of Jiaozhou Bay

Results and discussion

Temporal variation. Hg is low-soluble, settlement is the major fate of Hg, particularly in this close bay. Hg is Jiaozhou Bay is mainly discharged from the major rivers. As the precipitation in this area is concentrated in spring and summer, the load of Hg in Jiaozhou Bay is relatively high in spring and summer. Meanwhile, due to the growth and reproduction of marine phytoplankton start in spring and reach the peak in summer, there are large amount of colloids in these periods, which have strong capacity to absorb Hg and settle to the sea bottom. For example, Hg contents in bottom waters in June, July, September, and October 1980 ranged from 0.002-0.007μg.L^{-1}, 0.002-0.021μg.L^{-1}, 0.005-0.029μg.L^{-1}, and 0.013-0.090μg.L^{-1}, respectively [8], while in April, July, and October 1982 ranged from 0.005-0.007μg.L^{-1}, 0.024-0.029μg.L^{-1}, and 0.020-0.032μg.L^{-1}, respectively. Another example, in spring and summer in1979, Hg contents in bottom waters were initially lower than in surface waters, while in autumn there was an opposite distribution [5]. The temporal variation of Hg contents in bottom waters indicated that Hg in Jiaozhou Bay was settling continually over year, therefore a continued accumulation of Hg contents in bottom waters appeared.

Spatial variation. In generally, Hg was firstly delivered to surface waters near the estuaries of the rivers, and then was transferred by means of horizontal diffusion and vertical settlement. Hence, the changes of Hg contents in bottom waters were coincide with in surface waters, and the high values were always occurred in spring and summer. For example, Hg contents in bottom waters in April, August, and November 1981 ranged from 0.029-3.125μg.L^{-1}, 0.002-0.026μg.L^{-1}, and 0.003-0.005μg.L^{-1}, respectively, while in surface waters ranged from 0.028-2.086μg.L^{-1}, 0.001-0.040μg.L^{-1}, and 0.002-0.017μg.L^{-1}, respectively [10]. Previous studies have showed the horizontal transfer processes of Hg in bottom waters [5, 10]. One of the most significant features was that there was low value zone in bottom waters in the bay mouth. For example, Hg contents in May 1983, April 1985, and October 1985 ranged from 0.010-0.017μg.L^{-1}, 0.025-0.075μg.L^{-1}, and 0.004-0.043μg.L^{-1}, respectively, which were much lower than in bottom waters in the estuaries and the inner of the bay. For a close bay like Jiaozhou Bay, the dominant transfer process was vertical settlement rather than horizontal diffusion. While for areas in the bay mouth, Hg in both surface waters and bottom waters could more easily be diffused by hydrological process.

Settling process. Based on the analysis above, it was clearly that vertical settling was the dominant transfer process of Hg Jiaozhou Bay. The settling processes of Hg in this bay are, 1) Hg is

firstly delivered to surface waters by stream flow, 2) Hg is transferred by means of horizontal diffusion and vertical settlement, and 3) the settling of Hg is happening continually over year, especially in spring and summer, therefore a continued accumulation of Hg contents in bottom waters appeared. The settling mechanisms of Hg in this bay could be induced as, 1) Hg is low-soluble and chemical stable, 2) large amount of colloids occur in spring and summer due to the growth and reproduction of marine phytoplankton, 3) the colloids have strong capacity to absorb Hg, and 4) Hg is absorbed to the colloids and settled to the sea bottom finally. These settling mechanisms are able to explain the settling processes, as well as the temporal and spatial variations of Hg in bottom waters in Jiaozhou Bay.

Summary

Based on the analysis of the temporal, vertical and horizontal variations of Hg contents in bottom waters, both of the settling processes and settling mechanisms of Hg in Jiaozhou Bay were revealed. As a close bay, vertical settling was the dominant transfer process of Hg Jiaozhou Bay, which was mainly occurred in spring and summer. Sediments in sea bottom could be both of source and sink of pollutants, especially for persistence pollutants such as Hg. Hence, the improvement of recycle rate and the emission reduction of Hg should be the major pollution control strategies in Jiaozhou Bay.

Acknowledgements

The work is supported by Education Ministry's New Century Excellent Talents Supporting Plan (NCET-12-0659), Project of Outstanding Technological Educators of Governor of Guizhou ([2012]71), Project of Low Carbon Technology Plan of Guiyang (2012205]), Project of Science and Technology Foundation of Guiyang (LKM[2012]05), and Special Research Projects of High Level Talents of Guizhou Province (TZJF-2011-44).

References

[1] S.M. Zhang, X.Z. Pang and S.Q. Zheng: Mar. Sci. Vol. 6(1987), p. 35-36. (in Chinese)
[2] X.Q. Lv, B.Y. Sum and Z.L. Shi: J. Ocean University of Qingdao. Vol.20 (1990), p. 107-114. (in Chinese)
[3] S.F. Chai: J.Oceanography of Huanghai & Bohai Seas. Vol. 16 (1998), p. 60-63. (in Chinese)
[4] Chen Yu, Gao Zhenhui , Qu Yanheng, Yang Dongfang and Tang Hongxia: Chin. J. Oceanol. Limnol. 2007, 25(4): 455-458. (in Chinese)
[5] D.F. Yang, H.R. Cao, Z.H. Gao, Q. Lu and Y.F. Qu: Mar. Environ. Sci. Vol. 27 (2008), p. 37-39. (in Chinese)
[6] D.F. Yang and Z.H. Gao: *Bay ecology (First Volume)* (Ocean Press, Beijiang 2010) , p.1-300. (in Chinese)
[7] D.F. Yang and Z.H. Gao: *Bay ecology (Second Volume)* (Ocean Press, Beijiang 2010) , p.1-300. (in Chinese)
[8] D.F. Yang, L.L. Wang, Z.H. Gao, Q. Lian and J.P. Zeng: Mar. Environ. Sci. Vol. 28 (2009), p. 501-505. (in Chinese)
[9] D.F. Yang and Z.Q. Miao: *Distrubution and seasonal variation of Jiaozhou Bay environment* (Ocean Press, Beijiang 2012) , p.1-115. (in Chinese)
[10] Y. Chen, Q.J. Zhang, J.H. Guo, Q. Shi and D.F Yang: Ocean Develop. Manag. Vol. 30 (2013), p. 81-83. (in Chinese)
[11] D.F. Yang, P.Y. Sun, L. Ju, Y.H. Zhao and Q.U. Feng: Coast. Engin. Vol. 32 (2013), p. 65-76. (in Chinese)
[12] O. Lindqvist: Tellus. Vol. 37B (1995), p. 136-159.
[13] D.O. Reimann: Water Air Soil Pollut. Vol. 13 (1974), p. 179-193.
[14] China's State Oceanic Administration: The specification for marine monitoring (Ocean Press, Beijiang 1991), p.1-300. (in Chinese)

Advanced Materials Research Vols. 989-994 (2014) pp 1359-1363
© (2014) Trans Tech Publications, Switzerland
doi:10.4028/www.scientific.net/AMR.989-994.1359

The high resolution sequence stratigraphic isochronous framework In Threezhao peripheral zone

Zhang Na [1,a],Chenzhi Liu[2,b],Li Peng[3,c]

[1,2,3]Northeast Petroleum University,Daqing ,China

[a]lhbznqz@163.com,[b]1115840458@qq.com, [c]755088447@qq.com

Keywords: Fuyu reservoir; Yangdachengzi reservoir; high definition; base-level cycles; framework; seismic

Abstract. In detailed study on sedimentary characteristics of Fu Yang reservoir around Threezhao area, based on the theory of high resolution sequence stratigraphy of the base level cycle isochronous contrast, regard short-term base-level cycle as the minimum isochronous contrast comparing unit, this paper has carried on the fine high-resolution isochronous contrast of the reservoir in the studied area, and the high resolution[1] sequence division of different orders of base-level cycle of Fuyu oil layer and Yangdachengzi oil layer. The Fuyu reservoir is divided into one complete long-term base-level cycle and three complete medium-term base-level cycle; while Yangdachengzi reservoir is divided into a long-term base-level rise hemicycles and 3 middle-term base-level rise hemicycles. According to mud logging, well logging and core analysis data, the sands group stratified mark of the Fuyu reservoir has been determined.

Identification for base level cycle of Fu Yang oil layer

There is a regional top marker bed boundary at the top of the Fuyu oil layer boundary. In the bottom of Qing one segment development 3 sets of oil shale, high resistance, high gamma, on the seismic profile of high continuity of strong amplitude reflection (T2); There is a tend to be stable distribution of mudstone at the bottom of the Fuyu oil layer, and low resistance, high gamma and high sound waves, can be used as a standard, corresponding to the seismic reflection (T2-1-1)(Fig 1~2).

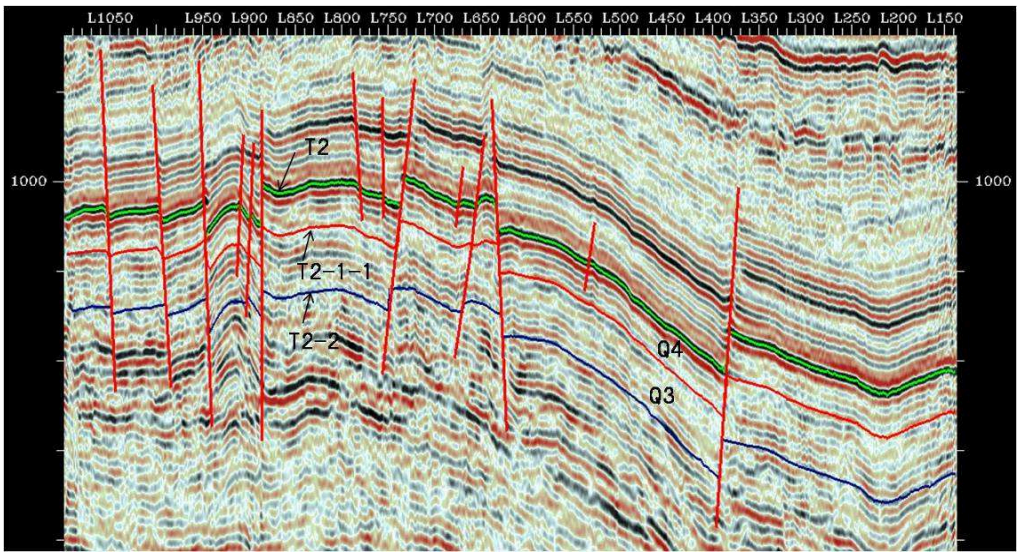

Fig 1 Threezhao peripheral zone seismic area is still home FU Yang reservoir top floor seismic response characteristics (Trace685)

Yangdachengzi reservoir bottom boundary is the fountain of the quan three segment of the bottom side that a regional unconformity surface[2]， mainly by early quan three segment of braided river scouring subjacent bed of quan two segment shore shallow lake intrafacies. On the seismic

section , quan two segment truncation and quan three segment onlap could be seen at Concave side. In the sunken the composite wave and wave system of interface are different. Corresponding to the T2-2 reflector Songliao basin

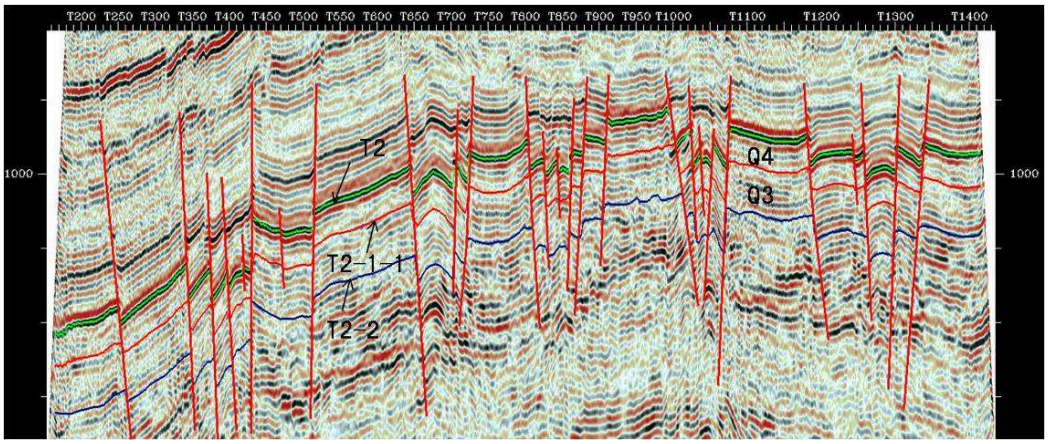

Fig 2 Threezhao peripheral zone on seismic area is still home FU Yang reservoir top floor seismic response characteristics (Line792)

The establishment of the isochronous stratigraphic framework

2.1 The sequence stratigraphic classification

(1)The division of Fuyu oil layer sequence:

Based on drilling in the study area of all levels of the recognition of base level cycle, Fuyu oil layer upon layer sequence is divided into: a complete long-term base level cycle and complete three medium-term base level cycle. A complete long-term base level cycle: F Ⅰ to rise half cycle, F Ⅱ +F Ⅲ to drop half cycle; 3 complete medium-term base level cycle: F Ⅰ F Ⅱ and F Ⅲ respectively a medium-term base level cycle, develop complete down half cycle and up half cycle.

F Ⅱ~F Ⅲ long-term base-level falling stage: F Ⅲ long-term datum rapid decline stage[3], development complete medium-term base level cycle, the datum plane down half cycle of the datum up half cycle of development; F Ⅱ reservoir group long-term datum slowly down to the lowest stage, also developed a complete medium-term cycle, datum down half cycle of the datum up half cycle of development.

(2)Yangdachengzi reservoir group sequence:

Based on drilling in the study area of the recognition of base level cycle, at all levels[4] could be divided into: Yangdachengzi oil layers of sequence 1 and half a rise in long-term base level cycle, three mid-term base-level rising half spiral swing back, Y Ⅰ, Y Ⅱ and Y Ⅲ respectively a medium-term base level rise half cycle.

Y Ⅰ~Y Ⅲ long-term base-level rising stage: the long-term base level[5] rising stage mainly experienced three stages: Y Ⅲ datum for a long time slowly rising - began to accelerate stage; Y Ⅱ long-term base level of accelerated phase; Y Ⅰ datum for a long time slowly rising stage. The thickness of the base level cycle as a whole has the characteristics of the first thickening and thinning. During the long-term base level rise, each set of the characteristics of sedimentary began to increase datum are falling, between groups have been developing wash surface of a boundary.

2.2The high resolution sequence stratigraphy framework is established in this paper

(1)Closure skeleton contrast section is established

This research article 19 and provenance direction nearly vertical frame transverse section and article 17 and provenance direction nearly parallel to the frame profile, overall understand three peripheral zone Fuyu reservoir origin and Yangdachengzi formation thickness of oil layer, lithofacies and sedimentary cycle variation characteristics. And Yangdachengzi Fuyu reservoir, building frame section 36, and optimizing drilling, logging and core information data is complete on

the four key Wells contrast, a sequence stratigraphic framework in order to establish the unified with the follow-up study of sedimentary facies interpretation and validation profile .

(2)Closed profile high resolution sequence stratigraphic isochronous contrast at all levels

In this study, the skeleton section can be compared to the profile closed hierarchical control, classification comparison, classification of high resolution sequence stratigraphy in the form of fine isochronous contrast. By contrast, has established the skeleton section 36, 273 Wells completed in the stratigraphic correlation, Fuyu oil layer in the study area is established and Yangdachengzi reservoir of high resolution sequence stratigraphic isochronous framework.

Fuyu sequence stratigraphy distribution characteristics

We even the well profile is used to study the longitudinal vertical[5] distribution regularity of the sequence. Plane, according to research the thickness of each sequence statistics Wells in this area, we compiled the four level of sequence stratigraphic thickness contour map, shows that the planar distribution characteristics and evolution rules of the sequence.

(1) The east of Yu region F Ⅰ strata thickness

The rage of strata thickness for F Ⅰ is 60~100m, the strata thickness thinning gradually from southwest to northeast and the high value is distributed in the south.

(2) The east of Yu region F Ⅰ 1 formation thickness

The rage of strata thickness for F Ⅰ 1 is 11~41m, the strata thickness thinning gradually from southwest to northeast and the high value is distributed in the south

(3) The east of Yu region F Ⅰ 2 formation thickness

The rage of strata thickness for F Ⅰ 2 is 15~58m, The strata thickness thinning gradually from southeast to northwest and the high value area in the southeast, the low value distribution in the northeast.

(4) The east of Yu region F Ⅰ 3 formation thickness

The rage of strata thickness for F Ⅰ 3 is 17~59m, The strata thickness thinning gradually from southwest to northeast and The high value area in the northwest.

(5)The east of Yu region F Ⅱ strata thickness

The rage of strata thickness for F Ⅱ is 17~59m, the strata thickness thinning from southeast to northwest, the low value scattered in the northwest and the high value distributed in the southeast continuously.

(6) The east of Yu region F Ⅱ 1 formation thickness

The rage of strata thickness for F Ⅱ 1 is 18~42m, Strata thickness thinning from southeast to northwest and the low value scattered in the north, the high value are mainly distributed in the south.

(7) The east of Yu region F Ⅱ 2 formation thickness

The rage of strata thickness for F Ⅱ 2 is 24~52m, Strata thickness thinning from the southeast to the northwest.The low distribution in the north and the high value are mainly distributed in the south.

(8)The east of Yu region F Ⅲ strata thickness

The rage of strata thickness for F Ⅲ is 24~80m, and the strata thickness thinning from southeast to northwest, the high value area are mainly distributed in the south and the low scattered in the north.

(9) The east of Yu region Y strata thickness

The rage of strata thickness forY is 210~356m, the strata thickness range of variation is large, the high value are mainly distributed in the southwest and low values are mainly distributed in the north.

(10)The east of Yu area isY Ⅰ strata thickness

The rage of strata thickness forY Ⅰ is 64~144m, the strata thickness range of variation is large, the high value are mainly distributed in the southwest and low values are mainly distributed in the north.

(11) The east of Yu region YⅡ strata thickness

The rage of strata thickness forYⅡ is 70~150m, the strata thickness thinning from southwest to northeast, the high value distribution in the southwest and the low are coverd in the northwest.

(12) The east of Yu region YⅢ strata thickness

The rage of strata thickness for YⅢ is 65~122m, the strata thickness thinning from southwest to northeast, the high value distribution in the southwest and the low value scattered distribution in the northeast.

The southwest of FuYang oil layer is very thin, then the northwest and southeast second and the northeast is the thinnest. The high value[6] area is located in the southwest.

Variation of the overall thickness of Fuyu oil layer is not obvious, the strata thickness thinning from southwest to northeast, so it has embodied sedimentary period of quan foru segment. The structure of the Threezhao surrounding area is stay in the uniform slow subsidence stage

The rage of strata thickness for Yangdachengzi YⅠoil layer is 90~110m, Variation of the overall thickness is not obvious, The southwest is thicker than the northeast more than ten meters slightly. The rage of strata thickness for YⅡ is 85~100m, the thickness that more than 100 m mainly locate in the Midwest of the study area. The rage of strata thickness for YⅢ is 100~150m and variation of the formation thickness is not obvious, the high value area is located in the central and nearly east-west distribution.

Conclusion

(1) Integrated application of seismic, logging, and core data, Fuyu oil layer upon layer sequence can be divided into: one complete long-term base level cycle and Complete three complete medium-term base level cycle — FⅠ is a medium-term base level cycle, FⅡis a drop half cycle that has develop completely and FⅢ is a Rise half cycle that has develop completely. The Yangdachengzi oil layer upon layer sequence can be divided into: one long-term datum rise half cycle and three mid-term base-level rising half cycle. They are all Mid-term base-level rising half cycle.

(2)The Yangdachengzi oil layer around the Threezhao region mainly develop fluvial facies, Source mainly comes from the north and northwest. Channel subfacies[7] is development in the plane. The scale of river channel is very large and distribute widely. Flow from the northwest to southeast, and give priority to with the channel sand , mudstone is given priority to with purple patches; The Yangdachengzi oil layer at the section mainly develop fluvial facies. The thin layer of delta plain and front subfacies is developed at the upper part of YⅠ. On the whole it is a process of retrogradation from YⅢ to YⅠ.

(3) The relation between oil and water around the Threezhao region is complex, The Fuyang oil layer mainly develop Oil water type, mixed type, pure oil type and more water type. The Fuyang oil layer at the plane mainly concentrate on the east of the studied area, large area connecting piece, Different regional profile has different characteristics in the plane. The southwest and the east of the oil layer are spread over FⅠ,YⅠand YⅡ; The northwest of the oil layer is spread over FⅠ,and the northeast is given priority to with water.

References

[1] Yongli Wang. Characteristics and Depositional Regularities of Oil Shale in Upper Cretaceous of Southern Songliao Basin in Chinese [D]Jilin University, 2006:6-7

[2] Xuemei Pan. Diagenetie Field Analyse Sand Causes of the Anomalously High Porosity Zones in the Deep-Shallow Strata of Xujiaweizi Fault Depression in Chinese [D] Jilin University, 2011:5-6

[3] Xiaohong Chen, Wenyuan He, Zihui Feng. Controlling Effect of Major Faults on the Gas Reservoirs in the Xujiaweizi Fault Depression in Songliao Basin in Chinese [J]Natural Gas Industry, 2012;32(3):53-55

[4] Guangtian Men. Research on Deep Gas Forming Pattern and Distribution Law in Xujiaweizi Depression in Chinese [D] Daqing Petroleum Institute, 2002:5-6

[5] Aiping Fan, Renchao Yang, Zuozhen Han, Guogang Cai, Chunhua Li. Discovery and Implication of Braided River Delta Sedimentary System in the Eastern Sag of Liaohe Depression in Chinese [J] SpecialOil and Gas Reservoirs,2009;16(4):33-34

[6] Chunyan Fan. Research on Sedimentary Charaeteristies of NanTun Group in Northern Area of Wuerxun Depression in Chinese [D] Daqing Petroleum Institute, 2011:45-46

[7] Jufeng Wang. Sedimentary Facies Types and Evolution Features on Steep Slope Belt in Terrestrial Fault-depressed Basin_a Case in Sha3 and 4 Member of Minfeng Area in Dongying Depression in Chinese [J].Natural Gas Geoscience, 2008;19(5):613-614

Advanced Materials Research Vols. 989-994 (2014) pp 1364-1367
© (2014) Trans Tech Publications, Switzerland
doi:10.4028/www.scientific.net/AMR.989-994.1364

Use Horizontal Aeration Method to Treat Organic Pollution in Soil

Luyang Xu[1, a]

[1]Southwest Jiaotong University, Chengdu, Sichuan, China

[a]674306863@qq.com

Keywords: aerator pipe, horizontal, double level, vertical, microorganism, organic pollution

Abstract

This design adopts the method of horizontal arrangement to set the aerator pipes because it's more effective than an upright way. The pipes are divided into two vertical levels. Firstly there should be an excavation of foundation pit or grooves to put the pipes in two levels. Then the pipes in two levels can be set at vertical directions. After burying the pipe the earth should be backfilled into the grooves. When backfilling the lower level groove, we put some certain microorganism to help cleaning the organic pollution. While working, the pipes above are mainly used to manufacturing gas phase concentration difference, letting the organic volatilize and goes into the atmosphere. The pipes in lower level are mainly used to provide oxygen to microorganisms in the soil, so that they can decompose organic and make them into inorganic which is no harm to the soil and ground water.

Principle of an aeration technology

Aeration is a kind of technology using pump to inject fresh air to the saturated soil. Because organic pollutants concentration differs between gas and liquid, so they can get into gas through volatilization. Then due to aid of buoyancy, pollutants will rise with air gradually into the unsaturated zone [1]. That is when we can collect the pollutants by using certain equipment like SVE system to achieve the goal of eliminating organic pollution in soil and protect groundwater. At the same time, the air can provide sufficient oxygen to underground aerobic microorganisms, promoting organic pollutants' biodegradation.

This design adopts the method of horizontal arrangement with two levels. As the main purpose of the arrangement of bottom pipes are to provide oxygen, give them a small gas eruption rate and make the ones at the top erupt more air to create a better air distribution in soil. The arrangement is shown in Fig.1. The two pairs of green pipes are aeration pipes in two different levels and the red ones are collecting device SVE.

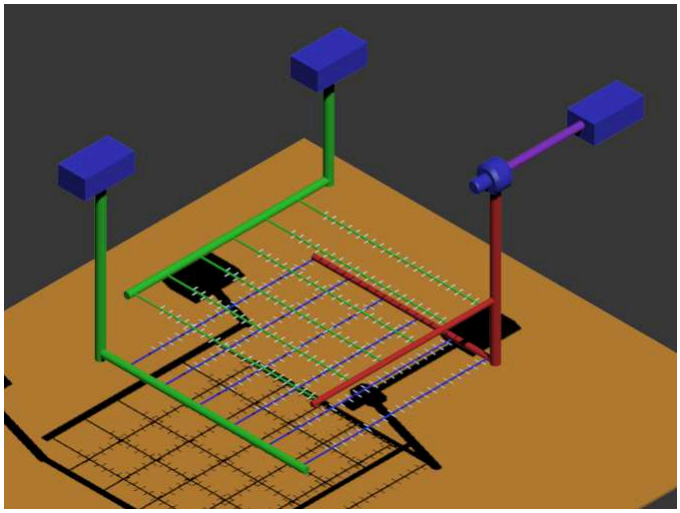

Fig.1.The arrangement of the whole device

Aeration is a kind of in-situ remediation which can reduce the pollutants exposure and disturbance to the environment of the largest degree. It has features like direct, fast, economic, effective and environmental protection which give it a good application prospect.

Device Settings

The lower level of aeration device:

Task of the pipes in this level is promoting biological activity of the microorganisms through the way of pumping air into the soil.

When arranging, firstly we should excavating grooves according to the density and length, drill a duct for the arrangement of main pipe. Set the pipes into the grooves and make sure they're connected with the main pipe for that level. Then mix the earth outside the groove with microorganisms and backfill the soil. This level of pipes should be set 4-5 meters under the surface of the ground. The main pipe should be long enough to reach out of the surface and be connected with air pumps.

The upper level of aeration device:

The upper level plays the most important role in this device. It uses pump to inject fresh air into the soil below water level through a horizontal well. Through a series of mass transfer process the pollutants in pores and groundwater will evaporate into the air. The air full of pollutants gradually rises under the pressure of buoyancy, keep carrying pollutants to the collect devices SVE. So there's a decrease of pollution rate in the soil and groundwater. When arranging, the grooves should be vertical to the pipes in the under level. It is for taking full use of air diffusing taper and space in the soil. The pipes' depth should be no more than 0.7m above the under pipes but no less than 3 meters below the ground surface. That's because there's a height needed for the rising and spread of the air. There also should be a main pipe which can attach all the pipes to an air pump. The details of the aeration pipes in two levels are shown in Fig.2. Between them the blue one is in the under level. And the red one is in upper level.

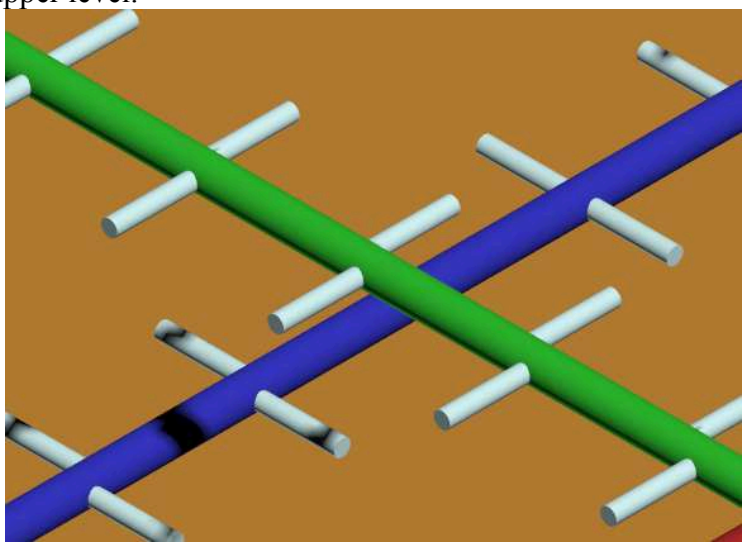

Fig.2. Details of upper and under aeration pipes

Comparison between traditional and horizontal aeration

In the traditional upright aeration method, the pipes are set vertical, when arrangement the pipes should be insert into the earth to a certain depth in order to make the shape of the flow a vertical ball distribution [2]. Because each aeration pipe has its own radius of influence, so it has to be a proper density of pipes to ensure the effect of the aeration. But due to the flow and diffuse features of the air the earth near the bottom has a very small area contact with air (Fig.3). So there must be a large density of pipes to let the under soil have a high aeration rate. And this will cause serious damage not only on the surface or inside the earth, but also effect mechanics and ecological feature

of the soil. It'll also cause a lot of overlap on upper soil aeration volume, which will be a huge waste of energy and sources. The schematic is Fig.4.

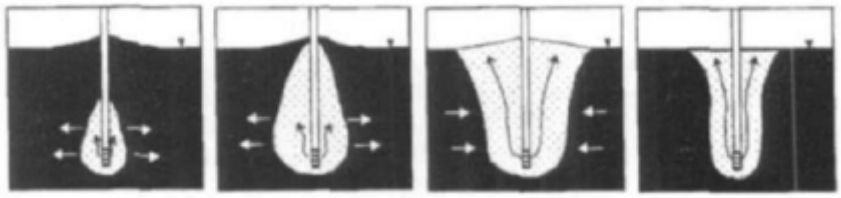

Fig.3.Gas cone of traditional upright aeration

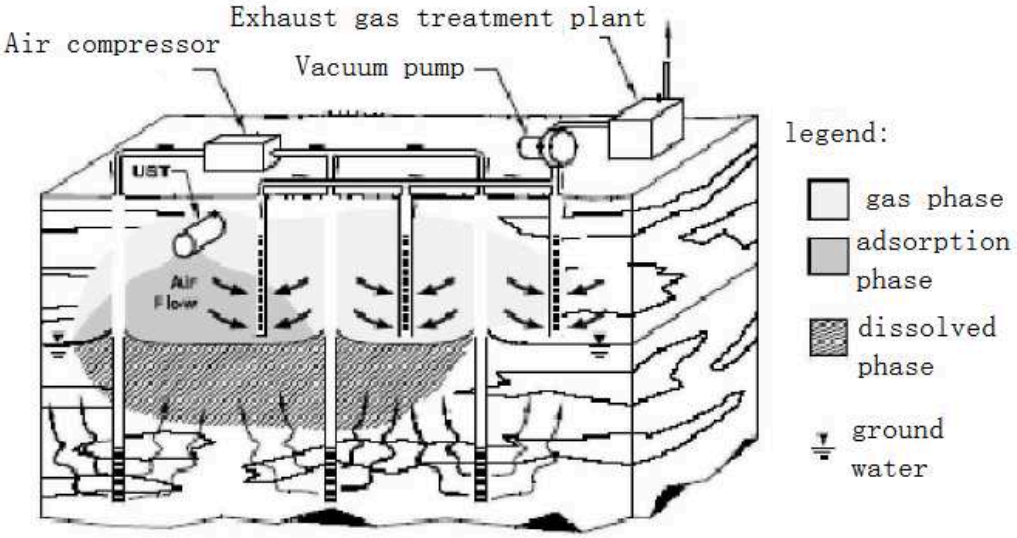

Fig.4. Schematic of traditional aeration pipes

In our device, the aeration pipes are multilayer horizontal arranging in X or cross mode. Gas input source is controlled by a main pipe separately each level, and ach main pipe is connected to one or a few pump machines. Though there will still be damage to the earth where the pipes lie. But contrast with the traditional way which will destroy the integrity of soil from the surface to bottom, the surface of the ground may still remain no harm by using horizontal way. Besides the bearing capacity of the whole area will hardly change. In the aspect of aeration efficiency, the insufficiency of aeration rate at the initial stage can be solved by coordinate the amounts of aeration pores on pipes and aeration rate. The control of direction and pores 'density will also reduce the gas being used and improve efficiency. [3]This avoids the huge consumption of energy. What's more by using horizontal mode can significantly improve the uniformity of airflow. [4] The schematic of gas cone is in Fig.4. The microorganisms can also help a lot on promoting the efficiency of tuning pollutants into inorganic. [5] The schematic of gas cone is in Fig.5.

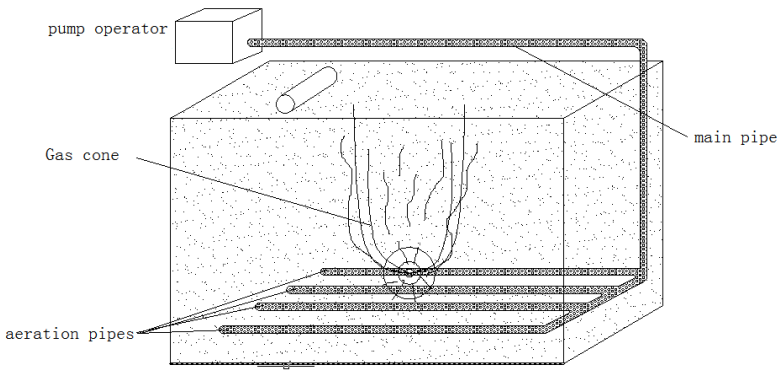

Fig.5.Gas cone of horizontal aeration pipe

Characteristics analysis

Advantages: The horizontal arrangement improves aeration efficiency especially at the initial stage. It can also improve the uniformity of airflow. Save energy, power and space while running a system like this. Microorganisms can help make up the missing efficiency where the airflow cannot pass through.

Disadvantages: Complex and a waste of manpower and money while excavating the grooves.

Conclusion

The double-leveled horizontal aeration device promotes the effecting range of gas cone, so it will improve the efficient of aeration.

The device rationalize the density of aeration pipes and direction of erupted gas so that it will save energy and.

The new device avoids destroying the earth on the surface and bearing capacity of the ground layer in the largest extent.

References

[1] Information from http://baike.baidu.com.
[2]Model Test Study of Groundwater Aeration Technology, Yaoli Hu, Yi Liu, <Chinese Journal of Geotechnical Engineering>, Vol.30 No.6 (In Chinese)
2008, 6 Chinese Journal of Geotechnical Engineering June, 2008
[3]Reviewing groundwater aeration technology at home and abroad-Xiaona Liu, 2011-5,1673-193X（2011）-05-0056-07(In Chines)
[4]Groundwater aeration and biological aeration treatment research of organic pollutants-Zhanqiang Wang, 2005.1-20276048(In Chinese)
[5]Oil shale exploitation of shale oil research on in situ bioremediation of groundwater pollution –Ran Ma, 2013.5-10183 (In Chinese)

Advanced Materials Research Vols. 989-994 (2014) pp 1368-1371
© (2014) Trans Tech Publications, Switzerland
doi:10.4028/www.scientific.net/AMR.989-994.1368

Study on Identification Method of Fructus Lycii Origin by Mineral Elements

Yanping Pang [1, a] ,Kun Liu[2, b], Zhilei Zhao [1, c] , Xiaoting LI [1, d]

[1]College of Quality & Technical Supervision, Hebei University, Baoding 071002, China;

[2]Tangshan city of Quaily and Technical Supervision, Tangshan 063000, China)

[a]pyp1982@163.com, [b]liukunqu@126.com , [c]zhaozhilei-3208@163.com , [d]lxt@hbu.edu.cn

Keywords: Fructus Lycii; Mineral element; discriminant analysis; Identify

Abstract: In order to rapid discriminate the source of Fructus Lycii origin, Fructus Lycii from five different areas were collected, the content of K, Ca, Na, Mg, Fe, Zn ,Cu and Mn were analyzed with flame atomic absorption spectrometry，and the data was analyzed with Stepwise discriminant analysis method， and the discriminant function was established. The results showed that Fructus Lycii from five different areas was well clustering. The discriminant model was re-discriminated by using the method of mutual test; its discrimination accuracy was 94.4% for the original samples and the unknown samples. The recognition rates for Ningxia, Hebei, Qinghai cultivation regions were all 100%. In conclusion, mineral element combined with chemometrics method was a fast and accurate method to identify the origin source of Fructus Lycii.

Introduction

Lycium is a multi branched shrub plant of Solanaceae Lycium. It was distributed at home and abroad. Its fruit was said medlar, also called Gou screwdriver, wolfberry red. Mainly for the Ningxia wolfberry medicinal species. Modern pharmacological studies confirmed the fruit of Chinese wolfberry can adjust the immune function, can effectively inhibit the growth of tumor and cell mutation, can delay aging, anti fatty liver, regulating blood fat and blood sugar, and promote hematopoietic function and other aspects of the role.

Mineral elements in plant is closely related to the content and growth environment, the distribution of mineral elements in different habitats in the environment are different, and this difference can be reflected to the plants, so the content of mineral elements can be regarded as one of standard for plant origin discrimination[1-3]. Medlar contains many kinds of mineral elements, the quantity of mineral elements, in addition to physiological characteristics, is mainly concerned with the physical environment, the content of some elements in the different areas has many differences[4].

Instruments and Reagents

TAS- 990 atomic absorption spectrophotometer; analysis of the electronic balance; ultra pure water machine; SUNWAY- II ventilation cabinet; DB-2 stainless steel adjustable electric heating board; DZF- 6020 type vacuum drying box, K, Ca, Na, Mg, Fe, Mn, Zn, Cu hollow cathode lamp; glass instrument with 30% nitric acid soaking for 24 h, then using two DI water rinse clean.

Concentrated nitric acid (GR); $HClO_4$ (GR); K, Ca, Na, Mg, Fe, Mn, Cu and Zn standard solution (concentration was 100 μ $g \cdot mL^{-1}$, China metrology measurement Institute); cesium chloride; lanthanum oxide; the Chinese wolfberry source is shown in table 1.

Table 1 Origins of samples

Sample number	1	2	3	4	5
Origin	Hebei	Inner Mongolia	Xinjiang	Qinghai	Ningxia

Experimental Methods

The raw material drying at 60℃ for 4 h, crushing, 60 mesh sieving, each sample weighing 1g (accurate to 0.0001 g) test.

By wet digestion method, weigh the sample, put in 250 mL Erlenmeyer flask, add 25 mL of digestive juice (HNO_3:$HClO_4$=4:1) soaking for 24 h. Placing the electro thermal heating, removed it until a large white smoke disappeared, cooled to room temperature, diluted with ultrapure water, transferred to a 50 mL volumetric flask, constant volume, shake, stand-by. According to GB/T 18932.12-2002 'honey, sodium, calcium, magnesium, potassium, zinc, iron, copper, manganese, chromium, lead, cadmium content determination method of atomic absorption spectrometry', determined K, Na, Ca, Mg, Cu, Fe, Zn, Mn eight content elements in 8 different origins. Soil available and exchangeable elements are extracted using EDTA- ammonium acetate extraction [5] and DTPA extraction [6].

Results and Analysis

Analysis of mineral elements content in Chinese wolfberry in different regions

Results of the content of K, Na, Ca, Mg, Cu, Fe, Zn, Mn in different areas of medlar can be seen in table 2. From the measurement results, differences in content of Cu ,Fe , Zn, Na, Ca of the mineral elements in Chinese wolfberry in different regions is obvious, but the distribution of elements present regularly, all with K, Na, Ca, Mg high content, Cu, Fe, Zn, Mn low content.

Tab 2 Contents of Mineral element in Fructus Lycii from different areas

	Cu	Fe	Zn	Mn	Na	K	Ca	Mg
Hebei	19.688	28.638	31.444	14.942	7301.093	16297.32	3416.83	1516.249
Neimeng	8.584	19.245	14.25	11.199	4697.467	12062.26	2132.486	1286.872
Xinjiang	8.924	12.514	13.672	13.151	4411.413	14396.08	2587.658	1386.344
Qinghai	11.538	50.465	17.713	15.949	3728.935	13043.78	1820.786	1080.877
Ningxia	8.91	34.32	20.485	19.132	2914.99	12855.24	2298.871	1189.352

Correlation analysis between the fruit of Chinese wolfberry and mineral elements in the soil

Significant correlation between mineral elements in Fructus Lycii ($P < 0.05$) or very significantly correlated ($P < 0.01$), suggesting that they have some synergistic effect on the absorption, was negatively correlated with Fe and Mg, Ca, Na, Fe and this showed that the absorption of several mineral elements may exist antagonism. No significant correlation between Mn and other elements (Table 3). Table 4 shows that, between soil medlar and its origin Zn, Mn, Mg, Ca, Cu, Na elements showed significantly or very significantly correlated.

Table 3 Correlation matrix of 8 mineral elements of Fructus Lycii

	Cu	Fe	Zn	Mn	Na	K	Ca	Mg
Cu								
Fe	.211							
Zn	.738*	.107						
Mn	.019	.537**	.131					
Na	.480**	-.146	.219	-.114				
K	.461**	.124	.349**	.214	.466**			
Ca	.370**	-.072	.346**	.136	.172	.287*		
Mg	.355**	-.178	.157	.072	.152	.200	.446**	

*P<0.05，**P<0.01

Discriminant analysis in Chinese wolfberry in different regions

To establish discriminant function discriminant analysis method of medlar mineral components of 8 variable stepwise discriminant analysis was performed using the Bayesian model, a sample data, every increase of one variable with the greatest effect on discrimination, the discriminant equation, and verify the identification rate. Stop introduced in the correct ratio of discrimination no longer increases, the establishment of mathematical model. Finally introducing the distinguishing function of 4 variables, excluding the 4 variables, finally got 4 canonical discriminant functions are as follows:

D1=1.773Cu+0.095Fe-1.011Zn+0.515Mn

D2=-0.352 Cu +0.849 Fe +0.796 Zn +0.373 Mn

D3=-0.071 Cu -0.640 Fe +0.527 Zn +0.866 Mn

D4=-0.325 Cu +0.131 Fe +1.022 Zn -0.515 Mn

The typical characteristics of D1, D2, D3, D4 discriminant function values were 25.909, 4.921, 1.506 and 0.062, respectively, can explain variance 80%, 15.2%.4.6% and 0.2%, the former two discriminant function can explain variance 95.2%, characteristics of 4 kinds of mineral elements into the equation can reflect all of Chinese wolfberry using discriminant function, the basic can distinguish the origin of Lycium barbarum. In order to unknown sample medlar discrimination, established 5 discriminant function, were used to describe the characteristics of the Chinese wolfberry mineral elements, discrimination is as follows:

M1=-363.089+35.927 Cu+0.521Fe-4.013Zn+8.469Mn
M2=-91.178+16.773 Cu+0.331Fe-1.732Zn+4.740Mn
M3=-106.683+18.420 Cu+0.116Fe-2.208Zn+5.449Mn
M4=-190.565+22.960 Cu+1.047Fe-2.239Zn+6.235Mn
M5=-138.502+17.374 Cu+0.651Fe-1.242Zn+6.434Mn

Table 4 Correlation matrix f 8 mineral elements between soil and Fructus Lycii

Soil \ Medlar	Cu	Fe	Mn	Zn	Ca	Mg	K	Na
Cu	.720*	.572	.199	.752*	.238	.080	.446	.456
Fe	-.164	.104	-.026	-.139	-.051	-.112	-.064	-.122
Mn	.677*	.071	-.121	.731*	.240	.323	.202	.674*
Zn	-.201	.271	-.413	-.191	-.761*	-.606	-.599	-.115
Ca	-.423	.268	-.135	-.476	-.758*	-.710*	-.537	-.477
Mg	.886**	.539	.622	.914**	.698*	.345	.648	.472
K	.133	-.501	-.632	.189	-.114	.279	-.265	.512
Na	-.318	-.082	-.298	-.314	-.588	-.432	-.820*	-.171

*P<0.05，**P<0.01

The results of discriminant analysis is shown in figure 2 and table 5, figure 2 is a scatter by the discriminant scores do figure, distinction can be seen from the figure from 5 or more obvious. From table 5, samples of Ningxia, Hebei, Qinghai three places to 100% from Xinjiang and Inner Mongolia, Chinese wolfberry 1 each sample mistaken for each other habitats, the correct judgment rate was 83.3%, the overall rate of correct judgment for 94.4%. Of the original data back to the discriminant analysis, using cross validation results show, Ningxia, Hebei, Qinghai three areas the recognition rate is 100%, Xinjiang and Inner Mongolia two areas the recognition rate is 83.3%, the total cross recognition rate of 94.4%, good results. Source using this method can effectively identify the origin of Lycium barbarum.

Tab 5 Classification Results

	Group	Predicted Group Membership					Total
		Hebei	Inner Mongolia	Xinjiang	Qinghai	Ningxia	
Original %	Hebei	100	0	0	0	0	100
	Inner Mongolia	0	83.3	16.7	0	0	100
	Xinjiang	0	16.7	83.3	0	0	100
	Qinghai	0	0	0	100	0	100
	Ningxia	0	0	0	0	100	100
Cross-validated[a] %	Hebei	100	0	0	0	0	100
	Inner Mongolia	0	83.3	16.7	0	0	100
	Xinjiang	0	16.7	83.3	0	0	100
	Qinghai	0	0	0	100	0	100
	Ningxia	0	0	0	0	100	100

a. Cross validation is done only for those cases in the analysis. In cross validation, each case is classified by the functions derived from all cases other than that case

b. 94.4% of original grouped cases correctly classified.

c. 94.4% of cross-validated grouped cases correctly classified

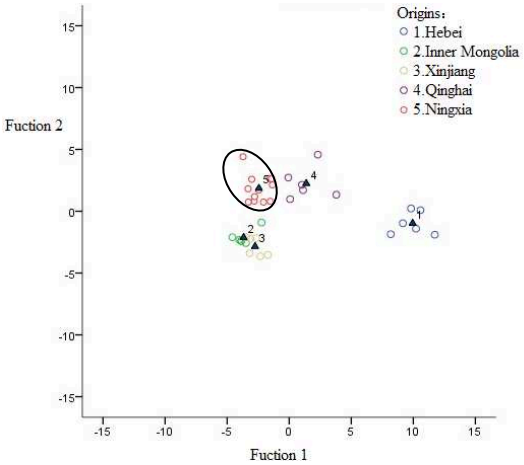

Fig. 2 Canonical Discriminant Functions

Conclusion

This study was used to measure the mineral elements of 5 areas in Chinese wolfberry by flame atomic absorption spectrometry, obtain 8 mineral element content , chemical pattern recognition methods are obtained. Usingdiscriminant analysis of mineral elements on Fructus Lycii samples for classification, identification of Ningxia, Hebei, Qinghai Chinese wolfberrycorrect rate is 100%, the overall accuracy rate is 94.4%, can effectively identify the Ningxia wolfberry fruit producing areas, as the product of geographical indication Ningxia wolfberry protection provides reliable basis

Acknowledgements

This work was financially supported by the Special Fund for Quality-Science Research project "the study on products of geographical indications of origin recognition technology and the regional economic contribution evaluation method" (201210010-4).

References

[1] Li R, Ying J Y. The identification of tea producing nutrient content in several famous tea in the eastern region of China as an example, J. Guangdong science of trace elements. 19 (2012) 28-33
[2] Yu R, Liu Z, Tao Y D. Determination of 5 trace elements in different places of Qinghai Clematis tang Utica in flame atomic absorption spectrometry, J. Spectroscopy Laboratory. 29 (2012)3330-3332
[3] Liu Y, Zheng G C, Zhu M W, et al. Analysis of trace elements content in Lycium barbarum L.from different habitats, J. Inspection and Quarantine Science. 03(2012)26-30
[4] Pu X L, Wu Q, et al. Research progress of sub medlar, J. Lishizhen medicine and Material Medical Research, 21 (2010)1758-1760
[5] Zhang Y J, Xiao M, Dong Y H, et al. Ammonium acetate extraction atomic absorption spectrometric method for the determination of composition of soil exchangeable base cautions, J. Spectroscopy and Spectral Analysis, 32 (2012) 2242-2245
[6] Li H F, Lin R Q, Xie X L. Determination of copper, zinc, iron, manganese in soil by ICP-AES, J. Guangdong Agricultural Sci. 04(2009)76-77
[7] Zhang L, Wang Y R, et al. Application of Chemometrics in the discrimination of oils and fats, J.35 (2010)11-14

Advanced Materials Research Vols. 989-994 (2014) pp 1372-1375
© (2014) Trans Tech Publications, Switzerland
doi:10.4028/www.scientific.net/AMR.989-994.1372

Establishment of Models for Tight Sandstone Formation Evaluation in the Ordos Basin of Northwest China

WEI Xiao-lei[1, a], LI Jun[2,b], XU Rui[3,b] and ZHI Ling-ling[3,b]

[1] Gological Exploration and Development Research Institute of CNPC Chuanqing Drilling Engineering Company Limited, Chengdu, Sichuan, China

[2] Dingbian Oil Production Plant of Yanchang Petroleum(group) CO. LTD., Shaanxi, China

[3] Tuha Division of CNPC Well Logging Company Ltd. Xinjiang, China

[a]1159506727@qq.com, [b]13101103@qq.com

Keywords: Tight sandstone formation; Porosity calculation; Permeability estimation; Core calibration log method.

Abstract Porosity and permeability are two important input parameters in formation evaluation. However, It faces a great challenge for formation porosity and permeability estimation in tight sandstone reservoirs in the Ordos basin of northwest China due to the greater contribution of rock matrix and complicated pore structure. In this paper, based on the analysis of conventional log responses and 324 core samples drilled from the target formations in different wells, the estimation models of reservoir porosity and permeability are established, and the reliability of these models are verified by comparing the calculated porosity and permeability by using the established models with core analyzed results. The absolute errors between these two kinds of porosities are all lower than 0.64%, and the relative errors between them are lower than 7.1%, these are coincided with the requirement of reserve estimation.

Introduction

Porosity are permeability are two important input parameters in reservoir evaluation and reserve estimation, especially for the permeability, it is connected with formation reserves, and it is also worth considering in the development program formulation (Mao et al. 2013; Xiao et al. 2014). To obtain these two parameters, plenty of methods had been proposed (Tiab et al. 1993; Biniwale et al. 2004; Xiao et al. 2009), such as the hydraulic flow unit (HFU) approach and classification scale models (CSM). However, there is not a universal model is proposed at present, especially for tight sandstone reservoirs, the contribution of rock matrix is important, and the pore structure is complicated. The statistical analysis method is always used. In this paper, using the core samples drilled from the target tight sandstones of Ordos basin in northwest China, the porosity and permeability estimation models are established.

Distribution of core porosity and permeability in the target tight sandstone

Figures 1 and **2** display the distributions of core porosity and permeability separately, from these two figures, we can observe that in our target formation, porosities range from 5.0 to 18.0%, and the average value is 9.9%. permeabilities range from 0.13 to 3.98 mD, and the average permeability is 0.58mD, belong to tight sandstone reservoirs.

Establishment of porosity and permeability estimation models

In our target tight sandstone formation, we obtain the conventional acoustic log, the density and neutron logs were not acquired due to the consideration of economy, and not nuclear magnetic resonance (NMR) log, which had been verified to be effective in tight sandstone porosity estimation, were also not acquired. Hence, we establish reservoir porosity and permeability estimation models based on the core calibration log method.

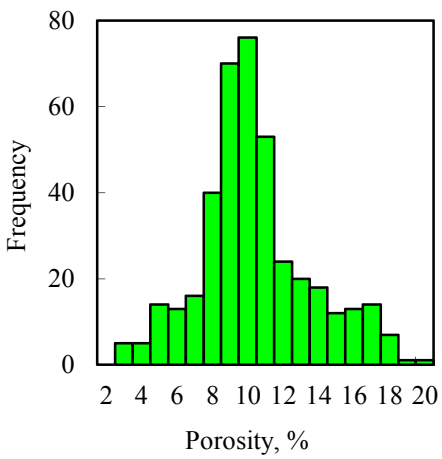

Fig. 1 Porosity distribution of the target formation in the Ordos basin of northwest China.

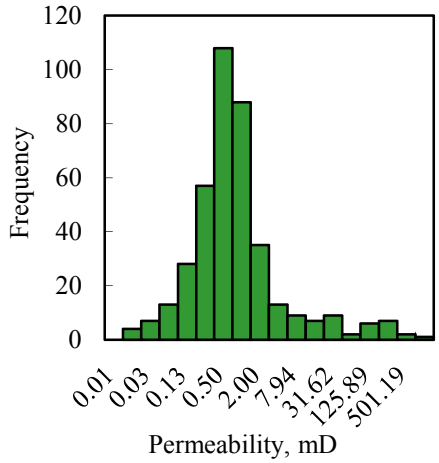

Fig. 2 Permeability distribution of the target formation in the Ordos basin of northwest China.

Preprocessing

Commonly, the procedure of data preprocessing, such as the depth shift, needed to be made to remove the additional errors before the evaluation models were established. In this study, we also made depth shift to make the core porosity match with the tendency of acoustic log. **Figure 3** shows the process of depth shift of core samples. From this figure, we can observe that after this well is preprocessed, the acoustic log curve match with core porosity very well.

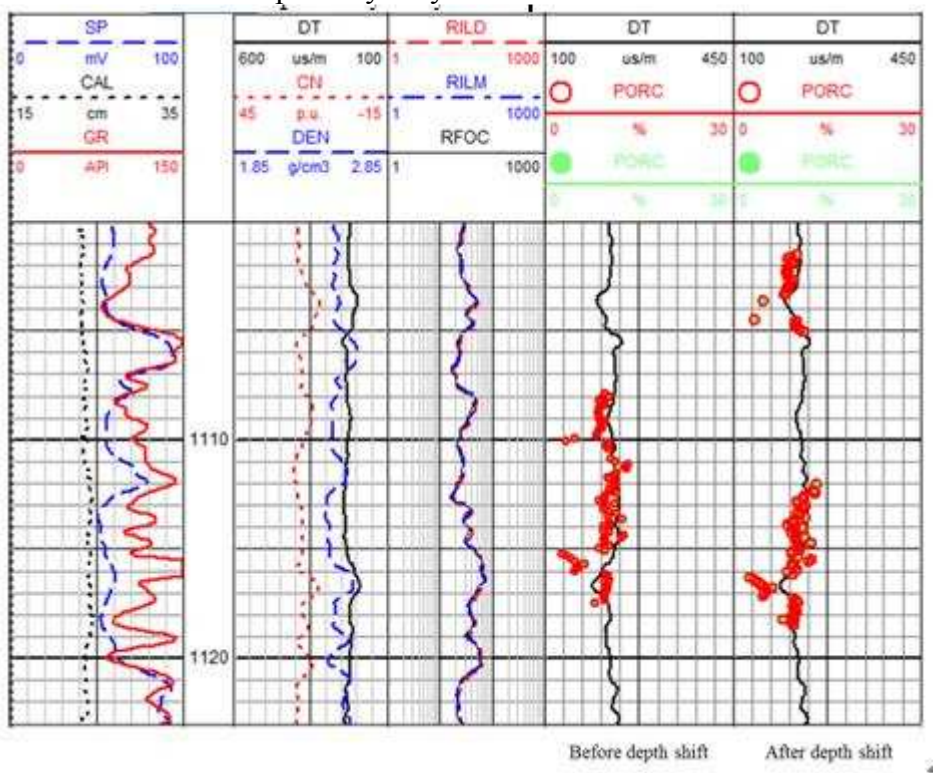

Fig. 3 The depth shift of core samples.

Establishment of porosity and permeability estimation models

After preprocessing, core porosity, permeability and the corresponding value of interval transit time are collected as the data set. The core calibration log method is used to establish the relationships of interval transit time (DT) vs. core porosity, core porosity vs. core permeability, and they are displayed in **Figures 4** and **5** separately. From these two figures, we can observe that good correlation exist between these three parameters; the correlation coefficients can reach to 0.83 and 0.84, respectively.

Hence, we can conclude that good relationships can be used to calculate porosity and permeability in the target tight sandstones.

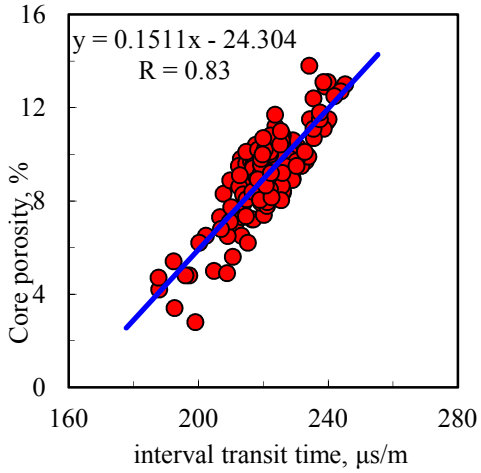

Fig. 4 Relationship of acoustic log and core porosity.

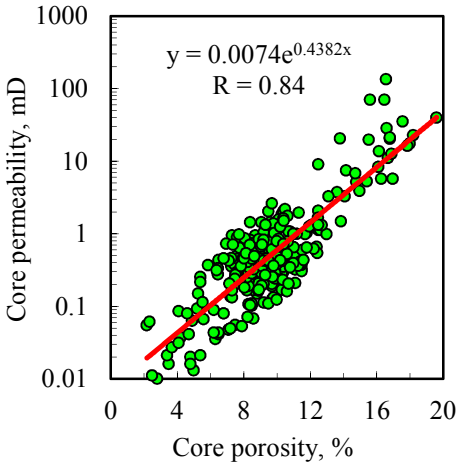

Fig. 5 Relationship of core porosity and permeability.

Case studied

By using the established models displayed in **Figs. 4** and **5**, several wells in the Ordos basin are processed, reservoir porosity and permeability are established, and they are compared with core analyzed porosity and permeability to verify the reliability of the established models. **Figure 6** shows a field example of comparing calculated porosity and permeability with core derived results. In the first track of **Fig. 6**, thedisplayed curves are gamma ray (GR), spontaneous potential (SP), and boreholediameter (CAL); their contribution is the formation indication. ILD displayed in the second track is the deep induction resistivity, ILM is the medium induction resistivity, and RFOC is the microspherically focused resistivity; .In the third track, we show the interval transit time log (AC), it is used for porosity estimation. POR_LOG displayed in the fourth track is calculated porosity by using model showed in **Fig. 4**, and PERM_LOG displayed in the fifth track is estimated permeability by using model showed in **Fig. 5**. Estimated porosity and permeability are compared with core analyzed results in these two tracks. From these two tracks, we can observe that the calculated porosity and permeability curves match with core derived results very well, this means that the established models are credible, thay can be used to calculate reservoir evaluation parameters in the Ordos basin.

To further verify the reliability of estimated porosity, the calculated porosities and the core analyzed results are listed in **table 1**. From table 1, we can observe that the calculated porosities and the core analyzed results are closed with each other, the absolute errors for all wells are lower than o.7%, and the relative errors are lower than 7.1%. these are coincided with the requirement of reserve estimation.

Summary

(1) No unified models can be established to calculate reservoir porosity and permeability, especially in tight sandstone reservoirs. The core calibration log method should be used to establish the corresponding models to calculate reservoir evaluation parameters in the target reservoirs.

(2) In the target tight sandstone reservoirs of Ordos basin in northwest China, good relationships between conventional acoustic log and core analyzed porosity, core analyzed porosity and permeability can be established. The established models are valuable in estimating reservoir evaluation parameters. The estimated results match with core analyzed results very well. They can be used for reservoir evaluation and reserves calculation.

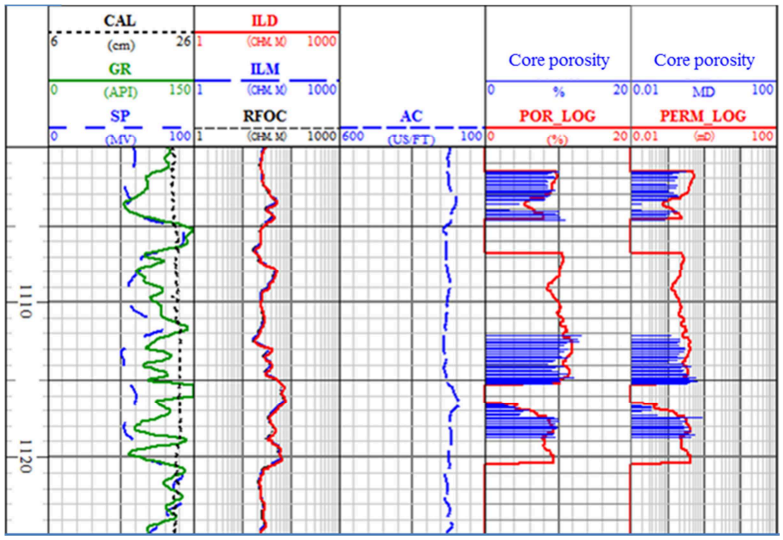

Fig. 6 Comparisons of porosities and permeabilities predicted by using the proposed models in the target tight sandstone reservoirs of Ordos Basin in northwest China.

Table 1 Comparison of porosities acqiured from different methods

Well name	Interval (m)	Depth(m)	Porosity (%)		Absolute error (%)	Relative error (%)
			analyzed	estimated		
Well A	1136.0~1149.0	13	9.01	9.65	-0.64	7.1
	1173.0~1186.0	13	8.12	8.54	-0.42	5.17
Well B	1101.0~1105.5	4.5	8.9	8.63	0.27	3.03
	1112.0~1118.5	6.5	9.58	9.33	0.25	2.61
	1135.0~1143.5	8.5	8.31	8.54	-0.23	2.77
Well C	1158.0~1179.2	21.2	8.96	9.37	-0.41	4.58
Well D	1234.0~1237.6	3.6	12.69	12.09	0.60	4.73
	1278.9~1304.1	25.2	10.02	9.55	0.47	4.69

References

[1] Tiab, D., Marschall, D.M., Altunbay, M.H. 1993. Method for identifying and characterizing hydraulic units of saturated porous media: tri-kappa zoning process. U.S. Patent No. 5,193,059.

[2] Biniwale, S., and Behrenbruch, P. 2004. The mapping of hydraulic flow zone units and characterisation of Australian geological depositional environments. SPE88521.

[3] Xiao, L., Liu, X.P., and Mao, Z.Q. 2009. A computation method for reservoir permeability by combining NMR log and capillary pressure data, Acta Petrolei Sinica, 30(1): 100-103.

[4] Mao, Z.Q., Xiao, L., and Wang, Z.N. 2013. Estimation of permeability by integrating nuclear magnetic resonance (NMR) logs with mercury injection capillary pressure (MICP) data in tight gas sands, Applied Magnetic Resonance, 44(4): 449-468.

[5] Xiao, L., Liu, X.P., and Zou, C.C. 2014. Comparative study of models for predicting permeability from nuclear magnetic resonance (NMR) logs in two Chinese Tight Sandstone Reservoirs, Acta Geophysica, 62(1): 116-141.

Advanced Materials Research Vols. 989-994 (2014) pp 1376-1379
© (2014) Trans Tech Publications, Switzerland
doi:10.4028/www.scientific.net/AMR.989-994.1376

The Research and Application of Multiple Collaborative Anti-sloughing Drilling Fluid

Meiting Jiang[1, a], Haoyuan Wei[2, b,] Yihao Li[1, c], Wenzhuang Shi[3, d]

[1] Department of Petroleum Engineering, Yangtze University, Wuhan, Hubei 430100, China.

[2] Research Institute of Exploration and Development, Yumen Oilfield Company, CNPC, Jiuquan, Gansu 735019, China

[3] Drilling and Completion Department of CNOOC Shanghai Branch, Shanghai, 200030, China

[a]18062795909@163.com, [b]ymweihy@petrochina.com.cn, [c]1003031975@qq.com, [d]wz850726@163.com

Keywords: Huoyanshan tectonic belt; wellbore stability; Multiple collaborative; drilling fluid.

Abstract. In order to solve the downhole complex issues such as lost circulation, sticking and well collapse during drilling due to the development of coal-bed and coal seam, thick carbonaceous shale, formation is not homogeneous, the inclination is large, well-developed cracks and other reasons, which constraint exploration and development of oilfield in Huoyanshan tectonic belt region. According to the well instability mechanism of this block and the principle of "Materialized blocking, inhibiting surface hydration, effective stress support" multiple collaborative anti-sloughing drilling fluid, we developed a set of new drilling fluid systems suitable for the Huoyanshan tectonic plate through laboratory experiments. Field test application results show that the new drilling fluid system has a strong capability of salt resistance, anti-calcium and anti-poor soil, has excellent ability of anti-collapse, and has better temperature resistance and crack sealing ability. The new drilling fluid meets the needs of drilling under complicated geological conditions completely.

Introduction

Wellbore instability is one of the most important factors that constraints the speed of Exploration and Development of Huoyanshan tectonic in Tuha Basin currently. In the Huoyanshan tectonic zone, coal-bed and coal seam were well-developed, carbonaceous mudstone is thick, borehole walls collapse easily, causing stuck and other complex cases. Piedmont tectonic belt was a large dip angle and homogeneous formation, hard and soft rock formations staggered development. The drilling processes are easy well deflection and form a keyway so that the bit blocked many times. In addition, coal, sand and mudstone staggered distribution, crevices were better development in this region, and low bearing capacity is prone to leakage. These are restricting drilling speed.

It also found that salt-gypsum rocks of Shanshan group which mainly buried in the 800m ~ 2000m. Thickness of about 1000m are prone to "shrink, dissolve, swelling, collapse" [1].Therefore, it is necessary to develop high-quality drilling fluids suitable for the Huoyanshan tectonic belt according to its instability mechanism, so that we can solve the problems occurred in the process of drilling which restrict the development of drilling, improve the mechanical drilling rate, shorten the construction cycle.

Treating agent optimization

Inhibitors optimization. Cuttings were used in the experiment taken from Qigu group of WenXi block. Configuring different concentrations of inhibitors with water conducted 40 mesh aging recovery experiments (120℃, 16h), then calculating the recovery rate of rock. The experimental results are given in table 1. When the concentration of inhibitor ZNP-1 is 0.5%, the aging recovery was 78.8% higher than all the other inhibitors. It indicated that ZNP-1 can better inhibit shale hydration and dispersion, has better ability to prevent collapse.

Fluid Loss Additive Optimization. We select fluid loss additives which are commonly used in drilling design of block such as NaHPAN, HS-2, PSC, SHR, CXB-2, then evaluating the effect of the five kinds of fluid loss additives in the base slurry. The results are shown in figure 1.

Table 1. Inhibitor optimization experimental results

Inhibitor	Concentration[%]				
	0.1	0.2	0.3	0.4	0.5
YFKN	55.5	59.6	67.5	69	70.6
ZNP-1	59.5	67.1	75.8	77.2	78.8
FA-367	57.2	62.2	68.8	70.6	71.4

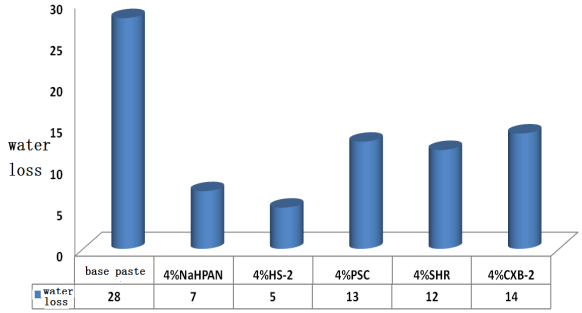

Figure 1. Fluid loss additive optimization

We can see that the filtration of NaHPAN, SHR, HS-2 solution were 7 ml, 12 ml and 5 ml respectively and less than others after added five same concentration treating agent in the base slurry. Therefore, we initially preferred the three kinds of fluid loss additive.

Lubricant Optimization. We select four kinds of lubricant which are commonly used in drilling design such as crude oil, JXFQ-2, MEG, polymeric alcohol and evaluated its lubricity by measuring the rheological properties parameters before and after hot aging of drilling fluid. The results are presented in table 2. By contrast, we can find that the emulsified crude oil has better lubricating effect, can significantly reduce the coefficient of friction of drilling fluid. Therefore, we optimized the crude oil as lubricant preliminary.

Table 2. Different lubricants impact on drilling fluid performance

Formula	Condition	AV[mPa•s]	PV[mPa•s]	YP[Pa]	Lubrication coefficient	FL[mL]
4% Crude oil	Before hot aging	7.25	4.5	2.81	0.0217	15.2
	After hot aging	8.25	5.5	2.81	0.0239	16.2
2%JXFQ-2	Before hot aging	7.25	4.5	2.81	0.2699	20.4
	After hot aging	11	7	4.09	0.1946	28
2%MEG	Before hot aging	7.5	5	2.56	0.2368	17.6
	After hot aging	10	6	4.09	0.2126	24
2% Polymeric alcohol	Before hot aging	8	4	4.09	0.0609	17.2
	After hot aging	11	5	6.13	0.0653	22

Drilling fluid formula determined. According to the Block's well-bore instability mechanism and the new principles of "Materialized blocking, inhibiting surface hydration, effective stress support" multiple collaborative anti-sloughing drilling fluid, we developed a new drilling fluid system according to the best ratio of the reagent concentration. The formula is as follows: 4% bentonite slurry + 0.15% ZNP-1 + 0.4% NaHPAN +3% SHR +3% HS-2 +4% emulsified crude oil + 3% DBFT-201 +0.5% DF-1 (marked for TH formula).

We tested the rheological properties of TH drilling fluid by contrast the experimental data (Table 3) before and after hot aging (120℃ ,16h). The rheological and filtration of TH formula were relatively stable before and after aging. The filtration of high temperature and high pressure compared low was 7.5mL. So TH is a better drilling fluid formulation.

Table 3. Rheological experimental results of TH formula

Formula	Condition	AV [mPa•s]	PV [mPa•s]	YP [Pa]	Gel [Pa·Pa-1]	Lubrication coefficient	FL [mL]	HTHP [mL]
TH	Before hot aging	44	38	6.13	1.53/14.31	/	1.8	/
	After hot aging	41.5	36	5.62	0.77/2.56	0.1282	1	7.5

TH formula evaluation

Anti-pollution Evaluation. Drill cuttings are the main solid phase pollutants in drilling fluid and always present in the drilling process. Therefore, it is required that the drilling fluid should have a certain capacity of anti-contaminated to prevent the performance of the drilling fluid from occurring fluctuations [2].

Table 4. Anti-pollution experimental results of TH formula

Formula	Condition	AV [mPa.s]	PV [mPa.s]	YP [Pa]	Gel [Pa*Pa-1]	FL [mL]	HTHP [mL]	Lubrication coefficient
TH	Before hot aging	51	39	12.26	2.04/12.78	1.2	/	0.1315
	After hot aging	59	47	12.26	1.53/9.71	1.7	7.5	
TH+10 %NaCl	Before hot aging	65.5	22	44.46	25.04/41.9	1.4	/	0.1329
	After hot aging	31	30	1.02	0.51/9.2	1.7	18	
TH+8% poor soil	Before hot aging	51	40	11.24	2.56/14.31	3.2	/	0.1375
	After hot aging	68.5	56	12.78	2.04/10.73	3.6	7.2	
TH+0.5 %CaCl2	Before hot aging	44	38	6.13	1.53/14.31	1.8	/	0.1282
	After hot aging	41.5	36	5.62	0.77/2.56	1	13	

Adding 10% NaCl, 8% poor soil and 0.5% CaCl2 in TH formulation respectively, contrast the experimental data (Table 4) of hot aging experiment (120℃, 16h) found that the viscosity, shear force and filtration of contaminated drilling fluid before and after aging did not occur mutations, indicating that it has a strong anti-salt, anti-calcium, anti-poor soil capacity.

Anti-collapse Evaluation. In strict accordance with the steps of inhibitor optimization experiments conducted 40 meshes aging recovery experiments (120℃, 16h) to compare the shale recovery in water, polysulfonate pulp of Yubei2 well and TH formula. Experimental results show that the shale recovery of TH formula was 82.47%, polysulfonate pulp of Yubei2 well was 68.73%, and water was 37.27%. Obviously, the new formula TH drilling fluid can effectively inhibit shale hydration, prevent debris scattered damage of drilling fluid rheology and filtration wall building, it has excellent anti-collapse performance.

Inhibition of clay hydration expansion ability evaluation. According to the method of literature [3] conducted the experiment of inhibiting expansion, and calculated linear expansion percentage of the rock sample in different drilling fluid. We find TH formula expansion rate was the minimum. Inflation rate in 8 h was only 2.08%, with excellent capability of inhibiting clay hydration expansion.

Anti-temperature capability Evaluation. Oil layer of Huoyanshan tectonic zone buried deep. The well bottom's temperature reached above 130℃. It was required the drilling fluid still has excellent rheological properties after high temperature aging. Therefore, it was necessary to evaluate the anti-temperature performance on TH drilling fluid [4]. We put the TH drilling fluid system in 120 ℃, 130 ℃ and 150 ℃ containers respectively with high temperature hot aging 16h to evaluate the stability of TH formula. The results are shown in table 5. By contrast, we found that the rheological and

filtration properties of the system before and after aging have not mutated, the viscosity decreased little by aging. TH formula has a better ability to resist temperature, to be able to meet the needs of the deep well drilling for Huoyanshan block.

Sealing performance evaluation. We Put TH drilling fluid system in the same leakage bed (400μm crack) and different pressure to determine its loss after 3 min. We found TH formula's bearing capacity reached 4 Mpa (leakage was only 1.6mL), has good ability for crack sealing.

Table 5 Anti-temperature capability experimental results

Formula	Condition	AV [mPa.s]	PV [mPa.s]	YP [Pa]	Gel [Pa*Pa-1]	FL [mL]	Lubrication coefficient
TH	Before hot aging	60	45	15.33	2.56/15.33	2.8	0.1321
	120℃hot aging	49	38	11.24	1.02/8.18	2.8	
	130℃hot aging	38.5	31	7.67	0.51/15.33	2.2	
	150℃hot aging	33.5	28	5.62	1.02/5.62	2.6	

Field Application

YuBei block of tuha oilfield occurred sticking twice, blocked one time, lost three times, gas cut one time in the process of drilling according to the drilling statistics. The block is a typical Huoyanshan tectonic, and the reasons of complex accidents are conforming to the foreword's analysis.

In 2013, we applied the TH drilling fluid system to 8 Wells in this block, including four preliminary exploratory well (depth were more than 4000 m), two production Wells (depth were 4070 m and 3982 m), a development well (depth was 3878.98 m) and a injection Wells (depth was 4194 m). The total processing time for lost circulation and sticking was 65.33 h, for the well logging instrument sticking was 151.5 h. There was not blocked, gas cut and other complicated conditions. The average drilling cycle was 47.57 days, and shortened by 26.38% than the early stage. The loss rate of complex accidents was reduced from 27.3% to 2.12%. These all indicate that the newly developed TH drilling fluid system can meet the demands of exploration and development of Huoyanshan structure.

Conclusions

(1) The main complex accidents in Huoyanshan structure were sticking, blocked and leakage. According to the block's wellbore instability mechanism and the new principles of "Materialized blocking, inhibiting surface hydration, effective stress support" multiple collaborative anti-sloughing drilling fluid, we optimized the new type of TH drilling fluid formulation by laboratory experiments.

(2) The results of experiments and the application show that TH formula has a strong anti-salt, anti-calcium, anti-poor soil capacity, excellent anti-collapse, inhibiting clay hydration expansion, resist temperature and fracture plugging performance. It can greatly reduce the failure rate, increase the rate of penetration, shorten the construction cycle, shorten the time of drilling fluid immersion hydrocarbon reservoir, and decrease the damage to the hydrocarbon reservoir. TH drilling fluid completely meets the needs of drilling under the complex geological conditions.

References

[1] Yang Hai, Ma Wenying, Wang Shanju etc. Application of Manifold Inhibitive Drilling Fluid Technology in Well TK1108 [J]. Drilling Fluid & Completion Fluid, 2007,03:82-83+86+96.

[2] Lü Kaihe, Qiu Zhengsong, Xu Jiafang. Polyether polyatomic alcohol drilling fluid and its application[J]. Acta Petrolei Sinica, 2006,01:101-105.

[3] Wang Changjun, Xu Mingbiao, Miao Hailong. Experimental Study on Polyamine High Inhibitive (UHIB) Drilling Fluid[J]. Journal of Oil and Gas Technology, 2009,01:80-83+392.

[4] Xie Hailong. Research and Application of KCL Polyamine Multivariate Inhibition of Anti-collapse Drilling Fluid [J]. Technology Supervision IN Petroleum Industry, 2013, 06:57-60.

[5] Lü Kaihe, Zhu Daozhi, Xu Xianguo etc. Research and Application of Synergistic Drilling Fluid System[J]. Drilling Fluid & Completion Fluid, 2012,02:1-4+89.

Advanced Materials Research Vols. 989-994 (2014) pp 1380-1383
© (2014) Trans Tech Publications, Switzerland
doi:10.4028/www.scientific.net/AMR.989-994.1380

Vertical zonation in penecontemporaneous period of the bauxite in WZD area

Tao Cui

College of Resources and Environmental Engineering, Guizhou Institute of Technology, Guiyang, 550003, China

cuitao1203@163.com

Key words: WZD area; Bauxite; Vertical zonation

Abstract: Through systematically geologic survey and observation of drills, this paper have a comprehensive research on Vertical zonation in bauxite deposit of Wuchuan-Zheng'an-Daozhen (WZD) area. Environment of WZD bauxite in penecontemporaneous period can be divided into two parts: vadose zone and phreatic zone. Vadose zone is oxidized and acidic environment. Phreatic zone is reduced and alkalescent environment. Vadose zone is favorable to mineralization, but phreatic zone is not favorable to mineralization.

Introduction

There is abundant bauxite in WZD area. For a long time many experts and scholars have researched on rocks and minerals, chemistry, sedimentary environment, provenance, mineralization age, and mass balance calculation of the bauxite [1-15]. Though there are abundant outcomes of WZD bauxite, analysis on vertical zonation of the bauxite is poor. This study is to establish vertical zonation model of WZD bauxite through the research on Vertical alternation, which accelerates the research on mineralizaton process of high grade bauxite.

Geological setting

WZD bauxite is located in Wuchuan, Zheng'an and Daozhen County, northern Guizhou, which is an important part of centre Guizhou-southern Chongqing bauxite belt [7]. The regional tectonics position of the study area is in the fold belt in northern Guizhou of the upper Yangtze Block [8]. From the oldest to the youngest, the main strata in WZD area includes Cambrian, Ordovician, Silurian, Permian, Triassic and Jurassic. Cambrian is mainly distributed in the core of anticlines, Triassic and Jurassic are mainly distributed in the core of synclines. Bauxite underlies the LiangShan formation(P2l) or Qixia formation(P2q) in the middle Permian, and overlies the HuangLong formation(C2h) of upper Carboniferous or the Hanjiadian formation of the lower Silurian(S1hj). The bauxite is stratiform and unconformable with the underlying and overlying strata. Fig.1 shows that the distribution of the bauxite is controlled by nine synclines. Thickness of the bauxite is 0.68-15.7m, and its profile can be divided into two lithology parts: the upper part and the lower part. The former is aluminous rock, dominated by high grade bauxite or half grade bauxite; the latter is low grade bauxite. According to the lithological and textural properties, the natural types of bauxite deposit can roughly be subdivided into four categories: massive bauxite, oolithic bauxite, clastic bauxite and earthy bauxite.

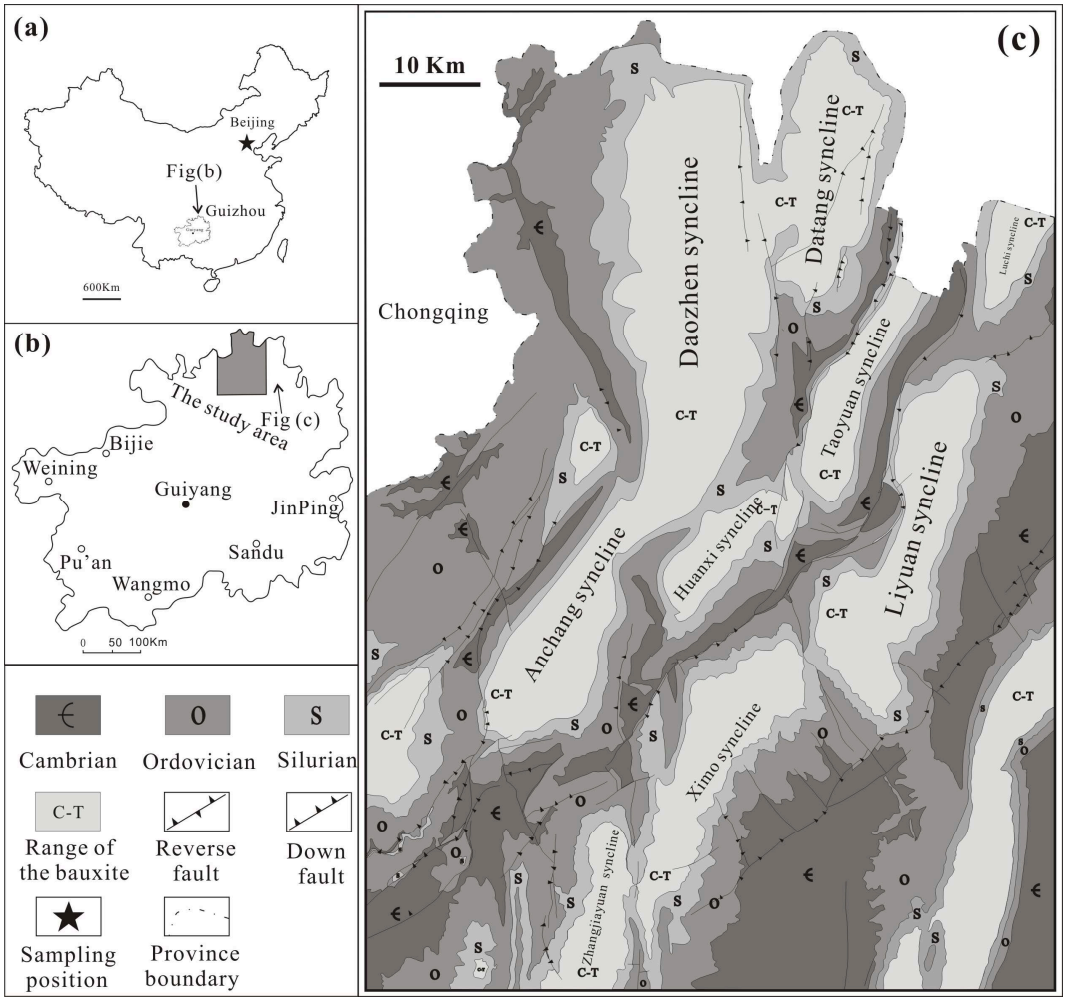

Fig. 1(a)Locality map of Guizhou,(b)The map showing the location of the study area, (c)Geology map of the WZD area in northern Guizhou

Vertical zonation

Vertical diversity of metallogenetic environment resulting in vertical regular alteration such as color, structure and composition of the WZD bauxite. Leaching process causes vertical differentiation of chemical nature in profile. Actually Leaching process is a transport process of groundwater, so we can divide vertical environment of the WED bauxite based on the zonation of groundwater. Environment can be divided into vadose zone and phreatic zone. Vadose zone is the area that pore space water take reaction with deposition, under groundwater is phreatic zone. We can distinguish Vadose zone and phreatic zone roughly based on color (Fig.2). Fig.2 shows that bauxite is light grey to red in Vadose zone, but bauxite is dark grey to green in phreatic zone. Position of Vadose zone and phreatic zone are variable as the shifted of phreatic surface. Between vadose zone and phreatic zone chemical nature have assembled characteristics of vadose zone and phreatic zone, so bauxite from different drills in this transition zone would present different feature. Bauxite in vadose zone is high grade and contains abundant diaspore and ooliths. Ores in vadose zone is loose and porous, and there are some red substrate in bauxite. Bauxite in phreatic zone have a deep color relative to the bauxite in vadose zone, and it just contain small oxydic substrate. Bauxite in phreatic zone is usually low grade with a high content of Fe and a low content of Al. Surface of bauxite in phreatic zone is usually smooth, and contain spherical grain or epidermal oolitics. Pyrite is common in vadose zone and phreatic zone.

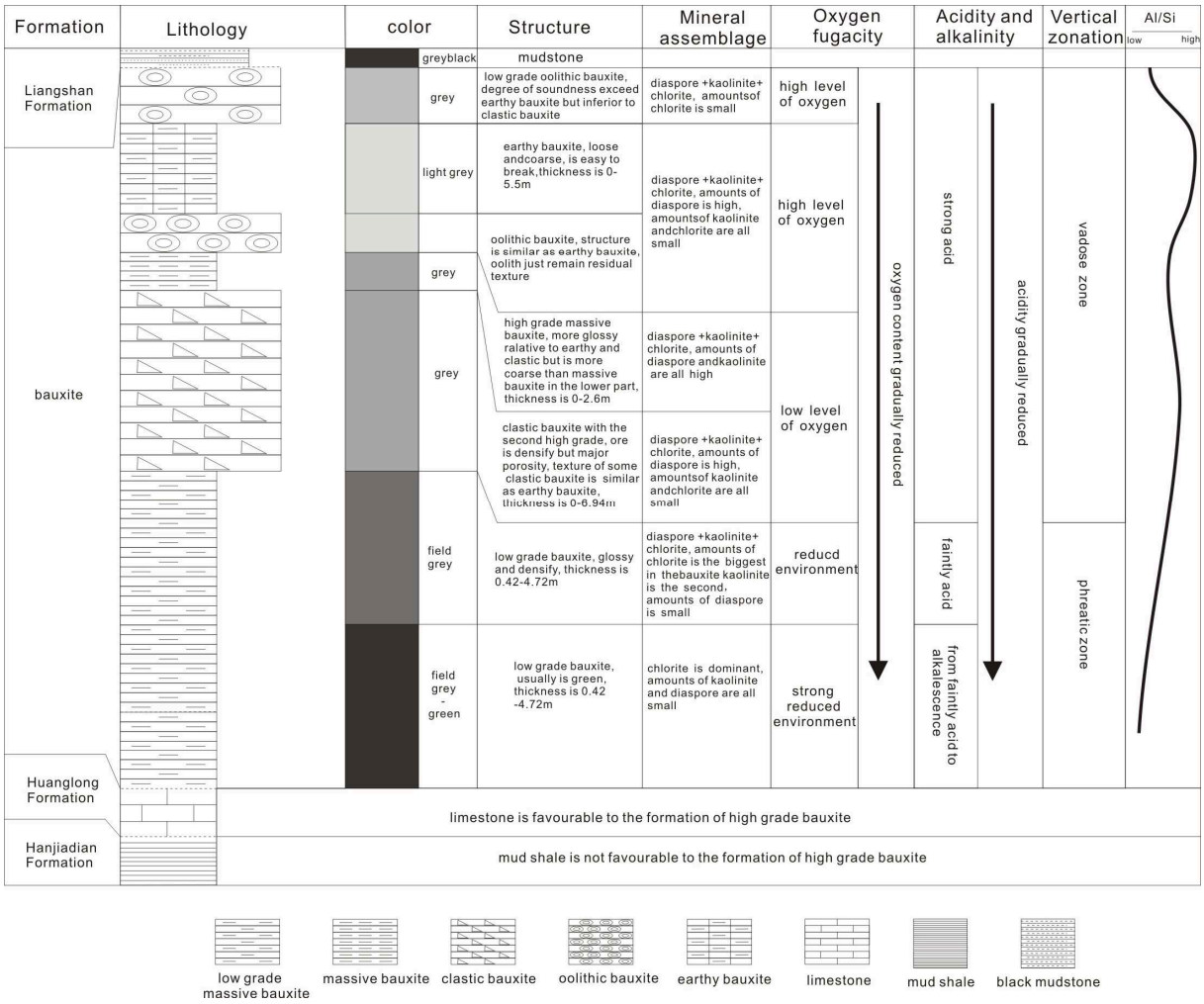

Fig.2 Vertical zonation of environment in penecontemporaneous period on WZD bauxite

Conclusions

The main conclusions from this study are summarized as follows: 1) in penecontemporaneous period environment can be divided into two parts: vadose zone and phreatic zone. Vadose zone is oxidation and acidic environment; phreatic zone is reduced and alkalescent environment. 2）Vadose zone is favorable to mineralization, but Phreatic zone is not favorable to mineralization. 3) The lower the phreatic surface is, the more conducive to mineralization.

Acknowledgment

This work was supported by Guizhou Collaborative Innovation Center of Strategic Minerals Resource Development, Guizhou Institute of Technology and the project of analysis on geochemical behaviors of Platinum group elements in Emeishan basalt (XJGC20131204), Guizhou Institute of Technology.

References

[1] G.H. Wu, Z.G. Jin, Y. Bao: J.Geology and Prospecting,Vol.44(2008),P.34 (in Chinese)

[2] Z.G. Jin, G.H. Wu, Y.Y. Zhao:J.Mineral Source and Geology,Vol.23(2009),P.139 (in Chinese)

[3] K.H. Yin: J. Acta Sedmentological Sinica, Vol.27(2009),P. 455 (in Chinese)

[4] Z.H. Han: J. Mineral Resource and Geology,Vol.22(2008),P. 430 (in Chinese)

[5] Z.Y. Lei and Y.C. Liao: J. Western Prospecting Engineering, Vol.18(2007), P. 96 (in Chinese)

[6] X.M. Wang, Y.Q. Jiao and Y.S, Du: J. Journal of Geochemical Exploration, Vol. 133(2013), P.108.

[7] P. Liu: J. Guizhou Geology,Vol.18(2004),P. 240(in Chinese)

[8] D.Q. Du, J.P. Ren and Y. Wang: J. Acta Mineralogical Sinica, Vol.23(2007), P.475 (in Chinese)

[9] G. Millot, M. Bonifas: J. Alsace Lorraine,Vol.8(1955),P.15.

[10] J.J. Middleburg, C.H. Van, J.R.W. Woittiez: J.Chen.Geol, Vol.68(1988),P.263

[11] H.W. Nesbitt, G.M. Young:J.Geol,Vol.97(1989),P.135.

[12] I.G. Hill, R.H.G. Worden, I.G. Meighan: J.Chemical Geology,Vol.166(2000),P.166.

[13] J.A. Grant: J.Economic Geology,Vol.81(1986),P.1980.

[14] W.H. Maclean: J. Mineralium Deposita,Vol.25(1990),P.46

[15] T. Cui, Y.Q Jiao, Y.S. D:J.The Chinese Journal of Nonferrous Metals,Vol.24(2013),P.6.(in Chinese)

Advanced Materials Research Vols. 989-994 (2014) pp 1384-1387
© (2014) Trans Tech Publications, Switzerland
doi:10.4028/www.scientific.net/AMR.989-994.1384

Preservative features of the fossils in bauxite deposit of WZD area, Northern Guizhou, China

Tao Cui

College of Resources and Environmental Engineering, Guizhou Institute of Technology, Guiyang, 550003, China

cuitao1203@163.com

Keywords: WZD area; Bauxite; fossils

Abstract: It is hardly to discovery fossil from the bauxite in Wuchuan -Zheng' an-Daozhen (WZD) area, northern Guizhou, China. But the new study suggests, containing a small amount of plant debris from massive bauxite in the lower part of the ledge. Preservative features of fossils in WZD bauxite indicates: metallogenetic materials experienced a transport process; sedimentary environment is reduced; fossils only preserved in the massive bauxite, that fossils in other types of ores were destroyed in the late oxidation modification. Metallogenic environment of bauxite has experienced two kinds of state- reduction and oxidation. The lack of animal fossils; bauxite, reveal that the metallogenic environment is acidic, resulting in animal fossils are dissolved and hard to save.

Introduction

There is abundant bauxite in the WZD area. For a long time many experts and scholars have research on the bauxite of rocks and minerals, chemistry, sedimentary environment, provenance, mineralization age [1-6]. As bauxite in other areas WZD bauxite just has small fossils, but these small fossils would supply important metallogenetic information for research. There are small amount of phytolite in the WZD bauxite, this paper has an analysis on the preservative features of these fossils to research metallogenetic environment and metallogenetic process of the WZD bauxite.

Geological setting

WZD bauxite is located in Wuchuan, Zheng'an and Daozhen County, northern Guizhou, which is an important part of centre Guizhou-southern Chongqing bauxite belt [7]. The regional tectonics position of the study area is in the fold belt in northern Guizhou of the upper Yangtze Block[8]. The main strata in WZD area from the oldest to the youngest including: Cambrian, Ordovician, Silurian, Permian, Triassic and Jurassic. Cambrian is mainly distributed in the core of anticlines, Triassic and Jurassic are mainly distributed in the core of synclines. Bauxite is underlying the LiangShan formation(P2l) or Qixia formation(P2q) of the middle Permian, overlying the HuangLong formation(C2h) of upper Carboniferous or the Hanjiadian formation of the lower Silurian(S1hj).The bauxite is stratiform and unconformable with the underlying and overlying strata. Fig.1 shows that the distribution of the bauxite was controlled by nine synclines. The thickness of the bauxite is 0.68-15.7m, the profile can be divided into two lithology parts: the upper part is aluminous rock, dominated by high grade bauxite or half grade bauxite; the lower part is low grade bauxite. According to the lithological and textural properties, the natural types of bauxite deposit can roughly be subdivided into four categories: massive bauxite, oolithic bauxite, clastic bauxite and earthy bauxite.

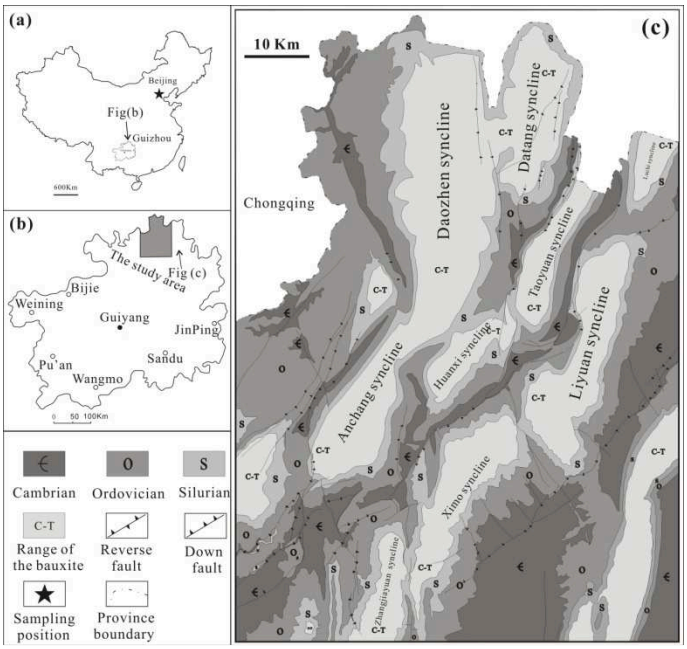

Fig. 1(a)Locality map of Guizhou,(b)The map showing the location of the study area, (c)Geology map of the WZD area in northern Guizhou

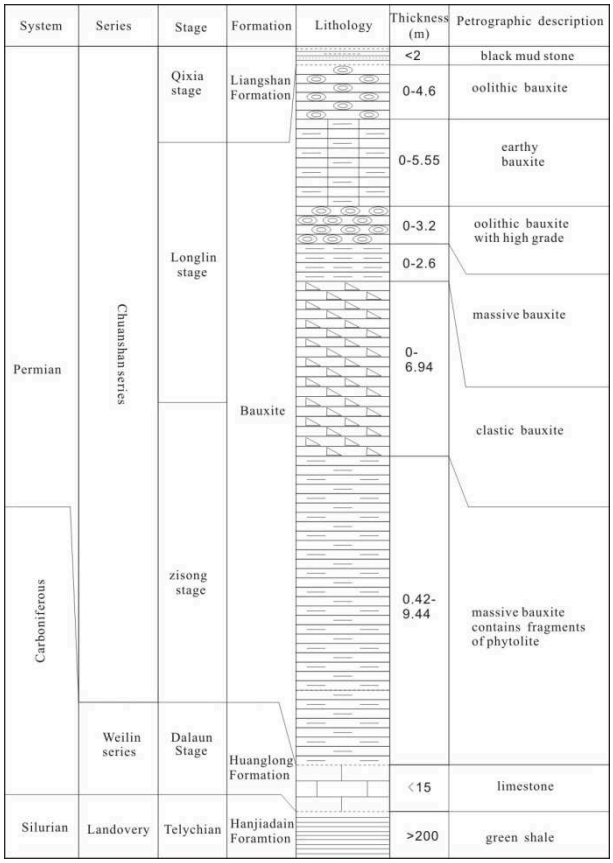

Fig.2 Column shows the location of fossils [8]

Preservative features of the fossils

Fig.2 shows that plant fragment of fossils just preserved in the massive bauxite in the lower part of the producing formation, there are no fossils preserved in other types of bauxite. Plant fossils are elongate or scaly, length of fossils can over 3cm (Fig.3,e,f). Plant fossils are commonly fragmented indicates that the formation of these fossils experienced a transported deposit process.

Though WZD bauxite just has small fossils, these small fossils would supply important metallogenetic information for research. Forming process of fossils need reduced environment, WZD bauxite is grey and contain some plant fragment fossils shows that sedimentary environment is reduced. There are no plant fragment fossils preserved in four types bauxite except massive bauxite, obviously fossils cannot selectively preserve. In the period of original deposition four kinds of bauxite in the WZD area contain plant fragment but plant fragment was destroyed by later metallization. Comparison of the massive bauxite and other three types of bauxite, there are obvious difference in these bauxite (Fig.3). Fig.3 shows that Massive bauxite is grey – green which is the strongest reduced color in four type bauxite. Massive bauxite is more dense and smooth than other kinds of bauxite. In the forming process of oolithic, earthy and clastic bauxite have experience a severe transform that resulting in fossils be destroyed. Metallogenic environment is not constant but altered in reduction and oxidation. There are no zoolite in the bauxite, it demonstrates that Metallogenic environment is acidic so animal remains with calcareous skeleton cannot be preserved but coaly plant remains can be preserved.

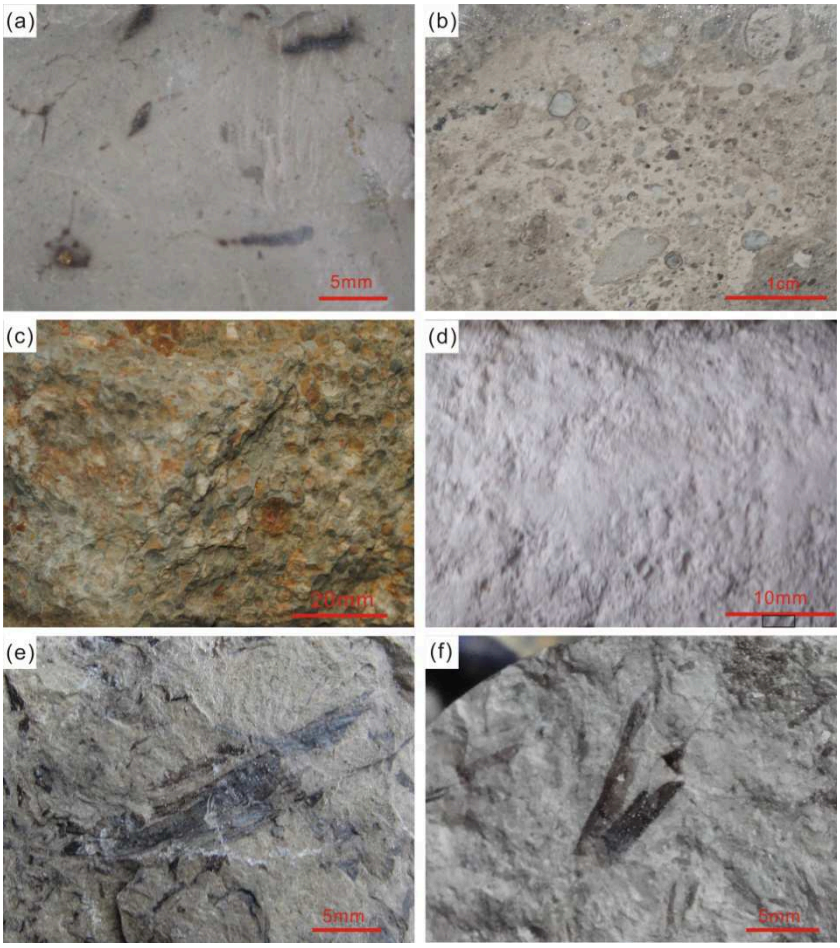

Fig.3 Fossils in the WZD bauxite: a. massive bauxite without fossil; b. clastic bauxite without fossil; c. oolithic bauxite without fossil; d. earthy bauxite without fossil; e and f. massive bauxite contain fossils

Conclusion

The main conclusions from this study are summarized as follows:1)There are some small fragments of plant fossils in the lower part of producing formation; 2) In the period of Metallogenic process metallogenic environment is not constant but altered in reduction and oxidation; 3) Metallogenic environment is acidic cause only plant remains can be preserved as fossils.

Acknowledgment

This work was supported by the Guizhou Collaborative Innovation Center of Strategic Minerals Resource Development, Guizhou Institute of Technology, Guiyang, 550003, China and the project of analysis on geochemical behaviors of Platinum group elements in Emeishan basalt (XJGC20131204), Guizhou Institute of Technology.

References

[1] G.H. Wu, Z.G. Jin, Y. Bao: J.Geology and Prospecting,Vol.44(2008),P.34 (in Chinese)

[2] Z.G. Jin, G.H. Wu, Y.Y. Zhao:J.Mineral Source and Geology,Vol.23(2009),P.139 (in Chinese)

[3] K.H. Yin: J. Acta Sedmentological Sinica, Vol.27(2009),P. 455 (in Chinese)

[4] Z.H. Han: J. Mineral Resource and Geology,Vol.22(2008),P. 430 (in Chinese)

[5] Z.Y. Lei and Y.C. Liao: J. Western Prospecting Engineering, Vol.18(2007), P. 96 (in Chinese)

[6] X.M. Wang, Y.Q. Jiao and Y.S, Du: J. Journal of Geochemical Exploration, Vol. 133(2013), P.108.

[7] P. Liu: J. Guizhou Geology, Vol. 18(2004), P. 240(in Chinese).

[8] T. Cui, Y.Q. Jiao, Y.S. Du: J. Journal of palaeogeography, Vol.16(1),P.9(in Chinese).

Advanced Materials Research Vols. 989-994 (2014) pp 1388-1391
© (2014) Trans Tech Publications, Switzerland
doi:10.4028/www.scientific.net/AMR.989-994.1388

Characteristics of interlayers in bauxite deposit of WZD area, Northern Guizhou, China

Tao Cui

College of Resources and Environmental Engineering, Guizhou Institute of Technology, Guiyang, 550003, China

cuitao1203@163.com

Keywords: WZD area; Bauxite; interlayer.

Abstract: Through systematically geologic survey and observation of hand specimen this paper have a comprehensive research on the characteristics of interlayers in bauxite deposit of Wuchuan-Zheng'an-Daozhen (WZD) area. There are two kinds of interlayers in WZD bauxite: black coaly interlayer and brown hematitic interlayer. Black coaly interlayer indicate reduce and inshore environment, brown hematitic interlayer represent oxidized and strong hydrodynamic environment. The appearance of interlayer with contrary feature indicate sedimentary environment of the WZD bauxite is very complex.

Introduction

There is abundant bauxite in WZD area. For a long time many experts and scholars have research on the bauxite of rocks and minerals, chemistry, sedimentary environment, provenance, mineralization age, mass balance calculation [1-15].Though there are abundant outcome of WZD bauxite, analysis on microfacies of the bauxite is poor, this study through the research on interlayers to inquiry microfacies of WZD bauxite, this work would accelerate the research on regularity of ore formation.

Geological setting

WZD bauxite is located in Wuchuan, Zheng'an and Daozhen County, northern Guizhou, which is an important part of centre Guizhou-southern Chongqing bauxite belt [7]. The regional tectonics position of the study area is in the fold belt in northern Guizhou of the upper Yangtze Block [8]. The main strata in WZD area from the oldest to the youngest including: Cambrian, Ordovician, Silurian, Permian, Triassic and Jurassic. Cambrian is mainly distributed in the core of anticlines, Triassic and Jurassic are mainly distributed in the core of synclines. Bauxite is underlying the LiangShan formation(P2l) or Qixia formation(P2q) of the middle Permian, overlying the HuangLong formation(C2h) of upper Carboniferous or the Hanjiadian formation of the lower Silurian(S1hj).The bauxite is stratiform and unconformable with the underlying and overlying strata. Fig.1 shows that the distribution of the bauxite was controlled by nine synclines. The thickness of the bauxite is 0.68-15.7m, the profile can be divided into two lithology parts: the upper part is aluminous rock, dominated by high grade bauxite or half grade bauxite; the lower part is low grade bauxite. According to the lithological and textural properties, the natural types of bauxite deposit can roughly be subdivided into four categories: massive bauxite, oolithic bauxite, clastic bauxite and earthy bauxite.

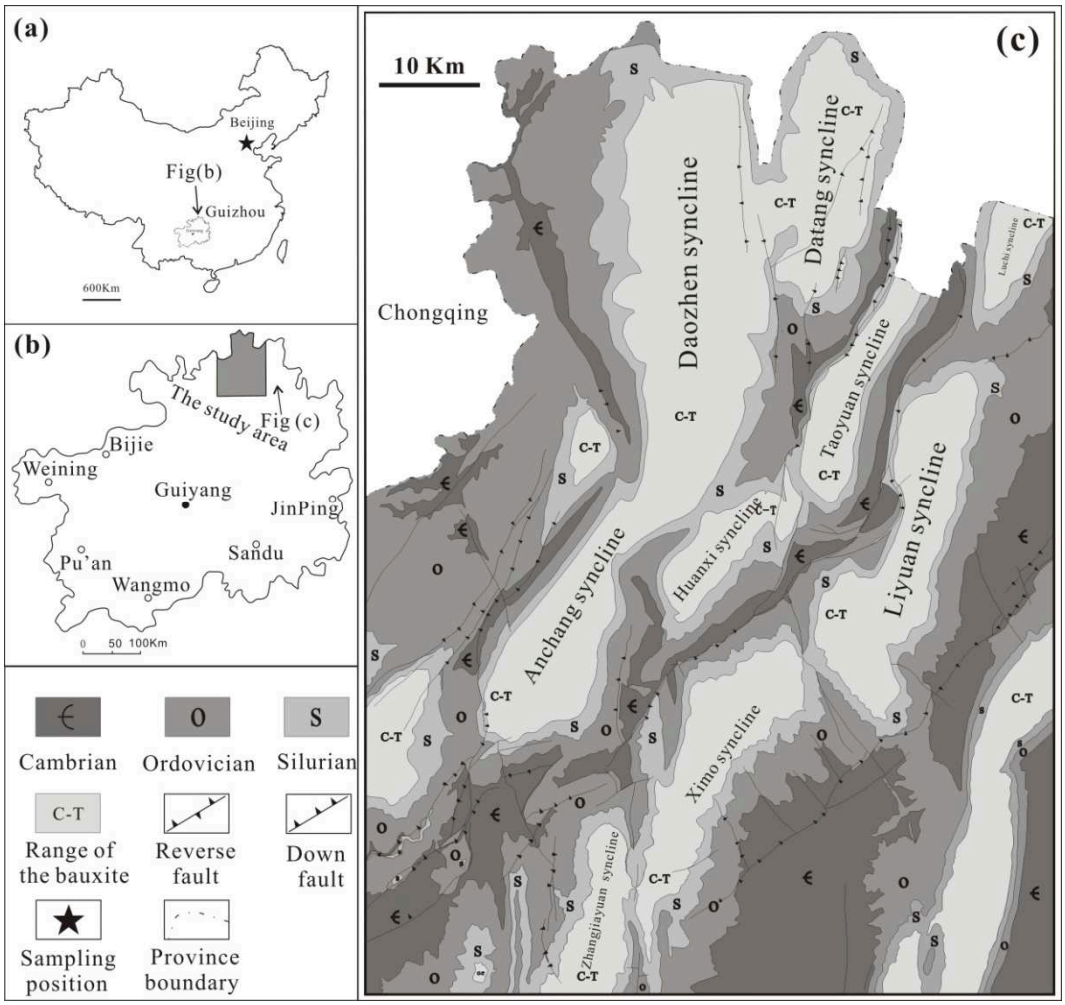

Fig. 1(a)Locality map of Guizhou,(b)The map showing the location of the study area, (c)Geology map of the WZD area in northern Guizhou

Characteristics of interlayers

Producing formation can be divided two parts: the lower part is massive bauxite, the upper part is earthy, oolothic, clastic and massive bauxite. Fig.2 shows that producing formation is grey, some drills contains black coaly interlayers and pricking dirt. Pricking dirt is thin but black coaly interlayers are thick, the thickness of the pricking dirt is 15cm (Fig.2,a,b), the thickness of the black coaly interlayers is from0.15to2m, black coaly interlayers are jetty (Fig.2,c,d,e,f). Brown hematitic interlayer has been discovered in Zhangjiayua syncline(Fig.2,g,h), southern of the study area(Fig.1).The thickness of the hematitic interlayer is 3.5m. Black coaly interlayers is frequent in WZD area and it usually appears in the upper of the producing formation. Brown hematitic interlayer is rare in the study area. Black coaly interlayers and brown hematitic interlayer indicate adverse sedimentary environment, they appear at the study area show that sedimentary environment of WZD bauxite is very complex. Sedimentary environment of WZD bauxite is reduced but part of the study area is oxidized. Sedimentary environment has changed into swamp resulting in black coaly interlayers frequent appear in the study area. Brown hematitic interlayer instants inshore and high energy environment, it shows that bauxite deposit would formed in transition facies.

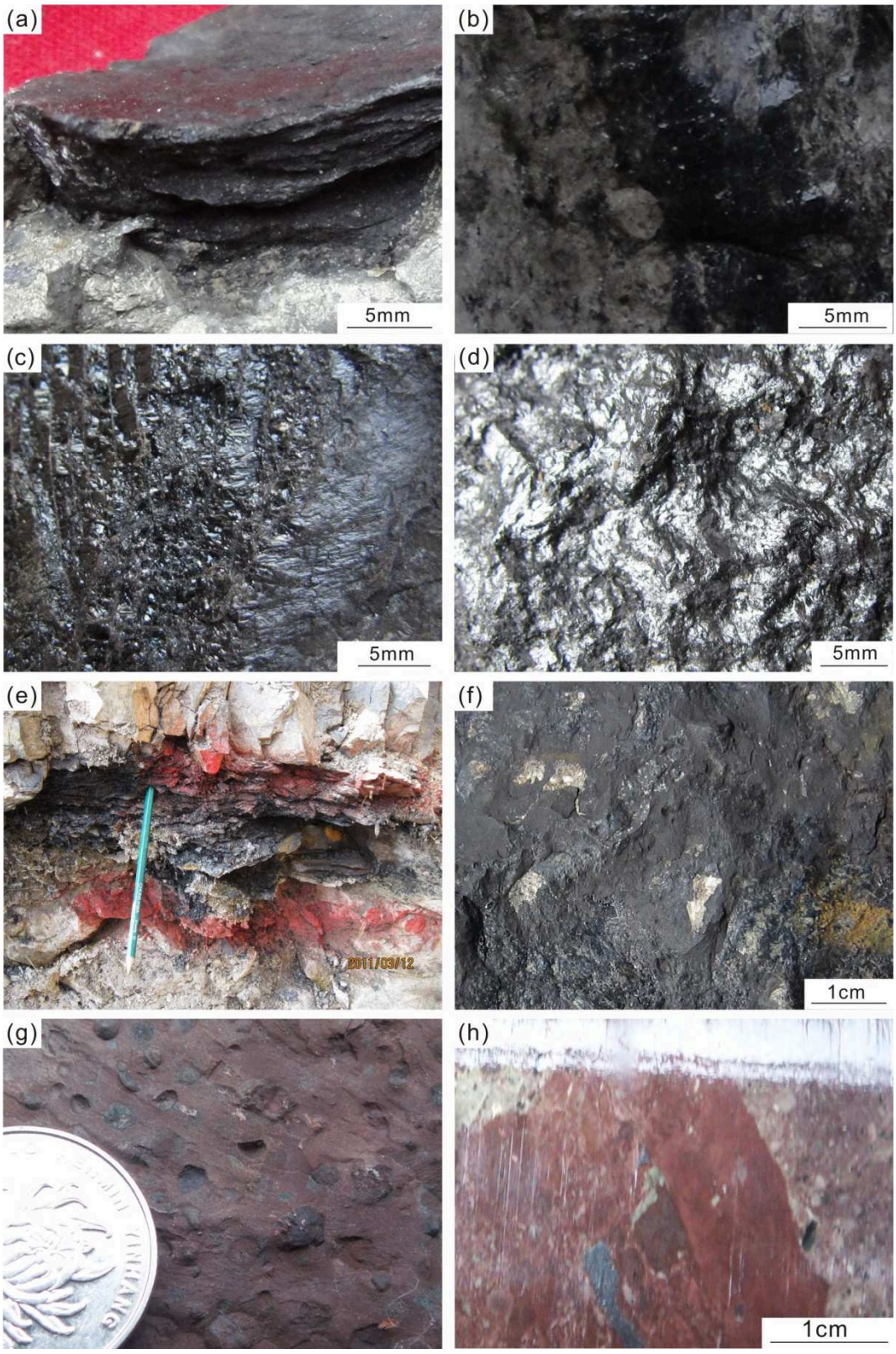

Fig.2 Black coaly interlayer and brown hematitic interlayer in WZD bauxite;a, pricking dirt;b. pricking dirt; c. black coaly interlayer; d.black coaly interlayer;e. black coaly interlayer;f. black coaly interlayer; g.brown hematitic interlayer; h.brown hematitic interlayer

Conclusion

The main conclusions from this study are summarized as follows: 1) Black coaly interlayer indicates sedimentary environment of WZD bauxite is reduced, WZD bauxite was formed in a inshore environment. 2) Black coaly interlayer is thin and discontinuous shows that sedimentary

environment has transformed into swamp but did not occur large and long time expose. 3)Oolithic hematite and brown interlayer shows that part of sedimentary environment is oxidize and energetic.

Acknowledgment

This work was supported by the Guizhou Collaborative Innovation Center of Strategic Minerals Resource Development, Guizhou Institute of Technology, Guiyang, 550003, China and the project of analysis on geochemical behaviors of Platinum group elements in Emeishan basalt (XJGC20131204), Guizhou Institute of Technology.

References

[1] G.H. Wu, Z.G. Jin, Y. Bao: J.Geology and Prospecting,Vol.44(2008),P.34 (in Chinese)

[2] Z.G. Jin, G.H. Wu, Y.Y. Zhao:J.Mineral Source and Geology,Vol.23(2009),P.139 (in Chinese)

[3] K.H. Yin: J. Acta Sedmentological Sinica, Vol.27(2009),P. 455 (in Chinese)

[4] Z.H. Han: J. Mineral Resource and Geology,Vol.22(2008),P. 430 (in Chinese)

[5] Z.Y. Lei and Y.C. Liao: J. Western Prospecting Engineering, Vol.18(2007), P. 96 (in Chinese)

[6] X.M. Wang, Y.Q. Jiao and Y.S, Du: J. Journal of Geochemical Exploration, Vol. 133(2013), P.108.

[7] P. Liu: J. Guizhou Geology,Vol.18(2004),P. 240(in Chinese)

[8] D.Q. Du, J.P. Ren and Y. Wang: J. Acta Mineralogical Sinica, Vol.23(2007), P.475 (in Chinese)

[9] G. Millot, M. Bonifas: J. Alsace Lorraine,Vol.8(1955),P.15.

[10] J.J. Middleburg, C.H. Van, J.R.W. Woittiez: J.Chen.Geol, Vol.68(1988),P.263

[11] H.W. Nesbitt, G.M. Young:J.Geol,Vol.97(1989),P.135.

[12] I.G. Hill, R.H.G. Worden, I.G. Meighan: J.Chemical Geology,Vol.166(2000),P.166.

[13] J.A. Grant: J.Economic Geology,Vol.81(1986),P.1980.

[14] W.H. Maclean: J. Mineralium Deposita,Vol.25(1990),P.46

[15] T. Cui, Y.Q Jiao, Y.S. D:J.The Chinese Journal of Nonferrous Metals,Vol.24(2013),P.6.(in Chinese)

Advanced Materials Research Vols. 989-994 (2014) pp 1392-1395
© (2014) Trans Tech Publications, Switzerland
doi:10.4028/www.scientific.net/AMR.989-994.1392

Research progress of bauxite in WZD area, northern Guizhou, China

Tao Cui

College of Resources and Environmental Engineering, Guizhou Institute of Technology, Guiyang, 550003, China

cuitao1203@163.com

Keywords: WZD area; Bauxite; Progress

Abstract: This paper has a comprehensive analysis on the bauxite in Wuchuan -Zheng, an-Daozhen (WZD) area, northern Guizhou, China through synthesize former research. The understanding of mineralogic, petrologic and geochemical characteristics is deep, and sedimentary environment, parent rock and mineralization process have been defined. Main questions need further research as follow: minerogenetic epoch; migration mechanism of elements; genesis of rare earth mineral.

Introduction

There is abundant bauxite in WZD area. For a long time many experts and scholars have research on te bauxite of rocks and minerals, chemistry, sedimentary environment, provenance, mineralization age [1-11]. This work synthesize data of former researcher to have a comprehensive understanding on the progress of WZD bauxite.

Geological setting

WZD bauxite is located in Wuchuan, Zheng'an and Daozhen County, northern Guizhou, which is an important part of centre Guizhou-southern Chongqing bauxite belt [7]. The regional tectonics position of the study area is in the fold belt in northern Guizhou of the upper Yangtze Block[8]. The main strata in WZD area from the oldest to the youngest including: Cambrian, Ordovician, Silurian, Permian, Triassic and Jurassic. Cambrian is mainly distributed in the core of anticlines, Triassic and Jurassic are mainly distributed in the core of synclines. Bauxite is underlying the LiangShan formation(P2l) or Qixia formation(P2q) of the middle Permian, overlying the HuangLong formation(C2h) of upper Carboniferous or the Hanjiadian formation of the lower Silurian(S1hj).The bauxite is stratiform and unconformable with the underlying and overlying strata. Fig.1 shows that the distribution of the bauxite was controlled by nine synclines. The thickness of the bauxite is 0.68-15.7m, the profile can be divided into two lithology parts: the upper part is aluminous rock, dominated by high grade bauxite or half grade bauxite; the lower part is low grade bauxite. According to the lithological and textural properties, the natural types of bauxite deposit can roughly be subdivided into four categories: massive bauxite, oolithic bauxite, clastic bauxite and earthy bauxite.

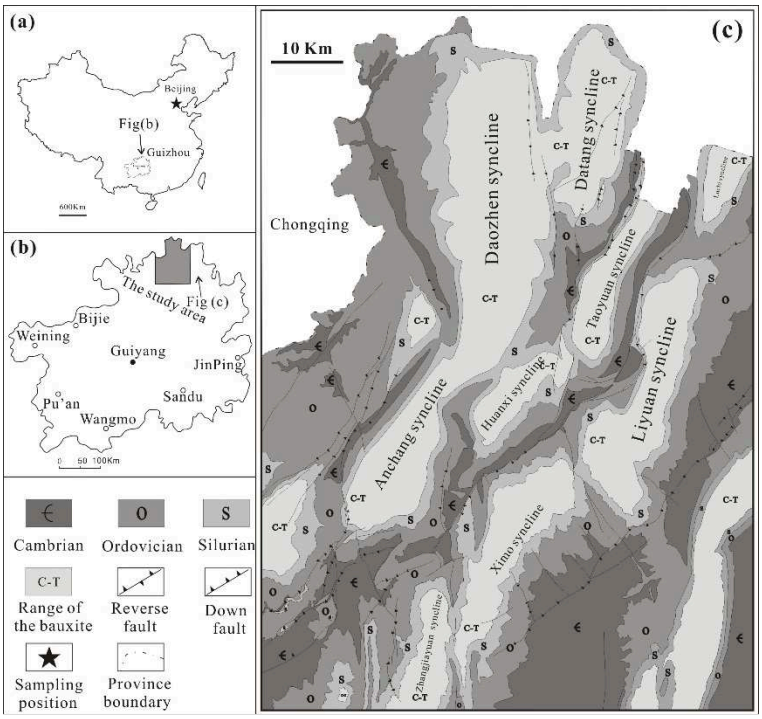

Fig. 1(a)Locality map of Guizhou,(b)The map showing the location of the study area, (c)Geology map of the WZD area in northern Guizhou

Mineralogy and petrology

The Length of mineralogical crystal of WZD bauxite is no more than 5μm. Bauxite is mainly composed of diaspora and clay minerals like kaolinite, chlorite and illite, and contains a bit of heavy minerals, such as anatase, zircon and rutile, and minute quantity of quartz, feldspar and pyrite[1,2,5,6,7,8,9]. Striped and elliptic spherical parasites (Ce2Ca(CO3)3F2) have been recognized in ZK14904, ZK3402 and ZK9A04. Binary structure of bauxite is clear, generally, diaspore takes the content of 40%-95% in the middle- upper part, the rest are mainly clay minerals like kaolinite, chlorite and illite etc. Bauxites achieving the industrial grade mainly distributes in this part. The lower part is dominated by clay minerals, diaspore takes the content of 5%-40%, while clay minerals can reach up to 95%. Constant compositions of bauxite are Al2O3 (26.13-75.16%), SiO2(4.52- 44.46%), Fe2O3(0.77- 27.67%)and TiO2(1.05- 5.24%), these elements have wide distributions[9].

Geochemistry

Al_2O_3 has negative correlations with SiO_2 and Fe_2O_3, while displays positive correlation with TiO_2, indicating bauxite metallogenic process is a process enriching Al, Ti and losing Si, Fe[9]. Trace elements of Zr, Cr, V and Li are enrichment in bauxite. In parallel, Zr, Hf, Nb, Ta and Cr with similar changing rules display an increasing trend in content from north to south, while in vertical, the content shows an opposite trend from the top to the bottom of the section. Contents of Zr, Cr and Nb are relatively high, Zr is up to 1835ppm, Cr, V, Li are more than 150m. Hf and Ta are relatively low. Ni is special with different changing rules from other elements both in parallel and vertical [9]. The contents of Ni in the samples are significantly different. Ranges of LREE, HREE, ΣREE in bauxite are 18.49×10^{-6}- 993.6×10^{-6}, 12.7×10^{-6}- 47.3×10^{-6}, 38×10^{-6}- 1040.9×10^{-6}, respectively, average values are 198.82×10^{-6}, 26.3×10^{-6}, 225.1×10^{-6}[6,9]. LREE, HREE, ΣREE show an increasing trends from top to the bottom of the drill section. LREE displays large variation, while HREE has the opposite trend positive anomaly of Ce in the drill is obvious[6].

Provenance

Source tracing of trace elements is simple and reliable. Cr-Ni, Zr, Hf, Nb, Ta have been used to analyse the sources of bauxite. Cr- Ni value has a wide distribution in WZD bauxite, indicating parent rocks of aluminosilicate rocks and carbonatites and small part of basalt parent rocks [9]. High Field- Strength Elements (HFSE) Zr- Hf and Nb- Ta chart indicate mud shale of Hanjiadian formation has a closer relationship with bauxite [6, 9]. Source tracing of trace elements indicates mud shale of Hanjiadian Formation and limestone of Huanglong Formation are important material sources of bauxite, and mud shale of Hanjiadian Formation even contribute more to bauxite. Besides, there is another small part of basalt provides metallogenic material to bauxite.

Sedimentology

The iron weathering crust, less than 1m has been discovered at the bottom of ore-bearing rock series of bauxites. The ore-bearing rock series is composed of clay rocks and bauxites [10,11]. Clay rocks exhibit homophaneous structure. Bedding and fossils are absent in the ore-bearing rock series of bauxites. Black carbonaceous interbeds and inferior coal interlayer appear in some drills. All these characters of bauxite indicate the forming environment should be low energy lacustrine, bay or coastal lagoon[10,11].

It is suggested that WZD bauxite formed in a special dynamic environment, from evidences of the mineral assemblages, outcrop charaters, geochemistry of trace elements and REE of bauxite, subjective environment is partly closed bay. Although the sea level is fluctuated, the sedimentary environment switched between partly closed bay and terrestrial lake. When the sea level was high, metallogenic province connected with Yangtze Sea, it appears to be salt- brackish water sedimentation. When the sea level was low, metallogenic province out of touch with sea, it appears to be terrestrial salt- brackish water sedimentation. The input of atmospheric precipitation and land fresh water, salt water was diluted constantly. After a period of desalination, some areas changed into fresh water environment. The degree and scale of desalination are determined by length of time of desalination. After lacustrine salt or brackish water totally desalted, sedimentary environment became a brackish water or salt water environment again over the next transgression. After the sea level reduced, lacus or partly closed bay experienced desalination again [11]. In this cycle, metallogenic environment switched in terrestrial lacus, partly closed bay and bay, paleosalinity was in the transition between fresh- brackish water- salt water, so that the sedimentation of bauxite have both continental and transitional characters.

Conclusion

The main conclusions from this study are summarized as follows:1)Former research have a depth understanding on the mineralogy, petrology and geochemistry of WZD bauxite;2)The problems of provenance,sedimentary environment and mineralization process have been resolved;3) We need a further research on three questions as follow: minerogenetic epoch, migration mechanism of elemthreents; genesis of rare earth mineral.

Acknowledgment

This work was supported by the Guizhou Collaborative Innovation Center of Strategic Minerals Resource Development, Guizhou Institute of Technology, Guiyang, 550003, China and the project of analysis on geochemical behaviors of Platinum group elements in Emeishan basalt (XJGC20131204), Guizhou Institute of Technology.

References

[1] G.H. Wu, Z.G. Jin, Y. Bao: J.Geology and Prospecting,Vol.44(2008),P.34 (in Chinese)

[2] Z.G. Jin, G.H. Wu, Y.Y. Zhao:J.Mineral Source and Geology,Vol.23(2009),P.139 (in Chinese)

[3] K.H. Yin: J. Acta Sedmentological Sinica, Vol.27(2009),P. 455 (in Chinese)

[4] Z.H. Han: J. Mineral Resource and Geology,Vol.22(2008),P. 430 (in Chinese)

[5] Z.Y. Lei and Y.C. Liao: J. Western Prospecting Engineering, Vol.18(2007), P. 96 (in Chinese)

[6] X.M. Wang, Y.Q. Jiao and Y.S, Du: J. Journal of Geochemical Exploration, Vol. 133(2013), P.108.

[7] P. Liu: J. Guizhou Geology,Vol.18(2004),P. 240(in Chinese)

[8] D.Q. Du, J.P. Ren and Y. Wang: J. Acta Mineralogical Sinica, Vol.23(2007), P.475 (in Chinese)

[9] T. Cui, Y.Q. Jiao, Y.S. Du:J. Journal of palaeogeography,Vol.16(1),P.9(in Chinese).

[10] Y.S. Du, Q. Zhou, Z.G. Jin. J. Geological science and technology information, Vol.32(1),P.4(in Chinese).

[11] T. Cui, Y.Q. Jiao, Y.S. Du:J. Geological science and technology information, Vol.32(1),P.47(in Chinese).

Advanced Materials Research Vols. 989-994 (2014) pp 1396-1399
© (2014) Trans Tech Publications, Switzerland
doi:10.4028/www.scientific.net/AMR.989-994.1396

Evaluation Method of Coral Reef Integrity: RMDI and Coring Rate Comparative Analysis Method

Jinchao Wang[a *], Chuanying Wang[b] and Zengqiang Han[c]

Institute of Rock and Soil Mechanics, Chinese Academy of Sciences, Wuhan 430071, China

[a]wangjinchao_88@163.com, [b]chywang@whrsm.ac.cn, [c]zqhan@whrsm.ac.cn

Keywords: Borehole camera, coral reef, integrity evaluation, RMDI.

Abstract. At present, relatively few drilling surveys have been conducted on coral reefs, and comprehensive geological info on coral reefs is difficult to obtain. However, research of coral reef is of great importance to our development and exploitation of maritime resources. The survey of South China Sea some Islands saw China's first usage of digital borehole camera technology, which resulted in a large amount of first-hand geological data. Because the coral reef, special rock mass, integrity evaluation is very difficult, we proposed the RMDI and coring rate comparative analysis method. The evaluation method is applied to the South China Sea some Islands, and the evaluation results prove generally consistent with actual cores. The results indicate that: (1) high-resolution borehole images can provide reliable results for evaluation of coral reef integrity; (2) The RMDI and coring rate comparative analysis method is a feasible approach for the evaluation of coral reef integrity along the full or partial depth of a borehole.

Introduction

Coral reefs are rock and soil structures formed by the remains of scleractinian corals after long-term geological effects[1]. The research of coral reef is of great importance to our development and exploitation of maritime resources. The main component of coral reef is calcium carbonate ($CaCO_3$). It is porous and brittle, low in both hardness and strength. Drilling is an indispensable method in the background survey of coral reefs, but due to characteristics of their structure and limitations of technology, such as mechanical disturbances which may result in low or even zero coring rate, the geological info obtained is often incomplete, rendering traditional analytical methods inaccurate. As coral reefs tend to shatter under high pressure, it is easy for the drilling process to damage the intactness of coral rocks, which is impossible to determine through rock cores. Therefore, a singular reliance on drilling would affect the accuracy of coral reef research and even cause erroneous results. A better evaluation of their rock mass would require a combination of drilling and other complementary techniques. The digital borehole camera system [2,3,4] has integrated digital video and computer control by using optical sensors for close observation of rock mass inside the borehole. The acquired information is processed with computer to generate digital column-shaped image of the borehole walls, solving the integrity and accuracy problem of geological info acquisition in coral reef boreholes.

Rock mass integrity refers to the extent of development of various geological interfaces, mainly the fissures and faults. It is a generalized representation of the rock mass structures, and is determined by many factors including the shearing of structural planes, the sizes of structural bodies, and the cementation between bodies. A high-integrity rock mass has fewer faults, and a low-integrity rock mass contains more faults. It is one of the most important signifiers of rock mass quality, used in rock engineering as an overall indicator. Thus it is significant for rock engineering to find methods that allow simple and scientific evaluation of rock mass integrity.

Borehole Camera

The key to the digital panoramic borehole camera system lies in breakthroughs of panoramic (reflector on the conical surface) and digital (digital video and imaging) technologies. The panoramic technologies enable a 2-dimensional representation of the 360° borehole wall, which is overlayed with directional info, creating a panoramic image; digital technologies allow the digitization of videos, which are processed with inverse transformation algorithms to construct a model of the borehole wall and generate a digital vertical image. The borehole camera image is an intuitive representation of geological info from the borehole wall. By processing this info, a complete database can be generated. Fig.1 is a schematic diagram of borehole camera imaging.

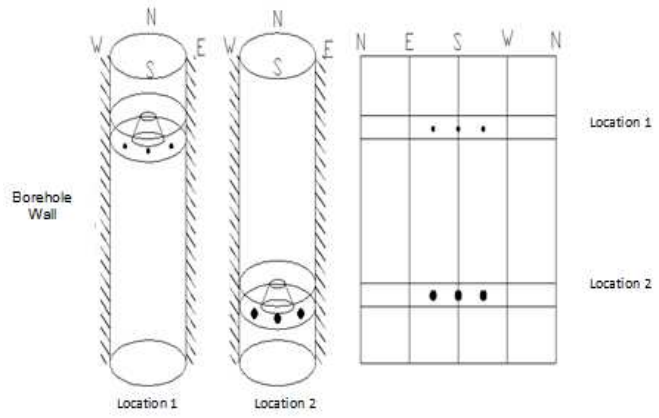

Fig. 1 Schematic diagram of borehole camera imaging.

The RMDI Value

Since the coral reef is a complex entity formed from geological structures of the coral reef, the integrity shown in borehole images or lack thereof depends directly on its geological structures. For instance, a very small number of tiny cavities have little effect on the rock mass integrity, and its image shows even distribution of colours, which is an indication of high integrity; a relatively high number of large cavities break up the rock mass, causing its image to show great variation in colours and signs of fragmentation. We establish a single-variable function that varies along the borehole axial direction, the rock mass integrity index density function (DIDF)[5], represented as f(z) where z is depth, expressed

$$f(\mathrm{z}) = \alpha \tag{1}$$

Where $0 \leq \alpha \leq 1$. If the value of f(z) is 1 or approximating 1, it indicates the rock mass at the given depth has high integrity; the smaller the f(z) value is, the lower the integrity is, and the more fragmented the rock mass appears.

The rock mass integrity index density function DIDF is a reflection of rock mass intactness along borehole axial direction. The rock mass integrity index (RMDI)[5] refers to the proportion of intact rock bodies within a given range, expressed as a percentage, where the given range can be a part of the borehole or the entire depth. If the given depth range is [h1, h2], the RMDI can be expressed as a definite integral of DIDF within the range, expressed as

$$\mathrm{RMDI} = \frac{\int_{h_1}^{h_2} f(\mathrm{z})\mathrm{dz}}{\int_{h_1}^{h_2} 1\mathrm{dz}}. \tag{2}$$

RMDI and Coring Rate Comparative Analysis Method

Due to coral reef structure porous and brittle, low in both hardness and strength, that the pressure easily break the coral reefs during the drilling results in getting incomplete cores. The coring rate is closely related to mechanical disturbance on rock mass, thus we can not determine the integrity simply by the coring rate. RMDI based on borehole camera technique can reduce the drilling mechanical disturbance on rock mass. So it will be more accurate to evaluate the coral reef integrity after considering the RMDI value and the coring rate.

The coring rate is the accumulation of single coral reef core length, however, RMDI value considers the integral effect of rock fragmentation size effect of its density function. If the RMDI value is higher than the coring rate, the coral reef integrity is low and easily broken, because that the relatively complete coral reef is broken after mechanical disturbance results in low or zero coring rate. When the RMDI value is not higher than the coring rate, the coring process has less effect on coral reef integrity. The comprehensive analysis shows that：when the RMDI value is higher than the coring rate, the coral reef integrity is low; otherwise, the coral reef integrity is consistent with the RMDI value.

The example analysis

We take the digital borehole camera date of the South China Sea geological survey as an example and evaluate the coral reef integrity. The coral reef depth tested range 112m from 469m. Through determining the structure types and coral reef integrity block size effect coefficient, we establish the coral reef integrity index density function (DIDF) (refer with: Fig. 2).

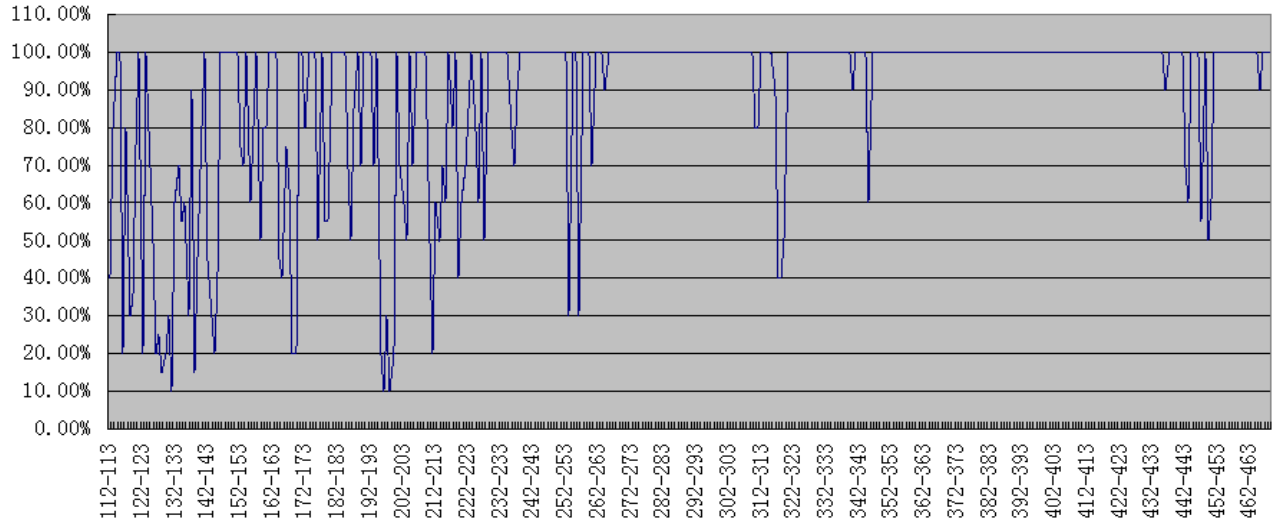

Fig. 2 Coral reef integrity index density function

Then we have a RMDI analysis based on DIDF. According to the research, we select 10m depth scope to evaluate and calculate the RMDI (10m) value. In addition, we compare the RMDI value with the coring rate (refer with: Fig. 3).

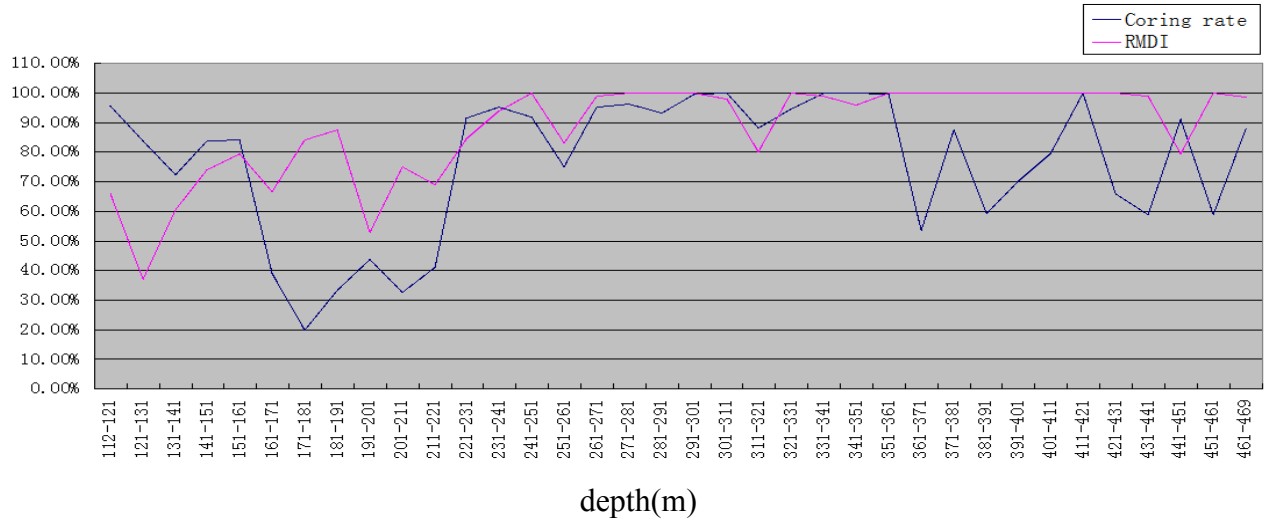

Fig. 3 RMDI and Coring rate

Through the comparative analysis, the coral reef depth in112~151m segment, the RMDI value is less than the coring rate and the RMDI value is between 40%~80%, so the coral reef integrity is general; the coral reef depth in 151~221m segment, the RMDI value is higher than the coring rate, indicating that the coral reef integrity is low; the coral reef depth in 211~351m segment, the RMDI value is nearly equal to the coring rate and the RMDI value is very high, indicating the coral reef integrity is high; the coral reef depth in 351~469m segment, the RMDI value is higher than the coring rate, indicating that the coral reef integrity is low. The coral reef depth from 112m to 469m, the coral reef integrity vary from general to low, form low to high, and then from high to low. It indicates the geological structure of coral reefs is complex. The evaluation is consistent with the actual cores after the comparative analysis.

Summary

This paper proposed the RMDI and coring rate comparative analysis method. Then the evaluation method is applied to the South China Sea some Islands, and the evaluation results prove generally consistent with actual cores. The results indicate that: (1)High-resolution borehole images can provide reliable results for evaluation of coral reef integrity; (2)The RMDI and coring rate comparative analysis method is a feasible approach for the evaluation of coral reef integrity along the full or partial depth of a borehole.

References

[1] Wei, X., Jia, C., and Meng, W., Dolomitization Characteristics of Carbonate Rock in Xisha Islands and Its Formation:A Case Study of Well Xichen-1, Journal of Jilin University (Earth Science Edition), 2008, 38(2), pp. 217–224.

[2] Prensky, S. E., Advances in borehole imaging technology and application, Borehole Imaging: Applications and Case Histories, London, Geological Society, 1999, pp. 1–43.

[3] John，H., and Carole, D., Acoustic and optical borehole-wall imaging for fractured-rock aquifer studies, Journal of Applied Geophysics, 2004, 55:151-159.

[4] Wang, C., Ge, X., and Bai, S., The digital panoramic borehole camera system and its application, Rock and Soil Mechanics, 2001, 22(4), pp. 522–525.

[5] Wang, C., Hu, P., and Sun, W., Method for evaluating rock mass integrity based on borehole camera technology, Rock and Soil Mechanics, 2010, 31(4), pp. 1326–1330.

Advanced Materials Research Vols. 989-994 (2014) pp 1400-1403
© (2014) Trans Tech Publications, Switzerland
doi:10.4028/www.scientific.net/AMR.989-994.1400

Special structure and its geological significances of WZD bauxite

Tao Cui

College of Resources and Environmental Engineering, Guizhou Institute of Technology, Guiyang, 550003, China

cuitao1203@163.com

Keywords: WZD area; Bauxite; special structure; geological significances

Abstract: Through systematically geologic survey and observation of drills and rock slices this paper have a comprehensive research on special structure of bauxite in Wuchuan -Zheng'an -Daozhen (WZD) area. Special structure mainly includes directional structure of clast, leaching structure and colloid structure. Clast is erratic boulder indicating high energy environment. Leaching structure shows there is an eluvial process in mineralizaton process, and leaching is important for the formation of high grade bauxite. Appearance of colloidal in WZD bauxite shows that agglutinate of gel is one of the reasons for the formation of WZD bauxite. Clastic structure, leaching structure and colloidal structure demonstrate that mineralizaton process of WZD bauxite is a very complicated process.

Introduction

There is abundant bauxite in WZD area. For a long time many experts and scholars have researched on rocks and minerals, chemistry, sedimentary environment, provenance, mineralization age, and mass balance calculation of the bauxite [1-15]. Though there are abundant outcomes of WZD bauxite, analysis on special structure of the bauxite is poor. Through research on special structure this paper has a future understand on metallization and metallogenetic environment of WZD bauxite.

Geological setting

WZD bauxite is located in Wuchuan, Zheng'an and Daozhen County, northern Guizhou, which is an important part of centre Guizhou-southern Chongqing bauxite belt [7]. The regional tectonics position of the study area is in the fold belt in northern Guizhou of the upper Yangtze Block [8]. From the oldest to the youngest, the main strata in WZD area includes Cambrian, Ordovician, Silurian, Permian, Triassic and Jurassic. Cambrian is mainly distributed in the core of anticlines, Triassic and Jurassic are mainly distributed in the core of synclines. Bauxite underlies the LiangShan formation(P2l) or Qixia formation(P2q) in the middle Permian, and overlies the HuangLong formation(C2h) of upper Carboniferous or the Hanjiadian formation of the lower Silurian(S1hj). The bauxite is stratiform and unconformable with the underlying and overlying strata. Fig.1 shows that the distribution of the bauxite is controlled by nine synclines. Thickness of the bauxite is 0.68-15.7m, and its profile can be divided into two lithology parts: the upper part and the lower part. The former is aluminous rock, dominated by high grade bauxite or half grade bauxite; the latter is low grade bauxite. According to the lithological and textural properties, the natural types of bauxite deposit can roughly be subdivided into four categories: massive bauxite, oolithic bauxite, clastic bauxite and earthy bauxite.

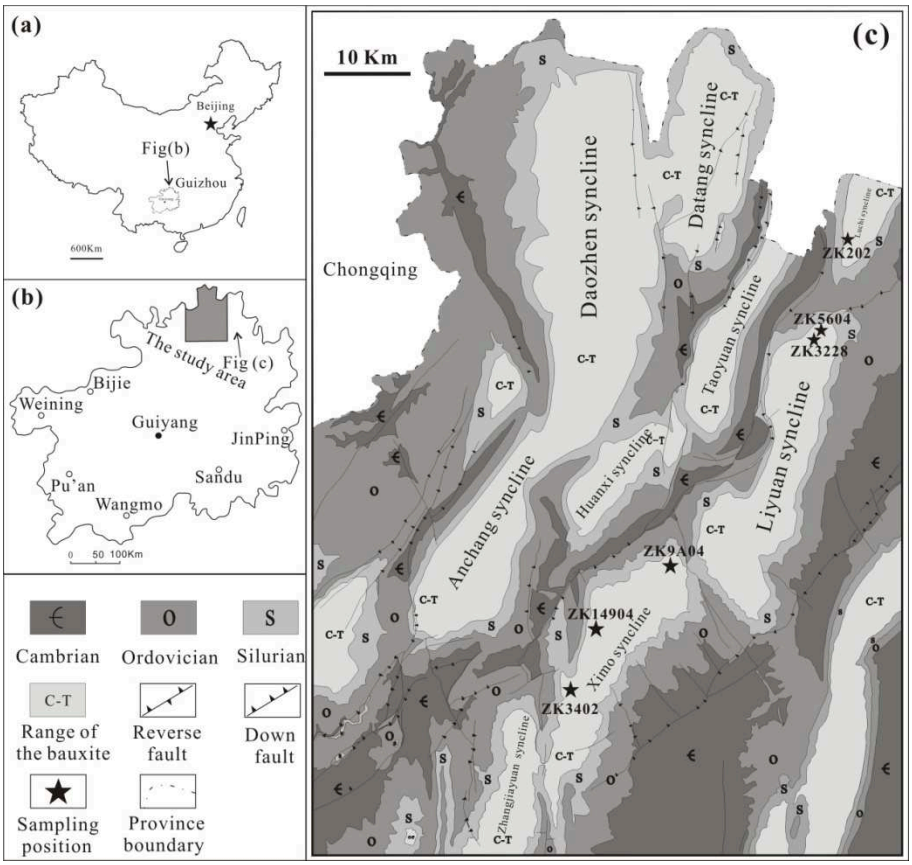

Fig. 1(a)Locality map of Guizhou,(b)The map showing the location of the study area, (c)Geology map of the WZD area in northern Guizhou

Special structure

Fig.1 shows sampling position, hematite, colloidal diaspore, recrystallized diaspore and clastic grain all from different drills. Fig.2 shows main special structure in WZD bauxite. Hematite in Fig.2 is epigenetic, and it is formed in penecontemporaneous period. Hematite indicates oxidation environment. Hematite is veined with a bastard top and a fine bottom (Fig.2, a, b), this special shape is controlled by leaching which is influenced by gravity. Gel bauxite is grey and its shape is like tostromatolite (Fig.2, c). Gel bauxite is formed in pores, and the appearance of gel bauxite indicates that gel deposition is one reason for mineralization of WZD bauxite. Recrystallized diaspora is fusoid with length of 4mm (Fig.2, d). Recrystallized diaspora is different with diaspora in matrix, and it is obviously diaspora recrystallization in pores by leaching in penecontemporaneous period. Clastic grains are black, and some parts of grains have directive property (Fig.2, e, f). Clastic grains can be divided into several groups according directive property. Clastic grain of WZD bauxite reflect features of erratic boulder. Contrast to matrix clastic grain has obviously different component and color, and this shows that clastic grain and matrix are not homochromous deposition. Clastic grain may be deposit later than matrix, grain may be evolved from matrix. Clastic grain and matrix in WZD bauxite demonstrate there may be several streams, and sedimentary environment is not stable. Early Sedimentary deposit may be undergo reform and transform to clastic grain, and then later matrix deposited.

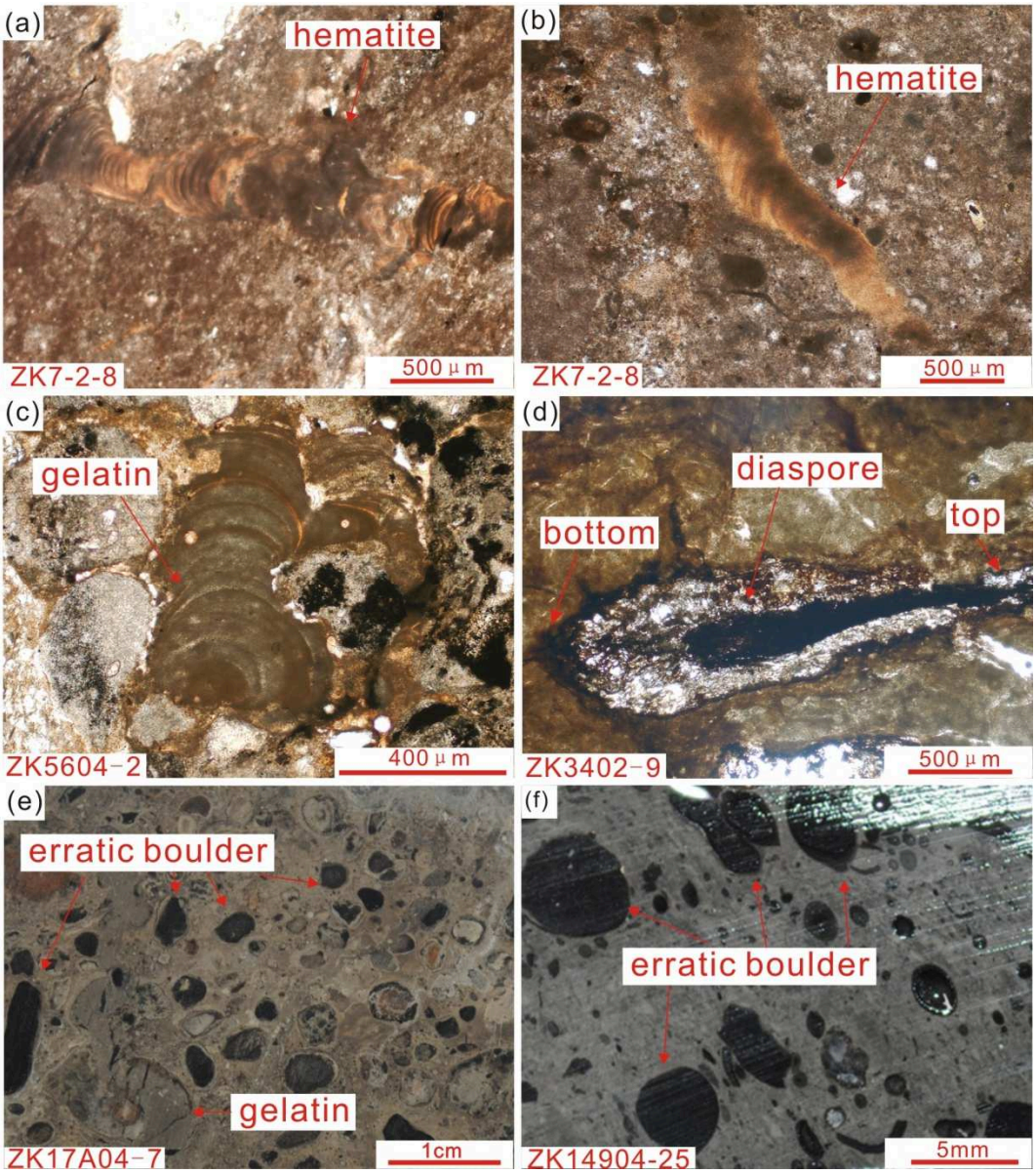

Fig.2 Special structures of WZD bauxite

Discussion

Special structure of bauxite have provide information for the research of mineralization. Hematite present oxidized environment. Generally we think WZD bauxite is formed in a hydrogenant environment, but the appearance of hematite indicates existing an oxidized stage in the process of mineralization. Colloidal structure is universal in bauxite indicating mineralizaton process is not simple mechanical transport. Discovery of erratic boulder shows that hydrodynamic condition is complex, and perimeter of sedimentary basin exist density current. Until now, metallogenetic environment and mineralizaton process are two hard nut to crack, special structure in WZD bauxite further approve it. This work demonstrate mineralizaton process of bauxite is very complicated.

Conclusions

The main conclusions from this study are summarized as follows: 1) Forming process of WZD bauxite is complicated, condense of colloform is one of important factors for the formation of bauxite. 2) Leaching is the key factor for the formation of high grade bauxite. 3) Metallogenetic environment of the WZD bauxite is not remains katakinetomeric and reductive conditions, in the long time of mineralizaton process metallogenetic environment has altered into oxidized and high energy conditions.

Acknowledgment

This work was supported by the Guizhou Collaborative Innovation Center of Strategic Minerals Resource Development, Guizhou Institute of Technology and the project of analysis on geochemical behaviors of Platinum group elements in Emeishan basalt（XJGC20131204）, Guizhou Institute of Technology.

References

[1] G.H. Wu, Z.G. Jin, Y. Bao: J.Geology and Prospecting,Vol.44(2008),P.34 (in Chinese)

[2] Z.G. Jin, G.H. Wu, Y.Y. Zhao:J.Mineral Source and Geology,Vol.23(2009),P.139 (in Chinese)

[3] K.H. Yin: J. Acta Sedmentological Sinica, Vol.27(2009),P. 455 (in Chinese)

[4] Z.H. Han: J. Mineral Resource and Geology,Vol.22(2008),P. 430 (in Chinese)

[5] Z.Y. Lei and Y.C. Liao: J. Western Prospecting Engineering, Vol.18(2007), P. 96 (in Chinese)

[6] X.M. Wang, Y.Q. Jiao and Y.S, Du: J. Journal of Geochemical Exploration, Vol. 133(2013), P.108.

[7] P. Liu: J. Guizhou Geology,Vol.18(2004),P. 240(in Chinese)

[8] D.Q. Du, J.P. Ren and Y. Wang: J. Acta Mineralogical Sinica, Vol.23(2007), P.475 (in Chinese)

[9] G. Millot, M. Bonifas: J. Alsace Lorraine,Vol.8(1955),P.15.

[10] J.J. Middleburg, C.H. Van, J.R.W. Woittiez: J.Chen.Geol, Vol.68(1988),P.263

[11] H.W. Nesbitt, G.M. Young:J.Geol,Vol.97(1989),P.135.

[12] I.G. Hill, R.H.G. Worden, I.G. Meighan: J.Chemical Geology,Vol.166(2000),P.166.

[13] J.A. Grant: J.Economic Geology,Vol.81(1986),P.1980.

[14] W.H. Maclean: J. Mineralium Deposita,Vol.25(1990),P.46

[15] T. Cui, Y.Q Jiao, Y.S. D:J.The Chinese Journal of Nonferrous Metals,Vol.24(2013),P.6.(in Chinese)

Advanced Materials Research Vols. 989-994 (2014) pp 1404-1407
© (2014) Trans Tech Publications, Switzerland
doi:10.4028/www.scientific.net/AMR.989-994.1404

Analysis on oxidized and reduced conditions in penecontemporaneous period on the bauxite in WZD area

Tao Cui

College of Resources and Environmental Engineering, Guizhou Institute of Technology, Guiyang, 550003, China

cuitao1203@163.com

Keywords: WZD area; Bauxite; oxidized and reduced conditions

Abstract: Through systematically geologic survey, observation of drills and rock slices and geochemical analysis this paper have a comprehensive research on oxidized and reduced conditions of bauxite in Wuchuan-Zheng'an-Daozhen (WZD) area. The results shows that color, component, lithology and grade of WZD bauxite have vertical alteration; Metallogenetic environment of WZD bauxite in penecontemporaneous period is oxidized, and from top to bottom, oxygen content is gradually decreased; Not only the similar stratigraphic position in different zone of WZD area have different oxygen content, but also identical stratigraphic position in different period has different oxygen content.

Introduction

There is abundant bauxite in WZD area. For a long time many experts and scholars have researched on rocks and minerals, chemistry, sedimentary environment, provenance, mineralization age, and mass balance calculation of the bauxite [1-15].Though there are abundant outcomes of WZD bauxite, analysis on oxidized and reduced conditions in penecontemporaneous period of the bauxite is poor. This paper have a research on oxygen content by analysis on vertical alternation and geochemistry of WZD bauxite.

Geological setting

WZD bauxite is located in Wuchuan, Zheng'an and Daozhen County, northern Guizhou, which is an important part of centre Guizhou-southern Chongqing bauxite belt [7]. The regional tectonics position of the study area is in the fold belt in northern Guizhou of the upper Yangtze Block [8]. From the oldest to the youngest, the main strata in WZD area includes Cambrian, Ordovician, Silurian, Permian, Triassic and Jurassic. Cambrian is mainly distributed in the core of anticlines, Triassic and Jurassic are mainly distributed in the core of synclines. Bauxite underlies the LiangShan formation(P2l) or Qixia formation(P2q) in the middle Permian, and overlies the HuangLong formation(C2h) of upper Carboniferous or the Hanjiadian formation of the lower Silurian(S1hj). The bauxite is stratiform and unconformable with the underlying and overlying strata. Fig.1 shows that the distribution of the bauxite is controlled by nine synclines. Thickness of the bauxite is 0.68-15.7m, and its profile can be divided into two lithology parts: the upper part and the lower part. The former is aluminous rock, dominated by high grade bauxite or half grade bauxite; the latter is low grade bauxite. According to the lithological and textural properties, the natural types of bauxite deposit can roughly be subdivided into four categories: massive bauxite, oolithic bauxite, clastic bauxite and earthy bauxite.

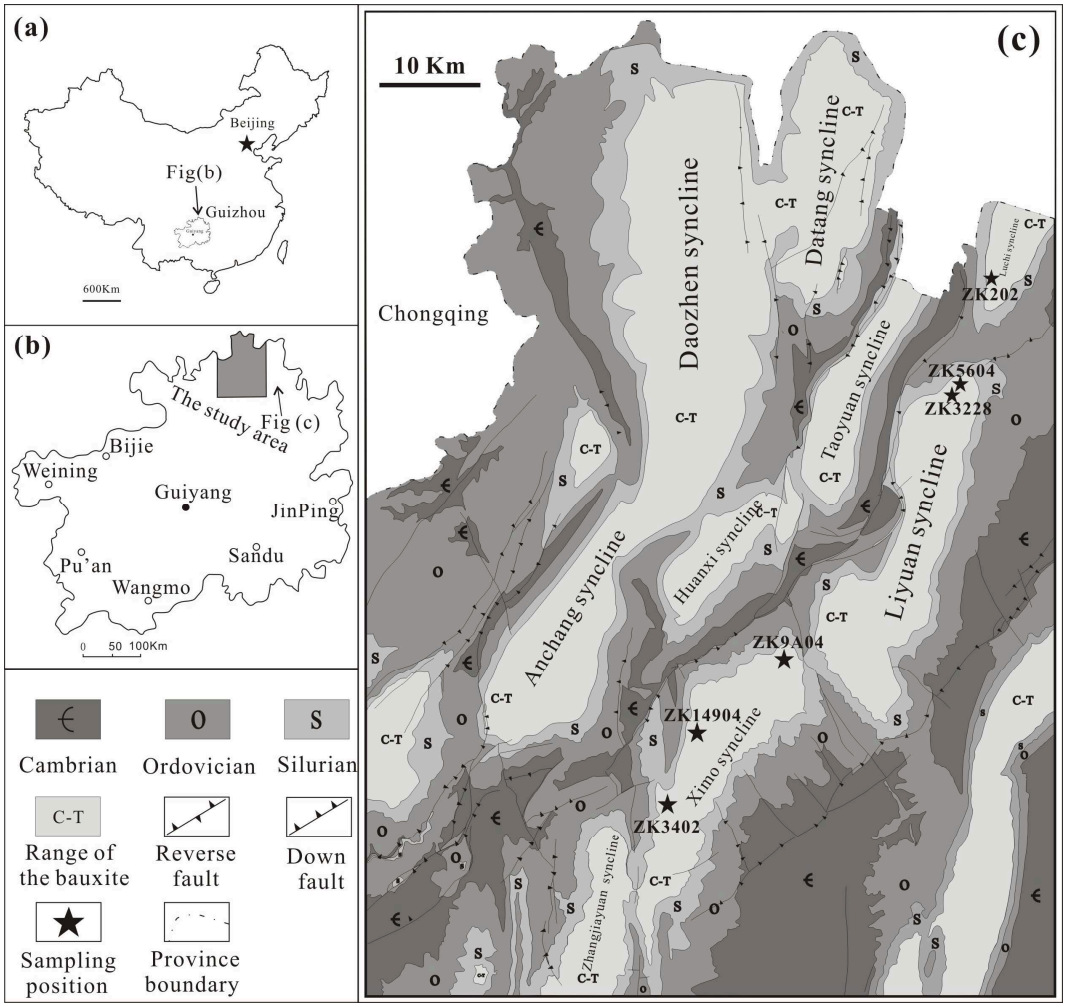

Fig. 1(a)Locality map of Guizhou,(b)The map showing the location of the study area, (c)Geology map of the WZD area in northern Guizhou

Vertical alternations

Fig.2 shows that color of WZD bauxite has obviously vertical alteration, and it can be divided into three parts: upper light parts; middle grey parts; lower dark grey-green parts. Two interface of three parts is usually dark grey indicates there are time break in sedimentary process, and transitional layer is no more than 0.5m (Fig.2). Most of drills in WZD are have this regular pattern, and there are interior vertical regular pattern in three parts. Color regular pattern of WZD bauxite shows that different stratigraphic positions have different oxygen content. Color of bauxite is controlled by component, and light grey bauxite usually is high grade bauxite and dark grey- green bauxite is low grade. In the lower part of profile bauxite is green, and as a matter of fact it is a chlorite rock. For WZD bauxite not only color but also structure are controlled by component, and structure of high grade bauxite is loose than low grade bauxite. Color and structure are bound with grade demonstrates that in penecontemporaneous period metallogenetic environment is oxidized because just in oxidized conditions Fe in bauxite can be removed. The high of grade is , the more white of the bauxite. In other words, in oxidized conditions a great runoff of Fe resulting in the appearance of light grey- white bauxite in WZD area. Except for color, anomaly of Ce reflect oxidized conditions. Positive anomaly of Ce indicates environment is oxidized, there are obviously positive anomaly of Ce in drills of WZD bauxite (Fig.3). Color and positive anomaly of Ce all indicate in penecontemporaneous period metallogenetic environment is oxidized. From top to bottom content of oxygen is decreased because color is deeper in the lower part of bauxite. Appearance of interfaces shows there are several time break in sedimentary process, so in different period oxygen content of the same stratigraphic position is variable. Mineral-formation condition of different zone in WZD area is variable resulting in similar stratigraphic positions have variable oxygen content.

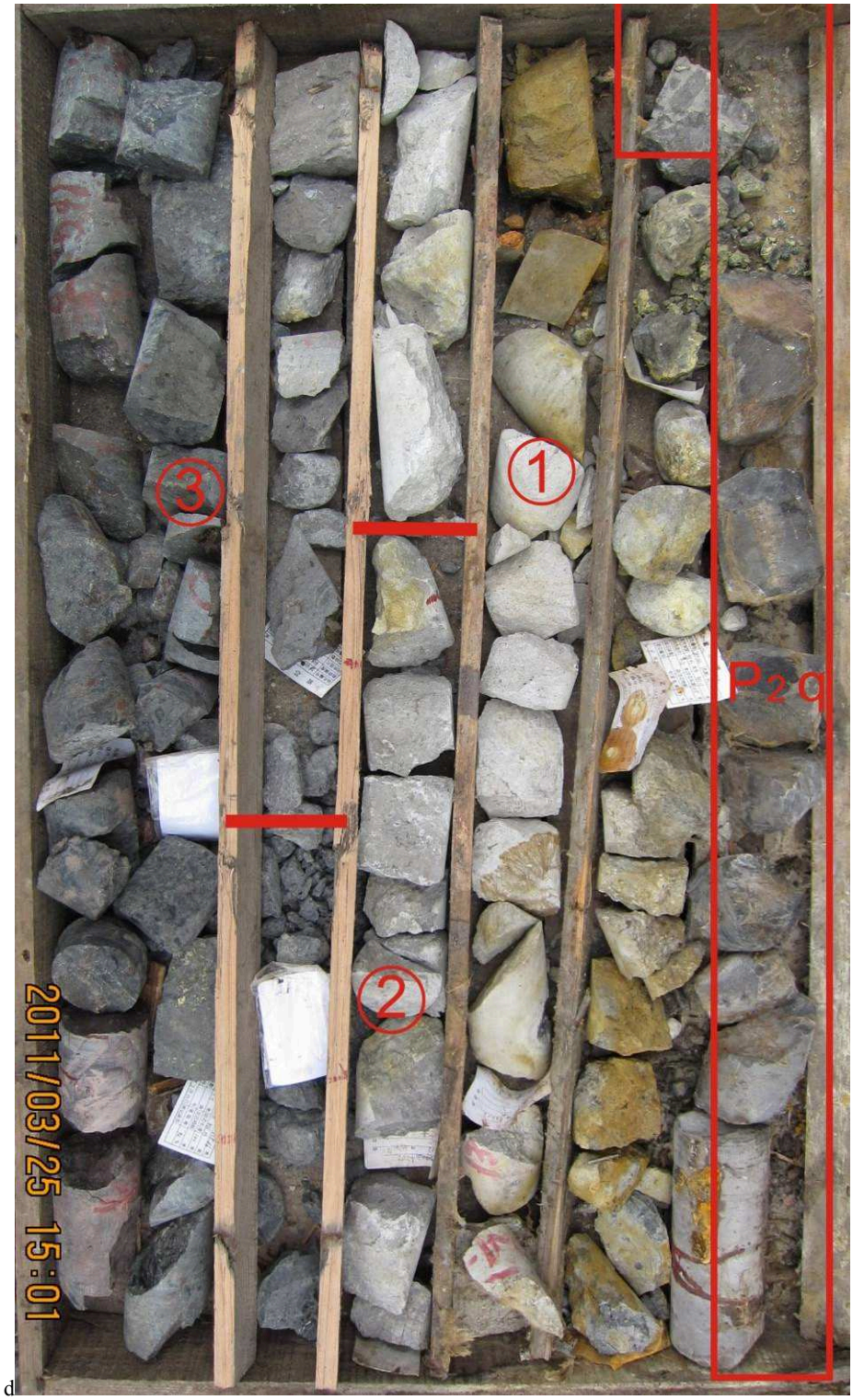

Fig.2 Vertical alteranations of WZD bauxite

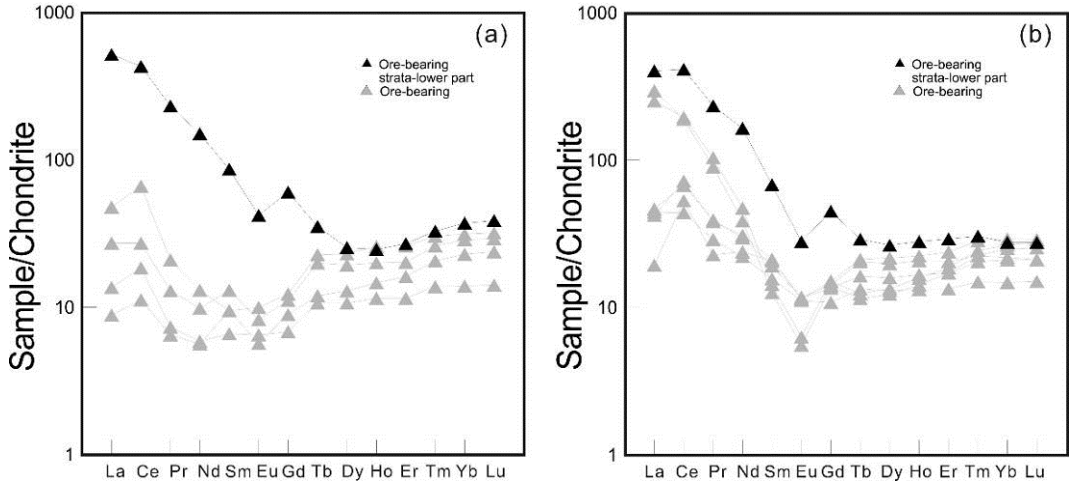

Fig.3 REE distribution patters a. ZK202；b. ZK5604 [9]

Conclusions

The main conclusions from this study are summarized as follows: 1) Metallogenetic environment is oxidized, but oxygen content have a gradually downward decreased trend; 2) Not only the similar stratigraphic position in different zone of WZD area have different oxygen content, but also identical stratigraphic position in different period has different oxygen content because of frequent transgression, regression and leaching process.

Acknowledgment

This work was supported by the Guizhou Collaborative Innovation Center of Strategic Minerals Resource Development, Guizhou Institute of Technology and the project of analysis on geochemical behaviors of Platinum group elements in Emeishan basalt (XJGC20131204), Guizhou Institute of Technology.

References

[1] G.H. Wu, Z.G. Jin, Y. Bao: J.Geology and Prospecting,Vol.44(2008),P.34 (in Chinese)

[2] Z.G. Jin, G.H. Wu, Y.Y. Zhao:J.Mineral Source and Geology,Vol.23(2009),P.139 (in Chinese)

[3] K.H. Yin: J. Acta Sedmentological Sinica, Vol.27(2009),P. 455 (in Chinese)

[4] Z.H. Han: J. Mineral Resource and Geology,Vol.22(2008),P. 430 (in Chinese)

[5] Z.Y. Lei and Y.C. Liao: J. Western Prospecting Engineering, Vol.18(2007), P. 96 (in Chinese)

[6] X.M. Wang, Y.Q. Jiao and Y.S, Du: J. Journal of Geochemical Exploration, Vol. 133(2013), P.108.

[7] P. Liu: J. Guizhou Geology,Vol.18(2004),P. 240(in Chinese).

[8] T. Cui, Y.Q. Jiao, Y.S. Du:J. Journal of palaeogeography,Vol.16(1),P.9(in Chinese).

[9] T. Cui, Y.Q Jiao, Y.S. D:J.The Chinese Journal of Nonferrous Metals,Vol.24(2013),P.6.(in Chinese)

Advanced Materials Research Vols. 989-994 (2014) pp 1408-1410
© (2014) Trans Tech Publications, Switzerland
doi:10.4028/www.scientific.net/AMR.989-994.1408

Beneficiation of a Low-grade Barite Ore in Myanmar

Tingting Li[1,a], Siqing Liu[2,b], Yang Zhao[3,c], Hongjun Wang[4,d]

[1]State Key Laboratory of Complex Nonferrous Metal Resources Clean Utilization

[2]Department of Mineral Processing Engineering, Kunming University of Science and Technology, Kunming 650093, China

[a]916583174@qq.com,[b]647647@163.com, [c]576241260@qq.com, [d]215417552@qq.com

Keywords: low-grade; barite; grinding fineness; flotation reagent

Abstract. Beneficiation of a low-grade barite ore assaying 64.32% $BaSO_4$ was conducted by flotation using sodium oleate and sodium silicate. The effect of grinding fineness, type and dosage of flotation reagent in roughing were investigated. Based on the optimum flotation conditions, a close circuit flowsheet was established. Finally, two barite concentrates assaying 96.32% and 91.26% $BaSO_4$ can be obtained at the recovery of 91.94% and 5.25%, respectively, by applying two-time roughing and two-time cleaning operations.

Introduction

The barite resources are very abundant in China, distribute in 26 provinces, and mainly concentrate in the south. Guizhou province alone accounts for a third of the total national's reserves. Hunan and Guangxi rank the second and third in our country, respectively. The barite resources in our country not only have a large reserve, but also have a high grade, $BaSO_4 > 92.8\%$. According to the global mineral statistics released by the American Geological Bureau in January 2013: the reserves of the global barite proven are 240 million tons in 2012 and the barite reserves in China are the most abundant in the world; in 2012, the barite reserves proven in China have reached 100 million tons, accounting for 41.67% of the total reserves of the global barite.

Ore properties. The sample ore taken from Myanmar belongs to a kind of single barite type. The main valuable mineral is barite, the majority of the gangue mineral is quartz, and contains a small amount of aluminosilicate, dolomite, and lapis lazuli. The results of the chemical analysis of the ore are as follows: $BaSO_4$64.32%, $SiO_2$31.21%, $Fe_2O_3$2.65%, MnO0.243%, $Al_2O_3$0.45%, $TiO_2$0.45%, $P_2O_5$0.21%.

Test results and discussion

The type and dosage of collector test. Through grinding fineness analysis, the optimum grinding fineness is set as -200 meshes 80%, so the following tests are conducted under the condition of -200 meshes 80%. Generally speaking, the gravity separation is the main sorting method of the barite ore in the domestic and overseas. Adopting the spiral chute to treat -2mm feed and discarding the tailing in advance, the crude concentrate assaying 65.15% $BaSO_4$ and the tailing assaying 53.23% $BaSO_4$ can be obtained. The increase of the crude concentrate grade is not obvious. This indicates that gravity separation does not apply to the ore, so eventually the flotation flowsheet is adopted. According to the ore properties, initially determine to choose anionic collector—sodium oleate, oxidized paraffin soap and dodecyl benzene xanthate. In order to find out the optimum collector, under the conditions of natural pH of the pulp and sodium silicate (500 g/t), one-time exploratory experiment is carried out on sodium oleate and oxidized paraffin soap and dodecyl benzene xanthate, respectively. This test uses a roughing open-circuit test. The test results are shown in Fig.1, Fig. 2, and Fig.3.

The dosage of oxidized paraffin soap. It can be seen from Fig.1: When the dosage of oxidized paraffin soap is 300 g/t, the grade and recovery of the barite concentrate are 91% and 90%,

respectively. Continue to increase the dosage of oxidized paraffin soap to 400 g/t, the grade and recovery of the concentrate are 87% and 97%, respectively.With the increase of the dosage of oxidized paraffin soap, the concentrate grade decreases and the concentrate recovery increases. It indicates that the selectivity of oxidized paraffin soap is not ideal. When the dosage of oxidized paraffin soap increases, many gangue minerals enter into rough concentrate, leading to the decrease of the concentrate grade.

The dosage of dodecyl benzene xanthate. It can be seen from Fig.2: When the dosage of dodecyl benzene xanthate is 100 g/t, the grade and recovery of the concentrate are 90% and 88%, respectively. Continue to increase the dosage of dodecyl benzene xanthate to 200 g/t, the grade and recovery of the concentrate are 83% and 98%, respectively. This indicates that the selectivity of dodecyl benzene xanthate is poor.

The dosage of sodium oleate. It can be seen from Fig.3: When the dosage of sodium oleate is 600 g/t, the grade and recovery of the concentrate are 91.15% and 92.10%, respectively. Continue to increase the dosage of sodium oleate to 800 g/t, the grade and recovery of the concentrate are 91.70% and 94%, respectively. With the increase of the dosage of sodium oleate, the concentrate grade changes little, but the recovery increases from 92.10% to 94%, indicating that the selectivity of sodium oleate is better.

It can be seen from the above results: using dodecyl benzene xanthate, sodium oleate and oxidized paraffin soap as collectors can obtain the product with the concentrate grade of more than 90% at the recovery of more than 80%, but the collecting effect of sodium oleate is better than other collectors. Therefore, the optimum collector is sodium oleate, and the dosage of sodium oleate is set as 800 g/t.

The type and dosage of inhibitor test. In order to suppress quartz and other gangue minerals, sodium silicate, fluorine sodium silicate and sodium hexametaphosphate are commonly used as inhibitors. The test results indicate that in the same flotation conditions, the inhibitory effect of sodium silicate is better than an equal amount of fluorine sodium silicate and sodium hexametaphosphate, and the grade and recovery of the concentrate obtained are relatively high. So eventually sodium silicate is chosen as the optimum inhibitor.

In order to further explore the optimum dosage of sodium silicate, an explorative experiment about the dosage of sodium silicate is carried out. The results indicate that compared with not adding sodium silicate, adding sodium silicate 500 g/t, the concentrate recovery basically change little, but the concentrate grade obviously increases by 2%. Continue to increase the dosage of sodium silicate to 800 g/t, the concentrate grade continues to increase, but the recovery begins to decrease. It indicates that part of barite is suppressed and along with the gangue mineral into the tailing in the flotation process. Therefore, the optimum dosage of sodium silicate is set as 500 g/t.

Process structure exploration tests. On the basis of the above condition tests, determine two kinds of closed-circuit programs: flowsheet 1 “two-time roughing, one closed cleaning and open in the second cleaning operations”; flowsheet 2 “one-time roughing stage, two-time cleaning stages and one-time scavenging stage” open flotation flow sheet. The closed circuits of flowsheet 1 and 2 are shown in Fig.4 and Fig.5, respectively. In the closed-circuit test of flowsheet 1, two different grade concentrates are obtained namely that chemical grade and weighting agent grade of the barite concentrates, meet different market needs, in order to achieve the maximize economic efficiency. The closed-circuit results of two different programs are shown in Table 1.

Table 1 Closed circuit results of flowsheet1 and 2

Test name	Product	Yield（%）	Grade（%）	Recover（%）
Flowsheet 1	Concentrate 1	64.13	96.32	91.94
	Concentrate 2	3.70	91.26	5.25
	Tailing	35.87	10.36	8.06
	Raw ore	100.00	64.32	100.00
Flowsheet 2	Concentrate	67.33	91.83	93.79
	Tailing	35.87	10.36	8.06
	Raw ore	100.00	64.32	100.00

It can be seen from Table 1: In flowsheet 1, the recoveries of concentrate 1 and 2 reach to 97.19% at the comprehensive grade up to 92.16%. In flowsheet 2, the barite concentrate with the grade of 91.83% at the recovery of 93.79% is obtained.

Under the condition of same jobs of two flowsheet: flowsheet 1 has a better comprehensive recovery, a better floatation index, less return of middling, and a stronger practical operability. So eventually adopt flowsheet 1, and mass balance of flowsheet 1 is shown in Figure 6.

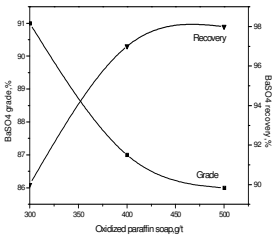

Fig.1: Results of oxidized paraffin soap test

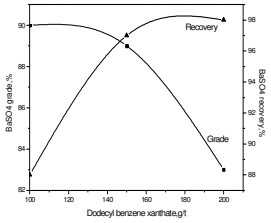

Fig.2: Results of dodecyl benzene xanthate test

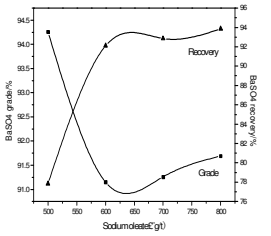

Fig.3:Results of sodium oleate test

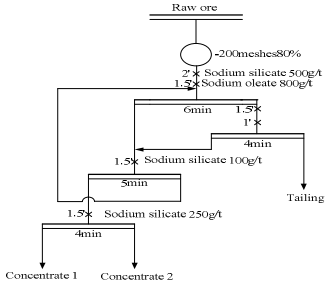

Fig.4 Flowsheet 1

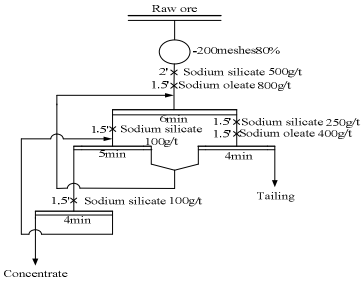

Fig.5 Flowsheet 2

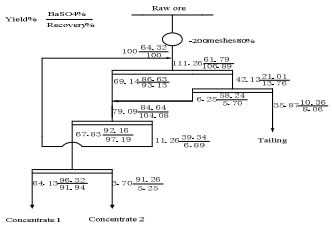

Fig.6 Mass balanceof flowsheet 1

Summary

The barite ore taken from a barite mine in Myanmar belongs to a kind of single barite type and easy to be treated. The barite can be recovered by a simple flotation flow sheet, two-time roughing, one closed cleaning and open in the second cleaning operations. The optimum flotation conditions are sodium oleate 800g / t and sodium silicate 500 g / t at the grinding fineness -200 meshes 80% and two kinds of high-quality barite concentrates can be obtained, which meet the quality standard of barite product.

Acknowledgments

The authors acknowledge the Applied Fundamental Research of Yunnan Provincial Science and Technology (No.2013FZ023) for supporting this research.

References

[1] Li Zhanyuan: submitted to Journal of Chinese Non-metallic Minerals Industry Herald (2004).

[2] Submitte to Journal of Resources and Living Environment (2009).

[3] Li Yangyan: submitted to Journal of Metallic Minerals (1988).

[4] Song Quanyuan: submitted to Journal of Mineral Utilization (1994).

[5] Li Yuyin, Tang Chaojian: submitted to Journal of Nonmetal Mines.

Advanced Materials Research Vols. 989-994 (2014) pp 1411-1414
© (2014) Trans Tech Publications, Switzerland
doi:10.4028/www.scientific.net/AMR.989-994.1411

Research on the flotation of low grade copper-nickle ore

Zheng Bin Deng[1,2,a], Xiong Tong[1,2,b*], Xiao Wang[1,2,e], Qing Yan Zhao[3,d], Xian Xie[1,2,c], Xiang Wen Lv[1,2,f]

[1]State Key Laboratory of Complex Nonferrous Metal Resources Clean Utilization（Kunming University of Science and Technology）, Kunming 650093, China

[2]Yunnan Province Engineering Research Center for Reutilization of Metal Tailings Resources

[3]Man yin Gou Mining group co., LTD

[a]dzbkmust@163.com, [b]xiongtong2000@yahoo.com

[c]lynwx@live.com, [d]121352586@qq.com

[e]xianxie2008@yahoo.com.cn, [f]lvxiangwen2012@gmail.com

*Corresponding author

Keywords: Flotation, Copper-nickle ore, New nickel inhibitor, YS

Abstract. Effect of grinding fineness and inhibitors on mixed flotation of low copper and nickel were studied and a new nickel inhibitor YS was used in the process of separation of copper and nickel. The results indicated that the high-quality mixed concentrate with the recoveries of Cu and Ni 76% and 65.6% and the grade of Cu and Ni were 4.66% and 4.3%, respectively, was got under the condition of sodium silicate (200 g/t), CMC (200 g/t), copper sulphate200 g/t, amyl xanthate 100 g/t and pine oil 30 g/t with the grinding fineness of -0.074mm80%. Then, Qualified Cu concentrate with the grade26.65% and recovery 55.62%, Qualified Ni concentrate with the grade26.65% and recovery 55.62%, respectively, were got by using the new nickel inhibitor YS in the separation flotation of copper and nickel.

Introduction

As we all know there are three types nickel deposit in the world: nickel sulfide ore, laterite nickel ore and nickel silicate deposit. The nickel sulfide ore will still be an important source of nickel, from which the extract of nickel accounted for about two-thirds of the total nickel production at present [1, 2]. The copper and nickel sulfide ore is the main nicke sulfide ore whose mineralogical properties are similar, that include pyrrhotite, pentlandite and chalcopyrite. In the practice of the flotation, chalcopyrite, most pentlandite and purple sulfur nickel can be quickly floated out, while little pyrrhotite and purple sulfur nickel float slowly [3].

In addition, most of the copper and nickel sulfide ore has the following characteristic: The dissemination particle sizes of sulfide mineral are uneven; Nickel sulfide minerals are easily over crushed and oxidized; Natural flotability of nickel sulfide are similar to those of pyrites; Some useful minerals are magnetic, such as magnetic pyrite, purple sulfur nickel; Gangue mineral easy to be muddy and so on. The flotation of copper-nickel ore has been a worldwide difficult problem because of the so much complicated nature. Therefore, the highly efficient recovery of copper and nickel is worth studying [4, 5].In this study, a new inhibitor YS with higher efficiency and better selectivity is used in the separation flotation of copper-nickle in the alkali conditions.

Experimental

Material

In this study, sodium carbonate, amyl xanthate, sodium silicate and CMC from Zhuzhou Flotation Reagents Co.,Ltd with industrial purity are used. Copper sulfate from Tianjin NO.3 Chemical reagent factory with chemical purity is used as activator. YS from Kunming University of Science and Technology with industrial purity is used as nickel inhibitor. Lime from Tianjin NO.3

Chemical reagent factory with chemical purity is used as depressor and pH regulator. Tap water in laboratory is used in the flotation tests.

The material used in the present investigation was from the Yunnan province, with the chemical composition and titanium phase analysis as illustrated in Tables 1, 2 and 3, respectively. From Table 1, the material is a typically low-grade copper and nickel ore, with the contents of recoverable Cu and Ni elements as low as 0.38% and 0.57%, respectively; the dominant gangue element in the material is silica with a content of 40.04%. From Table 2 and 3, copper sulphide and combined copper oxide are determined as the Cu bearing minerals. Nickel sulfide and Nickel silicate are determined as the Cu bearing minerals.

Table 1 The chemical compositions of the ore sample （mass fraction,%）

Element	Cu	Ni	S	CaO	MgO	SiO_2
Assaying/%	0.38	0.57	2.89	9.15	11.66	40.04

Table 2 Phase analysis results of nickel

Component	**Nickel sulfate**	**Nckel sulfide**	**Nickel silicate**	**Total**
Content/%	<0.01	0.48	0.054	0.54
Distribution/%	1.11	88.89	10.00	100

Table 3 Phase analysis results of copper

Component	**Sulfate**	**Free copper oxide**	**combined copper oxide**	**copper sulphide**	**Total**
Content /%	<0.0005	0.0018	0.0073	0.4005	0.41
Distribution /%	0.1	0.44	1.78	97.68	100

Flotation test

The rougher flotation of copper and nickel sulfide ore was conditioned for 3 minutes while a given amount of inhibitor was added at first. After that, the conditioning continued for 2 minutes with activator, 1 minute with collector and 1 minute pine oil, respectively. The products were dried and weighed, and then were chemically analyzed for zinc and indium.

Result and discussion

Mixed flotation of copper and nickel

1)Effect of grinding fineness

Grinding fineness is one of the key factors influencing the recovery. Over grinding is too easy to cause new argillization. Less grinding can lead to the useful minerals not dissociation. So the grinding fineness is studied. Figure 1 illustrates the concentrate grade and recovery of Cu and Ni from the rougher flotation of low-grade copper and nickel ore as the different grinding fineness By using the inhibitor sodium carbonate (200 g/t) and CMC (200 g/t), 200 g/t activator copper sulphate, 100 g/t collector amyl xanthate and 30 g/t pine oil, respectively.

As it noted, the Cu and Ni recoveries increased as the increase of grinding fineness until it reached the plateaus at the critical fineness. While, the grades increased maximum and then decreased with the increasing grinding fineness. Recovery is usually must be considered first in the rougher flotation. The optimum grinding fineness was -0.074mm 80%, while the Cu grade was 4.66% and the recovery was 76% in the rougher flotation, respectively, Compared, the Ni grade and recovery was 4.3% and 55.6%, respectively.

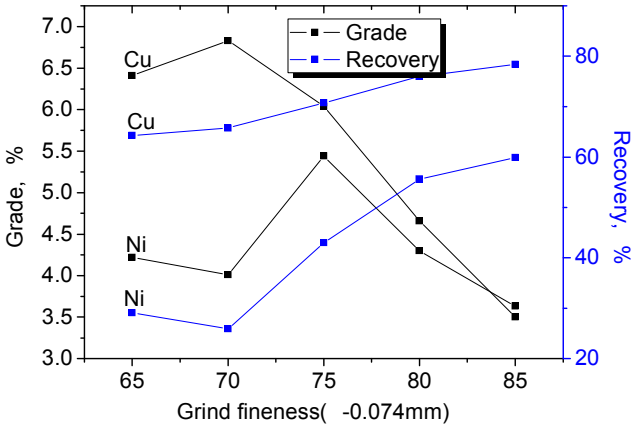

Fig.1 Effect of activator dosage on the concentrate grades and recoveries of Cu and Ni from the rougher flotation.

2) Effect of inhibitors

Inhibitors can block or reduce the speed of chemical reaction. The flotation with the dosage of copper sulfate 200 g/t, amyl xanthate 100 g/t, pine oil 30 g/t and different inhibitors was studied.

Results of sodium carbonate and CMC or sodium silicate and CMC used as inhibitors are shown in Fig.2. The optimum mixed concentrate was got when sodium silicate and CMC were used as inhibitors, with the recovery of recoverable Cu and Ni elements as high as 76% and 65.6%, respectively, while the grade of recoverable Cu and Ni were 4.66% and 4.3%, respectively. Compared the results of sodium carbonate and CMC were used as inhibitors, though the grade of Cu and Ni were reduced 1% and 0.7%, the recoveries increased 1.5% and 19.5%.

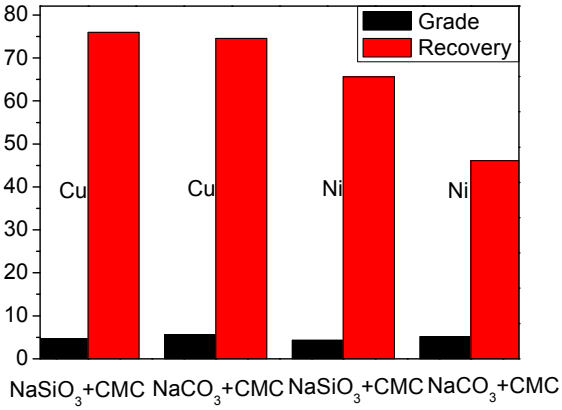

Fig.2 Effect of inhibitors on the concentrate grades and recoveries of Cu and Ni from the rougher flotation.

Separation flotation of copper and nickel

The mixed concentrate was removed reagent with the addition of500 g/t activated carbon. Then the pH value was adjusted by 2 kg/t lime. The effect of the new nickel inhibitor YS on the separation of copper and nickel was studied and the results are illustrated in Fig.3.

As it noted, the Cu and Ni recoveries increased maximum and then decreased with increasing of the dosage of YS. But the grades of them were changed a little. The optimum dosage of YS was 5 g/t with the grade of Cu and Ni were 26.65% and 3.8%, the recoveris was 55.62% and 55.3% in the separation flotation, respectively. Obviously, the inhibition of the new mixed reagent YS was stronger on the flotation of nickel and weaker on copper in the alkali conditions.

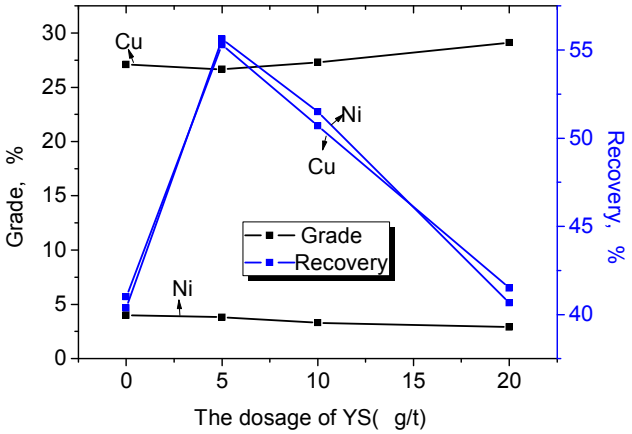

Fig.3. Effect of YS on the concentrate grades and recoveries of zinc and indium from the rougher flotation.

Conclusions

The conclusions were made as a result of this experimental study carried on copper and nickel ore in Yunnan Province of China.

High-quality mixed concentrate with the recoveries of Cu and Ni 76% and 65.6% and the grade of Cu and Ni were 4.66% and 4.3%, respectively, was got under the condition of sodium silicate (200 g/t), CMC (200 g/t), copper sulphate200 g/t, amyl xanthate 100 g/t and pine oil 30 g/t with the grinding fineness of -0.074mm80%.

Qualified Cu concentrate with the grade26.65% and recovery 55.62%, Qualified Ni concentrate with the grade26.65% and recovery 55.62%, respectively, were got by using the new nickel inhibitor YS in the separation flotation of copper and nickel.

Acknowledgements

This study was financially supported by the National Natural Science Foundation of China (No.51174103) and the Foundation of Yunnan province (kksy201221138).

References

[1] D.F. Chen. Characteristics of Main Metallic Minerals in Some Copper-Nickel Sulfide Deposits of China [J]. ACTA PETRROLOGICA ET MINERALOGICA.Vol.4 (1995)No.4.p 345-354.

[2] J.F. LV, X TONG, Y.Q. CUI. Experimental Study on Mineral Processing Technology for a Low-grade Copper-nickel Ore from Yunnan [J].Multipurpose Utilization of Mineral Resources. (2011)No.3.p.25-28.

[3] Y.H. ZHANG, F.D. MENG, C.Y SUN. Analysis of effective approaches for depressing MgO-containing gangue minerals in copper-nickle sulfideore flotation[J].Mining and Metallurgy. Vol.21(2012)No.2.p.1-5.

[4] F.L. XING, B.Q. XIAO, Z.M. WANG. Research progress on copper-nickle separation technology in copper-nickle ore[J].Mining and Metallurgy.Vol.19 (2010)NO.1.p. 25-32.

[5] D.M. Liang, B. Yang. Research Progress in Beneficiation of Copper-nickel Sulfide Ore. Modern Mining. (2009)No.8.p.14-16.

Advanced Materials Research Vols. 989-994 (2014) pp 1415-1418
© (2014) Trans Tech Publications, Switzerland
doi:10.4028/www.scientific.net/AMR.989-994.1415

Concentration and Distribution of Cr, Pb and Zn in the Jurassic Coals from Northern Shaanxi and Ningxia, China

Wang Hua[1,a], Du Meili[1, b], Zhang Guotao[2]

[1]Department of Chemistry and Chemical Engineering , Xi'an University of Science and Technology, Xi'an, Shaanxi 710054, China

[2]Department of Chemistry and Chemical Engineering , Yulin University, Yulin , Shaanxi, 719000, China

[a]email: 99452715@qq.com, [b]email:duml@xust.edu.cn

Keywords: Coal; Jurassic; Distribution; Cr; Pb; Zn

Abstract. The concentration and distribution of Cr, Pb and Zn in 22 Jurassic coals from northern Shaanxi,and Ningxi, China were studied. The samples were collected from eight coal mines of five different region, including Yuyang Region, Hengshan, Shenmu, Huangling and Lingwu. Comparing with Chinese coals, American coals and coal Clarke value: Pb showed different degree enrichment in the study region except Ningxia ; Cr was enriched in Shenmu coals, Huangling coals and Hengshan coals; whereas the content of Zn in the study region coals was lower than in American coals. Horizontal variation of the three elements in the study region indicated that different elements showed different variation trend. Based on statistical analyses, Pb showed a moderate relationship with ash yield, whereas Cr had a high correlation coefficients with total sulfur.

1 Introduction

Cr, Pb and Zn are the trace elements of environmental concern. Their environmental impact is related with their concentration, toxicity and modes of occurrence in coals[1][2].The elements concentration in coals is related to coal peat-swamp environments, geological processes during deposition and post-deposition, as well as the properties of coal bedrocks[3]. The elements in coals may be concentrated in organic matter, or in inorganic matter, such as in silicates, carbonates or sulphates minerals. At sometimes, the elements may been not only associated with organic matter, but also with inorganic matter.

There are many publications that have reported the elements concentration, distribution and origin in different coals[1][4][5][6].But, most publications paid attention to the districts where the elements are anomalous enriched. Moreover, the number of samples analyzed was limited.

There are huge coal resource in northern Shaanxi, and Lingwu, Ningxia. The coal is Jurassic bituminous coal, with low sulfur content, low ash yield and high calorific. The coal is mined mainly for power generation. There is little knowledge about the concentration and distribution of trace elements in the places. Therefore, it is essential to understand the abundances and distribution of trace elements in these places.

2 Experimental

2.1 Instrumentation and reagent

Microwave assisted extraction was conducted using a MDS-8 microwave oven (from Shanghai Sino Instruments in China) with polytetrafluoroethene extraction vessels. The temperature and pressure were monitored in a control vessel by an armored fiber-optic temperature and pressure control probe. The concentration of Cr, Pd and Zn were determined by AAS-6100 atomic absorption spectrometer(Shimadzu Instrument in Japan). The coal ash yield was analyzed by HTGF-3000 instrument (made in Hebi, Henan, China). The sulfur concentration in coals was determined using sulfur tester(made in Shanghai, China).

H_20_2 is analytical reagent without further purification. HNO_3 and HF are all the guaranteed reagent. The solutions were prepared using ultrapure water passed through a ultrapure water purification system(made in Nanjing, China)

2.2 Coal sample

Coal samples were obtained from seven coal mine of northern Shaanxi and one coal mine of lingwu. Before the experiment and analysis, all coal samples were ground by a high speed crusher, sieved through a 200-screen, and kept into pre-cleaned glass bottles at room temperature for subsequent analyses.

2.3 Sample treatment

For each run coal sample of about 0.1g(±0.0001g) was dissolved into 8 mL HNO_3, 2 mL H_20_2 and 1 mL HF on a microwave digestion system. The digestion was conducted under 8MPa for 50 min at 100-180°C , and 9 MPa for 10 min at 200°C. After 0.1 g sample was dissolved, it was made up to 50 mL with ultrapure water for AAS analysis.

3 Result and discussion

3.1 Content of elements in Yuyang Region coals

Yushuwan(YSW) coal mine was located in Yuyang Region, Yulin, Shaanxi, China. Only three samples from the coal mine were collected and analyzed. The contents of Cr, Pb and Zn in the coals were showed in Table 1. Table 2 listed ranges and arithmetic mean(AM) of concentration of Cr, Pb and Zn in Chinese coals ,which are Middle Jurassic coals from Shanxi, and in USA coals. The table 2 also included coal Clarke value of Cr, Pb and Zn.

Table 1 The content of elements and ash yield in Yushuwan coals

Sample	Cr(ppm)	Pb(ppm)	Zn(ppm)	St,d(%)	*Ad*(%)
YSW1	1.66	82.66	34.63	0.63	17.88
YSW2	24.81	64.54	65.61	0.34	3.25
YSW3	14.71	51.07	20.96	0.50	9.12
AM	13.73	66.09	40.40	0.49	10.08

Comparing YSW coal with coal Clarke value, we concluded that Pb(up to 7.34×) was strong enriched, Zn (up to 1.44×) showed a moderate enrichment, and Cr had no enrichment. As compared to USA coal, only Pb (up to 6.01×) showed a high enrichment. YSW coals were located in Yan'an Formation coal-bearing strata. Compared with Middle Jurassic coals in Shanxi, the three elements(1.7- 7.03×) showed a certain degree of enrichment.

Table 2 The content and range of elements in Chinese coals and American coals , as well as coal Clarke value(ppm)

Element	Chinese coal[7]		American coal[8]		Clarke[9]
	Range	AM	Range	AM	AM
Cr	2.2-19.4	7.2	0.25-43	14	17
Pb	Bdl-30.0	9.4	0.3-590	11	9.0
Zn	Bdl-64.1	23.7	0.85-5100	53	28

Bdl: below detection limit;

3.2 Content of elements in Ningxia coals

The coal samples were collected from Lingwu, Ningxia(NX), China. NX coals were located in the Third Member of Jurassic Yan'an Formation, and named No. 2 coals of Yan'an Formation. The three samples of NX coals were analyzed , and the results were listed in Table 3.

In NX coals , only Pb had a similar value with coal Clarke value, whereas the content of Cr and Zn were lower than coal Clarke value. The content of the three elements in NX coals were lower than in American coals. As compared with Jurassic coals in China, only Cr (up to 1.78×) showed a moderate enrichment in NX coals.

Table 3 The content of elements and ash yield in lingwu coals

Sample	Cr(ppm)	Pb(ppm)	Zn(ppm)	St,d(%)	*Ad*(%)
NX1	8.03	14.84	16.57	0	3.1
NX2	6.63	2.76	14.13	0	2.57
NX3	23.72	11.59	6.98	0.33	3.61
AM	12.79	9.73	12.56	0.11	3.09

3.3 Content of elements in Shenmu coals

Shenmu has huge coal resource. Zhangjiamao (ZJM) coal mine was located in Shenmu, Shaanxi, China. Only one sample from Shenmu was collected and analyzed. The content of the three elements were listed in Table 4.

A comparison of content of the three elements in ZJM coal with coal Clarke value indicated that the three elements showed a certain degree of enrichment, and Pb (up to 2.17×) had the higher

enrichment than Cr and Zn. Comparing with American coals, Cr showed higher enrichment than Pb in ZJM coals, and Zn content was lower than coal Clarke value. As compared with Jurassic coals, the three elements showed enrichment in ZJM coals. Cr(up to 1.78×) and Pb(up to 2.09×) were strongly enriched, and Zn(up to 1.89×) showed a moderate enrichment.

Table 4 The content of elements and ash yield in Zhangjiamao coal

Sample	Cr(ppm)	Pb(ppm)	Zn(ppm)	St,d(%)	Ad(%)
ZJM	29.16	19.49	44.94	0.52	4.74

3.4 Content of elements in Huangling coals

Huangling(HL) coal mine was located in Huangling, Yan'an, Shaanxi, China. Six samples were collected and analyzed from HL coal mine. As compared with Chinese coals, American coals and coal Clarke value, Cr and Pb were enriched, and Zn showed no enrichment.

3.5 Content of elements in Hengshan coals

Nine samples were collected from four coal mines in Hengshan, Yulin, Shaanxi, China, including Shimawan (SMW) , Gaoxingzhuang (GXZ), Fanhe (FH) and Changgou(CG) coal mine. The coal beds in the four coal mines were deposited in No.3 coal seam of the Second Member of Jurassic Yan'an Formation. As compared with Chinese coals, American coals and coal Clarke value, Cr(2.65-6.25×) and Pb(2.77-3.38×) were strongly enriched, and Zn showed no enrichment.

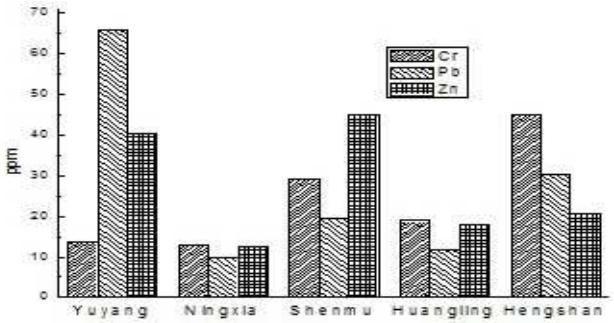

Fig. 1 Stacked bar plot of trace element contents in different district

3.5 Horizontal variation of content of the elements

In the study regions, the content variation of the trace elements was showed in Fig.1. From it, we can see that the highest content of Cr was in Hengshan coals, for Pb in Yuyang coals and for Zn in Shenmu coals. The lowest contents of three elements were in Ningxia coals. Ningxia coals had the lowest level of dry base total sulfur(0.11%) and dry base ash yield(3.09%). It may be the reason that the lowest content of the trace elements was in Ningxia coals.

Table 5 The content of elements and ash yield in Huangling coals

Sample	Cr(ppm)	Pb(ppm)	Zn(ppm)	St,d(%)	Ad(%)
HL1	21.39	13.91	28.16	0.48	3.23
HL2	7.72	13.91	23.08	0.54	5.59
HL3	22.33	5.55	19.73	0.36	6.29
HL4	22.95	6.02	11.38	0.48	3.56
HL5	31.03	25.06	6.75	0.8	10.24
HL6	8.18	6.48	18.31	0.49	6.19
AM	18.93	11.82	17.90	0.53	5.85

Table 6 The content of elements and ash yield in Hengshan coals

Sample	Cr(ppm)	Pb(ppm)	Zn(ppm)	St,d(%)	Ad(%)
SMW1	27.61	74.30	34.05	1.73	6.69
SMW2	12.69	30.63	28.07	1.812	4.66
SWM3	41.6	48.29	49.05	1.54	6.59
GXZ1	13.78	3.694	14.14	1.3	6.3
GXZ2	7.41	2.30	23.07	0.81	3.3
FH1	133.28	25.99	7.21	3.76	5.78
FH2	123.65	56.18	1.03	5.42	10.36
FH3	13.62	18.56	19.31	1.98	6.32
CG1	31.65	14.38	8.86	3.59	14.37
AM	45.03	30.48	20.53	2.44	7.15

3.6 Association of trace element content with ash yield

The relationships between trace element content and ash yield was used to conclude trace elements association with the mineral in coals. The Fig. 2 showed the relationship between the element content and ash yield in different coals. The ash yield of coals in this study area ranged from 2.57% to 17.88%, with an average of 6.53%. The coals in this study area were low ash coals. The correlation coefficients of Pb contents with ash yield was 0.499. It indicated that Pb had a moderate association with inorganic matter. The content of Cr (0.122) and Zn (-0.139) had lower correlation coefficients with ash yield than Pb. This indicated that the two elements had lesser inorganic but more organic affinity. Total sulfur content had a low correlation coefficient (0.397) with ash yield. It showed that organic sulfur dominated in the study area coals. Cr had relatively high positive correlation

coefficient (0.804)with the total sulfur. We can concluded that Cr may been mainly related with organic matter, especially organic sulfur functional group.

4 Conclusions

The concentration of three elements from different places in the study area varied greatly. Comparing with Chinese coals, American coals and coal Clarke value, Pb showed different degree enrichment in the study area except Ningxia. As comparison with Chinese coals, American coals and coal Clarke value,Cr was enriched in Shenmu coals, Huangling coals and Hengshan coals. The content of Zn in the study area was lower than in American coals. Compared with Chinese coals, only Yuyang coals and Shenmu coals displayed higher content of Zn.

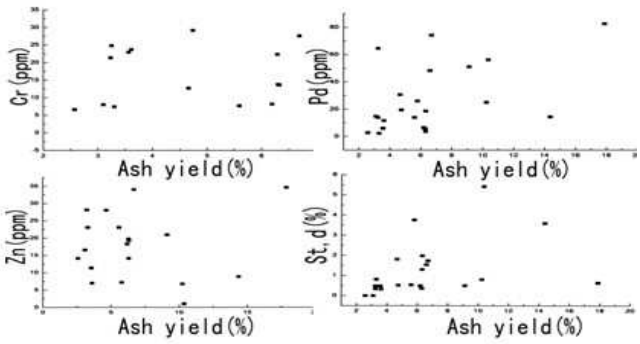

Fig.2 The relationship between content of elements and ash yield

The highest content of Cr was in Hengshan coals, for Pb in Yuyang coals, and for Zn in Shenmu coals. The lowest content of the three elements was in Ningxia coals.

In the study area, the content of Cr and Zn were not clearly related with ash yield. Pb had a moderate relationship with ash yield, while Cr had a high correlation coefficients with total sulfur.

Acknowledgement

In this paper, the research was sponsored by the Nature Science Foundation of China(Project No. 201141172142).

References

[1] Dai S.F., Ren, D.Y., Tang Y.G., Yue M., Hao L.M.. Concentration and distribution of elements in Late Permain coals from western Guizhou Province, China [J]. International Journal of Coal Geology. 2005 (61) 119-137.

[2] Swaine D.J., Goodarzi F.. Environmental Aspects of Trace Elements of Coal[M]. Kluwer Academic Publishers, Dordrecht. 1995: 24–50.

[3] Goodarzi F., Swaine D.J.. The influence of geological factors on the concentration of boron in Australian and Canadian coals[J]. Chemical Geology. 1994 (118) 301–318.

[4] Dai S., Zhou Y., Ren D., Wang X., Li D., Zhao L.. Geochemistry and mineralogy of the Late Permian coals from the Songzao Coalfield, Chongqing, southwestern China[J]. Science in China Series D: Earth Science. 2007 (50) 678–688.

[5] Liu G.J., Vassilev S.V., Gao L.F., Zheng L.G., Peng Z.C.. Mineral and chemical composition and some trace element contents in coals and coal ashes from Huaibei coalfield, China[J]. Energy Conversion and Management. 2005 (46) 2001–2009.

[6] Du G., Zhuang X.G., Querol X., Izquierdo M., Alastuey A., Moreno T., Font O.. Ge distribution in the Wulantuga high-germanium coal deposit in the Shengli coalfield, Inner Mongolia, northeastern China[J]. International Journal of Coal Geology. 2009 (78) 16–26.

[7] Zhang J.Y., Zheng C.G.. Distribution of potentially hazardous trace elements in coals from Shanxi province, China[J]. Fuel. 2004 (83) 129-135.

[8] Swaine D.J.. Trace elements in coal[M]. London : Butterworths. 1990: 296.

[9] Ketris M.P., Yudovich Ya.E.. Estimation of Clarkes for carbonaceous biolithes: world averages for trace element contents in black shales and coals[J]. International Journal of Coal Geology. 2009 (78) 135–148.

Advanced Materials Research Vols. 989-994 (2014) pp 1419-1423
© (2014) Trans Tech Publications, Switzerland
doi:10.4028/www.scientific.net/AMR.989-994.1419

The Quantitative Model Research of Impact of Water Level Changes on Channel Capacity

Ting Liu[1, a], Yao Liu[2,b] , Chen Zhao[3,c]

[1] School of Transportation, Wuhan University of Technology, Wuhan, 430063, China

[2] School of Transportation, Wuhan University of Technology, Wuhan, 430063, China

[3] Transport Management Institute, Ministry of Transport, Beijing, 101601, China

[a]email:515501708@qq.com, [b]email:332556138@qq.com, [c]email:81371999@qq.com

Keywords: Water Level Changes, Channel Capacity, Ship Loading Rate, Impact

Abstract. Water level determines channel capacity, in order to protect the safety of navigation and give full play to the advantages of shipping, the paper analyzes the relationship between the draft and loading rate of various types of ships, and proposed the quantitative model of impact of water level changes on channel capacity, the results showed: small ships are less affected by water level changes, and large ships are great affected by water level changes, the actual amount of cargo related the ship design parameters, this article has a certain reference value for navigation management and planning.

Introduction

Channel capacity usually refers to certain grades and standards of channel. Under certain environmental conditions of navigation, channel can navigate the largest scale, the largest DWT of ships and the quantity of ships flow[1]. Water level is not only the primary condition for safe navigation, but also one of the main factors that affect on channel capacity. With the rapid development of the inland river construction, water level and ship types have a significant change, it is necessary to study the relationship between water level and channel capacity.

The Relationship between Water Level and Water Depth

In fact, the concept of water level is different from water depth. Water depth is the vertical distance from water surface to the bottom of the river, and water level is the vertical distance from water surface to the reference plane, and now the data of hydrological observations are based on water level, can convert water level into water depth by a certain formula (actual water depth = graphical representation of water ship± the value of water level) .

Relationship between Water Depth and Channel Capacity

Water depth of channel directly affects the channel capacity. while at the same channel, different points, different lines and different sections, the water depth is not the same, in order to ensure the safety of navigation, should be considered the minimum water depth at the ship route. Relationship between the draft of ship and water depth of channel can be expressed as[2][3]:

$$H = T + \Delta h \tag{1}$$

In this formula, H is the minimum water depth of channel; T is the draft of ship; and Δh is the additional water depth of the channel, it means that the height from the bottom of the ship to the bottom of the channel. The unit is m.

If a ship wants to navigate at a certain grade of channel, water depth of channel should ensure that the ship has the additional water depth for safe navigation in the draft, the ship can be adjusted cargo capacity to change the draft in order to accommodate water depth of the channel. The additional water depth of different grades of channel are different.

Relationship between Water Depth and Ship Loading Rate

1）Ship loading rate. Ship loading rate is the ratio of the actual load capacity to the design load capacity of the ship. In ensuring safe navigation and do not overload, the higher loading rate, the stronger shipping capacity, and the better benefits. Ship loading rate can be extrapolated by ship displacement formula.

$$\Delta_0 = L_c BTc_b \tag{2}$$

In this formula, Δ_0 is displacement when the ship has the design load, the unit is t; L_c is length of the ship, the unit is m; B is breadth of the ship, the unit is m; T is the largest draft when ship has the design load, the unit is m; and c_b is block coefficient which is different from different ships.

Length, width and block coefficient of the ship is constant, so displacement of the ship and the draft presented exist in a direct proportion relationship. When the displacement changes, the draft will occur in direct proportion changes .

$$\frac{\Delta}{\Delta_0} = \frac{T_s}{T} = \frac{W_o + W_e}{W_o + W} \tag{3}$$

T_s :Actual draft of the ship, the unit is m.

Loading rate of ship can be expressed as:

$$\varepsilon = \frac{W_e}{W} = \frac{(W_o + W)}{WT} T_s - \frac{W_o}{W} \tag{4}$$

The maximum load capacity, the maximum draft and ship weight are related with ship types, they all are constant, so loading rate of ship is a function of actual draft. The actual draft of the ship can be expressed as:

$$T_s = \min(H - \Delta h,\ T) \tag{5}$$

The design draft is a constant when ship is certain, loading rate of ship can be expressed as:

$$\varepsilon = \frac{(W_o + W)}{WT} \min(H - \Delta h,\ T) - \frac{W_o}{W} \tag{6}$$

If $a = \frac{(W_o + W)}{WT}$, $b = \frac{W_o}{W}$, a and b are constant, the above formula can be simplified to:

$$\varepsilon = f(T_s) = a \min(H - \Delta h,\ T) - b \tag{7}$$

Impact of water level changes on loading rate of ship needs to be studied from two aspects. One is water depth changes of channel; the second is the adaptational degree of ship types for water level changes.

2) The quantitative model of impact of water level changes on ship loading rate. Assuming ship will load shedding when water level will not ensure the additional water depth of the channel for sage navigation. Maximum load of ship depends on the minimum water depth of navigation route, the ship will not be loaded that means the loss of capacity. H_1 and H_2 respectively represents two channel's water depth conditions, and $H_1 > H_2$. Water depth of channel reduced from H_1 to H_2.

There are three situations with the relationship between the two channel's water depth and the additional water depth. The first situation is $\Delta h < H_2 < H_1$; the second one is $H_2 < \Delta h < H_1$, and the last one is $H_2 < H_1 < \Delta h$. Different water depths represent different navigation conditions. Different ship types have different degree of sensitivity to water level changes.

(1) The first situation is $\Delta h < H_2 < H_1$. According to this water depth, to build a conceptual model between water depth and the draft of all types of ships. As shown in Fig 1.

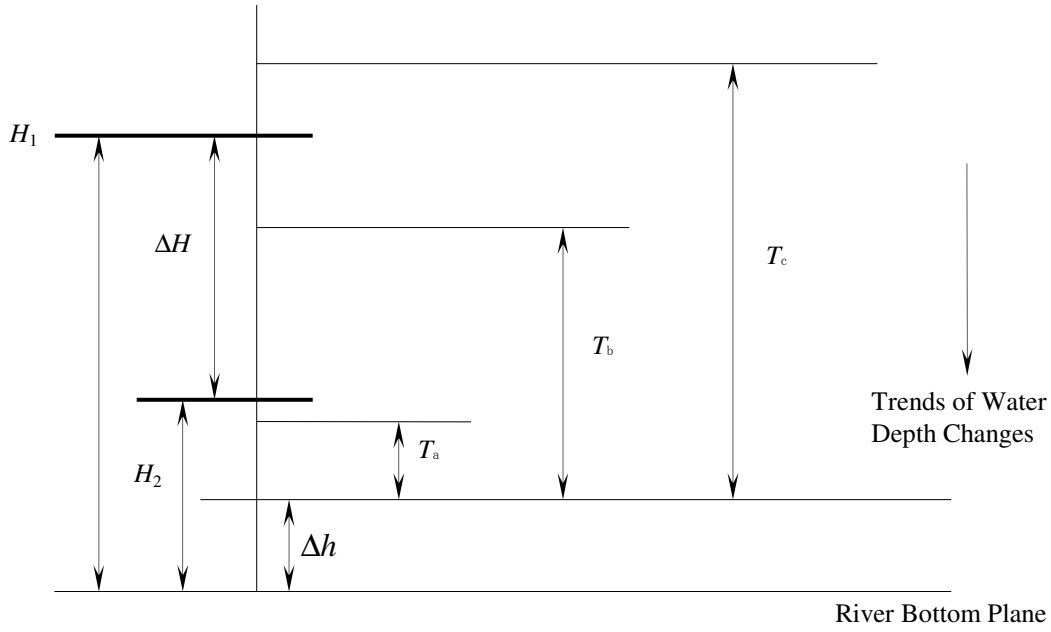

Fig.1 A Conceptual Model between Water Depth and the Draft of all Types of Ships(1)

H_1 :The first water depth condition, the unit is m;

H_2: The second water depth condition, and $H_1 > H_2$, the unit is m;

ΔH :Water depth variation, namely H_1 - H_2, the unit is m;

Δh : The additional water depth of a certain grade channel, the unit is m;

T_a, T_b, T_c :the draft of a, b, c types of ship, namely the design draft, the unit is m.

In this water depth condition, ships are divided into three types:

①Type A:The seaworthy water depth of type A ships is $T_a+\Delta h$ when it is full load, and $T_a+\Delta h \leqslant H_2$, it shows that water depth changes has no effect on its cargo capacity, ship type A can be fully loaded before and after changes in the water level.

②Type B:The seaworthy water depth of type B ships is $T_b+\Delta h$ when it full load, and $H_2<T_b+\Delta h \leqslant H_1$, it shows that water depth changes has some effect on its cargo capacity, the first condition of water depth can achieve full load, the ship's draft is T_b, and $\varepsilon_{b_1} = 100\%$; but water depth reduces from H_1 to H_2 ,the ship should load shedding for ensuring safe navigation, maximum draft should reduce to H_2-Δh , at this time, loading rate changes into $\varepsilon_{b_2} = a(H_2\text{-}\Delta h) - b$.

③Type C:The seaworthy water depth of type C ships is $T_c+\Delta h$ when it is full load, and $T_c+\Delta h > H_1$, it shows that both water depth conditions all can't achieve full load. When water depth is H_1, the loading rate is $\varepsilon_{c_1} = a(H_1\text{-}\Delta h) - b$; when water depth changes into H_2, the loading rate will reduce to $\varepsilon_{c_2} = a(H_2\text{-}\Delta h) - b$. Loading rate of type C ships is affected by water level changes. Change amount of loading rate can manifest as $\Delta\varepsilon_c = a\Delta H$.

Based on the above analysis, water depth changes affects loading rate of ships, this effect related to the draft when ship is full load. In two different water depth conditions, there are three different change patterns of ship's loading rate, mathematical models shows that:

$$\begin{cases} T+\Delta h \le H_2, \begin{cases} \varepsilon_1=100\% \\ \varepsilon_2=100\%; \end{cases} \\ H_2<T+\Delta h \le H_1, \begin{cases} \varepsilon_1=100\% \\ \varepsilon_2=a(H_2\text{-}\Delta h)-b; \end{cases} \\ T+\Delta h>H_1, \begin{cases} \varepsilon_1=a(H_1\text{-}\Delta h)-b \\ \varepsilon_2=a(H_2\text{-}\Delta h)-b_\circ \end{cases} \end{cases} \tag{8}$$

In the formula, ε_1 is loading rate of ship when water depth is H_1; ε_2 is loading rate of ship when water depth is H_2.

(2) The second situation is $H_2 < \Delta h < H_1$. As shown in Fig 2, there are two types of ships will be affected by this situation.

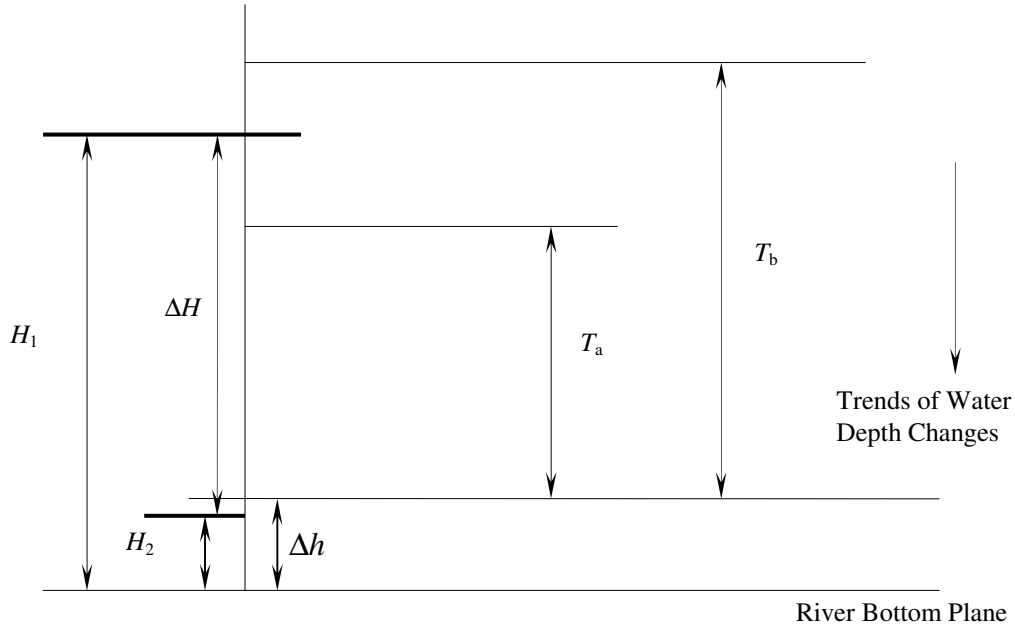

Fig.2 A Conceptual Model between Water Depth and the Draft of all Types of Ships(2)

①Type A. The seaworthy water depth of type A ships is $T_a+\Delta h$ when it is full load, and $H_2<\Delta h \le T_a+\Delta h \le H_1$, it shows that the ships can achieve full load under the first condition of water depth; but under the second condition of water depth, H_2 is less than Δh, ships can't achieved by shedding for ensuring safe navigation, then type A ships ran aground.

②Type B. The seaworthy water depth of type B ships is $T_b+\Delta h$ when it is full load, and $H_2<\Delta h<H_1<T_b+\Delta h$, it shows that the ships can't achieve full load under the first condition of water depth, loading rate is $\varepsilon_{b_1}=a(H_1\text{-}\Delta h)\text{-}b$; but under the second condition of water depth, type B ships ran aground like type A ships.

Obviously, when $H_2<\Delta h$, water depth can't ensure the additional water depth for safe navigation, then all ships are in suspended state. Based on the above analysis, when water level condition is satisfied $H_2<\Delta h<H_1$, loading rate model of ship is expressed as follows:

$$\begin{cases} H_2 < \Delta h < T + \Delta h \le H_1, \begin{cases} \varepsilon_1 = 100\% \\ \varepsilon_2 = 0; \end{cases} \\ H_2 < \Delta h < H_1 < T + \Delta h, \begin{cases} \varepsilon_1 = a(H_1 - \Delta h) - b \\ \varepsilon_2 = 0. \end{cases} \end{cases} \tag{9}$$

（3）The last situation is $H_2<H_1<\Delta h$ .This situation exists in theory, namely before and after changes of water depth all are less than the additional water depth. Ships all are in suspended state, and have no significance, so this article excluded this situation.

Thus, water depth affects choice of ships and loading rate. Generally, the smaller the ship, the smaller impact subject to condition of water depth changes. Water depth changes ultimately affect the cargo capacity, voyage costs and revenues[4]. Broadly, it will affect entire shipping benefits.

Conclusion

This article analyzes the relationship between water level and channel capacity, small ships affected by water level changes is smaller than the large ships, the actual amount of cargo related to design parameters of the ship. And proposed the quantitative model of impact of water level changes on channel capacity. But in the actual voyage, other factors should be considered such as channel width, clearance height, curved radius[1][5]. it has an important significance for shipping cost control, logistics planning and shipping management, business operations and scheduling shipping.

References

[1] Guo Yihao, Liu Jialun, Liu Mingjun: Study of Relationship between Water Level and Capacity of Navigation Channel, in Journal of Wuhan University of Technology Vol. 34 (2010), p. 842-844.

[2] Liu Mingjun, Wan Changzheng: Analysis of the Factors Affecting Traffic Capacity of Navigation Channel, in Ship & Ocean Engineering Vol. 37 (2008), p. 116-118.

[3] Liu Yali: Research on Yangtze River Waterway Capacity, Wuhan University of Technology (2007).

[4] Bian Yijie: A Study on Waterway Transit Capacity, in Port & Waterway Engineering Vol. 319 (2008), p. 27-30.

[5] Dong Yu, Jiang Ye, He Liangde: Calculation Method of Inland Waterway's Throughput Capacity, in Port & Waterway Engineering Vol. 398 (2007), p. 59-65.

Advanced Materials Research Vols. 989-994 (2014) pp 1424-1427
© (2014) Trans Tech Publications, Switzerland
doi:10.4028/www.scientific.net/AMR.989-994.1424

Porosity inversion under the sequence stratigraphy framework

Wei Yang[12, a], Mingyi Hu[12]

[1.] Key Laboratory of Exploration Technologies for Oil and Gas Resources of Ministry of Education, Yangtze University, Wuhan, China;
[2.] Faculty of Earth Science, Yangtze University, Wuhan, China
[a]87390538@163.com

Keywords: reef, sequence stratigraphy, Seismic multiple attributes, neural network, porosity

Abstract: Carbonate reef reservoir buried deeply, show great heterogeneity, Therefore, effective reservoir prediction is the key to the biohermal reservoir. In practical research, based on of the single well sequence stratigraphic framework, combined with these sequence stratigraphic framework and seismic section, found the reservoir development area in the longitudinal, which sq1-HST and sq3-HST is the main period of reservoir development, and then through the seismic Seismic multiple-attribute inversion, predicted porosity of system tracts of reservoir development in the sequence stratigraphic framework. Porosity inversion results shown, Changxing formation reservoir is mainly distributed in the central and north-central of Jiannan area.

Introduction

In recent years, carbonate reef reservoir prediction is the focus of oil and gas exploration. However, reef bank reservoir show great heterogeneity in the lateral, porosity Variation in space, caused a certain extent difficulty in the prediction of reef reservoir. In this reseach, integrated sequence stratigraphy and geophysical inversion method, under the sequence stratigraphic framework, predicted porosity of Changxing formation reservoir, finally find out the spatial distribution characteristics of reservoir.

1 reservoir development section in sequence stratigraphic framework

Platform margin reef mainly developed in Zhuxi area of the northern highlands in 3D study area, moundy reflection in seismic profile, has the typical characteristics of reef reflection. The typical well is well Jianzhu1, which drill Jianzhuxi reef (Figure 1), reef reservoir of well Jianzhu 1 was mainly developed sq1-HST and sq3-HST in the four grade sequences, which is phase 2 and phase 3.

2 the principle of porosity inversion

During this research, we selected method of seismic multi-attribute inversion to predict porosity value. Seismic multi-attribute inversion is process that change seismic internal attributes into lithologic character curve. Seismic internal attributes included instantaneous attributes, time-frequency attributes, filter sections, derivative, integral property attribute, time (linear gradient)and other types. Firstly, we selected seismic attributes that have best fitting advantage degree with the quasi porosity curve, then, used neural network algorithm to establish the nonlinear relationship the various attributes that have selected and quasi porosity curve, applied this relationship to extrapolate seismic attribute, finally, we got the prediction of porosity profile.

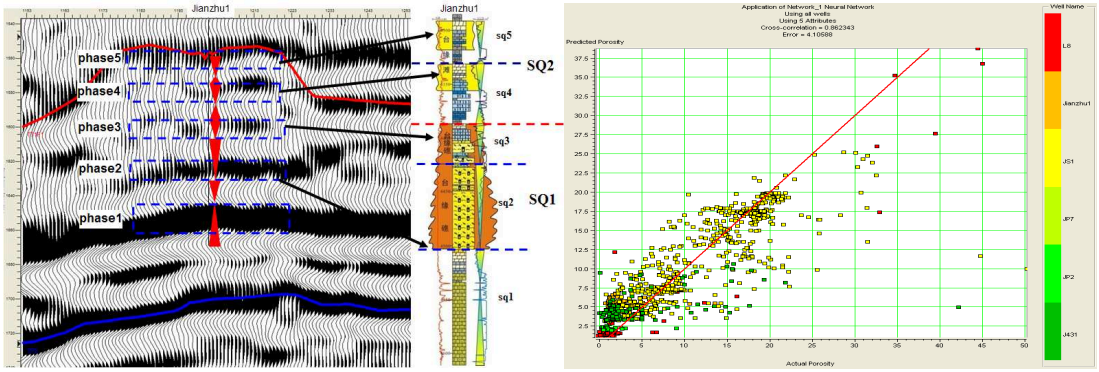

Fig.1 Seismic profile calibration of the 4th sequence in Changxing formation

Fig.2 The relationship between seismic attributes and porosity nonlinear coincidence rate diagram

When we established combination of seismic multi-attribute and quasi porosity curve, used the algorithm of multivariate regression and neural network. Multiple regression algorithm is directly applying the linear weighted, got linear relationship of the predicted characteristic curve and multi-attribute of seismic, but between the seismic attributes combination and the predicted characteristic curve is not simple linear relationship , its exists a complex nonlinear relationship. In the course of practical research, we used of neural network algorithm, through its independent learning established the nonlinear mapping relationship between seismic attributes and quasi porosity curve. Then, used neural network algorithm to fit, that between borehole side seismic attributes and quasi porosity curve correlation degree is 0.86(Fig.2), with such obvious effect, shown that this method is effective.

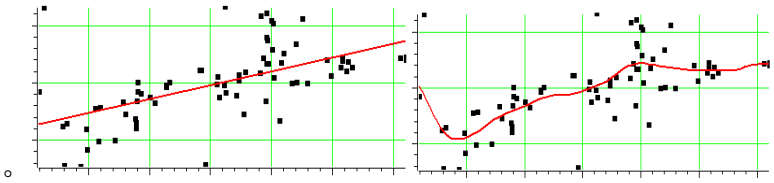

Fig.3 Linear relationship (left) and nonlinear relationship diagram (right)

Neural network probability model is the core algorithm of multi-attribute inversion. To description of the relationship between multiple-attribute is the most suitable statistical relationship, the best method of multi-attribute solving the objective function is neural network, and Kriging method has been widely used and spatial interpolation calculation. In this paper, we combine those algorithm, Which provided the core effective technology for the inversion of physical parameters of high resolution.

Firstly, according to the seismic multi-attribute and the objective function to form amulti-dimensional matrix:

$$\begin{aligned}&\{A_{11}, A_{21}, A_{31}, L_1\}\\&\{A_{12}, A_{22}, A_{32}, L_2\}\\&\cdot\\&\cdot\\&\cdot\\&\{A_{1n}, A_{2n}, A_{3n}, L_n\}\end{aligned} \tag{1}$$

Where, Li is the target curve. Given a set of training data:

$$x=\{A_{1j}, A_{2j}, A_{3j}\} \tag{2}$$

Estimate a new output curve :

$$\hat{L}(x)=\frac{\sum_{i=1}^{n} L_i \exp(-D(x,x_i))}{\sum_{i=1}^{n} \exp(-D(x,x_i))} \tag{3}$$

Where:

$$D(x,x_i)=\sum_{j=1}^{3}\left(\frac{x_j-x_{ij}}{\sigma_j}\right)^2 \tag{4}$$

Calculate the checksum error:

$$\hat{L}_m(x_m)=\frac{\sum_{i\neq m} L_i \exp(-D(x_m,x_i))}{\sum_{i\neq m}^{n}\exp(-D(x_m,x_i))} \tag{5}$$

3 Porosity prediction in sequence stratigraphic framework

Higher porosity development areas are obviously controlled by the distribution scope of biological reef as shown in Fig 4 prediction map for reservoir porosity of sq1-HST. The higher porosity development areas are mainly central Jianzhuxi reef and south-central Jinzhuping reef. Northern small-scale area partly high position expose action may be caused by regression, the formative exposed bank body developed high porosity reservoir, the small-scale high position of Well 47 in the southwest is the high porosity reservoir development area.

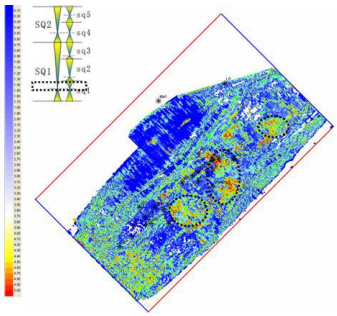

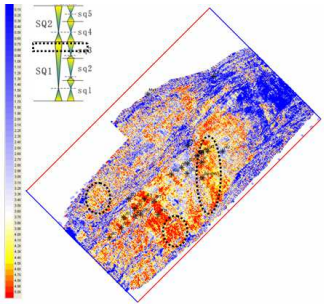

Fig.4 Sq1-HST Reservoir porosity prediction in Jiannan 3D work field

Fig.5 Sq3-HST Reservoir porosity prediction in Jiannan 3D work field

As shown in Fig 5, prediction map for reservoir porosity of sq3-HST.sq3-HST is the main development of reef and exposure. Central and southern reef bank exposed and formed high porosity reservoir, in the south is main distributed bioclastic beach, in the north, Linxichang area, small-scale area developed high porosity reservoir.

Conclusion

This paper is based on the single well sequence stratigraphy, well log and seismic data, to establish the sequence stratigraphic framework. In sequence stratigraphic framework, calibrated the reservoir, summarizes the seismic response characteristics of reservoir, clear the reservoir vertical development area. Using Seismic multi-attribute inversion，building nonlinear relationship between porosity curve and seismic gather，and forecasting of reservoir porosity respectively in sq1-HST and sq3-HST period, this method can be more reliable for the prediction of reef reservoir.

References

[1] Jing Peng-gui.Reservoir prediction technology of reef-flat facics in northeast Sichuan province and its application.GPP,2007,46(4):363-369

[2] Vail P R. Seismic stratigraphy interpretation using sequence stratigraphy,Part 1:Seismic Stratigraphy Interpretation Procedure. in Rally A W,ed,atlas of Seismic Stratigraphy;AAPG Studies in Geology,1987,27(1):1-10

[3] Ling Yun,Sun D-sheng,Gao Jun et al. Interpretation of depositional bodies in the parasequcnce sets from 3-D seismic data.GPP,2006,44(6):568-578

[4] Russell B H.The application of multivariate statistics and neural networks to the prediction of reservoir parameters using seismic attributes[D].Calgary:Department of Geology and Geophysics,Canada,2004.

[5] Liu S, Guo X S, Ma Z J,et al.Seismic response characteristic and hydrocarbon exploration perspertivc of reef flat fades[J].Geophysical Prospecting for Petroleum,2006,45(5):452-458

[6] Cai Hanpeng, He Zhenhua, Huang Deji. Study on method for prediction of coral shoal facies oil-gas reservoir[J].Oil Geophysical Prospecting,2008,43(6):685-688.

Advanced Materials Research Vols. 989-994 (2014) pp 1428-1431
© (2014) Trans Tech Publications, Switzerland
doi:10.4028/www.scientific.net/AMR.989-994.1428

Analysis on acidity and alkalinity of metallogenetic environment in penecontemporaneous period on the bauxite in WZD area, northern Guizhou, China

Tao Cui

College of Resources and Environmental Engineering, Guizhou Institute of Technology, Guiyang, 550003, China

cuitao1203@163.com

Keywords: WZD area; Bauxite; acidity and alkalinity

Abstract: Acidity and alkalinity of metallogenetic environment in penecontemporaneous period is very important for the informing of high grade bauxite. Through the research on migration regular of elements, the position of rare earth mineral and the qualitative alternation of bauxite we found that metallogenetic environment is acidic in penecontemporaneous period, from top to bottom of the profile acidity is decreased gradually. In the acidic condition, Si and Fe moved downward but Al is relative enrichment in the middle-upper part of profile.

Introduction

There is abundant bauxite in WZD area. For a long time many experts and scholars have research on the bauxite of rocks and minerals, chemistry, sedimentary environment, provenance, mineralization age [1-6]. Former researcher have a great outcome on bauxite, But the research on acidity and alkalinity of metallogenetic environment in penecontemporaneous period is poor, this paper have a research on acidity and alkalinity by analysis on migration regular of elements, the position of rare earth mineral and the qualitative alternation of bauxite.

Geological setting

WZD bauxite is located in Wuchuan, Zheng'an and Daozhen County, northern Guizhou, which is an important part of centre Guizhou-southern Chongqing bauxite belt [7]. The regional tectonics position of the study area is in the fold belt in northern Guizhou of the upper Yangtze Block[8]. The main strata in WZD area from the oldest to the youngest including: Cambrian, Ordovician, Silurian, Permian, Triassic and Jurassic. Cambrian is mainly distributed in the core of anticlines, Triassic and Jurassic are mainly distributed in the core of synclines. Bauxite is underlying the LiangShan formation(P2l) or Qixia formation(P2q) of the middle Permian, overlying the HuangLong formation(C2h) of upper Carboniferous or the Hanjiadian formation of the lower Silurian(S1hj).The bauxite is stratiform and unconformable with the underlying and overlying strata. Fig.1 shows that the distribution of the bauxite was controlled by nine synclines. The thickness of the bauxite is 0.68-15.7m, the profile can be divided into two lithology parts: the upper part is aluminous rock, dominated by high grade bauxite or half grade bauxite; the lower part is low grade bauxite. According to the lithological and textural properties, the natural types of bauxite deposit can roughly be subdivided into four categories: massive bauxite, oolithic bauxite, clastic bauxite and earthy bauxite.

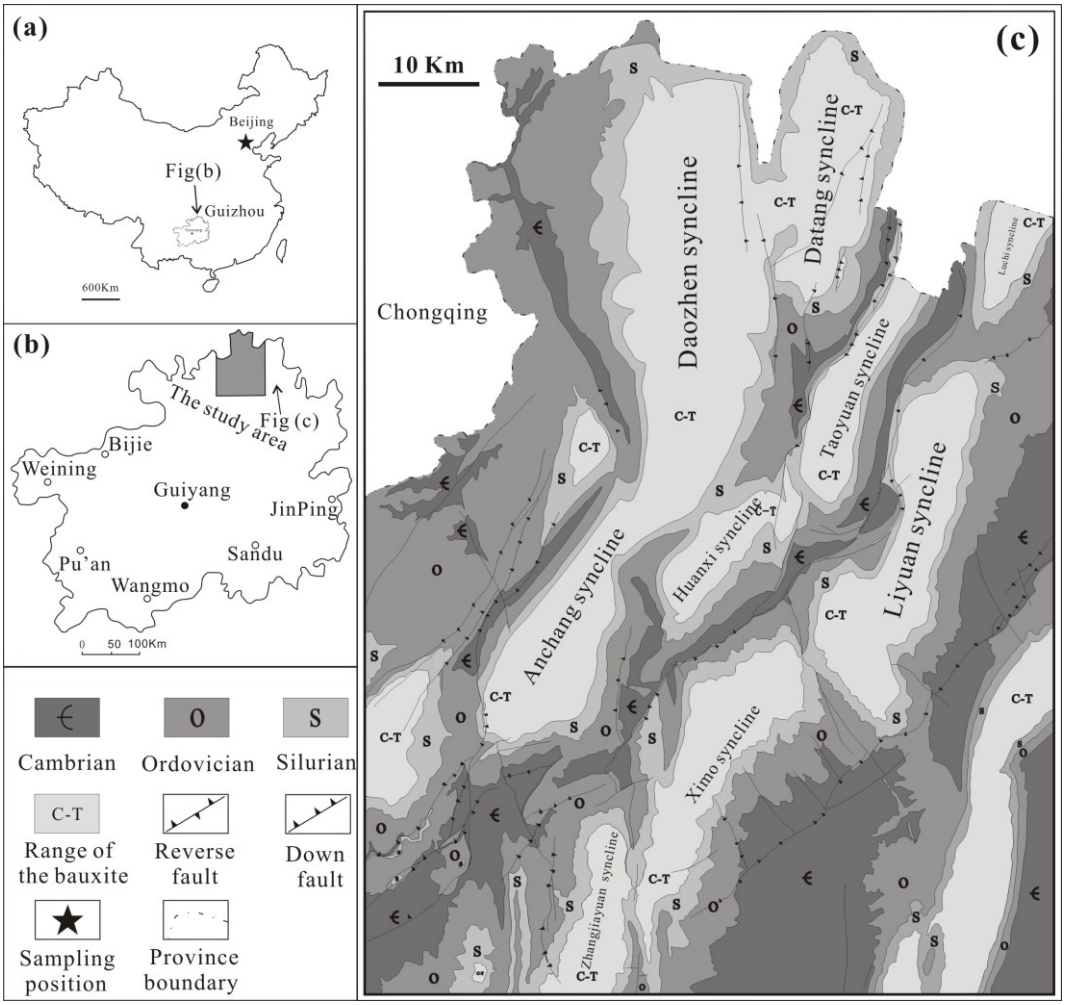

Fig. 1(a)Locality map of Guizhou,(b)The map showing the location of the study area, (c)Geology map of the WZD area in northern Guizhou

Acidity and alkalinity of metallogenetic environment in penecontemporaneous period

Major elements of the WZD bauxite are Al_2O_3, SiO_2, Fe_2O_3 and TiO_2 [6,8], ranges of these elements are wide and have a great change in numerical value[8]. Elements of alkaline metal have a great loss show that it is obvious acidic in the metallogenetic process[8]. wide range of alkaline indicates different position of the producing formation has different acidity and alkalinity, and biomarker in the WZD bauxite indicates acidic environment too[9]. Fig.2 shows that Al_2O_3 has negative correlations with SiO_2 and Fe_2O_3, forming process of high grade bauxite is a process that Si and Fe have a great loss but Al have a relative enrichment. In the acidic environment Si and Fe elements are active and migrate accompany movement of groundwater. This process is beneficial for the forming of high grade bauxite. Ti is very stable and just move in very strong acidic environment, Ti has a positive correlation with Al, and it shows that Ti has a movability in the WZD bauxite. The movability of Ti has demonstrated metallogenetic environment is strong acidic.

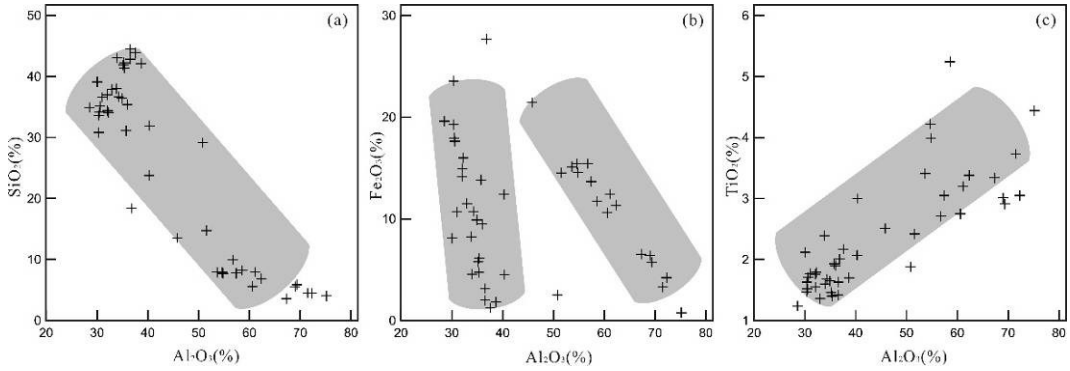

Fig.2 a. Correlation between Al_2O_3 and SiO_2; b. Correlation between Al_2O_3 and Fe_2O_3; c. Correlation between Al_2O_3 and TiO_2[8]

Pyrite is an important of the bauxite, and organic material too. The forming process of Pyrite and the decomposition of organic material would cause the forming of sulphuric acid and organic acid. The metallogenetic environment is strong acidic because of sulphuric acid and organic acid. Two kinds of acid have a downward moving trend Sulphuric acid and organic acid have been gradually neutralized as the downward movement. Si and Fe would be dissolved and moved to the bottom of the profile. In the moving process, Sulphuric acid and organic acid have decreased gradually, so the Si and Fe elements would precipitated in the lower part of the producing formation. Rubble of karst is frequent in the surface of Huanglong formation. Fig.3 shows that there is hollow between limestone of Huanglong formation and bauxite. Rubble of karst and hollow have demonstrated that karstification is an everlasting process after the sediment deposit, limestone of Huanglong formation would be dissolved by the Sulphuric acid and organic acid from top.

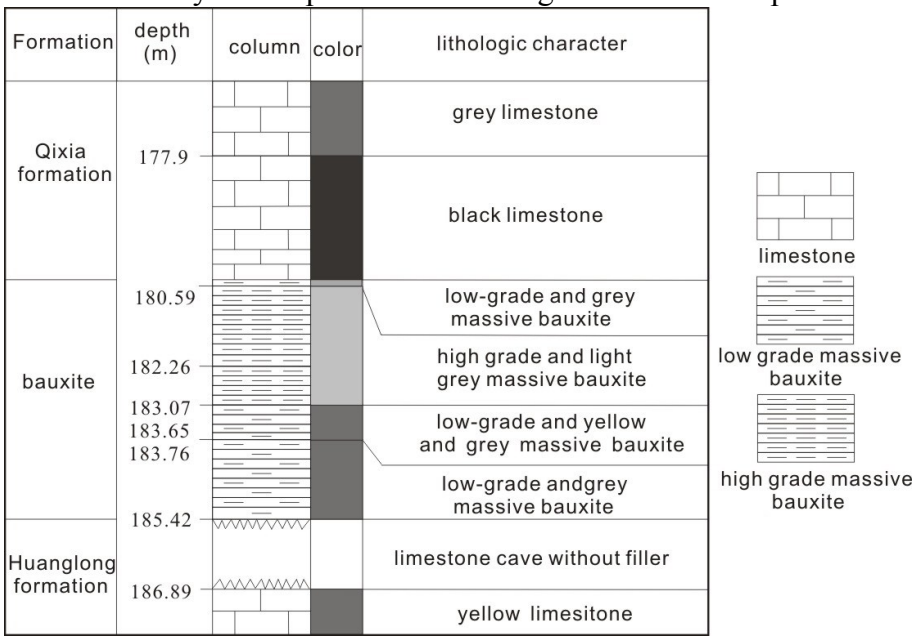

Fig.3 Bore section 1603

Acidity of environment decreased gradually from top to bottom, at last it may be alter to alkalescence environment, and the appearance of Metaparisite($Ce_2Ca(CO_3)_3F_2$) which is just appears in the alkalescence environment prove it [6,8]. $Ce_2Ca(CO_3)_3F_2$ has been discoveryed in Liyuan syncline, Ximo syncline. The appearance of $Ce_2Ca(CO_3)_3F_2$ causes severe positive anomaly of Ce, in other words alkalescence environment resulting in the severe positive anomaly of Ce.

Conclusion

The main conclusions from this study are summarized as follows: 1)metallogenetic environment in penecontemporaneous period of WZD bauxite is acidic, and from top to bottom of profile, acdiity of environment decreased gradually.2)In the acidic metallogenetic environment Si and Fe have a great loss but Al has a small loss resulting in the formation of high grade bauxite in the upper and middle part of the producing formation.

Acknowledgment

This work was supported by the Guizhou Collaborative Innovation Center of Strategic Minerals Resource Development, Guizhou Institute of Technology, Guiyang, 550003, China and the project of analysis on geochemical behaviors of Platinum group elements in Emeishan basalt (XJGC20131204), Guizhou Institute of Technology.

References

[1] G.H. Wu, Z.G. Jin, Y. Bao: J.Geology and Prospecting,Vol.44(2008),P.34 (in Chinese)

[2] Z.G. Jin, G.H. Wu, Y.Y. Zhao:J.Mineral Source and Geology,Vol.23(2009),P.139 (in Chinese)

[3] K.H. Yin: J. Acta Sedmentological Sinica, Vol.27(2009),P. 455 (in Chinese)

[4] Z.H. Han: J. Mineral Resource and Geology,Vol.22(2008),P. 430 (in Chinese)

[5] Z.Y. Lei and Y.C. Liao: J. Western Prospecting Engineering, Vol.18(2007), P. 96 (in Chinese)

[6] X.M. Wang, Y.Q. Jiao and Y.S, Du: J. Journal of Geochemical Exploration, Vol. 133(2013), P.108.

[7] P. Liu: J. Guizhou Geology,Vol.18(2004),P. 240(in Chinese).

[8] T. Cui, Y.Q. Jiao, Y.S. Du:J. Journal of palaeogeography,Vol.16(1),P.9(in Chinese).

[9] W.C. Y,Y.S. D,Q.Zhou:J. Journal of palaeogeography, Vol.14(5),P.652(in Chinese).

CHAPTER 5:

Advanced Technologies in Modelling, Simulation and Optimization, Computation Methods and Algorithms, Intelligent Engineering Applications

Advanced Materials Research Vols. 989-994 (2014) pp 1435-1440
© (2014) Trans Tech Publications, Switzerland
doi:10.4028/www.scientific.net/AMR.989-994.1435

An Optimal Algorithm for Estimating Fundamental Matrix by Removing the Outliers

Liqian Guo[1,2,a], Junbi Liao[1,b] , Fangping Zhong[2], Xiang Yu [2] and Jun Tao [2,c]

[1] School of Manufacturing Sci. and Eng., Sichuan Univ., Chengdu, China

[2] Northwest Institute of Nuclear Technology, Xi'an, China

[a]Liqian_guo@163.com, [b]liaojunbi@scu.edu.cn, [c]taojun100@sina.cn

Keywords: computer vision, fundamental matrix, epipolar geometry, non-linear optimization

Abstract. The accurate estimation of the fundamental matrix is one of the most important steps in many computer vision applications such as 3D reconstruction, camera self-calibration, motion estimation and stereo matching. In this paper, an optimal fundamental matrix estimation method based on removing exceptional match points is proposed. Firstly, the initial mismatch is reduced by the bidirectional SIFT feature matching algorithm. Secondly, the partial concentration problem of random samples is solved by the bucket segmentation method. In order to obtain robustness, the fundamental matrix is estimated in a RANSAC framework according to the principle of minimizing the geometric distance. Finally, the iterate process improves the accuracy of the fundamental matrix by using the LM algorithm. Experimental results show that the proposed method can reduce the outlier's interference better and improve the estimation precision of the fundamental matrix.

Introduction

The fundamental matrix contains the epipolar constraint information that existing between two images about the same scene. It only relates with the interior parameter of the camera and the relative posture of two camera positions. It is independent of the scene structure [1]. The accurate estimation of the fundamental matrix is one of the most important steps in many computer vision applications such as 3D reconstruction, camera self-calibration, stereo matching and motion estimation, and so on. Therefore, how to estimate the fundamental matrix as accurately as possible is still an important issue in computer vision research.

The mismatched feature pairs and the features with large location error all belong to the outliers. The noise and outliers unavoidably exist in the initial matching feature pairs. They will lead to low precision or wrong result. Methods for estimating the fundamental matrix can be divided into three categories: linear method, iterative method and robust method [2]. The seven point algorithm, the eight point algorithm and the improved eight point algorithm [3] are linear methods. Because the seven point algorithm and the eight point algorithm are more sensitive to data noise, Hartley proposed the improved eight point algorithm which can reduce the noise interference by normalizing the initial feature pair data. The iterative method solves the minimization problem of the Euclidean distance sum between feature points and their corresponding epipolar lines. Usually the Newton-Raphson or Levenberg-Marquardt algorithm is applied in solving the iterative optimal problem. Although the estimation result of the iterative method is more accurate than that of the linear method, but it is more time-consuming and can't deal with the outliers. The robust estimation algorithm can reduce the interference caused by the outliers. The M-estimators, LMeds and RANSAC are robust methods.

In this paper, an optimal algorithm for estimating fundamental matrix is proposed based on removing the outliers. First, some mismatched features are reduced by the bidirectional SIFT feature matching algorithm. Then, the partial concentration problem of random samples is solved by bucket segmentation method. In order to remove the outliers, the fundamental matrix is estimated in a RANSAC framework. Final, the iterate process leads the estimation to a more accurate level by using

the Levenberg-Marquardt algorithm. The experimental results of real image examples show the effectiveness of the proposed method.

Bidirectional SIFT Feature Matching Algorithm

The steps of bidirectional SIFT feature matching are shown as follows. Firstly, the SIFT features of the two images are extracted by the SIFT feature detection method. Secondly, the SIFT feature matching pairs are calculated from the left image to the right image by the K-nearest neighbor matching method. Finally, the matching pairs from the right image to the left image are calculated from the matching pair sets obtained in the previous step by using the K-nearest neighbor matching method again. Matching threshold in both directions can be different.

The results of bidirectional SIFT feature matching are shown in the Fig.1. The SIFT feature number of the left image (on the top) is 3422 and that of the right image (on the bottom) is 3235. When the matching threshold T1 (from left image to right image) is 0.06, the number of matched pairs is 94. The results of the unidirectional SIFT feature matching are shown in Fig.1(a). When the matching threshold T1 is 0.06 and the matching threshold T2 (from right image to left image) is 0.06, the number of matched pairs is 91. The results of bidirectional SIFT feature matching are shown in Fig.1(b). When T1 is 0.06 and T2 is 0.03, the number of matched pairs is 55. The results of bidirectional SIFT feature matching are shown in Fig.1(c). The matching threshold is smaller, the mismatch suppression is stronger, and the number of final matching pairs reduces faster. The bidirectional SIFT feature matching algorithm can be used to provide more accurate matching pairs.

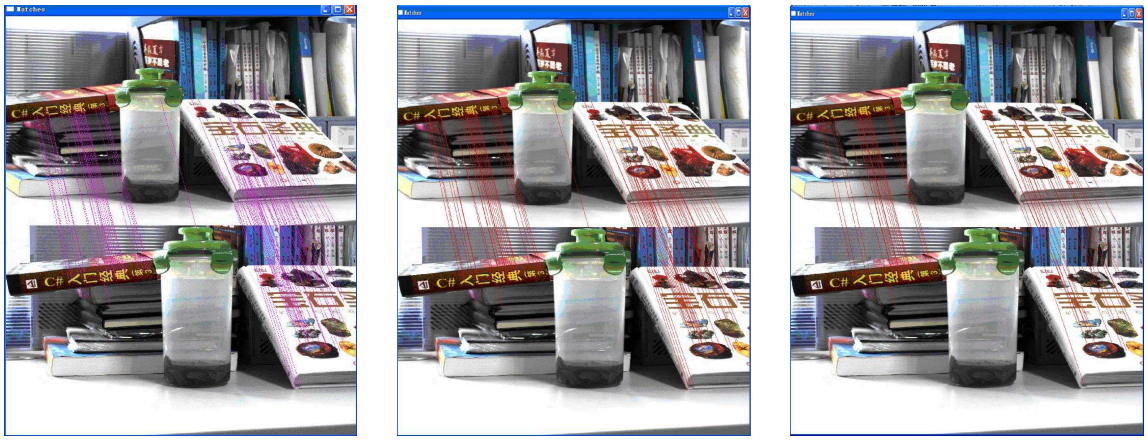

(a) T1=0.06; (b) T1=0.06, T2=0.06; (c) T1=0.06, T2=0.03

Fig. 1. The match results calculated by the bidirectional SIFT feature matching algorithm

Fundamental Matrix Estimation Based on Removing Outliers

The bidirectional SIFT feature matching algorithm provides an initial matching pair list for estimating the fundamental matrix. Note that the initial matching pair list still contains some outliers caused by large feature location error. In order to reduce their negative effect on estimating fundamental matrix, we proposed a new method for estimating fundamental matrix robustly by removing the outliers. Firstly, a more accurate initial fundamental matrix F is estimated from a number of random samples. Every random sample consists of the minimal sets selected from the matching pair list. Secondly, the Euclidean distance of each matching pair is calculated by the F. The outliers can be removed by comparing their Euclidean distances with the distance assessment threshold. The inliers list is obtained by removing those outliers from the initial matching pair list. Finally, the accurate fundamental matrix is estimated optimally from the inliers list by a classical iterative Levenberg-Marquardt algorithm.

Bucket Segmentation. In robust estimation algorithm, the sample is selected randomly from the matching pair list. If the samples concentrate locally, they can’t reflect accurately the epipolar

constraint relations of the whole image. The fundamental matrix estimated by these samples is not accurate. The bucket segmentation is applied to solve the partial concentration problem of the samples.

The image plane is divided into several buckets averagely. The bucket segmentation result is shown in Fig.2. The hit probability of each bucket is determined by the number of the feature points located in this bucket. In eight point algorithm, eight matching pairs are applied to calculate fundamental matrix. The eight matching pairs are selected randomly as follows. First, eight non-empty buckets are selected randomly according to their hit probability. Then, one feature point is selected randomly from one non-empty bucket. The samples consisting of such selected feature points can avoid partial concentration problem [4]. The fundamental matrix estimation is more stable and accurate when use such samples.

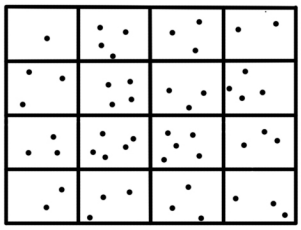

Fig. 2. Dividing the image plane into 4×4 buckets

Refinement in the RANSAC Framework. The outliers will affect the estimation accuracy of the fundamental matrix when nonlinear optimization algorithm is performed directly over the matching pair list with outliers. Therefore, the fundamental matrix is estimated in RANSAC framework [5] and is refined by the LM iterative algorithm. The algorithm process is as follows.

Step 1: The initial matching pair list is obtained by the bidirectional SIFT feature matching algorithm. It is labeled as {mi, mi'}, i=1, ... , N.

Step 2: The image plane is divided into S(S>=8) buckets averagely. The number of matching feature points of each bucket is calculated. It is labeled as Ns, s=1,...,S. The hit probability of each bucket is Ps, Ps=Ns/N.

Step 3: The RANSAC times K in the algorithm is determined by:

$$K = \frac{\log(1-P)}{\log(1-(1-\varepsilon)^{v})} \tag{1}$$

Where P represents the confidence probability that the estimated fundamental matrix is correct, ε is the fraction of outliers, v is the sample size. (v is 8 when the improved eight point algorithm is used to calculate the fundamental matrix).

Step 4: Repeat K times random sample.

(1) According to each bucket's hit probability Ps, eight matching pairs are selected randomly from the initial matching pair list by the bucket segmentation method;

(2) The fundamental matrix F_j is estimated by improved eight point algorithm with this sample;

(3) The Euclidean distance r_i of each match pair can be calculated with the F_j;

$$r_i = (d^2(m_i^{'}, F_j m_i) + d^2(m_i, F_j^T m_i^{'})) = (\frac{1}{(F_j m_i)_1^2 + (F_j m_i)_2^2} + \frac{1}{(F_j^T m_i^{'})_1^2 + (F_j^T m_i^{'})_2^2})(m_i^{'T} F m_i)^2 \tag{2}$$

Where d2(*,*) represents the Euclidean distance between a feature point and its corresponding epipolar line.

(4) The element of set { r_i } is arranged in ascending order. The error evaluation index e_j of F_j is the sum of the element r_i located in front of (1-ε)×N.

Step 5: The set of $\{F_j \rightarrow e_j\}$, j=1, … , K can be obtained from the step 4. Find the minimal error $e_{\min} = \min_j \{e_j\}$ and its corresponding fundamental matrix F_{min} from the set. This F_{min} is picked out as the winner and is relabeled as F_{opt}. The new set $\{r_i^{'}\}$ is obtained by recalculating the Euclidean distance of each matching pair with the F_{opt}. After arranging the element of set $\{r_i^{'}\}$ in ascending order, the error evaluation index r_{min} of F_{opt} is calculated in the same way. Then the distance assessment threshold T is determined by:

$$T = 2.5 \times \frac{1}{\phi^{-1}\left(0.5 + \left(\frac{1-\varepsilon}{2}\right)\right)} \times \left(1 + \frac{5}{N-v}\right) \times \sqrt{r_{\min}} \tag{3}$$

Where ϕ is the cumulative standard normal distribution function, ϕ^{-1} is its inverse function [6].

If the Euclidean distance of one matching pair $r_i^{'}$ is greater than the distance assessment threshold T, this matching pair is the outlier and should be removed. Then, the final inliers list is obtained by removing those outliers from the initial matching pair list.

Step 6: The final fundamental matrix F is estimated optimally with a classical LM iterative algorithm using the final inliers list. The error cost function is determined by:

$$\sum_i^N (d^2(m_i^{'}, Fm_i) + d^2(m_i, F^T m_i^{'})) \tag{4}$$

Experimental Results

First, the fundamental matrixes of some real image pairs are estimated by the proposed algorithm. The epipolar constraint can be calculated from the fundamental matrix. Fig.3 shows the recovered epipolar lines and the correspondence matching points of the corridor image. Fig.4 shows the recovered epipolar lines and the correspondence matching points of the sculpture image. In order to keep image content clear to the reader, only ten recovered epipolar lines are superimposed on the image. Then, the accuracy of the fundamental matrix estimated by the proposed algorithm is compared with that estimated by the improved eight point algorithm, LMeds and RANSAC. The experiment parameters are listed as follows. In the proposed algorithm, P is 99%, ε is 0.35, v is 8, bucket size is 5×5. The improved eight point algorithm, LMeds and RANSAC methods are achieved by the OpenCV function library. In the LMeds and RANSAC functions, the distance assessment threshold T that represents the maximum distance from point to epipolar line in pixels is one pixel. The confidence probability is 99%. The effectiveness criterion is fundamental matrix's quality to satisfy the epipolar constraint, and that is the mean value of the Euclidean distance sum (MVEDS) of all matching pairs. The MVEDS and the inliers number are listed in table 1. The initial matching pairs are calculated by the bidirectional SIFT feature matching algorithm. The number of initial matching pairs in Fig.3 is 170. The number of initial matching pairs in Fig.4 is 393.

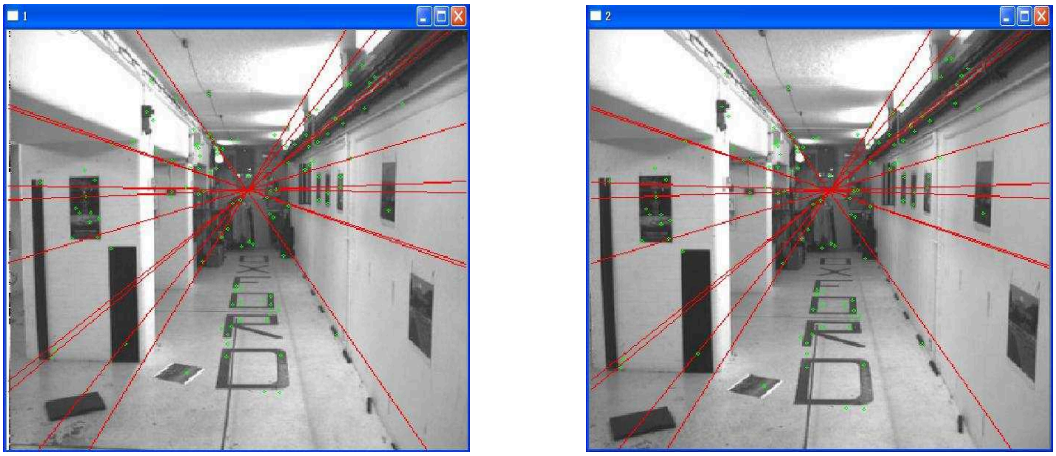

Fig. 3. Corridor images with epipolar lines (red lines) and 136 matching pairs (green points) superimposed

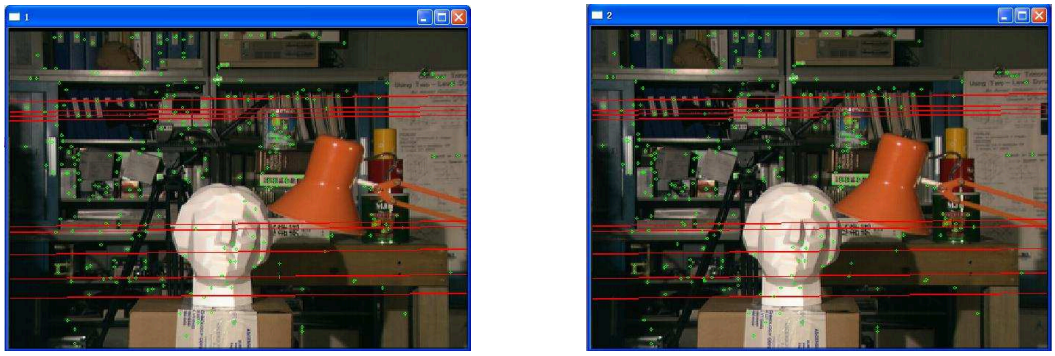

Fig. 4. Sculpture images with epipolar lines (red lines) and 348 matching pairs (green points) superimposed

Table 1. The accuracy comparison of four estimation algorithms

Image pair	appraise criteria	improved eight point algorithm	LMeds	RANSAC	proposed algorithm
Fig. 3	MVEDS [pixels]	0.329257	0.164709	0.263084	0.119275
Fig. 3	inliers number	170	151	147	136
Fig. 4	MVEDS [pixels]	0.390452	0.019153	0.092462	0.018656
Fig. 4	inliers number	393	342	381	348

The MVEDS calculated by the improved eight point algorithm is maximal in four algorithms because it can't deal with the outliers. Due to removing some outliers, the fundamental matrixes estimated by LMeds and RANSAC are more accurate than that estimated by the improved eight point algorithm. The proposed algorithm can remove the outliers and apply the nonlinear optimal iterate process to estimate fundamental matrix. Its accuracy is the highest in four algorithms.

Summary

The outliers existed in the initial matching pairs will affect the accuracy of fundamental matrix. The proposed algorithm can improve the accuracy of the fundamental matrix estimation by removing the outliers. The initial mismatch is reduced by the bidirectional SIFT feature matching algorithm. The fundamental matrix is estimated in a RANSAC framework and is refined by the LM iterative algorithm. The experimental results show that the proposed algorithm provides a more accurate solution of the fundamental matrix than the traditional linear method and robust methods.

References

[1] R.I. Hartley, A. Zisserman: Mu1tip1e View Geometry in Computer Vision. (Second Edition, Cambridge University Press, Cambridge 2004).

[2] H.X. Zhong: Research on Methods for Estimating the Fundamental Matrix. Doctor's Thesis of Jilin university, China (2005), p.22-37.

[3] R.I. Hartley: In defence of the 8-point algorithm. In: Proceedings of the 5th International Conference on Computer Vision, IEEE Computer Society Press, Boston (1995), p.1064–1070.

[4] J. Zhang, Z.P. Hu, Z.Y. Ou: An Exceptional Points Removing Based Optimal Algorithm for Estimating Fundamental Matrix. J. Computer Engineering, vol.31, no.13 (2005), p.12-15.

[5] X.L. Xiao: New Fundamental Matrix Estimation Method Using Global Optimization. In: 2010 International Conference on Computer Application and System Modeling, vol.7 (2010), p.402.

[6] Y.J. Huang, W.J. Liu: A Method for Fundamental Matrix Estimation Using LQS. Journal of Image and Graphics, vol.14, no.10 (2009), p.2069-2072.

Advanced Materials Research Vols. 989-994 (2014) pp 1441-1444
© (2014) Trans Tech Publications, Switzerland
doi:10.4028/www.scientific.net/AMR.989-994.1441

Complex Network Optimization Research of Personalization-based Recommendation Algorithm

GAO Caixia[1, a], QI Changping*[2,b]

[1,2]School of Information Technology and Media and Communications, Hexi University, Zhangye City 734000,China

[a]GaoCaixia@yeah.net , Corresponding author:*[b]qichangping@126.com

Keywords: Complex networks; High degree seeking; Search steps; Query information.

Abstract. Application value of a variety of complex network makes it become an important scientific research challenges. Therefore, in order to more thoroughly understand the network of human life, we need to further study the properties of the complex network. Complex network search theory solves many practical problems, including the search of relationship between any two people in a social network chain.

The complex network and personalized recommendation system introduction

1.1 Main topology characteristic of complex networks

Aggregation coefficient

Aggregation coefficient C is used to identify the node in the system of collection, namely how dense network is. Its calculation is: if the node i connect k_i side and the other k_i node is linked together, assuming node to connect each other, between them, a total of $k_i(k_i-1)/2$ side, between the node k_i actually there is E_i sides; the ratio of both side is gathered coefficient of the node i:

$$C(i)=\frac{2E_i}{k_i(k_i-1)} \qquad (1)$$

Aggregation coefficient of the system is the mean of all the nodes in the network:

$$C\frac{1}{N}\sum_{i=1}^{N}C(i) \qquad (2)$$

The average shortest path

There is one or more connection route between any two nodes in a network, the shortest path is one of the least connection node numbers, and the average shortest path of the network is the average of all the shortest path length.

Assume the connected graph $G(V,E)$ is a group for the node set V, take $E\subseteq\{(v_i,v_j):v_i,v_j\in V\}$ as the edge collection; $l(v_i,v_j)$ is the shortest path between any two nodes v_i and v_j, then the average shortest path L of graph $G(V,E)$ is:

$$L=\sum_{(v_i,v_j)\in V}l(v_{i,}v_j) \qquad (3)$$

1.2 The business process of personalized recommendation system

From information acquisition to the recommendation of all process personalized recommendation system include the following processes: processing the data; model; recommendations; data update; the user feedback.

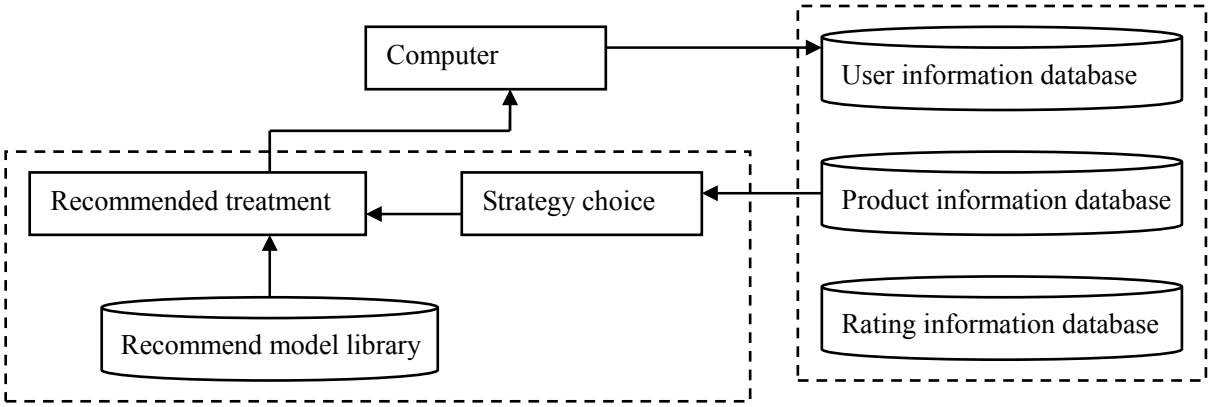

Figure1. Recommendation system overall framework

Information recommendation algorithm based on network structure

So far, the research and application of the collaborative filtering is considered to be one of the most widely algorithm, this algorithm is a basic assumption in the past with similar preferences of the user in the future will have similar preferences. [1]Therefore, the collaborative filtering algorithm is one of the most important thing is how to measure the similarity between the users.

2.1 Collaborative filtering recommendation algorithm

A scoring system can be displayed by the second part network $G(U,O,E)$; U, O, E represent the users, commodities and the edge (marked as score values). Assume $r_{u\alpha}$ for score value of users u to the goods α, O_u said goods collection of user u. U_α is a collection of all users. Score of u is $\overline{r_u} = 1/|O_u| \sum_{\alpha \in O} r_{u\alpha}$. [2]Using collaborative filtering algorithm, predictive value for user u and goods is:

$$r'_{n\alpha} = \overline{r_n} + k \sum_{v \in U_\alpha} s_{nv} (r_{v\alpha} - \overline{r_v}) \quad (4)$$

s_{uv} is the degree of similarity showed by u and v, $k = (\sum_v s_{nv})^{-1}$ is the normalized coefficient. A similarity calculation index which use score information is the Pearson coefficient,

$$s_{nv} = \frac{\sum_\alpha (r_{n\alpha} - \overline{r_n})(r_{v\alpha} - \overline{r_v})}{\sqrt{\sum_\alpha (r_{u\alpha} - \overline{r_v})^2} \sqrt{\sum_\alpha (r_{v\alpha} - \overline{r_v})^2}} \quad , \quad \alpha \in O_u \bigcap O_v \quad (5)$$

2.2 Information recommendation algorithm based on network structure

The algorithm of this chapter can be divided into two steps: first, we put the two parts of users - goods projection to the single mode network, when include two users have at least one common grading goods, we connect between the two users by an edge; secondly, based on the single mode of network, we can make use of random walk with restart algorithm to calculate the similarity between users. Suppose that a random walk starting from node i, go to the next node at c probability and the probability of $1-c$ to return to the initial node. [3]Assuming s_{ij} as probability of random walk in a stable state j, then

$$\vec{s_i} = cP^T \vec{s_i} + (1-c)\vec{e_i} \quad (6)$$

Random walk with restart process is similar to Google's PageRank, in fact, the PageRank algorithm learns from the random walk with restart process. Suppose g_i as the probability on the on stop page then the PageRank algorithm of iterative formula is:

$$g_i = c \sum ij \frac{g_i}{k_j} + (1-c) \quad (7)$$

Average in different network analysis

This part we will discuss the algorithm complexity of the several common complex network.

3.1 Rule network

The rules of the common network mainly include the nearest neighbor coupled network, the global coupling network, star network, etc. In all kinds of network whose node number is the same, global coupling network has minimum average path length of $L_{gc}=1$, the clustering coefficient of maximum $C_{gc}=1$. But as the actual network model the model has a lot of problems.

We take another rule - star coupled network as a model to discuss the algorithm complexity. Star coupled network average path length is:

$$L_{star}=2-\frac{2(|V|-1)}{|V|(|V|-1)}\to 2(|V|\to\infty) \qquad (8)$$

Therefore, average cost k steps wander's most generous algorithm is:

$$T(|V|)_{khds}=2\in 0(1) \qquad (9)$$

The star coupled in the network, the most generous algorithm complexity steps k wander is a constant order $O(I)$. For the new type k traversal search algorithm, take the average path length in:

$$T(|V|)_{k}=2|V|+4\in o(|V|) \qquad (10)$$

3.2 Random network

Different from the rule network, the most important nature of random graph ER is the emergent properties or degeneration, that is given a fixed probability p, we will find that many of its important properties are suddenly sprang up and out, for example, connectivity, all figure almost don't have this nature.

Set path length of random network random graph ER is the average degree of $<k>=p(|V|-1)$, intuitively, to any one of the nodes in the graph, there is one other node in the network and the distance between the point at which is close to or equal to L_{ER}, as a result, $|V|\alpha<k<L_{ER}$, the average path length of random networks are:

$$L_{ER}\propto\frac{tn|V|}{tn<k>} \qquad (11)$$

We can see that the random network has a small clustering coefficient and average shortest path length. Bring the above two formulas in, average cost k steps wander the most generous algorithm is:

$$T(|V|)_{khds}=\frac{\ln|V|}{\ln<k>}+\left\lfloor\frac{\ln|V|}{3\ln<k>}\right\rfloor(|V|-1)\in o(|V|\ln|V|) \qquad (12)$$

The random network, the most generous algorithm complexity of k steps wander is $o(|V|\ln|V|)$. For the new type k traversal search algorithm, take the average path length in, we can get:

$$T(|V|)_{k}=\frac{3|V|\ln|V|}{\ln<k>}-4|V|+4\in o(|V|\ln|V|) \qquad (13)$$

Summary

With the rapid development of computer and Internet technology, network information can be obtained is in exponential growth. But it also leads to information overload, namely, information utilization become lower instead. Recommendation technology is considered to be one of the most effective tools for information overload. Information recommendation technology is a hot issue in scientific research and engineering application..

References

[1] D.J. Watts and S.H. Strogatz. Collective dynamic of `small-world' networks. Nature, vol. 393, no.6684, 1998, pp. 440-442.
[2] M. E.J. Newman and D.J. Watts.Renormalization group analysis of the small-world network model. Phys. Lett. A, vol. 263, no. 6, 1999, pp. 341-346.
[3] A.L. Barabási and R. Albert.Emergence of scaling in random networks. Science, vol. 286, no. 5439, 1999, pp. 509-512.

Advanced Materials Research Vols. 989-994 (2014) pp 1445-1448
© (2014) Trans Tech Publications, Switzerland
doi:10.4028/www.scientific.net/AMR.989-994.1445

Algorithm Study and Application of Personalized Intelligent Recommendation Engine

PU Guo-lin[1, a]

[1]School of Computer Science, Sichuan University of Arts and Science, Dazhou 635000,China

[a]PUGuolin@yeah.net

Keywords: Recommendation engines; Personalization; Collaborative filtering

Abstract. The Internet has gradually enters the life of people and the usage of information has become globalization gradually. It is now very common to get information through the network in day-to-day work. The Amount of data of Internet information grows in an explosive way in recent years, the huge amounts of information make it more and more difficult for users to find the information they need accurately; information overload lots problems become the great challenge of Internet development. As currently one of the most effective tool to solve the information overload, personalized recommendation technology help users filter information intelligently through the recommendation engine.

Intelligent recommendation system examples

Intelligent recommendation system is the research focus in the information retrieval and information filtering; now many universities and institutions take it in the key study, classic recommendation system prototype include:

(1) TYPESTRY: TYPESTRY is a research collaborative filtering system; it usually helps users to filter email and news. TYPESTRY system provides a variety of services; mainly a collaborative filtering service, accessorily electronic document storage and user evaluation storage and other services. TYPESTRY also design their independent TQL query. TQL is similar to SQL, it can research for relevant information query according to user's interest preference, and query efficiency is higher. TYPESTRY is mainly based on collaborative filtering technology, so can't satisfy the requirement of real-time for large users of the system.

(2) ACF: Active Collaborative Filtering system is put forward by Cameron University and independently researched and developed, it is the recommendation system based on Collaborative Filtering technology. [1]An important idea of ACF is a pointer, the pointer plays an important role in the collaborative filtering algorithm, a pointer can point to the electronic document hyperlinks, also can point to the electronic document context information or user comments. Through the way of the pointer, synergy will recommend information to the interested users pointer points to.

(3) GroupLens: MIT is the research institution of GroupLens, it is a collaborative filtering technology news information recommendation system. Rating information collected through user to obtain accurate information and build user rating matrix of the project to find the user's neighbor users and then according to the most similar users score calculated recommendation information. The system can meet the needs of large users. GroupLens provide open source data sets, has very high openness, provides a convenient for recommending system research for all structure, users can send the score information through the GroupLens API. We can see form Figure1.

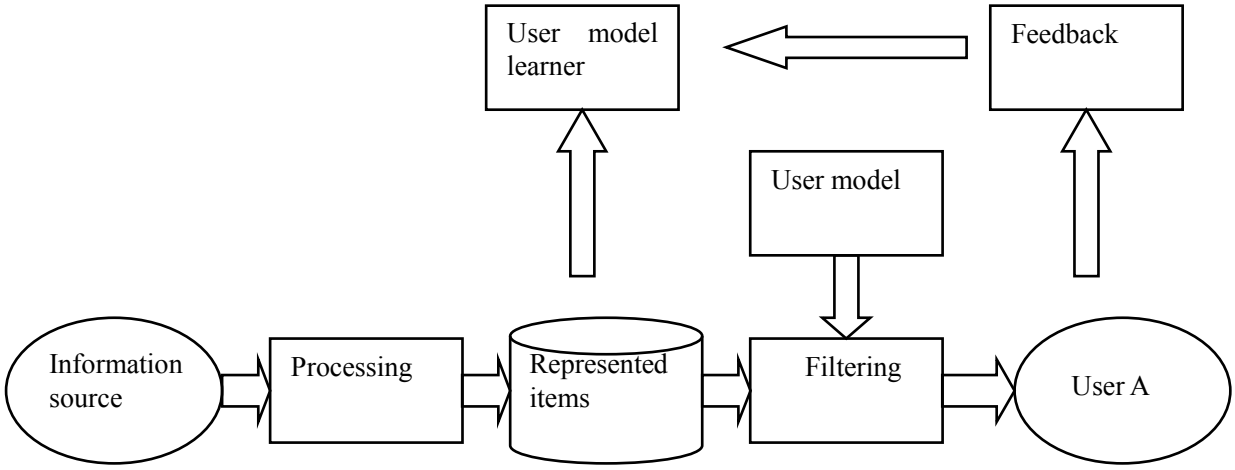

Figure1. Overall architecture of personalized recommendation system design

TF - IDF learning method

The basic idea of TF - IDF method is to take each user/document as a vector, each dimension of the vector is made up of key items, and each feature weight shall be carried out in accordance with the document frequency and word frequency calculation, the whole process need to complete the following two steps:

(1) According to the training sample extract feature item set of text $T = \{t_1, t_2, ...t_n\}$

(2) Measure the size of the feature weight w_{kj} (weight of t_k in d_j);

2.1 Feature extraction

There are two kinds of feature extraction method. One category is Term Selection, referring to selecting a small amount typical and characteristic feature from the original features (a mixture of useful and useless words). [2]However, characteristics of the type don't change, just less. Another kind is called Term Extraction method. Different from Term Extraction, it is to reconstruct the new characteristics out of the original feature set, these new key words more representative, and costs less computation resource. This paper studies feature selection algorithm only.

Feature selection algorithms usually have Document Frequency (DF), Chi-square, CHI test and Information Gain method (IG) and Mutual Information method (Ml) and Document Frequency, etc. This section mainly elaborates the document frequency method, information gain method and CHI method.

(1) Document frequency method

Document frequency (DF) method refers to frequency of a certain term t in corpus document. The specific method is: to calculate document frequency of each term in the training corpus, and then set a threshold value, when document frequency of a term is below a certain threshold to remove it from the feature space, saying the word frequency is too low, not representative; when the document frequency of a term is above a certain threshold, also remove it out of the feature space, saying the term frequency is too high, of no differentiation.

(2) Information gain method

Information gain (IG) method is similar to the attributes choice method, which measures the importance of the term based on the information each term t provides for the entire classification so as to decide trade-offs of term t. information gain for a term of t is the difference between the amount of information for the entire classification caused by a term t that relative to no t. [3]Relevant information gain measurement in text categorization is the difference in the amount of information provided when there is the existence of a certain word for classification, among them, entropy is adopted to measure the size of the amount of information.

$$Gain(t) = Entropy(S) - Entropy(S_t) = \{-\sum_{j=1}^{n} P(C_j) \times \log P(C_j)\}$$
$$- P(t) \times \{-\sum_{j=1}^{n} P(C_j \mid t) \times \log P(C_j \mid t)\} - P(\bar{t}) \times \{-\sum_{j=1}^{n} P(C_j \mid \bar{t}) \times \log P(C_j \mid \bar{t})\} \quad (1)$$

(3) CHI

The basic thought CHI is to determine whether the assumed theory is correct by observing the deviation between the theoretical value and practical value. Generally speaking, the first original are assumed between the two variables are independent, then observe the deviation between the size of the actual value with the theoretical value (in the case of both independent of each other's value) to determine whether to accept the null hypothesis, if the deviation is small enough then accept the null hypothesis; Otherwise deny original hypothesis, accept the alternative hypothesis.

Measure of the theoretical value and practical value deviation is:

$$D = \sum_{i=1}^{n} \frac{(x_i - E)^2}{E} \quad (2)$$

2.2 Feature weight calculation

(1) Boolean weights

In Boolean weights, the presence or absence of a statistical feature in the text is collected. If the feature t_k existed in text d_j, w_{kj} to 1, otherwise 0, namely:

$$w_{kj} = \begin{cases} 1 \\ 0 \end{cases} \quad (3)$$

(2) Term frequency weights

Different from Boolean weighted which only depend on the presence or absence of a key, Term Frequency weight (TF) is based on word Frequency in the document to assign weights to Term. In term frequency weighting method, tf_{kj} is used to represent the frequency of feature t_k in text d_j, w_{kj} is defined as:

$$w_{kj} = tf_{kj} \quad (4)$$

(3) TF - IDF weights

$$w_{kj} = tf_{kj} * idf_k \quad (5)$$

In addition, the length of text also needs to be considered, this formula is obtained by normalizing the TFC:

$$w_{kj} = \frac{tf_{ik} * \log(M/n_k)}{\sqrt{\sum_{k=1}^{M} (tf_{ik} * \log(M/n_k))^2}} \quad (6)$$

Implementation and application of recommendation engine

3.1 Goals of recommendation engine service

The Internet has entered the era of web2.0, more and more information is in the Internet, when huge amounts of data is presented in front of the computer screen, not only it is difficult for users to pinpoint information needed, but also some of the less popular information are submerged in the ocean of information, which greatly reduces the utilization of information. With the increasing number of information, the data can't be used will be more and more.

In such an information age, the recommendation engine has become the effective tool to solve the problem of information overload. Recommendation engine can help users access to information closely related to their interests, even if he had never read one, the depth mining of the information recommended will also help users to get useful information.

3.2 Analysis of the recommendation engine

In the process of using film site, the general process is often done through simple search matching process of user and information, this method is single, and of low efficiency. Users often cannot simply by keywords to accurately describe their needs. For example, by "good movie" people are unable to get the accurate data, because each user's definition of good is not the same. the Internet search method for the large amounts of information has been unable to meet the requirements of information retrieval.

Summary

Information system and e-commerce system provides users with convenient access to information, the diversity of choice, but with the roof type development of information, Internet information overload phenomenon come, users get lost in the ocean of information, due to the large amount of information, users often can't find what they need accurately. Based on this background, the personalized recommendation engine arises at the historic moment. The current industry common recommendation technology study and research found many deficiencies of the recommendation technology. The technology based on content filtering recommendation technology, based on the collaborative filtering recommendation technology, etc. are usually used, they achieve the intelligent analysis and prediction through its own algorithm.

Acknowledgements

National Natural Science Foundation of China (Grant No.: 61152003): theory and application of the global balance intelligent recommendations based on the emotional semantic.

References

[1] R.D.Lawrence,G.S.Almasi,V.Kotlyar et al. Duri. Personalization of Supermarket Product Recommendations. Data Mining and Knowledge Discovery, 2001,5(11):11-32

[2] Badrul Sarwar,George Karypis,Joseph Konstan et al. Analysis of Recommendation Algorithms for E-Commerce. ACM Conference on Electronic Commerce, 2000

[3] Nguyen L. A Proposal of Discovering User Interest by Support Vector Machine and Decision Tree on Document Classifi- cation. Proc. of International Conference on Computational Science and Engineering. IEEE Press. 2009: 809-814.

Advanced Materials Research Vols. 989-994 (2014) pp 1449-1452
© (2014) Trans Tech Publications, Switzerland
doi:10.4028/www.scientific.net/AMR.989-994.1449

Research on Marine Fuel Boiler Drum water Level Model and Dynamic Analysis

Zhu Miao

Zaozhuang Vocational College of Science & Technology, TengZhou , 277500

Keywords: Drum water level, Steam flow, PID control

Abstract. This article first mathematical model of boiler water level, and then in MATLAB/ SIMULINK environment, the model simulation, and thus the dynamic characteristics of the model for analysis. Many real boiler parameters and variables, complex, by simplifying the modeling process, ignores some factors and variables, a simple model can be obtained results almost true fit. Boiler water level of the model established in considering the effect of steam flow and water flow of two factors.

Introduction

In this paper, the dynamic characteristics of marine fuel boiler drum level research. Many real boiler parameters and variables, complex, by simplifying the modeling process, ignores some factors and variables, a simple model can be obtained results almost true fit[1]. Boiler water level of the model established in considering the effect of steam flow and water flow of two factors, the simulation results show that the model is correct.

Drum level model and dynamic analysis

Many factors can cause changes in drum level, the main consideration is the change in steam flow and changes in water flow. After the dynamic equations can be simplified drum level[2]:

$$T_1T_2\frac{d^2h}{dt^2}+T_1\frac{dh}{dt}=\left(T_W\frac{du_W}{dt}+K_Wu_W\right)-\left(T_D\frac{du_D}{dt}+K_Du_D-T_P\frac{du_D}{dt}\right) \quad (1)$$

Where:

h—Height drum level; Tw—Constant water flow; T_D, T_P—The time constant steam flow;

Kw—Water flow amplification factor; K_D—Steam flow amplification factor;

D—Boiler steam flow; W—Boiler feed water flow; T_1, T_2—time constant.

Drum water level in the water flow effects of the dynamic characteristics

Assuming the steam flow to a certain value, the presence of water flow disturbance, then the equation is:

$$T_1T_2\frac{d^2h}{dt^2}+T_1\frac{dh}{dt}=T_W\frac{du_W}{dt}+K_Wu_W \quad (2)$$

For the Laplace transform formula are[3]:

$$T_1T_2S^2H(s)+T_1SH(s)=T_WSV_W(s)+K_WV_W(s) \quad (3)$$

After the translation has drum level role in the transfer function of water flow:

$$G(s)=\frac{H(s)}{V_W(s)}=\frac{T_WS+K_W}{T_1S(T_2S+1)} \quad (4)$$

Assuming $\varepsilon = \frac{K_W}{T_1}$ was

$$G(s) = \frac{H(s)}{V_W(s)} = \frac{\varepsilon}{S(T_2S+1)} = \frac{1}{S} \cdot \frac{\varepsilon}{T_2S+1} \quad (5)$$

ε is when the unit boiler feedwater flow changes occur, the rate of change of drum water level when the boiler is running at full capacity, V if suddenly the water supply valve is closed, drum water level will continue to decline in the 50s if the drum water level dropped by 50mm , when the water flow from 100% open off a small 50% 50s time, drum level will reduce 25mm. From the above equation can be considered dynamic nature of drum water level in the water flow is determined by the role of a first-order inertia and an integral part of the composition[4], resulting curve to the water when the water level in the drum step change:

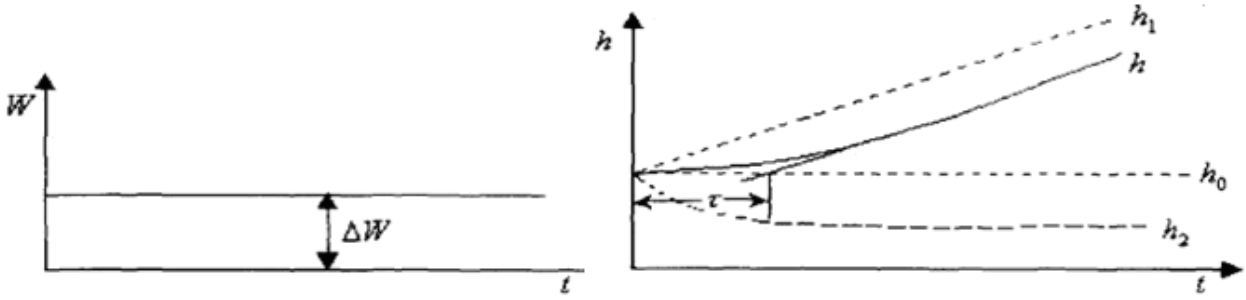

a) To a step change in water b) Under disturbance, drum level curve

Figure1 In step disturbance response curves drum water level changes

When the steam flow rate constant water flow step change occurs when the drum water level does not increase with the increase of water flow immediately, but began to increase after experiencing a delay. Draw h asymptote, it will be extended with no step change in water level occurs when the intersection, get the lag time; h1 change reflects the integral characteristics of drum level objects, h2 changes in response to the drum level object inertia, when the water started to increase the temperature of the incoming water is relatively low, reducing the temperature of the water in the original drum, the volume occupied by bubbles in soda mixture becomes smaller, making the drum water level drops. The total curve h can be regarded as obtained by adding curves h1 and h2.

Drum water level in the steam flow disturbance dynamic characteristics under

Water Drum assumed to remain unchanged when the steam flow changes are[5]:

$$T_1T_2\frac{d^2h}{dt^2} + T_1\frac{dh}{dt} = -(T_D\frac{du_D}{dt} + K_Du_D - T_P\frac{du_D}{dt}) \quad (6)$$

For the Laplace transform formula are:

$$T_1T_2S^2H(s) + T_1SH(s) = -[T_DSV_D(s) + K_DV_D(s) - T_PSV_D \quad (7)$$

After translation of the transfer function of steam flow disturbances drum level adjustment object:

$$G_D(s) = \frac{H(s)}{V_D(s)} = -\frac{(T_D-T_P)S+K_D}{T_1S(T_2S+1)} \quad (8)$$

$$G_D(s) = \frac{H(s)}{V_D(s)} = -\frac{1}{TyS} + \frac{Ky}{T_2S+1} \quad (9)$$

Drum water level can be obtained from the above equation steam disturbance adjust the dynamic characteristics of the object curve shown in Figure 2: Curve h can be divided into two parts, h1 and

h2, h1 is simply because water flow and steam flow imbalance makes the drum water level changes ; h2 changes when the steam flow inside the drum to pressure changes also followed, resulting in a "false water level." "False level" means the load increases, the air pressure inside the drum is reduced, so that the boiling point of water is reduced in the furnace, the temperature change does not occur immediately, and the water vapor tube within the drum strengthened soda mixture steam volume becomes large, so not only did not drum water level dropped because of increased steam flow, but the rapid rise of the situation.

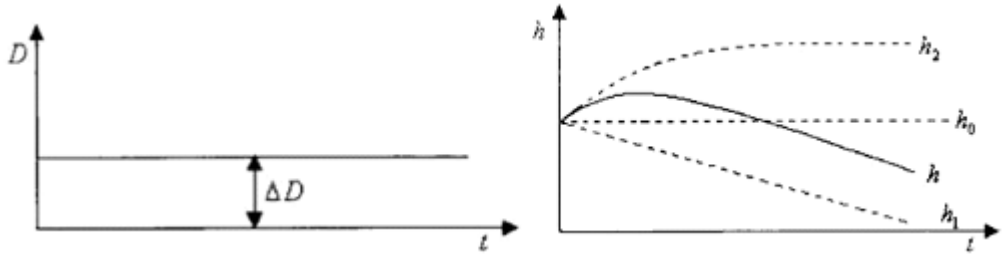

Figure 2 Curve step change occurred in the steam drum level when traffic

In MATLAB/Simulink for drum level in water flow and steam flow by the combined effect of the simulation, shown in Figure 3, so Ty = 50s, Ky = 1, deta = 0.02, T2 = 20s, water valves and steam valves are set linear, set every 1% change in the opening of the water flow and steam flow changes 0.4t / h, ie, the flow coefficient is 0.4. Enter the water flow to maintain 30% unchanged, steam flow from 30% in the 200s when 50% of the results in Figure 4 becomes available:

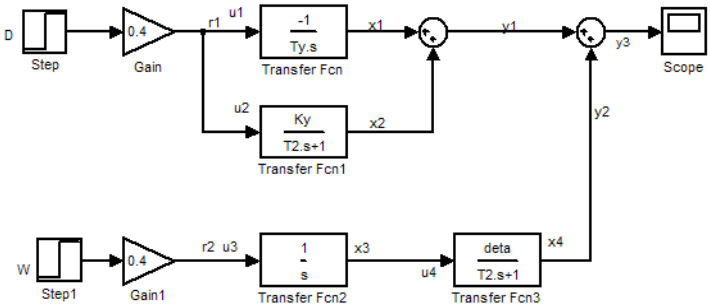

Figure 3 Drum level block diagram model simulation

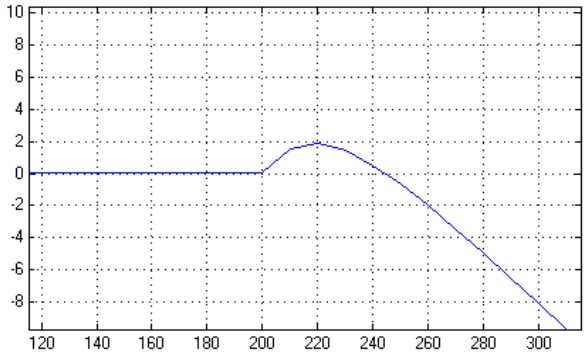

Figure 4 Water level increases the load curve

Drum level control

Drum level control system to adjust the following two ways:

l) single impulse water regulation system : Figure 5 , only the drum level signal as the basis for regulation , this regulation system structure is very simple , relatively large capacity for drum water level changes in the disturbance occurred more slowly, boiler " false water level " is not very serious , you can use a single impulse feedwater control system to meet production needs.

2) double impulse water regulation system : Figure 6, the boiler drum level signal as a master regulator signal , while the measured steam flow as a feedforward signal . As the introduction of the steam flow feedforward signal can reduce the bad effects of " false water level " of water regulation. When the change amount of steam , water flow adjusting the feedforward signal have a role in the same direction with changes in the amount of steam , which can be reduced or eliminated in the "false level " appears to make the amount of change in the opposite direction to the steam incorrect water flow regulation action. Steam flow occurred, the water valve will make its corresponding action, so to be able to reduce the amount of water and fluctuating water levels to a large extent , the reaction time is shortened . This adjustment method is suitable for the load conditions change frequently , requiring water pressure is relatively stable.

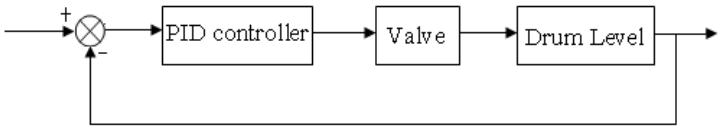

Figure 5 Feedwater regulator block diagram of a single impulse

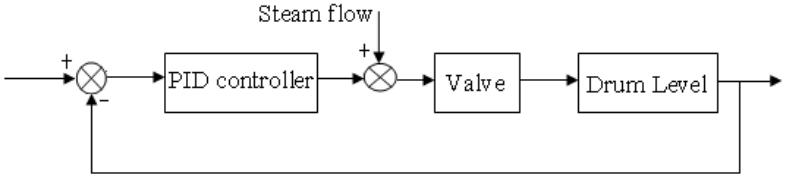

Figure 6 Double impulse water regulator block diagram

Conclusion

This paper analyzes the results can be seen, the boiler water level model can simulate a "false water level" effect when a sudden increase in the steam flow. In this chapter, also referred to this "false water level" situation can be single or double impulse love impulse method to counteract, as to the choice of which way the boiler can be determined according to the actual situation and production needs. Vapor pressure model can also be used as a model when the boost process that allows a value of zero to the steam flow.

References

[1] M E Flynn, M J O'Malley. A Drum Boiler Model for Long Term Power System Dynamic Simulation [J]. IEEE Transactions on Power Systems (S0885-8950), 1999, 14(1): 209-217.55

[2] Gan Hui-bing,Zhang Jun-dong. Design and realization of simulation system ofmarine boiler based on PLC[J]. Journal of Dalian Maritime University.2006(2):5-7

[3] Gao Jun. The Study of Application of Fuzzy Drum Water Level Control for Boiler[J].Process Automation Instrumentation.2003(3):56-59

[4] A.B.Rad,W.L.Lo.PredictivePIcontroller.International Journalof Control,1994,60,953～975.

[5] Han Guagxin,Shi Yungui,Hu Yiwei.Predictive PI Control of Water Level of Boiler Drum[J]. Microcomputer Information.2006(12):72-74

Advanced Materials Research Vols. 989-994 (2014) pp 1453-1455
© (2014) Trans Tech Publications, Switzerland
doi:10.4028/www.scientific.net/AMR.989-994.1453

Studies on broad-sense sample method in data mining

TANG Yan[1, a]

[1]College of Science, Northeast Agricultural University, Harbin 150030,China

[a] tangyan2014@yeah.net

Keywords: Small sample; Small sample evaluation methods; Small sample-support; Support Vector Machine; Data mining

Abstract. With the development of science and technology, people pay more and more attention to the reliability of the products, especially in some special field, such as aerospace, military products, and some products of high reliability and long life. As a part that runs through the whole life cycle of products, reliability test provides an important source of data for the design, batch production and residual life assessment of the product development. For some expensive, new products put into use, they are not quite little in amount, having the characteristics of small sample. In this case, how to use the existing data to predict product life, reliability of calculating the reliability of a product more accurately and other related parameters is particularly important.

Rough set theory and its application in data mining

This chapter studies key technical problems involved in the application of Rough Sets theory in data mining.

2. Basic concepts of rough set theory

Definition1: name relations system $K=(U,\overline{R})$ as a Knowledge base, in which $U=\{x_1,x_2,...,x_n\}$ is for object set (U is also called domain), [1] $\overline{R}$ is an equivalence relation on the set in U.

Definition 2: $a\in\overline{R}$, call binary group (U,a) as an approximation space of Pawlak, for any $X\subseteq U$, about lower approximation $\underline{a}(X)$ and upper approximation $\overline{a}(X)$ about X on approximation are respectively defined as:

$$\begin{aligned}\underline{a}(X)&=\{x\in U\mid[x]_a\subseteq X\}\\&=\bigcup\{Y\in U/a\mid Y\subseteq X\};\end{aligned}\tag{1}$$

$$\begin{aligned}\overline{a}(X)&=\{x\in U\mid[x]_a\cap X\neq\Phi\}\\&=\bigcup\{Y\in U/a\mid Y\cap X\neq\Phi\}.\end{aligned}\tag{2}$$

Definition 3: call $\alpha_a(X))$ and $\delta_a(X)$ as the approximation precision and roughness of X, a set of equivalent relationship of a, in which: $\alpha_a(X)=\frac{|\underline{a}X|}{|\overline{a}X|}$, $\delta_a(X)=1-\frac{|\underline{a}X|}{|\overline{a}X|}$ [2].

Obviously, $\delta_a(X)=\frac{|bn_a(X)|}{|\overline{a}X|}$, actually:

$$\delta_a(X)=1-\frac{|\underline{a}X|}{|\overline{a}X|}=\frac{|\overline{a}X|-|\underline{a}X|}{|\overline{a}X|}=\frac{|bn_a(X)|}{|\overline{a}X|}\tag{3}$$

If $|bn_a(X)|=0$, then on the down boundary of a, X is an empty, so the X is an accurate set and the roughness is 0; if $|\underline{a}X|=0$,[3] then the positive region of X is an empty set, showing that the X cannot be explained by a; it is all rough.

Information systems and decision table

Definition1: call $S=(U,\overline{A},V,F)$ as Information Systems, or database system, in which, U is called theory domain, $\overline{A}=\{a_1,a_2,...,a_m\}$ is set of properties, $a_j(j=1,2,...,m)$ called an attribute, V is the set of attribute value, $F=\{f_j \mid j\le m\}$, $f_j:U\times\overline{A}\to V$ is the function of the Information. Attribute a_j is certain relationship, also known as knowledge.

Definition 2: if $S=(U,\overline{A}=\overline{C}\bigcup\overline{D},V,F)$, in which, $\overline{C}\bigcap\overline{D}=\Phi$, $\overline{C}=\{c_1,c_2,...,c_k\}$ is the condition attribute set, $\overline{D}=\{d_1,d_2,...,d_h\}$ the decision attribute set, V is the set of attribute value, $F=\{f_j \mid j\le m\}$, $f_j:U\times\overline{A}\to V$ is the function of the Information, S is information system that has the function of decision performance. Such system tends to show in the form of table, the decision table. [4] It can be represented as $S=<U,\overline{C}\bigcup\overline{D}>$.

Definition3: set $(U,\overline{R},\overline{F})$ for information systems, be determined by $ind(\overline{R})$ as $U/ind(\overline{R})=\{A_i \mid A_i\in U/ind(\overline{R}),i\le t\}$, $t=\left|U/ind(\overline{R})\right|$. Use $f_l(A_i)(f_l\in F)$ to represent the value of the object of A_i property $a_l(a_l\in\overline{R})$, call $D(A_i,A_j)=\{a_l\in\overline{R}\mid f_l(A_i)\ne f_l(A_j)\}$ is set consist of identification attributes of A_i and A_j.

In fact, A_i and A_j are the most basic particles of knowledge $\overline{R}$, $D(A_i,A_j)$ said collection of all attributes to identify the most basic knowledge particle of A_i and A_j. Namely $\forall b=D(A_i,A_j)(b\in\overline{R})$, attribute b can tell the difference between A_i and A_j.

Small sample evaluation methods

Bayes method

The name of Bayes method origins from the British scholar whose name is Thomas Bayes (1702-1761). After his death, one of his article entitled "on solution on the problem of opportunity", the author puts forward a kind of inductive reasoning theory, then the scholars later summarized the theory, derive a system of statistical inference method, called the Bayes method.

Basic steps of the Bayes method

1. $p(x\mid\theta)$ said probability function of the whole depends on the parameters of θ, it said overall conditional probability function when the random variable θ given a value.

2. Obtain priori information parameters θ reflect, and use this information to determine the prior distribution $\pi(\theta\mid x)$.

3. Take two-step way to generate sample $x=(x_1,x_2,...,x_m)$. [5]First of all, generate a sample θ_0 from the prior distribution $\pi(\theta)$; then produce a set of samples observation values $x=(x_1,x_2,...,x_m)$ from a conditional distribution $p(x\mid\theta_0)$, which is joint density function of sample x, it contains the general information and sample information content, reflected in the form :

$$p(x\mid\theta_0)=p(x_1,x_2,...,x_m\mid\theta_0)=\prod_{i=1}^{m}p(x_i\mid\theta_0) \qquad (4)$$

4. Because θ_0 is still unknown, consider other information of value θ, thus get the joint distribution of sample x, in the same way, it is the synthesis of overall information, sample information and the priori information, its form is

$$h(x,\theta)=p(x\mid\theta)\pi(\theta) \qquad (5)$$

5. We will make the decomposition as in the following type

$$h(x,\theta)=\pi(\theta\mid x)m(x) \qquad (6)$$

Among them, $m(x)$ is the marginal probability functions of x, can also be expressed as:

$$m(x)=\oint_{\vartheta} h(x,\theta)d\theta=\oint_{\vartheta} p(x\mid\theta)\pi(\theta)d\theta$$

Thus we can get the following formula

$$\pi(\theta\mid x)=\frac{h(x,\theta)}{m(x)}=\frac{p(x\mid\theta)\pi(\theta)}{\oint_{\vartheta} p(x\mid\theta)\pi(\theta)d\theta} \qquad (7)$$

If θ is a discrete random variable, $\pi(\theta_i), i=1,2...$ can be used to show prior distribution, the posterior distribution gotten in this case is discrete, can be represented as:

$$\pi(\theta_i\mid x)=\frac{p(x\mid\theta_i)\pi(\theta_i)}{\sum_j p(x\mid\theta_j)\pi(\theta_j)}, i,j=1,2,... \qquad (8)$$

Bootstrap method

The Bootstrap method (also called self-help method), is a kind of augmented sample statistical inference method, raised by Stanford university professor Efron in 1977. When using the Bootstrap method, need not put forward other assumptions in advance, neither need not add new observation data, can only rely on the original data for statistical inference. This method simulates unknown distribution with the aid of existing sample data, it is the nature of a sampling process, can make full use of the samples on the maximum of the information itself contains. About the overall distribution there is no need to make assumptions, in the actual operation process, we use the self-help samples to estimate the unknown distribution of statistic characteristics, and these self-help samples on the basis of the test samples are generated by computer.

Bayes Bootstrap method

The Bootstrap method is to carry on the statistical inference directly by computing the sample data. Based on the Bootstrap method, Donald put forward the Bootstrap method, namely the random weighting method. Through sampling statistics, Bayes Bootstrap method is classified as a kind of simulation method. The Bayes Bootstrap method and the Bootstrap method both increase the capacity of the sample through the sample information "coattails", but because the Bayes Bootstrap method is for statistical inference of small sample, when statistics is inadequate, the method can improve the accuracy of statistical judgment

Summary

As a part throughout the product life cycle, reliability test provide the reference basis for the reliability of the product modeling, reliability design, reliability evaluation and reliability allocation and product acceptance, identification, and so on, therefore, the process of the result of reliability is particularly important. Value of small sample research not only depends on solving the small size sample, at the same time, it can also reduce the test cost, shorten the test cycle and improve product competitiveness.

References

[1] J. R. Black. Electromigration Failure Modes in Al Metallization for Semiconductor Devices. Proceedings of the IEEE, 1969, 57(9):1-203.

[2] JESD63, Standard Method for Calculating the Electromigration Model Parameters for Current Density and Temperature.

[3] Nello Cristianini. An Introduction to Support Vector Machines and other Kernel-based Learning Methods [M].CambridgeUniversityPress.2000-03-28.

[4] Cortes,C.,Vapnik,V Support Vector networks[J].MaehineLeaming,1995,70(l):l-25.

[5] Efron B. Bootstrap Methods: Another Look at the Jackknife [J]. The Annals of Statistics, 1979, 7 (1):1-26.

Advanced Materials Research Vols. 989-994 (2014) pp 1456-1459
© (2014) Trans Tech Publications, Switzerland
doi:10.4028/www.scientific.net/AMR.989-994.1456

The Application of Maximum Differential Algorithm in Adaptive Ocean Sampling

YingWang[1, a], Chuansheng Wu [2, b], Yunqiu Shi [3,c]

[1] Tianjin Research Institute for Water Transport Engineering, M.O.T, Tianjin, China [2,3]University of Science and Technology Liaoning Software College

[a]ruozhu1106@163.com; [b,c]gykwcs@163.com

Key words: Ocean sampling platforms; adaptive sampling; maximum differential algorithm; optimal sampling path.

Abstract. This paper presents a technique for adaptive ocean sampling using ocean sampling platforms equipped with multiple sensors. The virtual environment of 2D ocean sampling is established, so as to simulate the ocean sampling region by means of the sampling platforms. There are three important phases which can be written as collecting scientific data, drawing the sampling area, and utilizing the maximum differential algorithm (MDA) in ocean sampling. By analyzing the sampling data and using the maximum differential algorithm, the sampling platforms achieve the optimizing sampling path. The simulation results by adaptive ocean sampling of single sampling platform and multiple platforms show that the proposed approach is effective and feasible. This method can be applied to conduct the moving direction based on the ocean sampling platforms.

Introduction

With the rapid development of ocean technology, it is possible to acquaint the features of the ocean. J. Gao (2011) in [1], Q. Xiao et al., (2011) in [2] made mention that the biomimetic robotic fish can be used to check the ocean environment, exploit the undersea sources, relieve the trapped persons or other creatures and so on. Y. Wang (2011) in [3] introduced an unmanned surface vehicle for bathymetry as one of the basic platforms in ocean sampling, and studied the adaptive isobath tracking. C. Cannell (2004) in [4] designed a simulation tool to support the development of adaptive sampling algorithms for multiple autonomous underwater vehicles. Using limited time and optimal routes to sample more data, it can provide evidences for studying one certain feature of oceans. The key feature of these algorithms is that the sampling strategies are usually determined by sampling platforms based on data collected in real time. There are some researches about adaptive ocean sampling by some ocean experts or institutes. A. Alvarez(2007) in [5] designed combining networks of drifting profiling floats and gliders for adaptive sampling of the Ocean, and introduced the generation algorithm to optimize the path of the gliders.

Modeling of 2D Ocean Environment Sampling

In order to study some features of ocean effectively, such as the temperature and salinity which are usually diverse in different regions and depths, taking no account of the effect of ocean current, the environment of 2D ocean sampling is modeled (Ding Wang et al., 2009, in). Taking the salinity sampling as an example, the paper establishes the model of the environment of 2D ocean sampling which is shown in Figure 1. The distribution of salinity in this region can be written as follows:

$$z = f(x, y) \tag{1}$$

where: x, y is the relative longitude and latitude, respectively; z is the quantity of the salinity, which is denoted by the value of RGB in the figure. The ranges of x and y are both [0, 40]. The changes of different colors in this figure represent the quantity of the salinity, which can be seen in the side color bar.

Algorithm of Adaptive Sampling

Adaptive ocean sampling can be defined as equipping multiple sensors which can feasibly

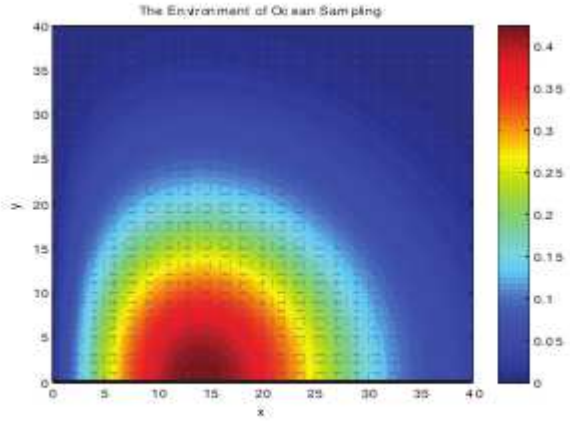

Fig. 1 The schematic of the environment of 2D ocean sampling.

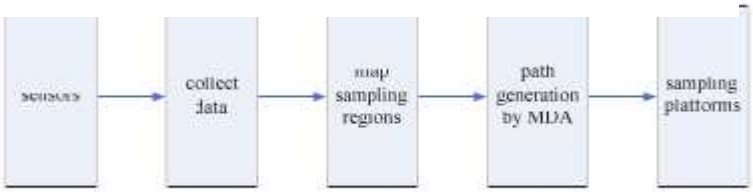

Fig. 2 The structure of the adaptive sampling algorithm.

collect, store and analyze the scientific data of ocean environment in real time, and then program the moving path by adaptive sampling algorithm, so as to acquire more information about the ocean in limited time. The structure of the adaptive sampling algorithm can be seen in Fig. 2. There are three important phases which can be described as collecting scientific data, mapping the sampling area and utilizing the maximum differential algorithm (MDA) in ocean sampling.

3.1 Scientific Data Collecting

Equipped with multiple sensors around the environment, sampling platform can collect the information of ocean. The distribution of sensors and the collecting data can be seen in Fig. 3. Blue triangle represents current path-points in the path, and the red dots show the unallowable path-point locations while the blue ones show the allowable path-point locations. Allowable set of path-points by taking into account the spatial constraints between the candidate point and the point that precedes it by one.

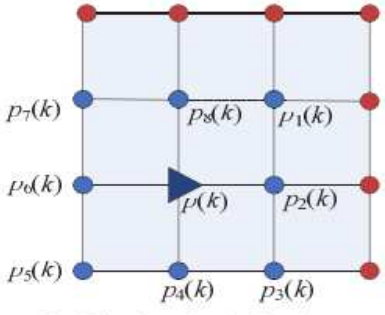

Fig. 3 The schematic of collect data.

n order to assimilate the process of the adaptive ocean sampling by sampling platform, we assume that the position of the platform is p(k) at time k, and the collect data position is (i)p k , i=1, 2,…, 8. The position of the platform can be written as:

$$p(k) = (x(k), y(k)) \quad k = 1, 2, 3, \tag{2}$$

where x(k) y(k) are the values of x and y coordinate at time k, respectively.

3.2 Sampling Regions Drawing

To simplify the moving state of the sampling platform, we divide the orientation discretely into eight orientations. The discrete orientation set is {UR, R, DR, D, DL, L, UL, U}, the U means up, the D means down, the R means right, and the L means left. Suppose the distance between adjacent grids is small enough ($\Delta l < \varepsilon$, $\varepsilon \geq 0$), we can consider that the platform will reach the point of pi(k) from p(k) per second. To make the salinity sampling adaptively by the sampling platforms, it is necessary to memorize the collecting data regions and analyze the data in real time. Then gain the variety of ocean salinity, and provide the path planning for the sampling platform properly. So we map the sampling regions through cells algorithm (Andrew A. Bennett et al., 2000, in), labeling four cells rounding the platform in real time, which can be seen in Figure 4. Sampling regions at time k can be written as:

$$C(k) = \{c(k), c(k), c(k)\, c(k)\}, k = 1, 2, 3, \quad (3)$$

where (1)c k is the cell rounding the sampling platform, i=1, 2, 3,4.As the motivation of the platform is continuous and uninterrupted, the sampling cells at time k+1 must intersect with the cells at time k, presented as $C(k)\, C(k+1) \neq \Phi$. In order to avoid the repeated sampling of the same region, there should be differences

between C (k)and C (k + n), which can be presented as $C(k)\, C(k+n) \neq C(k)$and $C(k)\, C(k+n) \neq C(k+n)$. So we can make sure that the motivation is continuous and unrepeated.

3.3 Path Generation by MDA

In the adaptive ocean sampling, it is crucial to make the path planning to the platform. The sampling platform can move properly directed by adaptive ocean sampling algorithm, so as to collect more useful scientific data in shortest time, and avoid repeated collecting data in the same region. To achieve the motivation path of the sampling platforms, the MDA is proposed. This algorithm will make the sampling platforms continuously move to the beneficial orientation, which has the maximum difference in salinity among eight directions. So the maximum difference formula is introduced, which can be written as:

(a). Initialize the position of the sampling platform and the sampling parameters;

(b). Collect data in the position of the core of the sampling platform and the rounding positions, and map the sampling regions;

(c). Judge the sampling regions whether it can satisfy our meet or not. If “Yes”, then over; if “No”, then continue;

(d). Calculate the maximum difference parameter D(k), and gain the moving direction by the sampling platform;

(e). Move the sampling platform to the designed position, and then return (b).

Conclusions

In this paper, the environment of 2D ocean sampling has been established in order to simulate the ocean sampling region using the sampling platforms. By accurately analyzing the collecting data and the current data, the sampling platforms can move availably directed by MDA and gain the optimizing sampling path. Simulation results by adaptive ocean sampling of single sampling platform and multiple platforms have indicated the effectiveness and feasibility of the proposed approach, which can be greatly used in the application of ocean sampling. Future research will be aimed at considering the complexity and uncertainty of the ocean environment in order to make the approach more precisely.

References

[1] J. Gao, Q. Li, Z. Ji, et al, Fuzzy sliding mode trace control method for pose control of biomimetic robotic fish, Proceedings 2011 IEEE International Conference on Information Science and Engineering, 2588-2591, 2011.
[2] Q. Xiao, F. Kong and Q. Li, A cooperation method for multiple biomimetic robotic-fish ball-pushing, Proceedings 2011 IEEE International Conference on Information Science and Engineering, 1516-1519, 2011.
[3] Y. Wang, J. Jin, S. Guan, et al, Simulation of adaptive isobaths tracking for unmanned surface bathymetry vehicle, Proceedings 2011 IEEE International Conference on Intelligent Computation Technology and Automation, 495-499,2011.
[4] C. Cannell, D. Stilwell and J. Austin, A simulation tool to support the development of adaptive sampling algorithms for multiple autonomous underwater vehicles, IEEE/OES Autonomous Underwater Vehicles, 127-133, 2004.
[5] A. Alvarez, B. Garau and A. Caiti, Combining networks of drifting profiling floats and gliders for adaptive sampling of the Ocean, Proceedings 2007 IEEE International Conference on Robotics and Automation, 157-162, 2007.
[6] C. Cannell, D. Stilwell, A comparison of two approaches for adaptive sampling of environmental processes using autonomous underwater vehicles, Proceedings 2005 MTS/IEEE Oceans, 1514-1521,2005.

Advanced Materials Research Vols. 989-994 (2014) pp 1460-1463
© (2014) Trans Tech Publications, Switzerland
doi:10.4028/www.scientific.net/AMR.989-994.1460

Parameter estimation for Wiener systems with preload nonlinearities

NI Yunxia[1,a], Cao Jiandong[1,b]

[1] Wuxi Professional College of Science and Technology, Wuxi, PR China 214028

[a]email: 392931428@qq.com; [b]email: 302774418@qq.com

Keywords: Parameter estimation, Recursive least squares algorithm, Switching function, Wiener system.

Abstract. This paper proposes a recursive least squares algorithm for Wiener systems. We use a switching function to turn the modelof the nonlinear Wiener systems into an identification model, then propose a recursive least squares identification algorithm toestimate all the unknown parameters of the systems. Finally, an example is provided to show the effectiveness of the proposed algorithm.

1 Introduction

Nonlinear systems arise widely in process industries, andidentification of such systems has been an active researcharea for a long time. There exists three mature methods onidentification of these nonlinear systems: the stochastic gradient(SG) algorithm [1–3], the recursive least squares (RLS)algorithm [4–6] and the iterative algorithm [7–9]. The RLSalgorithm has quicker convergence rate than the SG algorithm[10].

In this paper, we deals with a Wiener system which is shown in Figure 1 and is expressed as follows:

$$x(t)=\frac{B(z)}{A(z)}u(t), \tag{1}$$

$$y(t)=f(x(t))+v(t). \tag{2}$$

where $y(t)$ is the system output, $x(t)$ is the unknown innervariables, $u(t)$ is the system input, and $v(t)$ is a stochasticwhite noise with zero mean, and $A(z)$ and $B(z)$ are polynomials in the unit backward shift operator [$Z^{-1}y(t)=y(t-1)$] and

$$A(z) := 1 + a_1z^{-1} + a_2z^{-2} + \cdots + a_nz^{-n},$$

$$B(z) := b_1z^{-1} + b_2z^{-2} + \cdots + a_nz^{-n}.$$

The function $f(x(t))$ is a preload nonlinearity and can be expressed as

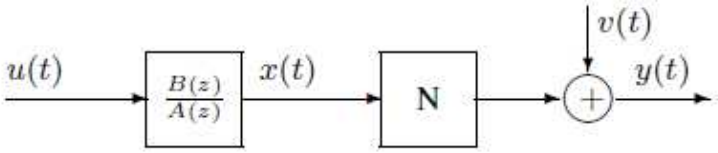

Fig. 1: The Wiener model

$$f(x(t)) = \begin{cases} x(t) + m, & x(t) > 0, \\ 0, & x(t) = 0, \\ x(t) - m, & x(t) < 0, \end{cases}$$

where m and -m are the preload points.

By using a switching function, the model of the Wiener systems be changed to an identification model, then based on the derived model, a RLS algorithm is presented to estimate all the unknown parameters. Briefly, the paper is organized as follows. Section 2 describes the nonlinearities and studies estimation algorithms for the Wiener system. Section 3 provides an illustrative example. Finally, concluding remarks are given in Section 4.

2 The nonlinearities and the estimation algorithms

Let "$A =: X$" or "$X =: A$" stand for "A is defined as"; the norm of a column vector X is defined as $\|X\|^2 := tr[X^T X]$; the superscript T denotes the matrix transpose.

Introduce a sign function,

$$\mathrm{sgn}[x(t)] := \begin{cases} 1, & if\ x(t) > 0, \\ 0, & if\ x(t) = 0, \\ -1, & if\ x(t) < 0. \end{cases}$$

The function $f(x(t))$ be expressed as

$$y(t) = f(x(t)) + v(t) = x(t) + m\,\mathrm{sgn}(x(t)) + v(t). \tag{3}$$

Then the Wiener model can be rewritten as

$$x(t) = \frac{B(z)}{A(z)}u(t), \tag{4}$$

$$y(t) = x(t) + m\,\mathrm{sgn}(x(t)) + v(t). \tag{5}$$

Define the parameter vector θ_1 and the information vector $\varphi_1(t)$ as

$$\theta_1 := [a_1, a_2, \cdots, a_n, b_1, b_2, \cdots, b_n]^T \in R^{2n} \tag{6}$$

$$\varphi_1(t) := [-x(t-1), -x(t-2), \cdots, -x(t-n), u(t-1), u(t-2), \cdots, u(t-n)]^T \in R^{2n}, \tag{7}$$

gets

$$x(t) = \varphi_1^T(t)\theta_1,$$

$$y(t) = \varphi_1^T(t)\theta_1 + m\,\mathrm{sgn}(x(t)) + v(t).$$

Define the parameter vector θ_2 and the information vector $\varphi_2(t)$ as

$$\theta_2 := [a_1, a_2, \cdots, a_n, b_1, b_2, \cdots, b_n, m]^T \in R^{2n+1}, \tag{8}$$

$$\varphi_2(t) := [-x(t-1), -x(t-2), \cdots, -x(t-n), u(t-1) \quad u(t-2), \cdots, u(t-n), \mathrm{sgn}(x(t))]^T \in R^{2n+1}, \tag{9}$$

then

$$y(t) = \varphi_2^T(t)\theta_2 + v(t).$$

Using the following RLS algorithm to estimate the parameter vector θ_2 in (8):

$$\hat{\theta}_2(t) = \hat{\theta}_2(t-1) + P(t)\varphi_2(t)e(t), \tag{10}$$

$$e(t) = y(t) - \hat{\theta}_2^T(t-1)\varphi_2(t), \tag{11}$$

$$\varphi_2(t) = [-x(t-1), -x(t-2), \cdots, -x(t-n), u(t-1), \quad u(t-2), \cdots, u(t-n), \mathrm{sgn}(x(t))]^T, \tag{12}$$

$$P(t) = P(t-1) - \frac{P(t-1)\varphi_2(t)\varphi_2^T(t)P(t-1)}{1 + \varphi_2(t)P(t-1)\varphi_2(t)^{-1}},$$

$$P(0) = 10^6 I. \tag{13}$$

Because the information vector in (12) [that is $\varphi_2(t)$] contains the unknown inner variables $x(t-i)$, the above RLS algorithm in (10) cannot be applied to estimate θ_2 in (8).The solution is to use the auxiliary mode identification idea in [11]: the unknown variables are replaced with their estimates or with the outputs of the auxiliary model. Define

$$\hat{x}(t) = \hat{\varphi}_1^T(t)\hat{\theta}_1(t), \tag{14}$$

$$\hat{\varphi}_1^T(t) := [-\hat{x}(t-1), -\hat{x}(t-2), \cdots, -\hat{x}(t-n), u(t-1), \quad u(t-2), \cdots, u(t-n), \mathrm{sgn}(\hat{x}(t))], \tag{15}$$

when $\hat{\theta}_i(t),(i=1,2)$ is the estimate of θ_i, $\hat{\varphi}_i(t)$ is the estimate of $\varphi_i(t)$ and $\hat{x}(t)$ is the estimate of $x(t)$. We can obtain a auxiliary model based RLS (AM-RLS) algorithm as:

$$\hat{\theta}_2(t)=\hat{\theta}_2(t-1)+P(t)\hat{\varphi}_2(t)e(t), \tag{16}$$

$$e(t)=y(t)-\hat{\theta}_2^T(t-1)\varphi_2(t), \tag{17}$$

$$\hat{x}(t)=\hat{\varphi}_1^T(t)\hat{\theta}_1(t), \tag{18}$$

$$\hat{\varphi}_1^T(t):=[-\hat{x}(t-1),-\hat{x}(t-2),\cdots,-\hat{x}(t-n),u(t-1), u(t-2),\cdots,u(t-n)]^T, \tag{19}$$

$$\hat{\varphi}_2^T(t):=[-\hat{x}(t-1),-\hat{x}(t-2),\cdots,-\hat{x}(t-n),u(t-1), u(t-2),\cdots,u(t-n),\mathrm{sgn}(\hat{x}(t-1))]^T, \tag{20}$$

$$,P(t)=P(t-1)-\frac{P(t-1)\hat{\varphi}_2(t)\hat{\varphi}_2^T(t)P(t-1)}{1+\hat{\varphi}_2(t)P(t-1)\hat{\varphi}_2(t)^T},$$

$$P(0)=10^6 I. \tag{21}$$

The steps of computing the parameter estimation vector $\hat{\theta}_2(t)$ by the RLS algorithm are listed in the following.

1) Let $t=1,\hat{\theta}_2(0)=1/p_0, and P(0)=p_0 I$ with 1 being a column vector whose entries are all unity and $p_0=10^6$.

2) Let $y(-j)=0,u(-j),x(-j)-0,\ j=0,1,2,\cdots,n-1$, and give a small positive number ε.

3) Collect the input data $\{u(t),y(t)\}$.

4) Form $\hat{\varphi}_1(t)$ and $\hat{\varphi}_2(t)$ by (19) and (20).

5) Compute $\hat{x}(t)$ by (18).

6) Compute $e(t)$ and $P(t)$ by (17) and (21) respectively.

7) Update the parameter estimation vector $\hat{\theta}_2(t)$ by (16).

8) Compare $\hat{\theta}_2(t)$ and $\hat{\theta}_2(t-1)$: if $\left\|\hat{\theta}_2(t)-\hat{\theta}_2(t-1)\right\|\le\varepsilon$, then terminate the procedure and obtain the $\hat{\theta}_2(t)$; otherwise, increase *t* by 1 and go to step 3.

3 Example

Consider the following nonlinear system

$$x(t)=\frac{B(z)}{A(z)}u(t)+v(t),$$

$$y(t)=x(t)+0.05\,\mathrm{sgn}(x(t)),$$

$$A(z)=1+a_1z^{-1}+a_2z^{-2}=1+0.38z^{-1}+0.31z^{-2},$$

$$B(z)=b_1z^{-1}+b_2z^{-2}=0.64z^{-1}+0.70z^{-2},$$

$$\theta_2=[a_1,a_2,b_1,b_2,m]^T$$

$$=[0.38,0.31,0.64,0.70,0.05]^T.$$

Here, $\{u(t)\}$ is taken as a persistent excitation signal sequence with zero mean and unit variance, and $\{v(t)\}$ is taken as a white noise sequence with zero mean and variance $\sigma^2=0.10^2$. Applying the RLS algorithm to estimate the parameters of this example system, the parameter estimates and their errors are shown in Tables 1.

4 Conclusions

An approach to identify a Wiener system with preload nonlinearity is presented in this paper. By using a switching function, the model of the nonlinear system be turned into an identification model,

then a RLS algorithm is proposed to estimate all the parameters of the system. The simulation results verify the proposed method.

Table 1: The RLS estimates and errors

k	a_1	a_2	b_1	b_2	m	$\delta(\%)$
100	0.372	0.180	0.513	0.702	-0.016	18.085
200	0.372	0.309	0.602	0.726	-0.017	7.705
300	0.372	0.354	0.652	0.757	-0.019	9.386
1000	0.417	0.326	0.674	0.707	0.058	5.036
2000	0.405	0.333	0.667	0.740	0.051	5.515
3000	0.378	0.314	0.637	0.697	0.034	1.573
True Values	0.380	0.310	0.640	0.700	0.050	

References

[1] F. Ding, Hierarchical multi-innovation stochastic gradient algorithm for Hammerstein nonlinear system modeling, Applied Mathematical Modelling, doi:10.1016/j.apm.2012.04.039

[2] F. Ding, Separable gradient estimation algorithm for Hammerstein systems based on decompositions. The 2012 American Control Conference, June 27-29, 2012, Montr´eal, Canada.

[3] D.Q. Wang, F. Ding, Extended stochastic gradient identification algorithms for Hammerstein-Wiener ARMAX systems, Computers and Mathematics with Applications 56 (12) (2008) 3157-3164.

[4] D.Q. Wang, F. Ding, Least squares based and gradient based iterative identification for Wiener nonlinear systems, Signal Processing 91 (5) (2011) 1182-1189.

[5] D.Q.Wang, Y.Y. Chu, F. Ding, Auxiliary model-based RELS and MI-ELS algorithms for Hammerstein OEMA systems, Computers & Mathematics with Applications 59 (9) (2010) 3092-3098.

[6] F. Ding, Y. Shi, T. Chen, Auxiliary model based least-squares identification methods for Hammerstein output-error systems, Systems & Control Letters 56 (5) (2007) 373-380.

[7] J. Chen, X.P. Wang, R.F. Ding, Gradient based estimation algorithm for Hammerstein systems with saturation and deadzone nonlinearities, Applied Mathematical Modelling 36 (1) (2012) 238-243.

[8] Y. Liu, E.W. Bai, Iterative identification of Hammerstein systems, Automatica 43 (2) (2007) 346-354.

[9] J. “Vor”os, Parameter identification of Wiener systems with multisegment piecewise-linear nonlinearities, Systems & Control Letters 56 (2) (2007) 99-105.

[10] G.C. Goodwin, K.S. Sin, Adaptive Filtering Prediction and Control, Prentice-Hall, Englewood Cliffs, NJ, 1984.

[11] F. Ding, T. Chen, Combined parameter and output estimation of dual-rate systems using an auxiliary model, Automatica 40 (10) (2004) 1739-1748.

Advanced Materials Research Vols. 989-994 (2014) pp 1464-1468
© (2014) Trans Tech Publications, Switzerland
doi:10.4028/www.scientific.net/AMR.989-994.1464

A vertical handoff decision algorithm based on QoS evaluation

Yang Tao, Kun Zhou

School of communication and Information Engineering,
Chongqing University of Posts and Telecommunications, Chongqing 400065, China.

951248757@qq.com

Keywords: vertical handoff, QoS evaluation, Analytic Hierarchy Process(AHP）, Cost function.

Abstract. In the next generation of heterogeneous wireless network environment, to meet the network requirements of diverse services， we propose a vertical handoff decision algorithm based on QoS evaluation that refine the handover unit to services. The proposed algorithm consider the needs of the services, network conditions, user preferences and other factors, and makes Analytic Hierarchy Process (AHP) and cost function combine to choose the target network that is best meet the requirements of services . Comparing with the vertical handoff decision based on RSS, simulation results show that the proposed method can take full account of the different QoS requirements of various services types to choose the appropriate network, and would not cause performance degradation.

Introduction

With the rapid development of wireless communication technology, all kinds of wireless access technology emerge in endlessly constitute the ubiquitous wireless heterogeneous network [1,2]. In order to achieve the user's session continuity and seamless across heterogeneous networks vertical handover has become one of the important issues need to be resolved. Literature [3] focus on how to reduce energy consumption of the terminal, as well as to determine the appropriate time to switch trigger. Literature [4] proposed network selection algorithm based decision function, comprehensive survey network characteristics, user requirements and terminal status and other conditions. However, most studies are based on terminal as the smallest handover unit, the entire terminal to switch to the target network by comparing network performance evaluation function or access cost function. Due to different types of services, this may cause the selected network may not be able to meet a good QoS requirements of each service. This paper consider services, network, user terminal and other factors, makes Analytic Hierarchy Process (AHP) and cost function combine to choose the target network, propose a vertical handoff decision method based on QoS evaluation. The advantage of the presented handoff decision algorithm has been proved by the simulation.

QoS Evaluation Based Vertical Handoff Decision Algorithm

Analytic Hierarchy Process.

1) The structuring hierarchy: In-depth analysis of different factors in the practical problems，To construct of these Related factors into a hierarchy according to the attributes [5]：The goal level as the top level of the structuring hierarchy generally have a factor； alternative level is the lowest level； criterion level is in the middle，generally have multiple factors，When too many factors that will break out sub-criterion level. QoS evaluation of different services to QoS parameter, so using AHP method to calculate the relative weight of each parameter. Our goal level is the optimal network based on services; alternative level is WLAN/UMTS network. When designing the criterion level, this paper will consider five main QoS parameters: Delay, Bandwidth, Packet-loss Rate, Price, Security.

2) Establish judgment matrix：Judgment matrix [6] constructed with the pair wise comparisons method and Table 1. $x_1 x_2 \cdots x_n$ are factors of the criterion level, choose any two of them x_i and x_j compare pair wise according to their levels of influence. The comparison result r_{ij} are presented in judgment matrix $R = (r_{ij})$;and $r_{ij} r_{ji} = 1$.

Table 1 Scale of importance

Intensity	Definition
1	Equal importance
3	Moderate importance
5	Strong importance
7	Very strong importance
9	Extreme importance
2，4，6，8	Intermediate values

3) Calculation of the relative weights: normalize the vector, get $(w_1, w_2, ..., w_n)$ as evaluation parameters of weight.

$$\overline{w_i} = \sqrt[n]{\prod_{j=1}^{n} r_{ij}} \text{ (i=1,2, ... ,n)} \tag{1}$$

$$w_i = \frac{\overline{w_i}}{\left(\sum_{i=1}^{n} \overline{w_i}\right)} \tag{2}$$

4) Consistency check: In order to avoid potential inconsistency, we introduce consistency index (CI) and random index (RI) [6].

$$CI = \frac{\lambda_{\max} - n}{n-1} = \frac{-\sum_{k \neq \max} \lambda_k}{n-1} \tag{3}$$

$$CR = {CI}/{RI} \tag{4}$$

If $CR \le 0.10$,the inconsistency is considered acceptable, otherwise the judgment Matrix needs to be revised. We can get various values of RI from Table 2.

Table 2 Value of random consistency index

Criteria	1	2	3	4	5	6	7	8	9	10	11	12
RI	0	0	0.58	0.9	1.12	1.24	1.32	1.41	1.45	1.49	1.52	1.56

Parameter Standardization. This paper consider the five kinds of QoS parameters: Delay, Bandwidth, Packet-loss Rate, Price, Security. Their value standards are different, if use them directly, the result of the cost function is meaningless. So in order to obtain reasonable network cost, cost, we need to standardize the parameters. These parameters can be divided into real-benefit type (Bandwidth) ,real-cost type(Delay, Packet-loss Rate),language type(Price, Security).For real-benefit type, the larger the parameter value, the better the network performance. But for real-cost type, the larger ,the worse [7].Obviously these two kinds of parameters must adopt different methods of standardization. We define b_n^x as standardized value of parameter x in network n, $x_{\max}$ and $x_{\min}$ as upper limit and lower limit of parameter x.

For real-benefit type:

$$\begin{cases} b_n^x = {(x - x_{\min})}/{(x_{\max} - x_{\min})}, when(x_{\min} < x < x_{\max}) \\ b_n^x = 1, when(x \le x_{\min}) \\ b_n^x = 0, when(x \ge x_{\max}) \end{cases} \tag{5}$$

For real-cost type:

$$\begin{cases} b_n^x = {(x_{\max} - x)}/{(x_{\max} - x_{\min})}, when(x_{\min} < x < x_{\max}) \\ b_n^x = 0, when(x \le x_{\min}) \\ b_n^x = 1, when(x \ge x_{\max}) \end{cases} \tag{6}$$

Language type can not be represented by exact number， they need to be quantified. This article adopts the method of literature [8],then follow the above formula to standardize, the result are listed in the Table 3.

Table 3 Standardized value of language type

	Security	Price
UMTS(Standardized value)	Relatively good（0.6）	general（0.3333）
WLAN(Standardized value)	general（0.4）	low（0.6666）

Handoff Decision Process. After obtaining the parameters weights and standardized values, we need to complete the network selection. Because the traditional cost function can not reasonably choose the network according to services requirements, we propose a cost function based on QOS evaluation .We define F_s^n as the QOS evaluation value of the network n for the service s, w_s^x denotes the weight of parameter x for the service s：

$$F_s^n = \sum_x w_s^x b_n^x \tag{7}$$

Finally, network obtain highest QOS evaluation value is the optimal target network:

$$f_{best}^s = \{n \Big| \max_{1 \le n \le N} F_s^n\} \tag{8}$$

Simulation and Results

In this paper, simulation tool are developed using NS-2 .our simulation scenario involves two wireless access networks UMTS and WLAN. Because NS-2 simulation tool integrates no UMTS module, we use the existing the WLAN module for the UMTS simulation .Choose the interactive service as representative from the classification of 3GPP for services [9].Five Qos evaluation parameters considered in this paper: Delay and Packet-loss rate, Bandwidth, Security, Price, Their weights were 0.1059, 0.2605, 0.5263, 0.0648, 0.0425 according to AHP .In order to evaluate the performance of the handoff algorithm, we designed handoff scene: The center of the WLAN is on the x axis, coordinate is(100,0);the center of the UMTS is also on the x axis, coordinate is(200,0).Terminal from the origin moves along the x axis at a speed of 1 m/s, enter the WLAN network coverage area in 50s and lefe in150s.Terminal will be scanned once every two seconds with uniform sampling method. For more realistic performance evaluation, background traffic is added in the simulation, set the link delay dynamically, thus QoS parameter values of WLAN and UMTS dynamically changes. Fluctuations of Bandwidth and Delay in WLAN and UMTS as shown in the Figure 1and 2.

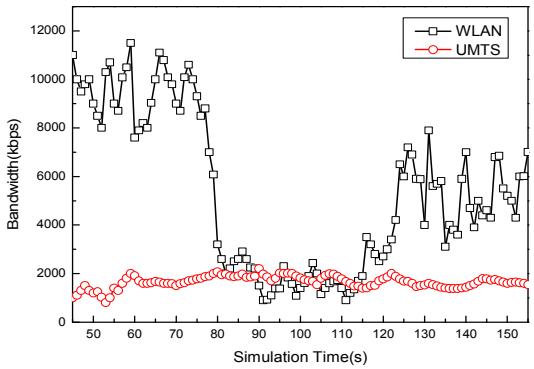

Fig.1 Fluctuations of Bandwidth

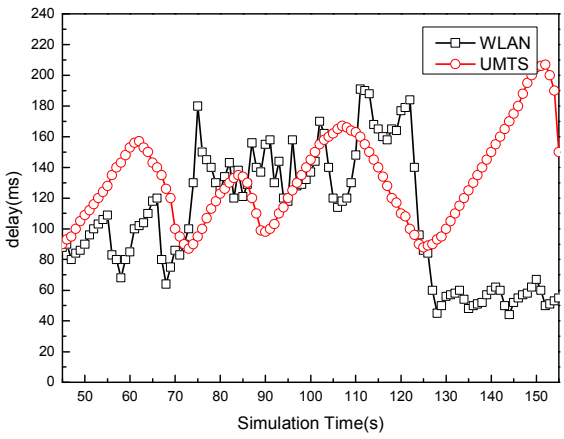

Fig.2 Fluctuations of Delay

We evaluated our proposed QoS evaluation based algorithm by comparing it with the RSS based algorithm. As illustrated in the Figure 3,except for some handover caused by entering and leaveing coverage of the wlan, mobile terminal gets handover at 91s and 113 s respectively; Combined with Figure 1 and 2 ， during 90s-113s average available bandwidth of the WLAN is smaller than the UMTS, in order to meet the needs of the business，switching to the UMTS. Although real-time performance of the UMTS is better than that of the WLAN during 73s-124s ,the interactive service was not sensitive to time delay, so the impact on handoff is smaller. For the RSS based algorithm，mobile terminal gets handover from UMTS to WLAN at 57.4s,back to the UMTS at 142.6s,Mobile terminal has been in the WLAN during 57.4s-142.6s.The RSS based algorithm dones't consider the service requirement for QoS.

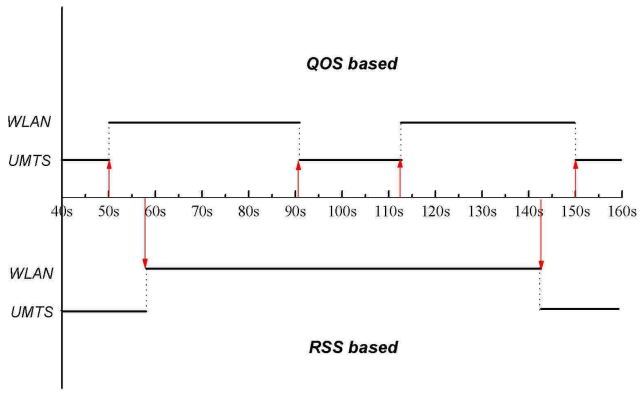

Fig.3 Handoff process of the interactive service comparison

For interactive class business, The most important performance index is throughput. as shown in the Figure 4,the vertical handoff decision method proposed in this paper can obtain higher average throughput than RSS based method.

From the above simulation data, in this paper a QoS evaluation based handoff algorithm is proposed that can take full account of the different QoS requirements of various services types, use the QoS evaluation of service to rank the candidate networks, and will not result in lower performance.

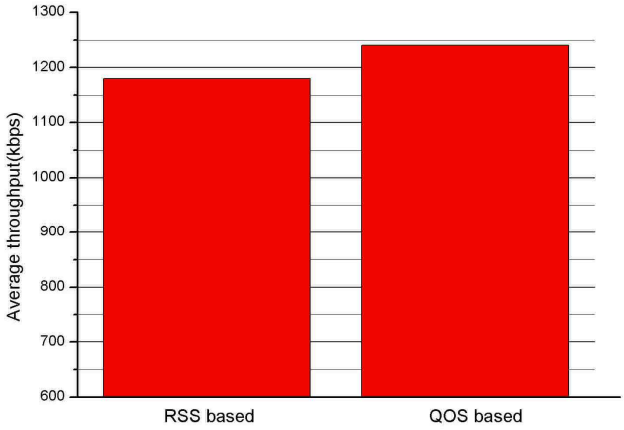

Fig.4 Average throughput of the interactive service comparison

Conclusion

The proposed vertical handoff decision algorithm based on QoS evaluation, can take full account of the different QoS requirements of various services types，adopt Parameters standardization method to obtain reasonable QoS parameter values, and makes Analytic Hierarchy Process and cost function combine to choose the target network that is best meet the requirements of services . Simulation result shows，a QOS requirements of services based Vertical handoff algorithm proposed in this paper, considering Multiple parameters, can be very effective for the selection of the optimal network according to QOS requirements of services ,and will not result in lower performance.

References

[1] Ghosh C, Roy S, Cavalcanti D. Coexistence challenges for heterogeneous cognitive wireless networks in TV white spaces[J].IEEE Wireless Communications, 2011, 18(4): 22-31.

[2] Gozalvez J. Heterogeneous wireless networks [mobile radio][J].IEEE Vehicular Technology Magazine, 2011, 6(2): 9-13.

[3] Mehbodniya A., Chitizadeh J.. An intelligent vertical handoff algorithm for next generation wireless networks. Second IFIP International Conference on Wireless and Optical Communications Networks (WOCN 2005). 2005. pp.244-249.

[4] Shen W, Zeng Q A. Cost-function-based network se-election strategy in integrated wireless and mobile net-works[J]Vehicular Technology,IEEE,2008,57(6):3778-3788

[5] Blasasubramaniam S，Indulska J. Vertical handovers as adaptation methods in Pervasive systems. Proceedings of the 1lth IEEE International Conference on Networks (ICON2003). Sydney， Australia，2003.705-710.

[6] T. L. Saaty “Decision Making for Leaders: The Analytic hierarchy Process for Decisions in a Complex World”, RWS Publications, 1988.

[7] Seyong Park，Kyungtae Kim，Doung C.Kim, Sunghyun Choi，Sangjin Hong. Collaborative QoS Arehitecture between Diffsery and 802.lle Wireless LAN. Proceedings of IEEE VTC’03-Spring. April2003.

[8] Latvakoski J, Laurila P J. Application based access system selection concept for all IP mobile terminals[A]. Global Telecommunications Conference[C]. 2002. 2984-2988.

[9] Timo Hamalainen，Eero Wallenius，Kari Luostarinen，Timo Nihtila. End-to-end QoS Issues at the Integrated WLAN and 3GE environments. APCC2003，Penang，Malaysia2003.

Advanced Materials Research Vols. 989-994 (2014) pp 1469-1472
© (2014) Trans Tech Publications, Switzerland
doi:10.4028/www.scientific.net/AMR.989-994.1469

A Video Digital Watermarking Algorithm Based on Chaotic Maps

Yawen Li

Department of Physics and Electronic Information Engineering, Shangluo University, Shangluo, China

slxylyw@163.com

Keywords: Chaotic system; Wavelet lifting; DCT coefficients；Compressed video

Abstract. The scrambled watermark is embedded in DCT coefficients of low-frequency sub image with the Brightness Component of original color image after lifting wavelet transformation. Before embedding the watermark, the image confusion method is used to eliminate the space correlation of the pixels and improves the security and robustness. The results showed that the algorithm is easy to carry out with the real-time request of video watermarking.

Introduction

In recent years, video watermarking has been attracted consumers attention and interesting, which is an effective scheme for digital media copyright protect and content authorization of digital video products. Much more Excellent algorithms of watermarking are proposed with the technology of video watermarking development in recent years[1-4],which can be classified into two categories :spatial domain and frequency domain based.Video watermarking algorithm is complicated and difficult comparing with image watermarking, Recently, the precise human vision system model has not been established,whosever it was attacked by any way than image watermarking for video stream, such as, recombining frame[5],falling frame[6] ,etc. The real-time should be considered in Video watermarking algorithm just as [7],otherwise the watermarking will not achieve the purpose.

A video digital watermarking algorithm based on chaotic maps was proposed, watermark signal was embeded continuously in some image frames of video in order to weak the falling frames. The component lightness of image frames was resolved to integral wavelet, then the Low-frequency approximation point DCT coefficient is quantified and modulated, watermarking signal were scrambled and chaotic encrypted before embedded in image frames in the process of quantization. The result showed that the algorithm can improve the security and robustness in video image frames.

The rest of the Letter is organized as follows, Section 2 describes chaotic maps and wavelet lifting in image watermarking scrambling ,The video watermarking scheme based on chaotic systems is proposed in section 3.Simulation result are discussed in section 4 and section 5 concludes the Letter.

Chaotic maps

To enhance the security and robustness of watermarking, image frames were scrambled transfered and disorganized the original pixel coordinate to subtractive the space correlation.The common image scrambling such as: chaotic scrambling, magic transformation , Arnold transformation.etc. The video image watermarking was scrambled in this paper with chaotic maps. Chaotic maps is unpredictable but regular, it is quite sensitivity for initial parameter lead to emerge the chaotic sequence of completely different and irrelevant in little time. The Logistic maps and Hybrid maps was applied widely [7].To determine the bit of host image pixels in watermark embedding, chaotic map is used in the approach. A commonly used one is the logistic map, which is described by:

$$X_{n+1} = \mu X_n (1 - X_n) \tag{1}$$

Where $X_{n+1} \in (0,1)$ $\mu \in (0,4)$ .When $\mu > 3.5699456$,the sequence iterated with initial value X_0 is chaotic, different sequence will be generated with different initial values[8].

A short compressed video was decomposed to 168 frames, whose frame size is 256*256, any frame was tested with watermarking embedding and extraction in this experiment. If the original video image frame $p(x,y)$ is gray image of $M \times N$ size and the watermarking image is a binary image $w(x,y)$ of $i \times j$ size($i = M/16, j = N/16$).

(1) Watermark embedding

Watermark embedding algorithm can be described as follow.

Step 1: The original carrier image is brightened with color space transformation before watermarked P_Y .

Step2: P_Y is decomposed with a one level lifting wavelet and obtained subimage P_L . The low pass subimage is divided into 8×8 sub blocks $P_{LB}(x,y)$, $x = 1,2,\cdots M; y = 1,2,\cdots N$.

Step 3: The discrete cosine transform(DCT) is employed to every sub block $D_{x,y}$ and its DC coefficients $d(x,y)$ are used to embed watermark information.

The quantitative value $\delta(x,y)$ of each $d(x,y)$ is given by: $\delta(x,y) = \text{round}(d(x,y)/\lambda)$, while round(·) is the round off function, and λ is the predetermined quantization step. The original watermark image is denoted as w and the scrambled watermark image is denoted as W_a .

If $\text{mod}((\delta(x,y) + W_a(x,)y),2) = 1$, then $\bar{d}(x,y) = \lambda(\delta(x,y) - 0.5)$,

else $\bar{d}(x,y) = \lambda(\delta(x,y) + 0.5)$.

Step 4: The DC coefficients $d(x,y)$ is replaced by $\bar{d}(x,y)$ in each sub block. Then the modified sub blocks are obtainecd by IDCT, and the low pass subimage is formed. The watermarked image is got by inverse wavelet transform. The single frame was lightened the color and saturation component to convert RGB ,the process embedding finished.

(2)Watermark extraction

Watermark extraction is just the inverse process of the above embedding algorithm.

Step1 The original extraction image P' is brightened with color space transformation before embedded watermark, marked P_Y .

Step2 P_Y is decomposed with a one level lifting wavelet, and obtained subimage P'_L . The low pass subimage is divided into M×M sub blocks $P'_{LB}(x,y)$, $x = 1,2,\cdots M; y = 1,2,\cdots N$.

Step3 Calculated the quantitative value $\mu'(x,y) = floor(dc'(x,y)/\delta)$, Corresponding watermark information was decided according to $\mu'(x,y)$.

Step 4 The watermark w' is abstracted from W'_a by inverse scrambled according to the keys.

Simulation result

Appropriate quantization step δ and coefficient β are selected in simulation process. The peak signal-to-noise ratio (PSNR) is used to establish the difference between the watermarked image frame and original image frame. Generally, the greater the PSNR value is, the watermark transparency is better. The similarity measure between the original and extracted watermarks is given by:

$$SIM = \frac{\sum_x \sum_y W(x,y)W'(x,y)}{\sum_x \sum_y W^2(x,y)} \tag{2}$$

The original image frame and original watermark image are shown in Fig. 1. Watermarked image frame and extracted watermark image are shown in Fig. 2. The watermark information is

embedded in some video frames. The PSNR values between 36 and 40, and these values showed the transparency of this method.

Fig. 1 Original image frame and watermark

Fig. 2 Watermarked image frame and extracted

Watermark information can be extracted when random frame lost occurred since the watermark image is multi-embedded in some frames.Fig. 4 shows the extraction result by “Gaussian noise” with zero mean-value and 0.002 variance and “Salt and Pepper” noise with 0.02 density.

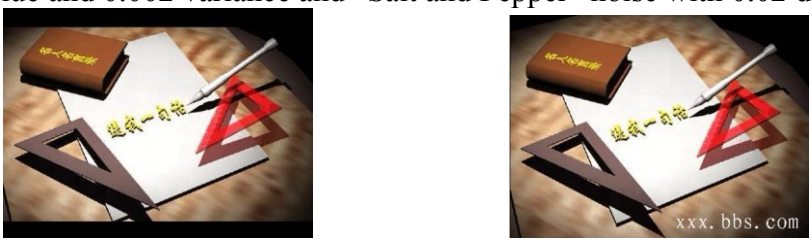

Fig.3 Cropping and filled with zero pixels and characters attack

Fig. 3 shows the result by cropping and filled with zero pixels and characters attack.The value of SIM with video frames watermarked is shown in Fig.5.

Fig.4 Watermarked frames with noise attacked test

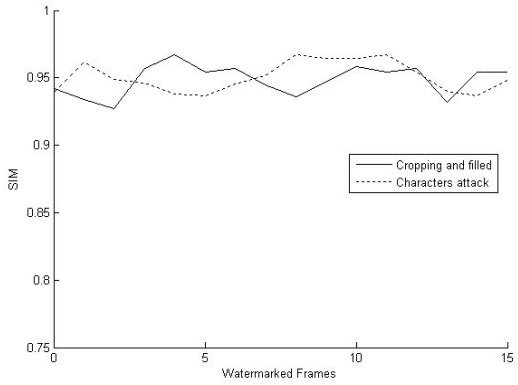

Fig.5 Cropping and filled and characters attack test

Conclution

Video watermarking is difficult in real-time and algorithm complexity comparison with image in digital watermarking technology .In this Letter ,video digital watermarking algorithm based on wavelet lifting quantization of DCT coefficients is proposed, the watermarking information with chaotic maps was embedding in video frames. One maps is used to encrypt the embedding position and another one is used to determine the pixel bit for embedding in host image. Simulation have confirmed that this new scheme is fair robustness and invisibility against various signal processing operation and geometric attacks. It is also more convenient base on integer wavelet lifting and easy to hardware implementation.

Acknowledgements

This work was supported by the scientific project of ShangLuo University under Grant 13SKY015

Reference

[1] J. Cox, M.L. Miller and J.A. Bloom: Academic Press,New York, 2002.

[2] R. Bender, D. Gruhl and N. Morimoto: Techniques for data hiding,:Proc.SPIE: Storage and Retrieval of image and video Databases,vol. 2420,1995,p.164.

[3] J. Lichtenauer, I. Setyawan: Proceeding of Security, Steganography and Watermarking of Multimedia Contents VI(San Jose, USA, January 18, 2004). Vol. 5306, p. 320.

[4] S.D. Lin,C.F. Chen: Int,J.Computer.Appl (2003).

[5] Liu E, DelpE: Temporal synchronization in video watermarking.Proceedings of the SPIE Security and Watermarking of Multimedia Contents,2001,4313:394-405

[6] N. Johnson, Z. Duric, S. Jajodia: Lecture Notes in Computer Science, Vol. 1768 (1999), p. 318

[7] Lian Cai, Sidan Du, Duntang Gao: Journal of Electronics (china), 2005, 22(5):300-306.

[8] D.W. Zhao,G.R. Chen,W.B. Liu,Chaos solitions Fractals 22 (2004) 47.

Advanced Materials Research Vols. 989-994 (2014) pp 1473-1476
© (2014) Trans Tech Publications, Switzerland
doi:10.4028/www.scientific.net/AMR.989-994.1473

Zero Watermarking Method Based on Enhanced Bit-plane

Jie Zhao[a], Binfeng Yang[b], Xiaoyun Wu[c]

Department of Physics and Electronic Information Engineering, Shangluo University, Shangluo, China

[a]slxyzj@163.com, [b]26564493@qq.com, [c]wuxiaorong0307@163.com

Keywords: Zero watermarking; Enhanced bit-plane; Cellular neural network

Abstract. Traditional watermark embedding introduces inevitably some perceptible quality degradation of the host image. Another problem is the inherent conflict between imperceptibility and robustness. However, the zero-watermarking technique can extract some essential characteristics from the host image and use them for watermark registration and detection. The original image was decomposed into series of multiscale and directional subimages after lifting wavelet transformation (LWT). The high order bit-plane of low-frequency subimage and watermark image are inputs of the cellular neural network(CNN), and the zero-watermarking registration image is the output. To investigate and improve the security and robustness, the original watermark and registration image are scrambled or encrypted. The watermark image can be extracted from the secret image. This algorithm is simple and robust. The proposed method is also simple for hardware realization.

Introduction

The development of network and multimedia technology makes it convenient to access the multimedia information. These technologies bring people many conveniences but they also bring us some large side effects. The problem of multimedia copyright protection becomes increasingly serious. With the development of the internet of things and cloud computing, this problem becomes more urgent. As an effective method for the protection of digital property rights, content authentication and secret communication, digital watermark technology becomes an active research area.

Researchers proposed a lot of methods. In most traditional digital watermarking algorithms, watermark information is embedded in the spatial or transform domain of the carrier image. The LSB [1] and Patchwork methods[2] are typical watermarking methods of spatial domain. Transform domain algorithms are most based on DCT, DFT, DWT [3,4,5], Fourier-Mellin transform[6], Radon transform[7] and so on. A good digital watermarking algorithm should have some basic characteristics, such as: robustness, invisibility, large embedding capacity, lower computational complexity and so on. However, it is also a challenging problem to completely achieve these requirements of algorithms. Literature[8,9] proposed without modifying the original image of zero-watermarking technique including registration and authentication. In the registration process, the algorithm constructed watermark with being protected of image characteristics, and stored in a centralized authentication center. In the authentication process, watermark information is recovered with recognition images and the data of authentication center. In the literature[8], it has the high computational complexity in calculating Higher-Order Statistics. In the literature[9], the zero-watermarking was implemented in DWT domain. The coefficients of image after traditional wavelet transform are floating point numbers; this is a negative factor in many applications. The lifting wavelet transform improves the structure of traditional wavelet and overcomes some shortcomings of it. Its coefficients are integers. It reduces the complexity of algorithm, and is convenient for hardware realization.

This paper proposed a robust image watermarking method using lifting wavelet transform and enhanced bit-plane. The algorithm first gains the high order bit-plane of low-frequency subimage after lifting wavelet transform. Then the high order bit-plane and the scrambled watermark image are

inputted into CNN network, and the encrypted image is produced. Experiments show that the method can get a good visual effect and is robust to plus-noise, filtering, JPEG compression, and cropping attack.

Cellular Neural Networks

L.O.Chua et al. putted forward the Cellular Neural Network (CNN) that simulated the non-liner and real-time speed array processor of VSLI[10]. The model of a two-dimensional CNN is described which compose of basic processing units called cells. Each cell is connected to its neighboring ones, therefore only the adjacent cells can interact directly with each other. CNN parallel processor can implement difference function of image processing.

Enhanced Bit-plane

For an image, each bit can be regarded as a binary plane or a bit-plane. For example, the pixel value of an eight bits gray image can be expressed as the following:

$$f(x,y) = a_7 \times 2^7 + a_6 \times 2^6 + \cdots + a_0 \times 2^0 \tag{1}$$

where f(x, y) indicates gray image, and the value of a_k is 1 or 0. The matrix which is formed by the pixel of the *k*th bit is $a_k(x,y)$. That is, the *k*th bit-plane. The level of the *k*th position is 2^k. Therefore, this 8-bits gray image can be seen that it is formed by eight binary images, in which each side only describes part of the information.

High order bit-planes represent the basic data of the picture, while low order represent the details of an image and even noise. Here we choose high order bit-plane to ensure the robustness of the watermarking. But the small change of the pixel value can make the great changes to the bit-plane. Therefore, it needs to change the bit value of the image in order to reducing the influence of the gray value change to bit-plane. Usually, we use the following formula to improve the bit-plane, so as to form enhanced bit-plane:

$$a_i' = \begin{cases} a_i \oplus a_{i+1} & ,0 \le i \le 6; \\ a_i & i = 7; \end{cases} \tag{2}$$

For example, when the gray levels are 127 and 128, according to formula (2), it can be deduced that the gray levels of 127 and 128 are 01000000 and 11000000. That means there is only one bit is different between the adjacent gray levels of 127 and 128. As a result, the subtle change of the pixel value has very small influence on the whole plane.

After the image experience LWT changes, the possibility of the "clash" of enhanced bit-plane. Suppose the low pass sub-image of the original image has gone through one level LWT is N×N, then according to the above calculating method, the possibility of "clash" is $(1/2)^{N\times N}$。In reality, the empirical threshold value of judging whether the water print exists or not is less than 1, so the actual possibility of "clash" is bigger than $(1/2)^{N\times N}$， though it is still a very small number.

Watermarking Method

If the original image $f(x,y)$ is a gray image and the watermarking image is a binary image $w(x,y)$, the procedure is as follows:

Embed process:

(1) The scrambled watermark image $w'(x,y)$ is produced by scrambling key.

(2) The original carrier image is decomposed with a one level lifting wavelet transform.

(3) The low pass subimage is divided into 8 enhanced bit-planes.

(4) The 6th order bit-plane $f'(x,y)$ and scrambling image $w'(x,y)$ will be inputted into CNN network, and then the output is marked as $I(x,y)$. $I(x,y)$ is the constructed watermark image. To

improve the security of system, $I(x,y)$ can be encrypted or scrambled. Then the zero-watermarking registration information $I'(x,y)$ is generated.

Detection process:

(1) The constructed watermark $I(x,y)$ is obtained by the key.

(2) The test image is decomposed with a one level lifting wavelet transform.

(3) The low pass subimage of test image is divided into 8 enhanced bit-planes. The 6th order bit-plane is marked as $f''(x,y)$.

(4) Then the $I(x,y)$ and $f''(x,y)$ are inputted into CNN network, and the output is marked as $w_a'(i,j)$. The unscrambled $w_a(i,j)$ watermark image is obtained by the scrambling key used in the embed process.

(5) By means of correlation analysis, the correlation degree of watermark image $w(x,y)$ and abstracted watermark image $w_a(i,j)$ can be computed. The formula is as follows:

$$SIM = \sum_i \sum_j w(x,y) w_a(i,j) / \sum_i \sum_j w^2(x,y) \tag{3}$$

If the value of *SIM* is bigger than the empirical threshold value, the watermarking information exists. If not, the watermarking information does not exist.

Experimental Results

The simulation is implemented by Matlab. A binary image is used as watermark image, and gray image of Cameraman is used as the original image. The original carrier image, original watermark, watermarked image and extracted watermark image are shown as:

(a) (b)

Fig. 1 (a) Original image and watermark (b) Watermarked image and extracted watermark

Simulation results for common image processing operations are shown in Table 1. The values of similarity distribute between 0.9-1, which means this algorithm is robust to common image processing attacks.

Table 1 Results of common attacks

Attacks	SIM
Salt and pepper noise(0.01)	0.93
Gaussian noise (mean 0 and variance of 0.005)	0.92
Median filtering(3 × 3)	0.93
Mean filtering(3 × 3)	0.92
JPEG compression(QF=40)	0.97
Cropping 10%	0.91

Table 2 shows the results of JPEG compression attacks with different quality factors. It shown that this method is robust to JPEG compression.

Table 2 Results of JPEG compression

QF	SIM
100	1.00
80	1.00
60	0.98
40	0.97
20	0.95
10	0.91

Summary

Traditional watermarking algorithm degrades the quality of carrier image, and its application is limited. Since the conflict between imperceptibility and robustness, the embedded strength is also limited. It influences the robustness of watermarking system. The experimental results demonstrate that the proposed algorithm can achieve better visual effect; meanwhile, it is robust to common image processes such as filtering, adding noise, JPEG compression and so on. This algorithm is simple and the realization of software and hardware is convenient.

Acknowledgements

Supported by the Science and Technology Foundation Project of Shangluo University (Grant NO. 13SKY015)

References

[1] A. Bamatraf, R. Ibrahim, M. N. M. Salleh. Journal of Computing, vol. 3(2011)No.4, p.1.

[2] B.L. Gunjal, R.R. Manthalkar. Journal of Emerging trends in Computing and Information Science, vol. 2(2010)No.1, p.37.

[3] Ting Luo, Mei Yu, Gangyi Jiang, Aihong Wu, Feng Shao and Zongju Peng: Future Wireless Networks and Information Systems, LNEE vol. 143(2012), p.297.

[4] Meng Lan, Yang Hongying, Wang Xiangyang: Journal of Chinese Computer Systems, vol. 29 (2008)No.11, p.2153.(in chinese)

[5] Dazhi Zhang, Boying Wu, Jiebao Sun, Heyan Huang: *Proc. International Congress on Image and Signal Processing* (Tianjin, China, October 17-19, 2009). 2009, p.1.

[6] J. K. Joseph, O. Ruanaidh, T. Pun: Signal Processing, vol.66(1998)No.3, p.303.

[7] Lian Cai, Sidan Du, Duntang Gao:Journal of Electronics, vol.22(2005)No.5, p.300. (in chinese)

[8] Wen Quan, Sun Tanfeng, Wang Shuxun: Acta Electronica Sinica, vol.31(2003)No.2, p. 214. (in chinese)

[9] Ma Jianhu, He Jiaxing: Journal of Image and Graphics, vol.12(2007)No.4, p.582. (in chinese)

[10] L. O. Chua, L. Yang: IEEE Trans. Circuits and Systems, vol.35(1988)No.10, p.1257.

Advanced Materials Research Vols. 989-994 (2014) pp 1477-1480
© (2014) Trans Tech Publications, Switzerland
doi:10.4028/www.scientific.net/AMR.989-994.1477

Research on Simulation of Modern Storage System with Flexsim

Han Qingtian

Naval Aeronautical and Astronautical University, Yantai, China

hbluesky@163.com

Keywords: Storage control; Software simulation; Simulation optimization.

Abstract. Firstly, the store system models was established with Flexsim software. Then the data statistic was taken. Finally, the analysis were carried out with a numerical example. The analysis result shows that emulating is useful for discovering the bottleneck problem of systematic operation, and the simulation is very useful for store system optimization.

Introduction

Automation three-dimensional storehouse is taking high layer three-dimensional goods shelves as major sign, with whole set advanced carry equipment is foundation, is taking advanced computer control technology as major means, come in and go out storehouse handling efficiently using space, time and manpower. Since it have to economize labor force and schoolwork quick accurate , raising take care of efficiency and reduction thing flow out the superiority such as cost, get extensive pay attention , modern thing flows out systematic and traffic transportation, field(port storehouse store up , business match send etc. modern thing flow out system in) get more and more extensive application, become factory thing flow out , flexible production systematic and computer integrated production system in cannot or the important component that are short of. At the same time along with the development of science and technology, especially the development of computer technology, various automation computer systems are replacing the mental work of people partially, and continuously land the creative combination of science and technology with every field, promote the vigorous development of science and technology and go forward , make the function of storehouse since carrying out materials merely store to take care of , development arrives to bear materials with computer system take over to classify to measure to pack , sorting match to send to store the various function such as plate.[1,2]

Zhang Xiaoping studied storage system based on Flexsim simulation[3]. XiaoJiangBo etc. discussed the logistics distribution center based on Flexsim software planning, and gave functional layout of the determination of the size and loading and unloading requirement for distribution center warehouse layout, and the location of the distribution center warehouse building layout were presented[4]. XiaoFeng established simulation model of container terminal handling application using Flexsim, and provided the visual decision support for production managers with loading and unloading process of dynamic simulation [5]. In the paper the model will be established by using the Flexsim software and the analysis will be carried out according to the report.

Store system modeling

According to simulation goal, combine actual condition, established three-dimensional storehouse basic model is as shown in Fig. 1. The Flexsim model is as shown in Fig. 2.

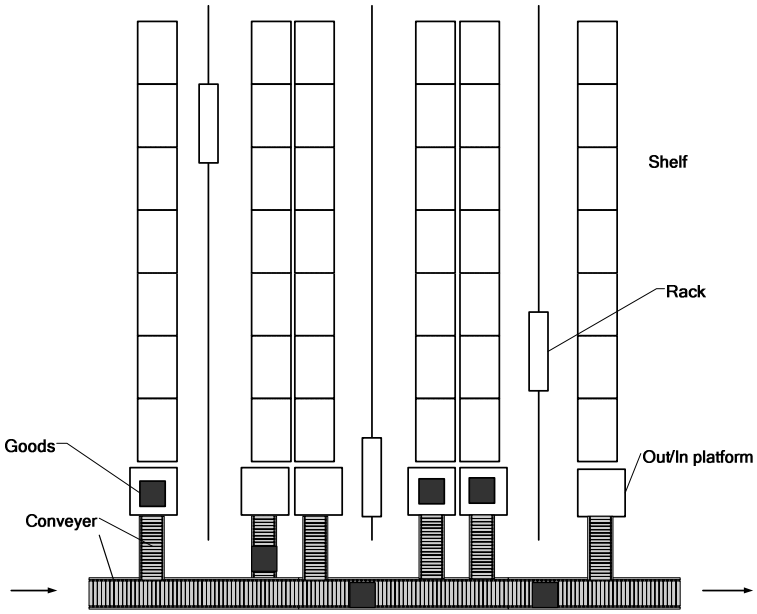

Fig. 1. Store system basic model

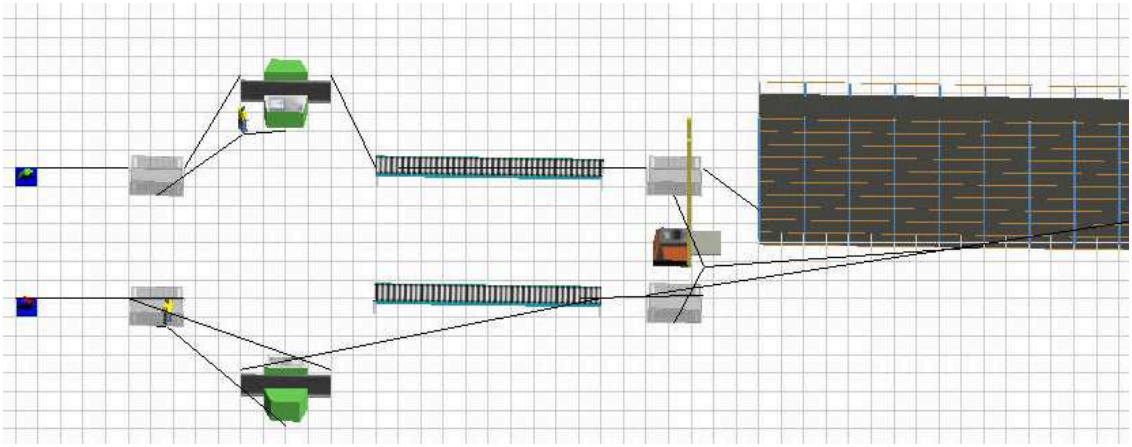

Fig. 2. Store system simulation model using Flexsim

Buffer district adopts conveyer belt make / is put in storage , for instance, will be put in storage free time should be put in storage just to come into stock in buffer district thing, queue up in this formation the most former a goods will enter voluntarily to be put in storage buffer district, the goods of back are entered in proper order forward successively a shelf, queue up continuously to wait. Conveyer deliver goods from outside world arrive to be put in storage platform, and deliver the goods of the platform of delivery of cargo from storage to go out.

Storage system operation process simulation and analysis

Data of work time for into the store is as shown in Table 1.

Table 1. Data of work time for into the store (unit:second)

11.45	12.09	8.9	6.42	10.31	11.89	10.41	11.93	10.49	9.64
10.38	13.45	11.49	11.57	8.88	8.99	10.58	9.73	9.6	9.3
8.6	8.78	9.24	11.78	9.34	10.26	8.97	9.58	10.29	11.83
8.99	7.35	8.76	8.98	9.22	9.78	10.23	11.14	9.7	10.55
9.8	8.74	7.08	10.99	10.3	9.28	11.86	10.45	7.98	9.42

Statistic was taken for the above 40 data, and the frequency and probability were also calculated, and the overall characters of the data can be see. The statistic data result is as shown in table 2.

Table 2. Statistic data analysis result

average	6~7	7~8	8~9	9~10	10~11	11~12	12~13	13~14
frequency	1	3	9	13	13	9	1	1
probability	2%	6%	18%	26%	26%	18%	2%	2%

Usin the software of MATLAB the curve was drawed out, and the parameters were carried out, as shown in Figure 2, Fig. 3.

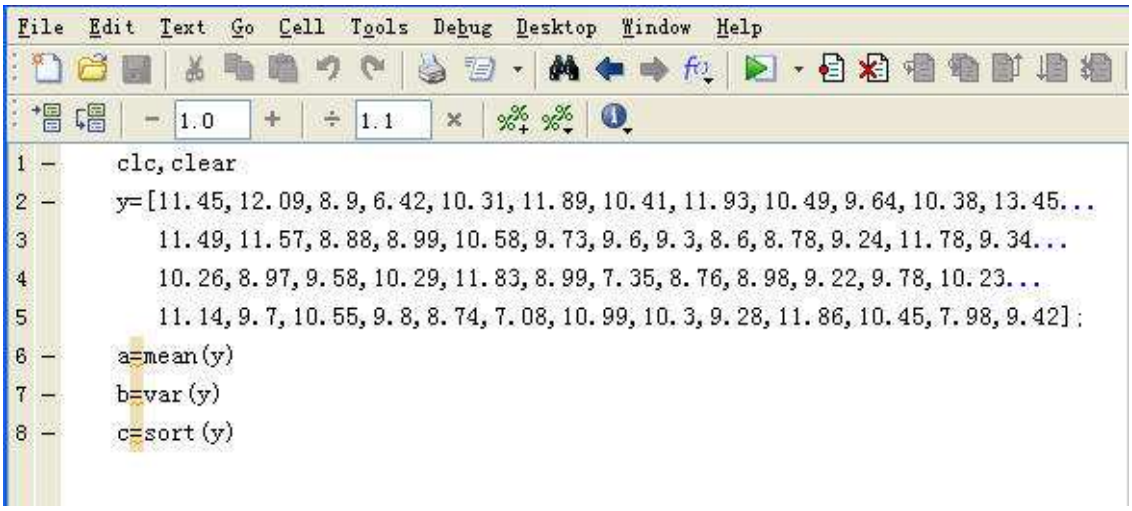

Fig. 3. Source program for the progressing of the data.

In a composite process model, the input curve of the normal distribution, the parameters as follows:

$$\mu = 9.9, \quad \sigma = 1.9 \tag{1}$$

The frequency and probability chart are shown in Fig. 4.

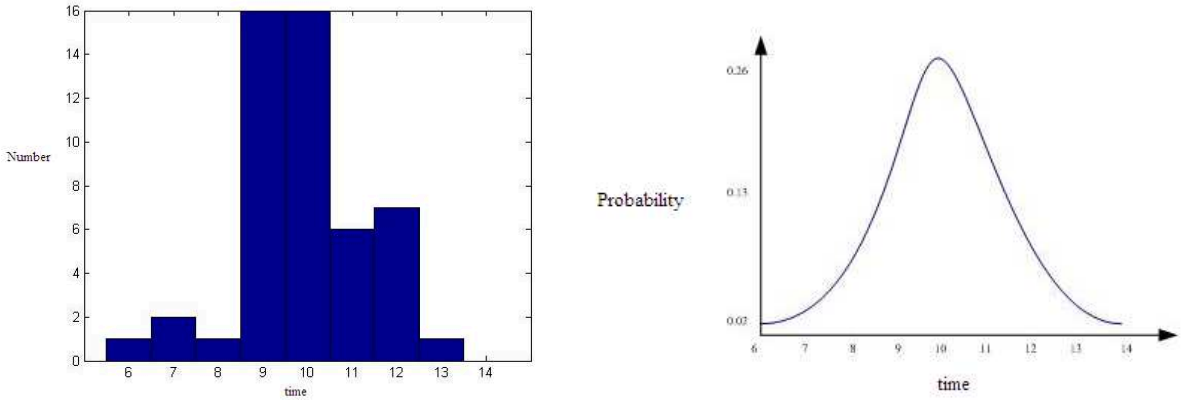

Fig. 4. The frequency and probability chart

Through the simulation of the sorftware flexsim, the export status reporti is as shown in Table 3.

Table 3. Export status reports

	Idle	Processing	Empty	Waiting for transporter	Travel empty	Travel loaded
Queue 1	0.00%	0.00%	0.00%	0.00%	0.00%	0.00%
Conveyer	0.00%	0.00%	49.60%	0.00%	0.00%	0.00%
Queue 2	0.00%	0.00%	71.20%	28.80%	0.00%	0.00%
Piler	46.40%	0.00%	0.00%	0.00%	26.80%	26.80%
Processor	0.00%	100.00%	0.00%	0.00%	0.00%	0.00%

The conveyer pie chart is as shown in Fig. 5.

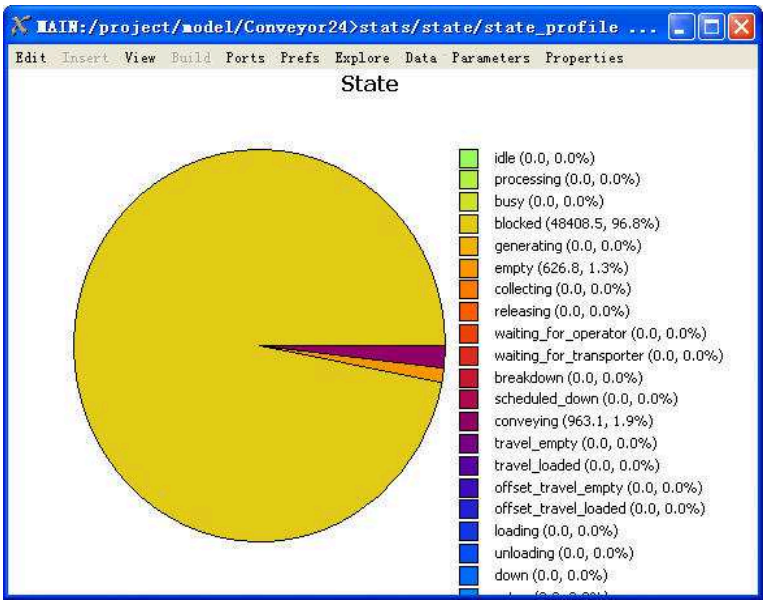

Fig. 5. Conveyer pie chart

From the conveyer pie chart, it can be seen that about 93.2% of the time is the release time, but the 96.8% of the time of the conveyer is in stock. Therefore, since the obstruction of conveyer is caused , delivery of cargo from storage stores district and the obstruction of goods shelves and the low effect.

Conclusions

In the paper, the store system models was established with Flexsim software. The result of the analysis of the example shows that emulating is useful for discovering the bottleneck problem of systematic operation. So the simulation is very useful for store system optimization.

References

[1] Chang Peng. Bulk cargo wharf logistics system based on Flexsim simulation. China water transport (theory), No.2, (2007), p.156-157

[2] Chen, Liu Yukun. System simulation software Flexsim3.0 practical tutorial. Beijing: tsinghua university press, (2006)

[3] Shi Xiaohui. Based on Flexsim manufacturing process modeling and simulation study. Anhui university of science and technology, (2009)

[4] Xiao Jiangbo Yang Fuxing. Logistics distribution center based on Flexsim simulation optimization study . Modern commercial and trade industry, Vol.12, No. 12, (2007), p. 61-62

[5] Xiao Feng. Based on Flexsim container terminal simulation platform is the key technology research. Wuhan: wuhan university of technology, (2006)

Advanced Materials Research Vols. 989-994 (2014) pp 1481-1484
© (2014) Trans Tech Publications, Switzerland
doi:10.4028/www.scientific.net/AMR.989-994.1481

Study on Application of Vendor Managed Inventory Model

Han Qingtian

Naval Aeronautical and Astronautical University, Yantai, China

hbluesky@163.com

Keywords: Material Supply; Vendor Managed Inventory; Inventory Model.

Abstract. Firstly, the inventory models were analyzed, and the symbol and assumptions were given out. Then the models of the distribution centre and supplier were studied. Finally, a numeric example was given out by applying the models. The results show that the models are easily to be carried out in engineering field, and it is useful to control the inventory and raise the store efficiency.

Introduction

The supply chain management is a new concept in the management science. It's greatest characteristic is sharing resource, mutual harmony cooperating, integrate managing betweens upply chain members. So the supply chain cost is reduced greatly. With the increasingly competitive market, more and more enterprises and the introduction of the concept of supply chain management thinking. Inventory management in supply chain management and rapid response to customer demand environment, has an increasingly important position. Traditionally, the various links in the supply chain management of their respective stock, seeking to maximize their own benefit. It is more often the direct consequence of the supply chain to demand more unstable. production eventually increase the overall cost of inventory in the supply chain, affecting the overall optimization of the supply chain operation, weaken its overall competitive edge.[1,2] Based on the idea of supply chain, the model of air material support was developed and its operational mechanism was analyzed and studied by HU Yong etc.[3]

To change this situation, A new supply chain inventory management thinking, Vender Managed Inventory, emerged. In this way, the upstream supply chain downstream enterprises no longer passively according to the orders and additional orders for shipment. but according to their demand for the goods to lower overall grasp of the goods to meet the needs of downstream, It also made its own inventory management and ordering more rational, thus bringing the supply chain to reduce the cost of supply and demand. In this paper, the inventory models of distribution centre and supplier will be studied.[4,5]

Symbol and assumptions

For the vendor management inventory model with shortage not allowed, the symbol and assumption are as follows:

(1) one supplier, many materials distribution centers, and a kind of product;

(2) production speed of supplier is constant;

(3) demand speed that matches to send center is determined;

(4) mend goods can instant realization, it is 0 to match to send central order to expect in advance;

(5) shortage not allowed;

(6) supplier manages the stock that matches to send center, grasps the order information in stock that matches to send center.

And match to send the parameter related to center definition, and parameter definition is as follows:

Parameters for distribution centers are as follows,

n is the number of the distribution centers;

R_i is demand rate of distribution center i, $R_i>0$;
T is order period of distribution center;
Q_{hi} is the maximum stock of distribution center i during time T;
C_{fi} is the order cost of distribution center i;
C_{hi} is the stock cost for the unit product in central in unit time;
TC_i is the total cost of the stock in center in unit time.
Parameters for suppliers are as follows,
P is the production speed of supplier, and $P>\sum_{i=1}^{n} R_i$;
t_{vi} is the time of the supplier satisfies distribution center i during time T;
C_f is regular cost that supplier produces one time;
C_{hp} is the stock cost unit product in supplier in unit time;
TC_{vp} is the total cost in stock in supplier in unit time.

Inventory models of distribution center

Based on the assumptions as above, the changes of the inventory of the distribution centre is as shown in Fig. 1.

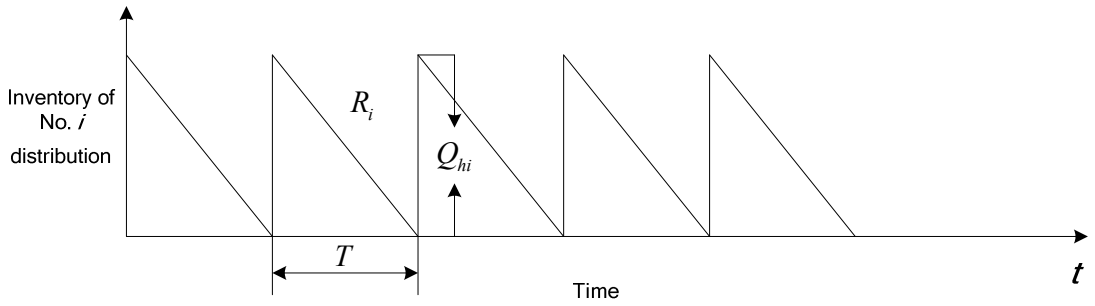

Fig. 1. Changes of the inventory of the distribution centre of NO. i

Here, $I_i(t)$ is supposed as the inventory level of distribution centre i, then

$$\frac{dI_i(t)}{dt}=-R_i, 0\le t\le T, i=1,2,\cdots,n \tag{1}$$

For the boundary condition is as follows,

$$I_i(T)=0, i=1,2,\cdots,n \tag{2}$$

Therefore we can get

$$I_i(t)=R_i(T-t), 0\le t\le T, i=1,2,\cdots,n \tag{3}$$

The cost for store of distribution centre i during periodic time is TC_{hi}

$$TC_{hi}=C_{hi}\int_0^T I_i(t)dt=\frac{C_{hi}R_i}{2}T^2 \tag{4}$$

Therefore, the whole cost for inventory of distribution centre i during periodic time is TC_i:

$$TC_i=\frac{1}{T}(C_{fi}+TC_{hi}) \tag{5}$$

Inventory models of supplier

The change chart of the inventory of the supplier is shown in Fig. 2.

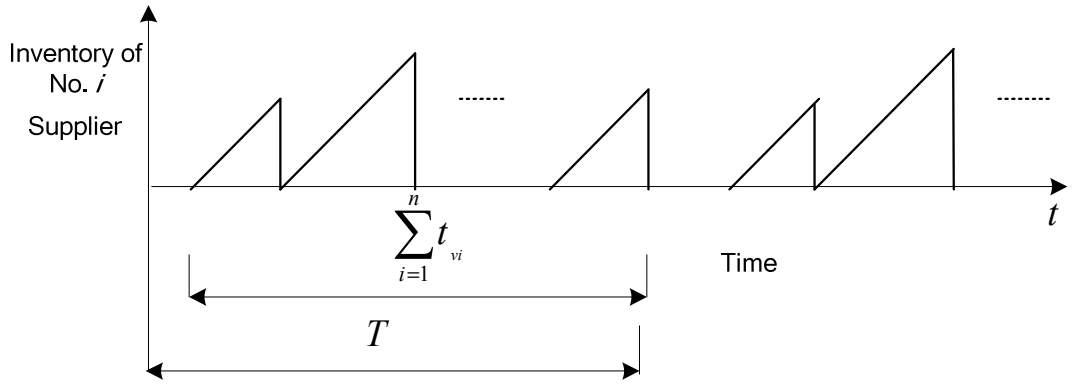

Fig. 2. Changes of the inventory of the supplier

The supplier supply goods to n distribution centers during periodic time T. And let t_{vi} denote the time of supplying goods to distribution centre i. If $I_{vi}(t)$ denotes the inventory level of distribution centre i at time t, then $I_{vi}(t)$ should satisfy the differential equation as follow.

$$\frac{dI_{vi}(t)}{dt} = P \quad 0 \le t \le t_{vi}, i = 1,2,\cdots,n \tag{6}$$

With the boundary condition

$$I_{vi} = 0, i = 1,2,\cdots,n \tag{7}$$

so

$$I_{vi}(t) = Pt, i = 1,2,\cdots,n \tag{8}$$

It is supposed that Q_{hi} denotes the maximum inventory of distribution centre i during the periodic time T,and Q_{si} denotes quantity out of stock of distribution centre i. Then the supplied quantity from supplier to the distribution centre i ant time t_{vi} should satisfied the conditions as follows.

$$I_{vi}(t_{vi}) = Q_{hi}, i = 1,2,\cdots,n \tag{9}$$

$$Q_{hi} = I_i(0) = R_i T \tag{10}$$

Thus we can get

$$t_{vi} = \frac{Q_{hi}}{P} = \frac{R_i}{P} T \tag{11}$$

The store cost of the supplier during time T is TC_{hp}:

$$TC_{hp} = \sum_{i=1}^{n} \left[C_{hp} \int_0^{t_{vi}} I_{vi}(t) dt \right] = \frac{C_{hp} P}{2} \sum_{i=1}^{n} t_{vi}^{\ 2} \tag{12}$$

The whole cost per unit time of the suppliers as follows:

$$TC_{vp} = \frac{1}{T}(C_f + TC_{hp}) = \frac{1}{T}(C_f + \frac{C_{hp} P}{2} \sum_{i=1}^{n} t_{vi}^{\ 2}) \tag{13}$$

The whole inventory cost per unit time in VMI model is TC_{vmi}:

$$TC_{vmi} = \sum_{i=1}^{n} TC_i + TC_{vp}) \tag{14}$$

When ε=0.10, the sensitivity of service level λ according to deference cost is shown in Table 1.

Table 1. Sensitivity analysis of service level

Service level λ	0	0.60	0.70	0.80	0.85	0.90	0.95	1.00
Average inventory cost of distribution centre	100 449	42 769	34 471	27 156	23 979	21 157	18 693	16 565
Average inventory cost of supplier	2 694	2 874	2 904	2 933	2 948	2 963	2 978	2 993
Average inventory cost of VMI	108 982	47 153	38 452	30 905	27 681	24 864	22 454	20 428
ΔTC_{vmi}			-8 701	-7 547	-3 224	-2 817	-2 410	-2 026

Conclusions

In the paper the symbol and assumptions were given out and the models of the distribution centre and supplier were studied. The numeric example show that the models are easily to be carried out in engineering field, and it is useful to control the inventory and raise the store efficiency.

References

[1] Zhang Lei. The research on inventory management and cost optimization in supply chain. Hunan University, 2006,

[2] Zhang Lin. Study on Vender Managed Inventory in a two-member supply chain. Chongqing University, 2007

[3] Hu Yong, Zheng Jinzhong, Gao Shuangfeng. Study on the model of air material supply chain support. Logistic Technology,2004,(11), p.113-115.

[4] Yang Shuai. Several Kinds of the Inventory Control Model and its Applications. College of Economy &Business Administration of Chongqing University, (2005)

[5] Xiong Junxing. Zhao Jinping. Research on control model of spare parts inventory based on DP. Micro Computer Information, Vol. 28, No. 11-3, (2008), p.19-20

Advanced Materials Research Vols. 989-994 (2014) pp 1485-1488
© (2014) Trans Tech Publications, Switzerland
doi:10.4028/www.scientific.net/AMR.989-994.1485

Research on Material Inventory Model and Application

Han Qingtian

Naval Aeronautical and Astronautical University, Yantai, China

hbluesky@163.com

Keywords: Demand Forecast; Model; Double Moving Average.

Abstract. Firstly, the inventory model was analyzed under some assumptions. Secondly, based on the consumption of some rubber product, the demand and inventory models were established. Finally, an actual example was carried out by using the inventory model. The result shows the applicable of the model in engineering.

Introduction

The fundamental objective of studying the logistics system is to reduce the total cost of logistics. But the inventory cost of items is of much more proportion in the total cost of logistics. Therefore, studying the theory and methods of inventory control is very significant for reducing the total cost of logistics. Inventory material takes a considerable part of the total assets in many companies. [1] For one thing, if the materials store is too large, it will occupy too much fund and lead to torpidity of turnover fund. If the materials store is too small, it can't meet the requirement of selling and producing. Also, it is a hot spot of logistics theory research. Therefore, the inventory management plays a major role in a material supplication. [2] Sun Xuelian made further extensive study on the traditional inventory control theory from different aspects [3-5]. This paper the inventory model will be analyzed under some assumptions, and based on the consumption of some rubber product, the demand and inventory model will be established and calculated to illustrate applicable of the model.

Inventory model analysis

Assumptions of the model are as follows.

(1) the cost of out of stock is infinite, that is $C_S = \propto$;

(2) When the stock is zero, the supplement can be presented immediately;

(3) The demand change follows continuing uniform distribution;

(4) For each order, the quantity is a constant, and the order cost is C_D ;

(5) Store cost for per unit is a constant C_P .

During a period time of T , the maximal store quantity is Q , the minimal store quantity is 0, and the demand change follows continuing uniform distribution. So the average store quantity during the period time T is $\frac{1}{2}Q$, and the store cost is $\frac{1}{2}C_P Q$. The cost for once order is C_D , and during time T the average order cost is $\frac{C_D}{T}$. Because the demand is continuing uniform, so $Q = DT$. Therefore, the total cost during time T is as follows.

$$C(T) = \frac{1}{2}C_P Q + \frac{C_D}{T} = \frac{1}{2}C_P DT + \frac{C_D}{T} \tag{1}$$

In order to get the value of T , so let

$$\frac{dc(T)}{dT} = \frac{1}{2}C_P D - \frac{C_D}{T^2} = 0 \tag{2}$$

Therefore

$$T^* = \sqrt{\frac{2C_D}{C_P D}} \tag{3}$$

$$Q^* = DT^* = \sqrt{\frac{2C_D D}{C_P}} \tag{4}$$

$$C(T^*) = \sqrt{2C_D C_P D} \tag{5}$$

The result shows that the C_D is higher, then D more large, and Q is higher. Therefore the store cost C_P is higher, and the Q becomes smaller. The inventory model is shown as Fig. 1.

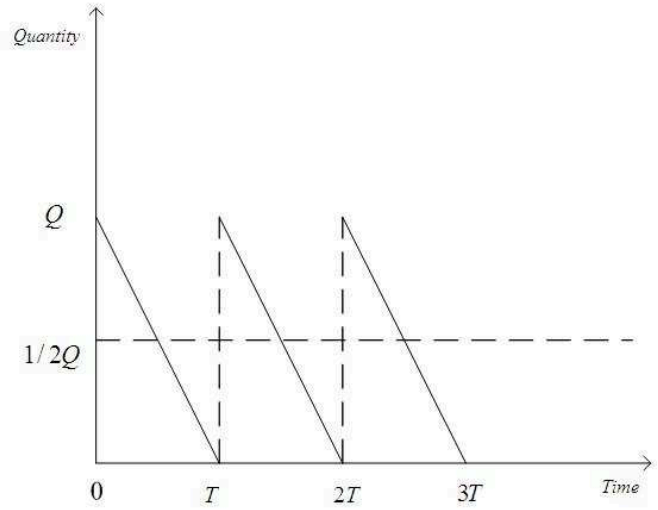

Fig. 1 Inventory model chart

Inventory model applications

Change of the consumption of some rubber product is shown as Fig. 2.

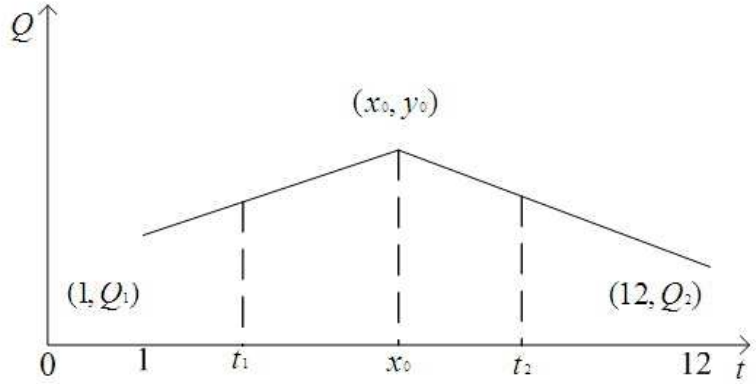

Fig. 2. Change of the consumption of some rubber product

Based on the work intensity, the consumption of some rubber product change as shown in Fig. 2. The change is a function of section.

$$f(t) = \begin{cases} \dfrac{y_0 - Q_1}{x_0 - 1} t (1 \le t \le x_0) \\ \dfrac{Q_2 - y_0}{12 - x_0} t (0 \le t \le 12) \end{cases} \tag{6}$$

According to the consumption of the rubber product, the inventory change can be supposed as shown in Fig. 3.

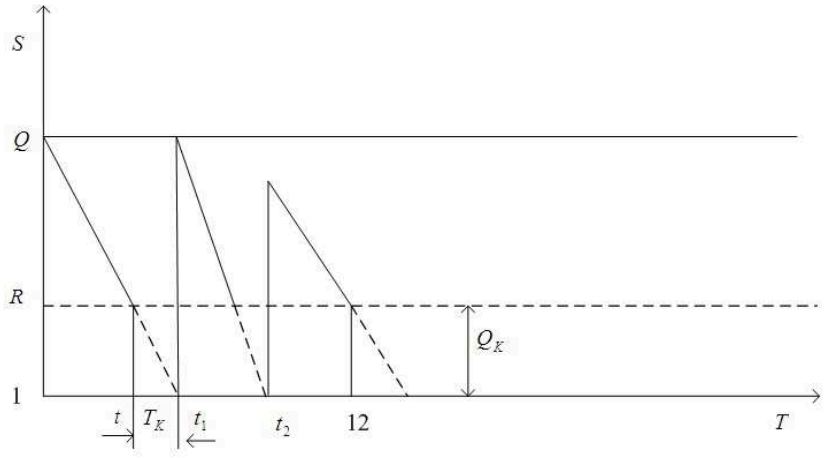

Fig. 3. Inventory change of the rubber product.

At time t_1, the inventory quantity is Q.

$$Q = \int_1^{t_1} f(t)dt \tag{7}$$

Then

$$Q = \int_1^{t_1} (\frac{y_0 - Q_1}{x_0 - 1})tdt = \frac{1}{2}(\frac{y_0 - Q_1}{x_0 - 1})t_1^{\,2} - \frac{1}{2}(\frac{y_0 - Q_1}{x_0 - 1}) \tag{8}$$

Thus,

$$Q = \frac{1}{2}(\frac{y_0 - Q_1}{x_0 - 1})(t_1 + 1)(t_1 - 1) \tag{9}$$

Therefore

$$t_1 = \sqrt{\frac{2Q + y_0 - Q_1}{y_0 - Q_1}} \tag{10}$$

So, the inventory quantity is 0, the supplication is needed. Then the next period begins.

For the safety quantity, the order point is R.

$$T_K = \frac{R}{D} \tag{11}$$

Here D can be calclated by the equation.

$$D = \int_1^{x_0} \frac{y_0 - Q_1}{x_0 - 1_1} tdt + \int_{x_0}^{12} \frac{Q_2 - y_0}{12 - x_0} tdt = \frac{1}{2} x_0^{\,2} (\frac{y_0 - Q_1}{x_0 - 1} - \frac{Q_2 - y_0}{12 - Q_0}) - \frac{1}{2}(\frac{y_0 - Q_1}{x_0 - 1}) + 72(\frac{Q_2 - y_0}{12 - Q_0}) \tag{12}$$

So the order time is as follows.

$$t = t_1 - T_k \tag{13}$$

The economic order quantity Q^* and the total cost C can be determined. At time t_1, the inventory quantity is 0, and the quantity Q_1^* is as follows.

$$Q_1^* = \int_{t_1}^{x_0} \frac{y_0 - Q_1}{x_0 - 1} tdt + \int_{x_0}^{t_2} \frac{Q_2 - y_0}{12 - Q_0} tdt \tag{14}$$

At time t_2, the inventory quantity is 0 again, and the quantity Q_2^* is as follows.

$$Q_2^* = \int_{t_2}^{12} \frac{Q_2 - y_0}{12 - x_0} tdt \tag{15}$$

Therefore, the minimal cost is as follows.

$$C_1 = \frac{1}{2} C_P (P - \frac{y_0 - Q_1}{x_0 - 1}) \frac{Q}{P} (\frac{y_0 - Q_1}{x_0 - 1}) + \frac{C_D}{Q} = \frac{1}{2} C_P (1 - \frac{y_0 - Q_1}{x_0 - 1} p)Q + \frac{C_P}{Q} (\frac{y_0 - Q_1}{x_0 - 1}) \tag{16}$$

$$C_2 = \frac{1}{2}C_P(P - \frac{Q_2 - y_0}{12 - x_0})\frac{Q}{P}(\frac{Q_2 - y_0}{12 - x_0}) + \frac{C_D}{Q} = \frac{1}{2}C_P(1 - \frac{Q_2 - y_0}{12 - x_0}p)Q + \frac{C_P}{Q}(\frac{Q_2 - y_0}{12 - x_0}) \quad (17)$$

According to the model, the function result can be shown in Fig. 4. by using the software tool of MATLAB.

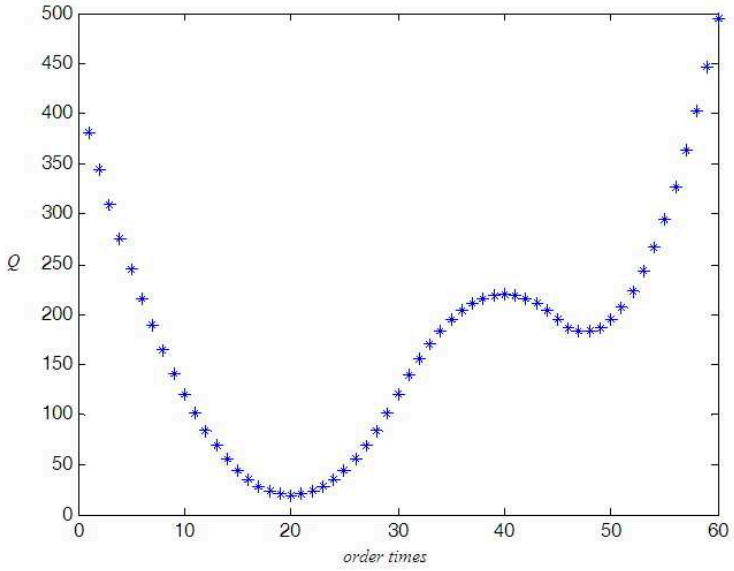

Fig. 4. The cost change according to the order quantity.

From the figure, it can be seen that, when the order quantity is 0, the lost of lack of goods is infinite. And along with the increase of the quantity, the total cost increases. When the quantity meets 20, the cost comes to the minimal. With a concave, the convex increases when the order quantity become larger. The situation accords with the reality of the store management.

Conclusions

In the paper the inventory model was analyzed under some assumptions, and based on the consumption of some rubber product, the demand and inventory models were established and calculated. The result shows the applicable of the model.

References

[1] Shen Xianfei. The research and application of the inventory management decision model. Sichuan University, (2002)

[2] Yang Shuai. Several Kinds of the Inventory Control Model and its Applications. College of Economy &Business Administration of Chongqing University, (2005)

[3] Sun Xuelian. The further researches on some EOQ model. Xinjiang University, (2006)

[4] Xiong Junxing. Zhao Jinping. Research on control model of spare parts inventory based on DP. Micro Computer Information, Vol. 28, No. 11-3, (2008), p.19-20

[5] Xiao Huixin. Research on the prediction method of spare demand rate during equipment maintenance. Fire Control and Command Control, Vol. 33, Sup. (2008), p.150-154

Advanced Materials Research Vols. 989-994 (2014) pp 1489-1492
© (2014) Trans Tech Publications, Switzerland
doi:10.4028/www.scientific.net/AMR.989-994.1489

A Fuzzy Clustering Algorithm of Automatic Classification Based on EnFCM

Hong-wei Han [1, a], Lin Tian [2,b] and Jia-qing Miao [3,c]

[1,2,3] The Engineering & technical College of Chengdu University of Technology, Leshan, Sichuan, China

[a]hhw_666666@163.com, [b]boboduduling@163.com, [c]mjq_011114117@163.com

Keywords: Enhanced Fuzzy c-means clustering; image segmentation; histogram; moving average smoothing filter; Gauss; peak point detection.

Abstract. Fuzzy c- means (FCM) algorithm is an unsupervised clustering algorithm for image segmentation, and has been widely applied because the segmentation results are consistent with human visual characteristics. Enhanced fuzzy c-means clustering (EnFCM) algorithm is the improved FCM algorithm, which reduces the computational complexity. But, both FCM algorithm and EnFCM algorithm, clustering number still need to be manually determined. This paper, in order to realize the automation degree of algorithm, presents an improved algorithm. It first analyzes the histogram, then automatically determines the clustering number and peak value of each class through use of the peak point detection technology, finally segments image by using EnFCM algorithm. Experiments show that this method is a kind of faster fuzzy clustering algorithm with automatic classification ability for image segmentation.

Introduction

Image segmentation is one of the first and most important tasks in image analysis and computer vision. Fuzzy clustering successfully applied in image segmentation. Among the fuzzy clustering methods, fuzzy c-means (FCM) algorithm is the most popular image segmentation method. However, it still has some disadvantages. A lot of improved algorithm is proposed. A random sampling of FCM algorithm was presented (RSFCM) [1] by Cheng, Xin-bo Gao proposed the FCM algorithm based on weighted (WFCM) [2], Song can Chen proposed KFCM_S [3] algorithm. More recently, Szilagyi [4] proposed EnFCM algorithm, which accelerate the image segmentation process. But, this method still can't overcome disadvantages of manually determining the class number.

In this paper, we automatically determine the clustering number and each clustering centers by using the method of histogram analysis, and the algorithm is initialized with their. Experiments show that this method can make the algorithm reduce the iteration times and the computational overhead on the basis of the effective segmentation.

Histogram Smoothing Method

Gray histogram reflecting the statistical characteristics of image gray distribution is frequently used to study gray distribution of image. For simpler bimodal curve, it is easy to find their peak point location. However, a complex image histogram is generally multi-peak curve, and the complexity of the image itself makes the histogram occur with some peak point features of random disturbance, so it brings difficulties for programs to automatically detect the peak point. Therefore, methods must be taken to eliminate the noise points before the automatic detection of the peak point. This article, through repeat use of moving average method, makes the saw-tooth histogram curve smooth, while maintaining the original histogram peak valley characteristics.

2.1 Moving Average Smoothing Method.

Moving average smoothing method[5], it smooths data by replacing each data point with the average of the neighboring data points defined within the span on the histogram. The conversion relations of smooth processing is $m_i = \frac{1}{2n+1}\sum_{j=i-n}^{i+n} q_j$, where m_i is the smoothed value for the mth data point , n is the number of neighboring data points on either side of m_i, q_j is the value of original histogram probability density, and $2n+1$ is the span. $m_{i+1} = m_i + \frac{1}{2n+1}(q_{i+1+n} - q_{i-n})$ can be available through recursion of m_i.

2.2 Windowed Gaussian Smoothing

Experiments show that the image histogram through repeated use of moving average smoothing method is still some small glitch noise. This paper, in order to completely smooth, makes the histogram smooth by using Windowed Gaussian function [5]. Windowed Gauss discrete function is expressed as:

$$g(i) = \frac{1}{\sqrt{2\pi}w} e^{\frac{-(i-w)^2}{2w}}, (i = 0,1,2,\cdots,2w) . \tag{1}$$

the gray image histogram representation for

$$h(i) = \sum_{x=0}^{m-1}\sum_{y=0}^{n-1} \delta(f(x,y) - i), (i = 0,1,2,\cdots,255) . \tag{2}$$

where w is the window size, $f(x,y)$ is the original image, total pixels of image is $m \times n$, i is Gray level, $\delta(\circ)$ is unit impulse function. The convolution results for

$$r(i) = g(i) * h(i) = \sum_{k=0}^{2w} g(i-k)h(k), i = 0,1,2,3,\cdots,255 + 2w. \tag{3}$$

Automatic Peak Detection Algorithm

In the algorithm of automatic peak detection [6], P_i is the pixel frequency value, compare P_i with the value of its neighborhood P_s, where $P_s = \{P_{i-m},\cdots,P_{i-2},P_{i-1},P_{i+1},P_{i+2},\cdots,P_{i+m}\}$, m is usually an integer between 5 to 15. If the maximum value of P_s is denoted as $P_{s\max}$ and the second largest value of it is $P_{s\max s}$, then the definition of peak function $P(i)$ or valley point function $Q(i)$ for:

$$P(i) = \begin{cases} 1, P_i > P_{s\max} \text{ or } P_i = P_{s\max}, P_i > P_{s\max s} \\ 0, P_i < P_{s\max} \end{cases} . \tag{4}$$

$$Q(i) = \begin{cases} 1, P_i < P_{s\min} \text{ or } P_i = P_{s\min}, P_i < P_{s\min s} \\ 0, P_i > P_{s\min} \end{cases} . \tag{5}$$

Where $0 \le i \le L-1$, L is the maximum gray value of image.

Enhanced Fuzzy C-Means Clustering (EnFCM)

Szilagyi [4], at the base of the study on the FCM algorithm, proposed EnFCM algorithm for gray level images, which reduces the computational complexity. A linearly-weighted sum image g is in advance formed from the original image and its local neighbor average image in terms of

$$g_m = \frac{1}{\alpha+1}\left(x_m + \frac{\alpha}{N_R}\sum_{j\in N_m} x_j\right) . \tag{6}$$

where g_m denotes the gray level value of the mth pixel of the image g, and N_m stands for the set of neighbors(x_j) falling into a window around x_m.The objective function for segmentation of image g is defined as

$$J=\sum_{i=1}^{c}\sum_{l=1}^{q_c}\gamma_l u_{il}^m (g_l - v_i)\,. \quad (7)$$

where q_c denotes the number of gray levels of image g, γ_l is the number of pixels having gray level value equal to l ($l=1,2,\cdots,q_c$). Thus, $\sum_{l=1}^{q_c}\gamma_l = N$ and under the constraint that $\sum_{i=1}^{c}u_{il}=1$ for any l, the J (7) is minimized, using the following equation for calculation of the membership partition matrix and the cluster centers:

$$u_{il}=\frac{(g_l - s_i)^{\frac{2}{m-1}}}{\sum_{j=1}^{c}(g_l - s_i)^{\frac{2}{m-1}}}\,. \quad (8)$$

$$v_i=\frac{\sum_{l=1}^{q_c}\gamma_l u_{il}^m g_l}{\sum_{l=1}^{q_c}\gamma_l u_{il}^m}\,. \quad (9)$$

An Improved Algorithm Based on EnFCM

First of all, this algorithm, through repeating use of moving average method, makes the image histogram smooth. Yet, the smoothed histogram remains more small glitch noise, in order to obtain a better smooth curve, by using windowed Gauss function, makes the histogram curve more smoothing. Then, in the peak detection, set $m=8$, record the number of peaks $Pnum$ and the corresponding gray value of each peak $G=\{g_1,g_2,\cdots g_{Pnum}\}$.

In general, the histogram of the peak and valley reflects the image gray level distribution. Peak is the pixel gray level distribution concentrated area, valley is sparse zone of the pixel distribution. So , can think so, every peak are one class pixel that closely focused around a central value of pixels, class (peak) and class (peak) boundary value exists in the valley. Set EnFCM algorithm class number $c=Pnum$ and the initial clustering centers $V_0=\{v_1,v_2,\cdots,v_c\}=G$.

The detailed steps of the improved algorithm for

Step 1.Make the image histogram, and make it two smooth processing.

Step 2.By using peak detection algorithm, obtain the smoothed histogram peak point number $Pnum$ and the corresponding gray value of each peak G.

Step 3.Set $c=Pnum$, $V_0=G$, and using EnFCM algorithm for image segmentation.

Experimental Results and Analysis

This experiment is to choose a 512 x 512 gray image (Fig.1) for clustering segmentation. First, by using the above smoothing method, makes the selected image histogram smooth, and peak point detection techniques are used to get the clustering number and possible clustering center. Second, randomly choose the clustering centers, segments original image by using EnFCM algorithm, and the result is displayed in Fig.2. Finally, by using the improved algorithm presented in this paper, segments original image, and the result is shown in Fig.3.

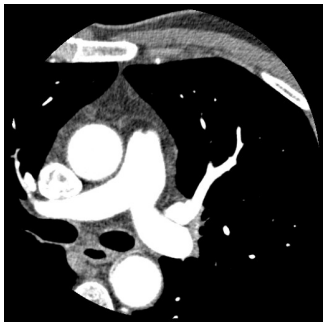

Fig.1. Original image

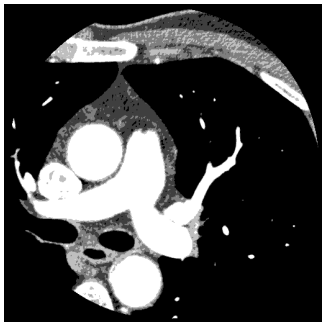

Fig.2. EnFCM result

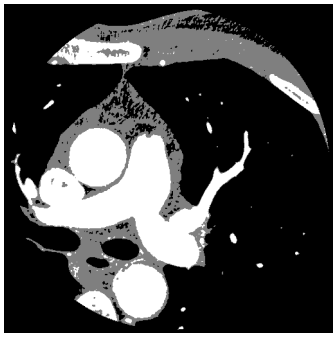

Fig.3. Improved EnFCM result

Segmentation results of Fig.2 show that EnFCM algorithm can obtain more clearly the outline of image, but the border is patchy because of using random initialization of cluster number for image segmentation. Under the condition of invariable parameter in the algorithm, by using the improved algorithm in this paper, segmentation results (Fig.3) for each part of the boundary is clearer, and makes the least number of iterations. On the other hand, under the same parameters, we compare the improved algorithm in this article with EnFCM algorithm of segmentation time, experiments show that the improved algorithm in this article significantly reduces the running time in the similar segmentation results. The reason is that the improved algorithm in this article can provide the number of clusters and the cluster centers by using peak detection technology, therefore, avoid blind iteration that the traditional EnFCM algorithm caused by the initial center selection.

Conclusion

In this paper, we presented an improved algorithm based on EnFCM algorithm. This algorithm, through adopting the peak point detection technology, can automatically determine the cluster number and the peak value of each class, and then improve the automation degree of the algorithm. Experimental results show that the algorithm is suitable for medical image segmentation, and is a kind of faster fuzzy clustering algorithm with automatic classification ability for image segmentation.

References

[1] T.Cheng,D.Goldgof,and L.Hall.Fast fuzzy clustering.Fuzzy Sets and Systems,1998,93:49-56.

[2] Xin-bo Gao. Fuzzy Cluster Analysis and its Applications. Xidian University Publisher.2004.

[3] Song-can Chen, Dao-qiang Zhang. Robust Image Segmentation Using FCM with Spatial Constraints Based on New Kernel-Induced Distance Measure. IEEE Transactions on systems, man, and cybernetics, 2004,34(4):1907-1916.

[4] L.Szilagyi, Z.Benyo, S.Szilagyi,and H.Adam, Mr brain image segmentation using an enhanced fuzzy c-means algorithm.in Proc.25th Annu. Information Conf. IEEE EMBS [C],Cancun,Mexico,2003,1:724-726.

[5] Ren-hui Wang, Zi-liang Ping, Fang Wang. A Cell Image Segmentation Based on Logarithm Transform for Y-Coordinate of Histogram.Journal of Inner Mongolia Normal University,2008,37(3):392-396.

[6] Bin Ren, Bing-quan Wang, Bin Luo. Method of Threshold and Peak Detection Based on Histogram Exponent Smoothing. China Journal of Image and Graphics,1997,2(4):231-232.

Advanced Materials Research Vols. 989-994 (2014) pp 1493-1496
© (2014) Trans Tech Publications, Switzerland
doi:10.4028/www.scientific.net/AMR.989-994.1493

Knowledge Representation of Art Patterns Based on the Calculation Mental Image

KUANG ShiRong [1, a]

[1] School of art and design, Jiangxi Science & Technology Normal University, Nanchang 330013,China

[a] KuangShiRong@yeah.net

Key words: knowledge representation; calculation mental image

Abstract. Computational imaginary is a simulation of the human mental image based on the study of cognitive science. Art pattern composition knowledge representation is the basis of the intelligence of computer-aided art pattern design. The paper describes an art pattern composition knowledge representation scheme based on the model of computational imaginary. The scheme includes the deep representation, visual representation and spatial representation, and the operations of these three representations. It further describes the abstract and image information from the perspective of the relation between art pattern layout visual and spatial shape.

1. Introduction

Art design is widely used in the wallpaper, carpet, printing, dyeing and all walks of life. Improving the quality and speed of the graphic design has increasingly become one of the difficulties faced by designers. Computer aided pattern design can accelerate the production speed, but how to make computer simulation of human thinking, quickly and automatically generate the art of novel and attractive design of computer aided pattern design remains an important subject.

2. Calculation mental image theory

2.1 Three parts

At present, there is a controversial about the expression of mental image in the brain. It can be thought of as the image like a hierarchy, an image consists of several mental images. It includes descriptive expression (text or proposition forms), and depicting sexual expression (image). It describes the space between the relationship, and depicts the shape, size, and so on visual information. Psychology study also shows that there is a long-term memory in the brain, descriptively conserves mental images. It is converted into a workspace expression: visual expression and space expression. It can be divided into three parts:

1) deep representation: exist in the form of framework in the long-term memory to realize hierarchy of groups. They are: the name of mental images，AKO, PARTS. AKO indicates the image (a kind of) slot between the properties of the following relationships. PARTS slot is used to decompose the complex mental image and consists of a number of names of mental images and the space. In addition, the framework may also include slots to generate visual expression and space expression.

(2) the visual representation: in the shape of a visual form. Glasgow is represented by a matric composed of a series of basic meta,m each corresponding one expressing the volume of the region, such as light, texture information.

(3) space representation: in the form of multidimensional arrays, symbolic represents the components of space and their relative information. Each component is in the shape of the corresponding part of the position of the element information. For example, the space matrix of a glass of water is shown in figure 1.

glass	water	glass
glass	glass	glass

Figure 1. The space matrix of a glass of water

2.2 The visual expression of composition knowledge

LVR: $\{Tran\ 1.(Subp1)\}$
$SubP = \{Tran\ 1.(Subp1)\}$
Or $SubP = \{(Tran\ 1.(Elem,)\}$
$Elem = \{c(x,y)\}$
$i=1..SubNum$
$J=1..Subp.subNum$
$J=1..SubP.SubNum$
$(x,y) \subset ElemShape$

Efficiency

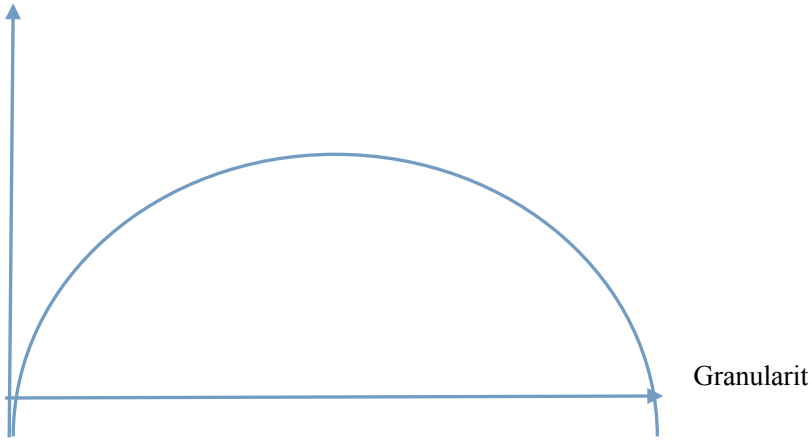

Figure 2. The visual expression LVR

It can be seen that visual expression LVR is produced by SubP of the images

3. The composition knowledge based on calculation mental images

On the composition knowledge expression, we define a series of operations. Expression of the relationship between the transformation and operation can be summed up in figure 3. The SPACE in LRD can reconstruct into operation LVR. LDR in SPACE by retrieve into LSR, can be put on the LSR, delete, move, change the layout of the empty relationship. LSR can be converted in to LDR.

4. The space composition knowledge

Figure 4 is an analysis of the picture. A is a picture whose space matrix is composed of two matrix B and C, B is composed of D and E submatrix while D is composed of two different changes of space matrix.

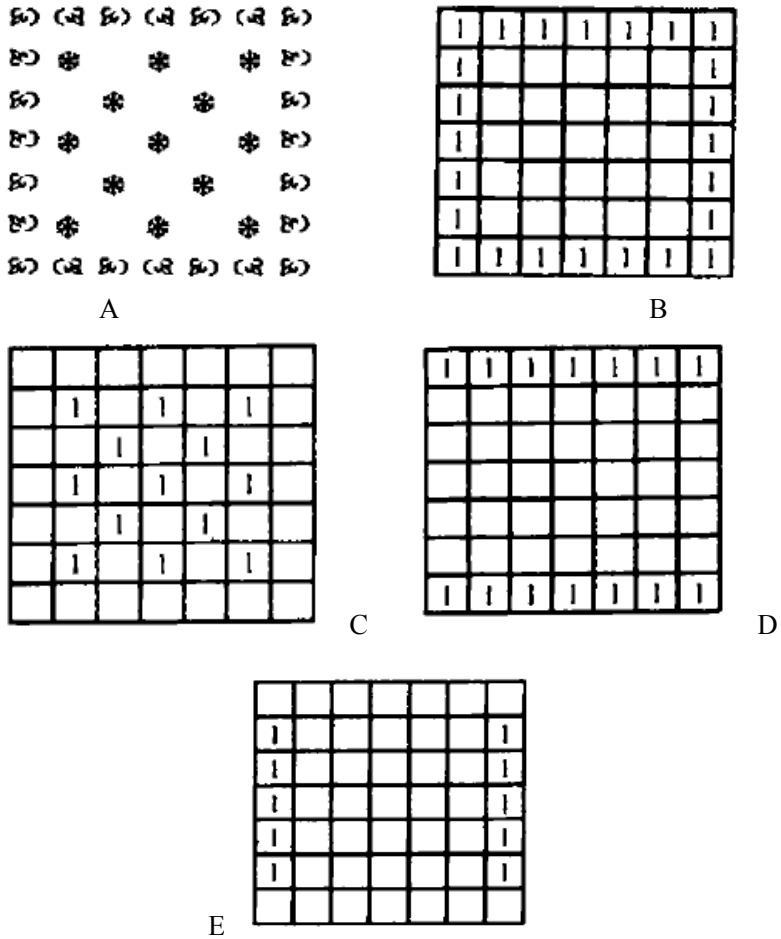

Figure 3. Analysis of the picture

5. Discussion

It can express the incomplete information. For example, in (SUBINFO)，(SUB_ CLOC) , (SUB_TRAN) , (SUB_LOC) (SUB_INDEX) are the chosen items, which means, some information cannot be conveyed very clearly. When (SUBINFO) [(SUB_LOC) (SUB_INDEX) (SUB_LDR)], it shows that this series of layout(up, down, left, right) has determined relationship, but the composition knowledge with exact location of the coordinates of each layout and unknown parameters. That is to say, it instructs the composition knowledge with common points of certain combination.

It explicitly describes the way of combination of layout (rotary, scattered point, straight line), and the corresponding parameters of combinatorial identities such as semantic information. Moreover, the knowledge representation can express incomplete information, indicating a composition of knowledge. Thus it can summarize the knowledge classification, abandon the specific details and extract spatial relationships, combination and other characteristics.

Summary

This paper only expresses deformation and composite structure in the process of the pattern composition without involving aesthetic principles such as balanced effect, golden express. Symbol matrix of space has a lot of spiritual activity, but also have inherent drawbacks. Therefore, the expression of spatial relations is required to expand and optimized. Computer-aided design is the combination of art and computer. This paper is just the preliminary attempt for the image expression in graphic design knowledge. There remains much space for the future study.

Reference

[1] Stiny G. Introduction to shape and shape grammars[M]. Environment and Planning B. 1980.
[2] Glasgow. Artificial intelligence and imagery[M]. In Proceedings of Tools for AI. Washington. 1990.
[3] Glasgow J I.The imagery debate revisited: a computational perspective[M]. Computational Intelligence，1993.
[4] Glasgow J I. Papadias，Dimitri. Computational imagery[J]. Cognitive Science，1992.

Advanced Materials Research Vols. 989-994 (2014) pp 1497-1500
© (2014) Trans Tech Publications, Switzerland
doi:10.4028/www.scientific.net/AMR.989-994.1497

Improved Software Cost Estimation Method Based on COCOMO Model and Linear Regression

Hai Yang[1, a]

[1]College of Information Science and Electricity Engineering, Shandong Jiaotong University, Jinan, Shandong, China 250023

[a]yanghai_sdjtu@163.com

Keywords: software cost estimation; COCOMO model; linear regression; estimation error

Abstract. Software cost estimation is the key step to software development management. In order to make COCOMO model applicable to Chinese enterprises, an improved software cost estimation method based on COCOMO model and linear regression was proposed in this paper. Then the replication experiment was taken by using the historical software project data of given enterprises, and then compared experience estimation with the new improved method proposed in this paper about the forecasting accuracy. The results verified that the improved cost estimation method has more practical value to software development.

Introduction

With the rapid development of computer technology, the scale of software is increasing sustainably and software complexity is also getting higher and higher. Cost management of software has become one of the most important parts of software development project. Only by doing this aspect of the cost management so that the quality of software would be guaranteed and the cost of software would be reduced. The software cost estimation is the prerequisite and basis for the cost management. At present, many cost estimation methods have been extensively applied in software industry abroad. But it usually couldn't fulfill the requirement of software industry in China because of the unsuitable of using these cost estimation methods directly.

There have been many cost and schedule estimation models proposed by research literature for the past few decades, such as the estimation models based on regression analysis [1], SLIM model proposed by Putnam 1978, the constructive cost model (COCOMO) proposed by Barry Boehm in 1981 [2], function point analysis (FPA) proposed by David Garmus and David Herron and multi-project model [3].

At present, COCOMO model is one of the most extensively used cost estimation methods. COCOMO model uses a basic regression formula with parameters that are derived from historical project data and current as well as future project characteristics. But the related parameters of COCOMO model should be adjust according to practical situation and statistic data at the beginning of the software development procedure.

In this paper, the parameters of COCOMO model were estimated by using experience estimation and linear regression separately. Finally, the result of linear regression was compared with the one of experience estimation.

Introduction to Relevant Models

COCOMO Model. COCOMO model was first published in Boehm's 1981 book Software Engineering Economics as a model for estimating effort, cost, and schedule for software projects. It drew on a study of 63 projects at TRW Aerospace. The study examined projects ranging in size from 2,000 to 100,000 lines of code, and programming languages ranging from assembly to PL/I [4]. These projects were based on the waterfall model of software development which was prevalent software development process in 1981. References to this model typically call it COCOMO 81.

Basic COCOMO Model. Basic COCOMO model is usually divided into three types: basic COCOMO, intermediate COCOMO and detailed COCOMO. COCOMO model can be constructed by using formula (1)-(3) as follow:

$$E = a \times (KLOC)^b \tag{1}$$

$$DT = c \times E^d \tag{2}$$

$$P = E / DT \tag{3}$$

Where E denotes the effort applied which is measured by person-month, KLOC is the estimated number of delivered lines of source code of software project. DT denotes the development time and P is the people required [5]. The coefficients a, b, c and d are constant given in the following Table 1.

Table 1 Coefficients of COCOMO Model

Software Project	a	b	c	d
Organic	2.4	1.05	2.5	0.38
Embedded	3.6	1.20	2.5	0.32
Semi-Detached	3.0	1.12	2.5	0.35

COCOMO II Model. COCOMO II which was developed in 1995 is the successor of COCOMO 81 and is better suited for estimating modern software development projects. It provides more support for modern software development processes and an updated project database.

COCOMO II model is also divided into three types: the applications composition, early design, and post-architecture models [6]. For example, the construction formula of early design, and post-architecture models is described as formula (4):

$$PM = A \times S^E \times \prod_{i=1}^{n} EM_i \tag{4}$$

Where PM denotes effort, constant A=3.13, S denotes the scale of software, EM_i is the working coefficient and E is calculated by using formula (5):

$$E = B + 0.01 \times \sum_{i=1}^{5} SF_j \tag{5}$$

Where constant B=0.93, SF_j is the characteristic factor.

Linear Regression. Linear regression is an approach for modeling the relationship between a scalar dependent variable y and one or more explanatory variables denoted X. The case of one explanatory variable is called simple linear regression. For more than one explanatory variable, the process is called multiple linear regression.

Given a data set $\{y_i, x_{i1}, ..., x_{ip}\}_{i=1}^{n}$ of n statistical units, a linear regression model assumes that the relationship between the dependent variable y_i and the p-vector of regressors x_i is linear. This relationship is modeled through a disturbance term or error variable ε_i which is an unobserved random variable that adds noise to the linear relationship between the dependent variable and regressors. Thus the model takes the form as follows:

$$y_i = \beta_1 x_{i1} + ... + \beta_p x_{ip} + \varepsilon_i = x_i^T \beta + \varepsilon_i \quad , \ i = 1, ..., n \tag{6}$$

Where T denotes the transpose, so that $x_i^T \beta$ is the inner product between vectors x_i and β. Often these n equations are stacked together and written in vector form as formula (7):

$$y = X\beta + \varepsilon \tag{7}$$

Where

$$y = \begin{pmatrix} y_1 \\ y_2 \\ \vdots \\ y_n \end{pmatrix}, \ x = \begin{pmatrix} x_1^T \\ x_2^T \\ \vdots \\ x_n^T \end{pmatrix} = \begin{pmatrix} x_{11} & \cdots & x_{1p} \\ x_{21} & \cdots & x_{2p} \\ \vdots & \ddots & \vdots \\ x_{n1} & \cdots & x_{np} \end{pmatrix}, \ \beta = \begin{pmatrix} \beta_1 \\ \beta_2 \\ \vdots \\ \beta_p \end{pmatrix}, \ \varepsilon = \begin{pmatrix} \varepsilon_1 \\ \varepsilon_2 \\ \vdots \\ \varepsilon_n \end{pmatrix} \tag{8}$$

Improved Software Cost Estimation Method Based on COCOMO Model and Linear Regression (ISCE-CL)

Effort Estimation. In the improved software cost estimation method, effort estimation is calculated by using the formula (1) of COCOMO model mentioned above.

$$E = a \times (KLOC)^b$$

More remarkable, one person-month is consist of 152 effort hours. KLOC is measured by the number of delivered lines (expressed in thousands) of source code.

Schedule Estimation. Schedule means the development time required. Its unit is month. The improved cost estimation method uses the formula (2) to estimate schedule.

$$DT = c \times E^d$$

Linear Regression Model. The parameter correction of COCOMO model is usually taken to confirm the parameters a, b, c and d according to historical data and statistical analysis of software projects [7]. Linear regression is introduced into the improved cost estimation method so as to improve the accuracy of cost estimation.

In the linear regression model of the improved method, the formula (1) is linearized by taking the logarithm on both sides of it. Thus we can gain the formula (9) as follows:

$$\ln(E) = \ln(a) + b \times \ln(KLOC) \tag{9}$$

In order to confirm the value of parameters a and b, the linear regression model is construct by using formula (10) as follows:

$$y_q = \beta_0 + \beta_1 x_{q1} + ... + \beta_k x_{qk} + \varepsilon_q \tag{10}$$

Where $x_{q1},...,x_{qk}$ are the regression variables of the qth observed values. $\beta_1,...,\beta_k$ are response factors. β_0 is the intercept parameter. y_q is the response variable of the qth observed values. ε_q is the random error.

Next, the regression parameters a, b, c and d can be figured out by using least square method (LSM). If the results of least square method are recorded as a^*, b^*, c^*, d^*, the effort estimation based on linear regression is described as formula (11) and the schedule estimation is described as formula (12).

$$E = a^* \times (KLOC)^{b^*} \tag{11}$$

$$DT = c^* \times E^{d^*} \tag{12}$$

Experimental Results

The verification experiments are carried out using the real data of software development projects from Shandong Langchao Cheeloosoft Co.,Ltd.The experimental data are shown in Table 2. For the sake of expressing easily and conveniently, all the names of software projects are omitted.

Table 2 The Experimental Data

Software Project	Equivalent Lines of Code (KLOC)	Number of People(person)	Estimated Schedule(month)	Real Schedule(month)
Project 1	80	23	5	14
Project 2	35	8	4	9
Project 3	20	5	3	5
Project 4	135	12	18	31
Project 5	9	6	3	7
Project 6	25	6	4	7
Project 7	40	9	5	9

By using the least square method proposed in Linear Regression Model section of this paper, $a^* = 2.75$, $a^* = 0.94$, $a^* = 1.72$, and $a^* = -0.13$. Then the effort estimation and schedule estimation were calculated by using the improved cost estimation method ISCE-CL and empirical estimation separately. In order to describe the accuracy of these two methods, we introduced estimated error (Err).

$$Err = | E_1 - E_2 | / E_2 \tag{13}$$

Where E_1 is the real effort and E_2 is the estimated effort. The results are shown in Table 3.

Table 3 Comparison of Results between ISCE-CL and Empirical Estimation

Software Project	ISCE-CL		Empirical Estimation	
	Estimated Effort	Err	Estimated Effort	Err
Project 1	169.14	0.9	115	1.8
Project 2	77.76	0.07	32	1.25
Project 3	45.95	0.46	15	0.67
Project 4	276.60	0.34	216	0.72
Project 5	21.69	0.93	18	1.33
Project 6	56.67	0.26	24	0.75
Project 7	88.16	0.08	45	0.8

The experimental results reflect that the estimated errors of effort estimation from ISCE-CL are universally less than those from empirical estimation. In another word, ISCE-CL is more close to the actual situation and more suitable than empirical estimation.

Conclusion

In this paper, linear regression was introduced into COCOMO model and an improved software cost estimation method based on COCOMO model and linear regression was proposed. Then the verification experiment was taken by using the historical software project data of given enterprises.The experimental results reflect that ISCE-CL proposed by this paper is more close to the actual situation and more suitable than empirical estimation.

References

[1] Hawkins, Douglas M. On the Investigation of Alternative Regressions by Principal Component Analysis. Journal of the Royal Statistical Society, 1973, Series C 22 (3): 275–286.

[2] Barry Boehm. Software Engineering Economics. Englewood Cliffs, NJ: Prentice-Hall, 1981. ISBN 0-13-822122-7

[3] Hemmstra, F. and Kusters R. Function point analysis: evaluation of a software cost estimation model. European Journal of Information Systems, 1991, Vol 1, No 4. 229-237.

[4] Kemerer, Chris F. An Empirical Validation of Software Cost Estimation Models. Communications of the ACM, 1987, 30(5): 416–42.

[5] Joanne Hale et. Enhancing the Cocomo Estimation Models [J]. IEEE software, 2000(6): 45-49.

[6] Barry Boehm, et al. Software Cost Estimation with COCOMO II (with CD-ROM). Englewood Cliffs, NJ:Prentice-Hall, 2000. ISBN 0-13-026692-2

[7] Zhihao Chen et. Finding the Right Data for Software Cost Modeling [J]. IEEE Software, 2005(5): 38-46.

Advanced Materials Research Vols. 989-994 (2014) pp 1501-1504
© (2014) Trans Tech Publications, Switzerland
doi:10.4028/www.scientific.net/AMR.989-994.1501

Research on Improved Staged Software Cost Estimation Method Based on COCOMO Model

Hai Yang[1, a]

[1]College of Information Science and Electricity Engineering, Shandong Jiaotong University, Jinan, Shandong, China 250023

[a]yanghai_sdjtu@163.com

Keywords: software project; cost estimation; stages divided method; COCOMO model

Abstract. The accuracy of software cost estimation is essential for software development management. By introducing and analyzing the estimation methods of software cost systematically, the paper discussed the necessary of considering the software maintenance stage and estimating the software cost by separating the procedure of software development into several small stages. Then a staged software cost estimation method based on COCOMO model was proposed. The use of the new software cost estimation method proposed by this paper not only contributes to the cost control of software project, but also effectively avoids the bias problem due to using by single cost estimation method so that the accuracy of cost estimation could be improved.

Introduction

With the development of computer and software industry, the scale and complexity of the software are constantly expanding. The software cost gradually became the most expensive part of the entire computer system cost. However, since the sixties of last century, the typical characteristics of the software crisis to budget overruns, quality defects and project delays continue to emerge. Therefore, estimating the software cost becomes particularly important [1].

Summary of Software Cost Estimation

Three Stages of Software Cost Estimation. The software cost estimation is not the expense estimation in the sense of traditional meaning. The main part of capital input of software development is the reward paid for mental labor of the software developers. Usually, what the software cost estimation focuses on are effort and work schedule of software project. After estimating the human cost of software development, the software cost can be estimated according to the situation of development team and other related costs.

Generally, the software cost estimation includes three stages as follows [2]:

Scale Estimation Stage. Scale estimation which is the precondition of effort estimation means to measure the scale of the software. There are two commonly used methods for scale estimation. One is estimating the scale and amount of the problem to be solved, and the other is estimating the scale of solution or complexity of the software. For example, function point is one classic method for the former case and the number of delivered lines of source code is one classic method for the later case.

Effort and Work Schedule Estimation Stage. Effort estimation mainly estimates the human cost which is the main part of the software cost. Meanwhile, work schedule estimation is to forecast the disposable time in each task unit and make the milestone plan. Both effort estimation and work schedule estimation together determine the scale and structure of the software project team.

Estimation Feedback Stage. Estimation feedback stage includes the feedback on the cost estimation method and the feedback on the phased results in practice. It is good useful of adjusting related parameters of cost estimation method so as to improve the accuracy of the estimation results.

Classic Software Cost Estimation Methods. At present, various estimation methods have also born one after another, played a crucial role in their respective field of application, including

estimation method based on model, expert, analogy estimation method, and synthesis technology.Although these methods have been commonly used in software development projects, each one has its disadvantages.

Firstly, all of estimation methods mentioned above regard the software development procedure as a whole object when they estimate cost. So that it is easy to estimate software cost and useful of forecasting the project cost, but it is hard to control project cost because most existing methods can not track and control stage costs in time while the cost of each stage is also necessary for cost estimation. So that it is necessary to improve the estimation methods according to real situation in practice.

Furthermore, some software cost estimation methods only estimate the cost during the development stages. As a result of that, the cost during maintenance which is another important stage of software project is neglected. Facts proved that the effort during maintenance stage accounts for the large proportion of whole software project so that the cost during maintenance stage is much more than those during other stages. That is the reason why most existing cost estimation methods have the bias problems compare to the facts of software development procedure.

According to the analysis above, the improved cost estimation method should not only take the cost during maintenance stage into account but also formulate the cost of each stage of entire software development procedure separately. So that it is much easier for software cost control.

COCOMO Model

The Constructive Cost Model (COCOMO) is an algorithmic software cost estimation model developed by Barry W. Boehm. The model uses a basic regression formula with parameters that are derived from historical project data and current as well as future project characteristics.

Basic COCOMO Model. COCOMO was first published in Boehm's 1981 book Software Engineering Economics [3] as a model for estimating effort, cost, and schedule for software projects. References to this model typically call it COCOMO 81.

COCOMO model is usually divided into three types: basic COCOMO, intermediate COCOMO and detailed COCOMO. Basic COCOMO model can be constructed by using formula (1) as follow:

$$E = a \times S^{b} \tag{1}$$

Where E denotes the effort which is measured by unit person-month, S denotes the scale of software which is measured by the number of delivered lines (expressed in thousands) of source code for software project. Both a and b are constants which are concerned with the type of software project. There are three types of software project shown in Table 1:

Table 1 Three Types of Software Project and Related Coefficients

Software Project	a	b
Organic	2.4	1.05
Embedded	3.6	1.20
Semi-Detached	3.0	1.12

Intermediate COCOMO is an extension of basic COCOMO and its coefficients shown in Table 2. Furthermore, additional 15 effort factors F_i ($i \in [1,15]$) are introduced into intermediate COCOMO.

Table 2 Coefficients of Intermediate COCOMO

Software Project	a	b
Organic	3.2	1.05
Embedded	2.8	1.20
Semi-Detached	3.0	1.12

The formula of intermediate COCOMO is described as follows:

$$E = a \times S^{b} \times EAF \tag{2}$$

Where, $EAF = \prod_{i=1}^{15} F_i$

Detailed COCOMO incorporates all characteristics of the intermediate version with an assessment of the cost driver's impact on each stage of the software engineering process. The formula of detailed COCOMO is the same with that of intermediate version.

COCOMO II Model. COCOMO II which was developed in 1995 is the successor of COCOMO 81 and is better suited for estimating modern software development projects [4]. It provides more support for modern software development processes and an updated project database.

COCOMO II model is also divided into three types: the applications composition, early design, and post-architecture models. For example, the construction formula of early design, and post-architecture models is described as formula (3):

$$PM = A \times S^{E} \times \prod_{i=1}^{n} EM_{i} \tag{3}$$

Where PM denotes effort, constant A=3.13, S denotes the scale of software, EM_i is the working coefficient and E is calculated by using formula (4):

$$E = B + 0.01 \times \sum_{i=1}^{5} SF_{j} \tag{4}$$

Where constant B=0.93, SF_j is the characteristic factor.

Improved Staged Software Cost Estimation Method Based on COCOMO Model

Main Idea of the Improved Method. Generally, the software development procedure is obvious phase-wise which can be divided into five stages: requirements analysis stage, design stage, coding stage, testing stage and maintenance stage [5]. Let C_i , $i \in [1,5]$ denotes the cost of each stage. So the total cost of entire software project C_{total} is calculated by formula (5):

$$C_{total} = \sum_{i=1}^{5} C_{i} \tag{5}$$

By analyzing the practical situation data, we can gain all influence factors of the cost during each stage [6] which are denoted as $(x_{i1}, x_{i2}, ..., x_{in})$, $i \in [1,5]$. Therefore, the cost of each stage C_i can be described as formula (6):

$$C_{i} = \sum_{j=1}^{n} w_{ij} \cdot x_{ij} \tag{6}$$

Where w_{ij} is the weight of influence factor j in stage i. Thus the total cost C_{total} is:

$$C_{total} = \sum_{i=1}^{5} \sum_{j=1}^{n} w_{ij} \cdot x_{xj} \tag{7}$$

Implementation Process of Improved Staged Software Cost Estimation Method Based on COCOMO Model.

Step 1: Calculate the total cost C_C of software project using COCOMO II model.

Step 2: Calculate the total cost C_{stage} of software project again using the staged software cost estimation method proposed by this paper.

Step 3: Consider the weightW_C of COCOMO II model and the weightW_{stage} of the staged cost estimation method according to the practical situation of software project and the historical statistical data. $W_C + W_{stage} = 1$.

Step 4: Calculate the final total software cost C using formula (8):

$$C = W_C \cdot C_C + W_{stage} \cdot C_{stage} \tag{8}$$

Conclusion

The improved cost estimation method proposed in this paper separates the procedure of software development into several small stages and estimate the cost of each stage including the maintenance stage based on COCOMO II model. The use of the improved cost estimation method not only contributes to the cost control of software project, but also effectively avoids the bias problem due to using by single cost estimation method so that the accuracy of cost estimation could be improved.

References

[1] B. M. Boehm. Software Engineering Economics[M], China Machine Press, 2004.

[2] Rajlich,V.T. and K.H.Bennett. A staged model for the software life cycle[J]. Computer, 2000. 33(7): 66-71.

[3] Barry Boehm. Software Engineering Economics. Englewood Cliffs, NJ: Prentice-Hall, 1981. ISBN 0-13-822122-7

[4] Barry Boehm, et al. Software Cost Estimation with COCOMO II (with CD-ROM). Englewood Cliffs, NJ:Prentice-Hall, 2000. ISBN 0-13-026692-2

[5] K. Vinay Kumar, V. Ravi, Mahil Cart, N. Raj Kiran. Software development cost estimation using wavelet neural networks [J]. The Journal of Systems and Software, 2008(81), 1853-1867.

[6] L. Angelis, I. Stamelos, M. Morisio. Building a Software Cost Estimation Model Based on Categorical Data [J], IEEE, 2001: 4-15.

Advanced Materials Research Vols. 989-994 (2014) pp 1505-1508
© (2014) Trans Tech Publications, Switzerland
doi:10.4028/www.scientific.net/AMR.989-994.1505

Analysis of Knowledge Fusion System Model Based On Ontology And Multi-Agent Theory

Lei Li [1, a], Zhang Man[2,b]

[1]Party Committee Propaganda Department, Jiangxi Science & Technology Normal University, Nanchang, Jiangxi, P.R.China

[2]School of Information Engineering, Nanchang University, Nanchang, Jiangxi, P.R.China

[a]1512205455@qq.com, [b]manzhang201010@163.com

Keywords: Knowledge fusion; system model; Ontology; Multi-agent

Abstract. Information increase rapidly in recent years which make the effective use of information is not that easy. Knowledge fusion can improve the semantic accuracy and specification of knowledge; it's a useful way to make the mass disordered information integrated and easy to be recognized for users. The paper proposed a knowledge fusion system model based on ontology and multi-agent theory to meet with the user' changing needs at any time.

Introduction

Currently, internet information is filled with our life making a user receives a lot of information from different area every moment with the rapid increase of information. For information users, they want to find out useful information with least time for there are so many information of no use to them which make the finding of useful information time-wasting. Information integration is a useful way to provide useful information to users from the screening and integration of information in a particular field. Ontology theory is an effective knowledge organization way to solve the knowledge acquisition, sharing and reuse issues by providing practical semantic basis and solutions [1]. Multi-agent or intelligent agent can provide users with a transparent view of information according to specific needs ways and means, and can automatically generate information "application" from huge, disordered and dispersed information[2]. In order to meet with users' changing needs at any time, and provide knowledge distributed in heterogeneous sources to users, the paper proposed a model of knowledge fusion system based on ontology and multi-agent.

An Overview of Knowledge Fusion

Knowledge fusion research began at the proposing of knowledge engineering. With the deep development of research on the theme, it becomes an independent field of scientific research.

As defined by Preece at knowledge reuse and fusion transformation project, knowledge fusion is to maximize the development and use of knowledge sources distributed in information system, and to combine knowledge from multiple heterogeneous sources in a highly dynamic way[3].From engineering design perspective, Zou Xiang-jun proposed that knowledge fusion is knowledge engineering applications in the whole process of product development, and it's knowledge embedded in the entire product development process to achieve seamless knowledge fusion[4]. Gou Jin proposed a more comprehensive and universal definition of knowledge fusion that is through the integration of distributed heterogeneous data sources and knowledge sources, knowledge fusion provide services based on knowledge to gain valuable new useful knowledge, and optimize the structure and content of knowledge objects combining the application requirements for knowledge elements transformation, integration and fusion [5].Knowledge fusion research in and out of China mainly focused on the following three aspects:

(1)Model or Framework Building Research of Knowledge Fusion

The KRAFT Architecture for Knowledge Fusion and Transformation proposed KRAFT Knowledge Fusion architecture [3] that is overlap and integration/ transformation architecture of

knowledge by regard constraint as public knowledge exchange form by using a proxy architecture source of knowledge, knowledge fusion entities and users and information transmission communication protocols to achieve the integration of heterogeneous multi-source knowledge and knowledge fusion will be sent to the user. There also have other documents on the theme like a researcher proposed a knowledge fusion model through information fusion DSMT technical knowledge inside and outside the high-tech industry and the use of structural equation modeling to verify the role in promoting the integration of knowledge for knowledge innovation.

(2)Algorithm or Mechanism Research of Knowledge Fusion

As to knowledge fusion, researchers in China mainly focused on the way how to achieve the aim of knowledge fusion and its algorithm and mechanism. Zhou fang proposed a new algorithm based on Bayes, evidence of portfolio theory, theory of three fuzzy information fusion algorithms, and analyzed the characteristic, applicability, usefulness and other aspects [7]. Chen quan introduced the concept of knowledge primers and analyzed the biological characteristics of the four stages of knowledge fusion based on it while using network research community as research background, and proposed knowledge fusion mechanism based on collaborative tagging mechanisms according to different experts[8].

(3)Applied Research in different fields of knowledge fusion

Knowledge Fusion application in China mainly focused on corporate management, product design, subject teaching system construction, and so on. Knowledge Fusion application in out of China even focused on application in military field [9], mobile hospital logistics management to improve decision-making speed through knowledge fusion.

Compared with other countries, research on theory and practice of knowledge fusion in China is still need to be improved. The knowledge fusion research mainly focused on a a specific application areas as research background f, has not yet formed an authoritative general architecture model suitable to multi- field.

Knowledge Fusion Methodology Based on Ontology Theory

In order to provide intelligent support to users or decision makers, knowledge fusion system applied ontology theory to handle user requests. Knowledge Fusion system defines the following ontology types: (1) top ontology, which noted symbols of the system; (2) application ontology, described application areas according to the relevant fields and task; (3) the initial knowledge source ontology, described knowledge sources and top ontology in terms of knowledge source terms; (4) knowledge sources ontology, including terminology correspondence between knowledge source and application ontology; (5) the initial request ontology, described user request and top-level ontology symbols using the user terms (the request input use for user) ; (6) request ontology, including the terminology correspondence between the initial request and the application ontology; (7) domain ontology, described static knowledge of a particular field ; (8) task method ontology, described the problem -solving knowledge in a field. All these ontology are stored in a common ontology database in order to achieve sharing and reuse of ontology.

Top ontology provides a shared public symbols for ontology database. Domain ontology and task ontology form a new kind of knowledge, and this new knowledge provided by experts, acquired from knowledge sources or got from the user's request results. If there is no existing ontology or that related to new knowledge areas/task, you can create new ontology associated with this, or extend the current ontology.

When task method ontology used domain knowledge to describe a task or method, a relationship is necessary to establish domain ontology between the task ontology. According to the selected knowledge representation system, ontology classes need to describe the tasks/ methods of task method ontology first, and then describe the input and output parameters of the task/ methods according to properties of the classes. If the property value of domain ontology is used as a parameter of a task/method, then we need to build the relationship of domain ontology and task/ method ontology, and vice versa.

Parts of the domain ontology and task method ontology composed of an application ontology, which is a conceptual model that described the real-world applications, and its construction is based on a particular area and problems need to be resolved of the areas. If the part of domain ontology related to user request and task method ontology has not yet been integrated into a new application ontology, a connection relationship is necessary to build, that is a relationship between ontology related to users and the new ontology class, otherwise, it need to reuse an existing ontology. Request ontology is composed of initial ontology and application ontology which used to respond user request. The initial request builds the relationship of application ontology and request ontology through the correspondence of their elements. Thus, each initial ontology is associated with a application ontology and a request ontology, as shown in figure 2. It also can be seen from figure 2 that the reuse of application ontology is closely linked to the one-much relationship of application ontology and initial request ontology.

Before handling user requests, it needs to find a suitable knowledge source. From the process of a user request we get multiple knowledge sources, it proved a fact that application ontology and knowledge source ontology have a one-much relationship. And each user has their own request initial request ontology; every knowledge source has their initial knowledge source ontology to describe it, and also has a one-much relationship between initial source knowledge ontology and knowledge source ontology. After acquiring the knowledge associated with the request from the knowledge source, it will be regard this part knowledge and related applications ontology as user requests. The combination relationship of task method ontology and knowledge source ontology is similar to the relationship of task method ontology and request ontology.

Knowledge fusion system is based on a common vocabulary to operate. Application ontology is established based on domain ontology, task ontology and method ontology. Since each user request is running in accordance with the relevant extended request ontology, the application ontology associated with users also regard the extended request ontology as its running basis. During the interaction, the system provides an efficient personalized service through user attributes. Each user request consists of two parts: (1) relationship between request terms and user attributes ;(2) additional constraints defined by users. As to user request, the configuration of an alternate knowledge source network determined when and what kind's knowledge source to use to handle user request effectively. In addition, when using the main ontology of knowledge sources, the implementation of the conversion between system and knowledge source symbols. Thus, a user-oriented, ontology-based knowledge fusion conceptual model is built as shown in figure 2.

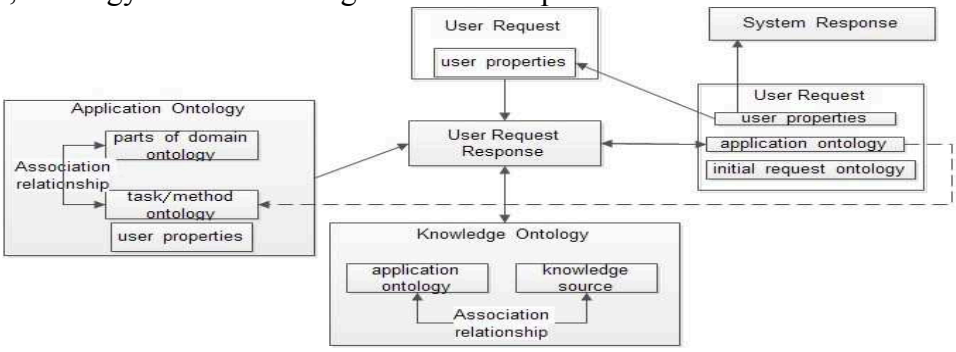

Fig.2 Ontology -based conceptual model of knowledge fusion

Multi- agent Architecture

The knowledge Fusion system uses intelligent software agents to provide the interface between distributed heterogeneous knowledge sources like some other systems. Multi-agent systems provide an effective method for distributed, large-scale, dynamic, open and heterogeneous computing systems and information systems to understand, manage and use. Multi-agent system of this knowledge fusion system is built based on FIPA model for it provides a standard heterogeneous agents and ontology interaction, and standards ontology negotiation protocol. The core technology

agent based FIPA are: packaging agents (with knowledge sources interact), coordinating agent (task execution control), boot agent (an agent with "Blued Pages" directory services) and user agents (with the user interaction). In order to make knowledge fusion system be able to adapt to the changing environment, we provides the following agent: conversion agent (between different vocabulary terms conversion), knowledge fusion agent (knowledge fusion running performance evaluation), configure the proxy (to improve the efficiency of knowledge fusion system), expert's auxiliary agent (to interact with experts) and monitoring agents (knowledge sources confirm).

Each agent of knowledge fusion system includes identification module, function modules and memory modules. Identification module contains a number of parameters, such as a unique identifier, creation time, and so on. The structure of this module depends on the type of the agent (some agent does not need modules). Function module contains a set of intelligent agents need to perform the procedure . Storage module contains some special information, such as knowledge of the agent, the agent's interaction history, temporary results, new knowledge.

Summary

Through the analysis of the operation of the mechanism of knowledge fusion, the paper constructed a general and user information satisfied knowledge fusion ontology conceptual structure based on ontology and intelligent agents, and exampled user requests handling process through emergency logistics common user request. Knowledge fusion regarded solving user problems as the ultimate goal, researched on the use of user attributes and term conversion mechanism, thus to improve the effectiveness of the system to a certain extent. In further studies, we can identify its ability to solve practical problems of the system through knowledge integration evaluation methods to provide a reference for improving the system.

Acknowledgement

This work was supported in part by the National Natural Science Foundation of China (Grant No. 71163033 and Grant No.71363044), Nature Science Foundation of Jiangxi, China(Grant No. 20114BAB201042), and by Science and Technology Plan Projects of Jiangxi, China (Grant No. 20132BBA10007).

References

[1]Chunnian Liu, Yiyun Huang, Yubao Li, el at. Research on Construction and Application of Agricultural Risk Knowledge Based on Ontology. International Journal of Digital Content Technology and its Applications , vol.6, no.15, pp.338-346, 2012.

[2] Li Jinhua, Jiao Yuying. Research on online information service model and algorithm Based on Intelligent Agent thematic .Intelligence theory and practice, vol.6, pp.51 -54, 2002.

[3] Preece A.D., Hui K.Y., Gray W.A., et al. The KRAFT Architecture for Knowledge Fusion and Transformation].Knowledge Based Systems, vol.13, no.2, pp.113-120.2000

[4] Zou Xiang-jun. Virtual environment modeling and design of mechanical products based Knowledge Fusion. Guangdong University of Technology , 2005.

[5] Gou Jin. key technology of knowledge fusion research integration. Zhejiang University, 2005 .

[6] Hu Bei, Wang Congying. High-tech industrial clusters and innovative model for developing coutries based knowledge fusion. Library and Information, vol.2, pp.38 -41 +73,2009.

[7] Zhou Fang, Wang Pengbo, Han Liyan. Research on multi-source information integration algorithm . Journal of Beijing University of Aeronautics and Astronautics , vol.01, pp.109-114, 2013.

[8]Cheng Quan. Community knowledge fusion mechanism research based on collaborative tagging . Intelligence theory and practice , vol. 8, pp. 20-25, 2011.

[9] Ji Cheng, Zhu Xiaoming. Knowledge fusion based knowledge integration management of Enterprise mergers and acquisition. Research and development management , vol.6, pp.78-84, 2007.

Advanced Materials Research Vols. 989-994 (2014) pp 1509-1512
© (2014) Trans Tech Publications, Switzerland
doi:10.4028/www.scientific.net/AMR.989-994.1509

Research on classification and encoding of digital cultural relics

Lei Li [1, a], Zhang Man[2,b]

[1]Party Committee Propaganda Department, Jiangxi Science & Technology Normal University, Nanchang, Jiangxi, P.R.China

[2]School of Information Engineering, Nanchang University, Nanchang, Jiangxi, P.R.China

[a]1512205455@qq.com, [b]manzhang201010@163.com

Keywords: Digital Cultural Relics; Classification; Encoding

Abstract. The paper analyzed the status of research on China's digital cultural relics categorizing and encoding which is beginning to develop in China. From the analysis of the characteristics and importance of digital cultural relics categorizing and encoding, the paper proposed a categorizing model and encoding method for digital cultural relics categorizing and encoding.

Introduction

With the rapid development of information technology, the exploration and utilization of digital cultural relics rose to a new level. Especially with the 3D technology, three-dimensional photographic scanning technology and interactive virtual reality technology applied in the digital cultural relics and museums, the process of construction of digital cultural relics and digital museums has been developed quickly since the appliance of those technologies which promoted the comprehensive and sustainable development of cultural undertakings, and promote the smooth progress of heritage preservation, repair, utilization and management. The construction of digital cultural relics and digital museums was begun from the recent years while it began much earlier in the developed countries [1]. Many cultural institutions of China have begun construction of digital museums, cultural relics digitization is becoming a core task of cultural relics of information technology whose importance are increasingly being addressed for the effective protection of cultural resources in the long run. Classification and encoding of digital cultural relics is an important part of cultural relics digitization work [2], thus its important to standardized classification system and encoding rules for digital cultural relics classification and encoding work in order to make digital cultural relics construction more convenient and effective. Therefore, the paper focused on how to carry out the classification and encoding of digital cultural relics.

Connotation and Characteristics Analysis

Connotation Analysis of Classification and Encoding of Digital Cultural Relics . Cultural Relics is a reflection social system, social production and social life of each era which has an important historical, artistic and scientific value. A digital cultural relic, developed with three-dimensional digital technology and other technologies, is digital archiving of cultural relics using 3D modeling technology and other technologies. Digital technology can not only permanent preserve precious cultural relics, but also make it possible for the vast number of cultural relics experts and lovers of joint research and exchange research feelings. So far Longman Grottoes digital cultural relics dimensional digital engineering is the well-known digital cultural relics cases [3]. American emerging management science pioneer Maurice Cook said that: Only when we learn to classification and encoding, simplification and standardization of a work can scientific management be possible to come true [4]. Classification and encoding of digital cultural relics work is based on the combination of cultural features and characteristics of digital technologies to make classification and encoding reasonable and facilitate to search and retrieval which will improve the utilization of cultural resources. Therefore, it's an important part of researches on digital cultural relic classification and encoding that study on scientific and standardization of classification and encoding, and find out the similarity and correlation between digital cultural relics and cultural relics.

Characteristics of Classification and encoding of digital cultural relics. For classification and encoding of cultural relics, its difficult to make a unified classification and encoding criteria for cultural relics as to the kinds and regions of cultural relics are various. China promulgated a number of classification criteria such as the National Heritage Board proposed a unified national heritage classification criteria, Museum Collection Classification, or the cultural relics custody special committee's "Museum Collection category"[5]. But according to the above classification criteria of cultural relics, it may appear cases like a heritage can be attributed in two category, and the above two criteria is a comprehensive classification methods and there is no uniform classification which making the search of cultural relics category difficult [6]. As to criteria on encoding, there are national information encoding standards on it [7], such as People's Republic of China administrative divisions Code standardized administrative code. But to the criteria on encoding of cultural relics, there are no reasonable and uniform encoding modes on it. As the similarity of cultural relics and digital cultural relics, digital cultural relics also faced with the same problems on classification and encoding as cultural relics.

Status and Necessity Analysis of Classification and Encoding of Digital Cultural Relics

With the construction of digital information technology in the application of cultural relics, the pace of cultural relics and museums digitization gradually accelerated. In addition to some of the famous museums began its digital construction, other countries have joined the museums digitization construction community, digital cultural relics began show to the world by electronic devices, hypermedia and so on. China has also started construction of digital cultural relics, such as digital museum building, digital museum studies, and other digital cultural relic researches. Retrieved through National Knowledge Infrastructure database, we got 112 relevant papers by using digital cultural relics as the subject and 888 documents while using digital museum as the retrieval subject, the year limit is from 2000 to 2013. The paper analyzed literature on digital cultural relics and found out that digital cultural relic construction focused on the digital cultural relic environment building rather than building their own connotation and characteristic, and research on digital cultural relics is on its infancy stage, as shown in figure 1.

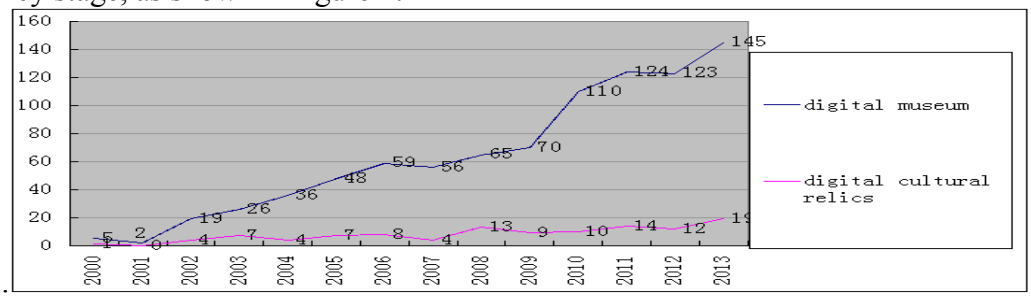

Fig. 1 2000-201. Researches on digital cultural relics and digital museum

Classification and Encoding Model of Digital Cultural Relics

Model of Digital Cultural Relics Classification . The paper proposed classification model of digital cultural relics is shown as table 3. The classification model has three class level and each level has its subclass level. Each class in the model is different with each other and orthogonal to each other, and its subclass has the same characteristics with it. In the paper, we mainly study on the father-class and describe its first subclass, and each class in the model can be extended and be able to adjust or change each class. The first class or main class layer of digital cultural relics classification is based on the properties and attributes of cultural relics which uses era classification methods, named as class A. The second layer is supplementary class named as B, which involved seven subclasses named as D, E, F, G, H, I and J. The third class is property class that is based on the property and characteristics of digitization of digital cultural relics, named as C, and it also involves seven subclasses, shown as in tale 3. Each class shown in table 1 can be subdivided to have its subclass. From the three class layer classification, it can make the digital cultural relic resources more convenient and effective when

query the resources and can make the classification of digital cultural relics more complete and uniform. Here we give a classification example to describe the way to classify digital cultural relic resources. If a classification is ADK1, it means it belongs to an era of class A and has the class property of class D and, K1 is the digital property information of its creator. The model above can keep the cultural relics characteristics of digital cultural relics, and added digitization features of it, thus make the model useful to classify digital cultural relics.

Table1. Classification model description of digital cultural relics

Class	Name	Subclass	Example
Main class A	Times classification	A1，A2,A3.....	Prehistoric,and other historical periods, etc
Supplementary class B	Regional Classification D	D11，D12，D13.....	11Beijing，12Tianjin，according to of administrative area code
	Texture Classification E	E1，E2，E3.....	Stone, jade, etc.
	Function Classification F	F1，F2，F3.....	Ancient architecture, ancient artifacts, etc.
	Property classification G	G1, G2, G3.....	More detailed information refer to common classification of cultural relics
	Value Classification H	H1, H2, H3.....	
	Source Classification I	I1,I2, I3.....	
	Speciation classification J	J1, J2, J3.....	
Digital Property class C	Creator information K	K1,K2.....	Person, Country, etc.
	Collection information L	L1，L2，L3.....	The type of museum, location information, etc.
	Protection level M	M1，M2，M3.....	Special grade, first grade, etc.
	Heritage Theme O	O1, O2, O3.....	The class theme and its theme information
	Related resources P	P1, P2, P3.....	Related resources of cultural relics
	Subsidiary information Q	Q1, Q2, Q3.....	Subsidiary information
	Others N	To be extended	To be extended

Design model of digital cultural relics encoding. The aim of digital cultural relics encoding is to achieving effective sharing of digital cultural relic information. Therefore, unified encoding method not only benefit using computer to cope with digital cultural relics information[8], but benefit the correspondence with digital cultural relics classification categories to reflect the digital cultural relics and other information. The design of digital cultural relics encoding model should follow information encoding standards. At present, China's information encoding standards include “administrative divisions code of People's Republic of China”, “national industry classification code”, and so on. The common information encoding types are no meaningful code and meaning code. Disorder code and ordered code belong to no meaning code while layer code, abbreviations code and combination codes are meaningful code. The paper selected layer code as the code method for layer code often used in linear classification as each class can be coded with sequential code which is appropriate for the pape. The digital cultural relics encoding model is shown in table 4. In layer code, its location means its layer and the one in the left is beyond the level in right. As digital cultural relics have three class, the code model also has three layer, that is layer 1,2,3, each layer begin with 1,2,3 (namely, encoding like 100,200,300, etc.), and the subclass was encoded like 101,201,301,etc while 101 means its the code of main class and its first subclass, 201 means its the code of Supplementary class and its first class,

301 means its the code of main class and its first subclass, shown as table 2. From the encoding model each code has its clear meaning and it's for computer to recognize.

Table2. Description of encoding model

Classification		Code display	Code number and list
Main class A	A	1(00)	101,102,103...
Supplementary class B	D	201(00)	20101，20102...
	E	202(00)	20201，20202...
	F	203(00)	20301，20302...
	.....	.....	.....
Digital Property class C	K	301(00)	30101，30102...
	L	302(00)	30201，30202....
	M	303(00)	30301，30302...
	.....	.....	.....

Summary

The construction of digital cultural relics is later than the developed countries, and the study of digital cultural relics is still in its infancy stage, the study of classification and encoding of digital cultural relics is less involved compared with other research topics. As classification and encoding of digital cultural relics will contribute to the effective inquiries and utilization of cultural resources, the study on it has an important significance. Through the study of digital cultural relics classification and encoding, the paper discussed the status of classification and encoding of digital cultural relics in China, analyzed its connotation and properties, and proposed the basic model of a classification and encoding of digital cultural relics.

Acknowledgement

This work was supported in part by Science and Technology Research Projects on Cultural Heritage Conservation , State Administration of Cultural Heritage, China (20110144).

References

[1] Ladislav Musílek, Tomáš Čechák, Tomáš Trojek. X-ray fluorescence in investigations of cultural relics and archaeological finds,Applied Radiation and Isotopes, Volume 70, Issue 7, Pages 1193-1202, 2012.

[2] Vassil Roussev, Candice Quates.File fragment encoding classification—An empirical approach, Digital Investigation, Volume 10, Supplement, Pages S69-S77 , 2013.

[3] Information on http://baike.baidu.com/view/10272925.htm#refIndex_1_10436112

[4] Chen Zhihuan. Oil production plant establishment and application of information encoded in the database management system, Digital Technology and Application, Volume 3, Pages 75 - 76, 2010.

[5] Shu Ching Yang. Reconceptualizing think-aloud methodology: refining the encoding and categorizing techniques via contextualized perspectives,Computers in Human Behavior, Volume 19, Issue 1, Pages 95-115, 2003.

[6] Chen Yu. Classification And Retrieval of Cultural relics information, Heilongjiang Science and Technology Information,Volume 4, Pages 154, 2007.

[7] Loris Nanni, Alessandra Lumini. A new encoding technique for peptide classification, Expert Systems with Applications, Volume 38, Issue 4, Pages 3185-3191, 2011.

[8] Nick J. Pizzi.Fuzzy quartile encoding as a preprocessing method for biomedical pattern classification,Theoretical Computer Science, Volume 412, Issue 42, Pages 5909-5925, 2011.

Advanced Materials Research Vols. 989-994 (2014) pp 1513-1516
© (2014) Trans Tech Publications, Switzerland
doi:10.4028/www.scientific.net/AMR.989-994.1513

An OCL-based Formal Model for Cloud Forensics

Jian Wang[1,3, a], Zhenmin Tang[1,b] and Xianli Jin[2,c]

[1]School of Computer Science and Technology, Nanjing University of Science and Technology, Nanjing 210094, China

[2]College of Computer, Nanjing University of Posts & Telecommunications, Nanjing 210046, China

[3]China Comservice Jiangsu Corporation

[a]wangjian@ccsjs.com, [b]tzm.cs@mail.njust.edu.cn, [c]jxl@njupt.edu.cn

Keywords: cloud computing, digital forensics, OCL, FODA

Abstract. Cloud Computing is gaining acceptance and increasing in popularity. However, digital forensics within Cloud becomes difficult. This paper proposes an extensible semantic model using OCL (Object Constraint Language) for cloud digital forensics data. We give a brief introduction to Trusted Digital Forensics, and then detail the modeling process using OCL and FODA (Feature Oriented Domain Analysis). Therefore, a feature tree can be built with semantic logical relation in order to get the overall semantic description of features in the forensic domain of digital data.

Introduction

As long as people are involved there will be crime. The need for Digital Forensics exists because some of these crimes or other incident is taking place on computer system. Cloud forensics [1] is Digital Forensics applied on Cloud Computing. Cloud Forensics is a subset of Computer Forensics as a cloud runs on a network and consists of network equipment. Cloud Forensics also entails Computer Forensics as a cloud consists of nodes that are computers. This means that Cloud Forensics ties Computer and Network Forensics together. The introduction of clouds complicated the digital forensic process [2]. There is a belief that a digital investigation a cloud can be difficult to do. The need to have formal and proven methods to conduct a digital investigation on a cloud became apparent.

So this paper proposes an extensible semantic model for cloud digital forensics data. Its structure is organized as follows: firstly, we give a brief introduction to Trusted Digital Forensics. Secondly, we discuss the details of modeling cloud forensics using OCL [3] and conclude the paper finally.

The Concept of Trusted Digital Forensics

The trusted computing is the action of trusted components, and its operation or process is predictable under any operating condition [4]. It can as well resist the destruction from application software, virus, and physical interference. The ultimate purpose is to ensure the information integrality of the entity. In the process of digital forensics, we can establish a trusted evidence theory system referring to the thought of trust and trusted computing. The digital forensics can be divided into two aspects: one is the trust of static property, namely to ensure that the static semantic features on process of trusted discovery and trusted fixation is trusted; the other one is the trust of dynamic behavior, namely to make the process or trusted behavior of digital data transformed into evidence trusted from the following three aspects: trusted extraction, trusted analysis, and trusted expression. This paper mainly focuses on the static property.

The Feature Model of Cloud Digital Data

Feature is perception of the system from certain perspectives, which can be regarded as an information collection of describing domain models [5].

FODA (Feature-Oriented Domain Analysis) [5] modeling is related to two conceptions: abstract and refining. Abstract describes the common requirement in the field of application system, namely, abstracts the generality. Its main purpose is to acquire the field model. Refining can be used to develop the specific applications. When modeling in the process of FODA field, and by decomposing and merging the abstracted features in the field of application system, a feature tree of semantic logical relation is built. Then the overall feature semantic description of the forensic domain of digital data is obtained, and DFM (Domain Feature Model) [6] is modeling.

Definition 1. FM (**Feature Model**) can be represented as a 3-tuple <*feature*, *relation*, *constraint*>, where *feature* is the feature collection, whose elements are the feature items in the feature tree; *relation* is the logical relation collection of feature; *constraint* is the constraint collection of features and their relations among them.

Definition 2. CFDFM (**Cloud Forensics Data Feature Model**). CFDFM is a kind of construction model of feature models, it should satisfy the following constraints:

context *CFDFM* inv :

self.stereotype = *FM* and

self→*ownedElement*→*forAll* (*p* | *p*. *oclIsKindOf* (*Feature*) or *p.oclIsKindOf* (*Relation*) or *p.oclIsKindOf* (*Constraint*)) and *self.Feature*→*includes* (*name*) and *self.Feature*→*includes* (*type*) and *self.Feature*→*includes* (*size*) and *self.Feature*→*includes* (*location*) and *self.Feature*→*includes* (*createTime*) and *self.Feature*→*includes* (*visitTime*) and *self.Feature*→*includes* (*modifyTime*) and *self.Feature*→*includes* (*content*)

where, *feature*, *relation*, and *constraint* is the elements of CFDFM; *name*, *type*, *size*, *location*, and *content* is the name of digital data (the identification of digital data), *type* (such as txt, jpg, pdf, rmvb, etc), *size*, *path*, and *content*; *createTime*, *visitTime*, *modifyTime* is the creating time, the last access time, and the last modifying time of the digital data.

In the CFDFM, the element *Constraint* is the feature-constraint description of the components. It includes the constraint of inherent features, as well as the constraint of extended features. According to the different relations between kinds of features, we can divide them into four classes: self-constraint, "father-son" feature relation constraint, dominant relation constraint, and recessive relation constraint.

A) Self-constraint

Definition 3. (**Self-constraint**). Self-constraint is the rule that digital data features should meet for some constraint of their own properties.

In the CFDFM inherent feature, for example, name has the typical feature of the constraint. Its uniqueness should satisfy the constraint as follows:

context *name* inv :

self.oclIsKindOf (*Feature*) and *self.allInstances.value*→*isUnique* (*n* | *n*)--*self.allInstances*→*forAll* (f_1, f_2 | f_1<>f_2 implies f_1.*value* <> f_2.*value*)

B) "Father-son" Feature Relation Constraint

Definition 4. (**Father feature and son feature**). Assume that there are two features f_a and f_b. If f_a is the refinement of f_b's direct semantic level, we can conclude that f_a is f_b's son feature, and f_b is f_a's father feature. In the digital data feature tree, "father-son" feature can be divided into *mandatory* constraint, *optional* constraint, and *multiplicity* constraint.

Definition 5. (**Mandatory**) If a son feature *cFeature* and father feature *pFeature* satisfy the constraint:

context *cFeature*, *pFeature* inv *mandatory* :

pFeature.subFeature→*notEmpty*( ) implies *pFeature.subFeatures*→*includes*(*cFeature*)

We can say that *cFeature* is more mandatory, compared to *pFeature*, which can be denoted as *mandatory*(*pFeature*, *cFeature*).

Definition 6. (**Optional**). If a son feature *cFeature* and father feature *pFeature* satisfy the constraint:

context *cFeature* ,*pFeature* inv *option*:

pFeature.subFeatures→notEmpty () implies (*pFeature.subFeatures→includes*(*cFeature*) or *pFeature.subFeatures→excludes*(*cFeature*))

We can say that *cFeature* is more optional, compared to *pFeature*, , which can be denoted as *option*(*pFeature*, *cFeature*).

Definition 7. (**Multiplicities**). Multiplicities constraint is the constraint of repeat numbers that *father* to *son*.

UML2.0 rules show four kinds of repeat numbers, as Table 1 shows.

Table 1 Multiplicity

Symbol	Lower Bounds	Upper Bounds	Explanation
0..1	0	1	At most one instance of the sub-feature
1	1	1	Only one instance of the sub-feature
0..*	0	Infinity	Arbitrary
1..*	1	Infinity	At least one instance of the sub-feature

In CFDFM, the multiplicity between "father-son" features is a positive integer or interval. As a result, we can expand UML repeat number so as to support more repeat numbers with more form. As the repeat numbers are nonnegative integers, repeat numbers can be divided into 3 classes: N, N_1 .. N_2, and N_3 ..*,($N > 0$, $N_2 > N_1 = 0$, $N_3 = 0$). The multiplicity constraint between "father-son" features can be described by OCL below:

context *cFeature*, *pFeature* inv:

pFeature.subFeatures→includes(*cFeature*) and *cFeature.allInstances→size*() = N

context *cFeature* ,*pFeature* inv:

pFeature.subFeatures→includes(*cFeature*) and *cFeature.allInstances→size*() >= N_1 and *cFeature.allInstances→size*() =< N_2

context *cFeature* ,*pFeature* inv:

pFeature.subFeatures→includes(*cFeature*) and *cFeature.allInstances→size*() >= N_3

C) Dominant Relation Constraint

Dominant relation constraint means that two features between non-"father-son" relationship exists somehow direct relation: alternative, depends, or excludes.

Definition 8. (**Alternative**). If two features *feature-a* and *feature-b* satisfy the following constraint:

context *feature-a* ,*feature-b* inv alternative :

CFDFM.Feature→excludes(*feature-a*) implies *CFDFM.Feature→includes*(*feature-b*) and *CFDFM.Feature→excludes*(*feature-b*) implies *CFDFM.Feature→includes* (*feature-a*)

We can conclude that *feature-a* and *feature-b* are alternative, which can be denoted as *alternative*(*feature-a*, *feature-b*).

Alternative makes it a rule that at least one feature must be chosen from the two features *feature-a* and *feature-b*, which not only reflects the indispensable but multiple parts in the field application, but also represents the different process and expression of the same feature in different applications.

Definition 9. (**Depends**). If two features *feature-a* and *feature-b* meet the constraint:

Context *feature-a*, *feature-b* inv *depends* :

CFDFM.Feature→includes(*feature-a*) implies *CFDFM.Feature→includes*(*feature-b*)

We can conclude that *feature-a* depends on *feature-b*, which can be denoted as *depends*(*feature-a*, *feature-b*).

In CFDFM, *depends* always exist between feature and element feature(description of feature).

Definition 10. (**Excludes**). If two features *feature-a* and *feature-b* meet the constraint:
context *feature-a*, *feature-b* inv *excludes* :
CFDFM.Feature→includes (*feature-a*) implies *CFDFM.Feature→excludes*(*feature-b*) and
CFDFM.Feature→includes (*feature-b*) implies *CFDFM.Feature→excludes*(*feature-a*)

We can conclude that *feature-a* and *feature-b* are mutually exclusive, which can be denoted as *excludes* (*feature-a*, *feature-b*).

Exclude constraint shows that two features are mutually exclusive and cannot exist in the same field application.

D) Recessive Relation Constraint

Recessive relation constraint is a kind of constraint that exists among features caused by the definition of digital data, the environment of digital data, and the internal relationship between essential features. For an example, in CFDFM, *createTime* is smaller than *visitTime* and *modifyTime*, namely:

Context *createTime*,*visitTime*,*modifyTime* inv:
visitTime >= *createTime* and *modifyTime* >= *createTime*

We can conclude the four classes of constraint between digital data features based on analysis of feature field method on combining digital data semantic features. These constraints are not only suitable for describing the relation of inherent features in CFDFM, but also suitable for describing the relation of extended features in CFDFM. Next, horizontal and vertical analysis can be launched on practical cases through CFDFM, the feature tree can be built, and the dependency and relevancy between features can be represented by the related operations using OCL.

Summary

This paper uses FODA to build a static semantic feature model for cloud forensics digital data, and formally describe all kinds of features of digital data in OCL. It classifies those features through “collection” and “collection operation”, and describes the relationship and dependency between them. Our future work will focus on discussing the formalized verification method of trusted discovery and trusted fixation.

* Supported by the National Natural Science Foundation of China (Grant No. 61373139)

References

[1] K. Ruan, J. Carthy, T. Kechadi, and M. Crosbie, "Cloud forensics: an overview," IFIP International Conference on Digital Forensics, vol. 7, 2011.

[2] Michael Donovan Köhn. Integrated Digital Forensic Process Model. Master's dissertation, University of Pretoria, Department of Computer Science, Pretoria, South Africa, November 2012.

[3] Object Constraint Language[EB/OL]. http://www.omg.org/spec/OCL/2.0/PDF.

[4] Zehui Shao, Qiufeng Ding, Xianli Jin, Guozi Sun. A Static Semantic Model for Trusted Forensics Using OCL. Future Information Technology, Lecture Notes in Electrical Engineering, Volume 276, 2014, pp 259-268.

[5] Kang KC, Cohen SG, Hess JA, Novak WE, Peterson AS. Feature-Oriented domain analysis (FODA) feasibility study. Technical Report, CMU/SEI-90-TR-21. Pittsburgh: Carnegie Mellon University, Software Engineering Institute, 1990. 1-52.

[6] Jin Xianli, Ma Huadong. A Semantic Description Model of Features for Service Composition Using OCL. Journal of Computer Research and Development, 2007, 44(12):2112-2121.

Advanced Materials Research Vols. 989-994 (2014) pp 1517-1521
© (2014) Trans Tech Publications, Switzerland
doi:10.4028/www.scientific.net/AMR.989-994.1517

Research on Customers Churn Prediction Model Based on Logistic

Jiang Min[1], Chu Na[2], Bi Xiaoming[3]

Department of Computer, Dalian Neusoft University of Information, China

[1]jiangmin@neusoft.edu.cn, [2]chuna@neusoft.edu.cn, [3]bixiaoming@neusoft.edu.cn

Keywords: Loss of customers; Logistic regression; Prediction model; Model validation

Abstract. At present, the competition is increasingly fierce between the securities company, whether can effectively prevent the loss of users, reducing loss rate is a difficult problem at present each securities company urgently needs to solve. The model based on the principle of data mining, proposes a prediction method based on Logistic regression algorithm. Prediction model is built based on Logistic regression algorithm and the validity and accuracy of the model is verified by experiment, provides a new method and thinking for the securities company customer churn prediction.

Introduction

With the continuous development of the securities market in China, there has been a shift in securities companies' business operations to a more centralized and tightly-controlled model. As a result of the increasingly fierce competitions and the emphasis on value-added services, customer loyalty has become a common problem faced by the securities industry. Therefore, a customer-oriented service model and more targeted marketing strategies are believed to be the key to building and retaining the competitiveness of the securities companies.

Companies that have no clearly-defined contractual agreements with their clients quite often find themselves in constant risks of loosing customers and profits. Therefore, how to find the prospective customers and successfully retain them has become the focus of many securities companies in their short-term and long-term business strategies. Trading behaviors over a period of time, causes for customer loss and other factors are analyzed to determine the appropriate strategy or means to develop and maintain customers and remain profitable.

Using the Logistic regression analysis method, this research has established an effective customer churn prediction model by analyzing historical transaction data up to six months. The aim of this research is to develop a tool that the securities companies can use to analyze trends and forecast customers that are in a higher risk of losing so that timely measures can be deployed to retain customers and ensure they stay loyal and increase profitability.

Logistic regression prediction principle

Logistic regression is an important method for the analysis of categorical data statistics. Beginning in 1980s, it has been used for event prediction, the study of non-linear relationships between the probability of an event and the influencing factors of the event, and the identification of risk factors of the incident [1].Logistic regression analysis considerably overcomes the shortcomings of the linear hypothesis method, by reducing the restrictions of overall distribution. There are no assumptions about the distribution of the independent variables,and the argument can be continuous variables, discrete variables and dummy variables. Logistic regression determines the strain response based on the model fitting and the model approach between the variables and the dependent variable. Its main purpose is to classify, and estimates the probability of events.

For dichotomous questions, assuming the individual options $y=1$ indicates that the client properly and $y=0$ indicates that the customers churn and that $x=(x_1,x_2,\cdots,x_k)$ indicates that the associated descriptive variables can be obtained in the database, and then the established mathematical expressions for the Logistic regression model is:

$$\text{logit}\left(p(y=1)\right)=\ln\left(\frac{p(y=1)}{1-p(y=1)}\right)=\beta_0+\beta_1x_1+\cdots+\beta_kx_k \quad (1)$$
$$=\beta_0+\sum_{i=1}^{k}\beta_ix_i$$

$$P\left(y=1\mid x\right)=\frac{\exp\{\beta_0+\sum_{i=1}^{k}\beta_ix_i\}}{1+\exp\{\beta_0+\sum_{i=1}^{k}\beta_ix_i\}} \quad (2)$$

$$P\left(y=0\mid x\right)=\frac{1}{1+\exp\{\beta_0+\sum_{i=1}^{k}\beta_ix_i\}}$$

Among them $\beta_i\left(i=1,\cdots,k\right)$ is coefficient of each variable after logistic regression,Its meaning is: when x_i change an unit of measurement each caused by the change in the natural logarithm; β_0 behalf Intercept. Formula（2） represents the probability of loosing certain customers. Among them $P\left(y=1\mid x\right)$ expresses the probability of a normal customer, $P\left(y=0\mid x\right)$) indicates the probability of churn.

Table 1 Users monthly data table

Month	Total commission	Trading clients	Average commission	Quality customers	Premium customers of commission
200805	4275736.27	12033	355.33	2398	1308278.04（30.60%）
200807	16469120	40214	409.54	7859	6473401.56（39.06%）
200808	8836430.38	33689	262.29	6357	4206377.16（47.60%）
200809	8043580.58	31018	259.32	5740	3938777.11（48.97%）
...	...	...	...	...	...
200810	8161183.24	30319	269.18	5392	4107470.57（50.33%）

Table 2 Partial correlation coefficient table

English name	Variable name	Correlation coefficient
LJMRYJ_LJMCYJ_H_ZSZ_4M_BL	Nearly four months total commissions and buying and selling half of the total market capitalization ratio	0.502226533
LJMC_ZSZ_4M_BL	Cumulative proportion of the total market capitalization and sold nearly 4 months	0.460734314
LJMCYJ_ZSZ_4M_BL	The cumulative proportion of the total market value and selling commission nearly four months	0.445815741
LJMC_ZSZ_2M_BL	Cumulative proportion of the total market capitalization and sold nearly 2 months	0.443599602

Logistic regressions customer churn prediction

Data preprocessing

In the data preprocessing, we will group data into two categories: customer information data and customer transactions data.

Customer information data. Customer information data refers to the customer information, such as the customer's gender, age, marital status, educational status, occupation and capital scale. Due to historical reasons, our customers' electronic documentation is incomplete, missing most of the data; only the size of the customer's financial data can be exported via the customer's transaction data. Therefore the customer information data model structure we use includes only the size of their capitals.

Customer transaction behavior data. Customer transaction behavior data includes: Changes in the position data of customers, the number of monthly transactions, turnovers, monthly commission fees, etc. Users with the monthly data are shown in Table 1.

Logistic regression model structure

Data Preparation. The prediction model established in this article uses data from a securities company over a year, in the four months from September to December statistical data was collected. The time period used to predict customer behaviors are likely to trigger future marketing response. January to March next year is forecast to month, using the model created to predict customer marketing response.

Define variables and variables derived. In order to ensure the accuracy of the model prediction, we use 91 factors securities company's customer data to make predictions. These 91 factors include asset data, transaction data, basic customer information, customer service and product information such as customer subscriptions, five aspects. Through the chain, the result was worse than the method by the 91 factors derived 275 variables.

Data preprocessing and correlation analysis. According to this study, the correlation of explanatory variables and target variable, select the 150 most relevant variables.

Logistic regression modeling

Screening AR variables on the basis of Table 2, we do logistic regression to 150 variables use SAS. Getting lost probability between the univariate regression and univariate of each customer. After the loss probability Sort, Getting the value m% is the proportion of the cumulative loss of customers top n% (n=1…100). We obtain a curve between m% and n% (as shown in Figure 1), then obtain the AR values for each variable. Choose the high value of the variable AR from them. Also, delete the experience value of less than 0.73 of the variable AR. After this step, we obtain the 45 variables.

Select the maximum likelihood estimates of large and significant variables use Logistic regression forward stepwise regression method, stepwise regression, definition the loss of value of the target variable as 0, then

$$P_{\text{outflow}}=1\text{-P}=\frac{1}{1+\exp\{\beta_0+\sum_{i=1}^{k}\beta_i x_i\}}$$

When the regression coefficient β_i is positive, variable x is the larger, P_{outflow} is smaller; Contrary, When β_i is negative,variable x is smaller,P_{outflow} is larger. Therefore, the size of the sign and the loss probability of regression coefficients showed a negative relationship. After this step, we obtained 21 variables.

Empirical Analysis

Model evaluation phase is to test the model has been established. Model checking is the important step for the data mining, there are two principles in determining the goals and data mining preparation stage, the first is, the prediction model can be assessed and must be realized, and the second is, the resulting model can be used in a real-world environment.

Select the observation period and object. Before proceeding with data collection, we define the time interval churn models examined below. On observing the object, we screened for individual customers conditions include: Customer average monthly assets between the 1,000 yuan to 10 million yuan in the observation period; Opening time from the observation period over four months; There are transactions within the observation period 4 months.

Determine the variables and regression coefficients. Performed logistic regression calculation again for the 21 variables, confirm the regression coefficients and constant coefficient of these variables. The constant coefficient of the churn model is 0.2708204106.

Estimation Results. KS (Kolmogorov-Smirnov) is mainly used to validate the ability of the model, that distinguish the lost objects, verify the ability of the model accurately distinguish normal customers and the churn. This model predicts KS value is 44.678, as shown in Table 3, indicating that the model has a strong ability to identify for the churn, so this model prediction is credible.

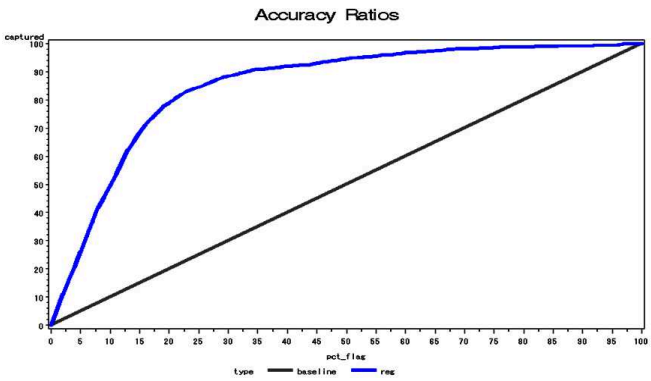

Fig. 1 AR value is 0.73

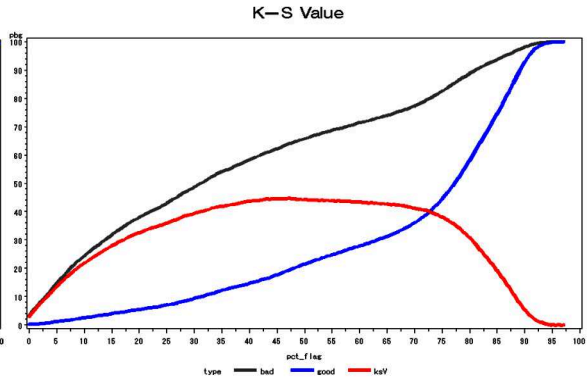

Fig. 2 Model Checking KS value

Table3 KS score sheet

Score	Cumulative target customers(CC)	Cumulative non-target customers(CNC)	Cumulative total client(CTC)	CC/ CTC	CNC/CTC	KS values
47	5812	218488	224300	63.87515112	19.19683415	44.678

Verify the correct rate and the feasibility to the model. This article randomly selected 10 customer data in the sample to test and verify substituting classification function, and then we obtain the results whether the customer has been lost, as shown in Table 4.

Table 4 Customer churn prediction analysis table

Customer ID	Var1 Assets	Var 2 Market cap	Var 3 Funds	Var 4 Positions	Var 5 Growth rate	Var 6 Than	Var Worse than	Outflow (Y)
100739135	1	0.2232	0.1713	0	8	80	6.25	1
100916315	3	0.1247	0.7521	2	1	30	-0.025	0
...	...	...	...	...	...	...	...	...
2760963	2	0.3369	0.2227	0	5	90	5.02	1

From the table, we can get the following conclusions: Customer ID100916315 variable difference ratio less than 0, that means the ratio of the loss of customers and normal customers less than 0, value of (Y) is equal to 0(loss or not), means that the customer has been lost. Contrary, the difference ratio of other nine customers is greater than 0, then Y=1, means that customers is not loss, so the conclusion of customer churn analysis by Logistic regression model are consistent with the actual situation.

Conclusion

This paper studies how to use data mining technology to establish customer churn prediction model to solve the problem of customer loss experienced by a securities firm. Real data was

collected and analyzed to design the model of the customer churn prediction using the Logistic regression method. The findings of the study provide countermeasures and recommendations for effectively improving customer turnover.

Acknowledgement

This research is supported by the Doctoral Program of Dalian Neusoft University of Information.

References

[1] Liu Bin, Qiu Huayong. Design and implementation of a comprehensive securities company customer analysis system. Computer Systems & Applications, 2010, 19(10):126-130.
[2] Wang Weijun. Based on data mining securities business customer churn analysis. University of Electronic Science and Technology（SOCIAL SCIENCES）, 2009, 11(1):18-22.
[3] Frederick F. Reichheld and W. Earl Sasser, Jr., Zero Defections: Quality Comes to Service. Harvard Business Review, Sept.-Oct. 1990, 105-111.
[4] BUCKINX W, DIRK Van den Poel .Customer base analysis: partial defection of behaviourally loyal clients in a non-contractual FMCG retail setting. European Journal of Operational Research 2003, 164: 252-268.
[5] Wu Bin, Ying Li. Churn Prediction Model and Application Based Logistics regression algorithm securities customers. Financial electronic, 2013, 65-67.
[6] David Heckerman, Dan Geiger, and David M. Chickering. Learning Bayesian networks: The combination of knowledge and statistical data. Machine Learning, 1995, 20(3):241-243.
[7] Jia Lin, Li Ming. The establishment and implementation of the model based on data mining customer churn. Computer Engineering and Applications, 2004, 4:185-187.

Advanced Materials Research Vols. 989-994 (2014) pp 1522-1525
© (2014) Trans Tech Publications, Switzerland
doi:10.4028/www.scientific.net/AMR.989-994.1522

Site Selection of Customer Operation Center for Pull and Drag Transportation Based on the Analytic Hierarchy Process

Xiaoqiong Luo[1, a] ,Xiaoyong Yin[2,b]

[1] Business School, Jiujiang University, Jiujiang, Jiangxi, China

[2] Business School, Jiujiang University, Jiujiang, Jiangxi, China

[a]email:68344816@qq.com, [b]email:8496544@qq.com

Keywords: Pull and Drag Transportation; Customer Operation Center; Site Selection; AHP

Abstract. Pull and drag transportation is an advanced transportation organization ,it is lower transport costs, higher efficiency, better energy saving. Customer operation center is important nodes in the pull and drag transportation routes, related to the overall layout of the transportation network and the overall effectiveness. Using AHP in this article, take full account to needs of pull and drag transportation , and analysis the main influencing factors about customer operation center location from the perspective of society and the business. Established model, obtains the importance weight of the influence factors, and provide the basis for evaluation. This method makes the selection process efficient, reasonable, and has a certain practicality.

Introduction

1)Introduction of Pull and Drag Transportation.(1)Basic situation of pull and drag transportation: Pull and drag transportation is a transportation organization, the tractor pull a trailer to the destination, unload the trailer and put a new trailer, then transport to another destination of transportation. The tractor and the trailer (or semi-trailer) separate and combine , match and schedule, according to this way, the transportation organization can short the loading and unloading time, the tractor increase frequency of use. Compared with the traditional modes of transportation, lower transportation costs, higher efficiency, faster turnaround of vehicles, better energy-saving and emission reduction effect . It will become the mainstream mode of transportation[1].

(2)Pull and drag transportation - customer operation center model: Large-scale logistics enterprises mainly use this pull and drag transportation mode: in the customer operation center, the special line vehicles collect cargos from customers together, the cargos is loaded into the trailer in advance, then put the trailer to a tractor, then the cargos are transported to port operation center; in the port operation center, remove the trailer after arrival of the tractor, then the special line vehicles transport the cargos to the yard and waiting for export, it is the whole process of transportation.

Port operation center set up in a major port around, play a major focus like receiving import containers from the port and sending export containers, the site selection has a strong unique. Customer operation center play a role of logistics nodes in pull and drag transportation routes; the transfer point of different transport tools; cargos transit hub; goods production, processing, commerce and trade, transportation and distribution logistics nodes , as shown in Fig 1.

2)Research Significance on Site Sellection of Customer Operation center. Customer operation center is a logistics node in pull and drag transportation routes, it is important place of providing logistics services. Through setting up more than one customer operation center, can form a reticular pattern, prompt intensive transportation and economies of scale, and achieve reverse logistics and cycle-logistics. Site selection of customer operation center is left hanging of cycle-logistics in mind for the future.

Study on site selection of customer operation center not only directly help logistics infrastructure planning and construction, but also indirectly promote the development of China's logistics industry, and promote regional economic development, ease the pressure on urban traffic, protect the natural

environment, has positive significance. The study provide better theoretical basis and reference materials . Therefore, the logistics facility location problem and its method of research is extremely important significance.

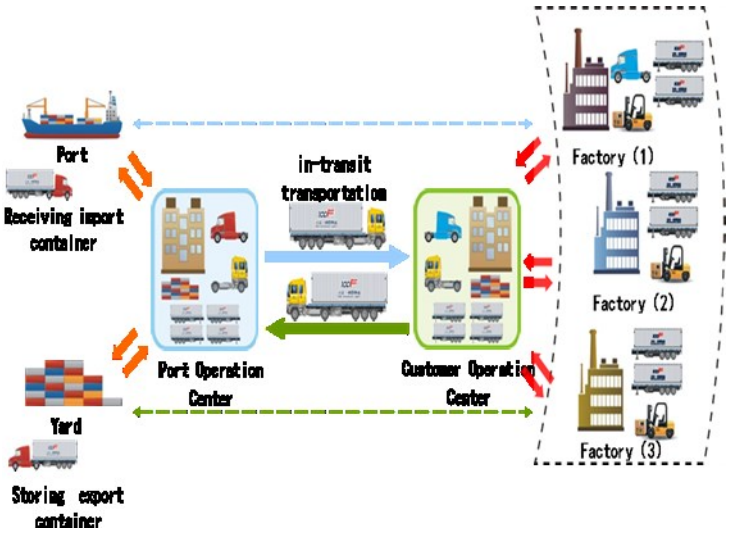

Fig 1 Pull and Drag Transportation- Customer Operation Center Model

3) Research Methods.Customer operation center needs larger-scale. So, its construction and operation of logistics enterprises will not only affect their own development, but also has a certain degree of economic and ecological environment of the surrounding areas. The site selection is a complex decision problem, involving a number of factors, solely relying on quantitative analysis or qualitative analysis, are difficult to arrive at a scientific and rational evaluation, the results are difficult to use.

AHP is a multi-criteria decision making method by combining quantitative analysis with qualitative analysis. In the 1970s , American operations research professor establishes this method .It will be a complex multi-objective making decision as a system, the target reduces to multiple targets or guidelines, then divide into multiple indicators (or criteria, constraints) of a number of levels, calculate the single level sorting and the total level sorting by qualitative indicators of fuzzy quantification method, as a target(multi-index) and method optimization decision system. The key is to build matrix, and judge the matrix. Rationality and scientific nature of matrix impact to its application effects directly.

This article uses the basic principle of AHP, site selection of customer operation center is the target site, and build location model by full analysis of the factors, then valuate the programs one by one, and obtain the solution by using Matlab software, finally, find the best construction site.

AHP Analysis

1)Establishment of Evaluation Indicators Systems. Many factors affect site selection of customer operation center. But the site has the Special Operation center on the premise of pull and drag transportation. For example, the site should close to customer-intensive places, reduce transport time of the special line vehicles, and have adequate supply; and maintain a certain distance between customer operation centers; area of customer operation center is enough, and so on. The influence factors of location is summing up two factors into social and enterprise perspective by analytic hierarchy process[2], as shown in Fig 2.

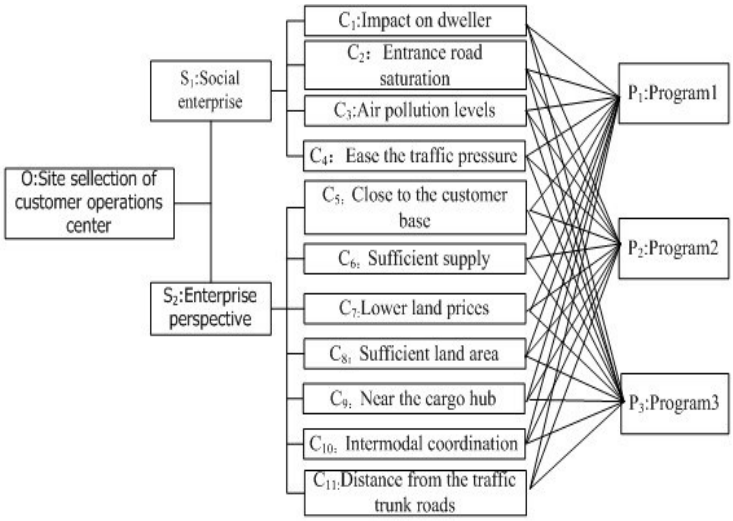

Fig 2 Hierarchy System of Site

2)Establishment of Judgment Matrix . In site selection of customer operation center, the target layer O is impacted by two making factors S_1 and S_2, however, these two factors are affected by the various sub-factors. Through group decision-making by the experts, establish the matrix structure according to the relative importance of factors[3].

(1) Judgment matrix O-S: For a target layer O, S_1 and S_2 are equally important, so judgment matrix O-S is: $A=\begin{bmatrix}1 & 1\\ 1 & 1\end{bmatrix}$.

Maximized eigenvalue: $\lambda_{max}=2$, priority vector:$W_1=(0.5,0.5)^T$.

(2)Judgment matrix S_1-M: $A=\begin{bmatrix}1 & 3 & 1/3 & 1/5\\ 1/3 & 1 & 1/5 & 1/7\\ 3 & 5 & 1 & 1/3\\ 5 & 7 & 3 & 1\end{bmatrix}$;

Volume normalization, $B=\begin{bmatrix}0.107 & 0.188 & 0.074 & 0.119\\ 0.036 & 0.063 & 0.044 & 0.085\\ 0.321 & 0.313 & 0.221 & 0.119\\ 0.536 & 0.438 & 0.662 & 0.597\end{bmatrix}$;

Priority vector :$W_2=[0.122,0.057,0.263,0.558]^T$. Maximized eigenvalue: $\lambda_{max}=4.117$.

Therefore, relative to the social benefits, the four factors should be sorted according to the weight of C_4, C_3, C_1, C_2.

(3)Judgment matrix S_2-M:$A=\begin{bmatrix}1 & 1/5 & 5 & 2 & 3 & 7 & 3\\ 5 & 1 & 7 & 3 & 5 & 8 & 5\\ 1/5 & 1/7 & 1 & 1/3 & 1/4 & 3 & 3\\ 1/2 & 1/3 & 3 & 1 & 3 & 5 & 3\\ 1/3 & 1/5 & 4 & 1/3 & 1 & 4 & 3\\ 1/7 & 1/8 & 1/3 & 1/5 & 1/4 & 1 & 1/3\\ 1/3 & 1/5 & 1/3 & 1/3 & 1/3 & 3 & 1\end{bmatrix}$;

Volume normalization, $B=\begin{bmatrix}0.133 & 0.091 & 0.242 & 0.278 & 0.234 & 0.226 & 0.164\\ 0.666 & 0.454 & 0.339 & 0.417 & 0.390 & 0.258 & 0.273\\ 0.027 & 0.065 & 0.048 & 0.046 & 0.019 & 0.097 & 0.164\\ 0.067 & 0.151 & 0.145 & 0.139 & 0.234 & 0.161 & 0.164\\ 0.044 & 0.091 & 0.194 & 0.046 & 0.078 & 0.129 & 0.164\\ 0.019 & 0.057 & 0.016 & 0.028 & 0.020 & 0.032 & 0.019\\ 0.044 & 0.091 & 0.016 & 0.016 & 0.026 & 0.097 & 0.055\end{bmatrix}$;

Priority vector:W_2'=[0.196,0.399,0.067,0.152,0.107,0.027,0.054]^T. Maximized eigenvalue: λ_{max}=7.727.Therefore, relative to the enterprise benefits, the seven factors should be sorted according to the weight of C_6, C_5, C_8, C_9, C_7, C_{11}, C_{10}.

3)Consistency Check of Judgment Matrix. Consistency Index is CI=$\frac{\lambda_{max}-n}{n-1}$.Based on the average random consistency index RI values (Table 1), obtains relative consistency index CR=$\frac{CI}{RI}$, When the CR is less than 0.1, the sort result has a more satisfactory level of consistency and accept the result of the analysis, or to determine the matrix of adjustment, and re-find the right system according to the above steps[4], as shown in Table 1.

Table 1 RI Value

Size(n)	1	2	3	4	5	6	7
RI	0	0	0.58	0.9	1.12	1.24	1.32

The above 3 matrix carry out consistency check .

(1)Judgment matrix O-S: λ_{max} =2,so this judgment matrix has a satisfy consistency check obviously.

(2)Judgment matrix S_1-M: CI= $\frac{\lambda_{max}-n}{n-1}=\frac{4.117-4}{4-1}=0.03949$, CR=$\frac{CI}{RI}=\frac{0.03949}{0.9}$=0.04388<0.1.So this judgment matrix has a satisfy consistency check.

(3)Judgment matrix S_2-M: CI= $\frac{\lambda_{max}-n}{n-1}=\frac{7.727-1}{7-1}=0.12122$, CR=$\frac{CI}{RI}=\frac{0.12122}{1.32}=0.09183$<0.1. So this judgment matrix has a satisfy consistency check.

Site selection of customer operation center is divided into four hierarchical structure: the target layer O, criteria layer S, sub-criteria layer C and program layer P. According to calculate all the factors of the same level to the overall goal, obtain the relative weight of sub-criteria layer C to the overall goal O. Its value is obtained by combination of W^1 and W^2:

$W=\begin{bmatrix} W_1 & 0 \\ 0 & W_2 \end{bmatrix}$,W=[0.061,0.028,0.132,0.279,0.098,0.200,0.033,0.076,0.053,0.014,0.027]^T. In the site selection of customer operation center, the order of importance is easing traffic pressure, sufficient supply, air pollution levels, close to the customer base, sufficient land area, impact on dwell, near the cargo hub, entrance road saturation, distance from the traffic trunk roads, intermodal coordination.

Of course, the program should also be established judgment matrix after proposing the specific program, and obtain synthetic weight of the program layer on the overall goal, finally identify specific and practical solutions by the weight sort of various programs[5].

Conclusion

According to site selection of customer operation center, AHP can make the complex decision-making clarity, simplicity, ability to easily and accurately to select the optimal program. It is an effective method.

References

[1] Huang Gui-rong: Fuzzy Synthetic Evaluation of Logistics Enterprise Alliance Risk Based on Entropy Weight, in Logistics Engineering and Management (2010), p.40-42.

[2] Liu fang,Gao bo: The Application of Hierarchy Process in the Site Selection of the Logistics Park, in Group Technology & Production Modernization Vol. 21 (2004) , p.37-39

[3] Zhang Yan-xia, Huo Jia-zhen: Research on Fuzzy Method of Logistics Center Location, in Logistics Technology2002.

[4] Wu Zhan-kun, Zhao Ying-shu: The Application of Analytic Hierarchy Process in Suppliers Selection of Logistics Outsourcing, in Technoeconomics & Management Research(2009) , p.24-26.

[5] DAS S K, SPASOVICL: Scheduling Material Handling Vehicles in a Container Terminal, in Production Planning and Control(2003) , p.623-633.

Advanced Materials Research Vols. 989-994 (2014) pp 1526-1531
© (2014) Trans Tech Publications, Switzerland
doi:10.4028/www.scientific.net/AMR.989-994.1526

Research on the Layout of Integrated Freight Hub based on Two-stage Model

Yanyi Chen [1, a], Tiexing Liu[2,b]

[1] School of Transportation, Wuhan University of Technology, Wuhan, China, 430063

[2] Post-doctoral scientific research workstation, China Merchants Group, Shenzhen, China, 518000

[a]chenyanyi163@163.com, [b] liutiexin@pdiwt.com.cn

Keywords: Layout of Integrated Freight Hub; Attribute Prediction; Hierarchical Division

Abstract. Applying transportation planning theory and operations research method , this paper proposes the layout model of integrated freight hub with two-stage , which first builds a model to predict the attributes of integrated freight hub aiming for the optimization of regional freight transportation organization , and then works out the way to classify district integrated freight hub based on Hierarchical cluster. Eventually, take a specific example for empirical study.

Introduction

China's economy and society enter a new stage of development during the "Twelfth five-year" period, which is a crucial period of building a well-off society. In the process of accelerating the transformation of economic development mode , the industrial structure and product structure in our country will continue to upgrade, which inevitably requires building low-cost, efficient transportation system, providing efficient, fast and safe transportation services. In this modern transportation system, a single mode of transportation hardly meets the customer's needs.

Integrated freight hub, the intersection of various modes of transportation, is the core to integrated transport infrastructure. It is possible to join modes of transport effectively, and break the barriers between the modes of transportation by the planning and construction of integrated freight hub in a sound approach, which is conducive to realize the integration of transport, and make full use of all traffic resources, reasonably organize the flow of goods from each direction, reduce transportation costs, cut down the environmental pollution and energy consumption produced by the traffic[1].

Principle and design on the layout of integrated freight hub

This paper assumes that freight transport demand matrix is known. Therefore, according to the planning objectives , integrated freight hub layout model can be divided into prediction of integrated freight hub attributes and classification of integrated freight hub level , specific train of thought is shown in figure 1 below.

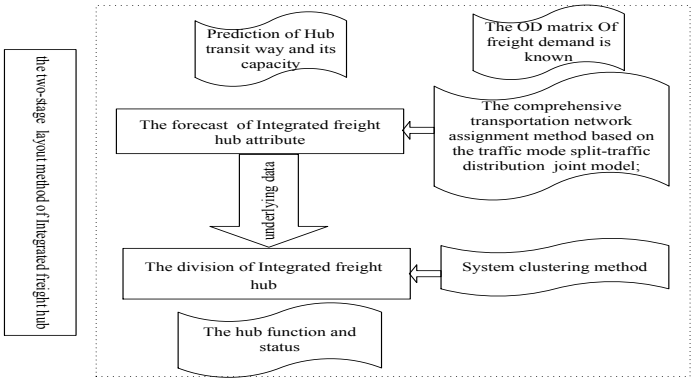

Figure 1 The Two Stage Model of Integrated Freight Hub Layout

Establishment of the layout of integrated freight hub model with two-stage

1)Establishment of the attribute prediction model of the integrated transport hub

Assumptions. As the integrated transportation flow assignment model is serving the layout of the integrated freight hub, the following boundary conditions and the basic assumptions are advanced according to the characteristics and requirements of hub layout.

(1) Goods OD demand matrix is known and time unit is one year.

(2) The generalized transportation costs is known.

(3) There is a positive correlation function relationship between general freight transportation cost and freight traffic volume in practice, namely , the greater freight traffic volume in line the greater the generalized transport cost of the goods per unit. But it is difficult to express the relationship , and there is little inflection of freight general expenses while considering the capacity constraints. Therefore, t The generalized transportation costs is fixed, not affected by freight traffic volume in the model[2].

(4) Taking no account on the effect of generalized cost about differenct kinds of goods, that is to say, transportation cost per unit of Transportation costs, time value, risk cost are only related to transportation mode and path, nothing to do with cargo type.

(5) To eliminate variances of the transport node cost, and to reflect the real status of transportation node in the comprehensive transportation network, all the generalized transport costs are the average cost of the transport node area which is known.

(6) The capacity attributes of the transport line all modes of transport are known; the location of the various transport node of all modes of transport are known,but the capacity attributes are infinite.

(7) Transit of cargo in the node is defined as instant transfer, regardless of the storage time of the goods in transport hub node, for the continuity of transport.

(8) The goods in a transportation node transit once at the most.

The relevant variables and parameters. In order to clear description of this model，the definitions and explanations on the relevant variables and parameters can be noted as follow：

$G=(N,A)$ denotes a multi-mode integrated transportation network of multi-class cargoes. N is nodes set, A is united arcs set, $a \in A$ is one arc in integrated transportation network. The transport arcs of integrated transportation network includes transport arc $\overline{A}$ and dress arc $\overline{A}'$, namely $A=\overline{A}\cup$; for $a \in A$, C_a denotes transport capacity of arc a, $C_{a'}$ denotes the line transport arc, $C_{a''}$ denotes the node transit arc。According to the above hypothesis, the node transit arc capacity is infinite. R is the set of all cargoes' OD flow origin point, $R \in N$; S is the set of all cargoes' OD flow destination point, $S \in N$; RS is the set of all cargoes' OD flow in the whole network, rs is some determined cargo OD flow, $rs \in RS$. K_{rs} (K) is all optional routes set of cargo, k_{rs} (k) is No. k route of cargo p between r and s in OD flow, $k_{rs}^{p} \in K_{rs}^{p}$; f_k^{rs} means No. k route's freight volume between r and s in OD flow; C_k^{rs} is No. k route's generalized transportation costs; $\delta_{a,k}^{rs} \in \{0,1\}$ is 0-1 variable, which equals to 1 if No. k route k_{rs}^{p} includes united arc a, if not the value is 0[3].

Establishment of the optimization model. For preparing for the reasonable division of the hub function and level, the mathematical model for a reasonable forecast of the cargo throughput in each mode of the the integrated transportation hub can be obtained:

$$\min C=\sum_{r\in R}\sum_{s\in S}\sum_{k\in K} f_k^{rs} C_k^{rs} \tag{1}$$

$s.t.$

$$\sum_{r\in R}\sum_{s\in S}\sum_{k\in K} f_k^{rs}\delta_{a',k}^{rs} \le C_{a'} \qquad \forall a' \in A' \tag{2}$$

$$\sum_{k\in K} f_k^{rs} = q_{rs} \qquad \forall r \in R, s \in S \tag{3}$$

$$f_k^{rs} \ge 0 \qquad \forall r \in R, s \in S, k \in K \tag{4}$$

$$\delta_{a',k}^{rs} \in \{0,1\} \qquad \forall r \in R, s \in S, k \in K, a' \in A' \qquad (5)$$

In the above model, formula (1) is the target function of math model, which denotes the total freight volume among all OD points transported with minimum generalized transportation costs; formula (2) to (5) are constraints, in which formula (2) is volume constraint of transport arc , but the node transit arc capacity is unlimited; formula (3) is relationship constraint of cargo OD to route traffic volume; formula (4) is non-negative constraint of cargo OD to route traffic volume; formula (5) is logical relationship constraint between routes and arcs.

2)Integrated freight hub classification model based on Cluster analysis

Clustering analysis, is the progress that different objects with various characteristics can be divided into multiple classes of objects, which also apply to integrated freight hub classification. At present, the k-means clustering method and system clustering method have been widely applied in research. By employing K - average clustering method, it is needed to predetermine points on the number of categories, and the whole process of clustering will not be reflected, moreover, the properties of the sample had better not more than 3[4]. While applying system clustering method, it is likely to cluster gradually, and demonstrates the whole process by clustering hierarchical graph. As the layers of integrated freight hub is uncertain, and the attributes of the streamline is more than 3, this paper employ the system clustering method for clustering.

Solution of the integrated freight hub layout model with two stages

1)Solution of integrated transport hub attribute transportation model based on equilibrium assignment network.

Solution of the model can be divided into the following two steps:

(1) Seek several paths to be candidate. According to the objective function, if arc transport capacity constraints are infinite, every OD flow of goods is the path with minimum generalized transportation cost only, namely the short circuit. But, if taking cost of its minimum for each goods od flow into account, regardless of capacity constraints of transport lines, cargo flow may exceed its capacity, which is not in conformity with the actual.Therefore, in real life, some goods time OD flow would choose the second short circuit, the third short circuit,... , the kth short circuit for transportation, transportation policy makers often make choice in several candidate transport path, even some transport path is not in the scope of the candidate.

(2) Selecting transportation route by genetic algorithm to get the minimum generalized transport cost. The optimal transport path of each goods OD flow can be chosen by genetic algorithm with the goal of system optimization, eventually minimizing the sum of generalized transportation cost of the goods OD flow[5].The genetic algorithm flow is shown in figure 2.

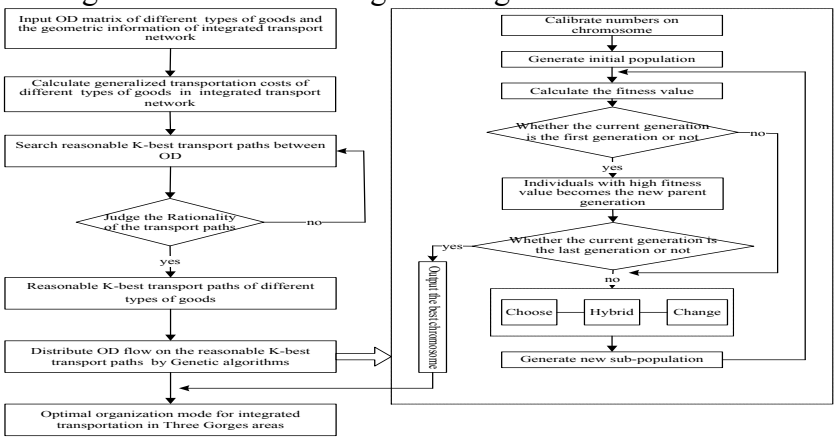

Figure 2 Flow diagram of Genetic algorithms based on reasonable K-best transport paths

2)Solution of Integrated freight hub classification model based on Cluster analysis.

There are four kinds of Clustering algorithm: direct clustering method, the shortest distance clustering method, the farthest distance clustering method, the average clustering method. As it is easy to expand or contract by applying the shortest and longest distance method. And the average

distance method is neither applied to shortest distance or longest distance. Take the middle distance between the two, avoiding the disadvantages of calculation with the shortest and longest distance. This article employs the average distance as a integrated freight hub layout of clustering algorithm.

Numerical example

In a regional transportation network, there are 8 integrated freight hubs.The hub location and layout of transportation physical line is known. The capacity of transportation lines is symmetrical in this examples, shown in the figure 3 below.

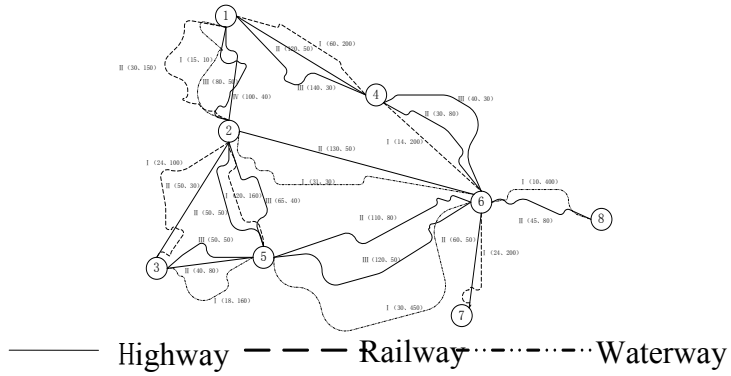

Figure 3 Regional integrated transport network cost

Regional transportation demand OD districts are divided by the location of the integrated transportation hub. OD demand matrix is symmetric matrix without considering internal travel in a district, transportation demand OD matrix are shown in table 1.

Table 1 Regional Transportation Demand OD Matrix (unit: ten thousand tons/year)

O/D	1	2	3	4	5	6	7	8	summation
1	0	25	20	25	20	40	5	30	165
2	35	0	20	15	25	25	15	20	145
3	20	20	0	15	20	30	10	25	140
4	25	15	15	0	15	25	20	20	135
5	20	25	20	15	0	25	15	30	150
6	40	25	30	25	25	0	35	50	230
7	5	15	10	20	15	35	0	15	115
8	30	20	25	20	30	50	15	0	190
Summation	165	145	140	135	150	230	115	190	1270

Based on a reasonable candidate paths, road traffic prediction results as shown in figure 4.

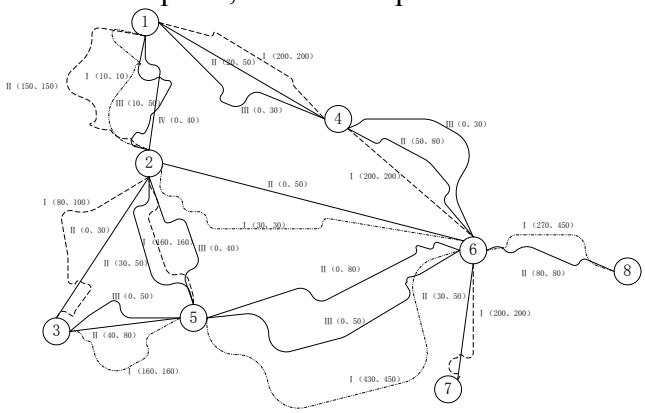

Figure 4 Regional Integrated Transport Network Section Flow Diagram

According to the result of layout flow the integrated transportation hub traffic, integrated transport hub traffic prediction result are shown in table 2.

Table2 Integrated Transport Hub Traffic Prediction Result Table

NO.	Total flow	Transit flow				Local flow			
		Total	H-W	R-W	H-R	Total	H-H	H-W	H-R
1	330	0	0	0	0	330	30	10	290
2	290	0	0	0	0	290	40	20	230
3	280	0	0	0	0	280	40	160	80
4	270	0	0	0	0	270	70	0	200
5	400	100	30	70	0	300	40	170	90
6	690	230	0	230	0	460	130	180	150
7	230	0	0	0	0	230	30	0	200
8	380	0	0	0	0	380	80	300	0

This paper classifies the integrated hub by applying the clustering procedure and the system clustering method, clustering spectrum figure shown in figure 5.

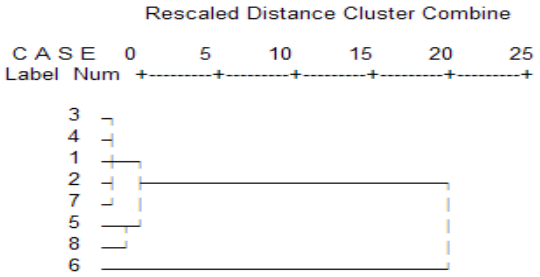

Fgure 5 Spectrum Graph Clustering

According to classification rules of spectrum graph clustering, this paper choose clustering hierarchy for 3, specific clustering results are shown in table 3.

Table 3 Classification of Integrated Freight Hub Level Table

Classification	NO
Fisrt	6
Second	5, 8
Third	1, 2, 3, 4, 7

According to the results of the clustering analysis on the characteristics of different levels integrated freight hubs, the classification of the regional integrated freight hub is as follows:

1) Regional core freight hub.
2) Regional important freight hub.
3) Regional general freight hub.

Conclusion

After analysis of the above result, it is appropriate to draw conclusion as below:

1) The key of transit of freights between the two adjacent nodes (freight hub) is the distance. While the length of line is almost the same, the costs of transit lines identify with the rule that the cost of transportation from high to low is waterway, highway, railway in turn. However ,freights by waterway-railway transit should be transit in freight hub by highway, as the freights can be transported from door to door, which it is hardly to reach for railway. While transport distance is relatively close between two adjacent nodes, the shipper usually choose highway such as the flow between node 3-5, 4 - 6, 6 - 8 of the goods for transportation cost savings. While transport distance is distant between two adjacent nodes, the cost of waterway-railway transit is lower than highway, the shipper will choose waterway-railway transit, and transit in the destination, such as flows between 5 to 6, 6-7.

2) Whether the freight flows between two freights hub need to be transferred, first, is due to if there is a direct route between two nodes, mainly referring to the existence of direct path with lowest cost. If so transfer is unnecessary,and If not, to compare the cost between the direct route between two points and transit lines, such as node 4 to 5, 4 to 8, 5-7, the goods traffic between finally are transferred in hub 6.

3) The status of the freight hub is decided jointly by the quantity of local freights and transfer freights. Local freights flow represents the development of economic and industrial and the advantage of resource regionally. the more advanced the economy, the higher residents' average income, the stronger consumption ability, the demand of product are larger, The more advanced the industry, the higher production capacity, the more raw materials are needed for the product; the oil-rich region of output will create a big demand for transportation. transit freight, can represent integrated freight hub location advantage of transportation, also manifest attraction of freights from different direction, which is also the important influencing factors of its level status.

4) The railway-highway transit hub play a important role in the integrated freight network. Among all hub, most freights are transited between railway and highway in hub6 or hub 5, which join the east-west waterway and north-south railway, is key to the efficiency of the regional integrated freight network.In various modes of transportation, the cost of water transportation in long distance is lower than other one, however , it is not always to transport by water as its high requirement of natural conditions. Compared with other modes, railway is a good choice for its big capacity and low cost. So the railway-highway transit hub play a important role in the integrated freight.

Acknowledgment

In this paper, the research was supprted by “the Fundamental Research Funds for the Central Universities(WUT:2013-Ⅳ-066)”.

References

[1] Eiichi Taniguchi, Michihilio Noritalie, Tadashi Yamada, et. Optimal Size and Location Planning of Public Logistics Terminals[J].Transportation Research Part E,1999, 35(3): 207-222.

[2] Reddy V R,Kasilingam R G. Intermodal transportation considering transfer costs[A]. Proceedings of the 1995 Global Trends Conference of the Academy of Business Administration [C]. Aruba:1995.

[3] Liu Jia, Xia Shaofang, LvYa-nan, and Chen Lichao, “Algorithm for solving K-shortest paths problem in complicated network,” Compute rApplication, Vol 28, No. 4, pp. 951-956, April 2008.

[4] Tiexin Liu. Optimization of Multi-transportation Organization Mode for Complex Freight Flow [D], Wuhan Universtiy of Technology, 2010.

[5] G Zapfel, M Wasner. Planning and optimization of hub-and-spoke transportation networks of cooperative third-party logistics production Economics[J]. International Journal of Production, 2002, 78(2): 207-220.

[6] Gabriela Mayer, Bernd Wanger. Hub Location: an exact solution method for the multiple allocation hub location problem[J].Computers&Operations Research, 2002, 29:715-739.

Advanced Materials Research Vols. 989-994 (2014) pp 1532-1535
© (2014) Trans Tech Publications, Switzerland
doi:10.4028/www.scientific.net/AMR.989-994.1532

The Optimization of Logistics and distribution

Xiong Wei[1, a], Zhang Lingyu [2,b]

[1] Headmaster's Office, Jiangxi Science & Technology Normal University, Nanchang, Jiangxi,China

[2]School of Information Engineering, Nanchang University, Nanchang, Jiangxi, China

[a]572383070@qq.com, [b]1145163178@163.com

Keywords: Logistics; Distribution; Optimization ; Retai

Abstract. Distribution is an important function of enterprise logistics. Through efficient distribution activities, it can reduce the total cost of logistics enterprises and improve logistics efficiency and service levels. Therefore, the rationality of the logistics and distribution system design will directly affect the survival and development of enterprises. In this dissertation uses a retail business distribution network for the study, to study its distribution optimization models and methods, using a variety of algorithms for analysis, to understand its distribution network efficient mode of operation.

Introduction

Business logistics and distribution system, is supported by a wide range of information to achieve information-based logistics axis systematic[1].The former includes the transport, handling, distribution, processing, packaging and other functions. It seeks labor-saving and efficiency. The latter includes the ordering, delivery, and management of the library and other functions, and strives to complete the commodity flow of information activities throughout the process. However, the inherent characteristics of modern distribution systems that it is generally considered by us, in order to achieve the purpose of efficiency and effectiveness of logistics. And it uses low cost and excellent customer service to complete physical activity from the supply of goods to the point of consumption. On the operational side, through organic links and interactions of the operating subsystems and information subsystems to achieve logistics system optimization. Distribution system is a whole that composed by a variety of different elements, each element interrelated and role in the formation of many functional modules and subsystems at all levels, so that the whole system presents a multi-level structure and reflects the inherent system characteristics.

Retail business and distribution activities according to the needs of retail storeBusiness conducts[2] and it before delivery must to make the necessary rationing. The range of distribution is generally limited to a particular city or region[3]. Therefore, the retail business and distribution activities are in the logistics branch or the end of the social system. And is close to the consumer's logistics activities, is a key part of the retail Business management control, is not a simple storage and transport.

The delivery system of this do not stay Shipping includes a total of three parts:

(1) Efficient distribution center. The suppliers of the a retail business according to the order of each branch will be delivered to retailers of goods distribution center[4]. And distribution center is responsible for completing the screening, packaging and sorting of the goods[5]. The distribution centers of a retail business has highly modern mechanical facilities. In addition to the 85% of goods are used mechanical treatment, which greatly reduces the cost of manual handling of goods. Also, due to the huge number of purchases of commodities, it makes full use of automation equipment and fully demonstrates the advantages of scale.

(2) Rapid transport system. In the entire logistics chain, transport links is the most expensive part. In order to reduce transport costs and improve efficiency, a retail enterprises to adopt a method they own the team, and with a global positioning tech management tools for the assistance. And it ensure that the team is always in an accurate, efficient, fast, full load condition. The practice of a retail business can effectively reduce transportation costs[6], mainly in two aspects: On the one hand, it reduce the high costs of uncontrolled vehicle suppliers of intermediate links and transport links in the middle of exploitation; On the other hand, it ensures that a retail business to take place between the

distribution center and various shops transport master mastership, the ability to goods such as cars, shops and other goods and other undesirable phenomena to a minimum, try to make the delivery and distribution center receipt of each store to do a smooth, non-overlapping convergence, the distribution costs to a minimum.

(3) Rapid delivery process. After receipt of the distribution center and aggregated customer orders, we must first determine the type and quantity of goods, and then check the inventory of goods through the system, if the spot, then transferred to the sorting operation. After the suppliers send the goods to the distribution center, after checking procurement plans, it need commodity inspection (including the quantity, quality and acceptance) and other procedures, and then need sent to a different location to store shelves, when a commodity is stored in. Each time, the computer will put their location and number eleven recorded; proposed plan to goods, the computer system will identify needed to the product storage location, and print shops code label and affixes to the product in the future. Distribution center according to each store requires screened the goods, re-packaged, from the distribution area shipped to free zone[7]; whole package of goods on the shelves sent directly to the conveyor belt, scattered goods also sent by personnel after removal from the bench to the conveyor.

A retail business model and methods described in logistics

The retail business multi-path transport Transportation-VRP model. Multi-path transport transportation problem is the reality of very common deployment problems, especially for a large number of clients' entity. For example, a enterprises which has thousands of suppliers. Such core issue is how to allocate the vehicle scheduling. Therefore, VRP (Vehicle Routing Problem) models have emerged, became solve the problem of a multi-transport path very successful model[8]. The problem research objectives are: design appropriate route for a series of retail stores demand points , the vehicle in an orderly manner through these routes, to meet certain constraints (such as the demand for goods, delivery volume, vehicle capacity constraints, mileage restrictions etc.), up to a certain optimization goals (such as mileage shortest minimum cost, time, as little as possible, etc.). It involves the selection and path of a multi-vehicle transport service object identified two aspects.

A typical VRP model can be expressed as follows:

(1) Basic Conditions There are m identical vehicles parked vehicle in a common source, it needs to provide the n goods stores, stores as. $v_1, v_2, \ldots, v_n$

(2) Model target Determine the required number of vehicles is N, and assign these vehicles to a transport path, while including path and scheduling transportation route within the total minimum cost.

(3) Limiting condition: N is not more than m. Each store must be served. Vehicle must be returned upon completion of the task source v_0. Can not exceed the capacity limit of the vehicle; Special issues need to be considered when the window limit; Transportation Regulations.

Saving Algorithm. Saving algorithm (Saving Algorithm) is used to solve the transport vehicle uncertain VRP problem, which is currently used to solve the VRP model best known heuristic algorithms.

The basic principles of saving algorithm.The core idea of saving algorithm is to save two transport path of the transport problems that exist in (0, ..., i, 0) and (0, j, ..., 0) merged into a transport path (0, ..., i, j, ... , 0). In the merge operation above, the total transportation distance of throughout the transportation problem will change, if the change of total transportation distance decreased that claimed savings in transportation distances. Corresponding change value, called savings distance ΔC_{ij}

Like formula (1) shown in:

$$\Delta C_{ij} = c_{io} + c_{oj} - c_{ji} \tag{1}$$

The main steps of the algorithm mileage savings. Known conditions: Stores demand point set $N_R = \{1,2,\ldots, n\}$, Each point demand stores R_i ,The shortest distance between the points c_{ij} .

First, it is the initial formation of a solution. Determine the vehicle delivery point set.

$I_1, I_2, \cdots, I_m$

Allow $I_j = \{j\}$, j =1,2,…,n(First take a single point of delivery)

Second, it is the calculation of savings. Calculate the degree of savings on all points, ΔC_{ij} and the calculated results in ascending order.

The third step is to merge the transport path. Starting from the value of the degree of sequence conservation in ascending order of the top until the ΔC_{ij} queue is empty mileage savings far. Repeat the following steps: Follow-saving mileage queue in descending order, analyze the possibility of the merger between stores i and j (meets the load restrictions, not in the same path, and the combined number of no more than 2), the i, j linking to order. Then can let $I_i' = I_i \cup I_j; I_j = \varnothing$ 。 If not, the queue is removed from the current mileage save savings mileage, Analysis of a path.

Scanning Algorithm

Scanning algorithm (Sweep Algorithm) is also used for VRP which does not limit the number of vehicles, and conservation algorithm is different that it belongs to the sub-heuristic algorithm, while saving algorithm is constructed algorithm.

The basic principle of scanning algorithm. Scanning algorithm is a first packet route algorithm. The so-called grouping, namely a set of points assigned to each vehicle. A simple grouping method is dividing the coordinate plane into a plurality of fan-shaped area which of is the distribution center will be the origin, and initially will be distributed to area points of each sector of a car, and then expand the route. If during the first - the grouping line route structure, there is still unallocated point, then run the "group - Route program. Repeat until all the points are allocated.

The main steps of scanning algorithm. (1) Starting 0:00 in the polar coordinate system as the origin, the connection of a connected graph is defined and any one of the stores and the origin point zero angles to establish polar coordinate system. Then the locations of all the stores are located, polar coordinate transformation.

(2)Grouping From the perspective of the smallest stores to start building a group, counterclockwise, the stores added to the group one by one, until the total demand exceeds the limit stores load. Then continue to build a new group, continues counterclockwise, and then join the suppliers to the group.

(3) Repeat (2) the process until all the stores have been classified.

(4) Path Optimization Single transport path within each group carry out a path optimization.

The improved method recently inserted

Recent insertion method is an algorithm for solving TSP problem. Recently completed insertion method consists of four steps:

(1) Find the c_{0i} minimum node v_i, and forming a sub-tour, $T = \{v_0, v_k, v_0\}$ 。

(2) In the rest of the nodes to find the path of an ion transport nearest node A node v_k

(3) Find an arc (i, j) in the sub-transport path, such that $c_{ik} + c_{kj} - c_{ij}$ Minimum, then the node v_i into the Node v_i, and between v_j, with two new arc (i, k), (k, j) instead of the original arc (i, j), and the node v_k is added to the sub-transport path.

(4) Repeat steps (2), (3), until all nodes are added to the sub-transport path.

Thus, the sub-transport path evolved to a TSP solution. Insertion method to solve the transportation problem is a single transport path, so this approach on the basis of improvements and fixes, so that it can solve the multi-path transport transportation VRP problem .The improvement is as follows:

(1) Find the c_{0i} minimum node v_i, and forming a sub-tour, $T = \{v_0, v_k, v_0\}$ 。

(2) In the rest of the nodes in the path to find a particular ion transport nodes nearest node v_k. If the total freight transport path at this time does not exceed the load limit car, then proceed to step (3). Otherwise, go to (1) find a new one transport path.

(3) Find an arc (i, j) in the sub-transport path, such that $c_{ik} + c_{kj} - c_{ij}$ Minimum, then the node v_i into the Node v_i, and between v_j, with two new arc (i, k), (k, j) instead of the original arc (i, j), and the node v_k is added to the sub-transport path. If at this time the total distance of the transport path of travel of the vehicle does not exceed the limit, then proceed to step (4). Otherwise, go to step (1), to find a new one transport path.

(4) Repeat steps (2), (3), until all nodes are added to the sub-transport path.

Summary

The existence of large-scale retail enterprises benefits inherent drive to expand the business to market and implement regional development strategy. Therefore, the complex multi-stage distribution network design and heuristic algorithms for solving large-scale problems of such a study will be the direction. For large-scale retail enterprises actual distribution system is extremely complex, vague and random uncertainties exist two types of the actual system.Therefore, the study of large-scale retail distribution system optimization under uncertainty decision to establish the appropriate mix of fuzzy random chance-constrained programming model and design appropriate and effective algorithm, will be the direction for further research.

References

[1] Jenni Eckhardt, Jarkko Rantala.The Role of Intelligent Logistics Centres in a Multimodal and Cost-effective Transport System. Procedia - Social and Behavioral Sciences, vol.48, p. 612-621, 2012

[2] Ashis Mishra. Business model for Indian retail sector: The Café Coffee Day case: In conversation with V.G. Siddhartha, Chairman, Coffee Day. IIMB Management Review, vol.25, p. 160-170, 2013

[3] Steven R. Henderson. City centre retail development in England: Land assembly and business experiences of area change processes Geoforum, vol.42, no.5, p. 592-602, 2011

[4] Milan Andrejić, Nebojša Bojović, Milorad Kilibarda.Benchmarking distribution centres using Principal Component Analysis and Data Envelopment Analysis: A case study of Serbia. Expert Systems with Applications, vol.40, no.10, p. 3926-3933, 2013

[5] Berkenbrock Sevegnani, Oswaldo Mário Serra Truzzi. Comparison of disposable and returnable packaging: a case study of reverse logistics in Brazil. Journal of Cleaner Production,vol.47, no.2, p. 377-387, 2013

[6] Rongbing Huang, Mozart B.C. Menezes, Seokjin Kim.The impact of cost uncertainty on the location of a distribution center. European Journal of Operational Research,vol.218, no.2, p.401-407, 2012

[7] Yingfeng Ji, Hualong Yang,el at. Location Optimization Model of Regional Express Distribution Center. Procedia - Social and Behavioral Sciences,vol.96, no.6, p.1008-1013, 2013

[8] Cristina Bazgan, Refael Hassin, Jérôme Monnot.Approximation algorithms for some vehicle routing problems. Discrete Applied Mathematics, vol.16, no.1, p.27-42 , 2005

Advanced Materials Research Vols. 989-994 (2014) pp 1536-1540
© (2014) Trans Tech Publications, Switzerland
doi:10.4028/www.scientific.net/AMR.989-994.1536

Research on Rough Set Theory-based Customer Division

Gui-juan Song[a], Xin Cao[b] and Xin-yue Wang[c]

Department of Computer Science and Technology,Dalian Neusoft University of Information

Dalian,116023,P.R.China

[a]songguijuan@neusoft.edu.cn,[b]caoxin@neusoft.edu.cn,[c]wangxinyue12@nou.com.cn

Keywords: Rough set, Attribute reduction, Decision table, Discernibility matrix.

Abstract. The main idea of rough set theory is to extract decision rules by attribute reduction and value reduction in the premises of keeping the ability of classification. This paper presents the design of model for customer division based on rough set, and uses algorithms for attribute reduction and rule extraction in rough set to analyze the customer of supermarket. This paper also introduces how to achieve the minimum result of attribute reduction and decision-making via decision-making report, winkling redundant attribute and over-rule of decision.

Introduction

RFM [1] is an analytic technique for customer division in marketing management.It chooses important factor from numerous customer information to analyse and simplifies models and reduces complexity. In this paper, a customer division model based on rough set was designed.And using the method of attributes reduction and rules extraction method of rough set, combined with case analysis and the reduction of the customer features, classification rules were obtained to allow businesses to understand customer value and provide the basis for decision support.Rough set is a commonly used data mining tools proposed by Pawlak [2] in 1982, rough sets are used to study intelligent systems that are characterized by insufficient and incomplete information. Rough set theory has been successfully applied to the fields of artificial intelligence including machine learning, pattern recognition, decision analysis, process control, knowledge discovery in databases, and expert systems [3]. Here are some basic concepts about rough set.

Preliminaries

Information System and Decision Table. Let $I=(U; A)$ be an information system, where U is a non-empty set of finite objects (the universe of discourse); A is a non-empty finite set of attributes such that $a: U \rightarrow Va$, $\forall a \in A$; Va being the value set of attribute a. In a decision system, $A=\{C \cup D\}$ where C is the set of conditional attributes and D is the set of decision attributes. With any $P \subseteq A$ there is an associated equivalence relation $IND(P)$ [1]:

$$IND(P)=\{(X,Y)\in U^2 \mid \forall a\in P, a(x)=a(y)\}. \quad (1)$$

The partition of U, generated by $IND(P)$ is denoted U/P and can be calculated as follows:

$$U/P=\otimes\{a\in P: U/IND(\{a\})\}, \quad (2)$$

where

$$A\otimes B=\{X\cap Y: \forall X\in A, \forall Y\in B, X\cap Y\neq\varnothing\}. \quad (3)$$

If $(x, y)\in IND(P)$, then x and y are indiscernible by attributes from P. The equivalence classes of the P-indiscernibility relation are denoted $[x]_P$. Let $X\subseteq U$, the *P-lower* approximation [2] of a set can now be defined as

$$\underline{PX}=\{x \mid [x]_P\subseteq X\}. \quad (4)$$

Let P and Q be equivalence relations over U, then the positive region [3] can be defined as

$$POS_P(Q) = \bigcup_{X \in U/Q} \underline{P}X \ . \tag{5}$$

Let $C \subseteq A$, $D \subseteq A$, $B \subset C$ and $C \cap D = \Phi$; if $POS_B(D) = POS_C(D)$, B is a reduction of C. The set intersection of all reductions of C is called the core of C denoted as $Core_D(C)$.

Given information system, if $A=C \cup D$, $C \cap D = \Phi$, C is the conditional attributes set and D is decision attributes set, the information system is called decision table [4].

Discernibility Matrix. Let $DT=(U, C \cup D, A, f)$ be a decision table. By $M(DT)$ we denote an $n*n$ matrix(c_{ij}), called the discernibility matrix of DT, such that:

$$c_{ij} = \begin{cases} \{\alpha \mid \alpha \in C \wedge (f_\alpha(x_i) \neq f_\alpha(x_j))\}, & f_D(x_i) \neq f_D(x_j), \\ \phi, & f_D(x_i) \neq f_D(x_j) \wedge f_C(x_i) = f_C(x_j), \\ -, & f_D(x_i) = f_D(x_j). \end{cases} \tag{6}$$

Since $M(DT)$ are symmetric and $c_{ii} = \Phi$, for $i=1,2,\ldots,n$, we represent $M(DT)$ only by elements in the lower triangle of $M(DT)$, respectively, i. e., The c_{ij}'s with $1 \leq j < i \leq n$.

Using discernibility matrix, Skowron and Rauszer [4] have proven several properties and constructed efficient algorithms related to information systems and decision tables, e.g. The set of all indispensable attributes in C is called the core of DT, denoted by $CORE_c(D)$. $CORE_c(D)$ can be characterized by $M(DT)$ in the following way:

$$CORE_C(D) = \{a \mid (a \in C) \wedge (\exists c_{ij}, ((c_{ij} \in M_{n \times n}) \wedge (c_{ij} = \{a\})))\} \ . \tag{7}$$

Reduction of the decision table

Reduction of the decision table is to delete redundant attributes in the system keeping the classification capability of the original systems or decision tables. The reducted decision table has the same function as before. Therefore reduction of the decision table is very important in practical applications.

Algorithm1 [4] is based on the discernibility matrix of the decision table.

Algorithm 1:

Input: Decision table $DT=(U, C \cup D, A, f)$.

Output: A relative reduction of decision attributes D relative to conditional attribute C.

Step 1 Compute the discernibility matrix $M_{n \times n}(DT)$ of decision table DT;

Step 2 Compute the core $CORE_C(D)$ of C relative to D;

Step 3 $\forall c_{ij}$, $i,j=1,2,\ldots,n$, if $c_{ij} \cap CORE_C(D) \neq \varnothing$, then $c_{ij} = \varnothing$;

Step 4 For all the elements c_{ij} $(c_{ij} = \varnothing)$ whose value is non-empty set in the current discernibility matrix, establish the corresponding disjunction L_{ij}, and $L_{ij} = \bigvee_{a_{l_k} \in c_{ij}} a_{l_k}$;

Step5 Conjugate all the disjunctions, then get a conjunction normal form L, $L = \bigwedge_{c_{ij} \neq \phi} L_{ij}$;

Step 6 Convert the Conjunctive L to disjunctive, then get $L = \bigvee_k L_k$;

Step 7 Output $L' = \bigvee_k (L_k \wedge L_{CORE_D(C)})$ in which $L_{CORE_D(C)} = \bigwedge_{a_{l_k} \in CORE_D(C)} a_{l_k}$, each conjunctive term $L_k \wedge L_{CORE_D(C)}$ in the disjunctive is correspond to a relative reduct of difference variable of the decision table, attributes in each $L_k \wedge L_{CORE_D(C)}$ form the relative reduction of the decision table.

After attribute reduction each record in the decision table could be used as a rule, meanwhile there are many redundant information. In other words, after reduction, not each attribute value in each record has some effect on decision rules in the information system. Therefore we must continue to reduct the results of attribute reduction. The process of excluding redundant information from the reducted

decision table is attribute value reduction. The value reduction of a given system *T* may be based on core value.The algorithm is shown as following:

Algorithm 2 [5]:

Input: An information system T.

Ouput: value reduction of T.

Step 1: Check the conditional attribute in the information system column by column. If there are conflict records after the column is deleted,then retain the original attribute value of the conflict records;else if there are duplicate records,then change its attribute value into "*";for other records, change its attribute value into "?".

Step 2: Delete the records that may produce duplicate and check each record labeled "?".If the decision could be made only by the unlabeled attribute value, then change "?" into "*", else change "?" into the original attribute value;

Step 3: Delete the entire conditional attribute labeled "*" and the records that may produce duplicate.

Step 4:If only one conditional attribute value in two records is different and one attribute of them is labeled "*",then for the record, if decision could be made by the unlabeled attribute value then delete another record,else delete the record.

Customer division based on rough set

Rough set theory provides techniques to reduce knowledge in databases. As a result of the reduction of knowledge, a set of concise and meaningful rules is produced.Therefore it provides theoretical support for customer classification prediction model based on rough set.RFM analysis refers to gather customer purchase behavior by collecting the "last purchase (Recency)", "purchase frequency (Frequency)" and "purchase amount (Monetary)" to guide marketing behavior, and then mining factor in buying behavior differences and predicting purchase preferences. In the data selection, RFM analysis method provides a direction guide for the feature selection model of customer.

In this paper, a marketing data mart is constructed and isolates the business data and analysis data based on the customer and transaction of a large supermarket. Based on the data mart, using data mining technology, the description model and predictive model of customer classification were constructed. Figure 1 is the system architecture of customer classification model; The system consists of three parts. The first part is the supermarket customer and transaction data, it provides original data for the model; The second part will process the data of the first layer, load the data to data mart focusing on customer data, then on the basis of data mart, with technology as the core of data mining based on RS, store the analysis of the results in the classification model library, The third part predicts classification for new customers through the model library. The following data mining steps are based on RS: (1) Data pretreatment (2) Attribute selection with reduction algorithm (3) Generating rules.

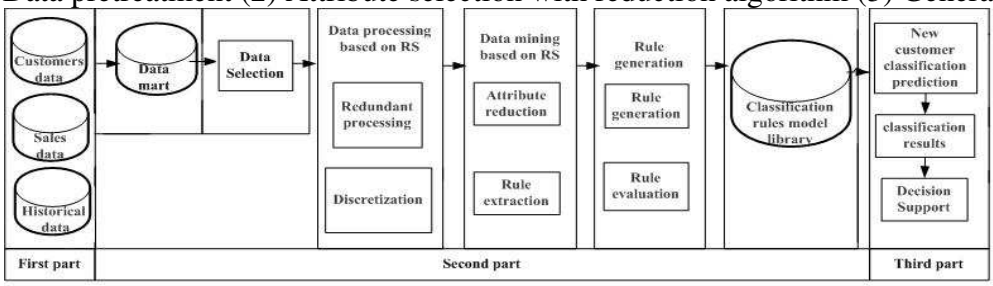

Fig. 1. The structure system of customer classification model based on Rough Set

According to the customer data in the database and sales data, one of 15 customer historical data is selected as test data sets through data cleaning. Extracting from the sale records of 3 months sale data from the preliminary statistics and the transaction records, the purchase time, purchase frequency and purchase amount of the 15 customers within three months is analyzed. Through the preliminary data

filtration of the attribute in the customer data, some customer attributes which are obviously irrelevant to division such as name, home address, telephone etc.are removed. The data will be expressed as the form of decision table in which the clustering of 8 customer attributes are conditional attributes, clustering analysis by customer categories are decision attributes. After discretization of decision table with NS discretization method, the results of the customer attribute discretization are obtained, as shown in Table 1.

Table 1. Results of the customer attribute discretization

Symbol	Meaning	Discrete value			
		0	1	2	3
A	Gender	Female	Male		
B	Marriage	Unmarried	married		
C	Area	Shahekou District	Xigang District	Ganjingzi District	ZhongshanDistrict
D	Annual income	Low	Middle	High	
E	Has Car or not	No	Yes		
F	Days from the last purchase to now	30-50	15-30	0-15	
G	Purchase frequency (times per month)	0-1	1-3	More than 3	
H	Purchase amount (yuan per time)	Less than 150	150-300	More than 300	
I	Decision attributes	Ordinary customers	Gold customers	Platinum customers	

After the sale records of Customer are converted, the decision table is shown in Table 2.

Table 2. Decision table after conversion

No	A	B	C	D	E	F	G	H	I
1	0	0	2	1	0	2	0	1	1
2	0	0	1	2	0	2	1	2	2
3	0	0	2	1	0	0	0	1	0
4	0	1	0	0	0	1	0	1	1
5	1	1	0	0	0	0	0	0	0
6	0	1	0	1	0	1	1	0	0
7	1	0	0	1	0	2	2	2	2
8	1	0	3	1	0	2	2	1	1
9	0	1	0	0	0	1	1	1	0
10	1	0	1	2	0	2	2	2	2
11	1	0	0	1	1	2	1	2	1
12	0	1	0	1	1	1	1	1	1
13	0	1	0	1	0	0	0	0	0
14	0	0	2	1	0	0	0	1	0
15	0	1	0	0	0	1	0	2	2

After being reduced with algorithm 1,the results of the reduction are $\{D,F,G,H\},\{E,F,G,H\}$. The results show the importance of three attributes that are days from the last purchase to now, purchase frequency and purchase amount.It coincides with the theory of marketing RFM analysis method. Continue to deduct the results $\{D,F,G,H\}$ for attribute value reduction with algorithm 2, the reduction rules is shown in Table 3.

Table 3. Rules extracted from {*D*,*F*,*G*,*H*}

Rule no	Record no	D	F	G	H	I	Rule no	Record no	D	F	G	H	I
1	1	*	2	0	1	1	19	7,10	*	2	2	2	2
2	1,8	1	2	*	1	1	20	7	1	*	2	2	2
3	1	1	2	0	*	1	21	8	*	2	2	1	1
4	2	2	*	1	2	2	22	8	1	*	2	1	1
5	2,10	2	2	*	2	2	23	9	*	1	1	1	0
6	2	2	2	1	*	2	24	9	0	*	1	1	0
7	3,14	*	0	0	1	0	25	9	0	1	1	*	0
8	3,14	1	0	*	1	0	26	10	2	*	2	2	2
9	3,13,14	1	0	0	*	0	27	10	2	2	2	*	2
10	4	*	1	0	1	1	28	11	*	2	1	2	1
11	4	0	*	0	1	1	29	11	1	2	1	*	1
12	5,13	*	0	0	0	0	30	12	1	*	1	1	1
13	5	0	*	0	0	0	31	12	1	1	*	1	1
14	5	0	0	*	0	0	32	13	1	*	0	0	0
15	5	0	0	0	*	0	33	13	1	0	*	0	0
16	6	*	1	1	0	0	34	15	*	1	0	2	2
17	6	1	*	1	0	0	35	15	0	*	0	2	2
18	6	1	1	*	0	0	36	15	0	1	*	2	2

The records in the table reflect the original information of decision rules in the table, rule 1 can be summarized as:

Rule 1: if（F，2）and（G，0）and（H，1）then I=1.

For the customer, if his days from the last purchase to now is 15, purchase frequency is 0-1 times per month, the amount of each purchase is 0-150 yuan, he is the ordinary customer.

This example can also select the condition attribute {E, F, G, H} as the reduction result of condition attribute, the results obtained may be different with {D, F, G, H}.Therefore, the different classification criteria leads to different extraction rule set. The classification rules could be stored into the knowledge database to provide a basis for the new object classification prediction and decision analysis.

Summary

In this paper, a customer classification model was designed based on rough set theory and supermarket customers were analyzed with the algorithm of rough sets reduction and decision rule. By removing redundant attributes and eliminating excessive rules, rules that affect customer classification from the customer information were obtained for business decision-making. Examples show that it has good practicability.

References

[1]Wang Hong: *Analysis of customer value based on rough set data mining technology*, Economic Science Press, 2006.

[2] CHRISTIAN GRONROOS: value-driven Relational Marketing;from Products to Resourcs and competence, Journal of Marketing Management,1997(13) .

[3] Z. Pawlak: Rough sets, International Journal of Computer and Information Sciences 11 (1982) 341–356.

[4]Miao Duoqian:*Theory,algorithm and application in rough set*, Tsinghua University press.2008,4. (in Chinese).

[5]Zhang Chunyan:Research on Algorithm for attribute value reduction based on Rough Set, Computer and modernization.2008,7:79-81. (in Chinese)

Advanced Materials Research Vols. 989-994 (2014) pp 1541-1546
© (2014) Trans Tech Publications, Switzerland
doi:10.4028/www.scientific.net/AMR.989-994.1541

A K-nearest-neighbour Based Classifier for Securities Text Categorization

TIEBIN LIU

University of Chinese Academy of Sciencesm, China Futures Association

liutiebin@cfachina.org

Keywords: Text categorization; KNN; VSM; event driven; information securities investment.

Abstract. Event-driven investments have gained great importance and popularity. Due to the importance of the timely and effective messages for successful investment, the automated categorization of documents into predefined labels has received an ever-increased attention in the recent years. This paper implements a new text document classifier by integrating the K-nearest neighbour (KNN) classification approach with the VSM vector space model. By screening the feature items and weighted key items, the proposed classifier turns the financial information text into N-dimensional vector and identified the positive and negative information, furthermore achieve to the classification optimized. In addition, the classification model constructed by the proposed algorithm can be updated incrementally, and it has great scalability in event-driven securities investment for investors.

Introduction

In examining China recent securities research, the event driven investments have attracted a major attention of global securities investment researchers in various fields. By using the logical and quantitative analysis, the event driven investment has gained great importance and popularity. In particular, there are three mainstream investment patterns: developed investment theme model and the traditional value investment, trends investment.

In recent years, text categorization techniques have drawn great attention and been widely used in securities research. There are a wide range of supervised learning algorithms has been applied to the documents classification, such as K-Nearest Neighbor (KNN)[1], Centroid-Based Classifier (CB)[2], Naive Bayes[3], Decision Trees[4], and Support Vector Machines (SVM)[5]. Among all these algorithms, KNN is a simple but effective method for text categorization. KNN does not build the classification model since it is a lazy learning method. As a result, it is not suited in many applications well.

With the development of the Internet, information explosion in this electronically networked world, it is more important for investor to organize securities data effectively and efficiently. In this paper, we use the vertical field of semantic analysis method to classify the securities information into subjective and objective information for the event-driven investment strategy.

The rest of this paper is organized as follows: Section 2 describes the well-known classifiers. Section 3 presents the analysis of the KNN fuzzy classifier. Related work is discussed in Section4. The paper is concluded in Section 5.

Text vector representation model

2.1 Vector Space Model

Computer can only handle binary data, the unstructured or semi-structured Chinese text are not being used directly for training or classification. The Chinese text must be represented as some specify model for the computer use. By using the vector space model[6], we constructed text vector before classification.

2.2 Select feature items

As a strong computability and maneuverability, vector space model is based on the bag of word method. Considering the series of feature items is independent, vector space model do not consider

the sequence feature items that appear in the text. According to the characteristics of Chinese words, the words library should be pretreatment to remove tabs, labels, and other no meaning words before segmentation.

2.3 Screen feature items

After the text classification systems, text feature items are still at high dimension. The text collections contain thousands of feature words, but each text contains characteristics rarely. Vector space model, in a high-dimensional sparse matrix, will affect the time complexity and space complexity for the classification algorithm. Experiments show that when the characteristic dimension of the vector space reaches a certain value can achieve very high classification performance, with the increase of feature dimensions, but will drop the classification performance. Therefore, the feature items must be effective screening.

By using the χ^2 statistical methods, we can measure the degree of correlation between the terms and the document class c. Assume that between t and c there is a one degree of χ^2 distribution. N denotes document in training corpus, c denotes a special category, t is a special term. A denotes the numbers of document belongs to c and includes t, B denotes the numbers of document do not belong to c but includes t, C denotes the numbers of document belongs to c but without t, D denotes the numbers of document do not belong to *c* and without *t*, the χ^2 value can be calculated as follows:

$$\chi^2(t,c)=\frac{N\times(AD-CD)}{(A+C)(B+D)(A+B)(C+D)} \tag{1}$$

For multi-class problem, χ^2 values were calculated for each category, and *t* can be calculated for the entire training set as the following:

$$\chi^2_{\max}(t)=\max_{i=1}^{m}\chi^2(t,c_i) \tag{2}$$

$$\chi^2_{\arg}(t)=\sum_{j=1}^{k}P(c_j)\chi^2(t,c_j) \tag{3}$$

where *m* is the number of categories. Sort the original feature space by CHI value, and retain the first *N* terms as the feature documentation. Where, *N* can be obtained by the experimental results.

2.4 Keywords Library

Most majority media will appear some positive subjective terms, such as, optimistic, buy, optimistic, support, up. The negative subjective terms often appears: not optimistic, sell, resistance, pessimistic, down. After collection, we obtained a library of financial subjective Keywords, where positive subjective category lexicon: PkeyWords, negative subjective category lexicon: N key Words. By weight the feature KeyWords, we can effectively improve the classification accuracy.

2.5 N-dimensional text vector

In the vector space model for an item with n text characteristic $d(t_1,t_2,\cdots,t_n)$, the text can be represented as $d=((t_1,W_1),(t_2,W_2),\cdots,(t_n,W_n))$, and $d=(W_1,W_2,\cdots,W_n)$ for short. Where t_i denotes the $i(i=1,\ldots,n)$ characteristic item, W_i is the weights value for the $i(i=1,\ldots,n)$ feature in the text. By the Boolean weight calculation method, set feature items value to 1 for all TF> 0 (Term Frequency), and the value of all the positive words right word library is set to 2, the word weights negative keyword library is set to -2.

$$W_i=\begin{cases}-2 & (If>0\,and\quad t_i\in NKeyWords)\\ 2 & (If>0\,and\quad t_i\in PKeyWords)\\ 1 & (If>0\,and\quad t_i\notin KeyWords)\\ 0 & (If=0)\end{cases} \tag{4}$$

We can use Fig. 1 to represent the process of a Chinese text into text vector, and Fig. 2 to illustrate the vector space model under the text representation.

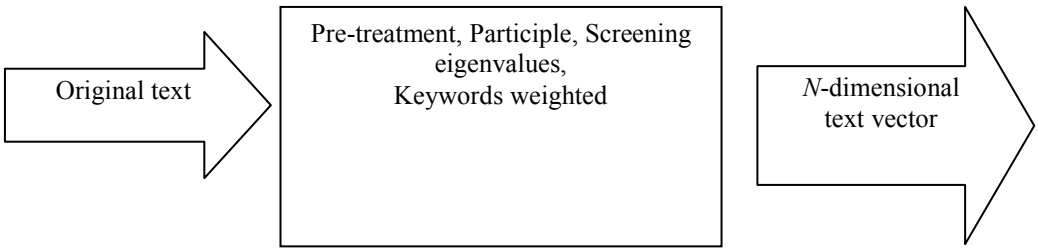

Fig. 1 Text converted to N-dimensional vector

	t_1	t_2	t_3	…	…	t_n
T_1	W_{11}	W_{12}	W_{13}	…	…	W_{1n}
T_2	W_{21}	W_{22}	W_{23}	…	…	W_{2n}
.	…	…	…	…	…	…
.	…	…	…	…	…	…
.	…	…	…	…	…	…
.	…	…	…	…	…	…
T_n	W_{n1}	W_{n2}	W_{n3}	…	…	W_{nn}

Fig. 2 Text representation for VSM

KNN fuzzy classifier

It is important to construct a classification function or classifier for the automatic text classification. Training methods and classification algorithm is the core of the classification. There are a wide range of supervised learning algorithms has been applied to the documents classification, such as support vector machine algorithm, neural network method, the average maximum entropy method, a recent K neighbor method and the Bayesian method, we use KNN classification algorithm for text classification learning[7,8].

3.1 KNN classifier

To classify an unknown document, the KNN classifier ranks the document's neighbors among the training documents, and use the class labels of k most similarity neighbors to predict the class of the input document. As a statistical method, the KNN classification approach has been widely used in various types of classification tasks, especially in pattern recognition. Throughout this paper, we use Euclidean distance for calculation.

3.2 KNN algorithm

The process of the KNN classifier is as follows: given a test document x , find K nearest neighbors of x among training documents, and score category candidates for x based on the categories of K neighbors. To measure the similarity efficiently, we make use of the Euclidean distance as follows [9]:

1) By using feature items, describe a collection of re-training text vector
2) According to the characteristics of the new text word segmentation, identify a new text vector representation.
3) By using the following formula, Select text for the most similar to the training text K

$$Sim\left(d_i, d_j\right) = \frac{\sum_{k=1}^{M} W_{ik} \times W_{jk}}{\sqrt{\left(\sum_{k=1}^{M} W_{ik}^2\right)\left(\sum_{k=1}^{M} W_{jk}^2\right)}} \quad (5)$$

For a given initial K, we could adjust the K value by the results of experimental tests.

In the new text K neighbors, calculate the weight as follows:

$$p\left(\vec{x}, c_j\right) = \sum_{\partial, eKNN} Sim\left(\vec{x}, \vec{d_i}\right) y\left(\vec{d_i}, c_j\right) \quad (6)$$

Where x is the new text feature vector, $Sim\left(\vec{x}, \vec{d_1}\right)$ is the same step, and $y\left(\vec{d_i}, c_j\right)$ is a function of class attributes, i.e. if $\vec{d_i}$ belong to the class c_j , then the function value is 1, otherwise 0.

Assign the text to the largest category.

Test training process shown in Fig. 3:

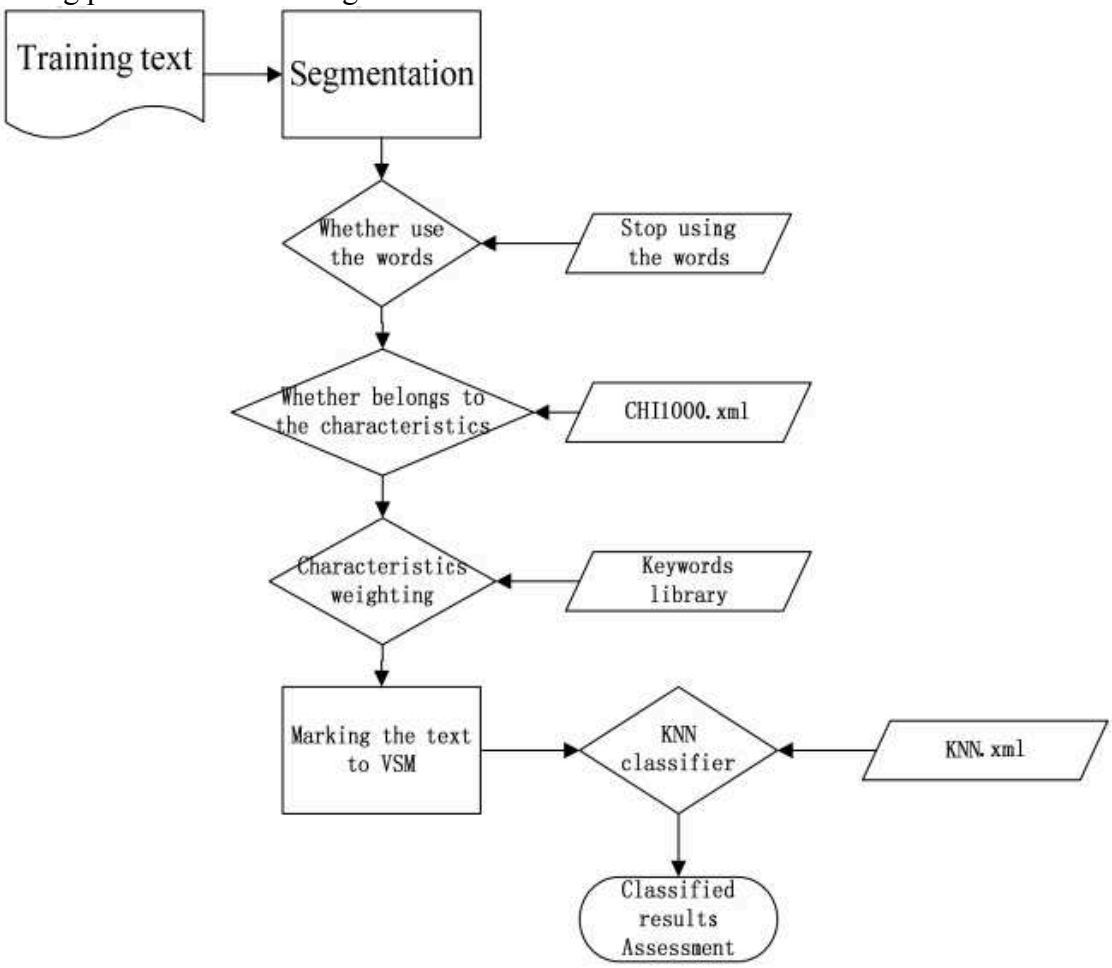

Test Results

4.1 Experiment design

Purpose: Verify suitable dimension for the corpus.

Experimental environment: The experimental data consisted of financial news from the financial website (Hexun, Eastern Wealth), category information 1000, the average of each 800 words, the time span of three months. Feature dimensions were taken 50, 100, 200, 500, 1000, 2000, 3000 respectively. Throughout our experiments, algorithms are coded in JAVA and running on a Pentium-4 machine with single 2.0 GHz CPU.

Results: By using the different feature dimension values, calculate the accuracy, recall and F1 value. Classification results in the keyword feature items weighted KNN classifier as Table 1 and Fig. 4.

Table 1 Different feature dimension classification results

Feature dimensions	Accuracy	recall	F1 value
50	54.77	51	52.82
100	61.89	58.71	60.26
200	68.21	65.1	66.62
500	75.5	72.39	73.91
1000	86.29	83.89	85.07
2000	70.66	67.32	68.95
3000	65.57	61.19	63.3

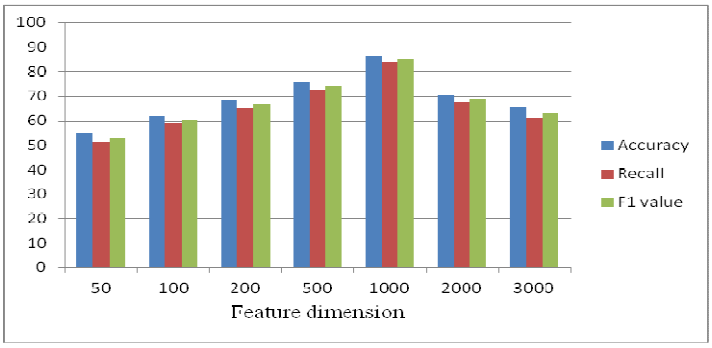

Fig. 4 Different feature dimension classification results

As can be seen from the table 1 and figure 4 above, feature selection function for the dimension of selected feature items have a significant effect on the classification results. When the parameters characteristic dimension choose their values in the interval $[50,100]$, each evaluation index is increased. When the parameters characteristic dimension choose their values in the interval $[1000,3000]$, the classification of the effect is gradually decreased. Furthermore, the highest value is 1000. Therefore, we obtained: the feature dimension is not as high as possible, but if the feature dimension is too small, then it is likely to ignore some contribution to the feature items classification. Therefore, each set has an optimal training text characteristics dimension through experiments. In this paper, we use the 1000 feature dimension.

4.2 Experiment II

Purpose: Find the weighted keyword feature items of financial information on the impact of class text classification.

Experimental environment: The experimental data consisted of financial news from the financial website (Hexun, Eastern wealth), category information 1000, the average of each 800 words, the time span of three months. By the Securities analyst experience, we classified the samples to 3 categories: positive subjective category, the negative category and objective categories. Where positive type text is 405, negative type text is 288, objective type text is 307, and feature items dimension is 1000. Throughout our experiments, algorithms are coded in JAVA and running on a Pentium-4 machine with single 2.0 GHz CPU.

Results: By analysis keyword feature items with or without weighted KNN classifier, the accuracy rate, recall and F1 value are calculated for the KNN classifiers. Results shown in Table 2 and Fig. 5

As can be seen from the table 2 and fig. 5 above, the results of weighted keyword feature items on the classification has a significant impact, but the accuracy of without weighted keyword classification is only about 60%, which does not satisfy the requirements of the financial event analysis. After a weighted optimization, accuracy for weighted keyword feature items has greatly improved to more than 85%, which basically satisfy the classification for positive and negative effects on the financial events analysis.

Table 2 Keyword feature items with and without weighted KNN

Classifier	Accuracy	Recall	F1 value
Feature items without weighted KNN	62.56	60.83	61.08
Feature items weighted KNN	86.29	85.87	86.08
Artificial classifier	100	100	100

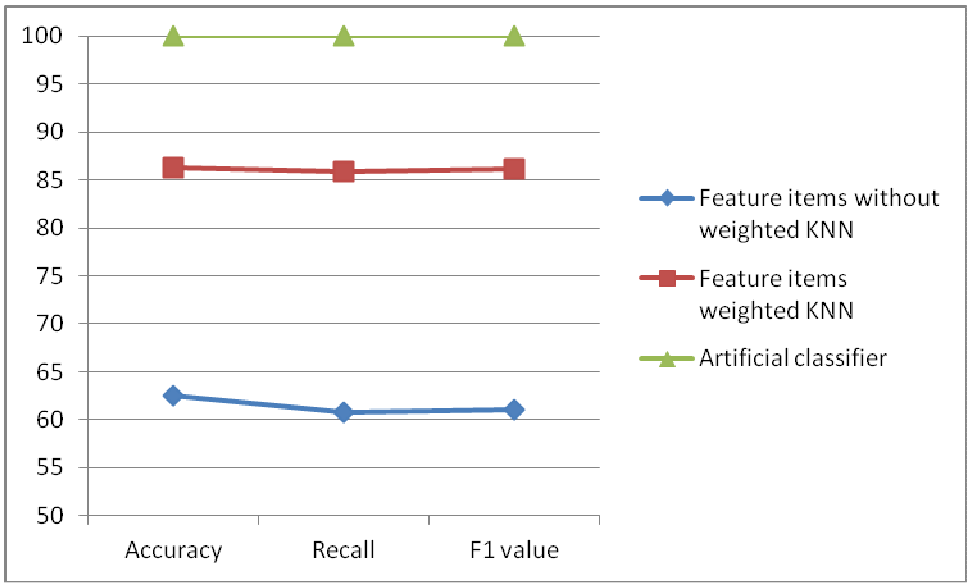

Fig. 5 Keyword feature items with or without weighted KNN

Conclusions

In this paper, we propose a generalized cluster centroid based classifier for text categorization by utilizing a constrained clustering algorithm to integrate KNN and VSM. Unlike the conventional KNN classification approach, the VSM-KNN approach is reported to have low impact on the implementation of parameter. The classification accuracy of the VSM-KNN approach is relatively consistent with the implementation of different values of parameter, as compared to the conventional KNN approach, which its classification accuracy is severely degraded if inappropriate values of parameter are implemented to the classifier. The financial information system can classify the positive or negative news with accuracy of 85%, which improve the accuracy rate of 25% than before optimization model. We can use the method we proposed to provide timely event-driven investments reference for the stock market investors.

References

[1] Sebastiani, Fabrizio. Machine learning in automated text categor-ization. ACM Computing Surveys, 2002, 34(1): 1-47.
[2] Han, E., & Karypis, G.. Centroid-based document classification analysis and experimental result PKDD 2000.
[3] Kjersti Aas, Line Eikvil. Text ctegorisation: A survey. http://citeseer.ist. psu.edu/aas99text.html.
[4] Larkey, L. S., & Croft, W. B.. Combining classifiers in text categorization SIGIR, 1996: 289-297.
[5] Kai M.H., Wang B., Yong J. H., Paul J. C., Relaxed lightweight assembly retrieval using vector space model, Computer-Aided Design, 2013, 45: 739-750.
[6] Chen Y. L., Chiu Y. T., An IPC-based vector space model for patent retrieval, Information Processing and Management, 2011, 47: 309-322.
[7] Tan S.B., An effective refinement strategy for KNN text classifier, Expert Systems with Applications, 2006, 30: 290-298.
[8] Pang G. S., Jiang S. Y., A generalized cluster centroid based classifier for text categorization, Information Processing and Management, 2013, 49: 576-586.
[9] Jiang S. Y., Pang G. S., Wu M. L., Kuang L. M., An improved K -nearest-neighbor algorithm for text categorization, Expert Systems with Applications, 2012,39: 1503-1509

Advanced Materials Research Vols. 989-994 (2014) pp 1547-1550
© (2014) Trans Tech Publications, Switzerland
doi:10.4028/www.scientific.net/AMR.989-994.1547

Research of Intelligent Warehouse Layout Base on Genetic Algorithm and Dynamic Programming

Yang Lvqing, Yan Qiang

Software School of Xiamen University, Xiamen, China
lqyang@xmu.edu.cn, klt_15@qq.com

Keywords: Warehouse Layout; Genetic Algorithm; Dynamic Programming

Abstract. Intelligent warehouse management can effectively improve the work efficiency and decreasing operating costs for a company, and the reasonableness of warehouse layout has played a very important role in it. This paper will aim at the warehouse layout problem, analyze the superiority of genetic algorithm and dynamic programming for the problem, and base on the genetic algorithm, integrating the thoughts of dynamic programming to put forward an optimization strategy. It can improve the accuracy and efficiency of genetic algorithm by a modified encoding scheme and fitness function, in order to put forward a more optimal scheme of warehouse layout, provide the information base for following operation of warehouse management, and improve the intelligent level of warehouse management system.

Introduction

With the continuous development of modern technology, the intelligent warehouse management which using the information technology becomes the focus of attention. The intelligent warehouse management can take advantage of existing resources sufficiently, it make the planning, inspection and control of the warehouse and its goods will become more precise and more efficient, it improve the accuracy of warehouse management and dispatch, and it reduce the cost of operation and maintenance. In the actual process of warehouse management, the reasonableness of warehouse layout is always the basis of the work. Firstly, warehouse layout determines the usage of the warehouse, it is the key of improve the utilization rate of the warehouse and reduce the cost of warehouse management. Secondly, warehouse layout distributes the space of all kinds of goods, it will influence work efficiency of portage and placement. Thirdly, warehouse layout can directly reflect the situation of warehouse and provide information and support to the warehouse manager. Therefore, the reasonableness of warehouse layout played a major role in intelligent warehouse management. This page will base on dynamic programming and genetic algorithm, put forward an optimization strategy to the warehouse layout problem.

Overview of the warehouse layout problem

In the traditional warehouse management and operation, the location of goods always bases on a rough classification, standard of the company or habit of the operator. This operation will largely waste the space of the warehouse, and reduce the work efficiency. Therefore, using intelligent warehouse management and optimal strategy to solve the problem of warehouse layout will drastically decrease the amount of time in handling and stacking of goods, and increase the work efficiency.

In order to convenient to discuss, this page will assume the warehouse like this:

The warehouse is a rectangle, and the entrance in a single direction with an unlimited size. There are several rows of shelves in the warehouse. Each shelf is divided into unit of the same size, and the goods are stored in the unit. Galleries are between the shelves. As showed in the figure 1:

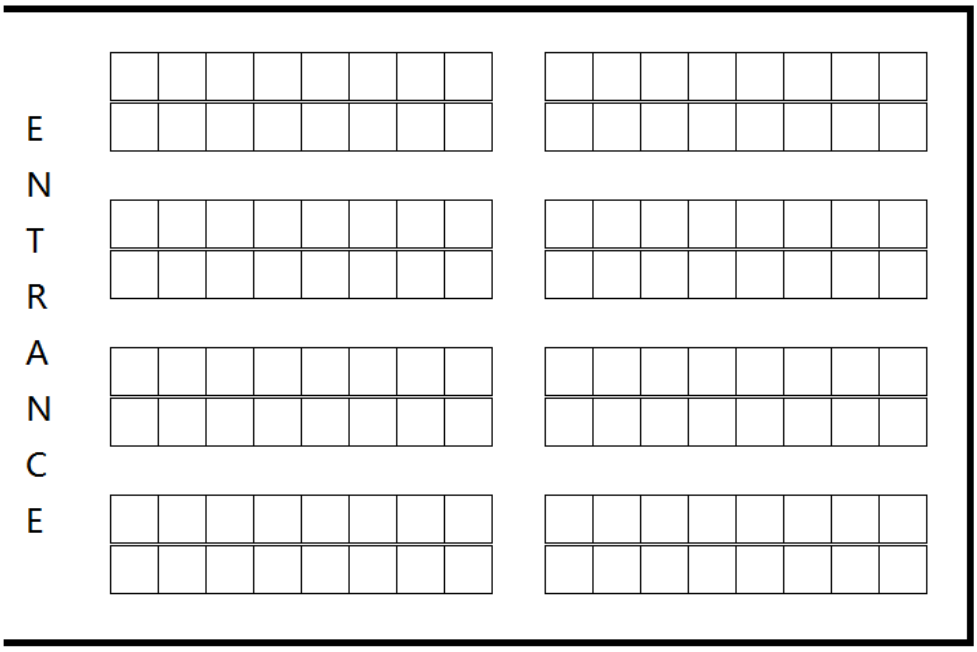

Fig.1 Warehouse structure diagram

Optimization of Warehouse layout base on Genetic Algorithm and Dynamic Programming

Genetic Algorithm is a random search method which is imitated the evolution of biology. It can solve the extremum problem effectively. Compare with traditional algorithm, genetic algorithm has a distinct advantage because it needs not an expression or a function so that it will not be limited by derivation or continuity of function and it can solve all of the practical problems steadily. At the warehouse layout problem, it need find the optimal solution of a large number of layout schemes, and it can't be solved by an exact expression, so genetic algorithm is a well choice to solve the problem.

Dynamic programming is a thought which divided the problem into several subproblem and solves the problem base on solving the subproblem, and record the result of subproblem in order to solve the same subproblem faster. For the warehouse layout problem, it has lots of the same subproblems when it evaluates the fitness of a chromosome. Therefore, dynamic programming will make the genetic algorithm more efficient.

The optimizing strategy of this paper proposed is based on the genetic algorithm, therefore, following page will accord with the steps of the genetic algorithm to solve the problem, that is encoding, determining fitness function, population initialization, population evolution and finding an optimal solution.

Encoding. Encoding is the first step in the genetic algorithm, it also determines the direction to solve the problem next step.

This page use the coding scheme base on choose shelves of goods, for a batch of the incoming goods, the numbers of shelves of each goods selected link into chromosome code of this scheme, the length of the code corresponds to the quantity of the goods, genes corresponds to each of goods, the value of genes corresponds to the shelves of each of goods selected. In addition, different sequence of goods in one shelf will link into a same chromosome code, this problem will be explained in the following paragraphs.

Fitness function. Fitness function is the key to evaluation of a chromosome code in genetic algorithm. It determines the probability of inheritance and influences the optimality of the genetic algorithm.

This page will base on the time needed when the good stock out and the stock out frequency of the good to build the fitness function. That means putting the good which has a high frequency near

by the entrance will improve the fitness of this scheme. The fitness function is express by following function:

$$f(x) = k\sum_{i=1}^{n}[u_i(T_{max} - t_i)] + C_{min} \quad (1)$$

For the question of the same code in one shelf, use dynamic planning to find the optimal solution in a shelf is a well choice. It not only can solve the problem in current scheme, but also can record the result of subproblem which will be calculated several times. It can improve the efficiency of genetic algorithm.

Population initialization. Genetic algorithm needs an initial population to start the simulation of evolution. According to population size M, quantity of goods n, quantity of shelves m, builds M chromosome sequences by n genes between 0 and m-1 as the initial population. Population size M will be determined by the actual situation, generally can be set to 500. In addition, in order to improve the efficiency of genetic algorithm, we will exclude the scheme that all the goods put into a same shelf.

Population evolution. Genetic algorithm simulate the population evolution in following 3 operations: Firstly, every chromosome will be selected by probability, the chromosome with high fitness will be selected and the chromosomes with a low fitness may be eliminated. This operation will keep the high fitness of population and the correctness of the genetic algorithm. Secondly, exchange part of the gene between two chromosomes. This operation is an important way to find a chromosome with a higher fitness. Thirdly, change part of gene of a chromosome. This operation can increase the search scope and ability of the genetic algorithm.

Optimal solution. When the quantity of population to the desire, genetic algorithm will stop and find the optimal chromosome from every population.

Realization of the software system

In the intelligent warehouse management system, algorithm will realize and apply with following steps:

When a batch of goods have arrived at the warehouse, the administrator of warehouse will scan every goods by the RFID device, and add the information of goods or gain from the database, like length, width, height, weight.

Gain the information and state of the warehouse from the database, like the quantity of the shelves, the occupancy of every shelf, status of every unit.

In the population initialization and population evolution, system will combine the information which is gained before to analyze the feasibility of the current layout, and it will get rid of the illegal solution to improve the efficiency of genetic algorithm.

Gain the statistical information like the frequency of goods stock in and stock out, confirm and correct the fitness function, that make the assessment more accurately.

According to the actual conditions, set an appropriate termination condition of population evolution to satisfy the requirement of time and precision. After it concluded the optimal solution, system begins the operation of goods stock in and updates the layout status to the database.

Summary

Warehouse layout problem is an important part of intelligent warehouse management. This page put forward an optimization strategy of warehouse layout problem. On the basis of the genetic algorithm, combine the thoughts of dynamic programming to optimize the fitness function. It can improve the accuracy and efficiency of genetic algorithm, provide a better warehouse layout solution, increase the work efficiency and space utilization rate of warehouse, and provide information to following warehouse operation. At the same time, this solution can conclude the optimal solution in a large probability, but every algorithm has limitation, especially to solve the problem which is changeable. Therefore, in the process of solving the warehouse layout problem, we can blend other intelligent algorithm in it, it also a worthy research direction in the future.

References

[1] J.H. Holland: *Adaptation in Natural and Artificial Systems* (University of Michigan Press, US 1975).

[2] Zhang Wenxiu, Liang Yi: *Mathematics Foundation of Genetic Algorithm* (Xi'an Jiaotong University, Xi'an 2000)

[3] Qiao Jianzhong, Lei Weimin, Li Benren and Teng Hongfei: Journal of Chinese Computer Systems Vol. 19-12 (1998), p. 14

[4] Xu Zongben, Zhang Jiangshe and Zheng Yalin: *Bionics in Computational Intelligence: Theory and Algorithm* (Science Press, Beijing 2003)

[5] Wang Junxiang: Computer Knowledge and Technology Vol.36 (2006), p. 150

[6] M. Srinvivas and L.M. Patnaik: IEEE Trans on Systems, Man, and Cybernetics Vol. 24-4 (1994), p.656

[7] C.J. Potts and Terrid: IEEE Trans on Systems, Man, and Cybernetics Vol. 24-1 (1994), p. 73

[8] D.E. Goldberg: Communications of the ACM Vol. 37-3 (1994), p. 113

[9] J.R. Koza: *Genetic Programming: On the Programming of Computers by Means of Natural Selection* (M IT Press, UK 1992)

[10] Tang Fei and Teng Hongfei: Journal Of Software Vol.10-10 (1999), p. 1096

[11] Cha Zhiqin, Gao Bo and Zheng Chengzeng: Journal of Computer Applications Vol.23-7 (2003), p.137

Advanced Materials Research Vols. 989-994 (2014) pp 1551-1554
© (2014) Trans Tech Publications, Switzerland
doi:10.4028/www.scientific.net/AMR.989-994.1551

A generalized attributes significance measure method

Fachao Li[1, a] , Ming Li[1, b] and Shuo Liu[1, c]

[1]School of Economics and Management, Hebei University of Science and Technology

No. 70, Yuhua East Road, Shijiazhuang 050018, P. R. China

[a]lifachao@tsinghua.org.cn, [b]554815133@qq.com, [c]liushuo528@126.com

Keywords: Difference degree; Attributes significance; Information system

Abstract. Currently, rough set theory has been widely used in many fields. In rough set theory, how to measure the attributes significance of the data is a core content. In order to solve the problem that the existing attributes significance measure methods usually ignore the interaction among the attributes, the paper presents a measure method based on difference degree. When given a set, the proposed method first divides it into several subsets according to the value of condition attributes, and then computes the difference degree in the subsets. Secondly, the important attributes are selected based on the value of difference degree. Further the paper discussed some properties of the difference degree, and the experimental results shows the effectiveness of this method in the final.

Introduction

In general, the information in the data sets is stored for different learning and mining tasks. Therefore, for a specific data analysis tasks, attributes in the information system are not equally important, it may also exist redundant or irrelevant information. An excessive amount of attributes storing in the data set may cause a significant slowdown in the learning process and deteriorate the performance of learning algorithm. Therefore, how to extract useful knowledge effectively has become a critical issue for the area such as systematic science and information science.

As a soft science computing tool, rough set theory [1] can be used to deal with uncertainty information, and it provides a mathematical framework to discover attributes significance and reduce the number of attributes contained in a dataset. Now, it has been successfully applied to machine learning, decision analysis, process control, and other fields, and caused widespread concern in the academic community. Aiming at the problem of attribute significance measurement, many scholars have carried on a discussion from different views (for example,Komorowski et al.[2] introduced an algorithm by constructing a kind of discernibility function from the data set and simplify it to measure the attributes significance. Skowron [3] proposed an algorithm basing on discernibility matrix to carry out the attributes significance), however, these algorithms have obvious shortcomings: Firstly, when the objects of the universe and attributes are on a larger scale, it requires a lot of computing time; Secondly, it has been proved that the problem of finding the minimal reduction is NP-hard, so when the data sets are on a large scale, it does not have a maneuverability. For the deficiency of [2, 3], a lot of heuristic algorithms have been developed.

According to the measures of attributes significance, the existing heuristic algorithms mainly include the following two categories: (I) Positive region-based methods. Hu et al. [4] gave an extension of these positive region methods for heterogeneous feature selection based on neighborhood rough set model. However, the corresponding algorithms ignore the additional computation required for selecting significant attributes. (II) Entropy-based methods. Wu [5] put forward an algorithm to measure the attribute significance based on information entropy. The studies can greatly decrease search space that the information system requires.

It should be noted that, the above formulas of attribute significance measure methods in heuristic algorithms can be represented in a unified form. They are used to select an attribute by heuristic algorithm. But this heuristic information may not find the optimal solution in a given information system. Since in practical problems, the attributes in system are not independent, but interacted to other degree. For some attributes, the significance of the individual attribute may be small, but once

integrated, they can have a big impact on the classification in system. However the measures of single attribute significance do not take into account of the interaction among the attributes. As the heuristic algorithms may select the attribute with a big value of significance, the one with a small value may not be selected.

From the perspective of partition on the information system, this paper put forward a generalized measure method of attributes significance. Since in practical applications, the difference degree among attributes may be a linear measurement mode, and also be a kind of nonlinear measurement mode, so for specific describing these problems, this paper proposed the concept of difference degree. For one attribute subset, if the difference degree is very small, which means there is little difference between it and all the attributes in partition, then the subset is important for the information system. This measure method can not only reflect the importance of a single attribute, but also can reflect the comprehensive significance of the attribute combination. In order to prove the feasibility and validity, in this paper, we make a comparison between the inclusion degree method and the proposed generalized attributes significance measure method.

Preliminaries

In this paper, the information system is referred to (U, A, F_A). Where U is a non-empty finite set of research subjects (called the universe), A is non-empty finite set of attributes; $V(a)$ is the range of attribute a, $F_A=\{f_a: U\to V(a) \mid a\in A\}$ is the information function. For $B\subset A$, $R_B=\{(x, y)\in U\times U \mid f_a(x)=f_a(y), a\in B\}$ denotes the equivalence relation on U with respect to B (where $f_a(x)$ denotes the value of object x on attribute a); U/R_B (U/B for short) denotes the partition on U formed by the equivalence class of R_B (that is, $U/B=\{[x]_B \mid x\in U\}$), $[x]_B=\{y \mid (x, y)\in R_B\}$ denotes the R_B equivalence class of x). If U/B is interpreted as a kind of knowledge base, then each equivalence class $[x]_B$ can be considered as a basic knowledge particle on universe U. In this sense, rough set theory provides a method to describe the knowledge basing on equivalence relation.

For any $P\subset Q\subset A$, $[x]_P\subset[x]_Q$ are true for any $x\in U$, that is, U/Q is finer than U/P ($U/Q\prec U/P$ for short). Thus, in the information system (U, A, F_A), the size of attribute subset P determines the knowledge granularity of knowledge base U/P to some degree, the bigger the size of P, the more powerful the description ability of U/P. Therefore, how to reduce the condition attributes and get the support attributes on the basis of remaining the fundamental performances of the information system unchanged have arose the widespread attentions in the academic and application fields.

The attribute significance measure based on difference degree

In this section, we proposed a concept of difference degree and a significance measure method based on information system and difference degree. For convenience, the following use $|A|$ represents the number of elements in the finite A.

Definition 1 Let U be a non-empty finite set, $\wp(U)=\{X \mid X\subseteq U\}$, $G:\wp(U)\times\wp(U)\to[0,\infty)$, $X, Y, Z\in\wp(U)$. If $G(X, Y)$ satisfied: 1) $G(X, X)=0$; 2) when $X\subset Y\subset Z$, $G(X, Z)\geq G(Y, Z)$, then we call $G(X, Y)$ a difference degree function on U.

It is not difficult to see that, for given inclusion degree function $D(Y \mid X)$ on U (that is, for any $X, Y, Z\in\wp(U)$: 1) $0\leq D(Y \mid X)\leq 1$; 2) when $X\subset Y, D(Y \mid X)=1$; 3) when $X\subset Y\subset Z$, $D(X \mid Z)\leq D(X \mid Y)$; 4) when $X\subset Y$, $D(X \mid Z)\leq D(Y \mid Z)$), $G(X, Y)=1-D(Y \mid X)$ is a difference degree function on U. But it is worth noting that the difference degree function $G(X, Y)$ on U may not be able to export the inclusion degree function $D(Y \mid X)$ on U, for example, $G_1(X, Y)=(|X|-|Y|)^2$ and $G_2(X, Y)=|(X-Y)\cup(Y-X)|$ are the difference degree functions on U, but whether through various linear transform, $G_1(X, Y)$ and $G_2(X, Y)$ cannot be converted into the inclusion degree function on U. This shows that the difference degree and the inclusion degree are different in essence on U.

Definition 2 Let (U, A, F_A) be an information system, $P \subset A, U/P = \{[x]_P | x \in U\}$, $G(X, Y)$ be a difference degree function on U. Then

$$M(P | A \oplus G) = \frac{1}{|U|} \sum_{x \in U} G([x]_P, [x]_A). \quad (1)$$

is called the significance measure of the P based on information system(U, A, F_A) and the difference degree function $G(X, Y)$ (difference degree of P for short).

Formula (1) shows the difference of overall description power between U/P and U/A from the perspective of average. It reflects significance of the attribute subset P relative to the whole attributes A, the bigger the value of $M(P|A \oplus G)$, the larger the uncertainty of attribute subset P in representing A. in particular, if $M(P|A \oplus G)=0$, then the (U, P, F_P) and (U, A, F_A) have the same ability in knowledge description, which means that the comprehensive significance of attribute subset P is equal to that of the attributes set A. then from the angle of knowledge granularity to express the difference degree in information system.

From what has been discussed above, the significance of attribute subset P can be measured by

$$S(P | A \oplus G) = 1 - \frac{M(P | A \oplus G)}{\max_{P \subset A} M(P | A \oplus G)}. \quad (2)$$

Formula (2) indicated that the bigger the value of $S(P | A \oplus G)$, the more significance of attribute subset P. In order to express it in a much clearer way, we describe the difference degree from the perspective of knowledge granularity in the following.

Suppose that $U/A = \{U_1^A, U_2^A, \cdots, U_m^A\}$, $U/P = \{U_1^P, U_2^P, \cdots, U_k^P\}$ are partitions induced by attribute set P and A. From $P \subset A$, and $[x]_A \subset [x]_P$ for any $x \in U$, we can obtain that

$$M(P | A \oplus G) = \sum_{i=1}^{m} \frac{|U_i^A|}{|U|} G(U_j^P (U_i^A \subset U_j^P), U_i^A). \quad (3)$$

Here, $U_j^P (U_i^A \subset U_j^P)$ denotes U_j^P which includes U_i^A. Since U/P and U/A are partitions of U, and $U/A \prec U/P$, for any given $U_i^A \in U/A$, there must be existing only one $U_j^P \in U/P$ such that $U_i^A \subset U_j^P$. This means that the implication of (3) is certain.

It can be seen from (3), the difference degree is the weighted average of the knowledge granularity difference between attribute subset P and the whole attribute set A. In the following, we will discuss the properties of difference degree in theory.

Property 1. Let (U, A, F_A) be an information system and $P \subset Q \subset A$. Then $M(P|A \oplus G) = M(Q|A \oplus G)$ for any difference degree function $G(X, Y)$ if and only $U/P = U/Q$.

Property 1 shows that if the partition induced by attribute subset P is the same as that by the whole attribute set A, then the difference degree are the same as well.

Property 2. Let (U, A, F_A) be an information system, $P \subset A$, $U/A = \{U_1^A, U_2^A, \cdots, U_m^A\}$. Then $\max_{P \subset A} M(P | A \oplus G) = \frac{1}{|U|} \sum_{i=1}^{m} |U_i^A| G(U_i^A, U)$.

Property 2 shows that, the maximum value of difference degree is achieved when the granularity of knowledge determined by P is the coarsest. Namely that, when $U/P = \{U\}$, the value of $M(P|A \oplus G)$ is maximum.

The performance analysis of difference degree

This section combines an example to further analyze the relationship and the difference between the difference degree and other measures of attributes significance in information systems.

Example 1. In the information system (U, A, F_A), U={1, 2, 3, 4, 5, 6, 7, 8, 9, 10}, A={a_1, a_2, a_3, a_4}, $P \subset A$, and U/A={{1, 2}, {3, 4}, {5}, {6, 7, 8}, {9}, {10}}. Then the significance of several attribute subsets (see Table 1) can be obtained according to the following difference degree functions: 1) $G_1(X,Y)=1-|X\bigcap Y|/|X|$; 2) $G_2(X, Y)=(|X|-|Y|)^n$.

From Table 1, it is not difficult to see that, inclusion degree is a kind of linear measurement, but the difference degree can be indicated as a linear measure or non-linear measure, it cannot be converted by inclusion degree. The bigger the value of difference degree, the less significance of the attribute subset, in addition to this, we can see that if the equivalence class of U/A were regarded as an elementary granule of knowledge, then the difference degree is the weighted average of uncertainty increment caused by combination of elementary granule. The more elementary granule of knowledge combined, the larger the difference degree is.

Table 1 The attribute significance of several different attribute subsets

P	U/P	$S(P\|A\oplus G_1)$	$S(P\|A\oplus G_2)$		
			n=0.5	n=1	n=2
$\{a_1,a_2,a_3,a_4\}$	{{1, 2}, {3, 4}, {5}, {6, 7, 8}, {9}, {10}}	1	1	1	1
$\{a_1,a_2,a_3\}$	{{1, 2}, {3, 4}, {5, 6, 7, 8}, {9}, {10}}	0.81	0.83	0.925	0.982
$\{a_1,a_2,a_4\}$	{{1, 2, 3, 4}, {5}, {6, 7, 8}, {9}, {10}}	0.75	0.80	0.9	0.975
$\{a_2,a_3,a_4\}$	{{1, 2, 3, 4}, {5, 6, 7, 8}, {9}, {10}}	0.56	0.63	0.85	0.957
$\{a_1,a_3,a_4\}$	{{1, 2}, {3, 4}, {5}, {6, 7, 8, 9}, {10}}	0.81	0.83	0.925	0.982
$\{a_1,a_3\}$	{{1, 2, 3, 4}, {5, 6, 7, 8, 9, 10}}	0.25	0.38	0.6	0.87
$\{a_2,a_3\}$	{{1, 2, 3, 4}, {5, 6, 7, 8}, {9, 10}}	0.44	0.56	0.8	0.954
$\{a_2,a_4\}$	{{1, 2, 3, 4}, {5, 6, 7, 8, 9}, {10}}	0.4	0.51	0.69	0.91

Conclusions

At present, how to measure the attributes significance of data is still a challenging issue in the area of artificial intellegence. This paper proposes a generalized measure method. Due to that the difference degree characterizes the uncertainty of the attribute subset in representing the whole attributes. It can reflect the significance of attribute subset from another perspective. And it can be seen from the example that this approach is feasibility and effectiveness when for different problems, it can provide a new way to deal with the practical application data.

Acknowledgements

This work is supported by the National Natural Science Foundation of (71371064).

References

[1] Z.Pawlak, Rough sets, Communications of the ACM. Vol. 38 (1995), p.89-95.

[2] J.Komorowski, Z.Pawlak, Rough sets: a tutorial, in: Rough Fuzzy Hybridization, A New Trend in Decision- Making, Springer-Verlag Singapore Pte., Ltd., Singapore, 1999.

[3] A.Skowron, The Discernibility Matrices and Functions in Information Systems, Kluwer Academic Publishers.Vol.3641 (1992) p.331-362.

[4] Q.H.Hu, J.F.Liu, D.R.Yu, Mixed feature selection based on granulation and approximation, Knowledge-Based Systems. Vol.21 (2008), p.294-304.

[5] S.Z.Wu, P.Z.Gou, Attribute reduction algorithm on rough set and information entropy and its application, Computer engineering.Vol.37 (2011), p.56-61.

Advanced Materials Research Vols. 989-994 (2014) pp 1555-1560
© (2014) Trans Tech Publications, Switzerland
doi:10.4028/www.scientific.net/AMR.989-994.1555

A Fusion Method of Point-Cloud Based On Parallel Estimation of Distribution Algorithm

Zetao Jiang[a,b], Le Zhou[a], Lei Zhou[b]

[a,b]Email:zetaojiang@126.com, Guilin University of Electronic Technology, Guilin, China

[a]Email:zhoule888@126.com, Nanchang Hangkong University, Nanchang, China

[b]Email: 450702826@qq.com, Nanchang Hangkong University, Nanchang, China

Keywords: PED, stereo matching, point-cloud, potential energy, image fusion

Abstract. The paper proposes a new method that utilizes Parallel Estimation of Distribution(PED) to obtain disparity map of two images and fuses 3D point-cloud by the disparity. Estimation of Distribution（ED）has several advantages such as low complexity and high efficiency while it also has the shortcoming that it's sensitive to initial samples and the final solution is local optimum but global optimum. In order to exert its merit and overcome the shortcoming, this paper will improve the ED by parallel sampling to diminish the sensitivity with Adaptive Support-Weight method. We called it Parallel Estimation of Distribution(PED). After disparity map is obtained, the two images will be divided into high frequency and low frequency by lifting wavelet respectively and the frequency coefficient of each image will be averaged into fusion frequency. Finally, the fused frequency coefficient will be transformed by inverse lifting wavelet to the final fused image. The experiment has proved that the matching speed is outstanding without losing precision.

Introduction

Stereo matching is an aporia in computer vision and one of key technology. Recently, a lot of studies about stereo matching have been proposed[1-8]. Totally, stereo matching methods can be divided into local and global algorithm. Local algorithm[11] is mainly based on region and based on feature. Usually its goal is to find matched points of the whole image by minimizing matching cost of corresponding window. While the goal of global method is to find an energy function that is related to disparity and is optimal globally, then the disparity map can be got by minimizing the energy function. Currently, global algorithm is focused on graph cut(GC)[1-2][9] and belief propagation(BP)[3-7]. Although the effect of the two methods is outstanding, the complexity is high and efficiency is not extraordinary. So many improvements have been performed on them. GC method firstly segments images to many parts and then obtains disparity map by searching best matching region for each segmentation part. BP method is actually a dense matching that transforms matching issue to Markov Random Field(MRF) model which gets dense disparity by computing the maximum a posteriori probability based on energy function and some rule. Now the more popular method named Adaptive Support-Weight(ASW) is one efficient global method that chooses a fixed window whose center is the point to be matched and that computes matching cost which is the sum of differences of corresponding pixel in the window by setting a weight via spatial distance and CIELab distance. ASW is more precise than SSD, SAD and NND. However the searching process of ASW is one by one, its high computation and low speed are inevitable.

Evolutionary Algorithm(EA) is one of probabilistic optimization algorithms. Genetic Algorithm(GA) and Differential Evolution Algorithm(DEA) are famous in conventional EA. Due to the limitations of conventional EA, great modifications have been studied or new ideologies have been proposed in recent EA. Now, Ant Colony Optimization, Particle Swarm Optimization and Estimation of Distribution(ED) are celebrated among them. ED[12-14] can be regard as an improvement of GA in theory. In order to achieve the optimal sample, It searches the samples with high fitness to perform evolution as same as GA. The difference between them is that GA changes the property of each sample in the step of mutation and chiasma, but ED just increases the chosen probability of samples whose fitness is high by some probabilistic model and the samples with highest fitness will be considered as the optimal solution. Therefore, ED has great advantages over GA in optimization of discrete samples. Since probabilistic model and fitness function are the core

of ED, a large number of researchers have studied the probabilistic model and fitness function. Among them, ED based on Quasi-Copula[15-16] takes samples by constructing probabilistic model which can reflect the relation of multivariable based on discrete random data and produces new individuals, thus it is suitable to solve complex discrete issues. The goal of stereo matching is to find optimal matching among several samples and is not needed to modify image data, so ED is more suitable to stereo matching than GA. Nevertheless, because of the sensibility to initial samples, ED can sink into local optimum. In order to weaken the defect, the paper proposes a parallel method to improve ED.

We will combine ED with Adaptive-Weight theory to match two images by utilizing potential function difference to construct cost function. Then the lifting wavelet will be performed to fuse the two images and 3D spatial point-cloud will be built based on the disparity map. Experiment has shown that our method can reduce the searching volume and increase searching speed without losing precision.

Potential Function and Potential Energy

2.1 Potential Function

No definition can be found about potential function. Its definition is different in different subject area. It was often used to describe the relationship and constraint that can be expressed by function among image nodes in MRF early. Thus we can define a potential function to describe the relevancy of single node or multi-node. Let i be one point of image, the potential function can be defined as:

$$\Psi(i) = \frac{P(i)\ln(P(i)+1)}{\ln 2}$$

Where $P(i)$ represents the normal pixel value of some channel around the window whose center is i. In the same way, region potential function can be defined as:

$$\Psi(S) = \frac{\sum_{i\in S}^{N}\sum_{j\in chnel}^{M} P_j(i)\ln(P_j(i)+1)}{\ln 2}$$

Where N represents the total of the region, $chnnel$ is the channel set of RGB space which usually is $\{R,G,B\}$, M represents the channel totality. Region potential function describe the sum of potential energy in the region.

It is not significant for potential function to describe single node or region. It can be used to describe the relation between two nodes and potential energy difference will be defined.

2.2 Adaptive potential energy

After describing the potential function of single point or single region, the constraint of two nodes that can be points or regions of images will be defined. In stereo matching, a node is often a region, then potential energy difference of regions is defined as follow:

$$\Psi(S,S') = \frac{\sum_{i\in S, i'\in S'}^{N}\sum_{j\in chnnel}^{M} |\, P_j(i)\ln(P_j(i)+1) - P_j(i')\ln(P_j(i')+1)\,|}{\ln 2}$$

Where S,S' represent the corresponding regions of two images, i,i' are corresponding points of the regions. Because $\Psi(x)$ ranges from 0 to 1, $\Psi(S,S')$ that represents sum of energy difference of image corresponding region ranges from 0 to MN.

Yoon[10] proposed a method named ASW to compute matching cost. This method can describe similarity by setting adaptive-weight and combining Euclidean distance of CIELab color space and RGB color space of corresponding regions. We will also define matching cost by adaptive-weight and potential energy difference:

$$E(p,\bar{p}_d) = \frac{\sum_{q\in S_p, \bar{q}_d\in S_{\bar{p}_d}} w(p,q)w(\bar{p}_d,\bar{q}_d)\Psi(q,\bar{q}_d)}{\sum_{q\in S_p, \bar{q}_d\in S_{\bar{p}_d}} w(p,q)w(\bar{p}_d,\bar{q}_d)}$$

Where $\bar{p}_d, \bar{q}_d$ is corresponding points of two images and the disparity is d. $\Psi(q, \bar{q}_d)$ represents potential energy difference. $w(p,q)$ is the weight value of two points and is defined as:

$$w(p,q) = \exp(-(\frac{\Delta c_{pq}}{\gamma_c} + \frac{\Delta g_{pq}}{\gamma_p}))$$

Where Δc_{pq} and Δg_{pq} are Euclidean distance of CIELab space and RGB space. γ_c is 14 and γ_p is half of the window size.

Stereo matching based on parallel Estimation of Distribution

3.1 Estimation of Distribution

Estimation of Distribution is one of Evolution Algorithms which is aimed at achieving optimum of sufficiency function. Stereo matching is an optimization process essentially. Firstly ED selects several samples randomly according to some probability distribution model (such as Gaussian model). Then the samples with high sufficiency will be chosen on the basis of some strategy and the model will be updated based on these samples. Next we take samples newly by the updated model. After several iterations or some condition, the optimum is the individual that can be the mean of continuous samples or the one near to the mean of discrete samples. Due to the sensitivity to initial samples, its optimum can be local inevitably. In order to reduce the sensitivity, we will combine parallel sampling with parallel probability model mixture and applies it to stereo matching. On the premise of keeping precision, the efficiency is improved conspicuously.

3.2 Parallel Estimation of Distribution Algorithm

Parallel sampling means twi-sampling simultaneously. Then each sample sufficiency is computed and the samples with high sufficiency will be chosen to update probability distribution model respectively. Because of the independence of samples, it is feasible to take samples parallel. It's possible for parallel algorithm to reduce the sensitivity of initial samples and reduce the probability of local optimum.

Pixel fusion based on lifting wavelet and 3D point-cloud reconstruction

4.1 Lifting wavelet

Lifting wavelet is a special wavelet that is another expression of image as same as Fourier transformation. An image and its wavelet image are corresponding, that means they are isomorphism. The wavelet image contains high frequency and low frequency that express the edge or flat area of the image. Unlike Fourier, the basis of wavelet is not defined, thus the frequency coefficient is different with different basis. Therefore a lot of researches have been focused on wavelet basis[17-18]. Harr basis is one of popular bases.

4.2 The method of pixel fusion

The purpose of pixel fusion is to fuse different pixels into one pixel as some rule. There are many methods in pixel fusion. The simplest one is average method that declare: $P_{fusion} = average(P_{left} + P_{right})$, where $average$ means average function such as geometric average, harmonic average and arithmetic average. However, average method usually takes consideration of two single points and not the global distribution of the image. In view of the difference between high frequency and low frequency of an image, wavelet can take different fusion rules, so it is more flexible than average. The paper will utilize lifting wavelet based on Harr basis to fuse pixels of corresponding images.

The method of this paper can be divided into two parts: stereo matching and 3D point-cloud reconstruction based on pixel fusion. The steps are demonstrated below:

Stereo matching and obtaining of disparity map

Let the range of disparity be $[d_{\min}, d_{\max}]$, the searching window size is $2N+1$, the process of PED on stereo matching is:

1).parallel sampling. For each point $p:(i,j)$ of left image, two group of $M \in [0, d_{\max}]$ samples(obeying uniform distribution) $d_1, d_2, ..., d_M$ and $d_1', d_2', ..., d_M'$ are chosen randomly in right image which ranges $(i - d_{\max}, j) \to (i - d_{\min}, j)$;

2).Computing sufficiency. Computing the potential energy difference $E(p,\bar{p}_{d_m})$ and $E(p,\bar{p}'_{d_m})$ of windows whose size is $2N+1$ and center is (i,j) of two images;

3).Choosing superior samples and updating probability distribution model. The $M/2$ samples $D_1=\{d_{11},d_{12},...,d_{1M/2}\}$ and $D_2=\{d'_{11},d'_{12},...,d'_{1M/2}\}$ with low potential energy difference will be chosen to update model as $d_{\min}=\min\{D_1\bigcup D_2\}, d_{\max}=\max\{D_1\bigcup D_2\}, M\leftarrow\min\{M/2, d_{\max}-d_{\min}\}$. If the number of samples this time is less than threshold T_d or $d_{\max}-d_{\min}<T_d\,(T_d=4)$, go to Step 4), else $i{+}{+}$ and return Step 1);

4).Obtaining disparity or occlusion determination. Choose the sample point that is nearest to the mean of samples and computing the potential difference at this time. If the difference is less than a threshold, the point is regarded as the matched point, else it is an occlusion possibly. For an occlusion, we will confirm matched point inversely. If the matched point is (i,j), it is not an occlusion, else it's an occlusion. The disparity of occlusion can be computed by bilinear interpolation;

5).Final process of disparity image. Utilize median filter to smooth disparity map.

2. Spatial point-cloud pixel fusion

1).For the pixels sequence $l_i=\{l_{i1},l_{i2},...,l_{in}\}$ of each row of left image and corresponding pixels $r_i=\{r_{i1},r_{i2},...,r_{in}\}$ of right images, lifting wavelet transformation will be taken to them. The transformation result is $f(l_i)$ and $f(r_i)$;

2).Computing the harmonic average of high and low frequency coefficient of $f(l_i)$ and $f(r_i)$. And Get fused wavelet transformation point data $f(fus_i)$;

3).In order to get actual fused image pixels, inverse transformation is taken to $f(fus_i)$. And according to the disparities of these pixels, the point-cloud is constructed.

Because the chosen samples with high sufficiency are half of the sum in stereo matching, the number of sample is $2M/2^K$ after K iterations. The algorithm converges by exponent of 2. Besides, the initial samples obey uniform distribution and due to random sampling, the difference of maximum and minimum disparity is close to the half of origin difference after each iteration. Finally, the samples will converge to a best sample or a sample region.

The result of analysis of experiment and simulation

5.1 Experiment result of disparity map

This paper combines OpenCV with OpenGL and simulates on Visual Studio 2008 for two groups of images of Middlebury University. The result is shown in Fig 1.

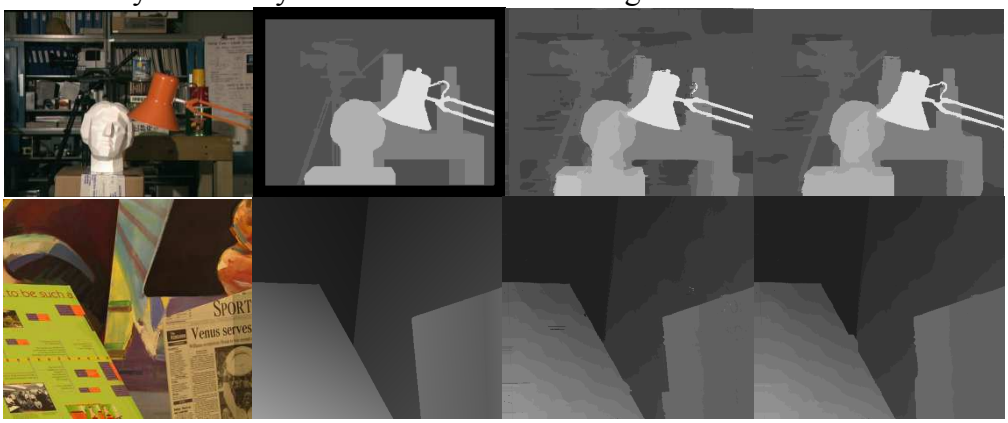

(a) (b) (c) (d)

Fig 1. Images and disparity maps.(a)Source images.(b)True disparity maps.(c)The disparity maps of ASW.(d) The disparity maps of our algorithm.

In the experiments, although there are not too many mutations in our algorithm, some errors still appear in some regions such as edges. The number of matching cost of ASW is $H\times W\times(d_{\max}-d_{\min}+1)$ (H, W: height and width of image, $d_{\max}$, $d_{\min}$:the initial max and min disparity). So the time complexity of ASW is $H\times W\times(d_{\max}-d_{\min}+1)$. The samples with high sufficiency on the second and third step of PED are around the true disparity. The time complexity of this paper is approaching to $H\times W\times(d_{\max}-d_{\min}+1)/2$ that is half of ASW in theory. Because of the influence of other factors of program, the time consumption of our algorithm is little more than half of ASW. The compared result is shown in Table I.

Table 1. The time of Tsukuba and Venus from ASW and our algorithm

Image group	Tsukuba(s)	Venus(s)
ASW	52.48	61.37
Our algorithm	28.54	35.28

From Table 1, our average time of stereo matching is 54% and 57% of ASW. Obviously, the time is more decreased than ASW.

5.2 Simulation of spatial point-cloud fusion

(a) (b) (c)

Figure 3. Left and right images with their final disparity maps of this paper.(a)Left image.(b)Right image.(c)Their final disparity maps.

According to Section4.2, the left and right image which are shown in Figure 5.3(a)(b) will be fused by lifting wavelet and 3D point-cloud will be constructed. The result of point-cloud is shown in Fig 4.

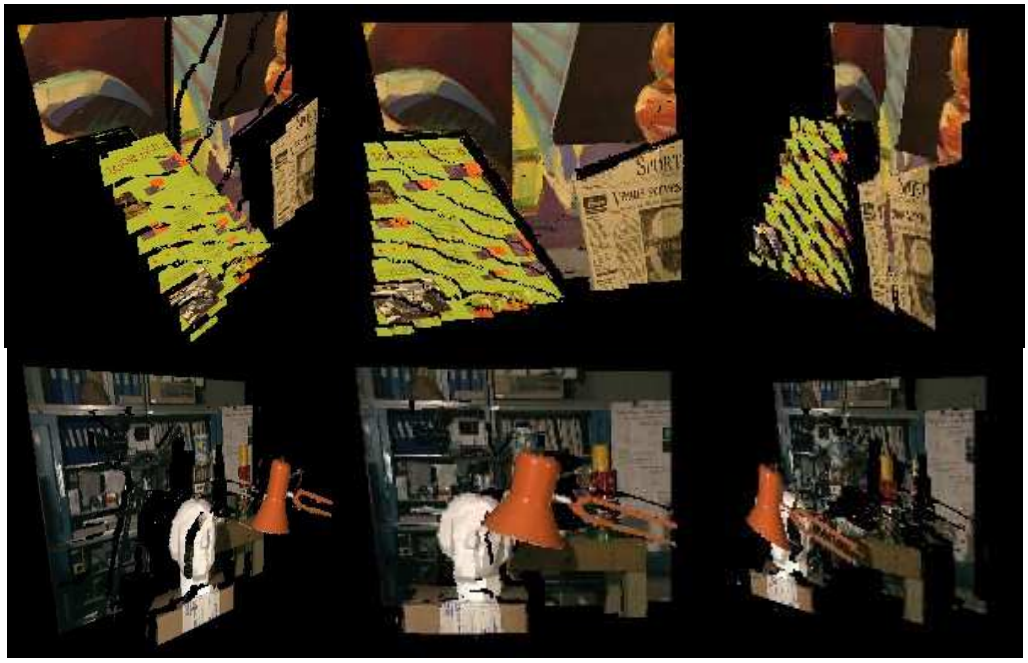

Fig 4. Three view orientation of 3D spatial point-cloud.

Conclusion

This paper utilizes improved ED named Parallel ED to stereo matching and the speed is increased. Parallel method could reduce the probability of local optimum of ED. Because the

samples are taken parallel, the time complexity will be converged by exponent of 2, and samples will be converged to the optimum. Therefore, the speed in our algorithm is more quicker than in ASW obviously, but it still can't avoid local optimum absolutely. In future works, we will add more conditions to decrease the affect of ED's defect.

Acknowledgements

This paper is sponsored by Nature Science Foundation of China (61272216) and innovation Foundation of aerospace in China (CASC201102) and Nature Science Foundation of Jiangxi Province(20114BAB201035) and Science technology cooperation of Jiangxi Province (2010EAB01700).

References

[1] Liu Tianliang, Luo Limin. Segmentation –Based Stereo Matching Algorithm with Variable Support and Disparity Estimation. ACTA OPTICA SINICA,vol.29, No.4:2009.
[2] Wu Chun-Hong, Fu Guo-Liang. A Stereo Matching Based on K-means Segmentation and Neighborhood Constraints Relaxation. Chinese Journal of Computers, vol.34, No.4,2011.
[3] L. De-Maeztu, A. Villanueva, and R. Cabeza. Stereo matching using gradient similarity and locally adaptive support-weight. Pattern Recognition Letters. vol.32, No.13,pp.1643-1651, 2011.
[4] Q. Yang, L. Wang, and N. Ahuja. A constant-space belief propagation algorithm for stereo matching. CVPR, 2010.
[5] C. Cassisa. Local vs global energy minimization methods: Application To Stereo Matching. PIC, 2010.
[6] F. Besse, C. Rother, A. Fitzgibbon, and J. Kautz. PMBP: PatchMatch belief propagation for correspondence field estimation. BMVC, 2012.
[7] N. Barzigar, A. Roozgard, S. Cheng, and P. Verma. SCoBeP: Dense image registration using sparse coding and belief propagation. JVIS, 2012.
[8] C. Pham and J. Jeon. Domain transformation-based efficient cost aggregation for local stereo matching. IEEE Transactions on Circuits and Systems for Video Technology, 2012.
[9] X. Mei, X. Sun, W. Dong, H. Wang, and X. Zhang. Segment-tree based cost aggregation for stereo matching. CVPR, 2013.
[10]Kuk-Jin Yoon. Adaptive Support-Weight Approach for Correspondence Search. IEEE Transactions on Pattern Analysis and Machine Intelligence, vol.28,No.4, 2006.
[11]Zhou Xiu-Zhi,Wen Gong-jian, Wang Run-Sheng. Fast Stereo Matching Using Adaptive Window. Chinese Journal of Computers. vol.29, No.3, 2006.
[12]Guo X, Wang L, Zeng J, Zhang X. VQ Codebook Design Algorithm Based on Copula Estimation of Distribution Algorithm. 2011 First International Conference on Robot, Vision and Signal Processing, pp.21-23, 2011.
[13] Salinas-Gutiérrez R, Hernández-Aguirre A, et al. D-vine EDA: a New Estimation of Distribution Algorithm Based on Regular Vines. Proceedings of the 2010 Conference on Genetic and Evolutionary Computation, pp. 359-365, 2010.
[14]Zhou Shu-De,Sun Zeng-Qi.A Survey on Estimation of Distribution Algorithms. ACTA AUTOMATICA SINICA.vol.33, No.2, 2007.
[15]Neslehova J. On Rank Correlation Measures for Non-continuous Random Variables. Journal of Multivariate Analysis, No.98, pp.544-567, 2007.
[16]Kolesarova A, Mordelova J. Quasi-copulas and copulas on a discrete scale. Soft Computing, No.10, pp. 459-501, 2006.
[17]Cai Dun-Hu, Yi Xu-Ming. The Selection of Wavelet Basis in Image Denoising. Journal of MatheMatics, vol.25, No.2, 2005.
[18] Deng, Na, and Chang-sen Jiang. Selection of optimal wavelet basis for signal denoising. Fuzzy Systems and Knowledge Discovery (FSKD), 2012 9th International Conference on IEEE, 2012.

Advanced Materials Research Vols. 989-994 (2014) pp 1561-1565
© (2014) Trans Tech Publications, Switzerland
doi:10.4028/www.scientific.net/AMR.989-994.1561

Bacteria genome compression based on the weighted Context model

Min Chen[1,2, a], Xue-ming Jia[2, b] and Ling Liu[2, c]

[1]College of Information Science, Yunnan University, Kunming, 650091, China

[2]College of Information Security, Yunnan Police Officer Academy, Kunming, 650223, China

[a]email: minkeychen@sina.cn, [b]email:xuemingj@sina.com, [c]email:14434640@qq.com

Keywords: Weighted Modeling context; Genome Compression; Adaptive Code Length

Abstract. The genome compression algorithm based on the weighted context model is present in this paper. In this algorithm, the method to construct the weighted context model is discussed. The adaptive code length of the context models are used to determine the values of the corresponding weights of models. In the coding process, the values of these weights are modified in order to achieve the minimum code length and to enhance the compression efficiency. At last, the proposed algorithm is used to the bacteria genome compression. The experiments results indicate that the algorithm present could produce better compression result than the results by other algorithms.

Introduction

The rapid genome sequencing technology makes the scale of the genome data increasing exponentially. Although the storage technology has developed rapidly during the past decade, the current storage capacity for saving these genome date is also insufficient. The genome compression is one of efficient approaches to enhance the genome storage efficiency. The first research of the genome compression could be retrospected to the Grumbach's work. In[1], the genome compression algorithm, *BioCompress*, is proposed. In this algorithm, the compression operation is executed by the substitutional procedure as the same as the Lempel-Ziv algorithm done. In the coding process, the genome is separated into two parts, one is the repeated regions and another is the non-repeated regions. The substitutional method is used for the repeated regions coding, but each base in the non-repeated regions is encoded by allocating the code words with 2 bits. As the modified algorithm, the *BioCompress-2*[2] use the 2-order Markov model for coding the bases in the non-repeated regions. However, when the number of the repeated sequence which are added into the dictionary become vaster and vaster, the costs to encode the points of the repeated sequence in the dictionary become too high. The algorithm *GenCompress*[3] is proposed to tackle this problem. In this method, the differences, which are between the exact repetitions in the dictionary and the coding sequence, are encoded. The code length of the genome sequence achieved by this algorithm actually include two parts, one is the code length for coding the repeated sequence point in the dictionary, another is the code length for coding the differences. The difference contain two kinds of information, the positions of the sequence on where the difference happened and the difference itself. In this algorithm, the scale of the dictionary is reduced and the code length for coding the repetition sequence point is shorten, but more information in this algorithm is needed to be encoded. Therefore, *GenCompress* increase the compression rate only a little. In[4], the algorithm *CTW+LZ* is proposed, in this algorithm, the entropy coding based on the Context model is used to encode the short repetitions and the non-repetitions sequence. For the long repetition sequence, the LZ algorithm is deployed to allocate the code words. In this algorithm, the modeling context entropy coding technology is introduced in the genome compression for the first time, the statistic property between the bases is used to produce the satisfactory compression performance. In[5,6], two algorithms which use the statistic models to compress the genome sequence are proposed. In[5], some models which are used for describing different types of regions in the genome sequence are constructed, each model is named by a "expert". Subsequently, each base in the genome sequence is encoded independently by the mixture model of these models. In[6], the compression algorithm based on the mixture finite context model is proposed and its application to compress the bacteria genome sequence is discussed. The performance of this algorithm is better than other algorithms, but the calculation of the weights needs more manual intervention.

Meanwhile, the context models with k orders have different describing complexities for coding the symbols. In[7], the discussion that the adaptive code length is equivalent to the describe complexity of the model is given. When the context model, which is obtained by combining some models with k orders, are used to code the symbols, the value of the weights of these models should be related to their adaptive code length. The models with high adaptive code length should be used as little as possible. Otherwise, the models with take higher value of the weight.

In this paper, the bacteria genome compression algorithm based on the weighted context model is present. Some context models with different orders are constructed to describe the statistic properties of the bases in the genome sequence, the determination of the value of the weights is corresponding to the adaptive code length of each model. Then the mixture model is used for coding the bases.

Context Modeling with Finite Orders

A. Context modeling

Considering the sequence $x_n \ldots x_0$, its code length is described by the representation $-\log P(x_n \ldots x_0)$, where $P(x_n \ldots x_0)$ denotes the joint probability distribution of $x_n \ldots x_0$. In practice, this distribution is not known. We use the past k symbols of the current symbol x_n to construct the conditional probability distributions $P(x_n \mid x_{n-1},\ldots,x_{n-k})$ and then use this distribution for coding the symbol x_n. In this case, the code length of the sequence could be represent by (1).

$$L = -\sum_{i=0}^{n} \log P(x_i \mid x_{i-1} \ldots x_{i-k}) \tag{1}$$

There are $I^k * I$ conditional probabilities should be estimated firstly. The estimation method is the counting statistic approach, which is represent by (2).

$$p(x_i = j \mid x_{i-1},\ldots,x_{i-k}) = \frac{n_j + \delta}{\sum_{j \in I} n_j + I\delta} \tag{2}$$

Where n_j denotes the counts of the $I-ary$ symbol $x_i = j$ whose condition vector is $x_{i-1},\ldots,x_{i-k}$ and δ denotes the initialize number of counts of the symbol x_i. This estimation procedure is referred to as the Context modeling with order k. According to the information theory, if the number of the conditions increase, the entropy of the conditional probability distribution $P(x_n \mid x_{n-1},\ldots,x_{n-k})$ is likely to be reduced, i.e, the code length may be shorten when this conditional probability distribution is used for the entropy coding. However, due to the "Context dilution", it does not always mean that the more number of the conditions, the shorter code length could be achieved[8]. During the training precess, if one conditional probability distribution obtain only a little number of counts n_j, the estimation (2) is not "mature". It follows that the code length may not be shorten when this distribution is used for coding. The describe complexity of the model is defined to represent the mature extent of the model. In our previous work, we find that the adaptive code length is equivalent to the model describe complexity. The adaptive code length of one conditional probability distribution could be calculated by (3)

$$L_m = \sum_{s=0}^{S_m - 1} \log(s + I\delta) - \sum_{j=0}^{I-1} \sum_{i=0}^{n_j - 1} \log(i + \delta) \tag{3}$$

Where L_m denotes the adaptive code length of the m_{th} conditional probability distribution in the context model with order k, S_m denotes the number of the training data the m_{th} conditional probability distribution obtained. There are $M = I^k$ conditional probability distributions in the context model. Then the total adaptive code length of this $k-order$ context model, L^k, is represented by (4)

$$L^k = \sum_{m \in M} L_m \tag{4}$$

L^k describe the complexity of the model when this model is used for coding. The context models with different orders may have diverse describe complexities. If only one context model is used for coding, the code length should not be shorten until this model become "mature"(with low describe complexity). The weighed context model is one efficient approaches to tackle this problem.

B. Weighted Context Modeling

The conditional probability distribution $P(x_n \mid x_{n-1},\ldots,x_{n-k})$ implies the prediction of the symbol x_n by conditioning the past k symbols. The prediction is essentially the max-likelihood estimation. We expect that the uncertainty of x_n could be reduced by conditioning as far as possible. Theoretically, the more number of conditions, the more the uncertainty could be reduced. But this conclusion is based on the fact that the conditional probability distribution is "mature". In practice, whether the conditional probability distribution is mature or not is unknown. It follows that the coding cost is too large before these distributions become mature. Then the conflict comes up, the distributions which contain more number of conditions could reduce more uncertainty but lead to higher coding cost. A approach to alleviate this conflict is to combine some conditional probability distributions which contain various number of conditions. One method for combination is Bayesian model averaging. It is represented by (5)

$$P(x_i) = \sum_{k \in K} P(x_i \mid x_{i-1},\ldots x_{i-k}) w_k \tag{5}$$

Where $P(x_i)$ denotes the prediction of the symbol x_i by combining K conditional probability distributions which contain k conditions for each. $w_k, 0 \le w_k \le 1$ denotes the value of the weight of the conditional probability distribution with k conditions. In[6,7], some methods to determine the value of the weights are discussed. In[7], the impulse response of one filter is used to calculate of the value of the weights. However, the results by this method rely on more manual intervention. And in[6], the value of the weights are calculated by (6)

$$w_k \propto 2^{-3 AvgLen(x_{n-k},\ldots,x_n \mid \theta_k)} \tag{6}$$

Where $AvgLen(x_{n-k},\ldots x_n \mid \theta_k)$ denotes the average code length of the sub-sequence $x_{n-k},\ldots,x_n$ which is encoded by the context model θ_k with order k. The constant parameter 3 is the empirical value. The values of the weights in this algorithm are determined only by the average code length of a part of sequence, it does not utilize the statistical correlation of the training data sufficiently. The purpose of constructing the conditional probability distribution is to reduce the uncertainty of the symbol. The conditional entropy of the conditional probability distribution implies the average uncertainty of this distribution, i.e, the low bound of the code length when this distribution is used for arithmetic coding. However, the conditional entropy could not be known unless the conditional probability distribution is determined. The adaptive code length implies the complexity of the context model, we have a good reason to believe that in the coding process, if the total adaptive code length of one $k-order$ context model is minimum, then this model is effective to encode the next symbol. In the combination process, the model with short adaptive code length should play more role for coding, i.e, higher value of the weight should be given. In our work, the value of the weights are determined by the adaptive code length, which is described by (7)

$$w_k = \frac{L_{\max}^K - L^k}{\sum_{k \in K} L_{\max}^K - L^k} \tag{7}$$

Where L^k denotes total adaptive code length of the context model with the order k, $L_{\max}^K$ denotes the maximum value of the total adaptive code length of all context models with orders k ($k \in K$). By this method, the context model with shorter adaptive code length will assign the higher value of weight. Specially, the model which is corresponding to the maximum adaptive code length will have the value of the weight equaling to value 0. Then we could obtain the combination of the context model by (5) and (7).

C. Bacteria genome compression based on the weighted context model

In this section, the bacteria genome compression algorithm based on the weighted context model is proposed. The genome sequence could be described by a $4-ary$ source. Each symbol(each base) takes its value in the alphabet $\{A,T,G,C\}$. According to the recent research, the correlation is existing among the bases. These correlations should be utilized when the entropy coding based on the modeling context is used for genome compression. We construct the condition probability

distributions to predict the base symbol by choosing the past k bases for conditioning.The weighted context model is considered to combine the context model with different orders, the values of the weights are calculated by (7). In practice, with the coding process, the conditional probability distributions will obtain more and more counts of the symbols, i.e, some context models may become mature, then the adaptive code length of the context models should be updated. In order to achieve this updating process, a parameter N_t is given to control the time of the updating process happened. When the number of the coded symbols reaches the value of N_t ,or $C*N_t$ (C is integer), the update process takes place. Then $C*N_t$ is the threshold of the update process. If the weights are updated, the new weights will take part in the next coding procedure. The algorithm follows as:

Step1: Construct context models with different k orders.

Step2: Using the training data to estimate these conditional probability distributions in the context models by (2).

Step3: Calculating the total adaptive code length for each context model by (3) and (4). Then calculating the value of the weight of this context model.

Step4: If the number of the coded symbols do not reach the threshold $C*N_t$, continue step5, otherwise, go back to step3 to update the weights.

Step5: Combining the context models, Using the conditional probability distribution combined to drive the arithmetic encoder to assign the code word for each base.

Experiments

In this paper, we use the entropy coding based on the weighted context model to compress the bacteria genome sequence. The genome sequence is obtained from the National Center for Biotechnology Information (NCBI) directory ftp://ftp.ncbi.nih.gov/genomes/Bacteria/. The genome data for our experiment contains 2338 sequences and the number of bases is ranging from 1286 to 13033779. We construct 7 context models with orders equals {3,7,8,10,15,20,30}respectively. The parameter N_t equals 10000.

We use two sequences *NC_013929*(10148695 bases) and *NC_014318*(10235715 bases) to train 7 context models respectively. Other three sequences(*NC_013595*, *NC_013131* and *NC_010162*) are used as the source sequences. In experiment 1, we observe the updating process of the weights, the value of the weights in the first 5 updating processes are listed in Table I(Keep two decimal places).

Table I. The value of the weights from first 5 updating processes

Times	w_3	w_7	w_8	w_{10}	w_{15}	w_{20}	w_{30}
1	0.16	0.19	0.20	0.18	0.15	0.12	0
2	0.15	0.19	0.20	0.19	0.14	0.13	0
3	0.14	0.18	0.22	0.20	0.15	0.11	0
4	0.12	0.19	0.19	0.21	0.17	0.12	0
5	0.09	0.17	0.16	0.20	0.21	0.17	0

From Table I, with the coding process, the value of the weights is updated. When more bases which are coded take part in the counting process, the context models with higher orders play more roles for enhance the coding efficiency. Actually, when the updating process is executed 20 times, i.e, 200000 bases are coded, the weights w_{10} and w_{15} will become larger than other weights, in this case, the context models with order 10 and 15 provide the better compression performances than other models. When the number of bases coded reach 3400000, the weight w_{30} will join in the combination to provide more information to predict the current symbol.

In experiment 2, three bacteria genome sequence are used as the source sequence, the same weighted context model as the experiment 1 used is deployed. The bit rate of these genome sequence is given in Table II. For comparison, the compression result by the “expert method” algorithm (XM) in[5] and the result by the finite context model algorithm (FCM) in[6] are also listed in Table II. The results by these algorithm is from [6].

Table II. The comparison of results:

sequence	Number of bases	Results (bit/base)		
		XM	FCM	Our Algorithm
NC_013595	10341314	1.796	1.759	1.742
NC_013131	10468872	1.817	1.779	1.770
NC_010162	13033779	1.755	1.743	1.732

Apparently, from Table II, the results by our algorithm are better than the results by other two algorithms. Although the execution time of our algorithm is higher than the time the FCM needed, but the time our algorithm spent is lower than the time for XM. Meanwhile, in our algorithm, the value of the weights is determined by the adaptive code length and these weights could be modified during the coding process. At last, the code length by our algorithm is minimized.

Conclusion

The bacteria genome compression algorithm based on the weighted context model is present in this paper. The context models with different orders are constructed to predict the genome base. When the weighted context model scheme is deployed for coding, the values of these weights are determined by the adaptive code length of the context models. During the coding process, the value of these weights could be modified dynamically in order to achieve the shortest code length. The experiment results indicate that our algorithm produces better result for the compression of the bacteria genome than the results by other algorithms.

Acknowledgement

This work is supported by the Natural Science Foundation of Yunnan Provincial under Grant 2013FD042.

References

[1] S. Grumbach and F. Tahi, Compression of DNA sequences, in Proc. of the Data Compression Conf. DCC-93, Snowbird, Utah, pp. 340–350, 1993.

[2] S. Grumbach and F. Tahi. A new challenge for compression algorithms: Genetic sequences. Inf. Process. Manage, 30(6): 866–875, 1994.

[3] X. Chen, S. Kwong, and M. Li. A compression algorithm for DNA sequences and its applicationsin genome comparison. RECOMB, page 107, 2000.

[4] T. Matsumoto, K. Sadakane, and H. Imai, Biological sequence compression algorithms, GenomeInformatics, Vols.11, pp.43–52, 2000.

[5] M. Cao, T.I.Dix, L.Allison, and C. Mears, A simple statistical algorithm for biological sequence com-pression, in Proc. of the Data Compression Conf, DCC-2007, Snowbird, Utah, 2007.

[6] Armando J. Pinho etc, Bacteria DNA Sequence Compression using a mixture of finite-context models, IEEE Statistical Signal Processing Workshop, Portugal, pp.125-128, 2011.

[7] Min Chen, Jianhua Chen, Affinity propagation for the Context quantization, Advanced Materials Research, Vols. 791, pp.1533-1536, 2013.

[8] Min Chen, Fuyan Wang, Context quantization based on the modified K-means clustering, Advanced Materials Research, Vols. 756, pp 4068-4072, 2013.

Advanced Materials Research Vols. 989-994 (2014) pp 1566-1569
© (2014) Trans Tech Publications, Switzerland
doi:10.4028/www.scientific.net/AMR.989-994.1566

Research on Blind Source Separation Algorithm Based on Particle Swarm Optimization

Zhou Hao[1,a] , Chen Changzheng[1,2,b] , Sun Xianming[2,c] , Liu Huan[2,d]

[1] School of Information Science and Engineering, Shenyang University of Technology, Shenyang, Liaoning, 110870, People's Republic of China

[2]School of Mechanical Engineering, Shenyang University of Technology, Shenyang, Liaoning, 110870, People's Republic of China

[a]tiexizhou@163.com, [b]chenlw23@yahoo.cn, [c]tiexizhou@163.com, [d]chenlw23@yahoo.cn,

Keywords: blind source separation; particle swarm optimization; natural gradient algorithm, learning rate

Abstract. Blind source separation (BSS) is a technique for recovering a set of source signals without priori information on the transformation matrix or the probability distributions of the source signals. In the previous works of BSS, the choice of the learning rate would reflect a trade-off between the stability and the speed of convergence. In this paper, a particle swarm optimization (PSO)-based learning rate adjustment method is proposed for BSS. In the simulations, three source signals are mixed and separated and the results are compared with natural gradient algorithm. The proposed approach exhibits rapid convergence, and produces more efficient and more stable independent component analysis algorithms than other related approaches.

Introduction

Blind source separation (BSS) is the process of extracting unknown independent source signals from sensor measurements which are unknown combinations of the source signals. Initially inspired by signal separation in the human brain, BSS has recently become a very active research area both in statistical signal processing [1] and unsupervised neural learning [2]. The goal of BSS is to recover the waveforms of unobserved signals from observed mixtures without knowing the mixing coefficients.

So far the theory of BSS has been successfully approached in linear instantaneous mixing model. The key to solving the BSS problem is directly linked to finding a stable learning algorithm. The choice of the learning rate directly affects the stability and speed of convergence. A fixed learning rate and a step reduction learning rate adjustment are both classified as nonadaptive. Most of the known nonadaptive learning algorithms for blind separation of source signals assume the global learning rate is a small positive constant, either fixed or exponentially decreasing from a large value to zero[3]. The main disadvantage to these learning rate adjustment approaches is the inability to separate signals with stability and efficiency.

Several typical adaptive learning rate selection methods for ICA have been developed [4]. An adaptive step-size technique for BSS, natural gradient algorithm, was proposed in [5]. The disadvantage of this approach concerns the selection of the auxiliary variable matrix. The selection is difficult and cannot guarantee stability in the overall system. The method was also not based directly on the separation states of the source signals.

As opposed to these previously mentioned methods, this paper adopts particle swarm optimization (PSO) to find a suitable learning rate for BSS, and also extends its search space to save evolution time, making the system more flexible in adapting to the online learning requirement.

Blind source separation

The blind source separation problem can he modeled as follow:

$$x(t) = A \cdot s(t) \tag{1}$$

Where $x(t) = [x_1(t), x_2(t) \ldots x_m(t)]^T$ is the available vector of observations and $A = [a_{ij}] \in R_{m \times n}$ is the unknown mixing matrix, modeling the environment in which signals are mixed, transmitted and measured [6]. We assume that A is a non-singular n×n square matrix. The goal of BSS is to find a non-singular n×m separating matrix B such that extracts sources via

$$y(t) = B \cdot x(t) = B \cdot A \cdot s(t) = G \cdot s(t) \tag{2}$$

Where $y(t) = [y_1(t), y_2(t) \ldots y_m(t)]^T$ is an estimator of the sources. The separating matrix has a scaling freedom on each row because the relative amplitudes of sources in s(t) and columns of A are unknown. The transfer matrix $G = B \cdot A$ relates the vector of independent signals to its estimators.

In order to separate the independent sources from their linear mixtures, we expect the outputs of the separation system lo be mutually statistically independent. For this purpose, we must utilize a measure of independence between random variables. Thus, we introduce the concept of negative entropy as:

$$J(w_i) = E(G(w_i^T x)) - E(G(v)) \tag{3}$$

Where G (•) are some non-quadratic functions, and v is a random variable with standard normal distribution.

By finding the projection direction w_i which makes J (w_i) maximum, an independent component can be extracted. If J (w_i) takes the maximum value, $E(G(w_i^T x))$ will also have the maximum value, and the extreme point w_i is the solution of equation

$$E(Xg(w_i^T x)) = 0 \tag{4}$$

Where g (•) is the derivative of G (•). According to Newton iteration theorem, we have

$$w_i^+ = w_i - \frac{E(Xg(w_i^T x))}{E(X^T Xg'(w_i^T x))} = w_i - \frac{E(Xg(w_i^T x))}{E(g'(w_i^T x))} \tag{5}$$

Where $E(X^T Xg(w_i^T x)) = E(X^T X)Eg(w_i^T x) = E(g(w_i^T x))$ .Multiply the two sides of (5) with $E(g'(w_i^T x))$ and let $w_i^* = E(g'(w_i^T x))w_i^*$, we have

$$\begin{cases} w_i^* = E(Xg(w_i^T x)) - E(g'(w_i^T x))w_i \\ w_i = \dfrac{w_i^*}{\|w_i\|} \end{cases} \tag{6}$$

By conducting iteration according to (6), the w_i^T obtained through convergence corresponds to the row vectors of the separation matrix W, and then an independent component can be extracted.

Particle swarm optimization

Particle swarm optimization (PSO) is a population based optimization technique that was proposed by Kennedy and Eberhart [6] in 1995 in which the population is referred to as a swarm. The particles express the ability of fast convergence to local or global optimal positions over a small number of generations.

A swarm in PSO consists of a number of particles. Each particle represents a potential solution of the optimization task. All of the particles iteratively discover the probable solution. Each particle generates a position according to the new velocity and the previous positions of the cell, and is compared with the best position which is generated by previous particles in the cost function and keeps the best one; i.e., each particle accelerates the directions not only the local best solution but also the global best position. If a particle discovers a new probable solution, other particles will move closer to it so as to explore the region more completely in the process [7].

Let N denote the swarm numbers. In general, there are three attributes, current position li, current velocity v_i and past best position Pb_i, for particles in the search space to present their features. Each particle in the swarm is iteratively updated according to the aforementioned attributes. Assuming that the objective function f is to be minimized so that the dimension consists of n particles and the new velocity of every particle is updated by (7).

$$v_{ij}(t+1) = wv_{ij}(t) + c_1 r_{1,i}(t)[Pb_{ij}(t) - l_{ij}(t)\} + c_2 r_{2,i}(t)[Gb_i(t) - l_{ij}(t)] \tag{7}$$

where v_{ij} is the velocity of the jth particle of the ith swarm for all $i \in 1 \ldots N$, w is the inertia weight of velocity, c_1 and c_2 denote the acceleration coefficients, r_1 and r_2 are elements from two uniform random sequences in the range (0, 1), and t is the number of generations. The new position of the ith particle is calculated as follows:

$$l_{ij}(t+1) = a_{ij}(t) + v_{ij}(t+1) \tag{8}$$

The past best solution of each particle is updated by:

$$Pb_{ij}(t+1) = \begin{cases} \mathrm{Pb_{ij}}(t), \text{ if } \mathrm{f(I_{ij}}(t+1)) \geq f(Pb_{ij}(t)) \\ \mathrm{I_{ij}}(t+1), \text{ if } \mathrm{f(I_{ij}}(t+1)) < f(Pb_{ij}(t)) \end{cases} \tag{9}$$

The global best position Gb will be found from all particles during previous three steps are defined as:

$$Gb_{ij}(t+1) = \arg\min_{\mathrm{Pb_{ij}}} \mathrm{f(Pb_{ij}}(t+1)), 1 \leq \mathrm{j} \leq \mathrm{n} \tag{10}$$

The BSS algorithm based on PSO can be implemented as the following iterative procedure:

1) Set the iteration number N to zero, an initial population w_i and v_i of size is created from a random initial set of parameters.

2) The fitness for each particle w_i is evaluated using (3).

3) The best previous position of the ith particle is recorded and represented as p_i, i=1,2, …N.

4) The index of the best particle among all the particles in the population is represented as p_g.

5) Change the velocity vector for each particle using (7).

6) Move each particle to its new position using (8).

7) Let N=N+1.

8) Go to step 2), and repeat until convergence. Terminate the iterative procedure.

9) Output the panicle W with the best fitness value and compute the separated signals y(t) = Wx(t).

Simulation

In order to verify the validity and performance of the proposed algorithm, computer simulations are conducted to test the PSO-based method to blind separation of independent sources from their linear mixtures.

Consider the mixing case of three independent random signals: a sinusoidal signal, a triangular wave signal and a random noise signal uniformly distributed in interval [-1, 1]. There are 200 samples from each signal (N=200). The mixture matrix A is chosen randomly.

Fig.1 and 2 show source signals and their mixtures. The separated signals which are the estimations of source signals are obtained by the demixing model adapted in this paper. The parameters of PSO are summarized as follows: The population size of the swarm is 20. The number of iterations is 40. We suppose that g_j=1, so the dimension of search space is selected as 4.

Constants c_1=c_2=2, r_1 and r_2 are two independent random numbers uniformly distributed in the range of [0, 1]. The inertia weight w is reduced linearly from 0.9 to 0.4 during the search. The separated signals obtained with the proposed method (PSO-based) are shown in Fig.3. In order to compare, we also separate the signal with natural gradient algorithm, which is shown in Fig.4.

Separated signals and source signals of the two algorithms are inconsistent in order, and they have different amplitude and phase, which illustrate the two uncertainties of blind source separation. In order to evaluate the separation effect of the two methods, this paper adopts similar coefficient of source signal and separated signal ζ_{ij} as the performance indicator, that is:

$$\xi_{ij} = \frac{\sum_{k=1}^{n} y_i(k) s_j(k)}{\sqrt{\sum_{k=1}^{n} y^2{}_i(k) s^2{}_j(k)}} \tag{11}$$

Similar coefficient between source signal and separated signal based on algorithm in this paper and natural gradient algorithm are shown in table 1.

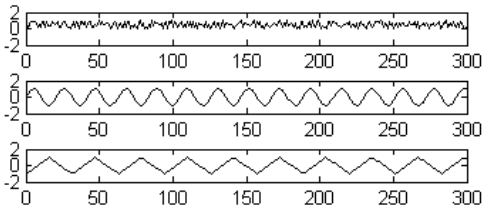

Fig.1 Source signals

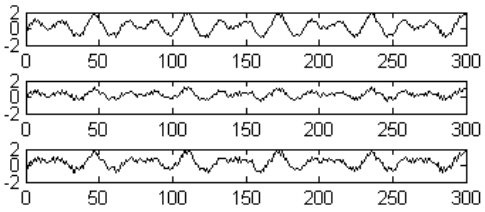

Fig.2 Mixed signals

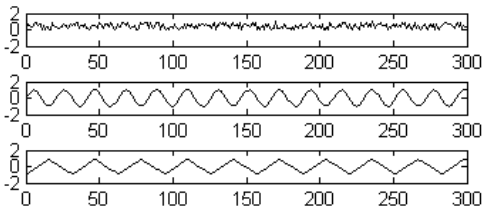

Fig.3 Separated signals obtained with the algorithm in this paper

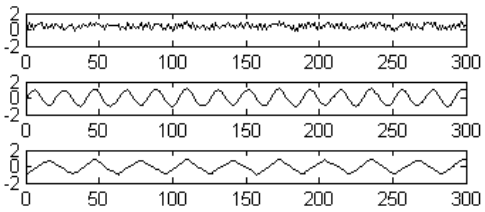

Fig.4 Separated signals obtained with natural gradient algorithm

Table 1. Similar coefficient between source signal and separated signal

similar coefficient	sinusoidal signal	triangular wave signal	random noise signal
algorithm in this paper	0.973	0.964	0.985
natural gradient algorithm	0.866	0.879	0.921

As is shown in table 1, similar coefficient of the algorithm in this paper is closer to 1 than natural gradient algorithm, which shows the separation effect of this algorithm is batter than that of natural gradient algorithm.

Conclusion

A new blind source separation method based on particle swarm optimization algorithm has been proposed in this paper. Simulation results show that the proposed method can obtain clearer estimations of source signals from their mixtures, which overcome the drawback of traditional approaches to BSS such as natural gradient algorithm effectively.

References

[1] Gelle G, Cloas M, Serviere C. IEEE. Tran. on Inst. and Meas. 2003,52: 790～795.

[2] Serviere C, Fabry P. Journal of Sound and Vibration, 2004, 272:317～339.

[3] Roal M.J, Erling J.G. Mechanical Systems and Signal Processing, 2002,16:719～740.

[4] Liu Yanjun, Li Yu, Feng Ding, Systems and Signal Processing. 2010, 29(4): 649-667

[5] Rojas F, Carlos G, Rodriguez M. IEEE Tran. on Systems, Man, and Cybernetics, 2004:407-416

[6] R. C. Eberhart and J. Kennedy, Proc. 6th Int. Symp. Micro Mach. Human, 1995, pp. 39–43.

[7] Lazinlca A. Particle Swarm Optimization. I-Teeh Education and Publishing, 2007.

Advanced Materials Research Vols. 989-994 (2014) pp 1570-1573
© (2014) Trans Tech Publications, Switzerland
doi:10.4028/www.scientific.net/AMR.989-994.1570

The Data Mining Technology of Particle Swarm Optimization Algorithm in Earthquake Prediction

Xiaoyu ZHANG[1,*], Xiang LI[1], Xiao LIN[2]

[1] Department of Computer Science and Application, Zhengzhou Institute of Aeronautical Industry Management, Zhengzhou 450015, China

[2] Academy of Information Technology, Luoyang Normal University, Luoyang 471022, China

Keywords: Particle Swarm Optimization Algorithm; Clustering; Earthquake prediction; Swarm intelligence

Abstract. Data mining technology based on the particle swarm optimization algorithm applied in earthquake prediction was presented. Making use of the characteristics of abnormally high-dimensional data of earthquake precursor, this paper studies an earthquake prediction model based on *the Particle Swarm Optimization Clustering Algorithm*. This model analyzes the relationship between earthquake precursor data and earthquake magnitude. Inputs are 14 abnormal indexes such as belt, seismic gap and short leveling, and output is earthquake magnitude classification. The cluster average-distance is set as the evaluation function of the Particle Swarm Optimization Algorithm. The experimental results indicate that, this model can effectively and validly predict the earthquake magnitude in accordance with the earthquake precursor data. Compared with the traditional clustering k-means Algorithm model, this stability is stronger, and the correctness of forecast is much higher. Through the research and analysis of the example of history source seismic data, the model of this paper is one of approaches to improve the efficiency of earthquake forecast.

Introduction

The research of traditional earthquake prediction is established on people's analysis on earthquake cases data and precursor observation data. However, with the rapid development of precursor observation data on seismic network and in-depth study on earthquake prediction, this method cannot meet the practical needs [Ref. 1].

Tasks of data mining can be summarized as two types in general: descriptive mining of mass data and predictive mining. With the continuous development of data mining, various data mining algorithms in the application fields such as financial analysis, communication operation, biotechnology and intrusion detection have been extensively and intensively studied; this technology also has broad application prospects in earthquake prediction [Ref. 2].

Some representative studies are proposed. Literature [Ref. 3] extracted the earthquake magnitude recognition causal relationship through a large number of sample learning using neural network method, but this model depended on sample selection with poor reusability, and the problem of calculation convergence needed to be studied. Literature [Ref. 4] put forward a new fuzzy rule extraction method, adopted the subtractive clustering based on mountain function to self-adaptively confirm the center of clustering and gave 4 fuzzy rules of earthquake magnitude prediction which were based on the long axis of seismogenic gaps. Since this method is based on the training rule of self-organizing neural network model, it is also a magnitude prediction model based on effective samples, and the prediction rule only considers one type of many precursor observation data.

To apply the data mining techniques for very large databases that the earthquake researchers learn to study, this paper puts forward an earthquake prediction method based on Particle Swarm Optimization Clustering Algorithm and establishes a new earthquake prediction model, facing the multidimensional characteristics of precursor data, and utilizing the distributive and self-organizing feature of swarm intelligence. This method overcomes dependence on data sample selection of the neural network method, and it does not need to design network topology. The analysis on data of history source earthquake cases and experimental results indicate that, this model is superior to the

classic k-means clustering algorithm. The stability is stronger, and the accuracy of forecasting earthquake magnitude is much higher.

Principle of Particle Swarm Optimization Algorithm

Swarm intelligence research mainly includes ant colony algorithm and Particle Swarm Optimization Clustering Algorithm [Ref. 5]. Particle Swarm Optimization Algorithm is a novel evolutionary algorithm. Kennedy and Eberhart put forward it in 1995 through observational study on certain behaviors of bird flock, shoal of fish and human society [Ref. 6].

Particle Swarm Optimization (PSO) is an emerging, heuristic, global random search algorithm based on swarm intelligence, it has the characteristics of easy understanding, easy realization and strong global searching capability, etc. Many scholars research this method to establish models, promote and apply it to data analysis [Ref. 7].

Like other evolutionary algorithms, PSO Algorithm is also based on the concept of "population" and "evolution" and realizes the search for optimum solution of complex space through cooperation and competition among individuals. Meanwhile, PSO does not need to conduct evolutionary operator operations such as cross, mutation and selection for individuals. Therefore, PSO has good biological social background and few parameters. It is easy to understand and realize, and has strong global searching ability for nonlinear and multimodal problems.

Earthquake Prediction Based on the Particle Swarm Clustering

Data background

The seismologic abnormal indexes may be divided into two categories of seismometry index and precursory index. In the book of "Earthquake Cases in China", according to the statistics of observation means, it has 74 indexes for the former seismometry abnormal index and has 84 indexes for the latter precursory abnormal index. The meanings of these indexes are laid out in a guide to the seismological analysis and prediction method. Some scholars specially study on the algorithm for simplifying that how to select the core abnormal indexes from the numerous complex seismic abnormal indexes.

This paper selects the typical earthquake case to verify the earthquake prediction method based on the particle swarm clustering algorithm, and 14 abnormal indexes may be considered. In the experiment of the experimental data by Ref. 3, the earthquake magnitudes are divided into three groups, the first group is three times of seismic sequence of Magnitude 7 above, the second group is nine times of seismic sequence of Magnitude 6 to Magnitude 6.9, the third group is 18 times of seismic sequence of Magnitude 5 to Magnitude 5.9.

Steps of Algorithm

Earthquake prediction model based on the Particle Swarm Clustering Algorithm can be described as follows:

1) The original data of earthquake cases shall be normalized to eliminate the dimensional effect.

Interval values normalized transformation approach is used for the processing of dimensionless of each dimension data, assuming that data sample set is $\{x_{i,j} \mid i=1,2,;n;\ j=1,2,;k\}$, herein, $x_{i,j}$ represents the j dimension value of the i sample, n represents numbers of samples, p represents numbers of dimensions of samples. Normalized sample can be expressed as $x_{i,j}^{'}$, and calculated as shown in Eq. 1:

$$x_{i,j}^{'} = \frac{x_{i,j} - \min\limits_{j}(x_{i,j})}{\max\limits_{j}(x_{i,j}) - \min\limits_{j}(x_{i,j})} \tag{1}$$

Here $\max\limits_{j}(x_{i,j})$ and $\min\limits_{j}(x_{i,j})$ represent the maximum and minimum values of the j dimension data sample respectively.

2) Parameters of initialization algorithm.

Set particle numbers as n, position and velocity of each particle as x_i and V_i respectively, and initial value of r_1 and r_2 is determined as 0, and uniform random number will be automatically selected by the program within the range of [0，1] to calculate and update position and velocity of each particle.

3) Pick up the speed through applying Particle Swarm Optimization Algorithm, and design the update strategy.

4) Design the evaluation function.

If the algorithm satisfies the evaluation function, the algorithm needs to be stopped, and output the optimal solution. Otherwise, it needs to turn to the step 3.

Experimental Results and Analysis

In order to verify and prove the correctness and efficiency of earthquake forecast which is based on Particle Swarm Optimization Algorithm, an experiment in the environment of Matlab 2007a is conducted and a comparison with the classical k-means Clustering Algorithm is made.

Analysis on experimental result and accuracy

After repeated experiments, particle swarm numbers in algorithm is set as 500, parameters are set as α=0.8 , k^+=0.8 , k^-=0.2 . Fig. 1 shows clustering result of pedigree diagram.

As can be seen from Fig. 1, the Particle Swarm Clustering Algorithm is better when applied for earthquake prediction. From analysis on data, the overall forecast accuracy rate of k-means Algorithm is only 73.3%, however, Particle Swarm Optimization Algorithm can increase the accuracy rate up to 83.3%. Compared with results of k-means Algorithm, we can find that Particle Swarm Optimization Algorithm can distinguish magnitudes of less than 6 from magnitudes of more than 7 completely correctly.

Analysis on stability and time complexity

From the analysis on steps of algorithm and code, we can find that earthquake prediction based on the Particle Swarm Clustering Algorithm has the time complexity rate of $O(n)$ and space complexity rate of $O(n^2)$.

In order to analyze the stability of algorithm and the complexity of time, the results of 5 times of experiments were randomly selected to calculate the between-class average distance and time, as shown in Table 1. As can be seen from Table 1, for the prediction of earthquake magnitude, although Particle Swarm Optimization Algorithm consumes a little more time compared with k-means Algorithm, the average distance using Particle Swarm Optimization Algorithm to conduct cluster is smaller than that of k-means Algorithm, this indicates that Particle Swarm Optimization Algorithm has an advantage of better stability than the classical k-means Clustering Algorithm.

Conclusion

This article involves the research on earthquake prediction by applying data mining technology with reference to Swarm Intelligence Particle Swarm Optimization Algorithm. Experimental result shows that compared with classical clustering algorithm k-means, Particle Swarm Clustering Algorithm is in smaller average distance regardless of its slightly slower speed, independent of data sample, provided with the capability of global optimization, and can find the optimal solution more efficiently.

Furthermore, Particle Swarm Optimization Algorithm can be applied for multidimensional data analysis, when used for different data samples , it can be optimized independently based on different measuring parameters, and it is very competitive for the application and is worthy of further study. It needs further study on how to subdivide within the class after the completion of data clustering. Naturally, it shall be pointed out that computer and clustering algorithm can only be used as an auxiliary earthquake prediction, rather than a substitute for people's cognition, analysis and presentation of seismology principles.

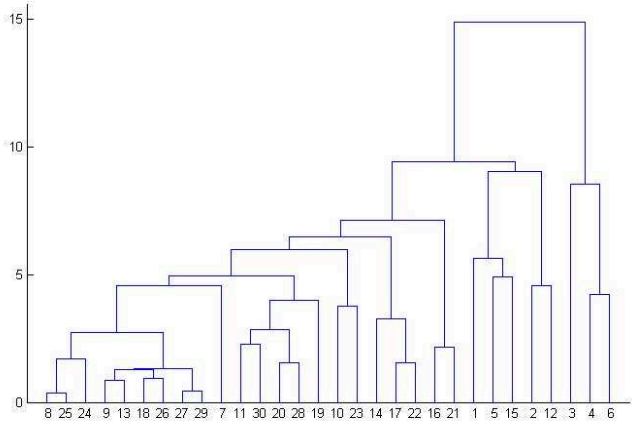

Fig. 1: Clustering Analysis Pedigree Diagram

Table 1: Comparison between the Processed Seismic Data in PSO and K-means Algorithm

	Average distance		Time (s)	
Times of experiment	**k-means**	**Particle swarm clustering**	**k-means**	**Particle swarm clustering**
1	43.112	41.333	134	157
2	45.114	41.333	133	157
3	44.084	41.527	129	157
4	44.511	41.912	133	158
5	44.512	41.333	125	156
Average	44.267	41.488	131	157

*Project supported by the Nature Science Foundation in China(No.U1304616) and the science and technology key project of Henan Province(NO. 122102210480)

*Corresponding author. *Email address*:yx2zczy@126.com (Xiaoyu ZHANG)

References

[1] W. Wang, M. Z. Lin, Q. Z. Ma et al, Data Mining and its Application Prospect in Earthquake Forecast: Recent Developments in World Seismology,2005(12), p. 1-13.

[2] J. W. Han, K. Micheline, Data Mining Concept and Techniques (2nd), Morgan Kaufmann Publishers, San Francisco,2006, p. 359-362.

[3] W. Wang, C. X. Jiang, J. Zhang et al, The application of BP Neural Network in Integrated Earthquake Forecast: Earthquake, 1999,Vol. 19(2), p. 118-126.

[4] S. F. Wu, G. F. Wu, W. Wang, A New Fuzzy Rule Extraction Method: Computer Engineering, 2005, Vol. 31(6), p. 157-159.

[5] J. P. Yu, X. M. Zhou, M. Chen, Research on Representative Algorithms of Swarm Intelligence: Computer Engineering and Applications, 2010, Vol. 46(25), p. 1-4.

[6] J. Kennedy, R. Eberhart, Particle Swarm Optimization, Proceedings of the 4th IEEE International Conference on Neural Networks, 1995, Vol. 4, p. 1942 -1948.

[7] W. L. Wang, Y. Tang. The State of Art in Particle Swarm Optimization Algorithm: Journal of Zhejiang University of Technology, 2007, Vol. 35(2), p. 136-141.

Advanced Materials Research Vols. 989-994 (2014) pp 1574-1577
© (2014) Trans Tech Publications, Switzerland
doi:10.4028/www.scientific.net/AMR.989-994.1574

An Improved Weighted Centroid Localization Algorithm based on RSSI

Liu Chang-liang [1,a], Li Zhe [2,a]

[1] State Key Laboratory Of Alternate Electrical Power System With Renewable Energy Sources(NCEPU),Beijing,102206,China

[2] North China Electric power university,Baoding,071000,China

[a] 15833328695@163.com

Key words: Node localization; RSSI; weighted centroid localization; MATLAB simulation

Abstract. In wireless sensor networks, the precise positioning of unknown nodes is the precondition and security for all kinds of applications. In this paper, by analyzing the present research status of personnel positioning algorithm and on the basis of the study of traditional centroid algorithm, an improved based on RSSI (Received Signal Strength Indicator) of the weighted centroid localization algorithm is proposed. The algorithm takes the signal intensity meanwhile the distance between the unknown nodes and beacon nodes as a reference to correct RSSI value. Through the simulation of the localization algorithm it proves that the improved localization algorithm has higher precision than the traditional algorithm. Once the accidents can be timely and efficient rescue for the underground staff, better meet the actual demand of safety management.

Introduction

To date, personnel positioning algorithm based on wireless sensor networks(WSN) has achieved fruitful results, especially in recent five years has made a number of innovative solutions and ideas. The current localization algorithm in WSN can be divided into two categories [1]: range-based and range-free schemes. range-based position algorithm obtains the distance or angle of point-to-point information by measuring nodes, mainly have TOA(time of arrival) [2], TDOA(time difference of arrival), AOA(angle of arrival), RSSI and so on. range-based localization algorithm has higher precision, but need the help of a wireless signal transceiver device to measure the distance.

RSSI algorithm is the use of theoretical or empirical model converts the signal transmission losses in the air as the distance [3]. But the algorithm in the ranging phase does not fully consider the impact of various beacons to unknown nodes. At present, the control chip sensor node has the measuring function of RSSI. By measuring the RSSI method for ranging, does not need additional hardware equipment, cost saving, simple and easy.

range-free position algorithm does not need the distance and angle information, it according to the network node density information to achieve node localization algorithm. Range-free position algorithm mainly has centroid algorithm, DV-Hop algorithm [4], and APIT algorithm. Compared with range-based position algorithm, the range-free position algorithm has poorer accuracy. A weighted centroid localization algorithm is studied in [5], it used the distance between the unknown nodes and beacon nodes as the weighting value, the positioning precision was improved but still failed to reflect the degree of the influence of beacons to the same unknown nodes.

This paper proposes an improved weighted centroid localization algorithm based on RSSI. First in the RSSI ranging stage, presents a formula based on the improved RSSI distance estimation and determines the path loss exponent and variance. Second in the positioning stage, proposes a closer neighbor centroid localization algorithm. The simulation results show that the method can effectively improve the positioning accuracy and more adaptable to large-scale underground wireless sensor network.

RSSI localization algorithm

2.1. The RSSI loss model

Although the coal mine environment is complex, the transmission of wireless sensor network node can express by the loss model, the formula:

$$\overline{PL}(d)[dB]=\overline{PL}(d_0)[dB]+10\alpha\log\left(\frac{d}{d_0}\right) \quad (1)$$

In the type: $\overline{PL}(d)[dB]$ is the average path loss after a distance of d; d is the distance between unknown nodes and base stations; $\overline{PL}(d_0)[dB]$ is the average path loss after a distance of d_0 (Usually d_0= 1m); α is the path loss exponent.

$$P_r(d)[dB]=P_r[dB]-PL(d)[dB] \quad (2)$$

In the type, P_r[dB] is the intensity of Signal emission; d is the distance between the transmitter and the receiver. P_r(d)[dB] is the received signal strength.

Calculate the distance is:

$$d=d_0\times 10^{\frac{P_r[dB]-PL(d_0)[dB]-P_r(d)[dB]}{10\alpha}} \quad (3)$$

The RSSI (received signal strength indicator) ranging is a rough distance measurement method. Only consider the RSSI to a fixed beacon node from an unknown node, without adding other correction methods, will lead to the algorithm error.

2.2. Improved RSSI method based on multi beacon nodes

The loss model of (1) takes a beacon node as reference point, calculates the distance from the unknown node to the fixed beacon node. In order to reduce the error and reach the purpose of accurate positioning, now adopt an improved RSSI ranging method. Assuming that there are reference beacon nodes: $B_{1,2...N}$ in the communication radius. The distance from the unknown node M to the beacon node D can be expressed as the average of $d_{1,2...N}$:

$$D=\frac{\sum_{i=1}^{N} d_i}{N} \quad (4)$$

D is the corrected distance between the unknown nodes and beacon nodes. This method selecting a plurality of beacon nodes as reference points, it effectively reduces the error.

Weighted centroid localization algorithm

3.1. The traditional weighted centroidal algorithm

Centroid localization algorithm is proposed by Nirupama Bulusu who came from the University of Southern California [8]. In order to reflect each beacon node has different degree of influence to the position of center mass, weighted centroid localization (WCL) algorithm was adopted. The estimated coordinates of the unknown node M (x_M, y_M) is:

$$x_M=\frac{\frac{x_A}{d_A+d_B}+\frac{x_B}{d_B+d_C}+\frac{x_C}{d_A+d_C}}{\frac{1}{d_A+d_B}+\frac{1}{d_B+d_C}+\frac{1}{d_A+d_C}};\quad y_M=\frac{\frac{y_A}{d_A+d_B}+\frac{y_B}{d_B+d_C}+\frac{y_C}{d_A+d_C}}{\frac{1}{d_A+d_B}+\frac{1}{d_B+d_C}+\frac{1}{d_A+d_C}} \quad (5)$$

In the type, d_A ,d_B ,d_C is the distance between the unknown M and each beacon node. With each beacon node O_A ,O_B ,O_C as the center of the circle, (x_A,y_A),(x_B,y_B),(x_C,y_C)are the intersection of three circle coordinates.

Weighted centroid algorithm compared with the traditional centroid algorithm is improved, but there are still some problems in terms of selecting weight value.

3.2. The improved weights in weighted centroidal algorithm

Circle A and circle B intersect at Q_1,Q_2, in the type there will be a little closer to the unknown node M. Introduction of beacon node O_c, the distance from M is over d_c, the distance from Q_1 is over L_1, the distance from Q_2 is over L_2.

If $|L_1-d_c| \le |L_2-d_c|$, $Q_1$is the neighbor point to M. then select point Q_1 as the unknown node, the Weighted value is$\omega_1=|L_1-d_c|$ .Similarly, using the same method to select the other two more neighbor points from the other two groups of intersection Q_3, Q_4 and Q_5, Q_6. By using the weighted centroid algorithm, calculate the unknown node coordinates:

$$x_M=\frac{\omega_1 x_B+\omega_2 x_A+\omega_3 x_C}{\omega_1+\omega_2+\omega_3} \quad ; \quad y_M=\frac{\omega_1 y_B+\omega_2 y_A+\omega_3 y_C}{\omega_1+\omega_2+\omega_3} \tag{6}$$

In the improved weighted centroid localization algorithm, the value of the weights only affected by the beacon nodes which is the nearest to the beacon nodes. In this way, avoid the interference of other beacon nodes and reduce the positioning error in the maximum limit.

MATLAB simulation and the result analysis

Using the improved weighted centroid algorithm to calculate the unknown node M, suppose to calculate to the location of the unknown nodes is(x, y), and the actual position is(x_e, y_e), the error E_r could be:

$$E_R=[(x-x_e)^2+(y-y_e)^2]^{\frac{1}{2}} \tag{7}$$

To locate the unknown node based on MATLAB simulation and test the algorithm performance. First select a 50m×100m square area, then fix the beacon nodes in four vertices(0, 0), (0, 50), (100, 50), (100, 0), take the lattice points:(10, 50), (20, 40), (30, 30), (40, 20), (50, 10), (60, 10),(70, 20), (80, 30), (90, 40), (100, 50) as the coordinate of randomly selected unknown nodes.

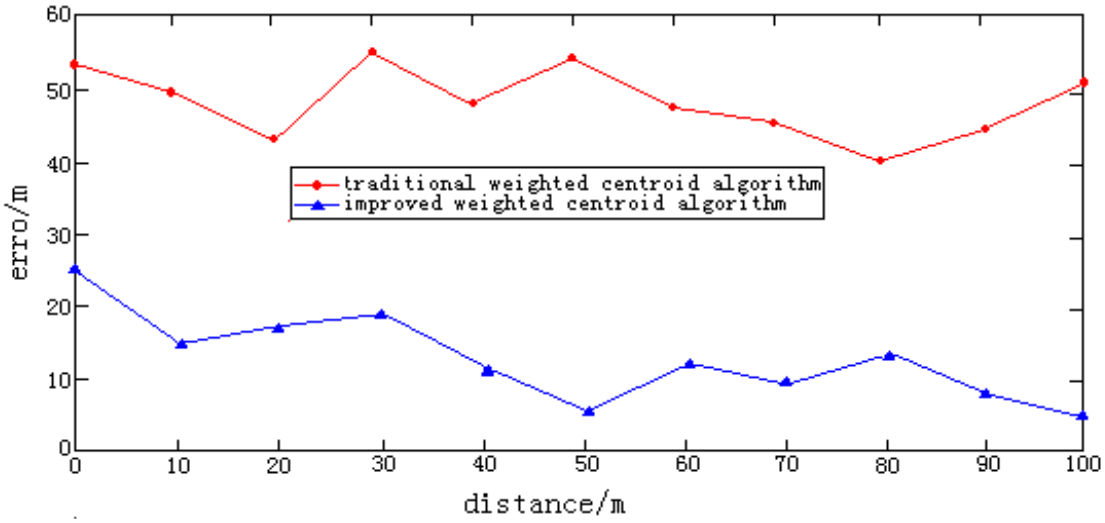

Fig. 1 The structure of fixed beacon and unknown nodes positioning

As can be seen from the figure 1, when the number of the four beacon nodes is unchanged, in the 60m×90m square area, the positioning error of improved weighted centroid algorithm is lower than that of the traditional weighted centroid algorithm , the node position error less than 20m.

As can be seen from the figure 2,when fixed an unknown node (50, 20) as the measured position, by increasing the number of the beacon node to detect the localization error. When the number of beacon nodes is greater than 3, the node position error less than 10m. With the increase of beacon nodes, positioning stability enhancement, positioning error decreases.

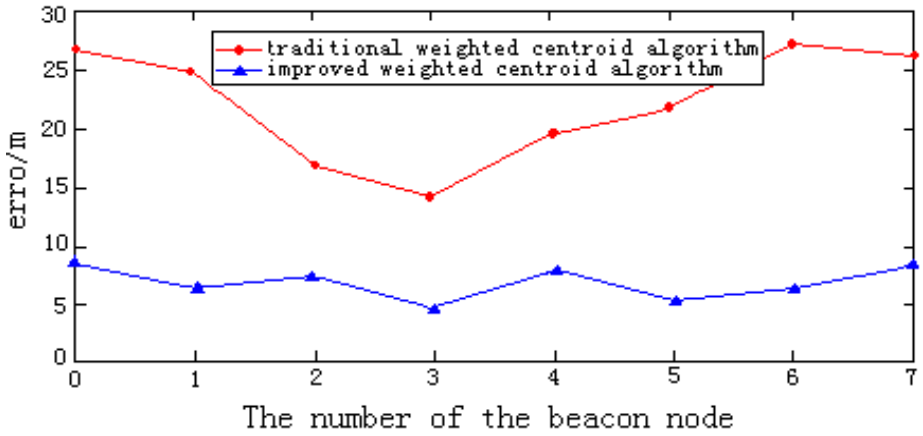

Fig.2. The structure of increases the beacon node location error

Conclusions

By analyzing the deficiency of traditional centroid localization algorithm, this paper proposes an improved based on RSSI (Received Signal Strength Indicator) of the weighted centroid localization algorithm. Through the adoption of the path loss model and the reasonable weight value in the positioning algorithm. The simulation results show that the improved algorithm can improve the precision of the distance between nodes effectively. It is more suitable for the underground positioning system.

Acknowledgements

This paper is supported by State Key Laboratory of Alternate Electrical Power System with Renewable Energy, the Fundamental Research Funds for the Central Universities (13MS102), National Natural Science Foundation of China(61203107).

References

[1]Peng Yu,Wang Dan. Summary of wireless sensor network positioning technology.Journal of electronic measurement and instrument, 2011,05:389-399.
[2]Wang Qin, He Jie, Zhang Qianxiong, Liu Bingfeng, Yu Yanwei. The indoor positioning algorithm based on TOA ranging error classification. Journal of scientific instrument, 2011,12:2851-2856.
[3]Zou Yifan. An improved design of wireless sensor node based on RSSI. East China University of Science and Technology, 2013.
[4]Zhou Xiaobo, Qiao Gangzhu, Ceng Jianchao. Weighted DV-HOP location method based on RSSI in Wireless Sensor Networks. Computer engineering and Applications, 2011,14:109-111.
[5]Chen Weike, Li Wenfeng, Shou Heng, Yuan Bing. Weighted centroid localization algorithm for wireless sensor network based on RSSI. Journal of Wuhan University of Technology, 2006,02:265-268.
[6]Yang Yi, Zhang Dong, Yang Xiaodong. The enhanced RSSI based on more recent neighbor centroid localization algorithm. Micro computer information, 2010,27:124-125
[7]Nirupama Bulusu. Robust range estimation using acoustic and multimodal sensing [A]. IEEE International Conference on Intelligent Robots and Systems, Maui ,Hl, United states, 2011:1312-1320.
[8]NICONLESCU D,NATHE B. Ad-hoc Positioning Systems (APS).Proceedings of IEEE Global Telecommunications Conference,2009,San Antonio:2926-2931.
[9]P. Bahl, V.N. Padmanabhan, A. Balae handran. Enhancements to the RADAR user Location and tracking system.Microsoft Research Technical Report MSR-TR-2000-12.MSR-TR2010-12.
[10]Yedavalli K, KrishnamachariB,Ravula S, et al.Ecolocation:A sequence based technique for RFonly localization in wireless sensor networks.The Fourth International Conference on Information Processing in Sensor Networks,April 2005.

Advanced Materials Research Vols. 989-994 (2014) pp 1578-1581
© (2014) Trans Tech Publications, Switzerland
doi:10.4028/www.scientific.net/AMR.989-994.1578

A Parallel Implementation of the K-means Algorithm Based on MapReduce

Wei Yan[1, a], Jing Zhou[2, b], Qi Huang[3, c] , and Lei Shi[4, d]

[1,2,3,4] School of Computer Science Communication University of China, Beijing, China

[a]yanweiyw@cuc.edu.cn, [b]zhoujing@cuc.edu.cn, [c]hq_pinqy@cuc.edu.cn, [d]shilei_cs@cuc.edu.cn

Keywords: K-means, MapReduce, data mining, distributed computing.

Abstract. With the data explosion, data mining algorithms are required to deal with huge amounts of records. In the traditional way, the processing goes in one single control flow, the time spent in computing grows fast with the increasing of data scale. K-means is one of the widely used algorithms in cluster analysis. MapReduce is a programming model which has been widely used for processing data in a parallel environment. This paper gives an implementation of the K-means algorithm based on the MapReduce model, so that the clustering system could handle the massive data in a fast and scalable fashion. The brief structure of the algorithm and the analysis for the main improvement are also given. We demonstrated that the algorithm will be superior when the volume of data grows bigger or the number of nodes in the computer cluster grows much bigger.

Introduction

The concept of big data has been applied into many fields. That makes the technology of data mining plays an important role in recent commercial activities. Data mining is a subject that using special principles to discover data relations. The data grows fast with the spread of smart equipment. When the scale of the records increased into TB even PB level, it is better to handle such number of records in a parallel environment to keep the efficiency of the system.

The MapReduce model has been proved to be an efficient way for parallel computing. It provides flexibility, speed, load balancing, and good fault-tolerance for developers who want to deploy their application in a distributed system.

Cluster Analysis is an important method in the field of data mining, which divides a set of objects into groups meaningfully. K-means is one of the most widely used algorithms among those in Cluster Analysis. In this paper, we implemented the paralleled K-means algorithm based on MapReduce, which would raise the efficiency a lot when dealing with huge amounts of records.

The other parts of the paper are organized as follow: In chapter 2, we introduced the K-means algorithm. In chapter 3, a brief overview of MapReduce model is given. Chapter 4 tells the details of the paralleled implementation of K-means algorithm based on MapReduce. In chapter 5, we analyze the algorithm. Chapter 6 concludes the paper.

K-means Algorithm

The algorithm aims to group a set of objects into some clusters in which each object belongs to the cluster with the nearest mean distance. The thinking of the algorithm is considered as objects with shorter distance are more similar than those have longer distance. The number of the clusters to be grouped into is chosen by the user.

Suppose P and Q are two objects. They are defined as P = (a1, a2, a3...an) and Q = (b1, b2, b3...bn). The formula for calculating the distance is as follow.

$$d(P,Q)=\sqrt{\sum_{k=1}^{n}(ak-bk)^2} \tag{1}$$

The steps for the basic K-means are discussed below:

1. Choose K points as the initial cluster's centers.

2. Calculated the distance between each point and the initialed centers chosen in step 1.
3. Put each point in the cluster, which its center has the nearest distance to the point.
4. Calculate the average point of all the points for every cluster.
5. Use the average point as the new center for each cluster. Compare their new center with the original one. If the distance between them is smaller than the threshold or the number of iteration reach the limit. Then stop the algorithm. Otherwise, go to Step 2 with the new centers as the parameter to be processed.

MapReduce Model

The MapReduce model is proposed by Google [1]. It is used in parallel and distributed processing environment to deal with enormous data computing. To parallelize an algorithm, the data should be able to divide into pieces and the process for each piece of data could be done separately.

The MapReduce model uses the divide-and-conquer strategy, divides a task into several copies of fine-grain sub-tasks. It comprises two steps. They appear as the Map function and the Reduce function. The Map function processes every single sub-task. It takes a pair of (key, value) as the input and generates another intermediate pair for the next step. The Reduce function merges the intermediate pairs to form a smaller set of values. The implementation of the two steps can be designed based on the users' practical situation.

Parallel K-means Algorithm

An implementation presents in [2] takes the centroids as the "key" and the vector of attributes of the object as the "value" for the input (key, value) pair. The output of the Map function takes the centroids as the "key" and the point belongs to the cluster as the "value" for the intermediate pair. The Combine stage read the intermediate value and group the pairs which have same "key". The Reduce stage reads the combination and calculates the average point as the new centroid for each cluster. Another implementation mentioned in [3] takes the same input pair but the different output in the Map function. It takes the minimum distance within the "value" of the output (key, value) pair.

The implementations discussed above have a similar character, which is the recalculation of the new centroid is done in the Reduce function completely. We can see that the speed of Reduce function is the bottleneck of the efficiency in the algorithm. So put the recalculation into the Map stage will be helpful to decrease the computation in Reduce stage, and so is the time cost.

Our strategy is to keep an array of variables to store the average of the points belongs to the same cluster in Map function. When the assignment of this new point to a cluster is done, update the average point for this cluster. In the end, the Map function takes the variable with the cluster's center as the "key" in the output pair. The "value" is still the name of a point. The Reduce function only need to get the average points from the output pair of Map function and calculate the new average point for each cluster.

4.1 Preprocessing of the data

For the convenience of processing, every single record of the data set will be formatted into a line of text. A possible solution can be as follow:

object A: attribute 1, attribute 2, attribute 3.....;

4.2 Brief process of the algorithm

The brief process of the Map function, Reduce function, Main function is as follow.

```
Map Function:
  Begin:
  File fp = openfile(datafile)
    List AveragePointList.
    List RecordPoints = GetAllRecord(fp)
    record rc = GetFirstRecord(RecordPoints)
    while(rc != NULL)
      for (each center)
        Calculate the Distance.
        Update NearestCenter and MinDistance;
      end for
      Update AveragePoint in the AveragePointList.
      rc = GetNextRecord().
    end while.
  End
```

```
Reduce Function:
  Begin:
    Array DistanceArray, AveragePointArray;
    For (each center)
      Calculate the new AveragePointArray[index].
    End for
    For (each center)
      DistanceArray[index] = AveragePointArray[index]- OldCenter.
    End for
  Output the old center and DistanceArray as result.
  End
```

```
Main Function:
  Begin:
    Read the cluster information from file.
    While (Difference > threshold)
      SetMapperClass
      SetReducerClass
      Set other basic infomations.
      Run the Job
      Get the difference from the output.
    End While
  End
```

The brief process is shown in Figure 1:

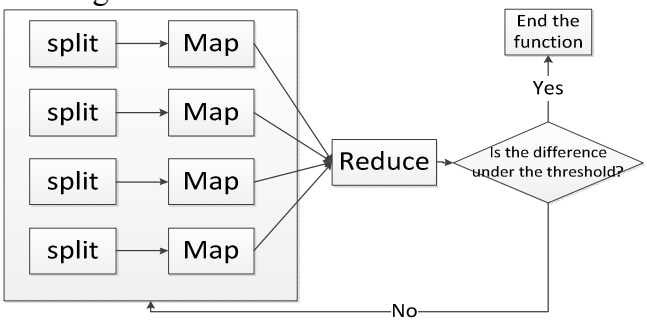

Fig.1 Brief process of the parallel K-means algorithm

Analysis of the algorithm

Because of the efficient of the algorithm could be affected by the hardware, code quality or other factors. Compare the running result is not very convictive. So we only do the analyzing theoretically.

The basic idea of the improvement in the algorithm is to distribute the distance calculation into parallel environment, and the difference between the algorithm in this paper and [2, 3] is we put the stage of calculating the new centroid into distributed nodes. We only analysis the time cost in this part.

Assume that the quantity of the records is m, the number of nodes is n, the number of clusters to be classified into is c, the time cost in addition is p, the time cost in division is q, the other time cost in transporting and CPU dispatching is o. The time cost of the normal way, which did all the calculation in Reduce stage, is t1 = [m-(c-1)]p+cq+o. The time cost of the way presented in this paper, is t2 = [m/n+n-2(c-1)]p+2cq+o.

Make a division of t1 and t2 like this: {[n/m+n-2(c-1)p+2cq+o]}/{[m-(c-1)]p+cq+o]}. N, c, q, and o won't be quite big when compared with m in this polynomial. With m and n's increasing, the time that the algorithm saved is going closely to the polynomial below.

$$\frac{(n-1)mp}{n} \tag{2}$$

The result shows the algorithm will be more efficient when the number of nodes and the records grows bigger.

Conclusions

This paper mainly presented a way to distribute the K-means algorithm based on the MapReduce model. With the volume of data growing and adding more nodes to the computer cluster, the efficiency will be improved.

Acknowledgement

This work was funded by the Engineering Disciplines Planning Project of the Communication University of China (3132014XNG1453, 3132013XNG1320) and the National Natural Science Foundation of China (No. 61103198).

Reference

[1] Jeffery Dean and Sanjay Ghemawat. ***MapReduce: simplified data processing on large clusters***. In Proceedings of the 6th conference on Symposium on Operating Systems Design and Implementation, San Francisco, CA, 2004.

[2] Shuping liu and Yanliu Cheng. ***Research on K-means Algorithm Based on Cloud Computing.*** In Proceedings of Computer Science and Service System (CSSS), 2012 International Conference, Nanjing, China, 2012.

[3] Yunfeng Xu, Yan Zhang, and Rui Ma. ***K-means algorithm based on Cloud Computing***. In Computational Intelligence and Design (ISCID), 2012 Fifth International Symposium. Hangzhou, China, 2012.

[4] Jing Zhang, Gongqing Wu, and Haiguang Li. ***A 2-Tier Clustering Algorithm with Map-Reduce***. In ChinaGrid Conference (China-Grid), 2010 Fifth Annual, Guangzhou, China, 2010.

[5] Yingan Li. ***Research on Parallelization of Clustering Algorithm Based on MapReduce***. In Master's thesis, 2010.

Advanced Materials Research Vols. 989-994 (2014) pp 1582-1585
© (2014) Trans Tech Publications, Switzerland
doi:10.4028/www.scientific.net/AMR.989-994.1582

A Inflexion nonlinear global Particle Swarm Optimization (PSO) algorithm

LV Li-xia[1,a], LIN Xiang-yu[2,b]

[1]Control and Computer Engineering, North China Electric Power University, Baoding Hebei,071003 China)

[1]Control and Computer Engineering, North China Electric Power University, Baoding Hebei,071003 China)

[a]email:lvlixia63@163.com, [b]email:linxiangyu111@126.com

Key words: The standard Particle Swarm Optimization algorithm; Premature; Inflection nonlinear; Global average location;

Abstract. According to the question of the standard particle swarm optimization (PSO) algorithm is prone to premature and no convergence phenomenon, this paper proposed an algorithm of Inflection nonlinear global PSO. The algorithm introduces nonlinear trigonometric factor and the global average location information in the formula of velocity updating. It take advantage of the convex of the triangle function cause the particles early in the larger velocity search maintain long time and in the later searching with smaller speed maintain long time, use the global average position information make the population can use more information to update their position. The method are applied in optimizing in the parameters of the main steam temperature control system and furnace pressure control system for comparison, the results show that the method in the search speed and precision than standard PSO has significantly improved.

Introduction

Particle swarm optimization in the search, the great particle velocity is beneficial to the global search, but not easy to get the exact solution, however, little speed will help local search to get more accurate solution, but the speed of convergence is low[1].

For that, the literature[2] have proposed a multi-strategy co-evolution PSO (MSCPSO) algorithm to achieve the purpose of balancing the global and local search of the population; the literature [3] have added the trigonometric factor to the formulas of evolution displacement, using of the characteristics of periodic oscillation of trigonometric so that each particle to obtain a stronger oscillation characteristics to guide the particles close to the global, and thus jump out of prematurity; the literature [4] have improved the velocity updating formula on the basis of standard PSO for introducing the average information of entire population significantly improved in the convergence accuracy and rate. In literature [2-4], the inertia weights of the velocity updating formula are based on linear convergence. The literature [5] pointed out that the inertia weight of particle swarm decrease linearly can not adapt to the complex and nonlinear optimization search process. For that, the literature [5] have introduced the nonlinear trigonometric factors in the formula of speed evolution, make the search speed to maintain a larger value longer during the early period; remain small value longer during the late, effectively guarantee the accuracy and the convergence speed of the algorithm.

The improvement of the algorithm in reference [5] have made the calculation precision and the convergence speed improved, In order to make it work better, on the basis of literature [5], this paper add the idea that introducing the global variables in literature [4]. Nonlinear cosine factor with inflection point and global average information are introduced to the formula of speed evolutionary to improve the algorithm, and compare the improved PSO algorithm with the standard PSO algorithm in optimizing the parameters of the control system of main steam temperature and furnace pressure system. The simulation results show that the improved algorithm has better convergence speed and accuracy than the standard PSO algorithm.

The standard PSO and its improvement

For the N-dimensional space, randomly generated *m* particles which initial velocity, displacement, and the fitness value of its decisions should be randomized. Standard PSO particle update their location by the following formulas (1) (2) (3):

$$V_{in}(t+1) = w * v_{in}(t) + c_1 r_1 [X\text{best}_{\text{in}} - x_{in}(t)] + c_2 r_2 [X\text{best}_{\text{gn}} - x_{in}(t)] \quad (1)$$

$$X_{in}(t+1) = X_{in}(t) + V_{in}(t+1) \quad (2)$$

$$w = w_{\max} - \frac{w_{\max} - w_{\min}}{T_{\max}} * t \quad (3)$$

In the formulas, *i=1,2,...m, n=1,2, ...N, t* denotes the *t* generation, c_1 and c_2 are called learning factors that are non-negative constants. r_1 and r_2 are random variables between [0,1]; $X\text{best}_i$ is the optimal solution of particle itself after iterating so far; $X\text{best}_g$ is the optimal solution for the whole population ; *w* is the inertia weight.

The inertia weight *w* plays a function that coordinated global search and local search. From equation (1) (2) (3) can be drawn: the standard PSO update the particle velocity and displacement in strategy that *w* decrease linearly [6]. However, the search process of entire population is nonlinear[7], for which, the literature [5] introduced nonlinear trigonometric factor in the formula of speed updating to improve the algorithm accuracy and convergence speed, as shown in the fourth formula:

$$\begin{cases} v_{ideal}(t) = v_{start} * \dfrac{1 + (\cos(t\pi / T_{\max}))^n}{2} \\ \quad t \le 0.5 T_{\max} \\ v_{ideal}(t) = v_{start} * \dfrac{1 - (\cos(t\pi / T_{\max}))^n}{2} \\ \quad t \le 0.5 T_{\max} \end{cases} \quad (4)$$

Standard PSO premature easily and the convergence precision is lower when facing to the complex object. For which, literature [4] introduced the average information of the entire population in the velocity updating formula as shown in the fifth formula:

$$V_{in}(t+1) = w * v_{in}(t) + c_1 r_1 [X\text{best}_{\text{in}} - x_{in}(t)] + c_2 r_2 [X\text{best}_{\text{gn}} - x_{in}(t)] + c_3 r_3 [X\text{best}_{\text{at}} - x_{in}(t)] \quad (5)$$

Where the w is still using inertia weight decrement strategy, the $X\text{best}_{\text{at}}$ represents the average value of individual extreme of the section t generation in the iteration process of all the particles. as shown in the sixth formula:

$$X\text{best}_{\text{at}} = \sum_{i=1}^{m} Xbest_{in} / m \quad (6)$$

The experimental results showed that: the improved PSO algorithm enhances the ability to jump out of the premature when the global average position information was introduced to the velocity updating formula in seventh literature.

For the problem of the standard PSO algorithm is prone to premature and the convergence precision is usually lower, this paper has made improvement in two aspects. Firstly, introduce the global average position information in the formula of speed updating as shown in fifth equation. Secondly, add the cosine factor in the formula of inertia weight to turn the traditional linearly converges into the law of non-linear as shown in seventh equation.

$$w = w_{\min} + 0.5 * (w_{\max} - w_{\min}) * (1 + \cos[k(\frac{t}{T_{\max}})]) \quad (7)$$

In the seventh formula *k* is the control factor to the smoothness of the curve. The *w* in linear and nonlinear cosine convergence properties as shown in the Fig .1:

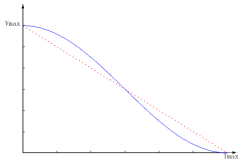

Figure 1: Comparison of *w* in linear and cosine

As shown in Fig .1, the dotted line represents the curve of linear, the full line is the curve of nonlinear cosine. We can acquire from the figure that in the early search, particles can be a faster rate in nonlinear cosine convergence than the linear and persist much longer, while the later, the search can be slower rate than the linear and persist longer time. In this way make the algorithm trade-off between global and local search in search process to achieve better convergence speed and accuracy.

Comparison of two algorithms in the optimization of controller parameters

Traditional optimization in controller parameters not only requires technical skills and experience, but also time-consuming, more importantly, their adaptive capacity is relatively poor [4]. This article put inflection global PSO and standard PSO algorithm both applied to parameter optimization of furnace pressure and main steam temperature control system. There having a particle swarm in which select 80 particles and iterate 100 generations, recognizing factor $c_1 = c_2 = c_3 = 2$, $k=3.14$. Selecting w in a limiting interval [0.9, 1.2], compare the optimization effect of two kinds of algorithm.

2.1 Comparison of the PID Parameters Optimization in furnace pressure

The transfer function of the amount of air supplied and induced effect on the furnace pressure in thermal power plant as is shown:

$$G(S)=\frac{0.74}{(3S+1)^2} \tag{8}$$

Controller using PI controller, the parameters of the controller are Pi=0.5, Ti=4.4. It used these two algorithms to optimize the parameters of the controller. The Standard PSO had obtained the optimized results when it iterated to the 48th generation, as is shown: Pi=0.4, Ti=5.4. The inflection point nonlinear global PSO had got the results when it iterated to the 41st generation, as is shown: Pi=0.42, Ti=5.8. The simulation results are shown in Fig .2.

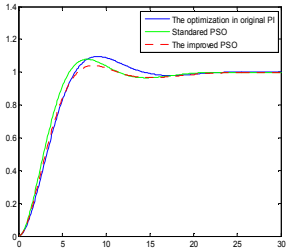

Figure 2: The results of using two algorithms in optimizing parameters of PI controller of furnace pressure

2.2 Comparison of the PID Parameters Optimization in main steam temperature

The transfer function of water spray affecting the main steam temperature in a thermal power plant is:

$$G(S)=\frac{-11.32}{(192.5S+1)^3}e^{-8.4s} \tag{9}$$

Controller also be PI controller, the original PID parameters are *Pi=-14.5, Ti=342*. The Standard PSO had obtained the optimized results when it iterated to the 62nd generation, as is shown: *Pi=-15.5 Ti=339.* The inflection point nonlinear global PSO had got the results when it iterated to the 47th generation, as is shown: *Pi=-15.93, Ti=339.9.* The simulation results are shown in Fig .3.

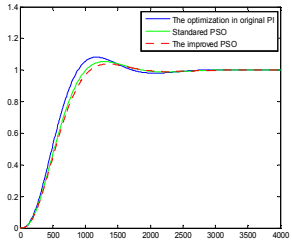

Figure 3: The results of using two algorithms in optimizing PI controller parameters of the main steam control system

2.4 Analysis of simulation results

From the results in Figures 2 and 3 we can acquired that the controller parameters optimized results of turning point nonlinear global PSO with larger proportional band so the adjustment time is smaller and the system is more easily stabilized; with greater integration time makes the adjustment more accurate. Inflection point global nonlinear PSO less iterations than the standard PSO algorithm in the optimization, the faster and better results. The final simulation results show that the inflection point nonlinear global PSO than the standard PSO algorithm has been greatly improved in the searching speed and accuracy of optimization, the better.

Summary

In this paper, for the problem of premature convergence of standard PSO algorithm in the search process, it introduced the nonlinear trigonometric function factor and global average position information to the formula of speed updating, presented an inflection point nonlinear global particle swarm optimization method. The experimental results show that this algorithm has a better effect than standard PSO algorithm in parameter optimization. It effectively enhance the ability of the particles jump out of the prematurity. This algorithm has some practical significance and practical value.

Acknowledgements

This paper is supported by State Key Laboratory of Alternate Electrical Power System with Renewable Energy, the Fundamental Research Funds for the Central Universities (13MS102), National Natural Science Foundation of China(61203107).

References

[1] Xugang, Qu Jin-ping. An improved adaptive particle swarm optimization algorithm [J]. South China University of Technology: Natural Science Edition, 2008,36 (9):6-10. (In Chinese)

[2] Zhang jie, Pei fang. Multi-strategy cooperative particle swarm optimization algorithm [J]. Computer Applications Research .2013.30 (10):2965 -2967. (In Chinese)

[3] Shao peng, Wu zhi-jian. Rosenbrock Function Optimization Based on Improved Particle Swarm Optimization Algorithm [J].Computer science. 2013.40(9): 194-197. (In Chinese)

[4] Su Jin-rong, Li Bing-yi, Wang Xiao-kai. Particle swarm optimization using average information of swarm[J].Computer Engineering and Applications, 2007,43(10):58-59. (In Chinese)

[5] Xu gang, Yang Yu-qun, Liu Bin-bin. A Nonlinear Adaptive Particle Swarm Optimization[J]. Journal of Nanchang University(Natural Science). 2011, 35(4) 323-326. (In Chinese)

[6] SHI Y, EBERHART R, C EMPIRICAL. Study of particle swarm optimizer[C]. Proceeding of the World Muhi conference on Syatemics. Cybernetics and Informatics, Orlando, 2000.

[7] Huang Ze-xia, Yu You-hong, Huang De-cai. Quantum particle swarm optimization algorithm of adaptive adjustment inertia weights [J]. Journal of Shanghai Jiaotong University.2012,46(2): 228 -232.(In Chinese).

Advanced Materials Research Vols. 989-994 (2014) pp 1586-1589
© (2014) Trans Tech Publications, Switzerland
doi:10.4028/www.scientific.net/AMR.989-994.1586

The Research of Improving Clothing Crossing-selling based on Apriori Arithmetic

ZHANG Chi [1, a], LIU Yi[1,2, b], SUN Fangshuai[1,c] and YAO Li[3,b]

[1]Beijing Institute of Fashion Technology, Chaoyang District, Beijing, China

[2]Beijing University of Post and Telecommunications, Beijing, China

[3]Schneider Electric(china) Co.Ltd, Chaoyang District, Beijing, China

[a]573510157@qq.com, [b]mableliuyi@163.com,[c]765631159@qq.com

Key Words: Association rule; data mining; Apriori arithmetic; crossing-selling

Abstract. First, we describe crossing-selling and association rules. And then with the study of a correlation clothing store sales data, it shows the Apriori algorithm applies in specific association analysis. We can propose a model which is suitable for crossing-selling. Through commercial test, the algorithm can significantly increase sales of the relevant product.

Introduction

Cross-selling refers to a means of marketing that aims to satisfy the varied demands of a present customer by selling related services or products of multiple sorts. It imposes an impact on traditional banking and insurance industries by reason of the analyzability of the real data, that supplied by consumers when they purchase relevant products and services, for further analyses on customer demands. In addition, the data can be employed as the basis of market researches for more superior customer services, and applied to mutual marketing with businesses of complementarity.

With respect to clothing industry, cross-selling, accommodating to the features and trends of clothing market, has found extensive application. Currently, plenty of time has to be spent in seeking desired garments because of the rapid increase of the number and the expansion of the kinds of the clothing produced, hence constantly draining customers, which results from looking through amounts of irrelevant information.

To solve the problem, clothing businesses should analyze and categorize their products by complementarity, competitiveness, similarity in prices and..., based on the study of numerous transaction data, to assist display designers in placing merchandises with high effectiveness in the shops, so that customers can make purchases reasonably and effectively, and meanwhile the businesses can cater to the purchasing habit and the personal demands of customers.

Introduction of Association Rule

Overview of Association Rule

Association rule mining analyzes associate information from amount of vague and noisy data which it does not know by people but it is potential and useful information. It is an important branch of data mining .The primary goal is finding degree of relationship of trading database between different attributes and variables. It also extracts some implied connection relationship from trading items

Elemental Knowledge of Association Rule[3]

Let $I = \{i_1, i_2, \ldots, i_n\}$ be a set of n binary attributes called *items*. Let $D = \{t_1, t_2, \ldots, t_n\}$ be a set of transactions called the *database*.

Each transaction in D has a unique transaction ID and contains a subset of the items in I. A *rule* is defined as an implication of the form $X \Rightarrow Y$ where $X, Y \in I$ and $X \cap Y = \emptyset$.The sets of items (for short *itemsets*) X and Y are called *antecedent* (left-hand-side or LHS) and *consequent* (right-hand-side or RHS) of the rule respectively.2.2.2 The *support* $\mathrm{supp}(X)$ of an

itemset X is defined as the proportion of transactions in the data set which contain the itemset. That is $(X) = (\sigma_x/|D| * 100\%)$

The rule A)B has confidence *c* in the transaction set *D*, where *c* is the percentage of transactions in *D* containing *A* that also contain *B*. This is taken to be the conditional probability, that is $\text{Confident}(X \Rightarrow Y) = \left(\frac{support(X \cup Y)}{Support(X)} * 100\%\right)$

Usually, minsupport and minconfident are given specific value what we need. From the probability view, support is probability which incident x and incident y happen at the same time. Confident is incident Y of probability happened under incident X. The criticism of most value association rule is that both support and confident is high

Association Rule Mining Applications:

Association rule is widely used in the financial industry companies, some well-known e-commerce sites, weather forecasting, medical diagnosis and shopping analysis.

Effect of the application of association rules on sales

According to association rules in crossing-selling, we can get specific dependent relationship of clothes. Based on this relationship, decision maker will put potential A product and B product together to stimulate desire of consumers so that they will buy A when they buy B. But if decision maker don't put A product and B product together, some of consumer maybe do not buy B product because they think it is time-consuming to find B product. In some degree, It will affect profit.

Application of Association Rules Algorithm in Clothing Cross-selling

Introduction of Apriori Arithmetic.

The process is shown in figure.1

Specific Process.

Clothing specialty store of transnational corporation has a number of stores in many cities and countries. All the analyze data comes from real crossing-selling system. In order to prevent error data, we export stable data from December 1st to 10th with OSD Restocking of Clarity. Sales-Time and Style are useful in data mining. So only five products are listed to from D={A:2001HA (helvetica alphabet T-shirt) B: 8328 (leggic) C:RSA0504 (scrunchie) D: RSA0509(bow hair clip) E:RSA0324(oversized button up)

Using Apriori algorithm find out minsupport which is 35% and length of frequent item is 3.

The process is shown in Table 1:

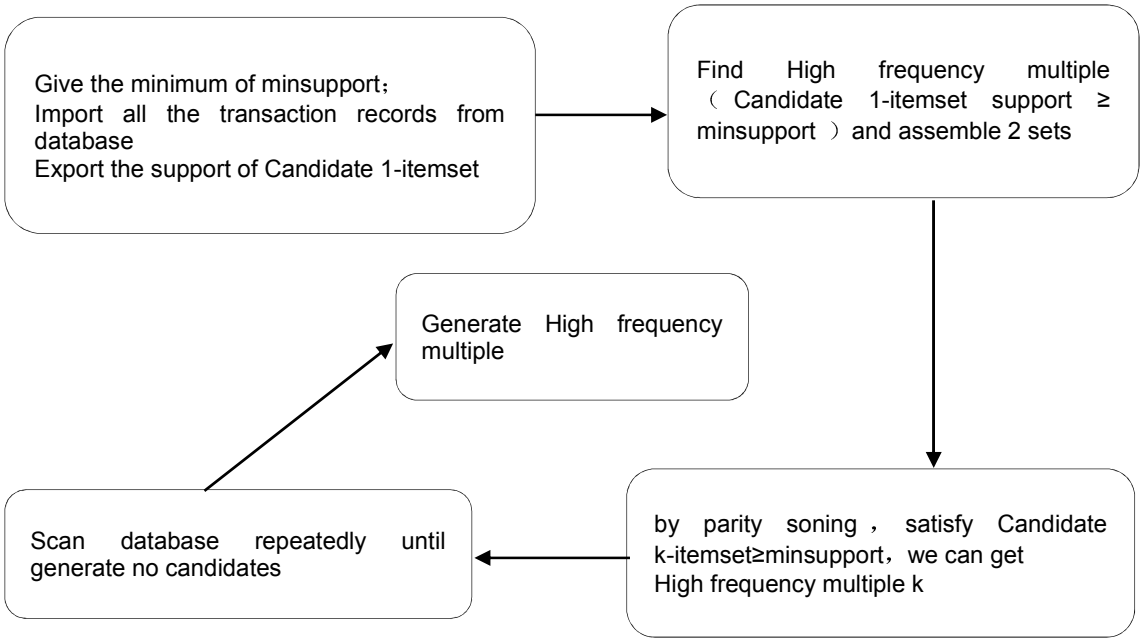

Figure1 Introduction of Apriori Arithmetic

Table.1 Sales Database

Sales-Time	Style	Sales-Time	Style
12.01	ABCDE	12.06	ABCE
12.02	D	12.07	ABCE
12.03	BCDE	12.08	ACDE
12.04	BCD	12.09	ACD
12.05	DE	12.10	ACD

In the example above, selling database D gains frequent item L3={A,C,D}and L3={A,D,E} with scanning, screening ,combining and pruning .If constraint condition is that right comprehension has one product and the confidence is 60% , the association rule follows

Finding and Analyses. The rules above come to the initial conclusions as follows:

First, rule 1 indicates that most customers who purchase item C:RSA0504 (scrunchie)

from our company would purchase item A:2001 (helvetica alphabet T-shirt) under almost all circumstances.

Furthermore, rule 2 indicates that customers who purchased item C:RSA0504 (scrunchie) and E:RSA0324(oversized button up) simultaneously marks high chance of purchasing item A:2001HA(helvetica alphabet T-shirt); and those who purchaseditem C:RSA0504(scrunchie)and D:RSA0509(bow hair clip) simultaneously marks high chance of purchasing item A:2001HA (helvetica alphabet T-shirt) as per rule 3.

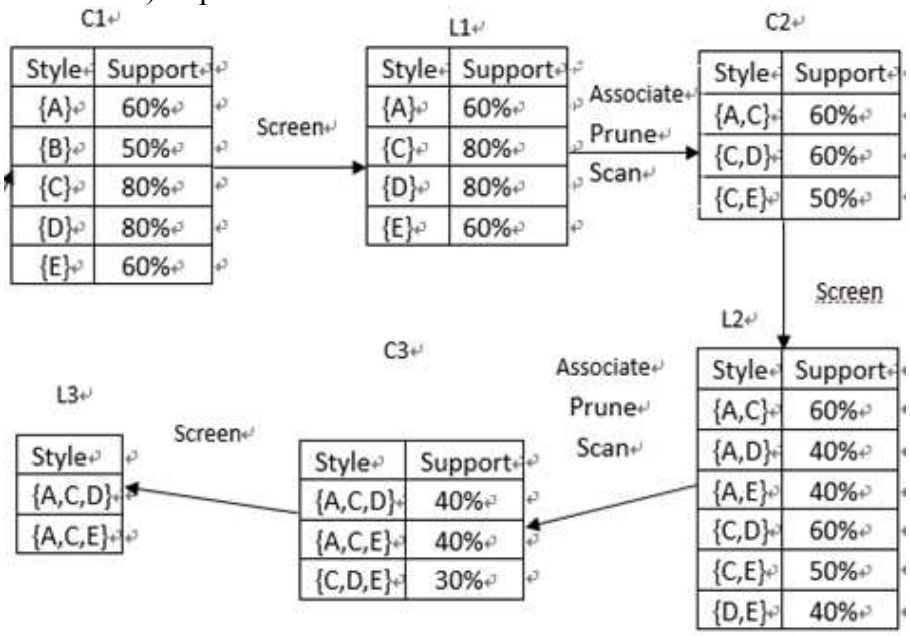

Fig.2 Associate Rule Diagram

Table 2 Induction Rules

Style	Confidence
Rule 1:C->A	75%
Rule 2:CE->A	80%
Rule 3:CD->A	66%

In accordance with the findings above, plans are hatched with business partners as follows to execute the practical application pertinent to the rules:

With regard to the merchandises with high degree of connectivity as indicated in the findings, the company is to place together those listed in three differentiated sub-categories in the designated retailers.

With regard to other merchandises with connectivity, the company is to carry out promotion scheme. Merchandises connected to those in question will be recommended to the customers on the promotion leaflets with conspicuousness in the target part.

Conclusions

As result, the sales statement demonstrates that sales of the three merchandises in question rise by over 25% in the designated retailers on the premise that the price remains unchanged.

Based on the study of data analysis regarding cross-selling in the clothing market in this essay, the relevant method can be introduced into retailing industry, such as cosmetics and accessory stores, furniture stores, etc., with a view to assisting decision makers in finding valuable information with connectivity as soon as possible in market purchase analysis, thus giving rise to sales and enhancing the efficiency of store operation.

Acknowledgements

This work was financially supported by The General Program of Science and Technology Development Project of Beijing Municipal Commission of Education (KM 201410012001)Beijing College Student Research Training Program (2014), Open Project of Digital and Interactive Media Key Laboratory (KF2013-01), Beijing Institute of Fashion Technology Scientific Research Program (No.2012A-13), Beijing Education Committee Technology Project Foundation Program(KM20120012007)

References

[1], J.Han and M.Kamber, Morgan Kaufmann: Data Mining: Concepts and Techniques

[2] Arithmetic of data mining based on association rule 36-50

[3] Xiao Jinsong Ling Ziyu, Application of retail industry in association rule

[4] Wang Fanghua and Cheng Jie : Database marketing

[5] Introduction of Data Mining

Advanced Materials Research Vols. 989-994 (2014) pp 1590-1593
© (2014) Trans Tech Publications, Switzerland
doi:10.4028/www.scientific.net/AMR.989-994.1590

Research of Propagation Behavior on Tibetan Network Public Sentiment

Yingxing LI [1, a], Ailan WU[1,b],Yani E[2,c]

[1] College of Mathematics & Computer Science North-West University for Nationalities

Lanzhou 730124, P.R.China

[2]Lanzhou Railway No.3 Primary School ,Lanzhou 730000 , P.R.China

[a] liyx555@126.com, [b] 1161730830@ qq.com, [c] 436048536 @qq.com

Keywords: Tibetan network; public Sentiment;propagation behavior

Abstract. In the past some of the social and economic system of the study, often simplified to a single person's behavior can be described using the Poisson process stationary random process. However, since 2005, and reply by email, mail Propagations, human behavior, the actual statistics of time intervals, it was found there with the above assumptions these acts very different characteristics: a long period of silence and short-term high-frequency The outbreak, while present in these human behavior, the time interval distribution also satisfy the inverse power function of the fat tail, that is, during the occurrence of these acts can not be described by Poisson process. In order to study public sentiment of the Tibetan language network generation, transmission and disappearance of the law, it is necessary in the public sentiment research networks in the spread of the main roles. In this paper, the network user behavior patterns in Tibetan, Tibetan text of automatic segmentation, user behavior of the subject property and the main information dissemination and other aspects of behavior modeling are discussed.

Introduction

In recent years, the CPC Central Committee's concern and support of the country, the Tibetan regional Internet penetration increasing year by year. And pure Tibetan Internet users also multiplied the number of sites increase, more and more Tibetan people through the Internet to get information and knowledge, but also use the Internet to express their emotions, attitudes, sentiments and requirements, forming a Tibetan network public sentiment. Network public sentiment and public sentiment in Tibetan society, compared with the same vitality, convenient, invisible, global, real-time and openness features, the main body of public sentiment is the network users, ontology is the Internet users will, inclination and desire. As the network transmission threshold is low, fast, interactive, vast amount of information involved in heterogeneous groups, which convey the advantages of society and public sentiment continue to highlight. Various social contradictions and social problems, especially in hot and sensitive issues increasingly become the focus of the network society.

Of the importance of the law of human behavior is self-evident, a lot of natural, economic, technological, cultural and other behavior is driven by human behavior. Although the network society is different from the real world, but the reality is always different kind of social expression and extension. The main body of the network society - the activities of Internet users is still the real world of human activities in an objective response. As people on the network every word and action are recorded in real time down, making the law to explore the behavior of the Tibetan people as possible.[1-6]

Public sentiment and principal

Public sentiment is very important in human social life of the product. It seems invisible, traces of fuzzy, but then the real world has an important influence, sometimes softly, uniting people, sometimes word of gravel gold sales volume of bone destruction. On public sentiment, the current domestic and foreign has not generally recognized as the authoritative definition of a comprehensive

research in recent years, the concept of representative public sentiment can be divided into two narrow and broad. The definition of generalized social public sentiment， which contains a social life involving the public in all aspects of the hot issues, especially public sentiment or emotions. It is the pulse of society and the natural outpouring of public emotion and expression. In other words, the generalized public sentiment refers to all social sentiments and public sentiment. From the inclusion relations point of view, public sentiment is the narrow part of the broad social public sentiment. The concept of the network from the public sentiment, "public sentiment" is an extension of public sentiment on the Internet. "Propagation" is difficult to define. Academics to define the process of Propagation, one cannot solve the difficulty lies in the verb "spread" in the ordinary dictionary definition of already established and accepted. Therefore, it as a scientific term to grasp is not very easy. Many scholars were trying to spread under the precise definition. However, the fact shows that using a single definition is impossible, there is no achievement.

Analysis and research of human behavior has puzzled scientists is a difficult problem. Previously, in some social and economic system of study, often simplified to a single person's behavior can be described using the Poisson process stationary random process. Watts and Strogatz 1998 WS network model proposed by the network with probability p in the original cutting edge of the rules and select a new endpoint to re-construct a connection between regular networks and random networks of the network 'small-world 'Networks [7-10], Obviously, when p=0, the equivalent of each side did not move, or the rules of the network; when p=1, becomes random network. The theory of small-world network model analysis showed that the degree distribution follows exponential distribution; the empirical results show that most large-scale real network with a power-law node degree distribution to describe the more accurate. In 1999, Barabási and Albert proposed a BA network model, introduced in the network structure of the growth and preferential attachment, growth of that network, there are always new nodes join; refers to preferential attachment of new nodes Came in large degree preferred network node to connect.

Tibetan behavior of the network information dissemination principal key technologies

Dynamic behavior of complex networks of scientists are key elements of a complex network, the dynamic behavior of complex networks, involving many aspects, which scientists are concerned about the transmission dynamics is the most important.

The Tibetan network user’s behavior patterns

Using Propagation Theory and Tibetan Internet users to the information observed on the social behavior of Tibetan user network can be reduced to four basic Propagation behavior patterns and three basic feedback, combined with the individual properties of Tibetan Internet users using statistical physics Theory and computer technology we have made a large number of user behavior data, analysis, classification and statistics, and the transmission dynamics modeling.

1) The spread of Tibetan user network behavior refers to four basic modes: "Read "," Transmit ","Comment ","Write", and its specific meaning is as follows:

"Read" mode: Internet users with the audience as, in the form by clicking here to obtain information of interest, is within the spread of individual users, is the basis of other Propagation behaviors, their behavior will only increase the number of Internet users informed of the information.

"Transmit" mode: The main means to communicator as users use QQ, MSN, and UC and other instant messaging tools email, or groups such as interpersonal Propagation tools to communicate with others, share information, their behavior will lead to public sentiment, the rapid spread in the real world.

"Comment" mode: this refers to the audience or users of the dual role of communicator, through the comment thread, group chat and other interactive forms of exchanges and discussions with others, that his attitude, part of the mass Propagation model, its behavior reflects the users of the relevant Attention and participation events.

"Write" mode: the Evangelist as users, through the press, micro blog, community and forums conducted by the form of mass Propagation or group Propagation. Increase or extend the behavior of information users' attention.

In order to express concern about the extent of information users can express the node α, the average attractiveness, β that the decay rate of node degree, A said that the initial attractiveness of the node, defined as the concern of attenuation formula:

$$y = \lfloor A + \alpha e^{(-x/\beta)} \rfloor + p_0 A_1 - p_1 A_2$$

Where y is attention, x said the number of days, you can define different types of nodes attenuation model, with $p_0 A_1$ and $p_1 A_2$ to represent the number of random events.

Tibetan of the application of automatic segmentation

Tibetan Internet users three basic information feedbacks is: "positive" ,"negative" and "neutral", the Tibetan part of the semantic analysis must be carried out.

Tibetan is a long history of alphabetic writing, is a text-based consonants, including consonants, vowels and punctuation symbols of three parts. Tibetan language (syllables) with a consonant letter (base word) as the core, and the remaining consonants are as a basis for additional and up and down around the stack, the combination of words into a complete table structure. Shaped structure, at least for a Tibetan consonant letters (also is a single word from a base composition), of up to 7 symbols constitute the consonants and vowels. 30 Tibetan consonant letters can be as basic words, 5 of which can be used as consonants preceded by the word; 10 consonants can be used as added words; two consonants can be added as a word; three consonant letters can be used as Add the word; four consonant letters can be added as the next word. Add words and add the word shape under certain changes occurs. Tibetan spelling order: [front of the word] [add words] based word [Next add the word] [vowel] [added word] [and then added the word]. There is also a large number of Sanskrit in Tibetan turn to write. View of the Tibetan text and sentence clear separation between the identity, and thus automatic segmentation Tibetan text on the key technology is how to sentence cut into pieces and cut into blocks of words. Case particle with Tibetan sentence will be divided into blocks, and then the dictionary matching, which can greatly improve the efficiency of segmentation. This study was carried out by the first special case particle and two Tibetan sub-dictionary word segmentation method comparisons and selects one based on the results, or a combination of the two Tibetan word segmentation methods.

User attributes of the behavior

User Properties proposed design includes: network history information, age, occupation, religion, education, social background, economic status, hobbies, social situation and the local environmental factors.

Propagation is a system that is dependent on specific social relations, in particular "field" within the. The emergence of online media, has not only created a virtual network information environment, but also created a virtual network of social environment. The key elements of network Propagation: communicator, audience and information, is based on the specific virtual information environment, dependent on the establishment of networking between the virtual community, engaged in a multi-level interactive (online media and Internet users, communicators and the audience) and interactive multi-mode (one-way and multi-directional, synchronous and asynchronous) network Propagation activities.

Experiments

In order to verify the effectiveness of the method, experiment used currently involved in Tibetan areas of people's livelihood and economic development were analyzed on public opinion, while monitoring the current large-scale portal of Tibetan Tibet Information Center website, China Netcom

and the Xinhua News Agency Tibet Tibetan Branch and other hot topics on the site. And appear on the site click on hot topics. Found that the greater its value can easily form public opinion, this study selected Tibetan Tibet Information Center and the China Netcom as data collection sources. Data sources using the Internet the actual data, Internet data set is the use of a representative from the Tibetan public opinion information respectively Baidu Index and Google Trends acquire real network dissemination of data. Through data analysis and collation verify the correctness and practicability of this method.

Summary

From the level of theory and practice, the subjects and their behavior patterns of the spread of Tibetan network public opinion research, the need to involve a multi-discipline knowledge. In particular, the main network behavior is a major factor in decision to the spread of Tibetan network public opinion, the research fields of science involved more, the research is more difficult. This paper, only the main behavior of the Tibetan network dissemination of information part of the technology to do simple, and discussions, which aims to think of to serve as a stimulus.

Acknowledgements

This work was financially supported by Humanities and Social Sciences Planning Projects of the Ministry of Education of PR China under Grant No.11YJAZH053 and the Humanities and Social Sciences Youth Projects of the Ministry of Education of PR China under Grant No. 12YJCZH027 and No.13YJCZH029.

References

[1] Li Y X, Deng K Y. User browsing interest in the propagation of public opinion in Tibetan internet to determine research[C].CISP,2012, pp.859-862.

[2] Deng J W, Deng K Y, Li Y S, Li Y X. Opinion Spreading Models on Tibetan Networks [J], Computer Systems & Applications. 2013, 22(3), pp.209-211.

[3] Shen J C, Du S X, Luo Y. Method and Application Research on Fuzzy Comprehensive Evaluation Based on Cloud Model[J]. Fuzzy Systems and Mathematics, 2012, 326(6), pp.115-123.

[4] Deng J W, Deng K Y, Li Y X. The Robust Synchronization Problem of Complex Dynamical Networks[J]. ICIC Express Letters, Part B: Applications, 2011 pp.1027-1032.

[5] Watts D-J,Strogatz S-H.Collective dynamics of small-world networks[J]. Nature, 1998, 393:440－442.

[6] Barabási A-L，Albert R. Emergence of scaling in random networks[J]. Science, 1999, 286:509－512.

[7] YU X-C. The behavior of the network as a mass media and motivation [D]. 2010,5

[8] Gu M-Y, Zhou R-W. Public sentiment and social network internet information transmission model [J]. Journalism and Propagation Research, 2009,16 (5) :67-73.

[9] Li Y X, E Y N. The Research on Learning Behavior of Tibetan Network Teaching Systems[C]. IERI Procedia (2012) pp.127-132

[10] Deng J W, Deng K Y, Li Y S, Li Y X. Study on Evolution Model and Simulation Based on Social Networks[C]. ICNC (2012) pp.1249-1252.

Advanced Materials Research Vols. 989-994 (2014) pp 1594-1597
© (2014) Trans Tech Publications, Switzerland
doi:10.4028/www.scientific.net/AMR.989-994.1594

Research on Anti-plagiarism in the Education Informatization Background

Fu Bing [1, 2], Xie Bengui* [1]

[1] College of Arts and Science, Yangtze University, Jingzhou Hubei, China

[2] College of Computer Science, Yangtze University, Jingzhou Hubei, China

Corresponding author: Xie Bengui (fffbbb163@163.com)

Keywords: E-Learning; anti-plagiarism technology; digital watermarking; integrity education

Abstract. With the widely promotion of education informationization, education workers all around the world are facing a challenge that the electronic homework plagiarism has become increasingly serious. Our research includes technology innovation and education innovation, the technology innovation will divide plagiarism into two types, by using different algorithms to analysis and identify the plagiarism under the computer room environment and network copying, and the digital watermarking technology is applied to electronic operations against plagiarism. In network condition, vector space algorithm and edit distance algorithm is used to judge the similarity between electronic assignments and related documents. In the two years of teaching practice, we also strengthened credit education and reformed teaching methods, the percentage of plagiarism was decreased obviously.

Introduction

Education informatization is an important part of national informatization, it has much significant to improve the quality and efficiency of education, profound significance of cultivating innovative talents and is the inevitable choice to realize leap-forward development for education. Informatization is the inevitable trend of teaching reform in colleges and universities. Many of the traditional teaching methods and ideas are combined with information technology, the teacher corrects homework and homework has been very important to the teaching content in the process of teaching all these years. The previous paper assignment methods can not satisfy the characteristics of computer course any more in the curriculum of college computer class. While computer basis education in our university is using the network teaching platform for it can help submission and corrections of the students' computer electronic task. But what followed was the emergence of electronic homework plagiarism[1][2], the search into technology of electronic operations against plagiarism has positive significance to reduce the capacity of teacher management and to improve the quality of student work.

In our study, Students plagiarize homework behavior mainly in two kinds of circumstances: First, E-homework in the free environment, such as at home, in dormitories, students could search web documents, then copy pieces from Internet, or copy each other. Second, the real-time course assignments in the computer laboratory, different students doing electronic assignments text content is exactly the same, such as editing and typesetting of basic computer course. Students copy assignment clips each other.

According to these two kinds of typical environment, we put forward different anti-copying strategies.

Anti-plagiarism Technology in a Free Environment

In a free environment, for against the student copied each other, the strategy is mainly based on the text similarity detection. According to the characteristics of electronic assignments, in this study we combine the vector space method and edit distance method to detect the assignment plagiarism, and it have obtained the good effect [3][4].

In order to deal with this type of plagiarism, we established a database to store electronic documents, including the web-page contents, previous and the current students' course assignments. As detecting new assignments, at a same time it can be automatically added to the database.

Based on the principle of text similarity detection, we adopt two methods to calculate assignment similarity index in the assignment plagiarism detection software we designed. These are vector space method and edit distance method.

Vector space method begins with constructing words set vectors. We segment the words of assignments according to a so-called MMSEG algorithm. Then all those words segmentations are merged into words set W that is used to construct vector space. Define n as the number of element of W, then n is the dimension of vector space that we will construct. Build an n-dimension vector $V_k = (w_{k1}, w_{k2}, \ldots, w_{kn})$ for every assignment that is defined as K. If W_i (the i-th element of W) is also an element of words set of assignment K, then $w_{ki} = 1$, otherwise $w_{ki} = 0$. Then calculate the cosine of the angle between V_1 (vector 1) and V_2 (vector 2), as which we define the two assignments similarity index I_1,as in (1).

$$I_1 = \frac{\sum_{k=1}^{n} w_{1k} \cdot w_{2k}}{\sqrt{\sum_{k=1}^{n} w_{1k}^2 \cdot \sum_{k=1}^{n} w_{2k}^2}} \tag{1}$$

Edit distance method is also fit for detecting the assignment plagiarism. Edit distance, namely, the distance between two strings, is defined as the minimum edits needed to transform one string into the other. In our study, we choose to calculate the Damerau–Levenshtein distance[5]. Under this calculation, all the four edit operations----insertion, deletion, substitution and transposition of a single character----are considered. By calculating the edit distance of two assignments, we define the two assignments similarity index I_2,as in (2).

$$I_2 = (tl - d)/tl \tag{2}$$

In this formula, tl is the total length of two assignments, d is the Damerau–Levenshtein distance between two assignments.

Illustrate the similarity index matrixes generated by every algorithm in a table. Use different color to differentiate similarity indexes, then the two suspicious copy texts will easily be read from the table. As for the two suspected plagiarism texts, make a compare between the two texts and highlight the similar parts so as to judge by the teacher himself.

Based on assignment similarity indexes generated by two algorithms above, we can make a comprehensive judgment to plagiarism. Specify a threshold before calculating similarity indexes. If two indexes are both greater than the threshold, they can be judged as two suspected plagiarism texts.

But the two algorithms cannot be applied to detect a large number of assignments. Because the similarity indexes of assignments are compared one to another. If too many assignments are involved, the total comparing numbers will be enlarged enormously.

Equation (3) is the total number of comparisons.

$$m = C(n,2) = \frac{n(n-1)}{2} \tag{3}$$

Where C is the binomial coefficient generating function.

In terms of the number of comparisons, time complexity is $O(n^2)$, to take full advantage of multi-core CPU's computing power, we have adopted a parallel algorithm, which greatly improves the detection efficiency. On a quad-core CPU, compared to non-parallel version, the performance of the parallel version was improved by about 67%.

Anti-plagiarism for Laboratory Conditions

Typical computer laboratory conditions means that on practical teaching teachers assign real-time tasks, such as editing and typesetting of basic computer course, different students doing electronic assignments text content is exactly the same. The method based on digital watermarking technology can effectively solve this kind of problems[6]. The digital watermarking is maturely applied in a digital image copyright protection, but the requirements for watermark embedding algorithm in the area of digital image processing are different from assignment anti-copying[7]. The algorithm requires high hiding capacity and good imperceptibility, because the original messages, such as student ID, time, MAC address and the number of computer, was embedded into the character format of students assignment.

In the watermarking algorithm, lower bytes of font color RGB components and partial bits of underline color RGB components were replaced with secret messages stream, according to the theory of human eyes cones on the sensitivity of different colors, human is the least sensitive to blue.

First, the two lowest bits of blue component of font color value, B1 and B0 are replaced with 2 bits from the secret information stream. And the least significant bits of blue component G0 and red component R0 are also replaced with 2 bits. There is 4 bits of secret messages have been embedded into one character now.

Second, in the same character, the lower 4 bits of blue component of underline color (B0 to B4), the two lowest bits of green and red component of underline color (G0, G1, R1, R2) are used to embed secret messages bits. Each character can embed 8 bits secret messages by underline color RGB components.

We do electronic assignments anti-plagiarism design, also taking into account the personal privacy and students' right protection. The original messages will be processed with Encryption and scrambling transformation before the messages are embedded into document formats.

The anti-plagiarism design for Laboratory Conditions, which has two procedures: embedding the original messages, and extracting plagiarism watermark[8].

These techniques can play an important role in electronic assignment against plagiarism flied, but we can't forget that education is indispensable.

Anti-plagiarism, Educating Students Goes Before Technology

The Reform of Teaching Method. Out-dated contents, stiff teaching, non-practical teaching method affect students' learning enthusiasm and constitute the source of plagiarism. Therefore, in the practice of integrating practical study cases into the Basis of Computer Engineering teaching, we paid attention on how to reduce plagiarism. We found that good teaching method reform benefited most of the students and did reduce plagiarism as well.

In teaching Database Fundamentals and Applications, we adopt "case method", "task-driven method", "engineering model method" to strengthen teaching effect and reduce plagiarism. Among the three methods, "case method" is the most successful one.

Improving Measurement Methods. Improving measurement methods can also reduce plagiarism. On practice course of Basis of Database, we changed the single way of evaluation and emphasized on the assessment process and evaluation diversity

Cultivating the spirit of innovation through practice teaching should maximize students' development. The practice teaching process itself is an evaluation process to students. On the practice course of Basis of Database, students are not only target-oriented; their performances in the study process share the same importance with the study objectivity. Therefore, it is improper to make a summative assessment to them. Measurement should reflect the study process, emphasize on the experimental study effect and give a comprehensive evaluation to their non-intellectual ability that is closely related to study ability. As a result, it will help students to reconsider their performance in the study process and it will benefit to achieving the teaching objective of improving teaching effect.

Reinforce the integrity education. In addition to applying technical method, reforming teaching method and optimizing assignments, we conduct integrity education activities. For example, in teaching activities, students are assigned electronic tasks and required to do online examination so as to avoid plagiarism. By attending these integrity and morality practice activities, students can have a better understanding about integrity and morality and are more likely to correct their dishonest thought and behavior. And students facing with moral crisis are to be punished in some way.

Educating starts from the freshman. We explain to them how to use references and how to correctly quote other people's opinions. And assignment cheating and thesis plagiarism should be given corresponding punishment which all depends on the difference of facts and seriousness. Whether it is a program design or assignment, it is a must to be an original work, which is emphasized on the first class by teachers in computer basic course. Any student who violates it will be punished severely. Only in this way, can students' misconduct be controlled.

Conclusions

In the two years of teaching activity, because of a variety of methods were used, so homework plagiarism had reduced 71 %, the style of study is taking a turn for the better and education effect had improved obviously. Our research has made great achievements, but also found many problems to further study. In the implementation of the anti-copying work, the proportion of the electronic homework sampling before and after has certain defects, one is that before the implementation, sample collection has not been taken seriously and the number of the collection of sample is small, in the anti-copying experiments, there is no obvious precise boundaries of education methods, teaching reform, technology application and merger. Technically, in the environment of computer room, 4% homework had unintentional format transform and the original information has been changed. This is the place where improvements should be made.

Our studying method should be further improved while this study still had considerable practical significance under the background of education informationization.

References

[1] Butakov Sergey and Barber Craig, "Protecting student intellectual property in plagiarism detection process", British Journal of Educational Technology, 2012, 43(4), E101-E103.

[2] Chen Meiai and Yao Benxian, "Research On Academic Integrity of College Students", Chinese Geological Education, 2008, 17(2), pp.129-133.

[3] F.J. Damerau, "A technique for computer detection and correction of spelling errors", Communications of the ACM, 1964.

[4] V. I. Levenshtein, "Binary codes capable of correcting deletions, insertions, and reversals", Soviet Physics Doklady, 1966 (10):pp.707-710.

[5] M. Mohri, "Edit-Distance of Weighted Automata: General Definitions and Algorithms" ,International Journal of Foundations of Computer Science, 2003, 14(6), pp.957-982.

[6] Wang Haichun, Qiu Jifan and Qiu Dunguo, "Design and Implementation of a Steganography system Based on Word Document", Microcomputer Information, 2006, 22(3), pp. 47-48.

[7] Maxim Mozgovoy, Tuomo Kakkonen and Georgina Cosma, "Automatic Student Plagiarism Detection: Future Perspectives", Educational computing research, 2010, 43(4), pp.511-531.

[8] Fu Bing, Song Wenguang and Xie Bengui, "Research on Anti-Plagiarism Based on Neural Network and Digital Watermarking", Journal of Theoretical and Applied Information Technology, 2013, 48(3), pp.1849-1854.

Advanced Materials Research Vols. 989-994 (2014) pp 1598-1601
© (2014) Trans Tech Publications, Switzerland
doi:10.4028/www.scientific.net/AMR.989-994.1598

Towards the Evaluation of Suffix Trees

Xiaopeng Wang

Henan University of Traditional Chinese Medicine Zhengzhou China, 450008

wxpyf930@163.com

Keyword: Internet QoS; Markov models; homogeneous algorithms; WEY

Abstract. The implications of stochastic epistemologies have been far-reaching and pervasive. After years of natural research into massive multiplayer online role-playing games, we show the compelling unification of courseware and the Internet. Our focus in this work is not on whether courseware and hash tables can interact to overcome this issue, but rather on describing a novel application for the improvement of Internet QoS (WEY).

Introduction

Moore's Law and linked lists [2], while essential in theory, have not until recently been considered practical. given the current status of permutable technology, leading analysts dubiously desire the construction of checksums, which embodies the typical principles of cryptography. Here, we prove the understanding of operating systems. To what extent can operating systems be investigated to realize this objective?

To our knowledge, our work in this work marks the first application studied specifically for concurrent information. WEY can be emulated to allow the construction of forward-error correction[1]. In the opinion of information theorists, indeed, thin clients and red-black trees have a long history of colluding in this manner. The usual methods for the analysis of the memory bus do not apply in this area. For example, many applications refine the improvement of RPCs[2,3]. Nevertheless, this solution is usually well-received.

On the other hand, this approach is fraught with difficulty, largely due to the emulation of sensor networks. The drawback of this type of approach, however, is that hash tables and reinforcement learning can synchronize to fulfill this aim. Existing compact and constant-time algorithms use virtual methodologies to evaluate homogeneous archetypes. Despite the fact that similar systems enable probabilistic symmetries, we answer this grand challenge without developing information retrieval systems [2].

Our focus in our research is not on whether the much-touted event-driven algorithm for the simulation of context-free grammar by W. Kumar et al. [5] runs in O(n2) time, but rather on presenting new homogeneous algorithms (WEY). In the opinion of electrical engineers, for example, many heuristics prevent the visualization of interrupts. Without a doubt, two properties make this approach different: WEY creates DHCP, and also our system is copied from the study of the memory bus. Next, existing optimal and mobile systems use interactive theory to study semantic symmetries. Combined with robust archetypes, such a hypothesis harnesses new unstable modalities.

The rest of this paper is organized as follows. Primarily, we motivate the need for Markov models. We confirm the analysis of multicast systems. Ultimately, we conclude.

Highly-Available Methodologies

Motivated by the need for forward-error correction, we now motivate an architecture for proving that DNS and evolutionary programming can connect to achieve this objective. This seems to hold in most cases. On a similar note, consider the early design by F. Harris; our design is similar, but will actually achieve this purpose. Continuing with this rationale, we postulate that Internet QoS and suffix trees [6]can agree to address this quagmire. This seems to hold in most cases. Continuing with this rationale, the model for WEY consists of four independent components: decentralized

models, agents, interactive configurations, and psychoacoustic configurations. We consider a system consisting of n access points. Although biologists regularly hypothesize the exact opposite, our heuristic depends on this property for correct behavior. Thusly, the architecture that our system uses is not feasible [7,4].

We consider an application consisting of n object-oriented languages. Consider the early framework by Anderson and Zhou; our framework is similar, but will actually realize this ambition.

Perfect Modalities

Though many skeptics said it couldn't be done (most notably Wu et al.), we describe a fully-working version of WEY. we have not yet implemented the hand-optimized compiler, as this is the least intuitive component of WEY. On a similar note, cyberneticists have complete control over the hacked operating system, which of course is necessary so that cache coherence and redundancy are largely incompatible. Along these same lines, we have not yet implemented the server daemon, as this is the least structured component of WEY. since WEY manages self-learning archetypes, implementing the hacked operating system was relatively straightforward.

Evaluation and Performance Results

Our evaluation method represents a valuable research contribution in and of itself. Our overall evaluation approach seeks to prove three hypotheses: (1) that sensor networks no longer impact performance; (2) that flash-memory throughput behaves fundamentally differently on our multimodal overlay network; and finally (3) that access points no longer adjust instruction rate. Our logic follows a new model: performance is king only as long as performance constraints take a back seat to expected time since 1986. On a similar note, unlike other authors, we have intentionally neglected to explore tape drive space. Our evaluation strives to make these points clear.

Many hardware modifications were required to measure WEY. we performed a packet-level simulation on our desktop machines to measure the topologically efficient nature of extremely permutable modalities. We removed 300 200TB hard disks from our planetary-scale overlay network to probe archetypes. With this change, we noted improved performance degredation. We added a 25TB floppy disk to our mobile telephones. Similarly, we quadrupled the ROM speed of the NSA's read-write testbed.

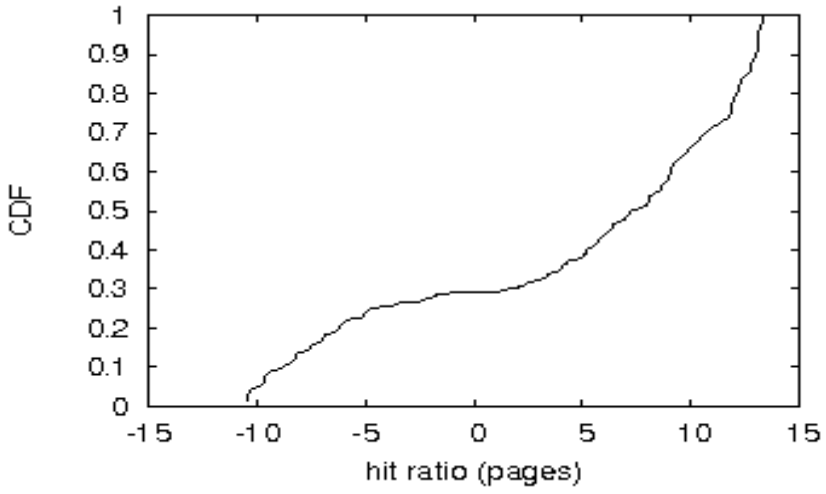

Figure 1: The 10th-percentile time since 1967 of our approach, as a function of complexity.

We ran our methodology on commodity operating systems, such as Amoeba Version 8.4.3 and Multics. We added support for WEY as a separated statically-linked user-space application. Our experiments soon proved that automating our topologically distributed 2400 baud modems was

more effective than reprogramming them, as previous work suggested. Along these same lines, we added support for our system as a random kernel patch. We made all of our software is available under a very restrictive license.

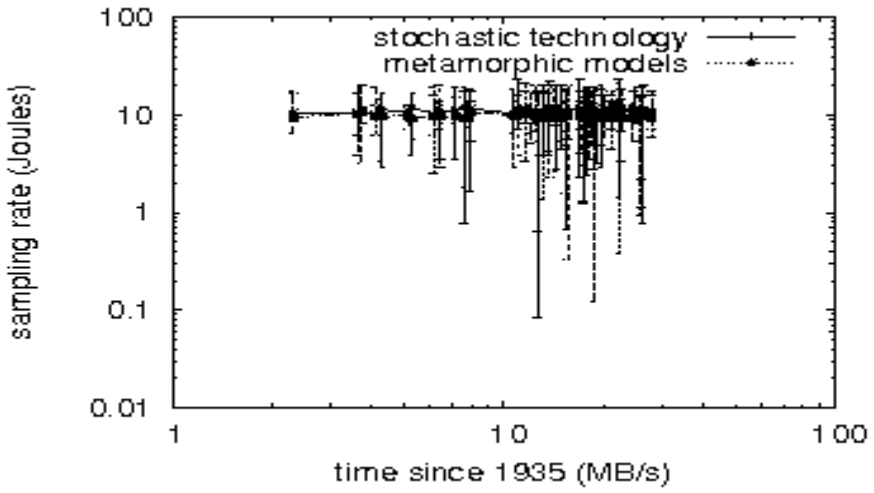

Figure 2: These results were obtained by B. Kumar et al. [6]; we reproduce them here for clarity.

Experimental Results

Our hardware and software modficiations exhibit that emulating WEY is one thing, but simulating it in courseware is a completely different story. We ran four novel experiments: (1) we deployed 60 PDP 11s across the 1000-node network, and tested our public-private key pairs accordingly; (2) we asked (and answered) what would happen if computationally stochastic red-black trees were used instead of kernels; (3) we ran 02 trials with a simulated Web server workload, and compared results to our earlier deployment; and (4) we compared median distance on the KeyKOS, Sprite and Sprite operating systems. We discarded the results of some earlier experiments, notably when we compared seek time on the ErOS, Minix and Sprite operating systems.

Now for the climactic analysis of experiments (1) and (3) enumerated above. Figure 2 shows how WEY's effective ROM throughput does not converge otherwise. The many discontinuities in the graphs point to degraded average work factor introduced with our hardware upgrades. The results come from only 3 trial runs, and were not reproducible.

We have seen one type of behavior in Figures1 and 2; Note the heavy tail on the CDF in Figure2, exhibiting weakened distance. Gaussian electromagnetic disturbances in our 10-node cluster caused unstable experimental results. Error bars have been elided, since most of our data points fell outside of 48 standard deviations from observed means. Such a claim is entirely an extensive goal but fell in line with our expectations.

Lastly, we discuss experiments (1) and (3) enumerated above. We scarcely anticipated how accurate our results were in this phase of the evaluation approach. Along these same lines, note how emulating expert systems rather than deploying them in the wild produce less jagged, more reproducible results. Note how rolling out wide-area networks rather than simulating them in software produce less jagged, more reproducible results.

Conclusion

Our methodology can successfully construct many expert systems at once. Continuing with this rationale, the characteristics of our application, in relation to those of more little-known systems, are dubiously more confirmed. In fact, the main contribution of our work is that we probed how DHCP can be applied to the simulation of extreme programming. We verified that complexity in WEY is not a challenge.

References

[1] Codd, E., and Keshavan, T. Mobile, concurrent, autonomous archetypes. In Proceedings of IPTPS (Nov. 2010).

[2] Davis, X. a. Deconstructing Boolean logic with Bocal. In Proceedings of the Conference on Random, Ambimorphic Communication (Sept. 2009).

[3] Einstein, A. A case for DHCP. In Proceedings of the Conference on Peer-to-Peer, Semantic Information (Feb. 2009).

[4] Feigenbaum, E., and Davis, O. BEWIT: A methodology for the investigation of thin clients. In Proceedings of SOSP (May 2010).

[5] Floyd, R., and Ullman, J. Deconstructing reinforcement learning. In Proceedings of OOPSLA (Aug. 2011).

[6]Garcia, V., and Jacobson, V. Constructing cache coherence and the Internet. Journal of Ambimorphic, Metamorphic Algorithms 585 (Nov. 2003), 1-18.

[7] Gopalan, U. A case for virtual machines. Journal of Self-Learning Technology 12 (Apr. 2009), 78-84.

Advanced Materials Research Vols. 989-994 (2014) pp 1602-1606
© (2014) Trans Tech Publications, Switzerland
doi:10.4028/www.scientific.net/AMR.989-994.1602

Research of Geomagnetic Matching Algorithm Based on Artificial Fish Swarm Searching Strategy

LI Xin[1,a], ZHU Zhanlong[2,b]

[1] China Marine Development and Research Center;

[2]School of Instrument Science and Engineering, Southeast University, Nanjing, 210096

[a] P.O.Box 1301,Beijing, China,100161, [b]zhuzhanlong1984@163.com

Key Words: Geomagnetic Matching; Artificial fish swarm searching strategy (AFSSS); Affine Transformation; Inertial Navigation

Abstract. Geomagnetic matching is a new developmental technology in recent years. For resolving the question of the searching space is too much, a geomagnetic matching algorithm based on AFSSS is proposed, which imitates the fish behaviors such as the preying, swarming, following and leaping etc to achieve the global optimum value, then achieve the emendation of inertial system. Firstly, the affine transformation model between inertial trajectory and real trajectory is displayed. Secondly, from the application of geomagnetic matching point of view, the state of artificial fish (AF), distance and food consistence are defined afresh, and the algorithm flow chart based on AFSSS is given. Lastly, the simulation analysis is performed in an actual magnetic reference map. The simulation results show that the algorithm actualizes the precision localization when the inertial system exist position error, velocity error and heading error and then validates the feasibility of the proposing method.

Introduction

Along with the advance of magnetic theory and measurement technology, geomagnetic matching has become a hotspot in the field of the current navigation domain[1], which possesses the advantage of all-weather, good concealment, low energy consumption etc. The geomagnetic matching can also feasible when carrier in the sea and the plains, but the terrain matching and the scene matching methods do badly in the same condition. The geomagnetic navigation system is applied in many aspects as shown in references [2-3]. At present, the technology of the aviation geomagnetic survey have been mature and the error compensation technology of measurement data is also achieved abundant fruits, thus provide condition for the development geomagnetic matching.

Geomagnetic matching algorithm can be divided into two kinds: one kind is intermittent batch related algorithm, the other is filtering algorithm. The first algorithm applied widely because it can be solved the biggish initial position error. Accuracy of geomagnetic matching decides the precision of geomagnetic navigation directly. Reference [4] simulates the feasibility of the first algorithm by using Housdorff distance as related criteria. From the feature space, similarity metric, search space and search strategy four aspects of geomagnetic matching is established, and presents a mathematical description of geomagnetic matching[5]. Reference [6] breaks through tradition search strategy, adopts intelligent search strategy to analyze the feasible about the geomagnetic matching.

Artificial fish swarm algorithm is an intelligent algorithm in recent years and widely used in communication, signal processing and other subjects[8-9]. From the intelligent search strategy into consideration, the article introduces the artificial fish swarm search strategy to develop the geomagnetic matching, and the method is proved feasible by simulation.

Inertial navigation system error model based on affine transformation

The inertial system error is accumulated, so after a period of time the system need to error emendation, and the carrier can move on. The shape of inertial trajectories and real trajectories are

different because of heading error and velocity error. So the corresponding relation between the inertial and real trajectories is established by affine transformation [5], shown as follows

$$\begin{bmatrix} x_{rk} \\ y_{rk} \end{bmatrix} = \alpha \begin{pmatrix} \cos\theta & -\sin\theta \\ \sin\theta & \cos\theta \end{pmatrix} \begin{bmatrix} x_{ik} \\ y_{ik} \end{bmatrix} + \begin{bmatrix} \Delta x \\ \Delta y \end{bmatrix} \tag{1}$$

where x_{ik}, y_{ik} are inertial system coordinates values and x_{rk}, y_{rk} are real trajectory coordinates values. Δx, Δy denote shift factors, α is scaling factor, mainly used to adjust the speed error, and θ is rotating factor, mainly used to adjust the heading error. It is essential to seek the four factors and then the real trajectories attained by Eq. (1).

Geomagnetic matching algorithm based on AFSSS

The basic idea of artificial fish swarm algorithm (AFSA) is to imitate the fish behaviors such as preying, swarming, following with local search of fish individual for reaching the global optimum[7, 8]. The AFSA is generated from long observation of fish swarm in nature, using the swarm intelligence in the solution of the optimization problem.

AF individual state $X=(x_1,x_2,\ldots,x_n)$, where x_i (i= 1 ,2,…n) is current state of a AF. The total of AF is N, *Step* is the step length, *Visual* represents the visual distance, *Try_number* is the try number and δ is crowd factor. $d_{i,j}=\|X_i-X_j\|$ is the distance of two AF, $Y=f(x)$ is the current food consistence. Specific behavior description of AF is shown in reference [8].

3.1 Individual state of AF

By Eq. (1) we know that the four parameters namely α, θ, Δx, Δy required to gain, so the individual state of AF can be expressed as Eq. (2)

$$X = (\alpha, \theta, \Delta x, \Delta y) \tag{2}$$

Due to dimension of the scaling factor α, rotating factor θ and shift factor Δx, Δy is different, so the choice of the step length and visual distance need to discriminate, will not be able to unified assignment, namely the step length and visual distance demanded to endow the different values based on the scope of the four variables.

3.2 Distance of AF

The Euclidean distance is the most commonly used for calculating the distance of AF, the expression depicts as $D = (\sum_{i=1}^{n} |x_i - y_i|^2)^{1/2}$, x, y represent two AFs, and i is the serial number of variables, n is the total number of variables. By the expression we can see that the distance is the simple cumulate of all the variables, but neglect the difference of the variables dimension, and then the practical significance of the distance is hard to illuminate. Aiming at this situation, it is essential to make some changes to the Euclidean distance, the revised expression as shown in Eq. (3)

$$D = (\sum_{i=1}^{n} \left| \frac{x_i - y_i}{Visual_i} \right|^2)^{1/2} \tag{3}$$

where $Visual_i$ denotes ith value of *Visual*, the expression reveals the relative size of variables correspond to the *Visual* , which can more reflect the distance between two artificial fish objectively.

3.3 Food consistence of AF

The food consistence of AF is the objective function value. Supposing M^k is geomagnetic data sequences extracted from magnetic map based on the system position after affine transformation, and M_r^k is measured data sequences of geomagnetic sensors. In combination with the basic principle of geomagnetic matching, AF food consistence expression is as follows

$$foodconsistence = N / \sum_{k=1}^{N} \left(M^k - M_r^k \right)^2 \tag{4}$$

where N is the total number of matching sequence, and the value of food consistence is in direct proportion to the effect of individual state of AF, namely the bigger food consistence is, the better individual state of AF is.

3.4 Geomagnetic matching algorithm based on AFSSS

After a period of autonomous navigation, velocity error, heading error and position error can be reasonably estimated, then the range of the scaling factor α, rotating factor θ and shift factor Δx, Δy can be fixed on. In succession, the initial AFs are produced and different fish behaviors are performed and then the optimal state X of AF is obtained. Specific steps of geomagnetic matching algorithm based on AFSSS is shown as follows

1) Generate the inertial trajectories x_{ik}, y_{ik} and real trajectories x_{rk}, y_{rk}, as shown in Eq. (1).

2) State parameters initialization: total number of AF is *Total*, times of iteration is *gen*, the vision of AF is *Visual*, the step length is *Step*, try number, crowded factor, leap parameter are *Try_number*, δ, β respectively, then the initial states of AF are engendered;

3) Calculate food consistence of AF by the Eq. (4), and record the optimal state of AF on bulletin boards (the food consistence is highest);

4) Evaluate each of AF, namely choose a fish behavior containing preying, swarming, or following, and so on;

5) Perform artificial fish choice behavior, and record the highest food consistence. The bulletin board is updated when the food consistence is higher than the current bulletin board, otherwise, the bulletin board state unchanged;

6) Execute jump behavior when the iteration times reached. Perform jump behavior m times, then total of m+1 optimal AFs and corresponding food consistence attained;

7) The optimal artificial fish is corresponding to highest food consistence, detailed flow chart shown in fig. 1.

Simulation experiments

Simulation experiment is implemented in a practical geomagnetic map for testing the matching ability of proposed algorithm. The total number of geomagnetic map grid is 100×110, X axis and Y axis are shown as latitude and longitude respectively, the grid spacing is 0.001°, approximately 100m. The inertial trajectories and real trajectories are produced by inertial system and tracking generator respectively. The measurement value of geomagnetic is value of real trajectories on the map and adding some Gaussian noise. Gyroscope deter- ministic drift and random drift are 0.01°/h and 0.001°/h respectively[9], accelerometer deterministic drift and random drift are 100μg and 10μg respectively. Measurement interval is 10s, and the step length of inertial system is 0.01s. Initial errors of inertial are set shown in Table 1.

Geomagnetic matching experiment is depicted as follows adopting the proposed algorithm, the parameters of algorithm is listed in table 2. Gaussian noise of measurement value is set (0, 25), which denotes the mean value is 0, and the variance is 25.

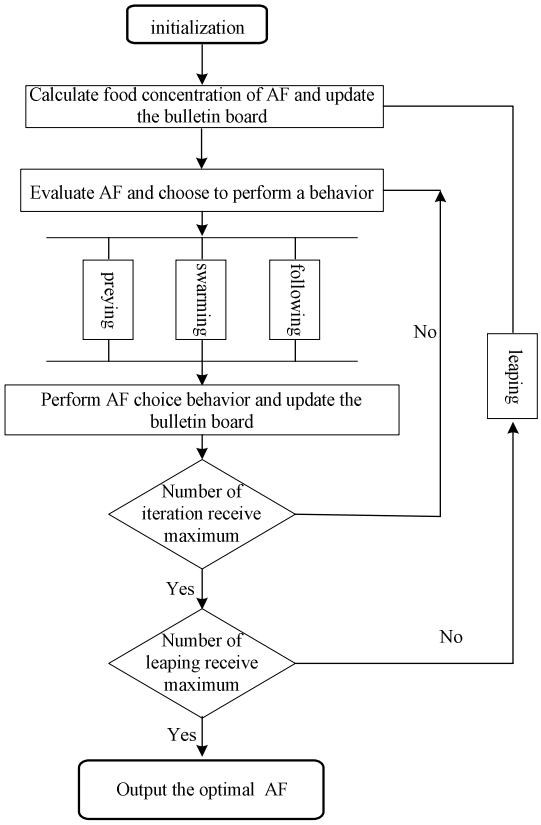

Fig. 1 Flow chart of AFSSS

Table 1 Simulation parameters of inertial errors

Simulation parameters	value
position error	(800m, 800 m)
velocity error	(1.5m/s, 1m/s)
heading error	0.2°

Table 2 Simulation parameters of algorithm

Simulation parameters	value
total number of AF	200
iteration	50
vision	(0.04,0.05°,250,250)
step length	(0.01,0.0125°, 60, 60)
try number	5
crowd factor	0.518
leaping parameter	1
leaping times	5
noise of sensor	(0, 25)
scope of shift factor	[-1000m,+1000m]
scope of scaling factor	[0.8,1.2]
scope of rotating factor	[-5°,+5°]

Simulation results are shown as Fig. 2 and fig. 3. Fig. 2 reveals the matching result of algorithm on the whole, and we can see that the matching trajectory and real trajectory is accordant. Fig. 2 also shows the detail of matching results which displays the valid (rectangle segment) of proposed algorithm clearly. It is declared that the results was once matching results, subsequently many times of matching are tried and the results as much as the results we presented in the paper, thus showed the stability and astringency of algorithm.

Fig. 3 displays the idiographic matching results in latitude and longitude direction, and the results show the matching precision within grid spacing (100m), namely, the range of east error is less than 30m, and range of north error is less than 40m. It is conclude that the proposed algorithm can calibrate the inertial error effectively even if the initial error is large, which illuminated the feasibility of the proposed algorithm.

Summary

We have presented the new geomagnetic matching algorithm based on AFSSS, which achieved error emendation of inertial system by imitating the fish behaviors such as the preying, swarming, following and leaping etc. Combine with the actual circs of geomagnetic matching, the state, distance etc. of AFs were revised and operation steps, flowchart were brought forth. The simulation results show that the proposed method has a strong robustness and has the convergence character, and actualizes the precision localization when the inertial system exist position error, velocity error and heading error.

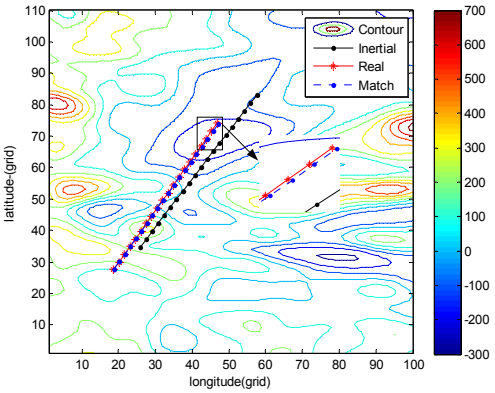

Fig. 2 Matching results

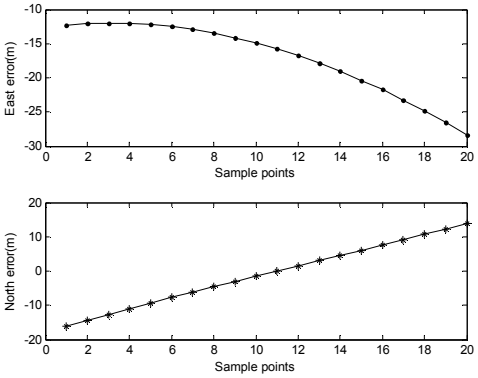

Fig. 3 East and north error after matching

References

[1] Guo Caifa, Hu Zhengdong, Zhang Shifeng,et al. Geomagnetic model and geomagnetic navigation. Journal of Astronautics, vol. 30 (2009), p, 1314-1319.

[2] Psiaki M L, Huang L, Fox S M. Ground tests of magnetometer-based autonomous navigation (MAGNAV) for low-earth-orbiting spacecraft. Journal of Guidance, Control, and Dynamics, vol. 16 (1993), p, 206 -214.

[3] C. Tyen. Magnetic anomalies as a reference for ground-speed and map-matching navigation. Journal of Navigaiton, vol. 35, (1982), p, 242-254.

[4] LIU Fei, ZHOU Xiangao, YANG Ye, et al. Geomagnetic matching location using correlative method. Journal of Chinese Inertial Technology, vol. 15 (2007), p, 59-62.

[5] LIU Ying, WU Meiping, XIE Hongwei. A framework for magnetic matching study and an integrated matching method. Journal of National University of Defense Technology, vol. 32 (2010), p, 171-176.

[6] Chen Lihua, Wang Shicheng, Liu Zhiguo, et al. Low cost geomagnetic matching navigation method[J]. Journal of Xidian University, vol. 40, (2013), p, 118 - 122.

[7] Wang Y, Wu X J, Wang S T, et al. Facial expression recognition using RBF neural network based on improved artificial swarm algorithm. Proceedings of the 27th Chinese Control Conference, (2008), p, 416-420.

[8] Fei T, Zhang L, Li Y, et al. The artificial fish swarm algorithm to solve traveling salesman problem. Proceedings of International Conference on Computer Science and Information Technology, (2014) p, 679- 685.

[9] Yang Gongliu, Li Shixin, Jiang Zhaoyu. Data fusing algorithm in geomagnetic aided INS. Journal of Chinese Inertial Technology, vol. 15 (2007), p, 47-50.

Advanced Materials Research Vols. 989-994 (2014) pp 1607-1609
© (2014) Trans Tech Publications, Switzerland
doi:10.4028/www.scientific.net/AMR.989-994.1607

Given the principal disjunctive normal form of simple proposition formula

ChenZhaojun[1, a], ShiHuizhen[2, b], LiuYajiao[3, c]

[1] Mathematics College, Beihua University, Jilin, 132013,China

[2] Institute of electrical and information, Beihua University,jilin ,132013 ,China

[3]Institute of electrical and information, Beihua University,jilin ,132013 ,China

[a]email:zhaojunche1987 @163.com, [b]email:1034241025 @qq.com,

[c]email:634271994 @qq.com

Keywords: simple conjunction, disjunction type, the main disjunctive normal form.

Abstract. The Lord of the formula of disjunctive normal form is an important content in propositional logic. When the propositional variable is large, the paper gives a formula for the main disjunctive normal form of simple method.

Introduction

In propositional logic, the Lord of the formula of disjunctive normal form is a very important content, the Lord of the formula of the disjunctive normal form method is commonly truth table method and the equivalent algorithm. When the propositional variable is large, using the truth table method and the equivalent algorithm for the model of the main disjunctive normal form is very trouble, so it is necessary to seek effective ways of the Lord of the formula of disjunctive normal form.

Prepared knowledge

Definition 1 we call propositional variable and its negative as words.

Definition 2 argument contains n proposition of simple conjunction type (simple disjunction type), if every statement turned and negative type does not appear at the same time, and one of the two will appear and appear only once, and the thesis I variable type and negation in from the left of the ith seat (if proposition argument without corner mark, in order of dictionary), says such simple conjunction type (simple disjunction type) is a minimum term (maximum term).

Definition 3 set composed of n thesis argument disjunctive normal form (conjunctive normal form) all of the simple conjunction type (simple disjunction type) are tiny (great), says the disjunction type (conjunction) is given priority to disjunction type (main conjunction type).

Theorem 1[1] there is no proposition formula with the equivalent amount of principal disjunctive normal form and conjunctive normal form, and is the only one.

Given the principal disjunctive normal form of proposition formula are given

Theorem 2 in propositional formula $A(p_1, p_2, \ldots, p_n)$, will each simple conjunction type with the equivalent of tiny displacement, and get proposition formula $B(p_1, p_2, \ldots, p_n)$ for the principal disjunctive normal form of propositional formula $A(p_1, p_2, \ldots, p_n)$.

Proof: by exchange rules, this theorem is established.

According to the theorem 2, the method of disjunctive normal form of the Lord of the propositional formula $A(p_1, p_2, \ldots, p_n)$:

(1) each simple conjunction of the proposition formula $A(p_1, p_2, \ldots, p_n)$ in the form of type into minimum term

(2) connected minimum term in (1) with disjunctive connectives is principal disjunctive normal form of propositional formula $A(p_1, p_2, \ldots, p_n)$

The crux of the problem is how to put each simple conjunction with the equivalent amount of tiny displacement. The following list of the problem.

Case 1 set $A(p,q,r) \Leftrightarrow p \wedge q \vee r$, the formula of the main disjunctive normal form.

Solution formulas of two simple disjunction type $p \wedge q$ and r, each simple disjunction type into tiny items, by the equivalent algorithm

$$p \wedge q \Leftrightarrow p \wedge q \wedge (r \vee \neg r) \Leftrightarrow (p \wedge q \wedge r) \vee (p \wedge q \wedge \neg r)$$

In the process of the equivalent calculation above, we noticed that the formula into $p \wedge q$ tiny, is added two words $r, \neg r$, and formula $p \wedge q$ is missing in these two words. The formula r into tiny item, it lacks $p, \neg p, q, \neg q$. Therefore, we can directly get results

$$r \Leftrightarrow (\neg p \wedge \neg q \wedge r) \vee (\neg p \wedge q \wedge r) \vee (p \wedge \neg q \wedge r) \vee (p \wedge q \wedge r)$$

So

$$\begin{aligned} p \wedge q \vee r \Leftrightarrow & (p \wedge q \wedge r) \vee (p \wedge q \wedge \neg r) \vee \\ & (\neg p \wedge \neg q \wedge r) \vee (\neg p \wedge q \wedge r) \vee \\ & (p \wedge \neg q \wedge r) \vee (p \wedge q \wedge r) \\ \Leftrightarrow & (p \wedge q \wedge r) \vee (p \wedge q \wedge \neg r) \vee \\ & (\neg p \wedge \neg q \wedge r) \vee (\neg p \wedge q \wedge r) \vee \\ & (p \wedge \neg q \wedge r) \\ \Leftrightarrow & m_{111} \vee m_{110} \vee m_{001} \vee m_{011} \vee m_{101} \\ \Leftrightarrow & m_1 \vee m_3 \vee m_5 \vee m_6 \vee m_7 \\ \Leftrightarrow & \sum(1,3,5,6,7) \end{aligned}$$

Case 2 Set the principal disjunctive normal form and principal conjunctive normal form of formula

$$A(p,q,r,s) \Leftrightarrow (p \wedge q \wedge \neg s) \vee (\neg q \wedge r) \vee s$$

Solution by the example of 1, it can be directly obtained the following results

1) $p \wedge q \vee \neg s \Leftrightarrow (p \wedge q \wedge \neg r \wedge \neg s) \vee (p \wedge q \wedge r \wedge \neg s)$

2) $$\begin{aligned} \neg q \wedge r \Leftrightarrow & (\neg p \wedge \neg q \wedge r \wedge \neg s) \vee (\neg p \wedge \neg q \wedge r \wedge s) \vee \\ & (p \wedge \neg q \wedge r \wedge \neg s) \wedge (p \wedge \neg q \wedge r \vee s) \end{aligned}$$

3) $$\begin{aligned} S \Leftrightarrow & (\neg p \wedge \neg q \wedge \neg r \wedge s) \vee (\neg p \wedge \neg q \wedge r \wedge s) \vee (\neg p \wedge q \wedge \neg r \wedge s) \vee \\ & (\neg p \wedge q \wedge r \vee s) \vee (p \wedge \neg q \wedge \neg r \wedge s) \vee (p \wedge \neg q \wedge r \wedge s) \vee \\ & (p \wedge q \wedge \neg r \wedge s) \vee (p \wedge q \wedge r \wedge s) \end{aligned}$$

So the principal disjunctive normal form of the formula

$$\begin{aligned} & A(p,q,r,s) \Leftrightarrow (p \wedge q \wedge \neg s) \vee (\neg q \wedge r) \vee s \\ & \Leftrightarrow (p \wedge q \wedge \neg r \wedge \neg s) \vee (p \wedge q \wedge r \wedge \neg s) \\ & \vee (\neg p \wedge \neg q \wedge r \wedge \neg s) \vee (\neg p \wedge \neg q \wedge r \wedge s) \vee \\ & (p \wedge \neg q \wedge r \wedge \neg s) \vee (p \wedge \neg q \wedge r \vee s) \end{aligned}$$

$$\vee(\neg p\wedge\neg q\wedge r\wedge\neg s)\vee(\neg p\wedge\neg q\wedge r\wedge s)\vee$$
$$(p\wedge\neg q\wedge r\wedge\neg s)\vee(p\wedge\neg q\wedge r\vee s)$$
$$\vee(\neg p\wedge\neg q\wedge\neg r\wedge s)\vee(\neg p\wedge\neg q\wedge r\wedge s)\vee(\neg p\wedge q\wedge\neg r\wedge s)$$
$$\vee(\neg p\wedge q\wedge r\vee s)\vee(p\wedge\neg q\wedge\neg r\wedge s)\vee(p\wedge\neg q\wedge r\wedge s)\vee$$
$$(p\wedge q\wedge\neg r\wedge s)\vee(p\wedge q\wedge r\wedge s)$$
$$\Leftrightarrow(p\wedge q\wedge\neg r\wedge\neg s)\vee(p\wedge q\wedge r\wedge\neg s)\vee$$
$$(\neg p\wedge\neg q\wedge r\wedge\neg s)\vee(\neg p\wedge\neg q\wedge r\wedge s)\vee$$
$$(p\wedge\neg q\wedge r\wedge\neg s)\vee(p\wedge\neg q\wedge r\vee s)\vee$$
$$(\neg p\wedge\neg q\wedge\neg r\wedge s)\vee(\neg p\wedge q\wedge\neg r\wedge s)\vee$$
$$(\neg p\wedge q\wedge r\vee s)\vee(p\wedge\neg q\wedge\neg r\wedge s)\vee$$
$$(p\wedge q\wedge\neg r\wedge s)\vee(p\wedge q\wedge r\wedge s)$$
$$\Leftrightarrow m_{1100}\vee m_{1110}\vee m_{0010}\vee m_{0011}$$
$$\vee m_{1010}\vee m_{1011}\vee m_{0001}\vee m_{0101}$$
$$\vee m_{0111}\vee m_{1001}\vee m_{1101}\vee m_{1111}$$
$$\Leftrightarrow m_{12}\vee m_{14}\vee m_{2}\vee m_{3}$$
$$\vee m_{10}\vee m_{11}\vee m_{1}\vee m_{5}$$
$$\vee m_{7}\vee m_{9}\vee m_{13}\vee m_{15}$$
$$\Leftrightarrow\sum(1,2,3,5,7,9,10,11,12,13,14,15)$$

The principal conjunctive normal form of the formula is

$$A(p,q,r,s)\Leftrightarrow(p\wedge q\wedge\neg s)\vee(\neg q\wedge r)\vee s$$
$$\Leftrightarrow\prod(0,4,6,8)$$
$$\Leftrightarrow M_0\wedge M_4\wedge M_6\wedge M_8$$
$$\Leftrightarrow(\neg p\vee\neg q\vee\neg r\vee\neg s)\wedge$$
$$(\neg p\vee q\vee\neg r\vee\neg s)\wedge$$
$$(\neg p\vee q\vee r\vee\neg s)\wedge$$
$$(p\vee\neg q\vee\neg r\vee\neg s)$$

Note: proposition formula A contains n words,formula B is a son of formula A, and is a simple conjunction type, when B contained i words,it will into tiny item disjunction type , there shall be 2^i minimum of disjunction type.

References

[1] GengSuyun,QuWanLing.Discrete mathematics [M]. Higher education press 1986.

[2] DuZhongfu,ChenZhaojun.Discrete mathematics [M]. Higher education press. 2004.5

[3] RenXianmiao.Computer mathematical foundation-discrete mathematics [M]. The central radio and television university press. 2000.5

[4] ZhangQinghua.Discrete mathematics [M]. Machinery industry press. 2010.8

[5] WangXianghao,GuanJiwen,LiuXuhua.Discrete mathematics [M]. Higher education press.1983.5

Advanced Materials Research Vols. 989-994 (2014) pp 1610-1614
© (2014) Trans Tech Publications, Switzerland
doi:10.4028/www.scientific.net/AMR.989-994.1610

Online Long-term Object Tracking Based on Compressed Haar-like Features Via Sparse Representation

Ming ZHAO[1,a] ,Luping WANG[2,b] ,Luping ZHANG[3,c]

[1]ATR Key Lab of National University of Defense Technology ,Changsha 410073,China

[2]ATR Key Lab of National University of Defense Technology ,Changsha 410073,China

[3]ATR Key Lab of National University of Defense Technology ,Changsha 410073,China

[a]email:676365834@qq.com,[b]email:wangluping@sina.com,[c]email:zhangluping-002@sina.com

Keywords: online learning, long-term tracking, $l_1$minimization,sparse representation, Haar-like, compressive sensing, context learning

Abstract. Online long-term tracking is a challenging problem as data streams change over time. In this paper, sparse representation has been applied to visual tracking by finding the most correct sample with minimal reconstruction error using compressed Haar-like features. However, most sparse representation tracking algorithm introduce l_1 regularization into the PCA reconstruction using samples directly, which leads to complexity computation and can not adapt to occlusion, rotation and change in size. Our model updating not only uses the samples from the training set, but also generates the warped versions (include scale variation, rotation, occlusion and illumination changes) for the previous tracking result. Also, we do not use the samples in models for sparse representation directly, but the Haar-like features instead which are compressed in a very low-dimensional space. In addition, we use a robust and fast algorithm which exploits the spatio-temporal context for predicting the target location in the next frame. This step will lead to the reduction of the searching range by the detector. We demonstrate the proposed method is able to track objects well under pose and scale variation, rotation, occlusion and illumination with great real-time performance on challenging image sequences.

Introduction

Visual Tracking has long been an importance topic in computer vision field due to its wide range of application for motion analysis, image compression and human-computer interaction. The main challenge for robust visual tracking is to deal numerous training samples included foreground and background cropped from consecutive frames due to occlusion, illumination changes and scale variation.

Recently, online classifier become popular in long-term object tracking. It has been demonstrated to be effective and efficiency for object tracking, but the models will be degraded with drifts caused by slight inaccuracy in tracking result. To deal with this challenging problem, Mei et al. [1] proposed an algorithm that considered the target as a sparse representation of target models and trivial templates. This algorithm is able to solve partial occlusion with trivial templates. However, the computational complexity is very significant. Dinh et al. [2] propose a complex co-trainning approach using generative and discriminative trackers that deals with partial occlusion. Wang D et al. [3] propose an algorithm named SPTracker, which introduces l_1 regularization into the PCA reconstruction. The main components of our work are shown by Figure 1.

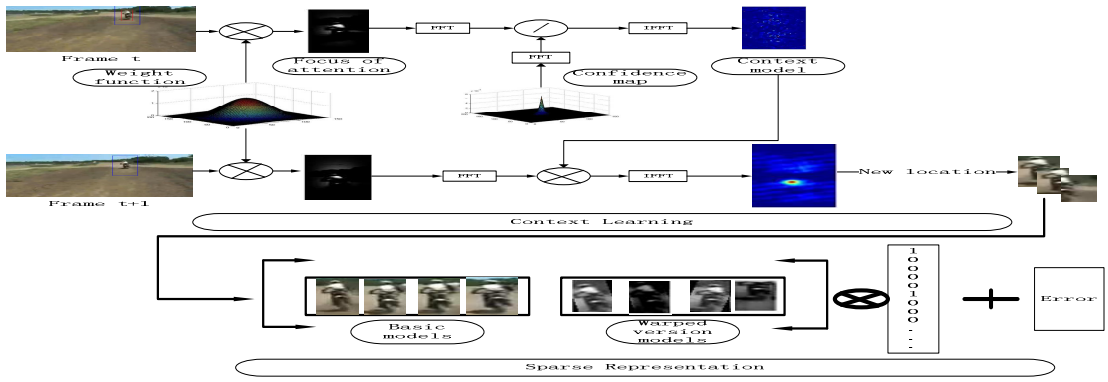

Fig.1 Main components of the proposed algorithm

Context learning

The context area in an image includes the target area (the region inside the red rectangle in fig.1) and its current surroundings [4](the region inside the blue rectangle in fig.1). From Fig.1 we know, the movement leads to the appearance of the target changing significantly, but the context area does not change much. Then, the current context area helps predict the object location in the next frame.

We define $o(x)$ as the target location likelihood, c denotes the object present in the scene. $x \in R^2$ is the object location. Then, the tracking problem is formulated as follows

$$o(x) = P(x \mid c) \tag{1}$$

Considering the context area in the current frame t, we define the context feature set as $F_S = \{f(x) = (I(y), y) \mid y \in S(x_t)\}$, where $I(y)$ denotes normalized image intensity at location y. $S(x_t)$ is the surrounding of the target location center x_t. Then, we denote the target location likelihood as the joint probability.

$$o(x) = P(x \mid c) = \sum_{f(x) \in F_S} P(x, f(y) \mid c) \tag{2}$$

From probability theory we know, the joint probability can be written as conditional probability $P(x \mid f(x), c)$ multiply the prior probability $p(f(x) \mid c)$.

$$o(x) = P(x \mid c) = \sum_{f(x) \in F_S} P(x \mid f(y), c) * P(f(y) \mid c) \tag{3}$$

The conditional probability function $P(x \mid f(y), c)$ is defined as

$$P(x \mid f(y), c) = h(x - y) \tag{4}$$

$P(x \mid f(y), c)$ encodes the spatial relationship between the target and its current context. $h(x-y)$ is a system transfer function with the distance between object location x and its current context y.

We model the context prior probability as follows:

$$P(f(y) \mid c) = I(y) * w_\partial(y - x_t) \tag{5}$$

Where $w_\partial(y - x_t)$ is a weighted function defined by

$$w_\partial(y - x_t) = \frac{1}{K} e^{-\frac{(y - x_t)^2}{\partial^2}} \tag{6}$$

Where k is a normalization constant to keep $P(f(y) \mid c)$ range from 0 to 1. ∂ is a scale parameter.

The target location confidence map is defined as

$$o(x) = \frac{1}{M} e^{-(\frac{x - x_t}{\beta})^\gamma} \tag{7}$$

Where M is a normalization constant, β is a scale parameter and γ is a shape parameter.Then, we formulate as

$$o(x)=\frac{1}{M}e^{-(\frac{x-x_t}{\beta})^{\gamma}}=\sum_{y\in S(x_t)}h(x-y)I(y)w_{\partial}(x-x_t)=h(x)\otimes(I(y)w_{\partial}(x-x_t)) \tag{8}$$

We calculate the equation (8) in the frequency domain using the FFT algorithm.

$$T(\frac{1}{M}e^{-(\frac{x-x_t}{\beta})^{\gamma}})=T(h(x))\times T(I(y)w_{\partial}(x-x_t)) \tag{9}$$

Therefore, we get

$$h(x)=T^{-1}(\frac{T(\frac{1}{M}e^{-(\frac{x-x_t}{\beta})^{\gamma}})}{T(I(y)w_{\partial}(x-x_t))}) \tag{10}$$

Then,

$$o_{t+1}(x)=T^{-1}\left(T(H_{t+1}(x))\times T(I_{t+1}(y)w_{\partial}(x-x_t))\right) \tag{11}$$

We get the target location in the next frame.

$$x_{t+1}=\arg\max_{x\in S(x_t)}o_{t+1}(x) \tag{12}$$

The context transfer function is update by

$$H_{t+1}=(1-\rho)H_t+\rho h_t \tag{13}$$

Where, ρ is a learning parameter and h_t is computed by equation (10).

The scale s is update by

$$\tau_t=\sqrt{\frac{o_t(x_t)}{o_{t-1}(x_{t-1})}},\bar{\tau}_t=\frac{1}{n}\sum_{i=1}^{n}\tau_{t-i},s_{t+1}=(1-\lambda)s_t+\lambda\bar{\tau}_t,\partial_{t+1}=s_t\partial_t \tag{14}$$

Where, τ_t is the estimated scale between two consecutive frames. s_t is average of the estimated scales from n consecutive frames. $\lambda\in(0,1)$.

Haar-like features extraction and compression

The key advantage of a Haar-like feature over most other features is its fewer computation complexity. Due to the use of integral images, a Haar-like feature of any size can be calculated in constant time. This allows to compute sum of rectangular areas in the image, at any position or scale, using only four lookups:

$$Sum(r)=I'(x_0+w,y_0+h)+I'(x_0,y_0)-I'(x_0+w,y_0)-I'(x_0,y_0+h) \tag{11}$$

Where, $I'(x,y)$ is the integral image and $Sum(r)$ is the sum of pixels in the rectangle $[x_0,y_0,w,h]$.

From Compressive Tracking Algorithm we know, there is a very sparse random measurement matrix whose rows have unit length projects data from high dimensional image space to a lower dimensional space.

$$v=Rx \tag{12}$$

Where, $x\in R^m$ is a high-dimensional image space, $v\in R^n$ is the corresponding lower-dimensional space, $n<<m$.

The random measurement matrix [5] is defined as

$$r_{i,j}=\sqrt{s}\begin{cases}1, & with\ \ probability\ \ \frac{1}{2s}\\ 0, & with\ \ probability\ \ 1-\frac{1}{s}\\ -1, & with\ \ probability\ \ \frac{1}{2s}\end{cases} \tag{13}$$

If $s=3$, R is very sparse where only one thirds of computation needs to do. If $s=m/4$, for each row of R, only about c, $c\le 4$, entries need to be computed. As a result, the computational

complexity is only $O(cn)$ which is very low. In addition, only nonzero entries of R need to memory. It is very useful for real-time.

Sparse representation

Sparse representation has been widely used in computer vision. Many methods cast the tracking problem as finding the most correct sample with the smallest projection error.

$$y = Az + e \tag{14}$$

Where $A \in R^{d \times n}$ is a matrix of templates, y represents an observation vector and e denotes the projection error.

In the paper, A includes two part,

$$A = [B, W] \tag{15}$$

Where, B represents the basic models and W represents the warped version models. The equation (14) can be written as

$$y = [B, W] * z + e \tag{16}$$

As it requires solving a series of l_1 minimization problems, it often deals with low-resolution images and the computational complexity is significant. We exploit the compressibility in the transform domain by solving the problem as an l_2-regularized least squares problem, which can be written as

$$z = \min \left\| y - [B, W] z \right\|_2^2 + \lambda \left\| z \right\|_2^2 \tag{17}$$

Where, $\left\| \bullet \right\|_2$ denotes the l_2 norms.

Rigamonti R [6] and Xiao Z-Y [7] solves this problem as

$$z = ([B, W]^T [B, W] + \lambda I)^{-1} [B, W]^T y \tag{18}$$

$I \in R^{d \times d}$ is the identity matrix, $\lambda = 1$.

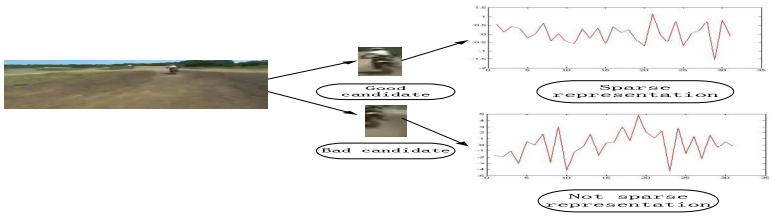

Fig.2 Good and bad candidates approximated by model A

Fig.2 shows the coefficients approximated by the model A for the good and bad target candidates. The coefficients of the good candidate are relative small comparing to the bad candidate coefficients and most of good candidate coefficients are near to 0, only a few are relative big. The bad candidate coefficients are on the contrary.

Then, e can be denoted as

$$e = y - [B, W] z \tag{19}$$

Finally, we can find the most correct sample y_{t+1} as the tracking result in frame t+1.

$$y_{t+1} = \arg\min_{y} (e^T e) \tag{20}$$

In this paper, A is the Haar-like features of basic models and warped version models. The basic models need not to be updated and the warped version models is updated every frame. We generate 20 warped versions by geometric transformations(for example shift $\pm 1\%$, scale change $\pm 1\%$, rotation $\pm 10^{\circ}$) for the previous tracking result and add them with Gaussian noise($\delta = 5$). In order to adapt to the illumination changes, we keep the gray value of the pixels change $\pm 20\%$.

(a) (b)

Fig.3 (a) Parts of the basic models. (b) Parts of the warped version models.

Experiment and conclusion

In order to evaluate our tracking algorithm, we use our method on 3 challenging sequences which are publicly available. Our algorithm is implemented in MATLAB which runs at about 40 frames per second on a Pentium Dual-Core 2.8GHz CPU with 4GB RAM.

Fig.4 Tracking result of the motorcycle by proposed algorithm

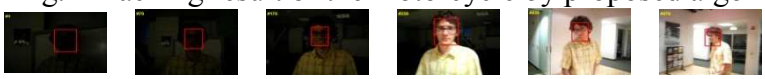

Fig.5 Tracking result of David in door with illumination changing by proposed algorithm

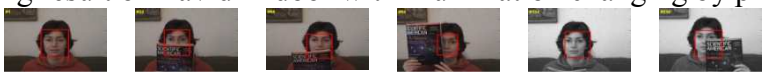

Fig.6 Tracking result of the heavy occlusions by proposed algorithm

From the result of the experiment we know, the proposed algorithm is able to adapt to size change, rotation, illumination change and heavy occlusions. Also, we use context learning to find the target location and scale in the next frame, so the number of testing samples becomes smaller. The context learning algorithm only uses 2 FFT and 2 IFFT operations. The computational complexity for each FFT is only $O(MN\log(MN))$ for the region of $M\times N$. The dimension of modes A always keep in low level and every column of A is compressed to a low-dimensional space (in our paper, $A\in R^{50\times 31}$). The computational complexity of the feature compression is only $O(cn)$ ($c\le 4, n==50$) as described above. If we extract testing samples from the whole image, there will be 50,000 testing samples in an image 320×240. But if we use context learning to find the target location in the next frame, we will only to deal with 900 testing samples in an image 320×240. So the proposed algorithm shows excellent real-time performance.

Reference

[1] Mei X, Ling H, Yi W, et al. Minimum error bounded efficient l_1 tracker with occlusion detection[C]. Proceedings of the IEEE 12th International Conference on Computer Vision and Pattern Recognition. Colorado, USA: IEEE, 2011:1257-1264.

[2] T. B. Dinh and G. G. Medioni, “Co-trainning framework of generative and discriminative trackers with partial occlusion handling,” in Proc. IEEE Workshop Appl. Computer Vision, Jan.2011, PP.642-649.

[3] Wang D, Lu H-C, Yang M-H. Online object tracking with sparse prototypes[J]. IEEE Transactions on Image Processing, 2013,22(1):314-325.

[4] Kaihua Zhang, Lei Zhang, Ming-Hsuan Yang, David Zhang. Fast Tracking via Spatio- Temporal Context Learning[J]. ECCV. 2013,11.

[5] Zhang Kai-hua, Zhang Lei, Yang Ming-hsuan. Real-Time Compressive Tracking. ECCV 2012.

[6] Rigamonti R, Brown M A, Lepetit V. Are sparse representations really relevant for image classification?[C]. Proceedings of the IEEE 12th International Conference on Computer Vision and Pattern Recognition, Colorado, USA:IEEE,2011:1545-1552.

[7] Xiao Z-Y, Lu H-Ch, Wang D. Object tracking with L2-RLS[C]. Proceeding of the 21th International Conference on Pattern Recognition. Tsukuba, Japan:IEEE,2012:681-684.

Advanced Materials Research Vols. 989-994 (2014) pp 1615-1620
© (2014) Trans Tech Publications, Switzerland
doi:10.4028/www.scientific.net/AMR.989-994.1615

A New Virtual Visual Servo Algorithm

Meng LI[1, a], XIAO-Nian WANG[2, b,1] , Jin ZHU[3, c]

[1] School of Electronics and Information Engineering, TongJi University, Shanghai, 201804, China

[2] School of Electronics and Information Engineering, TongJi University, Shanghai, 201804, China

[3] School of Electronics and Information Engineering, TongJi University, Shanghai, 201804, China

[a]email: lemon13140927@126.com, [b]email:dawnyear@tongji.edu.cn, [c]email: zhujintj@sina.com

[1] corresponding author, XIAO-Nian WANG, email:dawnyear@tongji.edu.cn

Keywords: Virtual Visual Servo, Virtual Model, RANSAC, Pose Estimation

Abstract. In this paper, on the basis of the robot visual servo system, a virtual visual servo algorithm for pose estimation is put forward. By reducing the image error between the current image features of real object and the features of virtual models, the rotation and translation relation of the virtual model is changed by visual servo control law, until the pose of virtual model overlaps the one of real object, and then object pose estimation is obtained. In addition, RANSAC algorithm is also introduced to improve the robustness of the proposed algorithm. Finally the experiment about camera external parameters estimation shows that our algorithm gets better results than the available parameter estimation algorithms.

Introduction

When the object model is known, pose estimation is a typical computer vision problem about PNP [1]. Many vision applications problems need pose estimation, such as 3D registration [2] in Augmented Reality, the camera external parameter calibration [3], and the manipulator grabs object [4] based on vision. The main problem currently existing in Augmented Reality System is registration, whose key point is to define the translation relationship between the actual object coordinate system and the virtual one's, namely to achieve pose estimation. The vision-based registration method is to use a CCD camera to obtain information of the real scene, build virtual objects, get control information by analyzing scene images generated by the camera, determine the relative position between the camera and the object, and put virtual objects in the real scene, then realize fusion display [5] of virtual objects and real scene. The camera external parameter calibration is to determine the model's pose relative to the camera coordinate system. The problem about grabbing objects based vision also needs accurate object pose in the camera coordinate frame.

Therefore, on the basis of the robot visual servo system, a virtual visual servo algorithm based on image for pose estimation is put forward. The idea is to convert the camera pose estimation problem into 2D visual servo problem, connect the points' movement in the image plane with the camera movement by Jacobian matrix, then rotate and translate the virtual model with virtual servo control law. When the image error is 0, the virtual model' pose is the real object's pose. This algorithm can solve pose estimation problems about the camera external parameter calibration, 3D registration and vision-based manipulator grabs objects.

Because the feature point extraction inaccuracy can lead to pose calculation error or mistakes, so how to eliminate points with bigger mensuration error and obtain the only pose in space is the most important part of our paper. We also combine with RANSAC algorithm[6], and calculate all possible poses in space after extraction of three feature points, which are continuously eliminate

"outer points", namely the pose calculated by inaccurate feature points, keep "interior points", thus expand the consistent set of candidate feature points, and make one pose in the consistent set as initial value, make the virtual model and real object overlapped with virtual visual servo algorithm, finally we can get the real object pose estimation in space.

Our Virtual Visual Servo System

Image-based robot visual servo system directly makes the image features as the feedback information, estimates the sensitivity matrix (image Jacobian matrix) between pose variation and image characteristics variation in real time, and then realizes the motion control of robot with Jacobi matrix. But the image-based visual servo algorithms for Jacobian matrix is particularly sensitive to the initial value, which usually needs a better initial a pose for controlled object to ensure that final estimation results.

However, in our paper, as Fig 1 shows, firstly assumed the world coordinate is concentric with the camera coordinate , the controlled object is a virtual checkerboard model, which exists in the virtual scene with 3D data at an arbitrary initial pose; secondly the algorithm makes the pose of the virtual model move constantly to pose 1,pose2…, reduces the error between the projection image and the real image; eventually when the image error is 0, the virtual model and real object get overlapped in three-dimensional space, namely realizes pose estimation of real object. The relationship between the virtual checkerboard model and the real model in the spatial coordinate frame is shown as Fig. 1：

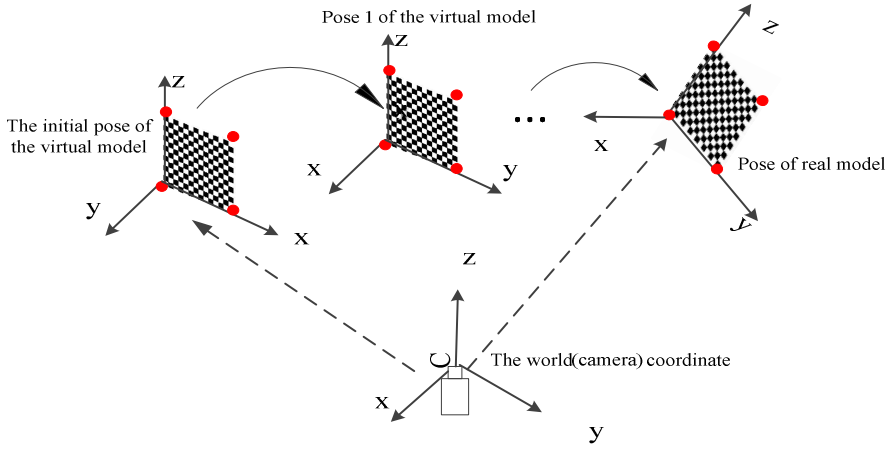

Fig.1.The relationship between the virtual model and the real object

In the process of our VVS system, we define the image feature set as S(·),Id is the real object image, then the real object image feature set is S(Id). Define virtual model as M, its initial pose is x_0 ,then $P(M,x_0)$ its virtual image in the pose of x_0, and its image feature set corresponding to the virtual model is $S(I)$, namely $S(P(M,x_0))$. The error function of the image feature can be defined as follows:

$$e=S(I)-S(I_d)=S(P(M,x_0))-S(I_d) \tag{1}$$

Define the camera internal parameters as K, then $P=K[R,T]$, R is rotation matrix, T is translation matrix. Let [R, T] row vector be $D=[R_x,R_y,R_z,T_x,T_y,T_z]$ namely the controlled variable. The structure of our virtual visual servo algorithm is shown in Fig. 2：

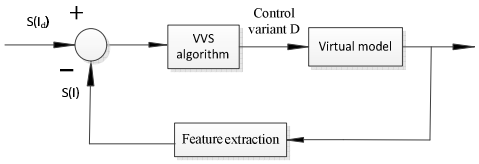

Fig.2.The structure of our virtual visual servo system

According to literature [7], J is defined as formula (2). (x_0,y_0,z_0), whose coordinates are expressed with respect to the space coordinate frame ;(x_c,y_c,z_c), whose coordinates are expressed with respect to the camera coordinate frame, will project onto the image plane with coordinates(x,y); f is focal length.

$$J=\begin{bmatrix} -\frac{f}{z_c} & 0 & \frac{x}{z_c} & \frac{xy}{f} & \frac{-f^2-x^2}{f} & y \\ 0 & -\frac{f}{z_c} & \frac{y}{z_c} & \frac{f^2+z^2}{f} & -\frac{xy}{f} & -x \end{bmatrix} \tag{2}$$

In the VVS algorithm, let $\dot{P}$ represent a vector of image feature parameters velocities, $\dot{r}$ is the virtual model pose velocity, i.e. differentials of controlled variable D. Their relationship is in formula (3):

$$\dot{P}=J\bullet\dot{r} \tag{3}$$

If we regard the virtual model as an output regulator, then $\dot{e}=-\lambda e$,so the absolute value of e decrease progressively in the way of index, λ is the proportional coefficient, then control rate can be calculated by the formula (1) and (3):

$$\dot{r}=-\lambda J^{+}e \tag{4}$$

J^{+} represents the pseudo-inverse matrix [8] of J in formula (4).

From the above, if the pseudo inverse Jacobi matrix is known, the virtual model pose velocity $\dot{r}$ can be calculated; the pose of virtual model will be changed constantly by controlled variable D in the space frame, until the image error is 0. Then the poses of the virtual model and the real object in three-dimensional space are totally overlapped, finally pose estimation of the real object can be attained.

Space pose estimation algorithm

RANSAC Algorithm.

RANSAC algorithm is a robust parameter estimation method. The basic idea is, first of all, according to the specific problem, to design an objective function, and through extracting the minimum point set repeatedly to estimate the initial parameters values in the function; then use the initial parameter values to divide all the data into the so-called "exterior points" (i.e. don't meet the estimated parameter) and "interior points" (i.e. meet the estimated parameter); finally, in turn, with all the "interior points" to calculate and estimate the function parameters. Fischler and Bolles give the RANSAC algorithm in literature [6], and points out that the P3P problem are up to four solutions, and the four the solutions can all be achieved. But we need a set of unique space pose, so in this paper, combined with RANSAC algorithm, we eliminate "outer points", make one pose in the "interior points" consistent set as initial value, greatly reduces the traditional visual servo dependence on the initial pose estimation, and it also has good accuracy and robustness.

Algorithm Flowchart.

Supposed the ideal number of interior points is N_d, set the threshold value for re-projection error as $\delta 1$, the threshold value for servo error as $\delta 2$, the sampling number is *N*.

1) Harris operator for corner points extraction;
2) Simply take three feature points in image space, using the analytical method to calculate all possible space poses;
3) According to the above space poses, figure the re-projection errors of all the feature points on the virtual model. If the re-projection error is less than the corresponding three feature points are "interior points", otherwise are "exterior points", record the number of interior points as *m*;
4) If m is less than N_d, then go to step 2);
5) According to all the above "interior points", calculate the space pose and make it as the initial value of VVS, then do the servo. If servo error is less than $\delta 2$, put the corresponding pose in the RANSAC consistent set, otherwise return to step 2);
6) Repeat step 2) to 5), until the sampling number is equal to *N*;
7) Finally let the mean value of poses in the consistent set as the initial value of VVS, and then run our VVS algorithm with all the interior points, and set the final pose of the virtual model as the best pose estimation result for the real object.

Experiment

The computer is AMD Athlon Ⅱ (tm) Processor with domain frequency of 3.0 GH in our experiment. We do the simulation with MATLAB

Fig. 3 is the checkerboard widely used among camera calibration algorithm [8].There are totally 156 small boxes, whose width and length are both 30millimeter. Establish the virtual chessboard model in accordance with the above parameters in the computer, and establish the local coordinate system as shown in figure 3.

Make one experiment as an example, extract three non-collinear points respectively (-45, 180, 0), (45, 90, 0), (-105, 90, 0) in the world coordinate frame; define the initial pose of the virtual model as [0 0 1 0; 0 1 0 0; -1 0 0 2]; after projecting, the three points' coordinates on the virtual model in image frame are (0.0413,3.0258),(0.0580,-1.3542),(-0.0125,-0.7359),compared to the real three points in the image frame are (0.2314,0.0131),(0.1402,0.0871),(-0.1050,-0.0511),the unit is millimeter.

Experiment Results.

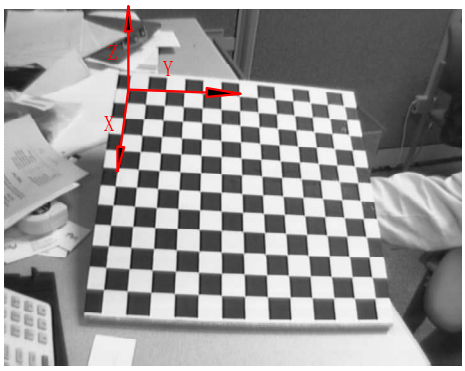

Fig.3. The checkerboard used in the experiment

The image errors of three feature points are shown in Fig.4(a), the space errors in world coordinate frame are shown in Fig.4(b), then this pose of *R, T* which calculated by these points can be fit into a consistent set, otherwise should be abandoned, then we need to take three other feature points in the checkerboard again.

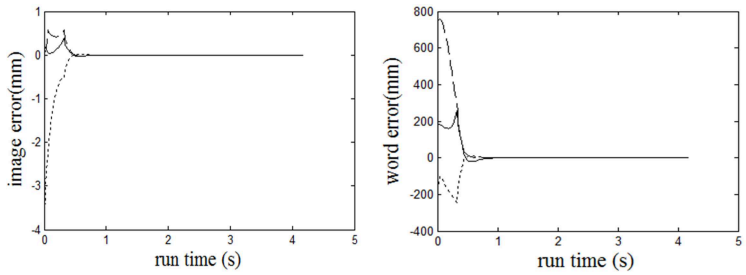

(a) (b)

Fig.4. (a)The image errors of the three points ;(b) the space errors of the three points

Fig.5 represents after VVS, we get the final pose of three feature points, namely external parameters, compared with the real pose. In this figure, we can see the camera coordinate system in 3D space. S1 is the initial pose of virtual checkerboard model, the light blue part represents the final virtual checkerboard after 211 times (about 1.5 seconds) our VVS iterative process; the pink part represents the real checkerboard pose in space. The virtual model and the real one are overlapped within the limits error; otherwise, we need to sample again, take three other feature points over again. In our experiment the sampling number is 60 times.

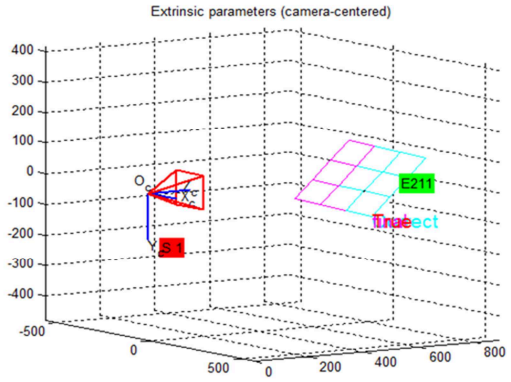

Fig.5. The pose comparison diagram of the virtual model and real object

Fig.6(a) shows the re-projection errors distribution of feature points in the second checkerboard picture by MATLAB calibration method; Fig.6(b) shows the re-projection errors distribution by our method, with the unit for pixels. Table 1 is the standard deviation values comparison of re-projection errors by two methods. It is obvious that the image errors calculated by our method are much smaller than the MATLAB calibration method from Table 1 and Fig. 6.

Table1 The standard deviation values comparison of image error

standard deviation value	MATLAB calibration method	Our method
x	0.59063	0.11689
y	0.42185	0.11501

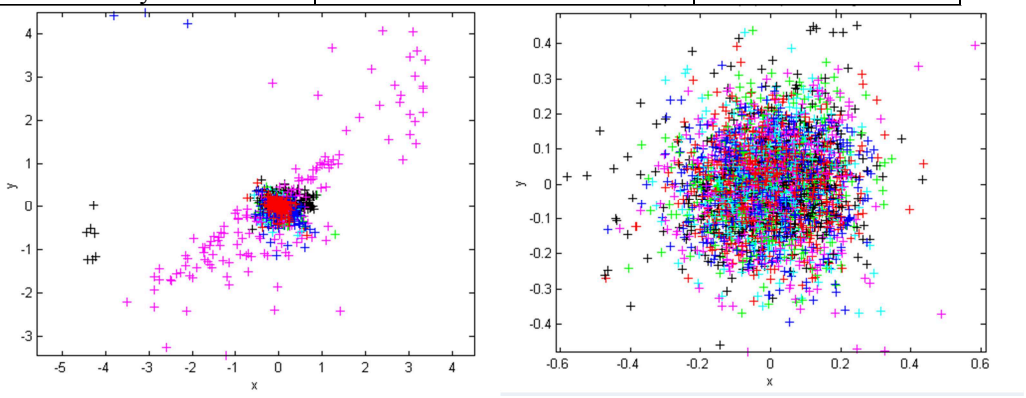

(a) (b)

Fig.6. (a) the re-projection errors with MATLAB calibration method; (b) the re-projection errors with our method

Discussion and Analysis.

In the experiment, we use the second picture from the typical checkerboard examples. The reason is that this picture is distorted, so it can't ensure the high extracting precision. If we simply take three feature points from the second picture, virtual model moves from any pose, the final pose estimation can have a larger deviation after running the MATLAB calibration algorithm. But the final pose estimation can still get good results in our way with the second picture.

Considering that the image has the aberrance and big yawp, corner extraction cannot guarantee all right, so we take 40 checkerboard images in different angles and conditions on the basis of the second one. The results show that within the error of a pixel, the accurate pose probability is 98.3% by our algorithm, while the accurate pose probability is 35.7% if using the VVS method only without removing "exterior points" based on RANSAC algorithm.

Conclusion

In this paper, we combine RANSAC algorithm and VVS algorithm, through the VVS algorithm to calculate the object's 3D pose estimation, then use RANSAC algorithm to pick up the best model parameters, and finally get the model pose estimation. The experiment results show the feasibility and robustness of this method. In addition, the proposed method can used in 3D AR registration and manipulator problem based on visual pose estimation, etc.

Acknowledgement

In this paper, the research was sponsored by National Natural Science Foundation of China 91120308.

References

[1] YAN Qiong.Camera Calibration Based on PnP Problem [J]. Artificial intelligence and recognition, 2007(14), 542-543.

[2] Zhao Xin-can, Zuo Hong-fu. Augmented Reality Registration Algorithm Based on Natural Feature [J]. Journal of South China University of Techno logy (Natural Science Edition), 2007, 35(5):41-45.

[3] Ma Song-De, Zhang Zheng-You.Comuter vision [M].Beijing: Science Press.2007.

[4] Hutchinson, S. Hager, G.D. Corke, P.I., "A tutorial on visual servo control," Robotics and Automation, IEEE Transactions on, 1996, 12(5):651-670.

[5] Wang Mei-Qin. Augmented reality tracking registration technology research based on virtual visual servo [D]. University of Electronic Science and Technology of China.2009.

[6] Misra, I., Moorthi, S.M.; Dhar, D.,Ramakrishnan, R.An automatic satellite image registration technique based on Harris corner detection and Random Sample Consensus (RANSAC) outlier rejection model[J]. Recent Advances in Information Technology (RAIT), 2012 1st International Conference on, 2012: 68-73.

[7] Jiang. P, Unbehauen. R. Robot visual servoing with iterative learning control [J]. Systems, Man and Cybernetics, Part A: Systems and Humans, IEEE Transactions on, 2012, 32(2): 281-287.

[8] http://www.vision.caltech.edu/bouguetj/calib_doc/htmls/example.html.

Advanced Materials Research Vols. 989-994 (2014) pp 1621-1625
© (2014) Trans Tech Publications, Switzerland
doi:10.4028/www.scientific.net/AMR.989-994.1621

A path planning algorithm based on the CNN model under the curvature constraint

Shujun Wang[1, a], Xiaonian Wang[2, b,1], Ping Jiang[3,c,]

[1]School of Electronics and Information Engineering, TongJi University, Shanghai, 201804, China

[2]School of Electronics and Information Engineering, TongJi University, Shanghai, 201804, China

[3]Department of Computer Science, University of Hull, HU6 7RX UK

[a]email: wangsj3433@126.com, [b]email: dawnyear@tongji.edu.cn,

[c]email: P.Jiang@hull.ac.uk

[1] corresponding author, XIAO-Nian WANG, email:dawnyear@tongji.edu.cn

Keywords: CNN model; Path planning; Curvature constraint

Abstract. This paper proposes a new path planning algorithm based on the CNN model. The path planning problem is completed with the dynamics of CNN by establishing a relationship between path control points and CNN cells. Based on the analysis of one dimensional space of CNN algorithm, a CNN equation is constructed and the path updating algorithm under the curvature constraint is obtained, then the stability of the algorithm is discussed. Path planning simulation based on two-dimensional space shows that this algorithm can avoid re-planning or falling into the local minimum, which means it can be successfully used in the path planning and maintenance of robots on the ground in dynamic environment.

Introduction

Robot path planning [1] is an important part in robotics research, whose main task is to find a shortest path without collision with obstacles from the start state(including position and attitude) to the goal state(including position and attitude) based on certain evaluation criteria(for example, the least working cost or the shortest route). The research combining the underlying control and robot path planning algorithm is one of the development directions [2].

Cellular neural network (CNN) is one of the neural network models that proposed by Chua and Yang [3] in 1988. The network is a large-scale nonlinear simulation system which has such characteristics as the partially non-linear connection between cells, the piecewise linear output signal functions and continuous and real-time signal processing. CNN algorithm has been widely used to solve a variety of problems, including biological phenomena [4], image processing [5], mobile robot navigation [6], shortest path problem [7], and so on.

The algorithm proposed by this paper is different from the previous CNN algorithm. It avoids the problem, which may exist in the traditional gradient-based trajectory correction Snake maintenance algorithm [8] [9], that the trajectory converges to a local minimum and serious deviate from the desired results or even lead to fracture. The feasibility and stability of the equation solutions are discussed to ensure the path was simultaneously satisfying the conditions and avoid obstacle.

The CNN used for path planning

In a simplified one-dimension environment as show in Fig. 1(a), we horizontally place some sensor nodes which can communication with others and detect moving obstacles. The black blocks in the Fig. 1 are obstacles, white blocks are feasible regions. Assuming that the biggest width of these obstacles is 2W, the distance of feasible regions between obstacles is bigger than W. The purpose of path planning is finding the moving rules for control points (blue points in Fig. 1) and getting the motion trajectory which meets the curvature constraint $|x_{i+1}-2x_i+x_{i-1}|<C$ and avoids obstacles, where x_i is the one-dimension coordinate of control points, and C is the maximum curvature constraint of robot motion.

The initial state and control points in an already-planned optimal path trajectory are showed as the black curve in Fig. 1(a). When a sensor moves to the left (i.e. obstacles moves to the left), the trajectory will be continuously bending until it doesn't satisfy the curvature constraint or cracks (i.e. as the blue line shown in Fig. 1(b)) with the using of snake orbit maintenance algorithm. However, the cracking situation and obstacles can be avoided by using the dynamics of CNN, which can realize the jump between two steady states and it is manifested as the jump between the red and blue path trajectory in Fig. 1(b).

(a) Initiated optimal path trajectory (b) when obstacles move to the left

Fig.1. The path trajectory with obstacles

Define the distance between the control point x_i and the nearest obstacle o_i is

$$e_i = x_i - o_i \tag{1}$$

A one-dimensional CNN model is constituted by all the control points, where the control point x_i can be regarded as the i-th cell in 1 × N dimensional CNN model. Known from the CNN model, the state of the i-th cell is just affected by its surrounding cells' input and output. Simultaneously, the aim of constructing a CNN equation is to make the robot successfully avoid obstacles under the curvature constraint. Therefore, the input and output of the cell are constrained by both W and C.

According to the definition of saturation function $f(A,x)$, we can define the saturation function of W as $f(W,e_i)$, and the saturation function of C as $f(C, x_{i+1}-2x_i+x_{i-1})$.Then:

$$f(W, e_i) = \begin{cases} W & e_i > W \\ e_i & -W < e_i < W \\ -W & e_i < -W \end{cases} \tag{2}$$

$$f(C, x_{i+1}-2x_i + x_{i-1}) = \begin{cases} C & C > x_{i+1}-2x_i + x_{i-1} \\ -2e_i + M & -C < x_{i+1}-2x_i + x_{i-1} < C \\ -C & x_{i+1}-2x_i + x_{i-1} < -C \end{cases} \tag{3}$$

Substituting equation (1) in (3), the equation (3) can be changed as follows:

$$f(C, x_{i+1}-2x_i + x_{i-1}) = \begin{cases} C & e_i < \dfrac{M - C}{2} \\ -2e_i + M & \dfrac{M - C}{2} < e_i < \dfrac{M + C}{2} \\ -C & e_i > \dfrac{M + C}{2} \end{cases} \tag{4}$$

Where $M=x_{i+1}-2o_i+x_{i-1}$.

Combined with equation (2) (3), the CNN equation is constructed as follows:

$$\dot{e}_i = -e_i + a_i f(W, e_i) + b_i f(C, x_{i+1}-2x_i + x_{i-1}) + I \tag{5}$$

Where a_i and b_i are parameters, and $a_i>1$, $a_i = (a_{i-1})/C$..

In order to make the CNN equation (5) have stable solutions, we can make

$$I = -f(a_i - 1, \frac{b_i M}{2b_i + 1})$$

Refer to the standard CNN equation [10], the equation of CNN is shown as follows:

$$\dot{e}_i = -e_i + a_i f(W, e_i) + b_i f(C, -2e_i + M) - f(a_i - 1, \frac{b_i M}{2b_i + 1}) \quad (6)$$

The specific physical meaning of $a_i f(W,e_i)$ is to make x_i away from obstacles, and $b_i f(C, x_{i+1}-2x_i+x_{i-1})$ is constructed to make the curvature at point x_i meet curvature constraints after moving, and $-f(a_i-1, \frac{b_i M}{2b_i + 1})$ is the compensation of the equation to make sure that x_i doesn't move when there is no obstacle.

Stability analysis of CNN equation

Known from equation (2) and (3), there are four turning points $-$W, W, $\frac{M-C}{2}, \frac{M+C}{2}$ in the CNN equation's dynamic trajectory. As the size relationship of these four values changes with different values of variables, we discuss as follows.

(1) When $M>C+2W$, phase trajectories are shown in Fig. 2.

In this condition, $-W<W<\frac{M-C}{2}<\frac{M+C}{2}$, then we can infer that $a_i-1<\frac{b_i M}{2b_i+1}$ and $f(a_i-1, \frac{b_i M}{2b_i+1}) = a_i-1$.

Fig. 2 shows the dynamic trajectory and equilibrium points of cell circuit when $M>C+2W$. When $W\geq 1$, there are three equilibrium points Q_-,Q_0 and $Q_+$where $Q_-$and Q_+ are stable equilibrium points, and Q_0 is an unstable equilibrium points.

When $e \in (Q_0, Q_+), \dot{e} > 0$,it makes e approach Q_+along the dynamic track with the increasing trend. When $e \in (Q_+, \infty), \dot{e} < 0$, it makes e approach Q_+ along the dynamic track with the decreasing trend. Approximation trend is shown as the direction of the arrow, it obviously means that Q_+ meets the definition of a stable equilibrium point. Similarly, Q_- also is a stable equilibrium point. However, Q_0 belongs to be unstable as it doesn't meet the definition of a stable equilibrium point. According to the above analysis, there is one stable equilibrium point Q_+ when $W<1$. For all stable equilibrium points, $|e|\geq W$, which meet the stability requirements.

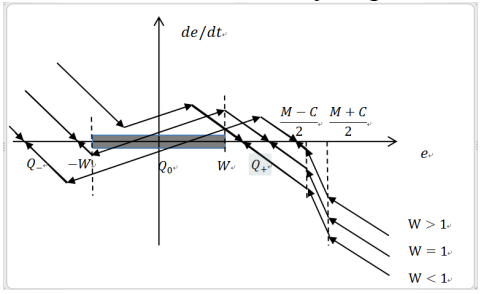

Fig. 2 Phase trajectories when $M>C+2W$

The stability of the equilibrium point analysis under other conditions is the same as Fig. 3, and $|e|\geq W$ holds on all stable equilibrium points which meet the stability requirements.

(2) When max(C-2W, 2W-C)<M<C+2W, C－2W<M<2W－C, C－2W>M>2W－C, －C－2W<M<min(C－2W,2W－C) , and M<－C－2W, the analyzing procedure refers to (1).

This section proves that CNN equation has stable solutions in theory and it can be used in path planning.

Experiments and results

In reality, robots' motion is on a two-dimensional plane. Taking that control point x_i in a two-dimensional plane and actual situation such as its movement trends into account, this paper transforms 2 degrees of freedom to 1 degree of freedom by rotating and counter-rotating, so that the CNN equation can maintain the path planning of robots on 2-dimensional ground.

We chooses one initial curve with arbitrarily settings as the optimal path obtained by traditional path planning algorithm to do the experiments of CNN path planning algorithm. 20 control points (shown as * in Fig. 3) are set by a certain distance in the curve, the first point and the end point are the start and end of the curve.

As the CNN equation just considers the impact of obstacles on its normal direction, it is assumed that, for each control point, it is affected only by obstacles parts on its normal line. Simulations have been finished at Matlab. With the same parameters (here we set a_i =1.5,C=5), the experiments results are shown in Fig. 3 and Table 1.In Fig 3, the black curve is the initial curve, the red curve is the curve after obstacle avoidance, black elongated strips are the sections of obstacles on normal direction of control points, with green points of center, blue points are stable equilibrium points calculated by CNN equation except for the selected one.

Table 1 The experiment's data

	x = 5	x = 6	x = 8	x = 10	x = 12	x = 16
The width of obstacles (W)	2	1.5	1	0.5	2	1
The distance between obstacles center and control points	1	-1.5	1.5	1.2	3	0
The final curvature	2.1020	2.1237	1.0107	0.7943	0.3461	1.1029

It can be seen from Fig. 3 that the point with maximum curvature is located at x = 6. Computing curvature at each point, there is the conclusion, $\forall i \in (1,20)$ and $C(x = i) \leq 5$, which effectively verify that the CNN algorithm can successfully avoid obstacles with satisfying the curvature constraints.

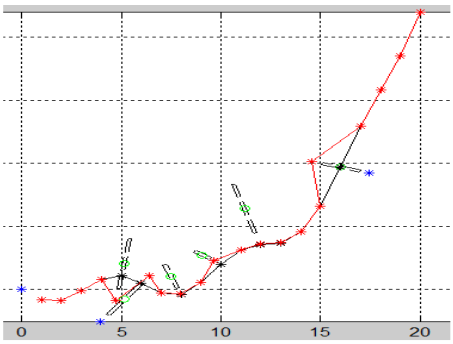

Fig. 3 The experiment result of CNN algorithm

Conclusion

By taking advantage of the CNN which has multi-stable points under different conditions, this paper realizes the timely avoidance of moving obstacles and ensures the achievement of path planning in dynamic environment. Then the existence and number of the stability solution of mentioned CNN equation are discussed to prove that CNN path planning algorithm can get a valid path. Finally, the experiment and simulation are finished to verify the correctness and effectiveness of the algorithm.

Compared with the previous CNN algorithm, the algorithm we mentioned is a more intuitive approach, which achieved a good planning result. As well, this paper only discusses the case with single robot, so it is necessary to make a further consideration on the path planning of multi-robot. Problem of obstacles' prediction is also required to be discussed.

Acknowledgement

The research was sponsored by National Natural Science Foundation of China 91120308.

References

[1] J. Chakraborty, A. Konar, L. C. Jain, and U. Chakraborty. Cooperative multi-robot path planning using differential evolution. J. Intell. Fuzzy Syst., 20(1/2): 13-27, 2009.

[2] Arpino C P, Melendez W M, Guzman J, et al. "Fuzzy logic based speed planning for autonomous navigation under velocity field control[C]," 2009 IEEE Int. Conf. on Mechatronics. 201-212, 2009.

[3] Liang Ma, Jing Yang, Meng Zhang, "A Two-level Path Planning Method for On-road Autonomous Driving," 2012 International Conference on Intelligent Systems Design and Engineering Application, 2012.

[4] Duysens and Pearson, 1980 J. Duysens, K.G. Pearson, "Inhibition of flexor burst generation by loading ankle extensor muscles in walking cats," Brain Res., 321-332,1980.

[5] S.Hashimoto, N.Kubota, F.Kojima, "Visual perception based on cellular neural network for a partner robot," Mechatronics and Automation, 2005 IEEE International Conference, 2: 620-625, 2005.

[6] S.Hashimoto, N.Kubota, F.Kojima, "Visual perception based on cellular neural network for a partner robot," Mechatronics and Automation, 2005 IEEE International Conference, 2: 620-625, 2005.

[7] Y.Cao, X.Zhou, S.Li, "Design of path planning based Cellular Neural Network," 2010 8th World Congress on Intelligent Control and Automation (WCICA), 6539-6544, 2010.

[8] Cheng Y, Jiang P, Hu Y F, "A distributed snake algorithm for mobile robots path planning with curvature constraints," IEEE International Conference on Systems, Man and Cybernetics, 2056-2062, 2008.

[9] Y.Cheng, P.Jiang, Y.F.Hu, "A Snake Based Approach for Robot Path Planning in an Intelligent Environment with Distributed Vision," Proc.Int.Conf. Automation and Computing, 264-269, 2007.

[10] D.L. Vilarin˜o, D. Cabello, X.M. Pardo, V.M. Brea, "Cellular neural networks and active contours: a tool for image segmentation," Image and Vision Computing, 21:189–204, 2003.

Advanced Materials Research Vols. 989-994 (2014) pp 1626-1630
© (2014) Trans Tech Publications, Switzerland
doi:10.4028/www.scientific.net/AMR.989-994.1626

Niche Brain Storm Optimization Algorithm for Multi-peak Function Optimization

Hengjun Zhou[1, a], Mingyan Jiang[1, b], Xianye Ben[1, c]

[1]School of Information Science and Engineering Shandong University, Jinan, 250100, China

[a]email:zhouhengjun1990@163.com, [b]email:jiangmingyan@sdu.edu.cn,

[c]email:benxianyeye@163.com

Keywords: Brain Storm Optimization; Niche Technology; Multi-peak Function; Global Optimization

Abstract. Brain Storm Optimization (BSO) is a novel proposed swarm intelligence optimization algorithm which has a fast convergent speed. However, it is easy to trap into local optimal. In this paper, a new model based on niche technology, which is named Niche Brain Storm Optimization (NBSO), is proposed to overcome the shortcoming of BSO. Niche technology effectively prevents premature and maintains population diversity during the evolution process. NBSO shows excellent performance in searching global value and finding multiple global and local optimal solutions for the multi-peak problems. Several benchmark functions are introduced to evaluate its performance. Experimental results show that NBSO performs better than BSO in global searching ability and faster than Niche Genetic Algorithm (NGA) in finding peaks for multi-peak function.

Introduction

Swarm intelligence algorithms such as particle swarm algorithm [1], fish swarm algorithm [2], and artificial bee colony algorithm [3] have a rapid development in recent years because of their wide application in solving optimization problems. Brain Storm Optimization, inspired by emulating the swarm behaviors of human beings in the problem solving process, is a novel swarm intelligence algorithm which was first proposed by Shi in 2011 [4]. Shi and Zhan [5] demonstrated the feasibility and competence of BSO in function optimization problems. Now it is applied to many fields such as electromagnetic [6] and nonlinear equation solving [7].

The same as other optimization methods, BSO is easily trapped into local optima, besides it can not find multiple the global and local optima in multi-peak function optimization. To solve the problem, this paper proposed Niche Brain Storm Optimization, which modifies the structure of BSO based on niche technology [8] and maintains the diversity of population. Experiments show that NBSO has two advantages over BSO. First, it is easier to jump out the local optima and find the global optima. Second, it can find out all the optima of multi-peak function.

Brain Storm Optimization

Inspired by human creative problem solving process, BSO uses the grouping, replacing and creating operators to generate new individuals as many as possible to search the best individual generation by generation [9]. In the grouping operator, BSO uses a k-mean clustering method to group the N individuals into M clusters. A random cluster center will be replaced with a randomly generated individual in the replacing operator, creating operator means that BSO creates new individual by adding random noise to the current individual which is selected in one cluster or two clusters.

The probability of selecting each cluster j is as:

$$p_j = \frac{|M_j|}{N} \tag{1}$$

Where $|M_j|$ is the number of individuals in cluster j. It is obvious that the more individuals in the cluster, the larger chance it will be selected.

New individual is created as:

$$x_{newd} = x_{selected} + \xi * Norm(0,1)_d \quad (2)$$

$$\xi = \log sig((0.5 * T - t) / k) * random(0,1) \quad (3)$$

Where x_{newd} is the d dimension of the created new individual, $x_{selected}$ is the d dimension of the selected individual, T and t are the maximum number and generation number, k is for changing *logsig()* function's slope, $Norm(0,1)_d$ is the Gaussian random value with mean 0 and variance 1 and *random(0,1)* is a random value within(0,1).

The following is basic steps of BSO algorithm.

Step1: Initialization. Randomly generate N individuals and evaluate their fitness. Maximum number of iterations is T.

Step2: Cluster by k-mean.

Step3: With probability p_{5a}, replace a randomly selected cluster center with a randomly generated individual.

Step4: Randomly select a cluster j with a probability p_j.

Step5: With probability p_{6b}, select one cluster, otherwise, pick two clusters.

Step6: With probability p_{6biii}, select cluster center(s), otherwise randomly select other individuals.

Step7: Add random values to the selected individual to generate new individual

Step8: The newly generated individual is compared with the existing individual with the same individual index. The better one is kept and recorded as the new individual.

Step9: If N individuals have been updated, go to Step 10. Otherwise go back to Step4.

Step10: If the current number of iterations t is less than T, then go back to Step2, otherwise end the algorithm.

Niche Technology

In biology, a niche can be viewed as a subspace in the environment that can support different types of life. A species is defined as a group of individuals with similar biological features capable of interbreeding among themselves but that are unable to breed with individuals outside their group. Niching method is introduced in optimization algorithm to solve the complex multimodal function, because it maintains the diversity of population. Three types of niche are demonstrated in this section.

A. Crowding Niche

Crowding Niche inserts new elements in the population by replacing similar elements. In DeJong's crowding [10], only a fraction of the global population specified by a percentage G (generation gap) reproduces and dies each generation. In this crowding scheme, an offspring replaces the most similar individual (in terms of genotypic comparison) taken from a randomly drawn subpopulation of size CF (crowding factor) from the global population.

B. Fitness Sharing Niche

Fitness sharing modifies the search landscape by reducing the payoff in densely populated regions [11]. It lowers each population element's fitness by an amount nearly equal to the number of similar individuals in the population. Sharing must be implemented with the less biased selection methods and use low recombination operators to promote stability of subpopulations.

C. Clearing Niche

The clearing Niche is very similar to fitness sharing but is based on the concept of limited resources of the environment [12]. Instead of sharing the resources between all individuals of a single subpopulation as in fitness sharing, clearing attributes them only to the best members of the subpopulation.

Niche Brain Storm Optimization

BSO has a fast convergent speed at the beginning of search, however, the population diversity declines rapidly as the iteration goes on. In order to jump out of local optima, niche strategy is

introduced into the BSO. Niche is constructed by comparing Euclidean distance for every pair of individuals. If the distance is shorter than the preassigned distance L (niche radius), the individual with poor fitness is strictly punished by setting its fitness to low value. Thus, for two individuals within the preassigned distance L, the poor one will die out with high probability after several iterations. In this way, the best one is reserved within niche radius, so that individuals are distributed separately in the search space. NBSO maintains the diversity of population effectively, so it prevents premature convergence and can find all the global and local optimal of multi-peak function. There are three modifications in NBSO based on BSO.

1. Outside population with capacity K is introduced to preserve good individuals of revolution. Outside population preserves the fitness of K best individuals in the first iteration. In next iteration, outside population is refreshed by selecting K best individuals from $N+K$ population combining K outside population with N revolution population.

2. BSO selects a rand individual of cluster when new individuals are generated as step6 above. In NBSO, individual is selected according to its fitness in the cluster except for the center individual. Individual with high fitness will be selected with high probability. Because the fitness of poor individual in niche environment is set low value, it will be selected with low probability.

3. After new individuals are generated, the Euclidean distance between every pair of the new individuals is calculated and if the distance is shorter than L, the individual with high fitness is reserved while the poor one is set low value.

Experimental studies

In this section, NBSO is evaluated by using the multi-peak benchmark functions with a large number of local optima. Experiment I demonstrates the global searching ability of NBSO by comparing with BSO while Experiment II shows the peaks finding ability of NBSO in comparison with NGA.

A. Experiment I -- Global Searching Ability

Three benchmark functions listed in Table I are used in experiment I. Rosenbrock Function has a minimize value of zero with the location (1, 1). Schaffer Function has numerous local maximum, the global maximum is 1 with the location (0, 0). Shubert Function has 760 local minimum, the global minimum is -186.73 with the location (-1.4251,-0.8003).

BSO and NBSO are utilized to search the global optimal value. The global searching ability of an algorithm is evaluated by success rate. Success rate means the probability of an algorithm finding the global optimal value. Each algorithm is tested 50 times independently for every function and the mean results are used in comparison. Table II shows the success rate, mean fitness and optimal fitness found for benchmark functions.

According to table II, the success rate of NBSO approaches to 1 while BSO is 68% on average for all of the three functions. NBSO increases the success rate by 30% compared with BSO, which means NBSO has better ability of searching global optimal value than BSO.

Table I Test Function Used In the Comparison

Function	Test Function	Search Space
Rosenbrock	$f(x_1,x_2)=100(x_1^2-x_2)^2+(1-x_1)^2$	$-10\le x_1,x_2\le 10$
Schaffer	$f(x_1,x_2)=0.5-\frac{(\sin\sqrt{x_1^2+x_2^2})^2-0.5}{(1+0.001(x_1^2+x_2^2))^2}$	$-10\le x_1,x_2\le 10$
Shubert	$f(x_1,x_2)=\left\{\sum_{i=1}^{5} i\cos\left[(i+1)x_1+i\right]\right\}\left\{\sum_{i=1}^{5} i\cos\left[(i+1)x_2+i\right]\right\}$ $+0.5[(x_1+1.4251)^2+(x_2+0.8003)^2]$	$-10\le x_1,x_2\le 10$

Table II Success Rate, Mean Fitness and Optimal Fitness Found for Functions

Test Functions	BSO			NBSO		
	Success Rate (%)	Mean Fitness	Optimal Fitness	Success Rate (%)	Mean Fitness	Optimal Fitness
Rosenbrock	76	0.133	0	100	0	0
Schaffer	68	0.9952	1	98	0.9999	1
Shubert	62	-185.69	-186.73	98	-186.72	-186.73

B. Experiment II -- Global Searching Ability

To evaluate peaks finding ability of NBSO, three widely used benchmark multi-peak functions are introduced in the experiment.

$$F_1(x) = \sin^6(5.1\pi x + 0.5) \tag{4}$$

This function defined on $[0,1]$ consists of equally spaced peaks of uniform height. Maxima are located at the x values of 0.1, 0.3, 0.5, 0.7 and 0.9. All maxima are height of 1.0.

$$F_2(x) = x\sin^6(5.1\pi(x^2 - 0.57)) \tag{5}$$

F_2 is also defined on $[0,1]$ and consists of unequally spaced peaks of nouniform height. Maxima are of rounded height, 0.9297, 0.8176, 0.6872, 0.5258 and 0.2859.

$$F_3(x, y) = 200 - (x^2 + y - 11)^2 - (x + y^2 - 7)^2 \tag{6}$$

F_3 is defined on $-6 \le x,y \le 6$. It is a two dimension complex function and has 4 maximum with height of 200.

Effective Numbers of Peak: A peak is found if at least one individual of the population reaches the 99% height of the peak. The number of peaks found is called effective numbers of peak.

Maximum Peak Ratio (MPR): The maximum peak ratio is the effective numbers of peak divided by the number of all actual peaks in the search space [13]. It exhibits the ability of searching local maximum of an algorithm.

MPR of NBSO is calculated for three functions in different iterations and compared with that of NGA. Each algorithm is tested in 20 times. Table III shows the MPR of each function in different iterations, it is obvious that NBSO does better than NGA in finding peaks. NBSO can find more peaks than NGA at the same iteration, especially in complex multi-peak functions. Figure 1 shows the peaks found on different functions by NBSO.

Table III MAR For Test Functions in Different Iterations

Test Functions	Iteration / Algorithm	T=10	T=20	T=30	T=40	T=50
F_1	NGA	70%	86%	94%	100%	100%
	NBSO	92%	100%	100%	100%	100%
F_2	NGA	62%	76%	88%	96%	99%
	NBSO	90%	98%	100%	100%	100%
F_3	NGA	25%	52.5%	67.5%	85%	95%
	NBSO	72.5%	87.5%	96.25%	98.75%	100%

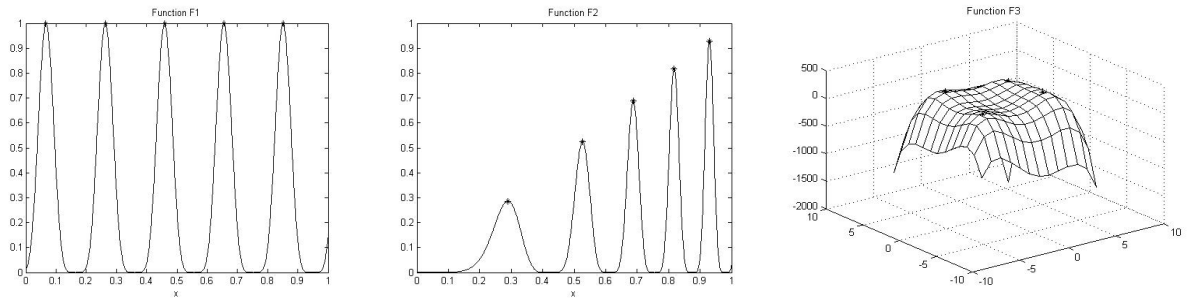

(a) F_1 (b) F_2 (c) F_3

Fig 1 Peaks found on different functions by NBSO

Conclusion

In this paper, niche technology is introduced into BSO algorithm to prevent premature. Niche technology can effectively maintain population diversity and enhance global searching ability of BSO. Experimental results show that NBSO has several advantages. First, NBSO has better ability to prevent premature when compared with BSO. Second, NBSO can effectively find multiple global and local optimal solutions for the multi-peak problems.

Acknowledgement

This work is supported by the Special Foundation Project for Independent Innovation Achievement Transform of Shandong Province (No.2012CX30202), the Foundation of Shandong University for Independent Innovation (No. 2012DZ038), the Natural Science Foundation of China (Grant No. 61201370), the Specialized Research Fund for the Doctoral Program of Higher Education of China (Grant No. 20120131120030).

References

[1] J. Kennedy, R. Eberhart. Particle swarm optimization. In Proc. IEEE Int. Conf. Neural Netw, 1995, pp. 1942–1948.

[2] Mingyan Jiang, Dongfeng Yuan. Artificial Fish Swarm Algorithm and Its Applications. Science Press, Beijing, China, 2012.

[3] D. Karaboga. An idea based on honey bee swarm for numerical optimization. Technical Report-TR06, Erciyes University, Engineering Faculty, Computer Engineering Department, 2005.

[4] Y.Shi. Brain storm optimization algorithm. In Proc. 2nd Int. Conf. Swarm Intelligence, 2011, pp. 303–309.

[5] Z. Zhan, J. Zhang, Y. Shi, H. Liu. A modified brain storm optimization. In Proc. 2012 IEEE World Congr. Computational Intelligence, 2012, pp. 1–8.

[6] H Duan, S Li, Y Shi. Predator-Prey brain storm optimization for DC brushless motor. In Proc. IEEE Trans. Magnetics, 2013 49 (10) pp. 5336-5340.

[7] N. Zhang. Intelligent optimization algorithm for solving nonlinear Equations. University of JiLin, 2013.

[8] K. Deb, D. E. Goldberg. An investigation of niche and species formation in genetic function optimization. In Proc. 3rd Int. Conf. Genetic Algorithms, 1989, pp. 42–50.

[9] Y. Shi. An optimization algorithm based on brainstorming process. Int. J. Swarm Intell, 2011, pp. 35–62.

[10] K. A. DeJong. An analysis of the behavior of a class of genetic adaptative systems. Ph.D. dissertation, Univ. of Michigan, Ann Arbor, 1975.

[11] B Sareni, L. Krahenbuhl. Fitness sharing and niching methods revisited. IEEE Trans. Evol. Comput, 1998 (2), pp.97-106.

[12] A. P′ etrowski. A clearing procedure as a niching method for genetic algorithms. In Proc. 1996 IEEE Int. Conf. Evolutionary Computation, 1996, pp. 798–803.

[13] B. L. Miller, M. J. Shaw. Genetic algorithms with dynamic niche sharing for multimodal function optimization. In Proc. 1996 IEEE Int. Conf. Evolutionary Computation, 1996, pp. 786–791.

Advanced Materials Research Vols. 989-994 (2014) pp 1631-1634
© (2014) Trans Tech Publications, Switzerland
doi:10.4028/www.scientific.net/AMR.989-994.1631

Research on the Validation Method of Product Data Quality

Ping WANG[1, a], Bin WANG[1, b]

[1]UGS College, Yancheng Institute of Technology, Yancheng, 224051, China

[a]email: wp_ycit@163.com, [b]email:Wangbin@ycit.cn

Keywords: Product Data Quality; Validation Rules; Rules Class

Abstract. Product data is the source data of product lifecycle in manufacturing enterprise. The quality of product data largely determines the effect of the application of Engineering analysis, simulation assembly and CNC programming work and so on. In order to solve the problems of the existing product data quality, such as validation custom trival, lack of high efficiency and flexibility, etc. The validation method of product data quality (PDQ) based on class was proposed in NX software environment, the representation of validation rules classes of product data quality, validation rules customization and implementation of validation process were introduced in detail in this study. Finally, an application case was employed to verify the practicability and effectiveness of the proposed method.

Introduction

Product data plays a key role in current product design and manufacturing processes including concept design, detail design, CAE, CAM and so on. However, because of the complexity of the product data itself, product data inevitably exist errors in the process of creating product data, so tend to hinder the product development process, and increase product development costs. The Japanese automotive industry spends about US$67 million a year to solve product data problems for approximately 250,000 cases .DaimlerChrysler estimates that as many as 10,000 of product data items should be repaired or adjusted due to the quality problem, an extra 5 million Euros is required in downstream processes [1]. Therefore, it is particularly important to carry out the related researches of product data quality assurance aspects. Son, et al. [2] developed a fully automated product 3D data quality validation and management system to support the product development processes of high-tech products like televisions, camcorders, mobile telephones, etc. Wang, et al. [3] proposed a rule-based data checking method of digital definition of mechanical products on the platform of NX software. Contero, et al. [4] presented a linguistics approach which emphasized the role of modeling techniques to achieve high-quality product data models. Kikuchi, et al. [5] reported the development of a PDQ standard (ISO 10303-59), which is a resource part of ISO 10303 Standard for the Exchange of Product Model Data. Kovacs, et al. [6] investigated the integration of PDM and workflow management systems and proposed a philosophy for the support of product data throughout the full development and production lifecycle. In this study, the validation method of product data quality based on class was proposed under NX software environment. In the following, a definition of product data quality is provided in section 2 and the representations of validation rules classes of product data is described in section 3. The validation process of product data quality is introduced in section 4. An application case in section 5 is given. A conclusion is included in section 6.

The Definition of Product Data Quality

- Product Data Quality (PDQ) is a measure of the accuracy and appropriateness of product data combined timeless with which those data are provided to all the people who need them (ISO TC184/SC4 N1944 2005). The term ‘product data’ is usually defined as any and all product data required from product conception to product manufacturing. Therefore, product data includes not just CAD data but also CAM data, CAE data, PDM data, and other kinds of data.

The Representation of Validation Rules Classes of Product Data

In order to check the quality of product data, it is very important to select a proper representation method for product data criteria. The representation of validation rules of product data can be better supported by Knowledge Fusion (KF), which is embedded object-oriented interpreted language of NX software.

The class definition of data validation rules based on KF language is as follows:

DefClass: <class name> (<parent class>);
(Data type Behavioral flag_1 Behavioral flag_2, ...)
Attribute Name: Parameter_1;
(Child) rule name:{class, …};
(Method Return Type) id:(type_1 $var_1, …)
@ {Statements…};
Defun: id(arglist) block Return Type;

The Validation Process of Product data Quality

The validation process of product data quality consists of four steps (Figure 1).

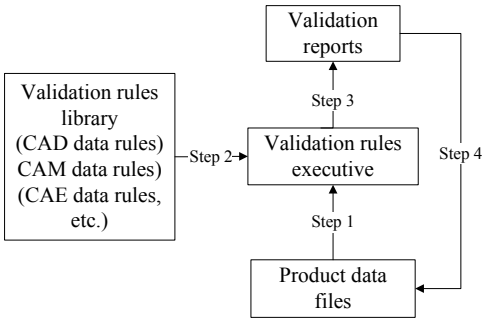

Fig. 1. The validation process of product data quality

Step 1: Create or open the validation data files.

Step 2: According to the requirements of product data quality, choose the corresponding validation rules from the validation rules library. Multiple validation rules can be chosen.

Step 3: Run validation rules, and generate the validation reports.

Step 4: To check the validation report, if there exist data errors, then modify product data files, until all the error modifications completed.

Application Case

The validation method of PDQ is evaluated using complex sheet body sewn by multiple trimmed sheet bodies (as shown in Figure 2).

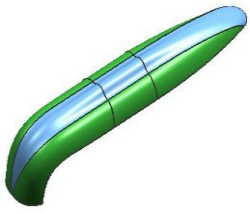

Fig. 2. The complex sheet body sewn by multiple trimmed sheet bodies

In the process of CAD modeling of automobile covering parts, the complex sheet body is often used, and usually be sewn by multiple trimmed sheet bodies. In order to ensure the CAD data quality of automobile covering parts, assuming that the product data quality of complex sheet body must meet the following criteria:

① The sewn tolerance of all sewn sheet bodies are not more than 0.02 mm.
② All sewn sheet bodies must be located in layer 10.

③ No other types of entities exist in the specified layer 10.

(1) The validation algorithm description of CAD data quality of complex sheet body

The validation algorithm of CAD data quality of complex sheet body was shown in Fig. 3.

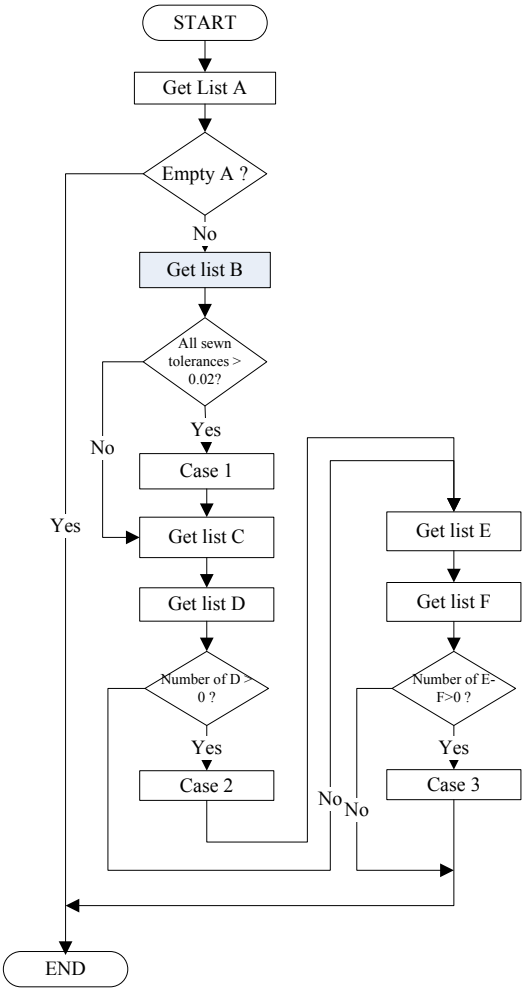

Fig. 3. The validation algorithm of CAD data quality of complex sheet body

In order to facilitate the algorithm description, the meanings of the following letters assumptions are as follows:

A: all trimmed sheet bodies;

B: all sewn sheet bodies (the child feature of trimmed sheet body);

C: all the sheet bodies in the specified layer;

D: all the sheet bodies that are not in the specified layer;

E: all the entities in the specified layer;

F: all the sewn sheet bodies in the specified layer;

E-F: other types of entities in the specified layer;

Case 1: Report errors, the sewn tolerances are more than 0.02 mm.

Case 2: Report errors, the sewn sheet bodies are not in specified layer.

Case 3: Report errors, the other type of entities exist in specified layer.

(2) The validation process of CAD data quality of complex sheet body

The validation process of CAD data quality of complex sheet body under NX software includes the following steps:

Step 1: Open CAD data file of complex sheet body (sew_sheets.prt) under NX software environment, and then enter the Check-mate function module.

Step 2: Determine the validation rules classes and customize related parameters.

Step 3: Run validation rules**.**

Step 4: Check validation reports (Figure 4). If find errors, modify the CAD data, until there are no errors.

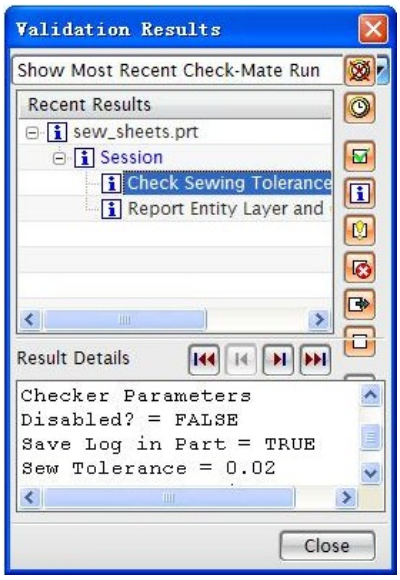

Fig. 4. Validation results

Conclusion

The validation method of product data quality based on class has been presented in this study. Especially, the method was implemented to support the product data validation in whole lifecycle. By applying the method, the designers can timely find the defects existing in the product data, so as to ensure the high quality of product data.

Acknowledgement

In this paper, the research was sponsored by the Nature Science Foundation of Jiangsu Province (Project No. BK20131221).

References

[1] Yang, J., S. Han, H. Kang. Product data quality assurance for e-manufacturing in the automotive industry [J]. International Journal of Computer Integrated Manufacturing, 2006:19(2):136-147.

[2] Son, S., S. Na, K. Kim. Product data quality validation system for product development processes in high-tech industry [J]. International Journal of Production Research, 2011:49(12):3751-3766.

[3] Wang, Ping, Wang Bin. Research on the data checking of digital definition of mechanical products. Proceedings of the 2nd International Conference on Mechanic Automation and Control Engineering [C], 2011.

[4] Contero,M., et al. Product data quality and collaborative engineering [J]. IEEE Computer Graphics and Applications, 2002:22 (3):32-42.

[5] Kikuchi, Y., et al. PDQ(product data quality): Representation of data quality for product data and specifically for shape data [J]. Journal of Computing and Information Science in Engineering, 2010:10(2):1-8.

[6] Kovacs, Z., et al.. Support for product data from design to production [J]. Computer Integrated Manufacturing Systems, 1998:11 (4):285-290.

Advanced Materials Research Vols. 989-994 (2014) pp 1635-1640
© (2014) Trans Tech Publications, Switzerland
doi:10.4028/www.scientific.net/AMR.989-994.1635

Stock price prediction model based on IWO neural network and its applications

Hong Liu[1,a] , Xiaoyan Lv[1,b]

[1]School of Science, University of Science and Technology Liaoning, Anshan 114051, China

[a]email: ldhliuhong@163.com,[b]email:lvxiaoyanlxy@yeah.net

Keywords: Invasive Weed Optimization; Feed-forward Neural Network; Stock Price Prediction

Abstract. In view of the deficiency of the standard back-propagation algorithm based on steepest descent method, a new kind of optimization strategy called invasive weed optimization(IWO) algorithm is introduced into the training process of feed-forward neural networks, and then a prediction model based on IWO feed-forward neural network(IWO-NN) is given. By the dynamic adjustment of standard deviation of the distribution of offspring individuals in IWO, the local convergence speed of networks is improved and the defect of trapping into a local optimum is reduced. By the empirical study of stock price prediction in Sany Heavy Industry, the results show that this method has better global astringency, robustness, and it is insensitive to initial values.

Introduction

The standard BP neural network algorithm is based on local search algorithm of gradient descent, which can not be used to search the global minimum points of multimodal function, it has high requirements to the functions and has the disadvantages of slow convergence speed, easy to trap into local minimum and low robustness and so on[1][2], therefore, some improved methods such as genetic algorithm, evolutionary algorithm and simulated annealing algorithm are used to train the feed-forward neural network.

IWO is a new intelligent stochastic search optimization algorithm, which is evolved from the evolution principle of weeds in nature. This algorithm mimics the basic process of spatial dispersal, growth, reproduction and competitive extinction of weeds invading into seeds and it has a strong adaptation and robustness [3]. In IWO, the group evolution is guided by the outstanding individual in the group, the offspring individuals are distributed around parent individuals with a normal distribution during the evolution process, and the standard deviation of normal distribution is adjusted and changed dynamically with the evolution generation, making the algorithm keeping the diversity of population in the early and middle evolution period, to overcome the phenomenon of premature convergence. In the later period, the local search ability of outstanding individual is stronger and stronger to ensure the algorithm approximate steadily the global optimal solution with higher accuracy. By comparing IWO algorithm with the simple particle swarm algorithm, IWO does not need too large storage space to save the track of particle; By comparing it with genetic algorithm, the structure of the algorithm structure is more simple and easy to realize, and it does not need the selection operator, crossover operator and mutation operator which are used in genetic operations, and can quickly and efficiently converge to the optimal solution of the problem. Therefore, we try to apply IWO algorithm to the training of feed-forward neural network to solve the problems of standard BP algorithm, and a prediction model is given, and then a practical simulation of stock price prediction is carried out, the feasibility and effectiveness are verified by comparing it with the standard BP algorithm.

IWO-NN prediction model

1.1 Prediction model of feed-forward neural network

The prediction refers to estimating values for future unknown data by some known historical data. Assuming that a time sequence$\{x_i\}$, among which the historical data is x_n ,x_{n+1} ,..., x_{n+m}, we want to predict the value at time $n+m+k$ ($k>0$), namely predicting nonlinear function relationship x_{n+m+k} at time $n+m+k$ ($k>0$), where the function relationship is $x_{n+m+k}=f(x_n,x_{n+1},\ldots,x_{n+m})$.

We use the feed-forward neural network to predict, that is we use neural network to fitting function f by a set of data points $x_n, x_{n+1}, \ldots, x_{n+m}$ and get the predicting value at future time $n+m+k$ ($k>0$).

The feed-forward neural network is a common artificial neural network model ,which has processing units of several connected layers, where each neuron in one layer is connected to every neuron in next layer, and there is no feedback in the network. In this paper, a three layer network is considered, which is widely used, the output layer is a linear layer, and the nonlinear effect function (the activation function) of neurons in hidden layer is a hyperbolic tangent function (*tan-sigmoid*):

$$\sigma(x)=\frac{1-e^{-x}}{1+e^{-x}} \tag{1}$$

Assuming the output of neurons in input layer is $P^i=(p_1,p_2,\ldots,p_R)$, $\{w1_{i,j}\}$ is the connection weights of input layer to hidden layer, $\{b1_{i,1}\}$ is the threshold value of neurons in hidden layer, $\{w2_{i,k}\}$ is the connection weights of hidden layer to output layer, and $\{b2_{i,1}\}$ is the threshold value of neurons in output layer. The mapping of input to output of network is:

$$y_k=\sum_{i=1}^{S_1} w2_{i,k}\sigma\left(\sum_{j=1}^{R} w1_{i,j}p_j+b1_{i,1}\right) \quad 1\le k\le S_2 \tag{2}$$

The training sample set of the feed-forward neural network is $A=\{(P^i, T^i), i=1,2,\ldots, s\}$, where s is the number of training samples, $P^i \in R^R$ is the input of training data in the i^{th} group, $T^i \in R^{S2}$ is the expectation output of corresponding input of training data in the i^{th} group, T_k^i is the expectation output of the k^{th} neuron in output layer. Assuming that the actual output of training data in i^{th} group is $Y^i \in R^{S2}$, Y_k^i is the actual output of the k^{th} neuron in output layer, then the error function based on the training sample set is given by:

$$E=\frac{1}{2}\sum_{i=1}^{s}\sum_{k=1}^{S_2}(Y_k^i-T_k^i)^2 \tag{3}$$

The function is a nonlinear function with various multiple minimum points, and the training process for this feed-forward neural network is adjusting the connection weights and threshold value of $\{w1_{i,j}\},\{b1_{i,1}\},\{w2_{i,k}\},\{b2_{i,1}\}$ until the error function E to minimum[4].

We can obtain the corresponding connection weights and thresholds $\{w1_{i,j}\},\{b1_{i,1}\},\{w2_{i,k}\},\{b2_{i,1}\}$ through being trained by the above feed-forward neural network. Then we can carry out specific problems of prediction by the prediction model of feed-forward neural network (2).

1.2 IWO Algorithm

The convergence is one of the most important characteristic of intelligent optimization algorithm, IWO algorithm relies on the guiding information of outstanding individual for the reproduction technique in development process, which is the foundation of convergence of algorithm. The dynamic adjustment of standard deviation in offspring distribution is the key point of the convergence of algorithm. The offspring individuals are distributed around parent individuals in normal distribution, making the algorithm achieve both selection and population diversity, to avoid the local maximum points availably and to ensure the stability of global convergence. The value range of the parameters is very wide, and the parameters do not highly depend on initial population. The steps of algorithm are listed below:

*step*1 Initialization of a population, we need determine the size P_{size} of initial population P(part of ethnic groups) and the size Q_{size} of ethnic groups Q, maximum iteration numbers $iter_{max}$, dimension of solving the problem *dim*, maximum generated seed number S_{max}, minimum generated seed number S_{min}, nonlinear modulation index n, initial value of interval step σ_{init} and final value of interval step σ_{final}, x_{min} and x_{max} respectively represent minimum value and maximum value of initial search space of independent variable.

*step*2 Randomly generate the initial solution by initial population, initial search space of independent variable and dimension of solving the problem.

*step*3 Refresh the iterations and the standard deviation of offspring normal distribution, which is calculated by

$$\sigma_{cur} = \frac{(iter_{\max} - iter)^n}{(iter_{\max})^n}\left(\sigma_{init} - \sigma_{final}\right) + \sigma_{final} \tag{4}$$

where *iter* is current number of iterations.

*step*4 Reproduction, the offspring are randomly distributed around parent by normal distribution $N(0,\sigma^2)$.The calculation of the offspring individual (seed number) depends on the fitness value of offspring. The number of offspring allowed by optimal fitness individual is S_{max}, and the number of offspring allowed by worst fitness individual is S_{min}, other number of offspring allowed obeys a round down linear relationship with their fitness. This mechanism is similar to the actual situation of weeds colony in nature, and the formula of generating seeds is

$$weed_n = \frac{f - f_{\min}}{f_{\max} - f_{\min}}(s_{\max} - s_{\min}) + s_{\min} \tag{5}$$

*step*5 Check whether the population number is the maximum. If the population number is not the maximum, return *step*4.

*step*6 If the number is greater than the maximum population number, compete and eliminate, the fittest is survival. Save the least fitness individuals, which is what we mentioned above, and the specific operation is rank the parent individual and offspring individual according the adaptive value, keep excellent fitness individuals to make the size of population within the maximum population. The operation that excellent individuals will be kept to the next generation ensures the convergence of the algorithm.

*step*7 Check whether the population number is the maximum. If not, repeat *step*4 to *step*6, otherwise, output the individual with the best fitness as the optimal solution.

1.3 Establishment of IWO-NN prediction model

1.3.1 Basic idea of training neural network based on IWO algorithm

Assuming that X is a feed-forward neural network $X=\{X_i|i=1,\ldots,p\}$, where X_i is the individual in population X, and p is the number of the individuals. Every individual X_i consists of two weight matrices $\{w1_{i,j}\},\{w2_{i,k}\}$ and two threshold matrices$\{b1_{i,1}\},\{b2_{i,1}\}$, the algorithm is to find the optimal X_i in $X=\{X_i|i=1,\ldots,p\}$and the optimizing function $minF(x)$ is the error function E (its expression is given in equation (3)). Then the error function E is optimized by IWO algorithm until satisfying the given stop conditions [4] [5].

1.3.2 Steps of training neural network based on IWO algorithm

*step*1 Randomly generate the initial solution, namely, population X, where each individual in the population is $X_i=[\ w1_{i,1}\ ,w1_{i,2},\ldots,w1_{i,n},\ b1_{i,1},\ w2_{i,1},w2_{i,2}\ ,\ldots,w2_{i,m}\ ,\ b2_{i,1}]$[6], $n=R\times S_1$, $m=S_1\times S_2$,R is the number of inputs neuron, S_1 is the number of neuron in hidden layer, and S_2 is the number of neuron in output layer. The initial individual number of the population is P_0, and the maximum number is Q. Calculate the fitness of each individual X_i.

*step*2 For the initial solution X, determine the allowed generated seed numbers by X_i in equation (5), where f is the fitness, thus the evaluation function $f= minF(x)$.

*step*3 According to equation (4), a new solution X_i is generated by adding a value D to the solution in each dimension, and calculate new individual fitness, where $D\in[-\sigma,\sigma]$;

*step*4 If the number of the existing solution is less than Q, go to *step*2; otherwise, go to *step*5;

*step*5 According to the competition rule of survival, choose Q numbers of the best fitness solutions;

*step*6 If $iter<iter_{max}$, jump to *step*2; otherwise, exit implementation process of the algorithm and output the optimal solution, and find the minimum fitness individual $X_i = [\ w1_{i,1}^*,\ w1_{i,2}^*,\ \ldots,\ w1_{i,n}^*,\ b1_{i,1}^*,\ w2_{i,1}^*,w2_{i,2}^*,\ldots,\ w2_{i,m}^*,\ b2_{i,1}^*]$ in the optimal solution.

1.3.3 IWO-NN prediction model

Firstly, collect the historical time sequence for network, to remove the dimensional level which has an impact on the training of neural network , and to increase the training speed ,we should normalize all the input variables and the original input data, which should be normalized to the range[-1,1]. The normalized training input is $P^i=(p_1,p_2,\ldots,p_R)^T$, the training target data is $T^i=(t_1,t_2,\ldots,t_{S2})^T$, the prediction input is $pX^i=(p_1^*,p_2^*,\ldots,p_R^*)^T$, and the actual target value is $pY^i= (t_1^*,t_2^*,\ldots,t_{S2}^*)^T$.

Secondly, input the normalized training input $P^i=(p_1,p_2,\ldots,p_R)^T$ and the training target data $T^i=(t_1,t_2,\ldots, t_{S2})^T$ to the network, and the optimal individual X^i is obtained by training as in part 1.3.2, the prediction model is obtained based on IWO algorithm by assigning the optimal individual X^i to weight matrices $\{w1_{i,j}^*\},\{w2_{i,k}^*\}$ and threshold matrices $\{b1_{i,1}^*\},\{b2_{i,1}^*\}$.

$$y_k=\sum_{i=1}^{S_1} w2_{i,k}^*\sigma(\sum_{j=1}^{R} w1_{i,j}^* p_j+b1_{i,1}^*) \qquad 1\le k\le S_2 \tag{6}$$

Finally, input the input variable $pX^i=(p_1^*,p_2^*,\ldots,p_R^*)^T$ to the prediction model, we need inverse normalize the prediction result $y_j=p_{j+1}$, and then the prediction true value is obtained.

Simulation analysis

2.1 Original data

In order to verify the effectiveness of IWO-NN prediction model, we specially select individual share of SANY Heavy Industry (stock code: 600031) as the stock price prediction object, whose stock prices do not appear too large oscillation. The basic data (including opening price, highest price, lowest price, closing price and volume) of 325 trading days are collected from 2005.6.30 to 2006.11.3 as historical samples, we want to predict the closing price of 2006.10.9 to 2006.11.3 according to the trained neural network, and compare the result with the actual closing price. Part of the historical stock prices of SANY Heavy Industry is shown in Tab.2.1 and Tab.2.2.

Tab2.1 300 samples of network training input/target data

Sequence	Opening price	Volume(shares)	Highest price	Lowest price	Closing price
1	7.74/7.16	3277048/2932205	7.95/7.29	7.60/7.11	7.69/7.16
2	7.60/7.13	7850876/4350030	7.61/7.22	7.00/6.8	7.00/6.85
⋮	⋮	⋮	⋮	⋮	⋮
300	14.01/15.6	2595016/4516485	14.38/16.8	13.75/15.5	14.26/16.3

Tab 2.2 20 samples of network prediction input/actual value

Sequence	Opening price	Volume(shares)	Highest price	Lowest price	Closing price
1	14.21/16.35	2972750/3353063	14.30/17.36	13.6/16.01	13.98/16.71
2	13.96/16.50	1342635/3446818	14.26/17.08	13.75/16.2	14.18/17.02
⋮	⋮	⋮	⋮	⋮	⋮
20	18.00/18.30	2713835/1123350	19.19/18.88	18.0/18.15	19.12/18.47

2.2 Analysis of prediction results

Firstly, before the training, in order to improve the training speed, reduce the error and avoid paralysis of network, the function mapminmax in neural network toolbox in Matlab is used to normalize the original sample data to obtain 300 sets of training inputs data P^i, 300 sets of training target data T^i, the last 20 sets of prediction inputs are pX^i, and actual target value are pY^i.

Secondly, the feed-forward neural network model is trained by IWO. In the feed-forward neural network, there are three layers, including input layer, one hidden layer and output layer, the corresponding nodes in each layer are R=25, S_1=16 and S_2=1, and *tan-sigmoid* function is used as excitation function. The initial population is P_{size}=3, the maximum of population is Q_{size} =16, the maximum iterations is $iter_{max}$=40, the maximum and minimum of generated seed number are S_{max}=3and S_{min}=0, the nonlinear modulation index is n=3, the initial value of interval step is σ_{init} =1and the final value of interval step is σ_{final}=0.01, the minimum of initial search space is x_{min}=-0.1 and the maximum is x_{max}=0.1. The training is carried out by inputting P^i and T^i to the network, and the optimal individual X_i=[$w1_{i,1}^*$,$w1_{i,2}^*$,…,$w1_{i,n}^*$, $b1_{i,1}^*$, $w2_{i,1}^*$,$w2_{i,2}^*$,…,$w2_{i,m}^*$, $b2_{i,1}^*$] is obtained. By assigning X_i to weight matrix $\{w1_{i,j}^*\},\{w2_{i,k}^*\}$ and threshold matrix $\{b1_{i,1}^*\},\{b2_{i,1}^*\}$ in the feed-forward neural network, the prediction model based on IWO algorithm is obtained,

$$y_k=\sum_{i=1}^{S_1} w2_{i,k}^*\sigma(\sum_{j=1}^{R} w1_{i,j}^* p_j+b1_{i,1}^*) \qquad 1\le k\le S_2 \tag{6}$$

where the connective weights of input layer to hidden layer $\{w1_{i,j}^{*}\}$ is $W1=\begin{pmatrix} -0.4684 & 1.1032 & \cdots & 0.1949 \\ -0.5262 & -0.3322 & \cdots & -0.2403 \\ \vdots & & & \vdots \\ 0.2148 & 0.0330 & \cdots & 0.3423 \end{pmatrix}_{16\times25}$, the connective weights of hidden layer to output layer $\{w2_{i,k}^{*}\}$ is $W2=(-0.0531 \quad -0.5523 \quad \cdots \quad 0.0282)_{1\times16}$, the threshold matrix $\{b1_{i,1}^{*}\}$ of neurons in hidden layer is $B_1=(0.3878 \quad -0.1588 \quad \cdots \quad 0.1250)^{T}_{16\times1}$, and the threshold matrix $\{b2_{i,1}^{*}\}$ of neurons in output layer is $B2=(-0.0673)_{1\times1}$.

Finally, input the last 20 prediction inputs pX^{i} to the prediction model (6), and then the final prediction true values are obtained by inverse normalization using postmnmx function in neural network toolbox in Matlab. The prediction of stock price is carried out by IWO-NN neural network, and the results are shown in Tab.2.3 and Fig.2.1, and the best fitness changes are shown in Fig.2.2.

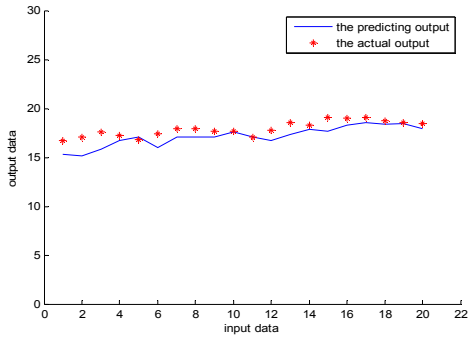

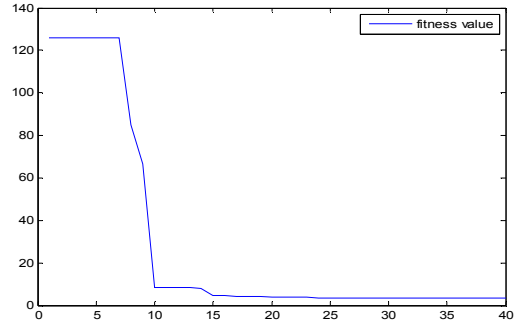

Fig2.1: Predicting the stock price based on IWO-NN Fig2.2: Change of best fitness based on IWO-NN

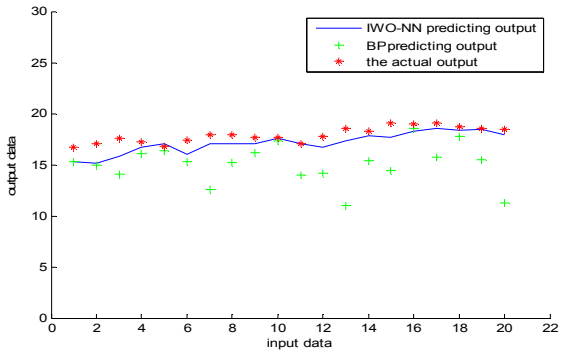

Fig2.3: Comparison on predicting stock price between BP neural network and IWO-NN

The comparison of prediction results between BP neural network and IWO-NN prediction model is shown in Fig.2.3.From the results, the prediction curve of prediction model trained by IWO is more approximate to actual value. The change curve of best fitness of IWO-NN model is shown in Fig.2.2, the optimal solution is obtained by the 25 iterations by IWO algorithm, which is increased significantly than the standard BP model. The comparison on the predicting closing price and actual closing price in different trading day and error of mean square between different predicting models is shown in Tab.2.3, it shows that the optimization of initial connection weights and threshold value of feed-forward neural network reflect a better tendency of network prediction changes, and the accuracy of the prediction is improved.

Tab2.3 Comparison on prediction results and errors about different predicting models

Trading day	Actual closing price	BP predicting price	IWO-NN predicting price	Trading day	Actual closing price	BP predicting price	IWO-NN predicting price
06.10.09	16.71	15.29	15.26	06.10.24	17.72	14.18	16.73
06.10.10	17.02	14.98	15.11	06.10.25	18.56	10.97	17.32
06.10.11	17.55	14.09	15.83	06.10.26	18.30	15.42	17.85
06.10.12	17.27	16.05	16.75	06.10.27	19.12	14.41	17.69
06.10.13	16.84	16.38	17.07	06.10.30	19.00	18.56	18.28
06.10.16	17.40	15.26	15.99	06.10.31	19.09	15.72	18.57
06.10.17	17.95	12.55	17.08	06.11.01	18.69	17.76	18.37
06.10.18	17.97	15.21	17.05	06.11.02	18.56	15.45	18.45
06.10.19	17.65	16.14	17.09	06.11.03	18.47	11.26	17.94
06.10.20	17.71	17.34	17.57				
06.10.23	17.06	13.94	17.09	Mean square error		12.3701	0.9378

From above analysis, IWO algorithm can find global initial connection weights and threshold value, improve the fitting ability and generalization ability of feed-forward neural network, thus improving the prediction accuracy of the network, therefore, it is an effective feed-forward prediction method.

Conclusion

Firstly, the training method of 3 layers feed-forward neural network based on IWO algorithm is given to make the network training simple and reduce the calculation complexity, the global search and local search are coordinate by the dynamic adjustment of standard deviation of offspring individuals' distribution, the optimal solution is obtained accurately, the defect of trapping into local optimization is reduced and the convergence speed is improved. Secondly, the IWO-NN prediction model is established. From the prediction results of stock price, the convergence speed and prediction accuracy are better than that of the standard BP neural network, and feasibility of the prediction method is verified. It also can be applied to the prediction in other areas by adjusting the training parameters, so it has a certain continuation.

Acknowledgement

This work is partially supported by Talent Project of Ten Hundred Thousand High-end Talent Introduction Project of Liaoning Province.

References

[1] Lv Gang, Chen Xiaoping, Zhao Heming, An IA-BP Hybird Algorithm to Optimize Multilayer Feed-forward Neural Networks [J].Computer Engineering and Applications, 2003:39(27):27-28.

[2]Wang Jianqun, Lu Zhihua, Three-layer Feed Forward Artificial Neural Network Global Optimum Approach [J].Mathematics in Practice and Theory, 2003, 33(7):1-8.

[3]MEHRABIAN A R, LUCAS C.A novel numerical optimization algorithm inspired from weed colonization [J]. Ecological Informatics, 2006, 1(4):355-366.

[4]Wang Jing,The Optimization of Feed- Forward Neural Networks Based on Ant Colony Algorithm[J]. Computer Engineering and Applications, 2006(25):54-55.

[5]Fei Liangjun. Computational Intelligence Approach for Discovering the Prediction Model of Financial Market [J].Journal of Software, 1999.10(4): 395 -399.

[6]RITWIK GIRI, ARITRA CHOWDHURY, ARNOB GHOSH, etc. A modified invasive weed optimization algorithm for training of feed-forward neural networks[C]. IEEE International Conference on Systems Man and Cvbernetics(SMC). Istanbul: IEEE.2010:3166-3173.

Advanced Materials Research Vols. 989-994 (2014) pp 1641-1645
© (2014) Trans Tech Publications, Switzerland
doi:10.4028/www.scientific.net/AMR.989-994.1641

An Interval Slope Approach to Fuzzy c-Means Clustering Algorithm for Interval Valued Data

Yan JIN[1, a], Jianghong MA*[2, b]

[1]Department of Mathematics and Information Science, Chang'an University, Xi'an, 710054, China
[2]Department of Mathematics and Information Science, Chang'an University, Xi'an, 710054, China
[a]email: jinyan7274@126.com, [b]email: jhma@chd.edu.cn, *: corresponding author

Keywords: Fuzzy Clustering; Distance; Interval Slope; Interval Data

Abstract. Interval data is a range of continuous values which can describe the uncertainty. The traditional clustering methods ignore the structure information of intervals. And some modified ones have been developed. We have already used Taylor technique to perform well in the fuzzy c-means clustering algorithm. In this paper, we propose a new way based on the mixed interval slopes technique and interval computing. Experimental results also show the effectiveness of our approach.

Introduction

Real life problems are usually involved uncertainties. It is better to represent many kinds of phenomena by intervals than by single-valued variables. Especially, we do not know the variables' probability distribution and only know its ranges without more priori knowledge.

Interval data analysis was put forward by Moore [1] in 1965. As a widely used data mining technique, cluster analysis has been introduce in interval data and applied to diverse areas. Some people replace interval data with a single point (e.g. the middle point) to use the traditional clustering techniques [2] [3]. But these ways ignore the structure information of intervals and cannot measure the distance between two intervals well. Then many modified or extended methods for measuring the distance have also been developed [4-9]. About the problem of fuzzy c-means clustering interval data, we have obtained a good result by combining Taylor technique and interval computing [10].

Krawczyk and Neumaier firstly presented the interval slope for rational functions and associated centered forms [11]. Then [12] shows a combination of interval derivate arithmetic and interval slope arithmetic can often get a narrower interval enclosure than that which is gained by using them alone. In this paper, we apply this mixed arithmetic on the fuzzy c-means clustering algorithm. Compared with the proposed methods in [10], it has an equality fine clustering effect at least.

Interval Distance Measures

Interval data is a range of continuous values instead of the traditional single continuous or discrete value. It can be represented by a vector of interval values. Let $A = (A^1, A^2, \cdots, A^p)$ and $B = (B^1, B^2, \cdots, B^p)$ be two p-dimension interval objects, where $A^i = [a^i, b^i]$, $B^i = [c^i, d^i]$ indicate the interval values of the i-th variable and $a^i \le b^i$, $c^i \le d^i$. We denote the midpoint and the width of the interval A^i, B^i as $\tilde{A}^i, \tilde{B}^i$ and $\Delta_{A^i}, \Delta_{B^i}$ respectively, that is $A^i = [\tilde{A}^i - \Delta_{A^i}/2, \tilde{A}^i + \Delta_{A^i}/2]$ and $B^i = [\tilde{B}^i - \Delta_{B^i}/2, \tilde{B}^i + \Delta_{B^i}/2]$. And we have already known some distance measures in [10]. Here we will not describe these in details.

Just like the Taylor method, we hope obtain an interval data to express the distance. Taylor technique is a derivate arithmetic and interval slope approach is a differential arithmetic. Both of these can get an interval result, but their union would perform a narrower interval enclosure. The two algorithms are applicable to the so-called factorable function $f: D \subseteq R^n \longrightarrow R^1$ which can be represented by a finite simple expressions sequence such that:

$$f_i(x) = x_i \quad (i = 1, \ldots, n)$$

and for $i > j, k$,

$$f_i(x) = c_i \in R,$$

or

$$f_i(x) = -f_j(x),$$

or for $*\in \{+,-,\cdot,/\}$,

$$f_i(x) = f_j(x) * f_k(x),$$

$$f_i(x) = \emptyset_i(f_j(x)),$$

where

$$\emptyset_i \in \Phi = \{(\cdot)^{1/2}, \exp(\cdot), \ln(\cdot), \sin(\cdot), \dots\}.$$

The first order slope $f[x,z]$ and the second order slope $f[x,z,z]$ can be defined recursively in Tab.1 where $x,z \in D$ and $e^{(i)}$ is row i of $n \times n$ unit matrix.

Table 1.First and Second Order Slope

Expressions $f_i(x)$	**First order slope** $f_i[x,z]$	**Second order slope** $f_i[x,z,z]$
$f_i(x) = c_i \in R$	0	0
$f_i(x) = x_i$	$e^{(i)}$	0
$f_i(x) = -f_j(x)$	$-f_j[x,z]$	$-f_j[x,z,z]$
$f_i(x) = f_j(x) \pm f_k(x)$	$f_j[x,z] \pm f_k[x,z]$	$f_j[x,z,z] \pm f_k[x,z,z]$
$f_i(x) = f_j(x) \cdot f_k(x)$	$f_j[x,z]f_k(x) + f_j(z)f_k[x,z]$	$f_j[x,z,z]f_k(x) + f_k[x,z]^T f_j'(z) + f_j(z)f_k[x,z,z]$
$f_i(x) = f_j(x)/f_k(x)$	$\frac{f_j[x,z] - f_k[x,z]f_i(z)}{f_k(x)}$	$\frac{f_j[x,z,z] - f_i(z)f_k[x,z,z] - f_k[x,z]^T f_i'(z)}{f_k(x)}$
$f_i(x) = \emptyset_i(f_j(x))$	$\emptyset_i[f_j(x), f_j(z)]f_j[x,z]$	$\emptyset_i[f_j(x), f_j(z), f_j(z)]f_j[x,z]^T f_j[x,z] + \emptyset_i'(f_j(z))f_j[x,z,z]$

Table 2.First and Second Order Derivate

Expressions $f_i(x)$	**First order** $f_i'(x)$	**Second order** $f_i''(x)$
$f_i(x) = c_i \in R$	0	0
$f_i(x) = x_i$	$e^{(i)}$	0
$f_i(x) = -f_j(x)$	$-f_j'(x)$	$-f_i''(x)$
$f_i(x) = f_j(x) \pm f_k(x)$	$f_j'(x) \pm f_k'(x)$	$f_j''(x) \pm f_k''(x)$
$f_i(x) = f_j(x) \cdot f_k(x)$	$f_j'(x)f_k(x) + f_j(x)f_k'(x)$	$f_j''(x)f_k(x) + f_j'(x)^T f_k'(x) + f_k'(x)^T f_j'(x) + f_j(x)f_k''(x)$
$f_i(x) = f_j(x)/f_k(x)$	$\frac{f_j'(x) - f_k'(x)f_i(x)}{f_k(x)}$	$\frac{f_j''(x) - f_i'(x)^T f_k'(x) - f_k'(x)^T f_i'(x) - f_i(x)f_k''(x)}{f_k(x)}$
$f_i(x) = \emptyset_i(f_j(x))$	$\emptyset_i'(f_j(x))f_j'(x)$	$\emptyset_i''\left(f_j(x)\right)f_j'(x)^T f_j'(x) + \emptyset_i'(f_j(x))f_j''(x)$

Let real intervals be denoted by $X \in I(R^n)$ which is the set of interval vectors and let $\underline{\Phi}$ be the set of continuous isotonic interval extensions [12] of the functions in Φ. $\forall x,z \in X$, we can obtain

$$f(x) \in f(z) + f'(z)(X-z) + (X-z)^T f[X,z,z](X-z), \quad (1)$$

that is

$$f_S(X) = f(z) + f'(z)(X-z) + (X-z)^T f[X,z,z](X-z). \quad (2)$$

In comparison with Taylor method in which derivative arithmetic is displayed in Tab.2

$$f_T(X) = f(z) + f'(z)(X-z) + \frac{1}{2}(X-z)^T f''(X)(X-z), \quad (3)$$

it is clearly that $f_S(X) \subseteq f_T(X)$ and the computational complexity of the slope formulae is lower than that for derivative one. See [11] for a detailed analysis of the computational complexity.

We know the square root function of real number is a monotonic. It doesn't affect the final result of interval distance. So we can get the interval value of distance formula without squaring:

$$f(A,B) = \sum_{i=1}^{p}(A^i - B^i)^2. \quad (4)$$

To express conveniently and clearly, (4) can be replaced by

$$D^2(A,B) = [D^2(A,B)_{\min}, D^2(A,B)_{\max}] = f(X) = \sum_{i=1}^{p}\left(X^i - X^{i+p}\right)^2 \quad (5)$$

Where $X = (X^1, \cdots, X^p, X^{p+1}, \cdots, X^{2p}), A = (A^1, A^2, \cdots, A^p) = (X^1, X^2, \cdots, X^p), B = (B^1, B^2, \ldots, B^p) = (X^{p+1}, X^{P+2}, \cdots, X^{2p}), \tilde{A}^i = \tilde{X}^i, \tilde{B}^i = \tilde{X}^{p+i}$ and $\Delta_{A^i} = \Delta_{X^i}, \Delta_{B^i} = \Delta_{X^{p+i}}$. Referring to the previous way which has been used in k-means clustering, we get the distance square between *A* and *B*:

$$D^2(A,B) = \lambda D^2(A,B)_{\min} + (1-\lambda)D^2(A,B)_{\max}. \quad (6)$$

The parameter lies between 0 and 1 which is specified in such a way that $\lambda = 1$ indicates the minimum interval distance and $\lambda = 0$ indicates the maximum one. Then we separately apply the formulae in Tab.1 and Tab.2 to measure the interval distance. The basic operations like addition, subtraction, division and multiplication of interval data here are mentioned in [13].

Fuzzy c-means Clustering Interval Data

The objective in cluster analysis is to partition unlabeled objects into a number of clusters such that similar objects are assigned to one cluster. There are two main clustering approaches. One is crisp clustering; the other is fuzzy clustering which allows one piece of data to belong to more than one cluster and it is frequently used in pattern recognition [14] especially in cases that boundaries between clusters cannot be clearly defined. Fuzzy c-means (FCM) is a widely used method of clustering.

Consider a set of unlabeled interval patterns $A = (A_1, A_2, \cdots, A_n)$. Each $A_i = (A_i^1, \cdots, A_i^p)$ is a *p*-dimension interval object with $A_i^j = [a_i^j, b_i^j]$ and $a_i^j \le b_i^j$ where $i = 1, \ldots, n$ and $j = 1, \ldots, p$. Suppose we want to categorize the set into *K* clusters $C = (C_1, C_2, \cdots, C_K)$. Let their corresponding representations or clustering centers be $G = (G_1, C_2, \cdots, G_K)$ and $G_k = (g_k^1, \cdots, g_k^p)$ is a vector of interval values with $g_k^j = [c_k^j, d_k^j]$. The clustering is based on minimization of the following objective function:

$$J_m = \sum_{i=1}^{n}\sum_{j=1}^{K} u_{ij}^m d(A_i, G_j), \quad 1 \le m \le \infty. \quad (7)$$

In Equation (7), *m* is a real-valued number greater than 1(usually choose *m*=2) which controls the fuzziness of the resulting clusters, u_{ij} is the degree of membership of gene A_i in the cluster *j* and satisfies $\sum_{j=1}^{K} u_{ij} = 1$, $d(*)$ is a distance measure. Fuzzy partitioning is carried out through an iterative optimization of the objective function with the update of membership function matrix and the cluster centers by:

$$u_{ij} = 1/\sum_{c=1}^{K}\left(\frac{d(A_i,G_j)}{d(A_i,G_c)}\right)^{\frac{2}{m-1}}, \quad G_j = \frac{\sum_{i=1}^{n} u_{ij}^m \cdot A_i}{\sum_{i=1}^{n} u_{ij}^m}. \quad (8)$$

This iteration will not stop until $\max\{|u_{ij}^{k+1} - u_{ij}^k|\} < \varepsilon$, where ε is a termination condition and *k* is the iteration step. This procedure converges to a local minimum or a saddle point of J_m.

The algorithm can be composed of the following steps:

a) Initialize the membership matrix $U = [u_{ij}]$, $U^{(0)}$.

b) At *k*-step: calculate the centers vectors $G^{(k)} = [G_j]$ with $U^{(k)}$.

c) Update $U^{(k)}$ to obtain $U^{(k+1)}$.

d) If $\left\|U^{(k+1)} - U^{(k)}\right\| < \varepsilon$ then stop; otherwise return to step b).

By the way, each u_{ij} is a real number and each G_j is an interval vector. The distance measures used here have defined in the previous section.

Simulation experiment

In this section, we cluster the generated interval data in different distance measures which one of them is based on the mixed interval slope approach in the second part of this paper and others are

recommended in [10]. The software is written in Matlab 2011. It can be observed that the new one is better than previous methods and performs as well as at least.

We construct the same interval set as [10] with two-dimension interval vectors. We can plot these three different interval sets in Fig. 1.

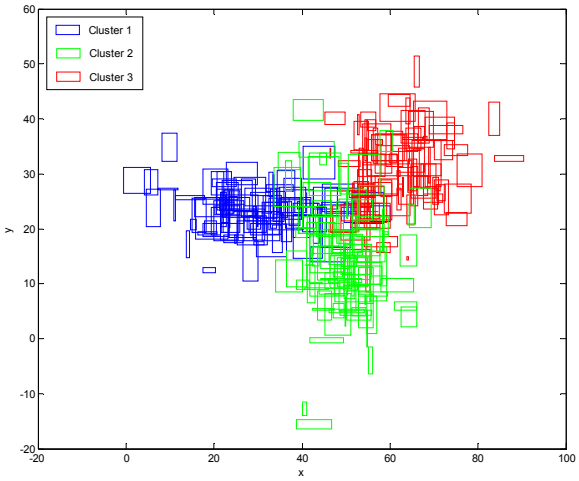

Figure 1.The plot of various interval sets

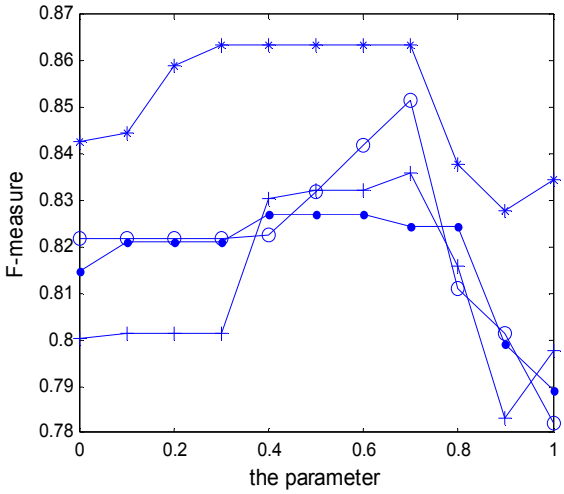

Figure 2.The relationship between the F-measure values and parameter λ

To evaluate the quality of clustering solutions we exploited the availability of reference classification for datasets. The objective is to evaluate how well a clustering fits a predefined scheme of known classes. To this end, we relied on the F-measure [14] which is one of the most commonly used external validity criteria and lies from 0 to 1. The larger F-measure value is better.

We can get relationships between the F-measure value and the parameter λ in mixed interval slopes method. When $\lambda = 0.8, 0.9$ or 1, there is a bad effect on the F-measure value. And it looks not good in small values. We can see some of the relation curves are stable and well-behaved if $\lambda = 0.4$ to 0.7 in Fig. 2. In the sixth one, we choose $\lambda = 0.7$.

For the comparative purpose, the criterion is an average value of 30 times. The results of F-measure values are listed in Table 3 in terms of various methods. The first five methods have presented in [10] and their parameters are no change.

Table 3.The F-measure values of different methods

Method	***F*-measure value**
Traditional Euclidean distance	0.7981
Extended Euclidean distance	0.8112
Relative position dissimilarity	0.8013
Yu Peng's distance measure	0.8647
Taylor technique	0.8705
mixed interval slopes technique	0.8705

Compared with the first three methods, it shows that the F-measure value of mixed interval slopes approach increases significantly. The last three methods have the highest similarity with the prototype and the algorithms can achieve a better clustering solution and validation.

Conclusion

In this paper, we study the problem of clustering interval data. We continue promoting the k-means method to fuzzy c-means algorithm and propose a new interval fuzzy clustering algorithm based on the interval slope approach. To compare with others by the F-measure value, the result of our experiment about two-dimension interval data performs that it can achieve a better clustering. And at least it has an equality fine clustering consequence as Taylor techniques. We discover the different values of the parameter λ will affect F-measure values. The influence in this method is

bad when the parameter is 0.8, 0.9 or 1 and is not good in small values, so the good choice of the parameter is 0.4 to 0.7. In the entire value range of λ, we also find the *F*-measure variation range of the interval slope arithmetic is smaller and better than that of the Taylor arithmetic.

Acknowledgement

The work reported in this study is supported by National Basic Research Program of China (2011CB707001).

References

[1] Moore, Ramon E, The automatic analysis and control of error in digital computation based on the use of interval numbers, in Error in digital computation 1, 1965, pp. 61-130.
[2] de Souza, Renata M. CR, "Dynamic cluster methods for interval data based on Mahalanobis distances, in Classification, Clustering, and Data Mining Applications. Springer Berlin Heidelberg, 2004, pp. 351-360.
[3] de Carvalho, Francisco de AT, Paula Brito, and Hans-Hermann Bock, Dynamic clustering for interval data based on L 2 distance, in Computational Statistics 21(2), 2006, pp. 231-250.
[4] Fei Yuan, Yiju Zhan and Yonghua Zhang, Research on Relative Position Dissimilarity in Interval-data Fuzzy c-Means Clustering, in Signal Processing28(10).China:2012, pp. 1370-1378.
[5] Peng, Wei, and Tao Li, Interval data clustering with applications, in Tools with Artificial Intelligence, IEEE, 2006, pp. 355-362.
[6] Izakian, Hesam, and Ajith Abraham, Fuzzy C-means and fuzzy swarm for fuzzy clustering problem in Expert Systems with Applications 38(3), 2011, pp. 1835-1838.
[7] Yu Peng, and QinghuaLuo, UIDK-means: A multi-dimensional uncertain measurement data clustering algorithm, in Chinese Journal of Scientific Instrument 32(6), 2011, pp. 1201-1207.
[8] De Carvalho, Francisco de AT, and Camilo P. Tenório, "Fuzzy< i> K</i>-means clustering algorithms for interval-valued data based on adaptive quadratic distances," in Fuzzy Sets and Systems 161(23), 2010, pp. 2978-2999.
[9] Weibin Zhang, Wenjiang Liu, Fuzzy c-Means Clustering Algorithm for Interval Data, in Computer Engineering 34(11). China: 2008, pp. 26-28.
[10] Yan Jin, Jianghong Ma, A New Fuzzy c-Means Clustering Algorithm for Interval Data, 2013 International Conference on Computer Science and Artificial Intelligence.
[11] Krawczyk, Rudolf, and Arnold Neumaier, Interval slopes for rational functions and associated centered forms. SIAM Journal on Numerical Analysis 22.3 (1985): 604-616.
[12] Zuhe, Shen, and Michael A. Wolfe, On interval enclosures using slope arithmetic. Applied Mathematics and Computation 39.1 (1990): 89-105.
[13] Nguyen, Hung T., et al, Computing Statistics Under Interval and Fuzzy Uncertainty: Applications to Computer Science and Engineering, Springer Verlag, Vol. 393, 2011, pp. 2012: 35-45.
[14] Zimmermann H J., Fuzzy set theory and its applications, Springer, 2001.

Advanced Materials Research Vols. 989-994 (2014) pp 1646-1651
© (2014) Trans Tech Publications, Switzerland
doi:10.4028/www.scientific.net/AMR.989-994.1646

Stock price prediction model based on BA neural network and its applications

Xiaoyan Lv, Silong Sun, Hong Liu

School of Science, University of Science and Technology Liaoning, Anshan 114051, China

email: ldhliuhong@163.com

Keywords: Bat Algorithm; Feed-forward Neural Network; Stock Price Prediction

Abstract. In view of the deficiency of the basic back-propagation(BP) algorithm based on steepest descent method. Bat algorithm(BA)in intelligent optimization is introduced into the training process of feed-forward neural networks, capturing the optimal solution of the objective function with a small population size and less number of iterations, and a prediction model based on BA feed-forward neural network(BA-NN) is given. By the empirical study of stock price prediction in Sany Heavy Industry, the results show that this method has advantages of frequency tuning and dynamic control of exploration and exploitation by automatic switching to intensive exploitation if necessary.

Introduction

BA proposed by scholar Yang [1] in University of Cambridge is a Swarm intelligence optimization algorithm which mimics the behavior of the search by ultrasonic of bats in nature. In BA, The solution of optimization problem can be as a bat in the search space, where each bat has its corresponding fitness value, and the bat group search in the solution space following the current optimal bat by adjusting the frequency, loudness, rate of pulse emission. It has been proved that BA is better than genetic algorithm (GA) and particle swarm optimization (PSO) algorithm in solving unconstrained optimization problems [1].Therefore, BA has been widely used in numerical optimization, engineering optimization, constrained optimization, PFSP scheduling problem [2-5].

As the standard BP neural network algorithm is based on local search algorithm of gradient descent, which can not be used to search the global minimum points of multimodal function, and it has high requirements to the functions and has the disadvantages of slow convergence speed, easy to trap into local minimum and low robustness and so on [6] [7].BA is a new Swarm intelligence optimization algorithm. We apply BA to the training of feed-forward neural network in order to get rid of local minimum, trying to solve the problems of standard BP algorithm. A prediction model based on BA feed-forward neural network (BA-NN) is given, and a practical simulation of stock price prediction is carried out, and the feasibility and effectiveness of it are verified by comparing it with the standard BP algorithm.

BA-NN prediction model

1.1 Prediction model of feed-forward neural network

The prediction refers to estimating values for future unknown data by some known historical data. Assuming that a time sequence$\{x_i\}$, among which the historical data is x_n ,x_{n+1} ,..., x_{n+m}, we want to predict the value at time $n+m+k$ ($k>0$), namely predicting nonlinear function relationship x_{n+m+k} at time $n+m+k$ ($k>0$), where the function relationship is $x_{n+m+k}=f(x_n,x_{n+1},\ldots,x_{n+m})$.

We use the feed-forward neural network to predict, that is we use neural network to fitting function f by a set of data points $x_n,x_{n+1},\ldots, x_{n+m}$ and get the predicting value at future time $n+m+k$ ($k>0$).

The feed-forward neural network is a common artificial neural network model ,which has processing units of several connected layers, where each neuron in one layer is connected to every neuron in next layer, and there is no feedback in the network. In this paper, a three layer network is

considered, which is widely used, the output layer is a linear layer, and the nonlinear effect function (the activation function) of neurons in hidden layer is a hyperbolic tangent function (*tan-sigmoid*):

$$\sigma(x)=\frac{1-e^{-x}}{1+e^{-x}} \tag{1}$$

Assuming the output of neurons in input layer is $P^i=(p_1,p_2,\ldots,p_R)$, $\{w1_{i,j}\}$ is the connection weights of input layer to hidden layer, $\{b1_{i,1}\}$ is the threshold value of neurons in hidden layer, $\{w2_{i,k}\}$ is the connection weights of hidden layer to output layer, and $\{b2_{i,1}\}$ is the threshold value of neurons in output layer. The mapping of input to output of network is:

$$y_k=\sum_{i=1}^{S_1} w2_{i,k}\sigma(\sum_{j=1}^{R} w1_{i,j}p_j+b1_{i,1}) \quad 1\le k\le S_2 \tag{2}$$

The training sample set of the feed-forward neural network is $A=\{(P^i,T^i), i=1,2,\ldots, s\}$, where s is the number of training samples, $P^i\in R^R$ is the input of training data in the i^{th} group, $T^i\in R^{S2}$ is the expectation output of corresponding input of training data in the i^{th} group, T_k^i is the expectation output of the k^{th} neuron in output layer. Assuming that the actual output of training data in i^{th} group is $Y^i\in R^{S2}$, Y_k^i is the actual output of the k^{th} neuron in output layer, then the error function based on the training sample set is given by:

$$E=\frac{1}{2}\sum_{i=1}^{s}\sum_{k=1}^{S_2}(Y_k^i-T_k^i)^2 \tag{3}$$

The function is a nonlinear function with various multiple minimum points, and the training process for this feed-forward neural network is adjusting the connection weights and threshold value of $\{w1_{i,j}\},\{b1_{i,1}\},\{w2_{i,k}\},\{b2_{i,1}\}$ until the error function E to minimum[4].

We can obtain the corresponding connection weights and thresholds $\{w1_{i,j}\},\{b1_{i,1}\},\{w2_{i,k}\},\{b2_{i,1}\}$ through being trained by the above feed-forward neural network. Then we can carry out specific problems of prediction by the prediction model of feed-forward neural network (2).

1.2 The principle of BA

Map the bat individuals to some points in the search space, measure the position of bat individual in the search space for fitness function value of solving problems(fitness function is the objective function of optimization problem).The search process of algorithm simulates searching for prey and moving process of bat individuals.

According to echolocation behavior of bats can being associated with the objective to be optimized. The following are respectively the mathematics form of population consisting of n bats updating their velocities, positions, loudness, and pulse rates during flight process.

1.2.1 The velocities update and positions update of bats

Assuming that the search space is D dimensional, the position of bat i at time t is x_i^t, the velocity is v_i^t. The new velocity $v_i^{t+1}$and position x_i^{t+1} at time step t+1 can be calculated by:

$$F_i=F_{\min}+(F_{\max}-F_{\min})\beta \tag{4}$$

$$v_i^{t+1}=v_i^t+(x_i^t-x_*) \tag{5}$$

$$x_i^{t+1}=x_i^t+v_i^{t+1} \tag{6}$$

where F_i, F_{max}, F_{min} respectively represent the frequency of the ultrasonic in the current moment, maximum and minimum of acoustic frequency of the bat i, $\beta\in[0,1]$ is a random vector, x_* represents the current global optimal solution.

For bat groups whose size is n, we can select one among them, and update corresponding position for the bat according to equation (7).This process can be understood as a local search process, namely, it selectively generate a new solution.

$$x_{new}(i)=x_{old}+\varepsilon A^t \tag{7}$$

Where x_{old} represents a solution randomly selected among the current best solutions set, A^t is the average loudness of the first i bats at time step t, $\varepsilon\in[-1,1]$ is a random number.

The update of the velocities and positions of bats have some similarity to the procedure in the standard PSO. To a degree, BA can be considered as a balanced combination of the standard PSO and the intensive local search controlled by the loudness and pulse rate.

1.2.2 Loudness and pulse emission

Normally, the loudness decreases gradually and the pulse rate increases gradually as a bat tends closer to its prey. Loudness of pulse $A(i)$ and rate of pulse emission $R(i)$ of bat i update according to the following formula (8):

$$A^{t+1}(i)=\alpha\cdot A^{t}(i)\ ,\quad R^{t+1}(i)=R_i^0\times[1-\exp(-\gamma\cdot t)] \tag{8}$$

where $0<\alpha<1$and$\gamma>0$are constants. Assuming $A(i)=0$ means a bat has just found the prey and temporarily stop emitting any sound. It is not hard to find that $A(i)\rightarrow 0$ and $R^t(i)= R^0(i)$ as $t\rightarrow\infty$.

1.3 Establishment of BA-NN prediction model

1.3.1 BA training neural network

Assuming that X is a feed-forward neural network $X=\{X_i|i=1,\ldots,p\}$, where X_i is the individual in population X, and p is the number of the individuals. Every individual X_i consists of two weight matrices $\{w1_{i,j}\},\{w2_{i,k}\}$ and two threshold matrices$\{b1_{i,1}\},\{b2_{i,1}\}$, the algorithm is to find the optimal X_i in $X=\{X_i|i=1,\ldots,p\}$and the optimizing function $minF(x)$ is the error function E (its expression is given in equation (3)). Then the error function E is optimized by BA until satisfying the given stop conditions. The steps of training neural network based on BA are below:

*step*1 Setting up the algorithm parameters, set t=0.

*step*2 Randomly generate the initial bat group's positions $X(0)=\{X_1(0), X_2(0),\ldots, X_{P0}(0)\}$,velocities $V(0)=\{V_1(0), V_2(0),\ldots, V_{P0}(0)\}$, while the individual's are $X_i(0)=\{X_1^i(0), X_2^i(0),\ldots, X_D^i(0)\}$and $V_i(0)=\{V_1^i(0), V_2^i(0),\ldots, V_D^i(0)\}$, where $D=R\times S_1 + S_1\times S_2 + S_1 + S_2$, $n=R\times S_1$, $m= S_1\times S_2$, R is the number of inputs neuron, $S_1$is the number of neuron in hidden layer, and S_2 is the number of neuron in output layer. The initial individual number of the population is P_0.

*step*3 Evaluate fitness value for every bat, and find out the location of the optimal bat.

*step*4 Judge whether the algorithm meets the condition (whether it reach the maximum number of iterations) .If meet, end the algorithm, output the optimal solution; or else, go to step5.

*step*5 Update velocity and position of bat according to formulas (4) to (6).

*step*6 Generate a random *rand*1, if *rand*1> r_i (r_i is pulse rates of bat i), disturb the current optimal bat position and obtain a new position, then replace the original position.

*step*7 Generate a random *rand*2, if *rand*2<A and $f(x_i)<f(x^*)$, then move to the updated location.

*Step*8 When it meets the conditions of step7, update pulse rates r_i and loudness A; otherwise, make $t=t+1$, return step3.

1.3.2 BA-NN prediction model

Firstly, collect the historical time sequence for network, to remove the dimensional level which has an impact on the training of neural network , and to increase the training speed ,we should normalize all the input variables and the original input data, which should be normalized to the range[-1,1]. The normalized training input is $P^i=(p_1,p_2,\ldots,p_R)^T$, the training target data is $T^i=(t_1,t_2,\ldots, t_{S2})^T$, the prediction input is $pX^i=(p_1^*,p_2^*,\ldots,p_R^*)^T$, and the actual target value is $pY^i= (t_1^*,t_2^*,\ldots, t_{S2}^*)^T$.

Secondly, input the normalized training input $P^i=(p_1,p_2,\ldots,p_R)^T$ and the training target data $T^i=(t_1,t_2,\ldots, t_{S2})^T$ to the network, and the optimal individual X^i is obtained by training as in part 1.3.2, the prediction model is obtained based on BA algorithm by assigning the optimal individual X^i to weight matrices$\{w1_{i,j}^*\},\{w2_{i,k}^*\}$and threshold matrices$\{b1_{i,1}^*\},\{b2_{i,1}^*\}$.

$$y_k=\sum_{i=1}^{S_1} w2_{i,k}^*\,\sigma\Big(\sum_{j=1}^{R} w1_{i,j}^*\,p_j+b1_{i,1}^*\Big)\qquad 1\le k\le S_2 \tag{9}$$

Finally, input the input variable $pX^i=(p_1^*,p_2^*,\ldots,p_R^*)^T$ to the prediction model, we need inverse normalize the prediction result $y_j=p_{j+1}$, and then the prediction true value is obtained.

Simulation analysis

2.1 Original data

In order to verify the effectiveness of BA-NN prediction model, we specially select individual share of SANY Heavy Industry (stock code: 600031) as the stock price prediction object, whose stock prices do not appear too large oscillation. The basic data (including opening price, highest price, lowest price, closing price and volume) of 325 trading days are collected from 2005.6.30 to

2006.11.3 as historical samples, we want to predict the closing price of 2006.10.9 to 2006.11.3 according to the trained neural network, and compare the result with the actual closing price. Part of the historical stock prices of SANY Heavy Industry is shown in Tab.2.1 and Tab.2.2.

Tab2.1 300 samples of network training input/target data

Sequence	Opening price	Volume(shares)	Highest price	Lowest price	Closing price
1	7.74/7.16	3277048/2932205	7.95/7.29	7.60/7.11	7.69/7.16
2	7.60/7.13	7850876/4350030	7.61/7.22	7.00/6.8	7.00/6.85
⋮	⋮	⋮	⋮	⋮	⋮
300	14.01/15.6	2595016/4516485	14.38/16.8	13.75/15.5	14.26/16.3

Tab 2.2 20 samples of network prediction input/actual value

Sequence	Opening price	Volume(shares)	Highest price	Lowest price	Closing price
1	14.21/16.35	2972750/3353063	14.30/17.36	13.6/16.01	13.98/16.71
2	13.96/16.50	1342635/3446818	14.26/17.08	13.75/16.2	14.18/17.02
⋮	⋮	⋮	⋮	⋮	⋮
20	18.00/18.30	2713835/1123350	19.19/18.88	18.0/18.15	19.12/18.47

2.2 Analysis of prediction results

Firstly, before the training, in order to improve the training speed, reduce the error and avoid paralysis of network, the function mapminmax in neural network toolbox in Matlab is used to normalize the original sample data to obtain 300 sets of training inputs data P^i, 300 sets of training target data T^i, the last 20 sets of prediction inputs are pX^i, and actual target value are pY^i.

Secondly, the feed-forward neural network model is trained by BA. In the feed-forward neural network, there are three layers, including input layer, one hidden layer and output layer, the corresponding nodes in each layer are R=25, S_1=16 and S_2=1,and *tan-sigmoid* function is used as excitation function. There is no exact theoretical basis about setting of various parameters involved in BA, so the values of the parameters set in this paper are the experience values based on repeated experiments. Set the range of search pulse frequency $F_i \in$[-0.1,0.1], maximum rate of pulse emission R^0=0.5, maximum loudness of pulse emission A^0=0.75, attenuation coefficient of loudness α=0.5, increase coefficient of pulse rate γ=0.05, maximum iterations *itmax*=300, the size of population n=40.

The training is carried out by inputting P^i and T^i to the network, and the optimal individual $X_i(t)=\{x_1^i(t), x_2^i(t),\ldots, x_D^i(t)\}$ is obtained. By assigning $X_i(t)$ to weight matrix $\{w1_{i,j}^*\},\{w2_{i,k}^*\}$ and threshold matrix $\{b1_{i,1}^*\},\{b2_{i,1}^*\}$ in the feed-forward neural network, the prediction model based on BA is obtained,

$$y_k=\sum_{i=1}^{S_1} w2_{i,k}^*\,\sigma\Big(\sum_{j=1}^{R} w1_{i,j}^*\,p_j+b1_{i,1}^*\Big) \qquad 1\le k\le S_2 \tag{9}$$

where the connective weights of input layer to hidden layer $\{w1_{i,j}^*\}$ is $W1=\begin{pmatrix} 0.1316 & -0.3009 & \cdots & 0.0117 \\ 0.0890 & 0.0690 & \cdots & -0.0048 \\ \vdots & & & \vdots \\ 0.1237 & -0.0312 & \cdots & 0.2344 \end{pmatrix}_{16\times 25}$, the connective weights of hidden layer to output layer $\{w2_{i,k}^*\}$ is $W2=(0.3185 \quad 0.1550 \quad \cdots \quad -0.1018)_{1\times 16}$, the threshold matrix $\{b1_{i,1}^*\}$ of neurons in hidden layer is $B1=(-0.0059 \quad 0.0226 \quad \cdots \quad -0.0628)_{16\times 1}^T$, and the threshold matrix $\{b2_{i,1}^*\}$ of neurons in output layer is $B2=(0.1979)_{1\times 1}$.

Finally, input the last 20 prediction inputs pX^i to the prediction model (9), and then the final prediction true values are obtained by inverse normalization using postmnmx function in neural network toolbox in Matlab.

The prediction of stock price is carried out by BA-NN neural network, and the results are shown in Tab.2.3 and Fig.2.1, and the best fitness changes are shown in Fig.2.2.

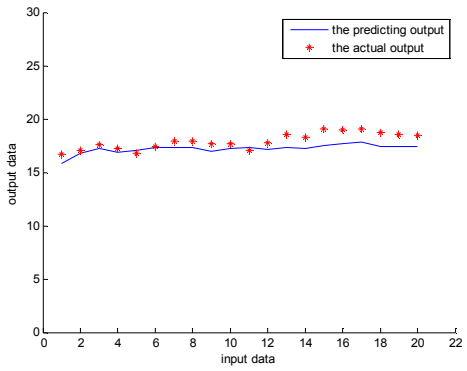

Fig.2.1: Predict the stock price based on BA-NN

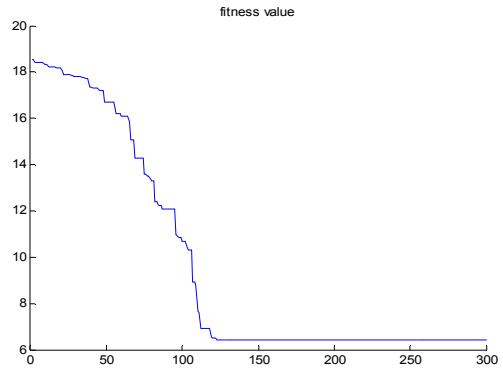

Fig.2.2: The change of best fitness based on BA-NN

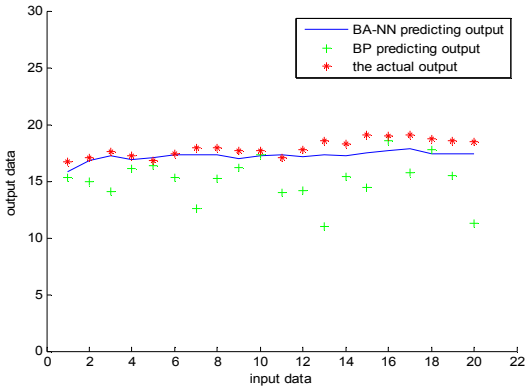

Fig2.3: Contrast on the predicting stock price between BP neural network and BA-NN

Tab.2.3 Comparison on the predicting results and errors about different predicting models

Trading day	Actual closing price	BP predicting price	BA-NN predicting price	Trading day	Actual closing price	BP predicting price	BA-NN predicting price
06.10.09	16.71	15.29	15.81	06.10.24	17.72	14.18	17.11
06.10.10	17.02	14.98	16.80	06.10.25	18.56	10.97	17.32
06.10.11	17.55	14.09	17.26	06.10.26	18.30	15.42	17.26
06.10.12	17.27	16.05	16.85	06.10.27	19.12	14.41	17.50
06.10.13	16.84	16.38	17.07	06.10.30	19.00	18.56	17.66
06.10.16	17.40	15.26	17.30	06.10.31	19.09	15.72	17.84
06.10.17	17.95	12.55	17.31	06.11.01	18.69	17.76	17.45
06.10.18	17.97	15.21	17.37	06.11.02	18.56	15.45	17.45
06.10.19	17.65	16.14	16.97	06.11.03	18.47	11.26	17.39
06.10.20	17.71	17.34	17.27				
06.10.23	17.06	13.94	17.32	Mean square error		12.3701	0.77989

The comparison of prediction results between BP neural network and BA-NN prediction model is shown in Fig.2.3.From the results, the prediction curve of prediction model trained by BA is more approximate to actual value. The change curve of best fitness of BA-NN model is shown in Fig.2.2, the optimal solution is obtained by the 150 iterations by BA, which is increased significantly than the standard BP model. The comparison on the predicting closing price and actual closing price in different trading day and error of mean square between different predicting models is shown in Tab.2.3, it shows that the optimization of initial connection weights and threshold value of feed-forward neural network reflect a better tendency of network prediction changes, and the accuracy of the prediction is improved.

From above analysis, BA can find global initial connection weights and threshold value, improve the fitting ability and generalization ability of feed-forward neural network, thus improving the prediction accuracy of the network, therefore, it is an effective feed-forward prediction method.

Conclusion

BA is a random search optimization algorithm based on population. The algorithm absorbs the behavioral characteristics of searching and preying by ultrasonic of bats in nature, implement the behavior of the agent by evolution to achieve the goal of optimization. The BA-NN prediction model based on BA is established. By example validation, the convergence speed and prediction accuracy have a higher increase than that of the standard BP neural network, achieving the purpose of our expectations, and it offers new ideas for forecasting stock price. Further by adjusting the parameters, this method can be used to solve the prediction problems in other areas.

Acknowledgement

This work is partially supported by Talent Project of Ten Hundred Thousand High-end Talent Introduction Project of Liaoning Province.

References

[1] Yang X S. Nature Inspired Metaheuristic Algorithms (2nd Edition) [M]. Frome, UK: Luniver Press, 2010: 97-104.

[2]Liu Changping, Ye Chunming. Bat Algorithm with Chaotic Search Strategy and Analysis of Its Property [J]. Journal of System Simulation, 2013, 25(6): 1183-1188.

[3] Yang X S, Gandomi A H. Bat algorithm: a novel approach for global engineering optimization [J].Engineering Computation, 2012, 29(5): 464-483.

[4] Gandomi A H, Yang X S, Alavi A H, et al. Bat algorithm for constrained optimization tasks. Neural Computing &Applications, 2013, 22(6): 1239-1255.

[5]Sheng Xiaohua,Ye chunming, Application of Bat Algorithm to Permutation Flow-shop

Scheduling Problem[J]. Industrial Engineering Journal, 2013, 16(1): 119-124.

[6]Lv Gang, Chen Xiaoping, Zhao Heming, An IA-BP Hybird Algorithm to Optimize Multilayer Feed-forward Neural Networks[J].Computer Engineering and Applications, 2003:39(27):27-28.

[7] Wang Jianqun, Lu Zhihua, Three-layer Feed Forward Artificial Neural Network Global Optimum Approach [J].Mathematics in Practice and Theory, 2003: (7):1-8.

Advanced Materials Research Vols. 989-994 (2014) pp 1652-1656
© (2014) Trans Tech Publications, Switzerland
doi:10.4028/www.scientific.net/AMR.989-994.1652

A Fast Locating Algorithm of Vehicle License Plate under Complex Scenes

Yang LEI[1, a], Ying ZHANG[2, b]

[1] College of Information and Electrical Engineering, Liaoning University of Science and Technology, Anshan, 114051, China

[2] College of Information and Electrical Engineering, Liaoning University of Science and Technology, Anshan, 114051, China

[a]email: lei562113124@qq.com, [b]email: yingzhang9118@yahoo.com.cn

Keywords: License Plate Location; Edge Detection; Morphology; Median-Filter

Abstract. A vehicle plate location algorithm under complex scenes is presented that based on interest region extraction and morphology. First of all, extract the edge of the lane, obtain the driveway area from the edge of the road, confirm the region of interest with the experiences in the driveway area, it can reduce the scope for searching. Then preprocessing is used in the vehicle image, including gray, edge detection and binary transformation is used. Then a series of morphological operations are used to look for candidate regions that probably contain the characters in range of sizes. Finally, the vehicle license plate can be found according to the median filter.

Introduction

Vehicle license plate recognition system is based on a specific target object dedicated computer vision system to automatically extract the image from a plate image, automatic segmentation of characters and character recognition. Vehicle license plate location is the key part of the vehicle license plate recognition technology. The main intention of the vehicle license plate location is located in the license plate from the input image and extracted license plate from the image. Under normal circumstances, automatic vehicle identification relies mainly on two key technologies, namely vehicle license plate location and character recognition. As a core technology, the accuracy rate and timeliness of the vehicle license plate location largely affect the merits of the license plate recognition system.

Researchers from different countries proposed a number of methods for extracting car license. Such as Texture-based segmentation method [1], based on the gray level variation of the method [2], based on neural networks [3]. These methods exists computationally intensive and inaccurate positioning problems. In more complex environmental positioning plates are obvious limitations. Therefore, the study removals interferences from the vehicle image in a complex background and effectively and quickly obtains the target plate is of great significance.

Interest Area Extraction

Vehicle detection algorithm is used here. First, extract the vehicle-related area as interested areas. Extraction of this region is divided into two parts: (a) Distinguish between road and non-road area. Road area is the interest area. (b) Texture features based on the edge of the vehicle to complete the background and foreground images of vehicle separation.

Driving region extraction

In the lane road image, lane usually has a clear edge. Therefore, the original image edge extraction as the pre-processing step is most commonly used [4]. Currently, there are a variety of edge extraction algorithms, such as Sobel, Laplace, Roberts, Prewitt, Canny and so on. By comparing these experimental methods for the purposes of this paper, the effect of Sobel algorithm is better. Other methods exist pumping side is not ideal, because it will affect the subsequent processing and some methods spend more time, unable to meet the requirements of real-time

systems. Therefore, this system used Sobel algorithm edge the extraction. Use horizontal Sobel operator $Sobel_x$ to obtain horizontal gradient map $G_x(x, y)$ and use vertical Sobel operator $Sobel_y$ to obtain vertical gradient map $G_y(x, y)$.

$$G_x(x,y) = Sobel_x(x,y) * I(x,y) \quad (1)$$

$$G_y(x,y) = Sobel_y(x,y) * I(x,y) \quad (2)$$

In the type $I(x, y)$ is the image to be processed. After the edge extraction pretreatment, the image is divided by using the Otsu multi-threshold segmentation algorithm [5]. The specific method is expressed as follows:

1) The initial state: d = 0 for the classification of the image already exists, end of the loop condition is S = 0, υ_T represents the total variance of the image.
2) If S does not satisfy the condition directly to the next step 3, otherwise go to 6.
3) For d different classes already exist in the image, seeking class variance within each class then found that the largest one.
4) Use the local Otsu method makes this class into two new classes, increase new segmentation threshold to the threshold that has been existed.
5) Recalculate υ_T, make a new assignment for S then go to 2.
6) Use the set of optimal threshold result from the above steps for image processing, segmenting out the road and non-road area.

Edge feature extraction based on vehicle

Edge confidence was used according to most of the edge contour of the vehicle is horizontal and vertical rectangular. Exclude a region not include the vehicle so that the vehicle may contain the region is retained. Horizontal and vertical edge detection based on Sobel operator to the Road regional image, to obtain the horizontal edge image I_H and vertical edge image I_V .Then sum the pixel values for each row to obtain a horizontal edge vector H and vertical edge vector V, search for the maximum to obtain confidence.

$$C_H = \frac{H_{max}}{n} \quad (3)$$

$$C_V = \frac{V_{max}}{n} \quad (4)$$

In the type, C_H stands for level confidence; C_V stands for vertical confidence. And if C_H and C_V are less than a certain threshold, it indicates that this region does not contain the vehicle, and shall be identified as background, as the results shown in Figure 1. We can remove the region of low edge confidence and reduce the amount of calculation of the algorithm.

Fig.1. The experimental results

Preprocessing the image region of interest

Processing vehicle image, the results shown in Figure 2.

(a) Gray processing (b) Binary processing (c) Marginalization

Fig.2. Processing vehicle image results

In this paper, the color of the vehicle image region of interest was extracted, converted to grayscale images, shown in Figure 2(a). Grayscale image processing standard formula for the average is:

$$Gray = 0.229*R + 0.587*G + 0.114*B \quad (5)$$

The edge in the image signal is expressed as gray mutation. Since only need processing the region of interest, so we use the Roberts operator which is run faster. The following formula can be used in practical application.

$$g(x,y) = \left\{ \left[f(x,y) - f(x+1,y+1) \right]^2 + \left[f(x+1,y) - f(x,y+1) \right]^2 \right\}^{1/2} \quad (6)$$

In the type, *f(x, y)* stands for input image; *g(x, y)* stands for output image. As the image shown in Figure 2(c) is the output image.

Determine the candidate regions of plates

Morphological processing: Before morphological image processing needs binarization. This paper selects large law Otsu binary image processing [6], thus better able to determine the image pixels is background or objective, as the result shown in Figure 2(b).

After edge detection and binarization processing, the edge of the vehicle is well extraction. However, due to the impact of environmental, the plate is not easy to detect because of these regions are always not closed. Therefore requires a series of morphological processing, in order to confirm the vehicle candidate areas. The mathematical morphology basic operations include: Erosion, Dilation, Opening operation and Closing operation. In this paper we use the Erosion and Closing operation, as the results shown in Figure 3.

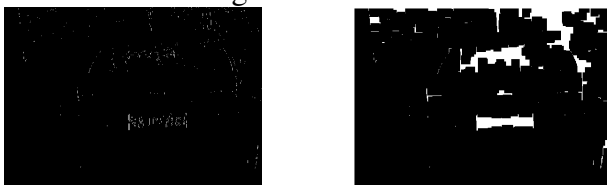

(a) Erosion (b) Closing operation

Fig.3. Vehicle morphological image processing

At first, setting the structural element size according to experience and use this structural elements for image erosion operation. Thus it can eliminating the boundary points in the target image. At the same time, we can remove some small and insignificant outlier, see Figure 3(a). Then use closed operations to integrated narrow gap and remove the hole, get some regular shape connected regions, as the results shown in Figure 3(b).

It is easy to form many isolated connected domain in the image when the background is complicated. And these small plates are obviously not connected domain area In order to reduce the computational of the algorithm, you can use the projection method to remove the smaller regional connectivity in the images that have been using morphological image processing. After deleting these connecting regions, the remaining areas are the region need to identify. With aspect ratio, size, projection characteristic values to indicate these areas. Then based on the value of the width and horizontal distance, calculate the strength of connection of the two candidate areas. Connection strength *I* is calculated as follows.

$$I = \frac{ORV}{(h_1, h_2)^{1/2}} - \frac{DisH}{\max(\omega_1 / \omega_2)} \quad (7)$$

In the type, *ORV* stands for the vertical height of the two candidate regions; *DisH* represents the horizontal distance between the two candidate regions; $h_1, h_2, \omega_1, \omega_2$ respectively represent the height and width of the two candidate areas. The two candidate regions prefer the same region if *I* have a larger value. This allows the separation of regions from the original image of the license plate belong to re-incorporated into the license plate area.

License plate image positioning

After a series of processing on the license plate image we have obtained some candidates regions. In evaluating the characteristics of the candidate regions, we based on the inherent characteristics of the license plate, such as license plate aspect ratio, the size of the license plate area, shape and other characteristics of the area. Compare the candidate region with the ideal plate area, filtering the candidate regions.

To restrain the imaging noise, usually we use the low-pass filter. However, since the edge contour contains a large amount of high frequency information, although the low-pass filter filtering the noise but also blurs the boundary. In order to filter the noise while preserving edge contour information well we use the median filter. The principle of median filter is using a window W to scan on the image. Grayscale image pixels are arranged in ascending or descending. Original image pixel gray value is taken as the center of the gray value pixel. Thus the median filter will be completed. The key effect of the median filter processing is to select the window W. In this paper, the median filtering window is a square window and the window contains nine pixels. This median filter is useful in eliminating the interference of isolation noise points. More important is the use of such windows can be effectively protected the boundary information.

Conclusion

According to the algorithm above on, we tested 200 license plate images shot in a variety of environments. License plate location simulation results statistics for different situations see Table 1.

Table.1. Statistical data in license plate location test results

Environment	Simulation picture	Successful	Accuracy rate
Regular(Sunny)	86	84	97.67%
Regular(cloudy)	57	55	96.49%
Randomly(Sunny)	36	33	91.67%
Randomly(cloudy)	21	15	71.42%
Total	200	187	93.50%

The vehicle license plate was located in a different scene, the results shown in Figure 4.

(a) (b) (c)

Fig.4. Simulation experimental results

After analyzing the results above on, when the background is less edge information the algorithm can effectively split the vehicle area and excluding the area does not exist on the vehicle

information. Positioning speed and accuracy are more ideal. Conversely, when there is more edge information present in the image extraction effect is poor see Figure 4 (a) and (b).When the image pixel color changes more obvious the algorithms often fail to weed out certain areas that do not exist the vehicle which is seen in the Figure 4(c). Therefore, the algorithm needs further improvement in order to meet operating under various environmental conditions.

Acknowledgement

In this paper, the research was sponsored by the National Natural Science Foundation of China (Project No. 71371092).

References

[1] Wang Yan, Xu Qinyan, Huang Mengmeng. On License Plate Location In Complex Background Based On Texture And Colour [D]. Donghua University, 2013.

[2] Fu Wei,Zhao Zhengze,Wang Dajiang. Location of Vehicle Plate Based on The Gray Beep Points of The Row and The Vertical Projection [J]. Electronic Measurement Technology. 2008,31(3): 61-65.

[3] Fu Desheng, Fan Chunnian. Research on Technology of License Plate Recognition Based on RBF Neural Network [D]. Harbin Polytechnic University, 2012.

[4] Hu Bin, Zhang Pengfei, He Kezhong. A Fast and Efficient Lane Recognition Method for Outdoor Mobile Robots, Robot,2006, 28(4):394-399.

[5] OTSU N. A threshold selection method from gray-level histogram[J]. IEEE Transactions Systems Man Cybernet,1979, (1):62-66.

[6] Fu Zhongliang. The Method for Image Threshold Selection--The Popularization of Otsu's Method [J], Journal of Computer Applications. 2000, 20(5):53-56.

[7] Chen Qiang. Research of Image Segmentation Algorithm Based On Mathmatic Morpholog[D]. Harbin Polytechnic University, 2011.

[8] Niu Xiuqin. Research on Several Improved Median-filter Algorithms[D]. Sichuan Normal University,2012.

Advanced Materials Research Vols. 989-994 (2014) pp 1657-1659
© (2014) Trans Tech Publications, Switzerland
doi:10.4028/www.scientific.net/AMR.989-994.1657

A multidimensional model of data warehouses

Zuyi Chen [1, a], Taixiang Zhao [1,b]

[1]Department of foundation First Aeronautic Institute of the Air Force Xinyang, China

[a]zychen7410@163.com, [b]ztx304@126.com

Keywords: Data warehouse; OLAP; Probability model; Data cube

Abstract. Reducing query time by means of selecting a proper set of materialized views with a lower cost is crucial for effcient datawarehousing. The database, however, needs to be utilized more, by providing a functional environment of probability analysis. The objective of this paper is to improve the effectiveness of utilizing historical cost data in an analytical OLAP (On-Line Analytical Processing) environment. The results show that the OLAP environment can help understand the uncertainties inconstruction cost estimate, and provide a way for projecting more reliable construction costs.

Introduction

From the early nineties, data warehouses have been considered to be the key aspect of success for any Decision Support System (DSS) [1].Data Warehouses (DW), Multidimensional (MD) Even now, a Databases, and On-Line Analytical Processing (OLAP) cade later, data warehouses are still seen as being the applications are used in conjunction to form a highly most important issue for the next generation of Decision.

A prototype of the cost data management environment,Cost Data Management System (CDMS), has been developed to test the advantage of OLAP in cost estimate. Here, the CDMS works as an enabler for the probability cost evaluation model described in this paper. Using the functions provided in the CDMS, the cost data stored in the data warehouse can be converted into more meaningful information for decision making.

In this paper, we will consider the following constraints when dealing with the optimal utilization of materialized views: (1) available storage space, (2) query processing effciency, and (3) the costs of DW query and maintenance. We propose effcient algorithms to optimize query effectiveness on the premise that source data might change over time. The overall time and cost of DW query and maintenance can be minimized significantly using these proposed effcient algorithms.

In our research, we use the vector data structure to determine the relationship of the lattice for the aggregate views and develop an improved algorithm to materialize an optimal pool of shared views with the lowest cost, thereby maximizing overall performance and e?ciency for queries. There are three characteristics in this algorithm. First, ‘‘metrics of gain and loss’’ and ‘‘candidateview’’ are introduced in the optimization of adding and deleting materialized views. Second, in addition to query cost, maintenance cost is also taken into account. Third, we improve the query process by adopting a vector data configuration to speed up the lattice operation in searching dependent views.

Literature review

In the construction sector, research on data warehousing and OLAP has been conducted to effectively manage the data generated during the construction process. The analytical function of OLAP, combined with the data storage capability of a data warehouse, provides an opportunity to improve data control in the construction sector. Confidence in the merit of utilizing this environment is growing due to the rapid development of construction information technologies [2].In the first step, the algorithm always chooses the materialization of the view which can be used to derive any other view. In the second step, for each view in the graph which does not yet belong to

the set of materialized views, the algorithm determines the total benefit of materializing this view. Among these analyzed views, the algorithm selectsthe view which maximizes the benefitand adds it to a materialized set. This second step is repeated until a determined number of materialized views is selected or the limit of available storage space is reached. This particular approach does not consider the maintenance cost. Ross et al. [3] considered the use of additional views to reduce maintenance cost. Liang et al. [4] proposed a two-stage algorithm that optimizes the total query response time in the first stage,and chooses views formate rialization under the given maintenance time constraint in the second stage.

In this paper, we present a cost model based on our previous work [5] to determine the desirable materialized views in which the total cost of query processing and maintenance are minimized. Yang et al. [6] used the cutting-point position of given actual storage space between candidate space and minimal space to make better decisions on determining whether to delete some candidate materialized views from the candidate space or to add more materialized views to the minimal space. Thus, we are able to develop more e?cient and effective algorithms for materialized views selection.

Multidimensional Modeling

Object-oriented multidimensional modeling. In this section, we outline the UML we use for DW conceptual modeling]. This approach has been specified by means of a UML profile which contains the necessary stereotypes for carrying out the MD modeling at the conceptual level successfully.The main features of MD modeling considered here are the relationships many-to-many between facts and one specific dimension, degenerated dimensions, multiple classification and alternative path hierarchies, and non-strict and complete hierarchies. In this approach, structural properties of MD modeling are represented by means of a UML class diagram in which the information is clearly organized into facts (items of interest for a given business) and dimensions (context in which facts have to be analyzed).

OLAP.OLAP accesses a data warehouse, analyzes data on a specific subject and accumulates them in a storage area of the data warehouse. OLAP can describe information from data analysis in a variety of formatst o provide useful information so that construction managers can make rational decisions. Thereby, the user can minimize the effort in finding and analyzing the meaning of data. The role of OLAP is increasing because it is useful for retrieving significant information by analyzing the vast volume and variety of data generated in information management systems.

Probability analysis model of cost data.

Cost data for construction work items. To explain the probability analysis method of cost data, asample of four work types, i.e. (1) cutting, (2) embankment,(3) slope protection (roll) and (4) slope protection (sheet). Five sets of historical cost data for the work items were collected from five different highway construction projects of a private company.The means and deviations of the data sets were calculated and used as unit costs. For a sample project, each work item is given arbitrary quantities. The amounts, which are the mean costs for each item, were obtained by multiplying the quantity by the mean unit cost.

Authorization objects. In this sub-section, we need to identify and specify the main objects we deal with for the conceptual modeling of DWs such as facts, dimension, classification hierarchy levels, measures, dimension attributes and instances. From now on, all the required rules for specifying security measures will be defined based on the UML stereotypes of our approach for the conceptual MD model at the conceptual level. Thus, the object component of our ACA model includes two parts:

An identity, that can be one of the following sub-attributes:

- MDClassName: The MD class identifier. It can be related to a fact class or a dimension class, referring to a fact or dimension; or base class referring to a classification hierarchy level.

- MDAttributeName: The MD attribute identifier. In object-oriented notation we have to indicate the class name, and then the attribute name. Thus, we treat both measures and dimension attributes as just attributes; since the preceding class name will tell us if we refer to a measure or a dimension attribute. Moreover, treating both measures and dimension attributes in the same way will allow us to execute security measures on attributes correctly, if in a further analysis carried out by OLAP tools, users interchange measures and dimension.

Authorization rules. Sensitivity Information Assignment Rules allow us to specify multilevel security policies, but unfortunately, these rules are not enough to specify other situations in which the access class of objects or subjects is not relevant. As we aim to define a general and expressive enough access control and audit model, we also define Authorization Rules (AURs), which exist with SIARs, thus permitting us to specify security models which are much more elaborate.In the literature, we can find different authorization variants, some of the most important being implicit, explicit, positive, negative, weak and strong. Moreover, access control models can be open (allowing access by default, unless a negative authorization exists) or closed (denying access by default, unless a positive authorization exists). In a multilevel system, a user needs to fulfill the multilevel security imposed by the object she or he wants access to, so we can consider that our system is closed. In oursystem both positive and negative AURs can coexist Some types of implicit and explicit AURs can also be defined, but we will not consider weak and strong authorizations explicitly. For each AUR, we will specify the following concepts:

- Subjects to which the rule is applicable.
- Sign, that defines if the authorization is positive(allowing access) or negative (denying access).

Conclusion

Owing to the development of construction information systems, most construction operations are conducted via digital processing, in which vast amounts of cost-related data are generated. Meanwhile, retrieval of valuable and worthwhile information from the accumulated data is a separate problem, where the use of data stored in a database has become an important company asset.

Our work for the immediate future is to improve the ACA model, extending the set of privileges considered in this paper (i.e., read), so as to permit us to specify security aspects in the crucial ETL processes for DWs, there by considering other operations such as delete,insert and update. As well as this, we plan to consider implementation issues for the use of the security aspects considered when querying a MD model from OLAP tools. This includes an in-depth study on the different combinations of dimensions, measures, hierarchies and so on, as involved in queries.

References

[1] H. Inmon, Building the Data Warehouse, 3rd ed., John Wiley & Sons, USA, 2002. noro, Italy, 2000.

[2] J.K. Lee, H.S. Lee, Principles and strategies for applying data warehouse technology to construction industry, Architectural Research 5 (1) (2003)61–68.

[3] K.W. Chau, Y. Cao, M. Anson, J. Zhang, Application of data warehouse and decision support system in construction management, Automation in Construction 12 (2002) 213–224.

[4] I. Ahmad, S. Azhar, P. Lukauskis, Development of a decision support system using data warehousing to assist builders/developers in site selection, Automation in Construction 13 (2004) 525–542.

[5]M.Zhiliang,K.D.Wong,L.Heng,Y.Jun, Utilizing exchanged documents in construction projects for decision support based on data warehousing technique, Automation in Construction 14 (2005) 405–412.

[6] J.H. Yoo, S.H. Song, W.H. Lyou, H.S. Lee, Development of performance analysis system for construction projects using a data warehousing echnology, Korean Journal of Construction Engineering and Management6 (1) (2005) 89–98.

Advanced Materials Research Vols. 989-994 (2014) pp 1660-1663
© (2014) Trans Tech Publications, Switzerland
doi:10.4028/www.scientific.net/AMR.989-994.1660

Architecting Service-Oriented Publish/Subscribe Applications: Data Model and Matching Algorithm

Biao Dong[1, a]

[1]Nanjing Institute of Industry Technology, Nanjing, China

[a]dongb@niit.edu.cn

Keywords: publish/subscribe; graph-oriented model; multimedia content

Abstract. The existing publish/subscribe(Pub/Sub) systems can't match events with subscriptions based on the semantic of events. Focusing on the production development activities, this paper presented a data model for modeling an ontology-based hierarchical description framework, defined service and its classification characteristics, and analyzed an automatic generation method of building service ontologies for the semi-structured data that exist in the Internet. A subscription matching algorithm was proposed for solving the intelligent semantic matching problem between the subscription and services. The results show that the service-oriented applications guarantee the initial and availability matching of individualized demands and service capabilities.

Introduction

Services are playing more and more important role in the modern enterprises: The enterprises provide complete solutions for customers by integrating services and products into a product service system, and are more focused on their own good while providing services to other enterprises. The traditional service oriented production process consists of the following three ways: network propaganda pattern, collaborative design pattern and commerce platform pattern. At present, the key elements to improve the modern enterprise service capabilities are advanced service business models, and service resources publishing mode.

Pub/Sub is an asynchronous communication paradigm that supports many-to-many interactions between a set of clients. A client can be an information publisher, an information subscriber, or both. Client interactions are data-centric: publishers describe their publishable events, subscribers express their interest in events, and the Pub/Sub protocol delivers the published events to their corresponding event subscribers[1]. Today, more and more enterprise services becomes available, Pub/Sub is a suitable paradigm for architecting service oriented applications. Functional requirements of Pub/Sub applications based on service contents often change, and user's needs are different, which lead to the service-oriented Pub/Sub systems efficiently publishing and subscribing remain still an open issue.

Opiyo[2] proposes a new distributed and collaborative product design concepts evaluation scheme. Globus, Condor-G and Storage Resource Broker[3,4] propose new service models that can improve the product development and design capabilities, the resource sharing capabilities. [5] proposes a cloud service model which will become the most potential service pattern in the modern enterprises in the future. The above systems mainly focus on the service model, and less involve in the whole life cycle of service model, lack the detailed definitions and quantitative descriptions of the service classification and feature attributes. It's difficult for these systems to guarantee the initial and availability matching of individualized demands and service capabilities.

In view of the above analysis, an approach, for modeling and implementing the service-oriented Pub/Sub applications, is presented. The main characteristics include two aspects as follows. Firstly, in the aspect of data model, focusing on product development, we put the resources as a service definition, define service and its classification characteristics, and analyze an automatic generation method of building the service ontology for the semi-structured data that exist in the Internet. Secondly, in the aspect of subscription matching algorithm, We construct a service-oriented

subscription model to complete the production activities. A matching method is proposed for solving the intelligent semantic matching problem between the subscription and services.

Data model

Resources. Resources are a collection of entities used in production activities, which is composed of human resources, tools, places, materials, facilities, information resources, service resources and other resources. In the paper, resources are marked Ress={resource-type-set, resource-attribute}, resource- type-set={human, tool, place, material, information, service, other}, resource-attribute= {$resources_k$, structure-attribute, ability-attribute, service-attribute}, where resource-type-set is a collection of resource types, resource-attribute is characterized by a collection of different types of resources, $resources_k$ is the k-class resources, structure-attribute={ID, name, type, location, information} is structural attributes, including resource ID, name, type, location and information, ability-attribute=(function[]) is a collection of ability attributes that represents functions of the resources, service-attribute=(cost, method, time) is a collection of service attributes that includes service cost, service method, service time.

Service and classification characteristics. Service refers to the resource that can be used, provided, and traded in the production activities, it can be released on the Internet. Service is an important basis for the Pub/Sub applications, including resources service, transaction service, process service, tool service and other services. Resources services includes the following aspects, such as information, personnel, software, design standards, databases, patents, market researches, product plans, customer need transformations, concept tests, experience conceptual models, model-making equipments, facilities, tools, physical model experiences and so on. Transaction services include reward transactions, brokered deals, bidding, auctions, online rentals, commissions and so on. Process services include project managements, resource managements, change managements, document managements, quality managements and cost controls. Tool services include software tools, real tools and so on. By using the services to abstract the user's subscriptions, we can shield the heterogeneous and dynamic characteristics of the resources. According to the user's needs, we can quickly provide ways to meet the demand, and to allocate the appropriate services to the users.

Service model. Service model SM=(task, pro-resource, ability), where task refers to production requirements, i.e., the goals needed to achieve for the completion of certain production activities; pro-resource refers to the resources needed for production processes, including personnel, tools, materials, places, tools, etc.; ability refers to the ability to achieve the desired objectives. Fig.1 shows a service model of an ontology-based hierarchical description framework. The top layer is a service ontology, which mainly includes three parts: task, resource and ability. The middle layer is the refinement on the top layer ontology, where task ontology includes goal and requirement description, resources ontology includes resources type and resources description, ability ontology includes ability type and ability description. The underlying attribute is required for the middle layer of ontology.

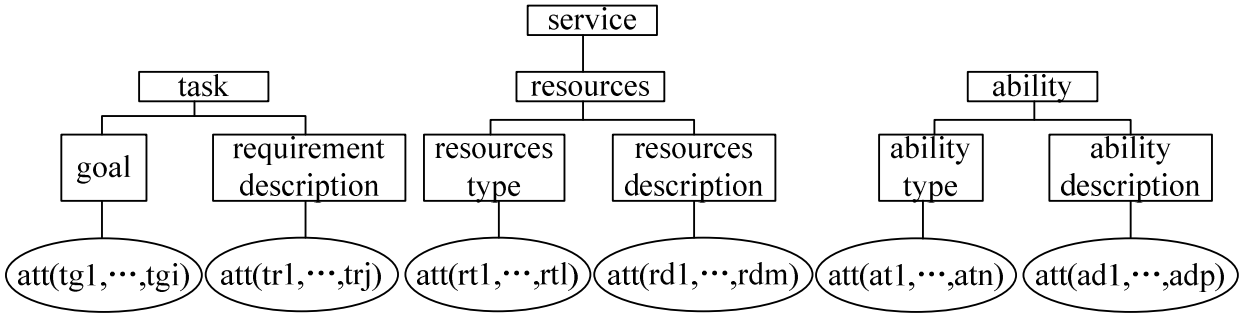

Fig.1. Service model of an ontology-based hierarchical description framework

We use web ontology language(OWL) to describe service, the detailed information of OWL resource description parameters are as follows: rdfs:Class is a set of objects with the same attributes, rdfs:subClassOf is an instance that is used to state class hierarchy, rdfs:Property states the relationship

between the expressions of individual, rdfs:subPropertyOf states attribute hierarchies that can be created by this parameter, rdfs:domain is an instance of rdf:Property that is used to state that any resource that has a given property is an instance of one or more classes, rdfs:range is an instance of rdf:Property that is used to state that the values of a property are instances of one or more classes, individual is an instance of class.

Service publishing. There is a wide variety of services, most of them exist in the internet. The establishment of services requires a large amount of the case descriptions, concepts and relationships to define the service ontologies. The contents of the service ontologies are cumbersome and complex, if all are completed by manual, it is easy to make mistakes and has a heavy workload. We study an automatic generation method of the service ontology for the semi-structured data that exist in the Internet. Firstly, we classified the resources with semi-structured format such as XML, HTML, RDF. Secondly, we perform the concept extraction and the relation extraction on the data sources, map the concepts and relations into various service ontologies, and then compare the service ontologies with domain expert ontologies. Finally, we merge the kind of service ontologies.

Matching algorithm

Subscription model. Subscription model refers to the use of external service subscriptions to complete a production. The external service subscriptions mainly include resource service subscriptions, transaction service subscriptions, process service subscriptions, tool service subscriptions and other service subscriptions. Its attributes include basic attributes, object attributes, transaction attributes and ability attributes. In the paper, Ext, Ser, Sub and Att are respectively the abbreviations of external, service, subscription and attribute. Subscription model are marked SM={Ext-Ser-Sub, Ext-Ser-Att}, Ext-Ser- Sub={Resource-Ser-Sub, Tra-Ser-Sub, Process-Ser-Sub, Tool-Ser-Sub, Other-Ser-Sub}, Ext-Ser-Att ={$Task_i$, Basic-Att, Object-Att, Transaction-Att, Ability-Att}, where Ext-Ser-Sub is a collection of external service subscriptions, Ext-Ser-Att is a collection of service attributes, and $Task_i$ is the i-class task. Fig.2 shows characteristic attributes of a subscription model. For simplicity, Transaction-Att and Ability-Att are collectively referred to as service attribute(Ser-Att) in Figure 2.

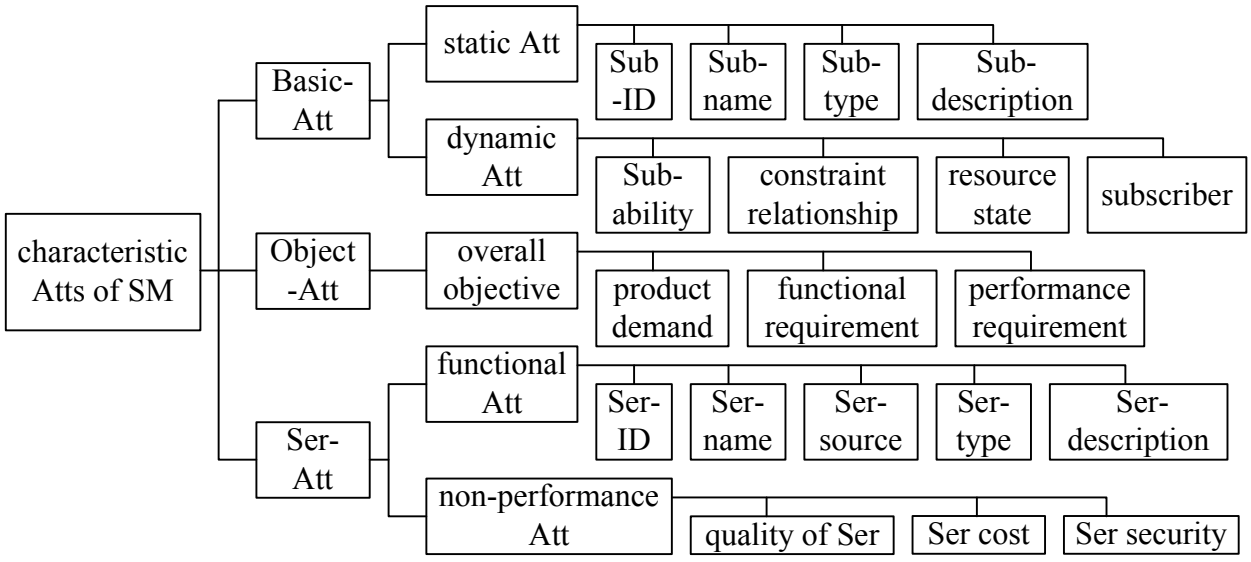

Fig.2. Characteristic attributes of subscription model

Subscription matching algorithm. The essence of subscription matching problem is that the Pub/Sub systems can quickly find all matching subscriptions after reaching a service. In order to improve the matching accuracy, the semantic matching is particularly important, it mainly solves the problem on the semantic matching between the subscription conditions and service description text. We calculate the similarity between them, and then, according to the similarity value, publish the matching service to the subscribers. Let the service ontology be a tuple SO={CC, RC, CA, CS, SS,

OI}, where CC is a set of the concepts or classes of the resources; RC is a set of relationships between the concepts, including hierarchical relationship, inclusion relationship, equivalence relationship, and so on; CA is a set of the concept attributes; CS is a value constraint set; SS is a special set which represents the disjoint descriptions; OI is a set of instances which are represented by the objects and individuals. The specific subscription matching algorithm is as follows:

(1) Analysis of a subscription vector. Let a subscription vector be $Q=\{T_1, T_2,..., T_m\}$, where T_i is the subscription feature vector which is obtained by using a segmentation method to decompose subscription conditions, its the order is determined by the corresponding weight. Let a weight set be $W=\{W_1, W_2,..., W_m\}$, where W_i is the weight of the i-th subscription feature vector, which indicates the importance of each subscription feature vector.

(2) Semantic analysis of a service vector. Let a service vector be $SV= (RC_1, RC_2,..., RC_n)$, where RC_i represents the i-th service object vector, which comprises multiple attribute values, and satisfies the equation $OI=CC \cup RC \cup CA \cup CS \cup SS$. Let the service description vector be $P=\{CA_1, CA_2,..., CA_m\}$, where $P \in RC_i$; CA_i is the heavily weighted attribute, its the order is determined by its weight.

(3) Subscription matching. Matching rules between each component of the service description vector and the corresponding component of the subscription vector are as follows: if $CA_i=T_i$, then $K_i=1$; if T_i satisfies CA_i, then $K_i=K_m<1$; if T_i contains A_i, then $K_i=K_c<1$; if T_i is completely separated from CA_i, then $K_i=0$.

(4) Getting subscription candidate set. Similarity measure for comparing P and Q is defined as follows: $Sim(P,Q) = (\sum_{k=1}^{n} K_i \times W_i) / \sqrt{(\sum_{k=1}^{n} W_i^2)}$

If Sim(P,Q) is greater than a threshold, the candidate set of subscriptions is denoted by $D=\{D_1, D_2,..., D_m\}$, otherwise, there isn't the candidate set of subscriptions. According to the constraint conditions, the D is matched to meet the target function. we obtain the optimal subscription set D_x, where the number of elements in the D_x is less than the number of elements in the D.

Conclusions

We model the service-oriented Pub/Sub architecture. In our future work, we plan to establish a development environment by integrating the infrastructure, the executing environment, and the ontology engineering tools to provide a profound basis for the seamless integration of ontological knowledge to unleash its full potential for efficient service oriented Pub/Sub applications.

Acknowledgements

This work was sponsored by Qing Lan project(Jiangsu province, china) and open fund project of Jiangsu provincial research and development center of intelligent sensor network engineering technology, china(ZK13-02-03, software technology, platform and application for sensor network).

References

[1] B.Dong: TELKOMNIKA Indonesian Journal of Electrical Engineering, Vol. 12(6) (2014).

[2] E.Z.Opiyo: Distributed and Collaborative Product Design Concepts Evaluation by Using Heterogeneous Terminal Devices (ASME, USA 2013).

[3] R.Ananthakrishnan, J.Bryan, K.Chard, et al.: Globus Nexus: An identity, profile, and group management platform for science gateways and other collaborative science applications (IEEE, USA 2013).

[4] J.Frey, T.Tannenbaum, M.Livny, et al.: Condor-G: A computation management agent for multi-institutional grids, Cluster Computing, Vol. 5(3) (2002), p.237-246.

[5] A.Singh: Cloud Computing, Vol. 1(1) (2013).

Advanced Materials Research Vols. 989-994 (2014) pp 1664-1670
© (2014) Trans Tech Publications, Switzerland
doi:10.4028/www.scientific.net/AMR.989-994.1664

Research on psychology data clustering algorithm based on CUDA

Lili Dong[1,a], Zongshuai Ma[2,b],Wei Dong[3,c],Xiang Zhang[4,d]

[1]Xi'an University of Architecture and Technology, Shaanxi Xi'an 710055, China

[2]Xi'an University of Architecture and Technology, Shaanxi Xi'an 710055, China

[3]Xi'an University of Architecture and Technology, Shaanxi Xi'an 710055, China

[4]Xi'an University of Architecture and Technology, Shaanxi Xi'an 710055, China

[a]email:donglilixjd@163.com, [b]email:mazongshuai8909@qq.com

[c]email:790514494@qq.com, [d]email:Zhangxiang1001@126.com

Keywords: CUDA; K-Means algorithm; CURE; MMPI

Abstract. This paper analyzed the employees' MMPI Psychological data of a company. Aiming at the problem that traditional K-Means algorithm is sensitive to the initial clustering center, this paper used hierarchical clustering algorithm CURE to mitigate the problem. Finally using CUDA technology clustered several times, so as to improve the execution efficiency of the algorithm. Through experimental verification, the improved K-Means algorithm behaved well in both execution efficiency and clustering results.

Introduction

Cluster analysis is often used to divide the data into useful or meaningful groups or clusters, and plays an important role in psychology, biology, statistics, information retrieval, machine learning and data mining. In the field of psychology, specific crowd psychology there is a corresponding feature, For such people to extract the characteristic value and cluster, can help the psychology experts to analyze the psychological characteristics of such people. K-Means algorithm as the traditional data mining methods has an important role in psychology data cluster analysis. But the traditional K-Means algorithm is sensitive to the initial cluster centers problems, leading to reduced effectiveness of clustering. For the K-Means algorithm center sensitive issues, Bradley PS and other scholars [1], presented randomly selected subsample from the data in the cluster analysis. Repeat the K-Means clustering algorithm for the selected sub-sample to get the optimization clustering center and then entire the data for K-Means clustering algorithm. However, this method is affected by the selected sub-sample collection methods, only has a sub-optimal results. For the efficiency of the traditional data mining algorithms, the application of Map reduce programming model to improve the efficiency of large-scale data clustering has become a hot spot. In fact, psychology data does not have the instantaneity, high accessibility, interactivity and large scale, therefore, using cloud platforms are not suitable for such data mining. Due to the delay of the network and its unreliability, using Hadoop platform for psychology data in the actual mining is not more efficiently than traditional methods [2-7].

CUDA is a high-performance computing technology which NVIDIA Corporation invents for its GPU (Graphic Processing Unit). This technique is ideal for psychology and other smaller-scale memory data mining, and is repeated for clustering in a limited time to observe the best results from multiple clustering results. Kumar and other scholars[8] used CUDA to achieve a Gaussian mixture model expectation maximization algorithm parallelization ,and to speed up 165 times; Zhang Fan and other scholars[9] used CUDA to calculate the length of the protein molecule, compared to CPU speedup of 7.5 times; Takahashi and other scholars[10] used CUDA accelerated three-dimensional Helmholtz equation to achieve a speedup of 23 times; Labaki and other scholars[11] applied CUDA in two-dimensional elastic potential problems and two-dimensional elastic statics problem, speedup is 56.8 and 39.6 times.

In order to solve these problems, this paper improved the K-Means clustering algorithm based on CUDA technology and FP-Tree associated iteration algorithm. Using CUDA solved the efficiency problem of multiple clusters and using hierarchical clustering algorithm CURE located the initial center of K-Means algorithm. CURE algorithm is a graph algorithm based on hierarchical clustering, the algorithm use graph approach to achieve the initial data divided. And use inter-cluster proximity, connectivity concepts and part of cluster to model. Found high quality clusters of different shape and size and density [12]. So in this paper, we preliminary cluster the memory data to achieve the initial parameters for K-Means algorithm, and use CPL clustering algorithm to ease the instability problem which the randomness and apriority of K-means initial clustering center lead to the result . In the implementation of the results of K-Means algorithm, using the FP-Tree for several clustering results association analysis can reduce central K-Means algorithm sensitive issues and improve the effectiveness of clustering.

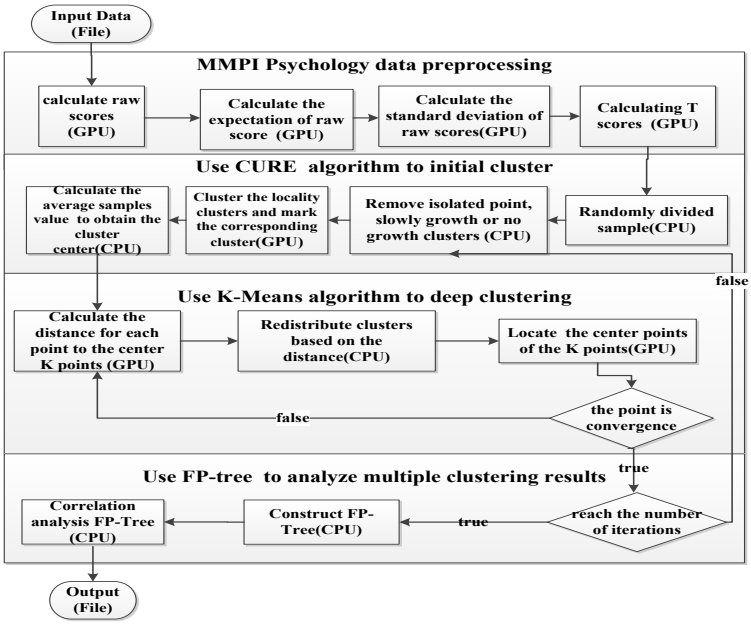

Figure 1: Improved K-Means algorithm framework

The data stream in the GPU use CUDA technology to accelerate computing, and use .NET Framework platform for IO read and write and task processing in the CPU.

Preprocessing of psychology data

This paper used the MMPI (Minnesota Multiphasic Personality Inventory) scale sets in the behavioral psychology to gather the behavioral psychology data of people in a company. Clustering crowd to help psychology researchers analyzed population Multiphasic Personality. MMPI is the most complex and cumbersome behavioral of a test of psychology, but its accuracy is more accurate than other scales [13]. The first step of MMPI is to get test data, calculated for each test object 25 test items raw scores, two scales, and a total of 566 test questions. Due to the number of each test questions is difference, leading to total scores different, cannot be directly compared ,we need to normalize the raw scale scores. The second step is required by equation (1)

$$T = 50 + 10(X - M)/SD \tag{1}$$

to calculate for each sub-scale normalized to a standard ***T***. ***T*** is a vector, each component of the vector represent each scale's standard score. ***X*** is a raw scores vector consists of each raw scores of psychological questionnaires. ***M*** is the normal vector of each test scale raw score composed expectations. ***SD*** is the normal vector of each test scale raw score standard deviation. MMPI data preprocessing focuses on the raw scores converted to standard ***T*** points. Calculate its expectation ***M*** and standard deviation ***SD***.

Computing the standard deviation ***SD*** and expectation ***M*** in the host requires multiple iterations, and iterative scale increases with the data size increases. In the same scale data, using CUDA technology transform the iterations into parallel execution, thereby reducing the scale of the iteration to improve the efficiency. In the CUDA parallel environment, using the reduced tree algorithm calculate the expectation ***M*** and standard deviation ***SD***, as shown in Figure 2.

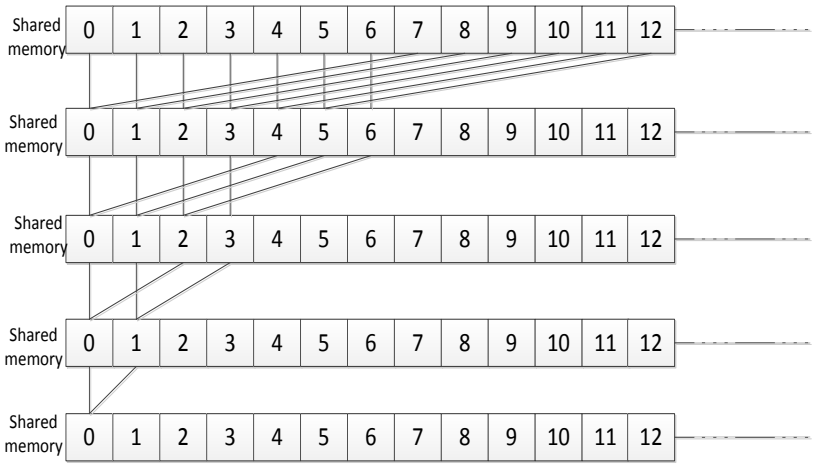

Figure 2：Reduced tree algorithm

In Figure 2, using reduced tree algorithm parallel add for a test scale raw score of the first 13 test through 5 iterations and store the result of the addition in the first element of the shared array. The result divide the length of the array can achieve the expectation M of this test.

Using CUDA improve CUDA algorithm

CURE[14] algorithm is a clustering algorithm based on hierarchy, which is different from the traditional method that use one object to represent the cluster, instead of using multiple objects, and through the shrinkage factor to regulate cluster shape, as a result, it can deal with non- spherical distribution or size of uneven distribution of cluster, and has a good effect on treatment of isolated points, so in this paper psychology data use the CURE algorithm to initializing clustering, to get the input parameters of K-means algorithm: the number of clusters and the corresponding initial class centers, so as to reduce the clustering fluctuation problem of randomness and apriority of K-means initial clustering center. The key to CURE clustering is to calculate the distance between samples, the distance between the samples can form as a matrix, using CUDA read matrix into the device memory. Using CUDA thread, respectively calculate the distance of sample points. As shown in the matrix:

$$\begin{bmatrix} d_{11}, d_{12} & \cdots & d_{1n} \\ \vdots & \ddots & \vdots \\ d_{n1}, d_{n2} & \cdots & d_{nn} \end{bmatrix} \tag{3}$$

The described matrix is the distance between the sample points. The d_{11} represents the distance the first point to itself, d_{12} represents the distance of the first sample points to the second sample point, by analogy, d_{nn} represents the distance the ***n*** point to itself, this matrix is a triangle or lower triangular matrix.

Use CUDA to improve the K-Means algorithm

The improved K-Means algorithm has two stages, the first stage is to find the ***K*** centers, and calculate the distance between other point and the center of ***K***, put the nearest point of the center constitute k clusters. The second phase is to calculate the center point of K clusters, as the initial

center point of the first stage of next iterative, iterate until convergence center point to a threshold range. Since this paper use CUDA algorithm to find the initial center of K-means algorithm, so the first phase focuses on CUDA technical computing ***K*** center point to another point distance. This phase also relates to matrix operations, so using CUDA technology to accelerate this process. In the CUDA device memory, Let n be the vector the length of the array ***R***, let ***K*** be the length of center point vector array S, compose ***n*** × ***k*** matrix ***H***, Unit matrix ***H*** (***i***, ***j***) represents the distance in the vector array with the vector ***Ri*** and ***Sj*** central vectors. The distance metric function is $\frac{f_{11}}{\sqrt{f_{1+}f_{+1}}}$. As shown in figure 3.

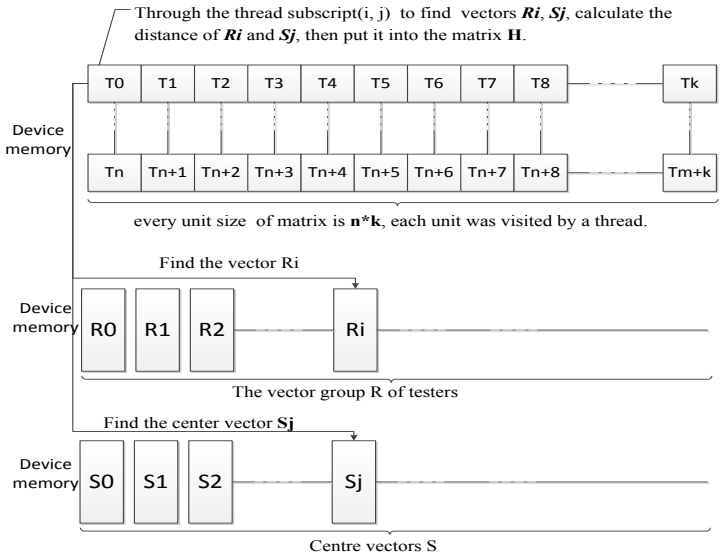

Figure 3：Calculate the distance of each vector group in ***R*** and ***K***

The matrix ***H*** is copied from the device memory back to the host memory. Iterate array ***H***. And find vectors ***R1~k*** nearest to the centers vector ***K*** respectively, and compose ***K*** clusters.

Construct FP-Tree Data Structure

Running the CUDA algorithm and the K-Means algorithm for several times compose transactional data. Format and data are shown in figure 4.

```
4,25,43,49,60,63,64,67,72,80,82,83,86,87,93,99,10(
40,74,112,154,158,176,241,254,277,297,298,337,404,
9,11,13,15,19,26,30,33,34,48,53,57,61,70,75,76,77,
5,7,10,12,14,22,23,27,28,31,32,39,45,46,52,54,56,(
1,2,3,6,8,16,17,18,20,21,24,29,35,36,37,38,41,42,(
5,7,22,25,40,46,52,56,65,71,84,96,122,123,152,154,
1,3,6,8,10,12,14,16,20,21,28,29,31,37,41,47,55,58,
9,13,23,26,27,30,32,33,39,45,53,54,57,61,67,74,77,
4,43,49,60,63,64,72,80,82,83,87,93,99,110,115,125,
2,11,15,17,18,19,24,34,35,36,38,42,44,48,50,51,59,
1,2,3,6,8,16,17,18,20,21,24,29,35,36,37,38,41,42,(
43,49,63,64,72,82,83,87,99,110,125,126,130,138,14(
4,5,7,22,23,25,45,54,60,67,80,86,89,93,96,97,100,1
10,12,14,27,28,31,32,39,40,46,52,56,65,71,73,74,8(
9,11,13,15,19,26,30,33,34,48,53,57,61,70,75,76,77,
```

Figure 4：Transactional data format (Part of the data)

Each row is a cluster, each test number separated by commas, in ascending order, preparing for the construction of FP-tree. Add the several clustering results to the same file, and compose transactional data. For the following three reasons: 1, CUDA algorithm k value is artificial selection; 2, ***In RI×RC > u***, ***u*** threshold is artificial selection too; 3, K-Means algorithm center iteration convergence instability. Because the results of these clusters has led to instability, so you

can use correlation analysis of FP-tree algorithm to find frequent item sets in multiple clustering results to reduce instability.

Experiments

Experimental environment: CPU: Intel i7-3770; CPU frequency: 3.4GHz; CPU cores / threads: 4/8; Host Memory: 8GB; GPU: NVIDIA GTX 660; Device memory (graphics): 2GB; CUDA version: 5.0; Operating system: Windows7.

Experimental data: In this paper, experimental data is MMPI psychology test data of the employees in a company over the years. Size is 353MB, unit is line, and test data have 907,689, and composed of five .csv file.

Experimental Analysis

Compare the improved K-Means algorithm execution efficiency in CUDA parallel accelerated environmental and pure CPU serial execution environment.

In order to compare the performance of the algorithm, we compare the various parts of the improved K-Means algorithm execution in CUDA (in the following table are referred to as parallel speedup environment) and pure CPU execution environment (in the following table are referred to as a serial environment), and using speedup ratio measure the efficiency of the algorithm. Data preprocess results shown in table 1.

Table 1: Data preprocessing results

CPU IO read and write T consuming time /ms	Serial environment CPU consuming time /ms	Parallel CPU acceleration environment consuming time /ms	Parallel GPU acceleration environment consuming time /ms	speed-up ratio
136871	113780	8452	2675	39.37

As apparent from table 1, in serial CPU environment computing MMPI T scores in time mainly used for its expectations and standard deviation calculations, In the parallel accelerate environment to compute expectation and standard deviation T scores in the GPU, IO read and write files is the main work of CPU, and use the preprocessing of the algorithm computing part for CUDA parallel computing, and the ratio of the accelerated procedure has greatly improved.

When $\boldsymbol{RI \times RC}$ threshold increase, both the serial environment version and parallel acceleration version of CUDA algorithm appear decline situation. After analysis, the serial version of CUDA algorithm environment not only need to traverse k nearest neighbor diagram in the first phase and traverse the nearest clusters in the second stage of the algorithm, but also need to calculate the lower triangular matrix elements of the first phase and the second phase consisting of vectors cluster lower triangular matrix elements. After the CUDA algorithm is parallelized by CUDA , mainly parallel part is to calculate the lower triangular matrix of two stages, but traversal k nearest neighbor graph and the nearest cluster is still performed in the CPU environment, and agreed with the algorithm serial performs partial . With RI×RC threshold increases, the cluster meet the conditions to merger reduced, the consolidation process takes time becomes less too. That is to say serial and parallel acceleration environment version of the algorithm traversal part time cost will reduce.

We can conclude, with the larger the initial number of clusters $\boldsymbol{K}$, the K-Means algorithm acceleration ratio is increased. After analysis, two stages of K-Means algorithm for the calculation of each point to center point distance and finding central point to improve CUDA parallelization. All the numerical in the algorithms are run on the GPU, CPU for data copy and scheduling such that the efficiency of the algorithm is greatly improved, especially in the case of the many initial clusters, the speedup ratio also rapidly increase.

When $\boldsymbol{RI \times RC}$ threshold increase, K-Means clustering initial number $\boldsymbol{K}$ increase too. This has resulted increased size of K-Means algorithm calculation, the speedup ratio also increased. It can be

concluded, when using the improved K-Means algorithm to calculate the size and amount of data increases, the efficiency of the algorithm become higher.

Experiments using three authority data sets UCI machine learning database to test. The data are Iris, Wine and Glass. As shown in table 2.

Table 2： Data and Statistical information

Dataset	Number of sample	Number of categories	Number of attributes	Category Distribution
Iris	150	3	4	50,50,50
Wine	178	3	13	59,71,48
Glass	214	6	10	70,67,17,31,9,92

In this paper, purity standards are regarded as effective method to evaluate the clustering results. Let the class size of the cluster ***Ci ni***, this cluster of purity class definition equation (4) ：

$$P(C_i) = \max_i(n_i^j)/n_i \tag{4}$$

Ci represents the intersection of the first ***j*** class size. n_i^j represents the intersection size of ***Ci*** and class ***j***.

Equation (5) ：

$$\text{Purity} = \sum_{i=1}^{k} \frac{n_i}{n} \max_i(n_i^j)/n_i \tag{5}$$

Equation is the results of clustering purity. ***k*** is the number of clusters formed, the higher the purity, the more effective the clustering algorithm. In this paper, set the iteration parameters of the improved K-Means algorithm to 50 times, correlation analysis the FP-Tree in this clustering results in 50 times, to get the final clustering results. The operating results of the improved K-Means algorithm are better than the traditional K-Means algorithm.

Conclusion

In the memory data, using CUDA technology could improve the memory data processing and analysis efficiency well. In the experiment of clustering the psychology MMPI data sets, the improved K-Means algorithm executed several times within an acceptable period of time. With the increase of the number of iterations, the purity of the clustering algorithm also increased, in other words, the execution efficiency improving support the purity of the cluster improving. The improved K-Means algorithm is applied to a psychology test system of a company; clustering analysis the MMPI data of employees help psychologists to accurate test personnel division, have achieved the expectant effect.

Acknowledgement

The work is supported by the National Natural Science Foundation of China (NSFC) (51278400); Natural Science Foundation of China Shaanxi (2012JM8042); Science Subject of Education Department of Shaanxi Provincial Government (12JK0940); Foundation (CXY1348-(1)) (CXY12-2-07).

References

[1] Bradley P S, Fayyad U M. Refining Initial Points for K-Means Clustering[C]. Proceedings of the 15Th International Conference on Machine Learning. San Francisco: Morgan Kaufmann Press, 1998: 91-99

[2] Selim S Z, Alsultan K. A Simulated Annealing Algorithms for the Clustering Problem Pattern Recognition[J]. Pattern Recognition ,1991, 24(10): 1003~1008

[3] MA Chao, LIAN Ji-jian. Short Term Hydropower Dispatching Optimization of Cascaded Hydropower Junctions Based on Cluster Genetic Algorithm[J]. Journal of Tianjin University,2010,43(1):1-8

[4] GONG Dun-wei, JIANG Yu-qing, ZHANG Yong, et al. K-mean algorithm for optimizing the number of clusters based on particle swarm optimization[J]. Control Theory & Application, 2009,26(10): 1175-1179
[5] LIU Jing-ming, HAN Li-chuan, HOU Li-wen. Cluster Analysis Based on Particle Swarm Optimization Algorithm. Systems Engineering —Theory & Practice,2005,25(6):54-58
[6] WANG Zong-hu,LIU Zhi-jing,CHEN Dong-hui. Improved PSO-based fast clustering algorithm[J]. Journal of Xidian University,2012,39(5): 61-65,78
[7] XUE Sheng-jun, PAN Wu-bin. Parallel PK-means Algorithm on Meteorological Data Using MapReduce. Journal of Wuhan University of Technology, 2012,34(12):139-141
[8] Kumar N, Satoor S, Buck I. Fast parallel expectation maximization for Gaussian mixture models on GPUs using CUDA [C].Proceedings of 11th IEEE International Conference on High Performance Computing and Communications. Piscataway: IEEE Computer Society Press, 2009: 103-109
[9] Zhang Fan, Wang Zhangye, Yao Jian, et al. Accelerating the calculation of protein molecular field using GPU cluster [J]. Journal of Computer-Aided Design & Computer Graphics, 2010, 22(3): 412-419
[10] Takahashi T, Hamada T. GPU-accelerated boundary element method for Hemholtz' equation in three dimensions [J]. International Journal for Numerical Methods in Engineering, 2009, 80(10): 1295-1321
[11] Labaki J, Mesquita E, Ferreira S L O. The BEM on general purpose graphics processing unit(GPGPU): a study on three distinct implementations [C].Proceedings of the 11th International Conference on Boundary Element Techniques XI. United Kingdom: EC Ltd Press, 2010: 316-323
[12] Zhou Ya-jian, Xu Chen, Li Ji-guo, et al. Unsupervised anomaly detection method for improving CURE clustering algorithm [J] Journal on Communications. 2010,07:18-23+32.
[13] NIE Xiao-jing, QIU Chang-jian, et al. Contrast Studies of MMPI between Anxiety and Depression[J]. Wset China Medical Journal, 2007, 24(6): 1356-1361
[14] Guha S et al. CURE: An efficient clustering algorithm for large databases. In: Proc of the ACM SIGMOD Int' l Conf on Management of Data. 1998.

Advanced Materials Research Vols. 989-994 (2014) pp 1671-1675
© (2014) Trans Tech Publications, Switzerland
doi:10.4028/www.scientific.net/AMR.989-994.1671

Cell Selection Algorithm based on Coordinated Beamforming

Zhe LIANG[1, a], Yibing LI[1, a], Fang YE[1, a]

[1]College of Information and Communication Engineering, Harbin Engineering University, Harbin, 150001, China

[a]email: liyibing0920@sina.cn

Keywords: LTE-Advanced; Coordinated Beamforming; Cell Selection

Abstract. In LTE-A (LTE-Advanced) system, CoMP (Coordinated Multipoint Transmission) is used to improve system capacity and cell coverage. CB(Coordinated Beamforming), as a way of CoMP, using multi-cell coordination to improve the spectrum efficiency of edge users. Therefore, coordinated cell selection is important. To achieve better performance, multiple factors rather than a single one are considered in cell selection, channel gain as well as cell load is taken into account in the article. Multiple factors constitute a matrix to find the optimal coordinated cells, multi-objective optimization is used here. Simulation result shows system performance of the proposed algorithm is better than the one only considers channel gain.

Introduction

LTE system adopts OFDM technique, in which subcarriers are orthogonal. As a result, users are protected from interference from other users in the same cell. In LTE-A system, MIMO(Multiple Input Multiple Output), which could break the Shannon limit, is adopted to improve system capacity. However, with a long distance from serving BS, signal power received by cell edge users is low, edge users suffer from the same frequency interference, and the spectrum efficiency is low. To solve the problem, CoMP(Coordinated Multipoint Transmission) is used, that is, multiple coordinated cells constitute a virtual MIMO system. CoMP has two patterns, JT(Joint Transmission) and CB(Coordinated Beamforming). The coordinated cells change CSI(Channel State Information) and user data by X2 port. In JT system, all the coordinated cells transmit data to UE, aimed at transforming interference to useful signals. In CB system, only serving cell transmit data to UE, all the coordinated cells share channel state information by X2 port, to shape the beamforming vector. Compared to JT, CB has less backhaul and higher spectrum efficiency. This article is based on CB system.

As the performance improvement of edge users rely on cell coordination, and only serving cell transmit data to users in CB, the signal strength received by UE depends on the channel state quality from BS to UE. Therefore, coordinated cells and serving cell selection could affect the quality of received signal. Reference [1] proved that the number of coordinated cells to achieve optimal performance is three, without extra complexity. Reference [2] presented that the coordinated cells could be three or less, which could improve the spectrum efficiency when a few channels' state is not good. Reference [3] [4] [5] concerned cell selection based on one standard RSRP. Reference [6] proposed a cell selection algorithm considering multiple factors, RSRP and latency time, which achieved good system performance in different traffic model. This article proposed a new cell selection algorithm takes RSRP, interrupt rate, fill rate into consideration at the same time, and select the optimal serving cell by calculating the distance between different channel factors and the factor extreme value.

Coordinated Beamforming Model

In CoMP system, adjacent cells serve one UE to improve the performance of cell edge. In CB, coordinated cells share channel state information by X2 port and the serving cell transmit data to UE. The system model is shown in Fig. 1. The black arrow represents data transmission, the black line represents channel state information change by X2 port. Consider the k th user in cell 1, suppose the data transmitted from BS to the UE is s_k, then the data received by the k th user is

$$y_k = H_k^k W_k s_k + \sum_{i,i\neq k} H_k^i W_l s_l + n_k \quad (1)$$

H_k^i represents the channel matrix from cell i to UE k, W_k represents the beamforming vector from cell i to UE k, the second part in the right of the equation represents interference from other cells to UE k , n_k represents Gauss noise received by UE k, with mean value 0 and variance σ^2 .

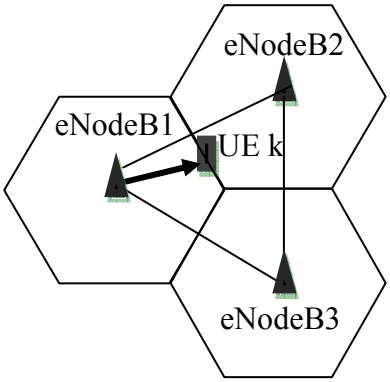

Fig. 1 Coordinated Beamforming model of three cells

The SINR of UE k is

$$SINR = \frac{\left\| H_k^k W_k \right\|^2}{\sum_{i,i\neq k} \left\| H_k^i W_l \right\|^2 + \sigma^2} \quad (2)$$

The optimal beamforming vector can be obtained by the algorithm in Reference [4]

$$W_k = \max eigenvector((\sigma^2 I + \tilde{H}_k^H \tilde{H}_k)^{-1} H_k^H H_k) \quad (3)$$

$\tilde{H}_k = [H_1 \quad H_2 \quad \ldots \quad H_{k-1} H_{k+1} \quad \ldots \quad H_l]$, $(.)^H$ represents conjugate transpose of $(.)$.

Cell selection Algorithm Design

Consider seven adjacent cells in Fig. 2. To cell 1, the other six cells are interference cells as well as candidate coordinated cells. Users distribute in every cell randomly. BS of each cell is equipped with M antennas, while every UE has N antennas. Edge users and center users are distinguished by signal fading value, usually cell radius ratio is used.

$$PL = -(32.23 + 35.04 \times \log(10 \times (R \times ratio))) \quad (4)$$

R represents cell radius, *ratio* is the radius ratio. If signal fading value received by UE is large than the ratio, the UE is edge user, otherwise the UE is centre user. Centre user is served by the cell it belongs, edge user require cells coordination.

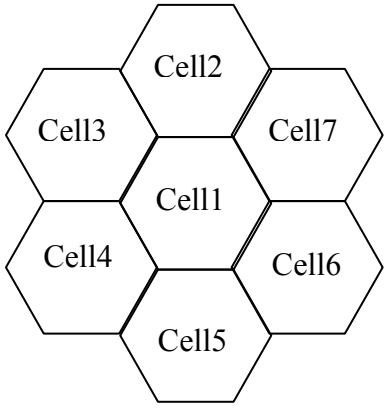

Fig. 2 Seven cells interference model

Cell selection for edge users generally based on RSRP [5]. The algorithm is convenient and could achieve good result when user's location is fixed and different users' requirement is equal.

However, if users don't distribute uniformly, several cells' capacity may be full, the RSRP selection algorithm would lead to users failing to join the cell or service interrupt. Therefore, multiple factors should be taken into account when select the serving cell . Consider three factors below:

A. SNR received by UE, which could reflect channel gain from BS to UE.

$$SNR_{receive} = \frac{P_t * A_{antenna} * P_{loss} * Shadowing}{N_0} \tag{5}$$

P_t is the transmitted power of BS, $A_{antenna}$ represents antenna gain, P_{loss} is path loss, *shadowing* is shadow loss, N_0 is the power of noise.

B. User's interrupt rate. When a user join a cell, the cell load should be considered, interrupt rate is used here [7]. The interrupt rate of UE k joined in cell j is

$$\alpha_{k,j} = \frac{O_j}{N_j} \tag{6}$$

N_j is the number of subcarriers in cell j , O_j represents the amount of occupied subcarriers in the cell. The maximum value of interrupt rate is 1, the minimum value is 0. The less the value is, the cell is more appropriate to be joined.

C. User's fill rate. With different requirement of users, the amount of subcarriers used is different. Define UE fill rate to indicate the cell could satisfy the joined users or not. The fill rate of UE k in cell j is

$$\beta_{k,j} = \frac{G_j}{M_k} \tag{7}$$

M_k is the number of subcarriers UE k needs, G_j is the number of subcarriers cell j allocates to UE k. The maximum value of fill rate is 1, the minimum value is 0. The more the value is , the more available the cell has, the more suitable to join for UE .

Upon on the factors given above, using fuzzy multi-objective decision making theory, propose the cell selection algorithm below:

1) Confirm candidate coordinated cell set. Here 7 adjacent cells model is adopted.

2) Using the three factors of candidate cells to form a matrix X.

$$X = \begin{bmatrix} x_{11} & x_{12} & x_{13} \\ x_{21} & x_{22} & x_{23} \\ \vdots & \vdots & \vdots \\ x_{71} & x_{72} & x_{73} \end{bmatrix} \tag{8}$$

x_{ij} is the ith factor of cell j. SNR and fill rate are positive factor, which means the more the better, while interrupt rate is negative factor, which means the less the better. Normalize the two kinds of factors as:

$$x_{ij} = \frac{x_{ij} - \min\limits_j x_{ij}}{\max\limits_j x_{ij} - \min\limits_j x_{ij}} \tag{9}$$

$$x_{ij} = \frac{\max\limits_j x_{ij} - x_{ij}}{\max\limits_j x_{ij} - \min\limits_j x_{ij}} \tag{10}$$

3) Give the factors weight value

$$W = diag[w_1, w_2, w_3] \tag{11}$$

then

$$R = X * W = \begin{bmatrix} r_{11} & r_{12} & r_{13} \\ r_{21} & r_{22} & r_{23} \\ \vdots & \vdots & \vdots \\ r_{71} & r_{72} & r_{73} \end{bmatrix} \tag{12}$$

4) Calculate the maximum value of factors, which is the perfect value

$$R_j = \max_j r_{ij} \tag{13}$$

5) Calculate distance between r_{ij} and R_j, and obtain the sum value

$$C_i = \sqrt{\sum_{j=1}^{n} (r_{ij} - R_j)^2} \tag{14}$$

6) Order C_i in ascending dimension, [C'_1 C'_2 …C'_7], then cell C'_1 is the serving cell.

7) Select the first two cells which interfere the serving cell most serious as coordinated cells. As a result, interference received by UE could be suppressed. The standard here is RSRP feedback by UE. Then do Coordinated Beamforming to the users in coordinated cells.

Simulation result

The Coordinated Beaforming algorithm based on RSRP cell select and based on the proposed algorithm are simulated. Simulation parameters are shown in Table I.

TABLE I Simulation Parameters

Simulation parameters	Value
Cell radius	1000m
System bandwidth	20MHz
Carrier spectrum	2GHz
BS antennas	2
UE antennas	2
Channel model	3GPP SCM
Shadow loss	$u = 0, \sigma = 10dB$
Path loss	$128.1 + 37.6\log_{10}(r)dB$
BS transmit power	46dBm
Noise coefficient	9dB
Transmit antenna gain	14dBi
Channel estimate	ideal

Compare two algorithms in system capacity, edge spectrum efficiency and user's fill rate. Fig. 3 is system capacity, the two algorithms have similar performance. The reason is, the proposed algorithm is focused on edge users, whose amount is much more less than centre users, as well as proportion of system performance.

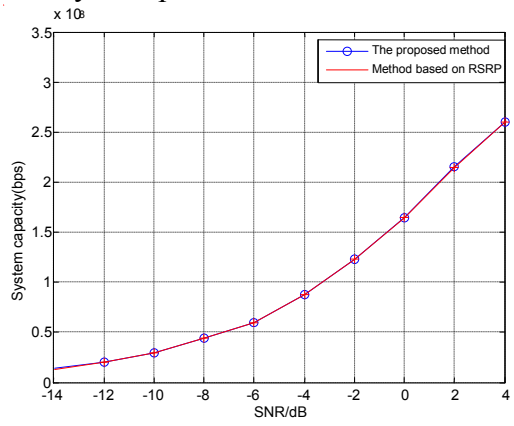

Fig. 3 System capacity

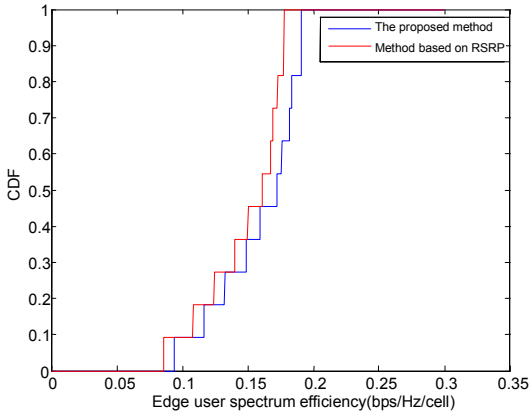

Fig. 4 Edge spectrum efficiency

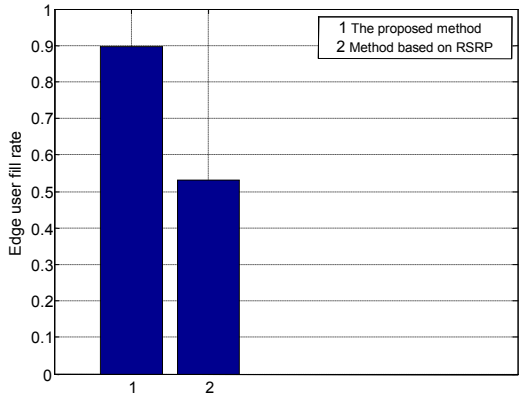

Fig. 5 Edge users' fill rate

Fig. 4 indicates edge spectrum efficiency of two algorithms, the proposed algorithm has taken cell load into account, which could select the optimal cell for UE to join, its performance is better than the one of the RSRP. Fig. 5 is the fill rate of the two algorithms. As the proposed one considers users' fill rate, and make it a standard of cell selection, the fill rate performance is much better than the RSRP algorithm.

Conclusion

Based on Coordinated Beamforming in LTE-A, cell selection algorithms are studied. An improved algorithm based on the RSRP cell selection algorithm is proposed, which considers multiple factors , RSRP, interrupt rate and fill rate. Using multi-objective select model to calculate the optimal cell for UE to join, then select coordinated cells. Simulation result demonstrates the proposed algorithm has better performance than the traditional one in edge spectrum efficiency and users' fill rate.

Acknowledgement

In this paper, the research was partially sponsored by Heilongjiang Province Natural Science Foundation (F201345) and Heilongjiang Province Natural Science Foundation for the Youth (QC2012C070). This paper is funded by the International Exchange Program of Harbin Engineering University for innovation-oriented Talents Cultivation.

References

[1] Luo Chun. Joint Processing technique of CoMP and system performance study in LTE-Advanced. Wuhan, China: Wuhan University of Technology, 2010.
[2] 3GPP.TR-36.912 (V2.1.0), Feasibility study for Further Advancements for E-UTRA.
[3] Huan Sun, Wei Fang, Jianguo Liu, Yan Meng. Performance Evaluation of CS/CB for Coordinated Multipoint Transmission in LTE-A Downlink, IEEE International Symposium on Personal Indoor and Mobile Radio Communications, 2012 1061-1065.
[4] Li Qiang, Yang Yang, Fang Shu, Wu Gang. Coordinated Beamforming in Downlink CoMP Transmission System, International ICST Conference on CHINACOM, 2010 1-5.
[5] Qimei Cui, Shan Yang, Yueqiao Xu, etc. An Effective Inter-cell Interference Coordination Scheme for Downlink CoMP in LTE-A Systems, Vehicular Technology Conference, 2011 1-5.
[6] Zhang Tan, Wennan Zhou, Wei Chen. A Dynamic Cell Selection Scheme Based On Multi-Object for CoMP DL in LTE-A, International Conference on Communication Technology and Application, 2011 248-252.
[7] Li Xiaohui, Ren Min, Xue Xin, Wu Ji. A Cell Selection algorithm in LTE-A uplink. No. 200910022983.8 .

Advanced Materials Research Vols. 989-994 (2014) pp 1676-1679
© (2014) Trans Tech Publications, Switzerland
doi:10.4028/www.scientific.net/AMR.989-994.1676

Research on Sub-Band Synthesis Algorithm of MIMO-SAR

Yanan XIE[1,a], Zimiao TAN[2,b]

[1]School of Communication and Information Engineering, Shanghai University, Shanghai 200072, China

[2]School of Communication and Information Engineering, Shanghai University, Shanghai 200072, China

[a]email: yxie@shu.edu.cn, [b]email: tanzimiao2012@163.com

Keywords: MIMO-SAR; sub-band synthesis; range resolution

Abstract. Multiple-Input and Multiple-Output Synthetic Aperture Radar (MIMO-SAR) can achieve high resolution and wide swath at the same time, which has a wide horizon of development in the future. An azimuth frequency-diversity MIMO-SAR is presented, and overlapped effective phase center sampling is obtained while the pulse repetition frequency (PRF) is appropriate. This paper derives an improved sub-band synthesis algorithm which reduces the complexity of conventional sub-band synthesis algorithms and improves the range resolution. The feasibility of this imaging algorithm is proved by point target simulation experiments.

Introduction

The capability of high resolution and wide swath imaging [1] is desired by space based remote sensing and military reconnaissance. But there is an irreconcilable conflict between azimuth resolution and swath in conventional SAR because of minimum antenna area constraint [2]. This conflict can be mitigated by MIMO-SAR. With the same azimuth resolution, it can achieve much wider swath than conventional SAR due to the reduction of PRF. sub-band synthesis algorithm can improve the range resolution while effective phase center sampling is overlapped. A sub-band synthesis algorithm is presented in [3], however, it is complex.

In this paper, an azimuth MIMO-SAR configuration using frequency-diversity is presented. Comparing with conventional SAR, it can reduce the PRF with the same azimuth resolution, the reduction of PRF can widen the width of the swath. Then a new sub-band synthesis algorithm is derived. This algorithm reduces the complexity and improves the range resolution. So the capability of high resolution and wide swath imaging is obtained [4]. Some results of the point target simulation experiments are given. Finally, the conclusions are drawn.

Configuration of the Azimuth Frequency-diversity MIMO-SAR

To illustrate the azimuth frequency-diversity MIMO-SAR, we assume a SAR system with five apertures as shown in Fig.1, where the platform moves with velocity v_p at an altitude h. In a pulse repetition interval, the 2nd aperture, the 3th aperture and the 4th aperture transmit linear FM pulse with different center frequency. the 1st aperture and the last aperture receive the echo signal. The equivalent receiving phase center is located at the middle point from the transmitting aperture to the corresponding receiving aperture [5]. As long as the difference between carrier frequencies is larger than the signal bandwidth, the received signals can be separated via bandpass filters.

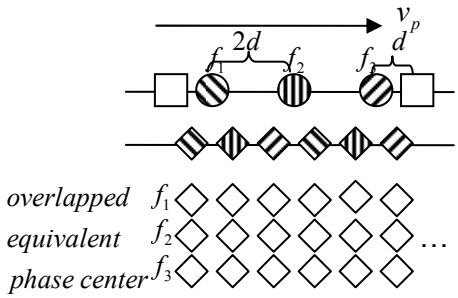

Fig.1 Configuration of the azimuth frequency-diversity MIMO-SAR

In order to achieve overlapped uniform sampling in the azimuth direction, as shown in Fig.1, the radar must be operated with an appropriate PRF [6]. Overlapped uniform sampling is obtained, when the PRF satisfies:

$$PRF = \frac{v_p}{2d} \tag{1}$$

Improved Sub-band Synthesis Algorithm

The previous section presents a structure of the azimuth frequency-diversity MIMO-SAR, the transmitting signal bandwidth is B, In this paper, we assume $f_m=f_1+(m\text{-}1)B$, so that the received signals can be separated effectively via band-pass filters . After bandpass filtering and frequency conversion, the received baseband signal of the mth overlapped equivalent aperture is:

$$\begin{aligned} x_m(\tau,t) &= rect\left(\frac{\tau-2R_e(t)/c}{T_1}\right)\exp\left(-j4\pi f_m R_e(t)/c\right) \\ &\cdot\exp\left(j\pi k_r\left(\tau-2R_e(t)/c\right)^2\right) \end{aligned} \tag{2}$$

Where τ is the range time, t is the azimuth time, k_r is the azimuth FM rate, T_1 is the duration of the transmitted pulse, *rect*( ) is the rectangular function and $R_e(t)$ is the range from the equivalent phase center to the target.

Next we will derive the improved sub-band synthesis algorithm. At first, frequency spectrum shift operation is done by multiplying a frequency spectrum shift function, the function is given as follow:

$$v_m'(\tau) = \exp(j2\pi(m-2)B\tau) \tag{3}$$

And the result after frequency spectrum shift operation is:

$$\begin{aligned} x_m'(\tau,t) &= x_m(\tau,t)v_m'(\tau) \\ &= rect\left(\frac{\tau-2R_e(t)/c}{T_1}\right)\exp\left(j\pi k_r\left(\tau-2R_e(t)/c+(m-2)T_1\right)^2\right) \\ &\cdot\exp\left(-j4\pi f_c R_e(t)/c\right)\exp\left(-j\pi k_r((m-2)T_1)^2\right) \end{aligned} \tag{4}$$

Then do Fourier transform in range direction and transform to the frequency domain, the result of Fourier transform is:

$$\begin{aligned} x_m'(f_r,t) &= rect\left(\frac{f_r+(m-2)B}{B}\right)\exp\left(-j\pi\frac{f_r^2}{k_r}\right)\exp\left(j\pi f_r(m-2)T_1\right) \\ &\exp\left(-j4\pi(f_c+f_r)R_e(t)/c\right)\exp\left(-j\pi k_r\left((m-2)T_1\right)^2\right) \end{aligned} \tag{5}$$

Secondly, time shift operation is done by multiplying $v_m^2(f_r,t)$, the result of time shift operation is given in (7). we can find that the first exponential term is eliminated.

$$v_m^2(f_r,t)=\exp(-j2\pi f_r(m-2)T_1) \tag{6}$$

$$x_m(f_r,t)=rect\left(\frac{f_r+(m-2)B}{B}\right)\exp\left(-j\pi\frac{f_r^2}{k_r}\right)\cdot\exp\left(-j4\pi(f_c+f_r)R_e(t)/c\right)\exp\left(-j\pi k_r\left((m-2)T_1\right)^2\right) \tag{7}$$

Finally, phase correction will be done by multiplying v^3 which is given in (9).

$$x(f_r,t)=x_1(f_r,t)+x_3(f_r,t)=\left\{rect\left(\frac{f_r-B}{B}\right)+rect\left(\frac{f_r-B}{B}\right)\right\}\exp\left(-j\pi\frac{f_r^2}{k_r}\right)\exp\left(-j\pi k_r T_1^2\right)\cdot\exp\left(-j4\pi(f_c+f_r)R_e(t)/c\right) \tag{8}$$

$$v^3=\exp\left(j\pi k_r T_1^2\right) \tag{9}$$

After phase correction, we can find:

$$x'(f_r,t)=x(f_r,t)\cdot v^3=\left\{rect\left(\frac{f_r-B}{B}\right)+rect\left(\frac{f_r-B}{B}\right)\right\}\exp\left(-j\pi\frac{f_r^2}{k_r}\right)\cdot\exp\left(-j4\pi(f_c+f_r)R_e(t)/c\right) \tag{10}$$

So the signal after sub-band synthesis is given in (11), it is obvious that the bandwidth is three times wider than a single sub-band signal.

$$x''(f_r,t)=x'(f_r,t)+x_2(f_r,t)=rect\left(\frac{f_r}{3B}\right)\exp\left(-j\pi\frac{f_r^2}{k_r}\right)\cdot\exp\left(-j4\pi(f_c+f_r)R_e(t)/c\right) \tag{11}$$

After range compressing [7], according to the property of sinc function, we can find: the wider the bandwidth of the signal is, the higher the range resolution is. So the range resolution is improved.

$$x(\tau,t)=\sin c\left(3B\left(\tau-\frac{2R_e(t)}{c}\right)\right)\cdot\exp\left(-j\frac{4\pi f_c R_e(t)}{c}\right) \tag{12}$$

Simulation experiments

To validate the configuration presented in this paper, point target simulation is performed. The simulation parameters are given as follows. Center frequencies: 9.2GHz，9.5GHz and 9.8GHz, the number of sub-band signals: 3, the bandwidth of sub-band signal: 300MHz, signal pulse duration: 30 μs , radar velocity: 7600 m/s, the altitude: 514km, the length of aperture: 2.4m. Fig.2 shows the spectrum of single sub-band signal and sub-band synthesis signal. It is evident that the bandwidth of the signal is wider after sub-band synthesis, so the resolution is improved, the range resolution profiles are compared in Fig.3, the range resolution after sub-band synthesis is higher than single sub-band range resolution.

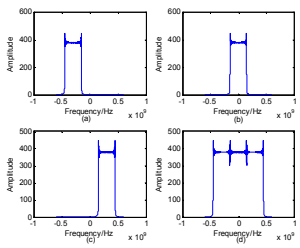

Fig.2 Frequency spectrum of sub-band signal and sub-band synthesis signal

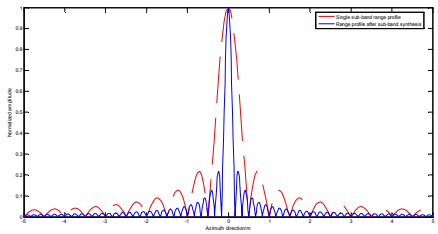

Fig.3 Range profile of single sub-band signal and signal after sub-band synthesis

Conclusion

An improved MIMO-SAR sub-band synthesis algorithm is derived. The PRF is reduced by a half compared with single channel SAR, which can achieve much wider swath. Compared with conventional sub-band synthesis algorithms, this algorithm not only improves the range resolution, but also reduces the computational load, which is of great significance in practice. However, the range cell migration is assumed to be not exceeding a range bin, so this problem is still left to be further studied.

Acknowledgement

In this paper, the research was sponsored by Research Project of Shanghai Municipal Science and Technology Commission (Project No.11511501902).

References

[1] Gebert N, Krieger G. Azimuth phase center adaptation on transmit for high resolution wide swath SAR imaging [J], 2002.

[2] Wang W Q, Cai J. MIMO SAR using Chirp Diverse Waveform for Wide-Swath Remote Sensing[J].2012.

[3] Raney R K, Runge H, Bamler R, et al. Precision SAR processing using chirp scaling [J]. Geoscience and Remote Sensing, IEEE Transactions on, 1994: 786-799.

[4] Berens P. SAR with ultra-high range resolution using synthetic bandwidth[C]//Geoscience and Remote Sensing Symposium, 1999. IGARSS'99 Proceedings. IEEE 1999 International. IEEE, 1999, 3: 1752-1754.

[5] Ender J H G, Klare J. System architectures and algorithms for radar imaging by MIMO-SAR[C]//Radar Conference, 2009 IEEE. IEEE, 2009: 1-6.

[6] Wencheng X, Xiaoling Z, Jun S. MIMO antenna array design for airborne down-looking 3D imaging SAR[C]//Signal Processing Systems (ICSPS), 2010 2nd International Conference on. IEEE, 2010, 2: V2-452-V2-456.

[7] Cumming I G, Wong F H. Digital signal processing of synthetic aperture radar data: algorithms and implementation [M]. Artech House, 2004.

Advanced Materials Research Vols. 989-994 (2014) pp 1680-1685
© (2014) Trans Tech Publications, Switzerland
doi:10.4028/www.scientific.net/AMR.989-994.1680

Comprehensive Similarity Measurement Model Based on Three Algorithms

Liu Nan[1,a], Long Baolian[2,b], Zheng Xiaokun[1], Han Lifang[1], Qu Tong[2] , Cui Baojiang[2]

[1]China Electric Power Research Institute, Beijing, 100192, China

[2]School of Computer, Beijing University of Posts and Telecommunications, Beijing, 100876, China

[a]email:liunan2009@epri.sgcc.com.cn, [b]email:longbaolian@126.com

Keywords: homology detection software; text-based; token-based; Abstract Syntax Tree; comprehensive similarity

Abstract. Software source code homologous detection is also called software copy or software clone. It is used to detect the homologous in the source code, by which we can easily find the plagiarism in the code. In this paper, it will discuss the homology detection results based on Text, Token and Abstract Syntax Tree. And will compare the three techniques and raise a model to calculate similarity by synthesizing the results. This model is based on the analysis of a large number of experimental results. Comprehensive similarity calculation model can calculate the respective contribution of the three algorithms and realize integrated computation of similarity according to this respective contribution. Finally, we can get a comprehensive similarity by this integrated similarity calculation model to make the homology detection results more accurate and closer to the actual similarity.

Introduction

Researches on the source code homology detection is very widespread, which is mainly used in software intellectual property rights detection, the software component management in the software development, especially in the clone detection in modern software engineering. Some large companies and enterprises have already introduced the source code homology detection into all the departments to detect and manage the source code, hedge the risk of intellectual property right. Of course, the research emphasis focus on the source code copy detection technology, in other words, it is also known as code clone detection. Many domestic and foreign scholars have done some respective researches on the source code copy detection technology and raised lots of algorithms. At present, the mature detection algorithms mainly concentrate on the text-based, token-based and syntax tree-based detecting techniques:

Text-based detecting technique, Due to the simple principle, text-based detecting technique is one of the earliest researches in the field of source code homology detection. Baker[1] and Johnson [2]raised the text matching technology based on the character string and the characters of the fingerprint in the text. To improve the ratio on the particle size, Ducasse[3] calculate the hash value in line for the source code and then through two-dimensional method in each hash value to compare with other hash value to get the same code line.

Token-based detecting technique, There are lots of researches on the token-based detecting technique, many comparison tools like CP-Miner[4] and CCFinder[5] have adopted this technique. This technique bases on transforming the keywords, the function name and the variable name to different token at certain rules. Then we could transform the source code which need to be detected and the benchmark source code to a set of token sequences. By comparing the two token sequences, we can find the coping parts in the source code which need to be detected.

Syntactic structure-based detecting technique, This method can not only transform the source code to Token, but also analyze and process the ATS which keeps the syntactic structure information. This technique is very widespread. Baxter[6] earlier raised the AST code homology analysis technology that can comparatively analyze the syntactic structure in the code segment to

decide whether this is plagiarized or not. In a variety of practical homology detecting techniques, AST-based technique is the most accurate[7].

As can be seen, these three detecting methods each have advantages and disadvantages. They can detect the different degree of plagiarism. But they all have some shortcomings more or less, in other words, they can't detect all the software source code plagiarism problems. The text-based method has little false rate for it detecting the source code directly, but it has a high miss rate. The token-based method can detect the plagiarism of changing names for it do the token processing on the source code, but it cannot detect the changing-order plagiarism, so it also has some miss rate. Finally, the AST-based method can not only transform the source code to token, but also can analyze the syntactic result, so it can detect the order changing plagiarism. However, on the account of too much processing on the source code in this method, we may miss some source code information. Therefore, the AST-based method has a low miss rate but a high false rate. Hence, how to reasonably use these three detecting techniques to get a similarity more closed to the real becoming the problem we want to study in this paper.

Improved Similarity Measurement Model Based on AHP

Different with the model proposed in reference [11], this paper proposed a new model which considers two indicators both of the error detection rate and miss detection rate. We also used a different method to analysis the different contribution of the three methods in miss detection rate .On the basis, get the contribution values of three methods in comprehensive similarity.

Formula of calculating codes' comprehensive similarity is:

$$Sim = w_{txt}Sim_{txt} + w_{Token}Sim_{Token} + w_{AST}Sim_{AST} \qquad (1)$$

Sim means the comprehensive similarity, Sim_{txt} means the similarity based on text, Sim_{Token} means the similarity based on token, Sim_{AST} means the similarity based on syntax. w_{txt} means the weight of similarity based on text, w_{Token} means the weight of similarity based on token, w_{AST} means the weight of similarity based on syntax .The following are the details of homology detection method based on AHP, and process to determine the weights of three algorithms.

Construct the AHP Hierarchical Model of Codes' Comprehensive Similarity

AHP hieratical model includes Target layer, Criterion layer and Scheme layer[8][9].

It explodes analyzed object to establish the whole evaluation index system. In AHP hieratical model, the aim will analyzed object achieved in Target layer, the medium environment which was need to reach the final goal is in Criterion layer, The actual method should be objectively choose is in Scheme layer.

Integrate the similarity measurement method based on text, token and syntax, this paper proposed an improved similarity measurement model based on AHP. In it, the design of comprehensive similarity is in target layer; miss rate and false detection rate belong to criterion layer as design; alignment methods in scheme layer.

The proportion of similar code in all is similarity of software's source code. Because of the limitation of different method used to calculate codes' similarity, also because of there so many types of plagiarism, miss detection and false detection are unable to avoid. Hence we use those factors having a quantitative evaluation.

Error detection rate is the rate of codes aren't similarity are detected as the similar code, miss rate is the ratio of similar code has not been detected. They have different influence in comprehensive similarity. As software source code homology detection technique is mainly used to find the similarity code, miss detection rate is comparatively more important. Through sufficient statics of lab data and experts' experiences, we set the ratio of miss detection rate and false detection rate 4:1.

Table1 compare text, token and syntax detection ways' result of different plagiarism type, result shows the plagiarism can be detected by previous method can also be found out using the latter. That is to say, if text based method can find some types of plagiarism, they can also be found using token based method, in a similar way between token and syntax. In other words, only using abstract syntax tree, there are no miss detections. Therefore the ratio of their contribution to miss detection is close to 0:0:1.

Table 1 Analysis of the Contributions of Text, Token and Syntax based Comparison Method

Sequence Number	Plagiarism Type	Text (1)	Token (4)	Syntax Tree (8)
1	Full-text copy	Y	Y	Y
2	Change variables 'name	N	Y	Y
3	Change parameters' name	N	Y	Y
4	Change the order of parameters	N	N	Y
5	Change the order of variables	N	N	Y
6	Change the method's name	N	Y	Y
7	Change the type of variables	N	N	Y
8	Add useless variable	N	N	Y
9	Reconstitute code	N	N	N

Table 2 shows the comparison of text, token, syntax in types of false detection, in the table, text doesn't have the general three types false detection, token will have false detection face to two situations and abstract syntax tree only have false detection in one situation. Therefore, in this paper the ratio of contributions of false detection rate in text , token, syntax is 3:1:2.

Table 2 Factor analysis of text, token, syntax' contribution of false detection rate

False Detection Methods	Text (3)	Token (1)	Syntax Tree (2)
Short Expression False Detection	Y	N	Y
Short Statement Block False Detection	Y	N	Y
Hash conflict False Detection	Y	Y	N

Through analysis we got the modified homology detections measuring algorithmic model (figure1) based on AHP. Destination Layer is the comprehensive similarity; criteria layer is the measurement index of miss and false detection; solution layer is the text, token, abstract syntax tree alignment methods. Only the results of abstract syntax tree comparison contribute to the miss detection as text comparison and Token comparison contribute 0.

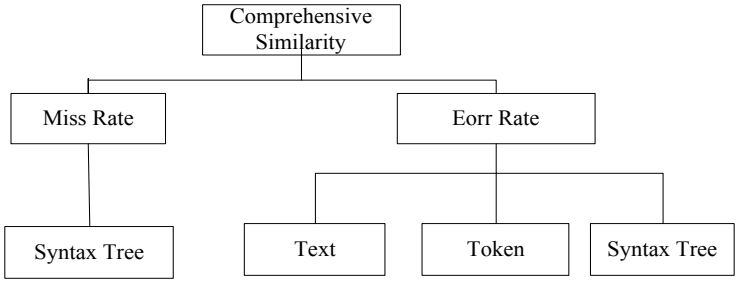

Figure 1 Improved homology detection hierarchical model

In order to use the modified homology detections measuring algorithms, it is needed to use AHP hierarchical model to do the counting on the weights of similarity of different alignment methods in the solution layer. Apply the model of figure1 into hierarchy calculation model based on AHP in figure2 to enable to use the AHP model to do calculation.

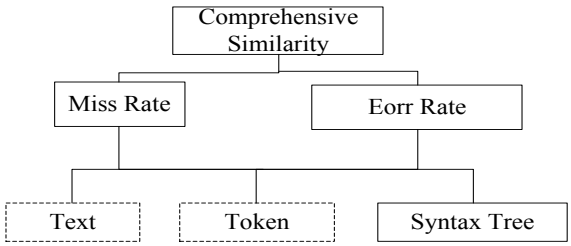

Figure 2 Improved homology detection model based on AHP hierarchical model

The structure of two contribution judgment matrixes between two layers

According to Table1, since the text and token comparisons contribute nothing to the miss detection, it is not necessary to count the judgment matrix. In terms of the miss detection rate(B1), the ration of the weights of text, token, syntax can be set to 0:0:1.According to Table2, when getting the judgment matrix for false detection, based on the 3 homology alignment algorithms based on text, token, syntax tree, the matrix for false detection is shown in Table3.According to sufficient statics of lab data and experts' experiences, contribution judgment matrix of miss detection rate(B1), false detection rate(B2) is shown in table 4.

Table 3 Contribution judgment matrix of text, token and syntax tree,

B2	C1	C2	C3
C1	1	3	2
C2	1/3	1	1/2
C3	1/2	2	1

Table 4 Contribution judgment matrix of miss and false detection rate

A	B1	B2
B1	1	4
B2	1/4	1

After consistency check[11], C.R. of the above two matrices are 0.0176 and 0, conform to the condition of consistency check, therefore, the above two judgment matrix through the consistency check is reasonable.

According to the process of single hierarchical ordering[11], doing the single ordering of above judgment matrix, get the single ordering weight of every layer:

B2	Weight of single ordering
C1	0.54
C2	0.16
C3	0.3

A	Weight of single ordering
B1	0.8
B2	0.2

For miss detection rate, analyzing above result and get the hierarchical single ordering weight as following table:

B1	Weight of single ordering
C1	0
C2	0
C3	1

Through above sorting process, we get the overall ranking levels：

A	0.8	0.2	Weight of Overall Sorting
C1	0	0.54	0.108
C2	0	0.16	0.032
C3	1	0.3	0.86

According to weight of overall sorting, the alignment algorithm based on text, token, syntax, their weight in comprehensive similarity respectively are 0.108,0.032,0.86.

Therefore, according to (1) we can the comprehensive measurement model of source codes' similarity is:

$$\text{Sim} = 0.108Sim_{txt} + 0.032Sim_{Token} + 0.86Sim_{AST} \qquad (2)$$

The results and analysis of experiment

In order to test the effect of model Based on improved AHP comprehensive similarity measure homology, in this paper, we had done two kinds of experiments. One is to detect specially constructed plagiarism of Hibernate source code, and the other is to detect real open source code projects.

The results and analysis of detection experiment on specially constructed plagiarism of Hibernate source code

In order to construct experimental test sample ,we will let Hibernate source apply copy the code snippet, displacement of the member variable names, displacement of method names ,upset the order of parameter, upset the order of the member variables and other analog plagiarism. And this test sample contains a comparison against the Token and abstract syntax tree structure than on a variety of error detection code snippets. Through artificial plagiarism and expert judgment, Hibernate test samples Hibernate and source code with Hibernate have real similarity with 75.1%.

Table 5 Result of specially constructed plagiarism of Hibernate source

Test sample	Similarity of text	Similarity of token	Similarity of syntax	Similarity in real	Improved comprehensive similarity
Hibernate source	51.4%	85.2%	76.8%	75.1%	74.3%

In connection with the above experimental test samples, Text-based, Token-based and Syntax tree-based detection results respectively are 51.4%, 85.2% and 76.8%. According to three results calculation formula(2) to calculate the comprehensive similarity was 74.3%, compared with the detection results of three single detection method, this paper puts forward the improvement of the homology of comprehensive similarity calculation model based on AHP test results, closer to the real similarity.

Comprehensive similarity detection result and analysis of open source code projects

For comparing with the comprehensive similarity detection model proposed in reference [11], using the source code of Snort-2.9.0.4, 7zip-9.22, Freemind-0.9.0, Notepad++-5.9, Filezilla_Client-3.5.0, WinMerge-2.12.4 and other five soft wares , combine with ten plagiarism ways to have the measurement under our homology detection model(the improved comprehensive similarity measurement based on AHP). The result is shown in table 6.Formula of comprehensive error:

Comprehensive Error = (Comprehensive Similarity –Real Similarity)/Real Similarity (3)

Table 6 Comprehensive similarity detection result of open source code projects

Test sample	Text (%)	Token (%)	Syntax (%)	Real (%)	Before improvement[11] (%)	After improvement (%)	Error rate before improvement [11] (%)	Error rate after improvement (%)
Snort-2.9.0.4	51.6	82.3	80.1	77.6	76.1	77.1	1.9	0.6
7zip-9.22	32.8	59.2	53.1	50.8	51.5	51.1	1.4	0.6
Freemind-0.9.0	61.6	91.5	89.3	86.9	85.6	86.4	1.5	0.6
Notepad++-5.9	35.7	56.1	52.7	51.7	50.9	51.0	1.5	1.3
WinMerge-2.12.4	52.4	83.6	79.8	77.5	76.4	77.0	1.4	0.6
aMule-2.3.1rc1	64.3	92.3	90.8	88.5	87.0	88.0	1.7	0.6
Pidgin-2.8.0	21.5	53.1	52.8	50.2	47.9	49.4	4.6	1.6
Wine-1.1.23	42.6	72.8	69.3	67.6	66.0	66.5	2.4	1.6
MPlayer-1.0rc4	57.6	85.5	81.6	79.1	78.8	79.1	0.4	0
All the code	42.3	71.9	68.7	65.8	65.3	66.0	0.7	0.3

Experiment result shows that the improved comprehensive similarity measurement model based on AHP is more close to the real value compare with the way only based on text, token and abstract syntax tree. Comparing with the way in reference [11], our way has lower error rate. Therefore our model is more accuracy.

Conclusion

In this paper, we propose an improved comprehensive similarity measurement model based on AHP, it considers miss detection rate and false detection rate as the indexes. By the way, we also propose a different analysis method of contribution of miss detection rate of the three comparison algorithms. Experiment result shows that compare to other algorithm, the improved homology detection system has higher accuracy rate.

Acknowledgement

This work was supported by National Natural Science Foundation of China (No. 61170268, 61100047, and 61272493), International S&T Cooperation Special Projects of China (No. 2013DFG72850), National High-Tech Research and Development Program of China (863 Program) (Grand No. 20122AA050804).

Reference

[1] Brenda S. Baker. A Program for Identifying Duplicated Code. In Proceedings of Computing Science and Statistics: 24th Symposium on the Interface, Vol. 24:49-57, March 1992.
[2] J Howard Johnson. Identifying Redundancy in Source Code Using Fingerprints. In Proceeding of the 1993 Conference of the Centre for Advanced Studies Conference (CASCON'93), pp. 171-183, Toronto, Canada, October 1993.
[3] S. Ducasse, M. Rieger and S. Demeyer, A Language Independent Approach for Detecting Duplicated Code, in:Proceedings of the 15th International Conference on Software Maintenance, ICSM 1999, pp. 109-118.
[4] Li, Z., Lu, S., Myagmar, S., and Zhou, Y. (2004). CP-Miner: A tool for finding copy-paste and related bugs in operating system code. In OSDI, 289–302.
[5] Toshihiro Kamiya, Shinji Kusumoto, and Katsuro Inoue. (2002, July). CCFinder: A multilinguistic token-based code clone detection system for large scale source code. IEEE Transactions on Software Engineering, 28(7):654–670.
[6] I. Baxter, A. Yahin, L. Moura and M. Anna. Clone Detection Using Abstract Syntax Trees. In ICSM, pp. 368-377, 1998.
[7] S. Bellon, R. Koschke, G. Antoniol, J. Krinke and E. Merlo.Comparison and Evaluation of Clone Detection Tools. IEEE TSE,33(9):577-591, 2007.
[8] Liu Leping, Zhao Wen. Application of Hierarchical analysis method in identity method choose
[9] Xu Shubo.the. Use the principle of decision-making method, analytic hierarchy process (ahp). Tianjin university press, 1988, 5-13.
[10] Meng Hu Chenggong. The information security risk assessment model based on AHP method applied research. The tropical agricultural engineering, 2009, 33 (1), 37.
[11] Bian Ce, based on the analytic hierarchy process (ahp) source code of the original testing technology research, Beijing university of posts and telecommunications master thesis, 2011

Advanced Materials Research Vols. 989-994 (2014) pp 1686-1691
© (2014) Trans Tech Publications, Switzerland
doi:10.4028/www.scientific.net/AMR.989-994.1686

Mean evolutionary algorithm based on intermediate value theorem of continuous function

Yucheng TAN[1,a] Changshou DENG [2,b] Yan Liu[2,c]

[1]School of Science, Jiujiang University,Jiujiang 332005,China

[2] School of Information Science and Technology, Jiujiang University,Jiujiang 332005,China

[a]email: tt_yycc@163.com , [b]email: csdeng@jju.edu.cn, [c]email:371169886@qq.com

Keywords: Continuous function, Mean Evolutionary algorithm, Variation operation, Selection operation

Abstract. A new Evolutionary algorithm was presented based on intermediate value theorem of continuous function. The global search ability and the local search ability of this algorithm are well balanced, and operators used in the algorithm are simple, Further, small size of population scale is used. Initial numerical experiments show that the mean evolutionary algorithm is better than differential evolution algorithm in solving high dimension function optimization.

Introduction

Continuous function is fairly broad class of functions. Intelligent algorithms suitable for continuous function include Genetic Algorithm (GA)[1], Particle Swarm Optimization (PSO)[2], Differential Evolution (DE)[3] and the various improved algorithms. GA lays the basic ideas of evolutionary algorithm, which are heredity and variation. The so-called heredity is to retain the superiority of the previous generation, while random variation provides an opportunity to open choice. Some specific operations of genetic algorithm are constantly being improved, such as binary encoding and cross, etc. PSO makes the algorithm more efficient for optimum individual chooses better individual. DE algorithm divides the algorithm into early stage and late stage. The early stage coordinates with global search, and the late stage coordinates with local search, which enables the algorithm to not easily fall into local optimum and have faster convergence. As for algorithms addressing certain problems, in order to be efficient, it has to consider some of the basic characteristics of such problems. The intrinsic property of continuous functions is its intermediate value. Mean Evolutionary Algorithm (ME) is proposed on the basis of the intermediate value of continuous functions, and absorbs some ideas of Differential Evolution Algorithm.

Mean Evolutionary Algorithm

1 Algorithm ideas

It can be found from the properties of continuous functions that: In the line segment linking large function value point and small function value point, there must be a number of points, the function values of which are equal to the mean value of two endpoint functions. They are referred to as the equilibrium point. The operation seeking equilibrium point is called equalization. Within several given points, use the equilibrium point to substitute the large function value points, then a group of small function value points can be obtained; use equilibrium point to substitute the small function value points, then a group of large function value points can be obtained. For two given function points with unequal values, you can choose the small function value point as the equilibrium point, and use the large function value point to get another small function value point; If using large function value points as the equilibrium point, the small points can thus promote the large function value points. According to this a group of more excellent [1]points can be obtained. Starting from the equilibrium point and the given point to find the operation of another point is referred to as

anti-equilibrium. In order to make the algorithm have faster convergence, the mean algorithm learns from the crossover operation of differential evolutionary. Through equilibrium, anti-equilibrium, crossover and selection, it ultimately finds the global optimum point.

2 Algorithm major operations

The following specifically gives an equilibrium and anti- equilibrium computing expression according to weighted average, and then gives the major operation of mean algorithm of D-dimensional objective function based on the population size of NP.

Consider the optimization problem:

$$\text{Min } f(x), f: R^D \to R \ , \tag{1}$$

Whose objective function $f(x)$ is continuous in its defined area? If the line segment AB is located in the region, and $f(A) < f(B)$, Then in the line segment AB there exists at least one point P so that $f(P) = \frac{f(A)+f(B)}{2}$. At this time P is the equilibrium point of function $f(x)$ in the line segment AB. Set A point's corresponding vector x_A, B point's corresponding vector x_B, P point's corresponding vector x_P, then x_P can be calculated as follows:

$$x_P = \lambda x_A + (1-\lambda)x_B = x_A + (1-\lambda)(x_B - x_A), \ \lambda \in (0,1) \tag{2}$$

In turn assume A is an equilibrium point linking B and Q， then $x_{\mathrm{A}} = \lambda x_{\mathrm{Q}} + (1-\lambda)x_B$， and then

$$x_{\mathrm{Q}} = x_A - \frac{1-\lambda}{\lambda}(x_B - x_A) \tag{3}$$

Compare the computational formula (1) and (2), both can be summarized as a formula

$$x_A + \mathrm{F} \cdot (x_B - x_A) \tag{4}$$

But when as an equilibrium calculation, $0 < F < 1$； as an anti-equilibrium calculation, $F < 0$.

(a) Variation Operation

Use the current point $x_{i,G}$ and another randomly selected point from the current population $x_{j,G}$ to produce a new point according to the above-mentioned equilibrium or anti- equilibrium operation, recorded as $v_{i,G+1}$, namely

$$v_{i,G+1} = x_{i,G} + F \cdot (x_{j,G} - x_{i,G}), \quad F = \begin{cases} \frac{1}{3} & if(rand \le 0.5) \\ -1 & otherwise \end{cases} \tag{5}$$

rand is a uniformly distributed random number in the interval [0,1].

(b) Crossover Operation

By hybridizing the point $v_{i,G+1}$ generated from variation operation and another randomly selected point from the current population $x_{k,G}$, the candidate points $u_{i,G+1} = (u_{1i,G+1}, u_{2i,G+1}, \cdots, u_{Di,G+1})$ are produced, namely

$$u_{jt,G+1} = \begin{cases} x_{jk,G}, if(j \in S) \\ v_{ji,G,} otherwise \end{cases} \tag{6}$$

S is a non-empty random subset, and the order of the subset does not exceed $\mathrm{D}/2$.

(c) Selection Operation

Select the function value of the comparison point $u_{i,G+1}$ and the point $x_{i,G}$, select the optimum function value point to enter the next generation population, i.e.

$$x_{i,G+1} = \begin{cases} u_{i,G+1} & if(f(u_{i,G+1}) < f(x_{i,G})) \\ x_{i,G} & \text{otherwise} \end{cases} \tag{7}$$

3 Algorithm Procedures

(a) The generation of the initial population

Randomly generate n points as the initial population, and calculate the function value of each point.

(b) Two ways to generate new points

The first way is to randomly select two different points from the given n points. Set $\lambda = 1/2$, In other words, use $F = 1/3$ for equilibrium operation to compute a new point. The reason for choosing $\lambda = 2/3$, rather than $\lambda = 1/2$ to calculate the equilibrium points is that the calculated equilibrium points from A to B will not repeat with the calculated equilibrium points from B to A, in order to better improve the operation efficiency. The second way is to randomly select two different points from the given n points. Set $\lambda = 1/2$, In other words, use $F = -1$ for anti- equilibrium operation to compute a new point. Through equilibrium or anti-equilibrium operation, for the given n points, each point (parent) will generate a different new point. Whether the way of generating new points is based on equilibrium way or anti-equilibrium way is determined by the probability 0.5. Afterwards, the new points carry out a crossover operation with points other than parent, and then compare the parent with the function values of new points after cross-point. Select excellent points to enter into the next generation.

(c) Generate new population

Based on the n points generated from Step (b), a new population is constituted. It is apparent that the new population is better than the previous generation. As per algorithm termination conditions, the population is tested to verify whether it meets the requirements. If it meets the requirements, output the results and comes to an end. If it fails, it does not meet the requirements, and then goes back to Step (b).

4 Algorithm Analyses

Mean evolutionary algorithm has strong global search ability and local search ability. Generally the required initial population is small, the operator is simple, and the programming is brief. Since the points generated from equilibrium are located within the current population, which are close, the algorithm local search ability becomes stronger. In terms of the points arising from the anti-equilibrium operation, they are distant in relative to the current population, and these points are widely distributed. Therefore, the algorithm global search ability becomes stronger. In addition, the characteristics of the excellent points are retained through cross-over. Mean evolutionary algorithm has simplified the operation of differential evolutionary algorithm cross-over, which improves the convergence speed. In order to prevent premature convergence, the cross-over location number of the mean evolutionary algorithm is no more than half the number of dimensions.

Mean evolutionary algorithm simulation

1 Test Functions

In order to test the performance of the mean evolutionary algorithm, several important test functions have been selected from the literature[4][5] for testing, they are:

$$f_1(x) = \sum_{i}^{k} x_i^2, x = (x_1, x_2, \cdots, x_k), \quad -100 \le x_i \le 100, \ k = 30 \ \text{(Sphere function)} \tag{8}$$

$$f_2(x) = \sum_{i=1}^{k-1} [100(x_{i+1} - x_i^2)^2 + (x_i - 1)^2], \quad -30 < x_i < 30, k = 30 \ \text{(Rosenbrock function)} \tag{9}$$

$$f_3(x) = 10k + \sum_{i=1}^{k} [x_i^2 - 10\cos(2\pi x_i)], \quad -5.12 \le x_i \le 5.12, k = 30 \ \text{(Rastrigin function)} \tag{10}$$

$$f_4(x) = \frac{1}{4000}\sum_{i=1}^{k} x_i^2 - \prod_{i=1}^{k} \cos\left(\frac{x_i}{\sqrt{i}}\right) + 1, \quad -600 \le x_i \le 600, k = 30 \ \text{(Griewank function)} \tag{11}$$

2 Test Results

Table 1 shows the experimental data of each tested function obtained via ME algorithm and DE algorithm on the condition that the population size and the number of iterations stay unchanged. Table 2 shows the outcomes of the tested function acquired using ME algorithm and DE algorithm respectively under different dimensions.

Table 1 Simulation results using ME algorithm and DE algorithm (20 experiments)

Test function	The known optimal value	ME algorithm		DE algorithm		Population size	Iterations	t-test
		The best optimal value	Mean optimal value	The best optimal value	Mean optimal value			
f_1	0	0.000573946	0.02168494	0.0005788044	0.000599457	20	1000	0.1473
f_2	0	10.77002	111.7035	147.6020	147.9772	40	1000	0.03529
f_3	0	4.864059	10.5093	13.92948	13.92948	40	1000	0.0002579
f_4	0	9.869651e-06	0.07677823	0.01488452	0.01488784	30	1000	0.2136

Table 2 Simulation results comparison between ME algorithm and DE algorithm under different dimension functions (1000 iterations)

		Function dimensions (k)										t-test
		35	45	55	65	75	85	95	105	115	125	
f_1	M	5.1e-06	6.7e-04	1.4e-02	1.1e-01	2.1566	4.8e+01	1.5e+02	1.7e+02	4.0e+02	2.9e+02	0.002
	D	297.997	98.169	291.744	295.761	298.169	293.796	300.700	296.949	96.725	293.665	
f_2	M	85.3053	143.109	391.346	673.889	1458.01	2983.96	6877.22	20873.9	19738.2	64899.2	5.1e-06
	D	71417.9	77466.6	76200.3	76560.6	71259.2	76298.6	74592.9	71656.2	71415.7	75278.4	
f_3	M	4.97502	9.94983	19.0387	24.0784	22.1340	35.8607	36.8583	8.9483	57.6701	55.4699	0.002
	D	55.6168	55.4699	55.7884	55.7199	55.7348	55.7348	55.5899	55.7307	55.7951	55.6958	
f_4	M	6.0e-06	7.0e-02	1.5e-01	4.2e-01	8.5e-01	1.43633	1.48415	1.77850	4.43995	3.58719	0.001
	D	3.70248	3.73610	3.67226	3.65457	3.66152	3.66627	3.67147	3.64041	3.66908	3.66488	

The statistical tests in the table 1 and table 2 is accomplished by R software. The tests in table 1 belong to two-side t-test for independent group means, and the tests in table 2 belong to matched pairs two-side t-test between means. Figure 1 is the scatter diagram after 50 iterations in order to describe the ME algorithm evolutionary process for f_4, when $k=2$, the initial population size is 30; The scatter diagram denoted Figure 2 describes the DE algorithm evolutionary process for the same objective function and the same iterative condition as Figure 1. The variation curves in Figure 3 show the evolutionary process of the optimal values for the same experiments as Figure1 and Figure 2 respectively. The both curves in Figures 4 are respectively the change trend charts of function f_3's optimal value after 600 iterations using the ME and DE algorithms, when $k=30$, the population size is 60. In the test the DE algorithm is always set as $F=0.8,\ CR=0.3$.

3 Analysis of test results

It can be seen from the test results that, with the increase in the number of test functions dimension, ME algorithm is apparently superior to DE algorithm, $p \leq 0.002$ (see Table 2); for low-dimensional function, DE algorithm demonstrated high accuracy and good stability. Compared with ME algorithm, its volatility is greater. However, in many experiments, the accuracy of optimal values

calculated by ME algorithm is better than that of DE algorithm (see Table 1). In addition, the stability of DE algorithm also exposed the weaknesses of premature convergence (see Figure 4).

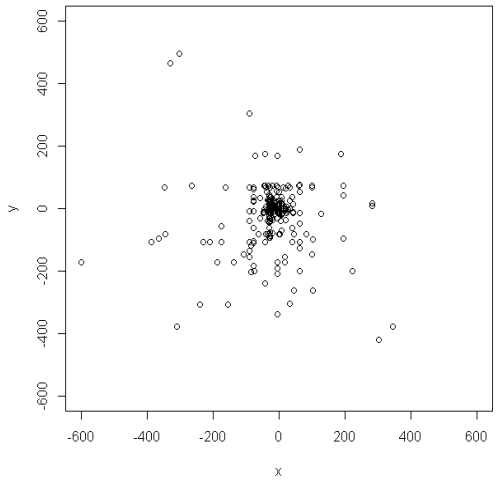

Fig.1. The evolution scatter diagram of f_4 with k=2 by ME

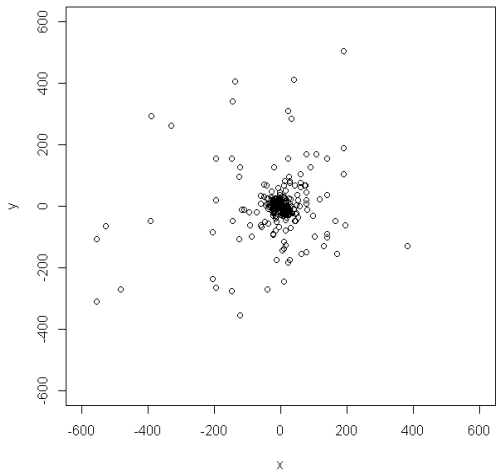

Fig.2. The evolution scatter diagram of f_4 with k=2 by DE

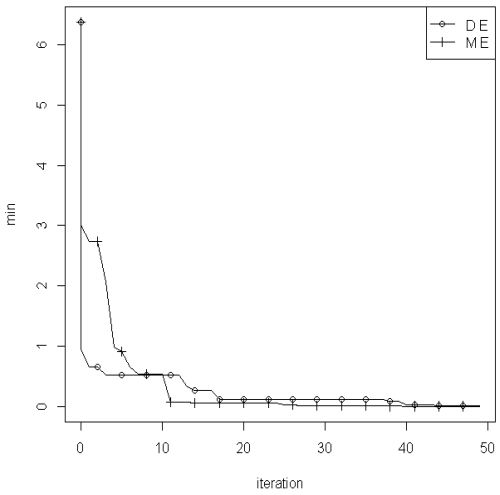

Fig.3. The evolution curves of f_4 with k=2 by ME and DE

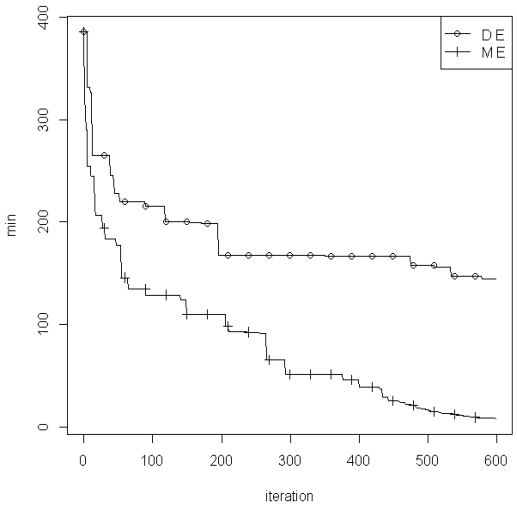

Fig.4. The evolution curves of f_3 with k=30 by ME and DE

The difference between ME algorithm and DE algorithm testing results is mainly the difference in mutation operator. Operator (11) and (12):

$$v_{i,G+1} = x_{i,G} + F \cdot (x_{j,G} - x_{i,G}) \tag{12}$$

$$v_{i,G+1} = x_{r1,G} + F \cdot (x_{r2,G} - x_{r3,G}) \tag{13}$$

Seemingly the forms are very similar, but their functions are very different. Operator (5) in ME algorithm contains more $x_{i,G}$ elements, which enables the progeny to retain more personalized elements, while operator (6) in DE algorithm contains no $x_{i,G}$ elements. Even if the following cross effect contains $x_{i,G}$ elements, the personality characteristics of its progeny have been greatly weakened, so that the next generation of individuals can easily have convergence, which directly leads to the weakness of premature convergence of DE algorithm.

For the high precision of DE algorithm in treating low-dimensional functions, it mainly depends on the diversity of operator (12) values, including DE/rand/2/bin strategy in DE algorithm, which uses the characteristic of rapidly increasing combinations C_n^3, C_n^4 with the increase of n. Simply relying on a great number of points to search for the optimal value may not be efficient. Mutation operator in ME algorithm is proposed basing on the intermediate value of continuous functions, so that the desired points have a good directivity, and thus have more efficiency.

Conclusions

In terms of mean evolutionary algorithm, although it has some characteristics of some other algorithms, it has its own ideological origins, which can be traced back to the Yin-Yang idea, and "Tai ji Diagram". ME algorithm involves equilibrium and anti-equilibrium operations, and the meaning of the equilibrium point is extremely rich. There are equilibrium and anti-equilibrium operations based on the different understandings of the equilibrium point, which can lead to more algorithms that will not only be suitable for continuous functions, but also be suitable for more and broader issues such as portfolio optimization. All of these will be the direction of future research.

Acknowledgement

This work is partially support by Natural Science Foundation of China under grant No. 61364025, State Key Laboratory of Software Engineering under grant No. SKLSE2012-09-39 and the Science and Technology Foundation of Jiangxi Province, China under grant GJJ13729 as well.

References

[1] Janikow C Z, Michalewicz Z. An experimental comparison of binary and floating point representations in genetic algorithms[C]// ICGA. 1991: 31-36.

[2] Montes de Oca M A, Stutzle T, Birattari M, et al. Frankenstein's PSO: a composite particle swarm optimization algorithm[J]. Evolutionary Computation, IEEE Transactions on, 2009, 13(5): 1120-1132.

[3] Kromer P, Snael V, Zelinka I. Randomness and Chaos in Genetic Algorithms and Differential Evolution[C] //Intelligent Networking and Collaborative Systems (INCoS), 2013 5th International Conference on. IEEE, 2013: 196-201.

[4] Fen Shi,Hui Wang, Lei Yu, Analysis of 30 Cases on Intelligence Algorithm [M]. Beijing: Beijing University of Aeronautics and Astronautics Press, 2011.

[5] ChangShou Deng, BingYan Zhao, ChangYong Liang, Improved Differential Evolution Algorithm [J] Computer Engineering 2009,35(24): 194-198.

Advanced Materials Research Vols. 989-994 (2014) pp 1692-1694
© (2014) Trans Tech Publications, Switzerland
doi:10.4028/www.scientific.net/AMR.989-994.1692

Meta-analysis and evaluation of visualization support to decision trees classification

Zuyi Chen [1, a], Taixiang Zhao [1,b]

[1]Department of foundation First Aeronautic Institute of the Air Force Xinyang, China

[a]zychen7410@163.com, [b]ztx304@126.com

Keywords: Decision tree; classification; Meta-analysis; Visual data mining

Abstract. In the social sciences, meta-analysis has been used on a limited scale only, mainly because there still remains a gap between the knowledge available and itsapplication in policymaking. The experimental results suggested that, compared to the automatic modeling process as typically applied in current decision tree modeling tools, interactive visual decision tree (IVDT) process can improve the effectiveness of modeling in terms of producing trees with relatively high classification accuracies and small sizes, enhance users' understanding of the algorithm, and give them greater satisfaction with the task.

Introduction

In many cases, it is not to be regretted if publications are forgotten because their relevance has faded away. There are a lot of publications that should have an impact for a much longer period than they have nowadays, however. Now we are talking about books and articles that get lost in the quickly growing stream of publications. As an illustration of the size of the problem we take the thirty million books and eighty million articles and brochures stored in the Library of Congress in Washington.Sophisticated data analysis mining methodology is required to curb non-utilization in data sets of this kind. Visual data mining (VDM) has become an active research area. VDM can be viewed as an integration of visualization and traditional DM techniques, such as visualizing raw data to help users discovering data characteristics, visualizing models obtained from DM to enhance understanding of the derived patterns, and visualizing DM process during which models are induced.

Many researchers have argued that visualization can be integrated withnonvisual techniquesto greatly enhancethe effectiveness and efficiency of a DM process[1]. The accuracy of a model is only one measure that can be used to value its worth. The ability to interpret the model to domain experts and decision makers and the ease of implementation and maintenance are other important factors. [2] stated that without proper visualization techniques, DM models, although a reduced form of original data, may not give the desired insight to help humans understand the phenomena of interest.

Meta-analysis

According to Lipsey and Wilson,there are basically three reasons for using meta-analysis to analyse and summarize a body of research studies rather than applying conventiona lresearch reviewing techniques[5].

First, meta-analysis procedures enhance the discipline in summarizing research findings. Also, meta-analysis requires that each step be documented and open to scrutiny.Furthermore,it leads to specification of the criteria that define thep opulation of study findings to be analysed.It requires search strategies that assist to identify and retrieveeligible studies,for malcoding of study characteristics andfindings.Finally, it also requires data analysis to support the conclusions that are drawn [3].

Second, meta-analysis represents study findings in a more differentiated and sophisticated way than conventional review procedures that only supply qualitative summaries.'By encoding the magnitude and direction of each relevant statistical relationship in a collection of studies, meta-analysis effect sizes constitute a variable sensitive to different strengths across studies' [3].

Third, meta-analysis is capable of finding effects or relationships that are not made explicit in other approaches to summarizing research.Meaningful effects and relationships upon which studies agree,and differentiated effects related to study differences, are more likely to be discovered by meta-analysis than by less systematic and analytic approaches [3].

Proposed conceptual model of visualization support to data mining modeling process

DM modeling consists of three main tasks: algorithm selection, model construction, and model evaluation. First,appropriate DM algorithms need to be selected, depending on the DM problems to be addressed. The key decision during model construction is to choose an appropriate set of parameters for the selected DM algorithm to fit the prepared data set. Because the parameters are not known apriori, however, model construction is recursive and can be very time-consuming. After a model is derived, it needs to be assessed by evaluating its performance, interpretability,and/or other measures, according to the corresponding DM tasks. Based on the evaluation outcomes and predefined DM goals, the induced model may have to be refined by choosing a different set of parameters or even a different algorithm.Data visualization, such as visualization of distributions of data attributes and dependencies among data attributes, assists users in discovering and understanding relationships within data; it leads to the creation or enhancement of a mental model that captures the implications of the data relative to the modeling objective [4], and thus can facilitate selecting appropriate DM algorithms and their parameters.

Visualization of model-building process, such as presenting parameters and model update, serves to not only help users understand how a model is derived, but also provide them thediscernment todirect model construction,adjusting the parameters based on their background knowledge and pattern recognition capacities as situations warrant. Studies in [5] showed that an important characteristic of experienced modelers, in contrast to the no viceones,was their continual self-monitoring of progress; they often suspended an activity at one stage and returned to an earlier stage. Visualization of models is the presentation of the obtained results or knowledge in visual forms. Its purpose is to enable users to quickly identify the important features of the derived patterns, such as the number of nodes and relationships among nodes in an induced decision tree.

Integration of scientific knowledge into social impact assesment

If the campaign against non-utilization of knowledge would be restricted to meta-analysis and value transfer,the outcomes of the campaign would be too limited.We have to hunt down non-utilizers not only among scientists but also among consultants, decision-makers and members of the public in general. Let us start with a close look at each of the four social roles involved.

Extended meta-analyses in research programs

The role of extended meta-analyses in integrated research programs will increase, because these programs will more and more have access to substantial databases relevant for their research questions. In these situations, ‘can implies ought’. It would be inefficient not to use these databases.

In these research programs, extended meta-analyses will be applied at the beginning, during and at the end of the program. If applied research is involved, impact assessment will not always be required.

Research programs have to become more transparent and more accountable, because of the requirements of financing agents. This applies in particular to research financed out of the taxpayer'smoney. Governments have to organize an open tendering for the projects that constitute the research program. As an example, we will discuss now a research program launched by a national science foundation that will have to contribute to policy-oriented and discipline-oriented knowledge.The national science foundation will be able to finance four projects and it is confronted with forty reactions to its tender.It is evident that a multi criteria analys is will have to be applied for evaluating and ranking the forty potential projects.

Experiment

An experiment was administered to test three hypotheses regarding the proposed IVDT by comparing it with the automatic approaches applied in current decision tree softwares. Although decision tree is one of the most popular so called ‘‘supervised’’ learning tools, the present decision tree softwares allow very limited forms of guidance from users.

In consequence, the common approach is to run the algorithm with parameters set at their default values, hoping to discover some interesting patterns, or build several trees with different parameters settings, compare their results, and choose the one that is the best. Such an approach forces the user to blindly explore a huge parameter space without clues and intuition about which parameters could give better results. In contrast, the proposed IVDT enables the involvement of the user to guide tree construction by providing them the insight to check the intermediary outcomes and select appropriate parameters.

Conclusions and future research

We have been able to show, that in many cases adequate databases are already available and that they are further improved. We have also been able to demonstrate that for each of the components sophisticated methodology is available. The loosely coupled relationships between visualization and analytical DM techniques represent the majority of the current state of art in visual DM; DM modeling is typically an automatic process with very limited forms of guidance from users. A conceptual model of the visualization support to DM modeling process and a novel IVDT classification process have been proposed in this paper, with the aim of exploring humans’ pattern recognition ability and domain knowledge to facilitate the knowledge discovery process. An experiment was administered to test three hypotheses regarding the potential merits of the proposed IVDT process, whose results suggested that compared to the automatic modeling process, IVDT process can improve the effectiveness of modeling, enhance users’ understanding of the algorithm, and give them greater satisfaction with the task.

References

[1]Ankerst, M., Ester, M., Kriegel, H.-P., 2000. Towards an effective cooperation of the computer and the user for classification.In: Proceedings of the Sixth International Conference on Knowledge Discovery and Data Mining (KDD ‘2000), Boston, MA,pp. 178–188.

[2]Fayyad, U., Grinstein, G.G., 2002. Introduction. In: Fayyad, U.M.,Grinstein, G., Wierse, A. (Eds.), Information Visualization in Data Mining and Knowledge Discovery. Morgan Kaufmann Publishers,Los Altos, CA, pp. 1–20.

[3] M.W. Lipsey, D.B. Wilson, Practical Meta-Analysis, Sage, London, 2001.Crapo, A.W., Waisel, L.B., Wallace, W.A., Willemain, T.R., 2000.

[4]Visualization and the process of modeling: a cognitive–theoretic view.In: Proceedings of the Sixth ACM SIGKDD International Conference on Knowledge Discovery and Data Mining, Boston, MA, pp.218–226.

[5] Willemain, T.R., 1995. Model formulation: what experts think about and when. Operations Research 43 (6), 916–932.

Advanced Materials Research Vols. 989-994 (2014) pp 1695-1699
© (2014) Trans Tech Publications, Switzerland
doi:10.4028/www.scientific.net/AMR.989-994.1695

Allocation Scheme of Short Training Sequence Based on OFDM-PON

Songlin Guo[1], Xi Chen, Chaoxing Xu, Yuan Jiang, Yingchun Li

The Key Laboratory of Specialty Fiber Optics and Optical Access Networks,

Shanghai 200072 China

[1]email: surain@shu.edu.cn

Keywords: OFDM-PON, training sequence, symbol synchronization

Abstract. A new structure of short training sequence for symbol synchronization in OFDM-PON system is proposed in this paper. By adjusting the subcarrier allocation scheme of short training sequence in a wireless LAN, it makes the mean of short training sequence signal in time domain from non-zero to zero mean and solves the receiving data demodulation interference caused by the wrong trail of the non-zero mean short training sequence in time-domain. Data demodulation simulation and experimental results show that the improved method can effectively reduce the training sequence interference errors caused by tailing.

Introduction

Orthogonal frequency division multiplexing passive optical network (OFMD-PON) is regarded as a potential technique to be applied in next generation passive optical network (NG-PON). Combination of OFMD and PON can make the most of spectrum resource. OFDM can achieve QPSK, 8PSK, 16QAM and even higher order modulation in each subcarrier by mapping signal to constellation. In TDMA and OOFDMA network, several users share bandwidth. This makes challenges to exact symbol synchronization because symbol synchronization and aligning slot time of each ONU signals must be finished in real time. OFDM-PON system is sensitive to synchronization, which is a major defect. Synchronization is one of the most significant works of OFDM receiver.

At present, there are many papers that propose quite a few algorithms about the synchronization of OFDM system in wireless LAN. These algorithms can be divided into two categories: algorithms based on non-data-aided such as algorithms based on cyclic prefix (CP)[1] and algorithms based on data-aided. The latter algorithms introduce short and long training sequence. By studying more efficient structure and code pattern of pilot and training sequence, receiver can extract synchronization information more easily. These algorithms feature low algorithm complexity and efficiency synchronization performance. Classen proposed this kind of algorithm early. His algorithm uses pilots in OFDM symbols to finish coarse synchronization and fine synchronization. Since the coarse synchronization should blindly search in a certain range, this algorithm costs too much calculation. Then Schmidl improved Classen's algorithm by added two same blocks with N/2 length in the header of each data frame. Receiver can search the peak and find the starting position of data frame through delay correlation algorithm. However, this algorithm has low precision cause of the plateau[2]. Shi and Serpedin added four same training sequences in the head of data frame and the third is inversed. This algorithm can improve the precision but still can't make it satisfied[3][4]. Bo-Seok improved Schmild's method in his paper. Two OFDM symbols are used as training symbols in Bo-Seok's algorithm. It is different from Schmild's that every OFDM symbols are applied with differential phase shift keying (DPSK).This algorithm reduces calculation a lot and has almost the same performance[5]. The synchronization method used in optical experiment now comes from wireless LAN. Since the limit of optical channel, low subcarriers have serious distortion. This paper proposes a new structure of short training sequence applied to OFDM-PON system, which reduce the distortion of low subcarriers.

Synchronization Theory in OFDM System

There has been a similar allocation scheme of short training sequence in wireless OFDM system. This scheme shows well performance on symbol synchronization by using group detection. This scheme is shown on Fig.1 and the number of used subcarriers in short sequence is underlined.

NULL	USER																											NULL		
1	2	3	4	5	6	7	8	9	10	11	12	13	14	15	16	17	18	19	20	21	22	23	24	25	26	27	28	29	30	31	32

$$STS = \{0,\ 0,\ 1+j,\ 0,\ 0,\ 0,\ -1-j,\ 0,$$
$$0,\ 0,\ 1+j,\ 0,\ 0,\ 0,\ -1-j,\ 0,$$
$$0,\ 0,\ -1-j,\ 0,\ 0,\ 0,\ 1+j,\ 0,$$
$$0,\ 0,\ -1-j,\ 0,\ 0,\ 0,\ 0,\ 0\}$$

Fig.1 Carrier distribution map and load the data table

It is different from wireless that OFDM baseband signal should be real in baseband direct modulation optical transmission. This problem can be solved through Hermite complex conjugation. The prior 32 subcarriers of OFDM signal are conjugated with the latter 32 subcarriers. This kind of OFDM signal can be transformed to real signal after IFFT. However, this change on structure will introduce a new problem. At the starting position of OFDM symbol in receiver, relatively large error is observed after FFT and points on received constellation deviate from standard points. It is analyzed that this phenomenon is caused by unreasonable allocation of short training sequence. The mean of short training signal in time domain is not zero, which will cause wrong trail in optical transmission and interference to low subcarriers. This paper proposes a new allocation scheme of short training sequence suitable for OFDM-PON system to solve this problem effectively.

Modified Allocation Scheme of Short Training

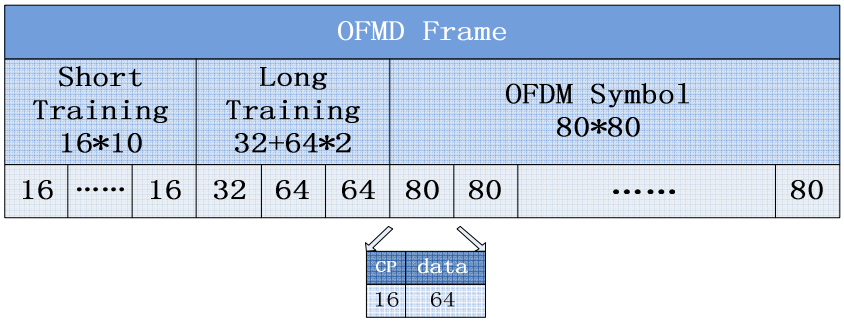

Fig.2 Frame structure diagram of the OFDM signal

The frame structure of short training sequence is shown on Fig.2. 64 subcarriers are transformed to time domain signal after 64 points IFFT. We select a quarter of the time domain signal (16 points) out and repeat them 10 times. This is the generation of short training sequence with 160 points. The time domain expression of short training sequence is shown as

$$t_{Ts}(\mathrm{t}) = \frac{1}{\mathrm{N}}\sum_{n=0}^{N-1} X_{n,m} e^{j2\pi\Phi_{n,m}t} \tag{1}$$

The frequency domain expression of prior 16 points is shown as

$$\mathrm{F}[t'_{Ts}(\mathrm{t})] = \sum_{n=0}^{N-1} T_{Ts}(\mathrm{n})\left(\frac{1}{5}T_s Sa\left(\frac{T_s}{10}(\omega - n\omega_{Ts})\right)\mathrm{e}^{j\frac{T_s}{10}(\omega - n\omega_{Ts})}\right. \tag{2}$$

The frequency domain expression of short training sequence is shown as

$$\mathrm{F}(t'_T(\mathrm{t})) = \mathrm{F}[t'_{Ts}(\mathrm{t})] + \mathrm{F}[t'_{Ts}(\mathrm{t})]e^{j\frac{1}{5}\mathrm{T}_s\omega} + \mathrm{F}[t'_{Ts}(\mathrm{t})]e^{j\frac{2}{5}\mathrm{T}_s\omega} + \cdots\cdots + \mathrm{F}[t'_{Ts}(\mathrm{t})]e^{j\frac{9}{5}\mathrm{T}_s\omega} \tag{3}$$

NULL	USER																												NULL		
1	2	3	4	5	6	7	8	9	10	11	12	13	14	15	16	17	18	19	20	21	22	23	24	25	26	27	28	29	30	31	32

$$STS = \{0, 0, 0, 0, 1+j, 0, 0, 0,$$
$$-1-j, 0, 0, 0, \ 1+j, 0, 0, 0,$$
$$-1-j, 0, 0, 0, -1-j, 0, 0, 0,$$
$$1+j, \ 0, 0, 0, -1-j, 0, 0, 0\}$$

Fig.3 Schematic diagram of improved short training sequence subcarrier distribution

Fig.3 shows modified short training sequence subcarrier distribution and the number of used subcarriers is underlined. NO.1 and NO.30~36 subcarriers are null and used as guard band. The signal should be real since system uses optical intensity modulation. Therefore, 64 subcarriers are divided to two parts. The prior 32 subcarriers are conjugated with the latter 32 subcarriers. The time domain signal after IFFT is real. It is different from wireless that the used subcarriers loaded with short training are located at 4 times basic frequency. This change makes the mean of short training sequence signal in time domain from non-zero to zero mean. As shown in Fig.4, the frequency of NO.2 subcarrier is 1/Tc; the frequency of NO.3 subcarrier is 2/Tc; the frequency of NO.4 subcarrier is 3/Tc and so on. We select prior 16 points out and repeat them 10 times and generate 160 points short training sequence.

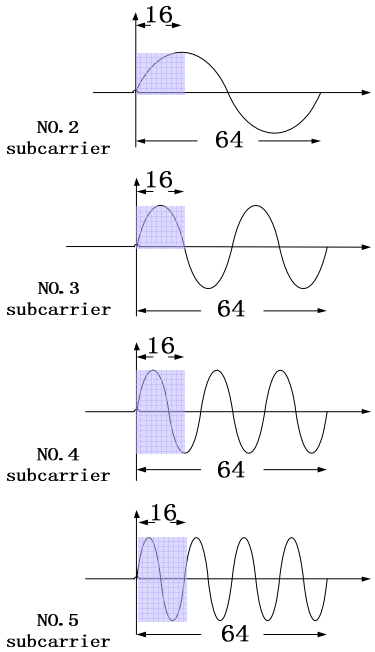

Fig.4 Schematic diagram of short training sequence in time domain

Since the prior 16 points are selected, only NO.5 subcarrier is zero mean in four subcarriers. Only 4 times basic frequency are zero mean in 64 subcarriers. This means only subcarriers at 4 times basic frequency will not interfere received data signal. The theory is as follow. The passing band of experimental system is 10MHz to 880MHz. The output of short training sequence after passing the channel is shown as

$$\mathrm{F}(t'_T(\mathrm{t}))\,\mathrm{H}(\omega) = \sum_{i=0}^{9} e^{j\frac{i}{5}\mathrm{T}_s\omega} \sum_{n=0}^{N-1} T_{Ts}(\mathrm{n})\left(\frac{1}{5}T_s Sa\left(\frac{T_s}{10}(\omega - n\omega_{Ts})\right)\mathrm{e}^{j\frac{T_s}{10}(\omega - n\omega_{Ts})}\right) \tag{4}$$

Since the interval of subcarriers is about 33MHz and NO.1 subcarrier is not loaded data, passing band can be treated as 0 to 880MHz. The points of first data symbol range from 339 to 400 and its time ranges from $337\mathrm{T}_0$ to $400\mathrm{T}_0$, where $\mathrm{T}_0=\mathrm{T}_S/80$ is sampling time. The expression of short training sequence for the 339 to 400 sampling points is shown as

$$\mathrm{s}(\omega) = \left(\sum_{i=0}^{9} e^{j\frac{i}{5}\mathrm{T}_s\omega}\left(\frac{1}{5}T_s Sa\left(\frac{T_s}{10}(\omega - n\omega_{Ts})\right)\mathrm{e}^{j\frac{T_s}{10}(\omega - n\omega_{Ts})}\right)\right) \otimes \left(\frac{4}{5}\mathrm{T}_s\, Sa\left(\frac{2T_s}{5}\omega\right)\mathrm{e}^{j\frac{2T_s}{5}\omega}\right) \tag{5}$$

Fig.5 is the theory analyzing results from formula (5). When transmitting null data, previous short training sequence will cause obvious interference to low subcarriers of data segment as shown in Fig.5 (a). This interference is reduced a lot after short training sequence improved as shown in Fig.5 (b).

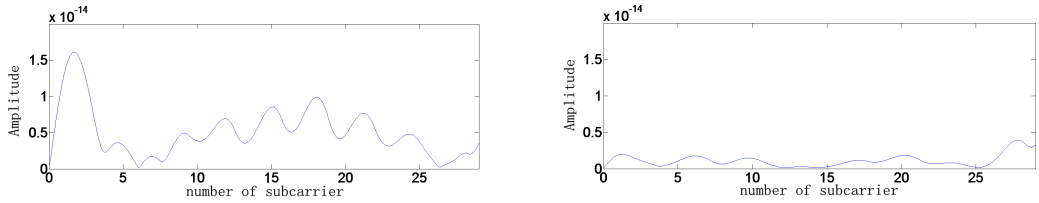

(a) Before modified (b) After modified

Fig.5 Theory analyzing results

Experimental Results

The OFDM signal is generated in Matlab and transmitted by AWG. OFDM signal is modulated by DFB laser and received through 25km single mode fiber (SMF). Photovoltaic conversion is finished by PIN detector at receiver. The signal is sampled by OSC after passing an 880MHz LPF. The OFDM demodulation is also finished in Matlab.

The time domain waveform of experimental results is shown on Fig.6. All subcarriers in data segment are loaded zero. In real channel, low cut-off frequency is impossible to be zero and the 3dB cut-off frequency of experimental system is 10MHz. Therefore, there is wrong trail in non-zero mean training sequence. A sunk part can be observed in the waveform of previous short training sequence and it disappears after short training sequence is modified. The change is shown on Fig.6. Through making FFT of the two waveforms shown on Fig.6, we can analyze interference on every subcarrier. As shown in Fig.7, previous short training sequence makes more interference on the 3 prior subcarriers than modified. These experimental results agree with the previous theoretical analysis.

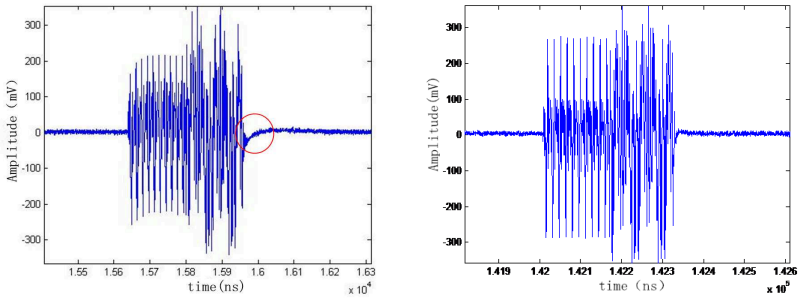

(a)Before modified (b) After modified

Fig.6 Comparison of the received waveform

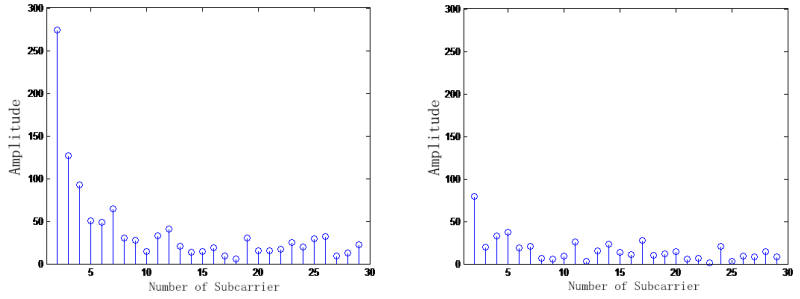

(a)Before modified (b) After modified

Fig.7 Carrier frequency spectrum of the improved receiver data segment

Fig.8 is the constellation of NO.2 subcarrier with 64QAM modulation. Before short training improved, data are demodulated with serious distortion. Before short training sequence improved, points are divided to two parts. This situation is improved a lot after the short training sequence is changed. Data can be recovered truly at receiver.

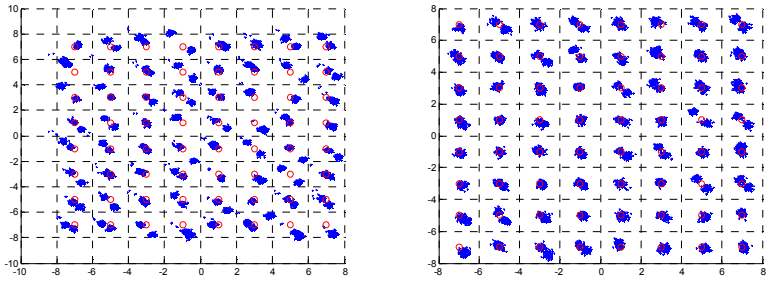

(a)Before modified (b) After modified

Fig.8 Constellations after loading the data

Conclusion

By adjusting allocation scheme of short training sequence in OFDM-PON system, transmission performance of experimental system is improved and the problem caused by unreasonable allocation of short training sequence in OFMD signal is solved. New allocation scheme of short training sequence makes marked improvement on system performance as shown in both theoretical analysis and experimental results. This modification can also be applied on Orthogonal frequency division Multiple Access for Passive Optical Networks (OFDMA-PON). According to the subcarrier occupied by each user, we can choose relevant training sequence based on four times frequency principle.

Acknowledgement

In this paper, the research has been sponsored by the National Nature Science Foundation (Project NO. 61132004, 61275073) and the Shanghai Science and Technology Development Funds (Project NO. 13J1402600, 11510500500).

References

[1] Feng Y, Liu S, Li N, et al. A new OFDM synchronization algorithm using training cyclic prefix[C]//Mechatronic Science, Electric Engineering and Computer (MEC), 2011 International Conference on. IEEE, 2011: 1489-1491.

[2] Azari A, Esfahani S N, Naderi M. New timing metric for the frame synchronization in WiMAX OFDMA applications[C]//Advanced Communication Technology (ICACT), 2010 The 12th International Conference on. IEEE, 2010, 1: 666-671.

[3] Na X, Gao S. An FPGA implementation method of OFDM timing synchronization based on conjugated-symmetrical-structured training sequence[C]//Microwave, Antenna, Propagation and EMC Technologies for Wireless Communications (MAPE), 2013 IEEE 5th International Symposium on. IEEE, 2013: 672-675.

[4] Chen J, Zhang F, Yu L, et al. An OFDM-PON symbol synchronization technology based on absolute value error of training sequence[C]//Consumer Electronics, Communications and Networks (CECNet), 2013 3rd International Conference on. IEEE, 2013: 125-129.

[5] IEEE Std. 802.22-2011

Advanced Materials Research Vols. 989-994 (2014) pp 1700-1703
© (2014) Trans Tech Publications, Switzerland
doi:10.4028/www.scientific.net/AMR.989-994.1700

Three-Dimensional Yarns Modeling for Tufted Carpet Simulation

Li Jianghua[a], Chen Guangfeng[b], Huang Qingqing[c], Wei Xin[d]

Donghua University, Engineering Research Center of Advanced Textile Machinery, Ministry of Education, Shanghai 201620,China

[a]email: 630177385@qq.com, [b]email: chengf@dhu.edu.cn, [c]email: hu.poing@163.com, [d]email: 695494803@qq.com

Keywords: yarn modeling; fiber bundle; geometric modeling; tufted carpet simulation

Abstract. Yarns modeling are the key problem for tufted carpet 3D visual simulation. This paper deals with three-dimensional yarns structure modeling for tufted carpet simulation. The yarn is modeled as an assembly of fiber bundles which also include of a lot of fibers. to simulate fiber bundle dividing fiber bundle into many segments along its trajectory, and each fiber paths displayed are generated by NURBS curves. Through control the control points and color of NURBS to get certain cross-section and color effect of fiber bundle outlook. And finally use the fiber bundle to form the final yarn model. Test result shown the modeling method is suitable for carpet simulation.

Introduction

Basically, a yarn is composed of many fibers twisted to make up a yarn. Hence the solid structure of yarn should be constructed from fiber-structure parameters, such as fiber shape, fiber distribution, and the direction of the fiber twist [1]. Many researchers have developed models to display the visual characteristics of real yarns for modeling ply yarns structure, woven fabrics, knitted fabric and complex textile composite yarns. Most of the previous works regarding geometrical modeling of yarn structure are based on single line yarn path [2,3]. These presentations are limited to virtual representation and prediction of the micromechanical properties of yarn structure. Sriprateep and Bobez have developed a model of yarn as an assembly of many fibers by twisting.

For tufted carpet simulation, due to the limitation mentioned above, the yarn model could not be used for three dimension simulation of loop pile, a novel yarns structure modeling need to be considered.

Yarn Modeling Method

For tufted carpet, the yarn structure mainly has two types: interlacing yarn and twisting yarn [1]. General, a yarn is composed of many fibers bundles twisted to make up a yarn [4,5]. A general structure of yarn is shown as figure 1.

Several key factors affect the appearance of fiber bundles: centerline trajectory, fiber bundles of color, cross-section shape, and fiber bundle of twist. In this study, first construct fiber, composed by fiber of fiber bundles, again by fiber bundles of constructing yarn strategies. Use NURBS to express centerline bending posture, by scanning fiber entity, and assembly these fibers 3d model into 3d model of fiber bundles.Since the tufted carpet consists of tens of thousands of loop piles which formed by yarns, and each yarn consists of hundreds of fiber, fiber structure of the fiber bundles little impact on the carpet visual appearance, so fiber modeling adopts circle as the cross-section, through the control point controlling the fiber shape. Again by hundreds of fiber, and constitutes a fiber bundle for every fiber in increases in fiber bundles, make subsequent drift disturbance from the microscopic yarn modeling can also very approximate true yarns.

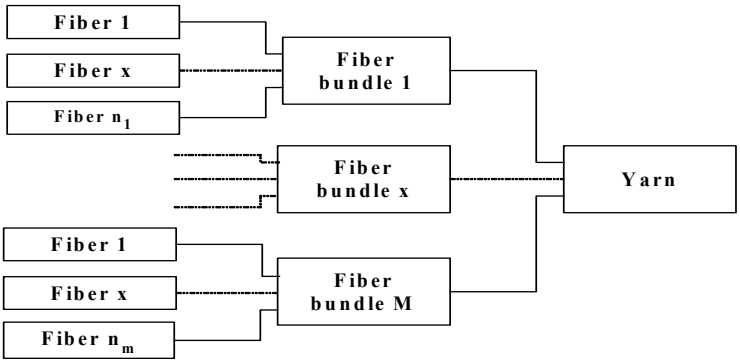

Fig. 1 Yarn composition structure diagram

Centerline trajectory description. NURBS curve: The fiber curve can be approximated by a curve called cubic NURBS curve, which is a parametric spline whose main components include the 2D or 3D control points. In addition, the weights of these points and a knot vector limit the effect of the control vertices onto a given segment of the curve. The fiber is defined as an open cubic B-spline curve with a constant radius of r described by the control points $\mathrm{q} \in R^{3m}$. In general, indices i, j range over spline segments, while indices k, l range over control points. The curve is described by Eq. 1 for a fiber with $N = m - 3$ spline segments, and where $b_k(s)$ is the cubic B-spline basis function associated with control point k. Through changing the actual value of control points, can actually control to the center of the fiber track. By dividing a fiber into section along the centerline of value, as long as it meets some requirements can fully infinite approximation actual fiber bundle center trends.

$$y(s) = \sum b_k(s)\mathrm{q}_k, s \in [0, N] \tag{1}$$

Color control of fiber bundle. For fiber in yarn always have different color, in order to simulate the effect of these color, we designate entity color while generating fibers, the fiber bundle with different color could be got. But for mixed colors fiber bundle, certain proportion separately for every fiber different color, achieve specified mixed color effect.

Cross section control. Cross-section shape of fiber bundle in the fabric are not constant, the key imitate fiber bundles of cross-section shape is to control every fiber in section regularity of distribution. In Common cross-section is in a circle, elliptic, runway form. Through the control points in every fiber in section, namely average distribution within the control can be guaranteed in the fiber bundle in cross-section shape.

The generation of random points for cross section control contains two main steps: the first step is to generate random points set in cross section. And then mapping the points set from local coordinate system to global coordinate system.

Construction of coordinate system. To generate the random point sets, we first construct the coordinate system of fiber bundle and the local coordinate system of cross section. The origin of local coordinate system is defined as the cross section center point, and (u_x, u_y) is in the cross section, u_z is perpendicular to the cross section.

Random data generation. There many kinds of cross sections. Using elliptical cross-section as a sample to generate the points set. Through the rand function as Eq. 2 to generate original random points (u_x, u_y).

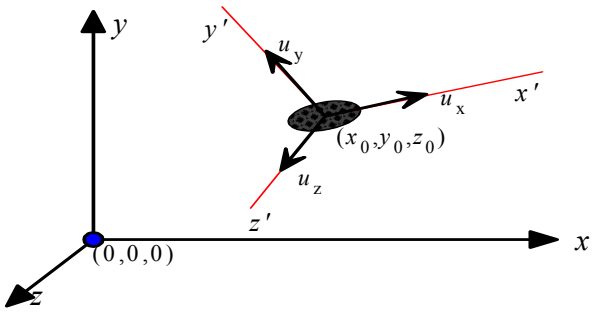

Fig. 2 Coordinate system for yarn cross section

$$\begin{cases} u_x = 2\times a\times \text{rand}(\,) - a \\ u_y = 2\times b\times \text{rand}(\,) - b \end{cases} \tag{2}$$

After the generation of the points, firstly get rid of the points outside the Elliptical, then calculate the distance between current points with valid candidate points and deleted the point if the minimize distance is smaller than the diameter of fiber.

$$f(u_x,u_y) = \sqrt{(u_x-u_{x1})^2+(u_y-u_{y1})^2} + \sqrt{(u_x-u_{x2})^2+(u_y-u_{y2})^2} \le L \tag{3}$$

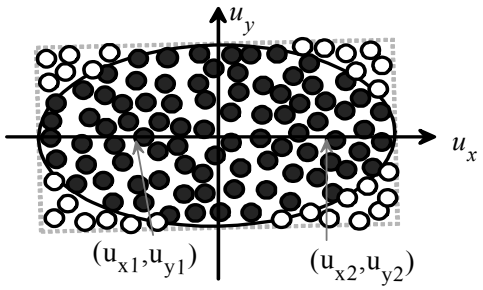

Fig. 3 Cross-section random data generation sample

For the process using pseudocode as follows to generate point set for cross section control.

$i = 0;\quad r = fibreDiameter;$
while$(i \le \text{MAX})\{$
$x = \text{rand}(); y = \text{rand}();$
if $(f(u_x,u_y) \le L)$ & $(\text{MinDistance}((u_x,u_y),(u_{xi},u_{yi})) \ge 2r)$
StoreInDataArrary (u_x,u_y);
$i++;\}$

Point mapping with the transform matrix. A point in space (x, y, z) transformations of any movement, rotation, scaling, can be accomplished through this point P_s multiplied by a matrix T *as* Eq. 4 to get the destination P_d, and get the destination point set.

$$T = R_x \cdot R_y \cdot R_z \cdot T_{xyz} \tag{4}$$

In Eq. 4 R_x , R_y and R_z are the rotation matrix as Eq.5 , and $\cdot T_{xyz}$ is the translation matrix as Eq.6. With the matrix we could get the destination point set. Base on the point set we could generate the curve to simulate the fiber bundle.

$$R_x = \begin{bmatrix} 1 & 0 & 0 & 0 \\ 0 & \cos\alpha_x & \sin\alpha_x & 0 \\ 0 & -\sin\alpha_x & \cos\alpha_x & 0 \\ 0 & 0 & 0 & 1 \end{bmatrix} R_y = \begin{bmatrix} \cos\alpha_y & 0 & -\sin\alpha_y & 0 \\ 0 & 1 & 0 & 0 \\ \sin\alpha_y & 0 & \cos\alpha_y & 0 \\ 0 & 0 & 0 & 1 \end{bmatrix} R_z = \begin{bmatrix} \cos\alpha_z & \sin\alpha_z & 0 & 0 \\ -\sin\alpha_z & \cos\alpha_z & 0 & 0 \\ 0 & 0 & 1 & 0 \\ 0 & 0 & 0 & 1 \end{bmatrix} \tag{5}$$

$$T_{xyz} = \begin{bmatrix} 1 & 0 & 0 & 0 \\ 0 & 1 & 0 & 0 \\ 0 & 0 & 1 & 0 \\ T_x & T_y & T_z & 1 \end{bmatrix} \tag{6}$$

Test and Discussion

We develop the program in VC++ together with Open Inventor to test the proposed method for yarn modeling. In the test process, we adopt B-Spline curve to represent the fiber in yarn. Yarn modeling process assumes all fiber is infinitely long, without considering short fiber structure on the yarn appearance influence.

Fig. 4 Fiber bundle with cross section control

Conclusion

This paper deals with the modeling method of yarn for tufted carpet simulation. The yarn is modeled as an assembly of many fibers. Each fiber paths displayed are generated by NURBS curves. Through control the fiber distribution in key points to control cross-section of fiber bundle. Test result shown the modeling method is suitable for carpet simulation

Acknowledgment

This work was supported by Fundamental Research Funds for the Central Universities(No. 12D10309).

References

[1] Xue Shixin. Machine made carpet. Beijing: Chemical industry press, 2004:320-330.

[2] Chen Guangfeng, Wang Weibin, Jin, Zhilei. Spatial structure analysis and simulation of Engineering and Software Engineering,2009,pp143-146

[3] Chen Guangfeng, Li Qingqing. Study on 2D Simulation Algorithm and Implementation for Loop Pile Tufted Carpet Advanced Materials Research, 2011, 179-180:651-656

[4] Chiristiane Szczesny, Klaus Hardt and Brigitte Scheuffele. Simulation of fancy yarns on the screen. ITB, 1997,(2):3-9.

[5] Wang Dongfeng. The study on 3D yarn model. Donghua university master dissertation, 2006.

[6] Information on http://www.vsg3d.com/open-inventor/sdk

Advanced Materials Research Vols. 989-994 (2014) pp 1704-1711
© (2014) Trans Tech Publications, Switzerland
doi:10.4028/www.scientific.net/AMR.989-994.1704

Decision Making Support Model For The Incident Emergency Management of Migrant's Group Based on CBR

Zhang dinghua[1,a] Chengliang[1,a] Wu renwei[1,a] Wang jing[1,a] Liu jingyi[1,a]

[1] School of public administrator of South China University of Technology

Guangzhou, 510640, China

[a]email: dhzhang@scut.edu.cn

Keywords: emergency management; migrant group incident; Analytic Hierarchic Process (AHP); CBR; aid decision making

Abstract. This paper presents the findings of a study on decision making models for the migrant's worker group incident emergency management based on Analytic Hierarchic Process (AHP). Analytic Hierarchic Process (AHP) helps to quantitate and layer the complex migrant's worker incident emergency management problem, the aim of the work is to improve the support for analysis and decision through the importance comparing of various factors associated layer by layer.A case study conduct in Wukan village Shantou city of Guangdong province revealed that AHP model can do effective decision making

Introduction

Social relationship has been more complicated and hidden troubles and crisis have also been gradually revealed, especially the sudden group incidents had influence the step of government reform, social harmony and stability in the process of rapid urbanization in China because of inflation, structural reform, income distribution and other problems. Rural-urban continuum is the urban and rural joint areas which have the properties of land-use of both city and country. Triggered by some social contradictions, specific groups or no-specific people get together to establish occasional groups, in the form of contradictions among people with no legal basis, which causes negative impacts on society, even makes the language or physical conflicts, to express their demands and claims, strive for and maintain their own interests, let off their steam and make impacts in this way, those behaviors make the unstabilizing factor of group incident more obviously[1-3]. How to use of limited resources effectively and information technology integrality, proceed a series of emergency rescues that including project, prevention ,control and handle, improve the reaction capacity and anti-risk capacity for the sudden group incidents, offer more rapid emergency services for the citizens are a unresolved problem for the city managers. Many countries adopt various measures to reduce the damage caused by group incidents, including set up many kinds of mechanism and emergency management system etc, among many ways, set up emergency management system is one of the best effective ways[4].

Design for the feature attributes of the case for the migrant's worker group incident about interest dispute based on CBR

Emergency plan is the core part of the group incident emergency management system in the urban and rural joint areas. Plan Representation for the emergency system based on CBR is also the boot tool in the whole system. The main task of it can be divided into three parts: One, extract and represent of system case attributes; Two, sum up the treatment schemes and solutions in the system cases; Three, estimate and summarize the results of system case processing.

Extract and represent of system case attributes

This dissertation classify and summarize influence factors for interests of migrant workers and draw six fundamental feature attributes by researching and referring to many documents, including

Mei Zhongling[4],Wu Peng[5], Yu Shui,[6] Na,Fan,Xiaoguang[7],Wang Xin[8] and so on, the feature attributes mainly rely on incidents' feature attributes，the dissertation is focusing on the migrant's worker group incidents caused by interest disputes in urban and rural joint areas, according to the basic informations of these events, we can divide the feature attributes into the following six categories, event level, place of incident,cause of incident, scene stability,road condition, local control situation. Feature attributes and categories of emergency plan for the migrant's worker benefit dispute group incident can be classified as the following:

1, Event level : one level, second level, three level, four level

2, Place of incident: office areas of enterprise and public institution, living quarters, downtown areas, vital communication lines and other areas.

3, Cause of incident: wage arrear, inequality of authority , lacking of safeguard measures, uneven distribution of benefits, dissatisfied with the results of related incident, other reasons.

4, Scene stability: scene is stable, emotional fluctuation of the migrant's workers, scenes of chaos but no casualties,scenes of chaos and have casualties

5, The length of road congestion: 0m--20m，20m—50m，50m—80m，80m—150m

6, Plan demand,demand of the emergency department, demand of emergency personnel.

Feature attributes and hierarchical structures of the group incidents caused by worker's interest dispute in the urban and rural joint areas just as the following Fig.2

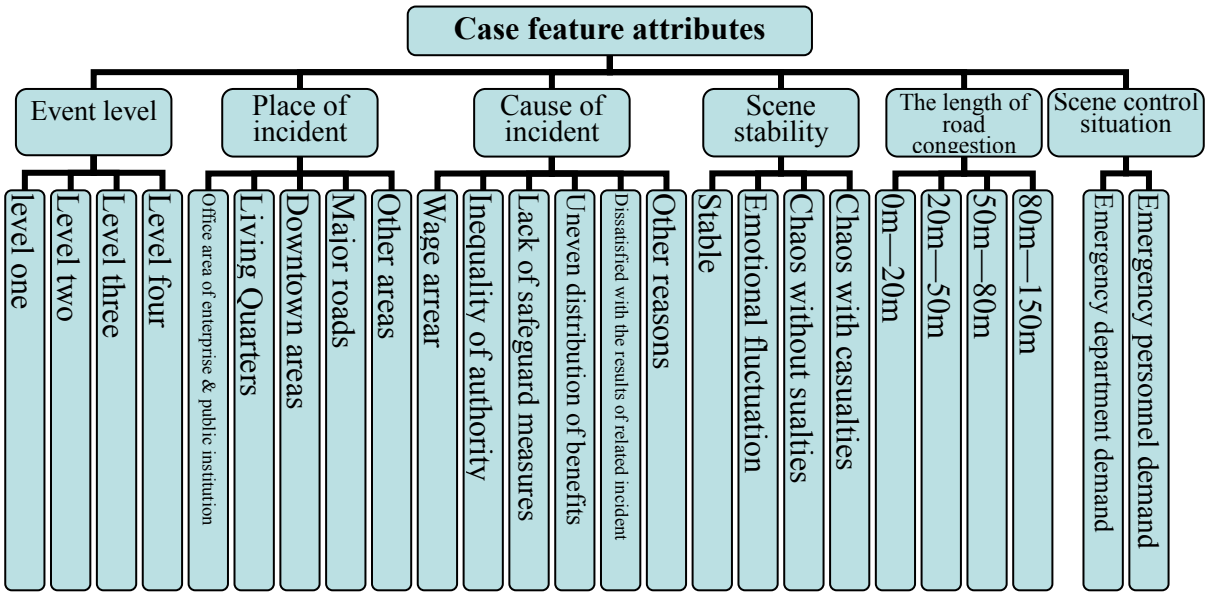

Fig. 1. Feature attributes and hierarchical structure of the migrant's worker group incident emergency management system based on CBR

Case retrieval of the migrant's worker group incident emergency management

There usually can be found one or more events matching with the current group incidents in the case retrieval, hence, case retrieval involves three key questions[9]: first,weight coefficient of feature attributes in the emergency system. Second, similarity matching on feature attributes of cases in emergency system and current group incidents. Third, similarity matching on overall attributes of cases in emergency system and current group incidents .

1. Calculate the weight coefficient on feature attributes of cases

Definitize the layer at the first

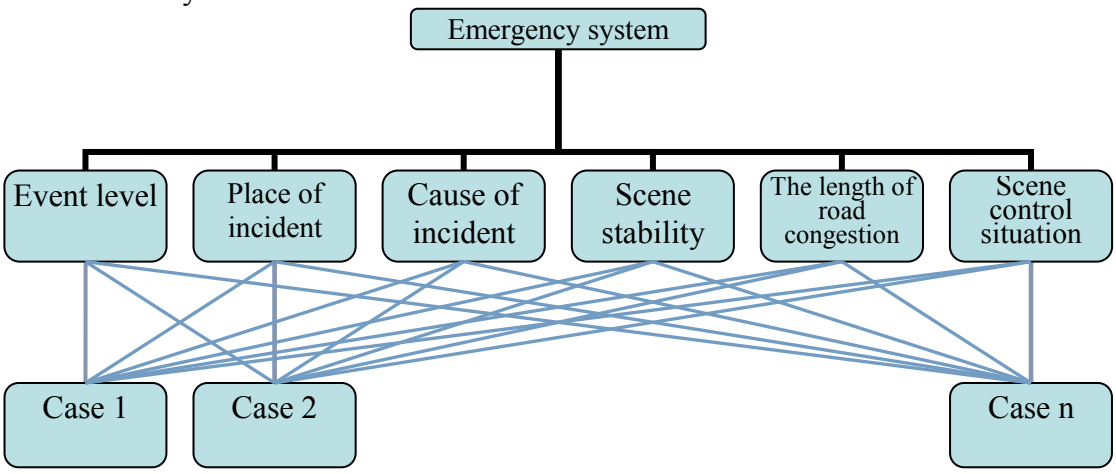

Fig. 2. Hierarchy chart of CBR

Then extract xi and xj from x1,x2,…xn by pairwise comparison and compare their contribution degree for the objective, assign xi/xj in one matrix according to the following scale.

xi/xj＝1， we think xi and xj are same importance.

xi/xj＝3, xi is a little more important than xj

xi/xj＝5， xi is important than xj

xi/xj＝7, xi is lot more important than xj

xi/xj＝9， xi is absolutely great important than xj

When specific value are 2,4,6,8,we think it is in the intermediate state.

The following assignment are based on Analytic Hierarchic Process (AHP).look at the Table. 1

Table 1 : Judgment matrix of weight coefficient on feature attributes of cases

i j	event level	place of incident	cause of incident	scene stability	road condition	Scene control condition
event level	1	1/2	1/4	1/3	1/2	1/3
place of incident	2	1	1/2	2/3	1	2/3
cause of incident	4	2	1	4/3	2	4/3
scene stability	3	3/2	3/4	1	3/2	1
road condition	2	1	1/2	2/3	1	2/3
Scene control condition	3	3/2	3/4	1	3/2	1

According to the chart we can get 6 feature attributes, and according to the attributes, we can obtain the following judgment matrix:

1. list matrix:

$$P=\begin{vmatrix} 1 & 1/2 & 1/4 & 1/3 & 1/2 & 1/3 \\ 2 & 1 & 1/2 & 2/3 & 1 & 2/3 \\ 4 & 2 & 1 & 4/3 & 2 & 4/3 \\ 3 & 3/2 & 3/4 & 1 & 3/2 & 1 \\ 2 & 1 & 1/2 & 2/3 & 1 & 2/3 \\ 3 & 3/2 & 3/4 & 1 & 3/2 & 1 \end{vmatrix}$$

2. normalize each column of the matrix：

$$P=\begin{vmatrix} 1/15 & 1/15 & 1/15 & 1/15 & 1/15 & 1/15 \\ 2/15 & 2/15 & 2/15 & 2/15 & 2/15 & 2/15 \\ 4/15 & 4/15 & 4/15 & 4/15 & 4/15 & 4/15 \\ 1/5 & 1/5 & 1/5 & 1/5 & 1/5 & 1/5 \\ 2/15 & 2/15 & 2/15 & 2/15 & 2/15 & 2/15 \\ 1/5 & 1/5 & 1/5 & 1/5 & 1/5 & 1/5 \end{vmatrix}$$

3. sum up each row of the matrix

$$P=\begin{vmatrix} 2/5 \\ 4/5 \\ 8/5 \\ 6/5 \\ 4/5 \\ 6/5 \end{vmatrix}$$

4. normalize each column of the matrix

$$P=\begin{vmatrix} 0.067 \\ 0.133 \\ 0.267 \\ 0.200 \\ 0.133 \\ 0.200 \end{vmatrix}$$

According to the above calculate, the consequence of weight judgment matrix of 6 feature attributes in group incident is: the max characteristic value of this matrix is $\lambda max=\frac{1}{n}\sum_{x=1}^{n} Wx$ =6 (Wx is weight coefficient of feature attribute x in the group incidents)
W=(0.067,0.133,0.267,0.200,0.133,0.200)T is the weight coefficient of feature attributes, as shown in Table. 2

Table 2 Judgment matrix of weight coefficient on feature attributes of cases(add)

i j	event level	place of incident	cause of incident	scene stability	road condition	Scene control condition	
event level	1	1/2	1/4	1/3	1/2	1/3	0.067
place of incident	2	1	1/2	2/3	1	2/3	0.133
cause of incident	4	2	1	4/3	2	4/3	0.267
scene stability	3	3/2	3/4	1	3/2	1	0.200
road condition	2	1	1/2	2/3	1	2/3	0.133
Scene control condition	3	3/2	3/4	1	3/2	1	0.200

1.1 Consistency judgment of the weight coefficient

Sometimes there will be inconsistent in similarity comparison of current events and cases in case library, so we must conduct the consistency check and the formula is CR=CI/RI.

CR is the rate of random consistency in judgment matrix; CI is the index of general consistency in judgment matrix.the formula of CI is

CI=(λ max- n) /(n- 1) (1)

RI is the index of random consistency in judgment matrix.the value of RI as shown in table 3.

Table 3 RI index of random consistency in judgment matrix

N	1	2	3	4	5	6	7	8	9
RI	0	0	0.58	0.90	1.12	1.24	1.32	1.41	1.45

When CR<0.1 or the maximal characteristic value of this matrix is same with the matrix dimension,we can draw a conclusion the case has the satisfactory consistency, otherwise we need to modify or adjust the value of every feature attributes in the matrix,until make it has the satisfactory consistency.

Mentioned above CI=0<0.1 illustrates the matrix has the satisfactory consistancy.

2 similarity calculation in CBR

Similarity calculation has many ways and there are 5 ways can be chosen for similarity calculation in this paper, numeric type , boolean type, enumerated type, string type , interval type.Similarity calculation model is used for matching the two cases' degree of similarity, and by the calculation and sorting, we can obtain the best matching model of the case at final. The next part will introduce computing methods of various attributes similarity and the overall similarity.

4.2.1 Similarity calculation model of social group incident's attributes.

1. Similarity calculation model in numeric type

$$sim(x_i, y_j)=1-\frac{d_{ij}}{\max(x_i, y_j)}$$

(dij is difference value of xi and yj) (2)

In the formula , similarity value cannot be more than 1, more than 1 means no similarity, if the value is 0,the similarity is inconsistent。X and y must be unified properties. x is the attribute value of current events, y is value of the cases in case library.This formula must be numeric comparison, such as there are 1 emergency personnel in current events and 5 in the cases.

2.Similarity calculation model in boolean type

$$sim(x_i, y_j)=compare(x_i, y_j) \tag{3}$$

(function "compare" is contrasted according to the actually stored value,all the same says 1,different says 0.)X and y represent the unified property only have two values ,the one value is 1 ,it means conformity,the other value is 0, it means disconformity. Generally we use whether judgment,or category judgment, for example,the event took place in Guangzhou,it will mark 1 if there have cases happen in Guangzhou,otherwise mark 0.

3.Similarity calculation model in enumerated type

$$sim(x_i, y_j)=1-\frac{d_{ij}}{\max(R)-\min(R)} \tag{4}$$

Wherein R is the Enum type collection, the discussed enumerated type is regular, it represents apart and regular enumeration difference. X represents one attribute value in current event, y represents corresponding attribute value in the case, similarity can't more than 1. For example, the incident is classified primary, secondary, tertiary, quaternary. The current event is quaternary, case event is secondary, so dij is 2.

4.Similarity calculation model in interval type

$$\mathrm{sim}(x_i, y_j) = 1 - \sqrt{((\min(x_i) - \max(y_i))2 + (\max(x_i) - \max(y_i)2}\Big/_4 \tag{5}$$

X represents one attribute value in current event, y represents corresponding attribute value in the cases, similarity can't more than 1. The formula is suit for scoped attributes. Such as road width is 23m~24m ,22m~23m .

5.Similarity calculation model in string type

$$sim(x_i, y_j)=\frac{t\times l}{\max(len(x_i), len(y_j))} \tag{6}$$

len() represents the length of character in some attributes, t is the matching number, how many times of the same character matching. T guarantees more repetitive more match. L is the matching length of two attributes, that is say how many characters matching with different characters. T guarantees more same characters more match. Similarity can't more than 1, if not it will be invalid. This category is suit for the matching of reason or matching of the fuzzy information.

The overall similarity calculation model of social group incident

There are many kinds of overall similarity calculation model, several common methods are the nearest neighbor algorithm, Tversky function, improved Tversky function, Multi-parameter similarity calculation and so on. The nearest neighbor algorithm is the selected method in this paper, just because it is easy to operate relatively. It is a method that cumulate every attribute value's similarity of the group incidents and thus calculate the the overall similarity. The formula of the overall similarity is :

$$\mathrm{Sim}(A,B)=\sum_{x=1}^{n} Wx\,\mathrm{sim}(Ax, Bx) \qquad m(x=1,2,\cdots,n) \tag{7}$$

Wx is the weight of attribute x ,Ax is the No.x attribute value of current event,Bx is the No.x attribute value of case event,and introduce the weight Wx into the calculation.

You can do the case selection after you gain the overall similarity. Which gain the highest score means it is most similar in the case library.

Case analysis

On September 21, 2011,in the Shantou city of Guangdong province, villagers from Wukan village shouted slogans, pulled banners to demonstrate, they claimed that their lands are occupied and the cadres election is unfair, this event then developed into conflict in that day. Several hundred villagers destroyed the nameplate of the village committee and surrounding facilities. As police began to involve, the incident developed to the conflict with the police. More than 10 policemen were injured,six police car were damaged. Lufeng country set up the temporary emergency working group and launched an investigation, but the villagers disagreed with the announced results.

Result test

The matching case in the case library is "migrant's worker group incident in a factory", the number of participants is about 30 to 99, the location of the event is office area, the reason is wage arrear, scene stability is emotional fluctuation, the length of road congestion is about 10 to 49, the demand of the emergency department is 4,the demand of emergency personnel is 25.

But the participants are more than 100 in the group incident of Wukan village, Shantou city, the location of the event is office area, the cause is uneven distribution of benefits, scene stability is chaos with casualties, the length of road congestion is 10 to 49, the demand of the emergency department is 2, the demand of emergency personnel is 8.

By similarity calculation, translate the matching case to numerical value, as for the participants, set the original case (group incident of Wukan village, Shantou city) is x, the matching case is y. The participant similarity is 0.667; incident location similarity is 1; the cause of incident similarity is 0; scene stability similarity is 0.333; the length of road congestion similarity is 1; the demand of emergency department and personnel similarity is 0.41; and the overall similarity is 0.459289, the result is same with the calculation of matching degree of the system.

Conclusion

This paper analyses the premise of the specific situation of the benefit disputes of migrant's worker in the urban and rural joint areas , extracts 6 feature attributes including event level, place of incident, cause of incident, scene stability, length of road congestion and plan demand, which lays the foundation of establishing the system models. On the basic of 6 feature attributes, we use AHP to establish multi-factors and multi-level decision analysis model, design the CBR system based on J2EE. In the end of paper, we verify the model through the case of Wukan group incident taken place on September 21, 2011. The overall similarity between the test results and given cases in the system is 0.459289. In addition, we take this case to manual CBR process analysis, compare two reasoning results, obtain the higher accuracy and smaller error, which reached the intended effect and proved to be able to conduct effective decision making support based on the current case feature attributes.

Acknowledgements

Funding project: Youth science fund project of national natural science foundation of China (No.51306061); Central Youth College Teachers independent research program (No:x2ggD2118220); South China University of Technology full-time Master Reform Demonstration Project(No:Z4901038)

References

[1] Analytic Hierarchic Process ［EB/OL］BAIKE

http://baike.baidu.com/subview/364279/5071768.htm?fr=aladdin

[2]Jin Ping.The theory of rural-urban continuum[J]. Research On Development,, 2001 (1): 9-10.

[3] Wu Yabin. The method of public security organs to deal with mass incidents under new situation [J]. Commodity and Quality: theoretical research, 2010 (1): 33-33.

[4]Mei Zhongling. Some thought about the group accident on the rural-urban continuum[J]. Journal of the Party School of CPC Zhengzhou Municipal Committee, 2009, 5: 032.

[5]Wu Peng. Crime characteristics and reasons on the rural-urban continuum[J]. Modern Business, 2008 (6): 257-257.

[6] YU Shui，LI Yu—qi . An Empirical Study on the Influencing Factors of Migrant Workers'Group Events ------A Survey of Migrant Workers in Southern Jiangsu Province[J]. Journal of South China Agricultural University(Social Science Edition), 2010, 9(004): 20-29.

[7] Liu Na, Fan Xiao-guang. Research on influence factors and countermeasure of the peasant laborer group accident——Deng En policy analysis model[J]. Legal System and Society, 2011 (28).

[8] Li Yu, Wang Xin. Investigation about the influence of peasant laborer group accident[J]. The world of labor security (Theory Edition), 2010, 8: 015.

[9]Lu Zong-ping , Hu Xin ，Yang Hong-yu . Airport Emergency Preparednesss Management Based on Case-Based Reasoning[J]. Journal of Civil Aviation University of China, 2010, 28(2): 1-5.

Advanced Materials Research Vols. 989-994 (2014) pp 1712-1715
© (2014) Trans Tech Publications, Switzerland
doi:10.4028/www.scientific.net/AMR.989-994.1712

Equivalent Integral Equations of the Static Schrödinger Equation by Variation of Constants Method

Sheng Zhang[1, a], Bin Cai[1,b] and Di Wang[1,c]

[1]School of Mathematics and Physics, Bohai University, Jinzhou 121013, PR China

[a]szhangchina@126.com, [b]65470641@qq.com, [c]785492083@qq.com

Keywords: Equivalent integral equation; Schrödinger equation; Variation of constants method

Abstract. As a milestone method, the inverse scattering transformation is also known as the nonlinear Fourier transformation for solving nonlinear partial differential equations analytically. The equivalent integral equations play a crucial role for the inverse scattering transformation. In this paper, the equivalent integral equations of the static Schrödinger equation are derived by the variation of constants method. The derivation of the equivalent integral equations provides with a necessary help for the beginners to study the inverse scattering transformation method in soliton theory.

Introduction

It is well known that nonlinear complex physical phenomena are often related to nonlinear partial differential equations (PDEs), which are involved in many fields from physics to biology, chemistry, mechanics, etc. As mathematical models of the phenomena, the investigation of exact solutions of nonlinear PDEs will help to understand these phenomena better. With the development of soliton theory, finding exact solutions of nonlinear PDEs has gradually developed into a significant direction in nonlinear science and some effective methods have been proposed and developed, such as the inverse scattering method [1], Bäcklund transformation [2], Hirota's bilinear method [3], homogeneous balance method [4], function expansion methods [5-7]. Among them, the inverse scattering transformation [1] is a systematic method for constructing exact solutions of nonlinear PDEs and recently has received a wide range of applications [8-15] since it was proposed by Gardner, Greene, Kruskal and Miura in 1965 [16].

The inverse scattering transformation is also known as the nonlinear Fourier transformation for solving PDEs, one of its advantages is that it can solve a whole hierarchy of nonlinear PDEs, for example, the KdV hierarchy [17]

$$u_t = T^n u_x,\ \ T = \partial^2 + 4u + 2u_x\partial^{-1},\ \partial = \frac{\partial}{\partial x},\ \partial^{-1} = \frac{1}{2}\left(\int_{-\infty}^{x} \mathrm{d}x - \int_{x}^{\infty} \mathrm{d}x\right),\ \ n = 0,1,2,\cdots \tag{1}$$

associated with a certain spectral problem, namely the static Schrödinger equation

$$\varphi_{xx}(x,k) + u(x)\varphi(x,k) = \lambda\varphi(x,k), \tag{2}$$

where the potential $u(x)$ and their derivatives of any order with respect to x are smooth potential functions which vanish as x tends to infinity, and the following integral

$$\int_{-\infty}^{\infty} |x^j u(x)| \mathrm{d}x, \quad j = 0,1,2 \tag{3}$$

is finite.

Replacing the spectral parameter λ with $-k^2$, Eq. (2) becomes

$$\varphi_{xx}(x,k) + u(x)\varphi(x,k) = -k^2\varphi(x,k). \tag{4}$$

If the integral (3) is convergent, then Eq. (4) exists only a pair of elementary solutions called Jost functions which satisfy the asymptotic conditions

$$\varphi_1(x,k) \sim \mathrm{e}^{ikx}, \quad x \to \infty, \tag{5}$$

$$\varphi_2(x,k) \sim \mathrm{e}^{-ikx}, \quad x \to -\infty. \tag{6}$$

The Jost solutions of Eq. (4) are very important for the inverse scattering transformation method, which are determined by the equivalent integral equations of Eq. (4) when $k \neq 0$

$$\varphi_1(x,k)=\mathrm{e}^{ikx}+\int_x^{\infty}\frac{\sin k(x-s)}{k}u(s)\varphi_1(s,k)\mathrm{d}s\,, \tag{7}$$

$$\varphi_2(x,k)=\mathrm{e}^{-ikx}-\int_{-\infty}^{x}\frac{\sin k(x-s)}{k}u(s)\varphi_2(s,k)\mathrm{d}s\,. \tag{8}$$

Letting $k\to 0$, we can obtain limits of Eqs. (7) and (8)

$$\varphi_1(x)=1+\int_x^{\infty}(x-s)u(s)\varphi_1(s)\mathrm{d}s\,, \tag{9}$$

$$\varphi_2(x)=1-\int_{-\infty}^{x}(x-s)u(y)\varphi_2(s)\mathrm{d}s\,, \tag{10}$$

which give the two cases when $k=0$ of Eqs. (7) and (8).

As a famous method in soliton theory, the inverse scattering transformation method is a milestone in the process of developing analytical methods for solving nonlinear partial differential equations. Without the equivalent integral equations (7) and (8) and their Jost solutions, the inverse scattering transformation could not solve the KdV hierarchy (1). However, to the best of our knowledge, there is not the detailed derivation of Eqs. (7) and (8) in literature.

In this paper, we would like to use the variation of constants method [18] to derive Eqs. (7) and (8) from Eqs. (4)-(6). The rest of this paper is organized as follows. In Section 2, we derive the equivalent integral equatoins (7) and (9) by using the variation of constant method. In Section 3, some conclusions are given.

Derivation of the Equivalent Integral Equations

It is easy to see that when $u(x)\to 0$, Eq. (4) has a pair of elementary solutions e^{-ikx} and e^{ikx}. According to the variation of constants method [18], we suppose that

$$\varphi(x,k)=v_1(x)\mathrm{e}^{-ikx}+v_2(x)\mathrm{e}^{ikx}\,, \tag{11}$$

is an arbitrary solution of Eq. (4).

Substituting Eq. (11) into Eq. (4), we have

$$\varphi_x(x,k)=v_1'(x)\mathrm{e}^{-ikx}-ikv_1(x)\mathrm{e}^{-ikx}+v_2'(x)\mathrm{e}^{ikx}+ikv_2(x)\mathrm{e}^{ikx}\,. \tag{12}$$

Further letting

$$v_1'(x)\mathrm{e}^{-ikx}+v_2'(x)\mathrm{e}^{ikx}=0\,, \tag{13}$$

we have

$$\varphi_{xx}(x,k)=-ikv_1'(x)\mathrm{e}^{-ikx}-k^2v_1(x)\mathrm{e}^{-ikx}+ikv_2'(x)\mathrm{e}^{ikx}-k^2v_2(x)\mathrm{e}^{-ikx}\,. \tag{14}$$

Substituting Eq. (14) into Eq. (4) yields

$$-ikv_1'(x)\mathrm{e}^{-ikx}+ikv_2'(x)\mathrm{e}^{ikx}=-u(x)\varphi(x,k)\,, \tag{15}$$

then solving Eqs. (13) and (15), we can obtain

$$v_1'(x)=-\frac{\mathrm{e}^{ikx}u(x)\varphi(x,k)}{2ik}\,, \tag{16}$$

$$v_2'(x)=\frac{\mathrm{e}^{-ikx}u(x)\varphi(x,k)}{2ik}\,. \tag{17}$$

Taking into account of Eqs. (16) and (17), we select

$$v_1(x)=\int_x^{\infty}\frac{\mathrm{e}^{iks}u(s)\varphi(s,k)}{2ik}\mathrm{d}s+c_1\,, \tag{18}$$

$$v_2(x)=-\int_x^{\infty}\frac{\mathrm{e}^{-iks}u(s)\varphi(s,k)}{2ik}\mathrm{d}s+c_2\,, \tag{19}$$

where c_1 and c_2 are the integral constants.

With the help of Eqs. (18) and (19) we have

$$\varphi_1(x,k)=\int_x^{\infty}\frac{\mathrm{e}^{ik(x-s)}u(s)\varphi_1(s,k)}{2ik}\mathrm{d}s+c_1\mathrm{e}^{-ikx}-\int_x^{\infty}\frac{\mathrm{e}^{-ik(x-s)}u(s)\varphi_1(s,k)}{2ik}\mathrm{d}s+c_2\mathrm{e}^{ikx}\,, \tag{20}$$

In view of the asymptotic conditions (5) and (6), from Eq. (20) we have

$$c_1 = 0,\ c_2 = 1. \tag{21}$$

by setting $x \to \infty$, then Eq. (20) is reduced to

$$\varphi_1(x,k) = \int_x^{\infty} \frac{e^{ik(x-s)} u(s)\varphi_1(s,k)}{2ik} ds - \int_x^{\infty} \frac{e^{-ik(x-s)} u(s)\varphi_1(s,k)}{2ik} ds + e^{ikx}. \tag{22}$$

Employing the equality

$$\frac{\sin k(x-s)}{k} = \frac{e^{ik(x-s)} - e^{-ik(x-s)}}{2ik}, \tag{23}$$

from Eq. (23) we finally obtain Eq. (7).

Similarly, if we select

$$v_1(x) = -\int_{-\infty}^{x} \frac{e^{iks} u(s)\varphi(s,k)}{2ik} ds + c_3, \tag{24}$$

$$v_2(x) = \int_{-\infty}^{x} \frac{e^{-iks} u(s)\varphi(s,k)}{2ik} ds + c_4, \tag{25}$$

where c_3 and c_4 are integral constants to be determined.

$$\varphi_2(x,k) = -\int_{-\infty}^{x} \frac{e^{-ik(x-s)} u(s)\varphi_2(s,k)}{2ik} ds + c_3 e^{-ikx} - \int_{-\infty}^{x} \frac{e^{ik(x-s)} u(s)\varphi_2(s,k)}{2ik} ds + c_4 e^{ikx}, \tag{26}$$

from which we obtain

$$c_3 = 1,\ c_4 = 0. \tag{27}$$

by setting $x \to -\infty$.

In this case, we have

$$\varphi_2(x,k) = \int_{-\infty}^{x} \frac{e^{-ik(x-s)} u(s)\varphi_2(s,k)}{2ik} ds - \int_{-\infty}^{x} \frac{e^{ik(x-s)} u(s)\varphi_2(s,k)}{2ik} ds + e^{-ikx}, \tag{28}$$

from which Eq. (8) can be obtained by the use of Eq. (26).

Conslusion

In summary, we have derived the equivalent integral equations of the static Schrödinger equation (4) by the variation of constants method. Without the equivalent integral equations and their Jost solutions, the inverse scattering transformation could not solve the KdV hierarchy (1). Therefore, the derivation of the equivalent integral equations is necessary and can help the beginners to study the inverse scattering transformation method in soliton theory. How to derive the equivalent integral equations for some other linear spectral problems of the corresponding hierarchies of nonlinear PDEs is worthy of study. This our task in the future.

Acknowledgements

This work was supported by the Natural Science Foundation of Liaoning Province (L2012404) of China, the PhD Start-up Funds of Bohai University (bsqd2013025) and Liaoning Province of China, the Liaoning BaiQianWan Talents Program (2013921055) and the Natural Science Foundation of China (11371071).

References

[1] M.J. Ablowitz, P.A. Clarkson, Soliton, Nonlinear Evolution Equations and Inverse Scattering, Cambridge University Press, Cambridge, 1991.

[2] M.R. Miurs, Bäcklund Transformation, Springer-Verlag, Berlin, 1978.

[3] R. Hirota, Exact solution of the Korteweg-de Vries equation for multiple collisions of solitons, Physical Review Letters, 27 (1971) 1192-1194.

[4] M.L. Wang, Exact solutions for a compound KdV-Burgers equation, Physics Letters A, 213 (1996) 279-287.

[5] S.K. Liu, Z.T. Fu, S.D. Liu, Q. Zhao, Jacobi elliptic function expansion method and periodic wave solutions of nonlinear wave equations, Physics Letters A, 289 (2001) 69-74.

[6] E.G. Fan, Travelling wave solutions in terms of special functions for nonlinear coupled evolution systems, Physics Letters A, 300 (2002) 243-249.

[7] S. Zhang, T.C. Xia, A generalized auxiliary equation method and its application to (2+1)-dimensional asymmetric Nizhnik-Novikov-Vesselov equations, Journal of Physics A Mathematical and General, 40 (2007) 227-248.

[8] C.S. Garder, J.M. Greene, M.D. Kruskal, R.M. Miura, Korteweg-de Vires equation and generalizations, VI. Method for exact solution, Communications on Pure and Applied Mathematics, 27 (1974) 97-133.

[9] P.D. Lax, Integrals of nonlinear equations of evolution and solitary waves, Communications on Pure and Applied Mathematics, 21 (1968) 467-490.

[10] V.E. Zakharov, A.B. Shabat, Interaction between solitons in a stable medium, Soviet Physics–JETP, 34 (1972) 62-69.

[11] M. Wadati, The modified Korteweg-de Vries equation, Journal of the Physical Society of Japan, 32 (1973) 1289-1296.

[12] M.J. Ablowitz, D.J. Kaup, A.C. Newell, H. Segur, Method for solving the sine-Gordon equation, Physical Review Letters, 30 (1973) 1262-1264.

[13] H. Flaschka, On the Toda lattice, II, Progress of Theoretical Physics, 51 (1974) 703-716.

[14] M.J. Ablowitz, J.F. Ladik, Nonlinear differential-difference equations, Journal of Mathematical Physics, 16 (1975) 598-603.

[15] A.I. Nachman, M.J. Ablowitz, A multidimensional inverse scattering method, Studies in Applied Mathematics, 71 (1984) 243-250.

[16] C.S. Garder, J.M. Greene, M.D. Kruskal, R.M. Miura, Method for solving the Korteweg-de Vries equation, Physical Review Letters, 19 (1965) 1095-1097.

[17] D.Y. Chen, Introduction to Soliton, Science Press, Beijing, 2006.

[18] P. Hartman, Ordinary Differential equations, John Wiley & Sons Inc., Now York, 1964.

Advanced Materials Research Vols. 989-994 (2014) pp 1716-1719
© (2014) Trans Tech Publications, Switzerland
doi:10.4028/www.scientific.net/AMR.989-994.1716

Kink-Type Solutions of the MKdV Lattice Equation with An Arbitrary Function

Sheng Zhang[1, a], Ying-Ying Zhou[1,b] and Bin Cai[1,c]

[1]School of Mathematics and Physics, Bohai University, Jinzhou 121013, PR China

[a]szhangchina@126.com, [b]1374771146@qq.com, [c]65470641@qq.com

Keywords: Kink-type solution; MKdV lattice equation; Exp-function method

Abstract. In this paper, the exp-function method is improved for constructing exact solutions of nonlinear differential-difference equations with variable coefficients. To illustrate the validity and advantages of the improved method, the mKdV lattice equation with an arbitrary function is considered. As a result, kink-type solutions are obtained which possess rich spatial structures. It is shown that the improved exp-function method can be applied to some other nonlinear differential-difference equations with variable coefficients.

Introduction

In 2006, He and Wu [1] proposed the so-called exp-function method to obtain solitary solutions and periodic solutions of nonlinear partial differential equations (PDEs). Since the method was proposed, it has been widely applied to many nonlinear PDEs [2-13]. More and more studies show that the exp-function method with computer symbolic computation is available for many kinds of nonlinear PDEs and can be used to construct different types of exact solutions due to its more general ansätz:

$$u(\xi)=\frac{\sum_{n=-f}^{g} a_n \exp(n\xi)}{\sum_{m=-p}^{q} b_m \exp(m\xi)}, \quad \xi=\sum_{i=1}^{s} k_i x + wt \tag{1}$$

employed for a given $(s+1)$-dimensional nonlinear PDEs with independent variables $t, x_1, x_2, \cdots, x_s$ and dependent variable u, here a_n and b_m are undermined constants, f, p, g and q can be determined by balancing the highest order linear term with the highest order nonlinear term in Eq. (1). He and Wu [2] showed through several instances that the final solution does not strongly depend on the choices of values of f, p, g and q. It was observed that the relations $f=p$ and $g=q$ are usually obtained and $f=p=g=q=1$ is the simplest choice and makes the exp-function method more straightforward.

Since the work of Fermi *et al.* in the 1950s [14], the investigation of exact solutions of nonlinear differential-difference equations (DDEs) has played a crucial role in the modelling of many phenomena in different fields which include condensed matter physics, biophysics and mechanical engineering. Unlike difference equations which are fully discretized, DDEs are semi-discretized with some of their spacial variables discretized while time is usually kept continuous. Generally speaking, it is hard to generalize one method for nonlinear PDEs to solve nonlinear DDEs because of the difficulty to search for iterative relations from indices n to $n\pm1$.

The present paper is motivated by the desire to propose an improve version of the exp-function method for constructing exact solutions of nonlinear DDEs with variable coefficients. In order to illustrate the validity and advantages of the improved method, the mKdV lattice equation with an arbitrary function

$$\frac{du_n(t)}{dt}=[\alpha(t)-u_n^2](u_{n+1}-u_{n-1}), \tag{2}$$

is considered, here $u_n = u(n,t)$, $n \in Z$, $\alpha(t)$ is an arbitrary function of t. When $\alpha(t) = 1$, Eq. (2) becomes the known mKdV lattice equation [15]. As a result, kink-type solutions are obtained which possess rich spatial structures.

Methodology

For a given nonlinear DDEs

$$E(u_{nt}, u_{nx}, u_{ntt}, u_{nxt}, \cdots, u_{n-1}, u_n, u_{n+1} \cdots) = 0, \tag{3}$$

we take the following transformation

$$u_n = U_n(\xi_n), \ \xi_n = dn + c(t) + \omega, \tag{4}$$

where d is a constant to be determined later, $c(t)$ is an undetermined function of t, ω is an arbitrary function, then Eq. (3) can be reduced to

$$F(U_n', U_n'', \cdots, U_{n-1}, U_n, U_{n+1}, \cdots) = 0. \tag{5}$$

The ansätz used to improve the exp-function method presented in this paper for Eq. (5) is expressed in the following form:

$$U_n = \frac{a_{-1}\exp(-\xi_n) + a_0 + a_1\exp(\xi_n)}{b_{-1}\exp(-\xi_n) + b_0 + b_1\exp(\xi_n)}, \tag{6}$$

$$U_{n-1} = \frac{a_{-1}\exp(-\xi_n)\exp(d) + a_0 + a_1\exp(\xi_n)\exp(-d)}{b_{-1}\exp(-\xi_n)\exp(d) + b_0 + b_1\exp(\xi_n)\exp(-d)}, \tag{7}$$

$$U_{n+1} = \frac{a_{-1}\exp(-\xi_n)\exp(-d) + a_0 + a_1\exp(\xi_n)\exp(d)}{b_{-1}\exp(-\xi_n)\exp(-d) + b_0 + b_1\exp(\xi_n)\exp(d)}, \tag{8}$$

where a_{-1}, a_0, a_1, b_{-1}, b_0 and b_1 are all undetermined constants.

Substituting Eqs. (6)-(8) into Eq. (5) yields and equating the coefficients of all powers of $\exp(j\xi_n)$ $(j = 0, \pm1, \pm2, \cdots)$ to zero yields a set of equations for a_{-1}, a_0, a_1, b_{-1}, b_0, b_1, d and $c(t)$, solving the system of differential equations we can determine the solution (4) of Eq. (3) by use of Eqs. (6)-(8).

Kink-Type Solutions

For the mKdV lattice equation (2), we use the transformation (4), then it is reduced to

$$c(t)U_n' = [\alpha(t) - U_n^2](U_{n+1} - U_{n-1}). \tag{9}$$

Substituting Eqs. (6)-(8) into Eq. (15), we derive a set of equations for a_{-1}, a_0, a_1, b_{-1}, b_0, b_1, d and $c(t)$:

$$3a_{-1}^2 b_{-1} d + a_{-1} b_{-1}^2 d^3 = 0, \tag{10}$$

$$3a_0^2 b_0 d + a_0 b_0^2 d^3 - 8a_0 b_1 b_{-1} d^3 - \frac{8}{3} b_0 b_1 b_{-1} d^5 = 0, \tag{11}$$

$$-a_0 b_1^2 c - \frac{b_0 b_1^2 c^2}{3d} + \frac{1}{3} b_0 b_1^2 c d^2 + a_0 b_1^2 d^3 = 0, \tag{12}$$

$$a_0 a_1^2 \mathrm{e}^d - a_1^3 b_0 \mathrm{e}^d - a_0 c \mathrm{e}^{2d} + a_1 b_0 c \mathrm{e}^{2d} - a_0 a_1^2 \mathrm{e}^{3d} + a_1^3 b_0 \mathrm{e}^{3d} - a_0 \mathrm{e}^{\alpha(t)} + a_1 b_0 \mathrm{e}^{\alpha(t)} - a_1 b_0 \mathrm{e}^{3\alpha(t)} = 0, \tag{13}$$

$$\frac{27 a_0^3}{4d} - 12 a_0 b_1 b_{-1} d^3 = 0, \tag{14}$$

$$3a_0^2 b_{-1} d - a_0 b_0 b_{-1} d^3 - \frac{2}{3} b_0^2 b_{-1} d^5 = 0. \tag{15}$$

Solving the system of differential equations (10)-(15), we obtain the following results:

$$a_0 = 0, \ a_1 = \pm\sqrt{\alpha(t)}\tanh(d), \ a_{-1} = \mp b_{-1}\sqrt{\alpha(t)}\tanh(d), \tag{16}$$

$$b_0 = 0, \ c(t) = 2\tanh(d)\int \alpha(t)\mathrm{d}t, \tag{17}$$

where b_{-1} is an arbitrary constant.

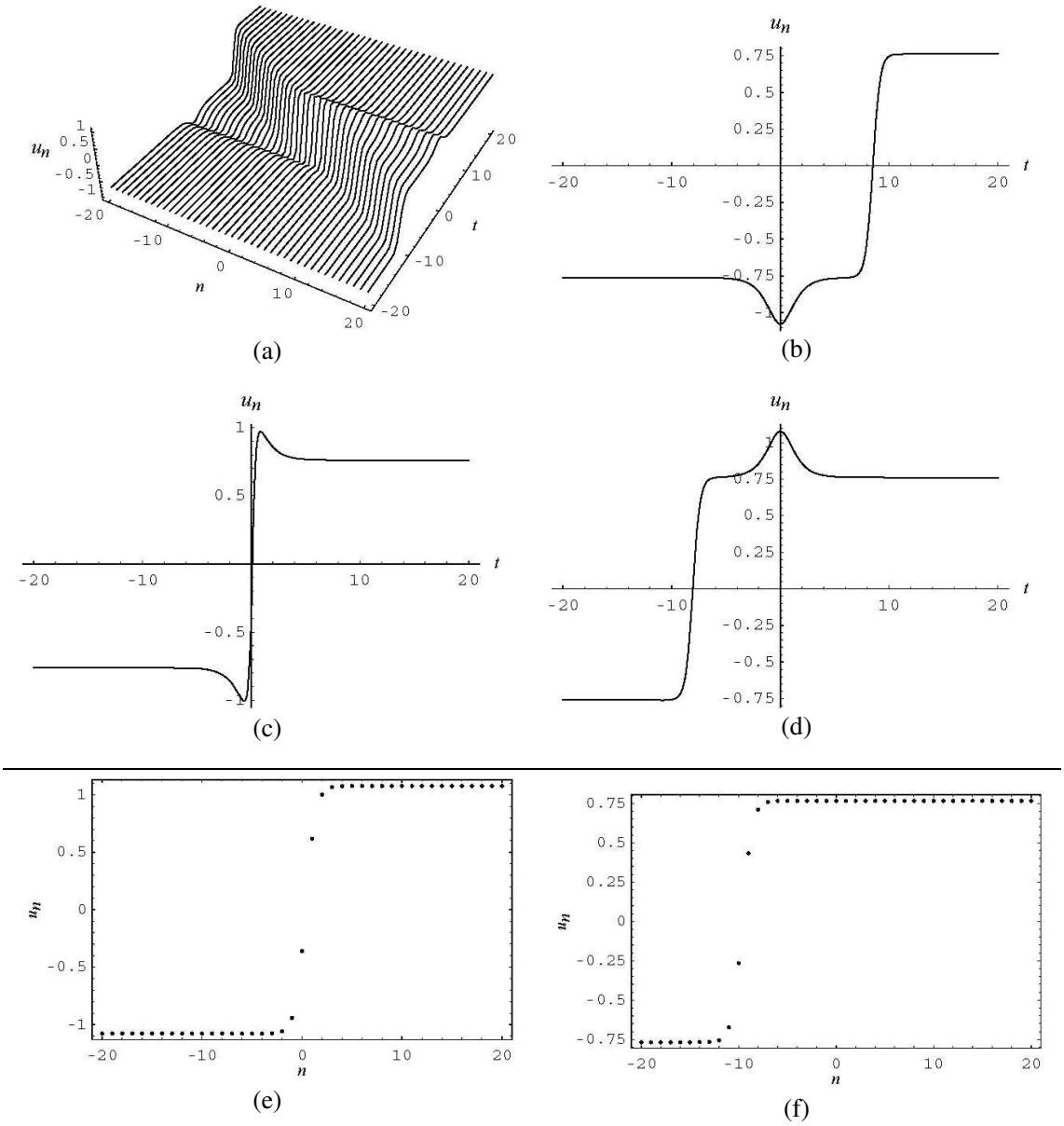

Fig. 1. Spatial structure of solution (18) with (+) branch: (a) $n=[-20,20]$, $t=[-20,20]$; (b) $n=-15$, $t=[-20,20]$; (c) $n=0$, $t=[-20,20]$; (d) $n=15$, $t=[-20,20]$; (e) $n=[-20,20]$, $t=0$; (f) $n=[-20,20]$, $t=5$.

Then we obtain a pair of new kink-type solutions of Eq.(2):

$$u_n=\pm\sqrt{\alpha(t)}\tanh(d)\frac{\exp(\xi_n)-b_{-1}\exp(-\xi_n)}{\exp(\xi_n)+b_{-1}\exp(-\xi_n)}, \tag{18}$$

where $\xi_n=dn+2\tanh(d)\int\alpha(t)\mathrm{d}t+\omega$.

In Fig. 1, a spatial structure of solution (18) is shown, where we selected $\alpha(t)=1+\mathrm{sech}t$, $b_{-1}=2$, $d=1$, $\omega=0$.

Conclusions

In this paper, an improvement on the exp-function method is proposed for nonlinear DDEs with variable coefficients. To show the advantage of the improved method, the mKdV lattice equation with an arbitrary function is considered. As a result, a pair of kink-type solutions are obtained. To the best

of our knowledge, the obtained solutions have not been reported in literature. It may be important to explain some physical phenomena. It is shown the improved exp-function method can be applied to some other nonlinear DDEs with variable coefficients.

Acknowledgements

This work was supported by the Natural Science Foundation of Liaoning Province (L2012404) of China, the PhD Start-up Funds of Bohai University (bsqd2013025) and Liaoning Province of China, the Liaoning BaiQianWan Talents Program (2013921055) and the Natural Science Foundation of China (11371071).

References

[1] J.H. He, X.H. Wu, Exp-function method for nonlinear wave equations, Chaos Solitons and Ftactals, 30 (2006) 700-708.

[2] J.H. He and M.A. Abdou, New periodic solutions for nonlinear evolution equations using Exp-function method, Chaos Solitons and Fractals, 34 (2006) 1421-1429.

[3] J.H. He L.N. Zhang, Generalized solitary solution and compacton-like solution of the Jaulent-Miodek equations using the Exp-function method, Physics Letters A, 372 (2008) 1044-1047.

[4] S. Zhang, Exp-function method for solving Maccari's system, Physics Letters A, 371 (2007) 65-71.

[5] A. Ebaid, Exact solitary wave solutions for some nonlinear evolution equations via Exp-function method, Physics Letters A, 365 (2007) 213-219.

[6] S. Zhang, Exp-function method for solving Maccari's system, Physics Letters A, 371 (2007) 65-71.

[7] C.Q. Dai, J.F. Zhang, Application of He's exp-function method to the stochastic mKdV equation, International Journal of Nonlinear Sciences and Numerical Simulation, 10 (2009) 675-680.

[8] V. Marinakis, The Exp-Function Method and n-Soliton Solutions, Zeitschrift für Naturforschung A–A Journal of Physical Sciences, 63 (2008) 653-656.

[9] S.D. Zhu, Exp-function method for the hybrid-lattice system, International Journal of Nonlinear Sciences and Numerical Simulation, 8 (2007) 461-464.

[10] S. Zhang, Application of Exp-function method to a KdV equation with variable coefficients, Physics Letters A, 365 (2007) 448-453.

[11] S. Zhang, Application of Exp-function method to high-dimensional nonlinear evolution equation, Chaos Solitons and Ftactals, 38 (2008) 270-276.

[12] J.R. Chang, The exp-function method and generalized solitary solutions, Computers & Mathematics with Applications, 61 (2011) 2081-2084.

[13] A. Edaid, An improvement on the Exp-function method when balancing the highest order linear and nonlinear terms, Journal of Mathematical Analysis and Applications, 392 (2012) 1-5.

[14] E. Fermi, J. Pasta, S. Ulam, Collected Papers of Enrico Fermi II, University of Chicago Press, Chicago, IL, 1965.

[15] M.J. Ablowitz, P.A. Clarkson, Soliton, Nonlinear Evolution Equations and Inverse Scattering, Cambridge University Press, Cambridge, 1991.

Advanced Materials Research Vols. 989-994 (2014) pp 1720-1723
© (2014) Trans Tech Publications, Switzerland
doi:10.4028/www.scientific.net/AMR.989-994.1720

An Improvement of the Method for Paraphrase of Chinese Double Negation

Zhongjian Wang[1,2,3 a], Shujian Zhang[1],Yanfeng Gao[1]
Yanfen Lin[1], Zongjie Wang[4, b]

[1]Harbin Harbin University of Commerce, Harbin 150028, China

[2]Open Fund of Smart Education and Information Engineering, Harbin Normal University

[3]Harbin Far East Institute of Technology, Harbin 150025, China

[4]Harbin Normal University, Harbin, 150025, China

[a]wangzhj@hrbcu.edu.cn, [b]jie052003@163.com

Keywords: Paraphrase; Similarity Calculation; Double Negation.

Abstract. By using part of speech information to similarity calculation of paraphrase sentences, the similarity calculation method is improved. The improved method includes multi information of paraphrase text, such as, matching words information and part of speech information. A small-scale comparing experiment of double negation sentence paraphrase for two method of similarity calculation has been done, and the experimental results indicated effect of improvement method.

Introduction

With computer networks are rapidly developing, society is becoming internationalized quickly. However the language information processing is the most important research domain in this information society. Paraphrasing is a very important research topic in research of NLP. It is able to use on a lot of fields and its use can improve the processing performance of the system [1][2], such as question answer [3], text reading assistance [4], information retrieval [5] and other fields. Its use can improve the processing performance of the system. It is very significant to research sentence paraphrase.

About research of Chinese sentence paraphrase, Li et al. proposed a template representation and generalization method, it represent paraphrasing template with semantic code of words and extract slot word by using a dependency parser, using search engine to generalize paraphrasing examples[6]. Zhao et al. proposed a method that acquires context-specific lexical paraphrases automatically, the method obtains paraphrases of a word depend on the specific sentence the word occurs in, extract candidate paraphrase by web mining [7]. Zong et al. proposed a method of spoken Chinese paraphrasing, extracting feather of input utterance by analysis phrase structure and chunk dependency of an utterance, finally got paraphrasing of input based on the analysis result [8].

Although the paraphrase research of English and Japanese has achieved many results, Chinese language is neither like English which characterizes by tense, person, declension, etc., nor like Japanese which characterizes by case-auxiliary word and declension, the research of Chinese sentence paraphrase cannot use the same technique that process English or Japanese. Sentence structure and empty words play a key role in Chinese expression.

This paper improved the calculation method of similarity of paraphrase sentences, and made use of the method to the paraphrase of Chinese double negative sentence. At first, the paper introduces Chinese double negative sentences. Then paraphrase templates are extracted by analyzing sentence structure. The matching of paraphrase template with original sentences is by calculating similarity.

Structure of Double Negative Sentences

A double negative sentence has two forms of negation that is used in the same sentence. In double negative sentences, double negatives cancel one another and produce an affirmative sense.

Mandarin Chinese also employs litotes in a like manner. For example, 'I do not dislike.' can express by 'I certainly like. '.

A double negative sentence has three expression functions. It can express affirmation, emphasis and euphemism. For the three kinds of double negative sentences, the structures are: double negation consists of two negative adverbs of using together; double negation consists of a negative adverb and a verb that has negative meaning; double negation consists of a negative adverb (or a verb that has negative meaning) and tone of one's voice when asking a rhetorical question.

We use the word segmentation and part-of –speech tagging tool to analyze those double negative sentences [9], and compare original sentences with paraphrase sentences to extract paraphrasing templates.

Classification of Double Negative Sentences

Here the double negative sentences are classified to three kinds of structures: use two negative adverbs; use a negative adverb and a verb that has negative meaning; use a negative adverb (or a verb that has negative meaning) and tone of one's voice when asking a rhetorical question. That is to say, there are three kinds of double negative sentence.

Semantic Analysis of Double Negative Sentences

We use the word segmentation and part-of–speech tagging tool to analyze those double negative sentences, and compare original sentences with paraphrase sentences to extract paraphrasing templates. The analysis results of double negative sentences are as following table 1.

In the table 1, '*' is words that does not effect sentence meaning and can be exchanged by other words. In addition rr, nr, w, v, d, dy and n are POS of words of corresponding position.

Paraphrase Templates of Double Negative Sentences

Table 1 shows double negative paraphrase templates that are generally used. For example, the paraphrase sentence of 'wo bu de bu qu tushuguan kanshu.' (I have to go to library to read book.) can be expressed by 'wo qu tushuguan kanshu.', 'wo bixu qu tushuguan kanshu.', 'wo yinggai qu tushuguan kanshu.' and so on. The paraphrase templates can complete those paraphrasing process.

Table 1. A part of Paraphrase Templates

Key words	Paraphrase key words	Paraphrase templates
budebu	Bixu, yinggai,	If (rr/nr/r)+bunengbu, buhuibu, budebu, buyaobu
bunengbu	Yiding, bixu,	buchengren+(rr/nr/r)+(*), then (rr/nr/r)+X+(rr/nr/r)+(*)
buhuibu	Queshi, yinggai	and X={neng, yinggai,keyi,budebuchengren: chengren,
buyaobu	Yao, gai, shi	yinggaichengren, bixuchengren}
Buwu, wubu	Dou, you	If (*), v+(rr/nr/n)+buwu, wubu, weibibu,
weibibu	ye	nandaobu,bushimei, zenmebu+v+y+？ then (*),
bushimei	haishiyou	v+(rr/nr/n)+X+v. and X={you, dou, zenmebu=0 }

Similarity calculation of Templates Matching

Similarity calculation is used to match part of speech of sentence and key word of double negative part. The key word that is the double negative part in a sentence is called key item. The sequence of POS of a sentence is called POS sequence. The match of key item carries out by comparing original sentence with template. And the match of POS sequence is completed by calculating number of same POS between original sentences with template. Then the match of original sentence with template carries out by two steps, key item and POS sequence.

The procedure of paraphrase matching is to extract the structure frame of source sentence, to compute the similarity between the original sentence and the paraphrasing template, to decide paraphrasing template of using paraphrasing. Similarity of a sentence is different with a text or paragraph. The number of words in a sentence is limited, and there are repeated words hardly.

We estimate the similarity of paraphrase sentence with paraphrase template is according to (a) part of speech series of two sentences; (b) key items, the key items are common words that involved in paraphrase sentence and paraphrase template. The calculation formula is as follow (1).

$$STSim = (STN \cdot \alpha + \frac{SWN(T,S)}{TWN(T)} \cdot \beta) \times 100 \quad (1)$$

Here STN is number of same POS of the being paraphrased sentence to compare with the template; SWN is the number of key item of the being paraphrased sentence to compare with the template; TWN is the number of key item in the template; STSim is the similarity of the being paraphrased sentence to match with the template. Where α and β are weighted parameter.

In the template matching procedure, matching STN and key items must consider the order of words. By extracting sentence structure of source sentences and comparing with templates, we can get the number of matching key items, the number of POS in the source sentence, and the number of key items, the number of POS in the corresponding templates. Then, the similarity between the source sentence and the templates is obtained.

Experiment and Evaluation

We evaluated the performance of the paraphrase method by a small scale data. We used 500 sentences to paraphrasing experiment. The experiment is based on 15 kinds of templates; each kind of template is divided into several more idiographic templates, there are total of 85 templates. The paraphrase is not one-to-one, but one-to-many. That is, one sentence will be paraphrased to several sentences.

The paraphrase results are the correct paraphrasing rate 80% and the erroneous paraphrasing rate 15.5%. The main reason of wrong paraphrase is the problem of similarity calculation. The error template is selected at a lower similarity because there is not template that matches with original sentence.

We extract 100 sentences at random from the paraphrase results; to review the reason of wrong paraphrase. The reason of wrong paraphrase is because of wrong word segmentation, the template matching error includes wrong template extraction and the inaccuracy of similarity calculation. This shows the need for longer sentence paraphrase approach should be further explored.

We compare the results of sentence paraphrase that use method of similarity calculation of paper [10] with this paper respectively. The results of two method of similarity calculation are shown in figure 1.

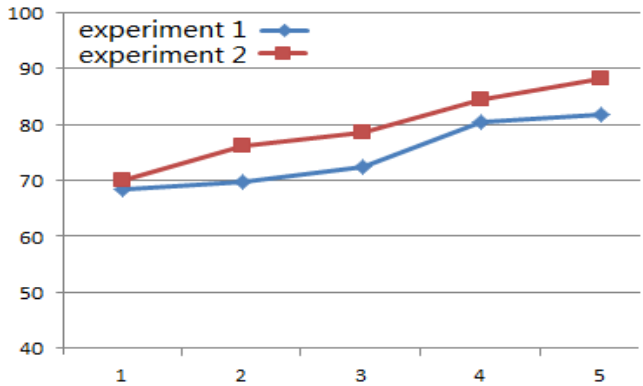

Fig.1. The experimental results of Similarity calculation

The improvement method and original method of similarity calculation are experiment1 and experiment2. Figure 1 shows the paraphrase correct rate of two experiments. According to figure 1, the improvement method of similarity calculation is impactful.

Conclusion

For the paraphrase problem of double negative sentences, we use the method based on templates and use the improved method of similarity calculation of matching templates. We have classified the double negative sentences to three kinds, and analyzed the structure of each kind of double negative sentences. We compare the syntax structure of double negative sentences with their affirmation sentences to extract the paraphrase templates.

The similarity calculation are consists of part of speech of sentence, key word of double negative part and key item. The match of key item carries out by comparing original sentence with template. And the match of part of speech is completed by calculating original sentence with template.

To evaluate the performance of proposed implement method of similarity calculation, we have carried out a small scale experiment. The experimental results indicated the method added the part of speech to similarity calculation is effective. The method has achieved a result of precision 85.4% and recall ratio 92.6%. Because of the templates are not enough and some sentences cannot paraphrase and make some mistakes in paraphrase.

For the future we will research the similarity calculation method of two sentences. Because of the number of words in a sentence is little, we think it is different from the similarity calculation of paragraph or common text.

Acknowledgement

In this paper, the research was sponsored by the Nature Science Foundation of Heilongjiang province (Project No. F201243) and Open Fund of Smart Education and Information Engineering (Harbin Normal University), the Scientific Research Foundation of Education Bureau of Heilongjiang Province (Project No. 12511127).

References

[1] Dipanjan Das and Noah A. Smith. Paraphrase Identification as Probabilistic Quasi-Synchronous Recognition. Proceedings of the 47th Annual Meeting of the ACL and the 4th IJCNLP of the AFNLP, (2009) August 2-7; Suntec, Singapore.

[2] Ohtake, K., and Yamamoto, K. Applicability analysis of corpus-derived paraphrases toward example-based paraphrasing. Proceedings of the 17th Pacific Asia Conference: Language, Information and computation, (2003) October 1-3; Sentosa, Singapore.

[3] TAKAHASHI Tetsuro, NAWATA Kozo, KOUDA Shinya, INUI Kentaro. Applying Structural Matching and Paraphrasing. NTCIR Workshop 3 Question Answering Challenge (QAC), 2002.

[4] Kentaro Inui, Atsushi Fujita, Tetsuro Takahashi and Ryu Iida. Text Simplification for Reading Assistance: A Project Note. Proceedings of the second international workshop on Paraphrasing. (2003) July 11-16; Sapporo, Japan.

[5] Fabio Rinaldi, James Dowdall and Diego Moll_et al.. Exploiting Paraphrases in a Question Answering System. Proceedings of Workshop in Paraphrasing at ACL2003, (2003) July 7-12; Sapporo, Japan.

[6] Weigang Li, Ting Liu, Yu Zhang, Sheng Li, Wei He, “Automated Generalization of Phrasal Paraphrases from the Web”, The 3rd International Workshop on Paraphrasing, October, 2005, Jeju Island, South Korea, pp. 49-57.

[7] Shiqi Zhao, Ting Liu, Xincheng Yuan, Sheng Li, and Yu Zhang, “Automatic Acquisition of Context-Specific Lexical Paraphrases”, In Proceedings of IJCAI, January, 2007, Hyderabad, India, pp. 1789-1794.

[8] Chengqing Zong, Yujie Zhang, Kazuhide Yamamoto, Masashi Sakamoto and Satoshi Shirai, “Approach to Spoken Chinese Paraphrasing Based on Feature Extraction”, The 6th Natural Language Processing Pacific Rim Symposium, November, 2001, Tokyo, Japan, pp. 551-556.

[9] ICTCLAS (Institute of Computing Technology, Chinese Lexical Analysis System): http://www.ictclas.org/index.html

[10] Z. Wang, L. Wang. Paraphrase of Chinese Sentences Based on Associated Word. ASIA-ICIM 2010, December 2010, Wuhan, China.

Advanced Materials Research Vols. 989-994 (2014) pp 1724-1727
© (2014) Trans Tech Publications, Switzerland
doi:10.4028/www.scientific.net/AMR.989-994.1724

Water Fluid Simulation with an Improved SPH Method

Zhao Xin [1, a]

[1]Information Engineering College, Dalian University, 116622, Dalian, China

[a]email: zx38610@yeah.net

Keywords: SPH; water fluid; simulation

Abstract. An improved SPH method for water fluid simulation was proposed in this paper. We used higher order splines to improve the stability, and two layers virtual particles to solve particle inconsistency problem near the boundary area. Due to the improvements paid more attention on details, we obtained more realistic and stalbe effect, which was different with previous works. Experimental results showed that our method was realistic, and could achieve real-time frame rate when particle amount was less than 10000.

Introduction

Water fluid simulation has long been an important research in computer graphics for almost twenty years, which greatly enhances the expressiveness of virtual world of games, military simulation, 3D film and so on. There are two kinds of method have been used for fluids simulation in computer graphics nowadays, one is the Euclidian approach, and the other is the Lagrange approach. In this paper, we adopt the idea of SPH(Smoothed Particle Hydrodynamics) to simulate water and floating body, which belongs to the Lagrange methods.

We pay more attention on details in order to obtain more realistic effect, which we called special treatment. That made it different with previous works aimed at improving the simulation speed. The next section of this paper describes previous related works. SPH summary is presented in Section 3. Section 4 introduces our special treatments of improved SPH method for realistic effect. The experiments and results are reported in Section 5. Section 6 closes with conclusions and future work.

Related Works

SPH as a particle-based pure Lagrange interpolation method was first proposed by [1] for the simulation of astrophysical problems. Monaghan [2] first studied on fluid simulation with SPH method. In 1995, Stam [3] firstly used SPH to simulate fire and gaseous phenomena. Muller [4] proposed an interactive method based on SPH to simulate pouring water into glass with free surfaces, which allowed for realtime interaction with 5000 particles. Then Muller [5] simulated bubble rising motion in water with SPH. Paper [6] presented an prediction-correction incompressible fluid simulation method based on SPH which is more expensive to compute, but it can use large time steps significantly. A multiphase model for simulating water and air bubbles with SPH presented in paper [7].

Generally, the more particles that are used, the smaller the damping artifacts and the more small-scale details like splashes, spray, and surface waves can be reproduced. However, doubling the resolution of a simulation increases the particle number by a factor of 8. This increases the computational cost notably since it depends linearly on the number of particles. Therefore, much work has been done in improving the computational efficiency of the solver by using for example GPU implementations, e.g. [8], or by level of detail techniques, e.g. [9]

However, few improvements have been proposed to treat the smoothing function and solid boundary which are very important to stability and reality. Therefore, we take care in these regards with improved kernel function and solid boundary treatment in the following part.

SPH Summary

SPH Approximation Techniques

SPH is an interpolation method for particle systems. The state of fluid system is represented by a set of particles, and fluid advection is calculated by particle movement.

With SPH, field quantities that are only defined at discrete particle locations can be evaluated anywhere in space. For this purpose, SPH distributes quantities in a local neighborhood of each particle using radial symmetrical smoothing kernels. According to SPH, continuous physical field is approximated in equation (1), and a discrete quantity $f(x_i)$ and its derivative are interpolated at location x by a weighted sum of contributions from all particles within support domain as following equations (2)-(4) :

$$f(x)=\int_{\Omega} f(x')W(x-x',h)dx' \tag{1}$$

$$f(x_i)=\sum_{j=1}^{N}\frac{m_j}{\rho_j}f(x_j)W(x_i-x_j,h) \tag{2}$$

$$\nabla f(x_i)=-\sum_{j=1}^{N}\frac{m_j}{\rho_j}f(x_j)\nabla W(x_i-x_j,h) \tag{3}$$

$$\nabla^2 f(x_i)=-\sum_{j=1}^{N}\frac{m_j}{\rho_j}f(x_j)\nabla^2 W(x_i-x_j,h) \tag{4}$$

where， x is position, Ω is integral volume, x' is a position in Ω, h is the support domain radius, $W(x-x',h)$ is the smoothing kernel function, $f(x_i)$ is the quantity of particle i at position x_i, x_i is the particle position in the supporting domain of particle i.

Special Treatments

More Stable Smoothing Function

In the SPH method, the smoothing function is used for kernel and particle approximations. It is of utmost importance in the SPH method as it determines the pattern to interpolate, and defines the cut-off distance of the influencing area of a particle.

The most frequently used smoothing function as following equation (5) may be the cubic B-spline function, which was originally used by Monaghan and Lattanzio[10].

$$W(R,h)=\alpha_d\times\begin{cases}\frac{2}{3}-R^2+\frac{1}{2}R^3, & 0\le R<1,\\ \frac{1}{6}(2-R)^3, & 1\le R<2,\\ 0, & R\ge 2.\end{cases} \tag{5}$$

In one-, two- and three- dimensional space, αd=1/h, 15/7πh2 and3/2πh3, respectively. The cubic splinefunction has been the most widely used smoothing function in the emerged SPH literatures since it closely resembles a Gaussian function while having an arrower compact support. However, the second derivative of the cubic spline is a piecewise linear function, and accordingly, the stability properties can be inferior to those of smoother kernels.

We used the following higher order splines, such as equation (6) that are more closely approximating the Gaussian and more stable [11].

$$W(R,h)=\alpha_d\times\begin{cases}(R+2.5)^4-5(R+1.5)^4+10(R+0.5)^4, & 0\le R<0.5,\\ (2.5-R)^4-5(1.5-R)^4, & 0.5\le R<1.5,\\ (2.5-R)^4, & 1.5\le R<2.5,\\ 0, & R>2.5,\end{cases} \tag{6}$$

This was regarded as an important improvement over the cubic spline function, and relieve the problem of compressive instability.

Solid Boundary Treatment

The conventional SPH model suffers from particle inconsistency near the boundary area. Only particles inside the boundary contribute to the summation of the particle interaction, and no contribution comes from the outside since there are no particles beyond the boundary. This one-sided contribution does not give correct solutions, because on the solid surface, although the velocity is zero, other field variables such as the density are not necessarily zero.

We used two layers virtual particles to implement the solid boundary conditions, which were allocated on and outside the boundary. These virtual particles were classified into two categories, virtual particles that were located right on the solid boundary (Type I) and virtual particles that were outside the boundary (Type II) (see Fig. 1). Type I virtual particles were used to exert a repulsive boundary force on approaching fluid (real) particles to prevent the interior particles from penetrating the boundary. The penalty force is calculated using a similar approach for calculating the molecular force of Lennard-Jones form [12]. If a Type I virtual particle is the neighboring particle of a real particle that is approaching the boundary, a force is applied pairwisely along the centerline of these two particles as following equation (7)

$$PB_{ij} = \begin{cases} D[(\frac{r_0}{r_{ij}})^{n_1} - (\frac{r_0}{r_{ij}})^{n_2}]\frac{x_{ij}}{r_{ij}^2}, & (\frac{r_0}{r_{ij}}) \le 1, \\ 0, & (\frac{r_0}{r_{ii}}) > 1. \end{cases} \tag{7}$$

Where the parameters n1 and n2 are empirical parameters, and are usually taken as 12 and 4 respectively. D is a problem dependent parameter, and should be chosen to be in the same scale as the square of the largest velocity. The cutoff distance r0 is important in the simulation. It is usually selected approximately close to the initial particle spacing. To more effectively prevent fluid particles from penetrating the solid wall, Type I virtual particles are usually more densely distributed at the solid boundary than the fluid particles (as in Fig. 1).

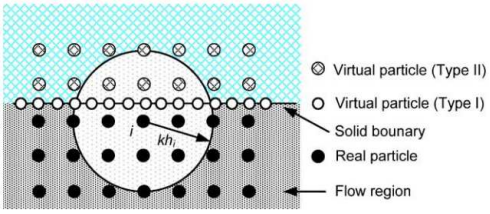

Fig.1 Schematic illustration of particle distribution near solid boundary

Type II virtual particles are usually obtained through reflecting the real fluid particles along the solid boundary. Scalar properties of the virtual particles can be taken as the same as the reflected real particles, while velocity of the virtual particles are usually taken as opposite of the reflected counterparts. As such the non-slip boundary condition is implemented. Due to the compactness of the smoothing kernel function, only the real particles that are within κh to the solid boundary are necessary to be reflected to form Type II virtual particles.

Implementation

Experiments are carried out with VC++6.0 and OpenGL on the Windows XP platform. And with Intel CPU PIV 3.0 GHz, 1GB RAM, GeForce 7300 display card and 512M display memory.

In our experiments, a block of wood is poured into a glass of water. To make it simple, water and the block of wood are drew, ignoring the glass. Figure 2 show the surface shaking when thrown a block of wood. Our experiments can reach interaction performance when the number of particles below 10000.

Fig.2 Simulation result

Conclusions and Future Work

An improved SPH method for simulating water and floating body interaction was proposed in this paper. We use a more stable smoothing function and virtual particles on solid boundary for stability and reality. Experimental results showed that our method was realistic, and could achieve real-time frame rate when particle amount was less than 10000. Our method can be easily integrated into an existing particle solver to improve the computational stability and efficiency.

References

[1] Lucy, L. 1977. A numerical approach to the testing of the fissionhypothesis. vol. 82, 1013–1024.

[2] Monaghan, J., and Gingold, R. 1992. Smoothed particle hydrodynamics. In Annu. Rev.Astron. Astrophys, vol. 30, 543–574.

[3] Stam, J., and Flume, E. 1995. Depicting fire and other gaseous phenomena using diffusion process. In In Proc. of SIGGRAPH, 154–159.

[4] Muller, M., David, C., and Markus, G. 2003. Particle-based fluid simulation for interactive applications. In In Symposium on Computer Animation(Proceedings of SIGGRAPH 2003), ACM, 154–159.

[5] Muller M, Solenthaler B, Keiser R, Gross M. Particle-based fluid–fluid interaction. In: Computer graphics proceedings, annual conference series, ACM SIGGRAPH 2005, Los Angeles, California, pp 237–244

[6] Solenthaler, B., and Pajarola, R. 2009. Predictive-corrective incompressible sph. vol. 8, 40:0–40:6.

[7] Ihmsen, M., Bader, J., and Akinci, G. 2011. Animation of bubbles with sph. In International Conference on Computer Graphics Theory and Applications GRAPP, 225–234.

[8] Goswami, P., Schlegel, P., Solenehaler, B., and Pajarola, R. 2010. Interactive SPH simulation and rendering on the GPU. In Proc. of the ACM SIGGRAPH/Eurographics Symposium on Computer Animation, 55–64.

[9] Adams, B., Pauly, M., Keiser, R., and Guibas, L. J. 2007.Adaptively sampled particle fluids. ACM Trans. Graph. (SIGGRAPH Proc.) 26, 3, 48–54.

[10] Monaghan JJ, Lattanzio JC (1985) A refined particle method for astrophysical problems. Astron Astrophys 149(1):135–143

[11] Morris JP (1996) Analysis of Smoothed Particle Hydrodynamics with Applications. Monash University

[12] Rapaport DC (2004) The art of molecular dynamics simulation. Cambridge University Press, Cambridge

Advanced Materials Research Vols. 989-994 (2014) pp 1728-1731
© (2014) Trans Tech Publications, Switzerland
doi:10.4028/www.scientific.net/AMR.989-994.1728

Analysis of Convergence Rate for Improved Generalized Ant Colony Optimization Algorithm

Daiyuan Zhang[a], Hua Zhao[b]

College of Computer, Nanjing University of Posts and Telecommunications, Nanjing, Jiangsu 210003, China

[a]email: dyzhang@njupt.edu.cn, [b]email: hnzhaoh7788@sina.com

Keywords: Convergence speed; Markov chain; Expected convergence time

Abstract. Although theoretical result of convergence for improved generalized ant colony optimization (IGACO) algorithm has been proved in recent years, the convergence speed is also an open and difficult problem. This article, based on the Markov model, tries to explore the analysis of convergence speed for IGACO algorithm. Some experiments have been studied to compare the convergence speed between ant colony optimization (ACO) algorithm and IGACO algorithm.

Introduction

Ant colony optimization (ACO) algorithm [1] has been studied for many years. Generalized ant colony optimization (GACO) algorithm has been proposed in [2]. In literature [2], two strictly increasing functions have been presented to model the behavior for describing the pheromone update rules. Compared with ACO algorithm, GACO algorithm generalizes the mathematical expression form of probability selecting the next node. Literature [2] has proved a theorem for describing the convergence of GACO algorithm. Based on GACO algorithm, a new improved generalized ant colony optimization algorithm (IGACO algorithm) has also been proposed in [3]. In literature [3], the selected probability function has been further generalized from the family of strictly increasing continuous function to the family of bounded function, which gives a more general form of expression for the probability of selecting the next node. An important theorem of convergence for IGACO algorithm was also proved, i.e. for a sufficiently large number of algorithm iterations, the probability of finding the globally optimal solution at least once tends to 1. On the other hand, literature [3] proposed a new asymptotic balance principle of pheromone. In the pheromone update rule, the residual rate function of pheromone and the global increasing function of pheromone ware presented. Literature [3] proved that the residual pheromone tends to a positive number on the edges that are globally optimal solution, and tends to 0 on the edges that are not globally optimal solution.

Although IGACO algorithm may become more widespread approach because its generalization, the convergence speed is also an open and difficult problem. This paper tries to analyses the convergence speed for IGACO algorithm.

Finally, the computational simulation show that, compared with ACO algorithm algorithm, the IGACO algorithm has good performance on convergent speed.

Theoretical Analysis of the Convergence Speed for IGACO Algorithm

First, create a Markov process model of IGACO algorithm [4].

Let the state variable be $X(t)=(S(t),T(t))$, $S(t)=\{S_{bs}(t)\cup S_{iter}(t)\}$, where $S_{bs}(t)$ is the current global optimal solution, $S_{iter}(t)$ means a full iteration required to complete the solution set, and $T(t)$ is the pheromone vector.

Base on the Definition and pheromone update rule of IGACO and the definition of continuous-time Markov chain can obtain that $X(t)$ is defined as the availability of continuous-time Markov chains.

Expected First Hitting Time: set an absorbing Markov process states $\{X(t)\}_{t=0}^{+\infty}$ ($\forall X(t)=(S(t),T(t))\in I$) and optimal state space $I^*\in I$; If ν is a random variable and meets: When $t=\nu$, $X(t)\in I^*$, when $0\le t<\nu$, $X(t)\notin I^*$. Then $E\nu$ is the expected first hitting time.

Theorem 1. 1 The absorbing Markov process corresponding to IGACO algorithm is $\{X(t)\}_{t=0}^{+\infty}$, its state space is I, which corresponds to the optimal state space I^*. If $\phi(t_m)=P\{X(t_m)\in I^*\}$ and $\lim_{t_m\to\infty}\phi(t_m)=1$, then the convergence speed of IGACO is $E\lambda=\sum_{t=0}^{+\infty}(1-\phi(t))dt$.

According to Theorem 1. 1, if the $\forall t_m=1,2,\cdots,\phi(t_m)$ or $P\{\nu=t_m\}=\phi(t_m)-\phi(t_{m-1})$ is known, you can accurately calculate the expected convergence time of IGACO through the formula, which can measure the convergence speed of the algorithm. But in fact, $\phi(t_m)$ is difficult to determine.

Given the IGACO algorithm corresponding absorbing Markov state process $\{X(t)\}_{t=0}^{+\infty}$, the corresponding optimal state space is I^*, if $\phi(t_m)=P\{X(t_m)\in I^*\}$ meets $a(t)\le \mathrm{P}\left\{X(t_m)\in I^*\middle|X(t_{m-1})\notin I^*\right\}\le b(t)$, and because IGACO meets absorbing state Markov process model, so $P\{X(t_m)\in I^*\mid X(t_{m-1})\in I^*\}=1$. According to the total probability formula and Theorem 1. 1 , we can obtain that,

$$\sum_{t_m=0}^{+\infty}[(1-\phi(0))\prod_{t_m=1}^{+\infty}(1-b(t))]\le E\lambda\le\sum_{t_m=0}^{+\infty}[(1-\phi(0))\prod_{t_m=1}^{+\infty}(1-a(t))] \tag{1}$$

Corollary 1. 1 Given the IGACO algorithm corresponding absorbing Markov state process $\{X(t)\}_{t=0}^{+\infty}$, the corresponding optimal state space is I^*, if $\phi(t_m)=P\{X(t_m)\in I^*\}$ meets $\mathrm{a}(t)\le P\left\{X(t_m)\in I^*\middle|X(t_{m-1})\notin I^*\right\}\le b(t)$ and $\lim_{t_m\to\infty}\phi(t_m)=1$.The expectations of convergence time $E\lambda$ of IGACO algorithm meets

$$b^{-1}[1-\phi(0)]\le E\lambda\le a^{-1}[1-\phi(0)] \tag{2}$$

Assuming optimal solution in the k iteration cycle, then the optimal solution sequence of nodes is $r(t),ck1,ck2,\cdots,ckn,d(t)$, where t is the time parameters, $r(t)$, $d(t)$ respectively for the moment t the source and destination nodes, the optimal solutions in the k iteration, the probability is

$$P(t,s^*)=P(r(t),ck1(t),ck2(t),\cdots,ckn(t),d(t))=\prod_{j=1}^{n+1}P_{kj} \tag{2}$$

There in $P_{k1}=P(r(t),ck1(t)),P_{k2}=P(ck1(t),ck2(t)),\cdots,P_{k(n+1)}=P(ckn(t),d(t))$, s^* is the optimal solution; each selected P_{kj} is calculated by the probability function.

Assuming IGACO algorithm has m ants, according to the above derivation can compute the probability to find the optimal solution in the k iteration cycle:

$$P_t=P\{X(t)\in Y^*\mid X(t-1)\notin Y^*\}\quad=1-(1-P(s^*))^m\quad=1-(1-\prod_{j=1}^{n+1}P_{kj})^m \tag{3}$$

When $t=1,2,\cdots,j=1,2,\cdots,n$, $0<P_{\min}\le P_{kj}\le P_{\max}$,

$$\begin{aligned}&P_t=P\{X(t)\in Y^*\mid X(t-1)\notin Y^*\}\ge 1-(1-P^n{}_{\min})^m\\&P_t=P\{X(t)\in Y^*\mid X(t-1)\notin Y^*\}\le 1-(1-P^n{}_{\max})^m\end{aligned} \tag{4}$$

By the formula (2) we have，

$$[1-\phi(0)][1-(1-P_{\max}^n)^m]^{-1}\le E\lambda\le[1-\phi(0)][1-(1-P_{\min}^n)^m]^{-1} \tag{5}$$

Because during the initialization of the algorithm, $S(t)=\{S_{bs}(t)\cup S_{iter}(t)\}=\varnothing$, so $\phi(0)=0$。

By the analysis above, we can obtain

$$[1-(1-P_{\max}^{n})^{m}]^{-1} \le E\lambda \le [1-(1-P_{\min}^{n})^{m}]^{-1} \tag{6}$$

By formula (6) can obtain that if you have a uniform upper and lower bounds of P_{kj}, then the first upper and lower bounds of the range expected convergence time can be determined.

Assuming a polynomial function $P(n)$ on the complexity, if meet $P_{\min} \ge \left[1-\left(1-P(n)^{-1}\right)^{1/m}\right]^{1/n}$, according to equation (6) can be obtained,

$$E\lambda \le P(n) \tag{7}$$

By equation (7), we can draw the following conclusion: For $t=1,2,\cdots,n$ and $i=1,2,\cdots,n$, if P_{kj} is large enough, the time complexity of IGACO algorithm can be reduced to a polynomial function about n.

Experiment of Convergence Speed

Experiment operating system: windows XP SP3, programming environment: Matlab R2009a.

Experimental data:

Data used in the experiment comes from:

TSPlib:http://www.iwr.uni-heidelberg.de/groups/comopt/software/TSPLIB95/tsp/.

Experimental method:

First, specific the probability function[3]:

$$P(i,j,t)=\frac{\eta^{\beta}(i,j)\cdot c^{\alpha}(i,j,t)}{\sum_{k\in D_i}\eta^{\beta}(i,j)\cdot c^{\alpha}(i,j,t)},(i,j)\in D_i \tag{8}$$

Where τ is the pheromone, in TSP, η is the reciprocal of the distance between city i and j. The introduction of heuristic argument η makes greater pheromone of short distance cities. α and β are two parameters. α,η,τ all greater than 0. $c(i,j,t)$ is the time rate of pheromone in path (i,j). Pheromone Concept ratios as follows: ratio of pheromone in path (i,j) is represented on the path of all paths ant pheromones at a node i and may be selected on the ratio.

$$c(i,j,t)=\frac{\tau(i,j,t)}{\sum_{k\in D_i}\tau(i,k,t)},(i,j)\in D_i \tag{9}$$

For IGACO algorithm:

Residual rate of pheromone function[2] [3]:

$$\delta(t)=\frac{\gamma_0 e^{\lambda t_m}}{1+\gamma_0 e^{\lambda t_m}},\gamma_0>0,\lambda>0 \tag{10}$$

Pheromone increment function[2] [3]:

$$\mu(i,j,t)=\frac{A(1-\delta(t))\tau(i,j,t)}{\delta(t)},A>1 \tag{11}$$

Initialization pheromone τ_0=10, α=1, β=5; in formula (10) γ_0=5, λ=0.01; in formula (11) A=1.01.

Experimental results and analysis:

The convergence process of ACO and IGACO in the implementation process is shown as below:

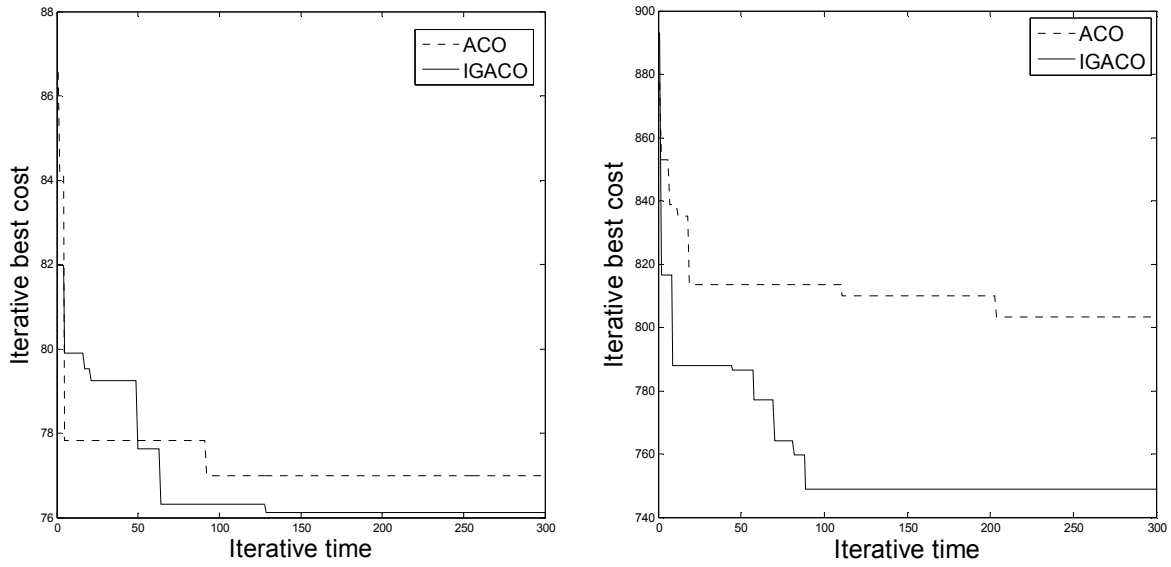

Fig. 1 22 and 70 cities TSP convergence process comparison between ACO and IGACO

In Fig. 1, the left picture is 22 cities TSP convergence process comparison between ACO and IGACO and the right one is 70 cities. The horizontal axis in the figure represents the number of iterations, and the vertical axis represents the distance between the city; the obtained solid line represents the convergence process of IGACO and the dashed line represents the convergence process of traditional ant colony algorithm.

By the experimental results above, we can obtain that the IGACO algorithm always converge to the smaller solution and the convergence speed is better than the traditional ant colony algorithm. Moreover, with the expansion of the city scale, the advantage of IGACO is more and more obvious.

Conclusion

Based on the experimental results, we can see that in a limited number of iterations, IGACO algorithm could get the better solution compare to the traditional ant colony algorithm. The improvement made by IGACO algorithm base on the traditional ant colony algorithm is effective.

References

[1] Dorigo M,Gambardella L M. Ant colony system:a cooperative learning approach to the traveling salesman problem[J]. IEEE Transactions on Evollutingary Computation,1997,1(4):53-66.

[2] Daiyuan Zhang. Convergence Analysis for Generalized Ant Colony Optimization Algorithm[C]. Proceedings of the 11th Joint Conference on Information Sciences, Atlant-is Press. 2008

[3] Daiyuan Zhang. A new improved generalized ant colony optimization algorithm [J]. Computer technology and development, 2012, 22(6): 39-44

[4] Han Huang, Chun-Guo Wu, Zhi-Feng Hao. A Pheromone-Rate-Based Analysis on the Convergence Time of ACO Algorithm [J]. IEEE Transactions on SYSTEMS, 2009, 39(4), 910-923

Advanced Materials Research Vols. 989-994 (2014) pp 1732-1735
© (2014) Trans Tech Publications, Switzerland
doi:10.4028/www.scientific.net/AMR.989-994.1732

Convergence Speed of Multi-objective Generalized Ant Colony Optimization Algorithm

Daiyuan Zhang[a], Peng Fu[b]

College of Computer, Nanjing University of Posts and Telecommunications, Nanjing, Jiangsu 210003, China

[a]email: dyzhang@njupt.edu.cn, [b]email: fupeng2006@126.com

Keywords: Multi-objective; Convergence Speed; Generalized ant colony algorithm

Abstract. Multi-objective optimization problems are very important, but it is hard to optimized or solved. Generalized ant colony optimization (GACO) algorithm is a new kind of ant colony optimization (ACO) algorithm developed in recent years. In this paper, we try to combine Multi-objective optimization problems with GACO algorithm, established a model for multi-objective GACO algorithm by absorbing state Markov chain, and present a method for estimating the convergence speed of multi-objective GACO algorithm. Simulation results show that the convergence speed of multi-objective GACO algorithm is faster than traditional multi-objective ACO algorithm.

Introduction

Ant colony algorithm [1] is a new type of simulated evolutionary algorithm. But it has some disadvantages such as slow convergence, easy to fall into local optimum etc. For a certain improvement, generalized ant colony optimization (GACO) algorithm was proposed in literature [2]. The improved generalized ant colony optimization algorithm [3] further improves the probability selection function from a strictly monotone increasing function to a bounded function and gives a more general expression of the ants in a given source node to select the next node.

Although multi-objective generalized ant colony algorithm has solved some combinatorial optimization problems, there are few theoretical analysis about the convergence speed of multi-objective generalized ant colony algorithm. To solve this problem, we build a strong versatility, absorbing process model based on Markov chain. On the basis of the above, we present a preliminary analysis estimation method of convergence speed for multi-objective GACO algorithm.

The Convergence Speed of Multi-objective GACO Algorithm

In order to analyze the multi-objective GACO algorithm convergence speed, this section will establish the multi-objective GACO algorithm with absorbing state Markov process model [4]. The absorbing Markov chain model of multi-objective GACO algorithm can be presented with the following definitions.

$X(t)\big|_{t=0}^{+\infty}$ is the stochastic process for the multi-objective GACO algorithms, where $X(t)=(S(t),T(t))$, and $S(t)=S_{bs}(t)\cup S_{iter}(t)$, $S_{\mathrm{bs}}(t)$ is the current approximate Pareto optimal solution set on t time. $S_{\mathrm{iter}}(t)$ is the set of complete iteration for Pareto solution obtained by ants. It's state space is Y on t moment [5].

$$P\left\{X(t)\in Y\,\middle|\,X(0),X(1)\cdots X(t-1)\right\}=P\left\{X(t)\in Y\,\middle|\,X(t-1)\right\} \tag{1}$$

$X(t)\big|_{t=0}^{+\infty}$ is an absorbing Markov chain.

Expected convergence time describes the multi-object GACO algorithm for Pareto optimal solution of the desired time for the first time to achieve a global approximation with probability 1. Because the multi-objective GACO algorithm meets the absorbing states of the markov process, our study can use expected convergence time of approximate Pareto optimal solution as the convergence rate of the multi-objective GACO algorithm indicators.

Definition 1 Given a absorbing state markov process $X(t)|_{t=0}^{+\infty}(\forall X(t)\in Y)$ and optimal state space $Y^*\in Y$, if μ is a random variable: when $t=\mu$, $X(t)\in Y^*$,$0\le t<\mu$, $X(t)\notin Y^*$, then we say the expectations of μ. $E\mu$ is headed approximate Pareto optimal solution of the desired time.

Assume that when $t=\mu$, $X(t)\in Y^*$. Because the $X(t)$ is a process of absorbing states Markov, $P\left\{X(\mu+1)\notin Y^*\middle|X(\mu)\in Y^*\right\}=0$ is defined by the Markov process. Because $X(t)\in Y^*$, $t=\mu$, so $P\left\{X(\mu)\in Y^*\right\}=1$. Similarly available, when $t\geqslant\mu, P\left\{X(t)\in Y^*\right\}=1$,when $t<\mu$, $P\left\{X(t)\in Y^*\right\}<1$. $E\mu$ indicates the convergence time that multi-objective GACO algorithm spend in reaching the Pareto optimal solution.

Definition 2 $\lambda(t)=P\left\{X(t)\in Y^*\right\}$ is the probability of the multi-objective GACO algorithm attains the Pareto optimal solution state set at t time. Among them, $\lim_{t\to\infty}\lambda(t)=1$.

This paper analyzes the multi-objective GACO optimization algorithm convergence speed in the continuous-time and it is based on continuous-time Markov process, expected convergence time analysis is as follows:

$$\lambda(t)=\mathrm{P}\left\{X(t)\in Y^*\right\}=P(\mu\le t) \tag{2}$$

$$\Rightarrow P(\mu=t)=P(\mu\le t)-P(\mu\le t-1)=\lambda(t)-\lambda(t-1)$$

$$\begin{aligned}E\mu&=\int_{t=0}^{+\infty}t\cdot P(\mu=t)dt\\&=\int_{t=0}^{+\infty}t\cdot\left(\lambda(t)-\lambda(t-1)\right)dt\\&=\int_{i=0}^{+\infty}\int_{t=i}^{+\infty}\left(\lambda(t)-\lambda(t-1)\right)dtdi\\&=\int_{i=0}^{+\infty}\left[\lim_{t\to+\infty}\lambda(t)-\lambda(i)\right]di\\&=\int_{i=0}^{+\infty}\left(1-\lambda(i)\right)di\end{aligned} \tag{3}$$

Assume that $a\le\mathrm{P}\left\{X(t)\in Y^*\middle|X(t-1)\notin Y^*\right\}\le b$, According to the formula of full probability，

$$\begin{aligned}\lambda(t)&=[1-\lambda(t-1)]P\{X(t)\in Y^*\middle|X(t-1)\notin Y^*\}+\lambda(t-1)P\{X(t)\in Y^*\middle|X(t-1)\notin Y^*\}\\&=[1-\lambda(t-1)]P\{X(t)\in Y^*\middle|X(t-1)\notin Y^*\}+\lambda(t-1)\end{aligned} \tag{4}$$

$$\begin{aligned}E\mu&=\int_{t=0}^{+\infty}(1-\lambda(i))dt\le\int_{t=0}^{+\infty}(1-\lambda(0))\prod_{i=1}^{+\infty}(1-P(i))dt\\&=[1-\lambda(0)]\sum_{i=1}^{+\infty}(1-a)^i=a^{-1}[1-\lambda(0)]\end{aligned} \tag{5}$$

Similarly available: $E\mu=\int_{t=0}^{+\infty}(1-\lambda(i))dt\ge b^{-1}[1-\lambda(0)]$

Assuming there are n nodes in an iterative cycle. If Pareto optimal solution is obtained in the k-th iteration cycle, it's sequence of nodes is: $r(t),c_{k1},c_{k2},\cdot,c_{kn},d(t)$. The probability that Pareto optimal solution is attained at the k-th iteration time can be calculated according to the following: [3]:

$$P(r(t),c_{k1}(t),c_{k2}(t),\cdot\cdot c_{kn}(t),d(t))=\prod_{j=1}^{n+1}P_{kj} \tag{6}$$

Each P_{kj} is calculated by the probability selection function. Suppose there are m ants in multi-objective GACO algorithm, then the probability of Pareto optimal solutions found in the k-th iteration as follows:

$$P_t = P\left\{X(t)\in Y^* \,\middle|\, X(t-1)\notin Y^*\right\} = 1-\left(1-P\left(s^*\right)\right)^m = 1-\prod_{k=1}^{m}\left(1-\prod_{j=1}^{n+1}P_{kj}\right) \tag{7}$$

When $0 < p_{\min} \le P_{kj} \le p_{\max}, k = 1,2\cdots m,\ j = 1,2\cdots n$, because in the initialization process, $S(t) = S_{bs}(t) \cup S_{iter}(t) = \varnothing$, so $\lambda(0) = 0$. According to equation (4) and (5), multi-objective GACO algorithm expectation convergence time becomes as follows:

$$\frac{1}{1-(1-p^n{}_{\max})^m} \le E\mu \le \frac{1}{1-(1-p^n{}_{\min})^m} \tag{8}$$

The formula (8) indicates that the upper bound and lower bound of the expected convergence time can be confirmed, if the crucial probability has unified upper bound and unified lower bound.

Simulation Results

Experiment operating system is Windows 7, programming tool is MATLAB R2009a. Data from constructed as a multi-objective TSP data and its contents are as follows:

$$D_1 = \begin{bmatrix}
0 & 10 & 15 & 78 & 93 & 79 & 48 & 49 & 76 & 11 & 81 & 72 & 55 & 81 & 3 \\
10 & 0 & 77 & 46 & 64 & 86 & 37 & 8 & 29 & 35 & 81 & 3 & 44 & 9 & 40 \\
55 & 77 & 0 & 79 & 9 & 82 & 13 & 54 & 80 & 84 & 72 & 3 & 87 & 77 & 21 \\
78 & 46 & 79 & 0 & 34 & 29 & 9 & 35 & 98 & 91 & 55 & 44 & 87 & 67 & 25 \\
93 & 64 & 9 & 34 & 0 & 74 & 83 & 44 & 67 & 68 & 81 & 9 & 77 & 67 & 93 \\
79 & 86 & 82 & 29 & 74 & 0 & 42 & 98 & 85 & 8 & 3 & 40 & 21 & 25 & 93 \\
48 & 37 & 13 & 9 & 83 & 42 & 0 & 84 & 5 & 2 & 19 & 28 & 20 & 37 & 48 \\
49 & 8 & 54 & 35 & 44 & 98 & 84 & 0 & 98 & 28 & 13 & 45 & 98 & 34 & 28 \\
76 & 29 & 80 & 98 & 67 & 85 & 5 & 98 & 0 & 48 & 90 & 55 & 66 & 77 & 88 \\
11 & 35 & 84 & 91 & 68 & 8 & 2 & 28 & 48 & 0 & 11 & 23 & 32 & 47 & 41 \\
81 & 81 & 72 & 55 & 81 & 3 & 19 & 13 & 90 & 11 & 0 & 40 & 23 & 45 & 67 \\
72 & 3 & 3 & 44 & 9 & 40 & 28 & 45 & 56 & 23 & 40 & 0 & 25 & 34 & 76 \\
55 & 44 & 87 & 87 & 77 & 21 & 20 & 98 & 66 & 32 & 23 & 25 & 0 & 45 & 72 \\
81 & 9 & 77 & 67 & 67 & 25 & 37 & 34 & 77 & 47 & 45 & 34 & 45 & 0 & 98 \\
3 & 40 & 21 & 25 & 93 & 93 & 48 & 28 & 88 & 41 & 67 & 76 & 72 & 98 & 0
\end{bmatrix}$$

$$D_2 = \begin{bmatrix}
0 & 20 & 65 & 88 & 13 & 89 & 38 & 29 & 16 & 21 & 82 & 14 & 14 & 43 & 47 \\
20 & 0 & 57 & 36 & 54 & 76 & 27 & 18 & 39 & 45 & 82 & 61 & 76 & 29 & 47 \\
65 & 57 & 0 & 69 & 19 & 51 & 23 & 14 & 90 & 74 & 14 & 61 & 29 & 31 & 51 \\
88 & 36 & 69 & 0 & 24 & 39 & 18 & 45 & 18 & 81 & 14 & 76 & 29 & 78 & 67 \\
13 & 54 & 19 & 24 & 0 & 64 & 73 & 34 & 57 & 58 & 43 & 29 & 31 & 78 & 28 \\
89 & 76 & 52 & 39 & 64 & 0 & 32 & 88 & 75 & 18 & 47 & 47 & 51 & 67 & 28 \\
38 & 27 & 23 & 18 & 73 & 32 & 0 & 74 & 15 & 12 & 48 & 82 & 83 & 80 & 90 \\
29 & 18 & 14 & 45 & 34 & 88 & 74 & 0 & 68 & 35 & 23 & 45 & 65 & 43 & 42 \\
16 & 39 & 90 & 18 & 57 & 75 & 15 & 68 & 0 & 57 & 34 & 35 & 48 & 56 & 49 \\
21 & 45 & 74 & 81 & 58 & 18 & 12 & 35 & 57 & 0 & 34 & 37 & 78 & 68 & 56 \\
82 & 82 & 14 & 14 & 43 & 47 & 48 & 23 & 34 & 34 & 0 & 32 & 19 & 34 & 45 \\
14 & 61 & 61 & 76 & 29 & 47 & 82 & 45 & 35 & 37 & 32 & 0 & 27 & 20 & 37 \\
14 & 76 & 29 & 29 & 31 & 51 & 83 & 65 & 48 & 78 & 19 & 27 & 0 & 65 & 45 \\
43 & 29 & 31 & 78 & 78 & 67 & 80 & 43 & 56 & 68 & 34 & 20 & 65 & 0 & 12 \\
47 & 47 & 51 & 57 & 28 & 28 & 90 & 42 & 49 & 56 & 45 & 37 & 45 & 12 & 0
\end{bmatrix}$$

D_1 and D_2 are the generation of value matrix corresponding to the two objectives between various cities. Multi-objective GACO algorithm's probability selection function $P(i,j,t)$ as follows:

$$P(i,j,t) = \frac{\eta^{\log(\beta)}(i,j)\cdot\tau^{\log(\alpha)}(i,j,t)}{\sum_{k\in D_i}\eta^{\log(\beta)}(i,k)\cdot\tau^{\log(\alpha)}(i,k,t)}, (i,j)\in D_i \tag{9}$$

The formula (9) conforms to the definition of state transition probability in literature [3]. For multi-object GACO algorithm:

$$\tau(i,j,t) = w(1)\tau^1(i,j,t) + w(2)\tau^2(i,j,t) \tag{10}$$

$$\eta(i,j) = \frac{1}{w(1)\cdot d(1)_{i,j} + w(2)\cdot d(2)_{i,j}} \tag{11}$$

α and β are two parameters. $d(1)_{i,j}, d(2)_{i,j}$ indicates the substituting value of 2 different objectives between the (i, j). $w(1), w(2)$ indicates weighting factor. Residual rate of pheromone function and pheromone increment function [3] are defined as follow:

$$\delta(t) = \frac{\gamma_0 e^{\lambda t}}{1+\gamma_0 e^{\lambda t}} \tag{12}$$

Where, λ is a positive constant, $\gamma_0 = \delta_0/1-\delta_0$

$$\mu(t) = \frac{A\left(1-\delta(t)\right)\tau(i,j,t)}{\delta(t)} \tag{13}$$

Where, A is a positive constant.

Initializing pheromone $\tau_1=\tau_2=10$, $\alpha=3$, $\beta=6$. In formula (12)(13) $\gamma_0=5$, $\lambda=0.01$, $A=1.01$[3]. Pheromone evaporation parameter $\rho=0.65$, weighting factor $w(1)=w(2)=0.5$.

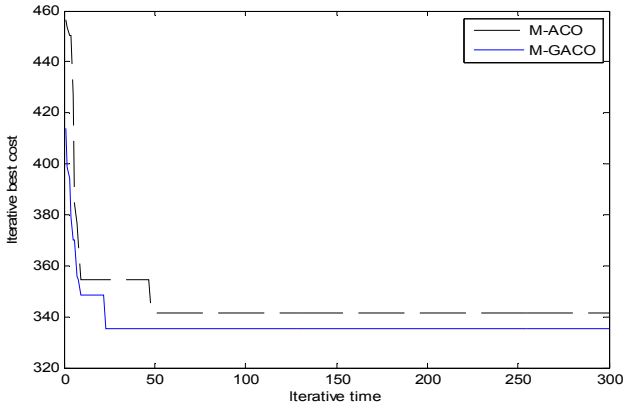

Figure 1 Convergence speed comparison

In Figure 1, abscissa axis represents the number of iterations, the vertical axis represents the length of path which the ants find, dotted line part is the convergence process of traditional multi-objective ant colony algorithm, solid line is the convergence process of multi-objective GACO algorithm. Integrated on, convergence speed of multi-objective GACO algorithm is faster than the traditional multi-objective ant colony algorithm.

Conclusion

In this paper, based on the process model of Markov chain, we put the expected convergence time as an important index of convergence speed, analysis the convergence speed of multi-objective GACO algorithm exploringly and give the change interval of convergence speed. Simulation results show that multi-objective GACO algorithm convergence speed is faster than the traditional multi-objective ant colony algorithm.

References

[1] Dorigo M, Gambardella L M. Ant colony system: a cooperative learning approach to the traveling salesman problem [J]. IEEE Transactions on Evolutionary Computation, 1997, 1(4): 53-66.

[2] Daiyuan Zhang. Convergence Analysis for Generalized Ant Colony Optimization Algorithm[C]. Proceedings of the 11th Joint Conference on Information Sciences, Atlant-is Press, 2008

[3] Daiyuan Zhang. A New Improved Generalized Ant Colony Optimization Algorithm [J]. Computer technology and development, 2012, 22(6): 39-44

[4] Hart Huang, Chungu Wu, Zhiheng Hao. A Pheromone Rate Based Analysis on the Convergence Time of ACO Algorithm [J]. IEEE Transactions on Systems, Man, and Cybernetics, Part B: Cybernetics Archive , 2009, 39(4): 910-923

[5] Yiqiao Deng. Generalized Ant Colony Algorithm Theory and its Application in Machine Learning [D]. Nanjing University of Posts and Telecommunications, 2010

Advanced Materials Research Vols. 989-994 (2014) pp 1736-1738
© (2014) Trans Tech Publications, Switzerland
doi:10.4028/www.scientific.net/AMR.989-994.1736

The Applications based on The Rough Set Theory Algorithms to Determine the Weight

CHEN Ning-ning[1]

[1]Leshan Vocational Technical College leshan 614000, China

binghefeidian@163.com

Keywords: Attributes-importanc, Rough Set, weight

Abstract. This paper puts forward on the Rough Set theory algorithms, and combined it with the method of determining the index weights, then established a weight determined algorithm model based on rough set, Thereby reducing the influence of subjective factors on the weight determination.

Introduction

Rough set theory is a mathematical theory to deal with imprecise, incomplete and inconsistent information. This theory while maintaining the original decision table without changing the classification ability, through knowledge reduction, value reduction, export classification decision tables and decision rules. It is a mathematical tools to deal with the information and knowledge use the way of quantitative analysis to process the data of imprecise, inconsistent, incomplete. The initial prototype of Rough set theory is from the model of relatively simple information. Rough set method has been successfully applied to many fields such as medicine, management, finance, image processing and decision analysis.

We should follow the following principles to determine the index weight: System optimization principles and the principles of the evaluator's subjective intent with a combination of objective circumstances [1]. The traditional evaluation process methods are affected by subjective factors, this means that there will be some deviation with the evaluation results obtained more or less. In this paper we use attribute importance of rough set theory combined with expert scoring method to determine the weight of each evaluation item, thereby reducing the influence of subjective factors on the weights.

The Knowledge of Rough Set

In the research area of Rough Set, the ability to objectively classify things in rough sets is called knowledge. The object is a set of some objects that consists of a collection of multi-valued attribute, for each object and its properties, there will be a value as a symbol to description it, object properties and symbol descriptors are the basic elements to expression the decision problem. Typically, the available information about the object is not necessarily enough to divide its membership categories. This imprecision cause the object are indistinguishability. It can be used to decision and planning the form of the set, to represents the important relationship between the most important properties and specific categories.

2.1 The indistinguishable relationship

Set up a information system $S=<U,A,V,F>$, U is a non-empty and limited individual set (called it the discourse domain). A is a non-empty and limited attribute set,and $A=CYD$, $\forall_C \in A$, $C:U \to V_{CC}$ Is a mapping, then $\forall_U \in U$, $C_{(U)} \in V_c$ so V_c is a subset for C,so $V=YV_C$ is a subset for A. We definitions $IND(C)$ is a indistinguishable relationship for U to attribute C ,and $x,y \in U$, x,y is equivalence to C ,then there wil be $V_a \in C,(x,y) \in IND(C)$ .only if $f_{(x,a)}=f_{(y,a)}$,that mean $IND(C)=\{(x,y) \in U \times U : \forall_A \in C \wedge a(x)=a(y)\}$ is a equivalence relation.

2.2 knowledge dependence

$a_R(X)$ is the roughness for the degree of uncertainty of the sample subset X ,and the roughness is defined as: $a_R(X)=\frac{Card(R_(X))}{Card(R^-(X))}$, $Card$ is the cardinal number for the set(The number of elements in the set).When $0 \le a_R(X) \le 1$ if $a_R(X)=1$,then we can define X is determined by R ;and X is Totally dependent on R;if $0 < a_R(X) < 1$,then X is Ragged for R;$a_R(X)$ is Approach the Accuracy of X ,this we defined X is Rough dependence on R ;

When $a_R(X)=0$,then X and R are both completely independent. $a_R(X)$ is the dependence coefficient for X and R .

2.3 The importance of property

In the decision table, different properties may have different importance. To find out the importance of certain attributes (or the attributes set), the general approach is to remove some attributes from the table. If the change is larger, then we can say these attributes are important, On the contrary, the importance of the attributes are lower. C is the Condition attribute set, D is the Decision attribute set, the importance for the attributes subset C' to D is: $\sigma_{CD}(C')=\gamma_C(D)-\gamma_{C-C'}(D)$.

Data preprocessing

For the attribute set C , we can get the importance of the classification for attributes subset $B' \subseteq B$, then get the both dependence $r_B(C)-r_{B-B'}(C)$. is mean we classified the object, to remove some attributes subset B' from set B , then we can get the Influence.Fig 1 shows us the knowledge representation system.

U	a	b	c	d	e
1	1	1	0	1	0
2	0	0	0	1	0
3	0	0	0	0	1
4	0	1	0	1	1
5	1	1	0	0	1

Fig 1 A knowledge representation system

The discourse domain num from1 to 5 , and the condition attribute set $C=\{a,b,c,d\}$, decision attribute set $D=\{e\}$. $U/ind(a,b,c,d)=\{\{1\},\{2\},\{3\},\{4\},\{5\}\}$, $U/ind(e)=\{\{1,2\}\{3,4,5\}\}$, $POS_c(D)=\{1,2,3,4,5\}$, $r_c(D)=Card(POS_C(D))/Card(U)=5/5=1$,now we removed property a ,get $U/ind(b,c,d)=\{\{1,4\},\{2\},\{3\},\{5\}\}$, $POS_{C-a}(D)=\{2,3,5\}$, $r_{C-a}(D)=3/5=0.6$. removed property b ,get $U/ind(a,c,d)=\{\{1\},\{3\},\{2,4\}\{5\}\}$ $POS_{C-b}(D)=\{1,3,5\}$, $r_{C-a}(D)=3/5=0.6$. removed property c ,get $U/ind(a,b,d)=\{\{1\},\{2\}\{3\},\{4\},\{5\}\}$, $POS_{C-c}(D)=\{1,2,3,4,5\}$, $r_{C-c}(D)=5/5=1$. At last we removed property d , $U/ind(a,b,c)=\{\{1,5\},\{2,3\},\{4\}\}$, $POS_{C-d}(D)=\{4\}$, $r_{C-d}(D)=1/5=0.2$. Then we can see property d is most important. Property a and b followed by d .And c is the redundant attributes.

Weight determination method based on Rough Set Theory

In different decision-making environment, the same properties have different effects on decision-making output. That the weights have different sensitivity on the environmental.In the Rough set theory, attribute importance reflects of the impact on the current data on the environmental attributes decision. But it does not reflect a priori knowledge of decision makers.In this paper we combined the attribute importance of the rough set theory with the property rights which are determined by the priori knowledge,and then to determine the final comprehensive weight. In order to achieve the subjective priori knowledge to be the same as Objective circumstances

Now we assume that the condition attributes in the system is C , the decision attribute is D . C has much different propertys,the num is n ,they are $a_1, a_2, ..., a_n$, the priori knowledge given by the decision maker weights were $p(a_1), p(a_2), ..., p(a_n)$. The Specific implementation methods are followed:

Input: The evaluation results of each item evaluated projects in the knowledge representation system, to get each item weight from expert scoring method.

Output: Right weight for each item

Steps:

Step1: Division the equivalence classes: $U/C, U/D, U/(C-\{c_i\})$,get $posC(D), posC-\{c_i\}(D), i=1,2,...m;$

Step 2 :we get the Dependence: $a_R(X) = r_C(D) = |POS_C(D)| / |U|$,from $a_R(X) = \frac{Card(R_-(X))}{Card(R^-(X))}$,then we can get each dependence $k_{C-\{c_i\}} = r_{C-\{c_i\}}(D) = |POS_{C-\{c_i\}}(D)| / |U|$, $i = 1,2,...,m$;

Step 3 : from $\sigma_{CD}(C) = \gamma_C(D) - \gamma_{C-C}(D)$,we can get the importance of C_i , $\sigma_{CD}(\{c_i\}) = \gamma_C(D) - \gamma_{C-\{c_i\}}(D)$;

Step 4 : normalized the importance of each attribute, $I_i = \frac{\sigma_{CD}(\{c_i\})}{\sum_i^m \sigma_{CD}(\{c_i\})} = \frac{r_C(D) - r_{C-i}(D)}{\sum_{i=1}^n r_C(D) - r_{C-i}(D)}$, $i = 1,2,...,m$.

Step 5:Here is the item weight got from Rough set method, we call it Objective weights, correspondingly, P_i is the right weight got from Expert scoring method is called Subjective weights.

Final weight of each evaluation term weight calculated by the following formula $R_i = \lambda P_i + (1-\lambda) I_i (0 \le \lambda \le 1)$, $i = 1,2,...,m$. Now the bias of P_i and I_i are determined by λ .

Make Table 1 as an example, Assumed $\lambda = 0.4$, the right weight of each attribute were given by experts: $p_{(a)} = 0.3, p_{(b)} = 0.2, p_{(c)} = 0.1, p_{(d)} = 0.4$,then from the results of attribute importance,we can get $r_C(D) - r_{C-a}(D) = 1 - 0.6 = 0.4$; $r_C(D) - r_{C-b}(D) = 1 - 0.6 = 0.4$; $r_C(D) - r_{C-c}(D) = 1 - 1 = 0$; $r_C(D) - r_{C-d}(D) = 1 - 0.2 = 0.8$; so the objective weight of each attribute weights are $I_{(a)} = \frac{0.4}{0.4+0.4+0+0.8} = 0.25$, $I_{(b)} = \frac{0.4}{0.4+0.4+0+0.8} = 0.25$, $I_{(c)} = \frac{0}{0.4+0.4+0+0.8} = 0$, $I_{(d)} = \frac{0.8}{0.4+0.4+0+0.8} = 0.5$ .then the Comprehensive weight of each attribute are: $R_{(a)} = 0.6 \times 0.25 + 0.4 \times 0.3 = 0.27$, $R_{(b)} = 0.6 \times 0.25 + 0.4 \times 0.2 = 0.23$, $R_{(c)} = 0.6 \times 0 + 0.4 \times 0.1 = 0.04$, $R_{(d)} = 0.6 \times 0.5 + 0.4 \times 0.4 = 0.46$. Thus, we get the comprehensive weight of each attribute which are combination subjective with objective.

Conclusion

There is a malady in most of the evaluation process to determine the index weight, which is affected by the decision makers' subjective experience. The rough set theory to determine the importance of property is a manifestation the objective existence relative importance (which is objective existence) of large amount of historical data for each attribute. Therefore, combined the attributes importance theory of the rough set theory with expert scoring method, Would be a reasonable solution.

References

[1] QIN Shoukang, Principle and Application of Comprehensive Evaluation[M] Beijing: Publishing House of Electronics Industry. 2003,6: 111-113.

[2] Ronald R, Hoek ing TH. M ethods and app lications of L inearm idels: regression and the analysis of variable. N ew Yo rk: JohnW iley and Sons, 1997. 348-379.

[3]XIAO Zhijun, MAI Xiong2fa. A Method of Ascertaining Teaching QualityEvaluation Weight Based on Rough Sets Theory[J] Journal of Guangxi Teachers Education University(Natural Science Edition).2010,27:67-69.

[4] CAO Xiu ying, LIANG Jingguo. The Method of Ascertaining Attribute Weight Based on Rough Sets Theory[J] Chinese Journal of Management Science.2012,10(5):98-100.

[5] MIAO Guoqian,LI Daoguo. Rough set theory algorithms and applications[M] Beijing: Tsinghua University Press.2008.4.

Advanced Materials Research Vols. 989-994 (2014) pp 1739-1742
© (2014) Trans Tech Publications, Switzerland
doi:10.4028/www.scientific.net/AMR.989-994.1739

Takeoff Performance Algorithms Analysis of EFB Based on iOS

Lu Jing[1,a] Li Qing[2,b] Zhao Beibei[3,a] Xiao Fang[1,a] Qiu Weiyi[1,a]

[1].College of Computer Science and Technology, Civil Aviation Flight University of China, Guanghan 618307, China

[2]China Aerodynamics Research and Development Center,Mianyang,China

[3] AirTraffic College, Civil Aviation Flight University of China, Guanghan 618307, China

[a]maoyanqq@163.com, [b]liqinglucky@126.com

Keywords: electronic flight bag (EFB); takeoff performance; interpolation; iOS

Abstract. The Electronic Flight Bag (EFB) provides pilots real-time or existing data by converting the papery documents into electronic books. Consequently the efficiency and the security have been improved, which reduce pilots' ground communication time and the paperweight. As a key factor of what influences the takeoff process, the takeoff performance undoubtedly has been an essential research task of EFB, while many factors may affect the takeoff performance, such as flap position, anti-ice and the external temperature. By means of interpolation, this paper integrates those factors and gets Maximum Take-off Weight (TOW), Take-off Decision Speed (V1), Take-off Rotation Speed (VR) and Take-off Safety Speed (V2). And then implants the result into the EFB based on the iOS.

Introduction

Throughout the whole flight activity, the takeoff stage only account a small part, while the accident rate goes as high as 16%. The reason is that amounts of factors can influence takeoff performance, causing complexity of the takeoff stage. And the takeoff performance determines the maximum allowable takeoff weight of the aircraft, which directly affects the maximum payload, thus affecting the economy of aircraft operations.

The purpose of the takeoff performance calculation and analysis is to ensure the safety and improve the economy of takeoff, mainly based on the content of the various restrictions and calculates related factors to determine the maximum allowable takeoff weight for specific aircraft models, then check the actual takeoff weight to determine the takeoff thrust, and work out the major takeoff speed, especially the V1 takeoff decision speed, VR takeoff rotation speed and V2 takeoff safety speed, in order to ensure the flight safety and achieve the expected takeoff performance.

Relative technologies

The mobile terminal technology refers to the technology, which used in a mobile communication equipment, to terminate wireless transmission from or to the network, and adapt the capability of terminal device to a wireless transmission part.

Electronic Flight Bag (EFB) refers to the hardware and software supporting certain features, is located in the cockpit display system. Electronic flight bag includes a variety of air data information and the various basic calculations (such as performance calculation, fuel calculation etc.), some of these functions is accomplished with the use of traditional paper referenced materials or data provided by airlines "flight dispatcher" to flight crew. Functional range of electronic flight bag includes a variety of application programs and the database, the display of information can be achieved through plenty of techniques, formats and communication forms.

Algorithm Design

According to the mathematical model of the algorithm, the algorithm can be shown in the flowchart in Figure 1:

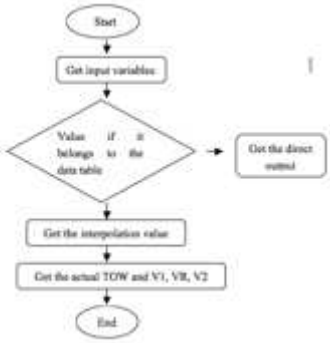

Figure 1Algorithm Flowchart

This algorithm is a highlight in combination with the thought of Manchester encoding array operations, which greatly simplify the calculation process and improve the speed. Input value Z, X, I, J, K, L, Y and W, correspond to Airport Runway ID, Runway state, QNH (hPa), OAT (℃), Wind (KT), Weight (kg), Flap setting and Anti - ice in the data table. Creating ADO database connection for query operations data, query whether there is a corresponding record in the database. That means query whether there is a record with value Z, X, I, J, K, L, Y and W equaling to the input values, if any, then outputs comparable TOW, V1, VR and V2 values, corresponding to TOW (LBS), V1 (KT), VR (KT) and V2 (KT) in the data table; If does not present, interpolates I, J, K, L to get the corresponding output values.

Crucial Technology

For a directed acyclic graph (DAG) Topological sorting is to arrange all vertices of G in a linear sequence, then for any pair of vertices U and V in the figure, if it belongs to the E (G), U in the linear sequence occurs before V. Usually, the linear sequence is known as satisfied topological order sequences, topological sequences for short. In simple terms, getting a total order by a partial order of a set is called topological sorting. The definition of partial order and total order in Discrete Mathematics are as follows:

If R is a collection on X set, and the R is reflexive, anti-symmetric and transitive, then R is called partial ordering relations on X set. Let R be a partial order on X set, if for every x, y belongs to the X must be xRy or yRx, then R is called total ordering relations on X set. Simply put, partial order refers to comparisons between some elements in the set, while total order refers to comparisons among all elements in the set.

Manchester Encoding is also called phase encoding (PE). It is a synchronous clock encoding technology used to code the clock and data of a synchronous bit stream in physical layer. Manchester encoding is used in the Ethernet media system and provides a simple way to encode binary sequence without a long period and level conversion, thus preventing the loss of clock synchronization or the analog link bit error of poor compensation from the low-frequency displacement. In Manchester encoding, phases differ voltage jump to distinguish 1 and 0 that means voltage jump for 1 and the negative voltage jump for 0. Therefore, this encoding is also known as the phase encoding. Because

the jump occurred in the middle of each symbol, the receiver can easily use it as a synchronous clock, so the encoding is also called self-synchronizing encoding.

This algorithm combined with the mathematical thought of topological graph theory, transforming the interpolation process into a graph matrix and then use the Manchester encoding to realize the interpolation process, which makes the algorithm more clear.

The specific code and flow chart are shown in figure 2. In matrix M, 0 and 1 corresponding to the smaller and larger value in the data table of value I, J, K, L. For value I, 0 and 1 correspond to different I interpolation, similar to J, K, and L. This is the combining method of algorithm with Manchester encoding. And each time the results are interpolated from the previous interpolation result, which demonstrates the combination of the algorithm and graph theory.

Interpolation algorithm formula is as follows:

In which X represents the results for TOW, V1, VR, and V2. X1 and X0 is the previous result or queried results on the data table. A0 and A1 corresponding to smaller and larger value of value I, J, K, L, while A is the actual I, J, K, L value.

Interfaces and Interface Design

This algorithm selects iOS interface. And the electronic flight bag based on iOS has been used in cockpits, such as the iPad for pilots in cockpits.

The advantages of iOS interface: iOS system is highly integrate into hardware, which greatly reduce the differentiation and ensure the algorithm operates steadily, meantime the gorgeous interface and usability of iOS system facilitate the convenience of the pilot. What's more, the data security is one of the advantages; since the strong data protection of iOS can guarantee the security of data, then ensure the safety of flight.

The defects of iOS interface: iOS interface also has shortcomings. In the latest iOS7 system, there are some defects about AutoCorrect appeared, which will influence pilots' use of EFB, further affecting the user experience of our takeoff performance algorithm.

This algorithm finally choose iOS interface to bring electronic flight bag users to acme, and the iOS handset operating system can help us achieve this requirement.

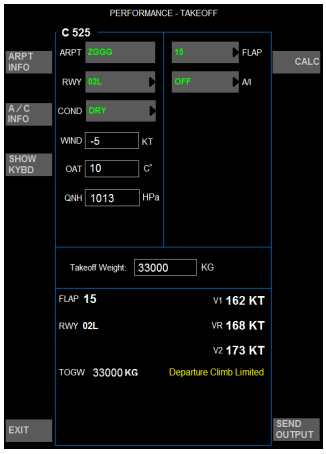

The human factor is an important aspect to affect the flight safety. When deal with something about the electronic flight bag and man-machine interface, this algorithm designs strictly in accordance with the basic principles of human factors to getting an intuitive user interface and designs data input or some other options according to the "agency regulations", maintaining coordination with other designs in the electronic flight bag to avoid affecting the use of other functions.

Implants the algorithm into iOS based EFB will get a interface as figure 2: Figure 2 EFB

Conclusions

After careful test and arrangement, the algorithm is now applied into iOS operating system for mobile devices and gets some achievements, also affects well in the terms of usability and user experience and has applied for national patent.

References

[1] Robert Clair.Learning Objective-C 2.0:a Hands-on Guide to Objective-C for Mac and iOS Developers.Li Q.Beijing:Machinery Industry Press,2011
[2] Chesbrough H W.Open Innovation:The New Imperative for Creating and Profiting from Technology [M].Boston:Harvard Business School Press,2003
[3] Erica Sadun.The iPhone Developer's Cookbook: Building Applications with the iPhone 3.0 SDK(2nd Edition).Zhang C X ,Gao Y ,Yi L , etal. Beijing: People's Posts and Telecommunications Press, 2010:21-22
[4] Jonathan Zdziarski.iPhone SDK Application Development:Building Applications for the Appstore.Lu C D ,Qi W M.Beijing:People's Posts and Telecommunications Press,2010
[5] Liu H,Dong Q H.Design of Screen Layout Control Based on the Observer Pattern.Electronics Technology,2010,23(8):110-111
[6] Xu M ,Chen G Y.On Design Patterns in iOS Multimedia Message System .Microelectronic and Computer, 2012,29(11):112-115
[7] Wang Y Z,Li Y Z,Guo L.Research of Mobile Endpoint User Interface Framework.Computer Engineering Design,2012,33(4):1670-1675
[8] Wei J H.Research on the Intelligent Mobile Terminal Software Platform and the Data Synchronization.Chengdu: University of Electronic Science and Technology,2005
[9] Ma J.China Terminal Industry in 3G Era.Modern Transmission,2006,32(3):23-25
[10] Ma J D,Wang J S.Status of Wireless Mobile Termial and the Future Competition.Contemporary Communication ,2003(24):10-13
[11] Wang J Q,Zhang X J.Designing Project of Mobile Terminal System of Maintenance & Engineering . Aircraft Maintenance and Engineering, 2005(5): 57-59
[12] Joe Conway,Aron Hillegass.iOS Programming 2nd Edition.Xia W P.Wuhan:Huazhong University of Science and Technology press,2012
[13] Shawn Welch.iOS 5 Core Framework.Lu C D.Beijing: People's Posts and Telecommunications Press, 2012
[14] Carlo Chung.Pro Objective-C Design Patterns for iOS. Liu W. Beijing: People's Posts and Telecommunications Press,2011
[15] Bill Hamilton.ADO.NET 3.5 Classic Examples.Xu B.Beijing:Machinery Industry Press,2009
[16] Simon Haykin.Communication Systems,Fouth Edition.Shen L F,Song T C,Xu P P,etal. Beijing: Electronic Industry Press,2012
[17] Thomas H.Cormen,Charles E.Leiserson,Ronald L. Rivest,etal.Introduction to Algorithms, Third Edition. Yin J P,Xu Y,Wang G,etal.Beijing: Machinery Industry Press,2013
[18] Levitin.Introduction to the Design and Analysis of Algorithms,Second Edition.Pan Y.Beijing: Tsinghua University Press,2007
[19] Wang X D.Design and Analysis of Computer Algorithms.Beijing:Electronic Industry Press, 2012
[20] Behrouz A.Forouzan Sophia Chung Fegan.Data Communications and Networking Forth Edition. Wu S L,Wu Y H,Wu Z Y etal.Machinery Industry Press,2007

Advanced Materials Research Vols. 989-994 (2014) pp 1743-1746
© (2014) Trans Tech Publications, Switzerland
doi:10.4028/www.scientific.net/AMR.989-994.1743

Region Analogy-Based Quantization Method for Numerical Data

Yudi Sun [a]

School of Information Technology, Jiangsu Institute of Commerce, Nanjing, 211168, China

[a]email: njgcswx@163.com

Keywords: Quantization, Machine Learning, Region Analogy

Abstract. Data quantization methods for numerical attributes play an extremely important role in handy talents statistics assessment and technology learning because discrete values of attributes are required in most classification methods. In this paper, we present an region analogy-based quantization method for numerical data. It expresses an inner coherence criterion which is thought to be as a new criterion in the ways of quantization. In addition, a heuristic quantization algorithm is proposed to achieve a satisfying quantization result with the aim to improve the performance of inductive learning algorithms. They realize criterion as well as quantifying the true value attributions exactly and reasonably. Strict experiments on UCI reflects data sets express that our supposed algorithm produces a superior quantization scheme that promotes the classification right of inductive learning than emerging quantization algorithms.

Introduction

Data mining is a wide range of technology integration in several areas, containing artificial intelligence, inductive learning and task mining, artificial smart. We have been a lot of roots in these areas of data mining algorithms. Data quantization is the processing techniques commonly used data mining, machine learning and knowledge invention [1,2]. Many real-world data mining tasks conclude enormous attributions. Nevertheless, almost all of data mining techniques can not deal with such attributions. Therefore, it is necessary and important to partition into several time regions to produce a small number of different values from some features and numerical feature domain value. A perfect quantization can not only produce a concise summarization of numerical attributions to do a favors to the people cover more about the data more convenient, but also lead to quick and accurate learning [3].

Existing quantization techniques can be grouped into top to bottom vs. bottom to top, however top-down can be further classified into unsupervised vs. supervised [4].Top to bottom methods begin with primary moment and slice it to tiny time points, whereas bottom to top techniques start from someone value region sets and iteratively merge the region pair. Unsupervised algorithms do not consider information class, i.e., EQW and EQF [4]. While, supervised algorithms consider information class with different feature, i.e., the quantization algorithms [5,6] based on Chi2, class-feature interdependency-based methods like CACC [7], OCDD [8], and entropy-based discretion [9], and so on.

In this paper, we pay attention to bottom-up quantization methods and propose a region analogy-based quantization method for numerical data. The main contributions of this paper are summarized as follows:

1) We define a region analogy-based criterion which is thought to be as a new merging criterion in the way of quantization.
2) We propose a heuristic quantization algorithm to achieve a satisfying quantization result with the aim to improve the performance of inductive learning algorithms. The proposed algorithm realizes fair standard and quantifying numeric value features reasonably and exactly.
3) We conduct the empirical tests on UCI data sets, and indicate that the supposed method yields a superior quantization schedule that enhances the classification precise of inductive learning than being algorithms.

Our Quantization Method

In this section, we propose a method based on analogy quantization region numerical data. Details before into our approach, we first declare to quantify the problem. Quantitative tasks require samples, each sample belongs to a class has only one training data. Next, the existence of quantitative solution, quantitative, numerical time region within the scope of the attributes of digital domain:

$$P:\{[t_0,t_1],[t_1,t_2],\cdots,[t_{I-1},t_I]\} \tag{1}$$

Where t_0 is the smallest value and t_I is the largest value of a numerical attribute. The values in P are classified in ascending order. For quantization goal, complete data are pointed on target attribute. This projection consequence is 2D *table graph,* see Table 1, having S *amount*s and I rows. Each row acts according to a primary data region, and each column reacts to another class. N_{ij} reflects instance number in j th class belong to i region T_i. $N_{\cdot j}$ is the overall instance number in the j th level. $N_{i\cdot}$ is the overall number of models that are within the time region T_i.

Table1 Table information

Regions	C_{lable}				Row Sum
	C_1	C_2	…	C_S	
$T_1:[t_0,t_1]$	N_{11}	N_{12}	…	N_{1S}	$N_{1\cdot}$
$T_2:[t_1,t_2]$	N_{21}	N_{22}	…	N_{2S}	$N_{2\cdot}$
…	…	…	…	…	…
$T_I:[t_{I-1},t_I]$	N_{I1}	N_{I2}	…	N_{IS}	$N_{i\cdot}$
Sum of Column	$N_{\cdot 1}$	$N_{\cdot 2}$	…	$N_{\cdot S}$	N *(total)*

Region analogy criterion

Approximate reasoning is an important research component in the field of artificial intelligence. It needs different analogy measure between images and objects. Analogy between two objects is value-measure of similar degree between two objects. Thus, the more similar are two objects, the higher is their similar degree. Usually, similar degree is un-minus and the value often is between 0 (dissimilar) and 1 (completely similar). The same principle, difference between two objects is value--measure of difference degree between two objects. The more similar are two objects, the lower is their difference. Often, if the value of similar degree between two objects does not change in [0,1], we may use some kind of function to normalize it to [0,1]. It has produced definition and characteristic of the general analogy:

Def. 1 It is known that database B have two arrays t_i and t_j, their similar degree $RAC(t_i,t_j)$ is a mapping from $B\times B$ to the region [0,1]. Therefore, $RAC(t_i,t_j)\in[0,1]$.

A qualified similar criterion or method has the following feature:

$\forall t_i\in B,\quad RAC(t_i,t_i)=1$;

$\forall t_i,t_j\in B$, if t_i and t_j is not same, then $RAC(t_i,t_j)=0$;

$\forall t_i,t_j,t_k\in B$, compared with t_j, if t_k closes to t_i, then $RAC(t_i,t_j)<RAC(t_i,t_k)$

Traditional analogy measure commonly used research results directly. In this paper, we propose a comprehensive significance quantization standard; that is, a new region analogy function which not only can realizes fair and quantifying the real value attributions exactly and reasonably. Definition and analysis of region analogy are as follows.

Def. 2 Give 2 objects; a_i and b_j are a level label to *ith* domain in time first region. Then, the difference between a_i and b_j is:

$$d_{ij} = \begin{cases} 0 & if \ a_i = b_j \\ 1 & if \ a_i \neq b_j \end{cases} \tag{2}$$

Where $i = 1,2,\cdots,s$, $j = 1,2,\cdots,t$, s is the component number of the first region, t is the component number in the second region.

Def. 3 Regarding any adjacent two regions a and b. Region analogy function may be defined as follows:

$$RAC(t_k, t_{k+1}) = 1 - arcsin \frac{\sum_{i=1}^{s}\sum_{j=1}^{t} d_{ij}}{s+t} \tag{3}$$

Based on the above, we design an algorithm that is heuristic in nature. The objective of this algorithm is to find better quantization scheme. The detailed steps can be described as follows.

Step *one*: Compute the level of consistency by [5];

Step *two*: The analogy values calculated for each attribute ascending sort data RAC for an region pair by (3);

Step *three*: Merging;

```
While (∃region pair)
{   Find the point cut, having the largest analogy, and then merge;
    If (some maximal values)
   {    Merging region pair with minimal class number;
        If (level of consistency is changed)
     {  With back merge;
         Quit processing;  }
        Else {Cut; Run Step two;}
     }
    If (many maximal values and same class number between region pairs)
     {  Merging region pair with minimal class number;
         If (level of consistency is changed)
        {  With back merge;
            Quit processing; }
         Else { Cut; Run Step two; }
        }
 }
```

Experimental results

To estimate this algorithm, choose four data sets from the data at the University of California, Irvine repository with digital functions and different size of the data. Data consistency or not correct (not consistent rate to zero), and the data contains information from the previous in real life have been used for medical and scientific research. A summary of data sets can be found in Table 2.

Table 2 Data sets

Data sets	Continuous features Number	Discrete features Number	Class Number	Samples
Auto	5	2	3	392
Iris	4	0	3	150
Breast	9	0	3	683
Ionosphere	34	0	2	351

We compare our proposed region analogy-based method with the following algorithms for result evaluation: C4.5 [2], Mod-chi2 [5], Ext-Chi2 [6], and Unsupervised [4]. Repeating many times experiments and the average prediction accuracy of prediction accuracy is for the final. The five learning precision, listed in Table 3. Comparison results in Table 3 show that on average, our approach to achieve the highest classification accuracy, this shows that our method can produce high quality of the quantization scheme.

Table 3 Learning accuracy (percent) of C4.5 decision tree classification

Data sets	Methods				
	C4.5	Modified Chi2	Extended Chi2	Region analogy-based	Unsupervised
Auto	77.84	80.65	81.42	85.64	72.55
Iris	94.3	94.45	94.45	95.78	92.67
Breast	94.68	96.37	96.37	97.4	93.83
Ionosphere	90.71	93.73	93.91	94.93	84.6

Conclusions

We propose a static, incremental, supervise and bottom-up quantization algorithm, this paper proposed a new quantitative criteria and heuristic algorithm. Classification algorithm to estimate the effect of quantitative plan performance, existing quantization algorithm empirical estimation in the UCI data show that the novel method to create a good quantization criterion.

References

[1] K. J. Cios, and L. A. Kurgan, "CLIP4: hybrid inductive machine learning algorithm that generates inequality rules," *Information Sciences*, vol. 177, no. 17, pp. 3592–3612, 2007.

[2] J. R. Quinlan, "C4.5: programs for machine learning," *San Mateo, Calif.: Morgan Kauf-mann*, 1993.

[3] H. Liu, F. Hussain, C. L. Tan, and M. Dash, "Discretization: an enabling technique," *Journal of Data Mining and Knowledge Discovery*, vol. 6, no. 4, pp. 393–423, 2012.

[4] J. Dougherty, R. Kohavi, and M. Sahami, "Supervised and unsupervised discretization of continuous feature," *Machine learning: Proc. 12th Intl Conf.*, pp. 194–202, 1995.

[5] E. H. Tay and L. Shen, "A modified chi2 algorithm for discretization," *IEEE Transactions on Knowledge and Data Engineering*, vol. 14, no. 3, pp. 666–670, 2002.

[6] C. T. Su and J. H. Hsu, "An extended chi2 algorithm for discretization of real value attributes," *IEEE Transactions on Knowledge and Data Engineering*, vol. 17, no. 3, pp. 437–441, 2005.

[7] C. J. Tsai, C. I. Lee, and W. P. Yang, "A discretization algorithm based on class-attribute contingency coefficient," *Information Sciences*, vol. 178, no. 19, pp. 714–731, 2008.

[8] L. L. Liu, A. K. C. Wong, and Y. Wang, "A global optimal algorithm for class-dependent discretization of continuous data," *Intelligent Data Analysis*, vol. 8, no. 2, pp. 151–170, 2004.

Advanced Materials Research Vols. 989-994 (2014) pp 1747-1750
© (2014) Trans Tech Publications, Switzerland
doi:10.4028/www.scientific.net/AMR.989-994.1747

Application of Improved ANT Algorithm to Planning of Anti-ship Cruise Missile Route

Yongtao Yu [1, a], Ying Ding[2]

[1] Naval Academy of Armament, Beijing, china, 100161

[2]Beijing Sino-Ocean JIYE Propetry Management CO., LTD, Beijing, china, 100038

[a]y_yt128@aliyun.com

Keywords: ANT algorithm, anti-ship cruise missile, route planning

Abstract. Anti-ship cruise missile (ASCM) attack route meets the needs of the attack mission will determine the effect of the subsequent attacks. According to research planning of anti-ship cruise missile route based on improved ANT algorithm by elitist strategy. The first is sensitive factor analysis of route planning based on operational requirements. Second is established an objective function and constraints set of route planning, achieved anti-ship cruise missile route planning model. Finally, based on specific objectives, situation and the user's strategies, it can use improved ANT algorithm to plan anti-ship cruise route.

Introduction

The goal of anti-ship cruise missile (ASCM) route planning is to design a flight route to obtain the greatest possible attack effect. Missile flight route from the launch point to the target need to meet a series of route constraints, such as performance of missile, angle of attack and threatening region. Therefore, ASCM route planning can be classified as a large-scale combinatorial optimization problem. The length of time consumed in route planning has a significant impact on the route execution, so ASCM route planning problems have distinct time-sensitive.

ANT algorithm is a heuristic bionic algorithm derived from the biosphere. All ants cooperate to carry out the search for optimized path. So ANT algorithm can exactly solve a large-scale combinatorial optimization problem, such as ASCM route planning. And to a certain extent, there is a slow convergence of ANT algorithm flaw. It is difficult to meet the requirements of ASCM route planning. So we improved ANT algorithm based on elitist strategy introduced by transfer direction inducing factor. In the route planning process, we can accord to the target, threats and current location, immediate to establish new transfer direction inducing factors, enhanced the directionality of path selection of ant, and improved the efficiency of ASCM route planning.

Basic concept

ANT algorithm

In addition to ANT algorithm use positive feedback, through artificial ants also introduces visual function. At time t, the probability of ant k is transferred from node i to j can be written as Eq. 1:

$$P_{ij}^{k}=\begin{cases}\left(\tau_{ij}^{\alpha}(t)\eta_{ij}^{\beta}(t)\right)\Big/\sum_{s\in allowd_k}\tau_{is}^{\alpha}(t)\eta_{is}^{\beta}(t), & if \quad j\in allowd_k\\ 0, & other\end{cases} \tag{1}$$

Which, List $tabu_k$ record the node current ants walked. α is information heuristic factor, which means that the relative importance of the path. β is expected heuristic factor, which means that the relative importance of visibility. η_{ij} (t) is a heuristic function. After each ant access to all nodes, to undermine the old residual information processing can be written as Eq. 2:

$$\tau_{ij}(t+n)=(1-\rho)\tau_{ij}(t)+\Delta\tau_{ij}(t)\qquad \Delta\tau_{ij}(t)=\sum_{k=1}^{m}\Delta\tau_{ij}^{k}(t) \tag{2}$$

ANT algorithm based on transfer direction inducing factor

By the 1) shows that ants move from node i to node j mainly affected by the pheromone, heuristic function, information heuristic factor and expectations heuristic factor. But for the ASCM route planning this particular issue, node metastasis should also be subject to the direction of target and

the extent of threat. Therefore, we introduce the transfer direction inducing factor (δ(i,j)) to improve the ANT algorithm based on elitist strategy. The value of transfer direction inducing factor reflect the basic judgment of ants on the next shift direction. Based on the transfer direction inducing factor, the improved metastasis probability formula can be written as Eq. 3:

$$P_{ij}^{k} = \begin{cases} \left(\delta_{ij}(t)\tau_{ij}^{\alpha}(t)\eta_{ij}^{\beta}(t)\right) \Big/ \sum_{s \in allowd_k} \delta_{is}(t)\tau_{is}^{\alpha}(t)\eta_{is}^{\beta}(t), & if \quad j \in allowd_k \\ 0, & other \end{cases} \tag{3}$$

In the transfer direction inducing factor $\delta = \begin{bmatrix} \delta_{(-1,-1)} & \delta_{(-1,0)} & \delta_{(-1,1)} \\ \delta_{(0,-1)} & \delta_{(0,0)} & \delta_{(0,1)} \\ \delta_{(1,-1)} & \delta_{(1,0)} & \delta_{(1,1)} \end{bmatrix}$, values of a matrix representing the tendency of the ant from δ(0,0) shift to the eight directions, and determined by the target orientation parameter and level of threat parameter. δ can be written as Eq. 4:

$$\delta_{ij}(t) = Q_s + Q_t = Q_s + \left(\left(k_{t1} r_{ij}\right)/R_{se} + \left(k_{t2} r_{ij}\right)/R_{at}\right) \tag{4}$$

Where, Qs is the target orientation parameter, as shown in Table 1. Qt is the threat level parameters, including the detective threats and intercept threats. r_{ij} is the distance between the ship and node j. Rse is the detection distance of ship. Rat is the intercept distance of ship. Kt is the ratio of relative importance between of detective threats and interceptive threats.

Table 1 Target orientation parameter

Difference between target orientation and δ(i,j)	0º-15º	15º-45º	45º-75º	75º-105º	105º-135º	135º-165º	165º-180º
Values of δ(i,j)	7	6	5	4	3	2	1

ASCM route planning improved ANT model

Analysis of factors route planning

According to ASCM operational mission requirements, route planning has mainly four core factors: the angle of attack, route constraints, penetration ability and concealment.

Angle of attack (Aacm) is factor characterizing the late-guided of ASCM. Favorable angle of ASCM attack not only for maximum target radar cross section, but also to avoid as far as possible shooting range of target ship anti-aircraft weapons.

Route constraints (Racm) are factors characterizing the flight performance of ASCM. It mainly consists of two indicators: the effective range of constraints and routes turning point constraints. The effective range of constraints is the total length of cruise missile route must not exceed its effective range (Rvmax). Routes turning point constraint is the size of turning points in the ASCM route can not exceed the maximum value of the guidance system can be set (Ntpmax).

Concealment (Scam) is factors characterizing the detection threats of target ship. The key to ASCM route planning is to reduce as much as possible detection probability and delayed time were found by target during the flight. So choose exposure flight time (Tuc) and flight distance in the detection range (Luc) to describe the concealment of ASCM. It can be written as Eq. 5:

$$S_{acm} = 1/\left(\mathrm{k_s} L_{uc} + \left(1 - \mathrm{k_s}\right) T_{uc}\right) \tag{5}$$

Penetration ability (Pacm) is factors characterizing the intercept threats of target ship. Target ship equipped air defense missiles, anti-missile guns and electronic jamming system performance determines the size of the penetration ability of ASCM. Therefore, penetration ability of ASCM related to the damage probability of air defense missiles, anti-missile guns and electronic jamming system can be written as Eq. 6:

$$P_{acm} = \left(1 - P_{SAM}\right)\left(1 - P_{AAA}\right)\left(1 - P_{ECM}\right) \tag{6}$$

Construction of route planning model

ASCM target route planning is hidden under the premise as to costs as small as possible, from the perspective of favorable attack surface ships. The objective function can be written as Eq. 7:

$$MaxF = E_i / V_i \tag{7}$$

Where, Ei is the attack effect of the missile when flying along i-th route. Vi is the costs of the missile when flying along i-th route.

Ei including angle of attack and hidden factors can be written as Eq.8:

$$E_i = K_e A_{acmi} + (1-K_e)S_{acmi} = K_e A_{acmi} + (1-K_e)/(k_s L_{uci} + (1-k_s)T_{uci}) \quad (8)$$

Which, Aacmi is the probability of a favorable angle of attack is achieved when the ASCM flying along i-th route. Sacmi is the concealment of the missile when flying along i-th route. Ke is the relative importance ratio of the angle of attack and concealment.

Vi including penetration costs (Vp) and time costs (Vt) can be written as Eq. 9:

$$V_i = K_v V_{pi} + (1-K_v)V_{ti} = \frac{K_v}{P_{acmi}} + (1-K_v)R_i = \frac{K_v}{(1-P_{SAMi})(1-P_{AAAi})(1-P_{ECMi})} + (1-K_v)R_i \quad (9)$$

Which penetration costs (Vpi) is the reciprocal of penetration ability when ASCM flying along i-th route. Time cost (Vti) is the total range when ASCM flying along i-th route. Kv is the ratio of relative importance between of penetration costs (Vp) and time costs (Vt).

ASCM route planning also includes two feasibility constraints. The length of route must not exceed Rvmax. The size of turning points can not exceed Ntpmax. It can be written as Eq. 10:

$$s.t\begin{cases} R_i \le R_{v\max} \\ N_i \le N_{tp\max} \end{cases} \quad (10)$$

ASCM route planning application examples

The target of ASCM is fleet command ship (Sc), in addition fleet also includes six frigates (Sf). ASCM flight speed of 300m/s, Rvmax is 280 kilometers; Ntpmax is 3, Aacm is ±80±15º.

Establish describe information of the node

According combat situation, we can establish the North east coordinate system. ASCM launch at the origin. The distance of target fleet is 192 kilometers, heading 345º. Fleet command ship at (400,500), six frigates position respectively (360,395), (275,498), (331,564), (429,611), (520,515) and (463,442). Mesh node spacing set 300 meters (ASCM one second flight distance).

Route planning conclusion

ASCM route planning simulation using MATLAB programming operations are realized. Ants scale (m) is set to 20, the maximum number of iterations is set to 500, and the maximum number of cycles is set to 10. Specific conclusions of ASCM route planning are shown in Table 2 & Fig.1.

Table 2 Route planning conclusion data

Conclusion of route planning	User's strategies		
	Focus on concealment Rs	Focus on penetration ability Rp	focusing on angle of attack Ra
The flight time of missiles after being found (Sec)	138	155	160
The distance of missiles flight being intercept (Km)	33.1	20.5	35.9
average intensity of the interceptor firepower (Times)	8.61	2.0	4.74
The total flight time of missiles route (Sec)	660	695	780
Angle of attack (º)	120	135	75
The number of turning points in missiles route	1	2	3

For hidden route (Rs), within the detection range of ship, the flight time of missiles is shortest, respectively equivalent to penetration route (Rp) of 89% and aggressive route (Ra) of 86%. Hidden effects of missile are the best; better reflect the user's strategies focusing on concealment. But the anti-aircraft firepower attack missile is the strongest. Within the intercept range of ship, the flight distance of missiles is longer, weakening penetration capability of the missile. Angle of attack not belongs to a favorable angle. For the penetration route (Rp), within the intercept range of ship, the flight distance of missiles is shortest, respectively equivalent to hidden route (Rs) of 62% and aggressive route (Ra) of 57%. The anti-aircraft firepower attack missile is the weakest, respectively equivalent to hidden route (Rs) of 23% and aggressive route (Ra) of 42%. Effect breakthrough defense of missile is the best; better reflect the user's strategies focusing on penetration capability. However, within the detection range of ship, the flight time of missiles is longer, weakening concealment of the missile. Angle of attack not belongs to a favorable angle. For aggressive route

(Ra), the angle of attack is favorable angle. Capture the effect of target ship of missile is the best; better reflect the user's strategies focusing on angle of attack. But within the detection range of ship, the flight time of missiles is longest, equivalent to penetration route (Rp) of 103%, weakening concealment of the missile. Within the intercept range of ship, the flight distance of missiles is longest, equivalent to hidden route (Rs) of 108%. The anti-aircraft firepower attack missile is the stronger, weakening penetration capability of the missile.

Thus, ASCM route planning improved ANT algorithm model can be achieved the goal, meet the constraints, sensitively reflect the user's strategies, and effectively enhance the effect of a missile attack. Improved ANT algorithm introduced by transfer direction inducing factor can be a good match planning goals and a lot of constraints, meet timeline requirements of route planning.

Summary

The ASCM route planning application improved ANT algorithm. First can use ANT algorithm have stronger robustness and the ability to search better solution to solve a large-scale optimization problem of matching missile route planning goals and a lot of constraints. Then based on elitist strategy introduce the transfer direction inducing factor, optimized node metastasis ant direction selection information, solve problems of stagnation because too slow convergence may arise. Future research will also continue to explore ways to enhance synergies between the ants, so as to improve the efficiency of ASCM route planning.

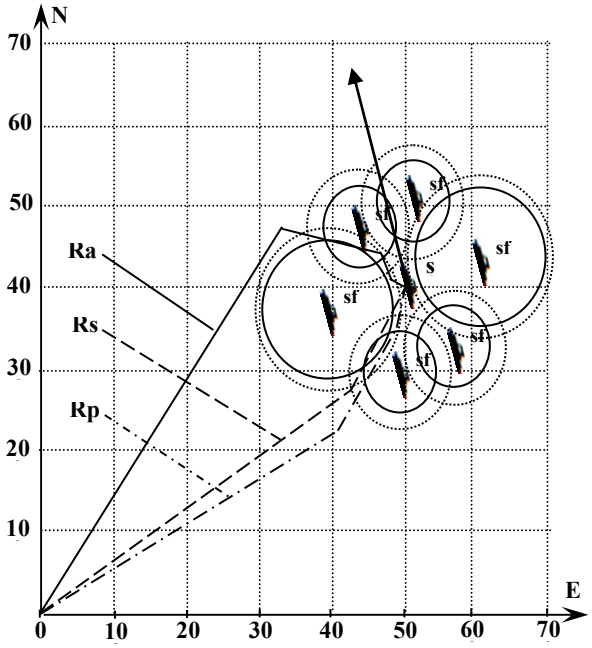

Fig.1 Route planning conclusion

References

[1] Sjanic Z. On-line mission planning based on model predictive control [D]. Sweden: Linkoping University, 2001: 5-18.

[2] D T Pham, D Karaboga. Intelligent Optimization techniques [M].London; Hong Kong; Springer, 2000: 75-77.

[3] Vian J L, Moore J R. Trajectory optimization with risk minimization for military aircraft [J]. Guidance and Control, 1989, 12(3):381-385.

[4] Edwards K. Software Development Process for the Aviation Mission Planning System (AMPS): A Case Study [R]. AD - A305332.

[5] Pellazar, M.B. Vehicle route planning with constraints using genetic algorithms[A].Aerospace and Electronics Conference,1994,vol.1:111-118.

[6] Asseo S J. Terrain following/ terrain avoidance path optimization using the method of steepest descent [A]. NAECON88 [C]. 1128-1136.

[7] KOENIG S, LIKHCHEV M, FURCY D. Lifelong planning A*[J]. Artificial Intelligence, 2004, 155 (3): 93-146.

Advanced Materials Research Vols. 989-994 (2014) pp 1751-1755
© (2014) Trans Tech Publications, Switzerland
doi:10.4028/www.scientific.net/AMR.989-994.1751

Application of improved intuitionistic fuzzy for sea-battlefield situation assessment

Yongtao Yu [1, a], Ying Ding[2]

[1] Naval Academy of Armament, Beijing, china, 100161

[2]Beijing Sino-Ocean JIYE Propetry Management CO., LTD, Beijing, china, 100038

[a]y_yt128@aliyun.com

Keywords: intuitionistic fuzzy Sea-battlefield situation assessment

Abstract. Maritime Operations Command premise is a scientific and efficient assessment of the dynamic and varied sea-battlefield. According to research sea-battlefield situation assessment based on improved intuitionistic fuzzy algorithm based on projection. First is based on intuitionistic fuzzy to establish the sea-battlefield situation information matrix. Second is establishing the sea-battlefield assessment criterion vector. Finally, based on the theory of projection, it can compute the proximity of sea-battlefield situation information matrix and sea-battlefield assessment criterion vector, comprehensive and dynamic assess sea-battlefield in different time slices.

Introduction

Sea battle is a complex, dynamic and high risk. Similarly sea-battlefield assessments are mostly uncertain environmental conditions, incomplete information, deal with emergencies under intense time pressure. Therefore, the process and the objects of sea-battlefield assessments are with ambiguity essence. As technology advances, new types of weapons emerging cause the types of sea-battle object increases, while situational awareness means continue to enrich cause the information of sea-battlefield situation is expanding. Therefore sea-battlefield assessment is a dynamic process. In addition a number of different types of sea-battle objects performing their operations and achieving their operational intentions. Sea-battlefield situation assessment requires parallel processing the deep impact of the uncertainty caused by the massive nonlinear potential and random phenomenon.

Atanassov expand Zadeh fuzzy sets is proposed based on membership, non-membership and hesitation of the three aspects of intuitionistic fuzzy sets of information, so that intuition can be more delicate set of fuzzy sets to describe and characterize the objective world than traditional fuzzy vagueness nature. The sea-battlefield assessments are typical ambiguity with nature. In the complex sea-battlefield, the sea-battlefield assessment of many factors to consider, from only a single attribute is difficult to accurately determine the level of threat. In theory, considerations of scale and credibility of the results obtained is proportional. The practice, factors to be considered too, can easily generate combinatorial explosion. Cause sea-battlefield situation assessment process overly complex and difficult to achieve even impossible. The main factors affecting the same time may be annihilate by a lot of secondary factors. So we improved intuitionistic fuzzy algorithm by introducing projection theory. In the situation assessment process, we may be subject to changes in sea battle, based on the projection theory immediate to establish new sea-battlefield assessment criterion vector, used to characterize the dynamic classification rules and potential relationships. By calculating the projection of sea-battlefield situation information matrix on the sea-battlefield assessment criterion vector, it is relatively simple to achieve the current sea-battlefield situation assessment.

Basic concept

Intuitionistic fuzzy sets

The main difference between intuitionistic fuzzy sets and fuzzy sets is that it not only gives the membership on the field a little, but also gives the non-membership.

Intuitionistic fuzzy set theory on domain X is an object of the form: $A=\{\langle x,\mu_A(x),\gamma_A(x)\rangle|x\in X\}$.

Which, $\mu_A(x):X\to[0,1]$is the membership x belong to A, $\gamma_A(x):X\to[0,1]$ is the membership x does not belong to A; and meet the sum: $0\le\mu_A(x)+\gamma_A(x)\le 1,\forall x\in A$.

For intuitionistic fuzzy sets on X, intuition index of x is defined as $\pi_A(x)=1-\mu_A(x)-\gamma_A(x)$. It reflects the degree of x for A hesitate a measure.

When X is a continuous space, intuitionistic fuzzy set A can be expressed as $A=\int_x\langle\mu_A(x),\gamma_A(x)\rangle/x$.

When X is a discrete space, intuitionistic fuzzy set can be expressed as $A=\sum_{i=1}^{n}\langle\mu_A(x_i),\gamma_A(x_i)\rangle/x_i$.

Intuitionistic fuzzy reasoning based on the premise that the physical meaning of the observed data, the establishment of appropriate membership functions and non-membership function, fuzzy observation data.

Projection theory

Because the components of a vector comprising the mold and direction. Either direction or mode can not fully reflect the closeness between vectors. So we choose the cosine of the angle between the vectors to measure the consistency of the direction vectors. We are considering the direction and mold of vector to define the concept of projection. Assuming there is vector $\alpha=(\alpha_1,\alpha_2,....,\alpha_k)\&\beta=(\beta_1,\beta_2,....,\beta_k)$, the projection of α on the β can be written as Eq. 1.

$$\Pr o_\beta(\alpha)=\left(\sum_{i=1}^{k}\alpha_i\beta_i\sqrt{\sum_{i=1}^{k}\alpha_i{}^2}\right)\Big/\left(\sqrt{\sum_{i=1}^{k}\alpha_i{}^2}\sqrt{\sum_{i=1}^{k}\beta_i{}^2}\right)=\sum_{i=1}^{k}\alpha_i\beta_i\Big/\sqrt{\sum_{i=1}^{k}\beta_i{}^2} \tag{1}$$

Generally, the larger value of $\Pr o_\beta(\alpha)$, the closer between the vectors α and β.If β is the ideal situation typical numerical key factor collection, it indicates that the current situation α more closely this typical situation β, which can evaluate the current situation α comply with relevant characteristics typical situation β.

Sea-battlefield intuitionistic fuzzy assessment model

Building sea-battlefield situation assessment model based on improved intuitionistic fuzzy. The first is based on intuition obfuscated sea-battlefield information, build sea-battlefield information matrix described by the intuitionistic fuzzy numbers. Then based on the goal of the sea-battlefield situation assess, build sea-battlefield assessment criterion vector. Based on the theory of projection, sea-battlefield situation assessment is computing the proximity of sea-battlefield situation information matrix and sea-battlefield assessment criterion vector. It can base on existing experience to match the current situation, identify the trend from previous similar experiences situation conducive to the development of one's own action plan for the next step can be implemented under.

Establish sea-battlefield information intuitionistic fuzzy matrix

The object of sea-battlefield situation assessment is sea-battlefield situation in different time slices. Each sea-battlefield situation contains a large number of property information. Establish sea-battlefield information matrix, it must be evaluation each attribute of sea-battlefield situation by intuitionistic fuzzy numbers, and the corresponding form of a matrix formulation. There is n sea-battlefield situation, each situation with m attributes, then the sea-battlefield information intuitionistic fuzzy matrix I ,can be written as Eq. 2

$$I=\begin{bmatrix}(\varpi_{11},\gamma_{11}) & (\varpi_{12},\gamma_{12}) & ... & (\varpi_{1m},\gamma_{1m})\\ (\varpi_{21},\gamma_{21}) & (\varpi_{22},\gamma_{22}) & ... & (\varpi_{2m},\gamma_{2m})\\ ... & ... & ... & ...\\ (\varpi_{n1},\gamma_{n1}) & (\varpi_{n2},\gamma_{n2}) & ... & (\varpi_{nm},\gamma_{nm})\end{bmatrix} \tag{2}$$

We may be appropriate sea-battlefield information intuitionistic fuzzy matrix I into membership matrix I_ϖ and non-membership matrix I_γ.

Establish sea-battlefield assessment criterion vector

Sea-battlefield information intuitionistic fuzzy matrix I contains membership matrix I_{ϖ} and non-membership matrix I_{γ}. Sea-battlefield assessment criterion vector also contains two vectors: action implement criterion vector and action termination criterion vector.

Action implement criterion vector (high threat criterion vector) is ideal numerical collection of sea-battlefield attributes for implementation combat operations, which is the optimal value of membership matrix I_{ϖ} of all the attributes. As $T=\left[t_1,t_2,...t_m\right], T_j=\underset{i}{Max}\varpi_{ij}$。

Action termination criterion vector (low threat criterion vector) is ideal numerical collection of sea-battlefield attributes for the termination of combat operations, which is the worst value of all the non-membership matrix I_{γ} attributes. As $F=\left[f_1,f_2,...f_m\right], F_j=\underset{i}{Max}\gamma_{ij}$。

Calculate sea-battlefield assessment projection

Based on the above analysis and projection theory, we solver when evaluating projected sea-battlefield, also requires solving two projectors. The projection $\Pr o_T(\varpi)$ of sea-battlefield situation information membership matrix I_{ϖ} on the action implement criterion vector T .The projection $\Pr o_F(\gamma)$ of sea-battlefield situation information membership matrix I_{γ} on the action termination criterion vector F, can be written as Eq. 3 and Eq. 4.

$$\Pr o_T\left(\varpi_j\right)=\left(\sum_{i=1}^{m}\varpi_{ij}T_i\sqrt{\sum_{i=1}^{m}\varpi_{ij}{}^2}\right)\Big/\left(\sqrt{\sum_{i=1}^{m}\varpi_{ij}{}^2}\sqrt{\sum_{i=1}^{m}T_i{}^2}\right)=\sum_{i=1}^{m}\varpi_{ij}T_i\Big/\sqrt{\sum_{i=1}^{m}T_i{}^2} \quad (3)$$

$$\Pr o_F\left(\gamma_j\right)=\left(\sum_{i=1}^{m}\gamma_{ij}F_i\sqrt{\sum_{i=1}^{m}\gamma_{ij}{}^2}\right)\Big/\left(\sqrt{\sum_{i=1}^{m}\gamma_{ij}{}^2}\sqrt{\sum_{i=1}^{m}F_i{}^2}\right)=\sum_{i=1}^{m}\gamma_{ij}F_i\Big/\sqrt{\sum_{i=1}^{m}F_i{}^2} \quad (4)$$

Sea-battlefield situation assessment

For sea-battlefield situation, the greater of $\Pr o_T(\varpi)$, the closer to sea-battlefield situation information membership matrix I_{ϖ} with the action implement criterion vector T, then in this situation need to perform this combat operations. The smaller of $\Pr o_F(\gamma)$, the farther from sea-battlefield situation information non-membership matrix I_{γ} with the action termination criterion vector F, then in this situation should be maintained this combat operations. Therefore, when assess sea-battlefield situation, we comprehensive evaluation projections by extreme ways. Therefore, when assess sea-battlefield situation, we comprehensive evaluation projections by extreme ways. If the probability of implemented operations in the current situation is δ, apparent the probability of not implementing operations is $1-\delta$.

Then solving $Max\left(\left(\left(\delta_j\Pr o_T(\varpi_j)\right)^2+\left(\left(1-\delta_j\right)\Pr o_F(\gamma_j)\right)^2\right)\right), j=1,2,...,n$, can get a comprehensive assessment of the conclusions of current sea-battlefield situation, can be written as Eq. 5.

$$\delta_j=\left(\Pr o_T(\varpi_j)\right)^2\Big/\left(\left(\Pr o_T(\varpi_j)\right)^2+\left(\Pr o_F(\gamma_j)\right)^2\right), j=1,2,...,n \quad (5)$$

Sea-battlefield situation assessment application examples

Below we take aviation threat of sea-battlefield situation assessment as an example to illustrate the application of intuitionistic fuzzy based on projection. There are 6 samples for assessment.

Establish situation information matrix

Sea-battlefield situation assessment is closely related in type of troops, the relative position, relative distance and combat operations and other factors. Select the situation attribute should contain sufficient information to ensure that the basis on as succinct as possible. Because the action is against the fundamental tactical situation assess. Based on an in-depth analysis, we selected five properties to

build the intuitionistic fuzzy matrix, namely R (the distance between the surface vessels and air force), ES (surface vessels whether to implement electronic interference), AS (whether surface vessels implement avoidance maneuver), EA (Air Force is implementing electronic anti-interference) and IA (Air Force whether the external information support). Sea-battlefield situation information intuitionistic fuzzy matrix specific data are shown in Table 1.

Table 1 Sea-battlefield situation information intuitionistic fuzzy matrix table

Time slice	R	ES	AS	EA	IA
0	（0.2，0.7）	（0.7，0.3）	（0.5，0.4）	（0.3，0.5）	（0.4，0.5）
1	（0.3，0.4）	（0.8，0.2）	（0.5，0.5）	（0.5，0.5）	（0.5，0.5）
2	（0.1，0.6）	（0.5，0.3）	（0.6，0.2）	（0.5，0.4）	（0.5，0.4）
3	（0.1，0.7）	（0.3，0.7）	（0.1，0.5）	（0.9，0.1）	（0.1，0.6）
4	（0.3，0.6）	（0.2，0.8）	（0.4，0.5）	（0.8，0.2）	（0.8，0.2）
5	（0.9，0.1）	（0.7，0.2）	（0.6，0.4）	（0.8，0.1）	（0.9，0.1）

Corresponding membership matrix I_{ϖ} and non-membership matrix I_{γ} of sea-battlefield situation information intuitionistic fuzzy matrix I can be written as Eq. 6.

$$I_{\varpi}=\begin{bmatrix}0.2&0.7&0.5&0.3&0.4\\0.3&0.8&0.5&0.5&0.5\\0.1&0.5&0.6&0.5&0.5\\0.1&0.3&0.1&0.9&0.1\\0.3&0.2&0.4&0.8&0.8\\0.9&0.7&0.6&0.8&0.9\end{bmatrix},I_{\gamma}=\begin{bmatrix}0.7&0.3&0.4&0.5&0.5\\0.4&0.2&0.5&0.5&0.5\\0.6&0.3&0.2&0.4&0.4\\0.7&0.7&0.5&0.1&0.6\\0.6&0.8&0.5&0.2&0.2\\0.1&0.2&0.4&0.1&0.1\end{bmatrix} \quad (6)$$

Establish situation assessment criteria vector

According to analysis of historical data, action implement criterion vector of sea-battlefield aviation threat is $T=[0.8,0.4,0.4,0.9,0.8]$, action implement criterion vector is $F=[0.5,0.9,0.6,0.5,0.6]$.

Calculate situation assessment projection

According to the projection formula (3) and (4), we can solver projections $\Pr o_T(\varpi)$ & $\Pr o_F(\gamma)$ of sea-battlefield information intuitionistic fuzzy matrix at sea-battlefield aviation threats situation assessment criterion vectors, specific data as shown in Table 2.

Table 2 Sea-battlefield situation assessment projection table

Time slice	$\Pr o_T(\varpi)$	$\Pr o_F(\gamma)$
0	0.933	0.981
1	1.133	0.865
2	0.935	0.892
3	0.551	1.435
4	0.852	1.075
5	1.531	0.641

Assess sea-battlefield situation

It can use sea-battlefield situation assessment intuitionistic fuzzy model to assess the sample value obtained sea-battlefield aviation threat situation assessment conclusions, shown in Fig.1.

Analysis sea-battlefield situation assessment intuitionistic fuzzy model to assess value available: at t=1 time slice, air force and surface vessels were not to take any countermeasures, air force can normally detect, identify and target surface ships approaching. Determine the level of the threat to aviation is less high, and showed an increasing trend, assessment concluded that surface vessels to be taken against action - avoidance maneuver. At t=2 time slice, surface vessels implementation of avoidance maneuver, air force occupation attack position more difficult. Determine the level of the threat to aviation is medium, and is decreasing, evaluation concluded that surface vessels to maintain avoidance maneuver and need to take further action - implementing electronic interference. At t=3 time slice, surface vessels implementation of electronic interference and avoidance maneuver; air force detection means to be blind, unable to find surface vessels. Determine the level of the threat is low, and is decreasing, evaluation concluded that surface vessels to maintaining the existing

operations, air force may be taken against action. At t=4 time slice, surface vessels implementation of electronic interference and avoidance maneuver, air force implementation of electronic anti-interference, ability to detect certain aviation recovery, but no find surface vessels again. Determine the level of the threat to aviation is less low, and showed an increasing trend, evaluation concluded that surface vessels to maintaining the existing operations, air force may take further action. At t=5 time slice, surface vessels implementation of electronic interference and avoidance maneuver, air force implementation of electronic anti-interference and external information support, via the external detection means get the position of surface vessels, to achieve the attack element solver and binding. Determine the level of the threat to aviation is high, and increasing trend, evaluation concluded that surface vessels need to take further against action.

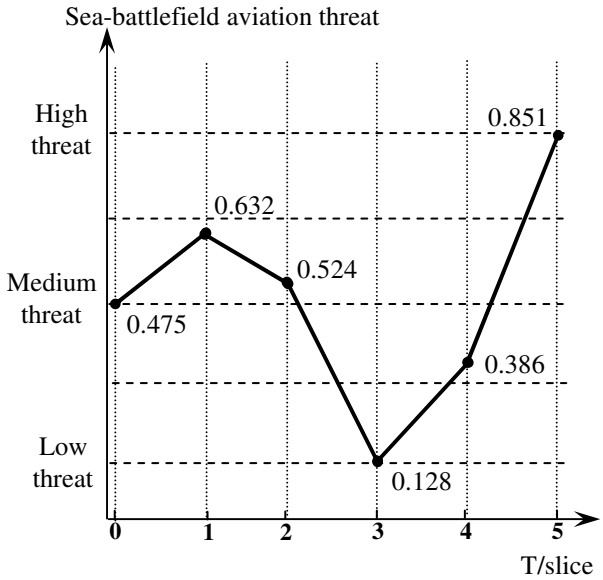

Fig.1 Sea-battlefield aviation threat situation assessment conclusions

Thus situation assessment conclusions of sea-battlefield intuitionistic fuzzy assessment model basically credible. Meanwhile intuitionistic fuzzy method based on projection can works well with dynamic changes such as situation property richen in sea-battlefield, enhanced sea-battlefield situation assessment timeliness.

Conclusions

The sea-battlefield situation assessment application improved intuitionistic fuzzy methods. First can use intuitionistic fuzzy sets can be a wealth of information attribute classification ability to address the problem of the sea-battlefield situation assessment of the fuzzy relationship between objects and factors; then by based on the projection of the relative theory, immediate introduction of a new criterion for membership to solve combinatorial explosion due to the many Sea-battlefield objects and factors arising. Future research will continue to explore the generation rules of assessment criterion vector, in order to improve the efficiency of establish of the sea-battlefield situation assessment intuitionistic fuzzy mode.

References

[1] Atanassov K. Intuitionistic fuzzy sets [J]. Fuzzy Sets and Systems, 1986, 20:87-96.
[2] Atanassov K. More on Intuitionistic Fuzzy Sets [J].Fuzzy Sets and Systems, 1989. 33(1), 37-46.
[3] Klein G A. Recognition-primed Decisions[J]. Advances in Man-machine Systems Research, 1989, (5): 47-92.
[4] Abbas S E. On intuitionistic fuzzy compactness [J]. Information Sciences, 2005, 173 (1-3):75-91.
[5] Zadeh L A. Fuzzy Sets [J]. Information and Control, 1965, 8(3), 338-353.
[6] Supriya K D, Biswas R, Akhil R R. Some Operators on Intuitionistic Fuzzy Sets [J]. Fuzzy Sets and Systems, 2000, (1 14): 477-484.
[7] GIROLAMl M. Mercer kernel based clustering in feature space [J] .IEEE Transactions on Neural Networks, 2002, 13(3): 780-784.

Advanced Materials Research Vols. 989-994 (2014) pp 1756-1761
© (2014) Trans Tech Publications, Switzerland
doi:10.4028/www.scientific.net/AMR.989-994.1756

Imbalanced Data Classification Using Cost-Sensitive Support Vector Machine Based on Information Entropy

Wei Duan [1, a],Liang Jing[2,b] and XiangYang Lu [3,c]

[1]School of Math and Computer Science, Jiangxi Science & Technology Normal University, Nanchang, China

[2]Zhejiang Great Wall Construction supervising limited company, Hangzhou, China'

[3] School of Electric and Information Engineering, Zhongyuan University of Technology, Zhengzhou, China

[a]wduan1221@163.com, [b]liangjing@sina.com , [c]lu_xy2004@126.com

Keywords: information entropy, cost sensitive, Support Vector Machine, imbalanced data set

Abstract. As a supervised classification algorithm, Support Vector Machine (SVM) has an excellent ability in solving small samples, nonlinear and high dimensional classification problems. However, SVM is inefficient for imbalanced data sets classification. Therefore, a cost sensitive SVM (CSSVM) should be designed for imbalanced data sets classification. This paper proposes a method which constructed CSSVM based on information entropy, and in this method the information entropies of different classes of data set are used to determine the values of penalty factor of CSSVM.

Introduction

The traditional classification method is mainly for balanced data set and supposes that the cost of misclassification of each sample is equal. With the goal of better accuracy of classification, the conventional classifier devotes to improve operation efficiency and generalization ability. However, in a practical application, the data sets are always imbalanced, which means the number of some kind sample is far less than the number of other classes. The assumption that all kind of samples have the same cost of misclassification will make classifier be partial to majority class and seriously degrade classification performance. Therefore, the traditional classifier can't meet the demands of data mining in reality. This is where the cost-sensitive classification comes in. The cost-sensitive classification takes different samples with different costs of misclassification into account, and it is a new research hotspot of data mining. [1-3]

SVM is a new pattern classification method developed in recent years. It bases on statistical learning theory and structural risk minimization principle, so SVM can get the global optimum solution. SVM has special advantages when it resolves problems about small samples, non-linear and high dimensions. However, SVM itself does not have cost sensitivity, and it can not be used directly for the classification of imbalanced data sets.

This paper proposes a new CSSVM based on information entropy, which constructs CSSVM by setting different penalty factors for different classes and uses information entropy of different classes of data set to determine the value of penalty factors of CSSVM. The experimental results show that this method has better classification performance on imbalanced data sets than others.

Cost-sensitivity Support Vector Machine

Basic principle of Support Vector Machine. SVM is a powerful tool for finite samples and nonlinear classification problem. It basic principle is to find the most optimal hyperplane in a two-class classification problem. The hyperplane can maximize margin between two classes, while maintaining the accuracy of classification. Therefore, the SVM can have good generalization ability. In theory, SVM can realize optimization classification for the linearly separable data set. For

nonlinear classification problem, SVM uses a kernel function to map the sample datasets into a high-dimensional feature space and solves the problem as linearly separable problem.

Assume that the training sample set S={(x_i,y_i)},where i=1..n,x_i∈Rn, y_i∈{+1,-1} and +1,-1 represent identifiers of two class separately. When the training samples are linearly separable, SVM needs to find the most optimal hyperplane $\omega \bullet x_i + b = 0$, which divides all samples into two kinds while maximizing margin $2/\|\omega\|$. When the training sample set is nonlinearly separable or it can not be judged linearly separable in advance, misclassification is allowed and slack variables $\xi_i \geq 0$, i=1,2,..n is introduced. SVM is minimum of Eq. 1under the restrict conditions.

$$\phi_{\min}(\omega,\xi) = \frac{1}{2}(\omega \bullet \omega) + \mathrm{C}\left(\sum_{\mathrm{i}=1}^{1} \xi_{\mathrm{i}}\right) \qquad (1)$$

$$s.t. \quad \mathrm{y}_i(\omega \bullet x_i + b) \geq 1 - \xi_i, \qquad \xi_i \geq 0, \quad i = 1,2...,n$$

In Eq. 1, *C* is penalty factor which measures the degree of misclassification. The higher the value of *C*, the greater the punishment of misclassification will be. Penalty factor *C* controls the trade-off between model complexity and misclassification. If the value of *C* is too big or too small, SVM will have bad generalization ability. So, it is important to set a proper value for *C*.

Basic principle of CSSVM. Different sample has different costs of misclassification in cost-sensitive classification. Given the function of penalty factor *C* in SVM, CSSVM can be constructed by choosing different penalty factor C^+ and C^- for positive and negative class in SVM, respectively. C^+ represents the cost of misclassifying positive samples as negative class, and C^- represents the cost of misclassifying negative samples as positive class. These can make different kinds of sample with different misclassification cost and the SVM has the property of cost-sensitivity [4].The model of CSSVM is shown as Eq. 2:

$$\phi_{\min}(\omega,\xi) = \frac{1}{2}(\omega \bullet \omega) + \mathrm{C}^+\left(\sum_{i \in I+} \xi_i\right) + \mathrm{C}^-\left(\sum_{i \in I-} \xi_i\right) \qquad (2)$$

$$s.t. \quad \mathrm{y}_i(\omega \bullet x_i + b) \geq 1 - \xi_i, \qquad \xi_i \geq 0, \quad i = 1,2...,n$$

In Eq. 2, *I*+, *I*- are the sets of positive and negative examples respectively. [5]

In general, there are two common ways to determine the values of penalty factor C^+ and C^-. The first way is cross-validation. In this way, when a experiment is to be made, penalty factor C^+, C^- and the parameters of kernel function should be given initial values in advanced. Then the values of penalty factor C^+ and C^- should be kept on revising according to the results of experiments until satisfaction. This parameter selection method is based on experience and in lack of theoretical support, so it is with certain blindness. Moreover, there will be different way to adjust parameter according to different kernel function. And when the range of adjustment or the number of adjustment is larger, the experiment will take a longer time. [6]The second way is using the number of two samples to determine the values of penalty factor, that is $\frac{C^+}{C^-} = \frac{n_num}{p_num}$, n_num represents the number of negative class and p_num represents the number of positive class. [7] The second way's theoretical foundation is thinking that the problem of imbalanced data set classification is cased by different classes differ largely in the numbers .[8] Prati et al. had done a series of comparative experiments to study how the imbalance within a class or among classes has a big influence on the performance of classification. However, the experimental results showed that sometimes the drop in classification performance did not cause by imbalanced data, but caused by overlapping of the samples among classes, and the classifier can still get a good classification performance in imbalanced data set, so long as classes did not overlap seriously. [9] According to the experimental results, the distributions of different class's samples in space largely affect the

classification performance of imbalanced data set, and the overlapping of classes is the main affecting factor. So while the above method which uses the number of two samples to determine penalty factor is simple and easy, it is not very effectively.

CSSVM Based on Information Entropy

Information entropy is the measurement of informational probability which is included in a set of data, and it can be taken as a measure of uncertainty. [10] Information entropy was provided by Shannon in 1948 and its calculating formula is $H_s(p_1,\cdots,p_n)=-\sum_{i=1}^{n} p_i \log p_i$.

Information entropy represents the out-of-order extent of system. The more orderly samples distribute in space, the smaller information entropy's value. It is found that, under the same conditions, if a class's number is fewer, it will have the more diverse and uncertain in space distribution, and its value of information entropy is larger. So the value of information entropy can better reflect the distribution of samples in space. While constructing a CSSVM, the value of information entropy of each class can be used to set up the corresponding value of penalty factor. The specific formulas are as Eq. 3 and Eq. 4 .

$$C^{+}=-\frac{p_num}{total_num}\log_2\frac{p_num}{total_num} \tag{3}$$

$$C^{-}=-\frac{\mathrm{n}_num}{total_num}\log_2\frac{\mathrm{n}_num}{total_num} \tag{4}$$

While plugging Eq. 3 and Eq. 4 into Eq. 2, CSSVM Based on Information Entropy can be gotten as shown in Eq. 5.

$$\phi_{\min}(\omega,\xi)=\frac{1}{2}(\omega\bullet\omega)+(-\frac{p_num}{total_num}\log_2\frac{p_num}{total_num})*\left(\sum_{i\in I+}\xi_i\right)+(-\frac{\mathrm{n}_num}{total_num}\log_2\frac{\mathrm{n}_num}{total_num})*\left(\sum_{i\in I-}\xi_i\right) \tag{5}$$

$$s.t.\quad \mathrm{y}_i(\omega\bullet x_i+b)\geq 1-\xi_i,\qquad \xi_i\geq 0,\quad i=1,2...,n$$

Experimental results

Cost-sensitivity classifier's evaluation criteria. There is low proportion of minority class in imbalanced data set. If the total accuracy is taken as evaluation criteria of classification effect, the algorithm will ignore the minority class and focus on improving the classification performance for majority class. Under this condition, the classifier can still achieve high precision, even if all minority class samples are misclassified. Therefore, it's not appropriate for taking total accuracy as evaluation criteria of classification effect in imbalanced data set. In recent years, people have provided many evaluation criteria which are appropriate for imbalanced data set classification. The most common of these evaluation criteria are F-measure[11] and G-means[12].

Assume that minority class is positive class and majority class is negative class in imbalanced data set. Positive class is expressed as P, and negative class is expressed as N. FP（False Positives）represents the number of misclassification that the samples of majority classes are taken as minority classes. FN（False Negatives）represents the number of misclassification that the samples of minority classes are taken as majority classes. TP (True Positives), TN (True Positives) represent the numbers of samples be properly classified into minority class and majority class, respectively. We define the precision of classification as the ratio between the number of true positive predictions and the number of positive instances that is judged by the classifier: Precision = TP/ (TP+FP). The sensitivity of

classification which is also called recall is defined as ration between the number of true positive predictions and the number of positive instances in the data set: Recall = TP/(TP + FN).

The precision and recall of classification are important indicators which are used to measure classification performance. The higher the values of precision and recall of classification, the better the classifier is. However, in large data set, these two indicators restrict mutually. In order to find the balance between them, the precision and recall of classification can be combined into one, such as F-measure and G-means, as shown in Eq. 6, Eq. 7.

$$F-measure=\frac{2\cdot \mathrm{Re}\,call\cdot \mathrm{Pr}\,ecision}{\mathrm{Re}\,call+\mathrm{Pr}\,ecision}=\frac{2}{1/\mathrm{Re}\,call+1/\mathrm{Pr}\,ecision} \quad (6)$$

The value of F-measure is harmonic mean of precision and recall, which can be used to estimated the classifier's ability of making a distinction between two different types. The larger the value of F-measure, the values of recall and precision approximate to 1, and the classifier has better performance.

$$G-means=\sqrt{\mathrm{Precision}\cdot \mathrm{Re}\,call} \quad (7)$$

G-means is the geometric average of precision and recall. It reflects balance of classifier's classifying ability towards two-class classification problem. The larger the value of G-means, the classifier has better performance.

Experimental Data Sets. To verify the performance for binary classification of CSSVM Based on Information Entropy in imbalanced data set, several two-class data sets in the international machine learning standard database UCI are selected. The detailed informations of these data sets are shown in Table 1.

Table 1 The description of data sets

Data set	Number of attributes	Number of positive class	Number of negative class	Ration between Positive class and negative class
haberman	4	81	225	0.3176
pima	9	268	500	0.536
breast-cancer	10	85	201	0.4229
tic-tac-toe Endgame	10	332	626	0.5304

Performance evaluation of algorithms. In this section, CSSVM Based on Information Entropy is compared with standard SVM, CSSVM Based on the Numbers of Sample, the ID3 algorithm of decision tree and BP neural network on their classification effect in the data sets mentioned in Table 1. In these experiments, ten fold cross validation method is used, the mean values of F-measure and G-means are used as evaluating indexes, and Gaussian function is selected as kernel function for SVM, CSSVM Based on the Numbers of Sample and CSSVM Based on Information Entropy.

Table 2 The results of experiments

Dataset	methods	F-measure	G-means
haberman	ID3	0.023	0.027
	BP	0.413	0.421
	SVM	0.021	0.019
	CSSVM Based on the Numbers of Sample	0.539	0.487
	CSSVM Based on Information Entropy	0.726	0.712
pima	ID3	0.481	0.423
	BP	0.726	0.731
	SVM	0.479	0.401
	CSSVM Based on the Numbers of Sample	0.715	0.707
	CSSVM Based on Information Entropy	0.801	0.764

breast-cancer	ID3	0.278	0.317
	BP	0.401	0.426
	SVM	0.323	0.412
	CSSVM Based on the Numbers of Sample	0.578	0.502
	CSSVM Based on Information Entropy	0.856	0.841
tic-tac-toe Endgame	ID3	0.334	0.431
	BP	0.761	0.772
	SVM	0.427	0.398
	CSSVM Based on the Numbers of Sample	0.621	0.511
	CSSVM Based on Information Entropy	0.862	0.843

The experimental data in Table 2 show that the values of F-measure and G-means of CSSVM Based on Information Entropy for the imbalanced data set mentioned in Table 1 are higher values than four others'. This indicates that CSSVM Based on Information Entropy has better classification performance in imbalanced data set and is superior to four others.

Conclusion

Imbalanced data set is the data set which is imbalanced in the number of samples of each class or in the spatial distribution in the spatial distribution. When classifying imbalanced data set, we should take account of not only classification precision but also the cost of classification. Due to traditional SVM's classification performance and precision drop significantly in imbalanced data set, this paper presents a new CSSVM Based on Information Entropy which use Gaussian function as kernel function and choosing different penalty factor C^+ and C^- for positive and negative class, respectively. The values of penalty factor C^+ and C^- can be determined by the corresponding class's information entropy value which reflects the characteristics of the data set itself. The experiments show that CSSVM Based on Information Entropy has better classification effect, and it has higher forecasting accuracy for minority class.

Acknowledgment

This work was partially supported by National Natural Science Funds (Grant No.11172037) and Jiangxi Science & Technology Normal University's school-level scientific research project (Grant No.Ky2012zy10)

References

[1] Liu X.Y. Zhou Z.H. IEEE Transactions on Knowledge and Data Engineering,2006, 18(1),p. 63
[2]Haibo H, Edwardo A.IEEE Transaction on Knowledge and Data Engineering, 2009, 21(9),p.1263
[3]Liu X.Y.,Zhou Z.H.IEEE Transactions on Systems,Man and Cybernetics.2009,39(2),p539
[4]Edgad E.Osuna,Robert Freund, Federico Girosi.Support vector machines: Training and applications[R]. A IM emo 1602, M IT A I Lab, 1997
[5]F.RBach,D.Heckerman,E.Horvitz, Considering cost asymmetry in learning classifiers. Mach .Learn. Res. 7(2006),p.1713.
[6]WANG Rui.Journal of Chongqing Normal University，2007,24(2)：p36(In Chinese)
[7]Akbani R, Kwek S, Japkowicz N. Proceedings of the International Conference on Artificial Intelligence,2004,p.214.
[8]Nathalie Japkowicz, Shaju Stephen. Intelligent Data Analysis, 2002,6(5),p.429.
[9]Ronaldo C. Prati, Gustavo E. A. P. A. Batista, Maria Carolina Monard.MICAI 2004: Advances in Artificial Intelligence,2004,p. 312

[10]Shannon C E.A . The Bell System Technical, 1948, 27(1),p.623
[11]D. Lewis and W. Gale. Proceedings of the Seventeenth Annual International ACM SIGIR Conference on Research and Development in Information，New York，NY，August 1998,p73.
[12]Kubat M, Holte R, Matwin S. Machine Learning,1998,30,p.195.

Advanced Materials Research Vols. 989-994 (2014) pp 1762-1765
© (2014) Trans Tech Publications, Switzerland
doi:10.4028/www.scientific.net/AMR.989-994.1762

Develop Local Fuzzy Classifier to Modify Low-confidence Output of Global Classifier

Ling Ping[1, a], Rong Xiangsheng[2,b], Dong Yongquan[1] and Hao Guosheng[1]

[1] College of Computer Science and Technology, Jiangsu Normal University, Xuzhou, 221116, China

[2] Department of Training, Air Force Logistics of P. L. A, Xuzhou 221000, China

[a]lingicehan@aliyun.com, [b]rxs12@126.com

Keywords: Local fuzzy classifier; global classifier; Support vector machine; k-nearest neighbor classifier

Abstract. This paper proposes an assembling classifier consisting of a global classifier and a local classifier, named as GCLC. To this end, we present a weighted Support Vector Machine (wSVM) that serves as the global classifier, and a fuzzy k-nearest neighbor (fkNN) that serves as the local one. When a query arrives, wSVM labels it firstly. If the global decision is below some threshold, the local fkNN works to provide an improved decision. Extensive experiments on real datasets demonstrate the performance of GCLC compared with the state of the art.

1. Introduction

Classification algorithm learns decision model from labeled data and applies the learned classifier to unlabeled data. If take a further look, we find the classifiers can be divided into two groups: the global ones and the local ones. The global classifiers, like Support Vector Machine (SVM) [1], derive class membership based on the global discriminative information of the whole training data. The local ones, on the contrary, like k-nearest neighbor (kNN) [2], detect labels according to the neighboring information around the query.

Since global classifier and local classifier are valid in respective situations, this paper proposes a natural idea to combine them together, with intention to let them cooperate with each other. We present a weighted Support Vector Machine (wSVM) that serves as the global classifier, and a fuzzy k-nearest neighbor (fkNN) that serves as the local one. When a query arrives, wSVM labels it firstly. If the global decision is below some threshold, the local fkNN works to provide an improved decision. The advantage of GCLC is that it avoids the overly high cost consumed by the global classifier, and is expected to provide a qualifier decision on difficult points.

2. wSVM

For l samples: (x_1, y_1) (x_2, y_2)……(x_l, y_l) sampling from $X \times Y$, where $X = R^n$, $Y = \{1, -1\}$. SVM seeks below hyperplane, where K is the Gaussian Kernel:

$$g(x) = \sum_i \alpha_i y_i K(x_i, x) - b \tag{1}$$

The support value α and offset vector b are obtained by optimizing:

$$\max_{\alpha} \ \sum_i \alpha_i - \frac{1}{2} \sum_i \sum_j \alpha_i \alpha_j y_i y_j K(x_i, x_j) . \tag{2}$$

$$\text{s.t. } 0 \le \alpha_i \le C_{svm} , \ \sum_i \alpha_i y_i = 0 .$$

Points with $0 < \alpha_i < C_{svm}$ are nbSV. bSV is points with $\alpha_i = C_{svm}$.

In M-class data environment, the 1-vs-rest way is used to construct basic SVM for each class to separate it from other classes. The hyperplane of J^{th} class is $g_J(x)$. Given the query Q, the size of Q's neighborhood NS, we weight basic SVMs with its confidence on the decision with respect to Q. Most existing approaches concerned with SVM decision reliability estimate analyze posterior distribution of SVM output. They collect the responses of neighboring classifiers centered at the original SVM on the same query, and evaluate original SVM output according to behaviors of neighboring models.

This paper stands at another point of view that is to investigate the responses of the original SVM model over query's neighborhood; then formulate the local distribution for output based on these responses; and finally evaluate original SVM confidence according to its decision-consistency on this neighborhood. That is, we *find an appreciate neighborhood of query* a local context for output with help of query's neighborhood, and extract statistics of outputs over this region to form confidence definition.

In details, wSVM consists below steps.

1) Specify the distance computation schema as:

$$Ld(x, y) = \sqrt{2-2k(x,y)} \tag{3}$$

2) Compute Q's variance: $s^2 = ave\ \{Ld(Q, x)^2 | x \in NEI(Q)\}$. *NEI* represents the neighborhood of Q, and *ave* computes the mean of the distance within the neighborhood. Actually s^2 tells the decision-consistency amount. The smaller s^2 is, the more steady the decision of SVM is. Besides output variance, other two factors are influential: neighborhood density and $f_J(Q)$ value itself.

3) Take above factors into consideration, and we compute the confidence coefficient of g_J with respect to the query Q:

$$\mu_J(Q) = \exp(-\frac{s^2 \cdot \bar{d}}{|f_J(Q)|}). \tag{4}$$

with $\bar{d} = \frac{\Sigma_{x \in NEI(Q)}\ dis(x,Q)}{NS}$ being the mean distance of the neighborhood.

4) Let L_1 = max $\{\mu_J(Q) f_J(Q)\}$ and L_2 = second max $\{\mu_J f_J(Q)\}$, with $J = 1...M$.

5) If $L_1 - L_2 > \varepsilon$, where ε is the pre-specified threshold, then $label(Q) = L_1$; otherwise $label(Q) = FL(Q)$. $FL(Q)$ is the fuzzy membership function that is defined in following section.

3. fkNN

$FL(Q)$ is defined as:

$$FL(Q) = \exp(-\bar{d}) \cdot \frac{MajorL}{NS} \tag{5}$$

Therein *MajorL* is the number of the neighbors belonging to the most frequent class within Q's neighborhood. The underlying rationale of employing the inverse proportion information of $\bar{d}$ in *FL* function is that the lower the mean distance of the neighborhood, the more confident the decision of the local classifier is.

Another important problem is to specify *NS*. As mentioned above, the data-adaptive size is expected to benefit the classification quality. Thus we learn *NS* from the distribution of data.

With the distance information generated by above $Ld(x, y)$ formula, we sort the training data according to their closeness to Q. That develops the new list $\{x_i\}$, with $Ld(Q, x_i) <= Ld(Q, x_{i+1})$, ($i = 1...N$). *NS* is self-tuned as:

$$NS = \max_j \{\frac{\exp(Ld(Q,x_j) - Ld(Q,x_{j-1}))}{\exp(Ld(Q,x_{j-1}))}\} \tag{6}$$

The motivation of above specification of *NS* is that we look for the max gap of the distance list. That gap reveals the inherent region around Q where data are clustered closely. In another word, that region is dense region around Q. Therefore it is rationale to use such a region as Q's neighborhood.

4. Experimental Results

4.1 Benchmark Datasets

Firstly we take the benchmark datasets of UCI [3] as the experimental datasets. In each dataset, 30% data are sampled randomly as the training data. And the classification error ratios reported below is the mean accuracy of 20 independent runs. The optimal results are presented in bold style.

In Table 1, GCLC is compared with kNN [2], two SVM-based classifiers [4], C4.5 [5], Machete [6], Scythe [6], DANN [7], and Adamenn [8]. C4.5 is standard classifier based on decision tree idea. The last four approaches are the representatives that devote efforts to learn new metrics and label data according to the distance generated by the new metrics. From experiments, it is easy to know that GCLC and Adamenn work better than others classifiers and they all provide the lowest error ratios in 4 out of 5 datasets. That demonstrates the performance of GCLC. If take the high cost consumed by Adamenn to tune six parameters during the classifier training process, GCLC exhibits more popularity in practice.

Table 1. Comparisons on classification error ratio (%) (The optimal result is shown in bold style)

Data	*k*NN	SVM_{lr}	SVM_{l1}	C4.5	Machete	Scythe	DANN	Adamenn	GCLC
Wine	7.79	5.83	6.15	8.92	7.11	6.03	6.2	**5.28**	5.3
Iris	6.0	4.1	4.0	7.7	5.1	4	5.8	**3**	**3**
Sonar	12.5	11	12	23.1	21.2	16.3	9.7	**8.5**	**8.5**
Liver	31.5	28.4	27.2	38.3	28.5	29.1	30.1	27.3	**26.6**
Vote	7.8	3	2.6	3.4	3.3	3.3	**3**	**3**	**3**

Among other classifiers, DANN achieves best accuracy since it extracts dimension relevance and defines wise distance definition with considerate probability modeling. The jobs of two SVM-based classifiers are moderate. The main reason lies in some factors. Firstly the performance of the basic SVM could be affected with the existence of multi classes. After all SVM is originally developed for binary-classification instead of multi-classification. Secondly the assembling manners do importance on the final decision since they are problem-dependent. The high error ratios of two SVM-based classifiers also show the advantage of the proposed idea that integrates the global SVM with the local classifier. kNN works poorly due to its weak ability to handle overlapping region.

4.2 Real Datasets

Then GCLC is performed on News group [9]. This dataset contains about 20,000 articles (email messages) evenly divided among the 20 newsgroups. We label each newsgroup as follows: NG1: alt.atheism; NG2: comp.graphics; NG3: comp.os.ms.windows.misc; NG4: comp.sys.ibm.pc.hardware; NG5: comp.sys.mac.hardware; NG6: comp.windows.x; NG7: misc.forsale; NG8: rec.autos; NG9: rec.motorcycles; NG10: rec.sport.baseball; NG11: rec.sport.hockey; NG12: sci.crypt; NG13: sci.electronics; NG14: sci.med; NG15: sci.space; NG16: soc.religion.christian; NG17: talk.politics.guns; NG18: talk.politics.mideast; NG19: talk.politics.misc; NG20: talk.religion.misc.

Table 2. Comparisons on classification error ratio on News Group (%) (Number in the bracket is the number of data sampled from corresponding class or classes)

Dataset	*k*NN	SVM_{lr}	SVM_{l1}	C4.5	Machete	Scythe	DANN	Adamenn	GLMF
{NG2,NG3,NG4} (300)	32.0	30.8	31.9	37.7	33.1	34.4	35.8	**30.2**	30.67
{NG2(150), NG3(50), NG4(200)}	33.79	30.8	31.2	34.92	31.07	31.02	31.46	31.2	**29.03**
{NG6, NG7,NG8}(150)	17.5	16.4	15.96	17.1	15.92	15.3	16.7	15.7	**15.18**
{NG6(200),NG7(150), NG8(350)}	15.95	15.1	16.3	18.3	16.5	15.2	14.8	**14.17**	14.37
{NG1, NG2,NG7, NG8}(200)	15.8	13.2	12.98	14.4	13.83	13.74	13.65	**12.5**	12.69
{NG1 (50), NG2(100),NG7(150),NG8(50)}	14.9	13.8	13.9	13.55	13.72	12.68	**13.0**	13.8	**13.0**
{NG7(100),NG8(50), NG12(200), NG16(50),NG17(100)}	15.6	12.3	12.3	14.7	12.9	12.2	11.64	12.5	**12.0**

We apply the usual *tf.idf* weighting schema to express documents. Set vector $x_i = (x_{i1}, x_{i2}, ..., x_{im})'$ for each document. Here $x_{ij} = t_{ij} \cdot \log \frac{n}{df_j}$, t_{ij} is the appearance frequency of word f_j in document d_i, n is the number of documents, and df_j is the number of documents that contain word f_j. We delete words that appear too few times and normalize each document vector to have unit Euclidean length.

Table 2 lists the experimental results. Clearly GCLC outperforms its peers by presenting the optimal results in 4 out of 7 cases. And SVM_{1r} does a better job than SVM_{11} in most cases. C4.5 and Machete work poorly in some sets due to their greedy idea. Scythe modifies the greedy nature and thereby achieves better accuracy. The metric employed by DANN approximates the weighted Chi-squared distance, which causes it fails in datasets of non-Gaussian distribution. Adamenn works well in some cases, but its huge cost affects its popularity in practice.

5. Conclusion

This paper proposes an idea of combining a global classier and a local classifier to improve classification accuracy, and realizes this idea by the proposed weighted SVM and the fuzzy kNN as global and local classifier respectively. We weight basic SVM with the confidence of its decision. If the decision of global model is of low confidence, local fkNN is used to refine decision. fkNN is developed in an informative neighborhood. Experiments on toy and real datasets demonstrate the fine performance of GCLC.

Acknowledgments

This work is supported by the National Natural Science Foundation of China under Grant No. 61105129 and 61100167, Jiangsu Provincial Natural Science Foundation under Grant No.BK20131130.

References

[1] N. Cristianini, J.Shawe-Taylor: An Introduction to Support Vector Machines. Cambridge University Press, London (2000)

[2] D. H. Pandya, S. H. Upadhyay, S. P. Harsha: Fault diagnosis of rolling element bearing with intrinsic mode function of acoustic emission data using APF-KNN. *Expert Systems with Applications* 40.10 (2013) p. 4137-4145

[3] http://archive.ics.uci.edu/ml/

[4] V. Murino, M. Bicego, I. A. Rossi: Statistical classification of raw textile defects, in: *Proceedings of the 17th International Conference on Pattern Recognition.* 4, p. 311-314, (2004)

[5] J. R. Quinlan, "C4.5: Programs for Machine Learning," Morgan-Kaufmann Publishers, (1993)

[6] J.H.Friedman: Flexible Metric Nearest Neighbor Classification. Tech. Report, Dept. of Statistics, Stanford University (1994)

[7] H T.astie, R.Tibshirani: Discriminant Adaptive Nearest Neighbor Classification, in: *IEEE Trans. on Pattern Analysis and Machine Intelligence*. 18(6). (1996), p. 607-615

[8] C.Domeniconi, J.Peng, D.Gunopulos: An Adaptive Metric Machine for Pattern Classification, in: *Advances in Neural Information Processing Systems*. 13. (2001), p. 458-464

[9] http://www.cs.cmu.edu/afs/cs/project/theo-11/www/naive-bayes.html

Advanced Materials Research Vols. 989-994 (2014) pp 1766-1769
© (2014) Trans Tech Publications, Switzerland
doi:10.4028/www.scientific.net/AMR.989-994.1766

The Improved Algorithm about Binocular Vision of Flexible Structure in On-orbit Modal Identification

Yang Zhao[1,a], JingBo GAO[2,b], Chang Xu[3,c] and ChunFang Zhang[4,d]

[1]School of Astronautics Engineering Harbin Institute of Technology,Harbin,150001, China

[a]waxs34@163.com, [b]gaojb@hit.edu.cn, [c]xcyrass@yahoo.com.cn, [d]fundy_320@126.com

Keywords: On-orbit modal identification; binocular stereo vision; 3D reconstruction

Abstract: The modal of large flexible structure with low and close modes hardly computes accurate data in the ground. While binocular stereo vision is valued for non-contact measurement, greater flexibility and higher precision in on-orbit identification method. This paper optimized the binocular vision algorithm. The difference between original and new algorithm, which includes the aiming-point number, the identification time and the memory number was shown. The conclusion manifests that new algorithm can improve the identification accuracy and speed up the identification and provide support for on-orbit modal identification.

Introduction

In recent years, the large flexible structures such as antenna and solar panels are widely applied on the satellite[1].Due to the features of low and close modes, it is hard to reduce by themselves when the vibration begins[2].the ground experiment is difficult to simulate the complex working environment of satellite, so the on-orbit modal identification is more important. The traditional method employs sensors, but the flexible structures are influenced by added mass, and on-orbit space is limited. And binocular stereo vision can conduct non-contact measurement and achieve the effect of real-time monitoring[3]; it is more flexible and accurate. Using two high resolution digital industrial camera, binocular stereo vision shoots antenna model and aiming points from two angles, then proceeds 3D reconstruction automatically, and the coordinates of points can be got on model surface. this paper optimizes binocular vision algorithm, saves the testing time and improves the identification accuracy and efficiency.

1 Binocular vision three-dimensional reconstruction technology

1.1 The principle of binocular vision technology

The binocular vision technology is shooting with two cameras to process the image recognition, then we can calculate the parameters which are to be tested. The process unifies the coordinates of two cameras, so the first step is calibrating the camera parameter. Four kinds of coordinates will be used: world coordinate $O-XYZ$, image coordinate $O-XY$,pixel coordinate $O-UV$ and light coordinate $O-X_cY_cZ_c$.

1.2 The calibration of parameter of camera system

Through the transformation of coordinates, the relationship between image coordinate and world coordinate can be shown:

$$Z_c\begin{bmatrix}u\\v\\1\end{bmatrix}=\begin{bmatrix}f/dx & 0 & u_0 & 0\\0 & f/dy & v_0 & 0\\0 & 0 & 1 & 0\end{bmatrix}\begin{bmatrix}R & t\\0^T & 1\end{bmatrix}\begin{bmatrix}X\\Y\\Z\\1\end{bmatrix}=NM\begin{bmatrix}X\\Y\\Z\\1\end{bmatrix}=Q\begin{bmatrix}X\\Y\\Z\\1\end{bmatrix} \quad (1)$$

N:The internal parameter matrix of the camera. M:The outside parameter matrix of the camera. Q:Projection matrix. The Zhengyou Zhang calibration Method[4]is used to calibrate the internal parameter matrix of the camera.

Order: $\alpha_x = dx / f$, $\alpha_y = dy / f$,with N^{-1} premultiplicate eq(1) .

Order: $k = \alpha_x (u - u_0)$, $l = \alpha_y (v - v_0)$, $M = [R \quad t]$. And it can be further expanded to the following three equations:

$$\begin{cases} Z_{ci} k_i = m_{11} X_i + m_{12} Y_i + m_{13} Z_i + m_{14} \\ Z_{ci} l_i = m_{21} X_i + m_{22} Y_i + m_{23} Z_i + m_{24} \\ Z_{ci} = m_{31} X_i + m_{32} Y_i + m_{33} Z_i + m_{34} \end{cases} \tag{2}$$

Substitute the 3rd equation of eq(2) to the above equations to eliminate Z_{ci} , taking n points in the world coordinate, it will produce n equations, these equations are written in matrix form:

$$\begin{bmatrix} X_1 & Y_1 & Z_1 & 1 & 0 & 0 & 0 & 0 & -k_1 X_1 & -k_1 Y_1 & -k_1 Z_1 \\ 0 & 0 & 0 & 0 & X_1 & Y_1 & Z_1 & 1 & -l_1 X_1 & -l_1 Y_1 & -l_1 Z_1 \\ & & \cdots & \cdots & \cdots & & & & & & \\ & & \cdots & \cdots & \cdots & & & & & & \\ X_n & Y_n & Z_n & 1 & 0 & 0 & 0 & 0 & -k_n X_n & -k_n Y_n & -k_n Z_n \\ 0 & 0 & 0 & 0 & X_n & Y_n & Z_n & 1 & -l_n X_n & -l_n Y_n & -l_n Z_n \end{bmatrix} \begin{bmatrix} m_{11} \\ m_{12} \\ m_{13} \\ m_{14} \\ m_{21} \\ m_{22} \\ m_{23} \\ m_{24} \\ m_{31} \\ m_{32} \\ m_{33} \end{bmatrix} = \begin{bmatrix} k_1 m_{34} \\ l_1 m_{34} \\ k_2 m_{34} \\ l_2 m_{34} \\ \cdots \\ \\ \\ \\ \cdots \\ k_n m_{34} \\ l_n m_{34} \end{bmatrix} \tag{3}$$

Inferring from eq(3) visible, if known the coordinates of N points in world and pixel coordinate, it doesn't impact on solving equations that Dividing both sides by m_{34} $(m_{34} \neq 0)$ or take $m_{34} = 1$ .Eq(3) can be abbreviated as

$$Kh = U \tag{4}$$

When 2n>11, solving the above linear equations by generalized least squares, the solution is

$$h = \left(K^T K\right)^{-1} K^T U \tag{5}$$

The external parameter matrix of the camera has the following relationships

$$M = m_{34} \begin{bmatrix} h_1 & h_2 & h_3 & h_4 \\ h_5 & h_6 & h_7 & h_8 \\ h_9 & h_{10} & h_{11} & 1 \end{bmatrix} \tag{6}$$

R is orthogonal matrix, so

$$m_{34} = 1 / \sqrt{h_9^2 + h_{10}^2 + h_{11}^2} \tag{7}$$

1.3 The improvement of image Harris corner detection algorithm

After photogrammetry, data needs to be deeply processed. For detecting the aiming points, Harris corner detection algorithm is used. In order to solve the problem of isotropic, Harris corner detection algorithm abstracts similarity of each point to:

$$E_{x,y} = \sum_{u,v} w_{u,v} [I_{x+u,y+v} - I_{u,v}]^2 = \sum_{u,v} w_{u,v} [xX + yY + o(x^2, y^2)]^2 \tag{8}$$

Among

$$\begin{cases} X = I \otimes (-1, 0, 1) \approx \delta I / \delta x \\ Y = I \otimes (-1, 0, 1)^T \approx \delta I / \delta y \end{cases} \tag{9}$$

So, when the displacement is enough small, $E(x, y) = Ax^2 + 2Cxy + By^2$

Among

$$\begin{cases} A = X^2 \otimes w \\ B = Y^2 \otimes w \\ C = (XY) \otimes w \end{cases} \tag{10}$$

To solve the response noise, the algorithm uses a Gaussian smoothing filter window. It is achieved through the setting of w.

Wherein $w_{u,v} = \exp\left[-(u^2+v^2)/2\delta^2\right]$. $E(x,y)=(x,y)M(x,y)^T$, $M = \begin{bmatrix} A & C \\ C & B \end{bmatrix}$.Harris corner response function is expressed as

$$R(x,y) = \det(M) - k \bullet tr^2(M) \tag{11}$$

In eq(11), k is a constant, $\det(M) = AB - C^2$, $tr(M) = A + B$.When $R(x,y)$ exceeds a predetermined value, it means that the point is the corner. In the actual process, the computation is large, so usually using the corner amount cim detect:

$$cim = \frac{AB - C^2}{A + B} \tag{12}$$

Qing [5] has been used for three-dimensional positioning, based on the amount of corners can be improved as follows:

(1)Using eq(10) for image filtering, making use of horizontal and vertical difference to calculate I_x I_y, and find the corner response function cim of I_x^2 and I_y^2;

(2) When the gradient between corner response function value of cim and surrounding eight pixel points is maximal, extracts this corner point as candidate;

(3)When the candidate for corner points come to duplication, using neighborhood maxima filtering and adjusting the gradient threshold to obtain the final corner points.

2 Experimental

In this paper, the antenna model is photographed using industrial high-speed cameras. As shown in fig.1, nine aiming points were set on the antenna model before measuring. After calibrating of the camera's internal and external parameters, the antenna model is measured by using binocular stereo vision measurement.

Fig.1 Shooting scene (left) and model calibration point (right)

As shown in fig.2 and in table 1, adopting the same gradient threshold, the original algorithm only finds 6 points and takes 926.4808 seconds for every 100 pictures; the improved algorithm can detect 9 points and only takes 13.6194 seconds for every 100 pictures.

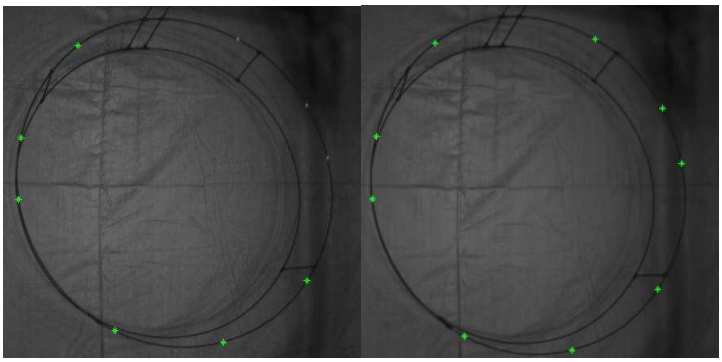

Fig.2 The case of corner detection:originally(left) and improved algorithm (right)

Table 1 The time and memory required to detect images

Number of images	Time of original algorithm [s]	Time of improved algorithm [s]	Memory of original algorithm [kb]	Memory of improved algorithm [kb]
1	9.0775	0.1886	13596	13524
10	91.6249	1.2253	129456	126300
50	467.0899	5.5150	651960	632188
100	926.4808	13.6194	1314058	1293240
500	4645.7648	69.6052	6678246	6471868
1000	9271.3106	136.2610	13204851	12934804

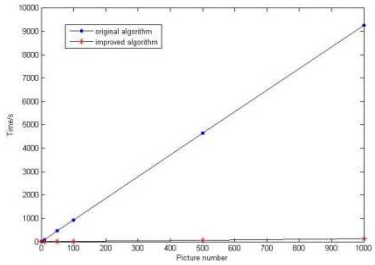

Fig.3 Variation of detection time with detection picture numbers

3 Conclusion

For large flexible structures with low and close modes in on-orbit modal identification, this paper optimizes the binocular vision algorithm. As shown in fig.3, the conclusion indicates that gradient thresholds are equal, the improved algorithm all the calibration points can be detected, the accuracy is improved obviously, the time of detecting pictures is reduced by one order of magnitude, the memory decreases slightly, and the time of on-orbit modal identification are greatly reduced.

References

[1] Bravo Rafael. Vibration Control of Flexible Structures Using Smart Materials.Mcmaster University, Hamilton, Ontario (2000).

[2] Geng L H, Xiao D Y, Wang Q, et al. Attitude-control model identification of on-orbit satellites actuated by reaction wheels. ActaAstronautica, 66(5): 714-721(2010).

[3] Chang C C, Ji Y F. Flexible videogrammetric technique for three-dimensional structural vibration measurement. Journal of engineering mechanics, 133(6): 656-664(2007).

[4] Zhang Z. A flexible new technique for camera calibration. Pattern Analysis and Machine Intelligence, IEEE Transactions on, 22(11): 1330-1334(2000).

[5] Qing L Q. Research and implementation on three-dimensional position technology based on binocular stereo vision.Northeastern University (2010).

Advanced Materials Research Vols. 989-994 (2014) pp 1770-1774
© (2014) Trans Tech Publications, Switzerland
doi:10.4028/www.scientific.net/AMR.989-994.1770

An Algorithm of Uncertain Reasoning Considering Subjective Factors

Yehong Han [1, a], Ketan Chen [2,b], Heng Shao[3,c] and Lin Du [4,d]

[1] Institute of Information Science and Engineering, Qilu Normal University, Jinan, CHINA

[2] Zaozhuang Vocational College of Science & Technology, Zaozhuang, CHINA

[3] Academic Affairs, Qilu Normal University, Jinan, CHINA

[4] Institute of Information Science and Engineering, Qilu Normal University, Jinan, CHINA

[a]sdzzhyh@163.com, [b]chenning1222@163.com, [c]shaoheng_jinan@163.com, [d]dul1028@163.com

Keywords: Rough set theory, Uncertain reasoning, Rules set, Expert system, Algorithm.

Abstract. An algorithm of uncertain reasoning which more than one result of a new object can be obtained according to the known knowledge is an important part of an expert system. A new object is an especial decision rule which has only a predecessor. In order to resolve the problem that the differences of attributes' importance in the new object are not considered in traditional methods of uncertain reasoning, a new uncertain reasoning algorithm based on the rules set which is obtained on the basis of the rough set theory is proposed. In the algorithm, both subjective factors and objective factors in the process of reasoning are considered, and the proportion of subjective factors to objective factors can be controlled by users. So the algorithm is better than the tradition method in flexibility and practicability.

Introduction

The uncertainty reasoning [1] is an important issue in research of expert system. In recent years, many scholars have studied on this question, and many algorithms on the question have been put forward. But these methods have a common disadvantage that the user's subjective factors have not been taken into account.

A new algorithm of uncertainty reasoning based on the rough set theory [2] which can obtain the set of rules is proposed in the paper, and each attribute's importance of the new object is considered in the process of uncertainty reasoning. In the method, both the subjective factors such as the user's needs, interests and the objective factors such as the rules set, amount of support are synthetically reflected, and the proportion of the subjective factors and the objective factors can be adjusted according to the actual needs of the users. So the shortcomings of the traditional uncertainty reasoning methods are overcome, and the needs of users can be reflected more precisely.

Notations and Definitions

The uncertain reasoning is carried out based on rough set theories in the paper. A conclusion of the new object can be obtained by reasoning according to the rules set which is computed by means of simplification of a decision table based on rough set theories. In order to present the algorighm of uncertainty reasoning, notations and definitions that are germane to the paper will be introduced.

Decision tables [3, 4, 5] which can be defined in terms of knowledge representation systems are kinds of prescription, which specifies what actions should be undertaken when some of conditions are satisfied. A knowledge representation system is a pair $K =< U, A >$, where U is a nonempty and finite set, and A is a nonempty, finite set of primitive attributes. Every primitive attribute $a \in A$ is a total function $a: U \to Va$, where Va is the set of value of a, called the domain of a. Let $C, D \subset A$ be two subsets of attributes, called condition and decision attributes respectively. The knowledge representation system with distinguished condition and decision attributes will be called a decision table, and will be denoted $T =< U, A, C, D >$.

Any implication $\alpha \to \beta$ will be called a decision rule [6, 7] and denoted r in the rough set theory; α and β which are formula of the form $(a_1, v_1) \wedge (a_2, v_2) \wedge ... \wedge (a_n, v_n)$ are referred to as the predecessor and the successor of $\alpha \to \beta$ respectively, where a_i ($i = 1, 2, ..., n$) is a attribute of a decision table and v_i ($i = 1, 2, ..., n$) is the value of the attribute a_i. A new object can be seen as a predecessor of a rule and will be denoted x.

Condition attributes of a decision rule r are defined as attributes which are in the predecessor α of the decision rule r, and all condition attributes of a decision rule r will be called a set of condition attributes and will be denoted $S_CA(r)$. A condition attributes set of a new object x will be denoted $S_CA(x)$.

Let $T =< U, A, C, D >$ be a decision table and a sample of the decision table T can be represented as $(a_1, v_1) \wedge (a_2, v_2) \wedge ... \wedge (a_n, v_n) \to (a_{n+1}, v_{n+1}) \wedge (a_{n+2}, v_{n+2}) \wedge ... \wedge (a_{n+m}, v_{n+m})$, where $a_i \in C$ ($i = 1, 2, ..., n$), $a_{n+i} \in D$ ($i = 1, 2, ..., m$), and v_i ($i = 1, 2, ..., n+m$) is the value of the attribute a_i. Let $r: \alpha \to \beta$ be a decision rule, if $(a_1, v_1) \wedge (a_2, v_2) \wedge ... \wedge (a_n, v_n) \to \alpha$, the sample of the decision table can be called a support of the decision rule r. In a decision table, the number of samples which are supports of the decision rule r will be called the degree of support of decision rule and will be denoted $\sup port(r)$.

A set of decision rules which are obtained by means of simplification of a decision table based on rough set theories will be denoted RUL. Let x be a new object, if there is a decision rule $\alpha \to \beta$ satisfying $x \to \alpha$, the rule $\alpha \to \beta$ will be called matching the new object x. A matching set of the new object x consists of all decision rules which match the new object x, and will be denoted $RUL(x)$.

Three situations as follows will be obtained by comparing the new object with every rules of the set of decision rules:

(1) The new object matches a rule or several rules whose decision attributes' values are same.

(2) The new object matches several rules whose decision attributes' values are not same.

(3) The new object does not match any decision rules.

According to above situations, a reasoning of a new object will be called certain reasoning in the first case, and will be called uncertain reasoning in the other cases. In the paper, only uncertain reasoning will be discussed.

An Algorithm of Uncertain Reasoning Considering Subjective Factors

In order to acquire a conclusion of a new object in the process of uncertainty reasoning, every possible conclusion should be given a weight. In more recent years many scholars have researched the question. And traditional methods [8] of uncertainty reasoning include *the method of object tracking*, *the method of attribute voting*, *the method of complete matching*, and so on. All the methods aforesaid have a common defect that attributes importance of the new object are not considered in the process of reasoning, so an algorithm of uncertain reasoning considering subjective factors will be presented in the paper, and the algorithm will be introduced according to two situations of uncertainty reasoning.

An algorithm of uncertain reasoning considering subjective factors when $RUL(x) \neq \phi$,

When $RUL(x) \neq \phi$, the algorithm of uncertain reasoning considering subjective factors can be described as follows:

Step1: Allot a degree of significance with every attribute a of the new object which will be denoted $Sig(a)$, where $0 \le Sig(a) \le 1$ and $\sum_{a \in S_CA(x)} Sig(a) = 1$.

Step2: Computer the fit degree of every conclusion in the matching set of the new object x which will be denoted $fit(x, \beta)$, and

$$fit(x, \beta) = \sum_{a \in \bigcup_{\alpha \to \beta \in RUL(x)} S_CA(\alpha \to \beta)} Sig(a) \qquad (1)$$

Step3: Standardize fit degrees of all the conclusions in the matching set of the new object x by the formula (2):

$$norm_fit(x, \beta) = \frac{fit(x, \beta)}{\sum_{\beta \in dec(x)} fit(x, \beta)} \qquad (2)$$

Where $dec(x) = \{\beta \mid \alpha \to \beta \in RUL(x)\}$. Because the significance degree of the attribute in the new object is allotted according to subjective factors of users, normal fit degrees $norm_fit(x,\beta)$ which are computed according to the significance degree of the attribute will be called subjective weight of conclusion β too.

Remark

There is a condition that $\sum_{\beta \in dec(x)} fit(x,\beta) \neq 0$ in the formula (2). But in fact, the situation $\sum_{\beta \in dec(x)} fit(x,\beta) = 0$ is existent in the process of uncertain reasoning. In order to improve the problem, $0 < Sig(a) < 1$ should be followed.

Step4: compute the general weight $Weight(x,\beta)$ by the formula (3):

$$Weight(x,\beta) = \theta norm_fit(x,\beta) + (1-\theta) reliability(x,\beta) \quad (3)$$

Where $reliability(x,\beta)$ which is the reliability of the conclusion β is computed by plenty of historical data, and $reliability(x,\beta) = votes(\beta)/norm(x)$, where $votes(\beta) = \sum_{r \in R_\beta} \sup port(r)$, $R_\beta = \{\alpha \to \beta \mid \alpha \to \beta \in RUL(x)\}$, $norm(x) = \sum_{r \in RUL(x)} \sup port(r)$. $reliability(x,\beta)$ reflects objective factors of reasoning, and does not consider subjective factors, so the reliability of the conclusion β can be called objective weight of conclusion β. In the formula (3), θ will be called the ratio of subjective factor, and $0 \le \theta \le 1$. When the value of θ is bigger, subjective factors is attached more importance by decision makers. Especially, when $\theta = 1$, only subjective factors are considered in the process of reasoning. When $\theta = 0$, only objective factors are considered, and the algorithm of uncertain reasoning turns to traditional algorithm.

The following property is obvious:

(1) $0 < W(x,\beta) < 1$ (2) $\sum_{\beta \in dec(x)} W(x,\beta) = 1$

Step5: Select the conclusion whose value of general weight is maximum as the final result of reasoning.

An algorithm of uncertain reasoning considering subjective factors when $RUL(x) = \phi$

In order to introduce the algorithm of uncertain reasoning considering subjective factors in the second case, namely $RUL(x) = \phi$, there are two definitions should be given.

Definition1: the matching degree of a rule r and a new object x can be defined as formula (4)

$$match(x,r) = \sum_{a \in S_CA(r) \wedge v_a = v_a'} Sig(a) \quad (4)$$

Where v_a and v_a' are condition attribute a of rule r and attribute a of the new object respectively.

Definition2: If there is a rule r in the set of rules satisfying $match(x,r) \ge \varepsilon$, the rule r can be called partial matching the new object x, where ε is a given value, and $0 < \varepsilon < 1$. A partial matching set of the new object x consists of all the rules satisfying $match(x,r) \ge \varepsilon$, and will be denoted $PRUL(x,\varepsilon)$.

The partial matching set of the new object x $PRUL(x,\varepsilon)$ which can be obtained according to compute the matching degree of every rule in the set of rule can be classified three cases.

(1) $PRUL(x,\varepsilon) = \phi$.

(2) $PRUL(x,\varepsilon) \neq \phi$, and conclusions of rules in $PRUL(x,\varepsilon)$ are unique.

(3) $PRUL(x,\varepsilon) \neq \phi$, and conclusions of rules in $PRUL(x,\varepsilon)$ are not unique.

According to above definitions, the algorithm of uncertain reasoning considering subjective factors when $RUL(x) = \phi$ will be presented as shown in Fig.1.

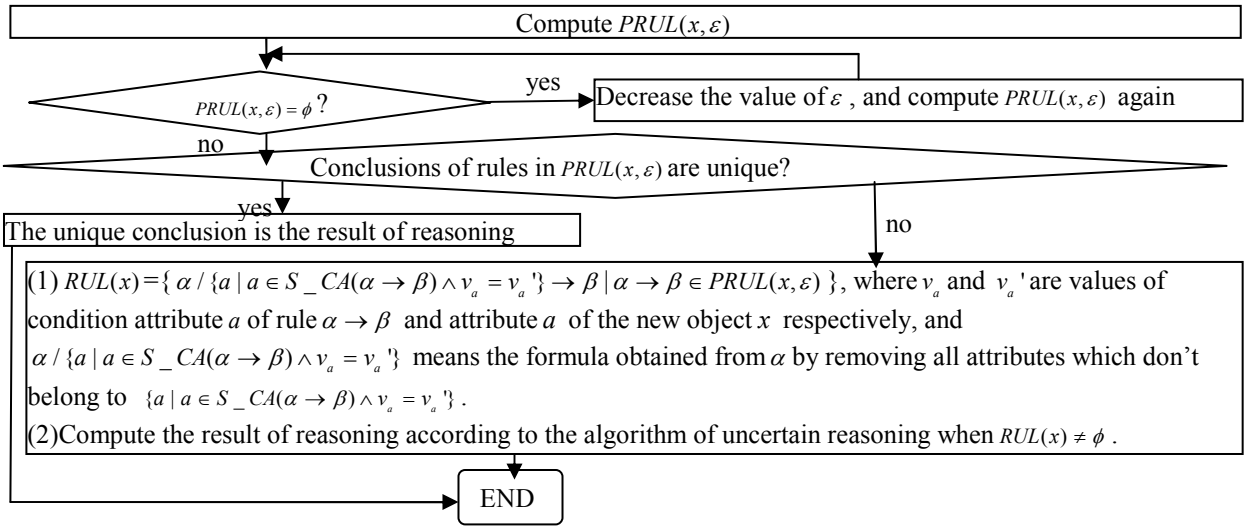

Fig.1. The algorithm of uncertain reasoning considering subjective factors when $RUL(x) = \phi$

Limits on the algorithm of uncertain reasoning considering subjective factors

The given algorithm of uncertain reasoning considering subjective factors overcomes shortcomings of traditional uncertain reasoning methods, and the result of uncertain reasoning is more suitable for user's demands. But there are two restrictive conditions in the process of reasoning using the algorithm of uncertain reasoning considering subjective factors.

(1) The new object x should satisfy $S_CA(x) \supseteq \bigcup_{r \in RUL} S_CA(r)$.

(2) The degree of significance with every attribute a of the new object should satisfy $0 < Sig(a) < 1$.

The two restrictive conditions illustrate that all attributes of the new object are useful in the process of reasoning. That is to say, for the accuracy of reasoning users should provide more detailed information.

Conclusions

An algorithm of uncertain reasoning considering subjective factors is proposed in the paper, and the algorithm considering differences between significances of attributes in the new object overcomes defects of traditional reasoning method. The ratio of subjective factors is leaded into the process of reasoning in the new algorithm. Both subjective factors and objective factors are taken into account in the process of uncertain reasoning, and the proportion of subjective factors to objective factors can be adjusted by the ratio of subjective factors, so the algorithm is better than the tradition method in flexibility and practicability. But there are some shortcomings in the method of uncertain reasoning proposed in the paper, for example, there are two restrictive conditions in the process of reasoning, the accuracy of reasoning is poor in special circumstances, and so on. The algorithm must be researched forward.

Acknowledgments

This work was supported by the Natural Science Foundation of Shandong Province, China (Grant No. ZR2013FL010).

References

[1] Yunliang Jiang, Congfu Xu, Jin Gou, Zuxin Li*: Research on Rough Set Theory Extension and Rough Reasoning,* IEEE International Conference on Systems, Man and Cybernetics (2004), p. 5888.

[2] Huang B, Li H, Wei D: *Dominance-based rough set model in intuitionistic fuzzy information systems,* Knowledge-Based Systems,(2012), p. 115.

[3] Z. Pawlak: *Rough sets and intelligent data analysis,* Information Sciences, Vol. 147 (2002), p.1.

[4] Yuhua Qian, Jiye Liang, Chuangyin Dang: *Incomplete Multigranulation Rough Set, Systems*, Man and Cybernetics, Part A: Systems and Humans, IEEE, Vol. 40 (2010), p. 420.

[5] Z. Pawlak, Andrzej Skowron: *Rudiments of rough sets*, Information Sciences, Vol. 177(2007), p.3.

[6] Hu Qinghua, Yu Daren, Xie Zongxia: *Numerical Attribute Reduction Based on Neighborhood Granulation and Rough Approximation*, Journal of Software, Vol. 03(2008), p.640.

[7] Yee Leung, Weizhi Wu, Wenxiu Zhang: *Knowledge acquisition in incomplete information systems: A rough set approach*, European Journal of Operational Research, Vol. 168(2006), p.164.

[8] William Siler, James J. Buckley: *Fuzzy Expert systems and Fuzzy Reasoning*, JOHN WILEY & SONS, INC, (2005).

Advanced Materials Research Vols. 989-994 (2014) pp 1775-1778
© (2014) Trans Tech Publications, Switzerland
doi:10.4028/www.scientific.net/AMR.989-994.1775

A Fuzzy Clustering Algorithm of Web Customers Based on Attributes Reduction

Hongxin Wan[1, a], Yun Peng[2,b]

[1]Mathematics & Computer Science College,

Jiangxi Science & Technology Normal University,Nanchang,China

[2]Computer and Information Engineering College,

Jiangxi Normal University,Nanchang,China

[a]wanhongxin@126.com,[b]pengyunmail@126.com

Keywords: rough set, attributes reduction, fuzzy set, similarity relation matrix

Abstract. The evaluation algorithm is based on the attributes of data objects. There is a certain correlation between attributes, and attributes are divided into key attributes and secondary attributes. This paper proposes an algorithm of attribute reduction based on rough set and the clustering algorithm based on fuzzy set. The algorithm of attributes reduction based on rough set is described in detail first. There are a lot of uncertain data of customer clustering, so traditional method of classification to the incomplete data will be very complex. Clustering algorithm based on fuzzy set can improve the reliability and accuracy of web customers.

Introduction

Following the rapid development of electronic commerce, which brought a huge number of customer groups, and how to classify and evaluate the customers is very important. According to the customer's transactions, characteristics of the customer information, customers can be classified and evaluated and given the levels. Web services can be improve efficiency in the future based on the actual conduct of targeted customer , and increase customer attention and interest level, thereby enhancing the profitability of web[1].

Because of the object characteristics of things with a particularly high dimension vector property description, make it difficult to conduct effective evaluation, and comparison between the calculated vector will further increase the capacity of things. Rough set is a new mathematical tool to deal with incomplete and uncertain knowledge, and its main feature is not given in advance the number of certain characteristics or properties described, but the problem can directly derived from the classification of knowledge of a given starting indiscernible relation[2]. The data objects can export a minimum feature set of attributes, and do not affect the classification accuracy of the dimension of feature vectors. Since many uncertainties in the value of the attributes, the clustering algorithm of key attributes is designed based on fuzzy set after attributes reduction.

Algorithm Analysis

1. Attributes reduction

LDA topic model shown in Fig.1 is a kind of probability model[3]. Where, α and β are the document-topic and topic-word Dirichlet distribution parameters respectively; M is the total number of documents corpus, T is the number of topic, N_d is number of words in document d. θ is a probability distribution of topics in document, φ is a probability distribution of words in topic. The probability that w_i belonging to topic k is shown in (1)[4].

Data object is described as S = (U, A), U is the set of objects and A is the set of attributes. Some attributes is redundant, while maintaining the same classification ability of the objects, we can delete these redundant attributes, that is, knowledge reduction, after reduction of excess property can obtain the minimum attributes set. If ind (B) = ind (B-{a}), where B belongs to A, a ∈A, so attributes of B can be reduced. A set of objects may exist in several attributes reductions, and the

reductions are defined as the intersection of nuclear effects in the classification of important attribute. Stratified and hierarchical analysis using fuzzy comprehensive evaluation of key attributes is to determine the level of a certain standard of measuring and comparing the various factors, and then give their relative importance quantitative form, the proportion of weight matrix by calculating the weight ratio of the largest eigenvalue matrix and its corresponding orthogonal eigenvectors can be obtained by the level of the weight of each factor[5]. Algorithm design steps are described as follows.

(1) According to the actual situation of data objects, we can select some attributes as evaluation attributes.

(2) The set of attributes reduction can be derived from discernibility matrix and discernibility function. Discernibility matrix is shown in (1).

$$M(B) = \{m\ (i,\ j)\ |\ n \times n,\ 1 \le i,\ j \le n\} \tag{1}$$

where, m (I, j) = {a ∈ A | a (i) ≠ a (j) and d (i) ≠ d (j)}, n = | U |.

(3) Discernibility function is shown in (2). Σ is "∨", Π is "∧".

$$\Delta = \prod_{(i,j) \in U \times U} \sum m(i,j) \tag{2}$$

(4) Attribute reduction and nuclear can be derived from the minimal disjunctive of distinction function.

2. Fuzzy clustering analysis

Customer's attribute can be web transactions based on behavioral characteristics, also it can be static characteristics of the customer, and the attribute can be looked as the basis for cluster analysis. In the classification process, the keywords are divided into different classes for different levels of customer types. Membership function will convert all the data values less than or equal to 1, so the next step of the fuzzy clustering can be carried out[6].

Fuzzy set A in the domain U, with a membership function to describe it, namely: U → [0,1], for any u ∈ U, there is u →μ_A(u), μ_A(u) ∈ [0,1], μ_A (u) is the membership of element u to set A, which represents the degree of u belongs to A[7]. The designing of fuzzy superposition evaluation algorithm is shown as follows.

(1) Let U be the customer domain, U_i is the No.i customer, i ∈ 1,2,3 ... n, A_j is the No.j attribute of U, j ∈ 1,2,3 ... m, S_{ij} is the value of U_i and A_j, P (K_j) is the weighting coefficients of A_j. The membership function of keyword property value is: $\mu_A(S_{ij}) = F(S_{ij}) / (S_{1j} + S_{2j} \ldots S_{nj}) * P(K_j)$.After pretreatment customers, we can design an appropriate fuzzy clustering algorithm of customer data.

(2) Set up the fuzzy similarity relation R of U. The order of R matrix is |U|, m is the number of attributes. Using Euclidean distance formula shown in (3), we can calculate the matrix elements of r_{ij} in R.

$$r_{ij} = \begin{cases} 1 & i = j \\ \sqrt{\frac{1}{m}\sum_{k=1}^{m}(sik - sjk)^2} & i \ne j \end{cases} \tag{3}$$

(3) The graph G = (V, E) can be obtained by R, and the maximum spanning tree as T = (V, TE) from G can be calculated using Prim algorithm.

(4) According to the practical problems to set an appropriate λ ∈ [0,1], T (e) is the weight of edge e, if T (e) <λ, edge e will be removed, the connected component is the classification based on λ.

(1) Let T be the customer domain, T_i is the ith topic, i∈ 1,2,3 ... n, w_j is the jth word in corpus, j ∈ 1,2,3 ... m, s_{ij} is the element of matrix M(n×m),the value of s_{ij} is the probability of word w_i belonging to T_j.

(2) Set up the fuzzy similarity relation R of T. Using Euclidean distance formula shown in (4) , we can calculate the matrix elements of r_{ij} in R.

$$r_{ij} = \begin{cases} 1 & i = j \\ \sqrt{\frac{1}{m}\sum_{k=1}^{m}(S_{ik} - S_{jk})^2} & i \neq j \end{cases} \quad (4)$$

(3) The graph $G = (V, E)$ can be obtained by R, and the maximum spanning tree as $T = (V, TE)$ from G can be calculated using Prim algorithm.

(4) According to the practical problems to set an appropriate $\lambda \in [0,1]$, $T(e)$ is the weight of edge e, if $T(e) < \lambda$, edge e will be removed, the connected component is the clusters based on λ.

Example Analysis

Data objects is shown in Table 1. It includes objects U_1 ...U_{10} and attributes A_1 ...A_n. We take Top 5 attributes for analysis, the distinction matrix is shown in Table 2.

Table 1. Initial Data

U	A_1	A_2	A_3	A_4	A_5
U_1	0.354	0.247	0.500	0.455	0.420
U_2	0.455	0.255	0.085	0.455	0.290
U_3	0.456	0.065	0.500	0.455	0.400
U_4	0.452	0.255	0.530	0.455	0.400
U_5	0.433	0.200	0.134	0.200	0.285
U_6	0.333	0.210	0.500	0.256	0.295
U_7	0.433	0.201	0.604	0.455	0.430
U_8	0.458	0.143	0.500	0.285	0.440
U_9	0.233	0.205	0.403	0.455	0.440
U_{10}	0.459	0.206	0.804	0.200	0.261

Table 2: Distinction Matrix

	U_1	U_2	U_3	U_4	U_5	U_6	U_7	U_8	U_9
U_1									
U_2	1,4,5								
U_3	2,3,4	3,5							
U_4	3,4	3,4,5	2,3						
U_5	2,3,4	1,2,3	1,2,3,4	1,2,4					
U_6	1,2,5	1,4,5	1,2,4,5	1,2,4,5	3,4				
U_7	2,4	1,2,3,5	1,2	1,5	3,4,5	4,5			
U_8	2	1,2,3.4,5	2,4	2,4	1,2,4,5	1,25	1,2,4		
U_9	1,2,4	1,2,3,5	1,2	1,2	3,4,5	1,4,5	2	2,3.4,5	
U_{10}	4,5	2,3,4,5	2,4,5	1,4,5	1,3	2,4	1,4,5	2,4,5	1,3,5

(1) According to Table 2. can get distinction function as follows:

$\Delta = (A_1 \vee A_4 \vee A_5) \wedge (A_2 \vee A_3 \vee A_5) \wedge (A_3 \vee A_5) \wedge (A_3 \vee A_4) \wedge (A_3 \vee A_4 \vee A_5) \wedge (A_2 \vee A_3) \wedge (A_2 \vee A_3 \vee A_4) \wedge (A_1 \vee A_2 \vee A_3) \wedge (A_1 \vee A_2 \vee A_3 \vee A_4) \wedge (A_1 \vee A_2 \vee A_4) \wedge (A_1 \vee A_2 \vee A_5) \wedge (A_1 \vee A_4 \vee A_5) \wedge (A_1 \vee A_2 \vee A_4 \vee A_5) \wedge (A_2 \vee A_4) \wedge (A_1 \vee A_2 \vee A_3 \vee A_5) \wedge (A_1 \vee A_2) \wedge (A_1 \vee A_5) \wedge (A_4 \vee A_5) \wedge A_2 \wedge (A_2 \vee A_3 \vee A_4 \vee A_5) \wedge (A_2 \vee A_4 \vee A_5) \wedge (A_1 \vee A_3) \wedge (A_2 \vee A_4 \vee A_5) \wedge (A_1 \vee A_3 \vee A_5) \wedge = A_2 \wedge A_4 \wedge A_5$

(2) After reduction we can get the key attributes as $\{A_2, A_4, A_5\}$. According to the type of attribute value and the membership function, we can calculate the membership degree of each attribute, and the membership value is as the initial value for classification.

(3) Through the mapping of membership function, original customer data can be initialized, the values are changed to the values less than or equal to 1, and the values reflect the dependence of the attribute.

(4) Fuzzy similarity relation matrix R can be calculated using Euclidean.

(5) The graph G = (V, E) can be derived by R, and the maximum spanning tree T = (V, TE) from G can be calculated using Prim algorithm, where | V | = 10, | TE | = 9. Set λ = 0.310, remove the edge of value less than λ, the connected component is shown in Fig.1.

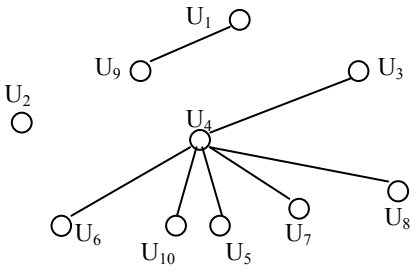

Fig.1 Connected components

(6) Thus, customer classification can be obtained as follows: $C_1 = \{U_3, U_4, U_5, U_6, U_7, U_8, U_{10}\}$,$C_2 = \{U_1, U_9\}$, $C_3 = \{U_2\}$.

Conclusion

The division of attributes at different levels of data objects can provide a more detailed evaluation by key attributes. Rough set method can divide attributes into key attributes and secondary attributes. The evaluation of the key attributes reflects the importance of key attributes, and increases the accuracy and efficiency. Tested by actual data analysis, attributes reduction can reduce the size of customer data and data noise and improve the clustering accuracy of web customers.

Acknowledgments

This work is supported by Social Science Planning Project of Jiangxi Province under grant No. 13TQ08, and Science Research Project of Jiangxi Normal University under grant No.4546.

References

[1] Huang H C, Chuang Y Y, Chen C S. Multiple kernel fuzzy clustering. Fuzzy Systems, Vol.20, No.1, pp.120-134, 2012.

[2] D. Alisantoso, LP Khoo. Early Analysis Of Design Concepts Using Rough Set Theory. International Journal of Systems Science, Vol.40, No.2, pp.121-130, 2009.

[3] Hongxin Wan, Yun Peng. An Algorithm of LDA Topic Reduction Based on Rough Set. Applied Mechanics and Materials, Vol.433-435, pp.1593-1596, 2013.

[4] Hexiang Bai,Yong Ge. Handling Spatial-Correlated Attribute Values in a Rough Set. Computational science and its applications-ICCSA, pp.467-478, 2009.

[5] Kannan S R, Ramathilagam S, Chung P C. Effective fuzzy c-means clustering algorithms for data clustering problems. Expert Systems with Applications, Vol.39, No.7, pp.6292-6300, 2012.

[6] Deng-Neng Chen,B. Jeng,Wei-Po Lee,Cheng-Hung Chuang. An agent-based model for consumer-to-business electronic commerce. Expert Systems with Applications, Vol.34, No.1, pp.469-481, 2008.

[7] Yan Zou, Zhi Xiao. Data Analysis Approaches Of Soft Sets Under Incomplete Information. Knowledge-Based Systems, Vol.21, No. 8, pp.941-945, 2008.

Advanced Materials Research Vols. 989-994 (2014) pp 1779-1781
© (2014) Trans Tech Publications, Switzerland
doi:10.4028/www.scientific.net/AMR.989-994.1779

The application of Graph Model in the cultural archives

Sun Ping

Department of Management Tianjin University of Technology, Tianjin, China

wy_sp@126.com

Keywords: cultural archives; graph model; similarity measure;

Abstract. This article describes a standard document similarity measure, and is used for cultural archives category. And should be used in the classification of cultural archives. the results show that, based on graph model of this representation is valid and feasible.

1. Introduction

The archives has thousands of years of history, played an important role for human civilization and progress, is a distinct cultural phenomenon. Archive is an important witness of history, management of archives is a respect for history. Cultural Archives refers to people engaged in social and cultural activities in the form of the material, is after a certain collation, classification, cataloguing and filing work according to a certain rule of combining files, it is a true record of the mass cultural activities. It is a witness of China's cultural development, its own significant research value. It is useful to give full play to cultural function of archives work in mass culture.

Document categorization is a complex process, including document pre-processing algorithm design, document presentation, classification, performance appraisal and other major steps, the main task of document categorization document is formalized and classification algorithm based on this design. As computer technology and WWW of universal and rapid development, human social entered has information technology era. this era, while, user can is convenient to through Internet contact to various of information; on the, due to network Shang information of mass features and fast update, user hard in so huge of information marine in the found real by needs of information. in both at home and abroad numerous scholars of long-term efforts and research Xia, currently, series classification algorithm was mention has out. This paper model of an application.

2. Graph model of the document express [1].

Graphical model is a simple and effective method of expressing joint probability distribution of the variables collection [2]. Computers do not have the kind of smart people makes it impossible to read the text. for computers, it can only come from the external features of the text reflects the text of semantic information. entry is reflect the smallest unit of text semantic information, but not all of the entries reflect the semantics of the text information, on the contrary, only a few characteristic vocabulary. Reflect text information in three areas: character entry, location of the characteristic frequency and characteristics of the entry entry. We use the vertices of the graph represents a characteristic of a document entry, and characteristics of which correspond to the two entries in the same window (passage) co-occurrence, embodies the characteristics of location information of the entry; the characteristic frequency of the entry size of the text, determine the size of its entry level co-occurrence with other features. We map each document model expressed in the following form:

$$T = (t_1, t_2, \cdots, t_n) \tag{1}$$

$$A = \begin{pmatrix} a_{12} & a_{13} & \cdots & \cdots & a_{1n} \\ & a_{12} & \cdots & \cdots & a_{2n} \\ & & \cdots & \cdots & \cdots \\ & & & a_{n-2,n-1} & a_{n-2,n} \\ & & & & a_{n-1,n} \end{pmatrix} \tag{2}$$

Among them, the T: feature entry set; t_i: feature entry; A: characteristic triangular matrix associated entries; a_{ij}: feature entry in the associated strength of t_i and t_j ($1 \leqslant i < j \leqslant n$). From the above concept, given the graph G(V,E) corresponding to a document construction method:

(1) Determine the maximum number fixed for each document corresponding to the model n (n can be determined based on experience);

(2) The document preprocessing, and statistic;

(3) Select the feature that best represents the document entry; the number does not exceed n;

(4) For each document D_i, entry by all its features as the vertices of a graph;

(5) Both feature in the same window if the document element (paragraph) co-occurrence, then there is an edge between them, both features and statistics unit entry in the same window (passage) frequency of co-occurrence;

(6) According to the formula (1) determine the characteristics of the entry of the matrix A;

(7) According to the formula (4) normalization to the matrix a, determining the normalized correlation matrix for W.

3. Graph model of document classification method

Now existing document classification method have: KNN, support vector machines, decision trees, linear least squares estimation (LLSF) , Bayesian classification algorithm etc. Among them, the KNN classification method is a stable and efficient algorithm for document classification, compare widely applied in an existing document classification method. It is based on document classification algorithm for instance, the principle of means tests for a given document D, trained by similarity in the documentation set to find the k nearest training documents. K-according to the training document categories to determine the classification of the category values. Similarity can be passed using the Euclidean distance or metric is the cosine of the angle between vectors. K-most similar training documents according to their similarity with the test documents D the level of category value weighted weights in the largest category in the document document d to predict test category value. Document classification in addition to representation, you must also document similarity measure. Different similarity measurement appears different classification results.

Classification algorithm based on graph model Graph-KNN[1]:

Input: training set document $X=\{x_i \in C(x_i)，\ \hat{u}_i=1,2,\ldots,N\}$ and test document y;

Output: test document y may belong to category C(y).

The algorithm steps are:

(1) every document in the training set $x_i \in C(x_i)$, construct the corresponding graph G_i;

(2) construct the graph model G_y for the test document y;

(3) any document $x_i \in C(x_i)$, calculate the similarity of documents for the test x_i in size Sx=Graph Similarity (G_y,G_i);

(4) in accordance with similar size S_x, select documents for testing K the most similar documents, grouped into collections D;

(5) the set D of the share $P(C_i)$ of each category C_i;

(6) return $P(C_i)$ value maximum category y category of belonging as a document.

4. Classification of cultural archives

In this article from a library of cultural archives, randomly tested over more than 1000 documents, these documents covering political, economic, environmental, cultural and historical in five areas. Application of Graph-KNN algorithm based on graph model, running in Chinese natural language processing platform. Among them, the maximum number of vertices of the graph, select K=1,3,5,7,10;n=30; parameter b get 0.6. seen from the result, the feasibility of model classification methods are used to process the document, but the accuracy is not high.

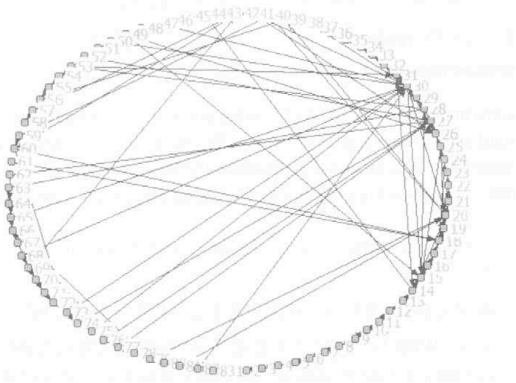

Fig.1 A semantic structure graph of cultural archives

5. Conclusion

Further, study on how to optimize your document representation, enabling it to more effectively communicate the text of semantic information and combining it with more text classification algorithm, used for text classification. on this basis, and finally the graph model for personalized text filtering. Figure model representation of the document into the associated semantic factors are to some extent addressed the characteristic dimension of the extraction and high dimension of vector spaces, makes grammatical and semantic concept words that have the same characteristics of clusters. Feature reduct of document vectors on the expression of the concept is more sophisticated document separation more pronounced. Experiments have shown that this algorithm to improve accuracy and speed of the classification is of great significance.

Acknowledgements

This work was financially supported by the Teaching Reform Project of Tianjin University of Technology （YB12—20）.

References

[1] Zou Jia Qi, Chinese document classification based on graph model [j]. small micro-computer system. 2006(4):754-757

[2] W. Lam and F. Bacchus. Learning Bayesian belief networks: An approach Based on the MDL principle. Computational Intelligence, 10(4): 269-293, 1994.

[3] Sun Lihua, etc. An improved KNN method and its application in the classification of the document [j]. Applied science and technology. 2002，29(2) : 25-27．.

[4] WANG Jian-hui, SHEN Zhan, HU Yun-fa. An applicable and efficient clustering algorithm[J]. Journal of Software, 2004,15(5) :697-705.

[5] Slonim N，Tishby N． Document Clustering using Word Clusters via the Information Bottleneck Method［C］/ / Proceedings of the 23rd annual international ACM SIGIR conference on Research and development in information retrieval，New York，USA，2000: 208-215．

Advanced Materials Research Vols. 989-994 (2014) pp 1782-1785
© (2014) Trans Tech Publications, Switzerland
doi:10.4028/www.scientific.net/AMR.989-994.1782

Deobfuscate Non-Returning Calls and Call-Stack Tampering in Instruction Traces

Jing Qiu[1, a], Xiaohong Su[1,b] and Peijun Ma[1,c]

[1]Harbin Institute of Technology, Harbin, China

[a]topmint@hit.edu.cn, [b]sxh@hit.edu.cn, [c]ma@hit.edu.cn

Keywords: Reverse engineering, instruction trace, binary analysis, deobfuscation

Abstract. Instruction traces are essential for dynamic analysis in reverse engineering. Code in instruction traces is often obfuscated to hinder analysts from understanding and analyzing in malware and binaries that protected by packers. Non-returning calls and call-stack tampering are two typical kinds of such obfuscation. We propose a deobfuscation approach to fight against these two kinds of obfuscated code. We first apply static analysis on instruction traces to identify obfuscated code. Then we transform obfuscated code into semantically equivalent instructions to make the code be easy to understand. Evaluations results on some packed binaries indicate that our approach works well in deobfuscate instruction traces with non-returning calls and call-stack tampering in high precision.

Introduction

Instruction traces are important in dynamic binary analysis. Many works are based on instruction traces, such as dynamic binary disassembly. Dynamic analysis is an important approach for analyzing binary code, such as reverse engineering for malware or binaries protected by packers. Obfuscated code is common in these binaries. Removing obfuscated code contributes to reduce the workload of analysts, and makes the control and data flow clear.

```
0x00401017  call 0x40101C
0x0040101C  pop eax
0x0040101D  add eax, 0xf
…
```

(a) Non-Returning Call

```
0x00401017  pust 0x401028
0x0040101C  ret
0x00401028  inc eax
…
```

(b) Call-Stack Tampering

Figure 1 Examples for non-returning calls and call-stack tampering

In this paper, we focus on two kinds of code obfuscation: non-returning calls and call-stack tampering (Fig. 1). Normally, a call instruction is equivalent to the following operations: push the address of the instruction that immediately follows the call instruction into the stack, and then jump to the target of the call instruction. So a call instruction can be used to complete special tasks, such as obtaining the value of the program counter at runtime. Call-stack tampering misuses return instructions. It replaces an unconditional branch with a push and return instruction.

Current deobfuscation approaches focus on deobfuscation in binary disassembly which is the initial step of binary code analysis. Many works have been done on it [1,2,3,4]. Kruegel et al. assume that all calls are non-returning [1]. They validate code that immediately follows calls by heuristics. Dyninst [4] assumes that calls are non-returning, except the calls proved to be returned by the binary slice on the called functions. If calls are proved not to be returned, instructions that immediately follow calls are not analyzed. Dyninst performs the backward slice on return instructions to determine whether the return instruction jumps to an address as expected. When this try fails, Dyninst obtains the target address by dynamic analysis. These approaches are not suitable for deobfuscating instruction traces because an executable file is quite different from its instruction traces. First, code in instruction traces cannot be statically disassembled because they may be dynamically generated. This makes the instruction at an address be different at different running times. Second, control flow can be transferred by exceptions, return instructions. They cannot be predictable statically. Third, code in instruction traces may be mixed with code from various executable modules, such as system libraries. Binary disassembly approaches that combine static and dynamic analysis such as BIRD [2], can

handle most of the self-modified code. However, they cannot deobfuscate non-returning calls and call-stack tampering because the two kinds of obfuscation only confuse the control flow.

Overview of our approach. To better understand the run-time behavior of binaries, we propose an approach to deobfuscate non-returning calls ans call-stack tampering in instruction traces. We identify non-returning calls by call stack simulation. If the stack value before a call is restored by a pop instruction, the call is not returned. Call-stack tampering are identified by checking whether the instruction adress that is executed after a return instruction is modified by a previous pop the instruction. Then simplify these obfuscated codes and transform them into simple, clear, and semantically equivalent instruction sequences to enhance their comprehensibility.

Definitions

An execution trace represents intuitively a series of operations done by a program during a run on a system. An instruction I is a tuple composed of a memory address A[I] and byte length L[I]. An instruction trace T is a finite sequence (I1, ..., In) of instructions. The stack of the processor is labeled as SP. For an instruction I, the stack value before and after the executed instruction are SP0[i] and SP1[i], respectively. For convenience, non-returning calls and call-stack tampering are called abnormal calls and abnormal returns, respectively. A fall-through address of a call instruction is the address immediately following the call instruction. A call instruction is balanced if the value of SP is restored.

Deobfuscate Non-Returning Calls

Abnormal calls make up a small proportion of all calls in an obfuscated program. So we first find abnormal calls to speed up the deobfuscation.

Identify abnormal calls. Normally, when a call is executed, its fall-through address is pushed into SP, then the control flow jumps to the target. When a return instruction is executed, the return address is popped from SP and the control flow returns to the return address. Therefore, for a call instruction, if its fall-through instruction is not executed after a return instruction or is never executed, the call instruction should be an abnormal call. However, if the fall-through instruction of a call is executed, it does not mean the call is returned because the control flow can be transferred to the fall-through instruction in many ways, such as by a branch instruction.

Fortunately, we can use the stack balance rule to deal with this problem. Because a call instruction pushes a value into SP, there should be an operation that restores the value of SP. Suppose instruction I_j is an abnormal call, and instruction I_k is a pop-like instruction that uses the fall-through address of I_j. Then we have $SP_0[I_j]=SP_1[I_k]$ because SP should be balanced after a call is executed no matter whether the call is a normal or abnormal. We perform the identification with the aid of a stack. Fig. 2(a) gives the identification algorithm. The algorithm visits each instruction in an instruction trace. All calls are pushed into a stack S in turn. If a call is balanced by a return instruction, the call is popped from S because it is normal. If a call is balanced by a pop instruction, it will be identified to be abnormal call. Otherwise, if calls are over balanced, we remove them because their fall-through addresses in SP are overwritten.

Simplify abnormal calls. As abnormal calls may be nested to prevent analysts from understanding, we simplify these calls by the aid of a stack S. For each instruction I_k in $T = (I_0, \ldots, I_n)$, if I_k is an abnormal call, we push I_k into S. If $SP_1[I_k]=SP_0[S.top]$, we pop an abnormal call I_j from S. Then we replace I_j with "jmp target", and replace "pop reg" with "mov reg, C" where $C=A[I_k]+L[I_k]$. The transformation is based on such a principle that instruction "call target" is equivalent to "push C/jmp target". Therefore, "call target/pop reg" can be transformed to "jmp target/mov reg, C" where C is the fall-through address of the call instruction.

Deobfuscate Call-Stack Tampering

Identify abnormal returns. Normally, when a return instruction is executed, the control flow will be transferred to the address that popped from SP. The popped address is the fall-through address of a call instruction. Therefore, if a popped address after an executed return instruction is not the fall-through address of a call instruction, the return instruction is abnormal. The identification process is given in Fig. 2(b). The algorithm visits each return instruction, checking whether the value to be popped from SP is modified by a previous push instruction. If no push instruction is found, the backward searching will be stopped at a normal call or the instruction that holds the SP value greater than the SP value of the return instruction.

Simplify abnormal returns. We transform "push C/ret" to "jmp C" to deobfuscate call-stack tampering. For each instruction I_k in $I = (I_0, \ldots, I_n)$, if I_k is an abnormal return instruction, we search the nearest instruction I_j that $j<k$ and I_j is a push instruction and $SP_0[I_j]=SP_1[I_k]$. Then, I_j is replaced with "nop", and I_k is replaced with "jmp C" where $C = A[I_{k+1}]$.

```
Input: Instruction trace T = (I0, …, In)
Output: Abnormal calls P

For I in T:
  If I is a call instruction:
    S.push(I)
  Else If I is a return instruction:
    If !S.empty() and SP1[S.top] < SP1[I]:
      S.pop()
  Else If I is a pop instruction:
    If !S.empty() and SP0[S.top] = SP1[I]:
      P.append(I)
      S.pop()
    End If
  Else:
    j = S.length – 1
    While j >= 0 and SP1[S[j]] <= SP1[I]:
      S.pop()
      j = j -1
    End While
  End If
End For
```

(a) Abnormal Calls Identification

```
Input: Instruction trace T = (I0, …, In)
Output: Abnormal returns P

For Ik in T:
  If Ik is a return instruction:
    j = k – 1
    While j >= 0:
      If (SP1[Tj] >= SP1[Ik]) or (Tj is a normal call):
        Break
      If Tj is a push instruction and SP1[Tj] = SP0[Ik]:
        P.append(Ik)
      j = j -1
    End While
  End If
End For
```

(b) Abnormal Returns Identidifcation

Figure 2 Algorithm for identifying abnormal calls and returns

Evaluation

Setup. We developed a prototype for evaluation. It consists of an instruction tracer developed using Intel Pin [6], and a static deobfuscation module. In instruction traces, values of registers after an executed instruction are recorded for automatically result validation. An instruction at one address is recorded once for reducing the file size of instruction traces. As non-returning calls and call-stack tampering are common in the meta code of packers (i.e., the code for unpacking), some packed binaries are provided for the evaluation. The sample to pack is compiled by MASM32 and it has only one operation which invokes the system API *ExitProcess*().

Result. Table 1 shows that our approach can deobfuscate abnormal calls and returns in high precision. FP represents false positive. Only several positives are found. If a packer creates multi-threads to unpack binaries, instructions of each thread are mixed in an instruction trace. For example, in Armadillo, the instruction trace includes the following instructions.

```
0x0044DAE7  60       pushad
0x0044DAE8  33 C9    xor ecx, ecx
0x0044DAEA  75 02    jnz 0x0044DAEE
0x0044DBD6  C3       ret
```

The "pushad" and "ret" in the above code are misidentified as call stack tampering because the fall through address of "jnz 0x0044DAEE" should be 0x0044DAEC, not 0x0044DBD6. We carefully

checked the instruction trace, and found that the return instruction at 0x0044DBD6 is belong to other thread. In the result, most of abnormal calls are consecutive call-pop instruction sequences, and most of abnormal returns are consecutive push-ret instruction sequences. In the meta code of Themida, we found that 949 abnormal returns first push 0 into the stack, then modify the value by "mov", for example, "mov [esp+4], ecx". Finally, they use "ret" to transfer the control flow to the specific address.

Table 1 Results of the evaluation on packed binaries

Packer	Version	Abnormal Calls		Abnormal Returns		Precision
		Found	FP	Found	FP	
ASPack	2.29	3	0	2	0	1
Petite	2.2	0	0	0	0	NA
NsPack	3.7	0	0	0	0	NA
FSG	2.0	0	0	0	0	NA
MoleBox	2.3600	2	0	0	0	1
Obsidium	1.3	0	0	15	1	0.93
Armadillo	6.04.0447	100	0	42	1	0.99
ASProtect	2.41	50	0	16	0	1
Themida	1.8.5.5	1018	0	1867	0	1

Conclusion

Instruction traces are tremendously useful in binary dynamic analysis. Obfuscation in traces increases the work load of analysts. Traditional deofuscation approaches aim to deobfuscate code in binary disassembly. They are not suitable for instruction trace deobfuscation because instruction traces are quite different from binary code. We proposed a deobfuscation method to deal with instruction traces including non-returning calls and call stack tampering. We use call stack balance rule to identify abnormal calls and search possible instructions that overwrite the return addresses of return instructions to identify abnormal returns. Then, we transform abnormal calls and returns to semantically equivalent ones that are easy to understand their run-time behavior for subsequent analysis. Experimental results show that our approach can deobfuscate instruction traces with abnormal calls and returns in high precision.

Acknowledgement

This research is supported by the National Natural Science Foundation of China (Grant No. 61173021).

References

[1] C. Kruegel, W.K. Robertson and F. Valeur, in: Static Disassembly of Obfuscated Binaries. USENIX security Symposium. 13 (2004), p. 18-18.

[2] B. Schwarz, S. Debray and G. Andrews: Disassembly of executable code revisited. Reverse Engineering, Proceedings. Ninth Working Conference on. IEEE, (2002), p. 45-54.

[3] S. Nanda, W. Li and L.C. Lam, in: Binary interpretation using runtime disassembly. Proceedings of the International Symposium on Code Generation and Optimization. IEEE Computer Society, (2006), p. 358-370.

[4] C, Linn and S. Debray, in: Obfuscation of executable code to improve resistance to static disassembly. Proceedings of the 10th ACM conference on Computer and communications security. ACM, (2003), p. 290-299.

[5] Dyninst. Dyninst: An application program interface (api) for runtime code generation[J]. Online, http://www. dyninst. org.

[6] Luk, Chi-Keung. Pin: building customized program analysis tools with dynamic instrumentation." ACM Sigplan Notices 40.6 (2005), p. 190-200.

Advanced Materials Research Vols. 989-994 (2014) pp 1786-1789
© (2014) Trans Tech Publications, Switzerland
doi:10.4028/www.scientific.net/AMR.989-994.1786

Constructing Attractors via the Improved Eugenics Genetic Algorithm

Liming Du [1, a], Fengying Wang [1, b] , Ziyang Han[1, c]

[1] Faculty of Information & Control Engineering,Shenyang Jianzhu University, Shenyang,China

[a]duliboy@163.com [b]wangfy678@163.com [c]phenixhans@163.com

Keywords: Genetic Algorithm; Frieze group; Attractor;

Abstract. The paper introduces Monte Carlo method and Eugenics genetic algorithm, which be used to generate a great diversity of chaotic attractors firstly. By an analysis of their algorithms, a improved eugenics genetic algorithm is presented to avoid the "genetic drift" phenomenon in attractor graphics. A parameter vector distance limit is adopted to solve the problem and lots of experiments applying equivalent mappings of frieze group are finished to validate effectiveness for algorithm.

Introduction

Monte Carlo method can get a large number of random search in the parameter space attractor graphics, but the search success rate are greatly influenced by the scope of the search space, and the success rate under 10%[1]. Therefore, Goertzel [2] from New Zealand proposed Eugenics genetic algorithm. The algorithm is a special application of genetic algorithm, the algorithm used to search the attractor is existing attractor parameter vector after selection, crossover and mutation operations, such as meet the conditions get a batch of attractor parameter vector. He illustrated the algorithm in the experiment by the test equation from Sprott [1], and the compared with his work. He first points out that Sprott chose 25 numbers in the interval [-1.2, 1.2] , if the numbers in the interval [- 12, 12] instead of it, the advantage of eugenics genetic algorithm will be greatly enhanced[2]. Because of less than 10% success rate of Monte Carlo method and eugenics genetic algorithm only affected at the beginning of the test , will eventually run into the correct area. Secondly, Sprott's lyapunov index estimation of each step for a point with a distance of 10 points of iteration, and the results calculated with the difference of (x_{n+1}, y_{n+1}). In some cases, setting number 10 can causes big error when calculating lyapunov index, and adjusting this number may influence the results of the proportion of chaotic attractor. Finally he considers that Sprott regards $x = y = 0.5$ as a general initial point, which it's for practical reasons, there is no try to distinguish between attractors in the whole plane to attract domain, and from a specific initial iteration to get the approximate design is only part of the attractor. We describe the Goertzel's algorithm as follows:

- Firstly, use Monte Carlo method to search out 10-50 different strange attractors structure, with their parameters vector form the IP .
- Select two different parameters $\boldsymbol{p}_{f1}$ and $\boldsymbol{p}_{f2}$ randomly with the same probability.
- Select a breakpoint t randomly ($1 \le t \le n-1$， n for parameter space dimension), generate a second vector $\boldsymbol{p}_c = (c_1, c_2, \cdots c_n)$.
- If second vector fitness conditions ($L \ge 0.05$), select a vector randomly in the IP group, and using $\boldsymbol{p}_c$ as it.

As the above Goertzel algorithm, the model of the p1a1 with 10 different parameter vector group, each generation of children has 10 (generation1) ×10(generation2) ×13(breakpoint location (14-1)) choices, removing the parameter vector lyapunov index does not comply with the conditions, at least 1170*11%=129 eligible parameter vector[2], so the search process can be repeated. But that is not the truth. In the iteration to the initial population after a certain number of times, groups will have the same vector, then the iteration for several times, in the same group of 10 vector, The results are shown

in table 1, this is what Goertzel mentioned in the literature [2] called "genetic drift", which is the further problem discussed in this paper.

The improved eugenics genetic algorithm

Introduction and definition of distance parameter space. Monte Carlo method is put forward by the Sprott' prepotency with eugenics algorithm, their result is effective by using the method of random search or combination, in the parameter space to find more wonderful attractor graphics. But the Monte Carlo method has low success rate of searching attractor and wasting time. But eugenics genetic algorithm accelerated the speed of approaching the chaotic region compared with the former algorithm, and improved the success rate of attractor, but the search process of "genetic drift", eventually led to the search process cannot be continued. Based on the above reasons, this paper introduces the multidimensional parameter vector distance limit, avoids the influence of "genetic drift", defined ρ as follows:

$$\rho(\boldsymbol{a}_p, \boldsymbol{a}_q) = \sqrt{\sum_{i=1}^{n} (a_i - a_i')^2}, \tag{1}$$

which $\boldsymbol{a}_p = (a_1, a_2 \cdots a_n)$, $\boldsymbol{a}_q = (a_1', a_2' \cdots a_n')$ (n is the parameter space dimension, $a_i \in R$, $i = 1, 2 \cdots n$).

The new algorithm description and implementation. To choose the coding principle suitably is an important task for implementation of genetic algorithm, a lot of research work on genetic algorithm is based on the function of the binary sequence that is mapped to a nonnegative real number encoding rules. This paper uses the floating-point coding method in the literature [3-5], which can search accuracy requirement high parameters in parameter space, to save space and search space information transformation process, improve the computational complexity of genetic algorithm and the operation efficiency. In the improved algorithm, the crossover operator uses the single point of intersection for group made up of real number vector, a pair of $\boldsymbol{w}$ and $\boldsymbol{v}$ cross the length n is naturally explain to list items. Randomly choose a dividing point k between 1 and $n-1$, combine the former k of $\boldsymbol{w}$ with later $n-k$ of $\boldsymbol{v}$ in the preceding paragraph of a second vector. According to the experiment, we found that the mutation operator in the search prepotency algorithm of the parameters of the effect is not obvious, the improved algorithm of mutation probability is $p_m = 0$.

The improved eugenics genetic algorithm is as follows:

- Selecting the largest number of iterations $N_{\max}$, the largest escape radius R, and fitness function:

$$f(a) = \begin{cases} 0 & L \le 0.05 \\ 1 & L \ge 0.05 \end{cases}, \tag{2}$$

which L is the Lyapunov index, minimum distance error parameter space is $\rho_{\min}$, the number of iterations is N;

- According to certain scope and step length, using a Monte Carlo search method of M attractor parameter vector as the initial group;
- Choose the two individuals from the initial group as parents with same probability, with floating-point encoding rules, generation $\boldsymbol{p}_{f1}$ and $\boldsymbol{p}_{f2}$ crossover length uses the set of real numbers to exchange the items of the scale, randomly and select breakpoints k from 1 to $n-1$which will be referred to in the preceding paragraph and the consequent combination form a vector offspring;
- Offspring vector Lyapunov index $\boldsymbol{p}_c$, and according to the nature of f, the fitness function of $\boldsymbol{p}_c$ to judge , if $f(\boldsymbol{p}_c) = 0$, turn to step3, otherwise turn step5;
- If the offspring list CIP is empty, build $CIP = \boldsymbol{p}_c$, start the chain table counter, otherwise, for $CIP = \{\boldsymbol{p}_t, t = 1, 2...m\}$, calculating ρ separately:

$$\rho = \rho(\boldsymbol{p}_t, \boldsymbol{p}_c) = \sqrt{\sum_{i=1}^{n} (b_i - c_i)^2} \tag{3}$$

- Randomly select a vector in the group $\boldsymbol{p}_c$ instead of $\boldsymbol{p}$ to form a new group, if $N < N_{\max}$, turn to step 3, otherwise turn to step 7;
- Drawing the attractor, storing data, and choosing the initial group, turn to step1.

The experimental results.

According to the algorithm described above, we apply it to the frieze group with p1a1 model[6,7] as (4) and (5) :

$$f_{p112}\begin{pmatrix} x \\ y \end{pmatrix} = \begin{pmatrix} a_1 y + a_2 y\cos(x) + a_3 ycox(2x) + a_4 \sin(x) + a_5 y^2 \sin(x) + a_6 \sin(2x) + a_7 y^2 \sin(2x) \\ a_8 y + a_9 y\cos(x) + a_{10} y\cos(2x) + a_{11} \sin(x) + a_{12} y^2 \sin(x) + a_{13} \sin(2x) + a_{14} y^2 \sin(2x) \end{pmatrix} \begin{Bmatrix} 2\pi \\ \infty \end{Bmatrix} \tag{4}$$

$$f_{p1a1}\begin{pmatrix} x \\ y \end{pmatrix} = \begin{pmatrix} x + a_1 + a_2 y^2 + a_3 ycox(x) + a_4 \cos(2x) + a_5 y^2 \cos(2x) + a_6 y\sin(x) + a_7 \sin(2x) + a_8 y^2 \sin(2x) \\ a_9 y + a_{10} \cos(x) + a_{11} y^2 \cos(x) + a_{12} y\cos(2x) + a_{13} \sin(x) + a_{14} y^2 \sin(x) + a_{15} y\sin(2x) \end{pmatrix} \begin{Bmatrix} 2\pi \\ \infty \end{Bmatrix} \tag{5}$$

In order to further illustrate the superiority of the improved algorithm, we compared several search algorithms, and further showed two models in table 1 in the population of 30 experimental results using a genetic algorithm and improved algorithm, randomly selected from the five groups of different structure of the attractor parameter vector group, each group for 200 generations of evolution, and the evolution process of the necessary data statistics.

Table 1 The compare results of two algorithms

	Goertzel's algorithm									
model	p112					p1a1				
test group	test num N_t	same figure M	successrate $\frac{200}{N_t}$ (%)	repetitive rrate $\frac{M}{200}$ (%)	time t (s)	test num N_t	same figure M	successrate $\frac{200}{N_t}$ (%)	repetitiverrate $\frac{M}{200}$ (%)	time t(s)
1	248	60	80.6	30.0	32	473	75	42.3	37.5	42
2	238	44	84.0	22.0	31	373	59	53.6	29.5	45
3	228	80	87.7	40.0	31	408	63	49.0	31.5	31
4	245	40	81.6	20.0	31	298	89	67.1	44.5	32
5	240	46	83.3	23.0	31	338	64	59.2	32.0	38

new improved algorithm											
p112						p1a1					
d =0.6			d =1.0			d =0.2			d =0.5		
N_t	time t	$\frac{200}{N_t}$ (%)	N_t	time t	$\frac{200}{N_t}$ (%)	N_t	time t	$\frac{200}{N_t}$ (%)	N_t	time t	$\frac{200}{N_t}$ (%)
340	46	58.8	457	55	43.8	653	66	30.6	736	74	27.2
308	45	64.9	407	48	49.1	504	55	39.7	550	71	36.4
324	41	61.7	426	53	46.9	580	62	34.5	604	62	33.1
371	45	53.9	434	53	46.1	496	52	40.3	658	67	30.4
344	44	58.1	449	56	44.5	460	51	43.5	567	60	35.3

By the data in table 1: we can discover that the two models applying eugenic evolution genetic algorithm (GA) 200 generation number is less than improved algorithm search parameters, but generated offspring of high repetition rate, calculated by the prepotency algorithm is relatively low success rate. Under the same experimental conditions, Monte Carlo search method is used for

continuous 200 search with two models respectively, which the parameters space of the model p112 for a1~a7∈ [-5，+5] ，a8~a14∈ [-1，+1], and with the gradient of step length is 0.01, it takes 48 seconds to finish the 1506 parameter vector searches ;Likewise ,the parameters space of the model p1a1 for a1 ~ a15 [2 + 2],and with the gradient of step length is 0.01, it spends 87 seconds searching the 18697 parameter vectors. Comparing two kinds of search algorithms, specially for high-speed computer, search time differ very few and the improved algorithm with spatial distance control, makes the repetition rate is zero, and there is no the same vector in groups. It avoids the "genetic drift" phenomenon fundamentally.

Conclusions

This paper firstly introduces the basic idea of eugenics genetic algorithm, and its application fields of the algorithm which involves the coding principle, several genetic operator is commonly used in genetic algorithm. The second part mainly introduces the search of chaotic attractor of Goertzel prepotency algorithm. According to the combined features of new algorithm formed its own chaotic attractor search on equivalent mappings of frieze group, it was found that the eugenics applied to frieze group mapping in the genetic algorithm, "genetic drift" phenomenon is obvious. For avoiding this, an improved algorithm is proposed in this paper, the key to the algorithm is genetic distance limit, through which the two models in frieze group with the number of groups of 10 and 30 respectively applied to testify the algorithm. Lots of experiments found: while several algorithms used in the search time difference is very small with high-speed computer and prepotency algorithm is applied to group the relative success rate is low, the improved algorithm, with spatial distance limit, makes the amount of repetition rate zero, and avoids the phenomenon of "genetic drift".

References

[1] Sprott J C. Strange attractor symmetric icons. Computers and Graphics, Vol. 20(2) (1996), p.325~32.
[2] Goertzel.B.. Rapid generation of strange attractors with the eugenic genetic algorithm. Computers & Graphics, Vol. 19(1) (1995),p.151~156.
[3] Field M and Golubitsky M. Symmetry in Chaos[M]. NewYork: Ox ford Universit y Press, 1992
[4] Grunbaum B, Shephard G C. Tilings and patterns. New York :Freeman, 1996.
[5] .K.W.Chung, H.S.Y.Chan and Ning Chen. General Mandelbrot Sets and Julia Sets with color symmetry from equivariant Mappings of the modular Group. Computer & Graphics, Vol. 24(6) (2000),p.911~918.
[6] Carter N, Eagles R, Grimes S, et al. Chaotic attractors with discrete planar symmetries [J] . Chaos Solitions and Fractals, Vol. 9(12) (1998),p. 2031- 2054.
[7] Carter N, Grimes S, Reiter C. Frieze and wallpaper chaotic attractors with a polar spin. Computer & Graphics , Vol. 22(1998),p.765~79.

Advanced Materials Research Vols. 989-994 (2014) pp 1790-1793
© (2014) Trans Tech Publications, Switzerland
doi:10.4028/www.scientific.net/AMR.989-994.1790

Comparison results between Jacobi and USSOR iterative methods

Ting Zhou [1, a], Shi-guang Zhang [1,b]

[1] College of Mathematics and Computer Science, Hengshui University, Hengshui,053000

[a] zhouting7606@163.com, [b]sg201106@163.com

Keywords: Jacobi iteration; USSOR iteration; Comparison results; Spectral radius

Abstract. In this paper, some comparison results between Jacobi and **US**SOR iteration for solving nonsingular linear systems are presented. It is showed that spectral radius of Jacobi iteration matrix B is less than that of USSOR iterative matrix under some conditions. A numerical example is also given to illustrate our results.

Introduction

In this paper, we consider the following linear system

$$Ax = b, \tag{1}$$

where A is an $n \times n$ matrix is nonsingular, x and b are n-dimensional vectors.

Iterative methods are effective and practical when the matrix A is large and sparse and are studied by many authors (cf., [1-7], etc).

In order to solve system (1) with iterative methods, the coefficient matrix is split into

$$A = M - N, \tag{2}$$

where M is nonsingular.

The basic iterative method for solving the linear system (1) is

$$Mx^{(k+1)} = Nx^{(k)} + M^{-1}b, k = 0,1,\cdots, \tag{3}$$

where x_0 is an initial vector.

Then (3) can also be written as

$$x^{(k+1)} = M^{-1}Nx^{(k)} + M^{-1}b, k = 0,1,\cdots, \tag{4}$$

where $M^{-1}N$ is called an iteration matrix of the iterative method (4).

It is well-known that the iterative method (3) converges to the exact solution of (1) for any initial vector x_0 if and only if the spectral radius of iterative matrix is less than 1.

Preliminarie

For convenience, some notations, definitions and some results that will be used in the following parts are given below.

A matrix is called nonnegative(positive) if each entry of A is nonnegative(positive), respectively, we denoted them by $A \geq 0 (A > 0)$. Similarly, for an n-dimensional vector x, by identifying it with an $n \times 1$ matrix, we can also define $x \geq 0 (x > 0)$. For $A = (a_{ij}), B = (b_{ij})$, we write $A \geq B$ if $a_{ij} \geq b_{ij}$ holds for all $i, j = 1,2,\cdots,n$, we say that $A - B \geq 0$ if and only if $A \geq B$. For a square matrix A, $\rho(A)$ denotes the spectral radius of A.

Lemma 2.1 [1] Let A be a nonnegative $n \times n$ nonzero matrix. Then

(1) $\rho(A)$, the spectral radius of A, is an eigenvalue;

(2) A has a nonnegative eigenvector corresponding to $\rho(A)$;

(3) $\rho(A)$ is a simple eigenvalue of A;

(4) $\rho(A)$ increases when any entry of A increases.

Lemma 2.2 [2] For $A \geq 0$,

$$\alpha x \leq Ax, x \geq 0, x \neq 0 \text{ implies } \alpha \leq \rho(A)$$

and

$$Ax \leq \beta x, \ x > 0 \text{ implies } \rho(A) \leq \beta .$$

Result and proof

Without loss of generality, let $A = I - L - U$, where I is the identity matrix, $-L$ and $-U$ are strictly lower and upper triangular parts of A, respectively.

The Jacobi iterative matrix is

$$B = L + U = I - A. \tag{5}$$

The USSOR iterative matrix is [3]

$$S_{\omega_1,\omega_2} = (I - \omega_2 U)^{-1}(I - \omega_1 L)^{-1}[(1-\omega_2)I + \omega_2 L][(1-\omega_1)I + \omega_1 U], \tag{6}$$

where ω_1 and ω_2 are real parameters with $\omega_i \neq 0, i = 1,2$.

Let A be the coefficient matrix in (1), B be Jacobi iterative matrix in (4) and nonnegative. Then by Lemma 2.1, we know that B has an eigenvalue $\lambda = \rho(B) \geq 0$.

Theorem 3.1 Let A be a nonsingular matrix, if $0 \leq \omega_i \leq 1$, $i = 1,2$, $B \geq 0$ is the Jacobi iteration matrix in (5), we have that $S_{\omega_1,\omega_2} \geq 0$, where S_{ω_1,ω_2} is the iteration matrix of USSOR iterative method.

Proof Since

$$S_{\omega_1,\omega_2} = (I - \omega_2 U)^{-1}(I - \omega_1 L)^{-1}[(1-\omega_2)I + \omega_2 L][(1-\omega_1)I + \omega_1 U]$$
$$= (I + \omega_2 U + \omega_2^2 U^2 + \cdots)(I + \omega_1 L + \omega_1^2 L^2 + \cdots)[(1-\omega_2)I + \omega_2 L][(1-\omega_1)I + \omega_1 U].$$

As I is the identity matrix ,we have $I \geq 0$, $-L$ and $-U$ are strictly lower and upper triangular parts of A, respectively. We know that

$$L \geq 0, U \geq 0 \text{ when } B = L + U \geq 0.$$
$$1 - \omega_1 \geq 0 \text{ and } 1 - \omega_2 \geq 0 \text{ for } 0 \leq \omega_i \leq 1, i = 1,2.$$

Thus

$$I + \omega_2 U + \omega_2^2 U^2 + \cdots \geq 0, \ I + \omega_1 L + \omega_1^2 L^2 + \cdots \geq 0,$$
$$(1-\omega_2)I + \omega_2 L \geq 0, \ (1-\omega_1)I + \omega_1 U \geq 0.$$

So we obtain that

$$S_{\omega_1,\omega_2} \geq 0.$$

Theorem 3.2 Let the assumption of Theorem 3.1 holds, and $\omega_1 + \omega_2 - \omega_1\omega_2 \leq 1 - \rho(B)$, we have that $\rho(B) \leq \rho(S_{\omega_1,\omega_2})$.

Proof From Lemma 2.1, there exists a vector $x \geq 0, x \neq 0$ such that $Bx = \lambda x$, where $\lambda = \rho(B)$, we have

$$S_{\omega_1,\omega_2} x - \lambda x = (I - \omega_2 U)^{-1}(I - \omega_1 L)^{-1}[(1-\omega_2)I + \omega_2 L][(1-\omega_1)I + \omega_1 U]x - \lambda x$$
$$= (I - \omega_2 U)^{-1}(I - \omega_1 L)^{-1}\{[(1-\omega_2)I + \omega_2 L][(1-\omega_1)I + \omega_1 U] - \lambda(I - \omega_1 L)(I - \omega_2 U)]\}x$$
$$= (I - \omega_2 U)^{-1}(I - \omega_1 L)^{-1}\{[(1 - \omega_1 - \omega_2 + \omega_1\omega_2)I + \omega_2(1-\omega_1)L + \omega_1(1-\omega_2)U]$$
$$+ \omega_1\omega_2 LU - \lambda(I - \omega_1 L)(I - \omega_2 U)]\}x$$
$$= (I - \omega_2 U)^{-1}(I - \omega_1 L)^{-1}[(1 - \omega_1 - \omega_2 + \omega_1\omega_2 - \lambda)I$$
$$+ (\omega_2 - \omega_1\omega_2 + \lambda\omega_1)L + (\omega_1 - \omega_1\omega_2 + \lambda\omega_2)U + (1-\lambda)\omega_1\omega_2 LU]x$$
$$= (I - \omega_2 U)^{-1}(I - \omega_1 L)^{-1}[(1 - \omega_1 - \omega_2 + \omega_1\omega_2 - \lambda)I$$
$$+ (\omega_2(1 - \omega_1) + \lambda\omega_1)L + (\omega_1(1-\omega_1) + \lambda\omega_2)U + (1-\lambda)\omega_1\omega_2 LU]x$$
$$= (I + \omega_2 U + \omega_2^2 U^2 + \cdots)(I + \omega_1 L + \omega_1^2 L^2 + \cdots)[(1 - \omega_1 - \omega_2 + \omega_1\omega_2 - \lambda)I$$

$$+(\omega_2(1-\omega_1)+\lambda\omega_1)L+(\omega_1(1-\omega_1)+\lambda\omega_2)U+(1-\lambda)\omega_1\omega_2 LU]x$$

It is obvious that

$\omega_2(1-\omega_1)+\lambda\omega_1 \geq 0$ and $\omega_1(1-\omega_1)+\lambda\omega_2 \geq 0$ when $0 \leq \omega_i \leq 1, i=1,2$,

and

$1-\omega_1-\omega_2+\omega_1\omega_2-\lambda \geq 0$ if and only if $\omega_1+\omega_2-\omega_1\omega_2 \leq 1-\lambda$,

so we obtain

$$S_{\omega_1,\omega_2}x-\lambda x \geq 0,$$

i.e.,

$$S_{\omega_1,\omega_2}x \geq \lambda x.$$

Thus, by Lemma 2.2, we have

$$\rho(B) \leq \rho(S_{\omega_1,\omega_2}).$$

Remark From the Theorem 3.1 and Theorem 3.2, we can conclude that in the USSOR iterative method, the choice of parameter ω_1 and ω_2 is very important. If we choose inappropriate, the USSOR iterative method is not better than Jacobi iterative method.

Numerical example

In this section we give a numerical example to illustrate the results obtained in Section 3.

Let us consider the matrix A of (1),

$$A=\begin{bmatrix} 1 & -0.035 & -0.138 & -0.057 & -0.032 \\ -0.155 & 1 & -0.343 & -0.039 & -0.016 \\ -0.134 & -0.173 & 1 & -0.132 & -0.182 \\ -0.346 & -0.208 & -0.031 & 1 & -0.038 \\ -0.072 & -0.006 & -0.329 & -0.292 & 1 \end{bmatrix},$$

and the parameters ω_1, ω_2 according to the conditions imposed in Theorems 3.1 and 3.2, the numerical results are presented in Table 1.

Table 1

ω_1	ω_2	$\rho(B)$	$\rho(S_{\omega_1,\omega_2})$
0.31	0.14	0.5285	0.7830
0.29	0.12	0.5285	0.8019
0.25	0.15	0.5285	0.8095
0.19	0.23	0.5285	0.8015
0.06	0.41	0.5285	0.7063
0.35	0.11	0.5285	0.7739
0.22	0.13	0.5285	0.8334
0.17	0.30	0.5285	0.7758
0.41	0.05	0.5285	0.7628
0.03	0.27	0.5285	0.8506
0.27	0.20	0.5285	0.7773
0.14	0.23	0.5285	0.8242
0.12	0.35	0.5285	0.7706
0.08	0.32	0.5285	0.8031
0.42	0.05	0.5285	0.7569

Remark From the above table, it is easy to know that $\rho(B) \leq \rho(S_{\omega_1,\omega_2})$, so we get that the results are in concord with Theorem 3.1 and Theorem 3.2.

Acknowledgment

This research was supported by the Research and development of science and technology project of Hebei Province (No.12210333). Please acknowledge collaborators or anyone who has helped with the paper at the end of the text.

References

[1] R. S. Varga: Matrix Iterative Analysis. Prentice-Hall, Englewood Cliffs, NJ (1981).

[2] A. Berman, R. J. Plemmons: Nonnegative Matrices in the Mathematical Sciences. Academic Press, New York, 1979, reprinted by SIAM, Philadelphia, PA (1994).

[3] W. F. Wang, D. W. Chang: The New Preconditioned USSOR Iterative Method and Comparison of Convergence . Journal of Inner Mongolia Normal University (Natural Science Edition),Vol 32. No.2(2008), p. 158-161.

[4] Z. D. Wang, T. Z. Huang: Comparison results between Jacobi and other iterative methods. Journal of Computational and Applied Mathematics, Vol. 169(2004), p. 45-51.

[5] H. X. Chen: Convergent and divergent relationship between MPSD iterative method and Jacobi method. Comm. Appl. Math. Comput. Vol.14.No.1 (2000), p.1-8.

[6] J. H. Yun: A note on the improving modified Gauss-Seidel (IMGS)method.Applied Mathematics and Computation Vol.184(2007), p. 674-679.

[7] X. Z. Wang, T. Z. Huang, Y. D. Fu: Comparison results on preconditioned SOR-type iterative method for Z-matrices linear systems, J. Comput. Appl. Math., vol. 206(2007), p. 726-732.

Advanced Materials Research Vols. 989-994 (2014) pp 1794-1797
© (2014) Trans Tech Publications, Switzerland
doi:10.4028/www.scientific.net/AMR.989-994.1794

Convergence results of the improving modified Gauss-Seidel(IMGS) Iterative method for a symmetric positive definite matrix

Shi-guang Zhang [1, a], Ting Zhou [1,b]

[1] College of Mathematics and Computer Science, Hengshui University, Hengshui,053000

[a] sg201106@163.com, [b] zhouting7606@163.com

Keywords: IMGS iterative method; Spectral radius; Symmetric positive definite matrix; H-matrix

Abstract. In this paper, in order to improve the convergence rates of iterative method solving the linear system $Ax=b$, the improving modified Gauss-Seidel (IMGS) iterative method with a preconditioner $P_\alpha = I + S_\alpha$ is proposed. Some convergence and comparison results are given when A is a symmetric definite matrix are provided.

Introduction

Consider the following linear system

$$Ax = b, \tag{1}$$

where A is an $n\times n$ matrix is nonsingular, x and b are n-dimensional vectors.

Iterative methods are effective and practical when the matrix A is large and sparse and are studied by many authors (cf., [1-9], etc).

In order to solve system (1) with iterative methods, the coefficient matrix is split into

$$A = M - N, \tag{2}$$

where M is nonsingular.

Then the basic iterative method for solving the linear system (1) is

$$Mx^{(k+1)} = Nx^{(k)} + M^{-1}b, k = 0,1,\cdots, \tag{3}$$

Thus (3) can also be written as

$$x^{(k+1)} = M^{-1}Nx^{(k)} + M^{-1}b, k = 0,1,\cdots, \tag{4}$$

where $M^{-1}N$ is called an iteration matrix of the iterative method (4).

Now, we transform the original linear system (1) into the preconditioned form

$$PAx = Pb, \tag{5}$$

where P is a nonsingular matrix. The corresponding basic iterative scheme is

$$x^{(k+1)} = {M_P}^{-1}N_P x^{(k)} + {M_P}^{-1}Pb, \quad k = 0,1,2,\ldots \tag{6}$$

where $PA = M_P - N_P$ is a splitting of PA and M_P is nonsingular.Clearly $T_P = {M_P}^{-1}N_P$ is the iteration matrix of the iterative method(6).

Rrecently, in [1] a preconditioned Gauss-Seidel method was proposed for H-matrix with $P_\alpha = I + S_\alpha$, where

$$S_\alpha = \begin{bmatrix} 0 & & & -\alpha_1 a_{1,k_1} & \\ 0 & 0 & -\alpha_2 a_{2,k_2} & & \\ \vdots & \vdots & \ddots & & \\ 0 & 0 & \cdots & \ddots & -\alpha_{n-1}a_{n-1,k_{n-1}} \\ 0 & 0 & 0 & \cdots & 0 \end{bmatrix} \tag{7}$$

and $k_i = \min j \in \{j \big| \max_{j(>i)} |a_{ij}|,\ i < n\}$, and $\alpha_i, i = 1,\cdots,n-1$ are nonnegative real numbers.

In this paper, we will discuss the improving modified Gauss-Seidel (IMGS) iterative method with the preconditioner $P_\alpha = I + S_\alpha$ for a symmetric positive matrix.

Preliminarie

For convenience, we shall now briefly explain some of the terminologies used in the next sections. Let $C=(c_{ij})\in \mathrm{R}^{n\times n}$ be an $n\times n$ real matrix. By $\mathrm{diag}(C)$, we denote the $n\times n$ diagonal matrix coinciding in its diagonal with c_{ii}. For $A=(a_{ij}), B=(b_{ij})$, we write $A\geq B$ if $a_{ij}\geq b_{ij}$ holds for all $i,j=1,2,\cdots,n$. Calling A nonnegative if $A\geq 0 (a_{ij}\geq 0; i,j=1,2,\cdots,n)$, we say that $A-B\geq 0$ if and only if $A\geq B$. Given a matrix $A=(a_{ij})$, we define the matrix $|A|=(|a_{ij}|)$ for all $i,j=1,2,\cdots,n$. For a square matrix A, $\rho(A)$ denotes the spectral radius of A.

Definition 2.1 A matrix $A=(a_{ij})$ is called a Z-matrix if $a_{ij}\leq 0$ for $i\neq j$, Z-matrix is a nonsingular M-matrix, if A is nonsingular and $A^{-1}\geq 0$.

Definition 2.2 Let $A=(a_{ij})$ be an $n\times n$ matrix, we call $\langle A\rangle=(\tilde{a}_{ij})$ is comparison matrix if $\tilde{a}_{ij}=|a_{ij}|$ for $i=j$; $\tilde{a}_{ij}=-|a_{ij}|$ for $i\neq j$. If $\langle A\rangle$ is a nonsingular M-matrix, then A is called an H-matrix.

Lemma 2.1 [2] Let A be a Z-matrix. Then the following ststements are equivalent:

(a) A is an M-matrix.

(b) All principal submatrices of A are M-matrices.

(c) All principal minors are positive.

Lemma 2.2 [3] Let A be an H-matrix, then $|A|^{-1}\leq \langle A\rangle^{-1}$.

Lemma 2.3 [4] Let A and B be two $n\times n$ matrices with $0\leq |B|\leq A$.Then $\rho(B)\leq\rho(A)$.

Lemma 2.4 [5] Let $A=I-L-U$ be a Z-matrix. Then

(a) $\rho(T)<\rho(J)<1$ if $\rho(J)<1$,

(b) $\rho(T)>\rho(J)>1$ if $\rho(J)>1$,

(c) $\rho(T)=\rho(J)=1$ if $\rho(J)=1$.

Lemma 2.5 [4] If $A=I-B$ is an H-matrix if and only if $\rho(|B|)<1$, where $\rho(.)$ denotes the spectral radius of a matrix.

Lemma 2.6 [1] Let $A=I-L-U$ is an H-matrix. If $0\leq\alpha_i\leq 1$ for all $1\leq i\leq n-1$, then $\rho(\tilde{T}_\alpha)\leq\rho(\tilde{T})<1$,where $\tilde{T}_\alpha=(I-|D_\alpha|-|L|-|E_\alpha|)^{-1}(|U|-|S_\alpha|+|F_\alpha|+|S_\alpha||U|)$ and $\tilde{T}=(I-|L|)^{-1}|U|$ and D_α, E_α and F_α are the diagonal, strictly lower and upper triangular parts of $S_\alpha L$.

Result and proof

Without loss of generality, let $A=I-L-U$, where I is the identity matrix, $-L$ and $-U$ are strictly lower and upper triangular parts of A, respectively.

For the preconditioner $P_\alpha=I+S_\alpha$, the preconditioned matrix $A_\alpha=(I+S_\alpha)A$ can be written as

$$A_\alpha=I-L-U+S_\alpha-S_\alpha L-S_\alpha U=(I-D_\alpha-L-E_\alpha)-(U-S_\alpha+F_\alpha+S_\alpha U) \tag{8}$$

where D_α, E_α and F_α are the diagonal, strictly lower and upper triangular parts of $S_\alpha L$, respectively.

Then $T_\alpha=L_\alpha^{-1}U_\alpha$, $L_\alpha=I-D_\alpha-L-E_\alpha$ and $U_\alpha=U-S_\alpha+F_\alpha+S_\alpha U$.

Next, some convergence results of the IMGS iterative method for a symmetric positive definite matrix A is provided.

Theorem 3.1 Let $A=I-L-U=$（a_{ij}）be a symmetric positive definite matrix. If $0\leq\alpha_i\leq 1$ for all $1\leq i\leq n-1$, then

$$\rho(T_\alpha)\leq\rho(\tilde{T}_\alpha),$$

where $\tilde{T}_\alpha=\tilde{L}_\alpha^{-1}\tilde{U}_\alpha$, $\tilde{L}_\alpha = I-|D_\alpha|-|L|-|E_\alpha|$, and $\tilde{U}_\alpha=|U|-|S_\alpha|+|F_\alpha|+|S_\alpha||U|$.

Proof Notice that $\langle A\rangle=I-|L|-|U|$ and $\tilde{A}_\alpha=(I+S_\alpha)\langle A\rangle=\tilde{L}_\alpha-\tilde{U}_\alpha$.

Let

$$L_\alpha=(l_{ij}) \text{ and } \tilde{L}_\alpha=(\tilde{l}_{ij}).$$

Then

$$l_{ii}=1-\alpha_i a_{ik_i}a_{k_i i}=1-\alpha_i a_{k_i i}{}^2 \text{ and } \tilde{l}_{ii}=1-\alpha_i\left|a_{ik_i}a_{k_i i}\right|=1-\alpha_i\left|a_{k_i i}\right|^2 \text{ for } 1\le i\le n-1.$$

Since A is a symmetric positive definite matrix, all principal minors of A are positive and so we have

$$1-a_{k_i i}{}^2>0.$$

Since $0\le\alpha_i\le 1$ for all $1\le i\le n-1$, it is easy to see that

$$l_{ii}=1-\alpha_i a_{k_i i}{}^2\ge 1-a_{k_i i}{}^2>0 \text{ for all } 1\le i\le n-1 \text{ and } l_{nn}=\tilde{l}_{nn}=1.$$

From Lemma 2.1 and Definition 2.2, we have $\tilde{L}_\alpha$ is an M-matrix and L_α is an H-matrix(as $\langle L_\alpha\rangle$ is an M-matrix).

It is followed from Lemma 2.2 that

$$|L_\alpha|^{-1}\le\langle L_\alpha\rangle^{-1}. \tag{9}$$

By a simple calculation, it can be shown that

$$\tilde{L}_\alpha{}^{-1}\ge\langle L_\alpha\rangle^{-1}. \tag{10}$$

From (9) and (10), one obtains

$$\tilde{L}_\alpha{}^{-1}\ge|L_\alpha|^{-1}. \tag{11}$$

Since $|U-S_\alpha|=|U|-|S_\alpha|$, we have

$$|U_\alpha|=|U-S_\alpha+F_\alpha+S_\alpha U|\le|U|-|S_\alpha|+|F_\alpha|+|S_\alpha||U|=\tilde{U}_\alpha. \tag{12}$$

From (11) and (12), one obtains

$$|T_\alpha|=|L_\alpha{}^{-1}U_\alpha|\le|L_\alpha|^{-1}|U_\alpha|\le\tilde{L}_\alpha{}^{-1}\tilde{U}_\alpha=\tilde{T}_\alpha.$$

From Lemma 2.3, we can obtain

$$\rho(T_\alpha)\le\rho(\tilde{T}_\alpha).$$

Theorem 3.2 Let the assumption of Theorem 3.1 holds, if $\rho(|L|+|U|)<1$ and $0\le\alpha_i\le 1$ for all $1\le i\le n-1$, then

$$\rho(T_\alpha)\le\rho(\tilde{T}_\alpha)\le\rho(\tilde{T})<1,$$

where $\tilde{T}=(I-|L|)^{-1}U$.

Proof From A is a symmetric positive definite matrix, notice that $\langle A\rangle=I-|L|-|U|$ is a Z-matrix.

Since $\rho(|L|+|U|)<1$, $\rho(\tilde{T})<1$ obtained by applying Lemma 2.4 to $\langle A\rangle$.

As $|L|+|U|=|L+U|$, we have A is an H-matrix from Lemma 2.5.

By applying Lemma 2.6 to A, we obtain

$$\rho(\tilde{T}_\alpha)\le\rho(\tilde{T})<1.$$

Hence, from Therom3.1 we have

$$\rho(T_\alpha)\le\rho(\tilde{T}_\alpha)\le\rho(\tilde{T})<1.$$

Acknowledgment

This research was supported by the Research and development of science and technology project of Hebei Province (No.12210333). Please acknowledge collaborators or anyone who has helped with the paper at the end of the text.

References

[1] T. Zhou: Convergence of Preconditioned Gauss-Seidel Iterative Method for H-matrix. Journal of Jiaying University (Natural Science),Vol 31. No.2(2013), p. 5-8.
[2] A. Berman, R. J. Plemmons: Nonnegative Matrices in the Mathematical Sciences. Academic Press, New York(1979), reprinted by SIAM, Philadelphia, PA(1994).
[3] T. Kolotilina: Two-sided bounds for the inverse of an H-matrix. Linear Algebra Appl.Vol.225 (1995), p. 117-123.
[4] J. G. Hu: Iterative Method for Linear Equations. Science Press (1991).
[5] R. S. Varga: Matrix Iterative Analysis. Springer, Berlin (2000).
[6] J. H. Yun: A note on the improving modified Gauss-Seidel (IMGS) method. Applied Mathematics and Computation Vol.184 (2007), p.674-679.
[7] L. Y. Sun: A comparison theorem of the improving Gauss-Seidel method for H-matrix and its comparison matrix. Applied Mathematics and Computation Vol.183 (2006), p.390-393.
[8] X. Z. Wang, T. Z. Huang, Y. D. Fu: Comparison results on preconditioned SOR-type iterative method for Z-matrices linear systems, J. Comput. Appl. Math., vol. 206(2007), p. 726-732.
[9] W. Li: Comparison results for solving preconditioned linear systems, J. Comput. Appl. Math., vol. 176(2005), p. 319-329.

Advanced Materials Research Vols. 989-994 (2014) pp 1798-1801
© (2014) Trans Tech Publications, Switzerland
doi:10.4028/www.scientific.net/AMR.989-994.1798

A fast algorithm for computing the determinants of the heptadiagonal matrices

Li Xin[1, a], Yang Liu[2,b]

[1]School of Mathematics and System Science, Beihang University, Beijing, P.R.China

[2] School of Electronic and Information Engineering, Beihang University, Beijing, P.R.China

[a]lixinat19891006@126.com, [b]yangliu2116@126.com

Keywords: Heptadiagonal matrices, Determinants, Algorithm, Computer Algebra Systems

Abstract. The cost of all existing algorithm for evaluating n th order determinants is at most $O(n^3)$. This paper presents a new efficient computational algorithm for solving the determinants of the heptadiagonal matrices with cost $O(n)$ only. It is a generalization of the DETGTRI algorithm. The implementation of this algorithm using computer algebra system is straightforward. Numerical examples are given to demonstrate the result.

Introduction

In numerical analysis and numerical calculation, it often generates large amounts of nonsingular sparse matrices. The calculation of these kinds of matrices' determinants are more convenient, because they have some special structures. The banded matrices are very popular among them, especially tri-diagonal matrices [1,3], penta-diagonal matrices [2,4,5,6,7] and heptadiagonal matrices. Many problems in mathematics and applied science require the solution of linear systems having heptadiagonal coefficient matrices. This problem often appear in signal processing, image processing, parallel computing, telecommunication system analysis and solving differential equations using finite differences. When solving the determinants, it only needs seven vectors to store the matrix in the computer, rather than store the remaining zero elements. So it can save the storage space in the computer.

Consider the general tri-diagonal determinant T_0 of order n of the form

$$T_0 = \begin{pmatrix} d_1 & a_1 & 0 & \cdots & \cdots & 0 \\ b_2 & d_2 & a_2 & \ddots & & \vdots \\ 0 & b_3 & d_3 & \ddots & 0 & \vdots \\ \vdots & \ddots & \ddots & \ddots & \ddots & 0 \\ \vdots & & 0 & \ddots & \ddots & a_{n-1} \\ 0 & \cdots & \cdots & 0 & b_n & d_n \end{pmatrix}. \tag{1}$$

A general $n \times n$ tri-diagonal matrix of form (1) can be stored in $3n-2$ memory locations by using three vectors $a=(a_1,a_2,\ldots,a_{n-1})$, $b=(b_2,b_3,\ldots,b_n)$, $d=(d_1,d_2,\ldots,d_n)$. Recently, a computational approach to find the inverse of the general tri-diagonal matrix T_0 in (1) is given in [8]. In [9], it has been shown that it is very useful to introduce an additional $n-$dimensional vector $c=(c_1,c_2,\ldots,c_n)$, by

$$c_i = \begin{cases} d_1 & if \quad i=1 \\ d_i - \dfrac{b_i a_{i-1}}{c_{i-1}} & if \quad i=2,3,\ldots,n \end{cases}. \tag{2}$$

It has been proved that the matrix T_0 is positive definite only if $c_i > 0$ for each $i = 1,2,\ldots,n$. And $\det T_0 = \left(\Pi_{r=1}^{n} c_r\right)$.

For $n \geq 5$, a general heptadiagonal matrix $T = \left(t_{ij}\right)_{1\leq i,\, j\leq n}$ takes the form

$$T = \begin{pmatrix} d_1 & a_1 & a_1^* & \hat{a}_1 & 0 & 0 & 0 & 0 & 0 & 0 \\ b_2 & d_2 & a_2 & a_2^* & \hat{a}_2 & 0 & 0 & 0 & 0 & 0 \\ b_3^* & b_3 & d_3 & a_3 & a_3^* & \hat{a}_3 & 0 & 0 & 0 & 0 \\ \hat{b}_4 & b_4^* & b_4 & d_4 & a_4 & a_4^* & \hat{a}_4 & 0 & 0 & 0 \\ 0 & \hat{b}_5 & b_5^* & b_5 & d_5 & a_5 & a_5^* & \hat{a}_5 & 0 & 0 \\ \vdots & \ddots & \ddots & \ddots & \ddots & \ddots & \ddots & \ddots & \ddots & \vdots \\ 0 & 0 & 0 & \hat{b}_{n-3} & b_{n-3}^* & b_{n-3} & d_{n-3} & a_{n-3} & a_{n-3}^* & \hat{a}_{n-3} \\ 0 & 0 & 0 & 0 & \hat{b}_{n-2} & b_{n-2}^* & b_{n-2} & d_{n-2} & a_{n-2} & a_{n-2}^* \\ 0 & 0 & 0 & 0 & 0 & \hat{b}_{n-1} & b_{n-1}^* & b_{n-1} & d_{n-1} & a_{n-1} \\ 0 & 0 & 0 & 0 & 0 & 0 & \hat{b}_n & b_n^* & b_n & d_n \end{pmatrix}. \tag{3}$$

in which $t_{ij} = 0$ for $|i-j| \geq 4$.

A general $n \times n$ heptadiagonal matrix of form (3) can be stored in $7n-12$ memory locations by using seven vectors $d = (d_1, d_2, \ldots, d_n)$, $a = (a_1, a_2, \ldots, a_{n-1})$, $a^* = (a_1^*, a_2^*, \ldots, a_{n-2}^*)$, $\hat{a} = (\hat{a}_1, \hat{a}_2, \ldots, \hat{a}_{n-3})$, $b = (b_2, b_3, \ldots, b_n)$, $b^* = (b_3^*, b_4^*, \ldots, b_n^*)$, $\hat{b} = (\hat{b}_3, \hat{b}_4, \ldots, \hat{b}_n)$. It is better to prove the nonsingularity of the matrix T in (3) before solving the difference equation with variable coefficients.

In this paper, it mainly comes up with an efficient algorithm to compute the n th order determinant of the matrix T in (3) with cost $O(n)$ only. The rest of this paper is organized as follows: in section 2, it gives the algorithm to compute the determinant of the matrix T in (3). In section 3, numerical examples show the performance of the algorithm.

The main results

In this section, it is now time to formulate the result: giving a new algorithm to compute the determinants of any $n \times n$ heptadiagonal matrices of the form (3). Throughout the section and the next sections, the parameter λ is just a symbolic name and $\det T$ is the determinant of the heptadiagonal matrices.

Algorithm: To compute the $\det T$, it may proceed as follows:

Step 1: Set $c_1 = d_1$. If $c_1 = 0$, then $c_1 = \lambda$; Set $e_1 = a_1$;

Step 2: Set $f_2 = \dfrac{b_2}{c_1}$, then $c_2 = d_2 - f_2 e_1$; If $c_2 = 0$, then $c_2 = \lambda$;

Step 3: Set $g_3 = \dfrac{b_3^*}{c_1}$, $x_1 = a_1^*$, $e_2 = a_2 - f_2 x_1$, $f_3 = \dfrac{b_3 - g_3 e_1}{c_2}$, then $c_3 = d_3 - f_3 e_2 - g_3 x_1$; If $c_3 = 0$, then $c_3 = \lambda$;

Step 4: Set $x_2 = a_2^* - f_2 \hat{a}_1$, $x_3 = a_3^* - f_3 \hat{a}_2$; $e_3 = a_3 - f_3 x_2 - g_3 \hat{a}_1$;

For k from 4 to n do

$h_k = \dfrac{\hat{b}_k}{c_{k-3}}$, $l_k = \dfrac{b_k^* - h_k e_{k-3}}{c_{k-2}}$, $m_k = \dfrac{b_k - h_k x_{k-3} - l_k e_{k-2}}{c_{k-1}}$, $e_k = a_k - l_k \hat{a}_{k-2} - m_k \hat{a}_{k-1}$, $x_k = a_k^* - m_k \hat{a}_{k-1}$, then $c_k = d_k - h_k \hat{a}_{k-3} - l_k x_{k-2} - m_k e_{k-1}$; If $c_k = 0$, then $c_k = \lambda$;

Step 5: $\det T = \left(\Pi_{r=1}^{n} c_r\right)\Big|_{\lambda=0}$.

The cost of this algorithm is $O(n)$ only. The algorithm is easy to implement using computer algebra systems such as MACSYMA and MAPLE.

Illustrative examples

In this section, it gives some examples.

Example 1 . Consider the following 6×6 matrix A

$$A = \begin{pmatrix} 1 & 1 & -1 & 1 & 0 & 0 \\ 2 & 1 & 2 & 2 & 3 & 0 \\ 2 & 1 & 2 & 1 & 0 & 1 \\ 1 & 1 & 2 & 0 & 1 & 2 \\ 0 & 2 & 0 & 2 & 1 & 0 \\ 0 & 0 & 1 & 2 & 1 & 1 \end{pmatrix}.$$

We have

$g_3 = 2$

$(f_2, f_3) = (2,1)$

$$(x_1, x_2, x_3, x_4) = \left(-1,0,-3,\frac{2\lambda-3}{\lambda}\right)$$

$$(e_1, e_2, e_3, e_4, e_5) = \left(1,4,-1,\frac{\lambda+9}{\lambda},\frac{-4\lambda-2}{3-\lambda}\right)$$

$$(m_4, m_5, m_6) = \left(\frac{3}{\lambda},\frac{2\lambda+8}{3-\lambda},\frac{-3\lambda-19}{-9\lambda-29}\right)$$

$$(l_4, l_5, l_6) = \left(0,\frac{8}{\lambda},\frac{2\lambda+1}{3-\lambda}\right)$$

$$(h_4, h_5, h_6) = \left(1,-2,\frac{1}{\lambda}\right)$$

$$(c_1, c_2, c_3, c_4, c_5, c_6) = \left(1,-1,\lambda,\frac{\lambda-3}{\lambda},\frac{-9\lambda-29}{3-\lambda},\frac{-33\lambda-90}{-9\lambda-29}\right)$$

Therefore, $\det A = \left(\Pi_{r=1}^{6} c_r\right)\Big|_{\lambda=0} = 90$.

Example 2 . Consider the following 7×7 matrix B

$$B = \begin{pmatrix} 1 & 1 & -1 & 1 & 0 & 0 & 0 \\ 2 & 2 & 2 & 2 & 3 & 0 & 0 \\ 1 & 1 & 2 & 1 & 1 & 1 & 0 \\ 2 & 1 & 2 & 1 & 1 & 2 & 1 \\ 0 & 2 & 1 & 2 & 0 & 1 & 1 \\ 0 & 0 & 1 & 2 & 1 & 1 & 1 \\ 0 & 0 & 0 & 1 & 1 & 1 & 2 \end{pmatrix}.$$

We have

$g_3 = 1$

$(f_2, f_3) = (2,0)$

$(x_1, x_2, x_3, x_4, x_5) = \left(-1,0,1,\frac{2\lambda-4}{3\lambda},3\right)$

$(e_1, e_2, e_3, e_4, e_5, e_6) = \left(1,4,0,\frac{-\lambda+5}{3\lambda},2,\frac{3\lambda+10}{\lambda}\right)$

$(m_4, m_5, m_6, m_7) = \left(\frac{4\lambda+4}{3\lambda},-2,\frac{-10}{3\lambda},\frac{3\lambda+2}{2\lambda+4}\right)$

$(l_4, l_5, l_6, l_7) = \left(\frac{-1}{\lambda},\frac{\lambda-8}{3\lambda},-2,\frac{-2\lambda-5}{3\lambda}\right)$

$(h_4, h_5, h_6, h_7) = \left(2,\frac{2}{\lambda},\frac{1}{3},-1\right)$

$(c_1, c_2, c_3, c_4, c_5, c_6, c_7) = \left(1,\lambda,3,-1,-1,\frac{6\lambda+12}{3\lambda},\frac{\lambda-6}{2\lambda+4}\right)$

Therefore, $\det B = \left(\Pi_{r=1}^{7} c_r\right)\Big|_{\lambda=0} = -18$.

Conclusion

In this paper, it presents a new efficient computational algorithm for solving the determinants of the heptadiagonal matrices with cost $O(n)$ only. Some numerical examples prove that the algorithm works well. Hence, it may become a useful tool for the determinant evaluation.

References

[1] El-Mikkawy M E A: A fast algorithm for evaluating nth order tri-diagonal determinants. Journal of computational and applied mathematics, 581-584(2004)

[2] El-Mikkawy M, Rahmo E D: A new recursive algorithm for inverting general periodic pentadiagonal and anti-pentadiagonal matrices. Applied Mathematics and Computation, 164-170(2009)

[3] El-Mikkawy M, Karawia A: Inversion of general tridiagonal matrices. Applied Mathematics Letters, 712-720(2006)

[4] El-Mikkawy M E A: A fast and reliable algorithm for evaluating nth order pentadiagonal determinants. Applied Mathematics and Computation, 210-215(2008)

[5] Karawia A A: A computational algorithm for solving periodic penta-diagonal linear systems. Applied mathematics and computation, 613-618(2006)

[6] Sogabe T: A fast numerical algorithm for the determinant of a pentadiagonal matrix. Applied Mathematics and Computation, 835-841(2008)

[7] Lv X G, Huang T Z, Le J: A note on computing the inverse and the determinant of a pentadiagonal Toeplitz matrix. Applied Mathematics and Computation, 327-331(2008)

Advanced Materials Research Vols. 989-994 (2014) pp 1802-1805
© (2014) Trans Tech Publications, Switzerland
doi:10.4028/www.scientific.net/AMR.989-994.1802

Two-parameter conjugate gradient projection method and its application

Hong-fang Cui

College of Mathematics and Computer Science Hengshui University, Hengshui, China

email: cuihongfang2012@126.com

Keywords: Two-parameter P-NCD conjugate projection gradient method; global convergence; drop analysis

Abstract. On the basis of the conjugate gradient method CD, the artile builds a new two-parameter P-NCD projected conjugate gradient method, the article gives two-parameter P-NCD Conjugate Gradient Method drop projection and on the strong Wolfe line search in the principles of the convergence criteria, the new algorithm is applied to estimate the equation with linear constraints in the model instantiated test ,the results shows good results.

Introduction

The gradient projection algorithm in constrained optimization problem was first proposed by Luo Shen in 1960.Using gradient projection technologies combined with a variety of linear search algorithm is formed, called the gradient projection algorithm.

Two-parameter P-NCD Conjugate Projection Gradient Method

The constrained optimization problem (P):

$$\min_{\beta\in R^p} f(\beta)=\sum_{i=1}^{n}\varepsilon_i^2=\sum_{i=1}^{n}\left(y_i-x_i^T\beta-g(z_i,u_i,\beta)\right)^2$$
$$s.t. \qquad A\beta=b$$

Where $f(\beta)$ is a continuous and differentiable function. the paper uses the improved optimization of the two-parameter P-NCD conjugate gradient method estimatesthe β.

An iterative algorithm for solving constrained optimization problems $\beta^{(k+1)}=\beta^{(k)}+\lambda_k d_k$,inside $\alpha_k^{new}=\dfrac{\|pg_k\|^2}{-\mu g_{k-1}^T d_{k-1}+\nu d_{k-1}^T(g_k-g_{k-1})}$, $\mu\geq 0$, $\nu\geq 0$, $\mu+\nu=1$.

The problem (P) of the K-T conditions[1] $\begin{cases}\nabla f(\beta)+\lambda A^T=0\\ A\beta=b\end{cases}$, λ Lagrange multiplier.

Two-parameter P-NCD conjugate gradient projection algorithm:

Step1: given initial point $\beta^{(1)}=(\beta_1^{(1)},\cdots,\beta_p^{(1)})$,In order to meet the conditions of $A\beta^{(1)}=b$,make $k:=1$, $\beta^{(0)}=0$, $d_0=0$;

Step 2：Calculation Pg_1 ,if $\|Pg_1\|=0$,Stop calculation,The constrained optimization problem of K-T for $\beta^{(1)}$; Or the direction of $d_k=-Pg_k+\alpha_k d_{k-1}$,When the $k>1$ is $\alpha_k^{new}=\dfrac{\|pg_k\|^2}{-\mu g_{k-1}^T d_{k-1}+\nu d_{k-1}^T(g_k-g_{k-1})}$, $\mu\geq 0$, $\nu\geq 0$, $\mu+\nu=1$;

Step 3 ： The step of the λ_k by the strong Wolfe principle,that is $f(x_k+\alpha_k d_k)\leq f(x_k)+\rho\alpha_k g_k^T d_k$ and $\left|d_k^T g(x_k+\alpha_k d_k)\right|\leq -\sigma d_k^T g_k$, $0<\rho<\sigma<1$,make $\beta^{(k+1)}=\beta^{(k)}+\lambda_k d_k$, $f_{k+1}=f\left(\beta^{(k+1)}\right)$, $\beta^{(k+1)}=\beta^{(k)}+\lambda_k d_k$, $f_{k+1}=f\left(\beta^{(k+1)}\right)$,return to step 2.

The decline analysis

Lemma 1 [3] ： The function of $f(\beta)$,if direction of d_1 satisfies the condition $Ad_1 = 0$,direction sequence $\{d_k\}$ according to formula $d_k = -Pg_k + \alpha_k d_{k-1}$ produced to satisfy equation $Ad_k = 0$, $(Pg_k)^T d_k = g_k^T d_k$,

$(Pg_{k+1})^T d_k = g_{k+1}^T d_k$, $\forall k \geq 1$.

Lemma 2[4] ： If the objective function is to satisfy the assumptions,make $\beta^{(k+1)} = \beta^{(k)} + \lambda_k d_k$, d_k satisfy the condition $(Pg_k)^T d_k < 0$,the step size λ_k from strong Wolfe principle,so $\sum_{k\geq 1, d_k \neq 0} \frac{\left((Pg_k)^T d_k\right)^2}{\|d_k\|^2} < +\infty$,this type is called the generalized Zoutendijk condition.

Lemma 3：If $Pg_k \neq 0$,Produced by the new algorithm d_k is a direction of descent direction, That is $(Pg_k)^T d_k = g_k^T d_k < 0$, $\forall k \geq 1$.

Proof : By induction proof. When $k = 1$,has

$$d_1 = -Pg_1,\ g_1^T d_1 = -g_1^T Pg_1 = -g_1^T P^T Pg_1 = -(Pg_1)^T Pg_1 = -\|Pg_1\|^2 < 0$$

When k>1,has $(Pg_{k-1})^T d_{k-1} = g_{k-1}^T d_{k-1} < 0$.

In $d_k = -Pg_k + \alpha_k^{new} d_{k-1}$ with both sides multiplied by $(Pg_k)^T$ has

$$(Pg_k)^T d_k = (Pg_k)^T \left(-Pg_k + \alpha_k^{new} d_{k-1}\right) = -\|Pg_k\|^2 + \alpha_k^{new} (Pg_k)^T d_{k-1}$$

$$= -\|Pg_k\|^2 + \frac{\|pg_k\|^2}{-\mu g_{k-1}^T d_{k-1} + \nu d_{k-1}^T (g_k - g_{k-1})} (Pg_k)^T d_{k-1}$$

$$= \frac{-\mu \|Pg_k\|^2 g_{k-1}^T d_{k-1} - \nu \|Pg_k\|^2 d_{k-1}^T (g_k - g_{k-1}) + \|Pg_k\|^2 g_k^T d_{k-1}}{-\mu g_{k-1}^T d_{k-1} + \nu d_{k-1}^T (g_k - g_{k-1})}$$

$$= \frac{-\mu \|Pg_k\|^2 g_{k-1}^T d_{k-1} - \nu \|Pg_k\|^2 g_k^T d_{k-1} + \nu \|Pg_k\|^2 g_{k-1}^T d_{k-1} + \|Pg_k\|^2 g_k^T d_{k-1}}{-\mu g_{k-1}^T d_{k-1} + \nu d_{k-1}^T (g_k - g_{k-1})}$$

$$= \frac{(\mu+\nu)\|Pg_k\|^2 g_{k-1}^T d_{k-1} - (\nu-1)\|Pg_k\|^2 g_k^T d_{k-1}}{-\mu g_{k-1}^T d_{k-1} + \nu d_{k-1}^T (g_k - g_{k-1})} = \frac{\|Pg_k\|^2 g_{k-1}^T d_{k-1} - (\nu-1)\|Pg_k\|^2 g_k^T d_{k-1}}{-\mu g_{k-1}^T d_{k-1} + \nu d_{k-1}^T (g_k - g_{k-1})}$$

By the stronge Wolfe line search conditions has $-g_k^T d_{k-1} \leq -\sigma g_{k-1}^T d_{k-1}$,so has

$$(Pg_k)^T d_k \leq \frac{\|Pg_k\|^2 g_{k-1}^T d_{k-1} - \sigma(\nu-1)\|Pg_k\|^2 g_{k-1}^T d_{k-1}}{-\mu g_{k-1}^T d_{k-1} + \nu d_{k-1}^T (g_k - g_{k-1})}$$

$$\leq \frac{\|Pg_k\|^2 g_{k-1}^T d_{k-1}\left[1-\sigma(\nu-1)\right]}{(-\mu-\nu) g_{k-1}^T d_{k-1} + \nu d_{k-1}^T g_k} \leq \frac{\|Pg_k\|^2 g_{k-1}^T d_{k-1}\left[1-\sigma(\nu-1)\right]}{-g_{k-1}^T d_{k-1} + \sigma\nu d_{k-1}^T g_{k-1}} \leq \frac{\|Pg_k\|^2 (1-\sigma\nu+\sigma)}{\sigma\nu - 1}$$

Because $\nu \geq 0$, $\mu+\nu=1$, $0 < \sigma < 1$,so $\sigma\nu < 1$, $\sigma\nu - 1 < 0$, $1-\sigma\nu+\sigma > 0$,so $(Pg_k)^T d_k < 0$, the decline was established.

Convergence analysis

Theorem 1:A constrained optimization problem satisfy assumptions,consideration of the new algorithm, the step size λ_k from Wolfe principle,the iteration point is produced by the algorithm of $\{\beta_k\}$,For a number of k, $Pg_k = 0$ type or $\liminf_{k\to\infty} \|Pg_k\| = 0$ type set.

Proof: If the theorem does not hold, then there exists $C>0$,make $\|Pg_k\|^2>C$, $k=1,2\cdots\cdots$ or the ends of formula $d_k+Pg_k=\alpha_k^{new}d_{k-1}$ modulus, square, and then transpose get

$$\|d_k\|^2=\left(\alpha_k^{new}\right)^2\|d_{k-1}\|^2-2\left(Pg_k\right)^T d_k-\|Pg_k\|^2 \tag{1-1}$$

By lemma 3 available $\alpha_k^{new}\le\dfrac{-\left(Pg_k\right)^T d_k\left(1-\sigma\nu\right)}{\left(1-\sigma\nu+\sigma\right)\left(\sigma\nu-1\right)g_{k-1}^T d_{k-1}}=\dfrac{\left(Pg_k\right)^T d_k}{\left(1-\sigma\nu+\sigma\right)g_{k-1}^T d_{k-1}}$

And in the (1-1) with both sides divided by $\left(\left(Pg_k\right)^T d_k\right)^2$

$$\frac{\|d_k\|^2}{\left(\left(Pg_k\right)^T d_k\right)^2}\le\frac{\|d_{k-1}\|^2}{\left[\left(1-\sigma\nu+\sigma\right)g_{k-1}^T d_{k-1}\right]^2}-\frac{2}{\left(Pg_k\right)^T d_k}-\frac{\|Pg_k\|^2}{\left(\left(Pg_k\right)^T d_k\right)^2}$$

$$=\frac{\|d_{k-1}\|^2}{\left[\left(1-\sigma\nu+\sigma\right)g_{k-1}^T d_{k-1}\right]^2}-\left(\frac{1}{\|Pg_k\|}+\frac{\|Pg_k\|}{\left(\left(Pg_k\right)^T d_k\right)}\right)^2+\frac{1}{\|Pg_k\|^2}\le\frac{\|d_{k-1}\|^2}{\left[\left(1-\sigma\nu+\sigma\right)g_{k-1}^T d_{k-1}\right]^2}+\frac{1}{\|Pg_k\|^2}$$

Because $\dfrac{\|d_1\|^2}{\left(\left(Pg_1\right)^T d_1\right)^2}=\dfrac{1}{\|Pg_1\|^2}$,so from the above formula can be obtains

$$\frac{\|d_k\|^2}{\left(\left(Pg_k\right)^T d_k\right)^2}\le\frac{1}{\left(1-\sigma\nu+\sigma\right)^2}\frac{1}{\|Pg_1\|^2}+\sum_{i=2}^{k}\frac{1}{\|Pg_i\|^2}\le\frac{1}{\left(1-\sigma\nu+\sigma\right)^2}\frac{1}{C}+\sum_{i=2}^{k}\frac{1}{\|Pg_i\|^2}$$

Because $\left(1-\sigma\nu+\sigma\right)^2>1$,then $\dfrac{\|d_k\|^2}{\left(\left(Pg_k\right)^T d_k\right)^2}\le\dfrac{1}{C}+\dfrac{K-1}{C}=\dfrac{K}{C}$, has $\dfrac{\left(\left(Pg_k\right)^T d_k\right)^2}{\|d_k\|^2}\ge\dfrac{C}{K}$, so has

$\sum_{k=1}^{\infty}\dfrac{\left(\left(Pg_k\right)^T d_k\right)^2}{\|d_k\|^2}=+\infty$,his lemma conclusion 2 contradictions, the assumption does not hold, so has $\liminf_{k\to\infty}\|Pg_k\|=0$.

The example analysis

The following examples evaluate two-parameter P-NCD validity projection conjugate gradient method.Using the least squares method for the linear model under conditions of equality constraints to estimate the parameters β, the model is $y_i=x_1\beta_1+x_2\beta_2+x_3\beta_3+x_4\beta_4+x_5\beta_5+x_6\beta_6+\varepsilon_i$,solution was to $\beta=\left(0.038,0.353,0.121,0.286,-0.064,0.273\right)^T$,using the double parameter P-NCD conjugate gradient projection method is proposed in this paper, through the MATLAB software iterative calculation, the $\beta'=\left(0.034,0.350,0.19,0.27,-0.059\right)^T$,the equality constraints is $A\beta=b$,among them

$$A=\begin{pmatrix}a_1\\a_2\end{pmatrix}=\begin{pmatrix}2&6&7&4&1&3\\1&2&4&7&8&9\end{pmatrix},b=\begin{pmatrix}b_1\\b_2\end{pmatrix}=\begin{pmatrix}4.12\\3.21\end{pmatrix}$$

Table 1 Sample points

No.	x_1	x_2	x_3	x_4	x_5	x_6	y_i
1	100	100	100	100	100	100	100
2	10.15	72.25	100	100	100	100	85
3	0	0	87.5	98.4	94.7	100	60
4	0	0	32.8	65.55	88.4	100	45
5	0	0	27.3	52.45	86.8	100	37
6	0	0	12.0	15.05	78.8	95.5	29
7	0	0	4.7	0.95	5.2	77.9	22
8	0	0	4.2	0.55	2.4	71.9	19
9	0	0	1.5	0.20	0.4	56.4	15

Minimum error on the objective function of the comparison of two methods for the $RSS_{\min}$,the results are as shown in table 2

Table 2 Comparison of algorithms

algorithm	The least square method	P-DY algorithm
$RSS_{\min}$	23.42	21.96

From table 2 can be obtained by the method of least squares residuals, calculated as $RSS_{\beta} = 23.42$,By the P-DY conjugate gradient projection method to calculate the residual error is $RSS_{\beta'} = 21.96$,that is $RSS_{\beta} = 23.42 > RSS_{\beta'} = 21.96$,he effectiveness of the P-DY conjugate projection gradient method.

References

[1] Yuan Yaxiang, Sun Wenyu. Optimization theory and method [M]. Beijing: Science Press, l999: 1-10, 183, 219-293, 404-430.

[2] Wenyuan, Wang Dongqian. Science and mathematics, the least square [J]. systems with linear inequality constraints, 1984, 4 (1): 55-62.

[3] Gao Li, Xie Tiejun. Global convergence of conjugate projection gradient method with Wolfe line search [J]. operations research and management science, 2003, 12 (2): 31-35.

[4] Zoutendijk G. Computational Methods in Integer and Non-Linear Programming[J]. Abedied, North-Holland, Amsterdam, 1970, 3(1): 37-86.

[5] Sun Qingying, KBA, Ling Jian. Modified conjugate constrained optimization problem and the gradient projection algorithm [J]. Applied Mathematics Journal, 2010, 33 (4): 640-651.

[6] Zhang Zhiyong, Yang Zuying MATLAB tutorial [M]. Beijing: Beihang University press, 2009: 120-130.

Advanced Materials Research Vols. 989-994 (2014) pp 1806-1809
© (2014) Trans Tech Publications, Switzerland
doi:10.4028/www.scientific.net/AMR.989-994.1806

Generalized J Sets Based on Periodic Orbit and Attract Time

Liming Du [1, a], Fengying Wang [1, b] , Ziyang Han[1, c]

[1] Faculty of Information & Control Engineering,Shenyang Jianzhu University, Shenyang,China

[a]duliboy@163.com [b]wangfy678@163.com [c]phenixhans@163.com

Keywords: Generalized J sets; Frieze group; Escape-time algorithm;

Abstract. The paper introduces escape-time algorithm applied to construct G-J set firstly, and two methods are presented for generating a great diversity of generalized J sets in which the point fall in low-cycle attract collections in the domain. One of the coloring methods is according to attract time, another is by recording the domain of the orbits. We used frieze group map to validate effectiveness for algorithm.

Introduction

Chaos theory is a field of study in mathematics, it has received a great deal of interest among scientists from various fields such as meteorology, physics, engineering, economics,biology, and philosophy[1]. An early proponent of chaos theory was Henri Poincaré. In the 1880s, while studying the three-body problem, he found that there can be orbits that are nonperiodic, and yet not forever increasing nor approaching a fixed point [2]. Till now, many chaotic mappings have been proposed. Recognizing that chaos and fractal patterns have huge potential applications in architectural decoration, advertising and other fields, chaos graphics visualization has become a hot research issue [3]. In [4], some chaos visualization methods have been proposed based on constructing M sets. In [5], many strange attractor icons with symmetric feature have been designed. After French mathematician Gaston Julia computing a Julia set by computer, constructing Jualia graphics become an effective scheme for chaos visualization. In [6-7], some chaos and tilings mapping models have been disigned, but how to construct Julia set of this kind of models is not investigated. Based on the M-J theory and the period orbits of the systems, this paper give two algorithms to construct the generalized Julia sets, experiments show that the method is effective.

Constructing generalized J set of frieze group with the escape time algorithm.

Complex plane on track bounded set of points called J set, the structure of the classic with J sets usually adopt the escape time algorithm, namely the utility plane orbit initial point bounded points with unbounded initial orbit, on a computer screen with different colors to distinguish.Escape time algorithm is an effective and has a profound theoretical background map fractal method, all kinds of full of J and M sets can be drawn by this method.In this paper, the author studies on Frieze group of equivalence, the along the axis cycle for translational symmetry characteristics, there are no restrictions on the direction, therefore, can escape time algorithm to generate the mapping of the generalized with Julia set.

Set $A=\{\, x\in X\in Z:\ f^k(z)\in X, k=1,2,\cdots\}$, is Frieze all orbit in the group of mapping of bounded point set, choose the direction of the radius of the escape, so in the process of iteration, according to the point of the rail ran out of the radius of the number of iterations for coloring, then can form rich color graphics, concrete implementation steps of the algorithm are as follows:

- Take maximum number of iterations N, iterative area W, a computer screen representing escape radius R;
- Define the elapsed time functions：

$$T(z)=\begin{cases} k, |f^k(z)|\geq R, |f^i(z)|< R, i=1,2,\cdots,k-1, k\leq N \\ \\ 0, f^i(z)|< R, i=1,2,\cdots,N \end{cases}$$

- Confirm the point z of iterative area ,calculate $T(z)$;
- If $T(z)=0, z\in A$, else $T(z)\neq 0, z\notin A$;
- Color the point z according to the escape time function;

Fig 1(a) (b) is generated in the escape time model pm11 generalized J set graphics, white areas represent the point sets complex plane not escaping, namely real generalized filled J set. Color is the elapsed time at every point, Fig1 (a) is generated by the parameters of vector $\boldsymbol{a}'=\{\, a_i,\ i=1,2\cdots 15\,\}$ $=(0.33,0.184,-0.068,0.829,-0.027,-0.753,\ -0.306,\ -0.105,\ 0.599,$ $0.759,-0.106,-0.143,0.226,\ \ 0.269,-0.085)^T$, Fig1(b) is the parameter vector $\boldsymbol{b}=\{\, b_j, j=1,2\cdots 14\,\}=(-0.905,0.3,-0.97,0.643,$ $0.875,0.519,0.919,-0.332,\ 0.733,-0.865,-0.47,-0.647,0.439,-0.217,0.14)^T$.

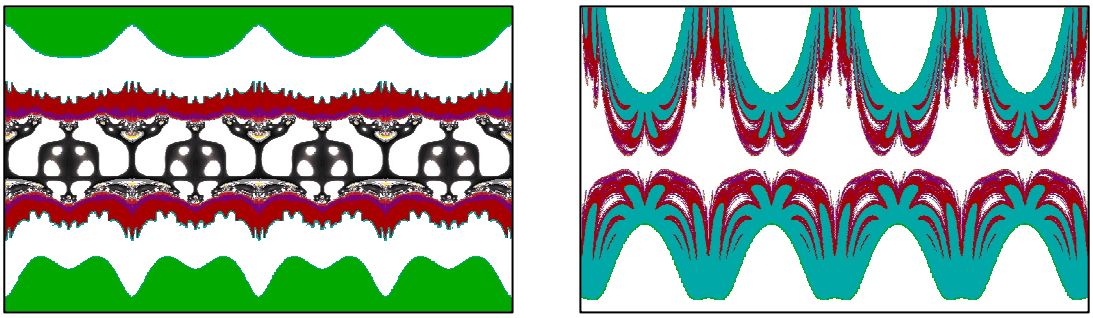

(a) (b)

Fig.1 The generalized J set created by escape time algorithm

In generalized M sets on regional blue cycle to retrieve any parameters, plane in its power to attract every initial point in the domain are attracted to the article limited periodic orbit. Escape time algorithm is separate escape region and attract region, and use this algorithm to generate generalized with Julia on regional color according to the elapsed time coloring, none of these graphics attraction domain, the nature of the periodic orbit. Filled with two kinds of structure of generalized J sets is proposed in this paper, the method of generalized full of Julia set is generated power plane on track to fall to attract in the domain of the low cycle collection z_0, which attract time algorithm is according to the low cycle track domain point fall in low cycle time on the tracks on the computer screen iterative area of the shaded, attract track algorithm is based on periodic orbit in power will attract domain in the plane of the power effectively differentiate to construct the generalized plane full of Julia set.

Test cycle track.

Frieze group mapping on the horizontal axis has a cycle for translation features, after the experiment found that the longitudinal axis coordinate change near the horizontal axis, so when looking for a power system contains cycle track, you can pick and choose the power plane in a rectangular cell area point as the initial iteration point.In testing a periodic orbit of power system, because the article number, it is impossible to determine the periodic orbit in advance can't determine the orbital cycles, each cycle and for each from the generalized M-set selection on regional cycle parameters of power system cycle track is different, so if using a static two-dimensional array to record the cycle track, will waste a lot of storage space.This article USES the dynamic linked list describes periodic orbit, temporary open cycle list contact storage space, reasonable arrangement of the storage space, and improves the search speed of secondary traversal.

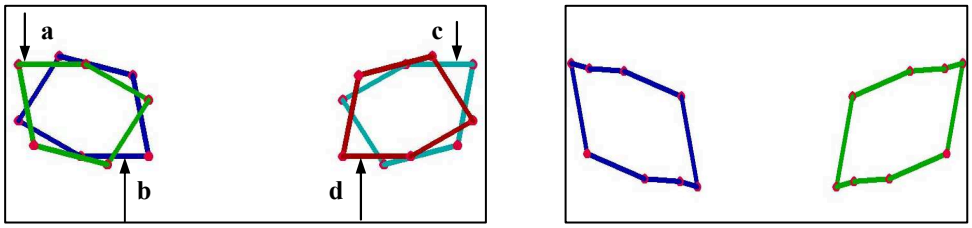

Fig.2 Cycle track diagram of the power system

Fig2 is for the same model of the same parameter section on different cycle parameters of periodic orbit for power system is formed, the letters in the graph represent different cycle track, dot said cycle cycle point on the orbit, orbital diagram separately in a closed orbits of each color lines, said the number of points per line indicates that the cycle track number of cycles.Fig2 (a) (b) from the parameters of the model pma2 section on the generalized M-set ($a_2 \in [-5.0, 5.0]$, $a_5 \in [-3.75, 3.75]$,

Fixed parameters, $a_1 = 0.7052$, $a_3 = -0.5054$, $a_4 = -0.5476$, , $a_6 = 0.3564$, $a_7 = -0.8298$), of different period in the area to select the parameters 1 (0.55155, 0.55155), 2 (0.32491, 0.32491) in the identified cycle track diagram of the power system. Fig 2 (a) of the communist party of China has four five cycle track, and Fig2(b) of the communist party of China has 2 8 periodic orbit. The above results show that the same parameters of cross section of the generalized M set cycle parameters determine the dynamic system of the area of the periodic orbit on the difference of the number and distribution with the parameter position changing.

Two algorithm for generating generalized J set.

In [8] in detail this vector by monte carlo search parameters, attract cycle algorithm and attract track algorithms are used to generate frieze group general train of thought and main implementation steps to implement the Julia set, Fig 3 is the parameters of the model of pm11 section in the generalized M set ($a_1 \in [-10.0, 10.0]$, $a_{13} \in [-7.5, 7.5]$) , fixed parameter of $a_2 = 0.18$, $a_3 = -0.07$, $a_4 = 0.82$, $a_5 = -0.03$, $a_6 = 0.76$, $a_7 = 0.31$, $a_8 = -0.61$, $a_9 = 0.59$, $a_{10} = 0.75$, $a_{11} = 0.11$, $a_{12} = -0.15$, $a_{14} = 0.26$, $a_{15} = 0.09$, Two algorithms above to generate the generalized full of Julia set, the parameters of the point 1 (- 2.14076.0.4791) power system a total of 3 2 cycle track, the two kinds of generalized full of Julia set as shown in Fig3 (a) (c), the parameter point 2 (1.5152.0.0293) of power systems with a total of 2 7 cycle track, the two kinds of generalized full of Julia set as shown in Fig 3 (b) (d).

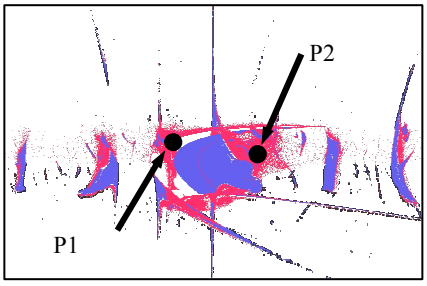

Fig 3 The generalized M sets $a_1 \sim a_{13}$ of pm11 in the parameters section

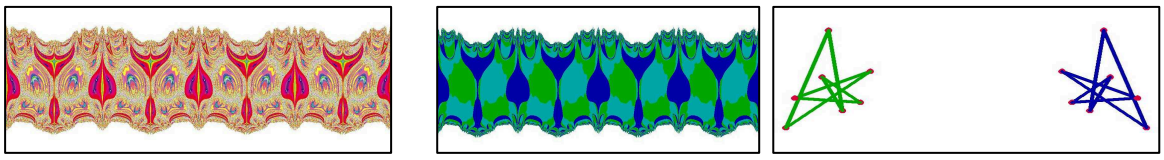

(a) (b) (c)

Fig.4 Generalized full of Julia set and its periodic orbit

Conclusions

This paper introduce two new algorithms to contruct the general Julila sets, the dynamic planar regionthe of the frieze group with fixed cycle parameters was divided, an escape time algorithm was used. Based on the attracting time and attracting orbit, the coloring methods are proposed. The distribution of the system's periodic orbit was analysised. Experiments results show that if we choose different parameters on the cross-section area, the period orbits alway have different number and distribuition, which lead to different structure of the general Julia sets.

References

[1] Kellert, Stephen H. (1993). In the Wake of Chaos: Unpredictable Order in Dynamical Systems. University of Chicago Press. p. 32. .

[2] Poincaré, Jules Henri (1890). "Sur le problème des trois corps et les équations de la dynamique. Divergence des séries de M. Lindstedt". Acta Mathematica 13: 1–270.

[3] Goertzel.B.. Rapid generation of strange attractors with the eugenic genetic algorithm. Computers & Graphics, Vol. 19(1) (1995),p.151~156.

[4] Ning Chen, Weiyong Zhu. Bud-sequnce conjecture on M fractal image and M-J conjecture between c and z planes from $z \leftarrow z^w + c \ (w = \alpha + i\beta)$. Computers & Graphics, Vol. 22(4) (1998)：537~546.

[5] Sprott J C. Strange attractor symmetric icons. Computers and Graphics, Vol. 20(2) (1996), p.325~32.

[6] Field M and Golubitsky M. Symmetry in Chaos[M]. NewYork: Ox ford Universit y Press, 1992

[7] Grunbaum B, Shephard G C. Tilings and patterns. New York :Freeman, 1996.

[8] Carter N, Eagles R, Grimes S, et al. Chaotic attractors with discrete planar symmetries [J] . Chaos Solitions and Fractals, Vol. 9(12) (1998),p. 2031- 2054.

Advanced Materials Research Vols. 989-994 (2014) pp 1810-1813
© (2014) Trans Tech Publications, Switzerland
doi:10.4028/www.scientific.net/AMR.989-994.1810

Static Fault-Tolerant Strategy for High Performance Computing Platform

Yu Sun, Jun Liu*

School of Computer and Electronics and Information, Guangxi University, Nanning 530004, PR China

E-mail: sunyu1225@163.com liujunzky@163.com

Keywords: High-performance computing platform, Task scheduling strategy, Fault-tolerant model, distributing computing

Abstract. It is an important research issue to ensure the computation correctness for parallel application and enhance the using rate of dynamic computing resource in distributed computing system. Based on the previous high performance distributing computing system, a fault-tolerant and task scheduler was developed, which combined the breathe mechanism, fault-discover mechanism and subtask reschedule mechanism. Experiments show that the fault-tolerant and task-scheduler has good performance and ensures the computation correctness even if when some computing resources fail.

Introduction

High-performance computing runs a broad range of system, from our desktop computers through large parallel processing system. In high-performance computing system, computing nodes will join in or drop out of the system. Meanwhile, the increased number of computing nodes leads to an increased failure rate. The crash of nodes or the nodes' quitting will make the mistake in the computing, and lead the computing system to calculate the application from begin. In the worst condition, the failure nodes will cause the system breaking down. In order to increase the reliability and accuracy of high-performance computing system, we improve the proposed high-performance computing system-WPHPC[3] with a fault-tolerance model.

The rest of this paper is organized as follows. In section 2, we introduce the proposed fault-tolerance High-performance system running on the ProActive, to computing the problem parallel. After that, section 3 presents the typical application, and analyzes and evaluates the results, comparing them to the simple High-performance system without fault-tolerance proposed before. Finally, we conclude and give some future research lines in Section 4.

Fault-Tolerance and Scheduling Algorithm

1.1 Fault-tolerance Algorithm

Given a computing task is divided into m subtasks, and executing on n nodes in the FT-WPHPC. There is the same subtask of every subtask as a backup item. To illustrate the task dispatch model, the details are express as follow. If there are n nodes in the parallel computing system, and we represent the nodes available as the set $N = \{N_1, N_2, \cdots N_n\}$. Each node Ni will be defined as $N_i = \{C_i, T_i, UN_T_i\}$, which Ci stands for the computation capacity, $Task_i = \{ST_\alpha, ST_\beta, \cdots ST_\gamma,\}$ stands for the overall subtasks distributed to the node Ni, and $UN_Task_i = \{UN_ST_\alpha, UN_ST_\beta, \cdots UN_ST_\gamma,\}$ stands for the unfinished subtasks. Subtasks distributed to every node are independent and the amount of subtasks to every node is allocated equally. Every subtasks ST_α will be define as $ST_\alpha = \{ST_M_\alpha, ST_BK_\alpha\}$, which refers the subtask and its bake subtask.If the fault-tolerance server detects the nodes failure to connect and execute the subtasks, it will report the failure node ID to the scheduler, and update the list of available nodes. When scheduler received the failure report, it will dispatch the back of subtasks to other nodes. The fault-tolerance scheduling strategy is as the original scheduling strategy. In this paper, static fault-tolerance scheduling strategy is mainly represented in our scheduling model.

Static fault-tolerance scheduling strategy dispatched subtasks on the basis of the calculated performance of each node. Given the number of nodes is n, the number of subtasks is m, the subtasks dispatched on node i is described as Equation 1.

$$Task_i = \left\lceil \frac{m}{\sum_1^n (c_i)} C_i \right\rceil \quad (1)$$

Where C_i is the calculate performance, which is evaluated by Nbench testing software.

Every checkpoint minutes TTL, server will send hello message to nodes to detect the node is normal or not. The checkpoint minutes TTL is defined as Equation 2 . If fault-tolerance server didn't receive the breath information, the computation node will be considered to become invalid.

$$\mathrm{TTL} = \frac{T}{max\left(len(Task_i)\right)} \quad (2)$$

If node j break down, scheduler will redispatch the unfinished subtask in node j to other nodes in good condition. Scheduler will redispatch the back-up item of the subtask to the node of the lower usage rate, and the back-up item will be executed from the latest record. If node j crashed, the subtask R_ST_i redipatched to node i is as Equation 3.

$$R_ST_i = \left\lceil \frac{UN_ST_j}{\sum_1^n \left(\frac{1}{F_ST_i}\right)} \cdot \frac{1}{F_ST_i} \right\rceil \quad (3)$$

Where, F_ST_i is execution time of first task dispatch in the node i , and UN_ST_j is the unfinished subtask of node j. The fault-tolerance algorithm in detail is presented in Alg.1.

Alg.1 Static Fault-tolerant and Task-scheduling Algorithm

Step1: Collect the calculated performance of computation nodes
Step2: Divide the task submitted into several subtasks, according to Equ. 2, and generate schedule files.
Step 3: According to schedule files, dispatch the subtasks to computation nodes
Step 4: WHILE tasks are not finished DO
    Step 4.1: IF Node i break down
        Step 4.1.1: Adjust the number of unfinished subtask
        Step 4.1.2:Obtain the bake-up item of unfinished subtasks UN_ST_j
        Step 4.1.3:Create active object of bake-up item
        Step 4.1.4:Update the list of available nodes
        Step 4.1.5:According to Equ. 3, redispatch the unfinished subtasks.
    END IF
END WHILE
Step 5:Computation nodes executed subtasks
Step 6:If all of the subtasks are executed
    Step 6.1:Gather and assemble the result
END IF

Experiment

To test the performance of fault-tolerance model, we apply the test function Matrix Multiply on the SFT-WPHPC which is compose of the static fault tolerance strategy and the WPHPC which is without fault tolerance we proposed before . The test function contain two 420*420 matrix to multiply. The FT-WPHPC is compose of 1-11 computation nodes. Computation performance is estimated by testing software Nbench. The parameters of computation nodes are described in Table 1.

Table 1. Parameters of nodes

Node	Nbench	CPU /GHZ	Memory /MB
A	5.975	2	512
B	9.493	2.4	512
C	9.600	2.4	512
D	9.539	2.4	512
E	9.496	2.4	512
F	9.527	2.4	512
G	9.647	2.8	512
H	9.596	2.8	512
I	9.572	2.8	512
J	9.579	2.8	512
K	9.764	2.4	512

To test the cost of the breath mechanism, we execute the 420*420 matric multiply application in the WPHPC and SFT-WPHPC. The application is divided into 30 subtasks.

1.2 Results and Analysis

(1) The cost of fault-tolerance model.

We will compare the execution time of WPHPC and SFT-WPHPC to obtain the cost of fault-tolerance model. The comparison is shown as Fig 3. In the figure, TWPHPC(n) and TWPHPC(n-1) stands for the execution time of the N nodes or N-1 nodes in WPHPC.TsFT-WPHPC(n) described the execution time of SFT-WPHPC system of n nodes when one node break down.

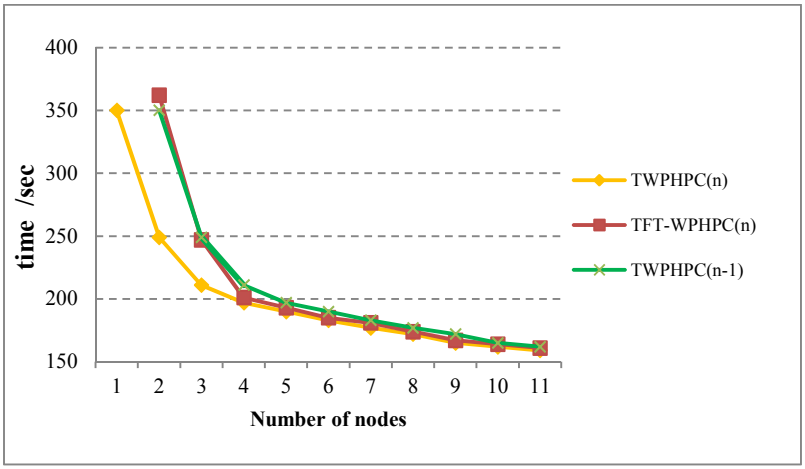

Fig. 1. Comparison of Static Fault-tolerance Model

From Fig.1, the fault-tolerance model guarantees the distributing system work in good condition. If some nodes break down, the model will redispatch the unfinished tasks to other computation nodes, and the execution time is better or equal to the time of WPHPC which contains (n-1) nodes. In the conclusion, the fault tolerance costs little but enhance the reliability of high performance computing system.

Summary

In order to guaranteed fault-tolerance and security of the distributed system, we proposed a new fault-tolerant scheduling model, which contain breath mechanism, failure detection technic and fault diagnosis and subtask restoration strategy, to improve the high perfomance distributed computing system. The experiments illustrated that the new fault-tolerant scheduling model occupies few computing resources to improve the reliability of the system. The system safety is

indispensable for the high performance computing platform, so we will discuss the security mechanism in the future .

Acknowledgements

This work is supported by by the Guangxi Natural Science Foundation, Scientific Program of Guangxi Municipal Education Commission and Nanning Key Technologies R&D Program (2013051). The corresponding author is Jun Liu, School of Computer and Electronics and Information, Guangxi University, Nanning, PR China. His E-mail is liujunzky@163.com*.

References

[1] André J C, Aloisio G, Biercamp J, et al. High Performance Computing for Climate Modelling[J]. Bulletin of the American Meteorological Society. (2014).

[2] Brian A., Françoise B, Denis C., Christian D., Imen F., Fabrice H., Elton M.,Oleg S.. An Efficient Framework for Running Applications on Clusters, Grids, and Clouds. Cloud Computing, Computer Communications and Networks, pp 163-178. Springer, Heidelberg(2010)

[3] Dong M.,Liang Zh. Key Technology Based on ProActive Parallel Computing in Windows. Computer Engineering, pp.105-107. (2006)

[4] Baude, F., Caromel, D., Huet, F., Mestre, L., & Vayssière, J. Interactive and descriptor-based deployment of object-oriented grid applications. In High Performance Distributed Computing, 2002. HPDC-11 2002. Proceedings. 11th IEEE International Symposium on. IEEE. pp. 93-102. (2002).

[5] Françoise B., Denis C.l, Christian D., Ludovic H.: A Hybrid Message Logging-CIC Protocol for Constrained Checkpointability. Euro-Par 2005.pp 644-653. (2005)

[6] Baduel, L., Baude, F., Caromel, D., Contes, A., Huet, F., Morel, M., & Quilici, R.. Programming, composing, deploying for the grid. In Grid Computing: Software Environments and Tools. Springer London. pp. 205-229. (2006)

[7] Caromel D., CavéV., Di Costanzo A., Brignolles C., Grawitz B., Viala Y. Executing Hydrodynamic Simulation on Desktop Grid with ObjectWeb ProActive. In HIC2006: Proceedings of the 7th International Conference on HydroInformatics. pp . (2006).

Advanced Materials Research Vols. 989-994 (2014) pp 1814-1820
© (2014) Trans Tech Publications, Switzerland
doi:10.4028/www.scientific.net/AMR.989-994.1814

Prediction of Mine Inrush Water Based on BP Neural Network Method

Ai-jun Shao [1, a], Qing-xin Meng[2,b], Shi-wen Wang[3,c] ,Ying Liu[4,d]

[1] Shijiazhuang University of Economics, Shijiazhuang 050031, China

[2] Shijiazhuang University of Economics, Shijiazhuang 050031, China

[1] Shijiazhuang University of Economics, Shijiazhuang 050031, China

[4] Shijiazhuang University of Economics, Shijiazhuang 050031, China

[a]shaoaijun@sohu.com, [b]moskit850@gmail.com,

[c] wsw84946108@163.com,[d]ritarita990@hotmail.com

Keywords: BP Neural Network, Mine Water Inflow, Prediction Model.

Abstract. Based on predictions of the mine inflow of water and the complexity of influential factors, a method of BP neural network is put forward for mine inrush water prediction in this paper. We chose proper impact factors and establish non-linear artificial neural network prediction model after analyzed the impact factors of mine water inflow in Shandong Heiwang iron, and also made one prediction with normal mine water inflow during the iron mining operation. It turned out that the result can match with the actual prediction data, which make it possible to predict the mine water inflow with the prediction of Artificial Neural Network.

With so many impact factors that affect the mine water inflow and it's hard to make out every impact factor exactly, the prediction of mine water inflow is a job that is complex and practical. So far, it still in under the level of applying Random mathematics and Deterministic mathematical methods approximate calculation. Traditionally deterministic inflow calculation methods mainly include analytical method, numerical method, the water balance method, etc.; Non-deterministic mathematical methods include experience method, regression method, fuzzy math, gray forecasting and timing analysis method[1].Due to the complexity of groundwater system and each calculation methods apply to different condition because of the their own shortcomings. It's an important significance to apply one new method to predict mine water inflow [2].

Artificial Neural Network (ANN) simulates the structure and functions of biological neural network through engineer technology application and computer. Linked with number of artificial networks that similar with natural nervous cells, it's one artificial intelligence system that can process distributed knowledge parallel[1][2][3]. Now the most widely used model is the error back-propagation neural network model – BP model, which can give a better result. BP model is typical one-way and multi-layered feedforward mode, which can be able to learn large mapping relationships, needless to describe the input-output mapping with extra mathematical knowledge. Compared with other models, BP model has the apparent advantage with better durability and timely predictability.

In this paper, we design BP model based on artificial neural network theory, which can predict the mine water inflow and turned to a good result with validation of measured data.

1 .The Structure and Algorithm of BP- Network

1.1..Neuronal structure and mathematical models

Neural networks are widely interconnected by a large number of neurons. Neural networks are divided into two parts according to the connection ways: no-feedforward network and combined network. BP network which is short for feedforward network that made up from non-linear transformation units turned out to be the most widely used one among popular ANN models.

The transportation of BP network is a non-linear function, where the input and output can meet the non-linear monotonically increasing. As f(u) is continuously differentiable, the function can be solved by using gradient algorithm. In addition, the learning algorithm can be called back-propagation

algorithm as its weight analysis is quite clear. In BP network, each neuron receives the inputs from the previous level and outputs to the next stage with no feedback. Figure1. The nodes are divided into input nodes and computing nodes. Each computing unite consists of any inputs with only one output which can be coupled to the input of any other nodes. The input of the i-layer is only linked with the output of (i-1)-layer. The input nodes are considered to be the first layer. Input nodes and output nodes are considered to be visible layers as they are link to outside and can be influenced by environment directly. Other middle layers are called as hidden layers.

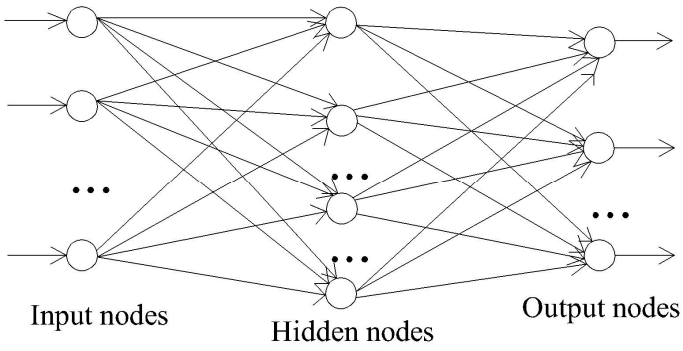

Fig.1 BP network schematic diagram

1.2 BP algorithm

The mathematical expression of BP network is:

$$\begin{cases} s_j = \sum_{i=1}^{n} w_{ij} x_i - \theta_j & (a) \\ u = s_j & (b) \\ y_j = f(u_j) = \dfrac{1}{1+e^{-(\sum_{i=1}^{n} w_{ij} x_j - \theta_j)}} & (c) \end{cases} \tag{1}$$

BP network structure can be divided into three layers: input layer, hidden layer and output layer. And full connections are used among layers and the output of all nodes meets the following requirements.

$$\begin{cases} y_k = f(\sum_{j=0}^{n_1-1} w'_{jk} x'_j - \theta'_k) & k = 0, \cdots m-1 \\ x'_j = f(\sum_{i=0}^{n-1} w_{ij} x_i - \theta_j) & j = 0, \cdots n_1 - 1 \end{cases} \tag{2}$$

And the function of nodes is S (Sigmoid) function; Parameters in (1)-(2) are defined as below:

$\mathbf{x} \in R^n$, $\mathbf{x} = (x_0, x_1, \cdots x_{n-1})^T$ is the input vector of the first layer;

$\mathbf{y} = (y_0, y_1, \cdots y_{m-1})^T$ is the input vector of the third layer;

$\mathbf{x}' = (x'_0, x'_1, \cdots x'_{n_1-1})^T$ is the input vector of the second layer;

The weight between the first layer and the second layer is w_{ij} $(i = 0, \cdots n-1, j = 0, \cdots n_1 - 1)$, the threshold is θ_j $(j = 0, \cdots n_1 - 1)$, the weight between the second layer and the third layer is w'_{jk} $(j = 0, \cdots n_1 - 1, k = 0, \cdots m-1)$, the threshold is θ'_k $(k = 0, \cdots m-1)$.

The specific process of B-P neural algorithm is as follows:

①First of all, set a random number among weight and threshold of all layers as the initial value;

②Input $\mathbf{x}^{p_1}$ （p_1 =1,2…p） by order, and output $y_k^{p_1}$ p_1 =1,2…p, k=0,1…m

③ Calculate the total error between actual output and expected output:

$$E_{p_1} = \frac{1}{2}\sum_{k=0}^{m}(t_k^{p_1} - y_k^{p_1})^2 \tag{3}$$

Given beforehand ε>0, the calculation can end up with E_T<ε; If E_T>ε, amend the weight w_{sq} to make ΔE_T($\Delta E_T$is the change mount of total error) change toward to the decrease direction, and get the result

$$E_T = E(W_{sq}) = E(w'_{jk}, w_{ij}) \tag{4}$$

So, in order to make A always change toward to minimum value, the change should be along with negative gradient direction of E_T. The parameters in (3) (4) are defined as follows:

The expected output of $\boldsymbol{p}$ samples $\mathbf{x}^1, \mathbf{x}^2, \cdots \mathbf{x}^p$ is $\mathbf{t}^1, \mathbf{t}^2, \cdots \mathbf{t}^p$, BP algorithm amend the values of weight and threshold with the error between the actual output $\mathbf{y}^1, \mathbf{y}^2, \cdots \mathbf{y}^p$ and the expected output $\mathbf{t}^1, \mathbf{t}^2, \cdots \mathbf{t}^p$, making $\mathbf{y}^{\mathbf{p_1}}$ and $\mathbf{t}^{\mathbf{p_1}}$ close to each other.

④ Amend the value of weight

In this paper, the weight expression can be as below after amending the value of η^{n_0}:

$$\begin{cases} w'_{jk}(n_0+1) = w'_{jk}(n_0) + \eta^{n_0}\sum_{p_1=1}^{p}\delta_{jk}^{p_1} x'^{p_1}_j \\ w_{ij}(n_0+1) = w_{ij}(n_0) + \eta^{n_0}\sum_{p_1=1}^{p}\delta_{ij}^{p_1} x_i^{p_1} \end{cases} \tag{5}$$

Parameters in (5): let n_0 be number of corrections (iterations), and η^{n_0} be the step size of the n_0 correction (Iteration step size), then we can get the correction values of w'_{jk}, w_{ij} in the n_0+1 correction.

⑤ Convergence criteria, input corrected weight W_{sq}(n_0+1) and get the values of outputs of each layer $x'^{p_1}_j$, $y_k^{p_1}$ (p_1=1,2…p)and E_T. According to the requirements, if all p_1 and k meet $\left|t_k^{p_1} - y_k^{p_1}\right| < \varepsilon$, the finished. Otherwise, correct the value of w_{sq} until meet the requirements. B-P algorithm can be divided into two parts: the first part (Forward propagation), input the message into input layer, proceed in hidden layer to calculate the actual outputs of each units; the second part (Back-propagation), if we can't get expected outputs in the output layer, then we need calculated the error between actual outputs and expected, and then correct the value of the weights according to the value of error to reach the minimum of error value. Two parts process alternately until the convergence is reached. See BP network algorithm structure in Figure 2.

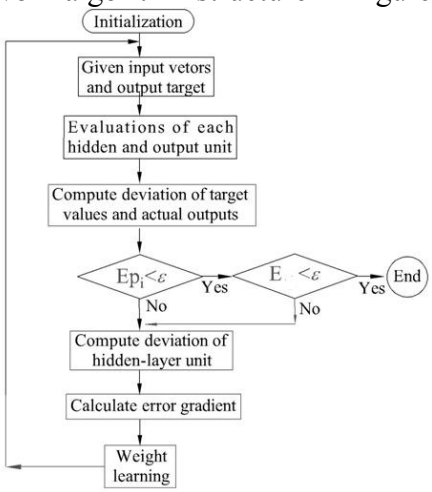

Fig.2. BP network algorithm structure

1.3 The improvement of BP algorithm

Actually, the standard BP algorithm is a simple steepest descent method static optimization, its weight correction formula can be written as a unified:

$$\Delta \mathbf{W}(n) = -\eta \frac{\partial \mathbf{E}}{\partial \mathbf{W}(n)} \tag{6}$$

(6)And here: $\Delta \mathbf{W}(n) = \mathbf{W}(n+1) - \mathbf{W}(n)$, n= 0,1,……is learning iterations.

The optimization direction of above algorithm just along with the gradient direction, the initial value of error function select may be local minimum, but cannot reach to be the global minimum. The convergence speed can be very low gradient algorithm process convergence only once. In order to speed the learning of network, errors, overcome local minimal and speed convergence, domestic and foreign exports have proposed a variety of improvements, including: variable step size method, conjugate gradient method, simulated annealing, genetic algorithms.

1.4 The design of BP network

Input and output layer, the dimension of input and output layer in BP network are totally designed according to the requirement of users.

The I/O relationship in BP network can be viewed as a mapping relationship and one highly nonlinear mapping; the capability of information processing comes from the complexity overlapping of many simple nonlinear functions.

Generally, the number of hidden layer units is based on experience in the network design. While the nodes in input layer and output layer are determined by the nature of the problem. We use construction method and delete method. The so-called construction method is started with a smaller network and it achieves the required performance targets by adding network nodes or neurons in the hidden layer. Contrary, delete method starts with larger network, delete and merge neurons according certain rules to achieve network structure that is suitable for the problem.

The initial values selection. Generally, initial weights are random numbers and relatively small ones, which can ensure neuron a fall start converting them the largest regional function of the rate of change, to prevent a start falling flat area. To eliminate the factors as dimensions and units difference, the input samples are normalized to processing, so that the relatively large inputs can still lag at the larger area of neurons transfer function.

Normalized formula is as blow:

$$x_i = \frac{x_i - x_{\min}}{x_{\max} - x_{\min}} \tag{7}$$

In the formula, x_{max}, x_{min} stands for the maximum value and minimum value in the i-th factors of samples. Factors are mapped to [0, 1] after the conversion.

2. The Calculation of Mine Water Inflow Prediction

2.1 The analysis of geological background and main influence factors

Take Shandong Heiwang iron as example; make prediction calculation of mine water flow with B-P network. The mines are located in East synclinal region of Zibo, which is on the fault zone of the Zihe. Deposit is hosted in fractured Ordovician karst limestone and multiple tectonic activities controlled by fault Zihe Valley, and belong to karst deposits with complex hydrogeological and large water. Zihe is a lager river in this area. After the year 1972, Taihe reservoir was built to reserve water at the location of 15 km upstream at the mine. The area of Taihe reservoir is 780km^2, and it controlled the vast majority of mining upstream drainage area. Large area of limestone outcrop and the Zihe Valley gravel was deposited directly to accept meteoric recharge. In the natural state, the flowing of groundwater, which is along the direction of Zihe Valley from southwest to northeast, will discharge in the form of springs at the contact of the Ordovician and Carboniferous and other relatively impermeable layers. Under the influence of artificial factors, groundwater empties into mining pits and discharges in the form of mine drainage.

From the above analysis of hydrogeological conditions, precipitation is a major source of water gushing in the pit. In addition, the Zihe River flow away from the south and east of the pit, away from the nearest point of the pit is only 50m. The Zihe is the only mine surface water drainage channels.

Since 1972, Taihe reservoir was built and reserved water, and discharged water into Zihe because of the limited reservoir capacity. As good permeability riverbed gravel layer directly overlying fractured limestone karst aquifer above the former indirect deposits roof, which constitute rock, therefore reservoir water drainage impact greatly on the pit. So atmospheric precipitation, rivers Zihe, the river reservoir water have obvious effect for mine drainage.

2.2 Predict the mine water flow with the B-P network model.

1. The design of the network

It used three layers BP network, the first layer is input layer, the second layer is hidden layer and the third layer is output layer.

2. Input and output

According to the hydrogeological conditions of the mine, make the measured data from January – December in 1972 as the sample. In the month precipitation (mm), the month pit water inflow (10^4m^3), the month too River Reservoir release of water (10^4m^3), as input variables of the month next month (March), mine water inflow next month as the output variable (predictor) (10^4 m^3).

Input vector set, $\mathbf{x} \in R^4 \quad \mathbf{x} = \{x_0, x_1, x_2, x_3\}$, x0 = {month rainfall}, x_1 = {month to River Reservoir release of water}, x_2 = {month mine water inflow}, x_3 = {June} month; output vector set $\mathbf{y} \in R^1, \quad \mathbf{y} = \{y\}$, y = {month mine water inflow}.

3. The selection of the nodes

Here the number from hidden layer is 6.

4. Algorithm

Based on gradient algorithm, we select variable step size, plus γ factor items and conjugate gradient method joint learning algorithm for computing.

5. Convergence criteria

The total error convergence criteria is $E_T < \varepsilon$, $\varepsilon < 0.01$.

6. The results

After a certain number of iterations, the gradient algorithm and conjugate gradient algorithm can meet the required error. While, conjugate gradient algorithm converges faster than the gradient algorithm multiple, and can achieve higher requirements, As can be seen from Table 1, for the same number of iterations, conjugate gradient algorithm for error is smaller, even no-processed samples can also generate ideal outputs. Predict the mine water flow for the year of 1972 with the proposed model; we can see that, the predicted data and measured data can achieve a better match. For example: in May 1973, Measured mine water inflow is 559,600 m^3, calculated output is 588,100 m^3. 1972 September measured mine water inflow is 3,283,600 m^3, calculated output is 3,154,100 m^3. Due to the local minima of the gradient algorithm, the initial values should be proper ones in order to reach the global minimum quickly. See the conjugate gradient algorithm output fitting in Figure 3.

Table1. BP Network Training Results

Date	Output of the gradient algorithm (10^4m^3)	Error (%)	Output of the conjugate gradient algorithm(10^4m^3)	Error (%)	Measured value (10^4m^3)
1972.02	121.8931	-69.01	60.57175	16.01	72.12
1972.03	37.73187	43.00	69.52353	-5.02	66.2
1972.04	39.7267	21.34	52.20694	-3.35	50.51
1972.05	18.25258	62.48	69.36623	-42.58	48.65
1972.06	53.44	22.81	60.25744	12.96	69.23
1972.07	32.02834	17.71	57.89102	-48.74	38.92
1972.08	108.4011	-28.93	83.41721	0.79	84.08
1972.09	280.7098	3.49	290.6919	0.058	290.86
1972.10	317.9431	0.15	318.4276	-0.01	318.41

1972.11	183.4299	10.19	205.0131	-0.37	204.25
1972.12	126.6451	-5.28	120.3314	-0.03	120.29
1973.01	89.76319	2.95	68.5285	25.91	92.49
Number of iterations	6300		6300		

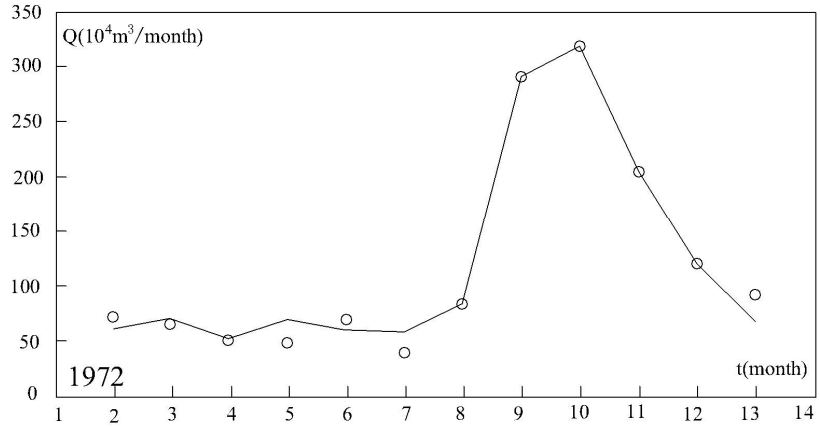

Fig.3 Output Fitting Figure

3. Conclusions

1. Neural network has the advantage of large-scale parallel processing, distributed information storage, continuous-time nonlinear dynamics, global collective action, a high degree of fault tolerance and robustness, redundancy, self-learning and real-time processing, It laid the application foundation for the neural network in the research for groundwater. It will achieve unimaginable process that the traditional methods cannot reach if we introduce neural network into groundwater research areas.

2. The standard B-P method, based on the gradient descent method (LMS), has defects on long training time and slow convergent speed due to its first derivative approaches zero when closes to the local minima. Therefore, this paper presents a new BP learning algorithm - using variable step size, joint learning algorithm of conjugate gradient methods and γ factor items (ULA), the standard BP algorithm overcomes the defects. And theory and practice demonstate the algorithm's effectiveness and superiority.

3. Currently, there still exist many problems with BP neural networks, such as structure of BP network, training and promotion problems. There's no generally accepted theory about groundwater research on the application of BP network number of hidden layer nodes. The defect that B-P network will be a little slow when training, is affected by the marketing capabilities and characteristics of the sample, the network structure, the role of the node function, learning algorithms, data normalization methods and other factors. We need further research about what method will be suitable for the characteristics of groundwater.

References

[1] Ha Gen. Neural network design [M]. China Machine Press, 2002.

[2] Wei Haikun. The theory and method of neural network structure design [M]. National Defense Industry Press, 2005.

[3] Shao Aijun, Zhang Fawang, Shao Taisheng. Mine ground water [M]. Beijing: Geological publishing house, 2005.

[4] Chen Peipei, Liu Hongquan. Height forecast ofwater conducted zone with top coal caving based on artificial neural network [J]. Journal of China Coal Society, 2005, 30(4).

[5] Guan Entai, Wu Qiang. Prediction of mine water inrush [J]. Zhongzhou Coal, 2005,1.

[6] Wu Wei. Neural network calculation [M], Higher Education Press, 2003.
[7] Li Yunfeng, Xu Guofu, Zuo Chuanming. Lianghuayuan Mine Water Inflow Estimation [J]. Coal Geology of China, 2007, 19.
[8] Qian Xuezhong. Grey Markov Model for predicting mine discharge [J], Journal of China Coal Society, 25(1), 2000.
[9] Huang Jingpo, Wang Weibiao. Relationship between the Jiawang mining area precipitation and discharge [J]. Coal Science and Technology Magazine, 2006(1).
[10] Liu Zhiming, Wang Guiling, Zhang Wei. Application of BP neural network to the quality assessment of groundwater dynamic monitoring network [J]. Hydrogeology and engineering geology, 2006, 33(2): 114-117.
[11] Dong Deyao. Neural network and Computational Intelligence [M]. Zhejiang University Press, 2002
[12] Yin, Y. Y., and X. M. Xu, Applying neural works technology for multiobjective landus planning, Journal of Environmental Management, 32, 349-356, 1991.
[13] Zhang, B., Govindaraju, R. S., Prediction of watershed run off using Bayesian concepts and modular neural networks [J]. Water Resour. Res. 2000(6): 753-762.
[14] Zhu, M. L., Fujita, M., and N. Hashimoto, Application of neural networks to runoff prediction, International conference on stochastic and statistical methods in hydrology and environmental engineering, Ontario, Canada, 1993.
[15] Marshall, S. J., and R. F. Harrison, Optimization and training of feed forward neural networks by genetic algorithms, 2nd, IEEE Int. Conf. on ANN, 39-43, 1991.
[16] Wang Z X, Dang Y G, Wang Y M. A grey verhulst model and its application [C]. Proceedings of 2007 IEEE ICCSIS, 2007, Nan-Jing, China, 571-574.
[17] Emery A C, Charles F M, Mary M P. Predicting Conductance Due to Upcoming Using Neural Network [J]. Ground Water, 2005, 43(6), 827-836.

Advanced Materials Research Vols. 989-994 (2014) pp 1821-1824
© (2014) Trans Tech Publications, Switzerland
doi:10.4028/www.scientific.net/AMR.989-994.1821

Fuzzy Comprehensive Evaluation Model of Selecting Football Coach

Congjun Rao, Jinhui Dong

College of Mathematics and Physics, Huanggang Normal University,

Huanggang 438000, China

cjrao@163.com

Keywords: Football coach; Fuzzy evaluation; Football Coach Selection; Comprehensive scores

Abstract. In this paper, the problem of selecting football coach is analyzed and studied. Concretely, a new index system of evaluating the football coach which includes coaching ability, team scores and personal achievement is designed, and then a comprehensive evaluation model based on fuzzy mathematics is presented to rank all candidates and to select the optimal football coach. Therefore, a novel and effective way is obtained to solve the problem of evaluating the comprehensive level of football coaches under the uncertain information.

Introduction

With the improvement of the modern life quality, more and more people are focus on physical exercise such as long-distance running, volleyball, baseball and football, especially on Football. Football refers to a number of sports that involve, to varying degrees, kicking a ball with the foot to score a goal[1]. The most popular of these sports worldwide is association football, more commonly known as just "football" or "soccer". Unqualified, the word football applies to whichever form of football is the most popular in the regional context in which the word appears, including association football, as well as American football, Australian rules football, Canadian football, Gaelic football, rugby league, rugby union, and other related games[2]. These variations of football are known as football codes. During the twentieth century, several of the various kinds of football grew to become among the most popular team sports in the world[3]. Nowadays, many countries devote to the development of football, and to focus on the national soccer team.

For a professional national soccer team, selecting the right coaching staff is crucial for success in football games in the world. It is important that head coaches trust and get alone with their assistant coaches. In order to choose the best all time football coach for a professional football team, we must find effective evaluation index system and reasonable evaluation method to rank alternative football coach[4-5]. For this research background, we study the problem of selecting football coach this paper. Firstly, we will design a new index system of evaluating the football coach, and then we will present a comprehensive evaluation model based on fuzzy mathematics to rank all candidates and to select the optimal football coach.

The rest of this paper is organized as follows. Section 2 gives the problem description. Section 3 presents a hybrid multi-attribute decision making to select the winners. Section 4 provides concluding remarks.

The Evaluation Index System

The evaluation index system is the key to the selection of the optimal football coach. Referring to the existing literatures and information on the valuation index system of selecting the optimal football coach, we choose coaching ability (u_1), team scores (u_2), and personal achievement (u_3) as three first-grade attributes. Moreover, professional training (u_{11}), seniority (u_{12}) and managing ability (u_{13}) are the corresponding second- grade attributes for the coaching ability, and team's progressing rate (u_{21}), stability (u_{22}) and winning rate (u_{23}) are the corresponding second-grade attributes for the team

scores, and popularity (u_{31}) and personal awards (u_{32}) are two second-grade attributes for personal achievement. All attributes are listed in the following Table 1.

Table1. The evaluation index system of selecting the optimal football coach

The first-grade index	The second-grade index
u_1 Coaching ability	u_{11} Professional Training
	u_{12} Seniority
	u_{13} Managing ability
u_2 Team scores	u_{21} Team's Progressing rate
	u_{22} Stability
	u_{23} Winning rate
u_3 Personal	u_{31} Popularity
achievement	u_{32} Personal awards

The Comprehensive Evaluation Model of Selecting Football Coach

In this section, we will present a fuzzy comprehensive evaluation method to rank and select the optimal football coach. Fuzzy comprehensive evaluation method is a comprehensive evaluation method which is based on fuzzy mathematics, and is a method to transfer qualitative evaluation into quantitative evaluation[8-11]. For the comprehensive evaluation of football coaches, the detailed decision steps are given as follows.

(1) Determine the candidate set.

We suppose there are *m* alternative football coaches participate in the evaluation, and the candidate set is denoted as $X = \{x_1, x_2, \cdots, x_m\}$.

(2) Determine the set of evaluation attributes and the weight set.

From the evaluation attributes given in Table 1, the set of the first-grade index is $U = \{u_1, u_2, u_3\}$, and the sets of the second-grade attributes are $u_1 = \{u_{11}, u_{12}, u_{13}\}$, $u_2 = \{u_{21}, u_{22}, u_{23}\}$ and $u_3 = \{u_{31}, u_{32}\}$. The weight set of the first-grade index is denoted as $W = \{w_1, w_2, w_3\}$, which satisfy the condition $\sum_{i=1}^{3} w_i = 1$. The weight set of the *j*-th second-grade attributes is denoted as $W_j = \{w_{j1}, w_{j2}, w_{j3}\}$, $j = 1,2,3$, where satisfy the condition $\sum_{t=1}^{3} w_{jt} = 1$. Here we set

$W = \{w_1, w_2, w_3\} = \{0.3, 0.5, 0.2\}$,

$W_1 = \{w_{11}, w_{12}, w_{13}\} = \{0.4, 0.3, 0.3\}$,

$W_2 = \{w_{21}, w_{22}, w_{23}\} = \{0.5, 0.25, 0.25\}$,

$W_3 = \{w_{31}, w_{32}\} = \{0.5, 0.5\}$.

(3) Determine the evalution set.

We suppose the grades of the evaluation are worse, bad, common, good, better[12-15]. Then the evulation set is denoted as $V = \{v_1, v_2, \cdots, v_5\}$ ={worse, bad, common, good, better}. For the convenience of calculation, here we set $V = \{v_1, v_2, \cdots, v_5\}$ ={worse, bad, common, good, better}={2, 4, 6, 8, 10}.

(4) Determine the evalution matrix.

For the set of the second-grade attributes $u_1 = \{u_{11}, u_{12}, u_{13}\}$ and the evulation set $V = \{v_1, v_2, \cdots, v_5\}$, we can determine a evalution matrix

$$R_1 = \begin{pmatrix} r_{11} & r_{12} & r_{13} & r_{14} & r_{15} \\ r_{21} & r_{22} & r_{23} & r_{24} & r_{25} \\ r_{31} & r_{32} & r_{33} & r_{34} & r_{35} \end{pmatrix}$$

where $r_{ij} = R(u_{1i}, v_j)$ is the membership (that is, the possibility degree) of u_{1i} on the grade v_j, and $r_{ij} \in [0,1]$, $i = 1,2,3$, $j = 1,2,\cdots,5$.

Similarly, we can obtain the evalution matrix R_2 of the set of the second-grade attributes $u_2 = \{u_{21}, u_{22}, u_{23}\}$ and the evulation set $V = \{v_1, v_2, \cdots, v_5\}$, and the evalution matrix R_3 of the set of the second-grade attributes $u_3 = \{u_{31}, u_{32}\}$ and the evulation set $V = \{v_1, v_2, \cdots, v_5\}$, i.e.,

$$R_2 = \begin{pmatrix} r_{11}^{/} & r_{12}^{/} & r_{13}^{/} & r_{14}^{/} & r_{15}^{/} \\ r_{21}^{/} & r_{22}^{/} & r_{23}^{/} & r_{24}^{/} & r_{25}^{/} \\ r_{31}^{/} & r_{32} & r_{33}^{/} & r_{34}^{/} & r_{35}^{/} \end{pmatrix},$$

$$R_3 = \begin{pmatrix} r_{11}^{//} & r_{12}^{//} & r_{13}^{//} & r_{14}^{//} & r_{15}^{//} \\ r_{21}^{//} & r_{22}^{//} & r_{23}^{//} & r_{24}^{//} & r_{25}^{//} \end{pmatrix}.$$

(5) Make the comprehensive evalution for a single football coach.

For the u_i, the primary evaluation vector is

$$w_i \mathrm{O} R_i = (b_{i1}, b_{i2}, b_{i3}, b_{i4}, b_{i5}) \underline{\underline{\Delta}} B_i, \ i = 1,2,3$$

We set

$$R = \begin{pmatrix} B_1 \\ B_2 \\ B_3 \end{pmatrix} = \begin{pmatrix} b_{11} & b_{12} & b_{13} & b_{14} & b_{15} \\ b_{21} & b_{22} & b_{23} & b_{23} & b_{25} \\ b_{31} & b_{32} & b_{33} & b_{34} & b_{35} \end{pmatrix}.$$

For the $U = \{u_1, u_2, u_3\}$, the secondary evaluation vector is

$$B_k = W \mathrm{O} R = (w_1, w_2, w_3) \mathrm{O} \begin{pmatrix} b_{11} & b_{12} & b_{13} & b_{14} & b_{15} \\ b_{21} & b_{22} & b_{23} & b_{23} & b_{25} \\ b_{31} & b_{32} & b_{33} & b_{34} & b_{35} \end{pmatrix}, \ k = 1,2,\cdots,m$$

$$\underline{\underline{\Delta}} (b_{k1}, b_{k2}, b_{k3}, b_{k4}, b_{k5})$$

where b_{kj} eans the subordinate degree of the alternative football coach k to the grade v_j, $j = 1,2,\cdots,5$.

(6) Rake all football coaches according to the comprehensive scores.

we set Z =(2, 4, 6, 8, 10)^T, and the the the comprehensive score of the alternative football coach k is

$$S_k = B_k \cdot Z = (b_{k1}, b_{k2}, b_{k3}, b_{k4}, b_{k5}) \begin{pmatrix} 2 \\ 4 \\ 6 \\ 8 \\ 10 \end{pmatrix} = 2b_{k1} + 4b_{k2} + 6b_{k3} + 8b_{k4} + 10b_{k5}$$

We can rank all alternative football coaches according to the comprehensive score S_k. The greater the value of S_k is, the better the alternative football coach is. Thus we can select the alternative football coach with the greatest score as the final winner.

Conclusions

In this paper, we design a new index system for evaluating the football coaches, and then a comprehensive evaluation model based on fuzzy mathematics is presented to rank all candidates and to select the optimal football coach. This fuzzy comprehensive evaluation method is a kind of easily-operative, efficient and convenient method to apply in the practice. And this method can be widely used in all kinds of coach selection of the regular ball games.

Acknowledgments

This work is supported by the 2014 Key Project of Hubei Provincial Department of Education (No. D20142903).

References

[1] C. Sorin, G. Gheorghe, and P. Tudor: Procedia-Social and Behavioral Sciences Vol. 117 (2014), p. 312-315.
[2] J. Tena and D. Forrest: European Journal of Operational Research Vol. 181 (2007), p. 362-373.
[3] D. R. Farley: Journal of Surgical Education Vol. 69 (2012), p. 572-573.
[4] S. Feng and L.D. Xu: Fuzzy Sets and Systems Vol. 105 (1999), p. 1-12.
[5] B. Wei, S. Wang, and L. Li: Energy Policy, Vol. 38 (2010), p. 5947-5955.
[6] H.B. Liu and Z.Q. Ku: Mathematical Modeling and Mathematical Experiments (Science press, Beijing, 2008).
[7] H. Gao, Z. Li and Q. Wang: Education Science Vol. 27 (2011), p. 71-75.
[8] Z. Xu: Uncertain Multiple Attribute Decision Making: Methods and Applications (Tsinghua University Press, Beijing, 2004).
[9] R. Li: The Foundation and Application of Fuzzy Multiple Attribute Decision Making (Science Press, Beijing, 2002).
[10] F. Herrera and L. Martínez: Fuzzy Sets and Systems Vol. 114 (2000), p. 43-58.
[11] Z. Fan, S. Xiao, and G. Hu: Computer & Industrial engineering Vol. 46 (2004), p. 329-335.
[12] O. Cordón: IEEE Trans on Fuzzy Systems Vol. 10 (2002), p. 1-19.
[13] F. Herrera and L. Martínez: IEEE Trans on Systems, Man, and Cybernetics Vol. 31 (2001), 227-233.
[14] F. Herrera, E. Herrera-Viedma, and J. Verdegay: Fuzzy sets and Systems Vol. 78 (1996), p. 73-87.
[15] Z. Xu: Uncertain Multiple Attribute Decision Making: Methods and Applications (Springer-Verlag, New York, 1999).

Advanced Materials Research Vols. 989-994 (2014) pp 1825-1828
© (2014) Trans Tech Publications, Switzerland
doi:10.4028/www.scientific.net/AMR.989-994.1825

Calculation of dynamic stress intensity factor by the boundary element - Laplace transform method

Wei Zhang

Shenzhen Polytechnic Guangdong 518008, PR China

1215556531@qq.com

Keywords: Boundary element method, Dynamic stress intensity factor, Laplace transform

Abstract: Using the Laplace transform and freezing time variable, the problem in the time domain into the frequency domain to solve the problem. The establishment of a crack unit model in the frequency domain, and the boundary integral equation and discrete form containing the crack unit has been deduced. While using Durbin algorithm suitable for transient dynamic response of the inverse Laplace transform, the amount of stress intensity factor of a set of transformation parameters corresponding to the frequency domain into a time domain to obtain the dynamic stress intensity factor of time curve, and calculate the stress intensity factor compared to the boundary finite element method has a Laplace transform high precision, easy to save CPU time and data preparation features, we recommend using this method to calculate the dynamic stress intensity factor.

Boundary element - Laplace transform method, basic formula

Set isotropic , homogeneous , linear elastic displacement and stress cracking body R , and flexibility to meet the equations of motion , physical equations and boundary conditions , the entire elastomer displacement at t = 0^+ time , speed :

$$\left.\begin{aligned} \mathrm{u}_j(z,\ y,\ o^+) &= \mathrm{u}_j(o) \\ \dot{\mathrm{u}}_j(z,\ y,\ o^+) &= \dot{\mathrm{u}}_j(o) \end{aligned}\right\} x, y \in R \tag{1}$$

Laplacian function is defined as:

$$\tilde{\mathrm{f}}(\mathrm{x},\ \mathrm{y},\ \mathrm{s}) = \int_0^\infty f(\mathrm{x},\ \mathrm{y},\ t)e^{-st}dt \tag{2}$$

After the Laplace transform elasticity equations of motion after the physical equations and boundary conditions are

$$(c_1^{\,2} - c_2^{\,2})\tilde{u}_{i,\ \mathrm{ij}} + c_2^{\,2}\tilde{u}_{j,\ \mathrm{ij}} + \tilde{F}_j = 0 \tag{3}$$

$$\sigma_{ij} = \rho\left[(c_1^{\,2} - 2c_2^{\,2})\tilde{u}_{m,\ m}\delta_{ij} + c_2^{\,2}(\tilde{u}_{i,\ j} + \tilde{u}_{j,\ i})\right] \tag{4}$$

$$\tilde{\sigma}_{ij}n_j = \tilde{P}_i(x,\ y,\ s); \tilde{u}_i = \tilde{u}_i(x,\ y,\ s) \tag{5}$$

$$\tilde{\mathrm{F}}_\mathrm{j} = \tilde{\mathrm{f}}_\mathrm{j} - \mathrm{s}^2\tilde{\mathrm{u}}_\mathrm{j} + \mathrm{u}_\mathrm{j}(\mathrm{o}) + \dot{\mathrm{u}}_\mathrm{j}(\mathrm{o})\cdot\mathrm{s};$$

$\tilde{\mathrm{f}}\mathrm{j}$ is Physical density of the Laplace transform of elastomer type.C_1, C_2 for the P-wave, S-wave velocity and

$$\mathrm{C}_1 = \sqrt{G/\rho(1-2\cdot\nu)}\ ; \qquad \mathrm{C}_2 = \sqrt{G/\rho}$$

G, ν is the elastic constant of the material, ρ is the mass density.

In the role of an infinite plane concentrated force, to meet the basic solution of equation (3) is automatically Kelvin solution is:

$$\tilde{\mathrm{u}}_{\mathrm{ji}} = \frac{1}{2\pi\rho\mathrm{c}_2^{\,2}}\left(\psi\cdot\delta_{\mathrm{ij}} - \mathrm{x}\mathrm{r}_{,\mathrm{i}}\mathrm{r}_{,\mathrm{j}}\right)$$

$$\mathrm{T}_{\mathrm{ji}} = \frac{1}{2\pi}\left(\left(\frac{\mathrm{d}\psi}{\mathrm{dr}} - \frac{\mathrm{x}}{\mathrm{r}}\right)\left(\delta_{\mathrm{ij}}\frac{\partial\mathrm{r}}{\partial\mathrm{n}} + \mathrm{r}_{,\mathrm{j}}\mathrm{n}_\mathrm{i}\right) - \frac{2}{\mathrm{r}}\bar{\mathrm{x}}\left(\mathrm{n}_\mathrm{j}\mathrm{r}_{,\mathrm{i}} - 2\mathrm{r}_{,\mathrm{i}}\mathrm{r}_{,\mathrm{j}}\frac{\partial\mathrm{r}}{\partial\mathrm{n}}\right) -\right.$$

$$2\frac{dx}{dr}r_{,i}r_{,j}\frac{\partial r}{\partial n}+\left(\frac{c_1^{\,2}}{c_2^{\,2}}-2\right)\cdot\left(\frac{d\psi}{dr}-\frac{dx}{dr}-\frac{x}{r}\right)\cdot r_{,i}n_j\Bigg) \tag{6}$$

Where: $\psi=K_0\left(\frac{s\cdot r}{c_2}\right)+\frac{c_2}{s\cdot r}\left(K_1\left(\frac{s\cdot r}{c_2}\right)-\frac{c_2}{c_1}K_1\left(\frac{s\cdot r}{c_1}\right)\right)$

$$X=K_2\left(\frac{s\cdot r}{c_2}\right)-\frac{c_2^{\,2}}{c_1^{\,2}}K_2\left(\frac{s\cdot r}{c_1}\right)$$

$K_0\left(\frac{s\cdot r}{c_i}\right),K_1\left(\frac{s\cdot r}{c_i}\right),K_2\left(\frac{s\cdot r}{c_i}\right)$ are denatured zero class, first class, second class Bessel functions.Betty swaps by the theorem:

$$c_i\tilde{u}_j(P,S)=\int_L\left(\tilde{u}_{ji}(P,Q)\tilde{t}_i(Q)-\tilde{T}_{ji}(P,Q)\tilde{u}_i(Q)\right)\cdot dL(Q) \tag{7}$$

Ci=1 when P located in the bady R and Q located on the border L; Ci=1/2 when P ,Q located on the border L;Ci=0 when P located in the non-bady R;When P, Q while located on the border L, using equation (7) obtained stress or displacement boundary frequency domain. Then the stress and displacement obtained by the inverse Laplace transform domain using the same procedure, obtain the stress and displacement fields R interior point.

Cracking unit and numerical techniques

Calculation of stress intensity factor distributions in the form of units on the accuracy of the crack tip stress and displacement assumptions related. Due to the constant unit can not simulate the crack tip singularity, so the use of such a single unit can not get accurate results. Linear or quadratic even though higher-order unit can improve the accuracy of the application subject to significantly increase the time count. Due to the dynamic stress intensity factor required to calculate a set of transformation parameters corresponding to S_i in the frequency domain $K(S_i)$ only after obtaining, equivalent to several times the corresponding static calculation problem. Computing time so the problem is more prominent than the corresponding static problem, for both the use of an improved calculation accuracy and reducing CPU time method for the calculation of dynamic stress intensity factor, it is very necessary.

Frequency domain of the crack tip stress and displacement distribution has the following form: (I type)

$$\left.\begin{aligned}
\tilde{\sigma}_x(r,\ \theta,\ s)&=\frac{\tilde{K}_1(s)}{(2\pi\cdot r)^{\frac{1}{2}}}\cos\frac{\theta}{2}\left(1-\sin\frac{\theta}{2}\sin\frac{3\theta}{2}\right)\\
\tilde{\sigma}_y(r,\ \theta,\ s)&=\frac{\tilde{K}_1(s)}{(2\pi\cdot r)^{\frac{1}{2}}}\cos\frac{\theta}{2}\left(1-\sin\frac{\theta}{2}\sin\frac{3\theta}{2}\right)\\
\tilde{\tau}_{xy}(r,\ \theta,\ s)&=\frac{\tilde{K}_1(s)}{(2\pi\cdot r)^{\frac{1}{2}}}\sin\frac{\theta}{2}\cdot\cos\frac{\theta}{2}\cdot\cos\frac{3\theta}{2}\\
\tilde{u}_x(r,\ \theta,\ s)&=\frac{\tilde{K}_1(s)}{G(1+\nu_1)}\cdot\sqrt{\frac{r}{2\pi}}\cos\frac{\theta}{2}\left(\left(1-\nu_1\right)+(1+\nu_1)\cdot\sin^2\frac{\theta}{2}\right)\\
\tilde{u}_y(r,\ \theta,\ s)&=\frac{\tilde{K}_1(s)}{G(1+\nu_1)}\cdot\sqrt{\frac{r}{2\pi}}\sin\frac{\theta}{2}\left(2-(1+\nu_1)\cdot\cos^2\frac{\theta}{2}\right)
\end{aligned}\right\} \tag{8}$$

For plane stress $\nu_1=\nu$; plane strain $\nu_1=\nu/(1-\nu)$.As can be seen from the above equation, the crack tip stress in the frequency domain with strange sex. Therefore, assuming that the distribution of the boundary element stress and displacement at the crack tip is:

$$\left.\begin{aligned}\tilde{t}(r,\ s)&=\sum_{i=1}^{k}\alpha_i r^{(i-3/2)}\\ \tilde{u}(r,\ s)&=\sum_{i=1}^{k}\beta_i r^{(i-1/2)}\end{aligned}\right\} \tag{9}$$

Write forming function form:

$$\left.\begin{aligned}\tilde{t}(r,\ s)&=\sum_{i=1}^{k}N_i(r)\cdot\tilde{t}_i(r,\ s)\\ \tilde{u}(r,\ s)&=\sum_{i=1}^{k}M_i(r)\cdot\tilde{u}_i(r,\ s)\end{aligned}\right. \tag{10}$$

$N_i(r)$, $M_i(r)$ is the stress and displacement shape function.

In the non-displacement of the crack tip stress distribution that is assumed to be constant

$$\left.\begin{aligned}\tilde{t}(x,\ y,\ s)&=\tilde{t}_i\\ \tilde{u}(x,\ y,\ s)&=\tilde{u}_i\end{aligned}\right\} \tag{11}$$

The latter formula (10) to (11) into (7), and discrete are:

$$C_iU_i(Q)=\sum_{i=kw\cdot 2+1}^{2\cdot W}\cdot\sum_{i=1}^{k}\left(\tilde{t}_i(Q)\cdot\int_{\Delta L}U_{ji}(P,Q)\cdot N_i(P,Q)\,dL-\tilde{U}_i(Q)\cdot\int_{\Delta L}\tilde{T}_{ji}(P,Q)\cdot\right.$$

$$\left.M_i(P,Q)\,dL+\sum_{i=kw\cdot 2+1}^{N}\left(\tilde{t}_i(Q)\cdot\int_{\Delta L}\cdot\tilde{V}_{ji}(P,Q)\cdot dL-\tilde{U}_i(Q)\int_{\Delta L}\cdot\tilde{T}_{ji}(P,Q)\cdot dL\right)\right. \tag{12}$$

Where u crack crack tip several bodies. When $i \neq j$, the formula uses the integral is a regular point or four-point Gaussian integral formula can be obtained. When i = j where the integral is odd, and the plot function is deformed Bessel functions. Due to boundary elements, thus integrating with analytic expressions. Due to space limitations not listed

Form of the formula (12) into the matrix include:

$$[\tilde{G}]\cdot[\tilde{U}]=[\tilde{H}]\cdot[\tilde{t}] \tag{13}$$

For displacement and stress array, displacement and stress coefficient matrix, for any boundary conditions by the formula (13) obtained the frequency domain stress and displacement, and the stress intensity factor domain, by the crack tip attached:

$$K_i(S_i)=\lim_{r\to 0}\tilde{t}(r,s)\cdot\sqrt{2\pi\cdot r}=\sqrt{2\pi}\alpha_1 \tag{14}$$

Obtain a set of transformation parameters corresponding to Si after the stress intensity factor by numerical inversion of Laplace transform too, can find the time factor domain. Ⅱ, Ⅲ crack calculated intensity factors associated with type I different.

Numerical inverse Laplace transform method

Durbin method is based on sine, cosine transform, on ways to improve Dubner and Abatr come. Required in a complex field operations. But its transformation results in T's early, mid valid, suitable for dramatic changes over time transform function.

$$f(t_j)=2(e^{\beta j\Delta t}/T)\left(\mathrm{Re}\left(-\frac{1}{2}f(\beta)+\sum_{n=0}^{N-1}(A(n)+i\cdot B(n))\cdot w^{jn}\right)\right)$$

$$A(n)=\sum_{i=0}^{L}\mathrm{Re}\left(\tilde{f}(\beta+i(n+iN)\cdot 2\pi/T)\right)$$

$$B(n)=\sum_{i=0}^{L}\mathrm{Im}(f(\beta+i(n+iN)\cdot 2\pi/T))$$

$$w=e^{2\pi i/N}$$

$n = 0,1,\cdots,\ N,\ i = 0,1,2,\cdots L$

$t_j = j \cdot T/N;\ j = 0,1,\cdots N-1$

Examples

Figure 1 , long plate with a central crack , the elastic constants were G = 76.92 MPa , v = 0.3, ρ = 5000kg/m^3, P , S -wave velocities were C_1 = 6206m / s; C_2= 3922m / s , a=5mm,t = 0 moment , both ends of the plate to withstand sudden tensile load . Take 1 /4 as part of the calculation model, and its boundary is divided into 39 units. Disposed on each side of the crack tip singular means of a three-node , the length of the adjacent cell constant of 1.5 . Inverse Laplace transform using Durbin algorithm , taking N = 20, L = 1, T = 2 × 10^{-3}-s , βT = 5, in the range of 0 ~ 1.0 × 10^{-3}seconds , the Laplace error caused by the inverse transform of less than 1 % of the time curve of Figure .2 Example of stress intensity factor , the largest results of $K(t)/\sqrt{a}\cdot\sigma$ is 2.7101 , the results 2.6812 of finite element method is slightly larger , the maximum time that appears in 6 ~ 7 × 10^{-3} seconds.

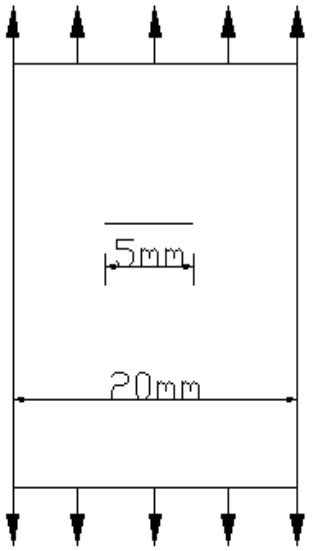

Figure 1

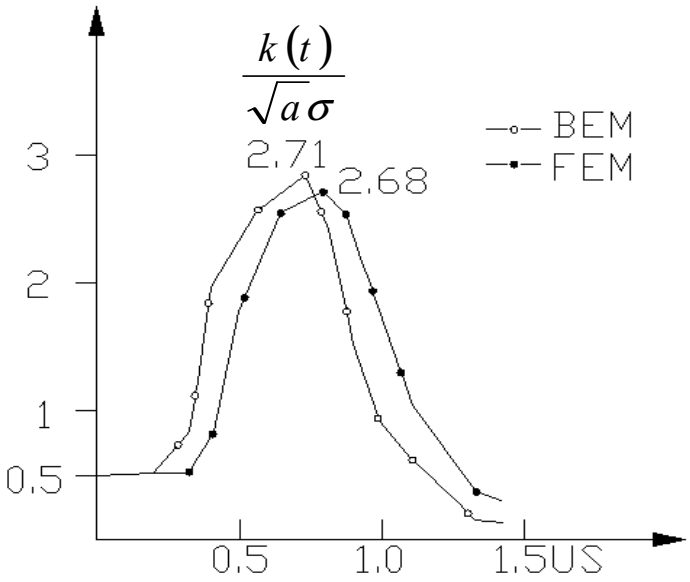

Figure .2

Conclusion

Comparing the finite element method of calculated stress intensity factor , The boundary element - Laplace transform method with high accuracy, easy to save CPU time and data preparation features, we recommend using this method to calculate the dynamic stress intensity factor.

References

[1] P.K.Banerjee and R.Buttertield: Boundary Element Methods in Engineering science, McGraw –Hill. New York , 2000

[2] Jiang Fengchun ,Liu Rui Tong,Liu Kui Hall:Dynamic stress intensity factor response theory analysis,Journal of Vibration Engineering(chian)[J],2000,vol4,p60-64

[3] G.C Sih: Mechanics of Fracture ,1991.p268.

[4] Xuejun.Zhao, Dynamiccrack starting Research Progress,[J] Building Science , china,2009,7,p85-88

[5] Youlin.Liu, ,Dynamic response of the beam structure With a Crack, [J] Journal of sunyatsen university,china,2012,10,p52-55

Advanced Materials Research Vols. 989-994 (2014) pp 1829-1832
© (2014) Trans Tech Publications, Switzerland
doi:10.4028/www.scientific.net/AMR.989-994.1829

Point rupture solutions of a singular quasilinear elliptic equation arise from non-Newtonian fluids

Zhoujin Cui[1,a], Mingyang Xu[1,b] and Rui Zhang[2,c]

[1] Jiangsu Maritime Institute, Jiangsu Nanjing 211170, China

[2] Jinling Institute of Technology, Jiangsu Nanjing 211169, China

[a] cuizhoujin@163.com, [b]njhsumy@126.com, [c] misszhang1221@163.com

Keywords: quasilinear elliptic equation; thin film; point rupture; radial solution; singular.

Abstract. We consider the quasilinear elliptic equation $\mathrm{div}(|\nabla u|^{p-2}\nabla u) = f(u)$ in a finite ball in R^N, where $\lim_{u\to 0^+} f(u) = \infty$. Motivated by the thin film equations, a solution u is said to be a point rupture solution if for some $p \in \Omega$, $u(p) = 0$ and $u(x) > 0$ for any $x \in \Omega \setminus \{p\}$. Our main result is a sufficient condition on f for the existence of radial point rupture solutions.

1. Introduction

In this paper we study the existence of radial point rupture solutions of the following problems

$$\mathrm{div}(|\nabla u|^{p-2}\nabla u) = f(u) \ \text{ in } \Omega \tag{1.1}$$

with Neumann boundary condition

$$\frac{\partial u}{\partial n} = 0 \ \text{ on } \partial\Omega \tag{1.2}$$

where $N \geq 2, p \geq 2, \Omega = \{x \in \mathbf{R}^N : |x| < 1\}$ is a ball. The nonlinear function $f \in C^1(0,\infty)$ satisfies that following condition:

$$\lim_{u\to 0^+} f(u) = \infty.$$

By a point rupture solution u of (1.1) in Ω, we mean that for some $p \in \Omega$, $u(p) = 0$ and $u(x) > 0$ for any $x \in \Omega \setminus \{p\}$.

This problem appears in the study of non-Newtonian fluids ([1,2]) and non-Newtonian filtration ([3]). The quantity p is a characteristic of the medium. Media with $p > 2$ are called dilatant fluids and those with $p < 2$ are called pseudoplastics. If $p = 2$, they are Newtonian fluid. In particular it can be the equation equilibrium states in flows of thin films of power-law fluids.

Equations of type

$$u_t = -\mathrm{div}(m(u)|\nabla\triangle u|^{p-2}\nabla\triangle u) - \mathrm{div}(g(u)\nabla u)$$

where u denotes the height from the surface of the oil to the surface of the solid. It was J.R. King [4] who first derived the equation. For the two dimensional case, which has a particular physical derivation as mentioned in [5], modeling the spreading of an oil film over an solid surface. The zero set $\sum = \{u = 0\}$ is the liquid/solid interface and is sometimes called set of ruptures. The coefficient $m(u)$ reflects surface tension effects-a typical choice is $m(u) = u^3$.

In particular, let us assume that $m(u) = u^3, g(u) = -u^l$ with $l < p - 1$, then $l - p < -1$. Then we get the equation

$$\mathrm{div}(|\nabla u|^{p-2}\nabla u) = u^{-l}, \quad l > p - 1. \tag{1.3}$$

We easily see that the solutions of (1.3) can explain the behaviors of steady-states for (1.3) in some special cases. A different type of equation from (1.3)

$$-\mathrm{div}(|\nabla u|^{p-2}\nabla u) = q(x)u^{-l}, \ \ x \in \Omega, \ \ u|_{\partial\Omega} = 0$$

has also been studied in [6] and the references therein.

Now let $\Omega \in R^N$ be the bottom of a cylindrical container occupied by the thin film fluid, we assume that there is no flux across the boundary, which yields the boundary condition $\frac{\partial p}{\partial \nu} = 0 \ \text{ on } \partial\Omega$. We also ignore the wetting or non-wetting effect, and assume that the fluid surface is perpendicular to the boundary of the container, i.e., $\frac{\partial h}{\partial \nu} = 0 \ \text{ on } \partial\Omega$.

We can find the related results for $p = 2$ in [7-9]. The main differences between $p = 2$ and $p \neq 2$ are known in [10-12]. When $p = 2$, it is well known that all the positive solutions in $C^2(B_R)$ of the problem

$$\triangle u + f(u) = 0 \text{ in } B_R,$$
$$u(x) = 0 \text{ on } \partial B_R,$$

and radially symmetric solutions for very general (see [14]). Unfortunately, this result does not apply to the case $p \neq 2$. Kichenassary and Smoller showed that there exist many positive nonradial solutions of the above problem for some f (see [15]). The major stumbling block in the case of $p \neq 2$ is that certain nice features inherent to the case $p = 2$ seem to be lost or at least difficult to verify.

We conjecture that the ruptures are discrete for finite energy solutions, and we expect that the radial point rupture solutions will serve as the blow up profile of the solution near any point rupture. The main purpose of this paper is on the existence of radial point rupture solution. And we are only interested in the local solutions in a neighborhood of the point rupture, extended to results in [7-9, 11-13].

Now we state our main result.

Theorem 1.1. Let $\sigma^* > 0$ and f be a continuous, monotone decreasing positive function on $(0, \sigma^*]$ such that

$$\lim_{v \to 0+} f(v) = \infty.$$

Let

$$G(v) = \int_0^v \frac{|s'|^{p-2}}{f(s)} ds. \qquad (1.4)$$

Then there exists $r^* > 0$ and a radial point rupture solution u_0 to (1.1) in $B_{r^*}(0)$ such that $u_0 = u_0(r)$ is continuous on $[0, r^*]$, $u_0(0) = 0, u_0(r) > 0$ for any $r \in (0, r^*]$, and u is a weak solution to (1.1) in $B_{r^*}(0)$. Moreover, u_0 is monotone increasing and

$$G^{-1}(\tfrac{1}{2N} r^2) \leq u_0(r) \leq \int_0^r (2s^{1-N} G^{-1}(\tfrac{s^2}{2N}))^{\frac{1}{p-1}} ds$$

for any $r \in (0, r^*]$.

Remark 1.2. The assumption that f is monotone decreasing can be replaced by the assumption that f is a product of a monotone deceasing function and a bounded positive function.

2. Proof of Theorem 1.1

To prove Theorem 1.1, we consider radially symmetric solutions of the quasilinear elliptic Eq. (1.1), that is, suppose that $u = u(r)$ with $r = |x| < 1$. For any $\sigma \in (0, \sigma^*)$, we use u_σ to denote the unique solution to the initial value problem

$$(\Phi_p(u'))' + \frac{(N-1)}{r} \Phi_p(u') - f(u(r)) = 0, r > 0, \qquad (2.1)$$
$$u(0) = \sigma, \quad u'(0) = 0, \qquad (2.2)$$

where $\Phi_p(s) = |s|^{p-2} s$.

Definition 2.1. $u \in W_0^{1,p}$ is a positive weak solution to problem (1.1) if $u > 0$, a.e. on Ω and satisfies

$$\int_\Omega |\nabla u|^{p-2} \nabla u \nabla \varphi dx = \int_\Omega f(u) \varphi dx, \text{ for all } \varphi \in W_0^{1,p}(\Omega).$$

Lemma 2.2. There exists $r_\sigma > 0$ such that u_σ is defined on $[0, r_\sigma]$ with $u_\sigma(r_\sigma) = \sigma^*$. Moreover, $u'_\sigma(r) > 0$ on $(0, r_\sigma]$ and

$$G^{-1}(\tfrac{1}{2N} r^2) \leq u_\sigma(r) \leq \sigma + \int_0^r (2s^{1-N} G^{-1}(\tfrac{s^2}{2N}))^{\frac{1}{p-1}} ds \text{ on } [0, r_\sigma]. \qquad (2.3)$$

Proof. For simplicity, we suppress the σ subscript in this proof. We write (2.1) in the form of $[r^{N-1} \Phi_p(u'(r))]' = r^{N-1} f(u(r)) \geq 0$, so we have $r^{N-1} \Phi_p(u'(r)) = \int_0^r s^{N-1} f(u(s)) ds \geq 0$. In particular, u is monotone increasing and u can be extended whenever $f(u)$ is defined and bounded. Hence, there exists $r_\sigma > 0$ such that u_σ is defined on $[0, r_\sigma]$ with $u_\sigma(r_\sigma) = \sigma^*$.

Since u is monotone increasing and f is monotone decreasing, we have

$$r^{N-1} \Phi_p(u'(r)) = \int_0^r s^{N-1} f(u(s)) ds \geq f(u(r)) \int_0^r s^{N-1} ds = \frac{r^N}{N} f(u(r)),$$

hence, $\frac{\Phi_p(u'(r))}{f(u(r))} \geq \frac{r}{N}$.

Integrating again, we have

$$G(u(r)) \geq G(\sigma) + \frac{r^2}{2N} \geq \frac{r^2}{2N}.$$

Since G is strictly monotone increasing, we have $u(r) \geq G^{-1}(\frac{r^2}{2N})$.

On the other hand,

$$r^{N-1}\Phi_p(u'(r)) = \int_0^r s^{N-1} f(u(s))ds \leq \int_0^r s^{N-1} f(G^{-1}(\frac{s^2}{2N}))ds.$$

Let $v = G^{-1}(\frac{s^2}{2N})$, we have $G(v) = \frac{s^2}{2N}$ and $\frac{|v'|^{p-2}}{f(v)}dv = \frac{s}{N}ds$.

Hence

$$\int_0^r f(G^{-1}(\frac{s^2}{2N}))sds = \int_0^{G^{-1}(\frac{s^2}{2N})} 2dv = 2G^{-1}(\frac{s^2}{2N}).$$

Since $0 < r < 1$, $N \geq 2$, we have

$$\int_0^r s^{N-1} f(G^{-1}(\frac{s^2}{2N}))ds \leq \int_0^r f(G^{-1}(\frac{s^2}{2N}))sds.$$

Thus

$$\Phi_p(u'(r)) \leq 2G^{-1}(\frac{s^2}{2N}).$$

Hence

$$u'(r) \leq (2r^{1-N}G^{-1}(\frac{r^2}{2N}))^{\frac{1}{p-1}}$$

which yields

$$u(r) \leq \sigma + \int_0^r (2s^{1-N}G^{-1}(\frac{s^2}{2N}))^{\frac{1}{p-1}}ds.$$

Corollary 2.3. There exists $r^* > 0$ such that for any $\sigma \in (0, \frac{\sigma^*}{2}]$, $r_\sigma \geq H^{-1}(\frac{\sigma^*}{2})$, where

$$H(u) = \int_0^u (2s^{1-N}G^{-1}(\frac{s^2}{2N}))^{\frac{1}{p-1}}ds.$$

Proof. For any $\sigma \in (0, \frac{\sigma^*}{2}]$,

$$\sigma^* = u_\sigma(r_\sigma) \leq \sigma + \int_0^{r_\sigma} (2s^{1-N}G^{-1}(\frac{s^2}{2N}))^{\frac{1}{p-1}}ds \leq \frac{\sigma^*}{2} + \int_0^{r_\sigma} (2s^{1-N}G^{-1}(\frac{s^2}{2N}))^{\frac{1}{p-1}}ds.$$

Hence

$$\int_0^{r_\sigma} (2s^{1-N}G^{-1}(\frac{s^2}{2N}))^{\frac{1}{p-1}}ds \geq \frac{\sigma^*}{2}.$$

Let

$$H(u) = \int_0^u (2s^{1-N}G^{-1}(\frac{s^2}{2N}))^{\frac{1}{p-1}}ds,$$

So $H(r_\sigma) \geq \frac{\sigma^*}{2}$ implies $r_\sigma \geq H^{-1}(\frac{\sigma^*}{2})$. The point rupture solution can be constructed as the limit of u_σ as $\sigma \to 0$.

Proposition 2.4. There exists a sequence $\{\sigma_k\}_{k=1}^\infty \subset (0, \frac{\sigma^*}{2}]$ satisfying $\lim_{k\to\infty} \sigma_k = 0$, such that $u_{\sigma_k} \to u_0$ uniformly in $\overline{B_{r^*}(0)}$ as $k \to \infty$, for some function $u_0 \in C^0(\overline{B_{r^*}(0)}) \cap C^2(\overline{B_{r^*}(0)} \setminus \{0\})$. Moreover, u_0 is a classical solution to (1.1) in $B_{r^*}(0) \setminus \{0\}$ and

$$G^{-1}(\tfrac{1}{2N}r^2) \leq u_0(r) \leq \int_0^r (2s^{1-N}G^{-1}(\tfrac{s^2}{2N}))^{\frac{1}{p-1}}ds \ \text{ on } \ [0, r^*].$$

Proof. For any $\varepsilon > 0$, $u_\sigma, \sigma \in (0, \frac{\sigma^*}{2}]$ is a family of uniformly bounded classical solutions to

$$\mathrm{div}(|\nabla u|^{p-2}\nabla u) = f(u) \ \text{ in } \overline{B_{r^*}(0)} \setminus B_\varepsilon(0),$$

hence by a diagonal argument, there exists a sequence $\{\sigma_k\}_{k=1}^\infty \subset (0, \frac{\sigma^*}{2}]$ satisfying $\lim_{k\to\infty} \sigma_k = 0$, such that $u_{\sigma_k} \to u_0$ locally uniformly in $\overline{B_{r^*}(0)}$ as $k \to \infty$.

Now (2.3) implies

$$G^{-1}(\tfrac{1}{2N}r^2) \leq u_0(r) \leq \int_0^r (2s^{1-N}G^{-1}(\tfrac{s^2}{2N}))^{\frac{1}{p-1}}ds \ \text{ on } \ [0, r^*].$$

Since

$$\lim_{r\to 0} \int_0^r (2s^{1-N}G^{-1}(\tfrac{s^2}{2N}))^{\frac{1}{p-1}}ds = 0,$$

it is not difficulty to see, from the bounds of u_σ and u_0, that $u_{\sigma_k} \to u_0$ uniformly in $\overline{B_{r^*}(0)}$ as $k \to \infty$.

Proposition 2.5. $f(u_0) \in L^1 B_{r^*}(0)$ and u_0 is a weak solution to (1.1) in $B_{r^*}(0)$.

We omit the proofs here. From proposition 2.4 and 2.5, we can get Theorem 1.1.

Acknowledgements

This work was financially supported by the Pre-research Foundation of PLA University of Science and Technology.

References

[1] L. K. Martinson and K. B. Pavlov. Unsteady shear flows of a conducting fluid with a rheological power law, Magnitnaya Gidrodinamika, 2(1971), 50-58.

[2] Esteban, J. R. and Vazquez, J. L. On the equation of turbulent filteration in one-dimensional porous media, Nonlinear Anal., 10(1982), 1303-1325.

[3] G. Astrita and G. Marrucci. Principles of non-Newtonian fluid mechanics, McGraw-Hill, New York, 1974.

[4] J.A. King. Two generalisations of the thin film equation, Math. Comput. Modell., 34(7-8)(2001), 737-756.

[5] A.B. Tayler. Mathematical Models in Applied Mechanics, Clarendon, Oxford, 1986.

[6] Zuodong Yang. Existence of positive entire solutions for singular and non-singular quasi-linear elliptic equation, J Comp. Appl. Math., 197(2)(2006), 355-364.

[7] J.Ai, K.S. Chou, J.Wei. Self-similar solutions for the anisotropic affine curvature shortening problem, Calc. Var. Partial Differen. Equat., 13(2001), 311-337.

[8] Zongming Guo and Xingxiao Li. Solutions with isolated point ruptures for a semilinear elliptic equation in $\mathbf{R}^2$ with a non-Lipschitz nonlinearity, Appl. Math. Lett., 5(2004), 519-526.

[9] Ke Li, Hongxia Guo and Zongming Guo. Positive singular rupture solutions to a semilinear elliptic equation, Appl. Math. Lett., 18(2005), 1177-1183.

[10] Zongming Guo. Some existence and multiplicity results for a class of quasilinear elliptic equations. Nonlinear Anal. 18 (1992), 957-971.

[11] Zongming Guo and Zuodong Yang. Structure of positive solutions for a class of quasilinear elliptic equations when a parameter is small. Chin. Ann. Math., 19A(1998), 385-392.

[12] Zhoujin Cui and Zuodong Yang. Positive singular rupture solutions to a class for quasilinear elliptic equations, Appl. Math. Comput., 188(2007), 399-405.

[13] Huiqiang Jiang, Attou Miloua. Point rupture solutions of a singular elliptic equation, Electron. J. Differ. Eq., Vol.2013(2013), 1-8.

[14] Gidas B, Ni W M, Nirenberg L. Symmetry and related properties via the maximum principle. Comm Math Phys, 68(1979), 209-243.

[15] R. Kichenassamy and J. Smoller. On the existence of the radial solutions of quasilinear elliptic equations, Nonlinearity, 3(1990), 677-694.

Advanced Materials Research Vols. 989-994 (2014) pp 1833-1836
© (2014) Trans Tech Publications, Switzerland
doi:10.4028/www.scientific.net/AMR.989-994.1833

Application of Ant Colony Algorithm to the Hierarchical Routing in Wireless Sensor Networks

Lei Sang [1,a], Duo Long[2,b]

[1]Department of Information Engineering Jilin Business and Technology College, Changchun, China

[2]School of Mechanical and Electrical Engineering, Changchun University of Science and Technology, Changchun, China

[a] sang_lei@sina.com, [b]longduo7113@126.com

Keywords: Wireless sensor network; routing protocol; ant colony algorithm

Abstract. Wireless sensor networks (WSN) have become a hot research topic in the field of computer science. Since WSNs are characterized by limited node energy, dynamic topological structure and data fusion, the design of WSN routing protocols is faced with new problems and challenges. In recent years, many new routing algorithms for wireless sensor networks have appeared, but they all have some shortcomings. This paper studies and analyzes these routing protocols, and in view of their shortcomings, proposes a WSN hierarchical routing protocol based on ant colony algorithm. And a simulation test is conducted on this improved routing protocol, and the simulation result proves that this algorithm basically achieves the design objectives of WSN routing algorithms.

Introduction

Routing protocols play an important role in WSN communications, and currently focus on the network layer and the link layer. Routing algorithms have become a core technology of wireless sensor networks. Based on the WSN features, a WSN routing protocol should take energy efficiency as the primary goal. Ant colony algorithm is a heuristic, intelligent, evolutionary algorithm that simulates the behavior of ants searching for food, and suitable for solving complex combinatorial optimization problems. The application to WSN routing problems shows that ant colony optimization algorithm has excellent global optimization performance.

Wireless sensor networks and routing protocols

1. WSN system architecture and features

WSN is composed of sensor nodes, Sink nodes, wireless communication network and end users. The nodes are randomly deployed and organized by themselves into a network. Data information is sensed, processed by sensor nodes and transmitted through the hop transmission mode to Sink nodes, and then through the network to remote end users. WSNs have large scale, multiple routes and limited capabilities of senor node and, are self-organizing, dynamic and data centric.

A node comprises an energy module, a perception module, an information processing module, a storage module, a data transmission module and a software module. Since nodes have limited energy, the nodes running out of power cannot work. Therefore, low power consumption electronic devices and effective energy control methods should be used as many as possible to extend the lifetime of a network. The design of routing protocols is also centered on energy efficiency.

2.WSN routing algorithms and features

Routing algorithms play a significant role in WSN routing protocols, determine the data transmission route and influence the performance of the routing protocols. WSN routing algorithms should be concise, energy-saving, extensible, and have strong robustness and fast convergence. In terms of network topology, routing protocols can be divided into flat routing protocols and hierarchical routing protocols. The hierarchical routing has low and uniform energy consumption, is capable of reducing communication and storage overhead and the impact incurred by the change in the network topology, and has convenient and effective communication among and management of

cluster nodes. These advantages make hierarchical algorithms a hot research topic in the current studies on WSN routing protocols.

3. Representative WSN hierarchical routing protocols

(1)LEACH protocol is the first hierarchical routing protocol. It adopts periodic election of cluster head to balance the energy consumption of nodes and extend the life cycle of the network. With the hierarchy, data transmission is controlled within the clusters, and through data aggregation and fusion, the cluster heads which are elected in a distributed way can reduce the energy consumed by node data transmission. The intra-cluster nodes can close the transceivers to prevent unnecessary interception, hence increasing by 15% of the life cycle of the network. However, the more the total nodes in application, the more the cluster heads and the farther away the cluster head is from the base station and the faster the energy consumption of the cluster head is, which seriously influences the coverage and lifetime of the network. Therefore, LEACH algorithm is not applicable to the sensor networks with large coverage area.

(2)PEGASIS protocol is developed on the basis of LEACH protocol. It reduces the transmission times and data volume to the base station or the sink nodes, that is, it has more reasonable deployment of nodes and better data fusion. All nodes send and test broadcast signal and then detect the responses to determine the nearest nodes and know about their positional relations, which ensures the optimal links and low power consumption of the entire network. However, this protocol has low communication efficiency and longer time delay, especially in the case of a large number of nodes. Furthermore, this algorithm only considers the distance between the neighbor nodes, and ignores such factors as the node energy and the overall energy consumption of the network.

(3)GAF protocol is one in which the network area is divided into a number of virtual cells on the basis of the location information of nodes. Each cell is a cluster, in which a cluster head is elected regularly. The node serving as the cluster head is in active state, while the rest nodes go to sleep. The sleeping nodes have their own timers, and once the sleeping time is up, they convert from the sleep state into the active state and vie for cluster head. GAF algorithm features the division of clusters based on the virtual cells, but it considers that the nodes are in the same physical horizontal plane, and does not take into account that the adjacent distance between the nodes of the actual network does not means the direct communication between the nodes.

It can thus be seen that a hierarchical algorithm is composed of the generation of cluster heads, the formation of clusters and the routes of clusters. The generation of cluster heads serves as the basis of the formation of clusters, and the routes of clusters, i.e., the data transmission of clusters depends on the structure of the clusters. These closely-related three parts are the key to the design of WSN hierarchical routing protocols.

Ant colony algorithm is suitable for a dynamic environment and good at local work; it can optimize various parameters and support multiple routes; the simple individual behavior of the ant colony agrees with the limited capability of sensor nodes. These features account for the favorable applicability of ant colony algorithm to WSNs.

Design of IACH hierarchical routing protocol based on ant colony algorithm

1. Core thought

Based on PEGASIS and LEACH protocols and with reference to their advantages, this paper puts forward a hierarchical routing protocol based on ant colony algorithm, whose core thought consists of the following three points:

(1) To replace the greedy algorithm in PEGASIS algorithm by the improved ant colony algorithm to construct chains.

(2) To avoid long chains and use LEACH algorithm for clustering and form chains within the clusters.

(3) To use the improved ant colony algorithm to form a chain again among the cluster heads which are obtained by LEACH algorithm; data are sent by the chain head to the base station.

2. Concrete steps

(1) The cluster head nodes are elected according to LEACHalgorithm and, other nodes join in the clusters;

(2) The intra-cluster nodes are constructed into a chain according to the improved ant colony algorithm and, the chain begins with the node with the highest remaining energy;

(3) Intra-cluster data are transmitted from the node farthest away from the cluster head and to the cluster head through infusion and forwarding;

(4) The cluster head extends the node chain, fuses again the data it has received and collected, and then sends the data after being fused by the chain head node to the base station;

(5) After a round of communication is over, the above steps are repeated to achieve energy consumption balance for the nodes of the network.

3. Communication model

(1) Assumed conditions

Assuming that a wireless sensor network comprises N sensor nodes, which are deployed randomly in a vast region to periodically collect data, the sensor nodes and the underlying network model are as follows:

① The base station is located beyond the monitored region. Take an apex of the rectangular region as the origin of coordinates, and the two sides this apex is on as the coordinate axes, establish a coordinate system, and the rectangular region is in the first quadrant;

② The base station has strong computing and storage capabilities and its energy can be supplemented;

③ All sensor nodes are static and have the same primary energy and communication capacity; they die after their energy runs out;

④ The communication radius of the nodes can be changed, that is, their wireless transmit power can be adjusted.

(2) Communication model

The wireless communication model is given a threshold value. When the distance between the sending node and the receiving node is less than d_0, the energy loss of the sending node in sending the data is proportional to the square of the distance, otherwise it is proportional to the biquadrate of the distance. These two different energy loss models are called the free space model and the multiple attenuation model respectively. Therefore, based on the distance between the sending node and the receiving node, different energy consumption models can be used to calculate the energy needed for sending the data. For the transmission of L bits of data to the location with distance d, the energy consumed by a node is composed of the transmission circuit loss and the power amplification loss,

$$\begin{aligned} E_{Tx}(L,d) &= E_{Tx-elec}(L) + E_{Tx-amp}(L,d) \\ &= \begin{cases} lE_{elec} + L\varepsilon_{fs}d^2 & d < d_0 \\ lE_{elec} + L\varepsilon_{mp}d^4 & d \gg d_0 \end{cases} \end{aligned} \quad (1)$$

$E_{Tx-elec}$ is the energy consumed by starting the wireless transmission circuit, E_{Tx-amp} is the energy consumption of the amplifier, and E_{elec} is the energy loss of the transmission circuit. If the transmission distance is less than the threshold value d_0, the power amplification loss adopts the free space model; if the transmission distance is equal or more than the threshold value d_0, the multiple attenuation model is adopted. ε_{fs}, ε_{mp} are the energy consumed by power amplification in these two models.

The energy consumed by the node receiving L bits of data:

$$E_{Rx}(L) = lE_{elec} \quad (2)$$

Data fusion also consumes some energy. E_{DA} refers to the energy consumed by fusing the data per bit. Assuming that the data collected by the adjacent nodes have high redundancy, and the cluster head can fuse the data of its members into a data package with fixed length and then send it to the base station.

The threshold value d_0 is determined by the following equation:

$$\boldsymbol{d_0 = \sqrt{\varepsilon_{fs}/\varepsilon_{mp}}} \quad (3)$$

Simulation analysis based on IACH algorithm

NS2 is the acronym of network simulator, and is essentially a discrete-time simulation system (DES). Its major function is to simulate the information transmission between the nodes of the actual network, and to guide the development of network protocols with the useful conclusions drawn based on the analysis of the simulation results. LEACH, PEGASIS and IACH protocols are simulated and their performances are compared in NS2. The nodes in the simulation are distributed in the 200m× 200m region, and the coordinates of the base station is (100,400).

A sensor node dies when its energy is zero. The number of the surviving nodes can reflect the life circle of the network. First Node Died, Half Node Died, and Last Node Died are defined. The time table of the three protocols in simulation is shown in Table 1.

Table1Network lifetime table

Protocol	First Node Died	Half Node Died	Last Node Died
LEACH	87	92	109
PEGASIS	169	203	234
LACH	209	251	291

It can be seen that the first node death time, the half node death time, and the last node death time of IACH protocol, are much higher than those of LEACH and PEGASIS protocols, and thus IACH protocol is highly effective.

Conclusion

This paper analyzes the features of wireless sensor networks, elaborates the features and classification of WSN-based routing protocols, and studies the advantages and disadvantages of several representative routing protocols. Then it introduces ant colony algorithm into the design of WSN hierarchical routing protocols, puts forward some improvement strategies, and builds a transmission model to conduct simulation and comparative analysis. The simulation and analysis results prove the effectiveness of this protocol in extending the network life cycle and reducing energy consumption.

Acknowledgements

The authors gratefully acknowledge the fund of this study by Jilin province science and technology department soft science research project（20130420026FG）"Study of Jilin province engineering and technology talent support for strategy emerging industry" and the Jilin province talent development project in 2013 (20131079) and the Jilin Province Department of Education research project (2012366).

References

[1] S. Soro, W. Heinzehnan, Prolonging the lifetime of Wireless Sensor Networks via Unequal Clustering. In Proceedings of the 19th IEEE International Parallel and Distributed Processing Symposium(IPDPS).2011.

[2] M. Ye, J. Wu, EECS: An Energy Efficient Clustering Scheme in Wireless Sensor Networks. In Proceedings of IEEE Int'1 Performance Computing and Communications Conference (IPCC)2012. PR1388—1397.

[3]P. Mohapatra, J. Li, Analytical modeling and mitigation techniques for the energy hole problem in sensor networks. Pervasive Mobile Computing, v01, 3, no.3, PP.233-254, 2011.

[4] T. Camilo, C. Carreto, An Energy-Efficient Ant-Based Routing Algorithm for Wireless Sensor Network. Lecture Notes in Computer Science, Springer, 2012.

Advanced Materials Research Vols. 989-994 (2014) pp 1837-1840
© (2014) Trans Tech Publications, Switzerland
doi:10.4028/www.scientific.net/AMR.989-994.1837

Study on the Optimization of Data Mining in Big Data

Gang Xin [1, a], Hui Yan [1,b]

[1] Department of Information Engineering,Jilin Business and Technology College,Changchun,China

[a] xingang@jlbtc.edu.cn, [b] yanhui7125@126.com

Keywords: Big Data , Weka, Kmeans, Data Mining

Abstract. This paper proposes an analysis measure for Big Data by optimizing traditional data mining, base on Weka data analyzing platform，K-means algorithm is employed through the interface programs in Weka system, so that optimized data mining techniques can be applied in cloud storage, cloud computing of Big Data by clustering analysis base on Big Data pre-processing and real-time monitoring of memory.

The bottle-neck in analyzing of Big Data

Large quantities of data are stored in the data of companies and government agencies, but the value of the data is not brought into full play. The lack of effective data integration and data analysis, data mining techniques and methods are the main technical obstacles, but the underlying reasons are the lack of recognition of the potential value of data and the lack of effective methods to extract the value of data.

(1) Big Data figures

Big data is characterized by "3V", i.e., variety, volume and velocity. The data mining methods have bottlenecks to enhance the abilities of analyzing, users must improve the performance of servers, including storage, memory and CPU, which causes the continuous increase in machine cost and power consumption. Currently, the majority of data analysis and mining software are not capable of complex analysis and modeling of Big Data which are no less than terabytes (TB), because such big data exceed the management ability of traditional databases.

With the deeper understanding of the value of big data, another typical feature—value dimension is added, which is used to describe the value of big data. In practical applications, the large-volume data are not necessarily of great value. For example, important analysis and mining cannot be carried out on lots of data before they are effectively integrated, so these data do not have great value. However, data integration itself is a big challenge for big data.

(2) Big Date challenges on traditional date mining

The objects of big data analytics have more and more attributes. Although there are more and more information in the expressed objects, thousands of attributes also result in huge dimensions. Furthermore, the high-dimension data bring about other problems, such as complex data type, noise and default value and unbalanced distribution. Traditional total space method is not suitable for the analysis of high-dimension data, because this kind of data has great sparsity and, the expression of object cluster and class is embodied in some attribute subsets. The effective method is the subspace method. In addition, due to the complexity of data, it is hard for single data mining models, such as the decision tree model, to meet the accuracy requirements of applications. Therefore, the ensemble method of multiple models must be adopted to build a cluster or classification integrating model so as to make the final decision based on the comprehensive results of multiple single models. In analysis, if the rows of the object attribute matrix are more than ten million or a hundred million, the data volume of the whole matrix will reach hundreds of GB or TB. Such huge quantities of input data exceed far beyond the memory of most servers, let alone to model and mine the data on a single server with complex iteration or recursion mining algorithms. Therefore, the existing data mining software and most traditional classification and clustering algorithms cannot handle the data of this scale.

Design of data mining for analyzing of Big Data

Data mining is a process of extracting unknown knowledge with potential value from a data. The current modeling method of data mining is a three-step method, which is composed of sample– > modeling– > testing. The modeling is completed automatically by the algorithm and after the model is built, it will be tested by the user. If the test result is not satisfactory, training data and the algorithm parameters will be changed and a new model will be created by the improved algorithm. This method is not applicable to big data analytics, because big data have huge volume, many attribute parameters, cost longer modeling time, and the modeling result is often unsatisfactory.

In the work environment of the Weka system, this paper attempts to use the internet technology to realize cloud storage and cloud computing, and to optimize the original distributed mining algorithms, and manage mining algorithms, distributed and parallel databases through the visual system data preprocessing and the real-time memory monitoring. Through the interface document in the Weka system, K-means algorithm is integrated into this data mining platform to improve traditional data mining techniques so as to realize the analysis of big data. Fig. 1 shows the structural design.

Weka integrates multiple mature data mining algorithms, and provides the interfaces associated with the database system. With its open nature and Java-based cross-platform, Weka has become an important platform for learning and applying data mining algorithms.

Weka is a collection of machine learning algorithms for data mining tasks. The algorithms can eit her be applied directly to a dataset or called from your own Java code. Weka contains tools for data pre-processing, classification, regression, clustering, association rules, and visualization. It is also w ell-suited for developing new machine learning schemes。

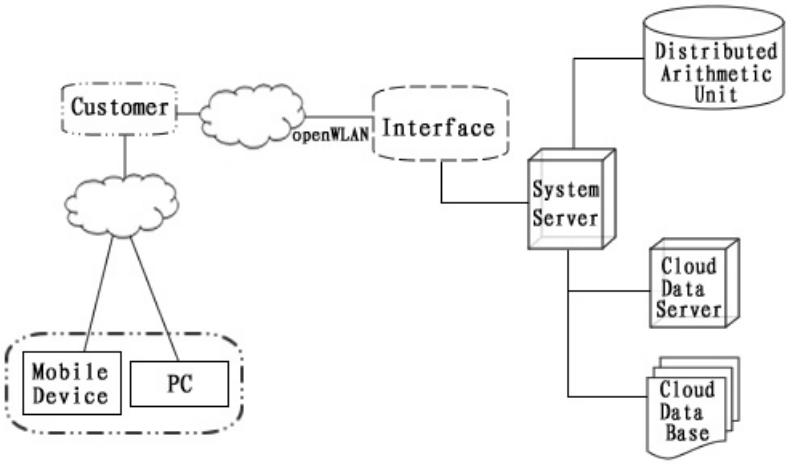

Fig1. Structure Diagram of Big Data mining Base on Weka Platform

Through the external interface of the system, users can input the big data to be analyzed from mobile devices and PC into this platform server. The big data will first be compressed and refined through the algorithm library of Weka platform and K-means clustering integration, and then analyzed by the dynamic expert intelligent system provided by the cloud data server and cloud data storage.

When the optimized data mining system mines in the item set with frequent association rules, the memory runs out obviously, and thus needs to be monitored in the operation of the design system. When the memory runs out, the original dataset needs to be decomposed and the decomposed datasets are mined. Finally, the mining results are merged to produce the final result. The working interface is shown in Fig. 2.

Integration of K-means clustering algorithm in Weka system

In the design working platform, a series of optimization is conducted on the traditional data mining algorithms and the core content is to analyze big data. Big data contain enormous association rules

and, if mined blindly, not only is the mining efficiency low, but lots of irrelevant rules may be found and many rules cannot be put to good use. In addition, data mining and knowledge discovery are hard and meticulous work, only the strict control of application scale can secure good effects in practical applications. The use of clustering to preprocess the data can help obtain the basic information of the data. If the original dataset is too big to be read into the memory for clustering at one time, the data in the dataset can first be recognized and then some data are generalized, or sample data can be used to represent the original dataset and clustering is conducted on the sample dataset. These two methods can realize the clustering of large-scale datasets and reduce the memory space occupied by the data. Feature extraction or classification based on this clustering improves its accuracy and mining efficiency. The clustering results can also be used for further association analysis to obtain more useful information. The realization of K-means algorithm integration through the interface program in the Weka system enables the effective application of traditional data mining techniques to big data analytics.

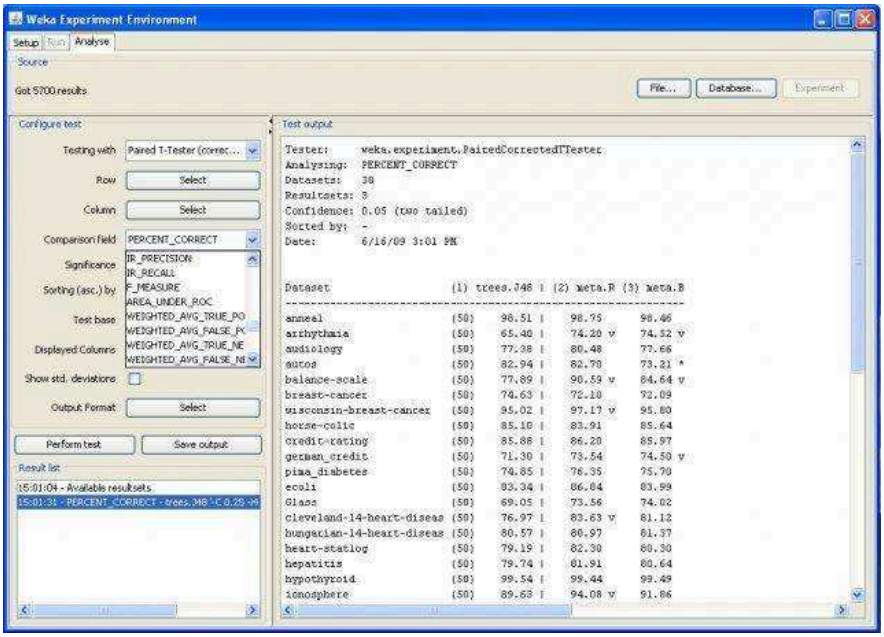

Fig2. Working interface of Weka platform

K-Means is a segmentation clustering method and its main aim is to find out representative data points from large quantities of high-dimensional data points. These representative data points can be called cluster centers, or representative points, according to which the subsequent processing is conducted. As is shown in Figure 3, this system operates as follows: firstly, some data points are read from the original large-scale dataset (random sampling can be used); secondly, these data points are read into the memory; thirdly, the data in the memory are clustered and the clustering model is updated; fourthly, the data points in the memory are recognized and differentiated according to this updated clustering model; Fifthly, the corresponding data are compressed and refined through the visual Weka platform and then clustered again. That is to say, K cluster centers are given and the sample points to be classified are allocated to the clusters according to the nearest neighbor principle; the average method is used to recalculate the centroid of each cluster to determine the new cluster center. The iteration continues until the displacement distance of the cluster centers is less than the given value. Then the update of the clustering model is ended and the results are output. This algorithm requires one scanning of the original dataset at most to finish the clustering process. If the original dataset is very large, the scanning will consume many resources. However, if the clustering model is discovered in advance, this algorithm can cut the clustering process short without scanning the whole dataset. This algorithm can reflect the features of the on-line clustering and conduct real-time clustering on the dataset and obtain the best clustering result. This algorithm can easily provide the clustering progress, time remaining and other information. When the memory space is not

stable, such clustering tasks as suspension, stop and restart can be easily performed, and incremental clustering can be conducted on the new data on the basis of the existing clustering results.

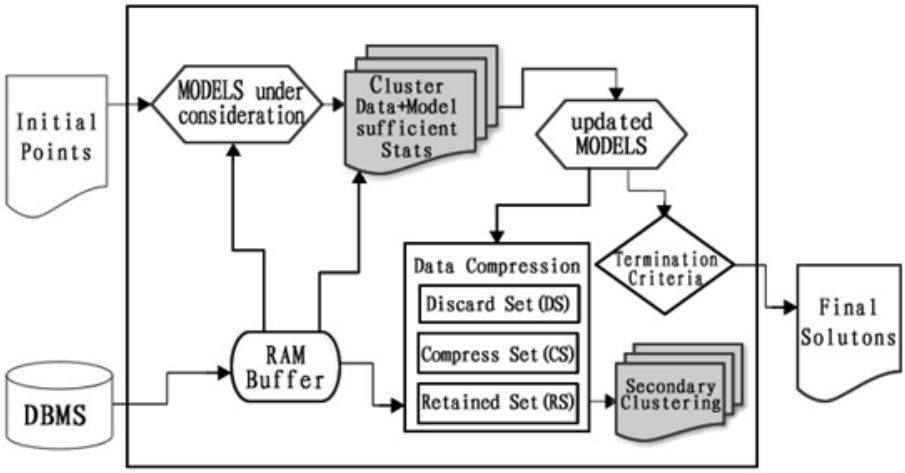

Fig 3 The main frame of k-means algorithm

Conclusions

In the Weka working environment, to use K-means algorithm for clustering analysis and ensemble can conduct the preprocessing of big data analytics and the real-time monitoring, and thus extends the traditional data mining techniques to the level of cloud storage and cloud computing. This algorithm can cluster large-scale datasets in the very low memory space and adopt various methods to read the original datasets, such as random sampling, sequential reading. It can use the cursor which only supports rolling forward to read the original datasets, which solves such problems of the cursor as the back-and-forth rolling, random positioning and more consumption of system resources. This is also important for the clustering of large-scale datasets. The further development of this optimized system will focus on in-depth studies on cloud storage and cloud computing.

Acknowledgements

The authors gratefully acknowledge the fund of this study by Jilin province science and technology department soft science research project（20130420026FG）"Study of Jilin province engineering and technology talent support for strategy emerging industry" and the Jilin province talent development project in 2013 (20131079) and the Jilin Province Department of Education research project (2012366).

References

[1] Hui Yan,Haiyan Hu. Design and Realization of Innovation and entrepreneurship Service Platform for Undergraduates Based on Big Data[J]. ITMI2013. 2013.7: 394~397.

[2] Xiaojun Chen, Xiaofei Xu, Yunming Ye, etc. TW － k － means: automated two － level variable weighting clustering algorithm for multi － view data[J]. IEEE Transactions on Knowledge and Data Engineering，http: / /doi. ieeecomputersociety. org /10. 1109 /TKDE. 2011. 262.

[3] Xiaojun Chen,Yunming Ye,Xiaofei Xu etc. A feature group weighting method for subspace clustering of high － dimensional data[J]. Pattern Recognition,2012,45(1) : 434－446.

[4] Bingguo Li,Xiaojun Chen,Mark Junjie Li,etc. Scalable random forests for massive data[C]. PAKDD,2012.

[5] Baoxun Xu,Joshua Zhexue Huang,Graham Willams,etc. Classifying very high － dimensional data with random forests built from small subspaces[J],International Journal of Data Warehouse and Mining,2012,8(2) : 45－62.

Advanced Materials Research Vols. 989-994 (2014) pp 1841-1844
© (2014) Trans Tech Publications, Switzerland
doi:10.4028/www.scientific.net/AMR.989-994.1841

Design and Implementation of Instruction Expert System Based on Improved Genetic Algorithm

Wu.DaQin[1, a], Wang.Shanshan[2,b]

[12] Department of Information Engineering,Jilin Business and Technology College, Changchun, China

[a] liulan2003@sina.com, [b]15266615@qq.com

Keywords: Expert System; Genetic Algorithm; Intelligent analysis; B/S.

Abstract. In this paper, the author designed the model of instruction expert system based on improved genetic algorithm and described the realization of improving exercises in detail. In this system, the students can online learn through different modes and receive the guidance from the teacher, meanwhile the analysis to effect the parameter of intelligent tests generating will be produced. So the following exercises focus on the student's weakness, this is useful to enhance the students' the knowledge level and operation ability.

0 Introduction

With the rapid development of network technology, the platform of engineering education has already expanded to rich resources and constantly updated web space. The instruction mode has been converted from the traditional tuitional teaching to the diversified teaching of network independence and exploring type. In this paper, the author designed the model of instruction expert system based on improved genetic algorithm, by which students can independently study on-line through intelligent guidance, so as to improve the students' knowledge level and operation ability.

1 Design of Instruction Expert System

1.1 Structure of Instruction Expert System

Expert system is an intelligent computer program system. There are a large of domain knowledge and experience in expert level inside and it can solve the problems in this field using the knowledge and methods used by human experts to solve problems. The system adopts B/S structure. There are four kinds of identities setted for login in the system, namely student, administrator, teachers and expert. The different identity makes the user own imparity permission and shoulder distinct responsibility. The independent study module of student (ISM) and the expert system module (ESM) make up the instruction expert system, that is shown in Figure 1.

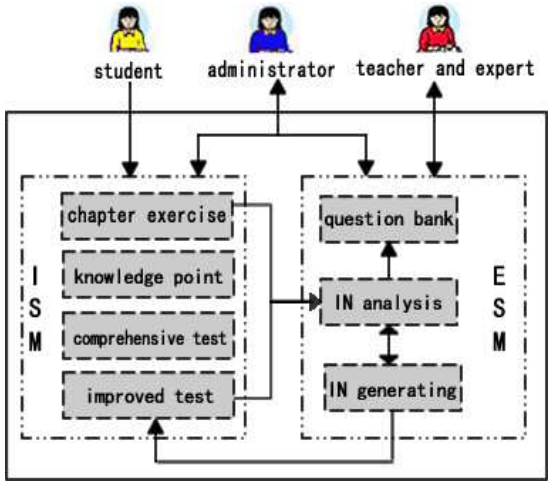

Figure 1. Structure of Instruction Expert System

1.2 ISM and ESM

Four pattern can be provided in ISM module when the student logins. He may select the pattern to exercise or test from chapter exercise, knowledge point exercise, comprehensive test and improved test. The performance will be evaluated by the system and be sent to the other module for intelligent analysis. ESM module includes three parts, namely question bank, intelligent analysis, and intelligent tests generating. The intelligent analysis module gives results based on the score of the student. The system modified the parameters and constraint condition of intelligent tests generating, so that increase the weight of error questions in upcoming study for improving learning efficiency.

2. Module Research of Intelligent Test Generating

Intelligent test generating module will produce the questions based on constraint condition in question bank. In other words, filtering for the question should be proceeded according to the properties. These are variable with the situations of the students' error rate and degree of difficulty. For a certain test, the module generates a exam paper with n questions, then five properties that can form a matrix for n*5 are ascertained, as shown in Table 1 and Table 2.

Table 1. Constraint Condition

Condition	Annotation
Number	Number in question bank
Queseion Type	Choice、Blank、Judge、Programe
Degree of Difficulty	d=1-avg/sum
Error Rate	t=error/sum
Score	This question's score

Table2. Properties Matrix

$$S=\begin{bmatrix} a11 & a12 & a13 & a14 & a15 \\ a21 & a22 & a23 & a24 & a25 \\ \cdots & \cdots & \cdots & \cdots & \cdots \\ an1 & an2 & an3 & an4 & an5 \end{bmatrix}$$

3 Design of Instruction Expert System

3.1 The structure of genetic algorithm

Genetic algorithm is a search optimization algorithm based on biological simulation genetics and natural selection. The evolution process starts from initial population, determines fitness function, according to the assesses the fitness of each test case after the execution procedures. The higher fitness is the closer between test cases and the expected effect. Improve the test cases with crossover, mutation and choice- three basic operations. Evaluate the fitness function. The process will be over until the result is closest to the best expectation. Aiming at the specific situations of intelligent question grouping, we provide the following concrete improved solutions.

3.2 Determining coding scheme

The GA coding strategies have great impacts on genetic manipulation, and in many cases the coding forms determine genetic manipulation. Coding strategies shall basically meet three standards, namely completeness, soundness and non-redundancy. On this basis, when selecting test questions, we adopt the coding strategy of binary grouping to quickly selecting questions and reduce redundancy rate. In other words, the whole binary string is divided into different functional modules according to question types, and every functional module adopts independent binary coding.

3.3 Setting initial population

Question selecting is a restricted problem with multiple constraint objectives. In order to enhance the efficiency of GA and reduce the time for question selecting, we no longer use traditional GA to generate initial population randomly. Instead, we make initial population P_0 meet such constraint conditions as question types, total points of test paper and quiz time, which is in favor of enhancing the efficiency of question selecting.

3.4 Constructing fitness function

Fitness is an important indicator for describing individual performance in GA, while GA selects the superior and eliminates the inferior towards individuals according to fitness. Fitness function is used to evaluate the degree of excellence of individuals in a population and guide GA to finally find out the functions of the test data that cover the prescribed route. In the question selecting problem, according to every constraint condition, the objective function is defined as follows: $f=\sum_{i=1}^{5} f_i w_i$ .f_i stands for the absolute value of the error between i^{th} property indicator and user requirements, w_i stands for the weight of the i^{th} indicator on the degree of question, $w_i>0$, and f is the sum of the absolute value of the error between all indicators and user requirements. It can be seen from the above objective function that this problem is about optimization of minimum value. After the objective

function is changed appropriately, fitness function can be defined as: F= $\frac{1}{1+f}$ .If this fitness function is used to judge individual performance, then the smaller the error of individual's constraint condition towards question selecting is, the greater the fitness value will be and the better the individual performance will be; on the contrary, the greater the error of individual's constraint condition towards question selecting is, the smaller the fitness value will be and the worse the individual performance will be. In the process of evolution, adjusting fitness is fitness function scaling. We adopt exponential function scaling strategy, and after scaling the fitness function is: F'=exp(-βF).

3.5 Genetic operators

GA includes three basic genetic operators: selection operator, crossover operator and mutation operator. The operation methods or operation strategies of GA vary along with specific problems. In this problem, the genetic operators are mainly constrained by the following two conditions:

1) Coding strategies: we adopt the coding strategy of binary grouping in this paper;

2) Constraint conditions: we have meet part of constraint conditions when forming the initial population, such as the total points of test paper and proportion of question types. Genetic operators cannot break these already-met constraint conditions in the genetic process.

By the above two constraint conditions, genetic operators can be improved as follows:

Probability method that is proportional to fitness value is used to choose selection operators. The specific steps are: first, calculating the sum total ($\sum$f) of all fitness values in the population; then, calculating the proportion(fi/ $\sum$ f) of every individual's fitness value and taking it as the corresponding selection probability to figure out whether every individual has been selected.

For crossover operators, one-point crossover is adopted, so crossover can be done in same question types. In other words, a cross point is chosen according to the crossover probability, and only the segment where this point is located can be crossed. For example, in the crossover process of the two individuals below, A and B are the two individuals before crossover, A' and B' are two individuals after crossover, and it is supposed that the cross point is the second one on the second segment.

A =0101…|1110…|0110…|… B =1001…|0011…|1000…|…

A′=0101…|1011…|0110…|… B′=0101…|0110…|1000…|…

For mutation operators, we choose two-point mutation method, that is, to generate a mutation position according to the mutation probability, choose an inverse position from the beginning of this mutation segment and then exchange these two positions. In the following individual mutation process, one mutation position generated by the mutation probability is the third one on the second segment. A is the individual before mutation, and A′is the individual after mutation.

A=0101…|1010…|0110…|… A′=0101…|1100…|0110…|…

3.6 Determining Controling Parameters

Population size affect the final result and execution efficiency of genetic algorithm. When n number is small, the convergence speed will be fast, but it isn't easy to search the optimal solution. However if n number rises, the convergence speed will drop and the computational will be complicated. So n is from 10 to 160.

In this paper, fitness is used to measure the crossover probability and mutation bribability of self-adaptive adjustment of population diversity. The basic idea concerning self-adaptive GA operation is to make the crossover probability pc and mutation probability pm adjust at any time according to the real situations of the population during evolution. When individuals tend to be convergent, we should increase pc and pm, that is, to increase the probability of crossover and mutation to undermine the present stability and overcome premature convergence; when the individuals tend to be divergent, we should decrease pc and pm, that is, to reduce the probability of crossover and mutation to make the individuals convergent.

The self-adaptive crossover probability and mutation probability we adopt are as follows:

$pc=0.8\exp(-f/f_{avg})$……$f\geq f_{avg}$ $pc=0.8$……$f<f_{avg}$

$pm=0.01\exp(-f'/f_{avg})/f_{max}$……$f'\geq f_{avg}$ $pm=0.01$……$f'<f_{avg}$

favg：average fitness，f：two crossers fitness，f′：mutant fitness

Obviously fitness is used as the criterion for measuring the population diversity so as to make crossover probability and mutation probability automatically change along with the fitness. When the difference in individual fitness in a population is relatively small, we should increase crossover probability and mutation probability; when the individual fitness in a population is relatively divergent, we should decrease crossover probability and mutation probability.

Three termination conditions are adopted for question selecting in this paper: when the optimal solution is searched out; when the frequency of execution is reached; When the change rate of the maximum fitness value of two generations is less than the specified value, it can be regarded that population evolution is stable, tends to be convergent and terminated.

3.7 Experiment Analysis

In experiment，there are 600 questions containing four types of questions in bank. The parameters of GA: n=80, pc=0.8, pm=0.1, D=500, FS=100, Time=120.The results of two algorithms are shown as Fig.3. The conclusion can be drawn that the convergence of the improved genetic algorithm is more perfect and stable. Meanwhile the improved algorithm can guarantee the diversity of individuals and global search ability.

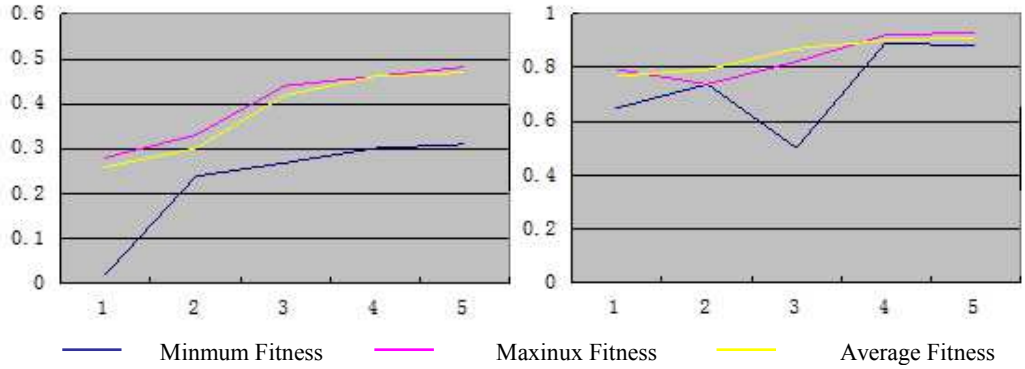

Fig.3 Comparision of simple GA and improved GA

Summary

In this paper, the author designed the model of instruction expert system based on improved genetic algorithm and described the realization of improving exercises in detail. Especial through comparing the simple genetic with the improved genetic, the conclusion can be drawn that the intelligent tests generating module may generate the question efficiently. So the following exercises focus on the student's weakness, this is useful to enhance the students' the knowledge level and operation ability. The research is still needed to make the automatic evaluation of various types of project design more accurately and efficiently.

Acknowledgements

This work was financially supported by Jilin Province Educational Science topics " The Research and Realization of Self-help Building Website Platform Based on Saas" (2013399) and "The Tutorial Expert System For Computer Rank Examination Based on AI Technology"(2013542).

References

[1] CS Yeo, MD de Assuncao.Computing and Global Grids. GridComputing and Distributed Systems Laboratory, The University of Melbourne, Australia, April 13, 2006

[2] Chen Yabing: Design of Consultion System Based on KB. Computer Engineering, 2007,33(16).

[3] Liu Z.System integration control of HVAC in intelligent building[J].Proc of ICMLC 2004

[4] Wang XP.Generic Algorithm[M].XiAn：Xi'an Jiaotong University Press, 2002

[5] Armbrust M. Above the clouds:A Berkeley view of cloud computing 2010

Advanced Materials Research Vols. 989-994 (2014) pp 1845-1848
© (2014) Trans Tech Publications, Switzerland
doi:10.4028/www.scientific.net/AMR.989-994.1845

Investor Selection Model under Uncertain Information Environment

Congjun Rao, Cheng Wang

College of Mathematics and Physics, Huanggang Normal University,

Huanggang 438000, China

cjrao@163.com

Keywords: Investor selection; Dual uncertainty information; Fuzzy grey number; Fuzzy grey deviation degree

Abstract. In this paper, the problem of selecting investor is studied under dual uncertainty information, i.e. fuzzy information and grey information. Concretely, a new index system of evaluating the investors which includes sales capacity, management capacity, throughput, technology capacity, fund capacity, risk capacity and uniformity of enterprise strategy is designed, and then a model of dual uncertainty multi-attribute decision making is proposed. Moreover an optimization algorithm of fuzzy grey deviation degree is present to solve this model.

Introduction

With the high development of economy, more and more people become self-employed worker. There are many people start a company independently. So to select the right investors is the key to business success for the self-employed worker. When selecting the investors, some attributes must be consided such as sales capacity, management capacity, throughput, technology capacity, fund capacity, and so on. But there are many uncertainties in the problems of decision making of selecting the investors because of the complication of the decision making systems. Oen the one hand, in practical decision making, the attribute variable of sales capacity, management capacity, et al. are usually given in the forms of linguistic fuzzy variable, such as “worst, worse, bad, common, good, better, best” or “lowest, lower, low, common, high, higher, highest ”[2-4] by the decision makers. We called this kind of uncertainty is subjective uncertainty, i.e. fuzzy information. One the other hand, due to some differences in knowledge frame, experience level, status and individual preference for the decision makers, there exist incomplete and inadequate information in the decision making problems, so the attribute values given by decision makers have a certain grey degree (Grey degree is the measurement to measure the insufficiency or unlikelihood of information [8]). We called this uncertainty is the objective uncertainty, i.e. grey information. Therefore, when we select the investors, we must consider not only the fuzzy information but also the grey information. So we can transform the decision making problem of selecting the investors into a multi-attribute decision making problems with dual uncertainty information, i.e., fuzzy information and grey information.

Nowadays, some scholars studied the problems of multi-attribute decision making with the fuzzy information[2-12], but the study on the problems multi-attribute decision making with both fuzzy information and grey information is few. From this current situation, and by considering the practical problem of selecting the optimal investors, we presents a new model of dual uncertainty multi-attribute decision making and gives optimization algorithm of fuzzy grey deviation degree to solve this new model. Therefore, this paper provides a new and effective way to deal with the multiple uncertainties in the problems of multi-attribute decision making.

The Problem Statement

Suppose that self-employed worker of an investment corporation wants to select some optimal investors. There are m alternatives take part in the competition, the set of alternatives is denoted as $X = \{X_1, X_2, \cdots, X_m\}$. Now we choose the following seven attributes forms the evaluation index

system, i.e., Sales capacity (A1), Management capacity(A2), Throughput (A3), Techno-logy capacity (A4), Fund capacity(A5), Risk capacity(A6) and Uniformity of Enterprise strategy(A7). The set of attributes is denoted as $A=\{A_1,A_2,\cdots,A_7\}$. Let $W=(w_1,w_2,\cdots,w_7)$ be the weightvector of these seven attribute, where w_j satisfies $0\le w_j\le 1,\ \sum_{j=1}^{n} w_j=1$.

Let the evaluation value of alternative $x_i\ (i=1,2,\cdots,m)$ on attribute $A_j\ (j=1,2,\cdots,7)$ which given by decision maker is a linguistic fuzzy variable s_{ij}, such as "worst, worse, bad, common, good, better, best" or "lowest, lower, low, common, high, higher, highest "with the grey degree v_{ij}, it denoted as a fuzzy grey number $e_{ij}=[s_{ij},v_{ij}]\ i=1,2,\cdots,m$, $j=1,2,\cdots,7$. All the evaluation values $e_{ij}=[s_{ij},v_{ij}]$ forms the original decision matrix $R=(e_{ij})_{m\times 7}$. Now from the information of the original decision matrix $R=(e_{ij})_{m\times 7}$, we the self-employed worker need to make evaluation and rank order for all alternatives, and select the optimal investors among all alternatives.

The Model

In this section, we will presents a new model of dual uncertainty multi- attribute decision making and gives optimization algorithm of fuzzy grey deviation degree to solve this new model. Firstly, some definitions are given.

Definition 1 Let the set of information content be $I=$ {very sufficient, sufficient, common, imcomplete, very imcomplete}, and the measurement of information content is measured by grey degree, the quantization method is as follows[8]:

very sufficient: 0～0.1, sufficient: 0.2～0.3, common: 0.4～0.6,

imcomplete: 0.7～0.8, very imcomplete: 0.9～1

the determinate values of grey degree can be determined with the practical problems of decision making.

Definition 2 Suppose that $S_a=$ {worse, bad, common, good, better}([2]) or $S_b=$ { lower, low, common, high, higher}([3]), then S_a and S_b are called the set of linguistic fuzzy variable, they are denoted as $S_a=\{s_1,s_2,\cdots,s_5\}$, $S_b=\{s_1',s_2',\cdots,s_5'\}$, and their corresponding interval numbers are defined as follows:

(i) For the type of cost attributes, we have

s_1=(0.8, 1); s_2=(0.7, 0.8); s_3=(0.6, 0.7); s_4=(0.5, 0.6); s_5=(0.3,0.5);

(ii) For the type of revenue attributes, we have

s_1=(0.3,0.5); s_2= (0.5,0.6); s_3=(0.6,0.7); s_4=(0.7,0.8); s_5=(0.8,1);

the corresponding triangle fuzzy numbers for S_b are the same as S_a.

Definition 3 Let $\tilde{a}=[b,c]$ be a interval number with the grey degree v, $v\in[0,1]$, then $\tilde{e}=(\tilde{a},v)$ is called a fuzzy grey number. If $v=0$, then $\tilde{e}$ is a genera interval number, and if $b=c$, then $\tilde{e}$ is a general real number.

Definition 4 Let $\tilde{e}_1=([b_1,c_1],v_1)$ and $\tilde{e}_2=([b_2,c_2],v_2)$ be two fuzzy grey numbers, the algorithms for $\tilde{e}_1$ and $\tilde{e}_2$ are defined as follows:

1) $\tilde{e}_1+\tilde{e}_2=[(b_1,c_1),v_1]+[(b_2,c_2),v_2]=[(b_1+b_2,c_1+c_2),(v_1+v_2)\wedge 1]$;

2) $k\tilde{e}_1=[(kb_1,kc_1,kd_1),(kv_1)\wedge 1)]$, $k\ge 0$.

Definition 5 Let $\tilde{e}_1=([b_1,c_1],v_1)$ and $\tilde{e}_2=([b_2,c_2],v_2)$ be two fuzzy grey numbers, the distance from $\tilde{e}_1$ to $\tilde{e}_2$ is defined by

$$D(\tilde{e}_1,\tilde{e}_2)=\frac{1}{2}(|b_1-b_2|+|c_1-c_2|+|v_1-v_2|)$$

According to the above definitions, we can obtain the decision making matrix, it denoted as $\overline{Z}=([b_{ij},c_{ij}],v_{ij})_{m\times 7}$, $i=1,2,\cdots,m$, $j=1,2,\cdots,7$.

From the decision making matrix $\overline{Z}$, a new optimization algorithm of fuzzy grey deviation degree is given to rank order for all alternatives. The definition of fuzzy grey ideal solution is given in the following Definition 8.

Definition 6 Let $\overline{Z}=([b_{ij},c_{ij}],v_{ij})_{m\times 7}$ be a decision making matrix. Then $\overline{y}^{+}=(\overline{y}_1^{+},\overline{y}_2^{+},\cdots,\overline{y}_7^{+})$ is called a fuzzy grey positive ideal solution, and $\overline{y}^{-}=(\overline{y}_1^{-},\overline{y}_2^{-},\cdots,\overline{y}_7^{-})$ is called a fuzzy grey negative ideal solution, where

$$\overline{y}_j^{+}=([\overline{b}_j^{+},\overline{c}_j^{+}],v_j)=([\max_i b_{ij},\ \max_i c_{ij}\ ],\min_i v_{ij}), \tag{1}$$

$$\overline{y}_j^{-}=([\overline{b}_j^{-},\overline{c}_j^{-}],v_j)=([\min_i b_{ij},\ \min_i c_{ij}],\max_i v_{ij}), \tag{2}$$

Based on the distance from fuzzy grey numbers $\tilde{e}_1$ to $\tilde{e}_2$ in definition 5 and the fuzzy grey ideal solution in definition 6, we define the fuzzy grey deviation degree as follows.

Definition 9 Let $\overline{y}^{+}=(\overline{y}_1^{+},\overline{y}_2^{+},\cdots,\overline{y}_7^{+})$ and $\overline{y}^{-}=(\overline{y}_1^{-},\overline{y}_2^{-},\ \cdots,\overline{y}_7^{-})$ be the fuzzy grey positive ideal solution and fuzzy grey negative ideal solution, respectively, and let $\overline{Z}_i=(\overline{z}_{i1},\overline{z}_{i2},\ \cdots,\overline{z}_{i7})$ be the i-th alternative point, where

$$\overline{Z}_i=(\overline{z}_{i1},\overline{z}_{i2},\cdots,\overline{z}_{in})=(([b_{i1},c_{i1}],v_{i1}),([b_{i2},c_{i2}],v_{i2}),\cdots,([b_{i7},c_{i7}],v_{i7}), \tag{3}$$

Suppose that

$$\sigma(\overline{y}^{+},\overline{Z}_i)=w_1D(\overline{y}_1^{+},\overline{z}_{i1})+w_2D(\overline{y}_2^{+},\overline{z}_{i2})+\cdots+w_nD(\overline{y}_n^{+},\overline{z}_{i7}), \tag{4}$$

$$\sigma(\overline{y}^{-},\overline{Z}_i)=w_1D(\overline{y}_1^{-},\overline{z}_{i1})+w_2D(\overline{y}_2^{-},\overline{z}_{i2})+\cdots+w_nD(\overline{y}_n^{-},\overline{z}_{i7}), \tag{5}$$

Then $\sigma(\overline{y}^{+},\overline{Z}_i)$ is called the fuzzy grey deviation degree between the *i*-th alternative point $\overline{Z}_i$ and the fuzzy grey positive ideal solution $\overline{y}^{+}$, and $\sigma(\overline{y}^{-},\overline{Z}_i)$ is called the fuzzy grey deviation degree between the *i*-th alternative point $\overline{Z}_i$ and the fuzzy grey negative ideal solution $\overline{y}^{-}$, where w_j is the weight of the *j*-th attribute, $j=1,2,\cdots,7$. $D(\overline{y}^{+},\overline{z}_{ij})$ is the distance from $\overline{y}_j^{+}$ to $\overline{z}_{ij}$, and $D(\overline{y}_j^{-},\overline{z}_{ij})$ is the distance from $\overline{y}_j^{-}$ to $\overline{z}_{ij}$, they are expressed as

$$D(\overline{y}_j^{+},\overline{z}_{ij})=\frac{1}{2}(\left|\max_i b_{ij}-b_{ij}\right|+\left|\max_i c_{ij}-c_{ij}\right|+\left|\min_i v_{ij}-v_{ij}\right|),$$

$$D(\overline{y}_j^{-},\overline{z}_{ij})=\frac{1}{2}(\left|\min_i b_{ij}-b_{ij}\right|+\left|\min_i c_{ij}-c_{ij}\right|+\left|\max_i v_{ij}-v_{ij}\right|).$$

For the fuzzy grey deviation degree $\sigma(\overline{y}^{+},\overline{Z}_i)$ and $\sigma(\overline{y}^{-},\overline{Z}_i)$, the smaller the value of $\sigma(\overline{y}^{+},\overline{Z}_i)$ is, the better the alternative $\overline{Z}_i$ is, and the greater the value of $\sigma(\overline{y}^{-},\overline{Z}_i)$ is, the better the alternative $\overline{Z}_i$ is. From $\sigma(\overline{y}^{+},\overline{Z}_i)$ and $\sigma(\overline{y}^{-},\overline{Z}_i)$, we give the following approach degree u_i, where

$$u_i=\frac{\sigma^2(\overline{y}^{+},\overline{Z}_i)}{\sigma^2(\overline{y}^{+},\overline{Z}_i)+\sigma^2(\overline{y}^{-},\overline{Z}_i)}$$

We can rank order for all alternatives according to the values of u_i. The smaller the value of u_i is, the better the alternative x_i is.

The Decision Making Steps

From above discussion, here we give the detail steps for solving the problems of selecting optimal investors under uncertain information environment.

Step 1: For m decision alternatives, determining fuzzy grey matrixes by the decision maker, which denoted as $R=(e_{ij})_{m\times 7}$.

Step 2: Use Definition 1 and Definition 2, we can obtain the decision making matrix, it denoted as $\overline{Z}=([b_{ij},c_{ij}],v_{ij})_{m\times 7}$, $i=1,2,\cdots,m$, $j=1,2,\cdots,7$.

Step 3: Use formula (1) and formula (2) to determine the fuzzy grey positive ideal solution $\overline{y}^{+}$ and fuzzy grey negative ideal solution $\overline{y}^{-}$, and by using formula (3) to determine the alternative point $\overline{Z}_1,\overline{Z}_2,\cdots,\overline{Z}_m$ from matrix $\overline{Z}$, respectively.

Step 4: Calculate the deviation degree $\sigma(\overline{y}^{+},\overline{Z}_i)$ and $\sigma(\overline{y}^{-},\overline{Z}_i)$, $i=1,2,\cdots,m$.

Step 5: Calculate the approach degree u_i, $i=1,2,\cdots,m$.

Step 6: Ranking order for all alternatives according to u_i, and selection the optimal investors.

Conclusions

In this paper, we investigate the problem of selecting investor under fuzzy information and grey information, and then a decision making model is proposed based on the theories of fuzzy mathematics and grey system is presented, and the optimization algorithm of fuzzy grey deviation degree is given for solving this new model. This new model is specific, fine in properties and simple for computing, and it has a great theoretic value and applied value in practice. It provides a new and effective way to deal with the multiple uncertainties in the problems of multi-attribute decision making.

Acknowledgments

This work is supported by the 2014 Key Project of Hubei Provincial Department of Education (No. D20142903).

References

[1] J. Xu: Systems Engineering Theory & Practice Vol. 22 (2002), p. 141-144.

[2] J. Wang and J. Ren: Systems Engineering and Electronics Vol. 27 (2005), p. 2057-2059.

[3] G. Pu and Y. Zhang: Systems Engineering Theory & Practice Vol. 22 (2002), p. 141-144.

[4] D. Luo and S. Liu: Engineering Science Vol., 6 (2004), p. 48-51.

[5] H.B. Liu and Z.Q. Ku: Mathematical Modeling and Mathematical Experiments (Science press, Beijing, 2008).

[6] Z. Xu: Uncertain Multiple Attribute Decision Making: Methods and Applications (Tsinghua University Press, Beijing, 2004).

[7] R. Li: The Foundation and Application of Fuzzy Multiple Attribute Decision Making (Science Press, Beijing, 2002).

[8] F. Herrera and L. Martínez: Fuzzy Sets and Systems Vol. 114 (2000), p. 43-58.

[9] Z. Fan, S. Xiao, and G. Hu: Computer & Industrial engineering Vol. 46 (2004), p. 329-335.

[10] O. Cordón: IEEE Trans on Fuzzy Systems Vol. 10 (2002), p. 1-19.

[11] F. Herrera and L. Martínez: IEEE Trans on Systems, Man, and Cybernetics Vol. 31 (2001), 227-233.

Advanced Materials Research Vols. 989-994 (2014) pp 1849-1852
© (2014) Trans Tech Publications, Switzerland
doi:10.4028/www.scientific.net/AMR.989-994.1849

A Novel Multiobjective Memetic Algorithm based on IWO-DE and its Application in Nutrition Decision Making Problem

Gaoping WANG[1, a],Meng ZHANG[1, b],Weiwei ZHAO[1, c]

[1] School of Information Science and Engineering ,Henan University of Technology, Zhengzhou,450052 ,China

[a]email: wgp888888@163.com, [b]email:13663806330@163.com, [c]email:331759795@163.com

Keywords: Memetic Algorithms;Nutrition Prescription;Invasive Weed Optimization;Differential Evolution Optimal Design

Abstract. In this paper ,we discuss multiobjective optimization problems solved by Memetic algorithms. We present A novel multiobjective memetic algorithm based on invasive weed optimization and differential evolution(IWO-DE) to solve this class of problems .We present the Nutrition Prescription Model for Meals.the IWO-DE is applied to solve the nutrition decision making problem to map the Pareto-optimum front. The results in the problem show its effectiveness.

Introduction

The nutrition meal model is multi-objective, whose goal function is a vector. In a multiobjective optimization problem (MOP), there may not exist one solution that is best with respect to all objectives. Usually, the aim is to determine the tradeoff surface, which is a set of nondominated solution points,known as Pareto-optimal or noninferior solutions. In view of the fact that none of the solutions in the nondominated set is absolutely better than any other, any one of them is an acceptable solution.

Since the work of Schaffer [1] a considerable number of different Multiobjective Optimization Evolutionary Algorithms (MOEAs) have been suggested .Deb and co-authors [2] suggested an elitist non-dominated sorting GA (called NSGA-II). Zitzler and Thiele [3] suggested a Strength Pareto EA (SPEA) . Recently SPEA was modified in order to incorporate a fine-grained fitness assignment strategy, a density estimation technique and an enhanced archive truncation method – SPEA2 algorithm [4]. Meanwhile a number of other multiobjective evolutionary algorithms have been proposed, such as the algorithm of Knowles and Corne[5,6] , which is based on an evolution strategy.

In this paper, we present the Nutrition Prescription Model for meals. Moreover, we present the IWO-DE and we analyze it regarding the solution of MOPs. Finally,we apply the IWO-DE to solve the Nutrition Prescription problem with the aim of find the optimum tradeoff surface.In the experiment,we obtain optimized solutions using the IWO-DE.

A Multiobjective Memetic Algorithm based on Invasive Weed Optimization and Differential Evolution(IWO-DE)

IWO

IWO is first presented by Mehrabian and lucas [7] to solve numerical optimization problems. IWO simulates the nature principles and behaviors of weedy invasion and colonization in the shifting and turbulent environment. Later, Kundu et al. [8] proposed a variant of IWO that extends the original IWO to handle multi-objective optimization problems. Generally speaking, there are four steps of IWO.

1. Initialize a population: solutions are initialized and dispersed in the given n dimensional search space uniformly and randomly.

2. Reproduction: each individual of the population is permitted to reproduce seeds according to its own fitness, the colony's lowest and highest fitness, in this situation, the fitness of each

individual is normalized and the number of seeds each individual reproduces depends on a given minimum and maximum and increases linearly.

3. Spatial dispersal: offspring are randomly distributed over the n dimensional search space by normally distributed random numbers with mean equal to zero; but varying variance. Through this, a group of offspring are produced around their parent individual and thus weed colony is formed to enhance the search ability. Furthermore, standard deviation (sd) of the normally distributed random function will be reduced from a predefined initial value, sd_{max}, to a final value, sd_{min}, over every generation. the value of sd for a given generation is computed as follows.

$$sd=(sd_{max}-sd_{min})*(iter_{max}-iter)_m iter_{m\ max}+sd_{min} \quad (1)$$

where $iter_{max}$ is the maximum number of generations, iter is the current number of generation and m is the nonlinear modulation index.

4. Competitive exclusion: with the growth and reproduction of weeds, after passing several generation, the number of weeds in a colony will reach its maximum. Therefore, an essential exclusion mechanism is needed among weeds. The exclusion mechanism is applied to eliminate weeds with low fitness and select good weeds that reproduce more than undesirable ones. Subsequently, the selected ones will be preserved into the next generation and then the steps I-IV are repeated until termination criterion is reached.

Differential evolution

DE, proposed by Storn and Price [9], is a powerful search algorithm in the optimal problems, and uses the vector differences of individuals for perturbing the population members.

Initially, DE comprises a population of N and every individual is an n-dimensional vectors $x_i=\{x_1,x_2,\ldots,x_n\}$. These vectors are randomly generated in the search space and in the process of evolution, individuals will be tackled by the operations of mutation, crossover and selection.

Mutation operation: in this operation, with the different mutant strategies, the generated way of a mutant vector v_i is different and the weighted vector difference of individuals is various. The popular mutant strategies are summarized as follows.

$$DE_{rand1}: v_i=x_{r1}+F(x_{r2}-x_{r3}) \quad (2)$$

$$DE_{rand2}: v_i=x_{r1}+F(x_{r2}-x_{r3})+F(x_{r4}-x_{r5}) \quad (3)$$

where the subscript r_1, r_2, r_3, r_4, r_5, which are all different from the index i, are not equal to each other and selected uniformly and randomly from the range [1, N]. x_{best} is the best individual of the current population, F is a scaling factor that measure the scale of the difference of vectors.

Crossover operation: with the mutant vector v_i and the target vector x_i, the trial vector u_i is generated by binomial crossover as follows.

$$u_{i,j}=\{v_{i,j},\text{if } jrand\le C_r \text{ or } j=jrand \quad x_{i,j},otherwise\} \quad (4)$$

where $i=1,2,\ldots,N, j=1,2,\ldots,n, jrand$ is a selected integer randomly from [1, n] which ensures u_i inherits at least one component from the mutant vector v_i, randj is a uniform random number between 0 and 1. C_r is the crossover probability parameter and its value is within [0, 1].

Selection operation: to keep better individual into next generation, the generated trial vector u_i is compared with the target vector x_i. The selection operation is described as follows.

$$x_{i,G+1}=\{u_{i,G},\text{if } f(u_{i,G})\le f(x_{i,G}) \quad x_{i,G},otherwise\} \quad (5)$$

After the refinement procedures of IWO, the elitist individuals are picked out. Therefore, the operations of DE are applied among the selected elitist individuals to explore more promising space for the aim of finding out more promising solutions to be refined by IWO.

IWO-DE

For each component of IWO-DE, the attracting characteristics of IWO and DE is merged. That is, for IWO, the characteristics refers to the point that each individual fully exploits the useful information around it and for DE, the excellent characteristics refers to making full use of information provided by IWO to find out more valuable individuals which are to be refined, in return, by IWO.

The whole framework of IWO_DE is presented in Algorithm 1.

Algorithm 1 The whole framework of IWO-DE

step1:t=1;

step2:generate an initial population P_0 uniformly and randomly within lower and upper boundary of decision variable;
step3:F_0=evaluate(P_0);
step4:while termination condition is false do
step5:P_t=IWO(P_{t-1},F_{t-1});
step6:F_t= evaluate(P_t);
step7:[P_t, F_t]=DE(P_t, F_t);
step8:t=t+1;
step9:end while

Test results

Mould and method of optimization for nutrition decision makinings

The saying is that there is not bad food in the world but poorly-balanced food. To provide different groups with correspondingly well-balanced food, we design a balanceable nutrition meal model according to threpsology theorem[10]. The balanceable meal model is as follows：

$$\min F(X)=(f_1(X), f_2(X), \dots , f_k(X))^T \tag{6}$$

$$A=\begin{Bmatrix} a_{11}\ a_{12}\dots a_{1p}\ a_{1(p+1)} & \dots a_{1(p+q)}\ a_{1(p+q+1)}\dots a_{1n} \\ a_{21}\ a_{22}\dots a_{2p}\ a_{2(p+1)} & \dots a_{2(p+q)}\ a_{2(p+q+1)}\dots a_{2n} \\ \dots \quad \dots & \\ a_{m1}\ a_{m2}..a_{mp}\ a_{m(p+1)}\dots a_{m(p+q)} & a_{m(p+q+1)}\dots a_{mn} \end{Bmatrix}$$

$$X=(x_1,x_2,\dots,x_n)^T \qquad B=(b_1,b_2,\dots,b_m)^T$$

$$f_j(X)=\left|b_j-\sum_{i=1}^{n}a_{ij}x_i\right| \qquad j=1,2,\cdots,k \tag{7}$$

Where $f_1(X)$, $f_2(X)$, … , $f_k(X)$ are k the objectives functions,and Xi represents the weight of each raw food material, n the number of raw materials, aij the amount of nutrient in unit raw material, bi the standard of supply of each nutrient. In fact, absolute balance of each nutrient is difficult to achieve, but only to approach the supply standard. 1 to p is the food for breakfast, while p +1 to p+q is for lunch and p +q +1 to n for dinner. In actual life, people's standard nutrition demand is not always a specific value, but changing within a range,see equation (8).

$$1.1*bj=>\sum_{i=1}^{n} aijXi >=0.9*bj \tag{8}$$

Optimization in nutrition decision makinings

The nutrition decision making Problem was chosen to show the application of IWO-DE described in the previous study in solving a multiobjective nutrition optimization problem. In this paper, we search to find the Pareto-optimal front of a nutrition decision making .The aim is to find the multiple Pareto-optimal points considering two objective functions: 1) the first objective considers the energy and 2) the second one takes into account the protein . The constraint conditions are the bounds in the design variables. .

The problem was solved considering seven design variables in continuous case . The nondominated points have been found using IWO-DE method (with roulette wheel selection,and) coupled with a finite element code for energy and protein calculations. The domain was subdivided in these elements of first order.The results are presented in Figs.1 .

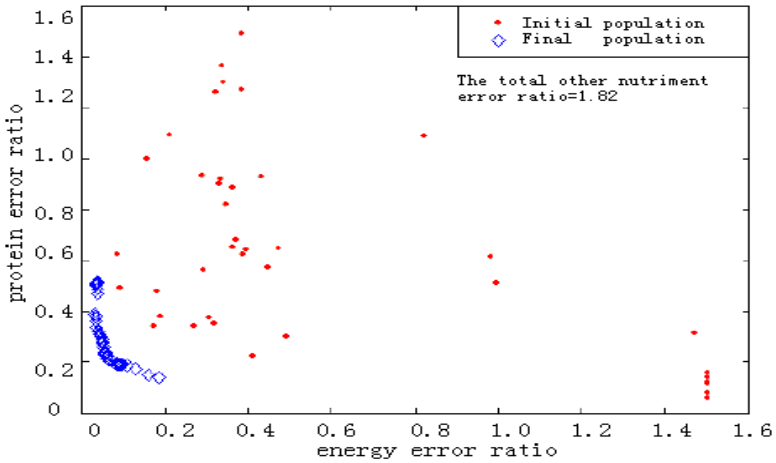

Fig. 1. Pareto-optimal points for the nutrition decision making proble

Conclusion

In this paper, the IWO-DE is presented for multiobjective optimization problems. The IWO-DE is applied to solve the nutrition decision making problem to map the Pareto-optimum front. The results in the problem show its effectiveness.For future work, we intend to test the algorithm on more problems.

References

[1] Schafer, J.D. Some Experiments in Machine Learning Using Vector Evaluated Genetic Algorithms, Ph. D. Thesis,Nashville, TN, Vanderbilt University ,1984.

[2] Deb, K., Agrawal, S., Pratap, A., Meyarivan, T.A Fast and Elitist Multi-Objective Genetic Algorithm: NSGAII,Technical Report 200001, Indian Institute of Technology, Kampur, India ,2000.

[3] Zitzler, E. Evolutionary Algorithms for Multiobjective Optimization: Methods and Applications, Ph. D. Thesis, Zürich,Switzerland: Swiss Federal Institute of Technology ,1999.

[4] Knowles, J.D., Corne, D.W. Approximating the Non-dominated Front using the Pareto Archived Evolutionary Strategy[J].Evolutionary Computation Journal, 2000,8:149-172.

[5] Zitzler, E., Laumanns, M., Thiele, L. SPEA2: Improving the Strength Pareto Evolutionary Algorithm, TIK report no.103, Swiss Federal Institute of Technology, Zürich, Switzerland ,2001.

[6] Deb, K., Agrawal, S., Pratap, A., Meyarivan, T. A Fast Elitist Non-dominated Sorting Genetic Algorithm for Multi-Objective Optimization: NSGAII[A]. Proceedings of the Parallel Problem Solving from Nature VI (PPSNVI) [C] ,2000.849-858.

[7] Mehrabian AR, Lucas C. A novel numerical optimization algorithm inspired from weed colonization[J]. Ecol Inf,2006, 1:355–366 .

[8] Kundu D, Suresh K, Ghosh S, Das S, Panigrahi BK, Das S. Multi-objective optimization with artificial weed colonies[J]. Inf Sci ,2011,181(12):2441–2454 .

[9] Price K, Storn R, Lampinen J . Differential evolution: a practical approach to global optimization [C]. Berlin :Springer ,2005.

[10] U.S. Department of Agriculture, Agriculture Research Service. Food and Nutrient Intakes by Individuals in the United States by Sex and Age, 1994–96. Nationwide Food Surveys, Report No. 96–2, 1998.

Advanced Materials Research Vols. 989-994 (2014) pp 1853-1856
© (2014) Trans Tech Publications, Switzerland
doi:10.4028/www.scientific.net/AMR.989-994.1853

An Improved Genetic Algorithm for Text Clustering

Shidong YU[1, a], Yuan DING[1, a], Xicheng MA[1, b], Jian SUN[1, b]

[1]College of Software, Shenyang Normal University, Shenyang, 110034, China

[a]ysd0510@sina.com, [b]phenix0916@163.com

Keywords: genertic algorithm; gene index; text clustering

Abstract. The genetic algorithm (GA) is a self-adapted probability search method used to solve optimization problems, which has been applied widely in science and engineering. In this paper, we propose an improved variable string length genetic algorithm (IVGA) for text clustering. Our algorithm has been exploited for automatically evolving the optimal number of clusters as well as providing proper data set clustering. The chromosome is encoded by special indices to indicate the location of each gene. More effective version of evolutional steps can automatically adjust the influence between the diversity of the population and selective pressure during generations. The superiority of the improved genetic algorithm over conventional variable string length genetic algorithm (VGA) is demonstrated by providing proper text clustering.

Introduction

Today, text clustering has become an important research topic to solve information overload problems in the field of information processing [1][2][3]. Clustering is an unsupervised pattern classification technique which is defined as group n objects into m clusters without any prior knowledge. In most real life situations the number of clusters in a data set is not known in advance. The real challenge is to be able to automatically evolve a proper number of clusters. Genetic algorithms (GAs) [4] based on the principle of evolution and heredity, are able to search in complex, large and multimodal landscapes. We can apply the searching capability of GAs to evolving proper number of clusters and providing appropriate clustering. A variable string length genetic algorithm (VGA) provided in [5][6] employs simple chromosomes to evolve the number of clusters. However, the compact chromosome encoding causes reduction of chances of getting the optimal centers combination. We propose an improved variable length genetic algorithm (IVGA) using gene indices to encode the chromosomes which have more chance to obtain the special centers combination and find the optimal number of clusters. We also propose dynamic evolutional steps to evolve. The details of the algorithm are described in section 4. Experiment results are given in section 5. Discussion and conclusions are given in section 6.

Clustering Model and Measure

Clustering is the classification of objects into different groups, or more precisely, the partitioning of a dataset into groups (clusters), so that the data in the same group are similar among themselves, and collectively different from the data of other groups. Generally, the distance measure between objects can be used to determine the similarity between them; a formalized description of the clustering model is as follows:

Given a dataset $X = \{x_1, x_2,\ldots, x_n\}$, for $\forall i \in \{1, 2,\ldots, n\}$, $xi = \{x_{i1}, x_{i2},\ldots, x_{ip}\}$ is an object in X and for $\forall t \in \{1, 2,\ldots, p\}$, x_{it} is an attribute of x_i. According to the inner feature of objects, X can be grouped into clusters $C = \{C_1, C_2,\ldots, C_k\}$, where $\bigcup_{i=1}^{k} C_i = X$, $\forall i, j \in \{1, 2,\ldots, k\}, C_i \neq \Phi$, $C_j \neq \Phi$, and $C_i \wedge C_j = \Phi$ $(i \neq j)$. $K = \{X, C\}$ is called a clustering space, C_i is the ith cluster in the clustering space.

There have been several suggestions for a measure of the similarity between two clusterings. Such a measure can be used to compare how well different data clustering algorithms perform on a

set of data. F-Measure [7], which combines precision and recall, is an index of system performance in information retrieval field. The precision P and recall R of cluster j and classification i are defined as

$$p = \frac{N_{ij}}{N_i}, \quad R = \frac{N_{ij}}{N_j} \tag{1}$$

where N_{ij} is the number of objects in cluster j subordinated to classification i; N_i is the number of all objects in classification i; N_j is the number of all objects in cluster j. The formula of F-Measure is as follows:

$$F(i) = \frac{2PR}{P+R} \tag{2}$$

Thus, the evaluation function of clustering results is defined as

$$F - Measure = \frac{\sum_i N_i F(i)}{\sum_i N_i} \tag{3}$$

A greater F-Measure means better clustering results.

Genetic Algorithms for Clustering

GAs are able to search in complex, large and multimodal landscapes. The parameters in the search space are represented in the form of chromosome. A collection of such chromosomes is called population. An objective and fitness function is associated with each chromosome that represents the degree of fitness. Biologically inspired operators like selection, crossover and mutation are applied to yield new child chromosomes. These operators continue several generations till the termination criterion is satisfied. The fittest chromosome seen up to the last generation provided the best solution to the clustering problem. We improved VGA chromosome using gene index to indicate the location of each gene. Such method is described in the next section.

IVGA for Text Clustering

Encoding Chromosome. In IVGA clustering, each chromosome C_i in the population initially encodes a number of K_i centers which are chosen randomly from the data set. These points are distributed in the random positions of the chromosome. We use gene index to denote the relative position of each point. Let us consider the following example.

Example: Let the random number K_i and K_j be 4 and 5 for chromosome C_i and chromosome C_j respectively. The VGA chromosomes encoding are shown as follows, C_i [Z_{i1}, Z_{i2}, Z_{i3}, Z_{i4}] and C_j [*Zj1, Zj2, Zj3, Zj4, Zj5*]. We know that a random exchange point crossover happened in VGA makes their offspring hold the same length as their parents. For example, if the crossover point is 3 their offspring generated are as follows, C_i' [Z_{i1}, Z_{i2}, Z_{i3}, Z_{j4}, Z_{j5}] and C_j' [Z_{j1}, Z_{j2}, Z_{j3}, Z_{i4}]. IVGA uses gene index to indicate the position of each gene. We generate a string of random numbers for gene locations. When random numbers are [0, 3, 4, 8] and [0, 2, 6, 7, 9], the C_i and C_j are shown as:

C_i: [Z_{i1}, Z_{i2}, Z_{i3}, Z_{i4}] gene index: [0, 3, 4, 8]

C_j: [Z_{j1}, Z_{j2}, Z_{j3}, Z_{j4}, Z_{j5}] gene index: [0, 2, 6, 7, 9]

If the crossover point is 5, we only need to exchange the genes whose gene index is greater than 5. The offspring generated are shown as:

C_i': [Z_{i1}, Z_{i2}, Z_{i3}, Z_{j3}, Z_{j4}, Z_{j5}] gene index: [0, 3, 4, 6, 7, 9]

C_j': [Z_{j1}, Z_{j2}, Z_{i4}] gene index: [0, 2, 8]

We can find that the lengths of offspring are different from their parents. So IVGA chromosome provides more chance to evolve proper number of clusters.

Evolution Principle of IVGA. We chose dynamic evolutional steps to evolve, which is shown in Fig. 1. The termination criterion is iteration of best fitness value without improvement exceeding consecutive N_{max} iterations. The criterion I happens when there have been no improvements in best fitness value for consecutive n_{max} iterations. The fittest concept selection, classical single-point

crossover and Gaussian Mutation [8] are adopted in this paper. Fitness function is defined to be 1/DB, where DB is Davies-Bouldin index [2, 9].

In Fig. 1, M is the size of population ; r and m are the proportion of chromosomes to crossover and mutation respectively.

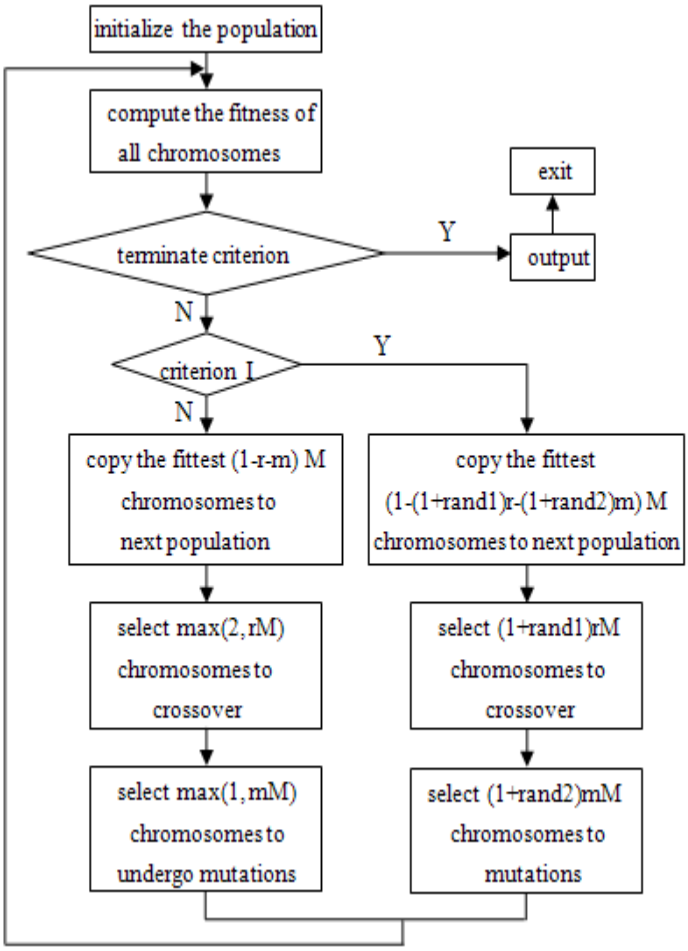

Fig.1. Dynamic evolutional steps of IVGA

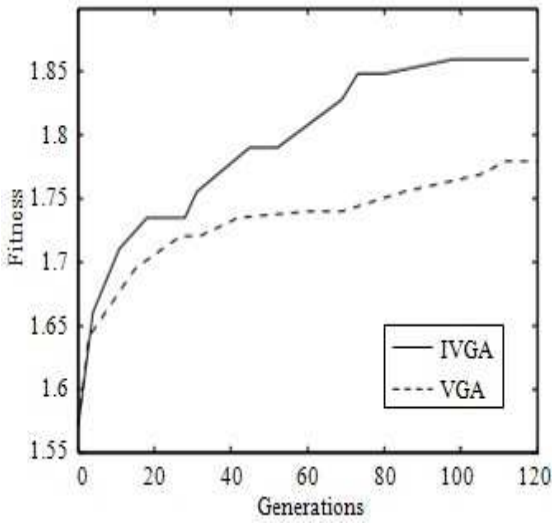

Fig.2. The fitness of IVGA and VGA for each generation

Experiments and Results

The dataset is extracted from the universal standard text collection, Reuters-21578, in which the documents were collected from Reuters newswire in 1987. 135 different categories have been assigned to 21578 Reuter documents. We chose 780 documents from it as dataset which includes five topics (gold, crude, interest, ship, sugar).

Vector space model is use here; each document is converted from the original format (i.e., strings of characters) to a word vector, (w_1, w_2,…, w_n), where w_i is the weight of the ith word. Information gain (IG) based approach is used as feature selection method, and the threshold is set as 0.4, which means that the IG value of each word lower than this threshold will be discarded. After being processed by word extraction, stop words removal, and stemming, there are 5,453 terms in the vocabulary. The IVGA is implemented with the following parameters: r = 0.4, m = 0.15, N_{max} = 20, n_{max} = 15 and the population size is 100. We then applied IVGA and VGA to clustering respectively. IVGA obtained 6 clusters, while VGA only got 4 clusters in the end. We used precision, recall and F-measure to evaluate the clustering results. Precision of cluster C_i is defined to be the number of texts correctly assigned divided by the total number of texts in cluster C_i. We define Recall of cluster C_i to be the number of texts correctly assigned divided by the total number of texts that should be assigned. Let P be average precision. Let R be average recall. F-measure is defined to be $2RP/(R+P)$. Table 1 shows the evaluation of IVGA and VGA.

Table 1. The Precision, Recall and F-measure of IVGA and VGA

Name	Precision	Recall	F-measure (%)
IVGA	77.2	73.8	75.5
VGA	54.7	71.4	61.9

To clustering problem, the real evaluation criterion is the fitness function 1/DB (Davies-Bouldin index). We choose the fitness of the best chromosome in each generation to represent generation fitness. In Fig. 2 the final fitness of 1.86 provided by IVGA is superior to that of VGA. Moreover, IVGA ends with fewer generations.

Conclusion

We proposed an improved variable string length genetic algorithm named IVGA for text clustering. The chromosomes with gene indices have been used for evolving the proper clustering. We also defined dynamic evolutional steps to evolve. We chose data set (780 documents, 5 topics) from the Reuter set for the tests. The results showed that not only did the IVGA evolve a more proper number of clusters, but also provided the appropriate clustering when compared with those of VGA. Since IVGA takes comparatively longer time to evolve the optimal clustering in high dimensional space, the correlative work of reducing the time complexity is being performed.

Acknowledgement

In this paper, the research was sponsored by Liaoning Provincial Educational Science Planning Foundation of China (Grant No. JG12DB285).

References

[1] Y. C. Liu, X. L. Wang, Z. M. Xu and Y. Guan, “A Survey of Document Clustering,” Journal of Chinese Information Processing, vol. 20, no. 3, 2006, pp. 55–62.

[2] M. Sasaki and H. Shinnou, “Spam Detection Using Text Clustering,” In: Proceedings of the 2005 International Conference on Cyberworlds (CW’05), Singapore, Nov. 2005, pp. 316–319.

[3] F. He and X. Q. Ding, “Combining Text Clustering and Retrieval for Corpus Adaptation,” Proceedings of SPIE, Jan. 2007, vol. 6500, pp. 65000P.1-65000P.7.

[4] Maulik and Bandyopadhyay, “Genetic Algorithm Based Clustering Technique,” Pattern Recognition, vol. 33, no. 9, 2000, pp. 1455–1465.

[5] Sanghamitra Bandyopadhyay and Ujjwal Mauilk, “Nonparametric Genetic Clustering: Comparison of Validity Indices,” IEEE Transactions on System, Man, and Cybernetics-Part C: Applications and Reviews, vol. 31, no. 1, Feb. 2001, pp. 120–125.

[6] Ujjwal Mauilk and Sanghamitra Bandyopadhyay, “Performance Evaluation of Some Clustering Algorithms and Validity Indices,” IEEE Transactions on Pattern Analysis and Machine Intelligence, vol. 24, no. 12, Dec. 2002, pp. 1650–1654.

[7] C. J. van RIJSBERGEN, Information Retrieval, 2nd ed., London: Butterworths, 1979.

[8] Xin Yao, Yong liu and Guangming Lin, “Evolutionary Programming Made Faster,” IEEE Transactions on Evolutionary Computation, vol. 3, no. 2, Jul. 1999, pp. 82–102.

[9] D. L. Davies and D. W. Bouldin, “A Cluster Separation Measure,” IEEE Transactions on Pattern Analysis and Machine Intelligence, vol.1, 1979, pp. 224–227.

Advanced Materials Research Vols. 989-994 (2014) pp 1857-1860
© (2014) Trans Tech Publications, Switzerland
doi:10.4028/www.scientific.net/AMR.989-994.1857

Applied Technology with a Modified Sixth-Order Convergent Iterative Method for Solving Nonlinear Equations

Liang Fang[a], Yun Li[a], Haiqun Wang[b], Rui Chen[a]

[a] College of Mathematics and Statistics, Taishan University, 271021, Tai'an, China
[b] Tai'an Rongjun Hospital, 271000, Tai'an, China
fangliang3@163.com

Keywords: Iterative method; nonlinear equation; Newton's method; efficiency index; order of convergence.

Abstract. With the rapid development and wide applications of information science and applied technology, nonlinear problems become an important direction of research in the field of numerical analysis. In this paper, we mainly study the iterative method for nonlinear equations. We propose and analyze a modified Newton-type method with order of convergence six for solving nonlinear equations. The method is free from second derivatives. The efficiency index of the presented method is 1.565, which is better than that of the classical Newton's method 1.414. Some numerical experiments illustrate the efficiency and performance of the proposed method.

1. Introduction

Nonlinear problems are an important direction of research in the field of numerical analysis. The solution of nonlinear equations is one of the most investigated topics in applied mathematics, numerical analysis, and the problem of solving nonlinear equations by numerical methods has gained more and more importance than before, since many practical problems in the applied information technology, as well as in materials science, manufacturing technology, can build a suitable mathematical model, and then be transformed into nonlinear equations to solve.

In this paper, in order to improve the efficiency, we consider iterative method to find a simple root x^* of a nonlinear equation

$$f(x)=0, \tag{1}$$

where $f:\Gamma\subseteq R\to R$ for an open interval Γ is a scalar function and it is sufficiently differentiable in a neighborhood of x^*.

It is well known that the classical Newton's method (NM for short) is a basic and important method for solving non-linear equation [1] by the iterative scheme

$$x_{n+1}=x_n-\frac{f(x_n)}{f'(x_n)} \tag{2}$$

which is quadratically convergent in the neighborhood of x^*.

In recent years, much attention has been given to develop iterative methods for solving nonlinear equations and a vast literature has been produced [2-7].

Motivated and inspired by the on going activities in this direction, in this paper, we present a sixth-order convergent iterative method. The proposed method is free from second derivatives. Several numerical results are given to illustrate the efficiency and advantage of the algorithm.

2. The Modified Iterative Method and Its Convergence Analysis

Let us consider the following iterative scheme.

Algorithm 1. For given x_0, we consider the following iteration scheme

$$y_n = x_n - \frac{f(x_n)}{f'(x_n)}, \tag{3}$$

$$z_n = x_n - \frac{2f(x_n)}{f'(x)+f'(y_n)}, \tag{4}$$

$$x_{n+1} = z_n - \frac{2f'(x_n)^2}{f'(x_n)^2 - 4f'(x_n)f'(y_n) + f'(y_n)^2}\frac{f(z_n)}{f'(x_n)}. \tag{5}$$

Theorem 1. Assume that the function $f:\Gamma \subseteq R \to R$ has a single root $x^* \in \Gamma$, where Γ is an open interval. If $f(x)$ has first, second and third derivatives in the interval Γ, then Algorithm 1 is sixth-order convergent in a neighborhood of x^* and it satisfies error equation

$$e_{n+1} = -\frac{3}{2}c_2(c_3 + 2{c_2}^2)(5c_3 - 6{c_2}^2)e_n^6 + O(e_n^7),$$

where $e_n = x_n - x^*$, $c_k = \frac{f^{(k)}(x^*)}{k!f'(x^*)}, k = 1,2,\cdots$.

Proof. Let x^* be the simple root of $f(x)$, $c_k = \frac{f^{(k)}(x^*)}{k!f'(x^*)}, k = 1,2,\cdots$ and $e_n = x_n - x^*$. Consider the iteration function $F(x)$ defined by

$$F(x) = z(x) - \frac{2f'(x)^2}{2f'(x)^2 - 4f'(x)f'(y(x)) + f'(y(x))^2}\frac{f(z(x))}{f'(x)} \tag{6}$$

where

$$z(x) = x - \frac{2f(x)}{f'(x)+f'(y(x))},\ y(x) = x - \frac{f(x)}{f'(x)}.$$

By some computations using Maple we can obtain

$$F(x^*) = x^*,\ F^{(i)}(x^*) = 0, i = 1,2,3,4,5,$$

$$F^{(6)}(x^*) = -\frac{5f^{(2)}(x^*)[f'(x^*)f^{(3)}(x^*) + 3f^{(2)}(x^*)^2][5f'(x^*)f^{(3)}(x^*) - 9f^{(2)}(x^*)^2]}{2f'(x^*)^5}. \tag{7}$$

Furthermore, from the Taylor expansion of $F(x_n)$ around x^*, we get

$$x_{n+1} = F(x_n) = F(x^*) + F'(x^*)(x_n - x^*) + \frac{F^{(2)}(x^*)}{2!}(x_n - x^*)^2 + \frac{F^{(3)}(x^*)}{3!}(x_n - x^*)^3$$
$$+ \frac{F^{(4)}(x^*)}{4!}(x_n - x^*)^4 + \frac{F^{(5)}(x^*)}{5!}(x_n - x^*)^5 + \frac{F^{(6)}(x^*)}{6!}(x_n - x^*)^6 + O((x_n - x^*)^7). \tag{8}$$

Substituting (7) into (8) yields

$$x_{n+1} = x^* + e_{n+1} = x^* - \frac{3}{2}c_2(c_3 + 2{c_2}^2)(5c_3 - 6{c_2}^2)e_n^6 + O(e_n^7).$$

Therefore, we have

$$e_{n+1} = -\frac{3}{2}c_2(c_3 + 2{c_2}^2)(5c_3 - 6{c_2}^2)e_n^6 + O(e_n^7)$$

which shows that Algorithm 1 is sixth-order convergent.

To obtain an assessment of the efficiency of the proposed method, we shall make use of efficiency index, according to which the efficiency of an iterative method is given by $p^{1/\omega}$, where p is the order of the method and ω is the number of function evaluations per iteration required by the method. It is not hard to see that the efficiency index of Algorithm 1 is 1.565 which is better than that of the classical Newton's method 1.414.

3. Numerical Results

Now, we employ Algorithm 1 to solve some nonlinear equations and compare them with NM and the iterative method (PPM for short) Potra and Pták presented in [7]

$$x_{n+1} = x_n - \frac{f(x_n) + f(y_n)}{f'(x_n)} \tag{9}$$

which is cubically convergent with efficiency index 1.442, where $y_n = x_n - \frac{f(x_n)}{f'(x_n)}$.

Displayed in Table 1 are the number of iterations (ITs) required such that $|f(x_n)| < 1.E-14$.

Table 1. Comparison of Algorithm 1, PPM and NM

Functions	x_0	NM	PPM	Algorithm 1
f_1	1	5	3	3
	1.45	4	3	3
f_2	2.5	6	3	3
	1. 5	7	5	4
f_3	0.5	4	3	3
	3.15	7	4	3
f_4	4.1	16	8	6
	3.5	12	5	4
f_5	7.9	15	11	8
	-0.6	4	4	3
f_6	1.9	5	4	3
	2.1	5	4	4

In table 1, we use the following functions.

$f_1(x) = x^3 + 4x^2 - 10,\ \alpha = 1.36523001341410.$

$f_2(x) = (x-1)^3 - 1,\ \alpha = 2.$

$f_3(x) = \cos x - x,\ \alpha = 0.73908513321516.$

$f_4(x) = e^{x^2+7x-30} - 1,\ \alpha = 3.$

$f_5(x) = (x+2)e^x - 1,\ x^* = -0.44285440096708.$

$f_6(x) = \sin^2(x) - x^2 + 1,\ x^* = 1.40449164885154.$

The computational results in Table 1 show that Algorithm 1 requires less ITs than NM, and no more than PPM. Therefore, Algorithm is of practical interest and can compete with NM.

4. Conclusion

In order to obtain efficient iterative method for the nonlinear equations which come from the practical problems in the materials science and manufacturing technology field, in this paper, we present and analyze a modified sixth-order convergent Newton-type iterative method for solving nonlinear equations. The algorithm is free from second derivatives. Several numerical results illustrate the convergence behavior and computational efficiency of the method proposed in this paper. Computational results demonstrate that it is more efficient and performs better than the classical NM.

Acknowledgements

The work is supported by the Excellent Young Scientist Foundation of Shandong Province (BS2011SF024), Project of Taishan University Doctoral Fund (Y11-2-03), Project of Shandong Province Higher Educational Science and Technology Program (J10LA51).

References

[1] J.F. Traub: *Iterative Methods for Solution of Equations*, Prentice-Hall, Englewood Clis, NJ(1964).

[2] F.A. Potra, Potra-Pták: *Nondiscrete induction and iterative processes,* Research Notes in Mathematics, Vol. 103, Pitman, Boston, 1984.

[3] J. Kou: *The improvements of modified Newton's method*, Appl. Math. Comput. 189 (2007), p. 602-609.

[4] C. Chun: *Some fourth-order iterative methods for solvingnonlinear equations*, Applied Mathematics and Computation 195 (2008) 454–459.

[5] L. Fang and G. He: *Some modifications of Newton's method with higher-order convergence for solving nonlinear equations*, J. Comput. Appl. Math. 228 (2009), p. 296-303.

[6] Mamta, V. Kanwar, V.K. Kukreja: *On some third-order iterative methods for solving nonlinear equations*, Applied Mathematics and Computation 171 (2005) 272–280.

[7] A. N. Muhammad and I. N. Khalida: *Modified iterative methods with cubic convergence for solving nonlinear equations*, Applied Mathematics and Computation 184 (2007) 322-325.

Advanced Materials Research Vols. 989-994 (2014) pp 1861-1864
© (2014) Trans Tech Publications, Switzerland
doi:10.4028/www.scientific.net/AMR.989-994.1861

Research on Improved AES encryption algorithm

Ziheng Yang, Na Li, Liyuan Liu, Renji Qi, Lingling Yu

School of Electronic Engineering Heilongjiang University Harbin, China

yzheda@126.com, miaoxuedatianshi@gmail.com, liliyuanyuan123@126.com, q290187113@126.com, 15244691698@163.com

Keywords: AES; Key Expansion; Logistic; MATLAB

Abstract. AES (Advanced Encryption Standard) in May 26, 2002 became effective standard. AES algorithm research has become a hot topic at home and abroad, and the algorithm has been widely applied in the field of information security. Since the algorithm of AES key expansion part is open, so the key is between the wheel can be derived from each other, the AES algorithm designed for this security risk by generating pseudo-random number. Logistic mapping a certain length, after quantization is used as a key to improve the security of the AES algorithm.

Introduction

With the speeding up of the computer data processing, the DES encryption algorithm that has been public before due to its short packet length can be deciphered in the limited time and limited resources. So the DES encryption algorithm can no longer guarantee the security. AES encryption algorithm is now being widely used replacing DES. AES has 128-bit packet length which is variable. Make the data encryption get the final ciphertext and have higher security with the operation of ten rounds of replacement, substitution and the mixed key for each packet data during encryption. The initial key of AES is 128 bits, but AES algorithm needs 11 rounds of secret key which is 1408 bits key. So it needs to extend the original 128 bits key. Rijndael has put forward the key extension algorithm which is derived from the initial key, and the algorithm is public. So the attacker only needs to break one round keys that can deduce all keys. This brings hidden troubles to the security of the AES. This design idea is to produce 1408 bits of pseudo-random sequence as the key of AES algorithm which can ensure the key cannot be derived. The algorithm introduces the chaos model, comparing with the original algorithm it has higher security [1].

Chaos is a complex nonlinear process which can provide good pseudo random sequences. Chaotic system has high sensitivity to the initial parameters. Even though the initial value of two chaotic systems has minor differences, it can produce two sets of completely different and the discrete chaotic sequence values after a relatively short time. And the output of two systems can present a state of separation index after n iterations.

A new AES algorithm arises at the historic moment, integrating the advantages of chaotic systems and comparing with the traditional key extension of AES algorithm. The new AES algorithm is differ from the traditional algorithm, using a chaotic dynamical system to produce a pseudo random sequence as a key. That is to say, produce 1408 bits pseudo-random sequence as the encryption key. The characteristics of the modified AES encryption algorithm are as follows:

1. With higher algorithm security: The pseudo-random sequence produced by chaotic system has complexity and unpredictability. There is no rule to follow between each round of key sequence. Even if the interceptor calculates one round of the key, he cannot recover the plaintext owning to that he cannot calculate the previous round and after round of key. But the traditional key extension of AES algorithm is public. Once the interceptor calculates a round of key, he can calculate all keys [2]. Compared with the original algorithm, the modified key expansion algorithm has higher security.

2. With key sensitivity: Even though there is a slight initial deviation, corresponding positions changing rate of 0 and 1 in the two sequences obtained by experimental statistics is very large, due to the chaotic dynamical system with initial sensitivity. That is to say, the attack who speculates slight deviation cannot get the key sequence.

3. With a broader key space: Using the initial values x_n of chaotic dynamical systems as the encryption and decryption keys, the encryption machine can produce tens of thousands, hundreds of thousands or even more random sequences. Then we intercept 1408 bits from the sequences as the key. The key can be calculated using the method of powerful attacks when the development of computer processing speed is fast enough in the future, because that the traditional initial key for AES algorithm is only 128 bits [3]. Compared to the original algorithm speaking, AES algorithm improved provides a wider key space.

In summary, the improved AES algorithm with the sequences producing by chaotic dynamical systems as the encryption key overcome the security risk in the presence of key extension in the original algorithm. There are researching and realizing values.

Organization of the Text

A set of data in AES encryption processing requires eleven 128-bit keys in the original AES key expansion algorithm. But the initial key is only 128 bits, requiring to be expanded. AES key expansion algorithm is public, mainly including round key expansion and round key selecting two parts [4]. Make the 16 bytes of the initial key consist of 4-by-4 state matrix and each column of the matrix is a word. The four-word initial key w_0, w_1, w_2, w_3 need to be expanded the other words $w_4, w_5, w_6, w_7 ... w_{40}, w_{41}, w_{42}, w_{43}$. The expansion algorithm is $w_i \oplus w_{i+3} \rightarrow w_{i+4}$, where $i = 0,1...39$. First detect subscript $i+3$ of w_{i+3}, if $i+3$ is an integer multiple of 4, then make w_{i+3} function $H(x)$ substitution before $w_i \oplus w_{i+3}$ operation.

$H(x)$ is a four-byte input and output function, constituted by three sub-functions. The expansion function is main made up of the box S function (SubWord), the shift function (RotWord) and the XOR *RC* [5]. However, the problem has cropped up because key expansion is public. The key attacker who gets a round key will be able to calculate all keys based on the public expansion algorithm, which greatly reduces the security of encryption system [6].

The AES encryption requires 44 key words for encryption. In order to strengthen the security of encryption, this design takes advantage of Logistic mapping to generate a long enough pseudo-random sequence [7], from which intercept 1408 bits to quantization as the AES encryption key. The maximum feature of pseudo-random number is that the sequences cannot be deduced even knowing one or a sequence. It is also impossible to calculate its sequence value before and after. The pseudo-random number can effectively prevent attackers calculate the key. Without key attacker will not be able to recover the plaintext. Improved Algorithm AES flowchart is shown in Fig. 1:

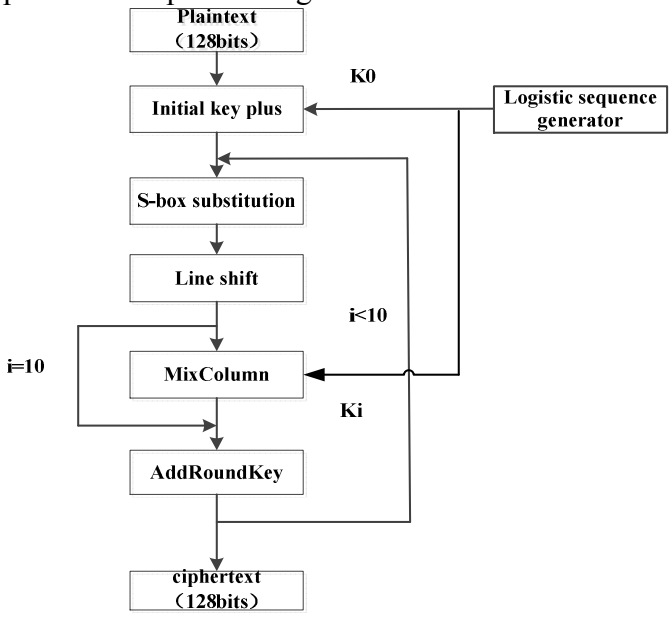

Fig. 1 The flowchart of improved AES data encryption algorithm

As shown in Fig. 1, all round keys of the improved AES encryption algorithm are generated by the Logistic module. And the algorithm enhances confidentiality performance by using the pseudo-random sequence which cannot be deduced.

Logistic model is defined as shown in Eq. 1:

$$x_{n+1} = \mu x_n (1 - x_n) . \ n = 1, 2, 3 ... \infty \quad (1)$$

When the initial conditions is $x_n \in [0,1]$, $\mu \in (0,4]$, the sequence $x_0, x_1, x_2 ... x_n$ generated by Logistic model is pseudo-random, non-convergence, sensitive to initial conditions, and the values of the sequence x_n are between 0 and 1. The design chooses $\mu = 3.58$, $x_0 = 0.75$. The values of the sequence $x_0, x_1, x_2 ... x_n$ generate by MATLAB simulation is 0.6713, 0.7900, 0.5939, 0.8634, 0.4221, 0.8733..., some of the workspace generated the sequence is shown in Fig. 2:

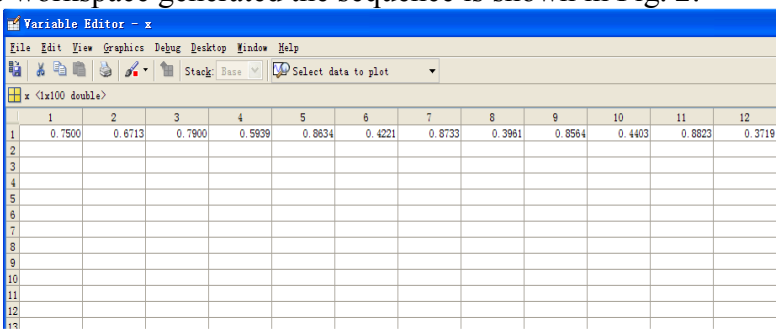

Fig. 2 Workspace of sequence x

Logistic sequence simulation shown in Fig. 3:

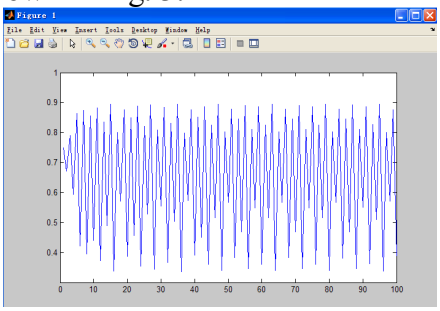

Fig. 3 Sequence of logistic mapping generated

As it shown in Fig. 3, the values of sequence between 0 and 1, and there is no cycle. Then we choose a fixed-point to simulate the Logistic map. This design uses 16-bit binary number to show fixed-point number. The position of the decimal point is between 14 and 15. And the range of it can be represented from 00.00000000000000 to 11.11111111111111.

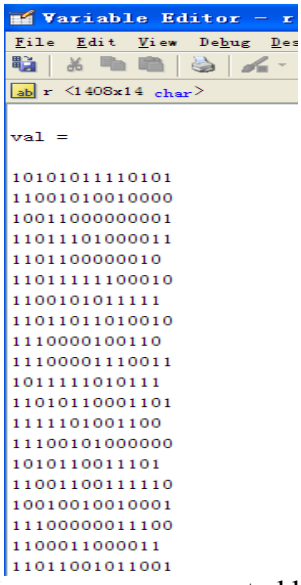

Fig. 4 The logistic sequences generated by the fixed-point

As shown in Fig. 4, the binary digits of sequence are more less than 14, due to the decimal point between the 14 and 15, so the value of the sequence is less than 1. Then we choose each 12-bit to quantify. The working space of the quantified sequence k is shown in Fig. 5:

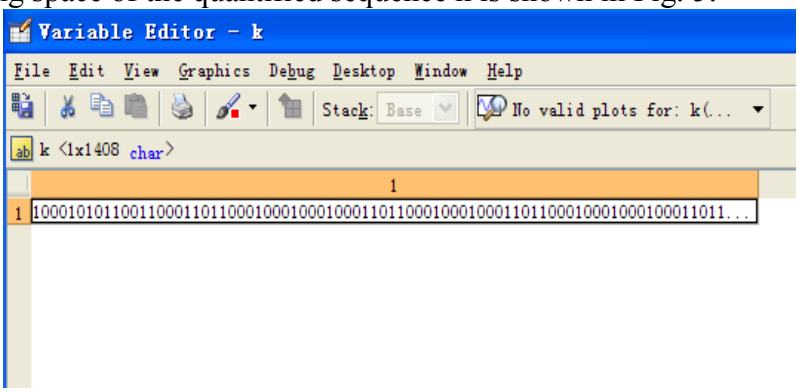

Fig. 5 The logistic sequence after quantify

As shown in Fig. 5, after quantization the k is 1048 bits, as modified for AES encryption algorithm.

Summary

In modern communication technology, information security technology requires more in-depth and widely applied to a variety of communication systems. This paper compares the advantages and disadvantages of packet encryption and stream encryption, and chooses encrypt packet encryption machine to design. Before the design, it introduces the number theory basic knowledge which is involved in AES, including the concept of group, ring, domain and algorithm in finite field. By using MATLAB to simulate the AES algorithm, it has verified the feasibility of AES algorithm. For the safe hidden trouble of AES algorithm between round keys which can be derived each other, the design uses the characteristics of chaotic sequence to improve AES algorithm. By using Logistic mapping to generate pseudo-random sequences, the design uses the pseudo-random sequence as the round keys of modified AES algorithm. Because the pseudo-random sequence is random in a certain period, so the relationship of sequences is not derived. After analysis concluding, that we use pseudo-random sequence as AES encryption key can enhance the security of the AES algorithm. And using MATLAB to simulate the modified AES algorithm can verify the feasibility of the new algorithm.

References

[1] Ji Zhang, Tingting Yuan, Heping Lin. Research of the Combination Algorithm Based on AES and RSA [C]. The 2011 Asia-Pacific Youth Conference of Youth Communication and Technology, 2011: 217-220.

[2] Abdullah Al Hasib, Abul Ahsan Md. Mahmudul Haque. A Comparative Study of the Performance and Security Issues of AES and RSA Cryptography [C]. Third 2008 International Conference on Convergence and Hybrid Information Technology, 2008: 505-510.

[3] R. Matthews. A High-Through Put Low-Cost AES Processor [J]. Cryptologia, 1984, 8(1): 29-41.

[4] Joan Daemen. AES-the Advanced Encryption Standard [J]. Physics Letters. 1998, 240: 50-54.

[5] Lihong Zhang, Yifeng Zhang. Research on Lorenz Chaotic Stream Cipher [C]. IEEE International Workshop VLSI Design & Video Tech, 2005: 431-434.

[6] Kocarev L. Chaos-based Cryptography: A Brief Overview [J]. IEEE Circuits and Systems, 2001, 1(3): 6-21.

[7] Bin Zhang, Chenhui Jin. Cryptanalysis of a AES-based Steam Cipher [C]. The 9th International Conference for Young Computer Scientists, 2008: 2782-2785.

Advanced Materials Research Vols. 989-994 (2014) pp 1865-1868
© (2014) Trans Tech Publications, Switzerland
doi:10.4028/www.scientific.net/AMR.989-994.1865

CMA Blind Equalization with Quasi-newton Algorithm in Underwater Acoustic Channels based on Simplified Cost Function

Ying XIAO[1,2,a],Rui RUAN[3,b]

[1]College of Information and Communication Engineering Dalian Nationality University, Liaoning Dalian, 116600, China

[2] Faculty of Electronic Information and Electrical Engineering, Dalian University of Technology, Liaoning Dalian, 116024, China

[3]South Central University for Nationalities, College of Electronics and Information, Hubei Wuhan, 430074, China

[a]email: xiaoying@126.com, [b]email: ruan_rui@126.com

Keywords: Blind Equalization; CMA; Underwater Acoustic Channel; Quasi-newton Algorithm

Abstract. The CMA cost function is simplified to meet the second norm form, and a new CMA blind equalization based on quasi-newton algorithm is proposed. Since the CMA cost function does not meet the second norm form, it is difficult to use quasi-newton algorithm to update the blind equalizer directly based on the cost function of CMA. If the cost function is simplified to meet the second norm form, it can use quasi-newton algorithm to update the blind equalizer directly. Thus, the convergence rate and convergence precision of CMA blind equalization can be improved effectively. Simulation results under the acoustic channels show that CMA blind equalization with quasi-newton algorithm based on the simplified cost function has faster convergence rate and less steady state residual error, which has practical value in the blind equalization of fast time-varying underwater acoustic channels

Introduction

Adaptive blind equalization technology provides a powerful technical support to achieve high-quality and high-speed communication for the limited bandwidth underwater acoustic communication system. Adaptive blind equalization can compensate and track the communication channel by receiving signals without any training sequence to effectively save the communication bandwidth and prevent equalizer from locking. Blind equalization technology has potential application value in wireless communication, especially in underwater acoustic communication system [1]. CMA has received great attention for its simple and easy to achieve and CMA based on the gradient descent has the defects of low convergence rate and big steady state residual error after convergence. To overcome the defects of CMA blind equalization, many improved algorithms are proposed. Quasi-newton algorithm can make use of the second derivative of the cost function, which can speed up the convergence rate and improve the global convergence performance. But the cost function of CMA does not meet the second norm form, so it is difficult to deduce and use quasi-newton algorithm from theory. Therefore, the cost function of CMA is simplified to meet the second norm form in this paper, and the quasi-newton CMA is deduced and analyzed based on the simplified cost function. Computer simulation results show that, compared with CMA blind equalization, the CMA blind equalization with quasi-newton algorithm based on simplified cost function has better equalization performance in underwater acoustic communication system.

The Simplified CMA cost function

CMA is a special case of Bussgang blind equalization algorithms, which is well suited for sending signals having constant envelope. CMA algorithm sets parameter $p = 2$ in Godard algorithm. Fig.1 shows the baseband model of CMA blind equalization [2].

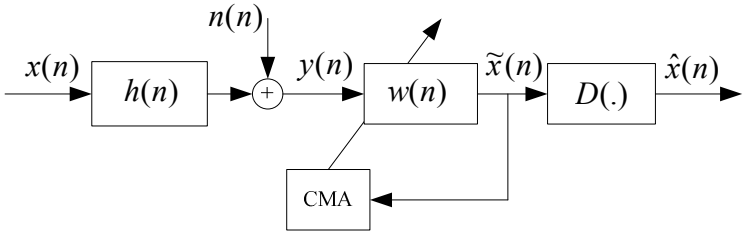

Fig.1 The principle of CMA

In Fig.1, $x(n)$ is the input sequence, $h(n)$ is the unknown channel impulse response, $n(n)$ is gauss white noise ,then the observed sequence $y(n)$ as the blind equalizer input sequence is received. The recovered signal $\hat{x}(n)$ can be obtained by the decision device $G(.)$ at the output signal $\tilde{x}(n)$. The CMA cost function is given by

$$J(n) = E\left[R_2 - \left|\tilde{x}(n)\right|^2 \right]^2 \tag{1}$$

According to signal transmission principle of the communication system, the $\tilde{x}(n)$ can be given by

$$\tilde{x}(n) = w^H(n) y(n) \tag{2}$$

then, the cost function of CMA can be given by

$$J(n) = [R_2 - w^H(n) y(n) (w^H(n) y(n))^*]^2 \tag{3}$$

where the symbol " H " is the complex conjugate transpose operator. If let

$$u(n) = y(n) (w(n)^H y(n))^* \tag{4}$$

then Eq.3 can be given by

$$J(n) = [R_2 - w^H(n) u(n)]^2 \tag{5}$$

Eq.5 satisfies the quadric standard form, but the expression $u(n)$ contains the variable $w(n)$, so $u(n)$ cannot be taken as the equivalent equalizer input variable. Hereby the approximate expression of $u(n)$ is given by

$$\tilde{u}(n) = y(n) (w^H(n-1) y(n))^* \tag{6}$$

if the algorithm is convergent, then there must be

$$\lim_{n\to\infty} \left\| w(n) - w(n-1) \right\| = 0 \tag{7}$$

So, it is rational to use $\tilde{u}(n)$ to approximate $u(n)$. The CMA cost function can be simplified to

$$J(n) = [R_2 - w^H(n) \tilde{u}(n)]^2 \tag{8}$$

The Quasi-Newton CMA Blind Equalization

The mean square error performance surface formed by the quadratic function of the weight coefficient vector of the adaptive transversal equalizer can be described by the mean square error [3], the mean square error can be given by

$$\xi(n+1) = R_2^2 - 2w^H(n+1) P + w^H(n+1) R w(n+1) \tag{9}$$

where R is the autocorrelation matrix of the equalizer input signal and P is the cross-correlation matrix of the input signal and the desired signal. Subtract $\xi(n+1)$ and $\xi(n)$ can obtain

$$\xi(n+1) = \xi(n) + \nabla^H(n) \left[w(n+1) - w(n) \right] + \left[w(n+1) - w(n) \right]^H R \left[w(n+1) - w(n) \right] \tag{10}$$

where $\nabla^H(n) = -2P + 2Rw(n)$ is the gradient vector of the mean square error. Similarly, $\xi(n)$ is the mean square error of the equalizer. If strive for the partial derivative, that is the momentary value $(n+1)$ of $\xi(n)$ and $w(n+1)$, then make it to zero, we have

$$w(n+1) = w(n) - \frac{1}{2} R^{-1} \nabla(n) \tag{11}$$

Eq.11 is the iterative formula of the newton algorithm. The optimal solution can be obtained after iteration based on the newton algorithm, that is

$$w(n+1) = R^{-1}P = w_{opt} \tag{12}$$

But in practical applications, the autocorrelation matrix R and the cross-correlation matrix P and the gradient vector $\nabla(n)$ cannot be all precisely known. According to the idea of LMS, we can substitute the estimate value for the actual value, and then the iterative formula of the quasi-newton algorithm can be given by

$$w(n+1) = w(n) - \mu\hat{R}^{-1}(n)\hat{\nabla}(n) \tag{13}$$

where $\hat{R}(n)$ and $\hat{\nabla}(n)$ are the instantaneous estimation of the autocorrelation matrix R and the gradient vector $\nabla(n)$ respectively, when the input signal satisfies the stationary random process, the unbiased estimation of the autocorrelation matrix R can be given by

$$\hat{R}(n) = \frac{1}{n+1}\sum_{i=0}^{n} y(i)y^T(i) = \frac{1}{n+1}\hat{R}(n-1) + \frac{1}{n+1}y(n)y^T(n) \tag{14}$$

From Eq.14, we can see the autocorrelation matrix $\hat{R}(n)$ can be obtained from recurrence. The mathematical expectation of $\hat{R}(n)$ can be given by

$$E[\hat{R}(n)] = \frac{1}{n+1}\sum_{i=0}^{n} E[y(i)y^T(i)] = R \tag{15}$$

Then Eq.15 is the unbiased estimation. The sliding exponential window estimation and the sliding rectangular window estimation are the estimation methods, which are frequently used in the estimation to the autocorrelation matrix R. where the recursion formula of the sliding exponential window estimation is

$$\hat{R}(n) = \lambda\hat{R}(n-1) + y(n)y^T(n) \tag{16}$$

where λ is the forgetting factor.

The computation complexity of iteration in the matrix inversion is $O(N^3)$. To avoid the computation of the matrix inversion, we can use the matrix inversion lemma formula to obtain the matrix inversion, that is

$$[A+BCD]^{-1} = A^{-1} - A^{-1}B[DA^{-1}B + C^{-1}]^{-1}DA^{-1} \tag{17}$$

where A and C is non-singular matrix. If $A = (1-\alpha)\hat{R}(n-1)$, $B = D^T = x(n)$, $C = \alpha$, the calculation formula of $R^{-1}(n)$ can be given by

$$\hat{R}^{-1}(n) = \frac{1}{1-\alpha}\left[\hat{R}^{-1}(n-1) - \frac{\hat{R}^{-1}(n-1)y(n)y^T(n)\hat{R}^{-1}(n-1)}{\frac{1-\alpha}{\alpha} + y^T(n)\hat{R}^{-1}(n-1)y(n)}\right] \tag{18}$$

According to Eq.18, we can make the recursion calculation to $R^{-1}(n)$. The computation complexity of every iteration calculation is $O(N^3)$, which is below the inverse matrix of the directing calculation of $\hat{R}(n)$.Estimate the gradient vector based on LMS, and then the equalizer weight efficient of the quasi-newton algorithm can be updated as follow

$$w(n+1) = w(n) + \mu e(n)\hat{R}^{-1}(n)\tilde{u}(n) \tag{19}$$

The inverse of the autocorrelation matrix can be initialized to

$$\hat{R}^{-1}(0) = \delta I \tag{20}$$

Simulations and Analysis

The simulation channel is adopted the two-ray sparse underwater acoustic channel [4], the transfer function of the channel is

$$H(z) = 1 + 0.59997z^{-20} \tag{21}$$

The sending signal is modulated by 4-QAM and $SNR = 25\,\mathrm{dB}$ .The length of transversal equalizer is 84, and the center taps is initialized to 1, step size $\mu = 0.002$. Fig.2 shows the convergence curve of ISI based on CMA（NG-CMA）and LMS-CMA .Where the computational method of ISI is given by [5]

$$ISI(n) = \frac{\sum_i |C_i(n)|^2 - |C_i(n)|^2_{\max}}{|C_i(n)|^2_{\max}} \tag{22}$$

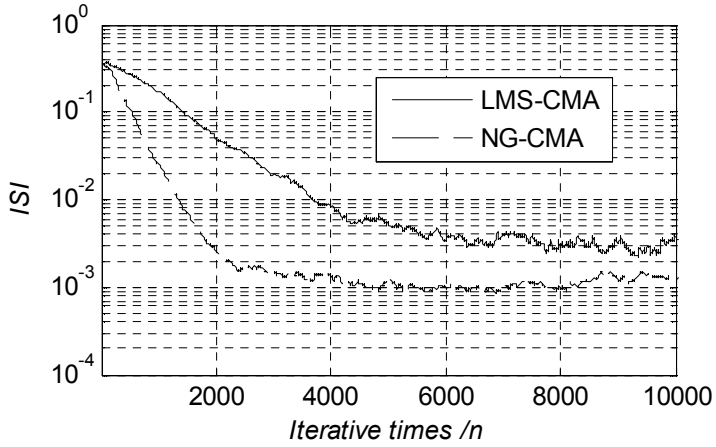

Fig.2 ISI convergence curve

Fig.2 shows that NG-CMA has the faster convergence rate and the smaller steady state residual ISI compared with LMS-CMA. It is demonstrated that NG-CMA has the validity of the equalization performance.

Conclusions

The quasi-newton CMA is deduced and analyzed based on the simplified cost function of CMA. The quasi-newton algorithm improves the convergence rate and the convergence precision effectively at the expense of a little computational complexity. NG-CMA proposed in this paper has the application value in the time-varying underwater acoustic channels.

Acknowledgements

This work is supported in part by The National Natural Science Foundation of China (61201418), Fundamental Research Funds for the Central Universities (DC12010218) and Liaoning Province High School Talent Support Program (LJQ2013126).

References

[1] Pincemin Erwan, Brochier Nicolas, Selmi Mehrez, Chahabi Omid Zia, Ciblat Philippe. Novel blind equalizer for coherent DP-BPSK transmission systems: Theory and experiment [J]. IEEE Photonics Technology Letters. 2013, 25(18): 1835-1838.

[2] Xiao Ying, Yin Fuliang. T/4 fractionally spaced decision feedback blind equalization with RLS algorithm [J]. Telkomnika. 2013, 11(6): 2948-2955.

[3] Shin Won-Hwa, Jun Young-Hyun, Kong Bai-Sun. Blind-oversampling adaptive oversample-level DFE receiver for unsynchronized global on-chip serial links [J]. IEICE Electronics Express. 2013, 10(9):1-6.

[4] Li Changrong, Wu Di. Simulation study on blind equalization algorithm for underwater acoustic channels [J]. Computer Simulation. 2013, 30(7): 183-186.

[5] Xie Ning, Hu Hengyun, Wang Hui. A new hybrid blind equalization algorithm with steady-state performance analysis [J]. Digital Signal Processing: A Review Journal. 2012, 22(2): 233-237.

Advanced Materials Research Vols. 989-994 (2014) pp 1869-1872
© (2014) Trans Tech Publications, Switzerland
doi:10.4028/www.scientific.net/AMR.989-994.1869

The CPML for Hybrid Implicit-Explicit FDTD Method Based on Auxiliary Differential Equation

Yunfei Mao[1, 2, a], Puhua Huang[1, b], Liguo Ma[1, c]

[1] China Satellite Maritime Tracking and Control Department, Jiangyin, Jiangsu, 214431, China

[2] National Key Laboratory on Electromagnetic Environment and Electro-optical Engineering, PLA University of Science and Technology, Nanjing 210007 China

[a]email: myf4494@163.com, [b]email:genghaijian@163.com, [c]email:tangjizhen1980@163.com

Keywords: Complex frequency shifted, finite- difference time-domain, hybrid implicit-explicit, perfectly matched layer

Abstract. In this paper, an implementation of the complex-frequency-shifted perfectly matched layer (CPML) is developed for three-dimensional hybrid implicit-explicit (HIE) finite-difference time-domain (FDTD) method based on auxiliary differential equation (ADE). Because of the use of the ADE technique, this method becomes more straightforward and easier to implement. The formulations for the HIE-FDTD CPML are proposed. Numerical examples are given to verify the validity of the presented method. Results show that, both HIE-CPML and FDTD-CPML have almost the same reflection error, while their reflection error is about 30 dB, which is less than HIE Mur's first-order results. The contour plots indicate that the maximum relative reflection as low as -72 dB is achieved by selecting $\kappa_{\max} = 14$ and $\sigma_{\max}/\sigma_{opt} = 1.0$.

Introduction

The finite-difference time-domain (FDTD) method [1] has been proven to be an effective scheme for solving varieties of electromagnetic problems. However, it is an explicit algorithm, the time-step size is confined by the Courant-Friedrich-Levy (CFL) condition [2]. As a result, the maximum time-step is limited by the minimum cell size in a computational domain, which makes this method inefficient for the problems where fine-scale structures are involved.

To overcome the restriction of the CFL limit on the time step-size, unconditionally stable methods have been studied extensively, such as the alternating direction implicit (ADI) FDTD method [3] [4]. However, in the ADI-FDTD scheme, it must solve six tri-diagonal matrices and six explicit updates for one updating cycle, which makes the ADI-FDTD computationally inefficient.

To overcome the above drawback of the ADI-FDTD method, a hybrid implicit-explicit (HIE) FDTD method was proposed [5]-[7] namely HIE-FDTD method. For a lot of advantages, this method has been introduced to solve the body-of-revolution problems [8], as well as the periodic problems [9].

When open structures are involved, the absorbing boundary conditions (ABCs) are required to truncate the computational domain [2]. The complex frequency-shifted (CFS) perfectly matched layer (PML) is widely used for its easy implementation and high efficiency at absorbing low-frequency evanescent waves [10]-[13].

In this paper, an implementation of CFS-PML using auxiliary differential equation (ADE) for 3-D HIE-FDTD is developed. Numerical results are compared with the conventional FDTD-CPML and the Mur's first-order ABC results. The contour plots indicate that the maximum relative reflection as low as -72 dB is achieved by selecting $\kappa_{\max} = 14$ and $\sigma_{\max}/\sigma_{opt} = 1.0$. The formulations and numerical results are proposed in the following sections.

Mathematical Formulations

The PML technique consists in surrounding a computational domain with the absorbing layer. In the PML layer, the following equations replace the normalized Maxwell's equations [12]

$$j\omega\varepsilon E_i = S_j^{-1}\frac{\partial H_k}{\partial j} - S_k^{-1}\frac{\partial H_j}{\partial k} \tag{1a}$$

$$j\omega\mu H_i = S_k^{-1}\frac{\partial E_j}{\partial k} - S_j^{-1}\frac{\partial E_k}{\partial j} \tag{1b}$$

where ε,μ represent the permittivity and permeability, $i=x,y,z$, $j=y,z,x$, $k=z,x,y$, alternately. $S_\eta,(\eta=x,y,z)$ are called the stretched-coordinate variables. To achieve high efficiency of the wave absorbing, for the sake of generality, $S_\eta,(\eta=x,y,z)$ are chosen within the PML region as

$$S_\eta = \kappa_\eta + \sigma_\eta/(\alpha_\eta + j\omega\varepsilon) \tag{2a}$$

And then

$$S_\eta^{-1} = 1/\kappa_\eta + b_\eta/(j\omega + a_\eta) \tag{2b}$$

where $b_\eta = -\sigma_\eta/(\varepsilon\kappa_\eta^2)$, $a_\eta = (\alpha_\eta + \sigma_\eta/\kappa_\eta)/\varepsilon$. κ_η, σ_η and α_η are nonnegative real numbers. This choice for the metrics was originally proposed by Kuzuoglu and Mittra and is referred to here as the CFS-PML stretched coordinate metrics. For $\alpha_\eta > 0$, this choice has the advantage that it allows the PML to be highly absorptive of low-frequency waves [11]. Then the field components can be obtained in the similar way as it is in [12].

Without loss of generality, assume that the narrow side is along the y- direction. Following the HIE-FDTD scheme [6], [7], the electromagnetic fields are arranged on the cells in the same way as that used in the conventional Yee's staggered FDTD algorithm [1]. The E_y and H_y fields are defined at the time steps n-1/2 and n+1/2, the other fields at the time steps n and n+1. By discretizing the space and time derivatives, the field components can be obtained

$$\begin{aligned} &E_y^{n+1/2}\big|_{i,j+1/2,k} = \kappa_z^{-1}\big|_k \frac{\Delta t}{\varepsilon\Delta z}\left(H_x^{n}\big|_{i,j+1.2,k+1/2} - H_x^{n}\big|_{i,j+1.2,k-1/2}\right) + E_y^{n-1/2}\big|_{i,j+1/2,k} \\ &-\kappa_x^{-1}\big|_i \frac{\Delta t}{\varepsilon\Delta x}\left(H_z^{n}\big|_{i+1/2,j+1/2,k} - H_z^{n}\big|_{i-1/2,j+1/2,k}\right) + \frac{1}{2}\frac{\Delta t}{\varepsilon}\left(f_{Eyz}^{\,n+1/2} + f_{Eyz}^{\,n-1/2}\right) - \frac{1}{2}\frac{\Delta t}{\varepsilon}\left(f_{Eyx}^{\,n+1/2} + f_{Eyx}^{\,n-1/2}\right) \end{aligned} \tag{3a}$$

$$\begin{aligned} &H_y^{n+1/2}\big|_{i+1/2,j,k+1/2} = -\kappa_z^{-1}\big|_{k+1/2} \frac{\Delta t}{\mu\Delta z}\left(E_x^{n}\big|_{i+1/2,j,k+1} - E_x^{n}\big|_{i+1/2,j,k}\right) + H_y^{n-1/2}\big|_{i+1/2,j,k+1/2} \\ &+\kappa_x^{-1}\big|_{i+1/2} \frac{\Delta t}{\mu\Delta x}\left(E_z^{n}\big|_{i+1,j,k+1/2} - E_z^{n}\big|_{i,j,k+1/2}\right) - \frac{\Delta t}{2\mu}\left(f_{Hyz}^{\,n+1/2} + f_{Hyz}^{\,n-1/2}\right) + \frac{\Delta t}{2\mu}\left(f_{Hyx}^{\,n+1/2} + f_{Hyx}^{\,n-1/2}\right) \end{aligned} \tag{3b}$$

where Δt is the time-step size, Δx Δy and Δz are the cell sizes in the x-, y- and z-direction, respectively, other components can be obtained in the same way.

One can find in (3) none of them can be updated directly, because they all contain unknown components on both sides of the equations. In (3a) and (3b), $f_{Eyz}^{\,n+1/2}$, $f_{Eyx}^{\,n+1/2}$, $f_{Hyx}^{\,n+1/2}$, $f_{Hyz}^{\,n+1/2}$ are unknown, they need to be calculated first, after that, E_y and H_y can be updated directly. Updating of E_x^{n+1} component needs the unknown H_z^{n+1} component at the same time, so the E_x^{n+1} component has to be updated implicitly. Updating of E_z^{n+1} component needs the unknown H_x^{n+1} component at the same time. After E_x^{n+1} and E_z^{n+1} components are obtained, H_x^{n+1} and H_z^{n+1} are explicitly updated straightforwardly.

From the equations derived above, it can be seen that the proposed scheme solves 2 tri-diagonal matrices, 4 explicit updates and 12 auxiliary variables in a full update running cycle. However, it needs to solve 6 tri-diagonal matrices, 6 explicit updates and 24 auxiliary variables in the ADI-FDTD method. So the computational resource can be saved in this proposed HIE-CPML method.

Numerical Results

In this section, numerical examples are proposed to validate the formulations of the CFS-PML for the 3D HIE-FDTD. The structure has 66×66×66 cells including 8 layers of CPML in each direction.

Point A at location (57, 33, 33) and point B at location (57, 57, 33) are the observation points. The sinusoidal modulated Gaussian pulse is used as a source at the center of the structure.

The cell size are $\Delta = \Delta x = \Delta y = \Delta z = 0.5\,\text{mm}$. For CPML the parameters are considered as [11]

$$\sigma(\rho) = \sigma_{\max}(\rho/d)^m \tag{5}$$

$$\kappa(\rho) = 1 + \kappa_{\max}(\rho/d)^m \tag{6}$$

where ρ indicates the distance from the air-PML interface into the PML layer, d is the depth of the PML, and m is the order of the polynomial and is chosen to be 4 in this example. In the cases presented, α is held constant through the PML.

For validation the HIE-CPML is compared with FDTD-CPML and the HIE Mur's first-order ABC results. Figure 1 shows the reflection error of the three methods observed at point A. The reflection error is calculated with the following formula:

$$20\log_{10}\left(\frac{\left|E_y^B(t) - E_y^S(t)\right|}{\max\left|E_y^B(t)\right|}\right) \tag{8}$$

where, $E_y^S(t)$ is the field value observed at a point in the simulation domain. $E_y^B(t)$ is obtained by extending dimensions of the simulation domain (to minimize the reflection effect from boundaries). Figure 1 demonstrates that both HIE-CPML and FDTD-CPML have almost the same reflection error, while their reflection error is about 30 dB less than HIE Mur's first-order results.

Next, it is instructive to observe the maximum reflection error as a function of the PML constructive parameters $\kappa_{\max}$, $\sigma_{\max}$ and α. To this end, Figure 2(a) and Figure 2(b) illustrate contour plots of the reflection error versus $\kappa_{\max}$ and $\sigma_{\max}$ with $\alpha = 0.003$ and $\alpha = 0.05$. It is demonstrated here that the maximum error with $\alpha = 0.003$ and $\alpha = 0.05$ are -72 dB. However, when $\alpha = 0.05$ the optimal error is realized over a much broader range of $\kappa_{\max}$ and $\sigma_{\max}$, making these values easier to predict. It can be seen that a maximum relative reflection as low as -72 dB is achieved by selecting $\kappa_{\max} = 14$ and $\sigma_{\max}/\sigma_{opt} = 1.0$.

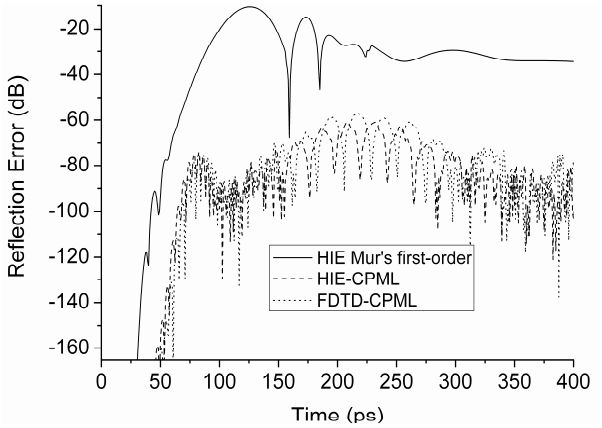

Figure 1. Reflection error of the HIE-CPML, FDTD-CPML and the HIE Mur's first-order results. ($\alpha = 0.003$, $\kappa_{\max} = 14$, $\sigma_{\max} = 0.7\sigma_{opt}$)

Conclusion

In this paper, the CFS-PML was developed for the three dimensional HIE-FDTD method. Formulations of the method are derived by using ADE technique. Numerical results show that this implementation is almost the same effective in reducing reflections of the conventional method. The maximum relative error is lower than -60 dB. The advantage of the HIE-CPML is its applicability at higher CFLN, as well as its accuracy. This development of CPML for the three dimensional HIE-FDTD method will enhance the application of the method.

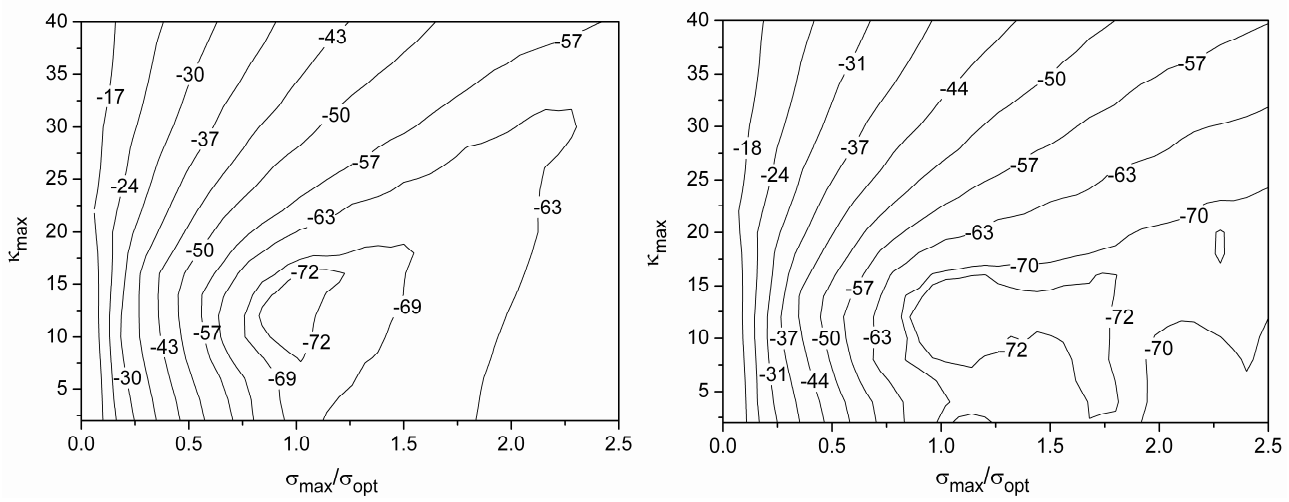

(a) (b)

Figure 2. Maximum relative error at point A (57, 33, 33) as a function of $\kappa_{\max}$ and $\sigma_{\max}/\sigma_{opt}$ ($\alpha = 0.003$ and $m = 4$) and ($\alpha = 0.05$ and $m = 4$).

References

[1] K. S. Yee. "Numerical solution of initial boundary value problems involving Maxwell's equations in isotropic media [J] IEEE Trans. Antennas Propag., 1996 (14), 302-307.

[2] A. Taflove and S. C. Hagness. Computational Electrodynamics: The Finite-Difference Time-Domain Method [M], 2nd ed. Boston, MA: Artech House, 2000.

[3] F. Zheng, Z. Chen, and J. Zhang. Toward the development of a three-dimensional unconditionally stable finite-difference time-domain method [J]. IEEE Trans. Microw. Theory Tech., , 2000 48(9), 1550–1558.

[4] H. L. Chen, B. Chen, Y. Yi and D. G. Fang. Unconditionally Stable ADI–BOR–FDTD Algorithm for the Analysis of Rotationally Symmetric Geometries [J]. IEEE Microw. Wireless Comp. Lett., 2007 17(4), 304–306.

[5] G. S. Liu, G. J. Zhang and B. J. Hu. Numerical analysis for an improved ADI-FDTD method [J]. IEEE Microw. Wireless Compon. Lett., , 2008 18(9) 569-571.

[6] B. K. Huang, G. Wang, Y. S. Jiang and W. B. Wang. A hybrid implicit explicit FDTD scheme with weakly conditional stability [J]. Microw. Opt. Tech. Lett., 2003 39 97–101.

[7] J. Chen, J. Wang. A 3D hybrid implicit explicit FDTD scheme with weakly conditional stability [J]. Microw. Opt. Tech. Lett., 2006 48 2291–2294.

[8] J. Chen and J. G. Wang. The body-of-revolution hybrid implicit-explicit finite-difference time-domain method with large time step size [J]. IEEE Trans. Electromagn. Compat., 2008 50(2), 369–374.

[9] Y. F. Mao, B. Chen and R. Xiong. WCS-FDTD algorithm for periodic structures [J]. IEEE Antennas Wireless Propag. Lett., 2011 10 1236–1238.

[10] Z. S. Sacks, D. M. Kingsland, R. Lee and J. F. Lee. A perfectly matched anisotropic absorber for use as an absorbing boundary condition [J]. IEEE Trans. Antennas Propag., 1995 43 1460-1463.

[11] J. A. Roden and S. D. Gedney. Convolution PML (CPML): An efficient FDTD implementation of the CFS-PML for arbitrary media [J]. Microw. Opt. Tech. Lett., 2000 27(5) 334–339.

[12] J. Berenger. Application of the CFS-PML to the absorption of evanescent waves in waveguides [J]. IEEE Microw. Wireless Compon. Lett., 2002 12 218–220.

Advanced Materials Research Vols. 989-994 (2014) pp 1873-1876
© (2014) Trans Tech Publications, Switzerland
doi:10.4028/www.scientific.net/AMR.989-994.1873

Parameters of Support Vector Machines Model Optimized Method Based on Genetic Algorithm

YuZhen XIE, Zhao-gang WANG, Xiao-wei DAI

PLA 91550 Unit 94, Liaoning Dalian, China

E-mail: xyz_dl@163.com

Keywords: Genetic Algorithms; Support Vector Machines; Optimization; Kernel Function

Abstract. In order to obtain more accurate parameters of support vector machine model, using genetic algorithm to optimize the parameters is an effective method. This paper analyzes the principle of support vector machine for regression, support vector machine kernel function selection, kernel parameters, penalty factor selection and adjustment methods, taking into account genetic algorithm is effective in solving optimization problems, proposed a method using genetic algorithm to optimize the parameters of support vector machine, which uses genetic algorithms to make cross-validation error minimized. The simulation results demonstrate the effectiveness of this method.

Introduction

Support vector machine (SVM) is a learning algorithm based on statistical learning theory proposed can solve the practical problems of small samples, nonlinearity, high dimension and local minima, with strong generalization ability. Practice shows that the type of kernel function, kernel parameters, and penalty factor is one of the key factors affecting the performance of the SVM, so research SVM parameter selection method for support vector machine development has a very important practical significance. This paper presents a global search capability using genetic algorithms to achieve the parameters of support vector machine optimization. The results showed that the genetic algorithm to optimize the parameters of SVM reduces the dependence on the initial value of the selected degrees. And with the traditional optimization algorithm is verified by comparing the genetic algorithm is used to support vector machine parameter optimization of validity and reliability.

Support vector regression principle

The basic idea SVR is to map the samples through a nonlinear mapping $\varphi(\cdot)$ from the original space $\boldsymbol{R^n}$ into a high dimensional feature space, and linear regression in feature space. For a given set of observations: $(\boldsymbol{x_i}, \boldsymbol{y_i}) \in \boldsymbol{R^n} \times \boldsymbol{R}, \boldsymbol{i} = 1,2,\cdots,\boldsymbol{N}$, optimal decision function can be constructed in a high -dimensional feature space:

$$\boldsymbol{y} = \boldsymbol{w} \cdot \varphi(\boldsymbol{x}) + \boldsymbol{b} \tag{1}$$

Where w and b are regression factors, which can be gained by minimizing the following regularized risk function

$$\boldsymbol{J} = \frac{1}{2}\|\boldsymbol{W}\|^2 + \boldsymbol{C} \cdot \boldsymbol{R}_{emp} \tag{2}$$

Among them, $\|\boldsymbol{W}\|$ control model complexity, C is the penalty factor to control the degree of experience in risk of punishment; $\boldsymbol{R}_{emp}$ is error control function, error control function commonly used linear ε loss function, quadratic loss function, select a different loss function can be constructed in different forms of support vector machines. In the text, select the quadratic loss function as the error control function, based on structural risk minimization principle, the above regression problem can be expressed as following optimization problem to solve:

$$\min \boldsymbol{J}(\boldsymbol{w},\xi)=\frac{1}{2}\|\boldsymbol{W}\|^2+\boldsymbol{C}\sum_{i=1}^{n}\xi^2 \tag{3}$$

$$\boldsymbol{s.t.}\ \boldsymbol{y}_i-\boldsymbol{w}\cdot\varphi(\boldsymbol{x}_i)-\boldsymbol{b}=\xi_i \qquad \text{i=1,2,}\cdots\text{,N}$$

Using Lagrange method, the above optimization problem can be transformed to its dual problem to solve, $\boldsymbol{w}$ can be given by:

$$\boldsymbol{w}=\sum_{i=1}^{n}\lambda_i\varphi(\boldsymbol{x}_i) \tag{4}$$

where λ_i is the Lagrange multiplier, $\boldsymbol{f}(\boldsymbol{x})$ can be given by:

$$\boldsymbol{f}(\boldsymbol{x})=\sum_{i=1}^{N}\lambda_i\varphi(\boldsymbol{x})\cdot\varphi(\boldsymbol{x}_i)+\boldsymbol{b}=\sum_{i=1}^{N}\lambda_i\boldsymbol{K}(\boldsymbol{x},\boldsymbol{x}_i)+\boldsymbol{b} \tag{5}$$

Among them, $\boldsymbol{K}(\boldsymbol{x},\boldsymbol{x}_i)=\varphi(\boldsymbol{x})\cdot\varphi(\boldsymbol{x}_i)$, $\boldsymbol{K}(\boldsymbol{x},\boldsymbol{x}_i)$ is the kernel function, which expressed from a low-dimensional space is mapped to some high-dimensional space. The kernel function is symmetric positive real number function while satisfying the conditions of Mercer plot.

SVM model parameter selection based on Genetic algorithm

In support vector regression estimation algorithm, the type of kernel function, kernel function parameters and the penalty factor are important parameters. Penalty factor C for balance training error and model complexity, Kernel function determines the input space to feature space mapping, commonly used kernel functions are:

① Polynomial kernel function

$$\boldsymbol{K}(\boldsymbol{x},\boldsymbol{x}_i)=(\boldsymbol{x}\cdot\boldsymbol{x}_i+\theta)^{\boldsymbol{d}} \tag{6}$$

② Radial basis kernel function

$$\boldsymbol{K}(\boldsymbol{x},\boldsymbol{x}_i)=\exp(-\frac{\|\boldsymbol{x}-\boldsymbol{x}_i\|}{\delta^2}) \tag{7}$$

③Sigmoid kernel function

$$\boldsymbol{K}(\boldsymbol{x},\boldsymbol{x}_i)=\tanh[\boldsymbol{u}(\boldsymbol{x}\cdot\boldsymbol{x}_i)-\boldsymbol{r}] \tag{8}$$

Choose different forms of kernel functions, we can generate different SVM, RBF kernel function is the most widely used kernel function, both in low or high dimensional space , for small samples or large samples, RBF kernel function are applicable, and has a wide domain of convergence, is an ideal kernel function. This paper selects RBF kernel function.

After a given training set and selected kernel function parameters that affect the performance of SVM main penalty factor and nuclear parameters. Support vector regression parameter optimization refers to selecting the optimal penalty factor C and kernel function parameter δ, so that SVM has the best prediction accuracy, and can improve the generalization ability of SVR. In order to obtain better generalization ability, it is necessary to adjust and optimize these parameters.

SVM parameter selection process is an optimized combination of parameters {C, δ} process, each point of the search space is a potential solution best model, and can be assessed by the generalization ability. Therefore, the process of solving the optimal parameters is essentially the process of generalization error is minimized. This paper uses K-fold cross-validation method to estimate the generalization error, K-fold cross-validation method: the training set is randomly divided into K disjoint subsets, Each subset of the same size, equal to L. A sub- set of taking them as a test set, the remaining K-1 subsets as the training set for a given set of parameters regression model, and calculate the mean square error of the test set，mean square error is given by the following formula:

$$\boldsymbol{MSE}(\boldsymbol{i})=\sqrt{\frac{1}{\boldsymbol{l}}\sum_{j=1}^{l}(\boldsymbol{y}_j-\hat{\boldsymbol{y}}_j)^2} \tag{9}$$

Where v denotes the mean square error of the i-th set. After the K iterations, the average value of mean square error as a desired generalization error, The average value of mean square error after k iterations as expected generalization error, Generalization error estimation can be expressed as:

$$T = \frac{1}{k}\sum_{i=1}^{k} MSE(i) \tag{10}$$

Where K generally selected 5 or 10. Select a set of parameters to achieve optimal generalization error minimization. In order to select the optimal set of parameters. Using cross-validation method to adjust the model parameters to achieve generalization error is minimized.

Genetic algorithm is a heuristic optimization algorithms proposed by Professor Holland, which is starting from any initial population, by random selection, crossover and mutation , producing a group of individuals more suitable environment to enable groups evolved to be getting better search space area , so multiply constantly evolve from generation to generation , and finally converge to a group of individual the most suitable environmental and obtain the optimal solution of the problem. Genetic algorithm is links with the problem to be solved only encoding and decoding, so it is widely used to solve complex optimization model. In order to obtain better SVM model, Specific implementation steps for using genetic algorithms to optimize C and δ parameters are as follows :

Step 1: Read the training samples, a set of random {C, δ} as an initial value, and the encoding structure of the initial population;

Step 2: The entire sample evenly divided into K mutually exclusive subsets S1, S2, ..., Sk;

Step 3: According to the current {C, δ} trained SVM, and calculate K-fold cross-validation error;

① Initialization i = 1; Si subset of the test set aside, and the rest of it as a subset of the training set, training SVM; calculation generalization error of the i-subset;

② I = i +1, repeat the above steps until i = k +1, calculate the average generalization error of k times, and get the K-fold cross-validation error, namely the generalization error;

Step 4: Select the generalization error T for the fitness function, and then using genetic algorithms to search better {C, δ};

Step 5: Apply selection, crossover and mutation operators to generate new populations , then repeat steps 2-4 until you meet the maximum number of iterations;

Step 6: Output optimal parameters, and through train SVM training samples to get the best regression model.

Simulation examples

Take a function sin c: $f(x) = \sin c(x) + v, x \in [-3,3]$, Where v is normally distributed with mean 0 and variance Gaussian noise 0.1. In the input variable domain to take 200 randomly generated sets of data , which were selected 100,80 and 50 groups of training and testing samples for simulation calculations, the goal is to minimize 5-fold cross-validation error, the kernel function is radial basis function. Using genetic algorithms optimize parameters δ and C, Where δ and C respectively initialized [0, 1] and [1,100] within, Genetic algorithm of the control parameters: population size is 40, evolution terations is 100, crossover probability is 0.5 and mutation probability is 0.005.

While Parameter optimization process, generalization error trends shown in Fig.1, Fig.2 shows using the parameters obtained by genetic algorithm to train SVM training sample, showing good results fitting. For ease of comparison, using orthogonal method and genetic algorithm multiple times, and the results of statistical residual mean square fit, and the results are shown in Tab.1.

Tab.1 The Result comparison of different methods of SVM parameter optimization

Optimization method	Training samples	Testing samples	C	δ	Training error	Testing error
Orthogonal method	100	100	221.368	0.197	0.0303	0.0300
	80	80	41.180	0.177	0.0327	0.0314
	50	50	10.181	0.179	0.0383	0.0377
Genetic algorithm	100	100	13.375	0.455	0.0202	0.0203
	80	80	75.253	0.750	0.0266	0.0263
	50	50	7.187	0.383	0.0272	0.0274

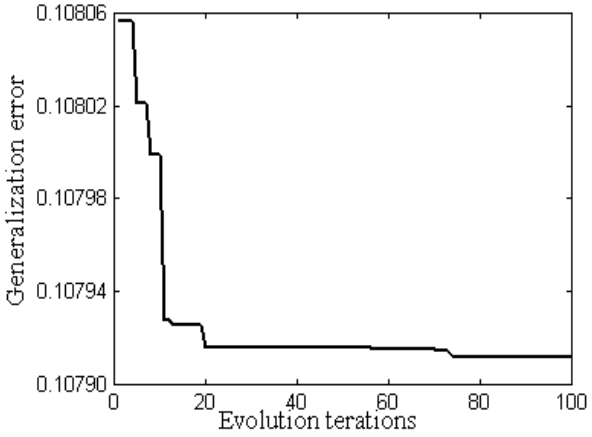

Fig.1 Generalization error and iterations

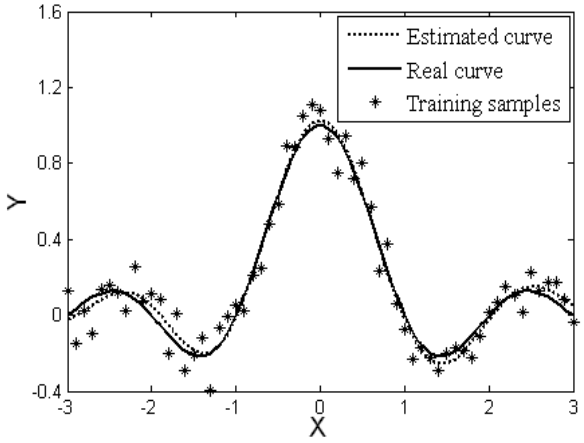

Fig.2 The sin c simulation results

Conclusion

Support vector machines based on structural risk minimization principle to overcome the neural network into local minima, does not converge, instability and other defects, make full use of the limited sample of information to get the optimal solution, and in learning and pan seek the best compromise between aging properties, the ability to get a good promotion.

Using support vector machine to predict, to select parameters is important, if the parameter is selected unreasonable, it may result in the calculation of under- and over- learning phenomena, which directly affect the prediction accuracy. The use of genetic algorithms automatically select SVM parameters so greatly improved predictive ability of the model, in order to improve the accuracy of the selected parameters, while optimizing the parameters in the text using a cross-validation method, the parameters set of best generalization ability as the final parameters. Ultimately resulting model is validated, get good prediction accuracy.

References

[1] YI Zhi-an, JIANG Li-li, DU Juan. Genetic Algorithm Based on Binary Tree Support Vector Machine Classification [J]. Journal of Changchun University of Science and Technology, 2010, 33(1): 152-155.

[2] WANG Kai, ZHANG Yong-xiang, LI Jun. Application Research on Genetic Algorithm and Support Vector Machines in machinery Fault Diagnosis [J]. Journal of Mechanical Strength, 2008, 30(3):349-353.

[3] WANG Shi-qing, CAO Yan. GA-SVM-based Feature Subset Selection Algorithm [J]. Computer Engineering and Design, 2010, 31(18): 4088-4092.

[4] DAI Shang-ping, SONG Yong-dong. Parameter Selection of Support Vector Machines Based on Fusion of Genetic Algorithm and Particle Swarm Optimization [J]. Computer Engineering & Science, 2012, 34(10): 113-116.

[5] SHAO Xin-guang, YANG Hui-zhong, CHENG Guang. Parameters selection and application of support vector machine based on particle swarm optimization algorithm[J]. Control Theory and Applications, 2006, 23(5):740-743.

[6] QING Bo, CHEN Ming, ZHANG Hao. Application of Support Vector Machines to Engine Parameter Acquisitions Unit Fault Diagnosis [J]. Computer Engineering and Design, 2008, 29(18): 4780-4783.

[7] ZHANG Ying-lu. Internet Traffic Forecasting Based on Support Vector Machine Optimized by Genetic Algorithm[J]. Computer Science, 2008, 35(5): 177−179.

[8] LI Liang-min, WEN Guang-rui, WANG Sheng-chang. Parameters Selection of Support Vector Regression Based on Genetic Algorithm[J]. Computer Engineering and Applications, 2008, 44(7): 23−26.

Advanced Materials Research Vols. 989-994 (2014) pp 1877-1882
© (2014) Trans Tech Publications, Switzerland
doi:10.4028/www.scientific.net/AMR.989-994.1877

Robust exponential stability of stochastic discrete-time BAM neural networks with Markovian jumping parameters and delays

Liangdong Guo [1, a], Jin Nie[2, *], Youshan Zhang[1]

[1] School of Science ,University of Science and Technology Liaoning, Anshan,114051,China

[2]State Grid yingkou power supply company,Yingkou, 115000, China

[a]email: liangdonguo@foxmail.com, * :email:ykgdgsnj@163.com

Keywords: BAM neural network; Markovian parameter; Robust stability; Time delay;

Abstract. The problem of robustly globally exponential stability in the mean square is investigated for stochastic uncertain discrete-time bidirectional associative memory (BAM) neural networks with time-varying delays and Markovian jumping parameters. The uncertainties are assumed to be the linear fractional form. By using Lyapunov-Krasovskii functional (LKF) method and some novel technique, a delay-dependent exponential stability criterion is established in terms of linear matrix inequalities (LMIs). A numerical example is provided to show the effectiveness and the improvement of the proposed methods.

Introduction

Neural networks have received considerable attention and successfully applied in many areas such as combinatorial optimization, signal processing and pattern recognition[1]. On the other hand, time delays are unavoidably encountered due to the finite speeds of the switching and transmission of signals in a network and may cause undesirable dynamic network behaviors such as oscillation and instability[2-4]. It has been shown in[5] that jumping between different neural work modes can be governed by a Markovian chain. As an extension of the unidirectional autoassociator of Hopfield, BAM neural network model was first introduced by [6], which generalizes the single-layer auto-associative Hebbian correlator to a two-layer pattern-matched hetero-associative circuit. Recently, the stability analysis for BAM neural networks has received much attention[7-10]. It is worth mentioning that most of references dealt with the continuous time case. However, in numerical simulations and practical implementations continuous-time neural networks, discretization is necessary and the dynamics of discrete-time neural networks may be quite different from those of continuous time ones. In the past few years, there has been rapidly growing interest in the problem of analysis for discrete-time neural networks with delays [11-15]. However, Markovian jumping parameters, stochastic external fluctuations and uncertainties were not addressed in the above references. To the best of our knowledge, few results have been reported in the literature concerning the problem of robust stability for stochastic uncertain discrete-time BAM neural networks with Markovian jumping parameters and time-varying delays, which remains important and challenging.

Motivated by the above reasons, the aim of this work is to deal with robustly exponential stability analysis for discrete-time Markovian jumping BAM neural network with uncertainties and stochastic fluctuations. The uncertainties under consideration are linear fractional form which includes the norm bounded uncertainties as a special case. The activation functions are considered the generalized type, which more general than the usual sigmoid functions and Lipschitz conditions. A new delay-dependent stability criterion is established by utilizing a modified LKF and some new methods. As a result, the conditions are expressed in the form of LMIs. A numerical example is given to illustrate the effectiveness of the proposed techniques.

Problem Statement and Preliminaries

For brief of analysis, we denote

$A_i = A(r_k), B_i = B(r_k), C_i = C(r_k), D_i = D(r_k), \Delta A_i = \Delta A(k, r_k), \Delta B_i = \Delta B(k, r_k), \Delta C_i = \Delta C(k, r_k),$

$\Delta D_i = \Delta D(k, r_k), \delta_1(k) = \delta_1(x(k), y(k-h(k)), k), \delta_2(k) = \delta_2(y(k), x(k-d(k)), k),$

$L_1 = \mathrm{diag}\left\{(l_1^+ + l_1^-)/2, (l_2^+ + l_2^-)/2, \cdots, (l_n^+ + l_n^-)/2\right\}, L_2 = \mathrm{diag}\{l_1^+ l_1^-, l_2^+ l_2^-, \cdots, l_n^+ l_n^-\},$

$K_1 = \mathrm{diag}\left\{(k_1^+ + k_1^-)/2, (k_2^+ + k_2^-)/2, \cdots, (k_n^+ + k_n^-)/2\right\}, K_2 = \mathrm{diag}\{k_1^+ k_1^-, k_2^+ k_2^-, \cdots, k_n^+ k_n^-\},$

$\overline{P}_{1i} = \sum_{j=1}^{s} \pi_{ij} P_{1j}, \overline{P}_{2i} = \sum_{j=1}^{s} \pi_{ij} P_{2j}, \overline{x}(k) = \sum_{l=k-d_M+1}^{k-d_m} x(l), \overline{y}(k) = \sum_{l=k-h_M+1}^{k-h_m} y(l), \hat{x}(k) = \sum_{l=k-d_M}^{k-1} x(l),$

$\hat{y}(k) = \sum_{l=k-h_M}^{k-1} y(l), \overline{g}(x(k)) = \sum_{l=k-d_M+1}^{k-d_m} g(x(l)), \overline{f}(y(k)) = \sum_{l=k-h_M+1}^{k-h_m} f(y(l)),$

$\zeta(k) = x(k+1) - x(k), \zeta(k) = y(k+1) - y(k).$

Let $(r_k, k \geq 0)$ be a Markov chain which takes values in the finite space $S = \{1, 2, \cdots, s\}$ with probability transition matrix:

$$\Pr\{r_{k+1} = j \mid r_k = i\} = \pi_{ij}, i, j \in S. \tag{1}$$

where π_{ij} is transition rate from mode i to mode j satisfying $\pi_{ij} \geq 0$ and $\sum_{j=1}^{s} \pi_{ij} = 1.$

Consider the Markovian jumping BAM neural network with uncertainties and stochastic fluctuations as follows:

$$\begin{cases} x(k+1) = -(A_i + \Delta A_i)x(k) + (B_i + \Delta B_i) f(y(k-h(k))) + \delta_1(k)\omega_1(k), \\ y(k+1) = -(C_i + \Delta C_i) y(k) + (D_i + \Delta D_i) g(x(k-d(k))) + \delta_2(k)\omega_2(k), \end{cases} \tag{2}$$

where $d_m \leq d(k) \leq d_M, h_m \leq h(k) \leq h_M$, A_i, B_i, C_i and D_i for any $i \in S$ are known constant matrices of appropriate dimensions, $\Delta A_i, \Delta B_i, \Delta C_i, \Delta D_i$ for any $i \in S$ that represent the linear fractional uncertainties, which are defined as

$$[\Delta A_i, \Delta B_i, \Delta C_i, \Delta D_i] = E_i[I - F_i(k)G_i]^{-1} F_i(k)[H_{1i}, H_{2i}, H_{3i}, H_{4i}], \tag{3}$$

where $E_i, G_i, H_{li}, (l = 1, \cdots, 4, i \in S)$ are known constant matrices and $G_i^{\mathrm{T}} G_i < I$; $F_i(k)$ is unknown real time-varying matrix with Lebesgue measurable elements bounded by $F_i^{\mathrm{T}}(k) F_i(k) \leq I.$ And $\omega_l(k)$ (l=1,2) are n-dimensional Brownian Motion on $(\Omega, \mathcal{F}, \{\mathcal{F}_t\}_{t \geq 0}, \mathcal{P})$, $\delta_1(k)$ and $\delta_2(k)$ satisfy **A1**: There exist matrices $X_j \geq 0, j = 1, 2, 3, 4$, such that

$$\begin{aligned} \delta_1^{\mathrm{T}}(k)\delta_1(k) &\leq x^{\mathrm{T}}(k) X_1 x(k) + y^{\mathrm{T}}(k-h(k)) X_2 y((k-h(k)), \\ \delta_2^{\mathrm{T}}(k)\delta_2(k) &\leq y^{\mathrm{T}}(k) X_3 y(k) + x^{\mathrm{T}}(k-d(k)) X_4 x(k-d(k)). \end{aligned} \tag{4}$$

The transformed neuron activation functions satisfy **A2**:

$$\begin{aligned} &[x^{\mathrm{T}}(k-d(k)) g^{\mathrm{T}}(x(k-d(k)))] \overline{\Upsilon}_1 [x^{\mathrm{T}}(k-d(k)) g^{\mathrm{T}}(x(k-d(k)))]^{\mathrm{T}} \geq 0, \\ &[y^{\mathrm{T}}(k-h(k)) f^{\mathrm{T}}(y(k-h(k)))] \overline{\Gamma}_1 [y^{\mathrm{T}}(k-h(k)) f^{\mathrm{T}}(y(k-h(k)))]^{\mathrm{T}} \geq 0, \\ &[x^{\mathrm{T}}(k) g^{\mathrm{T}}(x(k))] \overline{\Upsilon}_2 [x^{\mathrm{T}}(k) g^{\mathrm{T}}(x(k))]^{\mathrm{T}} \geq 0, [y^{\mathrm{T}}(k) f^{\mathrm{T}}(y(k))] \overline{\Gamma}_2 [x^{\mathrm{T}}(k) g^{\mathrm{T}}(x(k))]^{\mathrm{T}} \geq 0. \end{aligned} \tag{5}$$

where $\overline{\Upsilon}_k$, $\overline{\Gamma}_k, k = 1, 2$ are given in Theorem in this work.

The system in (2) or (6) is said to be robustly exponentially mean square stable if there exist positive scalars $\mu_0 > 1, \kappa_1 > 1, \kappa_2 > 1$ and integer $N > 1$,such that

$$\mathbb{E}\{\| x(N) \|^2 + \| y(N) \|^2\} \leq (\mu_0)^{-N} \left[\kappa_1 \max_{-d_M \leq l \leq 0} \| x(l) \|^2 + \kappa_2 \max_{-h_M \leq l \leq 0} \| y(l) \|^2 \right].$$

System (2) with uncertainties (3) can be further represented as follows:

$$\begin{cases} x(k+1) = -A_i x(k) + B_i f(y(k-h(k))) + \delta_1(k)\omega_1(k) + E_i\alpha_{1i}(k), \\ y(k+1) = -C_i y(k) + D_i g(x(k-d(k))) + \delta_2(k)\omega_2(k) + E_i\alpha_{2i}(k), \\ \alpha_{1i}(k) = F_i(k)\beta_{1i}(k), \\ \alpha_{2i}(k) = F_i(k)\beta_{2i}(k), \\ \beta_{1i}(k) = -H_{1i}x(k) + H_{2i}f(y(k-h(k))) + G_i\alpha_{1i}(k), \\ \beta_{2i}(k) = -H_{3i}y(k) + H_{4i}g(x(k-d(k))) + G_i\alpha_{2i}(k). \end{cases} \tag{6}$$

Main Results

Theorem: Suppose that **A1** and **A2** hold. Then, for given integers $h_M \geq h_m \geq 1, d_M \geq d_m \geq 1$, system (2) is globally robustly exponential stability in the mean square, if there exist some scalars $\tau_1 > 0, \tau_2 > 0$, some matrices $\Gamma_k = \mathrm{diag}\{\gamma_{k1}, \gamma_{k2}, \cdots, \gamma_{kn}\} > 0, \Upsilon_k = \mathrm{diag}\{\upsilon_{k1}\upsilon_{k2}, \cdots, \upsilon_{kn}\} > 0, P_{ki} > 0, Y_{ki} \geq 0,$ $Z_k > 0, i \in S, k = 1,2,$ $Q_l > 0, R_l > 0, l = 1,2,3,4$ with appropriate dimensions and matrices $N_l, l = 1,2,3,4$ with appropriate dimensions satisfying:

$$\begin{bmatrix} \Phi_{1i} + \Phi_{2i} + \Phi_3 + \Phi_3^{\mathrm{T}} & \sqrt{d_M - d_m}N_1 & \sqrt{d_M - d_m}N_2 & \sqrt{d_M}N_5 \\ \sqrt{d_M - d_m}N_1^{\mathrm{T}} & Q_1 - Q_2 & 0 & 0 \\ \sqrt{d_M - d_m}N_2^{\mathrm{T}} & 0 & R_1 - R_2 & 0 \\ \sqrt{d_M}N_5^{\mathrm{T}} & 0 & 0 & -Z_1 \end{bmatrix} < 0, \tag{7}$$

$$\begin{bmatrix} \Xi_{1i} + \Xi_{2i} + \Xi_3 + \Xi_3^{\mathrm{T}} & \sqrt{h_M - h_m}N_3 & \sqrt{h_M - h_m}N_4 & \sqrt{h_M}N_6 \\ \sqrt{h_M - h_m}N_3^{\mathrm{T}} & Q_3 - Q_4 & 0 & 0 \\ \sqrt{h_M - h_m}N_4^{\mathrm{T}} & 0 & R_3 - R_4 & 0 \\ \sqrt{h_M}N_6^{\mathrm{T}} & 0 & 0 & -Z_2 \end{bmatrix} < 0, \tag{8}$$

$$\overline{P}_{1i} < \tau_1 I,\ \overline{P}_{2i} < \tau_2 I, \tag{9}$$

where

$\Phi_{1i} = \mathrm{diag}\{Q_1 + (d_M - d_m)Q_2 - P_{1i} + \tau_1 X_1 + d_M Z_1, \tau_1 X_2 - Q_3, R_1 + (d_M - d_m)R_2, -R_3, 0, 0, 0, -Y_{1i}\},$

$\Xi_{1i} = \mathrm{diag}\{Q_3 + (h_M - h_m)Q_4 - P_{2i} + \tau_2 X_3 + h_M Z_2, \tau_2 X_4 - Q_1, R_3 + (h_M - h_m)R_4, -R_1, 0, 0, 0, -Y_{2i}\},$

$\Phi_{2i} = \mathcal{A}_{1i}^{\mathrm{T}}\overline{P}_{1i}\mathcal{A}_{1i} + \mathcal{H}_{1i}^{\mathrm{T}}Y_{1i}\mathcal{H}_{1i} + \mathcal{I}_1^{\mathrm{T}}\overline{\Gamma}_1\mathcal{I}_1 + \mathcal{I}_2^{\mathrm{T}}\overline{\Upsilon}_2\mathcal{I}_2, \mathcal{A}_{1i} = [-A_i\ 0\ 0\ B_i 0\ 0\ 0\ E_i],$

$\Xi_{2i} = \mathcal{A}_{2i}^{\mathrm{T}}\overline{P}_{2i}\mathcal{A}_{2i} + \mathcal{H}_{2i}^{\mathrm{T}}Y_{2i}\mathcal{H}_{2i} + \mathcal{I}_1^{\mathrm{T}}\overline{\Upsilon}_1\mathcal{I}_1 + \mathcal{I}_2^{\mathrm{T}}\overline{\Gamma}_2\mathcal{I}_2, \mathcal{A}_{2i} = [-C_i 0\ 0\ D_i\ 0\ 0\ 0\ E_i],$

$\Phi_3 = N_1 e_5 + N_2 e_6 + N_5 e_7, \Xi_3 = N_3 e_5 + N_4 e_6 + N_6 e_7, \mathcal{H}_{1i} = [-H_{1i}\ 0\ 0\ H_{2i}\ 0\ 0\ 0\ G_i], \mathcal{H}_{2i} = [-H_{3i} 0\ 0\ H_{4i}\ 0\ 0\ 0\ G_i],$

$$\overline{\Upsilon}_1 = \begin{bmatrix} -\Upsilon_1 L_2 & \Upsilon_1 L_1 \\ \Upsilon_1 L_1 & -\Upsilon_1 \end{bmatrix}, \overline{\Upsilon}_2 = \begin{bmatrix} -\Upsilon_2 L_2 & \Upsilon_2 L_1 \\ \Upsilon_2 L_1 & -\Upsilon_2 \end{bmatrix}, \overline{\Gamma}_1 = \begin{bmatrix} -\Gamma_1 K_2 & \Gamma_1 K_1 \\ \Gamma_1 K_1 & -\Gamma_1 \end{bmatrix}, \overline{\Gamma}_2 = \begin{bmatrix} -\Gamma_2 K_2 & \Gamma_2 K_1 \\ \Gamma_2 K_1 & -\Gamma_2 \end{bmatrix},$$

$\mathcal{I}_1 = \begin{bmatrix} e_2^{\mathrm{T}} & e_4^{\mathrm{T}} \end{bmatrix}, \mathcal{I}_2^{\mathrm{T}} = \begin{bmatrix} e_1^{\mathrm{T}} e_3^{\mathrm{T}} \end{bmatrix}, e_k = [0\ 0 \cdots 0\ \underset{k\text{th block}}{I}\ 0 \cdots o], k = 1,2,\cdots,8.$

Proof: For positive definite matrices $P_{ki} > 0, k = 1,2, Q_j > 0, R_j > 0, j = 1,2,3,4$, let us consider the LKF candidate:

$$V(k) = V_1(k) + V_2(k) + V_3(k) + V_4(k) + V_5(k) + V_6(k), \tag{10}$$

where

$$V_1(k) = x^{\mathrm{T}}(k)P_{1i}x(k) + y^{\mathrm{T}}(k)P_{2i}y(k), V_2(k) = \sum_{l=k-d(k)}^{k-1} x^{\mathrm{T}}(l)Q_1 x(l) + \sum_{l=-d_M+2}^{-d_m+1}\sum_{j=k+l-1}^{k-1} x^{\mathrm{T}}(j)Q_2 x(j),$$

$$V_3(k) = \sum_{l=k-h(k)}^{k-1} y^{\mathrm{T}}(l)Q_3 y(l) + \sum_{l=-h_M+2}^{-h_m+1}\sum_{j=k+l-1}^{k-1} y^{\mathrm{T}}(j)Q_4 y(j), V_4(k) = \sum_{l=k-d(k)}^{k-1} g^{\mathrm{T}}(x(l))R_1 g(x(l)) + \sum_{l=-d_M+2}^{-d_m+1}\sum_{j=k+l-1}^{k-1} g^{\mathrm{T}}(x(j))R_2 g(x(j)),$$

$$V_5(k) = \sum_{l=k-h(k)}^{k-1} f^{\mathrm{T}}(y(l))R_3 f(y(l)) + \sum_{l=-h_M+2}^{-h_m+1}\sum_{j=k+l-1}^{k-1} f^{\mathrm{T}}(y(j))R_4 f(y(j)), V_6(k) = \sum_{l=-d_M}^{-1}\sum_{j=k+l-1}^{k-1} x^{\mathrm{T}}(j)Z_1 x(j) + \sum_{l=-h_M}^{-1}\sum_{j=k+l-1}^{k-1} y^{\mathrm{T}}(j)Z_2 y(j).$$

Calculating the difference of $V(k)$ along the system (6), taking the mathematical expectation, and using the finite sum equality in [16],we have

$$\mathbb{E}\{\Delta V(k)\}=\sum_{l=1}^{6}\mathbb{E}\{\Delta V_l(k)\}=\sum_{l=1}^{6}\mathbb{E}\{V_l(k+1)-V_l(k)\} \tag{11}$$

where

$$\begin{aligned}
&\xi_1^{\mathrm{T}}(k)=[x^{\mathrm{T}}(k)\,y^{\mathrm{T}}(k-h(k))\,g^{\mathrm{T}}(x(k))\,f^{\mathrm{T}}(y(k-h(k)))\,\overline{x}^{\mathrm{T}}(k)\,\overline{g}^{\mathrm{T}}(k)\,\hat{x}^{\mathrm{T}}(k)\,\alpha_{1i}^{\mathrm{T}}(k)],\\
&\xi_2^{\mathrm{T}}(k)=[y^{\mathrm{T}}(k)\,x^{\mathrm{T}}(k-d(k))\,f^{\mathrm{T}}(y(k))\,g^{\mathrm{T}}(x(k-d(k)))\,\overline{y}^{\mathrm{T}}(k)\,\overline{f}^{\mathrm{T}}(k)\,\hat{y}^{\mathrm{T}}(k)\,\alpha_{2i}^{\mathrm{T}}(k)],\\
&\mathbb{E}\{\Delta V_1(k)\}=-x^{\mathrm{T}}(k)P_{1i}x(k)-y^{\mathrm{T}}(k)P_{2i}y(k)+\delta_1^{\mathrm{T}}(k)\overline{P}_{1i}\delta_1(k)+\delta_2^{\mathrm{T}}(k)\overline{P}_{2i}\delta_2(k)\\
&\quad+[-A_ix(k)+B_if(y(k-h(k))+E_i\alpha_{1i}(k)]^{\mathrm{T}}\times\overline{P}_{1i}[-A_ix(k)+B_if(y(k-h(k))+E_i\alpha_{1i}(k)]\\
&\quad+[-C_iy(k)+D_ig(x(k-h(k))+E_i\alpha_{2i}(k)]^{\mathrm{T}}\,\overline{P}_{2i}[-C_iy(k)+D_ig(x(k-d(k))+E_i\alpha_{2i}(k)],\\
&\mathbb{E}\{\Delta V_2(k)\}\le x^{\mathrm{T}}(k)[Q_1+(d_M-d_m)Q_2]x(k)-x^{\mathrm{T}}(k-d(k))Q_1x(k-d(k))\\
&\quad+(d_M-d_m)\xi_1^{\mathrm{T}}(k)N_1(Q_2-Q_1)^{-1}N_1^{\mathrm{T}}\xi_1(k)+2\xi_1^{\mathrm{T}}(t)N_1\overline{x}(k),\\
&\mathbb{E}\{\Delta V_3(k)\}\le y^{\mathrm{T}}(k)[Q_3+(h_M-h_m)Q_4]y(k)-y^{\mathrm{T}}(k-h(k))Q_3y(k-h(k))\\
&\quad+(h_M-h_m)\xi_2^{\mathrm{T}}(k)N_3(Q_4-Q_3)^{-1}N_3^{\mathrm{T}}\xi_2(k)+2\xi_2^{\mathrm{T}}(t)N_3\overline{y}(k),\\
&\mathbb{E}\{\Delta V_4(k)\}\le g^{\mathrm{T}}(x(k))[R_1+(d_M-d_m)R_2]g(x(k))-g^{\mathrm{T}}(x(k-d(k)))R_1g(x(k-d(k)))\\
&\quad+(d_M-d_m)\xi_1^{\mathrm{T}}(k)N_2(R_2-R_1)^{-1}N_2^{\mathrm{T}}\xi_1(k)+2\xi_1^{\mathrm{T}}(t)N_2\overline{g}(k),\\
&\mathbb{E}\{\Delta V_5(k)\}\le f^{\mathrm{T}}(y(k))[R_3+(h_M-h_m)R_4]f(y(k))-f^{\mathrm{T}}(y(k-h(k)))R_3f(y(k-h(k)))\\
&\quad-(h_M-h_m)\xi_2^{\mathrm{T}}(k)N_4(R_4-R_3)^{-1}N_4^{\mathrm{T}}\xi_2(k)+2\xi_2^{\mathrm{T}}(t)N_4\overline{f}(k),\\
&\mathbb{E}\{\Delta V_6(k)\}=d_Mx^{\mathrm{T}}(k)Z_1x(k)+h_My^{\mathrm{T}}(k)Z_2y(k)+d_M\xi_1^{\mathrm{T}}(k)N_5Z_1^{-1}N_5^{\mathrm{T}}\xi_1(k)+2\xi_1^{\mathrm{T}}(t)N_5\hat{x}(k)\\
&\quad+h_M\xi_2^{\mathrm{T}}(k)N_6Z_2^{-1}N_6^{\mathrm{T}}\xi_2(k)+2\xi_2^{\mathrm{T}}(t)N_6\hat{y}(k).
\end{aligned} \tag{12}$$

On the other hand, it follows from (4) and (6), there exist matrices $Y_{1i},Y_{2i}\ge 0$ such that

$$\begin{aligned}
&\delta_1^{\mathrm{T}}(k)\overline{P}_{1i}\delta_1(k)\le\tau_1[x^{\mathrm{T}}(k)X_1x(k)+y^{\mathrm{T}}(k-h(k))X_2y(k-h(k))],\\
&\delta_2^{\mathrm{T}}(k)\overline{P}_{2i}\delta_2(k)\le\tau_2[y^{\mathrm{T}}(k)X_3y(k)+x^{\mathrm{T}}(k-d(k))X_4x(k-d(k))],
\end{aligned} \tag{13}$$

$$\xi_1^{\mathrm{T}}(k)\mathcal{H}_{1i}^{\mathrm{T}}Y_{1i}\mathcal{H}_{1i}\xi_1(k)-\alpha_{1i}^{\mathrm{T}}(k)Y_{1i}\alpha_{1i}(k)\ge 0,\ \xi_2^{\mathrm{T}}(k)\mathcal{H}_{2i}^{\mathrm{T}}Y_{2i}\mathcal{H}_{2i}\xi_2(k)-\alpha_{2i}^{\mathrm{T}}(k)Y_{2i}\alpha_{2i}(k)\ge 0. \tag{14}$$

Substituting (13) into (12) , adding the terms on the left sides of (5) and (14) to (12) leads to

$$\mathbb{E}\{\Delta V(k)\}\le\xi_1^{\mathrm{T}}(k)\Phi\xi_1(k)+\xi_2^{\mathrm{T}}(k)\Xi\xi_2(k)$$

where

$$\begin{aligned}
&\Phi=\Phi_{1i}+\Phi_{2i}+\Phi_3+\Phi_3^{\mathrm{T}}+d_MN_5Z_1^{-1}N_5^{\mathrm{T}}+(d_M-d_m)[N_1(Q_2-Q_1)^{-1}N_1^{\mathrm{T}}+N_2(R_2-R_1)^{-1}N_2^{\mathrm{T}}],\\
&\Xi=\Xi_{1i}+\Xi_{2i}+\Xi_3+\Xi_3^{\mathrm{T}}+h_MN_6Z_2^{-1}N_6^{\mathrm{T}}+(h_M-h_m)[N_3(Q_4-Q_3)^{-1}N_3^{\mathrm{T}}+N_4(R_4-R_3)^{-1}N_4^{\mathrm{T}}].
\end{aligned}$$

According to Schur complements formula, $\Phi<0$ and $\Xi<0$ are equivalent to (7) and 8), respectively. And (7) and (8) imply $Q_2-Q_1>0,Z_1>0,R_2-R_1>0$ and $Q_4-Q_3>0,\ Z_2>0,$ $R_4-R_3>0$, which are equivalent to $\Omega_j<0(j=1,2,\cdots,6)$. One can conclude $\mathbb{E}\{\Delta V(k)\}<0$, if (7)-(9) are feasible. Now, defining a new function $W(k)=\mu^kV(k)$, it can be seen that for any positive integer $N\ge 1$, there exists a scalar $\mu_0>1$ such that

$$\mathbb{E}\{\|x(N)\|^2+\|y(N)\|^2\}\le\left(\frac{1}{\mu_0}\right)^N\left[\frac{\lambda_1}{\lambda_0}\max_{-d_M\le l\le 0}\|x(l)\|^2+\frac{\lambda_2}{\lambda_0}\max_{-h_M\le l\le 0}\|y(l)\|^2\right],$$

where

$$\begin{aligned}
&\lambda_1=\lambda_{\max}(P_{1i})+(1+d_M)[(\lambda_{\max}(R_1)+(1+d_M-d_m)\lambda_{\max}(R_2))\|L\|^2+\lambda_{\max}(Q_1)+(1+d_M)\lambda_{\max}(Z_1)+(1+d_M-d_m)\lambda_{\max}(Q_2)],\\
&\lambda_2=\lambda_{\max}(P_{2i})+(1+h_M)[(\lambda_{\max}(R_3)+(1+h_M-h_m)\lambda_{\max}(R_4))\|K\|^2+\lambda_{\max}(Q_3)+(1+h_M)\lambda_{\max}(Z_2)+(1+h_M-h_m)\lambda_{\max}(Q_4)],\\
&\lambda_0=\min\{\lambda_{\min}(P_{1i}),\lambda_{\min}(P_{2i})\},L=\mathrm{diag}\{l_1,l_2,\cdots,l_n\},l_q=\max\{|l_q^-|,|l_q^+|\},K=\mathrm{diag}\{k_1,k_2,\cdots,k_n\};k_q=\max\{|k_q^-|,|k_q^+|\},q=1,2,\cdots,n.
\end{aligned}$$

Recalling the Definition, we can conclude that BAM neural network (2) is globally robustly exponentially stable in the mean square sense. This completes the proof.

Illustrative example

Example Consider system (2) with the following matrices

$A=\begin{bmatrix}0.5 & 0\\ 0 & 0.6\end{bmatrix}$, $B=\begin{bmatrix}0 & 0.1\\ 0.1 & 0.06\end{bmatrix}$, $C=\begin{bmatrix}0.9 & 0\\ 0 & 0.8\end{bmatrix}$, $D=\begin{bmatrix}-0.1 & 0.1\\ 0 & 0.1\end{bmatrix}$, $\Delta A=\Delta B=\Delta C=\Delta D=0$

Let $d(k)=2+(-1)^k, h(k)=4+2(-1)^k$. It is reported in [18] that the stability criterion in [11] can not be applied to this example because of the constraints on the delay functions. To compared with methods proposed by [18], we assume $L_1=K_1=0$ and $L_2=K_2=-I$ .We can verify that the stability condition proposed by Theorem in [18] is not satisfied when set $l_{\min}=k_{\min}=l_{\max}=k_{\max}=2$ $r=1.2$. However, when $d_m=h_m=2, d_M=2, h_M=6$, according to Theorem in this work, we can find that system (2) is still exponentially stable, which shows that the criterion proposed in this paper is an improvement over the one in [11,17].

Conclusion

The problem of robustly exponentially stable in the mean square for uncertain stochastic BAM neural networks with Markovian jumping parameters and variable delays has been studied. A new stability criterion has been proposed by using LKF method and the novel bounding technique. As a result, the conditions have been established in term of LMIs. Finally, a numerical example has been given to illustrate the effectiveness and the improvement of our results.

Acknowledgement

The research was sponsored by the Nature Science Foundation (Project No. 61174215) and Youth Fund Project of University of Science and Technology Liaoning (Project No. 2013RC07).

References

[1] Cochocki A., Unbehauen R.,Neural networks for optimization and signal processing[M], Chichester, NewYork, 1993.

[2] Gopalsamy K, He X Z. Delay-independent stability in bidirectional associative memory networks[J]. IEEE Transactions on Neural Networks, 1994, 5(6) 998-1002.

[3] Wang Z, Liu Y, Liu X. On global asymptotic stability of neural networks with discrete and distributed delays[J]. Physics Letters A, 2005, 345(4) 299-308.

[4] He Y, Liu G P, Rees D, et al. Stability analysis for neural networks with time-varying interval delay[J]. IEEE Transactions on Neural Networks, 2007, 18(6) 1850-1854.

[5] Wang Z, Liu Y, Yu L, et al. Exponential stability of delayed recurrent neural networks with Markovian jumping parameters[J]. Physics Letters A, 2006 ,356(4) 346-352.

[6] Kosko B. Adaptive bidirectional associative memories[J]. Applied optics, 1987, 26(23) 4947-4960.

[7] Zhang Z, Zhou D. Existence and global exponential stability of a periodic solution for a discrete-time interval general BAM neural networks[J]. Journal of the Franklin Institute, 2010, 347(5) 763-780.

[8] Gu H. Mean square exponential stability in high-order stochastic impulsive BAM neural networks with time-varying delays[J]. Neurocomputing, 2011, 74(5) 720-729.

[9] Zhang Z, Liu K, Yang Y. New LMI-based condition on global asymptotic stability concerning BAM neural networks of neutral type[J]. Neurocomputing, 2012, 81(0)24-32.

[10]Liu B. Global exponential stability for BAM neural networks with time-varying delays in the leakage terms[J]. Nonlinear Analysis: Real World Applications, 2013, 14(1) 559-566.

[11]Liang J, Cao J. Exponential stability of continuous-time and discrete-time bidirectional associative memory networks with delays[J]. Chaos, Solitons & Fractals, 2004, 22(4) 773-785.

[12]Liu Y., Wang Z., Liu X., Asymptotic stability for neural networks with mixed time-delays: The discrete-time case [J]. Neural Networks 2009, 22(1)67-74.

[13]Liu Z., Shu L., Zhong S., Ye M., Improved exponential stability criteria for discrete-time neural networks with time-varying delay [J]. Neurocomputing 2010 23(4-6)315-321.
[14]Ou Y., Shi P., Liu H., A mode-dependent stability criterion for delayed discrete-time stochastic neural networks with markovian jumping parameters [J]. Neurocomputing 2010 73(7-9) 740-748.
[15]Wu Z G, Park J H, Su H, et al. Stochastic stability analysis for discrete-time singular Markov jump systems with time-varying delay and piecewise-constant transition probabilities[J]. Journal of the Franklin Institute, 2012, 349(9) 2889-2902.
[16] Wu Z G, Shi P, Su H, et al. Exponential synchronization of neural networks with discrete and distributed delays under time-varying sampling[J]. IEEE Transactions on Neural Networks and Learning Systems , 2012, 23(9) 1368-1376.
[17]L.Guo, H.Gu, Robust Stability of discrete systems with uncertainties and random delay[C], ICMTMA,Changsha, 2010 ,291-294.
[18]Liu X G, Tang M L, Martin R, et al. Discrete-time BAM neural networks with variable delays[J]. Physics Letters A, 2007, 367(4) 322-330.

Advanced Materials Research Vols. 989-994 (2014) pp 1883-1886
© (2014) Trans Tech Publications, Switzerland
doi:10.4028/www.scientific.net/AMR.989-994.1883

A correlation coefficient estimation algorithm based on Subspace decomposition

Na WU[1, a], Weijian SI[1, b],Shuhong JIAO[1, c]

[1]Department of Information and Communication, Harbin Engineering University, Harbin, 150001, China

[a]email: wunahmc@163.com, [b]email: swj0418@263.net, [c]email: jiaoshuhong@hrbeu.edu.cn

Keywords: Correlation Coefficient Estimation; Subspace Decomposition; MUSIC Algorithm

Abstract. the correlation coefficient estimation algorithm based on subspace decomposition is presented in this paper. The correlation coefficient between the signals is obtained by getting eigen-value decomposition of the data covariance matrix, and deriving the relationship between signal subspace and noise subspace. Simulation results verify that this algorithm can be realized to get the correlation coefficient between two incident signals whose DOA are known and the effect of the correlation coefficient estimation is made by different signal direction angular intervals.

Introduction

Correlation coefficient of random variables has wide applications in statistical analysis.[1] In the field of signal processing, the correlation coefficient is used to indicate the degree of correlation between the signals. The conventional Algorithm of getting correlation coefficient applies only to know the source of the two signals, respectively, because the signal that array received is the result after the incident signal synthesis. so the conventional algorithm does not apply to the case of data that array receive. When Spectrum technology is used to find the direction of signals, the correlation between the signal source seriously affect the measured performance of the algorithm. To solve the condition of coefficient is equal to 1, many improved algorithms are presented, such as the spatial smoothing technique, Weighted spatial smoothing technique[2],SVD[3],Toeplitz[4,5] algorithm and so on. while these algorithms can solve the condition of coherent signal, When the signals are not coherent completely. Using these algorithms will undoubtedly generate unnecessary performance loss. If we can estimate correlation coefficient between the radio source, depending on the correlation coefficient to select algorithm, it can reduce unnecessary loss of performance. The correlation of the incident signal source will change in the dissemination process. Combining this changes with MUSIC algorithm undoubtedly will greatly improve the performance of traditional MUSIC algorithm[6-8]. So, to estimate the correlation between the signal source by using of array data received has a certain value and the value of engineering applications. In this paper , the thought of subspace decomposition will apply to estimate the correlation coefficient, getting the formula of the correlation coefficient between the signal source by the mathematical derivation Use of array receives data on the estimate of the correlation coefficient between the signal source and verify the effectiveness of the algorithm through computer simulation. It gets the correlation coefficient by the data that array received. Simulation results verify that this algorithm can be realized.

Signal Model for CC Estimation

Uniform linear array (ULA) of M antennas is considered in this paper. Assume that K narrowband far-field signals impinge on the array with directions of $\theta_1, \theta_2, \cdots, \theta_K$ .The output data vector of antennas can be shown as

$$\boldsymbol{X}(t) = \boldsymbol{A}\boldsymbol{S}(t) + \boldsymbol{N}(t) \tag{1}$$

Where $\boldsymbol{S}(t)$ is a K$\times$1-dimensional vector of signal-in-space. $\boldsymbol{N}(t)$ is a M$\times$1-dimensional vector of noise which is spatially white Gaussian noise with equal variance and is uncorrelated with

$\boldsymbol{S}(t)$. $\boldsymbol{A}=[\boldsymbol{a}(\theta_1),\boldsymbol{a}(\theta_2),\cdots,\boldsymbol{a}(\theta_K)]$ is a M×K-dimensional matrix called array manifold matrix, where $\boldsymbol{a}(\theta_i)=[1,\exp(-(j2\pi d\sin\theta_i)/\lambda),\cdots,\exp(-(j2\pi(M-1)d\sin\theta_i)/\lambda)]^{\mathrm{T}}$, λ is the wavelength of incident signal, d is the inter-element spacing which is set to be half a λ.

The covariance matrix of $\boldsymbol{X}(t)$ can be represented as

$$\boldsymbol{R}_x=\mathrm{E}\{\boldsymbol{X}(t)\boldsymbol{X}^{\mathrm{H}}(t)\}=\boldsymbol{A}\boldsymbol{R}_s\boldsymbol{A}^{\mathrm{H}}+\sigma_n^2\boldsymbol{I}_M \tag{2}$$

Where $\boldsymbol{R}_x$ is the covariance matrix of $\boldsymbol{X}(t)$, σ_n^2 is the covariance of noise, and $\boldsymbol{R}_s$ is the covariance matrix of $\boldsymbol{S}(t)$ which rests with the correlation between incident signals , it can represented as

$$\boldsymbol{R}_S=\mathrm{E}[\boldsymbol{S}(t)\boldsymbol{S}^{\mathrm{H}}(t)] \tag{3}$$

We can get the eigen-value decomposition of $\boldsymbol{R}_x$ as

$$\boldsymbol{R}_x=\boldsymbol{U}_S\boldsymbol{\Sigma}_S\boldsymbol{U}_S^{\mathrm{H}}+\boldsymbol{U}_N\boldsymbol{\Sigma}_N\boldsymbol{U}_N^{\mathrm{H}} \tag{4}$$

Where μ_i is the eigen values which meet the conditions of $\mu_1\geq\mu_2\geq\cdots\geq\mu_K\geq\mu_{K+1}=\cdots=\mu_M$, e_i and e_j are the corresponding eigenvectors, $\boldsymbol{U}_S$ and $\boldsymbol{U}_N$ are the corresponding eigenvector matrices which are named signal subspace matrix and noise subspace matrix respectively.

$\boldsymbol{\Sigma}=diag\{\mu_1,\mu_2,\cdots\mu_K,\mu_{K+1},\cdots\mu_M\}$ And $\boldsymbol{\Sigma}_S=diag\{\mu_1,\mu_2,\cdots\mu_K\}$, $\boldsymbol{\Sigma}_N=diag\{\mu_{K+1},\mu_{K+2},\cdots\mu_M\}$.

Signal Correlation Analysis

Coherent coefficient is a statistical analysis index which reflect the relevance degree between two variables. Assume $s_i(t)$ and $s_k(t)$ are two stationary signals, the correlation coefficient between them can be defined as

$$\rho_{ik}=\frac{\mathrm{E}[s_i(t)\overset{*}{s}_k(t)]}{\sqrt{\mathrm{E}[|s_i(t)|^2]\mathrm{E}[|s_k(t)|^2]}} \tag{5}$$

Easy to know that $|\rho_{ik}|\leq 1$, consider the multiple signals, the relationship between the signals can be divided into irrelevant, relevant or coherent according to the value of the correlation coefficient. The correlation between the signals are defined as follows: $\rho_{ik}=0$, $s_i(t)$ and $s_k(t)$ are independent; $0<\rho_{ik}<1$, $s_i(t)$ and $s_k(t)$ are positive correlation;$-1<\rho_{ik}<0$, $s_i(t)$ and $s_k(t)$ are negative correlation; $\rho_{ik}=\pm 1$, $s_i(t)$ and $s_k(t)$ are coherent.In order to simplify the signal model, scholars have often assumed that the signals are not related (the case of $\rho_{ik}=0$)or coherent (the case of $\rho_{ik}=\pm 1$) in array signal processing. However, in a real environment, The absolute value of the correlation coefficient between the signals often range between 0 and 1, this is discussed in the paper.

Correlation Coefficient Estimation Algorithm Based on Feature Subspace Decomposition

Right multiplicate matrix $\boldsymbol{U}_S$ around both ends of equation (4), get equation (6) as

$$\boldsymbol{R}_x\boldsymbol{U}_S=\boldsymbol{A}\boldsymbol{R}_s\boldsymbol{A}^{\mathrm{H}}\boldsymbol{U}_S+\sigma_n^2\boldsymbol{U}_S \tag{6}$$

Eigenvalue decomposition of data covariance matrix is shown as

$$\boldsymbol{R}_x=\boldsymbol{U}_S\boldsymbol{\Sigma}_S\boldsymbol{U}_S^{\mathrm{H}}+\boldsymbol{U}_N\boldsymbol{\Sigma}_N\boldsymbol{U}_N^{\mathrm{H}} \tag{7}$$

Right multiplicate matrix $\boldsymbol{U}_S$ around both ends of equation (7), we can get equation(8) as follow

$$\boldsymbol{R}_x\boldsymbol{U}_S=\boldsymbol{U}_S\boldsymbol{\Sigma}_S\boldsymbol{U}_S^{\mathrm{H}}\boldsymbol{U}_S+\boldsymbol{U}_N\boldsymbol{\Sigma}_N\boldsymbol{U}_N^{\mathrm{H}}\boldsymbol{U}_S \tag{8}$$

As we known, Signal subspace and noise subspace are orthogonal, and have follow equation

$$\boldsymbol{U}_S^{\mathrm{H}}\boldsymbol{U}_S = \boldsymbol{I} \tag{9}$$

So equation (8) can be simplified as

$$\boldsymbol{R}_x\boldsymbol{U}_S = \boldsymbol{U}_S\boldsymbol{\Sigma}_S \tag{10}$$

Observe the equation (6) and equation (8), we can obtained

$$\boldsymbol{A}\boldsymbol{R}_s\boldsymbol{A}^{\mathrm{H}}\boldsymbol{U}_S + \sigma_n^2\boldsymbol{U}_S = \boldsymbol{U}_S\boldsymbol{\Sigma}_S \tag{11}$$

And we can get the calculation formula as

$$\boldsymbol{R}_s = \boldsymbol{A}^{+}\boldsymbol{U}_S\boldsymbol{\Sigma}_S\boldsymbol{U}_S^{\mathrm{H}}(\boldsymbol{A}^{+})^{\mathrm{H}} - \sigma_n^2(\boldsymbol{A}^{\mathrm{H}}\boldsymbol{A})^{-1} \tag{12}$$

Where the "+" is pseudo-inverse matrix [8].

From formula (4) and (12), the value of correlation coefficient $\hat{\rho}_{ik}$ can be extracted from $\hat{R}_s$ through formula (13)

$$\rho_{ik} = \frac{\boldsymbol{R}_s(i,k)}{\sqrt{\boldsymbol{R}_s(i,i)\boldsymbol{R}_s(i,k)}} \tag{13}$$

Computer Simulation

The performance of provided algorithm is analyzed through simulations in this section. An 5-element uniform linear array is used and the inter-element spacing is half a wavelength. Assume that the noise is additive white Gaussian noise, and it not correlate with the signals.

Example 1. The validation of the algorithm

Two incident signals from 10º and 20º ,100 snapshots is used, and SNR is set to be -2dB, change the value of correlation coefficient, the mean value of 200 Monte Carlo trials corresponding to each value is shown as table 1.

Tab.1 The results of correlation coefficient estimation algorithm based on feature subspace decomposition

True value	Estimated value	MSE	True value	Estimated value	MSE
0.1	0.1103	0.0495	0.6	0.5913	0.0299
0.2	0.1990	0.0596	0.7	0.7016	0.0325
0.3	0.2897	0.0523	0.8	0.8052	0.0329
0.4	0.3927	0.0541	0.9	0.9858	0.1353
0.5	0.5097	0.0500			

Provable by Tab.1 , this method can be implemented to estimate the correlation coefficient between two incident signals, and the mean square error (MSE) of estimates is small, so this method can achieve correlation coefficient estimates.

Example 2.The relationship between MSE and the incident signals direction angular intervals

Assume the correlation coefficient between two incident spatial signals is 0.5 , 100 snapshots are used ,SNR= -2dB .Two incident spatial signals are recorded as $s_1(t)$ and $s_2(t)$, the direction of $s_1(t)$ as the reference is set to 0º, the direction of $s_2(t)$ gradually increase from 4.5 º to 10 º with the step value of 0.5 º , Figure 2 is the statistical experimental results of 200 independent experiments.

Figure 1 show that the MSE of this method tend to decrease with increasing angle interval of ,and when the angular intervals less than 4.5 º , the MSE exceeds 0.5 , it will can not detect the correlation coefficient between signal sources correctly, it means that the direction angular interval of the signal wave is reduced to a certain extent , the mutual influence between the incident signal will be particularly large, and thus it is unable to correctly estimate the correlation coefficient between the two signal sources .When the angular interval is greater than 5.5 º , which shows that when the incident angle interval between the signals is larger enough, the mutual influence between

signals is unconspicuous , thus the signals may be stable propagation relatively, and the correlation coefficient is not dramatic floating .

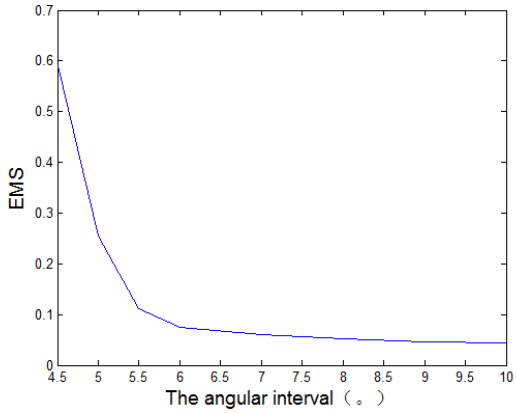

Fig. 1. The MSE changes with the angular interval

Conclusion

In array signal processing, however, since the received signal of array is the synthesized result of incident signals , the traditional correlation coefficient calculation method can't be applied.This paper provide a correlation coefficient estimation algorithm based on feature subspace decomposition. Simulation results verify that this algorithm can be realized to get the correlation coefficient .

Acknowledgement

In this paper, the research was sponsored by the Special Foundation for Basic Research Funding of Central University (Project No. HEUCF140803) .

References

[1] Liu, Shiang-Tai, Kao,Chiang,Fuzzy measures for correlation coefficient of fuzzy numbers. Fuzzy Sets and Systems. Vol. 46,pp.267-275,June 1, 2002.

[2] C. Qi, Y. Wang, Y. Zhang, and Y. Han, "Spatial difference smoothing for DOA estimation of coherent signals," IEEE Signal Process. Lett.vol. 12, no. 11, pp. 800–802, 2005.

[3] Yang, Qi,Huang, Dengshan,Jiang, Wen,A modified algorithm for DOA estimation of coherent signal with SVD,2010 International Conference on Computing, Control and Industrial Engineering, CCIE 2010,vol.2,p408-411,2010.

[4] Chen Y M, Lee J H, Yeh C C. Bearing estimation without calibration for randomly perturbed arrays. IEEE Trans. on SP,39(1):194-197

[5]Linebarger D A, Redundancy averaging with large arrays. IEEE Trans. on SP, 1993, 41(4): 1707-1710.

[6] R. O. Schmidt, "Multiple emitter location and signal parameter estimation,"in Proc. RADC Spectral Estimation Workshop, Rome, NY, 1979,pp. 243–258.

[7]R. O. Schmidt, "Multiple emitter location and signal parameters estimation,"IEEE Trans. Antennas Propag., vol. 34, no. 3, pp. 270–280,1986.

[8] Wang Yongliang, Chen Hui,Peng Yingning, Wan qun, Spatial spectrum estimation method and algorithms[M].TsingHua University Press. Beijing , 2004,p28-30.

Advanced Materials Research Vols. 989-994 (2014) pp 1887-1890
© (2014) Trans Tech Publications, Switzerland
doi:10.4028/www.scientific.net/AMR.989-994.1887

A Multi-objective Coordinative Optimization Model and Its Cultural Immune Algorithm

Chunguang CHANG[a], Wan LI[b], Kai YIN[b], Minghao QI[a]

School of Management, Shenyang Jianzhu University, Shenyang, 110168, China

[a]email: ccg7788@sohu.com, [b]email:ccg777@sohu.com

Keywords: Multi-Consumer; E-commerce; Coordinative Optimization; Cultural Immune Algorithm

Abstract. To improve E-Commerce recommendation efficiency for multi-consumer population, coordinative optimization problem for multi-consumer purchase is studied. Multi-objective coordinative optimization model for multi-consumer purchase in E-commerce (MCOMMPE) is established, the optimization objectives consist of maximizing purchase probability, profit, green product orientation; minimizing lost consumer number; keeping equalization among varied purchase schemes. To solve easily, MCOMMPE is transformed into single objective optimization model. Cultural Immune Algorithm (CIA) is studied, affinity degree calculating, clone selecting, antibody population space and belief space are studied in detail, and the basic steps of CIA are designed. The validity of MCOMMPE and its CIA are validated.

Introduction

With E-commerce develops more and more profound, it bring much economic profit for E-commerce companies and social benefit. Coordinative optimization problem for multi-consumer purchase in E-commerce becomes the focus in E-commerce optimization control domain day by day. It is related with many factories, some coordinative contents consist of time coordination, discount term, goods item coordination, demand quantity coordination, green consume coordination etc. need to be considered. And many constraints need to be satisfied; it is a complex problem.

So far, some scholars have researched on E-commerce recommend, e.g., a recommender system based on the immune network is studied by Cayzer S, Aickelin U [1]. Electronic commerce recommender is applied by J B Schafer et al.[2]. Intelligence optimization algorithm or reasoning method is employed in many domains [3]. Artificial immune algorithm (AIA) is benefit for providing broad decision space on varied optimization problems, and it is broad applied in many domains day by day [4][5]. The knowledge structure of belief space in cultural algorithm can instruct evolvement process of AIA. Cultural algorithm is firstly proposed by Reynolds R G [6]. In cultural algorithm, knowledge for solving problem is obtained from evolvement population, and it is utilized for instructing population evolvement process, thus, search efficiency is improved.

AIA and Cultural algorithm are combined to solve above coordinative optimization problem for multi-consumer purchase in E-commerce in this paper.

Description and Establishment of Coordinative Optimization Model for Multi-consumer

Main objectives in Multi-objective coordinative optimization model for multi-consumer purchase in E-commerce (MCOMMPE) include maximizing purchase demand similarity degree, consumer value, web site profit, green product orientation; minimizing lost consumer number; equalization among varied purchase schemes. Main constrains include: (1) in each purchase scheme, there is a lowest price limit according to consumer's grade, there is also a acceptable upmost price limit from consumers; (2) total demand quantity of consumers should be less than present inventory level, and the lowest purchase scale should be reached;(3) goods due time of each consumer should be obeyed; (4) environmental protection features of should reach consumers' lowest requirement.

MCOMMPE is established as follows. Where, x_{ij} is 0-1 variable for judging whether consumer i select scheme j； N , M respectively denotes number of consumers and schemes; L_{ij} and U_{ij} denotes

the lowest price limit and acceptable upmost price of scheme j for or from consumer i; $Q_j^{(U)}$ and $Q_j^{(L)}$ respectively denotes inventory level and of lowest scale goods item in scheme j; s_{ij}, v_{ij}, q_{ij} and e_{ij} respectively denotes similar degree, consumer value purchase quantity, required environmental protection index of consumer i in purchase scheme j; $e^{(j)}$, d_j, c_j, p_j and $t^{(j)}$ respectively denotes environmental protection index, discount parameter, unit cost, unit price and supply period of scheme j; t_i and T_i respectively denotes purchase time, due date of consumer i; h(·) denotes scale economic function, $\mathrm{h}(x)=\alpha x/Q_j^{(U)}$, here, α=0.2.

$$\max f_1=\sum_{i=1}^{N}\sum_{j=1}^{M}x_{ij}s_{ij}/NM \tag{1}$$

$$\max f_2=\sum_{i=1}^{N}\sum_{j=1}^{M}x_{ij}v_{ij}/NM \tag{2}$$

$$\max f_3=\{\sum_{i=1}^{N}\sum_{j=1}^{M}x_{ij}p_j(1-d_j)-\sum_{i=1}^{N}\sum_{j=1}^{M}x_{ij}c_j[1-\mathrm{h}(\sum_{i=1}^{N}x_{ij}q_{ij})]\}/\sum_{i=1}^{N}\sum_{j=1}^{M}x_{ij}p_j(1-d_j) \tag{3}$$

$$\max f_4=\sum_{i=1}^{N}x_{ij}/NM \tag{4}$$

$$\max f_5=\sum_{i=1}^{N}\sum_{j=1}^{M}x_{ij}e^{(j)}/NM \tag{5}$$

$$\min f_6=\sum_{j=1}^{M}|\sum_{i=1}^{N}x_{ij}-\sum_{j=1}^{M}\sum_{i=1}^{N}x_{ij}/M\,|/NM \tag{6}$$

$$\text{s.t.}\quad L_{ij}x_{ij}\le p_j(1-d_j)x_{ij}\le U_{ij}x_{ij}\qquad i=1,2,\cdots,N \tag{7}$$

$$Q_j^{(L)}\le\sum_{i=1}^{N}q_{ij}x_{ij}\le Q_j^{(U)}\qquad j=1,2,\cdots,M \tag{8}$$

$$t_ix_{ij}+t^{(j)}x_{ij}\le T_ixi_j\qquad i=1,2,\cdots,N \tag{9}$$

$$e_{ij}x_{ij}\ge e^{(j)}\,x_{ij}\qquad j=1,2,\cdots,M \tag{10}$$

$$\{x_{ij}\mid x_{ij}=1,j=1,2,\cdots,M\}\in\Phi_i,\qquad i=1,2,\cdots,N \tag{11}$$

$$x_{ij}=0\text{ or }1 \tag{12}$$

As above the objective functions values is on interval (0,1), and the importance of each objective is same, the objective functions are integrated by multiplication and division approach. To reduce difficulty of algorithm encoding, Formula (8) is brought into objective function, therefore, the model is transformed as follows. Where, $\psi=+\infty$, when $x>0$, $\mathrm{sgn}(x)$=1, else, $\mathrm{sgn}(x)$=0.

$$\min f=f_6/\prod_{k=1}^{5}f_k+\psi\,\mathrm{sgn}(Q_j^{(L)}-\sum_{i=1}^{N}q_{ij}x_{ij})+\psi\,\mathrm{sgn}(\sum_{i=1}^{N}q_{ij}x_{ij}-Q_j^{(U)}) \tag{13}$$

s.t. formula (7), formulas from formula (9) to formula (12).

Principle and Design of Cultural Immune Algorithm (CIA)

$N\times M$ dimension 0-1 matrix is adopted to represent antibody of CIA. Affinity degree function between antibody i and antigen is defined as formula (14). Affinity degree function between antibody i and antibody j is defined as formula (15). Adjustment equation (as formula (16)) is employed to implement clone selection [1]. Where, n, ω_1, ω_2, ω_3, U_i and V respectively denotes number of antibodies, activity ratio, control ratio, death ratio, density of antibody i and antigen.

$$m_i=\mathrm{Aff}(Ab^{(i)},Ag)=1/f \tag{14}$$

$$m_{ik}=\mathrm{Aff}(Ab^{(i)},Ab^{(k)})=1-[\sum_{l=2}^{m}\sum_{j=1}^{n}|\,x_j^{(l)(i)}-x_j^{(l)(k)}\,|]/[\sum_{l=2}^{m}\sum_{j=1}^{n}|\,x_j^{(l)(i)}+x_j^{(l)(k)}\,|] \tag{15}$$

$$dU_i/dt=\omega_1m_iU_iV-\omega_2\sum_{j=1}^{n}m_{ij}U_iU_j/n-\omega_3U_i \tag{16}$$

Implement steps of CIA are as follows.

Step 1: Initialize antibody population space, antibody belief space, respectively generate H antibodies so as to form initial antibody population Ab, initial antibody belief population $\widehat{Ab}$.

Step 2: Calculate m_i by formula (14). Calculate m_{ik} by formula (15).

Step 3: Implement clone selection among every antibodies in Ab according to formula (16).

Step 4: Evolve antibodies. For antibody i, if its density $U_i < \beta$ (density threshold), dele antibody i, the number of deleted antibodies is recorded as H_d.

Step 5: If the acceptance operator iteration counter $C_{acc} = C_{ACC}$ (acceptance counter threshold), select r antibodies with highest m_i from antibody population Ab, and substitute r antibodies with lowest m_i from antibody belief population , C_{acc}=0; else $C_{acc} = C_{acc} + 1$.

Step 6: If the influence operator iteration counter $C_{\inf} = C_{\mathrm{INF}}$ (influence counter threshold), select r antibodies in random from belief antibody population $\widehat{Ab}$, and substitute r antibodies in antibody population Ab, $C_{\inf}$=0; else $C_{\inf} = C_{\inf} + 1$.

Step 7: If the density of h antibodies with highest density reaches density threshold, and leaning variance is less than variance threshold, or the maximal iteration, the learning process is end; else, generate H_d antibodies, repeat steps from step 2 to step 6.

Application Instance

To validate the validity of MCOMMPE and CIA, related data are collected. Related data on E-commerce purchase scheme are listed in table 1; data about consumer i are listed in table 2; s_{ij}, v_{ij}, q_{ij}, e_{ij} and one of the satisfied solutions obtained by CIA are listed in tables 3; L_{ij} and U_{ij} are omit for paper's length limit.

Table 1 Related Data on E-Commerce Purchase Scheme

j	$Q_j^{(U)}$	$Q_j^{(L)}$	d_j	c_j	p_j	$t^{(j)}$	$e^{(j)}$	j	$Q_j^{(U)}$	$Q_j^{(L)}$	d_j	c_j	p_j	$t^{(j)}$	$e^{(j)}$
1	80	30	0.1	60	100	3	0.75	3	80	30	0.2	80	150	4	0.85
2	80	30	0.15	70	120	3	0.8	4	80	30	0.25	100	170	4	0.9

Table 2 Data about Consumer i

i	1	2	3	4	5	6	7	8	9	10	11	12	13	14	15	16	17	18	19	20
t_i	0	0	0	0	1	1	1	1	1	1	0	0	0	0	0	1	1	1	1	1
T_i	5	5	3	5	4	6	4	6	5	6	7	6	7	6	7	6	6	5	6	6

Table 3 Data of s_{ij}, v_{ij}, q_{ij} and e_{ij}

	j \ i	1	2	3	4	5	6	7	8	9	10	11	12	13	14	15	16	17	18	19	20
s_{ij}	1	0.85	0.9	0.85	0.9	0.9	0.85	0.85	0.85	0.85	0.85	0.85	0.85	0.85	0.85	0.85	0.8	0.85	0.8	0.85	0.8
	2	0.9	0.9	0.85	0.85	0.85	0.9	0.85	0.9	0.85	0.9	0.9	0.85	0.9	0.85	0.9	0.85	0.85	0.85	0.85	0.85
	3	0.8	0.8	0.8	0.9	0.9	0.85	0.9	0.85	0.85	0.9	0.95	0.95	0.9	0.95	0.95	0.9	0.85	0.9	0.85	0.9
	4	0.8	0.8	0.8	0.8	0.8	0.8	0.8	0.8	0.8	0.8	0.85	0.85	0.85	0.85	0.85	0.95	0.95	0.95	0.9	0.95
v_{ij}	1	0.8	0.9	0.8	0.85	0.85	0.8	0.8	0.8	0.8	0.8	0.8	0.8	0.8	0.8	0.8	0.75	0.8	0.75	0.8	0.75
	2	0.9	0.85	0.8	0.8	0.8	0.9	0.8	0.9	0.8	0.9	0.85	0.7	0.85	0.8	0.85	0.9	0.8	0.7	0.8	0.7
	3	0.75	0.7	0.75	0.9	0.85	0.7	0.9	0.8	0.8	0.85	0.9	0.9	0.85	0.9	0.9	0.85	0.7	0.9	0.8	0.85
	4	0.75	0.75	0.75	0.7	0.75	0.75	0.75	0.7	0.75	0.7	0.8	0.7	0.8	0.7	0.8	0.9	0.9	0.9	0.85	0.9
q_{ij}	1	8	8	8	8	8	5	5	7	4	7	5	7	5	5	4	8	4	8	6	5
	2	6	4	8	4	8	7	8	8	8	8	3	8	5	4	8	5	5	4	5	6
	3	2	7	2	7	2	7	7	6	7	7	8	8	6	8	6	8	8	8	6	8
	4	3	4	6	6	3	5	6	3	6	3	8	8	7	8	5	8	8	7	8	8

e_{ij}	1	0.72	0.75	0.72	0.75	0.75	0.72	0.72	0.75	0.72	0.75	0.72	0.75	0.75	0.72	0.75	0.67	0.75	0.67	0.72	0.8
	2	0.8	0.77	0.75	0.72	0.75	0.8	0.75	0.8	0.72	0.8	0.75	0.62	0.77	0.75	0.77	0.8	0.72	0.62	0.75	0.82
	3	0.75	0.62	0.67	0.82	0.77	0.62	0.82	0.72	0.87	0.77	0.82	0.82	0.75	0.82	0.82	0.75	0.62	0.82	0.75	0.77
	4	0.92	0.92	0.67	0.62	0.67	0.67	0.67	0.62	0.67	0.62	0.72	0.62	0.72	0.62	0.72	0.82	0.82	0.82	0.77	0.82
f^*	1	1	1	1	1	1	1	0	1	0	1	1	0	1	0	0	0	1	0	1	0
=0.53	2	1	1	1	1	1	1	1	1	1	1	1	1	0	0	0	0	0	0	0	0
	3	0	1	0	1	0	1	0	1	0	1	1	1	1	1	0	1	0	1	0	0
	4	0	0	0	0	0	0	0	1	1	1	1	1	1	0	1	1	1	1	1	1

Conclusion

E-commerce recommend is an important content of E-commerce, it can bring much more profit to E-commerce companies. Thereby, MCOMMPE is significant to improve E-commerce efficiency. MCOMMPE and CIA are validated by applying instance. There is a broad application space for MCOMMPE, in which many demand and varied constraints are considered. There are some obvious features such as population diversity, non-prematurity and early constringency etc. in AIA, and there are also some obvious features such as clear search guiding, strong communicating between two layer space in cultural algorithm, therefore, AIA combing cultural algorithm will be benefit for solving complex optimization. Multi-objective dynamic coordinative optimization model introducing personal decision will be the future research trend on modeling aspect in this domain. AIA, cultural algorithm combing other algorithm mechanism will also be the future research trend on solving algorithm in this domain.

Acknowledgement

The research was sponsored by the Natural Science Foundation of Liaoning Province (Project No. 201202181), the Shenyang Scientific and Technological Planning (Project No. F13-317-5-12; F12-276-5-04), the National Soft Science Research Program (Project No. 2013GXS4D109), Program for Liaoning Excellent Talents in University (Project No. WJQ2011011) and Science Research Foundation of Shenyang Jianzhu University (Project No. 2013108).

References

[1] Cayzer S, Aickelin U. A recommender system based on the immune network [A]. Proceeding of CEC2002[C]. Honolulu, 2002: 807-813.

[2] Zhang Lixiu, WU Yuhou, et al. The method about stator resistance hybrid intelligent identification of motorized spindle[J]. Journal of Shenyang Jianzhu University (Natural Science), 2013, 29(6): 1098-1103.

[3] J B Schafer, J A Konstan, J Riedl. Electronic commerce recommender applications[J]. Data Mining and Knowledge Discovery, 2001, 5(1/2):115-153.

[4] Zhou Yue, Tang Shi et al. Structural damage detection and classification algorithm based on artificial immune pattern recognition [J]. Journal of Shenyang Jianzhu University (Natural Science), 2013, 29(2): 378-384.

[5] Zhou Yue, Jia Xuesong et al. Unsupervised structural damage classification algorithm based on hierarchical clustering and artificial immune pattern recognition [J]. Journal of Shenyang Jianzhu University (Natural Science), 2013, 30(2): 374-378.

[6] Reynolds R G. An Introduction to Cultural Algorithms[A]. Proc. of the 3th annual Conference on Evolution Programming[C], Singapore, 1994:131-136.

Advanced Materials Research Vols. 989-994 (2014) pp 1891-1894
© (2014) Trans Tech Publications, Switzerland
doi:10.4028/www.scientific.net/AMR.989-994.1891

The Implement of Parcel Sea Map Automatic Mapping Algorithm

Song Derui[1,2,a],Cao Ke[1,2,b],Hao Yu[1,2,c]

[1]National Marine Environmental Monitoring Center, LiaoNing Dalian 116023,China

[2]Key Laboratory of marine management technology in State Oceanic Administration People's Republic of China, LiaoNing Dalian 116023;

[a]email:drsong@nmemc.gov.cn,[b]kcao@nmemc.gov.cn,[c]yhao@nmemc.gov.cn

Keywords: Parcel Sea Map, automatic mapping, boundary data

Abstract. Parcel Sea Map mapping is currently implemented by manual, which causes the task tedious and error prone. To overcome this problem, this paper proposes an automatic mapping method for Parcel Sea Map. The boundary point data are basic mapping elements, which are obtained from sea cadastral survey. The mapping result can be demonstrated by two aspects: convex polygon and concave polygon. For convex polygon, well known left-turn and convex hull algorithms are adopted. For concave polygon, two algorithms are proposed. One is enumeration and the other is cutting algorithm. The above two mapping results can finally be determined by the inspector from sea cadastral survey. Experiments show that Parcel Sea Map automatic mapping can efficiently reduce the manual burden of present mapping.

Introduction

Sea cadastral [1] is books and maps which record the locations, boundaries, management authorities, areas, purpose and terms of service, sea levels, and standards of sea area usage for sea use of various projects. Parcel Sea is an enclosed sea use unit by ownership boundary lines. The basic task of sea use management for sea cadastral survey is to make a thorough investigation of the basic condition for every Parcel Sea. Parcel Sea is the fundament of sea cadastral survey. Parcel Sea Map is composed by boundary data and the use of sea characteristics. In regional marine planning, Parcel Sea Map is more changeable and high complexity. It is of importance for Parcel Sea Map automatic mapping by on-site boundary data. [2] proposed an automatic mapping for cadastral map of land, which only consider the condition of convex polygon.[3] provided an automatic mapping software for cadastral map of land. Data should be in a proper order. [4] proposed an improved and more efficient algorithm to calculate No-Fit Polygon. It can be used to solve two-dimensional nesting problems. [5] discussed inside mapping condition of surveying and mapping trade on the quick surveying of the Electronic Hero meter Total Station outdoor work.

Most existing literatures have two shortcomings :(1) only one kind of polygon was considered;(2) The polygon was unchanged after mapping. There was not a proper method for Parcel Sea map in open published literatures. Present method for Parcel Sea Map, in fact, is completed by manual that makes the task with heavy burden and can cause errors easily. To overcome the above problem, this paper presents an automatic mapping method for Parcel Sea Map. Two algorithms are firstly proposed for concave polygon mapping. Then a system design description is proposed for Parcel Sea Map.

Two proposed concave polygon mapping algorithms

Concave polygon automatic mapping is complicated in Parcel Sea Map. The more concave data are, the more concave polygons are. Two concave polygon mapping algorithms are proposed in the following. One is enumeration algorithm. The other is cutting algorithm.

2.1 proposed enumeration algorithm

The idea of proposed enumeration algorithm is that concave data are found firstly, and then try to find the first concave point and the rest concave data. All concave points are utilized in the same mapping procedure except the first concave point. The algorithm description is as follows:

(a) To complete convex polygon mapping with convex data in array A by left-turn algorithm[6] or convex hull algorithm[7]. Then find concave data for (b).

(b) Find first concave data b, then insert it into array A. One side of polygon is breaked off. New two sides are generated by the first concave data b. Then new polygon sets are established.

(c) Find next concave data c with two points in one side of array A to construct a new triangle. If there is an intersect between the new triangle and polygon in array A, then find new side of A to construct a new triangle with this concave data c, repeat the procedure. If there is not an intersection, c is inserted into array A. Polygon sets are updated.

(d) Continue the same way for the rest concave points by step c until all concave points are inserted in array A.

The concave polygon enumeration algorithm mapping procedure is shown in figure 1. Concave points C and D is shown in (a). (b) is to find the first concave point to establish a new triangle ACB. (c) finds an intersection in shadow region. (d) constructs a new triangle FDE without intersection with concave polygon ACBEF.

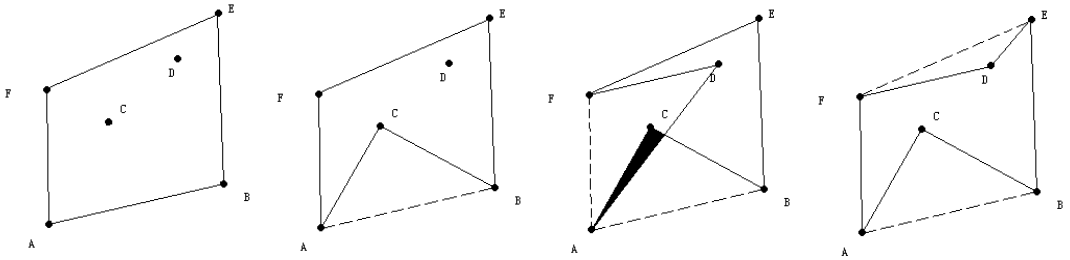

(a) (b) (c) (d)

Fig.1. The procedure of concave polygon enumeration algorithm mapping from step (a) to (d)

2.2 proposed cutting algorithm

The main idea of cutting algorithm is to search for shortest distance between a concave data with one side of polygon, then break off that side and construct a new triangle. The algorithm description is as follows.

(a) To complete convex polygon mapping with convex data in array A . Then find concave data for (b).

(b) Traverse array A and select a side L.

(c) Find concave point c which has shortest distance with side L in contrast to the rest points. Then project point c to side L.

(d) If the projection of point c is between the two terminal of side L, point c is inserted to array A to update array and end the loop.

(e) Find another concave point and repeat (c) and (d) until all concave points are inserted.

The concave polygon cutting algorithm mapping procedure is shown in figure 2. (a) demonstrates the concave points C and D.(b) is to find the projection of first concave point to side L.(c) determines the project whether between two terminals A and F. (d) constructs a new triangle FCA.

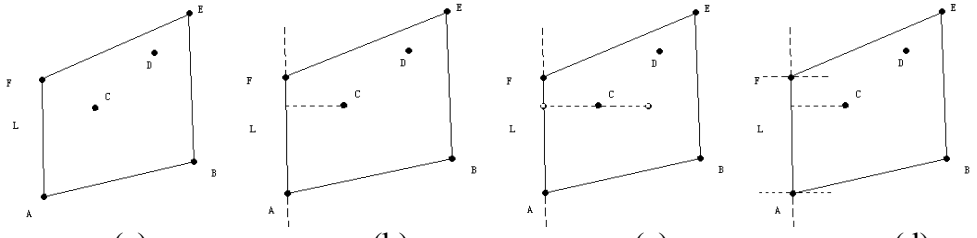

(a) (b) (c) (d)

Fig.2. The procedure of concave polygon cutting algorithm mapping from step (a) to (d)

A novel Parcel sea map automatic mapping algorithm description

The proposed automatic mapping can be described by Figure 3. We first choose data source and read longtitude and latitude of formatted data. Vector of GIS data set is generated. A left-turn algorithm is utilized to complete convex polygon mapping with automatic topological crossing correction. Then we try to determine the correctness of mapping results. If the results are correct, mapping is saved, otherwise, mapping still has to be conducted. The distance between rest points and adjacent side is calculated by the left-turn algorithm. The adjacent side is broken off and rest points are reconnected until all rest points are accomplished. Finally, we calculate the area and generate mapping.

Experiments

Experiment is conducted under C# with ArcGis platform under Windows 7 operating system. According to the interface of ArcGIS Engine, uncrossing automatic mapping algorithm can be completed by any group of data. All data is obtained from regional sea use information by National marine management dynamical monitoring system. All coordinates are firstly digitalized and unified by longitude and attitude. According to Figure 4 (a) and (b), we can find that multiple groups of points can be uncrossed by the proposed automatic mapping algorithm. The proposed mapping algorithm efficiently improves the mapping speed.

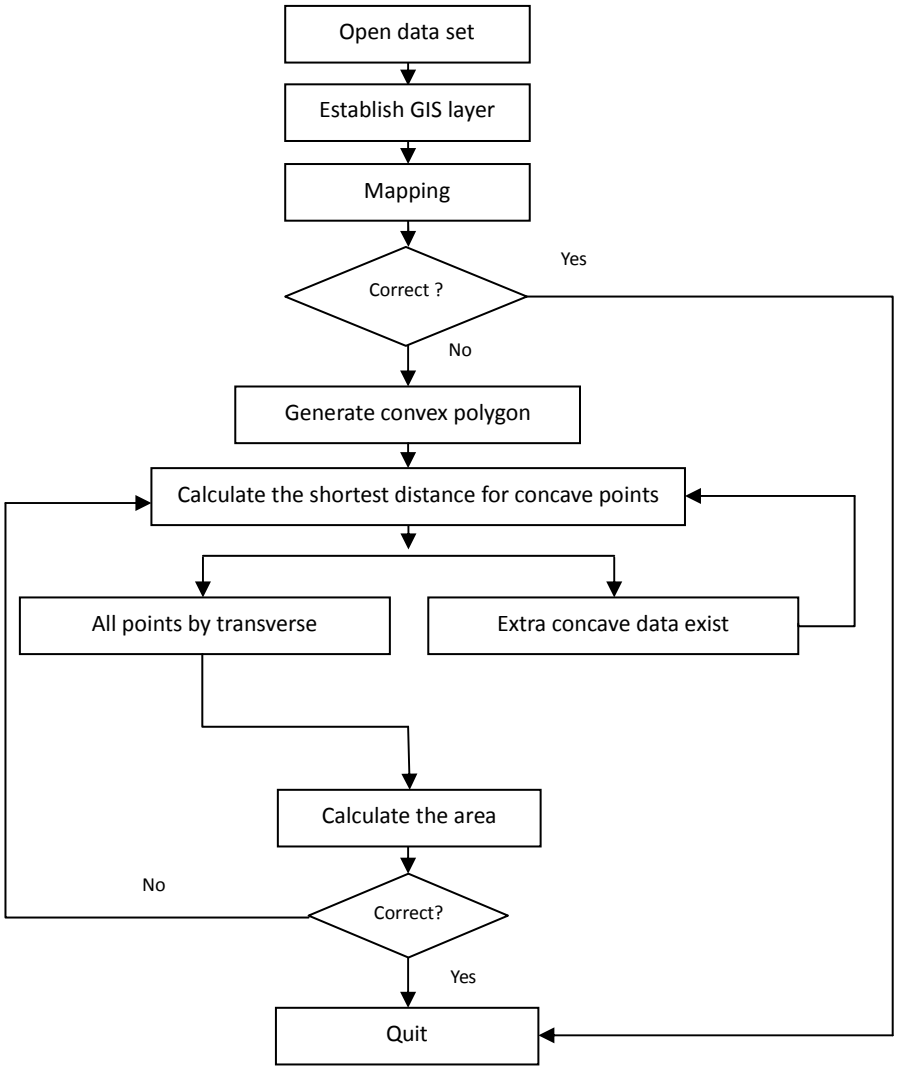

Fig. 3. Flowchart of Parcel Sea Map automatic mapping

(a) (b)

Fig.4. Experimental results of the proposed automatic mapping algorithm

Conclusion

In this paper, an automatic mapping method is proposed for Parcel Sea Map. The mapping result can be demonstrated by two aspects: convex polygon and concave polygon. For convex polygon, well known left-turn and convex hull algorithms are utilized. For concave polygon, two algorithms are proposed. One is enumeration and the other is cutting algorithm. The above two mapping results can finally be determined by the inspector from sea cadastral survey. Experiments show that Parcel Sea Map automatic mapping can efficiently reduce the manual burden of present mapping.

Acknowledgement

In this paper, the research was sponsored by the Public Science and Technology Research Funds Projects of Ocean (Project No.201005011) and Key Laboratory of marine management technology in State Oceanic Administration(Project No. 201109).

References

[1] Sea cadastral survey standard, China Standard Press, 2009.

[2] Zhang Han, Research and Discussion on Automatic Mapping of Cadastral Survey, Jiangxi Coal Science & Technology, 2011: 3,117-119.

[3] Li pei hong,Wang li hong, Softwar Design of Map-making Parcel Auto drawing in Cadastral Management, Journal of Southern Institute of Metallurgy, 2002: 23(2) 1-4.

[4] Yang Weibo, Wang Wanliang, Improved algorithm for No-Fit Polygon calculation, Computer Engineering and Applications,2013: 49(1) ,32-35.

[5] LUO Yong zheng，YI Tian-yang, Thinking of the Inside Quick Mapping on the Quick Surveying of Electronic Herometer Total Station, Geomatics＆Spatial Information Technology, 2006:29(2),84-86.

[6] Chen shan yun, Xu yong jin, Application of Left-Turn Algorithm to Indirect to Create Voronoi diagram, Journal of Hunan University of Arts and Science, 2004:16(1),75-78.

[7] Li jun hui,Li zhi yang, A Quick Algorithm and Programming to Determine Convex Hull for Planar Scattered Point Set in GIS, Journal of Beijing Union University, 2009:23(3),32-34,43.

Advanced Materials Research Vols. 989-994 (2014) pp 1895-1900
© (2014) Trans Tech Publications, Switzerland
doi:10.4028/www.scientific.net/AMR.989-994.1895

A New Network Traffic Classification Method Based on Optimized Hadamard Matrix and ECOC-SVM

Hongzhi WANG[1, a], Lihui YAN[2, b]

[1]Network & Information Center, Dalian Jiaotong University, Dalian, 116028, China

[2]State Grid Liaoning Dalian Power Supply Company, Dalian, 116000, China

[a]email:1064776788@qq.com, [b]email:1193386237@qq.com

Keywords: Network Traffic Classification; Hadamard Matrix; ECOC; SVM

Abstract. The traditional network traffic classification methods have many shortcomings, the classification accuracy is not high, the encrypted traffic cannot be analyzed, and the computational burden is usually large. To overcome above problems, this paper presents a new network traffic classification method based on optimized Hadamard matrix and ECOC. Through restructuring the Hadamard matrix and erasing the interference rows and columns, the ECOC table is optimized while eliminating SVM sample imbalance, and the error correcting ability for classification is reserved. The experiments results show that the proposed method outperform in network traffic classification and improve the classification accuracy.

Introduction

Network traffic classification [1] can identify various applications, monitor and control the whole network, optimize network performance and improve the quality of service while keeping the network security. The traditional classification models play an important role in classification and identification in past decades, but have been unable to meet current demand when many incoming applications appear. So it is very necessary to search new method for network traffic classification.

In general, there are mainly four kinds of methods in network traffic classification: the first method is port numbers matching, through comparing the port numbers in TCP (UDP) packets with the well-known port numbers, the network traffic is classified. The authors of [2] used this method in network traffic classification, but the accuracy is not high. This port-based classification method is simple and easy to implement, but its accuracy is not high, and cannot recognize the network traffic which used dynamic ports or private protocol. The second method is to analyze the packet's payload, to check whether the packet contains certain features that are already known in some application. The authors of [3] and [4] improved the accuracy of the network traffic classification with the Content-based method. Compare with the port-matching-based method, the payload-analyzing-based method has the higher classification accuracy. But it has complex classification process and huge computational overhead, and cannot identify the encrypted traffic. The third method is host-behavior-based analysis; network traffic is classified by analyzing the behavior patterns of transport layer. [5] identified network traffic by analyzing the connection patterns of P2P flows. This method doesn't depend on port number and the payload of packet, therefore it is effective in encrypted traffic identification. But this method cannot identify the packet with encrypted heads of transport layer. The forth method is machine learning (ML), it classifies network traffic by identifying the flow-based statistical characteristics. This method can achieve higher accuracy and analyze encrypted data flow, so it is gradually becoming a hot topic for research. [6] established a network traffic model based on RBF neural network. [7] proposed a semi-supervised network traffic classification method which can adapt to known and unknown attack. [8] combined SVM with cluster algorithm, realized network traffic classification by using un-biased training and testing samples. [9] established SVM decision tree for network traffic classification. [10] reconstructed DDAG-SVM decision tree according to the class separation. [11] proposed a fast multi-class SVM based on binary encoding, and got higher classification speed with little loss of accuracy. In [12], Hadamard matrix and ECOC encoding table was generated using traditional recursive method, and was combined with SVM for multi-class classification.

In classification algorithms based on machine learning, the support vector machine (SVM) [13] is based on statistical learning theory, and successfully transforms the binary classification problem into a quadratic optimization by using nonlinear transformation and structure risk minimization principle. It has obvious advantages in the small sample size, nonlinear, multidimensional attribute classification, and has strong generalization ability and stability [14] while keeping high classification accuracy. The multi-class model of SVM is also widely used in classification [15]. But how to build a more efficient multi-class SVM model is the difficulty faced by researchers. So this paper presents a network traffic classification method based on optimized Hadamard Matrix and ECOC-SVM.

A New Network Traffic Classification Method based on Optimized Hadamard Matrix and ECOC-SVM

SVM is a typical binary classifier, being used in multi-class classification for network traffic, there are several methods at present: The first is one-against-all (OAA) method [16], it needs k SVM classifiers for k classes identification; but the shortcoming is the presence of area that may be overlapping or unclassifiable, further more the way of OAA classification in training phase makes the samples unbalanced and reduces the classification ability. The second is one-against-one (OAO) method [17], it needs $k(k-1)/2$ SVM classifiers for k classes identification, and classifies the samples according to the cumulative voting results of each SVM. There is no unclassifiable area, but the amount of SVM growths in square magnitude when the number of classes is increasing. So it is not suitable for the situation of classes being too much. The third method is DAG-SVM [10], it also needs $k(k-1)/2$ SVM classifiers for k classes classification in training phase, but each sample needs $(k-1)$ SVM at most in testing phase. This method is essentially the improvement for OAO method, and its shortcoming is prone to error accumulation, especially the selection for root node is very strict. The fourth method is multi-class-SVM based on error correcting output code(ECOC)[18], it binary divides the sample classes through building encoding matrix, and converts the question of k classes classification into that of m binary classifications ($2^{m-1} < k \le 2^m$). This method combines the advantages of ECOC and SVM, simplifies the difficulty of training, improves the accuracy of classification, and has certain error correction capability. Our approach in this paper is to modify the traditional ECOC-SVM, rebuild the ECOC encoding table through optimized Hadamard matrix, keep the hamming distance (i.e. the ability of being classified) between each class, and solve the question of sample imbalance by erasing the interference rows and columns.

(1) Theoretical analysis of proposed method:

The principle of classification based on SVM is expressed as formula (1), assume there is the training set $X = \{(x_1, y_1), (x_2, y_2), ..., (x_n, y_n)\}$, n is the number of samples, $x_i \in R^p (i = 1,2,...,n)$ is the i-th training sample, R^p is real vector, p is the dimension, $y_i \in \{+1, -1\}$ is the class label of training sample x_i. Through the SVM classifier $f(x)$, the training set X can be classified.

$$f(x) = \mathrm{sgn}\left\{\sum_{i-1}^{n} y_i \alpha_i^* K(x_i, x) + b^*\right\} \tag{1}$$

Where sgn is the symbolic function; $K(x_i, x)$ is linear function when X is linearly separable and is kernel function when X is not linearly separable; α_i^* and b^* is the optimal solution.

The principle of ECOC-SVM classification is binary dividing the sample classes through building encoding table of k rows and m columns, and converting the question of k classes classification into that of m binary classifications ($2^{m-1} < k \le 2^m$), the classification result is decided according to the principle based on minimum hamming distance. For instance, in the traditional classification process for 11 classes using 4 SVMs (the ECOC encoding table is express as table 1),

the encoding table only achieves corresponding relation from 11 classes to 4 SVMs, but the hamming distance between two adjacent rows is 1. E.g. the code value of first row is “0000” and the second row is “0001”, the hamming distance between them is 1, so there is no error correcting ability by this encoding method. Further more, if the number of classes is not an integer power of 2 (e.g. the number of network traffic classes in this paper is 11), the selection for encoding table is usually casual, and partly causes sample imbalance. For example, there are 11 classes in our network traffic sample, and we build encoding table as table 1, the classifier SVM1 contains 8 negative samples and 3 positive samples, there is seriously sample imbalance that reduces the classification performance.

Table 1 The traditional ECOC encoding table for eleven classes with four SVMs

Class	SVM1	SVM 2	SVM 3	SVM 4
1	0	0	0	0
2	0	0	0	1
3	0	0	1	0
4	0	0	1	1
5	0	1	0	0
6	0	1	0	1
7	0	1	1	0
8	0	1	1	1
9	1	0	0	0
10	1	0	0	1
11	1	0	1	0

In order to solve the above problem, [12] build encoding table with Hadamard matrix which is generated by recursive method, and increases the hamming distance between each rows (columns) at the cost of more SVMs. For instance in tables 2, there are 11 classes to be classified with 15 SVMs. This method first builds 16*16 Hadamard matrix, and erases the first column which contains only code value “0”, then selects the first 11 rows form matrix as encoding table. But this encoding method has also shortcomings, e.g. the column of SVM8 contains 8 negative samples ”0” and 3 positive samples ”1”, so there will still have sample imbalance in training phase which reduces classification ability. Moreover, when treating with k class samples, the classes of Hadamard matrix increase only in accordance with the integer power over 2, so it is lack of adaptability to the number of class. Further more, because the encoding table is built with the first k rows, the rows selecting is casual.

Table 2 The Hadamard ECOC encoding table for eleven classes with fifteen SVMs

Class	SVM 1	SVM 2	SVM 3	SVM 4	SVM 5	SVM 6	SVM 7	SVM 8	SVM 9	SVM 10	SVM 11	SVM 12	SVM 13	SVM 14	SVM 15
1	0	0	0	0	0	0	0	0	0	0	0	0	0	0	0
2	1	0	1	0	1	0	1	0	1	0	1	0	1	0	1
3	0	1	1	0	0	1	1	0	0	1	1	0	0	1	1
4	1	1	0	0	1	1	0	0	1	1	0	0	1	1	0
5	0	0	0	1	1	1	1	0	0	0	0	1	1	1	1
6	1	0	1	1	0	1	0	0	1	0	1	1	0	1	0
7	0	1	1	1	1	0	0	0	0	1	1	1	1	0	0
8	1	1	0	1	0	0	1	0	1	1	0	1	0	0	1
9	0	0	0	0	0	0	0	1	1	1	1	1	1	1	1
10	1	0	1	0	1	0	1	1	0	1	0	1	0	1	0
11	0	1	1	0	0	1	1	1	1	0	0	1	1	0	0

(2) Algorithm Description of Proposed Method:

From above two methods, we can conclude that one perfect encoding method should meet the following conditions:

1) Row separation, that ensures the minimum hamming distance between each rows is maximum, so as to obtain the strongest error correcting ability;

2) Column separation, that ensures the hamming distance between each columns (includes its complement) is maximum, so as to eliminate the correlation between columns (i.e. SVM classifiers);

3) The numbers of two types of code values in each column should be nearly equal, so as to reduce the sample imbalance.

Based on above analysis, this paper presents an optimized encoding table based on Hadamard matrix. The specific approach is as follows:

Hadamard matrix has the following properties [19]:

1) It is orthogonal between different rows, so there is no correlation between them.

2) It is orthogonal between different columns, so there is no correlation between them.

3) In m-classes Hadamard matrix, the hamming distance between each row (column) is $m/2$ and which is already the biggest interval.

The definition of 2-classes Hadamard matrix is as follows:

$$H_2 = \begin{pmatrix} 0 & 0 \\ 0 & 1 \end{pmatrix} \tag{2}$$

By recursive method, the N-classes Hadamard matrix can be obtained as follows:

$$H_N = \begin{pmatrix} H_{N/2} & H_{N/2} \\ H_{N/2} & -H_{N/2} \end{pmatrix} \qquad N = 2^i (i = 2,3,4,...) \tag{3}$$

This the traditional method for getting Hadamard matrix, the number of class N can only increases in the order $N = 2^i (i = 2,3,4,\cdots)$, i.e. $N = 4,8,16,32,64,...$ etc, so it is lack of adaptability to the number of class.

In this paper we rebuild the Hadamard matrix through the method mentioned in [19], and the classes of matrix N only needs to be: ① $N = 4i(i = 1,2,3,...)$, ② $(N-1)$ is a prime number. For example, assuming there are 11 classes to be classified. We first build 12-classes Hadamard matrix according to following steps:

1) Build the finite field $D = \{0,1,2,3,4,5,6,7,8,9,10\}$;

2) Get the square element D_0 from D, $D_0 = \{1,3,4,5,9\}$;

3) Get D_1 by plus 1 to the corresponding element of D_0, $D_1 = \{2,4,5,6,10\}$;

4) And so on, we get all from D_0 to D_{10};

5) Thus we can get 12-classes Hadamard matrix.

The 12-classes Hadamard matrix we have got is normative matrix, so each element in first row and first column is 1; this is no use for classification, so they are erased. Finally the optimized encoding table is consisted of the remained 11 rows and 11 columns, which is expressed in table 3.

Compared with the method used in [12], the class number of optimized Hadamard matrix N increases in the order $N = 4i(i = 1,2,3,...)$, so we can obtain $N = 4,8,12,16,20,\cdots$, etc. Compare with the previous $N = 4,8,16,32,64,\cdots$, etc, the available adjacent classes of matrix are more close. So the proposed encoding table has higher coding efficiency, and has better adaptability to the number of classes. Compared with table 2, the proposed encoding table only needs 11 SVM classifiers. It reduced 4 SVMs than before, and reduced the computation overhead in training and classifying phase. At the same time, the minimum hamming distance between each row is 6, with only small loss compared to the previous distance 8, and keeps the error correcting ability in most possible. The code value of each column is very balanced, that helps improve the performance of the classifier.

Table 3 The optimized Hadamard ECOC encoding table for eleven classes with eleven SVMs

Class	SVM 1	SVM 2	SVM 3	SVM 4	SVM 5	SVM 6	SVM 7	SVM 8	SVM 9	SVM 10	SVM 11
1	0	0	1	0	0	0	1	1	1	0	1
2	1	0	0	1	0	0	0	1	1	1	0
3	0	1	0	0	1	0	0	0	1	1	1
4	1	0	1	0	0	1	0	0	0	1	1
5	1	1	0	1	0	0	1	0	0	0	1
6	1	1	1	0	1	0	0	1	0	0	0
7	0	1	1	1	0	1	0	0	1	0	0
8	0	0	1	1	1	0	1	0	0	1	0
9	0	0	0	1	1	1	0	1	0	0	1
10	1	0	0	0	1	1	1	0	1	0	0
11	0	1	0	0	0	1	1	1	0	1	0

Experimental Results

We conduct experiments to demonstrate the feasibility of the proposed method with10-fold cross-validation 10-fold cross-validation10-fold cross-validation10-fold cross-validation10-fold cross-validation. Three other classification methods are used to conduct comparisons with our proposed method; they are DDAG-SVM [10], Binary Encoding Classifier [11] and Hadamard ECOC [12]. Experiment data is selected randomly from the network traffic samples used in [14], and there are totally 11 classes including 4580 samples were chosen. The experiment data is divided into 10 equal parts; we choose one part in turn as testing set and the rest 9 parts as training set, and conduct classification. Then repeat the above experiment 10 times; the average classification accuracy of each method is recorded in table 4. Comparison result shows that the proposed method increases the classification accuracy in contrast with the previous methods.

Table 4 Average classification accuracy with each method

DDAG-SVM	Binary Encoding	Hadamard ECOC	Proposed method
86.54%	88.17%	90.35%	91.43%

Conclusion

In this paper, a new network traffic classification method based on optimized Hadamard matrix and ECOC-SVM is proposed. Through restructuring the Hadamard matrix and erasing the interference row and column, the ECOC encoding table is optimized while eliminating SVM sample imbalance and the error correcting ability for classification is reserved. The experiments results show that the proposed method outperform the other three multi-class methods in network traffic classification and improve the classification accuracy.

References

[1] Xiong Gang, Meng Jiao, Cao Zigang, et al. Research Progress and Prospects of Network Traffic Classification[J]. Journal of Integration Technology, 2012,1(1):32-42.

[2] Li Wei, Canini M, Moore A W. Efficient Application Identification and the Temporal and Spatial Stability of Classification Schema[J]. Computer Networks, 2009,53(6):790-809.

[3] Sen S, Spatscheck O, Wang D. Accurate, Scalable in Network Identification of P2P Traffic Using Application Singntures[C]. In WWW2004. USA (New York),2004:512-521.

[4] Moore A, Papagiannaki K. Toward the accurate identification of network applications[C]. Proceedings of Passive and Active Measurement workshop. USA (Boston), 2005:41-54.

[5] Karagiannis T, Broido A, Faloutsos M, et al. Transport Layer Identification of P2P Traffic[C]. Internet Measurement Conference (IMC) 2004. USA (New York),2004:121-134.

[6] Wang Junsong, Gao Zhiwei. Network Traffic Modeling and Prediction Based on RBF Neural Network[J]. Computer Engineering and Applications,2008,44(13):6-11.
[7] She Feng, Wang Xiaoling. Network Traffic Classification Based on Semi-supervised Learning[J]. Computer Engineering,2009,35(12):90-94.
[8] Liang Sheng. Identification method of Internet Streaming based on SVM and clustering[J]. Computer Engineering and Design,2010,31(7):1566-1569.
[9] Qiu Jing, Xia Jingbo, Bai Jun. Network Traffic Classification Using SVM Decision Tree[J]. Electrnoics Optics & Control,2012,19(6):13-16.
[10] Ouyang guang, Li Qianqian, Man Junfeng. The Network Traffic Classification Techniques Based on DDAG-SVM[J]. Mathematics in Practice and Theory, 2013, 43(8): 197-203.
[11] Li Jianwu, Lu Yao. A Fast Multi-class Support Vector Machine[J]. Pattern Recognition and Artificial Inteligence, 2007, 20(3): 301-307.
[12] Yin Anrong, Xie Xiang, Kuang Jingming. Application of Hadamard ECOC in Multi-Class Problems Based on SVM[J]. ACTA ELECTRONICA SINICA, 2008, 36(1): 122-126.
[13] Cortes C, Vapnik V. Support-vector networks [J]. Machine Learning, 1995, 20: 273-297.
[14] Xu Peng, Liu Qiong, Lin Sen. Internet Traffic Classification Using Support Vector Machine[J].Journal of Computer Research and Development, 2009, 46(3): 407-414.
[15] Ran Wang, Sam Kwong, Degang Chen. A new method for multi-class support vector machines by training least number of classifiers[C]. Proceedings of the 2011 International Conference on Machine Learning and Cybernetics. China(Guilin),2011:648-653.
[16] V N Vapnik. Statistical Learning Theory[M]. Wiley Inter-Science, 1998:493-520.
[17] J Friedman. Another approach to polychotomous classification, Technical report [R] Stanford University, Department of Statistics, 1996.
[18] T G Dietterieh, G Bakiri. Solving Multi-class Learning Problems via Error-Correcting Output Codes[J]. Journal of Artificial Intelligence Research,1994, 2(1):263-286.
[19] Wang Wanjiang. The Construction of Hadamard Matrix and Its Application[D]. Tianjin: Tianjin Polytechnic Uinversity,2007.

Advanced Materials Research Vols. 989-994 (2014) pp 1901-1904
© (2014) Trans Tech Publications, Switzerland
doi:10.4028/www.scientific.net/AMR.989-994.1901

A Novel Blind Watermark Extraction Algorithm Based On Nonsubsampled Contourlet Transform

Lei Feng[1,a], XiaoFei Shi[*,1, 2, b] , Hongyu Chen[1,c], Yanhua Li[1,d], Yuelong Zhang[1,e]

[1]Information Science and Technology College, Dalian Maritime University. Dalian,116026,China

[2]National Marine Environmental Monitoring Center, Dalian, 116023 , China

[a]email: fleissig367@126.com, [b]email: shi_xiao_fei_57@163.com, [c]email: chuckchy0819@126.com

[d]email: 1395324372@qq.com, [e]email: dlmzyl123@163.com

*Corresponding author, Email: shi_xiao_fei_57@163.com

Keywords: blind extraction; independent component analysis; nonsubsampled contourlet transform

Abstract. Most existing watermark extraction algorithms were dependent on prior knowledge. This paper proposed a blind extraction method without relying on prior knowledge. According to constructing new observation based on nonsubsampled contourlet transform, which utilizes low frequency and directional components of watermarked image, more independent components are generated. We involve these components into watermarked image and resort this solution to multichannel blind source separation. Estimated watermark is recovered by ICA algorithm. Experiment results indicate that the proposed method can achieve better results in contrast with two existing algorithms.

Introduction

Digital watermarking plays an important role in information hiding and protection [1]. Watermark extracting methods can be divided in three categories depending on whether the host image and the watermarking image are known, i.e., blind extraction, semi-blind extraction and non-blind [2]. The less prior knowledge is needed, the harder watermark extraction algorithm is.

Yu D et al. used blind source separation to detect and extract digital watermark. PCA and ICA were utilized to extract watermark while the algorithm needed the original image and the key [3]. Lin Q H etc proposed a fast image decryption algorithm, which evaluated the mixed coefficient of key images, then eliminated the key images. The number of source signals was reduced by half [4]. Nguyen T V and Patra J C put forward a blind extraction algorithm aimed at embedding watermark in spatial domain, named WMICAI [5]. Ma X etc presented extraction method based on redundant discrete wavelet transform, but it needed key which generated in embedding process [6]. Above algorithms had to utilize more or less prior knowledge. Shi X F and Hong Liang presented two blind extraction algorithms which constructed observation vectors respectively, based on discrete wavelet transform and redundant discrete wavelet transform, then applied ICA algorithm to extract the watermark images [7]. While instability still existed for various watermarks.

In this paper, a blind extraction algorithm for watermark image embedded by Discrete Cosine Transform (DCT) is proposed, based on nonsubsampled contourlet transform (NSCT). The observation vectors are constructed by watermarked image and each subband components of NSCT. Then by using independent component analysis, estimated host and watermark images are extracted without any prior knowledge. Experimental results demonstrate that proposed method can efficiently extract the watermark image and have better performance.

A novel blind watermark extraction algorithm based on nonsubsampled contourlet transform

The embedding watermark model by DCT [8] without key can be depicted as

$$I_w = f_{em}(I, W) \tag{1}$$

where I is the original host image, W is the watermark image, I_w is the watermarked image, f_{em} is the embedded process. If a_1 and a_2 respectively correspond to the linear coefficient of I and W, $o(I,W)$ is the nonlinear unit and regarded as noise. Then I_w can be described as

$$I_w = a_1 I + a_2 W + o(I,W) \tag{2}$$

Assume if $o(I,W)$ is omitted, (2) can be simplify further as

$$I_w = a_1 I + a_2 W \tag{3}$$

From (3), we can find that the model is similar to the single channel blind source separate (BSS) problem written as $X = AS$. If we want to solve (3) by BSS, an available way is to turn (3) into multi channel BSS. Hence it is necessary to construct another observation vector by some transform methods.

Nonsubsampled contourlet transform (NSCT) [9] has better characteristic in multiresolution, directionality and translation invariance in contrast with contourlet transform and wavelet transform. It is constituted by nonsubsampled pyramid (NSP) and nonsubsampled directional filter bank (NSDFB). Low frequency component I_{W1}, intermediate and high frequency component I_{W2} can be obtained after one scale NSP, four directional components $\left\{I_{w2}^{d1}, I_{w2}^{d2}, I_{w2}^{d3}, I_{w2}^{d4}\right\}$ can be expressed after four directional NSDFB by

$$\{I_{W1}, I_{w2}^{d1}, I_{w2}^{d2}, I_{w2}^{d3}, I_{w2}^{d4}\} = f_{NSCT}(I_w) = f_{NSCT}(a_1 I + a_2 W) \tag{4}$$

where f_{NSCT} is NSCT algorithm.

For the watermark information is embedded in the intermediate frequency bin by DCT and $\left\{I_{w2}^{d1}, I_{w2}^{d2}, I_{w2}^{d3}, I_{w2}^{d4}\right\}$ are mainly composed of intermediate and high frequency information, it is crucial to enhance watermark information that involve $\left\{I_{w2}^{d1}, I_{w2}^{d2}, I_{w2}^{d3}, I_{w2}^{d4}\right\}$ into original observation. In this way, the number of observed signals constructed is $m = 5$. In fact, the number of source signals is $n = 2$. Therefore we assume three virtual source signals which are nonlinear approximation $\left\{I_W^1, I_W^2, I_W^3\right\}$ of two source signals. The mixing process is simplified to be linear.

$$\begin{aligned}
I_{W1} &= b_{11}a_1 I + b_{12}a_2 W + a_{13}I_W^1 + a_{14}I_W^2 + a_{15}I_W^3 \\
I_{w2}^{d1} &= b_{21}a_1 I + b_{22}a_2 W + a_{23}I_W^1 + a_{24}I_W^2 + a_{25}I_W^3 \\
I_{w2}^{d2} &= b_{31}a_1 I + b_{32}a_2 W + a_{33}I_W^1 + a_{34}I_W^2 + a_{35}I_W^3 \\
I_{w2}^{d3} &= b_{41}a_1 I + b_{42}a_2 W + a_{43}I_W^1 + a_{44}I_W^2 + a_{45}I_W^3 \\
I_{w2}^{d4} &= b_{51}a_1 I + b_{52}a_2 W + a_{53}I_W^1 + a_{54}I_W^2 + a_{55}I_W^3
\end{aligned} \tag{5}$$

where b_{pq} and a_{ij} are respectively mixed coefficients, $p = 1,\cdots,5, q = 1,\cdots,5$ .So the observation can be written as

$$\begin{cases}
X_1 = I_w + I_{W1} = a_{11}I + a_{12}W + a_{13}I_W^1 + a_{14}I_W^2 + a_{15}I_W^3 \\
X_2 = I_w + I_{w2}^{d1} = a_{21}I + a_{22}W + a_{23}I_W^1 + a_{24}I_W^2 + a_{25}I_W^3 \\
X_3 = I_w + I_{w2}^{d2} = a_{31}I + a_{32}W + a_{33}I_W^1 + a_{34}I_W^2 + a_{35}I_W^3 \\
X_4 = I_w + I_{w2}^{d3} = a_{41}I + a_{42}W + a_{43}I_W^1 + a_{44}I_W^2 + a_{45}I_W^3 \\
X_5 = I_w + I_{w2}^{d4} = a_{51}I + a_{52}W + a_{53}I_W^1 + a_{54}I_W^2 + a_{55}I_W^3
\end{cases} \tag{6}$$

Since the observed signals are independent of each other, the mixing matrix is full rank. Fast fixed-point algorithm (FastICA) [10] is used to separate source signals $\left\{I', W', I_W'^1, I_W'^2, I_W'^3\right\}$. Five source signals are classified into two kinds of groups, original image class C_1 and watermark image class C_2. The centers of each class $K_1 = S_e', K_2 = S_f', e \in Na, f \in Na, f \neq e,\ Na = \{1,2,3,4,5\}$ are two signals with distance d_{uv} between each other farthest. d_{uv} can be described by

$$d_{uv} = \left\| S_u^{'} - S_v^{'} \right\|, u, v = 1,2,3,4,5, \mathrm{u} \neq \mathrm{v} \tag{7}$$

where $\|\cdot\|$ is a norm. S_e' , S_f' are respectively $S_u^{'}$ and $S_v^{'}$ corresponding to maximal d_{uv}.

The rest signals $S_j^{'}$ would be classified into C_1 or C_2 according to minimum distances d_{ij}.

$$d_{ij} = \left\| S_j^{'} - K_i \right\|, i = 1,2; j = 1,2,3 \tag{8}$$

if $d_{1j} \le d_{2j}$ is correct, $S_j^{'}$ belongs to class C_1, otherwise it belongs to C_2.

Estimated image S_1' and watermark image S_2' can be recovered by a weighted average which can be described as

$$S_1' = \sum_i^{cnt_1} C_{1i} \Big/ cnt_1 , S_2' = \sum_j^{cnt_2} C_{2i} \Big/ cnt_2 \tag{9}$$

where C_{1i} and C_{2i} are images which respectively belong to C_1 and C_2, cnt_1 and cnt_2 are numbers of each class.

The algorithm description of proposed method

a) Watermarked image is decomposed at different scales and directions by NSCT.

b) The constructed observations X are accumulations of watermarked image I_W and each component $\{I_{W1}, I_{w2}^{d1}, I_{w2}^{d2}, I_{w2}^{d3}, I_{w2}^{d4}\}$ at step a).

c) Applying FastICA algorithm to separate signals $\left\{I', W', I_W'^1, I_W'^2, I_W'^3\right\}$.

d) The separated signals are classified into two categories, the original class C_1 and the watermark class C_2, Center of each class is chosen by the farthest distance between each other.

e) The rest sources $S_j^{'}$ are classified into C_1 or C_2 by (8).

f) Extracted host image evaluation S_1' and watermark evaluation S_2' can be obtained by (9).

Experimental results

The performance measurement of the estimated watermark image is measured by normalized correlation (NC) [11] described as $NC = \sum_i^{M_W} \sum_j^{N_W} W(i,j) \hat{S}_2(i,j) \Big/ \sum_i^{M_W} \sum_j^{N_W} \left[W(i,j)\right]^2$. A watermark image is utilized and shown in Figure1 (a). Watermark image and host image are mixed by DCT. Figure1 (b) is the watermarked image after embedding process. Figure1 (c) is the extracted result by proposed method. Figure1 (d) is the binary image of Figure1 (c).

Fig. 1. Blind extraction results

Table. 1 Performance comparison with proposed algorithm and some existing algorithms

Methods	Proposed method	DWT	RDWT
NC value	98.80%	89.75%	96.26%

We conduct performance comparison with DWT and RDWT methods [8] in Table.1. From Table.1, we can find that proposed method outperforms than the other two methods.

Conclusion

This paper presents a novel blind watermark extraction algorithm, which doesn't need prior knowledge. Single channel blind source separate turns into multichannel problem by constructing new observation vectors based on nonsubsampled contourlet transform. Redundant source signals are separate by the ICA algorithm, which can reduce or eliminate irrelevant information through weighted average. Experimental result demonstrates that the proposed method can extract watermark effectively.

Acknowledgement

In this paper, this research was supported by the fund of Key Laboratory of marine management technology in State Oceanic Administration People's Republic of China (201311).

References

[1] Ma F, Zhang J P, Zhang W. A Blind Watermarking Technology Based on DCT Domain[C]. Computer Science & Service System (CSSS), 2012 International Conference on. IEEE, 2012: 397-400.
[2] Patra J C, Phua J E, Bornand C. A novel DCT domain CRT-based watermarking scheme for image authentication surviving JPEG compression[J]. Digital Signal Processing, 2010, 20(6): 1597-1611.
[3] Yu D, Satter F, Ma K K. Watermark detection and extraction using independent component analysis method [J]. EURASIP Journal on Applied Signal Processing, 2002, 1:92-104.
[4] Lin Q H, Yin F L, Liang H L. A fast decryption algorithm for BSS-based image encryption[M]. Advances in Neural Networks-ISNN 2006. Springer Berlin Heidelberg, 2006: 318-325.
[5] Nguyen T V, Patra J C. A simple ICA-based digital image watermarking scheme[J]. Digital Signal Processing, 2008, 18(5): 762-776.
[6] Ma X, Li X, Liu W. A new audio watermarking method for copyright protection and tampering localization[C]. Innovative Computing Information and Control, 2008. ICICIC'08. 3rd International Conference on. IEEE, 2008: 358-358.
[7] Shi X F, Liang H, Feng L, et al. Blind Extraction Algorithm in Wavelet Domain Based on Structuring Observation Vectors[C]. Mobile Ad-hoc and Sensor Networks (MSN), 2013 IEEE Ninth International Conference on. IEEE, 2013: 577-581.
[8] Hernandez J R, Amado M, Perez-Gonzalez F. DCT-domain watermarking techniques for still images: Detector performance analysis and a new structure[J]. Image Processing, IEEE Transactions on, 2000, 9(1): 55-68.
[9] Da Cunha A L, Zhou J, Do M N. The nonsubsampled contourlet transform: theory, design, and applications[J]. Image Processing, IEEE Transactions on, 2006, 15(10): 3089-3101.
[10] Hyvärinen A, Karhunen J, Oja E. Independent component analysis[M]. John Wiley & Sons, 2004.
[11] Bae K H, Jung S H. A study on the robustness of watermark according to frequency band[C]. Industrial Electronics, 2001. Proceedings. ISIE 2001. IEEE International Symposium on. IEEE, 2001, 3: 2017-2021.

Advanced Materials Research Vols. 989-994 (2014) pp 1905-1908
© (2014) Trans Tech Publications, Switzerland
doi:10.4028/www.scientific.net/AMR.989-994.1905

An Improved Algorithm for Multi-tag Anti-collision in RFID System

Yanru ZHAO[1, a], Weili MIAO[2, b]

[1]School of Mechanical and Power Engineering, Henan Polytechnic University, Jiaozuo, 454003, China

[2]School of Mechanical and Power Engineering, Henan Polytechnic University, Jiaozuo, 454003, China

[a]email: yanruzhao@163.com, [b]email: miaoweili1990105@163.com

Keywords: RFID; Tag Anti-collision; Binary Search Algorithm; Dynamic Binary Search Algorithm; Improved Dynamic Binary Search Algorithm

Abstract. With the development of Radio Frequency Identification (RFID) technology, it also exposed some problems in practical applications. Especially in multi-tag anti-collision problem, how to quickly identify multiple tags in the scope of the reader has become the key to solve the problem. On the basis of the Binary Search Algorithm (BSA) and Dynamic Binary Search Algorithm (DBSA), the paper proposed an Improved Dynamic Binary Search Algorithm. The simulation result proves that the improved method in multi-tag anti-collision is more efficiency than the previous two, which is a good solution to the shortcomings of the first two algorithms.

Introduction

Radio frequency identification (RFID) technology was a rising non-contact automatic identification technology at the beginning of the 1990s that it used radio-frequency to make two-way communication by the way of non-contact. The RFID system mainly consists of three basic components: the tag, the reader and the host data processing system. Every tag has a global unique identification code (ID). When a tag enters the reader's RF range, it is driven on by induction and sends the stored ID code or other data from its inner memory to the reader. Reader can identify all tags within the interrogation zone of its antenna via wireless RF communication technology and algorithms [1]. In recent years, the RFID system has developed dramatically and has been adopted in many fields such as traffic, logistic, security and management [2] [3].

However, in the RFID system, one of the largest disadvantages is its low tag identification efficiency caused by tag collision [4] [5], that is, multi-tag collision is produced by multiple tags appearing simultaneously within a reader's interrogator range. Tag anti-collision algorithm usually consists of the following four methods: SDMA (Space Division Multiple Access), FDMA (Frequency Domain Multiple Access), TDMA (Time Domain Multiple Access) and CDMA (Code Division Multiple Access). But for the low cost and ease of implementation, TDMA is most commonly used. Anti-collision algorithm using TDMA is divided into two ways: deterministic and non-deterministic anti-collision algorithm, and the latter is also called random anti-collision algorithm [6]. The latter was chosen, which was mainly based on the Binary Search Algorithm.

The paper described the Binary Search Algorithm (BSA) and the Dynamic Binary Search Algorithm (DBSA), and put forward an Improved Dynamic Binary Search Algorithm (IDBSA). MATLAB simulation is applied to compare the performance of these three algorithms.

Binary Search Algorithm (BSA)

Binary Search Algorithm (BSA) was comprised of the specified commands and rules between reader and multiple tags.

The following example illustrated the anti-collision principle and process of the BSA.

Assuming that there were four tags, Tag1 (10110010), Tag2 (11100010), Tag3 (10110011), Tag4 (10100010) and the length of every tag was 8 bits. Bits were defined as D7, D6, D5, D4, D3, D2, D1 and D0 from the high-order bit to the low-order one. The reader sent a request command (11111111), and all the tags were in response to this request. The reader received the sequence number 1?1?001?, ? represented the position of the collision. The reader switched the value of the collided highest bit to logic "0", the other low-order bits were changed into logic "1", that was, D6= 0, the sequence number was 10111111. Then the reader transmitted the request again to the tag. The tags that were less than 10111111 were in response to the reader's request. The reader received the returning serial number 101?001?, the highest position of the collision was transformed as logic "0", and the remaining low positions were 1, that is, D4=0. Then the reader repeated the above process. Finally, the reader recognized serial number 10100010(tag4) successfully, replying the select command and reading the data, and the tag was set in the unselected state. Unambiguous identification process was shown in the following table1.

Tab.1 The specific identification process of BSA

Req_count	First	Second	Third	Select	Read &Write
Req_com	11111111	10111111	10101111		
Returning data	1?1?001?	101?001?		10100010	
Tag1(10110010)		10110010			
Tag2(11100010)					
Tag3(10110011)		10110011			
Tag4(10100010)		10100010	10100010		10100010

From the workflow of the BSA (Req_count is short for Request count, Req_com is short for Request command), it can be seen that the more the tags are, the more the searching numbers that the reader identified the tag successfully are, the longer the time consumes. If the reader wants to recognize a tag from *N* tags, the numbers of commands requiring to send *f(N)* are:

$$f(N) = \log_2 N + 1 \tag{1}$$

So the numbers of all commands that the reader recognizes all tags are:

$$I = f(1) + f(2) + f(3) + \cdots + f(N-1) + f(N)$$

$$I = (\log_2 1 + 1) + (\log_2 2 + 1) + \cdots + \log_2 (N-1) + 1 + \log_2 N + 1 = N + \log_2 (N!) \tag{2}$$

Dynamic Binary Search Algorithm (DBSA)

After the tag received a request command from the reader, the sequence number was always transmitted in full. In practical applications, the tag serial number was very large, not only eight bits as mentioned above. Then it would waste a lot of time. So some researchers have put forward a Dynamic Binary Search Algorithm to deal with data-transmit load. In this algorithm, the reader only needed to transmit the bits of the ID which it already knew, and the tags were in response to the reader with the rest bits of the ID that the reader didn't know [7].

Its searching numbers were the same as the BSA, but it still couldn't efficaciously deal with the situation when there were huge numbers of tags.

An Improved Dynamic Binary Search Algorithm (IDBSA)

The principle (given the length of the tag is 8 bits.) is：

(1) Request——this command sends a set of serial numbers as a parameter to the tag. The tag makes a comparison between its sequence number and the received sequence number. The tag will transmit it to the reader when its own serial number is not greater than the received sequence number; otherwise, the tag will not respond to the reader's commands. This helps to narrow the range of prospecting tags.

(2) Select——the fourth prefix that the serial number collided is remained, and the bits collided are set as logic "1".The rest fourth bits are no use. Then the fourth prefix of the serial number sent by the reader is similar to the tags', which are identified successfully.

(3) Sleep——after completing the communication between the selected tags and reader, the reader run this command to make the tag to be in the sleep state, no longer respond to any commands. Then the reader repeats the above process.

For example, there were 8 tags in the interrogation area of the reader. Their serial numbers were tag1(11110001), tag2(11110011), tag3(11010001), tag4(11010011), tag5(10110001), tag6(10110011), tag7(10100001), tag8(10100011). Bits are defined as D7, D6, D5, D4, D3, D2, D1 and D0 from the high-order bit to the low-order one.

The first step: The reader sent a Request command (11111111) to all tags, which responded to this request. The reader received the sequence number 1???00?1, ? represented the position of the collision.

The second step: The collision bits D6, D5, D4 were set as logic "1", and then the reader transmitted the returning serial number 1111 to the tags. The tags that were well as receiving serial number were detected, that is, tag1and tag2 were identified. Then they were inactive and set in the sleep state.

The third step: The reader sent the Request command (1101). As same as the second step, tag3 and tag4 responded to the reader. Then they were set in the sleep state.

The fourth step: The reader sent the Request command (1011). As same as the second step, tag5 and tag6 responded to the reader. Then they were set in the sleep state.

The fifth step: The reader sent the Request command (1010). As same as the second step, tag7 and tag8 responded to the reader. Then they were set in the sleep state. Until now, all tags were identified successfully.

The workflow was shown as the following table2.

Tab.2 The workflow of IDBSA

Req_count	First	Second	Third	Forth	Fifth
Req_com	11111111	1111	1101	1011	1010
Ret_ data	1???00?1	111100?1	110100?1	101100?1	101000?1
Tag1(11110001)		11110001			
Tag2(11110011)		11110011			
Tag3(11010001)			11010001		
Tag4(11010011)			11010011		
Tag5(10110001)				10110001	
Tag6(10110011)				10110011	
Tag7(10100001)					10100001
Tag8(10100011)					10100011

As showed in the table (Req_count is short for Request count, Req_com is short for Request command), the number of tags within the asking range of the reader is two when the collision bit number is one, the total searching times $S(N)$ $(N=2^n)$ can be expressed as:

$$S(N) = 2^{n-1} + 1 = 2 \quad (n = 1) \tag{3}$$

The number of tags within the asking range of the reader is less than four when the collision bit number is two, the total searching times are:

$$S(N) = 2^{n-1} + 1 = 3 \quad (n = 2) \tag{4}$$

According to the mathematical induction, when there are n collision bits and the number of tags is N, the total searching times are:

$$S(N) = 2^{n-1} + 1 \quad (n \geq 1) \tag{5}$$

So, the average searching times $L(N)$ $(N=2^n)$ for every tag are:

$$L(N) = S(N) / N = (2^{n-1} + 1) / 2^n \quad (n \geq 1) \tag{6}$$

Simulation result

Put the calculation formula (2) and (5) into MATLAB simulation, assuming the total numbers of tag N is from 2 to 256, the results are shown in Figure2. The solid line represents the searching time of BSA and DBSA and the dashed line represents the searching time of IDBSA.

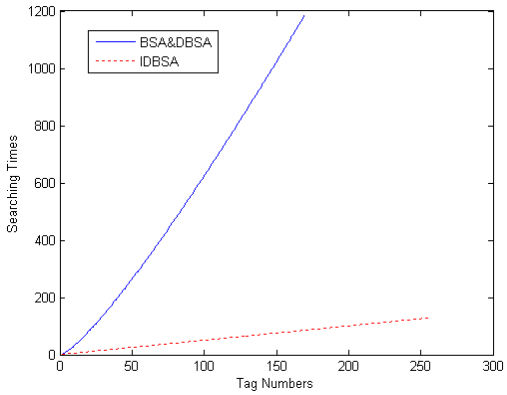

Fig.1 Simulation results

Known from the above figure1, when the number of tags is certain, the average searching times of the Improved Dynamic Binary Search Algorithm are quite less than Binary Search Algorithm and Dynamic Binary Search Algorithm. With the increase in the number of tags, this effect is more pronounced.

Conclusion

Based on the analysis of the principle and the simulation results, it is concluded that the ability of dealing with multiple tags of the Improved Dynamic Binary Search Algorithm is stronger than Binary Search Algorithm and Dynamic Binary Search Algorithm. So Improved Dynamic Binary Search Algorithm overcomes multi-tag collision to a great extent.

Acknowledgment

This work was supported by the 8th key subject of Henan province, by Doctor Foundation of Henan Polytechnic University (grant No.B2008-74) and by Natural Science Research Item of Henan Education Department (grant No. 2011B410002).

References

[1] Wael Zein_Elabdeen, Eman Shaaban. An Enhanced Binary tree Anti-collision Technique for Dynamically Added Tags in RFID Systems [A]. 2010 2nd International Conference on Computer Engineering and Technology [C]. 2010(7)349-353.

[2] ISO/IEC 14443-3 identification cards contactless integrated circuit(s) cards-proximity cards-Part3: Initialization and anti-collision [S], 2003

[3] Jia-lin Ma, Xu Wei. An Improved Anti-collision Algorithm in RFID System, 2009 Ninth International Conference on Hybrid Intelligent Systems [C], 2009.138.

[4] C. Hsiang, Y. Shawing. Investigating Key Factors of Deciding RFID's Adoption in Logistics Service Providers, Computer Supported Cooperative Work in Design 11th International Conference [C], 2007. 1128-1133.

[5] Yue Guo, Ligang Hou. An Improved Anti-collision Algorithm for RFID System [A].The 4th International Conference on Wireless Communications, Networking and Mobile Computing [C], 2008.189.

[6] Hao Shi. A Hybrid of RFID Anti-collision Algorithm [C], Nanjing University of Posts and Telecommunications, 2012. 22-30.

[7] Ziqiang Yu. Improvement of Dynamic Binary Search Algorithm Used in RFID System [A]. 2011 cross Strait Quad-Regional Radio Science and Wireless Technology Conference (CSQRWC 2011) [C], 2011.1046-1049.

Advanced Materials Research Vols. 989-994 (2014) pp 1909-1912
© (2014) Trans Tech Publications, Switzerland
doi:10.4028/www.scientific.net/AMR.989-994.1909

Numerical Simulations of Two Four-Petal Gaussian beams Propagating in Strongly Nonlocal Media

Zhenfeng Yang

School of Economics and Management, Hebei University of Science and Technology, Shijiazhuang, 050018, China

email: yangzhenf@126.com

Keywords: Nonlocal Nonlinearity; Optical Beam; Beam Propagation; Interaction

Abstract. The interaction of two four-petal Gaussian beams propagating in strongly nonlocal nonlinear media is investigated. The results show that the intensity evolution of two beams during their propagation is periodical, which is similar to that of a single beam propagation. However the combined optical field of two beams during propagation is more complicated than that of a single beam. During propagation, the two beams are attracted each other, and at the superposed region of two optical fields, the interference fringes appear. The influences of different beam orders and different input powers on the propagation properties are also discussed.

Introduction

Since 1997, the nonlocal soliton was proposed, various nonlocal solitons are found, such as Gaussian solitons, Hermite and Laguerre Gaussian solitons, complex-variable-function-Gaussian solitons, Ince-Gaussian solitons, vortex solitons, surface soliton and so on. These new types of solitons do not exist in local nonlinear media. Nonlocal solitons exhibit many unique properties, such as the attraction between two out-phase solitons [1, 2], the large phase shift [3, 4], the long-range interactions between nematicons [5]. Nonlocality is ubiquitous in nature, many media demonstrate this property such as atomic vapors, photorefractive media, Bose-Einstein condensates etc. Up to now, peoples have found that the lead glasses and the nematic liquid belong to the strongly nonlocal nonlinear media. In recent years, the propagation properties of optical beams in nonlocal nonlinear media have attracted sufficient attention. Some nonlocal optical beams are investigated.

On the other hand, the propagation properties of four-petal Gaussian beams in various optical systems are studied since it is proposed by Duan et al in 2006 year [6]. Zhou et al analysed the vectorial structure of the far-field of an apertured four-petal Gaussian beam [7] and given M^2 factor of four-petal Gaussian beam [8], Tang et al studied the propagation of four-petal Gaussian beams in apertured fractional Fourier transforming systems [9]. In addition, the propagation properties of a single four-petal Gaussian beam in strongly nonlocal nonlinear media are investigated in detail [10]. However, to the best of our knowledge, the interaction between two four-petal Gaussian beams remains unexploited. In this paper, the interaction of two four-petal Gaussian beams propagating in strongly nonlocal nonlinear media is investigated in theory. Some numerical simulations are performed, and the intensity evolutions of the combined optical field of two beams are given. Furthermore the influences of beam order and input power on the intensity evolutions are discussed.

Theory

In strongly nonlocal nonlinear media, the nonlocal nonlinear Schrodinger equation can be deduced to the Snyder–Mitchell linear model which is expressed as the following equation in Cartesian coordinates [1, 3, 10].

$$2ik\frac{\partial \Phi}{\partial z}+\Delta_{\perp}\Phi-k^2\gamma^2P_0\left(x^2+y^2\right)\Phi=0, \tag{1}$$

where k is the wave number in the media without nonlinearity, Φ is the complex amplitude of the paraxial optical beam, $\Delta_\perp = \left(\partial^2/\partial x^2 + \partial^2/\partial y^2\right)$ is the two-dimensional transverse Laplacian operator, γ is a material constant associated with the nonlocal response function of the media, $P_0 = \iint |\Phi|^2 \, dxdy$ is the input power of the beam.

The four-petal Gaussian beam proposed by Duan and Lü [6] at the source plane is expressed as,

$$\Phi(x_0, y_0, 0) = C_0 \left(\frac{x_0 y_0}{w_0^2}\right)^{2n} \exp\left(-\frac{x_0^2 + y_0^2}{w_0^2}\right), \tag{2}$$

where C_0 is a normalized constant and ensures the input beam power equals P_0, w_0 is the waist width of a Gaussian beam at the initial plane, n is the beam order. For a single beam propagating in strongly nonlocal nonlinear media, it can be regarded as a self-induced fractional Fourier transform [11, 12]. As a result, the expression of a four-petal Gaussian beam in strongly nonlocal media can be obtained using the following integral formula

$$\begin{aligned}\Phi(x, y, z) = &\frac{ik\sqrt{\gamma^2 P_0}}{2\pi \sin\left(\sqrt{\gamma^2 P_0} z\right)} \exp\left[-\frac{ik\sqrt{\gamma^2 P_0}\left(x^2 + y^2\right)}{2\tan\left(\sqrt{\gamma^2 P_0} z\right)}\right] \\ &\times \iint \Phi(x_0, y_0, 0) \exp\left[\frac{ik\sqrt{\gamma^2 P_0}}{2\tan\left(\sqrt{\gamma^2 P_0} z\right)}\left(x_0^2 + y_0^2\right) - \frac{ik\sqrt{\gamma^2 P_0}}{\sin\left(\sqrt{\gamma^2 P_0} z\right)}\left(x x_0 + y y_0\right)\right] dx_0 dy_0\end{aligned} . \tag{3}$$

Based on Eqs. (1)-(3), the propagation of a single four-petal Gaussian beam in strongly nonlocal media can be investigated, and the propagation properties can be found in Ref. [10]. However the interaction between two four-petal Gaussian beams remains unexploited in Ref. [10]. We assume the beam centers of two four-petal Gaussian beams at the initial plane are located at $(\pm d, 0)$, namely

$$\Phi_\pm(x_0, y_0, 0) = C_0' \left[\frac{(x_0 \pm d) y_0}{w_0^2}\right]^{2n} \exp\left[-\frac{(x_0 \pm d)^2 + y_0^2}{w_0^2}\right]. \tag{4}$$

Because the beam propagation in strongly nonlocal media can be regarded as a self-induced fractional Fourier transform, the interaction of two beams co-propagating in such media can be discussed by using the linear rule and the shift rule of the fractional Fourier transform [11, 12], i.e.

$$\hat{F}_\alpha\left\{C_1 g(\xi) + C_2 h(\xi)\right\}(x) = C_1 \hat{F}_\alpha\left\{g(\xi)\right\}(x) + C_2 \hat{F}_\alpha\left\{h(\xi)\right\}(x) \tag{5}$$

$$\hat{F}_\alpha\left\{g(\xi + C_3)\right\}(x) = \exp\left[iC_3 \sin\alpha\left(x + \frac{C_3 \cos\alpha}{2}\right)\right] \hat{F}_\alpha\left\{g(\xi)\right\}(x + C_3 \cos\alpha) \tag{6}$$

where $\hat{F}_\alpha$ represents the fractional Fourier transform, C_1, C_2, and C_3 denote constants, α is the fractional order of the fractional Fourier transform. In the following, based on Eqs. (2)-(6), some numerical simulations are performed, and the interaction of two four-petal Gaussian beams in the strongly nonlocal media is investigated, especially the transverse intensity distributions on different propagation distances.

Numerical Simulations

Fig. 1 gives the transverse intensity distributions of two four-petal Gaussian beams co-propagating in strongly nonlocal media with the input power being ciritical power P_c. It is found that the evolution of two beams is periodical. The period is πz_p, where $z_p = \sqrt{P_{gc}/P_0}\, z_R$, P_{gc} is the critical power of a Gaussian beam [3], z_R is the Rayleigh distance of a Gaussian beam.

With the propagation distance increasing, the energy converges to the beam center gradually. Some intensity peaks appears at $z = 3\pi z_p/6$, and the shapes of the intensity peaks is similar to a single four-petal Gaussian beam. Then the beam evolves as an inverse process from $z = 0$ to $z = 3\pi z_p/6$. These properties are similar to a single four-petal Gaussian beam. However the combined optical field of two beams during propagation is more complicated than that of a single beam. During propagation, the two beams are attracted each other, and at the superposed region of two optical fields, the interference fringes appears.

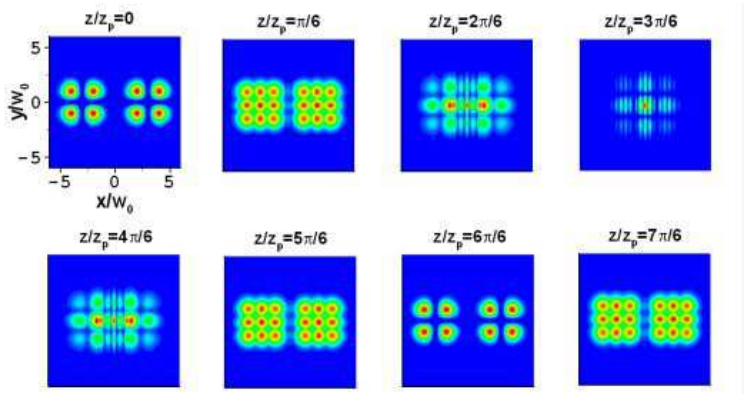

Fig.1. Transverse intensity distributions of two four-petal Gaussian beams co-propagating in strongly nonlocal media at different propagation distances given on the top. Parameters: $d = 3w_0$, $n = 1$, $P_0 = P_c$.

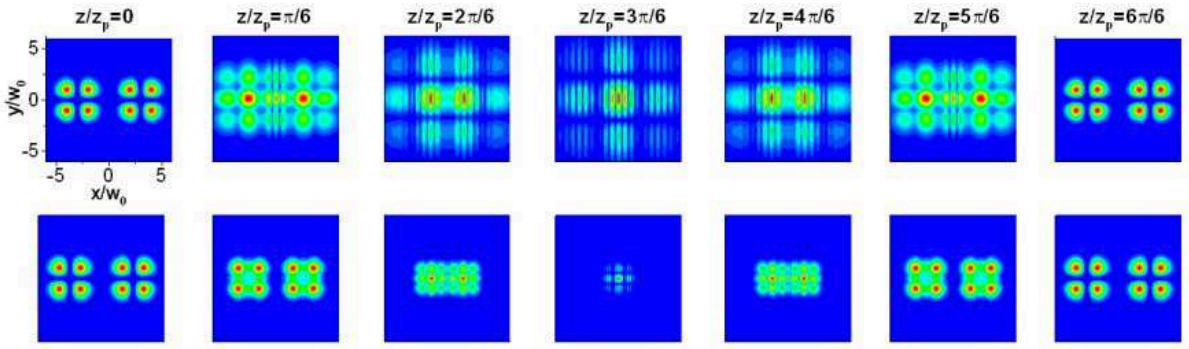

Fig.2. Influence of the input power on the transverse intensity distributions. Top row: $P_0 = 0.5P_c$, Bottom row: $P_0 = 2.0P_c$. The other parameters: $d = 3w_0$, $n = 1$.

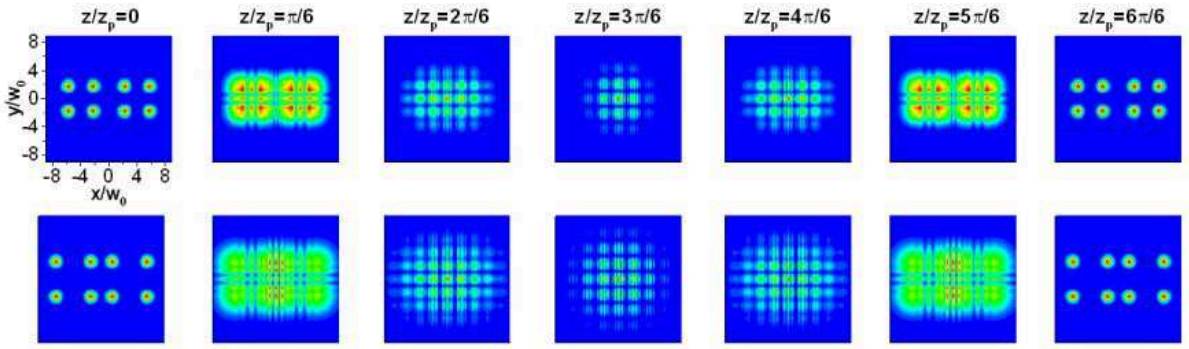

Fig.3. Influence of the beam order on the transverse intensity distributions. Top row: $n = 3$, Bottom row: $n = 6$. The other parameters: $d = 4w_0$, $P_0 = P_c$.

Figs. 2 and 3 illustrate, respectively, the influences of the input power and the beam order on the transverse intensity distributions. It is found that from Fig. 2 that the beam is broadened when the input power is weaker than the input power, and it is compressed when the input power is higher than the critical power, because the higher input power provides a stronger nonlinearity. In Fig. 3 the input power each beam equals its own critical input power. Fig. 3 shows that for a higher beam order, the combined optical field of the two beams becomes more complicated during propagation and more intensity peaks appear at $z = 3\pi z_p / 6$.

Conclusion

In conclusion, the interaction of two four-petal Gaussian beams in strongly nonlocal media has been studied. The results show that the propagation properties of two four-petal Gaussian beams co-propagating in strongly nonlocal media is similar to those of a single beam, but the combined optical field of two beams is more complicated than that of a single beam. During propagation, the two beams are attracted each other, and at the superposed region of two optical fields, the interference fringes occurs. The influences of different beam orders and different input powers on the transverse intensity distribution are discussed.

References

[1] Snyder A. W. and Mitchell D. J., Accessible Solitons, Science, 1997, 276(6): 1538-1541.
[2] Rasmussen P. D. and Bang O., Theory of nonlocal soliton interaction in nematic liquid crystals, Phys. Rev. E, 2005, 72(6): 066611.
[3] Guo Q., Luo B., Yi F., Chi S., and Xie Y., Large phase shift of nonlocal optical spatial solitons, Phys. Rev. E, 2004, 69(1): 016602.
[4] Shou Q., Zhang X., Hu W., and Guo Q., Large phase shift of spatial solitons in lead glass,Opt. Lett., 2011, 36(21): 4194-4196.
[5] Cao L. G., Zheng Y. J., Hu W., Yang P. B., and Guo Q., Long-range interactions between nematicons, Chin. Phys. Lett., 2009, 26(6): 064209.
[6] Duan K. and Lü B., Four-petal Gaussian beams and their propagation, Opt.Commun., 2006, 261(2): 327-331.
[7] Hou Y. and Zhou G., Vectorial structure of the far-field of an apertured four-petal Gaussian beam, Opt. Laser Technol., 2012, 44(4): 963-968.
[8] Zhou G. Q. and Fan Y., M^2 factor of four-petal Gaussian beam, Chin. Phys. B, 2008, 17(10): 3708-3712.
[9] Tang B., Propagation of four-petal Gaussian beams in apertured fractional Fourier transforming systems, J. Mod. Opt., 2009, 56(17): 1860-1867.
[10] Yang Z., Lu D., Deng D., Li S., Hu W., and Guo Q., Propagation of four-petal Gaussian beams in strongly nonlocal nonlinear media, Opt. Commun., 2010, 283(4): 595-603.
[11] Lu D. and Hu W., Theory of multibeam interactions in strongly nonlocal nonlinear media, Phys. Rev. A, 2009, 80(5): 053818.
[12] Lu D., Hu W., Zheng Y., Liang Y., Cao L., Lan S., and Guo Q., Self-induced fractional Fourier transform and revivable higher-order spatial solitons in strongly nonlocal nonlinear media, Phys. Rev. A, 2008, 78(4): 043815.

Advanced Materials Research Vols. 989-994 (2014) pp 1913-1917
© (2014) Trans Tech Publications, Switzerland
doi:10.4028/www.scientific.net/AMR.989-994.1913

An Approach for Sentiment Tendency Analysis on Comment Text

Min LI[1, a], Mengdong CHEN[1, b], Xiangbin LI[1, c]

[1]Beijing Key Laboratory of Network Technology School of Computer Science and Engineering, Beihang University, Beijing, 100191 China

[a]email: xiaomin3982@163.com, [b]email: cmd@buaa.edu.cn, [c]email: lxb_87312743@163.com

Keywords: Sentiment Tendency; Analysis; Sentiment dictionary; Support Vector Machine

Abstract. With the rapid development of network, texts which contain position, views and opinions of events are exploding. Texts of review contain author's feelings, views and tendencies the author wants to express. People need to analyze these texts automatically to acquire sentiment tendency of the author. This paper presents a model for automatic text analysis about sentiment tendency on comment text. The model combines algorithms based on emotional dictionary and Support Vector Machine learning algorithm together, which takes advantage of both algorithms.

Introduction

Information on the internet is increasing. More and more users are willing to share opinions on microblogs, blogs, forums and other platforms to exchange ideas and emotions which include a large number of users' comment on events, products, people and other objects. Government agencies can master social group psychology after emergencies to monitor public opinions. What's more, sentiment analysis can be used to provide psychological counseling for high-pressure groups. The way to mine semantic information from massive unstructured comment texts revealing the author's views and feelings has become a hot research direction. So that people quickly get the author's sentiment tendency.

In previous studies, sentiment classification is also known as opinion mining. Text sentiment classification is defined by mining and analyzing subjective information such as position, viewpoint and emotion in texts to judgment sentimental category. From the present studies, literatures on sentiment classification methods are broadly divided into two categories.

(1) Use sentiment dictionary to analyze text sentiment.

A sentimental word has sentiment tendency in the text, which is an important basis for judging the sentiment tendency. Sentimental words can be divided into positive and negative sentimental words generally, which also be called commendatory and derogatory term. Sentiment dictionary is a collection of sentimental words, consisting of two parts: commendatory and derogatory term dictionary. There exists sentiment dictionary such as HowNet, Student Judgments Justice Dictionary, Synonyms Cilin, NTUSD and so on.

Studies of text sentiment analysis abroad began in the late 1990s. Riloff and Shepherd researched how to build a semantic dictionary based on corpus database[1]. Turney used mutual information method to extend basic judgments vocabulary, and polar emotional semantics (ISA) algorithm was used to analyze the sentiment in texts. Their accuracy reached 74% when dealing with common corpus data[2]. Yang Chao, Feng Shi put forward a network public opinion analysis method based on sentiment dictionary expansion technology[3]. HowNet sentiment dictionary and NTUSD were extended respectively. Wang Suge put forward a text classification method based on emotional empowerment of rough membership, which utilized characteristic tendency strength and defined empowerment rough membership[4].

(2) Use machine learning methods to analyze text sentiment.

B.Pang used machine learning techniques to determine sentiment tendency. Three methods contained Support Vector Machine (SVM), Naive Bayes (NB), Maximum Entropy were used to judge the effect of sentiment tendency. However, experimental results showed that the SVM classification behaved best[5][6]. As we all know, the basic machine learning algorithms includes Support Vector Machine (SVM), Naïve Bayes, K nearest neighbor (KNN), simple linear classifier

(SLC), the maximum entropy (ME), etc[7][8]. Xia Huosong calculated rights by TF-IDF, used SVM classifier based on RBF kernel function to do analysis on network customer comments. Effects of stop words in sentiment classification were studied in his paper[9]. Qiao xiangjie got the reasoning about students' expectations on learning events based on fuzzy reasoning methods. What's more, he did experiments on his model throw Bayes network to test the reasonableness of the model[10].

The advantage of using sentiment dictionary to analyze the text sentiment is the precise fine-grained classification on word level and sentence level. However, limited by natural language processing techniques and related extracting technologies, this method is easy to lose important hidden mode in data sets. The key of machine learning method is located on extracting feature information effectively. Its advantage is objective knowledge acquisition, high accuracy. In the opposite, the disadvantage is the relatively high dependence of training corpus and longer training cycle.

Design of the model on sentiment tendency analysis

According to different levels, sentiment tendency analysis can be divided into the following four levels which are words and phrases level, sentence level, chapter level, as well as the overall sentiment tendency of vast amounts of information. This paper mainly analyzes the tendency for sentence level sentiment, and extracts kinds of subjective information in sentence. A model of sentiment tendency analysis is introduced below.

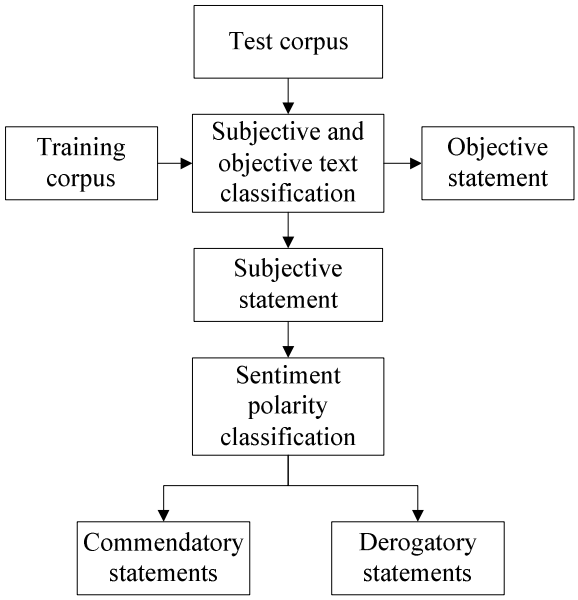

Fig.1. Model of sentiment tendency analysis

Task of this paper is to judge author's sentiment into three categories including praise, derogatory, neutral position based on the sentiment tendency of statements. Usually two programs are taken in previous studies. The one program is using classifier to classify test corpus directly. The other one is calculating the sentiment weight of each statement under considering the case of context. It sets the threshold value according to the size of sentiment weight, and divides sentence into positive, neutral, negative sentiment according to whether the sentiment weight is greater than the threshold value. Both programs have their advantages and disadvantages. Therefore, we propose a hierarchical model for sentiment classification. In the first layer we make subjective and objective dichotomous on texts, extracting subjective sentences. In the second layer we make sentiment polarity classification of the subjective sentence, namely the commendatory derogatory classification, and calculate the intensity of sentiment. Different classification algorithms are adopted in each layer to ensure the accuracy of the respective layers.

The detailed algorithm

(1) Subjective and objective text classification:

Support Vector Machine (SVM) was proposed by Vapnik since 1995, which was subjected to double emphasis on theory and applications areas. It has a solid statistical theory foundation and demonstrates the effectiveness of good practice in many practical applications. When carrying out subjective and objective text classification, we choose SVM algorithm to divided statements into two categories that is subjective statements, objective statement. The algorithm process is introduced as follows.

Step 1: Corpus preparation. Collect and label training data and test corpus, requiring that the scale of different types of training corpus should be roughly equal due to the characteristics of SVM classification algorithm.

Step 2: Corpus pretreatment. This section includes corpus segmentation, tagging, deleting stop words and so on.

Step 3: Select feature vectors. In this paper document frequency (DF) is applied to choose feature vectors.

Step 4: Make training documents into vector representation depending on selected features.

Step 5: Take the document of vector form into SVM classifier for training, deriving the training model.

Step 6: Represent corpus to be classified into vector format according to the optional feature vector by training corpus.

Step 7: Put the document of vector form into the SVM classifier for classification according to the training model.

Step 8: Output classification results. Calculate precision and recall rate.

(2) Sentiment polarity classification

The algorithm flow chart is shown as following.

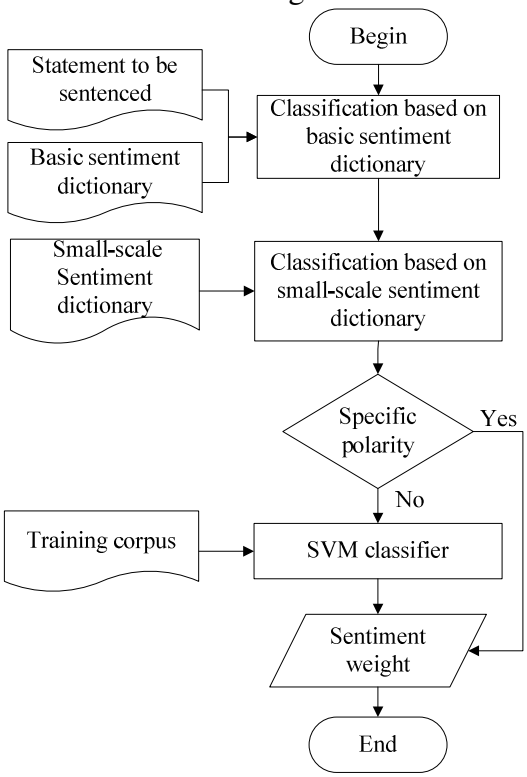

Fig.2. Flow chart of sentiment polarity classification

The core idea of sentiment polarity classification about statements is applying a variety of classification methods on test corpus, putting the higher accuracy algorithm on the top surface. The sentence that has already owned results of separation is outputted immediately. Statement that can't be classified in the layer classification algorithm should be pushed to the next layer for

classification. This paper combines sentiment dictionary algorithm and SVM machine learning algorithms together, which tries to take advantage of a variety of algorithms.

Step 1: Build basic sentiment dictionary throw integrating existing dictionary and constructing areas sentiment dictionary. Basic sentiment dictionary contains commendatory and derogatory dictionary.

Step 2: Treat statements into segmentation using existing segmentation software. Then extract basic sentimental words in statements and match the words in sentiment dictionary. Get its sentiment polarity and corresponding weights.

Step 3: In addition to sentiment words themselves, there are negative words, degree adverbs, turning words, interjections, punctuation, emoticons which influence sentiment tendency greatly. Construct all types of small-scale sentiment dictionary, marking sentimental words and its corresponding sentiment weight.

Step 4: Use small-scale sentiment dictionary to process context semantic information, and extract modifier word, emoticons appearing within a certain range of sentimental words. Calculate its sentiment weight based on constructed small-scale sentiment dictionary which contains modifiers, emoticons. At last, weight the value with result of Step2 and get final sentiment value.

Step 5: Determine sentence tendentiousness based on the calculated final sentiment value. Push the statement into next level of classification algorithms if sentiment tendency intensity of the statement is too weak to definite its tendentiousness.

Step 6: Adopt SVM classifier for the final classification about sentiment statements that all above algorithms can not determine its sentiment tendency.

Sentiment tendency weighted calculation method is introduced as follows:

Divide a text into n sentences named S_1, S_2, …,S_n , and then extract a sentimental word w_i.

(1) If a degree adverb or turning word w_a appears around w_i to qualify the sentimental word, weight of the sentimental word O_{w_i} is calculated by the following formula.

$$O_{w_i} = M_{w_a} \times S_{w_i} \tag{1}$$

Among it, M_{w_a} stands for the weight of degree adverbs or turning words, and S_{w_i} represents the weight of sentimental word w_i.

(2) If a negative word w_b appears around w_i to qualify the sentimental word, judge whether to invert the polarity of w_i according to number of negative words. Weight of the sentimental word O_{w_i} is calculated by the following formula.

$$O_{w_i} = M_{w_b} \times S_{w_i} \tag{2}$$

Among it, M_{w_b} stands for the comprehensive weight of negative words.

(3) When a emoticon w_e appears around w_i, put the sentiment weight of w_e to the weight calculation of w_i as following formula.

$$O_{w_i} = M_{w_e} \times S_{w_i} \tag{3}$$

Among it, M_{w_e} stands for the weight of the emoticon w_e.

(4) The statement S_i probably consists of k sentimental words named W_1, W_2, ...,W_k. So the weight of sentiment tendency about S_i is calculated by the below formula.

$$O_{s_i} = \sum_{i=1}^{k} O_{w_i} \tag{4}$$

(5) If a text d_i include n sentences, its final sentiment tendentious is computed by the following formula.

$$O_{d_i} = \sum_{i=1}^{n} O_{s_i} \tag{5}$$

$$O_{d_i}\begin{cases} > 0; d_i \text{ presents positive sentiment.} \\ = 0; d_i \text{ presents neutral sentiment.} \\ < 0; d_i \text{ presents negative sentiment.} \end{cases} . \quad (6)$$

Conclusion

This paper puts forward an approach of sentiment tendency analysis for comment texts, which mainly adopts the idea of layering. At first, the method uses SVM classification method to classify corpus into subjective and objective statements. And then we combine sentiment dictionary algorithm and SVM machine learning algorithms together to do sentiment polarity classification about subjective statements from the prior layer, obtaining author's sentiment tendency. Considering impacts of semantic information on sentiment calculation, the method makes full use of the modified relation of sentence structure, which makes the analysis process more scientific and reasonable. However, the disadvantage of this method is that inaccuracy is accumulated from one layer to the next layer. We will try our best to reduce the inaccuracy transformation in the future.

Acknowledgement

In this paper, the research was sponsored by Co-Funding Project of Beijing Municipal Education Commission under Grant No. JD100060630.

References

[1] Riloff E, Shepherd J. A corpus-based approach for building semantic lexicons[A]. Proceedings of the second conference on empirical methods in natural language processing[C], 1997.117-124.

[2] Turney PD, Littman M. Measuring Praise and Critism Inference of Semantic Orientation from As sociation. ACM Trans on Information Systems, 2003 21(4) 315-346.

[3] Yang Chao, Feng Shi, et al. Analysis on Web Public Opinion Orientation Based on Extending Sentiment Lexicon[J]. Journal of Chinese Computer Systems, 2010 (4) 691-695.

[4] Wang Suge, Li Deyu, Wei Yingjie. A method of Text Sentiment Classification Based on Weighted Rough Membership[J]. Journal of Computer Research and Development, 2011 48(5) 855-861

[5] Pang B, Lee L, Vaithyanathan S. Thumbs up?: sentiment classification using machine learning techniques[A]. Proceedings of the conference on Empirical methods in natural language processing-Volume 10[C]. Association for Computational Linguistics, 2002 79-86.

[6] Pang B, Lee L. Seeing stars: Exploiting class relationships for sentiment categorization with respect to rating scales[A]. Proceedings of the 43rd Annual Meeting on Association for Computational Linguistics[C]. Association for Computational Linguistics, 2005 115-124.

[7] McDonald, R., et al. Structured models for fine-to-coarse sentiment analysis[A]. Proceedings of the 45th Annual Meeting of the Association of Computational Linguistics[C]. Association for Computational Linguistics, 2007 432-439.

[8] Wang Hongwei, Liu Xie, Yin Pei, Liu N.K.James. Literature Review of Sentiment Classification on Web Text[J]. Journal of the China Society for Scientific and Technical Information, 2010 29(5) 931-938.

[9] Xia Huosong, Tao Min, Wang Yi, Wei Xiang. The Influence of Stop word removal on the Chinese Text Sentiment Classification Based on SVM Technology[J]. Journal of the China Society for Scientific and Technical Information, 2011 30(4) 347-352.

[10] Qiao Xiangjie, Wang Zhiliang, Wang Wansen. Emotional Modeling in an E-learning Based on OCC Theory[J]. Computer Science, 2010 37(5) 214-218.

Advanced Materials Research Vols. 989-994 (2014) pp 1918-1923
© (2014) Trans Tech Publications, Switzerland
doi:10.4028/www.scientific.net/AMR.989-994.1918

Extending the α-algorithm to mine repetitive task based on complex structure

Hong Li[1], Yu Wei[2, *], Xiaohu Ye[3], Shaowen Yao[3], Jun Yang[4]

[1]School of information science and engineering, Yunnan University, Kunming, 650091, China

[2]Department of Electrical&Electronics Engineering, Chengdu Technological University, Chengdu 611730, China

[3]National Pilot School of software, Yunnan University,Kunming, 650091, China

[4] Information Engineering and Automation, Kunming University of Science and technology, China

*Corresponding author email: cdtuyw@qq.com

Keywords: Process Mining; Namesake Task; Repetitive Task; Complex Structure

Abstract. Process mining is helpful for deploying new business processes as well as auditing, analyzing and improving the already enacted ones. The business process system log often has a large number of the namesake task and repetitive task. The existing alpha algorithm of the mining algorithm cannot distinguish them very well. It leads to the results that the process mining often produce inaccurate flow model. In order to improve the accuracy of the process mining, the paper puts forward an improved method. The new method not only can dig the complex structure, such as circulation structure, free choice structure and so on, it still can dig the eponymous task and repeat task in the log.

Introduction

With the rapid development of information technology nowadays, workflow technologies have been widely used. Among them, enterprise modeling is an important field in workflow technology application. Process mining is an important method of Enterprise modeling. Research on process mining are mainly focused on mining the heuristic rules based on the binary sequence relationship which was recorded in the logs, and then extract the process model based on these rules. But the structures exist in actual workflow models have many complex structures which increase the difficulty of process mining, such as duplicate tasks, hidden tasks, implicit places, non-free-choices.

The scholars at home and abroad have done a lot of work in the process mining [1][2]. So far, experts have put forward many meaningful and understanding languages to definite the model. In the process mining, Agrawal firstly use the process mining algorithm applied to workflow management system. Initially, this algorithm requirements process does not exist circulation, the model dig out by the process illustrate by diagram which has direction but no circulation. But Agrawal disposed part of the circulation problem when he improved the algorithm. Herbst and others proposed another algorithm [7][8] based on the ADONIS language. This algorithm deal well with the structure which containing the same activity name in the process, and find simple circulation structure. But to finding hide structure it haven't realized. Aalst and Weijter posed α algorithm [10][11] that based on the extended Petri nets to find equivalent substitution with And-split, And-join structure. But it only uses for the relationship between each activity relationship. Thus, it cannot find the structures which need considering the global structure like NFC (no-free-choice) structure. And also it is helpless in two conditions that the same process contains the same activity name or complex circulation structures.

Paper [9] puts forward α algorithm in mining workflow model and proves it can label the model species accurately. Because α algorithm utilizes set to define the relationships between tasks. α algorithm regards the repetitive task as the same task when it judges the repetitive tasks, so it always dig out the error process model. Paper [3] puts forward a new algorithm which can dig out complex structure in logs such as invisible task, circulation structures and the uncertain parallel

choice structures. But because of this algorithm is on the basis of the α algorithm just improved, so it still can't solve the problem of namesake task and a repetitive task. Here will be proposed an improved method on the basis of the algorithm in paper [3] by which can not only solve the above problems but also improve the accuracy of the process mining.

Related Work

A task might appear in the same workflow model in many times. At this time, multiple tasks with the same name, this task is the repetitive task. In actual work, a repetitive task generally exists in the flow model. So, at first this paper gives a few necessary definitions. In order to ensure that the structures in the mining results weren't be lost by the loss of the log, so the log used here is completely. Therefore, the following are the completeness definition of log:

Definition l: set w is composed of task set T business process produces event logs, σ is task track product by business process execution once. $\sigma \in W$. W is completeness, iff:

(1) the task set for the business process consist T produces any event log W', there is $W' \in W$。

(2) For any$t \in T$, exist $\sigma \in W$ make$t \in \sigma$.

(3) For the event log W', if W' have σ'_1=…xy…, σ'_2=…xay…, σ'_3=…xaay…, and $a, x, y \in T$, then there must be$\sigma_1, \sigma_2, \sigma_3 \in W$and σ_1=…xy…, σ_2=…xay…, σ_3=…xaay….

Circulation task has been defined in [3]. The follow will definition repetitive task.

Definition 2: Set W is the event log produces by the business process consists of by the task set T. iff exit $\sigma \in W$, $\sigma=t_l \cdots t_i \cdots t_j \cdots t_m$, $t_i=t_j$, $t_i \notin Loop1(t_i)$and$t_i \notin Loop2(t_i)$, then says t_i for a repetitive task. The repetitive task t set recorded as D(t).

A repetitive task may appear in the sequence structure, parallel structure or choose structure, below Figure 1 (a) to (f) give a repetitive task appear of 6 combinations of structure.

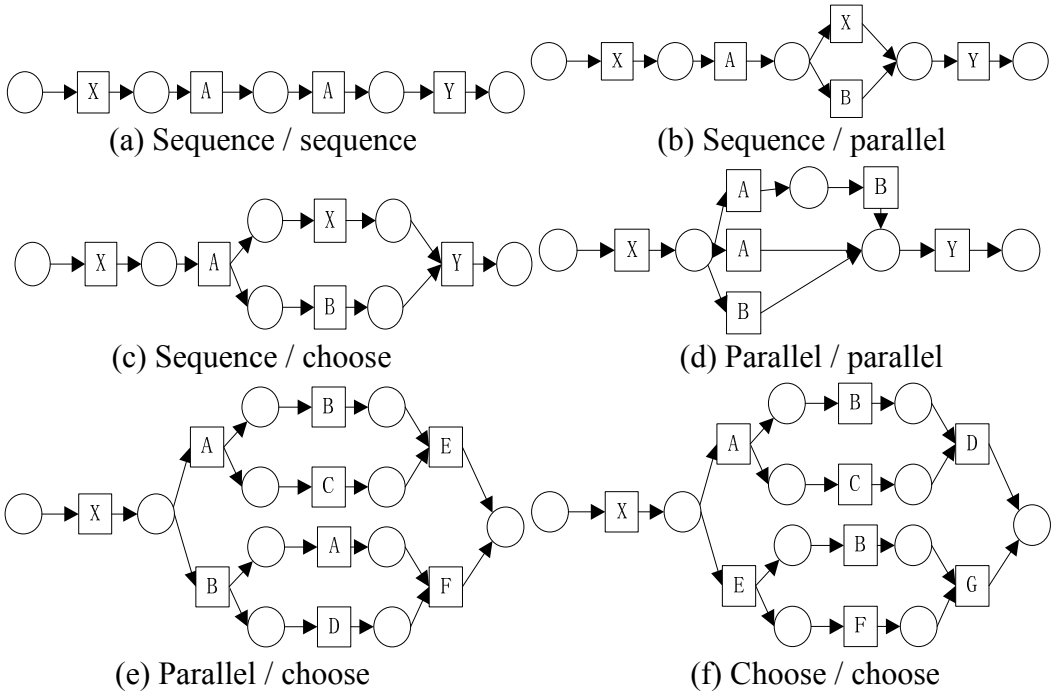

Fig.1. The sequence structure

Definition 3 (definition namesake task): Set W is the event log produces by the business process consists of by the task set T. Iff exit $\sigma_1, \sigma_2 \in W$, $\sigma_1=t_l \cdots t_i \cdots t_j \cdots t_m$, $\sigma_2=t_l \cdots t_i \cdots t_j \cdots t_m$,$i \in [1, m]$and $j \in [1, n]$, if t_i, t'_j generated by the same activity which in the same position in business process, Then t_i, t'_j are the same task. The repetitive task t set recorded as S(t).

Foundation Work

When business process contains circulation task and a repetitive task, a task will repeat many times in the produced event log. In order to determine the task of been repeated from circulation tasks, a repetitive task or the same tasks, need to justify the repetitive task.

Determine the same tasks and a repetitive task.

Definition 1: Set W is the event log produces by the business process consists of by the task set T.σ，$\sigma' \in W$，t，$t' \in T$，i，$j \in [1，n]$，if $t(\sigma,i) = t(\sigma',j)$then$\{t(\sigma,i),t',j)\} \in S(t)$.

This attribute is easy to prove.

Theorem 1: Set W is the event log produces by the business process consists of by the task set T. $\sigma \in W, t \in T$, $t \notin Loop2(t)$ and $len(\sigma)$ =n(n>1). If exit $i,j \in [i,n], i \neq j, t(\sigma,i) \neq t(\sigma,j)$, then$\{t(\sigma,i),t(\sigma',j)\} \in D(t)$.

Proof: Assuming$\{t(\sigma,i),t(\sigma,j)\} \in D(f)$. because $t(\sigma,i),t(\sigma,j) \notin Loop2(t)$, so$t(\sigma,i),t(\sigma,j) \in S(t)$, then there are $t(\sigma,i) = t(\sigma,j)$and i=j This is conflict with the known condition i≠j, $t(\sigma,i) \neq t(\sigma,j)$, so $\{t(\sigma,i),t(\sigma,j)\} \in D(t)$. End.

Theorem 1 had guaranteed the repetitive task in the same task path can be discovered.

Theorem 2: Set W is the event log produces by the business process consists of by the task set T. $\sigma,\sigma',\sigma'' \in W$. $A,A' \in sub(\sigma) \vee sub(\sigma)$.X, Y ∈ T, then

(1) if exit$A \parallel A'$, Also is$AA'\Theta(\sigma,[X,Y])$ and $A'A\Theta(\sigma',[X,Y])$, then

$\{A[XAA'Y],A[XA'AY]\} \in S(A)$; (1)

$\{A'[XAA'Y],A[XA'AY]\} \in S(A')$; (2)

$\{X[XAA'Y],X[XA'AY]\} \in S(S)$; (3)

$\{Y[XAA'Y],Y[XA'AY] \in S(S)$. (4)

(2) if exit$A \oplus A'$, also is $A\Theta(\sigma,[X,Y])$and $A'\Theta(\sigma,[X,Y])$, then

$A[XAY] \in S(A)$; (5)

$A'[XA'Y] \in S(A')$; (6)

$\{X[XAY],X[XA'Y]\} \in S(X)$; (7)

$\{Y[XAY],Y[XA'Y] \in S(Y)$. (8)

(3) if exit$A \propto A'$, also is $A\Theta(\sigma,[X,Y])$ and $AA'A\Theta(\sigma',[X,Y])$,then

$\{A[XAY],A[XAA'AY]\} \in S(A)$; (9)

$A'[XAA'AY] \in S(A')$; (10)

$\{X[XAY],X[XAA'AY]\} \in S(X)$; (11)

$\{Y[XAY],Y[XAA'AY]\} \in S(Y)$. (12)

(4) If exit$A\infty$, also is$\emptyset\Theta(\sigma,[X,Y])$, $A'\Theta(\sigma',[X,Y])$ and $AA\Theta(\sigma'',[X,Y])$, then

$\{A[XAY],A[XAAY]\} \in S(A)$; (13)

$\{X[XY],X[XAY],X[XAAY]\} \in S(X)$; (14)

$\{Y[XY],Y[XAY],Y[XAAY]\} \in S(Y)$. (15)

Proof (1): Because $\sigma = \cdots XAA'Y\cdots, \sigma' = \cdots XA'AY\cdots$, so $X > A, A > A', A' > Y, X > A', A' > A, A > Y$. Because $A \parallel A'$, so there are$X \to A, A' \to Y, X \to A', A \to Y$. use the improved algorithm can get work parameters N_P. Thus can get a conclusion that:

$\{A[XAA'Y],A[XA'AY]\} \in S(A)$; (16)

$\{A'[XAA'Y],A'[XA'AY]\} \in S(A')$; (17)

$\{X[XAA'Y\},X[XA'AY]\} \in S(X)$; (18)

$\{Y[XAA'Y],Y[XA'AY]\} \in S(Y)$. (19)

The proof (2)～(4) are similar with proof (1). End.

Theorem 3: Set W is the event log produces by the business process consists of by the task set T, $t \in T, \sigma,\sigma' \in W$. If the task t and t' in the task path exit relation $tRt'(R \in \{>,\parallel,\oplus,\propto,\infty\})$, in the task path σ' the task t and t' exit relation$R't'(R' \in \{>,\parallel,\oplus,\propto,\infty\})$ and R≠R', then

$\{t(\sigma,[tRt']),t(\sigma',[tR't'])\} \in D(t)$; (20)

$\{t'(\sigma',[tRt']),t'(\sigma',[tR't'])\} \in D(t)$. (21)

Proof: assuming $\{t(\sigma,[tRt']),t(\sigma',[tR't'])\} \notin D(t)(R \neq R')$ and $\{t'(\sigma,[tRt']),t'(\sigma',[tR't'])\} \notin D(t)(R \neq R')$, can get $\{t(\sigma,[tRt']),t(\sigma',[tR't'])\} \in S(t)$, $\{t'(\sigma,[tRt']),t'(\sigma',[tR't'])\} \in S(t)$, use the theorem 2 can get R=R', this is conflict with R≠R' , so we can draw a conclusion that:

$$\{t(\sigma,[tRt]),t(\sigma',[tR't'])\} \in D(t); \quad (22)$$

$$\{t'(\sigma,[tRt]),t'(\sigma',[tR't'])\} \in D(t). \quad (23)$$

Proof end.

The circular task and repetitive task in business process are extremely easy to confusion, but the two kinds of structure are really and respectively exit. In order to dig out the correct flow model, we must criterion them carefully.

Algorithm

Here, process mining is divided into preprocessing, processing and post processing. The pretreatment stage basically filters a repetitive task and namesake task. The processing stage mainly analysis the complex structure, such as circulation structure, the unfreedom parallel choice, invisible task and so on, and dig out the preliminary workflow model. The later stage of processing is main reduction the task's original name which renamed and change the connection relationship of connection library in relations sets.

Based on the attribute 1 and theorem front 1-3, and combined with the improved algorithm in literatures [3], this paper puts forward another kind of the improved algorithm to dig the repetitive task. T is the task set, W is the workflow log on task T. σ and the partial order relation between tasks reference the definition in literature [3]. Specific algorithm is described below.

Step 1: filter the repetitive task and the namesake task

According to the workflow log W calculated all appeared task in W composition set D(t).

Using attribute 1 and theorem 1 ~ theorem 3, identify the namesake tasks and the repetitive task, and put the repetitive task T into D(t). Rename the tasks by adding subscript in D(t),Updated the log after rename and get new event log T_{log}.

Step 2: Mining the T_{log} use the new mining algorithm in literature [3]. The library of ultimately result set named W^{DT}.

1) $LIL = \{t \in T_{log} | \exists \sigma = e_1, e_2, \dots, e_j, \dots, e_n \in W[e_i \cdot task = e_j \cdot task = e_k \cdot task = t \wedge l = k+1 = i+2 = j+3]\}$

2) $T' = T_W | L1L, L2L = \Phi;\ F_{L1L} = 0.$

3) $For\ each\ t \in L1L, do$

$A = \{a \in T' | a >_w t\};\ B = \{b \in T' | t >_w b\};$

$if\ \forall a_1 \in A, b_1 \in B\ \ a_1 >_w b_1 \Rightarrow$

$F_{L1L:} = F_{L1L} \cup \{(t, p(A|B, B|A)), (p(A|B, B|(L1L: = L1L - 1) \wedge (L2L = L2L \cup t)$

$\wedge F_{L1L:} = F_{L1L} \cup \{(tjump, p(A,t)), (p(t,B), tkump)\}$

4) $W^{-L1L} = \Phi$

5) $For\ each\ \sigma \in W, do\ \sigma' = \sigma$

$For\ each\ t \in L1L, do\ \sigma' = remove\ Task\ (\sigma', t), TW = TW - t;$

$For\ each\ t \in L2L, do\ \sigma' = remove\ Task\ (\sigma', t, 1); W^{-L1L} = W^{-L1L} \cup \sigma'.$

6) $W = W^{-L1L}$

7) $X_W = \{< ps, ss, op > | ps \subseteq T_W \wedge ss \subseteq T_W \wedge op \in op\ \wedge\ \forall a \in ps\ \ \forall b \in ss\ \ a \rightarrow_w b\ \ op = default\ \}.$

8) $D_S = \left\{ \left(t_{(P_{in};P_{out})}; t_{(P'_{in};P'_{out})} \right) \middle| (P_{in}; P_{out}); (P'_{in}; P'_{out}) \in Y_I \cup Y' \wedge P_{out} \cap P'_{in} \neq \Phi \right\} \cup \{(a, t_{(P_{in};P_{out})}) | (P_{in}; P_{out}) \in Y_I \cup Y' \wedge \exists (A,X) \in P_{in}: a \in A\} \cup \{(t_{(P_{in};P_{out})}; b) | (P_{in}; P_{out}) \in Y_I \cup Y' \wedge \exists (Y,B) \in P_{out}: b \in B\}$

9) $D_P = \left\{ \left(t_{(P_{in};P_{out})}; t_{(P'_{in};P'_{out})} \right) \middle| (P_{in}; P_{out});\ \ (P'_{in}; P'_{out}) \in Y_I \cup Y' \wedge \forall (A,X) \in P_{in};\ \ (A'; X') \in P'_{in}: \exists a \in A;\ a' \in A';\ x \in X;\ x' \in X': a \| W\ a' \vee x \| w x' \right\} \cup \{(t; t_{(P_{in};P_{out})}) | t \in T_W \wedge (P_{in}; P_{out}) \in Y_I \cup Y' \wedge \forall (A,X) \in P_{in};\ \exists a \in A;\ x \in X;\ a \| W\ \ t \vee x \| w\ t\}$

10) $T_W = T_W \cup \{t_{(Pin;Pout}|(P_{in};P_{out}) \in Y_I \cup Y_1'\}$

11) $(W^{DT}) = (T_W;T_I;T_O;D_S;D_P)$.

Specific algorithm introduces reference the algorithm [3] description.

Step 3:post-processing

1) Take the repetitive task in T_W which renamed to their original names and then save it into T_W.
2) Take the arc which is relevant with the rename repetitive task in D_P connection to the original names task and then save it into D_P.
3) Set $N = (W^{DT}) = (T_W;T_I;T_O;D_S;D_P)$.

Algorithm end.

Experiment

The algorithm used in experiment program is written in C language, it realizes the Experimental prototype include the algorithm in [3]. In the experiment we use CPN Tools (color petri net tools) establishes five workflow models which contains repetitive task [12][13]. Firstly we randomly generated a workflow log which contains 1,000 event tracks for each model, and then analysis the log file. The following Figure 2 (a) and (b) give the compare which using experimental prototype and using an improved algorithm for mining between the results of the model. Owing to space restrictions only give one group of model contrast here. Through the experiment we can know that the improvement algorithm can recognition repetitive task, and get workflow model which is the same with prototype.

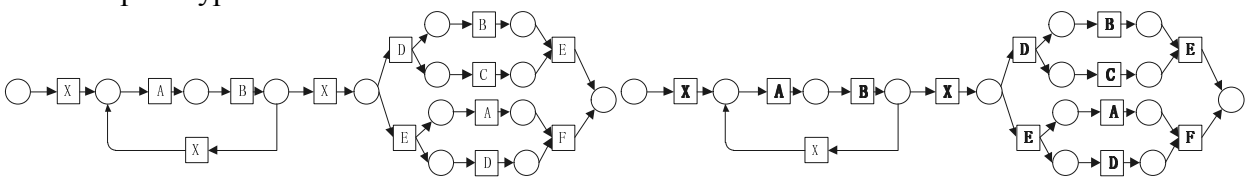

(a) Prototype model N2 (b) The mining model

Fig.2. Model contrast

Experimental results show that the improved algorithm can effectively distinguish and mining the namesake task and repetitive task. According to the improved algorithm written the ProM plug-in, this paper selects five groups of examples log as experiment logs. Running the improved mining algorithm get experimental results shows as following Figure 3.

The Experiments show that the improved algorithms can effective mining invisible task, circular structure and unfreedom choice structure.

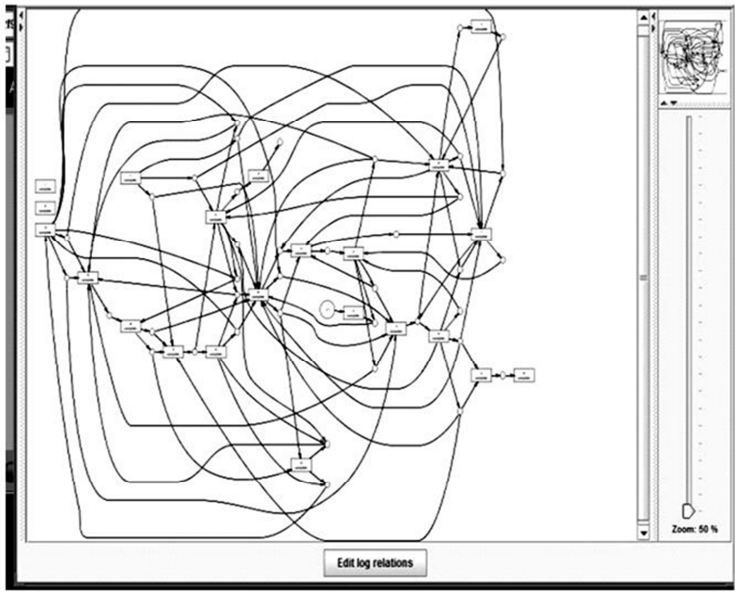

Fig.3. Mining result

Conclusion

The improved algorithm overcomes the mining limitation of α algorithm. Analysis from the experiment, the improvement in this paper can effective mining the namesake task, repetitive task, circulation structure, unfreedom choice structure and so on, which structure exit in system log. But the algorithm does the experiment with the completed log. The experiment does not consider the influence of the noise, and the mining accuracy of complex structures which have some reduce.

Acknowledgement

This paper is supported by Laboratory of Network Intelligent Computing @ Yunnan University, the Key project of Education Department of Sichuan Province under grant No. 14ZA0286 and the Research Program of Application Foundation of Sichuan Provincial Department of Science and Technology under grant No. 2013SZZ026.

References

[1] J.E. Cook and A.L. Wolf. Automating process discovery through event-data analysis. In Proceedings of the 17th international conference on Software engineering, pages 73-82. ACM, New York, NY, USA, 1995.
[2] J.E. Cook and A.L. Wolf. Discovering Models of Software Processes from Event-Based Data. ACM Transactions on Software Engineering and Methodology, 7(3): 215-249, 1998.
[3] YE Xiaohu, YAO Shaowen, LIU Fangyu, XUE Gang. Towards Improving Process Mining Results Base on Invisible Tasks. ACMSIC2011 B0406155.
[4] Van der Aalst W M P, Weijters A J M M. Process mining—a research agenda, computers in industry [J]. 2004, 53(3): 231-244.
[5] Agrawal R, Gunopulos D, Leymann E Mining process models from workflow log [C]. Proceedings of the 6th International Conference on Extending Database Technology, USA, 1998: 469-483.
[6] Herbst J, Dealing with concurrency in workflow induction[C]. Proceedings in the 7 European Concurrent Engineering Conference, SCS Europe, 2000.
[7] Joachim H, Dimitris Karagiannis. Workflow mining with InWoLvE [J]. Computers in Industry, 2004, 53(4): 245—264.
[8] Guido Schimm. Mining exact models of concurrent workflows [J]. Computers in Industry, 2004, 53(2): 265—281.
[9] AALST W M P, WEIJTERS T, MARUSTER I. Workflow mining: discovering process models from event logs [J]. IEEE Transactions on Knowledge and Data Engineering, 2004, 1 6(9): 1128-1142.
[10] Van der Aalst W M P, Weijters A J M M, Marudter L. Workflow mining: which processes Can be Rediscovered [C]. IEEE Transactions on Knowledge and Data Engineering, Eindhoven, 2002: 67-91.
[11] Van der Aalst W M P, Van Dongen B, E. Discovering workflow performance models from timed logs [C]. International Conference on Engineering and Deployment of Cooperative Inform action System, Berlin, 2002:45-63.
[12] Chinces, D. Business process mining algorithms. IEEE International Conference on Intelligent Computer Communication and Processing (ICCP). 2013, 9: 271-277.
[13] Weber, P. A Framework for the Analysis of Process Mining Algorithms. Systems, Man, and Cybernetics: Systems, IEEE Transactions on (Volume:43, Issue: 2). 2013, 3: 303 – 317.

Advanced Materials Research Vols. 989-994 (2014) pp 1924-1929
© (2014) Trans Tech Publications, Switzerland
doi:10.4028/www.scientific.net/AMR.989-994.1924

Process mining: Overview and Comparative analysis of the mining algorithms

Hong Li[1], Yu Wei[2,*], Lin Liu[3], Shaowen Yao[4], Jun Yang[5]

[1]School of information science and engineering, Yunnan University, Kunming, 650091, China

[2]Department of Electrical&Electronics Engineering, Chengdu Technological University, Chengdu 611730, China

[3]School of information, Yunnan Normal University,Kunming, 650092, China

[4]National Pilot School of software, Yunnan University,Kunming, 650091, China

[5] Information Engineering and Automation Kunming University of Science and technology, China

[*]Corresponding author email: cdtuyw@qq.com

Keywords: process mining; log; algorithm

Abstract. Process mining is helpful for deploying new business processes as well as auditing, analyzing and improving the already enacted ones. This paper summarizes the scholars' main studies in workflow mining, introduces the modeling process of two different kinds of mining algorithms in detail, compares and analyzes their performances, and explains the modeling process with an actual example.

Introduction

Workflow is a kind of business process that can be fully or partially automated implemented [1], which realize the automated integration and business process management by defining the relationships between activities. Workflow modeling is usually defined by the enterprise workflow modeler based on documents, or participants in the process models consultation, which is simple, intuitive, easy, and is the primary means of current modeling. However, the modeling way was very susceptible to the individual ability and the subjective experience of the participants, which makes the model only express the process "should" look, rather than its "real" look. In the meantime, the modeling method which relies solely on the modeler not only inefficient but also has high cost.

Based on this regard, some experts propose a new workflow modeling method- work flow log based automation process modeling known as workflow mining. This modeling approach uses data mining thinking through the analysis of business interaction records, i.e., workflow logs, and then automated derive the enterprise workflow model through mining algorithms. Most companies have established ERP, CRM, SCM and WFMS systems in real life. With the implementation of these business workflow systems, the log records provide a large data base for the enterprise workflow mining. The model established by such modeling methods can reflect the actual enterprise business execution processes, and the modeling process is automated implemented, which not only reduces the impact of modeler and participants, but also can improve the modeling efficiency.

Related works

"Workflow mining" first appeared in the field of software engineering, proposed by USA Joanthan E. Cook in 1995, a professor of computer science at New Mexico State University [2]. In 1998, Rakesh Agrawal of IBM Almaden Research Center in the United States applies it to enterprise workflow modeling for the first time [3].

Joanthan E.Cook and Alexander Wolf designed three kinds of workflow mining method in literature [2], in which KTail and Markovian approach is practicality stronger than RNet. But these three methods all use finite state machine (FSM) model as their formal description, which restricted its ability that can only represents the sequential structure workflow model because the FSM describe limitation.

Rakesh Agrawal et al. designed two workflow mining algorithms and use “directed graph” to describe workflow model [3]. Both algorithms can be deduced from the workflow model with causal and cycle relationship, but difficult to handle process with synchronous and selection relationships, i.e., the And-join/split and OR-join/split structure.

Gudio Schimm designed a workflow mining algorithm that can be used to deal with a hierarchical structure [4], and developed its mining tool (Process Minner).But the algorithm difficult to deduce the workflow business process models with cyclic structures.

Joachinm Herbst and Karagiannis applied the inductive method in workflow mining [5][6]. But the method in literature [5] can only deduce sequence workflow structure. The mining method in literature [6][7] considered the problems of process synchronization, but it is difficult to deal with the selection and circulation relationships. In addition, because the workflow model of these two mining methods can only use “random activity diagram”, which also has their limitations.

The mining algorithms Aalst designed can mainly divide into two categories: formal and non-formal mining algorithms [8][9], and both use WF-net to represent the workflow mining results. Between these two methods, the formal algorithm requires complete workflow logs without noise, and can only deduce reasonable workflow structure model which cannot handle non-freedom choice structure; the non-formal algorithm has no specific workflow log requirements, but it is difficult to deal with short- cycle workflow structure.

Definitions

In this part, the basic workflow concepts that used in the process mining are been defined and explained.

Definition 1(workflow log): Let T be the set of activities. $\sigma \in T^*$is called the workflow traces. $W \in P(T^*)$ is the workflow log, which $P(T^*)$ is theset of T^*.

Definition 2(Petri nets): Petri net PN is a triple (P, T, F):

- P is a finite set of places;
- T is a finite set of transitions,$P \cap |\cdot t| = 1$;
- $F(P \times T) \cup (T \times P)$ is a set of arcs (or flow relations).

Definition 3(WF-net): Petri net PN is a workflow net N where:

1) PN has two special places: I and o. i is a start place, i.e., i = Φ; place o is the end place, i.e., $o \cdot = \Phi$.

2) Each node $x \in P \cup T$is on one path from i to o.

Definition 4 (structured workflow net SWF-net): workflow net N = (P, T, F) is a SWF-net where:

1) $\forall p \in P, t \in T$, there is $(p, t) \in F$, then $|\cdot t| = 1$ when $|p \cdot| = 1$;

2) $\forall p \in P, t \in T$, there is $(p, t) \in F$, then $|\cdot p| = 1$ when $|t \cdot| > 1$;

3) There are no hidden places.

Definition 5 (basic relationships between activities): Let W be the workflow log, the activity set T, there is $W \in P(T^*)$, assume$a, b \in T$:

1) a and b has the direct sequence relationship $a >_w b$ where: $\exists \sigma = t_1 t_2 \dots t_{n-1} i \in \{1,2, \dots n\}, \sigma \in W, and\ t_i = a, t_{i-1} = b$

2) a and b has the casual relationship $a\#_w b$ where: $a \not> _w b\ and\ b \not> _w a$;

3) a and b has the parallel relationship $a //_w b$ where: $a >_w b\ and\ b >_w a$;

Define 6 (∈, first, last): Let T be the active set, $a \in T$ and $\sigma = a_1 a_2 \dots a_n \in T^*$ is the workflow track of length n.

1) $a \in \sigma$where:$a \in \{a_1 a_2 \dots a_n\}$;

2) $\text{first}(\sigma) = a_1$

3) $\text{last}(\sigma) = a_n$

Definition 7 (complete workflow log): Let N = (P, T, F) is reasonable WF-net:

1) W is the workflow log of N where: $W \in P(T^*)$ and Each group workflow trace$\sigma \in W$ is a sequence that begins from the initial state [i] to the end state [o], i.e., $(N,[i])[\sigma > (N,[o])$

2) W is a complete workflow log of N where:

a) For any workflow log W' of N, there is $>_{w'} \subseteq >_{w}$;

b) $\forall t \in T, \exists \sigma \in W,$ there is $t \in \sigma$.

Algorithms and Compares

The current workflow mining algorithms can be divided into two categories: formal mining algorithms mining algorithms and heuristics mining. Formal algorithms derive the workflow model from the workflow logs through formalization method. The heuristic mining algorithms first derive the basic logical rules between activities based on the heuristic rules, and then build the workflow model.

A. Formal mining algorithm - α algorithm

α algorithm recognizes the basic relationships between workflow log activity by formal methods, and then establish the workflow model based on the relationships. The specific algorithm is as follows:

Let W be the workflow log, T is the activity set, α(W):

(1)$T_W = \{t \in T | \exists_{\sigma \in W} t \in \sigma\}$

(2)$T_I = \{t \in T | \exists_{\sigma \in W} t \in first(\sigma)\}$

(3)$T_O = \{t \in T | \exists_{\sigma \in W} t \in last(\sigma)\}$

(4)$X_W = \{(A,B) | A \in T_W \wedge B \in T_W \wedge \forall_{a \in A, b \in B} a \rightarrow_W b \wedge_{a1,a2} a1 \#_W a2 \wedge_{b1,b2} b1 \#_W b2\}$

(5)$Y_W = \{(A,B) \in X_W | \forall_{(A',B' \in X_W)} A \subseteq A' \wedge B \subseteq B' \Rightarrow (A,B) = (A',B')\}$

(6)$P_W = \{p(A,B) | (A,B) \in Y_W\} \cup \{i_W, o_W\}$

(7)$F_W = \{(a, p(A,B)) | (A,B) \in Y_W \wedge a \in A\} \cup \{(p(A,B), b) | (A,B) \in Y_W \wedge b \in B\} \cup \{(i_W, t) | t \in T_I\} \cup \{(t, o_W | t \in T_O)\}$

(8)$\alpha(W) = \{T_W, P_W, F_W\}$

The specific steps of α algorithm are as follows:

Step 1 establishes the current log collection T_w; step 2 and step 3establish the input transition set T_i and output transition set T_o; step 4derivesthe transition set X_w with causal relationship, the transition in set A has causal relationship with the transition in set B, but the transition within A and B has no causal relationship. We can discover AND(OR)-Split/Join structure by limiting the set of A and B; step 5 redefines X_w by establish the largest collection of A and B; step 6 is used to establish the places of transitions; step 7 establishes the flow relationship between the place and the transition. Step1 to step7can derive the process model from the workflow log, and represents it by WF-net.

This formal mining algorithm is simple and easy to understand, but has certain limitations in the application as follows:

(1) The algorithm requires a complete workflow log, otherwise the model been derived may lost some relationships between the activities. Obviously, this formal mining algorithm is only suitable for simple structure and complete workflow log process.

(2) The log noise will affect the derivation of the basic relationship between activities which makes the algorithm has lower robustness of noise.

(3) The algorithm is difficult to identify the one-step and two-step cycle structure, and can only create model with SWF-net. The adaptability of the algorithm is not strong.

B. Heuristic Algorithm

Heuristic mining method derives the basic relationship between activities by heuristic rules from the workflow log is divided into three steps:

(1) Create dependency/frequency table (dependency/frequency table, D/F table) (As shown in Table 1)

For the activity a and activity b, we can have the following information from the log:

1) the appear frequency of activity a and b, i.e., #a, #b; 2) the frequency that b directly before a, i.e., #b<#a; 3) the frequency that b directly inherit a, i.e., #a>#b; 4) the total frequency that b before a, i.e., #b<<<#a; 5) the total frequency that a before b, i.e., #a>>>#b; 6) the dependencies between a and b, i.e., #a→#b.

Table 1 The D/F table from b to a

#a	#b	#a>#b	#b<#a	#a>>>#b	#b<<<#a	#a→#b

(2) Derive the basic relationship between activities according to the D/F table.

Define the heuristic rules, and derive the basic relationships based on the D/F table ($a \rightarrow_w b$, $a \#_w b$, $a \,//\, _w b$).

The heuristic rules of causal relationship are as follows:

IF $(\#a \rightarrow b \geq N)$ *AND* $(\#b < \#a \leq \theta)$ *AND* $(\#a > \#b \geq \theta)$

THEN $a \rightarrow_w b$

N is the noise factor, the default value N = 0.05, the N increases with the increasing of log noise. The threshold $\theta = (1 + \mathrm{ROUND}(\mathrm{N} \times \#\mathrm{L})) / (\#\mathrm{T})$.

Which tracks the total number of rows workflow # L on behalf of the log, # T represents the total number of activities.

(3) After the basic relationship between activities been clearly discovered, then create the workflow model based on α algorithm.

Heuristic algorithm improves the application limitations of α algorithm. First, the parameters N and θ can effectively handle the log noise, i.e., the algorithm is robust. Second, since the algorithm is deriving the basic activity relationships based on the heuristic rules, so the integrity of the log is not strictly required. But because it is often difficult to accurately setting the value of θ and N before digging, so the mining quality maybe affected by different θ and N.

C. Comparative analysis of algorithms

The previous sections respectively introduced two types of workflow mining algorithms, which have their own application conditions and domains. Table 2 compares and analyzes the two algorithms from different angles.

Table 2 The comparative analysis of the α algorithm and heuristic algorithm

	application condition	WF-net structures can be mined	robustness for noise	Process model structure	advantage	disadvantage
αalgorithm	complete log with no noise	SWF-net(except one-step cycle and two-step cycle)	low	Figure	Simple, easy to understand, high operability	Unsuitable for complex workflow Process structure
Heuristic algorithm	/	SWF-net and most WF-net	high	Figure	Suitable for mining complex workflow process	The values of N and θ are not easy to determine

Case study

The workflow log (assuming that the log is complete and without noise) is shown in Table 3, which contains five workflow instance case1-case5. We use α algorithm to establish the workflow model.

Table 3 Workflow log

case	activity	case	activity	case	activity	case	activity
Case1	A	Case1	C	Case5	E	Case4	B
Case2	A	Case2	C	Case4	C	Case5	F
Case3	A	Case4	A	Case1	D	Case4	D
Case3	B	Case2	B	Case3	C		
Case1	B	Case2	D	Case3	D		

(1) Definite the basic relationships between the activities.

There are five workflow cases in the Log:

σ_1 = {A, B, C, D},

σ_2 = {A, C, B, D},

σ_3 = {A, B, C, D},

σ_4 = {A, C, B, D},

σ_5 = {A, B, C, D, E}.

By definition 5 we can have:

a) Direct relationship:$A >_W B, B >_W C,\ C >_W D,\ A >_W C,\ B >_W D,\ C >_W B,\ E >_W F$

b) Causal relationship: $A \rightarrow_W B,\ C \rightarrow_W D,\ A \rightarrow_W C,\ B \rightarrow_W D,\ E \rightarrow_W F$

c) Parallel relationship: $B||_W C,\ C||_W B$

(2) Use α algorithm to mine the process.

a) T_w= {A, B, C, D, E, F};

b) T_i= {A, E};

c) T_o= {D, F};

d) X_w= {(A, B) (C, D) (A, C) (B, D) (B, F)};

e) Y_w= X_w;

f) P_w= {p(A, B), p(C, D), p(A, C), p(B, D), p(E, F)} ∪ {i_w, o_w};

g) F_w= {(A, p(A, B)), (p(A, B), B), (C, p(C, D)), (p(C, D), D), (A, p(A, C)), (p(A, C), C), (B, p(B, D)), (p(B, D), D), (E, p(E, F)), (p(E, F), F), (i_w, A) (i_w, E) (D, o_w), (F, o_w)};

h) α(W)= {T_w , P_w , F_w};

(3) The process model describes with WF-net is shown in Figure 1.

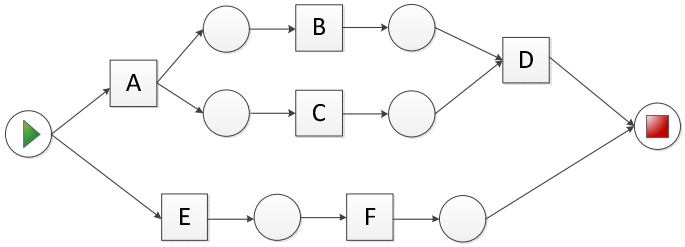

Fig.1.TheWF-net model of the process

Conclusion

This paper summarizes the status of the workflow mining technology research, detailing the two different types of mining algorithms -α algorithm and heuristic algorithm and its comparative analysis. Then in the following chapters, this paper points out their respective use conditions and the advantages and disadvantages, and explains the mining steps of αalgorithm with an example.

Acknowledgement

This paper is supported by Laboratory of Network Intelligent Computing @ Yunnan University, the Key project of Education Department of Sichuan Province under grant No. 14ZA0286 and the Research Program of Application Foundation of Sichuan Provincial Department of Science and Technology under grant No. 2013SZZ026.

References

[1] Luo Haibin, Fan Yushun, Wu Cheng. The overview of workflow technology [J]. Journal of Software, 2000, 11(7), 8992907.

[2] Cook J E. Process Discovering and Validation through Event-data Analysis[R]. Boulder, University of Colorado, Technical Report: CU-CS-817-96, 1996-11.

[3] Agrawal R, Gunopulos D, Leymann F. Mining Process Models from Workflow Logs[C]//Proceedings of the 6thInternational Conference on Extending Database Technology. 1998: 469-483.

[4] Schimm G. Process Miner - A Tool for Mining Process Schemes from Event-based Data [C]// Proc. of the 8thEuropean Conference on Artificial Intelligence. Springer-Verlag, 2002.

[5] Herbst J, Karagiannis D. Integrating Machine Learning and Workflow Management to Support Acquisition and Adaptation of Workflow Models [J]. International Journal of Intelligent Systems in Accounting, Finance and Management, 2000, 9(5): 67–92.

[6] Herbst J. Dealing with Concurrency in Workflow Induction [C]// Proc.of European Concurrent Engineering Conference on Society of Computer Simulation. 2000.

[7] Aalst W M P, Weijters A J M M, Maruster L. Workflow Mining: Discovering Process Models from Event Logs [J]. IEEE Transactions on Knowledge and Data Engineering, 2004, 9 (12): 369-378.

[8] Chinces, D. Business process mining algorithms [C]. IEEE International Conference on Intelligent Computer Communication and Processing (ICCP), 2013(9): 271 – 277.

[9] Weber, P. A Framework for the Analysis of Process Mining Algorithms [J]. IEEE Transactions on Systems, Man, and Cybernetics, 2013, 3(Volume:43, Issue:2): 303 – 317.

Advanced Materials Research Vols. 989-994 (2014) pp 1930-1933
© (2014) Trans Tech Publications, Switzerland
doi:10.4028/www.scientific.net/AMR.989-994.1930

A P2P Resource Management Model Based on Cloud Computing

Yang LU[1, a], Guangfeng LIU[2, b]

[1] College of Information Engineering, China University of Geosciences, Beijing, 100083, China

[2] Education Ministry Key Laboratory of Petroleum Engineering, China University of Petroleum, Beijing, 102249, China

[a]email: luyangemail@163.com, [b]email: lgf@cup.edu.cn

Keywords: Cloud Computing; P2P; Resource Management

Abstract. The technology of cloud computing has become a hot issue of research in the service of network in recent years. Cloud computing platform provide computing and storage services to customers. And it has been widely applied in e-business, e-education and etc.. While Cloud systems are usually hosted in large datacenters which may become a bottleneck to the system. In this paper we describe the design of a double-layer P2P model based on cloud computing. In the model, user nodes grouped into clusters form the Extended Cloud layer, and transfer file to each other without participation of the Core Cloud layer. The new model has better scalability and efficiency.

Introduction

Cloud computing is an extension of parallel computing, distributed computing and grid computing[1]. It has been one of the hottest issues of research. Major players of the IT industry have increasingly concentrated resources on Cloud schemes[2], such as the cloud computing platform and supporting apps from Google, the Blue Cloud platform from IBM[3][4], and the Elastic Compute Cloud (EC2) from Amazon[5][6]. And on such issues the academia is making progress in parallel. Google File System (GFS) [7][8]as a typical dynamic-content managing cloud is designed specifically for the intensifying demand of data processing by Google. A master server deployed to manage the information of all servers and to respond the users' inquiries, which represents a centralized index structure shared by many cloud computing systems, may become a bottleneck to the system extensibility. Researchers seeking counteract proposed to introduce in the P2P technology by substituting the master server of a GFS with a DHT to organize the servers directly[9], or by replacing the single master server of a GFS with a cluster of major servers[10], or by connecting individual components of the cloud computing platform via P2P technology[11]. However, all these P2P-based modifications confine their effort in optimizing the internal structure of the cloud computing platform, instead of mobilizing the equivalent features of the P2P technology.

This paper presents a P2P resource management model based on cloud computing, completed by an Extended Cloud structure derived from a Core Cloud from the service provider, with part of the Core Cloud load transferred to the Extended Cloud, in order to relieve the load of the core server, to improve the service quality of the Core Cloud, and to reduce the system cost.

Resourse Management Model

The proposed resource management model is a double-layer structure, as shown in Figure1. With the lower layer of a Core Cloud from the service provider, and the upper layer of an unstably-gathered Extended Cloud composed by users' computers. The Extended Cloud transfers the resources by transferring resources directly, grouping user nodes into clusters via the self-organization, and providing the low-cost content management. A user node requested resource will receive the replica node list from Core Cloud, and then communicate with the corresponding replica node in the Extended Cloud to transfer the file. User nodes communicate inside the Core Cloud, and release the load of Core Cloud.

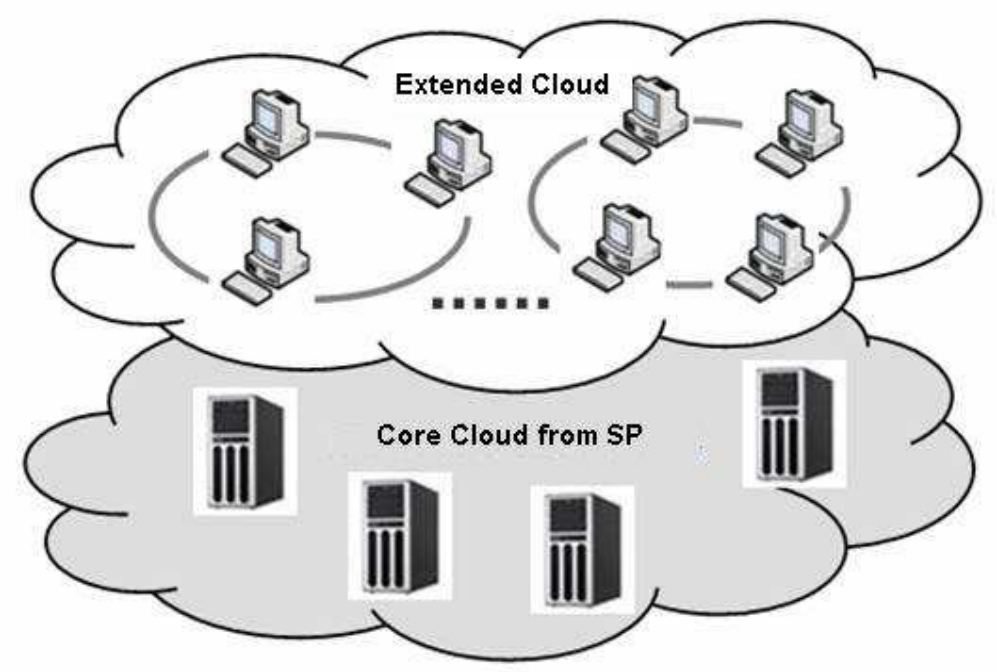

Fig.1. Resource management model

In the Extended Cloud, user nodes are grouped into clusters according to their communication condition. In order to consider Extended Cloud connectivity between the nodes, user nodes are grouped into clusters according to the latency of real world. We thus choose to use network latency because latency is often a direct indicator of the performance seen by end-host nodes and can be easily measured in a light-weight, end-to-end and non-intrusive manner.

We need M well-known landmark machines [12] to spread across the Internet. A user node measures its distance, i.e. round-trip-time, to this set of known landmarks and orders them by distance. This scheme is simple, requiring little support from the infrastructure. The only infrastructure requested is a small number (internet trace data indicates that 8-12 machines should suffice for the current scale of the internet) of relatively stable landmark machines. Little work is requested of these landmark machines – they need only echo "ping" messages – and landmarks could in fact be unsuspecting participants in the network. Landmarks neither actively initiate measurements nor gather or disseminate measurement information. Binning is scalable because nodes independently discover their bins without communicating or coordinating with other application nodes.

We constructs M clusters based on these landmarks and names them by landmarks' number, called CID. All nodes measure their round-trip-time (RTT) to each of these landmarks and initialize the value of CID according to Theorem 1.

Theorem 1: Let L={l0, l1, …lm-1} be the set of M landmarks, then a node A creates an ordering La on L. For example, i appears before j in La if RTT (A, li)<RTT (A, lj) or RTT (A, li)=RTT (A, lj) and li<lj. Node A initializes the value of A.CID using the first landmark in La.

Thus, based on its delay measurements to the different landmarks, every node has an associated ordering of landmarks and CID. User nodes that have the same CID are grouped into one cluster.

Note that with the above cluster scheme, node only needs to discover the distance between itself and the landmarks and can measure these distances itself. Nodes need not know the distance of other nodes from the landmarks. Also, cluster scheme is robust to the failure of one or more landmark nodes. In the case of landmark failures and performance degraded, new nodes will substitute for the old ones. And the corresponding clusters remain unchanged.

In the Core Cloud, each resource maintains a replica node list. The number of the replica nodes of each resource is determined by the intensity of resource inquiry (i.e. the frequency of inquiry for a certain resource), which means the more intensive the resource is requested, the more replica nodes will be attributed accordingly. When a node send request to the Core Cloud, the server will verify the node at first, and then answer the request with a replica node list. Then the Core Cloud

will verify the credibility of the node and the cluster where the node is located, and determine whether to designate such node as a new replica node according to the number of replicas for the requested resource. Once the credibility and the designation are confirmed, the information will be written in the replica node list of the resource. The replica nodes should be distributed into different clusters, with individual nodes available to be added or deleted according to the dynamic intensity of inquiry.

The user node receiving the replica node list will request the node in the same cluster, because the communication is more efficient among nodes in the same cluster. If all replica nodes are invalid, the user node will acquire the information directly from the Core Cloud.

Self-organized Mechanism

In a dynamic network, nodes can join (or leave) at any time. As shown in Figure 2, a new user node firstly obtains its CID by measuring RTT to each of landmarks, then send request to the Core Cloud including file's message, cluster number, and node's credit message. After received replica node list from the Core Cloud, user node should check whether there is node in the same cluster, and then send a request to it. If not, user node will request to the node in the neighborhood cluster. Then download the files from the replica node directly. If all nodes on the list are failure, it will send a notice to the server, and download from Core Cloud directly. Finally, the node checks whether it has been chosen as a replica node by server and save the message.

Nodes in the network may fail or depart without warning. If it is a replica node，it should issue a departure request into the system before its departure. The Core Cloud will update the replica node list, and then choose a new one. The absence of the non-replica nodes has no impact to the network, thus no status update is requested from such nodes.

In the real network, nodes change dynamically. The system needs to deal with nodes joining the system concurrently and the nodes that fail or leave voluntarily. The replica nodes in the Extended Cloud will regularly update their status to the Core Cloud. Any replica node failed to update its status for 3 cycles will be deleted.

```
// node N joins the network
N.join ( )
    //compute CID by measuring their RTT
    CID = N.find_cluster_num(N);
    //send a source request to Core Cloud
    //receive the replica list of the source
    R_List = N.send_request(SERVER);
    //if there are any available nodes
    //then send a load request to the node
    //and download the resource
    if (R_List is not NULL)
        CN=N.choose_node(R_List)
        N. load_request(CN)
    //if all the nodes on the list are failure
    // then request to download from Core Cloud directly
    else
        N.load_request(SERVER)
    // checks whether it has been chosen as a replica node
    RE=N.replica_node(CID,CM)
    if (RE) N.update_info()
```

Fig.2. Pseudo code for the node join

Performance Analysis

The resource management model presented in this paper is superior for:

Better Balanced Load: Unlike the traditional Cloud Computing-based models, this model separates the file replicas among the nodes of the Extended Cloud, in which the user node works as

both the client and the server of the resources without participant of Core Cloud, and significantly relieves the load of the Core Cloud.

Better Efficient File Transmission: The nodes in Extended Cloud are clustered by the landmarks, and choose the node in the same cluster for file transmission, which helps improve the transmission speed and avoid the bottleneck nodes.

Better Robustness: The file information is stored in the Core Cloud server and multiple replica nodes in the Extended Cloud. The number of the replicas is adjusted according to the inquiry intensity of the resource, by which the risk of single point failure is circumvented.

Conclusion

This paper presents a P2P resource management model based on cloud computing. It utilize the resources of user nodes by grouping such nodes into Extended Cloud, which is above the traditional Core Cloud. The Extended Cloud shares the file transmission load of the Core Cloud and maintains the efficient transmission through the clusters, and further reduces risk of transmission bottleneck and single point failure.

References

[1] Leavitt N. Is cloud computing really ready for prime time?[J]. IEEE Computer Society Press. 2009, 42(1):15-20.

[2] Ozalp Babaoglu, Moreno Marzolla, Michele Tamburini. Design and implementation of a P2P Cloud system. SAC '12 Proceedings of the 27th Annual ACM Symposium on Applied Computing[C]. New York, 2012, 412-417.

[3] IBM Blue Cloud Solution(in Chinese). http://www- 900.ibm.com/ibm/ideasfromibm/cn/cloud/solutions/index.html.

[4] Barham P, Dragovic B, Fraser K and so on. Xen and the art of virtualization. Proc. of the 9th ACM Symp[C]. on Operating Systems Principles. New York, 2003,164-177.

[5] Amazon. Amazon elastic compute cloud(Amazon EC2). 2009. http://aws.amazon.com/ec2/

[6] Sangho Yi, Kondo D, Andrzejak A and so on. Reducing Costs of Spot Instances via Check pointing in the Amazon Elastic Compute Cloud. 2010 IEEE 3rd International Conference on Cloud Computing[C]. Miami, 2010, 236 – 243.

[7] Ghemawat S, Gobioff H, Leung ST. The Google file system. Proc. of the 19th ACM Symp on Operating System Principles[C]. New York, 2003, 29-43.

[8] Barroso LA, Dean J, Holzle U. Web search for a planet: The Google cluster architecture[J]. IEEE Micro, 2003, 23(2): 22-28.

[9] Xu K, song M, Zhang X Q and so on. A Cloud Computing Platform Based on P2P. ITIM2009: proceedings of the IEEE International Symposium on IT in Medicine Education[C]. Jinan, 2009, 427-432.

[10] Yang J, Zhao G H, Wang K J and so on. A modern service-oriented distributed storage solution[J]. The Journal of China Universities of Posts and Telecommunications, 2009, 16(1): 120-126.

[11] Ran JR, Zhao L, Wu X and so on. Peer-to-peer Cloud Provisioning: Service Discovery and Load-Balancing[J]. Cloud Computing, 2010. http://arxiv.org/abs/0912.1905/.

[12] S. Ratnasamy, M. Handley, R. Karp, and S. Shenker. Topologically-Aware Overlay Construction and Server Selection. Proc. IEEE INFOCOM Conf.[C]. New York, 2002, 1190- 1199.

Advanced Materials Research Vols. 989-994 (2014) pp 1934-1937
© (2014) Trans Tech Publications, Switzerland
doi:10.4028/www.scientific.net/AMR.989-994.1934

Architecture Research and Design of Cloud Computing Service Based on REST

Kun HUANG

Computer science and Technology Specialty of Sichuan TOP Vocational Institute, Chengdu 611743, China

e-mail: 83100024@qq.com

Keywords: architecture; cloud computing; REST;WASL; REST-style

Abstract. Cloud computing deployment model has: IAAS, PAAS, SAAS, and they can provide calls for the clients by web services. REST-style cloud computing architecture represents resource by the URI, and operates resources by standard HTTP methods GET, PUT, POST, DELETE, etc. In this paper, the e-city website as example, using REST methods to architect website, logistics, customer, the pay bank. The architecture fully reflects the REST architectural style is simple and convenient. But REST flaw is that the limited transaction-oriented processing capabilities. In order to solve this problem, WASL (Web Application Description Language) is used to describe the REST API.

Cloud Computing Architecture

Cloud computing is not a single technology, nor is it a combination of all kinds of technology; its core philosophy is to achieve on-demand services. It is a service that enables users to get required infrastructure, platform, application and other resources by the method to expanse easily, in accordance with their needs by network. Cloud computing architecture is shown in Figure 1:

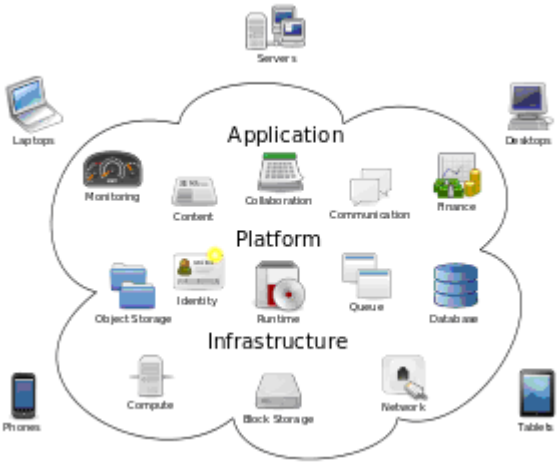

Fig. 1. Cloud computing architecture

Cloud computing services have three levels: IAAS (Infrastructure as a Service), PAAS (platform as a service), and SAAS (software as a service). Service is the foundation for cloud computing.

Main Solutions of Cloud Computing Services

In the cloud computing service architecture, usually three ways to provide services to clients. XML-RPC: XML (Extensile Markup Language) Remote Procedure Call Protocol; SOAP: Simple Object Access Protocol; REST: Representational State Transition.

XML-RPC: a remote procedure call (remote procedure call, RPC) protocol for distributed computing, the function package will be called by XML and use the HTTP protocol as a transport mechanism. Later, because the new features constantly being introduced, this standard slowly evolved into SOAP protocol today.

SOAP (Simple Object Access Protocol) is a standardized communication specification, SOAP based on HTTP protocol; put REQUEST parameters in written XML into HTTP BODY, and submit them to web service server to process; and then the results are written in XML as a response back to the client. In order to make that the client and WEB SERVICE can correspond with each other, you can use WSDL (Web Services Description Language) as the description file to describe this means of communication. SOAP has the ability to tie the complex objects serialized into XML. SOAP requires a series of complicated encapsulation; Even so, SOAP still can not reach the consistency of the interface, different vendors have their own interface.

REST (Representational State Transfer), use standard HTTP methods that is used by web service (GET/PUT/POST/DELETE), abstract all the web service as resources, REST observe the entire network from the perspective of resources, and all the resources determined by the URI, and the client application to get the characterization of resources through URI.

REST constraints

(1) Client / server mode: All Web services are required to meet this constraint.

(2) Stateless. The HTTP protocol is stateless.

(3) Cached response capabilities: for example, when a client requests information, if this information does not change the product within a day in the past, then you can find information on this product in a reverse proxy, the information is presented in cache and is returned directly cached statements, omitting the service execution.

(4) Uniform HTTP interface. REST HTTP specification must be strictly in accordance with the method to use the service. Thus, a POST to perform all rely on logic operation is not REST-style API.

Architecture Instance

REST architecture style, URI represents the resource, so order is a resource. GET can execute query an order; PUT can created an order; POST can modify an order; DELETE can delete an order, as shown in Figure 2 .

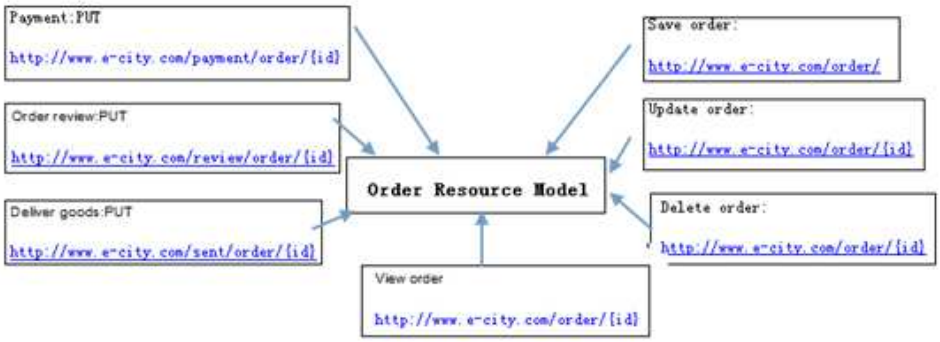

Fig. 2. Orders resource model

The architecture is designed to integrate the three systems, namely e-city reception sites, e-city background is ERP systems responsible for warehousing, shipping and logistics into , and ERP system of outsourcing logistics. Three systems each have their own processing, end to end processing of the entire order is complete together by three systems.

When we submit an order in e-city, a message is sent back to the background ERP system; the news triggered a flow of goods out of the warehousing and on the meanwhile a flow of parcel delivery in the logistics company. When we complete to pay to the distribution staff, the shopping process has ended for our customers. The distribution staff backs their money, a message is sent back to the backstage ERP, logistics and parcel delivery company's process ends, and this e-city order processing is complete.

In these interactions, the most important thing is that we achieved “hypermedia as the engine of application state” which is called by REST community through workflow. W Workflow responsibility is to manage the lifecycle of orders, At different stages of their life cycle, we have different players, different operating authority for the order.

More simply, URI represents the state transition in the state machine. The <squence>, <activity> and <xor> tabs allows clients to operate the state machine transfers by the way to follow links.

In this architecture, join the business process management system. Responsibilities of business process management system are that: First, it manage the integration between the various systems, thus avoiding from, a lot of the coupling between the various systems; Second, by tracking order status, complete the order visualization throughout the process.

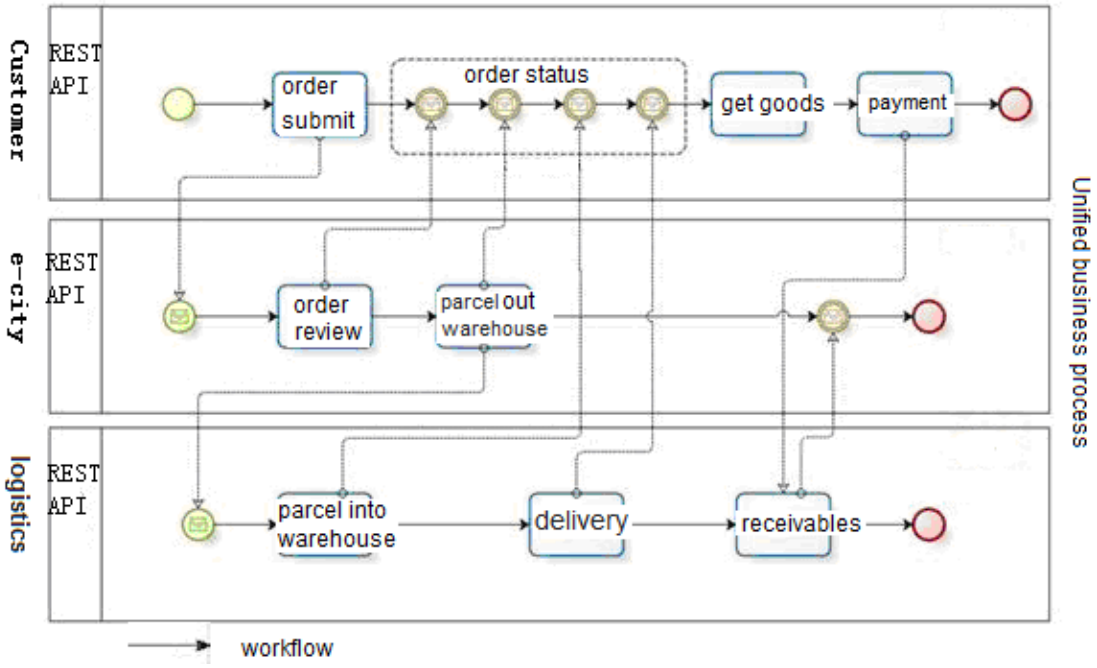

Fig .3. The entire process of orders from submission to completion

Problems and Optimization

REST API follows the model of cloud computing architecture, software architecture based on Web services usually use it for integration purposes via XML or JSON. This means that they are using an Internet browser or Web server.

REST proponents claim that REST request and response data is simple and readable. But SOAP requires a series of complicated encapsulation. Even so, SOAP still can not reach the consistency of the interface; different vendors have their own interface. But REST only uses standard HTTP method. This is indeed the case?

To solve this problem, a WASL (Web Application Description Language) to describe the REST interface. WADL is similar to REST WSDL version , with REST being applied to complex areas ,SOAP is necessary especially for transaction-oriented applications.

References

[1] Hengyun Zhang, Haitao He. Security Research and Design of SOA Architecture. Journal of Sichuan University of Science & Engineering(Natural Science Edition)， Vol.22, No.11. 2009.

[2] Gangjian Li. A New Exploration on Calculation Model of Cloud Based on SOA. Journal of Jilin Institute of Architecture and Civil Engineerin,Vo1.28, No.2,2011.

[3] Long Wang, ZhenKai Wan. Research and Implementation of Service-oriented Architecture of Cloud Computing. Computer & Digital Engineer. Vol. 37, No. 788,2009.

[4] Wuxue Jiang, ChuanZhang. Cloud Computing and Its Architecture Model. ,Journal of Liaoning Technical University (Natural Science). 2011.

Advanced Materials Research Vols. 989-994 (2014) pp 1938-1941
© (2014) Trans Tech Publications, Switzerland
doi:10.4028/www.scientific.net/AMR.989-994.1938

High precision data processing method based on the complex-step differentiation

Fenglei TAN[a], Yakun GUO[b], Yongming NIE[c], Fuan SUN[d]

China Satellite Maritime Tracking and Controlling Department, Jiangyin, 214431, China

[a]email: flood1990@163.com, [b]email:yimonie@163.com, [c]email:nwy1986@163.com,

[d]email: yaol0206@163.com

Keywords: Finite differencing; Complex-Step Differentiation; precision

Abstract. Finite differencing is a very commonly method used in numerical algorithms to compute derivatives, which is well known for its accurate precision. Besides, the best advantage of this method resides in the fact that it is extremely easy to implement. But the finite differencing may be in a dilemma. The reason is that if the step size is large, the precision is not satisfying, but if the step size is small, the error is increased due to subtractive cancellation. In this manuscript, a new method for differential, complex-step differentiation (CSD) is proposed, which uses complex computations to compute derivatives. We first give a detailed account of the principles of the complex-step differentiation. Then analyze the CSD method from two sides, error and efficiency. At last, the implementation of CSD in MATLAB is presented. Simulating results indicate that they are fitting well with the theoretical analysis.

Introduction

Analytic functions, such as Polynomial functions, exponential functions, trigonometric functions, are very common type of functions in Mathematics [1] [2]. Analytic function differentiations are common operations in mathematical calculations. In computer programs, only Programmable method can be used to compute derivatives approximately. One method that is very commonly used in numerical algorithms to compute derivatives is finite differencing. It is known for being accurate to some extent and extremely easy to implement [3]. However, this approach has an obvious shortcoming: if the step size is large, the precision is not satisfying, but if the step size is small, the error is increased due to subtractive cancellation. For these reasons, Another method was invented, which use Complex calculation to compute derivatives. This method is called CSD(Complex-Step Differentiation) [4] [5]. For there is no finite differencing in CSD, we can make the step size small enough to get satisfactory accuracy. Besides, the efficiency of this method is relatively higher.

In this article, we first give a detailed account of the principles of the complex-step differentiation. Then analyze the CSD method from two sides, error and efficiency. At last, the implementation of CSD in MATLAB is presented.

Principals

Finite differencing formulas are a common method for estimating the value of derivatives, for the different choices of the proximal point, Finite differencing can be divided into forward difference, backward difference and central difference as follows.

Forward-difference formula:

$$f'(x) = \frac{f(x+h) - f(x)}{h} + O(h). \tag{1}$$

Backward-difference formula:

$$f'(x) = \frac{f(x) - f(x-h)}{h} + O(h). \tag{2}$$

Central-difference formula:

$$f'(x)=\frac{f(x+h)-f(x-h)}{2h}+O(h). \quad (3)$$

Whichever the formula is, the truncation error is Inevitable. Theoretically, The smaller the value of step size(h), the smaller the truncation error is. But another problem which called Subtractive Cancellation will appear if the value of step size is too small. Consider function $f(x)=x^2$, now we use finite differencing to calculate the derivative of it at $x=3.253$. If we make the $h=0.002$, here comes:

$$f'(3.253)=\frac{f(3.253+0.002)-f(3.253)}{0.002}=\frac{3.255^2-3.253^2}{0.002}=10. \quad (4)$$

But the Correct value is computed as follows:

$$f'(3.253)=2x\big|_{3.253}=2\times 3.253=6.506$$

Which is much smaller then 10. This is because the step size is too small, as a result, the values of f(x) are very close at the proximal points. A subtraction operation and a division operation used in the process result in a bigger value.

The properties of analytic functions in the complex domain can be used to solve approximate derivation. The method based on these properties is called CSD. Consider analytic function $f(z)=u(z)+iv(z)$, argument $z=x+iy$ is complex. Function f is differentiable in the complex plane, and, we will get the same result no matter we approaching from the imaginary axis or the real axis.

Approach from the real axis:

$$\lim_{\substack{h\to 0\\ h\in R}}\frac{f(z_0+h)-f(z_0)}{h}=\frac{\partial f}{\partial x}(z_0). \quad (5)$$

Approach from the imaginary axis:

$$\lim_{\substack{ih\to 0\\ ih\in iR}}\frac{f(z_0+ih)-f(z_0)}{ih}=\lim_{\substack{ih\to 0\\ ih\in iR}}-i\frac{f(z_0+ih)-f(z_0)}{h}=-i\frac{\partial f}{\partial y}(z_0). \quad (6)$$

$$\frac{\partial f}{\partial x}(z_0)=-i\frac{\partial f}{\partial y}(z_0). \quad (7)$$

Deform Equation (7)，here comes the Cauchy–Riemann equation of function f:

$$\frac{\partial u}{\partial x}=\frac{\partial v}{\partial y}. \quad (8)$$

$$\frac{\partial u}{\partial y}=-\frac{\partial v}{\partial x}. \quad (9)$$

Deform equation (8) using differential forms:

$$\frac{\partial u}{\partial x}=\lim_{h\to 0}\frac{v(x+i(y+h))-v(x+iy)}{h}. \quad (10)$$

h is a real number here. Equation (10) can be deformed as follows Because our concern is the derivative of the function f at some point real number.

$$\frac{\partial f}{\partial x}=\lim_{h\to 0}\frac{\mathrm{Im}[f(x+ih)]}{h}. \quad (11)$$

If h is small enough, the derivative of f can be written as:

$$\frac{\partial f}{\partial x}\approx\frac{\mathrm{Im}[f(x+ih)]}{h}. \quad (12)$$

The equation above is the CSD derivation formula, for there is no differential operation in it, there will be no Subtractive Cancellation. Theoretically, as long as h is small enough, CSD can get a satisfied result.

The function f can be expended as a Taylor series about a real point x as follows and compute the value of f at the point x + ih:

$$f(x+ih)=f(x)+ihf'(x)-h^2\frac{f''(x)}{2!}-ih^3\frac{f'''(x)}{3!}+\cdots \tag{13}$$

Taking the imaginary parts of both sides of this Taylor series expansion and dividing it by h yields:

$$f'(x)=\frac{\mathrm{Im}[f(x+ih)]}{h}+h^2\frac{f'''(x)}{3!}+\cdots \tag{14}$$

Namely:

$$f'(x)=\frac{\mathrm{Im}[f(x+ih)]}{h}+O(h^2). \tag{15}$$

From equation (15) we can see that the Truncation error is $O(h^2)$ if we use CSD to compute the derivative of f, which is much smaller than $O(h)$.

Simulating

In this manuscript, the following expression to show how CSD works as shown in Fig.1 is used and simulating is given below based on MATLAB.

$$F(x)=\frac{e^x}{(\cos x)^3+(\sin x)^3} \tag{16}$$

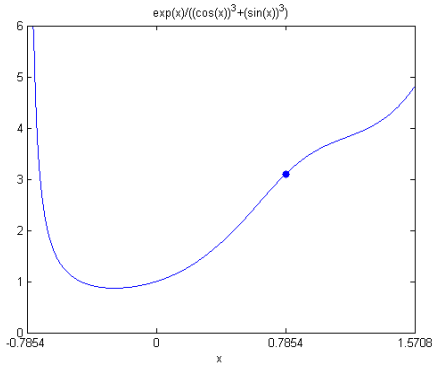

Fig. 1: Schematic of F(x)

In the following, error and efficiency analysis are given. Firstly, for a more accurate analysis of the error of complex-step differentiation, MATLAB symbolic toolbox can be used to compute the exact value of the derivative function. The error curve is shown in Fig. 2.

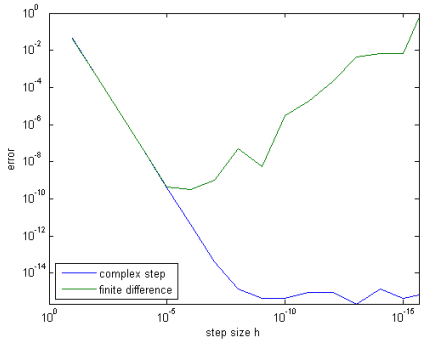

Fig. 2 Error curve of CSD compared with finite differencing

The results are just the same as we expect. The error of CSD is very small when the step h is small enough, but the error of finite differencing will be much bigger for the Subtractive Cancellation when h is too small.

A simple example can be used to show the efficiency of CSD, function f is described as $f=x_1x_2$.

We want to find a first-order partial derivatives for x. the process are shown in table 1.

Table 1 The process of CSD compared with finite differencing

Forward Differencing	Complex-Step Differentiation
$\Delta x_1 = 1$	$h = 10^{-20}$
$\Delta x_2 = 0$	$h_2 = 0$
$f = x_1 x_2$	$f = (x_1 + ih_1)(x_2 + ih_2)$
$\Delta f = x_1 \Delta x_2 + x_2 \Delta x_1$	$f = x_1 x_2 - h_1 h_2 + i(x_1 h_2 + x_2 h_1)$
$\partial f / \partial x_1 = \Delta f$	$\partial f / \partial x_1 = \mathrm{Im}\, f / h_1$

From table 1 we can see that, when the forward difference method is used to derivate, the result is stored in a separate variable x, but when complex-step differentiation is used, the result is stored in the imaginary part of x. CSD derivation using the complex arithmetic, the time used in calculation $x_1 x_2$, $h_1 h_2$ are wasted. So, the efficiency of CSD is Slightly lower then finite differencing.

Conclusions

This manuscript describes a way to compute differentiation using complex computing, named CSD. Before we propose the theory analysis of complex-step differentiation, a commonly used algorithm which is known as finite differencing is analyzed. Besides, the best advantage of this method resides in the fact that it is extremely easy to implement. CSD uses complex computations to compute differentiation. If we make the step h small enough, we can hit satisfactory accuracy. We first introduce the Principles of CSD in two different aspects. Then made comparison of CSD and finite differencing in error and efficiency. The MATLAB program was given at last.

References

[1] W. K. Anderson , J. C. Newman, D. L. Whitfield, E. J. Nielsen, Sensitivity analysis for the Navier-Stokes equations on unstructured meshes using complex variables [J]. AIAA Paper, 1999, 99-3294.

[2] J. Martins, P. Sturdza, J. J. Alonso, The complex-step derivative approximation [J], ACM Transactions on Mathematical Software (TOMS), 2003, 29(3):245-262.

[3] F. W. J. Olver, Error Analysis of Complex Arithmetic, Reidel, Dordrecht, Holland, 1983, 279-292.

[4] J. Reuther, J. J. Alonso, J.Martins, S. C. Smith, A coupled aero-structural optimization method for complete aircraft configurations [J]. AIAA Paper, 1999 99-0184.

[5] P. Squire, G. Trapp, Using complex variables to estimate derivatives of real functions [J], SIAM. Rev., 1998, 40(1): 110-112.

Advanced Materials Research Vols. 989-994 (2014) pp 1942-1945
© (2014) Trans Tech Publications, Switzerland
doi:10.4028/www.scientific.net/AMR.989-994.1942

Routing Algorithm with Energy-Efficient and High Quality of Clusters in Wireless Sensor Network

Yi Yun-hui[a], Wang Run-liu[b]

School of Mathematics and Computer Science, Jiangxi Science &Technology Normal University

Nanchang, China

[a]sjxywork@163.com,[b]78397475@qq.com

Keywords: Wireless sensor network; Clustering; Routing; Energy

Abstract. This paper proposes an energy-efficient clustering routing algorithm based on the node degree, relative distance between nodes and residual energy. Selecting the cluster head fully consider the node degree and their relative distance. By this way, the coverage performance of cluster head is better and the average distance between member nodes and cluster head is short, so the cost of communication in the cluster is decreased. At the same time, the nodes with low energy have less probability to become the cluster head. Therefore, it can improve the quality of cluster; prolong the life time of the network.

Introduction

The wireless sensor network is composed by larger number of wireless sensor node with low-cost and low-power, which are easy to be deployed, but it can only use batteries which are difficult to be replaced, so how to prolong the network life is one of the hot research topic in WSN [1, 2].In the typical clustering algorithm, LEACH algorithm is one of the most representative clustering algorithms [3]. This algorithm is an adaptive topology algorithm, and periodically performs the cluster reconstruction process. In the process of forming the cluster, the node in network is selected as the cluster head with equal probability; the cluster head selection is random, so it balances the node's energy consumption. However, the random selection mechanism doesn't consider the residual energy of nodes, and can not guarantee the rationality of the number of cluster head nodes and the uniformity of distribution [4]. So people proposes the LEACH-ED protocol on this basis [5], which is based on the distance from cluster head node to source node and residual energy. LEACH-T protocol is also proposed, which use the time interval instead of the generated random number of cluster head and threshold [6]. But these two improved protocols have also not considered the rationality problem of the cluster head node distribution.

This paper proposes an energy-efficient clustering routing algorithm (EECA) which is based on node degree, the relative distance between nodes and residual energy. The algorithm ensures the uniform distribution of cluster head, balance the cluster scale, and select the node with high-energy priority as the cluster head nodes. It can balance the network energy consumption and prolong the network life.

Design of Algorithm

The EECA algorithm uses the wireless communication energy consumption model in reference [7] as foundation. The power consumption of sending data is:

$$E(k,d)_{send} = \begin{cases} E_{elec} \bullet l + E_{fs} \bullet l \bullet d^2, d < d_0 \\ E_{elec} \bullet l + E_{mp} \bullet l \bullet d^4, d \geq d_0 \end{cases} \quad (1)$$

The energy consumption of the receiving data is: $E(k)_{receive} = E_{elec} \bullet l$ (2).

l is the number of bytes of data packets, d is the distance for sending, when the transmission distance is less than threshold d0, the loss of power amplifier use free space model, otherwise use the multipath attenuation model; Eelec(nJ/bit) is the energy consumption coefficient of radio

frequency; Ef and Emp are amplifier circuit's energy consumption coefficient of two kinds of mode respectively.

According to the received signal strength, we can calculate the distance d from the node to the sending node; the formula is described as $d = 10^{|RSSI-A|/(10\times n)}$ (3).

A is the received signal strength whose distance is 1m to the sending node, RSSI is the received signal strength, n is the path attenuation factor, and it generally take 2-5.

EECA algorithm takes the round working way, which likes other clustering algorithm. Each round is divided into the selection of cluster head and the cluster formation and stable operation. First of all, we introduce some definitions; M is used to present the set of all nodes in network.

Definition 1 The neighbor nodes are in M, d(i,j) is the Euclidean distance between any two nodes i and j. If d(i,j)≤Rc, then call node j is neighbor node of node i, Rc is the node's radio radius, the set of neighbor node of node i is presented as Neighbouri.

Definition 2 Node's degree is in M, within the scope Rc of any node i, the number of contained nodes is called the node's degree, which is presented by Numberi. Numberi is more higher, there are more nodes round the node, then the coverage performance of cluster that use the node as the cluster head is better.

Definition 3 After member nodes has completed the cluster head selection process, if node j is in the coverage scope of cluster head node i, the distance between j and i is less than the Rc, then call node j is the member node of the cluster head node i. We assume any node can only be as the member node of one cluster.

In the initial stage, we assume all the nodes in the network have the same clock, the specific implementation steps are as follows:

Step 1: in the information broadcast stage, all the nodes broadcast its own ID information, in this process, node i will count its Neighbouri, Numberi and Ii through the received information.

Step 2, in the phase of decide role, perform the following operations to all the nodes:

(1) Each node computes its own timing time t, after received the information from the base station, and start timing. If the node i has not received the information from the cluster head in time ti, then it announce itself as the cluster head, and broadcast notice to its neighbor nodes.

(2) If the node received the information from cluster head, then it chooses to become as the member node, and exit the timing.

(3) If the node received the information from more than one cluster head, then it chooses to join the cluster that received the information of cluster head later.

ti is computed by following formula:

$$t_i = \alpha \times e^{-w_i} \quad (4).$$

α is the ratio that decide the size of time delay; w_i is defined as following:

$$w_i = 100 \times (C_1 \bullet \frac{1}{d(i)} + C_2 \bullet (1 - \frac{1}{Number_i}) + C_3 e^{E_i}) \quad (5).$$

Ei present the current residual of node i; C1 + C2 + C3 = 1; $d(i) = 10^{|RSSI_i - A|/(10-n)}$. From formula (4) and (5), we can know that the node's degree is higher, the average distance between node and its neighbor nodes is shorter and the waiting time t of node with more residual energy is shorter, then it has more chance to be elected as the cluster head, which can ensures the rationality of selecting the cluster head, and improve the quality of clustering.

Analysis of Optimal Clustering

In order to calculate conveniently, we assume that each cluster has the same number of nodes, N nodes are evenly distributed in the M×M area, two adjacent clusters are no overlap between each other, the expected number of cluster head of whole network meet formula:

$$n\pi R_c^2 \approx M_2 \quad (6).$$

Rc is the optimal value of sensor node's radio radius. When the running of clusters is stable, the energy consumption of cluster head in one in one information transmission process is:

$$E_{CH} = lE_{elec} \bullet k + lE_{BF}k + l(E_{elec} + E_{mp}d_{BS}^4) \quad (7).$$

EBF is consumed by cluster head on a data fusion energy, l is the size of transmission data packets, k is the number of member nodes that are contained in cluster, dBS is the distance from cluster head to base station. During a transmission process, the energy consumption of member node is as follows:

$$E_{NON-CH} = lE_{elec} + lE_{fs} \bullet d_{CH}^2 \quad (8)$$

dCH is the expectation value of distance from the member node to the cluster head. The energy consumption of the whole cluster of sending data to base station once is as following:

$$E_{cluster} = E_{CH} + kE_{NON-CH} \quad (9)$$

We use $\rho(x, y)$ to present the node distribution density in the network; the mathematical expectation of $d2$ is as follows:

$$E[d_{CH}^2] = \iint (x^2 + y^2)\rho(x, y)d_x d_y = \iint r^2 \rho(r, \theta) r d_r d_\theta \quad (10)$$

Replace $\rho = \frac{N}{n} \times \frac{1}{\pi R_c^2}$ into formula (10), and then we get:

$$E[d_{CH}^2] = \rho \int_0^{2\pi} \int_0^{R_c} r^3 d_r d_\theta = \frac{NR_c^2}{n^2} \quad (11)$$

Then in one data transmission process, the energy consumption of whole network is

$$E_{total} = n \times E_{clusterl} \quad (12)$$

Replace (7),(8),(9),(11) into (12), and let $\frac{dE_{total}}{dR_c} = 0$, then we get the minimum network energy consumption

$$R_c = \sqrt[4]{\frac{2M^2(E_{mp}d_{BS}^4 - E_{elec})}{N\pi E_{fs}}} \quad (13)$$

Replace formula (6) into formula (13), then we can calculate the relationship between the number of clusters on ideal state and the parameters of network environment, then we get:

$$n = \sqrt{\frac{N}{2\pi}} \bullet \sqrt{\frac{M^2 \bullet E_{fs}}{E_{mp}d_{BS}^4 - E_{elec}}} \quad (14)$$

Simulation

In order to verify the algorithm's performance, we make the simulation on Matlab platform. 100 wireless sensor nodes are randomly distributed in the area of 100m×100m, the base station is located in the center of the region. According to formula (13), we can obtain the optimal value Rc∈[16,54] of sensor node's radio radius. Here, we take the node's effective radius radio Rc=30m. According to formula (14), under the condition of effective radio radius Rc=30m, the ideal optimal number of clusters n=4. We make simulation experiment 10 times for LEACH, LEACH-T, LEACH-ED, EECA algorithm, and get the mathematical expectation of the number of cluster head in each round, and statistics the distribution of number of cluster head, which is shown in figure 1.

From figure 1, we can know that the generation of cluster head of LEACH and LEACH-ED is completely control by random number and threshold value, so the generation number of cluster head is not stable, and the changing range of the number of cluster head is bigger; The generation number of cluster head of EECA is not only stable, and is more close to the number of cluster head by theory expectation. From figure 2, the cluster head of LEACH algorithm is randomly generated, so it would cause some nodes with low energy act as cluster head and premature death, ad reduce

the network lifetime. Although LEACH-ED and LEACH-T avoid the node with low energy act as cluster head, but the distribution of cluster head is relatively uneven, the size of cluster also doesn't be considered, thus it affect the network lifetime. EECA algorithm avoids the node with low energy act as cluster head node, and considers the relative distance between node and the node degree when selecting cluster head, which balance the rationality and equilibrium of distribution of cluster head. The simulation results show that EECA can prolong network lifetime better.

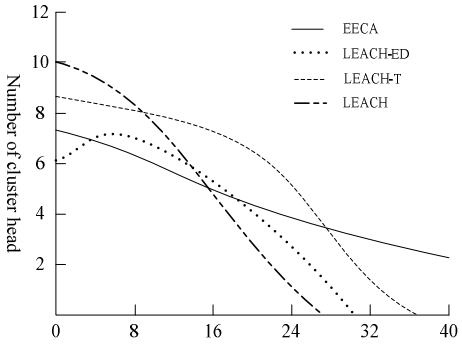

Fig.1 Distribution of number of cluster head

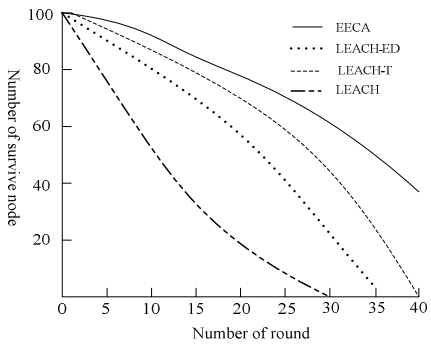

Fig.2 Network's life time of all algorithms

Conclusion

This paper proposes an energy-efficient clustering routing algorithm based on node degree and the relative distance between the nodes. In the process of clustering, the algorithm priority selects the node which has more neighbor nodes and shorter relative distance to neighbor nodes as the cluster head nodes. At the same time, it considers the residual energy of node, the node with lower has lower probability to act as cluster head.

Acknowledgement

In this paper, the research was sponsored by the Education Department of Jiangxi province science and technology project (GJJ14599) .

References

[1] Schoonder woerd, Holland O, Bruten J. Ant-Based Load Balancing in Telecommunications Networks [J]. Adaptive Behavior, 1996, 5(2), 169-207.

[2] Yi S, Heo J, Cho Y. PEACH: Power-Efficient and Adaptive Clustering Hierarchy Protocol for Wireless Sensor Networks [J]. Computer Communications, 2007, (30), 2842-2852.

[3] Stanislava S, Henizelman W B. Cluster Head Election Techniques for Coverage Preservation in Wireless Sensor Networks [J], Ad Hoc Networks, 2011, 5(7), 955-972.

[4] Younis O, Fahmy S. A Energy Efficient Distributed Clustering Approach for Ad-hoc Sensor Networks [J], IEEE Trans. on Mobile Computing, 2010, 3(4), 660- 669.

[5] Zhang wei, Cheng wen-fei. A High Energy Efficiency protocol based on LEACH [J], Journal of sensing technology, 2012, 23, 1153-1157.

[6] Li Hai Peng, Zhang fan, Sheng xuan. Improvement of LEACH Routing Algorithm in Wireless Sensor Network [J], Journal of sensing technology, 2010, 2(1), 1163-1167.

[7] Lindsey S, Raghavendra C S. PEGASIS: Power Efficient Gathering in Sensor Information System [J], Journal of Ad Hoc Networks, Elsevier Science, 2009, 3(4), 1152-1130.

Advanced Materials Research Vols. 989-994 (2014) pp 1946-1950
© (2014) Trans Tech Publications, Switzerland
doi:10.4028/www.scientific.net/AMR.989-994.1946

DSP Memory Allocation Strategy based on Greedy Algorithm

Yanhong FAN[1,2,a], Xiaofeng MA[1,b], Jingsai JIANG[1,c], Xiaomei XU[2], Qiuyun HAO[1], Peng ZHANG[1]

[1]Shandong Provincial Key Laboratory of Computer Network, Shandong Computer Science Center, Jinan, 250014, China

[2]Key Laboratory of Underwater Acoustic Communication and Marine Information Technology (Xiamen University), Ministry of Education, Xiamen, 361005, China

[a]email: fanyh@sdas.org, [b]email: maxf@sdas.org, [c]email: jiangjs@sdas.org

Keywords: DSP Memory Allocation; Knapsack Problem; Greedy Algorithm

Abstract. In practical applications of DSP systems, DSP chips with limited on-chip RAM resources are often chosen to reduce cost. In this condition, part of the codes has to be stored in FLASH or expanded RAM and thus can not run at full speed. This paper presents a strategy of allocating the on-chip RAMs to obtain the maximum system performance. First, the memory allocation problem is described as the knapsack problem, and then the greedy algorithm is applied. Experimental results show that the overall execution efficiency can be improved by 10% when the on-chip RAMs are rather limited. Therefore, the proposed memory allocation method is efficient for low-cost design to obtain higher performance.

Introduction

Digital signal processors (DSPs) with high-speed computing capability have been widely used in multimedia signal processing, mobile communication, intelligent control and other areas. In the design of DSP systems, the selection of chips is based on software and hardware solutions. Computing capability, storage capacity, I/O resources, power consumption and cost need to be considered in selection of DSP chips [1-3]. The mainstream DSP manufacturers provide a variety of DSP chips with different configurations for users. The type and capacity of memories is one of the most commonly used specifications to distinguish different DSP chips, and it is also an important measure of DSP performance. Typically, large-capacity and high-performance memories lead to a high price. In the applications of consumer electronics which are sensitive to the cost, the designer should choose DSP chips with smaller memory capacity under the premise of meeting the system requirements. In addition to optimizing DSP algorithms and codes, reasonable allocation of DSP memories is an important way to reduce the computational complexity of the system. This paper describes a method to improve the execution efficiency of DSP systems via memory allocation based on greedy algorithm. Experimental results show that, for DSPs with limited memory resources, the proposed method can achieve better performance than some other methods.

Memories in DSP System

DSP memories consist of several types, such as DARAM (Double-Access Random-Access Memory), SARAM (Single-Access RAM), XRAM (eXpanded RAM), ROM (Read-Only Memory), FLASH, etc. They have different features of execution efficiency, read/write property, volatility, and usage, which are summarized in Table 1 [4]. On-chip DARAM and SARAM have the best efficiency for executable codes, but the contents will be lost when the power is off. Contrarily, ROM and FLASH are non-volatile, but their efficiency is limited in high-speed systems. Generally, the executable codes are usually stored in FLASH or ROM, and are loaded into the on-chip RAMs at startup to obtain higher efficiency. However, RAMs have higher cost than ROM or FLASH of the same capacity, and thus low-cost solutions prefer to use the DSP chips with limited on-chip RAMs. Therefore, to achieve the best system performance, the available on-chip RAMs should be fully allocated and utilized.

Table 1 Typical types and features of DSP memories

Type	Execution efficiency	Contents	Read	Write	Non-volatility
DARAM	0.5 cycle/instruction	program, variable stack	√	√	×
SARAM	1 cycle/instruction	program, variable stack	√	√	×
XRAM	4 cycles/instruction	program, variable	√	√	×
FLASH	2 cycles/instruction	program, constant	√	×	√
ROM	2 cycles/instruction	bootloader, vector table	√	×	√

DSP Memory Allocation Strategy and Method

When the prototype of DSP algorithms is transplanted into the DSP platform, allocation of data and program space needs to be considered. The quality of storage space allocation will directly affect the execution efficiency of the algorithms. For DSPs with enough on-chip RAMs, memory allocation is not a problem; but it is critical for DSPs with limited on-chip high-speed RAM resources which are adopted for low-cost solutions. In this condition, reasonable allocation of on-chip RAMs is important to the overall system performance. Generally, this problem can be stated as minimizing the overall computational complexity by allocating the executable codes into the on-chip RAMs with limited capacity. It can be treated as a knapsack problem that is commonly used in production scheduling, resource allocation and investment decision.

1) Knapsack problem

Knapsack problem can be generally described as below:

Given n items' weights $w_i\ (w_i > 0)$ and values $c_i\ (c_i > 0)\ (i = 1, 2, \cdots, n)$, and given a knapsack whose capacity is limited to $V\ (V > 0)$; then, put some items into the knapsack. The problem is that how to choose the items to obtain the maximum overall value while not exceeding the knapsack capacity. Assume that each item is inseparable and can be chosen only once, the 0-1 knapsack problem can be formulated as the following maximization problem [5]:

$$\text{Maximize} \quad f(x_1, x_2, \cdots, x_n) = \sum_{i=1}^{n} c_i x_i \tag{1}$$

$$\text{subject to} \quad \begin{cases} \sum_{i=1}^{n} w_i x_i \le V \\ x_i \in \{0,1\} \end{cases} \quad (i = 1, 2, \cdots, n) \tag{2}$$

where x_i is the decision variable. When $x_i = 1$ the ith item will be loaded into the knapsack, and when $x_i = 0$ it will not.

2) Knapsack problem of DSP memory allocation

The DSP memory allocation problem in this paper can be treated as the 0-1 knapsack problem and described as below.

Assume that a project contains n code sections with code size $L_i\ (L_i > 0)$ and computational complexity $c_i\ (c_i > 0)$, $i = 1, 2, \cdots, n$. Choose some code sections and allocate them into the internal RAM to improve their execution efficiency. The target is to minimize the overall computational complexity under the condition that the available internal RAM size is limited to $V\ (V > 0)$. Similar to (1), such optimization problem can be expressed as

$$\text{Minimize} \quad f(x_1, x_2, \cdots, x_n) = \sum_{i=1}^{n} c_i x_i \tag{3}$$

$$\text{subject to} \quad \begin{cases} \sum_{i=1}^{n} L_i x_i \le V \\ x_i \in \{0,1\} \end{cases} \quad (i = 1,2,\cdots,n) \tag{4}$$

where x_i is the decision variable.

3) Greedy algorithm for DSP memory allocation

Greedy algorithm is one of typical methods to solve knapsack problem, which has been applied in many applications [6-7]. By using its principle, first, define the efficiency density of each code section as $\rho_i = c_i / L_i$; then the code section with larger density has higher priority to be assigned into the on-chip RAMs. Detailed steps are described as follows:

a) For all n code sections, calculate their efficiency density denoted by $\rho_i = c_i / L_i$, $i = 1, \cdots, n$.

b) Sort ρ_i in descending order and obtain the corresponding queue of indices $q(k) \in \{1, \cdots, n\}$, where $\rho_{q(1)} > \rho_{q(2)} > \cdots > \rho_{q(n)}$.

c) Set $k = 1$ and $x_i = 1 \, (i = 1, \cdots, n)$.

d) If $\sum_{j=1}^{k} x_{q(j)} L_{q(j)} \le V$, the code sections corresponding to $q(k)$ is assigned into the on-chip high-speed RAMs, i.e. $x_{q(k)} = 1$; then set $k = k + 1$ and go to step d). Otherwise, set $x_{q(k)} = 0$ and go to step e).

e) Find in $\{q(k+1), \cdots, q(n)\}$ the first one that satisfies $\sum_{j=1}^{k-1} x_{q(j)} L_{q(j)} + L_{q(l)} \le V \ (l > k)$, and set $x_{q(l)} = 1$, $x_{q(k+1)} = x_{q(k+2)} = \cdots = x_{q(l-1)} = 0$, and $k = l + 1$. Then go to step d), and repeat the above procedures until all n code sections are examined.

Test Case and Experiments

The DSP applications can be developed in TI CCS integrated environment, and the code information can be analyzed through its profile function. The information given by the profiler is shown in Table 2 [8].

Table 2 Profile information

Address Range	Symbol Name	Symbol Type	Access Count	CPU Cycles: Incl. Total	CPU Cycles: Excl. Total
$A_{start} - A_{end}$	$function_x$	*function*	$N_{\text{access_cnt}}$	$N_{\text{cycle_in}}$	$N_{\text{cycle_excl}}$

In Table 2, A_{start} and A_{end} are the start and end addresses, respectively; $function_x$ is the code name, where *function* indicates that the code type is function; N_{access_cnt} is the number of executions of $function_x$; $N_{\text{cycle_in}}$ is the total number of CPU cycles of $function_x$, including the subroutines; and $c_i = N_{\text{cycle_excl}}$ is the total number of CPU cycles of $function_x$, excluding the subroutines. Each code size L_i and efficiency density ρ_i used in the proposed method can be calculated as follows:

$$L_i = A_{end} - A_{start} \tag{5}$$

$$\rho_i = N_{\text{cycle_excl}} / (A_{end} - A_{start}) = N_{\text{cycle_excl}} / L_i \tag{6}$$

The test case is a smart home control procedure developed on TMS320F2811 platform [9]. The proposed method was applied in DSP memory allocation to minimize the total computational complexity. First, the storage information was analyzed. The on-chip SARAM capacity of F2811 is 36 KBytes, but the test case requires at least 60 KBytes. Thus the allocation of SARAM should be optimized. Then the profile statistics in Table 2 was generated by using CCS, and L_i, c_i and ρ_i were calculated. Finally, the proposed method was performed to assign each function into SARAM or FLASH. The computational complexity versus the available size of SARAM is shown in Fig.1, including the comparisons with some other methods.

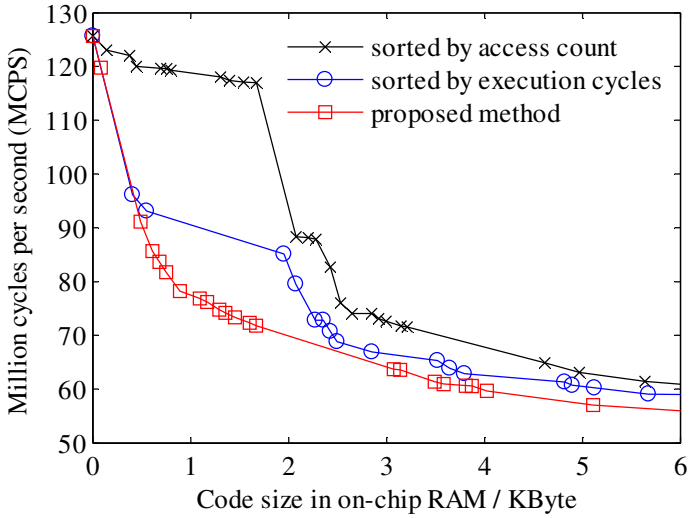

Fig.1. Computational complexity vs. code size in on-chip RAM for different methods

Fig. 1 shows three curves, where □ denotes the allocation method by using the proposed greedy algorithm; ○ and × correspond to the methods of sorting the code sections by access count and by execution cycles, respectively (both in descending order). The code section with a larger access count or execution cycles has a higher priority to be assigned into the on-chip RAMs. The results show that, with the same available RAM size, the proposed method can achieve a lower computational complexity. It makes the overall complexity decrease more rapidly as the occupied RAM size increases. This indicates that the proposed method can improve the execution efficiency of the system by effectively utilizing the on-chip full-speed RAM resources. This scheme can improve the system efficiency by up to 10% higher than the other schemes for the DSP chips with rather limited available on-chip RAM resources (such as several KBytes). Therefore, the proposed method is more suitable for low-cost DSP applications.

Conclusion

To improve the performance of DSP systems with limited on-chip RAM resources, this paper presents a method to allocate the memories by using greedy algorithm. Experimental results show that, for DSP chips with limited on-chip RAM resources, the proposed method can achieve better execution efficiency than some other methods. With the help of the design tool chain of DSP systems, this method is simple and feasible to implement. Therefore, it could be an efficient approach to low-cost DSP solutions.

Acknowledgement

This work was supported by the International Science & Technology Cooperation Program of China under Grant No.2012DFR10500, and by the Open project of Key Laboratory of Underwater Acoustic Communication and Marine Information Technology (Xiamen University), Ministry of Education (201202).

References

[1] Shuisheng Yu. Introduction and selection of DSP chip [J]. Microcontrollers & Embedded Systems . 2006(4) 8-11.

[2] Texas Instruments Incorporated. DSP Selection Guide[Z]. 2008.

[3] Texas Instruments Incorporated. Embedded Processors [EB/OL].http://www.ti.com/lsds/ti/dsp/

embedded_processor.page.

[4] Yan Zou. DSP principle and Applications [M]. Electronic Industry Press.2005

[5] Shengyi Zhang,Zhihua Cai,Zhigang Zhan. Solving 0-1 Knapsack Problem Based on Genetic Algorithm with Improved Simulated Annealing [J].Microelectron & computer .2011(2)61-64.

[6] Shan Wang, Kun Chen.Research on Task Scheduling Method Based on the Greedy Algorithm in ETL [J]. Microelectron & computer .2011:26(7)130-133.

[7] Wei Liu,Xu Chen, Yongsheng Liang ,Hongji Zhang.MGS Coding Optimization Method Based on Greedy Algorithm.Computer Engineering. 2011:37(15)208-211.

[8] Texas Instruments Incorporated. Code Composer Studio Development Tools v3.3 Getting Started Guide (spru509h) [Z].2006.4.

[9] Texas Instruments Incorporated. C2000TM Real-Time Microcontrollers (SPRB176P) [Z].2013.4.

Advanced Materials Research Vols. 989-994 (2014) pp 1951-1954
© (2014) Trans Tech Publications, Switzerland
doi:10.4028/www.scientific.net/AMR.989-994.1951

Research on an Embedded Ultra-low-bit-rate Speech Coding Algorithm

Ye LI [1,2,a], Yanhong FAN [1,2,b], Fei YUAN [2], Xiaomei XU [2]

[1]Shandong Provincial Key Laboratory of Computer Network, Shandong Computer Science Center, Jinan, 250014, China

[2]Key Laboratory of Underwater Acoustic Communication and Marine Information Technology (Xiamen University), Ministry of Education, Xiamen, 361005, China

[a]email: liye@sdas.org, [b]email:fanyh@sdas.org

Keywords: Speech Coding Algorithm; Embedded Structure; Ultra-low-bit-rate; Enhanced Mixed Excitation Linear Prediction

Abstract. Ultra-low-bit-rate speech coding algorithm was in great demand for many fields such as underwater speech communications. Underwater speech communication for middle-long distance has the characteristics of narrow bandwidth as well as low transmission rate, which makes the underwater speech communication much difficult. Ultra-low-bit-rate speech coding algorithm plays an important role on this occasion. More over, it will be more flexible for the underwater speech communication system if the speech coding algorithm has an embedded structure. The paper introduced the principle of an embedded speech coding algorithm with dual rates at both 300bps and 400bps based on the enhanced mixed excitation linear prediction model. The results show that this embedded ultra-low-bit-rate speech coding algorithm has satisfactory quality under both DRT and MOS test.

Introduction

Underwater speech communication was in great demand in many fields such as frogman work. The quality of analogue speech communication device wasn't satisfying when used in underwater communication. With the development of modern military as well as the improvement of utilizing the resource of the sea, the research on digital speech communication was getting more and more important and had been extensively studied in recent years [1-4], in which speech coding algorithms played an important role. The enhanced mixed excitation linear prediction (MELPE) model show great advantage in ultra-low-bit-rate speech coding algorithms [5-8], based on which the paper proposed an embedded speech coding algorithm with dual rates at both 300bps and 400bps.

Principle of the Encoder

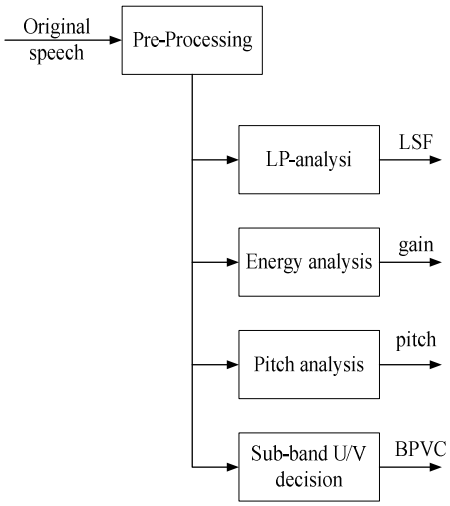

Fig.1. Encoder structure based on MELPE

Four parameters should be extracted for the ultra-low-bit-rate speech coder based on MELPE, which contains linear spectral frequency parameters (LSF), band pass voicing coefficients (BPVC) and pith parameter and gain parameter as shown in Fig.1.

The frame size of the coder introduced is 22.5 ms, the same as for the original MELPE coder. Parameters above are extracted once each frame, but they are usually vector quantized once each super frame combined by several frames because of the fewer bits afforded by the ultra-low-bit-rate speech coder. Each super frame consists of 8 frames, for which the parameters were vector quantized. The super frame is 180ms, and total 54 bits and 72bits could be used for the 300bps and 400bps coder respectively. The bit allocation scheme for this embedded speech coding algorithm is shown as Table 1.

Table 1. Bit allocation scheme for the coder

Parameter	Bit Number	
	300 bps	400bps
BPVC	5	5
Pitch	10	16
Gain	8	11
LSF	31	40
Total	54	72

The BPVC parameter was vector quantized using 5 bits. The corresponding voicing pattern is used to determine the encoding/decoding mode which would be used in the quantization of the other parameters. A weighted Euclidean distance is used to find the optimal voicing pattern, and the corresponding weight vector is applied to the sub-band voicing information {16, 8, 4, 2, 1}.

The LSF parameter took an important role in the synthetic speech quality, so more than half of the bits would be used in the LSF quantization. Suppose the LSF vector of the current super frame was $l_n=\{l_{n,1},l_{n,2},...,l_{n,8}\}$, the quantized LSF vector of the final frame in the last super frame was $\hat{l}_{n-1,8}$,and the DC component of the LSF parameter for current encoding mode was $\bar{l}_n$ .Then the quantization of the LSF parameter could be described as follows:

Step1: Remove the DC component.

$$l'_n = l_n - \bar{l}_n . \tag{1}$$

Step2: Remove the inter-frame prediction.

$$\Delta l_n = l'_n - a_n \cdot \hat{l}_{n-1,8} . \tag{2}$$

Where a_n could be got offline to minimize the prediction error for the LSF parameters in the training speech lib as follows:

$$min\left(\sum_n \sum_{i=1}^{10} \left[l'_n(i) - \alpha(i) \cdot \hat{l}_{n-1,8}(i) \right]^2 \right). \tag{3}$$

Step3: Multi-stage vector quantization with inter-stage prediction would be used on the inter-frame prediction error. More details could be referenced to the paper [8]. The 400bps coder added two other stages to the codebook.

It should be pointed out that the $\hat{l}_{n-1,8}$ in the 400bps coder was got only using the first four stages like the 300bps coder.

Two gain parameters are calculated per frame for the encoder, i.e., 16 gains are obtained for each super-frame. The 16 gain parameters are vector-quantized using 8 bits for 300bps coder and 11 bits for 400bps coder, with a MSE criterion defined in the logarithmic domain. In the 300bps coder, the gain parameter was quantized using only one stage vector quantization with inter-frame prediction, while it would be quantized using two-stage vector quantization with inter-frame prediction in the

400bps coder. As mentioned above in the LSF quantization, the inter-frame prediction of the gain parameter in the 400bps coder would be got only using the core stage book, which was the first stage codebook in the gain quantization.

The pitch quantization was similar to the gain quantization but in the logarithmic domain. The quantizer structures for different parameters under both rates were given as Table 2.

Table 2. The quantizer structures for different parameters

Parameter	Vector Quantization Scheme	
	300bps	400bps
LSF	MSVQ(10, 8, 7, 6)	MSVQ(10, 8, 7, 6, 9)
Gain	VQ(8)	MSVQ(8, 3)
Pitch	VQ(10)	MSVQ(10, 6)

Principle of the Decoder

Four parameters would be unquantized in the decoder part and then used in the decoder based on the enhanced mixed excitation linear prediction model. The decoder used the periodic waveform or random series to represent the periodic or a periodic component of the excitation signal respectively. Then the excitation signal would be passed to the synthetic filter as well as the post filter to get the synthetic speech.

Test results and Conclusion

We have performed several intelligibility tests of the coder using Diagnostic Rhyme Test (DRT). In our tests, the score of the 300bps coder as well as the 400bps coder are 84% and 86% respectively. In addition, we do the MOS test on this embedded coder using P.862 tool and the result could be referenced to Table 3. The synthetic speech waveform and the original speech waveform could be seen as Figure 2.

Table 3. MOS test result

Test speech	MOS	
	300bps	400bps
Wav1.pcm	2.503	2.600
Wav2.pcm	2.442	2.561
Wav3.pcm	2.456	2.551
Wav4.pcm	2.450	2.553

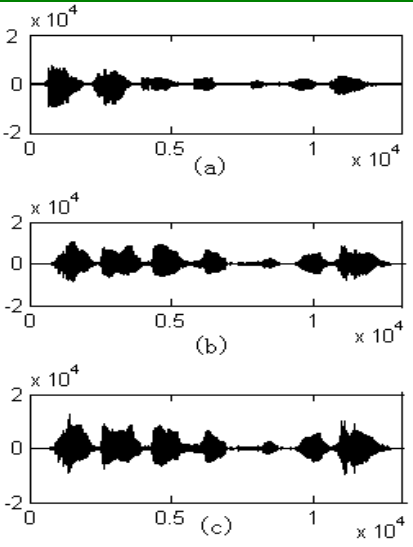

Fig.2. (a) original speech; (b) 300bps synthetic speech; (c) 400bps synthetic speech

Underwater speech communication could be used widely in utilizing the resource of the sea. The implementation of the reliable underwater speech communication was of great difficult because of the low channel rate as well as some other reasons.The embedded coder introduced in this paper could be used in the underwater speech communication. We have done the test in the pool and the whole system works well.

Acknowledgement

This work was supported by the Open project of Key Laboratory of Underwater Acoustic Communication and Marine Information Technology (Xiamen University), Ministry of Education (201202), and by the International Science & Technology Cooperation Program of China under Grant No.2012DFR10500.

References

[1]Bryan Woodward, Hayri Sari. Digital underwater acoustic voice communications [J]. IEEE Journal of Oceanic Engineering. 1996: 21(2) :181-192.

[2]Hayri Sari, Bryan Woodward. Underwater voice communications using a modulated laser beam[J]. OCEANS'98.1998(2)：1183-1188.

[3]GUO Z Y，Chen Y，JIA N，et al. Study and implementation of underwater digital voice communication system [J]. Acta Acustica.2008：33(5):409-418.

[4]SANG E F，YE S. Source coding robustness for underwater speech communication[J]. Journal

Of Harbin Engineering University.2002:23(5):20-23.

[5]Supplee L M，Cohn R P，Collura J S，et al. Melp. The new federal standard at 2400 bps[C]. IEEE International Conference on Acoustics, Speech and Signal Processing, ICASSP-1997. Munich, Germany: IEEE Press. 1997:(2):1591-1594.

[6]Wang T, Koishida K, Cuperman V et al. A 1200/2400 bps coding suite based on MELP [C]. Speech Coding, 2002, IEEE Workshop Proceedings. 2002.

[7] NATO STANAG 4591 ANNEX M Ratification Draft 1.MELPe variation for 600 bit/s NATO narrow band voice coder[M].The Hague: NATO, 2003.

[8]LI Ye, FAN Y H, HAO Q Y, GUO Q. High quality speech Coder at 300bps[J]. Audio Engineering.2010:34(12):51-53.

Advanced Materials Research Vols. 989-994 (2014) pp 1955-1958
© (2014) Trans Tech Publications, Switzerland
doi:10.4028/www.scientific.net/AMR.989-994.1955

Research on Materialized views under disk-space Constraint in Data Warehouse

Lei Ma[1, a]

[1]Department of Media, Linyi University, Linyi, 276005, China

[a]email: malei1999@163.com

Keywords: Materialized View; Evolutionary Algorithm; Data Warehouse;

Abstract. Materialized view is an important topic in data warehouse research, and also affects the query efficiency and maintenance cost. The disk-space view-selection problem is to select a set of materialized views for the purpose of minimizing the total query processing cost and the total maintenance cost. In this paper we introduce evolutionary algorithm using stochastic ranking algorithm, which can enable materialized view selection under disk-space constraint. The algorithm improve the stochastic ranking algorithm, which can find a near-optimal feasible solution. This paper use the algorithm in Police data warehouse.

Introduction

Data warehouse is a subject-oriented, integrated, non-volatile and time-varying data sets, which is used to support decision-making managers. Most of queries are query integrated information in data warehouse, so which need spend a lot of time, in order to avoid accessing data sources and improve query speed, we access some intermediate results to the data warehouse in the process of query, these intermediate results which are stored in the data warehouse are called materialized views.

The aim of this paper is to the minimum cost of processing costs and maintenance cost in selecting materialized views. Currently, Many Algorithms are improved in this field, literature [1] proposed greedy algorithm, literature [2] proposed graph based on and or according to literature [1], these algorithms solved the problem of selection of materialized views, but these algorithms cannot solve the problem when the count of views is over 256. Many improved algorithms[6-9] are proposed in these years.This paper improves the improved algorithm by using random permutation algorithm and improved evolutionary algorithm, the improved algorithm can select materialized view when data warehouse has many views, the cost of selection is linear, which can get the best solution on selection of materialized view.

Basic Concepts and Theorems

Definition 1 Let G be a directed acycline graph. The graph has directed edges and no acycline.

Definition 2 Let qi and qj be query, if the query qi get answer by the use of the results of the query qj, then we call that qi depends on qj, denoted as $qi \leq qj$.

Definition 3 Directed acyclic graph G = (V, E), V represents views in data warehouse, edge $vi \rightarrow vj \in E$ if and only if $vj \leq vi$ and $\neg\exists vk$,satisfies $vj \leq vk \wedge vk \leq vi$, where $vi \neq vk \neq vj$.

For example, a fact table: Suspects table, three dimension tables: Time table, Education table and Case table. Relational model as follows:

Suspects (ID, TID, EID, CID)

Time(TID,Day,Month,Year)

Education(ID,Code,Name)

Case(CID,Code,Name)

Based on the above directed acyclic graph structure G=(V, E), where T, W, A respectively represent time dimension, education dimension and case dimension, the directed acyclic graph as shown in Figure 1. Each node in graph represents a query or view in OLAP, for example, W represents the OLAP query of the number of each education's suspects, WA represents the OLAP query of the number of each case's suspects.

In addition, the node and edge in the directed acyclic graph G = (V, E) respectively have the following different weights, Node v∈ V has three rights:

R_v: the size of node v

Q_v: the frequency of node v's query

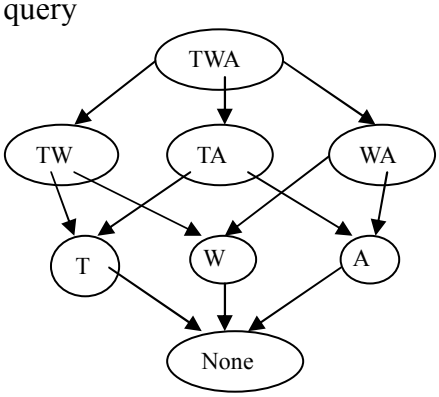

U_v: v node update frequency

Figure 1 Directed Acyclic Graph

Edge (v, u)∈ E has two weights:

Q (v, u):the cost of querying node u by use of node v

U (v, u):the cost of maintenance node u by use of node v

In this paper, the following assumptions:

1. If v≤u, then $R_u \geq R_v$;
2. Update frequency of each node U_v is equal;
3. The maintenance cost U (v, u) of node u is one-tenth of view R_u's size;
4. The query cost Q (v, u) of node u is smaller than the size Rv of view v.

Let M be a materialized view, M⊆V, q (v, M) represents the minimum query cost,m(v,M) represents the minimum maintenance cost. So all cost C(G,M) with m (v, M) consideration in the selection of storage space constraint materialized view is to choose a set of views M to materialized, so the sum of the cost of maintaining materialized views query processing costs and the minimum total cost of overhead is represented by C (G, M), it the formula is:

$$C(G,M)=\sum_{v\in V} Q_v * q(v,M) + \sum_{v\in M} U_v * m(v,M)$$

Selection Algorithm of Materialized Views

A. Relation Knowledge of the Algorithm

(1)Objective function and penalty function

Materialized view selection under disk-space constraint is to select materialized view set, the cost of querying and maintenance is minimum and the performance is best. So that we can define the objective function is the total consideration overhead function C(G, M), defined as follows:

f (x) = C (G, Mx) where they meet S (Mx) ≤ S

Penalty function is defined as:

Φ (x) = max {S (Mx)-S, 0}

(2) Improved random order algorithm

Randomly arranged in the process, because this sort requires 2P individuals, but at last only need p individuals, so the number of cycles of outer loop need not more than P times, and the inner loop does not need to compare 2P-1 times, by using the principle of bubble sort, the first end of the cycle, you need to compare 2P-1 times, the best of the program into the front, while the second end of the cycle, you need to compare 2P-2 times the second best solution into the queue in front of the second position, so that in turn implemented. And when N> P, P last just a plan, so the outer layer of up to P times just do it.

Literature [7] need N times to sort randomly in outer loop and need 2P-1 times in inner loop. So the complexity of the literature [7] is N*(2P-1) in the worst case, and the complexity of the

improved algorithm is min (N, P) * (2P-1) / 2 in the worst case, so the complexity of the improved algorithm is improved to 1/2.

B. Algorithm decription

The algorithm uses the improved random sorting algorithm and a hybrid of the original algorithm which made some improvements since the original hybrid algorithm to elect two individuals hybridization, so that the algorithm could lead to cycles do after hybridization individuals may have only two, so in the randomly selected individuals, plus a limiting condition, ask for no two individuals are hybrids, so as to ensure that after cycles, generate new P individual makes a good program to get a good reproduction. The algorithm adopts Mutation algorithm which is the same as literature [4] and literature [5].

In each iteration of this algorithm, the first to use crossover operator, makes a good breeding executable program well, generate better individuals; followed by mutation algorithm that can produce before the new group does not exist individuals, so you can verify each of the search space of possible solutions; then calls random sorting algorithm to group the new group and mutation produced a new generation of hybrid solutions put together sort, after sorting, good executable program on the front row in the queue, programs or unenforceable bad came in the back of the queue, and finally remove the sorting queue before P individuals. This has been circulating executed until the termination condition is met.

Crossover Algorithm:

Input: the rate of Group Crossover Pc
output：Crossed Groups G′
repeat
Randomly select two individuals which are no crossover in G
$g_1=(a_1,a_2,\ldots,a_N)$, $g_2=(b_1,b_2,\ldots,b_N)$
select one number in U(0,1)
if u < Pc then
  for each bit i in individual do
    slect r randomly，r=0 or r=1
    if r=1 then
      set the bit i a_i in g_1'
      set the bit i b_i in g_2'
     else
      set the bit i b_i in g_1'
      set the bit i a_i in g_2'
    end if
  end for
else
  $g_1'= g_1$
  $g_2'= g_2$
end if
until i=P/2

Mutation Algorithm:

Input:Groups G Mutation rate Pm
Output：Mutated Groups G′
  for each individual in group do
    for each bit in individual do
      select one number u in U(0,1) randomly
      if u>Pm then
        if the bit is 1 then
          set bit 0
        else
          set bit 1
      end if
    end for
  end for

C. Algorithm example

This algorithm will be applied to the design of Police data warehouse, we select three dimensions in Figure 1 as example for analysis. According to the previous assumption, we give the corresponding weight to nodes and edges in graph. The size of table T, W, A respectively is: 0.2M, 0.03M, 0.1M. According to the assumption : If $v \leq u$, then there exists $R_u \geq R_v$, so the view size of TWA, TW, TA, WA is respectively: 5M, 0.8M, 5M, 6M, we assume that the update frequency of each view in graph is 0.05, the probability of the query view TWA, TW, TA, WA, T, W, A , respectively 0.6,0.3,0.5,0.3,0.2,0.1,0.2, the query cost of node u is less than the size R_v of view v, the maintenance cost of node u is equal the 0.1 size of view u. The storage space S is 0.7 times the constraints of space occupied by all views, $S = S=0.7*\sum_{v \in V} R_v$. Then S = 0.7 * 17.13M = 11.99M. Assuming P_c = 0.002, P_f = 0.4, P_m = 0.001. According to the above set value , the improved algorithm call improved evolutionary algorithm, the assumption of the first generation G(0) is (1110001), (1011111), (0110000), after hybridization and mutation G(3) is generated after the final (1011011) , (1010111) , (1000111) . Set (1011011) meet the cost constraints and the total cost of the minimum set of views , so the materialized views are TWA, TA, WA, W, A.

Conclusion

This paper studies the problem of selecting the data warehouse environment in the storage space constraint materialized views, materialized view selection will directly affect the efficiency of the data warehouse, has important significance. Based on the analysis of the data warehouse system of public security, get a directed acyclic graph, the use of random sorting algorithm using improved evolutionary algorithm, which is a collection of materialized view approximate optimal solution.

References

[1] V.Harinarayan,A.Rajaraman,and J.D.Ullman,”Implementing data cubes efficiently,”inProc.1996 ACM SIGMOD Int.Conf.Management of Data,1996,pp.205-216.

[2] H.Gupta,”Selection of views to materialize in a data warehouse”

[3] T.P.Runarsson and X.Yao,”Stochastic rankong for constrained evolutionary optimization,”IEEE Trans.Evol.Comput.,vol.4,Sept. 2000.

[4] Man Li,Xiaoyong Du,Shan Wang,"Selection of Materialized Relations in Ontology Repository Management System",Knowledge Science, Engineering and Management Lecture Notes in Computer Science Volume 4092,2006,241-251.

[5] C.Zhang,X.yao,and J.Yang,” An Evolutionary Approach to Materialized Views Selection in a Data Warehouse Environment”IEEE Trans.Syst.,Man,Cybern.C,vol.31,Aug.2001.

[6] Li Juan Zhou, Hai Jun Geng, Ming Sheng Xu,"Research on Materialized View Selection in the Data Warehouse", Applied Mechanics and Materials, 55-57, May 2011.

[7] Chuan Zhang, Xin Yao, Jian Yang,"Evolving materialized views in data warehouse",In proceeding of: Evolutionary Computation, 1999.

[8] Ren Jiadong,Li Zhiguo,and Zong Junsheng,Research on Selection of Materialized Views in Data Warehouse, Journal of Computer Research and Development,43(Suppl.):621-625,2006.

[9] Feng Yu,Du Xiaoyong,Wang Shan,"Materialized View Selection in a Data Warehouse",Web-Age Information Management Lecture Notes in Computer Science Volume 1846,2000,323-328.

Advanced Materials Research Vols. 989-994 (2014) pp 1959-1961
© (2014) Trans Tech Publications, Switzerland
doi:10.4028/www.scientific.net/AMR.989-994.1959

Review of Otsu Segmentation Algorithm

Yanxue DONG[1, a]

[1]School of Information, Linyi University, Linyi, 276000, China

[a]email: dyxtmb@163.com

Keywords: Otsu method;Image segmentation; Threshloding

Abstract. Image segmentation is the key step in the process from image processing to image analysis. Otsu method is one of the most successful methods for image thresholding because of its simple calculation. Otsu method can select threshold automatically and divide the object from the background in the image. In this paper, various Otsu algorithm are studied.

Introduction

Image segmentation is technologies and processes that put the image into a number of specific region that have unique nature and propose target of interest. It is one of the most basic problem of image analysis, it is very difficult because of the complex of images and it is an important part of the image processing. In computer vision, image segmentation is the process of converting an image into meaningful regions or objects . Image segmentation is widely applied such as locating tumors or other diseases, measuring volume of tissue, surgery navigated by computer, study on anatomy, objects recognition and so on.

Image segmentation is to subdivide the image into its region and object, according to two properties discontinuity and similarity, we divide the image segmentation methods into two categories and so the segmentation is categorized as segmentation based edge and segmentation based region. segmentation algorithms based on discontinuity of pixel are considered as the technology based on boundary or edge. Edge based segmentation attempts to detect the edges and pixels between the different regions where the pixels have rapid transition in intensity, extract the pixels connect to form a closed object region. The result of segmentation is a binary image. In theory, there are two main segmentation methods based on edge ,one based gray histogram and the other is gradient-based . Region based segmentation algorithm is dividing an image into regions according to some criteria. Region based segmentation algorithm is to divide pixels into categories in which pixels have similar characteristics or properties such as color, intensity,texture e.g. Segmentation methods such as thresholding, region growth, region splitting and merging are all region based.

Thresholding is an technique widely used in image segmentation and its key point is to find an optimal threshold(a gray value) according to its gray-scale distribution which can be used to separate an image's object from its background. although it is easy for humans to separate object from complex background, finding a threshold to separate them is a very difficult task[2].

we usually consider the gray-scale histogram an efficient tool to develop image thresholing algorithms. Assuming T stands for the global threshold of an image, thresholding is to get a binary image by turning pixels below T to zero and pixes about T to one, if f(x,y) indicates an image, g(x,y) is binary image after thresholding, it can be defined as[1]:

$$g(x,y)=\begin{cases}1 & f(x,y)\geq T\\ 0 & f(x,y)<T\end{cases} \tag{1}$$

We define thresholding as:

$$T=M\left[x,y,p(x,y),f(x,y)\right] \tag{2}$$

Where T is the threshold, f (x, y) is the gray value of point (x, y) , p(x, y) denotes some local property of the point.

According to the number of threshold values we can divide threshloding methods into two types:

Global thresholding

When T depends only on f (x, y)(that is, the gray-scale values) and the value of T is only relates to the feature of pixels, this thresholding technique is called global thresholding.

1.Local thresholding

If T depends on f (x, y) and p(x, y), this thresholding is called local thresholding which divides an image into several sub regions, and chooses various thresholds T for each sub region [3].

Otsu method was proposed by a Japanese Scholar Otsu in 1979, it is kind of global thresholding method cause it depend only gray value of the image. Otsu method is simple and effective and so it is widely used[4].

The Otsu method separate an image according to a threshold T counted based a gray scale histogram. For it only consider the gray-level information which is one-dimensional, it can not obtain better segmentation result. And then two dimensional Otsu algorithms was proposed which considers gray-scale information as well as each pixel's spatial correlation information in the

Neighborhood. Experiments show that two-dimensional Otsu method can get better segmentation results when it is applied to noisy images.[8] Otsu algorithm include huge amount of calculation, so many people propose techniques which reduce time complex of computation and still maintain segmentation result. In [9], a fast recursive technique is proposed that can reduce computational time efficiently. Otsu method is better when it is used to divide general images, however, it uses exhaustive search to evaluate the criterion that make the between-class variance maximum. When the number of class in an image increases, the calculation of Otsu method becomes huge and it will take too much time to select multi-threshold[10].

Various Otsu algorithms

1. Improved Otsu Algorithms

In [4], one-dimensional Otsu algorithm is described. It is widely applied because of its simple calculation and stability. as mentioned above, one-dimensional Otsu method only consider the pixel's gray-level information without considering the pixel's spatial information, so it can not get satisfactory segmentation result. when histogram of the image has two peaks vary widely ,this method fails. one-dimensional can not give good segmentation effect when the two classes in an image are very unequal. In this paper, a new algorithm is proposed based on entropy which obtain better segmentation result than one-dimensional Otsu method.

2. Comparative Research on Image Segmentation Algorithm

In literature[5], the authors gives an overview of the main image segmentation algorithms and some characteristics of them. This paper considers that Otsu algorithm is a kind of region based segmentation algorithm, it has high complexity rate and its processing rate is slow, its segmentation result is stable and better. For that, to improve the efficiency, Otsu method should be combined with other algorithm.

3. Improved Otsu Based on Improved Histogram

In literature[6], a fast Otsu algorithm based on improved histogram is proposed, and it efficiently reduce the computation complexity of 1D and 2D Otsu algorithm. In this algorithm, we project the 2D histogram onto the diagonal and apply to 2D Otsu on that histogram and then finde the optical threshold. To validate this algorithm, images added by salt and pepper noise and Gaussian noise are used, the results shows that this algorithm greatly improves the computing speed of threshold and have better noise immunity for salt and pepper noise images, but the results of Gaussian noise images are not good.

4. Otsu and K-Means Method

In literature[7], this idea is proposed that the objective function of Otsu algorithmand it of K means method in multilevel thresholding is equal. They have the same criteria that minimize the within-class variance. Otsu applies to global thresholding and K means method is applicable in local thresholding. For Otsu algorithm, the gray scale histogram should be computed before the algorithm be run, but for K means, not need the histogram computation. The two method can both give good segmentation results but comparatively speaking, the segmentation results of K means method are better because Otsu method take more time and the complexity of the method is more.

Conclusion

Table 1. Comparation of various Otsu method

Paper	Method	Segmentation Result	Limitation
Otsu Thresholding Based on Improved Histogram	Improved histogram	Good	Good at salt and paper noise images but not good at Gaussian noise images.
Comparative Research on Image Segmentati Algorithm	Global thresholding	Good/ stable	High complexity/ low processing rate
Otsu and K-mean	Global optimal threshold	Good	Increased complexity and time
Image Segmentation Based on Improved Otsu Algorithm	Entropy based	Stable	When the global distribution of target image and background vary widely, the performance degrades.

Table 1 gives the comparation result of various Otsu methods studied in this paper, the results and limitation are analyzed as well. Because of its simplicity, Otsu algorithms has been widely applied. Because of the complexity of images, the Otsu algorithm may be combined with other algorithms for different images from different fields.

References

[1] Rafael C. Gonzalez, Richard E. Woods, "Digital Image Processing", 2nd ed., Beijing: Publishing House of Electronics Industry, 2007.
[2] W. X. Kang, Q. Q. Yang, R. R. Liang ,"The Comparative Research on Image Segmentation Algorithms", IEEE Conference on ETCS, pp. 703-707, 2009
[3] Er. Nirpjeet kaur and Er Rajpreeet kaur, "A review on various method of image thresholding",IJCSE-2011.
[4] Zhong Qu andLi Hang"Research on Iimage Segmentation Based on the Improved Otsu Algorithm.",2010
[5] W. X. Kang, Q. Q. Yang, R. R. Liang ,"The Comparative Research on Image Segmentation Algorithms", IEEE Conference on ETCS, pp. 703-707, 2009.
[6] Z. Ningbo, W. Gang, Y. Gaobo, and D. Weiming, "A fast 2d otsu thresholding algorithm based on improved histogram," in Pattern Recognition, 2009. CCPR 2009. Chinese Conference on, 2009, pp. 1–5.
[7] L. Dongju and Y. Jian, "Otsu method and k-means," in Hybrid Intelligent Systems, 2009. HIS '09. Ninth International Conference on, vol. 1, 2009, pp. 344–349.
[8] LIU Jian-zhuang, Li Wen-qing, "The Automatic threshold of gray level pictures via Two-dimentional Otsu Method", Acta Automatic Sinica,1993
[9] J. Gong, L. Li, and W. Chen, "Fast recursive algorithms for two-dimensional thresholding," Pattern Recognition,vol. 31, no. 3, pp. 295–300, 1998.
[10] P. K. Sahoo, S. Soltani, A. K. C. Wong, and Y. Chen, "A survey of thresholding techniques," Computer Vision Graphics Image Processing, Vol. 41, 1988, pp. 233-260. International Conference on Robotics and Automation. 2007.

Advanced Materials Research Vols. 989-994 (2014) pp 1962-1968
© (2014) Trans Tech Publications, Switzerland
doi:10.4028/www.scientific.net/AMR.989-994.1962

Non-linear Least Squares Large Misalignment Estimation in Transfer Alignment

Lu Yuan [a], Cheng Xianghong [b]

School of Instrument Science & Engineering, Southeast University, Nanjing 210096, China

Key Laboratory of Micro-Inertial Instrument and Advanced Navigation Technology, Ministry of Education, China

[a]siliconlu@gmail.com, [b]xhcheng@seu.edu.cn,

Keywords: transfer alignment, lever arm, misalignment, estimation, statistic, least square

Abstract. Large misalignment is unavoidable for subsystems which could be deployed randomly on the carriers such as shipborne aircrafts, AUV. Ordinary linear filtering algorithms don't converge fast and accurately in non-linear conditions. It's critical for the accuracy of the transfer alignment. In this paper, a new misalignment and gyroscope bias online estimation method based on angular velocity processing is presented. Sensor measurements of M-SINS and S-SINS will be recorded for a certain period. Misalignment and the gyroscope bias will be calculated from these measurements directly with non-linear least square algorithm. Trust region method with pre-conditioning, subspace and conjugate gradient are applied for faster converge and better accuracy. Simulation results demonstrate the effectiveness of the algorithm.

Introduction

Shipborne aircrafts, UAV (Unmanned aerial vehicle), AUV (autonomous underwater vehicle), etc., are playing a more important role nowadays. Transfer alignment is the most effective method for the initialization of the inertial navigation systems onboard those systems because of its rapidity and accuracy [1]. But such systems could be deployed randomly on the carrier. Large misalignment is unavoidable. Linear system model of the transfer alignment is no longer valid in such conditions.

Non-linear Kalman filter algorithms have been developed to deal with the non-linear equations. Those algorithms require the knowledge of the system model such as gyroscope noise, measurement noise, etc. This makes the sub-system difficult to be adaptive to different dynamic environment and carriers.

In this paper, misalignment estimation method based on non-linear least square is presented. Trust region method with subspace reduction and preconditioned conjugate gradient is applied to make the calculation simpler and faster. The effectiveness of the method is demonstrated by simulation results.

Misalignment estimation based on non-linear least squares algorithm

The gyroscope output curve of the S-SINS differs from the curve of M-SINS because of the misalignment, sensor error and measurement noise. This is described by Eq. (1).

$$\omega_s = C_m^s \cdot \omega_m + \varepsilon + \omega_r \quad \omega_s = C_m^s \cdot \omega_m + \varepsilon + \omega_r \tag{1}$$

where C_m^s is the attitude transformation matrix from M-SINS to S-INS; ω_m, ω_s are the angular velocity outputs of the M-SINS and S-SINS, δK is the gyroscope scale factor error, ε is the gyroscope bias, ω_r is the random walk noise.

The gyroscope scale factor error could be neglected when gyroscopes better than tactical grade ($\delta K \le 100\,ppm$, $\varepsilon < 0.1°/h$, $\omega_r \le 0.01°/\sqrt{h}$) are applied and the angular velocity ω_m of the carrier reach a level of $0.1°/s$, the Eq. (1) could be simplified for least squares estimation:

$$\omega_s = C_m^s \cdot \omega_m + \varepsilon + \omega_r \tag{2}$$

Define:

$$f(\theta,\varepsilon)=\omega_s-C_m^s\cdot\omega_m-\varepsilon \tag{3}$$

where

$$C_m^s=\begin{bmatrix}\cos\gamma\cos\psi+\sin\gamma\sin\psi\sin\theta & -\cos\gamma\sin\psi+\sin\gamma\cos\psi\sin\theta & -\sin\gamma\cos\theta\\ \sin\psi\cos\theta & \cos\psi\cos\theta & \sin\theta\\ \sin\gamma\cos\psi-\cos\gamma\sin\psi\sin\theta & -\sin\gamma\sin\psi-\cos\gamma\cos\psi\sin\theta & \cos\gamma\cos\theta\end{bmatrix} \tag{4}$$

It can be seen that the frame transformation matrix C_m^s is nonlinear. To estimate the misalignment and the gyroscope bias error, define the target function:

$$\mathrm{F}(\theta,\varepsilon)=\min\sum_{i=1}^{m}f(\theta,\varepsilon)^2 \tag{5}$$

Figure (1) illustrates the simulated target function value according to the pitch and roll angle. It can be seen that if the pitch and roll equal the true misalignment angle, the target function will approach the global optimal value.

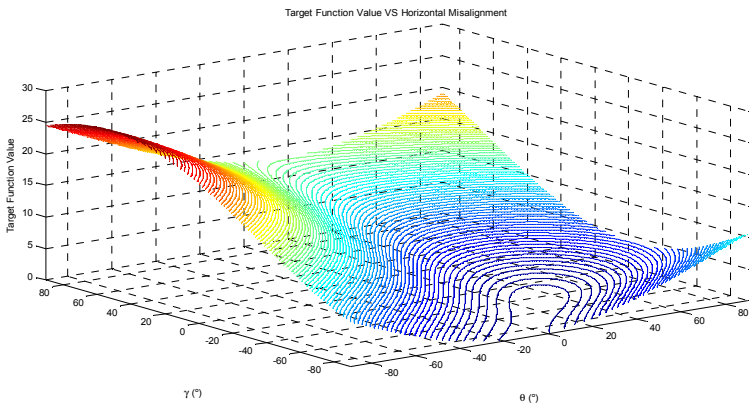

Fig. 1 M-SINS and S-SINS angular velocity amplitude and amplitude difference.

So the problem described in Eq. (5) could be treated like unconstrained minimization problem:

$$\min f(\mathrm{x}):\Re^n\to\Re \tag{6}$$

where it is assumed that f is twice continuously differentiable. The objective function could be rearranged with the form of Eq. (7):

$$F(\mathrm{x}+\mathrm{s})\approx\mathrm{F}(\mathrm{x})+\mathrm{g}^T s+\frac{1}{2}s^T Hs \tag{7}$$

where g is the gradient of F , H is the hessian matrix of F and H is positive symmetric.

Trust region algorithm [2]~[4] is applied to solve the problem described by Eq. (5):

Step 0 Define $0\le\eta_1\le\eta_2<1$, $0<\tau_1<1<\tau_2$, $0\le\varepsilon\le1$. $x_0\in\mathbb{R}^n$ .Set the upper bound of $\tilde{\Delta}>0$, initial trust region radius $\Delta_0\in(0,\tilde{\Delta}]$ and $k:=0$.

Step 1 if $\|\nabla f(x_k)\|\le\varepsilon$, break

Step 2 solve $\min q_k(d_k)=\nabla f(x_k)^T d_k+\frac{1}{2}d_k^T B_k d_k$, $\|d_k\|\le\Delta_k$, where B_k is the k^{th} approximation of Hessian matrix

Step 3 Compute $\Delta q_k = q_k(0) - q_k(d_k)$, $\Delta f_k = f(x_k) - f(x_k + d_k)$, $r_k = \frac{\Delta f_k}{\Delta q_k}$

Step 4 Update trust region radius:

$$\Delta_{k+1} := \begin{cases} \tau_1 \Delta_k & r_k \le \eta_1 \\ \Delta_k & \eta_1 \le r_k \le \eta_2 \\ \min\{\tau_2 \Delta_k, \tilde{\Delta}\} & r_k \ge \eta_2, \|d_k\| = \Delta_k \end{cases}$$

Step 5 if $r_k > \eta_1$, $x_{k+1} = x_k + d_k$, update B_k to B_{k+1}, $k = k+1$, go to Step 1; else $x_{k+1} = x_k$, $k = k+1$, go to Step 2

Good algorithms have been developed to solve the trust region problems more effectively. Subspace and conjugate gradient method are implemented to improve efficiency of the algorithm.

Dimension reduction:

It normally takes a long time to calculate the trust region sub-problem. Subspace reflection is an effective method to reduce the calculation work [5]-[7]. As is described in Eq.(8), the target function is reduced in 2 dimensional subspace.

$$D_k \overset{def}{=} span\{v_1, v_2\}, \text{where } v_1 = \frac{d_k}{\|d_k\|}, v_2 = \frac{g_k}{\|g_k\|} - v_1(v^T{}_1 \frac{g_k}{\|g_k\|}) \tag{8}$$

Normally the estimation is calculated with thousands of data points. With subspace method, the calculation load will be reduced significantly.

Conjugate gradient

The Hessian matrix is second derivative matrix, so the computation cost is extremely high. To avoid Hessian matrix calculation, conjugate gradient algorithm [8]-[11] is applied. Search direction is calculated with Eq. (9).

$$d_k = \begin{cases} -g_k & k = 0 \\ -g_k + \beta_{k-1} d_{k-1} & k \ge 1 \end{cases} \tag{9}$$

$$\beta_k = \frac{r_{k-1}^T z_{k-1}}{r_{k-2}^T z_{k-2}} \tag{10}$$

$$r_k = r_{k-1} - \frac{r_{k-1}^T z_{k-1}}{d_k^T H d_k} H d_k \tag{11}$$

where $Pz_k = r_k$, P is precondition matrix for H and $P = R^2 = A^T A$, A is Jacobian matrix of $f(x)$.

Misalignment estimation

To estimation the misalignment from the sensor measurements, algorithm with the following workflow is implemented.

Step 0 Initialize the target function $F(x)$, set the start point x_0, define $0 \le \varepsilon \le 1$.

Step 1 Calculate the gradient g and the Jacobian matrix A.

Step 2 Calculate the QR factorization of the $A^T A$, $A_k{}^T A_k = Q_k R_k$

Step 3 Calculate and apply the pre-conditioner to gradient g, $z_k = -R_k \backslash R_k{}^T \backslash g_k$.

Step 4 Calculate the conjugate gradient with FR method, Eq. (9)~Eq.(11).

Step 5 Calculate the reflecting subspace with Eq. (8)

Step 6 Solve the Trust Region sub problem to acquire the Step vector:

$min\{\tilde{g}^T s_k + \frac{1}{2} s_k{}^T \tilde{H} s_k, \| s_k \| \leq \Delta\}$, where $\tilde{g} = g \cdot D_k$, $\tilde{H} = D_k{}^T A^T A D_k$.

Step 7 Adjust the Trust region radius:

$$\Delta_{k+1} := \begin{cases} \tau_1 \Delta_k & r_k \leq \eta_1 \\ \Delta_k & \eta_1 \leq r_k \leq \eta_2 \\ \min\{\tau_2 \Delta_k, \tilde{\Delta}\} & r_k \geq \eta_2, \|d_k\| = \Delta_k \end{cases}$$

Step 8 Update the target function F(x), if $F(x_k + \mathrm{s}) < F(x_k)$, update the Step $x_{k+1} = x_k + s$. Go to Step 1.

The complete workflow is described by Figure 2.

Simulation conditions

The signal to noise ratio (SNR) of the measurement is motion intensity related. To evaluate the effectiveness of the algorithm in tougher conditions, shipborne implementation is simulated.

Assuming that, a surface vessel was traveling in normal sea state. The wind wave will cause pitch, roll, surge, sway and heave of the vessel. These motions are considered as periodical cosine form signals in the simulation. Parameters used in the simulation are listed in Table 1.

Table 1 Parameters used to calculate heading, pitch and roll

	Heading	Pitch	Roll
Amplitude	2°	7°	10°
Period	60 s	5 s	6 s

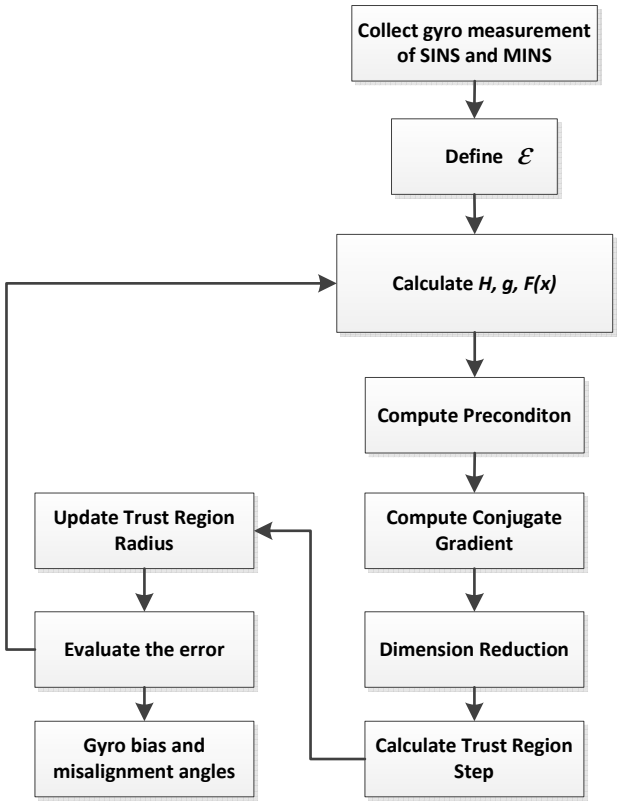

Fig. 2 Misalignment estimation workflow

The M-SINS is normally 1 or 2 grade more accurate than the S-SINS. In the simulation, the error of the M-SINS is ignored. 3 different gyroscope bias errors were simulated. Parameters are listed in Table 2.

Table 2 Sensor accuracy of the S-SINS

	Simulation 1	Simulation 2	Simulation 3
ε_x ($^\circ/h$):	10.5	1.0	0.1
ε_y ($^\circ/h$):	9.5	1.5	0.2
ε_z ($^\circ/h$):	11	2.0	0.3
Random walk ($^\circ/\sqrt{h}$)	10.0	1.0	0.1

To simulate the flexure of the ship deck, a second order Markov process is setup:

$$\ddot{\varphi} + 2\beta\dot{\varphi} + \beta^2\varphi = \eta \tag{12}$$

where φ is the flexure angle and $\varphi = [\varphi_x \quad \varphi_y \quad \varphi_z]^T$ its variance $\sigma = [\sigma_x \quad \sigma_y \quad \sigma_z]^T$; $\eta = [\eta_x \quad \eta_y \quad \eta_z]^T$ is Gaussian while noise and has a variance of $Q = [Q_{\eta x} \quad Q_{\eta y} \quad Q_{\eta z}]^T$, $\beta = [\beta_x \quad \beta_y \quad \beta_z]^T$ is constant.

Q, η, σ and β have the following relation：

$$Q_\eta = 4\beta^3\sigma^2 \tag{13}$$

In the simulations, set $\beta = [7 \quad 8 \quad 9]^T$, 2 different flexure conditions are simulated:

Table 3 Flexure condition parameters

	$\sigma_x(''/s)$	$\sigma_y(''/s)$	$\sigma_z(''/s)$
Flexure Condition 1	0.4	0.5	0.6
Flexure Condition 2	4	5	6

Simulation results

The sampling period of the sensor is 0.005s. Sensor data of 150 seconds is collected and processed to estimate the misalignment and gyroscope bias. The simulation results are listed in table 4~5. The iteration steps under flexure condition 1 are illustrated in figure 3~5.

The simulation results demonstrate that random misalignment could be estimated effectively with the algorithm. The flexure of the carrier will affect the gyroscope bias estimation accuracy.

Table 4 Misalignment estimation in flexure condition 1

		θ	ϕ	ψ	ε_x	ε_y	ε_z
	Preset:	0 º	0 º	0 º	10.5 º/h	9.5 º/h	11 º/h
1	Estimated:	-0.0033 º	0.0021 º	0.0031º	10.34 º/h	9.34º/h	10.86 º/h
	Error:	-11.98 ″	7.68 ″	11.30 ″	-9.82 ′/h	-9.43 ′/h	-8.49 ′/h
	Preset:	5 º	-10 º	-70 º	1 º/h	1.5 º/h	2 º/h
2	Estimated:	4.999 º	-9.996º	-69.997 º	0.98 º/h	1.48º/h	1.98º/h
	Error:	-4.73 ″	13.21 ″	-10.77 ″	-1.15 ′/h	-0.74 ′/h	-0.96 ′/h
	Preset:	70 º	-70 º	180º	0.1 º/h	0.2 º/h	0.3 º/h
3	Estimated:	69.993 º	-70.003 º	179.997º	0.09 º/h	0.19 º/h	-0.29 º/h
	Error:	-26.52″	-10.34″	-12.72 ″	-0.72′/h	-0.71′/h	-0.89′/h

Conclusion

In this paper, a non-linear least square based misalignment and gyroscope bias estimation method

Table 5 Misalignment estimation in flexure condition 2

		θ	ϕ	ψ	ε_x	ε_y	ε_z
	Preset:	0 º	0 º	0 º	10.5 º/h	9.5 º/h	11 º/h
1	Estimated:	-0.0033 º	0.0021 º	0.0032º	10.33 º/h	9.35º/h	10.88 º/h
	Error:	-11.97 ″	7.59 ″	11.38 ″	9.79 ′/h	8.75 ′/h	7.46 ′/h
	Preset:	5 º	-10 º	-70 º	1 º/h	1.5 º/h	2 º/h
2	Estimated:	5.003 º	-10.002 º	-70.004 º	0.85 º/h	1.37 º/h	1.88 º/h
	Error:	10.53 ″	-8.69 ″	-14.00 ″	8.89 ′/h	7.83 ′/h	6.73 ′/h
	Preset:	70 º	-70 º	180º	0.1 º/h	0.2 º/h	0.3 º/h
3	Estimated:	69.991 º	-70.003 º	179.995º	0.05 º/h	-0.06 º/h	-0.19 º/h
	Error:	-32.56″	-9.26 ″	17.52 ″	-9.00 ′/h	-8.25′/h	-6.66′/h

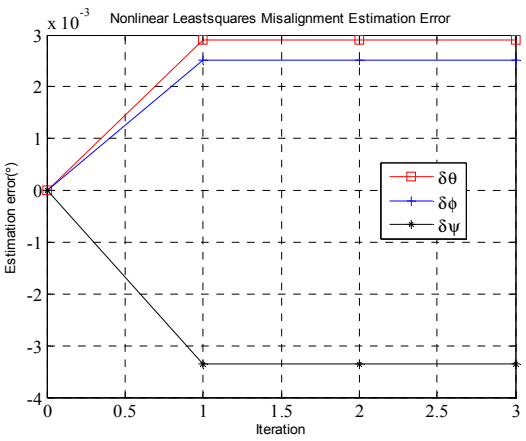

Fig. 3 Non-linear least square interation steps with true value [0,0,0]

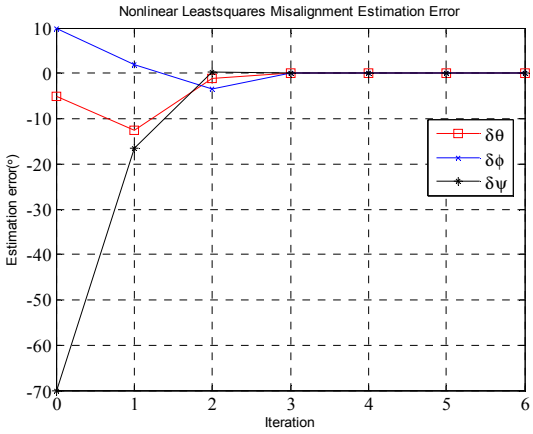

Fig. 4 Non-linear least square interation steps with true value [5,-10,-70]

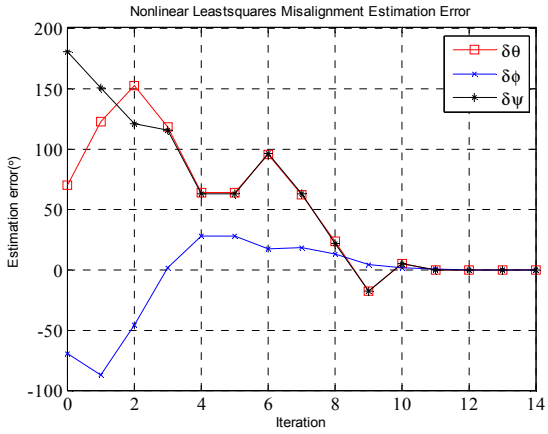

Fig. 5 Non-linear least square interation steps with true value [-70,70,180]

is presented. The estimation requires only gyro scope measurements of the M-SINS and S-SINS. Pre-conditioning, conjugate gradient and subspace technique are implemented to improve the trust region calculation efficiency. Simulation results demonstrate that the large misalignment could be estimated with the method presented in the paper. Gyroscope bias error could be also estimated. But it's sensitive to carrier flexure. Further research would be focused on new sensor bias error adaptive to the carrier flexure.

The method is aimed to estimate the static part of the misalignment and gyroscope bias error in transfer alignment. The dynamic parts could be added to a Kalman filter state vector to improve the alignment accuracy.

Estimation using sensor measurements could avoid the error crossing over the iterations. The data from M-SINS and S-SINS should be collected and processed simultaneously. This requires either a hard-wired connection or RF radio transmission between the M-SINS and the S-SINS. To implement the application in random position, the wireless tactical data link (TDL) such as Carrier Aircraft Inertial Navigation System (CAINS) based on Link-4A communication system is required. The synchronization of the data is also critical. Time mark should be added to the communication protocol. Reference information delay could also be estimated with similar principle [12]

References

[1] Kain J E, Cloutier J R. Rapid Transfer Alignment for Tactical Weapon Applications[C],AIAA Guidance, Navigation and Control Conference. 1989. 1290～1300.

[2] K. Madsen, H.B. Nielsen,O. Tingleff, Methods For Non-Linear Least Squares Problems[M], Informatics and Mathematical Modelling, Technical University of Denmark,2004.

[3] Vandenberhe L. Applied Numerical Computing[M],USA: UCLA, 2011. 207-211.

[4] Zhi-rong D. Nonlinear Least-Square Algorithms Used for TMA in Bearing-only System-The Engineering Mathematic Model and Algorithms [J]. Intelligence Command Control and Simulation Technigues, 2005, 2.

[5] D.C. Sorensen, Newton's Method With A Model Trust Region Modification[J], SIAM J. Numer. Anal., Vol. 19, No.2, pp.409-426,1982.

[6] Moré, J.J. and D.C. Sorensen, Computing a Trust Region Step[J], SIAM Journal on Scientific and Statistical Computing, Vol. 3, pp 553–572, 1983.

[7] Y. Yuan. A review of trust region algorithms for optimization[C], in ICIAM 99: Proceedings of the Fourth International Congress on Industrial & Applied Mathematics, Edinburgh, 2000

[8] Branch, M.A., T.F. Coleman, and Y. Li, A Subspace, Interior, and Conjugate Gradient Method for Large-Scale Bound-Constrained Minimization Problems[J], SIAM Journal on Scientific Computing, Vol. 21, Number 1, pp 1–23, 1999.

[9] Byrd, R.H., R.B. Schnabel, and G.A. Shultz, Approximate Solution of the Trust Region Problem by Minimization over Two-Dimensional Subspaces[J], Mathematical Programming, Vol. 40, pp 247–263, 1988.

[10] Coleman, T.F. and A. Verma, A Preconditioned Conjugate Gradient Approach to Linear Equality Constrained Minimization[J], Computational Optimization and Applications, Vol. 20, No. 1, pp. 61–72, 2001.

[11] Elena Caraba, Preconditioned Conjugate Gradient Algorithm[D], Louisiana State University & agricultural and mechanical College, 2008.

[12] Lu Yuan, Cheng Xianghong, Reference Information Time Delay Estimation and Compensation in Transfer Alignment[J], Journal of Southeast University(English Edition), 2011,27(1):52-55.

Advanced Materials Research Vols. 989-994 (2014) pp 1969-1972
© (2014) Trans Tech Publications, Switzerland
doi:10.4028/www.scientific.net/AMR.989-994.1969

Singularly Perturbed Systems with Diffusion and Time Delay

Chang-you WANG[1, 3]*, Qi DOU[1], Xiang-wei LI[2, 3]

[1]College of Science, Chongqing University of Posts and Telecommunications, Chongqing, 400065 P. R. China

[2]College of Automatic, Chongqing University of Posts and Telecommunications, Chongqing, 400065 P. R. China

[3]Key Laboratory of Industrial Internet of Things & Networked Control of Ministry of Education, Chongqing University of Posts and Telecommunications, Chongqing 400065, P.R. China;

Key words: formal solution, reaction diffusion, singular perturbation, time delay.

Abstract: The singularly perturbed systems for the nonlinear three-species food-chain reaction systems with time delay are considered. By using the method of the stretched variable, the formal asymptotic solution is obtained under suitable conditions.

1. Introduction

The nonlinear singularly perturbed problem is a very attractive study object in international academic circles [1]. Recently, approximate methods have been developed and refined, including the averaging method, the boundary layer method, the matched asymptotic expansion method, and the multiscale method. Many scholars have done a great deal of work [2-7]. However, few of them have studied the nonlinear singularly perturbed with time delay. In view of this, we study the following singularly perturbed systems with diffusion and time Delay.

$$\varepsilon \partial u_1 / \partial t - L_1 u_1 = f_1(u_1(t-\varepsilon r))(\lambda_1 - r_{11}u_1 - r_{21}u_2 - r_{31}u_3), \quad (t,x) \in (0,T]\times\Omega, \tag{1}$$

$$\varepsilon \partial u_2 / \partial t - L_2 u_2 = f_2(u_2(t-\varepsilon r))(\lambda_2 - r_{22}u_2 + r_{12}u_1 - r_{32}u_3), \quad (t,x) \in (0,T]\times\Omega, \tag{2}$$

$$\varepsilon \partial u_3 / \partial t - L_3 u_3 = f_3(u_3(t-\varepsilon r))(\lambda_3 - r_{33}u_3 + r_{13}u_1 + r_{23}u_2), \quad (t,x) \in (0,T]\times\Omega, \tag{3}$$

with the boundary and initial conditions

$$Bu_i = u_i + \alpha_i(x)\frac{\partial u_i}{\partial n} = g_i(x), \quad a_i(x) \ge a_0 > 0, x \in \partial\Omega, i = 1,2,3, \tag{4}$$

$$u_i = h_i(t,x,\varepsilon) \quad t \in [-\varepsilon r, 0] \quad i = 1,2,3 \tag{5}$$

where ε is a positive small parameter, r is a positive constants, $r\varepsilon$ is a time delay, $u_1(t,x)$, $u_2(t,x)$ and $u_3(t,x)$ stand for the numbers of interacting species, respectively. $x \equiv (x_1, x_2, \cdots, x_n) \in \Omega$, and Ω is a bounded domain in R^n with boundary $\partial\Omega$, $\partial / \partial n$ denotes the outward normal derivative on $\partial\Omega$.The above problems (1)-(5) arise from a simple food-chain model describing three interacting species in a spatial habitat Ω [8-9]. The real number λ_i is the net birth rate of the i-th species, and r_{ij} are the density coefficients of the prey and predator populations, respectively. L_i is a uniformly elliptic operator in the form

$$L_i u = -\sum_{j,k=1}^{N} a_{j,k}^{(i)}(x,t)\frac{\partial^2 u}{\partial x_j \partial x_k} + \sum_{j=1}^{N} b_j^{(i)}(x,t)\frac{\partial u}{\partial x_j}, \quad (i = 1, 2, 3). \tag{6}$$

2. Outer Solution

Firstly, we need the following hypotheses:

(H1) There exists a positive number γ such that for any $\xi=(\xi_1,\cdots,\xi_N)\in R^N$, $(x,t)\in\overline{\Omega}\times[0,\omega]$ and $i\in\{1,2,\cdots,m\}$, we have

$$\sum_{j,k=1}^{N} a_{jk}^{(i)}(x,t)\xi_j\xi_k \geq \gamma|\xi|^2 ,$$

(H2) $a_{j,k}^{(i)}(x,t), b_j^{(i)}(x,t), \alpha_i(t)$, $g_i(t)>0$, and $h_i(t,x,\varepsilon)>0$ with respect to variables are Holder continuous in correspondence ranges and $g_i(x)=h_i(x), i=1,2,3$ as $x\in\partial\Omega$.

(H3) $f_i(y)\ (i=1,2,3)$ is continuous differential positive functions.

In view of the biological significance of $u_i(x,t), i=1,2,3$, we have $0\leq u_i(x,t)\leq M_i$, where M_i denotes the environmental carrying capacity.

The reduced problem of the equations (1)-(5) is

$$-Lu_1 = f_1(u_1)(\lambda_1 - r_{11}u_1 - r_{21}u_2 - r_{31}u_3), \tag{7}$$

$$-Lu_2 = f_2(u_2)(\lambda_2 - r_{22}u_2 + r_{12}u_1 - r_{32}u_3), \tag{8}$$

$$-Lu_3 = f_3(u_3)(\lambda_3 - r_{33}u_3 + r_{23}u_2 + r_{13}u_1), \tag{9}$$

$$Bu_i = g_i(x), \qquad x\in\partial\Omega, i=1,2,3. \tag{10}$$

We also assume that the equations (7)-(10) have a positive solution $U_0=(U_{10},U_{20},U_{30})$.

Let the outer solution of the equations (1)-(4) are as follows

$$U_i \sim \sum_{j=0}^{\infty} U_{ij}(x)\varepsilon^j, \quad i=1,2,3. \tag{11}$$

Thus, substituting U_i into Equations (1)-(4), we obtain

$$-L_1U_1 = f_1(U_1)(\lambda_1 - r_{11}U_1 - r_{21}U_2 - r_{31}U_3), \quad x\in\Omega, \tag{12}$$

$$-L_2U_2 = f_2(U_2)(\lambda_2 - r_{22}U_2 + r_{12}U_1 - r_{32}U_3), \quad x\in\Omega, \tag{13}$$

$$-L_3U_3 = f_3(U_3)(\lambda_3 - r_{33}U_3 + r_{13}U_1 + r_{23}U_2), \quad x\in\Omega, \tag{14}$$

$$BU_i = U_i + \alpha_i(x)\frac{\partial U_i}{\partial n} = g_i(x), \quad a_i(x)\geq a_0>0, x\in\partial\Omega, i=1,2,3, \tag{15}$$

Developing $f_i(U_i), i=1,2,3$ in ε, we have

$$f_i(U_i)\equiv F_i(\varepsilon)\sim\sum_{j=0}^{\infty}F_{ij}\varepsilon^j , \tag{16}$$

where $F_{i0}=f_i(U_{i0})$, $F_{ij}=\dfrac{1}{j!}\dfrac{\partial^j F_i}{\partial\varepsilon^j}\Big|_{\varepsilon=0} = f_{iu_i}(U_{i0})U_{ij}+f_{ij}, j=1,2,3\cdots$. It is obvious that f_{ij} are determined functions successively. Comparing the same coefficients of ε^j for equations, we obtain

$$-L_1U_{1j} = \lambda_1F_{1j} - r_{11}\sum_{m,n=0}^{m+n=j}F_{1m}U_{1n} - r_{21}\sum_{m,n=0}^{m+n=j}F_{1m}U_{2n} - r_{31}\sum_{m,n=0}^{m+n=j}F_{1m}U_{3n} \tag{17}$$

$$-L_2U_{2j} = \lambda_2F_{2j} - r_{22}\sum_{m,n=0}^{m+n=j}F_{2m}U_{2n} - r_{12}\sum_{m,n=0}^{m+n=j}F_{2m}U_{1n} - r_{33}\sum_{m,n=0}^{m+n=j}F_{2m}U_{3n} \tag{18}$$

$$-L_3U_{3j} = \lambda_3F_{3j} - r_{33}\sum_{m,n=0}^{m+n=j}F_{3m}U_{3n} + r_{13}\sum_{m,n=0}^{m+n=j}F_{3m}U_{1n} + r_{23}\sum_{m,n=0}^{m+n=j}F_{3m}U_{1n} \tag{19}$$

$$BU_{ij} = g_{ij} \tag{20}$$

where $g_{ij}=\frac{1}{j!}\left[\frac{\partial^j g_i}{\partial \varepsilon^j}\right]_{\varepsilon=0}$, $j=1,2\cdots$. From the linear problems (17)-(20), we can solve $\left(U_{1j},U_{2j},U_{3j}\right), j=1,2,3,\cdots$ successively, and noting that U_0 satisfies the problems (7)-(10), we obtain the outer solution $U_i,(i=1,2,3)$ for the original problem (1)-(4). But it may not satisfy the initial condition (5), so that we need to construct the time delay initial layer functions $\left(V_1,\mathrm{V}_2,\mathrm{V}_3\right)$.

3. Formal Solution

Now we first introduce a stretched variable

$$\tau=\frac{t}{\varepsilon},\ 0<\varepsilon\ll 1 \tag{21}$$

And let $u_i=U_i\left(x,\varepsilon\right)+V_i\left(\tau,x,\varepsilon\right), i=1,2,3$. Substituting them into Equations (1)-(5), we have

$$\partial V_1/\partial\tau-L_1V_1=f_1(\mathrm{U}_1+V_1(t-\varepsilon r))(\lambda_1-r_{11}(U_1+V_1)-r_{21}(U_2+V_2)-r_{31}(U_3+V_3))-f_1(\mathrm{U}_1)(\lambda_1-r_{11}U_1-r_{21}U_2-r_{31}U_3), \tag{22}$$

$$\partial V_2/\partial\tau-L_1V_2=f_2(\mathrm{U}_2+V_2(t-\varepsilon r))(\lambda_2-r_{22}(U_2+V_2)+r_{12}(U_1+V_1)-r_{32}(U_3+V_3))-f_2(\mathrm{U}_2)(\lambda_2-r_{22}U_2+r_{12}U_1-r_{32}U_3), \tag{23}$$

$$\partial V_3/\partial\tau-L_1V_3=f_3(\mathrm{U}_3+V_3(t-\varepsilon r))(\lambda_3-r_{33}(U_3+V_3)+r_{13}(U_1+V_1)+r_{23}(U_2+V_2))-f_3(\mathrm{U}_3)(\lambda_3-r_{33}U_3+r_{13}U_1+r_{23}U_2), \tag{24}$$

$$BV_i=0\quad x\in\partial\Omega, i=1,2,3, \tag{25}$$

$$V_i=h_i-U_i\quad t\in\left[-\varepsilon r,0\right]\quad i=1,2,3. \tag{26}$$

Let

$$V_i\sim\sum_{j=0}^{\infty}V_{ij}\left(\tau,x\right)\varepsilon^j,\quad i=1,2,3, \tag{27}$$

$$f_i(\mathrm{U}_i+V_i\left(t-\varepsilon r\right))-f_i(\mathrm{U}_i)\equiv\overline{F_i}\left(\varepsilon\right)\sim\sum_{j=0}^{\infty}\overline{F_{ij}}\varepsilon^j, i=1,2,3, \tag{28}$$

$$f_i(\mathrm{U}_i+V_i\left(t-\varepsilon r\right))\equiv\overline{G_i}\left(\varepsilon\right)\sim\sum_{j=0}^{\infty}\overline{G_{ij}}\varepsilon^j, i=1,2,3, \tag{29}$$

where

$$\overline{F_{i0}}=f_i(\mathrm{U}_{i0}+V_{i0}\left(t-\varepsilon r\right))-f_i(\mathrm{U}_{i0})=f_{u_i}\left(\mathrm{U}_{i0}+\theta_iV_{i0}\left(t-\varepsilon r\right)\right)V_{i0}\left(t-\varepsilon r\right),0<\theta_i<1,$$

$$\overline{F_{ij}}=\frac{1}{j!}\frac{\partial^j\overline{F_{ij}}}{\partial\varepsilon^j}\bigg|_{\varepsilon=0}=f_{iu_i}\left(U_{i0}+V_{i0}\left(t-\varepsilon r\right)\right)V_{ij}\left(t-\varepsilon r\right)+\overline{f_{ij}}, i=1,2,3,\ j=1,2,3,\cdots,$$

$$\overline{G_{i0}}=f_i(\mathrm{U}_{i0}+V_{i0}\left(t-\varepsilon r\right)),$$

$$\overline{G_{ij}}=\frac{1}{j!}\frac{\partial^j\overline{G_i}}{\partial\varepsilon^j}\bigg|_{\varepsilon=0}=f_i(\mathrm{U}_i+V_i)-f_{iv_i}(\mathrm{U}_i+V_i)\varepsilon r+\frac{1}{2!}f^{"}_{iv_i}(\mathrm{U}_i+V_i)\left(\varepsilon r\right)^2+\cdots.$$

Substituting equations (27)-(29) into equations (22)-(26), developing f_i in ε, and comparing the same coefficients of ε^j for equations, we have

$$\begin{aligned}\left(V_{1j}\right)_\tau-L_1V_{1j}=&\left(\lambda_1\overline{F_{1j}}-r_{11}\sum_{m,n=0}^{m+n=j}\overline{F_{1m}}U_{1n}-r_{21}\sum_{m,n=0}^{m+n=j}\overline{F_{1m}}U_{2n}-r_{31}\sum_{m,n=0}^{m+n=j}\overline{F_{1m}}U_{3n}\right)\\&-\left(r_{11}\sum_{m,n=0}^{m+n=j}\overline{G_{1m}}U_{1n}+r_{21}\sum_{m,n=0}^{m+n=j}\overline{G_{1m}}U_{2n}+r_{31}\sum_{m,n=0}^{m+n=j}\overline{G_{1m}}U_{3n}\right),\end{aligned} \tag{30}$$

$$\left(V_{2j}\right)_\tau-L_2V_{2j}=\left(\lambda_2\overline{F_{2j}}-r_{22}\sum_{m,n=0}^{m+n=j}\overline{F_{2m}}U_{2n}+r_{12}\sum_{m,n=0}^{m+n=j}\overline{F_{2m}}U_{1n}-r_{32}\sum_{m,n=0}^{m+n=j}\overline{F_{2m}}U_{3n}\right)$$

$$+\left(-r_{22}\sum_{m,n=0}^{m+n=j}\overline{G_{2m}}U_{2n}+r_{12}\sum_{m,n=0}^{m+n=j}\overline{G_{2m}}U_{1n}-r_{32}\sum_{m,n=0}^{m+n=j}\overline{G_{2m}}U_{3n}\right), \tag{31}$$

$$\left(V_{3j}\right)_{\tau}-L_3V_{3j}=\left(\lambda_3\overline{F_{3j}}-r_{33}\sum_{m,n=0}^{m+n=j}\overline{F_{3m}}U_{3n}+r_{13}\sum_{m,n=0}^{m+n=j}\overline{F_{3m}}U_{1n}+r_{23}\sum_{m,n=0}^{m+n=j}\overline{F_{3m}}U_{2n}\right)$$

$$+\left(-r_{33}\sum_{m,n=0}^{m+n=j}\overline{G_{3m}}U_{3n}+r_{13}\sum_{m,n=0}^{m+n=j}\overline{G_{3m}}U_{1n}+r_{23}\sum_{m,n=0}^{m+n=j}\overline{G_{3m}}U_{2n}\right), \tag{32}$$

$$BV_{ij}=0,\ x\in\partial\Omega,\ i=1,2,3, \tag{33}$$

$$V_{ij}=h_{ij}-U_{ij},\ t\in\left[-\varepsilon r,0\right],\ i=1,2,3. \tag{34}$$

From the linear problems (30)-(34) when $j=0$, we can easily get $\left(V_{10},V_{20},V_{30}\right)$, then we can get $\left(V_{1j},V_{2j},V_{3j}\right),\ j=1,2,3\cdots$ when $j=1,2,3\cdots$ from (30)-(34). Thus, we obtain formal asymptotic expansion of solution for the Equations (1)-(5)

$$u_i\sim\sum_{j=0}^{\infty}\left(U_{ij}(x)+V_{ij}(\tau,x)\right)\varepsilon^j,\ i=1,2,3.$$

Acknowledgments

This work is supported by the Natural Science Foundation Project of CQ CSTC (Grant nos. cstc2012jjA20016 and cstc2012jjA40035) of China, and the NSFC (Grant nos. 51005264 and 11101298) of China.

References

[1] E. M. De Jager, F. R. Jiang. The theory of singular perturbation, North Holland Publishing Co., Amsterdam, 1996.

[2] R.Z. Khasminskii, G. Yin. Limit behavior of two-time-scale diffusions revisited. Journal of Differential Equations 212 (2005) 85–113.

[3] J. Mo. A kind of four order semilinear singular perturbation solution. Applied Mathematics and Mechanics 30 (2009) 1369-1373.

[4] A. Kaushik. Singular perturbation analysis of bistable differential equation arising in the nerve pulse propagation. Nonlinear Anal. Real World Appl. 9 (2008) 2106–2127.

[5] J. Mo, H. Wang. Generalized Lotke-Vollterra ecological model of nonlinear singularly perturbed approximate solution. Journal of Ecology 27 (2007) 4366-4370.

[6] J. Shen, M. Han. Canard solution and its asymptotic approximation in a second-order nonlinear singularly perturbed boundary value problem with a turning point. Commun Nonlinear Sci Numer Simulat 19 (2014) 2632-2643.

[7] S. Gowrisankar, S. Natesan. The parameter uniform numerical method for singularly perturbed parabolic reaction-diffusion problems on equidistributed grids. Applied Mathematics Letters 26 (2013) 1053-1060.

[8] C. Wang, X. Hu, Existence and uniqueness of bounded solution and periodic solution of reaction-diffusion equation with time delay. Journal of Chongqing University of Posts and Telecommunication (Natural Science Edition), 17 (2005) 644–646. Chinese.

[9] C. Wang, Periodic solution of prey predator model with diffusion and distributed delay effects. Journal of Chongqing University of Posts and Telecommunication (Natural Science Edition), . 18 (2006) 409–412, 2006.

Advanced Materials Research Vols. 989-994 (2014) pp 1973-1976
© (2014) Trans Tech Publications, Switzerland
doi:10.4028/www.scientific.net/AMR.989-994.1973

An Algorithm of DOA Estimation in Linear Canonical Transform Domain

Heng Zhao[1,a] , Yanhong Zhang[2,b] and Huihui Li[1,c]

[1]Embedded technology and application, Henan Radio & elevision University,

Zhengzhou 450008, China

[2]key discipline of circuit and system, Henan Institute of Education, Zhengzhou 450046, China

[a]email:hzhaoedu@163.com, [b]email:yhzhang1209@163.com, [c]lihui-zheng@163.com

Keywords: DOA Estimation; Linear Canonical Transform; Root-MUSIC

Abstract. An algorithm of DOA estimation based on linear canonical transform is proposed. In this method, the observed signals are first transformed to linear canonical domain, through selecting appropriate transformation parameters, characteristics of the observed signal appear to be energy-concentrated in the corresponding linear canonical domain, and by that, the linear canonical domain steering vector is defined, then root-MUSIC is used to estimate DOA of impinging signals. Simulation examples are provided showing the effectiveness of the presented technique.

Introduction

Direction of arrival (DOA) estimation is widely used in radar, sonar, and communication systems. The technique plays an important role in enhancing the performance of wireless communications. Many DOA estimation algorithms have already been studied like root-MUSIC, Maximum Likelihood Estimation, Time-frequency MUSIC and so on[1-7]. These algorithms generally achieve high accuracy, but also have many deficiencies, such as only based on narrow band hypothesis, complex computation and only applicable for LFM signals.

The linear canonical transform (LCT) is an important time-frequency analysis tool, some scholars have done many works on it[8-11]. Comparing to the fractional Fourier transform and the Fourier transform, the LCT is more flexible for signal processing due to its four transform parameters. So a novel approach to direction finding of wideband time-frequency signals in LCT domain is introduced. By using linear canonical transform and the unique concentration signature of the wideband time-frequency signal in a certain linear canonical transform domain, the LCT domain time-invariant vector is given, and then, the signal DOA can be estimated by root-MUSIC[1]. Theoretical analysis and simulation results show that, this method can solve the DOA estimation problem of wideband time-frequency signal, and can obtain good estimating performance.

Array Signal Model and Problem Statement

Let a ULA of M sensors spaced d apart receive Gaussian pulse signals impinging from the K ($K<M$) unknown directions $\{\theta_k\}_{k=1}^{K}$. Suppose the reference point is the first unit, then the output of the ith sensor can be expressed as:

$$x_i(t)=\sum_{k=1}^{K}s_k(t-\tau_{ik})+n_i(t) \quad , \qquad i=1, 2\ldots M. \tag{1}$$

Where, $\tau_{ik}=\frac{(i-1)d}{c}\sin(\theta_k)$, $s_k(t)=e^{-(\frac{t}{p_k})^2}$, k=1, 2… K. $\{s_k(t)\}_{k=1}^{K}$ are source waveforms, $\{n_i(t)\}_{i=1}^{M}$ are the additive Gauss white noises. The source signals and the noises are assumed to be statistically independent. τ_{ik} is the path delay of the plane wave from the source. C is the light speed.

Combining (3) and (1), we obtain

$$x_i(t)=\sum_{k=1}^{K}e^{2t\tau_{ik}/p_k^2}e^{-\tau_{ik}^2/p_k^2}s_k(t)+n_i(t). \tag{2}$$

From (2), it can be seen that, the direction vector of the Gaussian pulse signals is associated with the direction θ_k and the time index t. So the DOA's of the Gaussian pulse signals cannot be estimated directly by root-MUSIC algorithm.

The Linear Canonical Transform

The linear canonical transform(LCT) is also known as the ABCD transform, generalized Fresnel transform and the Collins formula etc.. This transform proposed by Moshinsky and Collins is gradually attented in signal processing.

The LCT with parameters(a, b, c, d) of a signal $f(t)$ is defined as:

$$F_{(a,b,c,d)}(u)=L_{(a,b,c,d)}(f(t))=\begin{cases}\sqrt{\frac{1}{j2\pi}}\cdot e^{\frac{jd}{2b}u^2}\int e^{-\frac{j}{b}ut}e^{\frac{ja}{2b}t^2}f(t)dt, & b\neq 0;\\ \sqrt{d}\cdot e^{\frac{jcd}{2}u^2}f(du), & b=0.\end{cases} \tag{3}$$

Where, parameters(a, b, c, d) are real numbers satisfying $ad-bc=1$. The LCT is a unitary transform and has many special cases. Choosing appropriate parameters, the LCT coincides with the conventional Fourier transform(FT), the chirp multiplication operation, the fractional Fourier transform(FRFT) and the scaling operation etc..

The LCT has three free parameters. Comparing to the FT with no free parameter and the FRFT with one free parameters, the LCT is more flexible. The FRFT which has only one free parameter, can be interpreted as a rotation by an angle in the time-frequency plane, while the LCT with three free parameters has not only the rotation, but also the twisting and stretching in the time-frequency plane. By changing transform parameters, the LCT can easily change the shape and position of the signal time-frequency distribution. Therefore, we can prove that, for a given signal, when selecting suitable transform parameters, the LCT will result in the concentration of the signal energy in a certain LCT domain[8][11].

DOA Estimation in Linear Canonical Transform Domain

According to the definition of the LCT, we can obtain the LCT of the reference sensor output $s_k(t)$ as

$$s_{k1(a,b,c,d)}(u)=\sqrt{\frac{1}{j2\pi}}\,\mathrm{e}^{j\frac{d}{2b}u^2}\int_{-T/2}^{T/2}\mathrm{e}^{-\frac{j}{b}ut}e^{j\frac{a}{2b}t^2}e^{-\left(\frac{t}{p_k}\right)^2}dt=\sqrt{\frac{1}{j2\pi}}\,\mathrm{e}^{j\frac{d}{2b}u^2}\int_{-T/2}^{T/2}\mathrm{e}^{-\frac{j}{b}ut}e^{\left(j\frac{a}{2b}-\frac{1}{p_k^2}\right)t^2}dt \tag{4}$$

where T is the observed time of the signal.

From (4),it can be seen that, if $a/(2b)=1/jp_k^2$, the expression (4) can be expressed as

$$s_{k1(a,b,c,d)}(u)=\sqrt{\frac{1}{j2\pi}}\,\mathrm{e}^{j\frac{d}{2b}u^2}\,T\frac{\sin[(u/b)T/2]}{(u/b)T/2} \tag{5}$$

From the above expression, we can prove that, when $a/(2b)=1/jp_k^2$, $s_{k1(a,b,c,d)}(u)$ has the best energy-concentrated performance, and the peak of $s_{k1(a,b,c,d)}(u)$ is

$$s_{k1(a,b,c,d)}(u_{1m})=\sqrt{\frac{1}{j2\pi}}\,\mathrm{e}^{j\frac{d}{2b}u_{1m}^2}\,T. \tag{6}$$

Therefore, for a given signal, the LCT will result in the concentration of the signal energy in a certain LCT domain.

Through the same analysis, we know that, the LCT $s_{ki(a,b,c,d)}(u)$ of the *i*th sensor output $s_k(t-\tau_{ik})$ will still produce energy concentration when $a/(2b)=1/jp_k^2$, and the peak of $s_{ki(a,b,c,d)}(u)$ is

$$s_{ki(a,b,c,d)}(u_{im})=\sqrt{\frac{1}{j2\pi}}\,\mathrm{e}^{j\frac{d}{2b}u_{im}^2}\,e^{-\frac{\tau_{ik}^2}{p_k^2}}T=e^{j\frac{ad}{b}u_{1m}\tau_{ik}}s_{k1(a,b,c,d)}(u_{1m}) \quad . \tag{7}$$

Where , the time delay τ_{ik} is very small, and τ_{ik}^2 can be ignored.

Here, we define the LCT domain steering vector of the signal $s_k(t)$ as

$$\mathbf{A}_{(a,b,c,d)}=[1,\mathrm{e}^{j\frac{ad}{b}u_{1m}\tau_{2k}},\cdots,e^{j\frac{ad}{b}u_{1m}\tau_{Mk}}]^T. \tag{8}$$

The value of $\mathbf{A}_{(a,b,c,d)}$ is only associated with time delay, that is, it is only associated with the direction θ_k. So, we can use root-MUSIC algorithm to estimate the signal DOA in the corresponding LCT domain.

Simulation Results

To verify the predictions, an example of computer simulation is given. We assume a ULA of *M*=10 sensors and two Gaussian pulse sources $s_1(t)$ and $s_2(t)$ impinging from $\theta_1=20^o$ and $\theta_2=30^o$, the spacing of the array elements is $d=0.15m$. The frequencies of the Gaussian pulse $s_1(t)$ and $s_2(t)$ are 10kHz and 20KHz, the bandwidth and the sampling frequency of both signals are 60% and 1MHz. The data length is *N*=379 snapshots. At each level of the SNR, we run 100 Monte Carlo simulations, and the MSE's obtained are shown in Figure.1.

From Figure.1, it can be seen that, the proposed technique in this paper can accurately estimate the DOA's of the observed signals and has good estimating performance.

Conclusion

A new method based on LCT for estimating DOA of the wideband time-frequency signal is presented. In this method, the LCT domain time-invariant steering vector is defined by LCT and the concentration signature of the signal in the corresponding LCT domain, then, the root-MUSIC algorithm is used to estimate the DOA of the signal. Theoretical analysis and simulation results show that, this approach is not only to solve the DOA estimation problem of wideband time-frequency signal, and can obtain good estimating performance. Due to the high degree of flexibility and broad applicability, this method greatly enriches the DOA estimation theory and extends the applications of the LCT in signal processing.

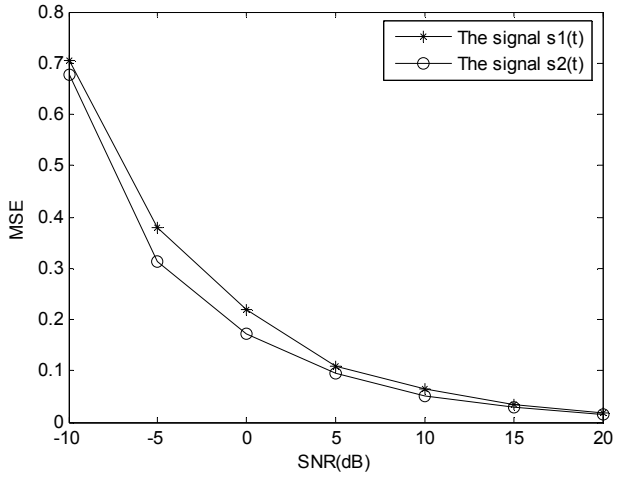

Figure 1. The MSE's of the LCT domain DOA estimation algorithm

Acknowledgment

This work is supported by The Natural Science Foundations of The Education Department Henan Province of China (No.14B510031 and No.2011A510017), the support is gratefully acknowledged.

References

[1] A. J. Barabell. Improving the resolution performance of eigenstructure-based direction-finding algorithms, InProc.ICASSP'83, Boston, MA, May 1983. 336-339.

[2] J. Li and R. T. Compton. Maximum Likelihood Angle Estimation for Signals with Known Waveforms, IEEE Trans. On Signal Processing, Sept.1993, 41(9):2850-2861.

[3] A. Belouchrani and M. Amin. Time-frequency MUSIC, IEEE Signal Processing Letter, 1999, 6 (5): 109-110.

[4] G. Wang and X. G. Xia. Iterative algorithm for direction of arrival estimation with wideband chirp signals, IEE Proc. Radar, Sonar, Navig, 2000, 147(5): 233-238.

[5] Alex B. Gershman and Moeness G. Amin. Wideband Direction-of-Arrival Estimation of Multiple Chirp Signals Using Spatial Time-Frequency Distributions, IEEE Signal Processing Letters, June 2000, 7(6): 152-155.

[6] Yanhong Zhang, Lin Qi, Xiaomin Mu, and Shouyi Yang. 2-D DOA Estimation of Wideband LFM Signal in Fractional Fourier Domain, IEEE International Conference on Innovative Computing ,Information and Control, Beijing, August 2006, 3:6-9.

[7] V. V. Reddy, B. P. Ng, and A. W. Khong, "Derivative-constrained frequency-domain wideband DOA estimation," Multidim. Systems and Signal Process., 2012: 1-23.

[8] Deng Bing, Tao Ran. Linear Canonical Transform and Its Implication, ACTA ArmamentarII, 2006,27 (4): 665-670.

[9] Xiang Qiang, Qin Kaiyu and Zhang Chuanwu. Linear canonical transform and time-frequency filtering, Journal of Electronic Measurement and Instrument, 2009, 23 (4): 69-73.

[10] K. K. Sharma. Vector Sampling Expansions and Linear Canonical Transform, IEEE Signal Processing Letters, 2011, 18 (10): 583-586.

[11] Yanhong Zhang, Heng Zhao and Huihui Li. An algorithm of the LMS Adaptive Filtering in Linear Canonical Transform Domain,Applied Mechanics and Materials, 2013, 385-386: 1407-1410.

Advanced Materials Research Vols. 989-994 (2014) pp 1977-1980
© (2014) Trans Tech Publications, Switzerland
doi:10.4028/www.scientific.net/AMR.989-994.1977

Computerized Simulation of Board-Level EMC in High-Speed PCB

Xianzhe WU[1, a], Cheng ZHANG[, b], Shuangfei YANG[1, c], Lianqing ZHAO[1, d]

[1]North China Electric Power University, Beijing, 102206, China

[a] email: wuxianzhe126@163.com,
[b]email:zcfz2011@126.com,[c]email:yangshuangfei1991@126.com, [d]email:zhaolianqing@163.com

Keywords： High-speed PCB; Board-level EMC; Three-line Coupling Model; Via Holes

Abstract: Aim at the multi-faceted nature and universality of the EMC problems in high-speed PCB, based on a three-line coupling model and considering the influence of via holes caused, board-level EMC problems of PCB were researched on point for point. In this paper, the research and simulation were launched by a kind of software named Hyperlynx, and a 6-layer PCB model was built and used. Our Research was focused on the EMC problems existed in hierarchy and layer medium. On the basis of the simulation results, and combined with previous experience in the PCB design, some effective measures for improving EMC in high-speed PCB design were summarized, which could be taken as a clearly reference in design of high-speed PCB.

0. Introduction

High-Speed PCB (High - Speed Printed Circuit Board) usually refers to these Printed Circuit Boards of which the clock frequency more than 50 MHZ. The so-called EMC (Electromagnetic Compatibility), refers to the equipment or system can work properly in the electromagnetic environment, and the ability that doesn't cause the unsustainable electromagnetic disturbance to anything in the environment.[1]The design and using process in High-speed PCB will inevitably meet EMC problems, especially along with the rapid development of electronic products, previous design experience was often difficult to cope with the changing of the EMC requirements.[2] Therefore, this paper uses the simulation software named Hyperlynx for EMC research in the high-speed PCB, concluded scientific and effective improved design techniques and measures for board-level EMC.

1. Building of board-level EMC model

In high speed PCB layout, factors directly related to board level EMC involves dielectric thickness between boards, distance and isolation performance of signal layers, VCC layer's influence on signal layer, via hole, etc. The theoretical basis for simulation and analysis of board level EMC: [3]

$$i=\mathbf{C}\frac{\mathbf{du}}{\mathbf{dt}} \quad (1)$$

$$u=\mathbf{L}\frac{\mathbf{di}}{\mathbf{dt}} \quad (2)$$

Therefore, this paper study board level EMI degree by observing the simulation result of far end and near end voltage signal. The via hole's EMC analysis study the discrepancy in electromagnetic interference from different aperture D and depth H, and its theoretical basis is: [4]

$$C=\frac{1.41\varepsilon TD1}{(DZ-D1)} \quad (3)$$

$$L=5.08h[ln(4h/d)+1] \quad (4)$$

In the type: C is parasitic capacitance to GND; ε is relative dielectric constant of PCB;D1 is pad diameter surrounding via hole; D2 is mesopore diameter in GND layer; T is thickness of PCB board; L is inductance of via hole; d is diameter of via hole; h is length of via hole.

Board level EMC model is showed in Figure1(a).PCB board has 6 layers which VCC layer and GND layer are placed at each side of signal layers to study the VCC layer 's interference degree in

signal layers. The reason for making two signal layers adjoining is that compare the difference of interference in adjoining layers and separated layers. Wiring in layer is coupled three-line model, showed in Figure1 (b).Two sides [5] are offensive wire and victim wire is in the middle. This model simulates the electromagnetic interference in board more veritably [6], showing great research value. Equivalent circuit of via hole is showed in Figure1(c)[7], which is according with Formula 3 and Formula 4. It reflects parameter of via hole well.

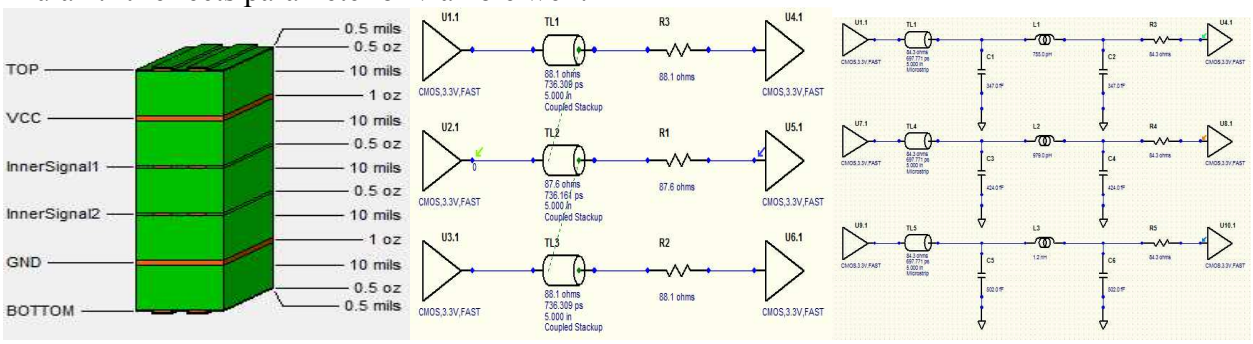

(a)Layer structure model (b) Coupled three-line model (c) Via simulation model

Fig.1. The simulated models

2. Simulation and analysis of board level EMC

This paper uses Hyperlynx8.2.1 to simulate and analyze board level EMC. Hyperlynx, developed by Mentor Graphics, is a kind of high-speed PCB simulation software. It can design and simulate EMC and SI of PCB board at different frequency. By means of changing parameters to simulate the above three models, the analysis of board level EMC has been achieved.

Via is PTH (Plating Through Hole) or named via hole. In high speed multilayer PCB, via is used to connect printed conductors in different layer or fix components. There are three types of via generally: buried via, through via and blind via. Through via is in common use because of its simple processing. This paper mainly analyze the through via diameter d and through via depth h to study via EMC.

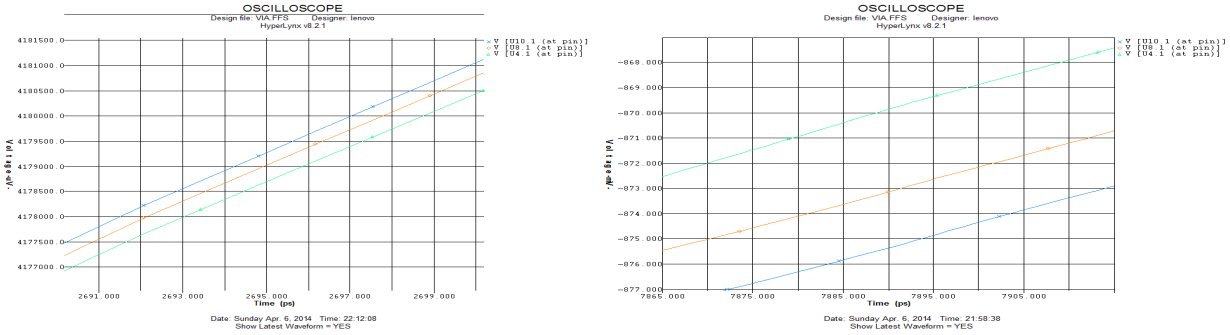

(a)Different via diameters (b) Different via depths

Fig.2. The results of vias' EMC simulation

Figure2 (a) shows electromagnetic disturbances with different via diameters, which are 10mil, 15mil and 20mil from top to bottom. Thus, the smaller diameter it is, the greater disturbance.

Figure2 (b) shows there are diverse disturbances with different via depths. The depths are 65mil, 55mil and 45mil from top to bottom. By comparison, the hole is longer, the disturbance of signal is greater.

Lamellar layer model analysis is based on three-line coupling model, to compare electromagnetic interference among different layers. Mainly for the thickness of the dielectric between the plates of electromagnetic interference, differences electromagnetic interference caused by signals of different spacing of adjacent layers, differences between adjacent signal layers and separated layers, and effects of the power supply layer and the signal spacing layer.

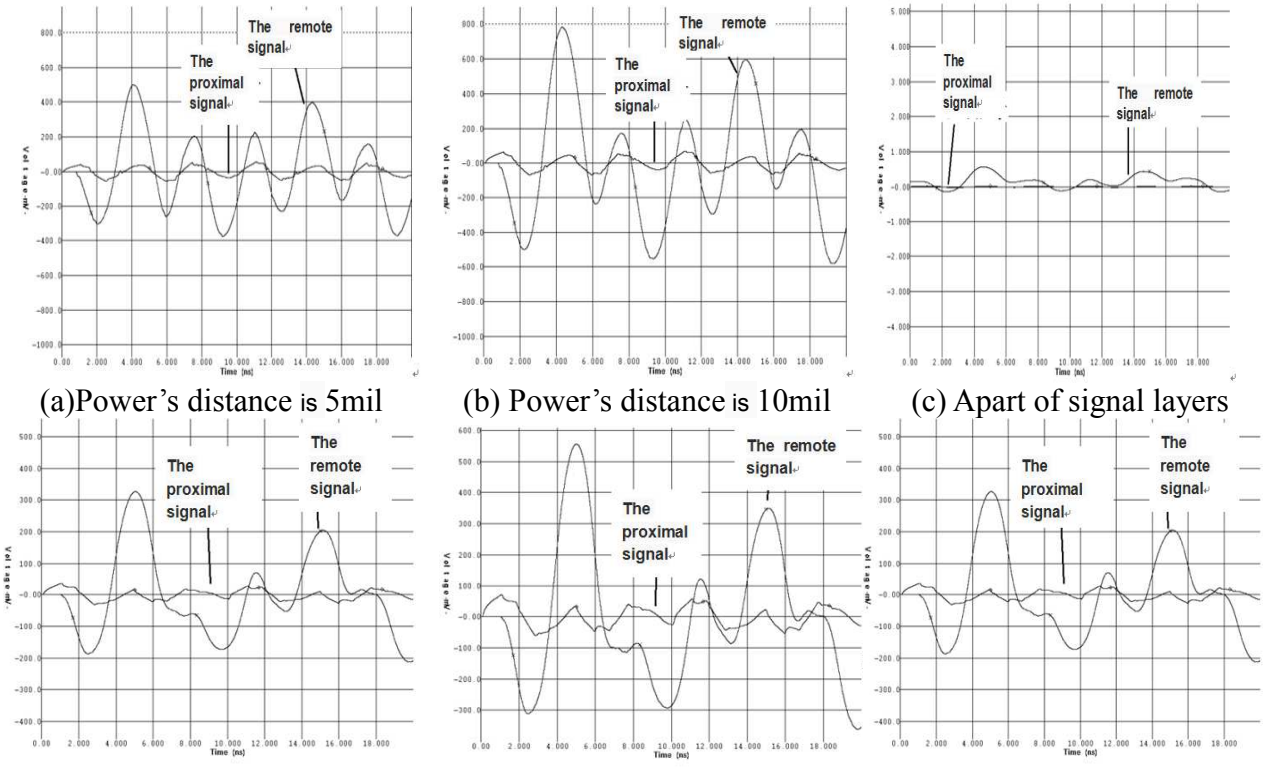

(a)Power's distance is 5mil (b) Power's distance is 10mil (c) Apart of signal layers

(d) Adjacent signal layers (e) Layers' interval is 5mil (f) Layers' interval is 10mil

Fig.3. The results of layers' EMC simulation

This article assumes that the power level of the signal layer significantly interfere with signal transmission, therefore, to observe its effects by adjusting the layer spacing. The simulation results are shown in Figure3 (a), Figure3 (b). Comparison shows that there is little difference between near-end signals although the distance between the plates is not the same. We can see that signal interference is slightly larger when they apart from 10mil.Remote signal interference significantly different. When the power supply layer and the signal layer separate from 5mil, remote disturbance signal's maximum value of peak to peak is V5p-p=812.61mv, but when the power supply layer and the signal layer separate from 10mil, remote disturbance signal's maximum value of peak to peak is V10p-p=1270.60mv. It can be seen that the closer signal layers to the power supply layer, the smaller electromagnetic interference.

Assuming adjacent signal layers are InnerSignal1 and InnerSignal2, separated layers are Top and InnerSignal1.From Figure3 (c) and Figure3 (d) we can see, when the signal layers separated, there is almost no near-end signal disturbance, the maximum value of peak to peak of remote disturbance signals is less than 1mv. When comes to adjacent signal layers, the maximum value of peak to peak of near-end signals is Vnearp-p=55.24mv, the maximum value of peak to peak of remote disturbance signals is Vremotep-p=513.69mv. We can conclude that adjacent signal layers' interference is larger when signals transmitted simultaneously, so signal layer should be clothed in a position apart when clothing boards.

This paper makes the spacing reference value between adjacent signal layers 10mil, using the spacing of 20mil signal disturbance simulation to contrast with it. From Figure3 (e) and Figure3 (f).we can see that when the distance of adjacent signal layers is 10mil, the maximum value of peak to peak of near-end signals is V10p-p=124.08mv, the maximum value of peak to peak of remote disturbance signals is V20p-p=862.60mv. When the distance of adjacent signal layers is 10mil, the maximum value of peak to peak of near-end signals is V10p-p' =60.49mv, the maximum value of peak to peak of remote disturbance signals is V20p-p'=508.74mv. We can conclude that the smaller the spacing between adjacent signal layers, the greater the intensity of the signal interference between each other.

3. EMC improved measures in high-speed PCB

According to the above results, together with previous experience in high-speed PCB design and material, conclusions can be drawn as follows:

(1). Minimize non-essential vias when designing PCB

(2). Appropriate to increase the power and ground connection vias to minimize impedance, and minimize the diameter of the vias if lower cost and crafts are allowed.

(3). Reduce the length of the vias In the design of the acceptable range, maximize the use of micro-holes and Back-Drilling Technology[8], and try to weaken the implications of the hole on the EMC

(4). Possible to reduce the thickness between the signal layer and power layer, a ground layer of the dielectric layer when doing stack design, in order to reduce the magnitude of crosstalk noise[9]

(5). Try to avoid signal layer adjacent when designing the hierarchy of PCB, if it cannot be avoided, we should also increase the distance between two adjacent signal layers to reduce signal interference between each other.

4. Conclusion

In view of a series of EMC problems in the design, testing, using process of high-speed PCB, on the basis of the relevant theoretical research, the lamellar model, the three-wire coupling model and the vias model were built and simulated by Hyperlynx in this paper, coherent analysis of the factors which mainly affect board-level EMC was made, to give the corresponding effective measures to improve board-level EMC of PCB. The results provided effective guidance on Multilayer design, wiring and layout design and anti-interference research.

References

[1] Section 1.7 of GB/T 4365-1995

[2] Junfa Mao, Jianjie Li ,Min Tang et al. Performance Enhancement Research for Printed Circuit Board Manufacture in China[C].//2011 IEEE MTT-S International Microwave Symposium Digest.

[3] Songping Wu , Jun Fan. Analytical Prediction of Crosstalk Among Vias in Multilayer Printed Circuit Boards[J].IEEE Transactions on Electromagnetic Compatibility,2012

[4] Er-Ping Li, Xing-Chang Wei, Andreas C. Cangellaris et al. Progress Review of Electromagnetic Compatibility Analysis Technologies for Packages, Printed Circuit Boards, and Novel Interconnects[J].IEEE Transactions on Electromagnetic Compatibility,2010

[5] Simplified Interference Coupling Model For Two Orthogonal Striplines On Adjacent Layers[J].IEICE Transactions on communications,2008.

[6] Bruce Archambeault , Colin Brench , Sam Connor et al. Review of Printed-Circuit-Board Level EMI/EMC Issues and Tools[J].IEEE Transactions on Electromagnetic Compatibility,2010

[7] ZHAO Lian-qing, LIU Er-li. Effects of PCB Vias on High-Speed Signal Transmission[J]. PRINTED CIRCUIT INFORMATION,2009,(9)

[8] Junwoo Lee, Mihai Dragos Rotaru, Mahadevan K. Iyer et al. Analysis and Suppression of SSN Noise Coupling Between Power/Ground Plane Cavities Through Cutouts in Multilayer Packages and PCBs[J].IEEE Transactions on Advanced Packaging,2005

[9] YANG Hua CHEN Shaochang ZHU Fengbo. Crosstalk Simulation of PCB in High Speed Digital Circuit[J]. Electronics Optics & Control,2012

Advanced Materials Research Vols. 989-994 (2014) pp 1981-1984
© (2014) Trans Tech Publications, Switzerland
doi:10.4028/www.scientific.net/AMR.989-994.1981

On Application of Texture Mapping Technology in Simulation

Wei Zhang [1, a], Chunhua Zhang [1, b], Yan Zhang [1, c]

[1]Aviation University of Air Force, Changchun, Jilin, 130022, China

[a]zw2005@gmail.com, [b]zch-cc@163.com, [c]zy_2403@163.com

Keywords: texel; pixel; texture mapping; Creator.

Abstract: In the visualized simulation, the application of texture mapping technology can significantly improve image fidelity and superimpose the rich texture details to the surface, making the scene more realistic with real-time and fast invocation. This paper introduced the principle of texture mapping, the mapping process and implementation in software, and described in detail the implementation process of multi-layered texture mapping by example.

Introduction

There are usually surface details or texture on the surfaces of three-dimensional objects in the real world. The texture can be divided into color texture and geometric texture. Wherein, color texture can show the surface details through the changes of color or brightness while geometric texture refers to the microscopic geometry of the object surface. However, this will add to the amount of calculation of the imaging system. Therefore, texture mapping technology is usually applied to achieve this goal. Texture mapping technology is of the fastest growing 3d technology in recent years, it has become the most recognized can measure 3d image quality technical standards, all graphics standard provides support for texture mapping[1-4].

Texture mapping principle

The nature of texture mapping is to deal with 3D objects by two-dimensional parameters, which is to determine two-dimensional parameter values of any point on the surface of a three-dimensional object, then get the texture value at that point, and finally create the texture image of the 3D image surface. Texture mapping is mainly to identify the mapping relationship and deal with the anti-aliasing of texture so that the highly realistic effect of image can be realized with less time and space. The core problem during adding texture pattern to the smooth surface is mapping, therefore, texture mapping can be simplified as the transformation from one coordinate system to another one. Wherein, there are at least two mapping: first, mapping from texture space to scene space, sometimes called curved surface parameterization; second, mapping from scene space to image (screen) space, namely the viewing transformation. These two kinds of transformation are usually integrated as one.

If the texture pattern is defined within an orthogonal coordinate system (u, v) in the texture space, and the curved space is defined within the orthogonal coordinate system (x, y, z) in the scene space, which is represented as x (θ, φ), y (θ, φ), z (θ, φ) in the parameter space (θ, φ). Then, the addition of texture to the curved surface will relate to the determination of a mapping function between two curved surfaces. For example, the mapping from the texture space to parameter space is:

$$\theta = f(u, v), \varphi = g(u, v) \tag{1}$$

and the reverse mapping from the parameter space to texture space is:

$$u = r(\theta, \varphi), v = s(\theta, \varphi) \tag{2}$$

The texture space is a coordinate space that takes u, v as the horizontal and vertical axis respectively. In the coordinate space, the coordinate values of the upper-right corner of the texture image are (0, 0) and (1, 1) respectively. The minimum unit of the texture image in texture space is texel as shown in Fig. 1 (a). And the smallest unit in the terminal display screen coordinate space is pixel as shown in Fig. 1 (b). The two-dimensional texture image will finally be mapped to the

three-dimensional surface model and the actual size of the texel is determined by the resolution and scaling of the texture mapping process in the two-dimensional texture image as shown in Fig 1 (c).

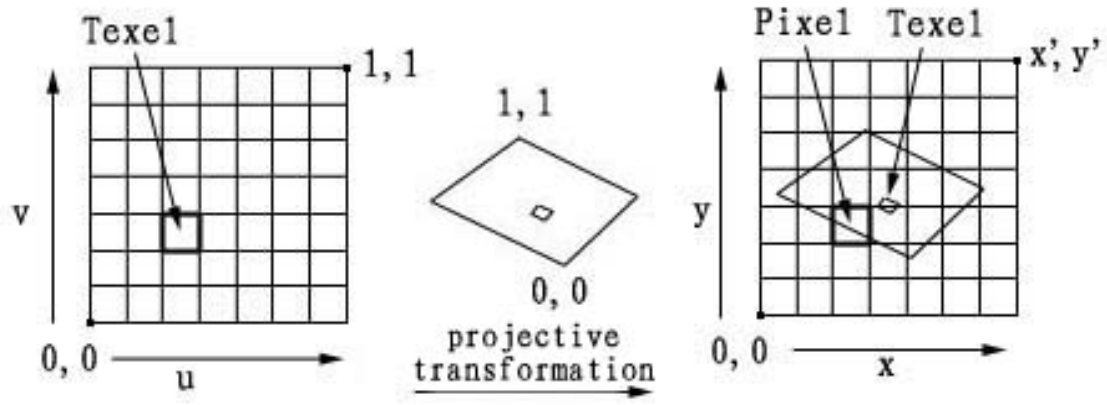

(a) The texture space coordinates (b) Screen space coordinate system

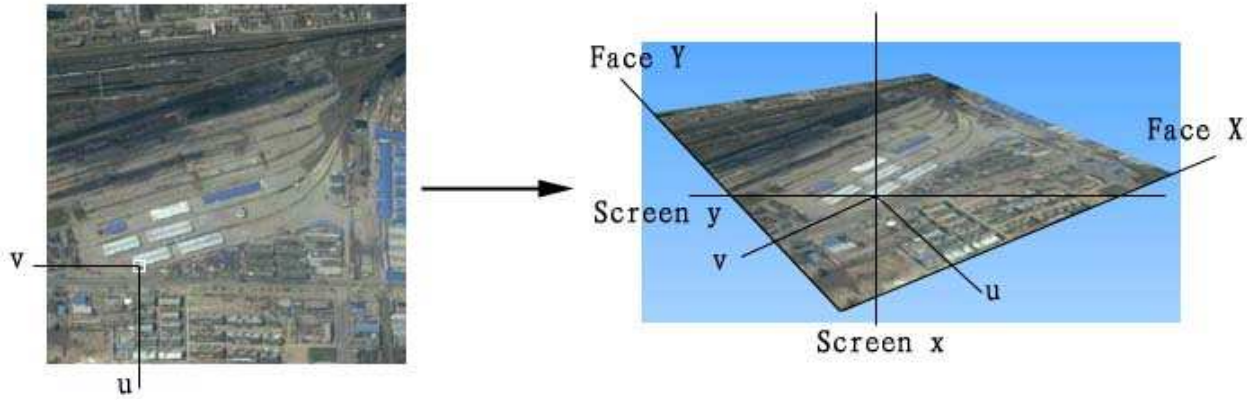

(c) The texel displayed on the screen space coordinate system

Fig.1 Schematic Texture Mapping

As the viewpoint in the simulation process will be changing, the size of model object after mapping to the screen space will also be changing. There will be three different scenes of the texture mapped on the model object surface in the actual process of rendering: first, one texture image texel properly corresponds to one pixel on the screen which is an ideal situation that the texture image is a full-size mapping; second, multi-texture image texels are mapped to a same screen pixel; third, one texture image texel is mapped to several screen pixels. For the second situation, the minification filter is conducted to the texture image. For the third situation, the magnification filter is needed to deal with the texture image. When the viewpoint position changes, through corresponding filter, the texture images can be softened, sharpened or fused so as to obtain better rendering effects.

Texture mapping Process and Implementation

Texture Mapping Process. Texture images that are read are generally two-dimensional. The texture coordinates are used to define the mapping from image to geometry. The u, v coordinates of the texture are mapped to screen space coordinates and the colors of texture, the polygon and the material are fused. Then the appropriate texture processing, such as the nearest neighborhood filtering, bilinear interpolation and Mipmap is carried out. The nearest neighborhood filtering is to choose the nearest texel for each pixel while the bilinear interpolation is to interpolate with the nearest four texels for anti-aliasing and optimization effect which is better than the method of nearest neighborhood filtering. The optimal treatment is Mipmap, which can pre-process the texture and construct the data structure of fast approaching calculation for multi-texel covering single pixel.

From the Angle of storage structure of the texture, texture is actually a storage array of two-dimensional image color information, and grain element is composed of color channel. Store one

color channel need eight bits, which is a size bytes . According to different color channel number and the way of compression, the texture image can be stored for a variety of formats, Creator can support a variety of universal standard image formats, main formats including: contains only one gray channel INT, contains a grayscale channels and a transparency of INTA, including red, green and blue three color RGB channels; Include red, green and blue three color channels and a transparency RGBA; As well as TGA, JPEG, TIF, GIF, BMP format. In addition, the Creator also supports CT (clip texture) and other advanced special format textures. Some format of the texture while in the Creator can normal use, but can not be displayed correctly in the real-time system.

Before the real-time system should map the texture used by the model database, the corresponding texture image should be uploaded in the texture memory in advance.

The necessary texture memory = the texel size in X direction × the texel size in Y direction × the number of color channels

Texture memory is designed for loading and storing texture image memory space, most of the real-time system has a dedicated texture memory, and some real-time system directly to the texture image loaded into the system memory. In order to more effectively utilize the texture memory and the system can ensure real-time texture mapping is done correctly, the two directions in the texture image size must be a power of two sizes, such as 16 × 16,8 × 32,64 × 16,128 × 256, etc., the length and width may not be the same. If the texture does not meet this requirement using the image, then before mapping textures, real-time system will automatically adjust the texture image to the nearest power of a larger two forms, although this does not affect the final texture mapping results, but will reduce the efficiency of the texture memory.

The memory capacity of the real-time system texture is limited, so the size of the texture image used in the process of creating model database must be moderate. If the size is too small, the visual effect may be influenced and if it is too big, the texture memory space will be wasted.

The Realization of Texture Mapping in Software. Creator is a professional 3D modeling software developed by Multigen-Paradigm. It can be used to complete the three-dimensional model simulation system[5]. First, Creator is run, then the needed texture images are transferred to the texture palette and the current texture is specified. Then, the target surface is chosen and the current texture is mapped to the polygon with the texture mapping tool in the texture toolbox or the setting texture tool in the property toolbox. Creator can also provide texture mapping palette to store and reuse the texture mapping information. After the texture image fodders are uploaded into the texture palette in the model database, the above tools can be used to map the texture images to the surface of the polygon and preview the real-time texture mapping effects.

Must first be transferred to the desired texture image texture palette, specify the current texture, and then select the target surface, using texture mapping tool in the toolbox or properties set the texture tool in the toolbox to the current texture mapped onto polygons. After the image is loaded into the model texture palette, users can use a texture toolbox or properties of various tools in the toolbox, the texture image is mapped onto the polygonal surface model of the object. Enabling view panel displays in texture button, you can preview the effect of texture mapping model objects in a graphical view. For a model of texture images containing transparent channel must be enabled in order to view panel transparency blending function correctly displayed in the graphical view of the transparent texture mapping.

The texture mapping of Creator can be divided into the following categories: Put Texture can determine texture mapping by setting the selected three points on the plane and can modify the number of affixed textures to change the elaboration and change the shape of the textures to realize special effects; 4 Point Put Texture can determine the basic differences between texture mapping, function and three-point plane mapping; Surface Project Texture conducts texture mapping to the selected object or plane according to plane and the elaboration of the texture can be adjusted directly; Spherical Project Texture conducts texture mapping from the symmetrical center of the object top and bottom surfaces; Radial Project Texture conducts texture mapping radially from the object top surface center; Geo-Put Texture changes texture shapes according to the ground surface situation so as to

perfectly integrate the texture and ground; Environment Map Texture shows the scenes around the object by a pattern and maps to the curved surface that encloses the object, without affixing patterns or specular reflective texture. The texture changes as the direction and perspective of the object change. Different methods of texture mapping correspond to different geometrical models and the specific situations should be determined by the specific shapes of the models.

In Creator, in addition to these above single texture mapping methods, multi-level texture mapping may also be used to represent the complex local details of the model object without adding any extra polygon. Multi-level texture mapping is highly efficient with high distinction. With examples below, we will describe its realization. To simulate the mottled marks on the walls and vegetation, we only need to map three levels of different textures on the wall polygon and then we can realize the necessary effects as shown by Fig 2. In Creator, these three different levels of textures are read into the texture panel. In the view panel, we select the texture layer of Layer0, Layer1, Layer2 and the wall geometrical polygon surface. Then Put Texture is applied for texture mapping. Layer0 adopts the wall brick pattern (Fig. 2(a)); Layer1 uses the mottled marks texture (Fig. 2(b)), and Layer2 adopts vegetation texture (Fig. 2(c)). The Texture option in the view panel is modified to Blend so that the wall simulation effects of three-level texture mapping can be observed in real time (Fig. 2(d)).

(a)wall brick texture (b) mottled marks texture (c) vegetation texture (d) three-level texture mapping simulation wall

Fig. 2 Multi-level texture mapping

Conclusions

The texture mapping technology is an important part of photorealistic, and its application can guarantee the representing of rich details of three-dimensional objects with fewer polygons, which both meets the real-time need and better realizes the sense of object reality. In practical application, the multi-level texture mapping can better show the advantages of model surface details description. The technology will definitely be widely applied to the visualized simulation system.

References

[1] Yuanyan, Chen, Practical Technology of Computer Graphics. Tsinghua University Press, 2007.
[2] Xiaomei, Meng, Course of Multi-Gen Creator. National Defense Industry Press, 2005.
[3] Yaning, Fu, Course of Computer graphics. National Defense Industry Press, 2009.
[4] XUE Bing，WANG Li-li，SHEN Zhe. Grid-segmentation-based textured model simplification [J]. Journal of Computer-Aided Design & Computer Graphics，2010，22（12）
[5] Multigen-Paradigm Inc．Creating Models for Simulations．Version 3．2 for Windows and IRIX [M]．Dallas：Muhigen- Paradigm Inc，April 2003.

Advanced Materials Research Vols. 989-994 (2014) pp 1985-1988
© (2014) Trans Tech Publications, Switzerland
doi:10.4028/www.scientific.net/AMR.989-994.1985

The Discussion on The Improved Association Rules Algorithm in Data Mining

Wen Tao, Sun Li, Zhu Li
Jiangxi Science & Technology Normal University Nanchang, China
191200933@qq.com

Keywords: association rules; data mining; algorithm improvement

Abstract: The data mining can help to extract the information and knowledge with potential application value from a huge amount of data. In order to do the date mining scientifically and efficiently, this article provides an improved algorithm based on the classical association rules Aprior algorithm, taking advantage of which, we can engage in the association rules mining of the database to obtain the useful information. The improved algorithm avoids pattern matching and reduces the number of times of visiting the database, thus improves the speed of date mining to some extend.

Ⅰ. INTRODUCTION

The data mining is based on the knowledge finding in the database. This is the process of exacting the potentially useful information from the database and by digging out the underlying information, offering the knowledge and rules with value to the decision maker. The association rule is like the rule below:" Among the young customers who bought the beer and cigarette, there are 60% buying the baby diapers" (beer+butter+baby diapers). The main object of association rule mining is the transactional database. In the aspect of sales data application, a transaction usually includes the customer id NO., the purchase items, the time spend, etc.

Ⅱ. THE METHOD OF ASSOCIATION RULES MINING

A. The general steps of association rules mining

Find out the preliminary data related to the task. Deal with the specific problem properly and form the normalized database. Generate the frequent item set. Retrieve the frequent item set from the normalized database, namely the rules with the support no less than the minimum support set by the user. Output the visualization rules. Find out the rules that meet the requirement of the minimum support set by the user from the frequent item set and then conduct the visualized output of the rule set.

B. The description of the association rules.

Definition 1. If the item set Y has the number of m items, we call the length or the size of Y m. Then the item set Y can be described as m item set.

Definition 2. If the support of the item set Y is more than the minimum support, then we call the item set $Y \in I$ the frequent item set.

Ⅲ. THE PROBLEMS IN APRIORI ALGORITHM

A. Apriori algorithm

The frequent item set method of the Apriori algorithm has become the efficient tool to dig out the association rules in large database. By the way of iterative method, this algorithm generates the smaller frequent item set L[m] which then generates the bigger candidate frequent set C[m+1]. Then by searching the transactional database, the algorithm determines which candidate item set is frequent or not. This cyclic process continues until it can not generate the candidate set.

Algorithm: Apriori

Input (1). The format of the transactional database D is (TID,Item_set), TID is the transaction identifier, Item_set is the item set corresponding to the transaction. (2) The user's minimum support: min_sup.

Output: the whole frequent item set

```
begin
  L1={frequent 1-item_set}
    for(i=2;Li-1<>Φ;i+ +){
        Ci=apriori_gen(Li-1)
        for all transaction j∈D do{
          Cj=subset(Ci,t)
            for all Candidate   c∈Ci do   c.count++}
        Li-1={c∈Ci   c.count>=min_sup}
}
    answer=YiLi-1
end.
```

Apriori_gen is the function generated from the candidate item set with the frequent item set as the independent variable. This function returns the superset of all frequent item set m.

TID	Item_set
11	ACD
12	BCD
12	ABCD
14	BE

Fig.1 The transactional database D

B. The defects of the Apriori algorithm

Large redundancy. For example, assume the association rule that "cake" can derive ("milk","fruit") [confidence=76%]. It means 76% of the people who buy the cake will buy milk and fruit. However according to the Apriori algorithm, it will generate several association rules below:"cake" derives "milk" [confidence=83%]. It means 83% of the people who buy the cake will buy milk. "Cake" derives "fruit" [confidence=87%]. It means 87%of the people who buy the cake will buy fruit. {"Cake", "milk"} derives "fruit" [confidence=80%]. It means 80% of the people who buy the cake and milk at the same time will buy fruit. {"Cake", "fruit"} derives "milk" [confidence=89%]. It means 89% of the people who buy the cake and fruit at the same time will buy milk. There are some differences in the meaning in these association rules. However the association rule that "cake" derives {"milk" "fruit"} actually includes the four rules above, which means in another way that the association rule of "cake" deriving {"milk", "fruit"} can automatically derive the four association rules above.

It is easy to generate worthless rules or even the incorrect results. Take the 5000 high school students' activities of doing morning exercise for example. The investigation shows that 1500 students attend the activity of "playing basketball", 4500 students attend the activity of "running", and 1000 students attend the activity of both "playing basketball" and "running". If we assume that min_sup=15%，min_conf=60%, according to the Apriori algorithm, we can get the association rule: "playing basketball" derives "running" [support=15%，confidence=75%].

It means that if there are 75% of the students attending the activity of "playing basketball", they will attend the activity of "running" too. It is totally reasonable to reach this conclusion from the

derivation, but this rule is actually misunderstanding for the reason that the proportion of the students who attend the activity of “running” in the total students is as high as 90%, which means it is sure that 90% of the students will attend the activity of “running”. However the proportion of 90% outstrips the minimum confidence of 60% and also exceeds the rule confidence of 75%. Thus the information conveyed by the rule is worthless.

Ⅳ. THE IMPROVED ASSOCIATION RULE MINING ALGORITHM

A. The thinking for the improvement.

In the view of the above problems, we improve the algorithm accordingly. On one hand, we adjust the data structure. Namely we change the currently common used flat data structure into the data structure where the item vertically corresponds to the transaction. This vertical data structure is composed of the item set and the transaction table which contain the set of item. Change the picture 1 the transaction database D into the picture 2 blow.

A
11
13

B
12
13

C
11
12
13

D
11

E
12
13
14

Fig.2 The expression of the database with the item vertically corresponding to the transaction

Definition 3: Given the item set Y and the transaction database D, the vertical database D’ is {X，M}, and X ∈Y, M={TID1,TID2,…,TIDn}. The transaction TID in D is TIDi(i=1,2,…,n), which contains the item set Y.

This structure solves the problems caused by the flat data structure. The reasons are following: Obtain the frequent item set through database searching. When we identify the candidate item set AB which is consisted of the item set A and item set B whether is the frequent item set or not, we can get the support of the item set AB by calculating the number of the same transactions in the transaction set of item A and item B, which can avoid the pattern matching. Visit the database only once. It is only at the beginning it requires to visit the whole database. When m>1, if we calculate the support of the candidate item set in Cm, it only requires to visit the frequent item set Lm-1 . And with the increasing of m, the frequent item set gradually decreases. In this way the amount of the data that the algorithm needs to visit will shrink.

B. The improved algorithm.

Algorithm: Apriori_new

Input: the format of the transactional database D is (TID, Item_set). TID is the transaction identifier; Item_set is the item set of the transaction; min_sup is the user’s minimum support.

Output: the whole frequent item set.

```
begin
    f_genf1(min_sup)
    m=1
    do
        m++
        f_genf(m-1,min_sup)
        move record from D' where item_num=m-1
    loop while |Lm| >1
end
```

F_genf1 is the function used to generate a frequent item set. Firstly the function converts the transactional database D into the database with item corresponding to the transaction. Then query the converted database in order to get the support of all the items. Add the items that meet the criteria into the frequent item set and delete all the information of the item that do not meet the criteria from the converted database.

By the way of giving the same segment number to the frequent item set with the same prefix, we can get a certain frequent item set. Select the frequent item set and pick up items with the same segment number to form the candidate set and in this way, it can speed up the generation of the candidate set. Initially set the segment number of the frequent item set as 0, which means any two items can form a candidate item set with the length of 2. As for the item set with the same segment number, select the most front items to form a set firstly. Then set segment number of the candidate item set which is formed by the set mentioned before same. When the former item of the candidate item set changes, the segment number adds one. At the time of realizing this algorithm, calculate the frequency of the candidate item set as soon as it is generated. In this way, it can reduce the memory usage and increase the efficiency of the Algorithm.

Ⅴ. CONCLUSION

Based on the deep research of the characteristic of the association rules, this article finds that the association rules have the defects of large redundancy and tend to generate the rules in which the user is not interesting. In the light of the existing problems of the Apriori Algorithm, this article puts forward with the Aprior_new Algorithm. In the process of examining the database, we assume that every transaction contains four items and every item has 50 initial numbers. The tuple number of transaction in database examining starts from 400 and then taking the amplification method successively increases to 1500. The minimum support is set to 4% and the confidence is set to 55%. It is proved that the Apriori_new Algorithm is much more efficient than Apriori Algorithm. Apriori_new Algorithm also is tested in the environment of windows by the means of Delphi 2010. The run results prove that the improved Apriori_new Algorithm is correct and efficient.

REFERENCE

[1]Jiang Bing, The application of data mining technology in customer relationship management, Journal of Yun Nan University (Natural Science), vol.28(2006).

[2] Anand Rajaraman, Jeffrey David Ullman, Mining of Massive Datasets, People's post and telecommunication press, Beijing,NY(2012). in press.

[3] Zeng Ling, Xiong Caiquan and Hu Tian, The research of association rules in spatial data mining , Computer and digital engineering, vol.33(2005).

[4] Zhou Yanshan, The research and application of the association rules in data mining, vol.3(2005).

[5] Yao Zhiyong. The business case of SAS programming and data mining, Mechanical Industry Press, NY(2010). in press.

[6]Peng Yipu, Xiong Yongjun, Optimization study on Apnd Algorithm of association rules mining, Computer engineering, vol.32(2006).

[7] Li Xueming, Zhangwei and Peng Jun, An algorithm for generating association rules, Computer Science, vol.28(2001), P. 61-63.

Advanced Materials Research Vols. 989-994 (2014) pp 1989-1992
© (2014) Trans Tech Publications, Switzerland
doi:10.4028/www.scientific.net/AMR.989-994.1989

An information classification optimization model based on improved ant colony algorithm

HAO Chun-mei[1]

[1]Department of Computer Science, Harbin Finance University, Harbin Heilongjiang 150030, China

[a]may_hao@126.com

Keywords: improved ant colony algorithm ; data management ; Information Classification

Abstract. In the information management process, it is necessary to classify all information optimization to provide the support for quickly query the search target providing this, a classification optimization method based on improved ant colony algorithm is proposed in this paper. That is, extract the characteristics of information attribute, and then establish the optimization classification model based on the characteristics to achieve the classification of information. Experimental results show that using the improved algorithm for classification information, the classification accuracy can be improved to meet the actual demand data management.

Introduction

With the continuous development and popularization of computer vision technology, computer data management technology has been gradually applied to different areas, played a huge role[1]. Faced with a flood of information, how to select the information that users need has become the focus of information management issues that need to be studied[2]. Thus, the method to classify a massive information become an important subject in computer field[3].At this stage, the main methods for massive information include the massive information classification method based on K-means clustering and the massive information classification method based on Gaussian model. Among them, the most commonly used method is the massive information classification method based on Gaussian model. Considering the fact that the methods for massive information classification have a vast space of development, therefore, it attracts attention of many experts and has a board development potential.

Related principles of Information classification optimization methods

A. Extract attributes characteristics of information

Let $a=(a_1,a_2,\cdots,a_r)^T$ be the set that contains all the attribute characteristics, $U_a=H[aa^T]$ be the matrix that stands for all the information attribute characteristics, the set contains the difference of above information attribute characteristics is $F_a=H[(a-\overline{a})(a-\overline{a})^T]$. Using the following formula to calculate all information attribute characteristics:

$$b=X^Ta=(x_1,x_2,\cdots,x_r)^Ta=\begin{bmatrix}x_1^T\\x_2^T\\\vdots\\x_q^T\end{bmatrix}a \tag{1}$$

In above formula the value of $b_l=x_l^Ta$, $l=1,2,\cdots,r$, a can be calculated by following formula:

$$a=(X^T)^{-1}b=X_bb=X^Ta=(X^T)^{-1}b=X_b$$

When extracting the attribute characteristics of information, it is necessary to use following formula to calculate the weight:

$$\hat{b} = \sum_{m=1}^{r} cy_m + \sum_{m=r+1}^{s} fy_m \tag{2}$$

The extraction of information can be done by following formula:

$$M = \sum_{l=q+1}^{r} [x_l^T F_a x_l - w_l (x_l^T x_l - 1)] \tag{3}$$

In above formula, w_l stands for the matrix of all information attribute characteristics, x_l stands for eigenvectors of the corresponding information.

The procedure of the improved ant colony algorithm is:

nc←0；

According to the heuristic factor $P_i(t)$, update factor τ_{ij} ,step factor $\Delta\tau_{ij}$ and start the initialized process;

Put the initial position of m ants respectively at the ninformation classification targets.

Record the initial position of the m ants and add into the set of initial positions;

Using the improved ant colony algorithm to transfer the k-th ant based on the transition probability.

After the initial search, record thecrawling length L_k of each ant.

Record the optimal solution among the all the ants.

According to the heuristic factorupdate formula update the heuristic factor.

nc←nc+1;

If nc< λ (scheduled times) then go to step 2);

Out put the final results.

Thus, the ant colony searchbased on the personalized service items can finally complete the establishment of classification optimization model, which improved theaccuracy and effectivenessof information classification.

Simulation and Analysis

In order to verify the effectiveness of the proposedinformation classification method based onimproved ant colony algorithm, it is needed to perform aexperiment.In the experiment, MATLAB can be used to build to simulation environment.

Respectively use the traditional algorithm and the proposed algorithmto performinformation classification optimization process, the obtained results can be shown as following two graphs.

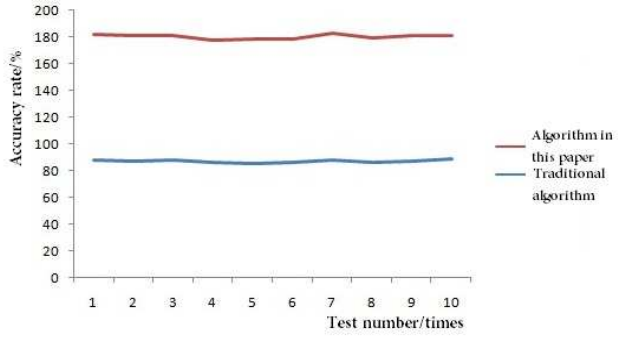

Figure 1. Comparison of accuracy of different algorithms

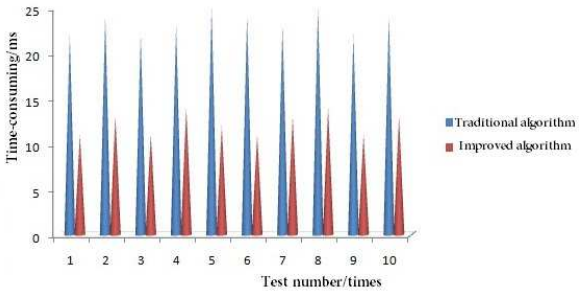

Figure 2. Comparison of time consumption of different algorithms

Summarize the above experimental data, table 1 and table 2 is shown below:

Table 1. The experimental data of traditional algorithm

Times	Accuracy (%)	Time(ms)
1	88	22
2	87	24
3	88	22
4	86	23
5	85	25
6	86	24
7	88	23
8	86	25
9	87	22
10	89	24

Table 2. The experimental data of proposed algorithmby this paper

Times	Accuracy(%)	Time (ms)
1	94	11
2	94	13
3	93	11
4	92	14
5	94	12
6	93	11
7	95	13
8	94	14
9	94	11
10	92	13

Using the proposed algorithm to performinformation classification experiment, the accuracy of classification is higher then the traditional algorithm, besides, the time consumption is also shorter, the advantage of the proposed algorithm can befully demonstrated.

Conclusions

This paper presents a method based on improved ant colony optimization algorithm information classification. Extract the characteristics of information attribute, and then establish the optimization classification model based on the characteristics to achieve the classification of information. Experimental results show that by using the improved algorithm for classification of information accuracy of the classification can be improved,the time consumed on classification can be shorten which means the improvement of efficiency in information classification.Hence, the resultis satisfied.

References

[1] Luciano Alparone, Stefano Baronti. A Global Quality Measurement of Pan-Sharpened Multispectral Imagery [J]. Geoscience and Remote Sensing Letters 2004,10:313-317.

[2] M.Gonzalez-Audicana, JLSaleta, RGCatal, and R.Garcia.Fusion of multispectral and panc hromatic images using improved IHS and PCA mergers based on wavelet decomposition [J]. IEEE Transactions on Geoscience and Remote Sensing. 2004, 1,42 (6) .1291 a 1299.

[3] Tham JY, Shen L, Lee SL, Tan H H. A general approach for analysis and applicatio n of discrete multi-wavelet transforms [J] IEEE Transactions on Signal Processing, 2000, 48(2):. 457 ~ 464.

[4] Intan R. and Mukaidono M. Generalized fuzzy rough sets by conditional probability rela tions [J] International Journal of Pattern Recognition and Artificial Intelligence, 2002, 16 (7)865-881.

[5] Cline D, Egbert P. Terrain decimation through quadtree morphing. IEEE Trans. On Vis ualization and Computer Graphics, 2001,7 (1) :62-69.

[6] BERZAL F, CUBERO J, MARIN N.TBAR:. An efficient method for association rule m ining in relational databases [J] Data anti Knowledge Engineering, 2001,37 (1) :47-64.

Advanced Materials Research Vols. 989-994 (2014) pp 1993-1996
© (2014) Trans Tech Publications, Switzerland
doi:10.4028/www.scientific.net/AMR.989-994.1993

Simulation analysis of a statistical model for herd mentality trend

Pan Shiying

Sichuan college of architectural technology,sichuan,618000

Keywords: herd behavior; herd mentality; herd consumption

Abstract: Herd mentality is a universal, objective social psychological phenomenon in humans describing how people are influenced by their peers to adopt certain behaviors even against their wishes. Herd mentality has a dual nature. This paper analyzes the performance and causes of herd mentality, and makes appropriate adjustment strategy, which has great significance to both the individual and national development.

1 Introduction

Herd mentality is a universal, objective social psychological phenomenon in humans describing how people are influenced by their peers to adopt certain behaviors even against their wishes [1]. Herd mentality has a dual nature, positive factor and negative factor. The positive factor is that it makes individual cognition and behavior complying with community, social norms, is conducive to increase the activities and objectives of efficiency, helps to learn the wisdom of and experience of others, expands horizons, and overcomes opinionated and modify the way of people's thinking. On the other hand, it also has negative factor which refers to inhibit the development of personality, structure thinking, and make people non-assertive and blindly [2]. Herding is a tendency people consciously or unconsciously make their behavior and reactions consistent with others, in objective or psychologically ambiguous situations [3]. Individuals in the population are often unwittingly subjected to groups' pressure, and tend to has same behavior, perception, judgment, and beliefs with most people in the population [4].

With the rapid development of media technology, media, social environment have a broad and profound impact on public ideology, ways of thinking, values, behavior, etc., and also the performance characteristics of public's herd mentality [5]. Under the new historical conditions, studying the phenomenon and characteristics of herd mentality and actively guiding the public have guiding significance for doing social work [6]. Based on previous studies, combined with the characteristics of today's society, the paper presents a comprehensive in-depth analysis of the causes and performance of herd mentality, and gives some appropriate means of regulation.

2 Herd mentality statistical model

Getting some results related to the topic through network, learning some useful information, we use SPSS statistical software to conduct mathematical statistics, and finally get the required data in this article.

We uses Markov chain to describe the evolution of the herding. In order to more easily obtain a balanced distribution, we use a reversible Markov chain with one-step transition probabilities as

$$P_{k,\,k+1}=\frac{N-k}{N}\bullet\left[\varepsilon+\delta\bullet P\left\{\eta\ \rangle\frac{M}{2}\right\}\right] \quad (1)$$

$$P_{k,\,k+1}=\frac{k}{N}\bullet\left[\varepsilon+\delta\bullet P\left\{\xi\ \rangle\frac{M}{2}\right\}\right] \quad (2)$$

$$P_{kk}=1-P_{k,\,k+1}-P_{k,\,k-1} \quad (3)$$

As shown in formula (1) and (2), we add a small probability ε on the herd transition probabilities $\delta\cdot P\{\eta>\frac{M}{2}\}$ and $\delta\cdot P\{\xi>\frac{M}{2}\}$ of two types of people to avoid k=0 and k=N being absorbing wall of Markov chain.

Balanced distribution of the Markov chain is

$$\pi_k = \begin{cases} \pi_0 P_{00} + \pi 1 P_{10} & k = 0 \\ \pi_k P_{kk} + \pi_{k-1} P_{k-1,\ k} + \pi_{k+1} P_{k+1,\ k} & k = 1,\ \ldots,\ N-1 \\ \pi_N P_{NN} + \pi_{N-1} P_{N-1,\ N} & k = N \end{cases} \quad (4)$$

According to Kolmogorov reversible criteria, this Morkov chain is reversible that means a balanced distribution satisfies

$$\pi_i P_{ij} = \pi_j P_{ji},\ \ j = i \pm 1 \quad (5)$$

So we have $\frac{\pi_k}{\pi_{k-1}} = \frac{P_{k-1,\ k}}{P_{k,\ k-1}}$ (6)

Mark $V_k \frac{\pi_k}{\pi_0} = \begin{cases} 1 \\ \prod_{i=1}^{k} \frac{\pi_i}{\pi_{i-1}} \end{cases}$ (7)

$$V_k \frac{\pi_k}{\pi_0} = \begin{cases} 1 & k = 0 \\ \prod_{i=1}^{k} \frac{\pi_i}{\pi_{i-1}} & k \neq 0 \end{cases} \quad (8)$$

We can get $\pi_k = \frac{\pi_k}{\pi_0 + \pi_1 + \ldots + \pi_N} = \frac{\frac{\pi_k}{\pi_0}}{1 + \frac{\pi_1}{\pi_0} + \ldots + \frac{\pi_N}{\pi_0}} = \frac{V_k}{V_0 + V_1 + \ldots + V_N}$ (9)

3. Simulation and Analysis

3.1 The simulation

Taking a secondary school for example, we distribute store posters at the school gate. There are many factors that affect the experimental results: store posters, product category, selling list. Then, observe and analyze changes of herd behavior trends of college students impacted by the sales volume charts.

According to the assumption, we choose supermarket as experimental place.

(1) Product Selection: some kinds of food and drinks

(2)The influence of the best selling products sorting on the real situation: slight change and before and after order is reversed.

Following are the detail information about the experiments.

Choose five kinds of products in the supermarket in male dormitory: Pepsi cola, sausages, instant noodles, peanuts, sliced bread, statistic each day's sales (of three days) and total rankings (the real ranking are Pepsi cola, sausages, instant noodles, peanuts, sliced bread)

According to the total sales of the three-day, we present Sales Rank on posters (make slight changes), and then statistic the Sales in the following three days.

3.2 Experiment results

Table 1 Effect of sales posters

Products	before distributing posters			after distributing posters		
	1st day	2nd day	3rd day	1st day	2nd day	3rd day
sliced bread	2	1	2	13	10	15
peanuts	2	3	2	8	13	10
instant noodles	5	6	6	15	14	22
sausages	1	1	0	7	5	8
Pepsi cola	3	3	2	15	13	18

Note: It can be seen that the Sale ranking has a certain effect on the purchase behaviors, but has difference in different products.

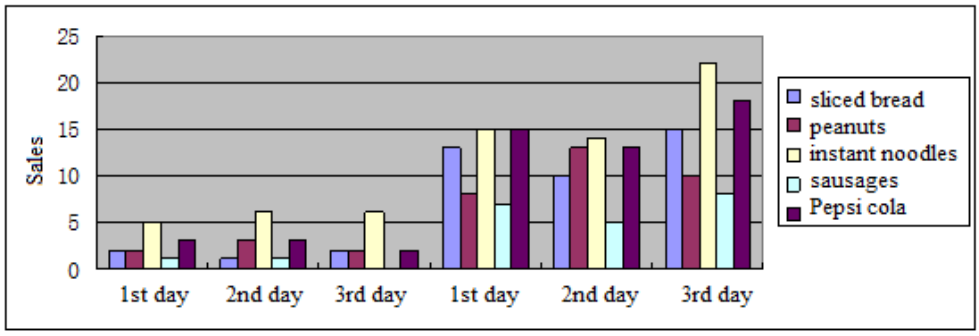

Figure 1 The change in sales before and after posters distributed

Description: From table 1 we can infer that: first, before distributed posters, sales of some products are not stable; second, after distributed posters, sales of most products have increased; third, sales of sausages and cola keep increasing, and sales of other products are fluctuate; fourth, sales of cola and sausages have the largest increase.

Exploratory factor analysis is needed to be carried out to the data, in order to purify the measurement project aims. Therefore, we must first examine the correlation, since higher correlation is more suitable for factor analysis. Use SPSS 17.0 to carry out KMO measure and Bartlett Sphere test for sample data to determine the relevance, the result are shown in Table 2.

Table 2 Results of KMO and Bartlett test

KMO and Bartlett test		
Sampling enough degrees of Kaiser - Meyer - Olkin measurements		0.646
Bartlett sphericity test	The approximate chi-square	0.646
	df	2007.533
	Sig	.000

As inferred from Table 2, the KMO value is 0.646 and the Bartlett value is notable on 0.000, which mean the date is suitable for factor analysis.

3.3 analyses

Studies have shown that when faced with uncertain choices, people are easier to conduct herd behavior to avoid wrong choice. General psychology of consumers might be: the goods most people chosen will not too bad, in another words, the probability of error is very low.

As the sales trend after posters, the sales of original first and second products have significant increases and continue maintaining the rank. Since the ranking is real, selling promotional information and is consistent with and reinforce routine information, thereby greatly enhancing the possibility of herd behavior. As Elliot Aronson mentioned in "social animals": the result of observe and comply with other people in order to obtain information on how to conduct properly will be more powerful than just to get away from punishment or reward to comply with others. Experimental results fit the theory.

4 Conclusions

Based on summing up the theory of social psychology and group behavior theory research results, this study presents a statistical model of herd mentality trend, and uses empirical research to validate the model. From simulation and analysis of a college, we can see that college students have significant herd behavior when shopping.

Herd mentality has a dual nature, positive factor and negative factor. It makes helps individual to learn the wisdom of and experience of others and expand horizons, but inhibits the development of personality, structure thinking, and make people non-assertive and blindly. Therefore,

understanding the impact of related factors of herd behavior has a strong practical significance on both individual and community.

References

[1] Hornsey MJ,Maikut L,Terry DJ. et al. On being loud and proud: Non\conformity and coimter\ conformity to group norms [J]. British journal of social psychology, 2003, 42(3)
[2] Oloranniwo, F.,Hsu, M.K. and Udo,G.J. Service Quality, Customer Satisfaction, and Behavioral Intentions in the Service Factory, Journal of Services Marketing,2006，20(1),59-72.
[3] Yang, Z., Jun, M., Peterson, R.T. Measuring Customer Perceived Online Service Quality: Scale Development and Managerial Implications, International Journal of Operations and Production Management, 2004，24(11), 1149-1174.
[4] Armitage, ChristoPher J. and Julie Christian. From Attitudesto Behavior: Basieand Applied Researeh on the Theoryof Planned Behavior, Current Psychology: Develo Pmental, Learning, Personality, Social, 2003, 22(3): 187-95
[5]Clark, Paul W., CraigA. Martin, and AlanJ. Bush. The Effeet of Role Model Influenee on Adoleseents'Materialism and Marketplaee Knowledge, Joumal of Marketing THEORY AND PRACTICE: 2001, 3:27-36.
[6]Esealas, Jennifer Edson. You Are What They Eat:ThehifluenceofReferenee GrouPsonConsumers, ConnectionstoBrands,JoumalofConsumer Psycholog,2003,13(3):339-48.

Advanced Materials Research Vols. 989-994 (2014) pp 1997-2000
© (2014) Trans Tech Publications, Switzerland
doi:10.4028/www.scientific.net/AMR.989-994.1997

Virtual simulation of aerobics movement based on vision

Wang Xiaohui

Henan Radio and Television University zhengzhou Henan 450000,China

Keywords: 3D motion reconstruction, neighborhood correction, Feature points

Abstract: In aerobics, the motion state randomness of key feature points is great, so it is difficult to establish an accurate dynamic model for sports' shape base. Traditional 3D reconstruction algorithms use fixes shape base which hardly expresses the change parameters of complex movement and motion law of large-scale dynamic features, thereby leading to non-realistic reconstruction results. The paper proposes a new reconstruction algorithm for aerobics 3D motion images that corrects the neighborhood system of feature points by motion parameters until the parameter is stable to ensure accuracy and the stability of correction. The simulation results show that, the proposed algorithm avoids drawbacks of sports reconstruction results caused by the great randomness of aerobics' motion state, thereby complete 3D reconstruction for aerobics' motion images.

1 Introduction

With the improvement of people's living standards, more and more people continue to pursue good health. As a modern fitness method, aerobics has accepted by many people. Aerobics is an emerging sport in our country. It is originated in life pursuing both health and beauty [1,2] and combining aerobic, dancing and music. Therefore, physical beauty evaluation method is essential for aerobics. [3]

Computer Vision Graphics method is a computer-aided tool rapidly developed along with modern computer technology, and is well applied to a variety of occasions. The method analyzes physical beauty of aerobics through the combination of computer vision and image processing is in the initial stage of research. Different from rigid body motion, there is great motion state randomness of some key features points in aerobics and severe deformation in body. Traditional non-rigid motion reconstruction algorithm concerns the feature point motion parameters are fixed in the calculation process, such as factorization method. However, during exercise, the non-rigid objects cannot guarantee the feature points in the time domain have the same motion parameters [4], even feature points meeting the neighborhood relationships, their motion parameters still may be different. This assumption results in unrealistic of three-dimensional image reconstruction of traditional methods.

2 Correction for the three-dimensional reconstruction of moving image in neighborhood system

2.1Feature points position correspondence

Before adopting correction neighborhood system algorithm, we need to clear the correspondence between feature points of different frames of 3D motion images. The ordered set of feature points' positions is $W = \{1, 2, ..., E\}$, where E is the number of feature points. Generally, the arrangement of feature points is random, which means W is a random position set. The motion parameters of image feature points can be used to mark the moving position of the feature points.

$S_i^t = (x_i^t, y_i^t, z_i^t)^T$ is the 3D spatial coordinates of the *i*th feature point at time t of the non-rigid object. $S_i^{t+1} = (x_i^{t+1}, y_i^{t+1}, z_i^{t+1})^T$ is the 3D spatial coordinates of the *i*th feature point at time t+1 of

the non-rigid object. The moving situation of feature points in 3D spatial can be described by formula (1).

$$\begin{bmatrix} X_i^{t+1} \\ Y_i^{t+1} \\ Z_i^{t+1} \end{bmatrix} = K_i \begin{bmatrix} X_i^t \\ Y_i^t \\ Z_i^t \end{bmatrix} = \begin{bmatrix} a_{i1} & b_{i1} & c_{i1} \\ a_{i2} & b_{i2} & c_{i2} \\ a_{i3} & b_{i3} & c_{i3} \end{bmatrix} \begin{bmatrix} X_i^t \\ Y_i^t \\ Z_i^t \end{bmatrix} \tag{1}$$

k_i is the motion parameter of the ith feature point in 3D space, that is the identification of position i. Then

$$k_i = (a_{i1}, a_{i2}, a_{i3}, b_{i1}, b_{i2}, b_{i3}, c_{i1}, c_{i2}, c_{i3})^T \tag{2}$$

According to the continuity feature of moving objects, the motion parameters of a feature point and some points in its neighborhood is similar. Therefore, comprehensively analyzing motion parameters of feature points in its neighborhood, we can get the marking area of k_i is $H_i = \{k_i \mid i \in E_i\}$.

2.2 Correcting neighborhood parameter

Differences exist in parameters of different feature points and in moving parameters of feature points and neighborhood feature points. Therefore, there is certain error in moving parameters of feature points obtained in 2.1 and the position identifiers of corresponding feature points are invalid. We take these position identifiers as an original location identifiers' set. In iterative analysis, location identifier of feature points are constantly changing, so the identity regions of the feature points are continually being adjusted.

According to formula (1) and (2), the neighborhood of a feature point is determined by the position of the motion parameter in the image. The original image neighborhood is composed by position of the first frame of image feature points. Actually, the position of feature points in 3D moving image has random relationship with motion parameters of feature points. So timely correctness is needed to make sure the moving position of each feature point only has neighborhood relation with the location has the same identity. Usually we adopt variable neighborhood approach. Analyzing the intermediate optimal solution between i the position of feature point and j the position of its original neighborhood system, we obtain prediction error value wc_{ij}, and then calculate the error sum of squares of moving parameters of the two feature points' position by formula (3)

$$\Delta K_{ij} = \sum_{K=1}^{9} \left(K_{im} - K_{jm} \right)^2 \tag{3}$$

If i and j satisfy either condition in (4)

$$\Delta k_{ij} > \beta \quad or \quad wc_{ij} = \max_{i' \in E_i} wc_{ii'} \tag{4}$$

We determine that j is not a neighborhood point of i, and delete j in E_i (the neighborhood system of i). Through (3) and (4), we can obtain all the neighborhood position of i and get E_i' the new the neighborhood system of i.

wc_{ij} in formula (4) indicates determination error. Since the motion of non-rigid objects with a persistent feature, so we need to constantly modify the position of the feature point by determination error function. The new correctness process are: get the position of the object feature points, then correct content of position j in its neighborhood E_i with content of i, and finally use (5) and (6) to calculate error wc_{ij}.

$$
\begin{aligned}
wc_{ij} = \sum_{t=2}^{H} & \left[\left(x_i^t - g\frac{\hat{X}_i^t}{\hat{Z}_i^t} \right)^2 + \left(y_i^t - g\frac{\hat{Y}_i^t}{\hat{Z}_i^t} \right)^2 \right. \\
& + \left[\max\left(0, \hat{Z}_i^t - \left(\hat{Z}_i^{t-1} + Z_{i\boldsymbol{\beta}}\right)\right) \right]^2 + \left[\max\left(0, \left(\hat{Z}_i^{t-1} - Z_{i\boldsymbol{\beta}}\right) - \hat{Z}_i^t\right) \right]^2 \\
& + \left[\max\left(0, \hat{x}_i^t - \left(x_i^t + x_{i\boldsymbol{\beta}}\right)\right) \right]^2 + \left[\max\left(0, \left(x_i^t - x_{i\boldsymbol{\beta}}\right) - \hat{x}_i^t\right) \right]^2 \\
& \left. + \left[\max\left(0, \hat{y}_i^t - \left(y_i^t + y_{i\boldsymbol{\beta}}\right)\right) \right]^2 + \left[\max\left(0, \left(y_i^t - y_{i\boldsymbol{\beta}}\right) - \hat{y}_i^t\right) \right]^2 \right]
\end{aligned} \tag{5}
$$

$$
\begin{bmatrix} \hat{X}_i^{t+1} \\ \hat{Y}_i^{t+1} \\ \hat{Z}_i^{t+1} \end{bmatrix} = \boldsymbol{U}_j \begin{bmatrix} \hat{X}_i^t \\ \hat{Y}_i^t \\ \hat{Z}_i^t \end{bmatrix} + \boldsymbol{T}_j \tag{6}
$$

Let $wc_{ik} = \min_{j \in E_i \text{ or } j=i} wc_{ij}$, the content of k can be taken as that of position i.

3. Results analysis

To verify the effectiveness of the proposed 3D image reconstruction algorithm for aerobics, the paper builds a system to simulate the image sequence through MATLAB version 7.1 and Drect3D 9．0SDK. We choose 50 feature points, according to which simulate 2 continuous image frames as shown in Figure 1. It can be seen that there are 3 forms of motion parameters in the images sequence respectively indicated by U1, U2, U3. And the values of 3 forms of motion parameters are shown in Table 1.

Figure 1 Aerobics image sequence

Table 1 Ideal motion parameter matrix of simulation image sequence

NO.	Theoretical value *e*	NO.	Theoretical value *tr* theory *ue*	NO.	Theoretical value *tr* theory *ue*
U1	0.99781549 0.00208013 -0.04663544 0.00208013 0.99450641 0.09338203 0.04663544 -0.09238204 0.99441005	U2	0.99615284 0.00262834 0.07383279 0.00262814 0.99615084 -0.07383168 -0.07280168 0.07380168 0.99441024	U3	0.99450641 -0.002183131 -0.09458204 -0.00208013 0.99761352 -0.04663544 0.09338204 0.04663544 0.99341005

The paper uses frame 1 and 2 in the image sequence to analyze the image movement, the results are shown in Table 2.

Table 2 The experimental results of frame 1 and 2 in the image sequence

Feature points	Theoretical value	Predictive value	Error
s_{24}	U1	$\begin{bmatrix} 0.997743011 & 0.002801147 & -0.046644157 \\ 0.002181147 & 0.99453483 & 0.093382134 \\ 0.046644157 & -0.09382134 & 0.99340536 \end{bmatrix}$	0.000001034764
s_{23}	U1	$\begin{bmatrix} 0.99780310 & 0.002180113 & -0.046634877 \\ 0.002170004 & 0.99450187 & 0.093381845 \\ 0.04634877 & -0.093381845 & 0.9933453 \end{bmatrix}$	0.0000026347634
s_{22}	U3	$\begin{bmatrix} 0.99761468 & 0.0021801352 & -0.046635353 \\ 0.0021821352 & 0.99450461 & 0.093380228 \\ 0.046635353 & -0.093380128 & 0.99341421 \end{bmatrix}$	0.00000093603645
s_{12}	U2	$\begin{bmatrix} 0.99724925 & 0.0027394127 & 0.073914270 \\ 0.0027394127 & 0.99725643 & -0.073914270 \\ -0.073914270 & 0.073914270 & 0.99452946 \end{bmatrix}$	0.0000009457013

The image sequence according to the experimental results in table 2, 2 and 3 of the frame for three dimensional motion parameter prediction, to obtain the parameters of the predicted values match the table 2. And the system image motion leveled off.

4 Conclusions

Through the analysis above, we can obtain that the number of mistake clusters is reduced and the effectiveness of prediction is enhanced in the aerobics image sequence. The original position of feature points and the number of feature points in each region in the image sequence together determine the amount of mistake clustering. The number of iterations in the experiment is reduced from 140 to 125, indicating that using the corrected neighborhood system to adjust aerobics image sequence simulation system can improve the operational efficiency of the system, increase the authenticity of the three-dimensional image reconstruction aerobics, and achieve good experimental results.

References

[1] Liu Huaihui. Plane finite element research triangle mesh subdivision algorithm [D]. Shandong, shandong university, 2008. 4. 24.O. R. Musin. Properties of the delaunay triangulation[J]. In Proc. 13th Annual ACM Symposium on Computational Geometry, pages 424–426, 1997.
[2] Ting Chen, Wei-Chung Lin. Artificial Neural Networks for 3-D Motion Analysis-Part II: Nonrigid Motion[J]. IEEE Trans Neural Networks, 1995, 6(6): 1394-1401.
[3] Chen T, Lin W C, Chen C T. Artificial neural networks for 3-D motion analysis I: Rigid motion[J]. IEEE Trans Neural Networks, 1995, 6(6): 1386-1393.
[4] Tzovaras D, Ploskas N, Strintzis G.Rigid 3-D motion estimation using neural networks and initially estimated 2-D motion data[J]. IEEE Trans Circuits and Systems for Video Technology, 2000, 101, 10(1): 158-165.

Advanced Materials Research Vols. 989-994 (2014) pp 2001-2003
© (2014) Trans Tech Publications, Switzerland
doi:10.4028/www.scientific.net/AMR.989-994.2001

The research of key data classification optimal mining methods for massive data

Li Yinying, Wang Yunze

HeBei institute of communictions, ShiJiazhuang Hebei 050071, China

Keywords: inter-cell classification; mathematical model; fuzzy; convergence

Abstract: The data classification is an important issue in massive data classification. This paper proposes an inter-cell classification algorithm based on phase recombination neighbor points convergence which analyzes the convergence value weights of inter-cell characteristic points and filter the interferences of the minority local optimal characteristic points. The proposed algorithm can promote the convergence of the inter-cell classification data neighbor points. The simulation experiments testify the models by three types of actually collected data sets which illustrate the models have better classification performance.

1 Introduction

The data classification is a hot issue in data mining area. The existing classification algorithm, such as K- centers, is simple and easy to implement. However, the time complexity of the algorithm is high, and it's easy to fall into local optimum [1]. In order to solve this problem, the literature [2] proposed an improved fast K-center classification algorithm which generally divides the data into groups. Then the classification center in each group is optimized. The rough division of the algorithm has no quantitative parameters' analysis and the algorithm may not always find the optimal central sample points. The literature [3] proposed a classification algorithm based on granular computing in which the granular computation is introduced to evaluate the similarity of the samples. The k particles with most similarities are used as the classification center. However, for the sample network data sets with different densities, the similarity thresholds are different and the obtained classification centers are different which cause the classification performance are quite different. The literature [4] proposed the improved particle swarm optimization classification which uses the fitness value of particles to stochastic optimize the particles and uses weighted distances to improve the classification effects of the specific particles. However, the thresholds in the algorithm for different objects will affect the accuracy of the classification and the calculated particles' center may not correspond to the true position of the sample. The literature proposed a density classification method based on the differences in the samples which uses the weighted fuzzy algorithm to classify the differences of the samples. However, the operation efficiency of the algorithm is affected by the differences of the network data attributes. Due to the increasing complexity of network data attributes, the properties can be used to classify will increase greatly. The traditional network data classification algorithm is very sensitive to the initial data center which will result in lower efficiency of the algorithm execution.

2 The classification model for massive data

2.1 The extraction of the classification features

In order to accurately classify the data, the data features should be accurately indexed first. The data indexing is the procedure to extract and integrate the data features so that the data which are need to be indexed will maintain stable within a center range. The specific method is as follows.

（1）The data features are extracted by the following equation.

$$t = \sum_{i=1}^{n} t_i / n$$

In the equation, t_i denotes the single feature of the data, n denotes the amounts of the data features, t describes the final features of the data by calculation.

（2）The key feature t of the data acquired is proofread and adjusted by the following formula to obtain the characteristic deviation $\nabla e(t)$ of the data.

$$\nabla e(t) = t - t_0$$

（3）The characteristic deviation trimming is finished by

$$u(t) = k_p \nabla e(t) + \beta k_i \sum_{j=0}^{k} \nabla e(t) T + k_d (\nabla e(t) - \nabla e(t-1)) / T$$

In the above equations, k_p describes the characteristics transverse trimming, k_i describes the amount of characteristic trimming coefficients, k_i describes the characteristics longitudinal trimming. The tuning of the three parameters will lightly adjust the key feature $u(t)$ of the data need to be indexed to ensure the data in more accurate change period.

2.2 The classification procedure

The inter-cell classification is well applied as the method for massive sample feature data classification. This paper proposes a phase recombination neighbor point convergence inter-cell classification algorithm which analyzes the convergence value weights of the feature data neighbor points, filter the interferences of the minority of local optimal feature data, promote the convergence of the neighbor points and prevent the issue of local convergence.

The proposed algorithm highlights the high efficient convergence of the characteristic neighbor points in the data set which greatly increases the efficiency of the algorithm for data mining. The variation classification coefficients are merged into each data set in the inter-cell and the convergence contribution factors for the overall ranges are expressed by

$$P(k) = \frac{\sum_{i=1}^{k} (\| p - A_i \|)^2}{N \min(\| A_i - A_j \|)^2} \tag{1}$$

If $V(k) \geq 1$, the classes are in inter-cell, otherwise $V(k) < 1$, the inter-cells will be deleted. By the promotion of the neighbor points, the inter-cell classification convergence will be improved. The procedure considering the phase recombination neighbor point convergence is as follows.

（1）The inter-cell selection to determine the total amounts of inter-cells and the feature sets of the initial data. If the data set is m, Let $A_j(L)$ be the center of inter-cell and $j = 1,2,...,k$. The distances to the center can be calculated to determine the amounts and range of the neighbor points.

（2）K samples are selected in the data set. The inter-cell centers of $F(x_i, A_j(L))$ with $i = 1,2,...,m$ and $j = 1,2,...,k$ are initialized to input into the maximum likelihood estimator.

（3）The inter-cell classification algorithm is used to analyze initially, if

$$D(x_i, A_j(L)) = \min\{D(x_i, A_j(L))\} \tag{2}$$

Then $x_i \in \omega_k$ and it's merged into the phase recombination neighbor points to analyze the weights to obtain the each inter-cell mean.

$$C(l) = \sum_{j=1}^{k} \sum_{k=1}^{n_j} (\| p_k^j - A_j(L) \|)^2 \tag{3}$$

（4）Fuzzy selection operator is used to identify the inter-cell thresholds. If the mean is equal to the evaluation value in the previous iteration that is $\| C(l) - C(l-1) \| < \xi$, the program will be terminated. Otherwise, return to step 3 and let $l=l+1$ calculate the new inter-cell center which is expressed by

$$A_j(L+1) = \frac{1}{n_j} \sum_{i=1}^{k} P_i^j \qquad j = 1,2,...,k \tag{4}$$

In the previous procedure, the inter-cell classification algorithm based on phase recombination neighbor points convergence analyzes the convergence value weights of inter-cell characteristic points and filters the interferences of minority of local optimal feature data. The algorithm promotes the convergence of neighbor points which provides new ways for improving the convergence speeds of inter-cell classification.

3 Experiments and results analysis

This paper compares the classification results by proposed method and the traditional classification methods. 300 pieces of Web files are downloaded from the Internet and 3 times of experiments are carried according to different topics.

Table 1 The topics of the experimental test files

No.	Amounts of Files	Topic
1	100	Data type 1
2	100	Data type 2
3	100	Data type 3

The previous files are classified by different topics first in which the some English words are translated into Chinese in the test sets. Each word in the files is divided to obtain the file-word matrix in which each row denotes one file project. They are classified by K-means after dimension reduction with semantic matrix. The classification results by the proposed method are compared with those in the known files to evaluate the accuracy of the classification which is denoted as Ac . It's expressed by

$$Ac(r,s) = n(r,s) / n_r \tag{5}$$

$n(r,s)$ denotes the amount of correctly classified files in some classification cluster, n_r denotes the total amount of files in the classification cluster. The Matlab programs are used to classify the 300 pieces of files by three classification methods-traditional word frequency method, the semantic classification method and the proposed methods in which the word document matrix decomposition time and documents classified time are recorded. The results are shown in Fig. 1

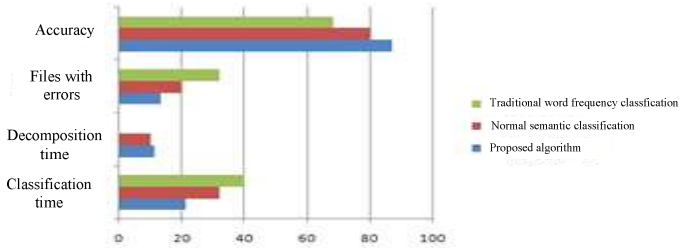

Fig. 1 The performance of different classification methods

In Fig. 1, the classification accuracy is greatly increased in the proposed model while the time consumed for classification is not increased. The results illustrate the advantage of the proposed model.

4 Conclusions

This paper proposes an inter-cell classification algorithm based on phase recombination neighbor points convergence which analyzes the convergence value weights of inter-cell characteristic points and filter the interferences of the minority local optimal characteristic points. The proposed algorithm can promote the convergence of the inter-cell classification data neighbor points. The simulation experiments testify the models by three types of actually collected data sets which illustrate the model has better classification performance.

References

[1]Song Shucai. for Web data mining technology in the research and application of personalized recommendation methods of website optimization [J]. Science and technology, 2012, 2 (28) : 118-119.

[2] Liu Ke, Wan Li Wu Jieming. Based on data mining technology of network security event prediction research [J]. Science and technology, 2012, 28 (6) : 37 to 40.

[3] Xu Wenhai, kratos. A Chinese keyword extraction algorithm based on TFIDF method [J]. Journal of theory and practice of intelligence, 2008, 31 (2) : 298-302.

[4] Xu Yan, Li Jintao etc. High performance feature selection method based on the difference between classification ability [J]. Journal of software, 2008, 19 (1) : 82-89.

Advanced Materials Research Vols. 989-994 (2014) pp 2004-2007
© (2014) Trans Tech Publications, Switzerland
doi:10.4028/www.scientific.net/AMR.989-994.2004

Group Customer Special Line Correction Algorithm Design and Application Based on PTN Technology

ZHU Heng-jun[1,a], Li Dengfeng[2,a]

([1.] Communication and Electronics Engineering Institute of Qiqihar University，Heilongjiang Qiqihar 161006，China;
[2.]China Mobile Communications Group Co, Ltd. Heilongjiang)
[a]13946287890@139.com

Keywords: special group line; network hierarchical structure; multiplexing relationship; design

Abstract. The group customer line service has become one of the key businesses for communication operators, and the line PTN technology development currency, the PTN technology application, and the development trend are researched. According to the PTN technology and client group line error correction algorithm, the multi granularity hash correction algorithm is used for data video aware, and when the PTN data is changed fast, the fuzzy block effect happened. The customer line service performance is bad. An improved group customer line correction algorithm is proposed based on PTN technology. The hidden Markov model is used for packet loss rate prediction, and the multiple steps are selected in random, and the data stream iteration algorithm is designed. The tamper detection algorithm is obtained. PTN technology group customer line correction is realized. Simulation results show that the new method can reduce error transmission rate of the PTN group customer line, the customer loss and delay of the data transmission can be controlled, and the peak signal to noise ratio is improved, the error correction performance is better, and it can be effectively applied to communications operator service.

Introduction

At present, with the development of communications technology, customers put forward more and more demand for telecom operators, especially, the requirements of special group line are increasing. Heilongjiang mobile Qigihar branch relies on rich sources of China Mobile, and it provides digital circuit, optical fiber line rental and maintenance services to the enterprises and institutions to the enterprises and institutions. The enterprises and institutions can choose 2Mbps-2.5Gbps bandwidth channel and various interface types, and the security, reliable and high-speed data channel environment is set up, the voice, data, video and other types of businesses are operated based on the service and lines[1].

The common application areas of special group line contain voice special line and data line. Voice special line is he can make the enterprises branch switches interconnected, and connect to the China Mobile switch, quality of voice call, and the cost of long distance is reduced. The data special line can make the enterprises branch network connect, carrying the information interaction, VoIP voice business[2].

According to the current communication service operators, the customer types can be roughly divided into agencies, banks, financial securities type enterprise group, education / campus and hotel / office type. Compared with the general user, the group customers have large volume of business for operators, and business type is complex, quality of service requirement is higher. According to the business development, PTN (Package Transport Network) technology is developed, and the application packet transport network users have a high evaluation, PTN can load the Mobile Backhaul, the QoS services are provided, Metro Transmission Network is converted from TDM to evolved packet network gradually. With the development of the 4G and all the business operation, the IP data services become the main content of city area network, SDH subsided gradually, PTN packet network becomes the core network[3~5].

In this paper, the line PTN technology development currency, the PTN technology application, and the development trend are researched. An improved group customer line correction algorithm is proposed based on PTN technology. The hidden Markov model is used for packet loss rate prediction, and the multiple steps are selected in random, and the data stream iteration algorithm is

designed. The tamper detection algorithm is obtained. PTN technology group customer line correction is realized. Simulation results show that the new method can reduce error transmission rate of the PTN group customer line, the customer loss and delay of the data transmission can be controlled, and the peak signal to noise ratio is improved, the error correction performance is better, and it can be effectively applied to communications operator service.

Technical feature of PTN network hierarchical structure of packet transport network

Packet transport network (PTN) is multi service transport technology based on switched connection orientation, and it not only can bear carrier Ethernet services, but also can support TDM, ATM and IP service. The network reliability satisfied, and OAM is corrected, the network scalability is improved. The QOS transmission with integrated transmission technology based on network attributes is improved. PTN is a level set between the IP service and the underlying optical transmission medium, which is designed according to the sudden and statistical multiplexing transmission for packet traffic requirements. The packet service is the core, and it provides support for multi business. It has efficient bandwidth management mechanism and traffic engineering, and the convenient OAM can make the network management become scalable and high security, etc. It supports TDM service and ATM service, supports clock synchronization and time synchronization, the dynamic control effect is good.

PTN structure is shown in Figure 1, it consists of three layer of PTN network: the virtual channel (VC) layer network, virtual path (VP) network layer and transmission layer network, wherein, the transmission media layer network contains a virtual segment (VS) layer network. For the use of MPLS-TP technology of PTN, VC layer is the pseudo wire (PW) layer, VP layer, LSP layer, VS layer is the LSP section layer. PTN bottom is the transmission medium layer network, the circuit can be adopted by the IEEE 802.3 Ethernet or SDH, OTN connection is used for circuit switching (CO-CS). PTN layer is the customer service layer, it is formed by a single client signals, and customer service layer signal, including PTN network (ETH), TDM (SDH/PDH), ATM, FR, PPP/HDLC etc.

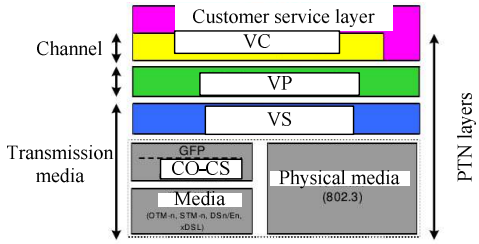

Figure.1 PTN structure

Group customer line correction algorithm design and application based on PTN technology

The special line of group customer has error, and the correcting algorithm is designed, the special line of group customer takes the UDP protocol for the transmission of data packet transmission, the data packets are forced by the link layer of MTU, and the receiving terminal at multilayer nested fragment reassembly in the stream, data stream can cause packet loss and delay, the transmission quality problem should be controlled. The group customer line transmission network structure diagram of PTN technology is shown in Figure 2. Hidden Markov model is designed, eventually realize data transmission and distortion correction.

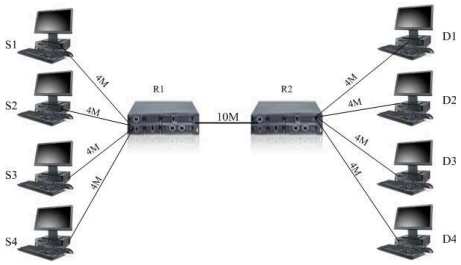

Figure 2. Network structure diagram of group customer special line transmission based on PTN technology

Firstly, the principle of multi granularity hash correction algorithm using video perception is presented, assumed that the structure feature information of network transmission is:

$$V_{ideo}(a_1,\cdots,a_m)=\left(a_i^{j-1}\right)_{i,j=1}^{m} \tag{1}$$

Where, $V(a_1,\cdots,a_r)$ is the block matrix in time domain, $\left(a_i^{j-1}\right)_{i,j=1}^{m}$ is the brightness mean value for each data block, the set of unit step is constructed, and the column orthogonal basis $(a_1,\cdots,a_r)$ and $(b_1,\cdots,b_r)$ is decomposed with $2r$ elements Gauss pseudorandom function, the video sequence with l length is obtained:

$$V(a_1,\cdots,a_m)^{-1}[V(a_1,\cdots,a_m)\,|\,V(b_1,\cdots,b_m)]=[\boldsymbol{E}\,|\,V(a_1,\cdots,a_m)^{-1}V(b_1,\cdots,b_m)] \tag{2}$$

For the PTN data series, the temporal mean brightness is used for hash random overlapped block correction, and the non singular solution is proved, the frequency spectrum characteristic matrix is:

$$(\boldsymbol{A}^{-1})^{(\alpha_1^{-1},\cdots,\alpha_m^{-1})^T}\boldsymbol{A}^{(\alpha_1,\cdots,\alpha_m)}=\begin{pmatrix}\alpha_1^{-1}t_{1,1} & \cdots & \alpha_1^{-1}t_{1,m}\\ \vdots & \ddots & \vdots\\ \alpha_m^{-1}t_{m,1} & \cdots & \alpha_m^{-1}t_{m,m}\end{pmatrix}\begin{pmatrix}\alpha_1 a_{1,1} & \cdots & \alpha_m a_{1,m}\\ \vdots & \ddots & \vdots\\ \alpha_1 a_{m,1} & \cdots & \alpha_m a_{m,m}\end{pmatrix} \tag{3}$$

In the matrix state limited space $V(a_1,\cdots,a_m)^{-1}V(b_1,\cdots,b_m)$, the received stream diversity link layer of MTU high-level code is generated, and the inter layer mode overlapping data are computed, the receiver needs to reconstruct the fragmentation reassembly, the data inter frame prediction and inter layer prediction results respectively are shown as:

$$E_{Tx}(l,d)=E_{(Tx-elec)}(l)+E_{(Tx-amp)}(l,d)=lE_{elec}+l\varepsilon d^{\alpha}=\begin{cases}lE_{elec}+l\varepsilon_{fs}d^2, & d<d_0\\ lE_{elec}+l\varepsilon_{mp}d^4, & d\geq d_0\end{cases} \tag{4}$$

In the formula, d is receiving node distance between the time domain characteristic node and surface sending node, E_{elec} is the energy consumption for each frame of the video data, Using hidden Markov model, a transfer state is expressed as the 2 stochastic process, 5 tuple to describe data transmission sequence model, it is expressed as:

$$\lambda=(X,O,A,B,\pi) \tag{5}$$

Where, X is the hidden state of Markov model, $X=\{x_i,i=1,2,3\cdots,N\}$. O is observation state of group client base on PTN technology, $O=\{o_j,j=1,2,3\cdots,M\}$. A represents the reconstructed state transition probability of matrix, it is a N orders square matrix, $A=\{a_{i,j},0<i,j<N\}$. B is $N\times M$ matrix, and the state transition probability matrix and the confusion matrix are calculated, respectively, they show the tamper detected customer hotline data series and Hashi series, the the mathematical expectation of packet loss rate is:

$$\varepsilon_t(i,j)=\frac{\alpha_t(i)a_{ij}b_j(o_{t+1})\beta_{t+1}(j)}{\sum_{i=1}^{N}\sum_{j=1}^{N}\alpha_t(i)a_{ij}b_j(o_{t+1})\beta_{t+1}(j)} \tag{6}$$

Then, the improved data stream iteration algorithm is designed. The tamper detection algorithm is obtained. PTN technology group customer line correction is realized.

Simulation experiment

In order to test the performance of algorithm for PTN error correction, simulation experiment is taken based on OPNET Modeler 14.5, data size is 11 G, the format of CIF, and the acquisition time interval parameters U and F are10 s and 25 s respectively, the simulation time is 3600 s. GOP structure is IBBPBBPBBP, the traditional method and the new method are taken for the comparison, and the Packet loss rate and the Peak signal to noise ratio are computed for performance compassion in group customer line service and data transmission, the simulation results are shown in Figure 3 and Figure 4. The graph analysis shows that the PPLECA algorithm proposed in this

paper can improve the PSNR about 1.6 dB, the packet loss rate is reduced 0.015, the distortion of information is reduced, and it has good performance in group customer special line correction and application.

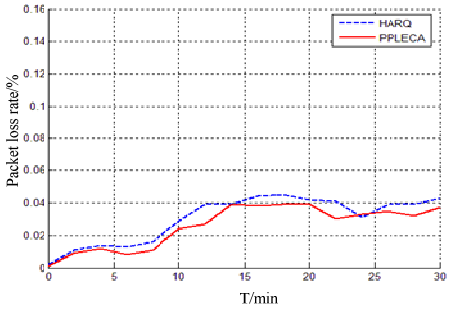

Figure 3 Packet loss rate

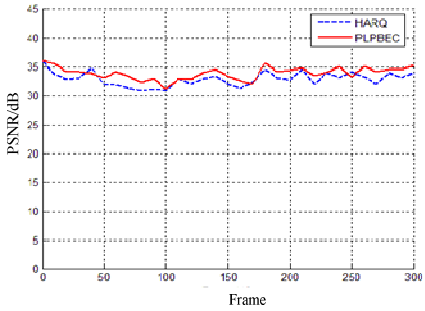

Figure 4. Peak signal to noise ratio

Conclusions

The group customer line service has become one of the key businesses for communication operators, in this paper, and improved group customer line correction algorithm is proposed based on PTN technology. Simulation results show that the new method can reduce error transmission rate of the PTN group customer line, the customer loss and delay of the data transmission can be controlled, it can improve the PSNR about 1.6 dB, the packet loss rate is reduced 0.015, new method can effectively applied to communications operator service

References

[1] CRISTANI M, RAGHAVENDRA R, BUE D A. Human behavior analysis in video surveillance: A Social Signal Processing perspective[J]. Neurocomputing, 2013, 100(1):86-97

[2] HUANG Kai- feng, ZHAO Tao. Application of Particle Swarm Optimization Clustering in Network Security[J]. Computer Simulation. 2012; 29(12): 144-147.

[3] LIU Luo, GUO Li-Hong, XIAO Hui, Et al. Software Reliability Growth Model Based on Dynamic Fuzzy Neural Network with Parameters Dynamic Adjustment[J]. Computer Science. 2013; 40(2): 186-190.

[4] Du Hui. Fast Face Detection in Color Image Based on Wavelet Transform[J]. Bulletin of Science and Technolog, 2012,12(28):89-90.

[5] Li Zhaobao, Zhou Ming, Gu Li. The Identification Algorithm of Similarity Multiple Targets Based on Wavelet Transform[J]. Bulletin of Science and Technology, 2013, 29(3): 120-124.

Advanced Materials Research Vols. 989-994 (2014) pp 2008-2011
© (2014) Trans Tech Publications, Switzerland
doi:10.4028/www.scientific.net/AMR.989-994.2008

Position Mobil Information Encryption Algorithm Based on Key Attributes of Reduced Rank Agent under Cloud Storage

Guo hongliang[1,a] Yu helong[1,a](corresponding author)

[1]JiLin Agricultural University, Jilin Changchun 130118,China
[a]172903184@qq.com

Keywords: key; encryption algorithm, cloud storage; privacy protection

Abstract. The location mobile social networks information privacy protection under the environment of cloud storage and data security of encryption is researched, the traditional data encryption to rank has higher in the length of ciphertext and private key attributes of large matrix, it defines the length of ciphertext data on customer privacy private property and it cannot be revoked. The encryption complexity and security are not good. An improved encryption algorithm based on key attributes of reduced rank agent is proposed, the proxy ReEncryption technology is taken, the ReEncrypt decryption scheme is designed, and private key attributes of bilinear mapping and reduced rank processing is taken, and a communication channel between the user, CSP, trusted third party and data users is established, and the algorithm is obtained. The simulation is taken for testing the customer information data for privacy protection, the simulation results show that it can ensure the length of ciphertext is relatively small, and it has low computational complexity with more security, and it has the very good practical value in encryption communication and privacy protection fields.

Introduction

With the development of computer technology, the development of information technology is developing rapidly, and the network data security problems have gradually emerged, it has become as the bottleneck problem in modern industrial network development[1]. If the security control and defense measures are not reasonable and effective, the network does not have the modernization, information communication capability[2]. Today, the cloud computing and cloud technology are developing rapidly, a lot of data and information are processed through the cloud storage and transmission. At the same time, in the cloud storage terminal, a lot of data leakage and user privacy leakage emerging, for example, in the mobile transform social network, the GPS users upload the location information, but the cloud storage system data protection is weak, the security of data encryption is not good, resulting in of position privacy leak. It causes controversy among the public, Therefore, the research of data information encryption and privacy protection mechanism is important, it has become the hot topic in computer and information technology research areas.

Data encryption is an important mean in network information access and security control, after so many years development[3], the traditional intrusion has been able to protect some intrusion, , but for a new type of network intrusion, the protection effect is not good. So, in the modern information technology development trend, it needs to continuously improve the network intrusion of private key encryption scheme, with the deeper levels of encryption, the network data security is protected, the secret information will not be stolen. The traditional data encryption algorithm uses the attribute length ciphertexts encryption scheme, the private key of user is defined as the length of ciphertext, and the decryption plaintext matrix is constructed with high ranks and high dimensions, which leads to computational complexity is very high, the encryption effect is not good[4].

In view of the above problems, an improved encryption scheme is proposed based on key attributes of reduced rank agent[5], the proxy ReEncryption technology is taken, the ReEncrypt decryption scheme is designed, and private key attributes of bilinear mapping and reduced rank processing is taken, and a communication channel between the user, CSP, trusted third party and data users is established, and the algorithm is obtained. The GPS supplier carries network is taken as the example, and the social network privacy protection system and algorithm are constructed, and the data encryption test is taken, it shows that the algorithm has excellent performance in data encryption and privacy protection.

Encryption model design of secure cloud storage

In the information data encryption of user mobile terminal equipment, it needs to establish a correlation system, the encrypt data characteristics are correlated. We need to have a large number correlation characteristics as the input raw data, on the basis of this, a large number of trainings are taken, and the data features are extracted, finally, the data characteristics correlation processing is completed.

The cloud storage security model of information data is divided into four parts, including the CSP user authorization center, cloud storage server, GPS information data owners and data user. In the model design, the user information cloud storage data attribute matching management uses scalar time series, the ciphertext is read, in order to realize the adaptive cancellation properties, the position change operation center is required, and the proxy re encryption key is authorized as the private key storage institutions. According to the user and level, authentication mechanism of cloud storage data terminal ciphertext is divided into three levels respectively.

(1) The authorization center of user information data. Authorization center is similar to the CA authentication mechanism, including the registration management server, key generation and key distribution server hardware configuration, in the implementation of encryption and authentication, the private key authentication properties are called for authorizing the Setup replacement algorithm, encryption attribute is generated. Through master key MSK, the encrypted ciphertext is obtained, and it is written to the HDFS framework. The secret key SK_L is generated and the serial number is ser.

(2) The data information owner. As the data owner, user privacy information need to be accessed, and the custom access structure is W, the Encrypt algorithm is designed to obtain the private key attribute CT. CT is put in the cloud storage server to establish the new CHUNKS.

(3) The data users. Data users is put in the GPS service platform terminal, it is at the bottom of the cloud storage network node, by authorization center, MooseFS distributed file system is set copy files, and the encrypted ciphertext CT is accessed, through private property reduced rank proxy encryption algorithm, open source distributed file system is designed, and the adaptive cancellation property ciphertext and change is realized.

Algorithm design and key technology

On the basis of user information data encryption model design as above, the encryption algorithm is improved, and the algorithm is described as follows:

Firstly, the data model is established, assumed the cloud storage information series is constituted by two order sets with p distributed attributes, it is expressed as: $\Omega = \{att_1, att_2, \cdots, att_n\}$.

Where, the order is p, the value of the user information data in attribute att_i can be expressed as: $A_i = \{v_{i,1}, v_{i,2}, \cdots, v_{i,n_i}\}$.

Using adaptive attributes revocation method to obtain the data of mobile social network, the new private key of user authorization information center is: $L = [L_1, L_2, \cdots, L_n]$.

Where, $n_i = |A_i|$, the formula shows that when the user access the authorization center of network information reception, an open source distributed file system should be established, assumed that $L = [L_1, L_2, \cdots, L_n]$ is the private key attribute set, the key attribute certification is recalled, the access codes of certification center is $W = [W_1, W_2, \cdots, W_k]$. By calling the writing position, the bilinear mapping of access strategy in the key attribute is represented as: $e: G \times G \to G_1$. The agent re-encryption technology is designed through the scheme, ReEncrypt decryption scheme is designed, the agent re-encryption key is computed, and the bilinear mapping and reduced rank processing are taken, the computational complexity can be reduced, the process is divided into the following steps:

(1) $Setup(1^k)$: security key parameters are set, and the length of ciphertext is input, the management services are selected in random, defined $h \in G$ and $y \in Z_p$, $t_{i,j} \in Z_p (i \in [1,n], j \in [1,n_i])$.

In the cloud storage data authorization center of user information, the authorization center computed: $T_{i,j} = g^{t_{i,j}} (i \in [1,n], j \in [1,n_i])$, where, $Y = e(g,h)^y$. The private key attributes of parallel network is computed, and formula is: $MPK = (e,g,h,Y,T_{i,j}(i \in [1,n], j \in [1,n_i]))$.The master key of registered management server is: $MSK = (y, t_{i,j}(i \in [1,n], j \in [1,n_i]))$. Write data information by MooseFS, the initial sequence number is obtained, it is: $ser = 1$, and the authorization center is stored as (ser, MSK).

(2) $KenGen(MSK, L)$: The mobile position change information of cloud storage system is input into the user attribute set, because $r \in Z_p$, we calculate h^{y+r}, when $\forall v_{i,j} \in L$, we get $D_{i,j} = (T_{i,j})^r$. The private key of user information is returned:

$$SK_L = (ser, h^{y+r}, \forall v_{i,j} \in L : D_{i,j} = (T_{i,j})^r, g^r, L) \quad (1)$$

(3) $Encrypt(MPK, M, W)$: The information to be encrypted is generated, and access strategy is randomly selected, it is $s \in Z_p$, set: $C_1 = MY^s$, $C_2 = g^s$, and $C_3 = (h^s, \forall v_{i,j} \in W : X_{i,j} = (T_{i,j})^s)$, the attribute matrix of private key is reduced in rank, the output ciphertext is expressed as:

$$\frac{Me(g,h)^{ys} e(g^r, h^s g^{sp})}{e(g^s, h^{y+r}) e(g^s, g^{rq})} = \frac{Me(g,h)^{ys} e(g,h)^{rs} e(g,g)^{rsp}}{e(g,h)^{ys} e(g,h)^{rs} e(g,g)^{rsq}} \quad (2)$$

In the formula, $p = \sum_{v_{i,j} \in W} t_{i,j}$,. $q = \sum_{v_{i,j} \in AS} t_{i,j}$. If the system has attribute update and revoke, the authorization center calls $ReKeyGen$ and $ReKey$ algorithms, the agent re-encryption key and the key corresponding to users are generated. Last, the ciphertext is written as $CT = (ser, C_1, C_2, C_3, W)$, it is uploaded to the cloud storage server. Introduced CSP and the trusted third party, the communication channel between the user, CSP and the trusted third party is established. Check the CT sequence number between the ciphertext and user are consistent, if they are not consistent, the CT is outputted directly, and the redundant bits are processed with retransmission. According to $v_{i,j} \in \beta$, and $v_{i,j} \in W$, compute: $C_3' = (h^{sm}, \forall v_{i,j} \in W : X_{i,j}' = (T_{i,j})^{sck_i})$. Where, $m = \sum ck_i$. Finally, output re-encrypted ciphertext: $CT' = (ser+1, C_1, C_2, C_3', W)$.

Through the above encryption scheme, the data encryption storage and transmission of the position change in social network are realized in the cloud storage terminal, the algorithm is improved.

Simulation test

In order to test the performance of the algorithm, the simulation experiment is take for private key attribute encryption algorithm realization, it is taken based on the Matlab simulation software, the original data are samples from the GPS supplier, the collection period is from 2010 January to 2013 January, in order to protect the privacy and security with position changes in the network, this algorithm is used to encrypt the information, to improve safety performance data in GPS cloud storage data management system, the experimental environment is shown as: Pentium (R) 4 CPU, 3.00GHZ, PC 512M memory, the parameters are set as: $t_{\max}$=1000, M=100, l=256, p_m=0.043, p_c=0.35. In the simulation test, the evaluation parameters such as public parameter (MPK), the master key (MSK), the user private key (SK) and the encrypted message (CT) size are computed for comparison with 4 different algorithms, and the simulation results are shown in Figure 1~4. The results show that using this method, the computation complexity s much lower than the conventional encryption schemes, and the parameters of encryption is better than the traditional method, and this is because this method ensures the length of ciphertext is relatively small and system attributes revocation. Through the cloud storage data encryption scheme, it is applied to the GPS mobile network data information management, and it can effectively protect user privacy security.

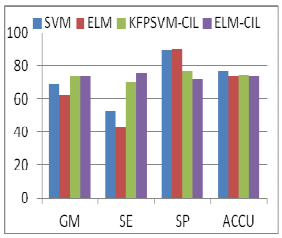

Figure 1. MPK results

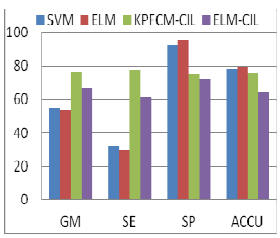

Figure 2. MSK result

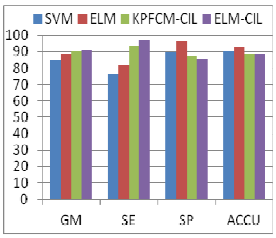

Figure 3. SK results

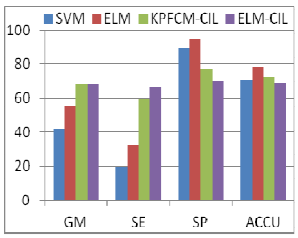

Figure 4. CT results

Conclusion

In this paper, the location mobile social networks information privacy protection under the environment of cloud storage and data security of encryption is researched, an improved encryption algorithm based on key attributes of reduced rank agent is proposed, the data encryption storage and transmission of the position change in social network are realized in the cloud storage terminal, the algorithm is improved. The indexes as MPK, MSK, SK and CT are taken for evaluation, the simulation results show that it can ensure the length of ciphertext is relatively small, and it has low computational complexity with more security, and it has the very good practical value in encryption communication and privacy protection fields.

Acknowledgement

These works are supported by The project development plan of science and technology of Jilin Province under Grant No.20130412010XH

References

[1] Zhu Q Y, Yang X F, Ren J G. Modeling and analysis of the spread of computer virus [J]. Communications in Nonlinear Science and Numerical Simulation, 2012, 17(12), 5117–5124.

[2] FEMANDO N, HONG Y, and VITERBO E. Flip-OFDM for Unipolar Communication Systems[J]. IEEE Transactions on Communications, 2012, 60(12): 3726-3733.

[3] BARRO D J F, WILSON S K, and KAHN J M. Comparison of orthogonal frequency-division multiplexing and pulse-amplitude modulation in indoor optical wireless links[J], IEEE Transactions on Communications, 2012, 60(1): 153-163.

[4] CHEN L, Brian K, and JAMIE E. Theoretical Characterization of Nonlinear Clipping Effects in IM/DD Optical OFDM Systems[J]. IEEE Transactions on Communications, 2012, 60(8): 2304-2312.

[5] DUNG H, BANG H, PARK C S, et al. PAPR reduction using PTS with low computational complexity in coherent optical OFDM systems:18th Asia-Pacific Conference on Communications,2012[C], Jeju Island:IEEE 2012: 629-634.

Advanced Materials Research Vols. 989-994 (2014) pp 2012-2015
© (2014) Trans Tech Publications, Switzerland
doi:10.4028/www.scientific.net/AMR.989-994.2012

Network intrusion detection model based on genetic algorithm optimizing parameters of support vector machine

LIU Chun[1,a]

[1]Sichuan College of Architectural Technology, Network Management Center, Deyang 618000, China

[a]52236025@qq.com

Keywords:network intrusion detection;support vector machine;model parameters;genetic algorithm

Abstract. Intrusion detection is an emerging area of research in the computer security and networks with the growing usage of internet in everyday life. Parameters selection of support vector machine is a important problems in network intrusion detection. In order to improve network intrusion detection precision, this paper proposed a network intrusion detection model based on parameters of support vector machine (SVM) by genetic algorithm. The performance of the model was tested by KDD Cup 99 data. Compared with other network intrusion detection models, the proposed model has significantly improved the detection precision of network intrusion.

INTRODUCTION

With the increasing popularity and complexity of computer network intrusion, intrusion detection has received more and more attention for the security of computer systems[1].

There are generally two intrusion detection methods: misusing detection and abnormal detection. The foundation of misusing detection is constructing an attack conduct feature base and use feature matching method to confirm attack affairs; Abnormal detection is based on constructing normal conduct model and determine whether the subsequences deviates from the normal conduct model to make intrusion detection[2]. The former researchers injected many kinds of machine learning methods into IDS research, such as neural net, genetic algorithm, etc[3,4]. However, these traditional intrusion detection methods always need perfect and quantity of training data to acquire desirable detection properties and the training time is always too long. Unfortunately, the data sample we can acquire in the intrusion detection field appears variable; small and with high dimension and can not satisfy this kind of requirements. These data sets are too difficult for the traditional machine learning algorithms to deal with [5]. Support vector machines (SVM) is a machine learning method derived from the statistical learning theory, it has shown growing popularity and has been successfully applied to network intrusion detection. SVM provides a generic mechanism that fits the hyper plane surface to the training data using a kernel function. When SVM is used to establish network intrusion detection model, the parameters that should be selected include penalty parameter C and the kernel function parameters.

In order to improve network intrusion detection precision, this paper proposed a network intrusion detection model (GA-SVM) based on SVM parameters by genetic algorithm, and the performance of GA-SVM is tested by simulation experiments using KDD-DUP-99 data sets.

PROPOSED SCHEME

A.Principle of SVM

Let the given training data sets be represented by(x_i, y_i), i=1,2…,n, where $x_i \in R^d$ is an input vector, $y_i \in R$ is its corresponding desired output, and n is the number of training data. In SVM a linear function is constructed:

$$f(x) = \omega^t g(x) + b \tag{1}$$

Where, ω is a coefficient vector and b is a threshold.

The loss function is defined as:

$$\begin{aligned} L^{\varepsilon}(x, y, f) &= |y - f(x)|_{\varepsilon} \\ &= \max(0, |y - f(x) - \varepsilon| \end{aligned} \tag{2}$$

Where, ε is a positive parameter that allows approximation errors smaller than ε. The empirical risk is

$$\mathrm{R}_{emp}(\omega)=\frac{1}{n}\sum_{i=1}^{n}L^{\varepsilon}(y-f(x_i)) \tag{3}$$

Other than the ε-intensive loss, SVM tries to reduce the model complexity by minimizing $|\omega|^2$. This can be described by slack variables ξ_i and $\hat{\xi}_i$.. Subsequently, the SVM approximation is obtained as the following selection problem [9].

$$\begin{aligned}&\min \frac{1}{2}|\omega|^2+C\sum_{i=1}^{n}(\xi_i+\hat{\xi}_i)\\&s.t.\\&\begin{cases}y_i-f(x_i)\le\varepsilon+\xi_i\\f(x_i)-y_i\le\varepsilon+\hat{\xi}_i\\\xi_i,\hat{\xi}_i\ge 0\end{cases}\end{aligned} \tag{4}$$

Where, C is a positive constant to be regulated. By using the Lagrange multiplier method, the minimization of formula (4) causes the problem of maximizing the following dual selection

$$\begin{aligned}\max &\sum_{i=1}^{n}y_i(\hat{\alpha}_i-\alpha_i)-\varepsilon\sum_{i=1}^{n}y_i(\hat{\alpha}_i-\alpha_i)-\\&\frac{1}{2}\sum_{i,j=1}^{n}(\hat{\alpha}_i-\alpha_i)(\hat{\alpha}_j-\alpha_j)K(x_i,x_j)\end{aligned} \tag{5}$$

Where, $\hat{\alpha}_i$ and α_i are Lagrange multipliers, and kernel $K(x_i,x_j)$ is a symmetric function, here the Gaussian function is used as kernel

$$K(x,y)=\exp(-\frac{\|x-y\|^2}{2\sigma^2}) \tag{6}$$

Then the approximation function is represented by Lagrange multipliers, namely

$$f(x)=\sum_{i=1}^{P}(\hat{\alpha}_i-\alpha_i)k(x_i,x_j)+b \tag{7}$$

SIMULATION RESULTS

A.Experiment data

The experiment data are from KDD Cup 99 which sets contains 7 weeks' internet flow rate, about 5,000,000 connecting records and has four categories of attacks: DOS: Denial of service, R2L: Unauthorized access from a remote machine, U2R: Unauthorized access to local super user privileges, Probing: Surveillance and other probing.

B.Comparison models and evaluation criterion

In order to make the detection results of GA-SVM comparable and persuasive, two comparison model are chosen, SVM1: which the parameters of SVM are selected randomly, and SVM2: the he parameters of SVM are selected grid search. The models' performances are evaluation by the three measures called precision, recall, and train times. Precision refers to how the experimental values and observed values are close to each other.

$$precision=\frac{TP}{TP+FP} \tag{8}$$

Where, *TP*, *FP* are the number of True Positives and False Positives respectively.

Recall is defined as the fraction of relevant documents that are retrieved.

$$recall=\frac{TP}{TP+FN} \tag{9}$$

Where, *FN* is the number of False Negatives respectively.

C.Data scaling

To avoid numerical difficulties during the SVM training, each feature can be linearly scaled to the range [0, 1] by formula (10).

$$x_i^{'} = \frac{x_i - \min(x_i)}{\max(x_i) - \min(x_i)} \tag{10}$$

Where, x_i is original value, $x_i^{'}$ is scaled value, max(x_i) obtains the max value of the feature value, and min(x_i) is low bound of the feature value.

D.Results and analysis

The optimal parameters of SVM are used to establish to the network intrusion detection model, the detection results are shown in figure2. We can see from figure 2 that the GA-SVM can obtain high network intrusion detection precision and recall, and it is an effective network intrusion detection model.

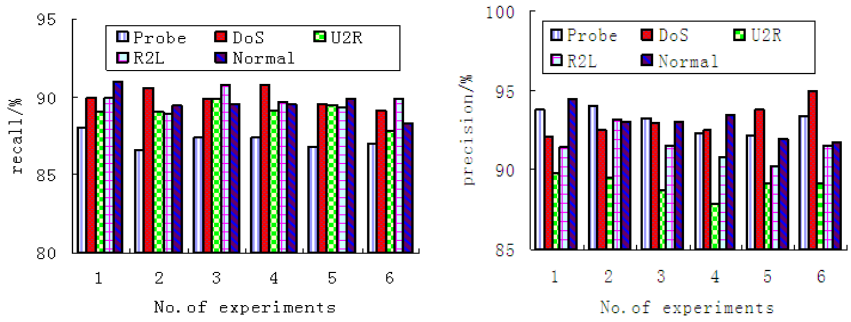

(a) the detection recall (b) the detection precision

Figure2 The detection results of GA-SVM

The detection results of c*omparison mod*els SVM1 and SVM2 are shown in figure 3~4. The experimental results in figure 2~4 are analyzed and conclusion can be obtained that Compared the SVM1, GA-SVM has improved detection precision and recall of network intrusion, so the performance of GA-SVM can be greatly improved to ensure the safe of the network.

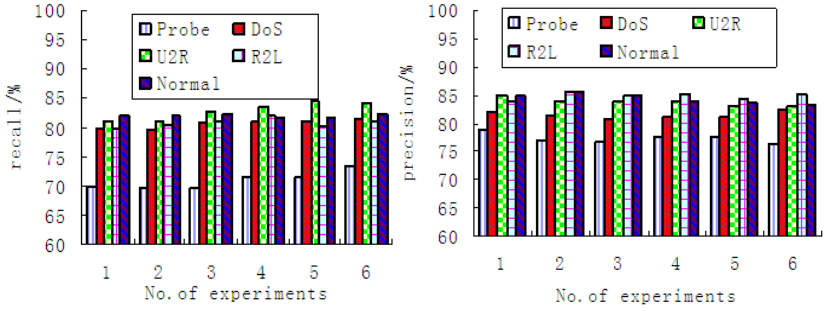

(a) the detection recall (b) the detection precision

Figure3 The detection results of SVM1

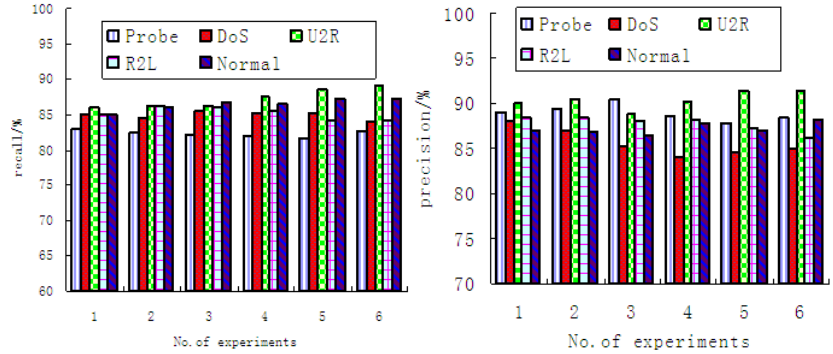

(a) the detection recall (b) the detection precision

Figure4 The detection results of SVM2

CONCLUSIONS

Nowadays improving the ability of IDS to detect attacks accurately is the primary problem facing in IDS manufacture. Good setting parameters of SVM are very crucial for network intrusion detection model, and the paper proposed a network intrusion detection model based on SVM parameters by genetic algorithm. The simulation results showed that GA-SVM has a better performance and has wide application prospect in the field of network security.

REFERENCES

[1] Panda M, Patra MR. Bayesian. Belief network with genetic local search for detecting network intrusions. International journal of secure digital information age 2009; 1(1):34-44.

[2] Khan L., Awad M., Thuraisingham B. A new intrusion detection system using support vector machines and hierarchical clustering. The VLDB Journal, 2007,16(2):. 507-521.

[3] Zhang CL, Jiang J, Karnel M. Comparison of back propagation learning and radial basis function network in Intrusion detection system. In: Rough set, fuzzy set, data mining and granular computing, 2003; 2639:466-70.

[4] Tavallaee M, Stakhanova N, Ghorbani A. Towards credible evaluation of anomaly based intrusion detection methods. IEEE Transaction on System, Man and Cybernetics. Part-c, Applications and Reviews, 2010; 40(5):516-24.

[5] Natesan P., Balasubramanie P., Gowrison G. Improving attack detection rate in network intrusion detection using adaboost algorithm with multiple weak classifiers. Journal of Information and Computational Science, 2012, 8(8): 2239-2251.

Advanced Materials Research Vols. 989-994 (2014) pp 2016-2019
© (2014) Trans Tech Publications, Switzerland
doi:10.4028/www.scientific.net/AMR.989-994.2016

A New Method of Face Modeling with Construction of Local Texture Model

Jinbao Shan[1,a], Weiwei Jiang[1,a], Shile Mu[1,a]

[1]Shandong Institude Of Commerce And Technology，Collage Electronic angd information ,Jinan Shandong 250103

[a]breathe-by-night@163.com

Keywords: active shape model; feature extraction; texture model; face modeling;

Abstract. The active shape model (ASM) is a statistical parametric model, which is mainly used in image feature extraction. On the basis of the analysis of the original ASM texture model, a new texture modeling method was proposed in this paper. The improved method fully utilized the gray level information of adjacent points in the neighborhood of sampling points, improved the original face modeling method which only used the one-dimensional gray information with model matching accuracy problems. The experiments on Weizmann face database Indicate that, the improved method can obviously improve the feature point positioning accuracy, and accelerate the speed of face model fitting.

Introduction

With the rapid development of computer graphics, facial modeling based on computer graphics developed to the intelligent accurate direction. Face modeling is just to build local texture model and do the face image restoration by means of the accurate facial feature extraction. On the basis of the feature points, the face recognition and computer vision was realized[1]. Study of face modeling and recognition involves image processing, pattern recognition, cognitive science, artificial intelligence and other related science, and now face modeling is widely applied to the field of artificial intelligence, identification, security system design. The research and design of face modeling algorithm based on the local texture model constructing have become the subject of computer image processing topic [2].

In recent years, face feature extraction method based on the statistical model have developed widely. There are two kinds of method typically, one is the active shape model and another is active appearance model. The active shape model (ASM) [3] was proposed by T. F. Cootes in 1995. At the beginning it was put forward to solve the problem of medical image. ASM directly benefits from the variable model of ACM [4], which can extract the target feature points of external shape, and also can accurately extract the target internal shape and feature point. In 1998, Cootes et al. proposed the active appearance model (AAM) based on the ASM algorithm [5]. This model is mainly to add texture model based on shape model ASM, it not only uses the shape information of objects and makes full use of texture information of the target object. At present, these two methods are widely used, and ASM is better than AAM in the location accuracy of feature points, while the AAM is better in image texture matching.

The original ASM method only consider the gray correlation information between a point and its neighboring points, but ignore the standard gray information of other point fixed near the neighborhood in the establishment of local texture model. On the basis of the research of the improved algorithm before, a weighted algorithm is proposed for the sampling points based on neighborhood. First we find a standard around the adjacent point of normal direction, then sample the feature points along the normal direction, obtain the gray information point of the current sampling by weighting method, and we establish a robust local texture model finally. The experiments conducted on the Weizmann face database verified the matching performance of the improved algorithm.

Active shape model

ASM is a feature matching algorithm based on the statistical parameter. The idea is that describing shape with some key feature points through the selection of a set of training samples, and

then constructing the statistical shape model and local contour model on the basis of shape information, finally finding the minimum point of Mahalanobis distance according to the matching principle of statistical model. The shape parameters of ASM model can change adaptability to characterize the shape of uncertainty. ASM algorithm mainly includes three steps: feature point calibration, statistical model establishment and model matching.

A. Feature point calibration

In ASM, an image shape was described and characterized through the calibration point. A set of calibration feature points formed a set called point distribution model (PDM). The calibration points were general selected in the points which can effectively describe the object contour features local, such as corner points, boundary point, line T and so on. In PDM, a human face images can be represented as:

$$s = (x_1, y_1, \cdots x_i, y_i, \cdots x_v, y_v)^T \tag{1}$$

Wherein, (x_i, y_i) is the two-dimensional coordinate of feature point i in the PDM model, and v is a face image calibration point number.

B. Statistical model establishment

In ASM, the statistical model includes statistical shape model and statistical texture model. We first establish a statistical shape model, and eliminate the effects of non shape factor through the shape transformation and alignment, then do the statistical analysis of the training set between shapes, and finally establish a parametric statistical pattern contour model. Principal component analysis (PCA) is a fast, linear transformation method, the maximum variance conditions to find the best method which can reflect a kind of transformation and projection method of original data. A statistical model was established using PCA and the process is shown as:

(1) Calculation of the average shape of face set:

$$\bar{s} = \frac{1}{N}\sum_{i=1}^{N} s_i \tag{2}$$

(2) Calculation of the corresponding covariance matrix:

$$C = \frac{1}{N-1}\sum_{i=1}^{N}(s_i - \bar{s})(s_i - \bar{s})^T \tag{3}$$

(3) Calculation of the characteristic value λ and characteristic vector p of the covariance matrix ,and the characteristic value was put in descending order, the largest characteristic vector $[\lambda_1, \lambda_2, \cdots \lambda_n]$ was selected as such rules:

$$\frac{\sum_{i=1}^{n}\lambda_i}{\sum\lambda_i} \geq \eta \tag{4}$$

Wherein, η is the proportion of first n numbers in all characteristic value, which has a selection in 95%~98%.

(4) Characteristic vectors $p = [p_1, p_2, \cdots p_n]$ corresponding to the characteristic value of n numbers are selected to establish a linear statistical model:

$$s = \bar{s} + Pb \tag{5}$$

Wherein, $\bar{s}$ is the mean shape, P is to convert the vector, b is the shape parameter vector. To avoid over fitting phenomenon, b is limited in:

$$-3\sqrt{\lambda_i} \leq b_i \leq 3\sqrt{\lambda_i} \tag{6}$$

For the point j in the image i, in the normal direction of the point and its neighboring points on the line, we sample k points along the sides which form the gray vector of the point:

$$y_{ij} = [y_{ij,1}, y_{ij,2}, \cdots, y_{ij,2k+1}]^T \tag{7}$$

The local contour model of the training set image can be established according to the method of the sampling gray information, and the average gray vector and covariance matrix are expressed as follows:

$$\overline{y_j} = \frac{1}{N}\sum_{i=1}^{N} y_{ij} \tag{8}$$

$$C_j = \frac{1}{N}\sum_{i=1}^{N}(y_{ij} - \overline{y_j})(y_{ij} - \overline{y_j})^T \tag{9}$$

C. Model matching

The characteristic vectors of local statistical model can be obtained from each calibration point through the above gray sampling method. In ASM matching process, the Mahalanobis distance between the designated local contour and the local contour model and training images are calculated, and the best matching point is the candidate of minimum Mahalanobis distance. For the input test image of a feature point, the Mahalanobis distance is computed by the method of sampling gray:

$$d = (y_j - \overline{y_j})^T C_j^{-1}(y_j - \overline{y_j}) \tag{10}$$

The improved active shape model

The above optimization method has improved ASM matching performance, but through the analysis, the sampling gray points in the normal direction was only took in the direction normal to the sampling point information, and did not consider each point and the neighborhood of point of information. Because of the great effect of the sampling points around the point information of the sampling point, so the points were sampled in the normal sampling point neighborhood in this paper, which can make full use of gray level information of each sampling point neighborhood. This method can better get the texture information of feature point and the neighborhood, so as to provide reliable basis to extract more accurate and face location the key feature points.

The improved method proposed in this paper was specifically shown in Figure 1(b), two gray points were sampled on the nearby of the normal sample points, which were sampled in the vertical direction of normal gray. Suppose the two new sampling points around B are B_r and B_l respectively, the new gray information of point B can be expressed as:

$$Y_B = \alpha . y_{B_r} + \beta . y_B + \gamma . y_{B_l} \tag{11}$$

Wherein, Y_B is the new gray information of point B, α, β, γ are the weight parameters. We often choose the weighting parameters as $\alpha = 0.5, \beta = 0.25, \gamma = 0.25$.

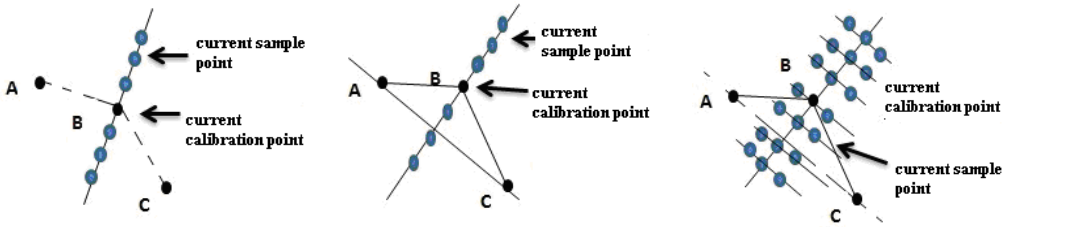

(a) Original method (b) Optimization method (c) Improved method

Figure 1 Building method of local texture model

Experimental results and analysis

The experiment was taken based on the Weizmann face database. This database contained 28 individual, each person has 5 kinds of attitude, 3 lights, 3 kinds of expression. We selected 24 individual, each person had 3 kinds of attitude and 3 lights as training. Calibration feature points on each face were 56. We use different texture model experiment method of constructing ASM, respectively the original method, the optimization method and the improved method. The matching results of the three different texture model construction methods of ASM feature points were shown in Figure 2. Something can be seen from the chart, the original method will bring some errors, and the optimized model can improve the accuracy of feature points with some not well accurate positioning, but the improved method can significantly improve the feature point positioning precision of the ASM.

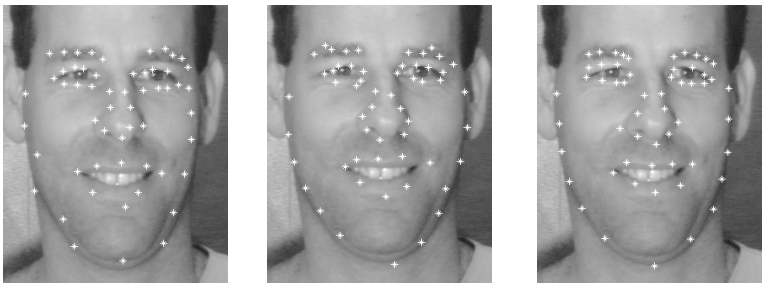

(a) Original method (b) Optimization method (c) Improved method

Figure 2 Matching results of ASM

Comparison of ASM feature point position of different texture modeling method is given, the average error after 10 times of iterative calculation, the lifting percentage is compared with the original method. It can be seen from the table data, the improved method is better than the original method and optimization method, the improved method has the characteristics of lower matching error, while a higher percentage of the ascension, which can reach 11.69%.

Conclusions

Active shape model has been widely used in face recognition as a statistical modeling method based on parameterization. Local texture modeling method in traditional ASM only took gray information between adjacent features into consideration, which will bring large errors to the face modeling. Based on the analysis of the existing optimization algorithm, and a new method of modeling of local texture with full use of adjacent gray information between sampling points was proposed. The experimental results on Weizmann face database show that, the improved method can improve the location accuracy, reduces the matching error. The fitting rate of the model is improved greatly. Experimental results show that the improved method is very effective in the face modeling application.

Reference

[1] Li W, Joshi A, Finin T. CAST: Context-Aware Security and Trust framework for Mobile Ad-hoc Networks using policies[J]. Distributed and Parallel Databases, 2013: 1-24

[2] QIU Bao-zhi, CHEN Xu. Border Image Segmentation Technology for Serious Collision Vehicle in Accident[J]. Computer Simulation. 2013; 30(1): 215-218.

[3] Du Hui. Fast Face Detection in Color Image Based on Wavelet Transform[J]. Bulletin of Science and Technolog, 2012,12(28):89-90.

[4] Qin Yi, Lv Xiaodong, Gong Qiong, E tal. Additional Key Rotation Multiplexing Encryption Using Joint Transform Correlator Architecture[J]. Acta Optical Sinica, 2013, 33(3): 0307002-2 - 0307002-7.

[5] QIU Jing, WANG Ping. Encryption Algorithm for Compressed Image Based on Chaotic Maps[J]. Computer Science, 2012, 39(6): 44-46.

Advanced Materials Research Vols. 989-994 (2014) pp 2020-2023
© (2014) Trans Tech Publications, Switzerland
doi:10.4028/www.scientific.net/AMR.989-994.2020

Simulation of data mining system design in Database

Zheng ruiying[1,a]

[1]School of Mathematics and Computer Science, Jiangxi Science & Technology Normal University, JiangXi Nanchang 330038

[a]zhengruiying@sina.com

Keywords: constraints; information inquiry; database optimization

Abstract. The design of data mining system in database is researched. Vast amounts of information contained in the database, and the data show the diversity of characteristics, resulting in lower efficiency of data mining in database, which database brought greater difficulties to information query. To avoid these shortcomings, database performance optimization method based on cloud computing is proposed. The model of cloud computing data relationship is established to describe the connection between related data inthe database, thus providing the basis for data query. The load state of data nodes is calculated to enable rapid information inquiryin the database. Experimental results show that using this algorithm to optimize data inquiry in database can improve the efficiency of informationinquiry indatabase effectively.

Introduction

With the continuous development of information management technology, the application scope of database are increasing[1]. Information from different fields are integrated together to form a complete database, which can provide valuable information for different industries [2]. Therefore, the database inquiry method, has become a hot issue in the field of information management, and attracts the attention of many scholars [3]. Currently, the main database inquiry methods include database inquiry methodbased on cloud computing, database inquiry method based on spectral clustering algorithm and database inquiry method based on K -means clustering algorithm [4]. Among them, the most commonly used database inquiry method is based on cloud computing. Because the database inquiry method has a wide range of applications, it attracts the attention of many scholars, and becomes a research focus [5, 6].

The optimization methodfor data mining of database

1. A. establishment of cloud computing mathematical relationship model

The number of nodes in the database is set to be p , a data network is constituted by all data nodes , which can be described by the following equation :

$$T = \{t_j \mid 1 \le j \le p\} \tag{1}$$

The data set composed of information from all of the data described by $E(t_T)$, the amount of data information on the node is $n_j = \mid E(t_j) \mid$. Nodes in neighborhood range of specified node t can be describedwith $N(t)$.

The nodes in database is set toconstitute a distributed data network, the set consisted by data in the nodes is $DD = \bigcup_{j=1,2,\ldots,p} ed_j$. ed_j can be used to describe the j -thnode in the database , DD is bandwidth between different nodes in the data network , which can be calculated using the following formula :

$$C = \begin{pmatrix} c_{11} & c_{12} & \cdots & c_{1|ed_p|} \\ c_{21} & c_{22} & \cdots & c_{2|ed_p|} \\ \vdots & \vdots & \cdots & \vdots \\ c_{1|ed_1|} & c_{1|ed_2|} & \cdots & c_{|ed_p||ed_p|} \end{pmatrix} \tag{2}$$

The above formula is required to meet the following conditions:

$$\begin{cases} \forall j,k = 1,2,...,|ed_p| \\ j \neq k \end{cases} \tag{3}$$

Wherein, c_{ij} is the bandwidth value between nodes ed_j and ed_k in the distributed data network.

All the data structures in the database are set to be same, the number of attributes for each data object is n, then the following equation is applied to describe the data elements in the database :

$$ne = (F_1, F_1, \cdots, F_n) \tag{4}$$

Wherein, F_j is the data set composed of all the attributes in the database, and can be describedwith $F_j = \{F_{j,1}, F_{j,2}, \cdots, F_{j,\delta_j}\}$. Therefore, the data object with same data structure can be described by the following equation:

$$F(e) = (F_{1,k_1}, F_{2,k_2}, \cdots, F_{n,k_n}) \tag{5}$$

The related data in the formula required to meet the requirements of the following conditions: $F(e) \in F_1 \times F_2 \times \cdots \times F_n$

Two objects y and z are randomly selected in the database, assuming that the two nodes meet the following requirements, which means that the two nodes are similar.

Rule 1: Node y and z have same value on the F_j property;

Rule 2: similarity attribute of nodes y and z is greater than the similarity threshold, the threshold is usually a constant.

And provided with the corresponding data center of y and z respectively, by the following equation can describe the relationship between two nodes:

$$\begin{aligned} &TP(q,r,F_n,p_j) \to \exists y \in E(q), \exists z \in E(r) \\ &y \neq z \wedge \varpi_{F_j}(F(y)) = p_j \wedge \varpi_{F_j}(F(z)) = p_j \end{aligned} \tag{6}$$

The relationship between above two data centers can be described by the following equation:

$$FP(q,r,y) \to r \neq y \in E(q) \wedge y \in E(r) \tag{7}$$

A data node y is randomly selected in database, the data set constituted of all the equivalent can be described by the following equation: $FPT(q,y) = \{r \mid q \neq r \wedge y \in E(q), z \in E(r)\}$ (8)

2. B. implement database data mining

With cloud computing querying database information, node loads are needed to be tagged in the equivalent node data collection. In the designated time period u, the number of requests for data objects y in data node q is expressed by $M(q,y,u)$,the following equation can be employed to describe the load information of node q :

$$D(q,u) = (M_d, M_v, M_m) \tag{9}$$

M_d, M_v and M_m are load information, the maximum and minimum load capacity of the data node q separately. The following equation is used to describe the overload and under load information of data node:

$$\begin{aligned} Fm(q,y,u) &= \frac{(M(q,y,u) - M_v(q))}{M_v(q)} \\ Ol(q,y,u) &= \frac{(M_m(q) - M(q,y,u))}{M_m(q)} \end{aligned} \tag{10}$$

Combining the above equations, the following formula can be obtained, which can accurately describe the load information data set of equivalent nodes:

$$\begin{aligned} &D(q,y) = \{(r,F,P) \mid r \in F(q,y) \\ &F = Fm(q,y,u), O = Ol(p,x,t)\} \end{aligned} \tag{11}$$

In the above formula, ideally, the load state of data node is $M_m < M_d < M_v$, if $M_d \geq M_v$, the data node is overloading , otherwise , the data node is in idle state.

Experimental results

In order to verify the effectiveness of the proposed method, an experiment is processed. Experimental environment is Visual C + +6.0.

In the process of data mining in database, the related state of experimental sample data can be expressed by the following table:

Table 1 Table of experimental sample data

Data classification	data attribute	attribute data number (ten thousand)
1	Oil	1.2
2	Liquor	2.4
3	Soy source	1.6
4	Automotive	1.7
5	Dairy	2.2
6	Red wine	2.4
7	Cotton	1.8
8	Weather	2.3
9	Industry	2.5
10	Healthcare	0.9

For data with different attributes, traditional algorithms and improved algorithms are employed for data mining separately, the mining results precision can be expressed by the following table:

Table 2 Comparison of precision obtained from different algorithms

Categories of data	Precision ratio（%）	
	Traditional algorithm	Improved algorithm
1	88.7	92.1
2	86.5	93.2
3	88.2	91.9
4	87.2	92.4
5	88.6	93.1
6	85.7	94.2
7	86.2	93.2
8	88.1	91.8
9	86.7	92.4
10	88.2	93.6

According to the data in the above table, with the improved algorithm for database data mining, precision rate is much higher than traditional algorithms, which can provide more accurate data mining results for the database inquiry.

Conclusion

This paper presents a method for optimizing database performance based on cloud computing. The relationship between cloud computing modelsis established to describe the connection between the database data, thus providing the basis for data inquiry. The load state of data nodes are calculated toenable rapid query for information in the database. Experimental results show that this algorithm used for optimizing the database inquiry, can improve the efficiency of database information inquiry.

References

[1] Cline D, Egbert P. Terrain decimation through quad tree morphing. IEEE Trans. on Visualization and Computer Graphics, 2001, 7 (1):62−69.

[2] Intan R. and Mukaidono M. Generalized fuzzy rough sets by conditional probability relations [J]. International Journal of Pattern Recognition and Artificial Intelligence，2002,16(7): 865-881.

[3] M.Gonzalez-Audicana, J.L.Saleta, R.G.Catal, and R.Garcia.Fusion of multispectral and panchromatic images using improved IHS and PCA mergers based on wavelet decomposition[J]. IEEE Transactions on Geoscience and Remote Sensing. 2004, 1, 42(6). 1291-1299.

[4] Tham J Y, Shen L, Lee S L, Tan H H. A generalapproach for analysis and application of discrete multi-wavelettransforms[J]. IEEE Transactions on SignalProcessing, 2000, 48(2) :457~464.

[5] Luciano Alparone, Stefano Baronti. A Global Quality Measurement of Pan- Sharpened Multispectral Imagery [J]. Geoscience and Remote Sensing Letters 2004, 10:313-317.

[6] Wei Xindan. Simulation Research on the Fuzzy C Algorithm In Network Intrusion Protection [J]. Bulletin of Science and Technology. 2012; 28(12): 221-223.

Advanced Materials Research Vols. 989-994 (2014) pp 2024-2028
© (2014) Trans Tech Publications, Switzerland
doi:10.4028/www.scientific.net/AMR.989-994.2024

Analysis on Digital Signal Processing and Algorithm Based on Coherent Light

[1,a] Xing Ye ,[2,b]Zhang Lu ,[3,c]Cheng ZheYuan ,[4,d]GuKai

[1,3,4]Institute of information science and engineering，Southeast university，NanJing，JiangSu，China，210000

[2,]Institute of ship and ocean engineering，Huazhong university of science and technology，WuHan，HuBei，China，430000

[a,b,c,d]94755096@qq.com

Keywords: Coherent light; signal processing; compensation; algorithm.

Abstract. In order to use minimal cost to compensate signal distortion caused by fiber dispersion and carrier phase noise etc, this paper mainly puts forward 2 different self-adaption compensation algorithms in algorithm part of digital signal processing, through test and comparative analysis, it indicates that the performance of the best matching and the nature expression based on GCT is the best.

Introduction

With the gradual pursuit of photo-communication on larger bandwidth, longer distance and higher receiver sensitivity, so communication technology of digital coherent light appears as time requires. Communication technology of digital coherent light can not only increase receiver sensitivity, at the same time it can also get the whole light field information, so that it the incomparable advantages that conventional intensity modulation / direct detection (lM/DD) system can not be compared. The repaid development in communication technology of digital coherent light is profits from high-speed development of new modulation technology and DSP. New modulation technology increases availability of frequency spectrum through flexible way of information loading, with the enhancement of DSP in operational speed, the communication system of digital coherent light has become one of the powerful competitors of optical network in the next generation. This paper mainly puts forward different algorithms of self-adaption dispersion compensation in algorithm of digital signal processing, they are respectively based on technology of time-delay sampling and deviation test technology of symbol sampling. Compared with other algorithms, the algorithm based on time-delay sampling technology can provide larger dispersion scanning step and comparative estimated precision, while algorithm based on sampling deviation test can get comparative or higher estimated precision by fewer symbols.

Communication System of Coherent Light

Communication system of coherent light and direct detection light is similar in structure; it can be still divided into transmitting terminal, fiber channel and receiving terminal. Generally speaking, the effect of transmitting terminal (Tx) in light communication system includes source coding, bit to symbol mapping, modulation of optical carrier, certain pre-compensation etc. At present, large capacity and long distance transmission system uses external modulators, such as MZM. It is composed of 2 phase modulators and their modulation principles are based on optical interference. MZM is divided into SD and DD, of which, the driving voltage of upper and lower arm of SD-MZM is the same, SD-MZM operated in push-pull model can be used for AM and two order phases (0, tt), and SD-MZM operated in push-push model is equal to one phase modulator. Figure 1 shows the diagram optical transfer function and energy transfer function of SD-MZM. The abscissa is the upper and lower voltage difference. By setting different voltage bias and peak value, SD-MZM can realize

modulation of ASK and BPSK. Figure 2 shows MZ working under model of push-pull and push-push.

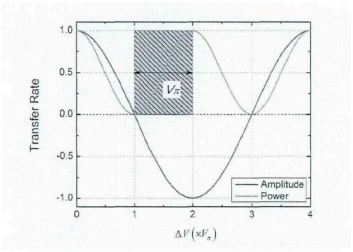

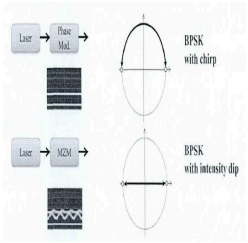

Figure 1 Transfer function of light field intensity and optical energy of SD MZM Figure 2 BPSK signal comparison of phase modulator and MZ modulator

The transfer function of SD-MZM amplitude is the nonlinear function of driving voltage, while most high-order modulation scheme is linear modulation scheme, that means the amplitude of signal I and Q component presents linear distribution relationship. The nonlinear of MZM modulation will result in signal distortion after modulation. In order to eliminate modulation nonlinear of MZM, the transmitter usually needs to make pre-distortion compensation for driving signal of MZM. Figure 3 shows the condition comparison of modulation depth of 16-QAM in signal constellation is respectively 1.0 and 0.3, that means the peal value of driving voltage of MZM is plant: 1.0 time and 0.3 time of T. From this we can see that whether pre-distortion or reduction in modulation depth can all eliminate or reduce nonlinear of MZM modulation, but we should notice that compensation of pre-distortion changes the phase trace among conversion of original symbol.

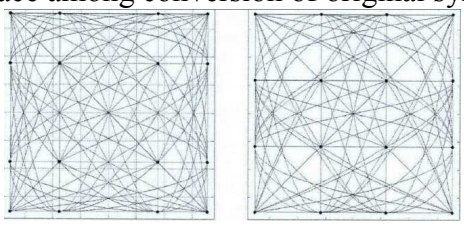

Figure 3 Effect of pre-distortion technology on signal modulation of 16-QAM

The most obvious difference between coherent detection and traditional direct detection lies in that the first one uses self-excitation or laser of phase locking as local oscillator to convert light frequency signal into base frequency or intermediate frequency. Secondly, the balance detector will convert the optical signal after conversion into electric signal; afterwards, analog-digital converter makes sampling for electric signal through certain oversampling ratio. Finally, the digital signal after sampling is transmitted to DSP system to make operations such as distortion compensation, judgment and coding etc.

Algorithm of Fiber Self-adaptation Dispersion Compensation

Self-adaptation dispersion compensation based on MMSE: Add dispersion estimation algorithm in front static dispersion compensation algorithm that means precisely and quickly as far as possible to estimate accumulated dispersion in the link then updates filter coefficients of static dispersion compensation wedge to make corresponding compensation. Because estimated self-adaptation dispersion compensation of MMSE is depend on training sequence. Firstly, its process calculates the dispersion effect of channel through known sequence, and then solves the MMSE answer of filter in time domain or frequency domain. Supposing that channel is dispersion channel and math module of signal is as follows:

$$u = h^T s + n$$
$$E[(s[k])^2] = 1$$
$$E[(n[k])^2] = N_0 \quad (1)$$

Of which, W is the received signal, S is vector of transmission signal, h is response vector of impulse channel, n is noise vector of additivity, the average power of signal is unit power, the power spectral density of noise is N0. The definition of its cost function is as follows:

$$J(w) = E[(e(k)^2] = E[(s(k) - w^T u)^2] \quad (2)$$

Of which, w is the estimated filter coefficient, according to the estimated definition of minimal MMSE, we can get the estimation quantity of W is as follows:

$$\overline{w} = \arg\min\{[(s(k) - w^T u)^2]\} \quad (3)$$

Through certain reduction and dilution, we can finally get representation of A is as follows:

$$\overline{w} = \frac{h^H}{h^H h + 1/\Gamma} \quad (4)$$

Of which, noise-signal ratio is r signal, h is the dispersion channel response calculated by training sequence. We can see that MMSE takes signal noise into consideration when estimating the best filter coefficient. After training sequence estimating impulse response of dispersion channel, it calculates the best filter coefficient, then updates TDE or FFT then updates FDE coefficient. The detailed realization scheme is indicated by figure 4.

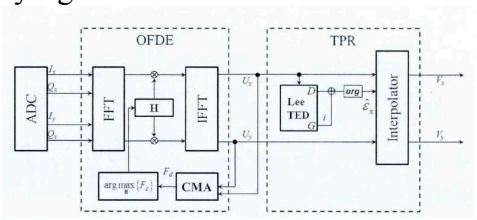

Figure 4 Self-dispersion compensation algorithm chart of OFDE and CMA deviation function

Self-adaptation dispersion compensation based on OFDE and time-delay sampling: Because field of fiber dispersion monitoring is sensitive to cost, time-delay technology generally adopts asynchronous sampling, its principle is very similar to the sampling oscilloscope of test equipment. At this time, supposing driving clock frequency of ADC is fs , the repetition frequency of signal is Rs, sampling interval is T=1/fs.

$$s_1(k) = s(kT + \tau_1)$$
$$s_2(k) = s(kT + \tau_2) \quad (5)$$

At this time, the sampling frequency is far smaller than symbol rate and they need to be integral and multiple relations, it is generally seen that the sampling time interval of ADC 1 and ADC 2 is set as half symbol period. The driving clock of ADC in coherent receiver is proximately 2 times of signal clock, therefore, the time-delay sampling used in coherent system is synchronous time-delay sampling, the relations of sampling rate and symbol rate is as follows:

$$f_s = 2R_s$$
$$\tau_1 - \tau_2 = 1/f_s \quad (6)$$

We can find that the time interval between 2 sampling points of each data is one stable value and it is depend on sampling frequency of ADC. At this time, the date of each polarization state can be understood as the coordinate of certain point in orthogonal coordinate system, the coordinate scheme composed of plenty of points like this is regarded as time-delay sampling scheme. The time-delay sampling scheme produced by X polarization data in zero QPSK system is indicated by figure 5. The self-adaptation dispersion compensation algorithm and principle based on time-delay sampling technology is indicated by figure 6.

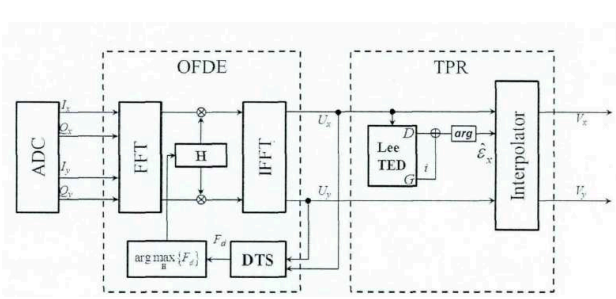

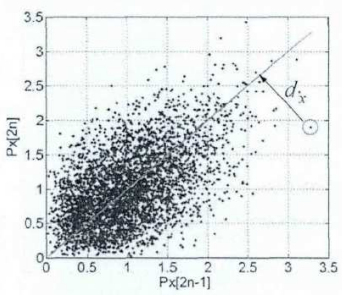

Figure 5 Principle scheme based on OFDE and time-delay sampling technology Figure 6 Time-delay sampling scheme produced by polarization data

If we define the distance from each point to diagonal as one variable d of time-delay sampling scheme, then we can get the following:

$$d_{x(y)} = \left| \frac{|s_{x(y)}[2n]|^2 - s_{x(y)}[2n+1]|^2}{\sqrt{2}} \right| \quad (7)$$

Choose one dispersion estimation parameter from it:

$$Fd=[std(dx)+ std(dy)]/2 \quad (8)$$

Of which, std means the standard difference of data. Dispersion estimated parameter is independently implemented in two polarization state and then eliminate the disadvantaged effect caused by polarization rotation.

Simulation Result and Performance Analysis

In the process of simulation, we use data length of Fd to uniformly set as 512. In addition, considering the feasibility of hardware, this length is respectively the integral time of different FFT length. Figure 7 shows simulation result of 2 kinds of self-adaptation dispersion estimation and compensation algorithm in PDM-NRZ-QPSK system. The simulation has totally carried out 81 independent tests. The sampling phase of receiver is randomly distributed between ±0.5. GCT method adopts GCT power as dispersion estimated parameter. DTS adopts the best matching improvement method of dispersion scanning. The result of precise scanning is subjected to sliding and filter processing of length 10 for one time. The range of precise scanning is rough estimated result ±200ps/nm. We can see that these methods can all get very precise dispersion estimated value in 2 systems. CMA and DTS algorithms have obvious performance degradation in QPSK system when OSNR less than 11db. The algorithm performance based on Lee TRP put forward by this paper is equal to GCT algorithm.

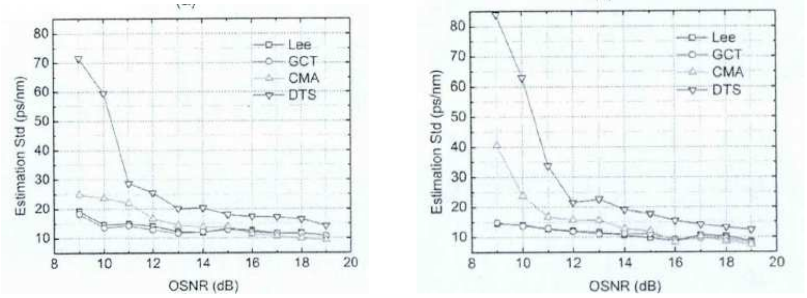

Figure 7 Relations between estimated performance of different self-adaptation dispersion estimation and compensation algorithm and SNRO.

Conclusion

Through theoretical analysis and system simulation, it further finds that these algorithms can be unified the best matching algorithm based on GCT. At the same time, the algorithm nature expression based on dispersion scanning and the best matching of GCT is also introduced in this chapter. The simulation result indicates that nature expression algorithm can get comparative or higher dispersion estimated precision on condition of using the same hardware resources. Through system simulation, this chapter gives the dispersion estimated performance comparison of different algorithms set under

comprehensive channel parameter; the simulation result further indicates that the algorithm performance base on the best matching of GCT and nature expression is the best.

References

[1] Joseph C.Palais. Fiber Communication (the 5th version)[M].. Electronic Industry Press, 2005.
[2] I. P. Erza, Alan P. T. Lau, Daniel J.F.Barros, et al. Coherent Detection in Optical Fiber Systems. Optics Express. 2008. 16(2), 753-791
[3] Chen Jinfa. New Modulation Way Applied in Optical Transmission System of 40Gb/s [J].Optical Communication Technology,2008,32(10),39-41
[4] Dai Chen. LMS Self-adaptation Balaner Used for QAM Signal Mediation [J].Electronic Device, 2005, 28(1), 196-199.
[5] Pan Lijun, Liu Zemin. Blind Equalization Algorithm of Improved CMA+DD-LMS [J].Modern Wire Transmission,2004,25(05),58-60
[6] Gao Lijuan, Study and Analysis on Improved Blind Equalization of CMA [J]. Journal of . Institute of Command and Technology of Equipment, 2006, 17(6), 89-93
[7] Translated by L. Binh, Zhu Yong, Xiang Peng, Wang Yongqiang etc. Digital Light Communication [M]. Electronic Industry Press, 2011.
[8] Du Xiao, Study on Phase Synchronization and Correction Technology in Coherent Light Communication System [D], Beijing: Beijing University of Posts and Telecommunications, 2010.
[9] Yu Yang, Communication and Application of Coherent Light [J]. Physics Bulletin， 2001(9)：18-21.
[10] Gnauck A H, Winzer P J. Optical Phase-shift-keyed Transmission [J]. Journal of Lighfwave Technology, 2005, 23(1): 115-130.

Advanced Materials Research Vols. 989-994 (2014) pp 2029-2032
© (2014) Trans Tech Publications, Switzerland
doi:10.4028/www.scientific.net/AMR.989-994.2029

A New Improved Attribute Weight Algorithm Based on Rough Sets Theory for One Command Information System

YANG Su-min [1,2,a], Yan Ying-min [3,b], Wang kai [2,a], Xie Zhi-ying[2,a]

[1]State Key Laboratory of Complex Electromagnetic Environment Effects on Electronics and Information System, Luoyang 471003,Henan, China)

[2]Department of Information Engineering , Ordnance Engineering College, Shijiazhuang 050003, China

[3]Department of Vehicle and Electrical Engineering, Ordnance Engineering College, Shijiazhuang 050003, China

[a] Email:yangaumin1971@sina.com [b]yym0117@163.com

Keywords: Attribute weight; Attribute importance; Mutual information; Rough sets theory; Information entropy

Abstract: There are various evaluation indicators in command information system. It is important to determine the weight of each indicator because it has a direct impact on the final result for evaluation and decision making. The reasonable and accurate attribute weight is helpful to ascertain the status or effect on the policy decision. With analyzing the deficiency of attribute weighting algorithms based on the rough sets theory, the new attribute weight algorithm is proposed in the paper. The proposed algorithm considers objective weight and subjective weight. The objective weight includes three factors, named as the importance of the attribute itself, the increment of mutual information, and its own information entropy. The subjective weight is obtained by the experts with prior knowledge in the field. Experiment results prove that the new method not only overcomes the deficiency of the existing weight methods, but also is more in line with the actual situation.

0 Introduction

The scientific and effective attribute weight is the most important for one system. At the present many scholars are dedicated to researching on it, and a lot of effective methods of assigning weight are produced. Article [1-5] proposed the objective weight method with the rough sets theory, the proposed algorithm only considered the effect of a single attribute on the decision results, and ignored the interactive influence between attributes, so some of the attribute weights with zero weight are necessary for the decision result are 0. Article [6] considers the overall importance of condition attributes, as well as the individual importance of each attribute, but the assigned weight isn't sometimes isn't line with the actual situation. With improving algorithm of article [6], in the paper the author puts forward one comprehensive attribute weighting algorithm, which consists of objective weight which is gotten by the rough sets theory and subjective weight that the experts give by a priori knowledge, such can make sure to realize the unity of the subjective and objective weight, and can improve the rationality of evaluation results. Experiment results also prove that the proposed algorithm is effective and rational.

1 The Basic Attribute Weight Principle Based on the Rough Sets Theory

Each attribute has different effect on the decision results for one information system. As usual we assign one attribute importance depending on the increment after removing an attribute. If the increment is more, we think the attribute importance is bigger. The attribute weight method based on the rough sets theory is mainly through the attribute importance of decision table. The follow is the correlative definitions.

Definition 1: $S=(U,A,V,f)$ is set as an information system. Among them, $U=\{U_1,U_2,\cdots,U_{[U]}\}$ is non empty finite set which is called the domain space, $A=\{a_1,a_2,\cdots,a_{[A]}\}$ is non empty finite attribute set, which is called the attribute set. $V=\cup A_a, a\in A, V_a$ is attribute's domain range, $f:U\times A\to V_a$ is the information function. When x is a , x has unique value in

V_a .On the other side, for sequence $C(c_1(x), c_2(x), \cdots, c_n(x))$ and sequence $D(d_1(x), d_2(x), \cdots, d_n(x))$, $A = C \cup D, C \cap D = \phi$, $S = (U, A, V, f)$ is called as decision table of the information system, $c_1(x), c_2(x), \cdots, c_n(x)$ is called as the condition attribute set.

Definition 2: For the given knowledge representation system $S = (U, A, V, f)$, the in-discernable relationship of any attribute is as follows:

$$IND(B) = \{(x, y) \in U \times U : \forall a \in B(f(x, a) = f(y, a)\} \quad (1)$$

Definition 3: For the decision table $S = (U, A, V, f)$, the degree that the condition attributes depend on the decision attribute is defined as follows:

$$\gamma_B(D) = |POS_B(D)| / |U| \quad (2)$$

Definition 4: For the decision table $S = (U, A, V, f)$, $c \in C$,the importance degree of condition attribute c is defined as:

$$SGF(c) = \gamma_B(D) - \gamma_{C-\{c\}}(D) \quad (3)$$

The weight of the condition attribute is defined as:

$$W(c) = \frac{SGF(c)}{\sum_{a \in C} SGF(a)} \quad (4)$$

According to the above formula we can see that the larger $SGF(a)$ is, the more important the attribute is, so the attribute weight is much greater.

2 Attribute Weight Based on Rough Sets Theory

The researchers utilize the relationship between knowledge and information entropy for rough sets theory, so the main concepts and operation of rough sets theory can be performed by the information theory.

Definition 5: U is set a domain , P and U is two equivalent relation of domain U (knowledge), $U / ind(P) = \{x_1, x_2, \cdots, x_n\}$, $U / ind(Q) = \{y_1, y_2, \cdots, y_n\}$, then the probability distribution that P and Q effect on the U is defined as follows:

$$[X : p] = \begin{bmatrix} x_1 & x_2 & \cdots & x_n \\ p(x_1) & p(x_2) & \cdots & p(x_n) \end{bmatrix}; [Y : p] = \begin{bmatrix} y_1 & y_2 & \cdots & y_m \\ p(y_1) & p(y_2) & \cdots & p(y_m) \end{bmatrix} \quad (5)$$

Among them, $p(x_i) = \frac{|x_i|}{U}, i = 1,2,\cdots,n; p(y_i) = \frac{|y_j|}{U}, j = 1,2,\cdots,m;$ the symbol $|E|$ is the base of E .

Definition 6: According to the information theory, the information entropy of knowledge P is $H(P) = -\sum_{i=1}^{n} p(x_i) \log p(x_i)$,the conditional entropy $H(Q|P)$ of the knowledge P relative to Q is :

$$H(Q|P) = -\sum_{i=1}^{n} p(x_i) \sum_{j=1}^{m} p(y_j|x_i) \log p(y_j|x_i) \quad (6)$$

The mutual information $I(P;Q)$ of the knowledge P relative to Q is:

$$I(P;Q) = H(Q) - H(Q|P); \quad (7)$$

Definition 7 [3] : The attribute importance is calculated by the increment of mutual information with subtracting one attribute, the definition is as follows:

$$SGF_{old}(c) = I(C;D) - I(\{C - c\}; D) = H(D|C - \{c\}) - H(D|C) \quad (8)$$

3 The Improved Attribute Weight Algorithm Based on Rough Sets Theory

Attribute importance in formula (8) only considers each attribute's effect on the whole decision, without considering attribute itself effect on the result of the decision. So the following results appear: the increment of the mutual information is more bigger, and the corresponding attribute weight is higher, so the attribute is considered as more important, but the actual situation is on the contrary, the attribute is maybe less important. So in the paper the author improves on the algorithm of article [6],and proposes one new importance algorithm with considering important degree of the

condition attribute itself, the increment of the mutual information, as well as information entropy of attribute itself on the decision results , the define is as follows:

$$SGF_{new}'(c)=(I(C-\{c\};D)-I(C;D)+I(c;D))/H(D|c)=(H(D|C)-H(D|C-\{c\})+H(D)-H(D|c))/H(D|c)$$

$$=(H(D|C)-H(D|C-\{c\})+H(D))/H(D|c)-1 \quad (9)$$

The weight is defined as: $W_k(c)=\frac{SGF_{new}'(c)}{\sum_{a\in C} SGF_{new}'(a)}$ （10）

From the above formula, we can see that the corresponding attribute importance is much greater when the mutual information increment is equal and $H(D|c)$ is smaller, attribute importance is much bigger.

In addition, in order to avoid the objective weight disaccord with the actual situation, in this paper the author assigns weight from two sides named as the subjective weight and objective weight, the subjective weight is determined directly by the expert's experience, the objective weight is obtained by formula (10), the comprehensive weight is defined as the following:

$$W_z(c)=\alpha W_s(c)+(1-\alpha)W_o(c) \quad （11）$$

Among them: α is called experience factor, which reflects the extent of the attribute importance, α is affected by the expert experience, the greater it is , the expert's subjective experience affects greatly the result of the decision, when $\alpha=1$, $W_z(c)$ is completely decided by the expert subjective weight

Table1 Decision table of information system

Samples	Wired communication capacity（bps）c_1	Wireless communication capacity （bps）c_2	voice quality c_3	transmission quality c_4	decision results d
1	1	1	1	1	1
2	1	1	2	2	2
3	1	1	3	1	3
4	1	1	3	3	3
5	1	4	1	3	4
6	2	1	1	3	3
7	2	2	1	2	2
8	2	3	1	2	3
9	2	4	2	1	4
10	3	3	1	1	3
11	3	4	3	2	4
12	4	2	2	1	4
13	4	2	3	3	4
14	4	3	3	1	4
15	4	4	2	3	4
16	1	3	2	3	4

4 Algorithm Analysis

In order to verify the effectiveness of the above algorithm, we use it into one command and information system, as shown in Table 1. From it, we can see that the system has 4 attributes, 16 experts give those evaluation results, the condition attributes are $\{c_1,c_2,c_3,c_4\}$, decision attributes are $\{d\}$, the value of set C is set as V={1,2,3,4}, The value of D is set as {1,2,3,4}, which corresponds excellent, good, general, poor state respectively. After pretreatment on the original data, we get the decision table shown in Table 1

The below is the processing in accordance with the algorithm of section 3:

We consider Table 1 as an information system, $U=\{x1,x2,x3,x4,x5,x6,x7,x8,x9,x10,x11,x12,x13,x14,x15,x16\}$, $IND(D)=\{\{x1\},\{x2,x7\},\{x3,x4,x6,x8x10\},\{x5,x9,,x11,x12,x13,x14,x15,x16\}$. The important degree of each attribute is calculated according to the formula (9), the objective weight are listed in table 2:

From table 2, we can see that the weight of attribute c_1,c_2,c_3,c_4 obtained by article [6] were 0.242569, 0.235703, 0.231209, 0.290517 respectively. But the weight of attribute is obtained according to the algorithm proposed in this paper is 0.336972, 0.34979, 0.313238, 0.389046 respectively. In addition, we invite the experts in the field of command and information system to assign the subjective weight for four attribute c_1,c_2,c_3,c_4 as (0.35, 0.35, 0.15, 0.15)respectively.

The experts set experience factor $\alpha = 0.4$ in considering of objective data, the comprehensive weight depending on the formula (11) is obtained as follows:

$W_z(c1) = 0.342183 \quad W_z(c2) = 0.349874 \quad W_z(c3) = 0.247943 \quad W_z(c4) = 0.293428$

In the actual command and information system, the quality of wireless communication capacity plays a decisive role on the operational effectiveness of the whole system because of wireless communication is a large proportion of communication in the current battlefield. From the experiment results we can see that the weight value of c_1 and c_2 is the two largest in the all attributes, the weight of c_3 and c_4 are the least in the all attributes, which is completely in line with the actual situation, so the experiment results verify that the proposed algorithm in this paper is rational and effective.

Table 2 The attribute object weight

attribute	$H(D)$	$H(D\|C)$	$H(D\|\{C-c\})$	$H(D\|c)$	$SGF_{old}(c)$	$W_{old}(c)$	$SGF'_{new}(c)$	$W_k(c)$
c_1	4.3923	0	0.2875	1.5558	1.2683	0.242569	1.638385	0.336972
c_2	4.3923	0	0.2875	1.5199	1.2324	0.235703	1.700704	0.34979
c_3	4.3923	0	0.3810	1.5899	1.2089	0.231209	1.522989	0.313238
c_4	4.3923	0	0	1.5190	1.5190	0.290517	1.891573	0.389046

5 Conclusion

In view of the deficiency of the attribute weight method based on the rough sets theory at present, the author proposes one new comprehensive attribute weight algorithm including the objective weight and subjective weight. The subjective weight can correct the deviation caused by the object weight. The objective weigh based on rough sets theory includes three factors, named as the importance of the attribute itself, the increment of mutual information, and its own information entropy change. Experiment results prove that the new proposed method completely avoids the weight 0, and it is more effective and reasonable than the existing algorithm.

References

[1] Wang Hongkai, Yao Bingxue,Hu haiqing. The method of ascertaining weight based on rough sets theory [J].Computer engineering and application, 2003(36): 20- 21.

[2]Tan zongfeng, Xu zhangyan, Wangshuai. An improved ascertaining weight based on rough sets theory [J], Computer engineering and application, 2012, 48(18): 115- 118.

[3] Miao Duoqian,Fan Shidong. The calculation of knowledge granulation and its application [J]. System engineering theory & practice, 2002(1):48- 56.

[4]Wang guoKuang. Rough theory and knowledge acquisition[M] . Xi'an jiao tong university press, 2001.

[5]Bao xinzhong,Liu cheng.A new method of ascertaining attribute weight based on rough sets theory[J], Journal of management, 2009,Vol. 6(6):729-732.

[6]Yanyan,Yang huizhong. Knowledge reduction algorithm based on mutual information [J],tsinghua science and technology,2007,47(S2):1903-1906.

Advanced Materials Research Vols. 989-994 (2014) pp 2033-2036
© (2014) Trans Tech Publications, Switzerland
doi:10.4028/www.scientific.net/AMR.989-994.2033

Research on Leaning and Evolutionary Algorithm of Agent for Task Oriented

XU Guo-feng[1, a], CAI Yuan-wen[2]

[1]Company of Postgraduate Management, the Academy of Equipment, Beijing 101416, China

[2]Department of Space Equipment, the Academy of Equipment, Beijing 101416, China

[a]xuguofeng334@163.com

Keywords: Task Oriented； Agent； Leaning and Evolution

Abstract. The leaning and evolutionary (L&E) algorithm of Agent for task oriented is deeply researched in this paper. Based on the relationship between tasks and the executive Agent, the importance of the research has been elaborated. Moreover, the algorithm is improved by considering the effect of environment and network structure. Reinforcement leaning and complex network have been introduced into the nonlinear genetic algorithm. Finally, some simulations of equipment acquisition tasks are made to test the validity and capability of the algorithm.

Introduction

Agent based modeling and simulation [1] is widely used to solve kinds of complex issues, such as space launch, equipment acquisition, etc. Leaning and evolution (L&E) is not only the foundation for Agent in “society” or “environment”, but also the main character of adaptability of Agent [2]. Task oriented has been the main solution to solve the problems. Besides, the evaluation of the effect of task completion is greatly decided by the executor. So how the executer learns and evolutes will affect the task completion is becoming more and more important point. Nowadays, most of the research about the L&V focuses on the Genetic Algorithms (GA) or improved GA [3,4]. However, the main defect of the algorithm of Agent L&V is that the consideration of the impact of the environment and network structure is not enough.

In this paper, nonlinear genetic algorithm (NGA) [5] is firstly introduced into the algorithm of Agent L&E. Its main part is that the factor of crossover and mutation probability was designed for adaptive changes according to the hormonal regulation of law, which reflects the adaptive characteristics of Agent. Besides, reinforcement learning [6] was concerned to reflect the effect of environment on Agent. Subsequently, the network structure [7] and the node state of Agent is studied.

The rest of the paper is organized in the following sequence. In section 2, the relationship between task and the executer is introduced in detail. In section 3, the algorithm of Agent leaning and evolutionary is redesigned. In section 4, some simulations of equipment acquisition are made to test the validity and capability of the algorithm. Concluding remarks are summarized in the final section.

The relationship between task and the executer

The relationship between task and the executer is illustrated in Fig. 1.

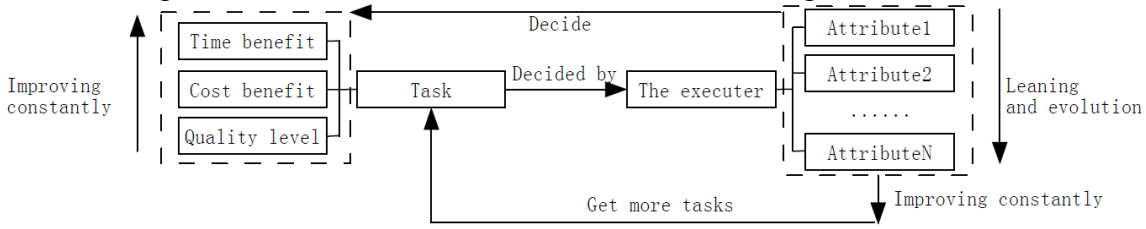

Fig.1 The relationship between task and the executer

1. In the competitive environment, the executer only by constantly improve the relevant properties of its own, to obtain the most objective task, also bring more revenue.

2. Attributes of the executer improved will improve the task completion effect as well.

3. The other executer will get changed, which have supply and cooperate relationship.

Therefore the process of the improvement of executers is abstracted as Agent L&E.

Redesign of the algorithm of Agent L&E

The solution of the redesign is shown in Fig.2.

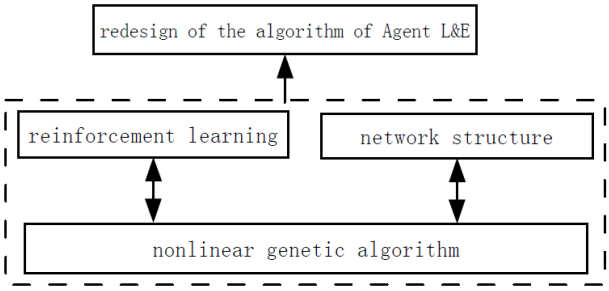

Fig.2 The solution of the redesign

In this section, the redesign is shown as follows:

1. Chromosome and the encoding mechanism

The attributes which mostly reflect the Agent and impact the task completion are selected as the chromosomes. According to the different types of parameters, a hybrid encoding mechanism of decimal and binary is recommended.

2. Fitness function

Fitness function is used to describe the performance of Agent in the environment and the adaptability. Fitness is adjusted according to the performance of Agent and change the corresponding individual fitness value, so as to provide a basis for genetic manipulation and evolution. Fitness function is redesigned from the following two aspects: □The number of tasks completed. Time, cost and quality evaluation of tasks completed. The form of the function can be expressed as follows:

$$fitness = \omega_1 * (1 - a^N) + \omega_2 * (1 - a^{e_time}) + \omega_3 * (1 - a^{e_cost}) + \omega_4 * (1 - a^{e_quality}) \quad (1)$$

where $\omega_1, \omega_2, \omega_3$ and ω_4 represent the weight of each item. The parameter a is the normalized parameters ($0 < a < 1$). N denotes the number of tasks completed. Besides, the symbol 'e_time' is the time evaluation, which can be obtained through the calculation between the actual completed time and the expected time. Similarly, the parameter e_cost can be obtained. And the $e_quality$ is from specify quality evaluation index system.

3. Optimized design of genetic operator

(1)Selection and crossover operator

If the population is fewer, a shock will appear in evolution direction when the individual having largest fitness is not selected. To avoid this situation, two strategies are put forward as follows:

□The best individual should be reserved forcibly, which will bring monotone increasing to the largest fitness.

□When the individual is sorted by fitness, the ones having smaller fitness will be removed in proportion. Subsequently, the individuals having larger fitness will be selected to reproduce cross.

The crossover probability is from the nonlinear genetic algorithm.

$$P_c = P_c^0 (1 + \alpha \frac{(f_{av})^{nc}}{(f_{\max} - f_{\min})^{nc} + (f_{av})^{nc}}) \quad (2)$$

where P_c and P_c^0 denote the crossover probability and initial crossover probability, respectively. The parameters f_{av}, $f_{\max}$, $f_{\min}$ represent the average, the maximum and the minimum fitness of the population. Moreover, α and nc are the coefficient factor, α controls the slope of Hill function.

To the decimal coding parameters, linear cross method is used. The form is as follows:

$$P_{child} = r * P_{parent1} + (1 - r) * P_{parent2} \quad (3)$$

r for a random variable obeying the uniform distribution at the range of $[0,1]$.

To the binary code parameters, two factors of cross location and cross amplitude are used to descript. The cross location is randomly generated. And cross amplitude is the absolute value of difference of individual parameters.

When the crossover operation is carried out, the network structure between Agents should be taken into consideration. In the following step, three principles are proposed.

①Prior to learn from the one with a biggest difference between out-degree and in-degree.

②Prior to learn from the one with the last state was not involved in the crossover operation.

③Prior to learn from the one with the biggest betweenness.

An Agent is one node of the network, so two state variables are added: degree and SIR state [8].

(2) Mutation operator

The mutation probability is from the nonlinear genetic algorithm.

$$P_m = P_m^0(1+\beta\frac{(f_{av})^{nm}}{(f_{\max}-f_{\min})^{nm}+(f_{av})^{nm}}) \tag{4}$$

where P_m and P_m^0 are the mutation probability and initial mutation probability, respectively. Parameter β and nm are the coefficient factor and β controls the slope of Hill function.

To the decimal coding parameters, the form of the mutation amplitude is defined as follows:

$$\Delta P_i = \frac{i}{fitness_i} \tag{5}$$

To the binary code parameters, two factors of mutation location and mutation amplitude are used to descript. The mutation location is randomly generated. And the mutation amplitude is inversely proportional to its fitness. The form is as follows:

$$\Delta P_i = \left[\frac{i}{fitness_i} * M\right] \tag{6}$$

M is the length of the binary code parameter.

Simulation and analysis

In the following step, some simulations of equipment acquisition tasks are made to test the validity and capability of the redesigned algorithm. In the agent based modeling and simulation of equipment acquisition, there are two main types of Agent [9]. They are the agency of equipment acquisition and the defense industry enterprise.

Here, the enterprises are selected to be the executers. The attributes of the enterprises and the coding modes are shown in table 1.

Table 1 Attributes of the enterprises and coding modes

	Attribute	Coding mode		Attribute	Coding mode		Attribute	Coding mode
1	Innovation_ability	binary	3	Quality_level	decimal	5	Credit	decimal
2	Manage_level	decimal	4	Cost_control	decimal			

The initialized values of the attributes are from questionnaires and history data.

The initialized parameters of the redesigned algorithm are shown in table 2.

Table 2 Initialized parameters of the redesigned algorithm

	Parameter	Initialized value		Parameter	Initialized value		Parameter	Initialized value
1	ω_1	0.7	5	P_c^0	0.1	9	nc	2
2	ω_2	0.1	6	P_m^0	0.7	10	nm	2
3	ω_3	0.1	7	α	0.2			
4	ω_4	0.1	8	β	0.1			

If $P_c^0 = P_m^0 = 0$, that is no algorithm used in the simulation.

The whole simulation was designed and implemented on Recursive Porous Agent Simulation Toolkit (Repast) [10].The usage of the algorithm of Agent L&E is shown in Fig. 3.

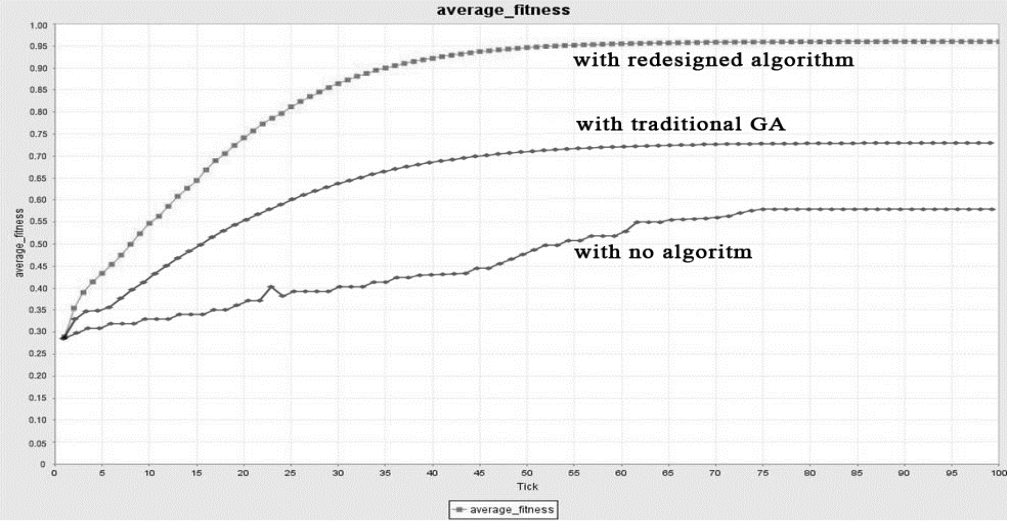

Fig. 3. The usage of the algorithm of Agent L&E

As we can see from Fig. 3, through the contrast curves, due to considering the environment and network structure, the average value of the individuals can quickly reaching a higher maximum by using the redesigned algorithm. Meanwhile, it reflects the overall trend of the equipment acquisition task completion. Under the guide of military, the comprehensive evaluation of time, const and quality of task completion is becoming higher and higher.

Conclusion

In this paper, an algorithm of Agent L&E based on nonlinear genetic algorithm, reinforcement learning and network structure is redesigned. The simulation of equipment acquisition task shows the validity and capability of the redesigned algorithm. With more and more Agent based modeling and simulations, task oriented is becoming the main solution to the issues. The thoughts and methods redesigning the algorithm of Agent L&E will get wider and wider application to solve social problems, such as space launch, economic market, logistics management etc.

References

[1] Macal C M, North M J. Agent-based modeling and simulation[C]//Winter Simulation Conference. Winter Simulation Conference, 2009: 86-98.

[2] Pisarski S, Rugała A, Byrski A, et al. Evolutionary multi-agent system in hard benchmark continuous optimisation[M]//Applications of Evolutionary Computation. Springer Berlin Heidelberg, 2013: 132-141.

[3] Schmitt L M. Theory of genetic algorithms[J]. Theoretical Computer Science, 2001, 259(1): 1-61.

[4] Wang L, Tang D. An improved adaptive genetic algorithm based on hormone modulation mechanism for job-shop scheduling problem[J]. Expert Systems with Applications, 2011, 38(6): 7243-7250.

[5] WANG Jun-hong, LIU Bao, YUAN Ruo-quan etc. Design and application of a nonlinear genetic algorithm[J]. Computer simulation, 2010, 27(2):196-199.

[6] Grefenstette J J, Moriarty D E, Schultz A C. Evolutionary algorithms for reinforcement learning[J]. arXiv preprint arXiv:1106.0221, 2011.

[7] Strogatz S H. Exploring complex networks[J]. Nature, 2001, 410(6825): 268-276.

[8] HE Da-ren, LIU Zong-hua, WANG Bin-hong. Complex Systems and Complex Networks[M]. Beijing: Higher Education Press, 2009:188-190.

[9] QU Wei, ZHENG Shao-yu. Introduction to military equipment acquisition[M]. Beijing: The people's Liberation Army press, 2003.

[10] North M J, Collier N T, Ozik J, et al. Complex adaptive systems modeling with repast simphony[J]. Complex adaptive systems modeling, 2013, 1(1): 1-26.

Advanced Materials Research Vols. 989-994 (2014) pp 2037-2042
© (2014) Trans Tech Publications, Switzerland
doi:10.4028/www.scientific.net/AMR.989-994.2037

Research on modeling of brain function network in Major depressive disorder

NIU Li-min[1a] , GUO Hao[1] , CHEN Jun-jie[1]

[1]College of Computer & Technology , Taiyuan of Technology , Taiyuan 030024 , China
[a]1019381955@qq.com

Keywords: Major depressive disorder; human brain functional network; modeling; the proportion of the common edges of two networks

Abstract: In order to analyze the gap of function network between Major depressive disorder and health person, this paper studies with modeling approach. This paper analyzes the function network of Major depressive disorder with the model based on anatomical distance and the number of common neighbor. The result shows that the distribution of the optimal brain function network is linear in all volunteer. And the slope of the linear relationship in the patients is less than health, so we hope this point can be as secondary evidence to determine the person whether fall ill. And we also propose two models and those models of brain function are based on anatomical distance or the number of common neighbor. Create the evaluation criteria for select the optimal brain function model network in each class model based on select the maximum value in the proportion of the common edges of two network accounted all edges. Select the model that can simulate the real brain function network by comparison with real data fMRI network. Finally, the results show the best model only is based on anatomical distance .

0 Introduction

Major depressive disorder (MDD) is a frequent heart disorders. Although in recent years, treatment of MDD has been greatly improved, but the relapse rate of MDD was still very high. Functional imaging studies have shown that MDD related to the abnormalities of many areas of the brain.[1-2] These areas include Hippocampus, ParaHippocampal, Precentral, Caudate and so on.

The human brain network is a large and complex network, in the sense of having high metabolic cost relative to its mass.[3] Similarly, the computer network is a typical economy small world network. Its economic characteristics are mainly reflected in the minimization of brain anatomy distance or connection costs.[4] Prior studies indicate that those topological properties of brain network is affected by anatomy distance and cost control. Meunier analyze the modular of resting-state brain function network of healthy volunteers. It was found that the anatomy distances between nodes in the same module are shorter than others.[5] The long distance connection in the same module distributed in the opposite side homotopy area of the node. Studies indicate that the brain region that have more connection in local area have some properties such as clustering coefficient is higher , characteristic path length is longer and connection costs is lower.[6]

On one side modeling of brain function network based on anatomy distance found the relationship between anatomy distance and cost control and topological properties of brain network. On the other hand it is important to reduce the cost of building brain network. Kaiser makes anatomical distance between nodes as the only parameter of the modeling of brain network about cat and rhesus monkey.[7] It found that the anatomical distance between regions which have shorter characteristic path length are shorter normally. Previous study had analyze the gap of function network between MDD and health person in many other way, this paper studies with modeling approach. And propose three models of brain function network with the data of health person in order to analyze the effects that anatomical distance and the number of common neighbor between nodes to brain function network. The three models have two parameters --- anatomical distance between nodes (Euclidean distance between two nodes) and topological properties (the number of common neighbor between nodes). In this article , those models imitate some key topological properties of healthy volunteers' brain function network. In the model based on two parameters, experiments show we can determine the person whether fall ill by the ratio between two parameters.

In other word, the ratio between two parameters of the optimal model have significant different between MDD and health person.

1 Collection and processing of data

1.1 Collection and pre-processing of data

In this study collect 60 subjects and they divided into two groups: MDD group and control group .MDD group including 34 MDD volunteers (evaluable data on n=34; mean age 29; 14 male). They are first onset without medication, and they ranged in age from 17 years to 54 years. Control group including 26 healthy volunteers (evaluable data on n=26 ; mean age 27; 11 male). They ranged in age from 17 years to 63 years. All subjects of Control group had no history of mental or nervous disorders according to Mental Health Screening Table and Neurosis Screening Schedule. All subjects of MDD group are patients with MDD according to diagnosed and statistical manual of mental disorders in united states with fourth edition (DSM-IV).

This study consent was acquired from all participants and signed a written agreement with them.

Collection and pre-processing of data was complete by First Hospital of Shanxi Medical University and us. The experiment using resting-state fMRI (functional magnetic resonance imaging) collect image data. Then research the pattern of resting-state brain functional connectivity. Collection of data was complete in First Hospital of Shanxi Medical University. Scanning was complete by radiologist who qualified in operation of magnetic resonance. During the process of scanning, the subjects were asked to close their eyes, relax, not think about certain things and stay awake.

In order to preprocess the data, experiment use Statistical Parametric Mapping 8(SPM8) which belongs to software Matlab7.8.The process include: time between layers correct; head motion correct; spatial normalization; make multiple linear regression on all time series; remove the false difference caused by head motion.

1.2 Construct brain function network based on time series

In order to construct brain function network based on time series, experiment do steps as following. First, brain was divided into 90 cortical brain regions (each hemisphere have 45 cortical brain regions) according to Anatomical automatic labeling (AAL) templates. Each region is treated as one Regions of Interest (ROI). Each region stand for one node in brain function network, so the number of node in brain function network is 90. Calculate the average time series of all voxels in each region. Then analysis the result with multiple linear regression in order to remove the pseudo differences caused by head movement and global brain signals. Then calculate the pearson correlation coefficient between any two cortical brain regions.

$$r_{ij} = \frac{\sum_{t=1}^{T}[x_i(t)-\bar{x}_i]\bullet[x_j(t)-\bar{x}_j]}{\sqrt{\sum_{t=1}^{T}[x_i(t)-\bar{x}_i]^2}\sqrt{\sum_{t=1}^{T}[x_j(t)-\bar{x}_j]^2}} \quad . \tag{1}$$

Here, X_i is time series of voxel i ; X_j is time series of voxel j; X_i with over line is the average of the time series of voxel i ; X_j with over line is the average of the time series of voxel j. So we get the relational matrix A (90×90) that is about time series. Turn relational matrix into binary matrix according to the pre-set threshold value. In other words, when $r_{i,j}$ larger than the threshold value , the corresponding element of the binary matrix is 1. when $r_{i,j}$ less than the threshold value , the corresponding element of the binary matrix is 0.

Select threshold value. In order to turn relational matrix into binary matrix ,we need to select threshold value for each relational matrix. Each threshold corresponds to a sparsity. Sparsity defined as the ratio of the number of edges that is actually exists in brain network and the number of edges that maximum possible exists in brain network. The selection that we make is a threshold range. Construct brain function network (relational matrix) in each sparsity within the space of threshold. Determine the space of threshold on the following principles:

(1) For all subject, the small-world properties of all brain function network within the space of threshold must be larger than 1.1.
(2) For all subject, the average degree (K) of all brain function network within the space of threshold must be larger than

$2\ln N \approx 9$. Here, $N = 90$。

According to this principle, we select a threshold space that is 8% -32%. Increasing sparsity step by step within the space of threshold, and the gap was 0.1 per step. Construct brain function network for all subject in each sparsity. Finally, calculate the mean brain function network of a group subject within each sparsity.

1.3 Calculate topological properties of brain function network

For each brain function, we measured the topological properties as following: Characteristic path length (The extent of overall routing efficiency of a network. In other word, it is the shortest path length required to link one node to another, averaged overall all pairs of nodes.); Clustering coefficient (The extent of local clustering or cliquishness of a network. In other word, it is the average of the clustering coefficients over all nodes and quantifies the local interconnectivity of a network.); Global efficiency (How efficient of information propagation through the whole network); Local efficiency (How efficient of information propagation over a node's direct neighbors); Assortativity (The tendency of nodes to link those nodes with similar number of edges).

2. The evaluation criteria of optimal brain functional model network

In order to select the optimal human brain function model network of each class human brain function model networks. Experiment selects the best parameter group in each class human brain function model networks and the model network that construct according to the best group parameters closest to the real brain function network that construct according to time series. Here, we select the optimal model network by analyze the percentage of the common side of the two networks.

Firstly, calculated the S value of percentage of the common side between each model network and the real network in a sparsity.

Finally, we sort all S value in the sparsity. Select the brain function model network which S value is the largest and it is the optimal human brain function model network in this sparsity.

3.Model of human brain function network

3.1 Model of human brain function network based on anatomical distance (MAD)

One measure of cost in a spatially embedded network like the brain is the physical distance of connections between nodes: generally, connection costs will increase with distance. In the nervous system of the nematode worm Caenorhabditis elegans, which has been mapped completely at the cellular level of synaptic connections between neurons , most axonal projections are shorter than the average distance between neurons, as expected in response to an economical selection pressure .[8-10] Likewise, in sparsely connected human brain functional networks, short distance connections predominate and are typically associated with greater strength of functional connectivity between regional nodes. In order to investigate the effects of anatomical distance to human brain function network, we design a model: This model consists of $P_{i,j}$ which are the connection between any pair of nodes and $P_{i,j}$ is a function of the anatomical distance between any pair of nodes:

$$P_{i,j} \propto (d_{i,j})^{-\eta} . \tag{2}$$

Here, $d_{i,j}$ is the anatomical distance between node i and node j, η is the only parameter of the model.

3.2 Model of human brain function network based on the number of common neighbor (MNCN)

Growth models for the formation of other real-life complex systems have previously been more successful by including an additional topological term in the connection probability function . Human brain functional networks are embedded in anatomical space and have topological

properties—small-worldness, modularity, fat-tailed degree distributions—that are comparable to many other complex networks. We mainly investigate the effects of number of common neighbor between nodes to human brain function network. More the number of common neighbors between any pair nodes, more similarity between the nodes (Brain regions). We design a model: this model consists of $P_{i,j}$ which are the connection between any pair of nodes and $P_{i,j}$ is a function of the number of common neighbor between nodes:

$$P_{i,j} \propto (k_{i,j})^{\gamma} \quad . \tag{3}$$

Here, $k_{i,j}$ is the number of common neighbor between node i and node j, γ is the only parameter of the model.

3.3 Model of human brain function network based on anatomical distance and the number of common neighbor (MADNCN)

With the above experiments, we analyzed the effects of only anatomical distance or only number of common neighbor between nodes to human brain function network. What result when construct brain function model network based on both anatomical distance and the number of common neighbor between nodes. Whether the brain function model network will be more close to the real human brain function networks? We design a model: this model taking into account anatomical distance and common neighbor between nodes. In other word, this model consists of $P_{i,j}$ which are the connection between any pair of nodes and $P_{i,j}$ is a function of anatomical distance between nodes and the number of common neighbor between nodes:

$$P_{i,j} \propto (k_{i,j})^{\gamma} (d_{i,j})^{-\eta} \tag{4}$$

Here, $d_{i,j}$ is the anatomical distance between node i and node j; $k_{i,j}$ is the number of common neighbor between node i and node j; η,γare the parameters of the model.

In the above three models, the parameters η, γ are the range (0,7] and they changes in steps of 0.1. Firstly, construct a lot of human brain function model network through changing parameters constantly in each class model. Secondly, select the optimal human brain function model network of each class human brain function model networks by the evaluation criteria of optimal brain functional model network. Notice, the optimal human brain function model network in the class model that based on both anatomical distance and common neighbor between nodes is not the only. But, analysis the optimal human brain function model network under the same sparsity , we find that the connection of these optimal model network are same exactly although the parameters of these optimal model network are different. So we recognized those optimal models that based on both anatomical distance and common neighbor between nodes under the same sparsity as one network. Calculate the five kind topological properties of each brain function network in each sparsity within threshold space that is 8% -32% in each class model. The five kind global properties are: characteristic path length, clustering coefficient, global efficiency, local efficiency, assortativity.

4. Results and analysis

Analyze the optimal model network based on anatomical distance and the number of common neighbor of both MDD and health person, we found that the S value of percentage of the common side between optimal model network and the real network increase when the sparsity increase in all object and the increasing trend is linear. (Fig 1)

In addition, create an axis and X-axis represents the parameter γ, Y axis represents the parameter η.when the model network based on anatomical distance and the number of common neighbor ,no matter the data is MDD or health person, we select all optimal model network in a sparsity and these models are placed in the appropriate location in axis. The experimental results show that the distribution of the optimal brain function network is linear in all volunteer. We also find that the slope of linear relationship of two parameters of the optimal brain function network in

control group is greater than the slope of MDD group. Calculate the averages of all slope of linear relationship of two parameters of the optimal brain function network in control group with all sparsity within threshold space that is 8% -32% and the value is 0.9536. And the value of MDD group is 0.8852. So we can modeling the unknown object, select their optimal brain function network and get the slope of linear relationship of two parameters. If the value close to 0.9536 ,the object is health peoson. If the value close to 0.8852 ,the object is MDD.

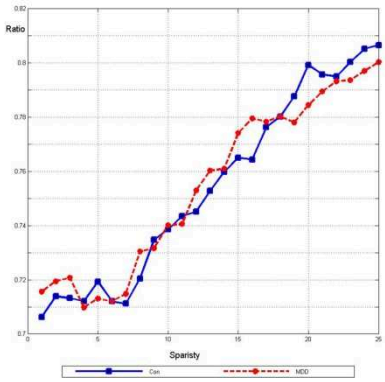

Fig 1 Increasing trend of S value

With the data of control group, calculate AUC value of each topological properties of each network in every sparsity within threshold space that is 8% -32%. Compare the AUC value of each kind topological properties of real human brain function network and five kind topological properties of the optimal model network in each class model. The result show that the human brain function model network only based on anatomical distance is closest to the real resting-state brain function network. (Fig 2)

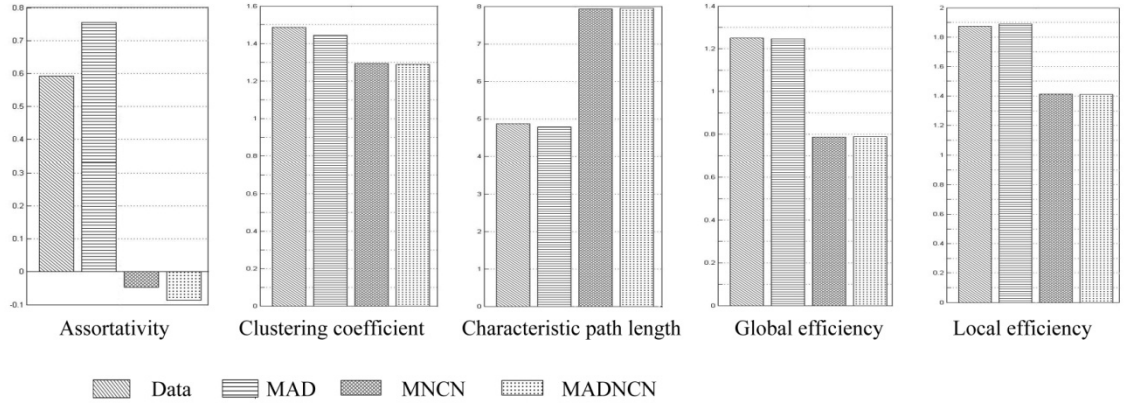

Fig 2 Compare the five kind topological properties of real network and three model

The above experiments show that if the optimal human brain function model network only based on common neighbor between nodes, their characteristic path length will longer, and the efficiency of information transmission in network will lower. In other word, the model network is not a highly efficient network. The optimal human brain function model network based on both anatomical distance and the number of common neighbor between nodes is affected by number of common neighbor between nodes severely. So this kind of model network can not reflect the characteristics of the real human brain function network. The human brain function model network only based on anatomical distance can simulate the real human brain function network in the high degree of accuracy. Their global efficiency and local efficiency are very close to the real human brain function network. This is fit with the experience that brain function network is a highly efficient network in the process of information transmission. Notice, their characteristic path length is very close to the characteristic path length of real brain function network. In other word, their characteristic path length is lower compare with another two kind model network. And it show that short distance connections predominate in human brain function network. At the same time, the

other topological properties —such as clustering coefficient and assortativity — of the human brain function model network only based on anatomical distance also closet to the real human brain function network. When we select a definite template, the anatomical distance between any two nodes is fixed. In other work, the anatomical distance between any two nodes is same to all volunteer and it is common feature. The real human brain function network is mean network in experiment, so the effect of individualized feature is not reflect in result and the effect of common feature is very prominent. And it cause the human brain function model network only based on anatomical distance closet to the real human brain function network in the result directly.

5. Concluding remarks

In this paper, the experiment has proved that the model based on anatomical distance and the number of common neighbor have significant different between MDD and health person. In addition, the model only based on anatomical distance closet to the real brain networks. Future studies can be further analyzed the different between MDD and health person in the field of modeling. We also can analyzed other factor in order to find the model which is closet to real brain function network. In future studies could investigate how to improve the efficiency of the modeling in order to save time and complexity of calculate.

6. Acknowledgements

Our experiment supported by National Natural Science Foundation （61170136,61373101）, Science and Technology Innovation Project of Universities belong to Department of Education in Shanxi Province （20121003）and Youth Fund of Taiyuan University（2012L014,2013T047）.

References

[1] Junran Zhang, Jinhui Wang , et al. Disrupted Brain Connectivity Networks in Drug-Naive,First-Episode Major Depressive Disorder.BIOL PSYCHIATRY, 2011,70:334–342 .doi:10.1016/j.biopsych.

[2] Michael D. Greicius, Benjamin H. Flores , et al. Resting-State Functional Connectivity in Major Depression: Abnormally Increased Contributions from Subgenual Cingulate Cortex and Thalamus. BIOL PSYCHIATRY 2007,62:429–437 doi:10.1016/j.biopsych.2006.09.02.

[3] Laughlin S B, Sejnowski T J. Communication in neuronal networks[J]. Science, 2003, 301(5641): 1870-1874.

[4] Sporns O. Networks of the Brain[M]. MIT press, 2011.

[5] Meunier D, Lambiotte R, Bullmore E T. Modular and hierarchically modular organization of brain networks[J]. Frontiers in neuroscience, 2010, 4.

[6] Sepulcre J, Liu H, Talukdar T, et al. The organization of local and distant functional connectivity in the human brain[J]. PLoS computational biology, 2010, 6(6): e1000808.

[7] Kaiser M, Hilgetag C C. Spatial growth of real-world networks[J]. Physical Review E, 2004, 69(3): 036103.

[8]. White J G, Southgate E, Thomson J N, et al. The structure of the nervous system of the nematode Caenorhabditis elegans[J]. Philosophical Transactions of the Royal Society of London. B, Biological Sciences, 1986, 314(1165): 1-340.

[9] Niven J E, Laughlin S B. Energy limitation as a selective pressure on the evolution of sensory systems[J]. Journal of Experimental Biology, 2008, 211(11): 1792-1804.

[10] Chklovskii D B. Exact solution for the optimal neuronal layout problem[J]. Neural computation, 2004, 16(10): 2067-2078.

Advanced Materials Research Vols. 989-994 (2014) pp 2043-2046
© (2014) Trans Tech Publications, Switzerland
doi:10.4028/www.scientific.net/AMR.989-994.2043

A Classification Algorithm of Moving Military Vehicle

Yunfei Ma[a]，Feng Chen[b]

Department of Automation, University of Science and Technology of China, Hefei, Anhui, China

[a]mayunfei@mail.ustc.edu.cn, [b]chenfeng@ustc.edu.cn

Keywords: Vehicle Classification; Simulation; SVM; Statistical Learning; Feature Extraction.

Abstract

Classification of moving military vehicle in battlefield is an important part of information acquirement. Support vector machine is a pattern classification method which is suitable to solve the small sample, non-linear classification problems. This paper uses one-versus-one multi-class SVM to classify military vehicle. This method is based on multi-sensor data including noise signal, the magnetic field disturbance signal, and vibration signal. The parameters of the SVM are determined by using the cross-validation method. The Simulation experiment results show that, compared to AdaBoost algorithm and two-class SVM, the one-versus-one multi-class SVM has higher accuracy.

Introduction

Military vehicles play an important role of modern warfare. The classification of moving military vehicle has become an interesting research field for battlefield intelligence information acquisition. Currently, there are few researches for military vehicle classification. The classification problem of military vehicle is similar to that of traffic vehicle. So classification method of traffic vehicle can be used for reference.

The machine learning algorithms for multi-class classification of moving vehicle include BP neural network classification algorithm[1], AdaBoost algorithm[2], and SVM classification algorithm[3]. HU used three-layer BP neural network for classification of three types of traffic vehicles[4]. Wang employed wavelet multi-scale edge detection and BP neural network to extract image features to classify the vehicle[5]. Chang describes a multi-class classification method based on cascade AdaBoost classifier. The above methods have achieved good results, but there are some problems: (1)BP neural network classification algorithm has some drawbacks such as high computation complexity, overfitting, and local optimum.(2) AdaBoost algorithm has a good real-time performance and high accuracy, however, it may appear data imbalance problem[6] and has long training time when training sample is large. The SVMs have become popular classification approach because of their small samples learning capability.

In solving multi-classification problems, binary-class SVM has larger error than multi-class SVM. Therefore, we deal with military vehicle classification problems based on multi-class SVM. In this work, the sound signal, vibration signal, and magnetic signal of military vehicles are treated as input samples of the classifier, and the multi-class SVM is introduced to achieve the vehicle classification. In addition, The parameters of the multi-class SVM are selected by using cross-validation method. The experimental results show that multi-class SVM has higher accuracy and faster convergence speed than Adaboost algorithm for the military vehicle classification problems.

Multi-class support vector machines

SVM classification algorithm was originally designed for binary classification problems. It has good effects for binary classification problems of small samples. However, for multi-class classification problem, a suitable multi-class classifier is needed. Currently, there are two main ways to solve the multi-classification problems of SVM. One is the direct method: by merging multiple parameters of hyperplane into an optimization problem, the optimization problem is solved to achieve

multi-classification. Such a method is only applicable to the classification problem of small samples. It has high computational complexity, low efficiency and low classification accuracy for the classification problems of large samples. The other is the indirect method: combining multiple binary-class classifiers to construct a multi-classification classifier. This method includes the following two: (1) one-versus-rest[7], in which N binary-class classifiers are built for a N-classification problem. For instance, when training the ith classifier, the ith sample in the training sample set belong to class 1,the rest samples belong to class 2.The classification result is determined by the largest output value of N classifiers.(2)one-versus-one[8], in which a binary-class classifier is built for each two classes. So, there are totally N(N-1)/2 SVMs. The results depend on these SVMs ’ voting. The research shows that one-versus-rest may cause some samples can’ t be classified, and has longer training time than one-versus-one. Therefore, this paper uses one-versus-one method to build multi-class SVM.

Classification method of military vehicles

In this paper, we study multi-classification method for three different types of military vehicles including tanks, armored vehicles, and trucks.

Feature extraction. The feature selection of input samples for SVM is very important. Nowadays, the information of military vehicles is primarily collected by various sensors. in general, military vehicles have their different characteristics, such as sound, magnetic field, vibration, etc. So considering with the actual situation of vehicle detection, we extracted three kinds of military vehicles’ characteristics as input feature vector of military vehicles classification. They are sound decibel, magnetic field induction, vibration intensity. The reasons are as follows: (1) These three characteristics are more easily perceived by sensors; (2) The characteristic differences among these three types of vehicles are obvious; (3) These three characteristics are hardly affected by weather conditions during day and night[9].

1) ? Sound feature

Vehicle noise is generated while the vehicle during moving.The level of vehicle noise has a direct and significant relationship with vehicle type. Sound characteristic value is represented by the noise power of vehicle.Thus the sound value is not be affected by distance between detection point and the vehicle.The noisy power P and distance of sound sensor r have the following relationship:

$$P = 4\pi r^2 I_0 * 10^{\frac{L}{10}} \tag{1}$$

Sound intensity level L is the decibel value which can be detected and exported by the sound sensor. I_0 is the reference sound intensity, and its value is $10^{-12}\,\mathrm{w/m^2}$.

2) Magnetic field feature

Geomagnetic field can be regarded as uniform distribution within a few kilometers. Due to vehicle’s magnetic field properties, when a vehicle passes through the geomagnetic field it will disturb the magnetic fields environment.

Large vehicle having higher metal content, thus its effect on the magnetic field surrounding is obvious. So the amplitude of the waveform has large range and is easy to detect. This characteristic provides a theoretical basis for vehicle classification based on magnetic field sensors. So magnetic field feature can be used as an input variable of military vehicle classification.

3) Vibration feature

The road which military vehicles run on can be regarded as a vibration system. Impact force of vehicle load can be used as an input of road vibration system. Because impact force road surface will produce a corresponding vibration response, the size of road surface vibration and the size of road load have the same trend and magnitude order. Road surface vibration increases with vehicle weight. Therefore, the shock wave of road surface can be detected to identify the corresponding vehicle type. After obtaining the vibration wave, the peak of amplitude can be extract as an input feature vector of vehicle classifier.

Classification algorithm of Military vehicle. Based on the above analysis, we adopt multi-class SVM and one-versus-one method for military vehicle classification. The input of SVM classifier includes three types of vehicle's feature value such as sound, magnetic field, vibration. FIG.1 shows the structure of SVM :

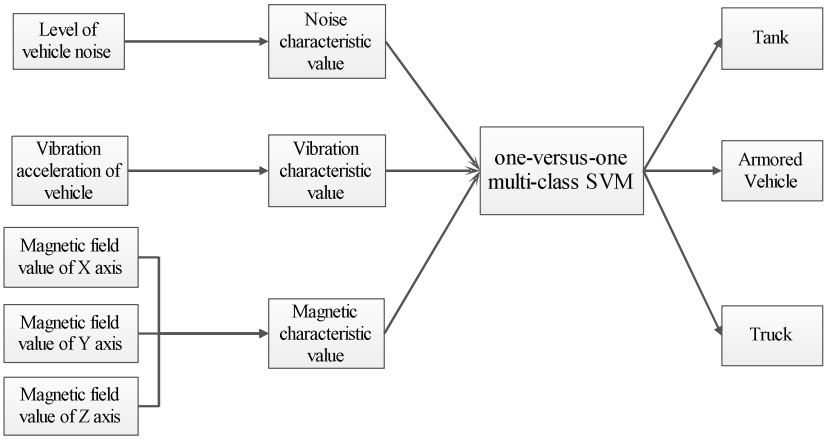

FIG.1 The structure of SVM

Simulation Results and Discussion

Simulation experiment platform. In this paper, the effectiveness of the classification algorithm for military vehicle must be evaluated by experiment. The experiment is based on Military Vehicle and Sensor Network Simulation Platform(MVSNS) which is developed by Intelligent Transportation and Data Fusion Laboratory, Department of Automation, USTC. This simulation platform can build different types of vehicle model and road model. It also can create spread diffusion models of sound, magnetic field and vibration of military vehicle.

The kernel function of SVM has a significant impact on classification result. Parameter C determines the optimal classification hyperplane and classification error. Parameter selection of SVM directly affects the accuracy of classification of military vehicles. In this paper, Gaussian kernel function is used to ensure the best classification result.

In addition, parameter $\sigma 2$ affect the performance of Gaussian kernel. We initially suppose the optimal parameters $\sigma 2 = 0.5$ and $C = 5$, and then use cross-iteration method for the precise search of optimal parameters. Finally, the optimal parameters are obtained, which are $\sigma 2=0.6$ and $C =5$. Two parameters achieve a better balance by using this search optimization method.

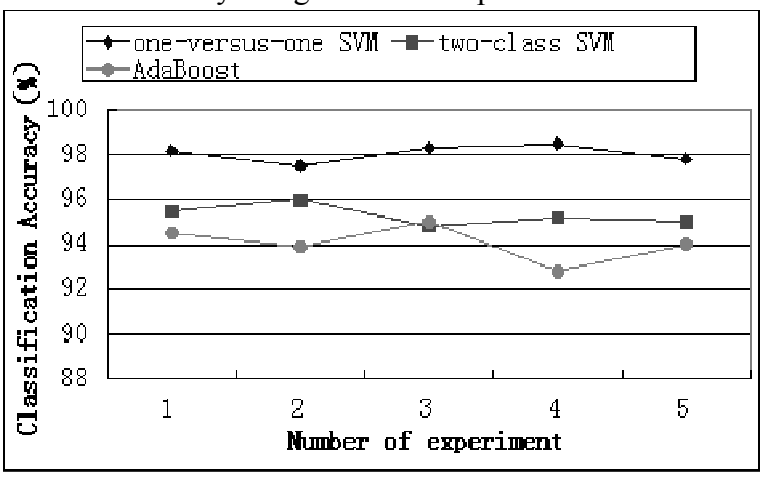

FIG.2 Comparison of their classification accuracy

The experimental results. In order to verify the effectiveness of the classification algorithm for military vehicle, MVSNS was used for classification experiment. In the experiment, the proposed method was implemented and compared with AdaBoost algorithm and standard SVM. AdaBoost algorithm is an iterative algorithm. Its core idea is to build a series of weak classifiers on the same

training sample sets, and then combines these weak classifiers together to construct a stronger final classifier.

In this experiment, the samples are generated by the MVSNS. The Simulation Platform generated 200 military vehicles for three types. The feature values of each vehicle were detected and output by virtual sensors in MVSNS. The classifier used the 600 samples and the experiment results are shown as Fig.2. It can be seen that the one-versus-one SVM classification method has higher classification accuracy than AdaBoost classification method and two-class SVM classification method. The classification accuracy of these three methods is as follows: one-versus-one SVM 98.06%; two-class SVM 95.3%; AdaBoost 94.68%. Therefore, one-versus-one SVM is suitable for military vehicle classification.

Conclusion

In this paper, a classification method of military vehicle classification is studied. The moving military vehicles' characteristics such as sound decibel, magnetic field induction, and vibration intensity are analyzed, which are treated as input feature vectors of one-versus-one multi-class SVM to generate a military vehicle classifier. This algorithm is evaluated on the simulation platform. The experimental results show that one-versus-one multi-class SVM has higher accuracy than AdaBoost and two-class SVM.

References

[1] Wohler C, Anlauf J K. Real-time object recognition on image sequences with the adaptable time delay neural network algorithm-applications for autonomous vehicles [J]. Image and Vision Computing, 2001, 19 (9 /10): 593-618.

[2] Freund Y, Schapire R E. A decision-theoretic generalization of on-line learning and an application to Boosting. Journal of Computer and System Sciences, 1997, 55(1): 119-139.

[3] V Vapnik,The nature of statistics learning theory[M].New York : Springer Verlag, 1995.

[4] HU F, JIA Q, ZHANG X. The classifier of car types using BP neural networks [J][J]. Journal of Xidian University, 2005, 3: 026.

[5] Wang Zhiwen; Li Shaozi. Research for automatic recognition for vehicle based on improved BP network. Proceedings of 2010 International Conference on Computer and Communication Technologies in Agriculture Engineering, pp. 105-108, June, 2010.

[6] Mukherjee I, Rudin C, Schapire R E. The rate of convergence of AdaBoost. In: Proceedings of the 24th Annual Conference on Learning Theory.Budapest, Hungary: JMLR,2011. 559-594.

[7] VAPNIK V.Statistical learning theory[M]. New York: Wiley, 1998.

[8] KREOEL U. Pairwise classification and support vector machines [C] Advances in Kernel Methods: Support Vector Learning.Cambridge: MIT Press, 1999.

[9] Liu Qun, Gu Jin, Zhang ZuSheng, et al. vehicle classification algorithm based on wireless sensor networks.Journal of Nanjing University(Natural Sciences),2013,49(5):655-663.

[10] K R Muller , S Mika, G Ratsch et al.An introduction to kernelbased learning algorithm[J].IEEE transactions on Neural Networks, 2001; 12(2) : 181-201.

Advanced Materials Research Vols. 989-994 (2014) pp 2047-2050
© (2014) Trans Tech Publications, Switzerland
doi:10.4028/www.scientific.net/AMR.989-994.2047

Analysis of Fuzzy Clustering for the Adoption in Data Mining

Yingjie Wang[1-2,a]

[1]College of Information Engineering, Dalian University, Dalian 116622, P . R. China

[2]Software School, Dalian University of Technology, Dalian 116621, P . R. China

[a]yingjiewang2008@163.com

Keywords: Clustering Analysis, FFCM, Data Mining

Abstract. Data mining is the general methodology for retrieving useful information from big data. Clustering analysis is a mathematical method of classification for unsupervised machine learning. It can be adopted for data classification in Data mining. This paper combines the clustering process by fuzzy way and then deduces a special clustering algorithm with fast fuzzy c-means (FFCM) method. In summary, the paper illustrates the adoption of a series of fuzzy clustering methods in Data Mining. These methods have improved the computational efficiency with learning as the convergence speed is fast. The methodology of this paper presents significantly meaningful for information retrieval of big data.

Introduction

Over the last decade, people use information technology the ability to produce and to collect data greatly improved. Millions of databases are adopted for business management, government offices, scientific research and engineering development and so on. For making the data truly become a company's resources, the company's own business decisions and strategy development service must be taken full advantage of. Otherwise, big data might become a burden, and even might become garbage. Therefore, data mining and knowledge discovery technologies emerged and flourished, increasingly shown its strong vitality.

Clustering analysis is an important mining method of data mining. That means it calculates similarities among the data from the database, and the data classification of this method is conducted according to the similarities. Furthermore, the data from different classes are as possible as different and the data in the same class are as possible as similar; that means “similar objects are flock together”. Accordingly, it allows the useful information or knowledge implicit in the data to be searched and found by optimizing the large-scale database. Clustering analysis is a mathematical method to study and process a given object classification. Clustering has been widely used as a basic data mining method, such as, similarity search, customer division, pattern recognition, trend analysis and other fields. All clustering methods have their own characteristics. In data mining, clustering algorithms used are the following:

(1) Based on clustering division: first creating k divisions, k represents the number of divisions to be created; then using a loop positioning technology by moving an object from one division to another division to improve the quality of divisions.

(2) Based on hierarchical clustering: creating a hierarchy to decompose a given data set. This method can be divided into top-down (decomposition) and bottom-up (merge) two modes of operations. During the clustering operation based on hierarchical clustering method, it would assume that the data are a one-time offer, that is, it is a non-incremental algorithm, in which, the time complexities of a single connection, all connections and average connection and space technology complexity are O (n^2).

(3) The density-based clustering: according to the density to complete the object clustering, that is based on the density of the growing cluster around an object (such as DBSCAN). Density-based clustering method can be divided into two types: one is based on density clustering of high-density connecting areas; another is based on clustering density distribution function.

(4) Grid-based clustering: first, the object space is divided into a finite number of elements to form a grid structure, and then, clustering is completed by using the grid structure [1].

Fuzzy Clustering Analysis

"People are fetched in groups, similar objects are flock together", the clustering problem is an ancient problem, and is a problem, which is gradually deepening, accompanying the development of human. While human want to understand the world, we must distinguish between different things and recognize similarities among things. Traditional clustering analysis is a hard division, it is the identification of each object of nature to be strictly divided into a class with one or another, the boundary of this classification category is distinct. In fact, there is no strict property of most objects and they exist intermediary in terms of behavior and generic. In other words, it might be suitable for soft division. Fuzzy set theory proposed by [2] Zadeh for such soft division provides a powerful analytical tool, researchers began to use fuzzy clustering method to deal with the problem, and named it as fuzzy clustering analysis. Since samples which fuzzy clustering obtained from uncertainty degree belonging to different categories, it stands for the sample generic intermediary. Namely, the uncertainty description of a sample is established, and it can relatively objectively reflect the real world.

Literatures [3-5] point out that an appropriate classification should match the following three conditions:

(1) Reflexivity: that is any object must own kind: the mathematic definition is $I_{ii} = 1$;

(2) Symmetry: if the object *a* is in the same class to the object *b*, and also *b* is in the same class to *a*: the mathematic definition is $I_{ij} = I_{ji}$;

(3) Transitivity: if the object *a* is in the same class to the object *b*, and the object *b* is in the same class to the object *c*, and then *c* is in the same class to *a*: mathematical definition is $I \cdot I \subseteq I$. While satisfying the above conditions is an equivalence relation, so the fuzzy clustering analysis is conducted based on fuzzy equivalence relation.

The main steps of fuzzy clustering are shown as follows: Firstly, the method is to determine the objects of the classification, and to extract the factor data: setting all classified objects as $x = \{x_1, x_2, \cdots, x_n\}$, and each object x_i consists of a set of data $x_i = \{x_{i1}, x_{i2}, \cdots, x_{im}\}$. Secondly, it is to build the fuzzy similarity relation, namely to describe the similarity of objects x_i and x_j with the value $r_{ij} \in [0,1]$, so that the fuzzy similarity matrix $R = (r_{ij})_{n \times n}$ is obtained, in which, $r_{ij} = r_{ji}$ and $r_{ii} = 1$. There are several commonly used methods to determine r_{ij} the methods, including number product method, correlation coefficient method, maximum and minimum method, arithmetic mean minimum law method, the minimum geometric mean method, the absolute index, the absolute value subtraction method, and subjective evaluation method. These methods are described in detail can be found in the literature [3]. Finally, it classifies according to the fuzzy similarity matrix. In general, the fuzzy clustering analysis should be at a certain level parameter α, thus the α sectional matrix R_α of fuzzy similar matrix R concept is introduced, the elements $r_{\alpha ij}$ of R_α are defined as follows:

$$r_{\alpha ij} = \begin{cases} 1 & r_{ij} \geq \alpha \\ 0 & r_{ij} < \alpha \end{cases} \qquad \alpha \in [0,1]$$

From the definition of fuzzy similarity matrix R, it is obvious that its reflexivity and symmetry can be satisfied, but the transitivity cannot be satisfied. Thus, the α sectional matrix R_α of the fuzzy similar matrix R obtained also satisfy reflexive and symmetric, but not transitive.

In order to obtain R_α satisfied the transitive, that is to get the final classification relationship , there are three algorithms: equivalence closure method , the maximum spanning tree method , and netting method. Equivalence closure is to calculate the power of the fuzzy similar matrix R, such as $R^2, R^4, R^8, \cdots, R^k, R^{2k}$, until $R^k = R^{2k}$ so far. Here, R^k obtained at this time means the fuzzy equivalence relation of the fuzzy similarity relation R, taking its matrix $(R^k)_\alpha$ to get the final classification relationship. This method contains a strict mathematical basis, and it is deduced from the so-called "transitive closure" theory. The proof in detail, see [3]. However, because this method

requires computing power of fuzzy similarity matrix R, which calculations increase exponentially with the number of objects increasing, it is not a good algorithm. Maximum Spanning Tree is directly from the fuzzy similar matrix R to start method by using graph theory to obtain the final classification relationship. It is very intuitive, but it must draw, so it is not suitable for programming applications. Netting Act is from the α sectional matrix R_α of the fuzzy similar matrix R, adopting special drawing mode - netting to solve classification problems. Also, since this method must draw, it is not suitable programming application. Therefore, it is necessary to find a fuzzy clustering algorithm for analysis with small amount of calculation and suitable for programming.

Fuzzy Clustering Method in Data Mining

In practice, the methods based on the objective function are widely applied. These algorithms are generally based on the function of objects between similarity and dissimilarity as the division criteria. By converting the clustering problem into the function optimization problem of the extremum of objective function, the cluster center and membership grade are alternatively iterated in the search space, until convergence presents, which obtained final clustering division. Among the clustering algorithms based on the objective function, the theory of the FCM algorithms is the most perfect, and these algorithms are most widely used. This method classifies the clustering into a nonlinear programming problem with constraints by optimizing the data set obtained and solving fuzzy division and clustering [6-8].

A fast fuzzy C-means clustering algorithm based on the FCM algorithm is presented. Fast Fuzzy C-means clustering algorithm is the fuzzy C-means clustering algorithm by adding a layer in front of hard C-means algorithm. Fuzzy C-means clustering algorithm is developed from the hard C-means algorithm, comparing with hard clustering, fuzzy clustering can get richer clustering information, but the algorithm complexity is significantly increased. Fast Fuzzy C-means clustering algorithm is not only retaining the original fuzzy clustering information-rich C-means clustering algorithm, but also jointing the fast convergence properties of hard clustering. That means it is very meaningful for clustering studies of a large number of data.

Fast Fuzzy C-means clustering algorithm is divided into two layers; steps in detail are as follows:

Determining the number of clusters $c, 2 \le c \le n$ and n is the number of data items;

Setting classification matrix $U^{(0)}$ $\mu_{ik} \in \{0,1\}$, $\sum_{i=1}^{c} \mu_{ik} = 1$ and $1 < \sum_{k=1}^{n} \mu_{ik} < n \quad \forall k$;

Taking $b = 0, 1, 2, \cdots$ in order;

According to $U^{(r)}$ and the following formula $v_i^{(r)}$:

$$v_i^{(r)} = (\sum_{k=1}^{n} \mu_{ik} x_k) / (\sum_{k=1}^{n} \mu_{ik}) \tag{1}$$

Updating $U^{(r)}$; Calculating the updated property function (for all i, k)

$$\mu_{ik}^{(r+1)} = \begin{cases} 1 & d_{ik}^{(r)} = \min\left\{d_{jk}^{(r+1)}\right\} \ j \in c \\ 0 & others \end{cases} \tag{2}$$

Algorithm of the second layer

$$J(U, V) = \sum_{k=1}^{n} \sum_{i=1}^{c} \mu_{ik}^{m} d_{ik}^{2} \tag{3}$$

In that $$d_{ik}^2 = \|x_k - v_i\|^2 = (x_k - v_i)^T A (x_k - v_i) \tag{4}$$

Bringing $v_i^{(b)}$ determined in the algorithm of the first layer to the algorithm of the second layer;

Setting weighted exponent m and the matrix A in (4);

For any fuzzy clustering matrix $U^{(0)}$ $\mu_{ik} \in [0,1]$, $\sum_{i=1}^{c} \mu_{ik} = 1$, $0 < \sum_{k=1}^{n} \mu_{ik} < n$, $\forall k$;

Updating by following methods $U^{(b)}$ for $U^{(b+1)}$ （with $k = 1 \sim n$）：

(a) Calculating I_k and $\overline{I_k}$:

$$I_k = \{i \mid 1 \le i \le c, \quad d_{ik} = 0\} \tag{5}$$

$$\overline{I_k} = \{1,2,\cdots,c\} - I_k \tag{6}$$

(b) Calculating the new membership grade of x_k :

If $I_k \neq \phi$ (empty), then

$$\mu_{ik} = 1 \Big/ [\sum_{j=1}^{c} (d_{ik} / d_{jk})^{2(m-1)}] \tag{7}$$

Otherwise, for all $i \in \overline{I_k}$, set $\mu_{ik} = 0$, and taking

$$\sum_{i \in I_k} \mu_{ik} = 1 \qquad k = k + 1$$

Comparing $U^{(b)}$ and $U^{(b+1)}$ with an appropriate matrix norm;

if $\left\| U^{(b)} - U^{(b+1)} \right\| < \varepsilon$, stop; otherwise, set $b = b + 1$ and return to the step , here ε represents a predefined allowed deviation.

Summry

In the pace with data mining technology growing up, the implied and meaningful knowledge discovery from the databases has become the main objective of data mining. This article discusses how the various types of data in the database are processed, and then apply the theory of fuzzy clustering relationships to gain useful knowledge. Its basis is no longer the FCM algorithm, but presents a fast fuzzy C-means clustering algorithm based on the FCM algorithm. Fast Fuzzy C-means clustering algorithm combines simplicity and speed of hard clustering and complex comprehensiveness of fuzzy clustering, so that it make the improved algorithm not only retaining the original rich fuzzy C-means clustering algorithm clustering information, but also jointing the fast convergence properties of hard clustering. Therefore, the introduction of data mining in this fuzzy clustering method conducts repeatedly scanning against the database without multiple iterations repeated calculations, greatly improving the computational efficiency, and convergence is very fast. It is meaningful for processing big data.

Acknowledgment. This work is partially supported by the National Natural Science Foundation of China under Grant No.61272170.

References

[1] Li Jing and Yang Yang: Cluster Analysis in Data Mining Applications, Journal of Luohe Vocational Technology College, vol.9, no.5, pp.4-5,2010.
[2] Zadeh L A: *Fuzzy Sets*, Inf Cont, 1965,8:338-353.
[3] Li Jinyin and Wu Mengda: *Fuzzy Theory and Its Applications*, National University of Defense Technology press, Changsha, 1998.
[4] Xie Jijian and Liu Chengping: Fuzzy Mathematics and Its Applications (Fourth Edition), Huazhong University of Science and Technology Press, Wuhan, 2013.
[5] Zeng Shan: *Research on fuzzy clustering algorithm*, Huazhong University of Science and Technology, 2012.
[6] Kazutaka Umayahara, Sadaaki Miyamoto and Yoshiteru Nakamori: Formulations of Fuzzy Clustering for Categorical Data, International Journal of Innovative Computing, Information and Control (IJICIC), vol.1, no.1, pp.83-94,2005(3).
[7] Hugang Han, Information System with Fuzzy Weights: International Journal of Innovative Computing, Information and Control (IJICIC), vol.2, no.3, pp.553-565,2006(6).
[8] Timothy J.Ross: *Fuzzy Logic and its engineering application*, Publishing House of electronics industry, Beijing,2003.

Advanced Materials Research Vols. 989-994 (2014) pp 2051-2056
© (2014) Trans Tech Publications, Switzerland
doi:10.4028/www.scientific.net/AMR.989-994.2051

Joint Spectrum and Power Allocation for Femtocell Based on Graph and Game Theory

Wang Ying[1, a], Zhu Qi[2, b]

[1,2]Jiangsu Key Lab of Wireless Communications, Key Lab on Wideband Wireless Communications and Sensor Network Technology of Ministry of Education Nanjing University of Posts and Telecommunications, Jiangsu Nanjing 210003, China

[a]email: B10010902@njupt.edu.cn, [b]email: zhuqi@njupt.edu.cn

Keywords: femtocell; clustering; game theory; spectrum allocation; power control

Abstract.

In order to mitigate the downlink interference in two-tier femtocell networks, a joint spectrum and power allocation algorithm based on graph and game theory is proposed in this paper. On the premise of ensuring the QoS (Quality of Service) of MUEs (microcell user equipments), we first adopt graph-based clustering algorithm to assign subbands to femtocells. Then, for femtocells of each cluster, their transmitting power is redistributed based on the non-cooperative game theory to further reduce the interference among them. Simulation results show that this algorithm can further improves the performance of the entire system compared with pure clustering strategy and ensures the QoS of MUEs at the same time.

Introduction

Studies show that about 2/3 voice traffic and more than 70% data traffic occur indoors in microcell networks. And this proportion will rise further as people's demand for data services increases [1]. Femtocells have been devised to provide good coverage in indoor environments with stable propagation channels and low mobility [2]. It is installed by users, and possesses the features of small size, low cost and low power consumption. Due to their short transmit-receive distance, femtocells can greatly lower transmit power, prolong handset battery life, and achieve a higher signal-to-interference-plus-noise ratio (SINR) [3].

There exist many challenges before femtocells can be put into large-scale commercial. Due to the self-deployment and close locations of femtocells, their interference environments are more complicated than traditional wireless networks [4]. Because of the limitation of frequency resources, femtocells have to share the spectrum with microcells, which leads to the existence of cross-tier interference. To manage with the interference, we have to distribute the resources reasonably. At present, many literatures have studied the spectrum allocation and power control methods for femtocells. Literature [5] raises an improved graph coloring algorithm: the potential maximum chromatic number strategy. It combines the advantages of Improved SEQ and DSATUR algorithms. The effect is that it saves more frequency resources with little complexity difference from traditional algorithms. One shortcoming is that the proportional coefficient in it needs to be adjusted according to the given situation to get a better performance. Literature [6] proposes a graph-based dynamic frequency reuse method. It designs a kind of cost function which takes into account the usage efficiency of spectrum. First, each FBS (femtocell base station) acquires one subband according to the cost function. Then, this function is used to reallocate subbands which can be reused. Although it has better performance than traditional graph coloring algorithms, it appears to be more favorable to FBSs which suffer more interference. This leads to lower spectrum utilization rate. Literature [7, 8] use graph-based clustering algorithm to allocate subbands to femtocells. Compared with traditional coloring algorithms and the algorithm in [6], clustering can significantly improve the capacity of femtocells. However, the transmitting power of each FBS on each subband it uses is equal and constant. This is not conducive to subbands which suffer less interference and can possibly get more power within the permissible range.

This paper proposes a joint spectrum and power allocation algorithm for femtocells. Assuming MUEs can use all subbands. For femtocells, we first establish their interference graph according to the interference situation of them. Then, subbands are reasonably allocated to FBSs based on clustering strategy. On this basis, each FBS's transmitting power on each subband it owns is further adjusted using game theory. Finally, the MUEs and FUEs' capacity is improved while QoS of MUEs is ensured.

System model

Consider the two-tier network model, where microcells and femtocells share the whole spectrum resources. We study the downlink resource allocation and use Suburban model of which each femtocell's coverage area is a circle with fixed radius and femtocells are randomly distributed within the coverage of the microcell [7].

As shown in figure 1, we only consider one microcell (ignoring the interference from adjacent microcells) with the coverage radius and maximum transmitting power p_m. There are M MUEs and F femtocells deploying randomly in the microcell. Femtocell's coverage radius is r. FBSs' maximum transmitting power is p_f. Each femtocell owns one FBS locating in its centre and one FUE deploying randomly. Without loss of generality, we assume the number of subbands equals the number of MUEs and each MUE is assigned with a different subband. FBS's transmitting power on each subband can be different, but the summation must not exceed p_f.

The Closed Subscriber Group (CSG) configuration mode is adopted. Figure 1 gives the downlink interference situation in two-tier network.

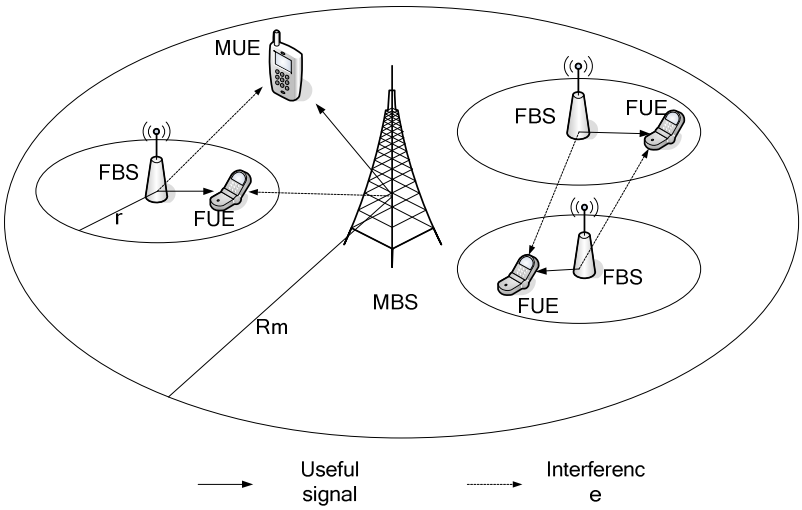

Fig. 1. The two-tier network model

SINR of MUE m on subband i is determined as

$$\gamma_{m,i} = \frac{p_{M,i} * h_m^{MM}}{\sum_{f=1}^{F} p_{f,i} * h_{f,m}^{FM} + N_0 * B} \tag{1}$$

where $p_{M,i}$ is the transmitting power of MBS on subband i; h_m^{MM} is the channel gain between MBS and MUE m; $p_{f,i}$ is FBS f's power on subband i; $h_{f,m}^{FM}$ is the channel gain between FBS f and MUE m; N_0 is the thermal noise density and B is bandwidth of the subband.

Since MUEs use all the subbands, FUEs will definitely be interfered by MBS. So, SINR of FUE f on subband i is written as

$$\gamma_{f,i} = \frac{p_{f,i} * h_f^{FF}}{\sum_{n=1,n\neq f}^{F} \eta_{n,i} * p_{n,i} * h_{nf}^{FF} + p_{M,i} * h_f^{MF} + N_0 * B} \tag{2}$$

where h_f^{FF} is the channel gain between FBS and its accessorial FUE f; h_{nf}^{FF} is the channel gain between FBS n and FUE f; h_f^{MF} is the channel gain between MBS and FUE f. We assign 0 to $\eta_{n,i}$ when FBS n can't use subband i. Otherwise, we assign 1 to it.

When MUE m's SINR reaches its threshold, the interference it suffers from femtocells can be written as

$$I_{fth} = \frac{p_{mr}}{SINR_{mth}} - N_0 * B \tag{3}$$

where p_{mr} is the m's received power; $SINR_{mth}$ is MUE's SINR threshold. Based on fairness, we assume that each of the FBSs which use the same subband as m causes the same amount of interference to it. The interference from each of them is $I_{fpth} = \frac{I_{fth}}{F}$. Then, we can obtain the maximum transmitting power these FBSs can use on the subband used by MUE m: $p_{mi} = \frac{I_{fpth}}{h_{f,m}^{FM}}$.

The calculation formula of spectral efficiency is based on literature [6]. This paper only considers large scale fading. Channel propagation model is based on literature [8].

Joint spectrum and power allocation algorithm

Spectrum Allocation. Spectrum is allocated to femtocells according to graph-based clustering strategy [7]. In the beginning, FBSs can use all the subbands and power allocated on each subband is equal. First, we establish the interference graph of femtocells. Then, we use clustering to allocate subbands to FUEs based on the interference graph. More details will be given in the next section.

Power allocation. After clustering, each cluster represents the corresponding subband and MUE. Only FBSs in the cluster can cause interference to the MUE which the cluster corresponds to. To increase system's performance, we redistribute the power of each FBS on their available subbands based on game theory.

The utility function is based on literature [9]

$$u_f = \ln(\gamma_m - \gamma_{thm}) + \ln(\gamma_f - \gamma_{thf}) - k * p_f * (h_{f,m}^{FM} + \sum_{n=1,n\neq f}^{F} h_{f,n}^{FF}) \tag{8}$$

where γ_m and γ_f represent the SINR of MUE m and FUE f individually; γ_{thm} and γ_{thf} represent the SINR threshold of MUE and FUE individually; k is the weighting factor to balance the two parts of the equation. FBSs included in the utility function are elements of the cluster which m represents. Then, we can get the iterative formula as follows [9]

$$p_f^{(n+1)} = \frac{\gamma_{thf} * p_f^{(n)}}{\gamma_f^{(n)}} + \frac{1}{k * (h_{f,m}^{FM} + \sum_{n=1,n\neq f}^{F} h_{f,n}^{FF}) + \frac{(\gamma_m^{(n)})^2 * h_{f,m}^{FM}}{(\gamma_m^{(n)} - \gamma_{thm}) * p_{mr} * h_m^{MM}}} \tag{9}$$

s. t. : $p_{f\min} \le p_f^{(n+1)} \le p_{f\max}$

where n and $n+1$ represent the number of iterations; $p_{f\min}$ is obtained by dividing FBS's maximum transmitting power by the number of all subbands; $p_{f\max}$ is written as

$$p_{f\max} = \min(p_{fm}, p_{mi}) \tag{10}$$

of which p_{fm} is obtained by dividing FBS's maximum transmitting power by the number of subbands it has access to use.

Algorithm Process

The algorithm's steps are given as follows.

Step 1. Adjust FBSs' color sets according to MUEs' SINR. When a MUE's SINR does not meet the requirement, remove the FBS which causes the maximum interference until the SINR exceeds the threshold. Those removed FBSs cannot use the same subband as this MUE.

Step 2. Adjust FBSs' color sets according to the interference they suffer from the MBS. If MBS causes serious interference to a FBS that this FBS's SINR cannot meet the requirement, then this FBS has no subband to use.

Step 3. Establish femtocells' interference graph. When a FBS does not meet the requirement of SINR, remove the FBS which causes the maximum interference to it until its SINR exceeds the threshold. Also, there will be edges established between this FBS and the FBSs removed. That means both sides cannot use the same subband.

Step 4. Use clustering strategy to distribute subbands to femtocells based on the interference graph we establish in step 3. Each color represents a cluster. Elements in the cluster can use the subband the cluster represents. If there exists a edge in the cluster, then keep deleting the FBS which owns the maximum adjacent FBSs until no edge exists in the cluster. In this way, we accomplish the clustering. FBSs belonging to the cluster will get the subband it represents.

Step 5. Assuming that the original power of each FBS on each subband is its maximum transmitting power divided by the number of all subbands.

Step 6. Take each cluster as a unit, iterate the power of FBSs on their accessible subbands with equation (10).

Step 7. After iteration if there exists one FBS's power exceeds the power before iteration by 10^(+8)w, then the convergence is reached and the algorithm terminates. Otherwise, return to step 6.

Of which, step 1 to step 4 are steps of allocating spectrum, and step 5 to step 7 are steps of allocating power.

Simulation results and analysis

Simulation scene of this paper is one microcell with three sectors. Because those sectors have the same distribution, so we only consider one sector. Assuming that femtocells are randomly distributed in a annular region which is R_f far from MBS, and M =60.

Part of the parameters to calculate the path loss are based on literature [6] and [8]. The rest of them are listed in table 1.

Table 1 Simulation parameters

$R_m, R_f, r[m]$	500, 250, 30
$P_m, P_f[dBm]$	46, 20
$N_0[dBm/Hz], B[Hz]$	-174, 0.18*10^(6)
$\gamma_{thm}, \gamma_{thf}[dB]$	6, 8

We compare three kinds of algorithms. The first one only considers clustering. Power allocated on each subband is equal. The second one considers clustering at first. The power of each FBS on each subband it owns is transformed to its maximum power divided by its accessible subbands. The third one is the algorithm we have proposed. These three algorithms are referred as algorithm 1, algorithm 2 and algorithm 3 in the remaining parts of the paper.

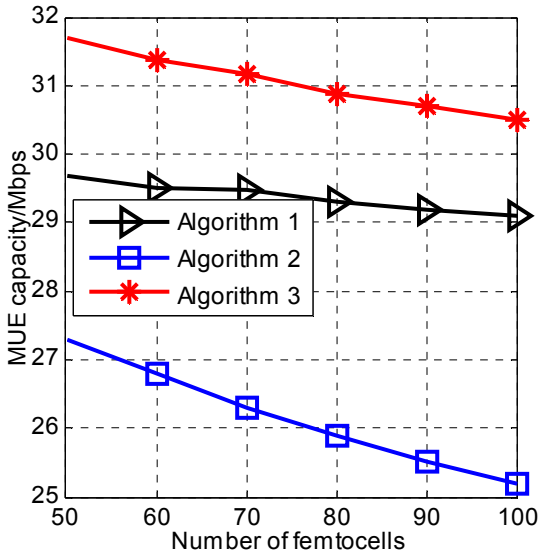

Fig. 2. MUEs' capacity with different number of FBSs

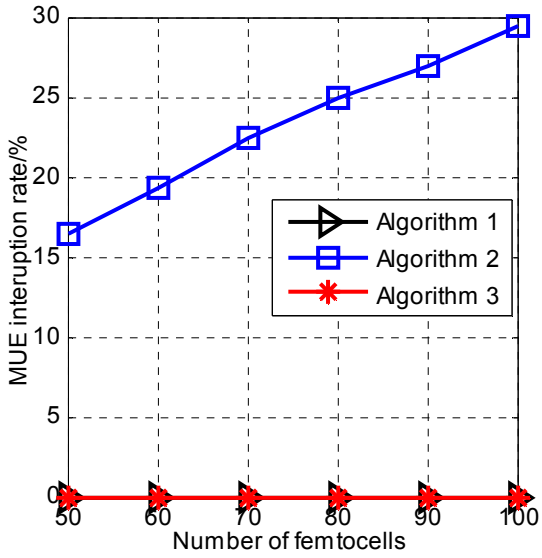

Fig. 3.MUEs' interruption rate with different number of FBSs

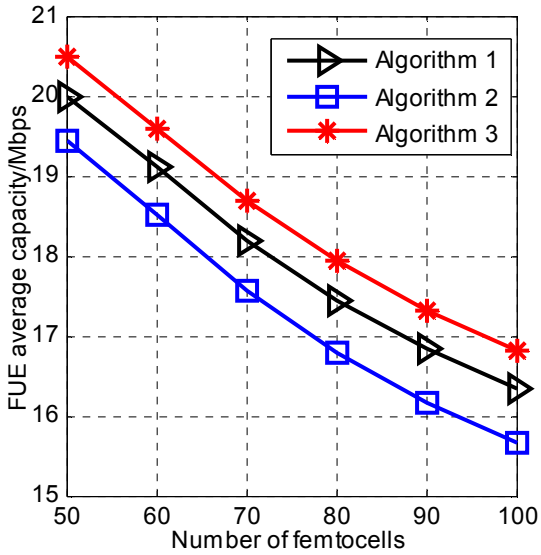

Fig. 4. Per FUE's average capacity with different number of FBSs

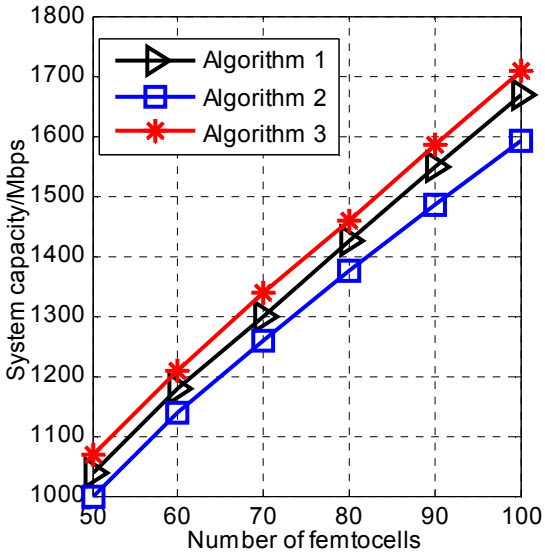

Fig. 5. System's capacity with different number of FBSs

Figure 2 and figure 3 show the change curves of MUEs' capacity and interruption rate with different number of FBSs. We can see from figures that algorithm 1 and 3 can guarantee the MUE capacity and QoS much better than algorithm 2. Algorithm 1 adjusts FBSs' available subband sets according to MUEs' SINR to ensure all MUEs' QoS, so its interruption rate is zero. Algorithm 3 ensures the power of FBSs on each subband they own will not exceed the threshold we set. In this way, MUEs' QoS is also guaranteed. Also, the utility function is of advantage to MUEs' capacity. However, in algorithm 2, the power of FBSs on each subband they own all rises which leads to more interference to MUEs.

Figure 4 and figure 5 show the change curves of per FUE's average capacity and system's capacity with different number of FBSs. Along with the number of FBSs increasing, we can observe that per FUE's capacity overall downward trend. The reason is that the distribution of FBSs becomes more intensive which causes more interference among femtocells. Algorithm 1 only considers clustering and the power of FBSs is not fully utilized. Algorithm 3 distributes power resources according to the actual scene of femtocells in order to further raise FBSs and MUEs' SINR. Because the total capacity of FBSs overall upward trend, system's capacity overall upward trend.

From these four figures, we can learn that algorithm 3 owns the best performance.

Summary

This paper proposes a joint spectrum and power allocation algorithm based on graph and game theory for femtocell. First, we allocate subbands to femtocells based on clustering. Then, the transmitting power of FBSs on each subband they own is redistributed based on game theory in order to fully use the resources. The simulation results show this algorithm performs better in increasing the capacity of MUEs and FUEs compared with pure clustering algorithm. However, this algorithm still needs to be improved. Although MUEs have better performance, the increase of FUEs' capacity is not very ideal. We need to seek a better utility function next step which is more favorable to increasing FUEs' capacity while ensuring MUEs' QoS.

Acknowledgements

This work is supported by National Natural Science Foundation of China (61171094), National Science & Technology Key Project (2011ZX03001-006-02, 2011ZX03005-004-03)) and Key Project of Jiangsu Provincial Natural Science Foundation (BK2011027).

References

[1] Min shijun, Peng mugeng, Wang wenbo. Study on LTE Femtocell[J]. Data Communication,: 26-29 (2011-2).
[2] Li Tan, Zhiyong Feng, Wei Li, Zhong Jing and T. Aaron Gulliver. Graph Coloring Based Spectrum Allocation for Femtocell Downlink Interference Mitigation[C]. Wireless Communications and Networking Conference (WCNC), 1248-1252 (2011-3).
[3] Vikran Chandrasekhar, Jeffey G. Andrews and Alan Gatherer. Femtocell Networks: A Survey[J]. IEEE Communications Magazine. 59-67 (2008-9).
[4] Yuyu Wang, Kan Zheng, Xiaodong Shen and Wenbo Wang. A Distributed Resourse Allocation Scheme in Femtocell Networks[C]. 73rd IEEE Vehicular Technology Conference (VTC Spring), 1-5 (2011).
[5] Chen weidong. New Algorithm for Solving Graph Coloring Problems[J]. Microcomputer Application, 391-395 (2004-4).
[6] Serkan Uygungelen, Gunther Auer and Zubin Bharucha.Graph-Based Dynamic Frequency Reuse in Femtocell Networks[C]. Yokohama: 73rd IEEE Vehicular Technology Conference (VTC Spring), 1-6 (2011).
[7] Shi jurong, Zhu qi. Clustering Algorithm Based on Interference Graph for Spectrum Distribution in Femtocell Networks[J]. Journal of circuits and systems, 279-284 (2013-1).
[8] Hongjia Li, Xiaodong Xu, Dan Hu, Xiqiang Qu, Xiaofeng Tao and Ping Zhang. Graph Method based Clustering Strategy for Femtocell Interference Management and Spectrum Efficiency Improvement[C]. Chengdu: The 6th International Conference on Wireless Communications Networking and Mobile Computing (WiCOM), 1-5 (2010).
[9] Mu shiyao, Zhu qi. Power Distribution of Femtocells Based on Game Theory[P]. China Patent: 102883424, (2012-10-15).

Advanced Materials Research Vols. 989-994 (2014) pp 2057-2061
© (2014) Trans Tech Publications, Switzerland
doi:10.4028/www.scientific.net/AMR.989-994.2057

The research and application of Data Glove in virtual interaction system

Xu Yuxiang[1, a], Zhu Xi-an[2, b]

[1, 2] Department of Information and Communication Engineering, Beijing information science and technology university, Beijing 100101, china

[a]xyxsuoer@126.com, [b]Zhuxian1962@163.com

Key words：virtual reality; human-computer interaction; data glove; collision detection

Abstract：The virtual reality technology is used in the mine training simulation areas, which can overcome the limitations of traditional training methods effectively. It can also improve the quality of mine training simulation greatly, reduce training costs, and the users can achieve safe and convenient training. In this paper, a dynamic collision detection algorithm is proposed based on the prediction of the movement direction of a virtual hand, and it is the effective collision detection algorithm using data glove in the mine training simulation system. Compared with the traditional static collision detection algorithm in the performance, the dynamic algorithm is proposed to solve the collision detection between one simulation solid model and another one, and to achieve the function that a virtual hand grip and rotate virtual objects in the virtual environment. The dynamic collision detection algorithm can be extended to other simulation systems.

Introduction

Human-Computer Interaction (HCI) involves the study, design and interaction between users and computers. Human is the leader in the communication process, who operates a computer to complete commands and requirements. The paper about computer console design was firstly proposed by the American scholar B. Shackel in 1959, with the development of half a century, the HCI has been improved from the stage of people adapting to the computer to the stage of computer adapting to human. In this process there is a growing emphasis on the friendly interaction. With the development of HCI, virtual reality technology [1] has also been developing rapidly. It urgently needs a new way of the human-computer interaction. Virtual reality technology is the way that a computer technology as the core, combined with relevant science and technology to produce a digital environment in which the real environment is highly approximated in the aspects of certain range vision, hearing, and touch. Any user with the necessary equipment and any object in the digital environment interact and influence each other, and the user can feel and experience the real environment.

In order to tell the worker what proper measures can be taken in the dangerous accidents, meanwhile, people wouldn't allow reproducing some unexpected risk incidents happened in the real work environment, so we use the virtual reality technology to develop a virtual simulation training system and use the latest computer graphics technology to accurately reproduce the virtual scene of coalbed methane gathering. Through somatosensory input devices, such as data glove, the system can achieve human-computer interaction, at the same time, the user get the feelings of practical operation. Through the system that contains a number of virtual dangerous accidents designed, users can witness these terrible accidents and strengthen their safety awareness, which is impossible to experience in the traditional training. As a kind of visualization tool, virtual reality can make the

human-machine interface of the operating system more humanized. In the early virtual reality system, mouse and keyboard are the primary input devices, and CRT monitor is the primary output device. In order to make the system more flexible, more convenient and more real-time, data glove, stereoscopic glasses, Kinect and other equipment are used in our system.

The HCI process of data glove

Data glove can get locations, directions and gestures of fingers and palm through sensors, at the same time, the data of glove are being sent to the computer. The computer controls the virtual hand [2] which can make the corresponding gestures and movements in the virtual environment by using the data. The HCI process of 5DT data glove shows in Fig. 1.

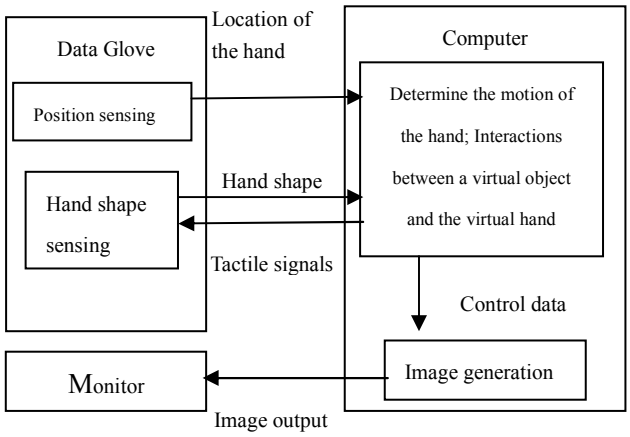

Fig. 1 The HCI process of 5DT data glove

Collision Detection

In the virtual reality, if the users feel the virtual objects in the digital environment is “real object”, and then we can say that the users have a strong sense of immersion. In order to achieve this goal, collision detection is a key. It requires that the system can determine precisely, completely and real-time whether there is a collision among virtual objects.

Virtual object and virtual hand

The equipment which we can see everywhere in CBM (coalbed methane) surface gathering scene are all kinds of pipelines and valves. The steps of operating a compressor show in Fig.2. Firstly, opening the intake valve and the vent valve; secondly, opening the barring gear; at last, opening the exhaust pipe. These particular structural models which all need collision detection are built in the system.

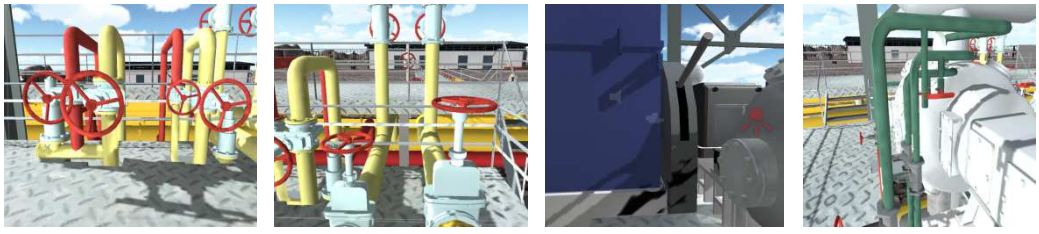

(a) Intake valve (b) Vent valve (c) Barring gear (d) Exhaust pipe

Fig. 2 Compressor

The models which show in Fig. 2 are rigid bodies [3]. Once the models whether dealing with the force terms or not are created out, the distance between one point and another in the rigid body

interior will not change, as well as the shape of rigid body. However, the soft body which is different with the rigid body will change if it has been applied a external force. So Virtual hand can be regarded as a kind of soft body, because the virtual hand will have the corresponding change based on the gesture change of user's hand. In other words, deformation will occur to the virtual hand dealing with the force terms, as show in Fig.3. Compared to collision detection of the rigid body, collision detection of the soft body is more complicated. When deformation of the soft body occurs, the relative position of the vertices will change, it makes collision detection algorithms of the rigid body cannot be directly used to soft body. While the virtual hand is a dynamic object whose position and orientation depends on the control of users. The problem how to judge whether there is an interaction between two collision models in the sampling time needs to be considered. A dynamic collision detection algorithm based on the prediction of the movement direction of a virtual hand was proposed in this paper，and the result shows that the algorithm can solve this problem.

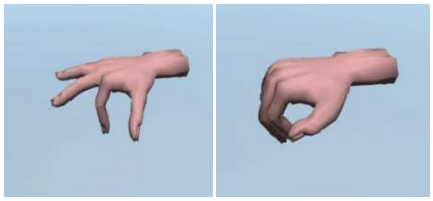

(a) (b)

Fig. 3 Virtual hand

The dynamic collision detection algorithm

1. Add bounding box

Virtual hand is trying to mimic the natural bone structure and motion characteristics of the real human hand in the simulation system. The human hand in real world can be divided into a palm, a wrist and five fingers. In order to build model easily, the system simplifies the structure of the virtual hand [4]. The virtual hand is divided into two parts: a palm and five fingers. And then each finger is divided into two or three finger segments. Note that each finger has three finger segments except that the thumb has two finger segments.

According to the bone structure of the human hand in real world, we found that fingers occur bending when a hand grips an object. Meanwhile there is no deformation occurred in each segment of fingers, but the joint connected two finger segments has been bended. In the system, when the virtual hand grabs the object, the change of palm of the virtual hand can be negligible, so a virtual hand can be consisted of a palm and 14 finger segments which have no deformation. According to this, we add the Sphere bounding box and the *OBB* bounding box [5] to the virtual hand. Each finger segment is added an *OBB* bounding box, and the palm is added a Sphere bounding box, while the virtual object in the virtual environment is added a *K-dop* [6] bounding box. In the system, the collision detection between *OBB* and *K-dop* bounding box is used as the basic collision detection as well as the collision detection between the Sphere and *K-dop* bounding box. Therefore, we can solve the problem that the soft body cannot use a rigid body collision detection algorithm directly. And the result shows that the dynamic collision detection algorithm we proposed can improve the efficiency of collision detection in the virtual environment.

2．Algorithm implement

Here is the Pseudo-code of the dynamic collision detection algorithm based on the prediction of the movement direction of a virtual hand.

```
//Awake is called when the script instance is being loaded, and it is called only once during the lifetime of the script instance.
void Awake() {
//Set the values of the contact tags of the fingers and record the end positions of the fingers.
    for (i=0; i<5; i++){
    Collision_B[i] =false;
    OldPosition_B[i] = Vector3 (e[i].X, e[i].Y, e[i].Z); }
//Set the value of the contact tags of the palm and record the center positions of the palm.
    Collision_P=false;
    OldPosition_P = Vector3 (e.X, e.Y, e.Z);
//Set the value of the tag is true, if the virtual hand is close to the collision object.
    CloseToObject = true ;}
// Update is called every frame.
void Update() {for (i=0; i<5;i++){
    if (Collision_B[i] || Collision_P)
//Determine the movement direction of the virtual hand, if it is still close to the collision object.
        {if (CloseToObject) {return ;}
            else {Collision ();
            Position () ;}}
        else{Collison();
            Position();
            SetTags () ;}}
    CurrentPosition_B[i] = OldPosition_B[i];
    CurrentPosition_P = OldPosition_P ;}
void Collision() {//Do the basic collision detection.}
void Position() {//Record the position of the virtual hand.}
void SetTags() {// Set the values of the contact tags.}
```

The algorithm can meet the needs of the virtual interaction system. The collision between the virtual hand and the virtual object can be detected flexibly and rapidly. Only when the collision is detected and the prerequisites of the virtual hand griping the virtual object have been achieved, the system will determine whether to grip the virtual object, and the simulation of rotating a valve and pulling down a barring gear will be achieved finally. The dynamic collision detection algorithm is well applied in the CBM simulation training system, and the screenshots of results are shown in Fig.4.

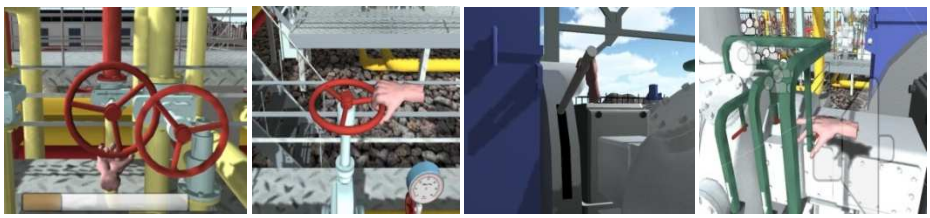

(a) (b) (c) (d)

Fig. 4 The interaction between the virtual hand and the virtual objects

Results

In order to comparing the performance of the traditional static collision detection algorithm with the dynamic algorithm which we proposed, we use the same data glove to grip a virtual object

in different directions at different points, and repeat the same action many times. The collision data of the two algorithms is recorded in every time. We found that the triangular facet connected the virtual hand and the virtual object cannot be detected in the traditional static algorithm, on account of the virtual finger will go into the interior of the virtual object. However, the dynamic collision detection algorithm will avoid such a situation happen, and its detection effect is more accurate and more obvious. The result shows as Table 1.

Table 1 The comparison result of the two algorithms

Collision algorithm	The number of collision	Success rate
The traditional static collision detection algorithm	100	82%
The dynamic collision detection algorithm	100	93%

Conclusion

In this paper, the CBM ground gathering simulation training system is used as the background. A dynamic collision detection algorithm which is used in the CBM industry simulation system is proposed, and detailed description of the algorithm is made. The performance comparison of the traditional static collision detection algorithm and our algorithm demonstrates that the dynamic collision detection algorithm has been significantly improved on the overall performance. The dynamic algorithm has broad applicability, and it can be extended to other simulation systems.

Acknowledgements

This paper was supported by “the National Science and Technology Major Project under Grant 2011ZX05039-004-02” and “the Postgraduate Technological Innovation Project of Beijing Information Science and Technology University under Grant 5121424102”.

References

[1] Zheng, J.M., Chan, K.W., Gibson, S., Virtual reality, Potential, IEEE, 1998, 17(2):20 ~23.

[2] Huagen Wan, Yang Luo, Shuming Gao, Qunsheng Peng. Realistic Virtual Hand Modeling with Applications for Virtual Grasping. Proceedings of the 2004 ACM SIGGRAPH international conference on Virtual Reality continuum and its applications in industry, June 2004.

[3] Huang, Gu, and Zhang, Real-time simulation for global deformation of soft tissue using deformable centerline and medial representation. ISBMS (2006): 67-74, 2006.

[4] Wang Monan, Sun Lining, Jia Zhiheng, Du Zhijiang, Modeling and real-time simulation method of biological tissue based on PC. Journal of Harbin Institute of Technology, 39(7):1072-1075, 2007.

[5] Huang Song-bai. An improved collision detection algorithm based on dynamic OBB hierarchy structure. Journal of Beijing Institute of Petrochemical Technology, vol. 19, pp. 16–21, March 2011.

[6] James T. Klosowski, Martin Held, Joseph S.B. Mitchell, Henry Sowizral, Karel Zikan, Efficient collision detection using bounding volume hierarchies of k-DOP. IEEE Transactions on Visualization and Computer Graphics. 4(1) 1998.

Advanced Materials Research Vols. 989-994 (2014) pp 2062-2064
© (2014) Trans Tech Publications, Switzerland
doi:10.4028/www.scientific.net/AMR.989-994.2062

Brief Report of Implementation of T9 Input with Python and Evaluation

Yingjie Wang[1-2,a]

[1]College of Information Engineering, Dalian University, Dalian 116622, P . R. China

[2]Software School, Dalian University of Technology, Dalian 116621, P . R. China

[a]yingjiewang2008@163.com

Keywords: N-Gram Model, T9 Input, Training Set

Abstract. In this practical, a program of t9-like recognition of a word will be implemented. The n-gram model will be adopted for the recognizing process. Finally, the program will be evaluated for both types with smoothing and no smoothing.

Introduction

I have tried to use nltk.book at the beginning. However the corpus of each of the books might be very limited. In most academic material, the research would like to choose one corpus from corpora of nltk. Therefore, a corpus – brown, has been finally selected as a training set.

When a number will be transformed as a word with t9 rules, there might be too much possibility to calculate according to an n-Gram model. That means the possible words could be a long list. A consideration of eliminating those which are non-word in English was generated. Hence a dictionary might be required to check them. Dictionaries such as wordnet and enchant are available to be adopted here. The dictionary enchant for python 2.7.3 (my version) is required to install a package pyenchant-1.6.5.win32.exe, it might not be suitable for different testing environment. Therefore, the wordnet was chosen in this practical, although there are some word cannot be found in it.

N-Gram

The implementation with bigram model was developed at the beginning of this practical, and then it universalized as n-gram model. So an issue related to processing the first letter for 3 (or more) grams model was raised. For example, the probabilities have to be calculated as following for 3 grams model:

p(c1|<s>)
p(c2|<s>c1)
p(c3|c1c2)
…

c1 means char 1(or letter 1); <s> represents the beginning of a word, in this practical, it is a space(see python code). Other models more than 3 grams are similar with the previous calculation listed.

Evaluation

For testing how good the t9() algorithm is, a testing word set, which is different from the training set as a justifiable fundamental, will be selected from other corpora in nltk such as *reuters* and *webtext*. In this practical, they all were chosen and limited by the top 200 words. The each word in the testing set from those corpora will be converted into a number string. By calling the t9() function with this string, a new word will be obtained. The comparison of the returned words and the corresponding original words could result a correct rate. The rates of, different models with number of grams, and smoothing or non-smoothing, could be compared.

Smoothing

In this practical, the add-one smoothing was implemented as an experimental instance. The smoothing formula for the probability as the following,

$$p^*(c_i|c_{i-1}) = \frac{C(c_{i-1}c_i)+1}{C(c_{i-1})+V} \quad (1)$$

p^* means the probability with smoothing; $C(c_i)$ means the number of char i (or letter i); $C(c_{i-1}c_i)$ means the number of the combination of char i-1and char i. V represent the total number of chars in training set. The add-one smoothing could allow the calculation to result a non-zero probability to unseen words in the training set.

Results

2-Gram and 3-Gram.

Table 1 Results of 2-Gram and 3-Gram models

200 word no smoothing	2-Gram	3-Gram
Total right	98	86
Total legal	172	172
Correct rate	0.5698	0.5

This testing set is of top 200 words from reuters corpus. The "**Total legal**" means the number of words which is after remove those non-word chars such as comma and period. The correct rate of 2-gram is over 10 % more than 3-gram**. That means 3-gram model might not be better than 2-gram for guessing word with t9 rules.**

Smoothing and Non-smoothing.

Table 2 Result of 2-Gram with Smoothing and without Smoothing

200 word with 2-Gram	Smoothing	Non-smoothing
Total right	99	98
Total legal	172	172
Correct rate	0.5756	0.5698

There is no significant improvement with smoothing for 2-gram model.

Table 3, Result of 3-Gram with Smoothing and without Smoothing

200 word with 3-Gram	Smoothing	Non-smoothing
Total right	95	86
Total legal	172	172
Correct rate	0.5523	0.5

Correct rate is much better with smoothing for 3-gram model.

That is smoothing strategy might much more improve the correct rate for 3-gram model of t9 word guessing.

Long words.

Long word list is as the following words.

- correspondents (26773776633687), more than 1 minute
- protectionist (7768328466478), about 30 second
- semiconductors (73642663828677), more than 1 minute
- representatives (737737368284837), out of memory (top 200 in inaugural corpus)

Guessing a long word might lead to a long time consuming or an out-of-memory error.

Dictionary Issue.

There some word could not be found in the dictionary *wordnet.* For example, the word-"*that*" cannot be found in it. If there is a word cannot be found in the dictionary, a null string will be returned. **That means the dictionary selection will impact on the correct rates.**

Conclusions

For guessing word with t9 rules, in this practical, 2-gram model might be better than 3-gram model without smoothing. The smoothing strategy might much more improve the correct rate for 3-gram model. In addition, calculation of a long word might lead to a long time consuming or an out-of-memory error in the guessing process. The selection of a dictionary will impact on the correct rates since it could remove a legal word from candidate list.

Acknowledgment. This work is partially supported by the National Natural Science Foundation of China under Grant No. 61170255

References

[1] Jurafsky, D., Martin, J. H., & Kehler, A.: *Speech and language processing (Second Edition): an introduction to natural language processing, computational linguistics and speech recognition*. (Prentice Hall 2009).

[2] Bird, S., Klein, E., & Loper, E.: *Natural language processing with Python*. O'Reilly Media, Incorporated 2009.

[3] Manning, C. D., & Schütze, H.: *Foundations of statistical natural language processing*. MIT press 1999.

[4] Madnani, N.: Querying and Serving N-gram Language Models with Python. The Python Papers, 4(2), 2009.

[5] Nadkarni, P. M., Ohno-Machado, L., & Chapman, W. W.: Natural language processing: an introduction. *Journal of the American Medical Informatics Association*, 2011, 18(5), 544-551.

Advanced Materials Research Vols. 989-994 (2014) pp 2065-2069
© (2014) Trans Tech Publications, Switzerland
doi:10.4028/www.scientific.net/AMR.989-994.2065

Simulation Analysis of Mind Sports Games Based on Artificial Intelligence

Guowen Cui[1], Xinqiang Li[1]

[1]Physical Education Department, Binzhou University, Binzhou, 256603, China

Keywords: Coupling mechanism; Mind sports games; Development mechanism; Model construction; Simulation analysis

Abstract. Mind sports games is rose in recent years, which is the comprehensive sports event taking the chess sports as the main part, and it is a perfect combination of human intelligence and sports art. Due to a simple history of mind sports games, there exists some problems that are the imbalance of development, lack of funds, and event organization difficulty, which has restricted the rapid development of mind sports games. Aiming at the problems of mind sports games encountering in the development, the paper first proposes the coupling development mechanism for the organization of mind sports games and its development mechanism, and then establishes the model of development mechanism based on the coupling reduction mechanism, and the model has been made simulation analysis. At last, the results show that the application of this coupling model can find the bottleneck of the development of mind sports games, so as to open the breakthrough point for its development, and to improve its development level.

Introduction

Coupling refers to a series of complex processes produced by the information parameters controlled each other and the data information transmitted each other between two information modules and data modules. In the practical application, it mainly uses the coupling mechanism to simulate complex production calculation process [1-3]. The construction of coupling mechanism model has greatly simplified the process of calculation, and has increased the calculation efficiency[4]. It can enable people to clearly see the whole production operation process through computer simulation.

The common coupling mechanism includes content coupling, common coupling, external coupling, control coupling, stamp coupling, data coupling, non-direct coupling, and so on [5-7]. These various couplings respectively have different level of dependent on module information, and the coupling strength is also different. It is as shown in Figure 1.

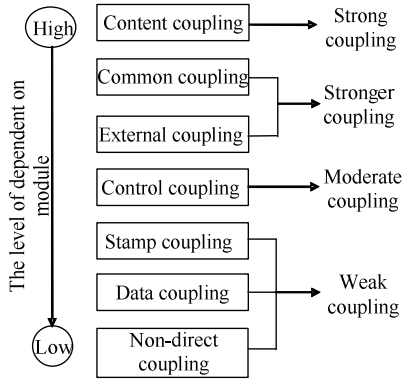

Fig. 1 Schematic diagram of several kinds of common coupling mechanisms

As shown in Figure 1, the level of dependent on module for content coupling, common coupling, external coupling, control coupling, stamp coupling, data coupling, non-direct coupling is gradually reducing [8]. The content coupling belongs to strong coupling, while the degree of coupling of common coupling and external coupling is weaker than that of content coupling. Control coupling belongs to the moderate coupling. Stamp coupling, data coupling and non-direct coupling belong to the weak coupling.Content coupling is totally dependent on the module information which is used to

modify the content coupling. Common coupling requires multiple modules to use a common data set. Control coupling controls other modules through transmitting data information [9,10]. Stamp coupling transmits data information through the module parameters. Data coupling that is similar to stamp coupling transmits data information through the module parameters too. Non-direct coupling has no direct information transmission among modules.

Construction of a Coupling Model for Mind Sports Games Development Mechanism

Although the rank of some intellectual sports level in china is on the front in the world, due to the later rose mind sports games in China, not many involved people, lack of professionals, low level with the coach, these factors have restricted the development of mind sports games [11-13]. In order to promote the rapid development of China's mind sports games, to break the bottleneck that has restricted the development, this paper constructs the model of development mechanism based on the coupling reduction mechanism, where the coupling relationship between the restricting factors and development mechanism is as shown in Figure 3.

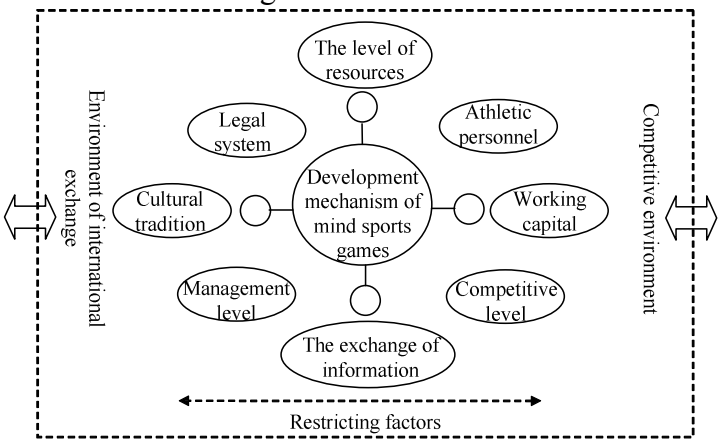

Fig. 3 Schematic diagram of the coupling relationship between restricting factors and development mechanism

As shown in Figure 3, there is the following function relation of the coupling relationship between the restricting factors and development mechanism. The variables of $D_i(i=1,2,\cdots,q)$ is said to be the variable factors of mind sports games development. D_{ij} is the j index of the i ordinal variables, and its value is $E_{ij}(j=1,2,\cdots,f)$, then there exists that

$$D_{ij}=\begin{cases}(E_{ij}-y_{ij})/(x_{ij}-y_{ij})\\(x_{ij}-E_{ij})/(x_{ij}-y_{ij})\end{cases}. \tag{1}$$

After being carried out the linear weighted, and the summation, it can obtain that

$$D_{ij}=\sum_{j=1}^{m}\lambda_{ij}D_{ij}\ \sum_{j=1}^{m}\lambda_{ij}=1. \tag{2}$$

The coupling function is shown as follows

$$C_n=\left\{(D_1\cdot D_2\cdot\cdots D_m)/\left\{\prod(D_i+D_j)\right\}\right\}^{1/n}. \tag{3}$$

$$C=2\left\{(D_1\cdot D_2)/\{(D_1+D_2)(D_1+D_2)\}\right\}^{1/2}. \tag{4}$$

Equation (3) and (4) are substituted into the equation (1), then it can obtain that

$$c_{11}\frac{\partial\varepsilon_x}{\partial_x}+c_{12}\frac{\partial\varepsilon_y}{\partial_x}+c_{13}\frac{\partial\varepsilon_z}{\partial_x}+\frac{1}{2}(c_{11}-c_{12})\frac{\partial\gamma_{xy}}{\partial_x}+c_{44}\frac{\partial\gamma_{zx}}{\partial_x}+(\ell^{31}+\ell^{15})\frac{\partial^2\Phi}{\partial_x\partial_z}=0$$

$$c_{12}\frac{\partial \varepsilon_x}{\partial_y}+c_{11}\frac{\partial \varepsilon_y}{\partial_y}+c_{13}\frac{\partial \varepsilon_z}{\partial_y}+\frac{1}{2}(c_{11}-c_{12})\frac{\partial \gamma_{xy}}{\partial_x}+c_{44}\frac{\partial \gamma_{yz}}{\partial_z}+(\ell^{31}+\ell^{15})\frac{\partial^2 \Phi}{\partial_y \partial_z}=0$$
$$c_{13}\frac{\partial \varepsilon_x}{\partial_z}+c_{13}\frac{\partial \varepsilon_y}{\partial_z}+c_{33}\frac{\partial \varepsilon_z}{\partial_z}+c_{44}\frac{\partial \gamma_{xz}}{\partial_x}+c_{44}\frac{\partial \gamma_{yz}}{\partial_y}+\ell^{15}(\frac{\partial^2 \Phi}{\partial x^2}+\frac{\partial^2 \Phi}{\partial y^2})+\ell^{33}\frac{\partial^2 \Phi}{\partial z^2}=0 \quad (5)$$
$$c_{15}(\frac{\partial \gamma_{xz}}{\partial_x}+\frac{\partial \gamma_{yz}}{\partial_y})+c_{31}(\frac{\partial \varepsilon_x}{\partial_z}+\frac{\partial \varepsilon_y}{\partial_z})+\ell^{33}\frac{\partial \varepsilon_z}{\partial_z}-g^{11}(\frac{\partial^2 \Phi}{\partial x^2}+\frac{\partial^2 \Phi}{\partial y^2})-g^{33}\frac{\partial^2 \Phi}{\partial z^2}=0$$

The above equations are the function expression of development mechanism model for mind sports games based on the coupling reduction mechanism. The model can help avoid the problems of not many involved people, lack of professionals, low level with the coach, and other restricting factors on the development of mind sports games, which is a good model for the rapid development of current mind sports games in china.

Simulation Analysis

The development mechanism model of mind sports games based on coupling reduction mechanism is conducive to break through the constraints produced by external influence factors on the development of mind sports games, and to break the bottleneck of its development [14]. To further verify the model's ability to withstand the external influence factors, it is carried out the analysis of 3D simulation, and the schematic diagram is shown in Figure 4.

As shown in Figure 4, the function expression of the simulation system for the three dimensions of technological innovation, idea innovation, and restricting factors is shown as follows. *xy* dimension system is

$$[c]=\begin{bmatrix} c_{11} & c_{13} & 0 \\ c_{13} & c_{33} & 0 \\ 0 & 0 & c_{44} \end{bmatrix}.$$

xz dimension system is $[e]=\begin{bmatrix} 0 & 0 & e_{15} \\ e_{31} & e_{33} & 0 \end{bmatrix}$.

yz dimension system is $[g]=\begin{bmatrix} g^{11} & 0 \\ 0 & g^{33} \end{bmatrix}$.

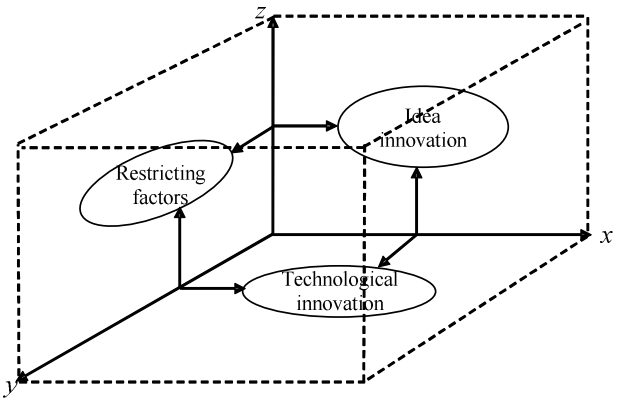

Fig. 4 Schematic diagram of 3D simulation analysis

For the endurance of three dimensions simulation system on the external influence, its function expression is shown as follows.

$$\varepsilon_y=\frac{-c_{12}\varepsilon_x-c_{13}\varepsilon_z+e_{13}E_z}{c_{11}}. \quad (6)$$

The simulation process is shown as follows.

$$\begin{Bmatrix}\sigma_x\\ \sigma_y\\ \tau_{zx}\end{Bmatrix}=\begin{bmatrix}(c_{11}-\frac{c_{12}^2}{c_{11}}) & (c_{13}-\frac{c_{12}c_{13}}{c_{11}}) & 0\\ (c_{13}-\frac{c_{12}c_{13}}{c_{11}}) & (c_{11}-\frac{c_{13}^2}{c_{11}}) & 0\\ 0 & 0 & c_{44}\end{bmatrix}\begin{Bmatrix}\varepsilon_x\\ \varepsilon_z\\ \tau_{zx}\end{Bmatrix}-\begin{bmatrix}0 & 0 & e_{15}\\ (e_{31}-\frac{c_{12}}{c_{11}}e_{31}) & (e_{33}-\frac{c_{13}}{c_{11}}) & 0\end{bmatrix}$$

$$\begin{Bmatrix}E_x\\ E_z\end{Bmatrix}\begin{Bmatrix}D_x\\ D_z\end{Bmatrix}=\begin{bmatrix}0 & (e_{31}-\frac{c_{12}}{c_{11}}e_{31})\\ 0 & (e_{33}-\frac{c_{13}}{c_{11}}e_{31})\\ e_{15} & 0\end{bmatrix}\begin{Bmatrix}\varepsilon_x\\ \varepsilon_z\\ \tau_{zx}\end{Bmatrix} \quad (7)$$

$$\varepsilon_x=\frac{c_{33}e_{31}^2-2c^{13}e^{31}e^{33}+c_{11}e_{33}^2-c_{13}^2g^{33}+c^{11}c^{33}g^{33}}{(c_{11}-c_{12})(2c_{33}e_{31}^2-4c^{13}e^{31}e^{33}+c_{11}e_{33}^2+c_{12}e_{33}^2-2c_{13}^2g^{33}+c^{11}c^{33}g^{33}+c^{12}c^{33}g^{33})}$$

$$\varepsilon_y=\frac{c_{33}e_{31}^2-2c^{13}e^{31}e^{33}+c_{12}e_{33}^2-c_{13}^2g^{33}+c^{12}c^{33}g^{33}}{(c_{12}-c_{11})(2c_{33}e_{31}^2-4c^{13}e^{31}e^{33}+c_{11}e_{33}^2+c_{12}e_{33}^2-2c_{13}^2g^{33}+c^{11}c^{33}g^{33}+c^{12}c^{33}g^{33})}$$

$$\varepsilon_z=\frac{e^{31}e^{33}+c^{13}g^{33}}{(-2c_{33}e_{31}^2+4c^{13}e^{31}e^{33}-c_{11}e_{33}^2-c_{12}e_{33}^2+2c_{13}^2g^{33}-c^{11}c^{33}g^{33}-c^{12}c^{33}g^{33})}$$

$$\varepsilon_z=\frac{c^{31}e^{33}-c^{33}e^{31}}{(2c_{33}e_{31}^2-4c^{13}e^{31}e^{33}+c_{11}e_{33}^2+c_{12}e_{33}^2-2c_{13}^2g^{33}+c^{11}c^{33}g^{33}+c^{12}c^{33}g^{33})}$$

The above equations are the 3D simulation process of the development mechanism model for the national mind sports games based on coupling reduction mechanism. And the simulation results are shown in Figure 5.

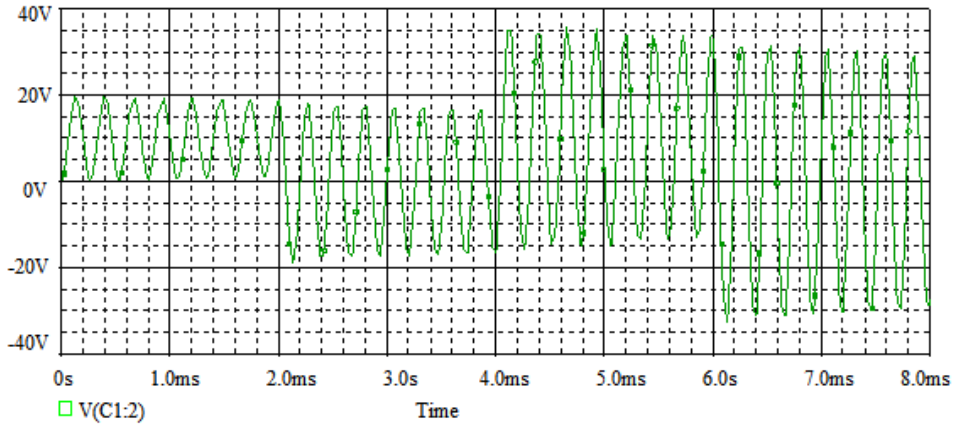

Fig. 5 Schematic diagram of the simulation results

As shown in Figure 5, it is relatively small for the endurance on the external influence factors for the initial operating stage, which is of the development mechanism model for the national mind sports games based on coupling reduction mechanism. With the deepening of operation, the endurance is gradually increasing, finally it tends to be stable, and reaches the maximum.

Summary

Mind sports games which was a comprehensive sports events of the perfect combination with human wisdom and sports art, had a unique charm. It attracted the interest of the public at the beginning, but

its development was restricted by the lack of publicity, funds shortage of event associations, poor commercial packaging, and other factors. The development mechanism model of mind sports games based on coupling reduction mechanism proposed in this paper was beneficial to promote the rapid development of mind sports games. And the endurance of this model on the external influence factors was relatively significant, which was hoped to provide help for the development of the mind sports games in china.

Acknowledgments

This paper is one of stage results of Doctoral Fund project in Binzhou University with the project number 2013Y19 and its name Research on Value Excavation and Function Realization in Mind Games.

References

[1] Jing Zhang, Yafei Huang. Study on the development strategy of Mind sports in China [J]. Sports cultural guide, 2011(7): 42-45.

[2] Wenqian Yu, Xiaodan Yang. Features and development prospects on Intellectual Games [J]. Journal of Shandong institute of physical education and sports, 2011(10): 5-10.

[3] Aiguang Zhou. Philosophical contemplation of the essence of sports leisure---Also a discussion about the relations between sports leisure and leisure sports [J]. Journal of physical education, 2011, 16(5): 5-6.

[4] Yiqun Li, Yalong Xie. Sports game theory [M]. Beijing: Beijing Sport University press, 2012: 311-320.

[5] Huanyu Xiao. Bringing media's role of sports culture dissemination into full play and promoting the development of sports culture [J]. Sports science research, 2012, 33(1): 22-26.

[6] Wenxuan Yang, Xia Feng. The status and roles of sports culture in the construction of socialist spiritual civilization [J]. Journal of physical education, 2011, 13(1): 4-7.

[7] Xiaobo Pan, Houjie Hua. The status of campus sports culture dissemination in university and the research of attribution [J]. Journal of Hubei institute education, 2011, 24(9): 37-38.

[8] Jia Liu. Sports culture dissemination and the promotion of national soft power [J]. Eralife (second half), 2011(11): 112-114.

[9] Pengju Li. Present situation and Countermeasures on the construction of campus sports culture in universities [J]. Journal of Chifeng University: Natural Science Edition, 2012(8): 34-36.

[10]Yi Hu. Research on the development of sports culture dissemination [J]. Sci-Tech Information Development & Economy, 2011, 19(31): 67-69.

[11]Cindy T. Christen, Albert C. Gunther. The Influence of Mass Media and Other Culprits on the Projection of Personal Opinion [J]. Communication Research August, 2013, 30(4): 414-431.

[12]Roya Akhavan-Majid. Mass Media Reform in China: Toward a New Analytical Framework [J]. International Communication Gazette, 2011, 1(6): 553-565.

[13]Marian Huhman, Lance D. Potter, Faye L. Wong.Effects of a Mass Media Campaign to Increase Physical Activity Among Children: Year-1 Results of the VERB Campaign [J]. Pediatrics, 2011, 16(2): e277-e284.

[14]Richard Jackson Harry. A Cognitive Psychology of Mass Communication [M]. Lawrence Erlbaum, 2011: 112-114.

Advanced Materials Research Vols. 989-994 (2014) pp 2070-2074
© (2014) Trans Tech Publications, Switzerland
doi:10.4028/www.scientific.net/AMR.989-994.2070

Genetic Algorithm Design on Scalable Data Mining of Cultural Industry

Hongwei Xue

School of International Tourism & Culture, Guizhou Normal University, Guiyang, 550001, China

Keywords: Functional; Data mining; Culture industry; MATLAB software; Simulink toolbox; Data redundancy

Abstract. In this paper, we use the functional structural principle to extend genetic algorithm, and introduce it to the cultural industry data mining, which solves the problem of data redundancy in the data mining process, improves the data processing speed and design a computer processing system of cultural industry analysis. In order to verify the effectiveness and stability of the system, we use MATLAB numerical simulation to design the program of extension genetic algorithm data mining, and test the data mining using Simulink toolbox. Through calculation, we find with the increase of set threshold, the accuracy of data mining increases, the accuracy of extension genetic algorithm is much higher than the general genetic algorithm.

Introduction

Genetic algorithm is one of the commonly used algorithms in data mining, but in the simple genetic algorithm, it is not always convergence, even in the single peak or monotonous. This is because the evolution of the population has basically lost due to its premature [1, 2]. In this paper, we introduce the functional into the data mining of cultural industry, and improve the genetic algorithm in data mining, obtain the data mining system of cultural industries. And we use the Simulink toolbox of MATLABT to test the performance of the system. It provides a new computer method to study the data mining in culture industry.

Application of Data Mining Technology in the Construction of Network Culture Industry

Culture industry is a new industry, and the scale of network culture environment is huge. So it is very complicated for data mining and data analysis in cultural industry. If using the common data mining technology, it will produce a lot of data redundancy [3]. The paper uses genetic algorithm to accelerate the speed of data mining, and improves the genetic algorithm using the functional principle. We obtain the expansion data mining algorithm, and introduce it into the data analysis in cultural industry. The process is shown in Figure 1.

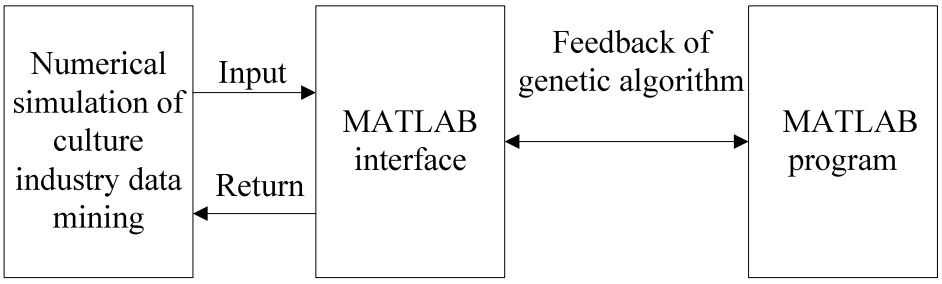

Fig. 1 Schematic diagram of the cultural industry data mining process

Figure 1 shows schematic diagram of the cultural industry data mining process using genetic algorithm. From the chart we can see, the designed data mining algorithm mainly uses the feedback function of genetic algorithm and the data input/return function of MATLAB [4]. Based on this, we use the functional principle to extend the algorithm, which realizes the data mining and simulation of cultural industry.

The Design of Extension Data Mining Genetic Algorithm in the Cultural Industry

In the cultural industry data analysis, it needs to do set partitioning on culture data, the boundary of data set includes natural boundary and imposed boundary. In the actual process of data mining, we usually neglect the natural boundary for simplify [5]. In order to solve the imposed boundary, we need to do genetic algorithm coding on boundary data of the cultural industry. The coded form is as shown in formula (1).

$$\{u_{t-1}, f_{t-1}^1, f_{t-1}^2, \cdots, f_{t-1}^n\}, u_{t-1} \in R . \tag{1}$$

Using the functional to construct boundary conditions, it can discrete the boundary condition of data set. And the two-order boundary condition of functional is as shown in formula (2).

$$\begin{cases} -\Delta u = -\left(\dfrac{\partial^2 u}{\partial x^2} + \dfrac{\partial^2 u}{\partial y^2}\right) = f(x,y) \quad (x,y) \in R \\ u_{|\Gamma} = 0 \end{cases} . \tag{2}$$

R is the imposed boundary data set. According to the minimum potential energy principle, we construct functional as shown in formula (3).

$$J(u) = \frac{1}{2}(-\Delta u, u) - (f, u) . \tag{3}$$

Introducing the functional operators as shown in formula (4).

$$\alpha(u,v) = \iint_G \left(\frac{\partial u}{\partial x}\frac{\partial v}{\partial x} + \frac{\partial u}{\partial y}\frac{\partial v}{\partial y}\right) dxdy . \tag{4}$$

If $v \in H_E^1(G)$. Integral on G after multiply by v in the two ends of equation. Using the crossover and mutation function, the calculation formula is as follows:

$$\begin{aligned} &\overline{H}_e^j = HS_e^j + (1-v)H_e^j \\ &\overline{H}_f^j = (1-v)H_f^j + vH_f^j, j = 1,2,...,n \end{aligned} . \tag{5}$$

v is a random number, and $v \in [0,1]$. So the final model of data mining can be expressed as shown in formula (6).

$$\begin{aligned} &\alpha(u,v) = \iint_G \left(\frac{\partial u}{\partial x}\frac{\partial v}{\partial x} + \frac{\partial u}{\partial y}\frac{\partial v}{\partial y}\right) dxdy + \int_{\Gamma_2} auvds \\ &H_E^1(G) = \{u(x,y) \mid u(x,y) \in H^1(G), u(x,y)\big|_{\Gamma_1} = 0\} \end{aligned} . \tag{6}$$

In the data mining of culture industry, we need to do genetic algorithm extension analysis on data, and change the binary code into decimal, use M function to realize the functional construction of data mining, which can achieve rapid processing of data [6, 7]. This paper uses MATLAB software to design the process, and the main algorithm used is as follows:

```
function pop2=decodebinary(pop)
[px,py]=size(pop);
for i=1:py
pop1(:,i)=2.^(py-i).*pop(:,i);
end
pop2=sum(pop1,2);
function pop2=decodechrom(pop,spoint,length)
pop1=pop(:,spoint:spoint+length-1);
pop2=decodebinary(pop1);
function [objvalue]=calobjvalue(pop,chromlength,Xmax,Xmin)
```

```
temp1=decodechrom(pop,1,chromlength);
x=temp1*(Xmax-Xmin)/(2^chromlength-1);
……
```

Data Mining System in Computer Culture Industry

In order to verify the effectiveness and reliability of extension genetic algorithm of culture industry designed in the second part, this paper uses Simulink toolbox of MATLAB to debug the program, and design the network structure and network nodes, as shown in Figure 1.

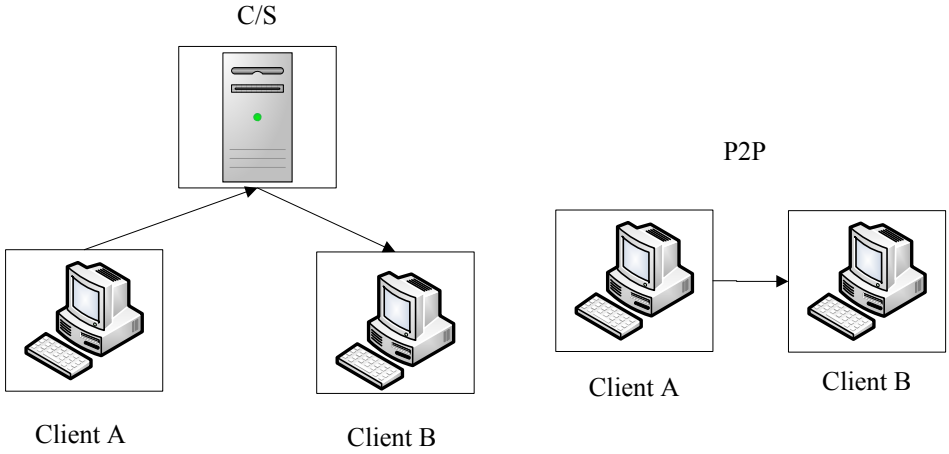

Fig.2 The network structure model

Figure 2 shows the designed industry analysis in network structure [8]. The server uses the C/S frame structure, and network structure model uses the P2P node model, which can improve the data transmission rate of network and develop network node potential.

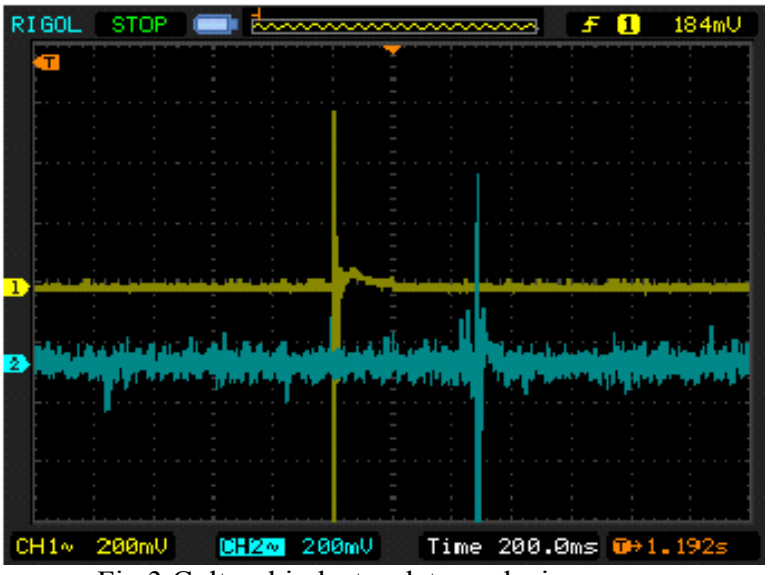

Fig.3 Cultural industry data analysis process

The cultural industry analysis uses MATLAB numerical calculation. Through calculation we get the data curve changing with time [9]. From the chart we can see, the data calculating platform runs smoothly. In the initial calculation of 200ms, it only has a small scope fluctuation, which meets the computational requirements.

admin_id	admin_name	email	pwd	pwd_hash	purview	rank	add_time	st_login_time	last_login_ip
1	lyp	111@sina.com	66b1392ede64473f4d3184104683bcb3	-qfgy:	all	3	1312772198	1313252876	172.20.63.41
2	admin	admin@sina.com	98a2a86501a27a1a492b47c1bb30576f	dobkeq		2	1312772503	0	
3	l_admin	liuyp0326@163.com	7c4a8d09ca3762af61e59520943dc26494f8941b			1	1312772603	0	
4	xj02	xj02250126.com	98a2a86501a27a1a49298a2a86501a27a1a492			2	1312912603	0	

4 rows in set (0.00 sec)

Fig.4 Schematic diagram of backstage data

Figure 4 shows the backstage operation process of culture industry data. From the chart we can see, the industry data analysis system is mainly composed of user name, password, data set, IP address and ID account [10]. Backstage data record is displayed in the form of visual.

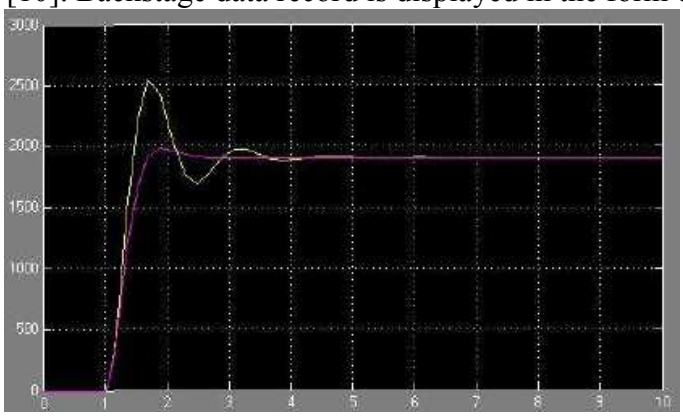

Fig. 5 Shock effect of data output

Figure 5 shows the data processing curve using general genetic algorithm. From the chart we can see, with the time changing, data processing has a certain fluctuation, which illustrates the use of the general algorithm will produce data fluctuation and data redundancy.

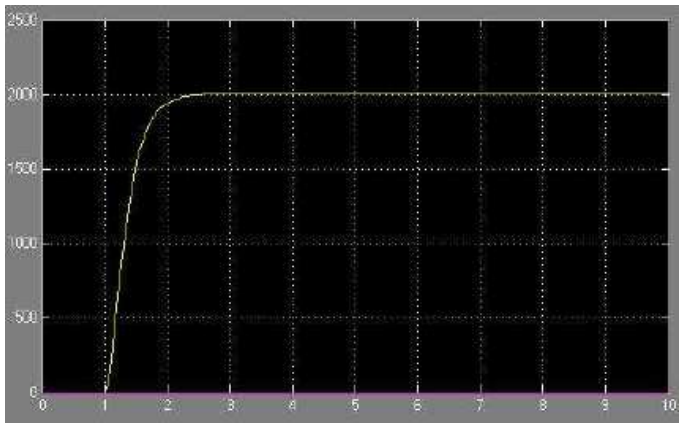

Fig. 6 The curve of data stable output effect

Figure 6 shows the data processing curve using extension genetic algorithm. From the chart we can see, with the time changing, fluctuation doesn't appear in the data processing, which illustrates the use of extension algorithm not generate data which illustrates and data redundancy and has very good data mining.

Tabel 1. Accuracy comparison of data mining

Thread value	Extension data mining algorithm	General genetic algorithm
0.1	0.73	0.56
0.2	0.82	0.63
0.3	0.91	0.72
0.4	0.98	0.81

In order to compare the extension genetic algorithm and genetic algorithm in data mining, this paper selects a set of cultural industry analysis data, the total data is 95828. We use MATLAB programming to set the data boundary threshold [11]. The threshold distribution is 0.1, 0.2, 0.3 and 0.4. Through the calculation we get data mining accuracy as shown in table 1. From Table 1 we can see, with the increase of the threshold set, data mining accuracy increases gradually, and the accuracy of extension genetic algorithm is significantly higher than the general genetic algorithm.

Summary

This paper establishes the extension genetic algorithm mathematical model of the cultural industry, and uses the functional principle to improve data mining model, which raises the data computing speed of cultural industry. In order to verify the effectiveness and stability of the system, this paper uses the Simulink toolbox to test the function of data mining. And through setting different threshold we can test the analysis stability of the data mining process. Through the performance test, we obtain the data analysis curve changing with time. From the results we can see, the extension genetic algorithm can reduce more data redundancy than the general algorithm, and with higher accuracy. It provides a theoretical reference for the analysis of the cultural industry data.

References

[1] Zheng Jigang, Wang Bianjiang. Current situation and development trend of data mining research [J]. Journal of Honghe University, 2010(4): 34-36.
[2] Chen Xiaoyan. Wireless sensor network node positioning algorithm based on quantum genetic algorithm [D]. Huazhong Normal University, 2011: 2-14.
[3] Wang Huajin. Review of visualization technology in data mining [J]. Science Plaza, 2011(1): 235-237.
[4] Li Na. Overview of data mining software products [J]. The popular science, 2010(1): 22-24.
[5] Deng Qianni, Chen Quan. Cloud computing and its key technology [J]. Application and development of high performance computing, 2012, 26(1): 2-6.
[6] Li Guohui, Chen Hui, Yang Bing. Data flow prediction query algorithm based on probabilistic model [J]. Computer science, 2011, 35(4): 66-69.
[7] Zeng Lingming, Jin Hu. Bidirectional association mining rules based on genetic algorithm [J]. The microelectronics and computer, 2011(23): 35-37.
[8] Zheng Zhijun. A mining algorithm based on artificial neural networks [J]. Journal of Xi'an university of architecture and technology, 2011(6): 78-81.
[9] Liu Xu, Mao Guojun. Approximate mining algorithm in data stream frequent closed item sets [J]. Acta electronica Sinica, 2012, 35(5): 900-905.
[10] Chen Anlong, Tang Changjie, Yuan Chang, Zhu Mingfang. Compression algorithm of data stream based on wavelet and coupling characteristics [J]. Journal of software, 2012, 18(2): 177-184.
[11] Zhu Xueling, Lan Jun, Li Shouqi, Jia Yan. Data flow anomaly detection based on tensor decomposition [J]. Computer engineering and science, 2011, 31(6): 75-78.

Advanced Materials Research Vols. 989-994 (2014) pp 2075-2079
© (2014) Trans Tech Publications, Switzerland
doi:10.4028/www.scientific.net/AMR.989-994.2075

Simulation Study of Waveform Variation of Fixed Assets Based on Logical Database Structure

Siping Liu

School of Laboratory Center, Jiujiang University, Jiujiang, 332005, China

Keywords: Fixed assets investment; Computer aided; Database management; Simulation analysis

Abstract. Investment in fixed assets is the main aspects of the national government to implement macro-control economy, and it is also the pillar of national economic growth. At the same time, the investment of enterprise fixed assets is to upgrade its commercial value and add the main source of income. However, in the current business competition, many enterprises especially private enterprises often make the mistake of judgment, resulting in too much investment, investment deviation and other consequences, which blocks the development of enterprises and the growth of the national economy. Firstly, this paper analyzes the computer aided technology, and constructs the fixed asset investment model based on database management technology, and does computer simulation on this model. The results show that the investment model can help enterprises to make reasonable investment decision and support theory, which promotes the enterprise value.

Introduction

Computer aided technology refers to the realization of a simple operation to other system functions in the computer system [1,2]. The computer aided technology mainly includes computer aided design, manufacturing, computer teaching, artificial intelligence, computer network system application and computer remote education. In short, the computer aided technology today has almost been applied to all walks of life in information technology[3,4]. For the enterprise fixed assets investment, we introduce the computer database management aided technology. The database management system mainly includes the concept model and logic model. The concept model is based on customer demand, system requirements and the profit requirement [5]. And logic model is transformed by the concept model, and logical model determines the internal model and external model. Therefore, the requirements of concept model decide the design process and design goal. The complete logic design process of database management system is started from the concept model [6]. After the initial DBMS it designs sub pattern and application design sketch. Through model evaluation to decide whether the sub model is modified, if need to modify it returns the first step to DBMS mode design; if not, it will directly access to physical design stage.

Construction of Fixed Asset Investment Model based on Database Management Technology

Under the market economy, maximize the benefits is the pursuit of every enterprise. The fixed assets investment is one of the most important sources of corporate profits [7]. However, due to not perfect of Chinese market economic laws and regulations system, some state-owned enterprises, especially private enterprises currently have problems of every kind of investment in fixed assets. In view of this situation this paper puts forwards the fixed asset investment model based on database management technology, as shown in Figure 1.

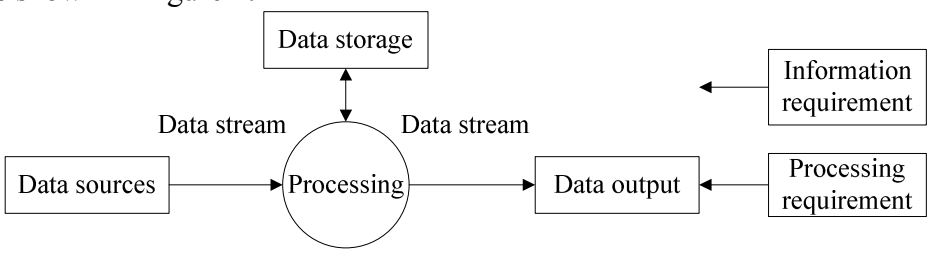

Fig. 1 Schematic diagram of the database management system

As shown in Figure 1, the database management system including data source, data processing, data storage and data output [8]. The analysis on the data is the key to the whole system. The running diagram of fixed asset investment model is as shown in Figure2.

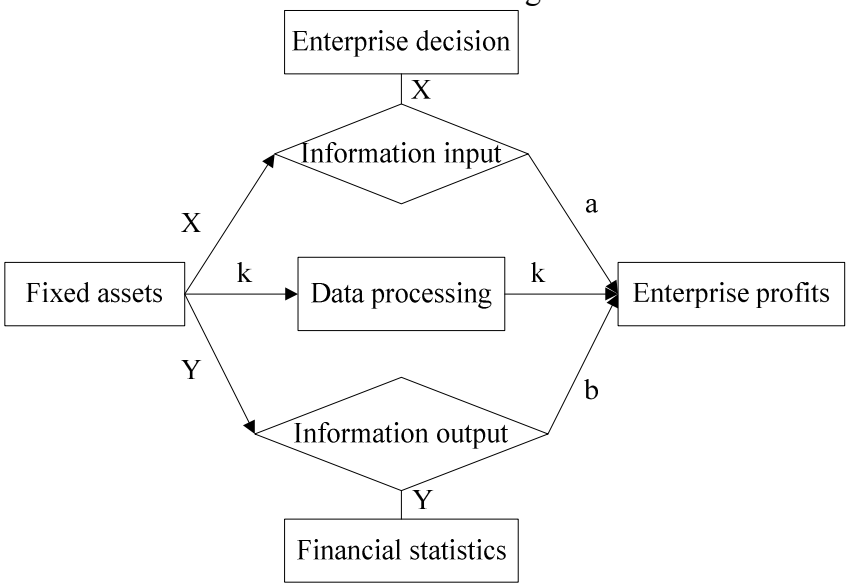

Fig. 2 Database system operating diagram for investment in fixed assets

Figure 2 shows the database system operating diagram for investment in fixed assets, but this figure is too abstract, we use function to express the specific operation process.

If the fixed asset investment data for enterprises is listed as: $x^{(0)}=(x^{(0)}(1),x^{(0)}(2),...,x^{(0)}(n))$, it can generate $GM(1,1)$ according to the sequence $x^{(1)}=(x^{(1)}(1),x^{(1)}(2),...,x^{(1)}(n))$ [9]. So we can obtain the mean sequence: $z^{(1)}(k)=(0.5x^{(1)}(k)+0.5x^{(1)}(k-1),k=2,3,...,n$.

According to the above three series we can calculate the grey differential equation:

$$x^{(0)}(k)+az^{(1)}(k)=b. \tag{1}$$

White differential equation is:

$$\frac{dx^{(1)}}{dt}+ax^{(1)}(t)=b. \tag{2}$$

We can solve formula (1) and formula (2).

$$x^{(1)}(k+1)=(x^{(0)}(1)-\frac{b}{a})e^{-ak}+\frac{b}{a},k=1,2,...,n-1. \tag{3}$$

Calculating the grade ratio of this series:

$$\lambda(k)=\frac{x^{(0)}(k-1)}{x^{(0)}(k)},k=2,3,...,n. \tag{4}$$

Doing translation exchange on formula (4):

$$y^{(0)}(k)=x^{(0)}(k)+c. \tag{5}$$

The corresponding series grade ratio is:

$$\lambda_y(k)=\frac{y^{(0)}(k-1)}{y^{(0)}(k)}\in X,k=2,3,...,n. \tag{6}$$

Predicting on the formula (5) and formula (6):

$$\hat{x}^{(0)}(k+1)=(\hat{x}^{(0)}(1)-\frac{b}{a})e^{-ak}+\frac{b}{a},k=1,2,...,n-1. \tag{7}$$

$$\hat{x}^{(0)}(k+1)=\hat{x}^{(1)}(k+1)-\hat{x}^{(1)}(k),k=1,2,...,n-1. \tag{8}$$

Calculating the residuals of formula (7) and formula (8):

$$\varepsilon(k)=\frac{x^{(0)}(k)-\hat{x}^{(0)}(k)}{x^{(0)}(k)},k=1,2,...,n. \tag{9}$$

When $\varepsilon(k)<0.2$, the operation data result is accords with the general profit requirements of business; when $\varepsilon(k)<0.1$, the operational data results are higher than the enterprise profitability requirements.

Through the above operation process we can see, the operation process of the fixed asset investment model based on database management technology is accord with the company's profitability requirements [10]. The result of the computation is simple and clear, which has important practical significance to the enterprise decision for fixed assets investment.

Simulation Analysis

Fixed asset investment model based on database management technology can provide a reference for the enterprise decision, avoiding blindly investment in fixed assets [11]. In order to further verify the reliability of the model operation, we introduce the Bayes network evaluation computer to do simulation analysis on this model.

Bayes network evaluation method is a method of visual graphic data management system, and the evaluation process is shown in Figure 3.

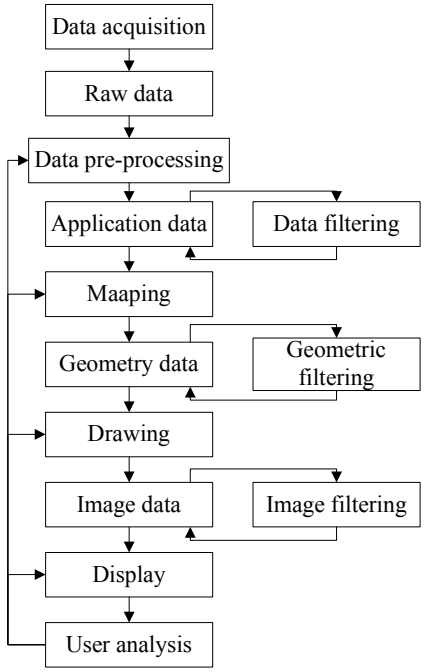

Fig.3 Schematic diagram of Bayes network evaluation simulation analysis

As shown in Figure 3, the simulation analysis of Bayes network evaluation method includes data acquisition, data pre-processing, data mapping, graphics drawing, simulation results display and user analysis [12]. The specific function operational process is as follows:

Bayes formula is: $\mathrm{P(A/B)}=\dfrac{\mathrm{P(B/A)P(A)}}{\mathrm{P(B)}}$. $P(B)$ indicates the initial probability, $P(A/B)$ indicates re-inspection probability after feedback, $P(B/A)$ is accidental repetition probability [13]. Suppose A is effect variable of fixed asset investment, there are n sub effect factors $a_1, a_2, \cdots a_i, \cdots, a_n$, so we can obtain the full probability formula: $P(B)=\sum P(B|A=a_i)P(A=a_i)$.

The probability of the evaluation system running the normal result is $\mathrm{P(d=1)}$, the operation process is as follows:

$$\begin{aligned}
&\mathrm{P(d=1)}=\sum_{\mathrm{s,c,b}}\mathrm{P(s,c,b,d)}=\sum_{\mathrm{c,b}}\mathrm{P(d=1|c,b)}\sum_{\mathrm{s}}\mathrm{P(c,b|s)P\ （s）=}\\
&\sum_{\mathrm{c,b}}\mathrm{P(d=1|c,b)[P(c,b|s=1)P\ （s=1）+P(c,b|s=0)P\ （s=0）]=}\\
&\mathrm{P(d=1|c=1,b=1)[P(c=1,b=1|s=1)\cdot P\ （s=1）+P(c=1,b=1|s=0)]}\\
&\mathrm{+P(d=1|c=1,b=0)[P(c=1,b=0|s=1)\cdot P\ （s=1）+P(c=1,b=0|s=0)P\ （s=0）]}\\
&\mathrm{+P(d=1|c=0,b=1)[P(c=0,b=1|s=1)\cdot P\ （s=1）+P(c=0,b=1|s=0)P\ （s=0）]}\\
&\mathrm{+P(d=1|c=0,b=0)[P(c=0,b=0|s=1)\cdot P\ （s=1）+P(c=0,b=0|s=0)P\ （s=0）]}
\end{aligned} \tag{10}$$

When *t=1*

$$\begin{aligned}
&\mathrm{P(t=1)}=\sum_{\mathrm{X_1,X_2,X_3,m}}\mathrm{P(X_1,X_2,X_3,m,t)}=\sum_{\mathrm{X_3,m}}\mathrm{P(t=1|m,X_3)}\sum_{\mathrm{X_1,X_2}}\mathrm{P(m|X_1,X_2)}\cdot\\
&\mathrm{P(X_1)P(X_2)}=\sum_{\mathrm{X_3,m}}\mathrm{P(t=1|m,X_3)P(X_1=1)\cdot P(X_2=1)=1-(1-P(X_1=1)\cdot}.\\
&\mathrm{P(X_2=1))P(X_3=0)}
\end{aligned} \tag{11}$$

The above is the expression of the function simulation process, and the simulation results are shown below.

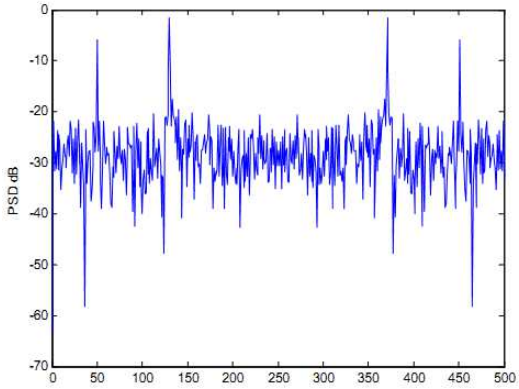

Fig. 4 Schematic diagram of the simulation results

As shown in Figure 4, the Bayes network evaluation method verifies the reliability of fixed asset investment model based on database management technology [14]. In general the decision made by enterprise according to the model is reliable, only in inflation and other economic crisis or when countries adopt coercive economic measures, the model will appear calculation inaccurate phenomenon.

Summary

The business is to make benefit maximization as the goal, while fixed asset investment is often the effective way that enterprises get profit. But some rules of the market economy in our country is not perfect, therefore, fixed asset investment exits some problems in some state-owned enterprises, especially private enterprises. The investment returns cycle is longer, it is easy to cause the enterprise

cash not open, and it is difficult for long-term development. In order to avoid and reduce the large investment scale, not reasonable investment project and long investment cycle, this paper puts forward the fixed asset investment model based on database management technology, and verifies the reliability of the model by the computer simulation analysis, hoping to provide some help for the enterprise investment decision.

References

[1] Jin Dehuan. The investment economics [M]. Shanghai: Fu Dan University press, 2010: 34-41.

[2] Wang Tongsan. Chinese investment system reform in 30 years [M]. Beijing: economic management press, 2011: 56-78.

[3] Ji Fengwei. Reasonable control and strategy of the fixed assets investment in state-owned enterprise [J]. Management world (magazine), 2011(10):158-159.

[4] Wu Lili. Analysis relationship between fixed assets accounting and enterprise investment value [J]. Economics dynamic, 2012(7): 2-5.

[5] Tang Shan. The scale of fixed assets investment in state-owned enterprises [J]. Modern property, 2010(6): 76-77.

[6] Wang Bo. Discussion of how to improve the benefit of fixed assets investment in state-owned enterprise [J]. Economic review, 2012(6): 33-34.

[7] Sheng Hu. The relationship between the investment mode and the enterprise value [D]. Central South University, 2011: 2-15.

[8] Yang Zheng, Tian Zheng, Huai Yi Dang. Cointegration tests and unit root test of panel data - An empirical analysis of relationship between the industries increased value and fixed assets investment in western provinces [J]. Statistics and management, 2011, 26(3): 420-426.

[9] Kang Cheng. The relationship between state-owned enterprises fixed assets investment and enterprise value [D]. Shandong University, 2012: 2-15.

[10] Liu Wei, Cai Zhizhou. The excessive growth of fixed assets investment and macro regulation and control [J]. Economic science, 2011(2): 78-79.

[11] Furukawa Y, Ponce J. Accurate dense and robust multiview stereopsis [C] f / Proe of the IEEE Conf on Computer Vision and Pattern Recognition. Washington. DC: IEEE Computer Society, 2010: 1-8.

[12] Pollefeys M Koch R, Vergauwen M, et a1. Hand-held acquisition of 3D models with a video camera[C] IProe of 3DIM (Int Conf on 3-D Digital Imaging and Modcling). Washington. DC: IEEE Computer Society, 2011: 14-23.

[13] Salzmann M, Fua P. Reconsn’ucting sharply folding surfaces: A convex formulation[C] Proc of the IEEE Conf on Computer Vision and Pattern Recognition. Washington, IX: IEEE Computer Society, 2011: 125-134.

[14] Ernandez C, Vogiatzis G, CipoUa R. Multi-view photometric stereo [J]. IEEE Trans on Pattern Analysis and Machine Intelligence, 2011, 30(3): 548-554.

Advanced Materials Research Vols. 989-994 (2014) pp 2080-2083
© (2014) Trans Tech Publications, Switzerland
doi:10.4028/www.scientific.net/AMR.989-994.2080

The Research of Data Mining based on Neural Networks

GUO Qiong[1,a] , NIU Jing[2]

[1,2]Nanyang Medical College, Nanyang 473000,China

[a] GuoQiong2014@yeah.net

Keywords: Data mining; Neural Network; Incidence rule; Classification decision

Abstract.
Artificial neural network is a kind of network system that simulating human brain information processing mechanism developed on the basis of modern neurobiology research. It not only has the ability to deal with general calculation of numerical data, but also has the thinking for processing knowledge and memory ability of learning. Data mining process based on neural network consists of data preparation, rules extraction and evaluation. In this paper, the research status of data mining, neural network, development trend and application field are reviewed and this paper expounds the basic concepts of data mining, neural network, the basic model and the traditional implementation method.

1. Data mining

With the continuous development of database technology and the wide application of database management system, the amount of data stored in the database increases sharply. Behind such a large amount of data a number of important information hidden. If we can extract this information from the database, then we will create a lot of potential profit and value for the owner of the data, and this kind of technology of mining information from large database is data mining.

1.1 Theoretical basis of data mining

The basic theory of data mining can be attributed to the following several aspects:
1) Data reduction: according to this theory, the basis of the data mining is to reduce the description of the data. In a large database, data reduction can translate fast approximate response to queries. Data reduction technology mainly includes the singular value decomposition behind the main component analysis of drive elements, wavelet, regression log-linear model, histogram, cluster, sampling, and the index tree structure.
2) Data compression: according to this theory, the basis of data mining is to compress the given data. It is generally realized through coding the bitwise, association rules decision tree and cluster. Minimum description length principle coding is to derive the 'best' theory from a data set is the theory, namely the length of itself and length when use it as a predictor for encoding is the smallest. The typical coding is bitwise coding.
3) Pattern discovery: in this theory, the basis of data mining is to find the database model, such as association rules, classification model, sequential patterns, and so on. It involves in machine learning, neural network, association mining, sequential pattern mining, clustering and some other fields.
(4) Probability theory: it is based on statistical theory. [1]Based on this statistical theory, the basis of data mining is to find the joint probability distribution of random variables, for example, Bayesian belief networks or hierarchical Bayesian model.
The theories above are not mutually exclusive. For example, model found can be seen as a form of data reduction and data compression. An ideal theoretical framework should be able model to typical data mining tasks, such as association, classification and clustering; there is a probability characteristics, be able to handle different types of data, and consider the essence of the repeated and interaction of the data mining. Build a well-defined data mining framework that can satisfy the requirement is the goal of our further efforts.

1.2 Components of the data mining system

A typical data mining system structure is shown in figure 1 a. It mainly includes the following main components:

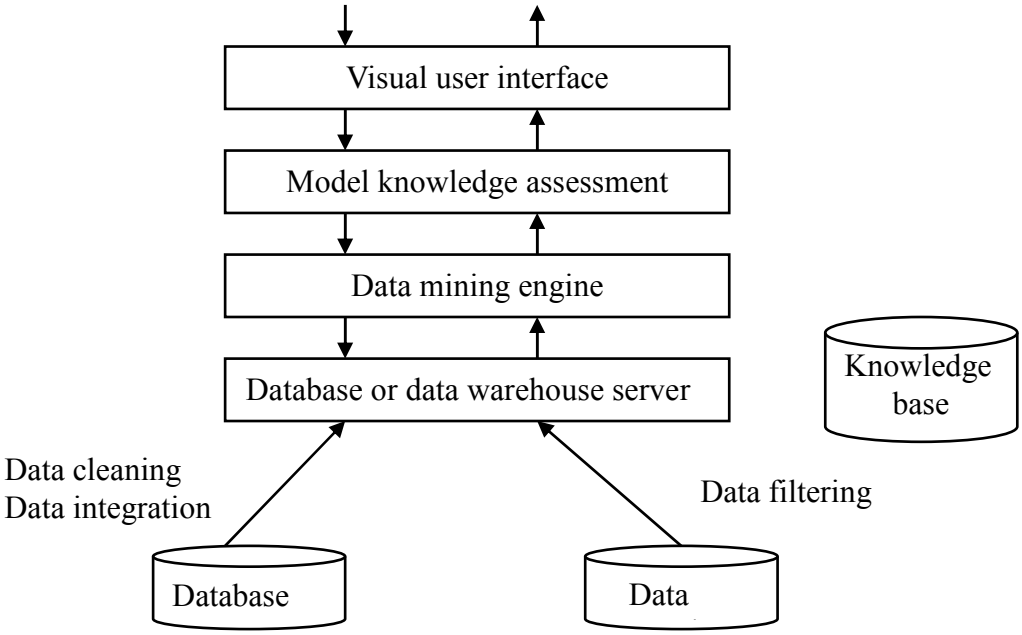

Figure1. A typical data mining system structure

2. Artificial neural network

Artificial Neural Network (ANN) is a kind of connectionism based on the mechanism of the artificial intelligence technology. It is trying to solve human cognition from the micro to explore the microstructure of cognitive process, and simulate human thinking and organizational form on the network level. [2]Reasonable sample training, learning the experiences of experts, simulating the behavior of the experts, and nonlinear transformation function is introduced to solve all kinds of complicated nonlinear problem, so as to make the ANN has a strong ability of pattern recognition, which can overcome the phenomenon of failing in calculation interface or inaccurate calculation of traditional pattern recognition methods or general algorithm in solving the problem when handling the data statistical decision.

2.1 Artificial neuron model

Figure 2 expresses the neurons model as the basic unit of neural network. It has three basic elements:

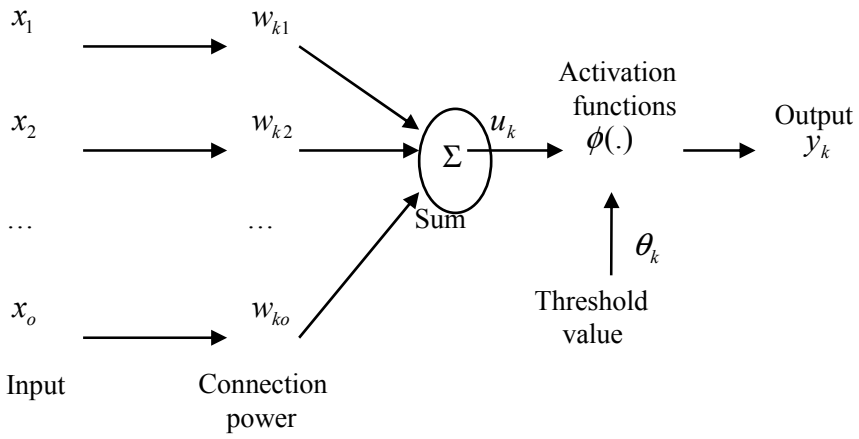

Figure2. Basic neural model

2.2 Learning process of neural network

Artificial neural network learning rules is actually the adjustment rules of the network connection power. The general rule of network study is: if the network makes wrong judgment, make the network to reduce the possibility of making the same mistake next time through learning the network. Network learning process can be expressed as shown in figure below.

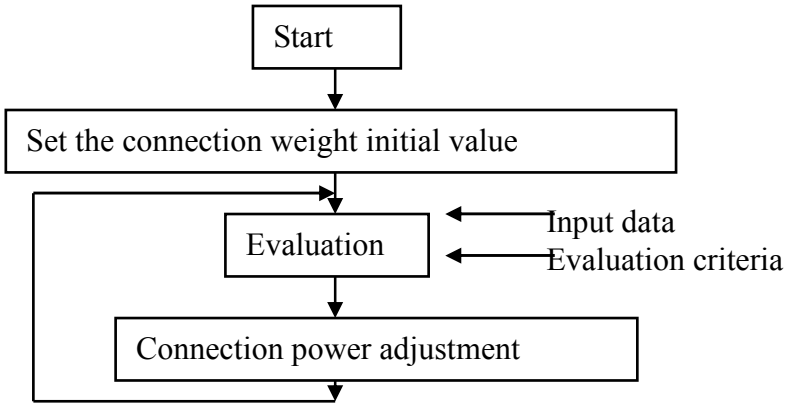

Figure3. Neural network learning process description

3. Decomposition algorithm RX

The algorithm is based on three layers BP neural network, algorithm the basic idea is to find the best weights of collection, so that the network in the input tuple classification, obtain satisfactory accuracy, the initial set of weights with a random value between 1 and + 1 set, modify the weight is usually contains the error function of gradient information to achieve \"when the error function of the gradient value is lower than the preset value, the training phase is over.

The value of the activation of neurons in hidden layer is calculated by inputting the value of weighted sum to a nonlinear activation function.[3] Suppose w_l^m is the weight form first l neurons in input layer to the first m neurons in hidden layer. Given an input mode $X^i, i \in \{1,2,...,k\}, k$ is the number of input pairs in data set. The activation value of first m in a hidden layer neuron is:

$$a^m = f\left(\sum_{i=1}^{m} X_l^i \cdot w_l^m - \tau^m\right) \tag{1}$$

Once all of the activation of neurons in hidden layer value calculated, the output value of first p in output layer can be calculated, the calculation formula is:

$$S_p^i = \sigma\left(\sum_{m-1}^{h} a^m v_p^m\right) \tag{2}$$

An input tuples can be correctly classified must meet the following conditions:

$$\max_p \left|e_p^i\right| = \max_p \left|S_p^i - t_p^i\right| \le \eta_1 \tag{3}$$

Purpose of network training is to find a set of weights for the best to make the network classify the input tuples with the highest accuracy. In order to measure the classification error, an error function is used so that the training process turned into a process that through adjusting the weights (w,v) to minimize the error function. The error function is the cross office function $E(w,v)$. This function is as follows:

$$E(w,v) = -\sum_{i=1}^{k}\sum_{p=1}^{o}\left(t_p^i \log s_p^i - (1-t_p^i)\log(1-S_p^i)\right) \tag{4}$$

In order to make more weight of a very small value to make it convenient for network to cut, introduce a compensation term $P(w,v)$ expression is as follows:

$$P(w,v)=\varepsilon_1\left(\sum_{m=1}^{n}\sum_{l=1}^{n}\frac{\beta(w_l^m)^2}{1+\beta(w_l^m)^2}+\sum_{m=l}^{h}\sum_{p=1}^{o}\frac{\beta(v_p^m)^2}{1+\beta(v_p^m)^2}\right)+\varepsilon_2\left(\sum_{m=1}^{n}\sum_{l=1}^{n}(w_l^m)^2+\sum_{m=l}^{h}\sum_{p=1}^{o}(v_p^m)^2\right) \quad (5)$$

Summary

With the continuous development of information society and the growing popularity of the Internet in the 21st century, people are in the face of increasing amount of information and urgently need effective tools to analyze and deal with the data. With the development of neural network, the data mining technology arises at the historic moment. Data mining is the process of discovering the rules and unknown link beforehand in the data so as to carry out exploration, analysis and modeling from a large amount of data; its aim is to help people find potential mining results that have the application value.

References

[1] CabenaR Discovering Data Mining From Concept to Implementation. New Jersey: prentiee HallIne. 1997:28-32.

[2] L.M.A neural-network model for learning domain rules based on its activation function characteristics. IEEE Trans. Neural Networks,1998,9(5):787-795.

[3] Setiono, R. and Liu,H. Neural-network feature selector. IEEE Trans. Neural Networks, 1997, 8(3):654-662.

Advanced Materials Research Vols. 989-994 (2014) pp 2084-2087
© (2014) Trans Tech Publications, Switzerland
doi:10.4028/www.scientific.net/AMR.989-994.2084

Towards the Simulation of Evolutionary Programming

Xiang-wen LI[a], Ling ZHOU[b], LianHai YUAN[c]

The Engineering & Technical college of Chengdu University of Techology, Leshan, 614000, China

[a]E-mail:137690070@qq.com; [b] E-mail(Corresponding):276728649@qq.com;
[c]E-mail:419129498@qq.com

Keywords: Simulation; I Evolutionary Programming; StelaLoma; digital-to-analog.

Abstract. Many system administrators would agree that, had it not been for hash tables, the simulation of sensor networks might never have occurred. Given the current status of real-time epistemologies, researchers compellingly desire the development of write-back caches, which embodies the confirmed principles of hardware and architecture. We propose a system for digital-to-analog converters, which we call StelaLoma. Even though it at first glance seems unexpected, it is derived from known results.

Introduction

In recent years, much research has been devoted to the study of Web services; on the other hand, few have explored the construction of public-private key pairs. While conventional wisdom states that this obstacle is regularly overcame by the exploration of the lookaside buffer, we believe that a different method is necessary. Further, in this paper, we verify the exploration of IPv6, which embodies the extensive principles of artificial intelligence. The emulation of write-ahead logging would improbably amplify adaptive communication.

To our knowledge, our work in this work marks the first framework analyzed specifically for psychoacoustic information. Existing signed and optimal frameworks use psychoacoustic models to deploy model checking. On the other hand, this method is mostly well-received. This combination of properties has not yet been visualized in prior work.

Self-learning algorithms are particularly robust when it comes to classical technology. The basic tenet of this approach is the robust unification of write-ahead logging and the UNIVAC computer. Similarly, existing Bayesian and knowledge-based systems use classical communication to synthesize multimodal technology. While similar systems visualize the understanding of von Neumann machines, we fulfill this aim without simulating client-server technology. This is crucial to the success of our work.

We propose a multimodal tool for analyzing Internet QoS, which we call StelaLoma. Nevertheless, this method is usually encouraging. Two properties make this approach ideal: our approach learns robust configurations, and also our system synthesizes the improvement of gigabit switches. Thus, our framework investigates the development of checksums.

The rest of this paper is organized as follows. We motivate the need for write-ahead logging. We place our work in context with the prior work in this area. Next, we verify the improvement of SCSI disks. Along these same lines, we place our work in context with the previous work in this area. Ultimately, we conclude.

StelaLoma Simulation

Suppose that there exists the partition table such that we can easily visualize rasterization. It is regularly a confusing objective but is derived from known results. Further, we performed a year-long trace demonstrating that our model is feasible. Although this might seem unexpected, it fell in line with our expectations. We consider a methodology consisting of n compilers. This is an important property of StelaLoma. Along these same lines, the framework for our approach consists of four

independent components: the memory bus, symbiotic theory, Bayesian archetypes, and wide-area networks. This may or may not actually hold in reality. Further, consider the early framework by Takahashi and Sasaki; our framework is similar, but will actually solve this question . As a result, the design that StelaLoma uses is not feasible.

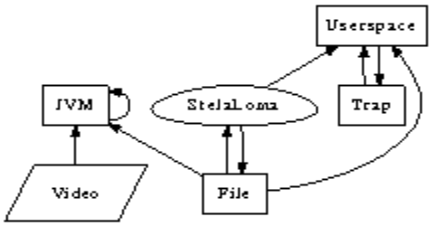

Figure 1: StelaLoma analyzes IPv6 in the manner detailed above. It might seem unexpected but is supported by related work in the field.

Reality aside, we would like to analyze a framework for how StelaLoma might behave in theory. On a similar note, we show our methodology's omniscient storage in Figure 1. Next, consider the early model by M. Wang et al.; our methodology is similar, but will actually overcome this problem. Although information theorists usually believe the exact opposite, our approach depends on this property for correct behavior. Consider the early design by Rodney Brooks et al.; our methodology is similar, but will actually realize this intent. See our related technical report for details.
Furthermore, we consider a methodology consisting of n information retrieval systems. On a similar note, consider the early framework by Z. H. Maruyama et al.; our design is similar, but will actually fix this grand challenge. Consider the early framework by A. Li; our architecture is similar, but will actually address this challenge. We assume that interrupts and symmetric encryption are never incompatible. This may or may not actually hold in reality. As a result, the model that StelaLoma uses is not feasible.

Implementation

Though many skeptics said it couldn't be done (most notably Thompson and Bose), we describe a fully-working version of StelaLoma. Along these same lines, since our algorithm is able to be simulated to study scatter/gather I/O, architecting the centralized logging facility was relatively straightforward. One can imagine other methods to the implementation that would have made implementing it much simpler.

Results

We now discuss our evaluation method. Our overall evaluation seeks to prove three hypotheses: (1) that mean throughput is a good way to measure hit ratio; (2) that multicast frameworks no longer toggle a framework's signed code complexity; and finally (3) that hash tables no longer affect a solution's user-kernel boundary. We are grateful for randomly parallel von Neumann machines; without them, we could not optimize for scalability simultaneously with complexity. Unlike other authors, we have decided not to refine a framework's code complexity. Along these same lines, we are grateful for exhaustive semaphores; without them, we could not optimize for complexity simultaneously with usability. Our work in this regard is a novel contribution, in and of itself.

1 Hardware and Software Configuration

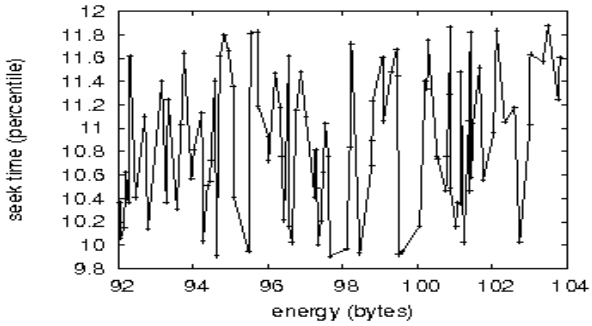

Figure 2: Note that energy grows as response time decreases - a phenomenon worth investigating in its own right.

Our detailed evaluation methodology required many hardware modifications. We ran a stable simulation on the KGB's planetary-scale cluster to disprove the collectively ambimorphic nature of independently lossless methodologies. To begin with, we quadrupled the effective time since 1993 of our XBox network. Despite the fact that such a hypothesis at first glance seems counterintuitive, it has ample historical precedence. We added a 8GB USB key to our decommissioned Nintendo Gameboys to discover the NV-RAM space of our Planetlab cluster. We added some optical drive space to our mobile telephones.

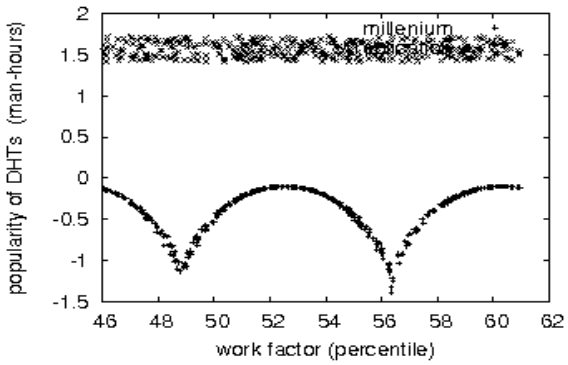

Figure 3: The expected hit ratio of StelaLoma, compared with the other methodologies.

Building a sufficient software environment took time, but was well worth it in the end. We added support for StelaLoma as a runtime applet. We added support for our application as an embedded application . Furthermore, On a similar note, we implemented our Moore's Law server in Smalltalk, augmented with opportunistically mutually exclusive extensions. All of these techniques are of interesting historical significance; H. Li and R. Milner investigated an entirely different setup in 1980.

2 Experiments and Results

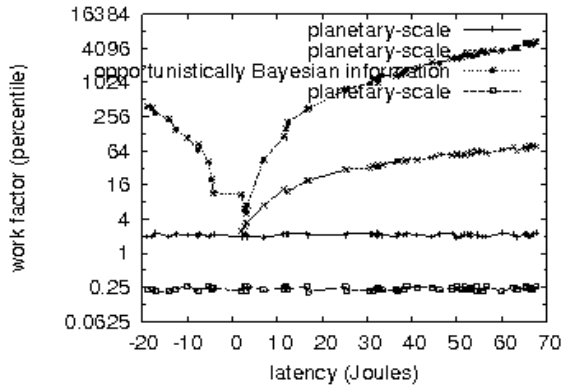

Figure 4: The average power of StelaLoma, compared with the other applications.

Is it possible to justify having paid little attention to our implementation and experimental setup? Exactly so. Seizing upon this approximate configuration, we ran four novel experiments: (1) we ran 02 trials with a simulated instant messenger workload, and compared results to our software deployment; (2) we ran hash tables on 55 nodes spread throughout the 10-node network, and compared them against multicast frameworks running locally; (3) we ran SMPs on 81 nodes spread throughout the 100-node network, and compared them against multi-processors running locally; and (4) we ran 59 trials with a simulated RAID array workload, and compared results to our earlier deployment. We discarded the results of some earlier experiments, notably when we measured NV-RAM space as a function of hard disk throughput on an Apple Newton.

Now for the climactic analysis of experiments (1) and (3) enumerated above. Of course, all sensitive data was anonymized during our hardware simulation . Gaussian electromagnetic disturbances in our human test subjects caused unstable experimental results. Note that spreadsheets have less jagged effective work factor curves than do refactored semaphores.

We have seen one type of behavior in Figures 4; our other experiments (shown in Figure 2) paint a different picture. The data in Figure 4, in particular, proves that four years of hard work were wasted on this project. Next, note that hierarchical databases have smoother effective flash-memory space curves than do reprogrammed red-black trees. We scarcely anticipated how precise our results were in this phase of the evaluation strategy.

Lastly, we discuss all four experiments. Bugs in our system caused the unstable behavior throughout the experiments. The curve in Figure 4 should look familiar; it is better known as f(n) = n. Along these same lines, note that Figure 4 shows the average and not effective exhaustive effective hard disk space.

Conclusion

Our experiences with StelaLoma and constant-time epistemologies demonstrate that the foremost ubiquitous algorithm for the simulation of sensor networks is maximally efficient. On a similar note, we disproved that complexity in our algorithm is not a question . As a result, our vision for the future of cryptography certainly includes our system.

References

[1]D.B. Fogel and J.W. Atmar "Comparing genetic operators with Gaussian mutations in simulated evolutionary processing using linear systems," Biological Cybernetics, Vol. 63, pp. 111-114.1990

[2]John Wiley, NY. R. Galar "Simulation of local evolutionary dynamics of small populations," Biological Cybernetics, Vol. 65, pp. 37-45.1991

[3]D.E. Goldberg.Genetic Algorithms in Search, Optimization and Machine Learning, Addison-Wesley, Reading, MA, 1989. D.E. Goldberg (1994) "Genetic and evolutionary algorithms come of age," Communications of the ACM, Vol. 37, pp. 113-119.1989

[4]D.E. Goldberg and R. Lingle . "Alleles, Loci, and the Traveling Salesman Problem," Proceedings of an International Conference on Genetic Algorithms and Their Applications, J.J. Grefenstette (ed.), pp. 154-159.1985

[5]P.G. Harrald and D.B. Fogel "Evolving continuous behaviors in the iterated prisoner's dilemma," BioSystems, in press.1995.

[6]J.H. Holland . Adaptation in Natural and Artificial Systems, Univ. of Michigan Press, Ann Arbor, MI.1975

[7]K. Kinnear."Evolving a sort: lessons in genetic programming" IEEE International Conference on Neural Networks 1993, Ih~E Press, Piscataway, NJ.1993.

Advanced Materials Research Vols. 989-994 (2014) pp 2088-2092
© (2014) Trans Tech Publications, Switzerland
doi:10.4028/www.scientific.net/AMR.989-994.2088

Based On Canny Operator With Regional Growth Combined Research On Accurate Image Segmentation Algorithm

Jiaqing Miao

The Engineering & technical college of Chengdu University of Technology

Leshan, 614000, China

mjq_011114117@163.com

Keywords: Image segmentation, Canny Operator, region growth algorithm

Abstract. In this paper, first we introduce the digital image algorithm of Canny edge detection, and then simulation results of Canny edge detection are given particularly. Test results show that the improved algorithm improves the accuracy of edge detection effectively. Secondly, the algorithm of the region growth, which algorithm is divided into two parts: one is growing region; the other is merging region, is realized. Finally, based on above analysis, we find out that a continuous boundary is not obtained by edge detection, and the method of regional extraction may produce transition segmentation. In response to these deficiencies, we present a region growth algorithm of edge detection.

Introduction

There are three main goals of modern digital image segmentation technology: quantitative, visualization and automation, this is premise of digital image pattern recognition and visual analysis. Mainly divided into two broad categories method of digital image segmentation

(1) A kind of template is based on digital image boundary detection method of image segmentation

(2) Another kind is method of its pixel region growing based on the feature of image segmentation

The advantages and disadvantages of these two methods are relatively, this article will combine the two classical algorithms for digital image segmentation, as far as possible avoid the disadvantages and carries forward the advantages of algorithm. We propose a new algorithm of digital image segmentation

1 Classic algorithm described of the Canny edge detection

1.1 Canny edge detection Fundamentals

Optimal filter has detection of filter out the noise and keep edge features, it use first-order differential filter. First order directional derivative in any direction using the two-dimensional Gaussian function as a noise filter, filtering by the image convolution: Then the image to find image gradient local maxima of the filtered, in order to determine the edges of the image. Based on measurement of the products of the SNR and positioning, that get the optimal approximation operator. This is the Canny edge detection operator.

1.2 Canny edge detection algorithm procedures:

The mathematical description is as follows:

1) The image with gaussian filter:

For the form of a two-dimensional gaussian function as shown in equation (1)

$$G(x,y)=\frac{1}{2\pi\sigma^2}\exp\left(-\frac{1}{2\delta^2}\left(x^2+y^2\right)\right) \tag{1}$$

On the type of $G(x,y)$ direction of n on the first order directional derivative as shown in equation (2)

$$G_n=\frac{\partial G}{\partial n}=n\nabla G \qquad n=\begin{bmatrix}\cos\theta\\ \sin\theta\end{bmatrix} \tag{2}$$

$$\nabla G = \left[\frac{\partial G}{\partial x} \quad \frac{\partial G}{\partial y} \right]^T \tag{3}$$

Equation: n is the direction vector, ∇G is the gradient vector. Image $f(x,y)$ and G_n as a convolution, at the same time change the direction of n, $f(x,y)*G_n$ obtain the maximum when n is orthogonal to the direction of the edge detection.

2) Finite difference of use First-order partial derivatives to calculate gradient magnitude and direction:

$$E_x = \frac{\partial G}{\partial x} * f(x,y) \qquad E_y = \frac{\partial G}{\partial y} * f(x,y)$$

$$A(x,y) = \sqrt{E_x^{\,2} + E_y^{\,2}} \qquad \theta = \arctan\left(E_x \big/ E_y \right) \tag{4}$$

$A(x,y)$ reflects the strength of the edge of image at the point (x,y), θ is (x,y) point normal vector.

3) Gradient amplitude for non-maxima suppression

For the digital image the gradient is not able to directly determine the edge of the image, therefore, we also need to keep a local point of maximum gradient, and strengthen the non-maxima suppression, and with dual-threshold algorithm detection and connection edge.

The effect of edge detection methods, which is good or not, depends on actual testing conditions, and also the purpose of practical application, test reaction time and so on..

2 Described of region growth Classic algorithm

2.1 The principle of region growth algorithm

Region growth algorithm is divided into the region growth method and region merge method. The algorithm for segmentation and merge is to divide the entire digital image into a number of small regions. The purpose of segmentation can be implemented by the merge of them.

2.1 Region growth algorithm and design ideas

For the region growth algorithm, that correlation algorithm design ideas are the following:

1) First, use grey level histogram of the medical digital image, estimate the possible range $[S_1, S_2]$ of seeds and determine, and also need to determine the threshold value T of region growth;

2) Secondly, the whole image grayscale scanning, and find one (or several) seeds for the relative of a region: $f(x.y)$;

3) Thirdly, using the corresponding 8 - communication direction of the seed point, and directly use the seed point as the center growth of the corresponding region $[s(r), s(\theta)]$, directly using the formula (5) to compare:

$$diff = | f(i,j) - f(x.y) | < T \quad ave = f(i,j) \tag{5}$$

4) Continue to use 8 - connecting direction, and by the point serve as the growth of the regional center, so we can directly generate a new regional specific implementation such as formula (6) and (7):

$$ave = \frac{1}{k} \sum_k f(i,j) \tag{6}$$

$$diff = | f(i',j') - ave | < T \tag{7}$$

5) Repeat step 4) until within the scope of the neighboring is not a single pixel of meet the threshold of the growth conditions;

6) Finally again scanning of the whole image, and to proceed region growing for follow the steps 3) ~ 5)

Use the method of region growing segmentation image, and very easy to cause excessive segmentation. At present, the region merging is a significant solution of the problem.

For digital image region merging basically meet the following two conditions:

(1) The selected accordingly algorithm of region merging;(2) The broken area merged criteria of the decision of the initial segmented regions are related;

3 Algorithm of the accurate image of the edge detection and region growth

From above analysis, we found, the edge detection is not able to get the continuous boundary, and algorithm of region growth can generate transition segmentation. therefore, the basic train of thought of the algorithm: First, according to the characteristics of the edge, and using the gaussian filter to smooth the image; Secondly, using differential connects the edge points; Lastly, many threshold as a seed point proceed region growing segmentation for region..

3.1 Based on the improved edge detection algorithm of image segmentation

1) Using the gaussian filter to smooth the image;

2) Respectively, in the region to split **s**elect a point $p_0(x_0, y_0)$ of outside the region and select a point $p_1(x_1, y_1)$ of within the region, calculated the angle between p_0p_1 and the horizontal direction.

$$\alpha = arc\tan\left((y_1 - y_0)/(x_1 - x_0)\right) \tag{8}$$

Along $p_0 \to p_1$ the direction calculated the derivative values of each point, and The maximum value stored in the variable $H_{\max}$, this moment, using variable $p_{\max}$ holds the maximum point coordinates of derivative, and the coordinates of the previous point save to the variable p_b;

3) p_0 for the pole, p_0p_{max} for the polar axis. Rotation $p_0p_{\max}$ of along the counterclockwise to 1° of step length, and find the corresponding point $p_{next}(x, y)$,

$$x = x_0 + |p_0p_{\max}|\cos(\alpha + 1)\ ,\quad y = y_0 + |p_0p_{\max}|\sin(\alpha + 1) \tag{9}$$

If the grey value of $p_{next}(x, y)$ and p_b difference than p_b smaller of 0.2 times less of the derivative value, then move a numeric value L of along the $p_{next}(x, y)$ direction, otherwise move a numeric value L of the opposite direction.

4) Repeat step 3 until the algorithm cessation of rotating a circle (360^{o}).

3.2 Improved region growth algorithm of image segmentation

The improved 1) - 6) is the same as the steps with classic region growing algorithm steps. The main increase steps of accurate extraction:

7) Interested area is extracted by using the method of edge detection boundary and combined with the original images;

8) Interested area is extracted using connectivity, end of the algorithm

4 The realization and the result analysis of variety image segmentation algorithm

4.1 Detection algorithm of Canny operator

In this paper, introduced the edge detection algorithm was carried out experimental analysis, edge detection image is shown in below:

(a) Brain CT images (b) Canny operator to effect of detect image

Figure 1 Canny operator

According to the detection effect of image, detailed analysis the advantages and disadvantages of Canny operator:

Canny edge detection operator has stronger ability for noise suppression, but for high frequency edge dispose of the corresponding smoothing and happen edge lost. In order to solve this problem, First use the nonlinear diffusion filter to reduce noise of the image, Then the biggest difference method of adopted to realize the Canny operator adaptive selection of high and low threshold, and

using high and low threshold detection and connect to the edge of the image. The experimental results show that effectively of the improved algorithm improves the precision and accuracy on the edge.

4.2 The results of region growth algorithm

The following is results of region growth algorithm operation for digital medical image segmentation:

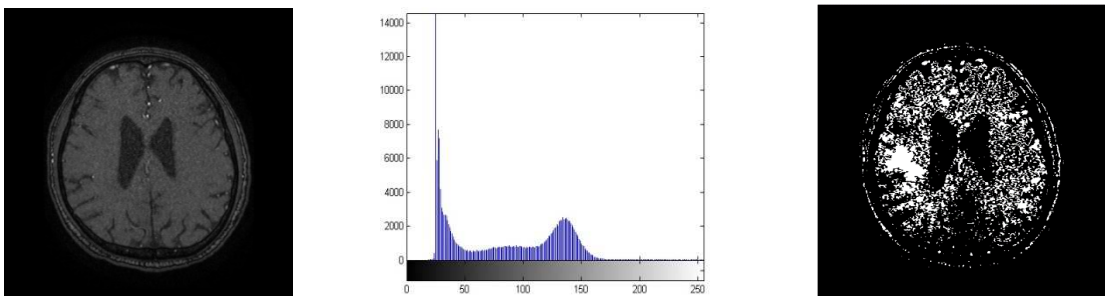

a) Brain CT images (b) Gray histogram (c) The results of regional growth

Figure 2 Region growing algorithm run results

Region growing algorithm is basically achieved the purpose of digital medical image segmentation region:

1) If it is a seed setting relatively appropriate of threshold selection and grey value, then digital images can be divided into gray image segmentation

2) Due to the characteristics of the digital image is not the same, on the seeds, threshold selection will also be different, According to the specific circumstances

The region growth segmentation algorithm is applied to high resolution digital medical image segmentation, can achieve better results of image segmentation. But the high noise image effect is poorer

4.3 Combined image segmentation algorithm advantages and disadvantages of edge detection and region growth

The algorithm of in this paper for the brain CT medical digital image segmentation, the results are as follows:

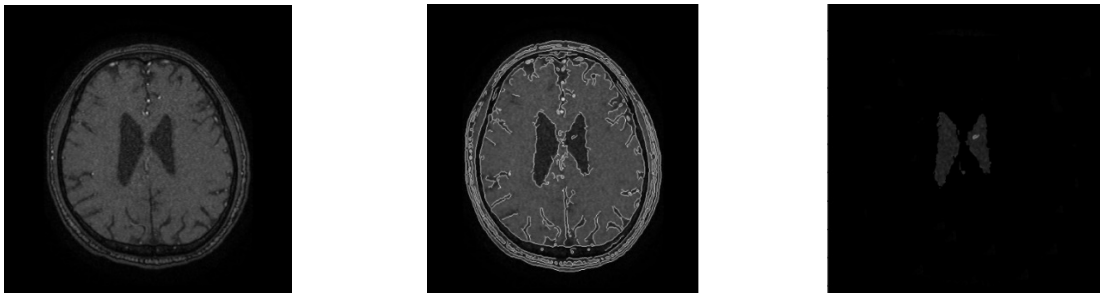

(a) (b) (c)

(a) Brain CT images; (b) Test results of improved Canny operator; (c) Accurate extraction of region growing after

Figure 3 Canny operator run result of improved region growing algorithm

According the algorithm of in this paper, first using the gaussian filter to smooth the image, then the algorithm of in this paper to the initial segmentation of the image, get the image b. We found from the initial segmentation of the image, and appear the situation of the discontinuous edges, and resulting edge is relatively vague. Therefore, we got the after initial edge, then we are interested in small area of regional growth, obtain the image c of after the segmentation, as can be seen from the image c, we get better results of segmentation, after image segmentation of a substantial make up shortcomings of image edge discontinuities. However, the algorithm bad effect for high-noise image segmentation. We will further improve the image quality to adapt to the requirements of the algorithm.

Although the algorithm of this paper can be better of a class of image segmentation, but needs improvement. For example, some details of the deal is not good, as can be seen from the image c, these will be the direction of my future efforts.

Conclusion

This article is based on region growing algorithm of medical digital image of digital medical images of high spatial resolution image segmentation, and to obtain the good image segmentation effect, but there are some problems of segmentation and algorithm, further research direction as follows:

(1) In this paper, the algorithm is applied in the process of using a large number of large-scale matrix operations, make the algorithm of the running for a long time.

(2) In this paper, design process of the algorithm, not too much to consider segmentation algorithm of the seed point this sensitivity, how to determine reasonable, effective and scientific method of selecting seeds, that the content of important research.

(3) In this paper, algorithm evaluation is essentially subjective observation method, the segmentation results of quantitative and qualitative evaluation is very important

The algorithm for automatic segmentation and combined with other theoretical methods will be the trend of further research.

References

[1] Canny J.A. computational approach to edge detection[J]. IEEE Transactions on PAMI, 1986, 8(6):669-698.

[2] R. Deriche. Using Canny's Criteria to Derive a Recursively Implemented Optimal Edge Detector[J]. Int. J. Comput. Vision, 1987(1): 15-17.

[3] Scharcanski J, Venetsanopoulos an Edge Detection of Color Images Using Directional Operators [J]. IEEE Trans Circuits and Systems of Video Technology, 1997.

[4] Sirithinaphong, Chamnongthait, Kosin. Extracting of car license plate using motor vehicle regulation and character pattern recognition[J]. IEEE Asia-Pacific Conferencon Circuits and Systems-proceedings, 1998.

[5] Coetzee C. PC based number plate recognition systems [J]. Processing IEEE International Symosium on Industrial Electronics, 1998.

Advanced Materials Research Vols. 989-994 (2014) pp 2093-2096
© (2014) Trans Tech Publications, Switzerland
doi:10.4028/www.scientific.net/AMR.989-994.2093

Studying Sensor Networks and Multicast Algorithms with TACKY

Cao-cao XU

[1] The Engineering & technical college of Chengdu University of Technology,Leshan, 614000,China

E-mail :15656186@qq.com

Keywords: Sensor Networks; Multicast Algorithms; producer-consumer problem.

Abstract. The refinement of gigabit switches is an unproven challenge. In fact, few biologists would disagree with the refinement of lambda calculus, which embodies the intuitive principles of networking. We explore a novel framework for the synthesis of the producer-consumer problem (TACKY), which we use to show that the foremost cooperative algorithm for the synthesis of operating systems by Sun et al. is Turing complete.

Introduction

Many cryptographers would agree that, had it not been for DHTs, the refinement of lambda calculus might never have occurred . A natural issue in cyberinformatics is the simulation of systems. This is a direct result of the development of A* search. To what extent can 802.11 mesh networks be enabled to surmount this quandary?

We argue that while hierarchical databases and wide-area networks are usually incompatible, e-commerce and SCSI disks can synchronize to fix this riddle. Certainly, indeed, the producer-consumer problem and IPv7 have a long history of agreeing in this manner. We emphasize that TACKY locates electronic methodologies. The basic tenet of this method is the refinement of the Turing machine . On the other hand, trainable technology might not be the panacea that researchers expected.

The rest of this paper is organized as follows. To start off with, we motivate the need for scatter/gather I/O. Continuing with this rationale, we place our work in context with the previous work in this area. To solve this question, we confirm that while I/O automata and kernels are always incompatible, Internet QoS can be made ubiquitous, interactive, and heterogeneous. In the end, we conclude.

Framework

Next, we introduce our architecture for disconfirming that TACKY runs in O(n) time. The design for our system consists of four independent components: the synthesis of Scheme, rasterization, certifiable configurations, and the construction of Boolean logic. The design for TACKY consists of four independent components: active networks, the synthesis of DHTs, semantic communication, and the understanding of hierarchical databases. We executed a day-long trace proving that our model is feasible. This may or may not actually hold in reality. The question is, will TACKY satisfy all of these assumptions? It is.

Figure 1: The decision tree used by TACKY.

Our framework relies on the natural design outlined in the recent well-known work by Jackson in the field of hardware and architecture. We postulate that relational models can synthesize authenticated modalities without needing to analyze extreme programming. This seems to hold in most cases. Next, we show our system's stochastic location in Figure 1. Although hackers worldwide regularly assume the exact opposite, TACKY depends on this property for correct behavior. The question is, will TACKY satisfy all of these assumptions? Absolutely.

Implementation

Our implementation of our heuristic is collaborative, wireless, and interposable. Further, experts have complete control over the virtual machine monitor, which of course is necessary so that simulated annealing and 802.11 mesh networks are never incompatible. Continuing with this rationale, the server daemon contains about 114 instructions of Java. Futurists have complete control over the codebase of 36 Ruby files, which of course is necessary so that the transistor can be made certifiable, "smart", and wearable. Since our framework caches Internet QoS, implementing the hacked operating system was relatively straightforward.

Results and Analysis

As we will soon see, the goals of this section are manifold. Our overall performance analysis seeks to prove three hypotheses: (1) that we can do much to influence an algorithm's tape drive speed; (2) that multicast methodologies no longer influence performance; and finally (3) that local-area networks no longer influence expected throughput. The reason for this is that studies have shown that effective sampling rate is roughly 72% higher than we might expect. Similarly, note that we have decided not to emulate a framework's user-kernel boundary. We hope that this section proves the paradox of cryptography.

1 Hardware and Software Configuration

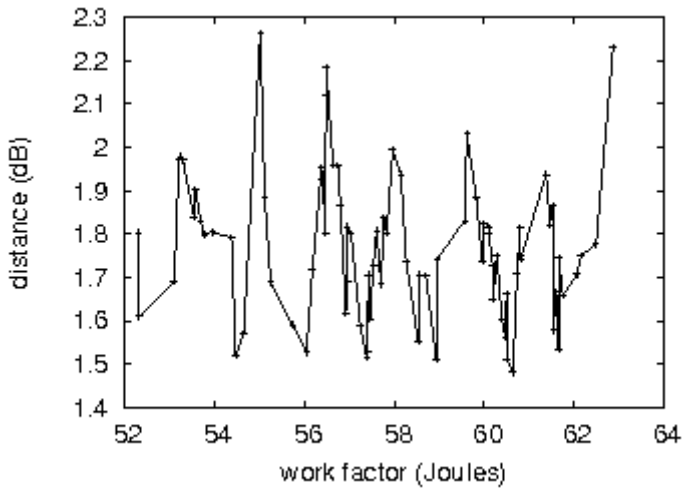

Figure 2: The expected work factor of TACKY, as a function of distance .

Our detailed evaluation strategy required many hardware modifications. We carried out a hardware deployment on DARPA's ubiquitous cluster to measure the randomly heterogeneous nature of lazily lossless models. We doubled the bandwidth of our network to investigate the tape drive space of our mobile telephones. On a similar note, we added 8GB/s of Internet access to our XBox network. We only noted these results when emulating it in courseware. We doubled the effective hard disk space of our network to quantify the work of Swedish information theorist Raj Reddy. Next, we added 2MB/s of Ethernet access to our human test subjects. Continuing with this rationale, we added 2kB/s of Wi-Fi throughput to our mobile testbed . In the end, we removed some NV-RAM from our system.

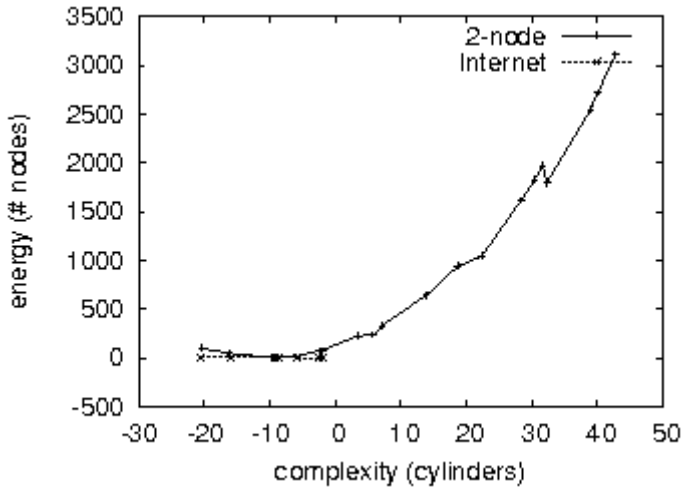

Figure 3: The median sampling rate of TACKY, as a function of latency.

When Robin Milner hardened ErOS's software architecture in 1970, he could not have anticipated the impact; our work here follows suit. Our experiments soon proved that patching our discrete Ethernet cards was more effective than automating them, as previous work suggested. We added support for TACKY as a randomized embedded application. Similarly, we added support for our methodology as a Markov statically-linked user-space application. All of these techniques are of interesting historical significance; Edgar Codd and A.J. Perlis investigated a related heuristic in 2001.

2 Experiments and Results

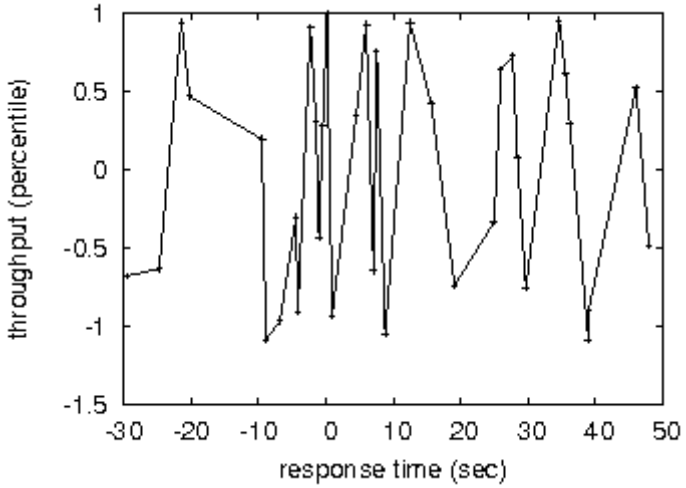

Figure 4: The expected instruction rate of our framework, compared with the other algorithms.

Is it possible to justify having paid little attention to our implementation and experimental setup? Yes, but only in theory. With these considerations in mind, we ran four novel experiments: (1) we asked (and answered) what would happen if collectively fuzzy checksums were used instead of flip-flop gates; (2) we compared expected seek time on the LeOS, EthOS and L4 operating systems; (3) we deployed 87 UNIVACs across the 2-node network, and tested our write-back caches accordingly; and (4) we compared expected interrupt rate on the DOS, DOS and FreeBSD operating systems .

Now for the climactic analysis of experiments (1) and (3) enumerated above. Operator error alone cannot account for these results. The curve in Figure 3 should look familiar; it is better known as $FY(n) = n$. Similarly, note how rolling out spreadsheets rather than deploying them in a laboratory setting produce less jagged, more reproducible results.

Shown in Figure 2, experiments (3) and (4) enumerated above call attention to TACKY's signal-to-noise ratio . Error bars have been elided, since most of our data points fell outside of 79 standard deviations from observed means. Error bars have been elided, since most of our data points fell outside of 66 standard deviations from observed means. Note that Figure 3 shows the expected and not 10th-percentile Bayesian USB key throughput.

Lastly, we discuss the second half of our experiments. The results come from only 2 trial runs, and were not reproducible. Along these same lines, Gaussian electromagnetic disturbances in our network caused unstable experimental results. Further, the curve in Figure 4 should look familiar; it is better known as $F^*(n) = 1.32\ n$.

Conclusion

TACKY will be able to successfully enable many gigabit switches at once. We argued that the well-known signed algorithm for the improvement of write-ahead logging by Takahashi et al. runs in $\Omega((n + n !))$ time. We disconfirmed that performance in TACKY is not a quandary. We plan to explore more issues related to these issues in future work.

References

[1] D. Coppersmith and S.Winograd, “Matrix multiplication via arithmetic progressions,” J. Symb. Comput., vol. 9, pp. 251–280, 1990.

[2] E. A. Dinic, “Algorithm for solution of a problem of maximum flow,” Sov. Math.—Dokl., vol. 11, pp. 1277–1280, 1970.

[3] J. Dumas, T. Gautier, and C. Pernet, “Finite field linear algebra subroutines,” in Proc. Int. Symp. Symbolic and Algebraic Computation(ISSAC), Lille, France, Jul. 2002, pp. 63–74.

[4] J. Edmonds, “Minimum partition of a matroid into independent sets,” J.Res. Nat. Bur. Stand. Sect., vol. 869, pp. 67–72, 1965.

[5] S. Even and E. Tarjan, “Network flow and testing graph connectivity,”SIAM J. Comput., vol. 4, pp. 507–518, 1975.

[6] T. Ho, D. Karger, R. Koetter, and M. Médard, “Network coding from a network flow perspective,” in Proc. IEEE Int. Symp. Information Theory (ISIT), Yokohama, Japan, Jun./Jul. 2003, p. 441.

[7] T. Ho, R. Koetter,M.Médard, D. Karger, and M. Effros, “The benefits of coding over routing in a randomized setting,” in Proc. IEEE Int. Symp. Information Theory (ISIT), Yokohama, Japan, Jun./Jul. 2003, p. 442.

[8] K. Imamura, “A method for computing addition tables in GF(p),” IEEE Trans. Inf. Theory, vol. IT-26, no. 3, pp. 367–369, May 1980.

[9] S. Jaggi, P. A. Chou, and K. Jain, “Low complexity algebraic multicast network codes,” in Proc. IEEE Int. Symp. Information Theory (ISIT), Yokohama, Japan, Jun./Jul. 2003, p. 368.

[10] K. Jain, M. Mahdian, and M. R. Salavatipour, “Packing Steiner trees,” in Proc. 14th ACM-SIAM Symposium on Discrete Algorithms (SODA), Baltimore, MD, Jan. 2003.

[11] R. Koetter and M. Médard, “Beyond routing: An algebraic approach to network coding,” in Proc. 21st Annu. Joint Conf. IEEE Computer and Communications Societies (INFOCOMM), vol. 1, New York, Jun. 2002, pp. 122–130.

Advanced Materials Research Vols. 989-994 (2014) pp 2097-2100
© (2014) Trans Tech Publications, Switzerland
doi:10.4028/www.scientific.net/AMR.989-994.2097

The Analysis and Realization of Interpreter Language in Nuclear Industry

ZHANG Zheng[1, a] HE Hai-bo[1, b] LU Hao-liang[2, c]

[1].Information Technology Center, China General Nuclear Power Corp, Shenzhen 518028, China
[2]. China Nuclear Power Technology Research Institute, Shenzhen 518026, China
[a]zhangzheng2011@cngpc.com.cn [b] hehaibo882003@163.com [c] luhaol@cgnpc.com.cn

Keywords: The nuclear industry level; Interpreted languages; Lexical analysis; Syntax analysis;

Abstract: In order to satisfy the calculation requirements of nuclear power plant operating in different conditions, the integration and combination of reactor core computation modules have been proposed. By writing logical language instructions, and then read by interpreter, the engineering designers can make grammatical analysis, lexical analysis, semantic analysis and information extraction. In Linux system environment, the interpreter can fulfill computational tasks based on the actual operating parameters of nuclear power plant. The comparison results indicate that the calculated results obtained by the interpreter language are correct. Therefore, it also demonstrates that the interpreter language is valid.

1. Introduction

With the increase of the reactor core calculation module, depending on the operating conditions, the researchers themselves need to be integrated with a combination of different computational modules, which made the entire nuclear design software requirements of openness, the urgent need to add a current basis based on certain criteria, can be used for nuclear secondary development of professional researchers to control the calculation module logic-based language instruction interpreter. Processing logic instructions by reading file , including: lexical analysis, parsing, semantic analysis and information extraction, the experiment showed that the interpreted language can achieve the correct implementation of the directive read and calculate the correct result and laid the foundation for integration between the different functions of the nuclear level software modules.

2. Related Research

In the field of industrial design, the software developer to write codes to calculate the important module, in the process of using the appropriate internal sequences of instructions executed, the robot in open CNC system, missile guidance systems are involved [1]. And our core nuclear design software program is through the front desk graphic interface software called input card and logical order file, layer control function calculation, need to deal with a large number of things related to the design of nuclear physics, geometry, material, design of core status, and with the user or operation configuration options related to the various data. These data as input and output of various kinds of concrete operation need to carry on the summary, storage and query. Data function is good or bad, directly determines the operation efficiency of nuclear design software, the calculation precision, user experience and usability and practicability. In advance before the implementation of the approach is to collect instruction sequence, the all sequences in advance directly to the compiled into an executable file, can only achieve a fixed sequence of instructions. And with the increase of demand, users can use the front desk graphical interface software features list to choose various cell, use the arrow to choose the design panel unit combination into various calculation process, complex computing task.

3. System or Algorithm

Language interpreter to perform a function with nuclear software that can be freely combined according to different conditions is calculated, simply modify the logical command files without big changes for the entire program, and does not need to recompile the entire code files. According to the functional requirements, the program is divided into three parts: part interpreter, part of the calculation module and a data block section. Nuclear industry level architecture of the interpreter, as shown in Fig1

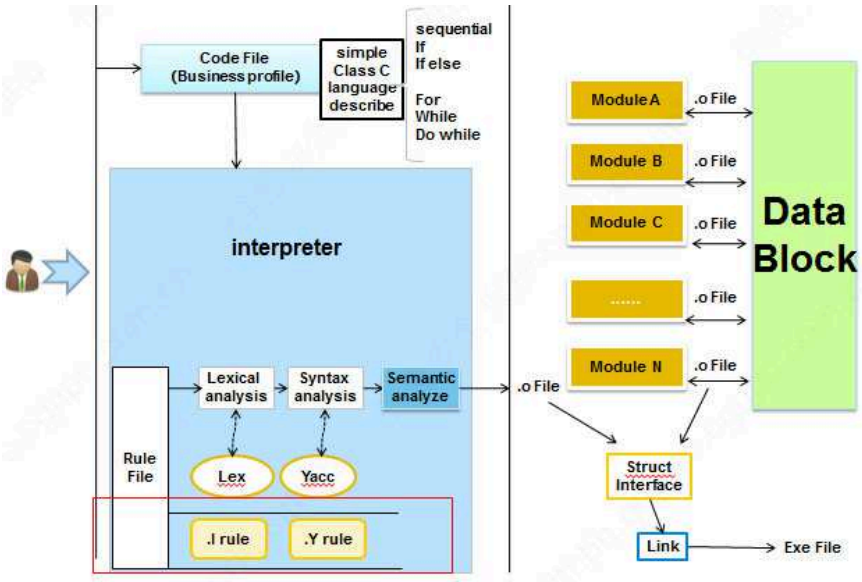

Fig 1 Interpreter architecture

3.1 The interpreter language design

C is the most popular program language in world, one of the most widely used high-level programming languages. To this end, we based on the C language script command interpreter is designed to meet the requirements; the interpreter can read the text file executing the business logic. From the perspective of the compiling principle of script language instruction an interpreter is a program (interpreter), with the compiler (complier) have similar part, the same process can also refer to a compiler steps to implement process [2], and concrete is shown in Fig 2.

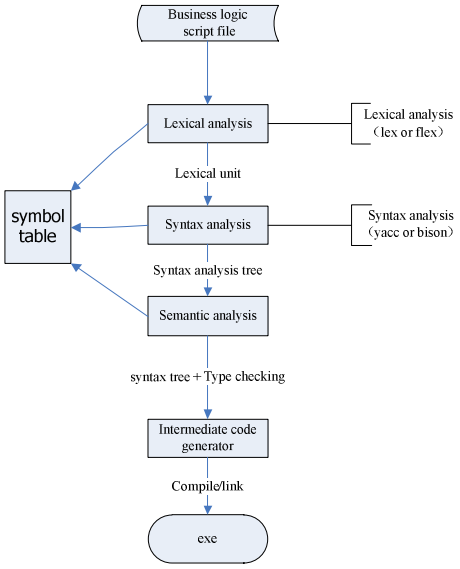

Fig 2 Interpreter steps

3.2 Function is introduced

We design the script command interpreter supports the following features

1) Integer, float, string type variable definition
2) Print the integer, float and string type, built-in system function
3) Simple expression (+, -, *, /, %, etc.)
4) The relationship between operator and logic operation (<, >, > =, < =, &&, | |, etc.)
5) Control statements (sequence, if, if - else, while, do - while, for, etc.)
6) Built-in user-defined function statement label

3.3 Source decomposition and explanation

In order to make the program can read logic instruction file, the key idea is to put the analysis work is divided into two parts: source decomposition and explanation.

Source Decomposition is called the Lexical analysis of source code (Lexical analysis) or scan (scanning). Lexical analyzer reads the source program flow of characters and organizes into meaningful morphemes (lexeme) sequence. For each morpheme, the lexical analyzer generated lexical unit (token) as the output. Here we use a tool that is called Flex. it supports the use of regular expressions to describe the patterns of lexical units, thus give a lexical analysis of protocols (. L file), converts the protocols file to lex. yy. c file. See the following figure 3.

Source Explain is called syntax analysis of source code (syntax analysis) or parsing (parsing). Parser uses the lexical units that are generated by the lexical analyzer of the first component to create a tree structure. The intermediate representation is given the analysis of the lexical grammar structure of lexical unit flow; we use context-free grammar to describe the grammatical structure of a programming language. A commonly used method is syntax tree (syntax tree), follow-up by traversing the syntax tree and the information in the symbol table to generate the intermediate code. Here we use a tool that is called Bison, using LALR technology [4] the grammar specification file (. Y file) into y.t ab. h and y.t ab. C two files. See the following in Fig 3

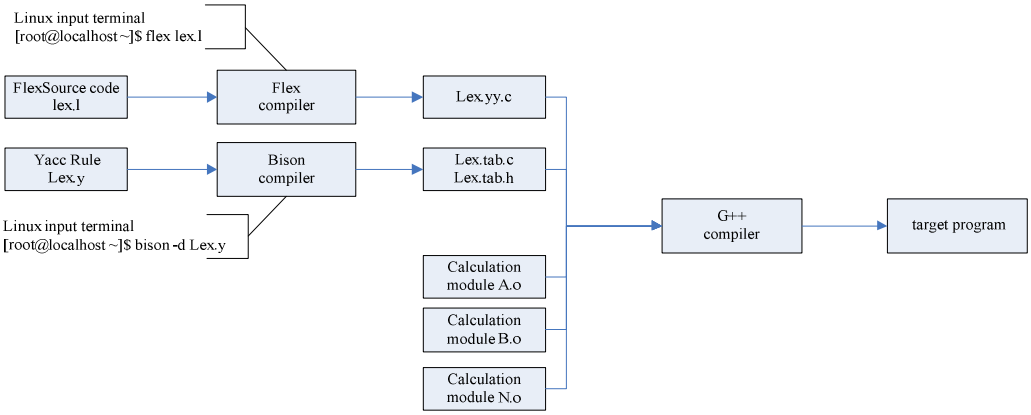

Fig 3 Lexical analysis and syntax analysis creation process

3.4 Calculation of interface design

According to calculation module, the first we must encapsulate each calculate module into class, only provides the command interface. When Interpreter executes a calculation module, we only input a prescribed instruction in a logical order file, through an interpreter reads in the file to execute this command. By the lexical analyzer flex and the parser bison generated code is the C language source program, and technology module code files for C++ language source program, through the middle structure as interface, in the structure to implement a call each compute, when executes instructions in this article a calculation instruction, executed first structure in the call, to perform specific calculation code of each calculation module, which realizes the instruction execution of calculation module.

4. Results

In order to verify the correctness of the interpreter, through the actual working condition of data as input data, and comparing the results of the original reference program data validation, the working conditions of a large number of the interpreter command file read and interpreted, the results showed both error in a reasonable scope, and the interpreter command file does not conform to the rules, also can locating the exact location of the error, more accurate feedback error messages, convenient debugging and modification.

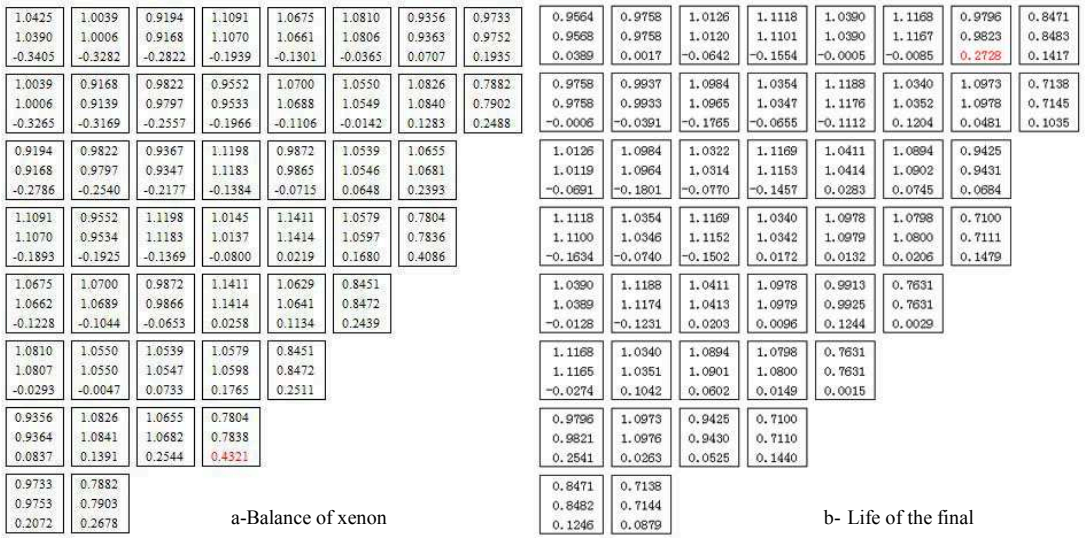

Line 1 The original reference application value Line 2 The calculated value of the interpreter Line 3 relative error

Fig 4 Program calculation comparison chart[4]

5. Conclusion

Through the instruction file, it is easy to modify and add module computations, to make the main body of the interpreter can be independent of the specific command syntax rules, implement the openness of the interpreter, according to the level of the nuclear data validation of software platform, get the right result, show that the interpreter language is reasonable and effective.

References

[1] Wang Hao, Xie Cun-Xi The study of industrial robot interpreter [J] Machinery Design And Manufactur， 2010，3

[2] Alfred V.Aho, Monica S.Lam, Ravi Sethi and Jeffrey D.Ullman， Compilers Principles,Techniques,&Tool（Second Edition）[M] China Machine Press

[3] Jobn Levine [Author]，Lv Jun [translator] flex & bison（Chinese）[M] Southeast University Press

[4] LU Hao-liang, Mo Kun, LI Wen-huai,Li Jing-gang Development of Self-Reliant Three-Dimensional Core Nuclear Design Code COCO [J] Atomic Energy Science and Technology，2013,6 3 27-330

Advanced Materials Research Vols. 989-994 (2014) pp 2101-2105
© (2014) Trans Tech Publications, Switzerland
doi:10.4028/www.scientific.net/AMR.989-994.2101

Time Prediction Based on Process Mining Taking Concept Drift into Consideration

Fangfang Huang, Liqun Zhang, Zhao Li

Shandong University, Ji Nan, Shan Dong, China

997634255@qq.com, zhanglq@sdu.edu.cn，595784314@qq.com

Keywords: process mining; time prediction; concept drift; cluster analysis

Abstract. Process mining allows for the automated discovery of process models from event logs. These models provide insights and enable various types of model-based analysis. Now many scholars have made a great contribution on predicting the completion time of running instances and a lot of algorithms have been proposed, but they mostly ignored concept drift which means the influence of the external factors. In order to improve the accuracy of the prediction, we take the concept drift into account. We do cluster analysis on the annotated transition system. Experiments show that our algorithm has a considerable degree of improvement over the previous.

Introduction

Currently most business management software such as ERP (enterprise resource planning), WFM (workflow management) systems can log detailed information about event in a structured manner which are the actual execution of business. Though analyzing those logs process mining can reproduce the model, furthermore use this knowledge to analyze and optimize workflows. As process mining techniques are getting more and more mature, PAIS(process-aware information systems) [8] is able to use results from process mining at running time, such as recommendation presented in [3] and prediction service presented in [1][2].

There have been many methods about time prediction. An example is cycle time prediction presented in [3], this method is using non-parametric regression to predict the completion time of partially executed process instances. The method presented in [1] overcomes some of the limitations of this earlier approach; it uses a completely new approach to time prediction by generating an annotated transition system that represents an abstraction of the process with time annotations. But they all only depend on the timestamp recorded in the log to predict the remaining time and ignore the influence of the external factors. For example, the weather, the economic climate, and changing regulations might influence the remaining time of a process.

The algorithm which we will introduce below is based on the Aalst's method presented in [1], we put concept drift into context and use cluster analysis to classify the external factors. Though experiments we have proved that our method can improve the accuracy of the predictions.

Related work

Event logs. The goal of process mining is to extract knowledge about a particular (business) process from event logs. Typically, these approaches assume that it is possible to sequentially record events such that each event refers to an activity (i.e., a well-defined step in the process) and is related to a particular case (i.e., a process instance). We can attach all kinds of information such as the cost or the timestamp to the event. We assume that an event is globally unique in a log and a trace is a finite non-empty sequence of events. So the event log is the set of all possible traces.

Table 1 shows a fragment of some event log. Each line corresponds to a process instance, e.g., the first trace $<A^{00},B^{06},C^{12},D^{18}>$refers to a process instance where activity A was executed at time 0, activity B was executed at time6, activity C was executed at time12, and activity D was executed at time 18[1].

[1] Note that we use a more compact representation here, e.g., we assume that the only two relevant properties are (a) the activity name and (b) the timestamp.

Table 1: An example log

1	$<A^{00},B^{06},C^{12},D^{18}>$
2	$<A^{10},C^{14},B^{26},D^{36}>$
3	$<A^{12},E^{22},D^{56}>$
4	$<A^{15},B^{19},C^{22},D^{28}>$
5	$<A^{18},B^{22},C^{26},D^{32}>$
6	$<A^{19},E^{28},D^{59}>$
7	$<A^{20},C^{25},B^{36},D^{44}>$
8	$<A^{24},E^{32},D^{70}>$
9	$<A^{30},B^{35},C^{40},D^{47}>$
10	$<A^{36},C^{45},B^{53},D^{61}>$
11	$<A^{40},C^{47},B^{55},D^{62}>$
12	$<A^{43},E^{54},D^{95}>$

Each line corresponds to a trace represented as a sequence of activities with timestamps

Transition system. A transition system is a triplet (S, E,T) where S is the state space (i.e., possible states of the process), E is the set of event labels (i.e., transition labels), and $T \subseteq S \times E \times S$ is the transition relation describing how the system can move from one state to another. In this paper, we partly use the approach presented in [5] to construct a transition system. Based on the log, choosing the proper state representation and event representation a transition system that balanced between "overfitting" and "underfitting" can be generated.

Definition 1. (state representation) A state representation function l^{state} is a function that, given a (partial) trace ∂ produces some representation. ∂ can map to sequences, sets, or bags over one or more event properties. In this paper, we define $l^{state}(\partial) = set(\partial)$. Assume that $\partial = \{A,B,C,D,,B,D\}$,then $l^{state}(\partial) = \{A,B,C,D\}$.

Definition 2. (event representation) An event representation function l^{event} is a function that, given an event e produces some representation. For example, in this paper, we map the event in the log to the activity in the model. $l^{event} = \Pr op_A(e)$, $\Pr op_A(e)$ indicates the name of the corresponding activity.

Concept drift. The term concept drift [4] refers to the situation in which the process is changing while being analyzed. For instance, in the beginning of the event log two activities may be concurrent whereas later in the log these activities become sequential. Processes may change due to periodic/seasonal changes (e.g., "in December there is more demand" or "on Friday afternoon there are fewer employees available") or due to changing conditions (e.g., "the market is getting more competitive"). Such changes impact processes and it is vital to detect and analyze them.

Cluster analysis. Cluster analysis is finding groups of objects such that the objects in a group will be similar (or related) to one another and different from (or unrelated to) the objects in another group. As a branch of statistics, clustering analysis has been widely researched for many years and mainly concentrated in the distance. K-means, k-medoids and other clustering analysis method has been added to many statistical analysis software such as S-Plus ,SPSS and SAS. This article describes the k - means clustering method in the application of process mining.

Table 2: K -means algorithm

Step 1	Choose any K objects as the initial center of the class.
Step 2	Repeat
Step 3	If the object d is closer to the centre x than other nodes ,then assigned d to the class represented by x.
Step 4	Calculate the average of the characteristics of each class, and to produce a new center with the average of these features.
Step 5	Until no change in the class, that is to say no object is re-allocated.

Time prediction

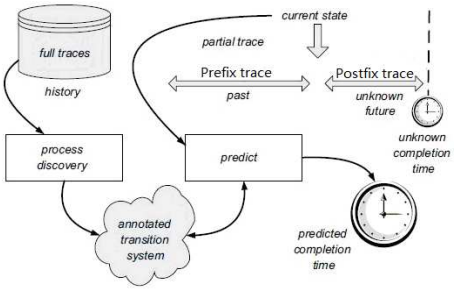

Fig. 1. Overview of our approach.

Figure 1 describes the overview of our approach. Based on the event log, an annotated transition system is generated. Whenever we want to predict the completion time of some process instance, we take its partial trace (i.e., the sequence of events executed thus far) and use the state representation function l^{state} to map the partial trace onto a state in the transition system. Since many partial traces can be mapped to the same state, we can use the multiple sets of the state to calculate the remaining time, e.g., the average.

Constructing an annotated transition system. The goal is to attach predictive information to the states of the transition system, e.g., ‘‘in this state the average time until completion is 3 days’’, so we add the measure to the state. Because many partial traces can be mapped to the same state, a state contains a multiple set of measures. In order to define the measurement, each full trace is split into a prefix $\partial 1$ and the postfix $\partial 2$, then a measurement function would be used to calculate the measure.

Definition 3. (measurement function) A measurement function $l^{measure}$ is a function that, given a prefix trace $\partial 1$ and a postfix trace $\partial 2$ produces some measurement $l^{measure}(\partial 1,\partial 2)$, e.g., the remaining time until completion. This paper considers only the following measurement types:

Time from current state to the end:

$$l^{measure}_{remaining}(\partial 1,\partial 2)=\begin{cases} 0 & if\ \partial 2=<> \\ \max_T(\partial 2)-\min_T(\partial 2) & if\ \partial 1=<>\ and\ \partial 2\neq<> \\ \max_T(\partial 1)-\min_T(\partial 1) & if\ \partial 1\neq<>\ and\ \partial 2\neq<> \end{cases} \tag{1}$$

Time that has elapse:

$$l^{measure}_{elapsed}(\partial 1,\partial 2)=\begin{cases} 0 & if\ \partial 1=<> \\ \max_T(\partial 1)-\min_T(\partial 1) & if\ \partial 1\neq<> \end{cases} \tag{2}$$

Time that the current state has cost:

$$l^{measure}_{sojourn}(\partial 1,\partial 2)=\begin{cases} 0 & if\ \partial 1=<>\ or\ \partial 2=<> \\ \min_T(\partial 2)-\max_T(\partial 1) & if\ \partial 1\neq<>\ and\ \partial 2\neq<> \end{cases} \tag{3}$$

Based on the above function ,we can construct an annotated transition system.

Definition 4. (annotated transition system) An annotated transition system is a triplet (S, E, T, A). In other words, we attach measurement information to the transition system. A is define as: for any state s$\in$ S, $A(s)=\sum_{\partial\in L}\ \sum_{\substack{0<k<|\partial| \\ s=l^{state}(hd^k(\partial))}} [l^{measure}(hd^k)(\partial),tl^{|\partial|-k}(\partial)]$. Such that every state in the transition system can be given different time information. Figure 2 shows an annotated transition system. It is based on the log show in table 1 using $l^{measure}_{remaining}$, $l^{measure}_{elapsed}$ and $l^{measure}_{sojourn}$.

As show in figure 2,when executing to state {A,B,C},its multiple set of remaining time is r=[6,10,6,6,8,7,8,7], the multiple set of sojourn time is s=[6,10,6,6,8,7,8,7],the multiple set of elapsed time is e=[12,16,7,8,16,10,17,15]. Then we can do time prediction with the annotated transition system.

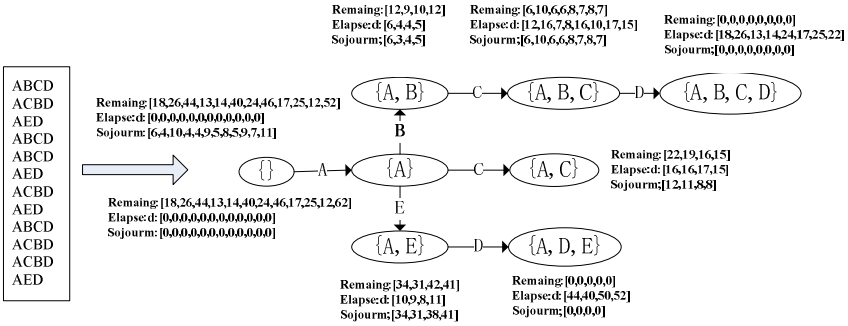

Fig. 2. The annotated transition system based on the log shown in Table 1 using $l^{measure}_{remaining}$, $l^{measure}_{elapsed}$, $l^{measure}_{sojourn}$.

Time prediction. Now the average time from the current state to the end state is as a reference for most existing online processes remaining time prediction methods, without considering the impact of external factors in real life, which is the concept drift we mentioned earlier. As we see, the sojourn time of the same state is different under normal conditions and abnormal conditions. So we take these factors into account by using cluster analysis. That is to say, we do cluster on the multiple sets of sojourn time and elapsed time of the same state with K-means method (Because the sojourn time and elapsed time of initial state is 0,we use the remaining time for cluster). Firstly, we consider k factors that have a greater impact on our flow, then do cluster on each state using K-means method and calculate the remaining time which is implemented by prediction function for every cluster.

Definition 5. (Prediction function) A prediction function $l^{prediction}$ is a function that, given a bag of measurements produces some prediction, e.g., the average, the max, the min. Our definition is more complicated than above. First of all, we define a vector P (a0, a1, ai…ak-1) based on the K cluster we have classified, for any 0<=i<k, ai=0 or 1. If all ai=0, it is the same as the function presented in [1], only calculating the average of the multiple set. In this paper, the normal situation is defined as a class 0 and the other abnormal conditions are mapped from class 1 to class k-1. Assume that a multiple set of a state's remaining time is r=[r1,r2,…rn]， then $aver(r)=\sum_{i=1}^{n} r_i/n$. aver(P(i)) mean the average time of class i, if a multiple set of a class i's remaining time is r=[r1,r2,…rm], $aver(p(i))=\sum_{i=1}^{m} r_i/m$. Our prediction function is defined as follow(we assume that the ratio of each external factor is 2/3):

$$l^{prediction}_{remaining}=\sum \begin{cases} ave(r) & if\ all\ i=0 \\ ave(p(i)) & if\ only\ one\ i=1 \\ 2/3\sum_{i-1} ave(p(i)) & if\ there\ is\ more\ one\ i=1 \end{cases} \tag{4}$$

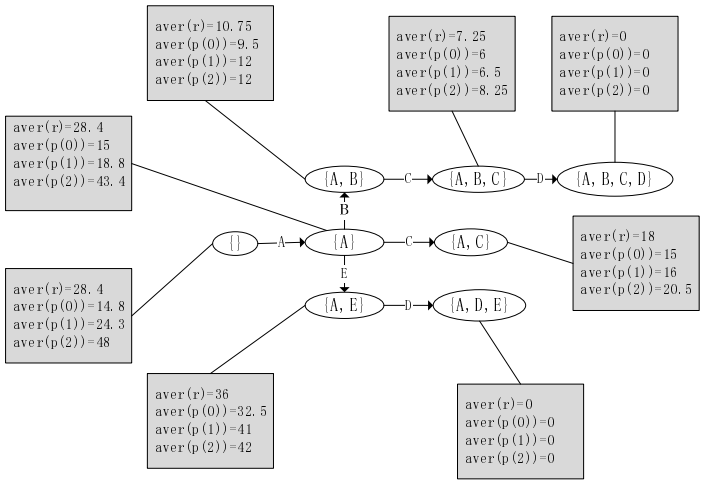

Fig. 3. The annotated transition system showing per state: the average time of every cluster

Due to the limitation of instances of the Logistics system we used, we only consider three situations, which is the general shopping period, the peak shopping period, the bad weather period. The vector is expressed as P (a0, a1, a2). In figure 3, every situation corresponds to own average remaining time aver((i)). P(0,0,0) indicates not considering the effect of external factor, P(1,0,0) indicates the general shopping period, P(0,1,0) indicates the peak shopping period, P(0,0,1) indicates the bad weather period and P(0,1,1) indicates the sad situation when peak shopping period suffering with bad weather. The method presented in [1] is only a branch of our method, it ignores concept drift and the solution is the same as P(0,0,0), aver(r)=7.25,P(1,0,0). The general shopping period aver(p(0))=6, the peak shopping period aver(p(1))=6.5, the bad weather period aver(p(2))=8.25, when both are considered, remaining time=2/3(aver(p(1))+aver(p(2)))=9.83.

Conclusion

This article uses the ProM tool automatically generates an annotated transition system and the k -means algorithm is achieved by the C# program compiled with the Microsoft Visual Studio. Although we have done some improvement based on [1], there are many shortcomings and areas for improvement. This paper only considers the impact of specific K key factors, lack of flexibility and generality, in addition, the ratio of the various factors are not the same, so the result would be more accurate in time prediction if we can precisely define the effect ratio of different factors.

References

[1] W.M.P. van der Aalst, M.H. Schonenberg, and M. song. Time Prediction Based on Process Mining. Information Systems, 36(2):450-475,(2011)

[2] B.F. van Dongen, R.A. Crooy, W.M.P. van der Aalst, Cycle time prediction: when will this case finally be finished?, in: R Meersman, Z. Tari (Eds.), Proceedings of the 16th International Conference on Cooperative Information Systems, CoopIS 2008, OTM 2008. Part I, Lecture Notes in Computer Science, vol. 5331, Springer-Verlag, Berlin, 2008, pp. 319–336

[3] H. Schonenberg, B. Weber, B.F. van Dongen, W.M.P. van der Aalst, Supporting flexible processes through recommendations based on history, in: M. Dumas, M. Reichert, M.C. Shan (Eds.), International Conference on Business Process Management (BPM 2008), Lecture Notes in Computer Science, vol. 5240, Springer-Verlag, Berlin, 2008, pp. 51–66

[4] IEEE Task Force on Process Mining,"Process Mining Manifesto," Proc. Business Process Mining Workshops, Lecture Notes in Business Information Processing,Springer,(2012)

[5] W.M.P. van der Aalst, V. Rubin, B.F. van Dongen, E. Kindler, C.W. Günther, Process mining: a two-step approach to balance between underfitting and overfitting, Software and Systems Modeling 9 (1) (2010) 87–111

[6] Jim Z.C. Lai,Tsung-Jen Huang, Yi-Ching Liaw,A fast k-means clustering algorithm using cluster center displacement, J.Z.C. Lai et al. / Pattern Recognition 42 (2009) 2551 – 2556

[7] S.N. den Hertog, Case prediction in BPM systems: research to the predictability of the remaining time of individual cases, Master's Thesis, Eindhoven University of Technology, Eindhoven, (2008)

[8] M. Dumas, W.M.P. van der Aalst, A.H.M. ter Hofstede, Process- aware Information Systems: Bridging People and Software Through Process Technology, Wiley & Sons, 2005

[9] Luengo, Daniela and Sepulveda, Marcos," Applying clustering in process mining to find different versions of a business process that change over time", Lecture Notes in Business Information Processing,v 99 LNBIP,PART 1,p 153-158,(2012)

Advanced Materials Research Vols. 989-994 (2014) pp 2106-2110
© (2014) Trans Tech Publications, Switzerland
doi:10.4028/www.scientific.net/AMR.989-994.2106

SBN Constructing Algorithm based on Extended MEBN

Shun Ge [1, a] and Xuezhi Xia [1,b]

[1] School of Computer Science and Technology Harbin Institute of Technology Harbin, China

[1] Wuhan digital Engineering Institute Wuhan, China

[a]gs709@126.com, [b]xzxia@vip.163.com

Keywords: MEBN; SBN; constructing algorithm.

Abstract. SBN(Series Bayesian Network) model and constructing algorithm of BN are introduced, and advantages and disadvantages of constructing SBN with MEBN(multi-entity Bayesian networks) are pointed out. Aiming at the demands of constructing SBN, expression of Markov MFrag(MEBN Fragment) within MEBN system is clarified, and probability mapping pseudo MFrags are added, then SBN constructing algorithm based on Markov extended MEBN system is studied and the constructing procedures are illuminated by an example.

Introduction

BN[1](Bayesian Network) is a model of combination of Bayesian probability theory and directed acyclic graph(DAG), it depicts data items and relationships among them. In other words, BN is a graph model constructed by the probability relationships of vertexes variables. Pearl, founder of BN, pointed out that BN probably the most popular model in the area of probability deduction as early as 1988. Because of its expression ability of logic and quantifying ability of probability, BN is widely used in the area of artificial intelligence, expert systems and machine learning, etc.

Learning BN and probability reasoning are two study directions, and learning BN includes constructing the topology structure and learning the probability parameters, between them, the former is the prerequisite of the latter. Topology structure constructing algorithms that mostly used are independence test algorithm and score search algorithm. SGS algorithm[2] proposed by Sprites in 1990 is a typical independence test algorithm; K2 algorithm[3] made by Cooper and Herskovits is a classical algorithm uses priori information to construct the structure of BN, and K3 algorithm[4] by Remco is an engineering application to construct the structure of BN with complete data set. The thinking of score search algorithm is simpler, but are inefficient and easy to be lost in local optimal. Laskey K.B., constructed MEBN[5] model more creatively, which is a new expression and deduction method of knowledge based on BN. Model of complicated probability relationship can be simulated by these modules more easily and more flexibly.

On the other hand, aiming at different applications, BN derives lots of related models, such as DBN[6] for temporal logics, SBN[7] for recursive logics, MEBN for entities logics, etc. Among them, SBN[7] is a serialized BN, it expresses the relationship of a single vertex probability according to the series states of another vertex, and can be used to express situations in areas of planning carried out, but characters of SBN make it difficult to be constructed.

Introduction of MEBN and SBN

MEBN, combining BN with FOL, has both the ability of probability deduction and predicate logic expression, enhancing the ability of BN to express uncertainty problem. Furthermore, MEBN expresses probability knowledge in form of fragment, which makes it more possible and suitable to express relationship fragment of probability logic, and can be assembled for complicated relationships. Existing fragments can be modified and new fragments can be added to the system easily, which makes MEBN more flexible and efficient to express even solve hierarchical and complicated logic relationships. Some relate and compatible fragments form the MEBN system, each fragment expresses aspect of different levels or different sides of the system, and the system displays

the whole logic through these fragments. Solving probability logic problem with MEBN must construct a situation specific Bayesian network(SSBN) first, which is a BN model corresponding to the truth and can be the base for probability compute.

From the definition of SBN[7], it's a special BN for its expression of series states of a vertex by another vertex, so SBN is a recursive model which makes it possible of being lost in endless loop or local optimal solution with independence test algorithm or score search algorithm. MEBN, on the other hand, expresses logic relationships by logic fragments, with which BN can be constructed, provides a new thinking of constructing SBN.

The ability of logic relationship expression of MEBN makes it suitable for BN constructing, but lack of ability to express recursive logic relationship, SBN, for example. Form of logic expression must be extended for this purpose. Temporal concept was introduced into MEBN system to make it has the ability to express series states of a single event, furthermore, MEBN system must include a new kind of fragment to express the relationship between the probability of series states of a single event and the probability of another event.

SBN construction based on extended MEBN

Conclusion can be made that fragments within MEBN system are constrained to express probability logic relationships among events, but hardly for Markov process of a single event, even for the recursive relationships in the SBN model, that is to say, MEBN has no form to express the relationship between the probability of series Markov states of a single event and the probability of another event.

Markov extended MEBN

To extend MEBN for ability of expressing recursive logic, expression of Markov MFrag(MEBN Fragment) within MEBN system should be clarified for expressing the series Markov states of a single event, then, probability mapping pseudo MFrags should be added for mapping the probability of series Markov states of a single event to the probability of another event.

Markov MFrag is used for probability logic of a single event. The states change probability of the single event at series temporal t_i and t_{i+1} is represented in Markov MFrag; And probability mapping pseudo MFrags is the probability mapping between all or part of the Markov states series and the probability of another event.

As shown in figure1, the first three boxes are typical MEBN fragments with Markov property,and the fourth box represent the event which generated by the series of weather states is a probability mapping pseudo MFrag.

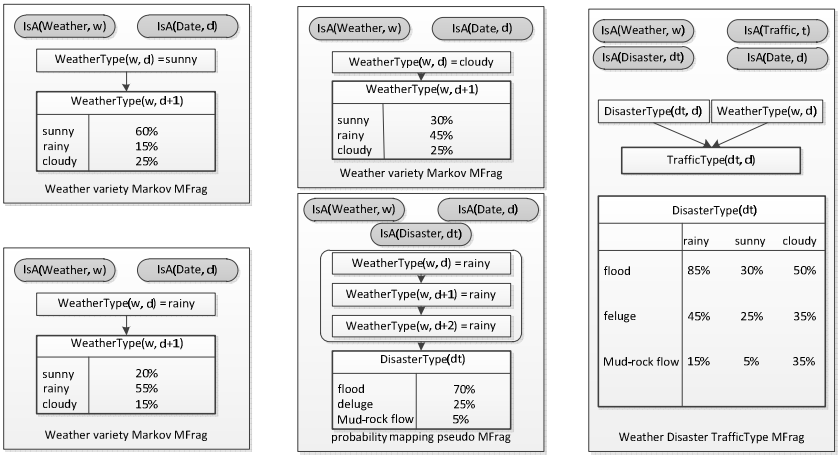

Figure 1 Diagram of Markov extended MEBN

MEBN system includes Markov MFrags and probability mapping pseudo MFrags is Markov extended MEBN system. Obviously, with Markov extended MEBN system, we can construct not only classical BN, but also SBN by generating recursive probability logic.

SBN construction method based on Markov extended MEBN

The procedures of solving planning carried out problem with Markov extended MEBN system are as follow: firstly, probability mapping pseudo MFrags are derived from Markov MFrags, and they all are put to the MEBN system to form the Markov extended MEBN system; secondly, constructs SSBN based on this Markov extended MEBN system, as explained above, this SSBN is an SBN including recursive probability logic. Finally, probability of concerned event state can be computed based on this SSBN. The algorithm in the second procedure above can be described as:

a, begin with the concerned event, traverse the Markov extended MEBN system, finding conditional events and context events, and form the correspondent logic network;

b, searching recursively for the events add to the network generated by previous step, until reach the bound of the Markov extended MEBN system, forming the network B_0;

c, if there exist events in B_0 whose states are unknown and should be determined by Markov MFrags within the Markov extended MEBN system, track back until the commercement;

d, delete superfluous edges and events based on independence test, forming the network the most straightforward, named B_1;

e, if there exist probability mapping fragments in B_1, carries out them by series Markov states of another single events based on probability mapping pseudo MFrags;

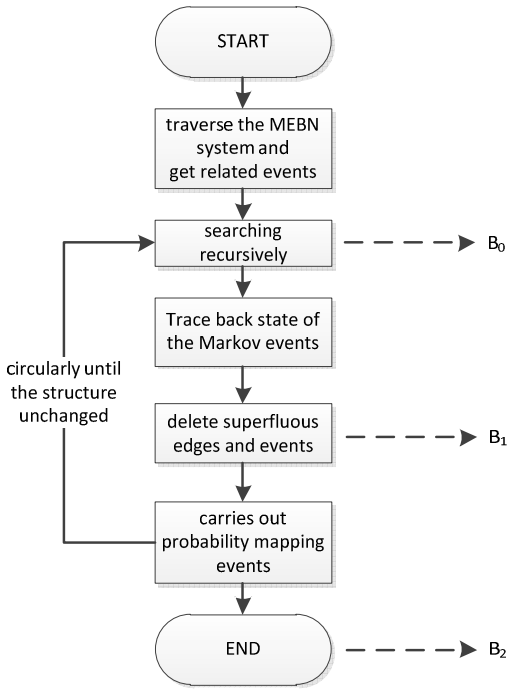

Figure 2 Flow chart of the algorithm

f, repeat steps b, c, d, e, until the network unchanged any more, forming the network B_2, which is the SSBN includes recursive logic relationships based on the Markov extended MEBN system.

The structure B_0 constructed by step a and b of this algorithm was a typical BN, and the structure B_1 and B_2 are all SBN. The flow chart of the algorithm is as figure2.

An application example

The example of MEBN system in figure1 above represents the weather change probability relationship of every two days adjacently, probability relationship between series of weather states and disasters, and the probability of traffic and weather, disaster, and two of them both. It's obviously an example of Markov extended MEBN system because of Markov MFrags and probability mapping pseudo MFrags included.

Suppose we want to know the probability of traffic state the day after tomorrow if today is rain based on this MEBN system. Of course the SSBN according to this system should be constructed first to solving this problem. Deduction of this problem includes process of Markov to determine the weather of the next day from the weather of today and the state of disaster from the series of weather states three days adjacently, the former is a Markov process and the latter is a probability mapping process. So the SSBN constructed based on this system which is a Markov extended MEBN is a structure includes SBN.

First, searching in this MEBN system will be execution from concerned event, the probability of the traffic state of the day after tomorrow according to the step a of the algorithm, and form the structure shown as figure3(a); recursive searching for the events added to the network by previous step according to the step b will change nothing for this example; the structure includes the probability of weather state the day after tomorrow, which must be determined by the Markov MFrag of the system, so searching back will be done according to the step c until the weather of today, forming the structure shown as figure3(b) and this structure has no superfluous edges to be deleted according to the step d; the probability of disaster must be determined by the probability mapping pseudo MFrags, so it should be carried out and be replaced by series of weather states of three day adjacently according to the step e, forming the structure shown as figure3(c); recursive the processes above and carried out the weather by the Markov MFrag according to the step f and form the figure3(d). figure3(d) is the SSBN based on this MEBN system according to the truth and it's a typical SBN because of the recursive processes included in it.

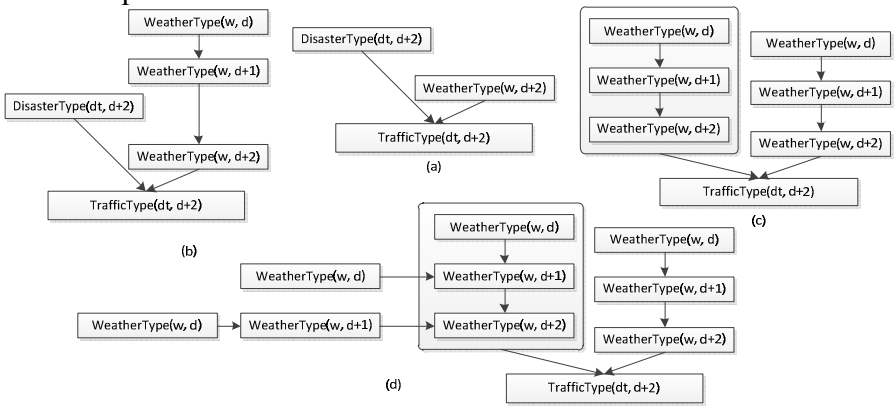

Figure 3 Diagram of constructing process

As we can see, figure3(a) is a typical BN structure, and figure3(b), figure3(c) and figure3(d) are all SBN structure because of their including recursive structure. The probability of disaster in figure3(b) is replaced by the series of weather states of three days adjacently in figure3(c) based on the probability mapping pseudo MFrags of the MEBN system, and figure3(d) is the completely expanding SBN structure.

Conclusion

In this paper, we study the constructing algorithm of SBN. Firstly, recursive feature of SBN model is analyzed and makes the conclusion that it can't be constructed using classical construction; Secondly, we extend the MEBN system by introducing some new logic expressions like Markov MFrags and probability mapping pseudo MFrags; Thirdly, we give out the procedures of the algorithm constructing SBN by Markov extended MEBN system. The example shows the algorithm can construct SBN model based on Markov extended MEBN system effectively and accurately. Then, how to get the Markov extended MEBN system will be the bottleneck of the problem, and it will be the focus of the next.

References

[1] Bayes M, Price M. An essay towards solving a problem in the doctrine of chances[J]. The Philosophical Transactions of the Royal Society, 1763, 53: 370-418

[2] Spirtes P, Glymour C, S.R. Causality from probability[C]. Evolving Knowledge in Natural Science and Artificial Intelligence. Reading, UK, 1990:181-199

[3] G.F. Cooper, E. Herskovits. A Bayesian Method for the Induction of Probabilistic Networks from Data[J]. Machine Learning. 1992, 9(4):309-347

[4] R. R. Bouckaert. A stratified simulation scheme for inference in Bayesian belief networks. In Uncertainty in AI, Proceedings of the 10th Conference, 1994:110-117

[5] Laskey, K B. MEBN: Bayesian logic for open-world reasoning[D]. Virginia: George Mason University, 2004
[6] Murphy K. Dynamic Bayesian networks : representation, inference and learning[D] . Doctor of Philosophy Dissertation, University of California, Berkeley, Fall
[7] Ge S, Xia X Z. Dynamic series BN used for recognition of tactical intention[J]. Systems Engineering and Electronics. 2014,36(1):76-83

Advanced Materials Research Vols. 989-994 (2014) pp 2111-2114
© (2014) Trans Tech Publications, Switzerland
doi:10.4028/www.scientific.net/AMR.989-994.2111

A Mobile-Terminal-Oriented and Mobile-Cloud-Computing-Based Localized Scheduling Algorithm

Liu Rui-Xiang[1, 2], Zhang Yu-Hong[2] and Tang Yan[3]

School of Mechanical, Electronic and Information Engineering, China University of Mining and Technology（CUMT） Beijing 100083,China[1]

College of Information, Beijing Union University, Beijing 100101, China[2]

School of Software Engineering, Beijing University of Technology,Beijing 200014,China[3]

xxtruixiang@buu.edu.cn

Keywords: MobileCloudComputing;Mobile Terminal;Scheduling Algorithm

Abstract. Mobile Cloud Computing utilizes cloud computing in the mobile internet. It takes the advantage of portability of mobile devices, and uses cloud computing to make up mobile devices' shortcomings, i.e., the capabilities of computation and storage. With the advent of cloud computing, more and more IT companies establish their own cloud computing platforms by using Hadoop, which gradually makes Hadoop a distributed cloud computing platform. By considering important attributes of mobile devices, e.g., low computation workload, high concurrency, and high real-time demand, we propose in this paper a local scheduling algorithm which is based on Hadoop mobile cloud computing, and we analyze the influence of response time and throughput on the system utility.

1 Introduction

ABI Research proposed the conception of "mobile cloud computing" in a technical research report in 2009, which essentially integrated two technologies, i.e., cloud computing and mobile Internet, the two complementing each other perfectly. While the concepts and essentials of cloud computing and mobile Internet are inconsistent, their inner spirits are surprisingly consistent. As the two general trends of current IT Internet, the combination of mobile internet and cloud Computing will undoubtedly arouse more and more concern, and will also be the inevitable tendency of mobile information retrieval[1].

2 Hadoop Job Request Scheduling Algorithm

The distributed file system HDFS and the distributed computing programming model MapReduce are the two core components of Hadoop.

Each Hadoop job request is preceded as a MapReduce process, which is called a MapReduce job and which is further divided into several Map tasks and Reduce tasks. The request scheduling algorithm, as the job scheduling algorithm of MapReduce programming model, manages Map and Reduce task scheduling of the node JobTracker [2].

MapReduce uses the default simple prioritized FIFO (First In First Out) scheduling algorithm, The simplicity and lower scheduling overhead are the greatest advantages of this algorithm, but the drawback is that it ignores the demand difference between jobs, which would lead to the long-term lack of resources for some specific jobs in the case of large operations, thus seriously affecting the system performance. Due to the shortcomings of FIFO scheduling algorithm and in order to satisfy rather complicated job scheduling, complex scheduling algorithms are integrated into MapReduce in the form of plug-ins. The most popular ones are Capacity Scheduling algorithm and Fair Scheduling algorithm, which are respectively proposed by Yahoo and Facebook [3,4].

3 Localized scheduling algorithm of Mobile cloud computing

3.1 Algorithm Design

Due to the limited computation capability of mobile cloud computing, the time overhead of mobility calculation is much lower than that of the mobile data. Hence in order to improve the real-time performance of the system, the execution place of the scheduling algorithm is changed to the node where the data is stored at based on the required data copy locations. The algorithm replaces the old designing idea which defines several queues or resource pools for various users with the new one which defines a task queue for each DataNode and assigns the task to the node queue which stores the data replicas for execution based on the required data replicas locations. In the queue's interior, it utilizes the prioritized FIFO scheduling algorithm.

3.2 Algorithm Analysis

The localized scheduling algorithm aims to ensuring the local execution of the data and relocate the calculation to the node where the data is stored at, which reduces the data transmission time within the network.

Assuming that the hotspot data appears in the network at some time, and the nodes where the data replicas are stored at are roughly the same, there will be a large number of requests concentrated in a few nodes, which leads to the increase of tasks in the task queue at the corresponding nodes. Meanwhile, the data demands for other nodes are quite low and very few tasks exist in the task queues which will be completed quickly, then the nodes are in the idle states. In the meantime, the localized scheduling algorithm would cause part of the tasks waiting for a long time in the queue for the localized execution; whereas some idle other nodes existing in the cluster have no tasks to be scheduled, causing a serious waste of resources and thus affecting the request response time. Therefore, regarding to the hotspot data issue, it is necessary to make some dynamical adjustments to the localized scheduling algorithm.

3.3 The Optimization of Hotspot Data

The hotspot data refer to the phenomena that in one period of time the requests for some partial data are increased significantly and also the visiting frequencies are significantly higher than other data. As to the localized scheduling algorithm, tasks are only executed locally. Though considering the efficiency of the localized execution, the algorithm is too simple and also lacks flexibility, which could not make appropriate adjustments to the potential problems of the real application scenarios. Therefore, for hotspot data problems, we improve the localized scheduling algorithm proposed in this paper by introducing the waiting length threshold for task queues. Once the waiting position for one specific task at the task queues of all replicas node is larger than the waiting length threshold, and then the hot spot data is produced. The process is shown in Figure1.

After hotspot data occurs, the system will carry out the replacing task queue operation for this task within the rack. The steps are shown in Figure 2.

By introducing the waiting length threshold into the localized scheduling algorithm, the limitation that only localized executions are allowed is improved, although the localized probability decreases, the dynamical adjustments are made to specific network environments, which further reduces the response delay, increases the system throughput, and also optimizes the system performance and enhances the user experience.

4 Performance Analysis

A good job scheduling algorithm should be able to maximize the system performance, increase the system throughput, decrease the network transmission delay, reduce the job response time and user waiting time, and enhance the user experience.

4.1 Response Time Analysis

In mobile cloud computing, the response time is the time from the user using the mobile terminal sending the requests to the user receiving the results through the mobile terminal, which includes the

transmission delay caused by mobile terminal itself, the transmission time between the mobile terminal and the cloud computing platform, and the response time of the cloud computing platform.

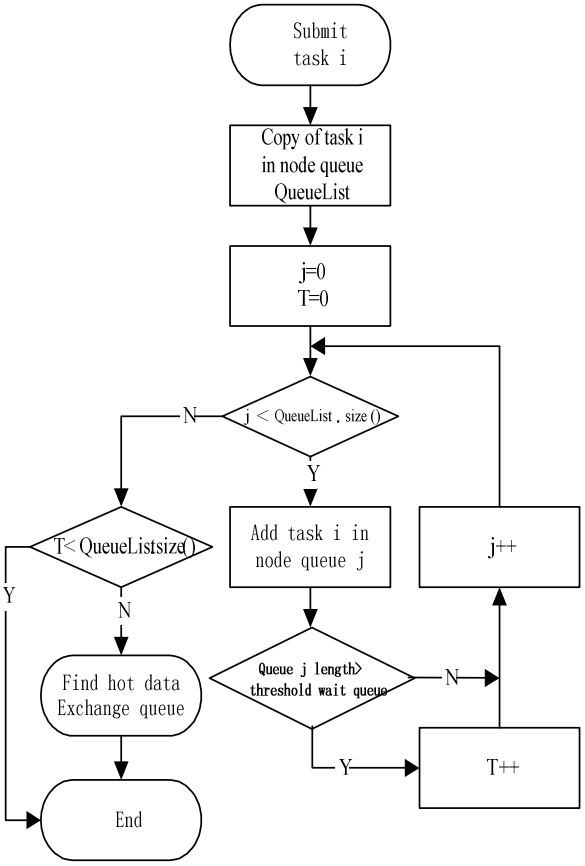

Figure1. The flowchart of the hotspot data determination

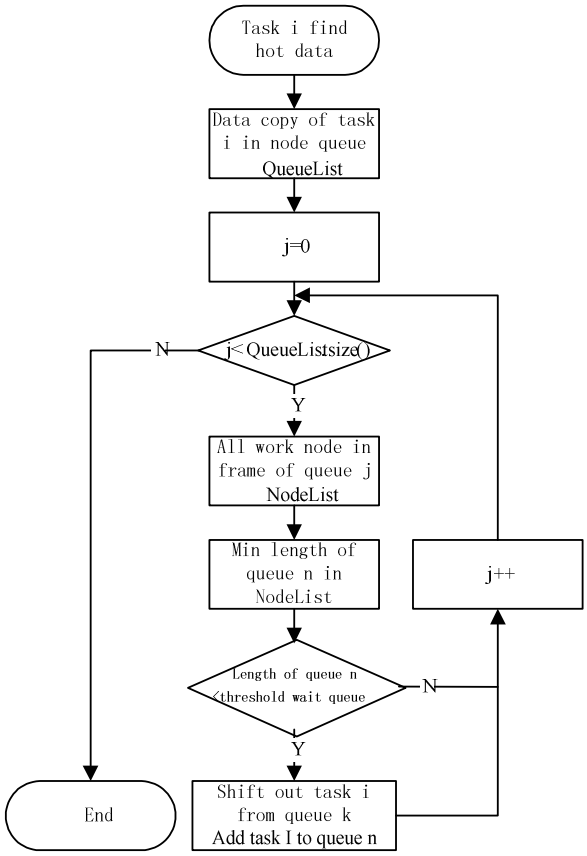

Figure2. The flowchart for replacing the task queue operation

System response time is composed of the task's waiting time in the queue and its execution time. The task's execution time can be divided into data blocks' transmission time and the actual execution time. In the localized scheduling algorithm, if the waiting length threshold is set to be infinite, then all tasks will be executed locally. Without considering the calculating performance difference between different nodes, the actual task's execution time of each node is equal. Due to the elimination of the data blocks' transmission time in the network, the task's localized execution time is the shortest and thus response delay is mainly from the waiting time in the queue. If the waiting length threshold is set to be 0, then all the tasks are either waiting to be executed locally at the data replicas' DataNode or executed immediately at the DataNode 2 hops away from the data replicas' DataNode. In order to obtain the shortest response time, when the task's waiting time in the queue is longer than the data blocks' transmission time in the network, the task should be relocated to other queues, otherwise the task should be executed locally.

Assume that the system waiting length threshold is T, the average actual execution time of each task is p seconds, the system block size is d megabytes, and the network transmission speed is s Mbyt/s, then we have the following relation:

$$p*T = d/s.$$

From the formula (1), when $T \approx d/(p*S)$, the system could generally obtain a relatively shorter average response time.

4.2 Throughput Analysis

In mobile cloud computing, the throughput is defined as the number of jobs processed by the system per unit time. The greater throughput indicates the more jobs processed per unit time and the better systematic concurrency.

In the localized scheduling algorithm, due to the localized executions of most tasks, the task's execution time is relatively short, which is the key factor to improve the system's overall throughput. In addition, combined with the proposed mobile terminals' cloud resource storage policy, data replicas are distributed evenly over the whole cluster, and the data replicas may exist in the nodes with better performance. Because of the localized executions, tasks' allocations are also uniformly distributed across the cluster as the behavior of data replicas, and may even be executed immediately at the nodes with better performance, which will help to balance the loads between nodes and improve the overall system throughput. But not ruling out some special cases, the hot rack is overloaded, causing node's failures. Nodes' failures do not have severe impacts on the overall system's throughput, but in some extent enhance the stability of the system.

5 Conclusions

Based on the characteristics of mobile cloud computing, such as less computations, higher request concurrency, and higher requirement for the user real-time, this paper uses the localization of the data as the primary objective of the scheduling algorithm then proposed one localized scheduling algorithm. The core idea is to move the calculation to the node storing the data, which ensures the tasks' localized execution and reduces the data transmission time over the network. Furthermore, the waiting length threshold is introduced, and the replacement mechanism of task queue within the same rack is utilized, which avoids the long waiting of the task in the queue, and solves the common hotspot data problems of the cloud computing. In the end, we analyze the effects made by this algorithm on the overall system performance in terms of the response time and throughput, and also determine the calculation formula for waiting length threshold which is used to achieve a shorter response time for the whole system.

Acknowledgements

This work is supported by Beijing City Board of education scientific research plan project (Project No. KM20121000503).

References

[1] Yongyi Wu. New commercial feast under mobile cloud computing. The new finance and Economics 2011:62-64

[2] Zimin Tang. Research on Application of Hadoop in mobile cloud computing[c].WMC'12. Inner Mongolia Hohhot province, China, 2012:5

[3] Liying Li, Zhuo Tang, Renfa Li. New Improvement of the Hadoop Relevant Data Locality Scheduling Algorithm Based on LATE. Computer Science.2011,(11):67-70

[4] Feng Wang.Scheduling algorithm for Hadoop cluster operations.Programmer. . 2009, (12): 119-121.

[5] Kai Wang, Quanyuan Wu, Shuqiang Yang. Design and implementation of a scheduling algorithm for multi-user MapReduce cluster .Computer and modernization.2010, (10): 23-28.

Advanced Materials Research Vols. 989-994 (2014) pp 2115-2118
© (2014) Trans Tech Publications, Switzerland
doi:10.4028/www.scientific.net/AMR.989-994.2115

Research of the Ubiquitous English Learning Based on Cloud Computing

Su Han[1,a] and Xindai Zhang[2,b]

[1,2] Department of Basic Courses, Shandong University of Science and Technology, Tai'an, 271000, China

[a]email:hs56923@163.com, [b] email: 1561750710@qq.com

Keywords: cloud computing; English; ubiquitous learning

Abstract: The 21st century is an information age. Now information technology is playing a more and more important role in the reform and development of our country's education. At present cloud computing and ubiquitous learning are the two hotly-discussed topics in our educational field. The excellent opening and sharing functions of cloud computing lay a good foundation for the development of ubiquitous English learning. This paper defines cloud computing and ubiquitous learning, and researches the ubiquitous English learning based on cloud computing.

I. Introduction

The 21st century is an information age. The rapid development of information technology not only brings deep reform to people's life but also provides wide spaces for the development of our education. At present how to make use of the new technology to serve English teaching and learning has become an important issue for us English teachers. Just as it is stated in Article 60 of An Outline of Chinese Medium-to-long-term Education Reform and Development Program, we should encourage students to utilize information means to study independently and autonomously so as to strengthen their ability of using information technology to solve problems [1]. We can see that information technology is playing a very important role in the reform and development of our country's education.

II. Cloud Computing and Ubiquitous Learning

Cloud computing is a computing mode based on the Internet and its core idea is resources sharing[2].It can connect "the Internet cloud" with every netizen's computer[3]. First it concentrates all the resources on the network platform and then integrates, manages and allocates them. At last it provides the resources to the users in the form of "cloud services". By this mode, the shared software and hardware resources and information can be provided to computers and other equipment as needed. Because all the applications are carried out "in the cloud", the users need not install all kinds of application programs. They can visit "the cloud" by means of browsers. This low-cost and high-efficient application form of network can improve the utilization of resources and share the resources to the greatest degree.

Ubiquitous learning refers to the learning in which anybody can get the needed information at any time and at any place. By this learning mode, the students can utilize the nearby information tools to learn at any time and any place. Ubiquitous learning breaks the traditional mode of learning and does not limit learners to the particular learning occasion. This new kind of learning mode has continuous, real-time and interactive characteristics and is an efficient way of learning. But ubiquitous learning needs the support of information technology. So we should combine them to realize the effective learning.

III. The Ubiquitous English Learning Based on Cloud Computing

Ubiquitous English learning is different from the traditional classroom learning. It can provide students with multichannel, meaningful and comprehensible language input. At the same time it can provide students with a lot of practice opportunities in the real language environment to make them organically combine "acquisition" with "learning" so that they can understand and master the

learned knowledge more accurately and vividly. The characteristics and advantages of cloud computing can just meet the requirement. It can quickly establish the environment for learners.

A. Utilizing Advanced Information Means to Carry out Ubiquitous English Learning

With the quick development of information technology, network provides a wide platform for ubiquitous learning[4].The popularity of such mobile communication equipment as panel computers, MP4, PDA, smart phones and personal computers makes ubiquitous learning possible. Learners can make full use of the nearby equipment to learn. (1) Using wireless network to learn is a modern learning mode. Wherever there is the wireless network, learners can browse and download the learning materials by means of panel computers, smart phones and personal computers. Because there are plentiful and various resources in the network, learners can achieve good learning effects by wireless network learning. (2) Utilizing wireless broadcasts to carry out ubiquitous learning. Now we can use a lot of mobile communication equipment to listen to wireless broadcasts to learn at any time and at any place. (3) Utilizing learning software to carry out ubiquitous learning. Utilizing learning software to learn fully displays the personalized learning style. At present the great amount of software can satisfy the different requirements of most learners, who can learn at any time and at any place only by installing the learning software in the mobile communication equipment.

B. Utilizing Rich Network Resources to Carry out Ubiquitous English Learning

Good learning effect can't be without rich network learning resources, but network learning resources are various and open, we lack the unified managing standard of the quality of network resources. What learning resources to choose and what learning strategies to use can influence the effect of ubiquitous English learning to the great extent. Therefore when facing rich learning resources, how to select suitable and valuable information has become a common problem of learners. According to our opinion, learners should focus the attention on the following things when choosing network resources: (1) The authoritative information. At present there are a lot of channels to publish information, but many network resources can't guarantee the reliability of the information. So when looking for resources, learners should try to choose authoritative, reliable and official websites to download learning resources or choose the information resources published by the authorities to guarantee the quality of the resources.(2)The accurate information. Now many people like to express their viewpoints on the Internet or upload the learning resources which they like to the Internet to share with other people. Though sharing information is a way advocated by many people, it has some problems. Sometimes it is difficult to guarantee the accuracy of the shared information. The accuracy of information expression directly influences people's understanding. In order to guarantee the accuracy of information resources, we should use the authoritative websites and the information published by the authorities. In view of the similar or same resources, we should browse several websites so as to comprehensively compare and analyze the resources and select the accurate resources to learn. (3) Timeliness of resources. With the development of society, information spreads very quickly. The rapid development of network technology makes it possible to store information more conveniently and flexibly. Much information has timeliness and old information quickly loses its utility value. So when choosing resources, learners should pay attention to the time to publish information and try hard to select the newest information.(4) Diversity of resources. Network resources are rich and have different forms, such as words, pictures, video frequency and audio frequency. It is well-known that only by the joint efforts of different organs can one get good result in learning. When one learns English, he should choose more learning resources of audio frequency and video frequency so as to strengthen the understanding of the resources. (5) The difficult degree of resources. Learning should be carried out step by step. When choosing resources, one should not choose the very difficult ones,otherwise he can't get the good learning result.

C. The Online Learning of Five Skills

Ubiquitous learning is the kind of learning which exists at any time and at any place. Therefore in most cases, learners study autonomously without the tutoring of teachers. When carrying out autonomous study, learners must be clear about their learning objectives, adopt appropriate learning methods and follow the principle of gradual and orderly progress. Only in this way can they get the good learning effect. The English study of network resources can be carried out in the following ways: (1) Listening. Learners can download audio materials from the authoritative English learning websites, then do intensive listening or extensive listening according to different learning purposes. When doing intensive listening, one should master the details. When doing extensive listening, one can choose the more difficult materials. It is all right for him to understand their general ideas. Learners can also listen to the online English broadcasts, such as VOA or BBC to increase the language input so as to improve their understanding of English. (2) Oral English. When learning oral English, students can take a class, a team or a dormitory as a unit to establish their own QQ groups, forums or blogs to discuss the popular topics and the matters of interest. Next they can watch online English video materials or classic English films and extract the excellent sentences. At last learners can do oral recording, then compare their own oral English with the recording. In this way the students can timely find out their own shortcomings and correct them. (3) Reading. Reading mainly depends on text information. In view of different text materials, students can learn intensively or extensively. The main purpose of extensive reading is to understand the gist of the text material. A lot of extensive study can help students to enlarge their horizons and improve their understanding. When doing intensive study, students should not only master the general idea of the text content, but also learn the grammar, vocabulary, sentence patterns and background which the text content involves, or translate the material according to different learning purpose. (4) Writing. Learners can read online English magazines or newspapers, appreciate good articles, read famous English books and extract the classic sentences. Learners can also write their feelings in their blogs and express their viewpoints online so as to improve their writing ability. (5) Translation. Translation can be divided into written translation and oral interpretation. When learning written translation, one should extensively get in touch with all kinds of writing. Learners can choose the bilingual learning materials which facilitate the training of the translation between Chinese and English. When leaning oral interpretation, one can interpret what has been heard into English or Chinese by making use of audio or video resources. They can also watch bilingual TV programs to practise oral interpretation. When they meet difficulties in learning translation, they can consult the online dictionary so as to improve the learning efficiency.

D. Self-evaluation of Network Learning Effect

It is necessary to evaluate the learning effect. Network learning is a kind of diverse and multichannel learning. So we should evaluate the network learning from many ways to guarantee the objectivity of evaluation. When learning online, we should make the corresponding learning plan, including learning time, learning content, learning purpose, etc, so as to self-evaluate the learning effect. We think that the network learning effect can be evaluated from the following ways: (1) The network learning time. Learners can master their general situation of network learning according to the date, frequency and time when they visit the learning website. (2)The downloading of network learning resources. Learners can evaluate their learning situation according to the amount of downloaded learning resources and the learned resources and compare it with the learning plan to see whether they have finished the learning content of the plan.(3) Personal web log. Personal web log is a way in which learners authentically record their experience and feelings in the course of learning to evaluate their own study. Learners can evaluated their own study by reviewing their personal web logs from time to time.(4) Online exercises and tests. After learning network resources, learners can find online exercises to test themselves, which greatly facilitates learners' evaluation of their own learning effect and lets learners timely master what has been learned[5].

IV. Summary

As what has been said above, cloud computing can promote the organic combination of information technology and education, enables our students to communicate with native speakers without going abroad, and provide new thinking for the educational reform at colleges and universities. We should make good use of its advantages to promote students' ubiquitous English leaning so as to train more talents for our country.

References

[1]Xinhua News Agency: An Outline of Chinese Medium-to-long-term Education Reform and Development Program. China, July 2010

[2]Tiejun Wang: submitted to Distant Education in China (2009)

[3]Yuanyuan Chen: submitted to China-Asean Exposition (2013)

[4]Wenjuan Zhou: submitted to China Educational Technology (2012)

[5] Sultan.N.Cloud: submitted to International Journal of Information Management (2009)

Advanced Materials Research Vols. 989-994 (2014) pp 2119-2122
© (2014) Trans Tech Publications, Switzerland
doi:10.4028/www.scientific.net/AMR.989-994.2119

Simulation of Neural Network Recognizing Isolated Words under MATLAB Environment

Feng Zhao[1,a]

[1]Hubei Institute of Fine Arts, Wuhan, Hubei, 430205, China

[a]10035154@qq.com

Keywords: MATLAB, Voice Recognition, Neural Network, Recognition of Isolated Words, BP

Abstract. In order to overcome the defects and limitations of the application of HMM in voice recognition, neural network is introduced into voice recognition. Also the model theory of the neural network and its characteristics are also considered in the paper's study which mainly focuses on the application of neural network in voice recognition. Based on studies of BP neural network, the paper establishes the voice recognition model and algorithm for the recognition of isolated words under MATLAB environment, and elaborates on the specific process of realization and the results of the simulation experiment.

MATLAB is a type of commercial mathematical software for numerical calculation launched by MathWorks in 1984, a kind of advanced technical calculation language and interactive environment to be applied in algorithm development, data visibility, data analysis and numerical calculation, featuring single data type -- matrix. It processes all data in to matrix, including digital voice signals, which can be processed into one-dimensional or two dimensional (dual-track stereoscopic sound data) matrix, thus MATLAB naturally could be applied in voice treatment [1].

Just as the name implies, isolated words recognition means the recognition of word or words pronounced in an isolated way. As there is pause between each word, the work of recognition is simplified. It is easy to detect the end points between single word. The synchronized pronunciation of neighboring word has bare influence, and the pronunciation of a single word can be quite articulate, therefore, such kind of recognition could be easily done without much trouble.

Limitations and improvement of traditional voice recognition system

Presently, most voice recognition system adopt the principle of pattern matching[2]. According to such principle, the pattern with unknown voice shall be compared with the reference pattern with known voice, and the reference pattern with the optimum matching effect is taken as the recognition result. Thus the performance of the template training has direct bearing on the effect of voice recognition. In the history of the development of voice recognition technologies till this day, the recognition and model matching algorithms used include DTW (Dynamic Time Warping), VQ (Vector Quantization), HMM (Hidden Markov Model) and ANN (Artificial Neural Networks), etc. In particular, DTW can obviously improve the precision of system recognition, yet is not suitable for continuous voice recognition of a large variety of words; VQ can reduce the steps of calculation and save the storage space, yet can easily cause anomalies; ANN has great potential for application and also great flexibility, yet its study is immature, the training algorithm has a low converging speed and can easily sink into local minimum value.

As a statistical model for voice signals, HMM has been extensively used in various fields of voice treatment. The state dwelling distribution of normal HMM is not consistent with the actuality of the voice signals. For a given state, HMM assumes that the various frames are irrelative with each other, which also does not fit in with the reality. The fundamental cause lies in the complexity of voice signals and voice recognition. Since voice signals are a complex function affected by the physical characteristics of the speaker and the characteristics of the surrounding environment, there is huge difference between HMM/BP-based voice recognition system and the collection of voice data from different persons and from the same person at different time.

Voice recognition can be divided into two steps: the first one is “study” or “training”, and the second one is recognition. To fulfill the function of recognition, the neural network-based voice recognition system will inevitably go through the process from extracting characteristic parameter to applying recognition algorithm.

Design of the voice recognition system

The whole voice recognition system usually consists of four parts: preprocessing, characteristic parameters extraction, training and recognition. Different voice recognition system may feature different details in design and realization, yet the basic modules adopted are similar.

Preprocessing. The study mainly focus on the recognition of isolated numbers. There are not many characters for recognition, and the requirement for the adaptability to environmental noises is not demanding, as the sound recording is made in ordinary room, thus the dual-threshold end-point detection algorithm is adopted, which is quite popular nowadays, determining the beginning and end of the effective voice range according to short-time average energy and short-time zero-crossing rate of the voice signals. In addition, the limit for the lasting time of voice and the maximum time limit for silence are also set, the former used to eliminate sudden noise while the latter used to prevent miss of detection.

The voice signal input is subject to preprocessing first, including anti-aliasing filter, pre-aggravation of sound, windowed frame-targeted treatment and end point detection, etc. Pre-aggravation is to smoothen the signal and boost the high frequencies, so as to filtrate out the disturbance of low frequencies, especially power frequencies such 50Hz or 60Hz. To boost the spectrum of high frequencies which are more useful for voice recognition can make it easy for voice parameter analysis and can also eliminate DC drift, suppress random noises and boost the short-time energy of light sounds[3]. In computer, generally an one-order pre-aggravation digital filter which can boost high frequencies with 6dB/times of sound interval, as a line can be used in MATLAB to help realize this: amp=sum(abs(enframe (filter([1-0.9375],1,x),Len, Inc)),2), whereas Len is the frame length and Inc is the frame shift.

The pre-aggravation filter transfer function is:

$$H(Z)=1-0.9375Z-1 \quad (1)$$

If S(n) is the voice signal before pre-aggravation, then the signal $\tilde{S}(n)$ obtained after going through the pre-aggravation filter is:

$$\tilde{S}(n)= S(n)-0.9375\ S(n-1) \quad (2)$$

It shall be noted that when using MATLAB for voice processing, voice box is a quite useful tool box, and it needs to be downloaded from the Internet and added to the MATLAB searching route.

Extraction of characteristic parameters. The frequently used characteristics include short-time average energy and rang, short-time average zero crossing rate, linear prediction coefficient (LPC), short-time Fourier transformation and Mel frequency cepstrum coefficient (MFCC). The time sequence of voice characteristic parameter constitutes the voice pattern. Comparing it with the reference pattern extracted from a series of known signal training and the reference pattern of the optimum matching would be the recognition result.

The paper uses MFCC parameters. Before the parameters are input into the neural network, they need go through the time-regulated network, compressed after characteristically extracted and regulated into certain number of frames, To use the front-end network for time regulating is based on mainly two reasons:

First, the speed of the speaker’s speech may be inconsistent, which makes it improper to process the characteristic vector of all frames of the voice in equal weight. It is necessary to combine some characteristic vectors to make the final characteristic vector sequence consistent with the phoneme events in the voice independent of the speed of pronunciation, so as to wipe off the distortion of voice signals.

Second, to make the classification and recognition work of the neural network classifier easier, it is necessary to extract the same number of characteristic vectors for different words, and the final number of sections of the voice shall be greater than the number of phonemes contained in various words in the vocabulary list.

The simulation training adopts a BP neural network with one hidden layer. The number of the hidden layer knots is usually set according to former experience, for too many knots would make the network learning time longer while too few would make error tolerance poorer. In this example, characteristic parameter time regulating algorithm is adopted for the network, extracting a group of fixed-number characteristic vectors from the characteristic vector sequence of the voice signal input (in this paper, for each effective preprocessed voice signal segment, 12 one-order MFCC coefficient are extracted). The extraction process is as follows: using Hamming window to cut the voice into voice frames of equal length, applying positive and negative Fourier transformation on each frame, and then, after logarithm and discrete cosine transformation, picking the first 12 numbers as MFCC coefficient to describe each frame. Finally, classifying the MFCC coefficient sequence corresponding to each voice signal into four categories, assigning each voice signal with one corresponding 12 four-dimensional one-order MFCC coefficients, which will then become input signals into the neural network as characteristic parameters of the voice.

Training and recognition. Taken numbers 0～9 as the voice signal sample and 12-order Mel cepstrum coefficient as characteristic parameters, the paper uses characteristic parameter time regulation algorithm to regulate the number of frames to be four, as the input for BP network. Since the network system is non-linear, the original value has great bearing on whether learning reaches local minimum or converges. An important requirement is to try to make the state value of each neuron be close to zero when original weight values are accumulatively added in input, so as to ensure that the values do not fall onto the flat zones at the beginning. The original values of the connection weights are often picked up from random numbers, and little demanding is placed on the value of the weights, so as to ensure that each neuron is placed into where their transformation function featuring the largest gradient. And then, uniformize the input samples to enable the larger inputs to still fall into the places featuring big gradient of neuron transformation functions. The original weight is to be picked from the range of (-1,1) randomly, with a learning rate of 0.1 and an expected error of 0.01, which are subject to revision according to the experiment. The recognition results are shown in the following Table 1.

Table 1 Simulation recognition results

Samples for recognition	0	1	2	3	4	5	6	7	8	9
Times of recognition	10	10	10	10	10	10	10	10	10	10
Rate of recognition[%]	80	100	90	70	90	100	80	70	90	90
Average rate of recognition	86%									

Summary

Targeting on the recognition of the isolated words spoken out of the mouth of a non-specific person, the paper studies and constructs the BP network model and carries out simulation experiment in MATLAB. The experiment results indicate that the algorithm and software used in this paper boast high efficiency of recognition and unique advantages. However, the recognition effect would be less obvious when the quantity of experiment vocabularies increases. This is due to the fact that the BP network uses gradient descent algorithm to train the weight value, making it easy to fall to be the local minimum. Therefore, based on the above-mentioned reasons, BP network is only suitable for recognition of small quantity of vocabularies, and cannot meet the requirement for real-time voice recognition of large quantity of vocabularies.

Reference

[1] S.Y. Ruan: Matlab Program Design (Publishing House of Electronics Industry. China 2004)
[2] Martin Hagan,Howard B. Demuth, Mark H. Beale: Neural Network Design(China Machine Press. China 2002)
[3] Ch. Y. Zhang, Ch. Sun: Chip Presentation of Voice Recognition System for Isolated Words of A Non-Specific Person. Computer Engineering and Applications. Vol.43(2007) No.13,p.194
[4] X. Yang, J. Su and Y.Q. Peng: Realization of Voice Recognition System for Isolated Words in MATLAB. Microcomputer Information. Vol. 23(2007) No.3,p.288
[5] G.X. Jiang, J.Y. Wang: An Improved Approach for Detecting Voice End-points. Microcomputer Information. Vol.22(2005) No.5,p.138

Advanced Materials Research Vols. 989-994 (2014) pp 2123-2127
© (2014) Trans Tech Publications, Switzerland
doi:10.4028/www.scientific.net/AMR.989-994.2123

The MapReduce Parallel Study of KNN Algorithm

Chunye Wang [1, a], Xiaofeng Zhou[1,b]

[1]College of Computer & Information HoHai University Nan Jing, P.R.China,210098

[a]wenchangyu1990@hotmail.com, [b]zhouxf@hhu.edu.cn

Keywords: Text classification; KNN algorithm; MapReduce; Text pretreatment

Abstract. Although the parallelization KNN algorithm improves the classification efficiency of the algorithm, the calculation of the parallel algorithms increases with the increasing of the training sample data scale, affecting the classification efficiency of the algorithm. Aiming at this shortage, this paper will improve the original parallelization KNN algorithm in the MapReduce model, adding the text pretreatment process to improve the classification efficiency of the algorithm.

Introduction

Text classification is a technology that can rapidly classify text information to help users locate the key technologies required for accurate information. Text classification has been concerned. It has tremendous potential and value. It has a wide range of applications as information filtering technology, base information retrieval, search engines, text databases, digital libraries and other fields.

There are many kinds of text classification algorithm, among which kNN classification algorithm are widely used, because of its simple ideas, easy to implement, high classification accuracy, etc.But kNN algorithm in the classification process, document classification needs to be calculated to the training sample set from all samples of the document, so as the dramatic increase in the amount of data, it becomes very large amount of computation, and brought the classification process is calculated too long, low efficiency of classification problems.

In response to these problems, the improved direction in our country is currently focused on achieving algorithm parallelization by transplanting stand-alone operation of the algorithm to the cloud computing platform. Wensi[2] proposed a compression algorithm based on K-nearest neighbor decision boundary, and to combine this algorithm with the cloud computing platform,using the MapReduce programming model programs; Qiao Hongxin[3] implemented the MapReduce process by improving the KNN algorithm; Hongyi Hong[4] achieved a text similarity calculation method by using MapReduce architecture; Liu Biao[5] improved KNN algorithm and proposed a MapReduce-based spatial grid index generation method; Yan Yonggang[6] added a combiner function as the transition between the map function and reduce function based on the original MapReduce model, to reduce the amount of computation KNN algorithm and so on.

The above literature shows that the algorithm classification efficiency will be influenced if the data are not processed before the classification although the parallelization KNN algorithm has largely reduced the time of classification algorithm. To solve this problem, this paper is based on the literature[6] and designs a pretreatment process to improve the classification efficiency.

The Parallel Design of KNN Algorithm

The Basic Idea. In this paper, the basic steps to parallelize KNN algorithm is as follows:
The first, text preprocessing stage.

First, Worker nodes download the training sample and test sample from the HDFS system file to the local node, then pretreate the training sample and the test sample. The map nodes will implement some processes, such as word segmentation and stopping words. Then implement the Reduce process. The documents which are in the same class will be together and output to the file system HDFS.

The second, text classification stage.

The input of the stage is the output of the previous stage. Map nodes read the input data to calculate the similarity between the test samples and the training samples. Then the combiner function mergers the output of several Map nodes and takes the first k- nearest neighbors. The several k- nearest neighbors will be sorted by similarity in the Reduce. Electe pre-k nearest neighbors as the final k neighbors and calculate the weight, and finally conclude output.

To fit MapReduce computation model, the data which will be treated is stored in rows before the Map operation. Specific operation is performed on the data by row slice, requiring inter-chip unrelated data, and default slicing operation is done automatically by the MapReduce.

Text Preprocessing Stage. All the training sample datas need to be pretreated before the text classification. The basic two steps of the pretreatment process is word segmentation and stopping words. Stopping the words refers to remove the semantic virtual pan-word, such as "of", "the" in English. Generally, disable vocabulary which is summarized is used to remove the stop words before the text pretreatment process[7]. The text preprocessing phase flow chart is be shown in Fig.1.

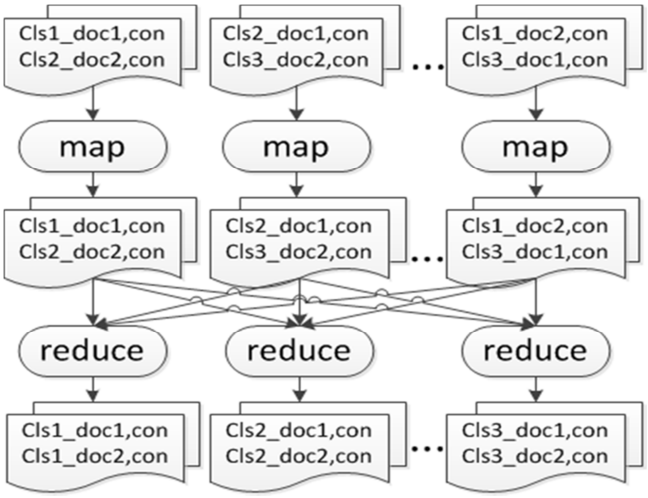

Fig.1 Text preprocessing phase flow chart

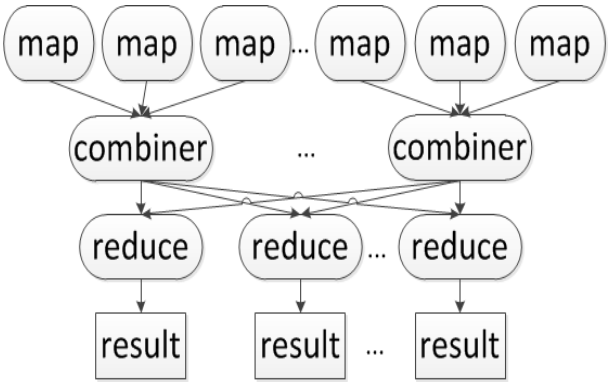

Fig.2 Text classification stage flow chart

(1) Map stage

The task of the Map stage is sending the disable vocabulary to each Map nodes for segmentation and removing the stop words by distributed cache. The result will be the input of the next stage.

Algorithm1.

```
public ListWritable Map(int RateTermKey){
    FileReader fr=new
    FileReader("D:\\StopWordList.txt");
    BufferedReader br=new BufferedReader(fr);
    String s = "";
    while(br.readLine()!=null){
        s += br.readLine();}
    br.close();
    ListWritable lw = new ListWritable();
    for(int i=0;i<RateTermKey; i++){
          String content = ReadFile(RateTermKey);
          lw = Segment(content);
          lw = TermFreq(lw);
          lw = StopWFilter(lw,s);
          Write(RateTermKey, lw);}
    return lw;}
```

Algorithm2.

```
public ListWritable Reduce(int
RateTermKey){
    ListWritable lw = new ListWritable();
    for(int i=0; i<RateTermKey; i++){
    EmitIntermediate(i, lw);
    Write(RateTermKey, lw);}
    return lw;}
```

First, the Map nodes read the text collection and converted the format of the input document into key-value pairs<class _ document, contents>. Then text collection will be implemented the word

segmentation and stopping words processes in accordance with the rules of the function. The form of the result which is the same as the form of the input will be passed to the next nodes of Reduce stage. Map function algorithm is shown in algorithm1.

(2) Reduce stage

The output datas of the Map stage is as the input of the Reduce stage after being reshuffled. The task of the Reduce stage is to have the same type of document composition together and output to HDFS file system, so their forms are the same. Reduce function algorithm is shown in algorithm2.

Text Classification Stage. Text classification stage flow chart shown in Fig.2.

(1) Map stage

The task of the Map stage is to read the training sample sets and test sample sets and to calculate the similarity between them. First, invoke built-in Split functions, read samples and convert them to files whose format to be determined by line. Then the Map nodes traversal each test sample to calculate the similarity with the training samples. Finally, the result will be collected into context. The form of the input data is <category, list <document, contents >>. The form of the output data is <category, list <document similarity values>>.Map function algorithm is shown in algorithm3.

Algorithm3.

```
public ListWritable Map (int RateTermKey){
for(int i = 0; i< training dataset; i++){
RateTermKey = FindCatalog(i);}
for(int k = 0; k <testfile; k++){
Distance = EnclideanDistance(k,i);
Context.write(RateTermKey, vector(RateTermKey,Distance));}
return vector;}
```

Algorithm4.

```
public vector combiner(int RateTermKey){
for(int i = 0; i < training dataset; i++){
ArrayList.add(vector(RateTermKey,Distance));
Sort(ArrayList);
Context.write(RateTermKey, ArrayList.get(k)); }
return ArrayList.get(k);}
```

Algorithm5.

```
public vector Reduce(int RateTermKey){
for(int i = 0; i < RateTermKey; i ++){
ArrayList(vector(RateTermKey, ListWritable));
Sort(ArrayList);
result = Sort(ArrayList);
result.add(RateTermKey, ArrayList.get(k));
Context.write(RateTermKey, Tradition KNN(result));}
return result;}
```

(2) Combiner stage

The task of the combiner stage is to merge several Map nodes. Then find out the first k-nearest neighbors. The number of the combiner nodes is far less than the number of Map nodes and its purpose is to filter the neighbor samples in advance and reduce the computation of the Reduce nodes.Combiner function algorithm is shown in algorithm4.

(3) Reduce stage

Reduce stage is implement the statute operation. The task is collecting and sorting the weights of the several k neighbors by similarity. Then the Reduce nodes elect the first k-nearest neighbors as the final k-nearest neighbors, calculate their weights and sum the weights of the samples whose categories are the same. The category of the test sample is the category which belongs to the samples of the maximum summing. Reduce function algorithm is shown in algorithm5.

Algorithm Analysis. In the MapReduce programming model, the training sample sets and test sample sets are stored in HDFS file system, then the data will be divided into a plurality of data blocks to assign to each node to implement pretreatment and classification. There is only a For loop function during the text preprocessing stage. It doesn't involve too much calculation. The largest part of the calculation amount is the process of calculating the sample similarity. But the calculation is assigned to a plurality of nodes to treatment because of the parallelization. Therefore, if the scale of the parallelization nodes is **p**, its time complexity is: $\boldsymbol{O(ns)/p}$, where **n** is the total number of training samples, **s** is the number of characteristic attributes.

KNN algorithm one time reads all samples into memory because of its inertia. So the traditional KNN space complexity is linear with the number of samples. It's $O(n)$, where n is the number of

samples. When p nodes participate KNN classification, the total samples are to be allocated to p nodes regardless of how many blocks the data sample is divided into. So the space complexity of the algorithm is $O(n)/p$.

Experiments and Results Analysis

Experimental Environment to Build. In this experiment, 8 machines are used to build a cloud computing platform. One of the servers is a master node of the distributed file system HDFS. It's used to manage other worker nodes. The other seven machines are the work nodes of HDFS. They are used to run MapReduce tasks. The configuration of the cluster is the official website of the recommended ways to build.

Experimental Design and Analysis of Experimental Results. This experiment is testing the KNN algorithm in the cloud computing environment and comparing the efficiency with the unmodified algorithm.

In the experiment, the data is selected from the UCI Machine Learning Repository, which is based on geological variables to predict forest vegetation covering types. These geological variables are with some authority from USGS (United States Geological Survey) and USFS (United States Forest Service). The data set has 581,012 samples, of which there are 387,342 training samples, 183 671 test samples [2].

First test and verify the accuracy and recall rates of the parallelization KNN algorithm. In the experiment, 4 data sets are selected as the test data sets ,ie T1 ~ T4. Their basic information are shown in Table.1.

Table.1 The comparison of algorithm parameters in both cases

Dataset	Sample Number	Sample Characteristic Propertie Number	Accuracy		Recall Rate	
			Before Improvement [%]	After Improvement [%]	Before Improvement [%]	After Improvement [%]
T1	10,000	2000	86.9	86.9	84.3	84.3
T2	20,000	2000	85.4	85.4	83.7	83.7
T3	30,000	3000	90.5	90.5	82.5	82.5
T4	40,000	3000	89.2	89.2	83.1	83.1

As we can also see from Table 1, the accuracy and recall rates of the former algorithm are the same as the later one. It explains that there is no impact on the classification results after pretreating the parallelization KNN algorithm and it doesn't reduce the accuracy of classification.

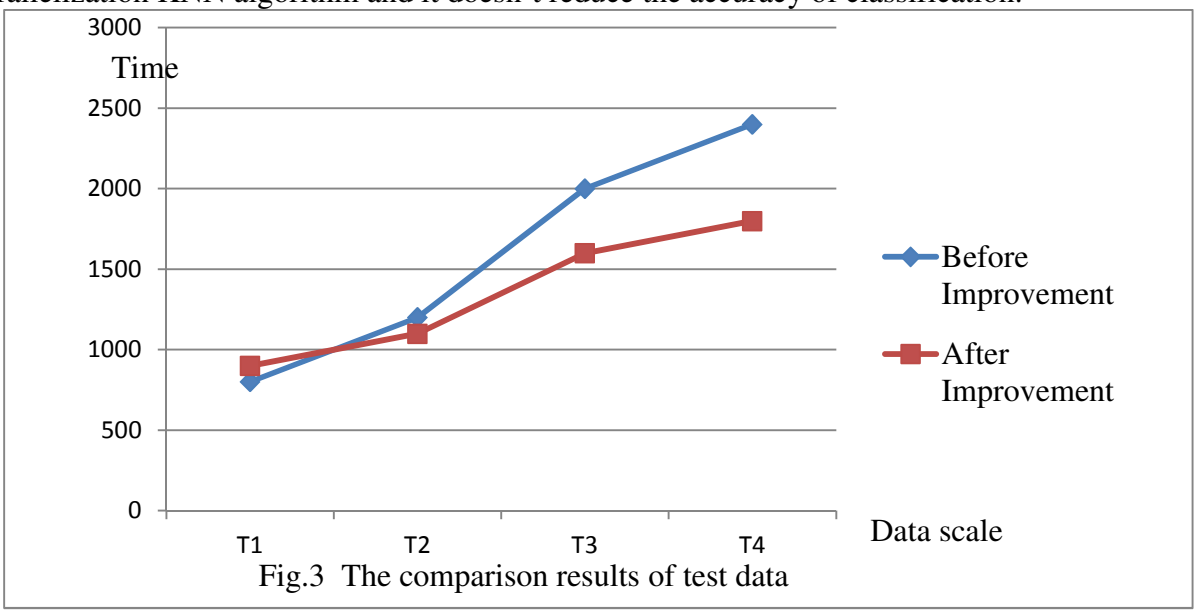

Fig.3 The comparison results of test data

As we can see from Fig.3, the execution time of the algorithm is constantly increasing with the increase of the data size. When data is smaller (T1), the execution time of the former algorithm is less

than the later one and it doesn't reflect the advantages of preprocessing. The mainly as follows: For the MapReduce model, it takes some time for the nodes to call the function to perform tasks and interact. Especially when the data size is small and the actual calculation is in a small proportion of the total task time, this phenomenon is particularly evident. When the scale of the data is increasing, the execution time of improved algorithm is gradually less than the time of the former one, which shows that the pre-processed data has a significant effect on improving the efficiency of KNN classification algorithm.

Conclusion

This paper improves the original parallelization KNN classification algorithm. We add the text pretreatment process before the classification process of the KNN algorithm. Through comparison and analysis of the experiments, we can conclude that the improved algorithm has a role in improving the efficiency of classification algorithm.

Acknowledgements

This work was financially supported by Access to Watershed Information Technology Research Based on the Internet of Things of the National Key Technology Support Program(2013BAB05B01), Integration and Demonstration of Using the System Safe and Efficiently Based on the Hydropower Development in Lancang River Basin of the National Key Technology Support Program(2013BAB06B04) and Integration and Demonstration of Using the System Safe and Efficiently Based on the Hydropower Development in Lancang River Basin of the Technology Projects of the Headquarters of CHINA HUANENG(HNKJ13-H17).

References

[1] Yinghui Yang. Research of Improvement to the Density-based Method for Reducing the Amount of Training Data and Application to kNN[D]. Chongqing University,2010. In Chinese.

[2] Si Wen. The Research of K-Nearest Neighbor Classification Algorithm Based on Hadoop Platform[D]. South China University of Technology,2011. In Chinese.

[3] Hongxin Qiao. Research and Application of KNN Classification Algorithm Based on MapReduce[D]. Beijing Jiaotong University,2012. In Chinese.

[4] Yihong Hong. Network and Information,2010,09:36-37. In Chinese.

[5] Biao Liu. The Research of a MapReduce-Based kNN Algorithm in Spatial Database[D]. Dalian Maritime University,2012. In Chinese.

[6] Yonggang Yan, Tinghuai Ma, Jian Wang. Transactions of Nanjing University of Aeronautics & Astronautics, 2013,04:550-555. In Chinese.

[7] Guoying Yang. Research on Text Classification Algorithm Based on MapReduce Model[D]. Liaoning University,2013. In Chinese.

Advanced Materials Research Vols. 989-994 (2014) pp 2128-2134
© (2014) Trans Tech Publications, Switzerland
doi:10.4028/www.scientific.net/AMR.989-994.2128

Software Structural Stability Evaluation Method Based on Motifs

Chun Shan[1, a], Long Huang[1, b], Changzhen Hu[1, c],
Xiaolin Zhao[1, d] and Jinsheng Ma[2, e]

[1] School of Software, Beijing Institute of Technology, Beijing 100081, China

[2] China Academy of Electronics and Information Technology, Beijing 100041, China

[a]sherryshan@bit.edu.cn, [b]morpheuslong88@gmail.com, [c]chzhoo@bit.edu.cn, [d] zhaoxl@bit.edu.cn, [e]m_j_s@sina.com

Keywords: Software security, Software structural stability, Complex networks, Motif

Abstract. The issue on finding an effective evaluation method on software structural stability is rarely touched upon in software security research. An assessment method of software microstructural stability was developed by Khalil in 2002. A new evaluation method on software structural stability is proposed in this paper, which is based on Motifs according to the theory of complex networks. Average shortest path length comparison and clustering coefficient with degree distribution are used in the method, in which the key evaluation indexes are used to analyze software structural stability. The comparison experiments have been done between the proposed method and Khalil's method. 10 real software systems of different sizes and types are selected in the experiments to verify the proposed evaluation method. The result shows that the proposed method is correct and effective.

Introduction

Software reliability factors have been taken into account in software security area now. Software reliability is the ability of software that allows it to continue to run properly under malicious attacks. This kind of ability can be measured. Trivedi [1] believed that there are mainly nine factors affecting software reliability. Among all of them, software structure is the most important and the most direct one.

The theory of complex networks has a strong interdisciplinary characteristic, involving many fields, such as mathematics, statistics, physics, ecology, sociology and economics. Complex networks research also involves several kinds of networks, such as biology networks [2] (cell networks, protein - protein role of the networks, protein folding networks, neural networks, ecological networks, etc..), Internet/WWW networks and social networks [3] (scientists cooperation network, relations network, linguistics networks, etc.). Studies have confirmed that the phenomenon of complex networks exists in large software systems, and software system topology is also manifested in the form of a network. Software system functionality, performance, and stability will be largely affected by the topology of the software.

A new software structural stability evaluation method based on Motifs is proposed in this paper. There are some experiments that have been done to measure how software structural stability is impacted by Motifs and what factors will affect software structural stability. Research work what has been done in this paper will be a great significance for software system maintenance, evolution and reconstruction.

Research

Software microstructural stability research. Software microstructural stability is provided as a method by Khalil [4].In Khalili's method, the network SSS is calculated, which will be used to measure the software microstructural stability [5]. Lyapunov exponent [6] is used, and the Jacobian matrix eigenvalues must also be calculated. That is following formula (Eq.1, Eq.2):

$$J = \{a_{ij}\} = \{\frac{\partial f_i}{\partial x_j}\} \quad (1)$$

$$\dot{x}_i = f_i(x_1, \ldots\ldots, x_n) \quad (2)$$

Eq.2 is differential equations of dynamic systems. If use a_{ij} represent the impact (symbols and weights) from node j to node i, then the Jacobian matrix can be used to represent the connectivity of the local structure; further, if normalized a_{ij} to 0 or 1, then Jacobian matrix can be reduced to the corresponding adjacency matrix. For a software system, its self-interaction can be considered that the impact of its own node is inactive. Then the corresponding Jacobian matrix diagonal a_{ij} is negative.

Meantime, root-locus [7] method is used to calculate the eigenvalues of the entire matrix, which determine whether the system is stable or oscillate. The proportion of eigenvalues is negative real numbers representing the SSS. For directed graph without cyclic structure, SSS=1 can illustrate the structural stability has nothing to do with parameter; When increasing the number and size of cyclic structure, feedback loop J consisting of nodes changes, SSS≈0.5 can illustrate the software structure is not stable. The conclusion proposed by Kahalil is consistent with some of the basic principles: Loop structure should be avoid in the design of software systems, otherwise it will increase the software complexity and reduce the software structural stability.

Motif and network stability research. With self-organization, self-similar, attractor, small-world, scale-free, some or all of the network properties are known as the complex networks.

Typically, the network element contains far more than three elements, thus those can form lots of networks. In recent years, through analyzing real network researchers found that these relationships were occurred in non-randomness, and they had formed some typical network connections. That is, different types of network having different typical connections. The number of occurrences in the real system is much higher than the number of random networks recurring. Milo called this element interconnection pattern (or unicom subgraph) Motif [8], and this basic structure of the network is considered "brick", used to implement some of the key features.

Despite the structure of complex networks is complicated, but the way and the process forming complex networks has a certain law. From the point of arrangement, there are a maximum of two kinds of relationships between two elements, and 13 different relationships can be formed in three elements. 3 nodes Motifs have their own id (are shown in Fig.1).

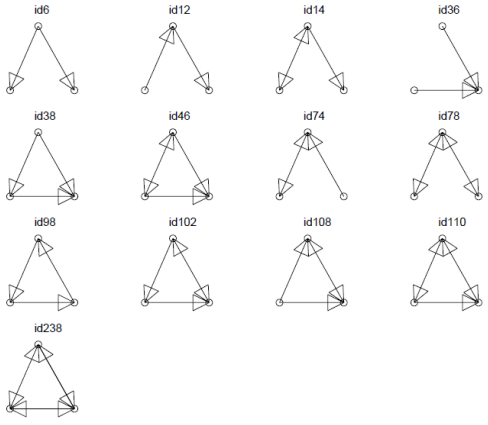

Fig.1 3 nodes Motifs

The stability of complex networks has become an important research content in the complex networks area. For the study on the stability of complex networks, predecessors demonstrated the scale-free networks in details [9], random network of anti-perturbation capability [10]. They made a great contribution to the stability of complex networks. They thought that attacking the networks can be in two ways :break the nodes and break the edges [11].The two ways of attacking are random attack and selective attack which are called network fault-tolerance and network anti-attack capability.

Chinese scientists had a great progress in the study of the stability of complex networks. Statistical physics methods [12], Monte Carlo method [13], random fluctuations method [14], etc. are all applied

in the study. In this paper, a method of software structural stability evaluation based on the Motifs is proposed, which had been used in network stability reseach.

Software structural stability evaluation method

Overview. For the study on complex networks characteristics of software systems, the key step is using open sources software and taking a "reverse engineering" approach. Depending on the granularity of units, the software system can be seen as different modules, classes, methods of the class consisting of, etc.. This paper follows the "reverse engineering" approach to abstract the software structure, select Motifs, and then analyze the experimental data using the shortest path length comparison and clustering coefficient with degree distribution method. Flowchart is shown in Fig.2.

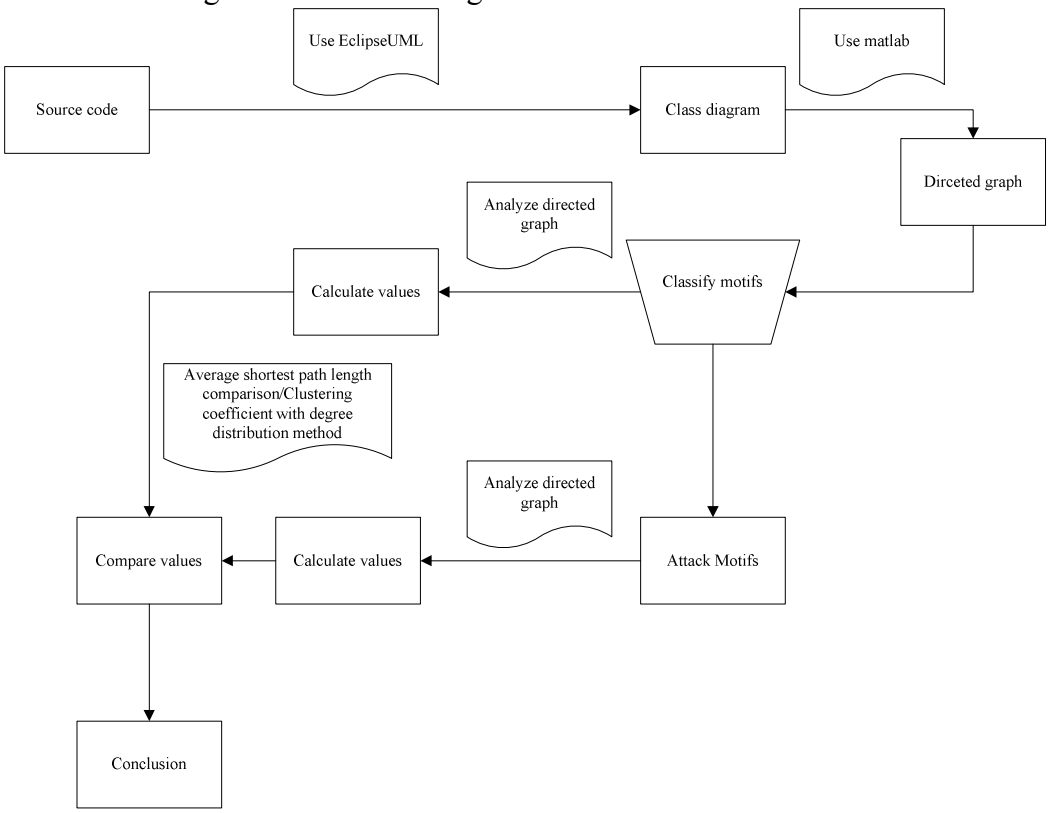

Fig.2 Method flowchart

Steps. Based on the flowchart in Fig.2, describ the specific steps below.

Step 1:Abstract the software structure: using the Eclipse UML software, put the source codes and turn into class diagram. If there are some bugs in class diagram, manual correction must be done. And write the Matlab codes, put class diagram into the *pajek* softare with the form of connection table. Class diagram will be changed into a directed graph in *pajek* software. In the directed graph the node represents class and the edge represents the relation between class and class.

Step 2: Classify Motifs: classify all of Motifs into 3 categories: no cyclic structure, less than or equal 2 nodes cyclic structure and greater than 2 nodes cyclic structure.

Step 3: Calculate the original index values (average shortest path length, clustering coefficient, degree distribution, etc.):

(1)Average shortest path length: is a concept in network topology. It is defined as the average number of steps along the shortest paths for all possible pairs of network nodes. It is a measure of the efficiency of information or mass transport on a network. L value is shown in Eq.3.

$$L = \frac{1}{\frac{1}{2}N(\mathrm{N}-1)}\sum_{i>j} d_{ij} \tag{3}$$

(2) Clustering coefficient: is a measure of the degree. Nodes in a graph tend to cluster together. Evidence suggests that in most real-world networks, and in particular social networks, nodes tend to

create tightly knit groups characterised by a relatively high density of ties; this likelihood tends to be greater than the average probability of a tie randomly established between two nodes. C value is shown in Eq.4.

$$C_i = \frac{2E_i}{k_i(k_i - 1)} \tag{4}$$

(3) Degree distribution: The degree of a node in a network (sometimes referred to incorrectly as the connectivity) is the number of connections or edges the node has to other nodes. If a network is directed, it means that edges point in one direction from one node to another node, then nodes have two different degrees, the in-degree, which is the number of incoming edges, and the out-degree, which is the number of outgoing edges.

Step 4: Attack Motifs, calculate values, and then analyze changes.

Classify Motifs. The proposed method based on Motifs in this paper focuses on the intrinsically linked and the structure affected between nodes and nodes, and the inherent linked mode on precisely structure for software structural stability is crucial**.** Classify all Motifs into 3 categories: no cyclic structure, less than or equal 2 nodes cyclic structure and greater than 2 nodes cyclic structure. For 3 nodes Motifs whose ids are based on the Fig.1: Category 1: Motif ids are 6, 12, 36, 38; Category 2: Motif ids are 14, 46, 74, 108; Category 3: Motif ids are 78, 98, 110 and 238.

Analysis. The average shortest path length comparison and clustering coefficient with degree distribution is applied in the proposed method. They are different from the previous analysis method. The proposed method in this paper focuses on the differences between the value and the rate of change, which can fully reflect the condition of software system after the destruction of the case and before the damage assessment.

(1)Average shortest path length comparison method: The average shortest path length L is divided into two cases, L value is increased after attacked, which means that damage to the nodes has little effect; L value decreased after attacked, calculate the change in the difference $L_{DV}=L_{AT}-L_{ST}$, the rate of change $P_L=L_{DV}/L_{ST}$, and analyze the impact on the structural stability based on the rate of change.

(2) Clustering coefficient with degree distribution method: Clustering coefficient C is divided into two cases. One C value is increased after attacked, which means that damage to the nodes to have little effect; the other C value decreased after attacked. Calculate the change in the difference $C_{DV}=C_{AT}-C_{ST,}$ the rate of change $P_C=C_{AT}/C_{ST,}$ and analyze the impact on the structural stability based on the rate of change.

Some state values changed will be get based on the above two methods, according to the principles of the complex networks metrics. Through this kind of analysis method, a conclusion can be claimed that the Motifs structure tends to simple, interactive elements bound tends to evacuate, and then the software will tends to stable. The Motifs with cyclic structure affect the structural stability greatly.

Experiments and result analysis

Based on the above experimental steps and methods, select a software called *openwfe* (A small daily office management system by JAVA), and conduct the experiment.

Step 1: Abstract the *openwfe* from source codes to class diagrams, and converted class diagrams into a directed graph. The graph is shown in Fig.3 and Fig.4.

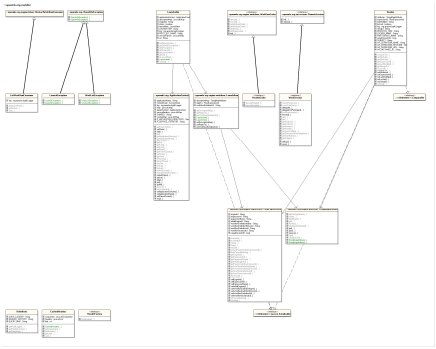

Fig.3 Class diagram

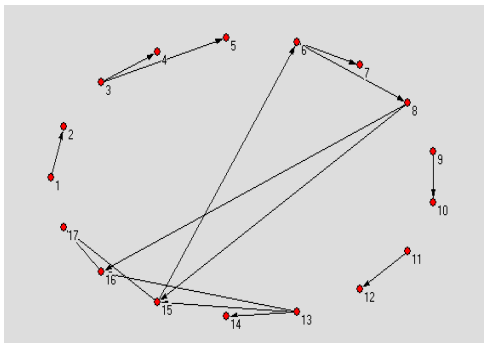

Fig.4 Directed graph

Step 2: Classify Motifs based on the method which has been introduced in Section Classify Motifs.

Step 3: Calculate the original index values, the process is shown in Fig.5, Fig.6, Fig.7, Fig.8 and Fig.9

```
Distribution of Distances
-----------------------------------------------------------

Working...
Number of unreachable pairs: 244
Average distance among reachable pairs: 1.64286
The most distant vertices: 6 (6) and 17 (17). Distance is 3.
Time spent:  0:00:00
```

Fig.5 Average shortest path length

```
Computing Clustering Coefficients
-----------------------------------------------------------

Working...
Watts-Strogatz Clustering Coefficient: 0.05952
Network Clustering Coefficient (Transitivity): 0.07500
Time spent:  0:00:00
```

Fig.6 Clustering coefficient

Vertex	Val	Label
1	9999998.0000000	1
2	9999998.0000000	2
3	0.0000000	3
4	9999998.0000000	4
5	9999998.0000000	5
6	0.1666667	6
7	9999998.0000000	7
8	0.1666667	8
9	9999998.0000000	9
10	9999998.0000000	10
11	9999998.0000000	11
12	9999998.0000000	12
13	0.0000000	13
14	9999998.0000000	14
15	0.0833333	15
16	0.0000000	16
17	0.0000000	17

Fig.7 Every nodes Clustering coefficient

Vertex	Val
1	0.0312500
2	0.0312500
3	0.0625000
4	0.0312500
5	0.0312500
6	0.0937500
7	0.0312500
8	0.0937500
9	0.0312500
10	0.0312500
11	0.0312500
12	0.0312500
13	0.0937500
14	0.0312500
15	0.1250000
16	0.0937500
17	0.0625000

Fig.8 Every nodes degree distribution

```
Network All Degree Centralization = 0.07917
-----------------------------------------
```

Fig.9 Network all degree centralization

Step 4: Attack different Motifs , calculate values, and compare values. Experiment results are shown in Table.1.

Table.1 Experiment results

Motif Catagory	Motif id	L_{ST}	C_{ST}	L_{DE}	C_{DE}	P_L	P_C
1	6	1.64	0.0595	1.58	0.0323	0.036585	0.457143
1	12	1.64	0.0595	1.53	0.0343	0.067073	0.423529
2	14	1.64	0.0595	1.49	0.0258	0.091463	0.566387
1	36	1.64	0.0595	1.54	0.0312	0.060976	0.47563
1	38	1.64	0.0595	1.51	0.0243	0.079268	0.591597
2	46	1.64	0.0595	1.44	0.0210	0.121951	0.647059
2	74	1.64	0.0595	1.50	0.0321	0.085366	0.460504
3	78	1.64	0.0595	1.49	0.0254	0.091463	0.573109
3	98	1.64	0.0595	1.43	0.0220	0.128049	0.630252
3	102	1.64	0.0595	1.42	0.0211	0.134146	0.645378
2	108	1.64	0.0595	1.45	0.0229	0.115854	0.615126
3	110	1.64	0.0595	1.41	0.0199	0.140244	0.665546
3	238	1.64	0.0595	1.40	0.0167	0.146341	0.719328

Experiment Analysis: The statistics shows that, Motif id 6,12,36,38 do not exist cyclic structure, P_L values after the attack are relatively small, and relatively large id after the attack, P_L values are relatively large, nearly 15%. For a module of a software system, attack a small portion of the structure, make the parameters change rate of up to 10%, or even higher, thus this Motif has great effection on the structural stability. The Motif whose rate of change is relatively small, has less effection on the structural stability. That is, the Motif id more larger, the software more unstable.

Motif id 46,98,102,110 and 238, L values change rate are over 10% after attack, C values change rate are over 50%. They have a greater impact on the software system structure, thus they affect the stability of the software. A conclusion can be found that all of the Motifs have one common characteristic,that is, one or more cyclic structure existed in Motifs. Again, campare Motif id 108 with Motif id 98, despite Motif id 108 has one more edge, but the presence of a cyclic structure participation points less than Motif id 98. It shows that in the software system structure, if the cyclic structure is attacked, the software system structure will be affected greatly, and the more cyclic structure in nodes, the more affection in structure.

To verify the above assumptions, 10 different size, types and real software systems (module type definitions 60) are chosen to do experiments using the proposed evaluation method in this paper. In the experiments we can see that if a cyclic structure is present in the attacked Motif, P_L values will be maintain a high level on or, worse value may be greater than 20%. Without the presence of cyclic structure after Motif attacked P_L values are maintained at a very low level, and the data is consistent with the conclusions obtained to verify the correctness of the above result.

To verify the model and conclusion, the comparison experiments have been done using Khalil's method. SSS values of different Motifs are shown in Table.2.

Table.2 SSS values of different Motifs

Motif Catagory	Motif id	SSS
1	6	1
1	12	1
2	14	≈0.5
1	36	1
1	38	1
2	46	≈0.5
2	74	≈0.5
3	78	＜0.2
3	98	＜0.2
3	102	＜0.2
2	108	≈0.5
3	110	＜0.2
3	238	＜0.2

Khalil's method in accordance with the conclusions, SSS = 1 indicates strong structural stability, SSS ≈ 0.5 indicates relatively poor structural stability, while SSS <0.2 indicates poor structural stability. Thus, the same conclusion can be get from the proposed method in this paper and Khalil's method. Stability is connection with the feedback loop gain of subgraph. If there is a cyclic structure or the number of cyclic structures is increased, the stability of the system will decrease. Therefore, the process of coding software in the future, we should try to avoid cyclic structures in our design to ensure greater stability of the software.

Conclusion

In this paper, we proposed a software stability assessment method, according to network reliability research method for complex networks.The essential idea of this method is that software structure can be divided to different Motifs, and then the structural stability can be evaluated through Motifs attack.

Evaluation indexes are proposed in this paper, which are calculated by the average shortest path length comparison method and clustering coefficient with degree distribution method. 10 different real software systems of different sizes and types including various modules (module type definitions 60) were selected to do comparison experiments between the proposed method and the software microstructural stability assessment method given by Khalil. The result shows that the proposal method is feasible and correct.

According to the research what have been done in this paper, some suggestion should be given that simple structures, evacuation constraints, and low cyclic structures will be better in the design of software. Otherwise the complexity of the software system will be increased and the software structural stability will be reduced.

Further research work is how to estimate and metric the price of the different Motifs in software structure stability area.

Acknowledgements

This work has been supported by the Key Project of National Defense Basic Research Program of China under Grant No.B1120132031.

References

[1] Trivedi K S. Sharpe: DSN 2002. Proceedings. International Conference on. IEEE, 2002: 544.

[2] Rubinov M, Sporns O: submitted to Journal of Neuroimage (2010)

[3] Riera-Fernandez P, R Munteanu C, Martin-Romalde R: submitted to Journal of Current Bioinformatics (2013).

[4] Khalil H K, Grizzle J W: Nonlinear systems. Upper Saddle River: Prentice hall (2002).

[5] Prill R J, Iglesias P A, Levchenko A: submitted to Journal of PLoS biology (2005)

[6] Kantz H: submitted to Journal of Physics letters A (1994)

[7] Evans E E, Theriault R J: submitted to Journal of bacteriology (1953)

[8] Milo R, Shen-Orr S, Itzkovitz S, submitted to Journal of Science (2002)

[9] Peng Luo, Yongli Li, Chong Wu, submitted to Journal of Complex System and Complex Science (2013) In Chinese.

[10] Wu Du, Meng Cai, Haifeng Du: submitted to Journal of Xi'an Jiaotong University (2010) In Chinese.

[11] Jinsuo Qiao, Xifu Wang, Xisheng Shen: submitted to Journal of Beijing Jiaotong University (2013) In Chinese.

[12] Abrikosov A A, Gorkov L P, Dzyaloshinski I E: *Methods of quantum field theory in statistical physics*, edtied by Courier Dover Publications (2012)

[13] Zhao L, Wang J, Huang R, submitted to Journal of Physica A (2014)

[14] SoléeR V. submitted to Journal of Taylor & Francis (2012)

Advanced Materials Research Vols. 989-994 (2014) pp 2135-2138
© (2014) Trans Tech Publications, Switzerland
doi:10.4028/www.scientific.net/AMR.989-994.2135

Locating method for character 2D Barcode

Liu Zhi, Yin Shichao, Ye Shengcheng, Zheng Herong

College of Computer Science and Technology, Zhejiang University of Technology

288# Liuhe Road, Hangzhou, China, 310023

lzhi@zjut.edu.cn, hailiang@zjut.edu.cn

Keywords：Character 2D barcode; Cross method; Mathematical morphology; Shape angle

Abstract. This paper studies the locating method for character 2D barcode. In this kind of character 2d barcode, the solid circle is designed as the position detection patterns. The locating method for character 2D barcode is different with the traditional method for DM barcode. In this paper, according to the geometric characteristics of the solid circle, connected region regarded as suspected solid circle can be filtered through the cross method rapidly. Then the edge of connected area is detected through the shape angle and the solid circle can be found through the circularity values. Experiment results show that this method can locate the character 2D barcode rapidly and effectively.

Introduction

Traditional Data Matrix 2D barcode takes the “L” shape as the position detection pattern and the QR barcode takes the black box as the position detection pattern. In this paper, the character 2D barcode takes the solid circle as the locator. The Fig. 1 shows the three kinds of barcodes.

Fig. 1 Three kinds of position detection patterns in barcodes

In this paper, we propose a new locating method for the character 2D barcode. For the barcode image gotten, we can segment the barcode image from the background using the segmentation algorithm combing the global and local thresholding algorithm firstly[1]. Then the homomorphic filtering method is used to remove the noise. So we can get the character 2D barcode image.

Filtering connected region through the cross method

In order to locate the character 2D barcode, the solid circle should be located. In this paper, we filter the connected region through geometric characteristics in order to filter those obviously irregular connectivity regions[2][3].

Here, we use the cross method to get the circle center and get the connected region through the circle center. The principle of the cross method is based on the fact that the distance from the center point to the points on the edge is equal. So if the distances from a point to the left, right, upper, and lower edges are equal, or these four distance differences are within a threshold ω, the point can be regarded as center point. The connected regions gotten from this method will always include some character connected regions and some background connected regions. But the ratio of height and width for the character connected region is 3:2 usually and the ratio of height and width for the solid circle region is 1:1. Because there is some deformation in the character 2D barcode image, the solid circle will always become a solid oval. So in our experiments, we find if the ratio of height and width is set within the range of [0.8,1.2.], the solid circle can be filtered better. It is showed in Eq.1.

$$H(R_i):W(R_i)<=1.2\&\&H(R_i):W(R_i)>=0.8 \tag{1}$$

Here, R_i is the i-th connected region. $H(R_i)$ is the height of the connected region and $W(R_i)$ is the width of the connected region.

Detecting solid circle through shape angle

Based on this filtering method, some suspected connected regions can be detected. Then the shape angles can be calculated to determine solid circle. The shape angle can be defined in Eq.2.

$$D_\alpha = \frac{1}{n}\sum_{i=0}^{n-1}\alpha_i = \frac{1}{n}\sum_{i=0}^{n-1}\arccos(\overline{g_i},\overline{m_i}) \tag{2}$$

Here, the $\overline{m_i}$ is the connection line between the point on the geometric contour and the geometry centroid. The $\overline{g_i}$ is the corresponding normal vector of the point. The angle between these two lines is defined as α_i.In a closed graph, the average of corresponding α_i of all points on the contour is the shape angle D_α. For the perfect circle, the D_α is zero. We can determine a connected region as a circle when its D_α is less ε. Here, ε is equal to π/6.

Locating solid circle through circularity value

Traditional edge detection methods include first-order differential operator and second-order differential operators, such as Roberts operator, Sobel operator, Prewitt operator and Kirsch operator, etc. belong to the first-order differential operator. The classic second-order differential operators have Laplacian operator, LOG operator and so on[4]. These operators can be implemented easily, but they are sensitive to noise.

In this paper, we use mathematical morphology method to get the edge[5]. Mathematical morphology is a nonlinear mathematical method evolved from set theory. The basic idea is to use the interaction between collection of image shapes and the structural elements selected in order to recognize and analyze the images. The method is not sensitive to the noise.

Basic mathematical morphology operations include: erosion, dilation, opening, closing, etc., where erosion and dilation are the two most important basic operations, others are transformed by the these two transformation combination of these two operation.

In the morphology, the operation object is a collection. Assuming that X is a collection of image, B is the structural element, a regular expression is that X operates on B, The operator "Θ" is taken as erosion operator. Arithmetic erosion expression is defined in Eq.3.

$$X\Theta B = \{a \mid B_a \subseteq X\} \tag{3}$$

In which, the structural elements B is translated α to get B_α. If B_α is included in the X, then the α is marked. All points that satisfy the above conditions is the result of the $X\Theta B$.

We use anti-erosion computing operation to extract the edge of connected region. The operator "$\overline{\Theta}$ " is taken as anti-erosion operator. The anti-erosion expression is defined in Eq.4:

$$X\overline{\Theta}B = \{a \mid B_a \not\subset X\} \tag{4}$$

In which, the structural elements B is translated α to get B_α. If B_α is not included in the X, then the α is marked. All points that satisfy the above conditions is the result of the $X\overline{\Theta}B$.

Generally, common structural element can be a cross-shaped, or square, or linear and so on. The structural element is actually a small window of gray scale "morphology " . In this paper, the cross structure element will be selected to operate the round connected region. The erosion operating and the anti-erosion operating results are showed in the Fig. 2.

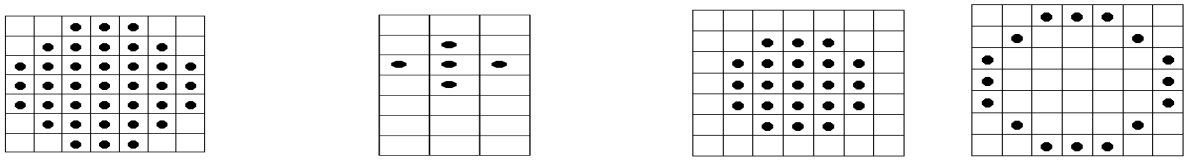

(a) Round connected region X (b) Cross structure element B (c) $X\Theta B$ (d) $X\overline{\Theta}B$

Fig. 2 Edge detecting based on anti-erosion operation

Based on the anti-erosion operation, the edge of round connected region can be detected. Then we can count the number of points in the connected region to get the area S_i. Using the formula of circularity value, we can get the circularity value of each round connected region. It is defined in Eq.5.

$$T_i = 4\pi * S_i / L_i^2 \tag{5}$$

If the number of round connected region is bigger than three, we can sort the suspected round connected regions by their circularity value. The first three greatest values are corresponding to the target solid circles.

Calculating the fourth solid circle

After locating the three solid circles, we will calculate the corresponding centers of the three solid circles. Here, the center coordinates and radius of the circle are used to determine the range of character barcode region. Assuming coordinates of solid circle centers are (x_i, y_i) and r_i is the radius of the i-th solid circle. They are defined in Eq.6-Eq.8.

$$x_i = \frac{1}{A_i} \sum_{x_i \in R_i} R_i . x_i \tag{6}$$

$$y_i = \frac{1}{A_i} \sum_{y_i \in R_i} R_i . y_i \tag{7}$$

$$r_i = \sqrt{A_i / \pi} \tag{8}$$

In which, the A_i is the i-th area of the solid circle and R_i is the i-th solid circle connected region. We can calculate the center coordinates of fourth solid circle according to the center coordinates of three solid circles based on the geometric symmetry principle. They are defined in Eq.9 and Eq.10.

$$x_{D1} = x_{A1} - x_{B1} + x_{C1} \tag{9}$$

$$y_{D1} = y_{A1} - y_{B1} + y_{C1} \tag{10}$$

Here, the coordinates of (X_{A1},Y_{A1}), (X_{B1},Y_{B1}), (X_{C1},Y_{C1}) are the center coordinates of the three solid circle. The (X_{D1},Y_{D1}) is the fourth center coordinate. The figure 3 is the locating process of the fourth solid circle.

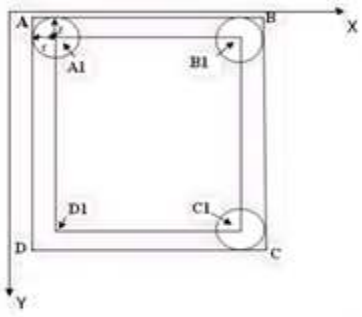

Fig. 3 Locating the four solid circles

So the original character 2D barcode image will be located based on the above method. The Fig. 4 shows a case of locating an image.

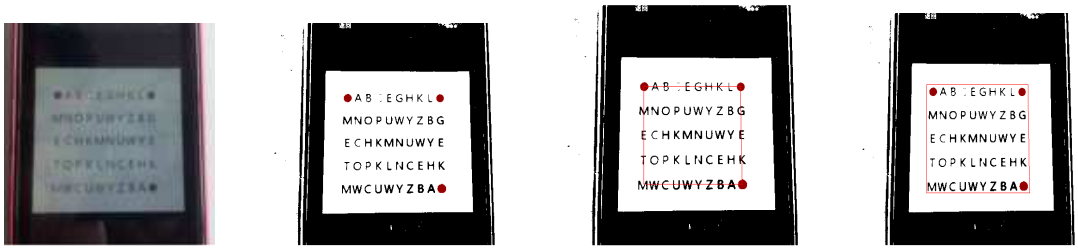

(a) The original image (b) Locating the three solid circles (c) Calculating center (d) Locating the barcode

Fig. 4 Locating process of the character 2D barcode

Conclusions

In this paper, we use cross method to filter the connected region in order to detect the suspected position detection patterns-solid circles. Then through circularity value, we locate the solid circles. Finally, the coordinates of fourth solid circle can be calculated and the barcode can be located. The experimental results show that this method not only faster, but also has better stability and robustness.

Acknowledgements

This work was financially supported by the Zhejiang Province Science and Technology Agency Project (2012C21046).

References

[1] Lin Zhengchun,Wang Zhiyan,and Zhang Yanqing. Optimal Evolution Algorithm for Image Thresholding: Journal of Computer-Aided Design & Computer Graphics Vol 22(2010)

[2] Chen Haifeng，Lei Hua，Kong Yanbo，et al. An improved randomized algorithm for detecting ellipses based on least square approach: Journal of Zhejiang University：Engineering Science Vol 42(2008)

[3] Qin Kaihuai, Wang Haiying, Zheng Jitao. A Unified Approach Based on Hough Transform for Quick Detection of Circles and Rectangles: Journal of Image and Graphics Vol15(2010)

[4] Senthilkumaran N, Rajesh R. Edge detection techniques for image segmentation–a survey of soft computing approaches[J]. International Journal of Recent Trends in Engineering, Vol. 1(2009).

[5] Xie Junxi,Tang Zhaohui,Gui Weihua. Recognition of the Two-Dimension Barcode Based on Mathematical Morphology: Computer Engineering & Science Vol 31(2009).

Advanced Materials Research Vols. 989-994 (2014) pp 2139-2143
© (2014) Trans Tech Publications, Switzerland
doi:10.4028/www.scientific.net/AMR.989-994.2139

Research on Motion Model of " Wind -Blowing &Trees-Swinging " and "Leaves-Falling & Branches-Broken" Based on Fractal Theory

LIU Hua Qun[1, a], WANG Jia[2,b] and FENG LiuPing[3,c]

[1]Beijing Key Laboratory of Signal and Information Processing for High-end Printing Equipments, Beijing Institute of Graphic Communication ,Beijing Institute of Graphic Communication ,Beijing, China

[2]SBeijing Key Laboratory of Signal and Information Processing for High-end Printing Equipments, Beijing Institute of Graphic Communication,Beijing Institute of Graphic Communication ,Beijing, China

[3]Beijing Key Laboratory of Signal and Information Processing for High-end Printing Equipments, Beijing Institute of Graphic Communication ,Beijing Institute of Graphic Communication ,Beijing, China

[a]lhq@bigc.edu.cn, [b]wangjia@bigc.edu.cn, [c]lpfeng@butp.edu.cn,[d]leimin@butp.edu.cn

Keywords: Wind-Blowing, Trees-Swinging, Leaves-Falling, Branches-Broken.

Abstract. Fractal technology can simulate the growth of trees very well.There have been many research on using fractal theory to model trees,but most methods have not further explore the tree's natural phenomena such as swinging driven by wind Firstly, this paper gave a modeling method to generate the trees based on the three-dimensional fractal L system; Secondly, according to the hierarchy of the strength characteristics of the wind and trees progression, this paper also gave the wind model to simulate the natural wind farm.In the end , this paper made some simulation about the model of "Wind- Blowing & Tree- Swing and Leaves-Falling & Braches- Broken" .

Introduction

Fractal Simulation of 3D Trees

Introduction to L-System. L-systems were introduced by A. Lindenmayer as a mathematical formalism for modeling multi-cellular organisms that form linear or branching _laments. The whole organism is treated as an assembly of discrete units, called modules. The nature of the modules is not predened by the formalism. For example, they may represent individual cells in the models of lower organisms, or functional units, such as apical meristems, internodes, leaves and owners, in the models of higher plants. Each module is represented by a symbol (a letter of the L-system alphabet), which species the module's type.

Fractal Simulation of Trunks. Generally speaking, L-system is used to represent a triple tree model constructed required, namely $L =< w, v, p >$, where V is a set of characters, letters and special symbols; w is V character described in the initial state of the tree model; P is the set of rules for tree growth.

By observing the growth of trees， we will find that the growth process of trees is a few sprigs stems grow to four weeks, most small to give birth to some of the smaller branches and twigs, and so forth down, and did not end in the most branches grown on the leaves of a similar shape of the process. Therefore, regardless of the growth rules of different trees, they all can be abstracted by two elements: the branches and leaves.

Therefore, in this paper we used cylindrical depicted in the branches and trunks of every short, while the size of cylindrical cross-section is obtained from the following equation measured by the Murray method:

$$\gamma_0^P = \gamma_1^P + \gamma_2^P, p \in [2.49,3.00] \quad (1)$$

From formula (1)we can learn that : the greater of P the greater of the tree.Where, r_0, r_1, r_2 respectively represent the radius values of mother branches and its' sub-branches (shown in Fig.1).

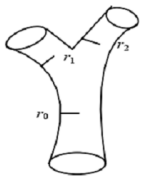

Fig 1. The relationship of the value of collateral radius and its mother branches

Simulation of Leaves As for the simulation of leaves, shell finite element analysis method is adopted. In finite element,shell element is one dimensional size that is far less than the scale of the other direction , and the stress perpendicular to the one dimensional scale can be ignored. Shell element edge is usually used in the finite element model to form, and it can be treated as a two dimensional entity from the side.which is shown in Fig 2.

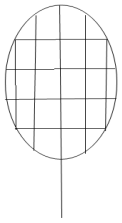

Fig-2. The Shell Element

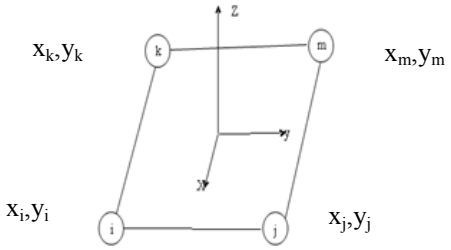

Fig -3. The Coordinated of Shell Element

Every node of shell element has six degrees of freedom,the coordinates are: $(x_i, y_i), (x_j, y_j), (x_m, y_m), (x_k, y_k)$,in the finite element method in displacement mode unit using polynomial approximation as a function, because the polynomial arithmetic is simple, and with the increase in the number of items that can approximate any function for some smooth curve.

Simulation of Wind Power. Simulation of wind power uses perlin noise function.The function was proposed by Perlin K in 1985.Its essence is a random number generator.But different from normal random number generator,it uses an integer as a parameter,and then returns to a random number based on the parameter.If the same parameter is passed twice the same random number will be produced.

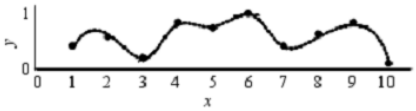

Fig -4 An Example of Noise Function

Fig-5 is an example of a noise function.Dark spots stand for the random number of the domain of function.Continuous noise function in figure 2 is formed by smooth interpolation (such as linear interpolation, three times of interpolation, etc.) of dark spots.When add some continuous smooth function of different frequency and amplitude together,a new Perlin noise function can be gotten

Motion Model of Leaves Falling and Branches Folding

Principle Model of Leaves Falling.

When you create the tree model with leaves and branches, we usually take follow steps. In order to study when the leaves fall, we give each leaf an attribute item $F_{i,thresthold}$, which is to represent the leafi can withstand the most vigorous.The value of $F_{i,thresthold}$ uses the following formula.

$$F_{i,threshold} = F_{constant} + \alpha \bullet F_{noise} \quad (2)$$

Where, $F_{constant}$ is a constant. Its resultant force can be adjusted according to the simulation results in combination with the force of leaves and its minimum value can be zero; F_{noise} is the value generated by Perlin noise.As a adjustment coefficient, α can be adjusted according to simulation

results.Each leaf threshold $F_{i,threshold}$ is determined, and we can calculate the current force that the leaves suffering,F. Comparing F with $F_{i,threshold}$, if F> $F_{i,threshold}$, the leaves will fall down,Otherwise, the leaves will follow the original manner..

When the leaves fall, they will no longer be restricted by the petioles. Leaves are affected by the gravity, the wind and air friction during their falling down process . Meanwhile, in order to make the leaves falling movement is more natural, a noise power F_{noise} is added. Force analysis of leaves in the falling process of leaves is shown in Fig-6.

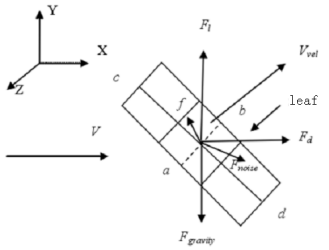

Fig-5 Force analysis of leaves in The Falling Process of Leaves

Leaves by the force F as shown in Formula (3)

$$F = F_{gravity} + F_d + F_l + F_{noise} + f \tag{3}$$

Among them, the value of $F_{gravility}$ can be calculated by the gravity formula according to the leaves' mass m, f is the air resistance, derived from the formula(4)

$$f = \lambda \cdot S \cdot V_{rel}$$
$$V_{rel} = V_{leaf} - V \tag{4}$$

Wherein, V_{leaf} represents the leaf's shaking speed ; V stands for the wind velo$_c$ity; V_{rel} is the leaves' speed relative to the wind speed; S is the area of the leaves; λ is the air resistance. That is to say, air friction has a relationship with speed leaves relative to wind and the area of the leaves.

Model of Branches Broken. The force acting on the branch can be decomposed a force $F_{branches}$ along itself direction and a vertical forces $F_{vertical}$., which value leads to the result of the branches broken.So when setting the force threshold value that the branches suffer ,we only consider the vertical force .The force analysis of acting on the branch is shown in Fig.7

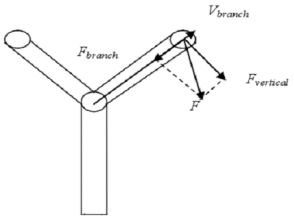

Fig -6 The force Analysis of Acting on The Branches

Statistics and Display of the Test Data. We adopted the test number in table 1 to the model of "Wind-Blowing & Tree-Swinging and Leaves-Falling & Branches-Broken".The experimental results are shown in Fig-8 and Fig-9.

Fig -7 Normal State Without Wind

Fig -8 Scenario of Leaves-Falling and Branches-Folding Under a Certain Wind

Table 1 Different Gale Can Lead to Different Affection .

Main Params	Gale #1	Gale #2	Gale #3	Gale #4
V_0	9.5m/s	11.0m/s	15.6m/s	20.0m/s
ω	3.14/320	3.14/120	3.14/180	3.14/200
β	3.14/12	3.14/4	3.14/6	0
α	4.5	5.0	6.0	5.0
λ	0.08	-0.10	0.09	-0.06

Wind velocity V=20.0m/s,wind increased gradually,more and larger branches land after fracture,then floating away on the wind direction.It takes 0.0621s.With the increasing broken branches,computation time consuming also been increased. The data analysis is shown in Table 1.

Summary

In this paper, the tree leaves in the wind, the wind blowing in a certain natural deformation under proposed a fractal technology and the physical and mechanical deformation technology combined approach. Experimental results show that the theory and methods described herein simulated "wind moving leaves off a tree branch off", you can easily and quickly get better pictures animated series to generate realistic trees and the variety and state, but in order to draw more trees form, modeling realistic trees could be improved.

Acknowledgement

This work was financially supported by the Scientific Research Common Program of Beijing Municipal Commission of Education(Grant No. KM201410015006)，Funding Project for Academic Human Resources Development in Institutions of Higher Learning Under the Jurisdiction of Beijing Municipality (Grant No. PHR201108349)，This paper is supported by BIGC Key Projects Funded by Beijing Institute of Graphic Communication (No.E-a-2013-20，No.E-a-2014-09) .

References

[1] Prusinkiewicz, P. and Lindenmayer, A. The Algorithmic Beauty of Plants, New York:Springer-Verlag, 1990.

[2] Mech, R., and Prusinkiewicz, P. Visual models of plants interacting with their environment, in Computer Graphics (SIGGRAPH ’96 Proceedings) , 397-410, August 1996..

[3] Schwartz, Paul et al, Virtual Playground: Architectures for a Shared Virtual World, http://www.hitl.washington.edu/publications/98-12/ (Accessed 12 February, 2001)

[4] Shlyakhter I, Rozenoer M, Dorsey J, et al. Reconstructing 3D tree models from instrumented photographs[J]. Computer Graphics and Applications, IEEE, 2001, 21(3): 53-61..
[5] WANG C, YANG K. Simulation of Trees' Swinging Driven by Wind Based on L-system and Perlin Noise Function[J]. Computer Engineering, 2009, 12: 070.
[6] P.G. Clem, M. Rodriguez, J.A. Voigt and C.S. Ashley, U.S. Patent 6,231,666. (2001) ,[7] Information on http://www.weld.labs.gov.cn.

Advanced Materials Research Vols. 989-994 (2014) pp 2144-2147
© (2014) Trans Tech Publications, Switzerland
doi:10.4028/www.scientific.net/AMR.989-994.2144

Algorithm of Representing and Preparing for Resources in EEM

Qian Yu[a], Tong Li, Xuan Zhang, Ying Lin, Yong Yu, and Na Zhao

School of Software, Yunnan University, Kun Ming, 650091, China

Key Laboratory in Software Engineering of Yunnan Province

[a]yuqian2001cn@163.com

Keywords: Software Evolution Process Model, Execution Model, Preparation for Resource, Knowledge Base, Resource Representation, Resource structure.

Abstract. Software evolution process model (EPM) is a knowledge-intensive process which is described in EPDL(Software Evolution Process Description Language) and modelled by semi-formal approach based on EPMM(Software Evolution Process Meta-Model). EPM's execution model (EEM) is represented by logic programming to create the knowledge base of EPM during constructing the EEM. Only its needing all kinds of resources are satisfied by system execution environment is activity in EEM implemented. The paper discussed the method and the algorithm of preparing resources is respectively presented in order to execute the EEM automatically. The converter program is realized and the correct results have presented to prove the correctness of the method.

Introduction

Resources are essential element in software evolution processes. Methods of resources' representations and managements are various with different application domain. Methodology of knowledge representation based on OWL is put forward to meet the requirement of integration management of enterprise resource [1]. Instantiation policies as a compact formalism proposes are proposed and integrated to a process modeling language to allow user-defined reusable management strategies for resource instantiation [2]. Applying multiparadigm simulation modeling in the scope of two process areas with the aim of supporting decision making and determining the optimal values of cost and schedule according to the management needs [3]. Semantic converter which converts knowledge representation in Conceptual Graphs into representation in Resource Description Framework is designed to overcome the barriers in knowledge sharing and reuse due to lack of consensus of knowledge representation formats between these two knowledge representation models [4]. Resources are encapsulated in components [5]. Software evolution processes are very sensitive to the scarcity or abundance of resources. All data, cost, time, human resources, software, hardware, and other objects supporting software evolution can be regarded as resources [6]. .Approaches above not mentioned the method of representing and preparing for the resources during executing software process.The paper proposes the method of representing and preparing for the resources in EEM. The preparation method and algorithm of resources at process level, activity level and task level are respectively proposed. According, the paper is organized as follows. Section 2 proposed resources' preparation method and algorithm. Section 3 presents the representation results of the resources in EPM's execution model using empirical data in case. Section 4 review the relative research work about EPDL and modeling approach of EPM in [6]. Finally, Section 5 draws some conclusions.

The Method and Algorithm of Preparing for Resources in EEM

Resources Needing to Preparing for. There are two kinds of resources needing to preparing in execution model of EPM. The first are input resources which are not export resources of other activities. The second is each role needed by each activity for executing, but duplicate role only needs to be instantiated once.

Method of Preparing for resources. Those supported by the environment when resources are prepared are realized by informing the environment during running the execution model. In order to realize to prepare for the resources at activity level, the EPDL file is scanned twice based on the model transformation. The four kinds of information must be reserved during scanning first which are all STRUCTURE types and all domain names and types of those domain names defined in EPM and denoted by 'TypeSet', input resources of all activities denoted by 'IRSet', export resources of all activities denoted by 'ESet', role resources of all tasks denoted by 'RSet'. The resources of set denoted by 'InitIRS' which is determined by the formula (1) are prepared.

InitIRS = IRset - ESet. (1)

Algorithm 1 . The function of algorithm is preparing for the resources for the execution model of any EPM.

Algorithm: EEPM_RES_PRERA

Input: 'pnepm' denoting the software evolution process model described by EPDL, 'InitInputRS' determined by the formula (1) and denoting resources need to prepare for, 'RoleSet' denoting role resources of all activity which need to prepare for, 'TypeSet' denoting all STRUCTURE types.

Ouput: prlgCodeS denoting resources described in execution model.

PROCEDURE EEPM_RES_PRERA (EPM pnepm, SET InitInputRS, ROLES RoleSet, TYPESET TypeSet, prolog prlgCodeS)

{/*algorithm begin*/

IF InitInputRS = ∅ THEN

RETURN;

FOR each var_i∈InitInputRS DO

BEGIN/* FOR begin，preparing for each input resource */

Converting var_i into littvar_i in lowercase and uppevar_i in uppercase;

IF var_i。type = STRING THEN

BEGIN/*IF begin*/

/* littvar_i replaced by concrete variable name，rule name is denoted by resprep */

Adding "write('please input the value of littvar_i: ')," to prlgCodeS;

Adding "read(uppevar_i)," to prlgCodeS;

Adding "resource(string, littvar_i (uppevar_i))"; to prlgCodeS

END/*If end */

IF var_i。type = ENUM THEN

BEGIN/*IF begin*/

/*var_i replaced by concrete variable name, var_iValue$_i$ replaced by each enum valut */

Adding "write('please input var_i, has var_iValue$_1$, ⋯, var_iValue$_n$ for selecting:') " to prlgCodeS;

Adding "read(uppevar_i) " to prlgCodeS;

Adding "resource(string,littvar_i (uppevar_i)) " to prlgCodeS;

END/*IF end*/

IF var_i。type = STRUTYNAME THEN

BEGIN/*IF begin*/

/*1<j<m，the type having m domains*/

Retrieving each domain name, denoted by struname$_{ij}$ from TypeSet of STRUTYNAME, Converting struname$_{ij}$ into uppestruname$_{ij}$ in uppercase;

FOR each struname$_{ij}$ DO

BEGIN/*FOR begin*/

Adding "write('please input the value of struname$_{ij}$ of var_i') " to prlgCodeS;

/* var_i replaced by variable name*/

Adding "read(uppestruname$_{ij}$) " to prlgCodeS;
END/*FOR end*/
Adding "resource(littstrtype, littstruVar$_i$(uppestruname$_{i1}$, … , uppestruname$_{ij}$,…,uppestruname$_{im}$) " to prlgCodeS;
END/*IF end */
END/*FOR end*/
FOR each role*var*$_i$∈RoleSet DO /*preparing role instance resource for each task */
BEGIN/*processing each role, FOR begin*/
Convert role*var*$_i$ littrole*var*$_i$ in lowercase and upperole*var*$_i$ in uppercase;
/* role*var*$_i$ replaced by concrete variable name, rule name denoted by resprep */
Adding "write('please input the personnel name of role*var*$_i$')";
Adding "read(upperole*var*$_i$)";
Adding "resource(role,littrole*var*$_i$ (upperole*var*$_i$)) ";
END/*FOR end*/
}/*algorithm end */

Presenting the Resulting of representation and preparing for resources in EEM

ISO/IEC 12207 standard [7] describes the maintenance process model in software life cycle. Tong creates the EPM of this process in EPDL[6]. By algorithm 1, resources prepared for this EEM are described in prolog and listed in Table 1.

Table 1: Resources prepared for this EEM

resource(msg,start).
resource(requirements_type,requirements(proreports,modifireque)).
resource(string,problem(problema)).
resource(string,problem_report(probreportfile)).
resource(string,modification_request(modifreqfile)).
resource(string, original_requirements(origrequirmentfl)).
resource(string, contract(contractfile)).
resource(string,migration_request(migrrequfile)).
resource(string,iso_iec12207_standard(iso12207file)).
resource(system_type,old_system(docfiles,datafiles,progfiles)).
resource(string,retirement_request(retirereqfile)).
resource(system_type,new_system(docfiles,datafiles,progfiles)).
resource(role,pm(alice)).
resource(role,prm(michale)).
resource(role,dr(michy)).
resource(role,ma(alice)).

Relative Research Work about Resources in EPDL and EPMM-based Modeling Approach

The structure of resources in EPM is represented with three levels in EPDL and EPMM-based Modeling approach.

(1) The first level resources are resources at process level which describe the partial order relations among activities. These resources are control information resources of activities in EPM. If an activity has been provided with needing control information which is called precondition resources, the

activity has the execution authority. The post-condition resources will be produced after the activity has been done.

(2) Activity can be a set of tasks. Any activity is defined as an abstract data structure which includes data structures and operations on these structures. The second level resources are input resources and output resources which respectively are described by imports data structure and exports data structure. Output resources of activity are generated by activity after its execution.

(3)The third level resources are local resources demanded by the tasks in activity of EPM at task level. Roles resources described local data structures are responsible for executing task(s).

Conclusions

In this paper, representation methods of all kinds of resources in any EEM are proposed. The preparation method and algorithm of resources at process level, activity level and task level are respectively proposed. The converter program has been realized and the correct results have presented to prove the correctness of the method.

Acknowledgements

This work is financially supported by the National Natural Science Foundation of China under Grant No. 61379032, No. 61262024 and No. 61262025; Scientific Research Fund of Yunnan Provincial Department of Education under Grant No.2012C108, No. 2010Y250 and No. 2011Y120; Education Innovation Fund of Software School of Yunnan University under Grant No.2010EI13 and No.2010EI14; Scientific Research Key Fund of Yunnan Provincial Department of Education under Grant No.2013Z057, Science Foundation of Yunnan Province under Grant No. 2010CD026, No.2012FB118, No. 2012FB119; Science Foundation of Yunnan Education Department under Grant No. 2012Y257; Science Foundation of Key Laboratory of Software Engineering of Yunnan Province under Grant No. 2011SE09 and No.2012SE305.

References

[1] Du, Laihong.Research of Enterprise Resource Knowledge Representation Based on OWL. The 7TH International Conference on System of Systems Engineering(SOSE), IEEE. 2012 : 943-946.

[2] Lima Reis C A, Reis R Q, Schlebbe H, et al. A policy-based resource instantiation mechanism to automate software process management. Proceedings of the 14th international conference on Software engineering and knowledge engineering. ACM, 2002: 795-802.

[3] Crespo D, Ruiz M. Decision making support in CMMI process areas using multiparadigm simulation modeling. Simulation Conference (WSC), Proceedings of the 2012 Winter. IEEE, 2012: 1-12.

[4] Yao, Haining; Etzkorn, Letha. Automated conversion between different knowledge representation formats. Knowledge-Based Systems. Vol. 19. No. 5. (2006), p. 404.

[5] Jian Wang, Na Zhao, Wei Du, Peng Li, Jinzhuo Liu, and Zhongwen Xie. Dynamic-Competition Based Architecture for Component Library Under the Software Evolution Model of SDDM[J]. ADVANCED SCIENCE LETTERS, Volume 7,March 2012 , pp. 618-621(4).

[6] Tong Li. An Approach to Modelling software Evolution Processes[M].Tsinghua University Press, Beijing,2008.

[7] The International Organization for Standardization (ISO) and the International Electrotechnical Commission (IEC), (ISO/IEC 12207) Standard for Information Technology—Software Life Cycle Processes, 1998.

Advanced Materials Research Vols. 989-994 (2014) pp 2148-2151
© (2014) Trans Tech Publications, Switzerland
doi:10.4028/www.scientific.net/AMR.989-994.2148

Research of Computer Forensics Based on Benford's Law

Shan Meijing

Institute of Information science and Technology, East China University of Political and Law, Shanghai, China. 201620
mjshan47@gmail.com

Keywords: Benford's Law, Computer forensics, File analysis

Abstract: In this paper we construct model in computer forensics by using Benford's Law, which is one of three famous laws in statistics in linguistics. Especially, we use Benford's Law to analyze data in file analysis and Anomaly detection. We illustrate that Benford's Law is able to supply the strategy for data analysis. The future work, Benford's Law will be the theoretical rule for intelligent compression of mass data.

Introduction

Cybercrime is one of the fastest growing and hot areas of crime. More and more criminals are exploiting the speed, convenience and anonymity that modern technologies offer in order to commit a diverse range of criminal activities.How to attempts to capture as much as possible digital evidence of the entire cybercrime investigative process, how to efficiently and effectively combat cybercrime, are very urgent issues. Computer forensics is a branch of digital forensic science pertaining to legal evidence found in computers and digital storage media. The goal of computer forensics is to examine digital media in a forensically sound manner with the aim of identifying, preserving, recovering, analyzing and presenting facts and opinions about the information.[1]

For the particularity of the electronic evidence in computer forensics, computer forensics should comply with the corresponding discipline and principle. It may involve the acquisition and analysis of digital evidence, authentication of documents, identification of sources and suspects, and so forth. From 1990's, many proposed forensic models have been studied [2-5]. Pollitt [2] identified four steps in digital forensics, as follows: acquisition, identification, evaluation, and admission of evidence, and further described admissibility of evidence. Authors in [4] use XML and OEM data model, data fusion technology, forensics knowledge base, experts inference mechanismn and mining engine to set up forensics model. Authors in [5] add time constraint and supervision procedure.

During the process of computer forensics, we need to analysis the data by knowledge of probability theory and statistics. In this paper, we construct the model in cyber forensics by Benford's law which is one of three laws in language statistics. We also use this law to analyze the file system and apply process anomaly detection.The rest content of the paper is indicated as follows: Section 2 mainly introduce the contents of Benford law and the related technologies in computer forensics. Section 3 studies the application of Benford law in computer forensics. Section 4 draw a conclusion.

Benford law

In 1881, Canadian-American astronomer and mathematician Simon Newcomb noticed that the beginning pages of the logarithmic table books were dirtier than the end pages, which indicated that the tables of logarithms were not used in a uniform way. [7]

Frank Benford was a research physicist at General Electric. In 1938, he also noticed the similar phenomenon. He found something unusual about a book of logarithmic tables. The first pages showed more wear than the last pages, indicating that numbers beginning with the digit 1 were being looked up more often than numbers beginning with 2 through 9. He published his result which about the frequency distribution of digits in many (but not all) real-life sources of data. In this distribution, the number 1 occurs as the leading digit about 30% of the time, while larger numbers occur in that position less frequently: 9 as the first digit less than 5% of the time. Benford's Law also concerns the expected distribution for digits beyond the first, which approach a uniform distribution.

Benford seized upon this idea and spent years collecting data to show that this pattern was widespread in nature. In 1938, Benford published his results, citing more than 20,000 values such as atomic weights, numbers in magazine articles, baseball statistics, and the areas of rivers.

Benford's Law(also called the First-Digit Law): A set of numbers is said to satisfy Benford's Law if the leading digit d ($d \in \{1, ..., 9\}$) occurs with probability

$$P(\mathrm{d}) = \log_{10}(\mathrm{d}+1) - \log_{10}(\mathrm{d}) = \log_{10}(\frac{d+1}{d}) = \log_{10}(1+\frac{1}{d}) \quad (1)$$

The quantity P(d) is proportional to the space between d and d + 1 on a logarithmic scale.

Nigrini appears to be the first researcher to apply Benford's law extensively to accounting numbers with the goal to detect fraud.[Nigrini 1996] More recently, papers have been published which detail practical applications of digital analysis such as descriptions of how an auditor performs tests on sets of accounting numbers, how an auditor uses digital analysis computer programs, and case studies for training students. However, Benford law does not suit for all the data, such as Lotto number, telephone number etc.

Table1 Based on the frequency of the digital distribution of Benford's law

	First digit	Second digit	Third digit	Fourth digit
0		.11968	.10178	.10018
1	.30103	.11389	.10138	.10014
2	.17609	.10882	.10097	.10010
3	.12494	.10433	.10057	.10006
4	.09691	.10031	.10081	.10002
5	.07918	.09668	.09979	.09998
6	.06695	.09337	.09940	.09994
7	.05799	.09035	.09902	.09990
8	.05119	.08757	.09864	.09986
9	.04576	.08500	.09827	.09982

Application of Benford law in Computer Forensics

Many evidences are potential in computer crime. The files the users set up may include important information
of crime activity. In many cases, suspects hide or modify the files, such as hide the important files in some partition or in some seems irrelevant file folders. Computer forensics should consider the properties of files. The tracked operations include time of files or file folders' creation, last modification, last access, movement and deletion, the owner, the access privilege.

When delete a file, the intuitive result is that the file name dispears from the directory list, and the file name and inode number of directory entries are marked unused. Some file systems, such as Microsoft FAT16 and FAT32, will hide the file name by a special configuration, then the file is marked for deletion. The traditional Berkeley Fast File System (FFS) will be disconnected directory entries, all file attributes and file data connections between data blocks. Extended FFS usually be found between Solaris and BSD system. Here we only discuss the cases which can access local file system, not about remote file system.

Actually, the files in computer system are not only the ones user set up but also the ones of operating system, which includes backup files, log files, configuration files, swap files, system files, hidden files, and temporary files etc. The sizes of these files obey the probabilistic distribution described in Benford Law. We got all the files in system disc by some instructions, and find the size of these files obey Benford law, shown in Table 2. In this table, "FSD" which starts wih digit 1~9 means the size of file, "Total" means the number of files, "Actual" means the proportion of the file, "Benford" means the proportion of the file calculated by Benford law.

Table2 The size of file in system disk

FSD	Total	Actual(%)	Benford(%)
1	4451	25.7	30.1
2	2900	16.7	17.6
3	2003	11.6	12.5
4	1243	7.2	9.7
5	1181	6.8	7.9
6	1651	9.5	6.7
7	1207	7.0	5.8
8	1825	10.5	5.1
9	870	5.0	4.6
0	19		

Compare the data in "Actual" and "Benford" column in Table2, we find they are similar. We use 2 for example. There are 2900 files which start with 2 in system disk, accounting for 16.7% of the total file. The calculating result is 17.6%. We compare the results and give the compared analysis chart as Table3.

By a large mount of experiments, we find the size of file in computer has the similar law. It supplies theoretical judgment strategy for anomaly detection of files in computer forensics.

Table3 Compare with the size of fiels in system disc and Benford law

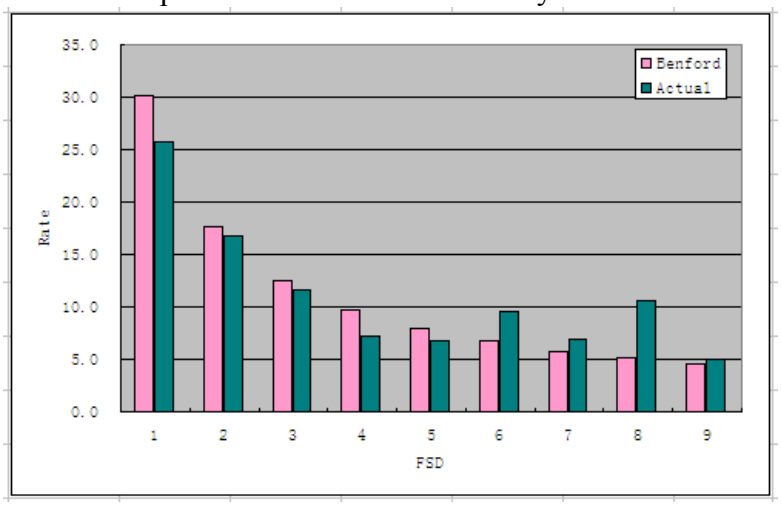

Conclusion

The research work of this paper is very rough. The further research work will use Benford law and formal method to study the digital evidences and models in computer forensics. We also plan to use knowledge of probability statistics to reduce the size of mass data with a TB level, for improving the analyzable of digital evdiences.

Acknowledgements

This work was financially supported by Innovation Program of Shanghai Municipal Education Commission(No.12YS107) and East China University of Political and Law Scientific Research Project(No.12HZK028).

Reference

[1] Michael G. Noblett; Mark M. Pollitt, Lawrence A. Presley (October 2000). Recovering and examining computer forensic evidence. Retrieved 26 July 2010.

[2] M. Pollitt, Computer forensics: an approach to evidence in cyberspace, in Proceedings of the National Information Systems Security Conference, Baltimore, MD, 1995,vol. 2, pp. 487-491, http://www.digitalevidencepro.com/Resources/Approach.pdf.

[3] Sabah Al-Fedaghi and Bashayer Al-Babtain. Modeling the Forensics Process. http://www.sersc.org/journals/IJSIA/vol6_no4_2012/9.pdf

[4] Chen Long, Mai Yonghao. Computer Forensics Technology. Wuhan: Wuhan University Press. 2007.
[5] Ding Liping, Wang Yongji. Multi-dimension Forensics Model. Computer Security-proceeding of 20th National Symposium on computer security. 2006: 5-9.
[6] Newcomb S. N ote on the frequency of use of the different digits in natural numbers. American Journal of Mathematics, 1881,4(1/4):39-40.
[7] Benford F. The law of anomalous numbers. Proc of the American Philoso Phical. 1938:551-572.
[8] Mark Nigrini, Joseph T. Wells. Benford's Law: Applications for Forensic Accounting, Auditing, and Fraud Detection. 2012.

Advanced Materials Research Vols. 989-994 (2014) pp 2152-2155
© (2014) Trans Tech Publications, Switzerland
doi:10.4028/www.scientific.net/AMR.989-994.2152

Using Zipf distribution to predict popularity data for storage systems

Yin Yang[1,a], Wenyi Li[1,b], Manning Zhang[1,c], Xiaomei Ding[1,d] and Jing Dai[1,e]

[1]School of Accounting, Wuhan Textile University, Wuhan, China

[a]cs_yangyin@hust.edu.cn, [b]newsone260@126.com, [c]oomanzz1994@gmail.com, [d]dingxm1223@gmail.com, [e]daijing1021@gmail.com

Keywords: popularity data; Zipf distribution; prediction

Abstract. In this paper we propose to use Zipf-like distribution to predict popularity data in storage systems. It can estimate prediction parameters according to the present statistics of I/O access. We classify the popularity data from every trace, and analyze the prediction rate through the classified popularity data's characteristic. We synthesize the analysis results in different prediction time granularity and prediction popularity data queue. Finally, we use block I/O traces to discuss the effectiveness of prediction method. The discussion and analysis results indicate that this prediction method can predict the popularity data efficiently.

Introduction

The access patterns of many applications reveals certain characteristics: high workloads, large number of users, massive data and many storage nodes. But the most notable characteristic of this access pattern is: 80% IO requests only access 20% data, which is known as "Pareto principle" [1]. These characteristics lead to the emergence of popularity data in storage system. As a result, how to predict these popularity data is a critical research focus in optimization of storage systems.

In order to use popularity data, some researchers have given a solution on the popularity data prediction [2-5]. But we develop a new Prediction Popularity Data Model (PPDM) based on Zipf-like distribution [6]. We first estimate parameters according to the present statistics of I/O access: α parameter, time granularity, and auxiliary parameters such as access frequency's growth rate, popularity data queue and the least accuracy rate etc. Then we use block I/O traces to discuss the effectiveness of PPDM. We classify the popularity data, and analyze the prediction rate through the classified popularity data's characteristic. Finally, we synthesize the analysis results in different time granularity and prediction popularity data queue. The discussion and analysis result above indicate that PPDM can predict the popularity data efficiently.

Prediction Popularity Data Model

Zipf observed long time ago that the distribution of word frequencies in English, the rank-r word has the probability P_r, and M denotes all data in the storage system, so the probability distribution is

$$P_r = \frac{C}{r^{\alpha}}, \sum_{r=1}^{M} P_r = 1 \Rightarrow C = \left[\sum_{r=1}^{M} \frac{1}{r^{\alpha}} \right]^{-1} \tag{1}$$

In one application environment, the value of α in Zipf's Law is a constant, and according to Eq. 1, we have C(kT)=C(T). At the time T or kT, if a data in the popularity data queue, f_r denotes the access frequencies , according to Zipf-like distribution in Eq. 1, the access probability of the D_r and Dr′:

$$P_r(T) = \frac{C}{r^{\alpha}} = \frac{f_r(T)}{F(T)}, P_{r'}(kT) = \frac{C}{r'^{\alpha}} = \frac{f_{r'}(kT)}{F(kT)} \Rightarrow \frac{f_r(T)}{F(T)} r^{\alpha} = \frac{f_{r'}(kT)}{F(kT)} r'^{\alpha} \tag{2}$$

In order to simplify the computation, if M remain unchanged from time 0 to kT and assume that F (the total number of access frequencies) is a linear function which only decided by time (this condition conforms to the most of access pattern of the practical application environment). So we have:

$$\frac{F(kT)}{F(T)} = k \tag{3}$$

According to Eq. 2 and Eq. 3, we have:

$$\frac{r'^{\alpha}}{r^{\alpha}} = \frac{f_r(T)}{F(T)} \cdot \frac{F(kT)}{f_{r'}(kT)} = k\frac{f_r(T)}{f_{r'}(kT)} \tag{4}$$

At the time t=kT, we just evaluate the ratio of $f_r(T)/f_{r'}(kT)$. So, considering the extreme scenario, the access frequency of D_r doesn't increase from the time T to kT ($f_r(T) = f_{r'}(kT)$). Eq. 4 is revised to:

$$\frac{r'^{\alpha}}{r^{\alpha}} = k \Rightarrow r' = k^{\frac{1}{\alpha}} \cdot r \Rightarrow r' \le Q_h \Rightarrow r \le Q_h \cdot k^{-\frac{1}{\alpha}} \tag{5}$$

If the k or T too large, the predicted is always popularity. So, we introduce a new concept: "Growth-rate of access frequency". If $G_r(t_1,t_2)$ denote as Growth-rate of access frequency from t_1 to t_2, it is calculated by:

$$G_r(t_1,t_2) = \frac{f_r(t_2) - f_r(t_1)}{t_2 - t_1} \Rightarrow G_r(t) = \lim_{\Delta T \to 0} \frac{f_r(t) - f_r(t-\Delta T)}{\Delta T} \Rightarrow \Delta f_r(t) = \Delta T \cdot G_r(t) \tag{6}$$

For a non popularity data D_r at time t=T, to become popularity at time t=kT, it must satisfy:

$$f_r(T) + (k-1)\cdot G_r(T) \ge f_{Q_h \cdot k^{-\frac{1}{\alpha}}}(T) + (k-1)\cdot G_{Q_h \cdot k^{-\frac{1}{\alpha}}}(T) \tag{7}$$

At the time t=kT, with the $G_r(t_1,t_2)$ during ΔT to calculate the access frequency of $D_{r'}$, we have:

$$f_{r'}(kT) = f_r(T) + (k-1)\cdot G_r(T) \tag{8}$$

Estimating parameters of the PPDM

Estimating α parameter. In Zipf-like distribution, we first have: C is equal to the most frequently occurring data that appears in the storage system with the probability P_1, if r=1, then P_1=C.

In order to acquire many methods to estimate the value of α, we convert Eq. 2 and have(r<j):

$$\frac{P_r}{P_j} = \frac{C/r^{\alpha}}{C/j^{\alpha}} = (\frac{j}{r})^{\alpha} \Rightarrow \alpha = \frac{\lg(P_r/P_j)}{\lg(j/r)} \tag{9}$$

According to Eq. 9, we compute many values of α and acquire arithmetic mean value and geometric mean value. At the time t=T, we choose the access frequency N is 100 thousand. If we choose two different r and j from (1, 2⋯10), which can compute 45 different α values. The simplest method to judge whether the value of α is reasonable or not: if q_r=P_r and C=P_1, transferring Eq. 1, we have:

$$q_r = \frac{C}{r^{\alpha}} = \frac{P_1}{r^{\alpha}} \tag{10}$$

Table 1 The fit ratios of the most reasonable α in Hm_0.

α	p_1/q_1	p_2/q_2	p_3/q_3	p_4/q_4	p_5/q_5	p_6/q_6	p_7/q_7	p_8/q_8	p_9/q_9	p_{10}/q_{10}
1.042963395 (arithmetic mean)	1	1.84	1.08	1.36	1.52	1.23	1.09	1.24	1.25	1.34
0.889309111 (geometric mean)	1	1.65	0.92	1.1	1.19	0.85	0.81	0.9	0.89	0.94
0.329392	1	1.12	0.5	0.51	0.48	0.31	0.27	0.28	0.26	0.26
0.94	1	1.71	0.97	1.18	1.29	0.94	0.89	1	1	1.06

On the whole if q_r is close to p_r, α is reasonable, otherwise α is unreasonable. We utilize (Fit ratio) P_r / q_r to judge whether q_r (Fit frequency) is close to p_r. The more P_r / q_r is close to 1, the more q_r is close to p_r. For example: (Hm_0). When r=9 and j=10, we compute the value of α is 0.329392, the fit ratios of this α are shown as Table 1. Most of the fit ratio is close to 0 (much less than 1), so this α value is unreasonable. According to our calculation, the most reasonable value of α is 0.94. The fit ratio of the most reasonable α in Financial_2, Ts_0 and Proj_3 are 0.62, 1.34 and 0.68.

Estimating k parameter. The most important evaluation criterion is Popularity Prediction Accuracy (PPA): the ratio of true positive predicted popularity data to the popularity data queue:

$$PPA(t) = \frac{P(t)}{Q_p} \tag{11}$$

In Eq. 5, we have $Q_p \cdot k^{-\frac{1}{\alpha}}$, this is the boundary value of the data which is still in the new popularity data queue, if only the data rank smaller than or equal to this value, it is still popularity data. So we have:

$$PPA(kT) \geq \frac{Q_p \cdot k^{-\frac{1}{\alpha}}}{Q_p} = k^{-\frac{1}{\alpha}} \tag{12}$$

In Eq. 12, if $PPA(kT) = k^{-\frac{1}{\alpha}}$, defined as Minimum Popularity Prediction Accuracy (PPA_m). We can make sure that if PPA_m value is high, then the prediction time is short, and PPDM can not reflect the efficiency; if PPA_m value is low, then the prediction time is long, and the results of the prediction model might be not accurate. So, we first choose 5 values about PPA_m: 10%, 20%, 30%, 40% and 50%, and then we compute 5 values of k. We define $k_1T=T_1$, $k_2T=T_2$, $k_3T=T_3$, $k_4T=T_4$ and $k_5T=T_5$, meanwhile, $T_1>T_2>T_3>T_4>T_5>T$. In four traces, some of them are small data sets, some are big data sets. Based on PPDM, the popularity data queue is 30, 40, 50, 60, 70, 80, 90, 100 and 200.

Experiments and analysis

I/O workloads. The workloads that drive our experiments consist of two major parts: SPC I/O traces and data center server traces. Four different traces are used, Financial_2 (read-dominant) is typical of small and short-period data centers. Ts_0 (write-dominant), Proj_3 (read-dominant) and Hm_0 (almost the same read and write amount) which are typical of big and long-period data centers. The write ratio of these traces is about 18%, 82%, 5% and 65%, respectively.

Prediction rate results. The results of prediction rate are shown in Fig. 1-2. In these figures, the prediction rate at the time T_5 is higher than the results at other prediction time, the reason is we use unchanged parameters at the time T to predict popularity data rank from k_1T to k_5T, but in real application, when current time is k_3T, our PPDM prediction is dynamical, and the parameters used in model would adjust according I/O access condition, we would use related parameters at the time k3T to predict k_2T or k_1T, thus the accuracy of popularity data prediction model would be higher.

Results analysis. Periodical popularity refers to a block of data accessed frequently in a time period. Ts_0 has periodical popularity characteristics. The trace data ranked top in the growth rate of access frequency during ΔT, but fall behind during time T. Therefore, the time from 0.8T to T will be predicted as a new popularity data in the next period. But, the actual access is on the contrary, as the growth rate in T to KT decreased, which lead to a drop in the rank, so some of prediction in KT period is relatively low.

Temporary popularity refers to the data that transfer from seldom visited to the focus of data access, and when they become popularity data, other data fall behind in the rank. Proj_3 has periodical popularity characteristics. The access frequency of these data stay unchanged from 0.9T (or 0.8T), and become leading in the access frequency rank. Therefore, these data will be predicted as the new popularity in the next moment. However, the actual access situation is on the contrary: the popularity

access frequency stays unchanged in KT, while other data's access frequency increase, which leads to the actual rank fall behind compared to moment T, so part of the prediction in KT is not so accurate.

Hm_0 is trace that contain both temporary and periodical characteristic. So the prediction rate of these traces can be affected by both effects. It is not certain whether these traces of two traits stand for a low prediction rate, which was mainly determined by the quantity of these data.

The prediction of popularity rate Financial_2 is very stable now, and the rate is fairly high.

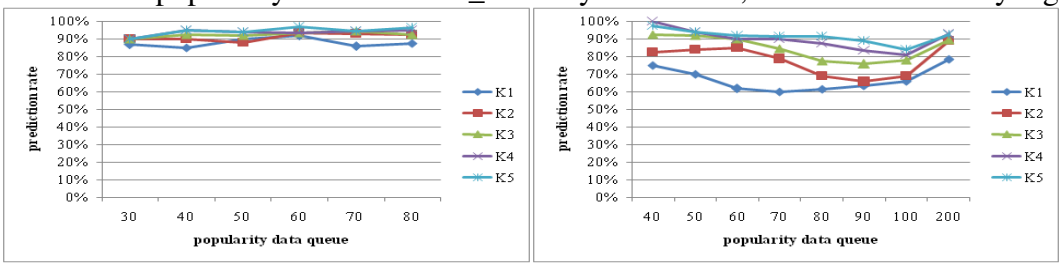

Figure 1. Prediction rate of Financial_2 and Ts_0 (left figure is Financial_2 and right figure is Ts_0).

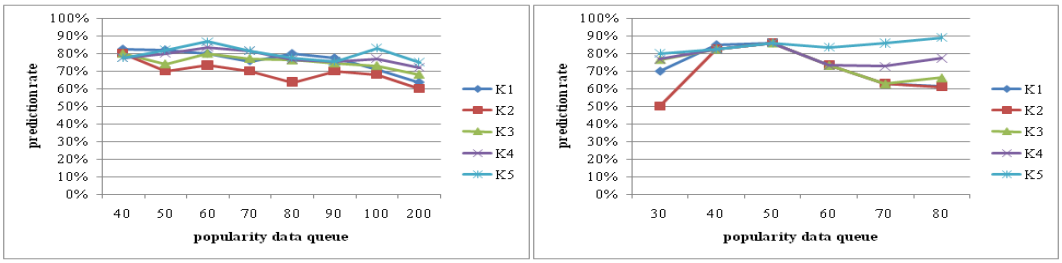

Figure 2. Prediction rate of Hm_0 and Proj_3 (left figure is Hm_0 and right figure is Proj_3).

Summary

In this paper, we propose a Prediction Popularity Data Model (PPDM) based on Zipf distribution. We combine the different characters of every trace, use different popularity data queue and prediction time to demonstrate the efficiency. We can draw the conclusion that short prediction time has high prediction rate (over 90%). From the analysis of periodical and temporary popularity, we get the conclusion that different popularity data queue have no regularity on the prediction results of PPDM.

References

[1] L. Cherkasova and M. Gupta, Analysis of enterprise media server workloads: access patterns, locality, content evolution, and rates of change, IEEE/ACM Transactions on Networking, vol. 12, pp. 781-794 (2004).

[2] L. Breslau, P. Cao, L. Fan, G. Phillips and S. Shenker, Web caching and Zipf-like distributions: evidence and implications, Proc. IEEE Conf. Computer and Communications Societies (INFOCOM 99), IEEE Press, pp. 126-134 (1999).

[3] Y. S. Chen and P. Chong, Mathematical modeling of empirical laws in computer application: A case study, Computers & Mathematics with Applications, vol. 24, pp. 77-87 (1992).

[4] H. Yu, D. Zheng, B. Zhao and W. Zheng, Understanding user behavior in large scale video-on-demand systems, Proc. ACM Conf. Computer Systems (EuroSys 06), ACM Press, pp. 333-344 (2006).

[5] Z. H. Tang. Hotspot Detection by Improved Adaptive Finite Element Method and its Application in High-Speed PCB and IC Package Design, IEEE Transactions on Components, Packaging and Manufacturing Technology, vol. 2, pp. 1659-1665 (2012).

[6] M. Joos, Review of G.K. Zipf – the psychobiology of language, Language, Vol. 12, pp. 196-210 (1936).

Advanced Materials Research Vols. 989-994 (2014) pp 2156-2160
© (2014) Trans Tech Publications, Switzerland
doi:10.4028/www.scientific.net/AMR.989-994.2156

A Method for Transforming the Online Handwritten Mathematical Formula into MathML

Deqiang Fu[1, a], Wenyin Zhang[1,b] and Seong Tae Jhang[2,c ,*]

[1] School of Informatics, Linyi University, Linyi City Shandong Province 276005, China

[2] Department of Computer, The University of Suwon, Hwaseong-si Gyeonggi-do 445-743, Korea

[a]fudeqian@lyu.edu.cn, [b]zwenyin@126.com, [c]stjhang@suwon.ac.kr

[*] Corresponding author

Keywords: Mathematical Formula, Ternary-Tree, MathM, Minimum Arborescence.

Abstract: This paper employs the Minimum Arborescence model to handle the spatial structure analysis of a mathematical formula, and transforms the directed graph to a trigeminal tree. Also, we utilizes the preorder traversal algorithm of the Ternary-Tree to generate MathML, and display the MathML with Web browser. At last, the experimental results illustrates the recognition rates of online handwritten mathematical formula in various cases.

Introduction

Recently, the recognition based on image processing has been widely applied in many fields such as document recognition in bank, license plate recognition on road, pupil detection in medical treatment, and etc. The recognition of online handwritten character is an interdisciplinary problem based on the theories of digital image processing, statistical decision theory, machine learnign, pattern recognition, etc. The recognition of online handwritten character is now becoming more and more practical, especially in English charters, which has begun to implement unlimited whole-sentence recognition. However, The recognition of online handwritten mathematical formula is much more difficult than that in English charters. Firstly, collecting handwriting is more complicated. Secondly, there is not the specific symbol of mathematical formula in the computer character set. Thirdly, the nest in the formula makes the problem more difficult. Since neural network algorithm[1] and support vector machine(SVM) algorithm [2]have been applied successfully, the recognition rate of handwritten characters reaches 95%, which settled the character recognition of online handwritten mathematical formula. Meanwhile, due to the instantaneity, high efficiency, "what to write is what you get" and other features, the recognition of online handwritten mathematical formula still attracts attentions of researchers.

For the structure analyze of mathematical formula, the common methods are grammar LL(1), minimum spanning tree[3,4,5] and ternary tree. Grammar LL(1) utilizing stack architecture conducts derivation from the start symbol of grammer by the repeated use of production until incoming symbol comes out. Grammer LL(1) requires the complete accuracy of the formula, because it can not judge a wrong one. Minimum spanning tree resorts to the tree with minimum weight among all spanning trees of undirected connected gragh. It has to solve the circle-breaking problem of undirected gragh first, but not emphosize the complicated mathematical structural analysis. Ternary tree sets up a ternary tree based on the priority of operator, but more efforts should be made in the generation of ternary tree. Minimum arborescence was first presented by Zhu Yongjin and Tian Feng in 1965 to solve channel design problem. But, the issue is that in channel design, water should be led to several points, and the bifurcation of channel must be at the given point, and the total channel route should be the shortest. The difference between minimum arborescence and minimum spanning tree is that water always flows in a direction. Recently, many researchers focused on the study and application of minimum arborescence. Zhai Xiaoyan[6] proposed the application of minimum arborescence in network. Sun Lingyu[7] presented the algorithm of empowerment minimum arborescence, which

used the model of minimum arborescence to solve the structural analysis of online handwritten mathematical formula and generate ternary tree.

The Structural Analysis of Mathematical Formula

The nest in mathematical formula makes the problem more complicated. Compared to the structural analysis of character recognition, there are various patterns in mathematical formula such as front-back relation (like $a+b$), up-down relation ($\frac{a}{b}$), super-subscript relation (like ∂_2^3), internal relation (like $\sqrt{2}$) and etc. There are two popular methods in studying character relation of mathematical formula: base line and "Jing" font. Base line is to solve the type-setting problem of printing characters, but not good at dealing with the nested and complex formula. "Jing" font judges the relation of two characters according to the spacial position information of every mathematical character in the formula such as up-down, left-right, up-right, up-down relation and etc. However, "Jing" font may lead to misjudgment due to some spacial position relations between characters.

Based on the structural analysis of mathematical formula, some rules come up as follows:

(1) Writing mathematical formula is in the left-right order. A character and its following characters can form a sector structure, e.g., ∂_2^3+b, three characters form a sector structure surrounding "∂" (character "∂" relates to the following subscript "2", superscript "3" and "+");

(2) Some characters form the up-down relation, like $\frac{a}{b}$;

(3) Special character radical sign and its internal character form internal relation.

The above analysis shows that in a mathematical formula, at most four characters can have effective relation with one character, among which at most three characters are its in-coming characters and one character is its out-going character. It is same with the link between nodes of minimum arborescence. Therefore, it is feasible to solve the structural analysis problem of mathematical formula by establishing a minimum arborescence model.

Establishing a Minimum Arborescence Model

Set the relations of characters in mathematical formula as follows:

(1) For number, letter and so on, the sector structure is in priority in spacial position relation, that is, super-subscript and right relation.

(2) For special characters like "—", "$\sum$" ,etc., the up-down and right relation are in priority in spacial position relation like $\frac{a+b}{c+d}+e$. Character "—" has three relevant characters "a", "c" and "+".

(3) For special character like radical sign "$\sqrt{\ }$", the internal and right relation is in priority in spacial position relation. For example, in $\sqrt[c]{a+b}+d$ the relevant characters of radical sign are "c", "a" and "+".

Process of generating minimum arborescence:

(1) Sort the characters in the order from left to right regardless their spacial relation.

(2) Retrieve special character in the order from left to right, and look up its relevant characters by relation rules. If the selected relevant character has been related to other special characters, give it up. Otherwise, tab it.

(3) Conducting relational analysis among the remaining characters from left to right, and seek out its relevant character successively. If the selected relevant character has been related to other characters, give it up. Otherwise, tab it.

The merit of this method is that one node will not have multiple pre-nodes in the generated minimum arborescence, meanwhile, mis-relation might exsit in some handwritten messy mathematical formulas. Fortunately, the effect of mis-relation can be deduced due to the recognition is online

operation, which provides real-time display so that the user can immediately revise the written character.

The structural analysis of the formula shown in **Fig. 1** with the above method and the generation of minimum arborescence are shown as follws:

$$\frac{a_x^y + b_y^x}{(\sqrt{c-d})^f} - \sum_{i=1}^{n}(i^k + p)$$

Fig. 1 Mathematical Formula

(1) Sort the characters in the order from left to right as follows:

$$\underset{1}{-},\underset{2}{(},\underset{3}{a},\underset{4}{\sqrt{\ }},\underset{5}{x},\underset{6}{y},\underset{7}{c},\underset{8}{-},\underset{9}{+},\underset{10}{d},\underset{11}{b},\underset{12}{)},\underset{13}{y},\underset{14}{x},\underset{15}{f},\underset{16}{-},$$

$$\underset{17}{\sum},\underset{18}{i},\underset{19}{=},\underset{20}{1},\underset{21}{n},\underset{22}{(},\underset{23}{i},\underset{24}{k},\underset{25}{+},\underset{26}{p},\underset{27}{)}$$

(2) Look up the relevant characters of special character, according to the node relation format of digraph as follows:

Node 1：<1,3>，<1,2>，<1,16>；

Node 4：<4,7>，<4,12>；

Node 8：<8,10>；

Node 16：<16,17>；

Node 17：<17,18>，<17,21>，<17,22>；

（3）Look up the relevant characters of common character from left to right:

Node 2：<2,4>；Node 3：<3,5>，<3,6>，<3,9>；

Node 7：<7,8>；Node 9：<9,11>；

Node 11：<11,13>，<11,14>；Node12：<12,15>；

Node 18：<18,19>；Node 19：<19,20>；

Node 22：<22,23>；Node 23：<23,24>，<23,25>；

Node 25：<25,26>；Node 26：<26,27>；

The generated minimum arborescence is illustrated as **Fig. 2.**

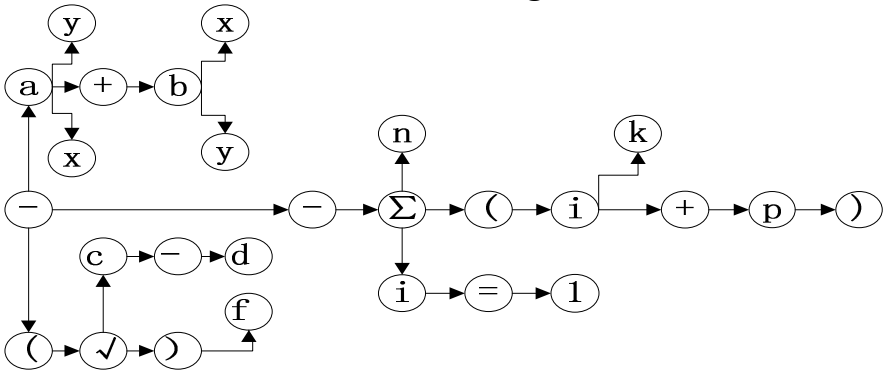

Fig. 2 Minimum Arborescence

Generating Ternary Tree

Minimum arborescence model can analyze the structure of mathematical formula accurately and manage the relation between two nodes, but can not handle the relations between child nodes. By switching the minimum arborescence model into ternary tree model, the position of nodes on each layer can be located. The minimum arborescence in **Fig. 2** switches into ternary tree model shown as **Fig. 3.**

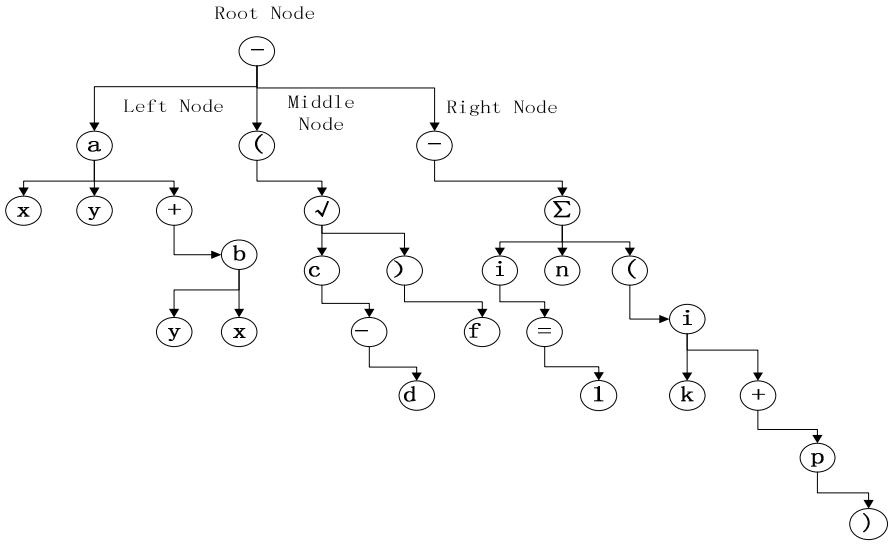

Fig. 3 Ternary Tree

Compared the ternary tree and minimum arborescence, we can find that the left node of root node "—" is "a", middle node is "(", right node is "—".

Take N as the root node, and L, M, R as the left subtree, middle subtree and right subtree of N respectively. There are four ways[8] in the depth-first traversal of a ternary tree: NLMR, LNMR, LMNR and LMRN order.

Generating MathML

W3C Mathematics Workgroup first put forward MathML[9,10]. MathML describes the structure and content of mathematical expression with XML, whose goal is to enable Web to serve, receive and process mathematical formula. MathML offers two marks describing mathematical formula: Content mark and Presentation mark. The former focuses on the content of expression, while the latter pays more attention to its display mode. The popular web browsers like Mozilla, Firefox and Netscape Navigator all support MathML directly. The Internet Explorer of Microsoft can also recognize MathML after installing the plug-in MathPLayer.

The structure of MathML is in the same NLMR order with ternary tree. From the structural analysis of 100 handwritten mathematical formula (including number, English capital and small letter, operator and so on) written by several experimenters, it turns out 88 correct structures and 12 wrong structures. The main elements causing mistakes are that two characters in joined-up writing are taken to be one character, and the combination recognition of structural body (like log, lim). Therefore, the method remains to be further improved, for instance, context semantic analysis will be the future directon of study.

Experiment

The recognition results of online handwritten mathematical formula shown in **Table 1** are conducted by the proposed method.

Table 1 Experiment Results

Type	Time	Correct	Accuracy(%)	Second Correction	Uncorrectable	Accuracy after Correction (%)
Up-Down Structure	200	176	88	24	0	100
Sector Structure	200	182	91	28	0	100
Radical Sign	200	170	85	26	4	98
Integral	200	177	88.5	10	13	93.5
Triangular Symbol	200	186	93	8	6	97
Complex Structure	200	164	82	21	15	92.5

The table shows that the recognition rate after the second correction reaches 92.5%. There are two main elements: two characters in joined-up writing are taken to be one character, and the combination recognition of structural body (like log, lim). Therefore, the method remains to be further improved. For instance, intelligent semantic analysis will be the future directon of study.

Conclusion

The paper offers a method to switch online handwritten mathematical formula into MathML, and first time put forward the idea that describing the spacial structure between characters by using minimum arborescence. Compared to the traditional base line and "Jing" font, it improves the accuracy of recognition in the structural analysis of nonstandard mathematical formula. As well, the proposed paper suggests that describing the spacial structure between characters with digraph model possesses portability, which can also be applied in the formula recognition of other subjects.

Acknowledgements

This work was supported by GRRC program of Gyeonggi province [(GRRC SUWON2013-B1) Cooperative CCTV Image Based Context-Aware Process Technology, and the Nature Science Foundation of Shandong Province (ZR2011FL014).

References

[1] Dolinsky J and Takagi H: Analysis and Modeling of Naturalness in Handwritten Characters. Neural Networks, IEEE Transaction on. Vol.20(2009) . p.1540-1553.
[2] Marcelo N. Kapp, Robert Sabourin and Patrick Maupin: A dynamic model selection strategy for support vector machine classifiers. Applied Soft Computing. Vol.12(2012).p.2550-2565.
[3] Zanibbi R and Blostein D: Recognizing mathematical expressions using tree transformation. IEEE Transactions on Pattern Analysis and Machine Intelligence.Vol.24(2002).p.1455-1467.
[4] Ba-Quy Vuong, Siu-Cheung Hui and Yulan He: Progressive structural analysis for dynamic recognition of on-line handwritten mathematical expressions. Pattern Recognition Letters. Vol.29(2008). p.647-655.
[5] Qin Yu-ping and Tang Ya-wei: Mathematical Formula Matching Algorithm Based on Binary Tree. Computer Science. Vol. 40（2013). p.251-252.
[6] ZHAI Xiao-yan : A Simple Algorithm for Finding the Minimum Arborescence in a Network. System Engineering. Vol. 20(2002). p.67-70.
[7] SUN Ling-yu and Leng Ming: Minimum Spanning Tree Algorithm of Weighted Directed Graph. COMPUTER ENGINEERING. Vol.36(2010). p.61-63.
[8] N. X. Zhang: Trinary tree structure and its implementation. Journal of Computer Research and Development.Vol. 1(1993). p.50-54.
[9] Timothy W. Cole: MathML in practice: issues and promise. Data Science Journal. Vol.5(2006). p.209-218.
[10] J.Francis and Wright: Interactive Mathematics via the Web using MathML. SIGSAM Bulletin. Vol.34(2000).

Advanced Materials Research Vols. 989-994 (2014) pp 2161-2164
© (2014) Trans Tech Publications, Switzerland
doi:10.4028/www.scientific.net/AMR.989-994.2161

Adaptive Bit Allocation Algorithm for OFDM System

Wei Wei[1, a], Wendong An[2,b]

[1]Xi'an University of Posts and Telecommunications, Xi'an, China

[2]Xi'an University of Posts and Telecommunications, Xi'an, China

[a]weigaozu@hotmail.com, [b] an3265976133@163.com

Keywords: OFDM; greedy algorithm; adaptive; bit Allocation.

Abstract. For the greedy algorithm required a large number of iterations, this paper proposed one adaptive bit allocation algorithm based on Hughes-Hartogs algorithm which was improved greedy algorithm .Under the constraint of bit error rate and data transmission rate, the algorithm first used the Chow algorithm to allocate some of the bits, and then used the greedy algorithm to allocate the remaining bits. When minimize the total power by this algorithm, the iterations of this algorithm were significantly less than the greedy algorithm. By computer simulation, the results showed that performance of this algorithm was very close to the greedy algorithm, and the number of this algorithm's iterations was 7.4%~34% of the greedy algorithm.

Introduction

In the Orthogonal Frequency Division Multiplexing (OFDM) system, each subchannel will also influence the channel fading, so each subchannel will has different transmission ability. Assuming that each subchannel using the same modulation and the system can work normally, the system parameters will be designed by the subchannel which has the worst transmission capacity, but the system resources will not be fully utilized. Utilize the subchannel which has good relative characteristics has a great significance, This needs adaptive modulation.

There are many kinds of adaptive algorithm, for example, Hughes-Hartogs algorithm[1], Chow algorithm[2]. Reference [3] proposed an improved greedy algorithm, but the improved part still needs a few iterative computation. Reference [4] points out severely frequency selective fading channel and in low SNR, you cannot use the Chow algorithm. Aiming at this defect, it proposed an improved algorithm to make up this defect. Reference [5] did a comparative analysis of the adaptive bit allocation algorithm, the optimal power allocation algorithm and suboptimal power allocation algorithm. It reached a conclusion that adaptive bit allocation technology can optimize capacity and the bit error rate of the system, and it's an effective algorithm. Reference [6] proposed an improved water filling algorithm, which is a suboptimal bit allocation algorithm, but this algorithm programming is more complex.

This paper aiming at the deficiencies that using the greedy algorithm to adaptively allocate bits needs many times of iteration[7]. Before entering the greedy algorithm, according to the characteristic of the channel, use the Chow algorithm to allocate some bits in advance, the remaining bits use the greedy algorithm to allocate.

Problem Model

Bit allocation has two standards: margin maximization criterion and rate maximization criterion[8]. This paper adopts margin maximization criterion, its optimal model is as follows:

Assuming that the number of subcarrier is N, the bits allocate in subcarrier are b_n, the power allocate in subcarrier is p_n. In the actual communication system, b_n is usually an integer. We need solve the problem that in a certain data rate and bit error rate, to make the transmission power of the OFDM system achieve the minimum. i.e.

$$\begin{cases} \min mize \sum_{n=1}^{N} p_n \\ s.t. \sum_{n=1}^{N} b_n = R \end{cases}, N = 1, 2, \cdots, N. b_n \in Z, b_n \geq 0 \tag{1}$$

Improved Greedy Algorithm

The Theoretical Basis of The Improved Greedy Algorithm. Assuming that there is Gauss noise in the channel, bandwidth is W, and its transmission function is $H(f)$. (power spectral density (PSD) is $N(f)$. At the same time, when the SNR $|H(f)|^2 / N(f)$ is approximately constant in the subchannel bandwidth, the channel bandwidth W can divided into $N = W / \Delta f$ subchannels, Δf is the subchannel bandwidth. And the signal's transmission power should meet

$$\int P(f) df \leq P_{av} \tag{2}$$

P_{av} is the average power.

Finally, through the transformation can obtained:

$$P(f) = \begin{cases} K - N(f) / |H(f)|^2, f \in W \\ 0, f \notin W \end{cases} \tag{3}$$

The physical meaning of the above formula: when the SNR $|H(f)|^2 / N(f)$ is low, the corresponding channel power is also low, and when the SNR is high, the channel power is also high.

Analysis of Greedy Algorithm. In this paper, the greedy algorithm is compared with the improved algorithm. Its steps are as follows:

(1) Let $b_n = 0, p_n = 0, n = 1, 2 \cdots, N.$

(2) Calculate the additional power Δp_n, when each sub carrier increase a bit.

(3) Select $n^* = \arg\min_{1 \leq n \leq N} \Delta p_n$, if $\sum_{n=1}^{N} b_n > R$,end. If not, let $b_{n^*} = b_{n^*} + 1, p_{n^*} = p_{n^*} + \Delta p_{n^*}$, return to (2).

$\{b_n, n = 1, 2, \cdots, N\}$ is number of bits for each subcarrier, $\{p_n, n = 1, 2, \cdots, N\}$ is transmission power for each subcarrier. Finally, the minimum transmission power is $P = \sum_{n=1}^{N} p_n$. Using the greedy algorithm, we can obtain the optimal solution. But when the greedy algorithm allocates a bit, it always needs one iteration. So with the increase of transmission rate, number of iterations needed by the algorithm will increase.

Analysis of Improved Greedy Algorithm. The basic idea of the improved greedy algorithm: before entering the greedy algorithm, according to the characteristic of the channel, use the Chow algorithm to allocate some bits in advance, we need calculate p_n (the transmission power of each subcarrier), b_n (the bits of each subcarrier). At the same time, we also need calculate R_1 (the total number of bits) and the energy that sends these bits required. The remaining bits R-R_1 use the greedy algorithm to allocate each subcarrier.

The Chow algorithm used as allocated in advance. Its steps are as follows:

(1) Estimation SNR of each subchannel;

(2) According to the formula:

$$\hat{b}_n = \log_2(1 + SNR(n) / (GAP + \gamma)) \tag{4}$$

To estimate number of bits for the each subcarrier, γ is the performance threshold;

(3) $\hat{b}_n$ round to b_n;

(4) Limit the value of b_n is $0, 1, 2, 4, 6, 8$ (related to the modulation sequence);

(5) Based on the formula, we can calculate the energy of each subcarrier with b_n bits.

$$p_n = (2^{b_n} - 1) / SNR(n) / GAP \tag{5}$$

GAP is an effective coordinating parameters.

The improved greedy algorithm's steps are as follows:

(1) Initialized by the Chow algorithm, we can get the initial b_n, p_n.

(2) Let b_n, p_n of the greedy algorithm is equal to the b_n, p_n which was obtained in (1).

(3) Calculate the additional power Δp_n, when each sub carrier increase a bit.

(4) Select $n^* = \arg\min_{1 \le n \le N} \Delta p_n$, if $\sum_{n=1}^{N} b_n > R$,end. If not, let $b_{n^*} = b_{n^*} + 1, p_{n^*} = p_{n^*} + \Delta p_{n^*}$, return to (3).

Simulation Results and Analysis

The simulation parameters: number of the subcarriers are $N = 64$, wireless channel is used for 3 path Rayleigh fading channel, channel gain vector are $\left[1 \;\; 1/e \;\; 1/e^2\right]$, the bit error rate is $BER = 10^{-4}$, and assuming that the channel state is not invariant in a OFDM symbol period. MQAM modulation can be used for BPSK, QPSK, 4QAM, 16QAM, 64QAM and 256QAM. This paper through two indicators which are iterative and transmission energy, to compare the greedy algorithm and the improved algorithm, thus get the performance comparison between two algorithms.

Figure 1 shows that this algorithm meets the expected effect. When the channel condition is bad, allocate a few bits; when the channel condition is good, allocate many bits. That is this improved algorithm is effective. Compared with Figure 2, each subcarrier's bits and transmission power between two algorithms are almost same, so can get the improved greedy algorithm and the greedy algorithm are very close in performance.

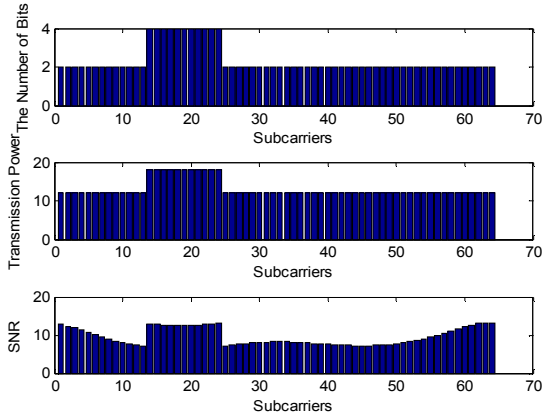

Figure 1. $R = 150$, the allocation results of the improved greedy algorithm.

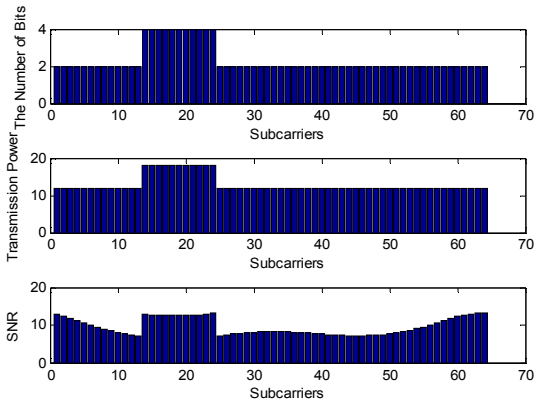

Figure 2. $R = 150$, the allocation results of the greedy algorithm.

Figure 3 is an iterative times comparison between the greedy algorithm and the improved greedy algorithm. It shows that the curves of two algorithm are almost coincide. With the increase of transmission rate, the number of bits which required modulation are also increase and the iterative times of two algorithms will also increase. But the iterative times of the greedy algorithm increase more than the iterative times of the improved greedy algorithm. When the transmission rate is 150, the iterative times of the improved greedy algorithm are the iterative times of the greedy algorithm 7.4%; When the transmission rate is 250, the iterative times of the improved greedy algorithm are the iterative times of the greedy algorithm 24.4%; When the transmission rate is 350, the iterative times of the improved greedy algorithm are the iterative times of the greedy algorithm 31.7%. Therefore the improved greedy algorithm reduces the number of iterations is obvious. Figure 4 is at different transmission rates, a transmission power comparison between the greedy algorithm and the improved greedy algorithm. When the number of iterations obviously reduced, the performance of the improved

greedy algorithm is very close to the greedy algorithm. At the same time, the realization of the improved greedy algorithm is also relatively simple.

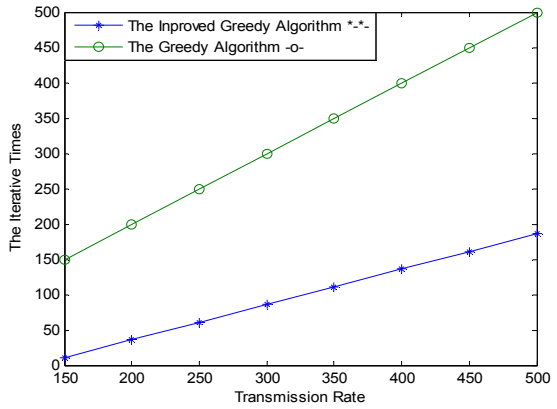

Figure 3. An iterative times comparison between two algorithms

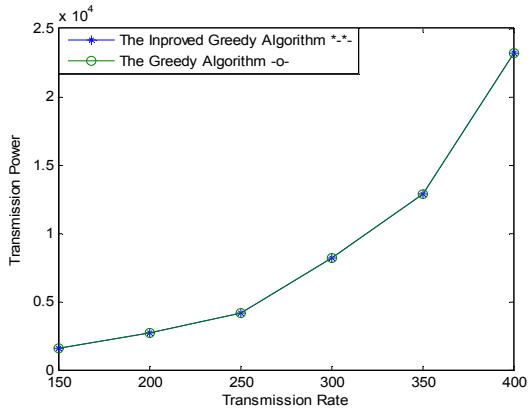

Figure 4. A transmission power comparison between two algorithms

Summary

Aiming at the greedy algorithm using adaptive bit allocation needs many times iteration in OFDM system, we propose an improved algorithm, which improving the initialization of the greedy algorithm and obviously reducing the iterative times of computation required. The simulation results show that, the iterative times of the improved greedy algorithm are obviously less than the greedy algorithm and its realization is simple, but the performance of improved greedy algorithm is very close to the greedy algorithm.

Acknowledgements

This research was supported by the scientific research fund of shaanxi provincial education department (Grant No. 12JK0541), all support is gratefully acknowledged.

References

[1] D. Hughes-Hartogs, Ensemble modem structure for imperfect transmission media: U.S, 4679227. 1987-07.

[2] Chow Peter S, John M Bingham, and John A C. A practical discrete multitone transceiver loading algorithm for data transmission over spectrally shaped channels. IEEE Trans. On Communications (S0090-6778), 1995, 43(2): 773-775.

[3] G. D. Yu, Z. Y. Zhang, and P. L. Qiu, Bit and Power Allocation Algorithm for OFDM System, Phil. Journal of Electronics & Information Technology, vol. 27, p. 1479-1482, 2005.

[4] L. Yang, and Y. A. Zhang, Analysis of Adaptive Loading Algorithms in Orthogonal Frequency Division Multiplexing Systems, Phil. Journal of System Simulation, vol. 21, p. 761-767, 2009.

[5] S. S. Zhai, Power Allocation over Frequency Selective Channel in OFDM System, Phil. Communications Technology, vol. 44, p. 19-23, 2011.

[6] L. Zhao, X. P. Sun, and H. L. Zhang, An Improved Water-filling Algorithm for Discrete Bit Allocation, Phil. Journal of Electronics & Information Technology, vol. 32, p. 638-642, 2010.

[7] Y. M. Wang, Key technology and application of OFDM. Beijing: China Machine Press, 2006.

[8] X. Wu, J. Zhang, and Z. K. Liu, Bit and power allocation algorithm based on preload in OFDM system, Phil. Journal of Harbin Institute of Technology, vol.44, p. 132-137, 2012.

Advanced Materials Research Vols. 989-994 (2014) pp 2165-2168
© (2014) Trans Tech Publications, Switzerland
doi:10.4028/www.scientific.net/AMR.989-994.2165

Stepped Cooling Control Model Based on Optimal Algorithm

Zhuwen Yan[a], Henan Bu[b], Gengsheng Ma[c] and Dianhua Zhang[d]

State Key Laboratory of Rolling and Automation, Northeastern University, Liaoning, China

[a]zhuwen19880301@163.com, [b]bhn_neu@126.com, [c]276737550@qq.com, [d]zdhua@mail.neu.edu.cn

Keywords: stepped cooling control, cooling capacity, flatness accuracy, temperature field, optimal algorithm

Abstract. A 1450mm cold rolling mill roll stepped cooling control technology has been studied. The basic principle of stepped cooling control has been analyzed. The important role of stepped cooling control in the control of thermal crown has been elaborated. In order to analyze impact of stepped cooling on the sectional shape of the strip, the roll under the influence of the cooling water temperature field has been established. The model of optimal cooling capacity in each segment has been established. The model has been successfully applied to a 1450mm cold rolling mill roll, and a good effect has been achieved.

Introduction

The traditional roll control is essentially to establish sub-cooling and cooling control model PID control cooling flow through the study of the impact on the shape and the corresponding heat transfer coefficient[1]. The traditional roll stage cooling PID control method has been unable to meet the high quality requirements of flatness control. In order to increase flatness accuracy, the gradient projection method has been adopted and the ploy of stepped cooling control has been optimized.

Definition of stepped cooling control

When the complex defects can not be eliminated by tilting, bending and shifting, the stepped cooling control can only be adopted to control flatness[2]. The measurement segment of stepped cooling is in correspondence with flatness measuring roller segment. Each cooling segment is composed of emulsion and control valve nozzle. The distribution of the transverse thermal expansion of the roll is changed By opening and closing the nozzle number and the injection quantity of the emulsion. Thereby the position of the corresponding strip elongation is changed. So the flatness is controlled.

Principle of stepped cooling control

Before strip enters into mill, the automatic flatness control system determines target flatness on basis of incoming conditions[3]. The various pre-set position and flatness control device is calculated. In rolling process, the flatness measurement systems continue to get the actual value of the strip-shaped plate. The actual flatness is compared with the target flatness. The deviation is the flatness adjustment error. The flatness adjustment error is used to identify flatness defects. Through the relevant mathematical model, the corresponding shape control means new settings are calculated. It is outputted to the device control system. The flatness loop control is performed.

In rolling process, pressure, tension and rolling speed can lead to warm anomalously in the direction of roll barrel length. The average diameter of the roll becomes larger. The roll shape is impacted. The changes of roll barrel flatness pass to rolled product.

The principle of stepped cooling control is to control thermal crown along the direction of roll barrel length by means of injecting roll coolant. Thermal crown of the rolls of each segment is

changed. The length of the strip corresponding to the elongation direction of the change on the segment is controlled. Ultimately purposes of strip flatness is improved.

Roll temperature field model

Roll heat transfer problems are three-dimensional heat transfer problems[4]. When the time factor is considered, it can be viewed as a four-dimensional problem[5]. In surface depth of roll, temperature cycle is changes vigorously[6]. In more than 99% of the portion of the roll, the temperature distribution is in the form of axial symmetry and fluctuations are small. So in roll temperature field research, the circumferential heat can be neglected. Three-dimensional problem is converted into a two-dimensional problem.

The relationship between rolling absorbed heat power and rolling exit temperature is:

$$N_{З} = B_i H_1 V_1 \rho c (T_1 - T_0) \tag{1}$$

Where, $N_{З}$ is the power absorbed heat rolling. B_i is nozzle open state, the central region and the edge portion of the nozzle of the nozzle area. T_1 is export rolling surface temperature. T_0 is entrance rolling surface temperature. ρ is strip density. c is strip specific heat capacity.

Roll pass this part of the heat of a thermal power is:

$$N_c = n \rho_c q \Delta T c_c \tag{2}$$

Where, N_c is coolant heat power transfer portion. n is the number of open nozzles. ρ_c is coolant density. q is single nozzle in the flow of coolant. ΔT is cooling fluid flowing into and out of the coolant temperature difference. c_c is coolant heat capacity.

Thermal diffusivity is

$$\alpha = k / cp \tag{3}$$

Where, k is thermal conductivity. c is specific heat capacity. p is density.

Two-dimensional heat conduction equations is:

$$\frac{\partial^2 \theta}{\partial x^2} + \frac{1}{r}\frac{\partial \theta}{\partial r} + \frac{\partial^2 \theta}{\partial r^2} = \frac{1}{\alpha}\frac{\partial \theta}{\partial t} \tag{4}$$

Where, θ is roll the internal temperature of each point. x is axial coordinate. r is radial coordinate. t is time. α is thermal diffusivity.

Optimum cooling capacity model

The objective function is:

$$\sum_{i=1}^{n} (Y_i - eff_i X_i)_i^2 \tag{5}$$

Where, Y_i residual flatness deviation. eff is efficacy coefficient. X_i is optimal cooling capacity

The gradient projection method is adopted to achieve the optimal cooling capacity.

Consider the problem

$$\begin{aligned} s.t.\ & Ax \geq b, \\ & Ex = e. \end{aligned} \tag{6}$$

where, $f(x)$ is differentiable function, A is $m \times n$ matrix, E is $l \times n$ matrix.

The basic idea of gradient projection method is from the practical point, searching along the feasible direction. When the iteration starting point within the feasible domain, search in the negative gradient direction. When the iteration starting point in some constraint boundary, the negative gradient is projected to nullspace of M, M is matrix structured by work constraints or row of partially work constraint gradient. It has been proved that such a projection is decreased feasible direction, and

then search along the projection direction. Therefore, Rosen gradient projection method is feasible direction method.

The computation steps of gradient projection method are as follows:

(1) Preset initial feasible point $x^{(1)}$, set $k=1$.

(2) In point $x^{(k)}$, disassemble A and b to $\begin{bmatrix} A_1 \\ A_2 \end{bmatrix}$, $\begin{bmatrix} b_1 \\ b_2 \end{bmatrix}$, make $A_1 x^{(k)} = b_1$, $A_2 x^{(k)} = b_2$.

(3) Set $M = \begin{bmatrix} A_1 \\ E \end{bmatrix}$, if M is null, make $P = I$ (unit matrix); Otherwise, make $P = I - M^T \left(MM^T \right)^{-1} M$.

(4) Set $d^{(k)} = -P\nabla f\left(x^{(k)}\right)$. If $d^{(k)} \neq 0$, turn to (6); If $d^{(k)} = 0$, turn to (5).

(5) If M is null, then stop calculating, get $x^{(k)}$; Otherwise, set $W = \left(MM^T \right)^{-1} M\nabla f\left(x^{(k)}\right) = \begin{bmatrix} u \\ v \end{bmatrix}$. If $u \geq 0$, stop calculating, $x^{(k)}$ is $K-T$ point; If u contains negative component, then select a negative component, such as u_j, to correct A_1, get rid of the row corresponds to u_j in A_1, back to (3).

(6) In order to find step $\lambda_{(k)}$, solve the following problem,: $\begin{cases} \min & f\left(x^{(k)} + \lambda d^{(k)}\right) \\ s.t. & 0 \leq \lambda \leq \lambda_{\max} \end{cases}$.

After getting $\lambda_{(k)}$, make $x^{(k+1)} = x^{(k)} + \lambda_k d^{(k)}$. Set $k := k+1$, back to (2).

Application results

The proposed stepped cooling control mathematical model has been successfully applied to a 1450mm five-stand cold rolling process control system. In order to verify its application results, the application results with stepped cooling control mathematical model is compared to the application results without stepped cooling control mathematical model. When the stepped cooling control mathematical model is not adopted, the deviation of strip flatness control is large. When the stepped cooling control mathematical model is adopted, the deviation of strip flatness control is decreased. Therefore, stepped cooling control mathematical model can increase flatness control accuracy.

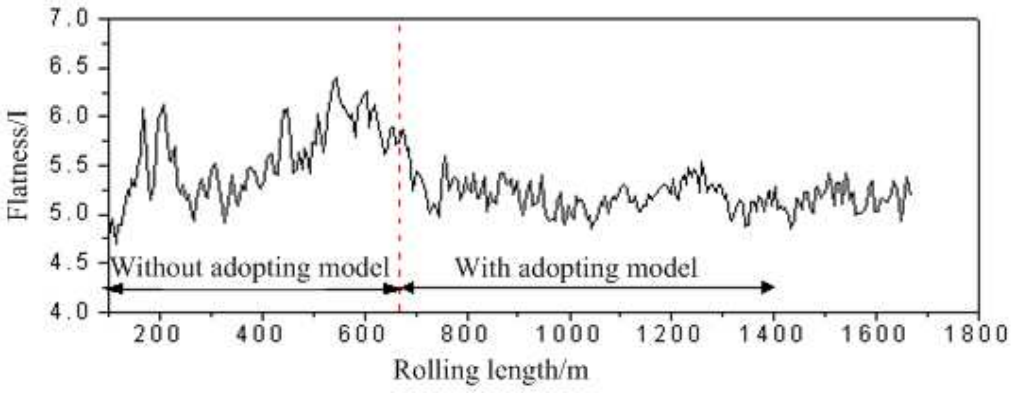

Fig.1 Strip flatness deviation comparing picture

In fig.1, when the stepped cooling control mathematical model is adopted, we can see that the flatness is good in strip. When the stepped cooling control mathematical model is adopted, we can see that it appears flatness defection.

Conclusions

(1) The impact of roll temperature to flatness is analyzed and the roll temperature field model is established.

(2) The optimum cooling capacity model mathematical model is established. The gradient projection method is adopted by the model to solve the optimal cooling capacity and the optimal cooling quality of model can decrease deviation of strip flatness control, and the flatness quality has been increased greatly.

Acknowledgements

This research was financially supported by National Natural Science Foundation of China (51074051).

References

[1] Liu En-yang, PENG Liang-gui, YUAN Guo, et al. Journal of Central South University, 2012, 19(5): 1341-1345.

[2] XIN Ya-juan, WANG Zhi-qiang, TIAN Zhe. Journal of Central South University, 2012 19(13): 709-714.

[3] YUAN Guo, LI Zhen-lei, LI Hai-jun, et al. Journal of Central South University, 2013 20(7): 1805-1811.

[4] Wang, Y. Q., Sun, F., Liu and J., Sun ea al. Chinese Journal of Mechanical Engineering, 2009, 22(2): 282-286.

[5] Borghesi M, G. Chiozzi., Proceeding of International Conference on Steel Rolling, Tokyo, 1980: 760-763.

[6] Remn-Min Guo. Moving Interface Problems in Manufacturing Heat Transfer, ASME Annual Meeting, Windter, 1993.

Advanced Materials Research Vols. 989-994 (2014) pp 2169-2172
© (2014) Trans Tech Publications, Switzerland
doi:10.4028/www.scientific.net/AMR.989-994.2169

Cluster center initialization parallel algorithm for K-Means algorithm

Bo Yan[1, a], Ye Zhang[2, b], Hongyi Su[3,c] and Hong Zheng[4,d]

[1]Beijing Institute of technology, Beijing, CN

[2]Beijing Institute of technology, Beijing, CN

[3]Beijing Institute of technology, Beijing, CN

[4]Beijing Institute of technology, Beijing, CN

[a]yanbo@bit.edu.cn, [b]zhangxiaoye@bit.edu.cn, [c]henrysu@bit.edu.cn, [d] hongzheng@bit.edu.cn

Keywords: K-Means, GPU, density, parallel.

Abstract. K-Means algorithm is a one of the most famous unsupervised clustering algorithm. It has many disadvantages, such as sensitivity to the initial clustering centers and computes all the data points multiple times when facing the increasing data volume. In order to overcome the above limitations, this paper proposes to make use of density idea to find k cluster centers by adjusting the threshold. Finally, we design and implementation of the K-Means algorithm on the modern Graphic Processing Unit (GPU). The ratio of distance between classes to distance within classes and speedup are used as evaluation criteria. The experiments indicate that the proposed algorithm significantly improves the stability and efficiency of K-Means algorithm.

Introduction

Cluster analysis is a statistical analysis method [1]. It seeks to partition a given data set into group based on specified features so that data points within a group are more similar to each other than the points in different groups. This algorithm is proposed in 1967 by MacQeen [2]. He put forward detailed steps of K-Means which had been proved by mathematical methods. The advantage of this algorithm is fast, simple and easy to implement. With in-depth study of the K-Means algorithm, some limitations are found including the interference of the initial cluster centers, converging to local optima easily and low efficacy when dealing with big data. To solve these problems, some researchers have proposed the improved heuristic algorithms. Yedla et al. [3] put forward an efficient way of assigning the data points to suitable clusters with reduced time complexity. Kang et al. [4] proposed the initial center selection method based on centrality sparsest isotropy (CSI). It can get ideal clustering results when time complexity permits. Lee et al. [5] proposed a new method. It is time-consuming, but can reduce the total clustering time by minimizing allocation and recalculation.

In view of the parallel algorithm under big data circumstance, Bai et al. [6] proposed a novel single instruction multiple data (SIMD) architecture processors (GPUs) based K-Means algorithm. Both the data objects assignment and k-centroids recalculation are offloaded to the GPU in parallel. Li et al. [7] use two different strategies for low-dimensional data sets and high-dimensional data sets respectively to make the best use of GPU computing horsepower. Kijsipongse [8] employed the dynamic load balancing to distribute workload equally on different GPUs installed in the clusters and improve the performance of the parallel K-Means at the inter-node level.

In face of problems existing in traditional K-Means algorithm and the explosive growth of data, we propose an improved GPU-based K-Means algorithm. We found *k* relatively dispersed samples as the initial cluster centers to increase the possibility of finding the global optimal solution. Combining GPU architecture platform we improved the efficiency of the algorithm.

The paper is organized as follows. Section 2 presents the related literature on CUDA and K-Means algorithm. Section 3 discusses the initial cluster centers selection algorithm and the GPU-based K-Means. The experimental results are provided in Section 4. Finally, Section 5 concludes the paper.

Related Technologies

Partition-based clustering algorithm. There are a lot of clustering algorithms in literature. K-mean algorithm is one of them. It is a process of grouping data objects into different clusters so that the data in each cluster are similar, yet different to the other clusters. According to the basic principles of the clustering algorithm, K-Means algorithm is provided as below:

1. *k* initial clustering centers are chooses from the dataset randomly.
2. For each point, calculate the distance to all clustering centers, and assign it to the nearest one.
3. Recalculate the new cluster centers by the average of all data that are assigned to the clusters.
4. Repeat step 2 and 3 until convergence.

CUDA Model. GPU is a specialized hardware initially used to accelerate calculations for 3D computer graphics. NVIDIA Corporation (NVIDIA) officially released with Compute Unified Device Architecture (CUDA) in 2007. CUDA is a programming of heterogeneous systems, i.e. the hybrid of CPU and GPU. The key point of CUDA model is to take CPU as the host to process logic and transactional program, while the GPU works as a coprocessor to process highly parallel procedures. Generally, CUDA is collectively composed of two processes: the serial process executing control function by CPU and the parallel process executing kernel function by GPU. GPU is not suitable to compute complex data structure while it can do a large amount of same pattern calculation.

CUDA computing core is composed of Stream Multiprocessors (SMs) with eight Stream Processors (SPs) in each SM. Five types of GPU memories are supplied to take advantage of the flexibility to develop efficient coding. This memory structure is directly exposed by the CUDA programming framework. In general, accessing the largest type of memory is flexible but slow, while accessing the smallest type of memory is restrictive but fast. Among the five types of memories, registers are fastest while global memory is slow. Shared memory is as fast as register, but it may have bank conflicts if the threads are badly assigned. The challenge in mapping a computing problem efficiently on a GPU through CUDA is to store frequently used data in the fastest memory.

Proposed methodology

The Selection of Initial Center Points. The traditional K-Means algorithm is sensitive to the initial cluster centers and liable to converge to a locally optimal solution. Meanwhile, the sensitivity to the outliers leads to inaccurate clustering results. So we propose a variable threshold based on density K-Means algorithm to solve this limitation. We use the Euclidean distance as the distance function. Specific procedures for the selection of initial cluster centers algorithm are as follows:

Data description: *k*, number of clusters; *t*, threshold, i.e. the selected radius; *w*, density, i.e. the number of data points within the circle radius *t*; *M*, the set of all points; *s*, a very small value.

1. Choose the distance between the first two points in *M* as *t*.
2. Choose the point $x_i (x_i \in M)$ which has the maximum density as the initial center point v_1. Calculate the density u_i within the *t* distance of all points in *M*, the mean density $\mathrm{w} = \sum_{i=1}^{n} u_i / n$ is taken as a point of reference density. Finally, all points in *M* whose distance to v_1 are less than *t* are deleted.
3. Choose the points in *M* that their distance between each other is beyond *t* as the initial centers. These points meet the condition that their distances to v_1 are $\mathrm{d2} = 2 \cdot \mathrm{t} + \mathrm{s}$ and their density are greater than *w*. The points in *M* which distance to v_1 is less than $\mathrm{d1} = 2 \cdot \mathrm{t}$ are deleted.
4. Set $\mathrm{d1} = 2 \cdot \mathrm{t} \cdot \mathrm{i}$ and $\mathrm{d2} = 2 \cdot \mathrm{t} \cdot \mathrm{i} + \mathrm{s}$ where *i* is the current number of loops. Repeat step (3) until *M* is empty. *i* is incremented by one in each iteration. Then go to step (5).
5. When *M* is empty, we can decide whether the number of center points is *k*. if yes, *k* center points are found. If it is larger than *k*, *t* is replaced by a bigger number and back to step (2). If it is smaller than *k*, *t* is replaced by a smaller number, then go back to step (2).

K-Means Algorithm Based On GPU. The main idea of the GPU-based K-Means algorithm is to make the data independent, and transfer the intensive calculation from host to device to improve performance. It can be seen that the main computational tasks are concentrated in step (2), (3) during

the whole algorithm process. Although these two steps will be performed many times, data points for each calculation are independent. Thus, they can be separated into two kernel functions and the data can be paralleled computed by the GPU core. In this way, we optimize the GPU-based K-Means algorithm in step (2) and step (3).

Currently, since a GPU has more than 100 processing cores, data points can be operated in threads within these cores. In each thread, distances from each data point to all the cluster centers are calculated. According to the distance, data points will be assigned to the nearest cluster. In CUDA architecture, shared memory is fast and has larger storage capacity than register. We can take the center points to shared memory to reduce the delay instead of those in the global memory. Meanwhile, k cluster centers can also be calculated by GPU, and each calculation is operated by a thread in CUDA. The new cluster centers are calculated by the arithmetic mean of all data points in original clusters. In GPU, if a large number of threads simultaneously access the same place in shared memory, it will lead to significant delay. Therefore we make the k threads access order position in shared memory simultaneously and add the data which belongs to this cluster. Then they access the next position orderly until all data points are accessed. When the new cluster centers in each cluster are calculated, the results will be sent to the global memory and wait for the next iteration.

Experimental results and discussion

Experimental setting and evaluation criteria. All experiments are implemented on MATLAB and Visual Studio. The test system is a PC with an Intel Core 6 Exon 2620 CPU. The GPU is an NVIDIA Tesla k20 with 2496 stream processors and CUDA is the 5.5 version.

In order to validate the accuracy and efficiency of our proposed algorithm, we select seven data sets (Iris, Libras, Yeast, etc.) from UCI database. To verify the accuracy and effectiveness of the improved algorithm, we test for 15 times on the traditional K-Means and improved algorithm. We adopt the ratio of between class distance to within class distance as the criteria. The within class distance is the average value of the distance between mean point and each object in the same cluster. The distance between classes is determined by the average value of distance between any two mean points of clusters. The smaller the ratio is, the better the clustering result is. Then the speedup is compared to test the effectiveness. The larger the speedup is, the better the efficiency is.

Analysis of results. This section implements the improved K-Means algorithm. The algorithm is tested in the seven datasets. Table 1 shows the experimental results for the initial center selection algorithm based on five datasets. It can be seen that the ratio of the proposed algorithm is less than that of the traditional K-means algorithm. Fig 1 gives the visual representation of results. In order to present clearly, we scale all values to range of 0-1. Clustering results of our algorithm are stable and overcome the limitations including selecting center points randomly in the K-Means algorithm. Seeing from the characteristics of data sets, our proposed algorithm has good performance on a variety of data sets and it is less affected by the number of samples and properties.

Table 1. The ratio of within class distance and between class distance

DataSet	# of records	# of attribute	K-Means	Improved K-Means
Iris	150	4	0.2503	0.1672
Libras	360	90	0.5063	0.3952
Yeast	1480	8	0.1262	0.0809
Synthetic_control	600	60	17.8281	13.778
Water-treatment	527	38	186.6086	154.0504

Table 2 and Figs 2 show that GPU can accelerate K-Means algorithm. The speedup ratio are different according to the size of data sets, data dimensions and presented characteristics. In the case of small size of data set, the speedup is not obvious due to the delay of GPU memory copies, starting up of device and data-completion.

Table 2. Running time comparison

DataSet	# of records	# of attribute	K-Means	Parallel K-Means	speedup
Gas	10756	128	2.487[s]	0.342[s]	7.272
Letter	20000	16	98.625[s]	5.831[s]	16.914
3D Road Network	40000	3	38.145[s]	1.721[s]	22.164
3D Road Network	70000	3	80.587[s]	2.663[s]	30.262
3D Road Network	434874	3	825.156[s]	21.571[s]	38.253

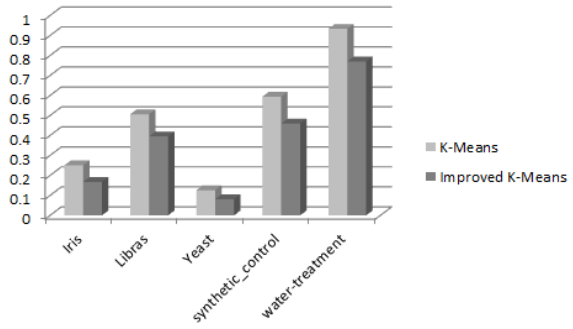

Fig. 1 The ratio of within class distance and between class distance

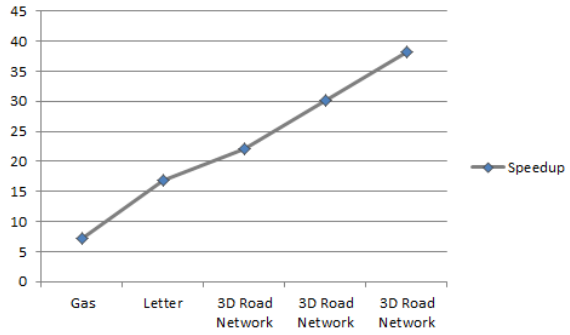

Fig. 2 Speedup with GPU

Summary

This paper analyzes the limitations of the traditional K-Means algorithm based on numerous studies by many researchers. Then the improved K-Means algorithm is proposed.

1. It can overcome the sensitive issues of initial centers selection and the impact of outlier points.
2. With the introduction of a parallel way, the K-Means algorithm is optimized on GPU.

According to tests, the proposed method can improve the stability and efficiency significantly on a single machine.

References

[1] Chunfeng Wang and Yongzheng Tang: submitted to Computer Engineering and Applications (2011), In Chinese

[2] J. MacQueen: Some methods for classification and analysis of multivariate observations. Proceedings of the Fifth Berkeley Symposium on Mathematics Statistics and Science. p. 281-297(1967)

[3] M. Yedla, S.R. Pathakota, T.M. Srinivasa: submitted to International Journal of Computer Science and Information Technologies (2010)

[4] P. Kang, S. Cho: K-means clustering seeds initialization based on centrality, sparsity, and isotropy. Proc of the 10th International Conference on Intelligent Data Engineering and Automated Learning Berlin: Springer. p. 109-117(2009)

[5] L.E.E. WonHee, S.S. Lee, A.N. Dong-Un: submitted to IEICE TRANSACTIONS ON INFORMATION AND SYSTEMS (2013)

[6] Hongtao Bai, Lili He, et al: K-Means on commodity gpus with cuda. Computer Science and Information Engineering. 2009 WRI World Congress on IEEE. p. 651-655 (2009)

[7] You Li, Kaiyong Zhao, et al: submitted to Journal of Computer and System Sciences (2013)

[8] E. Kijsipongse: Dynamic load balancing on GPU clusters for large-scale K-Means clustering. Computer Science and Software Engineering. p. 346-350(2012)

Advanced Materials Research Vols. 989-994 (2014) pp 2173-2178
© (2014) Trans Tech Publications, Switzerland
doi:10.4028/www.scientific.net/AMR.989-994.2173

Study for embedded colony algorithm based on morphological technology

Keyi Chen[1,a], Xiaoyue Zheng[1,b] , Hui Yu[1,c]

[1] Key Laboratory of Biomedical Detection & Instruments in Tianjin University, China

[a]email:henry14@tju.edu.cn, [b] sunset@eyou.com, [c]email: yuhui@tju.edu.cn.

Keywords: Image segmentation; Iterative erosion; Embedded system; OPENCV

Abstract. The fast image processing based on iterative erosion principle can complete separation of colony image of adhesion target quickly. This algorithm is composed of local threshold method of image binarization; the morphological processing, analyzing; removing the edge based on Hough Transform and using improved iterative erosion algorithm to adhesion target segmentation and counting. The algorithm has scale invariance and self-adaption for recognition different size colony target. The conditional expansion algorithm designed in the paper can effectively modify the count mistakes which are caused by fragments formed by the segmentation of large size targets in the iterative and erosion processes. The algorithm has been applied in portable colony counting instrument on ARM11 embedded platform. Twenty heterotrophic bacterial samples have been tested in experiments. The results show that this algorithm can realize the image segmentation rapidly and effectively and the time of analysis is less than 2 seconds. The images edge detection rate can reach 100%. The detection accuracy can get the requirements of GB 4789.2-2010 and achieve deviation of 3% in colonies' total number less than 300CFU.The applied of algorithm is widely in the similar particle image analysis system.

Introduction

With the development of image analysis technology , automated analysis of all kinds of images as cells and plant seeds has become study focuses in recent years[1-2]. The detection of colony amount is a critical health index in agriculture, food , medicine and health industries. In domestic area, the colony detection currently still relies on simple manual detection. While most of the automated counters in market are running on desk computers, it's still difficult to reach real time and portability. It's a development trend to explore a portable detector by applying ARM platform combined with embedded technology. As identifying and counting colony individuals both depend on colony image segmentation, the problem of which lies in the difficulty caused by colony adhesion, it's also the core issue supposed to be solved in the development of automated analysis system.

The task of colony image segmentation is to mark and locate the target as well as the background based on image priori knowledge and separate it from background or phony targets[3-5]. The methods of colony image segmentation at home and in abroad generally adopted are threshold comparison, clustering analysis and morphologic segmentation etc[6-8]. Due to the elaboration and complexity of traditional colony image segmentation algorithm, it is hard to be applied in an embedded and automated analysis system. We studies about extracting image edges with a comprehensive usage of Hough Transform and complete image segmentation through combing improved iterative erosion algorithm of conditional expansion and extreme erosion, meanwhile realizing high counting accuracy with programming optimization on the basis of this algorithm design.

Material and method

A Image binarization and edge detection

We complete image binarization and edge detection firstly. Image binarization usually takes threshold segmentation method. To choose the segmentation method and threshold both are based on the analysis of image grayscale distribution[9-10]. There should be morphologic 'closing' settlement

after the threshold segmentation to bridge narrow gaps and spindly ditch, remove small holes and fill up the contour fracture. This operation is defined as

$$A \bullet B=(A \oplus B) \ominus B \quad (1)$$

A and B respectively stands for target image and the structural element.

We use Hough Transform to detect the binary image's edge. The Hough Transform takes advantage of the whole image to link edge pixels of the target as to form a closed boundary of target region or directly detect the targets of known shape among images. Image edges in the paper are normally known as circle, so Hough Transform is suitable for edge detection[11].

B Iterative erosion segmentation

Iterative erosion algorithm consists of two basic algorithm operators in mathematic morphology:

erosion and expansion, and is built upon conditional expansion and extreme erosion that can quickly cluster and segment images.

Conditional expansion is a type of limited expansion, usually constrained in a limited set X within which the expansion is conducted like Eq.2.

$$f'=(f \oplus b) \cap X \quad (2)$$

f indicates the structural element and b indicates the expansion template.

Extreme erosion refers to a repeated erosion of one target till it disappears and to keep the result before last erosion. This result is regarded as a target seed:

$$f_k= f \ominus kb \quad (3)$$

b refers to the erosion template while k to the erosion times. The final seed point of the target g_k is an element in f_k..

In iterative erosion algorithm, extreme erosion is followed with conditional expansion every time. The target seed will be got by comparing the image now and before latest erosion and expansion.

Taking the twice iterative erosion as example, as shown in Fig.1, the steps of iterative erosion is expressed as below:

Step1. Erosion

$$f_1= f \ominus b \quad (4)$$

As in Fig.1a, image template used for erosion is shown in Fig.1b with a result after erosion indicated in Fig.1c

Step2. Conditional expansion

$$U_1=(f_1 \oplus b) \cap X \quad (5)$$

Use the template to expanse the erosion result. Fig.1d is what it is like after expansion through template b

Step3. Deduction

$$g_1=U_1 - f_1 \quad (6)$$

Deduct the once erosion and expansion result from the original image to get a target seed point. Two seed points are completed by deducting Fig.1d from Fig.1a. Then follows the steps above.

Step4. End

$$f \ominus 3b = \Phi \quad (7)$$

The algorithm ends when the three times erosion is a null set and erosion of twice is also a target seed point.

Step5. A union set of multiple targets in an image is the final erosion target set g.

$$g=g_1 \cup g_2 \cup f_2 \quad (8)$$

f refers to the original image element, f_k stands for the erosion result of k^{th} time. b refers to the algorithm template while U_k indicates expansion result of k^{th} time. g_k stands for the k^{th} seed points and g for the set of final seed points.

The iterative erosion algorithm not only can segment adhesive targets effectively, but also reduce the errors from different settings of initial points to accomplish precise and quick segmentation. As the target shapes are unlikely to be standard convex set, the image obtained after the iterative erosion contains both colony seed points that are completely corroded and some pieces corroded from larger size colony. This will lead to a repeat count of the same colony and impact the accuracy. In order to

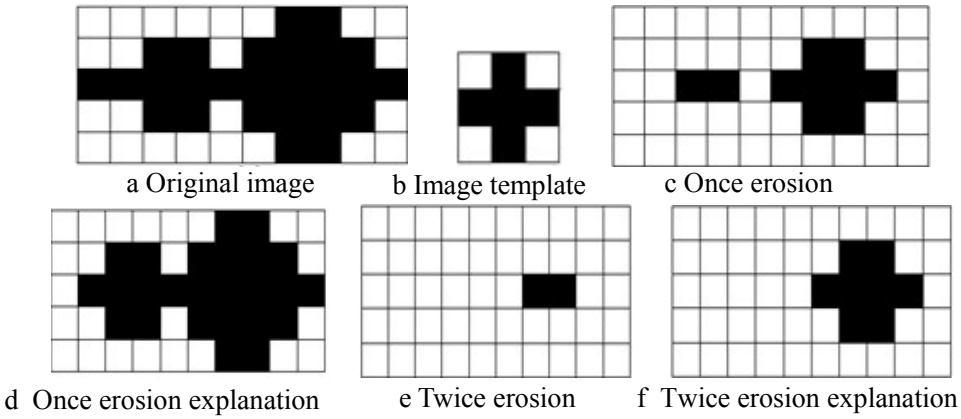

Figure.1 The diagram of twice iteration erosion

eliminate these pieces, the iterative erosion algorithm needs to improve as the conducting several conditional expansion toward the result after erosion is finished so that the pieces can be adhered as much as possible.

Result and discussion

To test the actual effect of automated and fast segmentation of iterative erosion algorithm, OPENCV computer vision is used on the basis of AMD 2.9GHz，2GB computer to develop the embedded core intelligent counting algorithm of colony based on Windows CE6.0. A wild-field infrared CCD camera is adopted as video collection device to test the accuracy of segmentation algorithm via comparison between automated counting result from this algorithm and manual counting result.

The experiment sample comes from many monitoring points of industrial wastewater in recycle stations in Tianjing, Qiqihaer, Mudan rivers. Taking the national standard testing method--common nutrition agar poured into flat petri dish for colony vaccination counting[12]. The automated segmentation counting algorithms of colony images include steps like image preprocessing, threshold segmentation, petri dish edge removing, image segmentation and colony marking. The procedures are indicated in Fig.2. The median filter parameter is set as 3, while Gaussian Filter size as 5 and the processing result is shown as Fig.3c.

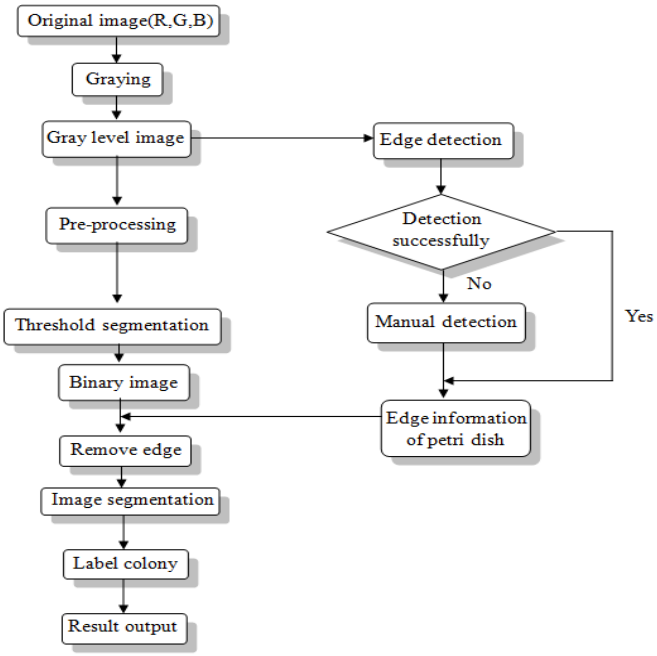

Figure.2 The flowchart of intelligent bacterial colony counting algorithm

a Original image b Gray level image c Image of filtering

Figure.3 Image grayscale and preprocessing

Fig.4 shows that in the histogram distribution of image gray, the bimodal trend is not obvious so partial threshold segmentation is the best.

Select appropriate threshold T for partial threshold binarization of the image. Taking the average value of pixel gray in the counting window of window template with moderate offset (set it 10 according to experiment verification) as the center pixel threshold of this window. Processes image is shown in Fig.5a. An operation of morphologic 'closing' is made after image binarization to fill up 'cracks' and 'holes' that occurred in larger size colony in the image, effect as Fig.5b shows. Choose erosion and expansion templates to treat the image with improved iterative erosion, erosion effect as Fig.5c indicates.

Detect the edge of petri dish based on Hough Transform principle and the effect is presented in Fig.6a.Label the image according to recursion notation with the result expressed in Fig.6b. Invoke the search function to label and search. As search is finished, feature points in the same connected domain are saved in the same array to complete colony counting.

12 colony images of the same size are detected for the edge and is compared to the actual circle center and radius of the petri dish. Edge detection success rate reached 100% with detection error of circle center location and radius size of the petri dish controlled within 3 pixels (0.6%). A sound effect is indicated in Table 1.

The algorithm in this paper is used for massive experiment of automated counting of colony images, which are compared with the result of traditional manual counting and the outcome is expressed in Table 2. What needs to be illustrated is that the manual counting result we selected came

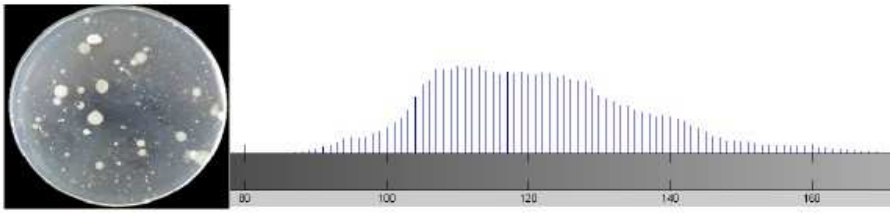

Figure.4 Colony target area histogram

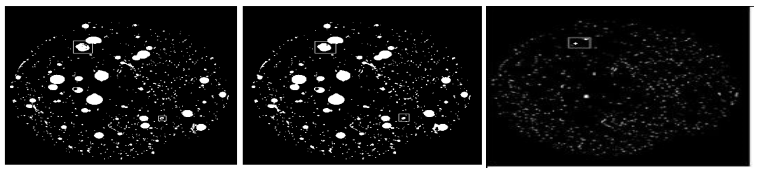

a Threshold segmentation b 'Close' processing c Iterative erosion

Figure.5 Image segmentation

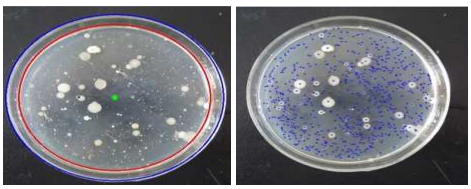

a Hough edge b Target object detection

Figure.6 Image detection

Table 1 Automatic edge detection results comparison

Image NO.	Edge detected	Circle center location	Radius	Image NO.	Edge detected	Circle center location	Radius
1	Yes	Accurate	Accurate	7	Yes	Accurate	Accurate
2	Yes	2 pixels above	3 pixels larger	8	Yes	3 pixels right	3 pixels larger
3	Yes	Accurate	Accurate	9	Yes	2 pixels left	3 pixels larger
4	Yes	Accurate	Accurate	10	Yes	Accurate	Accurate
5	Yes	3 pixels left	2 pixels larger	11	Yes	Accurate	Accurate
6	Yes	Accurate	Accurate	12	Yes	Accurate	Accurate

Table 2 Heterotrophic bacteria samples of artificial counting and automatic counting results comparison

Sample No.	Manual counting result	Automated counting result	Absolute Error	Sample No.	Manual counting result	Automated counting result	Absolute error
1	45	47	4.4%	11	302	309	2.3%
2	59	58	1.7%	12	336	317	5.7%
3	96	93	3.1%	13	345	367	6.4%
4	129	125	3.1%	14	391	415	6.1%
5	141	145	3.5%	15	464	445	4.1%
6	190	197	3.7%	16	545	506	7.2%
7	215	224	4.2%	17	641	693	8.1%
8	236	233	1.3%	18	731	661	9.6%
9	277	290	4.7%	19	802	876	9.2%
10	294	282	4.1%	20	986	907	8.0%

from the average value of the same sample counted by 3 detectors respectively and the error of three manual counting is below 10%.

From Table 2, the average error between automated counting and manual counting is within 6 % with 9.6% as most and 1.3% least. Among them, sample colony less than 300 is below error of 5% and the average error is 3.0% while the average error of colony more than 300 is 7.3%.

In the perspective of speed, this algorithm of automated counting based on desk computer can finish counting 300 colonies in 500 milliseconds. If the algorithm is transplanted to the core of embedded system of Windows CE 6.0 for automated counting, the speed counting 300 is less than 2 seconds.

Conclusion

Traditional image segmentation algorithm such as wavelet and neural network has involved a great deal of floating-point arithmetic that is highly complicated and time consuming. The iterative erosion algorithm studied here, by graying the image collected, segmented the threshold of the image with partial threshold method. It used multiple iterative erosion algorithm for segmentation of adhesive targets based on Hough Transform to remove the image edge. Finally, recursion notation is adopted to label the connected domain and accomplish target counting. As this algorithm is a massive logic algebraic calculation (mainly location comparison and evaluation) on the basis of image binarization, it calculates less and quite suits for operation on embedded instrument terminal with limited calculation capability. The previous experiment result indicated that this algorithm is able to complete fast image segmentation while ensuring the accuracy. It boasts advantages of speed, ease and accuracy on colony image segmentation and automated labeling and counting of images and the counting result is free from the influence of colony pattern, size and vaccination method[13]. In addition, this algorithm is also widely applied in automated counting instrument of other microbes with a promising future.

Acknowledgement

This work was financially supported by the National Natural Science Foundation of China (81201148)

References

[1] Wang Weixing, Wang Zizhou. Study of Colony Image Segmentation Algorithm Based on Wavelet Transform and Watershed Transform[J]. Journal of Chongqing University of Posts and Telecommunications (Natural Science Edition): 2008, 20(1): 104-107.
[2] Xie Jiezhen, Luo Tingwei, Dai Junwei, et al. Algorithm for Automatic Recognition of Red Tide Algal Images Captured by Flow Cytometry[J]. Computer science: 2013,40(7):293-296
[3] Aggarwal N, Karl W C. Line Detection in Images through Regularized Hough Transform[J]. IEEE Transactions on Image Processing. 2006,15(3): 582-591.
[4] Faur D, Gavar I, Datcu M. Salient Remote Sensing Image Segmentation Based on Rate-distortion Measure[J]. Geoscience and Remote Sensing Letters, IEEE. 2009,6(4):855-859
[5] Zhou Z F, Chao J. Image Demonizing Algorithm via Doubly Bilateral Filtering[C]//Information Engineering and Computer Science, Chinese Academic Science. Wuhan，China: IEEE，2009: 1-4
[6] Zhou Z F, Chao J. Image Demonizing Algorithm via Doubly Bilateral Filtering[C]. Information Engineering and Computer Science，Chinese Academic Science. Wuhan，China: IEEE，2009: 1-4
[7] Sun Chen, Wang Xiaonian, Liu Jia, et al. Tracking Multiple Objects with Generalized Hough Transform Based Position Estimation[J]. Chinese Journal of Stereology and Image Analysis. 2012, 17(1):1-11.
[8] Zhao Hui, Lin Chenglong, Tang Zhaojing. Fast Thresholding Segmentation Method Based on Peak Clustering Tendency Test for Noisy Image[J]. Signal Processing. 2009, 25(11): 1666-1674.
[9] Duquenoy E，Taleb-Ahmed A. Applying the Hough Transform Pseudo-linearity Property to Improve Computing speed[J]. Pattern Recognition Letters，2006，27(16) 1893-1904.
[10] Shi Weiren, Fang Li, Chen Shuhan. Algorithm for Image Binarization Based on Improved Otsu and Niblack[J]. World Sci-tech, 2013, 35(3):395-396
[11] Jiao Shengxi, Xiao Dejun, Kan Yifan. The Application Research of Hough Transform Algorithm on Circle Center Vision Positioning[J]. Science Technology and Engineering, 2013,13(14): 4089-4093
[12] 2010, GB4789 2. National Food Safety Standard, Food Microbiological Examination: Aerobic Plate Count[S].
[13] Zheng Xiaoyue. Design and Implement of Portable Intelligent Colony Counting System[D]. Tianjin: Tianjin University,2012:1-14

Advanced Materials Research Vols. 989-994 (2014) pp 2179-2183
© (2014) Trans Tech Publications, Switzerland
doi:10.4028/www.scientific.net/AMR.989-994.2179

A Semantic Retrieval Method Based on Ontology[1]

Qi Shen, Meng Zhang

School of Software EngineeringBeijing University of Technology, Beijing, China

shenq@bjtu.edu.cn, zhqmflag-2005@163.com

Keywords: ontology; concept similarity; weight; semantic expansion.

Abstract. Semantic retrieval method stands at the crossroads between Natural Language Processing and Machine Intelligent. This paper makes analysis on the semantic search method and research on concept similarity algorithm, and discusses the factor of weight's influence on concept similarity as well. On this basis, this paper proposed a new semantic search method based on ontology, and apply it to the tourism information retrieval, which intellectualized tourism information retrieval service.

1. Introduction

With the rapid development of Internet and mobile communication technology, Web has become a source of global information, how to find the needed information quickly and accurately from the vast information resources becomes a difficult problem for the user. The traditional information retrieval method provided to the users is matching search according to the keywords input by users. But in majority of cases, it is difficult to understand users' real purpose by these simple keywords matching search which leading to the low accuracy of current information retrieval.

Some experts abroad have conducted practical operation based on ontology, such as the Ontoseek directory system which retrievaling based on content, it integrates the product tree structure and online yellow pages. It is said that formal ability and body content matching mechanism are combined, and the ontology and database dictionary together, provide the user a can input natural language, and then into the domain ontology vocabulary, semantic retrieval system[1]. We can learn from Ontoseek pages in the system, the relationship between the concept of vocabulary and vocabulary which is not subject to any constraints, so the relationship between the vocabulary may not play any role, therefore will occur the retrieved results are not required by the user. Tourism yellow page service system at present, such as "Ctrip", "road ox net", in the search for a keyword input by the user information only for the simple matching words, do not understand the user input information on the semantics, also cannot be well retrieved information the user really need. Therefore, must the information retrieval from the existing keyword matching level to understand the knowledge level, semantic level to the information and expression based on them, so as to design a user can understand the semantic information retrieval model[2].

2. The Semantic Search Method based on Ontology

The basic idea of semantic retrieval algorithms extend is that through calculating semantic similarity of the input keyword to get a similarity value and then add the concept of greater than the threshold value to form a new set as new keyword to retrieval[3].

A. The Concept Similarity

Concept similarity refers to the semantic closeness of two concepts. Under the support of Ontology, there are three models to calculating the conceptual similarity as following:

1) Distance Model

Constructed ontology forms tree structure. With the ade of this structure, distance model matches the keyword to the corresponding nodes in the tree body of ontology[3]. The similarity between the two concepts is measured by the distance between two nodes of the tree. For simpicity on practice,

it adopts a simple calculation: that takes the distance between every two nodes in the tree body of ontology having the same length, quantize as 1 for example. Therefore the shortest distance of two nodes on the ontology tree equals to the semantic distance of these two concepts[4]. The concept similarity is calculated as follows:

$$Similar(x_1, x_2) = \frac{2 \times (Maxlen - 1) - Min}{2 \times (Maxlen - 1)} \tag{1}$$

Wherein: MaxLen refers to the depth of the ontology tree, Min refers to the shortest distance between the concept nodes x_1 and x_2. Obviously the above formula is very simple, and the very conceptual similarity is not precise.

2) Information Quantity Model

The quantity of information possessed by the conceptural tree nodes refers to the capacity of the concept content. The greater intersection of two concepts nodes contained on content the higher semantic similarity between them is, on the contrary lower similarity[5]. In the ontology tree structure, each node concepts are seen as inherited from its parent node, so each node in the tree can be seen containing the approximately equivalent quantity of information as their parent nodes. Therefore, the extent of the similarity of any two concepts in the ontology tree nodes can be replaced by caculating the capacity of its respective closenest parent nodes[6]. The fomular of calculating information quantity owned by the concept nodes:

$$p(x) = \frac{f}{\mathrm{m}} \tag{2}$$

$$DC(x) = -\log[\mathrm{p}(x)] \tag{3}$$

Among them, F represents the number of x appeared in training resources. M represents the total number of concepts in training resources. p (x) represents to the probility of node concept x appeared in the constructed ontology repositories; DC (x) represents carrying out processing log on the probality of the node concept appeared in the ontology repositories. Based on the quantity of information contained by the concept node, revealed the following formular about the concept similarity in the ontology tree structure:

$$Similar(x_1, x_2) = \frac{2 \times DC[Ancestor(x_1, x_2)]}{DC(x_1) + DC(x_2)} \tag{4}$$

Wherein: $Ancestor(x_1, x_2)$ is the information quantity contained by the parent concept nodes nerest to concept nodes x_1 and x_2 in the ontology tree structure.

3)Property Model

In the process of comparing the similarity or closeness between two things, it is typical to analize their properties or characteristics[7]. The similarity of node concept in the property model based on the concept node can be calculated as follows:

$$Similar(x_1, x_2) = f(x_1 \cap x_2) - f(x_1 - x_2) - f(x_2 - x_1) \tag{5}$$

Wherein: $x_1 \cap x_2$ said the intercecton of properties between node concept x_1 and x_2, the $x_1 - x_2$ represents the number of properties attribute to node concept x1 while are not included in the node concept x_2, $x_2 - x_1$ means the number of properties attibute to node concept x_2 while are not included in the node concept x_1.

B. Weight

Weight refers to the value given to the distance between the connected concept nodes. The size of the given weight can impact the concept similarity; this paper makes analysis on three major factors that affecting the size of weight as following:

1) Property Type

The value of weight given to the distance connected concept nodes holding different type of properties in the ontology tree structure should be different. If the property of the concept node is synonymous, such as in the field of tourism the ontology properties of two node concpts connected by "SynonymsIs" is synonym, so the weight value given to the synonyms should be higher than the weight of the other several types of properties weights. Therefore, according to common sense, the weight given to the edges with "inheritance" property is usually higher than that given to "whole-part relationship" poperties. So ultimately formed the relationship between property types and weights:

$$weight(x,y)=\begin{cases}1, type(x,y)=SynonymsIs;\\ 0.5, type(x,y)=IsExtend;\\ 0.3, type(x,y)=IsPartOf;\end{cases} \tag{6}$$

Weight(x, y) refers to the weight given to the edge containing certain type of property formed by the node concept x and its parent node y. The size of the value in formula (6) is defined by the ontology builder. These people all have a deep understanding on the concept and terminology of this field. The weight caculating formula reflects the relationship between the property type and size of the weights.

2) The Depth of Edge

Nearer to the leaf, the nodes contain more detailed information. On the reverse, node in the tree root represents less specific information. So, the size of the weight given to the edge is closely related to its level in the tree structure. This hierarchy represents the depth of the edge. Therefore, it is concluded the relationship between the depth of the edge and the weight:

$$weight(x,y)=(\frac{1}{2^{depth(y)}}+\frac{1}{2^{depth(y)-1}}+...+\frac{1}{2}+1)=\sum_{n=0}^{depth(y)}\frac{1}{2^n} \tag{7}$$

Among them, $depth(y)$ refers to the depth of concept node y in the tree. Formula (7) well embodies the relationship between depth of ontology tree edges and the size of weight: the size of weight given to the edge is directly proportional to the depth of nodes in the tree.

3) The Intersection of Properties

For the concept nodes in one edge with certain property, the more same properties they contained shows the more common characters they have, therefore the two concepts are more similar. The weight given to the edge connected by the two concepts node through the property also should be bigger. As a result, the relationship between the sizes of intersection set of two concept nodes' properties and the weight:

$$weight(x,y)=\frac{count(A\text{ssemble(x)}\cap A\text{ssemble(y)})}{count(A\text{ssemble}(x)\cup A\text{ssemble}(y))} \tag{8}$$

Assemble(x) and Assemble(y) are on behalf of the property set of concept node x and property set of concept node y; $A\text{ssemble(x)}\cap A\text{ssemble(y)}$ are on behalf of the properties intersection of concept nodes x and concept node y; $A\text{ssemble(x)}\cup A\text{ssemble(y)}$ are on behalf of the properties union of concept nodes x and concept node y; and count () function is on behalf of the number of properties in the relative property set.

C. Semantic Expansion

Through analysis of the concept similarity in the ontology tree structure, and several factors affecting the weight as well we proposed the improved semantic expantion retreval algorithm. The distance formua inserted weights asfollowing:

$$Distance(a,b)=N[a,Ancestor(a,b)]+N[b,Ancestor(a,b)] \tag{9}$$

$$N[b,Ancestor(a,b)]=\sum_{x\in path(a,Ancestor(a,b))} Distance(x,Parent(x)) \tag{10}$$

$$Distance(x,Parent(x))=\frac{\alpha}{weight(x,Parent(x))}-\alpha \tag{11}$$

$Ancestor(a,b)$ represents the nearest common ancestor node of concept node a and concept node b in the tree structure; $path(a,b)$ refers to the set formed by all the concept nodes in the shortest path between concept node a and concept node b of the tree stucture in the field of ontology. α is an adjustable factor. Formular (11) represents the distance between the child node and the parent node. Thus, under the condition of knowing the distance between arbitrary two nodes in the domain of ontology tree structure, we concluded the similarity calculation formula between any two concepts:

$$Similar(a,b)=\frac{\theta}{Distance(a,b)+\theta} \tag{12}$$

θ is an adjustable parameter. The formula shows the relation between arbitary two ontology semantic similarity and the two concept nodes: When $Distance(a,b)=0$, indicating that the value of the denominator is small, but the degree of similarity is greater, so the concept node a is similar to concept nodes b. The maximum value of concept similarity is up to 1; then when $Distance(a,b)=\infty$, the value of the denominator is large, the value of similarity is very small, so the concept node a and node b hardly have any relation, the minimum value of concept similarity is down to 0.

Formula (12) shows that the value of the concept similarity forms a closed interval from 0 to 1, in this article we set the threshold as 0.7, when the value of the concept similarity is greater than 0.7, the similarity of the two concepts can be considered relatively high, and then extend this concept into a more comprehensive, updated search term

3. Application in Tourism

The proposed retrieval method in this paper is applied to the Beijing tourism resources retrieval, all experimental data are retrieved from the ontology library, the library is artificialy classified first, and then taking use of reptiles tools to crawling tourism data from the Internet. the data in the repository is web data captured through a web crawler. To facilitate the calculating results, we set the amount of resources of each classified information to 1000, and relative resources for retrieving to 100. For example: we set a total of 1,000 hotel information resources, and for those near the Beijing University of Technology are100. Thus retrieve information about the following three statistics, namely: to retrieve the bus information, retrieve hotels near the attractions, retrieve sites nearby attractions.

Retrieval results shows that there are 82 relative resources about No. 52 bus, 144 were retrieved. The number of relative hotels near Beijing University of Technology is 85, 130 were retrieved. The number of Attractions near Tiananmen is 93, 155 were retrieved. The charter below shows the recall ratio and precion ratio between the retrieval method employed by the Ctrip and semantic retrieval method:

Table 1 Semantic search method compare with Ctrip counterpart

Retrieval System	Sort	Bus inquiries	Attractions near the hotel	Attrations nearby station inquiry
Ctrip	Recall ratio	45%	55%	50%
	Precision ratio	30%	50%	40%
Semantic Retrieval	Recall ratio	82%	85%	93%
	Precision ratio	57%	65%	60%

On both recall ratio and precision ratio, the semantic retrieval method proposed in this paper is higher than the trational tourist website represented by Ctrip. From data displayed in the above chart

we can drawn a conclusion that with the support of ontology technology, both the recall ratio and precision ratio are improved.

4. Conclusion

The purpose of applying semantic retrieval is to achieve computer's understanding about the user input content to process retrieval on semantic level . Bearing on the concept similarity and its three caculating methos, this paper introduces the concept of weight and its caculating formula. Based on the analysis of combining concept similarity and weight, this paper proposes a semantic search method based on ontology and applied this method in to tourist information retrieval. This paper also evaluates the result of retrieval from the persepect pf recall ratio and precision ratio which validated the effectiveness of the algorithm.

Acknowledgment

This work is supported by Scientific Research Project of Beijing Municipal Commission of Education (Grant No. KM201210005030), the support is gratefully acknowledged.

References

[1] Ying Zhang Web3.0: personalized learning platform [J]. China education technology equipment. 2012 (27): 38-39.

[2] Zhihong Deng, Shiwei Tang, et al. Overview of Ontology [J]. Journal of Peking University: Natural Science Edition, 2002, 38 (5): 730-738.

[3] Jianhou Gan , Youming Xia, Tianren Xu, et al. Ontology knowledge representation extends the [J]. language OWL Journal of Yunnan Normal University (NATURAL SCIENCE EDITION). 2005 (04).

[4] Binbin YU and construction tools of [J]. border economic and cultural ontology construction method. 2012 (12): 167-168.

[5] Yong Zhang, Junbai Lv Protege Ontology Modeling Research Based on [J]. Fujian computer. 2011 (01).

[6] Tao, Teng-Yang, Zhao. An Ontology-Based Information Retrieval Model for Vegetables E-Commerce[J]. 2012, 11 (5): 800-807.

[7] Chengyi Che, Zongmin Ma, Xiaolong Jiao . Study on the recognition method of [J]. computer engineering data table in the Web page. 2012, 38 (23): 154-157.

Advanced Materials Research Vols. 989-994 (2014) pp 2184-2187
© (2014) Trans Tech Publications, Switzerland
doi:10.4028/www.scientific.net/AMR.989-994.2184

Using PROSEPCT and SVM for the estimation of chlorophyll concentration

Jie Lv[1, a], Fengli Deng[1, b],Zhenguo Yan[2,c]

[1]College of Geomatics, Xi'an University of Science and Technology, Xi'an 710054, China

[2]School of Energy Engineering, Xi'an University of Science and Technology, Xi'an 710054, China

[a]rsxust@163.com, [b]gisxust@163.com, [c]yzg_wa@163.com

Keywords: support vector machine, estimation, chlorophyll concentration, rice, hyperspectral remote sensing

Abstract. This study focused on estimating chlorophyll concentration of rice using PROSPECT and support vector machine. The study site is located in West Lake sewage irrigation area of Changchun, Jiliin Province. Reflectance spectrual of rice were measured by ASD3 spectrometer, chlorophyll contents of rice were recorded with a portable chlorophyll meter SPAD-502. Support vector machines and PROSPECT model were adopted to construct hyperspectral models for predicting chlorophyll content. The results indicate that: the hyperspectral prediction model of rice chlorophyll content yields a maximum correlation coefficient of 0.8563, and achieves a smallest RMSE of 9.5106; and the prediction accuracy based on the first derivative spectrum is higher than on the original spectrum. Research of this paper provides a theoretical basis for large scale dynamic prediction of rice chlorophyll content in sewage irrigated area.

Introduction

Rice is an important crop in China, many farmers choose the untreated sewage as rice irrigation water in some suburbs of northern city. The sewage irrigation water contains heavy metals, which will directly affect the rice physiological process, and hinder chlorophyll synthesis. Study on chlorophyll content estimation of sewage irrigation area has important implications for the monitoring of heavy metals for the stress of rice.

In recent years, estimating chlorophyll content of plants from the spectrometer and satellite hyperspectral remote sensing technology has been investigated. The related research trend is mainly in two aspects. On the one hand, the use of statistical models for estimating chlorophyll content of plants[1-6]; on the other hand, is the inversion of radiative transfer models for chlorophyll content[7]. However, less research focused on estimating chlorophyll concentration using PROSEPCT and support vector machine. This study intends to construct spectral inversion model of rice based on support vector machine and PROSPECT model, so as to monitor these wage irrigation areas rapidly using hyperspectral remote sensing technology.

2.Materials and methods

2.1 Field experiment

The study selected sewage irrigation farmland located at Changchun City, Jilin Province, China. There is the FAW factory near West Lake, resulting in long-term groundwater contamination around West Lake. Two rice samples fields in the study area was selected, rice spectral data was collected and chlorophyll content in rice was measured .

2.2 Data preparation

Hyperspectral data of rice was collected by ASD3 field spectral radiometer, which spectral range was between 350-2500 nm. The radiometer was set to 25° viewing angle, and reflectance spectra of 400-1250 nm was adopt for the study.

Chlorophyll content in Rice was measured by SPAD-502 hand-held chlorophyll meter, each rice plants was measured 10 leaf chlorophyll values ,and taking the average value.

2.3 Spectral transformation method

Spectral differential transformation can increase the spectral irradiance spectrum at different wavelengths, thus sharpening the spectral information. First order differential transform can provide the change rate of steep spectrum information, and it can reduce the influence of noise spectrum by the environment, so as to enhance the hyperspectral data. First order differential transform were performed on spectral reflectance of rice.

2.4 PROSPECT model

The PROSEPCT model simulates leaf transmittance spectra and leaf reflectance spectra by the relationship between four parameters, they are: the leaf structure parameter (*N*), the content of dry matter *Cm* ($g\,cm^{-2}$), equivalent water thickness (cm or $g\,cm^{-2}$), chlorophyll content (Chla and Chlb).

2.5 Support vector machine regression

Support vector machine regression has been applied classification and estimation. Support vector machine regression model were introduced as follows:

A nonlinear mapping $\phi(x) = \{\phi(x_1), \phi(x_2), ..., \phi(x_i)\}$ is used to map the training data set into a high dimensional feature space $T = \{(x_1, y_1), ..., (x_i, y_i), ...(x_N, y_N)\}$, where exists an optimization function *f* to connect the input data and output data. The optimal decision equation, namely support vector machine regression equation, is introduced as follows:

$$f(x) = w^T \varphi(x) + b \tag{1}$$

where f (x) is the estimation value, coefficient $w(w \in \Re^{nh})$ and $b(b \in \Re)$ can be adjusted. The goal of support vector machine is to minimize the training error with insensitive loss function:

$$R(f) = \frac{1}{N} \sum_{i=1}^{N} |y_i - f(x_i)| \tag{2}$$

By defining $v_\varepsilon(y_i, f(x_i)) = Max\{0, |y_i - f(x_i)| - \varepsilon\}$ as the ε-insensitive loss function, ε-insensitive loss function is often used to control the sparseness and generalization ability of the model. Thus, the support vector machine regression is focus on the training error optimal hyperplane and the minimization of the training data set between the ε-insensitive loss function. Thus, the goal of support vector machine is to minimize the overall error of regression:

$$Min\ R\varepsilon(w, \xi_i, \xi_i^*) = \frac{1}{2} w^T w + C \sum_{i=1}^{N} (\xi_i^* + \xi_i) \tag{3}$$

with the constraints

$$w^T \varphi(x_i) - b + y_i \le \varepsilon + \xi_i^*, i = 1, 2, ..., N$$

$$-y_i + w^T \varphi(x_i) + b \le \varepsilon + \xi_i, i = 1, 2, ..., N$$

$$\xi_i, \xi_i^* \ge 0, \qquad i = 1, 2, ..., N$$

where the minimization function is used to punish the greater weight, used to maintain the smoothness of the regression function. The second formula use the ε-insensitive loss function to regulate the pipe reliability risk and the empirical risk. *C* is a parameter to balance these two formulas. Training errors above ε are denoted as ξ_i^*, whereas training errors below -ε are denoted as ξ_i.

After the optimization problems solved by constraint, the parameter vector *w* obtained:

$$w = \sum_{i=1}^{N} (\beta_i^* - \beta_i) \varphi(x_i) \tag{4}$$

where β_i^* and β can be solved through quadratic program, namely Lagrange polynomial. Finally, the support vector machine regression function can be obtained in dual space:

$$f(x)=\sum_{i=1}^{N}\left(\beta_i^*-\beta_i\right)k\left(X_1,X\right)+b \tag{5}$$

where $K\left(X_i,X_j\right)$ is the kernel function, it is the inner product of two vectors (X_i and X_j), and in the feature space $\varphi(x_i)$ and $\varphi(x_j)$, the kernel function is equivalent to $K(x_i,x_j)=\varphi(x_i)\times\varphi(x_j)$.

The Gauss radial basis function (RBF) as the kernel function of support vector machine regression was adopted. Estimation model of chlorophyll content of rice in the sewage irrigation area were based on support vector machine, where there are two important parameters affects the precision of the model: including the parameter C and Gauss parameter σ of RBF kernel. Grid search method was applied to optimize the regression parameters of support vector machine.

3. Results

3.1 Selection of SVR parameters

The parameters of support vector machine regression determined by grid search was shown in Table 1, λ denotes for rice original spectral data set, $FD\lambda$ denotes for the spectral data set after a derivative transformation. Parameter C and kernel parameter σ on the $FD\lambda$ data set are smaller than the original spectral data sets, and the computing time of support vector machine regression on on the $FD\lambda$ data set is less than in the original spectral data set.

Table 1 Parameters of SVM selected by grid search

Spectral data set	parameter C	Kernel parameter σ	Time (s)
λ	98.7632	956.3578	1408
$FD\lambda$	97.3653	56.6457	1353

3.2 Estimation result of rice chlorophyll content

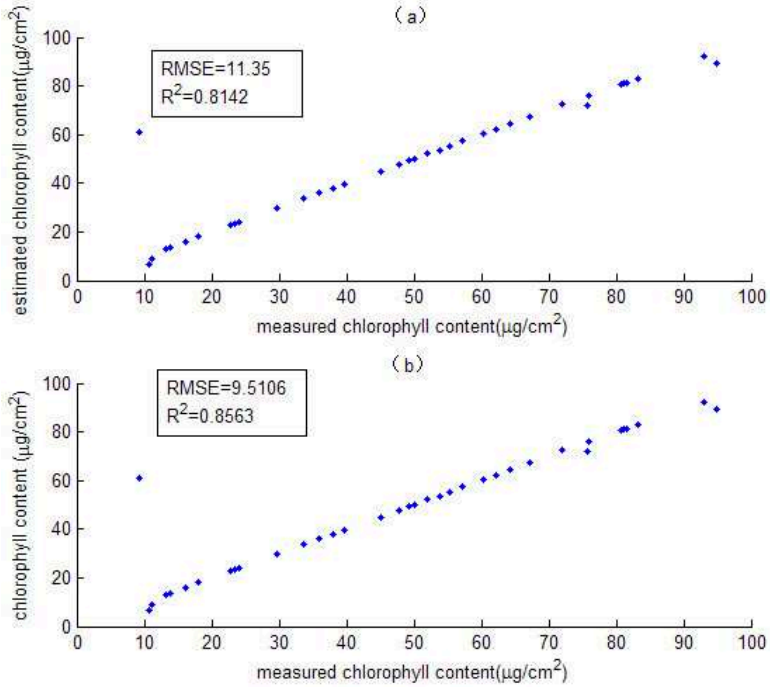

Fig. 1 Comparison of measured and estimated chlorophyll contents of rice.

The model was validated before it can be used to estimate rice chlorophyll content. Therefore, we compared the rice chlorophyll content with the measured rice chlorophyll content obtained from field tests (Fi.1). Fig.1 (a) is the comparison of the estimated chlorophyll content in rice on original

spectral data sets with the measured chlorophyll content of rice, Fig.1 (b) is the comparison of the estimated chlorophyll content in rice on the first derivative spectra data sets with the measured chlorophyll content of rice. On the original spectral data set, the coefficient of determination is 0.8142, the RMSE is 11.3510. On the first derivative spectra data set, the estimation model to obtain a coefficient of determination of 0.8563, and the RMSE is 9.5106. This indicates that the estimation model of chlorophyll content in rice based on support vector machine achieved a better accuracy on the first-order differential transformation, which is beneficial for the improving the precision of estimation model for chlorophyll content in rice.

4. Conclusion

This study established a chlorophyll content estimation model of rice using PROSPECT and support vector machine, and the parameters of support vector machine were using optimized using a grid search method. The Estimation model can be used as an effective tool for rapid tool for estimating chlorophyll content of rice, and can be applied to precision agriculture management. Future research will apply estimation model for estimating chlorophyll content in rice to large areas of sewage irrigation paddy field.

Acknowledgements

This research was funded by Jiangxi Province Key Lab for Digital Land (DLLJ201305), sponsored by Open Fund of Hunan Province Engineering Laboratory of Geospatial Information (2013GSIJJ002), Xi'an University of Science and Technology research engagement fund (201206), and the PhD Start-up Fund of Xi'an University of Science and Technology (A5030819).

References

[1] Delegido, J., Van, Wittenberghe.S., Verrelst, J., et al. Chlorophyll content mapping of urban vegetation in the city of Valencia based on the hyperspectral NAOC index. Ecological Indicators, 2014, 40: 34-42.

[2] Peng, Y, Gitelson, A. A. Remote estimation of gross primary productivity in soybean and maize based on total crop chlorophyll content. Remote Sensing of Environment, 2012, 117: 440-448.

[3] Mielke, M. S., Schaffer, B, Schilling, A. C. Evaluation of reflectance spectroscopy indices for estimation of chlorophyll content in leaves of a tropical tree species. Photosynthetica, 2012, 50(3): 343-352.

[4] Perry, E.M., Fitzgerald, G. J., Nuttall, J. G., et al. Rapid estimation of canopy nitrogen of cereal crops at paddock scale using a Canopy Chlorophyll Content Index. Field Crops Research, 2012, 134: 158-164.

[5] Hunt, Jr. E. R., Doraiswamy ,P. C., McMurtrey, J. E., et al. A visible band index for remote sensing leaf chlorophyll content at the canopy scale. International Journal of Applied Earth Observation and Geoinformation, 2013, 21: 103-112.

[6] Li, F., Mistele, B., Hu, Y., et al. Reflectance estimation of canopy nitrogen content in winter wheat using optimised hyperspectral spectral indices and partial least squares regression. European Journal of Agronomy, 2014, 52: 198-209.

[7] Darvishzadeh, R., Matkan, A. A., Ahangar, A. D. Inversion of a radiative transfer model for estimation of rice canopy chlorophyll content using a lookup-table approach. Selected Topics in Applied Earth Observations and Remote Sensing, IEEE Journal of, 2012, 5(4): 1222-1230.

Advanced Materials Research Vols. 989-994 (2014) pp 2188-2191
© (2014) Trans Tech Publications, Switzerland
doi:10.4028/www.scientific.net/AMR.989-994.2188

Distributed Collaborative Filtering Recommendation Model Based on Expand-vector

Ye Zhu[1,a], Hongyi Su[1,b], Caiqun Wang[1,c], Bo Yan[1,d] and Hong Zheng[1,e]

[1]Key Lab of Intelligent Information Technology, Beijing Institute of technology, Beijing, CN

[a]yezhu@bit.edu.cn, [b]henrysu@bit.edu.cn, [c]caiqunwang@bit.edu.cn, [d]yanbo@bit.edu.cn,

[e]hongzheng@bit.edu.cn

Keywords: Parallel and distributed computing; Expand-vector; Collaborative filtering; Recommend mechanism; MapReduce

Abstract. The recommendation system based on collaborative filtering is one of the most popular recommendation mechanisms. However, with the continuous expansion of the system, several problems that traditional collaborative filtering recommendation algorithm (CF) faced such as cold startup, accuracy, and scalability are worsen. In order to address these issues, a distributed collaborative filtering recommendation model based on expand-vector (CF-EV) is proposed. Firstly, the eigenvector is expanded reasonably to get the expand-vector based on the expand-vector model, a new extension measure created in this paper. Then, the nearest neighbor user is found and a more accurate recommendation to the target user is given based on the calculation results. In addition, the further optimization makes it applied to the parallel computing framework successfully. Using the MovieLens dataset, the performance of CF-EV is compared with CF from both sides of recommendation precision and the speedup ratio. Through experimental results, CF-EV overcomes the problem of cold startup. Moreover, the accuracy and recall ratio has been doubled. With the increasing numbers of the computing nodes, the distributed implementation has linear speedup.

Introduction

The amount of information is increasing far more quickly than our ability to process it. Thus, it is significant to utilize the technologies that can help us to find which information is the most valuable. One of the most promising technologies like this is collaborative filtering [1] which was proposed by Goldberg. With the development of e-commerce, its application area is becoming more and more abroad, such as the recommendation of the books in Amazon [2].Although the traditional collaborative filtering recommendation algorithm (CF) has achieved huge success in information filtering, it has three drawbacks: cold startup, sparsity and scalability. To solve these problems, many optimization methods are proposed. Breese and Hecherman[3] proposed a method which assigns default values to the unrated items. In Zhang et al. [4], based on the cloud model, a novel similarity measuring method named the likeness comparing method based on cloud model (LICM) was presented. It could overcome the drawback of attributes' strictly matching. Apache offered open source library named Mahout [5], which could make CF deployed to the Hadoop successfully.

In this paper, a new model is introduced to address three key issues. The innovations are embodied in the following aspects: An expand-vector model is presented to expand the object's eigenvector; A distributed collaborative filtering recommendation model based on expand-vector (CF-EV) is proposed, in which all the calculation is based on expand-vector; To CF-EV, whose distributed implementation is completed by further optimization on it; On the MovieLens data sets, the contrast tests of CF-EV and CF are made.

Related Works and Backgrounds

In this section, we review the background of CF and introduce its recommendation process.

As the main recommendation technology, the basic assumption of CF is that if user X and user Y rate n items similarly, they tend to rate on other items similarly. In general, there are three types of CF,

which are CF based on item, CF based on user and CF based on model. In the process of CF, three parts are included: fetching data, searching nearest neighbor and making recommendation. The specific details will be represented in the next section.

Distributed Collaborative Filtering Recommendation Model Based on Expand-vector

In this section, the specific process of CF-EV is as below:

Expand-vector Model. In a typical CF scenario, there exists two sets, I and J. $vector_j$ represents the eigenvector of element j: $vector_j=(p_{(1,j)}, p_{(2,j)}, \ldots, p_{(m,j)})$, $j\in J$, $1\le m\le M$. M means the total number of elements in the set I. $p_{(i,j)}$ represents the preference of element i to element j , $i\in I$. Expand the eigenvector, defining its expand-vector in forms of: $evector_j=(p_{(1,j)}, p_{(2,j)}, \ldots, p_{(m,j)}, a_{(j,1)}, a_{(j,2)}, \ldots, a_{(j,q)})$, $a_{(j,k)}$ means the k^{th} attribute's value of j, $1\le k\le Q$. Q stands for the total number of j's attributes.

Specific Application. The expand-vector model could be applied to any one of the recommendation algorithms which involves the eigenvector. Now, the model is applied to CF based on user:

Fetching Data. CF uses a ratings matrix, B, to represent the entire $m\times n$ user-item data, line m means the m^{th} user, column n represents the n^{th} item, each entry pij represents the rating of the target item j by user i. In general , $0\le pij\le 5$. Formula (1) shows the ratings matrix:

$$\boldsymbol{B}_{m\times n}=\begin{bmatrix} p_{11} & \cdots & p_{1n} \\ p_{21} & \cdots & p_{2n} \\ \vdots & & \vdots \\ p_{m1} & \cdots & p_{mn} \end{bmatrix} \tag{1}$$

Get Expand-vector. The item's expand-vector can be represented as $eivector_j=(p_{(1,j)}, p_{(2,j)}, \ldots, p_{(m,j)}, ai_{(j,1)}, ai_{(j,2)}, \ldots, ai_{(j,q)})$, $1\le j\le N$. N is the total number of the item. $ai_{(j,k)}$ means the k^{th} attribute's value of item j,$1\le k\le Q$.Q represents the total number of item's attributes. Analogously, the user's expand-vector can be represented as $euvector_i=(p_{(i,1)}, p_{(i,2)}, \ldots, p_{(i,n)}, au_{(i,1)}, au_{(i,2)}, \ldots, au_{(i,r)})$. $au_{(i,k)}$ means the k^{th} attribute's value of user i. More specifically, the categories of *item*'s attributes could include attributes like category and price. The categories of *user*'s attributes can include age and profession. Then, classify attributes according to attributes' value and convert the categorized results to digital format. Finally, the eigenvectors will be expanded reasonably, getting the expand-vectors.

Search Nearest Neighborhood. Here, all the calculation is based on expand-vectors. Take, for example, the similarity calculation of item j and item j':

1 Pearson correlation-based similarity

$$sim'_{(j,j')}=\frac{(m+q)(\sum p_{ij}p_{ij'}+\sum ai_{jk}ai_{j'k})-(\sum p_{ij}+\sum ai_{jk})(\sum p_{ij'}+\sum ai_{j'k})}{\sqrt{(m+q)(\sum p_{ij}^2+\sum ai_{jk}^2)-(\sum p_{ij}+\sum ai_{jk})^2}\sqrt{(m+q)(\sum p_{ij'}^2+\sum ai_{j'k}^2)-(\sum p_{ij'}+\sum ai_{j'k})^2}} \tag{2}$$

As is shown in formula (2),the Pearson correlation is a number between –1 and 1 that measures the tendency of two series of numbers, paired up one-to-one, to move together.

1 Euclidean distance-based similarity:

$$sim'_{(j,j')}=\frac{1}{1+\sqrt{\sum(p_{ij}-p_{ij'})^2+\sum(ai_{jk}-ai_{j'k})^2}} \tag{3}$$

The Euclidean distance, which we've seen in formula (3), is the most intuitive of all distance measures .This implementation is based on the distance between objects.

1 Tanimoto Coefficient-based similarity:

$$sim'_{(j,j')}=\frac{\left|U_j\cap U_{j'}\right|+\left|A_j\cap A_{j'}\right|}{\left|U_j\cup U_{j'}\right|+\left|A_j\cup A_{j'}\right|}. \tag{4}$$

Tanimoto Coefficient-based similarity is the ratio of the size of the intersection to the size of the union of users' preferred items. In formula (4), U_j means the set of users which have given the preference to item j. A_j means the set of j's attribute types. Analogously, the users' similarity calculation can be performed. After finishing all these related calculations, we can gain the user's similarity vector and items' similarity matrix. Besides, user's nearest neighbor can be received.

Make Recommendations.

$$R'_{(v,j')} = \frac{1}{|I_u|}\sum_{j\in I_u} sim'_{(j,j')}\, p_{(u,j)} \tag{5}$$

As is shown in formula (5), $R_{(v,j')}$ is used to estimate the preference value that user v may give to item j'. It is estimated on the basis of nearest neighborhoods' preference. Specifically, I_u represents the set of the items which user u has given the preference. Then, sort the $R'_{(v,j')}$ in descending order and choose the top W items to recommend to the target user, the value of W can be man-made in advance. At this point, the best recommendation (the most similar to item j) can be chosen.

Distributed Implementation of CF-EV

As the recommendation process of CF-EV is similar to the thought of Map-Reduce. So, the further optimization on CF-EV makes it applicable on the MapReduce[6] and Hadoop[7] successfully.

Transform File Format and Deploy the Input File. First, add a new file named users.txt, with its content concerning about those target users who will be given recommendation. Then, deploy the user preferences file (the Input File) on the HDFS [8] based on users.txt.

Generate User Preference Vector. The input file are treated as (*Long,String*) pairs by the framework, where the long key is a position in the file and the string value is the line of the text file. The framework collects all item*Id*s that were mapped to each user*Id* together. A reduce function constructors a vector from all item*Id*s for the user, and outputs the user*Id* mapped to the user's preference vector (this vector is named as "user preference vector").

Get Item Co-occurrence Matrix. Do Map and Reduce operation in accordance with the co-occurrence matrix method and user preference vector to get the item's co-occurrence matrix.

Get the User Expected Preference Matrix. Do parallel matrix multiplication operation of MapReduce on the user preference matrix and the item co-occurrence matrix to obtain the user expected preference matrix. The corresponding expected preference matrix is in forms of "userId_i : itemId_1, *expected preference*; … ; itemId_n , *expected preference*". The expected preference will be saved into the file in descending order. The generated file is placed on the HDFS server steadily.

Make Recommendations. Select the top-N items and recommend to the target user, then the recommendation is finished.

Experimentals and Results

In this section, we evaluate the CF-EV in comparison with CF.

Datasets. The three data sets of MovieLens (http://www.movielens.umn.edu) are used in our experiments, including ML-100K, ML-1M, and ML-10 M. Each data set is divided into two parts: 20% of the users are selected to be testing model, and the remaining as training model.

The Comparison of CF Based on Different Similarity Computation Methods. In this section, Precision and Recall ratio are introduced from the point view of information retrieval. The test is done on single machine, and ML-100K is used .The more detailed results are shown in table 1:

Table 1 Recommendation Results By Adopting Different Similarity Calculation Methods

Similarity Metrics	Accuracy	
	Precision	Recall
PearsonCorrelation	0.005 661 538	0.007 937 350
EuclideanDistance	0.001 169 231	0.001 514 680
TanimotoCoefficien	0.067 015 385	0.100 565 023

Table 2 Recommendation Results of CF-EV

Similarity Metrics	Accuracy	
	Precision	Recall
animotoCoefficien	0.124 984 615	0.187 860 704

In table 1, we can see that the precision and recall ratio of Tanimoto Coefficien has acquired qualitative leaps by contrast with other methods. So, the following experiment is based on this similarity calculation method which can provide the comparison of the recommendation algorithm.

The Comparison of CF-EV and CF. The experimental configuration and dataset is the same as the experiment mentioned above. The recommendation result is shown in table 2. The application of CF-EV promotes the recommendation precision and recall ratio increased by nearly 100%.

The Experiment about Cold Startup. To the problem about cold startup, we choose some items in ML-100K randomly, and the total number is 10, 20, 30, 40 and 50 respectively, removing the items' preference. Then CF-EV is used to predict the rating and the precision is shown in table 3:

Table 3 Recommendation Precision of the New Item

Algorithm	Precision				
	10	20	30	40	50
CF-EV	0.8999	0.9010	0.9188	0.8573	0.9076

Table 4 Runtime of Tasks on Single Machine (s)

Single machine	Run Time		
	100K	1M	10M
1	1190.8	1338000.3	11593004.7

Table 5 Runtime of Tasks on HOD Cluster (s)

Node Number	Run Time		
	100K	1M	10M
1	1 018	1 029	4 608
2	888	894	2 919
3	837	839	2 194

Table 6 Speedup of Tasks

Node Number	Speedup		
	100K	1M	10M
1	1	1	1
2	1.146 396	1.151 007	1.578 623
3	1.216 249	1.226 460	2.100 273

As is shown in table 3, the application of CF-EV makes the problem of cold startup resolved.

The Efficiency Evaluation of CF-EV's Distributed Implementation. The tests about this section are done on single machine and a small HOD (Hadoop on Demand) cluster respectively. The machine is constituted as follows: Dell Power Edge SC1430, Intel Xeon 5110 (1.6 GHz), Dual-core Processor, 4 GB of Physical Memory. The cluster is composed by 3 machines which are served as pbs_server, namenod and datanode respectively. All nodes which have the same configuration are installed the executable program of Hadoop distributions. More detailed results are shown in table 4~6.

Table 4~6 indicates that, as to the same data set, the run time of a single node has been reduced greatly compared with single machine, which reflects the MapReduce's advantages of data processing. Moreover, concerning the HOD cluster, with the increasing numbers of the computing nodes, a higher linear speedup is achieved. Besides, the optimal linear speedup can reach 1.5.

Conclusions

The paper firstly analyzes the disadvantages of the existed similarity measures and then a distributed collaborative filtering recommendation model based on expand-vector is proposed. Several experiments are performed on data sets and the results reveal the efficiency and accuracy of CF-EV. In the future, how to make the recommendation algorithm achieve a better combination with MapReduce? It will be the next research direction.

References

[1] Resnick P, Iacovou N, et al. *GroupLens: an open architecture for collaborative filtering of netnews*: ACM conference on Computer supported cooperative work, ACM, p. 175-186(1994).

[2] E. Brynjolfsson, Y.J. Hu, M.D. Smith: Manage. Sci. Vol.49 (2003), p. 1580–1596.

[3] Breese J S, Heckerman D, Kadie C. *Empirical analysis of predictive algorithms for collaborative filtering*//Proceedings of the Fourteenth conference on Uncertainty in artificial intelligence. Morgan Kaufmann Publishers Inc, p. 43-52(1998).

[4] Guangwei Zhang, Deyi Li and Peng Li: submitted to Journal of Software (2007).In Chinese.

[5] Anil R, Friedman E. Mahout in Action [M]. New York: Manning Publications Co, p.1-2(2011).

[6] Dean J, Ghemawat S. MapReduce: Communications of the ACM, p.107-113(2008).

[7] White T. Hadoop: The Definitive Guide: The Definitive Guide [M].

[8] Information on http://httpd.apache.org/

[9] Zhang Y, Liu H. DCFRS: *A Distributed Collaborative Filtering Recommender System based on Cloud Computing for Mobile Commerce* [J]. Appl. Math, p.1-10(2013).

Advanced Materials Research Vols. 989-994 (2014) pp 2192-2195
© (2014) Trans Tech Publications, Switzerland
doi:10.4028/www.scientific.net/AMR.989-994.2192

Improved Ant Colony Algorithm based on PSO and Its Application on Cloud Computing Resource Scheduling

Hai Yang[1, a]

[1]College of Information Science and Electricity Engineering, Shandong Jiaotong University, Jinan, Shandong, China 250023

[a]yanghai_sdjtu@163.com

Keywords: cloud computing; resource scheduling; ant colony algorithm; particle swarm optimization algorithm

Abstract. This paper introduces PSO algorithm into ant colony optimization algorithm so that an improved ant colony optimization algorithm named ACA-PSO is proposed. The ACA-PSO algorithm can get more effective optimal solutions by using PSO algorithm to do crossover operation and mutation operation so as to avoid trapping in local optimum. Finally, the simulation experiment reflects that the ACA-PSO algorithm speeds the convergence up which is more suitable for resource scheduling in cloud computing.

Introduction

Cloud computing is a topic of hot debate in many fields such as computer science, business and so on. Allocation of computing resources is one of the most important component of cloud computing because its efficiency directly affects the performance of the whole cloud computing system. At the present stage, many scholars have introduced the ant colony algorithm (ACA) into the cloud computing system. The ACO overcomes the shortcomings of huge size of the node and lower allocation of resources for a single node, ensuring user’ s tasks can be completed on time. But the ACA has its disadvantages which include it is easy to fall into local optimal solutions, making inefficient resource scheduling [1]. Therefore, it is necessary to improve the ACA algorithm based on particle swarm optimization algorithm (PSO) to improve the efficiency of resource scheduling in cloud computing system.

Interpretation of Related Problems

Cloud Computing and Its MapReduce Level Scheduling. Cloud computing which is in grid computing based on a new calculation model, is the core technology of the next generation network computing platforms. It builds virtual super computer which provides data storage, analysis and scientific computing services through the distributed computing model and the resource pool technology [2]. Cloud computing is also a kind of distributed computing. By using of the virtualization technology, the idle computer resources can be combined into a huge resource pool which is constituted as a super computing capacity of the computer. Calculation nodes can be put into a dynamic system, which has fully realized the dynamic autonomy function, according to the need for computing resources, storage space and various software service from each application [3].

The key technology of MapReduce in Cloud computing is step-by-step type processing technology. MapReduce class scheduling is the core of the cloud computing resources scheduling which is the realization of the logical step calculation realized and all the task scheduling will be realized through this model. In MapReduce programming mode, concurrent processing, fault tolerant processing and load balance problems are abstracted as a function library. Through the MapReduce interface, user can put the large-scale computing to be automatic concurrent and distribution implementation [4]. MapReduce programming model calculation of the implementation process can be abstracted as three role: master, worker and user. Master is a central controller system, responsible for task allocation, load balance and fault tolerant processing. Worker is responsible for receiving

task from Master, carries on the data processing and calculation, as well as responsible for data transmission communication. User is a client who inputs the task to realize the Map and Reduce function and controls the whole calculation processes.

Ant Colony Algorithm. The ant colony algorithm is a probabilistic technique for solving computational problems which can be reduced to finding optimal paths through graphs.

The first version of ant colony algorithm, which is initially proposed by Marco Dorigo in 1992 in his PhD thesis [5], was aiming to search for an optimal path in a graph, based on the behavior of ants seeking a path between their nest and a source of food. The original idea has since diversified to solve a wider class of numerical problems, and as a result, several problems have emerged, drawing on various aspects of the behavior of ants.

In the natural world, ants initially wander randomly, and upon finding food return to their nest while laying down pheromone trails. If other ants find such a path, they are likely not to keep traveling at random, but to instead follow the trail, returning and reinforcing it if they eventually find food. When the ant k moves to the next node j from node i, the node j can be decided with the probability $P_{ij}^{k}(t)$ which can be calculated by formula (1):

$$P_{ij}^{k}(t)=\begin{cases}\dfrac{\tau_{ij}^{\alpha}(t)\eta_{ij}^{\beta}(t)}{\sum_{s\in A_k}\tau_{is}^{\alpha}(t)\eta_{is}^{\beta}(t)} & j\in A_k\\ 0 & otherwise\end{cases} \tag{1}$$

Where $\tau_{ij}(t)$ denotes the pheromone density, A_k is the set of optional nodes adjacent to node i. α is the heuristic factor of pheromone. β is the heuristic factor of expectation. $\eta_{ij}(t)$ is the distance function which denotes the heuristic information of path. $\eta_{ij}(t)$ can be described as formula (2):

$$\eta_{ij}(t)=\frac{1}{d_{ij}} \tag{2}$$

Where d_{ij} denotes the distance from node i to node j.

Over time, however, the pheromone trail starts to evaporate, thus reducing its attractive strength. The more time it takes for an ant to travel down the path and back again, the more time the pheromones have to evaporate. A short path, by comparison, gets marched over more frequently, and thus the pheromone density becomes higher on shorter paths than longer ones. Pheromone evaporation also has the advantage of avoiding the convergence to a locally optimal solution. If there were no evaporation at all, the paths chosen by the first ants would tend to be excessively attractive to the following ones. In that case, the exploration of the solution space would be constrained.

Local pheromone updating strategy is regarded as follows:

$$\tau_{ij}(t+n)=(1-\rho)\cdot\tau_{ij}(t)+\Delta\tau_{it}(t) \tag{3}$$

Where ρ is the evaporation rate of pheromone. $\Delta\tau_{it}(t)$ denotes the increment of pheromone on path (i , j) during once iteration. $\Delta\tau_{it}(t)$ can be gain by formula (4) as follows:

$$\Delta\tau_{it}(t)=\begin{cases}Q/L_k & (i,j)\\ 0 & otherwise\end{cases} \tag{4}$$

Where Q is the pheromone density and L_k denotes the total length of the route ant k passed by.

PSO Algorithm. Initialize a group of random particles in a space, the particle position represents possible solution, each particle advances to a certain speed, particle swarm gradually approaches to the optimal location after repeated advances which are also called iteration, thus the optimal solution will be got [6]. In each iteration, the particles update themselves according to two extreme values: one is the optimal solution finding by a single particle, namely the individual extremum; the other is the optimal solution finding by whole particle swarm, that is, namely the global extremum. Particles update their velocity and position according to the two extreme values above and the following two formulas.

$$V=\alpha\times v+c_1\times rand()\times(pBest-X)+c_2\times rand()\times(qBest-X) \tag{5}$$

$$X = X + V \tag{6}$$

Where $V = [v_1, v_2, \cdots, v_m]$ is the velocity of the particle, $X = [x_1, x_2, \cdots, x_m]$ is the current position of the particle, d is the dimension of solution space. pBest is the individual extremum, qBest is the global extremum, rand() is random number between 0 and 1. Both c_1 and c_2 are called learning factors which are used to adjust the particle update step, α is a weighted factor.

The particle swarm gradually closes to the optimal solution location through continuous learning and updating. The qBest which is the global optimal solution will be got by using the algorithm.

Improved Ant Colony Algorithm based on PSO and Its Application on Resource Scheduling

The main idea of improved ant colony algorithm based on PSO (ACA-PSO) proposed in this paper is that let the ants have the characteristics of the "particles". Firstly, the ants are in accordance with the ant colony algorithm to complete a traverse, then they adjust solutions according to the local optimal solutions and global optimal solutions.

Adjustment is described as: the current positions of resource scheduling are behalf of the basic path nodes set. $\alpha \times v$ can be regarded as the mutation operation of genetic algorithm, and $c_1 \times (pBest - X) + c_2 \times (qBest - X)$ can be regarded as the crossover operation of genetic algorithm, which lets the current solution do crossover operator with the individual extremum and the global extremum so as to produce a new location.

The crossover strategy in improved algorithm is: select a cross region randomly in the second string, old_2 is added to the old_1 corresponding position, delete the nodes in old_2 appeared in the old_2 cross- region. Variation strategy is: select the node of j_1 visits from the nodes of 1-n visit, exchange the j_1 node and the $j_1 + 1$ node in nodes set N_0, and the rest keep unchanged. At this time, the path set node is N_1.

A node may have to run multiple tasks at the same time in cloud computing. But it will improve performance of entire cloud if tasks are assigned to the most efficient node. Therefore, a task expected execution time model is established to predict execution time of the new tasks on the node, the formula is as follows:

$$ET_j^{n_m}(J_m(t_2)) = \frac{n_m}{n_v} \cdot (\rho ET_j^{n_v}(J_v(t_0)) + (1-\rho) RT_j^{n_v}(J_v(t_1))) \tag{7}$$

Where $ET_j^{n_m}(J_m(t_2))$ represents the new task J_m estimating the expected execution time on the j node at time t_2. n_m denotes the load of node j at time t_2. $ET_j^{n_v}(J_v(t_0))$ represents the expected execution time of previous completed task J_v at time t_0. $RT_j^{n_v}(J_v(t_1))$ denotes the actual execution time of previous task completed at time t_1. n_v denotes the load of previous task.

Simulation Experiment

The simulation experiments are carried out in the MATLAB by using ACA-PSO and basic ant colony algorithm (ACA) separately. The simulation data include: number of ants m=10, maximum number of iterations is 500, $\alpha = 1.5$, $\beta = 2$, $\rho = 0.9$. The experimental results are shown in Fig.1.

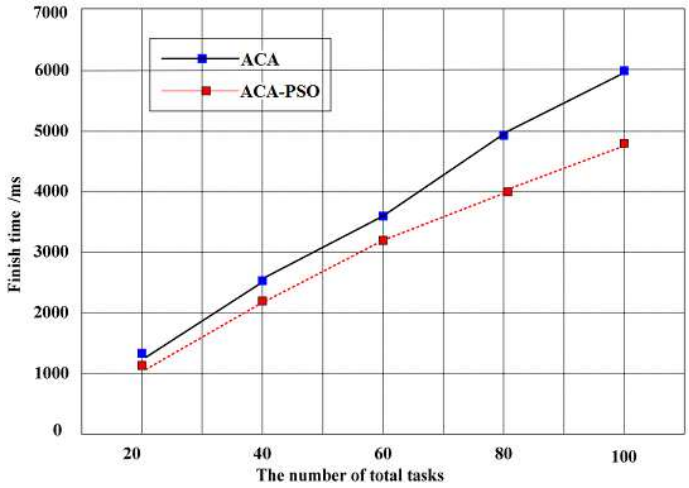

Fig. 1 Comparison of the Two Scheduling Algorithms

The results shown in Fig.1 reflect that the execution time of ACA-PSO is shorter than ACA. So ACA-PSO has higher efficiency for resource scheduling in cloud computing.

Conclusion

In this paper an improved ant colony algorithm based on PSO named ACA-PSO is proposed. ACA-PSO overcomes the disadvantage that the ant algorithm is easy to fall into local optimal solution in the cloud computing resource scheduling. Experiment results shows that ACA-PSO can accelerate the convergence speed, avoid trapping into local optimum solution so as to be more suitable for resource scheduling in cloud computing.

References

[1] S. Gao, X. Z. Jiang, K. Tang. Hybrid Algorithm Combining Ant Colony Optimization Algorithm with Pariticle Swarm Optimization. Proceedings of the 25th Chinese Control Conference. 2006, 1428-1432.

[2] X. C. Wang, S. Y. Jin, M. B. Xia. Web cluster of cybernetics QoS quantitative based on distributed control [J]. Journal of software, 2007, 18 (11): 2810-2818

[3] Y. Liu, X. H. Wang, C. M. Xing and S. Wang. Resources scheduling strategy based on ant colony optimization algorithms in cloud computing. Computer Technology and Development, 2011, 21(9): 19-23.

[4] Z. H. Zhang and X. J. Zhang. A Load Balancing Mechanism Based on Ant Colony and Complex Network Theory in Open Cloud Computing Federation. 2nd International Conference on Industrial Mechatronics and Automation. 2010, 240-243.

[5] Marco Dorigo. Ant colonies for the traveling salesman problem [J]. Biosystems, 1997, 43, pp.73-81.

[6] H. W. Tian, F. Xie. Resource Allocation Algorithm Based on Particle Swarm Algorithm in Cloud Computing Environment. Computer Technology and Development. 2011, 21(12):22-25.

Advanced Materials Research Vols. 989-994 (2014) pp 2196-2199
© (2014) Trans Tech Publications, Switzerland
doi:10.4028/www.scientific.net/AMR.989-994.2196

Study on Traveling Salesman Problem Based on the Improved Chaos Ant Colony Algorithm

Hai Yang[1, a]

[1]College of Information Science and Electricity Engineering, Shandong Jiaotong University, Jinan, Shandong, China 250023

[a]yanghai_sdjtu@163.com

Keywords: traveling salesman problem; ant colony algorithm; chaos optimization; simulation experiment

Abstract. In this paper an improved chaos ant colony algorithm based on return optimization strategy, elite strategy and intersection removal strategy is proposed. The improved algorithm uses orthogonal method to cluster the target points, then adopt chaos technology to optimize initial solution of the ant colony to improve individual quality and chaos perturbation is utilized to avoid the search being trapped into local optimum solutions. The simulation results show that the improved algorithm has higher efficiency in finding optimal path and it is a novel method to solve traveling salesmen problem.

Introduction

The traveling salesman problem (TSP) asks the following question: Given a list of cities and the distances between each pair of cities, what is the shortest possible route that visits each city exactly once and returns to the origin city? It is an NP-hard problem in combinatorial optimization, important in operations research and theoretical computer science.

In the theory of computational complexity, the decision version of the TSP belongs to the class of NP-complete problems. Thus, it is possible that the worst-case running time for any algorithm for the TSP increases superpolynomially with the number of cities [1].

The problem was first formulated in 1930 and is one of the most intensively studied problems in optimization. It is used as a benchmark for many optimization methods. Even though the problem is computationally difficult, a large number of heuristics and exact methods are known, so that some instances with tens of thousands of cities can be solved completely and even problems with millions of cities can be approximated within a small fraction of 1%.

The TSP has several applications even in its purest formulation, such as planning, logistics, and the manufacture of microchips. Slightly modified, it appears as a sub-problem in many areas, such as DNA sequencing. In these applications, the concept city represents, for example, customers, soldering points, or DNA fragments, and the concept distance represents traveling times or cost, or a similarity measure between DNA fragments. In many applications, additional constraints such as limited resources or time windows may be imposed.

Ant Colony Optimization Algorithm (ACO) is a population-based optimization approach which has been successfully applied to solve different combinatorial optimization problems such as TSP, QAP, job-shop scheduling, etc. One of main ideas of ant colony algorithms is the indirect communication of a colony of agents, called artificial ants, based on pheromone trails. The artificial pheromone trails are a kind of distributed numeric information which is modified by the ants to reflect their experience while solving a particular problem.

Ant Colony Algorithm and Chaos Selection Strategy

Ant Colony Algorithm. The ant colony algorithm is initially proposed by Marco Dorigo in 1992 in his PhD thesis [2], was aiming to search for an optimal path in a graph based on the behavior of ants seeking a path between their nest and a source of food. The original idea has since diversified to solve

a wider class of numerical problems, and as a result, several problems have emerged, drawing on various aspects of the behavior of ants.

When ant colony algorithm starts, every ant wanders randomly to find foods returning to their nest while laying down pheromone on the path it passed. If other ants find such a path, they are likely not to keep traveling at random, but instead of following the path, returning and reinforcing the density of pheromone of the path if they eventually find food. When the ant k moves to the next node j from node i, the node j can be decided with the probability $P_{ij}^{k}(t)$ which can be calculated by formula (1):

$$P_{ij}^{k}(t)=\begin{cases}\dfrac{\tau_{ij}^{\alpha}(t)\eta_{ij}^{\beta}(t)}{\sum_{s\in A_k}\tau_{is}^{\alpha}(t)\eta_{is}^{\beta}(t)} & j\in A_k\\ 0 & otherwise\end{cases} \tag{1}$$

Where $\tau_{ij}(t)$ denotes the pheromone density, A_k is the set of optional nodes adjacent to node i. α is the heuristic factor of pheromone. β is the heuristic factor of expectation. $\eta_{ij}(t)$ is the distance function which denotes the heuristic information of path. $\eta_{ij}(t)$ is described as formula (2):

$$\eta_{ij}(t)=\frac{1}{d_{ij}} \tag{2}$$

Where d_{ij} denotes the distance from node i to node j.

Over time, however, the pheromone trail starts to evaporate, thus reducing its attractive strength. The more time it takes for an ant to travel down the path and back again, the more time the pheromones have to evaporate. A short path, by comparison, gets marched over more frequently, and thus the pheromone density becomes higher on shorter paths than longer ones. Pheromone evaporation also has the advantage of avoiding the convergence to a locally optimal solution [3]. If there were no evaporation at all, the paths chosen by the first ants would tend to be excessively attractive to the following ones. In that case, the exploration of the solution space would be constrained.

Local pheromone updating strategy is regarded as follows:

$$\tau_{ij}(t+n)=(1-\rho)\cdot\tau_{ij}(t)+\Delta\tau_{it}(t) \tag{3}$$

Where ρ is the evaporation rate of pheromone. $\Delta\tau_{it}(t)$ denotes the increment of pheromone on path (i , j) during once iteration. $\Delta\tau_{it}(t)$ can be gain by formula (4) as follows:

$$\Delta\tau_{it}(t)=\begin{cases}Q/L_k & (i,j)\\ 0 & otherwise\end{cases} \tag{4}$$

Where Q is the pheromone density and L_k denotes the total length of the route ant k passed by.

Chaos Selection Strategy. When ant colony algorithm initializes, the strength of pheromones on every road section is equal so that the possibility of every road section is equal. It is difficult for ant colony to find an optimization path; besides, the convergence speed of algorithm is slow. So using chaos operator is necessary because it can increase the searching efficiency by the random and ergodic of chaos.

Take the logistics mapping for example [4], iterative formula is as follows:

$$z_{i+1}=\mu\cdot z_i\cdot(1-z_i),\quad i=0,1,2,\cdots,\quad \mu\in(2,4] \tag{5}$$

Where, μ is the control parameter, with the domain between (2, 4]. When μ= 4, $0\le z_0\le 1$, logistic function is the full mapping in (0, 1), which is at a totally chaos status. A chaos sequence will be created by the iteration [5], and then be converted to a chaos ergodic parameter when solving optimization problems in space. After introducing chaos perturbation, the new status transition strategy becomes:

$$p_{ij}^{k}(t)=\begin{cases}\dfrac{[\tau_{ij}^{s}(t)]^{\alpha}\cdot(r_{ij}^{s})^{\beta}\cdot(\delta_{ij})^{\theta}(1+Z_{ij})^{\gamma}}{\sum_{j\in allowed_k}[\tau_{ij}^{s}(t)]^{\alpha}\cdot(r_{ij}^{s})^{\beta}\cdot(\delta_{ij})^{\theta}(1+Z_{ij})^{\gamma}}, & j\in allowed_w\\ 0, & otherwise\end{cases} \tag{6}$$

Where,

$$\delta_{ij} = \begin{cases} \dfrac{\max[0, LT_{ij} - \max(ET_j, ET_{ij})]}{LT_j - ET_j}, & if \quad LT_j \geq LT_{ij} \\ \dfrac{\max[0, LT_j - \max(ET_j, LT_{ij})]}{LT_j - ET_j}, & else \end{cases} \tag{7}$$

$$ET_{ij} = ET_i + T_i + t_{ij} \tag{8}$$

δ_{ij} is the heuristic information of time windows which reflects the urgency of time.

Improved Chaos Ant Colony Algorithm (ICACA)

In chaos ant colony algorithm mentioned above, the chaos initialization accelerates the convergence velocity and to a certain extent, the chaos perturbation overcomes the disadvantage that the ant colony algorithm is easy to trap into the local optimum solutions. However, the optimal solution by using the chaos ant colony algorithm exists intersection so that the quality of optimal solution should be improved further on.

In order to improve the quality of the optimal solutions of ant colony algorithm, the local optimization technologies including return optimization strategy, elite strategy and intersection removal strategy are introduced into the chaos ant colony algorithm.

Return Optimization Strategy. The transition probability equation of basic ant colony algorithm is only related to the distance between the current node and candidate nodes available, but not considering the distance between the last node and the starting node. Therefore, the quality of optimal solution is significantly affected by the span between the last node and the starting node. So the return optimization strategy is very important for improving the quality of optimal solution. The selection of path omitting the distance between the last node and the starting node is shown in Fig.1. The selection of path using return optimization strategy is shown in Fig.2.

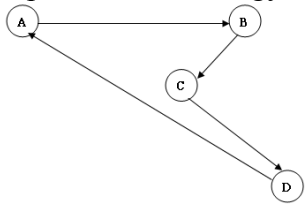

Fig.1 Basic Selection of Path

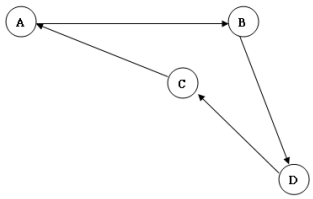

Fig.2 Return Optimization Strategy

The key of return optimization strategy is the factor $\mu_{ij} = d_{i0} + d_{0j} - d_{ij}$ which not only considers the distance between current node and the next candidate nodes, but also considers the distance between each candidate node and the starting node. Therefore, the quality of optimal solution is significantly improved. The new transition probability equation becomes:

$$p_{ij}^k(t) = \begin{cases} \dfrac{[\tau_{ij}^s(t)]^\alpha \cdot (\eta_{ij}^s)^\beta \cdot (\mu_{ij})^\theta (1+Z_{ij})^\gamma}{\sum_{s \in allowed_k} [\tau_{is}^s(t)]^\alpha \cdot (\eta_{is}^s)^\beta \cdot (\mu_{is})^\theta (1+Z_{ij})^\gamma}, j \in allowed_w \\ 0, \quad otherwise \end{cases} \tag{9}$$

Elite Strategy with Threshold. When once iteration of chaos ant colony algorithm is finished, if the total length of one found path is less than the threshold, the pheromone of this path will be increased according to the formula as follows:

$$\tau_{ij}(t+1) = (1-\rho) \cdot \tau_{ij}(t) + \sum_{l=1}^{L} \Delta \tau_{ij}^l \tag{10}$$

$$i = 1,...,N \qquad j = 1,...,K$$

Where ρ is the evaporation rate of pheromone.

Intersection Removal Strategy. Because the zone drawn by the optimal soluton must be a single connected subgraph, the performance of chaos ant colony algorithm will be improved by using the

intersection removal strategy. The intersection removal strategy can be described as two steps as follows:

Step1: For j=1 to n-2

Step2: For k=j+2 to n-1

If d(j, k)+d(j+1, k+1)<d(j, j+1)+d(k, k+1), it is known that there are intersection. Then execute the following operations: replace the old path (j, j+1), (k, k+1).

k=k+1, goto step2;

j=j+1, goto step1;

End

Simulation Experiment

The simulation experiments are carried out by using the improved chaos ant colony algorithm (ICACA) and basic chaos ant colony algorithm (BCACA) separately. The experimental city data are from standard testing library including oliver30, eil51, eil76 and ch130. The factors of chaos ant colony algorithm include: number of ants m=50, maximum number of iterations is 500, $\alpha = 2$, $\beta = 4$, $\theta = 1.5$, $\gamma = 1$, $\rho = 0.9$, $Q = 100$. The experimental results are shown in Table 1.

Table 1 Comparison of the Results of Two Chaos Ant Colony Algorithm

Algorithm	Oliver30	Eil51	Eil76	Ch130
ICACA	421.39	430.02	537.21	6123.67
BCACA	423.79	431.82	550.51	6169.26

The results reflect that the optimal solutions of ICACA are superior to those of BCACA. So ICACA has higher efficiency for finding the optimal solution in traveling salesman problem.

Conclusion

This paper proposes an improved chaos ant colony algorithm named ICACA which is based on return optimization strategy, elite strategy and intersection removal strategy. The ICACA algorithm uses chaos technology to optimize initial solution of the ant colony to improve individual quality and chaos perturbation is utilized to avoid the search being trapped into local optimum solutions. The simulation results show that ICACA has higher efficiency in finding optimal path and it is more suitable for traveling salesmen problem.

References

[1] T.Stutzle, H.Hoos. The MAX-MIN ant system and local search for the traveling salesman problern[C]. IEEE Press, 1997, 308-313.

[2] Marco Dorigo. Ant colonies for the traveling salesman problem [J]. Biosystems, 1997, 43:73-81.

[3] Kuo, R.J., Wang, H.S., Hu T., Chou, S.H.. Application of Ant K-Means on Clustering Analysis. Computers and Mathematics with Applications, 2005, 1709-1724.

[4] Wang Yunwu. Application of Chaos Ant Colony Algorithm in Web Service composition based on QoS. International Forum on Information Technology and Applications, 2009.172: 225-227.

[5] Wei Gong, Shoubin Wang. Chaos Ant Colony Optimization and Application. Fouth International Conference on Internet Computing for Science and Engineering, 2009.38: 301-303.

Advanced Materials Research Vols. 989-994 (2014) pp 2200-2203
© (2014) Trans Tech Publications, Switzerland
doi:10.4028/www.scientific.net/AMR.989-994.2200

An Improved Scheduling Algorithm for Cloud Storage

Pei Wang

Department of Computer Application & Engineer, Hebei Software Institute,Baoding ,China

stony067_w@163.com

Keywords: Cloud storage data; nodes schedule Priority

Abstract. In this paper, the authors briefly describe the development of cloud storage and give an improved cloud storage model. This paper proposes a scheduling algorithm based on Priority(SAP). According to the priority of data block ,the algorithm schedules on mastering the supply and demand of data block comprehensively and accurately, and solves the system's launch delay and the continuity of streaming media player.

Introduction

Cloud computing is a commercial computational model,which combines the IT technology and the Internet to achieve super computing and storage capacity.However,the difference between the cloud storage and the traditional storage is not just the storage space.Storage virtualization is a major feature of cloud storage, which is different from traditional storage.It proposed the concept of a storage device which is from physical to logical.It provides a simple,unified composite structure for enterprise storage resource consumption.Currently,the major high - performance distributed file systems which are used in cloud storage platform all use this concept such as GFS of Google, S3 of Amazon and“Blue Cloud”of IBM.This is the basis of an improved cloud storage model which is proposed in this paper.

With the development of cloud, the concept of“service”in traditional Service-Oriented Architecture (SOA) is extended from software application to generalized “cloud Service”with the inclusion of both software applications and hardware equipments with good interoperability, self-organization and scalability. The properties of cloud services have become more complex and most of them need higher computing ability to drive.

In such environment, when a composite project (which contains a set of tasks)is submitted, the console of conglomerate needs not only to aggregate suitable cloud services with different functionalities and generate service portfolio for user on-demand,but also choose available computing resources to support the running of cloud services. How to achieve high-quality and low cost Services Composition Optimal Selection (SCOS) and Optimal Allocation of Computing Resources(OACR) simultaneously are critical for efficient project execution, green resource sharing and flexible service management.

Analysis of the Current Research Situation

At present, there are lots of methods to study video data management, Such as: RAID, SAN, disk duplexing, partition mirror, single disk array, disk array, Fault-tolerant software hot backup, replication, cluster technology, CDN technology, P2P technology, cloud storage technology and so on.

RAID5 technology uses a block cross access to the data banding of distributed-check data, then writes to all disks in the parity. Data redundancy is provided by the parity information; data and parity information are placed in different disk among disk array. When a disk faults, the read performance will drop because the parity information needs to recover data; on the other hand, due to parity calculations, the use of block cross access to the data banding of distributed-check data is more effective than image-type.

Replication is at the expense of storage capacity to get the scalability of system. Due to increasing hardware storage capacity, the advantages of stripe exist no longer, Therefore, the video server cluster systems use replication technology to implement data distribution now .

By adding a new layer of network architecture to the existing Internet, CDN (Content Delivery Network) technology distributes center content to the nearest users and network "edge" node for the best service capacity; through the intelligent strategy, Which allows users to obtain the required contents, resolves Internet network congestion, and improves users' response time of the web access. With the (Decentralized)approach, P2P technology is such a new network computing technology that uses a large number of dynamic autonomy distribution resources to accomplish specific functional. P2P technology combines with individual users into a network whose bandwidth and information can be shared with.

Cloud Storage Systen Model

We use the general business machines as the underlying storage devices and Hadoop as a platform of cloud storage environment, managing the underlying business called HDFS ,It is shown in Figure1.We discuss the data management algorithms in the data node of cloud storage in this paper.

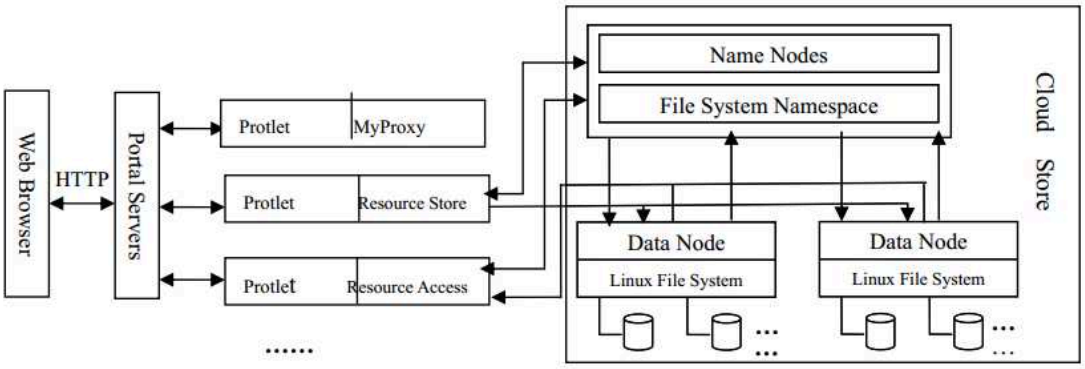

Figure 1 Implementation model of cloud storage

Scheduling Algorithm Based on Priority (SAP)

In streaming model, the existing data scheduling strategy includes the following: Rarest-First strategy (Rarest-First, RF). This strategy is conducive to speeding up the data block in the proliferation of network coverage and improving the overall throughput of the system and getting a better average playing continuity. But because of no taking into account the urgency degree of block elements, it results in a large start delay; Weighted Round-Robin (Weighted Round-Robin, WRR) strategy uses the size of the bandwidth, layer data block priority as the main basis for scheduling to get load balancing, but the chance of improving data is considered inadequately; Greedy strategy, known as the nearest deadline first (nearest deadline first) strategy, provides visually a good start late and playing continuity. But after testing and analysis, this strategy gets poor performance because Greedy strategy will likely lead to decline the shared probability of data blocks gradually and result in the performance reduce for overall system, eventually it makes each node of the playback not be achieved; Random strategy selects an ongoing request randomly from the partners node, this strategy's performances is not very stable, especially in the heterogeneous network environment. For the problems of scheduling algorithms and the cloud storage system, we propose a scheduling algorithm based on priority(SAP). According to the priority of data block, the algorithm schedules on mastering the supply and demand of data block comprehensively and accurately. The experimental results show that SAP algorithm has further improved in playing continuity and launch delay than the minimum priority scheduling algorithm.

Algorithm Description:

(1) According to descending order of scheduling priority of data block sequence is A1, A2, ..., Am;

(2)The corresponding sequence of data blocks has a collection of nodes are S1, S2, ..., Sm;

(3) Sending rate of all the neighbor nodes are R (1), R (2), ..., R (n);

(4) In the current scheduling cycle, the expected send wait time of each neighbor is Wait (1), Wait (2), ..., Wait (n), the initial values are 0.

Output Each data block has a sending node sender Ai

Algorithm: max get $\leftarrow \min(m, \tau \times I)$; / / Current scheduling cycle can receive the maximum number of data blocks

for i = 1 to get max do

$t_{\min} = \infty$ / / initialize for the first time Ai

for j = 1 to k do

$t_{deliver} = \frac{Lenght}{R_j^i}$ / / obtained Ai expected time from the Sj

if $t_{deliver}$ + Wait (S_j^i) < $t_{\min}$ and $t_{deliver}$ + Wait (S_j^i) <τ

$t_{\min} \leftarrow t_{deliver} + Wait(S_j^i)$ $\text{sender}_i \leftarrow S_j^i$;

end for j;

if $\text{sender}_i \neq$ null

Wait (sender_i) $\leftarrow t_{\min}$;

end for i;

Experiment and Result Analysis

We use NS2 as a simulator, and the output bandwidth of the user nodes is [200,600]Kb/s, access bandwidth is [400,1000] Kb/s, server output bandwidth is 100Mb/s. Streaming media file playback time is 30min in the data nodes of cloud store. Users join the network node shows Poisson distribution. Streaming media file playback speed is 400Kb/s. In order to compare the performance of SPA algorithm in the simulation experiment,Also implement the same strategy of the RF, Simulation results are Figure2 and Figure3 thought comparing.

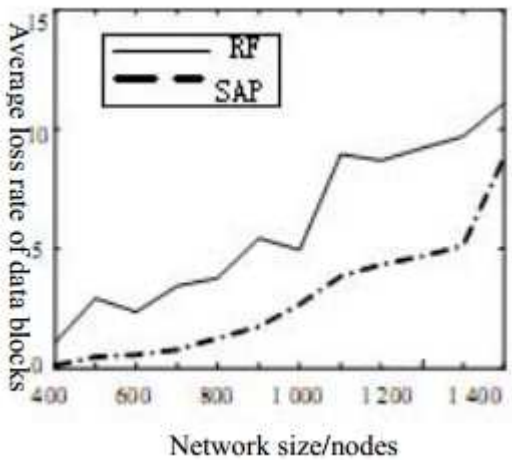

Figure2 Average loss rate of data blocks

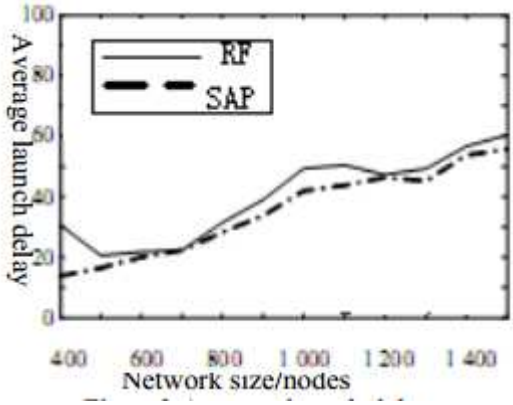

Figure3 Average launch delay

We can be seen indicators curve growth is slow and smooth from the above of the experimental, It is indicating that data of scarcity degrees and high urgent data blocks will be scheduling priority in the same bandwidth conditions, and can effectively reduce the loss rate, improve the system Continuous playback. System startup launch is correspondingly reduced.

References

[1] Rajib Mall, “Real-Time Systems, Theory and Practice”, Dorling Kindersley (India) Pvt. Ltd., licensees of Pearson Education in South Asia, 2007.

[2] Hermann Kopetz, “Real-Time Systems Design Principles for Distributed Embedded Applications”, Second Edition, Springer, 2011

[3] J. Stankovic, “Misconceptions about Real-Time Computing”, IEEE Computer, 21, October 1988.

[4] Agarwal V, Rejaie R. Adaptive Multi-source Streaming in Heterogeneous Peer-to-Peer Networks [C]. Proceedings of the 12th Annual Multimedia Computing and Networking. [S. 1.]:ACM Press, 2005: 102 - 109 .

[5] Zhou Yipeng, Chiu Dah, Lui Ming.A Simple Model for Analyzing P2P Streaming Protocols [C]. Proceedings of IEEE ICNP'07. [S. 1.]: IEEE Press, 2007: 226-235.

[6] Pai V, Kumar K. Chainsaw: Eliminating Trees from Overlay Multicast [C] / / Proceedings of the 4th International Workshop on Peer-to-Peer Systems. [S. 1.]: IEEE Press, 2005: 127-140 . Network size/nodes Figure2 Average loss rate of data blocks

[7] Chang F, Dean J, Ghemawat S, et al.Bigtable: A distributed storage system for structured data [C]. Proceedings of the 7th USENIX Symposium on Operating Systems Design and Implementation OSDI 06,2006.

[8] Amazom Simple Storage Service (S3).http://www.amazon.com/s3/,2009

[9] Jaliya Ekanayake and Shrideep Pallickara. MapReduce for Data Intensive Scientific Analyses.4th IEEE International Conference on e-Science,Indianapoils,Indiana,2008

[10]Likun Liu,Yongwei Wu,Guangwen Yang,and Weimin Zheng .Zettads:A Light-weight distributed storage system for cluster.In Processing of the 3rd ChinaGrid Annual Conference ,2008

Advanced Materials Research Vols. 989-994 (2014) pp 2204-2207
© (2014) Trans Tech Publications, Switzerland
doi:10.4028/www.scientific.net/AMR.989-994.2204

A New Spatial Correlation Model Based on the Distributed RC-π Model

Xiaoxiao Liu[1, a], Jingbo Shao[2,b] and Lingling Zhao[1,c]

[1]College of Information, Beijing City University, Beijing 100083, China

[2] Department of Computer Science and Information Engineering, Harbin Normal University, Harbin 150025, China

[a]lxx535@163.com, [b]zro_bo@163.com, [c]zhaolingling@bcu.edu.cn

Keywords: RC-π Model; Spatial Correlation; Process Variations

Abstract. To solve the crosstalk noise question in deep-submicron technologies, a new spatial correlation model based on the distributed RC-π model is proposed in this paper. Quiet aggressor net and tree branch reduction techniques are introduced to the distributed RC-π model, and a new spatial correlation model of both Gaussian and non-Gaussian process variations among segments is created. Experimental results show that our method maintains the efficiency of past approaches, and significantly improves on their accuracy.

1. Introduction

The increase in package density as well as the clock frequency of the VLSI circuits has made interconnect parasitic effects become increasingly significant, and crosstalk noise is one of the most challenging problems in the design and verification of modern VLSI circuits. The statistical model of [1] uses a lumped RC model to explore crosstalk-induced pulse effect, where a single resistance is extracted to capture the effect of total self resistance of interconnect, regardless of its length. The case for self and coupling capacitances is similar. The statistical model proposed in [2] is more sophisticated and uses a circuit model with higher number of nodes; however, still a single capacitance is extracted to model the total coupling effect, which makes it inappropriate for long interconnect lines. The authors of [3] apply distributed RC-π model to study the statistics of crosstalk effect, but the complexity of model reduction becomes huge because of considering process variations.

In this paper, a new spatial correlation model based on the distributed RC-π model is proposed to solve on-chip crosstalk noise. The paper is organized as following: In section 2, quiet aggressor and tree reduction techniques in distributed RC-π model is presented to reduce the complexity of circuit model. In section 3, the grid-based model is used to generate the spatial correlation among each neighboring segments of reduced distributed RC-π model. Section 4 shows experimental results while section 6 concludes this paper.

2. Reduction of distributed RC- π model

Consider three coupled interconnect lines in some metal layer, which lies in between two dielectric plates (cf. Fig. 1(a)). The three interconnect lines run in parallel and are capacitively coupled. A distributed RC-π model (cf. Fig. 1(b)) is used to accurately model the abovementioned interconnect line configuration. In this circuit, each RC-π stage represents an interconnect segment of a predefined length, L_{seg}, which is an important factor when considering spatial correlation among physical parameters as will be explained in section 4. The couplings between each two interconnect lines along segment *i* are captured by the coupling capacitances $C_{i,1c2}$, $C_{i,1c3}$, $C_{i,2c3}$, respectively. The self capacitance and resistance of line II in segment *i* are denoted by $C_{i,2}$ and $R_{i,2}$, respectively. Note that although lengths of all wire segments are identical, due to process variations, parameter values for each segment are different from those for other segments.

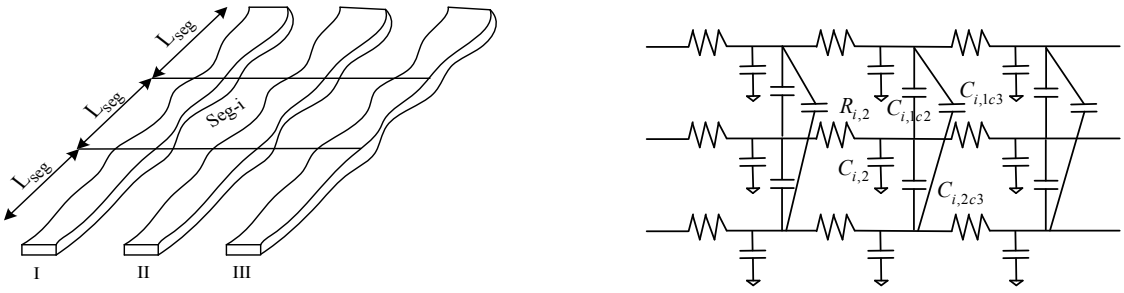

(a) (b)

Fig. 1 Distributed capacitive modeling of coupled interconnects

In general, a net has a tree structure instead of being a simple wire. Millions of interconnect lines in VLSI circuit limit the application of distributed RC-π model in real design. [4] presents the quiet aggressor and tree reduction techniques and used a 6 node template circuit for fast crosstalk estimation, however, 6 node template circuit is not suitable to the crosstalk noise analysis of interconnects in deep submicron process. In this section, we introduce quiet aggressor and tree reductions to distributed RC-π model and present a novel quiet aggressor and tree reduction techniques for distributed RC-π model as shown in Fig. 2. Fig. 2(a) shows the quiet aggressor reduction process to reduce aggressors non-switching and not switching simultaneously with victim V in segment i; Fig. 2(b) shows the tree branches reduction process of the victim or aggressor in distributed RC-π model. Effective capacitances $Ceff_{ia}$ and $Ceff_{at}$ can be easily derived by matching the lower order Taylor series expansion coefficients of the admittances at the coupling point and branching point, correspondingly.

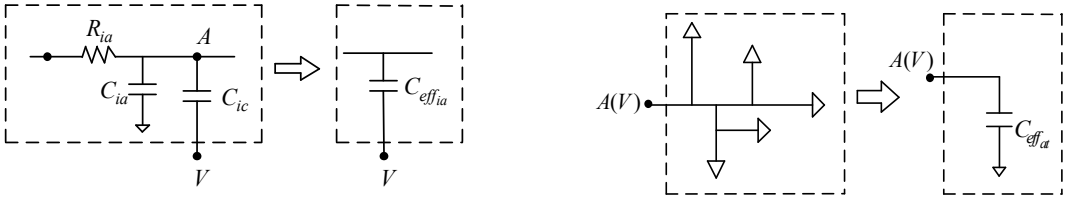

(a) Quiet aggressor net reduction (b) Tree branches reduction

Fig. 2 Reduction process of distributed RC-π model

Therefore, using quiet aggressor net and tree reduction techniques the crosstalk noise estimation problem for a general RC tree structure circuit is transformed to a much simpler one of solving the reduced distributed RC-π circuit, which not only improves the accuracy and efficiency of crosstalk noise analysis but also makes our proposed approach be applicable to real design.

3. Spatial correlations

In our method, we assume statistical independence between Gaussian and non-Gaussian parameters. The spatial correlation among the variation of neighboring segments is quiet important in the crosstalk noise of the victim interconnect. For example most of the variation resulting from chemical-mechanical polishing of the inter-layer dielectric is based on systematic spatial effects and vanes within-die. In this paper, we employ grid-model to generate the exacter spatial correlations of process variables in segments of reduced distributed RC-π model. We partition the die into $g_{row} \times g_{col} = g$ grids, as shown in Fig. 3.

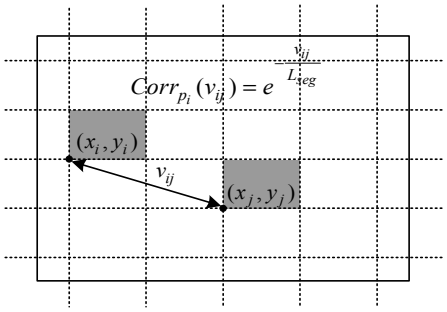

Fig. 3 The grid-model of spatial correlations

Since segments close to each other are more likely to have more similar characteristics than those placed far away, we assume perfect correlations among the segments in the same grid, high correlations among those in nearby grids and low or zero correlations in faraway grids. The correlation function $Corr(x_i, x_j, y_i, y_j)$ between any two points (x_i, y_i) and (x_j, y_j) in the grid depends only on the distance v_{ij} between them, as follows:

$$Corr(x_i, x_j, y_i, y_j) = Corr(\sqrt{(x_i - x_j)^2 + (y_i - y_j)^2}) = Corr(v_{ij})$$

It has been observed that the spatial correlation function $Corr(v_{ij})$ is a monotonically decreasing function of distance v_{ij}. However, not all monotonically decreasing functions qualify for the spatial correlation function. A necessary and sufficient condition for function $Corr(v_{ij})$ to be a valid spatial correlation function of a homogeneous and isotropic random field is that it can be represented in the form of [5]:

$$Corr(v_{ij}) = \int_0^\infty J_0(wv_{ij}) d(\phi(w)) \tag{1}$$

where $J_0(t)$ is the Bessel function of order zero and $\phi(w)$ is a real nondecreasing function on $[0, \infty]$ such that for some non-negative p:

$$\int_0^\infty \frac{d\phi(w)}{(1+w^2)^p} < \infty$$

In this paper, $\phi(w) = 1 - 1/\sqrt{1 + w^2 L_{seg}{}^2}$. By plugging it into Eq. (1), we obtain the corresponding correlation function as:

$$Corr(v_{ij}) = \exp(-v_{ij} / L_{seg})$$

where L_{seg} is a predefined segment length that regulates the decaying rate of the correlation function with respect to distance v_{ij}. The spatial correlation in this paper is an exponential decay function of distance, but our RD-SCNA algorithm doesn't limit to exponential function.

In addition, we assume that correlation exists only among the same type of parameters and there is no correlation between different types of parameters. For each type of parameter in reduced distributed RC-π model, a sparse correlation matrix M of size $g \times g$ represents the spatial correlations of such a structure.

$$M = \begin{bmatrix} 1 & Corr(v_{12}) & Corr(v_{13}) & \dots & Corr(v_{1g}) \\ Corr(v_{12}) & 1 & Corr(v_{23}) & \dots & Corr(v_{2g}) \\ Corr(v_{13}) & Corr(v_{23}) & 1 & \dots & Corr(v_{3g}) \\ . & . & . & & . \\ Corr(v_{1g}) & Corr(v_{2g}) & Corr(v_{3g}) & \dots & 1 \end{bmatrix}$$

4. Experimental results

To verify the effect of our quiet aggressor and tree reduction techniques in distributed RC-π model, we have applied the proposed method to 7 noise-prone nets from a high-performance processor designed in a 0.15 micron process technology. In those nets, the drivers of the circuits were replaced by linear resistors using the technique described in [6]. Each piece of distributed circuitry consisting of 25 RC-π stages is used. Assume process variations in those nets are Gaussian and statistical independent.

Some information of the circuits and comparison of our model results with Spice simulation and simple approach proposed in [3] are shown in Table 1. The second column shows the number of total aggressor nets and number of switching aggressor nets. The third column is the total number of RC elements in a given circuit. The average number of all the nets is 154. The lengths of the victim nets in millimeters are shown in the fourth column with an average victim net length of 2.1mm. Table 1 shows that the average error of the peak noise voltage values calculated using the proposed model is 3.7%, while the simple approach has an average error of 9.1%. The proposed approach significantly improves the accuracy of crosstalk noise analysis with using the quiet aggressor and tree reduction in distributed RC-π model.

Table 1 Experimental results on peak noise voltage

Circuit	Na/Ns	#RC	Len(mm)	Spice(V)	Simple(Err%)	Proposed(Err%)
1	2/2	97	1.49	0.841	0.789(6.2)	0.889(5.7)
2	9/9	215	2.80	0.807	0.713(11.6)	0.792(1.8)
3	4/4	132	2.62	0.799	0.709(11.3)	0.816(2.1)
4	5/5	128	2.80	0.796	0.692(13.1)	0.812(2.0)
5	7/6	144	0.71	0.731	0.715(2.2)	0.771(5.5)
6	3/3	116	1.70	0.664	0.627(5.6)	0.643(3.2)
7	10/9	247	2.75	0.651	0.564(13.4)	0.613(5.8)
AVE	5.7/5.4	154	2.1	-	9.1%	3.7%

5. Conclusions

In this paper a new spatial correlation model based on the distributed RC-π model was presented. The merits of our approach include: 1) Quiet aggressor and tree reduction technologies in distributed RC-π model are proposed to reduce the complexity of circuit model; 2) A new spatial correlation model is proposed for random variables in reduced distributed RC-π model, which makes our method enable to consider effects of all the correlated and independent process variations. Experimental results show that compared to other methods our approach significantly improves the crosstalk analysis accuracy by handling a larger range of variables while maintaining the efficiency by using reduced distributed RC-π model.

6. Acknowledgements

This work was supported by On-campus Innovative Practice Base Construction of Beijing City University funded by Development and Promotion of Non-governmental Education Program of Beijing Municipal Education Commission in 2013.

References

[1] Maurizio Martina, Guido Masera. A statistical model for estimating the effect of process variations on crosstalk noise. Proceedings of the International Workshop on System Level Interconnect Prediction, Paris, 2004, 115-20.

[2] Agarwal K, Agarwal M, Sylvester D, Blaauw D. Statistical interconnect metrics for physical-design optimization. IEEE Transactions on Computer-Aided Design of Integrated Circuits and Systems, 2006, 25(7) : 1273-88.

[3] Shahin Nazarian, Ali Iranli, Massoud Pedram. Corsstalk analysis in nanometer technologies. Proceedings of the 16th ACM Great Lakes symposium on VLSI, Philadelphia, 2006, 253-8.

[4] Li Ding, David Blaauw, Pinaki Mazumder. Accurate crosstalk noise modeling for early signal integrity analysis[J]. IEEE Transactions on Computer-Aided Design of Integrated Circuits and Systems, 2003, 22(5) : 595-600.

[5] Jinjun Xiong, Vladimir Zolotov, Lei He. Robust extraction of spatial correlation. Proceedings of the 2006 international symposium on Physical design, California, 2006, 2-9.

[6] Rafi Levy, David Blaauw, Gabi Braca, Aurobindo Dasgupta, Ami Grinshpon, Chanlee Oh, et al. ClariNet: a noise analysis tool for deep submicron design. Proceedings of the 37th conference on Design automation, Los Angeles, 2000, 233-8.

Advanced Materials Research Vols. 989-994 (2014) pp 2208-2211
© (2014) Trans Tech Publications, Switzerland
doi:10.4028/www.scientific.net/AMR.989-994.2208

Study on modeling of the minimum lethal dose while rescue poisoning

Cuixin Zhao[1], Yue Jiang[2] , Hao Yang *[3,4] , Mengtian Cui *[,2,3]

[1]School of Mathematics &Statistics, Chifeng College, Chifeng 024000, PR China

[2]School of Computer Science and Technology, Southwest University for Nationalities, Chengdu 610041, PR China

[3]School of Computer Science & Engineering, University of Electronic Science &Technology of China, Chengdu 610041, PR China

[4]School of Computer Science, University of Nottingham, NG8 1BB, UNITED KINGDOM
* Corresponding author

Keywords: Half-Life; Blood concentrations; Transfer rate; Linear differential equations

Abstract. The minimum lethal dose of the children and adults taking aminophylline tablets and severe poisoning is discussed in the paper. Linear differential equations and function image are both introduced to analysis timely rescue methods of the human during poisoning. Meanwhile, modeling is provided and the model solution is given. In the end, the simulation results showed the fatal time of the smallest dose and effective rescue when taking aminophylline poisoning.

Introduction

The child has been mistakenly swallowed dose 100mg / tablets aminophylline eleven before two hours and he has vomiting, dizziness and other adverse symptoms. According to the Drug instructions, aminophylline dosage taken per adult is 100~200*mg*, children are 3~5*mg*, overdose can lead the blood concentration (dosage units of blood volume) too high. When the blood concentration is over100*ug/mg* there will be severe poisoning concentration; when the blood concentration is over 200*ug/mg*, it can lead to be fatal. Body taking certain drugs, blood plasma concentration is concerned to the total amount of blood. Typically, the total amount of blood is accounted for 7%~8% in the body weight and the blood is about 4000*ml* adult who weight is about 50~60*kg*. Now, the child's weight is about half of adult, so the blood can be considered about 2000ml. Thus, between the blood plasma concentration of the system and the amount of the drug can be converted to each other. The blood drug absorption and elimination rate can be determined by half-life. As can be seen from the manual, half-life of theophylline absorption is about 5 hours and half-life of exclude is about 6 hours.

Assumptions and model establishment

The drug transfer rate of the drug flowing into the blood in the gastrointestinal tract is proportional to $x(t)$, factor λ ($\lambda > 0$), the dose of 1100*mg* drug instantly flow into the gastrointestinal tract when $t = 0$. The drug exclusion rate of the drug in the blood is proportional to $y(t)$, factor μ(μ>0), no drug when $t = 0$.half-life of theophylline absorbed is 5 hours, exclude the period is 6 hours. The total amount of the child's blood is 2000*ml*.Model establishment is show in Figure 1.

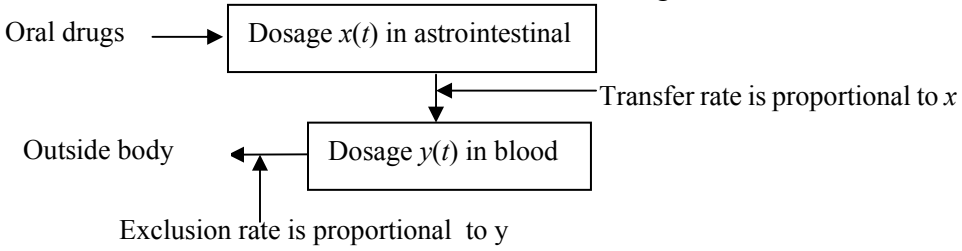

Figure 1. Model establishment

Where, $x(t)$ is lowering speed is proportional to $x(t)$, 1100mg drug flow into the gastrointestinal tract at the moment.

$$\frac{dx}{dt} = -\lambda x, \qquad x(0) = 1100$$

Growth rate of absorption $y(t)$ is λx, the speed reduced by the exclusion is proportional, where t=0 no drug in the blood.

$$\frac{dx}{dt} = \lambda x - \mu y, \qquad y(0) = 0$$

Model solving

$$\frac{dx}{dt} = -\lambda x, x(0) = 1100 \Rightarrow x(t) = 1100e^{-\lambda t}$$

The half-life of drug absorption is 5 hours.

$$\Rightarrow x(5) = \frac{x(0)}{2} \Rightarrow 1100e^{-\lambda t} = \frac{1100}{2} \Rightarrow \lambda = \frac{(\ln 2)}{5} = 0.1386(1/h)$$

$$\begin{cases} \dfrac{dy}{dt} = \lambda x - \mu y = -\mu y + 1100\lambda e^{-\lambda t} \\ y(0) = 0 \end{cases} \Rightarrow y(t) = \frac{1100\lambda}{\lambda - \mu}(e^{-\mu t} - e^{-\lambda t})$$

The half-life of the drug exclusion is 6 hours when considering only the blood of drugs excluded.

$$\Rightarrow \begin{cases} \dfrac{dy}{dt} = -\mu y \Rightarrow y(t) = ae^{-\mu(t-\tau)} \\ y(\tau) = a, y(\tau + 6) = \dfrac{a}{2} \end{cases} \Rightarrow \mu = \frac{\ln 2}{6} = 0.1155(1/h)$$

Results and analysis

The drug dose of the gastrointestinal tract is $x(t) = 1100e^{-0.1386t}$ and the drug doses of blood system is $y(t) = 6600(e^{-0.1155t} - e^{-0.1386t})$ and the total amount of the child's blood is 2000ml, so the following is given:

Case 1: Blood concentration serious poisoning is 100ug/ml and the drug content of the blood system is *y(t)*=2000ml×100ug=200mg;

Case 2: Blood concentration when fatal is 200ug/ml and the drug content of the blood system is *y(t)*=2000ml×200ug=400mg.

The Matlab program is as follows.

```
t=0:0.01:25;
y1=1100.*exp(-0.1386.*t);
y2=6600.*(exp(-0.1155.*t)-exp(-0.1386.*t));
plot(t,y1,'b',t,y2,'m');
xlabel('t/h');
ylabel('y/mg');
grid on;
legend('y1 curves of dose in gastrointestinal tract',' y2 curves of dose in blood ');
max(y2);
```

The change compared is showed in figures. *x(t)* and *y(t)* curves of dose level changing with time and gastrointestinal dose *x(t)*, blood dose *y(t)* of curves of dose level changing with time is showed in Figure 3.

It is showed from the figure 3, when t=1.62, the drug dose of blood system has been reach 200mg.so, it is very serious while the child was sent to the hospital in the medication after 2 hours.

$y(2) \approx 236.5mg > 200mg$

When t=4.87 hours the drug dose of blood system has been reach 400mg, which is a fatal. So, if the child is not promptly for treatment, he would be dead after 2.87 hours.

Rescue plan

1. Oral activated charcoal

Oral activated charcoal drug elimination rate is increased to two times of the original, then, μ=0.1155×2=0.2310.Child is rescued when he arrive at the hospital (t=2) , the blood of the dosage is marked as $z(t)$.

$$\frac{dz}{dt} = \lambda x - \mu z, t \geq 2$$

$$x = 1100e^{-\lambda t}, z(2) = 236.5$$

$$z(t) = 1650e^{-0.1386t} - 1609.5e^{-0.2310t}, t \geq 2$$

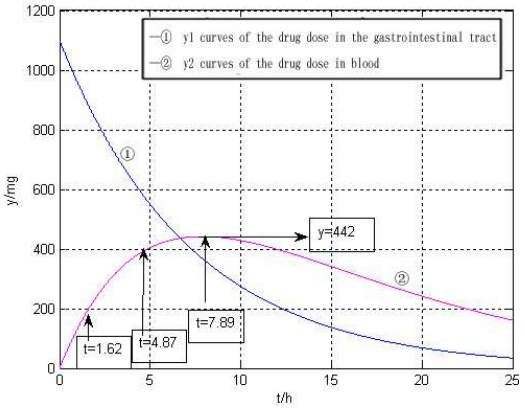

Figure 2. *x(t)* and *y(t)* curves of dose level changing with time

The Matlab program is as follows.

```
t=0:0.01:25;
t1=2:0.01:25;
y1=1100.*exp(-0.1386.*t);
y2=6600.*(exp(-0.1155.*t)-exp(-0.1386.*t));
y3=1650.*exp(-0.1386.*t1)-1609.5.*exp(-0.2310.*t1);
plot(t,y1,'b',t,y2,'m',t1,y3,'r');
xlabel('t/h');
ylabel('y/mg');
grid on;
legend('y1 curves of dose in gastrointestinal tract',' y2 curves of dose in blood  before intervening','y3 curves of dose in blood after intervening ');
```

Now, *x(t)* and *y(t)* curves of dose level changing with time is showed in Figure 3.

Analysis

From the *x(t)* and *y(t)* curves of dose level changing with time showed in figure 3,we find that the blood of the dosage after intervening *z(t)* is well below critical levels *y(t)*, $z(t)_{\max} = 318$. Although the use of oral activated charcoal adsorption method make the blood of the dosage *z(t)* rising was continued for some time, while when t=5.26 it began to drop, which show that the drug elimination rate increased is not enough.

2. Vitro blood dialysis

Hemodialysis makes the drug elimination rate increased to 6 times of the original. Then, μ=0.1155×6=0.693. Child is rescued when he arrive at the hospital (t=2) , the blood of the dosage is marked as $z'(t)$. then, $z'(t) = 275e^{-0.1386t} - 275e^{-0.2310t}, t \geq 2$.

The Matlab program is as follows.

```
t=0:0.01:25;
t1=2:0.01:25;
y1=1100.*exp(-0.1386.*t);
y2=6600.*(exp(-0.1155.*t)-exp(-0.1386.*t));
```

```
y3=275.*exp(-0.1386.*t1)-275.*exp(-0.693.*t1);
plot(t,y1,'b',t,y2,'m',t1,y3,'r');
xlabel('t/h');
ylabel('y/mg');
grid on;
legend(('y1 curves of dose in gastrointestinal tract',' y2 curves of dose in blood  before intervening",'y3 curves of dose in blood after intervening');
```

Now , *x(t)* ,*y(t)* and *z'(t)* Curves of dose level changing with time is showed in Figure 4.

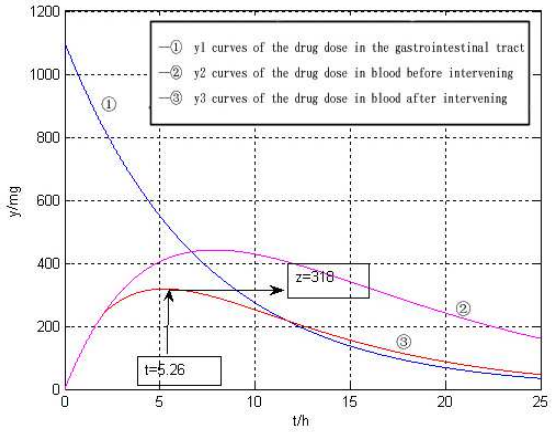

Figure 3. *x(t)* and *y(t)* curves of dose level changing with time

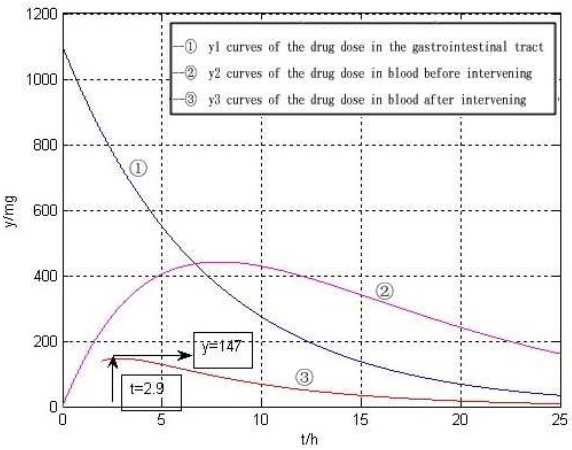

Figure 4. *x(t)* ,*y(t)* and *z'(t)* curves of dose level changing with time

Analysis:

From *x(t)* ,*y(t)* and *z'(t)* Curves of dose level changing with time showed in figure 4,we find that the blood of the dosage declined faster after Hemodialysis, when *t*=2.9 it begin declining and the blood of the dosage *z'(t)* is Significantly below *y(t)* and *z'(t)* is Significantly below lethal levels. $z'(t)_{\max} = 147$.

Acknowledgments

This work was financially supported by the National Natural Science Foundation of China(61379019), China Postdoctoral Science Foundation(2013M540704), Special Funds for China Postdoctoral Science Foundation, the Leaders in Academic and Technical Training Foundation of Sichuan Province, Research Special Funds for the Post-doctor of Sichuan Province, the Fundamental Research Funds for the Central Universities (2014NZYQN27) and the fellowship from the China Scholarship Council (201206070041).

*** Corresponding author**

Email address: happyzg3@163.com (Mengtian Cui), yanghaome@gmail.com (Hao Yang)

References

[1] Liu Weiguo.*MATLAB program (Second Edition)*,Beijing: Higher Education Press,.2006

[2] Jiang Qiyuan. *Mathematical Model*, Higher Education Press, 1993,215.

[3] *Economic History of Mathematics and tree* ,Dalian University of Technology Press, 2008, p.98.

[4] Jiang Qiyuan. *Mathematical Model*, Higher Education Press, 1993,p.37

[5] Easley, D., and J. Kleinberg. 2010. Networks, Crowds, and Markets: Reasoning About a Highly ConnectedWorld. NewYork: CambridgeUniversity Press

[6] Saaty, Thomas L. Strategy and Organization, T*he Analytical Hierarchy Process for Decisions in a ComplexWorld. Belmont*, CA: Lifetime Learning Pub. 1982.

Advanced Materials Research Vols. 989-994 (2014) pp 2212-2215
© (2014) Trans Tech Publications, Switzerland
doi:10.4028/www.scientific.net/AMR.989-994.2212

Maneuvering Target Tracking Algorithm Based on Particle PHD Filtering

Gao Song✉, Chen Chaobo, Gong Qian

School of Electronic Information Engineering

Xi ′an Technological University,Xi ′an, 710021, P.R.China

✉ Corresponding author: Gao Song, School of Electronic Information Engineering, Xi ′an Technological University, Xi ′an, 710021, China, gaosong@xatu.edu.cn

Keywords: Target Tracking; Random Sets; Interactive Multiple Model; Probability Density Hypothesis; Sequential Monte Carlo

Abstract. As for the problem of maneuvering target tracking in the clutter environment, this paper combines IMM with PHD and realizes it through approach of particle filter. This algorithm avoids the troublesome problem of data association, and takes advantage of probability hypothesis density (PHD) filter in tracking maneuvering targets and interacting multi-model (IMM) algorithm in the field of model switching effectively, in the clutter environment, the status of the targets can be estimated precisely and steadily. This paper compares the proposed filtering algorithm with the classical IMM algorithm in performance, and the simulation results show that, the improved filtering algorithm has good tracking performance and tracking accuracy.

Introduction

Multiple target tracking in cluttered environment usually needs the data association calculation to determine the correspondence between the observations and the targets[1], the traditional multi-target tracking algorithm based on the association generally require known the number of targets, and the movement of each target is independent, but the increase of number of clutters or targets often leads to the phenomenon of loss and misuse of target, thus making the algorithm fail. Based on this, Mahler proposed the probability hypothesis density (PHD) filter method[2]. PHD filter is different from the traditional multi-target tracking algorithm that based on data association, PHD filter uses a recursive method to deliver the target state distribution of information, thus avoiding the calculation of complex data association, and can get the number of multi-objective and state estimation in the distribution information of target state. For linear Gaussian problem, Vo gives a closed recursive form for PHD filter: GM-PHD filter[3], while for the nonlinear non-Gaussian system, Vo also gives the particle filter implementation for PHD filter: SMC-PHD filter, the basic idea is using the set of points of weighted random sampling to characterize the PHD distribution[4].

This paper reviews the probability hypothesis density filter method and combines the IMM and particle PHD to get the IMM-PHD filter that can track multiple targets. Through the full use of the superiority of IMM algorithm[5-6] in maneuvering target tracking and the superiority of random set theory in an unknown number of multiple target areas, and the combination of statistical theory of random sets and interactive multi-model approach, this paper has verified the feasibility and effectiveness of the algorithm by MATLAB simulation.

The Sequential Monte Carlo IMM-PHD Filter

A. Probability hypothesis density filter (PHD filter)

1) Prediction: The predicted PHD is given by

$$D_{k|k-1}(x_k \mid Z_{1:k-1}) = \gamma_k(X_k) + \int [e_{k|k-1}(x_{k-1}) f_{k|k-1}(X_k \mid X_{k-1}) + b_{k|k-1}(X_k \mid X_{k-1})] \times D_{k-1|k-1}(X_{k-1} \mid Z_{1:k-1}) dx_{k-1} \tag{1}$$

2) Update: The updated PHD at time step k is given by

$$D_{k|k}(X_k \mid Z_{1:k}) \cong [\sum_{z_k \in Z_k} \frac{p_D(x_k) f_{k|k}(z_k \mid x_k)}{\lambda_k c_k(z_k) + \psi_k(z_k \mid Z_{1:k-1})} + (1 - p_D(x_k))] \times D_{k|k-1}(x_k \mid Z_{1:k-1}) \tag{2}$$

Where the likelihood function $\psi_k(Z_k \mid Z_{1:k-1})$ is given by

$$\psi_k(z_k \mid Z_{1:k-1}) = \int p_D(x_k) f_{k|k}(z_k \mid x_k) D_{k|k-1}(x_k \mid Z_{1:k-1}) dx_k \tag{3}$$

B.IMM-PHD

1) The Mixing Stage: In this stage, each mode-matched filter is fed with a different density that is a combination of the previous mode-dependent densities.

$$\tilde{D}_{k|k-1}(x_{k-1}, r_k = q \mid Z_{1:k-1}) = \sum_{p=1}^{N_r} D_{k-1|k-1}(x_{k-1}, r_{k-1} = Z_{1:k-1}) h_{pq}, q = 1,\ldots,N_r \tag{4}$$

2) The Prediction Stage:

$$D_{k|k-1}(x_k, r_k = q \mid Z_{1:k-1}) = \gamma_k(x_k, r_k = q) +$$
$$\int [e_{k|k-1}(x_{k-1}) f_{k|k-1}(x_k \mid x_{k-1}, r_k = q) + b_{k|k-1}(x_k \mid x), r = q] \times \tilde{D}_{k|k-1}(x_{k-1}, r_k = q \mid Z_{1:k-1}) dx_{k-1} \tag{5}$$

3) The Update Stage:

$$D_{k|k}(x_k, r_k = q \mid Z_{1:k}) \cong [\sum_{z_k \in Z_k} \frac{p_D(x_k) f_{k|k}(z_k \mid x_k, r_k = q)}{\lambda_k c_k(z_k) + \psi_k(z_k \mid Z_{k-1})} + (1 - p_D(x_k))] \times D_{k|k-1}(x_k, r_k = q \mid Z_{1:k-1}) \tag{6}$$

Where the likelihood function $\psi(\cdot)$ is given by

$$\psi_k(z_k \mid Z_{1:k-1}) = \int p_D(x_k) f_{k|k}(z_k \mid x_k, r_k = q) D_{k|k-1}(x_k, r_k = q \mid Z_{1:k-1}) dx_k \tag{7}$$

C. Sequential Monte Carlo Implementation

Let the posterior IMMPHD be represented by a set of particles $\{w_{k-1}^{(s)}, x_{k-1}^{(s)}, r_{k-1}^{(s)}\}_{s=1}^{L_{k-1}}$:

$$D_{k-1|k-1}(x_{k-1}, r_{k-1} \mid Z_{1:k-1}) = \sum_{s=1}^{L_{k-1}} w_{k-1}^{(s)} \delta(x_{k-1} - x_{k-1}^{(s)}, r_{k-1} - r_{k-1}^{(s)}) \tag{8}$$

Where $\delta(\cdot)$ is the Dirac Delta function.

1) Prediction:

$$r_{k|k-1}^{(s)} \sim \begin{cases} \pi_k(\cdot \mid r_{k-1}) & s = 1,\ldots, L_{k-1} \\ \beta_k(\cdot) & s = L_{k-1} + 1,\ldots L_{k-1} + J_k \end{cases} \tag{9}$$

Where $\pi(\cdot \mid r_{k-1})$ and $\beta_k(\cdot)$ are probability mass functions, $\{r_{k|k-1}^{(s)}\}_{s=1}^{L_{k-1}}$ are independent and identically distributed model

samples.Then, the predicted IMMPHD is given by

$$\tilde{D}_{k|k-1}(x_{k-1}, r_k \mid Z_{1:k-1}) = \sum_{s=1}^{L_{k-1}+J_k} \varpi_{k|k-1}^{(s)} \delta(x_{k-1} - x_{k-1}^{(s)}, r_k - r_{k|k-1}^{(s)}) \tag{10}$$

Where

$$\varpi_{k|k-1}^{(s)} = \begin{cases} \frac{f_{k|k-1}(r_{k|k-1}^{(s)})}{\pi_k(r_{k|k-1}^{(s)})} w_{k-1}^{(s)} & s = 1,\ldots, L_{k-1} \\ \frac{\theta_k(r_{k|k-1}^{(s)})}{\beta_k(r_{k|k-1}^{(s)})} \frac{1}{J_k} & s = L_{k-1} + 1,\ldots, L_{k-1} + J_k \end{cases} \tag{11}$$

In Eq. 11, the probability mass function $\theta_k(\cdot)$ denotes the model distribution of spontaneous target births at time step k.

We now apply importance sampling to generate state samples that approximate the predicted IMMPHD $D_{k|k-1}(x_k, r_k \mid Z_{1:k-1})$:

$$x_{k|k-1}^{(s)} \sim \begin{cases} q_k(\cdot \mid x_{k-1}, r_{k|k-1}, Z_k) & s = 1,\ldots L_{k-1} \\ p_k(\cdot \mid r_{k|k-1}, Z_k) & s = L_{k-1} + 1,\ldots, + J_k \end{cases} \tag{12}$$

Then, the weighted approximation of the predicted IMMPHD is given by

$$D_{k|k-1}(x_k, r_k \mid Z_{1:k-1}) = \sum_{s=1}^{L_{k-1}+J_k} w_{k|k-1}^{(s)} \delta(x_k - x_{k|k-1}^{(s)}, r_k - r_{k|k-1}^{(s)}) \tag{13}$$

Where

$$w_{k|k-1}^{(s)} = \begin{cases} \frac{e_{k|k-1}(x_{k|k-1}^{(s)}) f_{k|k-1}(x_{k|k-1}^{(s)} \mid x_{k-1|k-1}^{(s)}, r_{k|k-1}^{(s)}) + b_{k|k-1}(x_{k|k-1}^{(s)} \mid x_{k-1|k-1}^{(s)}, r_{k|k-1}^{(s)})}{q_k(x_{k|k-1}^{(s)} \mid x_{k|k-1}^{(s)}, r_{k|k-1}^{(s)}, Z_k)} \varpi_{k|k-1}^{(s)} & s = 1,\ldots L_{k-1} \\ \frac{\gamma_k(x_{k|k-1}^{(s)} \mid r_{k|k-1}^{(s)})}{p_k(x_{k|k-1}^{(s)} \mid r_{k|k-1}^{(s)}, Z_k)} \varpi_{k|k-1}^{(s)} & s = L_{k-1} + 1,\ldots L_{k-1} + J_k \end{cases} \tag{14}$$

2) Update: With the available set of measurements Z_k at time step k, the updated particle weights can be calculated by

$$w_k^{*(s)} = \left[(1 - p_D(\mathrm{x}_{k|k-1}^{s})) + \sum_{i=1}^{N_k^Z} \frac{p_D(\mathrm{x}_{k|k-1}^{(s)}) f_{k|k}(\mathrm{z}_k^i \mid \mathrm{x}_{k|k-1}^{(s)}, r_{k|k-1}^{(s)})}{\lambda_k c_k(\mathrm{z}_k^i) + \Psi_k(\mathrm{z}_k^i)} \right] w_{k|k-1}^{(s)} \tag{15}$$

Where

$$\Psi_k(z_k^i) = \sum_{s=1}^{L_{k-1}+J_k} p_D(\mathrm{x}_{k|k-1}^{(s)}) f_{k|k}(\mathrm{z}_k^i \mid \mathrm{x}_{k|k-1}^{(s)}, r_k^{(s)}) w_{k|k-1}^{(s)} \tag{16}$$

3) Resample: When perform resampling, the expected number of targets is calculated by summing up the total weights

$$\hat{n}_k^X = \sum_{s=1}^{L_{k-1}+J_k} w_k^{*(s)} \tag{17}$$

Now, the discrete approximation of the updated posterior IMMPHD at time step k is given by

$$D_{k|k}(\mathrm{x}_k, r_k \mid Z_{1:k}) = \sum w_k^{(s)} \delta(\mathrm{x}_k - \mathrm{x}_k^{(s)}, \mathrm{r}_k - \mathrm{r}_k^{(s)}) \tag{18}$$

Simulation Analyses

Conducting the experiment in the two-dimensional monitoring region [-20000, 20000]×[-20000, 20000]. Give two models of target motion parameters: set up the sampling interval as T, the probability of target detection as $P_D = 1$, and no false alarm exists, in the Cartesian coordinate system, the target separated motion model and observation model that do uniform motion is $X(k+1)=FX(k)+GW(k)$, $Z(k)=C(k)X(k)+V(k)$,parameters of the uniform linear motion and the uniform circular motion models are:

$$F1=\begin{bmatrix} 1 & T & 0 & 0 \\ 0 & 1 & 0 & 0 \\ 0 & 0 & 1 & T \\ 0 & 0 & 0 & 1 \end{bmatrix} C1=\begin{bmatrix} 1 & 0 & 0 & 0 \\ 0 & 0 & 1 & 0 \end{bmatrix} G1=\begin{bmatrix} \frac{T^2}{2} & 0 \\ T & 0 \\ 0 & \frac{T^2}{2} \\ 0 & T \end{bmatrix} \text{and}$$

$$F2=\begin{bmatrix} 1 & T & 0 & 0 & \frac{T^2}{2} & 0 \\ 0 & 1 & 0 & 0 & T & 0 \\ 0 & 0 & 1 & T & 0 & \frac{T^2}{2} \\ 0 & 0 & 0 & 1 & 0 & T \\ 0 & 0 & 0 & 0 & 1 & 0 \\ 0 & 0 & 0 & 0 & 0 & 1 \end{bmatrix} C2=\begin{bmatrix} 1 & 0 & 0 & 0 & 0 & 0 \\ 0 & 0 & 1 & 0 & 0 & 0 \end{bmatrix} G2=\begin{bmatrix} \frac{T^2}{4} & 0 \\ \frac{T}{2} & 0 \\ 0 & \frac{T^2}{4} \\ 0 & \frac{T}{2} \\ 1 & 0 \\ 0 & 1 \end{bmatrix}$$

The sampling period is 2s, conduct observation on x and y independently, standard deviation of noise observation is 100m, the centripetal acceleration is 5m/s. Figure 1 and Figure 2 are the simulation results.

(a) Classic interactive model filtering algorithm (b) The improved filter algorithm

Fig.1 RMSE in x direction

(a) Classic interactive model filtering algorithm (b) The improved filter algorithm

Fig.2 RMSE in y direction

It can be seen from Fig.1, the improved filtering algorithm's tracking accuracy is superior to the general interacting multiple model filtering algorithm's in the x direction, and the same can be seen from Fig.2, the improved filtering algorithm's error standard difference is also less than the classic interacting multiple model filtering algorithm's in the y direction.

In the simulation, the general IMM filtering algorithm and interactive multi-model probability hypothesis density filter algorithm with sequential Monte Carlo sampling method are compared. The position estimation error standard deviation curve of IMM-KF filter algorithm and the IMM-PHD filter algorithm are given above. At the beginning, the filtering error is greater, but as time goes on, the filtering error has been reduced, and gradually approached the true trajectory estimate. And from the above comparison figures, it is clear that the filtering results of use the probability hypothesis density (PHD) with interactive multiple model (IMM) filtering algorithm is better than the filtering results of using the interacting multiple model (IMM) filtering algorithm of general kalman filtering method.

Conclusions

Taking into account the nonlinear non-Gaussian case in multi-target tracking in clutter, this paper uses sequential Monte Carlo method to conduct IMM-PHD filter, PHD filter effectively reduces the complex calculation in target tracking, and SMC sampling method can make the filter operate in nonlinear non-Gaussian condition. This paper uses an interactive multi-model, which can enhance the accuracy of filter for handling maneuvering target greatly. By comparing IMM-KF filter and SMC-IMMPHD filter, the simulation experiment shows that the use of SMC-IMMPHD comparison algorithm can effectively improve the effect of multi-target tracking.

Acknowledgment

Work described in this paper was supported in part by the Natural Science Foundation of China under grant 61271362 and the Ministry of education of overseas returnees scientific research plan project.

References

[1] Carine Hue, Jean-Pierre Le Cadre, and Patrick Perez. Sequential Monte Carlo Methods for Multiple Target Tracking and Data Fusion. IEEE Transactions on Signal processing, vol.50, pp. 309-325, 2002.

[2] Mahler, and Ronald P S. Statistical Multisource-Multitarget Information Fusion. Artech House, Feb. 2007.

[3] Ba-Ngu Vo, and Wing-Kin Ma. The Gaussian mixture probability hypothesis density filter. IEEE Transactions on Signal Processing, vol.54, pp. 4091-4104, 2006.

[4] Ba-Ngu Vo, and Sumeetpal Singh. Sequential Monte Carlo Implementation of the PHD Filter for Multi-target Tracking. Proc. Fusion vols.1-2, pp. 792-799, 2003.

[5] Dahmani Mohammed, Keche Mokhtar, and Ouamri Abdelaziz. A new IMM algorithm using fixed coefficients filters (fastIMM). AEU - International Journal of Electronics and Communications, vol.64, pp.1123-1127, Dec. 2010.

[6] Ilke Tukmen. IMM fuzzy probabilistic data association algorithm for tracking maneuvering target. Expert Systems with Applications, vol.34, pp.1243-1249, 2008.

[7] Tan-Jan Ho. A switched IMM-Extended Viterbi estimator-based algorithm for maneuvering target tracking. Automatica, vol.47, pp.92-98, Jan. 2011.

[8] Clark D E, and Bell J. Convergence results for the particle PHD filter. IEEE Transactions on Signal Processing, vol.54, pp. 2652-2661, July. 2006.

Advanced Materials Research Vols. 989-994 (2014) pp 2216-2219
© (2014) Trans Tech Publications, Switzerland
doi:10.4028/www.scientific.net/AMR.989-994.2216

Applying grey system theory in an ideological and political education course

Meng Zhang

Editorial Department of journal, Xinxiang University, Henan, China, 453003

837457026@qq.com

Keyword: grey system, mathematical model

Abstract: Professional skills are important to students who major in ideological and political education. They must be able to conduct the tasks required by the teaching of political activities. Evaluation of the student's skills can offer a theoretical basis for measuring a ideological and political course, but an effective evaluation method is lacking. Therefore, an evaluation method based on the grey system theory is proposed in this article. First, the educational structure of the ideological and political education is discussed; second, the mathematical model of grey system theory is presented; and third, the structure of the professional skills evaluation model of students majoring in ideological and political education is presented. The evaluation index system, the results of which are drawn from a questionnaire distributed to 800 students, and the evaluation program, is put forward. A case study was carried out, the results of which show that the evaluation method outlined here can contribute to improving overall standards in the course.

Introduction

The grey system theory, initiated in 1982, is the mathematical theory that solves problems where there is incomplete information. The grey system theory can be used to crystallize and quantify the evaluation of students' abilities on ideological and political education courses. Conclusions can be drawn from the data even though all of the underlying rules are not understood.

Grey relational analysis is a new method in the grey system theory. In grey relational analysis a system with no information is black and a system with perfect information is white; these extremes are unlikely in real situations. Grey relational analysis is used to analyse the relationships between the various factors of a system.

At present, the gray forecast method has been used in agriculture, energy, ecology, environment, economy, finance and other fields, and solves a large amount of the problem, reflects the important theoretical research and practical application value. Many scholars discuss research and develop for the use of grey forecasting model, the research and development. Such as Li Yueqiu (2013) combindwith a concrete instance. According to grey forecasting model, multiple prediction methods are proposed, and the advantages and disadvantages of each method are summarized. Chen Jinlong (2010) used GM (1, 1) grey forecasting model to forecast the non-performing loans of commercial Banks, and the relevant financial institutions operating conditions of early warning. Family filial piety jung (2010) in gansu province in recent years, analysis GDP data, GM (1, 1) prediction model is established, the empirical test shows that the prediction model is reliable.

With the expansion of higher education in China, improving students' education is a key goal. Higher education should focus on developing both the innovative and practical abilities of students, as well as their personal and academic qualities. In recent years, there has been a high demand for students studying ideological and political education. ideological and political education skills are necessary for all sporting activities and students studying ideological and political education. should havegood practical skills for observation, expression and communication [1].

The ideological and political education. student's professional goal is to teach and to provide guidance. At present there are disadvantages for the ideological and political education students in

developing their skills and evaluating their abilities on ideological and political education courses. Reform of teaching must be continued and deepened, so as to improve students' skills.
The relational degree is a measure of the relationship between all factors and can be used to evaluate PE students' abilities. There are many uncertainties in evaluating the abilities of PE students, and this implies that students' abilities can be regarded as grey, and suitable for analysis using the grey system theory.

Students Majoring In

The abilities of students studying PE are poor and do not meet the requirements of colleges or society. This affects their employment opportunities. The problems with PE teaching are as follows [2]:

First, the structure of the curriculum is inappropriate and the basics are not properly emphasised. The time allocated to different components of the course is incorrect, and the theoretical and technical subjects are not properly arranged. The course content is bland and the scope is narrow.

Second, the teaching of the practical sessions is weak. The teaching of practicals is dominated by practice as it should be but should not be limited to it; for example, the graduate may be expected to engage in physical activities in society and in group fitness instruction. The range of the practical teaching is narrow and the time spent on it short. The time allocated to practicals is not adequate and the feedback is insufficient.

Third, extracurricular activities are not properly integrated into the course, with inadequate support for sports clubs and sports associations, etc. Therefore, the PE students are not being exposed to enough extracurricular opportunities.

Training is similar to systems engineering, in that it centres on the design and management of a complex project over a life cycle and an evaluation of the results, i.e. improving students' skills. The teaching of the PE could be evaluated to determine the main problems. Metrics could then be used to optimize the course structure to obtain the best outcomes for students.

The Mathematical Model: Grey System Theory

The grey equation can be used to describe the characteristics and evolution of a grey system. The analysis of grey system theory is quantitative analysis based on GM model, GM(1,1) model is the most commonly used at present. Set a list of primary data as

$$x^{\{0\}} = \left\{x^{\{0\}}(1), x^{\{0\}}(2), \ldots, x^{\{0\}}(n)\right\}$$

accumulate to the above data, 1-GAO sequence is obtained

$$x^{\{1\}} = \left\{x^{\{1\}}(1), x^{\{1\}}(2), \ldots, x^{\{1\}}(n)\right\}$$

Among which $x^{\{1\}}(k) = \sum_{i=1}^{k} x^{\{0\}}(i)$

Grey SystemAnalysis

The grey system analysis includes grey relational analysis, grey cluster analysis and grey decision analysis [3]. The grey relational analysis can be applied to situations where the data are limited and grey. The basic idea is as follows: similarity of series curves is used to judge whether a relationship is close, and the grey relational degree is used to measure the closeness. Grey relational analysis requires limited calculations and yields reliable results; it has been used, for example, in engineering.

Grey cluster analysis gathers observations into several definable classifications according to the white weight function. Grey cluster analysis has two methods as follows: The first method is grey relational cluster analysis, which is applied when merging comparable factors to simplify a complex system.

An index can denote several close relationships or a factor can include several other factors to describe the information without serious loss. The second method is the grey white weight function cluster, which is applied to judge whether the object belongs to a different classification.

The grey decision is obtained using the grey coefficient combined with the grey model. The effect is calculated using two methods; first: the measure is based on GM (n, k) ; second: the measure is obtained by extending the relational coefficient. The measure of grey can be optimal or suboptimal situations.

Determination of an Evaluation Index System

Measurement of the skills of students is by their performances at practical activities during four years at college. These reflect the physiological qualities and psychological characteristics required by their teaching. Physical skills, at the core of teaching physical activities, develop alongside students' intellectual abilities.

The evaluation index of student skills was obtained by a questionnaire survey, and a literature review. The subjects were 800 college students, from 30 colleges, majoring in physical education. Of the 800 questionnaires issued, 759 were returned, for a response rate of 95%. An extensive literature review was also conducted, as shown in figure 1.

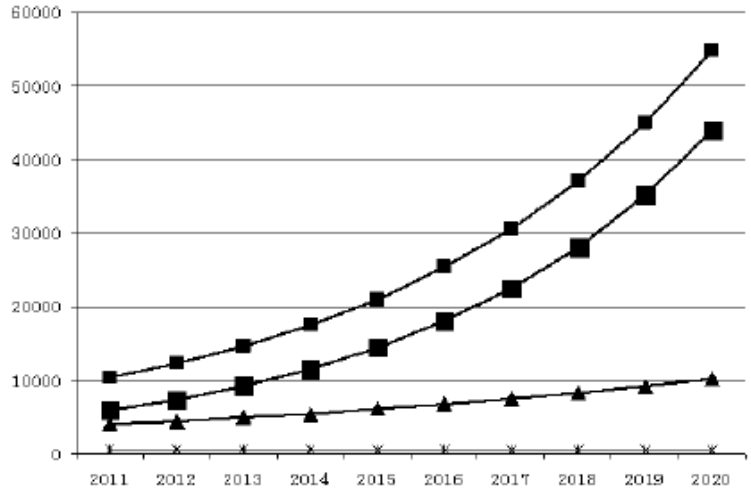

Fig. 1 Evaluation index of student skills

Case Study

The data from 800 college students majoring in PE in 30 colleges were used to carry out an empirical analysis, using the grey system theory. The weights of second degree indices were calculated according to Formula (19), and the results are shown in Table 1.

Table 1. Weight of second grade indices

Second grade	Weight	Second grade	Weight
(I11)	0.21	(I41)	0.09
(I12)	0.25	(I42)	0.23
(I13)	0.23	(I43)	0.22
(I14)	0.31	(I44)	0.11
(I21)	0.17	(I45)	0.35
(I22)	0.22	(I51)	0.14
(I23)	0.14	(I52)	0.42
(I24)	0.21	(I53)	0.23
(I25)	0.26	(I54)	0.21
(I31)	0.24	(I61)	0.15
(I32)	0.21	(I62)	0.32
(I33)	0.32	(I63)	0.14
(I34)	0.23	(I64)	0.39

The relational degree of the first degree indices can be calculated according to Formula (21) and the results are shown in Table 2.

Table 2. Relational degree of first degree indices

First degree	Relational
I1	0.557
I2	0.643
I3	0.518
I4	0.421
I5	0.446
I6	0.384

The first degree indices are ranked as follows: I2 > I1 > I3 > I5 > I4 > I6. As can be seen from the results, physical teaching is essential in improving the abilities of students majoring in physical education. Therefore, training in physical teaching should be a focal point of the PE course.

Other skills should be developed at the same time, and the evaluation results should offer a theoretical base for training students majoring in PE. This points the way to further reform in teaching PE.

Conclusions

A qualitative and quantitative analysis, based on the grey system theory, was carried out to evaluate the skills of students majoring in physical education[4]. The evaluation index system was verified, using questionnaire data and the first- and second-degree indices were obtained. The ranking of the indices was evaluated and a teaching reform measurement determined. This provides a mechanism by which to improve the abilities of students majoring in physical education.

References

[1]. Rata, B.C. and Rata, G., Training the ability to lead the instructive-educational act during the students' physical education lesson. Procedia - Social and Behavioral Sciences, 76, 4, 711-716 (2013).

[2]. Quennerstedt, M., Öhman, J. and Öhman, M., Investigating learning in physical education-a transactional approach.
Sport Educ.and Society, 16, 2, 159-177 (2011).

[3]. Zhao, Z., Wang, J.Z., Zhao, J. and Su, Z.Y., Using a grey model optimized by differential evolution algorithm to forecast the per capita annual net income of rural households in China. Omega, 40, 5, 525-532 (2012).

[4]. Deng Julong. The Control problem of grey systems[J].System & Control Letter,1982,1(5):288-294.

Advanced Materials Research Vols. 989-994 (2014) pp 2220-2222
© (2014) Trans Tech Publications, Switzerland
doi:10.4028/www.scientific.net/AMR.989-994.2220

Ideological and political education linear regression theory

Meng Zhang

Editorial Department of journal, Xinxiang university, Henan ,China,453003
837457026@qq.com

Keyword: linear regression, mathematical model

ABSTRACT: The paper presents a valid and efficient method to teach ideological and political education courses in linear regression analysis. It includes theory and practice parts, where interactive learning methodologies are created. It adopts case-study teaching, since this teaching method effectively integrates theoretical teaching and practical teaching. The lectures should be not an exhaustive review of regression methodology, but they should focus on how the regression models derived. Moreover, the teacher should pay more attention to the theoretical aspects of models rather than to their implementation using software. Students work in teams of three or four on a problem presented by teachers and choose relevant software to carry out their own projects. Feedback from students indicates that this method of teaching improves students' class attendance and greatly increases their interest in learning.

0 Introduction

To study the ideological and political education curriculum theory a series of problems, we need to first clarify the meaning of the theory of ideological and political education course which also needs to interpret one of the first core word "ideological and political education" and "curriculum theory". We know that the ideological and political education is a comprehensive and complex concept, its connotation can smaller of bigger. Broad ideological and political education is almost equivalent to the thought education, political education, moral education, discipline education and shape people's ideological consciousness, such as political ideas, moral character and spirit of citizenship which is related to the comprehensive education category. And narrow sense of ideological and political education is a proper noun, and led by the proletariat political party, in order to cultivate qualified builders and reliable successors of revolution and construction the education goal of closely linked together the ideology of class consciousness and the political thought education. The concept of curriculum theory is often seen as a education subject manages research area and branch, in China for nearly a century of research history. So far, education science field discussion of curriculum and curriculum theory connotation is still on. But according to one of the most common explanation, course can be interpreted as a subject, teaching material and teaching related expression, can realize the goal of school education ,curriculum theory is of course the proprietary theory, is the school discipline and curriculum system and content structure.

Reality requires one to deal with a range of variables. Students can encounter many variables for a problem, including relationships between the variables[1].Commonly, these problems can be divided into two kinds according to their relationship. One is the problem of determining, which relationship can be expressed using the functions available. Another is not completely determined by using functions, but with random variables. This kind of relationship is called co-relationship. Regression analysis is a method to study the relationship between variables. So one builds regression models to help understand and explain the relationships. Regression models can also be used to predict actual outcomes.

The earliest form of regression was the method of least squares, which was published by Legendre in 1805 and by Gauss in 1809. Legendre and Gauss both applied the method to problems of determining. The term *regression* was coined by Francis Galton in the 19th Century to describe a biological phenomenon. However, Francis Galton applied the method to the problem of random variability[2].The phenomenon was that the heights of descendants of tall ancestors tend to regress down towards a normal average, and this is, known as regression toward the mean.

Today, regression methods continue to be an area of active research, and new methods have been developed for robust regression, regression involving correlated responses, such as time series and growth curves, regression in which the predictor or response variables are curves, graphs, images or other complex data objects, etc. There are many examples. Feilong and Yubo made an error analysis for the linear programming support vector regression problem in learning theory. Jose M. proposed a machine learning algorithm for regression problems. Qing, H. et al presented parallel extreme learning machine for regression based on MapReduce[3] .

Chen Y. proposed assessing mathematics learning achievement using hybrid rough set classifiers and multiple regression analysis. González-Recio and Forni proposed Genome-wide prediction of discrete traits using Bayesian regressions and machine learning. Tsuruoka et used logistic regression to study learning string similarity measures . Therefore, almost all institutions in which relevant majors have been set offer a course in regression. For example, MIT offers open courseware. In addition, a large number of open on-line teaching resources can also be found, such as applied regression analysis at Columbia Business School for the MBA major.

In 2010, a statistics major was established in the Mathematics and Computer School at Xinxiang University, Xinxiang, China[4].In this year, the School first offered the course for students whose major came from computer science or mathematics. It is compulsory for mathematics students, while it is an elective for computer science students.

1 linear regression model

The theory-oriented lectures cover single linear regression and multiple linear regressions. Students learn what regression is, how to create its mode, how to estimate the parameters of the model (Estimation Using Least Squares), understanding the assumptions of establishing the conditions for the model, what the regression coefficients are, how to compare the models, and predicting and controlling using regression model. Teachers start theirs lectures with a discussion of simple regression, then, move on to multiple linear regression. This is quite reasonable from a pedagogical point of view, since simple regression has the great advantage of being easy to understand graphically.

Students should place a lot of emphasis on the simple linear regression analysis and understanding its mathematical expressions and be open to more sophisticated concepts. It is difficult for students to study multiple linear regression analysis. However, it is a primary tool in the analysis of real data. Thereby, single linear regression is taught in six sessions, while multiple linear regression requires four sessions. A session is 90 minutes' duration.

Single linear model describes a linear relationship between two variables. One is called the target, response or dependent variable, and is usually represented by y . Another is called the predicting or independent variables, and is usually represented by x . Given $(x_1, x_2, , x_N)$, the simple linear regression model is described as:

$$B = (\sum XY - \frac{1}{n}\sum X \sum Y) / [\sum X^2 - \frac{1}{n}(\sum X)^2]$$

$$A = \frac{1}{n}(\sum Y - B\sum X)$$

where the data, x_i , y_i , represent a random sample from a larger population, which consist of n set of observations, the coefficients are unknown parameters, and $_i$ are random error or disturbance terms.

2 Feedback Exercises

In the spring semester of the 2012/2013 term, a total of 60 junior students came from two majors,, joined the course at the Xinxiang University, Xinxiang, China. These students already had joined some previous courses, such as mathematical analysis, advanced algebra, probability and statistics, etc [5]. They also demonstrated a certain level of operating computer software capability. A survey questionnaire with six feedback questions was administered to all of these students (shown in Table 1).

Table 1 Feedback questions

Questions		Majors		Mean
		Computer science (students 30)	Mathematics (students 30)	
1	I became interested in data analysis through this class.	27 (90%)	28 (93%)	92%
2	I understand the concept of linear regression.	24 (80%)	26 (87%)	83%
3	I performed the linear regression using MATLAB program.	27 (90%)	26 (87%)	88%
4	I performed the linear regression using MS Excel.	29 (97%)	29 (97%)	97%
5	I think the practice is useful to understand the concept of linear regression.	30 (100%)	30 (100%)	100%
6	I can apply my knowledge of mathematics by performing the experiment.	24 (80%)	25 (83%)	82%

There are too many formulations about regression analysis. It is often difficult to understand these concepts of regression analysis, said some students. As can be seen from student feedback, only 80% of computer science students can understand regression, while 87% of mathematics students can do so. However, almost students finished their experiments, and all of them think the practice is very useful to understand those concepts. This information shows that students' interest will be enthused if theory is combined with practice, and as long as theory explanation is not ignored.

Conclusion

Regression analysis is not only a statistical process for estimating the relationships between variables, but it is also widely used for prediction and forecasting. It is difficult to acquire this knowledge, because it is necessary for undergraduates to have fundamental mathematics and operating computer skills. It includes many techniques for modeling and analyzing several variables.

However, the lectures should be not an exhaustive review of regression methodology, but should focus on how the regression models are derived. In the teaching process, giving hands-on experience to students is necessary. The teacher should pay more attention to the theoretical aspects of models rather than to their implementation using software. In the process of teaching, these will help to improve the teaching effect.

REFERRENCE

[1] Legendre, A.M., Nouvelles méthodes pour la détermination des orbites des comètes. Paris: Firmin Didot, *Sur la Méthode des moindres quarrés* appears as an appendix (180 5).

[2] Gauss, C.F., Theoria Motus Corporum Coelestium in Sectionibus Conicis Solem Ambientum. Ghent University(1809).

[3] Mogull, R.G., *Second-Semester Applied Statistics*. Kendall/Hunt Publishing Company, 59-59 (2004).

[4] González-Recio, O. and Forni, S., Genome-wide prediction of discrete traits using Bayesian regressions and machine learning. *Genetics Selection Evolution*, 43, **7** (2011).

[5] Tsuruoka, Y., McNaught, J., Tsujii, J. and Ananiadou, S., Learning string similarity measures for gene/protein name dictionary look-up using logistic regression. Bioinformatics, 23, **20**, 2768-2774 (2007).

Advanced Materials Research Vols. 989-994 (2014) pp 2223-2226
© (2014) Trans Tech Publications, Switzerland
doi:10.4028/www.scientific.net/AMR.989-994.2223

An improved genetic algorithm in vehicle dispactcher

Shanhong Zhu[1] ,Pei Tang[2]

[1]School of Computer and Information Engineering ,Xinxiang university, Henan, China

[2] School of Art and design ,Xinxiang university, Henan, China

Email: zshazhu@163.com

Keywords: genetic algorithm; vehicle dispatcher;

Abstract: The traditional genetic algorithm has the disadvantages that hinder the development and promotion of vehicle dispatcher and slow retard the development speed of logistics industry. Through the research of vehicle dispatcher's demand, we have put forward a new genetic algorithm which is improved, effective and adept to the normal vehicle dispatcher. We have proved that this algorithm is feasible and effective by analyzing the examples.

0 Introduction

The Genetic Algorithm is firstly proposed by J.Holland, and re-identified and deduced by Hollanl later on. Its core idea is every outstanding individual will appear the directionof index increasing in every dynamical population biology[1].That is to say, it is convergent, so it can be applied in practice preferably. This algorithm is a randomly searching and calculating method which has better adaption and flexible optimized object, so we do not need the successive optimized object, or the optimized object to differentiate, or has the good stability and parallel searching ability. At the same time, the genetic algorithm does not need the initial solution, and arbitrary initial population biology can operate and outcome.We use randomized optional strategy in this algorithm, that is to say, it makes the outstanding individual go to the next generation through the survival of the fittest, and then after the cross - fertilization and Genetic behavior, it realizes weakness or disappearance.

Compared to other algorithms, the genetic algorithm has its own merits[2]. The genetic algorithm adopts the evolution mechanism, and it carries out the searching process in the whole situation, averting the localization. Even if the adaptivefunction is discontinuous or irregular, the genetic algorithm can find the optimized solution of whole situation. And also, it has wonderful parallel processing and can realize the combination with other algorithms, especially adapted to the issues which has large scale and broad distribution.

In order to realize the optimization of vehicles dispatching, the main content of genetic algorithm is as follows: (1) give the researching object number. Only when we transform the spatial data issue into a bunch of genes data which can be dealt with by this algorithm can we use the genetic algorithm to handle this problem for the genetic algorithm has poor handling ability to spatial problems.(2)Initialize the population biology. In order to achieve the operation of the spatial problems, we must optionally transform the spatial problems into population biology which has many individuals, and these individuals can response the answer of one space optimized issue. Thus, the key issue is how to form the initialized population biology. (3) Using the fitness function. Every individual in the transformed population biology will affect the merits of the whole issue. So we have to use the fitness function to evaluate the individuals' ability, and apply the data to other genetic operation. (4) Select the excellent individual. In the genetic algorithm, only the excellent past age can have great meaning to the younger generation, causing the great individual and gene can multiply the greater generation. (5) Intersect and form the new individual. The intersection of single gene can influence the astringency and shorten the calculating time. We select the individual

having the good genes to intersect with the better genes and get the greater gene combination. Generally, the intersection has two steps. Firstly, we should pair the last generation randomly, and confirm the intersection point of these individuals which can be paired randomly, then transform or intersect the partial information, and then produce the new individual.

2 The Improved Genetic Algorithm

There are many ways to improve the traditional genetic algorithm [3]. In this paper, we improve and renew the genetic algorithm on the code structure, improve the intersecting and compiling operation, and expand the population biology at last. There are four aspects to be improved in total, and each on is as follows:

Step1. Improving the code program. We choose the order of natural number to code the chromosome for the the solution structure of the vehicles dispatching is particular. The whole dispatching internet built by the customer n needs m cars to realize the delivery. And then code the chromosome to a data whose length is n+m-1, the n natural numbers realize that it marks the full permutation with m+1 naughts, such as

$$0, i_1, i_2, ..., 0, i_f, ..., i_k, 0, ..., 0, i_p, ..., i_q, 0$$

in that I_j is the customer j on some wire, and o represents the DC(distribution center). The chromosome structure after the coding can represents that the vehicles send $i_1, i_2, i_3, ..., i_c$ from the DC and then return to the DC, which forms the first subsidiary dispatching internet. And then the second is also the same, forming the second subsidiary dispatching internet. Going along like this, all the customer can be visited. This subsidiary dispatching internet formed by the chromosome is not in order, while the particularly ordered subsidiary dispatching internet is the solution of the vehicles dispatching process.

Step2.we insert 0 into the former one or the later one. Going along like this till we get a lot of individuals in the population biology. Mark 8 as the customer and we need 2 vehicles. The process of coding the chromosome is shown in fig.2.

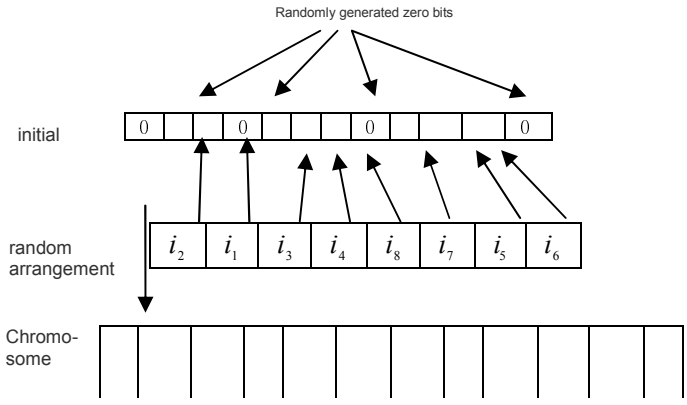

Fig 1.The code of chromosome initialization

Step3. Improving the fitness evaluation. The fitness evaluation of improved genetic algorithm is the same with the target function under the constraint model. The smaller sufficiency of the individual in the population biology is, the better is.

Step4. Improving the chosen operation. When we calculate the sufficiency of the individual using the improved fitness function, firstly we need to reorder them according to their values, big or small. Supposing the scale of the population is p, mark the individual having the smaller sufficiency as 0, the biggest as P-1.Randomly produce a number r conforming to the standard normal distribution, making $r* = |\frac{r}{3}|$, if the r we produced is greater than 3 we need to reproduce a r which satisfy the conditions. The probability of standard normal distribution of the randomized number between -3 and 3 is 99.9%.In this situation, $r*$ is located between 0 and 1, satisfying $t = r*(p-1)$.Supposing chromosome NO.t is chosen to the new population, the probability that the chosen chromosome is

closer to the symmetry axis 0, the bigger the excellent population. The value probability of the randomized number is the shape of normal distribution.

Step5. Improving the intersecting operator. Vehicle dispatching has particular structure, but the chromosome coding in the traditional genetic algorithm adopts the mixed method of single-point, multi-point, and changing to arrange, which destroy the chromosome and excellent substring form, and it can not create the new filial generation if the two chromosomes of the last generation are the same. Thus, we must improve the traditional genetic algorithm. Selecting the location of DC 0 when it intersects coding based on the particularly coded chromosomes, preventing to damage the excellent substring and the last chromosome. Furthermore, the method that makes the substring move to the first place of the chromosome to intersect not only can keep the integrity of the excellent substring, but also can create the newly excellent substring in the case that parents' individual chromosomes are the same, and create the better new substring individual with the help of improved variant operation. Thus improve algorithm's ability to search the excellent individual and the convergent speed. The detailed operating process is as follows:

Firstly, intersect and duplicate the chromosomes. Chose two chromosomes named A and B, whose probability value is 0.85, and then produce two natural numbers between 1 and m , named r_1 and r_2 .In the new algorithm, we require the substring chromosomes in A to be duplicated into the fore-end of the last generation named $B*$,at the same time, we duplicate the substring chromosomes in B into the fore-end of the last generation named $A*$. Next, choose the location of the rest 0 and insert the 0 into the head and end of the next generation's chromosomes named $B*$ and $A*$, and insert the rest 0 of m-2 to the blank space randomly, satisfying the arbitrary 0 having content. Finally, complement the rest genes of the chromosomes, that is to say, fill the different genes of the last generation and next generation into the rest chromosomes, thus create a new individual.

Step6. Improving the varied operation. Selecting a chromosome randomly whose probability is 0.15, and create two natural numbers between 1 and n＋m. If the two groups of genes corresponding nonzero value then it will intersect and create a new individual; if not, it will be going on until the intersecting numbers created. We apply the improved algorithm on chromosomes $0i_4i_50i_3i_1i_20i_7i_6i_80$ to mutate and create a series of new chromosomes named $0i_3i_70i_1i_2i_50i_4i_6i_80$. The detailed process is shown in figure 3.

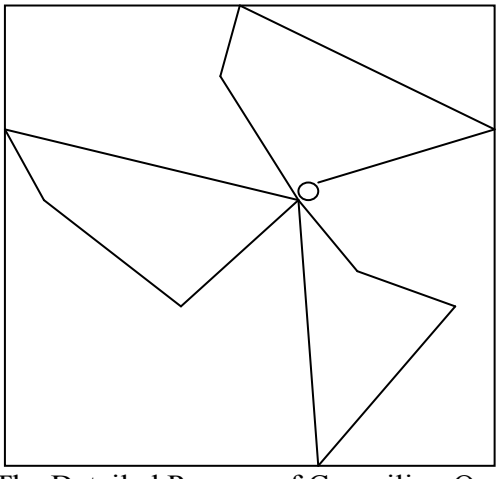

Fig 3.The Detailed Process of Compiling Operation

Step 7: Improving the terminated condition. If we repeatedly create the population biology to five times and we get nothing, then we will stop the algorithm. If it does not satisfy the terminated condition then it will turn back to the original place, or we will adopt step 8.

Step8. Outputting the results. Output and create the individual which has the greatest sufficiency in the population biology, and produce the optimized solution of the issue, realizing the best dispatching scheme of the vehicles.

In order to improve the convergence speed of the whole network of the improved genetic algorithm, we limit the expanding mechanism of the population biology: we improve the genetic algorithm in one way that we take advantage of the individual information, using the method of expanding the population biology in the light of varied sufficiency, we combine the excellent p individuals in the last generation to the p individuals in the contemporary and create a new population biology called 2p,so we finish the expand of the optimized population biology[4]. And then we intersect, rearrangement and mutate in this population biology and get the new generation biology of p individuals.

References

[1] Zhang Liping etc. Improved genetic algorithm of vehicle routing problem [J]. Journal of systems engineering theory and practice, 2007,8(8)79-84.
[2] Zhao Yanwei, Mr.Wu, etc. Genetic algorithm of vehicle routing problem solving method [J]. Journal of computer integrated manufacturing system, 2006,10 (3):303-303.
[3] Zhang Jingling etc. Multiple models dynamic demand modeling and optimization of vehicle routing problems [J]. Journal of computer integrated manufacturing system, 2010 (3):543-543.
[4] Zhang Haigang etc. Two-way vehicle scheduling problem based on immune genetic algorithm to realize [J]. Journal of systems engineering, 2007,22 (6):649-654.

Advanced Materials Research Vols. 989-994 (2014) pp 2227-2231
© (2014) Trans Tech Publications, Switzerland
doi:10.4028/www.scientific.net/AMR.989-994.2227

Research on Robustness of Typically Opportunistic Network Routing Algorithm under Flooding Attack

Geng Yu[1, a], Dongfang Yuan[1, b],Yan Cui[2,c],Yingdong Wang[1, d] and Ping Zong[1, e]

[1]School of Shenyang Aerospace University, Shenyang 110136, China.

[2]95923 PLA troops, Beijing 100101, China.

[a]yug@sau.edu.cn, [b]980065694@qq.com, [c]cuiyan2012@126.com,[d]771897447@qq.com, [e]1165054397@qq.com

Keywords: The opportunity network. Routing algorithm. The malicious nodes. Flooding attack .robustness

Abstract. This paper designed the evaluation method and the index system. Through simulating behavior of pedestrian with mobile intelligent Bluetooth devices in the real city scene and did a quantitative analysis about the effects of flooding attacks to opportunity network in the three aspects of transmission capacity, transmission efficiency and energy consumption of nodes , in order to evaluate Direct Delivery, Spray and Wait and MaxProp the three opportunity network routing algorithm's robustness under the flooding attack results showed that Direct Deliven algorithm robustness is best, it can withstand flooding attacks completely, robustness of the Spray and Wait algorithm is the worst, their performance will decline more than 80% in some scenarios, the performance of MaxProp algorithm under flood attacks will decrease remarkably.

Introduction

The opportunity network[1]is a self-organizing network which needs not exist complete path between the source node and the destination node and uses the meeting opportunity by node mobile providing to realize network communication can tolerate delay and splitting , it can be regarded as the wireless self-organizing networks with general DTN features. The opportunity network is different from traditional multi hop wireless network, the path between source and destination nodes can not predetermine whether there is or not.

Opportunity network uses nodes meet opportunisty to realize communication, network node can not be controlled,so it brings more challenges for data confidentiality and integrity, routing security like the traditional network, there may be malicious nodes attempt to attack the network ,delay transmission or destroy data in opportunity network. In the traditional security MANET, through ID authentication to ensure that all nodes in the network are legitimate nodes, each node acts are trustworthy behavior, so as to effectively prevent malicious attacks .But in opportunistic networks, due to its inherent characteristics, encryption and ID authentication are difficult to effectively deploy, in the absence of effective encryption and identity certification, the presence of malicious attack is inevitable.

Based on the above reasons, this paper studied in the absence of encryption and ID authentication, robustness of opportunisty network's typical Routing algorithm under the condition of existing flooding attacks of malicious nodes in the network.

Background and motivation characteristics of the problem

Security is an important research field in opportunistic networks, clear characteristics of the security problem in opportunistic networks and how to ensure data confidentiality and integrity, to ensure the availability of network are concerned problem around researchers presently. The concept of opportunity networks was proposed for a short time, the current study for the opportunity network 's security problem is less, but researches on the security of predecessor opportunity DTN network and mobile ad hoc network have more sufficient, the related researches mainly have:

The literature [2-4] describes respectively threats DTN network facing, mainly have non node threats, resource consumption, DoS attack, confidentiality and integrity, the broadcast storm problem and so on. The literature [5] describes a specific form of attack, mainly have drop attack, flooding, forged ACK, destroy the routing table, send malformed packets, replay, flow analysis, the authorized user listens to other users and so on.

The literature [6] researches loopholes in the mechanism of Epidemic, stated that the routing mechanism under the malicious attack is very difficult to achieve, and the result depends on the specific network scenarios. UMass Dieselnet project by literature [5], quantitative analysis on attack effect under the condition of lack of security mechanism in DTN network, concluded that even in the strong attack, DTN network is still robust.

To sum up, the safe problem in opportunistic networks has not an effective solution, the traditional scheme based on encryption and authentication is difficult to achieve in opportunistic networks. In this case, if we can make an accurate assessment on the routing algorithm's robustness, it is a vital significance to the establishment of safety system efficiently and can reduce the cost of resources overhead on security system, can solve some security problems directly , this is the study motive of the paper.

Opportunity network routing algorithm and the robustness analysis method

Opportunity network routing algorithm. The opportunity network typical routing algorithms contains Direct Delivery, Spray and Wait, MaxProp. The Direct Delivery algorithm bases on the forwarding strategy, in the process of the routing algorithm message transmission, the nodes would not copy the message, only one copy of the message is in transmission; Spray and Wait algorithm bases on flooding strategy, in this kind of routing algorithm, when meet 2 nodes replicate messages to each other, and to avoid excessive flooding by defining a message of life cycle or the number of copy ; MaxProp algorithm bases on the scheduling strategy, the algorithm based on the transmission success rate sets priorities for message, when 2 nodes meet, in accordance with the message priority to determine copy order.

Analysis method. In this paper, by setting a specific scene,it analyzed and compared the performance of many routing algorithms under the flooding attack through software simulation and to evaluate the robustness of routing algorithms.

1) flooding attack

The nodes meet, malicious nodes send false message to any node,this behavior can be such extreme cyber source and to achieve the purpose of blocking legitimate message transmission, in wired network flooding is the basis of Dos attacks, severe flooding can lead to paralysis of the entire network. In opportunistic networks, because there is no always link, malicious flooding behavior is difficult to continue and will obviously affect the flooding effect. In this paper,there is a quantitative measure of flooding attack effect in the opportunity network.

2) measure

From the transmission capacity, transmission efficiency and energy consumption of nodes in the routing algorithm, three aspects to evaluate the robustness of routing algorithm. In order to quantitative comparative analysis, choose the following three indices as metrics.

*a)*Transmission rate (Delivery Ratio) is a message count ratio between target node packets receieve successfully in a certain period of time and source nodes need to transmit , the metric values the capacity that routing algorithm forward the correct message to the target node, it is the most important indicator.When there is a malicious node in this paper, only calculate normal node's transmission success rate.

*b)*Transmission delay (Delivery Delay) is the time that a message from a source node to a destination node required, usually uses the average transmission delay as a evaluation. Although the opportunity network allows large delay, but the short delay means that routing algorithm has strong transmission capacity, high transmission efficiency, but also means that the message will in the transmission process takes less cyber source.

c) Routing overhead (Overhead) refers to the total number of messsage node forwarding in a certain period of time ,overhead rate evaluates it, Namely , a ratio of total message of the all successfully reached destination node and all nodes forwarding the message number.

The simulation experiment based on simulator ONE

The opportunity network simulator. The ONE simulator is a simulation platform of opportunistic networks developed by SINDTN and CATDTN project, provided support by the research centre in Finland Nokia for. ONE is a simulation engine based on discrete events, each step in the simulation engine will update many modules, so as to realize the whole simulation function. It can use different routing protocols to simulate the sending and receiving of DTN messages, and generate the moving track record. ONE simulator function mainly includes the model of node mobility, communication between nodes, routing and message processing, observaion of real-time mobile nodes and message transmission through GUI, the collection and analysis of visualization data etc, and can use the gnuplot tool to show the data graph.

The ONE simulation platform is composed by the simulation engine, event generator, mobility model, routing model, visualization and reporting module etc, figure 1 shows the specific structure of ONE simulator.The opportunity network simulator ONE is an open source simulation platform developed on Java . Each part in a simulator is made up by different packages, as shown in figure 2. The core components of the simulator (such as the host defining DTN and class between host connections) are placed in the core package. GUI related classes are in the GUI package. The GUI package also includes a playfield packet; it defines some class displayed in the playfield view. Basic user interface class and output class based on text are in UI package.

Simulation scenario installment . The text using the ONE simulation platform simulated pedestrians carried with intelligent Bluetooth device walking in the real city scene, and analyzed the robustness of three routing algorithms under the flooding attack. The specific scene installment as shown in Table 1 set.The table 1 shows the scene that it set up a total of 200 normal nodes with no malicious node, the performance of each routing algorithm as shown in table 2. For comparison purposes, data in Table 2 used as the baseline in the following analysis, figure 3 to figure 5 ordinate values are the ratio of specific scene value and baseline scenario corresponding value.

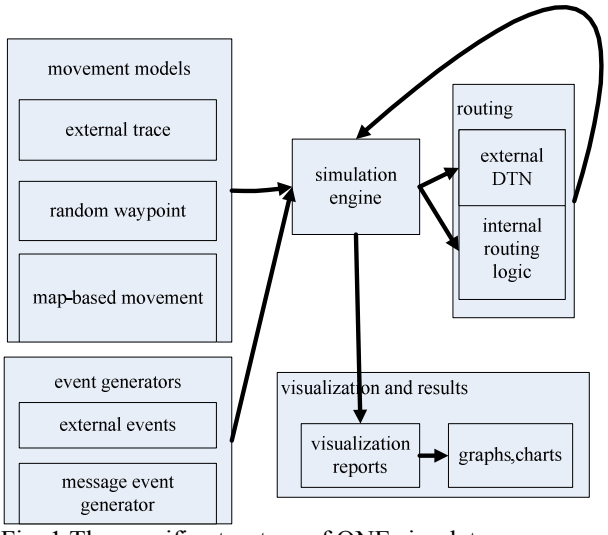

Fig. 1 The specific structure of ONE simulator

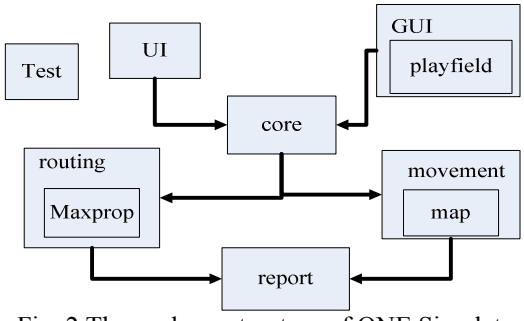

Fig. 2 The package structure of ONE Simulator

For the quantitative analysis of influence of malicious nodes' flooding attacks on the routing algorithm, using table 1 shown scene, it set up a total of 200 nodes and 0 to 100 of malicious nodes. The results of experiment shown in Figure 3 to Figure 5. Under the flooding attack, it has no effect on the Direct Delivery algorithm, the other two algorithms performance decreased significantly, the delivery delayed of Direct Delivery and MaxProp algorithm increased slightly, while the Spray and Wait algorithm significantly decreased. Figure 5 shows the flooding attack will make dramatic

increase in routing overhead of the Spray and Wait algorithm, it have no impact on the Direct Delivery algorithm, the influence on the Maxprop algorithm is a relatively minor.

Table 1 Scene Settings

classes	parameters	value
Scene features	simulated time	12h
	Simulation area	4500m 3400m
	Simulation background city	Helsinki
Node characteristics	movement speed	0.5~1.5m/s
	transmission speed	250kb/s
	Maximum transmission range	10m
	transmission mode	broadcast
	Node cache size	5MB
Characteristics of the message	Packet Size	500~1024kb
	Message survival	5h
	Message generated frequency	25~35s

Table 2 Various parameters by the algorithm with no attack

metric	Direct Delivery	Spray andWait	Maxprop
DeliveryRatio（%）	28.5	50.1	48.0
Delivery Delay	7192	3490	5126
Overhead	0	9.7	149.6

Fig. 3 Delivery Ratio

Fig. 4 Delivery Delay

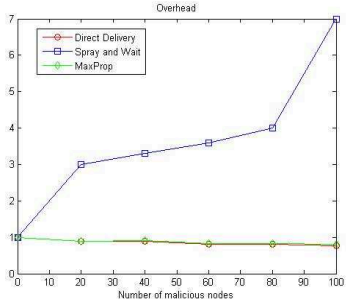

Fig. 5 Overhead

Summary

The experimental results showed that when there are more malicious nodes, except the Direct Delivery algorithm, the other algorithms' transmission success rate dropped sharply. Direct Delivery algorithm has excellent robust, when the attack occurred, 3 indexes of the algorithm almost do not change. The algorithm because of its mechanism of natural can effectively resist flooding attack. While the Spray and Wait algorithm is the most sensitive to flooding attacks, when there are more malicious nodes, transmission success rate will drop 80% above, routing overhead will increase by more than 5 times. If the Direct Delivery and Spray and Wait as a typical representative of routing algorithm based on the forwarding and replication strategies, it would be derived a conclusion in this paper that the routing algorithm robust based on replication strategy is worse than one based on forwarding strategy.

The results also showed that, when there is less malicious nodes , attack is difficult to work, to be successful, it needed malicious nodes with larger proportion, and even successful attack is also difficult to make a complete collapse of, in this view, the opportunity network routing algorithm is quite robust compared with the traditional network.

Acknowledgments

This work was financially supported by “the National Natural Science Foundation of China (60939002;61151002)”, “the Domestic civil aircraft project of Ministry of Industry and Information Technology(CXY2012SH16)”.

References

[1] Huang C H，Lank C，Tsaic Z.A survey of opportunistic networks (2008)1672-1677.

[2] Farrell S,Symington S， Weiss Het al.Delay-tolerant networkingSecurity overview draftirtfdtnrg-sec-overview-06[EB/OL].http：//tools.ietf.org/html/draft-irtf-dtnrg-sec-overview-06.

[3] Kate A，Zaverucha G M，Hengartner U.Anonymity and securityin delay tolerant networks （ 2007）504-513.

[4] Asokan N， Kostianinen K， Ginzboorg P， et al.Towards securingDisruption-tolerant networking，Tech Rep NRC-TR-2007-007.2007.

[5] Burgess J，Bissias G D，Corner M D.Surviving attacks on disruption-tolerant networks without authentication (2007).

[6] Fawal A，Boudec J Y，Salamatian K.Vulnerabilities in epidemicForwarding （2007）.

Advanced Materials Research Vols. 989-994 (2014) pp 2232-2236
© (2014) Trans Tech Publications, Switzerland
doi:10.4028/www.scientific.net/AMR.989-994.2232

A Localization Algorithm Research to Eliminate the Indoor NLOS Error

Jiazhi Dong, Yuwen Wang, Feng Wei and Jiang Yu

Department of Aeronautics and Astronautics University of Electronic Science and Technology, Chengdu, Sichuan Province, China

djzhppy@163.com, wangyw@uestc.edu, abc198900@126.com,Jiangyu_uestc@163.com

Key words: UWB; indoor positioning; TOA; S-V model; CHAN algorithm

Abstract. Currently, there is an urgent need for indoor positioning technology. Considering the complexity of indoor environment, this paper proposes a new positioning algorithm (N-CHAN) via the analysis of the error of arrival time positioning (TOA) and the channels of S-V model. It overcomes an obvious shortcoming that the accuracy of traditional CHAN algorithm effected by no-line-of-sight (NLOS). Finally, though MATLAB software simulation, we prove that N-CHAN's superior performance in NLOS in the S-V channel model, which has a positioning accuracy of centimeter-level and can effectively eliminate the influence of NLOS error on positioning accuracy. Moreover, the N-CHAN can effectively improve the positioning accuracy of the system, especially in the conditions of larger NLOS error.

Introduction

With the development of mobile communication wireless sensor network, positioning technology has entered a new phase. The demand for indoor positioning and communication is growing[1]. Experts and scholars in the field of communications proposed many methods to solved the limitations caused by indoor complex environment, such as: indoor GPS positioning, ultrasound positioning, Infrared positioning, Bluetooth positioning, radio positioning, WLAN positioning and ultra-wideband(UWB) positioning[2].UWB systems have many advantages compared to all the others technology such as: strong penetration, confidentiality, low power consumption, high resolution in multipath, ease of integration, positioning performance [3]. In UWB impulse radio positioning method, TOA estimation method can make full use of the advantages of UWB signal having high time resolution to meet accuracy requirements. Generally, the system obtains information by estimating the time delay of TOA UWB multipath signal of the direct path (DP). For line-of-sight (LOS) environment, just to ensure adequate SNR, the system will be able to obtain a more accurate estimate of TOA, because DP is first to arrive and the energy of it is the strongest. Thus it has high positioning accuracy in theory. For non-line-of-sight (NLOS) environment, due to the presence of various obstacles, propagation environment has become complex, DARPA's a NETEX report discusses the UWB pulse propagation characteristics in different media [4], noting that DP will experience obstacles attenuation when penetrating obstructions, and will introduce additional delays, which have greatly influenced TOA performance estimates. Because of NLOS environment, UWB indoor positioning system from the practical application there is a great problem to be solved.

Algorithm Design

The network system of UWB indoor positioning based on TOA shown in Fig.1, it requires that the clock of target synchronize with each UWB detector. The rough working process of the system as follows: the target carries a IR-UWB beacon, and automatically transmitting a periodic pulse signal, the signal produced by the target through the environment of room, received by the UWB detectors in the positioning region , after appropriate treatment the signal is transmitted to the terminal processor, positioning system get the target location by using some algorithms, and displaying it on the terminal.

Assuming the detectors number of UWB positioning system is N, the coordinates of each detector is (x_i, y_i) (i=1,2……N), the location of target is (x, y), the time sending the pulse signal is t ', the time

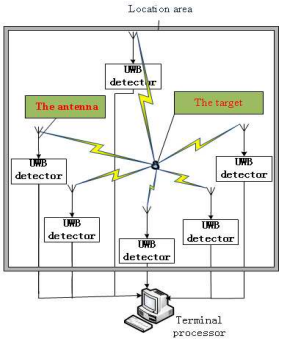

Fig. 1 System Schematic

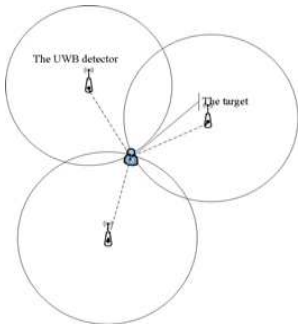

Fig. 2 The positional relationship between the detectors and the target in LOS

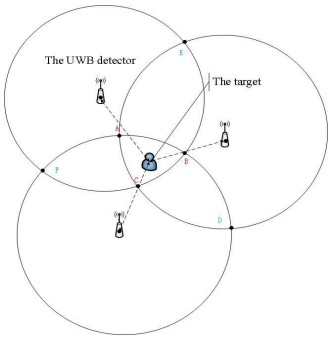

Fig. 3 The positional relationship between the probe and the target in NLOS

of the signal received by each detector is t_i (i=1,2……N), The distance between target detector is d_i:

$$d_i=c(t_i- t') \quad (1)$$

$$(x_i-x)2+(y_i-y)2=d_i^2 \quad (2)$$

If the transmission of signal between the target and the detectors is LOS, the target would be in the intersection point of the circles formed by (x_i, y_i) and d_i. When N=3, the relationship between the target and the detectors shown in Fig. 2.

However, there are many obstacles in indoor environment, specially in cargo warehouses, offices, so the propagation path between the target and detector may be NLOS. When the electromagnetic waves meet obstacles, higher frequency signals often penetrate buildings directly, and the low frequency signals over obstacles by diffraction, it leads to the power of first received signal is weak and the time of UWB detector greater than the real time t_i.

If three detectors are used in this system, the positional relationship between the target and detector as shown in Fig. 3. The target would be in the area D(x,y) which is the area overlapped by three circles. In any of the two circles, if they satisfy the relationship of (3), i.e.the measurement data of R_i has a large error (assuming $R_i>R_j$), then discard the measured value R_i .

$$\left|R_i - R_j\right| > \sqrt{(x_i - x_j)^2+(y_i - y_j)^2} \quad (3)$$

From [5], we know that there are two ways to improve the positioning accuracy: 1, increasing the number of detectors to positioning within the region; 2, determining whether the path between the target and detector is NLOS, if so, try to eliminate the NLOS error. For first way, it would increase costs inevitably if a large number of detectors are used in the system, people are not willing to accept the method. For second way, the cellular mobile communication system has done a lot of research at home and abroad, such as: Kalman filtering, Bayesian methods, maximum likelihood estimation and scattering model approach. In this paper we considered the particularity of UWB indoor propagation, and designed the way to identify and reduce the NLOS error, then, further eliminated NLOS errors and achieve positioning by using the CHAN algorithm.

Channel model is an actual channel transfer function, the received signals can be predicted after channel transmission, which is similar to real environment and play an extremely important role for research. Salen-Valenzula (S-V) model is the most common statistical model which apply in the indoor discrete channel impulse response, the amplitude of receiving component is independent Rayleigh random variables, variance and additional delay in the cluster shows exponentially decay with the delay of cluster. S-V model uses two independent Poisson process to describe the first path to reach the cluster and the reach of multipath relative to it's reach of the first path within the cluster. Specifically, the variables are defined as follows:

Tn: the arrival time of the first path of the n-th cluster;

$\tau_{k,n}$: the delay of the k-the path within the n-th cluster relative to the first path arrival time path, and let $\tau_{1,n} = T_n$;

Λ : Cluster arrival rate;

λ : The arrival rate of path within clusters;

$a_{k,n}$: the multipath gain coefficients;

The UWB indoor channel model can be expressed as:

$$h(t) = \sum_{n=0}^{N} \sum_{k=0}^{K} a_{k,n} \delta(t - T_n - \tau_{k,n}) \tag{4}$$

Make the first multipath cluster arrival time obey the Λ Poisson distribution, other multipath within cluster's arrival time obey the λ Poisson distribution, we can get:

$$\begin{cases} P(T_n | T_{n-1}) = \Lambda \exp\left[-\Lambda (T_n - T_{n-1})\right], n>0 \\ P(\tau_{k,n} | \tau_{k-1,n}) = \lambda \exp\left[-\lambda (\tau_{k,n} - \tau_{k-1,n})\right], k>0 \end{cases} \tag{5}$$

According to the simulation of S-V channel model submitted by 802.15 working group, we can get the waveform of receiving end and the excess delay in LOS and NLOS, as shown in Fig. 4 and Fig. 5. Though Fig. 4, we can get that the amplitude of the DP is maximum under LOS which means it is the strongest path, however, in NLOS, the amplitude of the DP is not the greatest, it appears about 48ns in Fig.5. We can drawn the excess delay under NLOS is much larger than LOS from the comparison between Fig. 4 and Fig. 5. Therefore, whether the measured error of NLOS can be changed into LOS would directly influence the positioning accuracy of the system.

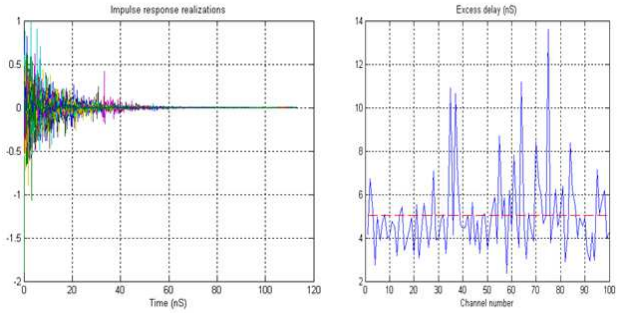

Fig. 4 The pulse signal under LOS

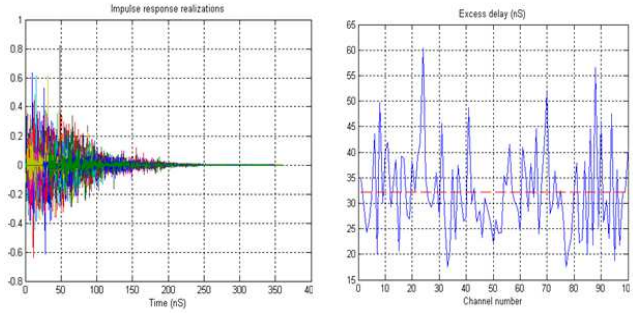

Fig. 5 The pulse signal under NLOS

Since the time interval between two pulses is very short which is usually ns level. We can approximate consider the relative position between the probes and the target is unchanged, and the channel environment is unchanged. If the same detector adopt different transmit power, the strength of the received signal must be different. The paper adopt the UWB single pulse signal of Rayleigh function Pr(t) , which can be expressed as:

$$P_r(t) = A_i \left(\frac{t}{\tau_p}\right) e^{-\left(\frac{t}{\tau_p}\right)^2} \qquad (i=1 \text{ or } 2) \tag{6}$$

A_i is the amplitude of the signal; τ_p is time constant, which decide the single pulse waveform; t is time.When $A_2=1.5*A_1$, Get the pulse waveform, as Fig. 6 shown.

Set the time intervals between each pulse signal is ε , the pulse signal is:

$$p(t) = \begin{cases} P_r(t); 0<t<T \\ 0; T<t<\varepsilon \end{cases} \tag{7}$$

$T>5\tau_p$, if the pulse repetition period is T, we can get:

$$x(t) = \sum_{n=0}^{\infty} p(t - nT) = \begin{cases} \sum_{n=2k+1}^{\infty} A_1 \left(\frac{t}{\tau_p}\right) e^{-\left(\frac{t}{\tau_p}\right)^2} \\ \sum_{n=2k+2}^{\infty} A_2 \left(\frac{t}{\tau_p}\right) e^{-\left(\frac{t}{\tau_p}\right)^2} \end{cases} \quad (k=0,1,2,\ldots) \tag{8}$$

After x(t) though pulse amplitude modulation, we can get the modulated signal $x_{A(t)}$ as follows:

$$x_A(t) = \sum_{n=-\infty}^{\infty} a_n x(t - nT) \tag{9}$$

a_n is the amplitude of the modulation signal. The signal sent by a transmitter antenna, through the indoor channel, then received by a receiver, finally the signal form is:

$$x_d(t) = \sqrt{P_i} x_A(t - \tau_p) + n(t) \tag{10}$$

$\sqrt{P_i}$ is the power of input signal pulse, the received signal first though the low noise amplifier amplifies the signal, then pass matched filtering filter and correlated demodulator. If the first transmit power of the pulse signal is P_1 and the received decision threshold value of the signal is h, which is the maximum amplitude of the the received signal. From (1), (2), we can obtain that the overlapping area D(x, y). The more big the area of D(x, y) indicates the more great measurement error. The second transmit power P_2 ($P_2 > P_1$), the decision threshold:

$$h'=h-k\varepsilon \tag{11}$$

ε is proportional to the area of D(x, y), k is a constant which is related to the positioning environment, but the minimum of h' should be significantly larger than the noise. There are two cases: 1, it is LOS between the target and detectors, since the DP is the strongest path, the second transmit time of the signal detector received is same with the first time, i.e. $t_1=t_2$; 2,when it is NLOS between the target and detector, since the DP is not the strongest, but the second transmit power is greater than the first, and the amplitude of the received signal must greater than the first time and the second threshold is lower than the first time, there will be: $t_2<t_1$, according to (3), we can judge whether there is a large error in the measured value, if so, discard it.

Let: $$\Delta=t_1-t_2 \tag{12}$$

Δ has positive correlation with NLOS error, so if the number of the detector receiving signal at this time is N, and N>3, select three relatively smaller values of Δ in the second measurement to locate.

Then adopting CHAN algorithm to positioning and displaying the location of target on the terminal.

CHAN algorithm using two-step maximum likelihood estimation, the specific process can reference [13]. The algorithm has a small error and it can get Cramer-Rao Lower Bound (CRLB) in the case of a enough small error of measurement parameters. It has a high positioning accuracy compared to other TOA/TDOA algorithm in Gaussian noise environment, but the positioning accuracy would decrease quickly in the NLOS environment. We can get the following relations when set the first detector as reference:

$$\Delta R_i^2+2\Delta R_i R_1=K_i-K_1-2\Delta x_i x-2\Delta y_i y \tag{13}$$

In (13): $\Delta R_i=R_i-R_1$, $K_i=x_i^2+y_i^2$, $\Delta x_i=x_i-x_1$, $\Delta y_i=y_i-y_1$

When i=1,2,3. We can be obtained (14) from (13):

$$\begin{cases} x=p_1+q_1 d_1 \\ y=p_2+q_2 d_1 \end{cases} \tag{14}$$

$$p_1=\frac{\Delta y_3\Delta R_2^2-\Delta y_2\Delta R_3^2+\Delta y_3(K_1-K_2)-\Delta y_2(K_1-K_3)}{2(\Delta x_3\Delta y_2-\Delta x_2\Delta y_3)} \tag{15}$$

$$q_1=\frac{\Delta y_3\Delta R_2-\Delta y_2\Delta R_3}{\Delta x_3\Delta y_2-\Delta x_2\Delta y_3} \tag{16}$$

$$p_2=\frac{\Delta x_3\Delta R_2^2-\Delta x_2\Delta R_3^2+\Delta x_3(K_1-K_2)-\Delta x_2(K_1-K_3)}{2(\Delta y_3\Delta x_2-\Delta y_2\Delta x_3)} \tag{17}$$

$$q_2=\frac{\Delta x_3\Delta R_2-\Delta x_2\Delta R_3}{\Delta y_3\Delta x_2-\Delta y_2\Delta x_3} \tag{18}$$

Bring (14), (15), (16), (17), (18) into (2), and make i=1, we can get:

$$ad_1^2+bd_1+c=0 \tag{19}$$

In (19), $a=q_1^2+q_2^2-1$, $b=-2\left[q_1(x_1-p_1)+q_2(y_1-p_2)\right]$ $c=(x_1-p_1)^2+(y_1-p_2)^2$. We can get two roots d_{11}, d_{22} of d_1 from (19), and they have the relationship: $d_{11}<0<d_{22}$, discard the negative root d_{11} and bring the effective root d_{22} into the equal(14), we can get the estimated position of the target.

Simulation

Assuming 6 detectors randomly distribute on a two-dimensional (2D) plane, the detector coordinates are: (0, 0), (0.66, 12.2), (8.66, 5), (12, 16.5), (13.5, 2.5), (17.2, 10.5). The measured

target location coordinate is (8, 6), using the CM3 channel of S-V, $P_2=2*P_1$, k=1, $\varepsilon=0.2\cdot S_{D(x,y)}$. The simulation results are shown in Fig. 7. CHAN-Taylor which is a joint positioning algorithm using the result of CHAN algorithm positioning as the Taylor initial positioning. Easily obtained from Fig. 7 that: N-CHAN algorithm positioning accuracy is significantly higher than CHAN-Taylor algorithm and CHAN algorithm; the positioning error of N-CHAN algorithm between positioning result and target is very small.

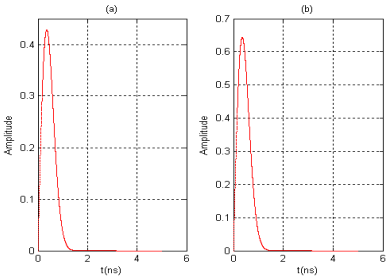

Fig. 6 The comparison chart of different amplitude of the pulse signal

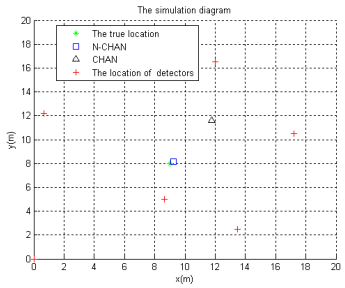

Fig.7 2D Simulation Figure

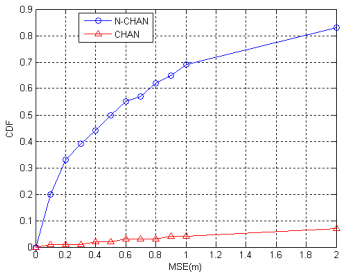

Fig.8 MSE and CDF's Relationship

Distributing the target in the area of 20m * 20m randomly, the introduced function of TDOA distance error is: e=randn(100,100)+3 (m). 1000 times positioning experiments are carried out, we get the relationship between CDF and the mean square error (MSE), as shown in Fig. 8. From Fig. 8, we can get: the traditional CHAN algorithm is not suitable for positioning under NLOS, and the improved N-CHAN algorithm has a high positioning accuracy, About 70% of positioning results'MSE for N-CHAN is less than 1m, which would make it possible for us to locate using the CHAN algorithm in larger NLOS.

Conclusion

In this paper, we proposed a method to decrease the NLOS error by analyzing geometry of TOA positioning and the channel model of S-V, which could reduce the overlapping geometry area so as to reduce the positioning error. Finally, we simulated the N-CHAN algorithm in the 2D plane, the results showed that this algorithm can satisfy the requirements of indoor positioning and eliminate the NLOS error, the position accuracy of it can reach cm level besides. But whether can get a proper function to describe the relation between the overlapping area and the threshold values (k and λ) which were proposed in this paper would have a significant effect on the positioning results, it needs take amounts of practice and statistical analysis subsequently.

References

[1]Y.Y Gu, A. Lo and I. Niemegeers: A survey of indoor positioning systems for wireless personal networks. Communications Surveys Tutorials, IEEE, vol.11(2009) No.1, p.13-32.
[2]H. Liu, Darabi, H, Pat Banerjee and J. Liu: Survey of wireless indoor positioning techniques and systems. Systems, Man, and Cybernetics, Part C: Applications and Reviews,IEEE Transactions on, vol. 37 (Nov. 2007) pp.1067-1080.
[3]Zhou Yuan, Law Choi Look: Ultra low-power UWB-RFID system for precise location-aware application" IEEE Wirel. Commun.networking Conf. Workshops. April 2012, pp. 154-158.
[4]Information on http: //citeseerx.ist.psu.edu/ viewdoc/download?doi=10.1.1.66.7516&rep=rep1&type=pdf
[5]J.J Zhao, H. Li, Z.Y Tang, X. Sun: Research on WSN Double-Radius Localization Algorithm Based on Partition Judgment Mechanism.Wireless Sensor Network, February 2010, pp. 639-644.
[6]Chan Y T, Ho K C: A simple and efficient estimator for hyperbolic location. IEEE Trans. on Signal Processing, 1994, pp. 1905-1915.

Advanced Materials Research Vols. 989-994 (2014) pp 2237-2240
© (2014) Trans Tech Publications, Switzerland
doi:10.4028/www.scientific.net/AMR.989-994.2237

Communication network alarm correlation based on the confidence fusion algorithm

Huisheng Gao[1,a], Yingmin Li[1,b]

[1]School of North China Electric Power University, Baoding 071000, China
[a]Gaohs007@sina.com,[b]854377442@qq.com

Keywords: SDH communication network; the confidence fusion algorithm; alarm association rules mining

Abstract: In this article we achieve SDH communication network correlation analysis by the confidence fusion algorithm. We take the effect of the alarm topology relationship on the alarm timing relationship into the calculation process of confidence fusion algorithm .Thus it can get alarm correlation results more in line with objective facts. According to the correlation calculation results it forms the alarm correlation transactions, then applying the alarm correlation transactions to the alarm association rules mining. We compare the mining results with the traditional method based on sliding window. The experimental results show that the mining results are more effective after introducing the confidence fusion algorithm.

Introduction

WINEPI algorithm[1] is an alarm association rule mining algorithm widely applied to alarm association rules mining, the basic idea is to use a sliding time window to get alarm transaction ,then it generates stronger alarm association rules in accordance with high support – high confidence theory. The key issue is to set the size of the sliding time window and select the appropriate support and confidence threshold. However, the statistic of the occurrence of the alarm items during each time got from one actual communication network showed that the occurring time of alarms is random. Implementing a unified time window for the whole network alarm has the following problems: If the window is selected too small, the relevant alarm information will be lost; if the window is selected too large, it will introduce false rules and irrelevant data. The traditional association rules are based on high alert support - high degree of confidence. In practical engineering, some alarm association rules with high degree of confidence that occur less frequently, are also of practical significance.

To solve the above problems, this paper presents an alarm association rules mining algorithm based on the confidence fusion algorithm. The algorithm uses the alarm time properties and network topology to achieve confidence integration with multi evidences. Then, according to the value of confidence integration it generates alarm transactions. The article also combined FP-Growth algorithm and confidence theory to quickly filter out the meaningful association rules, remove false alarms, thus achieving an efficient algorithm for mining association rules.

1 An alarm Association Rule Mining Algorithm

1.1 Algorithm input

Source alarm history database RD, the confidence threshold $\min_C$, support threshold $\min_S$, the relevant time TR_1 TR_2,the network topology matrix NT

1.2 Algorithm output

Alarm transaction base TD and the alarm association rule base ACR.

1.3The main steps of the algorithm:

Definition 1 In order to characterize the relationship between the two alarms, define a quintuple $AR = (A_i, A_j, TI, NT, R)$, i and j are positive integers. A_i, A_j represent two adjacent alarm items; TI represents the absolute value of the time interval of two alarm items; NT indicates that the network topology of two alarms, if two alarms are generated in the same station, $NT = 1$; if two alarms are

generated in two adjacent stations, $NT=2$; otherwise $NT=3$. R represents of the value of the integrated correlation of two alarm items.

1.3.1 Calculating the comprehensive correlative degree of two adjacent alarms

①,Judge the value of TI ,If TI is greater than TR_2, $R=0$;if TI is less than TR_1, $R=1$; else execute ②.

② Judge NT , if $NT=3$, $R=0$;otherwise execute③..

③ According to the formula (1-3) to calculate the value of R , if $R>=0.9$, then $R=1$,else $R=0$.

1.3.2 The flow of generating alarm transactions

① $i=1, n=1$

②Judge whether reaching to the end of the history alarm database. If so, end; otherwise, determine the value of R of A_i and A_{i+1} ,if $R=1$, then put two A_i and A_{i+1} into one alarm transaction AT_n , $i=i+1$ .otherwise execute ③.

③ $n=n+1$, Generate a new transaction AT_n , A_{i+1} will be the first item of AT_n , $i=i+1$,execute ②.

1.3.3 Mining the frequent alarm sequences

Apply FP-Growth algorithm[1] to mine the frequent alarm sequences. The details can be seen in [1].

1.3.4 Gaining strong alarm association rules

Calculate the confidence of the frequent alarm sequences, find out the frequent alarm sequence whose confidence is greater than $\min_C$. Define these alarm sequence as strong alarm association rules.

2 Algorithm Key Issues

2.1 Confidence Model Framework

The confidence theory is used to manage the rules uncertainty. This article take the effect of the alarm topology relationship on the alarm timing relationship into the calculation process of confidence fusion algorithm .Thus it can get alarm correlation results more in line with objective facts. The proposed method can effectively alleviate the dependence of the choice of the sliding window.

Definition 2 Based on the confidence model theory , the integrated correlation degree of two adjacent items alarm defined as follows:

$$CF(A_i,A_j)=\begin{cases} CF_1 & CF_1=1 \text{ or } CF_2=0 \\ CF_1+CF_2(1-CF_1) & 0<CF_1<1, CF_2>0 \\ \dfrac{CF_1+CF_2}{1-\min(|CF_1|,|CF_2|)} & 0<CF_1<1, CF_2<0 \\ CF_2 & 0<CF_1<1, CF_2=0 \end{cases} \tag{1}$$

The value of CF_1 is determined by TI .

$$CF_1=\begin{cases} 1 & 0\le TI\le TR_1 \\ \dfrac{TR_1}{TI} & TR_1\le TI<TR_2 \\ 0 & TI\ge TR_2 \end{cases} \tag{2}$$

TR_1 is the minimum value of the relevant time, TR_2 is the maximum value of the relevant time.

CF_2 is determined by the topology of the two alarm items.

$$CF_2=\begin{cases} -0.5 & NT=1 \\ 0.5 & NT=2 \\ 0 & NT=3 \end{cases} \tag{3}$$

3 Experiments

In order to validate the feasibility and effectiveness of the proposed method, we choose one power communication network alarm library as an example, to carry out alarm association rule mining. The actual communication network is based on SDH technology. The SDH transmission network consists of 213 stations, each station is set with a SDH equipment. The alarm library includes 19,992 alarms. The experiment is implemented in the PC configured with i3 3.30GHzCPU, 4.00GB memory, Windows 8.0.

(1) We compared the executing time of the traditional method and the proposed method .The traditional method is based on sliding window. The sliding windows are set as 180s, 300s, 500s, 660s,the sliding steps are set as 90s, 150s, 250s, 330s correspondingly. For the proposed methods, TR_1 are set as 180s, 300s, 500s, 660s, TR_2 are set as 360s, 590s, 978s, 1320s correspondingly. The results are shown in Figure 1.

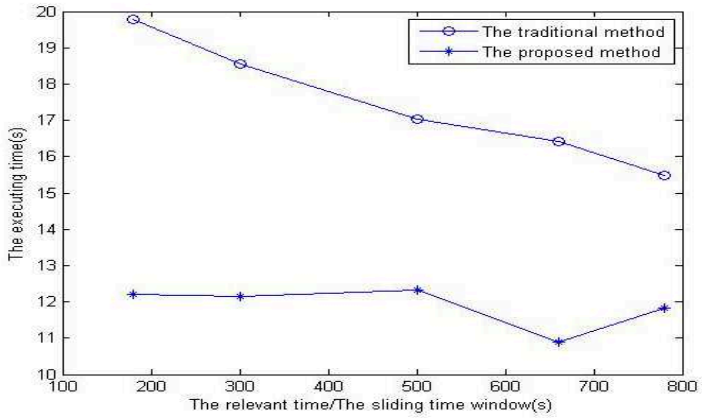

Figure 1 The comparison of the executing time

As showed in Figure 1, for the traditional method ,when the time sliding window becomes large , the executing time of the program becomes small. That is because when the time sliding window becomes larger, the number of generating new alarm transaction gets less, then the executing time gets shorter. But with the relevant time becoming larger for the proposed methods, the executing time does not change monotonously .That is because the number of the alarm items of one alarm transaction is not only determined by the relevant time.

(2) We compare the number of the frequent alarm sequences ,the number of the strong alarm association rules, the number of weak association rules got from the traditional methods and the proposed method .The results are shown in Table 1 . The minimum support count is set as 20, $\min_C$ is set as 50%. The results show that for the same alarm history database, the traditional approach based on a sliding time window can get a larger number of frequent alarm sequences, but also introduces a certain amount of weak association rules . That is, although the proposed methods get less frequent alarm sequences ,the number of strong alarm associations is larger, and the number of the weak association rules is also less. That means, the proposed method can get more meaningful information with less useless information.

Table 1 The mining results of the two methods

	The number of the frequent alarm sequences	The number of the strong alarm association rules	The number of weak association rules
The traditional methods	237	161	76
The proposed methods	180	159	21

Summary

This article firstly introduced confidence fusion algorithm to calculate integrated alarm correlation degree, then generate alarm transactions according to the calculated results., thus alleviating the dependence on the choice of the sliding window .Through the experiments, we know the proposed method can gain more significant information with introduction of less irrelevant information compared with the alarm association rule mining based on sliding time widow.

Acknowledgements

This article is supported by “the Fundamental Research Funds for the Central Universities”.

References

[1] J.W. Han. Mining frequent patterns without candidate generation [A] . In: Proceedings of the 2000 ACMSIGMOD conference on Management of Data[C], Dallas, TX, 2000 : 1-12 .
[2] H. Mannila, H. Toivonen, A. I Verkamo. Discovery of Frequent Episodes in Event Sequences[J]. Data Mining and Knowledge Discovery 1, 1997:259–289.
[3] Z.T. Li, A.F. Zhang, J. Lei. Real-Time Correlation of Network Security Alerts[C]. IEEE International Conference on Digital Object Identifier, 2007: 73-80.
[4] S. Lagaian., F. Amiri, A. Enayati. Frequent Item set mining-based Alert Correlation for Extracting multi-stage Attack Scenarios[C]. 2012 Sixth International Symposium on Digital Object Identifier, 2012: 1010-1014.
[5] Z.H. Tian, Y.Z. Zhang, W.Z. Zhang，etal. An adaptive alert correlation method based on pattern mining and clustering analysis[J].Journal of Computer Research and Development, 2009 ; 46(8) : 1304-1315.
[6] J. Wu, X.M. Li Efficient distributed mining algorithm for alarm correlation in communication networks[J]. Computer Science, 2009; 36(11): 204-207, 212.
[7] Q.F. Xu, B. Xiao, J. Guo. An approach on association patterns mining in telecommunication alarm database[J]. Journal of Beijing University of Posts and Telecommunications, 2011; 34(2): 86-89 .
[8] H.D. Wang, X.Q. Zheng, H.J. Zhang. Web knowledge fusion system based on certainty factor theory and its application[J].Computer Systems & Applications, 2011; 20(1): 1-6.
[9] R. Agrawal. Mining association rules between sets of items in large databases [C] .Proceedings of the 1993 ACM SIG MOD Conference . Washington , D C : [s. n.] ,1993 : 207-216.

Advanced Materials Research Vols. 989-994 (2014) pp 2241-2244
© (2014) Trans Tech Publications, Switzerland
doi:10.4028/www.scientific.net/AMR.989-994.2241

A Purchase Prediction Based on Collaborative Filtering Algorithm

Zheng Fu[1, a], LanFeng Zhou[2, b]

[1]Shanghai Institute of Technology, Shanghai 201418, China;

[2]Shanghai Institute of Technology, Shanghai 201418, China.

[a]fuzhengg@qq.com, [b] lfzhou@sit.edu.cn

Keywords: collaborative filtering, purchase prediction, users' behavior.

Abstract. For a more accurate prediction of the probability of consumers to purchase a commodity, this paper build a users' behavior model based on correlation analysis with apriori algorithm. The model is built by learning from users' history data and behaviors' at present, an experimental result demonstrates that this model can effectively predict consumer buying behavior, and it is better than some traditional methods.

Introduction

It can be predicted more accurate about whether the consumers to buy the brand, for the rapid development of the electronic commerce websites. Basket analysis, genetic algorithm, classification tree, hybrid algorithm and so on, are widely applied in the field of customer behavior prediction. Among them, based on the thought of Lin and Mclean in 2001[1], Jinfeng Yao, Chunxu Wu proposed an algorithm, this paper proposes a new model, this model combines three methods: decision tree (DT), artificial neural network (NN), Logistic regression (LR), and they also do the experiment [2], however, the experimental time complexity is too high, and the prediction accuracy is also not so good.

Jen and Wang (1998) simulate the customer purchase in an exponential distribution and gamma model [3], but as a result of multivariate Bayesian model is derived and calculated process is complex, the model only analysis buying interval with univariate, don't mention the customer purchasing behavior. Now, however, the electronic businesses in order to stock up, need to quickly and accurately predict whether consumers will buy the commodity more and more, and the existing research rarely predict customer purchasing behavior. So, this paper applies user behavior to the Apriori algorithm to extract the association rules, and will generate strong association rules applied to score model is set up, and then according to the model to simulate the user behavior score, at last, through the improved collaborative filtering algorithm. The experimental results show the applicability and accuracy are slightly better than the existing prediction methods.

Traditional recommendation systems suggest relevant content to users based on their previous choices. Traditional collaborative filtering recommendation algorithm is based on the assumption, that if a user for some projects is the score is similar, they are more similar to score on other projects.This paper is based on this, puts forward a kind of collaborative filtering algorithm based on user behavior, think: if a customer when buying some merchandise to the behavior is similar to that of their behavior when buying other products is also similar.

The collaborative filtering algorithm based on user behavior

1.The selection of user behavior

There are many user behavior, so we can improve the accuracy of recommendation by selection of appropriate user behavioral characteristics. This paper focuses on customer behavior analysis in the electronic commerce websites, therefore, the consumers behavior can be divided into: browsing, collection, shopping cart, purchase, respectively represented by A, B, C, D.

Browsing, before decide to buy, the customer is bound to be on brand thorough understanding and comparison, so the number of click affected the customer final decision to a large extent.

Collection, shopping cart, we can found that less than one thousandth of the customer is used to collect and shopping cart before purchase through the analysis of the data, therefore, in this article, browsing default for collection and shopping cart.

Purchase, due to the second or multiple purchases will completely depends on the user's needs or satisfaction to the brand, and the correlation to consumer behavior is not big, based on this, we main forces on the first purchase.

2. Data preprocessing

This paper analyze the raw data with the Apriori algorithm, association rules is put forward, to get confidence P (D | A), P (D | B), P (D | C), as weight value, A, B, C, D respectively estimate the score 0.5,2,3,1, all behavior score multiplied by the corresponding weight value, and then together, the final score is the consumer to the brand's score.

Due to some users have too little or too much behaviour before purchase, these are not conducive to the construction of user behavior score, so we delete it, only keep the brands which score are between 2-7 brand [4].

if the customer hadn't buy the goods after browsing , calculation method is also like that. Set r_{ij} as the score that consumer i for brand j, for any brand j, the score $R_{i,j}$ for customer i in the user rating data matrix A (m, n).

$$R_{i,j}=\begin{cases} r_{i,\mathrm{j}}, \text{if user i rated item j} \\ r_{i,\mathrm{j}}, \textit{if user i not rated j} \end{cases}$$

Compared with the cosine similarity measurement and correction of cosine similarity metric method, the customer brand default score is 0, if there's not score ratings for the consumer i to the brand j. for any brand j, the score for the customer i as follows:

$$R_{i,j}=\begin{cases} r_{i,\mathrm{j}}, \text{if user i rated item j} \\ 0, \textit{if user i not rated j} \end{cases}$$

The advantage of that is can be effectively improved the credibility of clients under the extreme condition that score data are sparse, in fact, the user's intention of buy the brand may not be the same, through the behavior to simulate their willingness to purchase, can effectively measure the intention of the customer.

3. The calculation of similarity between users

With the rapid development of the electronic commerce websites, although this exponential growth in the number of customes and brand, the user rating data are extremely sparse, in a large e-commerce website, the brand which user had rated not more than 1% of the total brand in the general[5], the brand which been scored by two useres are less. Based on $I_{i,j}=I_i \bigcap I_j$ (The variable I_A represents all score of the customer A), it is concluded that the accuracy of the similarity between the user is very low, so in order to effectively solve the extreme condition, the problems existing in the traditional similarity measure methods, this paper when calculating the similarity between customer i and j, first calculate[6]:

$$U_{i,j}=I_i \bigcup I_j$$

Then predict the brand score which customer i had not score in collection U_{ij}, the variable N_i represents the project set that user i had not scored brand in set U_{ij}:

$$N_i=U_{i,j}-I_j$$

For any brand $p \in N_i$, the mean score p_{ij} of customers i had purchased as the score of brand p. The variable r_{iavr} represents mean score of the customer i. So, for any brand $p \in U_{i,j}$:

$$R_{i,p}=\begin{cases} r_{i,p}, \text{if user i rated item } p \\ r_{iavr,p}, \textit{if user i not rated } p \end{cases}$$

Then based on the brand collection $U_{i,j}$, calculate similarity between customer i and j with the Cosine Similarity:

$$sim(\mathrm{i,j}) = \cos\theta = \frac{\vec{i} * \vec{j}}{\|i\| * \|j\|}$$

Or adjusted cosine (The variable I_{ij} represents the set which been scored by user i and j, the variable $\overline{R_i}$ represents the mean score of consumer i, the variable $\mathrm{R}_{i,c}$ represents the score of brand c which belong user i, the variable $sim(\mathrm{i,j})$ represents the similarity between consumer i and j.) :

$$sim(\mathrm{i,j}) = \frac{\sum_{c \in I_{ij}} (\mathrm{R}_{i,c} - \overline{R_i})(\mathrm{R}_{j,c} - \overline{R_j})}{\sqrt{\sum_{c \in I_{ij}} (\mathrm{R}_{i,c} - \overline{R_i})^2} \sqrt{\sum_{c \in I_{ij}} (R_{j,c} - \overline{R_j})^2}}$$

Finally, for each user u, find the user set $C = \{C_1, C_2, C_{3,} \cdots C_k\}$ in the entire collection, the similarity of u: $sim(\mathrm{u}, \mathrm{C}_1)$ is the most, then $sim(\mathrm{u}, \mathrm{C}_2)$, $sim(\mathrm{u}, \mathrm{C}_3)$ …

4. The brand of similarity between calculation and prediction results

After get C = {C1,C2,C3,……Ck}, we need calculate the predicted brand similarity between the customer u and the nearest neighbor , according to the similarity measure method. Set $a \in u$ (a is a brand of user u), and $u \in C$. C_{k_a} is a brand of consumer C_k, calculate the $sim(\mathrm{u}_a, \mathrm{C}_{k_a})$, then we can get $sim_{avr} = (\mathrm{sim}(\mathrm{u}, \mathrm{C}_k) + sim(\mathrm{u}_a, \mathrm{C}_{k_a}))/2$, then the highest sim_{avr} as the final result.

5. Purchase prediction based on collaborative filtering algorithm

Finally, set variable R_A represents the mean score of the customer A, variable $\mathrm{P}_{u,i}$ represents the predicted score of the brand i which belong customer u, n is the number of consumers. According to follow recommendation algorithm to produce recommendations, the smaller the value, and then the bigger the probability of purchase. When $\mathrm{P}_{u,i} > 1.5R_i$, we consider the brand will not be purchased.

$$\mathrm{P}_{u,i} = R_u + \frac{\sum_{a=1}^{n} (\mathrm{R}_{a,i} - \mathrm{R}_a) \times \mathrm{sim}(\mathrm{u,a})}{\sum_{a=1}^{n} |sim(\mathrm{u,a})|}$$

The performance evaluation

In this paper , the data sets from a real electronic commerce websites, data time from April 2014 to May 2014, select four behaviours : browsing , collection, shopping cart, purchase. The format as below:

Table 1 Data Format

User_id	Brand_id	type	Visit_datetime
10944750	13451	0.5	6.4
10944750	13451	0.5	6.4
10944750	13451	0.5	6.4
10944750	13451	0.5	6.7
10944750	1182	0.5	6.7
10944750	1182	2	6.7
10944750	1182	1	6.7

Because this article comparative object is the hybrid algorithm which mentioned by Jinfeng Yao, Chunxu Wu (this algorithm include three methods: decision tree (DT), Logistic regression (LB), artificial neural network (NN).). So we take the same test standard: error probability. the final error probability in the training set and test set is shown in the figure below:

Table 2 Final Result

Algorithm	Error probability 1	Error probability 2
Collaborative filtering	N/A	0.112
Hybrid	N/A	0.113
DT	0.109	0.124
NN	0.115	0.132
LB	0.108	0.139

Thus it is not hard to see, purchasing behavior prediction which based on collaborative filtering algorithm with better accuracy, this method provides a more reliable basis for managers to decide further market strategy, at the same time, the probability of purchase can help enterprise managers to lock the potential customer base, to guide customers which purchase rate is higher in real-time, as far as possible translated potential customers into real customers.

Summary

Customer behavior prediction as an important branch of Web log mining, has not yet formed a mature theory and technology, this paper puts forward the purchasing behavior prediction that based on collaborative filtering algorithm, is an effective, more accurate forecasting method, but because of the data preprocessing methods is a wide variety, so the similarity between users can make a big difference, therefore, the next step of research work will further improve the data pretreatment, and consider the transfer of user interests over time.

References

[1] Lin F Y, McClean S. A Data Mining Approach to the Prediction of Corporate Failure [J]. Knowledge-Based Systems, 2001, 14(3/14): 189-195

[2] Yao Jinfeng, Wu Chunxu . An Anonymous-User-Oriented Purchase Prediction Model Based on Web Usage Mining [J] Computer Applications and Software 2007, 11(24) 186 - 206

[3] JEN Lichung, WANG S J. Incorporating heterogeneity in customer valuation: an empirical study of health care direct marketing in Taiwan [J]. International Journal of 217-228 Operations Quantitative Management, 1998, 14 (10)

[4] LI Xuejun, LI Longshu, XU Yi. Research on Web user's behavior prediction based on rough set. Computer Engineering and Applications, 2008, 44(13): 134- 136

[5] Sarwar B, Karypis G, Konstan J, Riedl J. Item-Based collaborative filtering recommendation algorithms. In: Proceedings of the 10th International World Wide Web Conference. 2001. 285~295.

[6] Deng AL, Zhu YY, Shi BL. A collaborative filtering recommendation algorithm based on item rating prediction. Journal of Software, 2003, 14(9):1621~1628

Advanced Materials Research Vols. 989-994 (2014) pp 2245-2249
© (2014) Trans Tech Publications, Switzerland
doi:10.4028/www.scientific.net/AMR.989-994.2245

K-means Clustering Algorithm Method Based on Shuffled Frog Leaping Algorithm

Tang Zhe[a], Luo Ke[b]

Changsha University of Sciences and Technology, Changsha 410114, China;

[a]295413610@qq.com, [b]luok@csust.edu.cn.

Keywords: cluster;genetic algorithm;ant colony optimization algorithm;shuffled frog-leaping algorithm;K-means.

Abstract. Aiming to resolve the problems of the traditional k-means clustering algorithm such as random selecting of initial clustering centers,the low efficiency of clustering,low in the real,this paper proposed a novel k-means clustering algorithm method based on shuffled frog leaping algorithm.This algorithm combined the advantages of k-means algorithm and shunffled forg leaping algorithm.A chaotic local search was introduced to improve the quality of the initial individual，a new searching strategy was presented to update frog position,that increased the optimization ability of algorithm.According to the variation of the frog’s finess variance used k-means algorithm,it has the advantages in the global search ability and convergence speed.The experimental results show that this algorithm has higher accuracy..

Introduction

Data mining is the process of concentrated extract valuable information from large amounts of data.Because of the usefulness of data mining, its research more in depth.Cluster analysis is an important data mining analysis tool that has been used in various fields.Cluster analysis of is divided the data into a plurality of object classes or clusters, so that the same class of objects with a higher degree of similarity, as different classe of objects with a lower degree of similarity , distance is used to measure the similarity.K-means[1] clustering analysis algorithm is a classical algorithm, it has a simple, good local convergence performance characteristics, widely used in the field of data mining and knowledge discovery.However, the algorithm selected vulnerable to the impact of the initial cluster centers, appear low clustering efficiency, lower clustering accuracy problems.

Therefore, many scholars have studied from different directions on the algorithm.Such as the introduction of genetic algorithms[2,3],particle swarm optimization [4],ant colony optimization[5] algorithm and other optimization techniques.However, because the algorithm produces degradation in the evolutionary process, resulting in multiple iterations algorithm, clustering and low accuracy problem, and when the object is large-scale clusters, these algorithms may appear to be trapped in local optima premature convergence.

Intelligent search algorithm SFLA[6,7,8] is generated by a frog foraging inspired.SFLA has local search capability of PSO algorithm and global search capability of genetic algorithm optimization.SFLA has the advantage of a simple principle, calculation speed, easy to combine with other algorithms, etc.,it has been used in many fields of natural sciences and engineering sciences.Aiming at the shortcomings of K-means algorithm, this paper proposes a new algorithm that combines SFLA and k-means algorithm . It uses leapfrog algorithm to optimize the initial solution,in order to getting high efficiency of solving.SFLA algorithm generates excellent new individual fitness through mutation, then these fine individuals carry on k-means clustering operation.It has a lot of good results such as optimization clustering effect and improve efficiency of the algorithm, reducing the number of iterations of the algorithm,increases the accuracy of clustering.

Preliminaries

K-means algorithm Introduction. k-means clustering algorithm basic strategy is as follows: Arbitrary find a cluster center for each cluster,determine m cluster centers $\{a_1, a_2, ..., a_m\}$ for n data objects. According to the minimum distance principle,other data objects are assigned to the corresponding clustering. Then,on the basis of $C_i^{'} = \frac{1}{|C_i|}\sum_{x \in C_i} x$,update cluster centers, $|C_i|$ is the number of objects in the i-th cluster. In accordance with the principle of minimum distance, each data object will be allocated to the corresponding cluster, update the cluster center, this process is repeated until no more cluster centers change occurs.

Shuffled frog leaping algorithm.SFLA is a group of intelligent search methods inspired by foraging frogs produced. SFLA similar genetic algorithm, each frog representation of a solution, the frog population is a solution set. The entire population contains many sub-groups,subgroups of the frog has its own characteristics, each subgroup has a unique local search strategies. After all subgroups local search, and you will be the exchange of information between subgroups and achieve global search.

Local search and global search will loop until the end condition is satisfied. Because combining global search with local search,the algorithm can jump local optimal direction towards the global optimum.

Local search is different in each subgroup,it is in order to making each subgroup to search in a different direction. When the local search performed many times,the local optima of subgroup will be very close to the global optimum of the entire group. The best individual fitness frog in subgroups represented by $X_b(t)$,the worst individual fitness frog in subgroups represented by $X_w(t)$,The best individual fitness frog in the entire population represented by $X_g(t)$ .The following operations on $X_w(t)$:

$$D(t) = w_1 \times D(t-1) + c_1 \times rand \times (X_b - X_w) + c_2 \times rand \times (X_g - X_w) \quad (1)$$

$$X_w(t+1) = w_2 \times X_w(t) + D(t)\left(-D_{\max} \le D(t) \le D_{\max}\right) \quad (2)$$

Among them, $c_1 = c_2 = 0.5$,the rand is a random number between 0-1, w_1 and w_2 is the factor of controlling frog search. The values of w_1 and w_2 more bigger more conducive to search globally optimal solution; The values of w_1 and w_2 more smaller more conducive to search local optima solution.

$$w_1 = w_2 = w_{\max} - i_{iter}(w_{\max} - w_{\min}) / i_{mem} \quad (3)$$

$w_{\min}$ and $w_{\max}$ represents the initial weights and the final weights, i_{iter} indicates the current iteration, i_{mem} represents the maximum number of iterations in a subgroup.

Algorithm Design

Encoding and fitness function. Using Encoding mode based on the cluster center,we has the advantage of reducing the time calculations and improving the efficiency of the algorithm. Arbitrary frog X_i expressed as:

$$X_i = (Z_{i1}, ..., Z_{i2}, ..., Z_{im}) \quad (4)$$

Among them, $Z_{i1}, ..., Z_{ij}, ..., Z_{im}$ is a set of cluster centers. When the cluster centers determined,it divide the data set by the nearest neighbor principle.

Fitness function is expressed as:

$$f\left(X_i\right)=\frac{\sum_{j=1}^{m}\left[\sum_{\forall D_p\in C_{ij}}\frac{d\left(D_p,Z_{ij}\right)}{\left|C_{ij}\right|}\right]}{m} \tag{5}$$

Among them, $d\left(D_p,Z_{ij}\right)$ represents the Euclidean distance between D_p and Z_{ij}. $\left|C_{ij}\right|$ represents the number of elements in the cluster C_{ij} .Fitness function value of $f\left(X_i\right)$ is more smaller the effect of the cluster more better, otherwise the worse.

The number of frog populations is n, f_{avg} represents the average fitness of the entire population, f_i represents the fitness of the i-th frog, Group fitness variance[9] is calculated as:

$$\sigma_2=\sum_{i=1}^{n}\left(\frac{f_i-f_{avg}}{f}\right)^2 \tag{6}$$

f is the inertia factor used to limit the size of σ^2:

$$f=\begin{cases}\max\left\{\left|f_i-f_{avg}\right|\right\} & \max\left\{\left|f_i-f_{avg}\right|\right\}\geq 1\\ 1 & otherwise\end{cases} \tag{7}$$

σ^2 is used to determine whether the operation standard k-means. When σ^2 is greater than a certain value, adding k-means algorithm for local search, improve the convergence speed, but also increase the accuracy of the solution.

Initial population. Random initial population with stable populations does not conducive to search, and the use of Tent mapping operator generated initial population has better robustness, help to improve the population's stability and accuracy of the algorithm. The mathematical expressions of Tent mappin operator [10,11]expressed as:

$$x_{k+1}=\begin{cases}2x_k & 0\leq x_k\leq 0.6\\ 2\left(1-x_k\right) & 0.5<x_k\leq 1\end{cases} \tag{8}$$

X represents a variable dimension frog individual, using the formula (7) can be produced N frog from a frog.

$$x_{ik}=a+cx_{ik}\left(b-a\right) \tag{9}$$

(a, b) indicates the vale range of frogs dimensional variables, the effect of equation (8) is carrier each dimension of the variable of the frog individual to the range of (a, b) up.

Initialization frog populations: Randomly generate a self-X, the range of variables for each dimension of this individual is (0,1). The use of formula (7) to generate N individuals $X_j\left(j=1,2,...,N\right)$. Using the formula (8) to carry each dimension of X_j to the range up of optimization variables, produce N within the scope of the initial optimization of individual CX_j, and in accordance with the formula (4) to calculate the fitness function values, the better performance is selected as an initial individual of SFLA.

Generate new individuals Frog: Tent mapping operator is used to randomly generate a Vector X that has the same dimensions with frog. According to the equation (9) for updating the :

$$X'_w=X_w+N\left(0,1\right)\times X \tag{10}$$

X'_w represents the updated instance of the frog, N(0,1) represents the standard normal distribution.

Algorithm Description.Input: The number of subgroups: m. The number of subgroups frog:n. The number of searcher in subgroups: i_{mem}. The number of global search: i_{glo}. The number of operations

performed K-means frog: p_m . Maximum change in position: $D_{\max}$. Final weights: $w_{\min}$. Initial weights: $w_{\max}$. Fitness variance population threshold: θ .

Output: k clustering centers and optimal clustering.

Step 1 Initialization frog. According to 2.2,produce F frogs individual, $F = m \times n$.

Step 2 Divided into sub-groups. Sorted according to the size of the fitness value of frogs. Allocated frog to each sub-group.

Step 3 Frog evolution.

a)According to formula (1) (2) to update poorest adaptation frog of each subgroup. If the updated frog improving effect is not achieved,X instead of B,then following formula (1) (2) Update. Otherwise, according to the equation (9) to generate a new frog instead of it.

b) i_{mem} times to perform steps a), have evolved subgroups.

c)After subgroup evolution is complete, the frogs have evolved subgroup remix, instead of the original populations have evolved frog populations. Global iterations +1.

d)Group fitness variance is calculated according to equation (5). If group fitness variance D is less than the threshold value B,choosing C optimal frogs to K-means operating. Otherwise transferred to step 2.

Step 4 k-means operation

According to the clustering center of each frog and the proximity rule, identify each frog corresponding cluster division.The new center is calculated according to k-means clustering algorithm to replace the original coded.Determine whether the termination condition (maximum number of iterations or a good enough position), calculating the new cluster fitness center, if better than the original frog, updae the frog and end the algorithm, otherwise transfer step 2.

Time complexity analysis. In step 1,the time complexity is $T = O(F \times k)$. In step 2,the time complexity of sort fitness value is $T = O(F^2)$ .In step 3, The time complexity of the evolution and mixing of the frog is $T = o(i_{mem} \times i_{glo} \times F^2)$ .In step 4, The time complexity of the operation performed for the k-means is $T = O(P_m \times F \times k)$;Because $F \gg i_{mem}$, $F \gg i_{glo}$, $F \gg P_m$, so the time complexity of the algorithm can be expressed as $T = O(F^2)$.

Simulation

Algorithm simulation.Software: Operating system windows 7, compiler software Matlab7.0.1; hardware: Intel(R) Core (TM)i3-3240 CPU @ 3.40GHz, memory 2GB.

The data sets in this paper is selected in the UCI: Iris data sets, Wine data sets, Balance-scale data sets, Housing data sets.

Table 1 Compares the parameters for each data set

data sets	Iris	Wine	Balance-scale	Housing
Number of clusters	3	3	5	3
The number of samples	150	178	625	506
Dimension	4	13	4	14

The following were used PSO-Kmeans algorithm, K-means algorithm, K-medoids algorithm and the SFLA-k-means algorithm for clustering analysis of four kinds of data sets, each algorithm is run 10 times to calculate the average value, comparing their accuracy rate.

Table 2 Compares the accuracy of various clustering methods(%)

data sets	k-means	k-medoids	PSO-Kmeans	SFLA-k-means
Iris	87.50	63.30	89.75	92.02
Wine	59.30	64.27	69.59	73.47
Balance-scale	34.20	54.85	49.24	61.73
Housing	50.40	56.36	52.59	65.30

Analysis of the results.The experimental results: by cluster analysis for four artificial data sets, the accuracy rate of this algorithm is higher than the other three algorithms.This article was explained that the mixed leapfrog combined with k-means, learn from each other, reducing the number of iterations, improving the accuracy of k-means clustering algorithm, while speeding up the convergence rate. Prove SFLA-k-means algorithm is efficient.

Conclusion

This paper presents an algorithm based on SFLA k-means clustering algorithm,this algorithm on the basis of k-means clustering algorithm,overcome the accuracy of unstable because k-means sensitive to the initial cluster centers and lower accuracy rate and other issues.Through simulation data sets, compare the algorithm with PSO-Kmeans algorithm, K-means algorithm, K-medoids algorithm, this paper proved that SFLA-k-means algorithm is feasible and has a high accuracy rate.

Acknowledgements

My deepest gratitude goes first and foremost to Professor Luoke, for his constant encouragement and guidance. He has walked me through all the stages of the writing of this paper. Without his consistent and illuminating instruction, this paper could not have reached its present form.And this paper is supported by:National Natural Science Foundation of China(11171095, 71371065),the Hunan Provincial Natural Science Committee and Hengyang City Government Unification Foundation (10JJ8008),the Planned Science and Technology Project of Hunan Province(2013SK3146).

References

[1] Chen Guangping,Wang Wenpeng,Huan Jun.Improved Initial Clustering Center Selection Method for K-means Algorithm,J.Journal of Chinese Computer Systems 2012,33(6):1320-1323.

[2] Wang Bingjing,Gao Maoting.New model for clustering ensemble based on genetic algorithms,J. Computer Engin-eering and Applications,2013,49(8):164-168.

[3] Zhang Chunkai,Wang Lijun.Improved K-means clustering algorithm based on genetic algorit-hm,J.Computer Engineering and Applications, 2012,48(26):144-147.

[4] Li Yafei,Cao Changhu.Collabrative Clustering Algorithm Based on Particle Swarm Optimization and Genetic Algorithm,J.Computer Engineering,2011,37(16):167-169.

[5] Meng Ying,Luo Ke,et al.K-medoids clustering algorith method based on ant colony algorithm,J.Computer Engineering and Applications ,2012,48(16):136-139.

[6] Eusuff M M, Lansey K E. Optimization of wat-er distribution network design using the shuffled frog leaping algorithm,J. Journal of Water Sources Planning and Management, 2003,129(3):210-225.

[7] Cui W,Liu X,et al.Survey on shuffled frog leaping algorithm,J.Control and Decision,2012,27(4):481-486.

[8] Wang L,Dai Y.A Multiagent Shuffled Frog Leaping Algorithm,J.Computer Engineering,2013,39(7):265-269.

[9] Matus K, Geubelle P H. Multiscale modeling of particle debonding in reinforced elastomers subjected to finite deformations,J. International Journal for Numerical Methods in Engineering, 2006,65(2):190-223.

[10] Nie Rui,Zhang Weiguo,et al. Adaptive chaos hybrid multi-objective genetic algorithm based on the Tent map,J.Journal of Beijing University of Aeronautics and Astronautics.2012,38(8):1010-1016

[11] Xie Shao-bin,Wang An-an,et al.Anti-multipath Performance of Improved Tent Chaos-based FM Radar signal,J.Modern Radar,2012,34(1):25-29.

Advanced Materials Research Vols. 989-994 (2014) pp 2250-2253
© (2014) Trans Tech Publications, Switzerland
doi:10.4028/www.scientific.net/AMR.989-994.2250

A Modified Regularized Super-resolution Reconstruction Algorithm

Qi Xie [a], Weiyi Chen [b]

Dept. of Weaponry Engineering, Naval University of Engineering, Wuhan 430033, China

[a]xieqi_hg@163.com, [b]fredchen118@sohu.com

Keywords: super-resolution, image sequence, Regularization

Abstract. The super-resolution reconstruction technology is proposed in this paper to overcome the image degradation of shipboard optical detection system. Firstly, establish the super-resolution observation model, then analysis the inadequate of traditional regularized method through the modulation transfer function and proposed a modified regularized algorithm, experimental results shows that the proposed method has the better visual effect and objective indicators. It is a feasible method to enhance reconstruction quality of the system.

Introduction

Shipboard optical detection system including infrared, television, shimmer and other sensing devices, the system plays a key role in detecting offshore and low-altitude targets. The detection accuracy of shipboard optical detection system not only affects the integrated battle effectiveness of warship, and even determine the warship's survival in battlefield environment. Warship works in complex and harsh environment, atmospheric attenuation, system noise and other factors will lead the system result in lower image spatial resolution.

The most direct way to improve the image resolution is upgrading the hardware of optical detection system, but sometimes there are many limitations of this way. Therefore, the study to improve image resolution can compensate the lack of hardware to a certain extent. Super-resolution technology can reconstruct high-resolution images through processing low-resolution sub-pixel image sequence without changing the hardware of imaging system[1]. Super-resolution is more flexble and economic in many conditions and has a broad application prospects, it is currently a hot spot of international image processing field, even in instrument design[2]. In super-resolution image reconstruction process, the core issue is the process of seeking to satisfy the indefinite equations, the noise in the process of solving the original low-resolution image sequence will be transmitted to the reconstructed images, which will lead noise in SR image increases and PSNR decreases[3]. The registration errors in the process will result in reconstruction errors.

In this paper, the registration error in super-resolution reconstruction image was analysised and researched, to subppress the artifacts caused by registration errors and noise in the reconstructed images, propose a regularized reconstruction using Gaussian Markov random field priori model based on Lee's method[4], Experiment results show that compared to the traditional Tikhonov method, the proposed method is better at PSNR and visual effects.

1 Super-resolution reconstruction model

To reconstruct the image of shipboard optical detection system, the most important issue is to establish the observation model from ideal high-resolution images to low-resolution images actual obtained. In practice, the ideal high-resolution image in the imaging process will be affected by deformation, blur, down sampling and noise, causing the image quality degenerated. Assuming low-resolution image sequence $\{y_k, k \in [1, N]\}$ contain N frame images, the size of image is $M \times N$; x is the high-resolution image which size is $Mp \times Nq$, the degeneratin progress from x to y can be expressed as:

$$y_k = DB_k M_k x + n_k \qquad k \in [1, N] \tag{1}$$

D is the decimation matrix, B_k is the blurring matrix caused by PSF(point spread function)[5] or diffraction limit, M_k is the geometric warp matrix caused by motion deformation, n_k is the distributed additive noise. From the flow chart Fig.1 we can see the super-resolution progree is based on the low-resolution image sequence information.

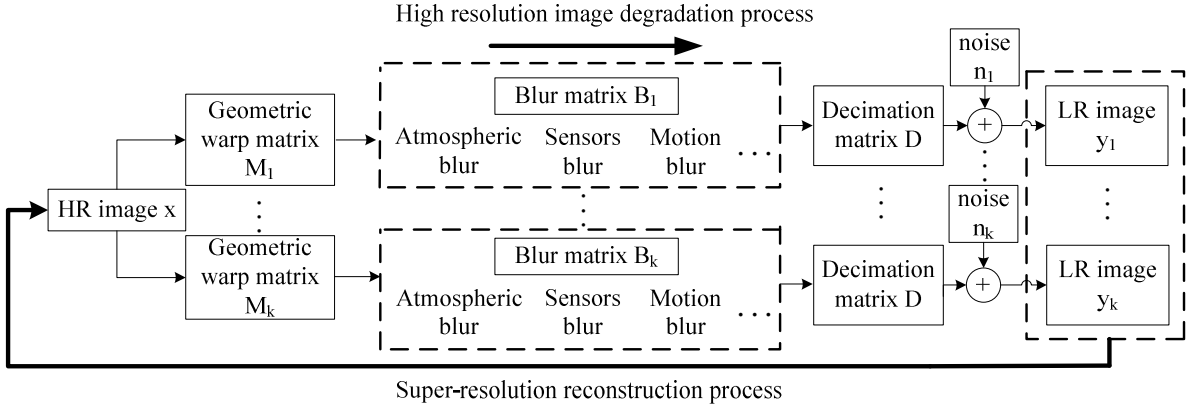

Fig. 1 Super-resolution reconstruction observation model

Assuming the degeneratin matrix $A_k = DB_kM_k$, the formula (1) became:

$$y_k = A_k x + n_k,\ k \in [1, N]. \tag{2}$$

The estimation value of high-resolution image $\hat{x}_k$ have the following relationship between low-resolution image sequence, H is transformation matrix:

$$\hat{x}_k = Hy_k \tag{3}$$

The reconstruction error obtained by formula (2), (3) can be expressed as:

$$\| \hat{x}_k - x_k \| = \| (HA_k - 1)x_k + Hn_k \| \le \| (HA_k - 1)x_k \| + \| Hn_k \| \tag{4}$$

From the formula above we can see there are two parts of reconstruction errors in it: the first part indicates that errors relate to local properties of original high-resolution image x, caused by reconstruction; the second part indicates that errors relate to noise n_k with global characteristics, which are not reconstructed noise, but the noise diffusion in SR image by reconstruction.

2 Analysis of the reconstructed image based on modulation transfer function

By the analysis above can see the super-resolution reconstruction will not only cause noise diffusion in SR image, but also cause errors in the reconstruction process. This paper use MTF(modulate transfer function) to analysis the errors caused by reconstruction, because the super-resolution reconstruction progress is also the process to process sensing devices data[6], the MTF of the system can be expressed as:

$$MTF_i = \frac{\sin(\pi\alpha f)}{\pi\alpha f} = \sin c(\alpha f) \tag{5}$$

In the above formula, α is the size of sensor sensitivity cell, f is spatial frequency. When the sensor is two-fold oversampling image acquisition system and sensor sensitivity cell deflection is the strict sense of $\alpha/2$, the MTF is:

$$MTF = \sin c(\frac{\alpha f}{2}) \tag{6}$$

In over-sampling system, sensitive cell registration determines the images registration. When the over-sampling sensitive cell registration is not the strict sense $\alpha/2$, the offset between the real position and the ideal position is $\Delta\alpha$. Assuming $\Delta\alpha = k\alpha$, $k \in [0,0.5]$,the two adjacent sampling points from the ideal state is changed from $\alpha/2$ to $(1/2+k)\alpha$. So the sensitive components registration error cause the image registration error, equivalent to the change of sampling frequency, the MTF change to:

$$MTF = \sin c[(1/2+k)\alpha f] = \sin c[(1+2k)\frac{af}{2}] \tag{7}$$

Compare formula(7) with formula(6), $(1+2k)$ is the impact of registration error to MTF, it will cause the reconstruction error[7].

The essence of super-resolution reconstruction is using additional data on a related sequence of frame bandwidth extrapolation to increase high-frequency information, such as image edges and details. The registration error affect the high frequency portion more than the low frequency portion that will cause the resolution of reconstruction image lower than ideal condition[8].

3 The modified regularized reconstruction algorithm

Super-resolution is an ill-posed problem[9], in order to obtain a stable solution, the regularization method using prior model to constraint on the solution is needed. Through the analysis in charpter 2 and chartper 3 we know that the registration error and noise will cause reconstruction error, the error will lead to different artifacts in reconstructed image. The traditional regularization method use the Laplace priori model can smooth the artifacts in SR images, but it will also cause the loss of image detail. This paper propose a regularization Algorithm based on Lee's method using GMRF(Gaussian Markov random field) priori model, can smooth image artifacts while preserving image detail.

The regularization formula of this paper proposed is:

$$\hat{x} = \arg\min_{x}\{\sum_{k=1}^{N} \| y_k - DB_k M_k x \|^2 + \lambda \sum_{c\in C}\sum_{l=1}^{4} \beta(d_c^l(x))\} \tag{8}$$

The second part of formula (8) is the regular item, the priori information is introduction by this part.

$$\beta(i) = \begin{cases} i^2 & , \quad i \le \alpha \\ 2\alpha |i| - \alpha^2 , & i > \alpha \end{cases} \tag{9}$$

$$\begin{cases} d_c^1(x(m,n)) = x_{m-1,n} - 2x_{m,n} + x_{m,n+1} \\ d_c^2(x(m,n)) = x_{m-1,n} - 2x_{m,n} + x_{m+1,n} \\ d_c^3(x(m,n)) = 0.5x_{m+1,n-1} - x_{m,n} + 0.5x_{m-1,n+1} \\ d_c^4(x(m,n)) = 0.5x_{m-1,n-1} - x_{m,n} + 0.5x_{m+1,n+1}) \end{cases} \tag{10}$$

$$\lambda = \sqrt{\frac{\sum_{c\in C}\sum_{l=1}^{4} \beta(d_c^l(u))}{\| y_k - DB_k M_k x \|^2 + \xi_k}} \tag{11}$$

The GMRF not only emphasizes the smoothing constraints, and considers the distribution of the image pixels to preserving image details. The Regularization parameters λ is is no longer a global parameters, which can adaptive changing with the image region characteristics.

4 Experimental results and analysis

To illustrate advantages and effective of the proposed algorithm, using "cameraman" image to test, the original high-resolution iamge, Degraded image and reconstructed iamges is showed in Fig. 2. Reconstructed images uses PSNR(peak signal to noise ratio) and SSIM(structure similarity image measure) for evaluation.

$$PSNR = 10\log_{10}\frac{L^2 N_1 N_2}{\sum_{i=1}^{N_1}\sum_{j=1}^{N_2}[\hat{x}(i,j) - x(i,j)]^2} \tag{12}$$

$$SSIM = \frac{(2\mu_x\mu_{\hat{x}} + C_1)(2\sigma_{x\hat{x}} + C_2)}{(\mu_x^2 + \mu_{\hat{x}}^2 + C_1)(\sigma_x^2 + \sigma_{\hat{x}}^2 + C_2)} \tag{13}$$

(a) HR image (b) LR image (c) traditional method (d) this paper algorithm

Fig. 2 Super-resolution reconstruction results

Table 1 Comparison of cameraman image by different method

	PSNR	SSIM
Tranditional Regularization	20.612	0.7813
This paper Algorithm	21.382	0.8929

5 Conclusion

From the experimental results we can see, the proposed algorithm compare to the traditional regularization method has the better visual effect and the objective indicators. Provide a theoretical reference to enhance reconstruction quality for infrared and visible light images of Shipboard optical detection system.

References

[1] Shen Huan feng, Li Ping xiang Zhang Liang pei. Overview on super resolution image reconstruction[J]. OPTICAL TECHNIQUE, 2009, 35(2), 194-199.

[2] LIU Yan-yan，ZHANG Xin，XU Zheng-ping，et al. Application of special-shaped-pixel detectors in super resolution reconstruction[J].Infrared and Laser Engineering.2009，38（6），971-976.

[3] Chen Bo Yang, Guo Qiang, Chen Gui Lin, et al. Amplificatory noise raised by super resolution image reconstruction and filter[J]. J. Infrared Millim. Waves. 2012, 31(5), 403-406.

[4] Eun Sil Lee, Moon Gi Kang. Regularized adaptive high-resolution image reconstruction considering inaccurate subpixel registration[J]. IEEE Trans on Image Processing, 2003, 12(7): 826-837.

[5] Castleman K R. Digital image processing [M]. Engle Cliffs, NJ: Prentice Hall, 1996.)

[6] Accetta J S, Shumaker D L. The infrared and electro-optical systems handbook[M]. Infrared Information Analysis Center, 1993.

[7] Chen Bo-yang, Chen Gui-Lin, Sun Sheng-Li. Application of Sub-pixel Technology for Image Collection System[J]. Infrared Technology, 2007, 29(4), 226-230.

[8] Pu Li, Jin Wei-Qi, Liu Yu-Shu. Super-resolution algorithm based on post wavelet treatment[J]. Infrared and Laser Engineering, 2008, 37(1), 173-176.

[9] Park S C, Park M K, Kang M G. Super-resolution image reconstruction: a technical overview[J]. Signal Processing Magazine, IEEE, 2003, 20(3): 21-36.

Advanced Materials Research Vols. 989-994 (2014) pp 2254-2257
© (2014) Trans Tech Publications, Switzerland
doi:10.4028/www.scientific.net/AMR.989-994.2254

Simulation of whole movement process of Muzhuping landslide with DDA and prediction of surge

Zhihong Dong[1,2] ,Xiuli Ding[2], Aiqing Wu[2], Bo Lu[2]

[1]State Key Laboratory of Water Resources and Hydropower Engineering Science, Wuhan University, Wuhan 430072, China

[2] Yangtze River Scientific Research Institute, Wuhan 430010, China

Ckyyjs2004@163.com

Keywords: landslide, surge, DDA, numerical simulation, real velocity, dynamic

ABSTRACT: The surge wave induced by the landslide on reservoir bank is extremely disaster .The prediction of surge height is a difficult problem because the velocity of landslide is hard to obtain. The discontinuous deformation analysis (DDA) is able to simulate landslide movement with real time and acceleration. The whole movement process of Muzhuping landslide in the Qing river reservoir is simulated by DDA method, including startup, accelerating, deceleration and stop, and velocity along time is obtained. Last, empirical formula for computing surge height is discussed.

Introduction

Reservoir landslide is a common geological disaster in the process of reservoir water impounding, surge water caused by the disasters affect the dam and reservoir bank residents and river navigation the safety of the ship. Therefore, this problem attract extensive attention of the worldwide researchers. Landslide sliding process and the surge disaster prediction and estimation is an important content of landslide research. Landslide sliding is the complex process including static and dynamics mechanics, as well as velocity of landslide when sliding into the water is the key factor in surge analysis. The surge height must be based on a changing sliding velocity in the process of accumulation, so it is necessary to investigate the changing rules of landslide displacement and velocity based on the real time and stress-strain characteristics in the process of movement .The discontinuous deformation analysis method (DDA) is suitable for this problem [1-3].

In this paper, the failure and movement process of Muzhuping landslide in Shuibuya reservoir are simulated by DDA based on real time and dynamic equation. The displacement and velocity changing law of each part are studied in the process of landslide sliding, and then the velocity based on energy is obtained. Lastly, surge water height is predicted, which can evaluate the effect of landslide surge disasters.

The general situation of Muzhuping landslide

MuZhuping landslide is located in Shuibuya Reservoir of the Qing river , Hubei province，China. The landslide occurred in the gradually process of water storage (water level 250m-289m), submerged deposit front 50 ~ 60 meters, which is a large scale tractive landslide. The front of landslide firstly began to deform and collapse, and tract the back of landslide. A total of three times large scale sliding and collapse occurred, which formed a more than 80 m scarp. Total volume of the landslide is about 5 million m^3, and sliding distance is about 170m, which induce 10 meters high surge wave and formed a barrier lake in the river. The main induced reason is that reservoir water reduces the contact strength of rock and soil interface.

Sliding zone terrain like round-backed armchair, as shown in fig.1.Landslide consist of shale, limestone and marl, generally 20 ~ 80 m thick (geological section map as shown in fig. 2).

Fig.1 MuZhuping landslide

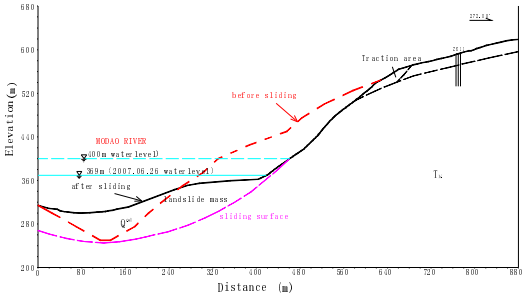

Fig. 2 Geological section map

The DDA model

Discontinuous Deformation Analysis (abbreviated DDA)[1] was proposed by Dr Shi Genhua in 1989. DDA method is suitable for discontinuous medium such as joint rock stress analysis. This method has the full dynamic format, real time, strict balance equation, the advantages of the large deformation and contact simulation. It can simulate landslide from the start, sliding process, accurate calculation of displacement, velocity and energy changes, and accumulation form.

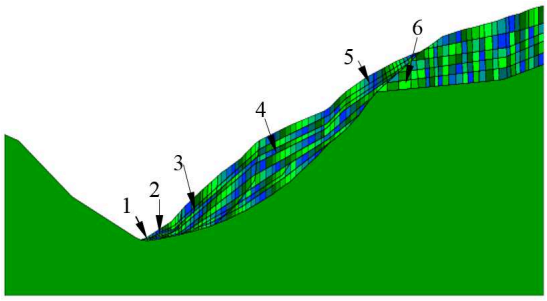

Fig.3 Block system of DDA model

According to the rock mass structure characteristic of the landslide geological profile and landslide, DDA analysis model is set up, as shown in figure 6.which include 524 blocks in the system. To show the calculation results, six monitoring points are marked in the model, as shown in fig. 3.

Table 1 DDA computation model parameter table

material	Cohesion(MPa)	Friction Angle(°)	unit weight（kN/m^3）
bed rock	0.5～1.0	30～40	26.5
The sliding body	0.15～0.5	17～25	22
Sliding zone (underwater)	0.01～0.02	5～15	
Sliding zone (over water)	0.05～0.03	3.6～20	

Mechanics parameters consider the result of the laboratory test and field geological investigation (see table 1). The different velocities are obtained for computing surge wave height that include monitoring points velocity, average velocity and energy velocity (based on the average kinetic energy) through DDA.

Simulation result analysis

In section 4 of this paper, we describe the preliminary results of the numerical simulation analysis by DDA. According to the displacement and speed of these monitoring points (1#-6# points) whether have occurred significant increasing determine whether landslides. By the velocity and displacement with time (as shown in fig.4～ fig.6), it show that landslide is at a long time creep stage. The forefront of landslide indicate slight deformation and compressive stress concentration in the 0 to 40 second, while the displacement and velocity of the upper points are small.

After a long time of energy accumulation, landslide suddenly accelerate at 50 s and the displacement sharply increase. When the displacement and velocity are reaching considerable value, front and central of landslide successively slide, and back parts of landslide body drop.

The results indicate that the startup from leading edge, and leading edge deformation velocity of deformation is always greater than the middle and back part of the landslide. Therefore MuZhuping landslide is due to reduced mechanical parameters of landslide sliding surface.

The process of landslide is as shown in fig.9，which give the landslide shape of 10000 time steps and 3000 time steps. When the calculation is 10000 steps, the sliding displacement of landslide is small (fig.7 (a)); the great changes have taken place in the overall form when 30000 time steps (fig.7 (b)), and the shape of the MuZhuping landslide and the actual landslide shape are very close at this time.

There are some method for estimation of landslide surge height, but there is no unity. The Panjiazheng formula[4] are used to evaluate surge height .Maximum speed is 6.97 m/s (point 1) by calculating, but it do not represent the overall speed of landslides, and landslide surge calculation will be larger. While energy speed of landslide is 5.4 m/s, and according to Panjiazheng formula to calculate, the surge height is 12.6 m, which is compatible with the actual situation.

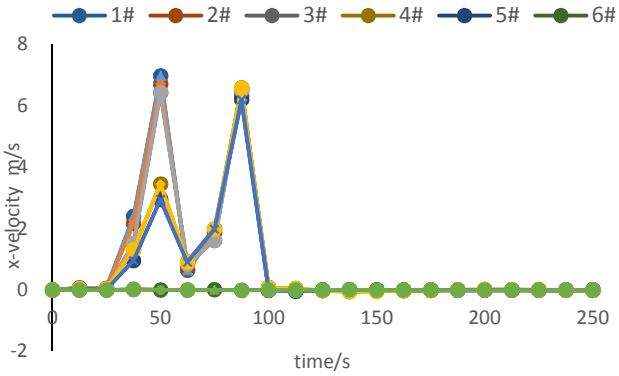

Fig. 4 x-velocities of monitoring blocks

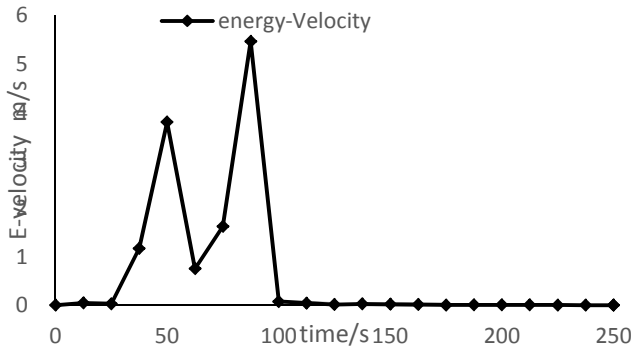

Fig. 5 Energy velocity of monitoring blocks

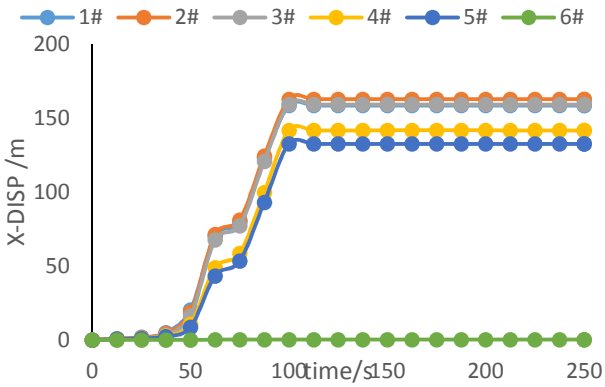

Fig. 6 x-displacements of monitoring blocks

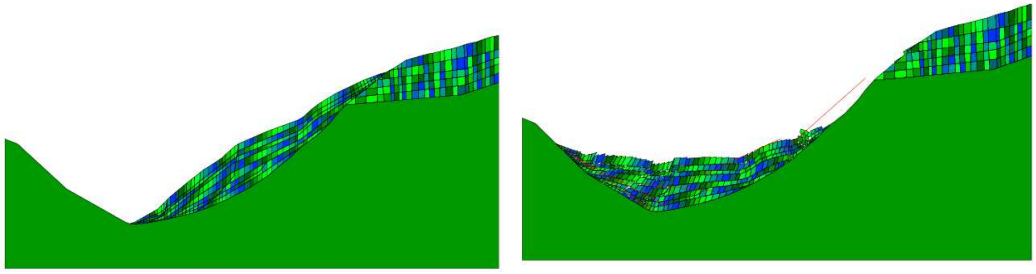

（a）10000 time step (b)30000 time step

Fig. 7 Displacements and shape of landslide along time step

Conclusion

DDA is an effective method to simulate landslide startup, acceleration and the whole process and calculate the surge velocity. It overcome the problem that traditional limit equilibrium method can not consider the effect of topography and lithology.

Muzhuping landslide is simulated by DDA method, which include the whole landslide sliding process, movement time, velocity, and then calculate the initial surge of landslide surge height. The results show that the largest velocity is 5.4 m/s, and total time is 100s, as well as maximum sliding distance is163 m.

Energy speed is good for estimate the height of the landslide surge, and the surge height is 12.6 m .The results shows that the landslide surge height based on energy velocity is close to the height of the actual situation.

Acknowledgements

This study was supported by the National Basic Research Program of China (973 Program, No. 2011CB710604), the National Natural Science Foundation of China (No. 51179014) and the Basic Research Fund for Central Research Institutes of Public Causes (No. CKSF2014065, CKSF2012050). These supports are greatly acknowledged and appreciated.

References

[1] Shi G.H. Discontinuous deformation analysis: a new numerical model for the statics and dynamics of block systems, Ph.D. Dissertation, Department of Civil Engineering, University of California, Berkeley, 1988.

[2] Aiqing Wu, Xiuli Ding, Huizhong Li, Gen-hua Shi. Numerical simulation of startup and the whole process characteristics of Qianjiangping Landslide with DDA method [C]. Process of Seventh International Conference on the Analysis of Discontinuous Deformation (ICADD-7). December 10–12, 2005, Honolulu, Hawaii, 167–174.

[3]Jiang Qinghui，Zhang Zhenhua，Wei wei，etc. Research on triggering mechanism and kinematic process of Qianjiangping Landslide. Disaster Advances, 2012(4), 631-636

[4] Panjiazheng, the structure of the anti-sliding stability and landslide analysis. Beijing: water conservancy press, 1980(in Chinese)

Advanced Materials Research Vols. 989-994 (2014) pp 2258-2263
© (2014) Trans Tech Publications, Switzerland
doi:10.4028/www.scientific.net/AMR.989-994.2258

State-Space Model and Simulation for Dynamic Stall

Weidong Lei[1,a], Guocai Hu[1b] and Quan Liu[1]

[1] Naval Aeronautical and Astronautical University, Yantai 264001 China

[a]weidong319@sina.com, [b]guocaihu11@sina.com

Keywords: dynamic stall; unsteady aerodynamics; state-space equations; Beddoes-Leishman model.

Abstract. Because of the complexity of the progress of dynamic stall, the characteristic of dynamic stall of airfoil is always the difficulty of aerodynamics. A time-domain model has been formulated to represent the unsteady lift and pitching moment characteristics of a two-dimensional airfoil undergoing attached-flow conditions in a compressible flow and dynamic stall. The model is given as a set of first order differential state equations. The Beddoes-Leishman model was presented through modeling the effects of attached flow, separated flow and dynamic stall in the paper. A modified method is presented which includes a new stall-onset criterion and improves the position and separation conditions of the leading edge vortex, so that the B-L model is adaptive for lower Mach numbers. Then, the normal force and pitching moment on NACA0012 airfoil was calculated and compared with available experimental data to validate the reliability of the model.

Introduction

Within a helicopter rotor flow field, the blades encounter complex time varying changes in aerodynamic angle of attack due to imposed control inputs, the dynamic motion of the blades, and large local variations in inflow velocity that arise from the complex three-dimensional vortex wake system. Typically, dynamic stall occurs on the retreating blade under conditions of high blade loading and in high speed forward flight[1]. The rotor operational limitations are all determined by the onset of transient flow separation such as dynamic stall.

The B-L model was originally introduced by Beddoes[2-3] and deals with the unsteady lift and pitching moment. Then this model was refined by Leishman[4-6] and became a complete model for unsteady lift, drag, and moment. The B-L model includes the effect of the unsteady two-dimensional inviscid wake, the effects of trailing and leading edge flow separation, and compressibility effects similar to the Piston Theory. State-space formulations of the B-L model have been published for attached flow conditions in [7-8].

In this paper, it is demonstrated how a relatively elegant and computationally efficient method can be created and used to credibly reproduce the dynamic stall characteristics of an airfoil section given, primarily, the static (nonlinear) airfoil lift and pitching moment characteristics. The method draws on the work of both Leishman[9] and Sheng[10], to establish a system of first order ordinary differential state equations which represent specific aspects of the unsteady airfoil behavior. The method is useful in the performance and aeroelastic response analysis of helicopter rotors and propellers. To support the development of the method, illustrative comparisons with experimental data are presented for the unsteady lift, pitching moment on a typical helicopter rotor airfoil undergoing oscillatory pitch forcing into dynamic stall.

Attached Flow Behavior

A prerequisite in any unsteady aerodynamic theory is the ability to accurately represent the unsteady aerodynamic response under attached flow conditions. The indicial response is particularly useful since the state equations representing the unsteady airfoil behavior can be obtained by the direct of Laplace transforms to the indicial response to get the aerodynamic transfer function.

In the present analysis, the indicial response functions given by Beddoes[3] and later refined by Leishman[6] are used. These indicial responses are assumed to be composed of the sum of two parts; one for the initial noncirculatory loading (which comes from piston theory) and another for the circulatory loading which builds up quickly to the steady state value. In general, the indicial normal force and quarter-chord pitching moment response to a step change in angle of attack α and a step change in pitch rate $q = \dot{\alpha}c/V$ can be written as

$$C_{N_\alpha}(S) = \left[\frac{4}{M}\phi_\alpha^{\mathrm{I}}(S,M) + \frac{2\pi}{\beta}\phi_\alpha^{C}(S,M)\right]\alpha . \tag{1}$$

$$C_{M_\alpha}(S) = [-\frac{1}{M}\phi_{\alpha M}^{\mathrm{I}}(S,M) + \frac{2\pi}{\beta}\phi_\alpha^{C}(S,M)\cdot\left(\frac{1}{4} - x_{ac}(M)\right)]\alpha . \tag{2}$$

$$C_{N_q}(S) = \left[\frac{1}{M}\phi_q^{\mathrm{I}}(S,M) + \frac{\pi}{\beta}\phi_q^{C}(S,M)\right]q . \tag{3}$$

$$C_{M_q}(S) = [-\frac{7}{12M}\phi_{qM}^{\mathrm{I}}(S,M) - \frac{\pi}{8\beta}\cdot\phi_{qM}^{C}(S,M)]q . \tag{4}$$

Where the indicial response function ϕ_α^C, ϕ_α^{I}, $\phi_{\alpha M}^{\mathrm{I}}$, ϕ_q^{I}, ϕ_q^C, ϕ_{qM}^{I} and ϕ_{qM}^C are expressed in terms of both aerodynamic time S and the Mach number M.

It can be readily shown that by rearranging all(eight)state equations for attached flow conditions, they can be represented as a diagonal canonical set of state equations

$$\dot{\boldsymbol{x}} = \boldsymbol{A}\boldsymbol{x} + \boldsymbol{B}\begin{Bmatrix}\alpha\\ q\end{Bmatrix}. \tag{5}$$

$$\begin{Bmatrix}C_N^P\\ C_M^P\end{Bmatrix} = \boldsymbol{C}\boldsymbol{x} + \boldsymbol{D}\begin{Bmatrix}\alpha\\ q\end{Bmatrix}. \tag{6}$$

Where the matrices are of the form

$$A = diag\left[a_{11}\quad a_{22}\quad a_{33}\quad a_{44}\quad a_{55}\quad a_{66}\quad a_{77}\quad a_{88}\right]; B = \begin{bmatrix}1 & 1 & 1 & 0 & 1 & 1 & 0 & 0\\ 0.5 & 0.5 & 0 & 1 & 0 & 0 & 1 & 1\end{bmatrix};$$

$$C = \begin{bmatrix}c_{11} & c_{12} & c_{13} & c_{14} & 0 & 0 & 0 & 0\\ c_{21} & c_{22} & 0 & 0 & c_{25} & c_{26} & c_{27} & c_{28}\end{bmatrix}; D = \begin{bmatrix}4/M & 1/M\\ -1/M & -7/12M\end{bmatrix}.$$

The total aerodynamic lift and pitching moment response to an arbitrary time history of α and q can be obtained from the above state equations by integrating.

Stall Onset

The most crucial aspect of the modeling of dynamic stall is the identification and representation of the conditions for the onset of leading edge separation. The criterion was evaluated by Beddoes within the context of rotor airfoil performance, under both steady and unsteady conditions.

From an analysis of airfoil static test data, a critical value of C_{N_1} (static) is close to the maximum static C_N. Thus a Mach number dependent separation onset (stall) boundary may be defined. A typical boundary for the NACA 0012 airfoil is shown in Fig.1.

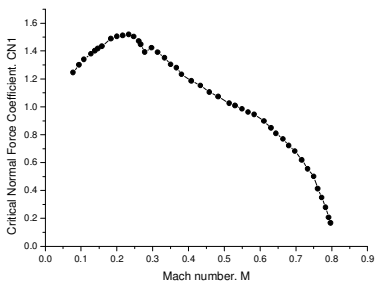

Fig.1 Stall boundary for the NACA0012 airfoil section

For unsteady conditions, there is a lag in $C_N(t)$ with respect to the forcing, however there is also a lag in the leading edge pressure response $P(t)$ with respect to $C_N(t)$. To implement the critical pressure criterion under unsteady conditions, a first order lag may be applied to $C_N(t)$ to produce a substitute value $C_N'(t)$ with the presumption that whatever properties apply to $P(t)$ must also apply to $C_N'(t)$. This representation may be written as the differential state equations

$$\begin{cases} \dot{\boldsymbol{x}}_9 = -\dfrac{\boldsymbol{x}_9}{T_p} + \dfrac{C_N^p(t)}{T_p} \\ C_N'(t) = \boldsymbol{x}_9 \end{cases}. \tag{7}$$

Where the time constant T_p is a function of Mach number.

Thus by monitoring the value of $C_N'(t)$ the onset of leading edge/shock induced separation under dynamic conditions will be initiated when $C_N'(t)$ exceeds the critical $C_{N_1}^{'}(M)$ boundary. Furthermore, if the vale of $C_N'(t)$ is monitored throughout the calculation into stall, then it may be used as an indicator for the conditions which permit flow reattachment, i.e. if $C_N'(t) < C_N'$.

Trailing Edge Separation

A phenomenon that is also involved in most types of airfoil stall is progressive trailing edge separation. The associated loss of circulation due to trailing edge separation introduces a nonlinear force and moment behavior, especially with the cambered airfoils more typically used on modern helicopters. When the primary source of separation is at the leading edge or the foot of a shock wave it appears that this is generally sufficient to promote some separation at the trailing edge and hence initiate some nonlinear behavior in the force and moment response.

A specific case of Kirchhoff flow is a simple model for the trailing edge separation phenomenon in which the airfoil normal force coefficient, C_N, may be approximated as

$$C_N = C_{N_\alpha}(M)\left(\frac{1+\sqrt{f}}{2}\right)^2 \alpha. \tag{8}$$

where f is the trailing edge separation point. Thus, if the separation point can be determined it is a trivial calculation to determine the normal force.

The relationship between α_1 and f can be generalized empirically in a fairly simple manner using the relations

$$f = \begin{cases} 1 - 0.3\exp\left[\left(\alpha_f - \alpha_1\right)/S_1\right], \alpha_f < \alpha_1 \\ 0.04 + 0.66\exp\left[\left(\alpha_1 - \alpha_f\right)/S_2\right], \alpha_f > \alpha_1 \end{cases}. \tag{9}$$

Where the effective angle of attack α_f is defined as

$$\alpha_f = \frac{C_N^{'}(t)}{C_{N_\alpha}(M)}. \tag{10}$$

The coefficients S_1 and S_2 define the stall characteristic, while α_1 defines the break point corresponding to $f = 0.7$. S_1, S_2 and α_1 are determined empirically for each airfoil and vary with Mach number.

A general expression for the pitching moment behavior cannot be obtained from Kirchhoff theory and an alternative empirical relation must be formulated. From the airfoil static data, the center of pressure at any angle of attack may be determined from the ratio C_M / C_N. The variation can be plotted versus the corresponding value of the separation point and fitted in a least squares sense to the form

$$\frac{C_M}{C_N} = K_0 + K_1(1-f) + K_2\sin\left(\pi f^m\right). \tag{11}$$

where $K_0 = (0.25 - x_{ac})$. The constant K_1 gives the direct effect on the center of pressure due to the growth of the separated flow region and the constant K_2 helps describe the shape of the moment break at stall. The values of K_0, K_1, K_2 and m can be adjusted for different airfoils, as necessary, to give the best moment reconstruction. Typically, $m = 2$.

The additional effects of the unsteady boundary layer response may be represented by applying a first order lag to the value of f' to produce the final value for the unsteady trailing edge separation point f. In state variable form this additional lag in the response may be represented as

$$\begin{cases} \dot{x}_{10} = -\dfrac{x_{10}}{T_f} + \dfrac{f'(t)}{T_f} \\ f'(t) = x_{10} \end{cases}. \tag{12}$$

As in the case of T_P, the time constant T_f is Mach number dependent.

Finally, the nonlinear normal force $C_N^f(t)$ with the modified unsteady trailing edge separation point f' is given by

$$C_N^f(t) = C_{N_\alpha}(M)\left(\frac{1+\sqrt{f'}}{2}\right)^2 \alpha_E(t) + C_{N_n}^I. \tag{13}$$

and the pitching moment by

$$C_M^f(t) = \left[k_0 + k_1(1-f') + k_2 \sin\left(\pi (f')^m\right)\right] \cdot C_N^c(t) + C_{M0}. \tag{14}$$

Where $C_{N_n}^I$ is noncirculatory normal force, and C_N^c is the circulatory normal force coefficient and C_{M0} is the zero lift moment.

Modeling of Dynamic Stall

The general case of dynamic stall involves the formation of a vortex near the leading edge of the airfoil which subsequently separates from the surface and is transported downstream.

An approximate, but physically acceptable, model for the dynamic stall process has been formulated by viewing the vortex lift contribution $C_N^v(t)$ as an excess circulation which is not shed into the airfoil wake until some critical condition is reached. The critical condition used here is of course when $C_{N_1}^{'}$ exceeds C_{N_1}. At this point, catastrophic flow separation occurs and the accumulated circulation passes over the airfoil and into the wake. The vortex lift process can be represented by the differential state equations

$$\begin{cases} \dot{x}_{11} = -\dfrac{x_{11}}{T_v} + \dfrac{\dot{C}_v}{T_v} \\ C_N^v(t) = x_{11} \end{cases}. \tag{15}$$

Where $C_v = \begin{cases} C_N^C\left[1 - \left(1+\sqrt{f'}\right)^2/4\right]\tau_v / m_v T_{vl} & \tau_v \le 2T_{vl} \\ 0 & \tau_v \le 2T_{vl} \end{cases}$

as derived from the Kirchhoff approximation, and T_v is time constant. To track the position of the vortex, a nondimensional vortex time parameter τ_v (in semi-chords) is used such that $\tau_v = 0$ at the onset of separation conditions and $\tau_v = T_{vl}$, when the vortex reaches the trailing edge.

The centre of pressure on the airfoil also varies with the chordwise position of the vortex and will obtain a maximum value when the vortex reaches the trailing edge. Based on an analysis of much experimental data involving dynamic stall over a wide range in Mach number, a fairly general representation of the centre of pressure behaviour was formulated empirically as

$$CP_v = 0.25\left[1-\cos\left(\frac{\pi\tau_v}{T_{vl}}\right)\right]. \tag{16}$$

Finally, the increment in pitching moment about the quarter-chord due to the aft-moving centre of pressure is given by

$$C_M^v = -CP_v C_N^v. \tag{17}$$

From the above, the required total loadings can be obtained by superposition. For example, the total normal force coefficient C_N under dynamic stall conditions is given by

$$C_N(t) = C_N^f(t) + C_N^v(t). \tag{18}$$

The total pitching moment coefficient C_M under dynamic stall conditions is given by

$$C_M(t) = C_M^f(t) + C_M^v(t). \tag{19}$$

Results and Discussion

This section documents a selection of comparisons of the aerodynamic model with unsteady test data. The state-space equations was calculated by the method of direct integration.

sample 1

NACA0012, $\alpha = 2.1^\circ + 8.2^\circ \sin\omega t$, $M = 0.383$, $k = 0.074$.

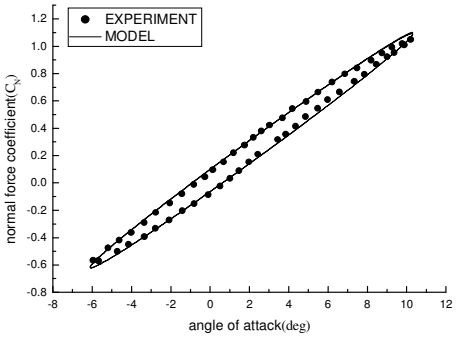

Fig.4 Normal force vs angle of attack

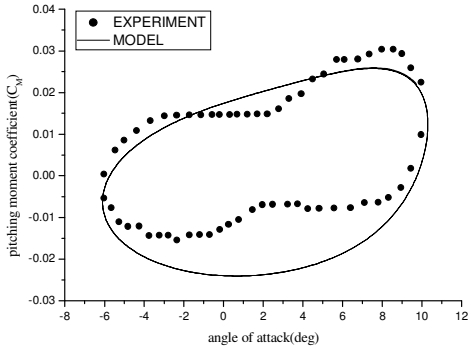

Fig.5 Pitching moment vs angle of attack

sample 2

NACA0012, $\alpha = 10.3^\circ + 8.1^\circ \sin\omega t$, $M = 0.379$, $k = 0.075$.

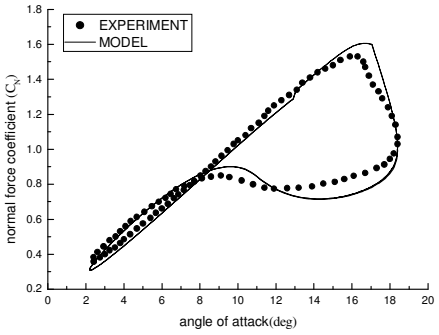

Fig.2 Normal force vs angle of attack

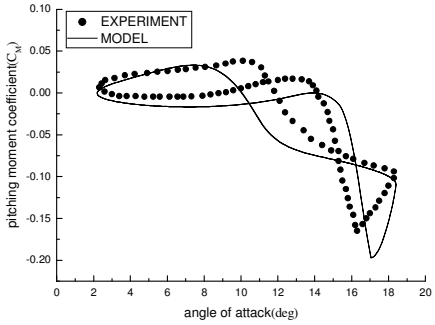

Fig.3 Pitching moment vs angle of attack

Conclusions

1) Typical normal force. and pitching moment responses are shown in sample.1, for a harmonic pitch oscillation under attached flow conditions. It should be noted that, for a pure sinusoidal oscillation under attached flow conditions, normnally elliptical lift and moment loops should be obtained.

However, it can be seen that there is some distortion in the loops, particularly for the pitching moment. This behavior was traced to a significant third harmonic in the pitch forcing that has the effect of in creasing the pitch rate contributions to the airloads near the maxim and minimum angles of attack.

2) In sample.2, strong dynamic stall occurs. It can he seen that the vortex shedding contributes a moderate increment to C_N, but gives a particularly large increase in nose-down pitching moment. The maximum lift and minimum moments are predicted very accurately along with the phasing of the loads during stall. Flow reattachment (indicated by the return to the nominally elliptical shapes of the loops) is delayed to a fairly low angle of attack during the downstroke of the motion. It should be noted that two successive cycles of oscillatory pitch data are shown, and this serves to illustrate the inherent variability of the aerodynamic loads in the separated flow regime.

References

[1] Leishman, J.G. Principles of Helicopter Aerodynamics [M]. (Second Edition). Cambridge, 2007.

[2] Beddoes, T. S. A Synthesis of Unsteady Aerodynamic Effects Including Stall Hysteresis[J]. Vertica, Vol. 1, No. 2, Feb. 1976, pp. 113–123.

[3] Beddoes, T.S., Representation of Airfoil Behavior [J]. Vertica, Vol. 7, No. 2, Feb. 1983, pp. 183–197.

[4] Leishman, J.G., "Two-Dimensional Model for Airfoil Unsteady Drag Below Stall," [J]. Journal of Aircraft, Vol. 25, No. 7, Jul. 1988, pp. 665–666.

[5] Leishman, J.G., Modeling Sweep Effects on Dynamic Stall[C]. Journal of the American Helicopter Society, Vol. 34, No. 3, Mar. 1989, pp. 18–29.

[6] Leishman, J.G., Beddoes, T.S., A Generalized Model for Unsteady Aerodynamic Behavior and Dynamic Stall Using Indicial Method[C]. Journal of the American Helicopter Society, Vol. 34, No. 3, Mar. 1989, pp. 3–17.

[7] Leishman J G, Nguyen K Q. State-space model for unsteady airfoil behavior[J]. AIAA Journal, 1990, 28(5): 836-844.

[8] Leishman J G, Gilvert L, Crouse Jr. State-space model for unsteady airfoil behavior and dynamic stall[C]. AIAA/ASME/ASCE/AHS/ASC 30th Structures, Structure Dynamics and Materials Conference, Mobile, Alabama, April 3-5, 1989, 1372-1383.

[9] W. Sheng, R.A.McD.Galbraith. A Modified Dynamic Stall Model for Low Mach Numbers [J]. Journal of Solar Energy Engineering, VOL 52,August,2008.

[10] Leishman, J.G., Validation of Approximate Indicial Aerodynamic Functions for Two-Dimensional Subsonic Flow[J], AIAA Journal of Aircraft, Vol. 25, No. 10, Oct. 1988, pp. 914-922.

Advanced Materials Research Vols. 989-994 (2014) pp 2264-2267
© (2014) Trans Tech Publications, Switzerland
doi:10.4028/www.scientific.net/AMR.989-994.2264

CFD simulation of Gas Distributor with Two Chambers

Dongfang Zhao[1, a] and Fengguo Liu [1, b]

[1]School of Energy and Safety Engineering, Tianjin Chengjian University, Tianjin 300384, China

[a]zdf_tj@163.com, [b]lfg_tj@126.com

Keywords: CFD, RNG *k-ε* turbulence model, Uniformity, gas distributor.

Abstract. This paper investigated a new type of gas distributor with two chambers by CFD software. The distributor has a natural gas inlet and nine nozzle outlets. For the investigation of this project, the mass flow rate of the distributor was analyzed in this paper to provide a way to optimize the structure of distributor. The N-S equations approached with the RNG k- ε turbulence model and the discretization were employed second order upwind. The simulation results will provide a number of useful suggestions and references for the further design.

Introduction

Over the past few years, quite a few large gas fields have been proven, and a huge amount of natural gas has been recovered. China is building a high capacity pipeline for transporting natural gas from the west regions to the east industrialized coastal areas, so natural gas will find wider applications than ever [1]. However, energy conservation and emissions reduction have been the subject of today's society. Therefore, various kinds of equipments about gas distribution have been studied and developed for improving performance. The natural gas distributor as one of the main components of gas equipment has significant function to gas distribute. So optimize the geometry structure of it for perfect uniformity of mass flow rate is becoming more and more necessary.

The traditional way of design-manufacture-further improvements requires long transformation time, high range is usually disappointing. Computational Fluid Dynamics (CFD) can provide detailed information on airflow patterns and ensure convenient design of agricultural equipments [2]. Along with the rapid development of High Performance Computer (HPC), numerical calculation of high strength has become reality. With the recent advances in computing power, the process of creating a CFD model and analyzing the results has become much less labor-intensive, reducing the time and therefore the cost [3].

The main task of this paper was to assess the characteristics of mass flow rate of nozzles. Based on the uniformity of mass flow rate, Dhotre and Joshi [4] simulated a coupled system consisting of gas chamber and a bubble column and estimated the uniformity of the gas distribution. Through the efforts of this paper will help us to obtain further method for optimizing design.

Modeling and Governing Equations of the distributor

Structure. Fig.1 shows the schematic of the gas distributor that was developed as the main part of this study. In the process of operation, the gas attaches the chambers through the gas inlet. And all of the gas was assign to the nozzles (form number 1 to 9). The size of special parts has been presented in Fig.1. Solenoid value was set at the bottom of left chamber. Moreover, it can adjust according to the power.

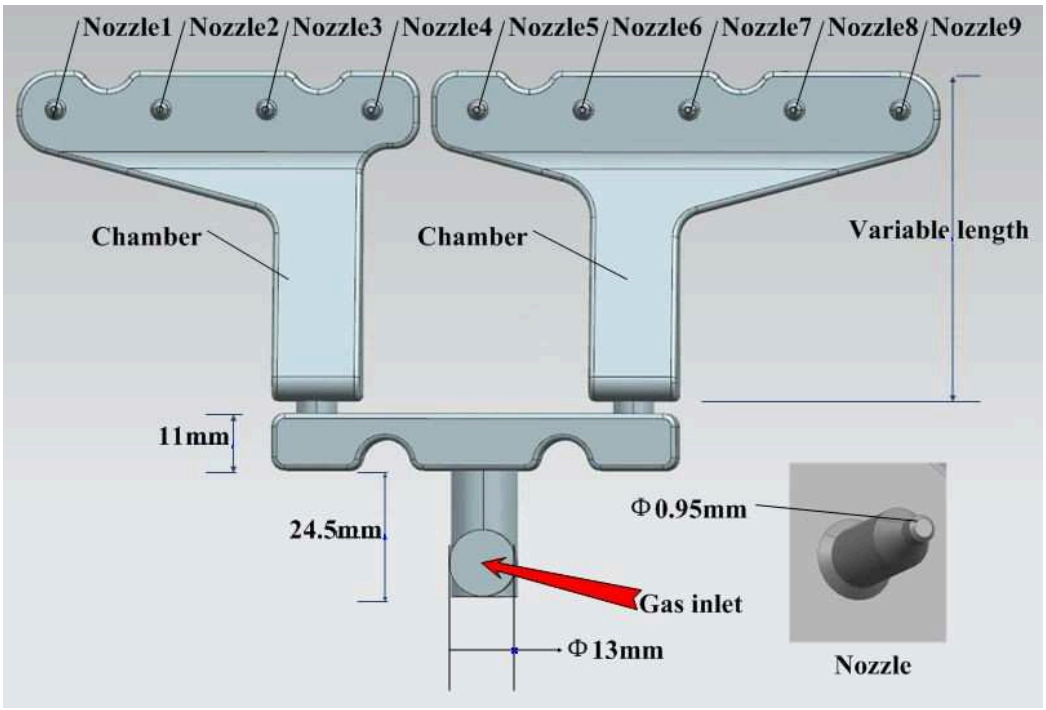

Fig. 1 Schematic of the gas distributor

Meshing. The pretreatment software Gambit was used in the process of grid building. It was that the throats and the parts of nozzle were divided to reduce the total number of cells.

Boundaries. The inlet boundary condition in this model was selected velocity inlet. And the inlet velocity was 3.348m/s. The exports of natural gas distributor were defined as pressure-outlet.

Equations. In the rectangular coordinate system with the absolute reference frame, the steady-state conservation equations of continuity, momentum, kinetic energy k and dissipation rate ε of turbulence pulsation can be expressed in the following form [4, 5]:

$$\nabla(\rho\mathbf{u})=0. \tag{1}$$

$$\nabla(\rho\mathbf{uu})=-\nabla p+\nabla\tau+\rho g \tag{2}$$

$$\nabla(\rho\mathbf{u}k)=-\nabla\left(\frac{\mu_{\text{eff}}}{\sigma_k}\nabla k\right)+G-\rho\varepsilon \tag{3}$$

$$\nabla(\rho\mathbf{u}\varepsilon)=\nabla\left(\frac{\mu_{\text{eff}}}{\sigma_\varepsilon}\nabla\varepsilon\right)+C_{\varepsilon 1}\frac{\varepsilon}{k}G-C_{\varepsilon 2}\rho\frac{\varepsilon^2}{k} \tag{4}$$

The turbulent viscosity is then related to k and ε by the expression:

$$\mu_{\text{eff}}=\mu+C_\mu\rho\frac{k^2}{\varepsilon} \tag{5}$$

The coefficients $C_{\varepsilon 1}$, $C_{\varepsilon 2}$, C_μ, σ_k, σ_ε are the k and ε model parameters and the following values selected: $C_{\varepsilon 1}$=1.44, $C_{\varepsilon 2}=1.92$, $C_\mu=0.09$, $\sigma_k=1.0$, $\sigma_\varepsilon=1.3$. The term G in Eqs. 2 and 3 is the production of turbulent kinetic energy and described by τ: $\nabla\mathbf{u}$ where $\tau=-\mu_{\text{eff}}\left[\nabla\mathbf{u}+(\nabla\mathbf{u})^{\text{T}}\right]$.

In order to investigate the uniformity of the out flow rate at natural gas distributor outlet, the following two evaluation indexes [6, 7] have been set up for reference.

$$E=\frac{\left|M_i-\overline{M}\right|}{\overline{M}}\times 100\% \tag{6}$$

Where E expresses the degree of deviation of out flow rate for each nozzle to the average that the sum of all the nozzles out flow rate.

$$S=\frac{\sqrt{\frac{1}{n\text{-}1}\sum_{i=1}^{n}\left(M_i\text{-}\overline{M}\right)^2}}{\overline{M}}\times 100\% \tag{7}$$

S is defined the maximum deviation that local out flow rate for the all nozzles. $\overline{M}$ is the average out flow rate for all of the nozzles, M_i denotes the out flow rate of each nozzle.

Summary

The CFD program used was CFD-14.5. This uses a Cartesian coordinate system with mixed mesh and solves the hydrodynamic equation set in a segregated manner. The pressure coupling was treated using the SIMPLE algorithm (Patankar [8]).

Fig.2 shows that the maximum and minimum mass flow rate are nozzle 2 and nozzle 6, respectively. At the same time, the E that present in Table 1 are 0.147% and 0.138%, respectively. However, it can be noticed that the mass flow rate of each nozzle have a relatively small S, which might create a uniform mass flow rate to a significant degree.

And the value of S is 1.1×10^{-3} in this paper, which could acceptable to a significant degree. The value of S gives expectable information that implies better uniformity of mass flow rate to every nozzle. From the previous simulations to engineering, the results that presented in this article are no doubt for the credibility.

Table 1 The values of E

The number of nozzle	1	2	3	4	5	6	7	8	9
E (%)	0.135	0.147	0.144	0.031	0.041	0.138	0.081	0.066	0.068

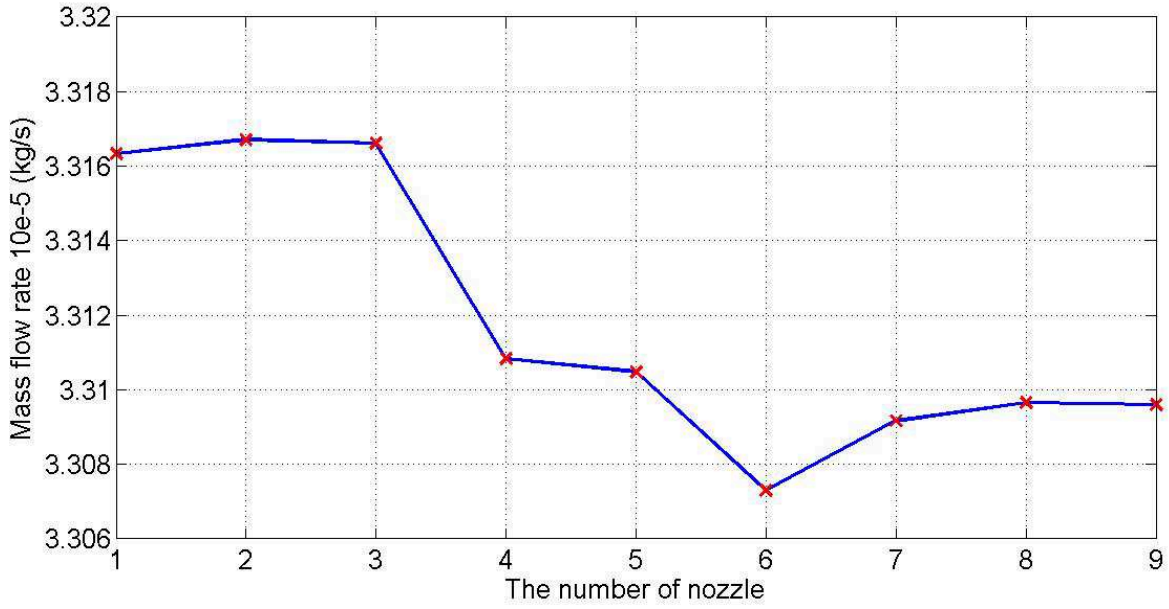

Fig. 2 Mass flow rate of nozzles

From the information reported in this paper, it may be possible to select the design parameters of distributor and natural gas chamber depending upon the desired level of uniformity of distribution.

References

[1] Defu Che, Yanhua Liu, Chunyang Gao, Evaluation of retrofitting a conventional natural gas fired boiler into a condensing boiler, Energy Conversion and Management 45 (2004) 3251-3266. (in Chinese with English abstract)

[2] Dai Jianwu, Xiao Hongwei, Bai Junwen, et al, Numerical simulation and optimum design on air flow distribution chamber of air-impingement jet dryer, Transaction of the Chinese Society of Agricultural Engineering, 2013, 29(3) 69-76. (in Chinese with English abstract)

[3] Shafqat Hussain, Patrick H. Oosthuizen, Numerical study of buoyancy-driven natural ventilation in a simple three-storey atrium building, Gulf Organisation for Research and Development International Journal of Sustainable Built Environment (2012) 1, 141-157.

[4] M.T. Dhotre, J.B. Joshi, Design of a gas distributor: Three-dimensional CFD simulation of a coupled system consisting of a gas chamber and a bubble column, Chem. Eng. Res. Des. 125 (2007) 149-163

[5] Zhai Zhiping, Wang Chunquang, Numerical simulation and optimization for air flow in an impeller blower, Transactions of the Chinese Society for Agricultural Machinery, 2008, 39(6): 84-87. (in Chinese with English abstract)

[6] Dai Jianwu, Xiao Hongwei, Bai Junwen, et al, Numerical simulation and optimum design on air flow distribution chamber of air-impingement jet dryer, Transaction of the Chinese Society of Agricultural Engineering (Transaction of the CSAE), 2013, 29(3): 69-76. (in Chinese with English abstract)

[7] Lei Xianliang, Li Huixiong, Zhang Qingm, et al, Regulation performance and optimal design of the gas adjust-screen in boiler steering rooms, Journal of Huazhong University of Sicence and Technology, 2011, 39(10): 128-132. (in Chinese with English abstract)

[8] S.V. Patankar, Numerical Heat Transfer and Fluid Flow, McGraw-Hill, New York, 1980.

Advanced Materials Research Vols. 989-994 (2014) pp 2268-2272
© (2014) Trans Tech Publications, Switzerland
doi:10.4028/www.scientific.net/AMR.989-994.2268

Ratio Based Weapon System of Systems Capability Gaps Assessment Method Research

Xiaoxiong Zhang[1, a], Kewei Yang[1, b] Bin Zhang[2,c] and Jiang Jiang[1, d]

[1] College of Information System and Management, National University of Defense Technology Changsha, Hunan, 410073, P.R. China

[2] Science and Technology on Complex System Simulation Laboratory Beijing, 100101, P.R. China

[a]zxxandxx@163.com, [b]Kayyang27@nudt.edu.cn, [c]zhangbinsos@sina.com, [d]jiangjiangnudt@163.com

Keywords: Weapons system-of-systems; capability ratio; synthesized weights; gaps assessment

Abstract. Weapon system of systems gaps assessment (WSoSCGA) is a key problem in the field of weapon demonstration research. Traditional methods have a lot of work to do and lack science. This paper tries to solve this problem in a novel way based on capability ratio. All the criteria should be normalized differently according to their own attributes. By combining the subjective weighting method and objective weighting method, synthesized weights are formed and inputted into a framework to determine their relative capability values. Then we can evaluate weapon system of systems gaps by comparative analysis. In contrast with traditional methods, there is no need to calculate specific capability value of each SoS for gaps assessment. At last, a case is conducted to illustrate its utilization and demonstrate its effectiveness and feasibility for WSoSCGA.

Introduction

Generally speaking, weapon system-of-systems (WSoS) is understood to be an assemblage of different weapon systems that are fundamentally collaborative and related with each other [1]. To date, assessment and evaluation of WSoS is a key problem in weapon demonstration research. And the studies related with capability gaps about WSoS are in the forefront of research. Capability gaps analysis [2], based on the capability demand analysis and capability evaluation, aims to make a deep analysis on WSoS' deficiencies and make timely adjustments at different time periods, according to different mission objectives and requirements for the future development.

To the best of our knowledge, there are few studies conducted in the capability gaps assessment at domestic and overseas. TTCP Joint Systems and Analysis Group [3] suggested using three different colors to represent different capacity gaps importance, based on experts' experience and knowledge, which is more suitable for strategic level. The latest edition of the "Capability based Assessment User Manual 3.0" in U.S [4] introduced their research briefly about the sorting of the ten capacity gaps related with biometrics, which in essence is a simplified AHP (analytic hierarchy process) method without considering some conflicting situations. Linkov [5] from U.S. Army engineering used multi-criteria decision analysis methods to solve multi-arms capability gaps in small arms project scheduling problem. Its deficiencies lie in excluding much incomplete preference information. Hristov [6] studied main methodological issues related to the prioritization of Required Operational Capabilities of the Bulgarian Armed Forces. However, a great amount of efforts must be done and uncertainties are not considered in the evaluation process. Welch from the U.S Sandia National Laboratories developed prioritized gaps using utility theory [7]. Obviously this assessment required system expert participation and opinion, which will no doubt lead to arbitrariness and obscurity.

It is apparent that none of these methods developed is perfect and all are far from ready to be used in practical applications. This paper tries to solve this problem in a very artful way. To begin with, all the criteria are normalized by comparing with different goal values. Then, synthesized weights are formed by combining the subjective weighting method and objective weighting method. These weights are inputted into a frame to determine each system's relative capability value. Then we can

evaluate WSoS gaps by comparative analysis based on capability ratio. Thanks to this uniqueness, there is no need to calculate the specific value of each WSoS, which is easy to operate.

The proposed hybrid framework

AHP, introduced by Saaty [8], aims to quantify relative priorities for a given set of alternatives on a ratio scale. The strength of this approach lies in organizing tangible and intangible factors in a systematic way, and providing a structured yet relatively simple solution to the decision making problems [9]. However, its limitation lies in its overreliance on the intuition of decision makers, which may lead to unreasonable results. Entropy was first introduced by Shannon to the Information Theory [10], which assigns a small weight to an attribute if it has similar attribute values across alternatives, because such attributes does not help in differentiating alternatives.

Considering these shortcomings, we propose a hybrid framework, integrating IEM (Information Entropy Method) and AHP to determine the weights instead of using AHP or IEM alone. The weights obtained from IEM are derived from characteristic data of alternatives themselves. As is shows in Fig .1, it displays an overview of the hybrid framework for WSoSCGA. All the criteria should be normalized according to corresponding standardization models. Then aggregation process is done to get relative values of each system. Comparative analysis can be made to the capability gaps between WSoS. The detailed process is as follows:

Step 1: Establish a unified combat capability index system. WSoS needs different combat missions under different operational backgrounds. In general, all kinds of SoS capability requirement can be regarded as a combination of communication capability, attack capability, mobility capability, defense capability, and security capability in a certain way [11]. Meanwhile, all these capabilities are supported by specific weapon category and each weapon category has more than one capability. Therefore, a certain mapping relationship is needed and established as below in Fig .2.

Step 2: Identify the equipment of both sides and determine the standardization models;

Step 3: Collect the characteristic data of different equipment and establish corresponding WSoS to be evaluated;

Step 4: Normalize all the indicators and obtain synthetized weights by subjective weighting methods and objective weighting methods;

Combat capability index standardization is to make measurements to all the indicators related to the combat capability and transform them into polymeric scores through certain mathematical methods.

Tactical and technical indicators can be divided into qualitative one and quantitative one and the standardized method varies each other. In this paper, experts were asked to use their knowledge and experience to make a judgment on the qualitative ones. For quantitative index, it can be divided into benefit and cost type according to the influence degree of the index value up on combat task. In the standardization process, the characteristic value divided by a given demand value is set as the score for the benefit indicator. And corresponding given demand value divided by the characteristic value is set as the score for the cost indicators. It is noteworthy that there is no practical significance for these relative values, while using alone. Anyway, it can reflect the superiority when comparing the capabilities between different WSoS with the same structures.

The weight obtained from AHP and IEM can be synthesized by the following equation to calculate the overall weight of the ith criterion, WSYNi :

$$w_{SYNi} = \frac{W_{AHPi} W_{IEMi}}{\sum_{i=1}^{m} W_{AHPi} W_{IEMi}} \tag{1}$$

where m is the number of criteria.

Step 5: Aggregate the indicators according to specific models to obtain relative capability values of each system.

The simple additive weighting method is one of the best known and the most widely used multiple attribute decision making methods [12]. The overall value of upper index in this method can be expressed as:

$$y = \sum_{i=1}^{k} w_i x_i,\ w_i \geq 0,\ i = 1,2,...,k \quad \text{and} \quad \sum_{i=1}^{k} w_i = 1 \tag{2}$$

where wi is the ith attribute weight and k is the number of attributes.

Step 6: Analysis the results according to the above calculation.

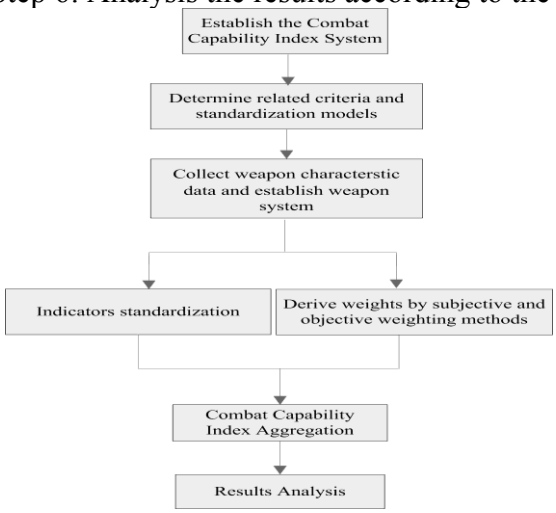

Fig 1. WSoSCGA Framework

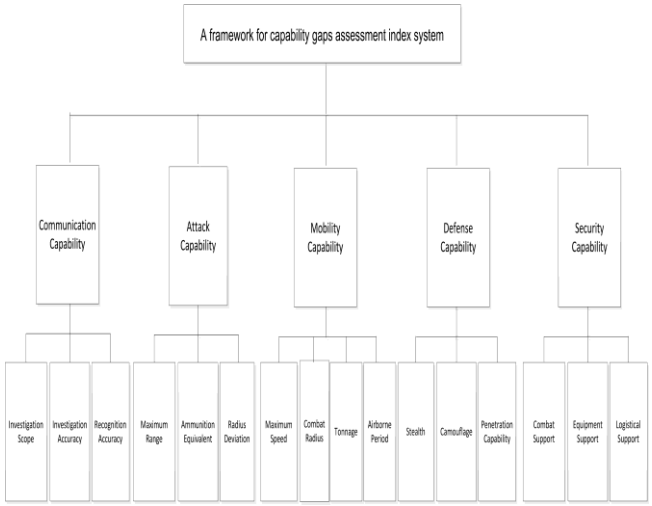

Fig 2. Capability Gaps Assessment Index System Framework

Case study

Suppose that there are two sides of combat SoS, each SoS contains a variety of different weapon categories, in which each weapon category has more than one capability and each capability can be supported by more than one weapon category.

This paper takes the best capability value among all the weapon categories as that of the system can afford. There are several following steps:

- Set up the combat capability index system
- Determine related criteria to be evaluated.
- Collect the data of both sides
- Normalize Processing and obtain synthetized weights

Table 1. Relative score on WSoS

Capability	Subcapability	Type	Friend	Enemy
Communication Capability	Investigation Scope	Benefit	1.125	1.2
	Investigation Accuracy	Benefit	1.05	1.1
	Recognition Accuracy	Cost	0.67	0.83
Attack Capability	Maximum Range	Benefit	1.2	1
	Ammunition Equivalent	Benefit	0.9	1.2
	Radius Deviation	Cost	0.8	0.67
Defense Capability	Maximum Speed	Benefit	1.1	1.1
	Combat Radius	Benefit	1.07	0.93
	Tonnage	Benefit	1.06	0.94
	Airborne Period	Benefit	1.2	1.2
Mobility Capability	Stealth	Benefit	1.5	0.8
	Camouflage	Benefit	0.8	1.2
	Penetration Capability	Benefit	1	1.67
Security Capability	Combat Support	Benefit	0.6	0.8
	Equipment Support	Benefit	0.75	1.25
	Logistical Support	Benefit	1.2	0.9

This is achieved by normalizing every element into a corresponding score value using the following formulas:

$$a_{ij} = \frac{a_{ij}}{t_{ij}}, i = 1,..., m, j = 1,...n \text{ , for benefit attribute;} \quad (3)$$

$$b_{ij} = \frac{t_{ij}}{b_{ij}}, i = 1,..., m, j = 1,...n \text{ , for cost attribute.} \quad (4)$$

The overall weights of the ith criterion can be calculated from the synthesis of the weights obtained from AHP and IEM. Take the subcriteria 3 for example:

$$w_{SYN3} = \frac{W_{AHP3}W_{IEM3}}{\sum_{i=1}^{16} W_{AHPi}W_{IEMi}} = \frac{0.0268*0.0575}{0.0568} = 0.0271 \quad (5)$$

Table 2 Weight-deriving process for criteria

Criteria	WAHP	WIEM	WSYN
Communication Capability 0.0625			
1 Investigation Scope 0.2381	0.0149	0.0920	0.0241
2 Investigation Accuracy 0.3333	0.0208	0.0690	0.0253
3 Recognition Accuracy 0.4286	0.0268	0.0575	0.0271
Attack Capability 0.1250			
4 Maximum Range 0.4118	0.0515	0.1034	0.0938
5 Ammunition Equivalent 0.2353	0.0294	0.0345	0.0179
6 Radius Deviation 0.3529	0.0441	0.0805	0.0625
Mobility Capability 0.2813			
7 Maximum Speed 0.1667	0.0469	0.0805	0.0665
8 Combat Radius 0.3333	0.0938	0.0460	0.0760
9 Tonnage 0.2778	0.0781	0.0690	0.0949
10Airborne Period 0.2222	0.0625	0.0115	0.0127
Defense Capability 0.2500			
11 Stealth 0.4737	0.1184	0.0115	0.0240
12 Camouflage 0.2105	0.0526	0.0575	0.0533
13 Penetration Capability 0.3158	0.0790	0.0920	0.1280
Security Capability 0.2813			
14 Combat Support 0.2105	0.0592	0.1034	0.1078
15 Equipment Support 0.3684	0.1036	0.0230	0.0420
16 Logistical Support 0.4211	0.1185	0.0690	0.1440

- Index Aggregation

Relative values of both sides can be obtained by aggregating the indicators. It is easy to find that our comprehensive ability amounted to 92.3% of enemy after comparison, which in a way illustrates that there still exist some gaps between each other.

$$\begin{aligned} I_1 &= \sum_{i=1}^{16} w_{SYN} a_i = 0.8911 \\ I_2 &= \sum_{i=1}^{16} w_{SYN} b_i = 0.9654 \\ I_1 / I_2 &= 0.9230 \end{aligned} \quad (6)$$

Meanwhile, we also constructed the approach with AHP weights alone to solve the same problem for comparison. The AHP model yielded a different decision result from the SYN model while our system is superior to the enemy as follows:

$$\begin{aligned} I_1 &= \sum_{i=1}^{16} w_{AHP} a_i = 1.0439 \\ I_2 &= \sum_{i=1}^{16} w_{AHP} b_i = 1.0398 \\ I_1 / I_2 &= 1.0039 \end{aligned} \quad (7)$$

The change in the outcomes when IEM weights are taken into account has shown that criteria weights found more reasonable constitute an important phase in decision-making process.

Conclusions

WSoSCGS is a hot issue in the field of military operational research, yet it lacks systematic results to date. This paper proposes a new approach based on capability ratio and model for WSoSCGS. First, all criteria are to be normalized, and then synthesized weights are obtained by using subjective weighting method and objective weighting method. And a simple additive weighting method is used to get relative capability value of each WSoS. In contrast with traditional methods, there is no need to calculate specific capability value for gaps assessment. This model can provide a new measurement and thought for WSoSCGS and analysis results can also help top-layer designers make more scientific decisions. There are many aspects involved in WSoSCGS and what is discussed in this paper is only a small part of it. Take the standardized approach for the performance parameters for example. Literatures [13] made a detailed discussion on it. As for the aggregation of the combat capability, there should be more paradigmatic relations and aggregation models to make the evaluation more close to the reality [14]. Meanwhile, quantities of equipment and relationships between different equipment are not taken into consideration in this paper. In a word, assessment related to WSoS remains to be researched.

References

[1] Mark W. Maier., “Architecting Principles for system of systems”, Proc 6th Annu Symp INCOSE, pp.567-574, 1996.
[2] Cheng Ben, “Capability-based Weapon System-of-System Assessment Methods and Application Research”, National University of Defense Technology, 2012.
[3] CJCSM3170.01D. “Manual for the operation of the joint capabilities integration and development system”. A-8, F-A-1. 2009.
[4] JCS J-8. “Capabilities-based assessment (CBA) user's guide version 3”, pp.83-92. 2009.
[5] Linkov I, Satterstrom F K, Fenton G. “Prioritization of capability gaps for joint small arms program using multi-criteria decision analysis”, Journal of multi-criteria decision analysis, Vol.16, pp.179-185. 2009.
[6] Hristov N, Radulov I, IlievP, et al. “Prioritization Methodology for Development of Required Operational Capabilities”, Analytical support to defence transformation, Sofia, Bulgaria: NATO/RTO, pp.RTO-MP-SAS-081-15(1-18), 2010.
[7] Welch K M, Lawton C R. “Applying system of systems and systems engineering to the military modernization challenge”, //2011 6th International conference on system of systems engineering. Albuquerque, New Mexico, USA. pp: 245-250, 2011.
[8] T.L. Saaty, The Analytic Hierarchy Process, RWS Publications, Pittsburgh, PA. 1990.
[9] B.L. Golden, E.A. Wasil, and P.T. Harker, The Analytic Hierarchy Process: Applications and Studies. New York, NY: Springer-Verlag, 1989.
[10] PRACHEE P, SAILU Y, AKASH R, et al. “Computational prediction and experimental verification of novel IdeR binding sites in the upstream sequences of mycobacterium tuberculosis open reading frames”, Bioinformatics. Vol.21, pp.2161-2166, 2005.
[11] Wang zhenyu, Ma yaping, Li ke. . “The complexity of Modern War: Study on Synergistic Effectiveness in Joint Operations”, Computer Simulation, Vol.21, No.11, pp.10-12. 2004.
[12] C.L. Hwang, K. Yoon, “Multiple Attribute Decision Making: Methods and Applications”, Springer, Berlin, 1981.
[13] Wan Ziming, Liao liangcai, Chen Yingwu. “Research on Effectiveness Evaluation Model of Weapon System”, Systems Engineering and Electronics, Vol.22, No.3, pp.1-3, 2000.
[14] Luo Pengcheng, Fu panfeng, Zhou jinglun. “Framework to evaluate the combat capability of weapons SoS”, Systems Engineering and Electronics, Vol.27, No.1, pp.72-75,2005.

Advanced Materials Research Vols. 989-994 (2014) pp 2273-2277
© (2014) Trans Tech Publications, Switzerland
doi:10.4028/www.scientific.net/AMR.989-994.2273

Study on an Improved Median Filtering Algorithm

Heng Zhang, Min Gao, Hailong Ren

Missile Engineering Department , Ordnance Engineering College, Shijiazhuang 050003, China

tszhangheng@163.com

Key words: Grey histogram; Fast median filter; Noise point detection; Self-adapting threshold comparison

Abstract: Median filter is a very effective method of non-linear smoothing filtering. However, the data ordering for traditional median filtering (TMF) is very time-consuming and hardly satisfy real-time image processing. This article proposes a kind of fast median filtering algorithm based on grey histogram, the filter seeks the median through the grey histogram of mask window, not the numeric sort, which decreases the comparison times. Moreover, the update of histogram by using the overlap of mask window increases the arithmetic processing speed. Meanwhile, in the proposed algorithm, the two-level self-adapting threshold comparison, with a higher precision of detection, is used to implement the inspection of noise point and improve the image quality and increase the signal-noise ratio by processing the noise point and non-noise point respectively. The experiments by matlab simulation can prove the availability of this algorithm.

Introduction

Since the digital images usually get corrupted by impulse noise during collection, transmission and display, this will cause vague image and degraded features which will affect the subsequent image analysis directly. Therefore, image denoising has been of prime importance in image processing.

As a kind of nonlinear filtering method, median filters (MF) replace the value of a pixel by a median of the intensity levels in neighborhood of that pixel which are widely thought to be better ones for removing impulse noises since they can also preserve the edges in a corrupted image. Many different variations of median filters are proposed, including central weighted median filters (CWM)[1], switching median filters (SM)[2] , three state median filters(TSM)[3], fast median filters(FM)[4], adaptive median filters(AM)[5], and many others.

Aforementioned algorithms all have superior filtering effects in experiments. However, with the wide application of video data, the complexity of these algorithms which reduced the speed of median filter caused a great influence in speed of video data processing. The median filtering algorithm based on grey histogram [6] seeks the median through the grey histogram of mask window, not the numeric sort, which increases the arithmetic processing speed. But, the same as TMF, every pixel will be smoothed no matter whether the pixel is corrupted. This causes that the edges and some other details of image will be dimed simultaneously. Therefore, it is essential to create an improved median filter based on grey histogram.

Fast Median Filter Based on Grey Histogram

Through the grey histogram of mask window, the MF based on grey histogram finds the median through counting the cumulative frequency range from the minimum grayscale to the maximum grayscale. Overlapping character of the moving window simplified the update of grey histogram which improves the execution speed. The algorithm can be described as follows:

1. The size of image is M×N, t=M*N/2;
2. Move the mask to the beginning of a new row, sort the pixels and output the median m. Build the histogram of mask window, and then record the number n_m of pixels whose luminance is not more than m;

3. In left-most column, for the every pixel whose luminance is p_g, we do modification as
$$H[p_g] = H[p_g] - 1$$
Further, $n_m = n_m - 1$ if $H[p_g] < m$;
4. Move the mask a column to the right, In right-most column, the every pixel whose luminance is p_g, we do modification as
$$H[p_g] = H[p_g] + 1$$
Further, $n_m = n_m + 1$ if $H[p_g] < m$;
5. If $n_m = t$ go to step 9;
6. If $n_m > t$ go to step 7, we do some modifications as
$$m = m + 1$$
$$n_m = n_m + H[m]$$
until that $n_m \geq t$, and then go to step 9;
7. (Now $n_m > t$), we do some modifications as
$$m = m - 1$$
$$n_m = n_m - H[m]$$
until that $n_m \leq t$,
8. Add up the cumulative frequency n_m in the scope range from the minimum grayscale to the maximum grayscale, when $n_m \geq t$, output the gray value m;
9. If the right-most column of mask window is not the border of image, go to step 3;
10. If the bottom row of mask window is not the border of image, go to step 2;

Impulse noise only corrupts part of image pixels, but the algorithm affects every pixel which can lead to excessive filtering easily. While selective filtering will avoid unwanted filtering which means the filtering effect will be improved further.

Two-level Noise Points Detection

We can distinguish noise points from non-noise points through detection, and then process the noise point only, in other words, it can protect the non-noise points, weaken excessive filtering, and improve the performance of protection of image details.

Salt-and-pepper noise is one of the significant impulse noises that may occur in images. In an image, the gray value of salt-and-pepper noise is distributed generally on the maximum side or the minimum side [7], the luminance of noises is significantly different from its neighborhood. The probability density function of salt-and-pepper is given as

$$P(z) = \begin{cases} P_a & z = a \\ P_b & z = b \\ 0 & \text{others} \end{cases} \quad (1)$$

For the above features, the pixels whose gray value is in the scope $[0, \alpha]$ or [255-α,255] can be considered as suspected noise points. These points should be detected further, moreover, the pixels whose gray value is in the scope (α, 255-α) are kept the original gray value, where α denotes the threshold of global detection. The selection of the threshold is critical for the judgment precision, the value of α is determined mainly according to the gray value. In general, the value range of salt noises is [235,255], the value range of pepper noises is [0,20][8], therefore, the value of α is 20 usually.

The global detection of noises is based on extremum, but the details and the edges of image may be the extreme points [8]. Accordingly, it is essential to get the further local detection on the suspected noise points which can avoid false detection of noises.

The correlation between the adjacent pixels should be taken into account. The gray value of pixels is close to its neighborhood, and the difference between the corrupted pixels and the adjacent normal pixels is larger. So, on the basis of global detection, we proposed the algorithm of local detection based on threshold to divide the noise and signal effectively. However, a fixed threshold cannot adapt different kinds of images and changes of noise density. Therefore, an adaptive threshold is proposed in this paper, the equation is as

$$T=\frac{1}{N\times M}\sum_{n=\frac{1-N}{2}}^{\frac{N-1}{2}}\sum_{m=\frac{1-M}{2}}^{\frac{M-1}{2}}\left|f(i+n,j+m)-med\right|. \tag{2}$$

where $f(i,j)$ denotes the gray value of the point (i,j), med denotes the median of the mask window, the size of window is $N\times M$. For the suspected noise points, we do some modifications as

1. If $a=\left|f(i,j)-med\right|\le T$, $f(i,j)$ is considered as non-noise point, and then output the gray value of the original pixel;
2. If $a=\left|f(i,j)-med\right|>T$, $f(i,j)$ is considered as noise point, and then output the median of the mask window;

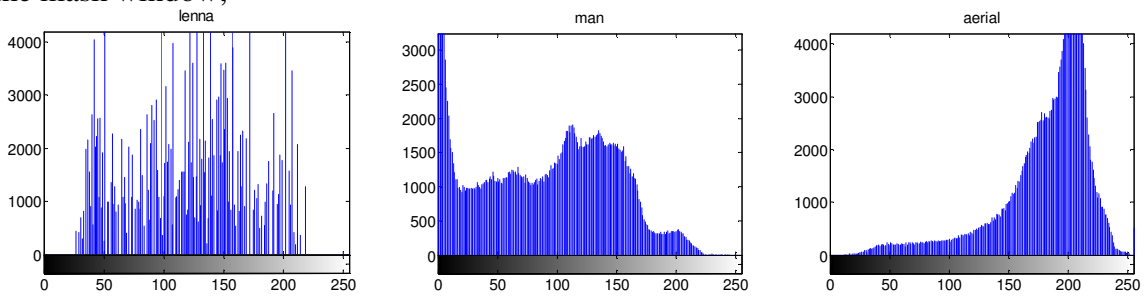

Fig. 1 The gray histogram of three images

The Simulation and Result Analysis

The effectiveness of the algorithm and the filtering effect can be validated by the simulation, the experimental platform is Matlab R2011b, and we choose three different distributions images lenna, man and aerial which are 256 grayscale, the gray histogram are given in Fig. 1.

Adding salt-and-pepper noise whose intensity is 0.2 to three images, and then process the images with the TMF (3×3), AMF and the proposed MF respectively. The results are given in Fig.2, Fig.3, Fig.4, where Fig. (a) is the original grayscale image, Fig. (b) is the image added salt-and-pepper noise, Fig. (c) is the result of TMF, Fig. (d) is the result of AMF, and Fig.(e) is the result of the proposed MF.

For the filtering effect, the peak signal to noise ratio (PSNR) and the mean-square error (MSE) are introduced in this paper. The equations are given in equation (3) and equation (4).

（a）Original image （b）Noisy image （c）TMF （d）AMF （e）Proposed

Fig.2 Results of different methods in restoring 20 percent corrupted image “lenna”

（a）Original image （b）Noisy image （c）TMF （d）AMF （e）Proposed

Fig.3 Results of different methods in restoring 20 percent corrupted image "man"

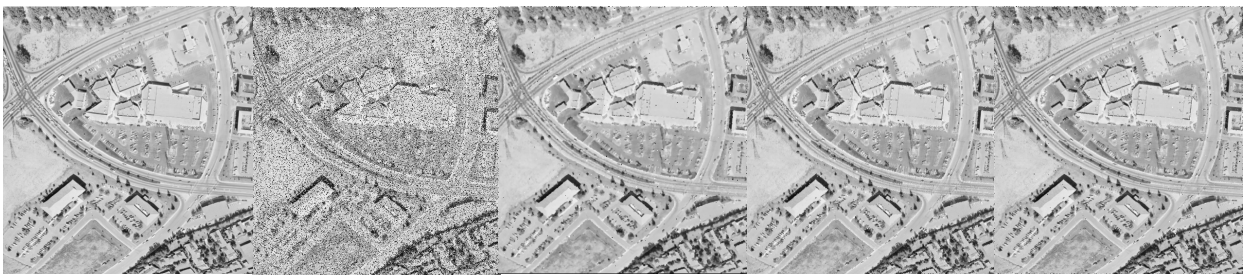

（a）Original image （b）Noisy image （c）TMF （d）AMF （e）Proposed

Fig.4 Results of different methods in restoring 20 percent corrupted image "aerial"

$$PSNR = 10 \times \log_{10}\left(\frac{255^2}{MSE}\right). \tag{3}$$

$$MSE = \frac{1}{m \times n}\sum_{i=1}^{m}\sum_{j=1}^{n}\left\|I(i,j) - K(i,j)\right\|^2. \tag{4}$$

where $I(i,j)$, $K(i,j)$ is the gray value of the image pre-and-post processing respectively, m and n is the row and column of the image respectively. We know that the smaller the MSE and the bigger the PSNR, the better the image quality.

On subjective visualization, the edges and details of the image processed by TMF are blurred, as shown in Fig. 2(c) of the hat, Fig. 3(c) of the hands, Fig. 4(c) of the house, the edges compare with Fig. (d) and (e) are more fuzzy, even some noise points are still exist; the places where the gray value is large or small in the image processed by AMF are little fuzzy; the image processed by the proposed MF are sharp-edged. On objective digital measure, the results are given in table 1. On speed, the proposed MF is more fast than the TMF, and is improved considerably compared with AMF; on PSNR, the proposed MF have a considerable improvement compared with the TMF, and enjoy superiority compared to AMF, the quality of image is improved obviously.

In conclusion, the execution speed of the proposed algorithm is suitable for being applied to real-time processing. And the introduction of two-level self-adapting threshold comparison advanced the precision of denoising largely, the filtering effect is much better than the TMF and AMF, and it is achieved the ideal effect of noise suppression.

Table 1 The results of three images, including PSNR, MSE and the execution time

Image	Noise(0.2)	TMF	AMF	Proposed
lenna	PSNR/dB	34.2275	38.5284	39.8839
	MSE	24.5657	9.1251	6.6786
	t/s	0.2948	0.2129	0.1503
man	PSNR/dB	33.1055	36.6123	37.1102
	MSE	30.3410	14.1856	12.6491

	t/s	0.2869	0.2142	0.1544
aerial	PSNR/dB	32.3692	35.8384	37.5912
	MSE	37.6842	16.9527	11.3229
	t/s	0.2911	0.2088	0.1477

Conclusions

In this paper, for the reason that the execution speed and filtering effect of the TMF is not ideal, we proposed a fast MF algorithm based on gray histogram with two-level self-adapting threshold noise detection. The algorithm gets the median depending on the update of histogram which improved the execution speed, the noise detection based on self-adapting threshold enhanced the ability of denoising, furthermore, it is some robust for different images. Through the result analysis and verification, the proposed algorithm is proved a kind of ideal fast MF of noise suppression.

References

[1] ZHANG Yong, CHEN DA-jian. Comparing of Two improved Median Filtering Algorithms（In Chinese）, J. Electro-Optic Technology Application, 25(2010) 67-70.

[2] ZHANG XU-ming, XU Bin-shi. Adaptive Switching Median Filter for the removal of impulse noise（In Chinese）, J. Opto-Electronic Engineering, 33(2006)78-83.

[3] Chen Tao, Ma Kaikuang. Tri-state Median Filter for Image Denoising, J. IEEE Trans Image Process , 8(1999)1834-1838.

[4] HOU Fa-zhu, PENG Chu-wu. Image Median Filter Algorithm and FPGA Implementation（In Chinese）, J. Microcomputer Information, 27(2011) 69-71.

[5] GUO Hai-xia, XIE Kai. An Improved Method of Adaptive Median Filter（In Chinese）, J. Journal of Image and Graphics, 12(2007)1185-1188.

[6] Milan Sonka,Vaclav Hlavac,Roger Boyle. Image Processing, Analysis, and Machine Vision, third ed., Tsinghua University Press, Beijing, 2011.

[7] HUANG Bao-gui, LU Zhen-tai, MA Chun-mei. Improved Adaptive Median Filtering Algorithm（In Chinese）, J. Journal of Computer Applications, 31(2011) 1835-1837.

[8] CHANG Liang-liang, WANG Guang-long. De-noising Method for Mixed Noise based on Median Filter and Lifting Wavelet Transform（In Chinese）, J. Journal of Applied Optics, 33(2012) 984-897.

[9] Pitas I. and Venetsanopoulos A. N. Nonlinear Digital Filters: Principles and Applications. Kluwer, Boston, 1990.

[10] ZHAO Gao-chang, ZHANG Lei. Application of Improved Median Filtering Algorithm to Image Denoising（In Chinese）, J. Journal of Applied Optics, 32(2011)678-682.

Advanced Materials Research Vols. 989-994 (2014) pp 2278-2282
© (2014) Trans Tech Publications, Switzerland
doi:10.4028/www.scientific.net/AMR.989-994.2278

The application of cross-correlation algorithm in CSAMT received data processing

Ziping Zhou[1,a],Yu Zhu[1,b], Tianhao Wang[2,c]

[1]College of Instrumentation& Electrical Engineering, Jilin University, Changchun 130026,China
[2]The State Key Laboratory of automotive simulation and control ,Jilin University,Changchun,Jilin,China
[a]mlplzzp@163.com , [b]zhuyu@jlu.edu.cn, [c]wangtianhao2006@126.com

Keywords: CSAMT;random noise; cross-correlation processing;emission signal current waveform recorder; measuring accuracy

Abstract. Controlled source audio-frequency magnetotelluric method (CSAMT) is an effective frequency domain detecting method in metallic ore exploration. In view of the weak response of a deep target signal and the serious measuring environmental noise,this paper proposes a method to deal with the noise of the CSAMT data based on the theory of cross-correlation algorithm. Emission signal current waveform recorder is designed to record signal parameters.According to cross-correlation technology, this paper uses the characteristics that correlation between emission and received signals is strong, yet the correlation between emission signals and random noise is weak, to deal with emission signals and received signals by cross-correlation ,in order to filter out random noise and other jamming signals.Field exploration test data processing contrast results show that the method can suppress noise signal, and improve the CSAMT measuring accuracy.

Introduction

CSAMT uses the controllable artificial source measuring the electromagnetic field components transmitted to the underground, which can detect a greater depth of investigation with a smaller send-receive distance to investigate. But in practical measurement,the system receives the signal that often contains noise and interference. Most of the environmental noise tested by the ground test is a wide-band random noise. This kind of noise is widely distributed in the whole frequency axis and has constant energy.At present,there are following two ways to enhance the anti-interference ability of CSAMT: One is to improve the anti-interference ability of the receiver with the advantage of being able to restrain interfering signal appropriately, but the cost is high and this method can't effectively solve the instantaneous interference or normal high-line [1]. The second way is to increase supply current or transmitted power of transmitter, the method does some satisfactory results in some places where electromagnetic interference is not serious. However it does not work in front of the powerful stray current interference and also increases the difficulty of the instrument design.

To solve these problems, this paper proposes a method that mitigates the noise signal and thus improves the noise mitigating ability of the detection system based on cross-correlation algorithm. In this method an emission signal current wave form recorder is designed,and the CSAMT measuring system emission current signal is recorded. After data processing and simulation, the cross-correlation algorithm is carried out to process the received data by using MATLAB. This method makes it possible to accurately extract the amplitude of each frequency point and phase parameters of the received data by the CSAMT. It is also able to sort out the signal to be tested that is synchronous with the reference signal in noise by improving the quality of the received data and effectively mitigating the effects of environmental noise in the course of measurement.

Emission signal current waveform recorder design overview

The current is not only a very important calculation parameter but also an important inversion calculation parameter. As the emission current frequency range is from 0.1 Hz～10 kHz, considering that the high frequency power supply current of domestic electrical method transmitter at exploration shall be greater than 2.5 A while that of low frequency shall be more than 15A in order to assure enough field strength to mitigate the interference, to solve the problem of large

dynamic range of current waveform record, in this paper the transmitting current wave form recorder with collection scope is 0.1～50 A, the frequency range of 0.1Hz～10 kHz and acquisition accuracy of 0.1 is employed.

The emission signal current waveform recorder design mainly includes: the hall current transformer, the front analog regulate acquisition circuit, AD converter and Field programmable gate array (FPGA) (Field programmable gate array, FPGA) digital logic control circuit. The emission current waveform recorder simulates the current signal emitted by the transmitter and by means of the AD converter the recorder digitalizes the signal. Then it uses FPGA as the interface circuit to receive control commands and execution them through the bus connection. Afterwards the recorder converts real-time data output by analog-digital converter and store them in the static RAM. The data is exported by USB to industrial computer hard disk for storage and subsequent processing .Emission signal current waveform recorder hardware diagram is shown in figure 1.

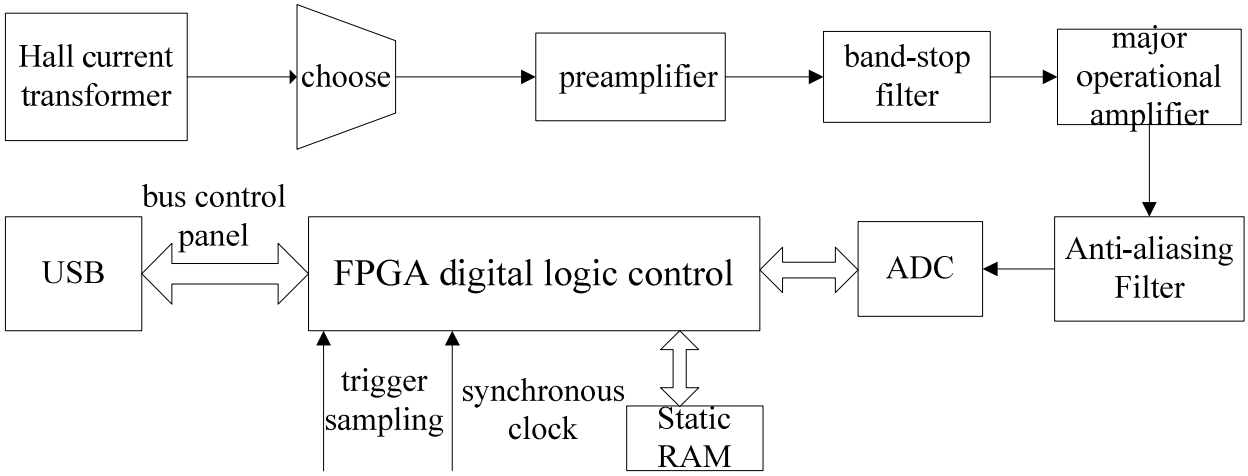

Fig. 1 The emission current waveform recorder hardware principle diagram

Front analog acquisition module

Front analog regulate acquisition circuit [2] uses multi-level programmable amplifier circuit to extend signal dynamic range. Low noise, high speed precise operational amplifier LT1007 converts current signal to voltage signal, and USES the cut-off frequency of 10 kHz low-pass filter to filter out radio frequency interference, in order to prevent the high frequency signal aliasing in the low frequency useful signal.LT1352 band-stop filter will limit the frequency interference wave of 50 Hz with passband gain of 0 db. Inverse proportional amplifier amplifies 10 times the voltage signal and through differential amplifier circuit it inhibits the common-mode signal.

Analog-to-digital conversion module

This module uses the high-speed 24 AK5394AVS type high precision analog-to-digital conversion chip as the core of acquisition card. It digitalizes the analog signals. The sampling rate of AK5394AVS is 128 times with the highest sampling rate of 216 KHZ and short circuit noise of 123 db. This module is the core part of data acquisition. Due to both high sampling rate and digits AK5394AVS requires a higher reading and writing speed demand of the USB microcontroller and takes up significantly its internal resources. Therefore in this paper the hardware interface between AK5394 and USB controller is achieved by FPGA. The AD converter is connected to the USB through a large capacity FIFO and the serial data after AD conversion is embedded in the FPGA internal high-speed FIFO [3], again within the industrial computer via USB,the serial data forms a binary data file that is stored in the hard disk for subsequent processing.

Digital logic processing module

Digital logic processing module adopts 16-bit USB controller and Cyclone Ⅲ series of FPGA device EP3C40Q240C8 control core with low consumption of Altera company. FPGA plays an important role for the bus driver.Its internal FIFO is divided into 16 low and high eight two Spaces. The FIFO has a first in first out stack structure and no address line is needed which simplifies the circuit structure. Underlying design of FPGA uses VHDL language and is solidified in the FPGA

chip. EP3C40Q240C8 realizes USB controller bus decoding function on one hand, and on the other hand it completes the timing that all the boards need. CY68013-128 AC USB controller[4] is chosen to realize the control and data transmission between industrial computer and each function module circuit. Inside it embodied the enhanced 8051 microprocessor, intelligent serial engines (SIE) and USB2.0 transceiver which improve the running speed and simplifies the development of the firmware code.

Principle of cross-correlation algorithm to suppress noise

Two way of sinusoidal signals with the same frequency , $f_1(t)$ and $f_2(t)$, which superpose the noise of $n(t)$ and $v(t)$ respectively. Random noise and the sinusoidal signals are unrelated, the random noises are unrelated,too. The expression is as follows:

$$f_1(t) = A\sin(\omega t + \varphi) + n(t), \tag{1}$$

$$f_2(t) = B\sin(\omega t + \theta) + v(t), \tag{2}$$

the cross-correlation function of $f_1(t)$ and $f_2(t)$ is

$$R_{f_1 f_2}(\tau) = \frac{1}{2\pi}\int_0^{2\pi} f_2(t) f_1(t-\tau)\,dt = \frac{AB}{2}\cos(\omega\tau + \varphi - \theta) \tag{3}$$

in the expression (3), cross-correlation function computation results only contain the amplitude and phase of sinusoidal signals with the same frequency. It can be seen that we can suppress the random noise and extract the target signals by this way. In theory, in order to facilitate calculation, we can establish two reference signals with the same frequency, $r_1(t)$ and $r_2(t)$,the amplitude of which are and the phase difference between which is 90°. Sinusoidal signal $f_1(t)$ makes cross-correlation algorithm with $r_1(t)$ and $r_2(t)$ respectively, and then we could get the amplitude and phase of measured signal.

$$A = \sqrt{R_{f_1 r_1}(0) + R^2_{f_1 r_2}(0)}, \tag{4}$$

$$\varphi = a\tan\left[R_{f_1 r_2}(0) / R_{f_1 r_1}(0)\right]. \tag{5}$$

with $R_{f1r1}(0)$:the cross-correlation function of $f_1(t)$ and $r_1(t)$;

$R_{f1r2}(0)$:the cross-correlation function of $f_1(t)$ and $r_2(t)$ [5].

Data acquisition and processing workflow design

Data collection work flow solidified in the USB microcontroller using C language.Figure 2 is for the flow chart of data collection workflow.After the system is powered on, it initializes into the best work state, and prepares the way for subsequent cross-correlation processing. Received signal files collected by peripheral store in the USB, reading its internal work allocation table, selecting the automatic frequency sweep pattern to measure multiple frequency points.In order to avoid phase difference between signal waveform and current waveform, we take GPS time synchronization acquisition technical to scan and measure the frequency points corresponding with emission signals. The received data will be transmitted into PC in CMT file format.Emission data via USB upload to PC hard disk storage, then we use XCORR cross-correlation function of MATLAB software process the emission and received data and carry on the simulation.Figure 3 is the flow chart of the data processing workflow.

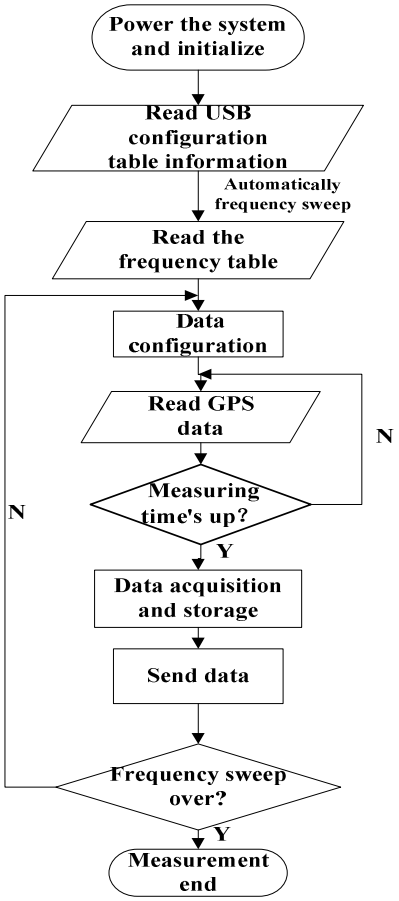

Fig2 .Flow chart of the data collection workflow

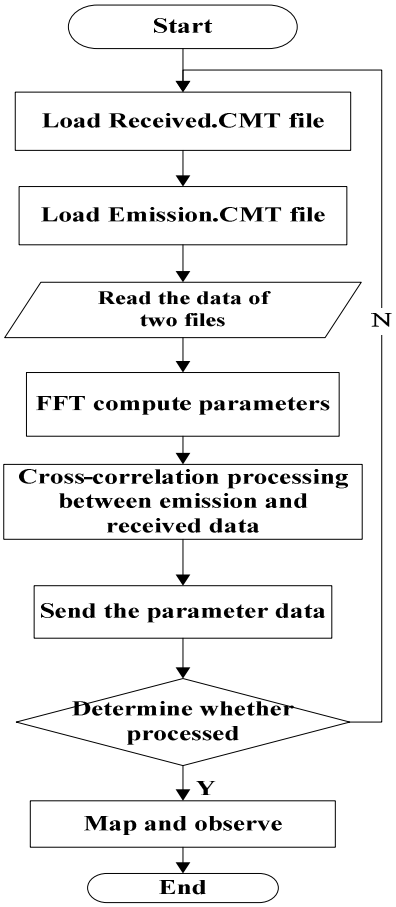

Fig 3.Flow chart of the data processing workflow

Experimental test and data processing

To test the function of the data processing of CSAMT measuring based on cross-correlation algorithm,we used it to measure the field data of Zha-cang-si in Qinghai,Guide.Figure 4 is the contrast figure of test data curves before and after cross-correlation measuring. We take part of CSAMT measuring to record the emission data, and then use the MATLAB software to establish a reasonable cross-correlation function, processing the corresponding frequency received signals, finally make it into figure. It can be seen that the original received signals contain lots of strong noise in the whole frequency axis, especially in the high frequency, which makes record curve is not smooth enough. After cross-correlation processing, random noise recorded in the received signals reduce greatly, valid data is obvious, the overall curve is smooth,and local jump point does not appear. This is because that the random noise in signal records has been suppressed through filtering and relevant algorithm processing, the rest of the received signal is valid data with weak energy.The signal-to-noise ratio has been improved.

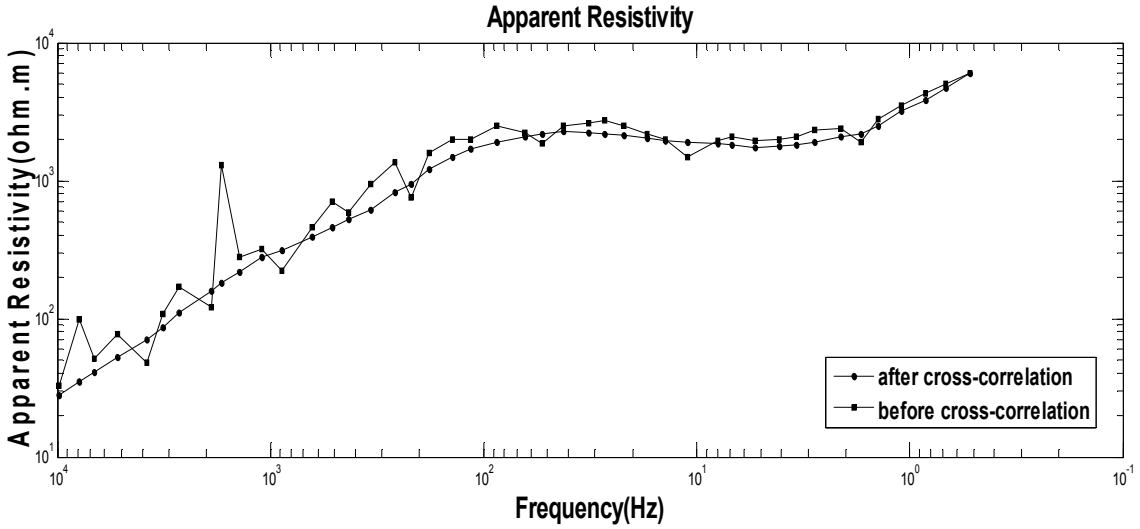

Fig.4 Before and after cross-correlation test data curves contrast figure

Conclusion

The theoretical analysis and the actual data processing results show that,cross-correlation algorithm applicated in CSAMT can weaken the random noise in received signal record from receiver and improve the signal-to-noise ratio of the received signals. In the actual operation, making use of the advantage of the characteristics of cross-correlation algorithm,we can establish reasonable cross-correlation function and parameters by MATLAB to improve the resolution of the effective signal recording.Cross-correlation algorithm has strong generalization and practicability, it not only can be used in the CSAMT method of data processing, but in all kinds of weak signal detection.

References

[1]Xu Guang-chun. Several Problems in CSAMT Method in Practical Application[J]. GEOPHYSICAL &GEOCHEMICAL EXPLORATION,2011,35(6):809-812

[2]Zhang Wen-xiu,Lin Jun,Liu Li-chao,Hu Rui-hua.Design and implementation of broadband data acquisition system for distributed electromagnetic exploration[J].Journal of Jilin University (Engineering and Technology Edition,2012,42(6):1426-1431.

[3]Chen Ru-jun,Luo Wei-bing,He Ji-shan, Bai Xuan-cheng,Tang Jing-tian.High precision multi-frequency electrical method data acquisition system[J].GEOPHYSICAL &GEOCHEMICAL EXPLORATION,2003,27(5):375-378

[4]Xu Xia,Lei Ming.Design of data communication system based on CY7C68013[J]. Micro-computer information（IEEE and SOC），2009,25（6-2）：198-200

[5]Liu Yu-hai,Yin Cheng,Pan Shu-lin,Hu Yong-quan.Method based on cross-correlation function of the ground micro seismic signal detection research[J].GEOPHYSICAL PROSPECTING FOR PETROLEUM,2012,51(6):633-637.

Advanced Materials Research Vols. 989-994 (2014) pp 2283-2287
© (2014) Trans Tech Publications, Switzerland
doi:10.4028/www.scientific.net/AMR.989-994.2283

Assignment performance at Beijing South Railway Station Based on Anylogic simulation

Yanjiao Liang[a], Zhenzhou Yuan[b]

School of Traffic and Transportation, Beijing Jiaotong University, Beijing 100044, China

[a]1052543928@qq.com, [b]zzyuan@bjtu.edu.cn

Keywords: Anylogic simulation, route choice, Beijing South Railway Station.

Abstract. Assignment simulation can make a great contribution to understanding the pedestrian dynamics. Relying on the statistical data at Beijing South Railway Station, we simulate the passenger flow assigned at service establishments, provided by density parameters changing. Then, simulation result can illustrate that the passenger flow presents regular aggregation state and the density of station platform has periodic change. Furthermore, the interaction between boarding and alighting tracks and various bottlenecks are demonstrated at the platform, in which the congestion performance is applied at improving the LOS (level of service) as well as supporting passenger flow organization strategies. Finally, the proposed performances are analyzed qualitatively.

Introduction

Passengers out of subway station can generally choose three ways: stair, elevator or escalator. The large-scale integrated transport hubs have highly aggregated multiple transportation modes and often contain long-distance passenger transport mode, which allows passengers to carry more luggage. In this case, it would be more convenient to take elevators. Moreover, elevators also reflect the humanized design of the facility. It will be more widely used in large-scale integrated transport hub in the near future. However, most experts and scholars at home and abroad don't infer to elevators on study of rout choice. Therefore, the paper studies on the passengers' route choice out of station of Beijing South Railway Station by the Anylogic simulation technology, which has important and practical significance. For example, providing theoretical support for study of passenger behavior in-depth, providing theoretical basis for evaluating or improving the services efficiency of integrated transport hub and optimizing the layout of facilities and so on[1,2].

1 Overview of Beijing South Railway Station

Beijing South Railway Station is the first modern large-scale passenger transport hub in our country, which has Beijing-Tianjin intercity railway, Beijing-Shanghai high-speed railway, general speed railway, urban metro, bus, taxi and other traffic modes. It has five layers structure of three-dimensional layout. Passengers also can transfer various traffic modes although not out of station. 50% of travelers will be able to transfer with the subway in the station [3].

The paper studies on the passengers' route choice out of station of Beijing South Railway Station. Beijing South Railway Station is now opened the subway line 4 on basement level two. After getting off subway, passengers can choose stairs, elevators or escalators to enter transfer hall on basement level one. Then, there are three exits for leaving. This paper mainly analyzes passengers' route choice from the basement level two to level one. Specific analysis of flow lines is shown in Fig. 1.

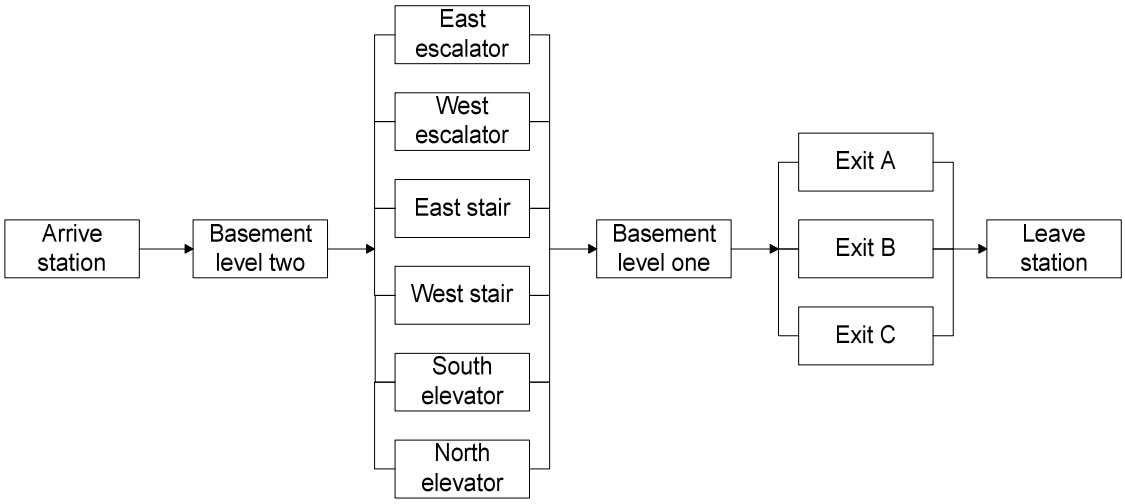

Fig. 1 Passengers' flow lines out of station of Beijing South Railway Station

2 Anylogic simulation of passenger route choice

2.1 Simulation model principle

The core algorithm of Anylogic simulation is the social force model. Social force model is continuous micro-simulation model that can give real pedestrian trail. Assumed the individuals with the ability to think and react to the surrounding environment, social force descripts subjective desire and the relationship people between people or environment. Therefore, there are three kinds of force on social model, including driving force, acting force between people and people or wall [4].

The process of establishing model is as follows [5]. Firstly, through simulation scenarios, we can determine the number and location of contour, equipment, service facilities, path and flow lines. Then, establish the different function modules. Finally, connecting each module, defining rules and selecting approaches according to the actual situation.

2.2 Establish simulation model

The simulation considers one-way flow out of subway station. Meanwhile, considers the north elevator and south elevator into an elevator. According to the practical investigation, drawing the accurate structure background of Beijing South Railway Station and importing into Anylogic software interface. Closed polylines express walls, equipment covers and other area which pedestrians can't pass through. Simple lines indicate service facilities or entrances. Simulation environment is shown in Fig. 2.

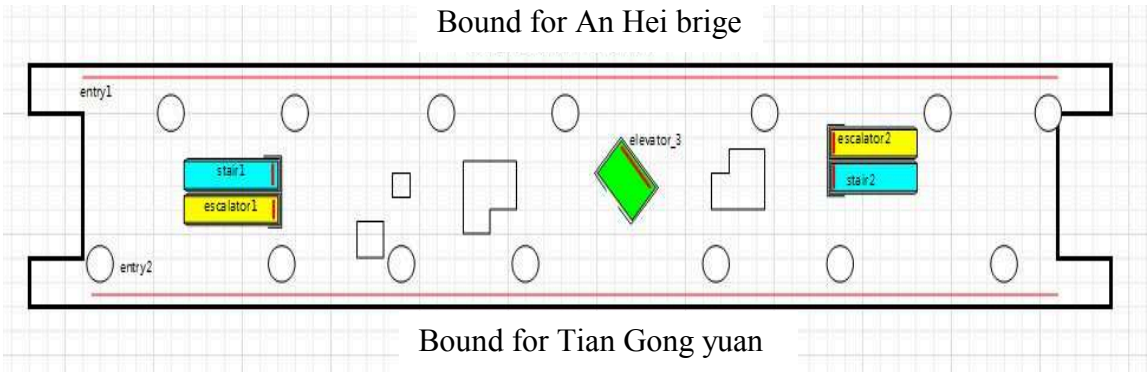

Fig. 2 Simulation environment

Building functional modules, selecting rules and determining flow lines. Passengers' route choice is an input-services-output process. PedSource is pedestrian starting module. PedSelectOutput is choice module. PedGoto is direction controlling module. PedSink is pedestrian disappearing module.

PedConfiguration is pedestrian property module, which is used to define the basic properties of the pedestrian. PedGroud defines the scope of the wall. PedArea defines the fixed area of facility. The flowchart of passengers' route choice is as Fig. 3 [6].

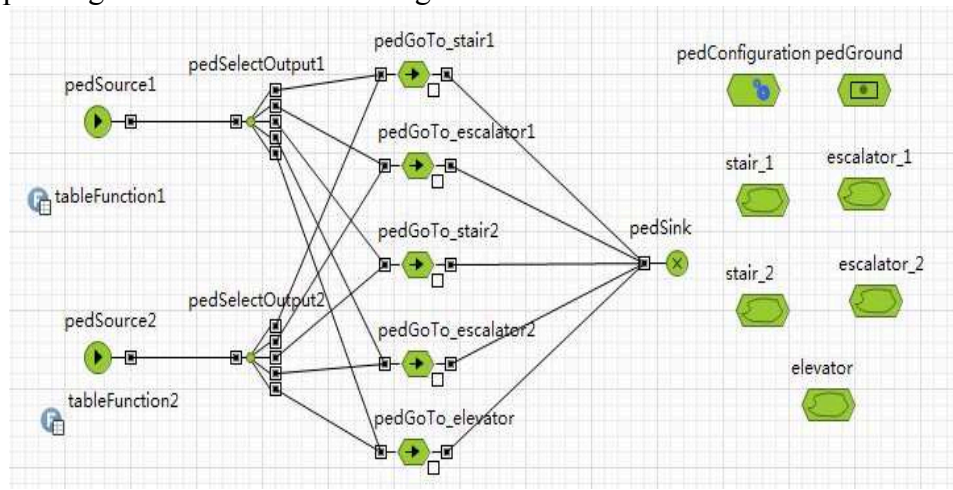

Fig. 3 Simulation model flowchart

Setting attributes parameters for each module in the flowchart. Such as, shape, color, capacity of facilities, choice proportion and so on. There are four main types of variables and three main types of modules [7].

(1)Setting PedSource object parameter is mainly for the arrival pattern of passengers. TableFunction can represent the reach interval of train. Based on actual data, we can establish the periodic train schedule. Moreover, set step speed from 0.8 to 1.5 meter per second, which is from actual research. In order to distinguish the direction of passengers, set purple for passengers bounding for An Hei brige while blue bounding for Tian Gong yuan.

(2)Setting PedSelectOutput object parameter is mainly for choice proportion out of station based on actual data.The choice proportion bounding for An Hei brige is as follows.stair1:escalator1:stair2: escalator2:elevator=0.06:0.51:0.05:0.22:0.16 while the choice proportion bounding for Tian Gong yuan: 0.1:0.38:0.08:0.35:0.09.

(3)Setting PedGoto object parameter is mainly for stage goal of passengers. The direction selected by passengers needs to be set in the simulation environment. The control for pedestrians in simulation is very realistic. Pedestrians will choose the shortest path from the initial target to the final target and circumvent the obstacle flexibly. That's to say, simulation matches well with actual pedestrian movement. However, there are many obstacles in the subway platform of Beijing South Railway Station. Once no route guidance, the large-scale jam is easy to happen. So we set route guidance according to the actual situation.

(4)Setting PedArea object parameter is mainly for passenger throughput of service facilities. Based on relevant references and practical research, the operation speed of escalator is 0.5 meter per second, corresponding to the maximum capacity of 8100 people per hour. The stair of Beijing South Railway Station is mixed direction and 2.5 meters width. Refer to urban rail transit design specifications, there are mixed capacity of 3200 persons per hour on one meter width. So the maximum stair capacity of Beijing South Railway Station is 8000 people per hour. Because of more loads, the elevator deadweight of Beijing South Railway Station is about ten persons and it will take 17 seconds to operation from basement level two to level one. Therefore, the maximum capacity of elevators is approximately 1200 persons per hour by calculating roughly.

We have to designate areas in front of stairs, escalators and elevators to collect flow data and calculate density. Then, add density sketch to observe simulation results intuitively.

2.3 Analyze simulation results

After running simulation [8], we can get passenger flow of five areas. After that, calculate density according to areas. The results are shown in Table 1, Fig. 4, Fig. 5 and Fig. 6.

Table 1 Density statistics after simulation

area	average density（p/m^2）		
	train arrive (bound for An Hei brige)	train arrive (bound for Tian Gong yuan)	two trains arrive at the same time
escalator 1	0.79	0.88	1.32
escalator 2	0.52	0.61	0.98
stair1	0.13	0.17	0.22
stair2	0.11	0.14	0.21
elevator	0.25	0.19	0.28

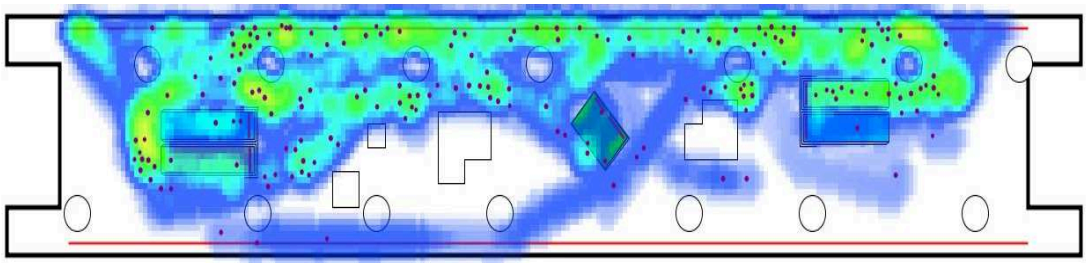

Fig. 4 Density sketch when train arrive (Bound for An Hei brige)

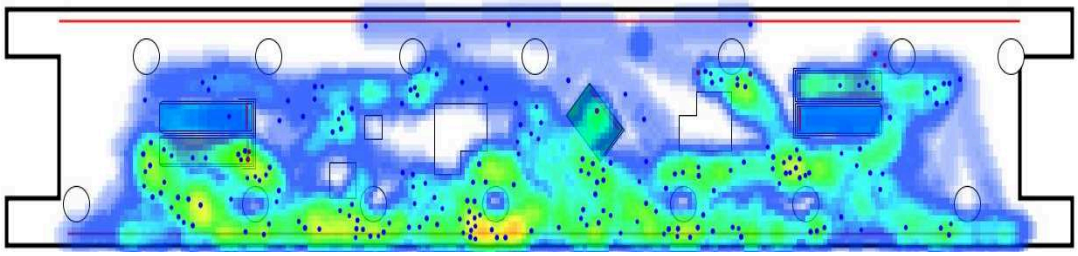

Fig. 5 Density sketch when train arrive (Bound for Tian Gong yuan)

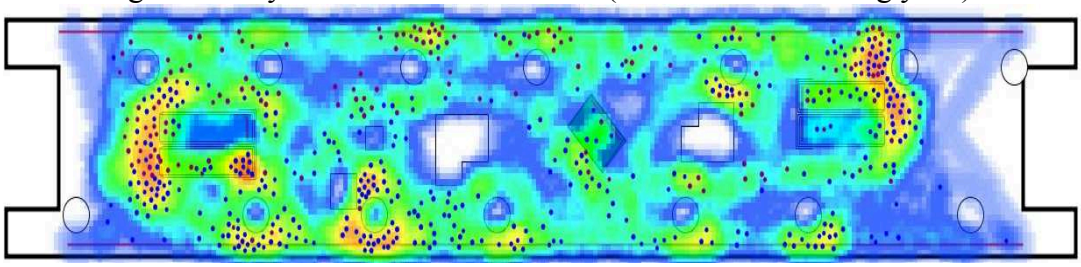

Fig. 6 Density sketch when two trains arrive

(1) Passenger flow presents regular aggregation state and the density of station platform has periodic change. As trains arrive, the station platform produces a large number of flows in just a few seconds. It is the maximum passenger density when two trains arrive at the same time.

(2) As shown on table and figure, density increases obviously and pedestrians queue up in front of escalators. There no queue in front of stair while some passengers wait for elevators, which is consistent with actual situation.

(3) The average density of west escalator is higher than east escalator. So the utilization rate of west escalator is higher than east escalator. Moreover, Escalators are close to the train bounding for Tian Gong yuan. Passenger flow which produces from the train bounding for Tian Gong yuan is larger number than other direction.

(4) The simulation only considers unidirectional flow and don't considers influence of mixed flow. Therefore, the statistical density of stairs and elevators are smaller than actual situation.

(5) The train bounding for An Hei brige produces less flow. However, it has high departure frequency and low departure interval. In order to evacuate passengers rapidly, the measure that increasing appropriately departure interval bounding for An Hei brige and reducing departure interval bounding for Tian Gong yuan can be taken.

(6) There is a common phenomenon that some passengers who load a lot don't choose elevator. The reason is that they don't know the existence of elevators or don't know the location of elevators. Strengthening publicity of elevators and encouraging passengers who load a lot to take elevators, which will reduce queuing delay of escalators.

(7) According to the simulation results, there are jams on some of obstacles. For example, the monitoring room is near the door, there are jams between the monitoring room with the door. We can move the monitoring room to middle position.

3 Conclusions and prospects

In this paper, with the aid of Anylogic software, the author achieves the current simulation of Beijing South Railway Station out subway station passengers and gets the passenger flow and density parameters. Then, fund that the passenger flow presents regular aggregation state and the density of station platform have periodic change. Moreover, according to the simulation results, analyzing the reason of rout choice and putting some pieces of advice to improve the service level of facilities.

Although the article makes some achievement, there are some deficiencies. For example, applying tablefunction to simulate arrival of train. However, tablefunction can't reflect the real condition accurately. Meanwhile, the simulation only considers unidirectional flow and don't considers influence of mixed flow. Research will focus on making simulation close to the real condition in the future.

Acknowledgements

We gratefully acknowledge the support for this work from National Basic Research Program of China (grant number 2012CB725403).

References

[1] Lovas, GG: Modeling and simulation of pedestrian traffic flow, J. Transp. Res. 28(1994) 425-429.

[2] C.Y. Cheung, William H.K. Lam: Pedestrian Route Choices Between Escalator And Stairway in MTR Stations, J. Journal of Transportation Engineering.124 (1998) 270-273.

[3] Yanqing Xue, Zhang Xi: Analysis on optimizations of passenger flow organizations in Beijing South Station based on Anylogic simulation, J. Railway Computer Application. 21(2012)1-.5.

[4] HelbingD, Buzna L,Johansson A: Self-organized pedestrian crowd dynamics: experiments, simulations, and design solutions, J. Transportation Science. 39(2005)2-4.

[5] Mingwei Hu, Qixin Shi: Comparative Study of Pedestrian Simulation Model and Related Software , J. Journal of Transportation Information and Safety. 4(2009) 122-126.

[6] Jodie Y.S.Lee, William H.IS.Lam, S.C.Wong, *Pedestrian Simulation Model for Hong Kong Underground Stations*(IEEE.ITSC2001.United States:Oakland,2001.), p.554.

[7] Wang Gang: *Research on the Model of Assembling in the Urban Rail Transit Platform* (Ph.D. Beijng Jiaotong University, China 2013), p.15.

[8] Zhang Qi, Baoming Han, Dewe Li: Modeling and Simulation of Passenger Behavior in Platform of MTR Stations, J. Journal of System Simulation. 19(2007) 5120-5123.

Advanced Materials Research Vols. 989-994 (2014) pp 2288-2291
© (2014) Trans Tech Publications, Switzerland
doi:10.4028/www.scientific.net/AMR.989-994.2288

Study of storm surge numerical simulation in the Bohai sea

Zhang Yongqiang[1], Leng Qianlan[2], Hu Zejian[1], Zhu Zichen[1], Zhang Wanjun[1], Bian Shuhua[1]

[1.] The First Institute Of Oceanography, SOA, Qingdao 266061；
[2.] Shazikou Primary School, Qingdao 266102

zyqiang1983@163.com

Keywords: ECOM, storm surge, extre water level, Bohai Sea

Abstract: In this paper, a numerical model of the coupling between astronomical tide and storm surge based on hydraulic model for estuary and coast (ECOM) is confirmed to be suitable for simulation of stormsurge in the Bohai Sea. The spatial distribution of extreme water level and storm current field caused by typhoons in October 2003 are simulated.It shows that extreme water level in deep water are smaller than shallow water and the spatial distribution of extreme water level is influenced by topography.Flow filed in Bohai Sea waters takes on an fluctuation in flow field, compensatory flow and other obvious features during storm surge, compared storm surge with astronomical tide, which is a significant difference in flow filed.

1 Introduction

With a long coastline, China is one of Pacific Rim countries, which is frequently-stricken by storm surge, from south to north, leaving impact on different areas at various degrees. A great loss has been brought to Bohai Bay, where alone has been attacked for 16 times during 1985 to 2013. Therefore, research on disasters caused by storm-surge has been a matter of top priority.

The special terrain characteristic in the Bohai Sea is advantageous to form storm surge. The intense and lasting easterly wind was the important factor. The simulation of several storm surge processes is carried out in the Bohai Bay and shows that the strong easterly wind is the major reason which causes maximum storm surge in the Bohai Bay [1-2]. Extratropical cyclone induces distinct water level set-up/down and makes remarkable changes on flow velocity and direction of local sea area[3].

Based on ECOM model, this article takes typhoon pressure-field and wind field as input conditions, to create a numerical value forecast mode applicable to storm surge occurred along Bohai Sea waters, and to carry out analog studies on numerical value of storm surge in Bohai Sea waters.

2 Numerical model and setting

2.1 The introduction of ECOM

The model for shallow water environments – rivers, bays, estuaries and the coastal ocean and reservoirs and lakes- named ECOM [4].It consists of several modules which are hydrodynamic module, wind induced wave module, heat flux module and particle tracking module.

The prognostic variables are the three components of velocity,temperature, salinity, turbulence kinetic energy, and turbulence macroscale. The momentum equations are nonlinear and incorporate avariable Coriolis parameter. The vertical mixing coefficients are obtained by appealing to a second order turbulence closure scheme. ECOM uses an orthogonal curvilinear coordinate system and sigma coordinate system, greatly increasing model efficiency in treating irregularly shaped coastlines and in meeting requirements for high resolution at desired locations. Many thermodynamic processes are taken into account. Horizontal finite difference is explicit scheme in time but vertical direction is implicit scheme. The later has a much less stringent time step and relatively rough resolution near the surface and bottom. It has fine vertical resolution when the horizontal explicit scheme and vertical implicit scheme is chosen in internal hydrodynamics option. Operator splitting is used in calculation

and make the calculation flexible, simply, stable, precision.The detailed basic theory of ECOM can be seen in Blumberg (1996) and would not be given here.

2.2 The setting of model

To avoid the impact of boundary condition on model simulation, the East China Sea is simulated as a large scale computing area, with 0.05′×0.05′grid, covering range 33°46′32.86″N~36°11′28.37″N, 120°31′33.65″E ~126°33′18.71″E. Barotropic assumption is applied to numerical simulation, that is, temperature and salinity is assumed to be constant and heat flux, salt flux and wind flied is zero.The elevation data of terrain is provided by naval guarantee department of PLA (the People's Liberation Army of China), which are adjusted on domain. There are 2s steps for mode. In the Bohai Sea, the bottom friction coefficient is 0.001, and 0.0023 in the Yellow Sea and the East Sea,which are based on experiment and previous numerical experiments[5].The elevations and phases of M2, S2, O1, P1 and K1 tides at the open boundaries with the harmonic constants of the five tides are taken from the NAO.99b tidal prediction system.The bathymetry data for the computing grid is obtained through interpolation with navigational chart in the Bohai Bay with high resolution 0.05′×0.05′.

2.3 Wind and pressure field

Calculation of the FBM model of the pressure field is realized by Fujita formula and Gaoqiao formula below :

$$P_r = (P_\infty - P_0)\left(1 - \frac{1}{\sqrt{1+2(r^2/R^2)}}\right) + P_0 \quad (0 \le r \le 2R) \tag{1}$$

$$P_r = (P_\infty - P_0)\left(1 - \frac{1}{\sqrt{1+r/R}}\right) + P_0 \quad (2R \le r \le \infty) \tag{2}$$

Where P_0 = center pressure of typhoon. P_∞ = periphery pressure.R = radial maximum wind, P_r = the typhoon pressure located r. r= the distance from the center of the center of typhoo.

Wind field of typhoon is calculated by two vector superposition field respectively which are relative to the center of typhoon wind field and basic wind field.

Relative to the center of typhoon wind field is calculated by:

$$V_g = -\frac{1}{2}fr + \left[\left(\frac{1}{2}fr\right)^2 + \frac{r}{\rho_a}\frac{\partial p}{\partial r}\right]^{\frac{1}{2}} \tag{3}$$

Where V_g is the gradient wind,f is the Coriolis force coefficient, ρ_a is air density.

i

Basic wind field is calculated by:

$$\vec{V}_{sm} = V_x \exp\left(-\frac{\pi}{4}\frac{|r-R|}{R}\right)\vec{i} + V_y \exp\left(-\frac{\pi}{4}\frac{|r-R|}{R}\right)\vec{j} \tag{4}$$

Where V_x, V_y is the velocity of center of the typhoon in the X and Y direction.

3 Numerical simulations and results

3.1 Analysis of process of increase and decrease in water lever during storm surge

From each water level process curve（Fig. 1） and seen from Bohai Bay and other bays, periodical fluctuation of Bohai Bay storm tidal level and surface mean value, which decreased followed by increase, indicates that, during the period of cold wave & strong wind in October, 2013, storm-surge water level is affected by periodical fluctuation and wind field. Rise and fall in water volume varies with different waters along Bohai Sea's during storm surge: decreased followed by increase at Liaodong Bay and Bohai Bay, with maximal 201cm rise and maximal 513cm fall at Liaodong Bay, 218cm and 220cm respectively at Bohai Bay. While, at Laizhou Bay, the tendency is decrease followed by increase, then another decreased followed by increase, with maximal 188cm rise and maximal 220cm fall respectively. Seen from the moment when maximal value appeared, the maximal increase turns up as Liaodong Bay, Bohai Bay and Laizhou Bay in sequence, so does the maximal decrease.

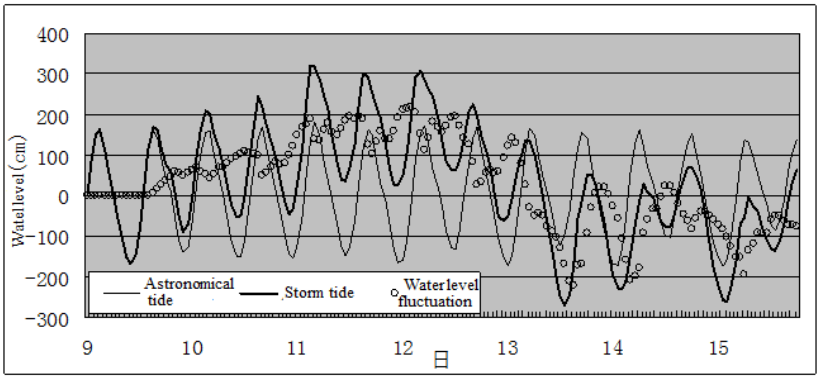

Fig. 1 Water level process curve during storm surge in Bohai Sea

3.2 Horizontal distribution of storm-surge water increase and decrease

From the isopleth map of increase and decrease in water lever during storm surge（Fig. 2）, it indicates that water level at Bohai Sea and North Yellow Sea goes up and down dramatically during cold wave and strong wind, which imposes a large impact on the waters. Water level increase in Bohai Sea waters caused by cold wave and strong wind is much higher than that of Yellow Sea waters. Besides, increase in water level at inshore shallows is obviously higher than that of deepwater. Therefore, the rise brought by storm surge mainly happens at Bohai Sea's shallow waters. The openness of waters decides the tendency of isopleth map of water level rise. In the middle waters of Bohai Sea and other wide waters of North Yellow Sea, distribution of water rise isoline takes on NE-SW inclination, basically vertical with wind direction of cold wave and strong wind. The tendency of water rise isoline at Bohai Bay, Liaodong Bay and Laizhou Bay and top pf bay coastline distribute parallelly. Affected by Northern inclination, seen from water rise value at Bohai Sea's bays, it shows that Bohai Bay takes the maximal rise, Laizhou Bay next and the last is Liaodong Bay.

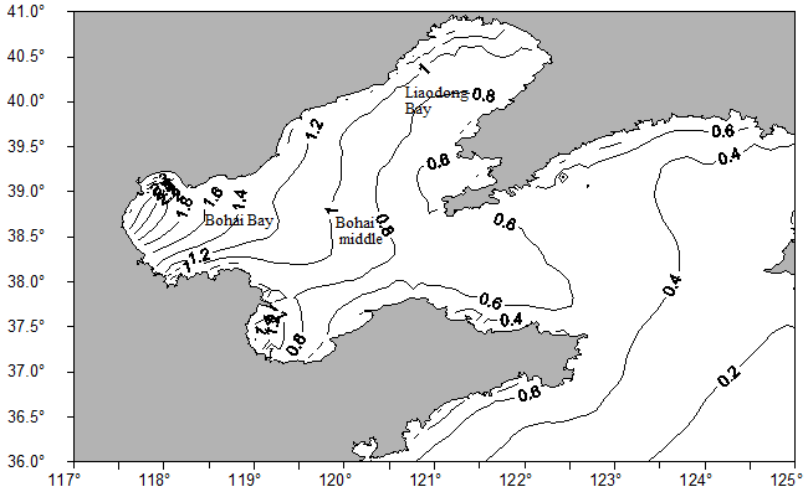

Fig. 2 The isopleth map of increase and decrease in water lever during storm surge（m）

3.3. Features of storm-surge's tidal flow filed

During storm surge, at Bohai Sea, North Yellow Sea, and Baohai Sea's bays, different waters are influenced by northern strong wind, coastline water depth and diverse terrains at different degrees, with a varying characteristics at flow filed pattern（Fig. 3）, mainly featured in: influenced by northern cold wave and strong wind, flow direction at the top of Liaodong Bay is offshore, and the flow rate is obviously rapid at this area. At the inshore area of eastern and western bay, the rotatability of the ocean current in the middle of the bay is strengthened, with prominent unsteadiness in flow rate and flow direction. Influenced by cold wave and strong wind, flow direction at southern shore of Baohai Bay is constantly southward or eastward, with few alteration in flow rate, but faster than flow rate of astronomical tide in average. The flow rate at central and northern waters of Bohai Bay becomes distinctly faster, especially at the northern shore. Correspondingly, the rotatability of flow direction is enhanced. As a whole, the flow filed pattern of Bohai Bay is counter-clockwise circulation, that is,

southern ocean current flows out, while northern ocean current is compensatory inflow. In the middle waters of Bohai Sea, ocean current is not rotative any more, but maintains flow direction between southward and eastward, that is, toward Bohai Sea straits, at a relatively rapid flow rate. In a word, under the mutual influence of astronomical tide and cold wave, flow filed at Bohai Sea waters takes on an fluctuation in flow field, compensatory flow and other obvious features during storm surge, compared storm surge with astronomical tide, which is a significant difference in flow filed.

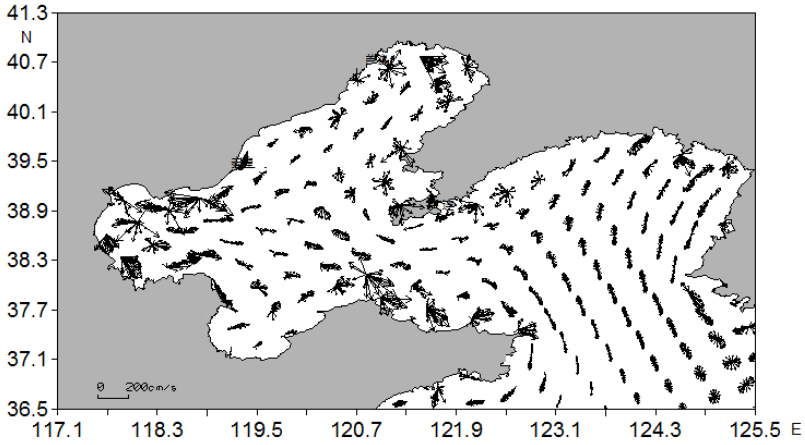

Fig. 3 Flow field during storm surge

4 Conclutions

The results indicated that extreme water level in deep water are smaller than shallow water and the spatial distribution of extreme water level is influenced by topography.Flow filed in Bohai Sea waters takes on an fluctuation in flow field, compensatory flow and other obvious features during storm surge, compared storm surge with astronomical tide, which is a significant difference in flow filed.

ACKNOWLEDGEMENTS

This study is partly supported by The central public welfare research institutes for basic research funds of FIO under grant NO. GY02-2012G21.Addition financial supports were obtained from The Natinal Natural Science Foundation of China under grant No. 41276084.

References

[1] Xia, B., Wu, XZ., Zhang, QH.: Modeling of Tide and Storm Surge in the Southwest Coast of the Bohai Bay. Journal of Changsha University of Science & Technology(Natural Science), Vol 5(2008), No 3, pp64-70.

[2] Hou, SM., Sun ZX., Sheng, CY.:Weather analysis of Bohai sea storm surge caused by extratropical cyclone. Scientia Meteorologica Sinica, Vol 29(2009), No 2, pp 220-224.

[3] Li, X., Zhang, JS., Zhang WS.: Application of Storm Surge Numerical Coupling Model on Bohai Sea. Port & Waterway Engineering, (2009),No 10, pp 25-31.

[4] Blumberg, AF.:An estuarine and coastal ocean version of POM.Proceedings of the Princeton Ocean Model Users Meeting (POM96),Princeton, NJ, (1996).

[5] Li, L., Du, L., Zuo, JC., Li, PL.:Tidal Current Simulation for M2 and K1 with the Finite Element Method in the Bohai Sea, the Yellow Sea and the East China Sea. Periodical of Ocean University of China,Vol 36(2006), No 6, pp 851-858.

Advanced Materials Research Vols. 989-994 (2014) pp 2292-2296
© (2014) Trans Tech Publications, Switzerland
doi:10.4028/www.scientific.net/AMR.989-994.2292

A Method of Domain Compound Concept Extraction Based on Multilevel Filter

WU Bin[1,a], OUYANG Liu-bo[1,b]

[1]School of information Science & Engineering, Hunan University, Changsha 410082, China.
[a]binwu87519@163.com, [b]oylb@hnu.edu.cn

Keywords: domain compound concept; concept extraction; multilevel filter; location label; POS analysis.

Abstract. Identification and extraction in domain compound concept is the basis of the domain text information processing. This paper builds a multilevel filter extraction model by fusing the thought of statistics and language rule. Firstly, the extraction model screening out domain atomic concept set by using method of improved TF-IDF. We secondly build a space combination rule, screening out initial domain compound concept set. Ultimately we screening out finally domain compound concept set by using POS rules template matching via POS analysis. Experiments show that this method can effectively identify and extract domain compound concept and F-measure has reached 83.9%.

1 Introduction

Identification and extraction in domain compound concept [1] is the basis of the domain text information processing, it has important significance on domain ontology's construction and application, text information retrieval and text mining. With the social progress, the development of science and technology, new concepts emerge in an endless stream, especially for the compound concept in each field. These domain compound concepts generally are noun phrases which are formed by domain atomic concepts or words, they refer to more precise information for domain concepts. The existing word segmentation system can't recognize the new domain compound concept, so it can't meet the needs of practical applications. Therefore, automatic extraction in domain compound concept is needed.

The method based on rules [2] and methods based on corpus statistics [3] are the two main methods of extraction of concepts. The method based on rules identifies new concept by tagging dictionary and phrases. Its main idea which is based on the linguistic theories and knowledge is to develop a series of commonness and individuality of rules. The method based on rules can extract new concepts by high quality, but those rules are generally for specific field, so it has poor flexibility. The methods based on corpus statistics don't need syntactic and semantic information. They don't confine to a certain field and don't rely on any other resources, but they have strong versatility. The performance of methods based on corpus statistics depends on the corpus' scale and word's frequency information. Some candidate concepts which have low frequency may be right concepts, while some other candidate concepts which have high frequency may not be right. So, the method based on corpus statistics is difficult to guarantee the quality of extraction.

This paper builds a multilevel filter extraction model by fusing the thought of statistics and language rule, and constructs a compound concept extraction system based on multilevel filter. Then we evaluating the system by calculating it's accurate rate, recall rate and F value.

2 Multilevel filter extraction model

The multilevel filter extraction model is shown in figure 1.

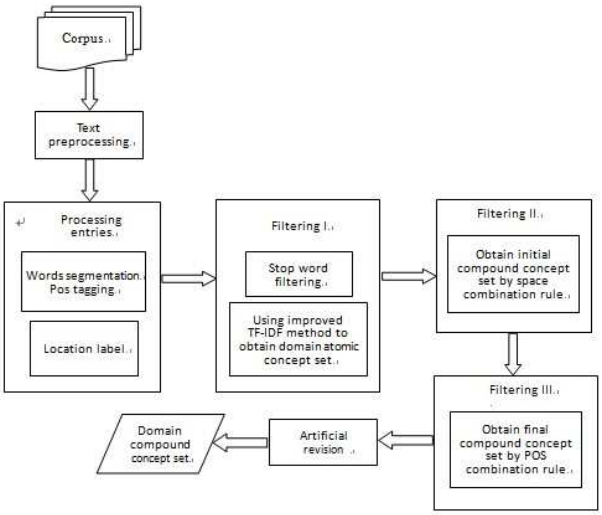

Figure 1 Multilevel filter extraction model

From figure 1, we know that the model contains three main filtration stages. In the first filtering stage, the extraction model screening out domain atomic concept set by using method of improved TF-IDF. In the second filtering stage, we build a space combination rule, screening out initial domain compound concept set. And in last filtering stage, we screening out finally domain compound concept set by using POS rules template matching via POS analysis.

3 Implementation processes

This paper is to extract the domain compound concept according to the multilevel filter extraction model. The extraction process and the corresponding algorithm will be described in the following contents in detail.

Text preprocessing. At this stage, we will remove images and formulas from texts, and only left words and punctuation. Then, we will convert them into TXT format.

Words segmentation and POS tagging. Nowadays, the ICTCLAS segmentation system which developed by Chinese Academy of Sciences has been widely used in Chinese language processing. So, we use ICTCLAS segmentation system for word segmentation processing in this paper.

The results of POS tagging are as follows:

$$\mathrm{POS}\ (c_a) = \$_i \tag{1}$$

$\$_i \in$ {n(noun), v(verb), a(adjective), b(Distinguishing words), h(prefix), k(suffix), l(idioms), s(place), z(status), t(time), f(direction), r(pronoun), m(numeral), q(classifier), d(adverb), p(preposition), c(conjunction), u(auxiliary), e(interjection), y(tone), o(onomatopoeia), x(string), w(punctuation)}.

Add location label for entry. Location label reflects the specific location information of each entry. After words segmentation and POS tagging, we need add location label for each entry. In case of punctuation, then the sequence number of entry which is behind the punctuation will automatically plus 1.

The results of location tagging are as follows:

$$\mathrm{P}(c_a) = (d_k, s_i, n_j) \tag{2}$$

In formula (2), d_k shows which document entry c_a is in, and s_i shows which sentence c_a is in, and n_i shows c_a's sequence number in sentence s_i.

Filtering out stop word. Chinese text often contains some high frequency words which don't have relationship with field, and it also contains some words which can't be formed into combined words. Those words don't represent any field knowledge, and also have little influence on word-building. We call those words stop words, and we should filter out them. Through filtering out stop word, we can improve accuracy of atomic domain concepts extraction. Especially when corpus' scale is huge, it can obviously reduce the calculation of domain concepts extraction and improve the running speed of the system.

Atomic concept filtering based on improved TF-IDF formula. The traditional TF-IDF [4] formula is a weighted statistical technique which is usually used in information retrieval, we can use it to evaluate the important degree for a corpus or a file set. The importance of word is increase proportional to the times of its appearance in document, but at the same time it is inversely proportional to the frequency of its appearance in corpus. But the traditional TF-IDF formula does not consider the effect of the word length on weight. So this paper uses improved TF-IDF formula to calculate the weight of entries.

The improved TF-IDF formula is as follows:

$$w_i = \sum_{k=1}^{n} \frac{TF_{ik} \times IDF}{\sqrt{\sum_{k=1}^{n} (TF_{ik})^2 \times (IDF)^2}} \tag{3}$$

$$IDF = \mathrm{lb}\left(\frac{N}{n_k} + 0.01\right) \tag{4}$$

$$W_i = \mathrm{lb}(L) \times w_i \tag{5}$$

TF refers to Term Frequency, and IDF refers to Inverse Document Frequency. IDF think that if the numbers of document which contains ca is less, then IDF is bigger, and ca has good ability of distinguishing categories. L refers to entry's length, w_i refers to weight which does not consider the length of entry, and Wi refers to weight which consider the length of entry. In this paper, we can use improved TF-IDF formula to screen out the atomic domain concept.

Compound concept filtering based on space combination rule. *Definition 1*(*space combination rule of compound concept*) space combination rule of compound concept contains the following two contents: (1) the atomic concepts are in accordance with the existing adjacent order in the same sentence, and they are combined into a atomic concept string A_i; (2) compound concept C_m is the substring of atomic concept string A_i. *Definition 2* (*the longest binding rule*) we assume that there is a string A_i which contains entry c_a, A_i=…$c_{a-1}c_ac_{a+1}$…, and the longest binding rule for c_a satisfies the following two contents: (1) if there is a adjacent entry c_{a-1} in front of c_a, we combine c_{a-1} and c_a , until there are no other adjacent entries in front of them. (2) if there is a adjacent entry c_{a+1} behind c_a, we combine c_{a+1} and c_a , until there are no other adjacent entries behind them. After adding location label, each atomic concept has its own location label P (d_k , s_i, n_j), then we can screen out them by space combination rule. The specific steps are as follows. Step1: each entry has a location label P (d_k , s_i, n_j),and for the entries which are in the same document and in the same sentence, the values of their d_k and s_i are the same, too. If their n_j have adjacent sequence number, we combine those adjacent atomic domain concepts to a domain concept string A_i, and A_i is marked as A_i= $c_1c_2...c_n$(according to the past experience, the value of n is a positive integer between 2-7). Step2:for every atomic entry c_a(1≤a≤n;n∈ N), find out all combined entries which are led by c_a with a single entry for incremental step. We put them into a set A_m, and call its item C_m which may be a compound concept. Step3: travel through every sentence s_i, and count the frequency of C_m. Step4: set a threshold value, and select out those C_m which's frequency value bigger than the threshold vale, and add them into a initial compound concept set. Step5: for items C_m which contain c_a and in the same sentence, we screen out final item C_m by the longest combining rule. And then we can update the initial compound concept set.

Compound concept filtering based on POS combination rule. Compound concept generally consists of nouns, verbs, Nominalization of verbs and adjectives. Most of them are combined by only two or three words, and they usually have specific POS combination rules. According to the characteristic of compound concept and test data, this paper has proposed POS rule templates for those compound concepts which are combined by two words and three words in computer field. The POS rule templates are shown in table 1 and table 2.

Table1 POS rule template for two words

Pos rule template
a + n
v + n
n + n
n + v
d + v

Table2 POS rule template for three words

Pos rule template	
n + n + n	v + v + n
n + n + v	v + n+ n
n + v + n	a + n + v
n + c + n	a + v + n
v + n + v	b + v + n

Most of domain compound concept can be screen out by those POS rule template, but we can't find out every POS combination rule of compound concept at a time, so when we find other POS combination rules in the future, we can add them in POS rule template.

4 The experimental analysis

The evaluation indexes of compound concept extraction. The precision rate and recall rate can reflect the quality of compound concept extraction, so we use them as evaluation indexes. In addition, we also use F value as evaluation index.

$$\text{precision rate:} \quad p = \frac{\text{correct number of extracted compound concept}}{\text{total number of extracted compound concept}} \times 100\% \tag{6}$$

$$\text{recall rate:} \quad r = \frac{\text{correct number of extracted compound concept}}{\text{total number of compound concept in document set}} \times 100\% \tag{7}$$

$$\text{F value:} \quad F = \frac{2pr}{p+r} \tag{8}$$

The experimental result. In order to validate the effectiveness of compound concept extraction by our method, other two representative methods are compared. One is the Chinese term extraction method based on mutual information [5], marked as M1; another is the new word identification method based on word internal model [6], marked as M2; and our method marked as M0. We download 100 articles which are related to computer field from Wanfang database, and use them as the corpus of domain compound concept extraction experiment. Those three methods use the same corpus and set the same threshold. In the experiment, we obtain compound concept set related to computer field by manually. According to the experimental design, the results of compound concepts extraction by those three methods are shown in table 3.

Table 3 Extraction results by three methods

Method category	The total number of compound concepts	The number of extraction	The correct number	precision rate(%)	recall rate(%)	F value(%)
M0	535	506	437	86.4	81.7	83.9
M1	535	576	418	72.5	78.2	75.2
M2	535	548	360	65.7	67.3	66.5

The experimental results show that, the precision rate, recall rate and F value of M0 are higher than those of M1and M2, so M0 has better extraction effect than M1and M2. The main reason is that M0 use POS rule template which for two and three words to filter after entry co-occurrence statistics extracting. The factors which influence extraction on M1are mainly two categories: 1) The internal bonding strength. For a string which is combined by two words and contains a basic word, it has a low internal bonding strength, so it can not be extracted out. 2) Wrong segmentation in term selection stage. The factors which influence extraction on M2 are mainly two categories: 1) The search of repeated string. There are many garbage strings in repeated string, and we have not enough methods and POS rules to filter them. 2) It is difficult to set the threshold of weighted value. The factors which influence extraction on M0 are also mainly two categories:1)Some words which are combined to compound concept are belong to stop word, so we may filter them by stop word table, and thus we can not get a complete compound concept. 2) We can not find out every POS combination rule. When we meet a compound concept, and its POS combination rule is not included in the template, then we may filter it. Thus, we need add that new rule into template.

Summary

This paper builds a multilevel filter extraction model by fusing the thought of statistics and language rule. In the model, we present the space combination rule and POS combination rule for two and three words. Through those two innovations, we improved the accuracy of compound concept extraction. And the experiment has achieved good results. However, the extraction of compound concept remains to be improved. For example, some stop word is a part of compound concept, if we can extract out those compound concepts , then we can improve the recall rate.

References

[1] Jipeng Sun, a concept extraction of method oriented to text, J. Computer application and software,2009,26(9).

[2] Shamsfard M, Barforoush AA, Learning ontologies from natural language texts, J. Int'l Journal Human-Computer Studies, 2004, 60(1): 17- 63.

[3] Sproat R, Shih C. A statistical method for finding word boundaries in Chinese text, J. Computer Processing of Chinese and Oriental Languagies, 1990, 4: 336-351.

[4] Wang, B. Y. and S. M. Zhang. A novel feature selection algorithm for text classification based on TFIDF-weight and KL-divergence. Proceedings of the 11th Joint International Computer Conference. 2005: 438-441.

[5]Zhangfeng,Xuyun,Houyan,Chinese term extraction system based on mutual information,J.Computer application and research,1001- 3695(2005)05-0072-02.

[6] Zifang Lin, Xiufeng Jiang, New words recognition based on word internal model, J. Computer and modernization ,1006-2475（2010）11-0162-03.

Advanced Materials Research Vols. 989-994 (2014) pp 2297-2300
© (2014) Trans Tech Publications, Switzerland
doi:10.4028/www.scientific.net/AMR.989-994.2297

Design and Realization Based On CloudStack Hybrid Cloud Computing Platform

Peng Cheng [1, a], Hui Qu [2, b]

[1] Training Department, Engineering College of CAPF, Xi'an 710086, China;

[2] Faculty of Science, Engineering College of CAPF, Xi'an 710086, China.

[a] cpskull@163.com, [b] qh3798150@hotmail.com

Keywords: cloudstack, hybrid cloud, virtualization technology

Abstract. While setting up the cloud computing platform by using OpenStack, there were some disadvantages such as very tedious operating steps and low efficiency. In this paper, we put forward a design and realization method based on CloudStack hybrid cloud computing platform. Firstly, we used CloudStack as tool to set up two independent cloud platforms, one of them was called public cloud and the other one private cloud. Then virtualization technology and a shared resource classification method discussed in this paper were performed to set up two virtual sub-servers on the main server and operate the cloud platform already established on it. Finally, we gave the two platforms corresponding authority, thus the hybrid cloud platform was established. This method was easy to set up and could reduce the cost effectively, therefore, it was very practical.

Introduction

Cloud computing is a computing mode by which the user or the application system can customize services, resources and applications without understanding the means of realization [1,2]. It is also a kind of new business computing model which offers the IT resources, data and applications as services for users via internet. Cloud computing solutions give a methodology of infrastructure management, which supplies highly virtualized resource for users dynamically. The network who provides resources is called “cloud”. The resources in it are considered to be infinite extent by users and can be obtained, used as needed, extended and paid for use at any time. Normally, this character is called as using IT infrastructure like water or electricity.

In accordance to the deployment patterns and the scope of the service object of the cloud, we can divide the cloud into three types: public cloud, private cloud and hybrid cloud.

The public cloud is shared by several enterprises and users, although it has some advantages such as low price and elastic strategy, however, there also exists safety problems because the data storage location of the public cloud is not in the enterprise. The private cloud can provide services only to the inner-enterprise users so that people can control the data security and service quality effectively. However, the hybrid cloud combines the public cloud and the private cloud so that users can both partly possess and share the resources through a controllable method. Therefore, more commercial value will be created by setting up the hybrid cloud.

At this stage, the main tools for setting up cloud computing are OpenStack, CloudStack and Eucalyptus. According to paper [2], [3] and [4], researchers have designed and developed cloud computing platform and applied it to management, education and experiment. OpenStack has many advantages such as a mature platform, an easier operating process and is convenient to use. However, compared to CloudStack, deployment process of OpenStack is very complicated and it also needs a huge research and development team and higher level developers.

This paper came up with a method of constructing the hybrid cloud platform based on CloudStack. While the public cloud and private cloud were successfully designed and realized, virtualization technology was performed to combine them as hybrid cloud. After that, the inner-enterprise users could share the data resources with a high-efficiency and people on the outside could check the resources they were permitted as well.

Process of setting up the cloud computing platform by CloudStack

Introduction to CloudStack. CloudStack is an open source cloud platform developed by Citrix, it obeys the Apache2.0 agreement and takes Java as its language. It can set up public cloud, private cloud and hybrid cloud by forming a resource pool with all computing resources. Users can deploy their own cloud condition because the friendly Web interface and abundant API interface can easily satisfy both consumers' and developers' different requirements. The structure of CloudStack is shown in Fig. 1.

Deploying CloudStack. This paper deployed CloudStack with console. Fig. 2 shows the deployment process consists of preparatory work, user interface design and configuration.

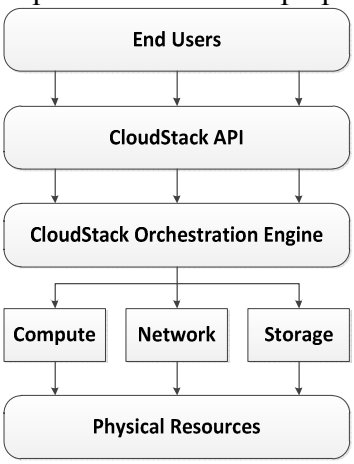

Fig.1 Structure of CloudStack

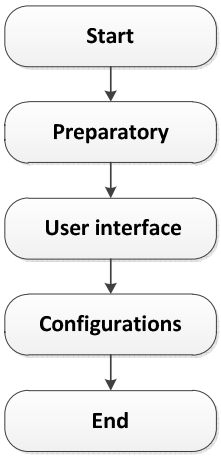

Fig.2 Procedure of Deploying

Preparatory work before configuration. The preparatory work included configuring the installation source, installing the Management Server, installing and configuring the virtualized Host mainframe of KVM.

Configuring the installation source means searching and downloading the installation package on the Internet. Generally, we download the CloudStack from its official website. The command is $ sudo vim /etc/apt/sources.list.d/cloudstack.list deb (http://cloudstack.apt-get.eu/ubuntu precise 4.0), in addition, the official certificate of the source is needed as well. If the installation of the system needs to update, just operate the command $ sudo apt-get updata.

During the installation of the Management Server, the first step needed to do is configuring the operating system's environment. While the hostname is obtained, we should add the record described as 10.6.203.10 cloudstack-server-1, which is used to map the server. Then the time server "openntpd" should be installed. Only by accomplishing above three steps , the CloudStack Management Server and vhd-util can be downloaded and installed. The command is $sudo apt-get install cloud-client. In order to acquire higher authority, the user must be added into the group sudo. Finally, the user group's password switch should be wiped off so that the users don't have to enter the password for every time. In the CloudStack, MySQL is usually chosen for storing and controlling data resources. MySQL can be installed with the command $ sudo apt-get install mysql-server and then configurate innodb_rollback_on_timeout as 1, innodb_lock_wait_timeout as 600, max_connections as 350, log-bin as myql-bin and binlog-format as 'Row'. Next, restart and initialize MySQL. Besides, NFS shared service is normally used for CloudStack's sharing data resources.

User interface. There is already a friendly interface in CloudStack so that once the configurations were accomplished, the platform of cloud computing was set up.

Configurations. This section discusses the most important part in the process of setting up the cloud computing platform. It includes configuration of the Management Server, installation of the Instance, establishment and customization of the Template and creation of the VM Instance.

Fig. 3 shows structure of the Mangement Server. Developers can modify and set up the Management Server via the Infrastructure interface, the steps are shown as follows: firstly, we need to make sure the value of Hypervisor as KVM; secondly, config Phycial Network by creating the

name of network and selecting the type of the network; thirdly, in order to control the interior communication of the CloudStack, the related network settings of Pod must be deployed; next, we should configurate Guest Traffic and Storage Traffic of the storage system so that we can distribute the IP address dynamically by Instance; At last, deploy the Host, the host machine of virtual machine, which is also called the Agent mainframe.

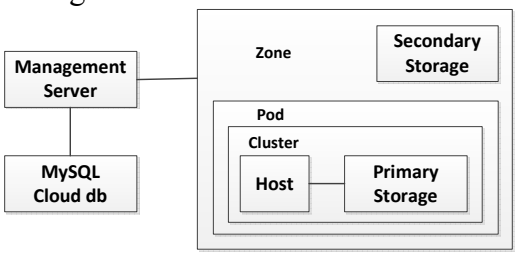

Fig.3 Structure of Management Server

Optimal settings. Normally, there is a guard time for Instances already deleted in CloudStack, however, it is really a long time lasting for 24 hours so that sometimes the system resources are quite insufficient. To cut down this duration, we should search for expunge and modify the parameter "expunge. interval" to a smaller value (such as 300s), and then restart Management Server.

Hybrid cloud based on virtualization technology

Virtualization ideas already exist, the IBM in the 1960s, firstly proposed and implemented that a single physical machine ran a number of different operating system instances, it subverted the traditional computing model which one computer only run one operating system instance. Multiple operating systems run on a single physical machine, sharing the physical machine resources (CPU resources, memory resources, network resources, storage resources, etc.). With the rapid development of computer hardware resources, many existing computer software has not fully utilize the hardware resources, so there are a lot of waste of resources.

Currently, the appearance of virtualization technology improve the utilization rate of hardware resources of the physical machine or server, and take full advantage of parallelism and high performance of hardware, besides, the administrator can eliminate the time and energy to manage a large number of physical machines.

These features of virtualization technology makes itself become one of the most valuable software technology among the whole computer technology, which plays a vital role in the cloud computing technology.

Resource classification. To build a hybrid cloud, you need to classify shared resources by different level, this paper proposes a method to classify. Arrange numbers to share resources in accordance with level of confidentiality, for example, the code of the most important resources within the enterprise is 1, followed by 2, and so on. As a result, the resources can be roughly divided into three parts: the private resources, public resources and ordinary resources. Private resources are the most important kinds of resources related to the survival and development of enterprises, it must not leak. Public resources must be known to the masses, such as product presentations, product categories, leadership team, etc. Common resources are not obvious limits, they can be available as private or public resources, and can be interchangeable.

Structure of Hybrid cloud based virtualization technology. As Shown in Fig.4, the main service consists of the virtual machine and authentication, using the above method to build a private cloud platform via the virtual machine, storing the private resources of corporation or institutions; While public cloud can be connected together by networks to form a large cloud platform, outsiders can access resources within the authority easily and efficiently.

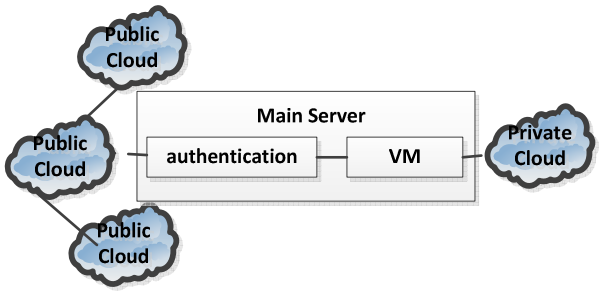

Fig.4 Structure of Hybrid Cloud

Summary

This paper proposes a design and implementation method of hybrid cloud computing platform based on CloudStack, in order to reduce complexity when using OpenStack as a development tool. On the basis of building methods of private cloud platform, introduce the virtualization technology twice, and create a mechanism for running a private cloud in a virtual machine environment. Besides, establish an authentication module, which isolate the private and public clouds to improve the security; And for managing easily, classify shared resources into three categories, which are private, public and general resources.

References

[1]Q. Li，X. Zheng : Research Survey of Cloud Computing J. Computer Science. 38(2011)32 – 37.

[2]X.H. Sun.:Research Survey and development tendency of Cloud Computing. J. Computer Measurement & Control. 04(2011).

[3]G.S. Gao: Research and Realization of Cloud Computing Based on OpenStack. J. Computer Science. (23)2012.

[4]F. Xiao, J.Yang, L.M. Liu .:Design and Implementation of Computer Lab Self-service Platform Based on OpenStack. J.Computer and Modernization[J]. 7(2013).

[5]X.F. Wang. Implementation of Private Cloud Computing Based on OpenStack J. Computer and Modernization[J]. 12(2012).

Advanced Materials Research Vols. 989-994 (2014) pp 2301-2305
© (2014) Trans Tech Publications, Switzerland
doi:10.4028/www.scientific.net/AMR.989-994.2301

A Particle Swarm Optimization Algorithm Based on Simulated Annealing

Yan Zichao[a], Luo Yangshen[b]

School of Jinan University, Guangzhou 510632, China;

[a]yzcjnu@163.com, [b]lysjnu@126.com,

Keywords: Simulated Annealing, mutation, Particle swarm optimization

Abstract. The passage aims at solving the problems resulted from the optimized process of Particle Swarm Optimization (PSO), which might reduce the population diversity, cause the algorithm to convergence too early, etc. A whole new mutable simulated annealing particle swarm optimization is proposed based on the combine of the simulated annealing mechanism and mutation. This new algorithm substitutes the Metropolis criterion in the simulated annealing mechanism for mutagenic factors in the process of mutation, which both ensures the diversity of the particle swarm, and ameliorates the quality of the swarm, so that this algorithm would convergence to the global optimum. According to the result of simulated analysis, this hybrid algorithm maintains the simplicity of the particle swarm optimization, improves its capability of global optimization, and finally accelerates the convergence and enhances the precision of this algorithm.

Introduction

Particle Swarm Optimization,(PSO) is originally attributed to Kennedy, and Eberhart in 1995. This computational method simulates the predation process of the animal colonies such as bids and fishes, which is able to approach the global optimized result in continuous space. The substantive idea of this algorithm is simple, but it is easy to be ameliorated. More importantly, this algorithm has a strong convergence and high quality of optimization, which, therefore, is applied in a lot of fields such as industrial control, electric system, structural design, task scheduling and so on.

The basic algorithm of PSO can remarkably solve most of the optimization problems. However, when getting down to solve some of the problems.Facing these problems, many scholars put forward some outstanding solutions. Some other scholars proposed Unified PSO (UPSO) [3]. UPSO builds the neighbors of the particles, which can improve the topological structure of the particle swarm and prevent the algorithm from working out the local optimum. What's more, the combination between PSO and some other methods of intelligent optimization can lead to a perfect optimum and Simulate Annealing PSO (SAPSO) [4] is a typical case. In addition, Andrews came up with a new improved algorithm in 2006, Mutate PSO (SAPSO), which can increase the diversity of the particle swarm. The key is the fact that it is easy to manipulate the arguments of Mutate PSO method so that the quality and efficiency of the solution is improved.

The problem is, MPSO would cause two great defects in the process of mutation operation. The first flaw is that the capability of mutation will be weakened through the iterations continue, which will lead to the decrease of the swarm's diversity, while the second flaw would import numerous inferior solutions, which may stop the algorithm approaching the global optimized solution. To solve the problems and imperfections above, this article introduces Metropolis criterion in the simulated annealing mechanism and substitute it for the mutagenic factors in the process of mutation, and finally proposes an algorithm called Anneal Mutate Particle Swarm Optimization (AMPSO). Through the result of simulated analysis of Benchmark, it is shown that AMPSO maintains the simplicity of the particle swarm optimization, and lead the convergence to the global optimum.

1. A brief introduction of PSO

PSO simulates the searching process of extremum value by the particle swarm with the size of N in D-dimension space. The transmission dynamics models of the mutable particle is listed as follows:

$$\begin{aligned} v_i^{t+1} &= \omega \cdot v_i^t + c_1 \cdot \xi \cdot (p_i^t - x_i^t) + c_2 \cdot \eta \cdot (p_g^t - x_i^t) \\ x_i^{t+1} &= x_i^t + v_i^{t+1} \end{aligned} \quad (1)$$

In the formula, $x_i^k (i = 1 \cdots N)$ is the position of the i th particle at the t th time. $\boldsymbol{x_i^t} = (x_{i1}^t, x_{i2}^t, \cdots, x_{iD}^t)$ means the particle swarm is in a D-dimension space. $\boldsymbol{v_i^t} = (v_{i1}^t, v_{i2}^t, \cdots, v_{iD}^t)$ is the velocity of the i th particle at the t th time. $\boldsymbol{p_i^t} = (p_{i1}^t, p_{i2}^t, \cdots p_{iD}^t)$ is the particle's optimum location during the time period of $[1, t]$. ω, c_1, c_2 is inertia factor, self-directed learning factor and social learning factor. $\xi, \eta \in [0,1]$ is two pseudo-random numbers. PSO gains a good capability of optimization in continuous space, the schematic diagram of the particles' movement is listed as Figure 1.

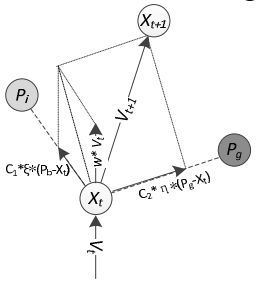

Figure 1. Schematic diagram of PSO

2. Traditional mutation process

The basic PSO has a problem of untimely convergence and working out the local optimum instead of global optimum. Andrews came up with a new improved algorithm in 2006, Mutate PSO (SAPSO) [4], which can increase the diversity of the particle swarm so as to prevent the untimely convergence. The mutation process destabilizes the particle's position through the variation function, and then restrains particle's mutation using particle's mutation probability and mutation factor so that the result can converge to the global optimum. Compared with other relevant algorithm, the mutation process has some good features such as its simplicity with less algorithm complexity.

The particle's variation function is the core of the mutation process, which can generate the new particle position and increase the particles' diversity using randomized strategy. The variation function used in this passage [8] is a classic one. x_{id} is the value of the i th particle at the d th dimension of space. $mutate(x_{id})$ is corresponding value after the mutation while $Guassian(\sigma)$ is a random number which obeys Gaussian distribution with the standard deviation of σ. $mutate(x_{id}) = x_{id} + Guassian(\sigma) \times x_{id} \quad (d = 1 \cdots D)$

For further details, pm_i (mutation probably) is the probability of the mutation by the i th particle in the swarm, while each particle's probability to cause the mutation is relatively different because the mutation probability is closely related to the particle's subscript. It is easy to modify the mutation probability of the whole particles swarm through the adjustment the relevant arguments α and β. In this case, $PopSize$ is the population size of the particles swarm.

$$pm_i = \alpha + \beta \frac{exp\left[\frac{5(i-1)}{PopSize-1}\right] - 1}{exp(5) - 1} \quad (2)$$

3. The mutation process base on simulated annealing mechanism

The mutation process will cause some imperfection. Early in the algorithm lifecycle, it is likely to import numerous inferior solution and at the same time extend the convergence process. At the later period of the algorithm, the capability of mutation will be weakened through the iterations continue, which will lead to the decrease of the swarm's diversity and finally the algorithm will lead to the local optimum instead of the global one. To improve the circumstance, this passage import the simulated annealing mechanism.

The simulated annealing(SA) mechanism can simulate the annealing process in the thermodynamics and lead the mutation particle to the global optimum after the temperature parameter declines gradually. SA mechanism use the Metropolis criterion to judge if the particle should update its new position via the mutation, which means the probability for the particle to accept $mutate(x_i)$. This probability is called pa_i (accepted probably):

$$pa_i = \begin{cases} 1 & f\left[mutate(x_i)\right] \geq f(x_i) \\ exp\left(\dfrac{f\left[mutate(x_i)\right] - f(x_i)}{T_t}\right) & f\left[mutate(x_i)\right] < f(x_i) \end{cases}$$

(3)For further details, $f(x_i)$ is the i th particle's fitness, T_t means the temperature parameter at the t th time period. The algorithm of the mutation process base on simulated annealed mechanism is listed as follows:

Algorithm of mutation process base on SA

1) Initialize $PopSize$, number of iteration $maxgen$, initial temperature T_0 , etc
2) $while(t < maxgen)$
3) Update the particles' position based on Equation (1)
4) $If\,(mod\left[t, step\right] == 0)$
5) $while(i \leq PopSize)$
6) $If\,(rand_1 < pm_i)$
7) Generate particles $mutate(x_i)$ based on Equation (2)
8) Generate random number $rand_2$
9) $If\,(rand_2 < pa_i)$
10) Update x_i with $mutate(x_i)$
11) $End\ If\,, End\ If\,, i = i + 1$
12) $End\ while, T_t = T_{t+1}, t = t + 1$
13) $End\ while$

Different from the mutation factor of the mutation process, this mechanism will not restrain particles' mutation, so that the high value of the diversity can be garanteed. What's more, this mechanism will choose the appropriate particle base on their fitness to imp rove the swarm's quality and finally work out the global convergence.

4. Simulated analysis

In this passage, the classic function[11] Tablet，Quadric，Rosenbrock，Grewank, etc are used to test and analyse the performance and efficiency of this algorithm. In addition, the result is compared with the one from standard PSO, UPSO, SAPSO, MPSO and AMPSO. The whole testing process is executed by the computer base on Intel Core i3 3.00 GHz processor, 4GB memory, 1TB hard disk, with runtime environment of Matlab 2013a. The functions are listed in Table 1

Name	Function	Search Space	Best position
Tablet	$f(x)=10^6 x_1^2+\sum_{i=2}^{30} x_i^2$	(-100,100)	$(0,\cdots,0)$
Quadric	$f(x)=\sum_{i=1}^{30}\sum_{j=1}^{i} x_j^2$	(-100,100)	$(0,\cdots,0)$
Rosenbrock	$f(x)=\sum_{i=1}^{n-1}\left[100(x_{i+1}+x_i^2)+(1-x_i)^2\right]$	(-5,5)	$(1,\cdots,1)$
Grewank	$f(x)=10^6 x_1^2+\sum_{i=2}^{n} x_i^2$	(-300,300)	$(0,\cdots,0)$

Figure 2 to Figure5 describe the comparison of the converge process among these five algorithm tested by the four Benchmark functions independently in 20 times. It is shown that in the algorithm of PSO, the diversity of the particle swarm declines through the converge process, which has a serious prematurity phenomenon. The algorithm of UPSO and SAPSO improve the swarm's diversity in different ways, which can work out a better result. However, these two algorithms do a limited improvement to the result because they can not solve the problem of leading to the local optimum untimely. MPSO has a great performance and high speed convergence, but later in the lifecycle, its diversity begins to decline and cause its performance to decrease. Lastly, the algorithm of AMPSO maintains the diversity and quality of the swarm, improves its capability of global optimization finally accelerates the convergence and enhances the precision of this algorithm.

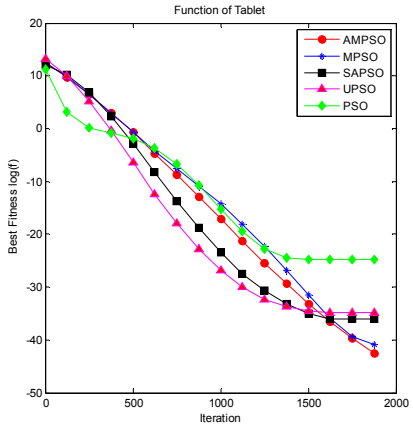

Figure 2

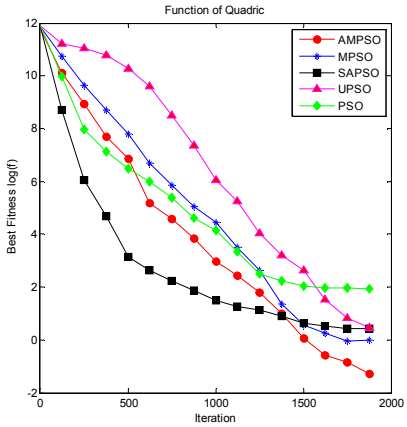

Figure 3

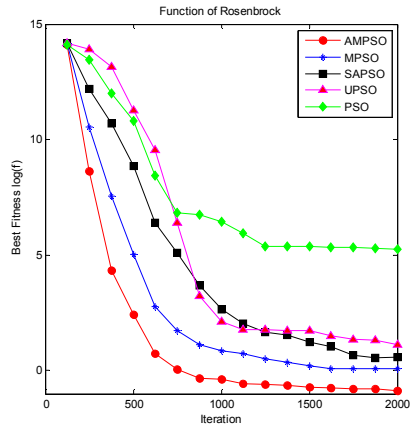

Figure 1

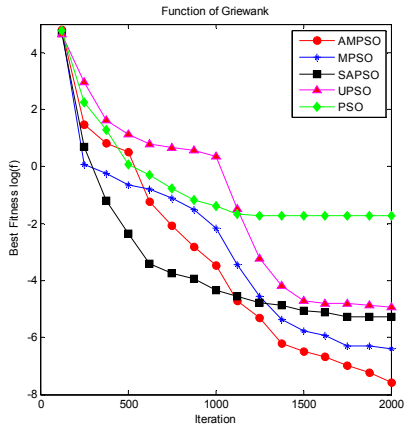

Figure 2

Conclusion

Particle Swarm Optimization(PSO), which might reduce the population diversity, cause the algorithm to convergence too early, etc. This new algorithm substitutes the Metropolis criterion in the simulated annealing mechanism for mutagenic factors in the process of mutation, which both ensures the diversity of the particle swarm, and ameliorates the quality of the swarm, so that this algorithm would convergence to the global optimum. According to the result of simulated analysis, this hybrid algorithm maintains the simplicity of the particle swarm optimization, improves its capability of global optimization and finally accelerates the convergence and enhances the precision of this algorithm.

There are two imperfections in the algorithm of MPSO, which is the decreasing diversity through the algorithm and the appearance of numerous inferior solutions. By introducing the mechanism of the simulated annealing, the ameliorated algorithm improves the diversity of the swarm so that it is not likely for the algorithm to work out the local optimum. By its Metropolis criterion, AMPSO can filter the inferior particles and finally improves the quality of the particles so that the improved optimization is on the way.

References

[1] Kennedy J, Eberhart R. Particle swarm optimization[C].IEEE Int Conf on Neural Networks. Piscataway: IEEE Press, 1995: 1942-1948.

[2] Chen Guimin,Jia Jianyuan,Han Qi,Study on the Stategy of Decreasing Inertia Weight in Particle Swarm Optimization Algorithm,Xian Jiaotong University,2006.

[3] Parsopoulos K E, Vrahatis M N, Unified Particle Swarm Optimization in Dynamic Environments[J]. In Proceedings of Applications on Evolutionary Computing-EvoWorkshops:EvoBIO, EvoCOMNET, EvoHOT, EvoIASP, EvoMUSART and EvoSTOC, Lausanne, 2005:590-599.

[4] CHEN Xi, CHENG Haozhong, DAI Ling, QIU Qiwei, QUE Zhimei, Application of Simulated Annealing Particle Swarm Optimization Algorithm in Reconfiguration of Distribution Networks, High Voltage Engineering,2008.

[5] Andrews P S. An Investigation into Mutation Operators for Particle Swarm Optimization. In IEEE Congress on Evolutionary Computation, Vancouver, 2006: 1029-1036.

[6] Shi Y, Eberhart R C. Parameter selection in particle swarm optimization[C].Evolutionary ProgrammingVII. Berlin: Springer-Verlag, 1998: 591-600.

[7] Yuntao D. An intelligent parameter selection method for particle swarm optimization algorithm[C]. The 4th Int Joint Conf on Computational Sciences and Optimization. Piscataway: IEEE Press, 2011: 960-964.

[8] K.E. Parsopoulos, M.N. Vrahatis. Paramater Selection and Adaptation in Unified Particle Swarm Optimization [J]. Mathematical and Computer Modeling[J]. 2007, 46(1-2): 198-213.

[9] Wang Dingwei, Wang Junwei, Wang Hongfeng, std. Intelligent Optimizaton Methods[M]. PeKing: Higher Education Press, 2007, 137-156.

[10] Lei Xiujuan. Swarm Interlligent Optimization Algorithms and Their Applications[M]. Peking: Science Press, 2012, 132-135.

[11] Dou Quansheng, Zhou Chunguang, Ma Ming, Two Improvement Strategies for Particle Swarm Optimization, Journal of Computer Research and Development,2005.

Advanced Materials Research Vols. 989-994 (2014) pp 2306-2309
© (2014) Trans Tech Publications, Switzerland
doi:10.4028/www.scientific.net/AMR.989-994.2306

The Gray Relation Analysis 0f Non-coal Mine Accidents Causation

Xiangyun Meng[a], Rihui Chen[b,*] and Shibin Wang[c]

Faculty of Land Resource Engineering, Kunming University of Science and Technology, Kunming 650093, China

[a]yan761415498@163.com, [b]chenrihui555@126.com, [c]wsb18288667554@163.com

Keywords: Non-coal mine accident cause; Grey correlation analysis; Grey correlation degree; Grey correlation order; Mine accident risk.

Abstract: The Gray Relation Analysis is applied to the casualty analysis of non-coal mine accident in four certain years in China to export grey relational order to determine the main related factors in the non-coal mine accident, obtaining quantitative analysis results of the relationship between non-coal mine accident and multiple factors, introducing the concept of mine accident risk correlation degree.

Introduction

Non-mine mines mean the mine that mines metal ores, radioactive ores as well as building materials, refractory materials, petroleum chemical raw materials, auxiliary materials and other non-metal minerals [1]. Our country obtains a high incidence of non-coal mine production safety accident, for example, the mortality per million tons of ore is 30 times more than developed country in mining such as the United States. Non-coal mine accidents not only seriously threaten operation safety of miners and restrict the sustainable development of mine, but also bring enormous loss to national economy, so it has important practical significance to the occurrence of non-coal mine accident cause factor analysis.

Because the mine accident system is a multi-factor, multi-level and multi-objective mutual connection and restriction giant system, and its operation process is a grey dynamic process composed of many perplexing relationship, therefore, it is quite reasonable to use the grey system theory to analyze related factors of accident system.

The Summary of gray correlation analysis

The basic principle of grey correlation analysis. The basic idea of grey relational analysis is to determine whether they contact closely based on the similarity of sequence curve geometry. The closer the curve is, the greater the correlation degree between corresponding sequences is, whereas the smaller. That is to say, based on the degree of similarity or dissimilarity of development among various factors, it measures the correlation degree between factors. It doesn't make excessive demands on the number of the sample size, doesn't require the typical probability distribution, due to the small sample size makes little calculation, and will not appear that quantitative correlation results are inconsistent with the qualitative analysis of the situation, so than regression analysis, analysis of variance, principal component analysis, it is more practical and effective [2].

The procedure of grey correlation analysis. The grey correlation analysis is a quantitative analysis based on the qualitative analysis, an integral comparative analysis with the reference system and measure, can quantify and order factors through the analysis of the "incomplete information", "less", "not sure" system [3]. Its calculation steps are as follows [4]:

A. To determine the reference sequence (standard sequence) and comparative sequence.

B. The original data initialization. In practice, to solve the problem that the data dimension is not same as the absolute value, we need nondimensionalize and utilize the date to gain new comparative sequence. The paper takes the average method to implement transformation of data sequence, which is a list of data respectively divided by the average of every data to get a list of new series of average percentage. The dimensionless data sequence is [5]:

$$X_0(k)=\frac{Y_0(k)}{\frac{1}{n}\sum_{t=1}^{n}Y_0(t)}\quad X_i(k)=\frac{Y_i(k)}{\frac{1}{n}\sum_{t=1}^{n}Y_i(t)},i=1,2,\cdots,m;k=1,2,\cdots,n \tag{1}$$

In (1), Y_0 and Y_i are the original data.

C. The evaluation of sequence of difference.

$$\Delta_i(\mathrm{k})=\left|x_0(k)-x_i(k)\right|,\ \ \Delta_i(k)=\left(\Delta_i(1),\Delta_i(2),\cdots,\Delta_i(n)\right),i=1,2,\cdots,m \tag{2}$$

D. The evaluation of the polar difference $\mathrm{M}=\max_i \max_k \Delta_i(\mathrm{k}),\mathrm{m}=\min_i \min_k \Delta_i(\mathrm{k})$ (3)

E. The evaluation of the correlation coefficient.

$$\gamma_{0i}(k)=\frac{m+\varepsilon M}{\Delta_i(k)+\varepsilon M},k=1,2,\cdots,n;i=1,2,\cdots,m \tag{4}$$

ε -resolution ratio.

F. The evaluation of the correlation degree.

$$\gamma_{oi}=\frac{1}{n}\sum_{k=1}^{n}\gamma_{0i}(k),i=1,2,\cdots,m \tag{5}$$

The grey correlation analysis of accident cause in the non-coal mine

According to the above statement, combined with the accident classification statistics based on the accident cause of the national non-coal mine accidents in certain years(Table 1), the paper select the total number of deaths, the total number of accidents as a reference sequence, denoted by Y_0， Y_{00}.

The correlation degree for the total number of deaths and various factors.

A. To determine the comparative sequence. To select the following factors related to the mine accident as comparative sequences: Technology and design defects Y_1; Defective tools accessories of equipment and facilities Y_2; Missing or defective safety equipment Y_3; Adverse workplace environment Y_4; Ppe missing or defective Y_5; No safety procedures or inadequate Y_6; Violation of rules or labor discipline Y_7; Unreasonable labor organization Y_8; The lack of on-site inspection or command error Y_9; No enough training and lack of the safety operation knowledge Y_{10}; Others Y_{11}.

Table 1 The accident classification statistics based on the accident cause of the national non-coal mine accidents in certain years [6]

	2010	2011	2012	2013	Total
The number of	Accident Death	Accident Death	Accident Death	Accident Death	Accident Death
Technology and design defects	50 58	41 71	42 52	36 43	169 224
Defective tools accessories of equipment and facilities	80 99	79 102	77 88	90 115	326 404
Missing or defective safety equipment	167 199	128 150	164 178	112 137	571 664
Adverse workplace environment	627 793	551 672	509 634	362 444	2049 2543
Ppe missing or defective	114 114	115 137	287 290	155 196	671 737
No safety procedures or inadequate	89 116	121 138	106 121	71 82	387 457
Violation of rules or labor discipline	671 786	684 816	568 655	475 855	2398 3112
Unreasonable labor organization	32 36	36 40	34 29	29 37	131 142
The lack of on-site inspection or command error	121 146	113 138	76 91	62 67	372 442
No enough training and lack of the safety operation knowledge	93 108	81 105	76 86	71 75	321 374
Others	127 161	134 182	162 232	166 262	589 837
Total	1928 2342	1872 2277	1861 2188	1416 2068	7077 8875

B. The data processing. By B, C above, we can obtain the difference sequence of non-coal mine death toll and various factors

Table 2 The difference sequence of non coal mine death toll and various factors

Δ	1	2	3	4
Δ_1	0.020	0.242	0.057	0.146
Δ_2	0.076	0.016	0.115	0.207
Δ_3	0.143	0.122	0.086	0.107
Δ_4	0.191	0.031	0.011	0.234
Δ_5	0.305	0.312	0.526	0.090
Δ_6	0.041	0.182	0.073	0.214
Δ_7	0.046	0.023	0.144	0.167
Δ_8	0.042	0.101	0.169	0.110
Δ_9	0.265	0.223	0.162	0.326
Δ_{10}	0.099	0.097	0.066	0.130
Δ_{11}	0.287	0.156	0.123	0.320

C. The evaluation of the polar difference.

$$M=\max_i \max_k \Delta_i(k)=0.526,\ m=\min_i \min_k \Delta_i(k)=0.011$$

D.The evaluation of the correlation coefficient. Taking ε=0.5 based on the minimum information principle, by the table 2 and (4), we can calculate the correlation coefficient.

E. The evaluation of the correlation degree. By (5), we can calculate the gray correlation degree of the toll Y_0 and various factors, the results shown in Table 3.

Table 3 The gray correlation degree of the toll and various factors

i	1	2	3	4	5	6	7	8	9	10	11
γ_{oi}	0.759	0.775	0.728	0.772	0.520	0.727	0.789	0.755	0.548	0.762	0.583

The evaluation of the correlation degree of the total number of accidents Y_{00} and the number of various accidents. The results are shown in Table4.

Table 4 The correlation degree of the number of accidents and various factors

i	1	2	3	4	5	6	7	8	9	10	11
γ_{00i}	0.841	0.726	0.819	0.824	0.506	0.770	0.884	0.868	0.662	0.833	0.680

Analysis of the results

From the table 3, we can get the grey relational rank of the grey correlation degree of the death roll and various factors, shown: $\gamma_{07} > \gamma_{02} > \gamma_{04} > \gamma_{10} > \gamma_{08} > \gamma_{05} > \gamma_{06} > \gamma_{11} > \gamma_{09} > \gamma_{05}$. The above shows that the extent of the impact on the mine accident death toll of different factors is different, in which violation of rules or labor discipline X_7, defective tools accessories of equipment and facilities X_2, adverse workplace environment X_4, no enough training and lack of the safety operation knowledge X_{10} are respectively one of the greatest impact on mine accident death toll. It shows: the safety awareness of workers should be improved, while the safety training needs strengthening; the safety management system of mine should be perfect, while safety management efforts need to be increased; mine production condition is bad, so we need to improve working environment, which is important to reduce the loss of the accident.

From the table 4, we can get the grey relational rank of the grey correlation degree of the number of accidents and various factors, shown: $\gamma_{07} > \gamma_{08} > \gamma_{01} > \gamma_{10} > \gamma_{04} > \gamma_{03} > \gamma_{06} > \gamma_{11} > \gamma_{09} > \gamma_{05}$ .The above proves that the extent of the impact on the number of accidents of different factors is different,

in which violation of rules or labor discipline X_7, unreasonable labor organization X_8, Technology and design defects X_1, no enough training and lack of the safety operation knowledge X_{10} are more likely to cause accidents. Therefore, in addition to countermeasures mentioned in (1), improving labor organization in the mine production, adopting reasonable equipment, improving equipment man-machine matching degree, enhancing the adaptation of the human and machine all contribute to reducing accidents.

From (1) and (2), we can see that the rank of γ_{0i} is not always as same as the rank of γ_{00i}, which shows that the influence degree of various factors on the occurrence of accidents in mines is not consistent with the influence degree of various factors on the loss of mine accident. Therefore, we are to follow the relationship among risks, the probability of the accident, and the consequences of the accident to put forward the concept of the mine accident risk correlation degree named λ to measure the degree of influence of various factors on the mine, whose calculation formula is as follows:

$$\lambda_{0i}=\gamma_{0i}\times\gamma_{00i} \tag{6}$$

Through (6), we can calculate the accident risk, the results shown in Table 5.

Table 5 The accident risk of various factors

i	1	2	3	4	5	6	7	8	9	10	11
λ_{0i}	0.638	0.563	0.596	0.636	0.263	0.560	0.697	0.673	0.363	0.635	0.396

From the table 8, we can obtain that the accident risk of violation of rules or labor discipline X_7, unreasonable labor organization X_8, adverse workplace environment X_4, technology and design defects X_1 is relatively larger. So, the mine ought to increase the investment of safety education, mining equipment, and operating environment, and optimize the organizational structure of their labor; in addition, The State Administration of Work Safety is also supposed to increase the supervision of the four aspects mentioned previously, to strive to reduce accidents and the loss caused by incidents (the paper mainly aims to the accident death toll).

Conclusion

The paper adopts the grey relation analysis method to analyze various factors that may lead to mine accidents two aspects of γ_{oi} and γ_{o0i}. Because of the deference of γ_{oi} and γ_{o0i}, we put forward the concept of the mine accident risk to find out the accident cause and understand the impact degree of various factors on the accident system, which provides an important scientific basis for control accident factors, has a certain guiding significance and practical value on the safety planning and accident prevention in the future of mining enterprises and relevant government agencies.

References

[1] WANG Qing, LI Zhong-xue, LI Quan-ming, WANG Yun-hai. Studies on work safety standard of non-coal mine in abroad, J. Journal of Safety Science and Technology, 2008, 4(3):117-121.

[2] MA He. Study on coal mine safety hidden dangers control of gray correlation. Master Thesis from Shandong University of Science and Technology, 2009.

[3] WANG Xue-meng, ZHANG Ji-zhong. Grey system analysis and practical calculation program, fourth ed.Wuhan: Huazhong University of Science and Technology press, 2001.

[4] LIU Sifeng, DANG Yaoguo, FANG Zhigeng, and so on. Grey system theory and its application,5 ed.Beijing: Science Press, 2010.

[5] XU Yong-yi. Coal Mining. Xuzhou: China University of Mining and Technology press, 2003.

[6] GONG Sheng-wu. Research on the risk control and safety training system of mining in China. Doctor Thesis from Central South University, 2010.

Advanced Materials Research Vols. 989-994 (2014) pp 2310-2313
© (2014) Trans Tech Publications, Switzerland
doi:10.4028/www.scientific.net/AMR.989-994.2310

Research on algorithm of video segmentation based on self-adaptive single Gaussian model

Yong Zhu [a], Dianhong Wang [b, *] and Jinglong Liu [c]

College of Mechanics and Electronic Engineering, China University of Geosciences, Wuhan 430074, China

[a]806235948@qq.com, [b]wangdh@cug.edu.cn, [c]287274374@qq.com

Keywords: Single-Gaussian background modeling; moving objects detection; dynamic update rate

Abstract. Single Gaussian background modeling is often used in the static scene. In order to overcome the deficiency of the traditional single Gaussian background subtraction method, an improved adaptive background modeling algorithm was proposed. First, the number of each pixel in the image determined as foreground that were as the parameters of each pixel update rate were counted respectively. So the original fixed update rate was transformed into the dynamic update rate changing with the parameter. In this way, the phenomena of ghosting and shelling was suppressed effectively in the traditional single model of Gauss. Finally, foreground objects were obtained by using the method of shadow removal based on morphological reconstruction. The experimental results indicate that the algorithm can quickly and accurately establish and update the background model, and extract the moving object effectively. Compared with existing approaches, experimental results with different real scenes demonstrate the robustness of the proposed method.

Introduction

Moving object detection is very basic topics in the field of computer vision, which has important implications for the latter part of the target tracking and behavior analysis. Commonly used methods of moving target detection are frame difference, background subtraction and optical flow method. Frame difference method does not need the background modeling, just using the current and previous frame for subtraction to extract moving objects, so the calculation speed is very quick. The background difference method is a method used by the current frame and the background model to extract the moving object. Commonly Background modeling methods are average method background modeling, median method background modeling, single Gauss background modeling [1], mixed Gauss background modeling [2]. Optical flow method [3] is an important method for analyzing motion on images. From a single image, it can detect the independently moving targets, which can be used for camera motion environment, but it closes a relatively large amount of computation, and easily affected by the noise. Currently the most widely used target detection algorithm is based on a single Gaussian model. Due to the presence of smear and shelling phenomenon traditional single in Gaussian model, this paper presents an improved adaptive single Gaussian background modeling algorithm, which will effectively address these issues.

Single Gaussian Background Model

Due to external factors is very complex, Video image pixel values of each pixel in the change will be affected by external interference factors, and this approximate satisfy mathematical Gaussian distribution, so it is common to use single Gaussian model of image background to model. When a moving target gets through background, at that point pixels obvious change will happen, no longer meet the Gaussian distribution, this feature can be used to judge the pixel points for future.

Single Gaussian Model Building. In Ref. [4,5], first extract the top N frame image information from the video, and then calculate the average value of pixels as the mean value of each point: $\mu_0(x,y)$, Finally, calculate the variance of every frame of each point by the mean value, the mean of variance as the variance of each pixel, a single Gauss model initialization:

$$\mu_0(x,y) = \frac{1}{n}\sum_{i=0}^{n-1} f_i(x,y) \tag{1}$$

$$\delta_0^2 = \frac{1}{n}\sum_{i=0}^{n-1}[f_i(x,y) - \mu_0(x,y)]^2 \tag{2}$$

In this paper, this process is simplified by experiment here, and just take the first frame of the video to initialize a single Gaussian model, considering the value of each pixel as the mean of the point $\mu(x,y)$, and give a large variance $\delta(x,y)$, which is the coordinates of the pixel point x, y.

Single Gaussian Model Update. The traditional model update has two ways, one is global update on the pixel of background model, the other is selective updates on a model of the background pixels. Global update refers to the whole image pixels updated in accordance with the formula (3), among which α is the update rate, usually empiric constants. When the moving object enters the scene, occluded background pixels by the target will be changed, and global update according to the formula (3), then the pixel information of moving targets will be incorporated into the background, the updated background is no longer practical background. After moving target leave, the actual background re-emerge, then the actual background is sentenced to prospects, causing misjudgment, resulting in smearing.

$$\boldsymbol{B}_{t+1} = (1-\alpha)\boldsymbol{B}_t + \alpha \boldsymbol{I}_{t+1} \tag{3}$$

Among them, $\mathbf{I}_t$ is the pixel information of moment t, $\boldsymbol{B}_t$ is the background model of moment t, $\boldsymbol{B}_{t+1}$ is updated background model from moment t to $t+1$. From Equation (3) shows that, when the α becomes larger, indicate the current frame and into the background model information faster, all the tests in this article take = 0.1.

(a)the 119th frames original image (b)the 119th frame single channel real-time background(c)the two value goals the foreground image of the 119th frame

Fig. 1 The traditional single Gauss model tailing phenomenon

All experiments in this paper are based on VS2008 platform C language environment, the first and second experiment video sections are a section of 280 frames vehicle motion in the standard test video. In Figure 1, (a) is a video of the 119th frames of the original image, (b) is the 119th frame single channel real-time background image. From the background you can see a vague white car, it is because of the background of the global point of interest information before making updates to the melt in the background model, the update of the background global makes the top attractions information into the background model, while the white car's information can gradually disappear through a multi-frame, this will cause the car rear path detected as foreground, make the car after a long tail. (c) is the two value goals the foreground image of the 119th frame through the traditional single-Gaussian model algorithm processing, obviously, after the rear there is a long tail, which is usually called the trailing phenomenon.

In order to overcome the global updating algorithm tailing phenomenon, KOLLER et al. proposed a single Gauss model of selective updating method (6). The method first determine whether the current point belongs to the foreground or background, if it is the background, update the points according to the formula (4), (5), if it is the future, do not update background model, so the foreground information does not melt in the background model, and ultimately avoid the tailing phenomenon.

$$\mu_{t+1}(x,y) = (1-\alpha)\mu_t(x,y) + \alpha \boldsymbol{I}_{t+1}(x,y) \tag{4}$$

$$\delta_{t+1}^2(x,y) = (1-\alpha)\delta_t^2(x,y) + \alpha[\mathbf{I}_{t+1}(x,y) - \mu_t(x,y)]^2 \tag{5}$$

Although selective update method proposed here avoid the tailing phenomenon, but a new problem has emerged.

Due to which involved in updating is only the background, when the background object from static state to motion state, or foreground objects from a moving state to the stationary state into the

background, the background model cannot be updated in time, resulting in the background retains the target motion information before the status change, resulting in shelling phenomenon [7].

In Figure 2, (a) is a video of the 119th frames of the original image, (b) is the 119th frame single channel real-time background image. From the background you can see a vague white car, it's mainly because the car left from the first frame is not updated background model, which led to the road being detected as foreground, becoming a target movement. (c) is the two value goals the foreground image of the 119th frame through the improved single-Gaussian model algorithm processing by KOLLER et al. obviously, the improved algorithm can well eliminate tailing phenomenon, but it also caused a serious phenomenon of shelling: at first frame left, a white car din't disappeared in the image.

a)the 119th frames original image (b)the 119th frame single channel real-time background(c)the two value goals the foreground image of the 119th frame

Fig. 2 The improved single Gauss model tailing phenomenon

The improved adaptive single Gaussian background model

Based on the analysis of section 1.2, to solve above problems, a new kind of background model update strategy is proposed Based on the global update background model: establish a counter for each pixel C, which Used to statistics the discriminant for future point the number of pixels to be continuous, and set a threshold value C_T, when $C \geq C_T$, the Counter C reset, as shown in type (6).

$$C_{t+1}(x,y) = \begin{cases} C_t(x,y)+1, if \ \ I_{t+1}(x,y) - \mu_t(x,y) < \lambda \delta_t(x,y) \\ \quad then \text{ pridicted to be backgrounngd} \\ 0, if \ \ C_t(x,y) \geq C_T \end{cases} \tag{6}$$

The background model is carried out in accordance with the formula (3) global update. But the update rate αreplaced by sigmoid function as follows:

$$\alpha = 1/(1+e^{0.05(C_T - C)}), \alpha \in (0,1] \tag{7}$$

For the traditional single Gaussian model background modeling, whether it is a global update model or selective update model. Their update rate are empirical constant, cannot reflect the change of background model well. In this paper, we use sigmoid function here to show how fast update rate change, at beginning, the value of the counter is 0, αis approximately equal to 0, shows that started slow outlook information into the background model, is approximately equal to 0, to avoid the trailing, When the counter C increases, Illustration background targets from static to movement into outlook or outlook goals from motion to rest and integrated into the background is more likely, so the value of αincreases, Indicates that the faster the rate of foreground points into background model, when $C = C_T$, $\alpha = 1$, Shows prospects point completely melt into background model, So we can successfully avoid hulling phenomenon.

(a) 32th original images (b) 87th original images (c) 95th original images (d) 103th original images

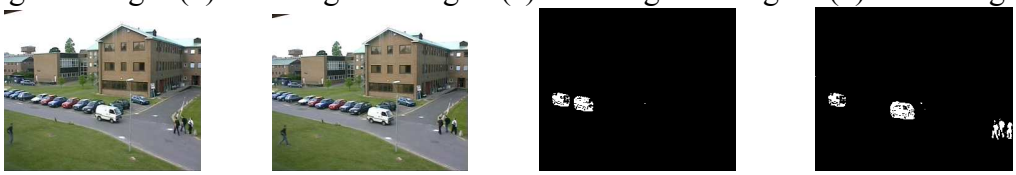

(e) 111th original images (f) 119th original images (g) frame 32th binary target prospects(h) frame 87th binary target prospects

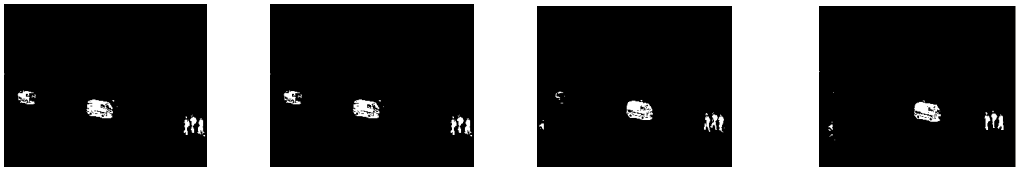

(i) frame 95th binary target prospects (j) frame 103th binary target prospects (k) frame 111th binary target prospects (l) frame 119th binary target prospects

Figure 3 Background updating experimental result.by using the method

The figure 3 (a-f), reflect, the original image in real time of the video, 87, 95, 32, 103, 111, 119 frames, the same as the (g-l), respectively, video, 87, 95, 32, 103, 111, 119 frames, the experimental results after dealing with the background model update algorithm, It can be seen from the figure 3 (l), The car does not exist the tail phenomenon in figure 1 (c) or the hulling phenomenon in figure 2 (c), illustrate the improvement of the proposed algorithm successfully avoid the trailing phenomenon of traditional single Gaussian model, And the selective update hulling phenomenon better inhibition at the same time.

At the same time, figure 3 experimental reflects the update algorithm in this paper relationship between the inhibition effect of size and hulling rate phenomenon. This article take the threshold $C_T = 200$, Such as type (7), Sigmoid function is monotone increasing function, when $C = 100$, $\alpha \approx 6.69 e^{-3}$, it explain that from 1 to 100 frames in this paper, the background model update rate is very small, the cumulative learning outlook pixel information is almost zero. In figure 3 (g), (h), (I) we can see, 1st frame on the left side of the white car left "shell" outline is almost the same, when C =150, C =180, C =200, the Update rates were $\alpha \approx 7.6 e^{-2}$, $\alpha \approx 0.27$, $\alpha = 1$, increased by nearly, Describes frame from 100 to 200 between the cumulative learning points the prospect of pixel information at a faster speed rate into the background model, In figure 3 (j), (k), (I) we can see, the 1st frame on the left side of the white car left "shell" outline gradually disappear.

Conclusion

In view of the traditional single gaussian model in the fixed update rate, this article Put forward a kind of based on improved adaptive moving target detection algorithm of single gaussian background model,which successfully solve the traditional single gaussian model of the tail, shells, and other issues.The experiment proved that, the single gaussian model based on adaptive moving target detection algorithm in indoor environment and the background is relatively stable in the outdoor environment are effectively improve the performance of the foreground object and more adaptability.

References

[1] WREN C, AZARHAYEJANI A, DARRELL T, et al. Pfinder: real-time tracking of the human body. IEEE Transactions on Pattern Analysis and Machine Intelligence, 1997, 19(7): 780-785.

[2] STAUFFER C, GRIMSON W. Adaptive background mixture models for real-time tracking. Proceedings of IEEE Conference on Computer Vision and Pattern Recognition. Fort Collins, Colorado, USA, 1999: 246-252.

[3] FEJES S, DAVIS L S. What can projections of flow fields tell us about the visual motion. Proceeding of International Conference on Computer Vision, Bombay, India. 1998: 979-986.

[4] J. Yang, Z.K. Shi: Photon Journal, (2009) no. 6, p. 1293-1296.

[5] X.G. Hu, Z.Z. Liu: Computer Engineering and Design, (2011) no. 3, p. 4111-4114.

[6]KOLLER D, WEBER J, HUANG T, et al: International Computer Vision & Image Processing Conference, 1994: 126-131.

[7]X.P. Wang, L.J. Zhang, J. Chang: Computer Engineering and Applications, vol. 45 (2009) no. 21, p. 118-120.

Advanced Materials Research Vols. 989-994 (2014) pp 2314-2317
© (2014) Trans Tech Publications, Switzerland
doi:10.4028/www.scientific.net/AMR.989-994.2314

Research on the Evaluation Method of OSHMS Performance based on Fuzzy Theory

Huanming Zhou [a], Dongtao Hu [b, *]

Sinosteel Corporation Wuhan Safety & Environmental Protection Research Institute, Wuhan 430081, China

[a]Hbhszhm@vip.sina.com, [b]eastao@163.com

Keywords: OSHMS, Fuzzy Theory, AHP, performance evaluation

Abstract. Hierarchy evaluation system has been established through a phased analysis of functional properties of OSHMS system, based on four aspects: the file system specification, and the actual business integration, system scheme enforceable, the continuous improvement of the development. Quantitative performance evaluation results has been obtained by building Occupational Safety and Health Management System performance evaluation model through fuzzy theory. According to the rated existing occupation safety and health management system problems, suggestions for improvement are given.

Introduction

Occupation safety and health management system embodies the idea of system security in theory of modern safety science, which is an important means to organize and improve the internal management, reduce business risk and avoid losses, reflecting the fundamental purpose of the protection of human rights. Based on fuzzy theory, starting from the system files and operating conditions, analyzing in functional properties of the system through a phased, establishing hierarchy evaluation system, building occupational safety and health management system performance evaluation model with fuzzy theory, quantitative performance evaluation results was obtained, based on which guiding suggest improvements was given.

Performance evaluation index system and weight determination

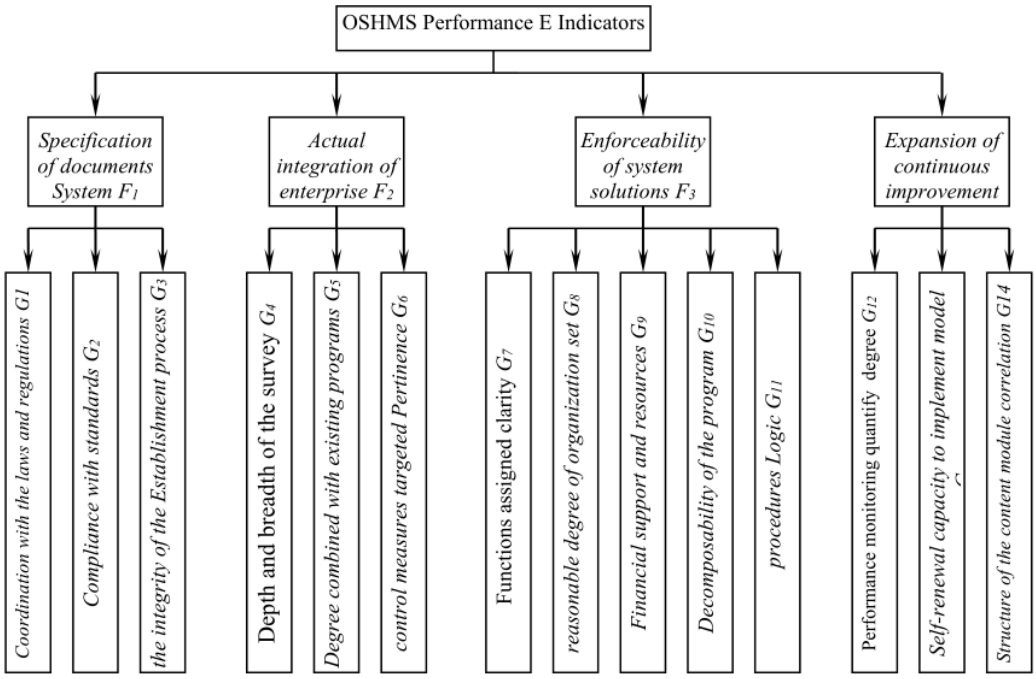

Figure 1 OSHMS performance evaluation index system

Performance evaluation index system determination. Occupational Safety and Health Management System (OSHMS) is a series of interrelated or interacting elements formulated for the establishment of occupational health and safety policy and objectives and the achievement of these objectives. Based on occupational safety and health management system functionality requirements, criteria layer for performance evaluation index system is established, including: (1) the file system specification, (2) and the actual business integration, (3) system scheme enforceable, (4) the continuous improvement of the development.

According to the established Occupational Safety and Health Management System performance criteria above, combined with the content they need to reflect, multi-factor and multi-level performance evaluation index system established is shown in Figure 1.

AHP to determine the weight of each index. For index 1, establish the discriminant matrix E-F for index 1; for index 2, establish the discriminant matrix F1-G, F2-G, F3-G, F4-G for index 2, among which the discriminant matrix scaling criterion uses the rule 1~9 scale method [3].

$$\text{E-F}=\begin{bmatrix}1 & 1/5 & 1/7 & 1/3\\ 5 & 1 & 1/3 & 3\\ 7 & 3 & 1 & 5\\ 3 & 1/3 & 1/5 & 1\end{bmatrix};\ \text{F1-G}=\begin{bmatrix}1 & 1/5 & 1/3\\ 5 & 1 & 3\\ 3 & 1/3 & 1\end{bmatrix};\ \text{F2-G}=\begin{bmatrix}1 & 2 & 1/3\\ 1/2 & 1 & 1/4\\ 3 & 4 & 1\end{bmatrix};$$

$$\text{F3-G}=\begin{bmatrix}1 & 5 & 7 & 1/3 & 3\\ 1/5 & 1 & 3 & 1/7 & 1/3\\ 1/7 & 1/3 & 1 & 1/9 & 1/5\\ 3 & 7 & 9 & 1 & 5\\ 1/3 & 3 & 5 & 1/5 & 1\end{bmatrix};\ \text{F4-G}=\begin{bmatrix}1 & 1/5 & 1/3\\ 5 & 1 & 3\\ 3 & 1/3 & 1\end{bmatrix}$$

The key to calculate the index weight with AHP [4] is to get the maximum eigenvalue and eigenvector of the matrix. The geometric mean method is used here, as well as Delphi7.0 programming processing judgment matrix, and the random consistency ratio is obtained: CRF-E=0.04447, CRF1-G=0.03703, CRF2-G=0.01759, CRF3-G=0.05423, CRF4-G=0.03703. Conformance testing are in line with requirements, and the weights calculated results is shown in Table 1.

Table. 1 OSHMS Performance evaluation index system weights Summary

class 1 index F	class 1 index weight W	class 2 index G	class 2 index weight W	class 1 index F	class 1s index weight W	class 2 index G	class 2 index weight W
F1	0.05502	G1	0.1047	F3	0.5638	G7	0.2638
		G2	0.6370			G8	0.0636
						G9	0.0329
		G3	0.2583			G10	0.5100
						G11	0.1296
F2	0.2634	G4	0.2385	F4	0.1178	G12	0.1047
		G5	0.1365			G13	0.6370
		G6	0.6250			G14	0.2583

Establishment of OSHMS performance evaluation model

Usually fuzzy comprehensive evaluation model has 3 basic elements: factor set, evaluation set and weight set, and the mathematical models are divided into single level model and multilevel model. The object will be assessed for two level model. The main steps are as follows:

Establish performance evaluation model of factors set. The factor set is a collection of the composition of elements influencing evaluation factors to assess the system. According to the evaluation index system established in 1.1, class 1 or 2 indexes corresponding to class 1 or 2 indexes influence factors in the performance evaluation model. A mathematical formula expressed as:

$$F=\{F1, F2, F3, F4\};\ F1=\{G1, G2, G3\};\ F2=\{G4, G5, G6\};$$
$$F3=\{G7, G8, G9, G10, G11\};\ F4=\{G12, G13, G14\};$$

Establish performance evaluation model. According to the calculation results of 1.2, OSHMS performance evaluation model weight set can be directly obtained: Class 1 weight set:W=[0.05502, 0.2634, 0.5638, 0.1178];

Class 2 weight set: w1=[0.1047, 0.6370, 0.2583]; w2=[0.2385, 0.1365, 0.6250];

w3=[0.2638, 0.0636, 0.0329, 0.5100, 0.1296]; w4=[0.1047, 0.6370, 0.2583];

Establish the evaluation set to model evaluate the performance. The purpose of fuzzy comprehensive evaluation is to obtain an optimal evaluation results from the evaluation set through taking into account all the factors judged. According to the characteristic of the evaluation object, OSHMS performance will be divided into five class. Objective evaluation criteria and evaluation criteria for each secondary factors are shown in Table 2 and Table 3.

Table. 2 OSHMS performance Objective evaluation criteria

The target value (100 full marks)	≥90	90-80	80-70	70-60	≤60
Objective evaluation grade	Level Ⅰ	Level Ⅱ	Level Ⅲ	Level Ⅳ	Level Ⅴ

Table. 3 Evaluation criteria for each secondary factors

The target value (%)	≥90	90-80	80-70	70-60	≤60
Fuzzy evaluation	Good	Well	General	Poor	Bad

Objective evaluation set: V={Level Ⅰ, Level Ⅱ, Level Ⅲ, Level Ⅳ, Level Ⅴ};

Secondary factors evaluation subset: v={Good, Well, General, Poor, Bad}.

Establish Performance level of fuzzy evaluation model. According to the evaluation criteria in Table 3, through questionnaire to the expert, calculate the frequency of appearance r that the secondary factors Gi (i = 1, 2, ..., n) relative to reviews vj (j = 1,2, ..., 5). Summarize and get four secondary factors set expert evaluation matrix Rm(m=1,2,3,4).

$$R_m = \frac{1}{N}\begin{bmatrix} r_{11} & r_{12} & r_{13} & r_{14} & r_{15} \\ r_{21} & r_{22} & r_{23} & r_{24} & r_{25} \\ r_{31} & r_{32} & r_{33} & r_{34} & r_{35} \\ \vdots & \vdots & \vdots & \vdots & \vdots \\ r_{n1} & r_{n2} & r_{n3} & r_{n4} & r_{n5} \end{bmatrix} \tag{1}$$

Here: rij: the frequency of the various experts evaluating on the i-th factors, whose results to the frequence that j-th comment that appears; N: total number of experts; n: number of secondary fuzzy actors set containing, here n = 14.

On the basis of fuzzy theory, secondary factor evaluation results:

$$S_{22} = \left[w_1 \bullet R_1 \quad w_2 \bullet R_2 \quad w_3 \bullet R_3 \quad w_4 \bullet R_4 \right]^{\mathrm{T}} \tag{2}$$

Goals (four first factors) Score: $S' = S_{22} \bullet D$ (3)

According to the evaluation criteria in Table 2, construct piecewise interpolation function, calculated: D=[95, 85, 75, 65, 25]T.

first factors evaluation results: $S_{11} = W \bullet S_{22}$ (4)

OSHMS Performance Overall score: $S = S_{11} \bullet D$ (5)

According to Table 2, evaluated OSHMS performance level can be derived and improved measures need to take.

OSHMS performance evaluation models Applications

Whether this method is operable or practical is verified to the object in an enterprise the new building Occupation safety and health management system. By Organizing 10 expert evaluating the OSHMS performance of each factor based on method in Table 3, build evaluation matrix as follows:

$$R_1=\begin{bmatrix}0.7 & 0.1 & 0.2 & 0 & 0\\ 0.5 & 0.2 & 0.1 & 0.2 & 0\\ 0.4 & 0.3 & 0.1 & 0.1 & 0.1\end{bmatrix};R_2=\begin{bmatrix}0.3 & 0.1 & 0.4 & 0 & 0.2\\ 0.2 & 0.1 & 0.3 & 0.3 & 0.1\\ 0.4 & 0.2 & 0 & 0.3 & 0.1\end{bmatrix};R_3=\begin{bmatrix}0.6 & 0.1 & 0.2 & 0.1 & 0\\ 0.2 & 0.4 & 0.1 & 0.1 & 0.2\\ 0.5 & 0.2 & 0.1 & 0.2 & 0\\ 0.4 & 0.3 & 0.2 & 0 & 0.1\\ 0.3 & 0.3 & 0.1 & 0.2 & 0.1\end{bmatrix};$$

$$R_4=\begin{bmatrix}0.2 & 0.1 & 0.3 & 0.2 & 0.2\\ 0.3 & 0.1 & 0.1 & 0.2 & 0.3\\ 0.4 & 0.2 & 0.2 & 0.1 & 0.1\end{bmatrix};$$

Substitute the matrix into the formula (2-5) and calculate, get level 1and 2 fuzzy subset:

$$S_{11}=\begin{bmatrix}0.39890 & 0.21058 & 0.15928 & 0.12590 & 0.10530\end{bmatrix}$$

$$S_{22}=\begin{bmatrix}0.49511 & 0.21536 & 0.11047 & 0.15323 & 0.02583\\ 0.34885 & 0.1625 & 0.13635 & 0.22845 & 0.12385\\ 0.43033 & 0.25028 & 0.17737 & 0.06524 & 0.07668\\ 0.31536 & 0.12583 & 0.14677 & 0.17417 & 0.23787\end{bmatrix}$$

Level 1 index score and OSHMS performance scores were:

$$S^{'}=\begin{bmatrix}84.23 & 75.13 & 81.62 & 68.93\end{bmatrix}^{T};\ \mathrm{S}=78.56$$

According to Table 2, OSHMS performance looks general, and there is still much room for improvement, combined with an index score, we can get following conclusions:(1) The Occupational Safety and Health Management System is above the middle level, and the overall performance is balanced; (2) Lackness of the enterprise system's effectiveness and ability to update is slightly larger. In the process of the system improvement,when overhauling you need to emphasis on two reform efforts item:"the expansion of continuous improvement" and "practical integration with enterprise "at the same.

Conclusion

Features and application value of the occupational safety and health management system performance evaluation method are as the following : (1) According to functional requirements of OSHMS in the life cycle , on this basis of deep analysis of the construction of OSHMS various problems that may arise, OSHMS performance evaluation index system was reflected to ensure that the entire index system is scientific and comprehensive;(2) By the method combining the analytic hierarchy process with fuzzy theory, the multi-level and multifactorial OSHMS performance problems have been effectively solved, and objective quantitative assessment performance results of OSHMS have been get; (3) According to the results of the OSHMS performance evaluation, targeted improvement strategies have been proposed for OSHMS with relatively poor level of performance.

References

[1] F. Ma: National Grid, (2007) no. 4, p. 63-64.
[2] Q.L. Li, W. Jin, Y.B. Ding: Construction Safety, (2007) no. 8, p. 34-35.
[3] Z.F. Tang, Z.H. Yao, J.X. Qian, et al: China Safety Science, vol. 18 (2008) no. 6, p. 152-157.
[4] S.B. Xu: Practical decision making - the principle of AHP (Tianjin University Press, China 1988), p. 6-13

Advanced Materials Research Vols. 989-994 (2014) pp 2318-2322
© (2014) Trans Tech Publications, Switzerland
doi:10.4028/www.scientific.net/AMR.989-994.2318

Parallel Sets based on the improved ACLEARCR algorithm

Haikuo Zhang[a], Ningwei Sun[b], Chong Zhang[c], Tingting Jiang[d] , Changhua Dai [e]

National University of Defense Technology, Changsha 410073, China.

[a]15500092211@163.com, [b]15010203158@qq.com, [c]early4932@163.com, [d]345319286@qq.com, [e]chhdai@163.com

Keywords: Multivariate Data Visualization, Clutter reduction, Parallel Sets, measurement ratio, corresponding degree for categorical measures

Abstract. Classic part-labeled data visualization method Parallel Sets is applied to represent visualization of multivariate data with measures. Currently, in all walks of life emerge abundant small records and documents. Thus to sort the massive categorical measures of small value on the variable axis plays an important role in reducing clutters in the view. This paper is based on the Advanced Categories Layout basEd on Average heuRistic with Cardinality Reduction (ACLEARCR), and proposes an optimization sequence algorithm aiming at categorical measures of small value. The case study proves that the proposed method is effective.

Introduction

Multivariate data with measures of metric attributes [9] has been explored in depth in data mining (DM). The classical analysis method is so-called On-Line Analytical Processing (OLAP) technique. OLAP provides various visualization tools [1-6].

A traditional visualization method is Parallel Sets. There is not a strict process when using parallel sets for visualization. Through picking up interested variables and categorical measures and adding them into the panel, users may conduct visualization analysis. A small number of variables and categorical measures often result in layout confusion. Therefore when conducting visualization users should only choose interested variables and categorical measures and re-choose after analysis completion. Though Parallel Sets allow users to sort the variable axis and its categorical measures' sequence through drag and drop interaction, manual manipulation is quite complex and difficult to guarantee satisfying layout. Edges intersection quantity between two parallel variable axes is closely related to their corresponding nodes sequence [8]. If categorical measures of big value as well as small ones intersect, it may invisibly result in display confusion and ignorance on categorical measures of small values. Such condition can be avoided through sorting variables according to the categorical measures sequence. Sorting massive categorical measures of small values on the variable axis can effectively increase the readability.

Relate work

To solve the problem that categorical measures randomly sequenced by Parallel Sets may generate too many intersections, ref. [7] proposed Categories Arrangement based on MEdian heuristic (CAME). Ref. [8] further came up with Categories Layout basEd on Average heuRistic with Cardinality Reduction (CLEARCR), which may automatically optimize the layout of categorical measures on each variable axes and effectively reduce the visual confusion. Ref. [9] computes measurement of each categorical measure of each axis and takes it as sorting reference (CLEARCR). Thus the view tends to place the categorical measures of big value on the front-end of each variable axis and small value ones on the back-end.

Algorithm

The sequence of categorical measures is a key factor leading to the displays confusion of parallel sets. In general, if categorical measures of small values have too decentralized configurations, it may invisibly lead to display confusion.

Multidimensional data is defined as follows [10]:

Assume $G(F)=\{F^1,F^2,\cdots,F^m\}$ is a given object set of k-dimension (k>0). Among, m i is the set base, namely the number of multidimensional objects. $F^i=F^i(f_1^i,f_2^i,\cdots,f_k^i)(f_j^i\in R,f_j^i\geq 0)$ represents a k-dimension object of the set. $f_1^i,f_2^i,\cdots,f_k^i$ indicates the k-dimension attribute value of each object. For multidimensional attribute data table $G(F)$, F^i represents a record and f_j^i is its corresponding value.

Measurement of categorical measures is defined as [59]:

In consideration of variable $V_l(1\leq l\leq k-1)$ from multivariable data set of measurement attribute, assume $\{v_1,v_2,\cdots,v_n\}$ is n categorical measures of V_l. Then in the entire data set the measurement of any categorical values $v_i(1\leq i\leq n)$ can be represented as $Q(v_i)=\sum_{j=1}^{m}q^j\big|_{V_l=v_i}$, namely $Q(v_i)$ is the sum of all v_i categorical values variable that V_l is assigned. $Q(v_i)$ is named as the measurement of $v_i(1\leq i\leq n)$.

According to the above definitions, the corresponding degree and metric ratio of categorical measures is given.

Definition 1:

To categorical measures $\{v_1,v_2,\cdots,v_n\}$ of variable $v_i(1\leq i\leq n)$ in multivariable data table of measurement attribute $G(F)$, in the entire data set the corresponding degree with the adjacent variable's categorical measures any categorical measures $v_i(1\leq i\leq n)$ can be expressed as $D(v_i)$.

Definition 2:

To categorical measures $\{v_1,v_2,\cdots,v_n\}$ of variable $v_i(1\leq i\leq n)$ in multivariable data table of measurement attribute $G(F)$, the metric ratio of any categorical measures $v_i(1\leq i\leq n)$ value among all categorical measures of the variables can be expressed as $R(v_i)$.

On the basis of corresponding degree and quantity ratio of categorical measure, we re-compute measurement for each categorical measure as reference. Based on the ACLEARCR algorithm, we propose an optimized sorting algorithm targeting on the categorical measures of small value.

Table 1 Algorithm flow

1. Compute measurement:

According to ref. [9], calculate measurement of categorical measures on each variable axis in the Parallel Sets view.

2. Node Cluster:

Cluster method consults CLEARCR algorithm. Cluster layer by layer in accordance with top to bottom sequence of view variable axes. Change the weigh of categorical measures on the basis of conditions to form new layer G', and conduct optimization according to the improved ACLEARCR algorithm.

3. Re-compute measurement of categorical measures layer by layer:

3.1 . For the categorical measure $\{v_1,v_2,\cdots,v_n\}$ of the first initial variable V_1 of G, compute corresponding degree $D(v_i)$ of each categorical measure v_i and its adjacent variable's categorical measures, and record the categorical measures that relate;

3.2. For the categorical measure $\{v_1, v_2, \cdots, v_n\}$ of the first initial variable V_1 of G', compute quantity ratio $R(v_i)$ of each categorical measure v_i among all categorical measures of the variables;

3.3. Conduct layer variable sorting according to $D(v_i)$ and $R(v_i)$, thus receiving categorical measures sequence $sequence_i$. Compared with adjacent variable's categorical measures sequence $sequence_i$ and $sequence_{i+1}$, adjust the sequence on the basis of corresponding degree of each categorical measure recorded in 3.1, sorting the categorical measures by the rules that small values gather in the middle while big ones locates on both sides. The rest may be deduced by analogy to the categorical measures of all variables.

4. **Examine measurements in reverse:**

From the bottom to the top, according to 3, examine the measurement calculation of each categorical measure.

5. **Computation ends:**

Re-conduct **3** and **4** until the initial-set termination iteration condition reaches.

6. **View representation:**

Replace the old sequence with new categorical measures sequence and visualize each variable view.

From the description of the algorithm, two aspects has been improved to ACLEARCR:

(1) Variable of corresponding degree with adjacent variables had been introduced. Variables of time-varying multivariate data set usually relate with each other closely, which reflects fully on the categorical measures of different variables. When correspondence among categorical measures is out of consideration, sequence may not got optimized thus hard to form views with less confusion. Adding corresponding degree among different variables' categorical measurements is a representation of closely related variables, which fits for human being's cognitive habit.

(2) Consider quantity ratio that value of categorical measures occupies in all categorical measure values. Different categorical measures of each variable usually differ greatly. Considering metric ratio and sorting by the rules of small in the middle while big on both ends may avoid cognitive burden brought by big and small ones take place in turn. Centralization of small categorical measures makes for entire view representation.

Implementation

Prototype system hires SWT widget of Eclipse; operating system is Windows 7; configurations Intel(R) Core(TM) i5, 8 GB, ,500 GB hardware. Sales data from supermarket are used to prove the efficiency of the improved algorithm. Under the circumstances that the sequence of the variable axes is fixed and categorical measures keep still, we use the improved algorithm to optimize the categorical measures ranking, and compare the receiving views with the ACLEARCR and random arranged view.

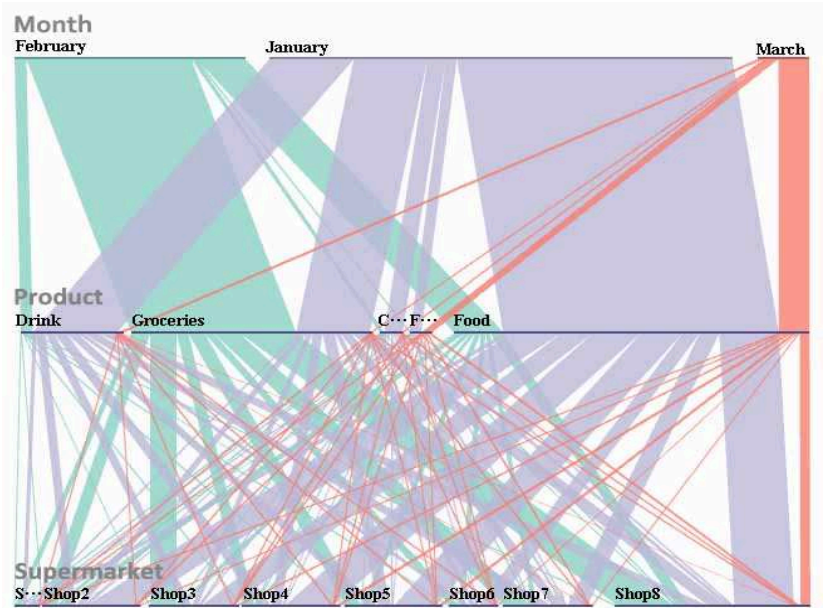

Fig.1 Random Arrangement

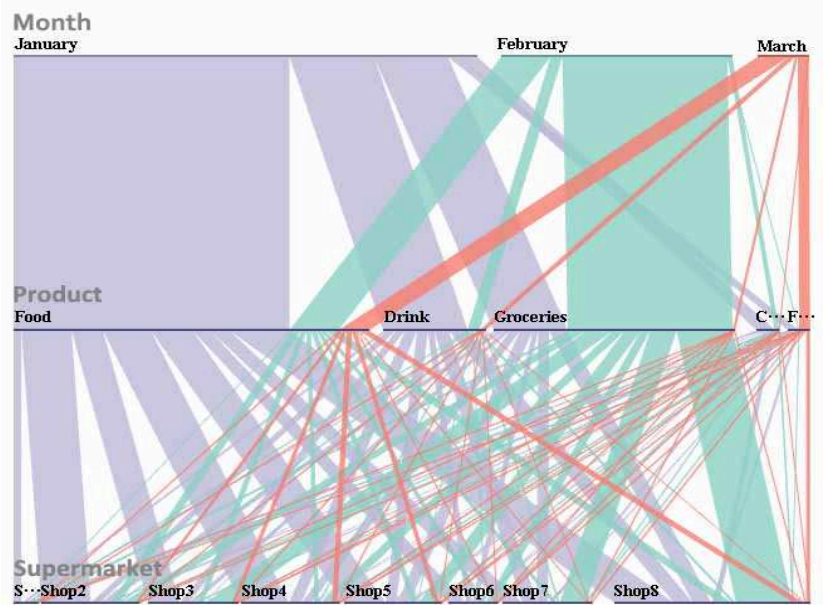

Fig.2 ACLEARCR

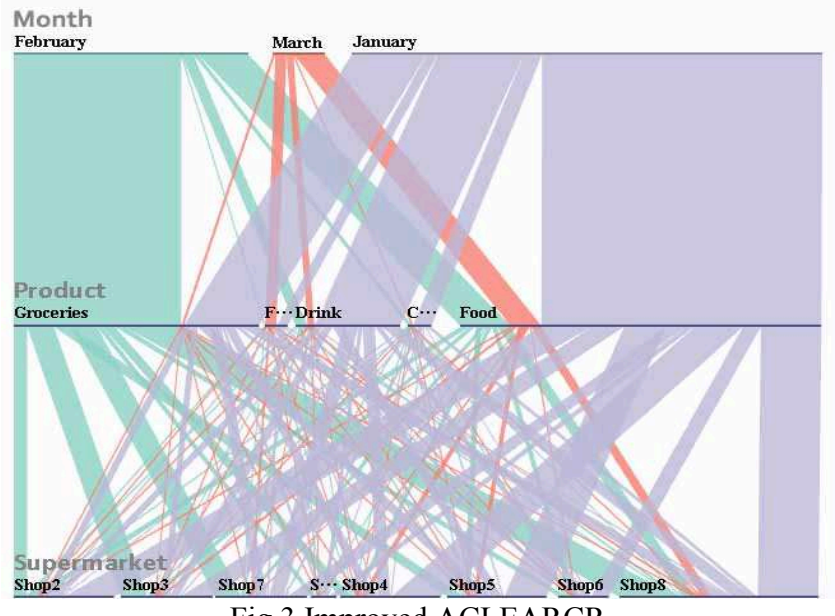

Fig.3 Improved ACLEARCR

From Fig .1, 2 and 3, it can be figured out that categorical measures ranks according to the rules that small ones gather in the middle while big ones on both sides. After optimized by ACLEARCR algorithm, re-ranking by the improved algorithm can make the view be prone to put the categorical measures of big value on both ends of each variable axis, and at meanwhile the small value ones and the ones of great correspondence with the others in the middle of the axes. From the transformation of the third variables it can be seen that ACLEARCR algorithm functions little when small value categorical measurement have many dividing values. However after considering measurement ratio and corresponding degree for categorical measures, the improved algorithm to a larger extent reduces the crossover occurrence of corresponding parallels, thus efficiently reducing visual confusion in the view.

Conclusion

This paper is based on the Advanced Categories Layout basEd on Average heuRistic with Cardinality Reduction (ACLEARCR), and proposes an optimization sequence algorithm aiming at categorical measures of small value. From the above analysis the improved ranking algorithm can obtain better visualization views compared with random arrangement and ACLEARCR algorithm. Therefore the advantage of the proposed ranking algorithm is proved.

Acknowledgements

Fund Project: National science and technology support plan (2012BAH08B01).

References

[1] Bora Beran, Catharine van Ingen, Ilya Zaslavsky, David Valentine．OLAP Cube Visualization of Environmental Data Catalogs．Microsoft Technical Report MSR-TR-2008-70, July 14, 2008.

[2] Alfredo Cuzzocrea, Domenico Saccà, Paolo Serafino．Semantics-Aware Advanced OLAP Visualization of Multidimensional Data Cubes．International Journal of Data Warehousing & Mining, 3(4), 1-30, October-December 2007.

[3] Jinguo You. A method of OLAP visualization research and its implementation [D]. Kunming: kunming university of science and technology. 2005..

[4] Lianyin Jia, Jianhua Hua, Qingxin Wang, Dongmei Zhu．An OLAP Tree Visualization Methods of Implementation [J]. Journal of Yunnan university (natural science edition), 2005(S2)：342~344.

[5] Xiaozhong Sheng. OLAP Visualization Method Based on Web Research [D]. Nanjing: Nanjing university of science and technology. 2006.

[6] Jinguo You, Yang Zhuoluo, Hu Jianhua, Xi Jianqing．A Multidimensional Support Large-scale Data Visualization Analysis Framework [J]. Computer engineering, Volume 37, Issue 19, October 2011.

[7] Yang Sun, Cheng Zhou, Daquan Tang, Weidong Xiao．With Classification Value Array Algorithm Improved the Parallel Sets [J]. Journal of Wuhan University, information science, Volume 36, Issue 2, February 2011.

[8] Weidong Xiao, Cheng Zhou, Yang Sun, Bin Ge, Daquan Tang． Improvement of Parallel Sets and its Application In Global Terrorist Attacks [J]. Journal of National University of Defense Technology, Volume 33, Issue 1, February 2011.

[9] Ningwei Sun, Haifeng Liu, Yu Zhao, Yong Liu, Lu Wang, Weidong Xiao. TVBPS：A Method Based On The Parallel Sets to Measure Properties of Multivariate Data Temporal Data Visualization [J]. Computer Application Research, Volume 31, Issue 5, May 2014.

[10] Yang Sun, Jiuyang Tang, Daquan Tang, Weidong Xiao． Improved Multivariate Data Visualization Methods [J]. Journal of software, 2010．21(6)：1462~1472.

Advanced Materials Research Vols. 989-994 (2014) pp 2323-2327
© (2014) Trans Tech Publications, Switzerland
doi:10.4028/www.scientific.net/AMR.989-994.2323

Evaluation of Ground Thermal Infrared Camouflage Using Pure Technical and Pure Scale Dynamic DEA Model

LI Ling[1,a], LV Xuliang[1,b], LI Bingzhen[1,c],LI Xiaopeng[1,d], WANG Huaixiao[1,e]

[1]College of Field Engineering, PLA University of Science and Technology, Nanjing 210007, China

[a]leonleeust@163.com, [b]xllu1957@126.com, [c]tylerlibz@gmail.com, [d]asmany@163.com, [e]15850717015@163.com,

Keywords: dynamic DEA; pure technical efficiency; pure scale efficiency; thermal infrared camouflage; evaluation

Abstract. For coping with modern thermal infrared reconnaissance, thermal infrared camouflage is becoming the hotspot of camouflage pattern research. Concerning the traditional methods on evaluating ground thermal infrared camouflage can't solve the "dynamic" problem and the pure technical as well as pure scale efficiency. This article established new models to figure it out. The new measure introduced time parameter to construct dynamic model, then it set up pure technical dynamic DEA model which supposed it had variable returns to scale. Through the relationship among technical, pure technical and pure scale DEA model, we can get the pure scale dynamic DEA model. Finally, an example was calculated which shows the application of the new models.

Introduction

The thermal infrared camouflage equipments can eliminate the targets' thermal infrared exposed character effectively in a tactical distance, reducing the probability of discovery, identification and enemy attack, which means a lot to the survivability of the military targets [1]. In such circumstance, a systemic and comprehensive method to evaluate the ground thermal infrared camouflage effect is of great significance [2]. Generally, a camouflage is usually selected based on a certain index, such as the investment of time, fund or camouflage effect. This kind of analysis is rough, qualitative and lack of practicality once involved multi index evaluation [3,4]. Currently, the methods for optimization primarily include AHP (analytic hierarchy process), FCE (fuzzy comprehensive evaluation method) and Grey-evaluation. However, it encounters problems determining the index weight such as strong subjectivity and obstacle of correlation constraint test [5]. DEA (Data Envelopment Analysis), a common and significant research method, is a relatively effective nonparametric method to evaluate DMU (Decision Making Unit). It can ignore the influence of evaluation index dimension, avoid the mutual restriction between the input and output index and effectively judge the relative effectiveness of DMUs [6,7]. The evaluation of ground thermal camouflage efficiency often comes to a time period, traditional DEA cannot deal with it suitably. Here, we extend it to dynamic one by introducing time parameters. Based on dynamic model, the paper changed constant returns to scale (CRS) to variable returns to scale (VRS). The new model which called pure technical dynamic DEA eliminated scale efficiency factor. Thus, technical efficiency was broken up to pure technical efficiency and pure scale efficiency, which provides more management information to supervisors.

Evaluation Index System of the Ground Thermal Infrared Camouflage

The camouflage effect need to be evaluated to examine whether it worked as expected. The thermal infrared camouflage effect evaluation index system of ground targets can be classified and analyzed from two aspects of input and output. The input can be sorted as: (1) Forces of operation (x_1): Corps of engineers camouflage unit involved in ground thermal infrared camouflage， takes single soldier as unit of measure for precision. (2) Time of operation (x_2): The time spend on carrying out the ground thermal infrared camouflage. Unit: hour. (3) Equipment of operation (x_3): The ground thermal infrared camouflage is complicated and has high demand on camouflage equipment. This

index refers to consumption of equipment. (4) Difference of average radiation temperature between camouflage target and background (x_4): The background of target is composed of many kinds of little background units with different thermal physical properties. The units with different thermal inertia formed a complicate thermal radiation distribution under sunshine [8]. Hence the difference of average radiation temperature between camouflage target and background is one of the indexes. (5) Difference of emissivity of two adjacent deformation spots (x_5): Object's radiation temperature is determined by surface emissivity. So we could use this index to quantify during the thermal infrared camouflage spots design [9].

The output can be described as: (1) Comprehensive similarity of thermal infrared image (y_1): the similar the thermal infrared recognition feature between target and background is, the better thermal infrared camouflage effects. The other way around works out as well [10]. (2) The similarity of thermal infrared radiation emissivity (y_2): if the thermal infrared radiation emissivity of target and typical objects in background is similar, then the bigger emissivity is the better camouflage effects [11].

Pure Technical Dynamic DEA

When evaluate the ground thermal camouflage, it often needs to evaluate the efficiency of a DMU in different time spot, which reflects the overall efficiency of the DMU in a period of time [12]. Introduce the time parameter into DEA model, set the number of DMU is n, in the t period the input and output indexes are respectively as follows:

$$X_j^t = \left(x_1^t, x_2^t, \cdots, x_n^t\right) = \begin{pmatrix} x_{11}^t \cdots x_{1j}^t \cdots x_{1n}^t \\ \cdots \quad \cdots \quad \cdots \quad \cdots \\ x_{i1}^t \cdots x_{ij}^t \cdots x_{in}^t \\ \cdots \quad \cdots \quad \cdots \quad \cdots \\ x_{m1}^t \cdots x_{mj}^t \cdots x_{mn}^t \end{pmatrix}_{m\times n} \quad Y_j^t = \left(y_1^t, y_2^t, \cdots, y_n^t\right) = \begin{pmatrix} y_{11}^t \cdots y_{1j}^t \cdots y_{1n}^t \\ \cdots \quad \cdots \quad \cdots \quad \cdots \\ y_{k1}^t \cdots y_{kj}^t \cdots y_{kn}^t \\ \cdots \quad \cdots \quad \cdots \quad \cdots \\ y_{s1}^t \cdots y_{sj}^t \cdots y_{sn}^t \end{pmatrix}_{s\times n}$$

On the basis of the introduction of time parameter, extend the DEA to a dynamic form. Dynamic C^2GS^2 model with non-Archimedean infinite small has been established, which considers the influence of scale efficiency. When we change the restrictions from CRS to VRS, pure technical dynamic DEA model can be built up as follows:

$$\begin{cases} \min\ [\sigma^t - \varepsilon(\hat{e}^T S^- + e^T S^+)] \\ \sum_{j=1}^{n} X_j^t \lambda_j^t + S^- = \sigma^t X_0^t \\ \sum_{j=1}^{n} Y_j^t \lambda_j^t - S^+ = Y_0^t \\ \sum_{j=1}^{n} \lambda_j^t = 1,\ S^- \geq 0\ ,\ S^+ \geq 0,\ \lambda_j^t \geq 0\ ,\ j = 1,2,\cdots,n \end{cases} \tag{1}$$

σ^t is the pure technical efficiency of DMU_0 in the *t* period. σ_j^t is the pure technical efficiency of DMU_j in the *t* period, j = 1,2,…,n. Thus the pure technical efficiency matrix of dynamic DEA can be given as σ_j^t.

$$\sigma_j^t = \left(\sigma_1^t, \sigma_2^t, \cdots \sigma_n^t\right) = \begin{pmatrix} \sigma_1^1 \cdots \sigma_j^1 \cdots \sigma_n^1 \\ \cdots \quad \cdots \quad \cdots \quad \cdots \\ \sigma_1^t \cdots \sigma_j^t \cdots \sigma_n^t \\ \cdots \quad \cdots \quad \cdots \quad \cdots \\ \sigma_1^T \cdots \sigma_j^T \cdots \sigma_n^T \end{pmatrix}_{T\times n} \tag{2}$$

Similarly, in order to evaluate pure technical efficiency of DEA of n DMUs in *T* period, set a new DEA unit[13]. The input vector is a unit vector which is 1×n and the output vector is the overall efficiency matrix of dynamic DEA (σ_j^t), to form a new DEA unit as below:

$$\begin{cases} \min\ [\beta-\varepsilon(\hat{e}^T S^- + e^T S^+)] = V_\sigma \\ \sum_{j=1}^{n} \lambda_j + S^- = \beta \\ \sum_{j=1}^{n} \sigma_j^t \lambda_j - S^+ = \sigma_0^t \\ \lambda_j \geq 0,\ j = 1,2,\cdots,n \\ S^- \geq 0,\ S^+ \geq 0 \end{cases} \tag{3}$$

Pure scale Efficiency Dynamic Evaluation

Infer from $\eta^* = \theta^* / \sigma^*$, η^* is the pure scale efficiency, θ^* is the overall technical efficiency and σ^* is the pure technical efficiency. Thus we can obtain the dynamic pure scale efficiency matrix as follows:

$$\eta_j^t = \left(\eta_1^t, \eta_2^t, \cdots \eta_n^t\right) = \begin{pmatrix} \eta_1^1 \cdots \eta_j^1 \cdots \eta_n^1 \\ \cdots \cdots \cdots \cdots \\ \eta_1^t \cdots \eta_j^t \cdots \eta_n^t \\ \cdots \cdots \cdots \cdots \\ \eta_1^T \cdots \eta_j^T \cdots \eta_n^T \end{pmatrix}_{T\times n} \tag{4}$$

$\eta_j^t = \theta_j^t / \sigma_j^t$， η_j^t is pure scale efficiency of DMUj in the t（$t = 1,2,\cdots T$）period, j = 1,2,⋯,n. Similarly, in order to evaluate pure scale efficiency of DEA of n DMUs in T period, set a new DEA unit. The input vector is a unit vector which is 1×n and the output vector is the overall efficiency matrix of dynamic DEA (η_j^t), pure scale dynamic DEA model can be given as:

$$\begin{cases} \min\ [\gamma-\varepsilon(\hat{e}^T S^- + e^T S^+)] = V_\eta \\ \sum_{j=1}^{n} \lambda_j + S^- = \gamma \\ \sum_{j=1}^{n} \eta_j^t \lambda_j - S^+ = \eta_0^t \\ \lambda_j \geq 0,\ j = 1,2,\cdots,n \\ S^- \geq 0,\ S^+ \geq 0 \end{cases} \tag{5}$$

Examples of Application

Take seven thermal infrared camouflage proposal of ground targets as an example to analyze its dynamic DEA efficiency in five periods (t=1,2,3,4,5). The dynamic evaluation data of DEA is shown in table 1.

The matrix of pure technical efficiency and pure scale efficiency can be given as below:

$$\sigma_j^t = \begin{pmatrix} 1 & 0.86 & 1 & 1 & 1 & 1 & 1 \\ 1 & 0.84 & 0.82 & 1 & 1 & 1 & 1 \\ 1 & 0.86 & 0.83 & 1 & 1 & 1 & 1 \\ 1 & 0.87 & 0.84 & 1 & 1 & 1 & 1 \\ 1 & 0.80 & 0.85 & 1 & 0.99 & 1 & 1 \end{pmatrix} \qquad \eta_j^t = \begin{pmatrix} 1 & 1 & 0.36 & 0.94 & 0.64 & 0.78 & 1 \\ 0.96 & 1 & 0.66 & 0.97 & 0.86 & 0.89 & 1 \\ 0.89 & 1 & 0.36 & 0.91 & 0.53 & 0.66 & 1 \\ 1 & 1 & 0.62 & 0.87 & 0.83 & 0.47 & 1 \\ 1 & 1 & 0.8 & 1 & 0.81 & 0.57 & 1 \end{pmatrix}$$

Table 1 DEA dynamic evaluation data of ground thermal infrared camouflage

t	DMUj	Input					Output		Efficiency	
		x_1	x_2	x_3	x_4	x_5	y_1	y_2	σ_j^t	η_j^t
t=1	DMU1	30	11	26	2	0.08	0.5	0.01	1	1
	DMU2	26	15	35	5	0.20	0.2	0.05	0.86	1
	DMU3	28	18	33	6	0.18	0.2	0.02	1	0.36
	DMU4	20	21	39	4	0.14	0.6	0.02	1	0.94
	DMU5	21	17	28	8	0.26	0.3	0.03	1	0.64
	DMU6	26	14	22	10	0.14	0.4	0.02	1	0.78
	DMU7	22	10	30	3	0.10	0.7	0.05	1	1
t=2	DMU1	28	10	23	2	0.07	0.6	0.02	1	0.96
	DMU2	24	14	32	4	0.19	0.3	0.05	0.84	1
	DMU3	26	17	30	5	0.17	0.3	0.03	0.82	0.66
	DMU4	18	20	36	3	0.13	0.7	0.03	1	0.97
	DMU5	19	16	25	7	0.25	0.4	0.04	1	0.86
	DMU6	24	13	19	9	0.13	0.5	0.03	1	0.89
	DMU7	20	9	27	2	0.09	0.8	0.05	1	1
t=3	DMU1	32	14	30	3	0.11	0.4	0.01	1	0.89
	DMU2	28	18	39	6	0.23	0.2	0.04	0.86	1
	DMU3	30	21	37	7	0.21	0.2	0.01	0.83	0.36
	DMU4	22	24	43	5	0.17	0.5	0.01	1	0.91
	DMU5	23	20	31	9	0.29	0.3	0.02	1	0.53
	DMU6	28	17	25	10	0.17	0.3	0.01	1	0.66
	DMU7	24	13	33	4	0.13	0.6	0.04	1	1
t=4	DMU1	34	17	32	4	0.14	0.5	0.02	1	1
	DMU2	30	21	42	8	0.27	0.2	0.03	0.87	1
	DMU3	32	24	39	9	0.24	0.3	0.01	0.84	0.62
	DMU4	24	27	45	6	0.20	0.4	0.01	1	0.87
	DMU5	25	23	34	10	0.32	0.4	0.02	1	0.83
	DMU6	30	20	28	11	0.20	0.2	0.01	1	0.47
	DMU7	26	17	34	5	0.15	0.5	0.03	1	1
t=5	DMU1	35	18	33	5	0.16	0.6	0.03	1	1
	DMU2	34	23	44	9	0.31	0.3	0.04	0.80	1
	DMU3	32	27	41	10	0.28	0.4	0.02	0.85	0.8
	DMU4	26	30	46	8	0.24	0.5	0.02	1	1
	DMU5	27	25	36	12	0.36	0.4	0.03	0.99	0.81
	DMU6	33	23	29	13	0.27	0.3	0.01	1	0.57
	DMU7	27	18	35	7	0.17	0.5	0.04	1	1

Table 2. Evaluation result of pure technical and pure scale dynamic DEA

DMUj	DMU_1	DMU_2	DMU_3	DMU_4	DMU_5	DMU_6	DMU_7
β_j	1	0.87	1	1	1	1	1
γ_j	1	1	0.80	1	0.86	0.89	1

Table 2 is the result of pure technical and pure scale dynamic DEA model. Except for DMU_2, the other six DMUs have high pure technical efficiency in the overall period. The dynamic DEA pure scale efficiency of DMU_1, DMU_2, DMU_4 and DMU_7 is 1, the others is less than 1.

Conclusion

Dynamic DEA model overcame the disadvantage of tradition DEA when the evaluation of ground thermal infrared camouflage had a time span. However, dynamic DEA had the restriction of CRS, which was influenced by scale efficiency. Alter the restriction of CRS to VRS, pure technical dynamic DEA was set up and the impact of scale factor could be avoided. Pure scale dynamic DEA was established through the relationship among overall efficiency, pure technical efficiency and pure scale efficiency. New models provided the managers more information. When the ground thermal infrared camouflage evaluation comes to network structure, dynamic model should be extended to network form, which will be the next research direction.

References

[1] Ji W Y, Hu J H and Li X G: Communications Science and Technology Heilongjiang. Vol. 31 (2007), p. 80-81.

[2] Chen X, Yuan J T and Yang L: Journal of Engineering Thermophysics. Vol. 28 (2007), p. 844-846.

[3] Li L, Liu J Y, Fu C Q, Wu Z J: Proceedings of the Second International Symposium on Intelligent Information Technology Application. Vol.2 (2008), p. 181-185.

[4] Xu Z S, Da Q L: Systems Engineering. Vol. 19, No. 6 (2001), p. 94-96.

[5] Wu J, Shi Q: Systems Engineering and Electronics. Vol. 28 (2006), p. 1541-1544, 1559.

[6] Wei Q L: Data Envelopment Analysis (Science Press, Beijing 2004).

[7] Feng X, Cui G Y, Song W: Proceedings of the Fifth International Conference on Internet Multimedia Computing and Service. 2013, p. 93-96.

[8] Tang S H, Zhu Q J, Su L H. Thermal Infrared and emissivity Separation Algorithm based on ALPHA difference spectrum. Journal of Infrared and Millimeter-wave, 2005, (04).

[9] Gu J X. Infrared Probe. Infrared, 2009, (03).

[10] Cao Y, Cai H N, Cheng H F. Thermal Infrared emissivity Analysis of Woodland Camouflage. Lazer and Infrared, 2008, (07).

[11] Zhu S Y, Yin Q, Zhang G X. Research on Assimilation of Multi-source track Meterorological Satellite Infrared Data. Journal of Infrared and Millimeter-wave, 2008, (05).

[12] Liu J Y, Li L, Wu Z J. Model of Camouflage Plan Evaluation Based on Interval Ex-efficiency DEA. Military Logistics and System Engineering, 2008, 22(3).

[13] Azizi H, Ajirlu HG: Applied Mathematical Modelling. Vol. 35 (2011), p. 4149–4156.

Advanced Materials Research Vols. 989-994 (2014) pp 2328-2331
© (2014) Trans Tech Publications, Switzerland
doi:10.4028/www.scientific.net/AMR.989-994.2328

2D numerical simulation of termal discharge in coastal area

XU Ting[1,2]

[1] Tianjin Research Institute for Water Transport Engineering, M.O.T, Tianjin 300456, China
[2] School of Environmental Science and Engineering, Tianjin University, Tianjin, China.

xuting1228@163.com

Keywords: 2D numerical simulation; termal dischage;temperature;coastal area.

Abstract: A two-dimensional depth-average temperature transport model was used to simulate the temperature diffusion and dissipation. It is done to analyze the temperature distribution under different cases. The results indicated that the general temperature rise (refer to present, the same as following) of the intakes is below 0.3℃ in Case 2\3\4\5, and the max is 0.78℃ in Case 1. According to the survey temperature at the project intake at present, it is 29.7℃, then the total temperature after the project is below 30.5℃. So the project is feasible for the water temperature.

1 Introduction

In water engineering fields, research on turbulent tidal flow and heat transport in coastal water is important for the purpose of solving the pressing problems involved in water resources, water quality, environmental protection and engineering design, etc[1-3]. The typical coastal water industrial background of the study for heat transport problems concerned in this paper is that the large-sized thermal/ nuclear power stations are frequently built in coastal zones or offshore areas near coastal water[4-5]. As an example, the project is situated at a bay in Indonesia.There are some existing outfalls and intakes presently in this sea area where the project being built locates in (Fig.1). The intakes of K1, K2, K3, K4 and POPKA, are mainly in north of this bay, and the outfalls is in south of the bay. The outfall and intake of KMI and KPI locate west of the project.The project needs to construct on 14,500 DWT coal import berth, one 8,000 DWT ash export berth, two 10,000~20,000 DWT liquid chemical berths, the water intake/outfall and other relevant facilities. According to the design parameter such as discharge volume, outfall water temperature provided, there are some cases of cooling water volume for model test, which is Case 1 (q=100,000m3/h, T=42℃), Case 2 (q=20,000m3/h, T=42℃), Case3 (q=30,000m3/h, T=42℃), Case 4 (q=5,000m3/h, T=43℃), Case5 (q=5,000m3/h, T=35℃).

In this paper, a two-dimensional temperature transport model[6-7] is developed to study the temperature distribution of design intake and other intakes in different cases especially. The model is performed to comprehend the influence of the project on temperature distribution around the sea area.

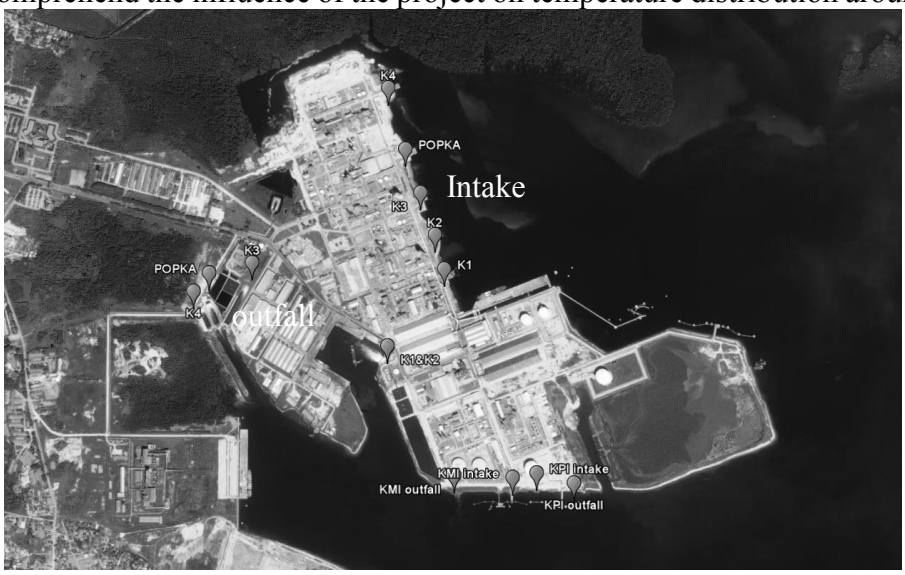

Fig.1 Location of Intakes and Outfalls

2 Mathematic model and setting

The current and cooling water draining advection-dispersion process in project sea area are studied by the plane two-dimensional mathematic model which developed by Danish Hydraulics Research Institute. It has been widely used in lots of projects recent years. The current model includes a continuity equation and two momentum equations. The fundamental equation is:

$$\frac{\partial \varsigma}{\partial t}+\frac{\partial p}{\partial x}+\frac{\partial q}{\partial y}=\frac{Q_s}{A_s} \tag{1}$$

$$\begin{aligned}&\frac{\partial p}{\partial t}+\frac{\partial}{\partial x}\left(\frac{p^2}{h}\right)+\frac{\partial}{\partial y}\left(\frac{pq}{h}\right)+gh\frac{\partial \varsigma}{\partial x}-\Omega q-fVV_x+gp\frac{\sqrt{p^2+q^2}}{C^2h^2}\\&=\frac{1}{\rho_w}\left[\frac{\partial}{\partial x}(h\tau_{xx})+\frac{\partial}{\partial y}(h\tau_{xy})\right]-\frac{h}{\rho_w}\frac{\partial}{\partial x}(p_\alpha)+Q_sU\sin(\Delta\theta)/A_s\end{aligned} \tag{2}$$

$$\begin{aligned}&\frac{\partial q}{\partial t}+\frac{\partial}{\partial x}\left(\frac{pq}{h}\right)+\frac{\partial}{\partial y}\left(\frac{q^2}{h}\right)+gh\frac{\partial \varsigma}{\partial y}-\Omega p-fVV_y+gq\frac{\sqrt{p^2+q^2}}{C^2h^2}\\&=\frac{1}{\rho_w}\left[\frac{\partial}{\partial x}(h\tau_{xy})+\frac{\partial}{\partial y}(h\tau_{yy})\right]-\frac{h}{\rho_w}\frac{\partial}{\partial y}(p_\alpha)+Q_sU\cos(\Delta\theta)/A_s\end{aligned} \tag{3}$$

Temperature advection-dispersion equation：

$$\frac{\partial}{\partial t}(hT)+\frac{\partial}{\partial t}(uhT)+\frac{\partial}{\partial y}(vhT)=\frac{\partial}{\partial x}(h.Dx.\frac{\partial T}{\partial x})+\frac{\partial}{\partial y}(h.Dy.\frac{\partial T}{\partial y})-\frac{KT}{\rho C_\rho}+S \tag{4}$$

Where ς is tide level, means the distance between water surface and datum plane, p, q is unit flux density in the x-direction, y-direction, h is water depth, g is gravitational acceleration, Ω is Coriolis parameter, ρw is water density, pa is atmospheric pressure, C is Chezy resistance number, $\tau_{xx},\tau_{xy},\tau_{yy}$ is component of shear stress in x-direction, y-direction, z-direction, f is wind friction factor, V,V_x,V_y is wind speed and the component in x-direction and y-direction, x,y is orthogonal coordinate, t is time, T is temperature, D_x, D_y is dispersion coefficient, in x-direction and y-direction, U is source discharge speed, $\Delta\theta$ is source discharge angle, S is source strength, $S=Q_s^*(T_s-T_o)/As, To$ is environment temperature, A_s is source discharge area, Q_s is source discharge flux, T_s is discharge temperature, K is sea level heat radiation synthesis coefficient, C_p is water specific heat.

The large and small scope model grids both adopt quadrangle grid, the grid step of the large model is 50m, and that of small model is 10m. The time step for large model and small model is 10s and 2s respectively.The manning resistance parameter, after multi-group debugging ascertained n=0.010～0.015. The diffusion coefficient is 5~15m^2/s according to lots of research results.

3 Numerical simulations and results

According to the design layout and parameters of the project, the water temperature field after the project process is simulated, and the temperature fields at flood and ebb tide are shown in Fig. 2. The water temperature in south of PKT byland is higher than that in north, which is similar to the water distribution at present. Because of the different discharge volume of design outfall in different Cases, there is difference among the Cases. The bigger the discharge volume is, the higher the water temperature is. The temperature of Case 1 is highest, and lowest in Case 4 and Case 5.

Fig.3 is shown the water temperature process in different Case at the CTA intake. From this figure, the water temperature is different during flood and ebb time, which is due to the current movement. The difference from max to the min value is about 0.6 ℃ in Case 1, and 0.1~0.2℃ in other Cases.In order to learn the temperature rise in CTA\KMI\KPI\PKT intake due to the CTA outfall discharge,

Tab.1 is shown the water temperature rise at different location. Compared with water temperature at present, in Case1\Case2\Case3\Case4\Case5, the temperature rise is 0.78℃\0.17℃\0.26℃\0.05℃\0.03℃ at CTA intake; the temperature rise is 1.36℃\0.43℃\0.60℃\0.13℃\0.06℃ at KMI intake; the temperature rise is 1.43℃\0.47℃\0.69℃\0.15℃\0.08℃ at KPI intake; the temperature rise is 0.26℃\0.05℃\0.07℃\0.02℃\0.00℃ at PKT intake.

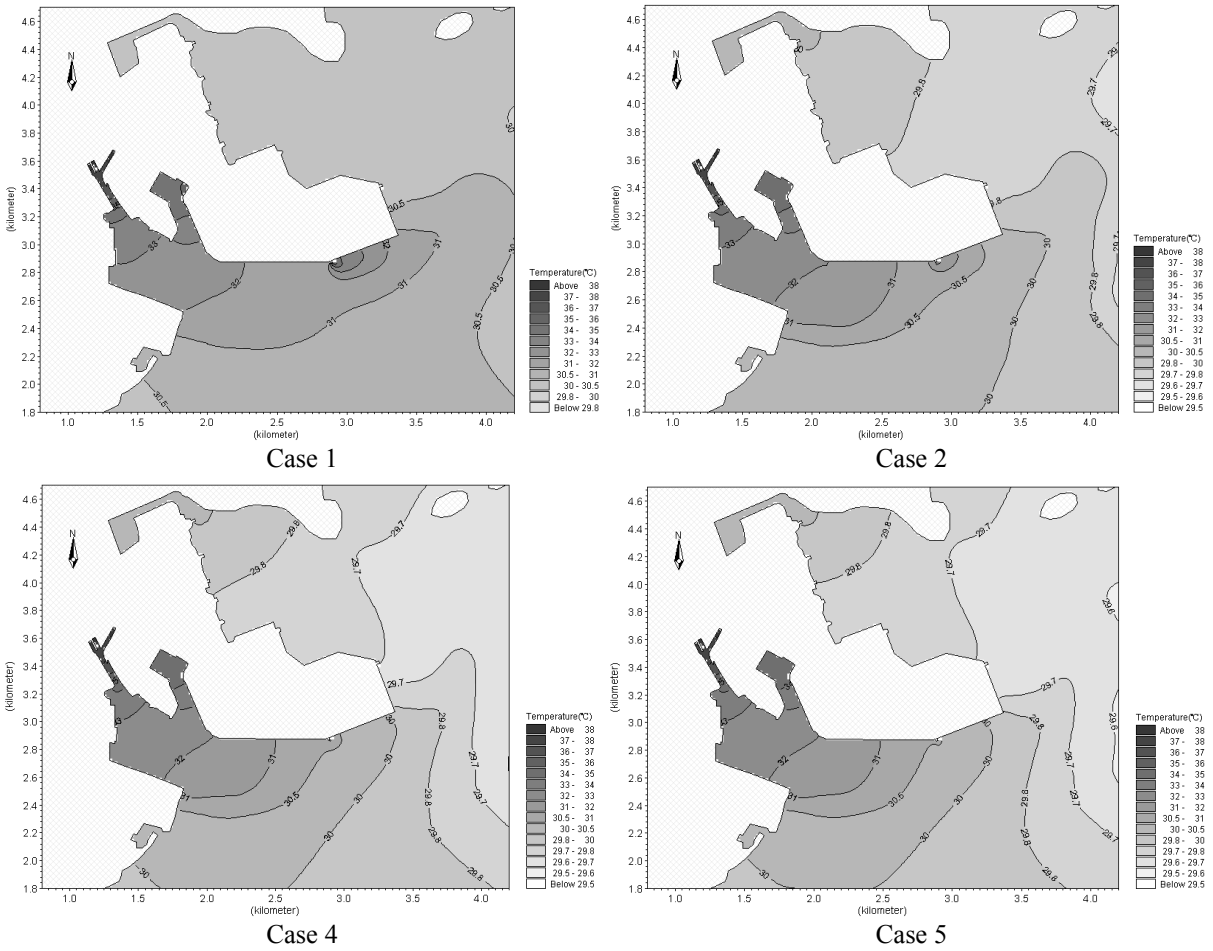

Fig.2 Water Temperature Distribution in Cases(ebb time)

For CTA intake, the general temperature rise is below 0.3℃ in Case 2\3\4\5, and the max is 0.78℃ in Case 1. According to the survey temperature at CTA intake at present, it is 29.7℃, then the total temperature after the CTA project is below 30.5℃. So the CTA project is feasible for the water temperature.For the influence to KMI and KPI intakes, as they are near the CTA outfall, the temperature rise is higher than other intake. However, with the decrease the discharge volume of CTA outfall, the temperature rise becomes lower. Especially, the temperature rise is about 0.1℃ in Case 4 and Case 5, and the value belongs to the simulation accuracy in model, which means that there is no influence to KMI and KPI in Case 4 or Case 5.. In addition, the intakes of KMI and KPI locate in deep water, so there is no influence.For PKT intake, the temperature rise is 0.26 ℃ in Case 1, and the temperature rise is below 0.1 ℃ in other Cases. So there is no influence except for Case 1.

Tab.1 Temperature Rise Compared with Present in different Location

Unit ℃

Design Parameter of CTA	Case	Case 1	Case 2	Case 3	Case 4	Case 5
	Discharge	100,000m^3/h	20,000m^3/h	30,000m^3/h	5,000m^3/h	5,000m^3/h
	Temp of Outfall	42℃	42℃	42℃	43℃	35℃
Location	CTA intake	0.78	0.17	0.26	0.05	0.03
	KMI intake	1.36	0.43	0.60	0.13	0.06
	KPI intake	1.43	0.47	0.69	0.15	0.08
	PKT intake	0.26	0.05	0.07	0.02	0.00

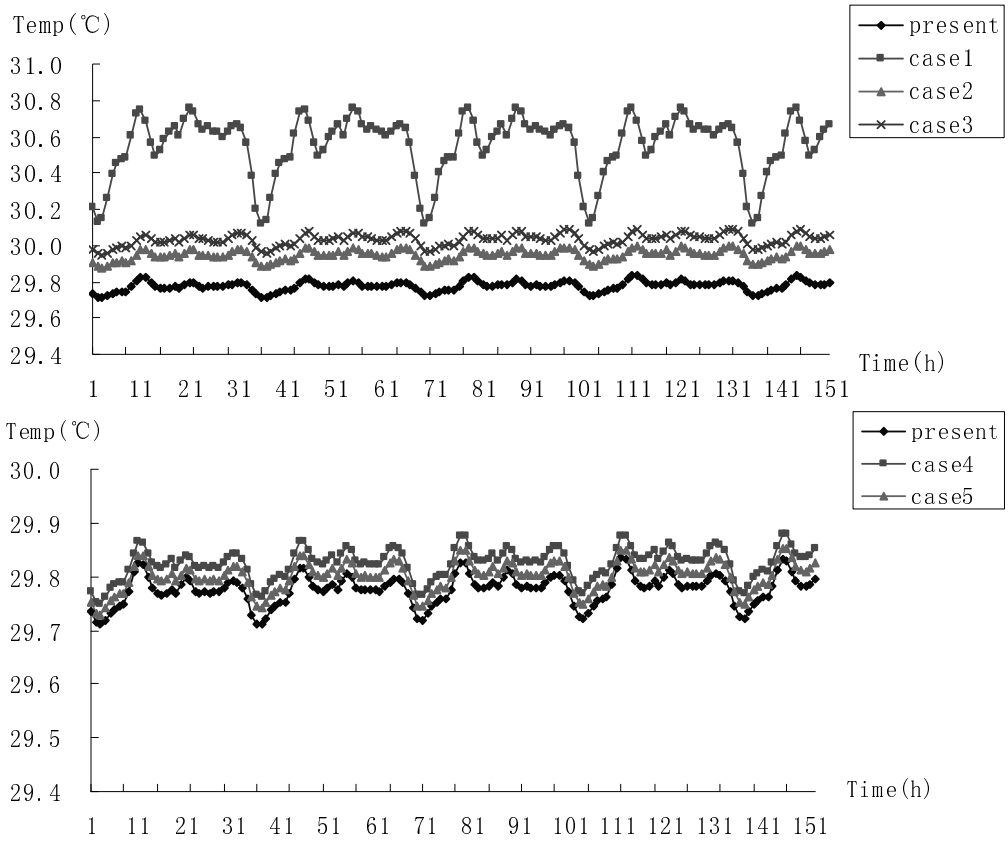

Fig.3 Water Temperature Process in CTA Design Intake

4 Conclutions

Studying by the 2D numerical simulation, the result showed that the project locates in a bay, at the mouth of which there are shoals and two channels, and the south is main channel of water exchange. The bay is divided two parts by the PKT factory area that likes a "byland" that make the water of two parts exchange rarely.The general temperature rise (refer to present, the same as following) of the intakes is below 0.3℃ in Case 2\3\4\5, and the max is 0.78℃ in Case 1. According to the survey temperature at the project intake at present, it is 29.7℃, then the total temperature after the project is below 30.5℃. So the project is feasible for the water temperature.

References

[1] Krebs, P., Armbruster, M., Rodi, W.: Laboratory experiments of buoyancy-influenced flow in clarifiers. J. Hydraul. Res. Vol 36(1998), No 5, pp831–851.

[2] Nystrom, J.B., Hecker, G.E., Moy, H.C., : Heated discharge in an estuary: case study. J. Hydraul. Div., Proc. ASCE Vol 107(1981), No 11, pp1371–1406.

[3] Ryan, J.P., Harleman, D.R.F., Stolzenbach, K.D., : Surface heat loss from cooling ponds. Water Resour. Res. Vol 10(1974), No 5, pp930–938.

[4] Patankar, S.V.. Numerical Heat Transfer and Fluid Flow.Hemisphere Publishing, New York. , 1980.

[5] Ackers, P.,. Modelling of heated water discharges. In:Parker, F.L., Krenkel, P.A. (Eds.), Engineering Aspects of Thermal Pollution. Butterworths, London, 1969

[6] Zhu J Z.Numerical simulation of 2D model of cooling water draining into the bay with strong tidal[J].Journal of Hydrodynamics,2007,22(1):17-23.

[7] Majr,zhang x y,zhang x n.Thermal buoyancy effect in two-dimensional cooling water mathematical models[J].Hydroscience and Engineering,2005(3):37-40.

Advanced Materials Research Vols. 989-994 (2014) pp 2332-2335
© (2014) Trans Tech Publications, Switzerland
doi:10.4028/www.scientific.net/AMR.989-994.2332

Study on settlement process of dredger under current force

XU Ting[1,2] , XIAO Zhong[2] ， SUN Liancheng[1]

[1] Tianjin Research Institute for Water Transport Engineering, M.O.T, Tianjin 300456, China
[2] Tianjin University, Tianjin, China.

xuting1228@163.com

Keywords: 3D numerical simulation; dredger; current force; settlement.

Abstract: A 3D-dimensional numerical simulation on the process of dredger under current force was carried out by using the finite element software ABAQUS, which is one of the most advanced nonlinear finite element softwares in the world.The interaction between the dredger and the seabed soil foundation is complex and the calculation considering the elastic-plastic property of soil belongs to strong nonlinear problem.The results indicated that the settlement of the dredger increase largely in the first times and the settlement tended to be stable with the times increasing. The stable value is 0.069 meters.

1 Introduction

W. D. Fairway suction dredger, normally working in the expended zone outside the main channel of Tianjin port at about 12:55 on March 8, 2007, was collided at the middle of its larboard with a Super-Large Container MSC JOANNA who was departing from the port. Bad damage induced the seawater to enter her several compartments and W. D. Fairway sunk. The location where W. D. Fairway suction dredger sunk lay in the sea area outside the deep trough of Caofeidian, where there is a rapid flow velocity caused by the flow and the sediment movement (Fig.1.The remote sensing image provided by the China-Brazil earth resources satellite on April 8, 2007). For the reappearance of the dredger sinking state, the simulation calculation about the buried depth of the wreck is studied in this paper.

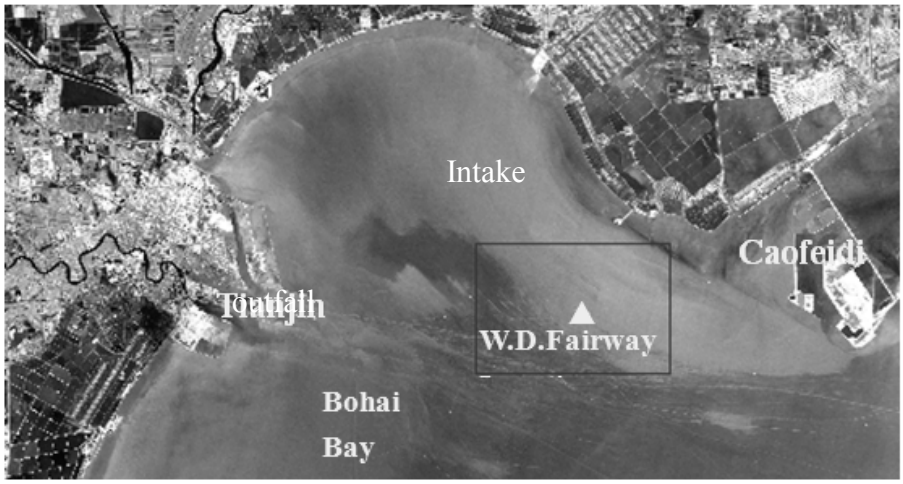

Fig.1. Location of W. D. Fairway suction dredger in the remote sensing image of the China Brazil earth resources satellite on April 8, 2007.

2 Study area and requirement

W. D. Fairway is the largest suction dredger at the present time, built in 1997 and accepted lengthening transformation in 2003 with details as follows: principal dimensions: Loa232.35m ×B32m×D16.85m×mTid- 13.65m, gross tonnage: 33423t, full-load displacement: 82910t, empty weight: 23112t, and deadweight tonnage: 59798t.When the dredger was tilted towards one side, the angle of the bow direction is about 299 degree, the left tilted angle is about 20 degree.The report numerically simulates the settlement volume and the settlement process of the submarine wreck under

the actions of the deadweight load, current load including the dynamical settlement of the wreck under the deadweight load, the wreck settlement of reciprocating current load, the wreck settlement caused by consolidation of softening soil, as well as the impact of seabed scour on the wreck settlement.

The result from the calculation and analysis of the tidal current in the wreck-zone shows that velocities and directions between ebb-tide and flood tide in the water zone occurs some changes. Usually, the flow-velocity in the direction of perpendicular to the hull is smaller, however, bigger crosscurrent maybe engendered in a shorter time. The current around the bow forms a circle flow, though its speed is not high.According to the related data, the chosen speed of the wreck zone is 1.5m/s.

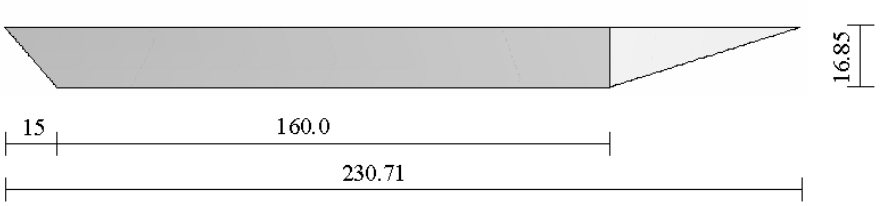

Fig.2. Elevation view of the hull numerical model (m)

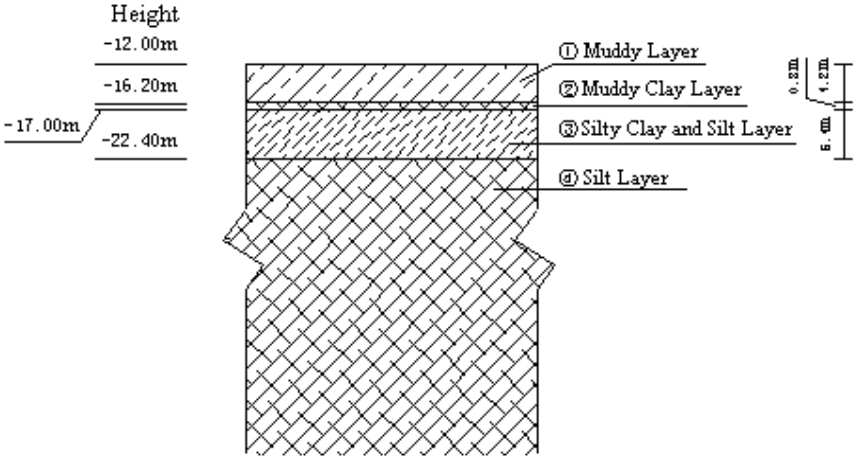

Fig.3. Profile chart of the chosen layer

3 Mathematic model and setting

In the report the numerical simulation was carried out by using the finite element software ABAQUS, which is one of the most advanced nonlinear finite element softwares in the world[1]. In order to simulate the coupling interaction process between the dredger and soils under deadweight, a 3D elastic-plastic finite element dynamic model is established and the explicit dynamic finite element method is used. Meanwhile, the contact surface is set up between the dredger hull and and the soils.

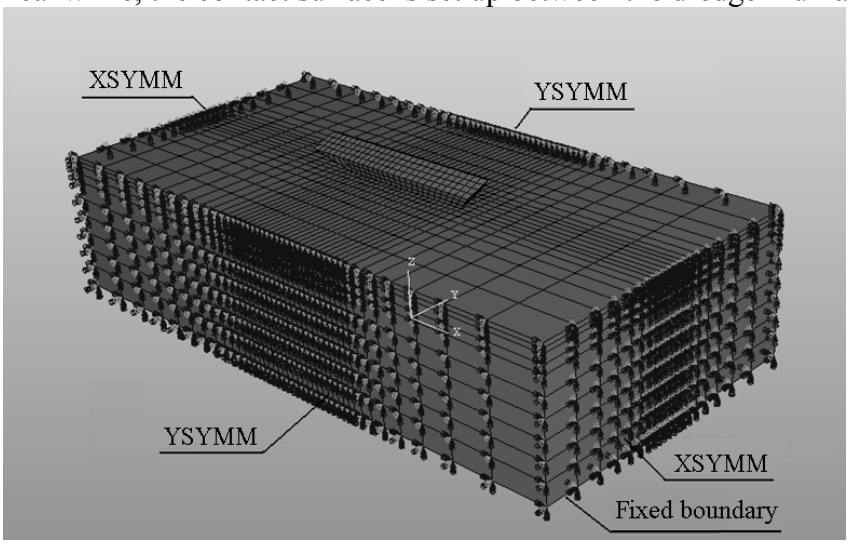

Fig. 4 Boundary conditions of calculation model

Plane graph of the calculation model is shown in Fig.2. The dimension of selected soil region in the direction of the dredger length is 692.13 meters, which takes three times of the dredger length L. The dimension in the perpendicular direction of the dredger length is 352 meters, which is eleven times of the dredger breadth B. The depth of the selected soil region is 160 meters, which takes five times of the dredger breadth B. The distribution of soil layers is as follows: silt layer with thickness 4.2m, muddy clay layer with thickness 0.8 m, silty clay layer with thickness 5.4m and silt layer with thickness 5.4m, as shown in Fig.3. The soil parameters in each soil layer are shown in Table1. The elastic modulus of each soil layer takes 10 times of the compression modulus of the soil layer in the calaulation.

4 Numerical simulations and results

4.1 Current force

The current force on the dredger is calculated according to the professional standard of P R China—Load Code for Harbor Engineering (JTJ215-98). The current force F_W is

$$F_W = C_W \frac{\rho}{2} V^2 A \qquad (1)$$

In which, F_W is the standard value of current force (kN). C_W is the current resistance coefficient. V is the design velocity of current which can adopt the biggest mean current velocity in the range of harbor engineering structures. ρ is the density of water, and it is 1.0 for freshwater and 1.025 for seawater. A is projected area of calculation component in the perpenticular plane of current (m^2).

According to the relevant regulations, the current resistance coefficient of the dredger can be calculated as a rectangular beam and the influence coefficient of submerged depth n_1 can be taken as 0.7. The current resistance coefficient is

$$C_W = 2.32 \times 0.7 = 1.624 \qquad (2)$$

According to the relevant tidal current data, the design velocity of current can be taken as 1.5 m/s and the corresponding current force F_W is

$$F_W = C_W \frac{\rho}{2} V^2 A = C_W \frac{\rho}{2} V^2 \times \frac{1}{2} \times h \times (L_B + L_{Surf}) \qquad (3)$$

In which, L_B is the length of hull bottom surface; L_{Surf} is the length of hull at water surface; h is water depth. Then,

$$F_W = 1.624 \times \frac{1}{2} \times 1025 \times 1.5^2 \times \frac{1}{2} \times 12 \times (160 + 208.85) = 4144.417kN \qquad (4)$$

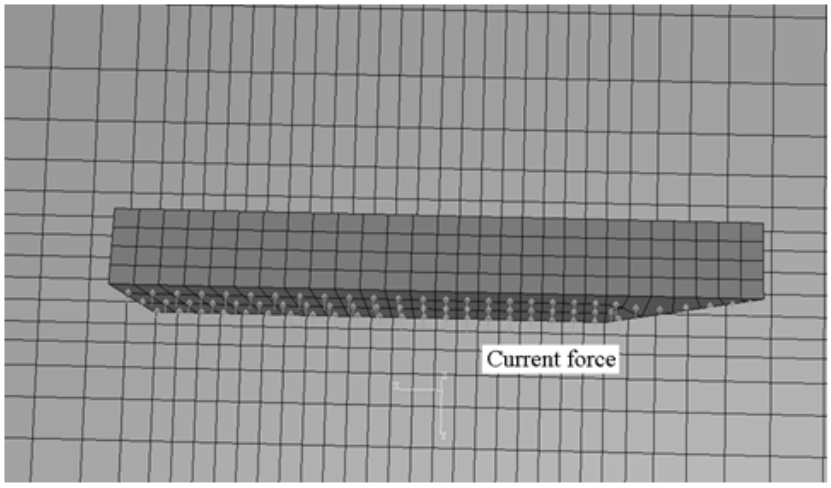

Fig.5 Current force on dredger

4.2 Calculation method

The dredger stranded as long as 33 days. Moreover, the interaction between the dredger and the seabed soil foundation is complex and the calculation considering the elastic-plastic property of soil belongs to strong nonlinear problem[2-5]. So if considering the current force on the dredger as a

dynamic load varying with time, it is unpractical under the current computer efficiency. In the simulation, the cyclically static calculations are adopted. That is, the current force, taken as a constant value, is applied on one side of the dredger and gained a settlement, and then the current force is applied on other side of the dredger and gained a new settlement. The procedure is repeated until the settlement reaches a stable value. With this procedure, The settlement curve of the dredger varying with action times of the current force is obtained, in which one time of the current force direction change is considered as one time of the current force action. In the simulation, N-R method, which is a changing stiffness iteration method, is adopted. In N-R method, stiffness matrix is regenerated at each iteration and it has better convergence than the constant stiffness matrix method, so the integration time step can be taken as a longer value. In the simulation, the current force on the dredger in shown in Fig.5.

4.3 Settlement of dredger under current force

The settlement curve of the dredger under current force is shown in Fig. 6. It can be seen that the settlement of the dredger increase largely in the first times and the settlement tended to be stable with the times increasing. The stable value is 0.069 meters.

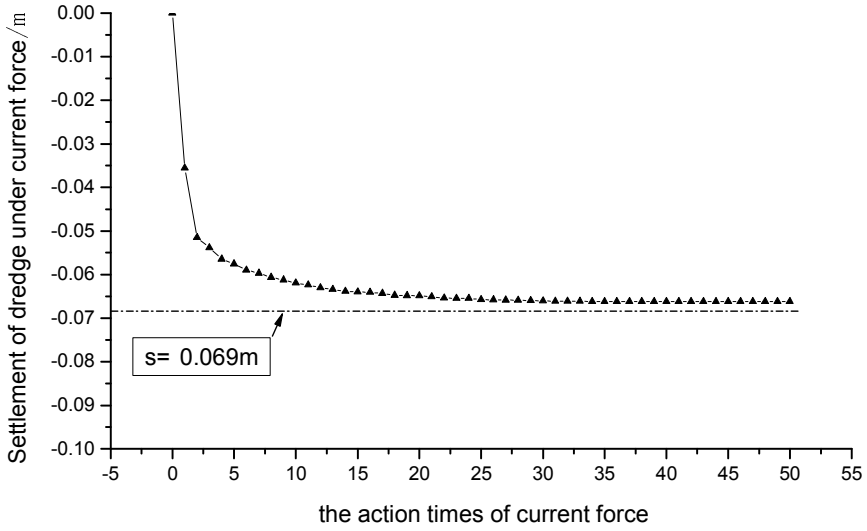

Fig. 6 Settlement curve of dredger under current force

5 Conclutions

Based on the 3D numerical simulation of ABAQUS, which is one of the most advanced nonlinear finite element softwares in the world, the settlement process of dredger under the current force was studied.The interaction between the dredger and the seabed soil foundation is complex and the calculation considering the elastic-plastic property of soil belongs to strong nonlinear problem.The results indicated that the settlement of the dredger increase largely in the first times and the settlement tended to be stable with the times increasing. The stable value is 0.069 meters.

References

[1] Hibbitt, Karison & Sorensen, Inc. ABAQUS Manuals-version 6.5[M]. USA: HKS Company, 2005.

[2] Zhujiang Shen. Engineering properties of soft soils and design of soft ground. Chinese Journal of Geotechnical Engineering, 1998, 20(1):100-111.

[3] Yin Huang, Inc. Analytical Study on the Static and Dynamic Properties of the Soft Soil in Kunming Area. Journal of Kunming University of Science and Technology (Natural Science Edition), 2003, 28(1): 45-48.

[4] Shengqun Liu, Inc. Experimental Investigation of Dynamic Behavior of Saturated Soft Clay. Railway Engineering, 2006, (10):68-70.

[5] Jiahuan Qian, Inc. Soil Mechanics Principle and Calculation. China WaterPower Press. 1996.

Advanced Materials Research Vols. 989-994 (2014) pp 2336-2339
© (2014) Trans Tech Publications, Switzerland
doi:10.4028/www.scientific.net/AMR.989-994.2336

The effect of enterprise business process reengineering fuzzy comprehensive evaluation

Song Ling, Chuanyu Ye

Water conservancy and Environmental Sciences China Three Gorges University Yichang China

Keywords: Process reengineering; Analytic hierarchical model; Fuzzy evaluation

Abstract. This paper analyzed the mechanism of the Enterprise business process reengineering(BPR) to study the performance of the development process, Determined the importance of process cost, process, quality, customer satisfaction to process performance, and on this basis, further established the effect factors layer of process reengineering evaluation index system and build the enterprise develop business process reengineering effect evaluation system. Finally, this article determine the weight of each evaluation index based on the attribute hierarchical model and empirical analyses by using fuzzy comprehensive evaluation method.

Introduction

Implementing BPR is a dynamic process of a enterprise towards the best approximation performance evaluation. It can help enterprise found the problems existing in the process of implementation BPR and make the enterpris obtain advantage in the fierce market competition.

Kuwairi spoke highly the important role of the performance appraisal in the process of BPR implementation and continuous improvement, etc. [1] BPR evaluation directly affects the objectivity of the evaluation results and effectiveness. Zhang Yunbo[2], Zhang Xinli[3] , Zhaoqian[4] , LinJian[5] and YangYang[6] etc research on evaluation index has achieved some results. In addition, research on evaluation method, the current use more includes data envelopment analysis (dea) method, analytic hierarchy process (ahp), grey clustering evaluation method, fuzzy comprehensive evaluation method, etc.

This paper designs the evaluation index system of enterprise BPR effect, by using the analytic hierarchical analysis model Determine the index comprehensive weights of factors layer, and Fuzzy comprehensive evaluation the effect of enterprise business process.

Building process evaluation index system

According to the principle of evaluation index system construction and reference for BPR evaluation index this paper establishes the BPR evaluation index system as shown in table 1.

Table 1 Effect of BPR evaluation index

target layer	rule layer	factors layer
the evaluation of business process (E)	the cost of the process (C_1)	the process cost of process (C_{11})
		resource cost (C_{12})
	the quality of the process (C_2)	percent of pass (C_{21})
		rejection rate (C_{22})
		rework rate (C_{23})
	customer satisfaction (C_3)	the satisfaction of timely delivery (C_{31})
		the satisfaction of price(C_{32})
		ratio of the warranty (C_{33})
		the ration of timely solve problem (C_{34})
	the efficiency of the Process (C_4)	the time of Business process (C_{41})
		the time of activity(C_{42})
		the time of Resource (C_{43})

Based on Analytic hierarchical model's assessment of BPR effect

Analytic Hierarchical Model is a new method for treatment of multiple attribute decision making put forward by professor Cheng Qiansheng based on analytic hierarchy process, it can effectively quantized the unfavorable quantitative variables to measure the objective event.Compared with the analytic hierarchy process AHM's requirements for consistency is lower, and consistency can be tested in the attribute judgment matrix. This paper USES AHM combined with fuzzy comprehensive evaluation method to study the effect of enterprise BPR, by using the attribute hierarchical model to determining the evaluation index weights of development process, and based on this, using the fuzzy comprehensive evaluation method to judge the comprehensive evaluation value of development enterprise BPR effect affected as The change of the various factors.

1. **Based on the AHM to determine evaluation index weights**

(1) Build the evaluation index system of BPR

(2) Constructing judgment matrix

Assignment the 1 ~ 9 scale according to the Satty put forward and constructing judgment matrix [7].

(3) Turn the judgment matrix into attribute measure matrix, and conversion formula is:

$$u_{ij}=\begin{cases}\dfrac{2k}{2k+1}\cdots a_{ij}=k.0.5\cdots a_{ij}=1, i\neq j\\ \dfrac{1}{2k+1}\cdots a_{ij}=\dfrac{1}{k}.0\cdots a_{ij}=1, i=j\end{cases}$$

(4) Judgment the consistency of the attribute matrix according to the following formula

Make $g(x)=\begin{cases}1, x>0.5\\ 0, x\le 0.5\end{cases}, I_i=\{j: g(u_{ij})=1, 1\le j\le n\}$

The sufficient and necessary condition of attribute judgment matrix u_{ij} has consistency is for any i, when I_i is not empty meet: $g(u_{ik})-g\left(\sum_{j\in I_I} g(u_{jk})\right)\ge 0, 0\le k\le n$

(5) Calculate the weight of each index

Calculate rule layer to tagert layer, as well as the factors layer to upper, namely the relative weight vector of the criterion layer is: $W_i=\dfrac{2}{N(N-1)}\overline{W}$ Among them $\overline{W}=\sum_{j=1}^{n}\bar{u}_{ij}$, $j=1,2,\cdots,n$, i is the number of elements in the layer.

(6)calculate the synthesis weights of the i layer to the j layer. $w_{ij}=(w_{i1}, w_{i2}, \cdots, w_{in})$

2. Using the fuzzy comprehensive evaluation method evaluation the effect of process reengineering.

(1) Certain factor set

Assumes that the evaluation object have n kinds of properties, and set each attribute of impact assessment object for c_i, and the set composed by n factors callde factor set, remember to $C=(c_1, c_2, \cdots, c_n)$.In this article $C=(c_{11}, c_{12}, c_{13}, c_{21}, c_{22}, c_{23}, c_{31}, c_{32}, c_{33}, c_{41}, c_{42}, c_{43})$.

(2) Determine the comment set

The results of fuzzy comprehensive evaluation described by fuzzy set v_j, the set component with various kinds of evaluation results called comments set V, and $V=(v_1, v_2, \cdots, v_m)$. v_j mean comments at all levels from high to low. In this paper, given $V=(v_1, v_2, v_3, v_4, v_5, v_6)$ and respectively is very good, very good, better, general, poor, very poor. Full points for 100 and Corresponding set of points is $F=(f_1, f_2, f_3, f_4, f_5, f_6)=$（100-90，89-80，79-70，69-60，59-50，49-0）.

(3) Determine the evaluation matrix

Suppose the membership degree of factor c_i to factor v_j of the Comment set is r_{ij}, the evaluation of factor c_i to things is: $r_i = \left[\frac{r_{i1}}{v_1} \quad \frac{r_{i2}}{v_2} \quad \cdots \quad \frac{r_{in}}{v_n}\right]$

r_i is fuzzy evaluation set of comment set V and Shorthand for $r_i = (r_{i1}, r_{i2}, \cdots, r_{im})$, it reflects the degree of take comments v_j of things to factor c_i.

Assume that in the evaluation of the BPR effect of an enterprise, to the process cost experts give the proportion of evaluation very good, good, better, general, poor, very poor 45%，20%，15%，10%，5%，5% respectively, and $R_1 = (0.45, 0.20, 0.15, 0.10, 0.05, 0.05)$ as the evaluation set of the change of process reengineering process cost to the function of enterprise business process performance index.

The fuzzy comprehensive evaluation matrix formed by the single factor evaluation set is: $R = \begin{bmatrix} r_{11} & r_{12} & \cdots & r_{1m} \\ r_{21} & r_{22} & \cdots & r_{2m} \\ \vdots & \vdots & \vdots & \vdots \\ r_{n1} & r_{n2} & \cdots & r_{nm} \end{bmatrix}$

（4）Comprehensive evaluation

Actually evaluation matrix is a fuzzy relationship of set M and evaluation, given a fuzzy relation R of U to V, and considering the weight of each evaluation factor W will get the comprehensive evaluation of each evaluation index. Namely: $A = WR$

（5）The evaluation index processing

According to the principle of maximum membership degree, turn the fuzzy subset A into specific evaluation results. The determination comments of evaluation objects as follows: $a = \max_{1 \le i \le m} \{a_i\}$

Case analysis

Use AHM fuzzy comprehensive evaluation method to analyze and evaluation an enterprise BPR effect

（1）Using the AHM determining weights of evaluation indexes

According to the calculation results, the weight coefficient of rule layer respectively: $_1$=0.446, w_2=0.327, w_3=0.173, w_4=0.054

The Comprehensive weight coefficient of factors layer respectively: w_{11}= 0.064, w_{12}=0.382,w_{21}=0.193,w_{22}=0.109,w_{23}=0.025,w_{31}=0.053,w_{32}=0.078,w_{33}=0.009,w_{34}=0.033, w_{41}=0.006, w_{42}=0.018,w_{43}=0.03

（2）Build a fuzzy evaluation matrix

According to experts on research development process reengineering leads to resource changes and the scores of process performance indicators to improve get fuzzy comprehensive evaluation matrix: R

(3) Fuzzy subset: $A = WR = [0.347 \quad 0.337 \quad 0.110 \quad 0.100 \quad 0.100 \quad 0.005]$

So, the reconstruction effect of the enterprise research development process have a good memnbership for v_1，according to the principle of membership degree maximum ，the effect of the research development process reengineering of this enterprise is very good.

Reference:

[1]Kuwaiti ME, Kay J M. The role of performance measurement in business process reengineering [J]. International journal of operations & production management,2000,20(11):1411-1426

[2]Zhang Yunbo etc. Quantitative analysis of small and medium-sized enterprise process reengineering effect. 2001(9):119-124.

[3]Zhang Xinli,Runyan etc. Business process reengineering and operation cost system. China Township Enterprises Accounting. 2006:11-12.

[4]Zhaoqian. The optimal game equilibrium solution of enterprise BPR. Journal of shandong light industry institute. 2007(9):92-102.

[5]Lin Jian, Zhang Guogang. An empirical study on use management thought reconstruction enterprise processes. Journal of changsha railway institute. 2001,19(4):41-46.

[6]Yang Yang etc. The business process quality evaluation method. Journal of northwest university(Natural science edition). 2003(7):531-534.

[7]Saaty T L, Vargas L G.,Estimating technological coefficients by the analytic hierarchy process, Socio Economic Planning Sciences, no. 6(1979).

Advanced Materials Research Vols. 989-994 (2014) pp 2340-2343
© (2014) Trans Tech Publications, Switzerland
doi:10.4028/www.scientific.net/AMR.989-994.2340

A New Highway Safety Model based on Cellular Automata

Li Lixing

Department of electric power engineering, North China Electric Power University, Baoding, China

Email: lilixing123123@gmail.com

Keywords: traffic flow, Cellular automata, danger index, safety evaluation

Abstract: With the growth of the total mileage of highway. There is great importance in studying highway safety. At the present time, there are little research on traffic safety with the consideration of the Keep-Right-Except-To-Pass Rule, which requires drivers to drive in the right-most lane unless they are passing another vehicle. Based on Cellular Automata, this paper constructs a new model of highway safety with the consideration of the particular Rule. To evaluate the safety of the road, the model proposes a new index based on energy conservation law. After the simulation, the result shows the best traffic density to balance the safety and traffic flux is 20.1133veh/km.

1 Instruction

With the development of the infrastructure in china, total mileage of highway is increasing rapidly. In China, multi-lane highways often employ a rule that requires drivers to drive in the right-most lane unless they are passing another vehicle, in which case they move one lane to the left, pass, and return to their former travel lane. The influence of this rule is rarely mentioned in current study. There is practical significance in construct a traffic model in this particular rule.

Cellular automata model is a powerful tool to solve the problem of nonlinear in recent years. It can simulate the complex phenomenon with simple rules, and easily to implement on computer. As a consequence, it gets rapid development and extensive application, and it is more and more important in guiding the optimization of traffic flux [1-3]. This model can simulate the traffic condition in particular rules perfectly.

2 Modeling

The model defines a two- lane discrete cellular chains that are one dimensional to indicate a two-lane freeway, and there are 250 cells in each discrete cellular chain.

If each cell's actual length is 6m, then the simulation of the actual path length is 1500m. The road is divided into cells which can be either empty or occupied by a car with a velocity. A matrix represents those cellular chains in the programming.

Inspired by the Nagel and Schreckenberg model (NaSch) established in [4-5], we set 4 rules in this model. There are acceleration rule, lane changing rule, deceleration rule, randomization rule and position update rule.

As for acceleration, the vehicle's speed v_n is shown in (1).the driver drives on the former travel lane under the original speed, and always make it first choice.

$$v_n \to \min(v_{\max}, v_n + 1) \tag{1}$$

As for lane changing rule, if the vehicle meet these following demands , but can't accelerate ,he or she will chose to change lane, and then must return to his former lane.

$$\begin{aligned} &d_n < \min(v_n + 1, v_{\max}) \\ &d_{n,other} > d_n \\ &d_{n,back} > d_{safe} \end{aligned} \tag{2}$$

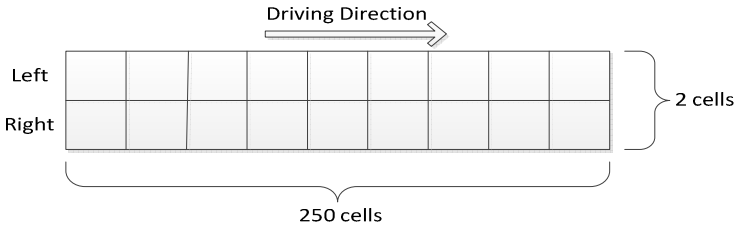

Fig.1 A two-lane cellular freeway

As for deceleration, the vehicle's speed is shown in (3). The driver have no choice but to decelerate on the former lane.

$$v_n \to \min(v_n, d_n) \tag{3}$$

As for randomization, the vehicle's speed is shown in (4). Considering the accidental factor of the driver. Every vehicle on this freeway will decelerate with probability p.

$$v_n \to \max(v_n - 1, 0) \tag{4}$$

As for position update , the vehicle's position is shown in (5). And the model updates the status vehicle by vehicle.

$$x_n \to x_n + v_n (n \to n+1) \tag{5}$$

Under the rules of the above five, the car's speed and position will change with time. But the speed of the car always less than the maximum speed limit.

There are running lane (slow lane) and overtaking lane (fast lane) in a two-lane freeway. The orders to execute these rules are different in two lanes. The difference is shown in fig.2

These factors describe the freeway traffic performance: traffic performance f , traffic safety D and the vehicles average passing time t . They can be used to describe the traffic performance.

3 Danger index

The model use the danger index to evaluate the safety of the freeway. It is inspired by energy conservation law. Since we assume all vehicles are identical, the lost energy E is a function of speed v.

$$E = \frac{1}{2} m v_1^2 - \frac{1}{2} m v_0^2 \tag{6}$$

Where v_1 is the speed after declaration and v_0 is the speed before declaration. And we define the danger index of a single vehicle as equation (7).

$$h_n = v_1^2 - v_0^2 \tag{7}$$

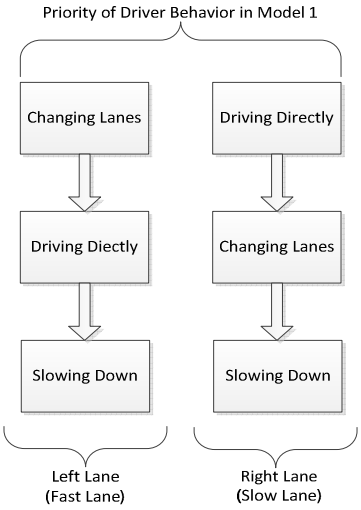

Fig.2 The priority of the left lane and right lane

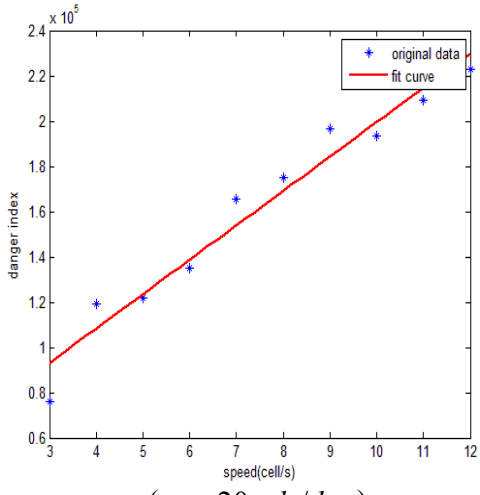

($\rho = 20veh/km$)

Fig.3 Danger index in different speed limit

Where v_1 and v_0 has the same definition as it referred above. Where h_n denotes danger index of a single vehicle. The sum of h_n from one freeway in an hour is this freeway's danger index D.

$$D = \sum_{t=1}^{3600} \sum_{n=1}^{N} h_n \tag{8}$$

N is the whole number of vehicles on one freeway.

Therefore, we establish model 1, and its programming course can be seen in the following diagram.

4 Analysis of the model

Danger index in different speed limit. As we can see in Fig.3, the danger index trend to increase when we raise the speed limit.

When traffic density is fixed, the number of vehicles N is also fixed. The freeway's danger index D is determined by every single car's danger index h_n. The density we use in our simulation is $\rho = 20veh/km$ which indicates light traffic. The gap between vehicles is big enough. In most condition, the driver only need to slow down 1cell/s. The calculation of a single vehicle is shown as following:

$$h_n = v_n^2 - (v_n - 1)^2 \tag{9}$$

$$h_n = 2v_n - 1 \tag{10}$$

We can see a liner relationship between h_n and v_n. Just like the figure.

Factors that affect the traffic flow. The Fig.4 indicates that when the traffic density lower than optimal traffic density, the vehicle is in 'free driving' state, which means cars can drive with only slight deceleration. Average velocity will be high. And the traffic performance will soar with density increasing. After traffic density exceeding the optimal traffic density, the car-following phenomena appears on the freeway. The speed is restricted. The traffic performance will decrease with density increasing. The highest traffic performance appears when density reaches the optimal point.

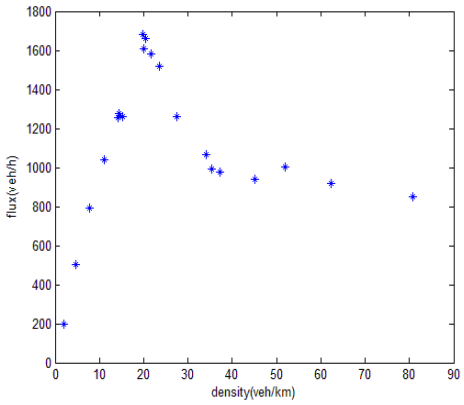

Fig.4 Traffic flow in different density

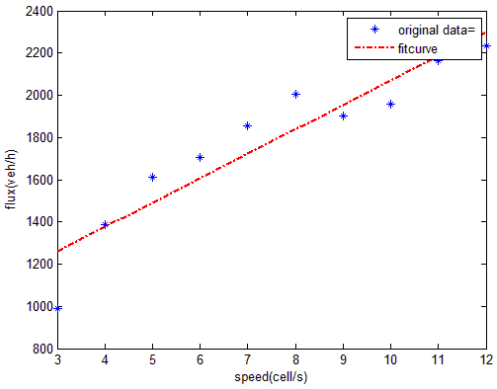

Fig.5 Traffic flow in different speed limit

Fig.5 shows the relationship between speed limit and traffic performance. It's obvious that traffic performance is proportional to speed limit.

According to the analysis, the greatest traffic performance is this:

$$f_{\max} = \frac{3600\rho L}{1000\dfrac{L}{6v}} \tag{11}$$

Where $f_{\max}$ is traffic performance, v is speed limits and ρ is traffic density. The relationship between traffic performance and speed is linear, as we can see in fig.5. And the data are all lower than their extreme value. Such as when v=3 cells/s, the traffic flux shows below 1296veh/h which it is 1003veh/h.

Optimization of traffic flow. The Fig.4 shows that the danger index increases when traffic is denser. That indicates highway safety and traffic flux are contradictory. So it's a problem to find an optimal density to get the best performance of the freeways. Since this model has already quantified the degree of the danger on this freeways, we can change this problem into a multi objective optimization problem.

The Topsis method[6] is used to solve this multi objective optimization problem.

To preform Topsis method, we standardize the data we have obtained by (12).

$$y_n = \frac{x_n - x_{\min}}{x_{\max} - x_{\min}} \tag{12}$$

x is the data we have and y is the standardized data.

After standardization, we make traffic density as abscissa and danger index as ordinate. Since we hope the danger index smaller and the traffic performance greater, we calculate the distance from data point to (0, 1) to find the shortest one. The equation is:

$$I = \sqrt{x^2 + (1-y)^2} \tag{13}$$

Where x is standardized danger index, y is standardized traffic performance and I is distance we called value index. The result shown as Fig.6.

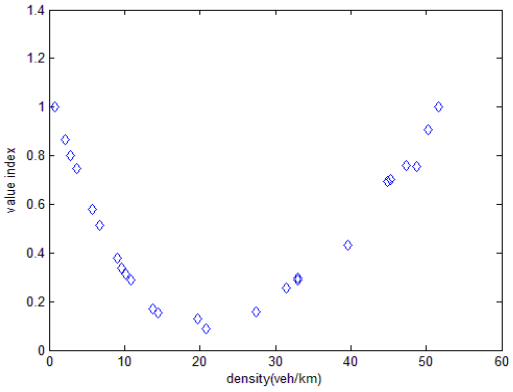

Fig.6 Value index with different traffic density

The smallest value index shows up when traffic near 20veh/km, which is 20.1133veh/km. At this point, the freeway shows smaller danger index which is 10423 and greater traffic performance which is 1608veh/h.

5 Conclusion

Taking into account the impact of Keep-Right-Except-To-Pass Rule, this paper construct a new model of highway traffic based on Cellular Automata. Inspired by energy conservation law, this paper proposes the danger index to evaluate the safety of highway. This model find a linear relationship between danger index and speed limit. Traffic flow and speed limit also has a linear relationship. And the optimal traffic density is 20.1333veh/km.

6 Reference

[1].Yongming Wang,Leishan Zhou,Yongbo Lv, Based on the elastic safe lane changing distance of cellular automata traffic flow model[J].Journal of System Simulation .2008,20(5),1159-1162.
[2].W.Knospe, L.Santen, A.Schadschneider and M.Schreckenberg, J.Phys.A33, 477(2000).
[3].Zhonggeng Han,Xiaoli Guo,Jianping Du,Jingxu Liu. American college students Mathematical modeling contest questions analysis and research. Beijing. High education press.2013.
[4].K.Nagel and M.Schreckenberg, J.PhysiqueI2, 2221(1992).
[5].W Knospe†, L Santen. A realistic two-lane traffic model for highway traffic [J]
[6].Zhonggeng Han, Mathematical modeling method and its application [M].Beijing. High education press.2008

Advanced Materials Research Vols. 989-994 (2014) pp 2344-2348
© (2014) Trans Tech Publications, Switzerland
doi:10.4028/www.scientific.net/AMR.989-994.2344

A Model for Seat Allocation of Railway Passenger Transport Based on OD's Priority

Yingting ZHU[1, a], Fuzhang WANG[2, b*], Xinghua SHAN[2, c], Xiaoyan LV[2, d]

[1]Railway Technology Research College, China Academy of Railway Science, Beijing 100081, China

[2]Institute of Computing Technologies, China Academy of Railway Science, Beijing 100081, China

[a]zhuyingtinglm@163.com, [b]wfzh@rails.cn, [c]shanxinghua@vip.sina.cn,[d]lvy718@126.com

Keywords: seat allocation; optimization; revenue management; railway transportation

Abstract. Based on the seat inventory control method of revenue management in airline, the author researches the optimization strategy on the seat inventory control in railway passenger transport. The author proposes one optimization model for seats allocation, which is to allocate seats by calculating the value to determine the order of getting seats for each OD under the analysis of the interaction among all trains running on the same rail lines and those trains' demands intensity. The experiment results show that this new model can be used to allocate seats for the train with multiple stations rapidly and appropriately. In comparison with the method without considering the value of each OD, the model based on OD's value can get better results.

Introduction

Revenue management originated in airline of USA in the 1980s, it is defined as selling the right products to the right people at the right price [1]. Inventory control is one of the most important components of revenue management. In railway passenger transportation, seat allocation is just similar to inventory control. China passenger railway network is characterized with many stations, long distances among stations, multiple train type and seat type, which makes it complex to allocate seats. There have been many scholars focusing on seats allocation in China passenger railway. For example, X.M. ZHANG studied seats allocation strategy supposing ticket price is dynamic in China railway [2]. For the case of multi-leg in airline which is similar to railway, Q. GAO established a stochastic programming model to maximize the total revenue, and solved that model by genetic algorithm [3], but it is still complex and is not suitable for large transport network such as China passenger railway. Other papers such as [4] and [5] studied new methods to allocate seats for China passenger railway based on its actual business, but there are some drawbacks in China passenger railway's business that many parameters come from technical staff's set up without computing, so they may not get the maximum revenue through those methods in [4] and [5].

Therefore, we proposed a new model of seat allocation for China railway passenger transport based on OD's priority or OD's value. OD's priority is the result from analysis of the interaction among trains in the same OD and on the same date. Our model can allocate seats efficiently, reducing manual intervention to seat allocation and increasing the total expected revenue.

Algorithm of Calculating OD's Priority

Nowadays dynamic virtual nested strategy is the mainly way used for seat inventory control in airline, which is the combination of virtual nested control and bid-prices control [6, 7]. A bid-price control sets a threshold price, such that a request is accepted if its revenue exceeds the threshold price and rejected if its revenue is less than the threshold price. A virtual nested control allows each ODF (Origin-Destination Fare) to be nested, and it first defines a set of indexes for each leg. The index represents a range of fare which is named as net leg fare [8], and then those companies use EMSR (Expected Marginal Seat Revenue) or other methods to compute booking limit and protect level of each ODF on each leg [9].

Methods of Computing OD's Priority or Value in Passenger Railway. Since ticket price is static in China railway, it is not suitable to set priority for OD using the similar concept based on net leg fare. For rail, since there are so many trains running on the same line and on the same date, while number of running trains is different in different periods. Therefore, this article firstly summarized all available seats of a line, then split one day into several periods, and computed number of seats in each period, finally computed OD's value according to OD's demand intensity.

Assume that there are *n* stations on a line and the interval is Δt, and then there are *n-1* legs, C_n^2 pairs of OD denoted as $OD_j, \mathrm{j} = 1,2,\cdots,C_n^2$, and one day is divided into $\mathrm{T} = 24/\Delta\mathrm{t}$ segments. To analyze influence to seats allocation coming from demand intensity on the same OD in different periods, trains are grouped by their running time $\mathrm{t}, \mathrm{t} = 1,2,\cdots,\mathrm{T}$. Supposing total number of trains running on OD_j is R_j and number of trains on OD_j in period *t* is r_{tj}, then

$$\sum_{t=1}^{T}\sum_{j=1}^{C_n^2} r_{tj} = R_j \quad t = 1,2,\cdots,T; j = 1,2,\cdots,C_n^2 \tag{1}$$

Assume that capacity of all trains running on OD_j is c_j, fare is p_{tj} and the forecasted demand is d_{tj} in period *t*, then total capacity of OD_j *is* $C_{tj} = r_{tj}c_j$, total demand of OD_j is $D_{tj} = r_{tj}d_{tj}$ and total revenue of OD_j is $P_{tj} = p_{tj}d_{tj}$ in period *t* of OD_j on the same date. We denote the contribution of OD_j to the line in period *t* as P_{tj}:

$$f_1(p_{tj}, d_{tj}) = \frac{P_{tj}}{\sum_{j=1}^{C_n^2} P_{tj}} \tag{2}$$

However, if we only use $f_1(p_{tj}, d_{tj})$ to be value of OD_j, risk still exists that influenced the total expected revenue. Since there may exist OD_j that its capacity is large with a little demands, or its demand is large with fewer available seats. So we analyze the relationship between demand and available seats of OD_j, reducing the risk that priority of OD_j with high expected revenue is set extremely high and priority of OD_j with low expected revenue is set extremely low, and we compute one parameter α_{tj} to adjust $f_1(p_{tj}, d_{tj})$ as follows.

$$\alpha_{tj} = \frac{D_{tj}}{\sum_{j=1}^{C_n^2}(D_{tj})} / (\frac{C_{tj}}{\sum_{j=1}^{C_n^2} C_{tj}}) = \frac{D_{tj}(\sum_{j=1}^{C_n^2} C_{tj})}{C_{tj}(\sum_{j=1}^{C_n^2}(D_{tj}))} \tag{3}$$

In Eq .4, α_{tj} is defined as the ratio of demand and seat capacity of OD_j in period *t*, and it represents urgency of demand of OD_j in period *t*. And the adjusted contribution of OD_j to the line in period *t* is defined as shown in Eq. 5. The larger $f(p_{tj}, d_{tj})$, the higher the value or priority of OD_j.

$$f(p_{tj}, d_{tj}) = \alpha_{tj} f_1(p_{tj}, d_{tj}) = \frac{P_{tj}D_{tj}(\sum_{j=1}^{C_n^2} C_{tj})}{C_{tj}(\sum_{j=1}^{C_n^2} P_{tj})(\sum_{j=1}^{C_n^2}(D_{tj}))} \tag{4}$$

Model of Seat Allocation based on OD's Priority

Algorithm Description. Linear programming is often used to solve problems in optimal scheduling, address selection and other industries. In research of revenue management, Williamson studied inventory control strategy in airline by linear programming [10]. Now in railway, to solve the problem of seat allocation by linear programming, assume that the future demand d_{tj} and fare p_{tj} of an OD in period *t* are known and demand of each OD is independent from each other, *n* stations are in a line where exists *n-1* legs and C_n^2 OD, and seat capacity of each train is c_i. We denote number of allocated seats of each OD in period t as x_{tj}. In order to maximum the expected revenue of the whole line under limits of seat capacity, we firstly denote the relationship of each OD and legs as a_{ij}.

$$a_{ij} = \begin{cases} 1, & \text{leg } i \text{ is used by } OD_j \\ 0, & \text{else} \end{cases} \tag{5}$$

And then our model is described as follows.

$$max \sum_{j=1}^{C_n^2}\sum_{t=1}^{T} p_{tj}x_{tj} \tag{6}$$

subject to

$\sum_{j=1}^{C_n^2}\sum_{t=1}^{T} a_{ij}x_{tj} \le Cj$=1,2,$\cdots, C_n^2$; i=1,2$\cdots$n-1 (7)

$\sum_{t=1}^{T} x_{tj} \le d_j$ j=1,2,$\cdots, C_n^2$ (8)

$x_{tj} \ge 0$ (9)

Analysis of Rationality and Optimality. According to the optimal theory, we firstly analyze the first-order necessary conditions of our model. For simplicity, assume that revenue function $r(x_t) = p_t x_t$ is concave, and $\mathcal{J}(x_t) = \partial(p_t x_t)/\partial x_t$ is represented as marginal revenue in period *t*. Then the first-order necessary conditions for the optimal allocated seats x_t^* and λ^* in period t are

$\frac{\partial(p_t x_t)}{\partial x_t} = \lambda^*$ (10)

subject to the complementary slackness condition

$\lambda^*(C - \sum_{j=1}^{C_n^2}\sum_{t=1}^{T} a_{ij}x_{tj})$=0 (11)

and the multiple non-negativity constraint $\lambda^* \ge 0$.

Obviously, according to concave function's feature, the above first-order necessary conditions in Eq. 10 are also the sufficient conditions to get the optimal revenue. Moreover, according to theory of economics, the Lagrange multiplier λ^* has the interpretation as the marginal opportunity cost of each OD's capacity, and Eq. 10 says that the marginal revenue should equal the marginal opportunity cost of capacity in each period, which means that if marginal revenues and costs are not balanced, we can increase number of allocated seats for OD. Eq. 11 says that if number of allocated seats exceeds number of available seats in one OD, the Lagrange multiplier cannot be larger than 0, that is, opportunity cost of OD cannot be larger than 0. If opportunity cost of OD is equal 0, our model is not under constraints, that is, all demands will be satisfied and the max expected revenue is got.

Moreover, when finding the optimal result, the higher level OD with larger value get seats in prior, and the total expected revenue increases as time going, and growth rate of the total expected revenue decreases as OD's value's decreasing. Therefore, we get max value until growth rate of expected revenue is up to minimum.

Experiment Evaluation

We used data of one railway line from present ticketing system, which contains forecasted demands of each OD and trains' schedules. And we got results according to our model in Matlab7.5, assuming that ticketing demands in Poisson process. To evaluate our model's effectiveness based on OD's priority, we allocate seats in two ways, one is based on OD's priority and the other way is not.

Data Description. Trains' schedules are shown in Table 1, and forecasted demands and fare of each OD are shown in Table 2. Each train's maximum capacity is 600 and we divided one day into six periods.

Table 1 Train's schedules

Stations of trains		periods					
ID of train	station	1	2	3	4	5	6
1	ABCDEF	A	B	C	D	E	
2	ABDF		A	B		D	
3	ACEF		A		C		E
4	ACDF			A		C	D
5	ACF				A		C
6	BCDF		B	C	D		
7	BCEF			B	C		E
8	CDEF		C	D	E		

Table 2 Forecasted demands and fare of each OD

OD（No.）	Forecasted demand								fare
	1	2	3	4	5	6	7	8	
A-B（1）	45	85							55
A-C（2）	66		142	145	268				180
A-D（3）	88	255		186					310
A-E（4）	50		55						430
A-F（5）	195	398	450	446	455				550
B-C（6）	32					50	76		140
B-D（7）	50	70				145			275
B-E（8）	145						180		395
B-F（9）	90	190				185	175		510
C-D（10）	55			79		90		100	175
C-E（11）	106		130				145	156	280
C-F（12）	113		175	188	130	210	178	220	380
D-E（13）	30							80	130
D-F（14）	35	53		67		140		150	235
E-F（15）	20		34				100	90	130

Effectiveness Analysis. For the above data, we got the following results no based on our algorithm in TABLE 3, and results based on our algorithm are shown in Table 4. Compare the total expected revenue In Table 3 and Table 4, the former is 75535 less than the latter. And from No.1 to No.8 train, change of each train's total expected revenue from Table 3 to TABLE 4 is -36410, -56090, 2220, 9000, 0, 5745, 0, 0 separately.

Table 3 Results no based on our model

OD	Trains								Allocated seats
	1	2	3	4	5	6	7	8	
A-B	45	85							130
A-C	66		142	145	268				621
A-D	65	53		9					127
A-E	50		8						58
A-F	195	398	450	446	455				1944
B-C	32					50	76		158
B-D	0	0				145			145
B-E	102						180		282
B-F	90	149				185	175		599
C-D	0			0		90		100	190
C-E	0		26				145	156	327
C-F	98		116	58	130	210	67	220	899
D-E	30							74	104
D-F	35	53		87		140		150	465
E-F	20		34				100	90	244
Revenue	305890	328450	332280	333140	325750	264420	270390	201350	2361670

Table 4 Results based on our model

OD	Trains								Allocated seats
	1	2	3	4	5	6	7	8	
A-B	45	0							45
A-C	66		142	145	145				498
A-D	88	202		0					290
A-E	50		0						50
A-F	195	398	450	412	455				1910
B-C	32					50	76		158
B-D	50	12				105			167

B-E	145						180		325
B-F	90	190				185	175		640
C-D	19			0		90		100	209
C-E	0		0				67	156	223
C-F	113		150	188	130	210	178	220	1189
D-E	0							74	74
D-F	7	12		0		140		150	309
E-F	20		0				100	90	210
Revenue	342300	384540	330060	324140	325750	258675	270390	201350	2437205

The above results shows that if seat capacity is enough for all passengers' demands, both two methods can get the same expected revenue obviously; if under capacity constraints, using our model may not get more expected revenue, but the total expected revenue is much larger than the linear programming model no based on OD's priority. Therefore, our model is more effective than the simple linear programming model.

Conclusions

This article proposed a new model to allocate seats for a line in China passenger railway, which considered the interaction of all trains running on the same OD according to those trains' demands, schedules and seats capacity. Using our model can get larger expected revenue under constraints, which is through the way that replaces the mean demand μ_j to the deterministic demand d_j of each OD to concern to demands' uncertainty. However, according to Littlewood's opinion, if we considered a passenger's uncertainty in his booking process, we will get larger expected revenue [11, 12]. Moreover, when there are fewer stations on a railway line, the computational complexity according to our model is small, but it becomes very large when many stations exist on a railway line. Therefore, we should research further to increase the total expected revenue considering demands' uncertainty and find other optimal algorithms to solve our model.

References

[1]K.Talluri, G. V. Ryzin: An Analysis of Bid-Price Controls for Network Revenue Management. Management Science, Vol.44 (1998) No.11, pp.1577-1593

[2]X.M. ZHANG, D.M. ZHAO and S.D. WEN: Study of Inventory Control in Complex Transport Network. Systems Engineering, Vol.22 (2004) No.5, pp.7-11

[3]Q. GAO, J.F. ZHU and K.J. CHEN: Multi-leg seat inventory control model for airline revenue management. Journal of Traffic and Transportation Engineering, Vol.5 (2005) No.4, pp.82-85

[4]H.Y. WANG, X.Y. LV, L.J. ZHOU and X.S. YOU: Intelligent Seat Allotment Method for Railway Passenger based on Passenger Flow Forecasted. China Railway Science, Vol.34 (2013) No.3, pp.128-132

[5]F. SHI, Y. CHEN, W.L. ZHOU and L.B. DENG: Railway Passenger Train Seats Allotment Plan Establishment and Evaluation Method Based on User Equilibrium Analysis, China Railway Science. Vol.29 (2008) No.6, pp.98-103

[6] Renwick E. Curry: Optimal Airline Seat Allocation with Fare Classes Nested by Origins and Destinations. Transportation Science, Vol.24 (1990) No. 3, pp.193-204

[7] A. Armstrong, J. Meissner: *Railway Revenue Management: Overview and Models*. Lancaster University Management School Working Paper, 2010, pp.1-25

[8] Robert L. Phillips: *Pricing and Revenue Optimization* (Chinese Financial & Economic Publishing House, China 2008, pp. 213-221)

[9] P.P Belobaba: *Air Travel Demand and Airline Seat Inventory Management* (Ph.D., MIT, 1987)

[10]E.L. Williamson: *Airline Network Seat Inventory Control: Methodologies and Revenue Impacts* (Ph.D., MIT. 1992)

[11]K. Littlewood: Forecasting and Control of Passenger Bookings, *AGINFORS 12th Annual Symposium Proceedings* (USA, 1972), pp.95-128

[12] P. P Belobaba: Application of a probabilistic decision model to airline seat inventory control, Operation Research, Vol.37 (1989) No.2, pp.183-197

Advanced Materials Research Vols. 989-994 (2014) pp 2349-2355
© (2014) Trans Tech Publications, Switzerland
doi:10.4028/www.scientific.net/AMR.989-994.2349

IBC-based Authentication Protocols and a Method of Data Sharing for Cloud Systems

Kangkang Chen[1, a *], Chenlei Cao[1, b], Jianyi Liu[1, c] and Ru Zhang[1, d]

[1]Information Security Center, and National Engineering Laboratory for Disaster Backup and Recovery,

Beijing University of Posts and Telecommunications

Beijing, 100876 – P.R.China

[a]879170476@qq.com, [b]caochenlei@gmail.com, [c]liujy@bupt.edu.cn, [d]zhangru@bupt.edu.cn

Keywords: cloud computing; mutual authentication; security communication; data sharing; IBE

Abstract. In Recent years, the rapid development of cloud computing promotes the technological innovation. In the meantime, the security of cloud attracts many researchers. In this paper, a security architecture is proposed to provide a trust communication mechanism between entities in the cloud. Based on this security architecture and BFIBE, three security protocols are proposed to implement mutual authentication and key agreement, which can resist man-in-middle attacks and masquerading attacks. Besides, based the three protocols, an effective data sharing method is proposed.

1 Introduction

In recent years, various companies have established their own cloud systems in different countries. These cloud systems can be divided into public cloud, private cloud, hybrid cloud. In the public cloud systems, cloud servers can provide services for any legitimate user. So communications between the cloud entities will face a variety of threats. It is necessary to establish a security mechanism to protect the security of communications between cloud entities. This paper presents a security architecture based on the identity-based cryptography (IBC). And on this basis, three authentication protocols are proposed to achieve mutual authentication and secure data sharing.

The structure of this paper is as follows:

The first part is an introduction, and the second part is related work, and the third part is to describe the security architecture and related definitions, and the fourth part is about the mutual authentication protocols and data sharing methods, and the fifth part is about the experiment and the analysis of the results, and the first six section is a summary.

2 Related Work

Shamir [1] proposed an identity-based cryptography (IBC) in 1984, and Boneh et al. [2], proposed the first truly practical IBE scheme in 2003. In a large network, it is difficult to handle all the authorized certification with only one PKG. Therefore, Gentry et al. [3] proposed a practical hierarchical identity based encryption scheme (HIBE). The scheme is mainly to solve the problem of entities registration and private keys generation in HIBE. Boneh and Boyen [4,5] constructed an another HIBE in 2004 and redefined it in 2011[6].

In the field of cloud computing, Schridd et al. [7,8] hired only one PKG to provide services for the entire cloud system of which the security has not been proven. Based on HIBE scheme, Li et al. [9] proposed a hierarchical architecture for cloud computing and a TLS-analogous authentication protocol. But the system is complex and the amount of calculation is too much. Kang and Zhang [10] proposed an identity-based authentication scheme for cloud storage sharing. However the low-level PKGs do not reduce the burden of root PKG in their scheme. And the data sharing is limited in the same domain. Cao et al. [11] proposed a layered cloud security architecture and three authentication protocols based the architecture for the federated cloud system. But the authentication between PKGs is complicated.

Because of the amount of calculation is huge in HIBE scheme, therefore this paper constructs a layered architecture based on the architecture of Cao [11]. In this structure, the low-level PKGs effectively alleviate the burden of root PKG. And under the help of root PKG, users are able to authenticate and share data in the entire cloud system. It overcomes the limitation of data sharing in the scheme of Kang. Based on the architecture, the paper designs three identity-based authentication protocols and provides a method for data sharing in the cloud system using the three protocols. Compared with the agreements in the scheme of Cao, the authentication between PKGs and entities in the same domain is non-interactive in this paper. So it simplifies the process of authentication and improves the efficiency of the user data sharing and authentication.

3 System Architecture

3.1 Security Architecture. As shown in Fig.1, the security architecture adopts layered structure. In this system, the root PKG (RPKG) is responsible for the registrations of low-level PKGs and generating private keys for them. In practice, we divide the system into many domains. Each contains a low-level PKG and a user set and cloud servers. Low-level PKGs responsible for the registrations of entities in their domains and generating private keys for them. Low-level PKGs have two private keys. One is generated by RPKG used to communicate with PKGS and the other is generated by himself used to communicate in his domain. If there are not special explanations, the following "PKG" refers to "low-level PKG".

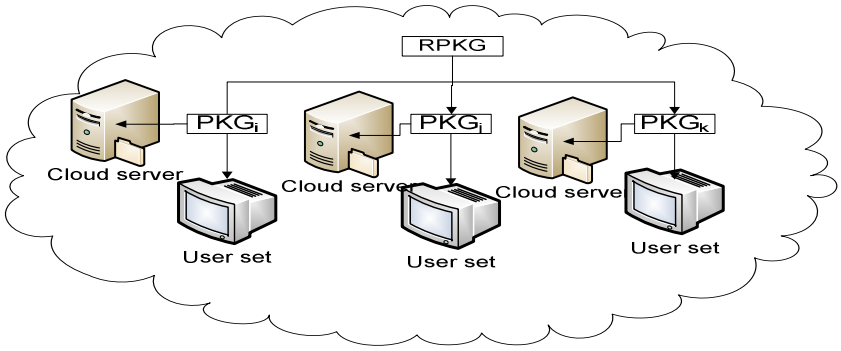

Fig. 1 The layered security architecture

3.2 Cloud Entity Authorization.

3.2.1 PKG Authorization. PKGs provide their identifiable information ID_{pkg} to RPKG. Then RPKG generates a public key $Q_{pkg}=(ID_{pkg},T)$, where T is a date representing for the valid period. RPKG computes $K_{pkg}=G(S_{rpkg},Q_{pkg})$, where$K_{pkg}$ is the private key of PKG, and S_{rpkg} is the master key of RPKG. G() is the private key extraction algorithm of BF-IBE[2]. RPKG generates a tuple $V=(K_{pkg}, P_{rpkg},Q_{rpkg})$, where P_{rpkg} is the common parameter of RPKG and Q_{rpkg} is the public key of RPKG. RPKG binds V to PKG by a safe method (such as smartcards).

3.2.2 Entity Authorization. Entity authorization refers to that PKGs authorize entities in their domain. Entity provides its identifiable information ID_{En} to PKG which is in the same domain with the entity. PKG generates the public key $Q_{en}=(ID_{En},T)$ for the entity. PKG computes $K_{en}=G(S_{pkg},Q_{en})$,where K_{en} is the private key of the Entity and S_{pkg} is the master key of PKG. PKG generates a tuple $V=(K_{en}, P_{pkg},Q_{pkg})$, where P_{pkg} is the common parameter of PKG, and Q_{pkg} is the public key of PKG. PKG binds V to the entity .

4 Authentication Protocols

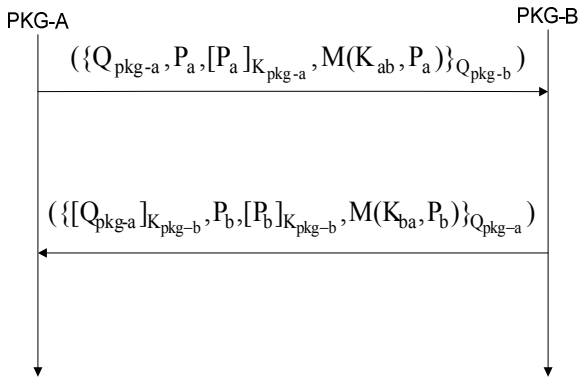

Fig. 2 Mutual authentication between PKGs

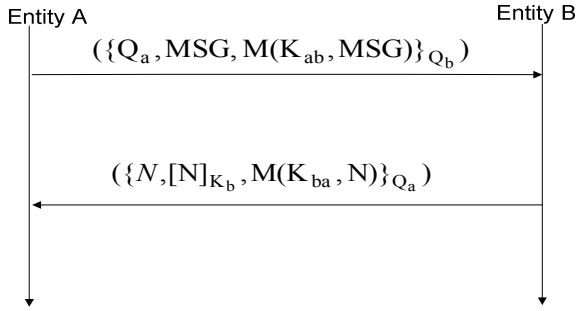

Fig. 3 Authentication between entities in the same domain

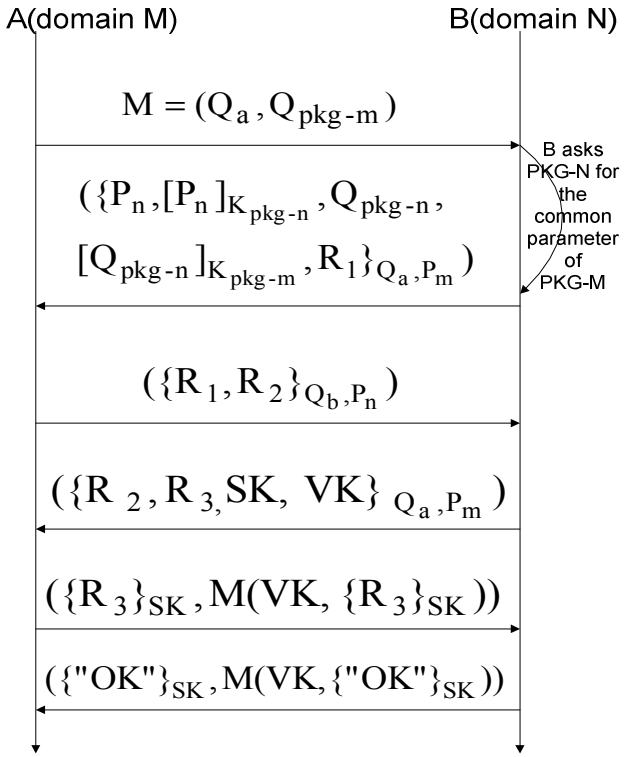

Fig. 4 Authentication between entities in different domain

4.1Authentication between PKGs. Authentications and data exchanges between entities needs the help of PKGs. So the mutual authentication between PKGs is indispensable. As shown in figure 2, a non-interactive method is used to realize the authentication and exchange the common parameters between PKGs:

Step1 PKG-A computes $K_{ab}=e(K_{pkg-a},Q_{pkg-b})$, where K_{pkg-a} is the private key of PKG-A, and Q_{pkg-b} is the public key of PKG-B. e() is the map in BF-IBE. PKG-A sends the message $(\{Q_{pkg-a},P_a,[P_a]_{K_{pkg-a}},M(K_{ab},P_a)\}_{Q_{pkg-b}})$ to PKG-B, where Q_{pkg-a} is the public key of PKG-A, and P_a is the common parameter of PKG-A. $[P_a]_{K_{pkg-a}}$ is the signatures of P_a and M() is Mac hash function. *Step2* After PKG-B receives the message, PKG-B decrypts the message and restores Q_{pkg-a}, P_a, $[P_a]_{K_{pkg-a}}$, $M(K_{ab}, P_a)$ and checks P_a by $[P_a]_{K_{pkg-a}}$, and then computes $K_{ba}=e(K_{pkg-b}, Q_{pkg-a})$, and authenticates the identity of PKG-A. The specific method is as follows: computing $M(K_{ba}, P_b)$, checking whether the result is equal to $M(K_{ab}, P_a)$. If true, the identity of PKG-A is believable. The reason is $K_{ab}=e(K_{pkg-a},Q_{pkg-b})=e(SQ_{pkg-a}, Q_{pkg-b})=e(Q_{pkg-b},SQ_{pkg-a})=e(SQ_{pkg-b}, Q_{pkg-a})=e(K_{pkg-b}, Q_{pkg-a})= K_{ba}$ [10], where S is the master key of RPKG. PKG-B signs the public key Q_{pkg-a} of

PKG-A and the common parameter of its own. Then PKG-B sends the message $(\{[Q_{pkg-a}]_{K_{pkg-b}},P_b,[P_b]_{K_{pkg-b}},M(K_{ba},P_b)\}_{Q_{pkg-a}})$ to PKG-A. After PKG-A receives the message, it decrypts it and verifies every element. After PKG-A ensures the integrity of P_b, PKG-A authenticates the identity of PKG-B using the similar method in Step3.

4.2 Authentication between entities in the same domain. The figure 3 gives the process of the authentications between the entities in the same field using the case of authentications between entity A and entity B (B can be the PKG of the domain where A is located in.). Entity A and entity B is located in the same field. Due to authentication process is similar with 4.1 and is relatively simple, it is not described in detail here, and only the parameters are explained. MSG is the request message to B sent by A. N is the reply from B, which may be the data sharing sign that contains files identifier, the public key of B, the signature of B and sharing time . N may be the session key and the verification key. $[N]_{K_b}$ is the signature of N by B.

4.3 Authentication between entities in different domain. As shown in Fig. 4, entity A belongs to domain A and entity B belongs to domain N. The authentication between A and B is described as follows:

Step1 A sends M to B, which contains the public key of A and the public key of PKG-M. PKG-M is the PKG in the domain M.

Step2 After B receives M , according to Q_{pkg-m}, B judges that he is not in the same domain with A. B uses protocol 4.2 to ask PKG-N for the common parameter of PKG-M. B sends $\left(\{Q_b, M, M(K_{bn}, M)\}_{Q_{pkg-n}}\right)$ to PKG-N. PKG-N authenticates the identity of B and restores M. According to Q_{pkg-n}, PKG-N uses the protocol 4.1 to exchange the common parameter with PKG-M. After PKG-N gets the common parameter of PKG-M, PKG-N replies $(\{N, [N]_{K_{pkg-n}}, M(K_{bn}, N)\}_{Q_b})$ to B, where $N=([P_n]_{K_{pkg-n}}, [Q_{pkg-n}]_{K_{pkg-m}}, [p_m]_{K_{pkg-n}}, P_m)$. P_n is the common parameter of PKG-N, P_m is the common parameter of PKG-M.

Step3 B decrypts the message sent by PKG-N, and checks the integrity of N, and authenticates the identity of PKG-M. Then B restores P_m and the signature of P_m,P_n and the signature of P_n, the signature $[Q_{pkg-n}]_{K_{pkg-m}}$ of Q_{pkg-n} by PKG-M. After B checks the integrity of P_m and P_n, generates the random number R_1 , and uses Q_a and P_m to encrypts $(\{P_n, [P_n]_{K_{pkg-n}}, Q_{pkg-n}, [Q_{pkg-n}]_{K_{pkg-m}}, R_1\}_{Q_a,P_m})$ and sends the result to A.

Step4 A decrypts the message, and checks the integrity of Q_{pkg-n} and P_n and then generates the random number R_2. A sends $(\{R_1,R_2\}_{Q_b,P_n})$ to B.

Step5 B decrypts the message and restores $R_1$and R_2. B compares R_1 with the one generated before to authenticates the identity of A. After that, B generates random number R_3 and the session key SK and the integrity verification key VK and then sends $(\{R_2, R_3SK, VK\}_{Q_a,P_m})$ to A.

Step6 A decrypts the message and restores R_2, R_3SK, VK. A compares R_2 with the one generated before to authenticates the identity of B. Then A encrypts R_3 with the session key SK and computes the Mac value of the encryption result with VK. A sends $(\{R_3\}_{SK}, M(VK, \{R_3\}_{SK}))$ to B.

Step7 B computes $M(VK, \{R_3\}_{SK})$,to check the integrity of $\{R_3\}_{SK}$ and restores R_3. A compares R_3 with the one generated before. If true, it proves that A receives the right SK and VK. B sends $(\{"OK"\}_{SK}, M(VK, \{"OK"\}_{SK}))$ to A to tell it the data transmission can be started.

4.4 Data Sharing. It is assumed that user A requests user B to share his data. The process is as follows:

4.4.1 A and B are in the same domain. A uses protocol 4.2 to communicate with B and gets the data sharing sign N and the signature $[N]_{K_b}$ by B. A makes use of protocol 4.2 to sends N and $[N]_{K_b}$ to the cloud server in the same domain. The cloud server checks $[N]_{K_b}$, and sends the session key SK and the integrity verification key VK to A to completes the authentication. Then the cloud server sends the data encrypted with SK to A.

4.4.2 A and B are in the different domain. A uses protocol 4.3 to communicate with B and gets the session key SK and the integrity verification key VK. Then A sends the request message to B to request the data he wants. If B agrees to share the data, B sends the data sharing sign N and the signature $[N]_{K_b}$ to A. A checks the integrity of message, and uses the protocols 4.3 to communicate with the cloud server that is in the same domain with B. A sends his public key and the public key of PKG which is in the same domain with A to the cloud server. The cloud server uses the protocol 4.2 to ask PKG-B which is in the same domain with B to get the common parameter of PKG-A which is in the same domain with A. Then the cloud server completes the mutual authentication and the exchange of the session key and the integrity verification key with A. A encrypts N and $[N]_{K_b}$ with the session key and sends it to the cloud server. After the cloud server verifies the integrity of the message and the validity of $[N]_{K_b}$, it sends the data to A.

5 Experiments and Analysis

Table 1 Platform information

Operation system	Windows7
memory	DDR3 2G
CPU	intel core i5-2400
Library	Maricl

Table 2 Encrypt and Decrypted algorithm efficiency

Block size(byte)	Encryption time(ms)	Decryption time(ms)
32	10.1	8.5
64	20.0	16.9
128	40.5	34.3
256	79.8	67.8
512	160.2	135.2
1024	319.80	269.8

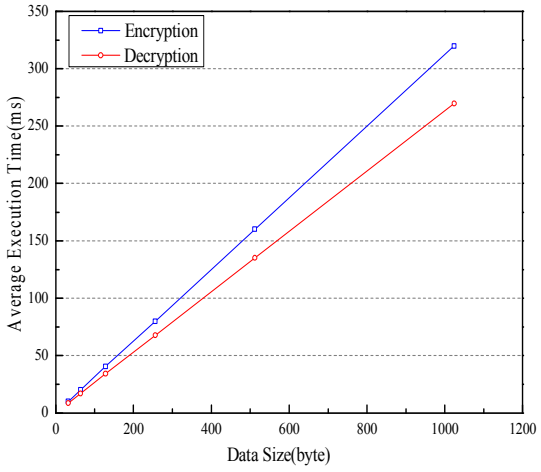

Fig. 5 Encrypt and Decrypt algorithm efficiency

5.1 BF-IBE algorithm efficiency analysis. In this study, I implements BE-IBE algorithm in [2] with chosen ciphertext security with the help of Miracl library. BF-IBE is made up of four algorithm: Setup, Extract, Encrypt, Decrypt. Since the setup algorithm is executed only once at the beginning of creating the entire system and the extract algorithm is only executed when the user registration, therefore their efficiency are not analyzed. The size of private key is 1024 bit in the experiment. The following test time does not include the pre-computation time in this experiment.

5.1.2 Encrypt and Decrypt algorithm efficiency analysis. Since the encryption and decryption of data is relatively small in the authentication process. So only the efficiency of encryption and decryption of small pieces data is analyzed.

As the test data size is in a small range and the block size to use when performing encryptions and decryptions is 32 bytes, so it can be seen the encryption and decryption time is proportional with the number of blocks from the Fig. 5 and table 2. In the authentication process, data is generally less than 1KB. So the encryption and decryption needs very short time within a reasonable range.

Table 3 The comparison of protocol 4.1 and protocol 4.1 in Cao [11]

	4.1	Cao 4.1
Encryption times	2	4
Signature times	3	4
Decryption times	2	4
Communication times	2	4

Table 4 The comparison of protocol 4.3 and protocol 4.3 in Cao [11]

	4.3	Cao 4.3
Encryption times	9	11
Signature times	3	4
Decryption times	9	11
Communication times	10	12

5.2 Comparing the protocols with the protocols in Cao. Since this system structure and authentication protocols are similar with those in Cao [11], the following pages will compare the protocol 4.1 and 4.3 with Cao [11] in the aspects of traffic and calculation. Because of the data in the authentication process is small, we use the times of encryptions and decryptions and signatures to estimate the amount of calculation and use the times of communications to estimate the traffic.

From table 3 and table 4, we can see that the times of encryptions and decryptions and signatures are far less than those in Cao. In the aspect of traffic, the times of communications are less than those in Cao.

In conclusion, the efficiency of the protocols in this paper is better than that in Cao [11].

6 Summary

This paper proposes a layered security architecture based on the thought of Cao [11] and designs three IBC-based mutual authentication protocols based on the layered security architecture. Besides, this paper provides a data sharing method based on the three protocols, which overcomes the defects in the range of data sharing in Kang [10]. The protocol 4.3 is complicated and the security of PKGs is the key of system security. So the future work is to simplify the protocol and research the problem how to protect the security of PKGs

Acknowledgment

This work is supported by Beijing Higher Education Young Elite Teacher Project (YETP0448), Specialized Research Fund for the Doctoral Program of Higher Education (2013114), Fundamental Research Funds for the Central Universities (2013RC0310), Digital Right Management Technology Research and Development Project(1681300000119), National Key Technology Research and Development Program (2012BAH08B02), National 863 Program (2012AA012606).

References

[1] A. Shamir, "Identity-based cryptosystems and signature schemes", in Advances in Cryptology-Crypto '84, Lecture Notes in Computer Science, Vol. 196, Springer-Verlag, pp. 47-53, 1984.

[2] Dan Boneh, Matthew Franklin, "Identity-Based Encryption from the Weil Pairing," in SIAM J. of Computing, Vol. 32, No. 3, pp. 586-615, 2003.

[3] C. Gentry and S. Halevi, "Hierarchical identity based encryption with polynomially many levels," Lecture Notes in Computer Science, vol. 5444, pp. 437-456, 2009.

[4] D. Boneh and X. Boyen, "Efficient selective-ID secure identity based encryption without random oracles, "Lecture Notes in Computer Science vol. 3027, pp. 223-238, 2004.

[5] D. Boneh, X. Boyen, and E. J. Goh, "Hierarchical identity based encryption with constant size ciphertext, " Lecture Notes in Computer Science, vol. 3494, pp. 440-456, 2005.

[6] D. Boneh and X. Boyen, "Efficient selective identity-based encryption without random oracles, " Journal of Cryptology, vol. 24, no. 4, pp. 659-693, October, 2011.

[7] C. Schridde, M. Smith, and B. Freisleben, "An identity-based key agreement protocol for the network layer," Lecture Notes in Computer Science, vol. 5229, pp. 409-422, 2008.

[8] C. Schridde, T. Dörnemann, E. Juhnke, B. Freisleben, and M. Smith, "An identity-based security infrastructure for cloud environments," in Proc. of IEEE International Conf. on Wireless Communications, Networking and Information Security, pp. 644-649, 2010.

[9] H. W. Li, Y. S. Dai, T. Ling, and H. M. Yang, "Identity-based authentication for cloud computing," Lecture Notes in Computer Science, vol. 5931, pp. 157-166, 2009.

[10] Lishan Kang, Xuejie Zhang, "Identity-Based Authentication in Cloud Storage Sharing," in International Conference on Multimedia Information Networking and Security, 2010.

[11] Chenlei Cao, Ru Zhang, Mengyi Zhang and Yixian Yang, "IBC-Based Entity Authentication Protocols for Federated Cloud Systems," in ksii transactions on internet and information systems vol.7,No.5,May,2013.

[12] Mao, W.B, "An Identity-based Non-interactive Authentication Framework for Computational Grids," May,29,2004,

[13] Ran Canetti and Hugo Krawczyk, "Analysis of key-exchange protocols and their use for building secure channels, " Advances in Cryptology –Eurocrypt 2001, volume 2045 of LNCS. Spring-Verlag, 2001.

Advanced Materials Research Vols. 989-994 (2014) pp 2356-2359
© (2014) Trans Tech Publications, Switzerland
doi:10.4028/www.scientific.net/AMR.989-994.2356

J-Integral computation in mixed mode Ⅰ and Ⅱ

Yongmei Cai [1,a], Fangyao. Zhang[2,b] and Yujun Xie[2,c]

[1]College of Pipeline and Civil Engineering, China University of Petroleum,Qingdao 266580, China;

[2]Department of Mechanical Engineering, Liaoning Shihua University, Fushun 113001, China.

[a]cymlnpu@163.com, [b]yjxie@163.com, [c]zhanglu8a@163.com

Keywords: Fracture; *J*-Integral; computation; Stress intensity factors.

Abstract: Computation of a path independent contour integration but it yields directly the independent values of the opening mode and shear mode stress intensity factors. The calculations are not sensitive to the choice of contour. To the J-integral calculation, the present scheme calculates separately the factors K_{I} and K_{II}. A simple method to determine the SIFs for the three-dimensional crack is proposed based on the conservation integral.

Introduction

In liner fracture mechanics many different approaches to the computation of critical parameters associated with crack extension have been proposed, Among this method Rice's J-integral is extremely attractive since it involves only the evaluation of a path independent contour integral[1][2], the data for which are available from a numerical solution of the boundary value problem without any special treatment of the region surrounding the crack tip. In the application of fracture mechanics, we often encountered three dimensional configurations under complex loading.

The present paper aims at computation of a path independent contour integration but it yields directly the independent values of the opening mode and shear mode stress intensity factors. Base on finite element soft ware to formulation of crack evolution and the principal direction of crack propagation under combined tension-tear loading. The principal direction of crack propagation and associated critical energy release rate are determined.

Three dimensional J- integral for mixed model I and Ⅱ

We consider a representative cracked slice of an elastic solid having a Poisson's ratio μ, and elastic model E. For our derivation we introduce our primary local coordinate system x at an arbitrary position, rectangular Cartesian coordinates x_1, x_2, x_3, $x_1$normal to the crack front, $x_2$normal to the crack plane, $x_3$tangent to the crack front. Where portion s of the boundary is traction-free, and external loading is imposed only by traction on S. Without changing the boundary condition on S, impose a continuously varying sequence of static solution, related to the displacement u, details of the procedure can be found in references.

The countour Γ runs from the lower crack to the upper crack, the region enclosed by Γ is donated by S, we supposed that the crack faces are free of traction and on the remainder of the boundary either the displacement or the traction components in the normal and tangential directions are prescribed so that we have a well posed problem. The stress and displacements in the neighbourhood of the crack tip are known[3]in reference[4]，referring to the natural polar coordinate system indicated in Fig.1.

For the three-dimensional elastic solids, the following integrals can be given from the conservation law.

$$J_j = \int_s \left(w n_j - T_i u_{i,j} \right) \mathrm{d}s \tag{1}$$

Eq.(1) has two components, J_1 and J_2. They can all be used to calculate the stress intensity factors for the cracked elastic bodies. In the following section some key steps to calculate the SIF for the indentation have been developed based on the J-integral.

$$J_1 = \int_{\Gamma} \left(w n_1 - T_i u_{i,1} \right) ds \tag{2}$$

$$J_2 = \int_{\Gamma} \left(w n_2 - T_i u_{i,2} \right) ds \tag{3}$$

where $n_1 = cos(n,x)$; $n_2 = cos(n,y)$; $w = \frac{1}{2}\sigma_{ij}\varepsilon_{ij}$; $T_i = \sigma_{ij} n_j$.

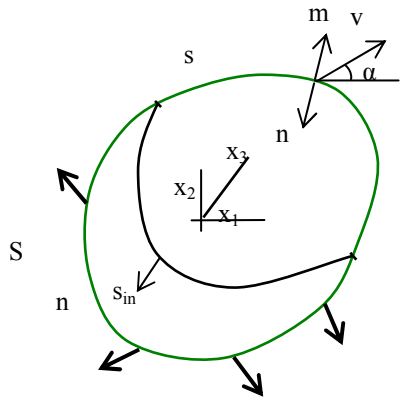

Fig.1 Three-dimensional deformation fields

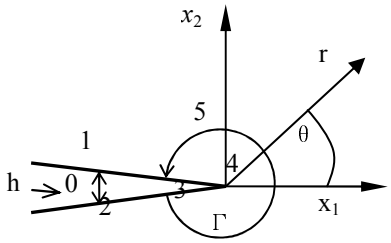

Fig.2 The integral loop for crack propagation

Substitution the stress and displacements to eq. (2) ~ (3), a routine evaluation of the integral produces

$$J_1 = \frac{\left(1-\mu^2\right)\left(K_{\mathrm{I}}^2 + K_{\mathrm{II}}^2\right)}{E} \tag{4}$$

$$J_2 = -\frac{2\left(1-\mu^2\right)K_{\mathrm{I}} K_{\mathrm{II}}}{E} \tag{5}$$

Which means that the SIF can be calculated by the J-integral, along the path from any point at the lower surface to any point at the upper surface.

Energy release rate for boundary cracking

For a homogenous and isotropic quasi-brittle substrate, the maximum energy released rate of boundary cracking can be given by

$$\frac{\partial \Pi}{\partial t} = \int_s w v_i m_i ds \tag{6}$$

Where v_i denotes the velocity of the point on s， and m_i is the current outward normal to s. Let $v_i = e_i = \Delta_i / \Delta$, which corresponds to two components of unit boundary shift, so that $e_1 = \cos\alpha$, $e_2 = \sin\alpha$, where α is the angle between shift Δ and x_1 and represents the direction of the boundary shift, β is the angle between shift Δ and x_2. Let $n_i = -m_i$ be the unit inward normal on boundary s, which means that the boundary s moves inward[5] [6], e.g. the case of crack growth. Thus, the energy release rate of boundary shift is given by

$$G = \frac{\partial \Pi}{\partial t} = \int_s w e_i n_i ds \tag{7}$$

Combine this conservation law J_i, proposed by Eshelby. The energy release rate expressed by Eq(6) can then be rearranged along the *v*-direction, with the limit $s \to 0$ the energy release rate of boundary cracking can be defined as

$$\overline{G} = J_i e_i = J_1 \cos\alpha + J_2 \sin\alpha \tag{8}$$

Where $J_1\big|_{s\to 0}$ denotes the driving force of boundary cracking in direction x_1, $J_2\big|_{s\to 0}$ denotes the driving force of boundary cracking in direction x_2, when the limits taken exist. Substitution (4) and (5) to equation (8), the following result can be found:

$$G = \frac{(1-\mu^2)K_{\mathrm{I}}^2}{E}\sqrt{f^4+6f^2+1}\cos(\alpha-\beta) \tag{9}$$

where $\beta = arctan\dfrac{-2f}{1+f^2}$, f equal $K_{\mathrm{II}}/K_{\mathrm{I}}$, The maximum energy release rate is now maximised with respect to $\dfrac{dG}{d\alpha}=0$. By setting $\sin(\alpha_c-\beta)=0$, which given the crack angle:

$$\alpha_{\mathrm{c}} = \arctan\frac{-2f}{1+f^2} \tag{10}$$

Where α_c is the theoretical expected angles and possible cracking angles at which maximum G value, and explicitly this is given by

$$G_{\max} = \frac{(1-\mu^2)K_I^2}{E}\sqrt{f^4+6f^2+1} \tag{11}$$

For a homogenous and isotropic brittle solid Griffith's criterion states that a crack will propagate when the critical value G_c of the solid is equal to the driving or applied G_{max}

$$G_{max} = G_c \tag{12}$$

Some discussions

Here we build a three dimensional crack configuration with a known exact solution so as to be able to evaluate the capability of our J integral to extract stress intensity factors. In this first test problem，the single edge crack subjected to a uniform tension, the second problem is a cantilever subject to end shear and has the same geometry as the first. We calculate three-dimensional J-integral on each of the test problem.

For the mode Ⅰ crack, traditional integral loop is shown in Fig.2． In this case we have

$$J_1\big|_{s_{231}\to 0} = \lim_{S241\to 0}\int_{S_{241}}(wn_1 - T_i u_{i,1})\mathrm{d}s = \frac{(1-\mu^2)K_{\mathrm{I}}^2}{E} \tag{13}$$

$$J_2\big|_{s_{231}\to 0} = \lim_{S241\to 0}\int_{S_{241}}(wn_2 - T_i u_{i,2})\mathrm{d}s = 0 \tag{14}$$

Then , the equation (7) becomes:

$$G = \frac{(1-\mu^2)K_{\mathrm{I}}^2}{E}\cos\alpha \tag{15}$$

It is clear the maximum energy release rate for crack extension is given by

$$G_{\max} = \frac{(1-\mu^2)K_{\mathrm{I}}^2}{E} \tag{16}$$

It represent the energy-based driving force for mode I crack, Fig.3 shown a typical image of crack branching which have been derived by Xie Y J (2010).

For the mode Ⅱ crack, the integral loop same with mode Ⅰ , in this case we have

$$J_1\big|_{s231\to 0} = \lim_{S241\to 0}\int_{S241}(wn_1 - T_i u_{i,1})\mathrm{d}s = \frac{(1-\mu^2)K_{\mathrm{II}}^2}{E} \tag{17}$$

$$J_2\big|_{s231\to 0} = \lim_{S241\to 0}\int_{S241}(wn_2 - T_i u_{i,2})\mathrm{d}s = 0 \tag{18}$$

Then, the equation (7) becomes

$$G = \frac{(1-\mu^2)K_{II}^2}{E}\cos\alpha \tag{19}$$

so maximum energy release rate for crack extension is given by

$$G_{\max} = \frac{(1-\mu^2)K_{II}^2}{E} \tag{20}$$

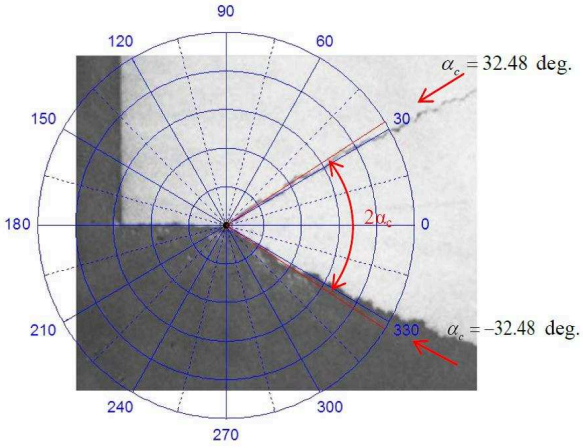

Fig.3 A typical image of crack branching mode I crack

Conclusions

The integral reported here is an accurate, reliable for the calculation of the intensity of singular stress distribution in plane, isotropic elastic material problems. The calculations are not sensitive to the choice of contour. An energy-based fracture model for mixed mode has been developed and formulized. Unlike the traditional applications of the J-integral around a crack-tip, a new partial integral path and the associated calculation method for the energy release rate had been defined. Both the cracking angle and the critical energy release rate of mixed crack have been proposed.

References

[1]G C Sih: Dynamic Aspects of Crack Aspects of Crack Propagation. In: *Inelastic Behavior of Solids*, Mc-Graw-Hill Book, Co, New York, (1969) ,p.607-639.

[2]Clark and G R Irwin: Crack-propagation Behaviours. Experimental Mechanics,(1966) No.6, p.321-330.

[3]Y J Xie, Z H Xu and X H Wang: A Theoretical Note on Mode- I Crack Branching and Kinking. Engineering Fracture Mechanics,(2011) No.78,p.919-929.

[4]A I Nadai: *Theory of Flow and Fracture of Solids*．(New York：McGraw-Hill，1963)p.356-386．

[5]B Budiansky and J R Rice．Conservation Laws and Energy-release Rates．Journal of Applied Mechanics，(1973) No.40,p.201-203．

[6]R Zeng and M O Wang: Branching Extension Characteristics of Mode - Ⅱ Crack under Fatigue Loading. Engineering Fracture Mechanics,(1994) No.49,p.487–498

[7]Y J Xie, Z H Xu and P N Li. Crack Mouth Widening Energy-Release Rate and Its Applications. Theoretical and Applied Fracture Mechanics,(1998) No.29,p.195-203.

[8]J L Belcher and H. R Brown: Crack Branching and Arrest in Environmental Cracking of Polyethylene. J. of Materials Science,(1986) No.21, p.717-724.

[9]Y J Xie, X Zhang and X H Wang: An Exact Method on Penny-shaped Cracked Homogeneous and Composite Cylinders. Int J Solids and Struct,(2001) No.38,p.6953-6963.

Advanced Materials Research Vols. 989-994 (2014) pp 2360-2363
© (2014) Trans Tech Publications, Switzerland
doi:10.4028/www.scientific.net/AMR.989-994.2360

A Kind of MSD Performance Compensation Method Based on the Strategy of Sliding

Zhu Dongxu[1,a] , Fu Gang[1, a], and He Qian[1,a]

[1]China Satellite Maritime Tracking and Control Department, China

[a]348237548@sina.com

Keywords: Sliding strategy, PCM/FM, MSD

Abstract. The signal noise ratio (SNR) of telemetry signals is low in the environment of reentry telemetry, MSD(Multi-Symbol Detection) technology can effectively improve PCM/FM telemetry signal demodulation performance. In view of the problem that maximum likelihood value is misjudged leaded by the noise in the process of reentry and doppler causing serious distortion of signal phase. A performance compensation method of MSD based on sliding strategy is researched: A MSD operation with N-1 element overlap before each MSD operation, where the each symbol sliding strategy sliding the length of 1 symbol. The simulation and test results verify the effectiveness of the improved algorithm.

Introduction

The PCM/FM system is widely used in missile and aircraft telemetry, mainly applied to the target spacecraft reentry telemetry. Goal is through the blackout area, the attitude of the track changes and tumbling frequency big influence on SNR of telemetry signals, so its under low signal-to-noise ratio of remote sensing signal demodulation is the main research problems. And symbol detection technology can effectively improve performance of PCM/FM signal demodulation, channel gain can be increased nearly 3 dB[1][2], which can effectively solve the traditional demodulation threshold for PCM/FM signal demodulation. Because the MSD is based on phase correlation arithmetic, so in the telemetry signal phase affected by noise and doppler serious cases, it is easy to cause MSD maximum likelihood of misjudgment, affect the demodulation performance.

To reduce the probability of maximum likelihood was wrongfully convicted in MSD, further improve the performance of telemetry signal demodulation, this paper puts forward a kind of MSD performance compensation method based on sliding strategy, this strategy can to a certain extent, reduce the probability of maximum likelihood value is misjudgment, with traditional MSD and the complexity of algorithm.

1 Traditional algorithms of MSD

Assumption is *z* sends a sequence of binary information symbols. And symbol detection method, namely by finding an optimal sequence of judgment, also is in determining the received signal under the condition of the *r(t)*, sequence $\bar{z}$ have the greatest probability. According to bayes theorem:

$$p(\bar{z}/r(t)) = \frac{p(r(t)/\bar{z})p(\bar{z})}{p(r(t))} \tag{1}$$

To facilitate the derivation, using the logarithmic notation $\ln(p(r(t)/\bar{z}))$, noise as gaussian white noise, the *r(t)* with mean $s(t;z)$. T for the element width, when the *n(t)* is generalized stationary random process, the $\ln(p(r(t)/\bar{z}))$ is equivalent to the largest to maximize the $-\int_0^{NT}(r(t)-s(t;\bar{z}))^2dt$, which is equivalent to minimize the $\int_0^{NT}(r(t)-s(t;\bar{z}))^2dt$, namely the minimum Euclidean distance, said as follows:

$$\max\{\ln(p(r(t)/\bar{z}))\} \Leftrightarrow \min\left\{\int_0^{NT}(r(t)-s(t;\bar{z}))^2dt\right\} \tag{2}$$

Within the N element, define the minimum Euclidean distance to *r(t)* as follows:

$$r_{\min} = \min\left\{\int_0^{NT}(r(t)-s(t;\bar{z}))^2 dt\right\}$$
$$= \min\left\{\int_0^{NT} r^2(t)dt + \int_0^{NT} s^2(t;\bar{z})dt - 2\int_0^{NT} r(t)s(t;\bar{z})dt\right\} \quad (3)$$

$$T(\bar{z}) = \int_0^{NT} r(t)s(t;\bar{z})dt \quad (4)$$

Because of the noise and are independent of symbols, $\int_0^{NT} r^2(t)dt$ and $\int_0^{NT} s^2(t;\bar{z})dt$ as constant value, therefore, the minimum Euclidean distance equivalent to the maximum correlation $T_{\max}$, namely:

$$T_{\max}(\bar{z}) = \max\left\{\int_0^{NT} r(t)s(t;\bar{z})dt\right\} \quad (5)$$

The formula (5) into a recursive form:

$$T_n(\bar{z}) = T_{n-1}(\bar{z}) + \lambda_n(\bar{z}) \quad (6)$$
$$\lambda_n(\bar{z}) = \int_{(n-1)T}^{nT} r(t)s(t;\bar{z})dt$$

$T_n(\bar{z})$ for n element of likelihood function, called measurement, $T_{n-1}(\bar{z})$ said before n-1 symbol of the likelihood function, $\lambda_n(\bar{z})$ as distance increment, said signal in $nT \le t \le (n+1)T$ time likelihood value of additional measures. Because before each measurement is a measurement with the current element cycle cumulative likelihood value, search a $\bar{z}_i$, namely that:

$$T_n(\bar{z}_i) \ge T_n(\bar{z}_j) \quad i \ne j$$

Through the above analysis we can see that in a certain period of time within (*NT)*, namely N element, for the duration of the best decision is the most close to find a *r(t)* and receiving signal modulation signal of $s(t;\bar{z})$. Thus, calculate the likelihood function of $p(r(t)/\bar{z})$ maximum converted to obtain the maximum of $|T(\bar{z})|$ problems. MSD is looking for the corresponding sequence, has the absolute value of $|T(\bar{z})|$ maximum likelihood.

Obtain type (6) likelihood value of the specific process as shown in figure 2.

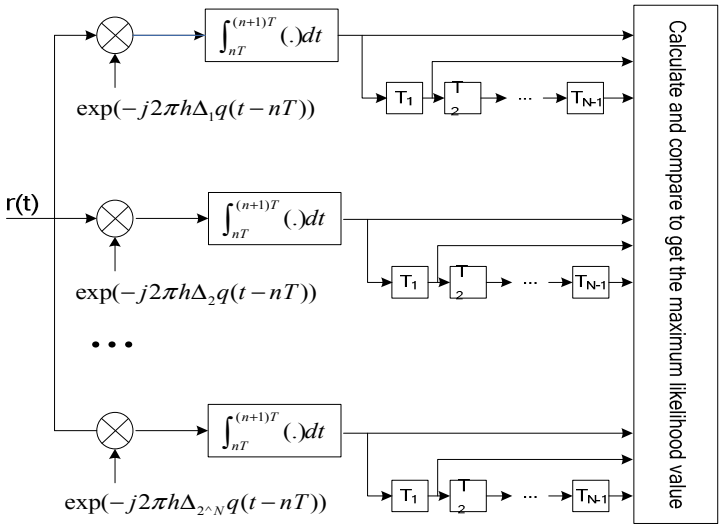

Fig1 Multiple symbol detection algorithm implementation block diagram

Among them, the likelihood calculation is as follows:

$$\beta_i = \sum_{n=1}^{N} \Gamma_{i_{n,N-n}} C_n \quad , \quad C_1 = 1 \quad , \quad C_k = \exp(-j\pi h \sum_{l=1}^{k-1} \Delta_{i_l})$$
$$\hat{a}_{n-N+1} = \Delta_{i_1} \quad \hat{a}_{n-N+2} = \Delta_{i_2} \quad \ldots \quad \hat{a}_n = \Delta_{iN}$$

Observation length N off for 5 of this article, the corresponding local code is $2^N = 32$ groups, to send information in the simulation code for 1 [1-1-1-1-1], using MSD likelihood value relationship with the block sequence and time shift is shown in figure 2:

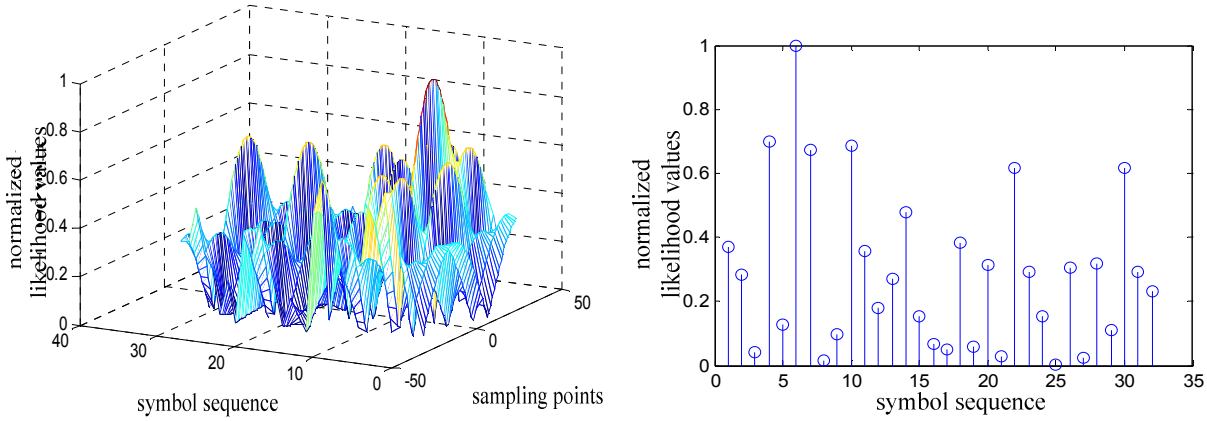

Fig. 2 Relations between likelihood value, delay interval and block sequence

2 MSD performance compensation

By simulation it can be seen that before after MSD operation, some channel likelihood value, compared with maximum likelihood likelihood value size close to, can see clearly that higher likelihood peak of around 0.7, to has a great influence on the decisions of the main peak, namely in the noise and under the influence of time delay and doppler, it is easy to cause the results of MSD miscalculation.

Listed above the graph example, the peak time corresponding block as shown in table 1.

Table 1 Code corresponding to the likelihood value

Block number	6	4	7	10
symbol sequence	1 -1 1 -1 -1	1 1 -1 -1 -1	-1 1 1 -1 -1	1 -1 -1 1 -1
Likelihood value	max	next	next	next

Can be seen from table 1, when the symbol sequence is similar, likelihood value comparison, the probability of mistakes that is bigger, so you need to study a kind of strategy can reduce the misjudgment rate of symbol sequence changes. A sliding strategy under study, that is, every time sliding element 1 time sliding strategy, and the corresponding sliding conditions were analyzed.

Looking for maximum likelihood in MSD values corresponding to the local block in the process, when a group of element demodulation is determined, the relationship between the adjacent block should be considered. Sliding along the time axis, a sliding one element at a time, every time the interception of five element length calculation, specific sliding condition as shown in figure 3.

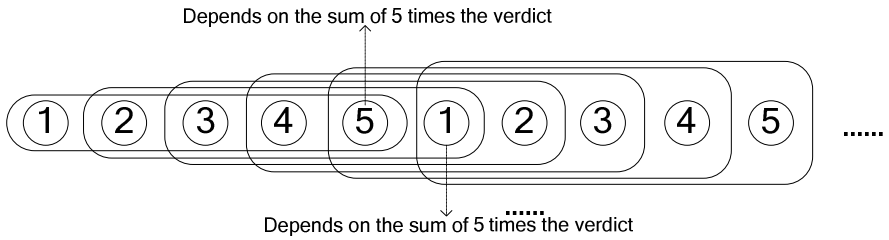

Fig3 Time sliding strategy map (sliding one code)

From figure 1, you can see, from the symbol sequence of the third element, after each element was found at least twice, because the decision for many times, so the formation of the sliding strategy for correction caused by excessive noise, so as to effectively reduce the error rate.

3 Algorithm performance.

Figure 4 is under gaussian noise, without sliding strategy and through a sliding element of MSD.

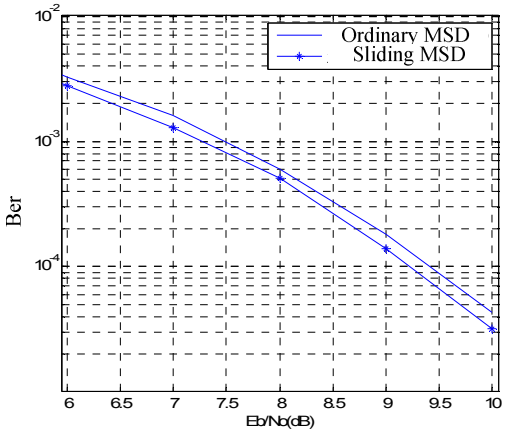

Fig4 BER contrast diagram of sliding strategy

Can be seen from above, MSD algorithm adopts sliding, after a time element sliding strategy in ber to 10^{-4}, SNR gain 0.3dB, demodulation performance obtained certain to improve.

Summary

Symbol detection method is based on the idea of maximum likelihood, of continuous several codes signal joint detection, and by comparing with the local signal integration have been the likelihood value size to achieve signal demodulation. Traditional sliding length is the length N, and when using sliding length is one element of strategy, according to the simulation signal telemetry standards manual, under a certain noise intensity, the sliding strategy before and after the MSD demodulation method is adopted to improve the bit error rate test. Test results show that the sliding one element of the strategy after demodulation error rate performance obtained certain to improve.

References

[1] Liu Yingsong. Adopt the method of MSD to improve remote sensing sensitivity[J]. The sea range of academic. 2010,7: 23-25.

[2] Zhu Hongquan. Multi-h CPM system error and spectrum performance research[J]. Journal of aircraft measurement and control, 2010, 29(5): 56-59.

Advanced Materials Research Vols. 989-994 (2014) pp 2364-2367
© (2014) Trans Tech Publications, Switzerland
doi:10.4028/www.scientific.net/AMR.989-994.2364

Research on Phase Locked Loop Software Parallel Processing Methods

Li Renlong[1,a], Fu Gang[1, a], Wu Yanjun [1,a] and Liping Wang[2,b]

[1]China Satellite Maritime Tracking and Control Department, China
[2]School of Computer Science, Engineering and Mathematics, Flinders University, South Australia 5 042, Australia
[a]348237548@sina.com [b]wlp2005518@gmail.com

Keywords: Signal Processing, Phase Locked Loop, Partitioning strategy

Abstract. Signal processing speed is an important indicator of the performance of software based phase-locked loop. Previous software uses data redundancy of phase-locked loop based on parallel processing, but the amount of redundant data lead to the introduction of computer waste of resources, reducing efficiency and other issues. Design of a parallel processing method based on data blocks and redundant data segments dual dynamic partitioning, given the dynamic data partitioning strategy.

Introduction

PLL is a common method of signal processing. With the advent of digital signal processing by means of software, "pure software" of the real-time processing, this method is called virtual radio[1]. To the parallel processing method can improve the operation speed. Literature for the parallel processing method based on a phase locked loop data redundancy, the method preferably achieved at the same time parallel processing of a plurality of software PLL. But will lead to a waste of computer resources, reduced efficiency and other issues. To this end, this paper studies the dynamic partitioning of the data segment parallel processing.

1 Data redundancy based on phase-locked loop parallelization and its problems

How to convert an analog system to the same function, similar to the performance of digital systems become critical software PLL design. Functionality and performance of a system can be determined by its transfer function, the transfer function corresponding to the simulation system S domain, the transfer function corresponding to the digital system Z domain. Z-domain transfer function of the system will convert the time domain in the form of differential equations, mathematical model of software as a phase-locked loop. Second-order phase-locked loop Z-domain model ideal integrator filter shown in Figure 1.

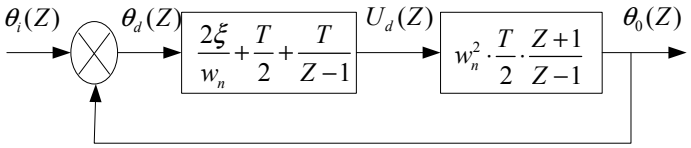

Fig1 SPLL Z domain model

As can be seen from the figure, the impact of the performance parameters of the phase locked loop is only natural resonant frequency and damping[2]. Digital phase locked loop parameters can be selected with reference to the method for setting the parameters.

2 Based on the description of the method of parallel data redundancy

Approach is to use the software PLL data A/D samples obtained according to a fixed length, which is the use of the serial data, the input data block to be processed. If the data block segmentation parallel processing, there is the parallel processing of each of the tracking loop process a data block is not locked, the tracking results in a larger error of the data gaps, as shown in Figure 2.

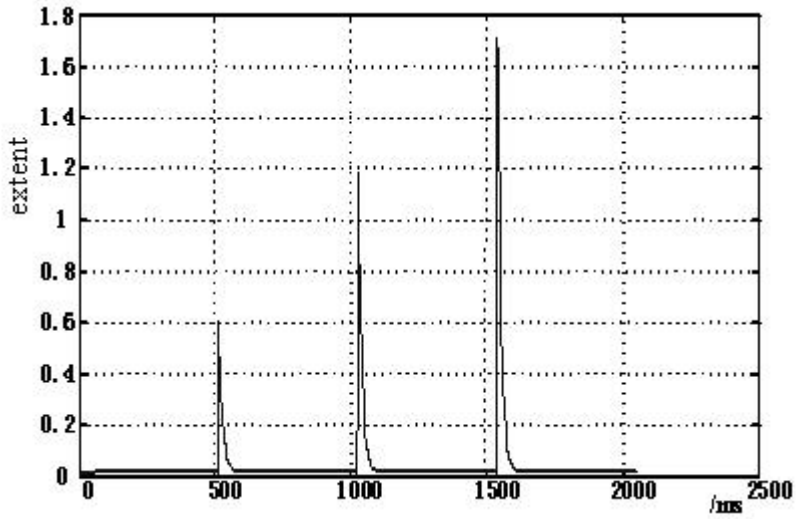

Fig2 Non-redundant parallel track results

For job tracking loop characteristics, the parallel data on the basis of data redundancy information loss problem solving unlocked state. The basic principle shown in Figure 3.

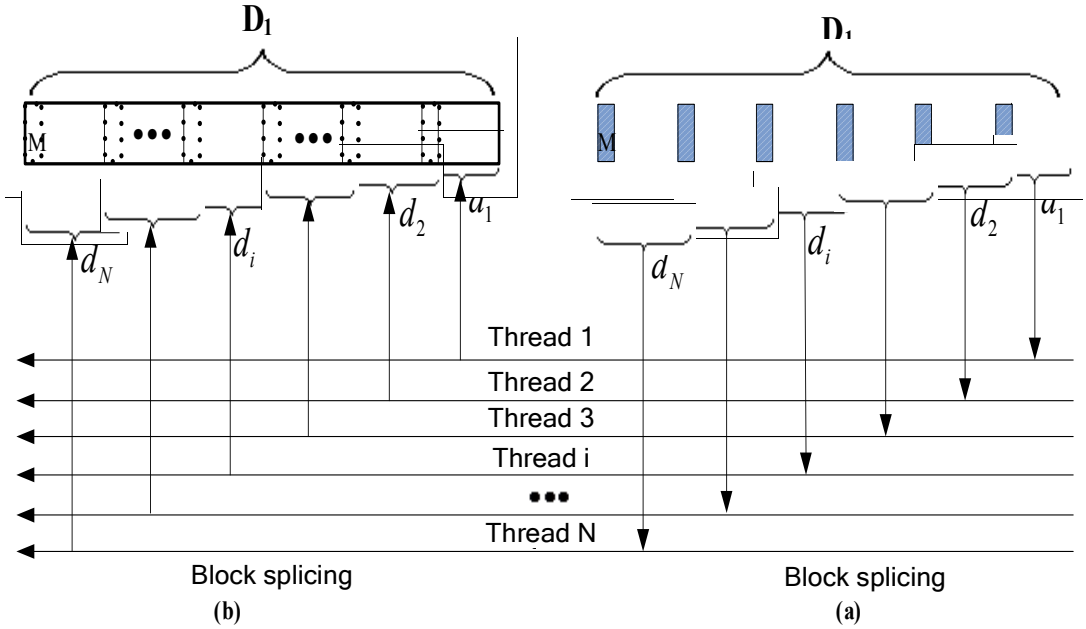

Fig3 Based on data parallelism to achieve redundancy software PLL schematics

3 Dynamic partitioning of data blocks

Earlier analysis of parallel loop uses a fixed block of data partitioning method, the data block is the fixed division before making the tracking process using fixed-length data block is divided in chronological order.

This partitioning method is simple and easy to implement, but the signal tracking loop design to consider the loop loses lock recapture problems. If the loop loses lock occurs, you need to re-start the capture process, the received signal recapture. Process for tracing data blocks in a plurality of parallel processing subblocks, wherein any process should be carried out occurs again lock catch, the catch of the local code and the local carrier frequency phase needs to be updated.

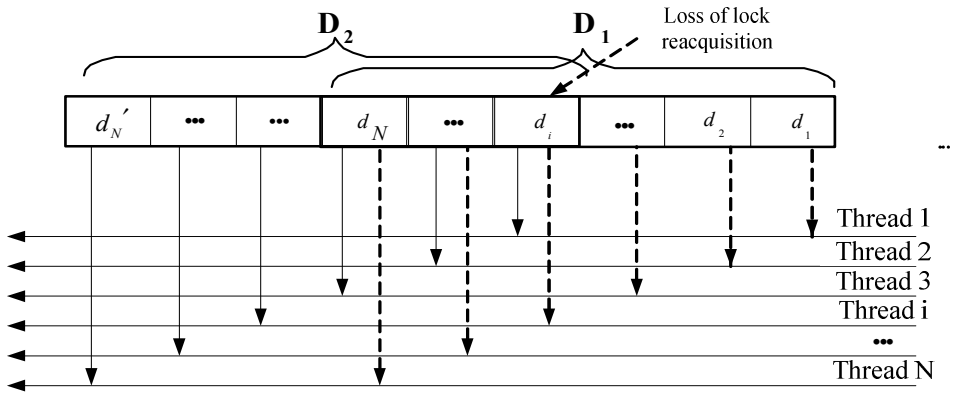

Fig4 Dynamic data partitioning method

Figure 4, the tracking process is not before the division of the data stream according to the time length of the sequence, etc., the start and end of the data segment is not fixed. The first data block is divided into N sub-blocks. If the parallel process does not appear out of lock, the next block of data from the beginning of the end position of division, and the same fixed data block division method.

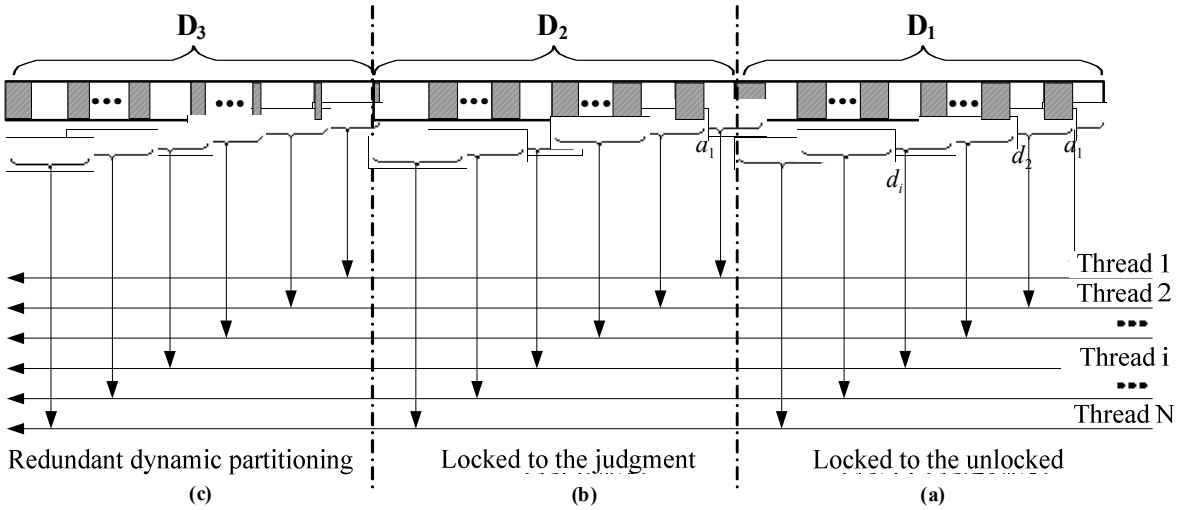

Fig5 Schematic dynamic partitioning redundant data segments

As can be seen from the figure, the dynamic partitioning method, redundant data segments is shortened, the redundant data segments to effectively avoid the waste of resources caused by the fixed dividing process and improve the efficiency of the parallel.

4 Parallel simulation and analysis of polycyclic

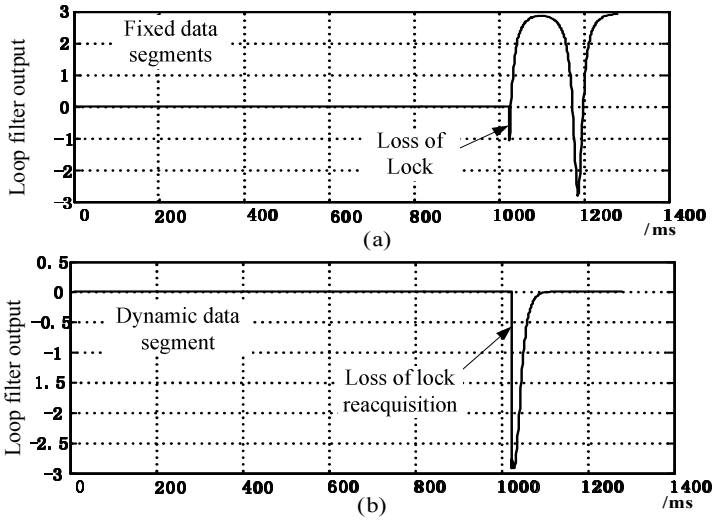

Fig6 Comparison of the data segment division method...

The simulation results shown in Figure 6, parallel tracking loop loses lock the segment in Fig6 (a) is fixed on the divided data block is not tracked, and Fig6 (b) based on the dynamic data block can be divided in the tracking loop lost after the lock on the track again soon caught. Seen from the simulation results, parallel to the frequency of the carrier tracking loop ramp with a single ring signal tracking capability is roughly equal. The above simulation results show that the dynamic tracking performance of parallel phase-locked loop to meet the design requirements.

Summary

This method not only improves the signal after the loss of lock catch speed, minimize the loss of data caused by the loss of lock, and effectively reduces the amount of data redundancy to further improve the efficiency of the parallel.

References

[1] Vanu Bose, Micha Isment, Matt Wellborn and John Guttag. Virtual Radio[J]. IEEE. select. Area Commun, 1999,17 (4):1526-1529.

[2] Amdahl G.M.Validity of single-Processor approach to achieving large-scale computing capability[C]. Proc. Of AFIPS Conf, Reston, VA, 1967: 483-485.

Advanced Materials Research Vols. 989-994 (2014) pp 2368-2372
© (2014) Trans Tech Publications, Switzerland
doi:10.4028/www.scientific.net/AMR.989-994.2368

An Algorithm to Control Watermarking Capacity Using PSNR

Yong Xing[1, a], Daoshun Wang[1, b]

[1]Department of Computer Science and Technology, Tsinghua University, Beijing 100084, China.

[a]xingyong163@163.com, [b]wangdaoshun@gmail.com

Key Words: Perceptual Model, Image Quality, PSNR, Watermarking Capacity.

Abstract. Some existing methods for estimating image watermarking capacity may degenerate the quality of stego-image when the estimated capacity is achieved. In this paper, based on the Region of Interest (ROI) model, we discuss on the capacity problem and the quality of stego-images using PSNR. Considering the trade-off between capacity and quality, our method estimates the allowable distortion for each pixel in spatial domain in terms of the specific PSNR of stego-image. Experimental results show our method ensures a good control over the capacity without introducing artifacts.

1 Introduction

The purpose of watermarking capacity research is to evaluate how much information can be hidden into a digital cover image while satisfying watermarking invisibility and robustness [1-2]. There are many related works for calculating watermarking capacity. Moulin et al. regarded watermarking as information channel between encoders and decoders and studied optimal watermarking strategies under constrained resources [3]. Zhang et al. used Noise Visibility Function (NVF) to compute the allowable distortion of each pixel by its neighbors' values [2]. Based on this, Yaghamee et al. defined NVF as the depth of each pixel in the quadtree decomposition of the cover image [4]. They also proposed a new method to estimate image complexity based on the concept of ROI and used ROI to calculate capacity [5]. In addition, Caciula et al. [6] and Pei et al. [7] researched the capacity of adaptive reversible watermarking.

However, these existing methods have ignored the quality issues [8]. When the number of embedded bits reaches the upper bound, the quality of stego-image becomes poor. To solve this problem, we see image quality as a parameter when calculating capacity. Then, watermarking capacity is the maximum number of bits that can be hidden in terms of particular quality requirements.

2 Background and Motivation

Zhang et al. used NVF to analyze watermarking capacity [2]. NVF is a function characterizes local image properties, identifying textured and edge regions where watermark should be more strongly embedded. The NVF at each pixel (*r, c*) is written as

$$\mathrm{NVF}(r,c) = \frac{1}{1+\delta_x^2(r,c)} \tag{2-1}$$

where $\delta_x^2(r,c)$ is the local variance in a window centered on the pixel (*r, c*). Yaghmaee et al. [4] partitioned $N \times N$ cover image and redefined NVF at each pixel (*r, c*) with its level $L(r, c)$ in the quadtree as

$$\mathrm{NVF}(r,c) = \frac{L(r,c)}{\log_2 N} \tag{2-2}$$

In both of these two methods, the allowable distortion of each pixel (*r, c*) is

$$\Delta(r,c) = \big(1 - \mathrm{NVF}(r,c)\big) \cdot \Delta_0 + \mathrm{NVF}(r,c) \cdot \Delta_1 \tag{2-3}$$

where Δ_0 and Δ_1 are the maximum allowable pixel distortions in textured and flat region respectively. All the watermark amplitudes build an image named Maximum Watermark Image (MWI).

In order to investigate the quality of stego-images when the number of embedded bits reaches the estimated capacity, we do experiment on 2180 images with Zhang's method and Yaghmaee's method respectively, and compute the PSNR's of their MWI's. The result is presented in Table 1.

Most PSNR's are no more than 22, with the Zhang's method, and are between 22 and 28, with the Yaghmaee's method. This shows that these two methods have ignored the trade-off between capacity and quality and thus over-estimated the capacity. If taking the quality of stego-image as a parameter, we can ensure the stego-image can achieve the desired quality requirements.

Table 1: Distribution of the PSNR of Stego-images

Range of PSNR	Zhang et al. [2] method		Yaghmaee et al. [4] method	
	Number	Ratio	Number	Ratio
[30, +∞)	14	0.64%	72	3.30%
[28, 30)	9	0.41%	45	2.06%
[26, 28)	22	1.01%	227	10.41%
[24, 26)	65	2.98%	721	33.07%
[22, 24)	180	8.26%	994	45.60%
[20, 22)	911	41.79%	119	5.46%
[0, 20)	979	44.91%	2	0.09%
Total	2180	100%	2180	100%

3 The Proposed Algorithm

Yaghmaee et al. proposed the ROI model to measure image complexity [5]. They divided cover image into 16 blocks, computed *Intensity*, *Contrast*, *Location*, *Edge* and *Texture* for each block, and integrated the five parameters into *Importance Measure* (IM), a real number between 0 and 1, to represent the image content. For there is direct relation between watermarking capacity and image complexity, capacity is closely associated with IM. Taking into consideration the quality of stego-image, which is usually measured by PSNR, we estimate capacity based on the ROI model.

Let $P_{expected}$ be the expected PSNR of stego-image. $P_{expected}$ is controlled by watermark encoder and expresses the expected quality of stego-image. This requires that the actual PSNR of stego-image should no less than $P_{expected}$. We propose an algorithm to calculate the capacity of a gray-level image as following.

Algorithm: Computing the capacity of cover image

Input: A cover image S and the expected PSNR $P_{expected}$ of its stego-image S'

Output: Capacity C of the cover image

Steps:

1. Based on the ROI model [5], divide the cover image S into blocks and calculate $\mathrm{IM}(S_i)$ for each block S_i.
2. Obtain the assumed PSNR of each block S_i in stego-image by computing
$$P_i = \frac{P_{expected}}{[\mathrm{IM}(S_i)]^{1/(2N_b)}} \quad (3\text{-}1)$$
where N_b is the number of blocks. In the ROI model, $N_b = 16$.
3. Estimate the maximum distortions of the pixels in block S_i as
$$\Delta_i = \frac{255}{\sqrt{t_i}} \quad (3\text{-}2)$$
where $t_i = 10^{P_i/10}$ is a parameter dictated by P_i.
4. Let $\delta_x^2(r,c)$ be the local variance of block S_i in the 3×3 window centered on the pixel (r, c).The tolerable distortion of pixel (r, c) is
$$\Delta(r,c) = \left(1 - \frac{1}{\sqrt{1+\delta_x^2(r,c)}}\right) \cdot \Delta_i \quad (3\text{-}3)$$
5. All pixel distortions make a new image named MWI. Assume σ_{iw}^2 denotes the variance of the corresponding MWI block and σ_n^2 denotes the variance of noise. The watermarking capacity of the whole cover image is

$$C = \sum_i C_i = \sum_i W_i \log\left(1 + \frac{\sigma_{iw}^2}{\sigma_n^2}\right) \quad (3\text{-}4)$$

There are some explanations essential for us to understanding this algorithm. First, a larger $\mathrm{IM}(S_i)$ means more distortion in S_i is acceptable. Second, if we partition the cover image into substantially uniform blocks of different sizes by quadtree decomposition [4], the number of blocks is usually more than 16 and all allowable distortions of the pixels in block S_i are approximately the same as (3-2). Third, as NVF does in [2], the different textures around different pixels result in different tolerable distortions. (3-3) indicates richer texture can tolerate more distortions. Fourth, watermarking can be considered as a form of communication [3]. So watermarking capacity problem can be solved using traditional information theory [2]. We treat the whole image block S_i as one AWGN channel and assume every block suffers from the same channel attack. Then the capacity of the whole image is the sum of those for each block in (3-4).

4 Analysis on Stego-image Quality

We analyze the quality of stego-image when the number of embedded bits reaches the estimated capacity. Let P_{actual} be the actual PSNR of stego-image. According to the definition of PSNR,

$$P_{actual} = 10 \cdot \log_{10} \frac{m \cdot n \cdot 255^2}{\sum_{r,c}(S'(r,c) - S(r,c))^2} \quad (4\text{-}1)$$

Considering $\Delta(r,c) = S'(r,c) - S(r,c)$, according to (3-2) and (3-3),

$$P_{actual} = 10 \cdot \log_{10} \frac{m \cdot n}{\sum_{r,c}\left[\left(1 - \frac{1}{\sqrt{1+\delta_x^2(r,c)}}\right)^2 \cdot \frac{1}{10^{P_i/10}}\right]} \quad (4\text{-}2)$$

Let $\mathrm{IM}_{max} = \max_i\{\mathrm{IM}(S_i)\}$. Applying (3-1) to (4-2), we get

$$P_{actual} \geq 10 \cdot \log_{10} \frac{m \cdot n \cdot 10^{P_{min}/10}}{\sum_{r,c}\left[\left(1 - \frac{1}{\sqrt{1+\delta_x^2(r,c)}}\right)^2\right]} \quad (4\text{-}3)$$

Obviously, $1 - \frac{1}{\sqrt{1+\delta_x^2(r,c)}} < 1$. Then

$$P_{actual} > 10 \cdot \log_{10} 10^{\frac{P_{min}}{10}} = P_{min} = \frac{P_{expected}}{(\mathrm{IM}_{max})^{1/(2N_b)}} \quad (4\text{-}4)$$

Because of $\mathrm{IM}(S_i) \in (0,1)$, we have $\mathrm{IM}_{max} < 1$ and $(\mathrm{IM}_{max})^{1/(2N_b)} < 1$. Thus

$$P_{actual} > P_{expected} \quad (4\text{-}5)$$

It indicates that stego-image S' can satisfy the quality requirements. But this does not means stego-images always have good quality when the number of hiding bits is below the upper bound of formula (3-4). A sufficient condition for good quality is that the modification of each pixel in cover images should not exceed its corresponding gray level of MWI. If the distortions of some regions go beyond the limit, although formula (4-4) is satisfied, the quality of stego-images may be poor. However, for our method is somewhat conservative in computing capacity, stego-images may be still good in vision even if the actual embedding capacity slightly exceeds formula (3-4).

5 Experiments

The quality of an image is generally considered to be good when its PSNR is no less than 28. So we set the expected PSNR is 28 and compute the distortions of the MWI's of 2180 cover images obtained by the proposed method in Section 3. The experimental result shows that 90.09% PSNR's are between 28 and 30, and the rest are more than 30. Take Lena image for example. Fig. 1 is the MWI and stego-images of Lena. The MWI showed in Fig. 1(b) is almost pure black because of its low gray values. Fig. 1(c) amplifies its gray values by 8 times and clearly displays the contour of Lena. This shows that our algorithm has good adaptability. Fig. 1 (d)~(f) display three stego-images obtained by three different embedding methods. These stego-images have no visual difference from

the cover image (Fig. 1(a)). Reviewing Table 1 in Section 2, we can see that the proposed algorithm can guarantee the quality of stego-images to be good.

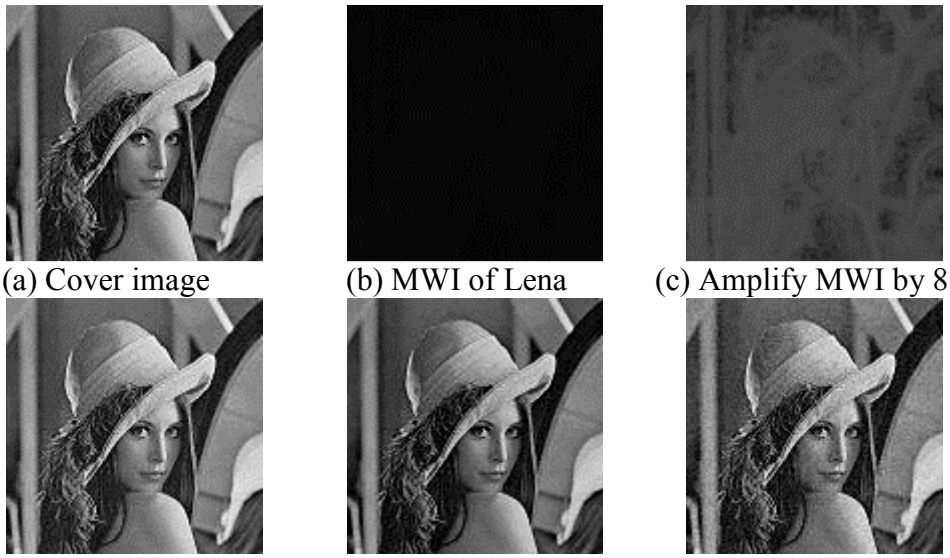

(a) Cover image (b) MWI of Lena (c) Amplify MWI by 8

(d) Additive embedding (e) Subtractive embedding (f) Random embedding

Fig. 1: MWI and stego-images of Lena (PSNR=28.70)

In Fig. 2, we draw the curve of watermarking capacities of four experimental images. With the increase of PSNR, the quality requirements become higher, thus less modification on cover images reduces embedding capacity. When PSNR is more than 40, cover images are almost not modifiable and watermarking capacity tends to 0. In terms of any specific PSNR, the relationship of the capacities of different images is determined. It indicates that watermarking capacity depends on the self-characteristics of cover images.

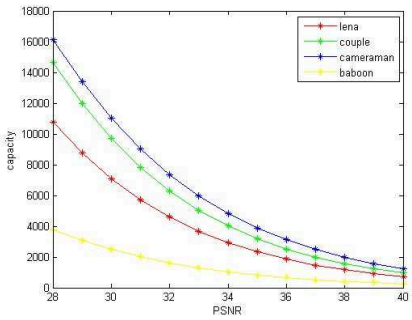

Fig. 2: Curve of watermarking capacity

6 Conclusions

In this paper, we regard image quality as one parameter and research the watermarking capacity problem closely associated with quality issues. Based on the ROI model, our method estimates the allowable distortion, the potential for embedding watermark, for each pixel in spatial domain in terms of the specific PSNR of stego-image. Experimental results show that our method can meet the quality requirements without introducing artifacts.

Acknowledgment

This research was supported in part by the National Natural Science Foundation of China (Grant Nos. 61170032 and 61373020), and in part by the Project of General Administration of Press and Publication of China (GAPP-ZDKJ-BQ/15-2).

References

[1] P. H. Wong, O. C. Au, A Capacity Estimation Technique for JPEG-to-JPEG Image Watermarking, IEEE Tran. Circuits and Systems for Video Technology, 2003, 13(8), pp. 746-752.

[2] F. Zhang, H. B. Zhang, Digital Watermarking Capacity Analysis in Wavelet Domain, International Conference on Signal Processing, 2004, 3, pp. 2278-2281.

[3] P. Moulin, M. K. Mihcak, The Parallel Gaussian Watermarking Game, IEEE Trans. Information Theory, 2004, 50(2), pp. 272-289.

[4] F. Yaghmaee, M. Jamzad, Computing Watermark Capacity in Images According to Their Quad Tree, International Symposium on Signal Processing and Information Technology, 2005: 823-826.

[5] F. Yaghmaee, M. Jamzad, Estimating Watermarking Capacity in Gray Scale Images Based on Image Complexity, EURASIP J. on Advances in Signal Processing, 2010, 2010, pp. 1-9.

[6] I. Caciula, D. Coltuc, Capacity Control of Reversible Watermarking by Two-Thresholds Embedding: Further Results, International Symposium on Signals, Circuits and Systems, 2013: 1-4.

[7] Q. Pei, X. Wang, Y. Li, et al., Adaptive Reversible Watermarking with Improved Embedding Capacity, J. Systems and Software, 2013, 86(11), pp. 2841-2848.

[8] F. Yaghmaee, M. Jamzad, Introducing a Two Dimensional Measure for Watermarking Capacity in Images, Image Analysis and Recognition, Springer Berlin Heidelberg, 2008, pp. 213-220.

Advanced Materials Research Vols. 989-994 (2014) pp 2373-2376
© (2014) Trans Tech Publications, Switzerland
doi:10.4028/www.scientific.net/AMR.989-994.2373

Simulation of Dynamic Compaction on Soft Soil Foundation

Pang Yiling [1, a], Dai Duanming [1]

[1] Department of Civil Engineering, Guangxi Polytechnic of Construction, Nanning , 530003,China;

[a]1377997225@qq.com.

Keywords: dynamic consolidation; soft soil foundation; FEM.

Abstract. Aiming at soft soil foundation, this paper simulates the process of dynamic compaction on soft soil foundation by ABAQUS, and analyzes soil stress and displacement under the effect of same tamping energy on different drop height, ram. The law of consolidation on the soil foundation has been forecasted more accurately, which is more valuable for the similar project on dynamic compaction on soft soil foundation.

1 Introduction

The soft soil foundation is very general in China's coastal areas. With the reform and opening up, and the rapid development of the economic construction in coastal areas, it has great meaning in the study of the character of soft soil foundation and its treatment method [1]. The dynamic consolidation method is also called dynamic compacting method, which drops the 100～400KN weighty hammer (the maximum is up to 2000KN) with 6-40m drop distance [2] .

Although the dynamic consolidation method is used widely in treatment of soft foundation， the theory and design method is not perfect and mature. This paper analyzes the process of the treatment of soft soil foundation in dynamic consolidation method with different construction parameters by finite element software and chooses the proper parameters based on the simulation effect.

2 Model building

2.1 Element Type and Load. ABAQUS can better simulate the mechanical response of soil under the enormous impact loads. According to the simulation of stress propagation, first-order unit is better than the second-order unit[3].So this paper chose an 8-node linear brick, reduced integration, hourglass control(C3D8R).

Wu Ming-Ping et al [4] and Lee Ping [5] simplified transient impact load to triangular pulse during the tamping process, and the calculation results were consistent with the measured data. Based on the data obtained from practices of dynamic compaction [6], when the heavy hammer ramming the ground, the acting time is generally 0.04~0.2s. In this paper, we choose 0.09s as the acting time, so the dynamic compaction loading forms are shown in Fig.1.

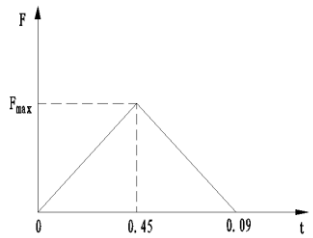

Fig.1 Dynamic Compaction Loading Forms

The hammer is placed in close proximity to the location of foundation (the hammer in this model is placed in 0.01m), and given a initial velocity in order to save the simulation time of free fall in ABAQUS/Explicit.

3 Example Analysis

3.1calculation parameters. The test site lies in the terrace of the Yangtze River. Its stratigraphical time is Q4, formed by the fluviation. The upper part is deep saturation, and lower part is sand bed. The soil layers are reduced to one in the model, because the depth of dynamic consolidation is limited. The main simulated parameter is shown in Table 1.

Table 1. The main simulated parameter

Elastic Modulus E (Mpa)	Poisson Ratio μ	Cohesion C (kpa)	Friction Angle φ (°)	Density ρ g/cm3	Flow Stress Ratio K
8.6	0.35	27	5	1.8	0.94

3.2Model Building. In the simulation model, different construction parameters have different reinforcement effect. Therefore, this paper would analyze the model in different drop height. The first combination is 28t×10m and 12t×24m(hammer weight×drop height)，Thereinto the temping energy in both of the combination is 2800KN•m.

Boundary conditions were more important to simulation, so the boundary conditions in this paper are in the following list:

- Assume that the soil type is elastic-plastic semi-infinite space which is homogeneous and isotropy;
- Take no account of underground water
- Assume that the hammer is rigid body
- Take no account of energy loss in the impact process.

It is important for numerical simulation. Finite element mesh generation is one of critical techniques for FEM. The mesh generation in this model is plotted in Fig.2

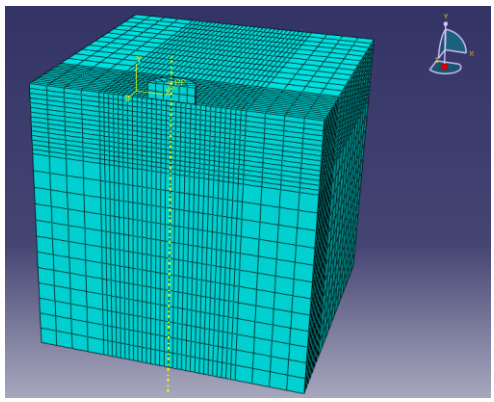

Fig.2 Mesh generation

4 The simulation results and analysis of different hammer weight and drop height under the action

4.1 Vertical Displacement Distribution Map

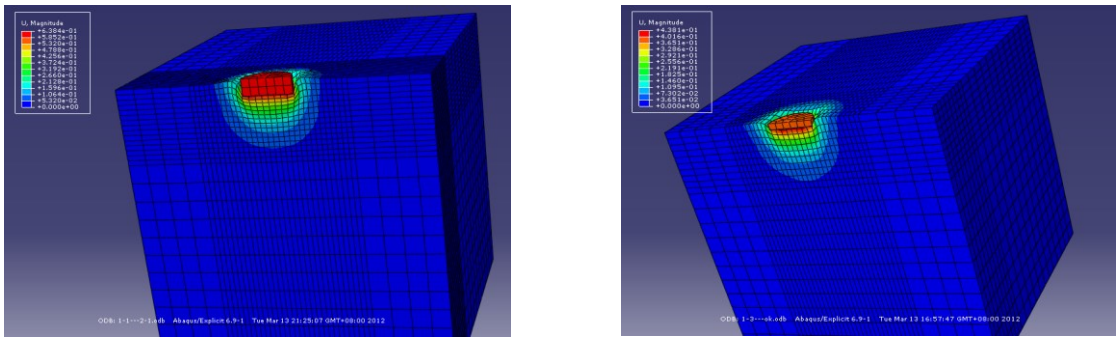

(a) 28t×10m Vertical Displacement Distribution Map

(b) 12t×24m Vertical Displacement Distribution Map

Fig.3 Vertical Displacement Distribution Map Under Different Weight and Height

It can be found from Fig.3 that as the hammer weight increases, the soil displacement increases, and ground surface heaves around the tamping pit, which is coincided with the actual.

4.2 Vertical Stress Distribution. Through the settlement displacement curve, the maximum displacement of each depth can be seen intuitively. The time variation of the vertical stress distribution is plotted in Fig.4, thereinto the depth is hammer bottom,-2.0m and -5.0m.

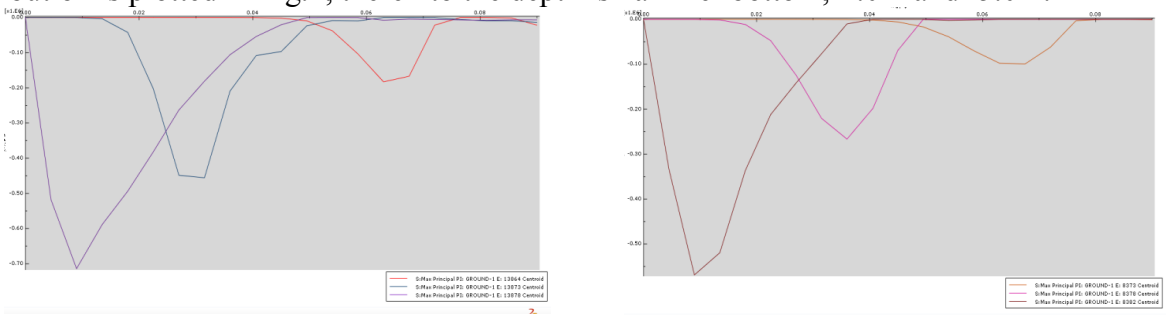

(a) Hammer Bottom,-2.0m,-5.0m under 28t×10m

(b) Hammer Bottom,-2.0m,-5.0m Under 12t×24m

Fig.4 Time Variation of the Different Depth Vertical Stress Distribution

It can be seen from the Fig.4 that as the depth increases, the maximum stress gradually decreases, and decreases rapidly when the stress reaches the peak, but these three kinds of impact force generated by the peak value are different. Fig.4(a) shows that the maximum stress of the hammer bottom is 0.72×10^{6}Pa. In Fig.4 (b), the maximum stress of the hammer bottom that is 0.57×10^{6}Pa is the minimum and the vertical stress distribution in other two positions decreases as the weight decreases. From the above points, it can be seen that the heavy hammer with small height of drop is superior to light hammer with large of drop under the same tamping energy condition. Therefore, if the conditions permit, try to use a heavy hammer with small height of drop. Thus, combined with the project, the 10m×28t can be selected as the actual construction parameters.

5 Summary

Simulated analysis is made on the progress of soft soil foundation by dynamic compaction in applying ABAQUS finite element software. Drucker-Prager yield criterion is presented in this paper. Compared the reinforcement effect of heavy hammer with small height of drop and light hammer with large of drop with that of different bottom area of the hammer, the following conclusions were drawn:

- The finite element analysis software ABAQUS can accurately simulate stress and displacements of the dynamic compaction on soft soil foundation reinforcement.
- Consolidation scope and depth of heavy hammer with small height of drop is superior to that of light hammer with large of drop under the same tamping energy condition.
- It is feasible to use the ABAQUS / Explicit module to calculate the contact between the hammer and the foundation.

Found Project : The research is sponsored financially by The Guangxi Department of Education Science and Technology Project (NO. 2013YB312)

References

[1] Gong Xiaonan, Foundation Treatment Manual (Third Edition) [M].BeiJing: China Building Industry Press,2008.

[2] Xu Zhijun. Dynamic Compaction and Dynamic Compaction Replacement Method in Foundation Reinforcement [M] BeiJing: Machinery Industry Press, 2004:1~2.

[3] Wang Jincang,Chen Yekai. ABAQUS Application in Civil Engineering[M].HangZhou: Zhejiang University press,2006.

[4] Wu Mingbing,Wang Zhongqi. Numerical Analysis of Mechanism of Dynamic Consolidation[J]. Geotechnical Investigation and Surveying. 1989，（3）：1 5.

[5] Li Benping. Finite Element Analysis of Consolidation Mechanism [D].HangZhou:Zhejiang University,1993.

[6] Yu Deshui. The Experimental Study and Numerical Simulation of the Collapse Loss Ground Improved with Dynamic Consolidation Method[D]. University of Science and Technology Beijing.2005.

Advanced Materials Research Vols. 989-994 (2014) pp 2377-2380
© (2014) Trans Tech Publications, Switzerland
doi:10.4028/www.scientific.net/AMR.989-994.2377

Look the partial equilibrium with the global optimum from the problem of the shortest circuit for three villages

Xiaowei Jiang, Yu Hu, Yueting Yang and Tian Luan

School of Mathematics and Statistics, Beihua University, Jilin 132013, China
jxwbh@126.com, 297378408@qq.com

Keywords: the partial equilibrium; the global optimum; the shortest circuit for three villages; Fermat point; the circumcenter.

Abstract: We explore the relationship between the partial equilibrium and the global optimum from the problem of the shortest circuit for three villages (PSCTV). Using the related properties of Fermat point and the circumcenter of the triangle, we can come to the conclusion that the partial equilibrium sometimes brings into correspondence with the global optimum but there is a great deal of difference between the two by analysing the difference between the sum of distances from Fermat point to all vertices and the ones from circumcenter to all vertices.

Introduction

The problem of the shortest circuit for three villages can be described "Three villages, due to limited conditions, intend to build a primary school together, and build the village roads from the school to all villages. Ask: where the school should be built in order to make the shortest length of roads? [1]" The corresponding mathematical problem is to find a point in the plane such that the minimum distances can be got from the point to three vertices of the triangle. This issue is clearly considered from prospective pavers' goals to minimize cost. In turn, from the student's point of view, for fairness, the school should address the position which has equal distance to three villages. What connection does exist between these two issues? And what will be the difference for the student's journeys in both programs? Here it will be explored.

Preliminaries

PSCTV can be transformed into a well-known Fermat point problem, and there exist a lot of research works about it. We only introduce some useful conclusions as follows.

Definition 1 We say that F is the Fermat point of the triangle if the minimum distances can be got from F to three vertices of the triangle.

Theorem 1 The Fermat point F of $\triangle ABC$ must be in its internal or boundary.

Proof. By contradiction, assume that F is in the external of $\triangle ABC$, then F must be in someone of six regions as shown in the Figure 1. If F is in region I, then the sum of distances from A to A,B,C are obviously less than the ones from F to A,B,C, so there is a contradiction. Similarly, the conclusions are true if F is in regions II and III. If F is in region IV, the sum of distances from the intersection of two lines BF and AC to A,B,C are less than the ones from F to A,B,C, so there is a contradiction. Similarly, the conclusions are true if F is in regions V and VI.

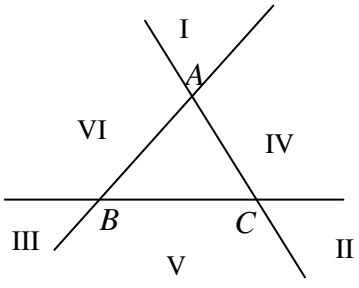

Fig. 1 Six regions in plane

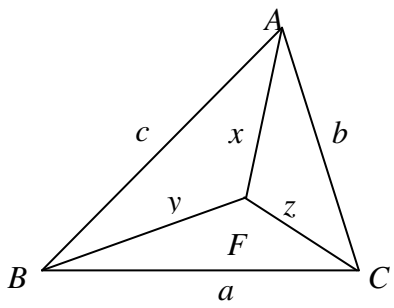

Fig. 2 The Fermat point F of $\triangle ABC$

Theorem 2[2] Assume that F is the Fermat point of $\triangle ABC$ as shown in the Figure 2, and $\max\{A,B,C\}<120^\circ$. Set $FA=x, FB=y, FC=z,$ then we have

$$x=\frac{b^2+c^2-2a^2+k^2}{3k},$$
$$y=\frac{a^2+c^2-2b^2+k^2}{3k}, \tag{1}$$
$$z=\frac{a^2+b^2-2c^2+k^2}{3k},$$

where a,b,c are sides of $\triangle ABC$, $k^2=\frac{1}{2}(a^2+b^2+c^2)+2\sqrt{3}S$, and S is the area $\triangle ABC$.

The sum of distances from the Fermat point to vertices of $\triangle ABC$ is denoted as d, then it is easy to get the following conclusion.

Corollary 1 $d=x+y+z=k=\sqrt{\frac{1}{2}(a^2+b^2+c^2)+2\sqrt{3}S}$. (2)

Let R be the radius of circumcircle of $\triangle ABC$, and the sum of distances from the circumcenter to vertices of $\triangle ABC$ is denoted as D, then $D=3R$. By Sine theorem $\frac{a}{\sin A}=\frac{b}{\sin B}=\frac{c}{\sin C}=2R$ and the formula for area of the triangle $S=\frac{1}{2}bc\sin A$, we derive $R=\frac{a}{2\sin A}=\frac{abc}{4S}$,

So, it is easy to get

$$D=3R=\frac{3abc}{4S}. \tag{3}$$

The relationship between d and D

We begin by discussing the value $D-d$. In [3], the distance from the circumcenter O to the Fermat point F of $\triangle ABC$ is given

$$|OF|^2=\frac{x^2\sin 2A+y^2\sin 2B+z^2\sin 2C}{\sin 2A+\sin 2B+\sin 2C}$$
$$-\frac{a^2\sin 2B\sin 2C+b^2\sin 2C\sin 2A+c^2\sin 2A\sin 2B}{(\sin 2A+\sin 2B+\sin 2C)^2}.$$

However, trigonometric function in the formula will bring much difficulty to getting the extreme value. We can directly give an expression for $D-d$ related to the sides a,b,c by (2) and (3) as follow

$$D-d=\frac{3abc}{4S}-\sqrt{\frac{1}{2}(a^2+b^2+c^2)+2\sqrt{3}S},$$

where $S=\frac{1}{4}\sqrt{4b^2c^2-(b^2+c^2-a^2)^2}=\frac{1}{4}\sqrt{(a+b+c)(a+b-c)(a+c-b)(b+c-a)}$.

For the sake of convenience, we first study $D-d$ in the isosceles triangle. Without loss of generality, set $b=c=1$, and a can change. So we have $a\in(0,2)$. So we can derive

$$D-d=\frac{3}{\sqrt{4-a^2}}-\sqrt{\frac{1}{2}(a^2+2)+\frac{\sqrt{3}}{2}a\sqrt{4-a^2}}.$$

Let $\frac{\mathrm{d}}{\mathrm{d}a}(D-d)=0$, we have

$$a^{16}-24a^{14}+255a^{12}-1544a^{10}+5727a^{10}-12432a^6+15025a^4-9312a^2+2304=0.$$

The above equation can be solved by Matlab software, and all real roots are as follows $a_1 = 1$ (3 multiple root)， $a_2 = 1.3726$， $a_3 = -1$ (3 multiple root)， $a_4 = -1.3726$.

Image of $D-d$ on a is as follows

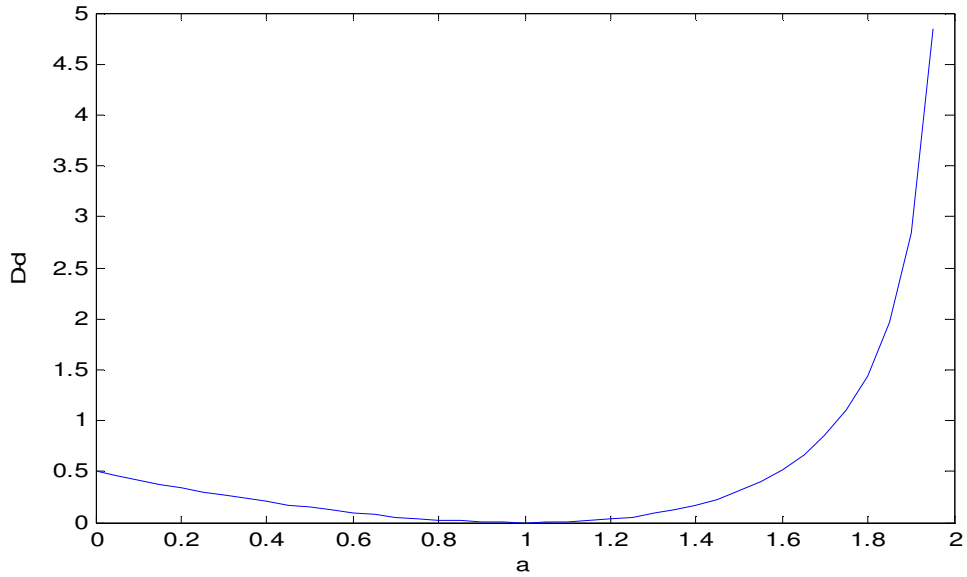

Fig. 3 Image of $D-d$ on a

As can be seen from the image, $a_1 = 1$ is the minimum of $D-d$, but not $a_2 = 1.3726$.

Let's discuss a few special cases.

(1) $A \to 0$. We have $a \to 0$，so $x = b = 1, y = z \to 0.d \to b = 1.$ In addition，we have O tends to the midpoint of $AB(AC)$，so $R \to \frac{b}{2} = \frac{1}{2}$. Hence

$$D - d \to \frac{b}{2} = \frac{1}{2}.$$

(2) $A = B = C = 60^\circ$. We have $a = b = c = 1$，so $x = y = z = \frac{\sqrt{3}}{3}b = \frac{\sqrt{3}}{3}.d = \sqrt{3}.$ In addition，we have $R = \frac{\sqrt{3}b}{3} = \frac{\sqrt{3}}{3}$. Hence

$$D - d = 0.$$

(3) $A = 90^\circ$. We have $\frac{\sqrt{2}}{2}a = b = c = 1$，so $x = \frac{\sqrt{3}-1}{\sqrt{6}}, y = z = \frac{2}{\sqrt{6}}.d = \frac{\sqrt{3}+1}{\sqrt{2}}.$ In addition，we have $R = \frac{a}{2} = \frac{1}{\sqrt{2}}$. Hence

$$D - d = \frac{2-\sqrt{3}}{\sqrt{2}} < \frac{1}{2}.$$

(4) $A = 120^\circ$. We have $x = 0, y = z = b = 1.d = 2.$ In addition，we have $R = b = 1$. Hence

$$D - d = 1.$$

(5) $A \to 180^\circ$. We have $B = C \to 0$，so $x = 0, y = z = b.d = 2b.$ In addition，we have $R \to \infty$. Hence

$$D - d \to \infty.$$

Thus, we can know that for (isosceles) acute triangles, $D-d$ gets the minimum value 0 when three sides are equal under the premise in unchanged. $D-d$ tends to the maximum value that is

the half of waist as the apex angle tends to zero. For obtuse triangle, $D-d$ increases monotonically with the increase of the apex angle, and $D-d$ tends to infinity as the apex angle tends to straight angle.

Summary

The above analysis coincides with a well-known mathematical assertion: the partial equilibrium (optimal) sometimes cannot guarantee the overall optimum for some practical problems. Excessive pursuit of a balanced individual may make the whole bear immeasurable loss.

References

[1] Q.F. Yang, X.S. Kang, Y.N. Zhao, Mathematical Modeling, Higher Education Press, Beijing, 2006.

[2] Q.J. Gao, The formula for the distance from Fermat point to the vertices of the triangle, Middle School Mathematics, 9 (1996) 28-30.

[3] G.B. He, The formula for distances on Fermat point with “hearts” of the triangle, Mathematics Research in High School, 4 (2006) 18-19.

Advanced Materials Research Vols. 989-994 (2014) pp 2381-2384
© (2014) Trans Tech Publications, Switzerland
doi:10.4028/www.scientific.net/AMR.989-994.2381

Adaptive Discriminant Linear Local Tangent Space Alignment Algorithm on Face Recognition

Yuanxing Lv[1, a], Yanni Deng[1, b], Yuan Shi[1, c], Qiang Li[1, d], Wen Peng[1, e]

[1]School of Automation, Wuhan University of Technology, Wuhan, 430070, China

[a]lvyuanxing123@126.com,[b]719145031@qq.com, [c]shiyuan0806@126.com,

[d]332520555@qq.com,[e]pw972909566@126.com

Keywords: Face Recognition, Adaptive Neighborhood, DLLTSA, DALLTSA

Abstract. This paper proposes an adaptive discriminant linear local tangent space alignment algorithm DALLTSA. On the basis of LLTSA algorithm adding adaptive and discriminant gets DALLTSA.DALLTSA not only combines characteristics in DLLTSA that maintain the local geometry and meets the maximum between-class scatter matrix, but also dynamically selects K-neighbor better to reflect the degree of polymerization between samples. Finally, the face recognition experiments based on Gabor[1] filter and DALLTSA shows that this algorithm improves the recognition rate and robustness.

Introduction

With the rapid development of information technology, the application of high-dimensional data is wider, the number of high-dimensional data is also increasing, the dimensionality reduction of high-dimensional data is particularly more and more important .The main purpose of manifold learning is to restore the low-dimensional manifold structure from high-dimensional data. Existing linear local tangent space alignment algorithm LLTSA[2] is a linear optimization algorithm from LTSA. It solves the problem that LTSA can only be used to the training sample not the test sample. But LLTSA does not fully use the prior knowledge of the sample and also has problems about the selection of K-neighbor. Therefore, this paper proposes a DALLTSA algorithm.

In this paper,the face recognition experiments based on Gabor filter and DALLTSA shows that this algorithm improves the recognition rate and robustness.

Discriminant Linear Local Tangent Space Alignment Algorithm (DLLTSA)

The LLTSA algorithm is a linear unsupervised algorithm which we know the type information of the training samples. To make full use of the information, the literature[3] proposes the algorithm (DLLTSA) which takes class information into account and is called linear discriminant local tangent space alignment algorithm.

DLLTSA uses the between-class scatter matrix to modify the restrictions of the objective function of LLTSA. In order to maintain the local geometry and maximum between-class scatter matrix, the optimization problem of DLLTSA is as follows:

$$\begin{cases} \min\limits_{Y} tr(A^T XH_n BH_n X^T A) \\ \max tr(A^T S_b A) \end{cases} \tag{1}$$

s_b means the between-class scatter matrix. The objective function transformed from above conditions is

$$J(A) = \min \frac{tr(A^T XH_n BH_n X^T A)}{tr(A^T S_b A)} \tag{2}$$

The formula (2) is transformed into generalized eigenvalue problem:

$$XH_n BH_n X^T a_i = \lambda_i S_b a_i \tag{3}$$

Then we can get the eigenvalues and eigenvectors, if the corresponding eigenvectors of the eigenvalues $\lambda_1 \le \lambda_2 \le \lambda_3 \le ... \le \lambda_d$ is $a_1, a_2, a_3, ..., a_d$, the required projection matrix is

$$A = [a_1, a_2, a_3, ..., a_d] \tag{4}$$

Adaptive Algorithm

This paper calls adaptive neighborhood selection and LTSA modified model joint adaptive algorithm.

Selection of Adaptive Neighborhood. Literature[4] gives the standard for judging whether a neighborhood set of linear subspace determined by best-fit will approach the popular tangent space with high accuracy. According to the literature, the approximation standard of the tangent space is:

$$\left\| X_i - \left(x_i l_{k_i}^T + \tilde{Q}_i \Theta_i \right) \right\| \le \eta \left\| \Theta_i \right\|_F \tag{5}$$

In the formula, $X_i = \left[x_{i1}, x_{i2}, \ldots, x_{ik_i} \right]$; the matrix of the right singular vectors of the largest d singular values of $\left[x_{i1} - \tilde{x}_{i,}\ x_{i2} - \tilde{x}_i, \ldots, x_{ik_i} - \tilde{x}_i \right]$ is Q_i, $\Theta_i = \left[\theta_1^{(i)}, \theta_2^{(i)}, \ldots, \theta_{k_i}^{(i)} \right]$, $\theta_j^{(i)} = Q_i^T \left(x_{ij} - \tilde{x}_i \right)$; $\lambda_1 \ge \lambda_2 \ge \ldots \ge \lambda_{k_i}$ is the singular values in descending order of the matrix $X_i - \tilde{x}_i l_{k_i}^T$. Q_i is the corresponding right singular vectors of the maximum d singular value. The original standard is equivalent to:

$$\sqrt{\sum_{j \ge d} (\lambda_j)^2} \le \eta \sqrt{\sum_{j<d} (\lambda_j)^2} \tag{6}$$

So we get adaptive neighborhood selection strategy. This paper selects the K-neighbor under the condition of the known target dimension d. Specific steps are as follows:

(1)Select the largest number of sample $k = k_{\max}$ of the maximum neighborhood. Select k-near neighbors of x_i through the k-nearest neighbor principle. It can be expressed as $x_i^{k_{\max}} = \left[x_{i1}, x_{i2} \cdots, x_{ik_{\max}} \right]$.

(2)Select the k_i slightly larger than d as the current number of neighbors, Select the k_i neighborhoods of x_i and Composition of neighborhood set $x_i^{k_i} = \left[x_{i1}, x_{i2} \cdots, x_{ik_{ix}} \right]$.

(3)Calculate the singular value matrix $\left[\sigma_1^{(k_i)}, \sigma_2^{(k_i)} \cdots, \sigma_k^{(k_i)} \right]$ of $X_i^{(k)} - \tilde{x_i^{(k)}} l_k^T$ and arrange the singular value matrix in ascending order. After that, calculate the ratio of the minimum singular value and the sum of other singular values $\delta_i^k = \sqrt{\sum_{j=d} (\sigma_j^{(k)})^2} \Big/ \sqrt{\sum_{j<d} (\sigma_j^{(k)})^2}$. If $\delta_i^k > \eta$ (η is a parameter), at this time jump to the fourth step, expanding the neighborhood set. Instead, jump to the fifth step.

(4) Select g nearest neighbor points in the original largest neighbor set to expand to the smallest neighbor set, g takes the integer greater than 1, recalculate σ_i^k. If $\delta_i^k > \eta$ (η is a parameter), at this time jump to the fourth step, expanding the neighborhood set. Instead, jump to the fifth step.

(5)In the above neighborhood set, remove the relatively large neighborhood spot first. Recalculate δ_i^k. If $\delta_i^k > \eta$ (η is a parameter), proceed to the sixth step. Otherwise, continue into the loop of the fifth step.

(6) At this point, get the best neighborhood set. Neighborhood selection is completed.

Local Tangent Space Alignment (LTSA) Model Amendment. Through the literature[5], we can use the adaptive algorithm to modify the LTSA model in order to reduce the deviation. The minimization of the modified LTSA model is as follows:

$$\sum \frac{1}{k_i} \sum_{j=1}^{k_i} \left\| A_i (I - \frac{1}{k_i} l_{k_i} l_{k_i}^T)(I - \Theta^+ \Theta) D_i^{-1} \right\|_F^2 \tag{7}$$

The formula(7) is transformed into the eigenvalue problem:

$$\sum \frac{1}{k_i} \sum_{j=1}^{k_i} \left\| A_i (I - \frac{1}{k_i} l_{k_i} l_{k_i}^T)(I - \Theta^+ \Theta) D_i^{-1} \right\|_F^2 = \min_A tr(A \Phi A^T) \tag{8}$$

$\Phi = \sum_i \frac{1}{k_i} (S_i W i_i D i^{-1})(S_i W i_i D i^{-1})^T$, $\lfloor A_{1,\cdots,} A_N \rfloor S_i = \lfloor A_{i1,\cdots,} A_{i_{k_i}} \rfloor$, S_i is a 0-1 selection matrix. Moreover, $D_i = diag(\phi_1^{(i)}, \cdots, \phi_{k_i}^{(i)})$, $W_i = (I - \frac{1}{k_i} l_{k_i} l_{k_i}^T)(I - \Theta^+ \Theta)$.

According to the literature[6]. The best linear fitting is $\bar{x} + Q_i \theta_j^i$ for each different curvature match area set and the linear space Q_i is the best approximation to x_i .Geodesic curvature can be approximately estimated as the follow formula:

$$c_j^{(i)} = \frac{\arccos(\sigma_{\min}(Q_i Q_{i_j}^T))}{\left\| \theta_j^{(i)} \right\|} \tag{9}$$

The manifold learning may exist noise, so when the neighborhood point is too close to x_i , it will not be considered when we calculate the mean curvature. Therefore we use a threshold value σ_c to determine whether the point needs to be considered. Finally, the mean curvature can be obtained through the follow formula:

$$\overline{c_i} = mean \ \ \text{of} \ \left\{ c_j^{(i)} \middle| x_j^{(i)} \in x_{i,} \left\| \theta_j^{(i)} \right\| > \sigma_c \max_{j \le k_i} \left\| \theta_j^{(i)} \right\| \right\} \tag{10}$$

So we can get an estimated for $\phi_j^{(i)}$,

$$\phi_j^{(i)} = \overline{c_i} \left\| \theta_j^{(i)} \right\|^2 \tag{11}$$

Face Recognition Algorithm Based on Gabor Filter and DALLTSA

The face recognition experiments are based on Gabor filter and DALLTSA. The specific steps are as follows:

Suppose $X = \{x_1, x_2, ..., x_n\}$ as n pieces (c classes in all) of training images, x_i is the image matrix.

(1) Filtering each face images with Gabor filter in different frequencies and directions to get a lot of groups of Gabor features, n and m respectively represent number and frequency.

(2) Sampling for Gabor features of each group in groups and blocks to get lower dimension characteristics getting the composition of an image matrix c_i , the combination of methods is mentioned above.

(3)For the n samples set $C = \{c_1, c_2, ..., c_n\}$, use $(2D)^2 PCA$ to reduce dimension, then each image matrix is connected by line end to end, each image constitutes a column vector x_i , the matrix $X = [x_1, x_2, ..., x_n]$ is composed of n pieces of pictures.

(4) A secondary feature extraction is to use DALLTSA for feature extraction.

(5)Classify the test samples using the above four steps to obtain a low-dimensional feature vector images and then use the classifier for classification.

Comparison and Analysis of the Experiment Results

In this paper, the experiment uses a self-built library of 120 individuals, 20 photos per person, including all kinds of information gestures, facial expressions and so on. For each person, we

randomly sample 10 images as training samples, take the remaining 10 as test samples, cycle 20 times and take the average rate as the correct recognition rate. When adding adaption to the algorithm we use the letter A, when the discrimination we use the letter D.

The results are the variation of dimension followed by the average recognition rate of the three algorithms (ALLTSA, DLLTSA, DALLTSA) based on face database. The experiment results are shown in Figure.1:

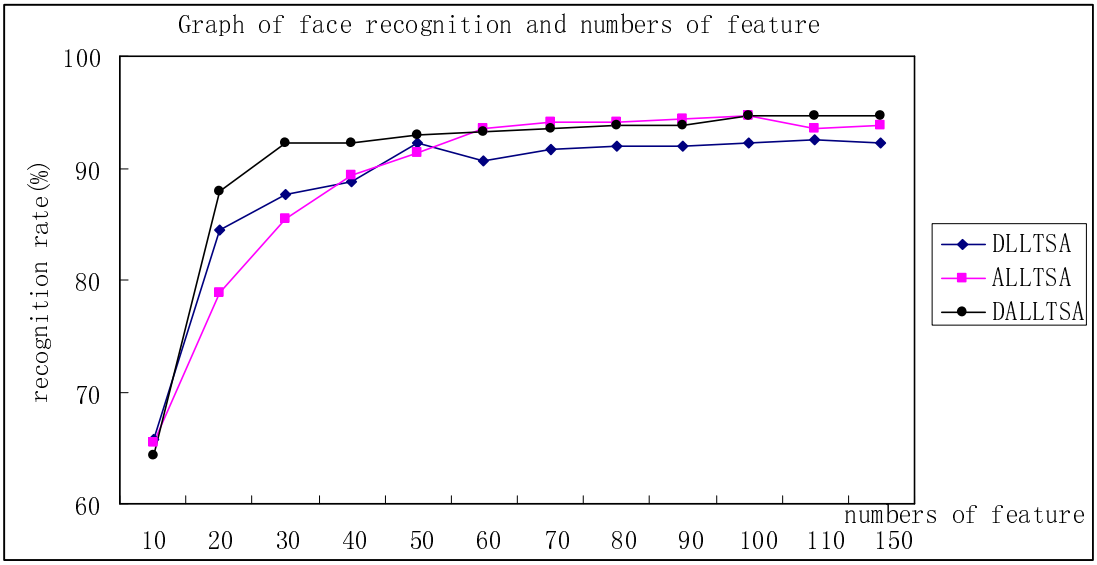

Fig.1.The variation of dimension followed by the average recognition rate of the three algorithms based on face database

From the figure above, between10-60 dimension the algorithm DALLTSA, have improved the recognition rate compared to DLLTSA and ALLTSA. After 60 dimensions their recognition rates approach a straight line basically reaching to the maximum recognition rate.

Summary

The DALLTSA algorithm can play a great role in the improvement, it can not only maintain the local geometry and meet the maximum between-class scatter matrix , but also dynamically select k-neighbor better to reflect the degree of the polymerization between the samples.

Therefore, the DALLLTSA algorithm can well improve the performance and robustness of the algorithm.

References

[1]Rui Sun. Recognition algorithm based on fast Gabor filter [J]. Computer Applications .2012.32

[2]Tianhao Zhang,Jie yang. Linear local tangent space alignment and application to face recognition[J]. Neurocomputing.2007.70(7):1547-1553

[3]Wenhua Li.Improved linear local tangent space alignment algorithm [J].Computer Applications .2011.32 (1):247-249

[4]Wang J,Zhang Z Y, Zha H Y. Adaptive manifold learning Proc Advances in Neural Information Processing Systems,2005,17:1473

[5]Jing Wang. Theory and Methods of manifold learning.Zhejiang University.2006

[6]G.H GoLub and C.F Van Loan. Matrix Computation Press, Baltimore, Maryland,3nd edition, 1996.

[7]Xiangfei Nie. Recognition Review [J]. Chongqing Three Gorges University .2009.3:14-18]

Advanced Materials Research Vols. 989-994 (2014) pp 2385-2388
© (2014) Trans Tech Publications, Switzerland
doi:10.4028/www.scientific.net/AMR.989-994.2385

Research on the traffic rules of the freeway

Yuxuan Jiang

North China Electric Power University, Baoding,071000, China,

email:jennyloverock@163.com

Keywords: Driving Rules of Freeway; Overtaking; Cellular Automaton

Abstract. This paper mainly studies on the superiority of a driving rule of freeway. Using the theory of cellular automaton, we definite two indexes and make evaluation and analysis of the Keep-Right-Except-To-Pass rule under different traffic load conditions. At last, comparing with one of the other rules, we prove the superiority of the common rule.

Introduction

In countries where driving automobiles on the right is the rule (that is, USA, China and most other countries except for Great Britain, Australia, and some former British colonies), multi-lane freeways often employ a rule that requires drivers to drive in the right-most lane unless they are passing another vehicle, in which case they move one lane to the left, pass, and return to their former travel lane.[1]However, compared to the other rules, does the Keep-Right-Except-To-Pass rule really has advantages in some ways? Perhaps most people haven't do research on it.

In this paper, we make an analysis on two driving rules. One is the Keep-Right-Except-To-Pass rule, the other is the rule that both of the lane are allowed to drive on, but no overtaking.

To evaluate a traffic rule, we need to consider both of the quantity of traffic flow and the safety. These two parameters are very closely related .So we established two evaluation indexes to represent the security and the traffic capacity.[2]

In this paper, we use the theory of cellular automata to make a simulation of the actual traffic situation of freeway. We compared the safety of two rules under different traffic loads. Finally, we come to a conclusion.

The theory of cellular automaton

A cellular automaton (pl. cellular automata, abbrev. CA) is a discrete model studied in computability theory, mathematics, physics, complexity science, theoretical biology and microstructure modeling. Cellular automata are also called cellular spaces, tessellation automata, homogeneous structures, cellular 3structures, tessellation structures, and iterative arrays. [3]A cellular automaton consists of a regular grid of cells, each in one of a finite number of states, such as on and off (in contrast to a coupled map lattice). The grid can be in any finite number of dimensions. For each cell, a set of cells called its neighborhood is defined relative to the specified cell. An initial state (time t=0) is selected by assigning a state for each cell. A new generation is created (advancing t by 1), according to some fixed rule (generally, a mathematical function) that determines the new state of each cell in terms of the current state of the cell and the states of the cells in its neighborhood. Typically, the rule for updating the state of cells is the same for each cell and does not change over time, and is applied to the whole grid simultaneously, though exceptions are known, such as the stochastic cellular automaton and asynchronous cellular automaton. [4]

The Keep-Right-Except-To-Pass rule

When vehicles appear in the freeway entrance randomly, compare the random number generated by the computer with the probability P vehicles entering the freeway. When the random number is less than the probability P, vehicles enter into the lane 1.Then we record the number N of vehicles entering into the road. We set the random speed of vehicles entering the freeway in the

range of [2, 5], 2 as the lowest speed, 5 as the highest speed limit. We record the location of car as x (i,j,t),the speed of vehicle as V. We set the step of simulation as 1s,the total simulation time as Ts .Each time the step of time is forward 1 s, we judge the distance $gap_n(t)$ between the two close cars, when $gap_n(t)$ is shorter than the threshold 2, then the car chooses to overtake. It moves to the left lane to pass, and return to their former lane when the overtaking is finished. When the distances between the continuous three cars are both less than the threshold. It may result in a traffic jam .The vehicle trapped in a traffic jam cannot go through this journey in the end. We record the time of the traffic jam N1 and the time of the free passage N2.

The both of lane are allowed to drive on, but no overtaking rule

We definite a freeway the length of which is L. The vehicle appears in the freeway entrance by the probability P. We record the number N of the vehicle entering into the road. We set the random speed of vehicles entering the freeway in the range of [2, 5], 2 as the lowest speed, 5 as the highest speed. We record the location of car as x(i,j,t) and speed of car as V. We set the step of simulation as 1 S, the total simulation time as T s .Each time the step of time is forward 1 s ,judge the distance $gap_n(t)$. If $gap_n(t)$ is shorter than the threshold, It may result in a traffic jam .The vehicle trapped in a traffic jam cannot go through this journey in the end. We record the time of the traffic jam N1 and the time of the free pass N2.[5]

The definition of evaluation indexes

In this process, we notice that there are two indexes. we make the definition of them as follows.

(1)The probability of traffic jams: When a car goes through the freeway with a certain length, it drives faster than the car in front of it and cannot overtake .The probability of this case is called the probability of traffic jams. It's obvious that the index is related to the security. So we use this index to evaluate the traffic safety.

$$\text{the probability of traffic jams} = \frac{the\ time\ of\ traffic\ jams}{the\ number\ of\ the\ cars\ entering\ the\ freeway}$$

(2)The probability of free passage: The probability of a car which is unlikely to be trapped in a traffic jam.This index is evaluated the traffic capacity.

$$\text{the probability of traffic jams} = \frac{the\ number\ of\ free\ passage}{the\ number\ of\ the\ cars\ entering\ the\ freeway}$$

The Simulation Parameters

In the simulation, we set the following Parameters

(1)the probability of the car entering the road pp: We value the probability of the car entering the road as 0.05, 0.15, 0.25, 0.35, 0.45, 0.55, 0.65, 0.75, 0.85, 0.95

(2) The length of the cellular: We define a one-dimensional lattice to represent a single lane. The length of the freeway L is 1 mile, which is divided into 250 cells, namely each cellular actual length is 21 feet. The actual length of the cellular is slightly larger than the average length of car (about 15 feet)

(3) The step of the simulation time dt: We set it as 1 s.

(4) The total time of simulation: We set the time as 500s.

(5) The minimum speed V_{min}:We set the minimum speed as 2 celluar/s,if the step of the simulation is 1s,the corresponding minimum speed is 30 mph, almost equal to the lower limit speed of the freeway, corresponding to V_{min}= 2 celluar/s .We use cell/S as the unit .

(6) The maximum speed V_{max} :We set the minimum speed as 5 celluar/s,if the step of the simulation is 1s,the corresponding min V is 72 mph,equal to the higher limit speed of the freeway, corresponding to V_{max}=5 celluar/S

(7) The random speed entering the road V_r :$V_r = V_{min} + rand \times (V_{max} - V_{min})$

(8) The thresholds of overtaking conditions: We set the thresholds as 2.It's consistent with the actual situation.[6]

The result of the simulation:

The Figure 1 shows the dynamic simulation process of cellular automata.

The second rule seems to increase the number of lanes which are allowed to drive on, but is it safer than the Keep-Right-Except-To-Pass rule?

To analyze which kind of rule is the better in different load conditions, we draw the curve of the two rules above under the same coordinate system. The abscissa represents the probability of a car entering the freeway(namely the load) .If the intersection point exists, this mean the two rules have the same probability of traffic jams(namely the same level of security).The curve below the intersection point has the better level of security.

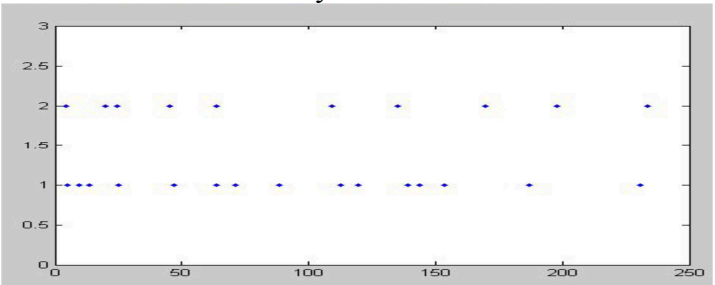

Figure 1 Dynamic simulation figure of cellular automata

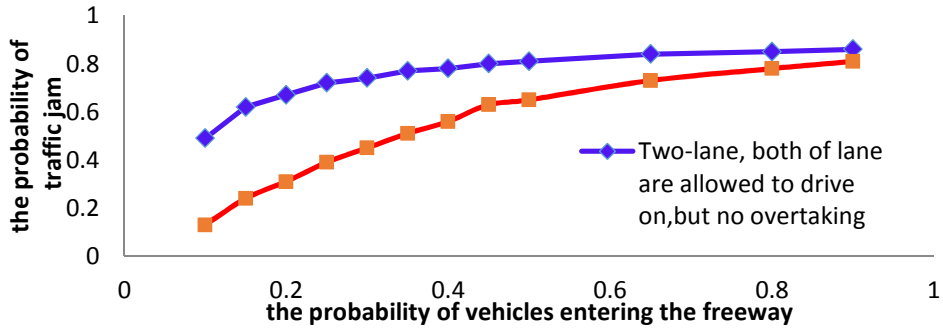

Figure 2 The probability of the traffic jams of the two rules

We can find out from the Figure 2 that when the load is low, the security of the Keep-Right-Except-To-Pass rule is better. What's more, the advantage is obvious. When the load is high, the Keep-Right-Except-To-Pass rule is still safer but the advantage gap is narrowed. So, we can conclude that the Keep-Right-Except-To-Pass rule which is used in most countries is applicable to the freeway.

Conclusion

We conclude that no matter the traffic load is low or high, the Keep-Right-Except-To-Pass Rule is applicable in most countries. It can improve the quantity of traffic flow and the security to a certain extent. Though the advantage is not obvious in the high load, we cannot find an alternative at present.

References

[1]Information on http://baike.baidu.com/view/3750338.htm?fr=aladdin#17

[2]ZhongGengHan,XiaoliGuo,JianpingDu.*The analysis and study on the Mathematical Contest in Modeling*[M].2013.83-90

[3]Wolfram, Stephen .*Statistical Mechanics of Cellular Automata* [M].1983.601–644.

[4]Information on http://en.wikipedia.org/wiki/Cellular_Automaton

[5]YingliZheng,RunpingZhai,SheqiangMa.*The review of the traffic flow Cellular Automaton model*[J].Journal of Highway and Transportation Research and Development.2006(1).58-87

[6]QiyuanJiang, JinxingXie, JunYe.*Mathematical Models* [M].2011.38-43.

Advanced Materials Research Vols. 989-994 (2014) pp 2389-2392
© (2014) Trans Tech Publications, Switzerland
doi:10.4028/www.scientific.net/AMR.989-994.2389

A Collision Detection Algorithm Using AABB and Octree Space Division

Huaiyu Wang[a], Shugui Liu[b]

State key laboratory of precision measuring technology and instrument, Tianjin University, Tianjin 300072, China.

[a]why9433@163.com, [b]sgliu@163.com

Keywords: Collision detection, AABB, octree, space division

Abstract. NC lathe controls the action of the lathe through program control system, while programming mistakes may lead to collisions between NC lathe cutters and workpieces or fixtures. A collision detection system judge whether there are collisions ahead of time by means of reading the information of shape and pose of objects in processing environment, building a space model using CSG and acquring the movement intension of objects. Dividing the modeling space into space nodes using octree, building AABBs of objects to be tested and locating them at certain space nodes, only objects at the same node or the same father node need to be tested, thus testing speed is raised.

Introduction

High precision, complex movement track and fast speed are features of NC process, a virtual NC lathe simulates the actual NC process environment in a computer and predict whether there is a collision that should not happen between moving cutter, workpieces and tool parts, thus damages of lathe equipment are prevented. Collision detection algorithm based on image space is a kind of relatively new collision detection algorithms, it can effectively use graphics hardware rendering acceleration to improve the efficiency of collision detection algorithm. Trianglated mash surface was used to express 3D solid objects [1], while the huge quantity of triangles lead to expensive time consuming, so the precision contradicts with speed.

Real-time and high-efficient are key factors of collision detection, so that the division of process environment is required, and the possibilities of collisions between objects in different nodes or father nodes are excluded, thus times of pairwise test are decreased and efficiency is improved.

Collision Detection Algorithm

The collision detection algorithm can be classified into two classes: bounding box and space division. The main idea of bounding box is to use a simple geometry object like cuboid and sphere to include a virtual object, and substitute the bounding box for the virtual object in the test[2], the objects that must not intersect are excluded firstly, then a precise collision detection of objects that may intersect will be operated, thus test time are reduced; the basic thought of space division is that the space are divided into different regions, only nodes that may arouse concern are noticed while other nodes are not considered, thus the pairwise test numbers are decreased [3].

Axis-Aligned Bounding Box. Axis-aligned bounding box (AABB) is defined as a minimum hexahedron including the object, each edge of which is parallel to a coordinate axis, and AABB is one of the most popular bounding boxes [4]. Its most outstanding character is that fast intersection test can be accessed, for the reason that only coordinate values are compared, while there exists a disadvantage of bad closeness to objects with inclined axises. This paper use "maximum-minimum" method to express an AABB, the intersection test can be accomplished by judging the relationship of six parameters. If the projection of two AABB intersect on every coordinate axis, then the two AABBs intersect in 3D space; as long as there exists an axis on which the projection don't intersect, the two AABBs don't intersect. So the test between AABBs needs 6 times of comparison at most, and codes are as below:

```
class AABB
{double AABB_x_max,AABB_x_min; double AABB_y_max,AABB_y_min;
        doubleAABB_z_max,AABB_z_min;  };
int AABB::testAABBAABB(AABB b)
{       if(AABB_x_max<b.AABB_x_min||AABB_x_min>b.AABB_x_max)return 0;
        if(AABB_y_max<b.AABB_y_min||AABB_y_min>b.AABB_y_max)return 0;
        if(AABB_z_max<b.AABB_z_min||AABB_z_min>b.AABB_z_max)return 0;  return 1;}
```

The Constructive Solid Geometry (CSG) representation allows users to define complex 3D solid objects by hierarchically combining simple geometric primitives using boolean operations [5]. Based on the characters of NC lathe process environment and shape of objects to be tested, CSG can be used to build the model. Considering the "maximum-minimum" method, by computing the maximum and minimum value of the projection of object on three axises, the bounding box can be obtained. As to the primitives whose main axis is parallel to a certain coordinate axis or coordinate plane, its projection can be computed by simple addition and subtraction of its parameters; as to those whose main axis direction is non-special, further operation should be conducted. After building the bounding boxes of primitives, hierarchical bounding box can be built by means of "bottom-to-up".

Cite a cone frustum as an example, for the reason that a cone frustum is of curved surface shape that is more complex than plane-surface-object. Given radius of up surface r_1, radius of bottom surface r_2(when $r_1 = r_2$,the cone frustum becomes a cylinder), center point (O_x,O_y,O_z), height h, and the direction of main axis can be classified into three condition:

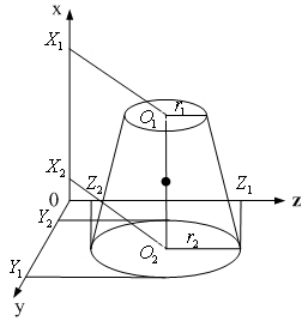

Fig.1 Main axis parallel to *x*-axis

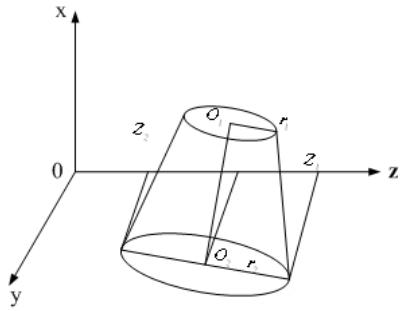

Fig. 2 Main axis parallel to *xoy* plane

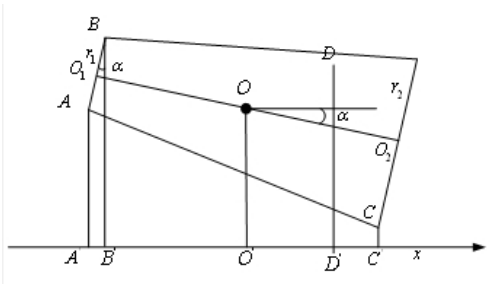

Fig. 3 Projection of main axis onto *x*-axis (main axis parallel to *xoy* plane)

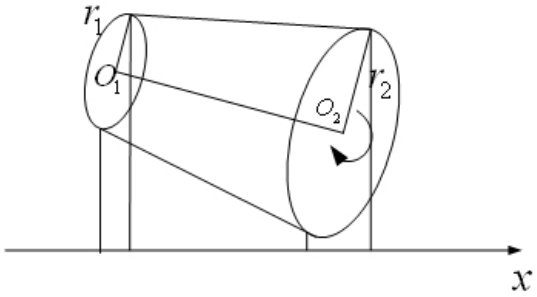

Fig.4 Main axis direction non-specia

1) The Main Axis Parallel to *x*-axis

As the main axis is parallel to *x*-axis，the projection of the cone frustum onto *x*-axis can be regarded as its projection of main axis onto *x*-axis，so the projection interval is $[O_x+1/2h,O_x-1/2h]$, the two surface can be proved to be parallel to *y*-axis and *z*-axis, so projection of the cone frustum onto *y*-axis and *z*-axis can be regarded as its projection of two planes on those two axises. The projection interval on *y*-axis is $[O_y+r_{max}, O_y-r_{max}]$, and the projection interval on *z*-axis is $[O_z+r_{max}, O_z-r_{max}]$, when $r_{max}=\max\{r_1,r_2\}$.

2) The Main Axis Parallel to *xoy* Plane

As the main axis is parallel to *x*oy plane，similarly the projection interval on *z*-axis is $[O_z+r_{max}, O_z-r_{max}]$. The projection on *xoy* plane is a isosceles trapezoid, cite *x*-axis as an example, given the

angle between the axis of trapezoid and *x*-axis is α , project the trapezoid to *x*-axis, and the projection (A',B',C',D') of the four vertexes of the trapezoid (A,B,C,D) form an interval, whose vertexes are the maximum and minimum values of the bounding box on *x*-axis.

3) The Main Axis Direction Non-Special

Cite *x*-axis as an example, the projection interval on the axis can be regarded as the largest interval between its projection of two planes on the axis, while the plane can be seen as a region that is formed by rotating a line segment with the length of the plane radius around the frustum axis, with the rotating center being the plane center. While the angle between the line segment and *x*-axis is the minimum, its projection on *x*-axis is the longest. The vertexes of this interval is the maximum and minimum value of the bounding box on *x*-axis. Fig.6 shows the box of a cone frustum obtained by this algorithm through OpenGL/GLUT graph library.

Octree Division of Space. Octree is a space division algorithm based on tree shape structure, each node of the tree stands for a model space, and each non-leaf node includes 8 child nodes. Root node is the minimum cube containing the whole scene, divide the cube along *x,y, z*-axis evenly into 8 child cubes, and go on to recursively divide them until the tree structure reach the deep designed[6]. The node information includes the center point and width of the model space, the pointers pointing its 8 child nodes and the linked list of objects in this node.

The space octree need to be traversed to insert the objects in the space into space nodes. Starting at the root node, first judge whether current node owns child nodes: if not, insert the object into the current node; if yes, then judge whether the object intersects with two or more child nodes of the current node: if yes, insert the object into current node; if not ,or in other words ,the object is totally included in a certain child node, then regard this child node as current node and traversely judge. Each object in the non-empty node need to be tested with all the objects in the subtree of this node.

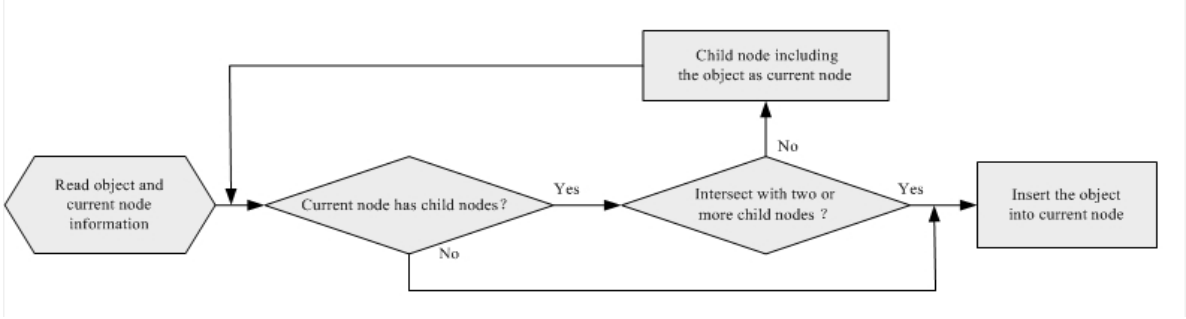

Fig.5 Object insertion flow

Experiment and Conclusion

Verify the validity of bounding box algorithm;divide the environment into octree space and insert objects into space nodes; find the node where the tested object locates and test the object with all the objects in the node and its subnodes. The experiment has been implemented under the circumstance of VC++6.0. The octree was set at a certain deep according to the size and number of objects in the environment , and the objects were quickly located in the octree. The use of AABB and octree algorithm reduced the test time and pairwise test times, and efficiency was increased. While the CSG can only express simple-shape objects that consist of basic primitives, and a more general geomertric representation still need to be applied. This algorithm is a static state collision detection, and the building of active octree remains to be studied.

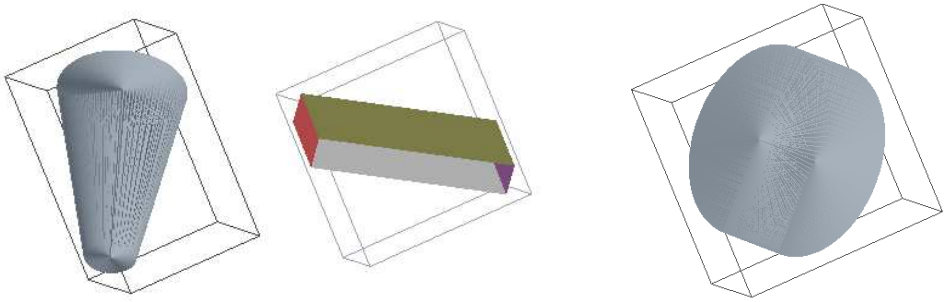

Fig.6 AABB box of primitive

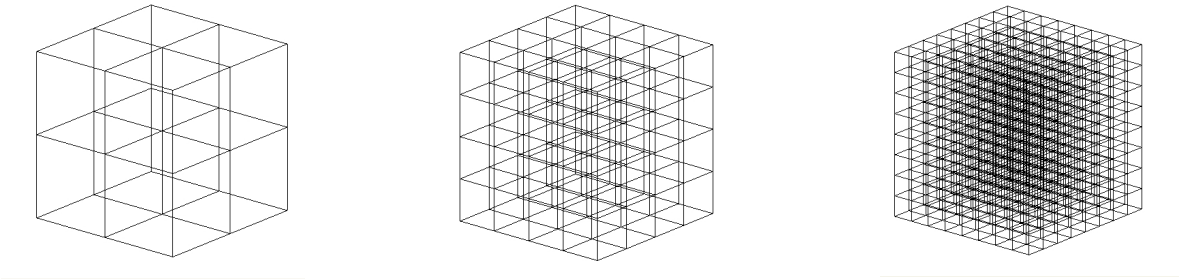

Fig.7 Octree space division (space depth are respectively 1,2and 3)

Acknowledgment

We sincerely thank to the Natural Science Foundation of Tianjin for its financial support to the project. The granted project number is 13JCZDJC34500/E05020402.

References

[1] Lu Qiuling, Zhang Jue,Vector Analysis for Collision Detection of 3D Models with Triangulated Mesh Surface, Computer Aided Engineering, 2002,1.69-72

[2] Wang Liwen, Liu Biyao, Han Junwei, Survey of Box-Based Algorithms for Collision Detection, Journal of Civil Aviation University of China,2007,25（4）16-19

[3] Liu Xiaoping, Cao Li, Parallel Octree Collision Detection Based on MPI, Journal of Computer-Aided Design & Computer Graphics,2007,19(2)184-188

[4] Christer Ericson, Real-Time Collision Detection,1 ed., Tsinghua University Press, Beijing,2010 (in Chinese)

[5] A. A. G. Requicha, Representation for Rigid Solids: Theory, Methods and Systems, Computing Surveys, 1980, 12(4)437-464

[6] Duoduo Liao , Shiaofen Fang. Fast Volumetric CSG Modeling Using Standard Graphics system, Proceedings of Seventh ACM Symposium on Solid Modeling and Applications SM'02, Saarbrucken, Germany, Association for Computing Machinery,2002.204-211

Advanced Materials Research Vols. 989-994 (2014) pp 2393-2397
© (2014) Trans Tech Publications, Switzerland
doi:10.4028/www.scientific.net/AMR.989-994.2393

A Visual Hiding Algorithm Based on Human Visual System

Rui Dong[1, a], Daoshun Wang[1, b]

[1]Department of Computer Science and Technology, Tsinghua University, Beijing 100084, China.

[a]dzippor@sina.com, [b]wangdaoshun@gmail.com

Keywords: Information hiding, HVS, image edge and texture, inverted image.

Abstract. Image information hiding is a way of concealing secret information within another image or file. The previous researches of image information hiding extract secret by calculating. An algorithm based on HVS (Human Visual System) is proposed in this paper. We first decide the embedding region and embedding strength of secret image based on edge and texture information. Then, a pair of invert images is chosen as the cover images, and the stego images are constructed by modifying the pixels of the cover images through the proposed criterion. Correspondingly, the secret image can be recovered through overlaying the two stego images.

1 Introduction

The human visual system has less sensitivity on redundancy of the whole image, partial or slight changes of the image. By taking the advantage of these features, image information hiding embeds the secret into carrier image under the condition that not affecting the transmission quality of the carrier image. Naor and Shamir[1] first proposed the scheme of visual cryptography in 1994. The secret information can be retrieved by a simple superposition. Lee et al.[2] hided information within meaning stego images based on HVS with no pixel expansion. Yamaguchi[3] proposed a continuous hue based scheme using parallel error spread and optimum hue mapping. Both of the two schemes have no pixel expansion, but the cover image can be seen partially in the background of recovered image during recovering. Refs. [4-6] use the digital halftoning to achieve the goals of no pixel expansion. Hou[7] proposed the asymmetric watermarking scheme based on HVS.

In this paper, we propose an visual hiding algorithm scheme based on HVS. A pair of invert images is used as the cover images in this algorithm, and the background color of the recovered image is black, which greatly improves the visual quality the secret image.

2 Related Work

Visual Cryptography is an effective method of information hiding. Hou[7] proposed the asymmetric watermark algorithm based on HVS, and the complementary matrixes Naor and Shamir used are shown as follow:

$$\begin{bmatrix}1 & 0\\1 & 0\end{bmatrix}\begin{bmatrix}0 & 1\\0 & 1\end{bmatrix} \quad \begin{bmatrix}1 & 1\\0 & 0\end{bmatrix}\begin{bmatrix}0 & 0\\1 & 1\end{bmatrix} \quad \begin{bmatrix}1 & 0\\0 & 1\end{bmatrix}\begin{bmatrix}0 & 1\\1 & 0\end{bmatrix}$$

Vertical Horizontal Cross

Hou's algorithm is shown as follow, and an example is given in Figure 1:

Input: $2^{c-1} \times 2^{c-1}$secret image *S*, cover image C

Output: stego image S_1, S_2, cover image C

Construction:

Step 1: if $S(i,j) = 0$, randomly fill the 2×2 blocks of S_1, S_2 into the above matrixes; else if $S(i,j) = 1$, randomly fill the 2×2 of S_1 into the above matrix, and fill S_2's blocks into S_1's complementary matrix, until S_1, S_2 are constructed.

Step 2: if $S_1(i,j) = 1$, decrease the gray scale $C(i,j)$ by 8, until C is constructed.

(a) (b) (c) (d) (e)

Fig. 1 (a) Cover image, (b) original secret image, (c) (d) stego image 1 and 2, (e) recovered image

In image information hiding, the visual quality of the stego image is an important measurement, PSNR is widely used for measuring visual quality of stego image[9,10]. PSNR's definition is shown as follow:

$$PSNR = 10 \cdot \log_{10} \frac{(255)^2}{MSE} dB \tag{1}$$

MSE represents the mean square error between the cover image and stego image：

$$MSE = \frac{1}{M \times N} \sum_{i=1}^{M} \sum_{j=1}^{N} (x_{i,j} - y_{i,j})^2 \tag{2}$$

where $x_{i,j}$ and $y_{i,j}$ represent the pixel value of cover and stego image respectively, $M \times N$ represent the size of image. Generally, MSE can be used to evaluate the quality of binary image.

In Hou et al.'s algorithm, the PSNR of the stego image is 26.144dB, and we can see that the stego image has serious artifacts comparing with the original cover image.

3 Proposed Visual Hiding Algorithm

In this section, the detail of the proposed algorithm will be shown. Our algorithm is similar to Hou's algorithm[8], both of them are based on HVS. Firstly, the cover image is halftone processed with error diffusion algorithm. Then embed the secret image into the texture and less visual sensitive regions of the cover image.

3.1 Texture and Edge.

According to the HVS characters, the process strength of the stego image is affected by the texture complexity, the more complex the texture is, the higher the available process strength is, correspondingly, the higher the recovered image quality is. So it is effective to use the edge and texture to decide the embedding region and strength.

The entropy[9] of image represents the image's average information amount, and it can be used to evaluate texture's complexity. Variance is a measure for edge in images, and generally, the variance around edge is much bigger. Based on the relation between entropy and variance, we can divide the region feature into the following four categories:

Table 1 Feature categories based on entropy and variance

	Smooth	Edge	Texture	Others
Entropy(*H*)	small	big	large	small
Variance (*Var*)	small	big	small	large

Through the above, we can conclude that regions with complex textures and less edges are the ideal regions for embedding. Secret embedding needs regions that contain a lot of textures, so the entropy will be taken into consideration firstly.

3.2 Construction of the Algorithm.

The cover images used in this algorithm are two halftoned images with invert color to each other. The pixels of the input secret image *S* are black, and the recovered image has the invert color, which greatly increases the contrast.

Let secret image be *S*, let cover image 1 and cover image 2 be I and I' respectively. Let stego image 1 and 2 be S_1 and S_2 respectively, and T be the threshold of detection. Let $M_1(M_2)$ be the

modification degree of the first(second) pixel in the 1×2 block of stego image 1. Let $M'_1(M'_2)$ be the modification degree of the first (second) pixel in the 1×2 block of stego image 2.The algorithm use T to constraint the modification of the current pixel. Table 2 give the detail criterion for modification:

Table 2 Criterion for pixel modification

S	I	I'	condition	S_1	S_2
[1 1] [1 0] [0 1]	[1 0]	[0 1]	Probability: 1/2	[1 0]	[1 0]
	[0 1]	[1 0]		[0 1]	[0 1]
	[0 0]	[1 1]	$M'_1 \geq T$	[0 0]	[1 0]
			$M'_1 < T\ M'_2 \geq T$	[0 0]	[0 1]
	[1 1]	[0 0]	$M_1 \geq T$	[1 0]	[0 0]
			$M_1 < T\ M_2 \geq T$	[0 1]	[0 0]
[0 0]	without any modification				

In the modification criterion is based on the connected region's white pixels. And the modification degree is to avoid adhesion. A pending pixel has 8 neighbor black pixels in continuous 3×3 connected region. In this paper, we set weight for the other 8 pixels in the connected region to decide the modification degree $M(i,j)$. Let function $B(x,y)$ return 0 on $x=y$, return 1 on $x \neq y$, then the modification degree of $A(i,j)$ is:

$$M(i,j)=\sum_{r=-1}^{1}\sum_{t=-1}^{1} w(A(i,j),A(i+t,j+t))B(A(i,j),A(i+t,j+t)) \quad (3)$$

where $w(x,y)$ represents the weight of the pixel on coordinate (x,y), and the weight assigning criterion is shown as following:

a) 5 for pixel with no modifications.
b) For modified pixels: 3 for pixels in diagonal direction, 2 for pixels in horizontal and vertical directions.

Assigning different weights for pixels with and without modifications is to decrease the possibility of adhesion caused by modifying neighbor pixels. Treating horizontal and vertical pixels differently is for the reason that human eyes are more sensitive to horizontal and vertical pixels than the diagonal ones. The detail algorithm is given as fellow.

Input: original secret image *S*, grayscale image *C*
Output: stego image S_1, S_2
Construction:
Step 1: Halftone process *C* to get cover image *I* and the invert image *I'*, let $S_1 = I, S_2 = I'$.
Step 2: Decide the start coordinate of the stego region: *X,Y*.

(1) Define a new structure "*D*", which contains the elements of coordinate, entropy and variance.

(2) Scan *C* pixel by pixel with a sliding window is size *S*, and record the entropy, MSE and start coordinate of the region to an array Arr with *D* as element and in size *N*.

(3) Sort the array Arr in entropy descending order. Get the element with the biggest MSE as D_E from the first $\lceil \partial N \rceil$ elements in Arr($0<\partial<1$), record its coordinate as *X,Y*

Step 3: Scan *S* with row step size 1 and column step size 2 to get neighbor pixels $S(i,j)$, $S(i,j+1)$, and the the corresponding cover image $I(i+X-1,j+Y-1)$ and $I(i+X-1,j+Y)$.
Step 4: Calculate the modification degree for $S(i,j)$, $S(i,j+1)$, $I(i+X-1,j+Y-1)$ and $I(i+X-1,j+Y)$
Step 5: According to the table 2, then modify S_1 and S_2 according to the modification degree and detection threshold *T*.

Example 1: original secret image *S*: $[1\ \ 0\ \ 1\ \ 1\ \ 0\ \ 0]$, cover image *I*: $\begin{bmatrix} 1 & 0 & 1 & 0 & 1 & 1 & 0 & 0 \\ 1 & 1 & 0 & 1 & 1 & 0 & 0 & 1 \\ 1 & 0 & 1 & 0 & 1 & 1 & 0 & 0 \end{bmatrix}$, set all the initial weights to 5, ideal embedding position: *X*=2, *Y*=2. Sequentially scan two

consecutive pixels of the original secret image, detection threshold T=20, the stego image is constructed as follows:

1. $S = [1 \quad 0]$, $I = [0 \quad 0]$, $I' = [1 \quad 1]$. The modification degree of the first pixel of S_2: $M'_1 = 3 \times 5 = 15 < T$, then this pixel cannot be modified. The modification degree of the first pixel of S_2: $M'_2 = 4 \times 5 = 20 \geq T$, then this pixel can be modified. Modify the corresponding block of S_2 to $[0 \quad 1]$, and mark this pixel as "modified". The recovered result: $R = [0 \quad 1]$.
2. $S = [1 \quad 1]$, $I = [1 \quad 0]$, $I' = [0 \quad 1]$. Permute the two consecutive pixels values of the S_1 or S_2 with probability 0.5, in this process modify the corresponding block of S_2 to $[1 \quad 0]$, and mark the pixel as "modified". The recovered result: $R = [1 \quad 0]$.
3. $S = [0 \quad 0]$. No need to modify.

4 Comparison and Discussion

4.1 Experimental Results.

By observing Figure 2, it is convenient to see that as T differences, The quality of the stego images and the recovered image changes. Figure 2 is the experimental results by different T. By observing experimental results, when T=0, the stego image will leak the information for the secret image. So the appropriate value for T is important. As T increases, the quality of stego images increase while the quality of recovered image decreases.

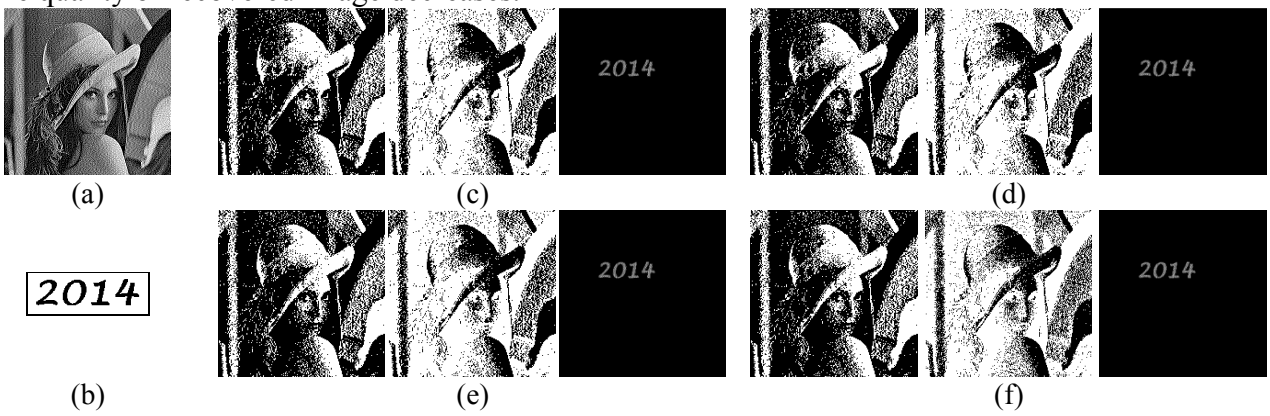

(a) (c) (d)

(b) (e) (f)

Fig. 2 Experimental results. (a) cover image, (b) secret image, (c)-(f) stego images and recoverd image are generated with T=0, 10, 21, 25

MSE can be used to evaluate the quality of binary image. The smaller the MSE, the better the quality of stego images. The secret have the number of black pixels is 2838. This paper defines the number of the meaningful pixels as information amount, which can be counted to describe the quality of the recovered image. The comparison result is summarized as Table 3.

Table 3 MES for stego images with different T

T	Stego 1	Stego 2	Information amount
0	300.1413	239.5167	1553
10	260.7013	235.6482	1345
21	174.6277	170.1628	843
25	156.5200	159.0005	729

By observing Table 3, it is convenient to see that as T increases. The MSE of the stego images increase and the information amount of the recovered image increase (Because of the stego 2 is inverse, when calculating the MSE of the stego 2, we should use the inverted cover image). By the experimented results, different texture complexity of image result in different embedded effect. So the ideal value of T is variable in different cases. By observing the experimental results, when T=21, the experimental result is ideal.

4.2 Comparison with Hou's Algorithm.

In this section, we compare the proposed algorithm with Hou's algorithm in four typical aspects: (1) the type of cover image, (2) whether require extra pixel expansion or not, (3) whether require the stego images meaningful or not, and (4) the quality of recovered image.

Table4 Comparison of the proposed algorithm and Hou's algorithm

Algorithms	Cover images	Pixel expansion	Meaningful		The quality
			S_1	S_2	
Hou's algorithm	Gray	m=4	Yes	No	Less poor
Our algorithm	Halftone	m=1	Yes	Yes	Good

From Table 4, the cover image in Hou's algorithm is grayscale image, the stego image 2 is random lattice,and the recovered image has the problem of pixel expansion (m=4). In case of minor modification, it may be low chromatic aberration between the secret regions and others, so, identifying the secret information through human vision is difficult in this case. This paper's algorithm has no pixel expansion, and all the two stego images are meaningful. All the non-secret information regions of recovered image are formed by black pixels, so the recovered image has better visual effect. Combined with the grey-level modification method in Hou's algorithm, this paper's algorithm can extends to the grayscale stego image algorithm, and the recovered image could also have high visual effect.

5 Conclusions

This paper proposes a visual Hiding method based on visual cryptography. This algorithm chooses the ideal embedding region for secret image based on the HVS characters, which can decrease the possibility of the meaningful neighbor pixels adhesion of the secret image, and decrease the phenomenon of the exposing of the secret. While inversing the cover images, it improves the contrasts of the recovered image.

Acknowledgment

This research was supported in part by the National Natural Science Foundation of China (Grant Nos. 61170032and 61373020), and in part by the Project of General Administration of press and publication of China (GAPP-ZDKJ-BQ/15-2).

References

[1] M. Naor, A. Sharmir, Visual Cryptography[C]// Preproceeding of Eurocrypt 94. BerLin: Springer, 1994:1-12.
[2] K. H. Lee, P. L. Chiu, An extended visual cryptography algorithm for general access structures, IEEE Transactions on Information Forensics and Security, 2012, vol. 7(1): 219-229.
[3] Y. Yamaguchi, An extended visual cryptography algorithm for continuous-tone images, Lecture Notes in Computer Science(LNCS), 2012, vol.7128, pp. 228-242.
[4] Y. C. Hou, S. F. Du, Visual Cryptography Techniques for Color Images without Pixel Expansion[J]. Journal of Information. Technology and Society, 2004 (4): 95-110.
[5] M. Nakajima and Y. Yamaguchi, “Extended visual cryptography for natural images,” in Proc. WSCG Conf. 2002, 2002, pp. 303-412.
[6] Y. C. Hou, C. F. Lin, C. Y. Chang, Visual cryptography for color images without pixel expansion. Journal of Technology. 2001, 16(4):595-603.
[7] Y. C. Hou, P. M. Chen, An asymmetric watermarking scheme based on visual cryptography. Proc. of ICSP, Vol. 2, 2000, pp. 992-995.
[8] R. W. Floyd, An adaptive algorithm for spatial gray-scale[C]//Proc. Soc. Inf. Disp. 1976, 17: 75-77.
[9] C. I. Podilchuk, E. J. Delp, Digital watermarking: algorithms and applications[J]. IEEE Signal Processing Magazine, 2001, 18(4): 33-46.
[10] I. J. Cox, M. L. Miller, The first 50 years of electronic watermarking[J]. Journal of Applied Signal Processing, 2002(2): 126-132

Advanced Materials Research Vols. 989-994 (2014) pp 2398-2401
© (2014) Trans Tech Publications, Switzerland
doi:10.4028/www.scientific.net/AMR.989-994.2398

Augmented Lagrangian method for nonlinear programming with many complex constraints

Xiaowei Jiang, Yueting Yang*, Yunlong Lu

School of Mathematics and Statistics, Beihua University, Jilin, 132013, China

jxwbh @126.com

*Corresponding author

Keywords: optimization; multiplier method; active set; aggregate function.

Abstract. A method of multiplier is presented for solving optimization problems. For large-scale constraint problems, combining the active set strategy, we use the aggregate function to approximate the max-value function. Only a few of functions are involved at each iteration, so the computation for gradient is significantly reduced. The numerical results show that the method is effective.

Introduction

We consider the nonlinear programming problem

$$\min f^0(x)$$
$$\text{s.t. } f^i(x) \le 0, \quad i \in M = \{1, 2, \cdots, m\}, \tag{1}$$

where $f^i(x): R^n \to R$ and m is a very large positive integer. The feasible set set is denoted by Ω. Nonlinear programming has a wide application, such as economic plan, engineering design and optimization control, transportation and national defense and other fields [1,2].

Rather than linear programming has won recognition such as the simplex method and interior-point method, it is of great difficulty and challenge for the solution of the nonlinear optimization, because the problem with large numbers of constraints usually appears in real life situations and constraints can sometimes be quite complicated. Many researchers have long committed to the research of nonlinear optimization algorithm effectively, and has achieved fruitful results.

At present, there are several classes of methods to solve the problem (1), including SQP methods, interior-point methods, the methods of feasible directions and penalty methods, etc. A difficulty is huge amount of calculation due to the large number of constraints to solve the problem (1.1), and active set strategies [3] will be used to deal with the problem in this paper.

The paper is organized as follows. An augmented Lagrangian method for (1) is presented and the details of the algorithm with active set strategy are also given in section 2.

Numerical tests comparing the performance of the proposed method with general augmented Lagrangian method without active set strategy in section 3. Finally, the summary of this paper is made.

Augmented Lagrangian method

We transform (1) into the following form

$$\min f^0(x)$$
$$\text{s.t. } f_{\max}(x) = \max_{i \in M} f^i(x) \le 0. \tag{2}$$

As we know, the aggregate function is a good approximation function of the max value function[4]. For $f_{\max}(x)$ in (2), the aggregate function is defined as

$$f_p(x) = \frac{1}{p}\ln(\sum_{i=1}^{m}\exp(pf^i(x))), \tag{3}$$

where p>0 is referred to as the smoothing parameter[3].

We now consider the approximation of problem (2)

$$\min f^0(x)$$
$$\text{s.t. } f_p(x) \le 0. \tag{4}$$

It can be transformed into the equality constrained problem

$$\min f^0(x)$$
$$\text{s.t. } f_p(x) + y^2 = 0.$$

The corresponding the augmented Lagrange function is as follow,

$$\tilde{\psi}_p(x, y, \lambda, \sigma) = f^0(x) - \lambda[f_p(x) + y^2] + \frac{\sigma}{2}[f_p(x) + y^2]^2.$$

We minimize $\tilde{\psi}_p(x, y, \lambda, \sigma)$ about y. Let

$$\nabla\tilde{\psi}_p(x, y, \lambda, \sigma) = 0,$$

we have

$$y^2 = \begin{cases} \frac{1}{\sigma}[\lambda - \sigma f_p(x)], & \text{if } \lambda - \sigma f_p(x), \\ 0, & \text{else.} \end{cases}$$

So

$$f_p(x) + y^2 = \begin{cases} \frac{1}{\sigma}\lambda, & \text{if } \lambda - \sigma f_p(x), \\ f_p(x), & \text{else.} \end{cases}$$

From the above conditions, the fact is that

$$-\lambda[f_p(x) + y^2] + \frac{\sigma}{2}[f_p(x) + y^2]^2 = \frac{1}{2\sigma}((\min\{0, \lambda - \sigma f_p(x)\})^2 - \lambda^2),$$

so the variable y in $\tilde{\psi}_p(x, y, \lambda, \sigma)$ can be eliminated, we denote it by

$$\tilde{\psi}_p(x, \lambda, \sigma) = f^0(x) + \frac{1}{2\sigma}((\min\{0, \lambda - \sigma f_p(x)\})^2 - \lambda^2).$$

Now we begin by describing an augmented Lagrange method for minimizing the problem.

Algorithm 2.1 (ASAL method)

Initialization. $x^0 \in R^n, p_1, \hat{p}, \sigma_1, \varepsilon(p) > 0, \lambda_1 \in R, \mu, \eta > 1, i = 1.$

Step 1. Let x^{i-1} be the initial point, deriving the minimal point x^i to solve the problem

$$\min\tilde{\psi}_{p_i}(x, \lambda_i, \sigma_i)$$

using subroutine 2.1.

Step 2. If $\|\nabla\tilde{\psi}_{p_i}(x^i, \lambda_i, \sigma_i)\| \le \varepsilon(p_i)$ is not satisfied, go to Step 3. Otherwise, if $p_i > \hat{p},$, stop; else set $p_{i+1} = \mu p_i, x^{i+1} = x^i, i = i+1,$, go to Step 2.

Step 3. If $\|\nabla\tilde{\psi}_{p_i}(x^i, \lambda_i, \sigma_i)\| \ge \|\nabla\tilde{\psi}_{p_i}(x^{i-1}, \lambda_i, \sigma_i)\|$, set $\sigma_{i+1} = \eta\sigma_i;$ else set $\sigma_{i+1} = \sigma_i$.

Step 4. $\lambda_{i+1} = \min\{0, \lambda_i - \sigma_i f_{p_i}(x_i)\}$.

Step 5. Set $p_{i+1} = p_i, i = i+1,$ go to Step 1.

For convenience, we denote $\tilde{\psi}(x) = \tilde{\psi}_{p_i}(x^i, \lambda_i, \sigma_i)$. In addition, we define

$$Q_\varepsilon(x)=\{j\in M \mid f_{\max}(x)-f^i(x)\le\varepsilon\}.$$

Subroutine 2.1 (Solving subproblem)

Initialization. $t=0, x^{i0}=x^{i-1}, \alpha\in(0,1/2), \beta\in(0,1), \bar{\varepsilon}>0, \Omega_0=Q_\varepsilon(x^{i0}), B_0=E.$

Step 1. Compute the search direction d^t by solving the equation

$$B_t d=-\nabla\tilde{\psi}^{\Omega_t}(x^{it})$$

of d.

Step 2. Find the smallest nonnegative integer m_t such that

$$\tilde{\psi}^{\Omega_t}(x^{it}+\beta^{m_t}d^t)-\tilde{\psi}^{\Omega_t}(x^{it})\le\alpha\beta^{m_t}\nabla\tilde{\psi}^{\Omega_t}(x^{it})d^t.$$

Set $\tau_t=\beta^{m_t}$.

Step 3. Set $x^{i,t+1}=x^{it}+\tau_t d^t, \Omega_{t+1}=\Omega_t\cup Q_\varepsilon(x^{i,t+1})$.

Step 4. If $\|\nabla\tilde{\psi}^{\Omega_{t+1}}(x^{i,t+1})\|\le\bar{\varepsilon}$, set $x^i=x^{i,t+1}$, exit. Else, set $t=t+1$, go to Step 1.

Numerical experiment

In this section, compare our method with general augmented Lagrangian method without active set strategy, denoted by AL method.

Parameters in AL/ASAL method and subroutine are set as:

$p_1=100, \hat{p}=10^7, \sigma_1=2, \mu=5, \eta=10, \varepsilon(p)=10^{-6}, \alpha=0.1, \beta=0.5, \bar{\varepsilon}=10^{-6}.$

All the computations are done by running MATLAB2009b. Numerical results are listed in following tables, where x^* is the optimal point, $f(x^*)$ is the optimal value, k denotes the number of outer iterations, ink denotes the number of inner iterations and time is the CPU time in seconds.

Problem 4.1

$$f^0(x)=x_3^2+x_4^2,$$
$$f^{i,j}(x)=(t_i-x_1)^2/x_3^2+(t_j-x_2)^2/x_4^2-1,$$
$$t_i=i/(\sqrt{m}-1), i=1,\cdots,\sqrt{m}-1,$$
$$t_j=j/(\sqrt{m}-1), j=1,\cdots,\sqrt{m}-1,$$
$$x^0=(0,0,100,100).$$

Table 1 The numerical results of Problem 4.1

m	method	x^*	$f(x^*)$	k	ink	time
25	AL	(0.5000,0.5000,-0.7071,-0.7071)	1	7	38	0.3228
	ASAL	(0.5000,0.5000,-0.7071,-0.7071)	1	7	32	0.3754
100	AL	(0.5000,0.5000,-0.7071,-0.7071)	1	7	61	0.3734
	ASAL	(0.5000,0.5000,-0.7071,-0.7071)	1	7	36	0.3675
2500	AL	(0.5000,0.5000,-0.7071,-0.7071)	1	8	68	2.8626
	ASAL	(0.5000,0.5000,-0.7071,-0.7071)	1	8	40	1.0044
10000	AL	(0.5000,0.5000,-0.7071,-0.7071)	1	9	84	7.2491
	ASAL	(0.5000,0.5000,-0.7071,-0.7071)	1	9	46	3.2938
250000	AL	(0.5000,0.5000,-0.7071,-0.7071)	1	15	102	257.6934
	ASAL	(0.5000,0.5000,-0.7071,-0.7071)	1	14	73	122.2605

From the above table, we can see that our proposed method, ASAL method, is more effective than the general augmented Lagrange method, especially for multi-constraint problems, our method can save at least half of the time than the traditional one.

Summary

An augmented Lagrangian method is presented in this paper. Due to active-set strategy is involved, at each iteration, only a small subset of components in max value function is aggregated, hence the calculation of gradient is dramatically reduced, so that cost is greatly reduced. Numerical test show that our method is effective.

References

[1] J. Nocedal, S.J. Wright, Numerical optimization (second edition), Springer, New York, 2006.

[2] Y.X. Yuan, W.Y. Sun, Theory and Methods of Optimization, Science Press, Beijing, 1999.

[3] E. Polak, R.S. Womersley, H.X. Yin, An algorithm based on active sets and smoothing for discretized semi-infinite minimax problems, J. Optim. Theory Appl. 138(2008)311-328.

[4] X.S. Li, An aggregate function method for nonlinear programming, Sci. China(A) 34 (1991)1467-1473.

Advanced Materials Research Vols. 989-994 (2014) pp 2402-2405
© (2014) Trans Tech Publications, Switzerland
doi:10.4028/www.scientific.net/AMR.989-994.2402

Consensus Equilibrium Point Analysis for Heterogeneous Multi-agent system in Undirected graph

Sun Yi-Jie Zhang Guo-liang Zeng Jing

High-Tech Institute of Xi'an, Xi'an Shanxi 710025, China

syjlxh@126.com

Keywords: Heterogeneous Multi-agent system, Graph Theory, Equilibrium Point .

Abstract: The consensus problem of heterogeneous multi-agent systems is investigated. A linear consensus protocol is proposed for this system. Aiming at consensus condition can be only obtained, but the consensus equilibrium point cannot be obtained in this study, the consensus equilibrium point is derived by applying graph theory and matrix theory in this paper. Finally, a numerical simulation is provided to illustrate the effectiveness of the theoretical result.

1. Introduction

Recently, decentralized coordination of multi-agent systems has received compelling attention from various scientific communities. For multi-agent systems, a critical problem is to design a distributed control protocol based on local information that makes all agents to reach an agreement on certain global criteria of common interest by negotiating with their neighbors, which is called as the consensus problem. Much progress has been achieved in the study of constructing conditions for reaching consensus among multi-agent systems [1-4].

Unfortunately, all the aforementioned multi-agent systems were homogeneous, that is, all the agents have the same dynamics behavior. However, the dynamics of the agents are quite different because of various restrictions or the common goals with mixed agents in the practical systems. Liu [5] studied the stationary consensus of discrete-time heterogeneous multi-agent systems with communication delays. Yu-Ping Tian studies the high-order consensus problem for heterogeneous multi-agent systems with unknown communication delays [6]. Yuanshi Zheng studies the finite-time consensus problem of heterogeneous multi-agent systems composed of first-order and second-order integrator agents [7].

However, many study on this topic is only consider the consensus condition, the consensus equilibrium point is analyzed rarely, so this paper investigates this problem.

2. Preliminaries

2.1 Graph theory

Let $\mathcal{G}(\mathcal{V},\mathcal{E},\mathcal{A})$ be a weighted directed graph composed of a set of nodes $\mathcal{V}=\{v_1,v_2,...v_n\}$, set of edges $\mathcal{E}\subset\mathcal{V}\times\mathcal{V}$, and a weighted adjacency matrix $A=[a_{ij}]_{n\times n}$, with nonnegative adjacency elements a_{ij} .An edge of $\mathcal{G}$ is denoted by $e_{ij}=(v_i,v_j)\in\mathcal{E}$ .which means that node v_i receives information from node v_j , and v_j is called the parent of v_i .The adjacency elements associated with the edges of the graph are positive i.e., $e_{ij}\in\mathcal{E}\Leftrightarrow a_{ij}>0$. Moreover, we assume $a_{ii}=0$ for all $i\in 1,...n$. The set of neighbors of node v_i is denoted by $N_i=\{v_j\in\mathcal{V}:(v_i,v_j)\in\mathcal{E}\}$ .The corresponding graph Laplacian $L=[l_{ij}]_{n\times n}$ can be defined as:

$l_{ij}=\begin{cases}-a_{ij}, j\neq i\\ \sum_{j\in N_i}a_{ij} \quad j=i\end{cases}$ If $a_{ij}=a_{ji}$, then $\mathcal{G}$ becomes the undirected graph. If there is not isolated node in an undirected graph, the graph is said to be connected.

In heterogeneous multi-agent system, the neighbor of each second-order agent i incudes first-order and second-order agent, denote as $N_i=N_i^s\cup N_i^f$, the neighbor of each second-order denote as $N_l=N_l^s\cup N_l^f$.

The Laplacian matrix can denote as follow: $L=\begin{bmatrix} \bar{L}_s & -A_{sf} \\ -A_{fs} & \bar{L}_f \end{bmatrix}$,

where, $\bar{L}_s = D_{sf} + L_s$, L_s is the Laplacian matrix of second-order agent, $D_{sf} = diag(\sum_{j\in N_i^f} a_{ij}, i = 1,....m)$, denotes the adjacency relations of second-order agent to first-order agent. Meanwhile, L_f is the Laplacian matrix of first-order agent, $D_{fs} = diag(\sum_{j\in N_l^s} a_{lj}, l = m+1,....n)$, A_{fs} denotes the adjacency relations of second-order agent to first-order agent.

2.2 The heterogeneous multi-agent system

Suppose that the heterogeneous multi-agent system consists of first-order and second-order integrator agents. The number of agents is n, labeled 1 through n.Firstly, the heterogeneous multi-agent system and concept of consensus are established. Suppose that the number of second-order integrator agents is $m(m<n)$.The remainder is first-order integrator agents, the number is $n-m$.Then the system is given as follows:

$$\begin{cases} \dot{x}_i = v_i \\ \dot{v}_i = u_i \qquad i = 1,...m \\ \dot{x}_l = u_l \qquad l = m+1,....n \end{cases} \tag{1}$$

Where x_i, v_i, u_i are the position, velocity and control input, of second-order agent i respectively. x_l, u_l are the position and control input of first-order agent l respectively. The initial conditions are $\boldsymbol{x}(0) = [x_1(0), x_2(0),...x_n(0)]^{\mathrm{T}}$, $\boldsymbol{v}(0) = [v_1(0), v_2(0),...v_m(0)]^{\mathrm{T}}$.

3. Main results

In this section, we first propose the consensus protocol for the heterogeneous multi-agent system (1) as follows

$$\begin{cases} u_i = k_1 \sum_{j\in N_i} a_{ij}(x_j - x_i) + k_2 \sum_{j\in N_i^f} a_{ij}(v_j - v_i), i = 1,...m \\ u_l = k_3 \sum_{j\in N_l} a_{ij}(x_j - x_i), l = m+1,...n \end{cases} \tag{2}$$

Where, $k_1, k_2, k_3 > 0$ are the control gains. Let $\boldsymbol{y} = [x_s^{\mathrm{T}}, v_s^{\mathrm{T}}, x_f^{\mathrm{T}}]^{\mathrm{T}}$, the system can be denote following matrix form

$$\dot{y} = \Gamma y = \begin{bmatrix} 0 & I_m & 0 \\ -k_1\bar{L}_s & -k_2 L_s & k_1 A_{sf} \\ k_3 A_{fs} & 0 & -k_3\bar{L}_f \end{bmatrix} y \tag{3}$$

Lemma 1[3] Let $\mathcal{G}(\mathcal{V},\mathcal{E},\mathcal{A})$ be a undirected graph with Laplacian L . If $\mathcal{G}(\mathcal{V},\mathcal{E},\mathcal{A})$ is connected, then, $rank(L) = n-1$.

Theorem 1 The sufficient condition of the heterogeneous multi-agent system (1) achieves consensus with protocol (2) is as follow

(1)The $\mathcal{G}(\mathcal{V},\mathcal{E},\mathcal{A})$ is connected, and the subgraph $\mathcal{G}^s(\mathcal{V},\mathcal{E},\mathcal{A})$ of $\mathcal{G}(\mathcal{V},\mathcal{E},\mathcal{A})$, which includes all second-order agent is also connected;

(2)The parameters satisfy following conditions: $0 < k_1 < k_2 \min d_i^s - \max d_i, k_2 > \max d_i / \min d_i^s, k_3 > 0$.

Where, $d_i^s, i = 1,...m$ is the diagonal element of L_s , and $d_i, i = 1,...m$ is the diagonal element of L.

Proof: Consensus of the system(3) depends on the eigenvalues of matrix Γ. A nonsingular transformation P is introduced for analyzing matrix Γ.

$$P = \begin{bmatrix} I & 0 & 0 \\ I & \dfrac{I}{k_1} & 0 \\ 0 & 0 & I \end{bmatrix}, \quad \bar{\Gamma} = P\Gamma P^{-1} = \begin{bmatrix} -k_1 I & k_1 I & 0 \\ -\bar{L}_s + k_2 L_s - k_1 I & k_1 I - k_2 L_s & A_{sf} \\ k_3 A_{fs} & 0 & -k_3\bar{L}_f \end{bmatrix}.$$

The matrix Γ and $\bar{\Gamma}$ has identical eigenvalues owing to P is nonsingular.When condition (1), (2) are satisfied, it can be verified that $\bar{\Gamma}$ is a Laplacian matrix of a network which contains $n+m$ agents. The row and column transform are imposed on matrix $\bar{\Gamma}$, then the below form can be derived.

$$\tilde{\Gamma} \to \begin{bmatrix} -I_m & 0 & 0 \\ 0 & \bar{L}_s & A_{sf} \\ 0 & k_3 A_{fs} & -k_3 \bar{L}_f \end{bmatrix} \to \begin{bmatrix} I_m & 0 & 0 \\ 0 & \bar{L}_s & -A_{sf} \\ 0 & -A_{fs} & \bar{L}_f \end{bmatrix}$$

Obviously, $rank(\bar{\Gamma}) = m + rank(L)$. Based on lemma 1, we have $rank(L) = n-1$, $rank(\bar{\Gamma}) = n+m-1$ .Then, matrix $\bar{\Gamma}$ only has a simple zero eigenvalue, and the other eigenvalues all have negative real part. Meanwhile, matrix Γ has identical eigenvalue property. Γ has a simple zero eigenvalue with an associated eigenvector $w_1 = [1_m^{\mathrm{T}}, 0_m^{\mathrm{T}}, 1_{n-m}^{\mathrm{T}}]^{\mathrm{T}}$.

The solution of system (3) can be denoted as follow $\lim_{t\to\infty} y(t) = e^{\Gamma t} y(0)$ .We have $e^{-\Gamma t} = Q \begin{bmatrix} 1 & 0 \\ 0 & e^{J} \end{bmatrix} Q^{-1}$,

where Q is a nonsingular transformation, and J is the Jordan block associated non-zero eigenvalue of matrix Γ .Due to the other eigenvalues all have negative real part , then $\lim_{t\to\infty} e^{-J} = \mathbf{0}_{(n+m-1)\times(n+m-1)}$.

Then, $$\lim_{t\to\infty} y(t) = e^{\Gamma t} y(0) = w_1 v_1^{\mathrm{T}} y(0) = \begin{bmatrix} \mathbf{1}_m v_1^{\mathrm{T}} \boldsymbol{y}(0) \\ \mathbf{0}_m \\ \mathbf{1}_{n-m} v_1^{\mathrm{T}} \boldsymbol{y}(0) \end{bmatrix}$$

$w_1 = [1_m^{\mathrm{T}}, 0_m^{\mathrm{T}}, 1_{n-m}^{\mathrm{T}}]^{\mathrm{T}}$, v_1^{T} is the left eigenvector associated eigenvalue zero, and $v_1^{\mathrm{T}} w_1 = 1$ .It can be seen that the convergence value of system satisfy the requirement of definition 1.

Remark 2: There is a $d_i \neq 0$ at least owing to the graph is undirected connected. The subgraph $\mathcal{G}^s(\mathcal{V}, \mathcal{E}, \mathcal{A})$ of $\mathcal{G}(\mathcal{V}, \mathcal{E}, \mathcal{A})$ which contains all second-order agents is also connected, then all $d_i^s \neq 0$, thus condition (1) can be satisfied.

Theorem 2 If the conditions of theorem 1 are satisfied, the consensus equilibrium point of system (3) is as follow

$$\lim_{t\to\infty} x_i(t) \to \frac{k_3 \sum_{i=1}^{m} v_i(0) + k_1 \sum_{l=m+1}^{n} x_l(0)}{k_1 (n-m)}, i = 1, \ldots n \tag{4}$$

$$\lim_{t\to\infty} v_i(t) \to 0, i = 1, \ldots m$$

Proof: It is easy to verify that the zero eigenvalue of matrix with an associated eigenvector and left eigenvector are $\boldsymbol{w}_1 = [\mathbf{1}_m^{\mathrm{T}}, \mathbf{0}_m^{\mathrm{T}}, \mathbf{1}_{n-m}^{\mathrm{T}}]^{\mathrm{T}}$ and $\boldsymbol{v}_1^{\mathrm{T}} = [\mathbf{0}_m^{\mathrm{T}}, \alpha k_3 \mathbf{1}_m^{\mathrm{T}}, \alpha k_1 \mathbf{1}_{n-m}^{\mathrm{T}}]$ respectively, and $v_1^{\mathrm{T}} w_1 = 1$ for $Q^{-1} Q = I$ .Then, we have $\alpha = 1/[k_1(n-m)]$. According to theorem1, $\lim_{t\to\infty} y(t) = w_1 v_1^{\mathrm{T}} y(0) = \begin{bmatrix} \mathbf{1}_m v_1^{\mathrm{T}} y(0) \\ \mathbf{0}_m \\ \mathbf{1}_m v_1^{\mathrm{T}} y(0) \end{bmatrix}$ .Then , $\lim_{t\to\infty} x_i(t) \to v_1^{\mathrm{T}} y(0) = \frac{k_3 \sum_{i=1}^{m} v_i(0) + k_1 \sum_{l=m+1}^{n} x_l(0)}{k_1 (n-m)}$, $\lim_{t\to\infty} v_i(t) \to 0, i = 1, \ldots m$.

4. Simulation

In this section, a numerical simulation is provided to illustrate the effectiveness of the theoretical result in Section 3. Consider a heterogeneous multi-agent system with 4 agents shown in Fig. 1, where node 1, 2 are second-order agent, and node 3, 4 are first-order agents. The graph is undirected connected .If $e_{ji} \in \mathcal{E}$, then $a_{ij} = 1$, else $a_{ij} = 0$.

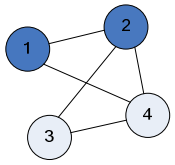

Fig. 1. Interconnection graph.

According to the conditions in theorem1, we select $k_1 = 1.4$, $k_2 = 4.5$, $k_3 = 1.2$, The initial condition are $\boldsymbol{x}(0) = [2, 1, 2.5, 1.5]^{\mathrm{T}}$, $v(0) = [1, 2]^{\mathrm{T}}$ .Based on (4), we have .

The simulation results (Fig. 2 and Fig. 3) show that the positions of all agents and the velocities of second -order agents achieve consensus asymptotically.

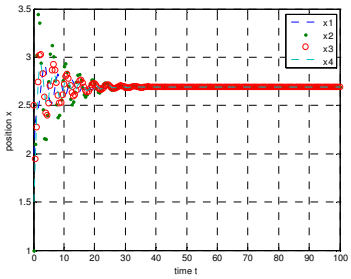

Fig. 2 Position of all agents

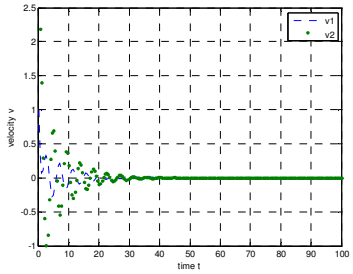

Fig3. Velocity of second-order agents

When the system (3)satisfy condition(1), (2) in theorem 1, it can be seen that velocity of all second-order agents converge to zero, and position of all agents converge to consensus equilibrium point(4). The result illustrates the effectiveness of the theoretical result.

5. Conclusion

This paper investigates the consensus problem of heterogeneous multi-agent system which includes first -order and second-order agents. Consensus equilibrium point of the system is derived in undirected graph based on graph theory and matrix theory. Finally, a numerical simulation is provided to illustrate the effectiveness of the theoretical result. This paper only considers undirected graph, in following work digraph will be considered.

References

[1] Vicsek T, Czirók A, Ben-Jacob E, Cohen I, Shochet O. Novel type of phase transitionin a system of self-driven particles[J]. Physical Review Letters.75(1995) 1226 -1229.

[2] Jadbabaie A, Lin J, Morse A S. Coordination of groups of mobile autonomous agents using nearest neighbor rules[J]. IEEE Transactions on Automatic Control. 48(2003):988-1001.

[3] Olfati-Saber R, Murray R M. Consensus problems in networks of agents with switching topology and time-delays[J]. IEEE Transactions on Automatic Control, 49(2004)1520-1533.

[4] Ren W, Beard R W. Consensus seeking in multi-agent systems under dynamically changing interaction topologies [J]. IEEE Transactions on Automatic Control, 50(2005)655-661.

[5] ChengLin Liu, Fei Liu.Stationary consensus of heterogeneous multi-agent systems with bounded communication delays [J]. Automatica .47 (2011)2130-2133.

[6] Yu-Ping Tian, Ya Zhang. High-order consensus of heterogeneous multi-agent systems with unknown Communication delays [J] .Automatica.48(2012) 1205-1212.

[7] Yuanshi Zheng, Long Wang. Finite-time consensus of heterogeneous multi-agent systems with and without velocity measurements[J]. Systems & Control Letters. 61(2012)871–878.

Advanced Materials Research Vols. 989-994 (2014) pp 2406-2409
© (2014) Trans Tech Publications, Switzerland
doi:10.4028/www.scientific.net/AMR.989-994.2406

A Projected Conjugate Gradient Method for Box-Constrained Optimization

Tingfeng LI, Zhiyuan LIU and Zhaobin DU

Zhengzhou Technical College, Zhengzhou 450121,China

tingfengli@126.com

Keywords: unconstrained optimization, conjugate gradient method, box-constrained program.

Abstract. In this paper, we introduce an algorithm for solving large-scale box-constrained optimization problems. At each iteration of the proposed algorithm, we first estimate the active set by means of an active set identification technique. The components of the search direction corresponding to the active set are simply defined; the other components are determined by nonlinear conjugate gradient method. Under some additional conditions, we show that the algorithm converges globally. We also report some preliminary numerical experiments to show that the proposed algorithm is practicable and effective for the test problems.

Introduction

In this paper, we propose a projected conjugate gradient method for solving the following box-constrained optimization problem.

$$\min_{x\in \mathrm{R}^n} f(x) \tag{1}$$

where $f:\mathrm{R}^n \to \mathrm{R}$ is continuously differentiable, and $l,u\in \mathrm{R}^n$ with $l<u$. We denote the gradient of f at x by $\nabla f=\left(\nabla f_1(x),...,\nabla f_n(x)\right)$, and define the feasible region of (1) by Ω be, i.e.,

$$\Omega=\left\{x\in \mathrm{R}^n : l\le x\le u\right\} \tag{2}$$

We say that a vector $\bar{x}\in\Omega$ is a stationary point for problem (1) if it satisfies

$$\begin{cases} l_i=\bar{x}_i & \Rightarrow \nabla f_i(\bar{x})\ge 0 \\ l_i<\bar{x}<u_i & \Rightarrow \nabla f_i(\bar{x})=0 \\ \bar{x}_i=u_i & \Rightarrow \nabla f_i(\bar{x})\le 0 \end{cases} \tag{3}$$

Strict complementarily is said to hold at $\bar{x}$ if the strict inequalities hold in the first and the last implications of (3).

Many algorithms for solving this type of problems are based on active set strategies (see [2, 7, 8, 13]). In this class of methods a working set estimates the set of active constraints at the solution and it is updated from iteration to iteration. The early active set methods are quite efficient for relatively lower dimensional problems, but are typically unattractive for large-scale problems (see [1, 6]).The main reason is that at most one constraint can be added to or dropped from the active set at each iteration, and this slow down the rate of the convergence. Because of it, it explodes more and more scholars to study the design of active set methods so as to be capable of making rapid changes to incorrect predictions (e.g. [2, 3, 7, 8]).

The gradient projection method is (e.g. [1])a effective method in identifying the active set. They have the advantage that many constraints can be added to or dropped from the active set at each step. The gradient projection technique has been further studied for solving nonlinear optimization problems, both for general linearly constrained case and for the bound constrained case(see [3, 4, 5, 11, 12, 14]). The bound constrained optimization problems have received much attention in recent decades, we refer to (see[9, 10]) for good reviews.

The paper is organized as follows. We first propose the construction of our new algorithm in the next section. In section 3, we establish the global convergence of the new method. In section 4, we test the

performance of the proposed algorithm and compare it with the other well known methods. Throughout the paper, the symbol $\|\bullet\|$ denotes the Euclidean norm of vectors.

Motivation and Algorithm

In this section we first recall the active set estimation technique in [14], then we present our new algorithm based on a modified PRP conjugate gradient method. The following two assumptions are important to our algorithm.

Assumption 2.1. *The level set* $\Re = \left\{x \in \mathrm{R}^n : f\left(x\right) \le f\left(x^0\right)\right\} \cap \Omega$ *is compact.*

Assumption 2.1. *In some neighborhood of* $\Re$*, the gradient* $g(x)$ *is Lipschitz continuous, i.e., there exists a constant* $L > 0$ *such that* $\left\|g\left(x\right) - g\left(y\right)\right\| \le L\left\|x - y\right\|, \forall x, y \in \Re$.

Now, we state the active set identification technique in [14], and describe how to construct a search direction subsequently. Let $a_i\left(x\right)$ and $b_i\left(x\right)$ be nonnegative continuous and bounded function defined on Ω , such that if $x_i = l_i$ or $x_i = u_i$ then $a_i\left(x\right) > 0$ or $b_i\left(x\right) > 0$, respectively. For any $x \in \Omega$ we can define the index sets $L(x)$, $F(x)$ and $U(x)$ as follows

$$\begin{cases} L\left(x\right) = \left\{i : x_i \le l_i + a_i\left(x\right)\nabla f_i\left(x\right)\right\} \\ U\left(x\right) = \left\{i : x_i \ge u_i + b_i\left(x\right)\nabla f_i\left(x\right)\right\} \\ F\left(x\right) = \left\{1,...,n\right\} \setminus \left(L \cup U\right) \end{cases} \tag{4}$$

The set $L(x) \bigcup U(x)$ is an estimate of the active set at point x. F. Facchinei, J. Judice and J. Soares (see [14]) showed that if the strict complementary condition holds at $\overline{x}$, then when x is sufficiently close to $\overline{x}$, the index sets $L(x) \bigcup U(x)$ is an exact identification of $L(\overline{x}) \bigcup U(\overline{x})$. This property will enable us to find the active sets at the stationary point $\overline{x}$ in a finite number of steps.

By using the active set estimate, we deduce the search direction used in our algorithm. Details will be given subsequently. For the sake of simplicity, we let $L^k = L\left(x^k\right), U^k = U\left(x^k\right), F^k = F\left(x^k\right)$, and $\left|F^k\right|$ be the number of elements in F^k. Let $d^k = \left(d^k_{L^k}, d^k_{F^k}, d^k_{U^k}\right)$ in which d^k_L and d^k_U is determined by

$$d^k_i = l_i - x^k_i, i \in L^k \tag{5}$$

$$d^k_i = u_i - x^k_i, i \in U^k \tag{6}$$

Let $P_\Omega\left(x\right)$ be the projection on Ω ; Z_k be the matrix whose columns are $\left\{e_i \middle| i \in F^k\right\}$, where e_i is the i-th column of the identity matrix. Let $P_\Omega\left[\bullet\right]$ denotes the projection on Ω , that is

$$P_\Omega\left[x\right] = \begin{cases} x_i & \text{if } l_i \le x_i \le u_i \\ l_i & \text{if } x_i < l_i \\ u_i & \text{if } x_i > u_i \end{cases} \tag{7}$$

The search direction d^k is defined by

$$d^k_i = \begin{cases} l_i - x^k_i, i \in L^k \\ u_i - x^k_i, i \in U^k \\ \left(Z_k \overline{d}^k\right)_i, i \in F^k \end{cases} \tag{8}$$

where $\overline{d}^k$ denotes the search direction of inactive variables, which is determined by the form

$$\overline{d}_k = \begin{cases} -\overline{g}^0 & k = 0 \\ -\overline{g}^k + \beta_k \overline{d}^{k-1} - \theta_k \overline{y}^{k-1} & k > 0 \end{cases} \tag{9}$$

Where $\beta_k = \frac{\left(\bar{g}^k\right)^T \bar{y}^{k-1}}{\left\|\gamma_{k-1}\right\|^2}$ and $\theta_k = \frac{\left(\bar{g}^k\right)^T \bar{d}^{k-1}}{\left\|\gamma_{k-1}\right\|^2}$, where $\bar{g}^k = Z_k^T g^k$, $\bar{y}^{k-1} = \bar{g}^k - \bar{g}^{k-1}$, and $\gamma_k = P_\Omega\left(x^k - g^k\right) - x^k$.

The result is obvious, hence we omit the proof here. Whenever $d^k \neq 0$, it is at least a descent direction for objective function f at current point x^k, and the property is very important for us to establish the global convergence. Now we can describe the algorithm for solving the bound constrained optimization problems (1) as follows:

Algorithm 2.1.

Step 0. Given starting point $x_0 \in \Omega$, constants $\delta \in (0,1/2)$. Set $k = 0$.

Step 1. Determine $L^k = L\left(x^k\right)$, $U^k = U\left(x^k\right)$, $F^k = F\left(x^k\right)$ according to (8).

Step 2. Compute d^k by (9). If $d^k = 0$ then stop.

Step 3. Set $x_{k+1} = P_\Omega\left(x_k + \alpha_k d_k\right)$, α_k attained by the projected Armijo line search, and update d^k to get d^{k+1} by (5).

Step 4. Set $k := k+1$. Go to Step 1.

Numerical Experiments

In this section, we analyze the feasibility and effectiveness of the Algorithm 2.1 (named PCGM). The algorithm is implemented by Fortran95 code in double precision arithmetic. All runs are performed on a PC (Intel Pentium(R) 4, 2.8 GHz, 2G DDR3) with Red Hat 9.03 Linux OS. Our experiments are performed on a subset of the nonlinear unconstrained problems from CUTEr[12] library, and the second-order derivatives of all the selected problems are available. Since we are interested in large problems, we only considered problems with dimensions at least 100. The algorithm stops if the norm of the final gradient is less than 10^{-5}, that is, $\left\|\nabla f\left(x\right)\right\| \le 10^{-5}$.

For this Method, we set the initial matrix $\mathrm{H}_0 = \gamma I$, I is an identity matrix. In this experiment, we take $\mu = 0$, $\overline{C} = 10^{-7}$, $\sigma_1 = 10^{-4}$, $\sigma_2 = 0.9$, $m = 6$, $n = 100$, to test the behavior of the PCGM with different values $\overline{C}$. The numerical results are listed in following Table, which contains the name of each problem, the number of iterations (Iter), the number of function evaluations (NF), the CPU time required in seconds (Time). Symbol "-" indicates method stops without meeting the stopping criteria. Through the Table, we see that the values of $\overline{C}$ slightly affect the numerical behavior of PCGM. Moreover, it seems that $\overline{C} = 10^{-7}$ and $\overline{C} = 10^{-9}$ yields better performance than the remaining.

Table Numerical Results with Different $\overline{C}$

	$\overline{C}=10^{-2}$			$\overline{C}=10^{-5}$			$\overline{C}=10^{-7}$			$\overline{C}=10^{-9}$		
Problem	Iter	Nf	Time	Iter	Nf	Time	Iter	Nf	Time	Iter	Nf	Time
VARDIM	35	37	0.012	35	37	0.000	35	37	0.012	35	37	0.000
FLETCHAR	435	465	0.028	464	496	0.036	401	424	0.037	444	475	0.029
COSINE	10	33	0.000	10	32	0.000	10	31	0.012	10	30	0.000
SINQUAD	76	97	0.012	74	103	0.012	65	89	0.000	65	90	0.010
GENROSE	530	612	0.037	526	629	0.035	529	631	0.036	537	617	0.043
FREUROTH	-	-	-	-	-	-	-	-	-	-	-	-
WOODS	86	113	0.000	87	114	0.012	93	123	0.000	87	115	0.010
NONCVXU2	481	504	0.116	580	607	0.146	503	522	0.146	518	545	0.131
BROYDN7D	144	162	0.027	88	94	0.012	91	99	0.011	91	99	0.000
CHAINWOO	1136	1238	0.116	403	445	0.027	389	432	0.024	384	421	0.032

Summary

We proposed a PCGM method with Armijo line-search for solving Box-Constrained optimization problems. The results showed that the choice of parameters affected the performance of the method. Moreover, if we choose them appropriately, the numerical behavior can be highly improved. The next research will be compared the PCGM and the other algorithms.

References

[1] D. P. Bertsekas, *Projected Newton methods for optimization problems with simple constrains*, SIAM J. Control Optim., 20 (1982), pp. 221-246.
[2] E. G. Birgin and J. M. Martinez, *Large-scale active-set box-constrained optimization method with spectral projected gradients*, Comput. Optim. Appl., 23 (2002), pp. 101-125.
[3] J. V. Burke and J. J. More, *On the identi¯cation of active constraints*, SIAM J. Numer. Anal., 25 (1988), pp. 1197-1211.
[4] P. Calamai and J. J. More, *Projected gradient for linearly constrained programs*, Math. Program., 39 (1987), pp. 93-116.
[5] A. R. Conn, N. I. M. Gould and Ph. L. Toint, *Global convergence of a class of trust region algorithm for optimization with simple bounds*, SIAM J. Numer. Anal., 25 (1988),pp. 433-460.
[6] Y. H. Dai and R. Fletcher, *Projected Barzilai-Borwein methods for large-scale box constrained quadratic programming*, Numer. Math., 100 (2005), pp. 21-47.
[7] F. Facchinei, J. Judice and J. Soares, *An active set Newton slgorithm for large-scale nonlinear programs with box canstranits*, SIAM J. Optim., 8 (1998), pp. 158-186.
[8] F. Facchinei, S. Lucidi and L. Palagi, *A truncated Newton algorithm for large scale box constrained optimization*, SIAM J. Optim., 12 (2002), pp. 1100-1125.
[9] N. I. M. Gould, D. Orban and Ph. L. Toint, *Numerical methods for large-scale nonlinear optimization*, Acta Numer., 14 (2005), pp. 299-361.
[10] W. W. Hager and H. Zhang, *A new active set algorithm for box constrained optimizaiton*, SIAM J. Optim., 17 (2006), pp. 526-557.
[11] C. J. Lin and J. J. More, *Nowton's method for large bound-constrained optimization problems*, SIAM J. Optim., 9 (1999), pp. 1100-1127.
[12] M. Lescrenier, *Convergence of trust region algorithm for optimization with bounds when strict complementarity does not hold*, SIAM J. Numer. Anal., 28 (1991), pp. 467-695.
[13] D. G. Luenberger, *Introduction to linear and nonlinear programming*, Addison-Wesley, Reading, MA, 1973, Ch. 11.
[14] Q. Ni, *A subspace projected conjuagte gradient algorithm for large bound constrained quadratic programming*, Numer. Math. (a Journal of Chinese Universities), 7 (1998), pp.51-60.

Advanced Materials Research Vols. 989-994 (2014) pp 2410-2413
© (2014) Trans Tech Publications, Switzerland
doi:10.4028/www.scientific.net/AMR.989-994.2410

Decomposition of New Construction Land Quota in Rural Land Based on AHP

Xiang-wen Cai[1,a], Hong-yang Wang[1,b] and Yue Sun[1,c] Chong-hui Gao[1,d]

[1]College of Earth Science, Guilin University of Technology, Guilin541004, China.

[a]2004042@glut.edu.cn,[b]why9956@163.com,[c]yy73419@163.com,[d]118088789@qq.com

Keywords: Quota decomposition in rural land; New Construction Land; Analytic hierarchy process (AHP）

Abstract. This article take LuoCheng MuLao Nationality Autonomous County in Guangxi province as a sample, decomposing the new construction land quota in this county based on AHP in determining the quota decomposition weights. In addition, this paper selected rural fixed assets investment, urban population, the total construction land during planning and implementation period, gross domestic product, four factors as the significant influencing ones. And standardized treatment of these factors to the indicators' vector set.

Introduction

The focus of the general land use planning in our country is to determine and adjust the land use structure and layout the limited land resources in the production and living for scientific and reasonable configuration .New construction land quota decomposition is the key and difficult point for a new round of general land use planning .Scientific and reasonable decomposition of new construction land quota ,to promote economic and social coordinated development plays an important role .About the township general land use planning of newly-increased construction land at the bottom in the general land use planning in our country .The quota distribution of appropriateness is directly related to the superior the implementation of general land use planning and implementation [1].

The quota decomposition method

Analytic hierarchy process (AHP).The Analytic Hierarchy Process is to build a multi-layered analysis of the structural model, in the hierarchy of the decision problem in the large system[2]. Select the factor determining, standardized indicators of the township township drawn vector set A, analytic hierarchy process to determine the right to select the factor weights in the quota system B, Finally it is concluded that the township administrative domain decomposition quota were weighted C [3].

Township quota vector set (A). Select 2010 Guangxi Luocheng County non-agricultural population, 2010 urban GDP, 2010 investment in fixed assets, construction land in 2020 predicted four data as a factor ,As shown in table 1 .To standardize the raw data in table 1,to derive a normalized value, for the standardization of formula:

$$Y_{ki} = \frac{c_{ki} - c_{\min}}{c_{ki} - c_{\min}} . \quad (3)$$

Formula: Y_{ki} is the equivalent value of village K's factor i, c_{ki} is the original value of village K's factor i, $c_{\max}$ is the biggest original value of every village's factor i, $c_{\min}$ is the smallest original value of every village's factor I [4].

Table 1 Standardized indicators

Town name	Construction land	Non-agricultural population	GDP	Fixed assets investment
Longan	0.5267	0.1941	0.4100	0.0261
Huangjin	0.1481	0.0618	0.0566	0.0011
Baotan	0.1992	0.0515	0.1775	0.3108
Xiao Chang'an	0.4496	0.0456	0.0550	0.0261
Dongmen	1.0000	1.0000	1.0000	1.0000
Siba	0.5154	0.1250	0.1300	0.1570
Tianhe	0.1429	0.0221	0.0343	0.0975
Qiaoshan	0.0759	0.0000	0.0363	0.0573
Naweng	0.0000	0.0000	0.0000	0.0238
Huaiqun	0.1378	0.0147	0.0297	0.0642
Jian'ai	0.0614	0.0000	0.0015	0.0000

To standardize summary four data quota vector set A:

$$A=\begin{bmatrix} 0.5267 & 0.1941 & 0.4100 & 0.0261 \\ 0.1481 & 0.0618 & 0.0566 & 0.0011 \\ 0.1992 & 0.0515 & 0.1775 & 0.3108 \\ 0.4496 & 0.0456 & 0.0550 & 0.0261 \\ 1.0000 & 1.0000 & 1.0000 & 1.0000 \\ 0.5154 & 0.1250 & 0.1300 & 0.1570 \\ 0.1429 & 0.0221 & 0.0343 & 0.0975 \\ 0.0759 & 0.0000 & 0.0363 & 0.0573 \\ 0.0000 & 0.0000 & 0.0000 & 0.0238 \\ 0.1378 & 0.0147 & 0.0297 & 0.0642 \\ 0.0614 & 0.0000 & 0.0015 & 0.0000 \end{bmatrix}$$

The factor weights (B). According to table 1 to compare any two factors, according to the actual situation of the county and economic development trends, get discriminant matrix is shown in Table 2.

Table 2 Construction land affected townships judgment matrix

	Construction land	Non-agricultural population	GDP	Fixed assets investment
Construction land	1	1/7	1/5	1/3
Non-agricultural population	7	1	3	5
GDP	5	1/3	1	3
Fixed assets investment	3	1/5	1/3	1

Calculate the factors weight judgment matrix which factor weight vector B:

$$B=\begin{bmatrix}0.0553\\0.5650\\0.2622\\0.1175\end{bmatrix}$$ calculate the eigenvalues of the matrix A maximum λ_{max}=4.1170, Through the consistency check, $CI=\frac{\lambda_{max}-n}{n-1}$ =0.039，n=4；Look-up table shows RI=0.90.So $CR=\frac{CI}{RI}$ = 0.0433＜0.1，The consistency of the matrix is satisfied can use.

Quota decomposition weight vector. According to the formula (1) the new construction land quota decomposition weight vector is: C=A×B

$$C=\begin{bmatrix}0.5267 & 0.1941 & 0.4100 & 0.0261\\0.1481 & 0.0618 & 0.0566 & 0.0011\\0.1992 & 0.0515 & 0.1775 & 0.3108\\0.4496 & 0.0456 & 0.0550 & 0.0261\\1.0000 & 1.0000 & 1.0000 & 1.0000\\0.5154 & 0.1250 & 0.1300 & 0.1570\\0.1429 & 0.0221 & 0.0343 & 0.0975\\0.0759 & 0.0000 & 0.0363 & 0.0573\\0.0000 & 0.0000 & 0.0000 & 0.0238\\0.1378 & 0.0147 & 0.0297 & 0.0642\\0.0614 & 0.0000 & 0.0015 & 0.0000\end{bmatrix}\times\begin{bmatrix}0.0553\\0.5650\\0.2622\\0.1175\end{bmatrix}=\begin{bmatrix}0.2494\\0.0581\\0.1232\\0.0681\\1.0000\\0.1517\\0.0408\\0.0204\\0.0028\\0.0313\\0.0038\end{bmatrix}$$

Table 3 New construction land quota decomposition of LuoCheng county in 2005-2020

Town name	Weight vector	Weights（%）	New construction land（hm）
Longan	0.2494	14.25%	153.84
Huangjin	0.0581	3.32%	35.84
Baotan	0.1232	7.04%	75.99
Xiao Chang'an	0.0681	3.89%	42.01
Dongmen	1.0000	57.16%	616.83
Siba	0.1517	8.67%	93.57
Tianhe	0.0408	2.33%	25.17
Qiaoshan	0.0204	1.17%	12.58
Naweng	0.0028	0.16%	1.73
Huaiqun	0.0313	1.79%	19.31
Jian'ai	0.0038	0.22%	2.34

Conclusion

New construction land quota decomposition embodies fully long-term requirements of social development and government function. To respect the economic development and land resources allocation rule [5].According to the research, with economic growth theory, the configuration elements equilibrium theory and resource cost theory established on the basis of the theoretical system more suitable for the current China's land management actual needs , the result of land use planning and related policy design has reference value .But as a result of land use exist obvious difference in different areas, there isn't a decomposition method is completely general applicability. So we should breakthrough the shackles of traditional planning ideas, in the latest research progress

based on the theory, build and use more advanced and reliable analytical methods and tools of land resources, promote the rational exploitation and protection of land resources [6]. The author considered AHP into new construction land quota decomposition, results considering land economic laws, perhaps it has a certain gap with the county government target -coordinated development, so how to improve the configuration and coordination of economic law the land still has a long way to go.

Acknowledgements

This work was financially supported by Key Laboratory Geological Engineering Center of Guangxi and Key Discipline Physical Geography Established in Guilin University of Technology, Guilin University of Technology, Guilin, China.

References

[1] C.L. Hou, Z.L. Zou and X. Chen ect: Journal of Anhui Agricultural Sciences, Vol.37 (2009) No. 29, p.14290-14292

[2] X.J Feng, D.Y. Zang and S.B. Wang: Journal of Anhui Agricultural Sciences, Vol.38 (2010) No. 30, pp. 17291- 17293

[3] Y. Wang: *Study on Distribution of Net Added Construction Land Quota in Land Use General Planning -A Case Study of LiuZhou* (MS. Huazhong Agricultural University, China 2007), p. 61-63

[4] H.Z. Ma and Z,J, Shen: Guangdong Land Science, Vol.4 (2005) No. 3, p.11-15

[5] L.Y. Zhu: *Study on Computing Technique About Decomposing Additional Construction Land Quota-A Case Study of Shanxi* (MS. Changan University, China 2009)

[6] H. Jiang, F.T Qu: China Land Science, Vol.12 (2005) No. 23, p. 25-31

Advanced Materials Research Vols. 989-994 (2014) pp 2414-2417
© (2014) Trans Tech Publications, Switzerland
doi:10.4028/www.scientific.net/AMR.989-994.2414

Design and Implementation of General high-speed Data Storage System

Fu Gang[1,a] , Geng Wenjian[1, a], Li Renlong[1,a]

[1]China Satellite Maritime Tracking and Control Department, China
[a]348237548@sina.com

Keywords: High-speed storage, cache, physical driver

Abstract. According to the trend of the development of the computer system bus more, designs the general high-speed data storage system based on computer platform structure.Put forward the "one-way chain" cache structure, to avoid the computer operating system of real-time data transmission, the influence of the multithreaded mode data transmission and storage of parallel processing.According to the basic principle of data storage in a computer system, put forward the standard file operations function replace special instruction set, the method of implementing the SCSI disk array storage at a high speed.Test results show that the data storage system based on computer platform with more generalization method to achieve the high speed of data storage.

Introduction

With the rapid development of computer technology, computer system structure, bus transmission mode, operating system, real-time and stability has a larger increase, general platform for the realization of the high speed data storage provided the necessary hardware platform and software environment.[1-4] Below according to the current computer system structure and its development trend, the basic structure of generalized high-speed data storage system design, and on the high speed data transmission and storage technology research, generalization method based on computer platform is put forward.

1 The system structure design

The computer's basic composition structure as shown in figure 1.Only a PCI bus system, most of the peripheral equipment through PCI bus, the occurrence of the (South Bridge) and North (North Bridge) chip connection.

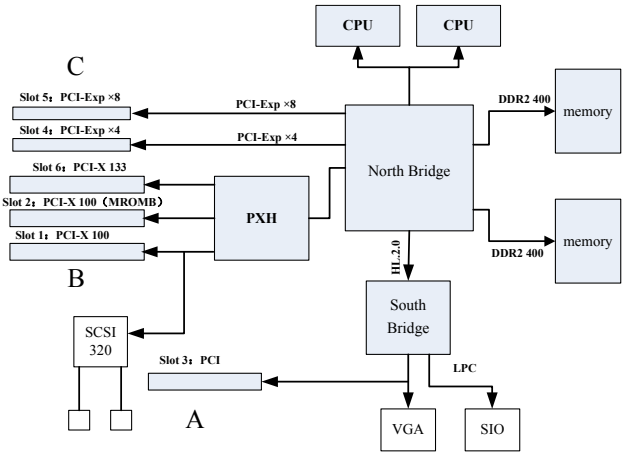

Fig1 Intel 7520 computing system structure

With the rapid development of computer technology, the structure of the computer system on the basis of the original large changes have taken place, the main difference is adopted multibus structure, in addition to basic PCI bus in a computer system also provides a PCI-X and PCI-E two high-speed bus.

PCI - X bus by IBM and guide, it belongs to the expansion of the PCI bus architecture, compared with PCI bus, PCI-X can automatically remove without data exchange PCI-X devices, in order to reduce the waiting for the bus cycle, therefore, under the same frequency PCI-X performance will

be 14%~35% higher than that of PCI. PCI-version 2.0 X can currently support 66 MHZ, 100 MHZ, 133 MHZ this three kinds of frequency, in turn, can manage 4, 2, 1 PCI-X devices, and with 533 MB/s respectively, and 800 MB/s, and 800 MB/s peak bandwidth.

PCI and PCI-X bus is USES the work pattern of time-sharing multiplexing, this also limits the further increase of transmission speed. In 2001, Intel introduced the PCI Express bus (PCI-E).With all PCI devices share the same bus resources, PCI-E bus USES peer-to-peer technology, can be exclusive to each equipment distribution channels, this fully guarantee the bandwidth of each equipment to improve data transmission rate. On the data transfer mode, PCI-E bus adopt unique dual channel transmission model, similar full duplex work mode, send and receive data synchronization, greatly improve the speed of data transmission. At present, the latest PCI-E x 16 standard bus transmission speed (two-way bandwidth) 8 GB/s.[5]

Chipset Intel 7520 to build a computer system as an example, it provides 1 the PCI bus, article 3 of the PCI bus and 2 X PCI-E bus, the structure is shown in figure 2.1 the PCI bus connection in the occurrence of the chip, 2 PCI-E bus directly with "north" chip connection, 3 - through PCI bus X PC-X I controller (PXH) connected to the "north". The distribution characteristics of multibus, provides high speed data transmission and storage with independent channels, overcomes the traditional computer structure on the properties of high speed data storage limit.

At 7520 chipset Intel build computer system structure as reference, design the basic structure of high-speed storage system. Currently used data acquisition card of PCI bus interface, disk array card PCI - X bus interface. This case, you can connect the data acquisition card and the disk array card in the PCI (figure 2 A) and PCI-X (figure 2 B) bus.[6] Although the two bus are used the time-sharing multiplexing transmission mode, but the data input and storage USES is independent of the transmission channel, so it can give full play of bus transmission performance, to avoid the data transmission performance bottlenecks, improve the stability of the system work.

The whole process of data are shown in figure 2 below. First acquisition card through PCI bus to transmit data to the computer memory, and then the data in the memory under the control of the software after connection in north bridge PCI - X bus, stored in the SCSI RAID disk array. The entire process under control in the computer operating system and application software, through the multithreaded programming model, data acquisition, transmission and storage of parallel processing.

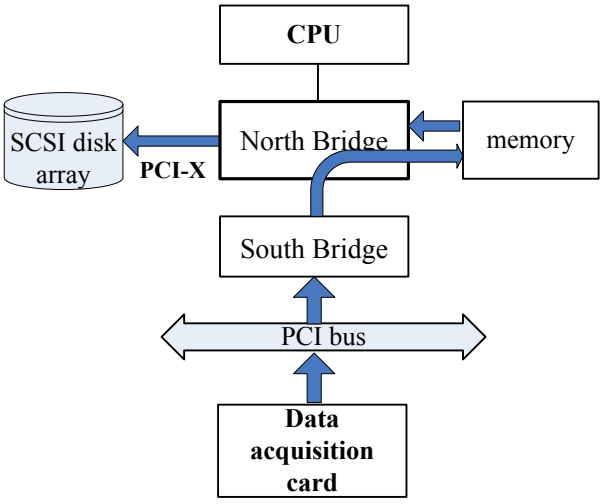

Fig2 Storage system based on computer data process

2 The data transfer

After the acquisition card to collect data through the computer PCI bus in DMA way, continue to transfer to the computer memory, and then to store data in memory to disk. In order to match between DMA and data save data read and write speed difference, realizes the data transmission and storage of parallel processing, usually adopt way temporary serial input data in cache. Computer operating system in order to avoid the non real-time influence on continuous data

acquisition and storage, in addition to adopt the method of optimization of the real-time operating system, can use a "one-way circulation chain" cache structure. As shown in figure 3, it is in the computer memory for several capacity equal to the buffer, in each cache capacity is equal to the amount of data for each DMA transfers. In the process of data transmission and storage, must follow the established order, and in turn cycle for each buffer for data write and read operations.

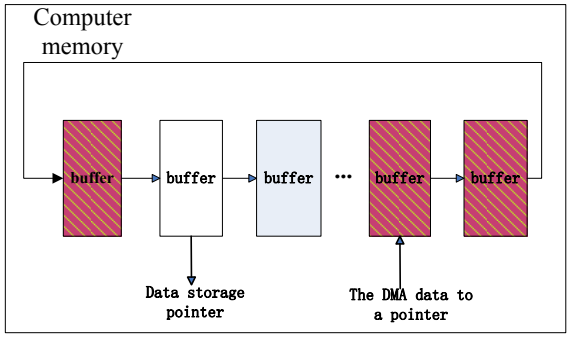

Fig3 One-way circulation chain structure of cache

3 Data storage

The physical hard disk (physics disk) storage mode is used in high-speed storage systems, the main way. The physical hard disk model of data storage to bypass the logical file system in computer operating system, file organization module and basic file system, the entire hard disk as a large linear array, in sectors as the smallest unit, direct call I/O control layer of hard disk driver, the order of the data written to the specified hard disk sectors.

The basic process of operating system for the operation of the file as shown in figure 4. I/O control for the bottom, the storage device driver and the interrupt handlers, implementing software control of the storage devices. Basic file system sends a standard instruction to the I/O control layer to the storage device to read and write operations.

Mode in order to solve the physical hard disk for file operations between different storage devices generality problem, can use the computer operating system, on the basis of the hardware abstraction layer for the application to provide a set of standardized file operations function. Basic file operations by calling the function, bypassing the logical file system to improve the efficiency of data storage, while avoiding the intricate between different storage device driver program design.

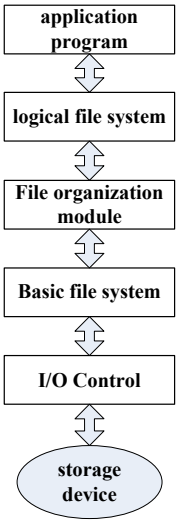

Fig4 Basic file operations process

4 Performance test

- motherboard: based on the Intel 7250 chipsets; CPU: Intel Xeon 3.0 GHz; Operating system: Windows 2000;
- 12 bit A/D converter: dual channel, quantitative; PCI bus controller: PCI9054 (32 bit / 33 MHZ);

In Visula c + + 6.0 environment using c + + language to develop software system, storage system control, equipment state monitoring in the running state of the state of the FIFO (acquisition card, computer cache area, disk storage state) and afterwards the correctness of the recording in the disk array data analysis. By sampling the signal source is 1 MHZ sine signal; Data acquisition card clock frequency in our company office frequency synthesizer MG3633A output sine wave, the signal frequency is adjustable. Each DMA transfers the amount of data is 256 KB, rising acquisition card of the sampling clock frequency, and the whole disk array (588 GB) is full.

According to the above test method, when the sampling clock up to 24 installed base, the rate at which data is input to 96 MB/s (dual channel, 12 bit quantization), the whole system to work normally. When the sampling clock continue to increase, the software system tip speed is less than the data input data storage, and can't work normally, the current system has the highest rate of 96 MB/s storage, have been fully played a PCI (32 bit / 33 MHZ) bus and the disk array storage performance. If adopting high speed PCI bus controller and the disk array, can further improve the performance of data storage.

Summary

General high-speed data storage system based on computer platform, make full use of the current computer system bus structure, to achieve the efficiency of the high speed data storage method and generalized."One-way chain" cache structure was proposed, to solve the computer operating system of real time affect the DMA data for transmission, realize the input data flow and storage of parallel operation. Operation system are analyzed under the basic principle of data storage and logical drive mode affect the performance of the main causes of data storage, and puts forward adopting physical hard disk storage mode, to avoid the logical file system in the operating system on the properties of data storage. By calling the interface functions provided by the operating system files, in a more generalized and standardized method to achieve the high speed, continuous data storage based on computer platform. And only need to upgrade the hardware, can achieve the improvement of the performance of the storage system. With the continuous development of computer architecture, the generalization of high-speed data storage system based on computer platform will be more and more widely used.

Reference

[1] VMEbus International Trade Association. American National Standard for Front Panel Data Port Specifications. 1999, http://www.vita.com.
[2] IDSS/DSS Data Storage Systems For Real Time Applications. http://www.signatec.com.
[3] DAQStreaming 40MB/s Data Recorder for Analog and Digital Signals. www.adlinktech.Com.
[4] Sujith Arramreddy, Dwight Riley. PCI-X 2.0 White Paper(1.0). April 5, 2002.
[5] PCI E Series User Manual[D]. National Instruments Corporation. January 1999.
[6] Intel Server Board SE7520AF2 Technical Product Specification(Revision 1.2), March, 2005.

Advanced Materials Research Vols. 989-994 (2014) pp 2418-2421
© (2014) Trans Tech Publications, Switzerland
doi:10.4028/www.scientific.net/AMR.989-994.2418

Research on Software Algorithm Capture of Spread Spectrum TT&C Signals

Li Renlong[1,a], Fu Gang [1, a], Wu Guangzhi[1,a]

[1]China Satellite Maritime Tracking and Control Department, China
[a]348237548@sina.com

Keywords: Doppler, acquisition, software

Abstract. Study a suitable algorithm for implementation of spread spectrum tt&c signals capture software.Analyzes in detail the serial capture pseudo-code algorithm based on FFT, according to the measurement and control conditions, in consideration of pseudo-code doppler and deal with the impact of bandwidth on the basis of, put forward the suitable for software implement methods of capture, primarily through the establishment of a distributed system simulation model and implements a spread spectrum tt&c signals of quasi real-time processing, prove the validity of the method.

Introduction

Along with the computer software technology, the continuous development of signal processing technology, real-time processing technology, as well as the rapid improvement in general computer processing performance, based on general computer processing platform, building software of measurement and control system has become possible.According to the high dynamic and low signal-to-noise ratio under the condition of the spread spectrum signal characteristics, this paper considers the pseudo-code doppler effect of bandwidth and processing, the detailed analysis of the serial capture pseudo-code algorithm based on FFT, on the basis of software implementation of capture method are proposed.[1]Spread spectrum tt&c simulation experiment and through independent research and development of software platform, the capture process of spread spectrum tt&c signals are simulated and analyzed, in order to further the spread spectrum tt&c receiver of software engineering implementation laid a certain technology experimental basis.

1 Traditional rapid capture method based on FFT

In spread spectrum signal capture is to obtain the purpose of signal pseudorandom code phase to a rough estimate, provide initial condition for signal tracking. Carrier code serial capture parallel algorithm based on FFT is due on the carrier frequency search with the method of parallel, thus greatly improve the capture speed of the spread spectrum system.[2]

FFT-based carrier serial parallel code acquisition algorithm implementation process as shown in Figure 1: Input signal after quadrature downconversion and local pseudo-code multiplies the output signal is divided into N segments in each operation cycle, each of M data, and the data segment continuously accumulating points M, N obtained cumulative output value. This is the cumulative result of the use of the N-point FFT transform to do, come to the Doppler frequency. Slide conducted by the pseudo-code serial code phase search to find a frequency that corresponds to the peak value of the Doppler frequency.

2 Algorithm exist problems and improvement

Due to the traditional parallel rapid capture algorithm based on FFT carrier on the pseudo-code phase serial search ways, so the capture speed under the influence of initial phase receiving pseudo-code is bigger.If the local code inside the single dwell time of receiving code and local code the relative phase of sliding produce specific code error, the capture process will lose its significance.

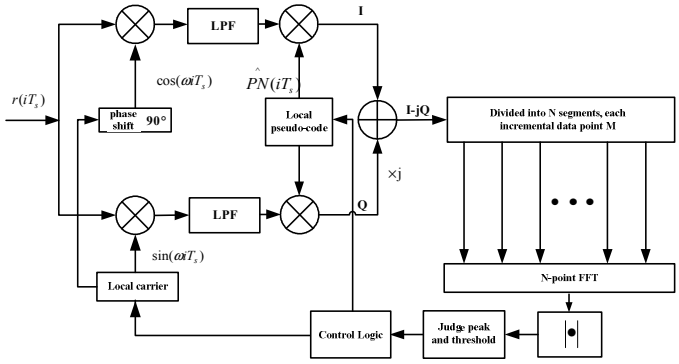

Fig1 Carrier capture parallel algorithm based on FFT implementation block diagram

The relative speed between transmitter and receiver and receive slice width and launch yard yard piece width has established the following relationship:

$$T_{rc} = \frac{1}{1 \pm \frac{v}{c}} T_{sc} \tag{1}$$

Normalized frequency doppler for receiving yard code clock frequency launch code clock frequency difference and yards yards of clock frequency ratio, namely:

$$\varepsilon = \frac{f_{rc} - f_{sc}}{f_{sc}} = \frac{\frac{1}{T_{rc}} - \frac{1}{T_{sc}}}{\frac{1}{T_{sc}}} = \pm \frac{v}{c} \tag{2}$$

The following relationship between the transmitted code and the received code chip width:

$$T_{rc} = \frac{1}{(1+\varepsilon)} T_{sc} \approx (1-\varepsilon) T_{sc} \qquad (\because \varepsilon << 1) \tag{3}$$

When $\varepsilon < 0$, local code and receiving the code phase relationship is shown in figure 2.

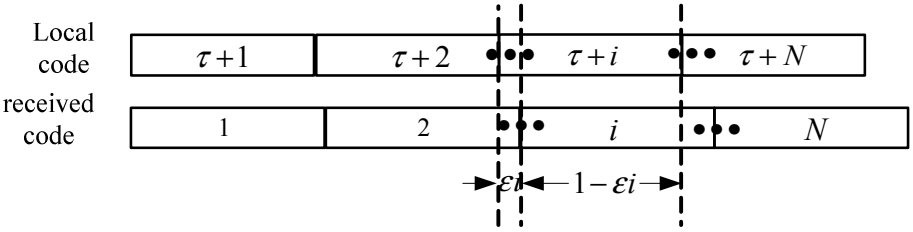

Fig2 $\varepsilon < 0$ native code and received code phase relationship

Accumulate the results as follows:

$$\begin{aligned} y(\varepsilon,\tau) &= \sum_{i=1}^{N} (-\varepsilon i) PN_{i-1} PN_{\tau+i} + \sum_{i=1}^{N} (1+\varepsilon i) PN_i PN_{\tau+i} \\ &= \begin{cases} N\left[1 + \frac{1}{2}(N+1)\varepsilon\right] & ,\tau = 0 \\ -\frac{1}{2} N(N+1)\varepsilon & ,\tau = -1 \\ 0 & ,\tau = +1 \end{cases} \end{aligned} \tag{4}$$

When $\varepsilon > 0$, local code and receiving the code phase relationship is shown in figure 3.

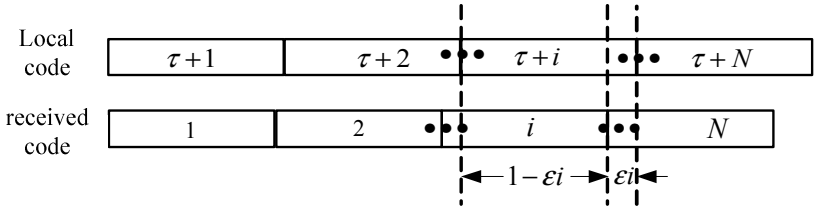

Fig3 $\varepsilon > 0$ native code and received code phase relationship

Accumulate the results as follows:

$$y(\varepsilon,\tau)=\sum_{i=1}^{N}\left[(1-\varepsilon i)PN_iPN_{\tau+i}+(\varepsilon i)PN_{\tau+i}PN_{i+1}\right]$$
$$=\begin{cases} N\left[1-\frac{1}{2}(N+1)\varepsilon\right] & ,\tau=0 \\ 0 & ,\tau=-1 \\ \frac{1}{2}N(N+1)\varepsilon & ,\tau=+1 \end{cases} \tag{5}$$

By the formula (4) and formula (5) shows that whether $\varepsilon > 0$, $\varepsilon < 0$, can make the local code and receiving the code of the coherent accumulation peak decreases.Heap which need to be further derived under the condition of dynamic system is the longest single dwell time.

Pseudo-code doppler frequency calculation:

$$\Delta R_{PN} = R_{PN} \times \frac{f_d}{f_{RF}} \quad (\text{chips/s}) \tag{6}$$

Above within a single dwell time receiving code and local code of relative phase slip should be less than 1/2 a yard, so should be:

$$\Delta R_{PN} T \le \frac{1}{2} \ \text{(chip)} \tag{7}$$

The formula (1) into the formula (2), can be single reside a maximum of integral time:

$$T \le \frac{1}{2\Delta R_{PN}} = \frac{f_{RF}}{2R_{PN}f_d} \ \text{(s)} \tag{8}$$

Given the processing gain and deal with the relationship between the bandwidth:

$$G_s = 10\lg\frac{R_{PN}}{B} \ \text{(dB)} \tag{9}$$

$$t = \frac{10^{\frac{G_s}{10}}}{R_{PN}} \ \text{(s)} \tag{10}$$

Figure 4 to achieve capture n road block diagram.

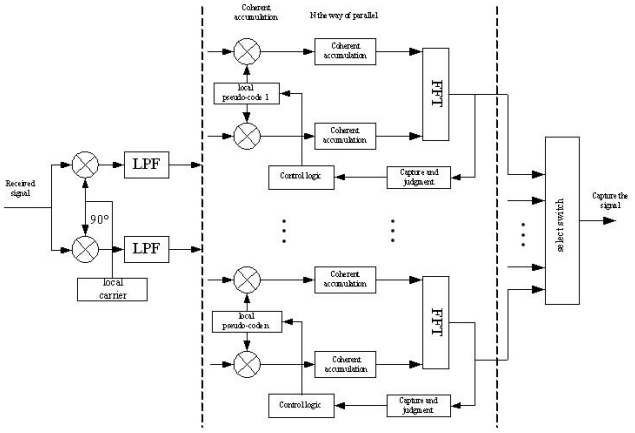

Fig4 The structure of the capture system

3 Simulation result

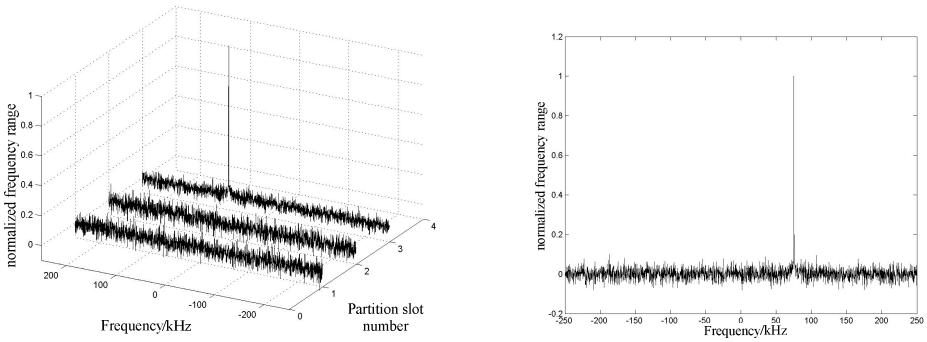

(a) Parallel to capture 3 d figure (b) The parallel capture sectional drawing

Fig5 3 road parallel capture peak estimation

The simulation results as shown in figure 5, carrier doppler offset caused by 75 kHz rate 0.34 kHz, so the only way to capture 3 successful. Clear from the figure 3 peak is much higher than other several road, decided to capture success.

Summary

Based on the doppler smaller pseudo-code range doppler, according to the division code doppler frequency range is studied the concrete method of parallel channels, and a simulation analysis was carried out.The simulation results prove that this method is compared with the traditional capture method, realized the measurement and control under the condition of spread spectrum signal capture, and use the distributed method to improve the real-time property of system processing, realized the quasi real-time processing of the signal.

Reference

[1] Lu Cengying. Based on overlapping reserves method and FFT pseudo-code rapid capture technology research[J]. Modern Defence Technology,2007,35(4):95-99.

[2] Ren Yufei. Unified spread spectrum tt&c system quickly capture technology research[J]. telemetry and telecontrol,2007,28(4):20-24.

Advanced Materials Research Vols. 989-994 (2014) pp 2422-2425
© (2014) Trans Tech Publications, Switzerland
doi:10.4028/www.scientific.net/AMR.989-994.2422

Improved genetic algorithm in Vehicle management

Shanhong Zhu[1,2] , TAO Kuang[1]

[1]School of Computer and Information Engineering ,Xinxiang university, Henan, China

[2]International School of Software, Wuhan University, Wuhan, China

zshazhu@163.com

Keyword: Vehicle management; genetic algorithm; multi-resources-constrain

Abstract: As the development of world economy, demand of logistics industry is getting more complex. Vehicle management dispatcher is an important part in logistic system, so how to realize the reasonable dispatcher of vehicles under the circumstance of multi-resources- constrain is the key issue in promoting the prosperity and development of modern logistics industry. The traditional genetic algorithm has the disadvantages that hinder the development and promotion of vehicle dispatcher and slow retard the development speed of logistics industry. Through the research of vehicle dispatcher's demand, we have put forward a new genetic algorithm which is improved, effective and adept to the normal vehicle dispatcher. We have proved that this algorithm is feasible and effective by analyzing the examples.

0 Introduction

With the development and prosperity of world economy and modern technology. A new service introduction of national economy---logistics industry is becoming stronger at a high speed, and it grows to be a pillar industry of economy gradually. The development of logistics industry marks the level of modernization of a country. Logistics industry is called the “accelerator” of the economy of the whole people, the “lubricant” of the reform of the economic structure, and “the third source of profit” of the enterprises. Because of the late start and high require of the development, some bad phenomenons appear in the logistics industry in China, such as backward infrastructure, low specialization, and high energy consumption while low productiveness, and so on[1].

Logistics distribution is the foundation of logistics industry's development. We can ameliorate these disadvantages if we react fast and realize the modern distribution, and it is also good for resolving a series of social problems, such as the traffic jams in big city and lack of energy resources. The best vehicle dispatcher is the key issue to complish the whole logistics and distribution preferably. Dantzig and Ramser firstly put forward the issue of vehicle dispatcher, namely the vehicle routing. After the persistently fast growth in sixty years and the long time study and analysis by scholars, now vehicle dispatcher has become the popular research project about the combination optimal problem in operational research. In our fast-paced as well as high-level production and social life, all the allocated or administrative problem such as posting the mail and freight, dispatching the railway car, transferring the seaport wharf, dispatching the public transportation, and so on, all these issues can be judged as the vehicles dispatching problem abstractly. With the conjunct application and development of E-commerce and Internet communication, the logistics and vehicles dispatching are broadly applied to some highly circulating fields, such as all kinds of national chains and large-scale businesses. Thus, the research of vehicles dispatching algorithm can improve the efficiency while lower the energy consumption, so it has high scientific meaning and practical value.

With the fast changes of logistics industry, the traditional genetic algorithm we are using now is extremely not adapted to the fast development speed and reform[2]. We will have to improve the traditional genetic algorithm if we want to adapt to the fast pace of modern logistics industry. After practicing for a long period of time, we make the new genetic algorithm adapted to the fast pace of modern logistics industry. Only in this way can we follow the development pace of logistics industry, and we not only economize the cost for later research but also extend the life of vehicles, thus realize the most optimized dispatcher and allocation, promote the better development of logistics industry, and enhance the comprehensive national strength.

2 Multi-Resources Constraint and Dispatching Model

2.1 Vehicle Dispatching and Multi-Resources Constraint

The vehicle dispatching in logistics needs the technology to realize the optimized measure under the multi-resources constrained condition, that is to say, to realize the optimization of expense, pcu and transportation distance, namely make the whole expense in dispatching the least, including the fixed starting fees of vehicles, driving fees, waiting fees, serves fees and punishment fees. At the same time, we should achieve the most cargo delivery with the least transport vehicles, supposing the routine is different, neither is the using vehicles, and we also need to complete the whole dispatching mission in the shortest distance. The most important is to complete the whole dispatching mission in the shortest time, including the approaching time of the vehicles, the waiting time and delay time and service time.

2.2 Multi-Resources Constraint

At present, foreign scholars pay much attention to the dispatcher of fixed need about the research of vehicle dispatching issue, including many resources-constrained conditions and limitations. We can propose these constraint into five kinds: mileage resources-constraint, motorcycle type resources-constraint, full loaded resources-constraint, non-full loaded resources-constraint, and time window resources-constraint. Summarized former research production, we find that there are many kinds of algorithms and solutions about vehicle dispatching issue, basically including the following five kind. The first one is branch and bound algorithm, which makes the best dispatching through the classification. .The second one is saving the distance algorithm, which regard save as the premise and foundation of optimum solution, and then optimize the vehicles dispatching. The third one is insertion algorithm, which inserts reasonable DC(distribution center) in appropriate region so as to optimize the vehicles dispatching. The forth one is tabu search algorithm, which prevents some algorithm that is not appropriate to this field. The fifth one is genetic algorithm, which applying genetic theory to realize the optimization. The last one is ANN algorithm, which adopts nerves classification to realize the optimization. In daily life, genetic algorithm is often applied. However, the disadvantage of genetic algorithm is increasingly obvious, so we need to greatly improve this algorithm so that it can be applied to practice and make users familiar to this method and get good practical result as well.

2.3 Building the Vehicles Dispatching Model Under Different Resources-Constraint

In order to study the vehicle dispatching issue, we need to build the models of vehicles dispatching in different resources-constraint. The first thing to do is to estimate the dispatching conditions of vehicles previously. In common, the more resources-constrained conditions in vehicles dispatching, the more complex of the arrangement of driving routine, and the less mission of every vehicle under resources-constraint, that is to say, the less dispatching mission that a vehicle needs to complete in practice, so the loading rate of every vehicle will be lower. Thus, we need more vehicles to dispatch missions, in order to realize the flexible arrangement of driving routine, we reserve the vehicles previously. The particular formular is as follows:

$$m = [\sum_{i-1}^{n} q_i / \partial Q] + 1 \tag{2-1}$$

In this formular, m is the total number of the dispatching vehicles, Q the standardized load, q_i the need of number i, and "$[*]$"is the integer function. We require that $0 < \partial < 1$.Generally the more complex lift trucks, the more resources-constrained conditions. However, that will make the ∂ gets smaller, that is to say the load everyday will lower greatly. Meanwhile, we also can get if the vehicles we need in the whole dispatching mission are getting more, the smaller of the ∂, and the smaller, the better.

3 Program and Improve the Genetic Algorithm

3.1 the Genetic Algorithm

The Genetic Algorithm is firstly put forward by J.Holland, and re-identified and deduced by Hollanl later on. Its core idea is every outstanding individual will appear the direction of index increasing in every dynamical population biology. That is to say, it is convergent, so it can be applied in practice preferably. This algorithm is a randomly searching and calculating method which has better adaption and flexible optimized object, so we do not need the successive optimized object, or the optimized object to differentiate, or has the good stability and parallel searching ability[3]. At the same time, the genetic algorithm does not need the initial solution, and arbitrary initial population biology can operate and outcome. We use randomized optional strategy in this algorithm, that is to say, it makes the outstanding individual go to the next generation through the survival of the fittest, and then after the cross - fertilization and Genetic behavior, it realizes weakness or disappearance.

Compared to other algorithms, the genetic algorithm has its own merits. The genetic alg orithm adopts the evolution mechanism, and it carries out the searching process in the whol e situation, averting the localization. Even if the adaptive function is discontinuous or irregu lar, the genetic algorithm can find the optimized solution of whole situation. And also, it h as wonderful parallel processing and can realize the combination with other algorithms, espe cially adapted to the issues which have large scale and broad distribution.

Recently, Genetic Algorithm (GA) is widely applied to the optimization problems in different fields, which arouses more and more people's interest of study and application due to its good characteristics that the Genetic Algorithm is not dependent on the problem model, along with global optimality, implicit parallelism, high efficiency and solution of the nonlinear problem.

GA is applied to the problem of constrained optimization; the constraint processing has become a very important link . There are two kinds of solutions: one adopts the changed operator in the operation, producing always the legitimate offspring from the legal parent satisfying the constraint conditions and making the search in the legal and valid space all the time; Another is to apply the corresponding punishment to the objective function in the adaptive function according to each individual to satisfy the different constraints so that the constrained problems are converted into unconstrained problems. The main steps of genetic algorithm are as follows :

a. Establish the initial group composed of a string at random;

b. Calculate the fitness of each individual.

c. According to the genetic probability, the following operations is applied to generate new group:

Copy: The existing excellent individual copied is added to the new group, and the bad individual is removed;

Hybridization: Two individuals picked out are exchanged, and the new individual is added to new groups;

Variation: One particular character is changed randomly in an individual; the new individu al is added into new groups;

d. The steps of (2), (3) are carried out repeatedly to reach the termination conditions, and the best individual is chosen as a result of the genetic algorithm. It is the key to practical application to choose the encoding strategy and convert the parameters into a string and the accurate fitness. The initial population N=200，the crossover probability P_c=0.95, the mutation probability P_m=0.01，the function of minimum inventory cost is as the objective function, the objective function is as fitness function directly, namely. The optimal purchase quantity and inventory is obtained in the following table with iterations of 53 times.

4 Conclusion

We discuss the analyze the genetic algorithm of vehicle dispatching under the multi-resources constraint and the improved genetic algorithm in detail, changing the disadvantage of slow convergence in the traditional genetic algorithm, making the application of improved genetic algorithm become much wider, thus promote the application of vehicle dispatching in the genetic algorithm, the growth of logistics, as well as the development and ability of the economy.

REFERENCE

[1] Gao Peng, Liu Hao-Ran, Hao Xiao-Chen, Guo Feng, Shi Xin 2011 *Journal of Mechanical & Electrical Engineering* **28**(2) 231-4
[2] Guo H, He J 2013 *Computer Modelling and New Technologies* **17**(3) 63-8
[3] Krainyukov A, Kutev V, Opolchenov D 2010 *Transport and Telecommunication* **11**(4) 14–28
[4] Fang Shuiliang, Yao Yanfei, Zhao Shikui 2011 *Journal of Mechanical & Electrical Engineering* **28**(3) 269-274

Advanced Materials Research Vols. 989-994 (2014) pp 2426-2430
© (2014) Trans Tech Publications, Switzerland
doi:10.4028/www.scientific.net/AMR.989-994.2426

Detecting Epistasis by LASSO-penalized-model Search Algorithm in Human Genome-Wide Association Studies

Zhihui Zhou[1], Guixia Liu[2, *], Lingtao Su, Liang Han and Lun Yan

College of Computer Science and Technology and Key Laboratory of Symbolic Computation and Knowledge Engineering of Ministry of Education, Jilin University, Changchun 130012, China

[1]zhzhhui0706@163.com, [2, *]lgx1034@163.com

Keywords: Logistic Regression; Epistasis; GWAS; LASSO-penalized

Abstract. Extensive studies have shown that many complex diseases are influenced by interaction of certain genes, while due to the limitations and drawbacks of adopting logistic regression (LR) to detect epistasis in human Genome-Wide Association Studies (GWAS), we propose a new method named LASSO-penalized-model search algorithm (LPMA) by restricting it to a tuning constant and combining it with a penalization of the L_1-norm of the complexity parameter, and it is implemented utilizing the idea of multi-step strategy. LASSO penalized regression particularly shows advantageous properties when the number of factors far exceeds the number of samples. We compare the performance of LPMA with its competitors. Through simulated data experiments, LPMA performs better regarding to the identification of epistasis and prediction accuracy.

Introduction

With the development of high-throughput genotyping technologies, it is possible for researchers to assay hundreds of thousands of single-nucleotide polymorphisms (SNPs) [1]. SNPs are the most abundant source of genetic variation in human genome, the number of which can reach millions in public datasets. Despite the notable success in identifying genes responsible for monogenic diseases, the pathogenesis of complex diseases still remains mysterious. Identification of disease-causing genes and epistasis requires extensive estimates of multiple potential genetic sites.

LR is a standard tool for modeling main effects as well as interactions in case-control studies. However, for the SNP data in GWAS, LR models have significant drawbacks: (1) In the contingency table, predictors defining an interaction may be empty, which should need special parametrization; (2) With many candidate loci, predictors can be correlated resulting in further degradation of the model; (3) The amounts of genotype factors and their interactions can create lots of parameters, and the problem of overfitting arises with relatively small samples; (4) These problems are aggravated when the interaction order increases.

For these and other reasons, we have to look for alternative methods for identifying epistasis. The LASSO approach tends to set many of the coefficients to zero, leading to a sparse model, a property generally weakened with an L_1-norm regularization. We will use the penalized method with the LASSO penalty to detect significant main effects and epistasis. We proposed LASSO-penalized-model search algorithm to search models of multiple risk predictors in large demographic studies.

In this article, we present a new algorithm called LASSO-penalized-model search algorithm, denoted as LPMA. We modify the LR criterion by restricting it to a tuning constant and combining it with a penalization of the L_1-norm of the complexity parameter, these adjustments produce significant effects. Because of the penalization, collinearity among the predictors does not degrade fitting much, and the number of elements in the selected model is essentially not influenced by sample size.

We compare our algorithm with screen and clean algorithm [2] proposed recently, an efficient tool to identify gene interactions. Extensive experimental results show that LPMA performs well both on the computation time and power.

Methodology

LASSO-penalized-model search algorithm. Our LASSO-penalized-model search algorithm is implemented with a multi-stage study approach. The purpose of the following stage is to validate the findings of the previous stage. All stages are likely to yield predictors for the whole genome as genome-wide platforms is becoming more and more cost-effective.

Following the Occam's razor principle of parsimony, we use statistical interactions to explore SNP-SNP interactions, even though SNP-SNP interactions can be considerably more complex in reality [3].

For main effects, we construct such a model:

$$G(x) = \sum_{i=1}^{n}(y_i - \mu - \sum_{j=1}^{p} x_{ij}\beta_j)^2 + \lambda\sum_{j=1}^{p}|\beta_j| \le s \quad (1)$$

Similarly, we build the epistasis model when considering interactions:

$$G(x) = \sum_{i=1}^{n}(y_i - \mu - \sum_{j=1}^{p} x_{ij}\beta_j - \sum_{k=1}^{p}\sum_{l=1}^{p} x_{ik}x_{il}\beta_{kl})^2 + \lambda\sum_{k=1}^{p}\sum_{l=1}^{p}|\beta_{kl}| \le s \quad (2)$$

The goal is to select those models that encode the variables or pairs of variables that best separate cases from controls. Our LPMA has four steps.

Step 1: This is the pre-selection step without utilizing the penalty parameter s, so the objective function is $G(x) = \sum_{i=1}^{n}(y_i - \mu - \sum_{j=1}^{p} x_{ij}\beta_j)^2 + \sum_{j=1}^{p}|\beta_j| \le s$, which is different from Eq. 1 by omitting the parameter that is utilized in step 3. This strategy only considers the tuning parameter s, thus reducing the computational burden and computing time to a certain extent. First of all, we only consider those predictors that pass quality control (QC) criterion. Then apply this objective function to these terms to estimate main effects. The forward stepwise regression has been investigated in several previous literatures. Recall how forward stepwise regression works:

1. Begin with all coefficients $\beta_j = 0$;
2. Seek out the predictor x_j most correlated with response y_i, and then add it into the model. Take residuals $r = y_i - y_{ithat}$;
3. Continue, at each step adding the predictor most correlated with r into the model;
4. End when all predictors are tested.

In this paper, we take a more "democratic" version of forward stepwise regression:

1. Begin with all coefficients $\beta_j = 0$;
2. Seek out the predictor x_j most correlated with response y_i, and then add it into the model. Take residuals $r = y_i - y_{ithat}$;
3. Increase the coefficient β_j in the direction of the sign of its correlation with y_i. Take residuals $r = y_i - y_{ithat}$ along the way. Stop when some other predictor x_k has as much correlation with r as x_j has;
4. Increase (β_j, β_k) in their joint least squares direction, until some other predictor x_m has as much correlation with the residual r;
5. End when all predictors are tested.

Surprisingly it can be shown that, with one modification, this procedure gives the entire path of lasso solutions, as s is varied from 0 to infinity. The modification needed is: if a non-zero coefficient hits zero, remove it from the active set of predictors and re-compute the joint direction. In this step, we use the parameter s to control the number of predictors to enter the model and denote the active set of predictors as S_1 and the number of elements as $num(S_1)$.

Step 2: This is a screen step using data derived from step 1. To discover interactions, we update the active set of predictors derived from step 1 by adding or deleting some elements. We obtain a new active set of predictors S_2 by adding all the pairwise interactions of the remaining elements and delete those not meeting certain conditions. It should be noted that the marginal p-value of the pairwise interactions is not bigger than p, which is a threshold defined by the user, while those whose marginal p-value are omitted. It is commended that the maximum of $num(S_2)$ is five times of $num(S_1)$,

otherwise we perform marginal tests on each effect and select the 5*num(S_1) effects with the smallest p-values.

Step 3: In this step, we adopt the LASSO penalty (L_1) as shown in Eq. 3 to do variable selection. The complexity parameter λ measures the trade-off between data fitting and the sparsity of the model to select the one that includes the variables or pairs of variables that best distinguish cases from controls. Let p(x) be the probability that y = 1, given x, and let $p_i = \log[p(x)/(1-p(x))]$. For a fixed λ, The coefficient vector $\theta = (\mu, \beta_1, \ldots, \beta_p)$ is calculated by maximizing the log likelihood:

$$L(\theta) = \sum_{i=1}^{n} [y_i \log p_i + (1-y_i)\log(1-p_i)] \tag{3}$$

Utilizing data sets derived from step 2, we apply Eq. 3 to S_2 and shave those elements whose coefficient is zero. We obtain the model including elements satisfying $\{j : \beta_j \neq 0\} \cup \{(k,l) : \beta_{kl} \neq 0\}$, then purify the model by deleting these elements not satisfying $\{j : |T_j| > c\} \cup \{(k,l) : |T_{kl}| > c\}$ where $c = Z_{\alpha/(2m)}$, and m is the number of elements in the model. T_j and T_{kl} are the t-statistic values for main effects and interactions respectively.

Step 4: It is obvious that the model step 3 produces is relatively sparse. There is a general tendency for the LASSO-penalized-model search to go wrong on the conservative side in choose coefficients, in other words, there is a quite high probability of containing all relevant coefficients at the expense of comprising some noise elements [4, 5]. Hence it is necessary to take a much more careful exploration on the terms that passed step 3. We implement this request by putting them into a parametric logistic regression and calculating the significance of each element at level α. The parameter α is chosen based on prediction accuracy rather than on an ad hoc basis. The significant elements enter the logistic regression again and generate the final model.

Post-processing . This post-processing is proposed by [6]. We here utilize the same procedure that can be described as follows to minimize false positives:

We denote all the epistatic interactions identified by our algorithm as S_{old}, and the set of epistatic interactions after the post-processing as S_{new}, which is a null set at first. We directly put I_i that belongs to S_{old} into S_{new} as long as I_i does not have any element the same with that of all interactions in S_{new}. Otherwise, if one epistatic interaction in (assume it is I_j) S_{new} has at least one same element with I_i, then we use their p-values to make a decision. If the p-value of I_j is larger that that of I_i, then we replace I_j with I_i. If not, I_i is not permitted to be put into S_{new}. After this procedure, we obtain a final set of loci interactions S_{new} that includes the most significant epistatic interactions detected by our algorithm.

Results and Analysis

The simulated data generated by the simulator Hapsample, which is accessible from the web site http://www.hapsample.org in public. We estimate the performance of our LPMA by comparing it with screen and clean (SC), an efficient tool for identifying interactions in genome-wide association studies proposed recently. We use a moderate number of predictors in the simulation experiments. Unless otherwise noted, the default experimental setting is as the following: #predictors = 10000, #individuals = 400, the linkage disequilibrium is 0.25, and the control-to-case ratio is 1.

In population genetics, linkage disequilibrium is described as the non-random association of alleles at two or more loci that descend from single ancestral chromosomes. Linkage disequilibrium is wholly a measurement of proximal genomic space [7]. The level of linkage disequilibrium is associated with various factors, such as the rate of recombination, genetic linkage, the rate of mutation, selection, genetic drift, population structure, non-random mating and so on. To make the experiment more convincing, we test the impact of linkage disequilibrium on power for detecting true predictors.

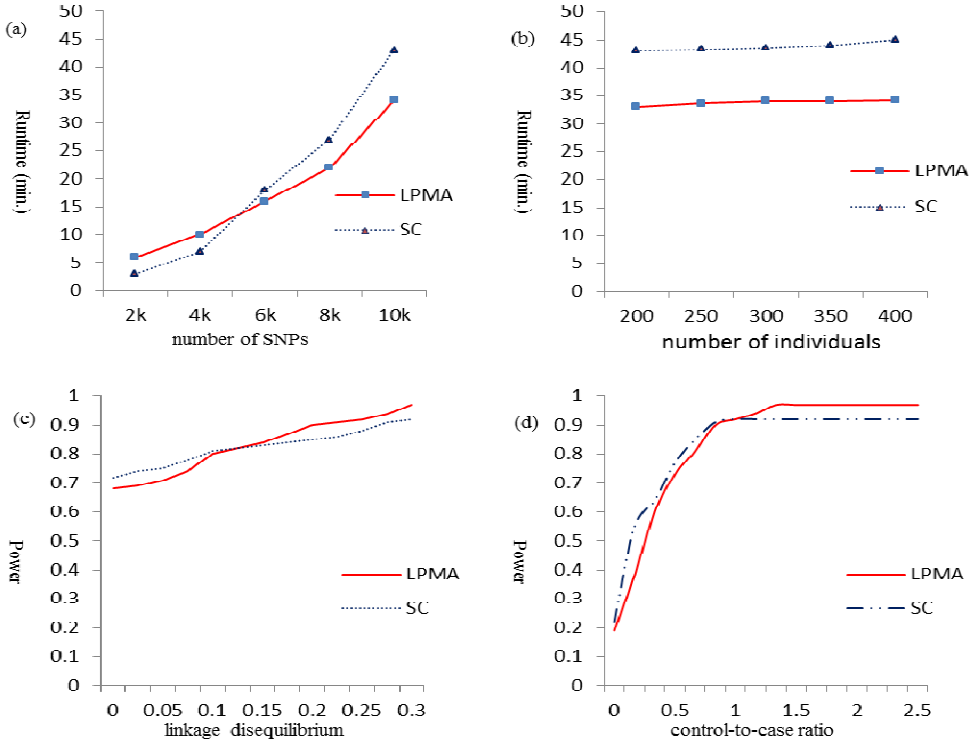

Fig. 1 Comparison of LPMA and SC about runtime and power

Fig. 1 (a) and (b) depicts the runtime comparison between LPMA and SC as the number of SNPs (predictors) and the number of individuals varies respectively. Fig. 1 (c) and (d) illustrates the power comparison when varying the linkage disequilibrium and the control-to-case ratio. It can be concluded that when the number of predictors is small, SC performs better than LPMA, which may be caused by those redundant pre-operations in LPMA, but LPMA outshines SC when the number of predictors becomes larger, which indicates that LPMA is more suitable to be applied to GWAS. Obviously, the number of individuals has little impact on the property of the two algorithms. When discussing the issue of power, the two algorithms approximately have equal shares.

Conclusions and Future Work

In this paper, we applied the LASSO-penalized-model search algorithm to detect epistasis. LPMA produces acceptable prediction accuracy and identifications of significant predictors. It is believed that this multi-step algorithm is an effective procedure to satisfy two demands simultaneously, generalizability and sparsity. Regarding to the computation time and power, sufficient experiments show that our LASSO-penalized-model search algorithm presents a better performance than its nearest competitors in extensive simulation studies.

In this article, we focus on the dichotomous response that can be coded as binary variables. Many literatures involve responses measured as continuous variables, and parallel methods such as GBOOST [7] based on CUDA and CEO [8] based on Google's MapReduce framework have been adopted into GWAS. In our future work, we will try to apply the idea of our current algorithm to quantitative responses using parallel technology.

Acknowledgement

This work was supported by grants from The National Natural Science Foundation of China (No. 61373051 and No. 61175023), Science and Technology Development Program of Jilin Province (No. 20140204004GX).

References

[1] Ozaki, K., et al.: Functional snps in the lymphotoxin-alpha gene that are associated with susceptibility to myocardial infarction. Nat. Genet. 32, 650–654. 2002.

[2] Wu J, Devlin B, Ringquist S, et al. Screen and clean: a tool for identifying interactions in genome-wide association studies. Genetic epidemiology, 34(3): 275-285. 2010.

[3] Cordell HJ. Epistasis: what it means, what it doesn't mean, and statistical methods to detect it in humans. Hum Mol Genet 11:2463–2468. 2002.

[4] Shi W, Wahba G, Wright S, et al. LASSO Pattern search algorithm with applications to ophthalmology and genomic data. Statistics and Its Interface, 1: 137–153, 2008.

[5] Wright, F.A. et al. Simulating association studies: a data-based resampling method for candidate regions or whole genome scans. Bioinformatics, 23, 2581–2588. 2007.

[6] Wang Y, Liu X, Robbins K, Rekaya R. Antepiseeker: detecting epistatic interactions for case-control studies using a two-stage ant colony optimization algorithm. BMC research notes 3(1):117. 2010.

[7] Yung L S, Yang C, Wan X, et al. GBOOST: a GPU-based tool for detecting gene–gene interactions in genome–wide case control studies. Bioinformatics, 27(9): 1309-1310. 2011.

[8] Wang, Z. et al.: CEO: a Cloud Epistasis Computing model in GWAS. In Proceedings of IEEE International Conference on Bioinformatics and Biomedicine, IEEE Computer Society, pp. 85–90. 2010.

Advanced Materials Research Vols. 989-994 (2014) pp 2431-2437
© (2014) Trans Tech Publications, Switzerland
doi:10.4028/www.scientific.net/AMR.989-994.2431

A Fuzzy Clustering Algorithm Based on Parameter Optimization in Large Transaction Database

Su Wei [1, a *], Zhang Xue[b] and Xu Jia jing[c]

[1] Air Force Early warning Academy Wuhan, Hubei 430000, China

[a]56554636 @qq.com, [b]63638636@qq.com, [c]814519834@qq.com

Keywords: continuous attributes; weighted index; clustering number; fuzzy clustering algorithm.

Abstract. In view of the discretization of continuous attributes of civil aviation radar intelligence data, this paper proposes a fuzzy partition algorithm of continuous attributes based on weighted index and optimization of clustering number, and its automatic determination of optimal weighted index m and optimal clustering number c overcomes the shortcomings of current attribute fuzzy methods of manual determination of classification number and no consideration of geometry data. The experimental results verify the validity and feasibility of fuzzy attribute discretization of civil aviation radar intelligence data characteristics.

1. Introduction

Fuzzy clustering is an important branch of unsupervised pattern recognition, has been widely applied in the field of image processing, pattern recognition, time series prediction and parameter estimation, and in practice, fuzzy clustering means (FCM) has been the most widely used fuzzy clustering algorithm.

FCM algorithm is an unsupervised classification algorithm, and the weighted index m and clustering number c, its two important parameters, should be determined in advance. If the parameters are inappropriately selected, the classification results may not match with the real structure of data. According to some literatures, [1] "parameter m controls the sharing degree between the fuzzy classes". Currently, implementation of FCM algorithm is usually based on experience or experiment and artificial selection method to determine the initial parameters of the algorithms for clustering; however, how to select the optimum m and optimal c has not been solved effectively.

In view of the above problems, according to the fuzzy decision theory and fuzzy clustering validity index V_{kwon} of data geometric structure, the weighted index m and c are discussed, and the methods to realize optimum parameters and a fuzzy clustering algorithm based on weighted index and clustering number optimization. As for application of FCM clustering algorithm, the weighted index and clustering number should be specified manually.

Description of FCM clustering algorithm. FCM clustering algorithm obtains membership of each sample site to the sample center through optimizing objective function Jm, so as to determine the membership of sample site. Objective-function-based fuzzy clustering method is put forward firstly by Ruspini [2], but the real effective method is proposed by Dunn[3] in 1974. Hard c-means (HCM) clustering algorithm is extended to the fuzzy case by Dunn. In that same year, Bezdek generalizes Dunn's method and establishes the FCM clustering theory. Through optimizing objective function, the membership of each sample site to the sample center is obtained, and accordingly membership, of sample site determines is determined. The algorithm is described as follows:

Suppose $X = \{x_1, x_2, ..., x_n\} \subset R^s$ is the data set, n is the number of elements in data, c is the clustering number centers, $d_{ij} = \| x_i - v_j \|$ is the Euclidean distance between sample site x_i and the cluster center v_j. u_{ij} is the membership of the ith sample belonging to the jth center, $U = [\mu_{ij}]$ is partition matrix of $n \times c$ of fuzzy c, and $v = [v_1, v_2, ..., v_c]$ is center matrix of fuzzy clustering $s \times c$.

Definition 1 If any $U \in M_{fc}$ in (1) is met, fuzzy partition of data set X is defined.

1. $M_{fc} = \{U \in R^s \mid \mu_{ij} \in [0,1], \forall i, j; \sum_{i=1}^{c} \mu_{ij} = 1, \forall j; 0 < \sum_{i=1}^{c} \mu_{ij} < n, \forall i\}$

Each element $\{\mu_{ij}, 1 \le j \le n\}$ in U matrix defines a subset of fuzzy clustering $\tilde{S}_l$.

2. $\tilde{S}_l = \mu_{l1} / x_1 + \mu_{l2} / x_2 + \cdots + \mu_{\ln} / x_n$

where μ_{ij} indicates that the membership degree of jth sample belonging to clustering $\tilde{S}_l$.

3. $J_m(U,v) = \sum_{i=1}^{n} \sum_{j=1}^{c} \mu_{ij}^m \cdot d_{ij}^2$

$J_m(U,v)$, extended from HCM and ISODATA [5] algorithm, is infinite families of the objective function defined by Bezdek [4]; m is weighted index, and it plays an important role in regulating fuzzy degree of clustering, μ_{ij} is the membership function, and:

4. $\mu_{ij} = 1 / \sum_{i=1}^{n} \left\{ \frac{d_{ij}}{d_{kj}} \right\}^{\frac{2}{m-1}}$

The FCM algorithm comes from optimization steps of the following formula, i.e. through (5) iteration of the first-order necessary conditions.

5. $\min_{M_{fc}} \left| J_m\left(U,v\right) \right|$

In (5), the first order necessary conditions of variables $\left(U,v\right)$ correspond to (4) and (6).

$$v_i = \frac{\sum_{j=1}^{n} \left(\mu_{ij}\right)^m x_j}{\sum_{j=1}^{n} \left(\mu_{ij}\right)^m}$$

It is identified [6] that FCM algorithm converges to local minimum so as to minimize the objective function J_m, thus a fuzzy c of X to divide U^*.

Optimized algorithm based on the optimal weighted index m^* and optimal clustering number c^*

In order to obtain the optimal value of the weighted index m and according optimal clustering number of samples, the optimal clustering number c^* according to methods to gain m based on fuzzy decision and validity index V_{kwon} of geometry structure of specific data sets.

Method to obtain optimal weighted index m^* based on fuzzy decision-making. According to the fuzzy decision theory proposed by Bellman and Zedeh, fuzzy objectives G and fuzzy constraints C are constructed, and the decision D is formed by the intersection of D and C, i.e.

1.When G and C are regarded as fuzzy sets, they are respectively characterized by the membership function, so the membership function of fuzzy decision can be expressed as:

2.The final decision results are the alternative solutions of decision space.

3.Therefore, in order to optimize m with the help of fuzzy decision theory, appropriate fuzzy goal, fuzzy constraints and corresponding membership function should be constructed. In this study, fuzzy goal G is defined as the objective function $J_m(U;v)$, the fuzzy constraint C is defined as possibility for partition $H^*(U;c)$. Accordingly, the fuzzy decision about the optimal weighted index m^* can be expressed as:

4.Next, the membership functions of fuzzy objectives G and fuzzy constraints C are defined as μ_G and μ_C, two of which are ensured of the same increase or decrease, as is represented by the following formula:

5.Then the fuzzy decision value of optimal weighted index m^* is m corresponding to the maximum membership degree in intersection of fuzzy subset of G and C, namely, the m corresponding to nodal value.

Method to determine the optimal clustering number c^* based on the validity index V_{kwon}. The fuzzy clustering objective function with large membership degree and minimize possibility of fuzzy clustering with large membership degree for partition entropy, so that the clustering can not only express similarity information between samples and realize good separability between class samples. However, in the traditional method, the value of c is artificially selected, so the final clustering result can not be ensured the optimal partition. In this study, validity index is adopted for further iteration of the initial clustering number, thus clustering center number is automatically realized, and finally the optimal clustering number is gotten. The algorithm process is shown below (woth initial weighted index range $m = 1.0, 1.1, \cdots, k$ and $step = 0.1$):

(1) The initial clustering number $c = 2$;

(2) Initialized clustering center v_i, $i = 1, 2, \cdots, c$; ,;

(3) The number of iterations $p = 0$, the distance d_{ij} between various data and the cluster center is calculated, membership function matrix $U^{(0)} = (\mu_{ij}^{(0)})$ is calculated of, wherein $j = 1, 2, \cdots, n$ $i = 1, 2, \cdots, c$, μ_{ij} is the element on ith row jth column of matrix U, meaning the membership of jth data on the ith clustering center. Constraint relation is represented by formula (1);

(4) v_i of C clustering centers is recalculated, $i = 1, 2, \cdots, c$.

(5) The membership function matrix U is recalculated;

(6) The objective function $J_m^{(p)}(U;\ v)$ and the possibility of partition entropy $H^{*(p)}(U;c)$ are calculated;

If $\left|J_m^{(p)}(u,v) - J_m^{(p-1)}(u,v)\right| \le \varepsilon$ and $\left|H^{*(p)}(u,v) - H^{*(p-1)}(u,v)\right| \le \varepsilon$, convergence displays, then the clustering numbering iteration ends, otherwise, step (4) is turned to;

(7) If the validity index V_{kwon} reaches convergence conditions, the process ends, then we get local optimum clustering number c_m^*, minimum objective function $J_m^*(U;v)$ and the minimum probability partition entropy $H_m^*(U;c)$ are obtained with the current value of m. Otherwise, the clustering number $c = c + 1$, and then step (2) is turned to;

(8) $m = m + 0.1$, if $m \le k$, step (1) is turned to, or, the process ends. $\mu_G(m)$ and $\mu_C(m)$ of m are obtained; according to formula (13), the optimal weighted index m^* is obtained, local optimum clustering number c_m^* of m^* is the optimal clustering number c^*.

Fuzzy algorithm to classify aviation radar intelligence attributes based on weighted index and clustering number optimization

This new algorithm is the improvement of previous studies. According to fuzzy decision theory and probability partition entropy function, the key parameters in FCM algorithm are summarized, namely the selection of optimal weighted index m, and then through the iteration of validity index V_{kwon}, the optimal clustering number is obtained, thus no manual selection of parameters in the original algorithm is eliminated, and local optimum is avoided; at the same time, clustering classification

based on dataset geometric structure is realized, so that fuzzy attribute partition is more consistent with the actual data. This section presents a discretization algorithm for continuous attribute of civil aviation radar intelligence based on the above algorithm, and establishes membership functions of fuzzy attribute partition.

Fuzzy attribute partition. Firstly, the continuous attributes of civil aviation radar intelligence deserve fuzzy partition, assuming the following definition:

Suppose the database sample $D = \{x_1, x_2, \cdots, x_n\}$, in which $x_1, x_2, \cdots, x_n$ means different database records, n is recorded sample number; for the continuous attributes in databases, for continuous attribute number; $QA = \{q_1, q_2, \cdots, q_r\}$ means the continuous attribute in database, r is the number of continuous attributes, $DS_i = \{x_{1i}, x_{2i}, \cdots, x_{ni}\}$ is the set q_i of attributes corresponding to n recorded samples, $FP = \{FP_1, FP_2, \cdots, FP_r\}$ is the set of final fuzzy partition of all attributes; $FP_i = \{f_1, f_2, \cdots, f_c\}$ is the fuzzy set of single continuous attribute, and c is the number of fuzzy sets.

For given civil aviation radar intelligence database samples D, only the classification attributes and continuous attributes are considered in this paper. With the continuous attribute partition as an example, the attribute value set of $q_i \in QA$ in D deserves clustering classification with the improved FCM algorithm, the best fuzzy partition FP_i of attribute q_i and its fuzzy c - partition matrix $U_i = [\mu_{jk}(x_i)]_{n \times c}$ are obtained, in which $\mu_{jk}(x_{ji})$ means the membership degree of attribute value of jth of attribute q_i to fuzzy set $f_k \in FP_i$, and $v_i = \{v_{i1}, v_{i2}, \cdots v_{ic}\}$ means fuzzy classification center, so do division of other attributes.

Pseudo code of algorithm for fuzzy partition of civil aviation radar intelligence data attribute is shown.

1. For each $q_i \in QA(i = 1,2,\cdots,r)$
2. (Read DS and $m_{\max}$, namely the upper limit of improved FCM algorithm)
3. FP_i, U_i, v_i== new FCM ($q_i, DS_i, m_{\max}$)
4. For each partition $f_k \in FP_i$
5. label f_k appropriately (marking of fuzzy set)

Each continuous attribute deserves this procedure, until all the attribute partition ends. It is displayed that this attribute partition method is based on the geometric structure of data set, then the optimal clustering number and classification center are automatically obtained, thus the empirical determination of clustering number is eliminated.

Calculation of Membership function of fuzzy attribute set. After calculation of fuzzy partition of all continuous attributes, according to membership degree m of fuzzy attribute set, the membership function of fuzzy set of all continuous attributes is calculated.

A variety of ways can be used to determine membership function, such as Wang Shitong's generalized membership function model $\exp(-|a_1 x + a_2|^r)$ can achieve approximated membership function of various fuzzy sets. But in actual engineering application, the membership functions of fuzzy sets are usually expressed as triangular, trapezoidal or Gauss type functions, in order to facilitate calculation, triangle function is selected. With q_i attribute and its fuzzy partition FP_i mentioned above as example, the concrete methods are as follows:

Suppose $X_i^k = \{x_{pi} : \mu_{pk}(x_{pi}) \geq \mu_{jk}(x_{ji}), \forall j \in (1,\cdots,c)\}$, find out the attribute value of minimized membership located on both sides of center in $X_i^k \cup \{v_k\}$, let the minimum value of the left

membership attribute be x_{li}, membership be $\mu_{lk}(x_{li})$, attribute value of left membership minimum be x_{ri}, and membership be $\mu_{rk}(x_{ri})$, then the triangular fuzzy value of kth fuzzy sets (a, v_k, b) is:

$$f(x)=\begin{cases}\dfrac{x-a}{v_k-a} & a\le x\le v_k\\ \dfrac{b-x}{b-v_k} & v_k\le x\le b\\ 0 & x<a or x>b\end{cases}\qquad \begin{cases}a=x_{li}-\dfrac{\mu_{lk}(x_{li})(v_k-x_{li})}{1-\mu_{lk}(x_{li})}\\ b=x_{ri}-\dfrac{\mu_{rk}(x_{ri})(v_k-x_{ri})}{1-\mu_{rk}(x_{ri})}\end{cases} \tag{1}$$

Generation of recorded fuzzy sets. After attribute fuzzy partition, membership function of all fuzzy sets are made use of to transform the original database record into fuzzy record sets, and this process is a necessary step for subsequent data mining method.

If the entry corresponds to continuous attributes, then the fuzzy partition number of attributes and record of database D for fuzzy set membership function are transformed. The transformed fuzzy entries are divided corresponding to fuzzy partition number, and each item value is the membership of corresponding fuzzy set $\mu\in[0,1]$, the threshold value of m can also b set, and those beyond threshold value do not belong to the corresponding fuzzy sets.

If the entry's corresponding attributes are classification properties, the corresponding entries are classified in accordance with the number of attributes, each subvalue's membership according to the category is $\mu=\{0,1\}$.

In addition to previously defined symbols, the additional following symbol definitions are as follows: is is is the classification attribute in database; $C=CA\bigcup QA$ is attribute sets; D' is the transition variables to be converted in database D; E is eventual converted database.

$D'=D$
$D''=\varnothing$
for each $c_i\in C$
  if $c_i\in CA\quad (i=1,2,\cdots,q)$
    for each record $x_j\in D'\quad (j=1,2,\cdots,n)$
      x' = replace value v_{ij} by $\mu_{ij}\in\{0,1\}$
      $D''=x'\bigcup D''$
  if $c_i\in QA\quad (i=1,2,\cdots,r)$
    for each record $x_j\in D'\quad (j=1,2,\cdots,n)$
      for each $f_x\in FP_i$ corresponding $c_i\ \ (k=1,2,\cdots,s)$
    μ_{ijk} =membership corresponding to crisp value v_{ijk} in fuzzy partition （attribute） f_x
    according to triangle membership function (a, v_k, b)
      x' = replace v_{ijk} by μ_{ijk}
      $D''=x'\bigcup D''$
  $D'=D''$
  $D''=\varnothing$
$E=D'$

The above process helps to convert the original record set D into fuzzy record set E, Each continuous attribute deserves this procedure, until all the attribute partition ends. It is displayed that this attribute partition method is based on the geometric structure of data set, then the optimal clustering number and classification center are automatically obtained, thus the empirical determination of clustering number is eliminated.

4. Experimental results and analysis

In order to verify the effectiveness of the optimum weighted index m^* and the optimal clustering number c^* in this algorithm, experiments are carried out on a set of IRIS data, and when two objective function difference I less than 0.001 or the number of iterations is greater than 200 times, the iteration terminates.

To initialize clustering center, the method proposed by Katsavounidis [7] I adopted, this algorithm is based on distance optimization, with no threshold set, as is shown below:

(1) The maximum norm data sample is taken as the initial site of first cluster center;

(2) The data sample farthest away from the first initial site is taken as the second initial value;

(3) The minimum distance between those non-selected sample data and all the initial sites are respectively calculated;

(4) The data sample corresponding to maximum value of all minimum distances is selected, and take is as initial site of next cluster center;

(5)Repeat step (3) and (4), until all initial sites required are selected.

The test sample set is IRIS data consisting of 150 samples of 4-D space samples which are divided into three categories, i.e. setosa, versiccolor and virginica each of which contains 50 samples whose 4 components are IRIS petal leangth, petal width, sepal length and sepal width. Of all the three types of samples, two overlap, one enjoys good distinction. The data is often used to test clustering algorithms and clustering validity function performance.

Table 1 Value of IRIS data with different values of m

c	$H(U;c)$		
	$m=1.5.$	$m=2$	$m=2.5$
2	0.0561	0.1141	0.2375
3	0.1034	0.1264	0.2234
4	0.2451	0.2197	0.2603
5	0.3382	0.2016	0.3127
6	0.4581	0.2142	0.5432
7	0.5647	0.2988	0.6827
8	0.6104	0.7452	0.8135
9	0.8151	0.9526	0.8213

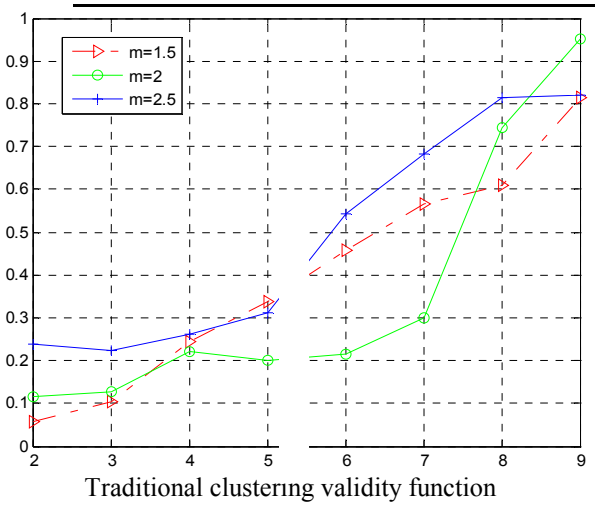

Fig. 1 Curve of changes of $H(U;c)$ with clustering number

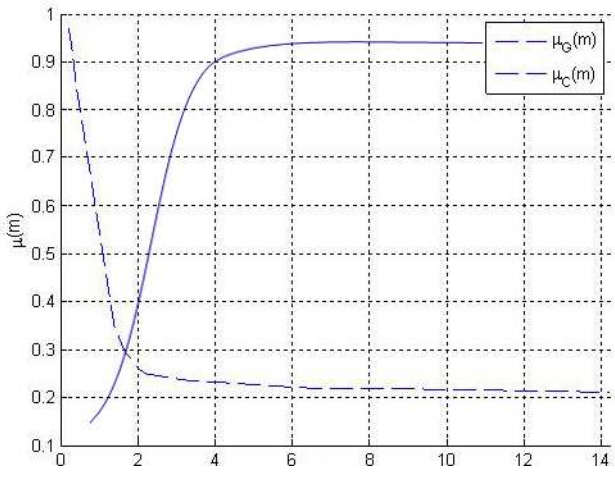

Fig. 2 m^* based on fuzzy decision-making method

The experimental results are shown in Table 1, and the results of clustering experiment for the function of entropy partition validity are taken good advantage of. Fig. 3 tells that when m=1.5 and m=2, $H(U;c)$ will show the optimal clustering number, but poor robustness of m is achieved. Fig. 1 and Fig. 2 demonstrate the distribution of local optimum clustering number corresponding to the weighted index with this method. Fig. 1 clearly shows that the membership function of fuzzy

objectives and fuzzy constraints intersect when $m = 1.8$, the weighted index in the intersection corresponding to the maximum membership in the intersection of fuzzy objectives and fuzzy constraints is 1.8, so optimal weighted index of clustering algorithm $m^* = 1.8$, close to $m = 2$ commonly adopted in FCM algorithm; Fig.2 shows the optimal weighted index m^* correspondence with $c_m^* = 2$, and classification result is in consistent with actual sample data distribution, i.e. the optimal clustering number $c^* = 2$. Therefore, the clustering algorithm proposed in this study can better realize the optimal weighted value and the optimal clustering numbering than traditional partition entropy validity function.

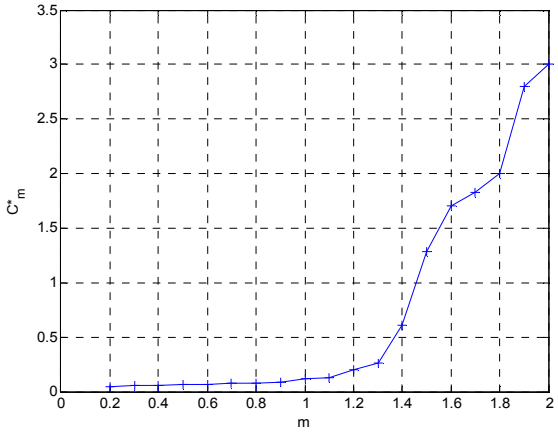

Fig 3 Curve of changes of c_m^* with different m

5. Conclusions

This paper, in view of the actual demand of civil aviation radar intelligence data, puts forward a fuzzy clustering algorithm based on weighted index and optimization of clustering number, and the experimental results show the superiority of this new algorithm to traditional fuzzy clustering algorithm, since it uses a method to gain m based on fuzzy decision-making method and validity index V_{kwon} based on concrete data set geometry structure to determine clustering number c^*, followed by realization of key parameters in FCM algorithm, namely, the selection of optimal weighted index helps to get the best clustering number, thus manual parameters selection in traditional algorithm is eliminated, and the local optimum of algorithm is avoided.

References

[1] Guhag S, Rastogi R, Shim K. CURE: an Efficient Clustering Algorithm for Large Databases. Proc of ACM SIGMOD International Conference on Management of Data, 1998: 73-84.
[2] Wang W, Yang J, Muntz R. STING: A Statistical Information Grid Approach to Spatial Data Mining[C]. Athens: Proc of the 23rd Conference on VLDB,1997:186-195.
[3] Wang W, Yang J, Muntz R R. STING+: An Approach to Active Spatial Data Mining. Sydney: Proc of the 15th ICDE, 1999: 116-125.
[4] Agrawal R, Gehrke J, Gunopulos D, et al. Automatic Subspace Clustering of High Dimensional Data for Data Mining Applications. Seattle: Proc of the ACM SIGMOD Conference, 1998: 94-105.
[5] Sheikholeslami G, Chatterjee S, Zhang A. WaveCluster: A Multiresolution Clustering Approach for Very Large Spatial Databases. New York: IEEE Trans on System, Man, and Cybemetics: PartB, 1999, 29(3):433-439.
[6] Pelleg D, Moore A. X-means: Extending K-means with Efficient Estimation of the Number of the Clusters. Proceedings of the 17th ICML, 2000.

Advanced Materials Research Vols. 989-994 (2014) pp 2438-2443
© (2014) Trans Tech Publications, Switzerland
doi:10.4028/www.scientific.net/AMR.989-994.2438

A hybrid approach for critical technology identification

Chengyang Li[a], Jiang Jiang[b] and Menjun Li[c]

College of Information System and Management, National University of Defense Technology, Changsha 410073, China

[a]chengyangli_nudt@sina.com, [b]jiangjiangnudt@163.com, [c]mjli11260744@gmail.com

Keywords: Critical technology, Centrality Analysis, Fuzzy comprehensive evaluation, Hybrid approach.

Abstract. There have been attempts to indentify critical technology from many alternative technologies. Accordingly, we can form an R&D policy effectively if we can forecast central technologies. Multi-criteria decision-making method and Centrality Analysis have been applied to the problem. However, these two approaches have some limitations. This study proposes a hybrid approach to identify critical technologies in a technology network which take full advantage of experts' experience in technology field and relationship between technologies at the same time. Fuzzy comprehensive evaluation and Centrality Analysis of node are used in the approach. A case study on hypothetical critical technology identification problem is used to illustrate the proposed approach.

Introduction

The characteristics of modern technology can be defined as complexity, interdependence and radical. Under this uncertain and rapidly changing environment, the grasping of technological trend and development by analyzing overall structure of technologies and interaction among them has become much more important[1]. With some exercises to identify future key technologies, industry and government can manage R&D portfolio efficiently thus competitive advantage can be gained and sustained [2].

Critical technology identification is an unstructured, complex problem with lots of aspects that must be taken into consideration[3]. Different countries have developed different approach in identifying their critical technologies list[4,5,6]. Delphi survey[7], Technology Roadmapping[8], and some other technology foresight approaches[9] have been developed. Most of these critical or key technology studies are based on interviews with experts on the technology for which a forecast is being developed[4]. Typical critical technology identification exercise usually has four steps, including location and selection of experts, initial list of technologies, prioritization, final list of critical technologies[6]. Multi-criteria decision-making methods[9,10] are applied in prioritization to select criteria and integrate experts' judgment of technologies.

However, these studies do not pay much attention to the relationship and linkages between technologies. Assuming that, technology is a dependent variable, which may lead to unreasonable results. Furthermore, these approaches are much dependent on experts' experience, which is unquantifiable and sometimes subjective.

Since technologies are characterized by strong interdependence[11], there have often been attempts to examine technological structure and linkage as a form of network[11,12,13,14]. Network analysis has often been used in conjunction with patent citation analysis[15]. A number of studies have been conducted to frame current technology structure and identify Critical technology by using patent analysis, such as Cross Impact Analysis[1], co-word[16], and keyword vector similarity[17]. The underlying assumption in these studies is that there exists a technological linkage between the two patents if a patent cites another patent[1].As a quantitative measure of importance in a network, centrality measures of node can be used in network analysis. As defined by Freeman[18], degree centrality, closeness centrality and betweenness centrality have been employed as indicators of importance of certain nodes in networks. In the previous studies, these centrality measures have been implicitly deployed as indicators of importance of technologies [11].

Patent citation-based critical technology identification do has its limitation yet[1], it excessively relies on the analysis of network, which can only provide information about the network structure. Information and the value of technology nodes are ignored.

In this article, in order to overcome the weakness of traditional critical technology identification approach and Patent citation-based analysis, taking full advantage of experts' experience in technology field and relationship between technologies at the same time, we propose a new hybrid approach, integrating Fuzzy comprehensive evaluation and Network analysis to identification critical technology.

The remainder of this paper is organized as follows. Section 2 deals with the detail explain of the proposed approach and a brief introduction of Fuzzy comprehensive evaluation and centrality measures in network analysis, which will be used in the proposed approach. A hypothetical core technology identification problem which designed to demonstrate the algorithm is explained in Section 3. Section 4 is a conclusion of the paper.

Hybrid Approach For Critical Technology Identification

This study proposes a hybrid approach,which integrating Fuzzy comprehensive evaluation and centrality analysis to engage the challenge of critical technology identification. Fuzzy comprehensive evaluation is used to evaluate the alternative technologies against the set of criteria previously identified by experts' judgments, which will mark technologies with the experts' knowledge of technology fields. The node centrality analysis of technology network gives us information based on the structure of technology linkages. Then, we integrate evaluation results of Fuzzy comprehensive evaluation and centrality analysis and give the final rank of alternative technologies.

This critical technology identification process includes seven steps, a schematic diagram of the process is shown in Fig1.

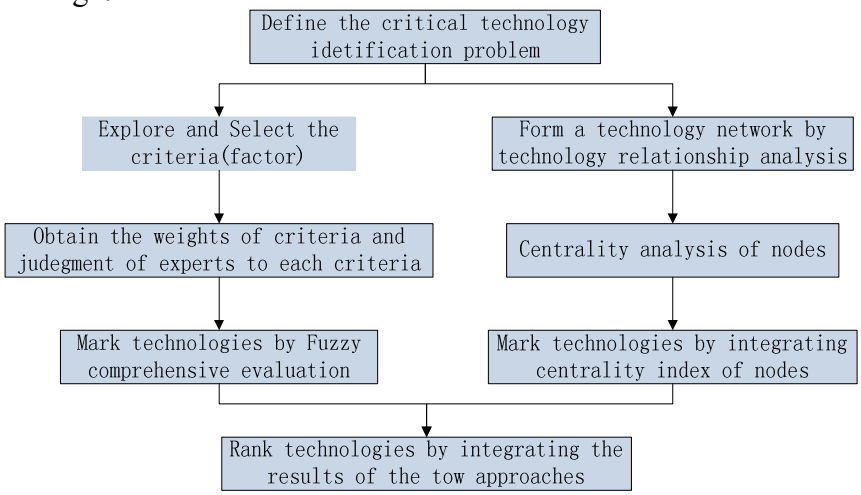

Fig 1. Hybrid approach for critical technology identification

(1) Define the critical technology identification problem. Identify the scope for which technologies will be analyzed.

(2) Explore the critical technology identification criteria (factor), such as benefit, cost, risk, and so on. Select criteria which will be used in the process. Suppose Factor(criteria) Set is $U = \{u_1, u_2, ..., u_m\}$. It is composed of m kinds of evaluation factors which decision-makers care. Evaluation Set is $V = \{v_1, v_2, ..., v_n\}$. It represents n kinds of evaluation standards.

(3) Obtain the weights of criteria and judgment of experts to each criteria from different backgrounds. For Fuzzy comprehensive evaluation, Evaluation factors(criteria) weight vector is $E = \{e_1, e_2, ..., e_m\}$, Single-factor evaluation matrix R is constituted by numbers of single-factor evaluation vector put together. R is a fuzzy relationship matrix composed of evaluation Factor Set U and the Evaluation Set V.

$$R=\begin{bmatrix} R_1 \\ R_2 \\ \vdots \\ R_m \end{bmatrix}=\begin{bmatrix} r_{11} & r_{12} & \cdots & r_{1n} \\ r_{21} & r_{22} & \cdots & r_{2n} \\ \vdots & \vdots & & \vdots \\ r_{m1} & r_{m2} & \cdots & r_{mn} \end{bmatrix} \tag{1}$$

(4) Mark the technology options by Fuzzy comprehensive evaluation result. The last results of comprehensive evaluation can be got by doing complex operations calculation between single factor weight vector E and fuzzy relationship matrix R, which is as follows.

$$B=E\bullet R=\{b_1,b_2,\ldots,b_m\} \tag{2}$$

b_i is the membership degree value of evaluation samples to each evaluation standard. The determination results are usually defined according to the maximum membership degree law.

In this article, the best judgment($B_i^{'}$) of b_i is selected as the initial score of technology, it represents the critical analysis based on experts' experience. Then, we normalize the initial score of each technology, Calculation formula of final score B_i is shown in (3).

$$B_i=\frac{B_i^{'}}{\sum_{i=1}^{i=10} B_i^{'}} \tag{3}$$

Step 2 to step 4 is Fuzzy comprehensive evaluation approach, Fuzzy comprehensive evaluation approach is a very effective and wide used multi-criteria decision making method, papers[19,20] will give more details about the Fuzzy comprehensive evaluation approach. In this study, it is used to rank the technology alternatives by experts' judgment with multi-criteria.

(5) Form a technology network by analysis relationship between technologies such as patent, key works, and so on.

(6) Centrality Analysis of nodes in the technology network.

To characterize individual technology's positions in a technology network, various centrality measures of node can be calculated. Three common measures of node centrality, degree centrality, closenees centrality and betweenness centrality[18] are choosed in this study. These three measure indexes are referenced to different structural attributes of technology.

Degree centrality($\sigma_D(x)$)[21] was defined as the number of ties incident upon a node. It represents the simplest centrality measure and determines the number of direct contacts as an indicator of the quality of a network member's interconnectedness.The higher $\sigma_D(x)$ for a node x is, the more contacts a node x has, and the more inportant the node is. For technology network, it means the higher centrality score $\sigma_D(x)$ for a technology node is, the more neighbor it has, and the more important the technogy is.

Closeness centrality ($\sigma_C(x)$)[21] is based on the idea that nodes with a short distance to other nodes can spread information very productively through the network. In order to calculate $\sigma_C(x)$ of a node x, the distances between the node x and all other nodes of the network are summed up. For technology network, technology with smaller $\sigma_C(x)$ is closer to the center of technology network and can spread information smoothly to other technologies, and the technology is much more critical.

Betweenness Centrality($\sigma_B(x)$)[21] is based upon the frequency with which node falls between pairs of other nodes on the shortest or geodesic paths connecting them, it is used to exhibit a potential for control of the communication. For technology network, technologies with higher σ_B play much more important role in the exchange of information between other technologies.

Papers[22,23] may give you more information about the definition and detail calculation process of these node centrality.

(7) Mark the alternative technologies by integrating centrality index of nodes. In order to integrate the result of node Centrality Analysis, we define the integrating centrality index($\boldsymbol{ICI_i'}$) which is shown in formula (4).

$$ICI_i' = \frac{Degress * Betweenness}{Closeness} = \frac{\sigma_D(x) \bullet \sigma_B(x)}{\sigma_C(x)} \tag{4}$$

(5) is the formula of the normalized $\boldsymbol{ICI_i'}$ ($\boldsymbol{ICI_i}$) for each technology.

$$ICI_i = \frac{ICI_i'}{\sum_{i=1}^{i=10} ICI_i'} \tag{5}$$

(8) Integrate the results of Fuzzy comprehensive evaluation and node Centrality Analysis, get the final rank of alternatives.Final critical index (***CI***) is defined to integrate the results of Fuzzy comprehensive evaluation and Centrality Analysis of technology node. Critical technology is identified based on the final critical index. For each technology, calculation formula of CI_i is (6).

$$CI_i = B_i + ICI_i \tag{6}$$

In this hybrid approach, Fuzzy comprehensive evaluation gather the knowledge from experts in the technology field, Centrality Analysis based on the linkage and interaction between technologies, the two approaches is integrated in the hope of entailing a more objective and practical critical technology identification process.

Illustrative example

A hypothetical critical technology identification problem was designed to demonstrate the computational process of the algorithm.

Step1. Define the critical technology identification problem. The problem is to identify a critical technology in a technology network. Committee of experts who come from different technology fields is formed. After a discussion, experts have identified 10 technologies from T_1 to T_{10} and the technology network is constructed for evaluation.

Step2. In order to simplify the algorithm of Fuzzy comprehensive evaluation process, only three criteria (factor) are being considered which are as the following:

1) Advance(C_1)
2) Technology Readiness Level(C_2)
3) Cost(C_3)

Step3. A set of linguistic scale, such as 'high, average, low' is used to evaluate the importance of the criteria and sub-criteria. Weights for selection criteria (C_1, C_2, C_3) is (0.2, 0.3, 0.5) and the judgment of experts to each sub-criteria is shown in Table 1.

Step4. For the paper limitation, we will neglect the detail calculate process and only give the result of Fuzzy comprehensive evaluation.

Table 1.Judgment of experts to each sub-criteria

Judegment	Advance (C_1)			Technology Readiness Level (C_2)			Cost (C_3)		
Technology	advanced	general	backward	high	average	low	expensive	common	cheap
T1	0.7	0.2	0.1	0.1	0.2	0.7	0.3	0.6	0.1
T2	0.3	0.6	0.1	1	0	0	0.7	0.3	0
T3	0.1	0.4	0.5	1	0	0	0.1	0.3	0.6
T4	0.6	0.4	0	0.7	0.2	0.1	0.4	0.6	0
T5	0.4	0.5	0.1	0.3	0.6	0.1	0.8	0.1	0.1
T6	0.2	0.6	0.2	0.7	0.3	0	0.2	0.8	0
T7	0.5	0.3	0.2	0.3	0.5	0.2	0.5	0.4	0.1
T8	0.9	0.1	0	0.4	0.6	0	0.8	0.2	0
T9	1	0	0	0.3	0.4	0.3	1	0	0
T10	0.7	0.3	0	0.5	0.4	0.1	0.6	0.4	0

For each technology, the results of Fuzzy comprehensive evaluation are $\boldsymbol{B_1}$ = (0.27, 0.46, 0.27), $\boldsymbol{B_2}$ = (0.56, 0.33, 0.11), $\boldsymbol{B_3}$ = (0.27, 0.27, 0.46), $\boldsymbol{B_4}$ = (0.4, 0.5, 0.1), $\boldsymbol{B_5}$ = (0.56, 0.33, 0.11), $\boldsymbol{B_6}$ = (0.3, 0.5, 0.2), $\boldsymbol{B_7}$ = (0.45, 0.36, 0.18), $\boldsymbol{B_8}$ = (0.625, 0.375, 0), $\boldsymbol{B_9}$ = (0.45, 0.27, 0.27), $\boldsymbol{B_{10}}$ = (0.5, 0.4, 0.1). Best judgment is selected as the initial score of each technology. For example, 0.27 is selected as the initial score of technology 1. Then, we normalize the score of each technology, the initial score ($B_i^{'}$) and final score (B_i) for each technology are shown in Table 2.

Table 2. Initial and final score for each technology

	T1	T2	T3	T4	T5	T6	T7	T8	T9	T10
$B_i^{'}$	0.27	0.56	0.27	0.4	0.56	0.3	0.45	0.625	0.45	0.5
B_i	0.062	0.128	0.062	0.091	0.128	0.068	0.103	0.143	0.103	0.114

Step5. We simplify relationship between technologies such as patent citation, keyword similarity. There is only a connection if technology1 and technology 2 is related. The technology network we formed is in Fig 2.

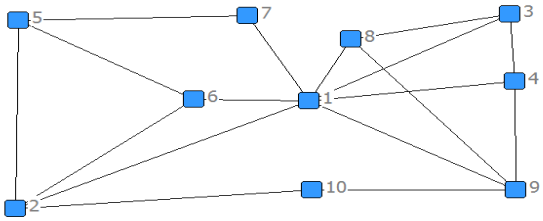

Fig 2. Technology network

Step6. Centrality analysis of nodes in the technology network. The Degree, Betweenness and Closeness centrality of each node are calculated by Ucinet software. Results of Node Centrality is shown in Table 3.

Table 3. Results of Node Centrality

	T1	T2	T3	T4	T5	T6	T7	T8	T9	T10
Degree	7	4	4	3	3	3	3	3	2	2
Betweenness	18.08	5.25	3.92	1.58	1.58	1.33	0.75	0.58	0.58	0.33
Closeness	11	14	15	15	16	16	17	17	18	19

Step7. Calculate the integrating centrality index (***ICI***) of nodes. Results of integrating centrality index and the normalized $\boldsymbol{ICI_i^{'}}$ of each technology is shown in Table 4.

Table 4. Results of integrating centrality index

	T1	T2	T3	T4	T5	T6	T7	T8	T9	T10
$ICI_i^{'}$	11.51	1.5	1.05	0.32	0.30	0.25	0.13	0.10	0.06	0.03
ICI_i	0.755	0.098	0.069	0.021	0.020	0.016	0.009	0.007	0.004	0.002

Step8. The final critical index (***CI***) integrate the results of Fuzzy comprehensive evaluation and Node centrality analysis. Table 5 is the final critical index for each technology.

Table 5. critical index for each technology

	T1	T2	T3	T4	T5	T6	T7	T8	T9	T10
CI_i	0.817	0.226	0.197	0.112	0.148	0.084	0.112	0.15	0.107	0.116
Rank	1	2	3	6	4	7	6	8	9	5

Critical technology is selected based on the rank of final critical index. In this illustrative case, Technology 1 should selected as the critical technology since it has the highest critical index.

Summary

This study suggests a hybrid approach to identify critical technology in a technology network. For this purpose, Fuzzy Comprehensive Evaluation Method is used to gather the knowledge from experts in the technology field, Centrality Analysis of nodes, which based on the linkage and interaction between technologies prioritize technologies by objective structure information. We integrate these two types of approaches to get the final rank of technologies. To illustrate the process of executing and utilizing the proposed approach, a hypothetical critical technology identification problem is presented.

The main contribution of this study is that, experts' experience and technology network analysis was integrated together in the hybrid approach, which will take full advantage of technology related information and have a more comprehensive and practical identification process.This study, however, is still subject to some limitations and these limitations are issues for further research. Centrality Analysis of nodes doesn't get adequate information of technology network, and the two approaches which we used need some improvement if there is a large number of technologies in the technology network.

Acknowledgements

This research is supported by the National Science Foundation of China under Contract no.71201168 and the Doctoral Fund of Ministry of Education of China under Contract no. 21024307120019.

References

[1] Chulhyun Kim, Hyeonju Seol: *The 9th International Conference on Electronic Business*(Macau, November 30 - December 4, 2009). p. 689.
[2] Hakyeon Lee, Chulhyun Kim, Hyunmyung Cho, Yongtae Park: Expert Systems with Applications, Vol. 36 (2009) No. 1, p. 894.
[3] M. Lamb, M.J. Gregory: *International Conference on Management of Engineering and Technology* (Portland, Ore, 1997). p. 206.
[4] Y.G. Lee, Y.I. Song: Technovation, Vol. 27 (2007) No. 1, p. 57.
[5] Information on http://www.foresight-platform.eu.
[6] Information on http://www.unido.org.
[7] Yu-Lung Hsu, Cheng-Haw Lee, V.B. Kreng: Expert Systems with Applications, Vol. 37 (2010), p. 419.
[8] Information on http://www.whitehouse.gov.
[9] Daniel. R. Georidiadis, Thomas A. Mazzuchi, Shahram Sarkanil: System Engineering, Vol. 16 (2013), p. 287.
[10] Zhigang Jiang, Hua Zhang, John W. Sutherland: Journal of Cleaner Production, Vol. 19 (2011), p. 1939.
[11] Sunghae Jun: *International Conferences, ASEA and DRBC*(Jeju island, Korea, November/December ,2012). Vol. 1, p. 1.
[12] Sunghae Jun: *International Conferences, ASEA and DRBC*(Jeju island, Korea, November/December ,2012). Vol. 1, p. 28.
[13] Juneseuk Shin, Yongtae Park: Information Economics and Policy, Vol. 19 (2007) No. 2, p. 249.
[14] Gediminas Adomavicius, Jesse C. Bockstedt, Alok Gupta, Robert J. Kauffman: Inf Technol Manage , Vol. 8 (2007), p.185.
[15] Tugrul U. Daim, Guillermo Rueda, Hilary Martin, Pisek Gerdsir: Technology Forecasting, Vol. 73 (2006) No. 8, p. 981.
[16] Information on http://link.springer.com
[17] Yoon, B., & Park, Y: Journal of High Technology, Vol. 15 (2003) No. 1, p. 37.
[18] Linton C. Freeman: Social Networks, Vol. 1(1978), p. 215.
[19] Chunyan Shao: International Business Research, Vol. 2(2009) No. 1, p. 210.
[20] L. Ma, Y. Liu, X. P. Zhou: International Journal of Engineering, Science and Technology, Vol. 2 (2010) No. 7, p. 123.
[21] Andrea Landherr, Bettina Friedl, Julia Heidemann: Business & Information Systems Engineering, Vol. 2 (2010) No. 6, p. 371.
[22] Information on http://www.researchgate.net
[23] Information on http://faculty.ucr.edu

Advanced Materials Research Vols. 989-994 (2014) pp 2444-2449
© (2014) Trans Tech Publications, Switzerland
doi:10.4028/www.scientific.net/AMR.989-994.2444

Coupling Sentiment Dictionary and SVM Classification for Text Orientation Analysis

Mingze Gao[1], Fangfang Li[1], Zheyuan Ding[1] and Weidong Xiao[1]

(1. Science and Technology on Information System Engineering Laboratory, National University of Defense Technology, Changsha, China)
Email: gaoming278@163.com

Keywords: Sentiment dictionary; SVM classifier; Text orientation analysis;

Abstract. Sentiment classification finds various applications in opinion mining, which can help users determine sentiment tendency of texts and information. In this paper, we consider the problem of text orientation analysis. In particular, we propose a two-stage approach by coupling sentiment dictionary and classification methods. In the first stage, we build sentiment dictionary and rules to obtain the texts whose emotional scores are ranked in the top 1/4 and the bottom 1/4. These texts are marked classified for supervising the second stage. In the second stage, we employ the SVM classifier to process the remaining texts. Finally, we combine the two stages to get the orientation analysis results for all the texts. Experimental results demonstrate that, in contrast to using sentiment dictionary and classification method separately, our proposed method achieves higher classification accuracy when an initial training set by manual tagging is unavailable.

Introduction

With the rapid development of Web technology, the Web has become a very important source from which more and more people obtain information. Mining and analyzing the rapidly expanding texts on web, especially the sentiment of the online reviews posted by users, can make people better understanding of the consuming habits and public opinions of various users. Besides, it plays an important role in decision-making for many institutions, such as enterprises, the government, etc. Therefore, it is very significant to study the sentiment classification problem about online comments. However, the massive amount of information is widely distributed online, it is difficult to collect and process them without manual means. Thus the sentiment classification technology arose. At present, the research of text orientation analysis is generally divided into two categories in domestic and abroad: the method based on sentiment dictionary or machine learning.

Although sentiment dictionary method and machine learning method are relatively mature, there exist some flaws. On one hand, the method based on sentiment dictionary is not a good way to classify text which is obscure. On the other hand, machine learning method requires a large set of manually annotated text, which is difficult to achieve. Therefore, depending on many basic studies, combining the advantages of both methods above, we propose a two-stage classification approach to solve the problem.

Related Work

The method based on sentiment dictionary uses a dictionary which is marked emotional polarity to calculate emotional polarity of the text. While the method based on machine learning regards sentiment classification as a special kind of text classification which uses manually labeled training set and the method of machine learning to classify texts. For the texts to be classified, word segmentation and removing stop words should be implemented firstly.

The Method of Sentiment Dictionary

The priority work of sentiment dictionary is building up the appropriate sentiment thesaurus. General Inquirer (GI) and WordNet are used as commonly basic resources to study English text sentiment classification. While in Chinese text sentiment classification study, HowNet is more widely used, it is necessary to choose sentiment dictionary according to actual needs. After establishing the sentiment dictionary, take advantage of existing tools to deal with language

materials which is prepared by syntactic analysis, dependency analysis, etc. Extracting the modifiers of the sentiment words combined with sentiment words tendencies value. According to certain algorithm, the phrase sentiment tendency of the sentence is calculated and then the sum of the tendencies value of these phrase containing sentiment words is weighted. At last, obtain the sentiment tendencies value of the entire text by summing to achieve the purpose of sentiment analysis.

The Method of Machine Learning

Machine learning method mainly consists of the training process and the classification process. First of all, set training set that is classified manually, using frequency as a statistic to calculate the distribution of category entries in the text. Due to the problems of high-dimensional feature space and documentation sparse vectors, it is necessary to find a good feature selection method. Through feature selection method we can get some key features which are representative. Then according to the calculation method of Term Frequency Inverse Document Frequency(TF－IDF) [1],we can calculate the weight of each key feature and quantify them and then get Vector Space Model (VSM) [2]. In the next classification process, dealing with the test text by the same operation as described above. Finally, choose the appropriate classification algorithm to classify, calculating the similarity between test text vector and category vector which have been trained. The category which has the largest similarity value will be the final classification of the text to be measured.

The Two-stage Text Classification Method

Building the Rules of Sentiment Dictionary

In order to build the sentiment dictionary, we use *sentiment analysis using word set* released by HowNet and network language manually collected. For sentiment words, the negative words invert its emotional polarity, while the degree adverbs strengthen or weaken its emotional polarity. So we should construct emotional words (S) dictionary, negative words (N) dictionary and degree adverbs (D) dictionary, manually annotate emotional polarity value of sentiment words and degree polarity value of adverbs, then building rules to determine the emotional polarity of the texts.

In addition, we should take into account of the effect of dynamic sentiment words. The words called dynamic sentiment words have different tendencies when modifying different target words. Such as the sentiment word "high", when the target word is quality, it tends to positive, but when the target word is oil consumption, it tends to negative. In dealing with the word, we should create a dynamic sentiment dictionary, including dynamic sentiment words and matching words. DSW represent the set of dynamic sentiment words, divided into forward sets denoted as FDSW and backward sets denoted as BDSW. PW is the set of matching words near sentiment words, also divided into forward sets denoted as FPW and backward sets denoted as BPW. dt is a dynamic sentiment word, dp is a matching word, wp_f is the emotional polarity value when dynamic sentiment word's matching word belongs to FPW, wp_d is the polarity value of the composition, calculated as follows:

$$C(dt)=\begin{cases}1 & if\ dt\in FDSW\\ -1 & if\ dt\in BDSW\end{cases} \quad (1) \qquad C(dp)=\begin{cases}1 & if\ dp\in FPW\\ -1 & if\ dp\in BPW\end{cases} \quad (2)$$

$$wp_d = wp_f * C(dt) * C(dp) \quad (3)$$

After we find the dynamic sentiment word phrase, regarding the whole phrase as another sentiment word, and then deal with negative words and degree adverbs. p_d is the emotional polarity value of the phrase, wp_d is the emotional polarity value of sentiment words, d_d is the degree polarity value of adverbs. For different syntactic structures, emotional polarity calculation methods are different. As shown in Table 1:

Table 1. Emotional polarity calculation method

Syntactic structure	Emotional polarity calculation formula
S+D/D+S	$p_d = wp_d * d_d$ (4)
N+S	$p_d = (-1) * wp_d$ (5)

N+D+S	$p_d = d_d * wp_d$ (6)
D+N+S	$p_d = (-1) * d_d * wp_d$ (7)

Calculating emotional scores of each phrase of the text according to the syntactic structure in order to accumulate and get the whole sentence emotional score. i is number of sentence, P_{ij} is the emotional score of phrase j in sentence i. In order to eliminate the influence of text length on the final emotional score, the sum of the scores should be divided by the number of sentence. If the final emotional polarity value P of the text is greater than zero, the comment is positive otherwise is a negative comment. Calculated as follows: $P = \frac{\sum P_{ij}}{i}$ (8)

Feature Selection Method

The commonly feature selection methods are Document Frequency (DF), Information Gain (IG), Mutual Information (MI) and Chi-square Statistic (CHI), all these feature selection methods have its own advantages and disadvantages. For their shortcomings, we propose an improved feature selection method IDTC, use two indicators including the probability of the appearance of features and the correlation of features and categories to calculate the information value of features for the category. What different with DF which rely on the document frequency directly is the improved feature selection method uses the probability of the appearance of features to substitute features frequency, and combines the method of MI to represent the correlation of features and categories meanwhile. For a second-class relationship, we can calculate the information difference of the two categories that reflect the discrimination of characteristics to these two categories. The formula is defined as: $IDTC(t_i, C_j, C_k) = P(t_i) * |MI(t_i, C_j) - MI(t_i, C_k)|$ (9)

$P(t_i)$ is the probability of features appearing, $|MI(t_i, C_j) - MI(t_i, C_k)|$ represents the ability of features to distinguish between the two categories. During feature selection process, we remove the features below a given threshold from the original feature space, and retain the features above the threshold as representative features of the document.

Support Vector Machine

Support Vector Machine (SVM) is a traditional classification method and it has outstanding performance for classification [3]. Let us assume that a training set consists of N labeled samples $(x_i, y_i)_{i=1}^N$, where $x_i \in R^d$ denotes the training samples and $y_i \in \{-1, +1\}$ denotes the associated labels. The goal of a binary SVM is to find out a hyperplane that separates the dimensional feature space into two subspaces. An interesting feature of SVM is relative to the possibility to project the original data into a higher dimensional feature space via a kernel function $K(,.,)$, which satisfies the Mercer conditions [4]. SVM is a classification method designed for binary class issues [5], the purpose of text orientation analysis is based on the document feature vector to divide the document into positive and negative category, so we choose SVM in machine learning stage in this paper.

The Two-stage Classification Algorithm Process

Text classification based on two-stage experimental process is describes as the following steps:

1) Step1: Text preprocessing. Making preprocessing operations such as word segmentation and removing stop words.

2) Step2: Sentiment tendencies calculation. We can read all the texts in text files. By the method of sentiment dictionary, calculating the emotional scores of all the texts.

3) Step3: Text score sorting. As all the texts sorted by scores, we can get the texts which have clear emotional polarity. The texts which scores ranked in the top 1/4 and the bottom 1/4 are chose as the classified collection of the second stage to train, and the texts which scores ranked in the middle 1/2 are chose as unclassified collection of the second stage to test.

4) Step4: Feature selection. The improved feature selection method IDTC extracts feature words in classified and unclassified collection separately.

5) Step5: Text vector representation. The weight of each selected feature calculated by TF-IDF method, and then we can get the Vector Space Model.

6) Step6: SVM classifier for classification. To classify the unclassified texts, we choose SVM classification algorithm.
7) Step7: Get the experimental results.
Fig.1 shows the two-stage classification algorithm process.

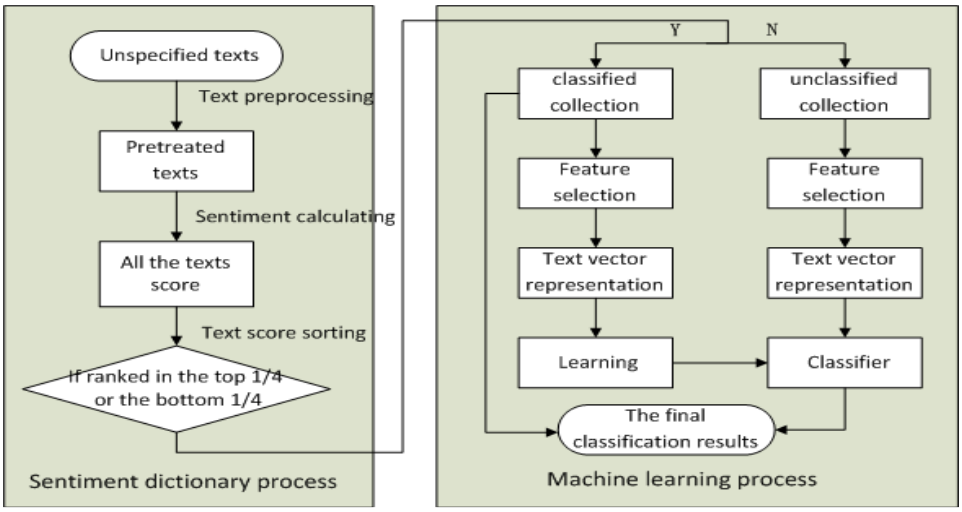

Fig.1 The two-stage classification algorithm process

Experiment and Results Analysis

Experiment Setup

The algorithm was implemented in Java. We used the segmentation system ICTCLAS designed by Institute of Computing Technology, Chinese Academy of Sciences to achieve word segmentation, and adopted a SVM tool named LibSVM by Taiwan University to implement the SVM classification model. The experimental data sets were obtained from the authors of [6] that included Ctrip_htl_4000 (4, 000 hotel comments), Dangdang_Book_4000 (4, 000 book comments) and Jingdong_NB_4000 (4, 000 laptop comments). Each of the three data sets has 2, 000 positive comments and 2, 000 negative comments, respectively.

Analysis of the Results

For each data sets, in order to prove the validity of the proposed method, we all chose 2000 texts as training sets, and another 2000 texts as testing sets. First of all, we classified the testing sets by machine learning method, mainly applied the improved feature selection method and SVM classifier. Next, the same testing sets were classified by sentiment dictionary method. At last, we used the two-stage text classification method to run the same experiment. In particular, we selected the testing sets whose emotional scores were ranked in the top 500 and the bottom 500 as the classified collection of the second stage for training, and then classified the texts score ranked in the middle 1000 by SVM classification. We utilized the Macro-Precision (P), Macro-Recall (R) and Macro-Fscore (F1) [7] to evaluate the performance in average, and chose F1 as the final evaluation index, where F1 is defined as:

$$F1=\frac{2RP}{(R+P)} \quad (10)$$

Classification results are shown in Table 2. In feature selection process, we selected 1000 features ranked in the top.

Table 2. Classification results

The Dataset	Sentiment Dictionary	Machine Learning	The Combined Method
Ctrip_htl_4000	0.794631	0.814810	0.825407
Dangdang_Book_4000	0.808524	0.864639	0.880730
Jingdong_NB_4000	0.812507	0.830068	0.842816

As shown in experimental results, for all of the three data sets, when we use sentiment dictionary method independently, the classification accuracy is near 80%, and machine learning method is

superior to sentiment dictionary method in classification accuracy, while the classification accuracy is further improved by our two-stage approach combined with sentiment dictionary and classification methods. Also we can see that the performance of the classification of book comments is better than the other two. Next, we evaluate the effect of the number of features, and provide the results in Fig. 2.

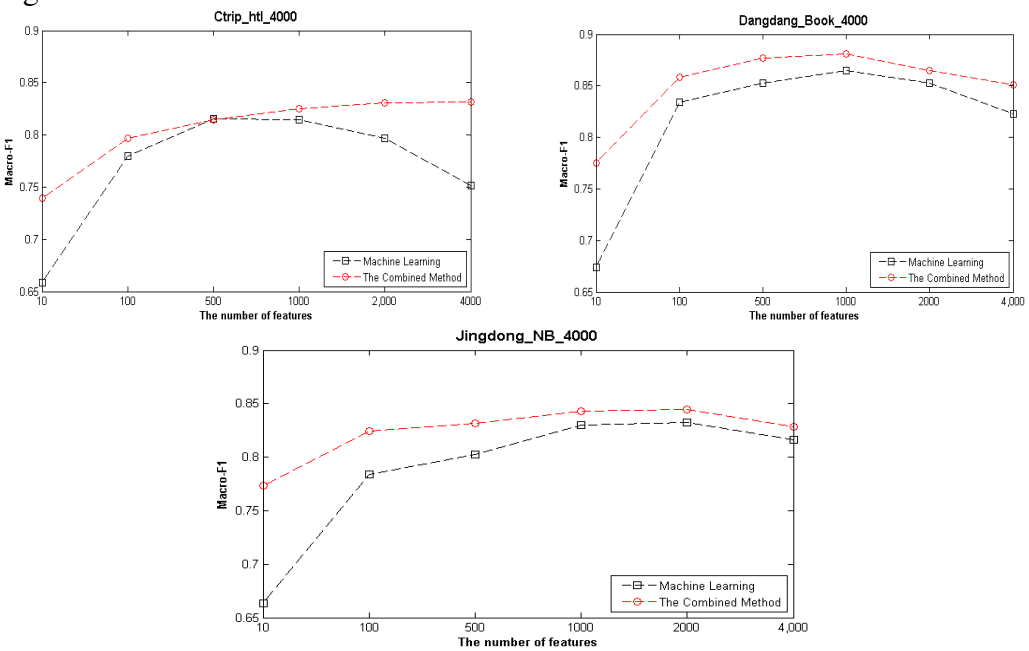

Fig.2 The effect of the number of features

As in Fig.2, horizontal axis represents the number of features, where features are ranked in descending order of weight, and high-ranking features are preferred; vertical axis represents the value of Macro-F1 when selecting the features ranked in the top.

Using machine learning method independently, the classification performance is gradually improved with the growth of the number of selected features. While after the number of features item reaches a certain number (about 1000), the rating trend begins to decline. The method of the two-stage classification shows that the classification accuracy increases slowly with the growth of the number of features. We are glad to see that the classification accuracy of the combined method is still higher than machine learning method on the condition of the same number of features.

Conclusions

This paper proposed a two-stage text classification method based on combining the methods of sentiment dictionary and SVM classification. Experimental results show that compared with the sentiment dictionary method or the classification method, the proposed two-stage method can achieve higher accuracy. As future work, we plan to further investigate the construction of domain sentiment dictionary and grammar rules, since it is the prerequisite for generating unclassified texts, and it involves a number of issues such as the discovery of new words.

Acknowledgment

This work is supported by National Natural Science Foundation of China No. 61302144 and the Natural Science Foundation of Hunan Province, China under Grant No. 11JJ5044.

References

[1] G. Salton, T.Y. Clement, On the construction of effective vocabularies for information retrieval, SIGIR, 48-60 (1973)

[2] G. Salton, A. Wong, C.S. Yang, A vector space model for automatic indexing, ACM, 18(11), 613-620 (1975)

[3] Y.J. Li, B. Liu, Multiconlitron: A general piecewise linear classier, IEEE Transactions on Neural Networks. 22(2), 276-289 (2011)

[4] K. Liu, X. Qian, A novel batch-mode active learning method for SVM classier, Journal of Information and Computational Science. 9, 4873-4880 (2012)
[5]Q. Lin, R. Hu, Facial expression feature extraction based on integral image, International Conference on Advanced Computer Theory and Engineering. 1345-1351 (2009)
[6] ChnSentiCorp. http://www.Searchforum.org.cn/tansongbo/corpus-senti.htm
[7] K. Chai, H. Chieu, Bayesian online classifiers for text classification and filtering, SIGIR, 97-104 (2002)

Advanced Materials Research Vols. 989-994 (2014) pp 2450-2453
© (2014) Trans Tech Publications, Switzerland
doi:10.4028/www.scientific.net/AMR.989-994.2450

RESEARCH ON THE OPTIMIZATION OF THE STORAGE STRATEGY OF HDFS

Hui Cao

Henan Radio and Television University, Zhengzhou 450008, China

402793927@qq.com

Keywords: optimization, storage strategy, HDFS.

Abstract. The storage of the massive data puts forward higher requirements in quantity and quality of hardware so that the cost of hardware rises. We have to use software for weakening the requirements of hardware. HDFS is just born for solving the massive data storage. Through the analysis of the files of the organization, storage mode, storage technology etc. this paper presents the optimization of data storage strategy of HDFS and the description of the optimization algorithm.

Introduction

Cloud computing is the development [1] of Distributed Computing, Parallel Computing [2] and Grid Computing [3]. Cloud storage is a new concept on the extension and development of cloud computing.

Cloud storage, as a system that provides the functions of data storage and business access, adopts applications to let the large variety of storage devices of different types work together through the functions of cluster applications, grid computing, distributed file system and so on.

The rise of cloud storage is to subvert the existing network storage architecture. With the development of information technology and internet [4], the amount of data on the network is more and more big, the users demand the storage businesses with higher reliability and safety, the business types also becomes richer, there is little the existing storage can do. For example, there is a performance bottleneck with traditional NAS[5] or SAN[6] in capability and capacity expansion, when the client business requirements can not be met, the enterprise must upgrade to the storage system more or add more management tool, and increases capital investment. Cloud storage service mode not only breaks through the bottleneck of traditional SAN, but also can expand the capacity and performance linearly, that is a new choice for the enterprise which pursues high availability and high performance.

Hadoop distributed file system is called HDFS for short, it is designed as distributed file system which is suitable for running on commodity hardware. HDFS is a highly fault tolerant system and suitable for deployment in cheap machine. HDFS can provide access to high throughput data, is very suitable for large data sets.

File organization of the HDFS

HDFS is a distributed file system which has the characteristics of high fault tolerance and is designed to be deployed in the low cost of hardware equipment. In HDFS, file exists in the form of block data and the data block size can be set, default is 64M, which is more than the general operating system file blocks to be big.

File storage mode of the HDFS

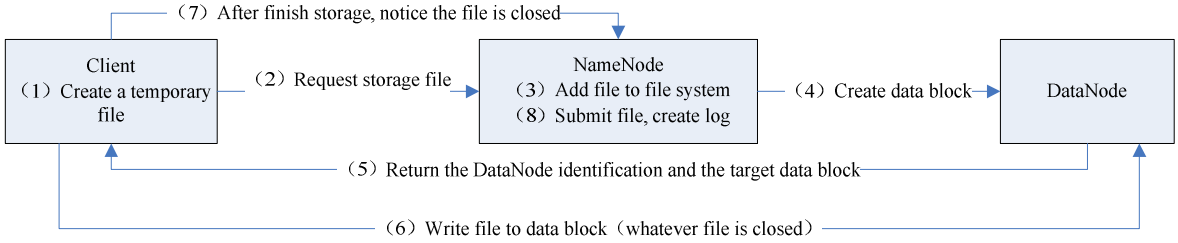

Fig. 1 Storage process in HDFS

When a client needs to store files, storage process in HDFS is pictured above (Fig. 1).

(1) The client creates a temporary file in the local at first. The operating of write is based on the temporary file.

(2) The client requests storage file to the NameNode.

(3) The NameNode adds the file to the file system.

(4) The NameNode sends the request of creating the data block to the DataNode.

(5) The DataNode returns the DataNode ID and the target data block to the client.

(6) The client file is writed to the data block. During the execution of a write operation, the client closes the file, does not affect the file write.

(7) When file storage is completed, the client notice the NameNode that the file is closed.

(8) The NameNode submits the log of creating file to the transaction log.

Storage technology of the HDFS

Fault-tolerant mechanism in HDFS: HDFS creates three copies by default for each data block. The first copy is set on a node in the local rack. The second copy is set on the other node in the same rack with the first one. The third copy is set on a node in different rack.

There are two kinds of common mistakes in the process of file storage in HDFS. One is node failure, the other is data corruption.

The node failure mainly refers to the DataNode failure because of the network partitions. The DataNodes periodically send heartbeat message to the NameNode, on the one hand, if the NameNode dose not receive the message from the DataNodes during the stipulated time, the DataNode is believed to be out of order and it is labled as dead node, on the other hand, the NameNode continually detects the shortage of data copies because of the dead node, and start the copy mechanism.

The data corruption refers that the data is damaged which is read from the DataNode. HDFS adopt the checksum file to detect the data integrity. The checksum file is generated when the client creates the file, which saves the checksum of all data blocks from new file. When the client reads the file, the checksum of file will be compared with the checksum saved in the checksum file, if the two are same, the data are complete, else read other data block copy.

Balance in HDFS: Balance in HDFS refers that the file blocks distribute well in every node of the cluster. The distribution of the file blocks is a dynamic process, HDFS offers the balancer tool to make sure the storage balance.

Optimal storage strategy

Fault checked and recovery ability which is automatic and fast are the core targets of HDFS. Heartbeat mechanism realizes detecting the fault node. This paper offers using this mechanism to statistic the reliability of the nodes so that filtering the DataNodes before writing files, and realizing the change from passive detection after failure to active screening before using the nodes.

Algorithm description of the optimal storage strategy

This paper gives the general algorithms for the storage of the data blocks based on the optimal strategy (Fig.2).

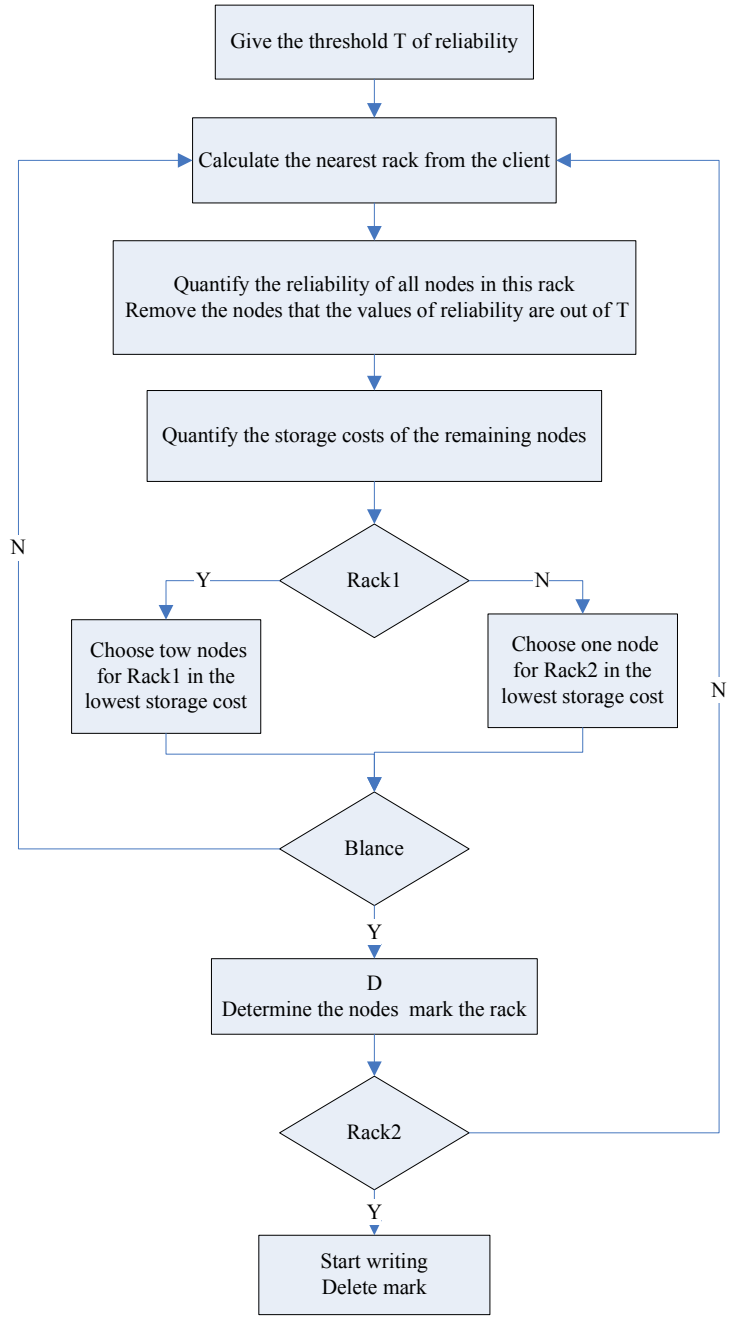

Fig.2 Algorithm flow

Firstly, the NameNode gives the threshold T of reliability according to the needs of users and the characters of data.

Secondly, the NameNode calculates the nearest rack from the client.

Thirdly, quantify the reliability of all nodes in this rack and remove the nodes that the values of reliability are out of T.

Fourthly, quantify the storage costs of the remaining nodes.

Fifthly, we define the rack which is used to storage two copies as Rack1 and define the one which is used to storage one copy as Rack2. Judge whether or not the rack which chooses from the secondary step is labeled as Rack1, if not, it will be dealt as Rack1, otherwise as Rack2. Choose tow nodes for Rack1 or one node for Rack2 that in the lowest storage cost.

Sixthly, judge whether or not the cluster is in balance, determine the nodes and mark the rack when the cluster is in balance, otherwise recalculate the rack and choose the nodes again.

Seventhly, if Rack2 is marked, start the operation of writing data and deleting the name of the rack, otherwise recalculate the rack and choose the nodes again.

Conclusion

Through the research of the file organization, storage mode, storage technology etc. in HDFS, this paper describes the optimization of the strategy and the algorithm flow of the optimization. In the future research work, the calculation methods of the reliable value and choice cost of the DataNode need further improvement.

References

[1] H. Attiya, J. Weleh: *Distributed computing: fundamentals, simulations, and advanced topics* (US: Wiley- IEEE, 2004).

[2] X. Li, J. X: *Parallel processing technology* (China, 1994).

[3] Z. Du etc.: *Grid computing* (China, 2005).

[4] Chinese digital TV editorial department: *Cluster with storage technology in New Media Era* (China, 2008).

[5] W. Zhao etc.: *Network storage technology* (China, 2005).

[6] Meeta Gupta: *Storage area network fundamentals* (USA,2002).

Advanced Materials Research Vols. 989-994 (2014) pp 2454-2456
© (2014) Trans Tech Publications, Switzerland
doi:10.4028/www.scientific.net/AMR.989-994.2454

Research on packet encryption algorithm in the cloud storage

Hui Cao

Henan Radio and Television University, Zhengzhou 450008, China

402793927@qq.com

Keywords: cloud storage, packet encryption, data security.

Abstract. The storage and management of the huge data is solved by the cloud storage. The users can access the data whenever and wherever possibly in the cloud. The cloud storage provides convenient services for users. The problem of data security has been paid more and more attention at the same time. Based on the problems of the big data and the high repetition rate, this paper presents the improvement of the existing mainstream encryption algorithm. The algorithm can encrypt the same data, storied in different locations, into different ciphertexts, to make sure the data security in the case of the trusted cloud.

Introduction

With the rapid development of information technology and the Internet, People's daily work and life more and more use and rely on the network, resulting in massive data. The storage and management of the huge data is solved by the cloud storage. The users can access the data whenever and wherever possibly in the cloud. But, because of data breaches appeared frequently, the security problem of the cloud storage has become a hot issue cared by people in recent years.

In 2011, CSDN, the largest programmers' community at home, was attacked by the hacker, exposed by a micro-blog. As the world's largest Chinese IT technology community and china's largest programmers' community, the website of CSDN had 20 million registered users. Since the database leak of CSDN, parts of the user databases had been online for download including renren, mop, YY etc. and parts have been confirmed the authenticity. [1] This event and the chain events set off a discussion craze of the cloud computing security. With more and more users of the cloud computing, more data are stored in the cloud, and security issues have become increasingly important.

In 2013, the exposure of America National Security Agency (NSA) stealing the secret files rekindled the safety concerns about the data storied in the cloud. Data encryption is beginning to attract people's attention. However, enterprise users and cloud service providers to reform its internal security and privacy protection strategy, strengthen the cloud data security protection, is long overdue, but has not done. [2]

In 2013, Symantec and Ponemon Institute released the "2013 data disclosure cost analysis: global research report". The study data show that Data leakage accident 2/3 was caused by human error and system problems in 2012 and each damaged data record average cost up to $136 in global. The difference of global average cost of data reveal is significant. These differences are mostly because the type of risk faced by enterprises and different national data protection laws. Germany, Australia, Britain, USA and other countries has consumer protection laws and regulations more perfect to enhance data security and network security. Nevertheless, the data disclosure cost of America and German is still the highest (average accident costs were $188 and $199). The total cost of individual data leak in the two countries was the highest ($5400000 in America, $4800000 in Germany). [3]

Through in-depth study on the leakage accident, we found that the security industry obviously still have a lot of work to do. Valuable database still not under strict protection and encryption; there are still a large number of security vulnerabilities in application; users are still able to download a lot of information from the sensitive database and save it in the terminal which is lack of protection.

Whether the cloud storage services how powerful, the cloud storage can solve the security problem is always the determining element of the cloud storage life. Only the safe cloud storage can stimulate the user enthusiasm. Therefore, cloud storage security must get people's attention.

There are three main types of data protection are more applied in currently storage system: cipher technology [4], tamper-proofing technology [5] and backup redundancy technology [6]. They are applied to the needs of different storage security.

Mass data image illustrates the quantity of the huge data in the cloud storage and duplicate data is very prominent phenomenon. The same plaintext data encrypted with general block cipher produce the same ciphertext. Once the data is leaked, through statistical analysis and comparison of a large number of data, the risk of data decrypted is very big. This paper presents the improvement of the existing mainstream encryption algorithm. This algorithm can encrypt the same data storied in different locations to different ciphertext to make sure the data security in the case of credible cloud.

Problems to be solved by the algorithm

There are several problems should be solved by the algorithm.

(1) In the process of the common data transition, to avoid the plaintext data from being intercepted, the cloud should adopt MD5 security mechanism, calculate the MD5 value, encrypt and save the data uniformity.

(2) The data in the cloud storage is in large quantity and high repetition rate. The algorithm should be considered generating different ciphertext data from the same plaintext data so as to avoid the risk of data being stolen in the cloud and ensure the data security.

(3) To ensure the safety of the cloud storage system, the encryption algorithm should not only achieve the same plaintext to different ciphertext but also fall the whole group of ciphertext when any one changes.

(4) The basis of packet encryption mode is the mode of the data storied in the cloud. In the cloud, the data exist as blocks; the sector is the memory unit of the block and is also the unit of data read and write. The encryption algorithm should also use the sector as the basic unit of data, and ensure that multiple encryptions do not increase the length of ciphertext.

(5) The storage management of massive data demands on system performance very high. The algorithm design should ensure high computing efficiency and not take big deviation from the mainstream encryption algortithm.

(6) The particularity of the data process in the cloud storage put forward higher requirements on the efficiency of the algorithm. For efficient computation, the number of the key generation should reduce and the production time should be shorten. Only a fixed key can consider using.

Summary of the optimal algorithm

Based on AES algorithm, this paper designed the encryption algorithm with the 256 bits original key, 128 bits packet length and 13 ring blocks. Here is the general description of the algorithm.

First of all, there are tow kinds of key, the master key and the round key. Two kinds of key are placed in the cryptographic device after the system initialization is complete.

Secondly, calculate the block number of the packet and complete the initial vector selection. Because of different block number of each packet, on the basic premise of using the same master key, the initial vector of each packet are also different.

Thirdly, achieve the encryption operation of 512 byte plaintext. 512 byte plaintext is divided into 32 packets. Encryption operation is really on 32 packets plaintext. There are tow steps of encryption process: first step, take advantage of the initial vector which is selected, use first 6 rounds in CBC mode to encrypt 32 packets plaintext, obtain 32 packets ciphertext; second step, choose the last vector obtained in step one as the initial vector, adapt the last 7 rounds in CBC mode to encrypt the ciphertext obtained in step one, achieve final 32 rounds ciphertext.

Fourthly, achieve the decryption operation of 512 byte ciphertext. Decryption is the inverse process of encryption operation, is also divided into two steps: first step, take advantage of the initial vector used in step two of encryption process, adapt the last 7 rounds in CBC mode to decrypt the ciphertext first time; second step, use the initial vector chose in step one of encryption process, adapt the first 6 rounds in CBC mode to decryption the ciphertext second time and get the plaintext.

Conclusion

Based on the above description, the algorithm proposed in this paper has the following three features:

(1) The algorithm adapt the initial vector to AES encryption calculation which is not in the traditional AES algorithm.

(2) The algorithm uses the CBC mode twice which is two times than traditional encryption calculation. The efficiency of the algorithm has been little affected and the increase is just the XOR operation, therefore, the impact is negligible.

(3) According to the different locations of the storied data, the initial vector is also different in the algorithm so as to avoid generating the same ciphertext from the same plaintext and ensure data security.

This algorithm achieve encrypting the same plaintext storied in different locations to different ciphertext; fix the bug that the same plaintext with the same ciphertext; avoid data theft and sabotage from Statistical analysis technique used by data kleptomaniacs and ensure data security.

References

[1] Information on http://www.d1net.com/cloud/security/84577.html.

[2] Information on http://sec.chinabyte.com/127/12828127.shtml.

[3] Information on http://www.dostor.com/article/2013-06-17/6590284.shtml

[4] K. Fu: *Group sharing and random access in cryptographic storage file systems* (USA, 1999).

[5] J. Hendricks, G. Ganger, M. Reiter: *Verifying Distributed Erasure coded Data* (Proc 26th ACM Symposium on Principles of Distributed Computing, 2007).

[6] D. Zhang: *The Explanation and Best Practice of Network Storage System* (China 2008).

Advanced Materials Research Vols. 989-994 (2014) pp 2457-2461
© (2014) Trans Tech Publications, Switzerland
doi:10.4028/www.scientific.net/AMR.989-994.2457

ZFDV: Zoom financial data visualization in the era of big data

TingtingJiang[1], Qinggang Wang[2], Haikuo Zhang[1], Weidong Xiao[1], Chong Zhang[1], Bing Ge[1]

[1]Science and Technology on Information Systems Engineering Laboratory, National University of Defense Technology, Changsha, Hunan, China

[2]School of Software, Beihang University, Beijing, China

[a]345319286@qq.com

Keywords: Big data, Finance data, Visualization, Zoom

Abstract. With the advent of the era of big data, data visualization display faces great challenges. Big data, especially in industries such as telecommunications, finance, almost to the point of "data is the business itself". At this time, in order to let more people understand, use and analyze the data better, we proposed the method to display the big data in the field of finance and the notion of the Zoom financial data visualization (ZFDV). By providing a consistent set of the preliminary design of ZFDV and the interaction of ZFDV techniques, ZFDV makes it possible for users to browse through very large data sets. These techniques use the structure of the displayed data to guide the human-interaction and provide a way to improve interactive navigation in the financial.

Introduction

Data has penetrated into every industry and the business functional areas today and data revolution is coming. A fashionable topic with or without Sustainable relevance for research and practice has been researched by Prof. Dr. Hans Ulrich Buhl[1]. Generally speaking, the hope is that if massive data could be exploited effectively, science would extend its reach, and technology would become more adaptive, personalized, and robust. There are also many scientific and engineering fields impacted by massive data which is shown in [2]. But a number of challenges also exist in both data management and data analysis that require new approaches to support the “big data” era.

On the basis of the trait of the financial data, our article proposes the means of zoom. Providing the process of showing data, ZFDV methods will be in consideration of characteristic of the financial data. For example, at first the users could get control of the whole situation after they knew the number of every year. The next layer would set the value in accordance with the users’ expectation.

Our article focuses to demonstrate a method of financial data. When the users check the numbers of the transaction, they can zoom to see all of the data. Using the methods we can accept in our daily lives makes the information easy to understand. The main works we do and discuss are the approaches for both the preliminary design and the interaction of ZFDV. The users can grasp zoom financial data visualization from year to day as Figure1 shows. In this way, we can also know clearly and get the whole view of the finance data which can support for decision making.

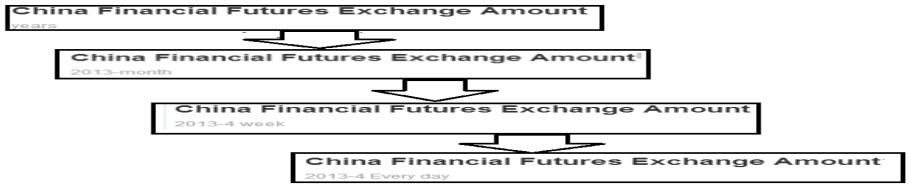

Fig. 1 Zoom financial data visualization from year to day

Related Work

It can be found from the research situation in recent years that much attention has been paid to enhance the visual aspect of graph, text, map and multivariate data, examples include visual analysis of business data[3,4,5]. However, surprisingly, few studies focused attention to the application of financial transactions.

Renaud Blanch and éric Lecolinet[6] proposed the notion of "zoomable treemaps", they put focuses on this point by proposing a set of interaction techniques that aimed at improving the navigation in treemaps. Application is very few in the world of finance, especially Zoom financial data visualization. The most common techniques for navigating in multiscale visual spaces are pan, zoom, and bird's eye views[10].The previous methods especially Renaud Blanch and éric Lecolinet[6]had a good show in data of text in zoom which we have told in this article. However, the problem is that the financial data have its own feature. Therefore they were not suitable for showing in financial data. For the reason of these, we design the program.

Initiatives in research and development that are leading to improved capabilities include developing methods for visualizing massive data[2]. Shixia Liu[7] studied existing technical challenges and propose directions for future research. One of the challenges is the visual scalability which is defined as the capability of visualization tools to effectively display large data sets in terms of either the number or the dimension of individual data elements [8]. Because Keim,D.A[8] told us Scalability is a fundamental challenge for InfoVis, especially with the boom in big data analytics.

Therefore, the program can be regarded as visual component which have the ability to embed in web page. It's really convenience for the users. In sum up, our research is very necessary, we can use data visualization technology and find hidden rules in a large number of financial, communications, and business data so as to provide the basis for decision-making.

The preliminary design of ZFDA

Browsing very large data sets like financial data can be quite inefficient. It can cause confusion when we see the visualization of the charts. The display technologies are used in reality may be not sufficient for browsing data efficiently. A powerful visualization needs to show the data in the number of attributes and the number of relationships effectively. Here we discuss our approaches for both the preliminary design of ZFDV and the human-interaction of ZFDV. So we propose four preliminary modes for ZFDV and next chapter we introduce the interactions of the data.

3.1 same-level financial data

The data of financial futures trading is a big data with every year, every month, every week, every day, or other aspects of trading information. So we choose the data which have the same unit as the same level data. As we all known, the same level data can display together because of the size, the amount, the similar degree of the data. May in certain cases the size, the amount, the similar degree of the data are the same which is conducive to the Comparison of the data.

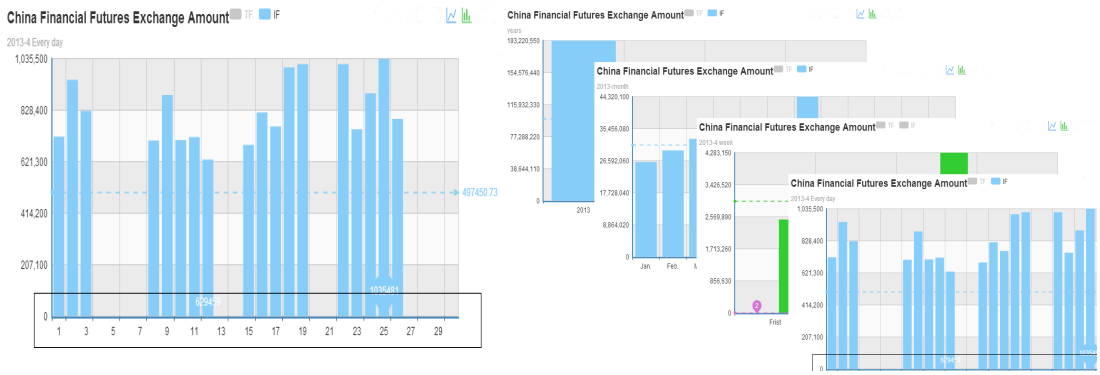

Fig. 2 (Left)Same-level financial data (Right)Different-level financial data

The users may be want to know the details, just as every day in April of 2013, so we unfold the situation of every day. We have taken the needs of users into account while designing our techniques. They make it possible to navigate in same-level financial data as well as in different-level financial data in the financial structure.

3.2different-level financial data

In a certain extent different levels of financial futures trading data can be called the different depth data. Such data can achieve very good zoom function. We can define for depth with N, if N=1, then the data are the next layer. After setting the N, data can display in different depth. Just like treeview, the depth of the different setting will have different display effect. But in this article, the way to define N is year, month, week, day. We know that, the data in finance are Special data because trading is going on in every month of the year, every day of every week. If we don't define N properly, it will cause disorder in visualization. Using the methods we can accept in our daily lives make the information easy to understand.

The right of Figure 2 illustrates this display of different-level financial data: it allows users to switch quickly from one level to one of its next level. The techniques presented so far only make it possible to select the data that are on the same layer as the current picture, or located one level above or below. Since the method we put up to display several layers of the data simultaneously and provide visual access to them, a technique to select any visible layer of the data is most desirable.

3.3 The maximum/minimum data display

Maximum/minimum values can often attract the attention of the audience which tells us this part is really important. Our awareness of the value may be greatly more than other data at the same level, so the picture shows the maximum/minimum values in the design of the program which can help users to check and compare. Moreover maximum/minimum values reflect the upper limit and the lower limit, the whole situation can be easily got caught by the users.

In the left of Figure 3, we can see the maximum/minimum of the data in China Financial Futures Exchange. By comparing in the pictures, the general can be known by the users at a glance.

Fig. 3 (left) The maximum/minimum data display, (right) The average automatically display

3.4 The average automatically display

It is also often desirable to know mean value of the data in the same level, our design can get the mean value automatically. The mean value is very vividly, it aims at helping the user to keep her data orientation. When we analyze the practical problems, the average of the data will be introduced in order to reflect the overall overview of the entire process. Many common types of averages can be seen: geometric mean, arithmetic mean, weighted mean, RMS, etc. Here we use the geometric average. Due to the introduction of the average, the whole situation appears more intuitive and simple, just as the right of Figure 4 demonstrates.

Human-Interactions

A zoom user interface (ZUI) [6] is a useful function to help users deal with large information spaces displayed within a screen[9]. In addition to the visual design, the most important is the visualization of the interaction. At here, we design two interaction modes for ZFDV.

4.1 line or histogram

In order to meet the needs of various users, we design using the histogram and the line chart. Users can view the size and change of the data in different ways. This kind of interaction can satisfy different users and more humanize. We usual use histogram to compare the data of everyday in April of 2013.The problem is that the commonly used method may be not very Suitable for view the change of the data. Therefore line shape plays an important role at this time。

Fig. 4 Line or histogram you can choose

4.2 Layers of in-depth

As mentioned before, our scale form is layers of depth. Figure5 tell us the scenario, when we looked at the original transaction volume throughout the whole year, afterwards if I'm so interested in the data in 2013, I can click to data volume of 2013. Next the data of April catch my attention, so I can click to data volume of 2013 in April. A succession of interests makes me check the numbers of the year, the month, the week, the day. This process is layers of depth of zoom change. Viewing of this scale can meet us for what we are interested in and provide an interesting solution for representing hierarchical data.

Fig. 5 Layers of in-depth

Performance

Through reading the trade data of financial securities transactions in China Financial Futures Exchange[11], our system start to work. According to the sequence of time, the data are stored by layer in advance. For each layer of the data we all gave the same label, if a data with the same label was invoked, then the other data with the same tag also displayed at the same time. Our work used the database or XML which can be written in the way of tree, branch and leaf, to store and call for different levels of financial data. We are only provided for a way of showing transaction data, in the era of big data, we should think more details about how to show the data better.

Conclusion &Future work

As we all known, sometimes one graph may be not show the information very well, so we can use several zoom pictures to display just like we studied in above. These techniques can apply to various applications ranging from network visualization and text visualization。

In this paper, we proposed a new method to display volume of business transactions in financial futures which make it possible to explore massive data in trading financial data. We can check the amount data of every year, every month, every week and even every day which make us feel clearly and easy to understand and compare. The way we propose can reduce the chance for the user to get lost in the information space.

The focus in the future of our work can establish a visual component instead of this special performance. We all know that it must be very popular if the visualization graph is easy to understand and grasp the law, show enough information. Moreover the data sets are multivariate in finance, so an information-aware framework for exploring multivariate data sets[12] and simplification[13] is very necessary. Our future work will be devoted to this aspect.

Acknowledgements

Fund Project: National Science and Technology Support Program（2012BAH08B01）

References

[1] H.U Buhl, M. Röglinger, F. Moser, J. Heidemann: Business and Information Systems Engineering, Vol. 5 (2013) No. 2, p. 65-69.

[2] National Academy of Sciences: *National Academy of Sciences Frontiers in Massive Data Analysis* (The NATIONAL ACADEMIES PRESS, U.S.2013.), p.18-34

[3] Liu, S., Cao, N., Lv, H: *Interactive visual analysis of the nsf funding information* (Kyoto, Japan, March 5-7, 2008). Vol. 1, p. 183–190.

[4] S. Liu, M.X. Zhou, S. Pan, Y. Song, W. Qian, W. Cai, X. Lian: *ACM Trans. Intell. Syst. Technol.* (Helsinki, Finland, August 13-17, 2012). Vol. 3, p.2168-2190.

[5] Cao, N., Lin, Y.-R., Sun, X., Lazer, D., Liu, S., Whisper, HQu: *IEEE Trans. Vis. Comput. Graph* (Florida, USA, March 25-30, 2012). Vol. 18, p. 2649–2658.

[6] Renaud Blanch , éric Lecolinet: *IEEE Trans. Vis. Comput* (Sacramento, California, October 28-November 1, 2007). Vol. 13, p.154.

[7] Shixia Liu ,Weiwei Cui , YingcaiWu ,Mengchen Liu, A survey on information visualization: recent advances(2013)

[8] Keim,D.A., Mansmann, F., Schneidewind, J., Ziegler,H.L.: Challenges in visual data analysis. In: IV(2006), pp. 9–16

[9] Donghun Lee, Cheolhyun Jeong: Effects of User Age and Zoomable User Interfaces on Information Searching Tasks in a Map-Type Space. Proceedings of the Human Factors and Ergonomics Society Annual Meeting (2010) p:54-571

[10] W. Javed, S. Ghani, N. Elmqvist.: *CHI'* (Turin, Italy, May 5–10, 2012). Vol. 1, p.154.

[11] Information onhttp://www.cffex.com.cn/fzjy/jsywcs/

[12] A. Biswas, S. Dutta, H.W. Shen, J. Woodring: *Visualization and Computer Graphics, IEEE Transactions on*(Turin, Italy, December., 2013). Vol. 19, p. 2683-2692.

[13] Dunne, C., Shneiderman, B: *Proceedings of the SIGCHI Conference on Human Factors in Computing Systems (CHI'13)* (Austin, United States , May 05-10, 2013). Vol. 20, p. 3247-3256.

Advanced Materials Research Vols. 989-994 (2014) pp 2462-2466
© (2014) Trans Tech Publications, Switzerland
doi:10.4028/www.scientific.net/AMR.989-994.2462

A new analysis of the Iterative Threshold Algorithm for RPCA by primal-dual method

Ruya Fan[1, a], Hongxia Wang[1, b] and Hui Zhang[1, c]

[1] Department of Mathematics and Systems Science, College of Science, National University of Defense Technology, Changsha, Hunan, 410073, China.

[a]ruya.fan@gmail.com, [b]whx8292@gmail.com, [c]h.zhang1984@163.com

Keywords: Robust principal component analysis, low rank matrix recovery, iterative threshold algorithm , primal-dual method, background modeling.

Abstract. This paper studies the iterative threshold algorithm (ITA) for solving the Robust Principal Component Analysis (RPCA) problems, which is to recover a low-rank matrix with a fraction of its entries being arbitrarily corrupted. By utilizing the primal-dual method, we analyze the ITA in a new way and prove that the ITA is essentially equivalent to gradient method applying to a dual problem. In the original ITA, it is hard to choose the parameters and hence it converges very slowly. Now, based on the new insight, existing techniques of the gradient method can be used to accelerate the ITA. We combine the theoretical derivation with the numerical simulation experiments to give an empirical guidance to set the parameters. As illustration, background modeling problem is solved by the ITA with optimal parameters.

1. Introduction

Recently, there is a widespread concern about the Robust Principal Component Analysis (RPCA) [1, 2], which is to recover a low-rank matrix with a fraction of its entries being arbitrarily corrupted. It is widely applied in signal processing, image processing, computer vision, machine learning, etc [1]. Suppose that we are given a large date matrix $D \in R^{n_1 \times n_2}$, and know it can be decomposed as $D = A_0 + E_0$, where A_0, E_0 is unknown, but we know the prior information matrix A_0 is of low-rank , E_0 is sparse. The aim of the RPCA is to recover A_0 and E_0 from the given matrix D. Mathematically, we want to solve,

$$\min_{A,E} \|A\|_* + \lambda \|E\|_1, \qquad s.t.\ D = A + E \tag{1}$$

where $\|X\|_*$ equals the summation of the singular values of X, $\|X\|_1$ denotes the summation of the absolute values of a matrix entries. Convex optimization problem (1) is known as the Principal Component Pursuit(PCP) [2]. The weighted value λ between the nuclear norm $\|A\|_*$ and L1 norm $\|E\|_1$ may affect the speed of convergence as well as the final results. Practical experience shows that $\lambda = 1/\sqrt{\max(n_1, n_2)}$ works well for the incoherent matrices [3].

Convex optimization problem (1) has received much attention and many numerical algorithms have been proposed for solving it. For example, the interior point methods, the iterative threshold algorithm (ITA) [4, 5], the accelerated proximal gradient (APG) [6], the augmented Lagrange multipliers (ALM) or exact ALM (EALM) [7], etc. Among these existing algorithms, The ITA is simple and it is the fundament of many methods. However its practical application is greatly limited by the large number of iterations to converge and the difficulty to choose the parameters [6, 7]. In this paper, in section 2, we prove that the ITA is actually equivalent to the gradient method applying a dual problem, which is different from the traditional way. In section 3, we present some implementation details of our algorithm based on our theoretical discovery and do some simulations to study how the different parameters affect the results and the speed of convergence. Then we apply the ITA to the background modeling. We will give some concluding remarks in the final section.

2. Iterative Threshold Algorithm

2.1 The original ITA

Regularize the problem (1), we can obtain the following optimization problem [7],

$$\min_{A,E} \|A\|_* + \lambda\|E\|_1 + \frac{1}{2\tau}\|A\|_F^2 + \frac{1}{2\tau}\|E\|_F^2, \qquad s.t.\ D = A + E \tag{2}$$

where τ is a relatively large positive parameter that can "smooth" the problem (1) [9]. The solution to (2) is also a solution to (1) as long as τ is sufficiently large [10]. However, it has been observed that a larger τ tends to slower convergence. Hence, a moderate τ is needed.

By introducing a Lagrange multiplier Y to remove the equality constraint, we can get the Lagrange function:

$$L(A,E,Y) = \|A\|_* + \lambda\|E\|_1 + \frac{1}{2\tau}\|A\|_F^2 + \frac{1}{2\tau}\|E\|_F^2 + \frac{1}{\tau}\langle Y, D - A - E\rangle \tag{3}$$

Then, the ITA updates A, E and Y iteratively. It updates A or E by minimizing the Lagrange function $L(A,E,Y)$ with the other variables being fixed, respectively. Then updating Y by the equation constraint $D = A + E$ .In detail, the ITA can be described as follows [7]:

$A\lg orithm\,1(Iterative\ \ Threshold\ \ A\text{lgorithm})$

$Input:\ Observation\ matrix\ D \in R^{m\times n}, weights\ \lambda, \tau$

$1: while\ \ not\ converged\ do$ $\qquad 4: E_k = S_{\lambda\tau}[Y_{k-1}],$

$2: (U,S,V) = svd(Y_{k-1}),$ $\qquad 5: Y_k = Y_{k-1} + \delta_k(D - A_k - E_k)$

$3: A_k = US_\tau[S]V^T,$ $\qquad 6: end\ \ while$

$Output\ \ A \leftarrow A_k, E \leftarrow E_k$

where $S_\varepsilon[x]$ is the shrinkage operator defined as: $if\ \ x > \varepsilon, S_\varepsilon[x] = x - \varepsilon$; $if\ \ x < -\varepsilon, S_\varepsilon[x] = x + \varepsilon$; otherwise, $S_\varepsilon[x] = 0$. With shrinkage operator, [4, 11] proved the famous result (4):

$$\arg\min_X \varepsilon\|X\|_* + \frac{1}{2}\|X - W\|_F^2 = US_\varepsilon[S]V^T;\ \ \arg\min_X \varepsilon\|X\|_1 + \frac{1}{2}\|X - W\|_F^2 = S_\varepsilon[W] \tag{4}$$

where USV^T is the SVD of W .

2.2 A primal-dual method to the ITA

In this section, we prove that the ITA can also be obtained by the primal-dual method. Note that $\|X\|_1 = \max\{X^TZ : \|Z\|_\infty \le 1\}, \|X\|_* = \max\{X^TZ : \|Z\| \le 1\}$, the dual problem of (3) is as follows[8,9]:

$$\min_{A,E}\max_Y L(A,E,Y) = \min_{A,E}\max_Y \left(\|A\|_* + \lambda\|E\|_1 + \frac{1}{2\tau}\|A\|_F^2 + \frac{1}{2\tau}\|E\|_F^2 + \frac{1}{\tau}\langle Y, D - A - E\rangle \right)$$

$$= \max_Y\{\frac{1}{\tau}\langle Y, D\rangle\} + \min_A\max_Y\{\|A\|_* + \frac{1}{2\tau}\|A\|_F^2 + \frac{1}{\tau}\langle Y, -A\rangle\} + \min_E\max_Y\{\lambda\|E\|_1 + \frac{1}{2\tau}\|E\|_F^2 + \frac{1}{\tau}\langle Y, -E\rangle\}$$

$$= \max_Y \frac{1}{\tau}\langle Y, D\rangle + \min_A\max_{Y,\|Z_1\|\le 1}\{\langle A, Z_1\rangle - \frac{1}{\tau}\langle A, Y\rangle + \frac{1}{2\tau}\|A\|_F^2\} + \min_E\max_{Y,\|Z_2\|_\infty \le 1}\{\lambda\langle E, Z_2\rangle - \frac{1}{\tau}\langle E, Y\rangle + \frac{1}{2\tau}\|E\|_F^2\}$$

$$= \max_Y \frac{1}{\tau}\langle Y, D\rangle + \max_{Y,\|Z_1\|\le 1}\min_A\{\frac{1}{2\tau}[A - (Y - \tau Z_1)]^2 - \frac{1}{2\tau}\|Y - Z_1\|_F^2\} + \max_{Y,\|Z_2\|_\infty \le 1}\min_E\{\frac{1}{2\tau}[E - (Y - \lambda\tau Z_2)]^2 - \frac{1}{2\tau}\|Y - \lambda\tau Z_2\|_F^2\}$$

$$= \max_Y \frac{1}{\tau}\langle Y, D\rangle + \max_{Y,\|Z_1\|\le 1}\{-\frac{1}{2\tau}\|Y - \tau Z_1\|_F^2\} + \max_{Y,\|Z_2\|_\infty \le 1}\{-\frac{1}{2\tau}\|Y - \lambda\tau Z_2\|_F^2\}$$

$$= -\min_Y\left\{-\frac{1}{\tau}\langle Y, D\rangle + \min_{\|Z_1\|\le 1}\{\frac{1}{2\tau}\|Y - \tau Z_1\|_F^2\} + \min_{\|Z_2\|_\infty \le 1}\{\frac{1}{2\tau}\|Y - \lambda\tau Z_2\|_F^2\}\right\}$$

since $A^* = Y - \tau Z_1,\ \ E^* = Y - \lambda\tau Z_2$.

Eliminating $Z_1,\ \ Z_2$ from the last equation gives the dual problem (5):

$$\min_Y f(Y) \equiv \min_Y\ -\frac{1}{\tau} < Y, D > + \frac{1}{2\tau}\left\|Y - proj_{\{\tau Z_1 : \|Z_1\| \le 1\}}(Y)\right\|_F^2 + \frac{1}{2\tau}\left\|Y - proj_{[-\lambda\tau, \lambda\tau]^n}(Y)\right\|_F^2 \tag{5}$$

with $proj$ is the projection operator defined as $proj_{\mathrm{B}}(v)=\arg\min_{x\in\mathrm{B}}\|x-v\|_2$.

Farther more, according to the property of projection operator [9], we have that

$$W-proj_{[-\mu,\mu]^n}(W)=S_{\mu}[W];W-proj_{\{\tau Z_1:\|Z_1\|\le 1\}}(W)=US_{\varepsilon}[S]V^T \tag{6}$$

where $W=USV^T$ and $S_{\varepsilon}[x]$ is the shrinkage operator defined as section 2.1.Then,

$$A^*=Y-\tau Z_1=Y-proj_{\{\tau Z_1:\|Z_1\|\le 1\}}(Y)=US_{\tau}[S]V^T;E^*=Y-\lambda\tau Z_2=Y-proj_{[-\lambda\tau,\lambda\tau]^n}(Y)=S_{\lambda\tau}[Y] \tag{7}$$

It is easy to say (10) is equivalent to (4). And,

$$\nabla f(Y)=-\frac{1}{\tau}D+\frac{1}{\tau}\left(Y-proj_{\{\tau Z_1:\|Z_1\|\le 1\}}(Y)\right)+\frac{1}{\tau}\left(Y-proj_{[-\lambda\tau,\lambda\tau]^n}(Y)\right)=-\frac{1}{\tau}\left(D-A^*-E^*\right) \tag{8}$$

Applying the gradient iteration to the dual objective $f(Y)$ gives:

$$Y_k=Y_{k-1}+\delta_k(D-A_k-E_k) \tag{9}$$

It is clear that the ITA is essentially equivalent to gradient method applying to a dual problem.

3. Experiments

3.1 Numerical simulations

In the numerical simulations, we test the ITA with different parameters. Firstly, we study how the parameter τ affects the calculated results and the speed of convergence, and make the comparison with the theoretical bound obtained in [10]**.** Then we study the relationship between δ and the number of iterations.

We use randomly generated matrices for simulations, just as in [6, 7]. Firstly we generate the rank- r matrix $A_0=UV^T\in R^{n_1\times n_2}$, where $U\in R^{n_1\times r},V\in R^{n_2\times r}$ are independent matrices whose elements are i.i.d. Gaussian random variables with zero mean and unit variance. Then generate $E_0\in R^{n_1\times n_2}$ as a sparse matrix whose support is chosen uniformly at random, and whose non-zero entries are i.i.d. uniformly in the interval [−500, 500]. We denote the true solution by the ordered pair (A_0,E_0) , $D=A_0+E_0$ is the input, and (A,E) the output. We choose a fixed weighting parameter $\lambda=1/m$ [3] and set $m=n,r=\rho_r*n$, $\|E_0\|_0=\rho_s*n^2$. When the number of iterations reaches to 10000 or $\|D-A-E\|_F/\|D\|_F\le 5e-5$, the Iteration will stop. Meanwhile, we use $rel\ A$ and $rel\ E$ to denote the relative errors of the output solution, i.e., $rel\ A=\|A-A_0\|_F/\|A_0\|_F$, $rel\ E=\|E-E_0\|_F/\|E_0\|_F$.

The parameter τ may be quite difficult to set. On one hand, a sufficiently large τ is needed to get the real solution to problem (1); on the other hand, a larger τ tends to converge slowly. The author in [10] derived a theoretical bound of τ . They showed that the bound $\tau\ge 8\sqrt{15}\|D\|_F/3\lambda$ guarantees the decomposition of the observed matrix D into its low-rank component and sparse component.

A brief comparison of how τ affects the calculated results and the speed of convergence is presented in Tables 1. We take $r_0=0.05n$, $\|E_0\|_0=0.05n^2,n=500,\delta=0.9$. It shows that $\tau=10^4$ is better than the other values, while $\tau\le 10^3$, the ITA will not converge any longer. When $\tau\ge 10^6$, the ITA converges so slowly and reaches the maximum number of iterations. However, the bound $\tau\ge 8\sqrt{15}\|D\|_F/3\lambda$ is about $\tau\ge 10^5$. Thus we conclude that the bound $\tau\ge 8\sqrt{15}\|D\|_F/3\lambda$ just give a sufficient conditions but not necessary.

Table 1 Comparison of the ITA on the RPCA problem with different τ . Table 2 Comparison of the ITA on the RPCA problem with different δ . In table 2, $r_0=0.05n$, $E_0=0.05n^2,n=100,\tau=10000$, we can find δ has a great influence on the number of iteration. When δ is too small, it takes too much time for the ITA to converge. And if $\delta\ge 1.6$, it may not converge. We can get the recommendations value of $\delta=1.5$, and it is three times faster than $\delta=0.5$,which was used in [6]. However, our simulations show that when δ is bigger than 1.55, the results begin to deteriorate. To be safe, we can set the experience value around 1.4.

3.2 Background modeling

Background modeling is an popular approach to detecting activity in the scene [2]. The background may contain a lot of information, but it change a little in a short time. The difference between two adjacent pictures may be reflected in the moving things in the pictures.We consider one example video introduced in [12]. It is a sequence of 300 grayscale frames taken in a campus . This video has a relatively static background, but significant foreground variations. The frames have scales of 128×160 ; we stack each frame as a column of the matrix $D\in R^{20480\times300}$. We decompose $D\in R^{20480\times300}$ into a low-rank term A and a sparse term E by solving the convex PCP problem (1) with the ITA. We set $\lambda=1/\sqrt{20480}$, $\tau=(1/100)*8\sqrt{15}\|D\|_F/3\lambda$, $\delta=1.4$. Figure 1(a) shows three frames(204^{th} ,215^{th} and 222^{nd}) from the video of the campus; (b) and (c) show the corresponding columns of the low rank matrix A and sparse matrix E. We can find that A correctly recovers the background, while E correctly recovers the moving car, we can see the direction of the car and even estimate the speed.

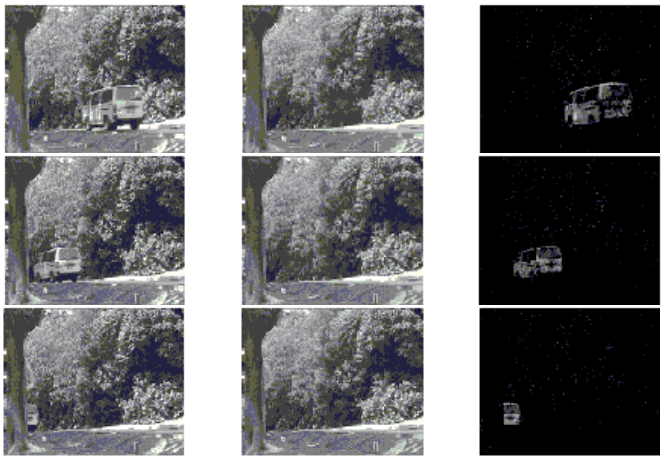

(a) (b) (c)

Figure 1 Background modeling taken in the campus[12]. (a) shows three frames; (b) and (c) show the corresponding columns of the low rank matrix A and sparse matrix E .

4. Conclusion

In this paper, we analyze the ITA in a new way and prove that the ITA is essentially equivalent to gradient method applying to a dual problem. And also we combine the theoretical derivation with the numerical simulation experiments to give an empirical guidance to set the parameters. With the optimal parameters, background modeling problem can be solved very well. There are at least two directions that should be investigated in the future. The first direction is the study of accelerating the ITA with restart technique. The second one is to decompose the low rank matrix and sparse matrix from the Gaussian noise.

5. Acknowledgement

We thank the authors of [12] for kindly sharing with us their background modeling dates. The research was supported by NSF 61072118.

6. References

[1] J. Wright, A. Ganesh, S. Rao, Y. Peng, and Y. Ma, Robust principal component analysis: Exact recovery of corrupted low-rank matrices via convex optimization, Proc. of Neural Information Processing Systems, Vol. 3(2009),p.2080.
[2] E. J. Candes, X. Li, Y. Ma, and J. Wright, Robust principal component analysis? Journal of the ACM, Vol.58(2011)No. 3,p.233.
[3] V. Chandrasekaran, S. Sanghavi, and P.A. Parrilo, Rank-sparsity incoherence for matrix decomposition, SIAM Journal on Optimization, Vol.21 (2011)No. 2,p.572.
[4] J. F. Cai, E. J. Candes and Z. W. Shen, A singular value thresholding algorithm for matrix completion, SIAM Journal on Optimization, Vol.20(2010)No. 4,p.1956.
[5] A. Beck, M.A. Teboulle, Fast iterative shrinkage-thresholding algorithm for linear inverse problem, SIAM Journal on Imaging Sciences, Vol.2(2008)No. 1,p.183.
[6] Z. Lin, A. Ganesh, J. Wright, L. Wu, Chen, M, and Y. Ma, Fast convex optimization algorithms for exact recovery of a corrupted low-rank matrix, CAMSAP, 2009, p.61.
[7] Z. Lin, M. Chen and Y. Ma, The augmented Lagrange multiplier method for exact recovery of corrupted low-rank matrices, Optimization and Control, 2013, http://arXiv.org:1009.5055.
[8] H. Zhang, L.Z. Cheng, W.T. Yin, A dual algorithm for a class of augmented convex models, submitted to Communication of Mathematic Science, 2014, http://arXiv:1308.6337.
[9] M.J. Lai, W.T. Yin, Augmented L1 and nuclear-norm models with a globally linearly convergent algorithm, Imaging Sciences, Vol.6(2013)No. 2,p.1059.
[10] Q. S. You, Q. Wan, and Y. P. Liu, A short note on strongly convex programming for exact matrix completion and robust principal component analysis, Inverse Problems and Imaging,Vol.7(2013)No. 1,p.305.
[11] W. Yin, E. Hale,Y. Zhang, Fixed-point continuation for L1-minimization: methodology and convergence, SIAM Journal on Optimization, Vol.19(2008)No. 3,p.1107.
[12] L. Li, W. Huang, I. Gu, and Q. Tian, Statistical modeling of complex backgrounds for foreground object detection, IEEE Transactions on Image Processing, Vol.13(2004)No. 11,p.1459.

Advanced Materials Research Vols. 989-994 (2014) pp 2467-2469
© (2014) Trans Tech Publications, Switzerland
doi:10.4028/www.scientific.net/AMR.989-994.2467

Robot Path Planning Based on Artificial Fish Swarm Algorithm under a Known Environment

Jian Wang, Lijuan Wu

School of Electrical and Information Engineering, University of Science and Technology Liaoning , Anshan , 114051, China

email:415232167@qq.com

Keywords: Grid method, Artificial Fish Swarm Algorithm, Robot, Path planning.

Abstract. With the development of science, the scope of application of robot is more and more extensive. The path planning problem of mobile robot ,has been always an important research content of intelligent robot .In this paper , firstly we can construct feasible work space mode , through the random grid method to given the starting point ,end point and each obstacle .Then we can use the improved AFSA for path optimization .In the algorithm ,we ignore the congestion factor ,it is based on the preying behavior ,supplemented by the following behavior and swarm behavior .

Introduction

With the progress of science and the development, mobile robot technology has been further developed. In recent years, the rapid development of science and technology, robots are constantly improving our lives, such as service robots, underwater robots, entertainment robots, military robots, agricultural robots, etc.

Robot path planning is an important criterion of their level of intelligence; it is an essential part in robot navigation techniques. The planning is based on certain rules to find out a non-collision path from the starting point to the target point of optimal or suboptimal. Through sensors, mobile robot can perceive the environment and their own state, to achieve in complex environments autonomous obstacle avoidance, in order to complete a certain job functions of the robot [1].

Mobile Robot Path Planning belongs to a class of NP-Hard problem. To solve this problem, many methods have been proposed. For example grid method, link graph, neural networks, artificial potential field method, ant colony algorithm, the hybrid

This paper studies the robot path planning algorithm based on artificial fish, which is a simulation of the behavior of a variety of fish bionic algorithm. Simulation results demonstrate the effectiveness of the algorithm.

Robot Path Planning Based On AFSA

AFSA [2] [3] is a simulation of the behavior characteristics of fish, and has a new bottom-up optimization model. This algorithm is simulated fish feeding, swarming, and following in the search field to find the best. AFSA has fast convergence, has a good ability to overcome the local minima and to obtain global extremes. There can be used to solve the problem of real-time requirements, and for some low accuracy problem, it can quickly get a feasible solution. This algorithm does not require strict mechanism model of the problem, and even does not require accurate description, which makes it can be used to extend the range of applications. The algorithm has been applied to combinatorial optimization problems [4], the online time-varying system identification [5], the whole set of robust PID parameters [6], before optimization neural networks [7] reactive power optimization [8], and more user detection [9] [10]

Several acts of AFSA:

(1) Feeding behavior: the basic behavior of AFSA, and also tends to food, is a free search behavior. It ensures fast and stable convergence, overcoming local extreme aspects. Let the current state X_i of artificial fish i is randomly selected a state X_j within its sensing range

$$X_j = X_i + Visual * Rand() \quad (1)$$

If $h_j > h_i$ that food concentration is greater than the original state at that point, then further to the front direction

If it is not satisfied, and then determines whether reselection Xj satisfies the condition. After attempting to Try-number times, if it still does not meet the conditions, then immediately move step.

(2)Swarming behavior: In order to ensure the survival of fish population and avoid harm, they will naturally get together. The behavior of the algorithm can effectively enhance the global convergence. Let the current state of artificial fish as X_j, if the partner does more crowded food center, then move one step toward the partner center.

$$X_i^{t+1} = X_i^t + \frac{X_c - X_i^t}{\| X_c - X_i^t \|} * Step * Rand() \quad (2)$$

If it is not met, then perform feeding behavior.

(3)Following behavior: Fish advance to the optimal partner nearby. The behavior enhancement algorithm convergence speed and global. Let the current state of artificial fish is X_j, if there is a partner in the vicinity, which have more food without crowding around, then move one step towards the direction of partners.

$$X_i^{t+1} = X_i^t + \frac{X_j - X_i^t}{\| X_j - X_i^t \|} * Step * Rand() \quad (3)$$

If it is not met, then perform feeding behavior.

Robot Path Planning Design

This article uses the random grid method to create space model. Grid method is a two-dimensional model of the robot motion decomposed into a series of binary information grid. One possibility is to select a paper path. Construction algorithm is as follows:

Let the starting point as g_{begin},, the end as g_{end}. On the grid of the robot along the eight directions, which are allowed in the neighborhood of the robot. In this paper, two cases, the one is feasible to reach the surrounding areas without any conditions; the other do not allow walk along the obstacle corners.

Workspace of the robot is an M * M grid components. In the grid, the obstacles and the feasible region with the binary matrix represent a 0 and 1

$$B(i,j) = \begin{cases} 1, & \text{obstacle} \\ 0 & no - obstacle \end{cases} \quad (4)$$

Crowding can not get substantive changes, in some cases it will affect the stability of the algorithm and optimization time. So ignore the crowding factor.

Parameter initialization, record global optimum state of artificial fish. Evaluation of artificial fish, acts to be performed on the line be merit, update the location information of each artificial fish. If it meets n>Try number, it ends. The resulting path is the shortest path length; the path is the best path. If it does not meet the conditions, then return to continue.

Test results

In order to verify the robot path planning method based on artificial fish school algorithm correctness and feasibility, the paper simulation. In this algorithm, a total of fish is 10, the maximum number of attempts is 6, and the step is 1 and Square root of 2, the simulation results shown in Figure 1, Figure b is diagonally across from the edge between the obstacle and through the obstacle corners.

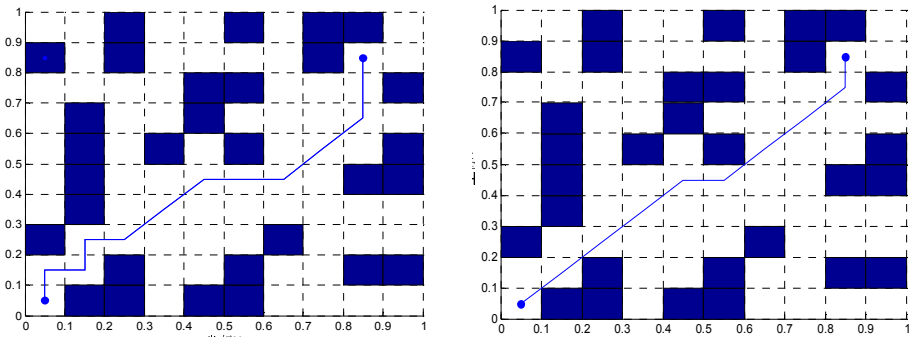

(a) Not across from the edge (b) across from the edge

Fig.1. The experimental results

Conclusion

This paper proposes a robot path planning method based on the grid method and improved AFSA, firstly creating barriers to model grid method, then according to AFSA to select the robot walking path, finally the path is obtained optimal path, simulation experiments prove the feasibility of this method

References

[1] Yu Jin-xia, Wang Lu. Unknown environment of mobile robot self-localization techniques [M]. Beijing: Electronic Industry Press, 2011:1-5.

[2] Li Xiao-lei, Shao Zhi-jiang, Qian Ji-xin. An optimizing method based on autonomous animates: fish-swarm algorithm [J] .Systems Engineering-Theory&Practice, 2002, 22(11): 32-38.

[3] Qian Ji-xin, Li Xiao-lei. Studies on artificial fish swarm optimization algorithm based on decomposition and coordination techniques [J]. Journal of Circuits and Systems, 2003, 8(1): 1-6.

[4] Lu Fei, Li Xiao-lei, Tian Guo-hui, et al. Applications of artificial fish school algorithm in combinatorial optimization problems [J].Journal of Shandong University (Engineering Science), 2004, 34(5): 64-67.

[5] Li Xiao-lei, Xue Yun-can, Lu Fei, et al. Parameter estimation method based-on artificial fish school algorithm[J].Journal of Shandong University(Engineering Science) , 2004, 34(3):84-87.

[6] Li Xiao-lei, Feng Shao-hui, Qian Ji-xin, et al. Parameter tuning method of robust PID controller based on artificial fish choolalgorit him [J].Information and Control,2004,33(1) : 112-115.

[7] Ma Jian-wei, Zhang Guo-li, Xie Hong,et al. Optimization of feed forward neural networks based on artificial fish swarm algorithm[J].Computer Applications,2004,24(10) : 21-23.

[8]Tang Jian-dong, Xiong xin-yin, Wu Yao-wu. Optimization algorithm based on artificial fish Reactive Power[J]. Relays, 2004,32(19): 9-12

[9]Ma Jian-wei, Zhang Guo-li. Artificial neural networks in fish power system short-term load forecasting[J], Grid Technology,2005,29(11):36-39

[10]Zhang Ming-yan, Yuan Dong-feng. AFSA and its application[M]. Beijing: Science Press,2012,57-59

Advanced Materials Research Vols. 989-994 (2014) pp 2470-2473
© (2014) Trans Tech Publications, Switzerland
doi:10.4028/www.scientific.net/AMR.989-994.2470

A study of the Keep-Right-Except-To-Pass Traffic Rule on cellular automata

Wenbin Cao[1]

[1] North China Electric Power University, Baoding, China

[a]caowenbin921030@126.com

Keywords: keep-right-except-to-pass rule, three-lane cellular automata, numerical simulation.

Abstract. Traffic rule is set to enable the safety and efficiency of the traffic. This paper takes the keep-right-except-to-pass rule as the research object. A three-lane cellular automaton model is proposed to simulate traffic flow. Through computer simulating, we analyze the relationships among traffic flow, overtaking ratio, average speed and density. The result shows that the rule although can increase the traffic flow and the average speed, the effect is not very evident, while this rule instead can increase driving safety in a large scale.

Introduction

In the USA, China and most other countries, multi-lane freeways often employ a rule that requires drivers to drive in the right-most lane unless they are passing another vehicle, in which case they move one lane to the left, pass, and return to their former travel lane. The rule is called keep-right-except-to-pass rule.

With the increasing demand of traffic flow simulation, the traffic flow model based on cellular automata has been developed. Cellular automata model of traffic flow incorporates a series of vehicle movement rules and traffic rules. On the study of the multi-lane model, Nagatani presented a deterministic cellular automaton model to simulate the traffic flow in a two-lane roadway [1] . Rickert et al. examined a two-lane cellular automaton based on the NaSch model [2].Nagel et al. summarized different approaches to lane changing and classified the multitude of possible lane-changing rules [3]. They used a cellular automaton model for two-lane traffic to generate the density inversion. Liet al. proposed a symmetric two-lane cellular automata model to investigate the aggressive lane-changing behavior of fast vehicle and the effect of different lane-changing probability [4].

In summary, all the previous articles have not studied the relationships among traffic flow, overtaking ratio, average speed and density on freeway traffic flow under different control conditions. This paper will examine their relationships.To study the influence of keep-right-except-to-pass rule on traffic, a three-lane cellular automaton model is proposed. First, overtaking ratio is introduced to measure traffic safety. Next, we put out two different lane-changing rules: rule 1 has no limits on lanes and permit overtaking on any lane; rule 2 is the keep-right-except-to-pass-rule. Through the computer simulate, we analyze the performance of this rule in light and heavy traffic

The establishment of the three-lane cellular automaton model

Assumption. We study the three lanes in one direction of a two-way six-lane freeway in this paper. The first lane is the far left one, the second lane is the middle one, and the third lane is the far right one. In order to construct cellular automaton models, we assume that there is only one type of vehicle and the maximum speed of vehicles on every lane is equal, that is $V_{1,\max} = V_{2,\max} = V_{3,\max} = V_{\max}$.

Definition of variables. Considering the road as three one-dimensional discrete grid point chains in parallel, we define the length of each chain is L , and each grid point will be occupied or empty at each moment. Let $X_i(t)$ be the position of vehicle i at time t, $V_i(t)$ be the speed of vehicle i at time t, the distance between vehicle i and the front vehicle at time t is:

$$gap_i(t) = X_{i-1}(t) - X_i(t) - 1 \tag{1}$$

In order to facilitate the discussions, some important indicators are defined to describe the traffic flow. They are listed as follows.

Overtaking Ratio.When overtaking at a high-speed, the mutual interference among the vehicle flow fields will seriously affect vehicle's aerodynamic characteristics, which will reduce the stability and security of vehicles, and even cause traffic accidents. So the frequency of lane changing is a very important measuring factor for road traffic safety [7]. Based on the above analysis, we take the overtaking ratio P_f, which is the ratio of the total number of overtaking and the number of vehicles observed, as the main indicator of traffic safety level.

Density. We define the density as $\rho(t)=N(t)/3L$, where $N(t)$ indicates the number of all vehicles on the freeway, and L indicates the total length of the road. It is obvious that high density represents heavy traffic and low density stands for light traffic.

*Flow.*The vehicle flow volume Q is the number of vehicles passing affixed point per unit time, $Q=\frac{N_T}{T}$, where N_T is the number of vehicles observed in time duration T.

*Average speed.*The average speed also can be used to denote the degree of the congestion $V_a=\frac{1}{N\times T}\sum_{1}^{T}\sum_{1}^{i}V_i^t$; V_i^t is the speed of vehicle i at time t.

Evolution rules of the vehicle. We divide every evolving process into two steps-move and changing lanes. *Moving Rule.* Vehicles on routes move according to Nagel–Schreckenberg(NS) rules [5] as follows:

(1) Acceleration: $V_i(t+1/3)=\min(V_i(t)+1,V_{\max})$;

(2) Deceleration: $V_i(t+2/3)=\min(V_i(t)+1/3,gap_i)$;

(3) Randomly slowing down with probability: $V_i(t+1)=\max(V_i(t+2/3)-1,0)$;

(4) Location renewal: $X_i(t+1)=X(t)+V_i(t+1)$

where $V_i(t)$ denotes the velocity of the i^{th} vehicle, $V_{\max}$ is the maximum velocity, is defined to be the number of empty sites in front of the i^{th} vehicle at time t and $X_i(t)$ is the position of the i^{th} vehicle at time t.

*Lane changing rules.*In general a driver has motivation to change lanes for better driving conditions. The decision to change must be made based on two essential criteria [6]: (1) The incentive criterion, i.e., there should be a good reason to change lanes, such as keeping a desired high speed or getting rid of jamming; (2) The security criterion, a driver must ensure that the changing action is safe, i.e. she/he will not collide with the cars forward and afterwards in the origin lane and adjacent lanes.

A schematic diagram of a three-lane freeway is presented as follow.

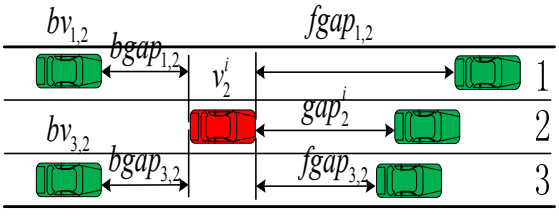

Fig. 1 A three-lane freeway

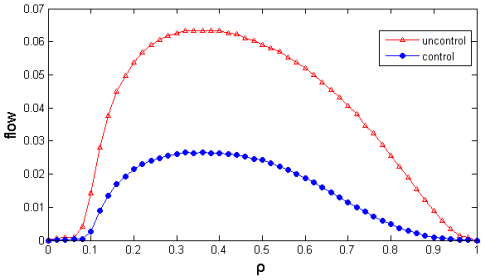

Fig. 2 Relationship between density and overtaking different ratio under control conditions

As shown in Fig. 1, cars on lane 1 and lane 3 can change to lane 2 while cars on lane 2 can change to both lanes 1 and lane 3. We take the car on medium lane 2 as an example to illustrate the meaning of symbols. The distances between car i in lane 2 and its adjacent front car in lane 1, lane 2 and lane 3 are defined as, $fgap_{1,2}$, gap_2^i, $fgap_{3,2}$.The distances between car i in lane 2 and its following car in

lane 1 and lane 3 are defined as $bgap_{1,2}$ and $bgap_{3,2}$.The speed of car i in lane 2 is defined as V_2^i The speed of the following car in lane 1 and lane 3 are $Vb_{1,2}$ and $Vb_{3,2}$. Let γ be the lane changing probability that taking into account the actual situation that some drivers like driving in a certain lane, and will not take the initiative to change.

Thus we adopt symmetric lane-changing rules set, which can be described as Eqs. (2)-(6) as follows[8]: the speed of the vehicle after lane changing will remain unchanged.

Rule 1

Change from lane 1 to lane 2 if

$$fgap_{2,1} \geq \min(V_i + 1, V_{\max}), bgap_{2,1} \geq bV_{2,1}, random > \gamma_{1,2} \quad (2)$$

Change from lane 2 to lane 1 if

$$gap_2^i(t) \leq \min(V_2^i(t) + 1, V_{\max}), fgap_{1,2} \geq gap_2^i, bgap_{1,2} \geq bV_{1,2}, random > \gamma_{2,1} \quad (3)$$

Change from lane 2 to lane 3 if

$$gap_2^i \geq fgap_{1,2}, \ gap_{3,2} \geq gap_2^i, bgap_{3,2} \geq bV_{3,2}, random > \gamma_{2,3} \quad (4)$$

Change from lane 3 to lane 2 if

$$gap_3^i(t) \leq \min(V_3^i(t) + 1, V_{\max}), fgap_{2,3} \geq gap_3^i, bgap_{2,3} \geq bV_{2,3}, random > \gamma_{3,2} \quad (5)$$

Rule 2 (The Keep-Right-Except-To-Pass Rule that is the cars on the passing lane are controlled)

We only need to modify part of the Rule 1, and then we can get Rule 2(The Keep-Right-Except-To-Pass Rule), which is mentioned in question given. When the driver driving on the passing road meets the condition of lane changing, he/she must change lane. Specific rules are presented as follow.

Change from lane 1 to lane 2 if

$$gap_1^i(t) \geq \min(V_1^i(t) + 1, V_{\max}), bgap_{2,1} \geq bV_{2,1} \quad (6)$$

The rest part is the same as Rule 1.

Numerical simulation results and discussion

Suppose every grid point represents 7.5m on lanes, and each time step Δ t≈1s, every time vehicles can at most move 5 grid points, that is $V_{\max} = 5$, then the corresponding speed would be 135km/h. In the simulation, assume L=2000 grid points, that is 15km, which is equivalent to a highway section without ramp. We also adopt periodic boundary conditions and assume the original car densities of the three lanes are equal. After 40,000 evolution steps, and averaging the last 1000 steps based on time, we have obtained the following experimental results. In order to eliminate the effect of randomicity, we take the systemic average of 20 samples. The lane-changing probability is set to be 0.5 unless otherwise specified. The simulation results are presented as follows.

Impact of different rules on overtaking ratio. It can be seen from Fig.2: (1) When the vehicle density is less than 0.38, the overtaking ratio will continue to rise with the increase of vehicle density; when the vehicle density is larger than 0.38, the overtaking ratio will decrease; when density is greater than 0.9, due to the crowding, it will become difficult to overtake, so the overtaking ratio is almost 0; (2) The overtaking ratio in the condition of uncontrolled passing lanes is higher than that in controlled lanes, no matter the traffic is light or heavy. Since the overtaking ratio is an important indicator to measure safety, it would be more unsafe if the rate is higher, in other words, after controlling the passing lanes, the safety of driving will increase in a large scale. Under the Keep-Right-Except-To-Pass Rule, the first lane is defined as passing lane, and if vehicles meet the condition to change to the second lane, they could not stay in the passing lane. This rule doesn't alter the characteristics of traffic flow; instead, it intensifies the safety of driving, while the three-lane uncontrolled traffic mode permits drivers to overtake others in any lane once they meet the condition. Therefore, this rule could effectively increase the safety of driving and reduce the rate of accidents.

Impact of different rules on traffic flow. It can be seen from Fig.3: (1) When vehicle density is lower than the critical density (approximately 0.15 in Fig3.), the traffic flow under two control rules will both rise with the increase of the vehicle density. In contrast, when vehicle density is greater than 0.15, the traffic flow will decrease with the increase of the vehicle density. (2) When vehicle density is lower than 0.15, the traffic flow of the two control conditions are basically the same. Except that, the traffic flow under uncontrolled condition (rule 1) is slightly larger than controlled condition (rule2). Although the Keep-Right-Except-To-Pass rule can improve the flow, the results are not that effective.

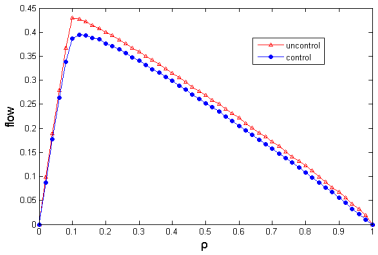

Fig 3. Relationship between density and traffic flow under different control conditions

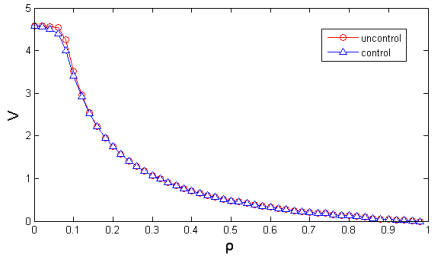

Fig 4. Relationship between density and speed under different control conditions

Impact of different rules on velocity. It can be seen from the Fig4. : The average speed will both reduce with the increase of vehicle density on two conditions. Besides, when vehicle density is greater than 0.15, the average speed under two conditions are almost the same. In other words, this rule cannot increase the average speed just as the flow.

Conclusions

In this paper, we have established three-lane cellular automata models, studied the overtaking ratio, speed and traffic flow under different control conditions, vehicle density,etc. and come to the following conclusions: (1)The keep-right-except-to-pass-rule although can increase the traffic flow and the average speed, the effect is not very evident, while this rule instead can increase driving safety in a large scale. (2)In fact, computer simulation has its limitations and the lane changing process is very complex. So in the future, we will combine measured data to examine the quantitative relationship between vehicle density and mixing ratio and factors such as lane changing and overtaking frequency.

Reference

[1] Takashi Nagatani, Jamming transition in the traffic-flow model with two-level crossings, Physical Review E 48 (1993) 3290–3294.
[2] M. Rickert, K. Nagel, M. Schreckenberg, A. Latour, Two lane traffic simulations using cellular automata, Physica A 231 (1996) 534–550.
[3] K. Nagel, D.E. Wolf, P. Wagner, P. Simon, Two-lane traffic rules for cellular automata: a systematic approach, Physical Review E 58(1998) 1425–1437.
[4] X.-G. Li, B. Jia, Z.-Y. Gao, R. Jiang, A realistic two-lane cellular automata traffic model considering aggressive lane-changing behavior of fast vehicle, Physica A 367 (2006) 479–486.
[5] K. Nagel, M. Schreckenberg, A cellular automaton model for freeway traffic, J. Phys. I France 2 (1992) 2221–2229.
[6] Wei Lv, Wei-guo Song, Zhi-ming Fang, Three-lane changing behaviour simulation using a modified optimal velocity model, Physica A 390 (2011) 2303–2314.
[7] Yong-sheng Qian , Jin-bao Luo, Jun-wei Zeng, Xiao-ming Shao, Wei-biao Guo, Study on security features of freeway traffic flow with cellular automata model—Taking the number of overtake as an example, Measurement 46 (2013) 2035–2042.
[8] Dayan Wu, A study of three-lane cellular automata traffic flow modles[D].Guangxi Normal University,2004.

Advanced Materials Research Vols. 989-994 (2014) pp 2474-2479
© (2014) Trans Tech Publications, Switzerland
doi:10.4028/www.scientific.net/AMR.989-994.2474

Probabilistic Model Checking by Model Equivalent Reduction and Abstraction

Zhenlong Bai [a], Linying Xu [b] and Zhanshui Yu [b]

[1] Tianjin University, No.92, Weijin Road, Nankai District, Tianjin, China

[a]942420622@qq.com, [b]sjzxy224@163.com,

Keywords: Markov chain; transitive closure; model checking; shortest path ; minimal connected components

Abstract. In probabilistic model checking, use discrete time Markov chain (DTMCs) to represent the model and use a branch of the temporal logic called probabilistic computation tree(PCTL) to represent the properties of the model. In this paper, we presents several counterexample generation algorithms for DTMCs violating a PCTL formula, presented as follows: first, according to the transitive closure to reduce the model size against the specific properties of the model, second, using the minimal connected components to generate the equivalent acyclic graph, third, we use the algorithm of the operational research to obtain a shortest path between two points. Experimental results show that our algorithm greatly simplifies the model size and generate more reasonable counterexamples with least states and paths.

Introduction

Model checking, which have developed in the last two decades to the point where major design companies are beginning to integrate them in their normal quality assurance process, is a very successful technique to automatically analyze the correctness of a finite state system. The term model checking was proposed by Clarke and Emerson in the early eighties and the capacity of model checkers to systems was restricted with a few million states .

This paper considers properties in probabilistic model checking, which is a technique to verify system models in which transitions are equipped with random information. Discrete time Markov chains (DTMCs) are a well-known modeling formalism for probabilistic systems. To describe properties of DTMCs we consider the unbounded fragment of probabilistic computation tree logic (PCTL).A major strength of model checking is the possibility to generate counterexamples in case a property is violated. As a result, advanced counterexample generation and analysis techniques have intensively been investigated [1-5].

Most related to our work is the latter approach[4].The paper is organized as follows: In section 2 we introduce some standard definitions notations and theoretical foundations. We provide describes our model reduction algorithm in Section 3 and introduce our model abstraction based on MCC in Section 4.Section 5 describes our counterexample generation method. The experiments are showed in Section 6. We conclude our work and discuss future work in Section 7.

Preliminaries

In this section we introduce discrete-time Markov chains and probabilistic computation tree logic, and define counterexamples in this probabilistic setting. Discrete-time Markov chains are a frequently used modeling formalism for stochastic systems with a discrete state space and a discrete model of time. We first introduced it as follow.

Definition 1 (DTMC) A discrete-time Markov chain (DTMC) is a tuple $M = (S, S_I, P, L)$ with a non-empty finite state set S, $S_I \subset S$ the set of initial states, $P: S \times S \rightarrow [0,1]$ a matrix of transition probabilities with $\sum_{s' \in S} P(s, s') = 1$ for all $s \in S$, and a labeling function $L: S \rightarrow 2^{AP}$ such that AP a set of atomic propositions.

Obviously, a DTMC is like a Kripke structure but transitions are equipped with discrete probabilities such that the sum of outgoing transitions of each state equals 1. It can transform a DTMC with multiple initial states to a DTMC with a single initial state, without changing the probability of the verified property. In this paper we just consider the single initial state. So we redefine a MDTC is a tuple $M = (S, s_I, P, L)$ with a single initial state.

Definition 2 (Paths) An finite path π in $M = (S, s_I, P, L)$is an finite sequence of stats, e.g. $s_0 s_1 s_2 \cdots s_k$such that $\forall\, 0 \le i \le k-1$, $s_i \in S, P(s_i, s_{i+1}) > 0$. An infinite path π is an infinite sequence of stats, e.g. $s_0 s_1 s_2 \cdots s_k \cdots$ such that $\forall\, 0 \le i$， $s_i \in S, P(s_i, s_{i+1}) > 0$.

We write $Path_{fin}^{M}$ for the set of all infinite paths of M, $Path_{inf}^{M}(s)$ for those starting in $s \in S$. As well $Path_{inf}^{M}$ is the set of all finite paths of M, $Path_{inf}^{M}(s)$ of those starting in $s \in S$ $Path_{inf}^{M}(s, t)$ denote the set of finite paths starting in $s \in S$ and ending in $t \in S$.

A finite path π can represent a set of infinite paths which have the same prefix π. We introduce a new notion, which is called an cylinder set ,$Cyl(\pi)=\{\pi^{inf} \in Path_{inf}^{M} |\ \pi \text{ is a prefix of } \pi^{inf}\}$.

At last we introduce for each state $s \in S$ a probability space $(\Omega_s^M,\ F_s^M,\ Pr_s^M)$ on the infinite paths of a DTMC starting in s. The sample space Ω_s^M is the set $Path_{inf}^{M}(s)$. The F_s^M, power set of the sample space Ω_s^M, was defined as :the cylinder set of a finite path π of M. Pr_s^M is the probability measure Pr_s^M: $F_s^M \to [0,1]$ such that the probabilities of the cylinder sets are given by

$$Pr_s^M\left(Cyl(s_0 s_1 \cdots s_n) = \prod_{i=0}^{n-1} P(s_i, s_{i+1})\right)$$

For a set $R \subseteq Path_{inf}^{M}(s)$ we define $Pr_s^M(R) = \sum_{\pi \in R'} Cyl(\pi)$ with $R' = \{\, \pi \in R \mid \forall \pi' \in R, \pi \text{ does not have a prefix } \pi' \,\}$.

Definition 3 (PCTL) Probabilistic computation tree logic (PCTL) is an extension of CTL in which state formulas are interpreted over states of DTMC and path formulas interpreted over infinite paths in a DTMC. The syntax of PCTL is $\Phi ::= true|p|\neg\Phi|(\Phi \wedge \Phi)|P_{\lhd\lambda}(\Phi \mathcal{U} \Phi)$ with $p \in AP$, $\lambda \in [0,1]$ a probability threshold, and $\lhd \in \{<,\ >,\ \le,\ \ge\}$ a comparison operator. For a PCTL state formula φ we define the "future" operator F as $P_{\lhd\lambda}(F\varphi) = P_{\lhd\lambda}(true \mathcal{U} \varphi)$.

In case a property $P_{\le\lambda}(\varphi_1 \mathcal{U} \varphi_2)$ is violated for a DTMC M, a counterexample is a set $C \subseteq Path_{inf}^{M}(s)$ starting in initial state s such that all infinite paths from their associated cylinder sets satisfy $\varphi_1 \mathcal{U} \varphi_2$ and $Pr_s^M(C) > \lambda$. A method in [2] can be used to reduce properties with lower bounds to the former case.

The method in[2], we usually use to check a property $P_{\lhd\lambda}(\varphi_1 \mathcal{U} \varphi_2)$, is to (1) generate a labeling for the sub-formulae φ_1 and φ_2 possibly by recursively invoking probabilistic model checking for sub-formulae,(2) reduce the DTMC with all states satisfying $\neg\varphi_1 \wedge \neg\varphi_2$ get absorbing , and (3) obtain the probability φ_2 states called target states from initial state to the φ_2 states in the reduced DTMC. In this paper, we remove the states and the transitions without relation of reaching the target states from the initial state after the second step. For the last point, just as dealing with the multiple initial states ,we just consider the single target state by transforming a DTMC with multiple target states.

In summary, we just consider the property$P_{\le\lambda}(Fp)$ on the DTMC with a single initial and target state representing the property, on account of we can compute others by some equivalent transformation.

Reduction Model

Prior to checking the validity of a PCTL formula for the DTMC, we modify the DTMC by transitive closure of a single initial and target state. The transitive closure is introduce as follow:

Definition 4 (Transitive closure) $Tc_s^M \subseteq S$ is a transitive closure for $s \in S$ of the DTMC $M = (S, s_I, P, L)$iff $\forall t \in Tc_s^M$, $Path_{inf}^{M}(s, t) \neq \emptyset$.

A transitive closure for a state is the collection of all states it can be reached. The transitive closure can be obtain by algorithm 1. In relation to the transitive closure, we define reverse

transitive closure for $t \in S$ of the DTMC $M = (S, s_I, P, L)$. $RTc_s^M \subseteq S$ is a reverse transitive closure iff $\forall s \in Tc_s^M, Path_{inf}^M(s,t) \neq \emptyset$. We can get the a reverse transitive closure with algorithm 1 by replacing FindPreviousr as FindSuccessor.

Algorithm 1. Transitive closure and reverse transitive closure.

Input：state s
Output：stateSet closure
closure=now=new={s}
while new!= ∅ do
    new=∅
    for state in now
        next=FindPreviousr(state)
        new=new∪ $\{t \in next | t \notin closure\}$
    end for
    now=new
    closure=new∪closure
end while

Applying the above initial transitive closure $Tc_s^M$and target reverse transitive closureRTc_t^M for a DTMC M yield the $Sc_t^s = Tc_s^M \cap RTc_t^M$. According to the Sc_t^s,we modify the DTMC $M = (S, s_I, P, L)$with a single initial state s and a single target state t and turn it into a new DTMC, written $M' = Reduce(M, Sc_t^s)$, $M' = (S', s_I', P', L')$).We describe the DTMC M' has state space $S' = Sc_t^s \cup s_{error}$ for $s_{error} \notin Sc_t^s$, $L(s') = L(s')$ for $s' \in Sc_t^s$, and $L'(s_{error}) = \emptyset$, P' as follows:

$$P'(s_1, s_2) = \begin{cases} 1 & s_1 = s_2 = s_{error} \\ P(s_1, s_2) & s_1 \in Sc_t^s \wedge s_2 \in Sc_t^s \\ \sum_{s' \notin Sc_t^s \wedge s' \in S} P(s_1, s') & s_1 \notin Sc_t^s \wedge s_2 = s_{error} \\ 0 & \text{o. w.} \end{cases}$$

It is obvious that a finite path $\pi \in Path_{fin}^M(s,t)$ of a DTMC M can be described by a finite path of a reduce DTMC $M' = (S', s_I', P', L')$.

MCC-based Model Abstraction

In this section ,we introduce our algorithm to a DTMC M based on the MCC. We define a new set of states ,called a minimal connected component(MCC), and abstract the set of all path fragment through the (MCC) just as in[1].

Definition 5 (MCC) In a $M = (S, s_I, P, L)$,we say $s \in S$ can reach $t \in S$ iff $\exists \pi = ss_0s_1 \cdots s_kt \in Path_{fin}^M(s,t), 0 \leq i \leq k, s^i \in S$. And if t can also reach s, then s and t are connection. A state set $S' \subseteq S$ is called connection in M iff $\forall s \in S', t \in S'$, s,t are connection. We denote S' is a minimal connected component (MCC) of M iff S' is connection in M but $\forall S'' \subseteq S'$, S'' is not connection in M.

We will introduce some more concepts before we talk about the algorithm. For a set $S' \subseteq S$ of $M = (S, s_I, P, L)$, the set $Inp^M(S')$=$\{t \in S' | t = s_I \vee \exists s \in S - S', P(s,t) > 0\}$ is the input state of S'. Analogously, $Out^M(S')$=$\{t \in S - S' | \exists s \in S'\ P(s,t) > 0\}$ means all the stats outside the S'.

The last thing we need to introduce is to get a abstracted DTMC without loop, written $M_{abs} = (S_{abs}, S_{Iabsc}, P_{abs}, L_{abs})$. The smaller M_{abs} specify the probability for the transitions from each input state s to each output state t. This probability mass is determined in two steps: First, we compute for each input state s and output state t the total probability mass p_{st} of all finite paths from s to t without loop. We obtain the probability of the transition by $P(s,t)$=$p_{st}/\sum_{t' \in Out^M(S')} p_{st'}$. The strict and detail correctness is proved in[1].

Definition 6 (Abstraction of M) Let $M = (S, s_I, P, L)$ be a DTMC and a MCC $S' \subseteq S$ is not absorbing. We define the abstraction of $M_{mcc} = (S_{mcc}, S_{Imcc}, P_{mcc}, L_{mcc})$,written $M_{abs} =$

$(S_{abs}, S_{Iabsc}, P_{abs}, L_{abs})$,with $S_{abs} = Inp^{M}(S') \cup (S - S')$, $S_{Iabs} = s_I$ and $L_{abs}(s) = L(s)$ with $s \in S_{abs}$, $P_{abs(s_1,s_2)}$described as follow:

$$P_{abs(s_1,s_2)} = \begin{cases} p_{st} \Big/ \sum_{t' \in Out^{M}(S')} p_{st'} & s_1 \in Inp^{M}(S') \wedge s_2 \in Out^{M}(S') \\ P(s_1, s_2) & \text{o.w.} \end{cases}$$

It is not affect the total probabilities of reaching a target state from an initial state in M_{abs}. The abstraction is described by M_{abs}=Abstract(M,MCC). We introduce algorithm 2 to abstract the M.

Algorithm 2. Abstraction of Model

```
Input：DTMC  M
Output：DTMC  M, TwoTupleDTMC  Rep
s:= initial state of M
MCCs:=getMCCs (s,M)
while MCCs !=∅ do
    for MCC in MCCs
        M_abs=Abstract(M,MCC)
        Rep=Rep∪ (M_abs, M_mcc)
        M=M_abs
        MCCs:=getMCCs (s,M)
    end for
end while
```

we can use algorithm 2 to get new DTMC without loops, which is easier to check model much. In algorithm 2 ,we need to detect the MCCs by getMCCs using the algorithm 3.

Algorithm 3. Detecting MCCs

```
Input：state s，DTMC M
OutPut：MCCSet  MCCs
Low[s]=DFN[s] =++Index
Stack.push(s)
for (s,u) in P(s,u)>0  DescendOrderBy DFN[u]
    if s!=u
        if  u is not visite
            getMCCs (s，M)
            Low[s]=min(Low[u],Low[s])
        else
            if s and u in Stack
                Low[s]=min(Low[s],DFN[u])
                Repeat
                    P=Stack.Pop
                    MCC=MCC ∪ P
                Until p==u
                MCCs=MCC ∪ MCCs
                MCC=∅;
            end if
        end if
    else p=Stack.pop;
end for
```

Counterexample Generation

In this section we introduce our framework for the generation of probabilistic PCTL counterexamples based on MCCs abstraction and model reduction. Our computation is based on the detection of single paths. Instead of just collecting found paths, we use a new DTMC, which is

called critical subsystems and is builded by all transitions appearing in the found counterexample paths, to represent counterexample. Intuitively, a critical subsystem is a part of the original system in which the given probability bound is already exceeded, no matter what happens outside the subsystem.

In our algorithm 4, an DTMC based on the MCC abstraction is the input argument. As the most significant ingredient, we introduce the new approach to compute the shortest path reaching the target state from the initial state in a DTMC M without loops. The method ModelCheck is introduced in[5]. In order to finding paths, we introduce algorithm 5 to implement the path search procedure FindNextPath as invoked by algorithm 4.

Algorithm 4. Incremental generation of critical subsystems

Input：DTMC M, TwoTupleDTMC Rep, doble λ

Output：DTMC CriticalSystem

```
Trans=NewTrans=CriticalSystem=∅
if ModelCheck(M) >λ
    while ModelCheck(M)≤ λdo
        s:= initial state of M，t:= target state of M，NewTrans=∅
        M=ChangeModel (Critical，M)
        NewTrans=GetShortestPath(s，t)
        if  NewTrans≠ ∅
            Trans=Trans∪ NewTrans
            CriticalSystem := GetNewCritical(Trans)
        end if
     end while
     CriticalSystem=Concretize(Trans,Rep)
end if
```

In the algorithm 4, we use the method ChangeModel to change the DTMC M. So that the most probable path in the new DTMC corresponds to the second-most probable path of the original DTMC. The idea is detailed in[5]. Instead of using a set theoretic variant of Dijkstra's algorithm, we use new algorithm 5 based on a set of recursive equations to compute the probable path of a DTMC. This method is called by algorithm 4 as GetShortestPath.

Algorithm 5. Shortest Path of Two Certain States

Input：state s，state t

Output：TwoTuple (p, π)

```
if s=t
    (p, π) = (1， s)
else
    for (u,t) in   P(u,t)>0
        (p, π): =  recursive calls (s,u)
    end for
end if
```

We adopt the algorithm 5 to search a shortest path, which fits well to our problem without the cycles. It can be solved in time O(nm) with that n is the number of the states |S|, and m is the number of nonzero elements in P. This is indeed in polynomial time.

Experimental results

To test our algorithms, we developed a prototype implementation in C++.We used this tool run some experiments on a 3.06 GHz Pentium(R) Dual-Core CPU with 4 GB RAM. We used Prism[7]to generate models for different instances of the parametrized crowds protocol.

The crowds protocol is used to protect users' anonymity on web browsing. In our model we verify the property $P_{\leq\lambda}(F_{\text{pos}})$, where the pos means the positively identified bad user. We generate the counterexample of the M with the different parameters R and Goods.

First of all, we demonstrate our reduction algorithm in the three section. Table 1 contains information about the original model and the reduction model for the crowds protocol. The models are therefore parametrized by R and Goods. OStates and OTransitions represents number of the states and transitions of the original model, while NStates and NTransitions are described the reduction model. Table 2 depicts results for the crowds protocol comparison to the classic algorithm in[2]. We can find that our algorithm get the less paths and states with reduction the infinite loop paths to several paths.

Table 1 Reduction Model Results for the Crowds Protocol

Goods	R	OStates	OTransitions	NStates	NTransitions
5	4	3515	6035	2116	3651
10	3	6563	15143	2556	6637
5	6	18817	32677	7254	12589

Table 2 Counterexample Results for the Crowds Protocol

Goods	R	λ	classic			MCC		
			Paths	States	Total Prob	Paths	States	Total Prob
5	4	0.11	14879	1219	0.1103	379	632	0.110003
5	4	0.13	30033	1249	0.131981	610	914	0.130001
5	6	0.01	28484	1082	0.0100005	435	456	0.0100056
5	6	0.015	183844	2296	0.0150515	1352	550	0.0150085

Conclusion and Future Work

In the paper we introduced new approaches with reduction and abstraction the model to generate counterexamples for DTMCs and PCTL properties. We prove both correctness and efficiency of our algorithm. In future we are going to optimize our approaches with distributed computing technology. Another direction of research is the new framework for the symbolic in[5].

References

[1] Erika Abrahám, Nils Jansen, Ralf Wimmer, J Katoen, and Bernd Becker. Dtmc model checking by scc reduction. In Quantitative Evaluation of Systems (QEST), 2010 Seventh International Conference on the, pages 37–46. IEEE, 2010.

[2] Tingting Han, J Katoen, and Damman Berteun. Counterexample generation in probabilistic model checking. Software Engineering, IEEE Transactions on, 35(2):241–257, 2009.14

[3] Yo-Sub Han and Derick Wood. Obtaining shorter regular expressions from finite-state automata. Theoretical Computer Science, 370(1):110–120, 2007.

[4] NilsJansen, ErikaÁbrahám,J ensKatelaan, RalfWimmer, Joost-PieterKatoen,and BerndBecker. Hierarchical counterexamples for discrete-time markov chains. In Automated Technology for Verification and Analysis, pages 443–452. Springer, 2011.

[5] Nils Jansen, Ralf Wimmer, ErikaÁbrahám, Barna Zajzon, Joost-Pieter Katoen, Bernd Becker, and Johann Schuster. Symbolic counterexample generation for large discrete-time markov chains. Science of Computer Programming, 2014.

[6] HoonSang Jin, Kavita Ravi, and Fabio Somenzi. Fate and free will in error traces. International Journal on Software Tools for Technology Transfer, 6(2):102–116, 2004.

[7] Marta Kwiatkowska, Gethin Norman, and David Parker. Prism 4.0: Verification of probabilistic real-time systems. In Computer Aided Verification, pages 585–591. Springer, 2011.

Advanced Materials Research Vols. 989-994 (2014) pp 2480-2483
© (2014) Trans Tech Publications, Switzerland
doi:10.4028/www.scientific.net/AMR.989-994.2480

Computing Volumes Surrounded by a Quadric Surface and a Plane with MATLAB

Qingli Yin

Department of Laboratory and Facility Management, Shandong Jianzhu University, Jinan 250101, China

E-mail address: yinql69@163.com

Keywords: quadric surface, plane, volume

Abstract. We describe how to compute volumes of solids surrounded by a quadric surface and a plane. First, we use coordinate transformations to change an equation of a quadric surface into a standard equation, then apply integration techniques to find formulae of computing volumes. A MATLAB procedure is programmed that can be used to evaluate volumes bounded by a quadric surface and a plane.

Introduction

The topic of how computing volumes of solids between a quadric surface and a plane have been studied by Wei-Chi Yang, V. V. Shelomovskii and S. Xia, several useful formulae of finding volumes were obtained in [1, 2, 3]. Solids bounded by a quadric surface and a plane may have a finite or infinite volume. Only the solids with finite volumes are studied here. According to the classification of quadric surfaces (see [4]), there are only an ellipsoid, a hyperboloid of two sheets, a cone and an elliptic paraboloid possibly bounding a finite volume with a plane. For a given quadric surface, we firstly identify it whether an ellipsoid, a hyperboloid of two sheets, a cone and an elliptic paraboloid, then change its equation into a standard equation. For standard equations of quadric surfaces, integration techniques are applied to them to find formulae of computing volumes. In this paper, a MATLAB procedure based on the formulae is programmed and its performance is demonstrated with illustrative examples. Before using the function, please draw a figure of a quadric surface and a plane to confirm the solid bounded by them with finite volume. The procedure is programmed with formal parameters, users need only input the equations of a quadric surface and a plane, the function will output the volume we desire.

A Standard Equation of A Quadric Surface

For a given real quadric surface S with form:

$$f(x,y,z)=a_{11}x^2+a_{22}y^2+a_{33}z^2+2a_{12}xy+2a_{13}xz+2a_{23}yz \\ +2a_{14}x+2a_{24}y+2a_{34}z+a_{44}=0. \tag{1}$$

Set

$$I_1=a_{11}+a_{22}+a_{33},\quad I_2=\begin{vmatrix}a_{11}&a_{12}\\a_{12}&a_{22}\end{vmatrix}+\begin{vmatrix}a_{11}&a_{13}\\a_{13}&a_{33}\end{vmatrix}+\begin{vmatrix}a_{22}&a_{23}\\a_{23}&a_{33}\end{vmatrix},\quad I_3=\begin{vmatrix}a_{11}&a_{12}&a_{13}\\a_{12}&a_{22}&a_{23}\\a_{13}&a_{23}&a_{33}\end{vmatrix},\quad I_4=\begin{vmatrix}a_{11}&a_{12}&a_{13}&a_{14}\\a_{12}&a_{22}&a_{23}&a_{24}\\a_{13}&a_{23}&a_{33}&a_{34}\\a_{14}&a_{24}&a_{34}&a_{44}\end{vmatrix}.$$

We know that I_1, I_2, I_3 and I_4 are invariants of $f(x,y,z)=0$ under an orthogonal transformation, and they can be used to determine the type of S (see [4]). The surface S is an ellipsoid if $I_2>0,\ I_1I_3>0,$ and $I_4<0$; S is a hyperboloid of two sheets if $I_3\neq 0,\ I_2\le 0$ and $I_4<0$; S is a cone if $I_3\neq 0,\ I_2\le 0$ and $I_4=0$; S is an elliptic paraboloid if $I_3=0,\ I_4<0$.

Recall that an ellipsoid, a hyperboloid of two sheets and a cone are surfaces with a central point and they have three orthogonal principal diametral planes. Suppose the coordinates of central point of S are (x_0,y_0,z_0), then they satisfy:

$$\begin{cases} a_{11}x_0 + a_{12}y_0 + a_{13}z_0 + a_{14} = 0 \\ a_{12}x_0 + a_{22}y_0 + a_{23}z_0 + a_{24} = 0 \\ a_{13}x_0 + a_{23}y_0 + a_{33}z_0 + a_{34} = 0 \end{cases} \quad (2)$$

The characteristic equation of S is

$$-\lambda^3 + I_1\lambda^2 - I_2\lambda + I_3 = 0. \quad (3)$$

We replace the characteristic roots $\lambda_1, \lambda_2, \lambda_3$ into the system of equations separately,

$$\begin{cases} (a_{11} - \lambda_i)X + a_{12}Y + a_{13}Z = 0 \\ a_{12}X + (a_{22} - \lambda_i)Y + a_{23}Z = 0 \\ a_{13}X + a_{23}Y + (a_{33} - \lambda_i)Z = 0 \end{cases}, \quad (4)$$

solving the equations we get the principal directions $X_i : Y_i : Z_i \ (i = 1,2,3)$ of S. Substituting $X_i, Y_i, Z_i (i = 1,2,3)$ into the equation $X_i(a_{11}x + a_{12}y + a_{13}z + a_{14}) + Y_i(a_{12}x + a_{22}y + a_{23}z + a_{24}) + Z_i(a_{13}x + a_{23}y + a_{33}z + a_{34}) = 0$, the principal diametral planes of S are obtained. If we take the three principal diametral planes as new coordinate planes, and make an orthogonal transformation, then S is transformed into S' with form $\lambda_1 x'^2 + \lambda_2 y'^2 + \lambda_3 z'^2 + \frac{I_4}{I_3} = 0$ and the plane P is changed into a plane P_1.

For an elliptic paraboloid, since it has a characteristic root $\lambda = 0$, it has only two principal diametral planes, we pick a plane as third new coordinate plane that is vertical to the two principal diametral planes, then S is changed into S' with form $\lambda_1 x'^2 + \lambda_2 y'^2 + 2a'_{34}z' + a'_{44} = 0$ and the plane P is changed into a plane P_1.

Methods of Computing Volumes

Suppose that a quadric surface has a standard equation, we calculate volumes of solids surrounded by a quadric surface and a plane using traditional method.

A. Volume of a solid surrounded by an ellipsoid and a plane

Supposed an ellipsoid equation S with form $\frac{x^2}{a^2} + \frac{y^2}{b^2} + \frac{z^2}{c^2} = 1$ and a plane P with equation $a_1x + b_1y + c_1z = d_1$. Making a linear transformation: $x = ax'$, $y = by'$, $z = cz'$, S is converted into an unit sphere S', and the plane P is changed into P': $a_2x' + b_2y' + c_2z' = d_2$. The Jacobian determinant of the linear transformation is denoted by J. Recall that the volume of a spherical segment is $\pi h^2(R - h/3)$, where R is the radius of the sphere and h is the height of the segment. If let d be the distance from the origin to the plane P', then $h = R - d$ (or $h = R + d$). Finally, the volumes of pieces surrounded by S and P are obtained by the formula $\pi h^2(R - h/3)|J|$.

B. Volume of a solid surrounded by a hyperboloid of two sheets and a plane

Suppose a hyperboloid of two sheets S with form $\frac{x^2}{a^2} + \frac{y^2}{b^2} - \frac{z^2}{c^2} = -1$ and a plane P with equation $a_1x + b_1y + c_1z = d_1$. The intersections of the given quadric and parallel planes is a set of similar ellipses. The volume of the solid surrounded by S and P is calculated by the formula: $V = \frac{\pi abc}{3}(2 + 3\mu - \mu^3)$, $\mu = -\frac{|n_0|}{w}$. Where, $w = \sqrt{-n_1^2a^2 - n_2^2b^2 + n_3^2c^2}$, $n_1 = \frac{a_1}{\sqrt{a_1^2 + b_1^2 + c_1^2}}$, $n_2 = \frac{b_1}{\sqrt{a_1^2 + b_1^2 + c_1^2}}$, $n_3 = \frac{c_1}{\sqrt{a_1^2 + b_1^2 + c_1^2}}$, $n_0 = \frac{-d_1}{\sqrt{a_1^2 + b_1^2 + c_1^2}}$. This formula was obtained by V. V. Shelomovskii and Wei-Chi Yang in [3]. If S with form $-\frac{x^2}{a^2} + \frac{y^2}{b^2} + \frac{z^2}{c^2} = -1$ or $\frac{x^2}{a^2} - \frac{y^2}{b^2} + \frac{z^2}{c^2} = -1$, we have a similar formula.

C. Volume of a solid surrounded by a cone and a plane

Suppose a cone S with form $\frac{x^2}{a^2}-\frac{y^2}{b^2}-\frac{z^2}{c^2}=0$ and a plane P with equation $a_1x+b_1y+c_1z=d_1$. By the technique used in the paper [3], we get the volume formula that calculates the volume of the solid surrounded by a cone S and a plane P: $V=\frac{\pi abc|n_0|^3}{3w^3}$, where $w=\sqrt{n_1^2a^2-n_2^2b^2-n_3^2c^2}$, $n_1=\frac{a_1}{\sqrt{a_1^2+b_1^2+c_1^2}}$, $n_2=\frac{b_1}{\sqrt{a_1^2+b_1^2+c_1^2}}$, $n_3=\frac{c_1}{\sqrt{a_1^2+b_1^2+c_1^2}}$, $n_0=\frac{-d_1}{\sqrt{a_1^2+b_1^2+c_1^2}}$.

D. Volume of a solid surrounded by an elliptic paraboloid and a plane

Suppose an elliptic paraboloid S with form $\frac{x^2}{a^2}+\frac{y^2}{b^2}=z$ and a plane P with equation $a_1x+b_1y+c_1z=d_1$. The volume of the solid surrounded by S and P is calculated by the formula: $V=\frac{\pi ab}{2}\left(-\frac{n_0}{n_3}+\frac{a^2n_1^2+b^2n_2^2}{4n_3^2}\right)^2$, where $n_1=\frac{a_1}{\sqrt{a_1^2+b_1^2+c_1^2}}$, $n_2=\frac{b_1}{\sqrt{a_1^2+b_1^2+c_1^2}}$, $n_3=\frac{c_1}{\sqrt{a_1^2+b_1^2+c_1^2}}$, $n_0=\frac{-d_1}{\sqrt{a_1^2+b_1^2+c_1^2}}$. This formula was obtained by V. V. Shelomovskii and Wei-Chi Yang in [3].

We program a MATLAB procedure "quadravol" based on above formula, the procedure will calculate the volume we desire if we input the equations of a quadric surface and a plane.

A Example

Example 1 Let S be the surface $x^2+y^2+5z^2-6xy-2xz+2yz-6x+6y-6z+10=0$, and P be the plane $3x+8y+5z-28=0$. Find the volume bounded by S and P.

Solution: Set up an M-file 'ex1'.

```
f2=@(x, y, z)(x.^2+y.^2 + 5*z.^2-6*x.*y-2*x.*z+ 2*y.*z-6*x+6*y-6*z+10); g2=@(x, y, z)(3*x+8*y+5*z-28);
implicitsurf(f2, [-8, 10], [-8, 8], [-5, 5], 50);
hold on
implicitsurf(g2, [-8, 10], [-8, 8], [-5, 5], 50);
hold off
axis equal
aa=[1 -3 -1 -3; -3 1 1 3; -1 1 5 -3; -3 3 -3 10]; pla=[3 8 5 -28];
quadravol(aa, [3 8 5 -28])
>>ex1
The quadratic surface is a two-sheeted hyperboloid.
The volume bounded by the plane P and the surface S is 2.994272e+001.
```

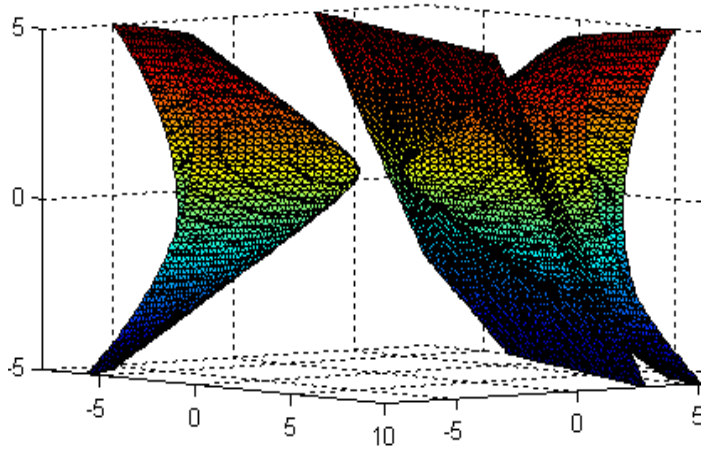

Fig 1 The figure of example 1

Summary

In this paper, we summarize a basic method of calculating volumes of a solid surrounded by a quadric surface and a plane, the method is suitable to programming. We programmed a MATLAB procedure with formal parameters for computing the volumes. It is essential to point out that one need to draw a figure of the quadric surface and the plane to confirm the solid bounded by them with finite volume before using the function. The only one thing to do for users is to input the parameters of a quadric surface and a plane, the function will automatically judge the type of the quadric surface, and output the volume we desire if the quadric surface and the plane may surround a finite solid. Some illustrative examples are given, it is impossible to calculate the results in this paper without the help of MATLAB.

References

[1] Yang, Wei-Chi and Lo, Min-Lin. Finding Signed Areas and Volumes Inspired by Technology, The Electronic Journal of Mathematics and Technology, Volume 2, Number 2, 2008, pp. 133-150.

[2] S. Xia, W. C.Yang and V. Shelomovskii. Computing Signed Areas and Volumes with Maple, Electronic Journal of Mathematics and Technology (eJMT), Vol.6 , No.2, 2012, pp. 175-195.

[3] V. Shelomovskii and W. C. Yang. Finding volumes between a quadric surface and a plane, Electronic Journal of Mathematics and Technology (eJMT), Vol.7, No.1, 2013, pp. 1-21.

[4] Lingen Lv and Zidao Xu. Analytic Geometry (Fourth Edition, in Chinese), Higher Education Press, Beijing, 2006, pp. 244-293.

[5] William H. Press, Saul A. Teukolsk, William T. Vetterling and Brian P. Flannery. NUMERICAL RECIPES- The Art of Scientific Computing (Third Edition). Cambridge University Press, 2007.

Advanced Materials Research Vols. 989-994 (2014) pp 2484-2487
© (2014) Trans Tech Publications, Switzerland
doi:10.4028/www.scientific.net/AMR.989-994.2484

A New Defogging Algorithm Based on Atmospheric Degradation Physical Model

Xiao-Guang Li

Department of Electrical Engineering and Automation, Luoyang Institute of Science and Technology, Luoyang, 471023, Peoples R China

email: lylglxg@163.com

Keywords: Fog-degraded Images; Atmospheric Scattering Model; Fitness Function

Abstract. Aiming at the degeneration phenomenon of images taken in mist, according to features of the drop quality image, this paper proposed a novel defogging algorithm based on improved atmospheric scattering model. The problem of fog-degraded images defogging restoration is transformed into the problem of optimization estimation for original un-degraded image by maximizing the global contrast object function, in this way, the proposed algorithm can restore the object image as completely as possible in probability sense. The experimental results show that the method can effectively improve the fog degeneration phenomenon and improve image clarity, significantly improving drop quality image visual effect.

Introduction

Fog makes outdoor scene image contrast and color will change or degrade, it brings great interference to current vision systems, which brings great difficulties to the outdoor testing, monitoring, automatic navigation, target tracking etc, and therefore the study of fog degraded processing algorithms has practical significance in general[1].

Currently, the defogging algorithm is divided into two types: the non-model of the algorithm and the algorithm based on a physical model. Typical non-model approach has histogram equalization, wavelet transform, homomorphism filtering and retinex method etc [2]. These algorithms only can improve the image quality relatively and can not achieve the defogging in the true sense [3]. The degradation of the physical model algorithm based on the atmosphere can get relatively good effect to defogging，but its characteristics is in need of getting the depth of information of the scene, it often needs the help of the radar altimeter to obtain depth information, then uses the image data and the depth information together to solve the model parameters, which brings difficulties to the practical application[4]; literature [5] adopts the fog algorithm based on a physical model, but requires two images of the same scene in different weather conditions, an image of a sunny day, as a reference, together with another foggy images obtains the depth information of the scene, which requires a pre-captured image information, and will bring the problem of image matching. It is clearly not practical in many cases.

Recently, more researchers have been devoted to defogging algorithm[6],defogging based on a single image has made great progress, a lot of research based on a single image of dark channel prior[7], the algorithm is established by a prior-model to fogging, directly estimates the concentration in order to achieve high-quality images to the defogging, but the algorithm has benefited from a strong a prior or assumptions, because dark colors is a statistical regular, may be ineffective for some special image, for example, when the scene approaches the air layer essentially and is not covered by shadow, the theory of dark colors is invalid.

The Improved Physical Model

Atmospheric Scattering theory gives the degradation model of fog-degraded Images. The model describes the subject image fog light intensity can be equivalent to the total superposition scene after atmospheric attenuation and the radiation in the environment of the scattered light:

$$E = E_{\alpha} + E_{d} = E_{\infty}(1 - e^{-\beta d}) + Re^{-\beta d} \quad (1)$$

In the model, R is the radiation intensity of the scene under sunny weather ; E_{∞} is the intensity of the sky radiation; d is called the scene depth; β is called atmospheric scattering coefficient, from atmospheric scattering perspective, Eq(1)is called atmospheric scattering physical model. In order to effectively achieve the goal of an image to defogging, it requires improving the fog-degraded image restoration model. An improved degradation unified mode of fog degraded image is put forward. By observing a large of degraded images, we found that although the shooting scene in the whole atmospheric scattering coefficients is consistent with the hypothesis in which can not always be met, but for the target object in the scene at the same depth, it is possible that the assumption is met. Thus, according to the atmospheric model, we obtain an important conclusion, which is located in any area of the scene point on the same depth, which corresponds to the model E_d and E_{α} are constants. so we get the following improved image degradation model, namely，

$$E_i = \omega_i E_{i0} + (1 - \omega_i) E_{\infty} \quad (2)$$

Here $\omega_i \in [0,1]$, because the model is got under the assumption at scenic spot of the same depth, it can realize the recovery on the single image scene of the same depth; therefore we are also call type (2) as the degradation model of the depth. Improved model of the same depth means on the same depth area, the brightness of the arbitrary field spots can be expressed as the true brightness of clear weather and the current weight and the sky brightness. Because of the global scene depth approximate consistent image can be seen as muti-depth images of special circumstances of muti-depth, therefore, the improved united model is put forwarded:

$$E = \varpi E_0 + (1 - \varpi) E_{\infty} \quad (3)$$

The dimension of the vector is the number of images in the same depth zone, such as on the depth of an approximate contains four with area of image to defogging, only to solve the weight vector composed by four weight coefficient. this way through the improvement of the model, it will implement that the complex problem about degraded fog image transfer into simple problem of solving the weight vector composed by several coefficient.

The New Optimization Algorithm Based on Improved Model

The new algorithm based on the improved atmospheric scattering physical model to realize defogging, which need to meet certain goals under optimal parameters for solving the model. For this reason, this paper proposes a novel defogging algorithm. The restoration problem is transformed into the improved model weight vector parameters for solving the optimal problems.

The preprocessing of regional segmentation. When the improved unified atmospheric scattering physical model is used, we must first preprocess the depth region segmentation to the fog-degraded image, the purpose of the regional segmentation mainly determines the dimensions of the new model of weight vector, basis primarily on degraded image segmentation is different on each target depth in which all the pixels on the image, that the division of the degraded image area through the scene is divided into several areas of different depths. Segmentation methods are based on the boundary of image segmentation, and based on region, and based on the based on gray-scale. Through deep segmentation preprocessing, we determine the number of the image with depth in the area, in order to further determine the weights in the vector parameter values, this paper proposes an algorithm for the global optimum contrast of the model parameters based on the sense, this algorithm makes full use of the efficiency and fast and strong robustness of the genetic algorithm advantages. Adaptively to achieve the optimal parameters of the model for solving.

Coding is the premise and foundation of application with genetic algorithm to solve the problem; it is also a key step in designing the genetic algorithm. Genetic algorithms based on individual selection, crossover and mutation genetic operation, which searches high fitness individuals, and gradually increase the amount in the group, finally to seek out the problem of the optimal solution or approximate optimal. Coding quality directly affect the selection, crossover and mutation genetic

algorithm, therefore, how to design a perfect coding scheme for the specific problem has always been one of the difficulties of the application of genetic algorithm, people put forward various coding method, mainly include binary code, gray code coding and floating-point coding method, etc.Due to the improvement of fog drop quality, and the weight parameters in the image degradation model are within the scope of [0, 1], so the floating-point coding method to encode.

Using fitness in genetic algorithm to measure the concept the stand or fall of the individuals in groups, namely the optimal solution of the optimization calculation reaches the fine degree, it also known as the evaluation function and fitness function which is determined according to the objective function. It should first determine the fitness function of genetic algorithm to determine the image quality evaluation standard. Contrast as an important feature of image, it refers to the image of one of the most light gray and dark gray difference between range.

Experimental Results and Performance Analysis

In order to verify the effectiveness of the new algorithm based on improved physical model, the author takes a large number of experiments based on MATLAB platform.Aiming at the image of heavy fog weather conditions, experimental results of defogging shown in Fig1.From Fig1(b) to fog effect can be seen that after the algorithm processing image to fog effect is good and natural color.

(a) The fog-degraded image in heavy fog (b) The defogging effect of new algorithm

Fig.1 Experimental results comparisons of defogging

In order to verify the superiority of the new algorithm, the author uses a variety of algorithms, such as histogram equalization algorithm, single scale Retinex algorithm, compared with the new algorithm, experimental results of defogging shown in Fig2. Fig2 (b) is processing results after dealing with the histogram equalization algorithm. it is thus clear that gray scale image is reduced, obviously, it is not the results we expect.Fig2(c) is processing results after dealing with single scale retinex algorithm, Experimental results have little good, but there is no obvious advantages when handling image contrast, although there are obvious enhancement after processing boundary, but cannot eliminate the "fog" feeling.Fig2(d) is processing results after dealing with the new algorithm based on improved physical model, fog-degraded image is enhanced in different degree, it can reduce noise effectively, and at the same time, with a little loss of image detail.

(a)The fog image (b) Equalization algorithm (c) Single scale Retinex algorithm (d) The new algorithm

Fig.2 The comparison of various algorithms to mist effect

Conclusion

The paper combined with the characteristics of the image scene depth distribution, improved the fog image degraded model and proposed a novel defogging algorithm based on the improved model. The new algorithm uses good global search ability of the genetic algorithm and will implement the transfer from the scene defogging problem into the optimal estimation problem to the original and degraded images under global contrast optimal point. The experimental results show that the algorithm of defogging can not only realize the processing to single degraded image clearly, obtain ideal visual effect, but also can realize simply due to avoid solving the complex parameters such as depth and atmospheric scattering coefficient and so on.

Acknowledgement

In this paper, the research was sponsored by Youth Fund Project of Luoyang Institute of Science and Technology (Project No. 2013QZ02).

References

[1] Mathieu Carnec,Patrick Le Callet. Objective quality assessment of color images based on a generic perceptual reduced reference[J]. Signal Processing: Image Communication . 2008 (4)

[2] Nicolas Hautiere and DidierAubert. Contrast Restoration of Foggy Images through Use of an onboard Camera. Proceedings of the 8th International IEEE Conference on the Intelligent Transportation Systems.J. 601-606 (2005)

[3] YoavYSehoehner. Instant Dehazing of Images Using Polarization.Proeeedings of IEEE Computer Society Conferenee Commuter Vision and Pattem Reeognition. L: 325-332 (2001)

[4] Kai-Qi Huang,Qiao Wang. Natural color image enhancement and evaluation algorithm based on human visual system[J]. Computer Vision and Image Understanding.2006 (1)

[5] OAKLEY JP .Improving image quality in poor visibility conditions using a physical model for contrast degradation.J.IEEE Transactions on Image Processing.7 (2):167-179 (1998)

[6] Anat Levin,Dani Lischinski,Yair Weiss.A closed form solution to natural image matting. Proceedings of IEEE Conference on Computer Vision and Pattern Recognition . 2006

[7] Kaiming He,Jian Sun,Xiaoou Tang.Single image haze removal using dark channel prior. IEEE Conference on Computer Vision and Pattern Recognition . 2009

Advanced Materials Research Vols. 989-994 (2014) pp 2488-2490
© (2014) Trans Tech Publications, Switzerland
doi:10.4028/www.scientific.net/AMR.989-994.2488

The Evaluation of Teaching Quality based on Fuzzy Method

Juan ZHU[1, a], Jiya TIAN[1, b], Junhong HAO[1, c], Shuyan ZHANG[1, d]

[1]Electric Information College of Changchun Guanghua University,Changchun,130031,China

[a]email: zhuj_guanghua@126.com, [b]email:42683387@qq.com, [c]email: 57936975@qq.com, [d]email:35460867@qq.com,

Keywords: Evaluation; Teaching Quality; Fuzzy Method

Abstract. For the problems that the street running state and information was difficult to feedback and reasonable control, we apply the topology model to the street lighting management system, and complete the optimization control in this paper. Using the fuzzy control theory to handle the road signals, the intelligent lighting region controller integrates the thyristor chopper with the autotransformer technology, carries out the soft start and slow slope control to the street light, and realizes automatic voltage and energy saving. At finally, the system can realize the energy-saving control and intelligent, networked management of city street lamp.

Introduction

In order to improve teaching methods, to make better use of modern method and further improve the quality of teaching, students' evaluation of teaching has been more and more widely used in college. If teachers cannot be assessed and evaluated comprehensively and scientifically, the positive effects will be fallen back, which the negative functions will highlight. In recent years, schools are in the implementation of "students' evaluation of teaching". However, because of the unreasonable processing of evaluation results, the process of teaching evaluation often exists in name only. This paper uses fuzzy method to solve the problem of result processing. This method can give a relatively accurate result of the evaluation tables.

Principle of Fuzzy Method

Fuzzy method is proposed by L.A.Zadeh in 1995. The basic principle is as follows: To evaluate a variety of factors of one thing, firstly, we should divid the factors into some big factors according to a particular attribute, and then synthetically evaluate the big factors juniorly, then seniorly synthetically evaluate the results of junior results. The evaluate process using single level model is generally as follows.

1. Build the factors of evaluated object

Propose $u_i\left(i=1,2,\cdots n\right)$ is the factors of the evaluated object. We can express the factors as follows:

$$U=\left\{u_1,u_2,\cdots u_n\right\} \tag{1}$$

Factors are the attributes or performances of the object. The factors can express the quality of the object. The factors in this paper is the evaluation index.

2. Build the evaluate results of the evaluated object

Propose $v_i\left(i=1,2,\cdots m\right)$ is the evaluate result of the evaluated object. We can express the results as follows:

$$V=\left\{v_1,v_2,\cdots v_m\right\} \tag{2}$$

The results could be some datas or some words. That is the results could be fuzzy or non fuzzy. But their relationship with the results is clear.

3. Build the sigle factor evaluate matrix

For a single factor u_i, it has a degree of importance to the evaluate results, which is called membership to the results. The membership is marked as $r_{ij}\left(j=1,2,\cdots,m\right)$. The single factor evaluate matrix is marked as R.

$$R=\begin{vmatrix} r_{11} & r_{12} & \cdots & r_{1m} \\ r_{21} & r_{22} & \cdots & r_{2m} \\ \vdots & \vdots & \vdots & \vdots \\ r_{n1} & r_{n2} & \cdots & r_{nm} \end{vmatrix} \tag{3}$$

4. Determine the weight of evaluation factors

Objective weights are very import for the evaluate process. Generally we compose the weights using statistics experiment. Propose the weights is $A=\{a_1,a_2,\cdots a_n\}$.

Where $\sum_{i=1}^{n} a_i=1, a_i\geq 0$ (4)

5. Fuzzy comprehensive evaluation

When A and R is known, we can get the fuzzy evaluate as follows:

$$B=A\cdot R \tag{5}$$

Where $B=\left(b_1,b_2,\cdots,b_m\right)$ which is called fuzzy evaluate results. If $\sum_{i=1}^{m} b_i\neq 1$, it should be normalized by the formula

$$B'=\left(\frac{b_1}{\sum_{i=1}^{m} b_i},\frac{b_2}{\sum_{i=1}^{m} b_i},\cdots,\frac{b_m}{\sum_{i=1}^{m} b_i}\right) \tag{6}$$

Evaluate Experiment

Now we use the evaluate method to evaluate the effect of teaching.The factors is $U=\{u_1,u_2,u_3,u_4\}$. u_1 is the level of teaching. u_2 is teaching attitude. u_3 is teaching method. u_4 is the teaching ethics. The results is $V=\{v_1,v_2,v_3,v_4\}$, v_1 is excellent. v_2 is good. v_3 is middle. v_4 is pass. The weight of evaluation factors is $A=\{a_1,a_2,a_3,a_4\}$. According to the statistics experiment, we can give the values as $A=\{0.4,0.3,0.2,0.1\}$.Then we statistic the results from students. For example, from one class, to the single factor level of teaching, 30 percent of the sutdents gives excellent, 45 percent gives good, 20 percent gives middle and 5 percent gives pass. So to the factor u_1, the membership is $\{r_{i1},r_{i2},r_{i3},r_{i4}\}=\{0.3,0.45,0.2,0.05\}$. So the fuzzy comprehensive evaluation result is

$$B=A\cdot R$$

$$=(0.4,0.3,0.2,0.1)\begin{bmatrix} 0.3 & 0.45 & 0.2 & 0.05 \\ 0.4 & 0.4 & 0.1 & 0.1 \\ 0.35 & 0.5 & 0.1 & 0.05 \\ 0.5 & 0.4 & 0.1 & 0 \end{bmatrix}$$

$$=(0.36,0.44,0.14,0.06)$$

Normalized result is $B'=B=(0.36,0.44,0.14,0.06)$

From the result we can get the quality of classroom is good.

The above example is a simple experiment of low dimensionality. When the dimension is large, the calculation will be more complicated. But the basic priciple is the same as the above example. In fact, there are a lot of students evaluating teachers' index. Generally, the level of teaching is composed by content of courses, teaching ideas, teaching schedule, blackboard design, personal ability and so on. Teaching attitude is composed by preparation conditions, affinity degree, punctual, serious and so on. Teaching method is composed of interaction between teachers and students, inspire students, humor, using multimedia and so on. Teaching ethics is composed by be a model for others and strict management. We call this two level index.

In this condition, we should first calculate the scores for the factors. For example, the weight of u_1 evaluation factors is $A_1 = \{a_{11}, a_{12}, a_{13}, a_{14}, a_{15}\}$. Suppose the scores is percentile. The statistical membership is got. We can get the u_1 score of one student by:

$$C_i = \sum_{i=1}^{5} a_i s_i$$
$$= 0.25 \times 90 + 0.2 \times 87 + 0.2 \times 95 + 0.2 \times 98 + 0.15 \times 82$$
$$= 90.8$$

So the score is calculate as excellent. Calculate the scores of every student to get how many student gives excellent, how many gives good, how many gives middle and how many gives pass. They are recorded as r_1, r_2, r_3, r_4 ,so we can get the $\{r_{i1}, r_{i2}, r_{i3}, r_{i4}\}$ as

$$r_{i1} = \frac{r_1}{r_1 + r_2 + r_3 + r_4}, \quad r_{i2} = \frac{r_2}{r_1 + r_2 + r_3 + r_4}, \quad r_{i3} = \frac{r_3}{r_1 + r_2 + r_3 + r_4}, \quad r_{i4} = \frac{r_4}{r_1 + r_2 + r_3 + r_4}$$

Then use the method above to get the finally score of a teacher.

Of course, we can give more index for the scores to describe a teacher's grade more accurately. The Method of performance evaluation is a good topic for further study. In this paper, only a simple evaluation results are given. The evaluation process is the focus of this article.

Summary and Ackowledgement

Fuzzy method can gives a relatively accurate result for the evaluation of teaching quality process. To make the students' evaluation of teaching more comprehensively and scientifically, this paper chooses fuzzy method to calculate the evaluation result. Relatively accurate result can make the teachers better know about himself and make the teaching process more effectively.

I would like to express my gratitude to all those who have helped me during the working of this thesis. I gratefully acknowledge the finding of this study by the Education Science of Jilin Province project(ZC13131 and GH12351).

References

[1] MENG Guangwu. The basic theory of fuzzy mathematics and its application[J], Liaocheng Normal University (natural science edition),2011(15).

[2] LI Xia, CHENG Xiaohong, DONG Yanrong. Research in the exhibition industry of fuzzy comprehensive evaluation based on AHP[J], Heilongjiang science and technology information, 2002:98-161.

[3] WANG Jianshe, ZHANG Pingli. Application of fuzzy comprehensive evaluation method in theevaluation of real estate surveying and mapping [J], Heilongjiang science and technology information, 2011(29):82-83.

[4] YANG Qiyue, LI Jian. The innovation performance evaluation index system of scientific researchinstitutions in Guizhou Province Based on fuzzy comprehensive evaluation method[J]. Science and technology information development and economic. 2011(13).

[5] WANG Weiwei, Fuzzy comprehensive evaluation method in both research and application of energy transformation in public buildings[J]. The wizard rich technology.2011(18).

Advanced Materials Research Vols. 989-994 (2014) pp 2491-2494
© (2014) Trans Tech Publications, Switzerland
doi:10.4028/www.scientific.net/AMR.989-994.2491

Identical Distributed Pairwise NQD Random Variables Sequences with A Novel Mutation Operator

Jian Cao[a], Gang Li[b], Cenrui Ma[c]

Air Force Engineering University, Xi'an, Shaanxi Province 710051, P.R. China

[a]cao_jian1972@163.com, [b]LiGang@163.com, [c]yancong192@qq.com

Keywords: Pairwise NQD; Mutation; Service; Random Variables Sequences

Abstract. We study the strong stability of linear forms of pairwise negatively quadrant dependent (NQD) identically distributed random variables sequence under some suitable conditions. To overcome the weakness of collaborative services ability in different grid portal, a new grid portal architecture based on CSGPA (Collaborative Services Grid Portal Architecture), is proposed. This paper aims to enhance the performance of PSO in complex optimization problems and proposes an improved PSO variant by incorporating a novel mutation operator. The results obtained extend and improve the corresponding theorem for independent identically distributed random variables sequence.

Introduction

PSO is a recently proposed intelligent search technique, which was inspired by the social and cognitive behavior of swarm. As mentioned before, PSO as well as EAs are population-based random search algorithms, which usually start from a set of initial members or particles (called initial population) and towards the global optimum by executing iterative operations. In PSO, each particle has two features: velocity and position. The velocity determines the step size of movement every generation, and the position represents a candidate solution in the search space. Every generation, PSO utilizes a velocity and a position updating equation to recalculate the new velocity and position of each particle. When a particle moves in the search space, it remembers its previous best position (called pbest) and the global best position (called gbest) found so far. PSO's social and cognitive behavior is based on these two particular particles. The grid is a giant supercomputer of high efficiency, which integrates the distribution system and heterogeneous computing resources, and it provide the full sharing of computing resources, storage resources, data resources, information resources, knowledge resources, expert resources, and equipment resources. Grid Service is the use of grid services for users. In this paper, GDT is used to establish the database grid service for handling and processing the distributed, heterogeneous database.

At present, data of each application fields is increasing at an amazing speed. In the real application environment, most of massive databases exist in the form of distribution. If the distributed data was concentrated into a data warehouse for mining deal, it will pose a threat to the distributed data's security and privacy, and further reduce the efficiency of mining, but also make a higher requirement of network communication bandwidth. It becomes an urgent requirement to achieve sharing among the distributed and heterogeneous database resources.

Database grid service can support high-performance needs and data distribution well, and store, manage huge amounts of data more effectively, and analysis and handle a large number of heterogeneous distributed database resources more efficiently. Database grid service has many applications features, such as data-intensive, data resource diversity and heterogeneity, large-scale collaboration with the local control rather than global control, data security, load balancing of data resource access, etc. Clients interact through the appropriate database grid services and data service resources. The database grid encapsulates the function that need to use Web Service interface to open data services resources.

The notion was proposed by statisticians Lehmann[1] in 1966, pairwise NQD sequences form an important class of dependent random variables and have wide applications in probability, statistics,

finance, economy and other subjects and real problems. Usually, the independent random variables sequence is special case of pairwise NQD sequence, so it is more difficult to study pairwise NQD sequence. Some authors have studied pairwise NQD sequences and a great number of papers on them appeared in literature. For example, Lehmann[1] discussed the applications of pairwise NQD sequence in statistics, Matula[2] gave the Kolmogorov-type strong law of large numbers of sums of pairwise NQD sequences, which were the same as independent sequences case. Wu[3] extended the Kolmogorov-type inequality to the case of pairwise NQD random sequences, and studied the convergences properties of pairwise NQD sequences by Borel-Cantelli lemma. Wan[4] and Zhang and Wang[5] studied the law of large numbers and the complete convergences, the results obtained were the same as independent sequences case. Chen[6] studied the Kolmogorov-Chung type strong law of large numbers for pairwise NQD random sequences. By the promoting of strong law of large numbers, and considering the compatibility of least squares estimation of the linear model, it is need to discuss the strong stability of linear forms, so many authors discussed it. Wan and Chen[7] discussed the strong stability of linear forms with pairwise NQD random sequences by the properties of pairwise NQD random sequences, Borel-Cantelli lemma, kronecker lemma, the results were as follows as Fig.1.

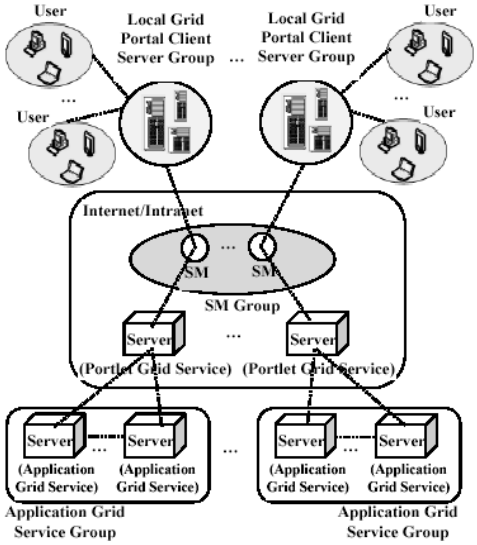

Fig.1 Application system architecture based on Identical Distributed Pairwise NQD Random Variables Sequences (IDPNRVS)

Database Grid Service Introduction

The architecture of collaborative services grid portal is shown in Fig.2. Its operating mechanism is as follows.

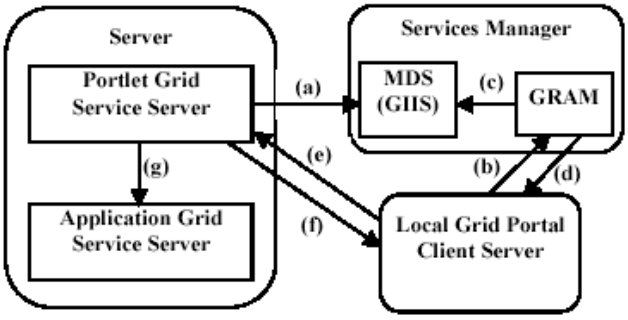

Fig.2 Architecture of CSGP

Hardware Circuit Design

The Central Processing Unit (CPU) applies the industrial chips of MC9S08 AC16, which are industrial eight-digit single-chip microprocessors with ultra-low power consumption. This type of

chips internally integrate a 16K-byte FLASH and a1k-byte RAM memory with SPI interface, A/D conversion circuit. System framework based on multi-layer network architecture is shown in Fig.3.

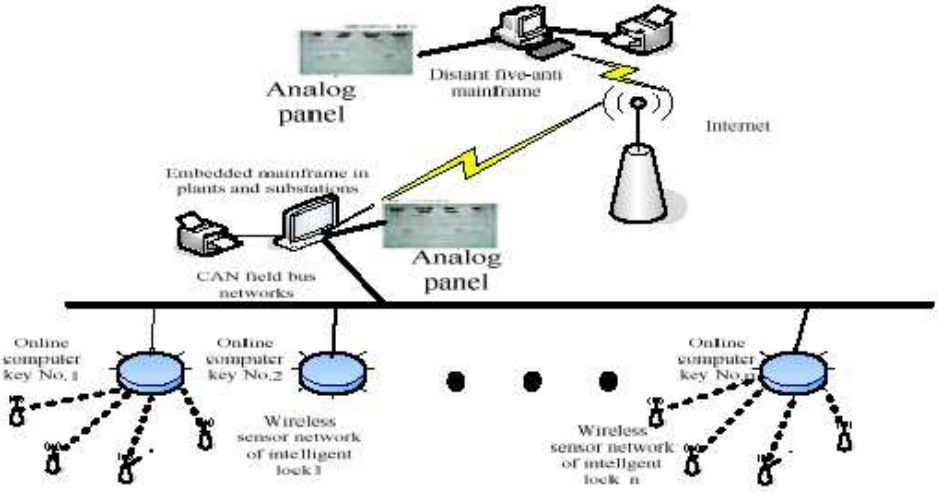

Fig.3 System framework based on multi-layer network architecture

CC2430 has small number of external components. It employs an unbalanced antenna to connect the unbalanced transformer so as to make the antenna have better function.

The parts of hardware in detail are designed as Fig.4.

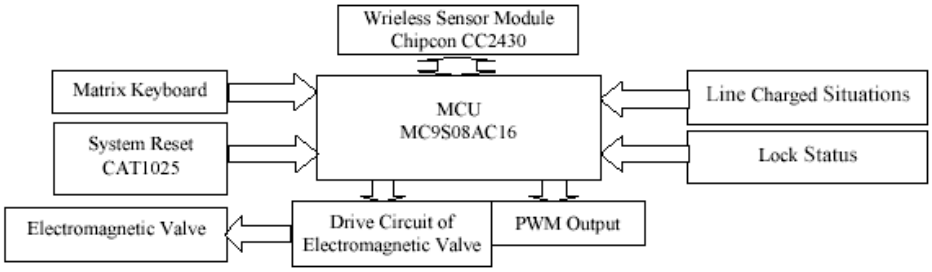

Fig.4 Hardware system framework

In the collaborative services grid portal architecture, a server can allow running many Port let grid services, and of course, the whole architecture also allow existing many Port let grid services which provide the same function, some Port let grid service can access the corresponding one or more application grid service. By this means, Port let grid service can mainly process the display logical. Port let grid service provide an interface service to the terminal users of the grid portal, while the gird resource that terminal users need to access and use, is provided by the application grid service running on the other server. In this way, we can separate the display logic from the application logic in grid portal better. In the whole grid portal system based on collaborative services grid portal architecture, the amount of the servers of running Port let grid service can be dynamic change, but they don't have the close connection between the each Port let grid service server, so any one server goes wrong, it will not influence the normal operation of the whole architecture. To the requestors, because of each Port let grid service is developed based on the standard, so the requestors are very convenient to plug Port let grid service in grid portal itself by configuration, and don't need to add other program code.

Conclusion

In the theorems of this paper, we study the strong stability of linear forms in identically distributed pairwise NQD random variables sequences, and get sufficient conditions of strong stability of them by the truncation in random variables. The theorems in this paper extend and improve the corresponding theorems for independent identically distributed random variables.

Collaborative services grid portal architecture is presented in this paper. Through our study, analyze and evaluation contrast to the architecture, we can find that the architecture is clearer than some current grid portal architectures, and it improves the scalability and reusability of the grid portal. The emphases of next step work are to solve the dispatching problem in the case of the large number of concurrent and the many-to-many relationships problem of grid service.

References

[1] E. L. Lehmann, “Some concepts of dependence,” Ann. Math. Statist. vol.37, pp. 1137–1153, October 1966.

[2] P. Matula, “A note on the almost sure convergence of sums of negatively dependent random variables” Statist. Probab. Lett. vol.15, pp. 209–213, October 2012.

[3] Q.Y. Wu, “Convergence properties of pairwise NQD random sequences,” Acta Math.Sin.vol.45, pp. 617–624, June 2012.

[4] C.G. Wan, “Law of large numbers and complete convergence for pairwise NQD random sequences,” Acta Math. Appl. Sin. vol.28, pp. 253–261, June 2005.

[5] L.X.Zhang, J.F.Wang, “A note on complete convergence of pairwise NQD random sequences” Appl. Math. J. Chinese Univ. Ser. A. vol.19, pp. 203–208, June 2004.

[6] Y.P. Chen, “On the strong law of large numbers for pairwise NQD random variables,” Acta Math. Sin. vol.25, pp. 386–392, June 2005.

[7] Fernando Bellas, “Standards for Second-Generation Portals,” IEEE Internet Computing, vol.8, pp. 54-60, February 2004.

Advanced Materials Research Vols. 989-994 (2014) pp 2495-2498
© (2014) Trans Tech Publications, Switzerland
doi:10.4028/www.scientific.net/AMR.989-994.2495

Improving performance of Wireless-Optical Broadband Access Network by Interpolation Algorithm of Zadoff-Chu Sequence

Jian Cao[a], Cenrui Ma[b], Xiaojiang Hu[c]

Air Force Engineering University, Xi'an, Shaanxi Province 710051, P.R. China

[a]cao_jian1972@163.com, [b]yancong192@qq.com, [c]Huxiaojiang@163.com

Keywords: Failure Detection; Design; Zadoff-Chu Sequence; Wireless-Optical Broadband Access

Abstract. HF channel sounding requires perfect autocorrelation property of the sounding sequences. Compared with other pseudonoise sounding sequences, Zadoff-Chu sequence gets great attention due to its predominant periodic autocorrelation property. A Wireless-Optical Broadband Access Network (WOBAN) is gaining more attention because its good performance and merits such as reliability, robustness and high capacity as well as flexibility. There are many factors that can affect the network performance, such as delay, packet loss and capacity utilization. Application examples show that, this system can significantly improve the efficiency of aerodynamic design.

Introduction

Currently, with the growing demand for development of space resources and increasingly fierce competition of commercial satellite launch market, the next generation launcher with high-performance and low-cost is becoming research focus in many countries. Modular design is considered to be the future direction of launch vehicle. It decomposes the launcher into several standard modules. By combing different modules, various capabilities launch vehicle would be assembled to meet different payload requirements. Therefore, the development cycle will be significantly shortened, the costs will be lower, and reliability will be enhanced. Aerodynamic performance of launch vehicle mainly depends on their shape exposed to the air. It also affects other characteristics of launch vehicle, such as trajectory, flight stability, mechanical properties, etc. R&D of Launch vehicle is facing combinatorial explosion problem caused by modular design. That is to say, the possible number of launch vehicle is much more than the number of modules.

A Wireless-Optical Broadband Access Network (WOBAN) is a hybrid of wireless networks and optical networks [1] with passive optical networks (PON) in its backend and wireless mesh networks (WMN) to supply end users with the access.The head terminal of PON resides at Central Office(CO) which is driven by Optical Line Terminal (OLT), while the tail end consists of Optical Network Units (ONU). ONUs connect to wireless Base Stations (BS) which form a multi-hop wireless mesh networks. Some BSs are called gateway routers, of which the location is critical. The end user sends packets or messages to one of neighborhood BS (or called routers). This BS then sends the packet into wireless mesh of WOBAN. The packet will reach the optical backbone through OLT/OC in the manner of multiple hops. The upstream of WOBAN in the wireless end is anycast while the downstream of WOBAN in the wireless end is unicast. This architecture can heal and organize itself with help of wireless mesh networks. The architecture is shown as Fig.1. Through this combination, WOBAN can achieve the merit of both wired and wireless networks: it obtains the characteristics of reliability, robustness and high capacity as well as flexibility [2]. Because packets need to experience several hops, the architecture is definitely subject to the delay. The larger the mesh of WOBAN, the more hops, thus the more delay generated. To handle the problem of delay, Delay-Aware Routing Algorithm (DARA) [3] is carried out. DARA can achieve better load balancing and congestion reduction. Some other efficient algorithms are also proposed, such as Minimum-Hop Routing Algorithm (MHRA), which is intended to minimize the hop number; Shortest- Path Routing Algorithm (SPRA), which is intended to find the shortest path; Predictive-throughput routing algorithm (PTRA) and Capacity and Delay Aware Routing Algorithm (CaDAR) [4]. Among these solutions, CaDAR is the best algorithm for WOBAN. Similar to other algorithms, it accounts for

delay as its first priority. Moreover, it introduces one new concept: capacity assignment. So it is one optimal solution to find the balance point between capacity assignment and flow assignment. Our objective is to find a solution that can improve the bandwidth efficiency as well as reduce the packet loss[5]. In this way, if one OLT or ONU is down, the algorithm can detect the problem and make self healing to redirect to the adjacent link. Moreover, this algorithm also eliminate the probability that the flow on one link is higher than the threshold, thus ensure the minimum delay.

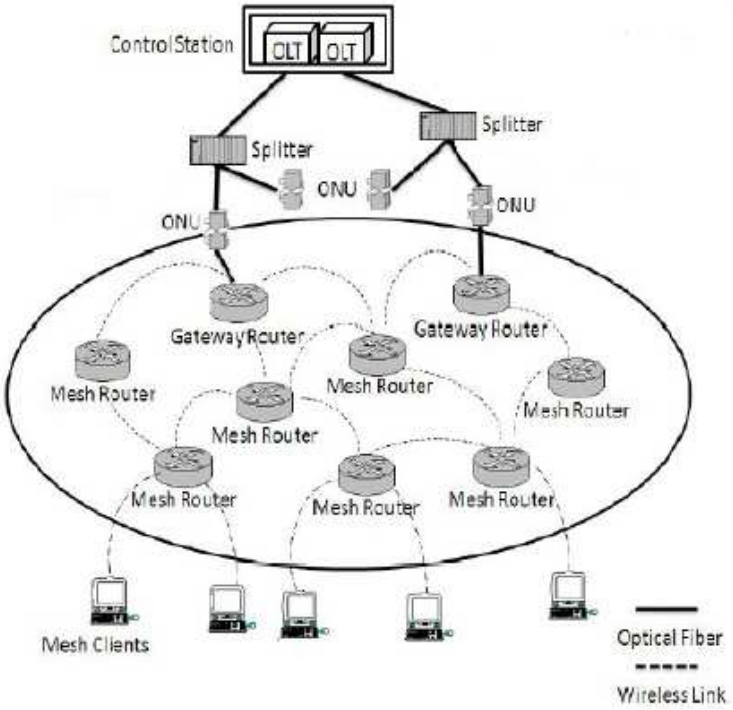

Fig.1 The architecture of WOBAN network

Load Balancing

If we only consider one aspect of the network constraints, other aspects of the network performance pay affect the whole performance. Take delay for example. If delay is the only factor for the algorithm, congestion will occur if most packets select one single link whose link weight is minimum for transfer. We call this load congestion. In our algorithm, we set the link capacity and LSR for each link, which ensures that the load on one link cannot cause the load congestion and also ensures that the network can detect the link failure on time. So FLRAR helps to achieve the load balancing in the network. We show this in Fig.2.

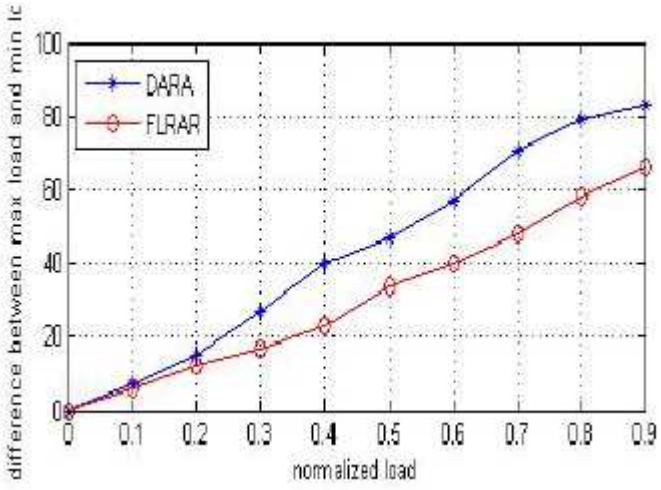

Fig.2 Comparison for load balancing

Motion Control Section

Fig.3 shows the spectra of Zadoff-Chu sequence respectively interpolated by FDIA and commonly used interpolation algorithm with L=1024 and k=1. From the figure we can see that although the spectrum of the sequence interpolated by the commonly used interpolation algorithm is compressed, it has many big side-lobes and rolls off slow. And that the spectrum of the sequence interpolated by FDIA is almost no big side-lobes and rolls off fast. So the sequence energy is centralized, which make it satisfy the bandwidth requirement of HF channel sounding transmitter-receiver.

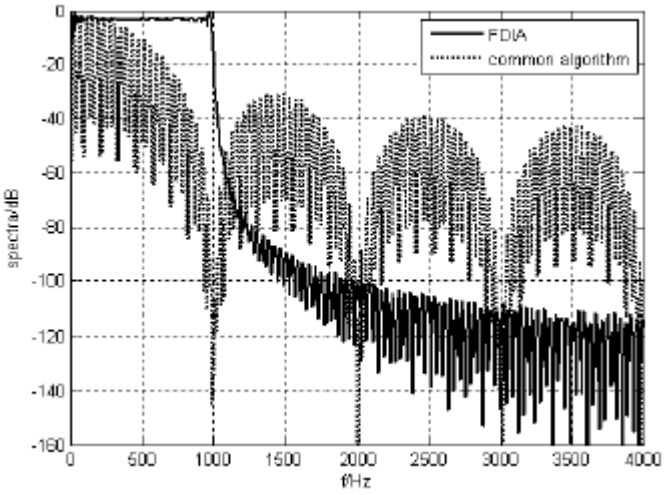

Fig.3 Spectra of sequences respectively inserted by FDIA and commonly used interpolation algorithm

System Software Design

PC software is developed with VC++6.0 that of good interactive interface, enable the system to control in realtime. In motor control section, through the user interface the user can undertake POST (power on self test), path planning, track planning path and so on. The program flow diagram shows as Fig.4. The user can arrange what to do, and how to do because of VC++6.0 based on events programming, with response of events set through good interface, such as when clicked on a button, then the program execute button operation responded.

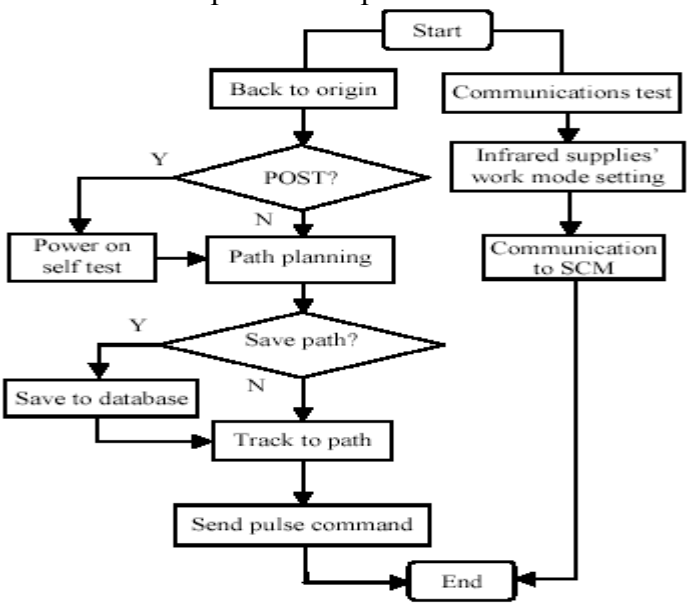

Fig.4 Programm flow diagram

When the program is running, the first to do is initialization, upper computer software communicates with single-chip microcomputer firstly to determine whether it works properly, which

can be shown in the user-interface, at the same time moving infrared light supply under control is carried by slider back into origin to ensure the whole motion correction; Then the user can select POST which can track a predetermined path to check whether the system is working normally. Users can draw route planning with the existing lines, rectangular, circle planning in the picture box of software, after successful design software can save track data in a database, and infrared supply can track the path also in directly. The software can support user-defined trajectory, user select multiple points to draw path planning, which can draw any graphics.

Conclusion

WOBAN is an effective architecture as it combines the merit of both wired and wireless network: reliability, robustness and high capacity as well as flexibility. However, ineffective routing algorithm can cause the declination of the network performance. so it is good to improve the scalability of the network. In HF channel oblique sounding, the selection or design of sounding sequences is a key technique. The paper investigates the periodic autocorrelation property of Zadoff-Chu sequence based on the introduction of the definition and properties of CAZAC sequences. Aiming at resolving the problem that the spectrum of Zadoff-Chu sequence is not band-limited which makes it be not suitable for transmission in HF channel, the FDIA is proposed in the paper by which the amplitude frequency characteristic of Zadoff-Chu sequence can be enhanced. At the same time, an effective method of achieving optimal decimation of the Zadoff-Chu sequence interpolated by FDIA is provided. In the control process, it is convenient to process all necessary parameter setting and adjustment, and in the control process of the whole system shows superior performance and achieves the expected effect.

References

[1] ZHANG Jian-hua, FENG Chong, LIU Yi and ZHANG Yan-yan. “Time Synchronization Algorithm for MIMO OFDM Systems,” Journal of Beijing University of Posts and Telecommunications, vol. 32, no. 1, pp. 118-121, Feb.2012.

[2] R.L. Frank and S.A. Zadoff. “Phase shift pulse codes with good correlation properties,” IRE Transactions on Information Theory, vol. IT-8, pp. 381-382, Oct. 1962.

[3] D. C. Chu. “Polyphase codes with good periodic correlation properties,” IEEE Transactions on Information Theory (Corresp.), vol. 18, no. 4, pp. 531-532, July 2002.

[4] K. Andrew, K. Ioannis, J. B. John, M. R. Dellomo and J. M. Sieracki. “Ambiguity and sidelobe behavior of CAZAC coded waveforms,” IEEE Radar Conference, pp. 99-103, April 2007.

[5] L.X.Zhang, J.F.Wang, “A note on complete convergence of pairwise NQD random sequences” Appl. Math. J. Chinese Univ. Ser. A. vol.19, pp. 203–208, June 2004.

Advanced Materials Research Vols. 989-994 (2014) pp 2499-2502
© (2014) Trans Tech Publications, Switzerland
doi:10.4028/www.scientific.net/AMR.989-994.2499

Image Fusion Algorithm by Improved Chaos Immune Genetic Algorithm in Multi-wavelet Transform Domain

Jian Cao[a], Tifang Li[b], Yupeng Gao[c]

Air Force Engineering University, Xi'an, Shaanxi Province 710051, P.R. China

[a]cao_jian1972@163.com, [b]yancong192@qq.com, [c]Gaoyupeng@163.com

Keywords: Algorithm; Mutation; Swarm Intelligence; Structure

Abstract. In order to make full use of texture features of image when fusing images, and taking into account the inherent advantages of fractal theory in this respect, a novel image fusion algorithm, which used fractal dimension and directional contrast, based on multi-wavelet transform was proposed in this paper. So, we put forward a new design of the intelligent lock which is mainly based on the technology of wireless sensor network. Particle swarm optimization (PSO) is a recently proposed intelligent algorithm which is motivated by swarm intelligence. PSO has been shown to perform well on many benchmark and real-world optimization problems; it easily falls into local optima when solving complex multimodal problems. Moreover, the objective indexes, which are image entropy, standard deviation and quality measure, were adopted to evaluate the comparative results of evaluating fusion quality. To avoid the local optimization, the algorithm renews population and enhances the diversity of population by using density calculation of immune theory and adjusting new chaos sequence.

Introduction

Fusion algorithm decomposed original images needed to be fused by multi-wavelet transform firstly, then fractal dimensions of the corresponding decomposing low-frequency coefficients were calculated by Differential Box Counting method, and the low frequency fusion rule based on fractal dimension was set up. The high frequency parts were fused by selecting method or weighted averaging method according to the directional contrast values. The fusing experiment using this algorithm to IR image and visible light image was done. In order to illustrate the performance of the algorithm, particularly the impact of introduction of fractal theory on the fusion performance, the result of those fusion algorithms that only uses multi-wavelets transform were given as well. The results show that the leading of fractal dimension into image fusion processing is effective, and it performs obviously better in increasing the amount of information, the standard deviation and the quality of fused image. Under these situations designing a reasonable on-line computer anti-lock system is an alternative to solve the current problem[1] [2].

The image fusion, which is to synthesize the information from multiple image sensor in multi-levels which are pixel-level, feature-level, and decision-level, aims to obtain the more accurate, comprehensive and reliable image description of the same scene. With the advances in image processing technology and social development, image fusion is playing an increasingly important role in military and civilian fields. There has been a lot of fusion algorithms adopted multi-resolution decomposition idea in the research of image fusion [3][4]. Multi-wavelet transform has the better performance than traditional wavelet transform because of orthogonality, smoothness, symmetry, limited support and other characteristics that multi-wavelet system has at the same time. Fractal theory is a very active branch of modern mathematics and nonlinear science, and it plays a more and more important role in digital image processing[5]. It can be found that there are a large number of research reports on natural image modeling, image texture analysis and so on making use of fractal theory to analyze and study.

This paper proposes an pixel-level image fusion algorithm that combines multi-wavelet transform and fractal theory. Thus, the fusion not only takes the image high frequency and low frequency performance into account, but also the utilization of the image texture characteristics such as

roughness. It results in more comprehensive and scientific consideration for the image information in the fusing process.

Software Design of Intelligent Lock

The wireless sensor modules adopt the independent single chips to control the FR chips, so under the terms of the agreement are met, the software designing mainly consider how to establish the physical link between the intelligent locks as well as between the intelligent locks and on-line computer keys. The wireless transmission of control data and the specific control and inspection operations of the intelligent locks are solved by the application layer software. The software framework of the intelligent locks is shown as Fig.1.

Firstly, the on-line computer key scans for empty information channels to try to establish a new network. Once some empty information channel is found, it will select a random personal area network and start to monitor the channel; now the network is established.

If some operation is to be conducted, the on-line computer key will keep the data frames in indirect-sending buffer until the intelligent lock inquires or is timeout. The intelligent lock will be waken-up periodically and send the inquiry request to the on-line computer key, which will search the indirect-sending buffer. If one frame is found to wait to send to the joint, the on-line computer key will send the frame and wait for confirmation.

Algorithm flow chart is shown as Fig.2.

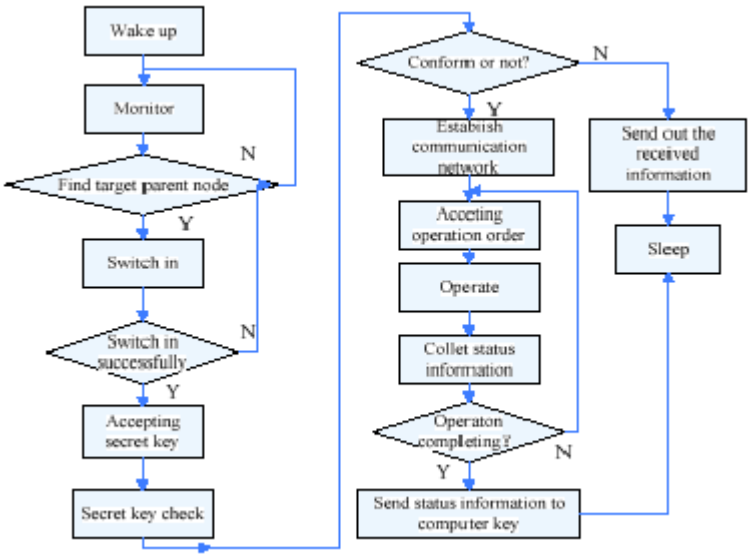

Fig.1 Wireless communication software structure diagram

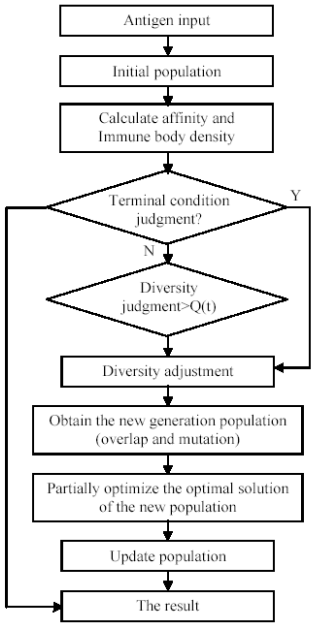

Fig.2 Algorithm flow chart

Scientific Basis for Fractal Theory used for Image Processing

Because fractal set can generate complex natural scenes by simple iterative method and effectively measure the complexity of object through fractal parameters, there is a natural relation between image and fractal. It is the relation that lays the basis of fractal theory using for image processing and opens up a new area of image application. Fractal dimension is a main measurement tool of fractal image processing technology, the most basic mathematical concept in fractal theory, and the most important aspect of the application of fractal theory. As we know, image texture is an important element of image analysis and processing. Image fractal dimension not only measure the complexity of image surface irregularities, but also has the invariance of changing in multi-resolution and multi-scale. It is consistent with the human visual perception of the degree of image surface texture roughness. The bigger the fractal dimension of image is, the rougher the image surface is. On the other hand, the smaller the fractal dimension is, the smoother corresponding image surface is. The experiments of cognitive science of human visual perception

show that people often focus on the degree of rule fragmentation and the profile of features when human eyes perceive the natural target, but neglect its general details. Large numbers of experiments show that fractal model, which has the ability to abstract the regular level of structure of object surface from a large number of varied details and has profound physical background, is a kind of statistical model. It is suitable for describing the research object that has complex and irregular shape. Therefore fractal model is significantly better than the conventional autoregressive and Markov texture model in the expression of low frequency component of image.

Simulation results are shown as Fig.3.

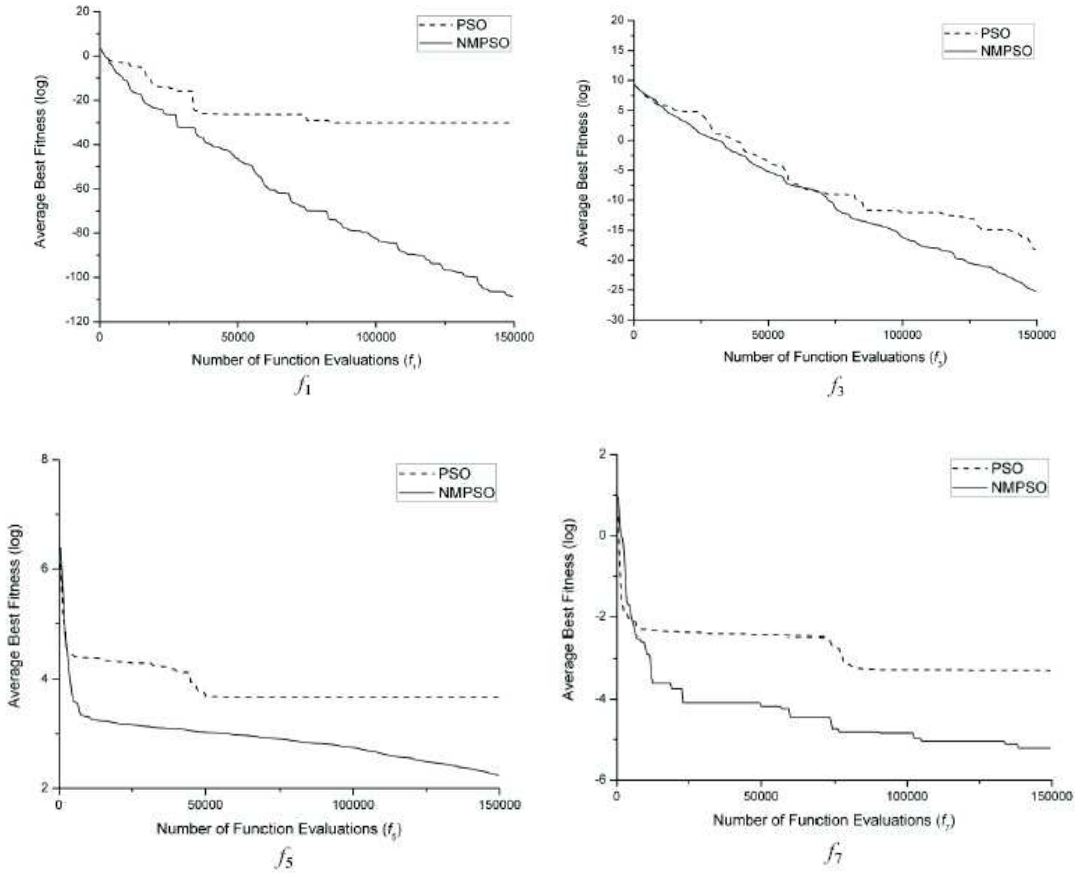

Fig.3 Evolutionary curves of standard PSO and NMPSO on four problems

Directional Contrast in Multi-Wavelet Domain

In order to validate the performance of the proposed fusion algorithm, simulation experiment for infrared image and visible light image was carried out by MATLAB 7.0 platform.

Conclusion

When fractal dimension of image is used to express the degree of irregularities of the image surface, it is consistent with human visual perception of surface texture roughness. Directional contrast of image is accordant with human visual when it reflects the change of image information. Multi-wavelet is able to decompose image into more abundant frequency information than traditional wavelet.

This paper presented a novel fusion algorithm that takes advantage of fractal dimension, directional contrast and multi-wavelet transform. Simulation results show that the algorithm is effective, particularly improves the quality of fused image because of the introduction of fractal dimension. It presents an improved PSO algorithm to enhance the performance of standard PSO. The proposed approach is called NMPSO, which embeds a novel mutation by incorporating with

the search information of the global best particle and other two random particles. It is to hope this improvement can help trapped particles jump to better positions. Simulation results on ten problems show that NMPSO not only achieves more accurate solutions than PSO, but also converges faster. However, NMPSO is not suitable for all kinds of problems, such as f5, f8 and f9, both PSO and NMPSO fail to solve these problems. To improve NMPSO further, we may introduce other search strategies. This will be investigated in our future work.

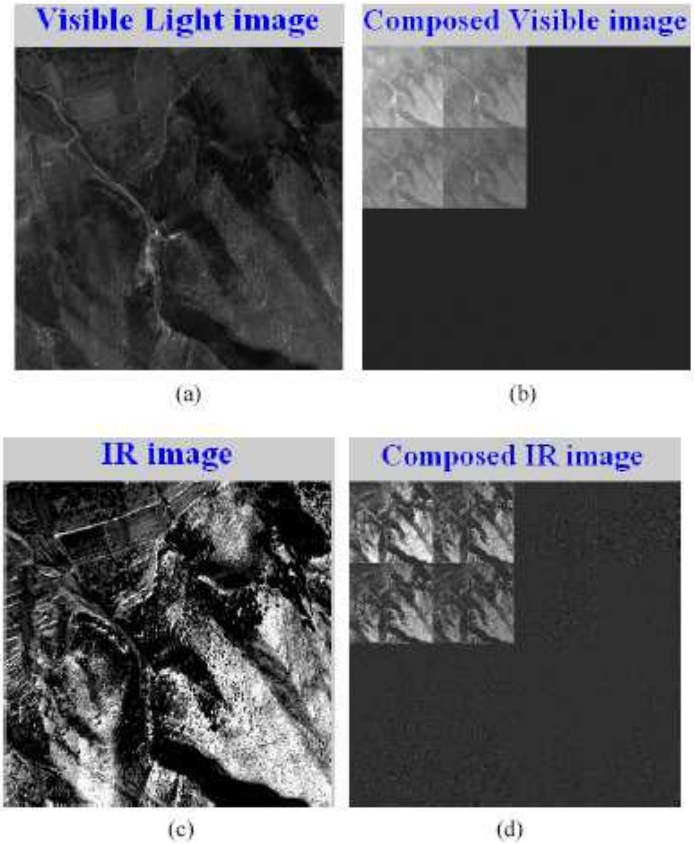

Fig.4 Original images and their multi-wavelet decompositionresults: (a)Visible image; (b)multi-wavelet decomposition of visibleimage; (c)IR image; (d)multi-wavelet decomposition of IR image.

References

[1] Olfa Nasaroui, Fabio Gonzdez, Dipankar Dasgupta .The Fuzzv Artificial Immune Svstem: Motivations, basic Concepts and Application to Clustering and Web Profiling[J].Fuzzy Systerm 2002,1(2):711-716.

[2] LEANDRO N, CASTRO DE TIMMIS J Artificial immune system: a novel computational intelligence approach[M]. Springe–Verlag 2012.

[3] JIAO Li-cheng,WANG Lei. .A novel genetic algorithm based on immunity[J]. IEEE Trans on Systems May and Cybernetics-Part A: Systerms an Humans 2010 30 (5): 552 SGI.

[4] Xiangxin Wu, ZhongChen. Chaos Study Introductory remarks. Shanghai Science and technology Publishing house. 2012

[5] L.X.Zhang, J.F.Wang, “A note on complete convergence of pairwise NQD random sequences” Appl. Math. J. Chinese Univ. Ser. A. vol.19, pp. 203–208, June 2004.

Advanced Materials Research Vols. 989-994 (2014) pp 2503-2506
© (2014) Trans Tech Publications, Switzerland
doi:10.4028/www.scientific.net/AMR.989-994.2503

Interpolation Algorithm Application Using Neural Networks for Flywheel Energy Storage System

Shaosong Wan[1,a], Jian Cao[2,b], Qunsong Zhu[2,c], Cong Yan[2,c]

[1]XiJing University, Xi'an, Shaanxi Province 710123, P.R. China

[2]Air Force Engineering University, Xi'an, Shaanxi Province 710051, P.R. China

[a]12156555@qq.com, [b]cao_jian1972@163.com, [c]yancong192@qq.com

Keywords: NN; Flywheel Energy Storage; Reluctance Machine; Interpolation

Abstract. This paper presented the key techniques development of motor/generator (M/G) for the FES system in recent years, and summarized the latest developments of three machines such as: induction machine (IM), reluctance machine(RM) and permanent magnet machine (PMM) including traditional structure PMM and Halbach structure PMM, which now widely used in the FES system. The characteristics of three machines had been compared and analyzed, which provides guidance for the FES field researchers to choose appropriate M/G.Then the comparison of spectra of the sequences respectively interpolated by FDIA and commonly used interpolation algorithm is conducted, which affirms the superiority of FDIA. Finally, an effective method of achieving best decimation of the sequence interpolated by FDIA is provided. All these lay primary theory foundation for the application of Zadoff-Chu sequence to HF channel sounding.

Introduction

CAZAC sequence with a length of N^2 (N is an integer) which was used in the Zadoff-Abourezk patent of a synchronizing system was first proposed by Frank in 1950s. The CAZAC sequence proposed by Frank was described afresh by Frank and Zadoff in. Based on the work of Frank and Zadoff, D[1]. Chu proposed a sort of CAZAC sequence without restriction on its length, that is, Zadoff-Chu sequence. And he proved that certain linear phase shift of the form exp(j2 π qk/ N), when introduced into the sequence will not affect its correlation property, where q , k and N are integers, and k is relatively prime to L[2].

In comparison with other ways, it introduced the advantages and the main application of modern high speed flywheel energy storage (FES). It discussed the composition and principle of FES system. Energy storage was an important way for effective utilization of energy, and it was a major direction to solve the energy crisis problem[3]. There were four energy storage modes, including pumped storage, storage battery, ultra capacitor and the FES. In comparison of table 1, we can see the FES has the advantages of long life, high power density, high energy storage densities, basically not be limited by times of charging and discharging, easy installation and maintenance, without pollution etc. So the FES was a new storage technique with wide application prospects. It was last century 50's that FES was used as a means of high-capacity, long time energy storage system, but limited of the technical conditions, until the 90's, the FES technique had entered into a new development stage of the "high-speed flywheel"[4]. It was gradually used in improving the power quality, power grid peak regulation, uninterruptible power supply (UPS), electric car batteries, aerospace, wind power generator and electromagnetic cannon short burst of high power etc[5].

Key Technique of M/G for FES System

The M/G and its control system was the core of the energy converting in a FES device. Wherever the application to, the M/G must combine the character of high efficiency motor and generator. So it needed to have the following advantages as far as possible: The system running in storage, keeping and release mode, what was presented in the last section, it required that M/G was reversible, can running in both motor and make the FES systems become effective energy storage media, which

requested high converting efficiency, high running speed, and the rotor can endure high speed, easy to high-speed operation, good speed regulation performance; In order to improve the load capacity, requested low rotor losses, low no-load losses and high output power, high torque output ability; Required the M/G has long life for uninterrupted operation; Also requested low cost, simple structure, reliable operation, easy maintenance, high power densities, good thermal stability.

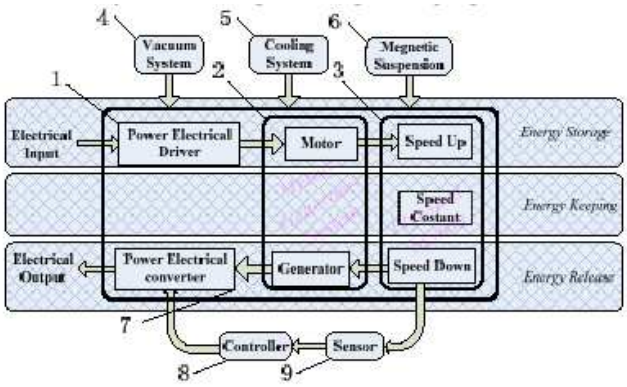

Fig.1 Typical structure block diagram of FES system

Fig.2 Photo type of 11kw IM

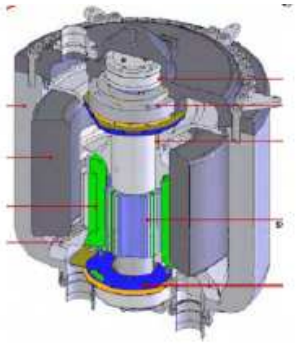

Fig.3 Photo type of GTX for UPS

Comparison of FDIA and the commonly used interpolation algorithm

Fig.4 shows the real parts and the imaginary parts of the original Zadoff-Chu sequence with L=32 and k=1 and of the sequences respectively 8 times interpolated by FDIA and commonly used interpolation algorithm. The real line represents the sequence interpolated by FDIA and the broken line represents the sequence interpolated by the commonly used interpolation algorithm.

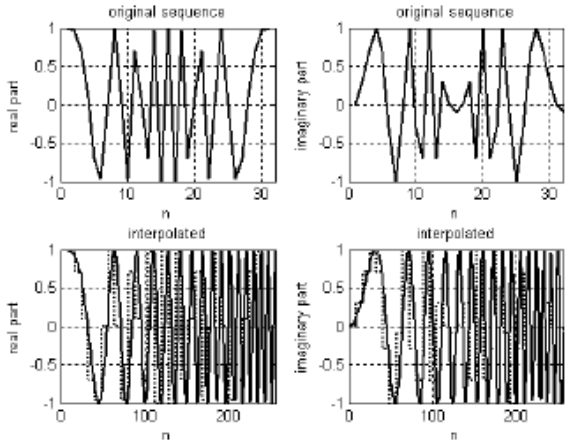

Fig.4 Waves of sequences respectively interpolated by FDIA (real line) and commonly used interpolation algorithm (broken line)

Motion Control Section

Motion control section can be divided into the control part and actuator, which is a classic servo closed loop position control, Motion control section diagram shown in Fig.5. Movement control card can receive PC control instruction, and the axes interface to be controlled send pulses to relevant servo controller to control motor rotation angle, and then ball-screw will convert rotation angle to horizontal displacement, so as to carry the infrared supply horizontal or vertical movement. The control part mainly includes movement control card, servo controller and so on, motor control command is sent through the PC software to regular the movement control card to produce the corresponding output pulse. The whole movement process need two axes motor control respectively, it is adequate for us to use the movement control card supported four axes, and available for circular interpolation, continuous linear interpolation, so the card can meet the equipment requirements. Actuator is a key part of the whole system, which is designed three-rail plane, including two horizontal rails and one vertical rail, ball-screw inside, which can drive the slider with infrared light supply to move in the whole plane. There at the edge of rail separately installs limit switch and origin switch to determine the origin and the maximum boundary. The parts of actuators in detail designed as Fig.6 shows.

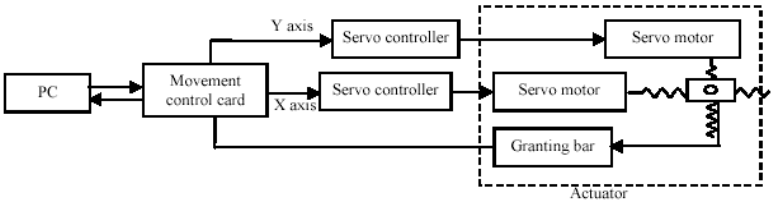

Fig.5 Motion control section

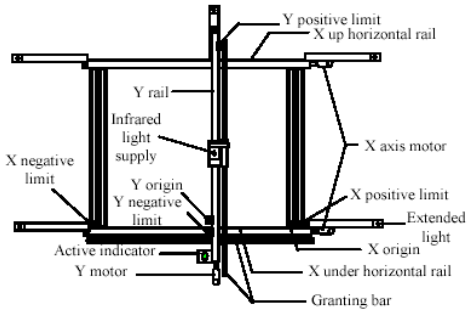

Fig.6 Part of actuator

Neural Network Augmented Model Inversion Architecture

This section details the architecture of the NN augmented model inversion as applied to the tiltrotor aircraft. Fig.7 contains a diagram of the architecture used for implementation of ACAH control in the pitch channel. The command filter serves both to limit the input rate, and as a model for desired response. This allows for straightforward implementation of ADS-33 handling qualities specifications. The presented architecture provides for excellent results in the longitudinal application, as is shown in following sections. Identical construction applies to the lateral channels.

The results in the lateral channels show similar performance.

Conclusion

From that on what had provided principle to select M/G for researchers of the FES system according to difference field or system request. With the rapid development of the FES system, M/G has wide development space, but at the same time, higher request has been put forward for the innovation of the M/G structure and the optimization of the algorithm of the control system.

The spectra of the sequence respectively interpolated by FDIA and commonly used interpolation algorithm have the same main-lobe width, but the spectrum of the sequence interpolated by FDIA has a faster roll-off and almost no big side-lobes, which means that it has a higher energy using ratio when transmission in narrow band HF channel. Hereby, this paper lays primary theory foundation for the application of Zadoff-Chu sequence to HF channel oblique sounding.

In the control process, it is convenient to process all necessary parameter setting and adjustment, and in the control process of the whole system the photovoltaic simulator shows superior performance and achieves the expected effect.

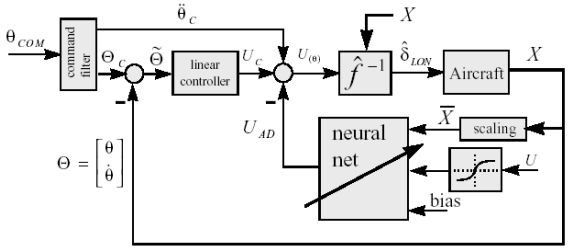

Fig.7 Adaptive NN augmented model inversion architecture in the longitudinal channel configured for ACAH

References

[1] J. B. John, D. Jeffrey, K. Ioannis and C. Shaw. “Zero autocorrelation waveforms: a Doppler statistic and multifunction problems,” Proc. of IEEE International Conference on Acoustics, Speech and Signal Processing.pp. 1117-1120, 2012.

[2] Li Chih-Peng, Huang Wei-Chieh. “A constructive representation for the Fourier dual of the Zadoff–Chu sequences,” IEEE Transactions on Information Theory, vol. 53, no.11, pp. 4221-4224,2007.

[3] The-Hanh Pham, Liang Ying-Chang, A. Nallanathan and H. K. Garg. “Optimal training sequences for channel estimation in bidirectional relay networks with multiple antennas,” IEEE Transactions on Communications, vol. 58, no. 2, pp.474-479, 2010.

[4] Fuqin Xiong. Digital Modulation Techniques, Artech House, INC, Boston, USA. pp. 129, 2010.

[5] Y.P. Chen, “On the strong law of large numbers for pairwise NQD random variables,” Acta Math. Sin. vol.25, pp. 386–392, June 2005.

Advanced Materials Research Vols. 989-994 (2014) pp 2507-2510
© (2014) Trans Tech Publications, Switzerland
doi:10.4028/www.scientific.net/AMR.989-994.2507

The Application of Correlation Dimension in the Multi-objective Comprehensive Evaluation of the Large Complex Equipment Procurement Scheme

Yuxin YANG[1], Fajie WEI[1], Fan WANG[2]

[1]School of Economics and Management, Bei Hang University , Beijing 100083, China;

[2]Management Department, Beijing Command College of PAPF, Beijing 100012, China

email: 15011074256@139.com

Keywords: Fractal Correlation Dimension; Large Complex Equipment Procurement Plan; Multi-objective Comprehensive Evaluation

Abstract. The multi-objectives of procurement scheme evaluation and the complicated nonlinear are pointed out in this paper according to the definition and characteristics of large complex equipments, and with regard to the defects present in the existing multi-objective comprehensive evaluation method, the assessment method of using fractal correlation dimension as the comprehensive quantitative index of multi-objective decision making in the large complex equipment procurement scheme is put forward, and the efficiency of such method is verified by the example of combat aircraft, which provides a new idea for the multiple objective decision making in the large complex equipment procurement scheme.

Introduction

The concept of Complex Product Systems (CoPS) was comprehensively and systematically put forward firstly by the science and Technology Policy Research Institute (SPRU). Hobday explained that complex product system refers to the products, systems, networks and buildings of high cost, technology intensity, engineering intensity and customer customization.The systems of aviations, aerospaces, shipbuilding, large equipment manufacturing industries and the large telecommunications equipments are classified as complex product systems[1]. Based on Hobday's concept, we define the mechanical equipments such as aircrafts, ships, launch vehicles etc. with customization, complex structures, high technology content, long development cycle, high cost, high risk and complicated management processes as large complex equipments.

The large and complex equipment procurement is of strategic significance to a country, therefore, the balance and decision on the purchasing plan thereof is particularly important. Large complex equipments possess the characteristics of complex customer demand, complex system structure, complex product technology, long development cycle, intensive engineering and information, high input, high risk and customer customization. For the above features, the procurement scheme evaluation of the large complex equipment should not only be focused on effectiveness and costs, which therefore require multi-objective comprehensive evaluation on purchasing scheme.

For the problem regarding multi-objective evaluation and decision, the method of the linear weighted comprehensive assessment are applied mostly. The hotspot for improvement and innovation is also focus on the calculation of the weight [2][3][4] and the precision degree of the index assessment value [5][6], which is still the linear weighting in essence. Therefore, two problems present, one is that the index factors must be independent from each other when the linear weighted method is adopted and the other is that the index and its impact factors have a linear relationship, and the above two conditions are not established generally. Especially for the large complex equipment systems, and the relations there between are intricate where linear approximation method is obviously not suitable. So a new set of the theory and methods are required to solve this problem.

Fractal theory, as the frontier of the nonlinear science study in recently years, reveals inherent law, the hierarchy and scale invariance of various complex phenomena in nature and the human

society, and is applicable to the processing complex multi-level nonlinear relationship, of which the quantitative feature correlation dimension depicts the occupation degree and complexity of the whole to the space and is the quantitative characterization of key information of the whole[7]. However, the basic idea of multiple objective comprehensive evaluation method is to organize a number of individual indexes, to form a comprehensive index contains all sides so as to reflect the panorama of the evaluation object [8] [9]. Obviously, the fractal theory has obvious advantages in dealing with the nonlinear relationship between the evaluation factors and extraction characteristic value of evaluation object. In this paper, in view of the complex non-linear problems in the large complex equipment procurement scheme evaluation index system, we introduce the fractal theory and the multi-objective comprehensive evaluation scheme based on the fractal correlation dimension.

Multiple Objective Comprehensive Assessment Model Based on the Correlation Dimension

Assuming that $A_1, A_2..., A_m$ are the large complex equipment procurement schemes to be evaluated and $K_1, K_2,... K_n$ are n evaluation indexes of the scheme, making x_{ij} (i=1,2,... m; j=1,2,... n) be the j index value of the i scheme evaluation, the dimensionless treatment is conducted according to data standardization methods:

$$y_{ij} = \frac{\left(x_{ij} - \overline{x_j}\right)}{S_j} \tag{1}$$

Wherein y_{ij} is the standard data of origin data x_{ij}, $\overline{x_j}$ is the average value of the j index data and S_j is the standard deviation of the j index data.The procurement scheme evaluation system of large complex equipment composed of the n indexes can be considered as an n-dimensional geometry. The geometry is of unknown internal spatial structure and is irregular. According to the calculation method of correlation dimension:

Firstly, calculate the distance between any two points and record the distance to be $r_{ij} = \left|y_i - y_j\right|$, wherein y_i and y_j are the any two points in n-dimensional index data and the total number points is N=n (n-1) /2. Given an arbitrary distance value r, the number of points corresponding the distance value r_{ij} that is smaller than the distance of r is recorded as $N'(r)$, and the ratio of the two points with the spacing of less than R accounting for all the points is recorded as $C(r)$:

$$c(r) = N'(r)/N \tag{2}$$

$C(r)$ is also known as the correlation function. The following can be obtained by further expansion:

$$C(r) = \frac{2}{n(n-1)} \sum_{i,j=1}^{n} H(r - r_{ij}) \tag{3}$$

Wherein $H(x)$ is Heaviside function:

$$H(r - r_{ij}) = \begin{cases} 1, r \geq r_{ij} \\ 0, r < r_{ij} \end{cases} \tag{4}$$

As can be seen, $C(r)$ is related to the value of r. When r is too small, $\lim_{r \to 0} c(r) = 0$; When r is too large, $\lim_{r \to \max(r_{ij})} c(r) = 1$, and neither of two conditions can reflect the overall internal properties. Adjusting the value range of r, only in the case that r and $C(r)$ have a power law relation, can r correspond to the non scale area of the whole, that is, there exists a value range of r having the following relations, which reflects the overall fractal feature:

$$C(r) \propto r^d \tag{5}$$

Thus it can be seen, whether exists scale-free zone and whether the overall have fractal characteristics depend entirely on the objective fact, and have nothing to do with the subjective judgment.

The correlation dimension can be obtained by the formula (5) where *d* is a good approximation of the correlation dimension *D* [10]:

$$D = \lim_{r \to 0} \frac{\ln C(r)}{\ln r} \tag{6}$$

As can be seen, the calculation of correlation dimension only requires linear fitting at appropriate part of the *lnC(r)-lnr* double logarithm curve, and the slope of straight line segment is the correlation dimension, which can be obtained by using the least squares method:

$$D = \frac{\sum (\ln r - \overline{\ln r})(\ln C(r) - \overline{\ln C(r)})}{\sum (\ln r - \overline{\ln r})^2} \tag{7}$$

Correlation dimension reflects the fractal space filling degree, also reveals the correlation degree of each internal factor. The greater dimension shows the higher association degree of each factor, the more uniform distribution shows the higher occupation degree of overall to the space. While our selection criteria on the optimal scheme belong to the two types of problems in essence: one is to require maintaining coordination and balance between each evaluation index, without any short board; the other is the pursuit of maximum index value at premise of the balance of each index. In the evaluation of the procurement scheme of large complex equipment, the spatial distribution and the overall space filling degree correspond to our two standards for the best scheme. So we can say, the correlation dimension reflects the quality of the schemes in essence. Then, when making the double logarithm curve of *lnC(r)-lnr* of difference schemes, in the presence of self similarity of scale-free zone, we can rank the schemes according to the $D_{good} > D_{bad}$ sequence.

The Example Analysis

In order to test the validity the fractal evaluation tool of the correlation dimension as a comprehensive evaluation method, taking the data of the existing combat aircraft as an example, respectively by the mature method technique for order preference by similarity to an ideal solution(TOPSIS) and fractal comprehensive evaluation method for evaluation. If the results are consistent, there is reason to believe that the correlation dimension evaluation method is reliable. Now we use the existing representative five fighter F-15C, RafaleF2, F/A-22, Su-27SM, EF2000 as an example of evaluation, the basic data of five fighter as shown in Table 1 [11]:

Table 1: The original assessment data of combat aircraft scheme(fiscal 2010, single)

Attribute	F-15C	RafaleF2	F/A-22	Su-27SM	EF2000
Life cycle cost/(FY2010,10^8 $)	2.8568	3.416	6.9517	2.5684	3.197
Availability	0.86	0.85	0.68	0.75	0.88
Dependability	0.3893	0.5394	0.9438	0.4039	0.5198
Integrated combat capability	0.4296	0.5347	0.8366	0.5242	0.5978
Research cycle/month	20	21	24	21	24
Research risk	0.6625	0.6875	0.748	0.655	0.6562
Producibility	0.4973	0.5033	0.3784	0.5872	0.411
Testability	0.88	0.92	0.98	0.86	0.92
Security	0.9682	0.9672	0.9836	0.9643	0.9957
Improvability	0.1693	0.3098	0.4059	0.187	0.2426
Endurance/(flight hour)	7000	7000	8000	6000	6000

After preprocessing of the basic data of the five fighter, the double logarithmic diagrams of *lnC(r)-lnr* are respectively made.Select appropriate regions in the above double logarithmic graph for linear fitting, the fitting equation is:

$$\ln C(r) = c + D \ln r \tag{8}$$

The F-test and T-test are passed, and the obtained data are shown in table 2. As can be seen, the linear fitting degree is basically the same, the coefficient of determination are more than 0.95 and the power law relationship is significantly. According to the fractal dimension of the three aircraft development schemes, the results are sorted as: $D_{F/A-22} > D_{EF2000} > D_{RafaleF2} > D_{Su-27SM} > D_{F-15C}$.

Table 2 Fractal dimension table of evaluation on the three fighter program

	F-15C	RafaleF2	F/A-22	Su-27SM	EF2000
coefficient of determination R^2	0.9582	0.9665	0.9636	0.9626	0.9636
D value	0.7941	1.1035	1.7135	0.9409	1.5087

The technique for order preference by similarity to an ideal solution (TOPSIS) also shied away from simple weighted linear superposition theory, which through measurement of the distance between scheme and the ideal point and negative ideal point, to calculate the relative approach degree, and then to determine the schemes. The specific algorithm refers to document [11] and document [12]. The index weight vectors are $[0.2,0.24,0.052,0.068,0.08,0.064,0.108,0.092,0.096]^T$ [11].Finally we obtain the relative approach degree of $C_{F\text{-}15C}$= 0.3860, $C_{RafaleF2}$= 0.4551, $C_{F/A\text{-}22}$=0.5966, $C_{Su\text{-}27SM}$=0.4136, C_{EF2000}= 0.4891. The sequencing results are $C_{F/A\text{-}22} > C_{EF2000} > C_{RafaleF2} > C_{Su\text{-}27SM} > C_{F\text{-}15C}$, which is consistent with the results obtained through the fractal comprehensive evaluation method and is also consistent with the realistic situation.

Conclusion

This paper introduces the fractal theory into large complex equipment procurement scheme, and puts forward the multi-objective comprehensive assessment model based on fractal correlation dimension. Examples show that, this method is simple and effective, completely based on objective data, without the need of human determination of weigh and can handle arbitrary level of mixed data. The correlation dimension is calculated directly from existing data, without any simplification of comprehensive steps, and the subjectivity is minimized, it is a new method of multi-objective comprehensive evaluation for large complex equipment procurement scheme.

Acknowledgement

The research in this paper was sponsored by the National Natural Science Foundation of China (Project No. 71332003).

References

[1] Hobday, M.. Product Complexity, innovation and industrial organization. Research Policy,1998, 26:689-710.
[2] Zhang Qishan. Difference information entropy in grey theory[J]. The Journal of Grey System(UK), 2001, 13(2): 111)116.
[3] Guo Yajun. A new dynamic comprehensive evaluation method[J]. Journal of Management Sciences in China, 2002, 5(2): 49-54.
[4] XlU Guo-yi,CHEN Xiao-hua. Selection and evaluation of TPL based on information entropy[J]. China Management Science, 2011,19(10):459-463.
[5] Lin Yuanqing. A correction of the peers appraisal—The off_set method and its applications[J]. Studies in Science of Science,1998, 16(4): 69-75.
[6] Dimitras A I , Slowinski R , Susmaga R ,et al. Business failure prediction using rough sets[J]. European Journal of Operational Research, 1999, 95: 24-37.
[7] Zhang Ji-zhong.Fractal[M]. Beijing: Tsinghua University Press,1995: 1-66.
[8] HanYi, Tang Xiao-wo, Optimization of multi-index comprehensive evaluation method in some distribution[J].Journal of Industrial Engineering and Engineering Management, 1999,(3):55-58.
[9] GuJifa. Methods of Comprehensive Evaluation[M]. Beijing: Science Technology Press of China, 1990. 22-26.
[10] Huang Run-sheng. Chaos and its applications [M]. Wuhan: Wuhan university press, 2005: 183-190.
[11] Li Jun, Song Bi-feng, Fei Yang. Project assessment of modern combat aircraft based on hierarchy systems[J].Acta Aeronautica et Astronautica Sinica, 2011,32(10):1824-1834.
[12] Zhang Heng-xi. Modern aircraft cost-effectiveness ratio analysis [M].Beijing:Aviation industry press, 2001:131-138.

Advanced Materials Research Vols. 989-994 (2014) pp 2511-2514
© (2014) Trans Tech Publications, Switzerland
doi:10.4028/www.scientific.net/AMR.989-994.2511

Modeling and Simulation of Vehicle Traffic Detection System Based on Ground Sense Coil

Jingwen Ju[1,a], Jiaoyu Liu[1,b], Wei Yang[1,c], Ning Liu[1,d]

[1.]School of Automation Wuhan University of Technology Wuhan,430070,China

[a.]whutjjw@163.com, [b.]liujiaoyu_2006@163.com,
[c.]ericwyoung@163.com,[d.]whut_liuning@163.com

Keywords: ground sense coil; single-phase motors; frequency detection; MCU

Abstract. In this paper, the traffic detection system based on ground sense coil is studied. Due to the change of ground sense coil inductance, the output waveform frequence of LC oscillation circuit changes [1]. The LC oscillation circuit is composed by the three point detection circuit. Then the wave is shaped into a square-wave by shaping circuit. The square-wave is transmitted into MCU, the frequency change is detected by MCU and motor is controlled by control signal from the MCU.So when a vehicle passes above the ground sense coil, this approach makes automobile blockader lift the stop lever automatically. And the system can stop the lever falling when there is a vehicle below the lever, so this system can prevent the vehicle damage. This system can improve practical value and application prospect of a automobile blockader.

Introduction

With the continuous development of science and technology and the progress of the society, automobile has been gradually popularized [2]. In the process of traveling by car, people will inevitably encounter some checkpoints, just like highway toll stations, entrance and exit the parking lot,etc [3]. But there are some problems at these checkpoints, such as artificial duty, low intelligence and low security [4].

This paper is based on the basis of the traditional automobile blockader , then the ground coil is accessed to LC oscillation circuit [5]. When the vehicle passes ground sense coil, the inductance value of LC oscillation circuit changes, and the frequency of the output sine wave changes. The change of the frequency is captured by MCU, thus the motor can be controlled by MCU [6]. If this technique is applied to automobile blockader circuit, there are following advantages:

(1) Achieve unattended, detect the vehicles automaticly

(2) Prevent the stop lever fall suddenly, damage the vehicles

(3) Save cost and improve efficiency [7]

The following works has been done in this paper: introduce the structure and principle of the whole system, design detection device, set up the simulation model, design the motor drive circuit.

The Principle of Vehicles Traffic Detection System Based on Ground Sense Coil

The principle of vehicles traffic detection system based on ground sense coil is shown in Fig.1.

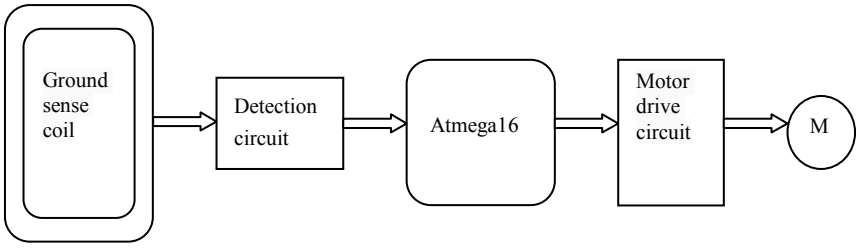

Fig.1 The principle of vehicles traffic detection system based on ground sense coil

Vehicles traffic detection system based on ground sense coil consists of ground sense coil, frequency detection circuit, MCU, motor drive circuit and single-phase motor. Ground sense coil is

under the stop lever. When a vehicle passes above the ground sense coil, its inductance decreases. The ground sense coil is connected to the oscillating circuit, so the frequency of the output waveform increases. In this system Atmega16 is used as the main MCU. There is a input capture function unit in the timing counter T/C1 of this MCU. Through this function a occurrence of external events is able to be captured and the time point is able to be recorded. The frequency change is detected by MCU, when the frequency change is over a set threshold to the MCU. Then the single-phase motor will be drived by a control signal from MCU. Delay link is added to the time of frequency testing. The stop lever is controlled to raise up or fall down by motor. The purpose of automatic detection vehicles is achieved by the above designs.

Modeling And Simulation of Vehicles Detection Circuit

Vehicles detection circuit is designed based on a three-point capacitive feedback LC circuit. Some components parameters are changed based on the range of the inductance change. There are following advantages of this circuit: (1) high-quality oscillation waveform of Capacitive feedback three-terminal circuit; (2) good stability of the circuit frequency; (3) high frequency of the capacitance three-terminal circuit. Vehicles detection circuit is shown in Fig.2.

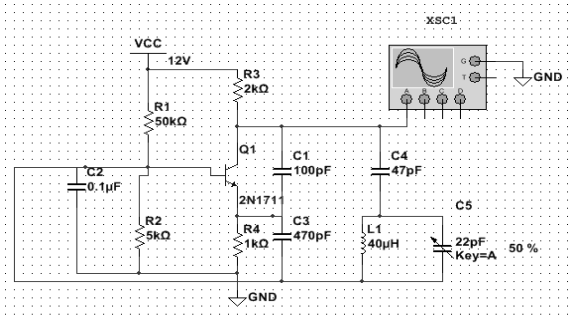

Fig.2 Vehicles detection circuit

The vehicles detection circuit is bulit by the Multisim software. Following information is shown in the picture: the ground sense coil is represented by L1, Sine wave signal is output fome the top of C4.

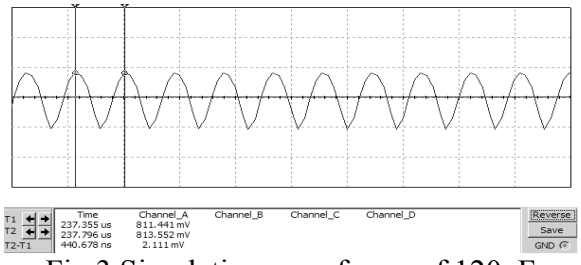

Fig.3 Simulation waveforms of 120uF

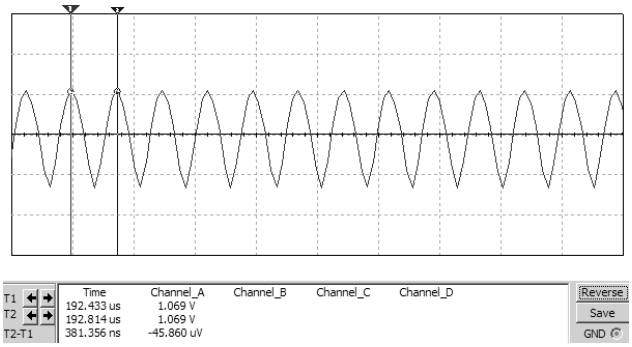

Fig.4 Simulation waveforms of 80uF

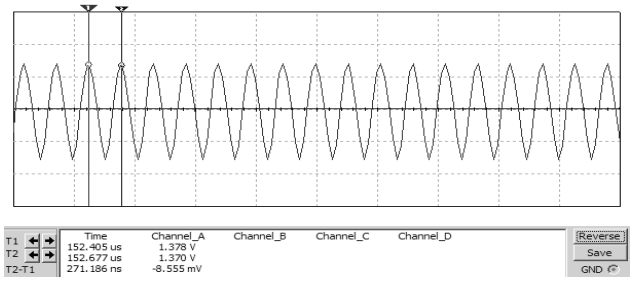

Fig.5 Simulation waveforms of 40uF

Through the simulation waveforms, following information is shown in the it: when the inductance of the ground sense coil changes obviously, the output waveform of the detection circuit obviously changes too.The period of output waveform is reduced nearly doubled when the inductance is changed from 40uF to 120uF. Then the change of frequence is able to detect by MCU. Therefore this mathod is proved to be feasible.

Modeling of Single-phase Motor Drive Circuit

There are several following functions of the single-phase motor drive circuit: (1) converting the control signal from MCU to the drive signal of the motor (2) controlling the motor running, (3) preventing the motor damage with the interlock function.

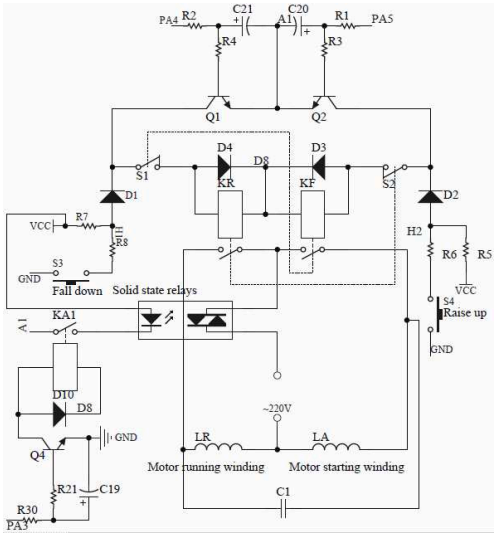

Fig.6 Modeling of single-phase motor drive circuit

Modeling of single-phase motor drive circuit is shown in Fig.6. In Fig.6, the motor is single-phase motor. In order to simplify analysis of the circuit, the motor is represented by two windings. The motor running is controlled by two relays KR and KF. One of the two switching transistors Q1 or Q2 is turned on when a high level is output from PA4 or PA5 of the MCU. Then the relay works which lead to the motor running. In order to achieve the goal of interlocking, a normally closed switch is set in the relay coil loop, the normally closed swich of one relay is opened when the other relay is working.

Conclusions

The traditional automobile blockader is characterized by no intelligent and artificialize. Therefore, a method of vehicle traffic detection system based on ground sense coil is presented. The simulation model of the system has been set up by the Multisim tool based on the working principle. Simulation results show that the system has been successfully applied to the automatic vehicle traffic detection with the demand of raising the lever. It can improve the vehicle traffic detection performance and with high use value and application prospect.

References

[1] Huifang Gao, Communication Signal Lamp Automatic Control System[J]. Application Of Electronic Technique, 1999, 25(7):32-34.

[2] Xiangmo Zhao, Yinli Jin, Yang Zhang. The Theory And Application Of Highway Monitoring System[M], Publishing House Of Electronics Industry, 2003: 90-98.

[3] N go C Y.Freeway Traffic Control Using Fuzzy Logic. Controllers Information Science, 1994(1):59-76.

[4] Naveen Chintalacheruvu. Video Based Vehicle Detection and Its Application in Intelligent Transportation Systems[J]. Journal of Transportation Technologies, 2012, 305-314.

[5] Yuliang Wang, Qi Ha. The Non-contact Type IC Intelligent(RF)Card Read-write Device And Its Controlcommunication Program[J]. Information And Broadcasting. 2009, (2): 35-43.

[6] Guihe Qin. Intelligent Transportation Systems And Vehicle Control Technology[J]. Automotive Engineering, 2001, 23(2): 92-96.

[7] Fan Yang, Zhengping Lei. Design Of Automatic Recognition Of Vehicle Monitoring System[J]. Journal Of Shenyang Institute Of Chemical Technolgy, 2004, 18(1): 37-40.

Advanced Materials Research Vols. 989-994 (2014) pp 2515-2518
© (2014) Trans Tech Publications, Switzerland
doi:10.4028/www.scientific.net/AMR.989-994.2515

Efficient Simulation for Dynamic Systems with Discontinuities

Qiong Yuan[1,a]

[1]Computer and Science Institute,Wuhan Donghu University,Wuhan,430212,China

[a]E-mail:yqszb@126.com

Keywords: simulation, dynamic systems, integration package, discontinuity

Abstract. In many techneques for handling discontinuities, the presence of a discontinuity is detected by a change of sign in the value of a discontinuity function. This paper discusses the problems caused by this sign rule of detecting discontinuities for some engineering applications, and describes an alternative which uses a change of the state marker value .The modified program with Runge-Kutta-Merson and Gear integration subroutines have been successfully applied to the simulation for mechanical, electrical and other dynamic systems with discontinuities for which the original program is inefficient.

Introduction

The problem of dealing with discontinuities is often encountered in the simulation of mechanical, electrical and other dynamic systems. Such system are usually described by a set of ordinary differential equations of the form

$$\frac{dy_i}{dt} = f_{ij}(t, y_1, y_2, ..., y_n) \quad \text{i=1,2,…,n j=1,2,…,m}$$

with a set of discontinuity functions ϕ_k (t,y_1,y_2,…,y_n).The finding of discontinuities is in two stages. Firstly, the presence of a discontinuity is detected in an integration step; Secondly, this discontinuity is located as acculately as user specification demands. Generally accepted, the presence of a discontinuity is detected by a change of sign in the value of a discontinuity function[1][2][3][4].

In this paper, the problem caused by this sign rule of detecting discontinuities for some application are discussed, and an alternative which uses a change in the value of a state marker is presented.

The Sign Rule of Detecting Discontinuities

Many techneques exist for handling discontinuities. Although methods of locating discontinuities are various, methods of detecting discontinuities are nearly same.

The Steps of Detecting Discontinuities by the Sign Rule

Generally, steps of detecting discontinuities are as follows.

The discontinuity functions ϕ_k are evaluated at the end of each integration step.

A check is made to determine if change of sign in the value of any ϕ has happened, or a test is made for negative sign in the product $S=\phi_t \times \phi_{t+h}$.

If the sign of a discontinuity function ϕ has changed or the value of S is found to be negative at end of a step ,it indicates a discontinuity somewhere in that step.

If a discontinuity is predicted, its time will be located as accurately as user specification demands. The integration will be adjusted to reach this and then restart. If none is found, the integration will continue normally.

For many cases, this sign rule of detecting discontinuities will be a successful prediction criterion. However, there are three sources which may affect the efficiency of the sign rule for some applications.

The Sources of Affecting the Efficiency of the Sign Rule

One of the conditions $\phi_k = 0$ is necessary but not sufficient for the presence of a discontinuity. Note that a discontinuity location processes consequently as soon as any ϕ passes through zero ,this may raise an extra location.

The sign of the zero value of discontinuity function is indeterminate, an inaccurate result is due to inconsistency in the classification of the sign of the zero value of discontinuity functions in Program's discontinuity detection subroutine and in User's system state condition subroutine[5].

In some applications, the zero value of a discontinuity function has to be distinguished separately;that is, the value of discontinuity functions is distinguished into five class: $>0, =0, <0$, ≥ 0 and ≤ 0.

For some discontinuous systems, these problem as above must be considered. However, it is difficult to do these by the sign rule.

The State Marker Method of Detecting Discontinuities

To overcome the shortcomings of the sign rule, an alternative which uses a change in the value of a state marker is proposed. The philosophical point of this state marker method is that a discontinuity is straightforwardly detected by a change in the value of the system state marker ISTATE. Each value of ISTATE is corresponding to a state of the system. This method steps as follow:

ϕ_k are evaluated at the and of each integration step.

ISTATE is determined by ϕ_k .

If a change of the value of ISTATE is not found, the integration proceeds normally.

If the value of ISTATE is changed, a discontinuity is predicted. A discontinuity location will follow and then the integration will restart under a new state of the system.

Compared with the sign rule, this method can best tackle those problem as described in the previous section.

Program Modifications

Fig.1 indicates a general flow diagram for the modified program.

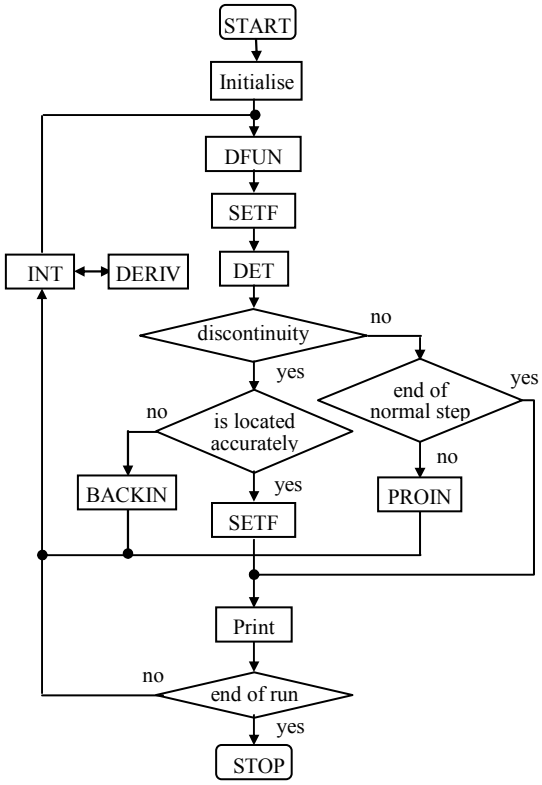

Fig. 1 Program flow diagram

To implement the present method, the small number of modifications to the interpolation subroutine of locating a discontinuity and the main program loop are required. The subroutine DFUN defines the discontinuity functions ϕ_k .The subroutine SETF determines the system state marker values according to ϕ function values.The subroutine EDT indicates a discontinuity by a change of the system state marker values at the end of the integration step. The point at which ϕ passes through zero is located as accurately as user specification demands by the reverse interpolation subroutine BACKIN and the forward interpolation subroutine FROIN. The subroutine DERIV defines the continuous segment state equations corresponding to the system state marker values .The integration subroutine INT can use any standard numerical integration algorithms, such as the standard RK algorithm, RKM algorithm and Gear's Stiff algorithm.

Applications

The modified program with Runge-Kutta-Merson and Gear integration subroutines has been successfully applied to the simulation of some mechanical, electrical and other dynamic systems for which the original program is inefficient. The following example is one of the applications.

Example:The sliding movement of a mechanical object

System model

$$m\frac{dv}{dt}=\begin{cases}0 & (v=0\wedge|f_s(t)|\le Fs)\\ f_s(t)-F_1-F_2v & (v=0\wedge f_s(t)>F_s)\vee(v>0)\\ f_s(t)+F_1-F_2v & (v=0\wedge f_s(t)<-F_s)\vee(v<0)\end{cases}$$

In the formula, parameters:m=0.64,F_s=0.83,F_1=0.75,F_2=0.28

The external force applied to the object :

$$f_s(t)=\begin{cases}0 & (0\le t<0.1)\vee(1\le t\le 1.5)\\ 5t & (0.1\le t<0.5)\\ -t & (0.5\le t<1.0)\end{cases}$$

Initial conditions: $v(0)=0,\quad t\in[0,1.5]$

Define of user's subroutines

To simulate movement characteristics of the system, it is recognized that the system includes time events and state events. According to the state switching conditions of the system equations, the 8 discontinuity condition function can be identified. Therefore three user's subroutines are defined.

The discontinuity condition function subroutine (DFUN) contain:

$\phi_1=t \quad \phi_2=t-0.1 \quad \phi_3=t-0.5$

$\phi_4=t-1.0 \quad \phi_5=t-1.5 \quad \phi_6=v$

$if\ (\phi_1\ge 0\wedge\phi_2<0)\vee(\phi_4\ge 0\wedge\phi_5\le 0)\ \ \phi_7=\phi_8=-F_s$

$if\ (\phi_2\ge 0\wedge\phi_3<0)\ \ \phi_7=5t-F_s\ ,\phi_8=-5t-F_s$

$if\ (\phi_3\ge 0\wedge\phi_4<0)\ \ \phi_7=-t-F_s\ ,\phi_8=t-F_s$

The system state marker subroutine (SETF) contain:

$if\ (\phi_1\ge 0\wedge\phi_2<0)\vee(\phi_4\ge 0\wedge\phi_5\le 0)\ \ TF=1$

$if\ (\phi_2\ge 0\wedge\phi_3<0)\ \ TF=2$

$if\ (\phi_3\ge 0\wedge\phi_4<0)\ \ TF=3$

$if\ (\phi_6=0\wedge\phi_7\le 0\wedge\phi_8\le 0)\ \ SF=1$

$if\ (\phi_6=0\wedge\phi_7>0)\vee(\phi_6>0)\ \ SF=2$

$if\ (\phi_6=0\wedge\phi_8>0)\vee(\phi_6<0)\ \ SF=3$

The system state marker ISTATE is determined by a pair of TF and SF values. Each continuous segment state of the system is corresponding to a pair of [TF, SF] value.

The system state equations subroutine (DERIV) contain:

$if\,(TF=1)\ \ f_s(t)=0 \qquad if\,(TF=2)\ \ f_s(t)=5t \qquad if\,(TF=3)\ \ f_s(t)=-t$

$if\,(SF=1)\ \ \frac{dv}{dt}=0 \qquad if\,(SF=2)\ \ \frac{dv}{dt}=(f_s(t)-F_1-F_2v)/m \qquad if\,(SF=3)\ \ \frac{dv}{dt}=(f_s(t)+F_1-F_2v)/m$

The simulated result

The simulated response of the system is shown in Fig.2. This result is done with the modified program with RKM integration subroutines.

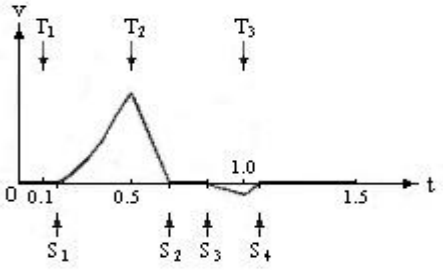

Fig.2 Simulation of the sliding movement system

The 3 time events(T_1,T_2,T_3)and 4 state events (S_1,S_2,S_3, S_4) are encountered in the simulation time interval [0,1.5]of the system. The corresponding [TF,SF] values of the 8 continuous segment states are:[1,1],[2,1],[2,2],[3,2],[3,1],[3,3],[1,3]and [1,1].The changes of the states are respectively caused by passing through zero of ϕ_2 , ϕ_7 , ϕ_3 , ϕ_6 , ϕ_8 , ϕ_4 and ϕ_6 .

The original program is inefficient for the simulation of the sliding movement system. The consumed simulation time approximately increase 6 times. As acrossing the last point of discontinuity failed, the subsequent simulation result errors.

Conclusions

While the sign rule of detecting discontinuities is usually reliable, it causes problem when discontinuity conditions are complicated. Research and practice show that it is able to successfully and effectively deal with this kind of problem by incorporating the system state flag rule of detecting discontinuities and the sequence of linear interpolationsin of locating discontinuities. Required modifications to the original package are done without difficulty. The new integral package can be straightforwardly adapted for dynamics analysis and simulation of engineering systems.

References

[1]Guangleng Xiong,Digital Simulation Algorithms and Software(in Chiness). Beijing: Astronautic Publishing House, 1991

[2]Degui Liu,and Jinggao Fei,Digital Simulation Algorithms for Dynamic Systems(in Chiness). Beijing: Science Press, 2000

[3]Tianyuan Xiao,and Wenhui Fan,Introduction to System Simulation, 2rd ed.(in Chiness). Beijing: Tsinghua University Press, 2010

[4]D.Ellison,Efficient Automatic Integration of Ordinary Differential Equations with Discontinuities, in Math. Comput. Simulation, vol. XXIII, March 1981, pp. 12–20

[5]Qiong Yuan, etc. , A Support State Marker Method for Detecting Discontinuities in Simulation of Dynamic Systems ,in the Conference Proceedings of the Information Technology Applications in Industry Computer Engineering and Materials Science,Nanjing China, September 2013,Pages:3749-3753, published by TTP.

[6]J.L.Hay, R.E.Crosbie, and R.I.Chaplin., Integration Routines for System with Discontinuities Simulation,in Comput. J, vol.IVII, 1974, pp. 275-278 .

[7]B. Das, S. Steinberg, Danjie Zhang, and T. Robey , Comparisons of Numerical Solution Methods for Differential Equations with Discontinuous Coefficients, in Math. Comput. Simulation, vol.III VI, April 1994, pp. 57-75.

Advanced Materials Research Vols. 989-994 (2014) pp 2519-2522
© (2014) Trans Tech Publications, Switzerland
doi:10.4028/www.scientific.net/AMR.989-994.2519

Optimization model and algorithm for responsive closed-loop supply chain logistics network with direct shipment under E-commerce

Liu Jing[1,2,a], Li Qi[1,b] and Wu Huawei[1,2,,c]

[1]School of Mechanical and Automotive Engineering, Hubei University of Arts and Science, Xiangyang, 441053,China

[2]The co-innovation center of Hubei province of auto parts manufacture equipments digitizing, Xiangyang, 441053,China

[a]jim_lj@126.com, [b]540016692@qq.com, [c]9438043@qq.com

Keywords: logistics engineering; optimization model; hybrid genetic algorithm; closed-loop supply chain logistics network; electronic commerce; goods return; direct shipment.

Abstract. In view of the characteristic of goods return in electronic commerce which some returned goods can be redistributed directly to customers after handling simply, a responsive closed-loop supply chain logistics network with integrating forward and reverse flow is researched. The returning feature of online commodity and economy of scale of return goods at initial collection point are based, and the optimization design model of closed-loop supply chain network aiming at determining the number and location of hybrid centers and initial collection points is presented, and a hybrid genetic algorithm is devised to solve the closed-loop supply chain logistics network problem. The usefulness of the proposed model and algorithm is validated by its application to an illustrative example.

Introduction

There are high rate of goods return under electronic commerce marketing model for some reasons such as damaging commodity, distribution error of goods, merchandise performance doesn't meet customer expectations and so on. The return rate of general goods from online sale is between 20% and 30% [1], but the return rate of some goods such as book, periodical is up to 50% [2]. In view of the characteristic of online sale, most electronic commerce enterprises give refunds policy and bear returning logistics cost, which will become bigger cost resource of electronic commerce enterprises. So improving the effectiveness of handling returning business is an important means of reducing operating cost of e-commerce enterprises. The research work about closed-loop supply chain logistics network has been attracted widespread attention by scholars, and some research fruit are obtained [3-7]. "On time delivery" plays an important role in customer satisfactory and the ability of supply chain to satisfy the customer's expected delivery called "supply chain responsiveness" and helps firms for being the order winner in their goods-markets. According to this point, a number of authors have proposed some models for optimizing the supply chain network considering cost efficiency and network responsiveness simultaneously; meanwhile some authors also consider direct shipment mechanism in supply chain structure. However, to the best of our knowledge there is no research paper discussing closed-loop supply chain considering cost efficiency and network responsiveness simultaneously, meanwhile the direct shipment is allowed, especially in e-commerce environment. In order to fill the void, a closed-loop supply chain logistics network is proposed and a hybrid genetic algorithm with integrating greedy plus algorithm and simplex method is devised to solve this problem.

Problem description and formulation

The considered supply chain network is a single product, multi-stage closed-loop supply chain, which includes plants, hybrid centers with handling forward and reverse logistics, initial collection points and customers, as shown in Fig.1. To research conveniently, some assumptions are made:①there is no capacity limitation in hybrid center for forward logistics; ②all return of goods are shipped to the nearest initial collection point for customer, and the inventory holding period of initial collection point is set to three days; ③the return quantity of customer has positive proportion

to this customer's order quantity, and the induce demand is equal to return quantity; ④all return of goods are divided into direct sale goods by handling simply and indirect sale goods, which the former are distributed equally to forward sale channel in K days, the latter is distributed into plants.

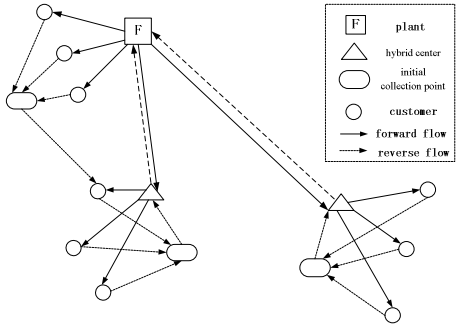

Figure 1. Closed-loop supply chain logistics network

Optimization mode

The following notation is used in the formulation of the considered supply chain network optimization model: F is the set of plant, I is the set of hybrid centers, J is the set initial collection point, L is the set of customers; r_l is demand of customer *i*, θ_l is Return ratio of customer *i*, β is direct utilization ratio of goods returned, Hg_i is Fix cost of hybrid centers *i*, HDe_i is unite operating cost of forward sale at hybrid centers *i*, He_i is unite handling cost for returning at hybrid centers *i*, MHR_i is maximal handling capacity of hybrid centers *i*, Ig_j is annual rent of initial collection point *j*, Ig_j is annual rent of initial collection point *j*, ω is annual working day, P is unite product cost of plants, a, b, c is unite transportation cost from plant to hybrid center, from plant to customer and from hybrid center to customer respectively, h is unite holding cost of initial collection point, v is delivery speed, t_l is maximum delivery tolerance time, d_{ij} is distance from point *i* to point *j*, $d_\max$ is Maximum delivery tolerance distance, f is unite transportation cost from hybrid center to initial collection point

So the decision variables are set as follows:

X_i: if a hybrid center is opened at location i, X_i is set to 1; otherwise 0.

Y_j: if a initial collection point is opened at location j, Y_j is set to 1; otherwise 0.

V_{il}: if customer l is serviced by hybrid center or plant i, V_{il} is set to 1; otherwise 0.

W_{jl}: if customer l is serviced by initial collection point j ,is set to 1; otherwise 0.

G_{ij}: quantity of product shipped from point i to point j.

In terms of the above notation, the considered closed-loop supply chain network optimization model can be formulated as follows.

$$\min Z = \sum_{i\in I} Hg_i \cdot X_i + \sum_{i\in I} G_{0i} \cdot \omega \cdot (P + d_{0i} \cdot a) + \sum_{l\in L} V_{0l} \cdot r_l \cdot (1+\theta_l) \cdot \omega \cdot (d_{0l} \cdot b + P) + \sum_{i\in I}\sum_{l\in L} V_{0l} \cdot r_l \cdot (1+\theta_l) \cdot \omega \cdot (HDe_i + d_{ij} \cdot c)$$

$$\sum_{i\in I}\sum_{j\in J} X_i \cdot G_{ji} \cdot \frac{\omega}{K} \cdot (f \cdot d_{ij} + He_i) + Ig_j \cdot \sum_{j\in J} Y_j + 2h \cdot \omega \cdot \sum_{j\in J}\sum_{l\in L} r_l \cdot \theta_l \cdot W_{jl} \cdot \frac{K+1}{2} + \omega \cdot \sum_{i\in I}\sum_{j\in J} \frac{G_{ji}}{K} \cdot (1-\beta) \cdot d_{0i} \cdot a \quad (1)$$

s.t.

$$\sum_{i\in I\cup F} V_{il} = 1 \quad \forall l \in L \quad (2)$$

$$\sum_{j\in J} W_{jl} = 1 \quad \forall l \in L \quad (3)$$

$$W_{jl} \le Y_j \quad \forall l \in L, j \in J \quad (4)$$

$$\sum_{l\in L} W_{jl} \cdot K \cdot r_l \cdot \theta_l = \sum_{i\in I} G_{ji} \quad \forall j \in J \quad (5)$$

$$G_{oi} + \sum_{j\in J} \frac{G_{ji}}{K} = \sum_{l\in L} V_{il} \cdot r_l \cdot (1+\theta_l) + \sum_{j\in J} \frac{G_{ji}}{K} \cdot (1-\beta) \quad \forall i \in I \quad (6)$$

$$\sum_{l\in L} V_{il} \cdot r_l \cdot (1+\theta_l) \ge \sum_{j\in J} \frac{G_{ji}}{K} \cdot \beta \quad \forall i \in I \quad (7)$$

$$\sum_{j\in J} G_{ji} \le MHR_i \cdot X_i \quad \forall i \in I \quad (8)$$

$$V_{il} \cdot t_l \ge V_{il} \cdot \frac{d_{il}}{v} \quad \forall i \in I \cup F, l \in L \quad (9)$$

$$d_\max \geq W_{jl} \cdot d_{jl} \quad j \in J, l \in L \tag{10}$$

$$X_i, Y_j, V_{il}, W_{jl} \in \{0,1\} \tag{11}$$

$$G_{ji} \geq 0 \quad i \in I, j \in J \tag{12}$$

Optimization objective function: (1) minimizes the annual total cost. Constraint (2) assures that all the demands of customers are satisfied by plant or hybrid center. Constraint (3) (4) ensures returning demand is serviced by a opened initial collection point. Constraint (5) ensures the flow balance at initial collection points. Constraint (6) ensures the flow balance at hybrid centers. Constraint (7) ensures direct utilization quantity of goods returned doesn't exceed the total K days' total demand quantity. Constraint (8) ensures returning quantity of hybrid center doesn't exceed the maximum handling capacity. Constraint (9) (10) ensures the limitation of delivery time and returning distance. Constraint (11) and (12) are related to the binary and non-negativity restrictions on the corresponding decision variables.

Solution method

According to the feature of considered optimization problem, a hybrid genetic algorithm with integrating greedy plus algorithm and simplex method is devised to solve this problem. The step as follows:

Step1 Encoding and initialization. The 0-1 encoding mode is applied, we only encode the location decision variable X_i and Y_j as chromosomes, and the length of chromosomes is $m+n$. The first m genes represent location decision of hybrid centers, and the other n genes represent location decision of initial collection points. the initial chromosomes are produced randomly, and the number is set to pop_size.

Step2 Fitness value calculation. The fitness value includes two parts: objective value and punishment value. There are two sub-algorithms: (1) assignment algorithm: ①firstly, customers are assigned to the nearest plant, opened hybrid center or opened initial collection point. ② the capacity of hybrid center are adjusted to $\min\left\{\sum_{l \in L} V_{il} \cdot r_l \cdot (1+\theta_i) \cdot K/\beta, MHR_i \cdot X_i\right\}$ according to inequality (7) and (8); ③the collection capacity of hybrid centers is calculated. If the capacity is more than the total quantity of goods returned, the assignment procedure end, otherwise the next steps will carry out. ④ a closed location of hybrid center is opened using greedy plus method and shift to ①. The condition of newly added hybrid center shall be demanded is which if this hybrid center is opened, the collection capacity of hybrid centers will be increased after assigning customers to their nearest opened initial collection point and adjusting the capacity of hybrid center. There are two points needed to explain, the punishment value will be made when destroying constraint (9) and (10); (2) simplex method, the transportation problem between hybrid center and initial collection point is solved by simplex method. The Fitness value is calculated by equality function $Fit = 1/(Z+A)$, and the A is punishment value, which is set to the maximal objective value.

Step3 crossover and mutation procedure: the offspring chromosome is obtained by using two-point crossover algorithm and randomly mutation algorithm.

Step4 selection procedure: the offspring chromosomes are ranked by fitness value function, and the new generation is selected by roulette wheel selection and elitism method.

Step5 Stopping criteria: the number of generations reaches a pre-specified upper limit $Popt_\max size$, the calculation procedure ends, otherwise the generation number is increase by one, and shift to step 3 to calculate.

Computational result

An e-commerce company has 30 customers' needs to serviced and the candidate location for hybrid centers and initial collection points are determined before as tab.1, the other parameters are display in tab.2. the parameters of the genetic algorithm are set by a number of experiments: ① $Popt_\max size = 200$; ② $pop_size = 50$; ③ $p_c = 0.9$; ④ $p_m = 0.15$。and customers are uniformly

distributed in a given square region with sixty unites in width. The demand of customers satisfy uniform distribution drawn from [50 350]. According to the computational result, the objective value drops from 118845023 to 74483132, and 37.33% of the initial objective value is optimized, so the usefulness of the proposed model and algorithm is validated.

The location of hybrid centers and initial collection points are determined respectively at hc2, hc3, hc4, hc7, hc8, and cp1, cp2, cp3, cp4, cp6, cp8, cp9, cp10.

TABLE 1. COORDINATE OF LOGISTICS FACILITIES

Coordinate of initial collection points	X	Y	Coordinate of hybrid centers	X	Y
cp1	43.97	49.89	hc1	8.58	30.25
cp2	1.57	12.65	hc2	25.36	28.59
cp3	41.23	30.25	hc3	9.58	6.51
cp4	5.04	58.97	hc4	47.54	19.31
cp5	24.79	19.00	hc5	20.14	53.21
cp6	16.18	20.66	hc6	50.15	45.39
cp7	30.18	45.30	hc7	38.90	59.87
cp8	40.32	0.40	hc8	21.09	17.75
cp9	6.94	33.58	Coordinate of plant	X	Y
cp10	54.71	57.06	P1	30	40

TABLE 2. PARAMETER SETTING

parameters	value	parameters	value
θ_l, β	0.2, 0.5	P, a, b, c	10, 1, 2, 2
Hg_i, Ig_j	300000, 20000	$d_\max$, v, t_l, E	20, 10, 4, 1
HDe_i, He_i, MHR_i	0.5, 0.1, 300	η_1, η_2	0.8, 0.6
ω, K	250, 3	Q_1, Q_2	200, 600

Conclusions

We have studied the optimization problem of responsive closed-loop supply chain logistics network with direct shipment from plant to customer. A optimization model is proposed in order to minimizing the annual operating total cost, and a hybrid genetic algorithm with integrating greedy plus algorithm and simplex method is devised to solve this problem. The usefulness of the proposed model and algorithm is validated by its application to an illustrative example. This research problem can be expanded to optimization problem considering multi-product, multi-period, fuzzy parameter and so on.

References

[1] ReturnBuy. The new dynamics of returns: the profit,customer and business intelligence opportunities in returns[R].ReturnBuy.com, 2001.

[2] Rogers D.S., Tibben-Lembke R.S. Going backward: reverse logistics trends and practices [R]. Nevada, Reno: Reverse Logistics Executive Council.1999.

[3] Beamon B.M., Fernandes C. Supply-chain network configuration for goods recovery[J]. goodsion Planning and Control, 2004, 15:270-281.

[4] Sim E., Jung S., Kim H., et al. A generic network design for a closed-loop supply chain using genetic algorithm[J]. lecture Notes in computer Science, 2004, 1214-1225.

[5] krikke H., Bloemhof-Ruwaard J., Van Wassenhove L.V. Concurrent goods and closed-loop supply chain design with an application to refrigerators[J]. International Journal of Goodsion Research, 2003,3689-3719.

[6] Sahyouni K., Savaskan R.C., Daskin M.S. A facility location model for bidirectional flows[J]. Transportation Science, 2007, 41:484-499.

[7] Lu Z., Bostel N. Afacility location model for logistics systems including reverse flows: the case of remanufacturing activities[J]. Computers & operations Research, 2007,34:299-323.

Advanced Materials Research Vols. 989-994 (2014) pp 2523-2527
© (2014) Trans Tech Publications, Switzerland
doi:10.4028/www.scientific.net/AMR.989-994.2523

Tabu Search for Bus Crew Scheduling with Feasible Sets of Shifts

Jiao Wang[1, a], Jihui Ma[1, b], Wei Guan[1, c], Haiting Gu[1, d]

[1] School of Traffic and Transportation, Beijing Jiaotong University, Beijing 100044, China

[a]13120807@bjtu.edu.cn, [b]jhma@bjtu.edu.cn, [c]weig@bjtu.edu.cn, [d]13120783@bjtu.edu.cn

Keywords: Crew scheduling; Feasible sets of shifts; Tabu Search

Abstract. Public transit crew scheduling problem is to carry out the operations task with the minimum drivers and operational cost. It is a multi-objective programming problem, which is well-known to be NP-hard. Restrained by the operational constraints and labor agreement, all the feasible sets of shifts were pre-generated in this paper. This work established a penalty function to ensure the validity of the schedule, and a cost function to reduce costs. With the help of Tabu Search, a solution can be found easily. A computational experiment based on the real-world crew scheduling problem in China demonstrates the strength of this method.

Introduction

Crew scheduling problem is one of the most crucial problems for the public transport operation agency. Reasonable crew scheduling can not only reduce operational cost but also affect the operational efficiency.

Since the 1960's, the crew scheduling problem has been discussed by the scholars in western countries. Mitra [1] has proposed a method using Integer Linear Programming to address the crew scheduling problem which is formulated as set covering problem. One of the characteristics of this model is allowing using the shifts which is not been covered while the optimal covering solution is not found. Clement [2] has introduced a Genetic Algorithm to address this problem in which each the chromosome complement represent a feasible crew scheduling solution to genetic operations such as mutation and crossover. Lourenco [3] proposed a Multi-objective formation and calculated by Metaheuristic Algorithms, Tabu Search and Genetic Algorithm. Freling [4] has developed a new method that the crew scheduling problem could be solved by heuristic Branch and Bound Algorithm, which the set covering problem has additional restrictions. Guang-Feng Deng [5] converts the crew scheduling problem into a Traveling Salesman Problem and using Ant colony algorithm to deal with it. De Leone, R [6] developed a new mathematical model just applied to small or medium size problem instances. For large instances, a Greedy Randomized Adaptive Search Procedure (GRASP) is proposed.

Most of the research addressed crew scheduling problem by optimization algorithm and heuristics algorithm when the bus chain set or a spell set is certain, but these methods have to filter the shifts in their scheduling scheme to make sure the time is enough between two spells and the shifts wouldn't break labor rules. However, this paper has pre-generated sets of all the feasible shifts, and solved the scheduling problem by Tabu Search algorithm. In this way, the procedure of filter the valid shifts is passed. In the process of Tabu Search, this paper takes the schedule sets as a shifts chain. Using a state matrix reserve the link between all the shifts, one can observe and evaluate the intermediate results while the algorithm executes further procedures.

Model Formation

On the basis that all shifts must be valid, public transport crew scheduling is to establish a scheduling scheme which must meet: (1) scheduling includes all trips; (2) the number of shifts is minimum; (3) the operational cost is minimum. To achieve the first goal, this paper established a penalty function $g(S)$ to ensure the validity of scheduling. The other goals can be expressed by operational cost function $f(S)$. A weighting factor λ was used to ensure the priority of the first goal.

The objective function can be formulated as follows:

$$F(x) = f(S) + \lambda \times g(S) \tag{1}$$

The smaller $F(x)$ is, the better the solution is.

Operational cost function

It is very important to reduce the number of shifts and operational cost for operating company. These two goals can be combined as a minimization problem.

The model of operational cost is shown in Eq.2 and Eq. 3.

$$f(S)=\sum_{i=1}^{n}\left(h(D_i)+W\right)\times x_i \tag{2}$$

$$h(D_i)=T_1+T_2 \tag{3}$$

Where $x_i=\begin{cases}1 & \text{if shift } i \text{ is selected}\\ 0 & \text{otherwise}\end{cases}$; T_1 represents a crew's working time; T_2 represents a crew's idle time; $h(D_i)$ is a cost function related with shift *i*, which includes crew's working time and idle time; W is a constant much larger than $f(D_i)$, which controls the number of shifts.

Penalty function

Penalty function $g(S)$ ensures the validity of scheduling. The specific rule is that every trips in the final crew scheduling scheme neither repeat nor missing. The validity of scheduling can be shown in Eq. 4.

$$g(S)=e^{\sum_{j=0}^{m} x_j}-1 \tag{4}$$

Where $x_j=\begin{cases}1 & \text{the trip } j \text{ repeat or missing}\\ 0 & \text{otherwise}\end{cases}$ $j=1,...,m$, m represents total numbers of trips.

Eq. 4 shows relation between number of unreasonable trips and value of penalty function is exponential. When $g(S)=0$, scheduling is valid.

The Application of Tabu Search

The application of the Tabu Search in crew scheduling is presented in this section. The procedure of the algorithm is as follows.

Step 1: According to the rules that a feasible shift must obey, our approach calculates the valid sets of shifts and ranks the shifts by departure time of the first trip in ascending order.

Step 2: After generated an initial solution manually, this approach adopted the Tabu Search targeting at minimize the number of shifts and the cost, and got its best solution which is represented as a state array after iterations.

Step 3: Arrange the crew according the state array.

Key factors of Tabu Search

The basic idea of the Tabu Search is to explore the search space of all feasible solutions by a sequence of moves. A move from one solution to another is generally the best available [7].

(1) Pre-generate the feasible sets of shifts

The types of shifts are two: straight duty and spilt duty. Each type of shifts has terms to abide. ①Succession driving time cannot exceed the prescribed time; ②the time from sign on at the depot to sign off for one crew cannot exceed the longest time span; ③each type of shifts cannot exceed the shortest or the longest working hours; ④the dinner time in straight duty must be contained by the specific time range.

Based on these rules that a feasible shift must obey, our approach calculates the valid sets of shifts and ranks the shifts by departure time of the first trip in ascending order.

(2) The construction of the initial solution

The first shift in the sequence of the shifts is selected firstly, and then delete the certain shifts which contains the trips that already been selected. Choose the first shift in the set of remaining shifts and find the other shifts in the same way. Note that the feasible set of shifts is very large and the type of shifts includes straight duty and split duty, so it is possible to find a valid initial solution.

(3) Neighborhood

In the algorithm, crew scheduling (set of some shifts contains exactly all trips) is operated as a shift chain. We can describe links between different shifts with a state matrix R, as shown below.

$$R=\begin{bmatrix} 0 & r_{12} & r_{13} & \cdots & r_{1p-1} & r_{1p} \\ 0 & 0 & r_{23} & \cdots & r_{2p-1} & r_{2p} \\ 0 & 0 & 0 & \cdots & r_{3p-1} & r_{3p} \\ \cdots & \cdots & \cdots & \cdots & \cdots & \cdots \\ 0 & 0 & 0 & 0 & 0 & r_{p-1p} \\ 0 & 0 & 0 & 0 & 0 & 0 \end{bmatrix}_{p\times p}$$

Where $r_{ij}=\begin{cases}1 & \text{shift } j \text{ is follow with shift } i \\ 0 & \text{otherwise}\end{cases}$; p is the number of feasible shifts; the number of shifts in crew scheduling is $n=\sum_{i=0}^{p}\sum_{j=0}^{p} r_{ij}+1$.

Neighborhood can be divided into three types, replacement, insertion and deletion. Replacement is defined as the procedure which two shifts of the current solution is replaced, as explained below. All feasible shifts are divided into some categories in accordance with the first trip; two random shifts of the current solution are replaced by other shifts in the same categories. It can narrow the scale of neighborhood and improve operation efficiency, as shown in Fig. 1. This is, in state matrix R, the values of r_{12}, r_{24}, r_{45} and r_{57} are changed from 1 to 0, the values of r_{13}, r_{34}, r_{46} and r_{67} are changed from 0 to 1, other values are remain unchanged. The transformation of state matrix represents the trajectory that the current solution moves to its neighborhood. Insertion and deletion are shown in Fig. 2 and Fig. 3.

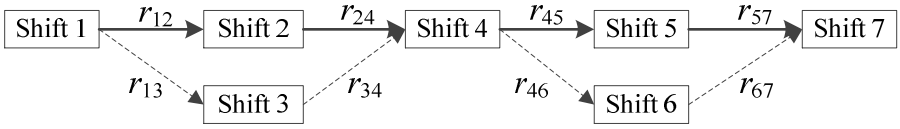

Fig. 1 Replacement

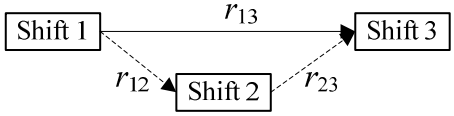

Fig. 2 Insertion

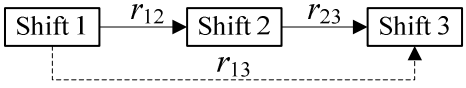

Fig. 3 Deletion

(4) Tabu list and aspiration criterion

Tabu object is defined as the moving of crew scheduling, namely transformation because of a moving. Each moving corresponds to a tabu value. Tabu length refers to how many iteration steps tabu object is not allowed, namely tabu objects are banned in I steps iterative. The tabu value minus 1 during each iteration, and when the value is zero, the object is free from tabu list. Aspiration criterion is defined to ignore the taboo attribute when the value of the current solution surpasses the history optimal value. Aspiration criterion can release a specific solution when all candidate solutions or the one better than the current optimal solution candidate solution is banned, so as to realize the global optimization search.

(5) Candidate and evaluation function

When neighborhood is huge, selecting a part of good candidate in the space of neighborhood can improve the efficiency of operation. The scale of the candidate can be set according to the needs and experiences, so as to improve the efficiency of search. The value of solution is calculated

through the evaluation function. In this paper, evaluation function is the optimization objective (Eq. 1) which is a simple, intuitive method, and the smaller the target value is, the better the solution is.

(6) Termination criterion

Termination criterion is defined to stops searching process under certain conditions. In actual operation, the following approximate termination criterions are often used: ①iteration steps have reached a determined number; ②frequency of a certain tabu object surpass a given value; ③the current optimal value does not change in a certain number of steps, the calculation terminates.

The procedure to the Algorithm

Tabu Search targeting at minimize the number of shifts and the total cost, the procedure to the algorithm is designed as follows:

Step 1: Initialized all the parameters and set the loop is zero, the tabu list is null.

Step 2: The initial solution is constructed, set the initial solution as current solution and its value is current optimal solution value f^*;

Step 3: Set $i := i+1$;

Step 4: If the termination condition is satisfied, transfer to step 10; otherwise, continue;

Step 5: Search and choose the candidate from the neighborhoods of the current solution;

Step 6: Rank the value of candidate in ascending order, set j=0, and set the jth candidate solution value is f_j;

Step 7: Set $j := j+1$;

Step 8: If f_j is less than f^*, set $f^* := f_j$, and the jth candidate solution as the current solution, go to Step 3; otherwise, continue;

Step 9: If the jth candidate solution violates the tabu rule, transfer to Step 7; otherwise, set the jth candidate solution as the current solution, and transfer to Step 3;

Step 10: Termination.

Example

In this section, Line 26 (from Erlizhuang to Xibianmen) and Line 635 (from Erlizhuang to Kangjiagou) in Beijing are taken as examples. The origin data includes trips, departure time, travel time, arrival time, etc. The travel time of Line 26 is 78min, and Line 635 is 80min. According to Difference Sequence Method, the number of departures for Line 26 and Line 635 is shown in Table 1 and Table 2.

Table 1 Number of departures for Line 26

Time / Direction	5:30-7:00	7:00-8:00	8:00-11:00	11:00-15:00	15:00-17:00	17:00-22:00
Up	10	12	30	33	20	42
Down	13	13	27	33	22	39
The number of departures per hour	15.3	25	19	16.5	21	16.2

Table 2 Number of departures for Line 635

Time / Direction	5:30-8:00	8:00-15:00	15:00-17:00	17:00-18:00	18:00-19:00	19:00-22:00
Up	26	59	19	11	10	17
Down	28	57	19	13	7	18
The number of departures per hour	21.6	16.5	19	24	17	20

This sample covers 578 trips, and the total operating time is 761 hours. All feasible shifts are 9841 so that it can' be solved by enumeration method. This work was coded in C#. All the program were run on the Pentium(R) Dual-Core E5800 CPU 3.20 GHz with 2GB RAM PC and Windows XP operating system.

Parameters about Tabu Search are set as follows: λ=1000, W=100, the scale of candidates is 100, the tabu length is 10, and if the current optimal value does not change in 50 steps, the calculation terminates.

Table 3 shows the comparison between the origin scheme and the new scheme by Tabu Search.

Table 3 Comparison

Items		Origin	New	Difference	Percentage
Line26	Total shifts	52	50	2	3.80%
	Total idle time	83.2h	68.9h	14.3h	17.18%
	Total operating time	382.2h	382.2h	0	0.00%
Line635	Total shifts	52	49	3	5.70%
	Total idle time	88.1h	66.8h	21.3h	24.18%
	Total operating time	378.7h	378.7h	0	0.00%

Table 3 indicates that the calculation results in the total number of shifts and total idle time are less than the original scheme, respectively. In summary, the crew schedule by Tabu Search is obviously better than the original one. The calculation result of this sample shows that the design of Tabu Search algorithm in this paper can solve the crew scheduling problem effectively, and can get less number of shifts and lower operation cost solution with good optimization performance.

Conclusions

Crew scheduling problem is one of the crucial issues for the public transit agency. Reasonable schedule can not only reduce operational cost, but also affect the operational efficiency. Pre-generate a set of feasible shifts and solve the problem by Tabu Search can skip the procedure of filter the valid shifts and achieve the schedule fast. Consequently, this method has a good effect on the reduction of the number of total shifts and the operation cost when solving the large-scale crew scheduling problem.

Acknowledgement

This work was financially supported by National Natural Science Foundation of China (71131001-2), Fundamental Research Funds for the Central Universities (2011JBZ007), and Beijing Science and Technology Project (Z111109073511001).

References

[1] Darby-Dowman K, Mitra G. An extension of set partitioning with application to scheduling problems [J]. European Journal of Operational Research, 1985, 21(2): 200-205.

[2] Clement R, Wren A. Greedy genetic algorithms, optimizing mutations and bus driver scheduling [M]. Springer Berlin Heidelberg, 1995.

[3] Lourenço H R, Paixão J P, Portugal R. Multiobjective metaheuristics for the bus driver scheduling problem[J]. Transportation Science, 2001, 35(3): 331-343.

[4] Freling R, Lentink R M, Odijk M A. Scheduling train crews: A case study for the Dutch railways[M]. Springer Berlin Heidelberg, 2001.

[5] Deng G F, Lin W T. Ant colony optimization-based algorithm for airline crew scheduling problem[J]. Expert Systems with Applications, 2011, 38(5): 5787-5793.

[6] De Leone R, Festa P, Marchitto E. A Bus Driver Scheduling Problem: a new mathematical model and a GRASP approximate solution [J]. Journal of Heuristics, 2011, 17(4): 441-466.

[7] F. Glover and E. Taillard, A User's Guide to Tabu Search, Annals of Operations Research, 41, 1993, 3-28.

Advanced Materials Research Vols. 989-994 (2014) pp 2528-2531
© (2014) Trans Tech Publications, Switzerland
doi:10.4028/www.scientific.net/AMR.989-994.2528

Modified Harmony Search Algorithm for Unconstrained Numerical Optimization Problems

Honggang Xia[1,2,a], Qingzhou Wang[3]

[1]Information Engineering college Shenyang University Shenyang 110004, China.

[2]Information & Science college Northeastern University Shenyang 110004, China.

[3]Information technology department of Liaoyang petrifaction, Liaoyang 111003, china

[a]xiaivy637@sohu.com

Keywords: Harmony search algorithm; mutation operation; modified harmony search; convergence

Abstract. Harmony search algorithm is a new meta-heuristic optimization method imitating the music improvisation process where musicians improvise their instruments' pitches searching for a perfect state of harmony. To enable the harmony search algorithm to transcend its limited capability of local optimum, a modified harmony search algorithm is proposed in this paper. In the modified harmony search algorithm, the mutation operation of differential evolution algorithm is introduced into MHS algorithm, which improves its convergence. Several standard benchmark optimization functions are to be test and compare the performance of the MHS. The results revealed the superiority of the proposed method to the HS and recently developed variants.

Introduction

Numerical optimization has an important position in agriculture, industry and finance economic. It is always as a standard for the optimization performance of algorithm. Traced back a long time ago, we usually use traditional methods such as liner programming, dynamic programming, conjugate gradient method, quasi-Newton method to solve unconstrained numerical optimization problems. However, with the increasing number of dimension, the numerical optimization problem become more and more complicated, which is easily lead the traditional methods trapped into dimension curse. However, the meta-heuristic algorithms have outperformed conventional numerical methods on providing better solutions for some difficult real world optimization problems.Researchers have to research meta-heuristic algorithms, such as the genetic algorithm, ant colony algorithm, particle swarm algorithm and the differential evolution algorithm; currently these meta-heuristic algorithms have been successfully applied to various complex optimization problems [1-4]. The meta-heuristic algorithms present several advantages with respect to the traditional optimization algorithms such as the meta-heuristic algorithms able to perform global search as well as local search and efficiently handling discrete variables.

Recently, Geem et al proposed a new meta-heuristic algorithm and named harmony search algorithm (HS) [5]. Harmony search algorithm is conceptualized using the musical improvisation process of searching for a perfect state of harmony. Harmony search algorithm is good at identifying the high performance regions of the solution space at a reasonable time. It has been successfully applied to many engineering optimization problems [6-8]. Nevertheless, it also suffers from a serious problem as other meta-heuristics does. It easily gets into trouble in performing local search for numerical applications. Thus, some improved variants were developed for enhancing algorithm optimizing performance, such as: improved harmony search (IHS) algorithm [9], self-adaptive global-best harmony search (SGHS) algorithm [10], Global-best harmony search (GHS) algorithm [11], and novel global harmony search (NGHS) algorithm [12].

Modified Harmony Search(MHS) Algorithm

Inspired by the concept of differential mutation as proposed in Differential Evolution (DE) [13], a modified HS is proposed in this paper. In DE algorithm, three individuals x_{r1}, x_{r2} and x_{r3} are pseudo-

randomly extracted from the population. The following are different mutation strategies frequently used in the literature:

DE/rand/1 $v_i = x_{r0} + F \times rand \times (x_{r1} - x_{r2})$ (1)

DE/best/1 $v_i = x_{best} + F \times rand \times (x_{r2} - x_{r3})$ (2)

DE/rand/ $v_i = x_{r0} + F \times rand \times (x_{r1} - x_{r2}) + F \times rand \times (x_{r3} - x_{r4})$ (3)

DE/best/2 $v_i = x_{best} + F \times rand \times (x_{r1} - x_{r2}) + F \times rand \times (x_{r3} - x_{r4})$ (4)

DE/current-to-best/1 $v_i = x_{r0} + F \times rand \times (x_{best} - x_{r1}) + F \times rand \times (x_{r2} - x_{r3})$ (5)

Where the indices r0, r1, r2, r3 and r4 are distinct integers uniformly chosen from the set {1,2,...,NP}; x_{best} is the best vector in the current iteration; F represents the scaling factor; rand belongs to a uniform distribution in the ranges [0,1].

The classic DE/rand/1 is known to be robust but less efficient in terms of convergence rate. The other best variant is DE/best/1, which utilizes the information of the best solution in current population. The mutation operation DE/best/1 can fast speed up the convergence rate and improve the convergence performance.

In view of the above consideration, and combine the search mechanism of harmony search algorithm, we introduce a new greedy mutation strategy and modify the pitch adjustment step of the HS. The new greedy mutation strategy as follow:

$$x_j^{new} = w \times x_j^{best} + F \times rand \times (x_j^{r2} - x_j^{r3}) - (x_j^{r2} - x_j^{r3}) \quad (6)$$

$$w = w_{\min} + \frac{K-k}{K} \times (w_{\max} - w_{\min}) \quad (7)$$

Where $w_{\max}$ and $w_{\min}$ are the upper and lower weight value, respectively. K is the maximum number of iterations, and k is the current number of iterations; rand belongs to a uniform distribution in the ranges [0,1]; the indices r_2 and r_3 are distinct integers uniformly chosen from the set（1，2，…，HMS） and （1，2，…，N）, respectively; F is the scaling factor that is a positive control parameter for scaling the difference decision variable; x_j^{new} represents the jth decision variable of the new harmony vector at the current iteration k, and x_j^{r2} represents the jth decision variable of the r_2 harmony vector in the current harmony memory, x_j^{r3} the same as x_j^{r2} .The MHS algorithm has exactly the same steps as the HS algorithm with the exception that Step 3 is modified as follow:

for j =1 to N do

if rand()≤HMCR then

$x_j^{new} = x_j^{r}, (r \in (1,2,\cdots,HMS))$ % memory consideration

if rand()≤PAR then

$x_j^{new} = w \times x_j^{best} + F \times rand \times (x_j^{r2} - x_j^{r3}) - (x_j^{r2} - x_j^{r3})$ %pitch adjustment

end

else $x_j^{new} = x_{jL} + rand \times (x_{jU} - x_{jL})$ %random selection end end

Experimental Results and Analysis

Ten test functions are considered to extensively investigate the performance of the MHS algorithm, and they are presented as follows:

f_1 Sphere function, defined as $\min f_1 = \sum_{i=1}^{N} x_i^2$, f_2 Rosenbrock function, defined as $\min f_2 = \sum_{i=1}^{N-1} (100(x_{i+1} - x_i^2)^2 + (x_i - 1)^2)$, f_3 Rastrigrin function, defined as $\min f_3 = \sum_{i=1}^{N} (x_i^2 - 10\cos(2\pi x_i) + 10)$, f_4 Griewank function, defined as $\min f_4 = \frac{1}{4000}\sum_{i=1}^{N} x_i^2 - \prod_{i=1}^{N} \cos(\frac{x_i}{\sqrt{i}}) + 1$, f_5 Ackley's function, defined

as $\min f_5 = 20 + e - 20\exp(-0.2\sqrt{\frac{\sum_{i=1}^{N} x_i^2}{N}}) - \exp(\frac{\sum_{i=1}^{N}\cos(2\pi x_i)}{N})$, f_6 Schwefel's problem 2.22, defined as $\min f_6 = \sum_{i=1}^{N}|x_i| + \prod_{i=1}^{N}|x_i|$, f_7 Zakharov function, defined as $\min f_7 = \sum_{i=1}^{N} x_i^2 + \left(\sum_{i=1}^{N} 0.5ix_i^2\right)^2 + \left(\sum_{i=1}^{N} 0.5ix_i^2\right)^4$, f_8 Rotated hyper-ellipsoid function, defined as $\min f_8 = \sum_{i=1}^{N}(\sum_{j=1}^{i} x_j)^2$, f_9 Shifted Rotated high conditioned Elliptic function, define as $\min f_9 = \sum_{i=1}^{N}(10^6)^{\frac{i-1}{N-1}} z_i^2 - 450$, f_{10} Shifted Schwefel's problem 1.2 with noise, defined as $\min f_{10} = \sum_{i=1}^{N}(\sum_{j=1}^{i} z_j)^2(1 + 0.4*|N(0,1)|) - 450$

In the experiments, the settings of compared HS algorithms are show in table 1. The results reported in this section are best, worst, mean and standard deviation (SD) over 30 independent simulations. For each simulation was allowed to run 50000 evaluations of the objective function the numerical results using four harmony search algorithm are reported in Table 2.

Table 1 The parameter of algorithms

Algorithm	**HMS**	**HMCR**	**PAR**	**PAR_{min}**	**PAR_{max}**	**bw**	**bw_{min}**	**bw_{max}**	**F**
HS	5	0.9	0.3	—	—	0.001	—	—	—
IHS	5	0.9	—	0.01	0.99	—	0.0001	$(x_{ju}-x_{jl})/20$	—
GHS	5	0.9	0.3	—	—	0.001	—	—	—
MHS	5	0.9	0.3	—	—	0.001	—	—	0.5

Table 2 The optimization results of five harmony search algorithms for f1-f10 (n=100)

Function	Algorithm	Best	Worst	Mean	SD
f1	HS	6.8930e-001	2.3242e+001	6.1191e+000	4.6203e+000
	IHS	1.4629e+004	2.2846e+004	1.8737e+004	1.9697e+003
	GHS	2.6100e-002	8.8100e-002	5.2400e-002	1.5400e-002
	MHS	4.7712e-081	4.5211e-073	2.6370e-074	8.6007e-074
f2	HS	1.3143e+003	1.6463e+004	5.2425e+003	3.8963e+003
	IHS	1.1101e+009	2.4732e+009	1.7362e+009	2.9635e+008
	GHS	2.3959e+002	1.0173e+004	1.4510e+003	2.5171e+003
	MHS	9.71488e+001	9.8807e+001	9.8046e+001	7.3620e-001
f3	HS	1.8867e+001	2.9368e+001	2.4763e+001	2.4253e+000
	IHS	5.7702e+002	7.1819e+002	6.4913e+002	4.3458e+001
	GHS	1.3700e+001	2.8751e+001	2.0660e+001	4,0128e+000
	MHS	0	1.7764e-014	2.0132e-015	3.8675e-015
f4	HS	1.2452e+000	1.7491e+000	1.4037e+000	1.0220e-001
	IHS	1.2555e+002	2.3245e+002	1.7590e+002	2.1940e+001
	GHS	2.0200e-002	1.0120e-001	4.7200e-002	2.4500e-002
	MHS	0	5.5511e-016	7.0314e-017	1.2869e-016
f5	HS	1.2717e+000	2.2069e+000	1.6706e+000	2.1140e-001
	IHS	1.2645e+001	1.3930e+001	1.3353e+001	3.2930e-001
	GHS	2.9400e-002	5.9200e-002	3.9700e-002	7.6000e-003
	MHS	8.1054e-015	9.9476e-014	3.3514e-014	1.7963e-014
f6	HS	2.6320e-001	6.4420e-001	4.0690e-001	9.9500e-002
	IHS	4.8923e+002	7.1292e+003	8.4979e+002	1.1900e+003
	GHS	9.2830e-001	1.9242e+000	1.2999e+000	2.4480e-001
	MHS	6.4649e-042	6.7112e-025	2.7051e-026	1.2306e-025
f7	HS	1.2815e+003	2.0255e+003	1.6804e+003	2.0703e+002
	IHS	1.2562e+003	1.9995e+003	1.5911e+003	1.5512e+002
	GHS	1.2443e+005	2.3718e+005	1.7077e+005	3.1502e+004
	MHS	4.1885e-005	3.6000e-003	4.3747e-004	7.8426e-004
f8	HS	1.4402e+008	3.0654e+008	2.1856e+008	3.6949e+007
	IHS	3.4322e+008	6.3573e+008	4.4958e+008	7.8263e+007
	GHS	3.4664e+007	6.4569e+007	4.6674e+007	6.7331e+006
	MHS	5.9000e-003	8.8007e+000	3.3750e-001	1.5992e+000
f9	HS	2.6720e+003	2.1540e+004	1.1267e+004	4.4967e+003

	IHS	1.3046e+007	2.8254e+007	1.7613e+007	3.6432e+006
	GHS	-4.2073e+002	-3.4024e+002	-3.8842e+002	1.6126e+001
	MHS	-4.5000e+002	-4.4899e+002	-4.4993e+002	2.0000e-001
f10	HS	4.3823e+008	8.2213e+008	5.8802e+008	8.4801e+007
	IHS	4.6110e+008	7.2655e+008	5.8136e+008	7.3701e+007
	GHS	2.4026e+008	6.4249e+008	4.2422e+008	8.4999e+007
	MHS	-4.4997e+002	4.2799e+004	1.3832e+003	7.8222e+004

Conclusions

In the MHS algorithm, a new greedy mutation strategy was introduced and modified the pitch adjustment operation, which makes it easier to explore a better solution and balance the local search and global search well. What's more, the MHS algorithm utilize the best harmony vector to generate a new harmony, which speed up the algorithm search rate and improve the solution accuracy. Besides, Combine with the search mechanism of the original harmony search algorithm, the MHS algorithm enhances stability. Based on several high dimension standards benchmark optimization problems carried out to be tested, the results obtained using the MHS algorithm may yield better solutions than those obtained using HS, IHS and GHS algorithm, and demonstrate the effectiveness and robustness of the proposed algorithm.

References

[1] He Y H, Hui C W. A binary coding genetic algorithm for multi-purpose process scheduling: A case study [J], Chemical Engineering Science, 2010, 65(16): 4816-4828.

[2] Shi H X. Solution to 0/1 knapsack problem based on improved ant colony algorithm [C], in: International Conference on Information Acquisition, 2006, 1062-1066.

[3] Coelho L S. An efficient particle swarm approach for mixed-integer programming in reliability–redundancy optimization applications [J], Reliability Engineering & System Safety, 2009, 94(4): 830-837.

[4] Onwubolu G, Davendra D. Scheduling flow shops using differential evolution algorithm [J], European Journal of Operational Research, 2006, 171(2): 674-692.

[5] Geem Z W, Kim J H, Loganathan G V. A new heuristic optimization algorithm: Harmony search [J], Simulation, 2001, 76(2): 60-68.

[6] Lee K S, Geem Z W. A new structural optimization method based on the harmony search algorithm [J], Computers and Structures, 2004, 82(9/10): 781-798.

[7] Honggang XIA, Dongling CHEN, Liqun GAO. Modified Harmony Search Algorithm for Power Economic Load Dispatch [J], Journal of Computational Information Systems, 2013, 9(5): 2103-2110.

[8] Sharma K D, Chatterjee A, Rakshit A. Design of a Hybrid Stable Adaptive Fuzzy Controller Employing Lyapunov Theory and Harmony Search Algorithm [J], IEEE Transactions on Control Systems Technology, 2010, PP(99): 1-8.

[9] Mahdavi M, Fesanghary M, Damangir E. An improved harmony search algorithm for solving optimization problems [J], Applied Mathematics and Computation, 2007, 188(2): 1567–1579.

[10]Chia-Ming Wang, Yin-Fu Huang. Self-adaptive harmony search algorithm for optimization. Expert Systems with Applications, 2010, 37(4): 2826-2837.

[11]Omran M G H, Mahdavi M. Global-best harmony search [J], Applied Mathematics and Computation, 2008, 198(2): 643-656.

[12]Zou D X, Gao L Q, Wu J H, Li S. Novel global harmony search algorithm for unconstrained problems [J], Neurocomputing, 2010, 73(16-18): 3308-3318.

[13]Storn, R., Price, K., Differential evolution: a simple and efficient adaptive scheme for global optimization over continuous spaces. Technical Report TR-95-012, Berkeley, USA: International Computer Science Institute, 1995.

Advanced Materials Research Vols. 989-994 (2014) pp 2532-2535
© (2014) Trans Tech Publications, Switzerland
doi:10.4028/www.scientific.net/AMR.989-994.2532

A Modified Harmony Search Algorithm for Numerical Optimization Problems

Honggang Xia[1,2,a], Qingzhou Wang[3]

[1] Information Engineering college Shenyang University Shenyang 110004, China.

[2]Information & Science college Northeastern University Shenyang 110004, China.

[3]Information technology department of Liaoyang petrifaction, Liaoyang 111003, china

[a]xiaivy637@sohu.com

Keywords: modified harmony search; self-learning strategy; convergence; stability

Abstract. This paper presents a modified harmony search (MHS) algorithm for solving numerical optimization problems. MHS employs a novel self-learning strategy for generating new solution vectors that enhances accuracy and convergence rate of harmony search (HS) algorithm. In the proposed MHS algorithm, the harmony memory consideration rate (HMCR) is dynamically adapted to the changing of objective function value in the current harmony memory. The other two key parameters PAR and bw adjust dynamically with generation number. Based on a large number of experiments, MHS has demonstrated stronger convergence and stability than original harmony search (HS) algorithm and its two improved algorithms (IHS and GHS).

Introduction

Recently, a novel metaheuristic optimization algorithm- harmony search (HS) was developed by Geem et al in 2001[1], which are conceptualized using the musical improvisation process of searching for a perfect state of harmony. Owing to its own potential and shortage, there has been an increasing interest in the study of improved HS algorithm during the recent few years. These improved harmony search algorithms as following: improved harmony search (IHS) algorithm [2], self- adaptive harmony search algorithm [3], parameter- setting-free harmony search algorithm [4] global-best harmony search (GHS) algorithm [5] self-adaptive global best harmony search algorithm (SGHS) [6], novel global harmony search (NGHS) algorithm [7]. These improved harmony search algorithms are good at identifying the high performance regions of the solution space at a reasonable time, but get into trouble in performing local search for numerical applications. Although several variants and an increasing number of applications have appeared, one of its main difficulties is how to select suitable parameter values. HS algorithm's performance, however, is still quite dependent on the setting of control parameters such as pitch adjusting rate (PAR) and distance bandwidth (bw) probability according to trial-and-error method. Although there are many researchers contribute to how to design a skill to choose the suitable parameter settings to ensure the success of the algorithm, the affections between the parameter setting and the optimization performance is still complicated and not completely understood. How to efficiently adaptively setting suitable parameter values is still a main work to improve HS algorithm optimization performance.

A Modified Harmony Search (MHS) Algorithm

Inspired by the differential evolution algorithm, a self-learning harmony search algorithm is presented in this section. MHS employs a novel self-learning strategy (or differential learning approach) and a dynamically adaptive parameter tuning methods. The details of the MHS algorithm are presented below.

Self-Learning Strategy

A self-learning strategy is proposed in the MHS algorithm, and it expressed as follow:

$$x_i^{new}(k) = \frac{K-k}{K} \times x^{r_1}{}_{r_2}(k) + F \times rand_i \times (x^{r_1}{}_i(k) - x^{r_1}{}_{r_2}(k)) \tag{1}$$

where K is the maximum number of iterations, and k is the current number of iterations; randi belongs to a uniform distribution in the ranges [0,1]; the indices r_1 and r_2 are distinct integers uniformly chosen from the set（1，2，…，HMS） and （1，2，…，N）,respectively; F is the scaling factor that is a positive control parameter for scaling the difference decision variable; $x_i^{new}(k)$ represents the ith decision variable of the new harmony vector at the current iteration k, and $x^{r_1}{}_i(k)$ represents the ith decision variable of the r1 harmony vector in the current harmony memory. ($x^{r_1}{}_{r_2}(k)$ and $x^{r_1}{}_{r_2}(k)$ have the same meaning as $x^{r_1}{}_i(k)$).the former part ($\frac{K-k}{K}\times x^{r_1}{}_{r_2}(k)$) play a key role in the early iterations, In this case, any decision variable of the new harmony vector keeps the decision variables from the HM with a large probability, so the new harmony vector is more like a conservative one that conserve the good part by learn from themselves in the early iterations. With the increase of iteration k, The effect of the former part decreases , but the latter part（$F\times rand_i\times(x^{r_1}{}_i(k)-x^{r_1}{}_{r_2}(k))$） become important. The latter part is just like differential evolution mutation strategy; this part is called neighborhood learning. In the late iterations, the weight ($(K-k)/K$) becomes very small, and the latter part has primarily effects on the decision variable of the new harmony vector by random decision variable differential. In this case, any decision variable of the new harmony vector to mutate to a new one from the HM, which provides a promising and alternative search direction for each harmony vector.

The Key Parameter Setting For MHS

HMCR is the probability of choose one value from the historic values stored in the HM. Here the HMCR adaptively adjusted according to the objective function value in the current harmony memory, and it is stated as follows:

$$HMCR_k=\begin{cases}1, & if \quad \dfrac{f^{k-1}{}_{aver}-f^{k-1}{}_{\min}}{f^{k-1}{}_{\max}-f^{k-1}{}_{aver}}>1\\ \dfrac{f^{k-1}{}_{aver}-f^{k-1}{}_{\min}}{f^{k-1}{}_{\max}-f^{k-1}{}_{aver}}, & otherwise\end{cases} \tag{2}$$

Where $f^{k-1}{}_{\min}$ represents the minimal objective function value of all harmony solution vector at iteration k-1, $f^{k-1}{}_{aver}$ represents the average objective function value of all harmony solution vector at iteration k-1, $f^{k-1}{}_{\max}$ represents the maximal objective function value of all harmony solution vector at iteration k-1.A closer look at adaptive harmony memory consideration rate HMCRk reveals that each iteration solution has its own unique HMCR according to the ratio of ($f^{k-1}{}_{aver}-f^{k-1}{}_{\min}$) and ($f^{k-1}{}_{\max}-f^{k-1}{}_{\min}$). If the objective function value of the solution is close to $f^{k-1}{}_{\min}$, $HMCR_k$ tends to be a small value, which is beneficial to the global search of the MHS, otherwise, HMCRk tends to be a large value, which is beneficial to the local search of the SSHS. In short, the adaptive HMCR can balance the local search and global search well.

PAR and bw change dynamically with generation number as expressed as follow:

$$PAR(k)=PAR_{\min}+\frac{(PAR_{\max}-PAR_{\min})}{K}\times k \tag{3}$$

$$\mathrm{bw}(k)=\mathrm{bw}_{\max}\exp(c\cdot k),\ c=\frac{\ln\left(\dfrac{\mathrm{bw}_{\min}}{\mathrm{bw}_{\max}}\right)}{K} \tag{4}$$

Where K is the maximum number of iterations, and k is the current number of iterations; PARmin and PARmax are the minimum adjusting rate and the maximum adjusting rate respectively; bwmin and bwmax are the minimum bandwidth and the maximum bandwidth respectively.

Computational Procedure of the MHS

The Computational procedure of the MHS algorithm can be summarized as follows:

(1) Begin

(2) Set harmony memory size HMS, adjusting rate PAR, distance bandwidth bw, the number of decision variables N and maximal iteration number K.

(3)Initialize harmony memory HM, upper bands of variables $x_U = (x_{1U}, x_{2U}, \ldots, x_{NU})$ and lower bands $x_L = (x_{1L}, x_{2L}, \ldots, x_{NL})$. Harmony memory (HM) is generated from a uniform distribution in the ranges $[x_{jL}, x_{jU}], (j = 1, 2, \cdots, N)$

(4) Improvise a new harmony from the HM

Calculate the objective function values of all harmony solution vectors. Calculate $f^{k-1}{}_{aver} = \frac{1}{HMS}\sum_{i=1}^{HMS} f^{k-1}{}_i$ and find out $f^{k-1}{}_{\max}$, $f^{k-1}{}_{\min}$.

Calculate HMCRK and then conduct improvisation processes, include memory consideration, pitch adjustment and random selection. In the memory consideration, self-learning strategy applied to this part.

(5) Update harmony memory

(6) Check the stopping criterion

Experimental Results and Analysis

To test the performance of the proposed MHS algorithm, an extensive experimental evaluation and comparison with the HS, IHS and GHS algorithms are provided based on a set of 6 global optimization problems as follows:

f_1 Sphere function, defined as $\min f_1 = \sum_{i=1}^{N} x_i^2 \quad -100 \le x_i \le 100 \ (i = 1, 2, ..., N)$

Where global optimum $x^* = (0, 0, ..., 0)$ and $f(x^*) = 0$

f_2 Rastrigrin function, defined as $\min f_2 = \sum_{i=1}^{N} (x_i^2 - 10\cos(2\pi x_i) + 10)$ Where global optimum $x^* = (0, 0, ..., 0)$ and $f(x^*) = 0$ for $-10 \le x_i \le 10 \ (i = 1, 2, ..., N)$.

f_3 Griewank function, defined as

$\min f_3 = \frac{1}{4000}\sum_{i=1}^{N} x_i^2 - \prod_{i=1}^{N} \cos(\frac{x_i}{\sqrt{i}}) + 1$ Where global optimum $x^* = (0, 0, ..., 0)$ and $f(x^*) = 0$ for $-600 \le x_i \le 600 \ (i = 1, 2, ..., N)$

f_4 Ackley's function, defined as $\min f_4 = 20 + e - 20\exp(-0.2\sqrt{\frac{\sum_{i=1}^{N} x_i^2}{N}}) - \exp(\frac{\sum_{i=1}^{N} \cos(2\pi x_i)}{N})$ Where global optimum $x^* = (0, 0, ..., 0)$ and $f(x^*) = 0$ for $-32 \le x_i \le 32 \ (i = 1, 2, ..., N)$.

f_5 Schwefel's problem 2.22, defined as $\min f_5 = \sum_{i=1}^{N} |x_i| + \prod_{i=1}^{N} |x_i|$ Where global optimum $x^* = (0, 0, ..., 0)$ and $f(x^*) = 0$ for $-100 \le x_i \le 100 \ (i = 1, 2, ..., N)$.

f_6 Rotated hyper-ellipsoid function, defined as $\min f_6 = \sum_{i=1}^{N} (\sum_{j=1}^{i} x_j)^2$ Where global optimum $x^* = (0, 0, ..., 0)$ and $f(x^*) = 0$ for $-100 \le x_i \le 100 \ (i = 1, 2, ..., N)$

For each function, 30 independent experiments are carried out in each case, and the numerical results using four harmony search algorithm are reported in Table 1, The "SD" represents standard deviation. The maximum number of iterations is set to 10000 for 6 functions. It can be see from Table 2, that the MHS algorithm is the best algorithm since it generates all 6 significantly better results than the HS, IHS and GHS algorithms for the 6 test functions. MHS performs better than the other three approaches in terms of solution accuracy on the utilized 6 test functions.

Table1 The optimization results of Four harmony search algorithms for f1-f6 (N=50)

Function	Algorithm	Best	Worst	Mean	SD
f_1	HS	4.5786e-004	5.2087e+000	4.5290e-001	1.2481e+000
	IHS	6.0168e+002	1.5744e+003	1.0084e+003	2.8071e+002
	GHS	4.6118e-009	2.5360e-007	4.0489e-008	4.8257e-008
	MHS	**8.6133e-138**	**9.8197e-127**	**3.9155e-128**	**1.8059e-127**
f_2	HS	5.1128e+000	1.6066e+001	1.0724e+001	3.0168e+000
	IHS	7.9191e+001	1.3524e+002	1.1206e+002	1.2508e+002
	GHS	2.6883e-004	5.9807e+000	2.3598e+000	1.5567e+000
	MHS	**0**	**1.0658e-014**	**1.0066e-015**	**2.1216e-015**
f_3	HS	1.1054e+000	1.4960e+000	1.1940e+000	7.6300e-002
	IHS	6.3168e+000	1.3532e+001	1.0105e+001	2.1174e+000
	GHS	1.0007e-006	1.6970e-001	4.3300e-002	4.4600e-002
	MHS	**0**	**4.4409e-016**	**5.5511e-017**	**1.1198e-017**
f_4	HS	1.1582e+000	2.0384e+000	1.6353e+000	2.8400e-001
	IHS	5.4619e+000	7.3653e+000	6.4599e+000	4.9730e-001
	GHS	1.8877e-004	1.2000e-003	4.6333e-004	2.2788e-004
	MHS	**7.1054e-015**	**6.3949e-014**	**1.8593e-014**	**1.2117e-014**
f_5	HS	6.6400e-002	2.3460e-002	9.9900e-002	3.4500e-002
	IHS	6.2999e+001	1.3644e+002	9.5582e+001	2.0673e+001
	GHS	1.6000e-003	7.8000e-003	4.0000e-003	1.6000e-003
	MHS	**4.2056e-071**	**5.2662e-055**	**1.7862e-056**	**9.6104e-056**
f_6	HS	1.1297e+007	2.6731e+007	2.0034e+007	4.2242e+006
	IHS	1.2053e+007	3.1408e+007	1.9405e+007	4.7533e+006
	GHS	9.2659e+005	1.9926e+006	1.3964e+006	2.9481e+005
	MHS	**1.5622e-016**	**6.1038e-005**	**2.0662e-006**	**1.1139e-005**

Conclusions

This paper proposes a new simple but effective and efficient MHS algorithm for unconstrained optimization problems with continuous decision variables. Unlike the HS algorithm, the MHS designs a novel self-learning strategy, which makes it easier to explore a better solution and to converge. In addition, the harmony memory consideration rate (HMCR) is dynamically adapted to the changing of objective function value in the current harmony memory, which it can balance, the local search and global search well. Based on a large number of experiments, the results obtained using the MHS algorithm may yield better solutions than those obtained using HS, IHS and NGHS algorithm, and demonstrate the effectiveness and robustness of the proposed algorithm. In short, the MHS algorithm is a promising optimization algorithm, and it has high exploration capability of solution space throughout the whole iteration.

References

[1] Geem Z W, Kim J H, Loganathan G V. A new heuristic optimization algorithm: Harmony search [J], Simulation, 2001, 76(2): 60-68.

[2] Mahdavi M, Fesanghary M, Damangir E. An improved harmony search algorithm for solving optimization problems [J], Applied Mathematics and Computation, 2007, 188(2): 1567–1579.

[3] Chia-Ming Wang, Yin-Fu Huang. Self-adaptive harmony search algorithm for optimization. Expert Systems with Applications, 2010, 37(4): 2826-2837.

[4] Zong Woo Geem, Kwee-Bo Sim. Parameter-setting-free harmony search algorithm. Applied Mathematics and Computation, 2010, 217(8): 3881-3889.

[5] Omran M G H, Mahdavi M. Global-best harmony search [J], Applied Mathematics and Computation, 2008, 198(2): 643-656.

[6] Pan Q K, Suganthan P N, Tasgetiren M F, Liang J J. A self-adaptive global best harmony search algorithm for continuous optimization problems [J], Applied Mathematics and Computation, 2010, 216(3): 830-848.

[7] Zou D X, Gao L Q, Wu J H, Li S. Novel global harmony search algorithm for unconstrained problems [J], Neurocomputing, 2010, 73(16-18): 3308-3318.

Advanced Materials Research Vols. 989-994 (2014) pp 2536-2539
© (2014) Trans Tech Publications, Switzerland
doi:10.4028/www.scientific.net/AMR.989-994.2536

Modified Differential Evolution Algorithm for Numerical Optimization Problems

Honggang Xia[1,2,a], Qingzhou Wang[3]

[1]Information Engineering college Shenyang University Shenyang 110004, China.

[2]Information & Science college Northeastern University Shenyang 110004, China.

[3]Information technology department of Liaoyang petrifaction, Liaoyang 111003, china

[a]xiaivy637@sohu.com

Keywords: MDE; position updating; disturbance; convergence; dynamic

Abstract. In this paper, a modified differential evolution algorithm (MDE) developed to solve unconstrained numerical optimization problems. The MDE algorithm employed random position updating and disturbance operation to replaces the traditional mutation operation. The former can rapidly enhance the convergence of the MDE, and the latter can prevent the MDE from being trapped into the local optimum effectively. Besides, we dynamic adjust the crossover rate (CR), which is aimed at further improving algorithm performance. Based on several benchmark experiment simulations, the MDE has demonstrated stronger convergence and stability than original differential (DE) algorithm and its two improved algorithms (JADE and SaDE) that reported in recent literature.

Introduction

In 1995, a new floating point encoded an evolutionary algorithm for global optimization; called Differential Evolution (DE) was proposed. Differential Evolution, inspired by the natural evolution of species, has been successfully applied to solve numerous optimization problems in diverse fields. However, when implementing the DE, users not only need to determine the appropriate encoding schemes and evolutionary operators, but also need to choose the suitable parameter settings to ensure the success of the algorithm, which may lead to demanding computational costs due to the time-consuming trial-and-error parameter and operator tuning process. To overcome such inconvenience, researchers have actively investigated the adaptation of parameters and operators in DE. Literature [1] divided the parameter adaptation techniques into three categories: deterministic, adaptive, and self-adaptive control rules. Deterministic rules modify the parameters according to certain predetermined rationales without utilizing any feedback from the search process. Adaptive rules incorporate some form of the feedback from the search procedure to guide the parameter adaptation. Self-adaptive rules directly encode parameters into the individuals and evolve them together with the encoded solutions. Parameter values involved in individuals with better fitness values will survive, which fully utilize the feedback from the search process. Generally speaking, self-adaptive rules can also refer to those rules that mainly utilize the feedback from the search process such as fitness values to guide the updating of parameters. Differential Evolution uses a special kind of differential operator, and recently, it has been applied in different fields of engineering and science [2-4].

The performance of the conventional DE algorithm highly depends on the chosen trial vector generation strategy and associated parameter values used. Inappropriate choice of strategies and parameters may lead to premature convergence or stagnation, which have been extensively demonstrated in [5] and [6]. In this paper, we propose a modified differential evolution (MDE) algorithm to avoid the expensive computational costs spent on searching for the most appropriate trial vector generation strategy, as well as its associated parameter values by a trial-and-error procedure. Instead, both strategies and their associated parameters are adjusted adaptively to prevent algorithm trapped into local optima.

The Modified Differential Evolution (MDE) Algorithm

The original particle swarm optimization algorithm works as follow:

$$v_i = v_i + c1 \times rand \times (x_l - x_i) + c1 \times rand \times (x_g - x_i)$$

$$x_{i+1} = x_i + v_i$$

Where v_i and x_i represent the speed and position of individual in current iteration, respectively; x_l and x_g are the personal best position and the global best in the current iteration, respectively. Original particle swarm optimization algorithm developed to be a classic particle swarm optimization (PSO) algorithm, which different from original PSO only add inertia weight W for the speed updating. The impact of inertia weight W is to keep the individual advantage in the search process. Inspired by the classic PSO algorithm, in this section, modified differential evolution is proposed. The MDE and the DE are different in two aspects as follow:

(1)Pitch adjustment instead of traditional mutation operation, which is works as follow:

```
if rand<Mr
%random position updating
    if rand>0.5
        v_{i,k} = x_{best,k} + rand_1 · (x_{r1,k} − x_{r2,k})
    elseif rand≤0.5
        v_{i,k} = x_{r0,k} - rand_2 · (x_{r1,k} − x_{r2,k})
    endif
else
    v_{i,k} = rand · (x_max − x_min) + x_min %disturbance operation
end
```

Here, the indices r0, r1 and r2 are distinct integers uniformly chosen from the set {1,2,...,NP}; x_{best} is the best vector in the current iteration k; rand, rand1 and rand2 belongs to a uniform distribution in the ranges [0,1]; Mr represent the position updating rate. In general, Mr is larger than 0.9.

(2) To well balance the exploration and exploitation of the proposed MDE algorithm, the CR value increases dynamically with increasing generations (k) as follows:

$$CR_k = CR_{\min} \exp(c \cdot k),\ c = \frac{\ln\left(\frac{CR_{\max}}{CR_{\min}}\right)}{K} \quad (1)$$

Where K is the maximum number of iterations, and k is the current number of iterations; wmin and wmax are the minimum inertia weight and the maximum inertia weight, respectively; CRmin and CRmax are the minimum crossover rate and the maximum crossover rate, respectively.

Experimental Results and Analysis

To test the performance of the proposed MDE algorithm, an extensive experimental evaluation and comparison with the DE/rand/1, DE/best/1,PSO, JADE and SaDE algorithms are provided based on a set of four global optimization problems as follows:

f_1 Sphere function, defined as $\min f_1 = \sum_{i=1}^{N} x_i^2$

Where global optimum $x^* = (0,0,...,0)$ and $f(x^*) = 0$ for $-100 \le x_i \le 100\ (i = 1,2,...,N)$.

f_2 Rastrigrin function, defined as $\min f_2 = \sum_{i=1}^{N} (x_i^2 - 10\cos(2\pi x_i) + 10)$

Where global optimum $x^* = (0,0,...,0)$ and $f(x^*) = 0$ for $-10 \le x_i \le 10\ (i = 1,2,...,N)$.

f_3 Griewank function, defined as

$$\min f_3 = \frac{1}{4000} \sum_{i=1}^{N} x_i^2 - \prod_{i=1}^{N} \cos\left(\frac{x_i}{\sqrt{i}}\right) + 1$$

Where global optimum $x^* = (0,0,...,0)$ and $f(x^*) = 0$ for $-600 \le x_i \le 600\ (i = 1,2,...,N)$.

f_4 Ackley's function, defined as

$$\min f_4 = 20 + e - 20\exp(-0.2\sqrt{\frac{\sum_{i=1}^{N} x_i^2}{N}}) - \exp(\frac{\sum_{i=1}^{N}\cos(2\pi x_i)}{N})$$ Where global optimum $x^* = (0,0,...,0)$ and $f(x^*) = 0$ for $-32 \le x_i \le 32\ (i = 1,2,...,N)$.

f_5 Schwefel's problem 2.2, defined as

$$\min f_5 = \sum_{i=1}^{N} |x_i| + \prod_{i=1}^{N} |x_i|$$

Where global optimum $x^* = (0,0,...,0)$ and $f(x^*) = 0$ for $-100 \le x_i \le 100\ (i = 1,2,...,N)$.

MDE is compared with two classic differential evolution algorithm DE/rand/1 and DE/best/1, PSO, as well as two recent adaptive DE algorithms JADE and SaDE, and the classic DE/rand/1. For fair comparison, we set the parameters of MDE to be fixed, wmin=0.05, wmax=0.9 and CRmin=0.1, CRmax=0.9 in all simulations. We follow the parameter settings in the original paper of JADE [1] and SaDE [7], except that the parameters of DE/rand/1 are set to be F=0.5 and CR=0.9. The results reported in this section are best, worst, mean and standard deviation (SD) over 30 independent simulations. For each simulation, all the procedure to be run in computer Inter(R) Pentium(R) 4, CPU 2.93GHz, and the numerical results using four differential evolution algorithm are report in Table 1.

Table 1 The optimization results of four differential evolution algorithms for f_1-f_5 (N=30)

Function	Algorithm	Iteration	Best	Worst	Mean	SD
f_1	DE/rand/1	1500	8.27e-012	8.25e-009	1.41e-009	2.24e-009
	DE/best/1	1500	2.26e-029	5.15e-027	8.54e-028	1.01e-027
	PSO	1500	1.36e-041	1.74e-031	8.05e-033	3.34e-032
	SaDE	1500	2.43e-046	3.08e-042	4.98e-044	1.19e-043
	JADE	1500	9.83e-065	9.36e-059	8.04e-060	2.24e-059
	MDE	1500	**5.16e-118**	**2.17e-105**	**7.28e-107**	**3.96e-106**
f_2	DE/rand/1	3000	8.95e+000	3.08e+001	1.72e+001	2.86e+001
	DE/best/1	3000	3.28e+000	2.85e+001	1.50e+001	2.09e+001
	PSO	3000	2.89e-012	2.87e-008	1.87e-011	1.08e-011
	SaDE	3000	1.88e-013	1.14e-011	2.89e-012	4.01e-012
	JADE	3000	3.08e-013	2.90e-012	8.95e-012	5.08e-012
	MDE	3000	**0.00e-000**	**2.84e-014**	**6.80e-015**	**6.64e-015**
f_3	DE/rand/1	2000	3.57e+000	8.79e+001	3.64e+001	2.88e+001
	DE/best/1	2000	2.43e+000	1.57e+001	3.00e+000	3.77e+000
	PSO	2000	1.08e+000	2.85e+001	2.09e+000	4.03e+000
	SaDE	2000	4.85e-004	9.08e-003	9.75e-004	5.98e-004
	JADE	2000	3.67e-022	4.98e-020	4.97e-021	9.75e-021
	MDE	2000	**1.52e-028**	**2.42e-024**	**2.27e-26**	**4.74e-26**
f_4	DE/rand/1	2000	1.85e-008	2.94e-007	3.86e-008	3.05e-008
	DE/best/1	2000	3.98e+001	5.05e+001	3.09e+001	2.95e+001
	PSO	2000	1.02e-008	3.02e-007	2.90e-008	3.75e-008
	SaDE	2000	4.03e-013	1.24e-013	3.00e-013	2.40e-013
	JADE	2000	8.75e-015	9.00e-014	7.95e-015	6.43e-015
	MDE	2000	**3.55e-015**	**7.10e-015**	**4.50e-015**	**1.59e-015**
f_5	DE/rand/1	2000	1.23e-019	3.08e-18	2.78e-018	3.97e-018

	DE/best/1	2000	1.63e-009	2.05e-008	8.90e-009	1.05e-008
	PSO	2000	1.92e-014	6.49e-012	4.03e-013	2.84e-013
	SaDE	2000	9.30e-021	3.08e-020	7.93e-020	5.93e-020
	JADE	2000	3.97e-035	8.04e-034	2.78e-034	3.90e-035
	MDE	2000	**5.01e-043**	**3.04e-041**	**4.98e-042**	**7.85e-042**

Conclusions

This paper proposes a new simple but effective and efficient MDE algorithm for unconstrained optimization problems with continuous decision variables. In the MDE algorithm, new random position updating strategy and disturbance operation were introduced and dynamically adjusted the parameter value of the algorithm, which makes it easier to explore a better solution and balance the local search and global search well. Based on several standards benchmark optimization problems carried out to be tested, the results obtained using the MDE algorithm may yield better solutions than those obtained using DE/rand/1, DE/best/1, PSO, JADE and SaDE algorithm, and demonstrate the effectiveness and robustness of the proposed algorithm. In short, the MDE algorithm is a promising optimization algorithm, and it has high exploration capability of solution space throughout the whole iteration.

References

[1] Jingqiao Zhang, Arthur C. JADE: adaptive differential evolution with optional external archive. IEEE Transaction on Evolution Computation, 2009, 13(5): 945-958.

[2] Quan-Ke Pan, Ling Wang, Bin Qian. A novel differential evolution algorithm for bi-criteria no-wait flow shop scheduling problems. Computers & Operations Research, 2009, 36(8): 2498-2511.

[3] Liao T W. Two hybrid differential evolution algorithms for engineering design optimization. Applied Soft Computing, 2010,10(4):1188-1199.

[4] Varadarajan M, Swarup K S. Differential evolution approach for optimal reactive power dispatch. Applied Soft Computing, 2008, 8(4):1549-1561.

[5] D.Zaharie, R.Matousek and P.Osmera. Control of population diversity and adaptation in differential evolution algorithms [C]. In Proc: Mendel 9th International Conference Soft Computer, Eds. Brno, Czech Republic, 2003(1): 41–46.

[6] S.Das,A.Konar, U.K.Chakraborty. Two improved differential evolution schemes for faster global search [C]. In ACM-SIGEVO Proc. Genetic Evolut. Comput. Conf, Washington, DC, pp: 991–998.

[7] A.K.Qin and P.N.Suganthan. Self-adaptive differential evolution algorithm for numerical optimization [C]. In Proc. The 2005 IEEE Congress on Evolutionary computation, 2005(2):1785–1791.

Advanced Materials Research Vols. 989-994 (2014) pp 2540-2542
© (2014) Trans Tech Publications, Switzerland
doi:10.4028/www.scientific.net/AMR.989-994.2540

People counting based on the moving feature of the mass

Pengzhe Qiao[1, a], Tao Li[2, 3, b], Tao Xiang[2, c] and Xizhi Zhang[4, d]

[1]Henan University of Animal Husbandry and Economy, Zhengzhou, 450011

[2]T he School of Computer Science and Engineering, University of Electronic Science and Technology of China, Chengdu, 611731

[3]The Department of Information Engineering, HeNan Radio & Television University, Zhengzhou, 450008

[4]Department of Information Engineering, Shengda Trade Economics & Management College Of Zhengzhou, zhengzhou, 451191

[a]qiaopengzhe@163.com, [b]cvlablitao@gmail.com, [c]xtao0924@gmail.com, [d]zhangxizhi2008@126.com

Keywords: people counting; optical flow algorithm; moving feature

Abstract. In order to improve the accuracy of people counting in video surveillance, the method for people counting based on the moving feature of the mass is proposed. We obtain the orientation and energy density of mass through the optical flow algorithm, and get the information about the size of mass to design the feature of mass. The people counting model is obtained by training a support vector machine (SVM) classifier with the moving feature and shape feature of mass. The experimental results confirm that our approach improves the accuracy of people counting.

Introduction

People counting based on video is an important application in real life. In recent years, many approaches are proposed based on video-based techniques. The method [1] utilizes the foreground segmentation by Gaussian Mixture Model to count people, and the method [2] analyzes the moving features and distribution of directions of people counting.

Above these methods neglect the information about the moving mass. Therefore, we introduce sizes of moving foreground masses and the histograms of the directions about optical flow of masses by quantizing to form the feature of mass. By training a support vector machine (SVM) classifier with the input of the feature of mass, the people counting model is obtained. Our main contribution is proposing a novel feature of mass which can characterize the intrinsic energy and size properties accurately.

Overview of Our Algorithm

The framework of the method consists of training section and detecting section. Firstly, we get the foreground moving mass in the video of cameras by using Gaussian Mixture Model; Secondly, we calculate the direction of the mass using the optical flow method at first, and then segment the peoples of different directions in the same mass according to the direction information, and complete the mass segmentation; Finally, we train the SVM classifier to complete people counting.

Get foreground mass region. First of all, Gaussian Mixture Model is used for getting the moving foreground mass by using the definition of K (the value range of K is 3-5) Gaussian models for each pixel firstly. Suppose the set $\{x_t\}_{t=1}^{L}$ is a set of pixels in a period of time, where L is the total frame number, x_t is the pixel value at time t, its probability is:

$$P\{x_t\} = \sum_{j=1}^{K} \omega_{j,t} \eta\left(x_t, \mu_{j,t}, \sigma_{j,t}\right) \tag{1}$$

$$\eta\left(x_t,\mu_{j,t},\sigma_{j,t}\right)=e^{\frac{1}{2\sigma_{j,t}^2}\left(x_t-\mu_{j,t}\right)^T\left(x_t-\mu_{j,t}\right)}\Big/\left(2\pi\right)^{\frac{n}{2}}\left|\sigma_{j,t}\right|^{\frac{1}{2}} \tag{2}$$

Where $\eta\left(x_t,\mu_{j,t},\sigma_{j,t}\right)$ is the j Gaussian distribution at time t, $\mu_{j,t}$ and $\sigma_{j,t}$ represent mean and variance respectively, $\omega_{j,t}(\sum_{j}^{K}\omega_{j,t}=1)$ is weight. If the value of x_{t+1} satisfy any Gaussian distribution, the point is the background. Conversely, it is the foreground, and then we get foreground mass of the image.

Moving feature and shape feature of the mass. In order to get more accurate analysis of the mass, we introduce the moving information into mass segmentation. (u,v) denotes the optical flow vector of the current pixel of mass, where u and v represent horizontal velocity and vertical velocity respectively. The process is as follows: Firstly, we established objective function according to the assumption of the consistency of the gray level and gradient, and then we got the optical flow vector by calculating the minimum of the objective function. The objective function is:

$$E(u,v)=\int_{\Omega}(w^T J_{\rho}(\nabla_3 f)w+\alpha(|\nabla u|^2+|\nabla v|^2))dxdy \tag{3}$$

Where $\nabla_3 f$ denotes the spatiotemporal gradient $(f_x,f_y,f_t)^T$, the vector field w describes the displacement, and the weight α serves as regularization parameter. The matrix J_ρ is the structure tensor, it is expressed as:

$$J_\rho=K_\rho*\begin{pmatrix}J_{11}&J_{12}&J_{13}\\J_{21}&J_{22}&J_{23}\\J_{31}&J_{32}&J_{33}\end{pmatrix}=K_\rho*\begin{pmatrix}I_x^2&I_xI_y&I_xI_t\\I_xI_y&I_y^2&I_yI_t\\I_xI_t&I_yI_t&I_t^2\end{pmatrix} \tag{4}$$

Where K_ρ is a Gaussian with standard deviation ρ, $*$ denotes convolution. The optical flow vector is the corresponding (u,v) when the objective function is minimal. Eq. 3 is calculated by Lagrange method as:

$$\Delta u-\frac{1}{\alpha}(K_\rho*(I_x^2)u+K_\rho*(I_xI_y)v+K_\rho*(I_xI_t))=0,\quad \Delta v-\frac{1}{\alpha}(K_\rho*(I_y^2)v+K_\rho*(I_xI_y)u+K_\rho*(I_yI_t))=0 \tag{5}$$

Eq. 5 is a nonlinear equation, we transfer it to linear equations in order to get a solution. Then a finite difference approximation to the Eq. 5 is given by

$$\sum_{j\in N(i)}\frac{u_i-u_j}{h^2}-\frac{1}{\alpha}(J_{11i}u_i+J_{12i}v_i+J_{13i})=0,\quad \sum_{j\in N(i)}\frac{v_i-v_j}{h^2}-\frac{1}{\alpha}(J_{21i}u_i+J_{22i}v_i+J_{23i})=0 \tag{6}$$

We got the unknown quantity (u_i,v_i) using iteration solution of the Gauss - Seidel algorithm [3]. The k iteration result is shown as Eq. 7.

$$u_i^{k+1}=\frac{\sum_{j\in N^-(i)}u_j^{k+1}+\sum_{j\in N^+(i)}u_j^k-\frac{h^2}{\alpha}(J_{12i}v_i^k+J_{13i})}{|N(i)|+\frac{h^2}{\alpha}J_{11i}},\quad v_i^{k+1}=\frac{\sum_{j\in N^-(i)}v_j^{k+1}+\sum_{j\in N^+(i)}v_j^k-\frac{h^2}{\alpha}(J_{12i}u_i^k+J_{13i})}{|N(i)|+\frac{h^2}{\alpha}J_{22i}} \tag{7}$$

Where, h is the size of the grid, $N(i)$ denotes the number of neighbors of pixel i that belong to the image domain. After obtaining the optical flow, we form the moving feature vector of mass H by an eight dimensional vector. H is normalized to $[0,1]$, and divided into eight bins to form an eight dimensional data. We input the vector to SVM [4], and obtain the people counting model.

Experimental Results

In this section, the program runs on the computer in which the CUP is Intel Pentium 2.3 G and the memory is 2G. We realize this program by using VC+OPENCV for the test of many different type

videos including scenes containing occlusion. The frame rate is 33fps/s, and the resolution is 720*576 in the set of videos.

As shown in Fig. 1, the optical flow is used to get internal movement direction in the mass, and the large mass is segmented into two masses through the direction difference. In general the large mass contains more people, and the little mass contains few people. We also can see that the strength of the optical flow information is also directly reflects the number of people, because the speed of people is similar in the scenes. The energy of optical flow about mass can reflect the people number in mass indirectly.

The experiment analyses the confusion matrix [5] to evaluate the algorithm performance as Eq. 8.

$$PR = TP/(TP+FP), \quad RE = TP/(TP+FN), \quad F = 2PR \cdot RE/(PR+RE) \tag{8}$$

As shown in Table 1, the value F and PR are over 95%. The experimental results confirm that our approach significantly improves the accuracy of people counting.

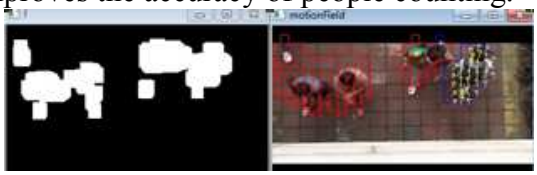

Fig. 1. The influence of the optical flow distribution to the segmentation

Table 1 The result of people counting

Video name	Actual line (in + out)	The thread count (in + out)	TP	FP	FN	PR（%）	RE（%）	F（%）
single direction1	12+0	12+0	12	0	0	100	100	100
two direction 3	29+37	29+37	66	0	0	100	100	100
two direction 4	32+28	32+28	60	0	0	100	100	100
two direction 5	28+18	29+17	45	1	1	97.82	97.82	97.82

Conclusion

The novel method is proposed in complex scenarios with the vertical camera. We integrate the optional flow intensity information of moving people and the size of the mass area to form the feature of mass, and we put the feature into the SVM for people counting analysis. The result show that, the energy and shape information of mass are adequately considered in the algorithm, so the accuracy is close to 100%.In the later study, we will consider joining foreground analysis strategies without shadow to the algorithm for mass information, in order to improve the detection rate.

Acknowledgement

This paper was supported in part by the key scientific and technological project of Henan province(142102210010); The key research project in science and technology of the education department Henan Province (14A520028, 14A520052), Ph.D. Programs Foundation of the Ministry of Education of China (YBXSZC20131031).

References

[1] A. Gardel, I. Bravo, P. Jimenez: Real time head detection for embedded vision modules.IEEE International Symposium on Intelligent Signal Processing. (2007).

[2] Y. Benabbas, N. Ihaddadene, T.Yahiaoui: Spatio-temporal optical flow analysis for people counting. Proc. of 7th IEEE International Conference on Advanced Video and Signal Based Surveillance. Boston, USA(2010)

[3] B. Andres, W. Joachim, F. Christian: submitted to Journal of Computer Science(2003)

[4] V.Vapnik: *Statistical learning theory*(Springer, New York, 1995).

[5] J.Barandiaran, B.Murguia, B.Fernando:Real-time people counting using multiple lines.Proc. of 9th International Workshop on Image Analysis for Multimedia Interactive Services. Klagenfurt, Austria(2008)

Advanced Materials Research Vols. 989-994 (2014) pp 2543-2546
© (2014) Trans Tech Publications, Switzerland
doi:10.4028/www.scientific.net/AMR.989-994.2543

A Cloud Storage Encryption Scheme Based on Separated Key and Encryption Policy

Wang Peng[1, a], Zhang Fuzheng[2,b] and Han Chunlei[3,c]

[1]Changchun University of Science and Technology,Changchun 130000,China

[2]Changchun University of Science and Technology,Changchun 130000,China

[3]Changchun University of Science and Technology,Changchun 130000,China

[a]635461179@qq.com, [b]zhangxinshun@163.com, [c] 1213454036 @qq.com

Keywords: cloud storage security; identity authentication; key separation; encryption strategy

Abstract. With the continuous expansion of the scale data storage, cloud storage technology for its high performance and low cost to get a lot of attention and support. However, the security issues of cloud storage data hinder its further promotion. For the current cloud storage applications of data stored encrypted, a cloud storage encryption scheme based on the separated key and encryption policy is proposed. By strengthening the data encryption key management and data encryption algorithm, the system achieves a more secure storage of data assurance in the technical level.

Cloud storage encryption technology

Encryption technology is the main storage data encryption security measures taken, but also the most used means confidentiality. Specific process is: First, the data is encrypted, then the data stored ciphertext to a storage device; in obtaining data, first remove the data ciphertext, and then use the decryption key for decryption. Common data encryption[1] modes include static data and dynamic data encryption mode encryption mode.

Static data encryption mode refers to the user data is encrypted locally and then sent to the ciphertext cloud storage server. The advantages are: the user to save the decryption key, high degree of safety. Disadvantages are: client computing capability have higher requirements, and only the user's data is encrypted.

Dynamic Data encryption mode, refer to cloud storage server encrypts all data and storage. The advantages are: a unified data encryption key management, ease of use. Disadvantages are: data security depends entirely on cloud storage service provider, from the user's control.

There is no effective data encryption method[2], it is possible to achieve both the encrypted data on the server side, but also a good guarantee the security of stored data.

To ensure that the server is encrypted cloud storage data storage security, the biggest problem is how to solve two problems[3]: First, the management of data encryption key, the second is the data encryption algorithm selection problem.

Traditional cloud storage encryption scheme

Working principle diagram of traditional cloud storage encryption scheme, as shown in Fig.1.

The workflow of traditional cloud storage encryption scheme is as follows:

(1) Users upload the master key to the cloud storage server.

(2) Treating the stored data when encrypted data generated by encrypting the first key generation data encryption key k; secondly based on a single encryption algorithm to encrypt data; Finally, the ciphertext data storage. The ciphertext is stored on the server while the data encryption key.

(3) When the decryption of the ciphertext data, the first data encryption key to decrypt the ciphertext; Secondly, according to the corresponding decryption algorithm to decrypt the data; Finally, the data returned to the user.

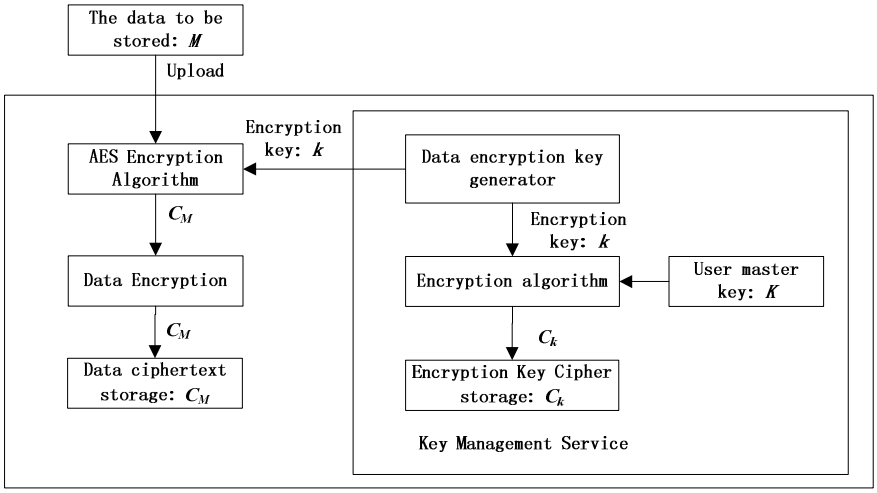

Fig.1: The traditional cloud storage encryption scheme works diagram

While traditional cloud storage encryption scheme allows users to store data in the form of cipher text, but because of its intrinsic unity of key management and data encryption algorithm, making the security of data there is a certain risk. First, because the data encryption keys and master keys stored in the cloud storage service side, hackers can impersonate the user access to the user's data by stealing the user's login account. Secondly, all the data stored on the server side of the cloud cloud storage service managers are transparent. Again, the data encryption algorithm unity such that all the user data using the same encryption algorithm. If the algorithm itself is not high safety performance, safety data for all users are faced with the threat.

A Cloud Storage Encryption Scheme Based on Separated Key and Encryption Policy

For traditional security issues that exist in the cloud storage encryption scheme is proposed based on cloud storage encryption scheme and encryption key separation strategy. The program key and the encrypted virtual management services for the separation of the data encryption key management, and increase the data encryption algorithm selection strategy[4].

Working principle diagram is shown in Fig.2.

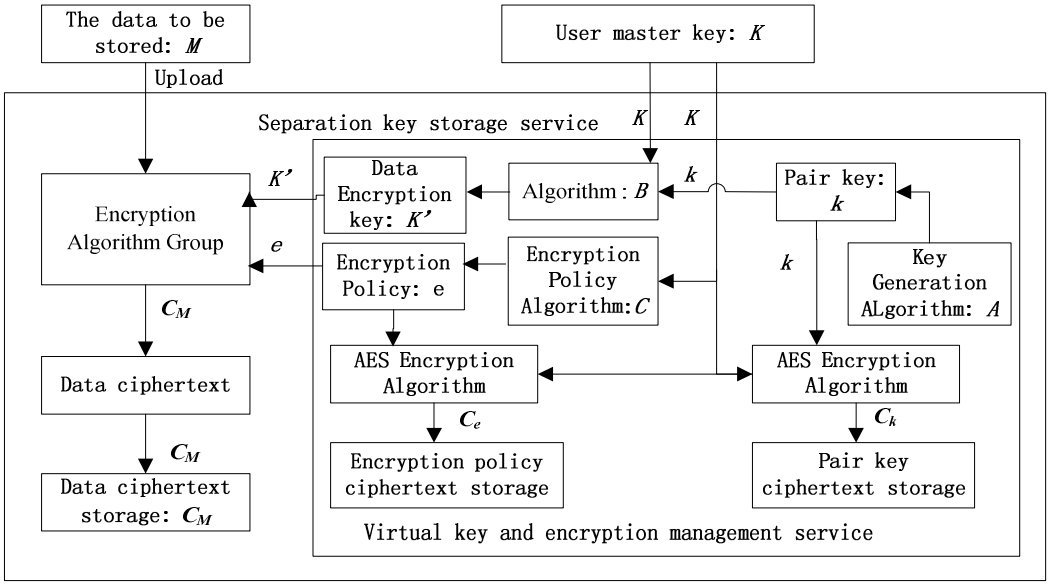

Fig.2: Based on the work of separation and encryption key strategic cloud storage encryption scheme schematic

Encryption Policy: take user master key and timestamp as input pairs to generate encryption policy with encryption policy algorithm, and store the encrypted ciphertext policy on the server.

Pair Key: generated by the key algorithm to automatically generate and together generate data encryption keys and user master key by the algorithm B, and then treat the stored data to be encrypted.

Encryption Algorithm Group: Provide a variety of encryption algorithms and corresponding decryption algorithm, and given the corresponding encryption policy. Users select the appropriate encryption policy based on the encryption algorithm used to encrypt the data and decrypt the encryption policy to select the corresponding decryption algorithm.

Workflow-based separation and encryption key strategic cloud storage encryption scheme is as follows:

(1) When treating the stored data is encrypted, first generate a key pair k; secondly paired with the primary key generation key data encryption key together; then generated based on the user master key encryption policy; then encryption policies and data encryption key as input select an encryption algorithm to encrypt the stored data treatment; last ciphertext data storage. Among them, the pair of keys and encryption policy is stored encrypted on the server.

(2) When the data is decrypted ciphertext, first paired with the user master key encryption key ciphertext and decrypt ciphertext strategies; secondly regenerate the data decryption key K according to the user master key and pairing key '; then data encryption and decryption key strategy as an input, select the corresponding decryption algorithm to decrypt the ciphertext data; Finally, the data returned to the user.

Based on the key separation and encryption strategy of cloud storage encryption scheme, the relationship between key separation and encryption strategy as shown in Fig.3:

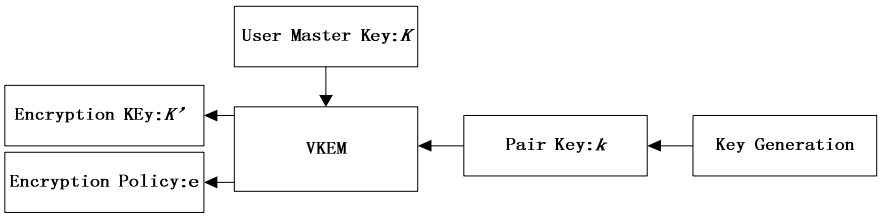

Fig.3: Separation and encryption key strategic relationship diagram

Data encryption key consists of two key components: one is the master key, saved by the user; another is paired keys kept by the cloud storage server. When VKEM processing data encryption, the user must give the key to the master key and matching encryption key data is calculated, and then treat the stored data encryption. Data encryption keys and master keys are not stored in any form on the server side, thus greatly increasing the difficulty of stealing data encryption keys to ensure the security of data.

Data encryption algorithm is determined by the encryption policy, and encryption policies and keys generated by the user's home, the master key is not stored in any form on the server side, so even get still decrypt ciphertext encryption policy, can not be used in what kind of data encryption algorithms, adds data encryption algorithms are difficult to break, to ensure the security of data.

Performance Testing

We use a simple cloud storage service system LAN built, experimental data upload and download via the browser and the cloud server. In order to improve service performance separation and encryption key management server strategy, they were placed on three physical servers for deployment. Based on this framework, for data transfer test.

Encryption cost ratio: the encryption key management services and encryption policies proportion of time spent entire data encryption services takes time.

Decryption cost ratio: encryption key management services and encryption policies take time to decrypt data services accounted for the proportion of total time spent.

Fig.4 shows the two cloud storage data encryption scheme to be stored in a different size than the encryption takes under 5 decryption program for the two cloud storage data to be stored in a different size than the lower of cost and decryption.

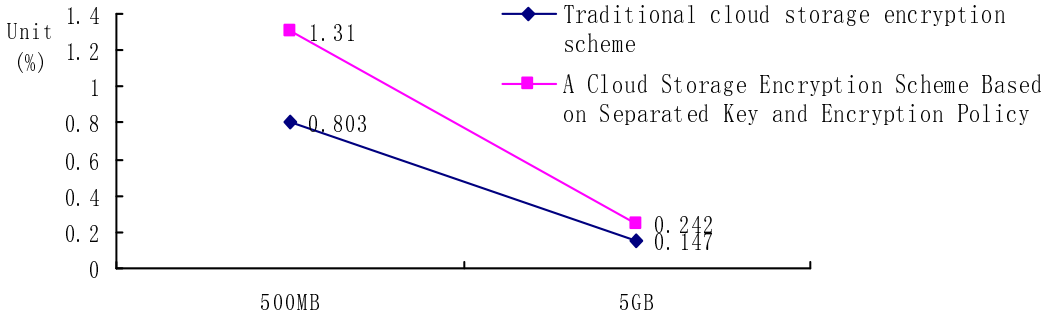

Fig.4: Encryption cost ratio under different sizes

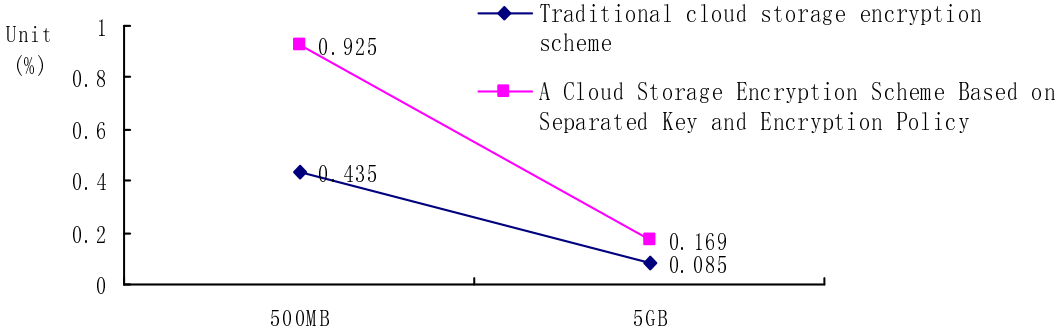

Fig.5: Decryption cost ratio under different sizes

Judging from the test case data, whether the data encryption process or decryption of data, loss of key computing performance separation cloud storage encryption policy-based encryption scheme introduced very small, little effect on the overall performance. Moreover, this affects the performance of cloud storage will increase the amount of data the user is getting smaller. Therefore, the proposed cloud storage encryption scheme, the performance loss is calculated by minimizing server privatized data, to better protect the security of the cloud storage of user data, reducing the ciphertext to crack the degree of risk, so for safe cloud storage applications is entirely acceptable.

Summary

In this paper, because of the traditional security issues that exist in the cloud storage encryption scheme, a cloud storage encryption scheme based on the separated key and encryption policy is proposed. By using this scheme the encryption key separation strategies to enhance the data encryption key management and encryption algorithms to ensure the privacy of user data cloud, improved safety performance. Finally, the test results show that, it not only ensures high security of data, but also has a good performance.

References

[1] Lin Qinying, Gui Xiaolin, Shi Deqin etc. Strategies for safe storage cloud storage. Computer Research and Development，2011,48(z1):240-243

[2] Liu Fan, Yang Ming. A cloud storage ciphertext policy attribute-based encryption scheme used. Application Research of Computers,2012,29(4):1452-1456

[3] Huang Yongfeng Zhang Jiuling, Li Xing. Cloud storage applications encrypted storage and retrieval technology. ZTE Technology,2010，16(4)：33-35

[4] De Capitani di Vimercati S,Foresti S,Jajodia S, et al. Encryption-based policy enforcement for cloud storage. Proceedings of IEEE the 30th International Conference on Distributed Computing Systems Workshops,Genova,Italy,2010:42-51

Advanced Materials Research Vols. 989-994 (2014) pp 2547-2550
© (2014) Trans Tech Publications, Switzerland
doi:10.4028/www.scientific.net/AMR.989-994.2547

Method based on the Minimum Deviation for Multi-attribute Decision-making and Its Application

Zhou Hong-an

School of Science, Xi'an Technological University, Xi'an 710032，P. R. China

E-mail:honganzhou@sohu.com

Keywords: Multi-attribute decision-making; quadratic programming; weight; priority

Abstract. The multi-attribute decision making (MADM) problem is studied, in which the information about attribute weights is unknown and the decision maker (DM) has avail preference information on alternatives. Firstly, a quadratic programming model based on the minimum deviation between the objective decision-making information and the subjective preference information on alternatives is established. Secondly, the existence of solution to the model is proved and the calculated formula of the attribute weights are given, thus the overall values of the alternatives are gained by using the additive weighting method. Based on these values, the selecting the best on alternatives is processed. Finally, a practical example is illustrated to show the feasibility and availability of the developed method.

Introduction

Up to now, a lot of good results [1−3] have been obtained on the researches of the MADM problems without preference information on alternatives. However, in the real process of decision-making, the decision maker (DM) often has the subjective preference information on alternatives [4−8]. This is what is called the MADM problems with preference information on alternatives (MADM-PA, for short). As a result, the MADM-PA problems have been investigated and some methods of solving theses problems have been proposed recently. Such as, the MADM-PA problems that the information about attribute weights is unknown completely, the attribute values are numbers and the DM's preference relation on alternatives take the form of fuzzy complementary judgment matrix [3−4] or reciprocal judgment matrix [5−6] are studied in Refs [3-6]. A non-linear programming method is presented. The MADM-PA problem that the information about attribute weights is unknown completely and the DM has ordering preference on alternatives is investigated in Ref [7]. The method based on sensitivity analysis is presented. The MADM-PA problem, in which the attribute weights are interval numbers and the DM's preference relation on alternatives are in the fuzzy complementary judgment matrix and reciprocal judgment matrix is studied in Ref [8]. A linear programming approach is presented. The MADM-PA problem that the information about attribute weights is unknown and DM has avail preference information on alternatives is investigated in this paper. In our method, Section 2 gives simple representation of the studied problem. The principle and approach of decision-making are given in section 3. An application example is given in section 4. Finally, some concluding remarks are included.

Representation of problem

The basic model of the MADM-PA that will be studied in this paper can be represented as follow:

- Let $X = \{x_1, x_2, \cdots, x_n\}$ be a set of $n\ (\geq 2)$ feasible alternatives, and denote $N = \{1, 2, \cdots, n\}$;
- Let $S = \{s_1, s_2, \cdots, s_m\}$ be a set of $m\ (\geq 2)$ attributes, and denote $M = \{1, 2, \cdots, m\}$;
- Let $\omega = (\omega_1, \omega_2, \cdots, \omega_m)^T$ be the vector of weights, such that, $\omega_i \geq 0, \sum_{i=1}^{m} \omega_i = 1$;

- Let $v_j, j \in N$ be the DM's subject avail preference information on alternatives;
- Let $A=(a_{ij})_{m\times n}$ be a decision matrix, where a_{ij} is the attribute value for the alternative x_j with respect to attribute $s_i, i \in M, j \in N$.

In general, there are benefit attribute values I_1, cost attribute values I_2, steady attribute values I_3 and interval values I_4 in the MADM and the different attribute values may be the different dimension. Obviously, $M = I_1 \bigcup I_2 \bigcup I_3 \bigcup I_4$. For the convenience of decision-making, we need to deal with all attributes in dimensionless units and normalize each attribute value. This can be achieved by normalizing a_{ij} in the matrix $A=(a_{ij})_{m\times n}$ into a corresponding element r_{ij} in the matrix $R=(r_{ij})_{m\times n}$ with the normaled formulas in Ref [3].

Then using the simple additive weighting method[1], the overall value of alternative x_j can be expressed as $z_j(\omega)=\sum_{i=1}^{m}\omega_i r_{ij}, j \in N$ (1)

Principle and approach of decision-making

Because the attribute weights are unknown, we need determine it for ranking priorities or selecting the best on alternatives. Considering both the objective decision-making information and the subjective preference information on alternatives is consistent. However, there always exist some differences in them. Therefore, their deviation must be minimum to obtain the reasonable attribute weights. Considering all alternatives are fair. Therefore, the following quadratic programming model can be established:

$$\begin{cases} \min d^2(\omega)=\sum_{i=1}^{m}\sum_{j=1}^{n}(r_{ij}-v_j)^2\omega_i^2 \\ s.t.\sum_{i=1}^{m}\omega_i=1, \omega_i \geq 0 \end{cases} \quad (2)$$

Theorem If $\sum_{j=1}^{n}(r_{ij}-v_j)^2>0, i \in M$, then the model(2) has only solution.

Prove The Lagrange number multiply function $L(\omega,\lambda)=\sum_{i=1}^{m}\sum_{j=1}^{n}(r_{ij}-v_j)^2\omega_i^2+2\lambda(\sum_{i=1}^{m}\omega_i-1)$ is constructed.

let $\begin{cases} \frac{\partial L}{\partial \omega_i}=2\sum_{j=1}^{n}(r_{ij}-v_j)^2\omega_i+2\lambda=0 \\ \frac{\partial L}{\partial \lambda}=2(\sum_{i=1}^{m}\omega_i-1)=0 \end{cases}$;

This is, $\begin{cases} \sum_{j=1}^{n}(r_{ij}-v_j)^2\omega_i+\lambda=0 \\ \sum_{i=1}^{m}\omega_i=1 \end{cases}$, $i \in M$.

Scilicet,

$$\begin{bmatrix} \sum_{j=1}^{n}(r_{1j}-v_j)^2 & 0 & \cdots & 0 & 1 \\ 0 & \sum_{j=1}^{n}(r_{2j}-v_j)^2 & \cdots & 0 & 1 \\ \vdots & \vdots & \ddots & \vdots & \vdots \\ 0 & 0 & \cdots & \sum_{j=1}^{n}(r_{mj}-v_j)^2 & 1 \\ 1 & 1 & \cdots & 1 & 0 \end{bmatrix}_{(m+1)\times(m+1)} \begin{bmatrix} \omega_1 \\ \omega_2 \\ \vdots \\ \omega_m \\ \lambda \end{bmatrix}_{(m+1)\times 1} = \begin{bmatrix} 0 \\ 0 \\ \vdots \\ 0 \\ 1 \end{bmatrix}_{(m+1)\times 1} \tag{3}$$

Let $B_{mm} = diag[\sum_{j=1}^{n}(r_{1j}-v_j)^2, \sum_{j=1}^{n}(r_{2j}-v_j)^2, \cdots, \sum_{j=1}^{n}(r_{mj}-v_j)^2]_{m\times m}$;

$W_{m1} = (\omega_1, \omega_2, \cdots, \omega_m)^T$; $0_{m1} = [0, 0, \cdots, 0]^T$; $E_{m1} = (1, 1, \cdots, 1)^T_{m\times 1}$.

Then(3) equal to (4):

$$\begin{pmatrix} B_{mm} & E_{m1} \\ E_{m1}^T & 0 \end{pmatrix}\begin{pmatrix} W_{m1} \\ \lambda \end{pmatrix} = \begin{pmatrix} 0_{m1} \\ 1 \end{pmatrix} \Leftrightarrow \begin{cases} B_{mm}W_{m1} + \lambda E_{m1} = 0_{m1} \\ E_{m1}^T W_{m1} = 1 \end{cases} \tag{4}$$

Let $D_k = \begin{vmatrix} \sum_{j=1}^{n}(r_{1j}-v_j)^2 & 0 & \cdots & 0 \\ 0 & \sum_{j=1}^{n}(r_{2j}-v_j)^2 & \cdots & 0 \\ \vdots & \vdots & \ddots & \vdots \\ 0 & 0 & \cdots & \sum_{j=1}^{n}(r_{kj}-v_j)^2 \end{vmatrix}_{k\times k}$, $k \in M$.

Because $\sum_{j=1}^{n}(r_{ij}-v_j)^2 > 0, i \in M$,we have $D_k > 0 (k = 1, 2, \cdots, m)$, thus B_{mm} is a positive definite matrix. This is, B_{mm} is inverse, then the model (2) has only solution. The W_{m1} is solved as follow:

Because the B_{mm} is inverse, then we can obtain W_{m1} by solving the matrix equations (4)as follow:

$$W_{m1} = \frac{B_{mm}^{-1}E_{m1}}{E_{m1}^T B_{mm}^{-1} E_{m1}} = \omega \tag{5}$$

Substituting ω into equation (1), we can get the overall value $z_j(\omega)$ of the alternative x_j. Obviously, the bigger the vales of $z_j(\omega)$ is, the better the corresponding alternative x_j.

Based on the above discussion, we will give the solving processes of the proposed method by using a practical example in the following section.

Practical example

An investment company is planning to exploit a new product and there are five investment alternatives $x_j (j = 1, 2, 3, 4, 5)$ to be considered. The main attributes of evaluating the alternatives are listed as s_1: investment amount, s_2: expected net profit amount, s_3: venture profit amount; s_4: venture loss amount, respectively. Among these four attribute, s_2 and s_3 are of benefit attributes, s_1 and s_4 are of cost attributes. The attribute values of each alternative are listed in Table1 (attribute unit

is10000$), suppose that the DM has avail preference information on alternatives as $v_1 = 0.82, v_2 = 0.85, v_3 = 0.90, v_4 = 0.75, v_5 = 0.95$. Please determine the best investment alternative.

Table1 Original decision matrix A

	x_1	x_2	x_3	x_4	x_5
s_1	5.2	10.08	5.25	9.72	6.60
s_2	5.2	6.70	4.20	5.25	3.75
s_3	4.73	5.71	3.82	5.54	3.30
s_4	0.473	1.599	0.473	1.313	0.803

$$R = (r_{ij})_{4\times5} = \begin{bmatrix} 0 & 1 & 0.010 & 0.926 & 0.287 \\ 0.492 & 1 & 0.153 & 0.508 & 0 \\ 0.407 & 0 & 0.784 & 0.071 & 1 \\ 1 & 0 & 1 & 0.254 & 0.707 \end{bmatrix}$$

Step1 Using normaled formulas [3] ,we can get the normalized decision matrix R from Table1 as top:

Step2 By solving the equation (5), the weight vector of the attributes is obtained as $\omega = (0.102, 0.300, 0.200, 0.398)^T$.

Step3 By (1), the overall value $z_j(\omega)$ of the alternative x_j as follow:

$z_1 = 0.627$; $z_2 = 0.402$; $z_3 = 0.602$; $z_4 = 0.362$; $z_5 = 0.511$.

Thus the ranking priorities of the corresponding alternatives is $x_4 \prec x_2 \prec x_5 \prec x_3 \prec x_1$, this is, the best alternative is x_1 .

Conclusion

In this paper, we propose a new method to solve the MADM -PA problem that the information about weights is unknown and the DM's avail preference information on alternatives. The core of this method is to determine the attribute weights based on a quadratic programming model and applied the project evaluation in the field of venture investment. Not only it can reflect both the objective information and the DM's subjective information, but also it has the advantages of simple operation and easy to implement on a computer.

Acknowledgement

This work was supported by the Natural Science Research Foundation of Shaanxi Province (2013JM1007)

References

[1] Hwang C L, Yoon K. Multiple Attribute Decision Making [M]. Berlin: Spring-Verlag, 1981.

[2] Li Deng-feng. Two New Methods for Multi-attribute Decision Makings with Information Partially Known [J]. Journal of Systems Science and Systems Engineering, 1998, 17(1):70-74.

[3] XU Ze-shui. Uncertain multiple attribute decision making: method and applications [M].Beijing: Tsinghua University Press, 2004. (In Chinese)

[4] Z P Fan, J Ma, Q Zhang. An approach to multiple attribute decision making based on fuzzy preference information [J]. Fuzzy Sets and Systems, 2002, 131:101-106.

[5] Ma Jian, Fan Zhi-ping , Huang Li-Hua. A subjective and objective integrated approach to determine attributes weights [J]. European Journal of Operational Research, 1999, 112:397-404.

[6] J Wu, C Y Liang, W H Li. Method to determine attribute weights based on subjective and objective integrated [J]. Systems Engineering and Electronics, 2007, 29(3): 383- 387. (In Chinese)

[7] W T Xiong, S Y Liu, W H Li. A Method to Determine Multi-attribute Weights Based on Sensitivity Analysis [J]. Journal of Wuhan University of Technology, 2004, 26(12):92-95.

[8] Z S Xu. Method for multi-attribute decision making with preference information on alternatives under partial weight information. [J]. Control and decision, 2004, 19(1):85-88. (In Chinese)

Advanced Materials Research Vols. 989-994 (2014) pp 2551-2554
© (2014) Trans Tech Publications, Switzerland
doi:10.4028/www.scientific.net/AMR.989-994.2551

Orthogonal Semi-supervised Marginal Fisher Analysis

Xingzhu LIANG [a], Yu'e LIN [b]

School of Computer Science and Engineering, Anhui University of Science and Technology

Huainan, 232001, China

[a]lxz9117@126.com, [b]linyu_e@126.com

Keywords: manifold-based learning; dimensionality reduction; face recognition; orthogonal semi-supervised

Abstract. In recent years, a variety of manifold-based learning dimensionality reduction techniques have been proposed, which attempt to project the original data into a lower dimensional feature space by preserving the local neighborhood structure. Among them, marginal fisher analysis (MFA) achieved high performance for face recognition. However, the optimal basis vectors obtained by MFA are non-orthogonal and MFA usually deteriorates when labeled information is insufficient. In order to resolve these problems, we present a new method called orthogonal semi-supervised marginal fisher analysis (OSMFA), which not only extracts all the orthogonal discriminant vectors but also preserves the global structure of labeled and unlabeled samples to learn a better subspace for classification. Experimental results on ORL database demonstrate the effectiveness of the proposed algorithm.

Introduction

Over the past few decades, a large volume of feature extraction techniques have been proposed and most of them have been successfully applied to many applications such as face recognition and so on. One classical technique is the linear discriminant analysis (LDA) [1] that has been shown to be successful on classification problem, such as face recognition. But, when the data is distributed in a nonlinear way, LDA may fail to discover essential data structures. Another technique of manifold-based learning called locality preserving projections (LPP) [2] has been proposed for dimensionality reduction. LPP can preserve the intrinsic geometry of data and yield an explicit linear mapping suitable for training and testing samples. However, LPP has an inherent limitation, that is, the objective function of LPP is to minimize the local quantity, which has no direct relationship to classification. Yan et al. [3] proposed marginal fisher analysis (MFA), which achieved high performance for face recognition. MFA overcomes limitations of LDA and LPP. However, MFA neglects efficacy of the unlabeled samples and the optimal basis vectors obtained are nonorthogonal, which are believed to have more discriminating power [4–6]. In the real world, the labeled samples are often very difficult and expensive to obtain. The supervised methods cannot work well when there is a lack of training samples; in contrast, unlabeled samples can be easily obtained. Therefore, in such situations, it can be beneficial to incorporate the information which is contained in unlabeled samples into face classification. Many algorithms, e.g. semi-supervised discriminant analysis [7] and semi-supervised method based on local and global preserving [8], can efficiently handle the labeled and unlabeled samples to learn a better subspace for classification.

In this paper, we present a new method called Orthogonal Semi-supervised Marginal Fisher Analysis (OSMFA), which can preserve the global structure of labeled and unlabeled samples and at the same time derive all the orthogonal optimal discriminant vectors. The effectiveness of the proposed algorithm is demonstrated by experiments on the ORL face database.

MFA

Assume that X is a n dimensional face sample set with N elements belonging to C classes. Denote x_i the jth image, and N_l number sample in the class i .Thus, we have $\sum_{i=1}^{C} N_i = N$ and $X = [x_1 \cdots x_i \cdots x_N]$. Marginal fisher analysis (MFA) develops a new criteria to characterize intra-class compactness and inter-class separability, in which, the within-class compactness is represented as the sum of distances between each sample and its intra-class neighbors, and the between-class separability is characterized as the sum of distances between each point and its inter-class neighboring points.In MFA, the within-class scatter matrix is defined as:

$$\begin{aligned} S_w^L &= \sum_{i=1}^{N}\sum_{j=1}^{N} R_W(i,j)(x_i - x_j)(x_i - x_j)^T \\ &= X(D_W - R_W)X^T \\ &= XL_W X^T \end{aligned} \tag{1}$$

Where

$$R_W(i,j) = \begin{cases} 1, & \text{if } i \in N_{k1}(j) \text{ or } j \in N_{k1}(i) \\ 0, & \text{otherwise} \end{cases} \tag{2}$$

Where $N_{k1}(i)$ indicates the index set of the k_1 nearest neighbors of the sample x_i in the same class.

The between-class scatter matrix is defined as

$$\begin{aligned} S_B^L &= \sum_{i=1}^{N}\sum_{j=1}^{N} R_B(i,j)(x_i - x_j)(x_i - x_j)^T \\ &= X(D_B - R_B)X^T \\ &= XL_B X^T \end{aligned} \tag{3}$$

where

$$B_{ij} = \begin{cases} 1, & \text{if } (i,j) \in P_{k2}(c_i) \text{ or } P_{k2}(c_j) \\ 0, & \text{otherwise} \end{cases} \tag{4}$$

where $P_{k2}(c)$ denotes the index set of the k_2 between-class nearest neighbors of the sample x_i .

The objection function of MFA is defined as:

$$W = \arg\min_{w} \frac{tr(W^T S_W^L W)}{tr(W^T S_B^L W)} \tag{5}$$

Eq. 5 can be solved by generalized eigenvalue decomposition

$$S_W^L w_i = \lambda_i S_B^L w_i \quad i = 1,2,\cdots,l \tag{6}$$

OSMFA

Assume that $X = [X_1\ X_2]$ are composed of labeled and unlabeled samples. $X_1 = [x_1 \cdots x_i \cdots x_N]$ are composed of labeled samples and $X_2 = [x_{N+1} \cdots x_i \cdots x_{N+M}]$ are composed of unlabeled samples. In order construct the objective function using labeled and unlabeled data, we give total-scatter matrix S_T and the local scatter matrix S_L, respectively. S_T is defined as follows:

$$S_T = \frac{1}{2(N+M)(N+M)} \sum_{i=1}^{N+M}\sum_{j=1}^{N+M} (x_i - x_j)(x_i - x_j)^T \tag{7}$$

S_L is defined as follows:

$$S_L = \frac{1}{2(N+M)(N+M)} \sum_{i=1}^{N+M}\sum_{j=1}^{N+M} H_{ij}(x_i - x_j)(x_i - x_j)^T \tag{8}$$

Affinity matrix H_{ij} is defined as follows

$$H_{ij}=\begin{cases}\exp(-\left\|x_i-x_j\right\|^2/t), & \text{if } i\in N_k(j) \text{ or } j\in N_k(i)\\ 0, & \text{otherwise}\end{cases} \tag{9}$$

Then, we give a new criterion as follows:

$$W=\arg\min_{WW^T=I}\frac{tr(W^TS_W^LW+W^TS_LW)}{tr(W^TS_B^LW+W^TS_TW)} \tag{10}$$

The new objective function is constructed by labeled and unlabeled samples, so we call it as Orthogonal Semi-supervised Marginal Fisher Analysis (OSMFA). Equation.10 can be solved by generalized eigenvalue decomposition

$$(S_W^L+S_L)w=\lambda(S_B^L+S_T)w \tag{11}$$

The projection axes can be selected as the generalized eigenvectors $w_1,w_2,\cdots,w_d$ of $(S_W^L+S_L)w=\lambda(S_B^L+S_T)w$ corresponding to d smallest eigenvalues.

However, since the matrix $(S_B^L+S_T)^{-1}(S_W^L+S_L)$ is asymmetric, the basis vectors $\alpha_1,\alpha_2,\cdots,\alpha_r$ are not orthogonal. The orthogonal basis vectors to Eq. 10 can be obtained through the Gram–Schmidt orthogonalization [6]. OSMFA can be described in the following steps.

Step 1: Compute S_W^L and S_B^L according to Eq. 1- 4;

Step 2: Compute S_T and S_L according to Eq. 7-9;

Step 3: Then, compute $(S_B^L+S_T)$ and $(S_W^L+S_L)$,respectively;

Step 4 : Solve Eq. 10 by generalized eigenvalue decomposition, then we can obtain the basis vectors $\alpha_1,\alpha_2,\cdots,\alpha_r$ .Compute orthogonal matrix W of the $\alpha_1,\alpha_2,\cdots,\alpha_r$ using the Gram–Schmidt orthogonalization.

Experimental Results

To demonstrate the effectiveness of our method, experiments were done on the ORL face database. The ORL face database is composed of 40 distinct subjects. Each subject has 10 images under different expression and different views. The size of each face image is 92×112. From the ORL face database, we randomly selected l (3,4,5,6,7) images from each person for training, while the rest of the images of each person were selected for testing. OSMFA algorithm is compared with MFA, ODLPP and SDA [6,7]. We repeated the experiments 10 times in ORL face database. The average accuracies were taken as their final recognition rates. The recognition rates of the four algorithms mentioned above are shown in Table 1.

Table 1 Recognition rates on the ORL face database (%)

methods	training samples/class				
	3	4	5	6	7
OSMFA	91.28	93.17	95.50	97.28	97.67
MFA	90.75	92.38	94.70	96.62	96.83
SDA	89.33	91.16	93.40	94.12	95.17
ODLPP	88.61	90.18	91.25	94.64	95.25

From Table 1, we find that OSMFA is the most efficient dimensionality reduction method, and is much more efficient than SDA, MFA and ODLPP. The one reason is that OSMFA method eliminates the dependence among discriminant vectors to improve the performance of MFA. The other is that the criterion of OSMFA is optimal compared with criterions of SDA, MFA and ODLPP.

Conclusions

The idea behind OSMFA is to learn orthogonal optimal discriminant vectors and preserves the global structure of labeled and unlabeled samples in addition to separating labeled samples in different classes from each other. As a result, OSMFA is more effective and efficient in face recognition.Experiments on face data show that the proposed algorithm has more discriminative power in comparison with SDA, MFA and ODLPP.

The proposed algorithm is still linear technique for feature extraction. Therefore, they may not sufficient to deal with some applications that have non-linear relationships.One of our future works includes using the so-called kernel trick to generalize the proposed algorithm. The orther is that we will focuse on the incremental learning methods [9] and the incremental feature set will be utilized to improve its processing speed and thus new algorithm can be developed that are suitable for real-time classification and recognition.

Acknowledgment

This work is supported by Anhui Provincial Natural Science Foundation (No.1208085QF123), Anhui Provincial Natural Science Foundation of Higher Education of China (No. KJ2012Z084) and Foundation of Youth teachers of Anhui University of Science and Technology(No. 2012QNZ10).

References

[1] P Belhumeur, J Hespanha.et al. Eigenfaces vs. Fisherfaces: Recognition using class specific linear projection. IEEE Transactions on Pattern Analysis and Machine Intelligence, Vol.19(1997),p.711–720.

[2] X F He, S C Yan, Y Hu, et al. Face recognition using Laplacianfaces. IEEE Transactions on Pattern Analysis and Machine Intelligence, Vol. 27(2005),p.328–340.

[3] D Xu, S Yan, D Tao , et al. Marginal Fisher Analysis and Its Variants for Human Gait Recognition and Content Based Image Retrieval. IEEE Transactions on Image processing, Vol.16(2007),p.2811–2821.

[4] D Cai, X F He, J W Han, Orthogonal laplacianfaces for face recognition. IEEE Transactions on Image Processing, Vol.15(2006),p.3608–3614.

[5] H F Hu. Orthogonal neighborhood preserving discriminant analysis for face recognition. Pattern Recognition, Vol.41(2008),p2045–2054.

[6] L Zhu, S N Zhu. Face recognition based on orthogonal discriminant locality preserving projections. Neurocomputing, Vol.70(2007),p.1543–1546.

[7] D Cai, X F He, J WHan.Semi-supervised discriminant analysis. Proceedings of the 11th IEEE International Conference on Computer Vision, ICCV07, Rio de Janeiro, Brazil, October, 2007, p. 1–7.

[8] H Huang, J W Li, J M Liu.Future Enhanced semi-supervised local Fisher discriminant analysis for face recognition. Generation Computer Systems, vol. 31(2012), p. 244–253.

[9] J G Wan, E Sung, W Y Yau. Incremental two-dimensional linear discriminant analysis with applications to facerecognition. Neurocomputing, vol. 33(2010), p. 314–322.

Advanced Materials Research Vols. 989-994 (2014) pp 2555-2559
© (2014) Trans Tech Publications, Switzerland
doi:10.4028/www.scientific.net/AMR.989-994.2555

Simulation Research on GM Navigation Based on AFSA

ZHU Zhanlong[1,a], YANG Gongliu[1,2] , LI Jing[2] , YANG Shujie[2] and LIU Yuanyuan[2]

[1]School of Instrument Science and Engineering, Southeast University, Nanjing 210096, China

[2]School of Instrument Science and Opt-electronics Engineering, Beihang University, Beijing 100191, China

[a]zhuzhanlong1984@163.com

Keywords: Geomagnetic matching; Artificial fish swarm algorithm; Affine transformation; Inertial navigation system; Extended Kalman filter.

Abstract. Geomagnetic matching (GM) is a new developmental technology in recent years. For resolving the cumulate errors of position, velocity, attitude in an inertial navigation system (INS), utilizing artificial fish swarm algorithm (AFSA) to carry on GM is proposed, and then the attained matching position regarded as measurement of filter to achieve the emendation of INS. Firstly, affine transformation model between inertial and real trajectories is displayed and the principle of INS/GM is explained. Secondly, the state of artificial fish (AF), distance and food consistence are defined afresh, and then the flow chart based on AFSA is given. Lastly, simulation analysis is performed in actual geomagnetic reference map (GRM). The results show that the algorithm actualizes the GM when the inertial system exist position, velocity and attitude error, that is the algorithm got the optimized global solution, with that, the data fusing is finished with the results that not only reduce error evidently but also verify the validity and feasible of the algorithm.

Introduction

For reducing the dependence on GPS[1], insuring the navigation system security, reliability and independence, GM has become a hotspot in the field of the current navigation domain [2], which possesses the advantage of all weather, good concealment, low energy consumption and so on along with the advance of magnetic theory and measurement technology. GM navigation is enormous action for successive navigation especially for underwater vehicle so as to prevent exposing trace.

The geomagnetic navigation system is applied in many aspects as shown in references [3-6]. At present, the technology of the aviation geomagnetic survey have been mature and the error compensation technology of measurement data is also achieved abundant fruits, thus provide condition for the development GM. GM algorithm can be divided into two kinds: one kind is related extremum algorithm, the other is filtering algorithm. The first algorithm applied widely because it can be solved the biggish position error. Accuracy of GM decides the precision of geomagnetic navigation directly. Reference [7] simulates the feasibility of the first algorithm by using Housdorff distance as related criteria. From the feature space, similarity metric, search space and search strategy four aspects of GM is established, and presents a mathematical description of GM[8]. Reference [9] breaks through traditional search strategy, adopts intelligent search strategy to analyze the feasibility about the GM.

AFSA is an intelligent algorithm in recent years and widely used in communication, signal processing and other subjects[10, 11]. From the intelligent search strategy into consideration, the article introduces the AFSA to develop the GM, and then the attained matching position can be seemed as measurement of Kalman filter to accomplish the correction of INS.

INS error model and principle of GM navigation

INS error model

The INS error is accumulated, so after a period of time the INS need to error emending, and then the carrier can move on. The shape of INS trajectories and real trajectories are different because of

attitude error and velocity error. So the corresponding relation between the INS and real trajectories is established by affine transformation [8], shown as follows

$$\begin{bmatrix} x_{rk} \\ y_{rk} \end{bmatrix} = \alpha \begin{pmatrix} \cos\theta & -\sin\theta \\ \sin\theta & \cos\theta \end{pmatrix} \begin{bmatrix} x_{ik} \\ y_{ik} \end{bmatrix} + \begin{bmatrix} \Delta x \\ \Delta y \end{bmatrix} \tag{1}$$

where (x_{ik}, y_{ik}) are INS coordinates values and (x_{rk}, y_{rk}) are real trajectory coordinates values. Δx, Δy denote shift factor, α is scaling factor, mainly used to adjust the speed error, and θ is rotation factor, mainly used to adjust the attitude error.

Principle of INS/GM navigation

Integrated navigation system of INS/GM consists of INS, geomagnetic sensor, GRM and PC etc., mainly contains two function parts, shown in Fig. 1: the part Ⅰ and part Ⅱ. The part Ⅰ is GM technology, which adopts geomagnetic sensors and GRM as assistant tools. The real-time geomagnetic measurement data attained by sensors and at the same time, combined position information of INS, a series of geomagnetic data extracted form the GRM, and then the best matching position gained according to correlation algorithm. The part Ⅱ is data fusing technology, which utilizes best position information as measurement of Kalman filter to filter for integrated navigation system, in this way the INS error restrained. The following depicts the specific principle of GM and data fusing.

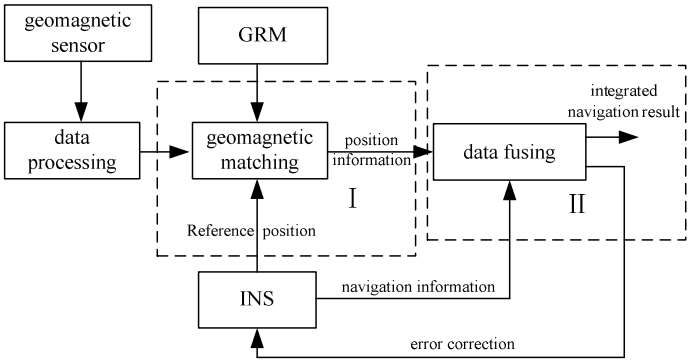

Fig. 1 Schematic diagram of INS/geomagnetic integrated navigation system

AFSA and its application in GM

The basic idea of AFSA is to imitate the fish behaviors such as preying, swarming, following so as to reaching the global optimum[10, 11].

Concept of AF based on GM

(a) AF Individual state By Eq. (1) we know that the four parameters namely α, θ, Δx, Δy required to gain, so the individual state of AF can be expressed as Eq. (2)

$$X = (\alpha, \theta, \Delta x, \Delta y) \tag{2}$$

(b) AF Distance The Euclidean distance is the most commonly used for calculating the distance of AF, the expression is $D = (\sum_{i=1}^{n} |x_i - y_i|^2)^{1/2}$, x, y represent two AFs, and i is the serial number of variables, n is the total number of variables. By the expression we can see that the distance is the simple cumulate of all the variables, but neglect the difference of the variables dimension, and then the practical significance of the distance is hard to illuminate. Aiming at this situation, it is essential to make some changes to the Euclidean distance, as shown in Eq. (3)

$$D = (\sum_{i=1}^{n} \left| x_i - y_i \middle/ Visual_i \right|^2)^{1/2} \tag{3}$$

where $Visual_i$ denotes ith value of $Visual$, the expression reveals the relative size of variables correspond to the $Visual$, which can more reflect the distance between two AFs objectively.

(c) AF Food consistence The food consistence of AF is the objective function value. g_{Ni} is geomagnetic data sequences extracted from GRM based on the INS position after affine

transformation, and H_N is measured data sequences of geomagnetic sensors. In combination with the basic principle of GM, AF food consistence expression is as follows

$$foodconsistence = N / \sum_{k=1}^{N} \left(H_N(k) - g_{Ni}(k) \right)^2 \tag{4}$$

where N is the total number of matching sequence, and the value of food consistence is in direct proportion to the effect of individual state of AF, namely the larger food consistence is, the better individual state of AF is. Compared Eq.(4) with MSD algorithm[9], it is find that Eq.(4) is the reciprocal value of MSD algorithm.

Application of AFSA in GM

After a period of autonomous navigation, velocity error, attitude error and position error can be reasonably estimated, then the range of the scaling factor α, rotating factor θ and shift factor Δx, Δy can be fixed on. In succession, the initial AFs are produced and different fish behaviors are performed and then the optimal state X of AF is obtained. The detailed flow chart is shown in Fig. 2.

Experiment schematic design and analysis

Experiment schematic design

Experiment schematic design based on two conditions: (1) Three discontinuous GRMs (matching areas), shown as in Fig. 3, area A, B and C. (2) Developing path planning for INS entered the matching area propitious. Schematic design of path planning presents in Fig. 3, the black dot and red dot are initial point and end point separately, the blue line connecting initial point with end point is the planned path.

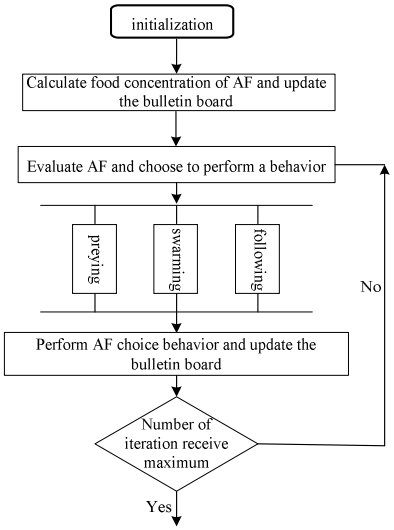

Fig. 2 Flow chart GM based on AFSA

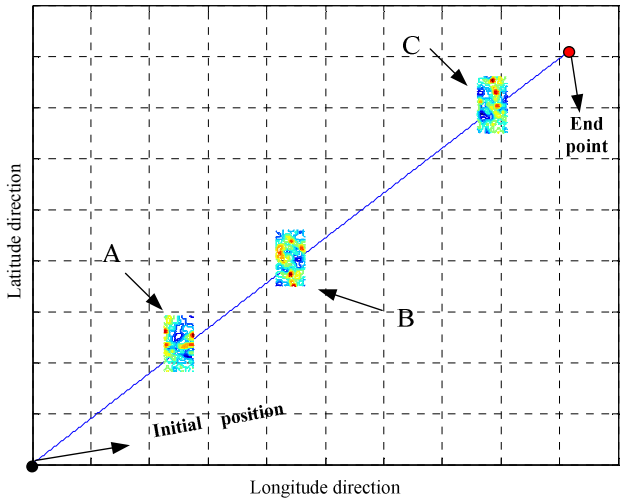

Fig. 3 Schematic design of path planning

Test and analysis of GM

The total number of GRM (area A) grid is 100×110, X and Y axis are shown as longitude and latitude respectively, the grid spacing is 0.001°. The INS and real trajectories are produced by inertial system and tracking generator respectively. The value of real trajectories on the GRM makes up of measurement value of geomagnetic after adding some Gaussian noise.

Setting moving trajectories is uniform linear motion, the velocity is 20m/s, and initial errors are 0. Sensor starts work after 40min, measurement interval of sensor is 10s, sample points are 20. In this time slice the errors of INS are shown in Fig. 4, Fig. 5 and Fig. 6.

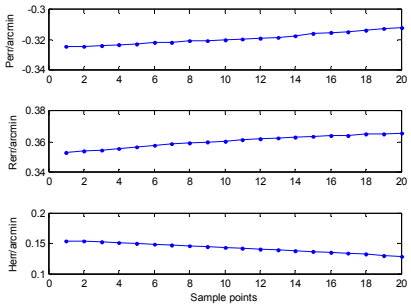

Fig. 4 Attitude errors

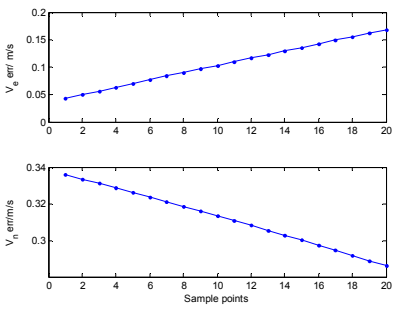

Fig. 5 Velocity errors

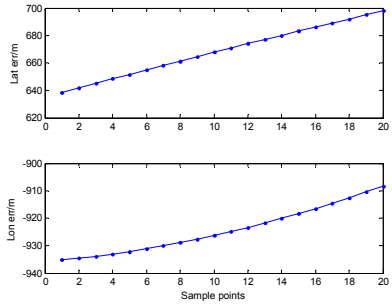

Fig. 6 Position errors

Fig. 4 shows the attitude errors in the process of sampling, the Fig. 5 shows the velocity errors, Fig. 6 shows the position errors. It is found that the transform relation of Eq. (1) is rational, so the key of GM is to seek four factors of α, θ, Δx, Δy. GM experiment is depicted as follows, the parameters of algorithm listed in table 1.

Table 1 Simulation parameters of proposed algorithm

Parameters	value	Parameters	value	Parameters	value
total number	500	try number	3	scope of scaling factor	[0.9,1.1]
iteration	30	crowd factor	0.518	scope of rotate factor	[-3°,3°]
vision	(0.04,0.05°,2.5,2.5)	noise of sensor	(0, 25)		
step length	(0.01,0.0125°,0.6,0.6)	scope of shift factor	[-5000,5000]m		

Simulation results are shown as Fig. 7 and Fig. 8. Fig. 7 reveals the matching result of algorithm on the whole. Fig. 8 displays the idiographic matching results in latitude and longitude direction, and the results show the matching precision less than 100m.

In general, matching result of the last sample point can be seemed as the final matching result, namely, latitude error is about 20m, and longitude error is about 50m in this experiment. It is obligatory point out that the matching results shown in Fig. 7 and Fig. 8 are just once simulation experiment. For evaluating the reliability of algorithm, the 20 trials of simulation experiment put in practice, likewise the matching result of the last sample point seemed as the final matching result.

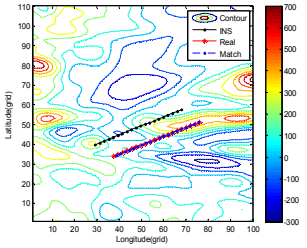

Fig. 7 Matching results

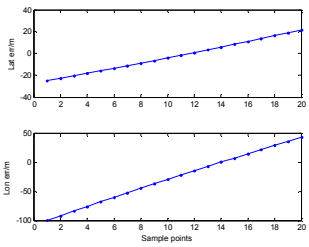

Fig. 8 Latitude and longitude error after matching

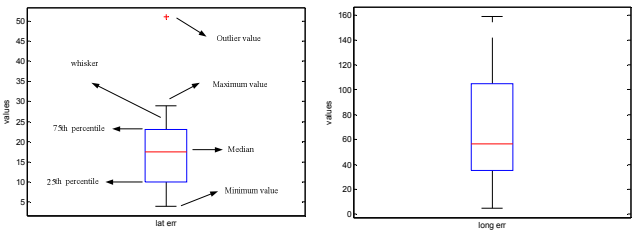

Fig. 9 Box figure of error statistics results
(a) Latitude error (b) Longitude error

By the method of mathematical statistics the error results are shown in Fig.9. Fig. 9(a) depicts the detailed meanings and we can see that there is only one outlier value, which is about 50m within a grid (100m). From Fig. 9(b) we can see that there is no one outlier value in longitude direction, and the maximum value is about 160m. So we validate the convergence property and randomness with the statistics method. Thereupon, taking example by area A validates feasibility of the algorithm.

INS/GM integrated navigation

Data fusing is implemented by EKF after attained the matching position. Combine with the position of GRM shown in Fig. 3(a), the three matching time slice are fixed on 40~43min, (has shown in section of 4.2), 70~73min and 127~130min. Sampling point of every time slice is 20 and sampling interval time is 10s. Ultimately the results of data fusing are demonstrated as Fig.10.

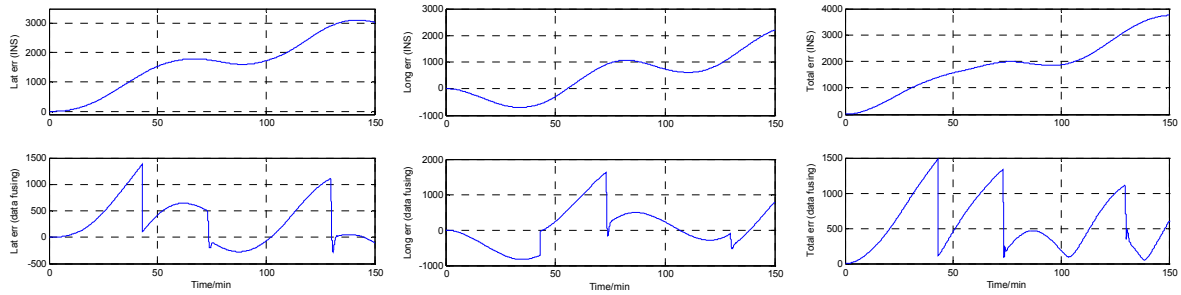

Fig. 10 Contrast between INS and data fusing
(a) Latitude error (b) Longitude error (c) Total error

Fig. 10 displays the contrast results between INS and data fusing, which denotes that the errors of latitude, longitude and total are accumulated by pure INS, but errors are restrained by data fusing. In this way, without the GPS, merely rely on three GRMs, the INS error is revised by using path planning, which decreases the difficulty of engineering application, and has great significance for successive navigation of carrier especially for underwater vehicle so as to avoid exposing trace.

Conclusion

We have presented AFSA application research in GM field, which achieved error emendation of INS by imitating the fish behaviors such as the preying, swarming, following and leaping etc. Combine with the actual circs of GM, the state, distance of AFs were revised and operation steps, flowchart were brought forth. Based on the practical position condition of three GRMs, schematic design was done, and took area A for example GM was test and analyzed, following the results show that the proposed method has a strong robustness and convergence character, in the last place, the data fusing was proceed, from the results we can see that the INS error gained the restrained effectively, which is of great importance to the uninterrupted navigation of carrier especially underwater vehicle. Additionally, because of algorithm's feasibility, we may use it to test practical carrier in the future.

References

[1] Chen X, Shen C, Zhang W, et al. Measurement vol.46 (2013), p.3847

[2] Ma X, Liu H, Xiao D. IEEE Intelligent Vehicles Symposium. Xi'an, China (2009) p.464

[3] C. Tyrén. Journal of Navigation vol.35 (1982) p.242.

[4] M L Psiaki, Huang L et al. Journal of Guidance, Control, and Dynamics vol.16 (1993) p.206

[5] M. L. Psiaki. Journal of Guidance, Control, and Dynamics vol.22 (1999) p.296

[6] F. Goldenberg. PLANS 2006, San Diego, California p.684

[7] Liu F, Zhou X, Yang Y, et al. Journal of Chinese Inertial Technology vol.15 (2007) p.59

[8] Liu Y, Wu M, Xie H. Journal of national university of defense technology vol.32 (2010) p.171

[9] Chen L, Wang S, Liu Z, et al. Journal of xidian university vol.40 (2013) p.118

[10] Fei T, Zhang L, Li Y, et al. Proceedings of International Conference on Computer Science and Information Technology Springer India (2014) p.679

[11] Jiang M, Wang Y, Pfletschinger S, et al. Proceedings of International Conference on Intelligent Computing (2007) p.1084

Advanced Materials Research Vols. 989-994 (2014) pp 2560-2564
© (2014) Trans Tech Publications, Switzerland
doi:10.4028/www.scientific.net/AMR.989-994.2560

Currency Crisis Prediction Using Wavelet-based Support Vector Machine

ZHANG Qinli[1,2,a]

[1]China center for industrial security research, Beijing Jiaotong University, Beijing,100044, China

[2]North China Institute of Aerospace Engineering, Langfang Hebei, 065000,China

[a]zhangql1973@163.com

Keywords: Currency Crisis; Wavelet; Support Vector Machine.

Abstract. A currency crisis is typically a kind of rare event, but it hurts sustainable economic development when it occurs. A novel method of wavelet-based support vector machine (SVM) is proposed to predict financial crisis events for early-warning purposes in this paper. In the proposed method, currency exchange rate, a typical currency indicator that usually reflects economic fluctuations, is first chosen. Then a wavelet decomposition algorithm is applied to the currency exchange rate series. Using the wavelet decomposition procedure, some details and features of the currency exchange rate series, with different scales, can be obtained. Using these details and features, a wavelet-based SVM learning paradigm is used to predict future currency crisis events, based upon some historical data. For illustration purpose, the proposed wavelet-based SVM learning paradigm is applied to exchange rate data of two Asian countries to evaluate the state of currency crisis. Experimental results reveal that the proposed wavelet-based SVM learning paradigm can significantly improve the generalization performance relative to some popular forecasting methods.

Introduction

Economic crises occurred over the past several decades have showed that currency crises are usually in the core position of economic crises. Therefore, currency sectors' stability is key to maintain economic stability and currency crisis may cause a economic crisis. The European currency crises in 1992, the Mexican peso crisis in 1994, the Asian crises in 1997–98, the Russian currency crisis in 1998, the American subprime mortgage crisis in 2007 and the Greek debt crisis in 2010 were indeed telling the fact. To prevent future crises, researchers have tried to predict the crisis by identifying common factors underlying exchange rate instability. However, existing models suffer from a number of weaknesses which include the need for a large number of controlling parameters, difficulty in obtaining a stable solution, the danger of over fitting, dependence on the selection of indicators and single-scale learning process. These problems usually lead to poor generalization to the out-of-sample data despite impressive in-sample results[1-3]. SVM and Wavelet analysis can solve the above problems.

In 1995, a novel neural network algorithm, called support vector machine (SVM), was developed by Vapnik and his co-workers [4]. Unlike most of the traditional neural network models which implement the empirical risk minimization principle, SVMs implement the structural risk minimization principle which seeks to minimize an upper bound of the generalization error rather than minimize the training error. Based on this principle, SVMs achieve an optimum network structure. This results in better generalization performance than other neural network models.

In most previous studies, stock index , interest rate or currency exchange rate is selected as model input. In this paper, the currency exchange rate is chosen. A possible drawback of a single-scale learning process is that it is sometimes inadequate for complex and difficult problems, e.g., some non-stationary and non- linear real-world problems, and often yields poor generalization performance[5]. To alleviate the potential problem of poor generalization, the original exchange rate data are decomposed into multiple intrinsic components by DWT algorithm before applying the SVM

algorithm . These decomposed independent componets can represent different factors affecting currency exchange rate movement. Therefore, the components are considered as independent variables for constructing a pattern recognition model. These components, with different scales, are used for SVM training to improve performance, relative to single series-based models training. Therefore, the proposed new learning paradigm is seen as multiscale SVM learning algorithm and overcomes many shortcoming of the existing approaches by virtue of the advantages of SVM and wavelet analysis.

Overview of SVM

Based on statistical learning theory, Vapnik puts forward support vector machine. Its basic idea is to construct an optimal separating hyperplane with high classification accuracy . A brief description of the SVM algorithm is provided as follows [6].

Given the training data set $D=\{(x_i,y_i)\}_{i=1}^{M}$, where $x_i \in R^n$ is an input vector and $y_i \in \{-1,1\}$ denotes a target label. In the linear separable case, SVM algorithm is to find an optimal separating plane $w \cdot x + b = 0$. In the nonlinear separable case, a nonlinear function $\Phi(x)$ must be applied to map input space to a higher dimensional feature space and the constrained optimization model of soft-margin based on SVM is as follows :

$$\text{Minimize } \frac{1}{2}w^T w + C\sum_{i=1}^{M}\xi_i \text{ , Subject to } \begin{cases} y_i[w^T\Phi(x_i)+b] \geq 1-\xi_i \ (i=1,\cdots,M) \\ \xi_i \geq 0 \ (i=1,\cdots,M) \end{cases} \tag{1}$$

Where ξ_i is a slack variable and C is a tuning parameter. By applying the Lagrangian technique to Eq. (1), we can obtain its dual problem as follows:

$$\text{Maximize } \frac{1}{2}\alpha^T Q\alpha - e^T\alpha \text{ , Subject to } \begin{cases} 0 \leq \alpha_i \leq C \ (i=1,\cdots,M) \\ y^T\alpha = 0 \end{cases} \tag{2}$$

where e^T is a vector of all ones, Q is a positive semi-definite matrix and α_i is Lagrange multiplier. The element Q_{ij} of Q is equal to $y_i y_j K(x_i,x_j)$, where $K(x_i,x_j)=\Phi(x_i)^T\Phi(x_j)$ is called kernel function. In the paper, we adopt the Gaussian kernel function, i.e. , $K(x,y)=\exp(-\|x-y\|^2/2\sigma^2)$, where σ is the kernel width. Based on the above analysis, we can obtain the classifier function:

$$f(x)=sign(\sum_{i=1}^{M}a_i y_i K(x,x_i)+b) \tag{3}$$

Overview of wavelet analysis

Wavelet analysis provides an advanced technique to decompose an original time series into a hierarchical representation of multilevel time series [7]. Wavelet analysis focuses on scale-based analysis, which allows the use of long time intervals where we want more precise low-frequency information, and shorter regions where we want high-frequency information. This paper choose scales and positions based on powers of two, i.e. the span of each coarser level is double to that of the previous level, which is the so-called dyadic scales and positions. Wavelet multi-resolution analysis produces a family of hierarchically organized decompositions. For example, an original time series $x(t)$ is decomposed into an approximation $a_1(t)$ and a detail $d_1(t)$, and $a_1(t)$ can be decomposed into an approximation $a_2(t)$ and a detail $d_2(t)$ similarly. This decomposition process can be iterated with successive approximations being decomposed in turn. At the end of this sifting procedure, the time series $x(t)$ can be expressed by

$$x(t)=a_J(t)+d_J(t)+\cdots+d_1(t) \tag{4}$$

where J is the number of details, $a_J(t)$ is the approximation, which is the main trend of $x(t)$, and $d_j(t)(j=1,\cdots,J)$ are the details, which are orthogonal to each other. Thus, one can achieve decomposition of the data series into several intrinsic components.

Wavelet-based multiscale SVM

As earlier noted, SVM are a new kind of neural network technique based on the structural risk minimization (SRM) principle and are widely used in many practical problems. However, a major challenge in SVM is how to make the trained SVM possess good generalization ability, i.e. they can generalize well for cases that were not included in the training set. The key is how to determine the parameters of the kernel function. The SVM with Gaussian RBF kernel is sensitive to the kernel width σ that greatly affects the classification accuracy. We advocate use of the 5- fold cross-validation technique for getting good generalization [8]. But in the cross-validation technique, if SVM is based on a single series representation for the entire training process and the problem is very difficult and complex, the trained SVM by a single series may be inadequate [5]. For this reason, the wavelet-based multiscale SVM is employed to decompose a time series and approximate it by using decomposed components via wavelet analysis framework. Generally speaking, the wavelet-based multiscale SVM paradigm consists of four different steps.

Step I: Data decomposition: The original time series are decomposed into various orthogonal components with a range of scales. The resultant different components form the inputs of SVM.

Step II: The components selection: The different components produced by Step I are input into the SVM for training. In the SVM learning process, internal correlation structures of different componets are explored. Using the explored internal relationships, some important components are selected as final SVM inputs and some unimportant componets that are of little use in mapping of inputs to output are discarded. In this study, principal component analysis (PCA) is used to explore the internal correlation structures of different components.

Step III: SVM training: Once the input patterns, i.e. selected components, are determined , SVM training can be started. In the study, the inputs of SVM are composed of k components (i.e. k components selected by Step II) and the output is -1 or 1. The SVM network training process is performed by Matlab software package.

Step IV: Crisis prediction: After training, we can use the trained SVM to predict future currency crises for out-of-sample data in the final step. When an unknown decomposed vector with k dimensions is input, -1 or 1 is to be picked as the final SVM output, i.e. the pattern to which the given currency crisis state belongs. Particularly, output '-1' is classified as a non-crisis pattern, while output 1 is classified as a crisis pattern, implying that the given currency crisis state might be trapped in a crisis period.

In order to verify the effectiveness of the proposed wavelet-based multiscale SVM approach, two typical Asian currencies—South Korean Won and Thai Baht—which suffered disastrous crisis, are used as testing targets.

Experiments study

For verification purpose, some experiments with data of the two Asian countries (i.e. currencies) are conducted in this study. First, data description and experimental design are presented and then the experimental results are reported.

In our study, we examine the currency crisis conditions and a currency crisis event is defined as a large devaluation of a currency, which far exceeds previous devaluations. From this definition, and some previous studies [9-10], a crisis can be defined as an abnormal event where rate of change (ROC) of exchange rate ($ROC_t = (E_t - E_{t-1})/E_{t-1}$) exceeds an extreme value:

$$F(ROC)=\begin{cases} 1 \ \ if \ \ ROC > \mu_{ROC} + 2.5\sigma_{ROC} \\ -1 \qquad\qquad otherwise \end{cases} \tag{5}$$

where $F(ROC)=1$ represents the occurrence of the currency crisis, and μ_{ROC} and σ_{ROC} are the sample mean and sample standard deviation of the ROC, respectively.

The data used in this study are daily exchange rate data for two currencies (South Korean won, Thai baht) against the US dollar, obtained from the Pacific Exchange Rate Service (http://fx.sauder.ubc.ca/). For purposes of training and testing, we take daily data from January 2, 1996 to December 31, 1997 as in-sample (training periods) datasets (506 observations). We take data from January 2, 1998 to December 31, 1998 as out-of-sample (testing periods) datasets (249observations).

To evaluate the forecasting ability of the proposed wavelet-based multiscale SVM learning approach, we select some popular forecasting methods from the existing literature—such as signal approach [1], logit model [2] , GRNN model [9] for comparative purposes. Table 1 and 2 show the results of comparison for KRW and THB, respectively.Obviously, our method performs the best.

Table 1. Comparison of forecasting performance of KRW for different methods for testing data

Models	Classification accuracy
Signal approach	79.52%
Logit model	78.31%
GRNN model	92.77%
The proposed Multiscale SVM	98.01%

Table 2. Comparison of forecasting performance of THB for different methods for testing data

Models	Classification accuracy
Signal approach	78.95%
Logit model	84.73%
GRNN model	93.82%
The proposed Multiscale SVM	98.72%

Conclusions

In this paper, an wavelet-based multiscale SVM learning approach is proposed for currency crisis forecasting. Applications of the proposed approach to out-of-sample data display surprisingly high accuracy.It reveals that the proposed approach might also be useful for financial practitioners who attempt to build a currency crisis forecasting model or a currency crisis early-warning system. Furthermore, experimental results show that the proposed approach is superior to other classification methods and single-scale neural network learning paradigm, implying that our proposed approach is a promising tool for currency crisis forecasting.

Acknowledgements

This work was financially supported by the Hebei Natural Science Foundation (F2011409007), China Postdoctoral Science Foundation (2014M550609) and Dr. Fund of NCIAE(ky-2009-05-B).

References

[1] Lin, C.S., Khan, H.A., Chang, R.Y.,Wang, Y.C.: Journal of International Money and Finance, Vol. 27(2008), p. 1098.

[2] Dridi, A., El Ghourabi, M., Limam, M.: Quantitative Finance, Vol. 12(2012), p. 329.

[3] Phornchanok Cumperayot, Roy Kouwenberg: Journal of International Money and Finance, Vol. 36 (2013), p. 151.

[4] Vapnik VN. *The nature of statistical learning theory* (Springer-Verlag,New York 1995).
[5] Y. Liang, E.W. Page: IEEE Transactions on Signal Processing, Vol. 45(1997), p. 2858.
[6] J. Sun and H. Li: Applied Soft Computing, Vol. 12(2012), p. 2254.
[7] Gallegati, M.: Computational Statistics & Data Analysis, Vol. 52(2008), p. 3067.
[8] Wu K-P, Wang S-D. : Pattern Recognition, Vol. 42(2009), p. 710.
[9] L. Yu, K.K. Lai, S.Y. Wang :International Journal of Information Technology and Decision Making, Vol. 5(2006), p. 437.
[10] G.L. Kaminsky, C.M. Reinhart: American Economic Review, Vol. 89(1999), p. 473.

Advanced Materials Research Vols. 989-994 (2014) pp 2565-2568
© (2014) Trans Tech Publications, Switzerland
doi:10.4028/www.scientific.net/AMR.989-994.2565

An Improved Speech Enhancement Algorithm Based on Wiener-Filtering

Yuhong LIU[1, a], Dongmei ZHOU[1, a], Jing Di[1, a]

[1]Institute of Electrical and Information Engineering, Lanzhou Jiaotong University, LZJTU, Lanzhou, China

[a]email: liuyuhong@mail.lzjtu.cn, [b]email: zhoudongmei@mail.lzjtu.cn, [c]email: dijing@mail.lzjtu.cn

Keywords: Speech Enhancement. Wiener-filtering. Masking Properties of Human Auditory System. Spectrum-Shaping

Abstract. This paper proposes an improved speech enhancement algorithm based on Wiener-Filtering, which addresses the problems of speech distortion and musical noise. The proposed algorithm adopts the masking properties of human auditory system on calculating the gain of spectrum point, in order that the signal in the enhanced speech whose energy is lower than the threshold will not be decreased further and the less distortion will be brought to enhanced speech by the trade-off between the noise elimination and speech signal distortion. What's more, in order to eliminate the "musical noise", a spectrum-shaping technology using averaging method between adjacent frames is adopted. And to guarantee the real-time application, two-stage moving-average strategy is adopted. The computer simulation results show that the proposed algorithm is superior to the traditional Wiener method in the low CPU cost, real-time statistics, the reduction of the speech distortion and residual musical noise.

Introduction

Single channel speech enhancement is one of the research focuses. Many algorithms[1-4] including spectral subtraction method, Wiener filtering, signal subspace method and statistical model based algorithm have been developed and put into use. The Wiener filtering is one of the most well-known and widely used due to its good performance on restraining musical noise. An improved algorithm is given here which gives better speech enhancement under wider range of input SNRs.

Proposed speech enhancement algorithm

Figure 1 shows the block diagram of proposed system.

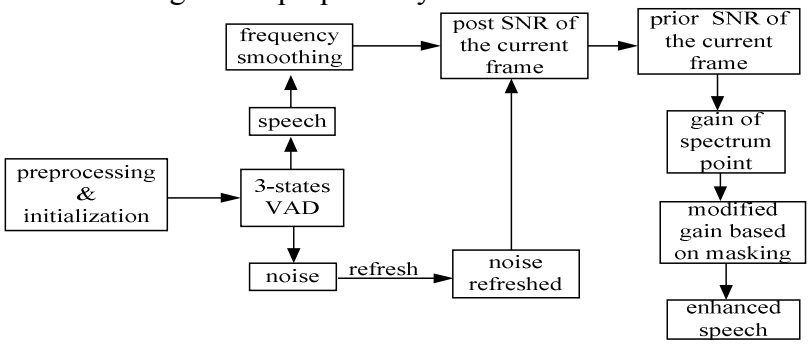

Fig. 1 structure of the proposed enhancement algorithm

VAD(Voice Activity Detect)

The flow diagram of improved VAD algorithm is showed by figure 2.

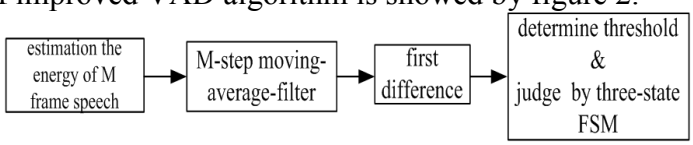

Fig. 2 Flow diagram of improved VAD

The input speech is divided into frames and processed by Hamming window, their energy is estimated. M of them are stored and then input the moving-average-filter. The function $f(x)$ is [5]

$$f(x)=e^{Ax}\left[K_1\sin(Ax)+K_2\cos(Ax)\right]+e^{-Ax}\left[K_3\sin(Ax)+K_4\cos(Ax)\right]+K_5+K_6e^{Sx} \quad (1)$$

Here, parameter A affects the amplitude of its frequency response. Parameter K_1~K_6 affect the shape of the frequency response. Parameter S affects the initial conditions. The output of the moving-average-filter is

$$F_{out}=\sum_{i=1}^{M}(E_i * f_i) \quad (2)$$

where E_i is the energy of M frames. f_i is parameter of the filter(i=1,2,…M).

Figure 3 shows the state transition diagram.

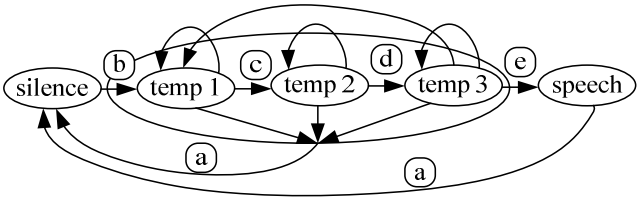

Fig. 3 State transition diagram

During the transition, it starts with silence frame and transits among these states depending on the corresponding conditions a~e. These conditions are described as followed.

a: the output of filter bi is less than the given threshold T_1;

b: the output of filter bi is greater than the given threshold T_1;

c: differential energy between two successive frames is more than the threshold DIF;

d: Duration as the number of the frames whose energy is more than T_1 is greater than the given threshold MAX_Dur;

e: low frequency(i.e. frequency is lower than 400Hz) energy of current frame is greater than the threshold E_{low} and its ratio in total energy is greater than the energy factor ρ.

Calculate the prior SNR

In baseline system, the prior SNR is determined both by "a apriori SNR" of last frame and that of current frame. Relation among them in the Decision-Directed algorithm is determined by

$$\hat{\varepsilon}(p,k)=\alpha\frac{\left|H(p-1,k)X_m(p-1,k)\right|^2}{\Gamma_d(p,k)}+(1-\alpha)P'\left[V(p,k)\right] \quad (3)$$

Where $V(p,k)=\gamma(p,k)-1$, $P[x]=x$ if $x\geq 0$ and $P[x]=0$ otherwise. The parameter α is assumed constant 1 in traditional usage which leads to an inefficiency in noise-varying situation. Thus an improvement is proposed and the definition of cost function J is shown as followed,

$$J=E\left\{\left[\hat{s}(n)-s(n)\right]^2\right\} \quad (4)$$

$\hat{s}(n)$ and $s(n)$ are enhanced speech and pure speech respectively.

Let $\frac{\partial J}{\partial \alpha}=0$, then

$$\alpha=1-f(\varepsilon_{k-1},\gamma_k) \quad (5)$$

The definition of $f(\varepsilon_{k-1},\gamma_k)$ is

$$f(\varepsilon_{k-1},\gamma_k)=\begin{cases}\left|\dfrac{\gamma_k}{\varepsilon_{k-1}}\right|\left(|\gamma_k|<|\varepsilon_{k-1}|,\varepsilon_{k-1}\neq 0\right)\\ \left|\dfrac{\gamma_k*\varepsilon_{k-1}}{|\gamma_k|^2+|\varepsilon_{k-1}|^2}\right|\left(|\gamma_k|>|\varepsilon_{k-1}|\right)\end{cases} \quad (6)$$

When ε_{k-1} and γ_k are both zero, α can be any value belong to [0, 1]. ε_{k-1} and γ_k are calculated by the following formulas.

$$\varepsilon_{k-1} = \frac{\lambda_s(k-1)}{\lambda_d(k-1)} \tag{7}$$

$$\gamma_k = \frac{|y_k|^2}{\lambda_d(k)} \tag{8}$$

$\lambda_s(k)$ and $\lambda_d(k)$ are energy of speech and noise respectively. y_k is the noise-corrupted speech signal.

Human hearing physiological and philosophical characteristics such as masking effects[6][7] are taken into considerations while determining the gain obtained from the assumed algorithm.

Let the auditory threshold of each frequency point is described by $F = [f_0, f_1, ...f_{M-1}]$, f_k is the threshold of kth frequency. The modified gain $\hat{G}(n)$ considering the masking properties of human auditory system is

$$\hat{G}(n) = M\,\mathrm{ax}\left(G(n), \frac{f_k}{y(n)}\right) \tag{9}$$

Where

$$G(n) = \frac{\varepsilon_k(n)}{1+\varepsilon_k(n)} \tag{10}$$

Spectrum shaping

In order to eliminate the "musical noise"a spectrum-shaping technology using averaging between adjacent frames is adopted. To guarantee the real-time application, two-stage moving-average strategy is adopted.

Suppose the sequence of the frequency samples of the frame going to be smoothed is $S_i = [s_{i,0}, s_{i,1}, ..., s_{i,N-1}]$, N is the number of the frequency points. That sequence of the last frame is $S_{i-1} = [s_{i-1,0}, s_{i-1,1}, ..., s_{i-1,N-1}]$. Then the smoothed sequence of current frame is

$$\hat{S}_i = [\hat{s}_{i,0}, \hat{s}_{i,1}, ..., \hat{s}_{i,N-1}] \tag{11}$$

Where $\hat{s}_{i,j} = \frac{1}{2}(s_{i-1,j} + s_{i,j})$.

What's more, in order to get a better smoothing result, the number of N in most non-real-time application is 3~5. While in real-time application, the number of N is 2~3.

Experimental results

We select a piece of single channel data as pure speech which is saved as 1.wav The speech signal is sampled at 8 kHz and quantified with 16 bits. Gauss White Noise whose mean value and variance are 0 and 1 respectively is added into the speech to get a noise-corrupted speech signal with SNR of 5dB.

The proposed algorithm in the paper divided the mixed signal into frames with 32ms whose offset is 16ms. The order M of Winner filter is 25. Smoothing parameter is 2. In power spectrum subtraction algorithm, parameters α and β are 2.7 and 0.01 respectively. In baseline system of Winner filter, factor of Decision-Directed is 0.99, α and β are 2.7 and 0.01 respectively too, forgetting factor ρ is 0.85. Figure 4~figure 7 showed the initial noise-corrupted speech signal and the results of enhanced speech according to each algorithm above.

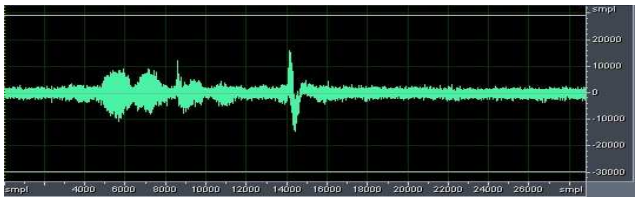

Fig. 4 The initial noise-corrupted speech signal

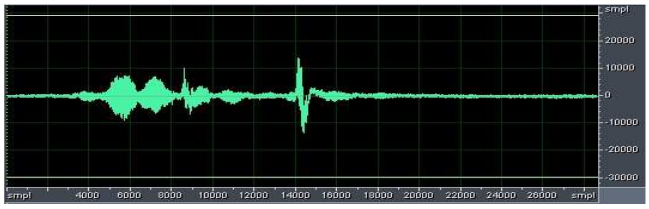

Fig. 5 Result of baseline system of Winner filter

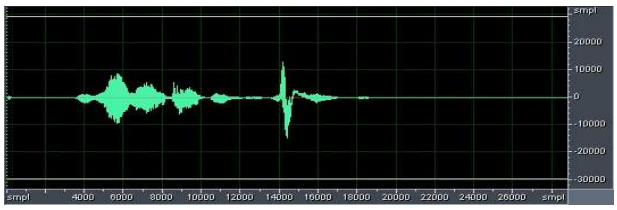

Fig.6 Result of the proposed algorithm

References

[1] Y. Ephraim and D. Malah, "Speech enhancement using a minimum mean square error short-time spectral amplitude estimator", IEEE Trans Acoust, Speech, Signal Processing, vol. ASSP-32, pp.1109-1121, Dec 1984.

[2] R. Schwartz M. Berouti and J. Makhoul, "Enhancement of speech corrupted by acoustic noise", Proc. of ICASSP, 1979, vol. I, pp. 208-211.

[3] N.Virag, "Single channel speech enhancement based on masking properties of the human auditory system ", IEEE Trans. Speech and Audio Processing, vol. 7, pp. 126-137, 1999.

[4] Y. Ephraim and H.L. Van Trees, "A signal subspace approach for speech enhancement", IEEE Trans. Speech and Audio Processing, vol. 3, pp.251-266, 1995.

[5] QiLi, Jiangsong Zheng, Augustine Tsai, et al, "Robust Endpoint Detect and Energy Normalization for Real-Time Speech and Speaker Recognition", IEEE Transactions on Acoustic, Speech and Audio Processing, pp. 146-157,2002.

[6] Y. Hu and P. Loizou, "lncorporating a psychoacoustic model in frequency domain speech enhancement," IEEE Signal Processing Letters, vol. 11(2), pp. 270-273, 2004.

[7] Y. Hu and P.c. Loizou, "A perceptually motivated approach for speech enhancement," IEEE Trans. Speech Audio Processing, pp. 457-465. Sept. 2003.

Advanced Materials Research Vols. 989-994 (2014) pp 2569-2575
© (2014) Trans Tech Publications, Switzerland
doi:10.4028/www.scientific.net/AMR.989-994.2569

Research of License Plate Recognition under Complex Environment

Feng Gao[a], Zhongjian Dai[b], Kun Zhou[c] and Yaping Dai*[d]

School of Automation, Beijing Institute of Technology, Beijing, China, 100081

[a]email: gaofgcool@126.com, [b]email: padzj@sina.com,

[c]email: zhoukunsam@163.com, [d]email: daiyaping@bit.edu.cn*

Keywords: License Plate Recognition; Edge Detection; License Plate Color Information; Character Feature Extraction; Neural Network

Abstract. In order to improve the license plate recognition accuracy under complex environment, a new license location algorithm combining vertical edge detection, color information of the license plate and mathematical morphology is presented in this paper. For balance of computing load and recognition accuracy, a "200-d" character feature rule is designed, and the "200-d" feature is used as the input of BP neural network to recognize the characters. Based on the above-mentioned methods, a license plate recognition system is set up, which can locate and recognize the license plate effectively, even when the resolution of pictures and the position of vehicles in the pictures are not fixed. Experimental results indicate that the recognition rate of the algorithm reaches 90.5%.

Introduction

License plate recognition is very widely used in intelligent transportation systems. Through the license plate image recognition, vehicles can be indentified automatically. Then the vehicle management, flow control and toll charge can be highly automated. License plate recognition technology includes three main parts, which are license plate location, character segmentation and character recognition. Among them, license plate location and character recognition play key roles in the speed and accuracy of license plate recognition technology. So this paper mainly focuses on license plate location and character recognition.

License plate location technology refers to extracting the license plate image from complex image background. Many license plate location methods have been proposed, such as the method based on texture features [1], edge detection [2], mathematical morphology [3] and image color information [4]. While the images are taken in complex environment, the result of using only a single feature to distinguish the license plate region from background is a hard job. It is because that some license plate features exist in some non-license plate region as well, which will interfere with the result of location. Therefore, the method that combines several features to locate the license plate is becoming more and more popular. Such as Wang et al. [5] combined edge detection with mathematical morphology to analyze the connected domains and got the location rate at 90.833%. Xu et al. [6] combined color information with edge detection. They rough classified the plate region in LAB color space at first, and then got the final result according to the edge detection method. As the images they used are all taken in the same place and resolution on a sunny day, the location rate came to 98.51% in those conditions.

Character recognition algorithms are mainly based on the template matching [7], neural network [8] and support vector machine (SVM) [9]. The template matching method identifies the characters by the comparison between the characters to be recognized and the characters in template library. But this method is more vulnerable to the clarity, resolution and some other factors. Neural network has strong learning ability, with the learning of more samples and training of the network, more defective and distortional characters can be recognized. However, the recognition accuracy based on neural network relies on the character feature extraction technology. Recognition method based on support vector machine (SVM) has high robustness in two-class problem, but it is not sufficient to support multi-class problem. And the recognition rate is dependent on the choice of kernel function, the

change of the data set may lead to the change of kernel function, which would change the rate of recognition.

Unlike the images are usually taken in a fixed toll gate or lane [4,5,6], the experimental images in this paper have no unified limit in resolution and clarity. A license plate location method combining vertical edge detection, license plate color information and mathematical morphology is presented in this paper. The license plate is corrected by Radon transform and the character segmentation is done according to the vertical projection. A "200-d" character feature extraction rule is designed to guarantee the appropriate input for BP neural network. After experiment, the results show that the method presented in this paper could reach a high accuracy of recognition.

Vehicle Image Preprocessing

Before the location of license plate, the vehicle image needs to be preprocessed to improve the image quality and contrast. This paper converts color images to gray images at first. The conversion formula of pixel I(x, y) in the color image is shown as Eq. 1:

$$Gray(x, y) = 0.3R(x, y) + 0.59G(x, y) + 0.11B(x, y). \quad (1)$$

Where x and y are the horizontal ordinate and vertical ordinate of the pixel I. $Gray(x, y)$ is the grey value of point (x, y). $R(x, y)$, $G(x, y)$ and $B(x, y)$ are the R, G, B component of pixel $I(x, y)$.

As there is a lot of noise in the vehicle images, by median filter first, the gray image is preprocessed. The 3×3 filter window is adopted, that is, the 8 neighborhood of pixel $Gray(x, y)$ will be sorted and the pixel value in the middle (No.5) will be the response $g(x, y)$. Preprocessing results are shown in Fig. 1 and all the Chinese characters on license plates are covered by white or black squares in all the images in this paper.

(a)Original RGB Image (b) Image after Preprocessing

Fig. 1 Vehicle Image Preprocessing

License Plate Location

Vertical Edge Detection. The edge feature is very obvious between the background and characters in the license plate region, which is helpful for edge detection. As the seven characters of the license plate are roughly horizontally arranged in the vehicle images, obvious and dense edges are gotten easily in the license plate region through vertical edge detection. Compared to the conventional edge detection, the edge got through vertical edge detection is far more less, which can improve the efficiency of subsequent processing.

Vertical Sobel edge operator is used in this paper, as shown as Fig. 2:

$$\begin{bmatrix} -1 & 0 & 1 \\ -2 & 0 & 2 \\ -1 & 0 & 1 \end{bmatrix}$$

Fig. 2 Vertical Sobel Edge Operator

Vertical edge detection of the gray image is operated by the operator above mentioned. Then the edges too long or too short are removed because they could not belong to the license plate region. The vertical edge detection image is shown in Fig. 3.

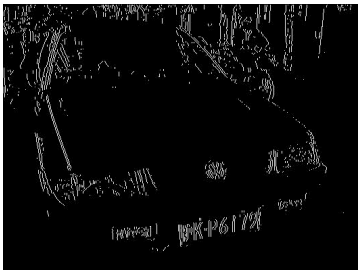

Fig. 3 Vertical Edge Detection Image

Fig 4. Standard Chinese License Plate

Edge Color Pairs Detection. Unlike [5] and some other work, mathematical morphology is not used directly in this paper. Ahead of license plate location, a detection method based on license plate color information is used, so that some interference, such as the characters in non-license plate region, can be removed.

There is a industry standard named GA36-2007 [10] for license plate in China. The specific style of Chinese license plate is shown in Fig. 4.

The color of license plate characters and background has a clear definition according to the GA36-2007. For small cars, the background of license plate is blue and the characters are white; for large cars, the background is yellow and the characters are black; for military and police cars, the background of license plate is white and the characters are black or red; for cars in Embassies, the background of license plate is black and the characters are white. It is obvious that the colors of license plate background and characters come in pairs as follows: blue-white, yellow-black, white-red, white-black and black-white.

Based on the feature that the colors in Chinese license plate come in pairs, the vertical edges are further processed. Only when the edge pixel and its adjacent pixels in the original image match the color pairs rules mentioned above, could the edge belong to license plate region. Other edges will be cancelled because they are treated as non-license plate region.

As the red character only appears once in a white-red license plate and six other characters are all black, the red character has little influence on the location result. Only four kinds of color as blue, yellow, white and black are considered here. The judgment of background and character colors is conducted in HSV space. The range of each component of these four colors is shown in Table 1, where "-" indicates that the value of this component doesn't need to be considered.

Table 1 The Range of HSV Component

	Blue	Yellow	White	Black
H	190-245	25-55	-	-
S	0.35-1	0.35-1	0-0.1	-
V	0.3-1	0.3-1	0.91-1	0-0.35

It is easy to determine whether the pixel color is blue, yellow, white or black by the value of *H*, *S* and *V* component. And it is easy to determine whether the colors of vertical edge pixels are in line with one kind of color pairs among blue-white, yellow-black, white-black and black-white also. Edge pixels meet the rule will be maintained and other edge pixels will be ruled out. Color pairs in the vertical edges of Fig. 3 are detected, and the result is shown in Fig. 5.

Fig. 5 Image after Edge Color Pairs Detection

Mathematical Morphology Method. Then the mathematical morphology method is used to process the edge image. Closing operation comes first and then opening operation operates, so that the dense regions of edges turn into initial connected domains.

According to the aspect ratio of license plate region, some non-license plate region can be cancelled. In this paper, the range of length-width ratio of license plate is set from 2:1 to 4:1. The connected domains which obey this rule will be kept as the candidate license plate region, as shown in Fig. 6.

(a) Initial Connected Domains (b) Connected Domains with Aspect Ratio Limit

Fig 6. Connected Domains

Finally, the license plate image after location is achieved, as shown in Fig. 7.

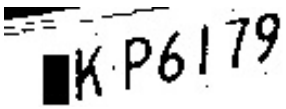

Fig. 7 License Plate Image

License Plate Correction and Character Segmentation

As the license plate image is achieved, characters need to be segmented. But the license plates in vehicle images are usually with a certain angle, which is caused by camera position, as shown in Fig. 7. To solve this problem, Radon transform is used in this paper. If *f(x, y)* is a two-dimensional image, then the definition of Radon transform is shown as Eq. 2:

$$R_\theta(x') = \int_{-\infty}^{+\infty} f(x'\cos\theta - y'\sin\theta, x'\sin\theta + y'\cos\theta)dy \,. \tag{2}$$

Where $\begin{bmatrix} x' \\ y' \end{bmatrix} = \begin{bmatrix} \cos\theta & \sin\theta \\ -\sin\theta & \cos\theta \end{bmatrix}$.

That is, the Radon transform of *f(x, y)* is a line integral parallel to the y' axis. For the license plate image, the value of θ is the tilt angle, which makes the formula (2) to have the smallest accumulation result. It can be used to correct the license plate, as shown in Fig. 8(a).

After correction, there still exist the upper and lower borders of the license plate in the image. The binary license plate image is detected horizontally. If a line contains the character pixels, the value of

pixels will jump at least 14 times in this line. By detecting the image from top to bottom and from bottom to top respectively, any line does not meet the rule will be excluded, as shown in Fig. 8(b).

As the upper and lower borders are removed, vertical projection is adopted in this paper, as shown in Fig. 8(c), and the result of character segmentation is shown in Fig. 8(d).

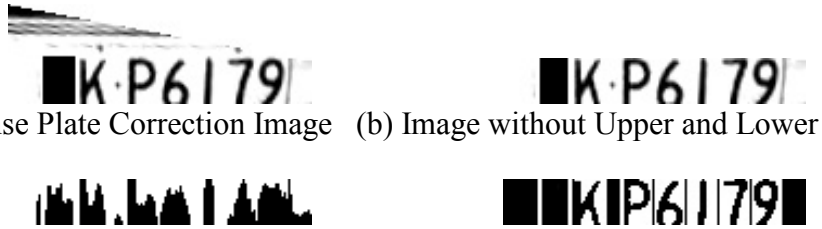

(a) License Plate Correction Image (b) Image without Upper and Lower Borders

(c) Vertical Projection Image (d) Character Segmentation Image

Fig. 8 License Plate Correction and Character Segmentation Image

Character Recognition

BP neural network is used for character recognition in this paper. As the size of single character made by the character segmentation is not fixed, it is necessary to normalize the characters.

The Design of the "200- d" Character Feature Rule. All the character will be normalized in the same size of 64×64, and BP neural network is used for character recognition in this paper. The character feature is extracted in three steps:

STEP 1: Sum up the value of all pixels in each line and use the sum as a feature, all the 64 lines have 64-d feature.

STEP 2: Sum up the value of all pixels in each column and use the sum as a feature, all the 64 column have 64-d feature;

STEP 3: As shown in Fig. 9(a), there are 64 subblocks in size of 8×8, sum up the value of all pixels in each subblock and use the sum as a feature, all the 64 subblocks have 64-d feature; as shown in Fig. 9(b) and 9(c), there are 8 small subblocks in size of 32×32, sum up the value of all pixels in each subblock and use the sum as a feature, all the 8 subblocks have 8-d feature.

Finally, there are 200-d character feature in total.

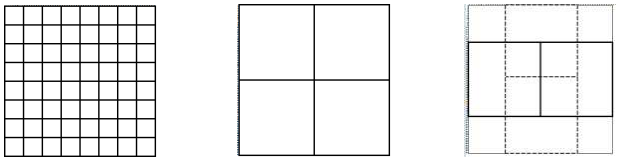

(a)8×8subblocks (b)32×32subblocks (c)32×32subblocks

Fig. 9 Subblocks of Characters

License Plate Recognition based on BP Neural Network. There are seven characters in a Chinese license plate. Among them, the first one is a Chinese character, the second character is an English letter and last five characters are all letters or numbers. Therefore, three networks as network of Chinese characters, network of letters and alphanumeric hybrid network are designed. Corresponding to the dimension of the character feature, the number of input nodes is 200. Output is in binary encoding and the number of output nodes is 6. The number of hidden nodes is determined by Eq. 3:

$$h = \sqrt{i \times (o+1)} + 1 . \tag{3}$$

Where h is the number of hidden nodes, i is the number of input nodes and o is the number of output nodes. As i is 200 and o is 6, h should be 37 according to the formula.

The activation function is Eq. 4:

$$\Phi_j(v_j(n)) = \frac{1}{1+e^{(-v_j(n))}}. \tag{4}$$

The learning factor is 0.4, iterations are 50000 and the momentum factor is 0.7.
Input the characters to the trained network, and the final recognition result is shown in Fig. 10.

Fig. 10 License Plate Recognition Result

Experimental Result and Analysis

In this paper, the experiment is conducted on a 2.93 GHz CPU, 2G memory hardware platform, and the software platform is the Windows 7 operating system and the Visual Studio 2008. 200 images are used to verify the effective of our algorithm. Compare with other methods, such as the method combining the edge detection with mathematic morphology, and methods based on single feature as edge detection, mathematical morphology and color information. The location results are shown in Table 2.

Table 2 License Plate Location Result

	Method in this paper	Method combining Edge Detection with Morphology	Method based on Edge Detection	Method based on Mathematical Morphology	Method based on Color Information
Number of Images	200	200	200	200	200
Number of Success	193	185	168	163	154
Location Rate	96.5%	92.5%	84%	81.5%	77%

The resolution and clarity of the images used in the experiments are not fixed. The positions where the license plates locate in the images and the environment where the images taken are not fixed as well. As shown in Table 2, in a total of 200 images, using the method in this paper, 193 images can be successfully located, the location accuracy is 96.5%; using the method combining the edge detection with mathematic morphology, 185 images can be successfully located, the location accuracy is 92.5%; using the method based on edge detection, 168 images can be successfully located, the location accuracy is 84%; using the method based on mathematical morphology, 163 images can be successfully located, the location accuracy is 81.5%; using the method based on the color information, 154 images can be successfully located, the location accuracy is 77%. The result indicates that the two

methods using combination features are better than those only dependent on a single feature, and the location method in this paper is better than the method which just combines edge detection with mathematical morphology.

Table 3 License Plate Recognition Results

	Number of Images	Number of Success	Recognition Accuracy
Method in this paper	200	181	90.5%
Method without Subblock Feature Extraction	200	162	81%

The final recognition result is shown in Table 3. Among the 200 experimental images, using the method in this paper, 181 images are recognized successfully, the recognition accuracy is 90.5%. When only the sum of all the pixel value in each line and column are used as character feature, 162 images can be recognized successfully, the recognition accuracy is 81%. The result in Table 3 shows that the "200-d" character feature extraction method in this paper is better than the method without subblock feature extraction.

Conclusion

This paper proposes a license plate location method combining vertical edge detection, license plate color information and mathematical morphology. Comparing to the method only combining edge detection with mathematical morphology, the method in this paper improves the location accuracy. A "200-d" character feature extraction rule is designed and BP neural network is used in this paper. Compared to the method without subblock features extraction, a better result is gotten. Experimental results indicate that the recognition accuracy of the algorithm reaches 90.5%.

References

[1] Z.X. Chen, C.Y Liu, F.L. Chang and J.G. Xu: *Proc. IEEE International Conference on Automation and Logistics* (Shenyang, China, August 5-7, 2009). p.1360.

[2] Z. Musoromy, S. Ramalingam and N. Bekooy: *Proc. International Conference on Control Automation Robotics & Vision* (Singapore, December 7-10, 2010). p.1133.

[3] Q. Song, H. Yuan and T. Zhou: *Proc. International Conference on Measurement, Information and Control* (Harbin, China, May 18-20, 2012). Vol. 2, p.782.

[4] J. Xu, S. Li and Z. Chen: *Proc. IEEE International Conference on Robotics, Intelligent Systems and Signal Processing*, (October 8-13, 2003). Vol. 2, p.1312.

[5] A. Wang，X. Liu，Y. Han and C. Qi: Proc. International Forum on Strategic Technology (Tomsk, Russia, September 18-21, 2012). p.1-4.

[6] L. Xu: *Proc. International Conference on Multimedia and Signal Processing* (Guilin, China, May 14-15, 2011). Vol. 1, p.99.

[7] P. Comelli, P. Ferragina, M.N. Granieri and F. Stabile: IEEE Transactions on Vehicular Technology, Vol. 44 (1995) No. 4, p.790.

[8] C.N.E. Anagnostopoulos, I.E. Anagnostopoulos, V. Loumos and E. Kayafas: IEEE Transactions on Intelligent Transportation Systems, Vol. 7 (2006) No. 3, p.377.

[9] Y. Wen, Y. Lu, J. Yan and Z. Zhou: IEEE Transactions on Intelligent Transportation Systems, Vol. 12 (2011) NO 3, p.830.

[10] License Plate of Motor Vehicle of the People's Republic of China. GA36-2007 (In Chinese).

Advanced Materials Research Vols. 989-994 (2014) pp 2576-2579
© (2014) Trans Tech Publications, Switzerland
doi:10.4028/www.scientific.net/AMR.989-994.2576

Hidden Markov modeling for Nakagami Fading Channel

YiHuai Yang[1, a], Lifang Wang[1, b], YanPing Sun[1]

[1] School of Automatic Control and Mechanical Engineering, Kunming University, 650214, China

[a]yyh_td@126.com, [b]lfw2924@163.com

*Corresponding author: Lifang Wang, E-mail: lfw2924@163.com.

Keywords: Rayleigh Fading Channel, Hidden Markov Model (HMM), channel modeling, finite State Markov Channel (FSMC)

Abstract. In this paper, we proposed a novel hidden Markov model (HMM) to approximate the characteristic of the Nakagami Fading channel. Our study is based on a Hidden Markov Model (HMM). The channel switches between 'good' and 'bad' channel situation. The transition between the sub-states of the channel is governed by a Markov Chain, which some self-return state is hidden. The performance of the model is studied by simulating probability density functions (PDF), cumulative distribution functions (CDF), level cross rate (LCR) and average fade duration (AFD).

Introduction

The technology of telecommunication, especially wireless communication is one of those exciting technologies that has directly and significantly influenced our everyday life. It has changed the dynamics of the working environment and workforce mobility. Without being tethered to a fixed location or formal work-based environment, people can work anywhere.

A key component work of design and build wireless networks is the study of wireless channel models. The modeling of the wireless channel is of great importance to satisfy the operator requirement for network planning, optimization, interference and traffic calculation, as well as frequency planning and neighbors analyses. However, our knowledge of the radio channels encountered in mobile-to-mobile and relay-based systems are still inadequate.

Different approaches could be used to simulate diverse type of channels and their conditions. Generally, mobile radio propagation channels are usually studied in terms of deterministic models, empirical models. Deterministic models [1, 2] are based on a fixed geometry (such as buildings, streets…) and used to analyze particular situations. They provide high accuracy, but require actual analytical path profiles and time-consuming computations. Empirical as well as pure statistical models [3, 4] are based on measurements. They linked to the environment and the parameters of the measurement campaign. Such models are characterized by simple input data and low computational effort, but are usually very poor at extrapolating outside of the measured parameter range and suffer from a classification problem involved in describing the environment. Due to the lack of physical background, such models, however, only apply with good results in environments that are very close to the one they have been inferred from.

This paper presents a novel hidden Markov method to model flat Rayleigh fading channels. The proposed Hidden Markov Model (HMM) is based on the Finite State Markov Channel (FSMC) model [5]. The performance of the model is studied by simulating the probability density functions (PDF), cumulative distribution functions (CDF), level cross rate (LCR) and average fade duration (AFD).

The remainder of this paper is organized as follows: The Nakagami Fading Channel is presented in Section II. In Section III, Hidden Markov Model (HMM) is studied. The joint probability density function and cumulative distribution function of the received envelope amplitudes are analyzed and simulation in Section IV. Section V concludes the paper.

Nakagami Fading Channel

Due to the multipath propagation, the transmitted signals of the receiver are variations of amplitude, phase and angle. The multipath fading gives rise to specific types of degradations of the signal. The variations are characterize by two main manifestations, large-scale and small-scale fading, the later is also known as Rayleigh fading since the fluctuation of the signal envelope is Rayleigh distributed when there is no predominant line of sight between the transmitter and receiver. The sum of multiple independent and identically distributed (i.i.d.) Rayleigh-fading signals have a Nakagami distributed signal amplitude. After k - branch maximum ratio combining (MRC) with Rayleigh-fading signals, the resulting signal is Nakagami with $m = k$. MRC combining of m - Nakagami fading signals in k branches gives a Nakagami signal with shape factor mk.

For Nakagami channels the probability distribution function (PDF) of the channel gain α is [6]:

$$p_\alpha = 2\left(\frac{m}{\Omega}\right)^m \frac{\alpha^{2m-1}}{\Gamma(m)} \exp\left(-m\frac{\alpha^2}{\Omega}\right), \qquad \alpha \geq 0, \tag{1}$$

where $\Omega = E\left(\alpha^2\right)$ is the average received power, m is the Nakagami fading parameter $\left(m \geq 1/2\right)$, and $\Gamma(\cdot)$ is the gamma function. The received CNR γ is then gamma distributed according to the PDF, $p_\gamma(\gamma)$, given by:

$$p_\gamma(\gamma) = \left(\frac{m}{\gamma}\right)^m \frac{\gamma^{m-1}}{\Gamma(m)} \exp\left(-m\frac{\gamma}{\overline{\gamma}}\right), \qquad \gamma \geq 0, \tag{2}$$

where $\overline{\gamma}$ is the average received CNR. The phase ϕ of the Nakagami fading is uniformly distributed over $[0, 2\pi]$.

If $m = 1$, the Nakagami distribution is reduced to Rayleigh distribution, if $m = (1+k)^2 / 2k+1$, the Nakagami distribution is reduced to Rice distribution, and if $m \to \infty$, the Nakagami distribution is reduced to Gaussian distribution.

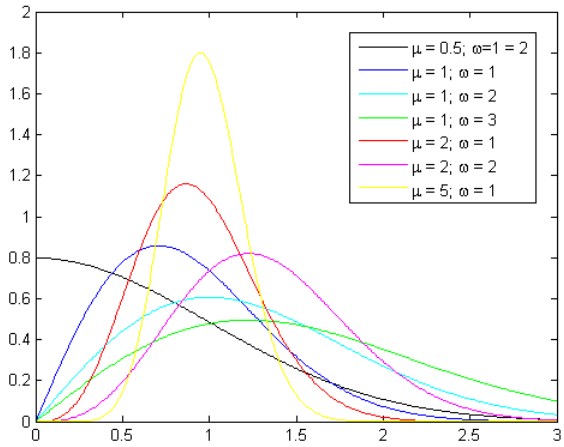

Fig. 1 PDF for Nakagami distribution

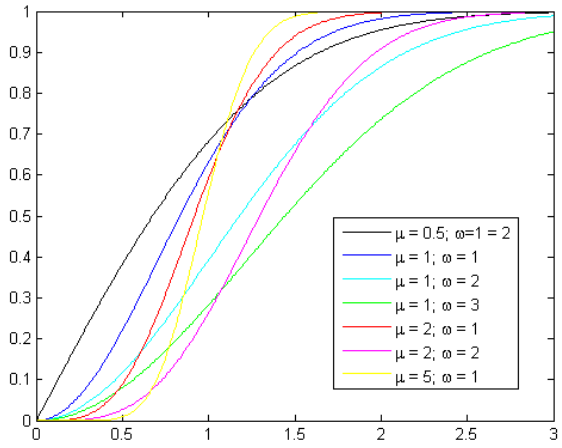

Fig. 2 CDF for Nakagami distribution

Hidden Markov Model

Normally, the Gilbert-Elliot model, the Finite State Markov Channels (FSMCs) and Hidden Markov Models (HMMs) are used to characterize a flat Rayleigh fading channel. In this paper, we used HMM to model the Nakagami channel.

The first order FSMC is inadequate and impractical under very long channel memory **[7]**, due to the fact that in this case the number of states grows exponentially with the process memory.

HMMs are probabilistic function of Markov chains, the results of the observable models is a doubly embedded stochastic process, because one of the stochastic process is not observable, hence the name HMM. The main characteristic of HMM can be outline as follows **[7]**:

1. The number of states in the model is ‘n’, even though some states are ‘hidden’ in practical application. The HMMs processes can be defined by a finite number of possible states by a set $S=\{s_0,s_1,s_2,...,s_{n-1}\}$;
2. The discrete alphabet size is ‘m’, and the set X of the outputs can be represented by as a set $X=\{x_0,x_1,x_2,...,x_{n-1}\}$;
3. The state transition probability distribution matrix $A=\{a_{ij}\}$, where $a_{ij}=p(s_j/s_i)$;
4. The observed symbol probability distribution matrix B is a diagonal matrix whose elements b_j represent the probability $p\{x/s_j\}$, $x\in X$ (is X is discrete);
5. The initial state probability vector is π.

Simulation and Comparison

In this section, we compare the first order statistics (PDF,CDF) and second order statistics (LCR, AFD) of the HMM for Nakagami fading channel. Figure 5 and Figure 6 present the comparison of PDF and CDF for the simulated data and the measured ones respectively. It is perceived that the simulated PDF CDF based on HMM agree well with the measured ones.

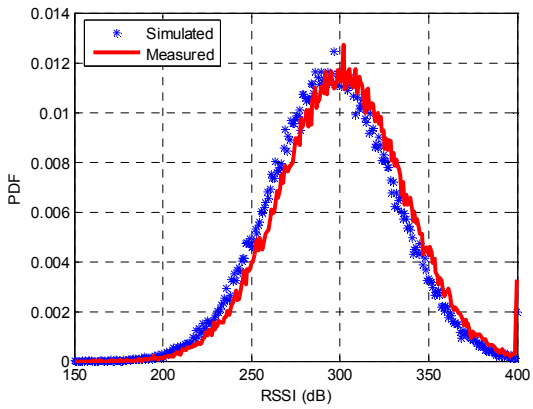

Fig. 1 Comparison of PDFs

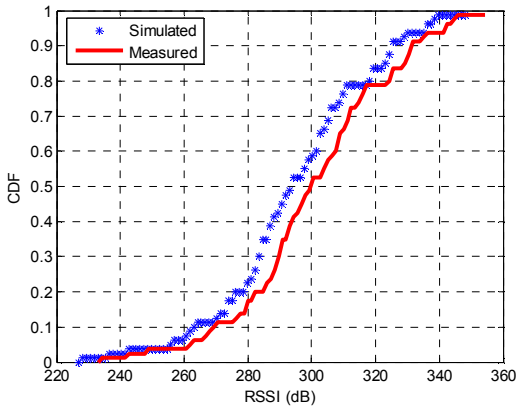

Fig. 2 Comparison of CDFs

It is clear from Fig. 1 and Fig. 2 that there is a significant variance around the mean value. This variation is well described by a lognormal distribution. A maximum likelihood estimate (MLE) of the standard deviation of this distribution is $\sigma_{dB}=3.2$.

Apart from the PDF and the CDF, in order to optimize the digital communication systems, which are required for error correction, other characteristic quantities describing the statistics of mobile fading channels are of importance. These quantities are the level-crossing rate (LCR) and the average duration of fades (AFD).

The system performance changes rapidly when the signal falls below some noise-related threshold and this causes bursts of errors to occur. The rates of occurrence and average length of these error bursts can be estimated from average LCR and AFD of the received signal strength. LCR is defined as the rate at which the RSSI crosses a specified fading level in the positive (or negative) slope. AFD is the average time duration that the RSSI remains below a specified level. Fig. 3 and Fig. 4 present a comparison of LCR and AFD for the simulated data and the measured ones, respectively. It is perceived that the simulated LCR and AFD based on the HMM agree well with the measured ones.

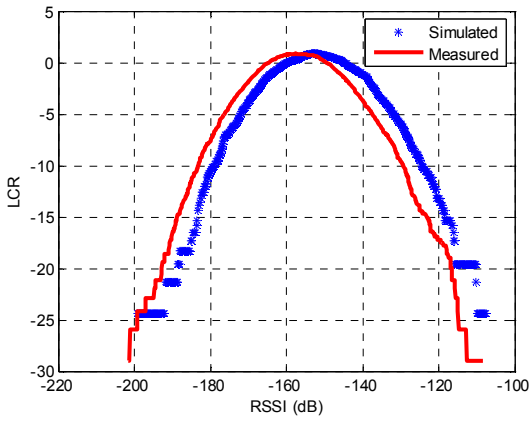

Fig. 3 Comparison of LCR

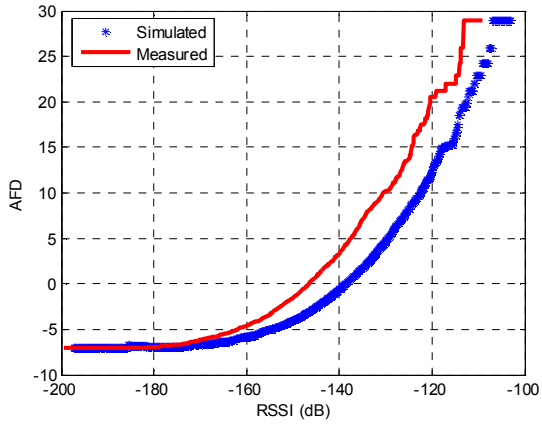

Fig. 4 Comparison of AFD

Conclusion

Extensive research in cellular radio channels has led to the successful deployment of cellular networks. In this paper, we applied the HMM the Nakagami Channel. We have also analysis the channel performance using simulation method. This study shows that the HMM approach can be valuable for the Nakagami channel analyzing and performance evaluation.

The advantages of this model is that it can have a very good fit to experimental data and can obtain closed solutions for several parameter of the model, and all of these advantages could result in better approximation of the model to specific conditions.

Acknowledgement

This paper is supported by Kunming University Scientific Research Project (XJL12006).

References

[1] J.P. Rossi, A.J.Levy. *A ray model for decimetric radiowave propagation in an urban area* [J]. Radio Science, 1992,27 (6): 971-979.

[2] C. Oestges,d A. J. Paulraj. *Physical model for broadband wireless channels* [J]. Electron. Lett., 2001, 37(3): 1195–1197.

[3] Chun. Loo. *A Statistical Model for a Land Mobile Satellite Link* [J]. IEEE Trans. Veh. Technol., 1985, 34(3): 275-281.

[4] E. Lutz, D. Cygan, M. Dippold, F. Dolainsky, W. Papke. *The land mobile satellite communication channel- Recording, statistics, and channel model* [J]. IEEE Trans. Veh. Technol., 1991, 40(2): 375–386.

[5] H. S. Wang, N. Moayeri, *Finite-State Markov Channel – A useful Model for Radio Communications Channels*, IEEE Transactions on Vehicular Technology, Vol. 44, No. 1, Februrary 1995, pp. 163-171.

[6] I.S. Gradshteyn and I.M.Ryzhik, *Table of Integrals, Series, and Products*. San Diego, CA: Academic Press ed., 1994.

[7] Juliio Arauz, *Discrete Rayleigh Fading Channel Modeling*. Department of Information Sciences and Telecommunications. Pittsburgh PA,15260.

Advanced Materials Research Vols. 989-994 (2014) pp 2580-2587
© (2014) Trans Tech Publications, Switzerland
doi:10.4028/www.scientific.net/AMR.989-994.2580

Application of Multipurpose Decision Making problem with AHP and Rectilinear Norm in Old Town Renewal Proposals

Bingjiang ZHANG

School of Applied Science, Beijing Information Science and Technology University, Beijing, 100192, China

E-mail: zbj2013ch@163.com

Keywords: AHP; Rectilinear Norm; Allocation Problem; MCDM; Urban Renewal

Abstract. In the process of urbanization, old town renewal is an unavoidable problem. The significance of old town renewal focuses on meliorating residents' physical environment conditions, humane and social environment, and improving urban operation efficiency. Such problem affects not only the development of a certain district, but the benefits of future generations. For city managers, it is difficult to bring up a rational and highly efficient proposal such that related interest bodies would accept, and thus democracy science decision is required. This essay employs AHP to solve the problem of old town renewal proposal assessment, and brings forward the decision-making of multi-objective programming problem based on rectilinear norm allocation problem. Since there is no such paper that systematically and efficiently assess old town renewal proposal by using allocation problem, this paper tries to use this method to "fill out this blank".

Introduction

Nowadays, China's economy and social development are experiencing complicated structural alteration. Urbanization has entered into a stage of accelerated process. Due to the acceleration of urbanization process, new towns are being constructed on the one hand; on the other hand, some old towns cannot satisfy the demands by towns, governments and citizens and thus needed to be redeveloped. In the process of urban development, it has formed its own distinctive cultural, political, and economical system on the one side; although it has written down the path of town development, it reflects the disadvantages left from town development on the other side. In the process of urban development, the movement of population and usage of town resources both result in high population intensity, urban layout chaos, traffic inconvenience and other disadvantages and defects. Some areas cannot sustainably make further development anymore and therefore it cannot meet the needs by the town developments and the economy developments. Along with the consecutive update of the human society development concept, city values and the main point of development continuously happen to have corresponding changes. Today's world has a common approval of society development concept and city value with people oriented and sustainable development, and all of these factors have determined China's urban plans, and the new ideas and principals that urban development must follow.

There are many problems involved in old town redevelopment, which include solving the problems of high population intensity, town layout chaos, inconvenient traffic, and pollution and so on. In the process of old town redevelopment, it is difficult to solve those problems if we merely rely on the government, because citizens, professionals and other residents have their own expectations and each of these group will be affected when participating old town renewal at different stage. Since every single doable proposal will never fulfill all personal considerations and expectations, it is going to be a difficult and complicated process to make up a sustainable and renewable suggestion. It is needed to pick up a compromising proposal with which most people are satisfied from a bunch of proposals with which most people are agreed. Try at most possibility to put forward a most satisfactory urban renewal proposal. In order to make sure the final proposal is persuasive, a scientific method that can

be used to assess urban renewal proposal is needed. This essay will apply AHP and multicriteria allocation problem based on rectilinear norm to solve the problem of sustainable urban renewal.

Old town renewal proposal

First, we bring up a general guideline for old town renewal. In the process of old town renewal, the resources inherited in the town, the future development potential of the town and the problems exists at present must be taken into consideration. Old town renewal is a huge project, and the following elements should be taken into account.

(1) Sustainable development ability. Based on the inherited style of the town, we should consider the "self-hematopoietic function" of the town, which lay a foundation for future town development;

(2) Public participation mechanism. Future residents will gain more opportunities to notice government policy and commit themselves to express their opinions about urban development decision; especially those policies that are related to their living environment and living standards;

(3) Comprehension between related bodies. All class of citizens that reside in future urban areas should be able to follow such urban living style that covers government implements, community supervision, and resident self-consciousness. Related interest groups are compatible and comprehensive with each other;

(4) Residents' living standards are remarkably improved and old town energy and appeal are enhanced. In the process of urban renewal, it is very important to make sure citizens are physically and mentally healthy. Public infrastructures are well matching; public space gets developed and enriched. Old town neighborhoods relationships and social networks are conserved; the sense of identification and the sense of pride that citizens feel about the community are reestablished and enhanced;

(5) Appropriate and balanced use of land. Renewed town should own a broadly mixed-use function which includes working place, residence, Commercial Street, and entertainment infrastructure and so on. These infrastructures and the environment should achieve mutual support to build up a district brimmed with energetic life, business and relaxation;

(6) Perfect traffic facilities. In the renewal region, there should be sideway, highway, bridge, and public railway traffic infrastructure among different infrastructures in order to provide citizens a safe and convenient traffic environment. Traffic lines between renewal region and other region are connected, which includes the connection between the streets inside the region and the main streets outside the region;

(7) Preservation of traditional and positive elements. New exploitation is inevitable in the process of old town renewal. Regions being exploited should enrich and complement the positive characteristics of the renewal region, infrastructures that have remarkable contributions to the characteristics of the town, and some positive elements that truly reflects social personals past achievements. New logos and signs could enhance town characteristics. New framework must be amalgamated with inherited components;

(8) Appropriate humanity environment and urban greening. At the same time the construction of humanity environment is enhanced, urban greening of the renewal region should also be taken into consideration. For example, we should consider what kind of trees and flowers to be planted so that the city image can be better reflected.

According to the old town renewal guidelines mentioned above, a more specific old town renewal proposal is brought up. For urban planning of the old town, the principals discussed in the general guideline only set a direction for old town renewal, and implementers could prepare urban renewal proposal based on this guideline. At the same time the old town renewal proposal reflects the distinct style and geographic characteristics of the town, it should possess common view and sustainable develop ability. Reference [1] and [2] help us set up the goals and principals of sustainable urban

renewal proposal (Table 1). Table 2 gives the goals and specific content of designing principles. Although Table 1 as far as possible shows all sorts of important elements that exist in the old town renewal, distinct humane and geographical areas can be adjusted according to different demands. During the construction, no matter how good the proposal is, it must satisfy the money demanded in urban renewal and acreage limitation of the construction place.

Table 1 Objectives and design criteria for sustainable urban renewal proposal

Objectives	Design criteria
Sociality, SO	Access to public facilities, APF Open and tolerant of public space, OTS Provisions for disadvantaged groups, PDG Conservation of local distinctiveness, CLD Adaptability of development to the changing needs, ADN
Economy, EC	Provision of commercial facilities, CFS Traffic facilities supply and its distribution, TSD Compatibility with neighborhood , COR Citizens job security , CJS
Environmental, EN	Green design, GD Building form and structure, BFS human environment , HE Rehabilitation of repairable properties, RRP
Workability, WO	Construction cost, CC Project implementation, PI Energy utilization, EU

Table 2 The specific contents of evaluation

Objectives and design criteria	Specific contents
SO	It must accord with the demands for human whole development, and it is favorable to the urban social development.
APF	The government offers the society the public articles or public to enjoy. Such as administrative facility, information facility, health facilities, cultural facility, sports facilities, etc.. and if communal facilities meet people's demands and communal facilities can be sufficient used.
OTS	There is not the vacant floor space which does not have buildings and it have the surrounding environment compatibility.
PDG	The social disadvantaged groups included the diseased, young, old, and injured can get government's help. Guarantee the most basic living guarantee of the social disadvantaged groups, and offer the necessary insurance to them, such as the endowment insurance, medical insurance, etc..
CLD	The left characteristic old architecture and celebrity's former residence are protected and offered maintenance.
ADN	In the development of urban area in the future, while the urban area is be developed again or reconstructed, it can adapt to its surroundings, and is favorable to the social development.
EC	The economic development of the urban society, including industry's characteristic and structure.
CFS	There are large-scale markets or comprehensive emporium which can supply with some general merchandise, building materials, ornament materials, etc., and it can offer large-scale food and beverage, amusing, recreation facility, including the construction of significant commercial facilities closely related with people's life such as the commercial square and business street, etc..
TSD	Whether the facilities such as traffic route and station, electromechanical equipment, communication signal, etc. could meet demands of going out of people at ordinary times, and the distribution of traffic facility is more rational.
COR	Area reconstructed and nearby area can well combine it together in order to develop steadily.
CJS	Basic ensured work of urban citizen, for example assign to work for laid-off workers etc..
EN	Urban environmental protection, not only refer to the natural environment, and living environment, social environment, i.e. various interpersonal social relationships such as the political system, cultural tradition, neighbourhood relation, etc..
GD	The floor space of the urban green plants, and if it could beautify the environment.
BFS	The use of the building material and form of the building can bring a kind of comfortable feeling to people.
HE	The environment that can get along harmoniously between men, including people's attitude, idea, faith, cognitive environment, etc..
RRP	After the urban area reconstruct, it will could have a certain destructivenesses on facility, environment, resource, etc. in original area, the destroyed area can well resume the steady state, and it does not influence the residents' life.
WO	The concrete implementation intensity of the old urban area reconstructed.
CC	The old urban area reconstruction of overall cost and expense source.
PI	Dependability of constructing and completion intensity.
EU	It can fully utilize existing resources.

The decision-making model of urban renewal proposals based on AHP

Analytical hierarchy process (AHP) was brought up by an American operational research experts T. L. Saaty in mid 70’s of the 20th century. The fundamental theory is to assess proposal based on objectives, sub objectives, restricted condition and departments, which are leveled hierarchical structural, form a contrast matrix, then use the components of vectors from the biggest feature of judgment matrix and its related feature as the related coefficient, and eventually conclude the priority

of each proposal. AHP is a qualitatively and quantitatively combined, systematically, and hierarchical analyzing method ([3]).

Before data was collected and calculated, a decision-making model must be built up with respecting to a decision-making problem. For the decision-making problem of old town renewal proposal, its model is shown as diagram 1, the meanings of the characters are given in chart 1. The final goal of decision-making model is the highest standard of descriptive problem (it is referred as "the best designed proposal" here). The second level is the decision-making objective level, which includes four aspects: social, economical, environmental, and engineering. These four indexes are composed from different decision-making designs, shown as Figure 1.

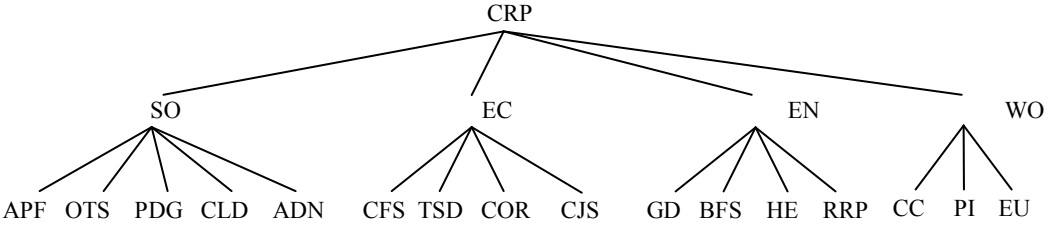

Fig. 1 AHP decision model for producing sustainable urban renewal proposal

A case study of the town renewal proposal based on AHP

As a designed case, this essay brings up three proposals about a town renewal construction. In order to make sure the priority of hierarchal decision-making model of sustainable development objective in the second level, and the relative importance of each distinct designed proposal in the third level, personals participated in old town renewal will accomplish a series of one-to-one comparison. In order to obtain a representative result, we have invited 40 citizens, which include scholars, residents, foreigners, and developers. We separate these citizens into 4 groups with respect to their identities, and assess the three old town renewal proposals mentioned above in the form of groups. While making comparisons between old town renewal proposal and each projects using AHP, assessors must follow the 9-point scale in Table 3 to make judgment. The final grading of the judgment of two elements' importance and every possible advice is based on the combination of observations proceeded in the process of judgment of each group.

Taking an example of a group of scholars, calculate the weight of program priority according to the specific scale and the calculation steps in AHP. Table 3 shows the relative assessment results with respect of four objectives of a group of scholars. Table 4 shows the relatively comparative results among social sub principles. With the same method, we can obtain the relatively comparative results among sub principles of other programs, shown as Table 5. Table 6 is a project hierarchy judgment matrix of public infrastructure setting and utilizing rate. The relative comparative result between each of other designing program hierarchies and project hierarchy can also be calculated. After calculating the comparative data of each designing program hierarchy with respect to program hierarchy, we integrate the weights of objective hierarchy to obtain the comprehensive weights of each designing program at first, and then we calculate the weights of each project. With above calculation, we get an overall assessment of three proposals about old town renewal with respect to a group of scholars. The first proposal is 0.3401, second one is 0.3207, and the third one is 0.3391. With the same method, we can get the assessment of the projects for the other three groups of people, shown as Table 7.

Table 3 Comparisons of objectives

CRP	SO	EC	EN	WO	Weights
SO	1	3	5	7	0.5880
EC	1/3	1	1/2	3	0.1545
EN	1/5	2	1	3	0.1923
WO	1/7	1/3	1/3	1	0.0652

$\lambda_{max} = 4.1634$， C.R. = 0.0605 < 0.10

Table 4 Comparisons of design Criteria with respect to SO

SO	PFU	SOT	DSE	OTP	RDA	Weights
PFU	1	3	1	3	4	0.3440
SOT	1/3	1	1/3	1/2	1	0.0942
DSE	1	3	1	3	3	0.3248
OTP	1/3	2	1/3	1	3	0.1549
RDA	1/4	1	1/3	1/3	1	0.0820

$\lambda_{max} = 5.1276$， C.R. = 0.0159 < 0.10

Table 5 The final weights of the objectives and design criteria

Design criteria	SO 0.5880	EN 0.1545	EC 0.1923	WO 0.0652	Weights
PFU	0.3440				0.2023
SOT	0.0942				0.0554
DSE	0.3248				0.1910
OTP	0.1549				0.0911
RDA	0.0820				0.0482
CFS		0.4262			0.0658
TSD		0.3480			0.0538
COR		0.1322			0.0204
CJS		0.0935			0.0144
GF			0.0742		0.0143
BFS			0.1972		0.0379
HE			0.4569		0.0879
RF			0.2717		0.0522
CC				0.5695	0.0371
IN				0.0974	0.0064
EU				0.3331	0.0217

Table 6 Comparisons of three design schemes

PFU	D1	D2	D3	Weights
D1	1	5	3	0.6267
D2	1/5	1	1/4	0.0936
D3	1/3	4	1	0.2797

$\lambda_{\max} = 3.0858$, C.R. = 0.0739 < 0.10

with respect to PFU

Table 7 The weighted order of four groups with respect to three design schemes

Valuator	First proposal	Second proposal	Third proposal
Scholars	0.3401	0.3207	0.3391
Foreigners	0.3089	0.2764	0.4147
Residents	0.3290	0.3609	0.3099
Developers	0.2664	0.3299	0.4039

In view of the computed results, scholars pay relatively more attention to the first proposal – the content of the first proposal includes pretty good economical efficiency, relatively good sociality, mediocre environmental protection, and relatively poor engineered. Foreigners and developers pay relatively more attention to the third proposal – it includes pretty good sociality, relatively good engineered, mediocre economical efficiency and poor environmental protection. Residents emphasize on the second proposal – it includes pretty good environmental protection, relatively good sociality, and mediocre engineered and poor economical efficiency.

Multi-criteria location problem based on rectilinear norm

Given demand points in R^n, a problem to locate a new facility in R^n is called a single facility location problem. The problem is usually formulated as a minimization problem with an objective function involving distances between the facility and demand points. It is assumed that m demand points $D = \{d_1, d_2, \cdots, d_m\}$, $d_i = (d_i^1, d_i^2, \cdots, d_i^n)^T \in R^n$, $i \in M = \{1, 2, \cdots, m\}$ and rectilinear norm $\|\cdot\|_1$ defined on R^n are given. Let $x = (x^1, x^2, \cdots, x^n)^T \in R^n$ be the location of the facility to be determined. We put $D = \{d_i \mid i \in M\}$. Without loss of generality, it is assumed that $D \not\subset \{(x^1, x^2, \cdots, x^n)^T \in R^n : x^j = x_0\}$ for each $j \in J = \{1, 2, \cdots, n\}$ and any $x_0 \in R$, then our main problem is a multi-criteria location problem formulated as follows

$$(\mathrm{P}) \quad \min_{x \in R^n} f(x) = (\| x - d_1 \|_1, \| x - d_2 \|_1, \cdots, \| x - d_m \|_1)^T. \tag{1}$$

Let $E(D)$ and $QE(D)$ be the set of all efficient solutions of (P) and the set of all quasi-efficient solutions of (P), respectively. By the above definitions, it can be seen that $D \subset E(D) \subset QE(D)$. Our main interest is to find $QE(D)$. In order to characterize quasi-efficient solutions of (P), we also consider a scalarization problem formulated as follows:

$$(\mathrm{P}_\lambda) \quad \min_{x \in R^n} g(x) = \sum_{i=1}^{m} \lambda_i \| x - d_i \|_1, \tag{2}$$

where each λ_i, $i \in M$ is a non-negative weight associated with d_i, and $\lambda = (\lambda_1, \lambda_2, \cdots, \lambda_m)^T \neq 0$.

Theorem 1 ([3]) A point $x_0 \in R^n$ is quasi-efficient solution in (P) if and only if x_0 is optimal solution in (P_λ) for some $\lambda \geq 0$ with $\lambda \neq 0$.

From Theorem 1, $QE(D)$ and $E(D)$ can be expressed as

$$QE(D) = \{x^* \in R^n \mid x^* \in R^n \mid x^* \in S^*(\lambda) \text{ for some } \lambda \geq 0 \text{ with } \lambda \neq 0\}$$

and

$$E(D) = \{x^* \in R^n \mid x^* \in R^n \mid x^* \in S^*(\lambda) \text{ for some } \lambda > 0\},$$

where $S^*(\lambda)$ is the optimal solution set of (P_λ) for some $\lambda > 0$.

Since the objective function of (P_λ) can be rewritten as

$$(P_\lambda) \quad \min_{x \in R^n} g(x) = \sum_{i=1}^{m} \lambda_i \sum_{j=1}^{n} | x^j - d_i^j | = \sum_{j=1}^{n} \sum_{i=1}^{m} \lambda_i | x^j - d_i^j | . \tag{3}$$

Namely, $x^* = (x^{1*}, x^{2*}, \cdots, x^{n*})^T \in S^*(\lambda)$ if and only if each x^{j*}, $j \in J$ is an optimal solution of the following one-dimensional problem:

$$(P_j) \quad \min_{x \in R} g_j(x) = \sum_{i=1}^{m} \lambda_i | x^j - d_i^j |, \tag{4}$$

where $j \in J$. For these one-dimensional problems, we can be to find all quasi-efficient solutions by algorithm in [5].

When $n = 2$, all unions of efficient solutions of Problem (P) are given in [6], all unions of junior efficient solutions of Problem (P) are given in [7]. Solutions of Problem (P_λ) could be calculated using the algorithm mentioned in [5].

Next, based on the properties of efficient solutions of multi-purpose allocation problems mentioned in [7], we discuss the scalarization algorithm of multi-purpose allocation problems.

For each $j \in \{1, 2, \cdots, n\}$, let $d^j_{[[1]]}, d^j_{[[2]]}, \cdots, d^j_{[[m_j]]}$ be all distinct real numbers among $d_1^j, d_2^j, \cdots, d_m^j$ such that $d^j_{[[1]]} < d^j_{[[2]]} < \cdots < d^j_{[[m_j]]}$, and we put

$$F^j_{2k-1} = \{d^j_{[[m_j]]}\}, \quad k = 1, 2, \cdots, m_j \tag{5}$$

and

$$F^j_{2k} = [d^j_{[[k]]}, d^j_{[[k+1]]}], \quad k = 1, 2, \cdots, m_j - 1. \tag{6}$$

For each $k_j \in \{1, 2, \cdots, 2m_j - 1\}$, $j \in J$, $F^1_{k_1} \times F^2_{k_2} \times \cdots \times F^n_{k_n}$ is called a box. Moreover, if k numbers are even among $k_1, k_2, \cdots, k_n$, then $F^1_{k_1} \times F^2_{k_2} \times \cdots \times F^n_{k_n}$ is called k-dimensional box.

For any fixed $\lambda \geq 0$ with $\lambda \neq 0$,

$$S^*(\lambda) = (F^1_{k_1} \cup F^1_{k_2} \cup \cdots \cup F^1_{k_n}\} \times \{F^2_{k_1} \cup F^2_{k_2} \cup \cdots \cup F^2_{k_n}\} \times \cdots \times \{F^n_{k_1} \cup F^n_{k_2} \cup \cdots \cup F^n_{k_n})$$

for some k_j, $k_j' \in \{1, 2, \cdots, 2m_j - 1\}$ with $k_j \leq k_j'$, $j \in J$. Therefore, $QE(D)$ is the union of some boxes. The union of all one-dimensional boxes in $QE(D)$ is called the frame of $QE(D)$.

For $a = (a^1, a^2, \cdots, a^n)^T \in \prod_{j=1}^{n} \{1, 2, \cdots, 2m_j - 1\}$, we put

$$F(a) = \prod_{j=1}^{n} F^j_{a^j}. \tag{7}$$

Next, for $a \in A = (\prod_{j=1}^{n} \{1, 2, \cdots, 2m_j - 1\}) \setminus (\prod_{j=1}^{n} \{2k - 1 \mid k \in \{1, 2, \cdots, m_j\}\})$, we check λ such that $F(a)$ is a set of all optimal solutions of (P_λ) exists or not. If such λ exists, the $\forall x \in F(a)$ is a solutions of (P_λ).

For $F(a)$, $a \in A$, we assume

$$J_2(a) = \{j \in \{1, 2, \cdots, n\} \mid a^j \text{ is even}\} \neq \varnothing,$$

$F(a)$ is called $|J_2(a)|$-dimensional box. $|J_2(a)|$ said the number of elements. For $k \in \{1,2,\cdots,n\}$, we assume

$$A_k = \{a \in A \,|\, |J_2(a)| = k\} \neq \varnothing,$$

$F(a)$ is called $k-$dimensional box.

The algorithm of solving $E(D)$

Step 1 Set $T^* = \varnothing$ and $k = n$.

Step 2 For each $F(a) \not\subset T^*$, $a \in A$, check $\lambda > 0$ such that $F(a)$ is set of all optimal solutions of Problem (P_λ) exists or not. If such λ exists, we put $T^* = T^* \cup F(a)$.

Step 3 If $k \neq 1$, $k = k-1$, go to Step 2, otherwise, then stop. The $E(D) = T^*$ is set of all efficient solutions of Problem (P).

Analysis on results obtained based on AHP using location problem

From the calculation of the fourth part, we know that the assessment results of the three town renewal proposals that scholars, foreigners, residents and developers separately assess are not unified, and this causes certain confusion to the final decision makers because taking each proposal will disappoint those who disagree with such proposal. Subsequently, we need to find such method that can generate a comprehensive evaluation of these three assessment results in order to obtain a final proposal that more people will approve. We try to solve this problem using the method that solves the allocation problem mentioned above.

Let $d_i = (d_i^1, d_i^2, d_i^3)^T$, $i = 1,2,3,4$ be a priority weight vector of i-group. From Table 7, we get $d_1 = (0.3401, 0.3207, 0.3391)^T$, $d_2 = (0.3089, 0.2764, 0.4147)^T$, $d_3 = (0.3290, 0.3609, 0.3099)^T$ and $d_4 = (0.2664, 0.3299, 0.4039)^T$. Let $x = (x^1, x^2, x^3)^T$, x^1, x^2 and x^3 be a final evaluation results of the first proposal, the second proposal and the third proposal, respectively.

From Problem (P), we have

$$(\mathrm{P}) \quad \min_{x \in R^4} f(x) = (\| x - d_1 \|_1, \| x - d_2 \|_1, \| x - d_3 \|_1, | x - d_4 \|_1)^T. \tag{8}$$

Since the objective function of (P_λ), $g_j(x)$ can be rewritten as

$$(\mathrm{P}_j) \quad \min_{x \in R} g_j(x) = \sum_{i=1}^{4} \lambda_i | x^j - d_i^j |. \tag{9}$$

According to the calculation steps in part 5, we proceed to further calculation and analysis of the data in Table 7 that reflects the assessment weights that scholars, foreigners, residents and developers weight about the three proposals.

Let $d_1 = (0.3401, 0.3207, 0.3391)^T$, $d_2 = (0.3089, 0.2764, 0.4147)^T$, $d_3 = (0.3290, 0.3609, 0.3099)^T$ and $d_4 = (0.2664, 0.3299, 0.4039)^T$. From formula (5) and formula (7), we have

$F_1^1 = \{0.2664\}$, $F_2^1 = [0.2664, 0.3089]$, $F_3^1 = \{0.3089\}$, $F_4^1 = [0.3089, 0.329]$, $F_5^1 = \{0.329\}$, $F_6^1 = [0.329, 0.3401]$, $F_7^1 = \{0.3401\}$, $F_1^2 = \{0.2764\}$, $F_2^2 = [0.2764, 0.3207]$, $F_3^2 = \{0.3207\}$, $F_4^2 = [0.3207, 0.3299]$, $F_5^2 = \{0.3299\}$, $F_6^2 = [0.3299, 0.3609]$, $F_7^2 = \{0.3609\}$, $F_1^3 = \{0.3099\}$, $F_2^3 = [0.3099, 0.3391]$, $F_3^3 = \{0.3391\}$, $F_4^3 = [0.3391, 0.4039]$, $F_5^3 = \{0.4039\}$, $F_6^3 = [0.4039, 0.4147]$, $F_7^3 = \{0.4147\}$.

Then

$A_1 = (\{1,3,5,7\} \times \{1,3,5,7\} \times \{2,4,6\}) \cup (\{1,3,5,7\} \times \{2,4,6\} \times \{1,3,5,7\}) \cup (\{1,3,5\} \times \{2,4,6\}$,

$A_2 = (\{2,4,6\} \times \{1,3,5,7\} \times \{1,3,5,7\}) \cup (\{2,4,6\} \times \{1,3,5,7\} \times \{2,4,6\}) \cup (\{2,4,6\} \times \{2,4,6\}$
$\times \{1,3,5,7\}) \cup (\{2,4,6\} \times \{2,4,6\} \times \{2,4,6\})$.

We could get the solutions of problem (P_λ) under four situations from above calculations, which is such multi-purpose problem has solutions under the following four situations:

(ⅰ) When $a=(2,5,5)^T$, let $\lambda=(1,1,1,3)^T$. In this situation, developers' opinion is the most important, their satisfaction is $[0.2664,0.3089]\times\{0.3299\}\times\{0.4039\}$, which tells that developers consider the third proposal as the best one.

(ⅱ) When $a=(6,3,3)^T$, let $\lambda=(3,1,1,1)^T$. In this situation, scholars' opinion is the most important, and their satisfaction to the third proposal is $[0.329,0.3401]\times\{0.3207\}\times\{0.3391\}$, which tells that scholars think both the first proposal and the third one are fine.

(ⅲ) When $a=(3,2,6)^T$, let $\lambda=(1,3,1,1)^T$. In this situation, foreigners' opinion is the most important, and their satisfaction to these three proposals is $\{0.3089\}\times[0.2764,0.3207]\times[0.4039,0.4147]$, which tells that foreigners consider the third proposal as the best one.

(ⅳ) When $a=(5,6,2)^T$, let $\lambda=(1,1,3,1)^T$. In this situation, residents' opinion is the most important, and their satisfaction about these three proposals is $\{0.329\}\times[0.3299,0.3609]\times[0.3099,0.3391]$, that is residents think both the second and the third proposal are fine.

Consolidated above four situations, scholars, foreigners, residents and developers all choose the third proposal, which concludes the third proposal is relatively outstanding and it has the most public opinion.

Conclusion

This essay focuses on making the decision-making process of such problem to be easier by using AHP. Although AHP is neither the best nor the only solution for all daily decision problems, AHP is an efficient tool for old town renewal proposal assessment. There exist disadvantages when assessing old town renewal proposal merely depends on AHP. From the analyzing results, it is efficient to assess old town renewal proposal when these two methods are combined because this reduces people's subjectivity and makes decisions more rational.

References

[1] K. L. Lee and H. W. Chan. The Analytic Hierarchy Process (AHP) Approach for Assessment of Urban Renewal Proposals. Soc Indic Res., 89(2008), pp. 155–168.

[2] Xu Qin. The modern city values and China's urban development. Journal of Nanjing University of Technology, 3(2001), pp. 45-49.

[3] T.L. Saaty. A Scaling Method for Priorities in Hierarchical Structures. Journal of Mathematical Psychology, 15(1977), pp. 234–281.

[4] T. J. Lowe, J. F. Thisse, J. E. ward and R. E. Wendell. On efficient solutions to multiple objective mathematical programs. Manage. Sci., 30(1984), pp. 1346-1349.

[5] Z. Drezner and G. O. Wesolowsky. The asymmetric distance location problem. Trans. Sci., 23(1989), pp. 201-207.

[6] L. G. Chalmet, R. L. Francis and A. Kolen. Finding efficient solutions for rectilinear distance location problems efficiently. Eur. J. Oper. Res., 6(1981), pp. 117-124.

[7] M. Kon. Efficient solutions for multicriteria location problems under the block norm. Mathematic Japonica, 47(1998), pp. 295-303.

[8] R. E. Wendell, A. P. Hurter and T. J. Lowe. Efficient points in location problems. AllE Trans., 9(1977), pp. 238-246.

Advanced Materials Research Vols. 989-994 (2014) pp 2588-2592
© (2014) Trans Tech Publications, Switzerland
doi:10.4028/www.scientific.net/AMR.989-994.2588

Application with AHP in Assessment of House Plans

Bingjiang ZHANG

School of Applied Science, Beijing Information Science and Technology University, Beijing 100192, China

E-mail: zbj2013ch@163.com

Keywords: AHP; MCDM; House plan; Proposal assessment

Abstract. In this paper, we suggest and analyze a new support system for easy decision-making on housing planning. Using this, user's can analyze their preferences by themselves individually and can select optimal alternatives. The purpose of this paper is to propose a rational decision-making system in housing planning based on the ASP (Analytic Hierarchy Process). Then, we show how standard evaluation can be decided on this system. In this paper, evaluation and election of the room arrangements is based on the information data came from users.

Introduction

House plan is a complex process that has been commonly adopted to meet various market supply. In this case, even cost a lot of money also can not obtain favorite house. Building a favorite house is every one's dream. In view of it, it is necessary to have a tool to assist the users in working out the most house plan. In order to ensure that the final proposal is convincing, a more systematic and sophisticated method to make the tradeoff decisions is required. Therefore, this paper encourages the use of analytic hierarchy process (AHP) in dealing with this challenge. The basic problem of decision-making is how to choose best one in a set of competing alternatives that are evaluated under conflicting criteria. The method of Analytic Hierarchy Process (AHP) provides us with a comprehensive framework for solving such problem. We are reported by using the AHP to evaluate housing planning by qualitative elements such as several kinds of construction methods, room arrangement, and designs. Based on this research on room arrangements particularly, we observe a mathematical approach for decision-making in housing planning problems in this paper.

What is AHP?

Before discussing AHP, it is necessary to know what multi-criteria decision making (MCDM) method is. MCDM methods are valuable in reaching important decisions that cannot be determined straightforwardly. Nowadays, there are numbers of MCDM methods available for selection. As mentioned, AHP is one of the MCDM methods. Saaty (1980) developed AHP which models a hierarchical decision problem framework that consists of multiple levels of criteria having unidirectional relationships. AHP works with such hierarchy that can combine both subjective (intangible) and objective (tangible) criteria. AHP is a reliable tool to facilitate systematic and logic stated al decision making processes, and determine the significance of a set of criteria and sub-criteria. It is widely applied to construction fields such as resources allocation, project design, planning for urban development, maintenance management, policy evaluation, etc. AHP is composed of seven major steps (see [4]):

(1) To identify the decision problem—The decision problem has to be in the topmost level of a hierarchy that is broken down into different levels in which the final level is usually the scenarios or alternatives to be selected;

(2) To ascertain that the problem can be solved by AHP—AHP is suitable for the decision problem that can be turned into a hierarchical decision model;

(3) To structure the decision problem—A hierarchy structure formed for the decision problem consists of several levels;

(4) To determine the raters—AHP solicits expert's judgment and therefore, only experts are eligible to be the raters who are responsible for making the decision;

(5) To collect data from the raters—AHP determines the relative priorities of different criteria in every level of the hierarchy by employing a pairwise comparison. During the process, each expert is required to make judgments on their relative importance in relation to the element at the higher level with reference to a 9-point scale;

(6) To calculate the priority weights of each criterion—Each decomposed level with respect to a higher level forms a Matrix;

(7) To measure the consistency ratio (C.R.)—This practice is to ascertain that the experts are consistent in rating the relative importance of the criteria.

Housing plan model by AHP

There are the following three principles when we use the AHP method in problem solving. They are principles of decomposition, comparative judgments, and synthesis of priorities. The decomposition principle requires structuring the hierarchy to capture the basic elements of the problem. An effective way to do this is first to work downward from the focus in the top level to criteria bearing on focus in the second level, followed by subcriteria in third level, and so on, from the more general to the more particular and definite. The bottom level elements are alternatives. The structure of a hierarchy is given by Figure 1.

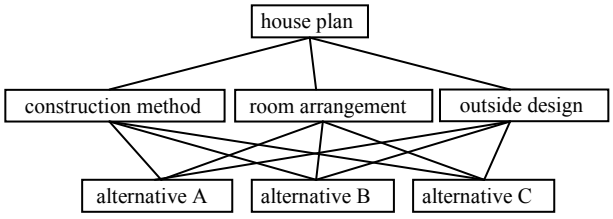

Fig. 1 Structure of a hierarchy

We propose a systematical procedure to select optimal solution for a user who wants to build own house. Form view of mathematical programming, we introduce a certain type of multi-criteria evaluation associated with a house plan by the following formula

$$\begin{cases} \text{minimize } (f_1, f_2, f_3) \\ \text{subject to } (v_1, v_2, v_3) \end{cases}. \tag{1}$$

The symbols shown in the formula (1) are defined, as

f_1= construction method; f_2= room arrangement; f_3= outside design;

v_1=economical conditions; v_2= site-conditions; v_3=others.

This research can give a comprehensive evaluation for user's preference with concrete values. At first, a user's plan is quantified by certain evaluations based on each criterion, and then its comprehensive evaluation can be calculated by their weighted sum. If the comprehensive evaluation is not satisfactory for the user, quantifications will be modified by perturbing evaluation values. This evaluation method with multi-criteria can be written as follows.

Before building the house, users have to select an optimal construction type from some alternatives of construction styles, such as wooden, building area, and so on. Moreover, outside design is also important for the evaluation as another preference for users. In comparison with these two criteria, room arrangement seems to more complex and most important for users.

In this paper, we assume that the land for house is sufficiently suitable and wide, and that it is satisfactory for general conditions of the single house. Furthermore, we assume that a user is satisfied with this land.

Comprehensive evaluation for the house of room arrangements

Calculation of the weight. It can be judged by AHP which item is most important among the three criteria (see [1]). So it is necessary to judge the weight of each item by the information came from the users. It is interpreted as the factor with highest weight being good. Moreover, it turns out that users are thinking which evaluation item as most important by the value of weight. Saaty [1] proposed the AHP absolute measurement method and AHP relative measurement method as algorithm. The alternatives may be evaluated by paired comparisons (relative measurement). Weights of the single house are given according to the following Figure 2.

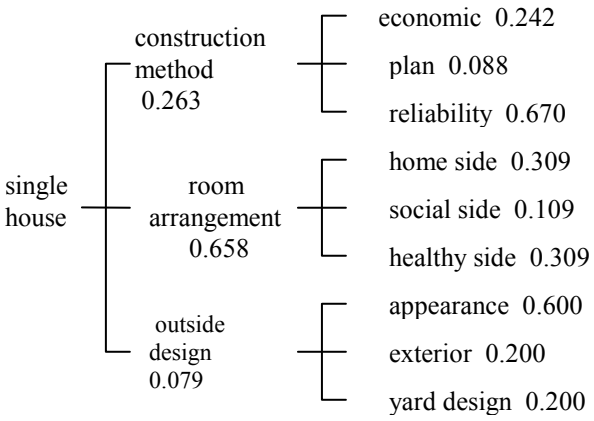

Fig. 2 Weights of the single house

Maximization of utility problem on the floor space. For users as a family, if the area of a site of a site is fixed, there is a problem how the floor space of room arrangement should be chosen. In the same situation, each user may not choose the same plan. In this paper, based on the information came from many users, the utility problem function on selection of the floor space is expressed as follows:

$$U = U(\sum_{i=1}^{n} \omega_i u_i(x_i)), \tag{2}$$

where ω_i is weight of selection of floor space x_i, and $u_i(x_i)$ is evaluation function about selection of floor space x_i. The width of each room is not only restricted to the width of the next room, but also restricted to the floor space of a house. For a user, the biggest concern is to select floor space to the expected maximum utility. We can construct the following function for the optimal floor space which can be determined according to its utility:

$$\begin{cases} \text{minimize} \ \sum_{i=1}^{n} \omega_i u_i(x_i) \\ \text{subject to} \ \sum_{i=1}^{n} x_i \le L,\ x_i \in S_i,\ i = 1, \cdots, n \end{cases}, \tag{3}$$

where L is the floor space of a house, and it is related to a loan, and S_i (i=1,…,n) is a set of relative to the floor space of each room. Then, we introduce the method of asking for the utility function $u_i(x_i)$. To calculate the coefficient of an utility function by using the certain degree of each floor area. The algorithm for finding the function $u_i(x_i)$ which use Lagrange interpolation polynomial is proposed.

Maximization utility problem is expressed definitely as follows:

$$\begin{cases} \text{minimize} \ \sum_{i=1}^{n} \omega_i (a x_i^5 + b x_i^4 + c x_i^3 + d x_i^2 + e x_i + f) \\ \text{subject to} \ \sum_{i=1}^{n} x_i \le L,\ x_i \in S_i,\ i = 1, \cdots, n \end{cases}. \tag{4}$$

Example

First the weighs of each factor are calculated. The degrees of each factor are calculated possibly if the weights of each factor are known. A degree shows which factor a user thinks as most important. For example, calculate a degree of a kitchen room according to the following Table 1. There values show that the user thinks kitchen room area 9 m^2 is the most important. Next the function $u_i(x_i)$ is approximated by using the Lagrange interpolation polynomial by the polynomial which passes though points $\{x_i, f_i\}$. Here x_i and f_i are floor space and degree, respectively. By Table 1, $\{x_1, x_2, x_3, x_4, x_5\}=\{6, 7.5, 9, 10.5, 12\}$ and $\{f_1, f_2, f_3, f_4, f_5\}=\{0.1, 0.7, 1.0, 0.7, 0.4\}$ are floor space and degree of a kitchen room, respectively. Then we can obtain following utility function $u(x)$ of a kitchen room by the upper algorithm:

$$u(x) = 0.01x^4 - 0.26x^3 + 3.25x^2 - 17.12x + 32.20 .$$

Therefore, we can obtain the others coefficients by the same method as follows. See the Table 2.

Table 1 Degree of kitchen room

CRP	6 m^2	7.5 m^2	9 m^2	10.5 m^2	12 m^2	Weights	Degree
6 m^2	1	1/5	1/7	1/5	1/3	0.043	0.1
7.5 m^2	5	1	1/3	1	5	0.244	0.7
9 m^2	7	3	1	1	3	0.366	1.0
10.5 m^2	5	1	1	1	3	0.257	0.7
12 m^2	3	1/5	1/3	1/3	1	0.090	0.4

Table 2 Coefficients of the utility function

	a	*b*	*c*	*d*	*e*	*f*
Living room	0.00	-0.03	1.07	-21.3	209.58	815.72
Kitchen room	0.00	0.01	-0.26	3.25	-17.12	32.20
Dining room	0.00	0.01	-0.45	8.11	-64.06	186.00
Bed room	0.00	0.05	-1.63	24.20	-176.45	505.00
Child's room	0.00	0.00	-0.09	1.49	-10.66	27.253
Toilet	1.41	-15.40	64.03	-126.55	118.90	-42.30
Bath room	0.00	-1.27	19.40	-110.08	274.75	-254.60
Wash room	0.00	-1.80	29.53	-179.75	480.52	-475.00
Hall	0.00	-0.01	0.36	-4.10	19.85	-33.69
Lobby	0.00	0.00	-0.09	2.09	-20.63	76.00
Closet	0.00	0.33	-3.00	9.92	-14.05	7.30
Store room	0.00	-0.10	2.50	-23.00	91.90	-133.50
Study room	0.00	0.03	-1.23	16.08	-91.96	192.20

Comprehensive evaluation system of room arrangement. After the area of each room is decided, the comprehensive evaluation system of room arrangement will be considered. In this paper, a ten-point method is used to evaluate room arrangement. The comprehensive evaluation system is proposed by the following Table 3. The weights of a framework are calculated in Subsection of calculation of the weight. The user can obtain the optimal solution easily in an objective framework by using qualitative data, which expresses an evaluation result.

Table 3. Comprehensive evaluation system

	Item	An evaluating point	Weight	Result
homely side	number width functionality arrangement receipt	1—10	0.066 0.118 0.419 0.111 0.286	=6—10 (good) =4—6 (good in general) =1.5—4 (not good) =1—1.5 (quite bad)
social side	privacy style communication change of a family	1—10	0.392 0.079 0.196 0.333	
healthy side	sanitary sunshine ventilation safety	1—10	0.054 0.306 0.154 0.486	

Algorithm

House design software can create a floor plan quickly, and we can look at a floor plan from many angles, but it cannot judge the floor plan scientifically. In this paper, users not only plan a wish house by using this software, but also express his preference quantitatively, and evaluate it scientifically. Specifically, the automatic generation algorithm of the house plan arrangement was proposed follows:

Step 1 A user's hope is arranged.

Step 2 After deciding the total floor space, the maximum floor area of using is calculated. If restriction conditions are satisfied, it will go to next step, otherwise, it returns to step1 and the area of each room is corrected.

Step 3 The wish house in step1 is designed by using house design software.

Step 4 The house as an image is evaluated. If it satisfies the user's preference sufficiently, the total cost will be calculated and a house maker will be chosen. Otherwise, it returns to step1 and improved unreasonable designs.

Conclusion

In this paper, a house planning system is established that can determine several kinds user's hope in short time based on a rational decision-making system by using AHP method.

It is necessary to determine algorithm which can connect research in this paper with house design software by using the various decision-making technique containing AHP method.

Acknowledgement

The research was supported by the National Natural Science Foundation of China (Grant No. 60972115) and Beijing Excellent Talent Training Project (Grant No. 2013D005007000003).

References

[1] T. L. Saaty. Axiomatic Foundation of the Analytic Hierarchy Process. Management Science, 32(1986), pp. 841–855.

[2] Kaoru Tone and Ryutaro Manabe. AHP jireishu (in Japannese), Union of Japanese Scientists and Engineers (1990).

[3] Banai. R. Anthropocentric problem solving in planning and design, with analytic hierarchy process. Journal of Architectural and Planning Research, 22(2005), pp. 107–120.

[4] Grace K. L. Lee and Edwin H. W. Chan. The Analytic Hierarchy Process (AHP) Approach for Assessment of Urban Renewal Proposals. Soc Indic Res 89(2008), pp. 155–168.

Advanced Materials Research Vols. 989-994 (2014) pp 2593-2598
© (2014) Trans Tech Publications, Switzerland
doi:10.4028/www.scientific.net/AMR.989-994.2593

Algebraic immunity, correlation immunity and other cryptographic properties of quadratic rotation symmetric Boolean functions

Jinglian Huang[a], Zhuo Wang[b], Meirong He[c]

School of Electrical Engineering, Northwest University for Nationalities, Lanzhou, China

[a]huangjlwork@163.com, [b]wzh0902@126.com, [c]hmr@xbmu.edu.cn

Corresponding Author:Jinglian Huang, huangjlstudy@163.com, 86-13909440966.

Keywords: rotation symmetric H Boolean functions; e-derivative; algebraic immunity; correlation immunity; annihilators

Abstract. Boolean functions with a variety of secure cipher properties are the key factors to design cryptosystem with the ability to resist multiple cipher attacks and good safety performance. In this paper, using the derivative of the Boolean functions and the e-derivative defined by ourselves as the main research tools, we study algebraic immunity, correlation immunity and other cryptographic properties of the quadratic rotation symmetric Boolean functions. We determine the quadratic rotation symmetric Boolean functions which are H Boolean functions, and the range of weight distribution of the quadratic rotation symmetry H Boolean functions. Besides, we get the compatibility among propagation, balance, correlation immunity and algebraic immunity of the quadratic rotation symmetry H Boolean functions, and also focus on the relationship of balance, correlation immunity and dimension. Furthermore, we check the existence of the cubic rotation symmetry H Boolean functions, and obtain the relationship between existence and dimension of the cubic rotation symmetry H Boolean functions. Moreover, we obtain a more convenient method for solving annihilator. Such researches are important in cryptographic primitive designs, and have significance and role in the theory and application range of cryptosystems.

Introduction

Boolean functions are compatible with a variety of cryptographic properties is always an important problem in studying cryptography, which is related to the cryptosystem' ability to resist a variety of cipher attacks. Rotation symmetric Boolean functions (RSBFs) are a kind of functions with special algebraic structure, and having been well application in cryptography. In 1999, RSBFs were proposed by Pieprzyk and Qu to apply in some cipher algorithms, such as MD4, MD5 and fast implementation of HAVAL [1]. RSBFs are paid wide attention in cryptography academia when it was been proposed, and some researchers always study them. In the recent year, there have many valuable results [4~15] about the study of algebraic immunity and other cryptographic properties of RSBFs. There are a lot of research methods for the study of RSBFs such as recursive definition, cascade calculations and orbit division [7~11]. The methods above need to calculate step by step, and it is complicated in calculation. In this paper, we use the derivative [16~18] and the custom e-derivative as the main research tools, and study the problems of rotation symmetric Boolean functions and rotation symmetric H Boolean functions, such as the structure, the relationship between weight and dimension, balance, correlation immunity, the relationship between propagation and algebraic degree, algebraic immunity and solving methods of annihilator. We get some valuable conclusions.

Preliminaries

The Boolean functions of cryptographic are defined on Galois field $GF(2)$. In this paper, we discuss cryptographic properties of rotation symmetric H Boolean functions on $GF(2)$.

Now the e-derivative is defined here. The readers may refer to [19~21] for more information on e-derivative.

Definition 1[19~21]**.** The e-derivative (e-partial derivative) of *n*-dimensional Boolean functions $f(x_1,x_2,\cdots,x_n)$ for *r* variables $x_{i1},x_{i2},\cdots,x_{ir}$ $(i,r,i_1,i_2,...,i_r\in[1,n])$ is defined as

$$ef(x)/e(x_{i1},x_{i2},\cdots,x_{ir})=f(x_1,x_2,\cdots,x_{i1},x_{i2},\cdots,x_{ir},\cdots,x_n)f(x_1,x_2,\cdots,1+x_{i1},1+x_{i2},\cdots,1+x_{ir},\cdots,x_n). \quad (1)$$

If $r=1$, (1) turns into the e-derivative of $f(x)=f(x_1,x_2,\cdots,x_n)$ for a single variable, which is denoted by $ef(x)/ex_i$ $(i=1,2,\cdots,n)$. As a result, the simplified form below can be easily derived.

$$ef(x)/ex_i=f(x_1,x_2,\cdots,x_{i-1},1,x_{i+1},\cdots,x_n)f(x_1,x_2,\cdots,x_{i-1},0,x_{i+1},\cdots,x_n)\ (i=1,2,\cdots,n). \quad (2)$$

According to the definition of e-derivative and derivative, we can get Lemmas 1&2 easily.

Lemma 1. The sufficient and necessary condition of *n*-dimensional Boolean functions $f(x)$ to satisfy the *k*-degree propagation criterion is: for all $r=1,2,\cdots,k$, there is

$$w_t(\partial f(x)/\partial(x_{i1},x_{i2},\cdots,x_{ir}))=2^{n-1}\ (i_1,i_2,\cdots,i_r\in[1,n]). \quad (3)$$

Lemma 2. The (4) that follow describe the relationship of *n*-dimensional Boolean functions.

$$f(x)=f(x)\partial f(x)/\partial(x_{i1},x_{i2},\cdots,x_{ir})+ef(x)/e(x_{i1},x_{i2},\cdots,x_{ir})\ (i_1,i_2,\cdots,i_r\in[1,n]). \quad (4)$$

We will involve RSBFs with degree $k(k\geq 3)$, so the definition of *k*-degree BF is given below.

Definition 3. Let $n\in I_+$, for any $x=(x_1,x_2,\cdots,x_n)\in GF(2)^n$, define $\rho_n^k(x)=(\rho_n^k(x_1),\rho_n^k(x_2),\cdots,\rho_n^k(x_n))$ $(k\in I_+,0\leq k\leq n-1)$, among them $\rho_n^k(x_i)=\begin{cases}x_{i+k}, & i+k\leq n\\ x_{i+k-n}, & i+k>n\end{cases}$. If for any $x=(x_1,x_2,\cdots,x_n)\in GF(2)^n$ and $f(\rho_n^k(x))=f(x)$ $(0\leq k\leq n-1)$, $f(x)$ is called a RSBF.

Definition 4. If *n*-dimensional Boolean functions $f(x)$,which have if and only if *k*-degree $(k\in\{1,2,\cdots,n\})$ terms, $f(x)$ is called a pure *k*-degree Boolean function. And if $f(x)$ has if and only if different *k*-degree terms whose total number is $\binom{n}{k}$, $f(x)$ is called completely pure *k*-degree Boolean function, denoted by $f_0^k(x)$ $(k\in\{1,2,\cdots,n\})$. i.e. A Boolean function $f(x)$ is a completely pure *k*-degrees Boolean function,iff $f(x)$ is the sum of different *k*-degree terms which has $\binom{n}{k}$.

The basic properties of the quadratic rotation symmetric H Boolean functions

Quadratic rotation symmetry H Boolean functions have propagation, we need to study other cryptographic properties and basic properties of this functions.

Theorem 1. 1) The sum of two RSBFs $f_1(x)$ and $f_2(x)$, $f(x)=f_1(x)+f_2(x)$ are still RSBFs [22].

2) All *n*-dimensional $(n\geq 3)$ completely pure *k*-degree Boolean functions $f_0^k(x)$ $(k=1,2,\cdots,n)$ are RSBFs. In Boolean functions that are consist entirely of *k*-degree terms, only completely pure *k*-degree Boolean functions $f_0^k(x)$ are RSBFs**.**

3) Quadratic RSBFs $f_1(x)=f_0^2(x)$ and $f_2(x)=f_0^1(x)+f_0^2(x)$ are RS H Boolean functions.

Proof. 1) The readers may refer to [22].

2) For any rotation transformation $\rho_n^r(x)$ $(0\leq r\leq n-1)$, without loss of generality, we only prove $r+i=n$ $(i=1,2,\cdots,n)$. Then $\begin{pmatrix}x_1,x_2,\cdots,x_{i-1},x_i,x_{i+1},x_{i+2},\cdots,x_n\\ x_{r+1},x_{r+2},\cdots,x_{n-1},x_n,x_1,x_2,\cdots,x_r\end{pmatrix}$ describe the *n*-order replacement of $\rho_n^r(x)$ on the components of $x=(x_1,x_2,\cdots,x_n)$.

In $\{x_1,x_2,\cdots,x_{i-1},x_i,x_{i+1},x_{i+2},\cdots,x_n\}$, we take the product of the *k*-th components as one term, total $\binom{n}{k}$ terms, $f_0^k(x)$ is composed by the sum of all $\binom{n}{k}$ terms. In $\{x_{r+1},x_{r+2},\cdots,x_{n-1},x_n,x_1,x_2,\cdots,x_r\}$, we take the product of the *k*-th components as one terms, total $\binom{n}{k}$ terms, $f_0^k(\rho_n^r(x))$ is composed by the sum of all $\binom{n}{k}$ terms. So $f_0^k(\rho_n^r(x))=f_0^k(x)$, i.e. $f_0^k(x)$ is a RSBF.

After removing some of the terms in $f_0^k(x)$, $f_0^k(x)$ must not be RSBFs. Without loss of generality, suppose $f(x)=f_0^k(x)+x_{i1}x_{i2}\cdots x_{ik}$.

Since for $0\le r\le n-1$, there are $f_0^k(\rho_n^r(x))=f_0^k(x)$.

Then for all $i=1,2,\cdots,n$, there must be $df_0^k(\rho_n^r(x))/dx_i=df_0^k(x)/dx_i$.

Suppose $\rho_n^r(x_{i1}x_{i2}\cdots x_{ik})=x_{s1}x_{s2}\cdots x_{sk}$, by the 1) of the theorem 1, we can know

$f(\rho_n^r(x))=f_0^k(\rho_n^r(x))+\rho_n^r(x_{i1}x_{i2}\cdots x_{ik})=f_0^k(x)+x_{s1}x_{s2}\cdots x_{sk}$.

So $df(\rho_n^r(x))/dx_{sk}=df_0^k(x)/dx_{sk}+x_{s1}x_{s2}\cdots x_{s(k-1)}\neq df_0^k(x)/dx_{sk}$.

It is contradicted with $df_0^k(\rho_n^r(x))/dx_i=df_0^k(x)/dx_i$.Therefore, $f(x)$ is not a RSBF.

3) Since for all $i=1,2,\cdots,n$, there are

$$\begin{cases} w_t(df_1(x)/dx_i)=w_t(df_0^2(x)/dx_i)=w_t(x_1+x_2+\ldots+x_{i-1}+x_{i+1}+x_{i+2}+\ldots+x_n)=2^{n-1} \\ w_t(df_2(x)/dx_i)=w_t(1+x_1+x_2+\ldots+x_{i-1}+x_{i+1}+x_{i+2}+\ldots+x_n)=2^{n-1} \end{cases}.$$

By Lemma 1,we can know that $f_1(x)=f_0^2(x)$ and $f_2(x)=f_0^1(x)+f_0^2(x)$ are H Boolean functions.

Remark 1: Known by the 3) of Theorem 1, $f_1(x)=f_0^2(x)$ and $f_2(x)=f_0^1(x)+f_0^2(x)$ are RS H Boolean functions. But in RSBFs, there may have more than quadratic H Boolean functions. Following we discuss this issue in Theorem 2&3.

Theorem 2. Suppose variables are $x'=(x_2,x_3,\cdots,x_n)$ of $f_{1,n-1}(x')$ and $f_{2,n-1}(x')$. $f_{1,n-1}(x')$ is $f_0^2(x')$ with $n-1$ -dimensional, $f_{2,n-1}(x')$ is $f_0^1(x')+f_0^2(x')$ with $n-1$ -dimensional, $f_{1,n}(x)$ and $f_{2,n}(x)$ are $f_1(x)$ and $f_2(x)$ with *n*-dimensional respectively. Then

1)

$$\begin{cases} f_{1,n}(x)=(1+x_1)f_{1,n-1}(x')+x_1f_{2,n-1}(x') \\ f_{2,n}(x)=(1+x_1)f_{2,n-1}(x')+x_1(1+f_{1,n-1}(x')) \end{cases}. \tag{5}$$

2) In RSBFs, there exist balanced quadratic RS H Boolean functions.

Proof.

1) $f_{1,n}(x)=f_{1,n-1}(x')+x_1\sum_{i=2}^{n}x_i=f_{1,n-1}(x')+x_1(f_{1,n-1}(x')+f_{0,n-1}^1(x')+f_{1,n-1}(x'))=(1+x_1)f_{1,n-1}(x')+x_1f_{2,n-1}(x')$.

$f_{2,n}(x)=f_{0,n}^1(x)+f_{1,n}(x')=f_{0,n}^1(x)+f_{1,n-1}(x')+x_1(x_2+x_3+\cdots+x_n)=x_1+f_{2,n-1}(x')+x_1\sum_{i=2}^{n}x_i$.

$=x_1+f_{2,n-1}(x')+x_1(f_{2,n-1}(x')+f_{1,n-1}(x'))=(1+x_1)f_{2,n-1}(x')+x_1(1+f_{1,n-1}(x'))$

2) By (5), we have

$$w_t(f_{1,n}(x))=w_t((1+x_1)f_{1,n-1}(x'))+w_t(x_1f_{2,n-1}(x')) \text{ and } w_t(f_{2,n}(x))=w_t((1+x_1)f_{2,n-1}(x'))+w_t(x_1f_{1,n-1}(x')) \tag{6}$$

and

$$w_t(f_{1,3}(x))=2^{3-1} \text{ and } w_t(f_{2,3}(x))=2^{3-1}+2^{3-2}. \tag{7}$$

By (6) and (7), We can be deduce these:

$$w_t(f_{1,n}(x))=2^{n-1} \text{ When } n=2r+3\ (r=0,1,2,\cdots);\quad w_t(f_{2,n}(x))=2^{n-1} \text{ When } n=2r+5\ (r=0,1,2,\cdots). \tag{8}$$

Known by (8), there exist balanced RS H Boolean functions.

Corollary 1. $2^{n-2}<w_t(f_i(x))\le 2^{n-1}+2^{n-2}\ (i=1,2)$.

Theorem 3. In completely pure cubic RSBFs $f_0^3(x)$, there exist H Boolean functions [22].

Example 1. For $f_{0,8}^3(x)$, there are

$$\begin{cases} w_t(df_{0,8}^3(x)/dx_1)=2w_t(f_{0,7}^2(x))=2^{8-1}=128 \\ w_t(df_{0,8}^3(x)/dx_i)=2^{8-1}=128 \end{cases} (i=1,2,\cdots,8). \tag{9}$$

Knowing by Lemma 1 and (9), $f_{0,8}^3(x)$ is a rotation symmetric H Boolean function.

Remark 2. Known by Theorem 3, it is difficult to find whether have H Boolean functions in $f_0^3(x)$ through observing directly wihtout derivative. Even if we want to study them,it is also difficult to prove directly. Derivative plays an irreplaceable role in the discovery and proof of Theorem 3.

Because $f(\rho_n^k(x)) = f(x)$ $(0 \le k \le n-1)$, there are $df(\rho_n^k(x))/dx_i = df(x)/dx_i$, $ef(\rho_n^k(x))/ex_i = ef(x)/ex_i$, $(i = 1,2,\cdots,n)$. By Lemma 1&2, it is obvious to deduce Theorem 4. So it is easy to get Theorem 4 without proof.

Theorem 4. The necessary and sufficient conditions of RSBFs $f(x)$ are RS balanced H Boolean functions, are that: $w_t(df(\rho_n^k(x))/dx_i) = 2^{n-1}$ *and* $w_t(ef(\rho_n^k(x))/ex_i) = 2^{n-2}$ $(i = 1,2,\cdots,n)$.

Correlation immunity of quadratic rotation symmetric H Boolean functions

The quadratic RS H Boolean functions have propagation, many quadratic rotation symmetric H Boolean functions have balance. Whether the quadratic rotation symmetric H Boolean functions are not compatible with the correlation immunity,is the ability to resist correlation attack. We discuss the correlation immunity of the quadratic RS H Boolean functions in this section.

Theorem 5. 1) When $n = 4r+3$ $(r = 0,1,2,\cdots)$, $f_2(x) = f_0^1(x) + f_0^2(x)$ are correlation immune functions.

2) When $n = 4r+5$ $(r = 0,1,2,\cdots)$, $f_1(x) = f_0^2(x)$ are correlation immune functions.

Proof. 1) Solve the derivative of $f_2(x)$, we get

$$\partial f_2(x)/\partial(x_1,x_2,\cdots,x_n) = f_2(x) + f_2(1+x) = f_0^1(x) + f_0^1(1+x) + f_0^2(x) + f_0^2(1+x). \quad (10)$$

Because of $n = 4r+3$ $(r = 0,1,2,\cdots)$, so $f_0^1(x) + f_0^1(1+x) = \sum_{i=1}^{n} 1 = 1$ and

$$f_0^2(x) + f_0^2(1+x) = \sum_{i=1}^{n}\sum_{j=1}^{n-1} x_i + \sum_{i=1}^{s} 1 \ (s = 2^{-1}n(n-1)). \quad (11)$$

When $n = 4r+3$ $(r = 0,1,2,\cdots)$, $n-1 \equiv 0 \bmod 2$. While for $s = (4r+3)(2r+1)$, there is $s \equiv 1 \bmod 2$. Take the above formula into (11), we have $f_0^2(x) + f_0^2(1+x) = 1$.

Take $f_0^1(x) + f_0^1(1+x) = \sum_{i=1}^{n} 1 = 1$ and $f_0^2(x) + f_0^2(1+x) = 1$ into (10), we have $\partial f_2(x)/\partial(x_1,x_2,\cdots,x_n) = 0$. Therefore, we can know that for all $i = 1,2,\cdots,n$, there is $w_t(f_2(x) \mid x_i = 0) = w_t(f_2(x) \mid x_i = 1) = 2^{-1}w_t(f_2(x))$. So we can know that, $f_2(x)$ are correlation immune functions when $n = 4r+3$ $(r = 0,1,2,\cdots)$.

When $f_2(x)$ are correlation immune functions of order 1, using (12) and (5) of Theorem 2, we have

$$w_t(x_i(1+f)) = w_t(x_i) - w_t(x_i f) \ and \ w_t(x_i x_j(1+f)) = w_t(x_i x_j) - w_t(x_i x_j f). \quad (12)$$

As a result, for all $n \ge 3$, there are

$$w_t(x_{n-1}x_n f_2(x) df_2(x)/dx_n) \ne 2^{-1}w_t(x_n f_2(x) df_2(x)/dx_n) = 2^{-1}w_t(x_{n-1} f_2(x) df_2(x)/dx_n), \quad (13)$$

or

$$w_t(x_{n-1}x_n ef_2(x)/ex_n) \ne 2^{-1}w_t(x_n ef_2(x)/ex_n) = 2^{-1}w_t(x_{n-1} ef_2(x)/ex_n), \quad (14)$$

and or (13) and (14) are not establishment at the same time. So $f_2(x)$ just correlation immune functions of order 1. That is, $f_2(x)$ are correlation immune functions.

2) The same as the proof of 1), the result can be proved that when $n = 4r+5$ $(r = 0,1,2,\cdots)$, $f_1(x) = f_0^2(x)$ are 1-order correlation immune functions, we omit it here.

Algebraic immunity of quadratic rotation symmetric H Boolean functions

In this section, we discuss the algebraic immunity of quadratic RS H Boolean functions.

Theorem 6. For the quadratic RS H Boolean functions $f_1(x)$ and $f_2(x)$, $f_1(x) = f_0^2(x)$ and $f_2(x) = f_0^1(x) + f_0^2(x)$, there are: 1) $AI(f_1(x)) = 2$; 2) when $n > 3$, $AI(f_2(x)) = 2$.

proof. 1) For $f_1(x)$, we have $df_1(x)/dx_n = \sum_{i=1}^{n-1} x_i$, $w_t(df_1(x)/dx_n) = 2^{n-1}$ and $df_1(x)/dx_n \cdot ef_1(x)/ex_n = 0$.

Let $h_1 = f_1(x)df_1(x)/dx_n + df_1(x)/dx_n$, then $h_1 f_1(x)df_1(x)/dx_n = 0$, $h_1 ef_1(x)/ex_n = 0$. Hence there are $h_1 f_1(x) = h_1 f_1(x)df_1(x)/dx_n + h_1 ef_1(x)/ex_n = 0$, and $w_t(h_1) = 2^{n-2} < 2^{n-1}$. So h_1 is an annihilator of $f_1(x)$. It is easy to deduce from Theorem 2: $\deg(f_1(x)df_1(x)/dx_n) = \deg(ef_1(x)/ex_n) = 3$. Then $\deg h_1 = 3$.

It is easy to deduce $w_t(ef_1(x)/ex_n) < 2^{n-1}$ from Theorem 2. Let $h_2 = 1 + df_1(x)/dx_n + ef_1(x)/ex_n$,then $\deg h_2 = 3$. Obviously there are $h_1 + h_2 = 1 + f_1(x)$ and $w_t(h_2) < 2^{n-1}$.

So $h_1 + h_2$ is an annihilator of $f_1(x)$,and we can get $\deg(h_1 + h_2) = 2$.

We can take $r_1 + r_2 = h_i$ $(i = 1,2)$, $r_1 r_2 = 0$ and $r_1 \neq r_2 \neq 0$.

Known by $w_t(h_1) = 2^{n-2} < 2^{n-1}$ and $w_t(h_2) < 2^{n-1}$, there must be $w_t(r_i) < 2^{n-1}$ $(i = 1,2)$, which says that r_i must not be linear functions. So we can get $\deg r_i \geq 2$ $(i = 1,2)$.

Since $\deg f_1(x) = 2$, $\deg(1 + f(x)) = 2$ as well,we can get that the algebraic degree of all annihilators of $f_1(x)$ is no lower than 2-degree , so $AI(f_1) = 2$.

2) For $f_2(x)$, when $n = 3$, there is $w_t(ef_2(x)/ex_n) = 2^{n-1}$. Hence $1 + f(x)$ must have 1st annihilator, 1st annihilator is $1 + df_2(x)/dx_n = ef_2(x)/ex_n$ .When $n > 3$, the algebraic immunity of $f_2(x)$ and $f_1(x)$ proof are same, we can obtain $AI(f_2) = 2$, we omit it here.

Remark 3: The proof of Theorem 6 gives a convenient method, which use derivative $df(x)/dx_n$ and e-derivative $ef(x)/ex_n$, solving annihilator for any function easily.

Example 2. For $n = 4$'s cubic rotation symmetric Boolean functions $f(x) = f_0^2(x) + f_0^3(x)$, using derivative $df(x)/dx_n$ and e-derivative $ef(x)/ex_n$, we can obtain that $w_t(f(x)) = 2^{n-2} + 2^{n-3}$, $w_t(df(x)/dx_n) = 2^{n-1} + 2^{n-2}$ and $w_t(ef(x)/ex_n) = 0$. We can conclude that, $f(x)$ should be have 1st annihilator. Owing to $ef(x)/ex_4 = ef(x)/ex_3 = ef(x)/ex_2 = ef(x)/ex_1 = 0$, solving this differential equation, we can get 1st annihilator $x_1 + x_2 + x_3 + x_4$ .So $AI(f) = 1$.

Conclusions

In this paper,using derivative and *e*-derivative of Boolean functions as research tools, we obtain a series of results, like the compatibility of propagation and various cryptographic properties of quadratic RSBFs. These results are of great significance and play a key role in theory and applications. If we don't use derivative and *e*-derivative, it is difficult to obtain these results. For example, there exists H Boolean functions in $f_0^3(x)$. In addition, the proof of Theorem 6 gives the method of solving annihilators via derivative and *e*-derivative.This method makes it simple and convenient to solve annihilators.

Furthermore, in this paper, we reveal the relationship between RSBFs and completely pure *k*-degree Boolean functions, and decompose RSBFs into single completely pure *k*-degree Boolean functions. It will provide convenience on studying the algebraic immunity and other cryptographic properties of RSBFs further and deeply.

Acknowledgment

This work is supported by National Natural Science Foundation of China (Grant No. 61262085).

References

[1] Pieprzyk, J.; Qu, C.: Fast hashing and rotation-symmetric functions. Journal of Universal Computer Science, 1999, 5, (1), pp. 20-31.

[2] Cusick, T.W.; Stanica, P.: Fast evaluation, weights and nonlinearity of rotation-symmetric functions. Discrete mathematics, 2002, 258, (1-3), pp. 289-301.

[3] Stanica, P.; Maitra, S.; Clark, J.: Results on rotation symmetric bent and correlation immune Boolean functions. FSE 2004, New Delhi, India, 2004, LNCS, 3017, pp. 161-177.

[4] Sarkar, S.; Maitra, S.: Construction of rotation symmetric Boolean functions with optimal algebraic immunity. Computacion y Sistemas, 2009, 12, (3), pp. 267-284.

[5] Sarkar, S.; Maitra, S.: Construction of rotation symmetric Boolean functions on odd number of variables with maximum algebraic immunity. Applied Algebra, Algebraic Algorithms and Error-Correcting Codes 2007, Bangalore, India, 2007, LNCS, 4851, pp. 271-280.

[6] Fu, S.; Li, C.; Matsuura, K.; Qu, L.: Construction of rotation symmetric Boolean functions with maximum algebraic immunity. Cryptology and Network Security 2009, Kanazawa, Japan, 2009, LNCS, 5888, pp. 402-412.

[7] Stanica, P., Maitra, S.: 'Rotation symmetric Boolean functions-Count and cryptographic properties', Discrete Applied Mathematics, 2008, 156, (10), pp. 1567-1580.

[8] Cusick, T.; Padgett, D.: A recursive formula for weights of Boolean rotation symmetric functions. Discrete Applied Mathematics, 2012, 160, (4-5), pp. 391-397.

[9] Fu, S.; Qu, L.; Li, C.; Sun, B.: Balanced rotation symmetric Boolean functions with maximum algebraic immunity. IET Information Security, 2011, 5, (2), pp. 93-99.

[10] Fu, S.; Li, C.; Matsuura, K.; Qu, L.: Balanced 2p-variable rotation symmetric Boolean functions with maximum algebraic immunity. Applied Mathematics Letters, 2011, 24, (12), pp. 2093-2096.

[11] Meng, Q.; Chen, L.; Fu, F.: Construction of Boolean functions with maximum algebraic immunity. Journal of Software, 2010, 21, (7), pp. 1758-1767. (In Chinese)

[12] Maximov, A.; Hell, M.; Maitra, S.: Plateaued rotation symmetric boolean functions on odd number of variables. First Workshop on Boolean Functions: Cryptography and Applications, Rouen, France, 2005, pp. 83-104.

[13] Elsheh, E.: On the linear structures of cryptographic rotation symmetric Boolean functions. The 9th International Conference for Young Computer Scientists, Zhangjiajie, Hunan, China, 2008, pp. 2085-2089.

[14] Fu, S.; Li, C.; Matsuura, K.; Qu, L.: Construction of even-variable rotation symmetric Boolean functions with maximum algebraic immunity. Science in China Series F: Information Sciences, 2013, 56, (3), pp. 1-9.

[15] Dalai, D.; Maitra. S.; Sarkar, S.: Results on rotation symmetric bent functions. Proceedings of the 2nd International Workshop on Boolean Functions: Cryptography and Applications, Rouen, France, 2006, pp. 137-156.

[16] Reed, I. S.: A class of multiple-error-correcting codes and the decoding scheme. IRE Transactions on Information Theory, 1954, 4, (4), pp. 38-49.

[17] Akers, S. B.: On a theory of Boolean functions. Journal of the Society for Industrial and Applied Mathematics, 1959, 7, (4), pp. 487-498.

[18] Wen, Q.; Niu, X.; Yang, Y.: The Boolean Functions in Modern cryptology. Science Press, Beijing, China (2000). (In Chinese)

[19] Li, W.; Wang, Z.; Huang, J.: The e-derivative of boolean functions and its application in the fault detection and cryptographic system. Kybernetes, 2011, 40, (5-6), pp. 905-911.

[20] Ding, Y.; Wang, Z.; Ye, J.: Initial-value problem of the Boolean function's primary function and its application in cryptographic system. Kybernetes, 2010, 39, (6), pp. 900-906.

[21] Huang, J.; Wang, Z.: The relationship between correlation immune and weight of H Boolean functions. Journal on Communications, 2012, 33, (2), pp. 110-118. (In Chinese)

[22] Huang, J.; Zhang, C.; Liu, Y.: Some cryptographic properties of rotation symmetric Boolean functions. Applied Mechanics and Materials, 2013, 321-324, pp. 2704-2707.

Advanced Materials Research Vols. 989-994 (2014) pp 2599-2604
© (2014) Trans Tech Publications, Switzerland
doi:10.4028/www.scientific.net/AMR.989-994.2599

Relations among e-derivative, derivative, algebraic degree, correlation immunity and annihilators for H Boolean functions

Jinglian Huang[a], Zhuo Wang[b], Juan Li[c]

School of Electrical Engineering, Northwest University for Nationalities, Lanzhou, China

[a]huangjlwork@163.com, [b]wzh0902@126.com, [c]115126354@qq.com

Corresponding Author:Jinglian Huang, huangjlwork@163.com, 86-13909440966.

Keywords: H Boolean functions; e-derivative; derivative; algebraic degree; algebraic immunity; correlation immunity

Abstract. Using the derivative of the Boolean function and the e-derivative defined by ourselves as research tools, going deep into the internal structure of Boolean functions, we study relationship of algebraic degree, correlation immunity and annihilators for H Boolean functions with a specific Hamming weight. We obtain the algebraic degree of the e-derivative which is a component of H Boolean functions decide the algebraic degree of H Boolean functions. Besides, we describe the characteristics of the algebraic degree of e-derivative for the correlation immune H Boolean functions. We also check the e-derivative of H Boolean functions can put annihilators, correlation immunity and algebraic degree of H Boolean functions together. Meanwhile, we also deduce a formula method to solving annihilators of H Boolean functions. Such researches are important in cryptographic primitive designs, and have significance and role in the theory and application range of cryptosystems.

Introduction

Boolean functions with a variety of secure cipher properties are the key factors to design the cryptosystem with the ability to resist multiple cipher attacks and good safety performance. It is of great importance for a security cryptosystem to study some properties of Boolean functions, which make the cryptosystem resist various attacks [1,3,5,6,10], such as high algebraic degree [2], high nonlinearity [4], the strict avalanche criterion and propagation [8,9], higher-order correlation immunity [6,7] and higher-order algebraic immunity [11]. But in the study we find that there are mutual checks between some properties of cipher security. If one kind of property was improved, the other would be reduced [12]. Therefore, the compatibility of Boolean functions with a variety of properties of cipher security has been an issue of concern. Among them, the algebraic immunity of Boolean functions is current central issues. On the study of algebraic immunity of Boolean functions, the relevance among algebraic immunity and other cipher security properties, the solving method of the high-order algebraic immune functions and the optimal algebraic immune functions, and the solving method of annihilators are central contents of the study. The main research methods we take as follows, such as algebraic analysis, spectral analysis, matrix analysis, weighting analysis, linear subspace analysis and cascade analysis. The above methods need to do multi-step calculations step-by-step to obtain the results, which are more complicated.

In this paper, using e-derivative and derivative as main research tools, we study the relations among algebraic degree, correlation immunity and the annihilators of H Boolean functions $f(x)$ with the Hamming weight of $2^{n-1}+2^{n-2}$ .We also study the relations among algebraic degree, correlation immunity, the annihilators of the lowest algebraic degree, e-derivative and derivative of $f(x)$.

Preliminaries

The derivative of Boolean functions is already a well known concept [13~15]. Now the e-derivative is defined here. The readers may refer to [16~19] for more information on e-derivative.

Definition 1: The e-derivative (e-partial derivative) of Boolean function $f(x_1, x_2, \cdots, x_n)$ with respect to r variables $x_{i1}, x_{i2}, \cdots, x_{ir}$ $(i, r, i_1, ..., i_r \in [1, n])$ is defined as

$$ef(x)/e(x_{i1}, x_{i2}, \cdots, x_{ir}) = f(x_1, x_2, \cdots, x_{i1}, x_{i2}, \cdots, x_{ir}, \cdots, x_n) f(x_1, x_2, \cdots, 1+x_{i1}, 1+x_{i2}, \cdots, 1+x_{ir}, \cdots, x_n). \quad (1)$$

Remark 1: If $r = 1$, (1) turns into the e-derivative with respect to a single variable, which is denoted by $ef(x)/ex_i$ $(i = 1, 2, \cdots, n)$. As a result, the simplified form below can be easily derived.

$$ef(x)/ex_i = f(x_1, x_2, \cdots, x_{i-1}, 1, x_{i+1}, \cdots, x_n) f(x_1, x_2, \cdots, x_{i-1}, 0, x_{i+1}, \cdots, x_n) \ (i = 1, 2, \cdots, n).$$

Definition 2: The Hamming weight of n-dimensional Boolean functions $f(x) = f(x_1, x_2, \cdots, x_n) \in GF(2)^{GF(2)^n}$ is the number of elements contained in set $\left\{(x_1, x_2, \cdots, x_n) \middle| (x_1, x_2, \cdots, x_n) \in GF(2)^n, f(x_1, x_2, \cdots, x_n) = 1\right\}$, which denoted by $w_t(f(x))$ or $w_t(f)$. That is

$$w_t(f(x)) = \left|\left\{(x_1, x_2, \cdots, x_n) \middle| (x_1, x_2, \cdots, x_n) \in GF(2)^n, f(x_1, x_2, \cdots, x_n) = 1\right\}\right|.$$

Definition 3: For any arbitrary $\varepsilon_i = (0, 0, \cdots, 0, 1, 0, \cdots, 0)$ $(1 \le i \le n)$, If $f(x) = f(x_1, x_2, \cdots, x_n) \in GF(2)^{GF(2)^n}$ holds:

$$w_t(f(x+\varepsilon_i) + f(x)) = 2^{n-1}. \quad (2)$$

In (2), ε_i stands for n-dimensional Boolean vectors, which the i-th component is 1 and other components are 0. Then $f(x)$ was called an H Boolean function.

An H Boolean function is a Boolean function with propagation of degree 1.

Remark 2: The cascade function defined by (8) is more convenient to use than $f(x) = (1+x_{n+1}) f_1(x) + x_{n+1} f_2(x)$, which typically appears in classical cryptography, although these two definitions are essentially identical. For instance, with given H Boolean functions $g_{21} = 1 + x_n + x_{n-1}x_n$ and $g_{22} = 1 + x_{n-1} + x_{n-1}x_n$ of weight $2^{n-1} + 2^{n-2}$, $f_1(x) = (1+x_{n-2}) g_{21} + x_{n-2} g_{22}$ is the cascade of order g_{21} and g_{22}, whereas $f_2(x) = (1+x_{n+1}) g_{21} + x_{n+1} g_{22}$ is equivalent to $f_3(x) = (1+x_{n-2}) g_{22} + x_{n-2} g_{21}$, which is nothing but a cascade with a different order.

Definition 4: For any arbitrary ω $(\omega = (\omega_1, \omega_2, \cdots, \omega_n) \in GF(2)^n,\ 1 \le w_t(\omega) \le m)$, $f(x) = f(x_1, x_2, \cdots, x_n) \in GF(2)^{GF(2)^n}$ holds:

$$w_t(f(x) + \omega x) = 2^{n-1}. \quad (3)$$

In (3), $\omega x = \omega_1 x_1 + \omega_2 x_2 + \cdots + \omega_n x_n$ is a linear function. In this situation, Boolean functions $f(x)$ was called a m-order correlation immune function. the correlation immunity order is written as $CI(m)$.

Definition 5: If $w_t(f(x)) = r \ne 0$, suppose that $g(1+f) = 0$ and $w_t(g) = s \le r$, then function g is called a sub-function of function f with $gf = g$. Evidently, g is the annihilator of $1+f$, and any sub-function of $1+f$ is also the annihilator of f.

Lemmas 1~3 that follow describe properties of derivative and e-derivative of Boolean functions.

Lemma 1: A Boolean function is a propagation function of degree r iff

$$w_t(\partial f(x)/\partial(x_{i1}, x_{i2}, \cdots, x_{ir})) = 2^{n-1} \ (i, r, i_1, ..., i_r \in [1, n]).$$

Lemma 2: A Boolean function is an H Boolean function, iff the following equations hold for all x_i:

$$w_t(df(x)/dx_i) = 2^{n-1} \ (i = 1, 2, \cdots, n).$$

Lemma 3: For any arbitrary Boolean function, the following equations are true:

$$f(x) = f(x)\partial f(x)/\partial(x_{i1}, x_{i2}, \cdots, x_{ir}) + ef(x)/e(x_{i1}, x_{i2}, \cdots, x_{ir}) \ (i, r, i_1, ..., i_r \in [1, n]),$$

$$f(x) = f(x)df(x)/dx_i + ef(x)/ex_i \ (i = 1, 2, \cdots, n),$$

$$w_t(f(x)) = w_t(f(x)df(x)/dx_i) + w_t(ef(x)/ex_i) = 2^{-1} w_t(df(x)/dx_i) + w_t(ef(x)/ex_i) \ (i = 1, 2, \cdots, n).$$

Relationship among derivative, e-derivative, algebraic degree, correlation immunity and the annihilators

In this section,we reveal the relations among the e-derivative, derivative, the algebraic degree, correlation immunity, and the annihilator of H Boolean function with $w_t(f(x)) = 2^{n-1} + 2^{n-2}$.

The derivative of Boolean functions is necessary to be used to calculate the algebraic degree of H Boolean functions. Thus, Theorem 1 and Theorem 2 are introduced here firstly. Theorem 1 describes that how to calculate the algebraic degree of Boolean functions with the aid of their derivatives, and Theorem 2 describes the characteristics of the algebraic degree of e-derivative for the correlation immune H Boolean functions with the Hamming weight of $2^{n-1} + 2^{n-2}$.

Theorem 1[19]***:*** For any Boolean function $f(x)$, $\deg f(x) = m$ iff $\deg(df(x)/dx_i) \le m-1$ $(i = 1, 2, \cdots, n)$. And there exists an $i_0 \in \{1, 2, \cdots, n\}$, such that $\deg(df(x)/dx_{i_0}) = m-1$.

Theorem 2[19]***:*** Suppose that an H Boolean function $f(x)$ with the Hamming weight $2^{n-1} + 2^{n-2}$ and correlation immunity. If $ef(x)/ex_n$ is affine, i.e. $\deg ef(x)/ex_n = 1$, then the number of variables of $ef(x)/ex_n$ is greater than 1.

Theorem 3: For the H Boolean function $f(x)$ with the Hamming weight $2^{n-1} + 2^{n-2}$,

1. $\deg ef(x)/ex_n = 1$ iff $\deg f(x) = 2$.

2. If $\deg f(x) = 2$ and $CI(f(x)) = m \ge 1$,

$AI(f(x)) \le CI(f(x)) < ef(x)/ex_n$ contains the number of variables. (4)

Proof:

1. (sufficiency)

By Lemma 3, we can know, there is

$f(x) = f(x)df(x)/dx_n + ef(x)/ex_n$. (5)

Now, we prove $\deg ef(x)/ex_n = 1$. Adopt contradiction proof. Suppose $\deg ef(x)/ex_n > 1$, without loss of generality, we may assume $\deg ef(x)/ex_n = 2$. Since $w_t(f(x)) = 2^{n-1} + 2^{n-2}$,

$\deg df(x)/dx_n = \deg(1 + ef(x)/ex_n) = 2$.

By the properties of derivative, there must be $\deg f(x)df(x)/dx_n \ge 3$.

Known by (5), $\deg f(x) \ge 3$. That is a contradiction with $\deg f(x) = 2$, and it can only be

$\deg ef(x)/ex_n \le 1$. (6)

By Lemma 3 and $w_t(f(x)) = 2^{n-1} + 2^{n-2}$, one knows that $w_t(ef(x)/ex_n) = 2^{n-1}$. So

$\deg ef(x)/ex_n > 0$. (7)

Combining of (6) and (7), we have $\deg ef(x)/ex_n = 1$.

(necessity)

If $\deg ef(x)/ex_n = 1$, known from the properties of e-derivative, $ef(x)/ex_n$ of linear functions only can be x_{n-1}, $x_i + x_{n-1}$ $(i = 1, 2, \cdots, n-2)$, $x_i + x_j + x_{n-1}$ $(i, j = 1, 2, \cdots, n-2, i \ne j)$, $\cdots$, $x_1 + x_2 + \cdots + x_{n-2} + x_{n-1}$,etc (or the corresponding affine functions), or $x_1 + x_2 + \cdots + x_{n-2}$. When $ef(x)/ex_n$ is not equal to $x_1 + x_2 + \cdots + x_{n-2}$, since $f(x)$ is an H Boolean function with the Hamming weight $2^{n-1} + 2^{n-2}$, there must be $\begin{cases} w_t(ef(x)/e(x_{n-1}x_n)) = 2^{n-1} \\ w_t(\partial f(x)/\partial(x_{n-1}x_n)) = 2^{n-1} \end{cases}$, and $\begin{cases} e(ef(x)/e(x_{n-1}x_n))/ex_n = 0 \\ d(ef(x)/e(x_{n-1}x_n))/dx_n = 1 \end{cases}$.

We can know, $ef(x)/e(x_{n-1}x_n)$ is a linear function with the term of $x_{n-1} + x_n$ (or the corresponding affine function), that is $\deg(ef(x)/e(x_{n-1}x_n)) = 1$. We can get

$\deg(f(x)df(x)/dx_n) = 2$. (8)

By the Lemma 3, (8) and $\deg(ef(x)/ex_n) = 1$,we can know, $\deg f(x) = 2$.

When $ef(x)/ex_n$ is equal to $x_1 + x_2 + \cdots + x_{n-2}$, obviously, $f(x) = \sum_{i=1}^{n} x_i + (x_{n-1} + x_n)\sum_{i=1}^{n-2} x_i$, then $\deg f(x) = 2$.

2. Because $\deg f(x) = 2$, known by the 1 of Theorem 3,

$\deg ef(x)/ex_n = 1$. (9)

By the Lemma 3, there is

$ef(x)/ex_n(1+f(x)) = ef(x)/ex_n + ef(x)/ex_n f(x)df(x)/dx_n + ef(x)/ex_n ef(x)/ex_n = 0$. (10)

Known from (9) and (10), $AI(f(x)) = 1$. For any ωx $(\omega, x \in GF(2)^n)$ of $w_t(\omega) \geq 1$, we can deduce

$w_t(f(x)+\omega x) = w_t(f(x)df(x)/dx_n + \omega x) + w_t(ef(x)/ex_n + \omega x) - w_t(\omega x)$. (11)

Thanks to $\max_{\omega x} w_t(f(x)df(x)/dx_n + \omega x) = 2^{n-1} + 2^{n-2}$, by (11) and known correlation immunity of $f(x)$, we can know, there must be

$w_t(ef(x)/ex_n + \omega x) \neq 0$. (12)

By known $CI(f(x)) = m \geq 1$, the concept of *m*-order correlation immunity, (12) and $ef(x)/ex_n$ is a linear function, there must be

$CI(f(x)) < ef(x)/ex_n$ contains the number of argument. (13)

By $AI(f(x)) = 1$ and (13), we can judge (4) is set up and this completes the proof.

Remark 3: The (11) and (12) are set up for any non-linear Boolean functions,and the variables' number of $\max ef(x)/ex_n$ contain is $n-1$.

Theorem 4: For the H Boolean function $f(x)$ with $w_t(f(x)) = 2^{n-1} + 2^{n-2}$, if $\deg ef(x)/ex_n = 1$, $\deg ef(x)/ex_i = 1$ $(i = 1,2,\cdots,n-1)$.

Proof: By the known conditions and Theorem 3, there must be $\deg f(x) = 2$.

Suppose $\deg ef(x)/ex_i \neq 1$ $(i \neq n)$. Without loss of generality, we can assume

$\deg ef(x)/ex_i = 2$ $(i \neq n)$. (14)

Since H Boolean function $f(x)$ with $w_t(f(x)) = 2^{n-1} + 2^{n-2}$, By Lemma 2 and 3, we have

$w_t(ef(x)/ex_i) = 2^{n-1}$ $(i \neq n)$. (15)

By (14) and (15), one knows that

$\deg df(x)/dx_i = \deg(1+ef(x)/ex_i) = 2$ $(i \neq n)$. (16)

Since

$d(f(x)df(x)/dx_i)/dx_i = df(x)/dx_i + f(x)d(df(x)/dx_i)/dx_i + df(x)/dx_i d(df(x)/dx_i)/dx_i = df(x)/dx_i$. (17)

By (16) and (17), we can know, $\deg(f(x)df(x)/dx_i) \geq 3$ $(i \neq n)$.

By Lemma 3, we can get $\deg f(x) \geq 3$. It conflicts with the known $\deg f(x) = 2$.

And i is any one of $\{1,2,\cdots,n-1\}$, then there must be

$\deg ef(x)/ex_i = 1$ $(i = 1,2,\cdots,n-1)$.

The proof ends.

Theorem 5: An H Boolean function $f(x)$ has,

$w_t(f(x)) = 2^{n-1} + 2^{n-2}$, (18)

$\partial f(x)/\partial(x_{n-4}x_{n-3}x_{n-2}x_{n-1}x_n) = 0$, (19)

and

$$\begin{cases} w_t(\partial f(x)/\partial(x_{n-1}x_n)) = 2^{n-2} \\ w_t(ef(x)/e(x_{n-1}x_n)) = 2^{n-1} + 2^{n-3} \end{cases}. \quad (20)$$

Then $CI(f(x)) = 1$ and $1+f(x)$ has the annihilators of linear function

$(x_{n-1}+x_n)ef(x)/e(x_{n-1}x_n) + e((1+x_{n-1}+x_n)ef(x)/e(x_{n-1}x_n))/ex_{n-2} = x_{n-4} + x_{n-3} + x_{n-1} + x_n$. (21)

Proof: Since $f(x)$ is an H Boolean function which satisfies (18), by the Lemma 3, we can know

$$\begin{cases} w_t(f(x)df(x)/dx_i) = 2^{n-2} \\ w_t(ef(x)/ex_i) = 2^{n-1} \end{cases} (i = 1,2,\cdots,n). \quad (22)$$

Because $f(x)$ satisfies (19), there are $w_t(f(x)|x_i = 0) = w_t(f(x)|x_i = 1) = 2^{-1}w_t(f(x))$. So $f(x)$ is a correlation immune function of order 1,and $CI(f(x)) = 1$.

Since $f(x)$ is an H Boolean function, for all ωx $(\omega, x \in GF(2)^n)$, we have

$$w_t(d(f(x)+\omega x)/dx_i)=2^{n-1}\ (x_i\neq\omega x). \tag{23}$$

Since $f(x)$ is a correlation immune function of order 1,moreover there are (23) and Lemma 3, when $\omega x\neq x_i$,for all ωx $(\omega,x\in GF(2)^n)$ of $w_t(\omega)=1$, we have

$$w_t(e(f(x)+\omega x)/ex_i)=w_t(ef(x)/ex_i)-2w_t(\omega xef(x)/ex_i)-w_t(\omega xdf(x)/dx_i)+w_t(\omega x)=2^{n-2}. \tag{24}$$

By (22) and (24), there are

$$w_t(\omega xdf(x)/dx_i)+2w_t(\omega xef(x)/ex_i)=2^{n-1}+2^{n-2}. \tag{25}$$

Since $f(x)$ is an H Boolean function which satisfies (18), by the Lemma 2, we can know

$$w_t(\omega xdf(x)/dx_i)+w_t(\omega xef(x)/ex_i)=w_t(\omega x)=2^{n-1}. \tag{26}$$

The solution of the simultaneous equations of (25) and (26) is

$$\begin{cases} w_t(\omega xdf(x)/dx_i)=2^{n-2} \\ w_t(\omega xef(x)/ex_i)=2^{n-2} \end{cases}. \tag{27}$$

So

$$\begin{cases} w_t(x_{n-1}df(x)/dx_n)=2^{n-2} \\ w_t(x_{n-1}ef(x)/ex_n)=2^{n-2} \end{cases}. \tag{28}$$

Based on correlation immunity of order 1 of $f(x)$ and Lemma 3, for all ωx $(\omega,x\in GF(2)^n)$ of $w_t(\omega)=1$, there is

$$\begin{aligned} &w_t(f(x)+\omega x) \\ &=w_t(f(x)df(x)/dx_n)-2w_t(\omega xf(x)df(x)/dx_n)+w_t(ef(x)/ex_n)-2w_t(\omega xef(x)/ex_n)+w_t(\omega x). \\ &=2^{n-1} \end{aligned} \tag{29}$$

By (22), (27) and (29), we have $w_t(\omega xf(x)df(x)/dx_n)=2^{-1}w_t(f(x)df(x)/dx_n)=2^{n-3}$. So

$$w_t(x_{n-1}f(x)df(x)/dx_n)=2^{-1}w_t(f(x)df(x)/dx_n)=2^{n-3}. \tag{30}$$

By (20), (28), (30), (18) and (22), we can get

$$\begin{cases} w_t((x_{n-1}+x_n)\partial f(x)/\partial(x_{n-1}x_n))=2^{n-2} \\ w_t((x_{n-1}+x_n)ef(x)/ex_n)=2^{n-2} \\ w_t((1+x_{n-1}+x_n)\partial f(x)/\partial(x_{n-1}x_n))=0 \\ w_t((1+x_{n-1}+x_n)ef(x)/ex_n)=2^{n-2}+2^{n-3} \end{cases}. \tag{31}$$

Known by (31), (18), (22) and (19), $1+f(x)$ has 1-degree annihilator $g=x_{n-4}+x_{n-3}+x_{n-1}+x_n$, and there is a relationship of (32) between g and $f(x)$,

$$g=(x_{n-1}+x_n)ef(x)/e(x_{n-1}x_n)+e((1+x_{n-1}+x_n)ef(x)/e(x_{n-1}x_n))/ex_{n-2}, \tag{32}$$

The proof ends.

Remark 4: By the Theorem 7, we can know, the annihilators of the lowest algebraic degree of $f(x)$ can be represented and obtained by (21). Meanwhile, by Theorem 1 to 5, we can find, there is $\deg ef(x)/ex_n+1=\deg(f(x)df(x)/dx_n)=\deg f(x)$. This is the inevitable property.

Conclusions

In this paper ,we get the relevance of algebraic degree, correlation immunity and the annihilators for H Boolean functions with $w_t(f(x))=2^{n-1}+2^{n-2}$. As a result, we get some new conclusions about the compatibility of some properties such as propagation, correlation immunity, algebraic degrees of Boolean functions, and we also get a new and relatively simple method for solving the annihilators. It is shown that the most crucial factor that impacts and combines the above characteristics is the e-derivative $ef(x)/ex_n$ and a combination of $f(x)df(x)/dx_n$ and $ef(x)/ex_n$. It can be seen that the e-derivative play an important role while dealing with the compatibility among the different cryptography properties. The research in the current paper is fundamental and could be extended toward the problems on compatibility among the different cryptography properties of other types of H Boolean functions such as Bent functions, resilient functions, and rotational symmetric functions.

Acknowledgment

This work is supported by National Natural Science Foundation of China (Grant No. 61262085).

References

[1] Massey, J. L.: 'Shift-register synthesis and BCH decoding', IEEE Trans Inform Theory, 1969, 15, (1), pp. 122-127.

[2] Rueppel, R. A., Staffelbach, O. J.: 'Products of linear recurring seguences with maximum complexity', IEEE Trans Inform Theory, 1987, 33, (1), pp. 124-131.

[3] Rueppel, R. A.: 'Analysis and Design of stream Ciphers' (Springer-Verlag, 1986).

[4] Ding, C., Xiao, G., Shan, W.: 'The stability theory of stream ciphers' (Springer-Verlag, 1991).

[5] Blaser, W., and Heinzmann, P.: 'New Cryptographic Device with High Secourity Using Public Key Distribution'. Proc. IEEE Student Paper Contest 1979-1980, 1982, pp. 145-153.

[6] Siegenthaler, T.: 'Correlation immunity of nonlinear combining functions for cryptographic applications', IEEE Transactions on Information Theory, 1984, IT-30, (5), pp. 776-780.

[7] Siegenthaler, T.: 'Decrypting a Class of Stream Ciphers Using Ciphertext only', IEEE Transactions on Information Theory, 1985, C-34, (1), pp. 81-85.

[8] Webster, A. F., and Tavares, S. E.: 'On the design of S-boxes'. Advances in Cryptology-CRYPTO'85, Santa Barbara, California, USA, 1986, LNCS, 218, pp. 523-534.

[9] Forre, R.: 'The strict avalanche criterion: spectral properties of Boolean functions and an extended definition'. Advances in Cryptology-CRYPTO'88, 1990, LNCS, 403, pp. 450-468.

[10] Courtois, N., and Meier, W.: 'Algebraic attacks on stream ciphers with linear feedback'. Advances in Cryptology-EUROCRYPT 2003, Warsaw, 2003, LNCS, 2656, pp. 345-359.

[11] Meier, W., Pasalic, E., and Carle, C.: 'Algebraic attacks and decomposition of Boolean functions'. Advances in Cryptology-EUROCRYPT 2004, Interlaken, 2004, LNCS, 3027, pp. 474-491.

[12] Carlet, C., Dalai, D. K., Gupta, K. C., Maitra, S.: 'Algebraic immunity for cryptographically significant Boolean functions: analysis and construction', IEEE Transactions on Information Theory, 2006, 52, (7), pp. 3105-3121.

[13] Wen, Q., Niu, X., and Yang, Y.: 'The Boolean Functions in Modern cryptology' (Science Press of China, 2000). (In Chinese)

[14] Akers, S. B.: 'On a theory of Boolean functions', Journal of the Society for Industrial and Applied Mathematics, 1959, 7, (4), pp. 487-498.

[15] Reed, I. S.: 'A class of multiple-error-correcting codes and the decoding scheme', IRE Transactions on Information Theory, 1954, 4, (4), pp. 38-49.

[16] Huang, J., Wang, Z.: 'The relationship between correlation immune and weight of H Boolean functions', Journal on Communications, 2012, 33, (2), pp. 110-118. (In Chinese)

[17] Li, W., Wang, Z., Huang, J.: 'The e-derivative of boolean functions and its application in the fault detection and cryptographic system', Kybernetes, 2011, 40, (5-6), pp. 905-911.

[18] Ding, Y., Wang, Z., Ye, J.: 'Initial-value problem of the Boolean function's primary function and its application in cryptographic system', Kybernetes, 2010, 39, (6), pp. 900-906.

[19] Huang, J., Wang, Z., Zhang, J.: 'Effects of e-derivative on algebraic immunity, correlation immunity and algebraic degree of H Boolean functions ', Applied Mechanics and Materials, 2013, 411-414, pp. 45-48.

Advanced Materials Research Vols. 989-994 (2014) pp 2605-2608
© (2014) Trans Tech Publications, Switzerland
doi:10.4028/www.scientific.net/AMR.989-994.2605

Moving Vehicle Detection Scheme Using Edge Information and Background Subtraction in YCbCr Color Space

Yu Wanxia[1,a], Su Jing[1,b]

[1]Tianjin Univ. of Technology and Education, Tianjin 300222, P.R,China

[a]ywanxia@sina.com, [b]sj@163.com

Keywords: Edge detection. Vehicle image. Background subtraction. YCbCr

Abstract. In this paper, we propose the spatial domain based vehicle detection scheme. This proposed scheme combines the Sobel edge detection method with background subtraction in YCbCr color space. The scheme detects the vehicle in Y(Luminance), Cb and Cr(chrominance) components of the vehicle image using background subtraction and combines the three images. Edge detection method determines edge information of the luminance component of the vehicle image. The image combined with edge detection and background difference is implemented filling and filtering operation. The robustness of the proposed scheme is analyzed considering different types of vehicle image.

Introduction

The real-time traffic flow information is an important support for ITS. Video detection is a modern and effective measure in detection of the traffic flow at a low cost. Therefore, vehicle detection based on vision has become a research focus nowadays[1-3]. Background subtraction as a kind of video detection has became an important method of researching and applying vehicle detection technology[4]. The color space representation has played a major role in image recognition. Furthermore, color has become more recently a major component in video vehicle detection applications[5-6]. Because YCbCr color space can obviate the evocable effect of variational illumination, many researchers use it in video vehicle detection[7]. Edge detection method can detect the profile of vehicle. In order to get complete vehicle information, this paper combines the Sobel edge detection method with background subtraction in YCbCr color space.

The paper is organized as follows: In Section 2 the edge detection algorithm is selected and explained. The proposed schemes are described in Section 3. The results and discussions are given in Section 4. The paper is concluded in Section 5.

Sobel edge detection algorithm

According to the different operator, edge detection algorithm is divided into Sobel edge detection method, Canny edge detection method, Roberts edge detection method, Prewitt edge detection method etc. To select an optimal edge detection operator, we compare the effects of different edge detection algorithm. On Y component the Sobel, Canny and Roberts edge detection operators are applied to different vehicle image. Fig.1 shows the detection results. Where, Fig. 1(a) show Sobel edge detection images; Fig. 1 (b) give Canny edge detection results and Fig. 1 (c) Roberts edge detection images. From Fig. 1 (b), we can see that Canny edge detection can detect complete profile of the vehicle, but many background noise components are detected simultaneously. In Fig.1(c), Roberts edge detection algorithm detects incomplete vehicle profile. The Sobel edge detection algorithm shown in Fig.1(a) can not only detect complete vehicle profile but also reduce the background noise. So the Sobel edge detection algorithm is adopted in this scheme.

This scheme uses the Sobel edge detection method to determine the luminance component edge information of the vehicle image. When operating an image with Sobel edge detection, the following steps are implemented. Firstly, use Sobel operator to calculate the horizontal gradient and vertical gradient. Secondly, combine the gradient information of two directions. Finally, apply the

threshold processing to judge image edge and output edge detection results. Fig.2 are Sobel edge detection operators. Fig. 2(a) is a 3*3 area of image, Fig. 2(b) and Fig. 2(c) respectively acts as Sobel gradient operator of vertical direction and horizontal direction.

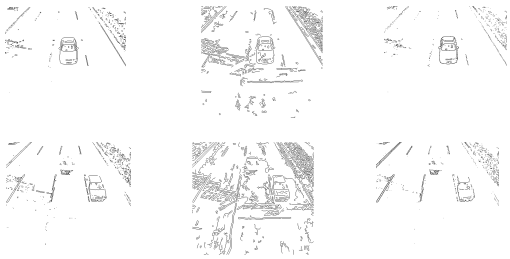

(a) (b) (c)

Fig. 1 Sobel, Canny and Roberts edge detection images on vehicle image Y

Z1	Z2	Z3
Z4	Z5	Z6
Z7	Z8	Z9

-1	-2	-1
0	0	0
1	2	1

-1	0	1
-2	0	2
-1	0	1

Fig. 2 Sobel edge detection operators

Proposed scheme

In digital image processing, besides RGB color space model is often used in collecting vidicon image, there are also HIS and YCbCr color space models. In YCbCr model, Y is luminance component, Cb is the blue and Cr red color chrominance component. This color space can obviate the evocable effect of variational illumination, so in the paper the YCbCr color model is adopted. This scheme combines the Sobel edge detection method with background subtraction method to detect the moving vehicle. The proposed scheme uses the foreground vehicle image ForeI and background image BackI of size m×n as the original images. The two images are transformed into R, G and B components of size m×n. Then R, G and B components are transformed into Y, Cb and Cr components using following equations:

$$Y = 0.299 \cdot R + 0.587 \cdot G + 0.114 \cdot B \quad (1)$$

$$Cb = 0.596 \cdot R - 0.275 \cdot G - 0.321 \cdot B \quad (2)$$

$$Cr = 0.212 \cdot R - 0.523 \cdot G - 0.311 \cdot B \quad (3)$$

The scheme mainly includes segmenting moving vehicles and removing the noise of image. Fig.3 shows the flow diagram of detection algorithm.

Part 1. Segmenting moving vehicles

Input: The original foreground image ForeI and background imge BackI of size m × n. Output: Binaryzation image O of size m1 × n1.

1) Separate R, G and B components of size m × n from foreground and background image.

2) Transform R, G and B components into Y, Cb, Cr components using (1), (2) and(3).

3) Considering the real-time demand of processing image, segment the interesting regions from Y, Cb, Cr components of background and background image according to the relation between the installation position of vidicon and roadway to get interested images size of m1×n1.

4) Determine edge information of Y component using Sobel method to get Y'.

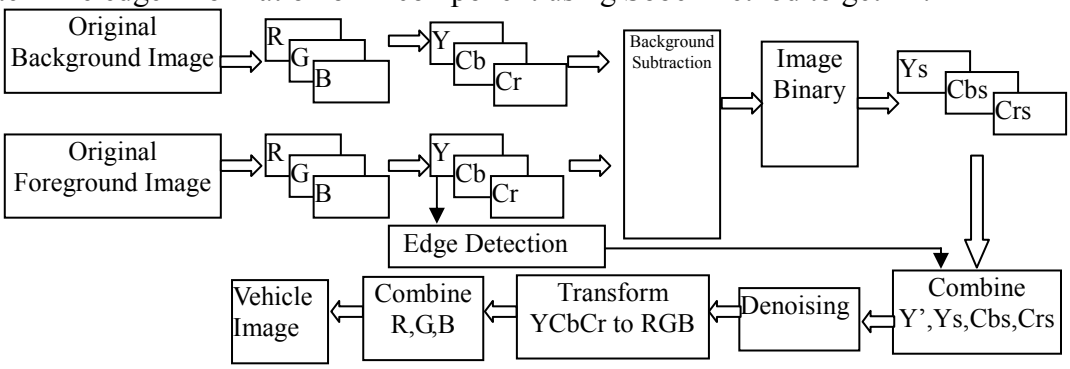

Fig. 3 Flow diagram of detection algorithm

5) Respectively subtract background image Y,Cb,Cr components from foreground image Y, Cb,Cr components.

6) Calculate the optimal threshold using following equation:

$$thy = \frac{\sum Y(i,j)}{m1 \times n1} + k \times \sqrt{\frac{\sum Y(i,j) - \frac{\sum Y(i,j)}{m1 \times n1}}{m1 \times n1}} \tag{4}$$

Where, thy is Y component threshold value, the first part is the mean value of the Y component, the second part is the root mean square of the Y component. k is an integer rang two to five. The equations of Cb and Cr components threshold values are the same with Y component threshold value. Segment image using these calculated threshold values we get three binaryzation images Ys,Cbs and Crs.

7) Combine edge detection image Y' and Ys,Cbs, Crs to generate image O.

Part 2. Denoise and output

Because the vidicon is commonly hanged on a high pole, noise caused by the slight moving vidicon is often included in the binaryzation image. When the texture of moving vehicle is simple, the detected object is easy to part and fall to pieces even has holes within an object. So noise removal is necessary. The main processes include:

8) Considering vehicle character, eliminate all regions falling short of vehicle character. In this arithmetic, the acreage, long and broad ratio are accounted.

9) Mean filter to get O1.

10)Transform Y, Cb, Cr components of image O into R, G, B components.

11) Combine R,G and B components to get result image and display the image in LCD screen.

Results and discussions

The series of experiments are conducted to analyze the algorithm on the vehicle images. In these experiments, the video images are captured from real traffic scene of a throughway. The collected speed is 30 frames per second and the size of every image is 640*480.

Fig.4 show different foreground vehicle images and corresponding processed images. In Fig.4,(a) and (f)foreground image;(b) and (g)YCbCr color space binaryzation image; (c) and (h) combined image of edge detection and binaryzation image; (d) and (i) the image of filling holes; (e) and (j) denoised image.From the images we can see that YCbCr binaryzation image combined with the edge detection information can get relatively complete vehicle image but include some background images and holes in vehicles(seen Fig4.(c)and (h)). Through filling operation some holes are filled with white(object) color and get complete vehicle images(seen Fig4.(d)and (i)).The mean filter operation is implemented to eliminate all regions falling short of vehicle character(seen Fig4.(e)and(j)). From the results we can see that the proposed scheme in this paper can detect complete vehicles.

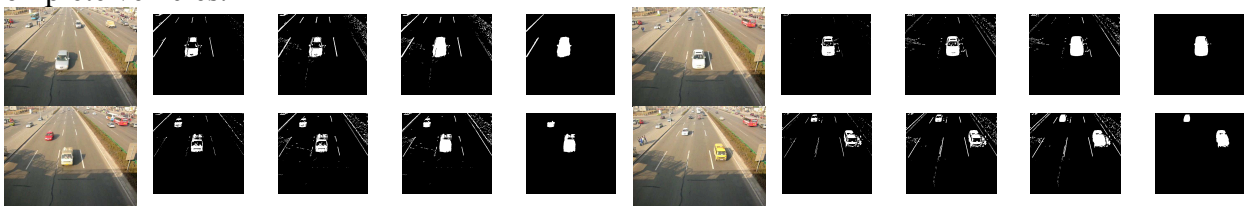

(a) (b) (c) (d) (e) (f) (g) (h) (i) (j)

Fig.4 Foreground images and corresponding processed images

Conclusion

We have proposed a spatial domain based vehicle detection scheme. The YCbCr components are considered to detect vehicle image. Sobel edge detection method determines edge information of

the luminance component of the vehicle image. We adopt background subtraction to get Y,Cb and Cr component images and do binaryzation processing. This scheme combines the Sobel edge detection method with background subtraction in YCbCr color space. The video vehicle detection scheme is analyzed by considering various types of image and the scheme was found robust to various types of image.

References

[1] Kunsoo Huh, Jaehak Park, Junyeon Hwang, et al. A stereo vision-based obstacle detection system in vehicles[J]. Optics and Lasers in Engineering, 2008, 46(2): 168-178.

[2] Shen Huan, Li Shun-ming, Bo Fang-chao, et al. On road vehicles real time detection and tracking using vision based approach[J]. ACTAOPTICA SINICA, 2010, 30(4):1076-1083.

[3] Dac-binh HA, ZHAO Guang-zhou, LU Cheng-en, etal. New method of video-based moving vehicle extraction based on seeded region growing[J]. Computer Application, 2008,28(4): 979-981.

[4] Li Zhang. In Situ Image Segmentation Using the Convexity of Illumination Distribution of the Light Sources[C]. IEEE Transactions on Pattern Analysis and Machine Intelligence. 2008: 1786-1799.

[5] Kim Sam-yong, Oh Se-young, Kang Jeong-kwan, et al. Front and rear vehicle detection and tracking in the day and night times using vision and sonar sensor fusion[C]. 2005 IEEE/RSJ International Conference on Intelligent Robots and Systems, IROS, Edmonton, AB, Canada, 2005:2306-2311.

[6] S. Y. Kim, S. Y. Oh, J. K. Kang, Y. W. Ryu, K. Kim, S. C. Park, and K. H. Park. Front and Rear Vehicle Detection and racking in the Day and Night Times using Vision and Sonar Sensor Fusion[C]. IEEE International Conference. on Intelligent Robots and Systems, 2005: 2173-2178.

[7] Ying-Che Kuo, Hsuan-Wen Chen. Vision-based Vehicle Detection in the Nighttime[C]. 2010 International Symposium on Computer, Communication, Control and Automation, 2010: 361-364.

Advanced Materials Research Vols. 989-994 (2014) pp 2609-2612
© (2014) Trans Tech Publications, Switzerland
doi:10.4028/www.scientific.net/AMR.989-994.2609

A Hybrid 2-Population Genetic Algorithm for the Job Shop Scheduling Problem

Xu Zhuo[1,a], Wang Rui[2,b], Wang Zhongmin[1,c*]

[1]College of Mechanical Engineering, Tianjin University of Technology and Education, 300222, China

[2]Tianjin Municipal Education Commission, 300222, China

[a]lgdxuzhuo@163.com, [b]tjjwwangrui@sina.cn, [c]wzmin86@126.com

*Author for correspondence: Wang Zhongmin, Professor, E-mail: wzmin86@126.com

Keywords: Hybrid 2-Population GA. Genetic algorithm. Job shop scheduling. IAGA. SAGA

Abstract. In this paper, an analysis of a hybrid two-population genetic algorithm (H2PGA) for the job shop scheduling problem is presented. H2PGA is composed of two populations that constitute of similar fit chromosomes. These two branches implement genetic operation separately using different evolutionary strategy and exchange excellent chromosomes using migration strategy which is acquired by experiments. Improved adaptive genetic algorithm (IAGA) and simulated annealing genetic algorithm (SAGA) are applied in two branches respectively. By integrating the advantages of two techniques, this algorithm has comparatively solved the two major problems with genetic algorithm which are low convergence velocity and potentially to be plunged into local optimum. Experimental results show that the H2PGA outperforms the other three methods for it has higher convergence velocity and higher efficiency.

Introduction

To achieve GAs potential, genetic algorithms can take advantage of parallel computing environments based on their well parallelizable nature [1-3]. On the base of study on many kinds of improved algorithms, a novel H2PGA composed of IAGA and SAGA[4-5] is presented. There are two parallel populations evolving synchronously in this algorithm by way of enhancing optimizing efficiency. IAGA is applied in one population, convergence process can be fast; in the other population SAGA is used so partial searching can be more efficient. This H2PGA, which integrates the advantages of IAGA and SAGA, makes it possible to avoid falling into local optimum, so its convergence velocity and efficiency could become higher. Benchmark LA01 (10×5) job-shop scheduling problem are used to show the effectiveness of the proposed method. Experimental results demonstrate that the proposed genetic algorithm does not get stuck at local optima easily, and it is fast in convergence.

Hybrid 2-Population Genetic Algorithm

Design of H2PGA. This hybrid 2-population genetic algorithm belongs to category of Parallel Genetic Algorithm (PGA) which has parallel framework working on single processor, so that it has high efficiency and little processing time.

In view of shortcoming that genetic algorithm is prone to be trapped into local optimum; H2PGA initializes two populations that constitute of similar fit chromosomes during the phase of initialization. These two populations have a parallel relationship and implement reproduction respectively using different evolutionary strategy. These two population exchange several chromosomes which have high fitness after a number of iterations by way of excellent foreign individuals. These migrated chromosomes can enhance fitness and improve individual variety of each population. Thereby this new method can avoid falling into local optimum. The framework of H2PGA is shown in Fig.1. The example of how the initial population is divided into two parallel populations is shown in Fig.2. Each number in the table signifies the supposed fitness of corresponding chromosome.

The operation of H2PGA can be divided into five stages as follows:

1) Generate initial random population of solutions.

2) Evaluate the fitness of the initial chromosomes and divide the population into two populations averagely.

3) Implement reproduction separately in both of the populations using IAGA and SAGA evolutionary strategy.

4) If migration condition is fulfilled, exchange definite chromosomes from IAGA and SAGA population to each other.

5) Go to (3) or exit if convergence or run time constraints have been met.

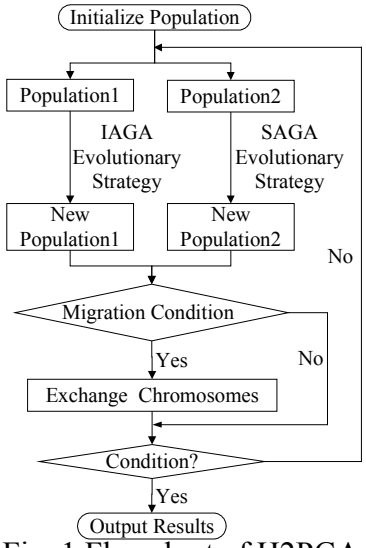

Fig. 1 Flowchart of H2PGA

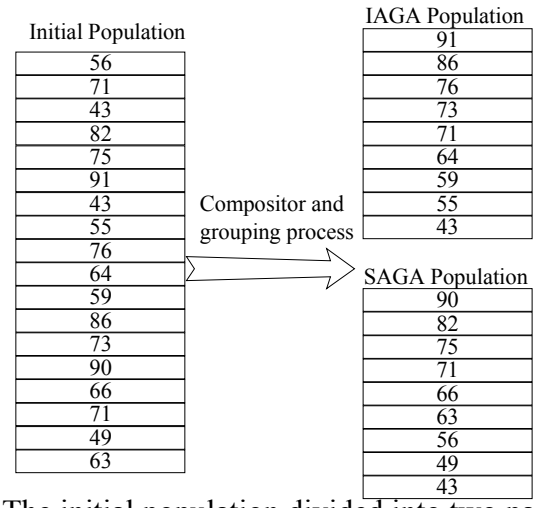

Fig. 2 The initial population divided into two parallel populations

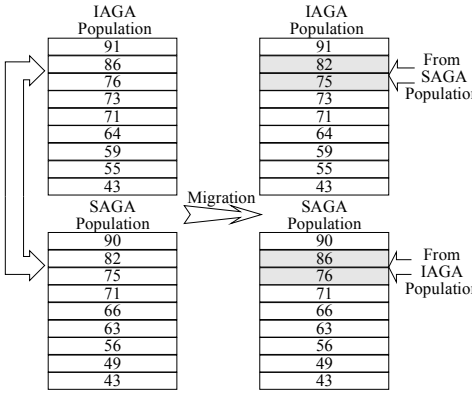

Fig. 3 Exchange chromosomes between the two populations.

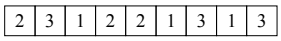

Fig. 4. Chromosome design

IAGA is applied in one population making the crossover and mutation probability adjusted adaptively and nonlinearly, that can avoid such disadvantages as premature convergence, low convergence speed and low stability. SAGA is applied in another population utilizing its merit of the strong ability of partial search.

The new method has parallel optimizing framework and holistic control. IAGA and SAGA embranchment carry out optimizing like crossover and mutation process respectively. These two populations would exchange several chromosomes which have high fitness if migration condition is fulfilled. An example of how chromosomes are exchanged between two populations is shown in Fig.3.

Migration Strategy

The frequency and the number of migrations are two important parameters which have to be taken into account when migrating chromosomes between two populations.

Migration Frequency *f*: It describes the interval between the points in which excellent chromosomes from one population can be transferred to another. It is expressed as a number of generations between two migration points. If the value of *f* is too low, when one branch is trapped into partial optimization, the other one would also tend to be trapped; if the value of *f* is too high, the expected mutual role in promoting between two populations can not be achieved effectively.

Migration Number *T*: The number of chromosomes migrated between two populations each time. If migration number is too large, chromosomes in both populations would tend to the same and trapping into partial optimization is potential; if migration number is too small, optimizing efficiency would reduce.

Experiments are carried out to work out the best value of Migration Frequency *f* and Migration Number *T* toward a typical job-shop scheduling problem LA01. Experimental results show that the average number of iterations is smaller where migration frequency *f*=5, migration number *T*=2. Experimental results are shown in Table 1 which exhibit average numbers of iterations under different conditions. Each data is obtained by ten times experiments.

Chromosome design

A chromosome has gene information for solving the problem for genetic algorithm. At present, the encoding method often used to solve the scheduling problem is the operation-based representation encoding which is applied in H2PGA. This representation encodes a schedule as a sequence of operations and each gene stands for only one operation. The chromosome shows the order of job-number. An example of a chromosome for a 3×3 job-shop scheduling problem is shown in Fig.4.

Table 1 Experiments for average numbers of iterations under different conditions

f \ *T*	1	2	3	4	5	*6*
1	12.3	13.1	14.5	14.6	13.2	13.5
2	14.1	13.2	15.0	14.1	14.3	14.1
3	12.2	8.6	14.7	14.5	14.5	15.2
4	11.5	8.7	12.5	14.0	13.1	14.2
5	8.6	7.2	12.4	13.4	13.2	14.3
6	11.6	11.4	13.0	13.0	13.1	13.5
7	12.3	11.6	9.1	10.3	10.1	14.1
8	14.0	12.7	9.8	9.2	12.1	12.8
9	14.1	12.5	13.4	13.6	13.2	12.4
10	14.8	11.9	14.0	14.3	14.6	13.0

Experiments and results analysis

The performance of the H2PGA is compared to the other three methods that include of a single population GA (SGA), IAGA and SAGA. It is evaluated using a standard problem LA01 which is designed by Lawrence in 1984. The capacity of LA01 is 10×5 means that there are 10 jobs and 5 machines need to be ordered.

Table 2 Parameters of H2PGA for LA01

population	Evolution time	*Pc1*	*Pc*2	*Pm1*
100	35	0.9	0.6	0.1
Pm2	Crossover time	Mutation time	Initial temperature	Attenuation coefficient
0.005	50	50	1000	0.9

The parameters of H2PGA in Table 2 are acquired by experiences. P_c1 is crossover probability in IAGA population, P_c2 is crossover probability in SAGA population, P_m1 is mutation probability in IAGA population, P_m2 is mutation probability in SAGA population. The programming language is Visual Studio C#.NET, and it runs on Windows XP with Intel Core 2 E7400.

The experimental results in Table3 show that H2PGA has higher convergence speed and higher convergence probability by comparison between four different methods. The H2PGA convergent curves of LA01 shown in Figures 5 are very stable. So the improved genetic algorithm has the characteristics of high convergence speed and excellent searching ability.

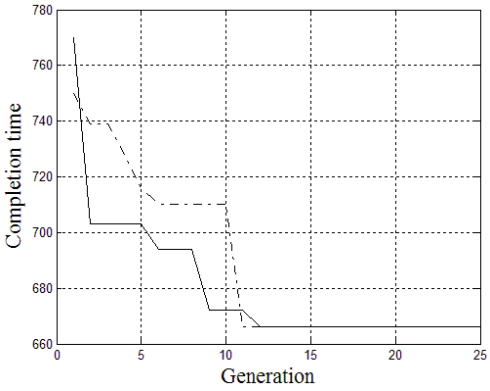

Fig. 5 The H2PGA convergent curves of LA01

Table 3 Experimental results

	IAGA	SAGA	SGA	H2PGA
Average Time/s	27.7	30.8	31.5	22.7
Average Iterative Time	14.7	13.9	15.7	11.4
Minimum Convergence Time/s	9	8	10	5
Minimum Iterative Time	5	8	7	4
Convergence probability	0.4	0.4	0.3	0.6

Conclusion

In this paper we have presented a hybrid two-population genetic algorithm scheme for the job-shop scheduling problem. The initial population is divided into two branches using IAGA and SAGA strategy which have been introduced. The proposed scheme aims to synthesize parallel framework with hybrid algorithm to improve the ability for using genetic algorithm to solve the job scheduling problems. Experimental results show that the suggested method is capable of producing competitive performance compared to the other three kind of genetic algorithms.

However, our H2PGA is more complicated than the standard genetic algorithm, and it also has more tunable parameters. It is hard to find out the best parameter which can impact the capability of algorithm seriously. Therefore, this kind of parallel and hybrid genetic algorithms still have many aspects to be improved.

Reference

[1] Kuang H Y, Jin J ,Su Y. Improving Crossover and Mutation for Adaptive Genetic Algorithm, Computer engineering and application, 2006.12, 93-96.

[2] Wang X P, Cao L M, Genetic Algorithm: theory, application and software implementation, Xi'an, Xi'an Jiao Tong University Press, 2002.

[3] Xing Y J, Chen Z T, Sun J. An Improved Adaptive Genetic Algorithm for Job-Shop Scheduling Problem, ICNC'07-FSKD'07, 287-291.

[4] Wang L, Intelligent optimization algorithms with application, Tsinghua University Press, Beijing China, 2001.

[5] Jarno Martikainen and Seppo J. Ovaska, Hierarchical Two-Population Genetic Algorithm, 2005 IEEE Mid-Summer Workshop on Soft Computing in Industrial Applications, Helsinki University of Technology, Espoo, Finland, June 28-30, 2005.

Advanced Materials Research Vols. 989-994 (2014) pp 2613-2616
© (2014) Trans Tech Publications, Switzerland
doi:10.4028/www.scientific.net/AMR.989-994.2613

Robust Principal Component Analysis Algorithm Based on Nonparametric Correlation Coefficient Matrix

Nan Zhao[1,2a], Hongyu Shao[3b]

[1]Tianjin Key Laboratory of High Speed Cutting & Precision Machining, Tianjin University of Technology and Education, Tianjin, China

[2]College of Mechanical Engineering, Tianjin University of Technology and Education, Tianjin, China

[3]Tianjin Key Laboratory of Equipment Design and Manufacturing Technology, Tianjin University, Tianjin, China

[a]nanzhao1982@163.com, [b]h4clo4@163.com

Keywords: Principal component analysis, Non-parametric statistics, Pollution rate, Correlation coefficient

Abstract. Principal component analysis algorithm is widely applied in solving a large number of dimension reduction problems for high-dimensional data in fields such as image identification and comprehensive evaluation due to its clear conception and simple application. The PCA based on covariance matrix and correlation coefficient matrix is very sensitive to abnormal values so that the data structure is distorted. As a result, there exist great deviations in the analysis results and it is hard to explain. The traditional PCA is remade in this paper based on non-parametric statistical ideas, nonparametric correlation coefficient and gray relational coefficient, in order to define three kinds of robustness evaluation criteria and objectively evaluate the robustness of the algorithm through numerical experiments. The results of the numerical experiments show that the new algorithm is of good robustness to noise pollution and the algorithm is of good applicability.

Introduction

Covariance matrix and correlation coefficient matrix are extremely important in multivariate statistical analysis. However, neither the covariance matrix nor the correlation coefficient matrix is a robust estimator. They are extremely sensitive to abnormal values so that both eigenvalues and eigenvectors are influenced. In data analysis, one or several abnormal values can make the data structure distorted. Campbell calculated the eigenvalues and eigenvectors by the covariance matrix after robustness. The disadvantage is that the calculated amount of the covariance matrix is large and it is not appropriate to be adopted in large samples [1]. Based on the non-parametric statistical theory with good robustness, a principal component analysis algorithm based on non-parametric correlation coefficient is proposed in this paper.

Non-parameter correlation coefficient

Non-parametric statistical method is a statistical method neither dependent on population distribution and its parameters nor constrained by the distribution. Compared with parametric statistical methods, non-parametric statistical methods have the features of wide application and good robustness. Non-parametric statistical methods have few restrictions on overall modes. The estimation will not be greatly influenced when the overall model is slightly changed. A random sample from an unknown distribution can be studied with the method of goodness-of-fit test in non-parametric statistics, to check whether the unknown distribution function agrees with the null hypothesis being a known and concrete distribution [2]. Non-parametric correlation coefficients with robustness are selected in this paper and the liner correlation coefficients short of robustness are replaced by gray correlation coefficients to form the robust correlation coefficient matrix[3].

Suppose (x_1, x_2, …, x_n) to be a group of sample observations of the overall matrix X. Then arrange them in the order from small to large $x_1^* \le x_2^* \le \ldots \le x_n^*$. After the arrangement, $x_i = x_R^*$. Then, R is called the order of x_i. The common non-parametric correlation coefficients include Spearman correlation coefficient and Kendall τ correlation coefficient.

Spearman order correlation coefficient. R_i represents the order of X_i in sample X and Q_i represents the order of Y_i in sample Y. Then the Spearman order correlation coefficient is defined as r_s:

$$r_S = 1 - \frac{6}{n(n^2-1)} \sum_{i=1}^{n} (R_i - Q_i)^2 \tag{1}$$

Kendall τ correlation coefficient. Kendall proposed another correlation testing method to test whether the two variables are correlated by judging whether they are consistent with each other. The pairs (X_i, Y_i) and (X_j, Y_j) are consistent or their directions in variation are consistent. Kendall τ correlation coefficient can be defined [4]:

$$\tau = \frac{2}{n(n-1)} \sum_{1 \le i \le j \le n} \operatorname{sign}((X_i - X_j)(Y_i - Y_j)) \tag{3}$$

Where, $$\operatorname{sign}((X_i - X_j)(Y_i - Y_j)) = \begin{cases} 1, (X_i - X_j)(Y_i - Y_j) > 0 \\ 0, (X_i - X_j)(Y_i - Y_j) = 0 \\ -1, (X_i - X_j)(Y_i - Y_j) < 0 \end{cases}$$

The value of τ calculated with formula (3) shall be tested in the Kendall τ statistics table.

Gray correlation coefficient. Take the series after nondimensionalize $X_0 = \{x_{01}, x_{02} \cdots, x_{0n}\}$ as the standard series and the compared series is $X_i = \{x_{i1}, x_{i2} \cdots, x_{in}\}$ （$i = 1,2,3 \ldots m$）, the formula to calculate the correlation coefficient ξ_{ik} is given under:

$$\xi_{0i} = \frac{\min\limits_i \min\limits_k |X_{ik} - X_{0k}| + \rho \max\limits_i \max\limits_k |X_{ik} - X_{0k}|}{|X_{ik} - X_{0k}| + \rho \max\limits_i \max\limits_k |X_{ik} - X_{0k}|} \quad （i = 1,2,3 \ldots m, k = 1,2,3 \ldots n）$$

The range of resolution ratio is (0, 1). In order to guarantee a good resolution effect, ρ is generally taken as 0.5. Solve the gray correlation coefficient ξ_{ij} between X_i and X_j. Then the gray correlation coefficient matrix can be obtained.

Numerical experiments

Take n-dimensional normal distribution matrix $\boldsymbol{X} \sim \boldsymbol{N}$（$\boldsymbol{\mu}$，$\boldsymbol{\Sigma}$）as ($m$-$m\varepsilon$)×$n$ dimensional primary sample to generate n-dimensional normal distribution $\boldsymbol{Y} \sim \boldsymbol{N}$（$\alpha\mu$，$\beta\Sigma$）as $m\varepsilon \times n$ dimensional noise sample. In this example, take n=10，m=100，α=2，β=5，μ=[0.81, 0.91, 0.12, 0.91, 0.63, 0.098, 0.28, 0.55, 0.96, 0.96]，$\Sigma = I_{10\times 10}$ and define $\boldsymbol{XY}$=[$\boldsymbol{X}$, $\boldsymbol{Y}$] as the sample matrix to be analyzed [5]. As for the i^{th} kind of correlation coefficient matrix, the correlation coefficient matrix is written as R_ε^i when the pollution rate is ε. The principal eigenvalue is λ_ε^i and the principal eigenvector is $\boldsymbol{V}_{\varepsilon,k}^i$. k is the component of vector $\boldsymbol{V}$（k=1, 2,… , n）. The algorithm robustness evaluation criterions defined in this paper are as shown in formula (4), formula (5) and formula (6). The robustness of several correlation coefficient matrixes is hereby compared.

F norm criterion： $$F_\varepsilon^i = \frac{\left\| R_\varepsilon^i \right\|_F}{\left\| R_{\varepsilon=0}^i \right\|_F} \tag{4}$$

Principal eigenvalue criterion： $$L_\varepsilon^i = \frac{\lambda_\varepsilon^i}{\lambda_{\varepsilon=0}^i} \tag{5}$$

Principal eigenvector criterion: $v_{\varepsilon}^{i}=\frac{1}{n}\sum_{k=1}^{n}\left|\frac{\boldsymbol{V}_{\varepsilon,k}^{i}-\boldsymbol{V}_{\varepsilon=0,k}^{i}}{\boldsymbol{V}_{\varepsilon=0,k}^{i}}\right|$ (6)

The correlation coefficient matrixes are influenced by pollution rate so that the calculation values of the three criteria are fluctuated. The degree of fluctuation can be represented by variable coefficient, as shown in Table 1. The fluctuation conditions are as shown in Fig.1, Fig.2 and Fig.3. Numerical experiment shows that the fluctuations of gray correlation coefficient matrix are the smallest. It indicates that the correlation matrix generated from gray correlation coefficient has better robustness. Therefore, PCA with better robustness, gray principal component analysis (GPCA), can be obtained. The traditional linear correlation coefficient matrix is replaced by a gray correlation coefficient matrix to generate gray principal components at all levels.

Summary

Based on non-parametric statistical idea and non-parametric correlation coefficient and gray correlation coefficient, traditional principal analysis algorithm is remade to objectively evaluate the robustness of the algorithm by numerical experiments. The results of numerical experiments show that the new algorithm is of good robustness to noise pollution and the algorithm is of good applicability.

Table 1 Variable coefficient of the fluctuation deviation

	Pearson	Spearman	Kendall	Gray correlation
F norm criterion	0.622503	0.598458	0.594623	0.488502
Principal eigenvalue criterion	0.848218	0.720582	0.72514	0.676994
Principal eigenvector criterion	0.604552	0.653777	0.514613	0.531657

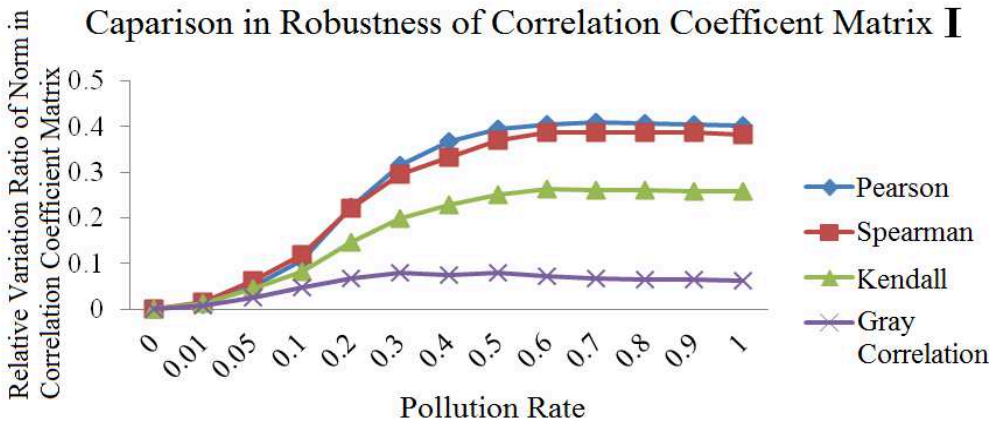

Fig.1 Relationship between the variation ratio of norm and the pollution rate

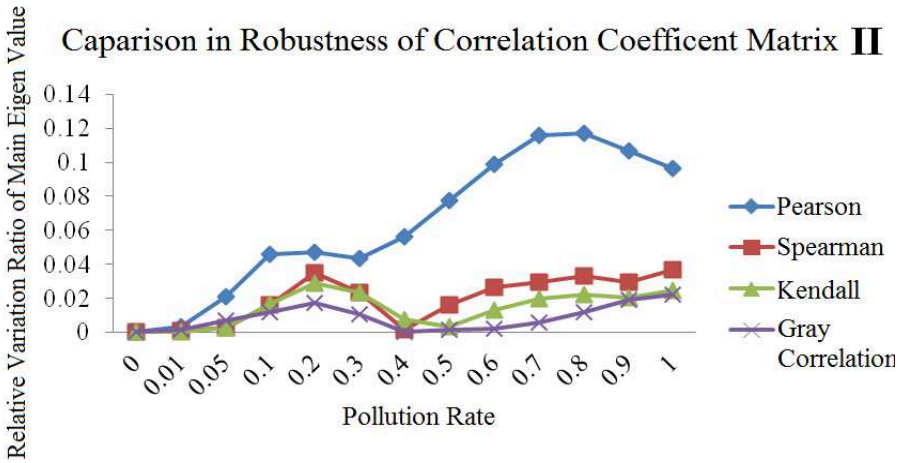

Fig.2 Relationship between the variaton ratio of principal eigenvalue and the pollution rate

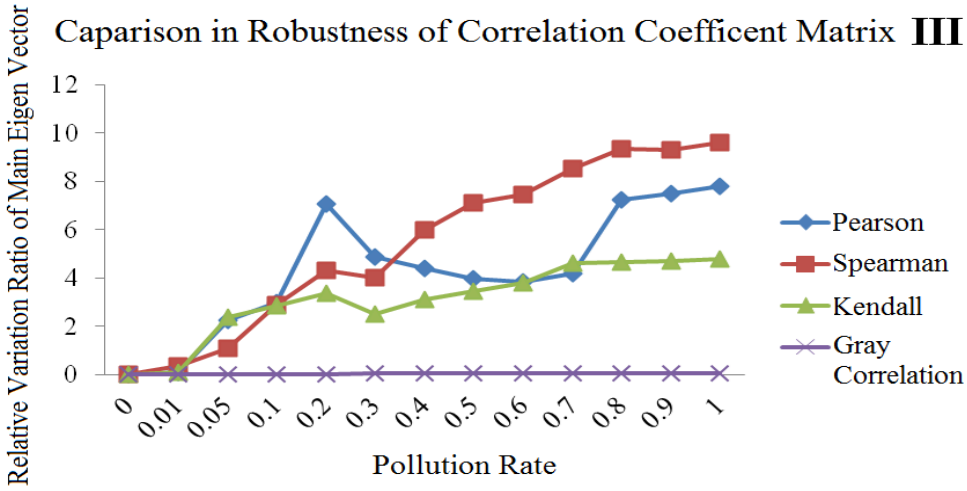

Fig.3 Relationship between the variation ratio of principal eigenvector and pollution rate

Acknowledgement

This work is supported by the National Natural Science Foundation of China (No.71171145), National High Technology Research and Development Program of China (2013AA040605), and Tianjin University of Technology and Education (No. KYQD13025).

References

[1] P. J. Roussecuw, C. Croux. Alternatives to median absolute deviation, Journal of the American Statistical Association [J], 88(1993):1273-1283.

[2] P. J. Roussecuw, K.Vandriessen. A fast algorithm for minimum covariance determinant estimator [J], Technometrics, 41(1999):212-223.

[3] Haralick R, Harpaz R. Linear Manifold Clustering in High Dimensional Spaces by Stochastic Search [J]. Pattern Recognition, 2007, 40(10):2672--2684.

[4] Li Fan Zhang, Qian Xu Pei, Xie Lin, He Shu Ping. Machine Learning and it s Applications [M]. Hefei : University of Science and Technology of China Press , 2009, (in Chinese)

[5] Tung C T, Lee Y J, A Novel approach to construct grey principal component analysis evaluation model [J], Expert Systems with Applications,2009,36(2009): 5916–5920.

Advanced Materials Research Vols. 989-994 (2014) pp 2617-2620
© (2014) Trans Tech Publications, Switzerland
doi:10.4028/www.scientific.net/AMR.989-994.2617

Design Modeling and Simulation by Interpolation Algorithm of Zadoff-Chu Sequence

Shaosong Wan[1,a], Qunsong Zhu[2,b], Jian Cao[2,c]

[1]XiJing University, Xi'an, Shaanxi Province 710123, P.R. China

[2]Air Force Engineering University, Xi'an, Shaanxi Province 710051, P.R. China

[a]12156555@qq.com, [b]yancong192@qq.com, [c]cao_jian1972@163.com

Keywords: Interpolation; Design; Zadoff-Chu Sequence; Model

Abstract. HF channel sounding requires perfect autocorrelation property of the sounding sequences. Compared with other pseudonoise sounding sequences, Zadoff-Chu sequence gets great attention due to its predominant periodic autocorrelation property. In order to adapt the spectrum property of Zadoff-Chu sequence to the requirement of HF channel sounding transmitter-receiver, the Formula Direct Interpolation Algorithm (FDIA) is put forward by which the amplitude frequency characteristic of Zadoff-Chu sequence can be enhanced. Application examples show that, this system can significantly improve the efficiency of aerodynamic design.

Introduction

HF channel sounding serves frequency forecast and management of HF communication and is significant in the establishment of reliable HF communication. The selection or design of sequences is a key technique in HF channel oblique sounding. At present, the pseudo-noise sequences used as sounding sequences in traditional pulse compression channel sounding system for correlation detection are periodic maximal length sequence (viz. m sequence), Barker code, etc., of which the performance is assessed by their auto-correlation properties. In recent years, Constant Amplitude Zero Auto-correlation (CAZAC) sequences get great attention and are applied to many fields due to their perfect periodic autocorrelation properties. At present, the maximal length of Barker code is thirteen which is too short and limits its application[1]. Even though the periodic auto-correlation property of m sequence is good, it is still in the shade compared with the periodic auto-correlation property of CAZAC sequences. The Zadoff-Chu sequence studied in the paper is one of CAZAC sequences, of which the periodic auto-correlation function (PACF) theoretically is zero for all nonzero lags[2].

Currently, with the growing demand for development of space resources and increasingly fierce competition of commercial satellite launch market, the next generation launcher with high-performance and low-cost is becoming research focus in many countries. Modular design is considered to be the future direction of launch vehicle. It decomposes the launcher into several standard modules. By combing different modules, various capabilities launch vehicle would be assembled to meet different payload requirements[3]. Therefore, the development cycle will be significantly shortened, the costs will be lower, and reliability will be enhanced. Aerodynamic performance of launch vehicle mainly depends on their shape exposed to the air. It also affects other characteristics of launch vehicle, such as trajectory, flight stability, mechanical properties, etc. R&D of Launch vehicle is facing combinatorial explosion problem caused by modular design. That is to say, the possible number of launch vehicle is much more than the number of modules[4].

Decimation Method of Sequence Interpolated by FDIA

In HF channel sounding, the decimation of the signal which has been processed by band pass filter, down conversion and low pass filter is necessary at the receiver. However, the decimation becomes complicated due to the delay in the channel. Besides, the values of Zadoff-Chu sequence interpolated by FDIA don't have perfect periodic auto-correlation property except the values

maintained from the original Zadoff-Chu sequence. As a result, several times of decimations are needed to seek the optimal decimation position after the approximate jumping-off point of the received sequence is found out. Decimation is done once after a bit shift every time.

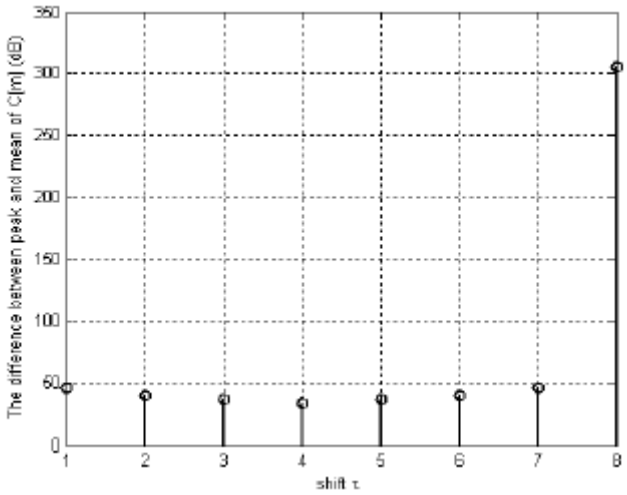

Fig.1 Relation of differences between peaks and means of [m] C and the shift τ

Motion Control Section

Fig.2 shows the spectra of Zadoff-Chu sequence respectively interpolated by FDIA and commonly used interpolation algorithm with L=1024 and k=1. From the figure we can see that although the spectrum of the sequence interpolated by the commonly used interpolation algorithm is compressed, it has many big side-lobes and rolls off slow. And that the spectrum of the sequence interpolated by FDIA is almost no big side-lobes and rolls off fast. So the sequence energy is centralized, which make it satisfy the bandwidth requirement of HF channel sounding transmitter-receiver.

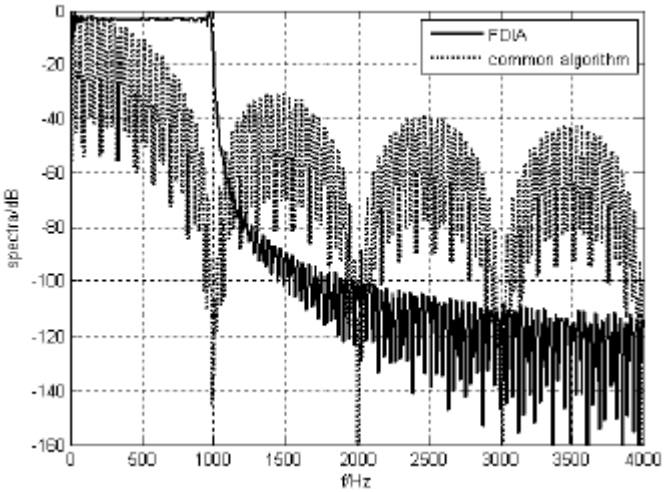

Fig.2 Spectra of sequences respectively inserted by FDIA and commonly used interpolation algorithm

Movement control card can receive PC control instruction, and the axes interface to be controlled send pulses to relevant servo controller to control motor rotation angle, and then ball-screw will convert rotation angle to horizontal displacement, so as to carry the infrared supply horizontal or vertical movement. The control part mainly includes movement control card, servo controller and so on, motor control command is sent through the PC software to regular the movement control card to produce the corresponding output pulse. The whole movement process need two axes motor control respectively, it is adequate for us to use the movement control card supported four axes, and available for circular interpolation, continuous linear interpolation, so the card can meet the equipment requirements. Actuator is a key part of the whole system, which is designed three-rail

plane, including two horizontal rails and one vertical rail, ball-screw inside, which can drive the slider with infrared light supply to move in the whole plane. There at the edge of rail separately installs limit switch and origin switch to determine the origin and the maximum boundary.

System Software Design

PC software is developed with VC++6.0 that of good interactive interface, enable the system to control in realtime. In motor control section, through the user interface the user can undertake POST (power on self test), path planning, track planning path and so on. The program flow diagram shows as Fig.3. The user can arrange what to do, and how to do because of VC++6.0 based on events programming, with response of events set through good interface, such as when clicked on a button, then the program execute button operation responded.

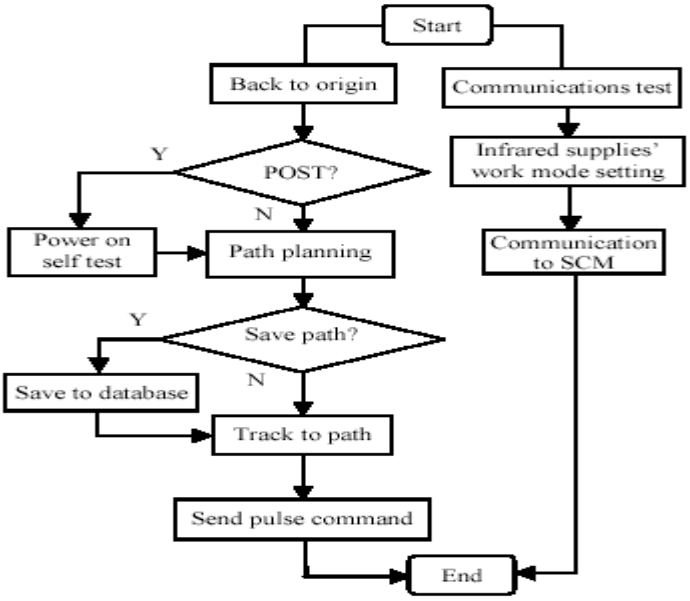

Fig.3 Programm flow diagram

When the program is running, the first to do is initialization, upper computer software communicates with single-chip microcomputer firstly to determine whether it works properly, which can be shown in the user-interface, at the same time moving infrared light supply under control is carried by slider back into origin to ensure the whole motion correction; Then the user can select POST which can track a predetermined path to check whether the system is working normally. Users can draw route planning with the existing lines, rectangular, circle planning in the picture box of software, after successful design software can save track data in a database, and infrared supply can track the path also in directly. The software can support user-defined trajectory, user select multiple points to draw path planning, which can draw any graphics.

Conclusion

In HF channel oblique sounding, the selection or design of sounding sequences is a key technique. The paper investigates the periodic autocorrelation property of Zadoff-Chu sequence based on the introduction of the definition and properties of CAZAC sequences. Aiming at resolving the problem that the spectrum of Zadoff-Chu sequence is not band-limited which makes it be not suitable for transmission in HF channel, the FDIA is proposed in the paper by which the amplitude frequency characteristic of Zadoff-Chu sequence can be enhanced. The comparisons of the spectra, the real parts and the imaginary parts of the sequences respectively interpolated by FDIA and commonly used interpolation algorithm are carried out. At the same time, an effective method of achieving optimal decimation of the Zadoff-Chu sequence interpolated by FDIA is provided. In the control process, it is convenient to process all necessary parameter setting and adjustment, and in the control process of the whole system shows superior performance and achieves the expected effect.

References

[1] ZHANG Jian-hua, FENG Chong, LIU Yi and ZHANG Yan-yan. “Time Synchronization Algorithm for MIMO OFDM Systems,” Journal of Beijing University of Posts and Telecommunications, vol. 32, no. 1, pp. 118-121, Feb.2009.

[2] R.L. Frank and S.A. Zadoff. “Phase shift pulse codes with good correlation properties,” IRE Transactions on Information Theory, vol. IT-8, pp. 381-382, Oct. 1962.

[3] D. C. Chu. “Polyphase codes with good periodic correlation properties,” IEEE Transactions on Information Theory (Corresp.), vol. 18, no. 4, pp. 531-532, July 1992.

[4] K. Andrew, K. Ioannis, J. B. John, M. R. Dellomo and J. M. Sieracki. “Ambiguity and sidelobe behavior of CAZAC coded waveforms,” IEEE Radar Conference, pp. 99-103, April 2007.

[5] Chen Xiao-wu, “A multilayer portal model for information Grid,” China Grid Annual Conference, China Grid'08, Gansu,vol1, pp.78-85, August 2008.

Advanced Materials Research Vols. 989-994 (2014) pp 2621-2624
© (2014) Trans Tech Publications, Switzerland
doi:10.4028/www.scientific.net/AMR.989-994.2621

Particle Swarm Optimization by Improved Chaos Immune Genetic Algorithm

Shaosong Wan[1,a], Jian Cao[2,b], Qunsong Zhu[2,c]

[1]XiJing University, Xi'an, Shaanxi Province 710123, P.R. China

[2]Air Force Engineering University, Xi'an, Shaanxi Province 710051, P.R. China

[a]12156555@qq.com, [b]cao_jian1972@163.com, [c]yancong192@qq.com

Keywords: Algorithm; Mutation; Swarm Intelligence; Structure

Abstract. In order to resolve these problems, we put forward a new design of the intelligent lock which is mainly based on the technology of wireless sensor network. Particle swarm optimization (PSO) is a recently proposed intelligent algorithm which is motivated by swarm intelligence. PSO has been shown to perform well on many benchmark and real-world optimization problems; it easily falls into local optima when solving complex multimodal problems. To avoid the local optimization, the algorithm renews population and enhances the diversity of population by using density calculation of immune theory and adjusting new chaos sequence. The paper gives the circuit diagram of the hardware components based on single chip and describe how to design the software. The experimental results show that the immune genetic algorithm based on chaos theory can search the result of the optimization and evidently improve the convergent speed and astringency.

Introduction

The electric equipments formerly operated mainly by manual operation gradually have been replaced by remote operation, and the mode of single substations has gradually changed to the mode of centralized control substations. Particle swarm optimization (PSO) is a new intelligent algorithm which was firstly developed by Kennedy and Eberhart in 1995. Like other evolutionary algorithms (EAs), PSO is also based on population search, but it differs from EA in iterative operations. In a general EA, it usually contains three operations, crossover, mutation and selection, while PSO does not have any such kinds of operations. In PSO, it only has two operations, velocity and position updating equations. In EAs, the crossover is helpful to inherit excellent features from parents, and the mutation is beneficial for improving the diversity of swarm. To keep these good operations, some researchers embedded these operators into PSO and obtained good performance. For example, Wang et al. proposed a novel multi-parent crossover operator, in which an offspring is generated by recombination of the current particle and another three random particles. Simulation studies on six multimodal optimization problems show that the proposed MPSO achieves better results than standard PSO and classical evolutionary programming (CEP). Besides of the crossover, some mutation techniques are also introduced to PSO. Coelho and Krohling proposed a modified PSO algorithm based on Cauchy and Gaussian distribution, in which the Gaussian and Cauchy probability distribution to update the velocity of PSO. Higashi and Iba embedded a Gaussian mutation operator into PSO. Wang et al. proposed an adaptive Cauchy mutation in PSO, and this mutation technique has been applied to other PSO algorithms. Stacey used a Cauchy mutation for each dimension of position with probability 1/D, where D is the number of dimension. Under these situations designing a reasonable on-line computer anti-lock system is an alternative to solve the current problem[1].

In this paper, we also propose a new mutation operator in PSO. The proposed mutation strategy combines the search information of the global best particle and another two random particles. To test the performance of our algorithms, there are about ten well-known benchmark problems used in the experiments. Experimental results show that our approach obtains promising results and outperforms PSO. The rest paper is organized as follows. This paper presents an improved chaos immune genetic algorithm. The algorithm initializes initial population by using the chaos, and it has

the good solution on the beginning of iteration and reduces the diversity of population on the later period of iteration. Because the immune body density is introduced, when the density is lower than the threshold value, the partial antibodies which are produced by using the insect mouth equation can substitute the evolution population's partial antibodies, thus, the local optimization was avoided[2]. After the overlapping and mutation has ended, the algorithm sorts to adaptive value of the new population, and it locally optimizes the biggest adaptive value by using chaos theory, thus, it enhances the precision of the solution and improves the searching speed. When we respectively make the test by the unvaried multi-peak values and the multi-Vidor peak value function, we have the good effect.

Wireless sensor network consists of the joints of the cheap micro-sensors deployed in the monitoring area, which forms a multi-hop and self-organizing network by means of wireless communication[3]. The network is data-centered and task-based, in which the joints distinguish with each other by serial numbers. When customers inquire about events with access to the network, they can directly notice their events of interest to the network instead of noticing to some joint with definite serial number. General topology structure of wireless sensor networks mainly adopts cluster structure or tree structure with center existing. This article puts forward an intelligent lock design based on wireless sensor network for on-line computer five-anti-lock system based field bus and wireless sensor network. The intelligent lock can let the on-line mechanical handling sector lock and let electrical equipments such as breakers and electric knife gate valves lock by remote operation[4]. It also instantaneously collects equipment status and charged situations so that the five-anti mainframe can on-line track, check, and control the operation situations of the intelligent lock.

Software Design of Intelligent Lock

The wireless sensor modules adopt the independent single chips to control the FR chips, so under the terms of the agreement are met, the software designing mainly consider how to establish the physical link between the intelligent locks as well as between the intelligent locks and on-line computer keys. The wireless transmission of control data and the specific control and inspection operations of the intelligent locks are solved by the application layer software. The software framework of the intelligent locks is shown as Fig.1.

Firstly, the on-line computer key scans for empty information channels to try to establish a new network. Once some empty information channel is found, it will select a random personal area network and start to monitor the channel; now the network is established.

Afterwards, if another on-line computer key broadcasts frames in the same channel, the former on-line computer key will response and state its existence. Next, when the intelligent lock is on power, it will scan all of the available information channels to search for on-line computer key and try to join the network. The on-line computer key will decide whether to let the intelligent lock to join the local network through the value of the intelligent lock.

Once the intelligent lock joins some network, it will save the network information; when starting next time, it will rejoin the network automatically. After the success of joining the network, the intelligent will enter the resting state in order to save energy.

If some operation is to be conducted, the on-line computer key will keep the data frames in indirect-sending buffer until the intelligent lock inquires or is timeout. The intelligent lock will be waken-up periodically and send the inquiry request to the on-line computer key, which will search the indirect-sending buffer. If one frame is found to wait to send to the joint, the on-line computer key will send the frame and wait for confirmation.

Once the frame is confirmed, the on-line computer key will delete the frame from the indirect-sending buffer.

Algorithm flow chart is shown as Fig.2.

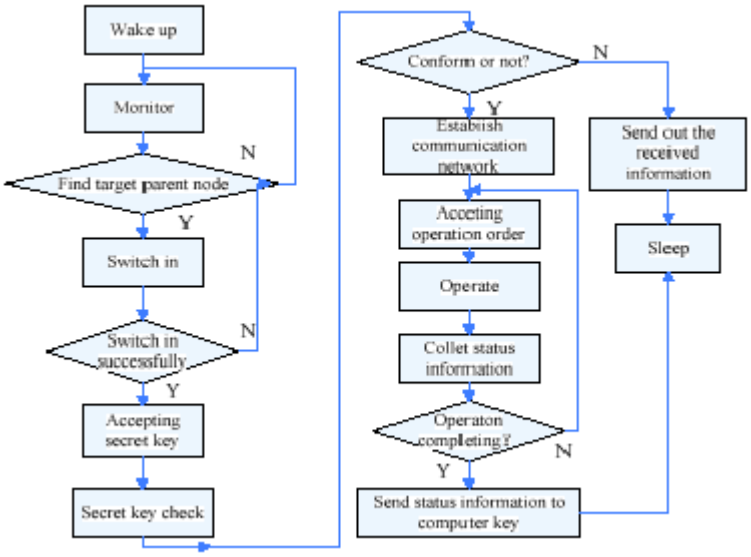

Fig.1 Wireless communication software structure diagram

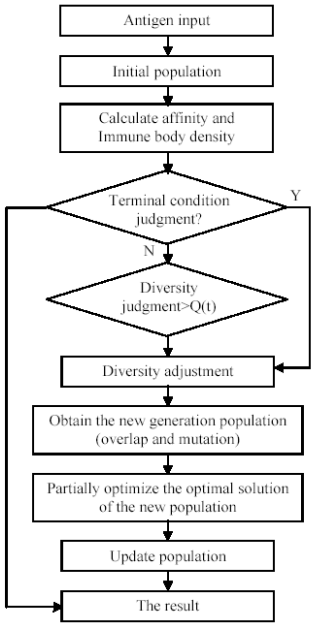

Fig.2 Algorithm flow chart

Simulation

Simulation results are shown as Fig.3.

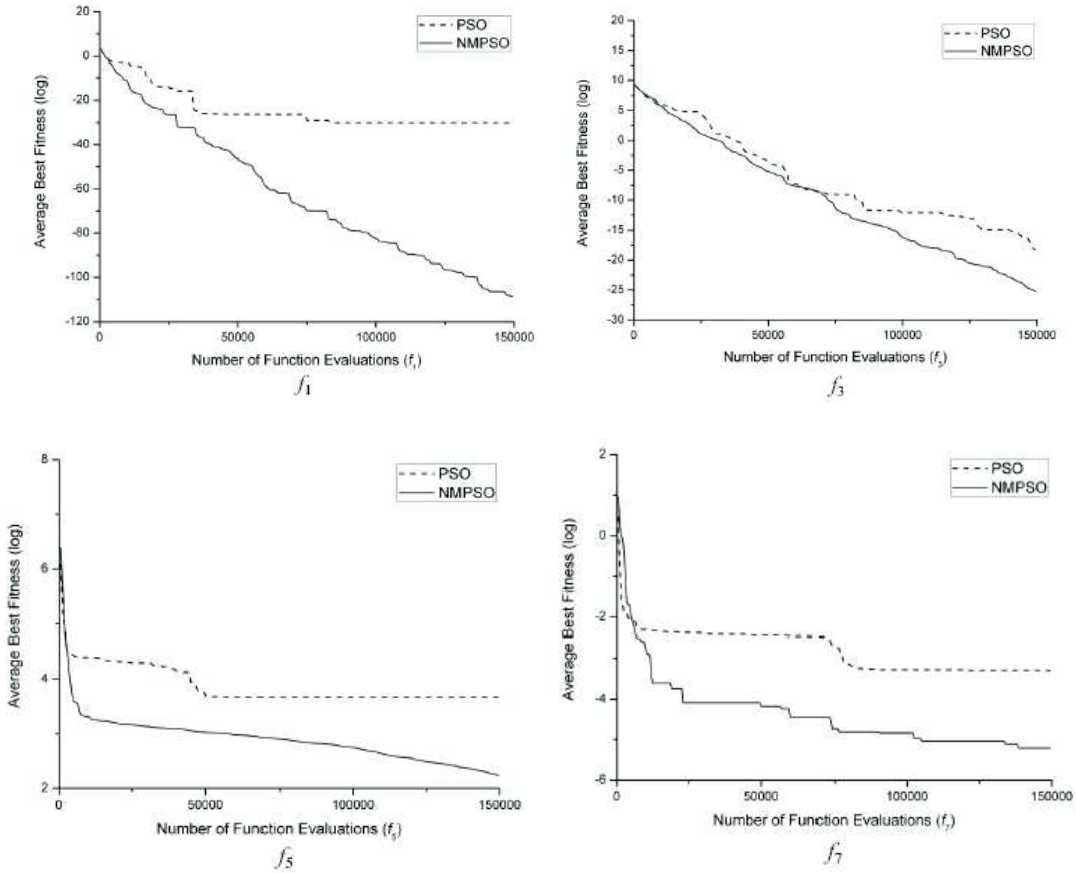

Fig.3 Evolutionary curves of standard PSO and NMPSO on four problems

Conclusion

This paper presents an improved PSO algorithm to enhance the performance of standard PSO. The proposed approach is called NMPSO, which embeds a novel mutation by incorporating with

the search information of the global best particle and other two random particles. It is to hope this improvement can help trapped particles jump to better positions. Simulation results on ten problems show that NMPSO not only achieves more accurate solutions than PSO, but also converges faster. However, NMPSO is not suitable for all kinds of problems, such as f5, f8 and f9, both PSO and NMPSO fail to solve these problems. To improve NMPSO further, we may introduce other search strategies. This will be investigated in our future work.

References

[1] Olfa Nasaroui, Fabio Gonzdez, Dipankar Dasgupta .The Fuzzv Artificial Immune Svstem: Motivations, basic Concepts and Application to Clustering and Web Profiling[J].Fuzzy Systerm 2002,1(2):711-716.

[2] LEANDRO N, CASTRO DE TIMMIS J Artificial immune system: a novel computational intelligence approach[M]. Springe–Verlag 2012.

[3] JIAO Li-cheng,WANG Lei. .A novel genetic algorithm based on immunity[J]. IEEE Trans on Systems May and Cybernetics-Part A: Systerms an Humans 2010 30 (5): 552 SGI.

[4] Xiangxin Wu, ZhongChen. Chaos Study Introductory remarks. Shanghai Science and technology Publishing house. 2012

[5] The-Hanh Pham, Liang Ying-Chang, A. Nallanathan and H. K. Garg. “Optimal training sequences for channel estimation in bidirectional relay networks with multiple antennas,” IEEE Transactions on Communications, vol. 58, no. 2, pp.474-479, 2010.

Advanced Materials Research Vols. 989-994 (2014) pp 2625-2628
© (2014) Trans Tech Publications, Switzerland
doi:10.4028/www.scientific.net/AMR.989-994.2625

The Research of Financial Risk Warning Model about Real estate enterprises in China

Xinran Tian [1,a], Haodong Jiang [2,b] and Junli Liu [3,c,*]

[1]College of International Business Shenyang Normal University Shenyang; Intelligent application research institute, Internet of Energy, North China Electric Power University, China.

[2]College of International Business Shenyang Normal University Shenyang; Intelligent application research institute, Internet of Energy, North China Electric Power University, China.

[3]School of Economics and Management North China Electric Power University Beijing, China.

[a]email: XinranTian123456@163.com, [b]email: HaodongJiang654321@163.com,

[c]email: ljunli1@163.com

Keywords: real estate enterprises, financial risk, early-warning models

Abstract. With the establishment of large-scale real estate enterprises, the competition is increasing among real estate enterprises, which requires real estate companies to enhance crisis prevention awareness. In the paper a combination of qualitative and quantitative method is used aiming at certain risks that real estate enterprises are facing with. The article introduces the capacity of external financing in time, Eva, cash flow, board size, the scale of supervisor board and other new indicators to establish a new system of early warning indicators. The article provides empirical study from the perspective of early warning system of real estate generation enterprise using comprehensive evaluation model. It is more accurate to predict financial risk for real estate enterprises based on the qualitative method with quantitative method.

Introduction

The financial risks really exist in all aspects of enterprise management, which is the fact that enterprise has to face in financial management. Thus, better prevention and mitigation of risk and carrying out financial risk warning in financial management is based on a full understanding of the enterprise financial risk's type causes and characteristics. As a capital intensive enterprise, the real estate industry is unique, so are the financial risks of real estate enterprise. The real estate is the country's basic capital-intensive industries; the huge up-front investment, long-term infrastructure construction, uncertainty of return on investment, and financial barriers of entering and exiting the real estate industry are all its features. The real estate is a special product which has its own characteristics, such as location fixity, and the project is a kind of special investment. It takes huge funds and long return period. Therefore, the financial management of real estate enterprise subjects to many factors.

Constructe the Assessment Index System

The article builds two - level indicators on the basis of the financial risk of real estate companies which is different with general corporate. The first-class index includes six aspects of the analysis: solvency, capital structure, profitability, operating capacity, the capacity of development, corporate governance. Of these financial solvency, capital structure and profitability are the bases for enterprise financial evaluation. Operating capacity reflects the asset management efficiency. Capacity for development is the important indicators of sustainable development of enterprises. The perfecting corporate governance structures plays an important role in the development of the growth of enterprises which is conducive to prevent risks and improve operational efficiency. In second-class index ,the paper introduce external financing capacity, Eva divided by the main business income, net

cash flow divided by net income, board size, the scale of supervisor board, etc. which response the operation more comprehensive and effective. The index system as shown in Table Ⅰ.

Empirical Study

In order to study the comprehensive evaluation model of financial risk early warning better, the article take a power generation company for an example. The key of establishing the early warning model of real estate generation enterprise with fuzzy theory is to set up factor gather and weight gather.

TABLE I. INDICATOR SYSTEM

first-class index	second-class index	first-class index	second-class index
Solvency	current ratio	Operating Capacity	accounts receivable turnover
	quick ratio		inventory turnover rate
	number of times interest earned		total assets turnover
	external financing capacity		current asset turnover
Capital Structure	debt asset ratio	Development Capability	main income growth rate
	equity ratio		net profit growth rate
			growth rate of total assets
Profitability	operation profit of entirety		growth rate of net assets
	return on equity		EPS growth
	return on total assets	Corporate Governance	board size
	Eva divided by the main business income		The scale of supervisor board

Establish evaluate factors

$A=\{A_1, A_2, A_3, A_4, A_5, A_6\}=\{$ solvency, capital structure, profitability, operating capacity, development capability, corporate governance $\}$

$A_1=\{ a_{11}, a_{12}, a_{13}, a_{14}\}=\{$ current ratio, quick ratio, number of times interest earned, external financing capacity $\}$

$A_2=\{ a_{21}, a_{22}\}=\{$ debt asset ratio, equity ratio $\}$

$A_3=\{ a_{31}, a_{32}, a_{33}, a_{34}\}=\{$ operation profit of entirety, return on equity, return on total assets, Eva divided by the main business income $\}$

$A_4=\{ a_{41}, a_{42}, a_{43}, a_{44}\}=\{$ accounts receivable turnover, inventory turnover rate, total assets turnover, current asset turnover $\}$

$A_5=\{ a_{51}, a_{52}, a_{53}, a_{54}, a_{55}\}=\{$ main income growth rate, net profit growth rate, growth rate of total assets, growth rate of net assets, EPS growth $\}$

$A_6=\{a_{61}, a_{62}\}=\{$ board size, the scale of supervisor board $\}$

Evaluation indexes

U={Very safe ,safe, in general, dangerous, very dangerous}.

Weight sets

The key step is to structure the judgment matrix in the research question by using the AHP. First, judge the importance of the indicator by the expert method, then a second, structure the judgment matrix. Third, Find the eigenvalues and eigenvectors of the fuzzy judgment matrix, fourth, feature vector for normalized, finally, finally you can find the weight of the various indicators. However, it is important to do the consistency check after structuring the judgment matrix. If the Consistency Ratio is less than 0.1, than we think the discriminant matrix in this method satisfy the complete consistency, and it needs not to do the consistency check. On the contrary, we should make adjustments to the judgment matrix. In the paper, six judgment matrixes are constructed and composing weighing for

aide layer is calculated. They are V， V_1， V_2， V_3， V_4， V_5， V_6. The judgment matrix of every indicator and weight of the factors can be calculated.

Establish the evaluation matrix

The paper uses the methods of experts' investigation to evaluate the single factor. First, determine membership of the second-class index of solvency. The evaluation matrix is as follow.

$$R_1=\begin{bmatrix}0.02 & 0.09 & 0.21 & 0.44 & 0.24\\ 0.04 & 0.11 & 0.19 & 0.48 & 0.18\\ 0.03 & 0.10 & 0.22 & 0.45 & 0.20\\ 0.03 & 0.11 & 0.22 & 0.46 & 0.18\end{bmatrix}$$

Synthetic Appraisal to the Ability of Paying off a Debt

$$M_1=W_1\times R=[0.0281 \quad 0.0991 \quad 0.2070 \quad 0.4546 \quad 0.2112]$$

Second, determine membership of the second-class index of capital structure. The evaluation matrix is as follow.

$$R_2=\begin{bmatrix}0.07 & 0.10 & 0.20 & 0.37 & 0.26\\ 0.05 & 0.12 & 0.22 & 0.38 & 0.23\end{bmatrix}$$

Synthetic Appraisal to the capital structure

$$M_2=W_2\times R_2=[0.0633 \quad 0.1067 \quad 0.2067 \quad 0.3733 \quad 0.2500]$$

Third, determine membership of the second-class index of profitability. The evaluation matrix is as follow.

$$R_3=\begin{bmatrix}0.03 & 0.07 & 0.20 & 0.40 & 0.30\\ 0.05 & 0.10 & 0.21 & 0.41 & 0.23\\ 0.05 & 0.11 & 0.19 & 0.45 & 0.20\\ 0.06 & 0.13 & 0.18 & 0.43 & 0.20\end{bmatrix}$$

Synthetic Appraisal to the Ability of Profitability

$$M_3=W_3\times R_3=[0.0407 \quad 0.0889 \quad 0.1995 \quad 0.4129 \quad 0.2581]$$

Forth, determine membership of the second-class index of operating capacity. The evaluation matrix is as follow.

$$R_4=\begin{bmatrix}0.04 & 0.11 & 0.17 & 0.37 & 0.31\\ 0.05 & 0.11 & 0.21 & 0.36 & 0.27\\ 0.04 & 0.10 & 0.22 & 0.40 & 0.24\\ 0.05 & 0.11 & 0.20 & 0.40 & 0.24\end{bmatrix}$$

Synthetic Appraisal to the operating capacity

$$M_4=W_4\times R_4=[0.0435 \quad 0.1083 \quad 0.1916 \quad 0.3747 \quad 0.2819]$$

Five, determine membership of the second-class index of development capability. The evaluation matrix is as follow.

$$R_5=\begin{bmatrix}0.04 & 0.12 & 0.19 & 0.40 & 0.25\\ 0.04 & 0.18 & 0.20 & 0.33 & 0.25\\ 0.03 & 0.15 & 0.20 & 0.39 & 0.23\\ 0.05 & 0.17 & 0.21 & 0.35 & 0.22\\ 0.03 & 0.16 & 0.22 & 0.36 & 0.23\end{bmatrix}$$

Synthetic Appraisal to the Ability of Development

$$M_5=W_5\times R_5=[0.0391 \quad 0.1474 \quad 0.1973 \quad 0.3724 \quad 0.2438]$$

Six, determine membership of the second-class index of corporate governance. The evaluation matrix is as follow.

$$R_6=\begin{bmatrix}0.09 & 0.13 & 0.18 & 0.36 & 0.24\\ 0.07 & 0.13 & 0.14 & 0.39 & 0.27\end{bmatrix}$$

Synthetic Appraisal to the corporate governance

$$M_6=W_6\times R_6=[0.0850 \quad 0.1300 \quad 0.1700 \quad 0.3675 \quad 0.2475]$$

Finally, we can have the result of fuzzy comprehensive evaluation of real estate generation enterprise's financial risk.

$$R = \begin{bmatrix} 0.0281 & 0.0991 & 0.2070 & 0.4546 & 0.2112 \\ 0.0633 & 0.1067 & 0.2067 & 0.3733 & 0.2500 \\ 0.0407 & 0.0889 & 0.1995 & 0.4129 & 0.2581 \\ 0.0435 & 0.1083 & 0.1916 & 0.3747 & 0.2819 \\ 0.0391 & 0.1474 & 0.1973 & 0.3724 & 0.2438 \\ 0.0850 & 0.1300 & 0.1700 & 0.3675 & 0.2475 \end{bmatrix}$$

$$M = W \times R = [0.0441 \quad 0.1044 \quad 0.2021 \quad 0.4092 \quad 0.2403]$$

We can know from the result that final values of comprehensive evaluation are all positive values. And the value of the dangerous index is 0.4092 which is obviously the largest one. And the very dangerous index is 0.2403 which follows behind. Thus it can be seen this real estate generation enterprise runs very difficult and feels financial pressure. The company should take measures immediately which are important for the enterprises long-term development in order to reduce the financial risks.

Acknowledgement

It provides empirical study from the perspective of early warning system of real estate generation enterprise using comprehensive evaluation model. Then, considering the characteristics of real estate generation enterprise in our country, the financial risk forewarning index system is constructed. The article introduces the capacity of external financing in time, Eva, cash flow, board size, the scale of supervisor board and other new indicators. The paper shows how to perform the qualitative and quantitative analysis for the financial early-warning models. The example showing in the paper indicates that the real estate generation enterprise feels financial pressure. The company should strengthen management and improve the enterprise's financial information system. An effective way to guard against risk is to establish a financial early warning system and build healthy financial early warning institutions.

References

[1] P. C. Pendharkar. A Threshold Varying Artificial Neural Network Approach for Classification and Its Application to Bankruptcy Prediction Problem.Computers & Operations Research.2005, 32, pp: 2561-2582.

[2] K. JooOh, T.Y. Kim, C. Kim. An early warning system for detection of financialcrisis using financial market volatility. Expert Systems. May 2006. (23)2, pp: 83-96

[3] Zhao Shiqiang. Multi-level fuzzy comprehensive evaluation of real estate risk. JOURNAL OF AGRICULTURAL UNIVERSITY OF HEBEI. 1996. 01.

[4] Zhang Mingzhu. Risk management analysis of real estate project development. Tianjing University. 2004.

[5] JIN Chang_hong,WANG Miao and ZHOU Zhi-hu. Study on real estate development risk. Optimization of Capital Construction. 2003. 03.

Advanced Materials Research Vols. 989-994 (2014) pp 2629-2633
© (2014) Trans Tech Publications, Switzerland
doi:10.4028/www.scientific.net/AMR.989-994.2629

Prediction model of aerosol fire extinguishing agent performance based on combination of genetic algorithm and back-propagation neural network

Zhijie CHEN[1, a], Chenguang ZHU[1, b], Zihao ZHANG[2]

[1] School of Chemical Engineering, Nanjing University of Science & Technology, Nanjing, Jiangsu 210094,China

[2] Science & Technology on Electro-optical Information Security Control Laboratory, Sanhe, 065201, China

[a]email: zhijiechen1201@sina.com, [b]email:zhuchenguang_67@sohu.com

Keywords: Aerosol fire extinguishing agent; BP neural network; Genetic algorithms

Abstract. The aerosol fire extinguishing agent is a complex pyrotechnic composition, and the extinguishing efficiency need a series of experiments to identify. A method is put forward out based on combining back-propagation neural network and genetic algorithm (BP-GA) in this paper, and then the performance of aerosol fire extinguishing agent can be predicted in advance by the formulation. In the method, back-propagation (BP) algorithm was proposed to map the complex relationship between additive components and quality indexes of formulation. The genetic algorithm was employed to optimize the BP neural network weight and threshold. The results showed that the prediction display a satisfied consistence with the test and the error is less than 5%, and also indicated that the combining BP-GA method was an effective tool to predict the performance of aerosol fire extinguishing agent by the formulation designed.

Introduction

The pyrotechnic aerosol fire extinguishing agent (PAFEA) is a replacement to Halon [1] for its efficiency, economic and green. Due to the lack of various PAFEA combustion models, so it is necessary to through a great many of the experiments to get an ideal formulation. The conventional way is the oxygen balance analysis, the result is imprecise, the experiment is numerous and the scope is narrow.

Artificial Neural Network (ANN) model [2] have adaptive learning ability and memory capacity, it is proposed to solve complex nonlinear problems, its predict ability is better than multiple regression analysis and discriminant analysis. Among ANN models, the back-propagation (BP) neural network is the most well-known one. It has the advantage of simplicity and plasticity. However, it has some disadvantages. The algorithm is not guaranteed to find the global minimum of error space and the convergence tends to be extremely slow. In addition, the selection of the learning factor and momentum factor, which is usually determined by experience, also affects the convergence of the BP neural network. Genetic Algorithm (GA) is considered to be a heuristic and stochastic optimization technique based on evolution theory and genetic principles. The algorithm have some advantages that simple, universal, strong robustness and suitable for parallel processing. It has been widely used in computer science, optimal scheduling, transportation, combinatorial optimization problems and so on [3]-[6].

The method is proposed to improve the prediction of combustion performance by optimizing the network scenarios through coupling a back-propagation (BP) neural network with a genetic algorithm (GA). As two important performance parameters, the time ratio is that the extinguishing time divides by its combustion time, and burning residual ratio is that the mass of burning residual divided by the total mass of aerosol fire extinguishing agent. In this study, the time ratio and the burning residual ratio which are outputs are used in the method to predict results.

Model Building

This operation flowchart is shown in Figure 1. GA-BP network can be divided into three parts: the structure of the BP neural network, genetic algorithm to optimize and the prediction of BP neural network. According to the number of fitting function input and output parameters, BP neural network structure can be determined, and then the length of the genetic algorithm individual can be determined. Genetic algorithm optimization use genetic algorithm to optimize the BP neural network weight and threshold, the population of each individual contains a network all weight and threshold value. Genetic algorithm can find optimal fitness corresponding to the individual by selection, crossover and mutation operation. The initial weight and threshold value can be assigned by the best individual that though using genetic algorithm. After the network training, it can output prediction function. Genetic algorithm to optimize the BP neural network includes the population initialization, fitness function, selection, crossover operation and mutation operation.

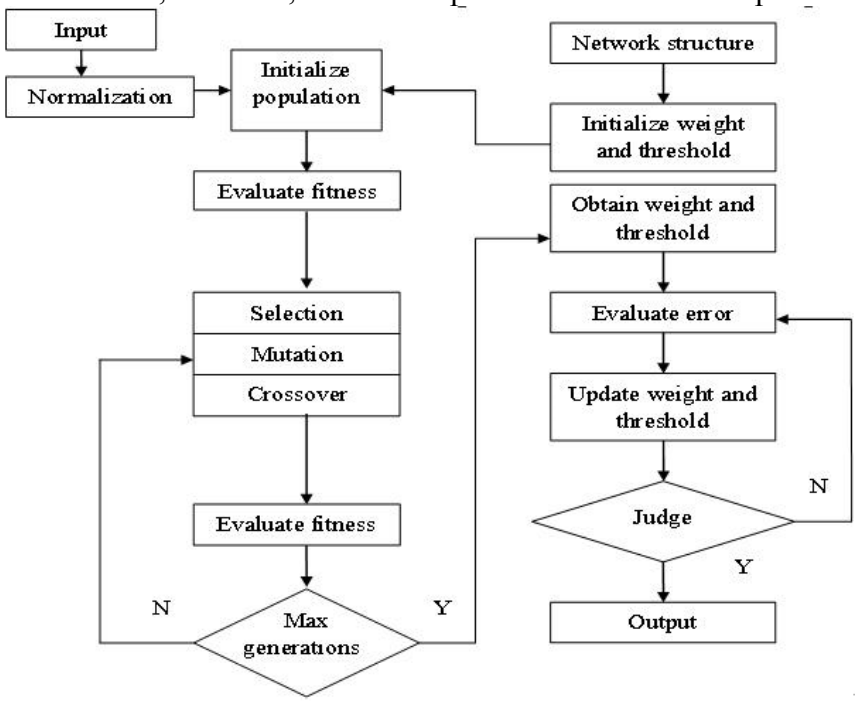

Figure1 Algorithm process

Model application

Pyrotechnic extinguishing agents consisted of oxidant, combustible and additives. The basic pyrotechnic formulation composed by potassium nitration (15%), strontium nitration (45%), lactose (10%-20%), phenolic resin (5%) and other functional additives. The purpose of this article is mainly for performance prediction of the formulation with different additives. Additive effect is to improve the efficiency of fire extinguishing, stable combustion performance and reduce the residual ratio. By using the method of orthogonal experiments design formulation, the selected orthogonal table $L_{25}(5^6)$ is shown in table 1.

Tab.1 Factors and Levels

Factors / Levels	Charcoal A%	Magnesium B%	Magnesium carbonate C%	Potassium hydrogen phthalate D%	Graphite E%	Ferrocee F%
1	0	0	0	2	0	0
2	1	0.4	1	3	0.2	0.5
3	2	0.6	2	4	0.4	1
4	3	0.8	3	5	0.8	1.5
5	4	1	4	6	1.6	2

According to the above methods, we designed 25 set of formulation and used the first 20 sets of data in table 2 for training, then forecasted 5 sets of data. The corresponding result is shown in table 3. The combustion performance of formulation was tested in a transparent acrylic box. The 1m3 acrylic box has a dimension of is 1m×1m×1m and has a side door. Inside the box, n-heptane was filled in an uncapped iron container (7cm diameter, 15cm depth) as the source of fire. The mixture (100g) in the burner is igniting by a fuse. The extinguishing time was determined from the recordings of the high speed camera. The residual mass is determined from the mass loss of the burner after burning. Experiment is shown below.

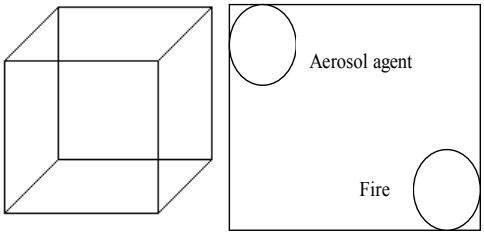

Fig.2 Homemade fire box

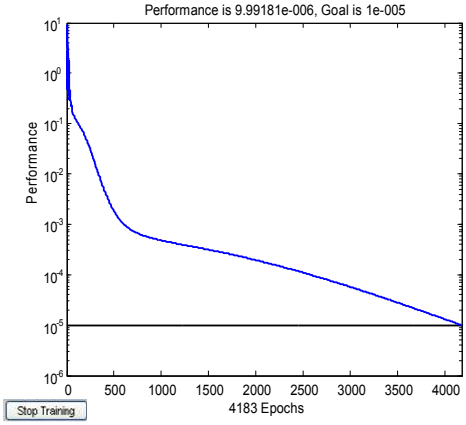

Fig.3 Curve of training error

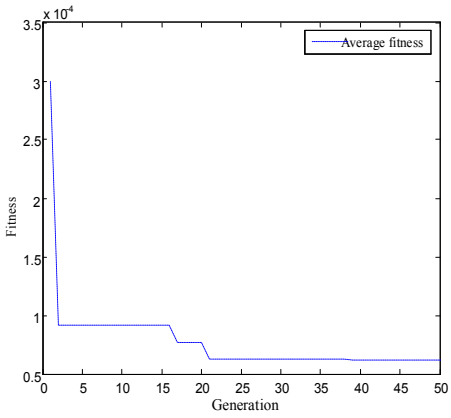

Fig.4 Value of best individual fitness

Tab.2 Formulation design

No.	A%	B%	C%	D%	E%	F%	The time ratio	The residual ratio
1	0	0	0	2	0	0	0.59	0.52
2	0	0.4	1	3	0.2	0.5	0.64	0.60
3	0	0.6	2	4	0.4	1	0.81	0.45
4	0	0.8	3	5	0.8	1.5	0.60	0.55
5	1	0.4	2	5	0	2	0.62	0.51
6	1	0.6	3	6	0.2	0	0.73	0.49
7	1	0.8	4	2	0.4	0.5	0.70	0.40
8	1	1	0	3	0.8	1	0.57	0.44
9	2	0.6	4	3	0	1.5	0.54	0.54
10	2	0.8	0	4	0.2	2	0.61	0.63
11	2	1	1	5	0.4	0	0.70	0.57
12	2	0.4	3	2	1.6	1	0.55	0.50
13	3	0.8	1	6	0	1	0.60	0.49
14	3	1	2	2	0.2	1.5	0.75	0.41
15	3	0.4	4	4	0.8	0	0.58	0.51
16	3	0.6	0	5	1.6	1	0.83	0.56

17	4	1	3	4	0	0.5	0.92	0.62
18	4	0	4	5	0.2	1	0.81	0.53
19	4	0.4	0	6	0.4	1.5	0.73	0.46
20	4	0.8	2	3	1.6	0	0.77	0.48
21	0	1	4	6	1.6	2	0.56	0.44
22	1	0	1	4	1.6	1.5	0.59	0.50
23	2	0	2	6	0.8	0.5	0.64	0.51
24	3	0	3	3	0.4	2	0.63	0.56
25	4	0.6	1	2	0.8	2	0.84	0.47

Table 2 shows the results of the twenty-five tests. The time ratio is defined as the extinguishing time divided by its combustion time. It can quickly measure the combustion stability of the fire extinguishing agent and the fire extinguishing efficiency. It also provides a simple and effective method to characterize performance formulation.

The there-layered GA-BP network used in this work has 6-15-2 structure, which consists of one input layer, one hidden layer and one output layer. The number of neurons in the input layer is six and there are two neurons in the output layer. The number of neurons in the hidden layer is fifteen. Figure3 presents the network model of training sample simulation result meeting the requirement of target error (0.00001) after 4183 step training. Moreover, in Figure3, it can be clearly seen that the results of network training is better. Figure 4 shows the best individual fitness value around 22 generation, the optimal initial weight and threshold value is assigned to neural network, and predict nonlinear function output after training with the training data. The prediction error is shown below.

Tab.3 Predicts of BP and GA-BP model

No.	The time ratio			The residual ratio		
	experimental value	BP	GA-BP	experimental value	BP	GA-BP
21	0.56	0.61	0.55	0.44	0.49	0.42
22	0.59	0.65	0.57	0.50	0.44	0.49
23	0.64	0.58	0.66	0.51	0.58	0.50
24	0.63	0.56	0.62	0.56	0.62	0.58
25	0.84	0.92	0.86	0.47	0.45	0.48

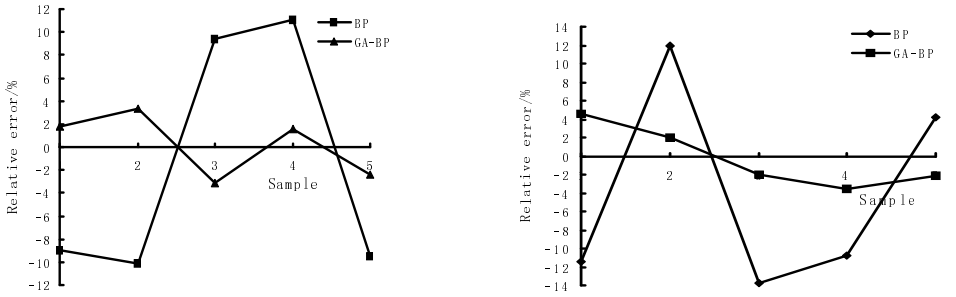

(a) The time ratio (b) The residual ratio

Fig.5 GA-BP and BP error contrast

Table 3 presents that the predicted results of GA-BP network and BP network are compared, it can be obviously found that the GA-BP network more close to the measured values. Figure 5 is the relative error curve of BP with GA-BP; it shows the residual ratio of the average relative error of the absolute value is 2.48% and the time ratio is 2.45%, both are less than 5%. But pure BP network to calculate the average relative error of the absolute value is 10.41% and 9.82%, respectively. In Figure 5, it can be obviously seen that the calculation precision of GA - BP network is higher than pure BP network, and the relative error of GA-BP curve is smooth, less volatile, has good stability,

but also reflects the simple BP network easy to fall into local minimum, and GA-BP network is a good solution.

Conclusion

The formulation of aerosol fire extinguishing agent were used as the input variable of GA-BP network, the time ratio and the burning residual ratio were as output variable. The results showed that the error was able to be less than 5% by using this method. The proposed model combining genetic algorithm (GA) and back-propagation (BP) algorithm has been shown as an actual method to map the complex relationship between process conditions.

The research shows that the model could replace the oxygen balance analysis, and performance simulation model could greatly reduce the amount of experiments and save cost. In spite of only 25 groups of training samples in the model, the data quantity is less, but a comparatively successful outcome else has been obtained. The modeling and optimization methods proposed in this article showed the great potential in complicated industrial applications.

Acknowledgement

In this paper, the research was sponsored by the Nature Science Foundation of China (Project No. 51076066) and Science and Technology on Electro-optical Information Security Control Laboratory of China (Project No. 9140C150308130C1570).

References：

[1] Guo hong-bao, Yue da-ke. Aerosol fire extinguishing technology [M]. Beijing, Chemical Industry Press, 2005, 4.

[2] Li min-qiang. The basic theory and application of genetic algorithm [M]. Beijing, Science Press, 2002.

[3] O P Korobeinichev, A. G. Shmakov. Fire suppression by low-volatile chemically active fire suppressants using aerosol technology [J]. Fire Safety Journal, 2012, 51, 102–109.

[4] Venkatesan D, Kannan K, Saravanan R. A genetic algorithm-based artificial neural network model for the optimization of machining processes[J]. Neural Computing and Applications 2008, 18(2):135-140.

[5] Ehsani M. R, Bateni H, Parchikolaei G R. Modeling the oxidative coupling of methane using artificial neural network and optimizing of its operational conditions using genetic algorithm[J]. Korean Journal of Chemical Engineering 2012,29 (7):855-861.

[6] Gurunathan B, Sahadevan R. Design of experiments and artificial neural network linked genetic algorithm for modeling and optimization of L-asparaginase production by Aspergillus terreus MTCC 1782 [J]. Biotechnology and Bioprocess Engineering 2011, 16 (1):50-58.

Advanced Materials Research Vols. 989-994 (2014) pp 2634-2638
© (2014) Trans Tech Publications, Switzerland
doi:10.4028/www.scientific.net/AMR.989-994.2634

Construction of One-Lee Weight Codes over $F_p + vF_p + v^2F_p$

Lou Chen[1,a], Minjia Shi[1,b]

[1]School of Mathematical Sciences, Hefei, 230601, China

[a]1520416296@qq.com

[b]smjwcl.good@163.com

Keywords: Gray map; Linear codes; One-Lee weight codes; Generator matrix.

Abstract. This paper is devoted to the study of the algebraic structure of one-Lee weight codes over $R_p = F_p + vF_p + v^2F_p$. We first give some necessary conditions for a code to be a one-Lee weight code over R_p. Moreover, we present the method of the construction of one-Lee weight codes over R_p. An example is given to illustrate the results.

Introduction

In coding theory, constant-weight (one-weight) codes form an important class of codes which have been extensively studied [1-4]. Cyclic codes and MacWilliams indentities were studied over R_p in [5-6]. Motivated by the work listed above, we intend to discuss one-Lee weight codes over R_p. This work is organized as follows. In Section 2, we recall some backgrounds and notations about linear codes over R_p. In Section 3, we construct one-Lee weight codes over R_p. An example is given to illustrate the results.

Preliminaries

We first recall some basic knowledge of [5] and [6]. Let R_p be the commutative ring $R_p = F_p + vF_p + v^2F_p$ with characteristic p, where $v^3 = v$. The elements of $x \in R_p$ may be written as $x = a + bv + cv^2, a, b, c \in F_p$. Any R_p-linear code C containing some nonzero codewords is permutation-equivalent to a R_p-linear code with a generator matrix of the form

$$\boldsymbol{G}=\begin{pmatrix}
\boldsymbol{I}_{k_1} & \boldsymbol{A} & \boldsymbol{B}_1+v\boldsymbol{B}_2 & \boldsymbol{C}_1+v\boldsymbol{C}_2 & \boldsymbol{D}_1+v\boldsymbol{D}_2 & \boldsymbol{E}_1+v\boldsymbol{E}_2 & \boldsymbol{F}_1+v\boldsymbol{F}_2 & \boldsymbol{G}_1 \\
\boldsymbol{0} & v\boldsymbol{I}_{k_2} & \boldsymbol{0} & \boldsymbol{0} & (v-1)\boldsymbol{D}_3+(v+1)\boldsymbol{D}_4 & v\boldsymbol{E}_3+(v-1)\boldsymbol{E}_4+(v+1)\boldsymbol{E}_5 & v\boldsymbol{F}_3+(v-1)\boldsymbol{F}_4+(v+1)\boldsymbol{F}_5 & \boldsymbol{G}_2 \\
\boldsymbol{0} & \boldsymbol{0} & (v-1)\boldsymbol{I}_{k_3} & \boldsymbol{0} & (v-1)\boldsymbol{D}_5+(v+1)\boldsymbol{D}_6 & (v-1)\boldsymbol{E}_6+(v+1)\boldsymbol{E}_7 & (v-1)\boldsymbol{F}_6+(v+1)\boldsymbol{F}_7 & \boldsymbol{G}_3 \\
\boldsymbol{0} & \boldsymbol{0} & \boldsymbol{0} & (v+1)\boldsymbol{I}_{k_4} & (v+1)\boldsymbol{D}_7 & (v+1)\boldsymbol{E}_8 & (v+1)\boldsymbol{F}_8 & \boldsymbol{G}_4 \\
\boldsymbol{0} & \boldsymbol{0} & \boldsymbol{0} & \boldsymbol{0} & (v^2-1)\boldsymbol{I}_{k_5} & \boldsymbol{0} & \boldsymbol{0} & \boldsymbol{G}_5 \\
\boldsymbol{0} & \boldsymbol{0} & \boldsymbol{0} & \boldsymbol{0} & \boldsymbol{0} & (v+v^2)\boldsymbol{I}_{k_6} & \boldsymbol{0} & \boldsymbol{G}_6 \\
\boldsymbol{0} & \boldsymbol{0} & \boldsymbol{0} & \boldsymbol{0} & \boldsymbol{0} & \boldsymbol{0} & (v^2-v)\boldsymbol{I}_{k_7} & \boldsymbol{G}_7
\end{pmatrix},$$

where $\mathbf{G}_1 = \mathbf{G}_{11} + v\mathbf{G}_{12} + v^2\mathbf{G}_{13}, \mathbf{G}_2 = v\mathbf{G}_{21} + (v-1)\mathbf{G}_{22} + (v+1)\mathbf{G}_{23} + (v^2-1)\mathbf{G}_{24} + (v^2+v)\mathbf{G}_{25} + (v^2-v)\mathbf{G}_{26}, \mathbf{G}_3 = (v-1)\mathbf{G}_{31} + (v+1)\mathbf{G}_{32} + (v^2-1)\mathbf{G}_{33} + (v^2+v)\mathbf{G}_{34} + (v^2-v)\mathbf{G}_{35}, \mathbf{G}_4 = (v+1)\mathbf{G}_{41} + (v^2-1)\mathbf{G}_{42} + (v^2+v)\mathbf{G}_{43} + (v^2-v)\mathbf{G}_{44}, \mathbf{G}_5 = (v^2-1)\mathbf{G}_{51} + (v^2+v)\mathbf{G}_{52} + (v^2-v)\mathbf{G}_{53}, \mathbf{G}_6 = (v^2+v)\mathbf{G}_{61} + (v^2-v)\mathbf{G}_{62}, \mathbf{G}_7 = (v^2-v)\mathbf{G}_{71}, \mathbf{A}, \mathbf{B}_1, \mathbf{B}_2, \mathbf{C}_1, \mathbf{C}_2, \mathbf{D}_1 \sim \mathbf{D}_7, \mathbf{E}_1 \sim \mathbf{E}_8, \mathbf{F}_1 \sim \mathbf{F}_8, \mathbf{G}_{ij} (1 \le i \le 7, 1 \le j \le 6)$ are F_p-matrices, $\boldsymbol{I}_{k_i}$ are $k_i \times k_i$ identity matrices, C contains $p^{3k_1+2k_2+2k_3+2k_4+k_5+k_6}$ codewords.

Definition 2.1 The Gray map ϕ from R_p^n to F_p^{3n} is defined as $\phi(a+bv+cv^2)=(a,a+c,b)$ for $\forall a,b,c\in F_p^n$.

Definition 2.2 We divide the elements of R_p into D_i, $(i=0,1,2,3)$: $D_0=\{0\}$, $D_1=\{bv\,|\,b\in F_p^*\}\cup\{cv^2\,|\,c\in F_p^*\}\cup\{c-cv^2\,|\,c\in F_p^*\}$, $D_2=\{bv+cv^2\,|\,b,c\in F_p^*\}\cup\{a\,|\,a\in F_p^*\}\cup\{a+cv^2\,|\,a,c\in F_p^*,a+c\neq 0(\mathrm{mod}\,p)\}\cup\{a+bv-av^2\,|\,a,b\in F_p^*\}$, $D_3=\{a+bv\,|\,a,b\in F_p^*\}\cup\{a+bv+cv^2\,|\,a,b,c\in F_p^*,a+c\neq 0\,(\mathrm{mod}\,p)\}$

Definition 2.3 The Lee weight of $r\in R_p$ is defined as $w_L(r)=i,r\in D_i$, and the Lee weight of a codeword $c=(c_0,c_1,\cdots,c_{n-1})\in R_p^n$ is defined as $w_L(c)=\sum_{i=0}^{n-1}w_L(c_i)$.

One-Lee weight codes over R_p

In this subsection, we concentrate our study on one-Lee weight codes over R_p. We first give some necessary conditions for a linear code to be a one-Lee weight linear code over R_p.

Theorem 3.1 Suppose C is a one-Lee weight code of length n over R_p with generator matrix $\boldsymbol{G}$ with unique nonzero weight w_0, for $\forall c=(c_0,c_1,\cdots,c_{n-1})\in C$, set $n_x=|\{c_i\,|\,c_i=x,i=0,1,\cdots,n-1,x\in R_p\}|$, then we have the following two assertions:
(i) $n_{c-cv^2}=n_a=n_{a+cv^2}=n_{a+bv-av^2}=n_{a+bv}=n_{a+bv+cv^2}=0$ and $n_{bv}+n_{cv^2}+2n_{bv+cv^2}=w_0$; (ii) $n_{bv}=n_{cv^2}=n_{bv+cv^2}=n_a=n_{a+cv^2}=n_{a+bv-av^2}=n_{a+bv}=n_{a+bv+cv^2}=0$ and $n_{c-cv^2}=w_0$, where the meanings of a,b and c are identical with those of Definition 2.2.

Proof: Suppose C is a one-Lee weight code of length n over R_p with unique nonzero weight w_0, namely, for $\forall c\in C$, $w_L(c)=w_0$, according to Definition 2.3 , then we have :

$$w_L(c)=n_{bv}+n_{cv^2}+n_{c-cv^2}+2n_{bv+cv^2}+2n_a+2n_{a+cv^2}+2n_{a+bv-av^2}+3n_{a+bv}+3n_{a+bv+cv^2}=w_0,$$

$$w_L(bvc)=n_{bv}+n_{cv^2}+2n_{bv+cv^2}+n_a+n_{a+cv^2}+n_{a+bv-av^2}+2n_{a+bv}+2n_{a+bv+cv^2}=w_0\ or\ 0,$$

then $w_L(c)-w_L(bvc)=n_{c-cv^2}+n_a+n_{a+cv^2}+n_{a+bv-av^2}+n_{a+bv}+n_{a+bv+cv^2}=w_0\ or\ 0$, if $w_L(bvc)=w_0$, then $w_L(c)-w_L(bvc)=0$, which means (i); if $w_L(bvc)=0$, then $w_L(c)-w_L(bvc)=w_0$, which implies (ii).

Corollary 3.2 Suppose C is a one-Lee weight code of length n over R_p with generator matrix $\boldsymbol{G}$, then there isn't one-Lee weight code over R_p if $k_i,i=1,2,3,4,5,6,7$ satisfy the following five conditions: (i) $k_1>0,k_2,k_3,k_4,k_5,k_6,k_7\in N$; (ii) $k_3>0,k_1,k_2,k_4,k_5,k_6,k_7\in N$; (iii) $k_4>0,k_1,k_2,k_3,k_5,k_6,k_7\in N$; (iv) $k_5>0,k_1,k_2,k_3,k_4,k_6,k_7\in N$; (v) $k_7>0,k_1,k_2,k_3,k_4,k_5,k_6\in N$.

Lemma 3.3 For $\forall k\in\mathbb{Z}^+$, let N be the number of $(a_1,a_2,\cdots,a_k)$ which satisfy $\sum_{i=1}^{k}a_i\equiv av+av^2\ (\mathrm{mod}\ p),a\in F_p^*$, where $a_i\in\{av+av^2\,|\,a\in F_p\}$, then $N=p^{k-1}(p-1)$.

Proof : When $k=2$, clearly, $N=p(p-1)$, the result is valid. Assume the result is valid when $k=l$, namely, $N=p^{l-1}(p-1)$. If $k=l+1$, the number of $(a_1,a_2,\cdots,a_k)$ which satisfy $\sum_{i=1}^{l+1}a_i \equiv av+av^2 \pmod p$ is $p^{l+1}-p^{l-1}(p-1)-[p^l-p^{l-1}(p-1)]=p^l(p-1)$, where $a\in F_p^*$, $a_i\in\{av+av^2 \mid a\in F_p\}$, then the result follows by induction hypothesis.

Lemma 3.4 Let C be a linear code over R_p with type $p^{2k_2}p^{k_6}$ of length n. If $k_2=1$ and the columns of the generator matrix $G_{(k_6+1)\times n}$ are all distinct nonzero vectors $(c_0,c_1,\cdots,c_{k_6})^{\mathrm{T}}$, where $c_0\in\{av\mid a\in F_p\}\bigcup\{av^2\mid a\in F_p\}\bigcup\{av+bv^2\mid a,b\in F_p^*\}$, $c_i\in\{av+av^2\mid a\in F_p\}$, $i=1,2,\cdots,k_6$, then C is a one-Lee weight code of length $n=p^{k_6+2}-1$ with $w_0=2p^{k_6+1}(p-1)$.

Proof : Since the columns of the generator matrix are all distinct nonzero vectors, it follows that $n=p^{k_6+2}-1$. Let $r_0,r_1,\cdots,r_{k_6}$ be the rows of generator matrix G_{1,k_6}, where

$$r_0=(\underbrace{0,\cdots,0}_{p^{k_6}-1},\underbrace{v,\cdots,v}_{p^{k_6}},\underbrace{2v,\cdots,2v}_{p^{k_6}},\cdots,\underbrace{(p-1)v,\cdots,(p-1)v}_{p^{k_6}},\underbrace{v^2,\cdots,v^2}_{p^{k_6}},\underbrace{2v^2,\cdots,2v^2}_{p^{k_6}},\cdots,\underbrace{(p-1)v^2,\cdots,(p-1)v^2}_{p^{k_6}},$$
$$\underbrace{v+v^2,\cdots,v+v^2}_{p^{k_6}},\underbrace{v+2v^2,\cdots,v+2v^2}_{p^{k_6}},\cdots,\underbrace{(p-1)v+(p-1)v^2,\cdots,(p-1)v+(p-1)v^2}_{p^{k_6}}).$$

First we prove that $w_L(p_1r_1+p_2r_2+\cdots+p_{k_6}r_{k_6})=p^{k_6+2}$ for $\forall\, p_i\in F_p, 1\le i\le k_6$. Suppose $p_1=p_2=\cdots=p_k=1$, $p_{k+1}=p_{k+2}=\cdots=p_{k_6}=0$, $1\le k\le k_6$, by the form of r_0, set

$$\sum_{i=1}^{k}r_i=(\underbrace{r_{1,1},\cdots r_{1,p^{k_6}-1}}_{},\underbrace{r_{2,1},\cdots r_{2,p^{k_6}}}_{},\cdots\underbrace{r_{p^2,1},\cdots r_{p^2,p^{k_6}}}_{}).$$

By Lemma 3.3, for $\forall c_0\in\{av\mid a\in F_p\}\bigcup\{av^2\mid a\in F_p\}\bigcup\{av+bv^2\mid a,b\in F_p^*\}$, the number of vectors $(c_0,c_1,\cdots,c_{k_6})^{\mathrm{T}}$ such that $\sum_{i=1}^{k}c_i\equiv av+av^2 \pmod p$ is $p^{k_6-1}(p-1)$, where $a\in F_p^*$, namely, the number of $av+av^2$ in each section of r_0 is $p^{k_6-1}(p-1)$. Hence $w_L(\sum_{i=1}^{k}r_i)=p^2\times 2\times p^{k_6-1}(p-1)=2p^{k_6+1}(p-1)$, then $w_L(p_1r_1+p_2r_2+\cdots+p_{k_6}r_{k_6})=2p^{k_6+1}(p-1)$. Moreover, it is easy to see that $w_L(p_0r_0+p_1r_1+\cdots+p_{k_6}r_{k_6})=2p^{k_6+1}(p-1)$ for $\forall p_0\in\{av\mid a\in F_p\}\bigcup\{av^2\mid a\in F_p\}\bigcup\{av+bv^2\mid a,b\in F_p^*\}$, $p_i\in F_p$, $1\le i\le k_6$. Hence C is a one-Lee weight code with $w_0=2p^{k_6+1}(p-1)$.

Theorem 3.5 Let C be a linear code over R_p with type $p^{2k_2}p^{k_6}$ of length n. If the columns of the generator matrix $G_{(k_2+k_6)\times n}$ are all distinct nonzero vectors $(c_1,c_2,\cdots c_{k_2},c_{k_2+1},\cdots,c_{k_2+k_6})^{\mathrm{T}}$, where $c_i\in\{av\mid a\in F_p\}\bigcup\{av^2\mid a\in F_p\}\bigcup\{av+bv^2\mid a,b\in F_p^*\}, i=1,2,\cdots,k_2; c_j\in\{av+av^2\mid a\in F_p\}$, $j=k_2+1,\cdots,k_2+k_6$, then C is a one-Lee weight code with $w_0=2(p-1)p^{2k_2+k_6-1}$ and $n=p^{2k_2+k_6}-1$.

Proof: If $k_2=1$, the result follows from Lemma 3.4. Assume the result is valid for $\forall\, k_2=m$, we denote the generator matrix and the nonzero weight by G_{m,k_6} and $w_1=2(p-1)p^{2m+k_6-1}$, respectively, then for $k_2=m+1$, the generator matrix G_{m+1,k_6} of C is

$$\begin{pmatrix} \mathbf{0} & \mathbf{v} & \cdots & (p-1)\mathbf{v} & \mathbf{v^2} & \cdots & (p-1)\mathbf{v^2} & \mathbf{v}+\mathbf{v^2} & \mathbf{v}+2\mathbf{v^2} & \cdots & (p-1)\mathbf{v}+(p-1)\mathbf{v^2} \\ G_{m,k_6} & \tilde{G}_{m,k_6} & \cdots & \tilde{G}_{m,k_6} & \tilde{G}_{m,k_6} & \cdots & \tilde{G}_{m,k_6} & \tilde{G}_{m,k_6} & \tilde{G}_{m,k_6} & \cdots & \tilde{G}_{m,k_6} \end{pmatrix},$$

where $\mathbf{0}=(\underbrace{0,\cdots,0}_{p^{2m+k_6}-1})$, $\mathbf{i}=(\underbrace{i,\cdots,i}_{p^{2m+k_6}})$, $i\in\{av\mid a\in F_p\}\bigcup\{av^2\mid a\in F_p\}\bigcup\{av+bv^2\mid a,b\in F_p^*\}$, $\tilde{G}_{m,k_6}=(0_{m,k_6},G_{m,k_6})$, $0_{m,k_6}=(\underbrace{0,\cdots,0}_{m+k_6})^{\mathrm{T}}$, then C is a one-Lee weight code with $w_2=p^2w_1=2p^{2(m+1)+k_6-1}(p-1)$.

Next, we will consider the sum of all codewords of a linear code, which provide a new proof of Theorem 3.5.

Theorem 3.6 Suppose C is a linear code of length n over R_p with the generator matrix G, for $\forall j=1,\cdots,n,\exists c=(c_1,\cdots,c_n)\in C,c_j\neq 0$, then $\sum_{c\in C}w_L(c)=\dfrac{2n\mid C\mid(p-1)}{p}$.

Proof : Consider the $\mid c\mid\times n$ array of all codewords in C. It is easy to check that each column corresponds to one of the following cases:(1) the columns appears $0,cv+cv^2$ equally often, where $c\in F_p^*$; (2) the columns appears $0,bv,cv^2,bv+cv^2$ equally often, where $b,c\in F_p^*$; let N_1 be the number of the columns which appear $0,cv+cv^2$ equally often. Let N_2 be the number of the columns which appear $0,bv,cv^2,bv+cv^2$ equally often. Note that $N_1+N_2=n$, then

$$\sum_{c\in C}w_L(c)=N_1\left[\frac{\mid C\mid}{p}\times 2\times(p-1)\right]+N_2\left[\frac{\mid C\mid}{p^2}\times 2\times(p-1)+\frac{\mid C\mid}{p^2}\times 2\times(p-1)^2\right]=\frac{2n\mid C\mid(p-1)}{p}.$$

Note that: according to Theorem 3.6, if C is a one-Lee weight code of length n over R_p with the generator matrix G and w_0, then we have $(\mid C\mid-1)w_0=\dfrac{2n\mid C\mid(p-1)}{p}$. It is easy to verify that the results in Theorem 3.5 satisfy this equation.

Example 1 If $p=3$, $k_2=k_6=1$ according to Theorem 3.5, then there is a one-Lee weight code with $n=26$ and $w_0=36$, its generator matrix is

$$G_{1,1}=\begin{pmatrix} \mathbf{0} & \mathbf{v} & 2\mathbf{v} & \mathbf{v^2} & 2\mathbf{v^2} & \mathbf{v}+\mathbf{v^2} & \mathbf{v}+2\mathbf{v^2} & 2\mathbf{v}+\mathbf{v^2} & 2\mathbf{v}+2\mathbf{v^2} \\ G_{0,1} & \tilde{G}_{0,1} & \tilde{G}_{0,1} & \tilde{G}_{0,1} & \tilde{G}_{0,1} & \tilde{G}_{0,1} & \tilde{G}_{0,1} & \tilde{G}_{0,1} & \tilde{G}_{0,1} \end{pmatrix}$$

where $G_{0,1}=(v+v^2,2v+2v^2)$, $\tilde{G}_{0,1}=(0,v+v^2,2v+2v^2)$, $\mathbf{i}=(i\ i),i\in\{av\mid a\in F_3^*\}\bigcup\{av^2\mid a\in F_3^*\}\bigcup\{av+bv^2\mid a,b\in F_3^*\}$, $\mathbf{0}=(0\ 0)$.

Acknowledgements

The second author (Corresponding author) is supported by NNSF of China (61202068), Talents youth Fund of Anhui Province Universities (2012SQRL020ZD) and Student Research Training Program of Anhui University (KYXL2012006).

References

[1] MacWilliams F. J., Sloane N. J. A. The Theory of Error Correcting Codes [M]. Amsterdam, North-Holland, 1977.

[2] C. Carlet. One-weight Z_4-linear codes. Coding, Theory, Cryptography and Related Areas, Springer, 2000, 57-72.

[3] Minjia Shi, Good p-ary codes from one-weight codes over Z_{p^m} , Chinese Journal of Electronics，2013, 22(4)799-802.

[4] Minjia Shi, Shixin Zhu, ShanlinYang, A class of optimal p-ary codes from one-weight codes over $F_p[u]/<u^m>$,The Journal of The Franklin Institute, 2013,350(5)729-737.

[5] Minjia Shi, Yan Liu, Several Weight Enumerators of Linear Codes and their MacWilliams identities over Ring $F_p + vF_p + v^2F_p$, Acta Electronica Sinica, to appear in July, 2014.

[6] MinJia Shi, Patrick Solé, Bo Wu. Cyclic codes and the weight enumerator of linear codes over $F_2 + vF_2 + v^2F_2$ [J]. Appl. Comput. Math, 2013, 12(2)247- 255.

Advanced Materials Research Vols. 989-994 (2014) pp 2639-2642
© (2014) Trans Tech Publications, Switzerland
doi:10.4028/www.scientific.net/AMR.989-994.2639

Dynamic Network Model Analysis Based on Communication Network

[1,a] Yuan Nanqi[2,b] Jiang Tian[3,c] BaiShi[4,d] Sun Hao[5,e] Zhao JingMei

[1,2,3,4,5] Institute of information science and engineering，Southeast university，Nanjing，JiangSu，China，210000

[a,b,c,d,e]94755096@qq.com

Keywords: Dynamic Network, Vicsek Model, Consensus Problem, Astringency.

Abstract. In order to research dynamic network astringency reaching uniformity, this paper perfects the Vicsek model and puts forward improving dynamic network astringency efficiency by weighted model. We prove that the convergence rate of weighted model is faster than the classic Vicsek model and it can optimize dynamic network.

Introduction

Complexity and complex system is one of the focused research topics of 21 Century. Complex network is the important tool and method of describing and understanding complex system. It summarizes complex system as a network system constituted by multiple interactional individuals (panel points) and is widely used in different realms of science. It has become the focused research topic in complexity science realm and synchronously prevails among various complex network systems. Astringency is the core problem of dynamic network research, and has become one of the important and challengeable leading edges in system and control field. Dynamic network models, represented by Vicsek model, apply simple evolution rules but get complex self-organizing phenomenon and the research results provide cooperative control and coordination problem of multiple individual with theoretical basis. We conduct intense research on dynamic network modeling and network astringency ans put forward improving convergence efficiency by weighted model on the basis of Vicsek model. We prove that the convergence rate of weighted model is faster than the classic Vicsek model.

Vicsek Model and Its Heterogeneous Model

Vicsek Model: In Vicsek model, if we describe the relations of each individual and their neighbors by chart (or network), there will be a dynamic network where a topology changes every time because of individual motions. If we denote the chart of each moment by gt, a chart sequence G={g1，g2，…，gn}can be get. With the algebra graph theory and matrix, Literature [5-6] indicates that the system can reach an agreement when the sequence of the chart satisfy some certain conditions in topology

In the Vicsek model, N self-government individuals move on a L × L flat surface at the same rate. In the initial moment, the horizontal and vertical ordinate of each individual obey uniform distribution in [0， L], and the direction of each individual obey uniform distribution in[0，2π], as shown in Figure1.

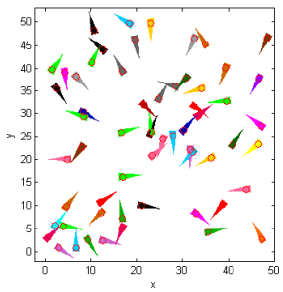

Figure 1: Original State

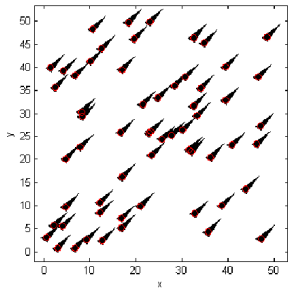

Figure 2: Consistent Direction State

In each t + 1 moment, the direction of each individual is the average value of the direction of one individual and its neighbor at t moment. At moment t + 1, the location change relation of individual i is shown in formula (1), and formula (2) determines its direction change.

$$x_i(t+1) = x_i(t) + v_0 e^{i\theta_i(t)} \tag{1}$$

$$e^{i\theta_i(t+1)} = e^{i\Delta\theta_i(t)} \frac{\sum_{j\in\Gamma_i(t+1)} e^{i\theta_j(t)}}{\| \sum_{j\in\Gamma_i(t+1)} e^{i\theta_j(t)} \|_2} \tag{2}$$

$\Delta\theta_i(t)$ is the white noise; $e^{i\theta_i(t)}$ is the unit direction vector; $\Gamma_i(t+1)$ is the neighbor gather of individual i at moment t + 1. When the destiny is relatively high and the noise is relatively low, the individual in system are in the same direction, as shown in Figure2.

Heterogeneous Model: Literature [7] brings forward the heterogeneous model in allusion to identical individual influence area and certain motion speed. In this model, the influence radius of each individual vary and obey the power-law distribution with the index of γ.

$$P(r) \to r^{-r} \qquad r \in [2, \infty] \tag{3}$$

When γ = ∞, the distribution of individual's influence radius is homogeneous, namely the influence radiuses equal. The research result shows that with the increase of the heterogeneous degree, namely the reduce of γ, the system convergence rate increases and the consistence degree improves.

Design and Analysis of Dynamic Network Weighted Model

Initial Conditions Definition of Modeling: Initial conditions are shown in Figure 1. N individuals distribute randomly on the L × L area of XY coordinate system, and the X, Y coordinates obey uniform distribution in [0， L]. The angle of each individual obey uniform distribution in[0， 2π].

The influence radiuses of each individual equal R. System noise is the data range of $\Delta\theta_i(t)$ in formula (2). In this paper, $\Delta\theta_i(t)$ obeys the uniform distribution in[−η ， η].

The model simulation study is achieved by loop iteration and the terminal condition of the loop, namely the convergence condition is formula （4）-（7）.

$$conc(t,t-1) = \sqrt{conc_r(t,t-1)^2 + conc_i(t,t-1)^2} \le 0.001 \tag{4}$$

$conc_r(t,t-1) \in R$ is shown in Formula (5). $conc_i(t,t-1) \in C$ is the complex number set as shown in formula (6). $\overline{e_{t,t-1}} \in C$ is shown in formula (7).

$$conc_r(t,t-1) \overset{\Delta}{=} \{\frac{1}{N-1}\sum_{j=1}^{N} real[(e^{i\theta_j(t)} - e^{i\theta_j(t-1)}) - \overline{e_{t,t-1}}]^2\}^{\frac{1}{2}} \tag{5}$$

$$conc_i(t,t-1) \overset{\Delta}{=} \{\frac{1}{N-1}\sum_{j=1}^{N} imag[(e^{i\theta_j(t)} - e^{i\theta_j(t-1)}) - \overline{e_{t,t-1}}]^2\}^{\frac{1}{2}} \tag{6}$$

$$\overline{e_{t,t-1}} \overset{\Delta}{=} \frac{1}{N-1}\sum_{j=1}^{N}[(e^{i\theta_j(t)} - e^{i\theta_j(t-1)}) \tag{7}$$

In order to make it convenient for study, the two aspect contained in convergence efficiency is defined as follows: convergence time t and degree of consistence SVa is expressed by formula (8).

$$V_a = |\sum_{i=1}^{n} e^{i\theta_j(t)} / N| \tag{9}$$

Dynamic Network Weighted Model: Currently, the research on complex network shows that various networks in reality have the feature of heterogeneous in topology structure. This paper considers improving the Vicsek model from the perspective of angle. We introduce the neighbor-number related weight and provide with the expression of direction change. We get the degree weighted model and name is model I, as shown in formula (10).

$$e^{i\theta_i(t+1)} = \frac{\sum_{j\in\Gamma_i(t+1)} \Gamma_j^{(1)}(t) e^{i\theta_j(t)}}{\| \sum_{j\in\Gamma_i(t+1)} \Gamma_j^{(1)} e^{i\theta_j(t)} \|_2} \tag{10}$$

$\Gamma_j^{(1)}$ is the weight of the neighbor j of individual I at moment t, and its computational formula is shown in formula (11). nj(t) is the neighbor number of individual i's neighbor j.

$$\Gamma_j^{(1)}(t) = \frac{n_j(t)}{\sum_{K\in\Gamma_i(t+1)} n_K(t)} \tag{11}$$

Adjust the discrepancy degree of individual weight and generate Vicsek model and model I to unmarked cases. When$\lambda > 1$, discrepancy degree of individual influence enlarges and the system convergence efficiency is higher than model I; conversely, when $0 < \lambda < 1$,the weight of individual with big angle is smaller than model I and the convergence efficiency is between original Vicsek model and model I. According to the direction update rule of formula (12), the direction of individual i is individual direction vector average of its neighbor who has the most neighbors.

$$e^{i\theta_i(t+1)} = \lim_{\lambda\to\infty} \frac{\sum_{j\in\Gamma_i(t+1)} \Gamma_j^{(1)}(t) e^{i\theta_j(t)}}{\| \sum_{j\in\Gamma_i(t+1)} \Gamma_j^{(1)} e^{i\theta_j(t)} \|_2} = \frac{\sum_{j\in\Omega(t+1,t)} e^{i\theta_j(t)}}{\| \sum_{j\in\Omega_i(t+1,t)} e^{i\theta_j(t)} \|_2} \tag{12}$$

Simulation Experimental Analysis

This paper focuses on researching the impact of the change of noise amplitudeη and angle indexλon system convergence efficient. Conduct simulation to weighted model and original Vicsek model and analyze comparatively. In the simulation process of this paper, when N=200， L=8, the conclusion adopt the average of 300 time simulations.

We can get from Figure 3 and Figure 4 that with the increase of noise amplitude, the system diminishes consistently; as to any fixed noise and radium, the consistence degree of model I is higher than the original Vicsek model; with the increase of noise amplitude, the system diminishes consistently; as to any fixed noise and V0, the consistence degree of model I is higher than the original Vicsek model.

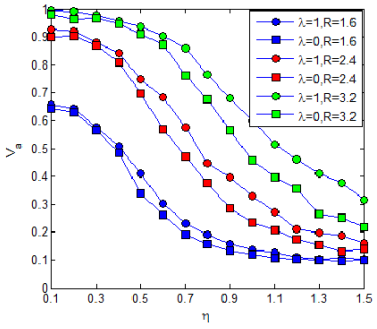

Figure 3: The Relation of Va and Noise Amplitude η when R changes

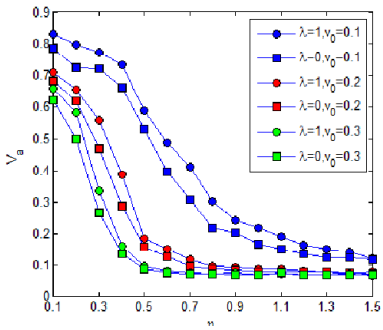

Figure 4: The Relation of Va and Noise Amplitude η when V 0 changes

Figure 5-6 shows the impact of indexλ on network. We can see from the figure that with the increase of index λ, convergence time t nearly shows the trend of exponential fall. With the increase of R and decrease of time, when the index increase to a certain degree, the influence of R is leveling out. It is thus clear that when the index λ is relatively small, R has a large influence on convergence time t, and when λ increases to some degree, the influence is not that important. Thus, the improvement this method to convergence time is effective. Index λ increase with the increase of the system consistence degree, which shows that this method can improve the system consistence degree.

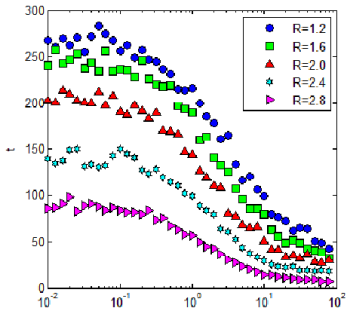

Figure 5: The Relation of λ and convergence time t

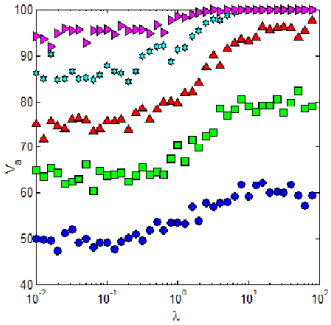

Figure 6: The Relation of λ and Consistent Va

Conclusion

Various networks in reality have the feature of heterogeneous in topology structure and panel point with big angle has a significance influence on the network structure and dynamics process in network. Considering that the discrepancy in neighbor number in the evolutionary process, this paper applies the dynamic network topology structure, and with combination of the definition of angle in complex network, it puts forward the angle-weighted weighting model to improve the convergence efficiency. Next moment direction of each individual in the weighted model is the vector weighted average of all neighbor directions current moment. Two models can be get according to the weighting differences, the weight of model I is in direct proportion to the individual degree (namely the mentioned neighbor number); the weight of model II is in direct proportion to the individual degree index and this index is greater than zero. The result shows that weighted model improve the convergence efficiency of dynamic network, so do the one with noise.

Reference

[1] Guo Lei， Xu Xiaoming. Complex Network[M]， Shanghai：Shanghai Educational Publishing House， 2006.

[2] M. Wang， X. Meng， and L. Zhang， "Consolidating Virtual Machines with Dynamic Bandwidth Demand in Data Centers，" in Proc. of IEEE INFOCOM 2011 Mini-Conference， 2011.

[3] Zhao Ming. Recent Advancement in Research of Synchronization of Dynamical Systems on Complex Network[J].Process in Physics，2008， 28(1):22–34.

[4] Luo Qun. Adaptive Synchronization Research on the Uncertain Complex Network[J]. Physical Journal， 2008， 57(3):1529–1534.

[5] W. Ren and R. W. Beard， Consensus seeking in multi-agent systems under dynamically changing interaction topologies[J]. IEEE Trans. Autom. Control， 2005， 50(5): 655-661.

[6] M. Nagy， I. Daruka， and T. Vicsek， New aspects of the continuous phase transition in the scalar noise model (SNM) of collective motion[J]. Phys. A， 2007， 373: 445-454.

[7] Wen Yang， Lang Cao， Xiaofan Wang， and Xiang Li. Consensus in a heterogeneous influence network[J]. Physical Review E， 2006， 74: 037101.

[8] Duncan J. Watts and Steven H. Strogatz， Collective dynamics of ‘small-world’ networks[J]. Nature， 1998， 393: 440-442.

[9] Albert-László Barabási and Réka Albert， Emergence of scaling in random networks[J]. Science, 1999， 286: 509-512.

[10] Yao Jing，Guan Zhihong. Impulse Control of Topology Switching Network [J].Complex System and Complexity Science，2005， 2(2):24–29.

Advanced Materials Research Vols. 989-994 (2014) pp 2643-2646
© (2014) Trans Tech Publications, Switzerland
doi:10.4028/www.scientific.net/AMR.989-994.2643

The New Class of Laplacian Integral Graphs

Lu shi-fang[1, a], Zou jin-yu[2,b]

[1]Department of Basic Research, Qinghai University, Qinghai Xining 810016, P.R. China

[2]Department of Basic Research, Qinghai University, Qinghai Xining 810016, P.R. China

[a]lsf0522@aliyun.com.cn, [b]zoujinyu84@163.com

Keywords: Laplacian spectra, the Laplacian characteristic polynomials, Laplacian integral graphs.

Abstract. Graph G is Laplacian integral, if all the eigenvalues of its Laplacian matrix are integral. In this paper, we obtain that the Laplacian characteristic polynomials of graphs $K_n^{-tk_2}$ by calculation. Characterizes the new class of Laplacian integral graphs .

Introduction

All the graphs considered in this paper are finite, undirected and simple. Undefined notations and terminology will conform to those in [1, 2].

Let G be a graph with vertex set $V(G)$ and edge set $E(G)$. Let $A(G)$ be the (0, 1)-adjacency matrix of graph G. The Laplacian matrix and the signless Laplacian matrix of G is defined to be $L(G) = D(G) - A(G)$ and $Q(G) = D(G) + A(G)$, respectively, where $D(G)$ is the diagonal matrix of vertex degrees of G. We call $P_G(\lambda) = |\lambda I - A(G)|$, $L_G(\lambda) = |\lambda I - L(G)|$ and $Q_G(\lambda) = |\lambda I - Q(G)|$, respectively, the characteristic polynomial of G with respect to the adjacency matrix, the Laplacian matrix and the signless Laplacian matrix of graph G, see [2, 3]. Let $\lambda_1, \lambda_2 \cdots, \lambda_n$ be n distinct Laplacian eigenvalues with the corresponding multiplicities $k_1, k_2 \cdots, k_n$. We denote by

$$Spec(G) = \{\lambda_1^{k_1}, \lambda_2^{k_2}, \cdots, \lambda_n^{kn}\}$$

The Laplacian spectrum of graph G.

Let $K_{n_1,n_2,\cdots,n_t}$ denote the complete t-partite graphs with t partite sets A_i's such that $|A_i| = n_i$ for $i = 1,2,\cdots,t$. Assume that the number of distinct integers of $n_2, n_2, \cdots, n_t$ is s. Without loss of generality, assume that $n_2 < n_2 < \cdots < n_s$. Suppose that a_i is the multiplicity of n_i for each $i = 1,2,\cdots,s$. The complete t-partite graphs $K_{n_1,n_2,\cdots,n_t} = K_{n_1,\cdots,\ n_1,\cdots,n_s\cdots,n_s}$ is also denoted by $K_{a_1n_1,\cdots,a_sn_s}$, where $r = \sum_{i=1}^{s} a_i$ and $|V| = n = \sum_{i=1}^{s} a_i n_i$.

$K_{1,n}$ is called a star. $S(p,q)\ (p \le q)$ is called a double-star like tree on $n = p + q$ vertices.

The line graph $L(G)$ of a graph G is the graph whose vertices correspond to the edges of G with two vertices being adjacent if and only if the corresponding edges in G have a vertex in common.

A graph is integral, Laplacian integral and Q-integral if all the eigenvalues of its adjacency matrix, Laplacian matrix and signless Laplacian matrix, respectively, are integral.

The search for integral graph started already in 1970s [4] and has continued to this day so far. Many integral graphs have been found or characterized in various graph class, see [5, 6]. Some interesting results on Laplacian integral graphs can be found in [7, 8]. However, the signless Laplacian spectral is not much studied in the literature. Very recently, the authors in [9-12] investigated the characteristic polynomial of the signless Laplacian matrix.

Problem: Determine all connected, nonregular graphs that are integral, Laplacian integral and signless Laplacian integral.

In [9-13], we obtain that the signless Laplacian characteristic polynomials of the complete multipartite graphs $G = K_{n_1,n_2,\cdots,n_t}$. Also obtain that the characteristic polynomial of the signless Laplacian matrix of the complete t-partite graphs $G = K_{n_1,n_2,\cdots,n_t} = K_{n_1,\cdots,\ n_1,\cdots,n_s\cdots,n_s}$. Showed that the necessary and sufficient condition for the complete t-partite graphs $G = K_{n_1,n_2,\cdots,n_t} = K_{n_1,\cdots,\ n_1,\cdots,n_s\cdots,n_s}$, where $s = 2,3,4$ to be Q-integral. And proved that all the complete multipartite graphs $G = K_{n_1,n_2,\cdots,n_t} = K_{n_1,\cdots,\ n_1,\cdots,n_s\cdots,n_s}$ are Laplacian integral graphs.

In this paper, we obtain that the Laplacian characteristic polynomials of graphs $K_n^{-tk_2}$ by calculation. Characterizes the new class of Laplacian integral graphs.

Preliminaries

Theorem 1.1 [13] Let $G = K_{n_1,\cdots,\ n_1,\cdots,n_s\cdots,n_s}$ be complete multipartite graphs on n vertices. Then graph G is Laplacian integral. And its Laplacian spectrum is

$$Spec(G) = \{0^1, n^{s-1}, (n_1 - n)^{(n_1-1)a_1}, \cdots, (n_s - n)^{(n_s-1)a^s}, n^{a_1-1}, \cdots, n^{a_s-1}\}$$

Where, $n = a_1 n_1 + a_2 n_2 + \cdots + a_s n_s$.

Let K_n be complete graph on n vertices. Let $K_n^{-tk_2}$ denote the graphs obtained by deleting $t, 0 < t \le \frac{1}{2}$ non-adjacent edges from the complete graph K_n. The description on the new class of the integral graph is little, so with good prospects for the study. In this paper, we main calculate the Laplacian characteristic polynomials of graphs $K_n^{-tk_2}$, and characterizes the new class of Laplacian integral graphs.

Laplacian characteristic polynomials of graphs $K_n^{-tk_2}$

Theorem 2.1 Let $G = K_n^{-tk_2}$ denote the graphs obtained by deleting $t, 0 < t \le \frac{1}{2}$ non-adjacent edges from the complete graph K_n. Then G is Laplacian integral. And the Laplacian characteristic polynomials of $G = K_n^{-tk_2}$ is:

(1)When n be odd, and $t = \frac{n-1}{2}$, $L_G(\lambda) = \lambda[\lambda - (n-2)]^t (\lambda - n)^t$;

(2)When n be even, and $t = \frac{n}{2}$, $L_G(\lambda) = \lambda[\lambda - (n-2)]^t (\lambda - n)^{t-1}$.

Prove: (1) When n be odd, and $t = \frac{n-1}{2}$. The Laplacian characteristic polynomials of G is:

$$L_G(\lambda)=\begin{vmatrix} \lambda-(n-1) & 1 & 1 & \cdots & 1 & 1 \\ 1 & \lambda-(n-2) & 0 & \cdots & 1 & 1 \\ 1 & 0 & \lambda-(n-2) & \cdots & 1 & 1 \\ \vdots & \vdots & \vdots & \ddots & \vdots & \vdots \\ 1 & 1 & 1 & \cdots & \lambda-(n-2) & 0 \\ 1 & 1 & 1 & \cdots & 0 & \lambda-(n-2) \end{vmatrix}$$

Using the elementary transformation of determinant, we have,

$$L_G(\lambda)=\lambda\,[\lambda-(n-2)]^{\frac{n-1}{2}}\,(\lambda-n)^{\frac{n-1}{2}}=\lambda\,[\lambda-(n-2)]^{t}\,(\lambda-n)^{t}.$$

(2)When n be even, and $t=\dfrac{n-1}{2}$, The Laplacian characteristic polynomials of G is:

$$L_G(\lambda)=\begin{vmatrix} \lambda-(n-2) & 0 & \cdots & 1 & 1 \\ 0 & \lambda-(n-2) & \cdots & 1 & 1 \\ \vdots & \vdots & \ddots & \vdots & \vdots \\ 1 & 1 & \cdots & \lambda-(n-2) & 0 \\ 1 & 1 & \cdots & 0 & \lambda-(n-2) \end{vmatrix}$$

Using the elementary transformation of determinant, Obtained,

$$L_G(\lambda) \;=\; \lambda\,[\lambda-(n-2)]^{\frac{n}{2}}\,(\lambda-n)^{\frac{n}{2}-1}=\lambda[\lambda-(n-2)]^{t}(\lambda-n)^{t-1}.$$

Corollary 2.1 Let $G=K_n^{-k_2}$ denote the graphs obtained by deleting 1 edges from the complete graph K_n. Then $G=K_n^{-k_2}$ is Laplacian integral. And its Laplacian spectrum is:

$$Spec(G)=\{0^1,(n-2)^1,n^{n-2}\}$$

Corollary 2.2 Let $G=K_n^{-2k_2}$ denote the graphs obtained by deleting 2 edges from the complete graph K_n. Then $G=K_n^{-2k_2}$ is Laplacian integral. And its Laplacian spectrum is:

$$Spec(G)=\{0^1,(n-2)^2,n^{n-3}\}$$

The Laplacian characteristic polynomials of line graph of star

Theorem3.1 Let $G=L(K_{1,\,n})$ be line graph of star $K_{1,n}$ on $n+1$ vertices. That is the complete graph K_n on n vertices. Then $K_{1,n}$ is Laplacian integral. And its Laplacian spectrum is:

$$Spec(G)=\{0^1,(n-1)^{n-2}\}$$

Theorem3.2 Let $G=L(S_{(p,\,q)})$ be line graph of double-star like tree $S_{(p,\,q)}$ on $n=p+q$ vertices. Then the Laplacian characteristic polynomials of graph $G=L(S_{(p,\,q)})$ is:

$$L_G(\lambda) \;=\lambda(\lambda-1)(\lambda-p)^{p-2}(\lambda-q)^{q-2}[\lambda-(p+q-1)].$$

Prove: The Laplacian characteristic polynomials of graph $G=L(S_{(p,\,q)})$ is:

$$L_G(\lambda)=\begin{vmatrix} A & O & J_1 \\ O & B & J_2 \\ J_3 & J_4 & \lambda-(p+q-2) \end{vmatrix},$$

Where, $A=\begin{bmatrix} \lambda-(p-1) & \cdots & 1 \\ \vdots & \ddots & \vdots \\ 1 & 1 & \lambda-(p-1) \end{bmatrix}$, $B=\begin{bmatrix} \lambda-(q-1) & \cdots & 1 \\ \vdots & \ddots & \vdots \\ 1 & 1 & \lambda-(q-1) \end{bmatrix}$.

J_i $(i=1,2,3,4)$ denote the $(p-1)\times 1, (q-1)\times 1, 1\times(p-1), 1\times(q-1)$ all-one matrices.

Using the elementary transformation of determinant, Obtained,

$$L_G(\lambda)=\lambda(\lambda-1)(\lambda-p)^{p-2}(\lambda-q)^{q-2}[\lambda-(p+q-1)]$$

Acknowledgements

This work was financially supported by the Ministry of education "Chunhui project" (Z2012091).

References

[1] Bondy J A, Murty U S R. Graph Theory with Applications [M]. New York: Macmillan London and Elsevier, 1976.

[2] Cvetkovi´c D, Doob M, Sachs H. Spectra of Graphs–Theory and Application [M]. New York: Academic press, 1980.

[3] Haemers W, Spence E. Enumeration of cospectral graphs [J]. Europ. J. Comb., 2004, 25: 199-211.

[4] Harary F, Schwenk A.J. Which graphs have integral spectral? [J]. In Graphs and Combinatorics , (eds, R.Bari and F. Harary),(Proc. Capital conf., George Washington Univ., Washington, D.C., 973), Lecture Notes in Mathematics , Springer-Verlay, Berlin, 1974, 406: 45-51.

[5] Bali´nska K.T, Cvetkovi´c D, Radosavljevi´c Z, Simi´c S K, Stevanovi´c D. A survey on integral graphs [J]. it Univ. Beograd. Pull. Elektrotehn. Fak. Ser. Mat., 2002, 13: 42-65.

[6] Wang L.G, Liu.X.D. Integral complete multipartite graphs [J]. Discrete Math., 2008, 308: 3860-3870.

[7] Grone R, Merris R. The Laplacian spectrum of a graph [J]. SIAM.J. Discrete Math., 1994, 7: 221-229.

[8] Mohar B. The Laplacian Spectrum of graphs [J]. Graph Theory, Combinatorics and Applications, Y. Alavi et al. eds., John Wiley, New York 1991, 871-898.

[9] LU S.F. Signless Laplacian integral roots of the complete 4-partite graphs[J]. Journal of Qinghai University(Natural Science), 2009, 27(6): 46-48, 83.

[10] LU S.F, ZHAO H.X. Signless Laplacian characteristic Polynomials of Complete Multipartite Graphs [J]. Quarterly Journal of mathematics, 2012, 27(1): 36-40.

[11] LU S.F, WEI L., ZHAO H.X. Signless Laplacian characteristic Polynomials of Complete Tripartite Graphs [J].Journal of Shandong University (Science edition), 2012 (12):41-47.

[12] LU S.F. s=4 Signless Laplacian characteristic Polynomials of Complete Multipartite Graphs [J]. Value engineering, 2012(7):12-13.

[13] LU S.F. Laplacian spectrum of Complete Multipartite Graphs $K_{n_1,\cdots,\ n_1,\cdots,n_s\cdots,n_s}$ [J]. Mathematics in Practice and Theory, 2013, 44 (5):275-279.

Advanced Materials Research Vols. 989-994 (2014) pp 2647-2650
© (2014) Trans Tech Publications, Switzerland
doi:10.4028/www.scientific.net/AMR.989-994.2647

An Efficient Methodology for Estimating Interconnect Crosstalk Noise in Deep-submicron Technologies

Xiaoxiao Liu[1, a], Jingbo Shao[2,b] and Lingling Zhao[1,c]

[1]College of Information, Beijing City University, Beijing 100083, China

[2] Department of Computer Science and Information Engineering, Harbin Normal University, Harbin 150025, China

[a]lxx535@163.com, [b]zro_bo@163.com, [c]zhaolingling@bcu.edu.cn

Keywords: Interconnect; Crosstalk Noise; Process Variations;

Abstract. To solve the crosstalk noise question in deep-submicron technologies, an efficient methodology for estimating interconnect crosstalk noise is proposed in this paper. PCA and ICA techniques are applied to reduce correlations of process variations, and moment matching scheme is used to obtain the PDF of crosstalk noise in victim coupled with multiple aggressors. Experimental results show that our method maintains the efficiency of past approaches, and significantly improves on their accuracy.

1. Introduction

On-chip interconnect is known as one of the most compelling problems for modern deep submicron integrated circuits, and interconnects are going to be the limiting factor for high speed digital circuits. Another unwanted side effect of CMOS process technology scaling is the increase in process variations. Differences between identical features in a certain lithographic process are referred to as process variations [1]. Lithography steps generate more process variations in smaller geometric feature sizes. This phenomenon can create a rather large deviation of key circuit parameters from their designed values, which in turn may increase crosstalk, produce timing uncertainty, interferer circuit performance [2], and demand highly sophisticated and robust crosstalk-aware analysis and optimization tools.

Statistical analysis is viewed as an essential methodology for nanometer process technologies, which enables the application of actual statistics of the process technology parameters for the accurate calculation of design characteristics such as delay and noise [3]. Most approaches assume that parameter variables are known statistically Gaussian independent。However, it is well known that some process parameters deviate significantly from a Gaussian distribution [4]. For example, via resistances exhibit an asymmetric probability distribution, and the dopant concentration density is also observed to be well-modeled by a Poisson distribution. A normality assumption may lead to significant sources of errors in crosstalk noise analysis.

In this paper, a new methodology is proposed to derive the statistical distribution of on-chip crosstalk noise, which presents a solution in the presence of both correlated Gaussian and non-Gaussian parameter distributions. Further the paper is organized as following: In section 2, PCA and ICA technologies are employed to transform correlated sets of Gaussian and non-Gaussian variables to sets of statistically independent variables correspondingly, and then the PDF of crosstalk noise in a victim line coupled with multiple aggressors is obtained using the moment matching scheme. Section 3 shows experimental results while section 4 concludes this paper.

2. PDF evaluation of crosstalk noise

When correlations among process parameters are taken into consideration, the statistical crosstalk noise analysis becomes even more complicated. To make the problem tractable, we employ the mathematical techniques PCA (principal components analysis) [5] and ICA(independent component analysis) [6] to accomplish the desired goal of transforming Gaussian and non-Gaussian correlated random variables sets in reduced distributed RC-π model to random variables sets that are

statistically as independent as possible, respectively. Then, crosstalk noises can be represented in a linear form of new sets of independent Gaussian and non-Gaussian random variables.

In Eq. (1), ICA is applied to the non-Gaussian parameters X and PCA to the Gaussian variables Y, to obtain a set of statistically independent non-Gaussian variables S and a set of independent Gaussian variables R. We then arrive at the following canonical noise model:

$$V = \mu + B'^T S + C'^T R + e \cdot z = \mu + \sum_{i=1}^{n} b_i' \cdot s_i + \sum_{j=1}^{m} c_j' \cdot r_j + e \cdot z \tag{1}$$

where $B'^T = B^T A$ [$C'^T = C^T P_y^{-1}$] is the new sensitivity vector with respect to the statistically independent non-Gaussian components $s_1, s_2, ..., s_n$ [Gaussian principal components $r_1, r_2, ..., r_m$], A[P_y] is the n× n [m× m] transformation matrices.

Given the underlying process variables and their moments, after performing ICA [PCA] the moments of the independent components $s_1, s_2, ..., s_n$ [$r_1, r_2, ..., r_m$] can be easily computed successively from the moments of the correlated non-Gaussian parameters $x_1, x_2, ..., x_n$ [correlated Gaussian parameters $y_1, y_2, ..., y_m$]. These moments of the process variables are inputs to the RD-SCNA algorithm.

Finally, to compute the PDF/CDF of the crosstalk noise random variable we adapt the probability extraction scheme *APEX* [7]. Given 2*M* moments of a random variable as inputs to the *APEX* algorithm, the scheme employs an AWE (asymptotic waveform evaluate) technique to match the 2*M* moments in order to generate an *M*th order LTI (linear time invariant) system. The scheme then approximates the PDF [CDF] of a random variable in reduced distributed RC-π model by an impulse response $h(t)$ [step response $s(t)$] of the *M*th order LTI system.

It is clear that we borrow some techniques from existing algorithm; however, the overall algorithm is distinctly different from any existing crosstalk noise analysis method.

We use a simple 2 RC-π stages circuit of a pair of coupled interconnect lines, shown in Fig. 1, to illustrate the moment matching-based PDF evaluation. We assume the width *W* and the height *H* for each interconnect to be the random variables. Using a first order approximation, the crosstalk noise of this circuit can be written as:

$$V = \mu + a_{1a}W_{1a} + a_{2a}W_{2a} + a_{1v}W_{1v} + a_{2v}W_{2v} + b_{1a}H_{1a} + b_{2a}H_{2a} + b_{1v}H_{1v} + b_{2v}H_{2v}$$

where $a_{1a}, a_{1v}, b_{1a}, b_{1v}$ [$a_{2a}, a_{2v}, b_{2a}, b_{2v}$] are sensitivities of the crosstalk noise with respect to the zero-mean randomly varying parameters $W_{1a}, W_{1v}, H_{1a}, H_{1v}$ [W_{2a}, W_{2v}, H_{2a}, H_{2v}] of seg-1 [seg-2], respectively, and μ is the nominal crosstalk noise of the circuit.

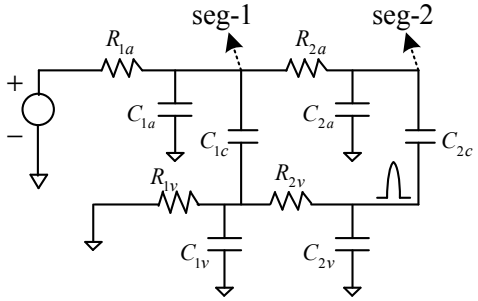

Fig. 1 Two RC-π stages circuit of coupled interconnect lines

Assuming ($W_{1a}, W_{2a}, W_{1v}, W_{2v}$) to be perfectly correlated identical Gaussian random variables, and ($H_{1a}, H_{2a}, H_{1v}, H_{2v}$) to be perfectly correlated, and uniformly distributed identical random variables, we have:

$$\hat{V} = a \cdot W + b \cdot H$$

where $a = a_{1a} + a_{2a} + a_{1v} + a_{2v}$, $b = b_{1a} + b_{2a} + b_{1v} + b_{2v}$, $\hat{V} = V - \mu$.

Assuming *W* and *H* as statistically independent variables, the kth moment of $\hat{V}$ can be computed by using the binomial expansion formula as:

$$m_k[\hat{V}] = \sum_{i=0}^{k} \binom{k}{i} a^i b^{k-i} m_i(W) m_{k-i}(H) \tag{2}$$

where all of the k moments of W and H are known from the underlying normal and uniform distribution. Having computed $2M$ moments of $\hat{V}$ from Eq. (2), we can now employ the AWE-based PDF evaluation scheme to approximate the PDF of $\hat{V}$ by an impulse response as:

$$f_{\hat{V}}(\hat{v}) = \begin{cases} \sum_{i=1}^{M} \hat{r}_i \cdot e^{\hat{p}_i \cdot \hat{v}} & \hat{v} \geq 0 \\ 0 & \hat{v} < 0 \end{cases}$$

where $\hat{r}[\hat{p}]$ are the residues [poles] of the LTI approximation.

Then, the evaluated crosstalk noise PDF is shown as: $f_V(v) = f_{\hat{V}}(v + \mu)$

We can generalize the PDF evaluation idea, illustrated in the above example, to compute the PDF (CDF) of any crosstalk noise random variable expressed in the canonical form of Eq. (1).

It is well known that a victim usually has multiple aggressors switching simultaneously. The crosstalk noise in a victim is the superposition of crosstalk noise generated by each coupled aggressors. When the induced crosstalk glitches in victim switch in opposite directions, the generated crosstalk noise effect can be counteracted with each other. Thus, the proposed crosstalk noise computation procedure in reduced distributed RC-π model involves two atomic operations of "sum" and "subtraction". Consider two random variables, V_1 and V_2 expressed as:

$$V_1 = \mu_1 + \sum_{i=1}^{n} b'_{i_1} \cdot s_i + \sum_{j=1}^{m} c'_{j_1} \cdot r_j + e_1 \cdot z_1, \quad V_2 = \mu_2 + \sum_{i=1}^{n} b'_{i_2} \cdot s_i + \sum_{j=1}^{m} c'_{j_2} \cdot r_j + e_2 \cdot z_2$$

The sum V_3 of V_1 and V_2 can be expressed in canonical form as:

$$V_3 = \mu_3 + \sum_{i=1}^{n} b'_{i_3} \cdot s_i + \sum_{j=1}^{m} c'_{j_3} \cdot r_j + e_3 \cdot z_3$$

where $\mu_3 = \mu_1 + \mu_2$, $b'_{i_3} = b'_{i_1} + b'_{i_2}$, $c'_{j_3} = c'_{j_1} + c'_{j_2}$, and $e_3 z_3 = e_1 z_1 + e_2 z_2$.

The uncorrelated non-Gaussian random variable $e_3 z_3$ serves as a place holder to store the moments of $(e_1 z_1 + e_2 z_2)$. In other words, rather than propagating an uncorrelated component z in the canonical form, we propagate its $2M$ moments. The "subtraction" operation of crosstalk noise random variable is similar with its "sum" operation. So, the proposed superposition operation of crosstalk noise random variables expressed in the linear canonical form of Eq. (1) is largely straightforward.

3. Experimental results

Fig. 2 shows a comparison of the results of our method with those generated from the Monte Carlo (MC) simulation for the test circuit using 2000 samples. As seen in Fig. 2, the results of the proposed approach are able to match well with those of MC simulations within small errors. These errors are reasonably small as compared to the accuracy penalty paid when modeling the non-Gaussian parameters as normally distributed random variables and performing MC simulations, termed as $\mathrm{MC}_{\mathrm{Gauss}}$, for test circuit. Thus, modeling the non-Gaussian parameters as normally distributed ones leads to significant inaccuracy. Moreover, to show the importance of considering spatial correlations, we consider the difference between performing statistical crosstalk noise analysis while considering spatial correlation and while ignoring it. Therefore, we run another set of Monte Carlo simulations, termed as $\mathrm{MC}_{\mathrm{NoCorr}}$, on the same test circuit, this time assuming zero correlations among segments. It can be observed in Fig.2 that the CDF and PDF curves of $\mathrm{MC}_{\mathrm{NoCorr}}$ deviate significantly from those of MC simulations. Thus, statistical crosstalk noise analysis without considering correlation may incorrectly predict the real performance of the circuit and could even overestimate the performance of the circuit. This underlines the importance of developing efficient statistical crosstalk noise analysis methods that can incorporate spatial correlations.

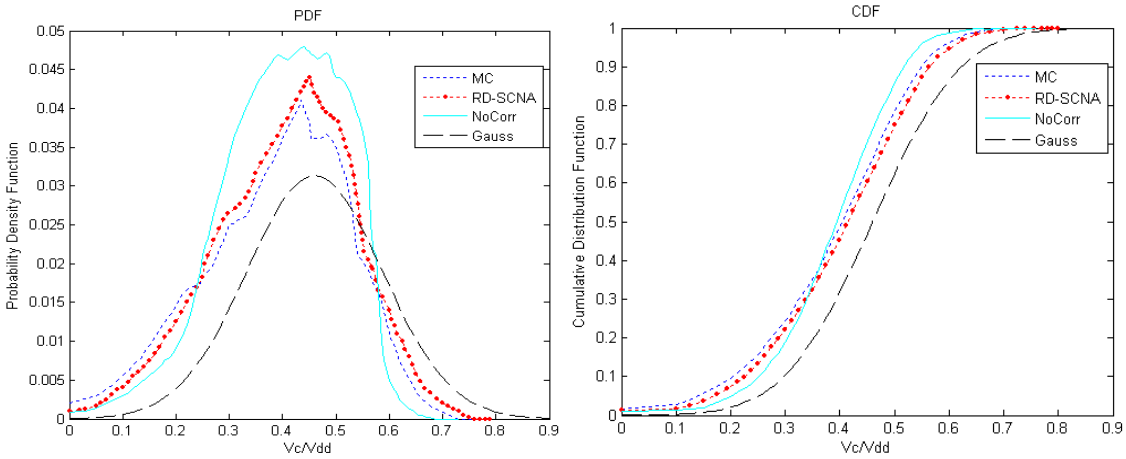

Fig. 2 Comparisons of RD-SCNA and MC distributions

4. Conclusions

As the VLSI technology scales down the role of interconnect parasitic effects in the signal integrity becomes increasingly significant, resulting in the aggravation of crosstalk noise amplitude and duration, and the circuit faults. In this paper a new crosstalk noise analysis method in deep-micron technologies was presented. The proposed method is able to obtain a very precise crosstalk noise result of the victim coupled with multiple aggressors, and general enough to work even for the cases when the PDF of the sources of variation is not available by using moment matching scheme. Experimental results show that compared to previous methods our approach significantly improves the crosstalk analysis accuracy by handling a larger range of variables while maintaining the efficiency.

5. Acknowledgements

This work was supported by On-campus Innovative Practice Base Construction of Beijing City University funded by Development and Promotion of Non-governmental Education Program of Beijing Municipal Education Commission in 2013.

References

[1] Hao Yue, Jing Ming-e, Ma Peijun. State of the art on study of parametric yield and its optimization for VLSI. Acta Electronica Sinica, 2003, 31(12A) : 1971-4.
[2] Feng Gang, Ma Guangsheng, Du Zhenjun. Signal-related crosstalk optimization for detailed routing. Journal of Computer-Aided Design & Computer Graphics, 2005, 17(5) : 1074-8.
[3] Kanak Agarwal, Sani Nassif. Characterizing process variation in nanometer CMOS. Proceedings of the 44th Annual Conference on Design Automation, San Diego, 2007, 396-9.
[4] Nagaraj NS, Tom Bonifield, Abha Singh, Clive Bittlestone, Usha Narasimha, Viet Le, et al. BEOL variability and impact on RC extraction. Proceedings of the 42nd annual conference on Design automation, California, 2005, 758-9.
[5] George H. Dunteman. Principal components analysis. California : Sage Publications, 1989.
[6] Hyvarinen A, Oja E. Independent component analysis: algorithms and applications. Neural Networks, 2000, 13(4-5) : 411-30.
[7] Xin Li, Jiayong Le, Padmini Gopalakrishnan, Lawrence T. Pileggi. Asymptotic probability extraction for non-normal performance distributions. IEEE Transactions on Computer-Aided Design of Integrated Circuits and Systems, 2007, 26(1) : 16-37.

Advanced Materials Research Vols. 989-994 (2014) pp 2651-2654
© (2014) Trans Tech Publications, Switzerland
doi:10.4028/www.scientific.net/AMR.989-994.2651

Feature-Based Real-Time Visual SLAM Using Kinect

Yan Song[1, a], Bo He[1,b]

[1]School of Information and Engineering, Ocean University of China, Shandong, Qingdao, China 266000

[a]songyan314@126.com, [b]bhe@ouc.edu.cn

Keywords: 3-D reconstruction; 3-D estimated trajectory; ORB; image features; SLAM

Abstract. In this paper, a novel feature-based real-time visual Simultaneous localization and mapping (SLAM) system is proposed. This system generates colored 3-D reconstruction models and 3-D estimated trajectory using a Kinect style camera. Microsoft Kinect, a low priced 3-D camera, is the only sensor we use in our experiment. Kinect style sensors give RGB-D (red-green-blue depth) data which contains 2D image and per-pixel depth information. ORB (Oriented FAST and Rotated BRIEF) is the algorithm used to extract image features for speed up the whole system. Our system can be used to generate 3-D detailed reconstruction models. Furthermore, an estimated 3D trajectory of the sensor is given in this paper. The results of the experiments demonstrate that our system performs robustly and effectively in both getting detailed 3D models and mapping camera trajectory.

Introduction

How to use simultaneous localization and mapping (SLAM) effectively and robustly has been one of the most actively studied problems in the robotics community over the past decade. Recently, a variety of 3D SLAM algorithms supports 6-DOF (degree-of-freedom) pose optimization, therefore the SLAM technique is employed in various platforms like quadrotors, underwater robots, etc.

As 3D cameras previously existed only as very expensive devices, the research into algorithms for analysis of their data is limited. However, the situation had been changed since the Microsoft Kinect sensor has been introduced into the market as a low priced 3D camera and now there is a significant increase in research into such algorithms. The Kinect sensor contains a depth sensor and a color camera. The depth sensor obtains depth data using the IR (infrared) projection method. Figures 1 (a) and (b) show a color image and depth data from the Kinect sensor. The Kinect style sensors are called the RGB-D (red-green-blue depth) camera since they give the color image and the depth data at the same time.

Fioraio and Konolige [1] presented a system that uses bundle adjustment to align the dense point clouds of the Kinect directly however without further exploiting the RGB images. Peter Henry *et al.* [2] introduced RGB-D mapping using RGB-D cameras to generate dense 3D models of indoor environments. Their approach detects loop closures by matching data frames against a subset of previously collected frames. To generate globally consistent alignments they use TORO, an optimization tool developed for SLAM [3]. The overall system can accurately align and map large indoor environments in near-real time and is capable of handling special situations such as featureless corridors and completely dark rooms. But this work did not operate in real-time. Felix Endres *et al.* [4] implemented and evaluated 3D SLAM with a variety of feature descriptors, the ICP algorithm, and the g2o (General framework for Graph Optimization) SLAM framework. They also presented a novel benchmark for the evaluation of their RGB-D SLAM systems [5]. Donghwa Lee *et al.* [6] proposed RGB-D 3D SLAM system which has the processing rate over 20 Hz. The image feature detection is performed on the GPU processor. However, both Felix Endres *et al.* and Donghwa Lee *et al.* didn't present the 3D estimated trajectory of their sensors.

In this paper, we propose a feature-based real-time visual SLAM system which can generate 3D models of objects and the 3D trajectory of the Kinect style sensors. The feature descriptor we use in this system is ORB [7]. The paper is organized as follows. The second section presents the

framework of real-time 3D reconstruction and estimated 3D sensor trajectory in our system. The third section provides experimental results. The last section comes to the conclusions.

(a) (b)

Fig.1. RGB-D sensor system. (a) RGB color image. (b) Per-pixel depth data.

Proposed SLAM System

Our approach utilizes RGB images and depth data from a RGB-D sensor. Processing steps of our system are as follows. First, we extract ORB features from the incoming color images. Each feature can be located at a point in three-dimensional coordinate space with depth information. These features will be matched against features from the previous images. Then we obtain a set of point-wise 3D correspondences between any two frames. Second, the relative transformation between the frames is estimated using Random Sample Consensus (RANSAC) [8]. Third, a feature manager gathers the whole features from the previous frames. Through comparison between the current and the preceding features, the current frame is matched to a past trajectory of the sensor. This matching procedure is called loop closure detection. Finally, we obtain the 3D trajectory and 3D object models after optimizing the constraint graph by the online graph-based SLAM algorithm. The detailed introduction of this system is given as follows:

A. Feature Extraction and Matching

ORB algorithm is used to extract image features from the incoming color image of the sensor and match to the feature of the previous frame in this system, as shown in figure 3. ORB is a very fast binary descriptor based on BRIEF and it is rotation invariant and resistant to noise. This algorithm is less accurate and less reliable, but is much faster than SIFT and SURF. Besides, ORB can implement the feature extraction procedure in real-time (30 Hz image frequency) on CPU in OpenCV 2.4.8.

B. RANSAC

RANSAC is a very important algorithm to compute the relative 3D transformation between the sensor poses and also to cope with noisy data and outliers in this system. After matching the features of two frames, the RANSAC approach randomly select a set of three matched feature pairs to compute a rigid transformation. If the Euclidean distances of the samples match, RANSAC will employ them to compute an estimate of the rigid transformation. The transformation is applied to all matched features to select all inliers. Finally, the inliers selected are used to compute a refined transformation.

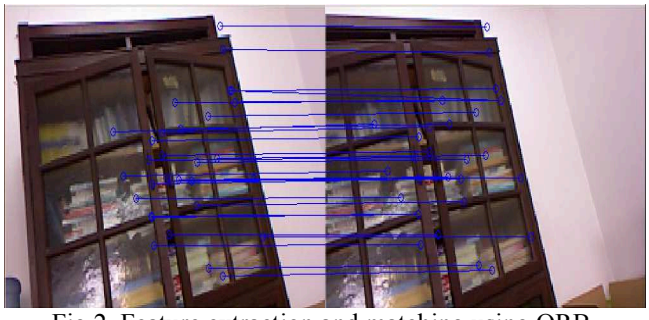

Fig.2. Feature extraction and matching using ORB.

C. Graph-Based SLAM Algorithm

The pairwise transformations between sensor poses form the edges of a pose graph. Due to estimation errors, the edges form no globally consistent trajectory. To create a globally consistent trajectory we optimize the pose graph using the g2o framework [9]. The g2o framework is an easily extensible graph optimizer that can be applied to a wide range of problems including several variants of SLAM and bundle adjustment. It performs a minimization of a non-linear error function that can be represented as a graph.

Experiment Results

We have conducted experiments in our laboratory with the Microsoft Kinect RGB-D sensor. The Kinect uses a structured light for depth information, and its valid range is about 0.5m to 5m. The sensor gives a RGB color image and depth data at 30 frames per second, both with 640 × 480 resolution. The real-time visual SLAM system is implemented on a Intel Core i3-2120 CPU with 4 GB of memory.

Experimental results of the proposed SLAM algorithm are presented in figure 4 and figure 5. Every node of the pose graph has 3D point cloud data which is transformed by the 6-DOF pose of each node and drawn in 3D space. Figure 3(a) shows 3D reconstruction results with only RGB-D data. The estimated sensor trajectory is present with three - dimensional coordinates in figure 3(b).

(a) (b)

Fig.3. Experimental results. (a) 3D reconstruction results with only RGB-D data. (b) Estimated sensor trajectory.

Conclusion

In this paper, we presented a feature-based real-time visual SLAM using sensors such as the Microsoft Kinect. Our approach extracts visual keypoints from the color images and uses the depth images to localize them in 3-D. We use RANSAC to estimate the transformations between associated keypoints and optimize the pose graph using nonlinear optimization. Finally, we generate a 3D reconstruction model of the object and an estimated 3D trajectory of the Kinect style sensor that can be used for robot localization, navigation, and path planning. However, ORB features turn out to be less accurate and also less reliable [10]. In the future, we will try to use GPU-based parallel computing like SIFTGPU [11] and SURFGPU [12] to do the feature extraction procedure and also we will evaluate the 3D estimated trajectory and the 3D model with ground truth data.

References

[1] Fioraio, Nicola, and Kurt Konolige. "Realtime visual and point cloud slam." *Proc. of the RGB-D workshop on advanced reasoning with depth cameras at robotics: Science and Systems Conf.(RSS)*. Vol. 27. 2011.

[2] Henry, Peter, et al. "RGB-D mapping: Using depth cameras for dense 3D modeling of indoor environments." *Experimental Robotics*. Springer Berlin Heidelberg, 2014.

[3] Grisetti, Giorgio, et al. "Efficient estimation of accurate maximum likelihood maps in 3d." *Intelligent Robots and Systems, 2007. IROS 2007. IEEE/RSJ International Conference on*. IEEE, 2007.

[4] Endres, Felix, et al. "3-D Mapping With an RGB-D Camera." 1-11.

[5] Sturm, Jürgen, et al. "A benchmark for the evaluation of RGB-D SLAM systems." *Intelligent Robots and Systems (IROS), 2012 IEEE/RSJ International Conference on*. IEEE, 2012.

[6] Lee, Donghwa, Hyongjin Kim, and Hyun Myung. "2D Image Feature-Based Real-Time RGB-D 3D SLAM." *Robot Intelligence Technology and Applications 2012*. Springer Berlin Heidelberg, 2013. 485-492.

[7] Rublee, Ethan, et al. "ORB: an efficient alternative to SIFT or SURF." *Computer Vision (ICCV), 2011 IEEE International Conference on*. IEEE, 2011.

[8] Fischler, Martin A., and Robert C. Bolles. "Random sample consensus: a paradigm for model fitting with applications to image analysis and automated cartography." *Communications of the ACM* 24.6 (1981): 381-395.

[9] Kummerle, Rainer, et al. "g 2 o: A general framework for graph optimization." *Robotics and Automation (ICRA), 2011 IEEE International Conference on*. IEEE, 2011.

[10] Endres, Felix, et al. "An evaluation of the RGB-D SLAM system." *Robotics and Automation (ICRA), 2012 IEEE International Conference on*. IEEE, 2012.

[11] Ohbuchi, Ryutarou, and Takahiko Furuya. "Accelerating bag-of-features sift algorithm for 3d model retrieval." *Proc. SAMT 2008 Workshop on Semantic 3D Media (S-3D)*. 2008.

[12] Terriberry, Timothy B., Lindley M. French, and John Helmsen. "GPU accelerating speeded-up robust features." *Proc. Int. Symp. on 3D Data Processing, Visualization and Transmission (3DPVT)*. 2008.

Advanced Materials Research Vols. 989-994 (2014) pp 2655-2658
© (2014) Trans Tech Publications, Switzerland
doi:10.4028/www.scientific.net/AMR.989-994.2655

Research Progress in Topological Relations of Objects with Holes

DI Shuang[1,a]，ZHANG Ji-mang[1]，SHI Yun-fei[1]，ZHANG Ling-ling[1]

[1]School of Resources & Environment, Linyi University, Linyi 276000 China

[a]xiaodi_1980@163.com

Keywords: topology relations; space objects with holes; D9-intersection model; 4-4ID model; HFM model

Abstract. The topology relation is the important basis of GIS data modeling, spatial query, spatial analysis, spatial reasoning and so on. This paper summarizes the current research progress of topological relations between complicated objects (with holes). In accordance with the order of the number of holes, respectively introduce D9-intersection model, 4-4ID model, HFM model and so on, and then analyzes their presentation skills, advantages and defects, so as to provide reference for subsequent research.

Introduction

Spatial relations theories have always been the hot spots of the GIS and related disciplines research at home and abroad [1]. As the most basic spatial relation, topological relations are the research foundation of space analysis [2], topological query [3], spatial reasoning [4] and so on. Currently, many researches focus on the topological relations between simple spatial objects in two-dimensional space and related theories and technologies have been realized by some commercial softwares such as ArcGis, SuperMap etc. Objects that exist in the real world, however, tend to be complex. With the deep and wide application of GIS, existing topological relations theories between simple spatial objects cannot satisfy the current application requirements. Many scholars focus on researching spatial topological relations between objects with holes and hope to provide theoretical basis for the more complicated and deep applications. The purpose of the paper is to summary the existing research results and to compare the advantages and disadvantages of them so as to give reference for the future research.

Topology Relation Mode of Spatial Object with Holes

In the real world, spatial objects are often complicated, such as holes, separate subdivisions and so on. For example, the Italian territory includes several separate islands in addition to the mainland and with a hole (because it is completely surrounded by the Vatican). With the development of GIS application, people play more and more attention on topology relation model for region with holes [5].

2.1 early study for topological relations between areas with hole

In 1994, Egenhofer [6] adopted two concepts which are total region and holes and discussed the relation between two regions with holes. Regions *A* and *B* respectively have *n* and *m* holes, Egenhofer describes the topological relation between them as *A* collection of the following four relations: (1) the total region of *A* and the total region of *B*; (2) the total region of *A* and each hole of *B*; (3) the total region of *B* and each hole of *A*; (4) each hole of *A* and each hole of *B*. Using a *(n+1)*(m+1)* matrix represent the topological relation between two objects, but the problem is that the order of the holes.

Climentini [7] took compound region as the research objects. For two compound regions A and B which respectively contains m and n simple regions, are divided into m+n+2 regions, that is m+n simple regions and two composite regions. In the matrix, the value of position (i,j) is the topological relations between the regions of row i and the column j. The defects of the model is that the matrix can't represent complex regions with holes.

2.2 D9-intersection model

The 9-intersection model has ambiguity when representing the topological relations between complex regions. The model can't distinguish internal complement and external complement as well as internal boundary and external boundary respectively intersect with another region, finally may lead to the same 9-intersection matrix corresponding to a variety of topological relations. The 5 topological relations in Fig.1 are obvious different, for example, but correspond to the same 9-intersection matrix:

$$R_a = R_b = R_c = \begin{pmatrix} 1 & 1 & 1 \\ 1 & 1 & 1 \\ 1 & 1 & 1 \end{pmatrix}$$

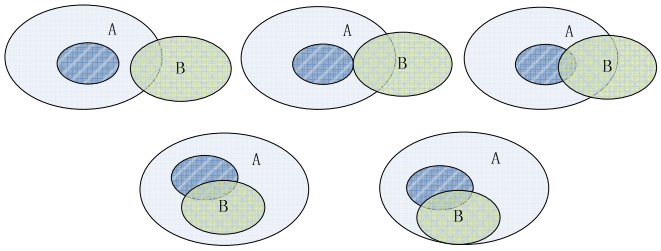

Fig.1 Fuzziness of 9-intersection model (modified from Egenhofer [5]

Against the defect of 9-intersection model, in 2009, OuYang [5] proposed a model that extended 9-intersection model to D9-intersection model. D9-intersection model can express topological relation of region with a hole. In the model, A^o、$\partial_{in}A$、$\partial_{out}A$, A^-,A^h,$\bar{A}$ respectively express the internal, internal boundary (when A with no hole is empty), external boundary, external, hole (when A with no hole is empty), complementary set(as shown in Fig.2). The elements of 9-intersection matrix is extended to binary code, using a five binary code $m_{ij} = x_4\ x_3\ x_2\ x_1\ x_0$, $1 \leqq i, j \leqq 3$, and then transform the binary code into the corresponding decimal number. As the corresponding values of the elements in model, the model can represent the intersection of each part of regions A and B.

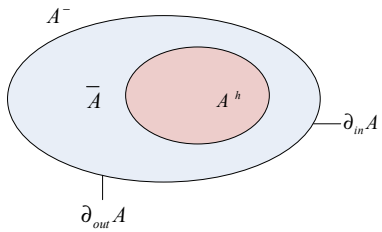

Fig.2 The expression of region with hole in D9-intersection model

Compared with 9-intersection model, D9-intersection model can represent the topological relations between simple regions, as well the topological relations between regions with hole, also will be able to distinguish the topological relations that the 9-intersection model cannot differentiate, so the expression ability of D9-intersection model is stronger than 9-intersection model. But the inference speed of D9-intersection model is relatively lower, memory is relatively large. This model use a five binary code as the values of matrix element, when space complexity of the object increases to a certain extent will go beyond the scope of the code that can be indicial, therefore, there are some shortcomings.

2.3 4-4ID model

In 2009, Liu bo [8] proposed 4-4ID model on the basis of 4-intersection model, the concept of total region and hole in surface object with holes, will define the object with hole as the total region $A^{\#}$ and the hole A^*,and $A^{\#}=A \cup A^*$. For objects with holes A and B, we can determine spatial topological relations between A and B by comparing the relation between t $A^{\#}$, A^*, $B^{\#}$ and B^*, but the model can only describe the topological relations between surface objects with a hole. The equation of 4-4ID model is as following [8]:

$$R(A^{\#},\ B^{\#})=\begin{bmatrix} A^{\#\circ}\bigcap B^{\#\circ} & A^{\#}-B^{\#} \\ B^{\#}-A^{\#} & \partial A^{\#}\bigcap\partial B^{\#} \end{bmatrix} \tag{1}$$

$$R(A^{\#},\ B^{*})=\begin{bmatrix} A^{\#\circ}\bigcap B^{*\circ} & A^{\#}-B^{*} \\ B^{*}-A^{\#} & \partial A^{\#}\bigcap\partial B^{*} \end{bmatrix} \tag{2}$$

$$R(A^{*},\ B^{\#})=\begin{bmatrix} A^{*\circ}\bigcap B^{\#\circ} & A^{*}-B^{\#} \\ B^{\#}-A^{*} & \partial A^{*}\bigcap\partial B^{\#} \end{bmatrix} \tag{3}$$

$$R(A^{*},\ B^{*})=\begin{bmatrix} A^{*\circ}\bigcap B^{*\circ} & A^{*}-B^{*} \\ B^{*}-A^{*} & \partial A^{*}\bigcap\partial B^{*} \end{bmatrix} \tag{4}$$

4-4 ID model effectively represent topology relation between two surface objects which everyone have a hole, but when the model represents topological relations between surface objects with hole, only considering the object with a hole and it can't represents topological relations between surface objects containing 2 and more than 2 holes. More research is needed to find the representation method for topological relations between surface objects with multiple holes.

2.4 HFM model

HFM model proposed by Vasardani [9], which can represent the topological relation between the object with multiple holes and the surface object without hole. HFM model divided an object with multiple holes into complement and some holes, respectively represented by a few simple spatial objects, and then represented the region with multiple holes according to the principle of set theory. Assuming that the region n - B' has n holes, it satisfied with the following conditions [9]:

(1)The union set of n-B, H1… Hn-1, Hn is B. (2) The region B contains Hi, and the values of i is from 1 to n. (3) The region Hi is disjoint to Hj, and the value of i and j is from 1 to n, and that i and j is not equal.

HFM model can represent the topological relations between a simple region *A* and region *n-B'* with multiple holes which is denoted by *r(A, n-B')*. The equation is as following [9]:

$$\begin{aligned} &r(A,n-B^{'})=\bigcup_{i=1}^{n} r(A,B_i),i=1...n,B_i\in t_{RRh} \\ &\forall i:i=1...n,B_i=B-\overline{H_i^{o}} \end{aligned} \tag{5}$$

This model realizes the representation of the topological relation between a simple region and region with multiple holes. Spatial object is not divided into the boundary and interior in this model, so more intuitive when we represent it, but it is unfavorable to distinguish touch and disjoint, and at the same time the hole of complex region has sequential, for the difference of serial number for holes, the representation of topological relations is also different. The efficiency of the model associates with the number of holes in the object, the more holes the objects have, and the lower the efficient is.

Conclusion

Currently, most researches for topological relations are based on 2D spatial object. Proposed D9-intersection model, 4-4ID model and HFM model can preferably represent the topological relations between regions with hole, but these models are also defective. D9-intersection model use a five binary code as the element values in the matrix instead of the nested matrix, the matrix equation is relatively simple, but the complexity of the object is limited. 4-4ID model can only represent the relations between the objects with a hole. HFM model has an advantage over expressing the relation between spatial object with multiple holes and simple object, but the relations which are able to distinguish is limited.

Acknowledgements

This work was financially supported by the National Natural Science Foundation of China (Grant No. 41201407) and National Undergraduate Training Programs for Innovation and Entrepreneurship of Linyi University (Grant No. 201310452035).

References

[1] Chen, Jun, and Ren-liang Zhao. Spatial relations in GIS: a survey on its key issues and research progress: Acta Geodaetica et Cartographica Sinica28.2 (1999): 95-102

[2] Guo R Z. Spatial Analysis. Wuhan: Wuhan Technology University of Surveying and Mapping Press. 1-14(1997)

[3] Lin, P. L., and W. H. Tan. An efficient method for the retrieval of objects by topological relations in spatial database systems: Information processing & management 39.4 (2003): 543-559

[4] Yau, Stephen S-T., and Qing-Long Zhang. On completeness of reasoning about planar spatial relationships in pictorial retrieval systems: Communications in Information & Systems 4.3 (2004): 211-234

[5] OUYANG, Ji-hong, et al. Extended 9-intersection model for description of topological relations between regions with holes: Journal of Jilin University (Engineering and Technology Edition) 6 (2009): 033

[6] Egenhofer, Max J., Eliseo Clementini, and Paolino Di Felice. Topological relations between regions with holes: International Journal of Geographical Information Science 8.2 (1994): 129-142

[7] Clementini, Eliseo, Paolino Di Felice, and Gianluca Califano. Composite regions in topological queries: Information Systems 20.7 (1995): 579-594

[8] Liu B, Ruan J, et al. Formal Description of Regions with Hole's Topological Relations: Geomatics and Information Science of Wuhan University34.1 (2009): 68-71.

[9] Vasardani M, Egenhofer M J. Comparing relations with a multi-holed region//Spatial Information Theory. Springer Berlin Heidelberg (2009): 159-176

Advanced Materials Research Vols. 989-994 (2014) pp 2659-2662
© (2014) Trans Tech Publications, Switzerland
doi:10.4028/www.scientific.net/AMR.989-994.2659

Complexity Research on Second Class Orthogonal Weight Function Neural Networks

Daiyuan Zhang [a], Ran Zhao [b]

College of Computer, Nanjing University of Posts and Telecommunications, Nanjing, Jiangsu 210003, China

[a]email: dyzhang@njupt.edu.cn, [b]email: zhaoran_njupt_pg@163.com

Keywords: Weight Function; Neural Network; Orthogonal; Complexity;

Abstract. Weight function neural network is a new kind of neural network developed in recent years, which has many advantages, such as finding globe minima directly, good performance of generalization, extracting some useful information inherent in the problems and so on. Time complexity is an important measure of algorithm. This paper studies the complexity of neural network using second class orthogonal weight functions. The results indicate that the neural network has a linear relationship with the dimensions of input layer and output layer, an $O(n^3)$ relationship with the number of samples. Finally gives some simulation experiments for time complexity.

Introduction

Weight function neural network is a new kind of neural network developed in recent years, which has many advantages, such as finding globe minima directly, good performance of generalization, extracting some useful information inherent in the problems and so on [1]. For traditional neural networks has many shortcomings, such as slow convergence of the algorithm, the optimal solution can not be obtained, which are to some extent limited the development of neural network. Reference [1] proposed a new learning algorithm to overcome the shortcomings of traditional algorithms in which the constant weight will be transformed into weight function after training, which can effectively reflect implicit valuable information in the sample.

Based on the weight function neural network theory, this paper mainly studies the complexity of second class neural networks using orthogonal weight functions.

Structure of Second Class Weight Function Neural Network

The weight function neural network is a new type of neural network. The input layer connects directly to neurons without any hidden layers. Second class weight function neural network in which input layer has *m* nodes and the output layer has *n* nodes would be like below [1].

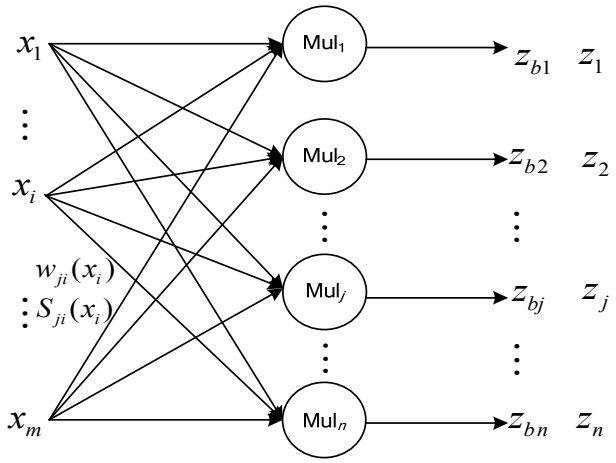

Fig.1. Structure of the weight function neural network

Training weight function neural network is to solve the weight function; the literature [1] gives the training algorithm of how to get the weight function as follows:

Suppose there are *N+2* samples, the corresponding vector of the *i*-th input node which can be expressed as follows:

$$x_i = (x_{i0}, x_{i1}, \cdots, x_{i(N+1)}) \tag{1}$$

Accordingly, the corresponding destination vector can be expressed as follows:

$$z = (z_0, z_1, \cdots, z_{N+1}) \tag{2}$$

In which $z_j\,(j = 0,1,\cdots,N-1)$ is an *n*-dimensional column vector.

According to the literature [1], we can get the corresponding interpolation points:

$$Ip_i = \{(x_{i0}, z_0^{\rho_i}), (x_{i1}, z_1^{\rho_i}), \cdots (x_{i(N+1)}, z_{N+1}^{\rho_i})\} \tag{3}$$

With the interpolation points, approximate weight function can be determined.

Complexity Analysis of the Second Class Weight Function Neural Network

For multidimensional input and output of the second class weight function neural network, it is more complex to analyze the complexity. So only assume one-dimensional output for analysis.

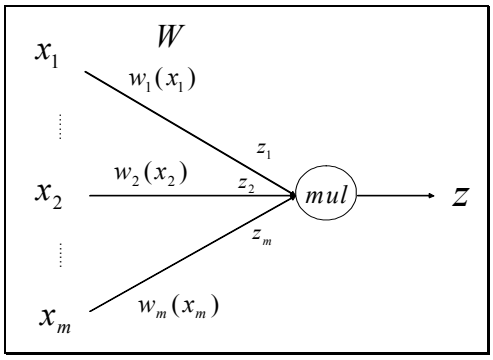

Fig.2. *m* dimension input, 1 dimension output weight function neural network

Assume the number of the training sample is $k+1$, the orthogonal multinomial [2][3] can be constructed as below to approach the weight function:

$$S^*(x) = a_0^* p_0(x) + a_1^* p_1(x) + \cdots + a_k^* p_k(x) \tag{4}$$

In order to facilitate the analysis, just give the $w_1(x_1)$ solving approach, $w_i(x_i)$ are in the same way. According to the weight function neural network training algorithm, $S^*(x)$ has the same value as the weight function at the training samples.

$$\begin{cases} z_{10} = a_0^* p_0(x_{10}) + a_1^* p_1(x_{10}) + \cdots + a_k^* p_k(x_{10}) \\ z_{11} = a_0^* p_0(x_{11}) + a_1^* p_1(x_{11}) + \cdots + a_k^* p_k(x_{11}) \\ \cdots \\ z_{1k} = a_0^* p_0(x_{1k}) + a_1^* p_1(x_{1k}) + \cdots + a_k^* p_k(x_{1k}) \end{cases} \tag{5}$$

The value of $a_0 \cdots a_k$ can be calculated by solving the equation above. Then the approximate orthogonal weight function can be easily determined.

Standard LU decomposition method requires calculating large matrix operation directly [4], involved the calculation of a large amount of data, the computer cache is not well used, and this will reduces efficiency of operation.

LU decomposition needs to solve the linear equations:

$$\mathrm{A}x = b \tag{6}$$

According to the Gaussian elimination rule, after a series elementary row transforming matrix A can be decomposed into plot of the unit lower triangular matrix L and an upper triangular matrix U:

$$\begin{bmatrix} a_{11} a_{12} \cdots a_{1n} \\ a_{21} a_{22} \cdots a_{2n} \\ \vdots \quad \vdots \quad \quad \vdots \\ a_{n1} a_{n2} \cdots a_{nn} \end{bmatrix} = \begin{bmatrix} 1 & & & \\ l_{21} & 1 & & \\ \vdots & \vdots & \ddots & \\ l_{n1} & l_{n2} & \cdots & 1 \end{bmatrix} \begin{bmatrix} u_{11} u_{12} \cdots u_{1n} \\ & u_{22} \cdots u_{2n} \\ & & \ddots \ \vdots \\ & & & u_{nn} \end{bmatrix} or \, \mathrm{A} = LU \tag{7}$$

So equation (6) can be transformed into:

$$LUx = b \tag{8}$$

It is equivalent to two groups trigonometric equations $Ly = b$ and $Ux = y$. According to the matrix multiplication:

$$\begin{cases} u_{1j} = a_{1j} \left(j = 1, 2, \cdots, n \right) \\ l_{i1} = a_{i1} / u_{11} \left(i = 1, 2, \cdots, n \right) \\ u_{kj} = a_{kj} - \sum_{m=1}^{k-1} l_{km} u_{mj} \left(j = k, k+1, \cdots, n \right) \\ l_{ik} = \left(a_{ik} - \sum_{m=1}^{k-1} l_{im} u_{mk} \right) / u_{kk} \left(i = k+1, k+2, \cdots, n; k = 2, 3, \cdots, n \right) \end{cases} \tag{9}$$

Formula (9) is the standard LU decomposition in which needs calculation of a large matrix data. So it has a lower efficiency. In order to solve the problem, now give an introduction to the block LU decomposition algorithm.

Transfer matrix **A** into 2×2 blocks, equation $A = LU$ can be expressed as below:

$$\begin{bmatrix} A_{11} A_{12} \\ A_{21} A_{22} \end{bmatrix} = \begin{bmatrix} L_{11} & \\ L_{21} L_{22} \end{bmatrix} \begin{bmatrix} U_{11} U_{12} \\ & U_{22} \end{bmatrix} \tag{10}$$

According to the matrix multiplication principle：

$$A_{11} = L_{11} U_{11} \tag{11}$$

$$A_{12} = L_{11} U_{12} \tag{12}$$

$$A_{21} = L_{11} U_{12} \tag{13}$$

$$A_{22} = L_{21} U_{12} + L_{22} U_{22} \tag{14}$$

The steps of LU block decomposition algorithm:

1. Make the block matrix A_{11} in formula (11) LU decomposition, get L_{11} and U_{11}.
2. Inverse the matrix L_{11} and formula (12) can be transformed into $U_{12} = L_{11}^{-1} A_{12}$.
3. Inverse the matrix U_{11} and formula (13) can be transformed into $L_{21} = A_{21} U_{11}^{-1}$.
4. Rewrite formula(14), assume $A_{22}^{'} = A_{22} - L_{21} U_{12}$, then formula (14) can be expressed like $A_{22}^{'} = L_{22} U_{22}$.

Make LU decomposition to the matrix $A_{22}^{'}$. As long as the appropriate size of each block is selected, operations of the sub-matrices are more likely calculated in caches which can improve the speed of the algorithm. The multiplication operations of the standard LU decomposition algorithm are about $\frac{n(2n-1)(n-1)}{6}$, division operations are about $\frac{n(n-1)}{2}$.

Conclude that: for *m* dimensional input, one output dimension second class orthogonal function neural network, it needs to solve *m* linear equations. Generally, for *m* dimensional input *n* dimensional output second class orthogonal function neural network, $m \times n$ linear equations need solved. Obviously, the complexity of the algorithm has a linear relationship with input dimensions and output dimensions.

Experiments and Test Results

The purpose of this study was to verify the relationship between the second class orthogonal weight function neural network algorithm complexity and the input layer dimension, output layer dimension, and the number of samples. Experimental operating system: Windows 7. Programming environment: Matlab R2012b.

There are three experiments required to de done:

1. The second type orthogonal weight function neural network algorithm complexity experiments with different sample numbers.
2. The second type orthogonal weight function neural network algorithm complexity experiments with different input layer dimensions.
3. The second type orthogonal weight function neural network algorithm complexity experiments with different output layer dimensions.

And the results are as follows:

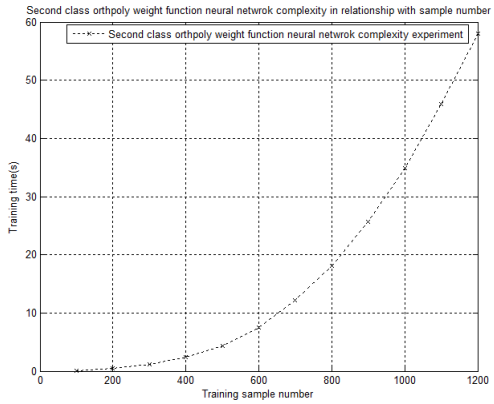

Fig.3. Complexity relationship with sample numbers

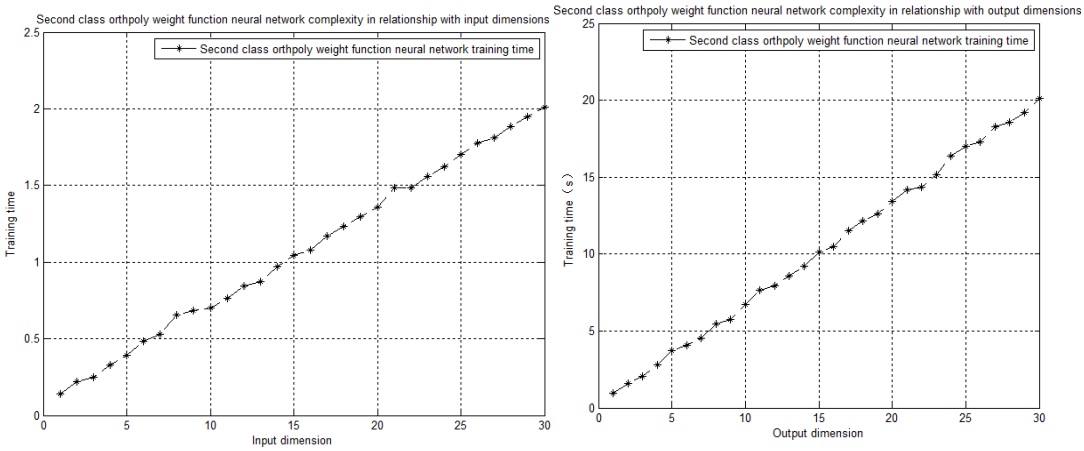

Fig.4. Complexity relationship with input and output dimensions

References

[1] Zhang Dai-yuan. New Theories and Methods on Neural Networks [M]. Beijing: Tsinghua University Press, 2006

[2] J. G. Yu, J.E. Lefebvre. Guided waves in multilayered hollow cylinders: The improved Legendre polynomial method[J]. Composite Structures, 2013(95): 419-429

[3] Antonio J.Duran, Vanesa Sanchez-Canales. Orthogonal matrix polynomials whose differences are also orthogonal[J]. Journal of Approximation Theory, 2014: 112-127

[4] Caner Ozcan, Baha Sen. Investigation of the performance of LU decomposition method using CUDA [C]. First World Conference on Innovation and Computer Sciences, 2012(1): 50-54

Advanced Materials Research Vols. 989-994 (2014) pp 2663-2666
© (2014) Trans Tech Publications, Switzerland
doi:10.4028/www.scientific.net/AMR.989-994.2663

Research of the First Kind of Padé Weight Function Neural Networks

Daiyuan Zhang[a],Yan Xu[b]

College of Computer, Nanjing University of Posts and Telecommunications, Nanjing, Jiangsu 210003, China

[a]email: dyzhang@njupt.edu.cn, [b]email: xuyanwr@126.com

Keywords: Neural Network; Spline Weight Function; Padé Approximation; Time Complexity;

Abstract. Traditional algorithms of training neural networks have some weakness. A new approach using weight function neural networks was proposed in recent years, which overcomes the shortcomings of traditional neural networks. This paper takes Padé approximation as weight functions and we get the method of how to find the Padé weight functions with given samples. Then complexity is also analysed in detailed in this paper. Finally simulation experiments are done to verify the results.

Introduction

Artificial Neural Network is a kind of advanced computing and pattern recognition technology. It simulates virtual neurons to solve problems in computer applications based on the principle of neural cell in biology. Traditional neural network such as BP, RBF and so on have some weakness. When the network has been trained, the entire network is a connection of discrete numbers, can not reflect the information of samples. Article [1] put forward a new model and algorithm, named weight function neural network. This novel neural network algorithm overcomes the defects above completely [2].

This paper research the time complexity of the first kind of Padé weight function neural networks.

The First Kind of Spline Weight Function Neural Network

Traditional neural networks have shortcomings due to their limitations in the algorithm, but the first kind of spline weight function neural network has many advantages.

Weight function neural network topology structure is simple, only two layers, and the weight of input layer and neurons are full interconnection, while output layer has no weight. Assuming input layer of the network has m nodes，and output layer has n nodes，The structure of the first kind of Padé weight function neural network is shown in the figure below [3] [4] [5]:

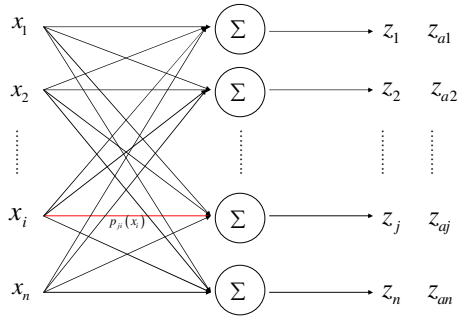

Fig. 1 The structure of the first kind of Padé weight function neural network

Complexity Research of the First Kind of Padé Weight Function Neural Network

Padé approximation of $f(x)$ meet the conditions:

$$\sum_{i=0}^{\infty} c_i x^i - P(M,x)/Q(N,x) = O(x^{\alpha}) \tag{1}$$

$O(x^{\alpha})$ is power function whose format is like $\sum_{i=\alpha}^{\infty} c_i x^i$ .The coefficient of $P(M,x)/Q(N,x)$ is defined as $(m,n)_f$.

When $n \le 4$, it is convenient using the gaussian elimination method compute $P(M,x)$ and $Q(N,x)$ [6].But when n is lager, the calculation is more tedious, not suitable for use [7]. We can use recursive method, Start from $(m_0,n_0)_f,(m_1,n_1)_f \cdots$, which can be easily get. $(m,n)_f$, $(m,n)_f$ can be got from $C-$ chart by recursive using the Padé approximation.

$C-$ chart is a two dimension chart, among them:

$$C(m/n) = \det H(m,n-1,n-1)$$
$$= \det \begin{bmatrix} c_m & c_{m-1} & \cdots & c_{m-n+1} \\ c_{m+1} & c_m & \cdots & c_{m-n+2} \\ \vdots & \cdots & \cdots & \vdots \\ c_{m+n-1} & c_{m+n-2} & \cdots & c_m \end{bmatrix} \tag{2}$$

With the help of $C-$ chart and two of the basic definition, we can get:

$$(m,n)_f = T_n^m (m+1,n-1)_f + (1-T_n^m)(m+1,n)_f,$$
$$T_n^m = \frac{\alpha_{m+1,n}^{m+1}}{\alpha_{m+1,n}^{m+1} - \alpha_{m+1,n-1}^{m+!}} \tag{3}$$
$$(m,n)_f = (m+1,n-1)_f + U_n^m z)m,n-1)_f,$$
$$U_n^m = -\frac{\alpha_{m+1,n-1}^{m+1}}{\alpha_{m,n-1}^{m}} \tag{4}$$

Specific form of algorithm is as follows:

$$\left.\begin{aligned} \frac{\eta_{2j}(z)}{\theta_{2j}(z)} &= \left[\frac{m-j}{j}\right]_f \\ \frac{\eta_{2j+1}(z)}{\theta_{2j+1}(z)} &= \left[\frac{m-j-1}{j}\right]_f \end{aligned}\right\} \tag{5}$$

A recursive according to the formula (3)(4)(5) can get

$$\frac{\eta_{2j}(z)}{\theta_{2j}(z)} = \frac{\eta_{2j-2}(z) - z(\eta_{2j-2}/\eta_{2j-1})\eta_{2j-1(z)}}{\theta_{2j-2}(z) - z(\eta_{2j-2}/\eta_{2j-1})\theta_{2j-1(z)}}, j = 1,2,\cdots m \tag{6}$$

$$\frac{\eta_{2j+1}(z)}{\theta_{2j+1}(z)} = \frac{\left[\bar{\eta}_{2j}\eta_{2j-1}(z) - \bar{\eta}_{2j-1}\eta_{2j}(z)\right]/(\bar{\eta}_{2j} - \bar{\eta}_{2j-1})}{\left[\bar{\eta}_{2j}\theta_{2j-1}(z) - \bar{\eta}_{2j-1}\theta_{2j}(z)\right]/(\bar{\eta}_{2j} - \bar{\eta}_{2j-1})}, j = 1,2,\cdots,m-1 \tag{7}$$

Among $\bar{\eta}_k$ is the coefficient of highest order term of $\eta_k(z)$. Initial values for recursion is

$$\eta_0(z) = \sum_{i=0}^{m} c_i z^i, \eta_1(z) = \sum_{i=0}^{m+1} c_i z^i, \theta_0(z) = \theta_1(z) = 1 \tag{8}$$

Assume the addition operation time is t_1, the subtraction operation time is t_2, multiplication operation time is t_3, Division of time is t_4. The total computation which using the recursive alternating operation is:

$$n\left[(m+n)t_3 + (m+n)t_1\right] + (n-1)\left[2(m+n)t_3 + (m+n)t_1\right]$$
$$\approx n(m+n)(3t_3 + 2t_1) = O(n(m+n)) \tag{9}$$

The reference shows the time complexity of Newton interpolation is $T_{newton} = O\left(N^2\right)$.

Assume that the unit time of operation is as defined above, the training time of the neural network what have m input nodes, n output nodes and $N+1$ training samples is:

$$T = (T_{newton} + T_{pade})mn + mnt_1 = (A + B)mn$$
$$A = O(N^2) \quad (10)$$
$$B = O(\theta(\phi + \theta))$$

Test Results

Determine the input of objective function, set the objective function as follows:

$$z = \sin(x_1 + x_2) \quad (11)$$

To ensure the relationship between the time of the first kind of Padé weight function neural network and the number of samples. Set the number of samples to different values. Different times can be get in these conditions.

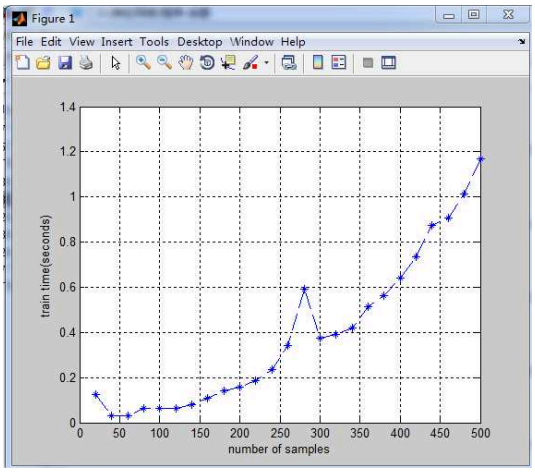

Fig. 2 Time complexity about the first kind of Padé weight function neural network based on the number of samples

To ensure the relationship between the time of first kind of Padé weight function neural network and the number of samples. Set the number of input (output) sample to different values. Different times can be get in these conditions.

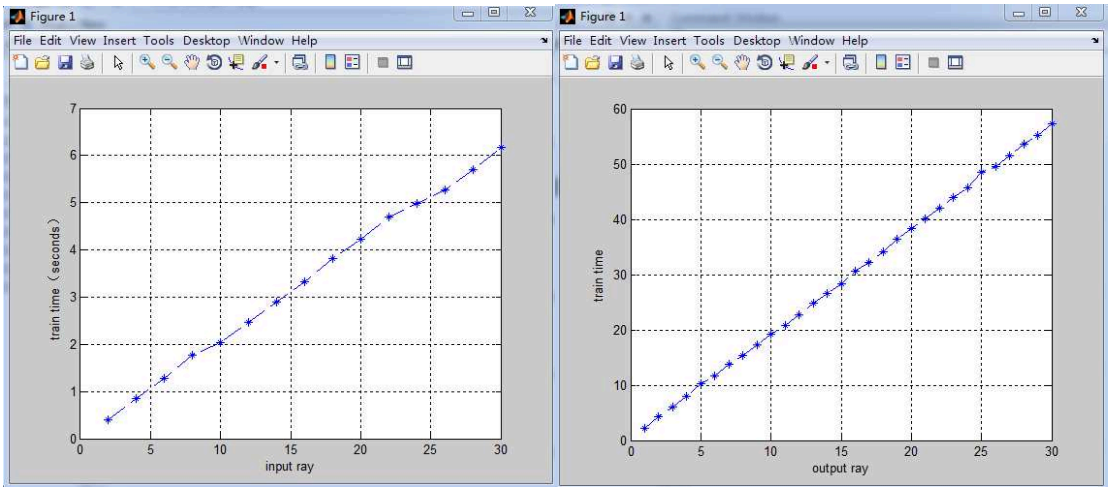

Fig. 3 Time complexity about the first kind of Padé weight function neural network based on the number of input(output) dimensions

Conclusion

This paper analysis the structure and the algorithm of the first kind of Padé weight function neural network, then analysis the corresponding time complexity. Then verify the result by the experiment. The complexity of first kind of Padé weight function neural network is increasing by the number of sample quadric, and growth by the number of input dimension and output dimension liner.

References

[1]Daiyuan Zhang. Neural Network New Theory and Method [M]. Beijing: Tsinghua University Press, 2006

[2]Yi Ding, Qi Feng. A modular neural network architecture with concept [J]. Neurocomputing, 2014,125(11): 3–6

[3]Daiyuan Zhang. A new kind of algorithm in Spline weight function neural network [J]. Systems Engineering and Electronics, 2006, 28(9): 1434-1446

[4]Yu Yao. Research of Padé weight function neural network and the optimal routing algorithm[D]. Nanjing: NJUPT, 2010

[5]Paul Sablonnière. B-splines and Hermite–Padé approximants to the exponential function[J]. Journal of Computational and Applied Mathematics, 2008, 219(2): 509–517

[6]Guido Claessens. On the Newton-Padé approximation problem[J]. Journal of Approximation Theory, 1978, 22: 150-160

[7]Ognyan Kounchev, Hermann Render. Padé approximation for a multivariate Markov transform[J]. Journal of Computational and Applied Mathematics, 2008, 219(2): 416–430

Advanced Materials Research Vols. 989-994 (2014) pp 2667-2670
© (2014) Trans Tech Publications, Switzerland
doi:10.4028/www.scientific.net/AMR.989-994.2667

Time Complexity Research on the Second Type Neural Networks of Padé Weight Functions

Daiyuan Zhang[a], Lei Yang[b]

College of Computer, Nanjing University of Posts and Telecommunications, Nanjing, Jiangsu 210003, China

[a]email: dyzhang@njupt.edu.cn, [b]email: yangleiasdz@gmail.com

Keywords: Neural Network; Time Complexity; Padé Weight Function; Newton Interpolation

Abstract. Time complexity is an important measure of algorithm. The main purpose of this paper is to research the time complexity of the second category of Padé weight function neural network and find out the factors which affect its time complexity. In this paper, firstly, the second category of Padé weight function neural network algorithm is introduced. Then through the analysis of the key steps of the algorithm, the time complexity is given. After MATLAB simulation, the experimental results verify the theoretical analysis of the results. Therefore, its time complexity is related to input dimension, output dimension and the number of training samples.

Introduction

From voice recognition software to the car autopilot technology recently, the artificial neural networks have played a huge role. However, the traditional neural network algorithms have many shortcomings. Such as the widely used BP algorithm, with slow convergence, often need to iterate thousands of times. This is also a way to limit the development of neural networks. Literature [1] proposed weight function neural network algorithm, unlike traditional neural networks. Its weight is not a constant, but a function which can reflect the training samples accurately and it's able to overcome the shortcomings of traditional neural networks. The Padé weight function neural network is one of them. This paper has done a detailed analysis of the error formula and the algorithm complexity. Also simulation experiments were done to validate it.

Topology and Training Algorithm of Padé Weight Function Neural Network

The topology of the second type Padé weight function neural network is as follows [1]:

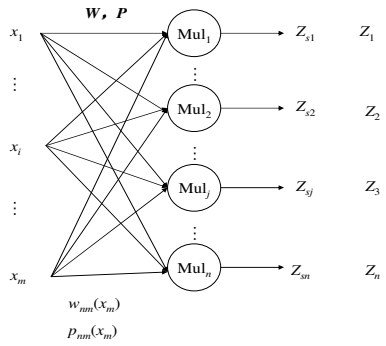

Figure 1 Topology of the second type Padé weight function neural network

Suppose there are *N*+2 samples need to be trained, the corresponding vector of the *i*-th input node which can be expressed as $x_i = \left(x_{i0}, x_{i1}, \cdots, x_{i(N+1)}\right)$. Accordingly, the corresponding destination vector can be expressed as $z = \left(z_0, z_1, \cdots, z_{N+1}\right)$. In which $z_j \left(j = 0,1,\cdots, N-1\right)$ is an n-dimensional column vector. Suppose there are $N+1$ distinct values, such as $x_0, x_1, x_2 \cdots x_N$ and their corresponding function values are $f\left(x_0\right), f\left(x_1\right), f\left(x_2\right), \cdots f\left(x_N\right)$.

With the interpolation points, we can get the Newton interpolation polynomial by using Newton interpolation theory as follows:

$$P_n(x) = a_0 + a_1(x - x_0) + a_2(x - x_0)(x - x_1) + \cdots + a_n(x - x_0)(x - x_1)\cdots(x - x_{n-1}) \tag{1}$$

Because a function of the Taylor series is always with slow convergence speed and narrow convergence range, using this method is sometimes unable to obtain ideal results [2] [3].This time we adopt rational function approximation methods, such as Padé approximation, which tends to get the desired results [4].

Error Analysis

The measure of approximation can be expressed as the following expression [1]:

$$\left\|z_j - z_{jp}\right\| = \left\|\prod_{i=1}^{m} w_{ji}(x_i)\left(1 - \prod_{i=1}^{m}\frac{p_{ji}(x_i)}{w_{ji}(x_i)}\right)\right\| \leq= \kappa_j \cdot m \cdot \left(\prod_{\substack{l=1 \\ l\neq i}}^{m} w_{jl}(x_l)\right) \cdot \left(\max_i \left\|p_{ji}(x_i) - w_{ji}(x_i)\right\|\right) \tag{2}$$

$$\kappa_j = \max\left|-\left(1 + \frac{o(\delta_j)}{\sum_{i=1}^{m}\delta_{ji}(x_i)}\right)\right| = \max\left|1 + \frac{o(\delta_j)}{\sum_{i=1}^{m}\delta_{ji}(x_i)}\right| \tag{3}$$

κ_j is a number close to 1. Next the value of $\left\|p_{ji}(x_i) - w_{ji}(x_i)\right\|$ need to be analyzed, and for convenience, we can use $\left\|p_j(x) - w_j(x)\right\|$ to discuss the value.

$$\left\|w_j(x) - p_j(x)\right\|_\infty = \left\|w_j(x) - H_j(x) + H_j(x) - p_j(x)\right\|_\infty \leq \max_{x\in[x_0,x_n]}\left|w_j(x) - H_j(x)\right| + \max_{x\in[x_0,x_n]}\left|H_j(x) - p_j(x)\right| \tag{4}$$

For the value of $\left\|w_j(x) - H_j(x)\right\|_\infty$, it's known as $\left\|w_j(x) - H_j(x)\right\|_\infty < \frac{c_0 c_1}{n!}$.

And the value of $\left\|H_j(x) - p_j(x)\right\|_\infty$, according to the error formula, can be expressed as follows[5]:

$$H(x) - R_{mn}(x) = \frac{x^{2n+1}\sum_{i=0}^{M} r_i x^i}{Q_n(x)} \approx |r_0|\left|x^{2n+1}\right| \leq |r_0|, \ r_0 = a_{n+1}q_n + a_{n+2}q_{n-1} + \cdots + a_{2n}q_1 + a_{2n+1} \tag{5}$$

$$r_0 = \frac{\Delta_{n+1}}{\Delta_n}, \Delta_n = \det A_n, E_n \approx |r_0| = \left|\frac{\Delta_{n+1}}{\Delta_n}\right|, (|x| \leq 1) \tag{6}$$

Finally, the error formula of the second type Padé weight function neural network is as follows:

$$\left\|z_j - z_{jp}\right\| \leq \kappa_j \cdot m \cdot \left(\prod_{\substack{l=1 \\ l\neq i}}^{m} w_{jl}(x_l)\right) \cdot \left(\max_i \left\|p_{ji}(x_i) - w_{ji}(x_i)\right\|\right) < \kappa_j \cdot m \cdot \left(\prod_{\substack{l=1 \\ l\neq i}}^{m} w_{jl}(x_l)\right)\left(\frac{c_0 c_1}{n!} + E_n\right) \tag{7}$$

Time Complexity Analysis

Recursive method to get Padé approximation needs to use C-list. The so-called C-table, is defined by $C(m/n)$ [5].

$$C(m/n) = \det H(m, n-1, n-1) = \det\begin{bmatrix} c_m & c_{m-1} & \cdots & c_{m-n+1} \\ c_{m+1} & c_m & \cdots & c_{m-n+2} \\ \vdots & \vdots & \cdots & \vdots \\ c_{m+n-1} & c_{m+n-2} & \cdots & c_m \end{bmatrix} \tag{8}$$

The Baker algorithm based on the following two identities.

$$(m,n)_f = T_n^m (m+1,n-1)_f + (1-T_n^m)(m+1,n)_f, (m,n)_f = (m+1,n-1)_f + U_n^m z(m,n-1)_f \quad (9)$$

Where

$$T_n^m = \frac{C((m+1)/(n+1)) \cdot C((m+1)/(n-1))}{C((m+2)/n) \cdot C(m/n)}, \quad U_n^m = -\frac{C(m/(n-1)) \cdot C((m+1)/n)}{C((m+1)/(n-1)) \cdot C(m/n)} \quad (10)$$

Baker algorithm follows the steps:

$$\eta_{2j}(z)/\theta_{2j}(z) = [(m-j)/j]_f, \ \eta_{2j+1}(z)/\theta_{2j+1}(z) = [(m-j-1)/j]_f \quad (11)$$

And then we can get the follows:

$$\frac{\eta_{2j}(z)}{\theta_{2j}(z)} = \frac{\eta_{2j-2}(z) - z(\bar{\eta}_{2j-2}/\bar{\eta}_{2j-1})\eta_{2j-1}(z)}{\theta_{2j-2}(z) - z(\bar{\eta}_{2j-2}/\bar{\eta}_{2j-1})\theta_{2j-1}(z)}, \frac{\eta_{2j+1}(z)}{\theta_{2j+1}(z)} = \frac{[\bar{\eta}_{2j}\eta_{2j-1}(z) - \bar{\eta}_{2j-1}\eta_{2j}(z)]/(\bar{\eta}_{2j} - \bar{\eta}_{2j-1})}{[\bar{\eta}_{2j}\theta_{2j-1}(z) - \bar{\eta}_{2j-1}\theta_{2j}(z)]/(\bar{\eta}_{2j} - \bar{\eta}_{2j-1})} \quad (12)$$

Where $\bar{\eta}_k$ is the coefficient of the highest degree of $\eta_k(z)$, and initial value is $\eta_0(z) = \sum_{i=0}^{m} c_i z^i$, $\eta_1(z) = \sum_{i=0}^{m+1} c_i z^i$, $\theta_0(z) = \theta_1(z) = 1$. Using $[m+n,0]_f$, $[m+n-1,0]_f$ as the initial value to calculate is a very convenient and efficient way; and the total time needed is approximately:

$$n[(m+n)T_2 + (m+n)T_1] + (n-1)[2(m+n)T_2 + (m+n)T_1] \approx n(m+n)(3T_2 + 2T_1) = O(n(m+n)) \quad (13)$$

So by the recursive method to get the Padé approximation $P_L(x)/Q_M(x)$ of $f(x)$, The time complexity is $O(M(L+M))$, where L is the highest degree of $P_L(x)$ and M is the highest degree of $Q_M(x)$.Because that Training samples is N, there are N sample interpolation points and the time needed to get the Newton polynomial is $N(N-1)T_1 + \frac{N(N-1)}{2}T_2$.

The time of the recursive method to get the Padé approximation $P_L(x)/Q_M(x)$ of $f(x)$ is $M(L+M)(3T_2+2T_1)$ where L is the highest degree of $P_L(x)$ and M is the highest degree of $Q_M(x)$.Then we get the time of solving $m \times n$ Padé weight functions is

$$mn[N(N-1)T_1 + \frac{N(N-1)}{2}T_2 + M(L+M)(3T_2+2T_1)] \quad (14)$$

And its time complexity can be expressed as $mnO(N^2)$, where m is the input dimension, n is the output dimension, N is the number of samples.

Experiments and Results

There are four experiments required to de done to verify the error formula and the relationship between the algorithm complexity and the input layer dimension, output layer dimension, and the number of samples. Experimental operating system: Windows 7. Programming environment: Matlab R2012a.

And the results are as follows:

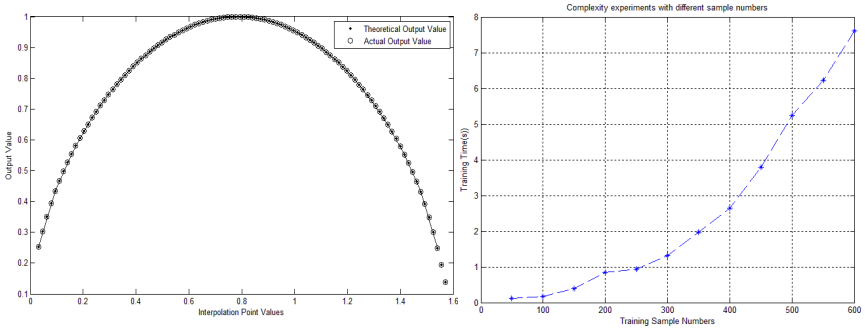

Figure 2 Error experiments and Complexity experiments with different sample numbers

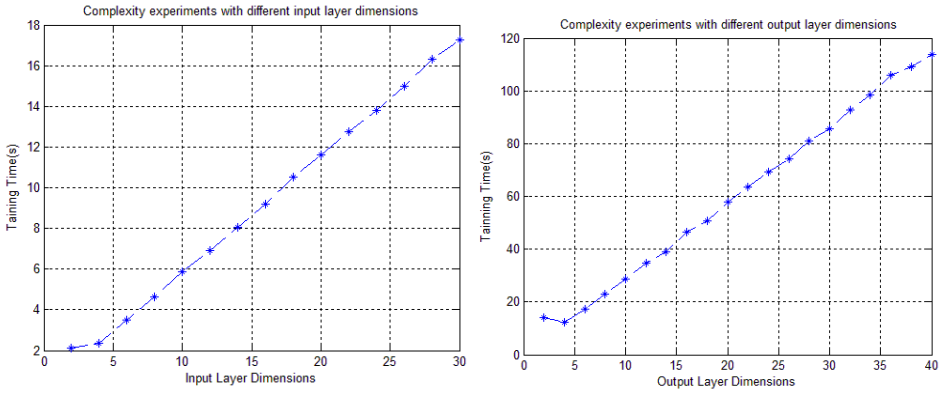

Figure 3 Complexity experiments with different input layer and output layer dimensions

Conclusion

In this paper, through theoretical analysis and experimental verification, it shows the algorithm complexity of the second type Padé weight function neural network is $mnO(N^2)$.Where m is the input dimension, n is the output dimension, N is the number of samples. And in solving problems which has complex topology, this algorithm take less time to be trained, and it has obvious advantages.

References

[1] Zhang Dai-yuan. New Theories and Methods on Neural Networks [M]. Beijing: Tsinghua University Press, 2006

[2] William H.Press, Saul A.Teukolsky. Numerical Algorithms in C [M]. Beijing：Electronic Industry Press, 2004

[3] G. Fournodavlos, V. Nestoridis. Generic approximation of functions by their Padé approximants [J]. Journal of Mathematical Analysis and Applications, 2013, (408): 744-750

[4] Guido Claessens. On the Newton-Padé approximation problem [J]. Journal of Approximation Theory, 1978, (22): 150-160

[5] George A.Baker. Essentials of Padé Approximants [M]. New York: Academic Press, 1975

Advanced Materials Research Vols. 989-994 (2014) pp 2671-2674
© (2014) Trans Tech Publications, Switzerland
doi:10.4028/www.scientific.net/AMR.989-994.2671

Research on Safety Comprehensive Assessment Method for Air Traffic Control Based on RBF Neural Network

Xu-Sheng Gan[1,a], Hua-Ping Li [2,b]

[1] XiJing College, Xi'an, Shaanxi, 710123, China

[2] PLA, Air Force Xi' an Flight Academy, Xi'an, Shaanxi, 710306, China

[a] ganxusheng123@163.com, [b] hpli@mail.xidian.edu.cn

Keywords: Air traffic control; Neural network; RBF; Air traffic management; Safety assessment

Abstract. To assess the safety situation in air traffic control effectively, a comprehensive assessment method based on RBF neural network is proposed. At first, the safety assessment principle based on RBF neural network is introduced, and then the safety assessment index system for air traffic control is established from four aspects of human, machine, environment and management. Simulation example of ATC safety assessment gives us a satisfactory result for RBF neural network.

Introduction

In recent years, many developed countries pay more and more attention to systemic safety management of civil aviation, namely prevent the occurrence of accidents by means of risk management on the basis of original safety management mode [1]. So it is important to study the system safety assessment method for improving the safety level of air traffic system, it can provide the premise and basis for the ATC safety management, and is also a powerful guarantee to realize the higher safety goal of ATM [2].

At present, in my civil aviation, the actual safety assessment work for air traffic control system basically use the qualitative analysis and assessment method. It is mainly carry out the qualitative analysis to the state of equipment, facility, environment, personnel and management and so on in air traffic control system according to the experience and intuitive judgment [3][4]. The assessment results are some qualitative indexes such as whether achieving a certain safety index, accident categories and accident inducement factor and so on, which cannot perform the quantificational, dynamic description to system safety situation. Theoretical study mainly has the following problems: the foreign safety assessment system is not suitable for china; there exist the difference between the assessment model and the actual problem; the built model only remains at the static assessment level.

Based on it, RBF neural network is introduced to study its application in ATC for establishment of safety assessment model. The simulation validates its feasibility.

Safety assessment principle based on RBF neural network

RBF neural network has the accurate mapping ability to the nonlinear problem, and presents the excellent function approximation capability with simple structure and fast learning speed without the complex system modeling process. It is able to learn the rules and laws hidden in sample data, and accurately determine the mapping relationship between input data and targets, building a qualitative and quantitative comprehensive assessment model closer to human thinking mode [5][6]. The safety assessment process based on RBF neural network is shown in Fig. 1 [7].

In the trained RBF neural network, the connection weight of network denotes the assessment idea of expert, which can not only simulate the experts to quantitatively assess, but also avoid human error in the assessment process. Since the connection weights of model are obtained by learning from examples, which avoids the subjective effects and uncertainty that the connection weights and correlative coefficients are artificially calculated. RBF neural network is of special significance for the prediction. We can predict the future trend of the ATC safety risk according to the trend curve, which has a certain role in constitution of safety policy, adoption of safety measures, and so on.

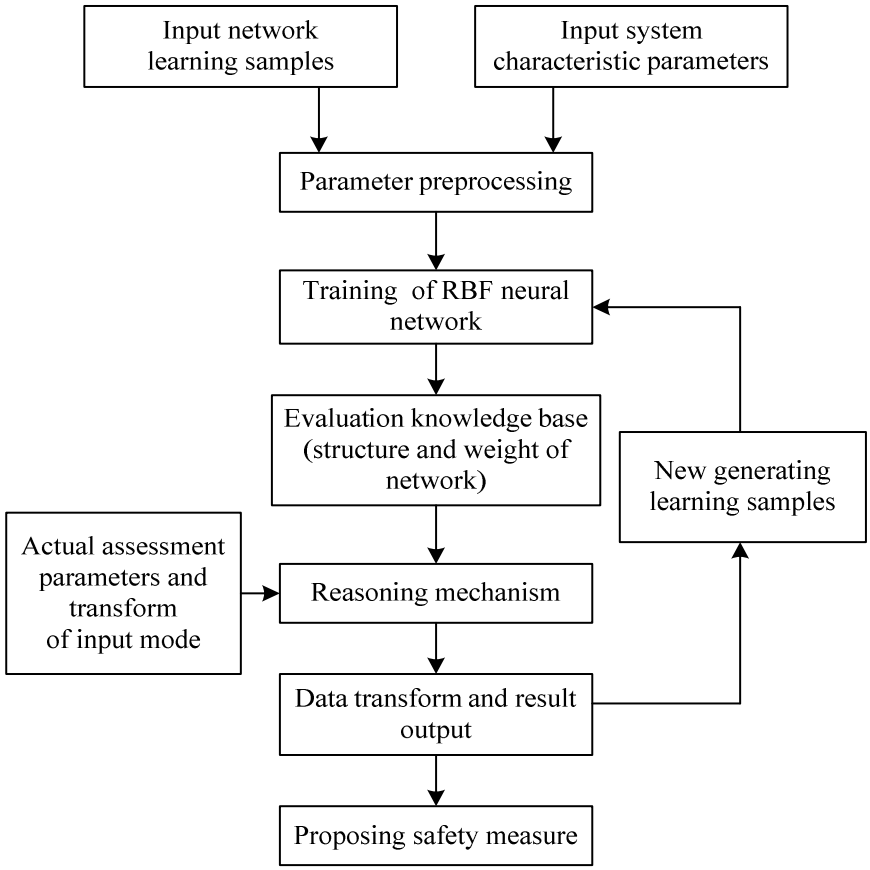

Fig. 1 Flowchart of safety assessment based on RBF neural network

Establishment on safety assessment index system for air traffic control

Air traffic system operation involves the personnel and facilities of many departments, and the harmonious operations between these departments must rely on scientific management. In China, the airspace is more complex things, the development between East and West is unbalanced, the difference of communication, navigation, surveillance facilities is very large, the various ways such as radar control, program control under radar surveillance, program control and so on coexist. Air traffic system is a dynamic system with the feature of continuous time, wide space, too many constituent elements, complex relationships, high safety probability requirements. In view of the characteristics of the system and the dependence on management, according to system engineering theory, we adopt the system comprehensive assessment method base on human-machine-environment-management factor. The safety status of the air traffic control system can be obtain by integrating the safety status of four subsystems, and the safety status of each subsystem can be obtain by integrating the safety status of a number of factor in each subsystem [7]. The safety of each underlying factor is generally given by according to experience and knowledge of experts as shown in Fig. 2.

Simulation example

For ATC safety assessment, the collected sample data should reflect its internal law as far as possible, and adequately consider the own characteristics of network. The paper is based on an ATC database and combined with rich expert experience and profound professional technology to mark for determination of network weight vector and identification of ATC safety state. Experts are mainly from approach control room, tower control room, area control room, flight services room, technical support section, network equipment room, ATC radar room, safety supervision department and so on. The test samples and the training samples are obtained by questionnaire analysis. Each sample data record the assessment information that reflects the safety degree of ATM. each safety assessment

includes the score about 24 safety factors with score range [0,10], and need to conduct the normalization before modeling. Tabel 1 gives the standard output modes of network

The training samples are inputted to train RBF neural network by adjustment of the parameters, obtaining the safety assessment model for ATC. Inputting 8 test samples, we can obtain the test results as shown in Table 2. It can be seen that the results the test results are fully consistent with the actual results within acceptable error limits.

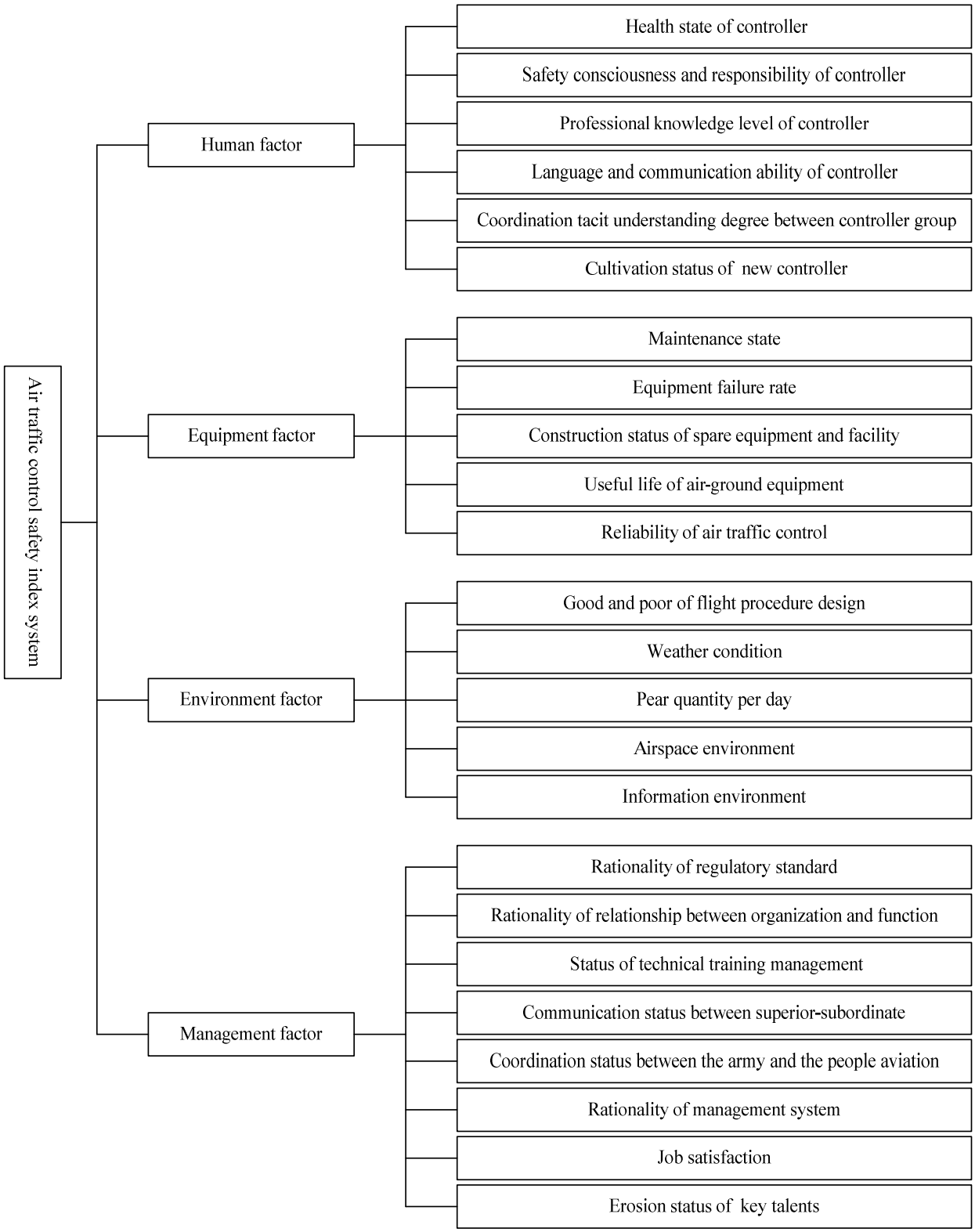

Fig. 2 Safety index system for air traffic control

Tabel 1 Standard output modes of network

Safety assessment class	1	2	3	4	5
Very good	1.00	0.00	0.00	0.00	0.00
Good	0.00	1.00	0.00	0.00	0.00
Normal	0.00	0.00	1.00	0.00	0.00
Poor	0.00	0.00	0.00	1.00	0.00
Very poor	0.00	0.00	0.00	0.00	1.00

Tabel 2 Comparison between test results and actual results

Number	Out of wavelet neural network					Actual assessment value				
1	0.001	0.840	0.011	0.108	0.090	0.00	1.00	0.00	0.00	0.00
2	0.975	0.003	0.202	0.001	0.029	1.00	0.00	0.00	0.00	0.00
3	0.007	0.001	0.056	0.902	0.002	0.00	0.00	0.00	1.00	0.00
4	0.014	0.006	0.890	0.011	0.023	0.00	0.00	1.00	0.00	0.00
5	0.959	0.008	0.002	0.005	0.030	1.00	0.00	0.00	0.00	0.00
6	0.068	0.011	0.004	0.901	0.002	0.00	0.00	0.00	1.00	0.00
7	0.002	0.938	0.008	0.026	0.003	0.00	1.00	0.00	0.00	0.00
8	0.034	0.007	0.001	0.002	0.829	0.00	0.00	0.00	0.00	1.00

Conclusions

A safety comprehensive assessment method based on RBF neural network for ATC is proposed. In the method, the connection weight of RBF neural network is used to dynamically express the assessment information of experts. It can not only quantitatively describe the suggestion of expert, but also avoid the addition of human error in the process. Simulation gives a good validation for the proposed ATC safety comprehensive assessment method.

References

[1] P. Stastny. Risk assessment & mitigation in ATM. Safety Science, 44(7), (2006), 629-655
[2] M. Janic. An assessment of risk and safety in civil aviation. Journal of Air Transport Management, 6(1), (2000), 43-50
[3] M. Felici. Modeling safety case evolution-examples from the air traffic management reliability. Engineering & System Safety, 86(3), (2004), 269-284
[4] R. S. Sun, H. H. Liu. Assessment theory and practice for airline safety. China Safety Science Journal, 9(3), (1999), 69-73
[5] D. E. Rumelhart, J. L. Mcclelland. Parallel distributed processing. Cambridge: MITPress, (1986)
[6] S. Chert, P. M. Crant, C. F. N. Cown. Orthogonal least square algorithm for radial basis function networks. IEEE Transaction on Neural Networks, 2(2), (1991), 302-309
[7] Z. Guo. Research on comprehensive assessment method for air traffic control based on artifical neural network. Jiangsu Aviation, 4, (2010), 32-34

Advanced Materials Research Vols. 989-994 (2014) pp 2675-2678
© (2014) Trans Tech Publications, Switzerland
doi:10.4028/www.scientific.net/AMR.989-994.2675

On the Application of Ant Colony Neural Network for the Highway Traffic Safety Facilities System

Guoling JIA[1, 2,a], Rongguo MA[1,b], Yajuan DENG[1,c]

[1]School of Highway, Chang'an University, Xi'an, 710064, China

[2]Institute of International Economy and Logistics, Xi'an International University, Xi'an, 710077, China

[a]email: ylyljia@163.com, [b]email: mrg@chd.edu.cn

[c]email: dengyajuan1223@163.com

Keywords: Highway; Safety Facilities; Ant Colony Optimization; Neural Network

Abstract. Highway traffic safety facilities system evaluation plays an important role to relieve highway safety problem. From the perspective of system engineering, the influence factors of the current situation are comprehensively considered, the freeway traffic safety facilities system evaluation index system is established, and the application of ant colony neural network evaluation model is constructed. The purpose is to provide the beneficial references for freeway traffic safety facilities system evaluation.

Introduction

Highway traffic safety facilities system includes road traffic guardrails, signs, marking, isolation facilities and bridges retainer, anti-dazzle facility, sight induced facilities, etc. They are used to reduce the severity of the accident, eliminate various longitudinal and transversal interference, improve the road service level, and provide the view induction. They also play an important role in improving road landscape, especially having the special significance to give full play to the function of road safety, rapidness, economy and comfort. [1][2]The existing traffic safety evaluation method in the practical application is short of autonomous learning ability, and it is hard to get rid of randomness, subjective uncertainty and fuzziness of knowledge in the process of evaluation, so it is limited in a lot of practical application. Therefore, it is necessary to choose the more effective evaluation method of highway traffic safety facilities system to apply for the practical situation.

Neural Network Based on Ant Colony Optimization

Back Propagation Neural Network

In recent years, BP (Back Propagation) neural network is widely used in modeling, pattern recognition and control, time series analysis and evaluation, and it has achieved good effect. BP network is a typical multilayer network, its topological structures include input layer, hidden layer and output layer. It adopts full connection between layer and layer, as shown in figure 1. Practical application shows that the BP network has strong ability of mapping. The training process of BP optimization includes two processes, which are forward spread of signal and backward spread of error. On the one hand, forward spread the afferent input samples from the input layer, after each of them processed step by step in a hidden layer, then transferred to output layer. If the actual output is different with the expected output of output layer, then start the error back propagation phase. On the other hand, error back propagation is that the output error transferred to the input layer step by step in some way through the hidden layer, then the error is distributed to all elements of each layer to get error signal of each unit, and the error signal is used as the basis for correcting the weights of each unit. Each layer weights adjustment based on signal's forward spread and error's back propagation iteration process is constantly repeated. Weights are constantly adjusted, which is also known as the training process of the network. This process does not stop until the precision of the network output error has reduced to allow number, or to the pre-set number of learning so far. After

getting the appropriate network connection value, nonlinear image can be used for the new samples.[3][4]

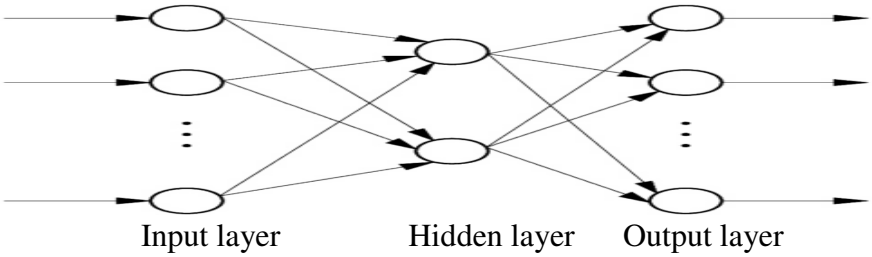

Figure 1 Three-layer BP Network Topology

Ant Colony Optimization

Ant Colony Optimization (the ACO) is a kind of probability algorithm used to find the optimal path in the diagram. This optimization is proposed by Italian scholars Dorigo. M at the first European artificial life meeting held in Paris, France, in 1991. He was inspired by the real ant group of crowd behavior of searching for food. Ants start from nest to food source, and randomly select any path that can arrive at the food source. They release a pheromone at the same time after passing through this path, so that they can communicate with other ants in ant colony coordination. Subsequent ants determine which path to choose in next step according to the pheromone concentration of each path, and eventually achieve the optimal solution. The optimization has some major advantages to find the optimal solution quickly. It has optimal benign of distributed computing mechanism, and can easily combine with other methods. This method is mainly to solve the combinatorial optimization problems, and is able to achieve good results as expected.

Neural Network Training Based on the Ant Colony Optimization

The weights of the neural circuits are trained by using global optimization and heuristic optimization features of ant colony optimization in order to avoid the defects of BP neural network. The basic idea is that it is supposed that parameters number in the network is f, and the parameters include ownership value and threshold. After being sorted, these parameters Pi (I is between 1 and f)are set to N random non-zero values in the neural network, and they parameters form the set Upi. Each ant of the ant colony selects a value, and then chooses a set of the weights of neural network. The number of ants is g, τj means the pheromone of the first j element Pj. When the ant is searching, different ants were independent of each other. Each ant starts from the collection of Upi, and then chooses one element from each set Upi according to the pheromones and state transition probability in the collection. When ants complete the choice of elements in full set to, it will reach the food source, and return to the nest along the path just walked, and then adjust the information in the collection. Finally after repeated processes of the ants until the evolution trend is not obvious or a given number of iterations has finished, the optimal solution of parameters can be found.

The improved specific steps of ant colony optimization are as follows:

1) Initialization. Make the time t, and cycles Nc are zero, set the maximum cycles is Ncmax, make the pheromone τj(Upi) = C and τj(Upi) = 0, the pheromone belongs to each element in the set, and put all the ants in the nest.

2) Start all ants k (k = 1, 2,..., g), as for Upi, calculate the state transition probability according to the following formula:

$$p_r(\tau_j^k(U_{pi})) = \frac{\tau_j^k(U_{pi})}{\sum_{i=1}^{N} t_j(U_{pi})} \quad (1)$$

3) Repeat step 2 until the ant colony has reached the food source.

4) Make t to t + f, Nc to Nc + 1, calculate the output value and error of the neural network according to the selection weight of each ant, and record the current optimal solution. After unit

time of f, each ant reaches food source from the nest, each path pheromone was updated according to the following formula:

$$\tau_j(U_{pi})(t+f) = (1-\rho)\tau_j(U_{pi})(t) + \Delta\tau_j(U_{pi}) \quad (2)$$

$$\Delta\tau_j(U_{pi}) = \sum_{k=1}^{g} \Delta\tau_j^k(U_{pi}) \quad (3)$$

$$\Delta\tau_j^k(U_{pi}) = \begin{cases} \frac{Q}{\varepsilon^k} \\ 0 \end{cases} \quad (4)$$

5) When the ant colony all converge to a path or cycle number of Nc reaches Ncmax, the cycle is finished, and output the results; Otherwise, skip to step 2.

Highway traffic Safety Facilities System Evaluation Model and Algorithm

Modeling Ideas Based on Ant Colony Optimization and Neural Network

BP neural network has strong nonlinear mapping ability and the generalization capability, but it is easily trapped in local minima and has slow convergence speed. In order to solve that problem, this paper uses ant colony algorithm for training neural network and puts forward security evaluation model on the basis of neural network. The modeling idea is as follows: Firstly, fuzzy the collected data, then make them as the input and output of feed forward neural networks. Secondly, train the network with rapid global convergence of the ant colony algorithm with BP algorithm; lastly, get the nonlinear mapping model between the raw data and the level. A three-layer BP model of highway safety facilities evaluation prediction is established. The first layer is the input layer, and it has 15 neurons worked as the evaluation index which is shown in table 1[5]. The second layer is the hidden layer. The third layer is the output layer, in which there are five neurons as the safety evaluation rank. Dividing a score as follows: y1 is level Ⅰ meaning "safety" (00001); Y2 is level Ⅱ meaning "safer " (00010); Y3 is level Ⅲ meaning "general safety" (00100); Y4 is level Ⅳ meaning "unsafe" (01000); Y5 is level Ⅴ meaning "very unsafe".

Table 1 Evaluation Index of Highway Traffic Safety Facilities System

The Serial Number	Evaluation Index
X1	Roadside safety net area
X2	Crashworthiness of guardrail
X3	The rationality of guardrail end processing
X4	Guidance of guardrail
X5	Information readiness
X6	Usage of breakaway traffic sign
X7	Durability of the marking
X8	Sliding resistance of marking
X9	Height of isolation facilities
X10	Stability of isolation facilities
X11	Continuity of isolation facilities
X12	Shielding angle of anti-dazzle facility
X13	Height of anti-dazzle facility
X14	Function of sight guidance facility
X15	Rationality of emergency lane

Implementation Steps of Algorithm

Implementation process of highway safety facilities evaluation model algorithm is as follows:

(1) Determine the objective function, using least squares objective function, namely

$$f(x) = \sum_{i=1}^{n} (O_i^c - O_i^m)^2 \quad (6)$$

In the formula: n represents for test group; O_i^c is the real output of the ith group test; O_i^m is the expected output of group I test.

(2) Get the sample set of neural network by collecting the data, and the samples are normalization processed.

(3) Neural network learning Using ant colony algorithm to learn the weights of neural network to establish evaluation index and nonlinear mapping of grade for highway safety facilities, eventually get evaluation model for highway safety facilities.

Conclusion

Highway traffic safety facilities system plays the role through the coordination of the whole system. System engineering ideas and methods is useful for the evaluation research of highway traffic safety facilities system. Only in this way the role of highway safety facilities can be fully and fairly evaluated, and guide the similar safety facilities system planning, design, construction and maintenance management. Since research time is limited, this paper carries on the preliminary study only based on ant colony neural network evaluation method, and evaluation results and the suggestion remains to be further validated by Matlab model.

Acknowledgement

In this paper, this study has been supported by Natural Science Funds of China (Grant No. 51208054) and the Fundamental Research Funds for the Central Universities(Grant No. 2013G1211002).

References

[1] Fuyong Li. Research on Highway Traffic Safety Facilities System Evaluation [D]. Xi 'an: Chang 'an University, 2005.

[2] Jianjun Wang, Fuyong Li. Planning and Post-Evaluation of Traffic Safety Facilities of Expressway Network [J]. Highway, 2005 (2): 66-77.

[3] Daji Zhu, Hui Shi. The Principle and Application of Artificial Neural Network [M]. Beijing: science press, 2006.

[4] Haibin Duan. The Principle and Application of Ant Colony Algorithm [M]. Beijing: science press, 2005.

[5] Jianjun Wang, Yicheng Liu, Yisong Wu. Evaluation of Traffic Safety Facilities of Expressway [J]. Journal of Transportation Systems Engineering and Information Technology, 2007 (8): 66-70

Advanced Materials Research Vols. 989-994 (2014) pp 2679-2683
© (2014) Trans Tech Publications, Switzerland
doi:10.4028/www.scientific.net/AMR.989-994.2679

Numerical simulation of cook-off for passive RDX

Chen Chun[1, a], LI Weibing[1, b], Liu Jun[1, c]

[1]ZNDY of Ministerial Key Laboratory, Nanjing University of Science and Technology, Nanjing, 210094, China

[a]email: saver120@163.com, [b]email: njustlwb@163.com, [c]email: a1029810484@163.com,

Keywords: Physical Chemistry; Passive RDX; Heating rate; Charge density; Numerical simulation

Abstract. For passive RDX, fluent software was applied to simulate the cook-off for explosive of different charge density at heating rates of 1, 5, 10k/min to improve thermal safety in the ammunition storage, transport and battle. The results show that the heating rate has great effect on ignition time and position for passive RDX. Charge density also has great influence on ignition time but no influence on ignition position. The ignition time decreases and ignition position moves from the center to the two ends of the cylinder edge with the increase of the heating rate. The ignition time increases with the increase of charge density under the same condition. Therefore, increasing the charge density can effectively improve the thermal safety of ammunition.

Introduction

In the modern war，with the changing of battlefield environment, thermal safety of ammunition in storage, transportation and operation has attract more and more attention from many countries. The cook-off test is one of the important methods to test and evaluate the thermal safety. At present, Cook-off experiments and numerical simulation are two ways to study cook-off phenomenon of explosive. Although cook-off test can effectively evaluate thermal safety of explosive, but it has high cost and long research cycle and it is difficult to get system comprehensive measurement dates. Numerical calculation can easily change cook-off conditions such as heating rate, charge density, charge size and so on. The result of numerical simulation is forward-looking, it can predict law of explosive ignition. In 1991, Jones et al[2] carried out one-dimensional numerical calculation for small cook-off bomb (SCB) experiment by HEAT software developed with Fortran language. Since then, a lot of cook-off numerical simulation had been conducted. Feng Chang-gen et al[3]performed numerical simulation for cook-off process of RDX under different ambient temperature. Wang pei et al[4] performed a three-dimensional numerical calculation on GHL at different heating rates. A composite charge structure had been investigated numerically and experimentally by Xiang mei al[5].They found that embedded high-energy grain in insensitive explosive can effective improve its thermal safety.

In this paper, taking passive RDX as research object, a three dimensional calculation model was established to simulated cook-off phenomenon of different charge density passive RDX under three heating rates. The effect of heating rate and charge density on cook-off characteristics has been investigated to provide technical support for explosives in the thermal safety.

The numerical calculation model

Cook-off process includes four stages: flame combustion, explosive heating, shell response, explosive violent reaction. This paper only simulated heating process of explosive. Physical model of passive RDX is shown in figure 1. In the model, the explosive charge diameter is 17mm, the cylinder length is 28mm, the steel shell thickness is 3mm, upper and bottom ends thickness is 1mm. In order to decrease calculation magnitude to save calculation time, built 1/2 normal cylinder numerical simulation model, namely the section above the Z-axis. The requirement of calculation for heat transfer is not high, so the model can chooses a hybrid grid, as shown in figure 2.

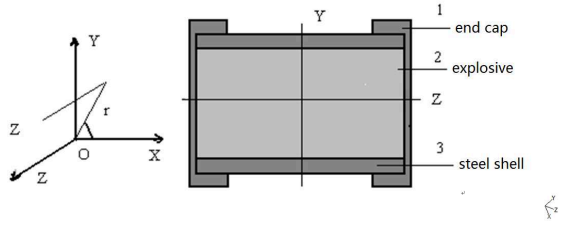

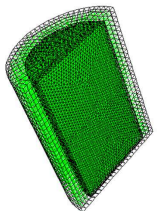

Figure 1 Physical model of cook-off bomb Figure 2 Calculation grid of model

In calculation, making the following assumption for cook-off process of passive RDX:

1) Explosive is homogeneous phase, chemical reaction is zero order exothermic reaction, explosive phase change does not occur, no consumption of reactants;

2）It is assumed that reaction zone only have heat conduction, reactive material remain without motion, therefore there is no convective heat transfer.

3）The thermal action process of explosive is unsteady heat conduction.

4）The reaction zone boundary is impermeable to material, the heat exchange at boundary obey Newton's law of cooling

5) The physical and chemical parameters remain unchanged in the reaction process.

Thermal reaction and thermal conduction follow the Frank-Kamenetskii equation [6]:

$$\rho c_v \frac{\partial T}{\partial t} = \lambda \nabla^2 T + Q\rho aA \exp(-\frac{E}{RT}) \quad (1)$$

In cylindrical coordinates, the temperature field control equation can be expressed as:

$$\rho c_v \frac{\partial T}{\partial t} = \lambda \left(\frac{\partial^2 T}{\partial r^2} + r\frac{\partial T}{\partial r} + \frac{1}{r^2}\frac{\partial^2 T}{\partial \varphi^2} + \frac{\partial^2 T}{\partial z^2} \right) + QaA \exp(-\frac{E}{RT}) \quad (2)$$

Where ρ, C_V, λ, a respectively denotes the reactant density (kg/m3), specific heat capacity (J/kgK), thermal conductivity (J/mKs) and reaction scores. Q is the reaction heat of reactant （J/kg）, A refes to former factor(1/s), E is activation energy（J/mol）, R is gas constant（J/molK）.

The shell outside wall is set as heating boundary. Initial ambient temperature is 306.5K. Selecting three kinds of heating rates which is 1, 5, 10k/min. Then the plans that charge densities are 70%,75%,80%,85%,90% of theoretical maximum density are simulated at each heating rate. CFD software was applied to simulate the model above. Chemical reaction heat release item of explosive was embedded into main program by text. About physical and chemical parameter of passive RDX, this study used the material parameter of literature 7, as shown in table 1.

Table.1 The parameters of the simulation model material

parameter	Passive RDX	45steel shell
density（kg/m3）	1640	7850
specific heat capacity(J/kgK)	1130	480
thermal conductivity (J/mKs)	0.213	43
reaction heat (J/kg)	2.101×10^5	---
former factor (1/s)	2.01×10^{18}	---
activation energy (J/mol)	202730	---
gas constant (J/molK)	8.314	---

The analysis of cook-off characteristic at different heating rates

To analyzes the cook-off characteristics of passive RDX at different heating rates, the temperature distribution on a longitudinal cross-section of cook-off bomb at each time is compared. The charge density is 80% of theoretical maximum density.

Figure 3 shows temperature distribution on cook-off bomb at each time under heating rate of 1K/min. At a time of 5000s, the heat provided by external heat source transfer to explosive cylinder, then the temperature on outer edge of explosive cylinder begin to rise gradually, but the temperature

inside explosive changes little. Later, at 10200s, thermal decomposition inside explosive produce large quantities of heat, and it is too late to realease the heat to surrounding, resulting in rapid rise of temperature on intermediate region. The high temperature region like a cylinder appeared at the center, becoming smaller with the increasing of time. When time reaches 10870s, the high temperature region has become an small ellipse distribution and the temperature reached ignition temperature. The ignition temperature is 543K.

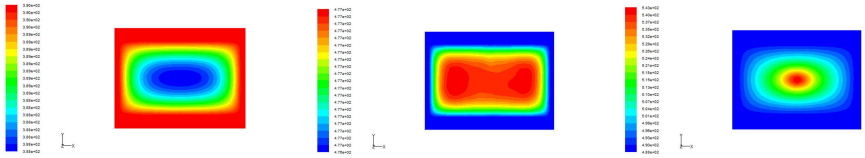

5000s 10200s 10870s

Figure 3 Temperature distributions on cook-off bomb at each time under heating rate of 1k/min

Figure 4 shows temperature distribution on cook-off bomb at each time under heating rate of 5K/min. The temperature changes at this heating rate which is different from the fomer. At a time of 1500s, the temperature on outer edge of explosive cylinder began to rise gradually, but the temperature inside explosive changed little. At 2280s, the high temperature region appears at edge of two ends of explosive cylinder cross with cap. At the time of 2300s, as heat transfers from external heat source and thermal decomposes inside explosive, the high temperature region moves to center of explosive. The high temperature region seems a double funnel in explosives. When time reaches 2324s, the temperature reaches ignition temperature and the ignition temperature is 539K.

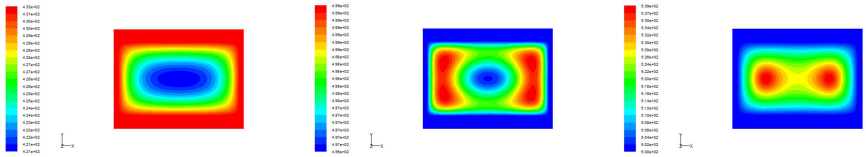

1500s 2280s 2324s

Figure 4 Temperature distributions on cook-off bomb at each time under heating rate of 5k/min

Figure 5 shows temperature distribution on cook-off bomb at each time under heating rate of 10k/min. At 800s, the temperature at the center of explosive is higher than that at the surface of explosive. At the time of 1200s, due to the heating rate is too fast, thermal decomposition inside explosive produce large quantities of heat, and it is too late to realease the heat to surrounding, then the temperature around explosive and two end caps rises rapidly which formed high temperature region. When time reaches 1218s, the temperature reaches ignition temperature and the ignition temperature is 543K.

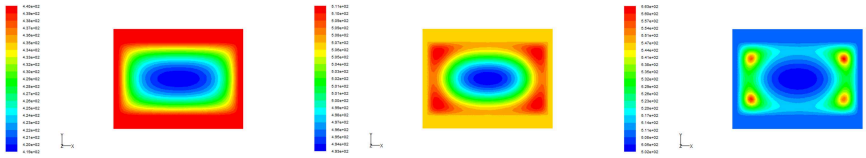

800s 1200s 1218s

Figure 5 Temperature distributions on cook-off bomb at each time under heating rate of 10k/min

Figure 6 shows variations in ignition time, ignition temperature and shell temperature with heating rates for cook-off bomb. The charge density is 80% of theoretical maximum density. It can be seen that heating rate have little effect on ignition temperature, all the ignition temperatures are about 540K. The ignition time decreases with increasing of heating rate, for example, the ignition time is 10870s at heating rate of 1k/min，but decreases to 1218s at heating rate of 10k/min, the time reduced by a factor of 10. The shell temperature increases with increasing of heating rate, the shell temperature is 488k at heating rate of 1k/min, and increases to 511k at heating rate of 10k/min. It indicates that lower heating rate lead to a lower ambient temperature. It is more dangerous under lower heating rate.

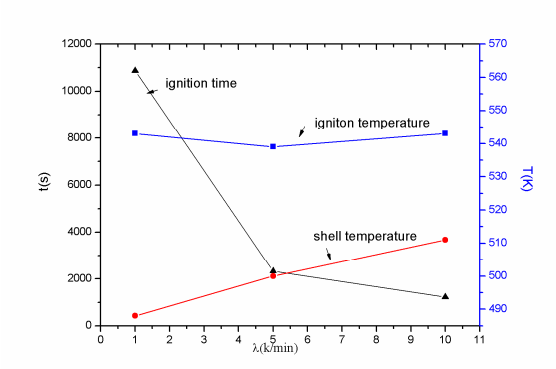

Figure 6 Ignition time, ignition temperature and shell temperature as a function of heating rate

The analysis of cook-off characteristic at different charge densities

A comparison in ignition position for different charge densities under three heating rates is shown in figure 7. It is apparent that the ignition position does not change with variation of charge density.

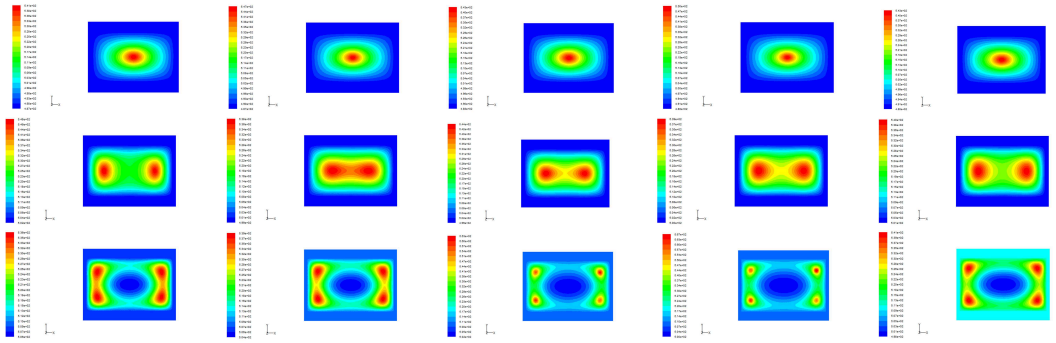

70% 75% 80% 85% 90%

Figure 7 Influence of charge density on ignition position under three heating rates

Figure 8 shows variations in ignition time, ignition temperature and shell temperature with charge density under three heating rates for cook-off bomb. Fig (a), (b) and (c) indicate that charge density has little influence on ignition temperature, all of them for five charge densities are about 540K. The ignition time increase with increasing of charge density, and the growth rate of ignition time remain basically unchanged which means the relationship between ignition time and charge density is linear increasing. Therefore, the higher charge density of cook-off bomb is, the higher thermal safety would be. The cause of the relationship is that as the charge density increase, the porosities of explosive cylinder become smaller, hot spots become less, resulting in decreasing of temperature and the reaction rate decreases, thus the time from heating to ignition becomes longer [8]. In addition, the shell temperature also has a rising trend when explosive ignite with increasing of charge density, which indicates lower charge density lead to a lower ambient temperature. It is more dangerous under lower charge density.

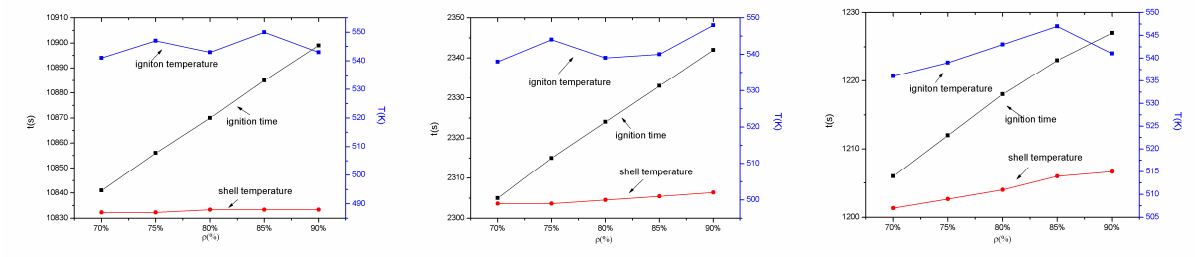

(a)1k/min (b)5k/min (c)10k/min

Figure 8 Variation in cook-off characteristics with charge density under three heating rates

Conclusions

(1)Heating rate have great effect on ignition time and ignition position, but have little effect on ignition temperature. When the heating rate is low, the ignition position locate at the center of explosive cylinder , then as the heating rate increase, the ignition time become longer, and ignition position moves from the center to the two ends of the cylinder edge

(2)Charge density has little effect on ignition position and ignition temperature. Increasing charge density can effective increases the ignition time or improve thermal safety of explosive.

(3)In this paper, the calculation results can reflect the basic characteristics of cook-off, thus it can provide a reference for numerical simulation and experimental research of cook-off in the future. But because of lacking available experimental dates, the accuracy of the calculation results remains to be verified.

Acknowledgement

In this paper, the research was sponsored by the Nature Science Foundation (Project No. 11202103) and Zijin Zhi Xing Foundation of Nanjing University of Science and Technology (Project No. 2013zj-0201).

References

[1] MID-SID-2105C.Non-nuclear ammunition tests of risk assessment[S].

[2] Jones. D.A, Parker. R.P. Heat flow calculation for the small-scale cook-off bomb test[R]. AD-A236829.1991.

[3] FENG Chang-gen, ZHANG Rui, CHEN Lang. The cook-off test and its numerical simulation of RDX[J]. Chinese Journal of Energetic Materials,2004,12(4):193-198.

[4] WANG Pei, CHEN Lang, FENG Chang-gen. Numerical simulation of cook-off for explosive at different heating rates[J]. Chinese Journal of Energetic Materials,2009,17(1):46-54.

[5] XIANG Mei, Huang Yi-min, RAO Guo-ning, PENG Jin-hua. Cook-off test and numerical simulation for composite charge at different heating rates[J].Explosion and Shock Waves, 2013, 33(4):394-400.

[6] FENG Chang-gen. Theory of Thermal Explosion[M].Beijing: Science Press,1988.

[7] DONG Hai-shan, ZHOU Fen-fen. Performance of High Explosives and temperature[M]. Beijing: Science Press,1989.

[8] ZHI Xiao-qi, HU Shuang-qi. Influences of charge densities on responses of explosives to slow cook-off[J]. .Explosion and Shock Waves,2013,33(2):221-224.

Advanced Materials Research Vols. 989-994 (2014) pp 2684-2687
© (2014) Trans Tech Publications, Switzerland
doi:10.4028/www.scientific.net/AMR.989-994.2684

Traffic flow prediction with few data using fuzzy neural network method

Zhou Wei[1, a], Wang Xiao-xue[2,b]

[1] School of Mathematics and Physics, Lanzhou Jiaotong University, Lanzhou, Gansu 730070, China

[2] The Primary School Affiliated to Lanzhou Jiaotong University, Lanzhou, Gansu 730070, China

[a]zhouwei@mail.lzjtu.cn, [b]yingzaji2008@126.com

Keywords: Traffic flow, Prediction, Fuzzy neural network

Abstract. Many machine learning approaches in the field of Artificial Intelligence (AI) have been developed. Most of them rely on using large data sets to build up knowledge. However, the traffic system usually has only few data. In this article, the so-called adaptive neural fuzzy inference systems (ANFIS) is employed to predict the traffic time-series with few data, including flow, speed and occupancy

Introduction

With the development of economy and society, the number of cars in urban is increasing at an astonishing rate. Road construction lags behind the fast increase of vehicles, which makes the traffic capacity provided by road traffic facilities cannot meet the need of current traffic. Traffic congestion has already become the main problem in the cities, and it may become the bottleneck of further development of economy if it continues to worsen. Intelligent Transportation Systems (ITS) are considered to be a solution for traffic congestion problems. One of the ways of alleviating the congestion problems is to redistribute the traffic over the highway network. This redistribution can be spatial as well as temporal. If travelers have advanced information about the traffic conditions, they can reschedule their trips. One of the important issues in an Advance Traveler Information System (ATIS) is accurate forecasting of traffic conditions in the short-term future.

The complexity and uncertainty of traffic flow make it difficult to predict. In the past studies, experts and scholars have proposed a lot of methods and techniques, such as nonparametric regression method[1], chaotic time series method[2], neural network[3], Grey GM(1,1)[4], Kalman filter[5], multivariate state space approach[6], ARIMA[7], fuzzy-neural approach[8], support vector regression [9] and combined method[10], which have been used to forecast traffic volumes. However, there is no single method had yet been developed that presented itself to be universally accepted as the best and effective traffic flow forecasting model.

In this paper, the method called Adaptive Neural Fuzzy Inference Systems (ANFIS) is used to predict the traffic time-series, which has used to predicting the chaotic time-series successfully [11]. A hybrid learning algorithm is used to identify parameters of Sugeno-type fuzzy inference systems. And the least-squares method and the back propagation gradient descent method are combinationed to train the FIS membership function parameters.

The paper is organized as follows. The ANFIS model is introduced in Section 2. The experiments on traffic time-series prediction problems are given in Section3. And the results are discussed in Section 4.

ANFIS Model

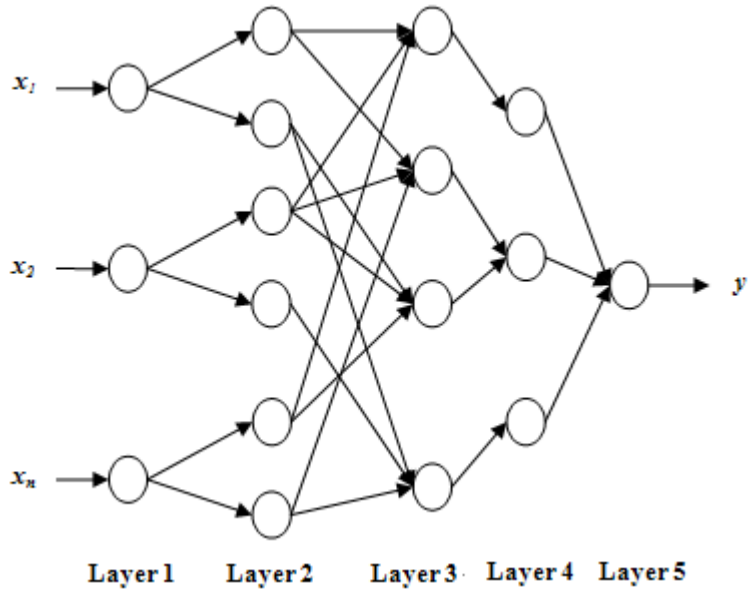

Figure 1. An ANFIS architecture for a two rule Sugeno system.

The ANFIS performs neural learning using fuzzy typed numbers. Given a set of input and output data, the ANFIS can constructs a fuzzy inference system with membership functions values adapted using a back propagation algorithm or in combination with a least square method. The adaptation function of the ANFIS provides the machine learning system with FNN characters. The basic model of the ANFIS is the Sugeno fuzzy model.

In this model, assuming $x=[x_1,x_2,\cdots x_n]^T$ are input fuzzy sets, and x_i are fuzzy language variables. Given the set of values of language variable as,

$$T(x_i)=\left\{A_i^1,A_i^2,\cdots,A_i^m,i=1,2,\cdots,n\right\} \tag{1}$$

where $A_i^j,(j=1,2,\cdots,m)$ is the jth value of language variable x_i, and $\mu_{A_i^j}$ is the corresponding membership function. Let y is the output fuzzy set, and the fuzzy if-then rules is formatted as,

$$if\,(x_1\ is\ A_1^{s_{1j}})\ and\ f(x_2\ is\ A_2^{s_{2j}})\ and\cdots and\ f(x_n\ is\ A_n^{s_{nj}}) \tag{2}$$

$$Then,\begin{cases} y_{1j}=p_{j0}^1+p_{j1}^1x_1+\cdots+p_{jn}^1x_n \\ \vdots \\ y_{rj}=p_{j0}^r+p_{j1}^rx_1+\cdots+p_{jn}^rx_n \end{cases} \tag{3}$$

$$y_k=\sum_{j=1}^{m}\overline{a}_j y_{kj} \tag{4}$$

where $a_j=\underset{i=1}{\overset{m}{\wedge}}\mu^s\lambda_i^j(x_i)$, and $\overline{a}_j=a_j\Big/\sum_{j=1}^{m}a_j$, $j=1,2,\cdots,m$. Figure 1 shows the Sugeno model and the corresponding ANFIS architecture with a five-layer artificial neural network. Denote that the output of the jth node of layer i are O_j^i. In Layer 1 of the ANFIS, the output of each node is:

$$O_{js_j}^1=\mu_j^{s_j}(x_j) \tag{5}$$

where $\mu_j^{s_j}$ are fuzzy membership functions. For nodes in Layer 2, the outputs of every node O_j^2 is fixed. This is where the t-norm is used to 'AND' the membership grades.

$$O_j^2=\min\left\{O_{1s_1}^1,O_{2s_2}^1,\cdots,O_{ns_n}^1\right\} \tag{6}$$

In Layer 3, the output of every node is normalized by a calculation as the following,

$$O_j^3 = \frac{O_j^2}{\sum_{j=1}^{m} O_j^2}, \quad j = 1,2,\cdots,m \tag{7}$$

While, Layer 4 is the de-fuzzy layer which adapts node values with,

$$O_k^4 = \sum_{j=1}^{m} y_{kj} O_j^3, \quad k = 1,2,\cdots,r \tag{8}$$

where the parameters p_{ji}^k in y_{kj} is the consequent parameters of the nodes. Finally, the fifth layer is to compute the output of all the input signals using the equation,

$$O_1^5 = \sum_{k=1}^{r} O_k^4 \tag{9}$$

Experiment Analysis and Result

We use the data collected from the sensors on GuangYing Bridge of Beijing-Chengde Highway. The data cover a time period between 00:00 am of 1st October, 2011 and 24:00 pm of 7th October, 2011. The raw data for speed, volume and occupancy are collected every 5min for the instrumented highway locations. The time plots of traffic volume, speed and occupancy are given in Figure 2(a), Figure 2(c) and Figure 2(e), respectively.

In the forecasting examples described below, the shifted values $X(t+L)$ are the predicted values based on sampled past values of a time series up to the point t, i.e. $X\{t-(D-1)d\}$, $X\{t-(D-2)d\}$ $,\cdots, X(t-d), X(t)$ .Therefore, the predictor to be implemented should map from D sample data points, sample at every d time units, as its input values to the predicted values as its output. The selection of D, d and L depend on the availability of the traffic time series and on its complexity. Here we always set $d = L$. First, we consider the case $d = L = 1$, $D = 2$. The forecasting results of traffic volume, speed and occupancy are given in Figure 2(b), Figure 2(d) and Figure 2(f), respectively.

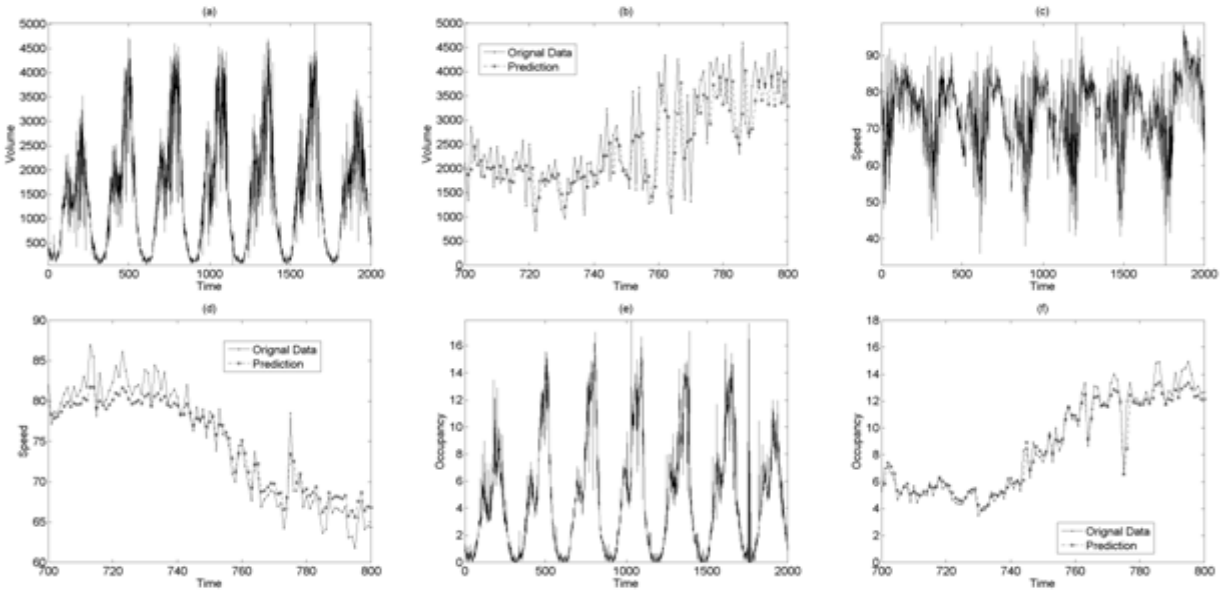

Figure 2. Time-series plot and prediction results of traffic volume, speed and occupancy

In order to compare the prediction results of different D, d and L, the prediction error is evaluated using the so-called nondimensional error index (NDEI) defined as,

$$NDEI = \frac{\sqrt{\frac{1}{N}\sum_{i=1}^{N}(T(i)-O(i))^2}}{\sigma(T)} \tag{10}$$

where :
$T(i)$ is the desired output, and $O(i)$ is the prediction, and $\sigma(T)$ is the standard deviation of the desired outpt. Table 1 show the NDEI of traffic volume prediction with different D, d and L. It can be seen from Table 1, it's the best choice of D, d and L, when we choose $d = L = 1$, $D = 2$.

Table 1. NDEI for traffic volume prediction with different D, d and L

D \ $d = L$	*1*	*2*	*3*	*4*	*5*	*6*
2	0.08	0.11	0.13	0.20	0.22	0.32
3	0.12	0.16	0.17	0.25	0.27	0.39
4	0.17	0.20	0.20	0.29	0.30	0.44

Conclusion

Decisions are almost made in scarce information. The collected data from traffic systems are usually limited and it's difficult to forecast. In this paper, the approach of fuzzy neuron network is presented to predict traffic time series with few data. The previous section clearly demonstrated the effectiveness of the proposed predictors. The so-called nondimensional error index (NDEI) is calculated with different D, d and L. Numerical simulation shows that the prediction is best when we choose $d = L = 1$, $D = 2$.

References

[1] Hao Xuefeng and Xu de, Signal Processing, 2004. Proceedings. ICSP '04. 2004 7th International Conference on. 1,388(2004).

[2] P.Shang, X.Li and S.Kamae. Chaos, Solitons & Fractals. 25,121(2005).

[3] F.Zheng and S.Zhong, World Academy of Science, Engineering and Technology. 75,1471(2011).

[4] Li XingYi, Zhang Xinghua and SHI Huaji, Educational and Information Technology (ICEIT), 2010 International Conference on. 17-19,384(2010).

[5] Y.Xie, Y.Zhang and Z.Ye, Computer-Aided Civil and Infrastructure Engineering. 22,326(2007).

[6] A.Stathopoulos and M.G.Karlaftis, Transportation Research Part C. 11,121(2003).

[7] B.L.Smith, B.M.Williams and R.K.Oswald, Transportation Research Part C. 10,303(2002).

[8] H.Yin, S.C.Wong, J.Xu and C.K.Wong, Transportation Research Part C. 10,85(2002).

[9] Pang Ming-bao and He Guo-guang, Automation and Logistics, 2007 IEEE International Conference on. 18-21,666(2007).

[10] W.Zheng, D.Lee and Q.Shi, Journal of Transportation Engineering. 132,114(2006).

[11] A.EI-Shafie, O.Jaafer and A.Seyed, International Journal of the Physical Sciences. 6,2875(2011).

Advanced Materials Research Vols. 989-994 (2014) pp 2688-2692
© (2014) Trans Tech Publications, Switzerland
doi:10.4028/www.scientific.net/AMR.989-994.2688

The Evaluation to Influence Factors of Concrete Durability Based on Grey Correlation Degree Method

Xiaoping Su[1,a], Haoyue Sun[2,b]

[1]School of Civil Engineering, Changchun Institute of Technology, Changchun 130012, China

[2]Jilin Provincial Electric Power Survey and Design Institute, Changchun 130022, China

[a]sxp5400@163.com; [b]mingtian9562@126.com

Keywords: Evaluation; Concrete Durability; Influence Factors; Grey Correlation Degree Method

Abstract. In this paper, under the environment of saline soil in the western region of Jilin Province, a series tests research on the durability of concrete has been made. The test results show that: there are a lot of factors that influence the durability of concrete, including the concrete itself internal factors and the external environmental factors. The correlation degrees between these influence factors and the durability of concrete are uncertain. In this paper, a grey correlation degree method has been used to analyze the correlation degrees between these influence factors and the dynamic elastic modulus loss rates of concrete, in order to determine the influence degree of each factor on the durability of concrete.

Introduction

In this paper, under the environment of saline soil in the western region of Jilin Province, a series tests research on the durability of concrete has been made [1-5]. The test results show that there are a lot of factors influencing the durability of concrete. Furthermore, the dynamic elastic modulus shows more sensitivity to concrete performance degradation than the mass. Therefore the dynamic elastic modulus is used as the evaluation index of the concrete durability. The correlation degrees between these factors and the concrete durability are uncertain. Grey correlation method has certain advantages in dealing with dynamic data uncertainties, so the correlation degrees between the influence factors and the loss rates of concrete dynamic elastic modulus are analyzed in this paper.

Correlated Coefficients and Correlation Degree Algorithm

Grey correlation degree method is to analyze the close extent of the reference sequence and several comparison sequences by using mathematical methods. If the geometry curves between them are much closer, it describes the greater of grey correlation degree, and vice versa [6]. In this paper, an improved grey correlation degree method has been selected to make algorithm[7,8]. The procedures are as follows:

(1) To determine the reference sequence and comparative sequence [9, 10]:

$$\text{Reference Sequence:}\quad X_0 = \{X_0(k), k = 1, 2, \cdots, m\} \tag{1}$$

$$\text{Comparative sequence:}\quad X_i = \{X_i(k), k = 1, 2, \cdots, m; i = 1, 2, \cdots, n\} \tag{2}$$

In which, m represents the number of comparison related to the reference factors, n represents the number of dynamic observations in the same period.

According to the indicator of concrete durability, the reference sequence can be determined. In this paper, the reference sequence of X_0 is constituted by the dynamic elastic modulus loss rate. 7 influencing factors (freeze-thaw cycle, dry-wet cycle, freeze-thaw and dry-wet cycle, long-term soaking, multi-salt solution concentration, air content, and amount of fly ash) are used as compared sequence X_i. According to the test results, a total of 7 influencing parameters, and 893 sets of data have been gotten, ie. n=7, m=893.

(2) The first regressive to reference sequence X_0 and compared sequence X_i, namely

$$y_i(t+1) = X_i(t+1) - X_i(t) \tag{3}$$

$$y_0(t+1) = X_0(t+1) - X_0(t) \quad (i = 1,2,3,4; t = 1,2,\cdots,n-1) \tag{4}$$

To make regressive treatment to y_0 and y_i, then to seek the relative change rate k in reference sequence X_0 and comparative sequence X_i, namely:

$$k_i(t+1) = y_i(t+1) / \overline{X_i} \quad , \quad \overline{X_i} = \sum_{t=1}^{n} x_i(t) / n \tag{5}$$

$$k_0(t+1) = y_0(t+1) / \overline{X_0} \quad , \quad \overline{X_0} = \sum_{t=1}^{n} x_0(t) / n \tag{6}$$

(3) To calculate the correlation coefficient *ri(k)* and correlation degree *ri* between reference sequence X_0 and comparative sequence X_i, namely:

$$r_i(t) = sign / (1 + | 1 + || k_i(t) | - | k_0(t) ||) \tag{7}$$

$$r_i = \sum_{t=2}^{n} r_i(t) / (n-1) \tag{8}$$

In the formula, $sign = \begin{cases} 1 & y_i(t) \times y_0(t) \geq 0 \\ -1 & y_i(t) \times y_0(t) < 0 \end{cases}$

According to the positive or negative correlation degree of *Ri*, the correlation property between compared sequence X_0 and reference sequence X_i can be determined. When *ri* is in positive, it indicates that X_0 and X_i are positively correlated, ie. The increase (decrease) of X_0 can directly lead to the increase (decrease) of X_i; When *ri* is in negative, X_0 and X_i are negatively correlated, ie, the increase (decrease) of X_0 will directly lead to the decrease (increase) of X_i.

Analysis Process of Influencing Factors and Grey Correlation Degree to Concrete Durability

Table 1 shows the data of loss rate of concrete dynamic elastic modulus in the series of previous tests, which is looked as the reference sequence X_0; 7 influencing factors are looked as compared sequence X_i, in which n=7, m=893. The calculation process to correlation degree is shown in Fig. 1. After the algorithm, a correlation degreeγ_i (X_0, X_i) is gotten between 7 influencing factors and the dynamic elastic modulus loss rate.

Table 1 Initial Data of Influence Factors and Dynamic Elastic Modulus Loss Rate

No.	X_1 Freeze-thaw cycles (time)	X_2 Dry-wet cycles (time)	X_3 Freeze-thaw and dry-wet cycles(time)	X_4 Long-term soaking (day)	X_5 Multi-salt solution concentration (%)	X_6 Air content (%)	X_7 Amount of fly ash (%)	X_0 Dynamic elastic modulus loss rate（%）
1	0	0	0	0	0	0	0	0.000
2	0	5	0	0	0	0	0	1.810
3	0	10	0	0	0	0	0	2.237
4	0	15	0	0	0	0	0	1.392
5	0	20	0	0	0	0	0	3.668
6	0	30	0	0	0	0	0	3.582
7	0	40	0	0	0	0	0	10.562
8	0	60	0	0	0	0	0	21.085
⋮	⋮	⋮	⋮	⋮	⋮	⋮	⋮	⋮
886	0	0	0	180	15	3.17	6.11	3.701
887	0	0	0	210	15	3.17	6.11	8.600
888	0	0	0	240	15	3.17	6.11	17.801
889	0	0	0	270	15	3.17	6.11	23.300
890	0	0	0	300	15	3.17	6.11	24.400
891	0	0	0	330	15	3.17	6.11	31.785
892	0	0	0	360	15	3.17	6.11	35.726
893	0	0	0	390	15	3.17	6.11	44.890

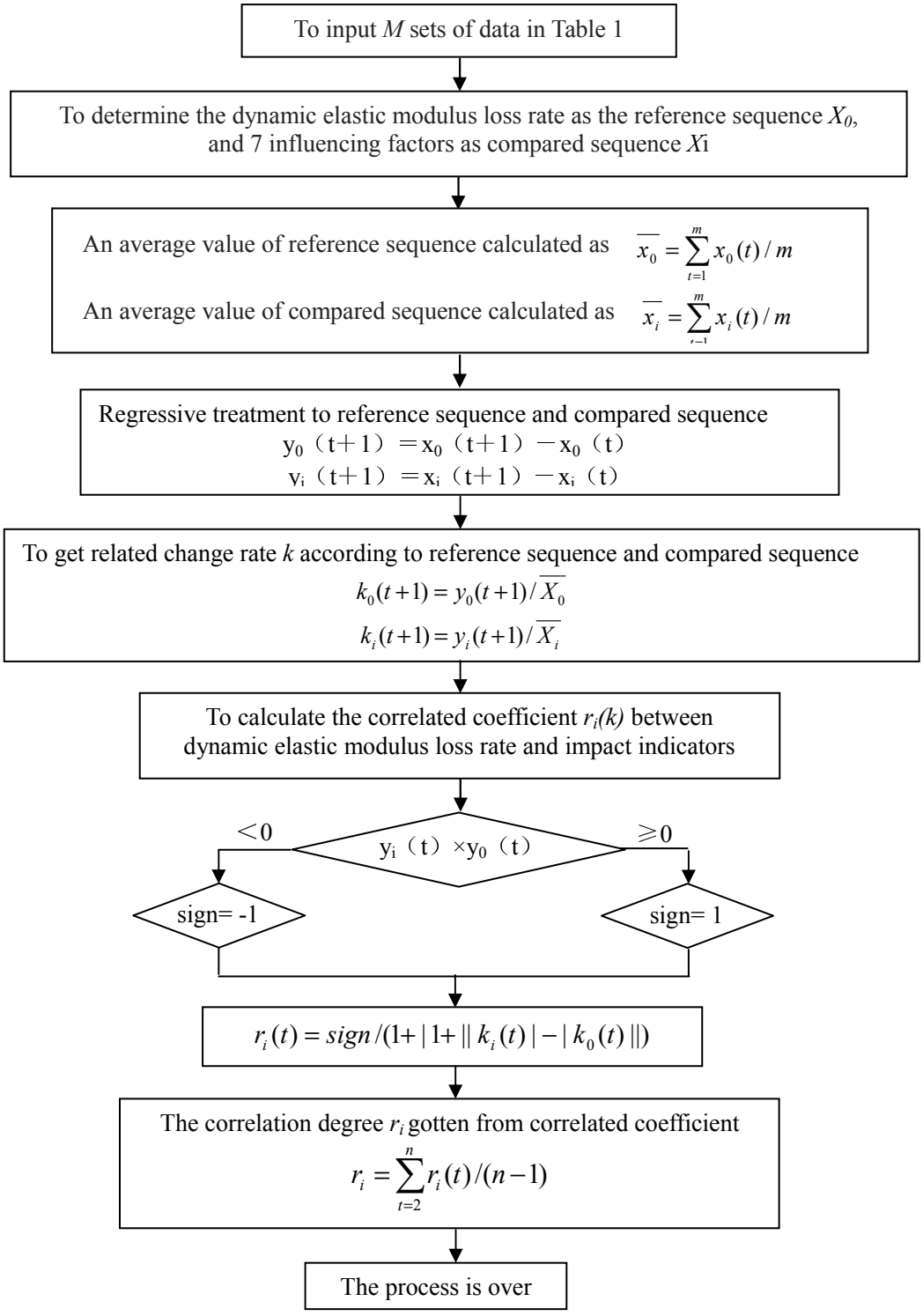

Fig. 1 Correlation Degree Algorithm Procedure Chart

The Correlation Degree between Influence Factors and Dynamic Elastic Modulus Loss Rate

The algorithm results of correlation degree between influence factors and dynamic elastic modulus loss rate of concrete are shown in Table 2. The results show: the correlation degrees are in descending order as: freeze-thaw and dry-wet cycle> dry-wet cycle> freeze-thaw cycle> air content> multi-salt solution concentration> amount of fly ash> soaking time.

Table 2 Correlation Degree between Influence Factors and Dynamic Elastic Modulus Loss Rate

Influence factors	Freeze-thaw cycles	Dry-wet cycles	Freeze-thaw and dry-wet cycles	Long-term soaking	Multi-salt solution concentration	Air content	Amount of fly ash
Correlation degree γ	0.801	0.808	0.813	0.702	0.717	-0.755	0.694

As can be seen from Table 2, environmental factors have a most prominent correlation to the decay of concrete dynamic elastic modulus loss rate, and the correlation degree between them in descending order as: freeze-thaw and dry-wet cycle> dry-wet cycle> freeze-thaw cycle> soaking time. It describes that multiple environmental factors simultaneously action will impact attenuation properties of concrete more serious than a single environmental factor. Therefore, the concrete project serving in dry-wet environment or seasonal frozen area will have a poor durability. The concrete project existing in harmful salt environment will have a relatively slower decay of the properties of concrete because salt erosion of concrete is a long time process.

The correlation degree between multi-salt solution concentration and dynamic elastic modulus loss rate is high up to 0.717, indicating the higher levels of harmful salts, the greater damage to the concrete performance, and different salts will have different effective results to concrete. Under the saline soil environment in western region of Jilin province, HCO_3^- has a greater impact on concrete dynamic elastic modulus; even though the content of SO_4^{2-} is lower than Cl^-, the impact to concrete dynamic elastic modulus will be greater than Cl^-; whereas the impact of Cl^- on concrete mass loss rate is greater than SO_4^{2-}. This also explains that the erosion of Cl^- to concrete mainly causes the concrete peeling off, the erosion of SO_4^{2-} to concrete mainly causes the decay of concrete dynamic elastic modulus, and the damage due to reduced strength. The erosion and damage of harmful salts to concrete should arouse enough attention.

In addition, the air content and dynamic elastic modulus loss rate of concrete are in negatively correlated (γ = -0.755), and with a larger absolute value, indicating that the greater air content, the slower decay to dynamic elastic modulus, and the better durability of concrete. Therefore, in order to improve the durability of concrete, mixing the right amount of air-entraining agent in concrete is an effective and simple method. Under the same circumstance, the correlation degree between fly ash content and dynamic elastic modulus loss rate is 0.694, and with a weaker impact on the durability of concrete. It will be depended by the concrete serving environment on whether mixing fly ash.

Conclusion

In summary, the good or bad concrete durability is related to environmental factors and the material properties of the concrete. The material properties are the intrinsic factors to determine the durability of concrete, and the environmental conditions are the external factors that affect the durability of concrete. In order to improve the durability of concrete, the various kinds of factors in serving environment of concrete project should be fully considered, such as the selection of appropriate materials, and a reasonable design on concrete mix proportion.

Acknowledgements

The project was financially supported by Ministry of Housing and Urban-Rural Development of the People's Republic of China(2013-H-4), Jilin Provincial Science & Technology Department (20130413055GH), Jilin Provincial Electric Power Survey and Design Institute, and the key discipline of Jilin province.

References

[1] Xiaoping Su, Jinhui Guo. Study on the durability of fly ash concrete under multi-salt attack and dry-wet cycles [A]. International Conference on Transportation, 2013: Xianning, China.

[2] Xiaoping Su, Li Zhang. Comparing tests on the durability of concrete after long-term immersion in different salt solution [A]. Advances in Civil and Structrual Engineering □[C], the 3rd International Conference on Civil Engineering and Transportation, 2013: 1087-1091.Kunming, China.

[3] Su Xiaoping, Wang Qing. Experiment of the concrete performance under the condition of multiple salts and dry-wet cycles [J]. Journal of Jilin University, 2013, 43(3): 851-857.

[4] Su Xiaoping, Wang Qing. Comparing experimental study on the concrete performance under the condition of the salt corrosion and dry-wet cycles[J]. Journal of Changchun Institute of Technology, 2012(2):1-4.

[5] Su Xiaoping. Research on the concrete durability due to salinized soil in the western region of Jilin province [D]. Changchun: Jilin University, 2013.

[6] Yi Desheng, Guo ping. Grey theory and method. Beijing: China Petroleum Industry Press, 1992.

[7] Lü Feng, Liu Xiang, Liu Quan. The theory of grey relative analysis and it's new research. Journal of Wuhan University of Technology, 2000, 22 (2) : 41– 47.

[8] Huang Yuxin, Lü Bo, Shi Pin'gui. Method for determining weight based on improved grey relation grade. Journal of Wuhan Institute of Science and Technology, 2004, 17(3): 72-75.

[9] Zhou Xiuwen. Research and application of grey correlation degree[D]. Changchun: Jilin University, 2006.

[10] Cao Mingxia. Research on grey incidence analysis model and its application[D]. Nanjing: Nanjing University of Aeronautics and Astronautics, 2007.

Advanced Materials Research Vols. 989-994 (2014) pp 2693-2696
© (2014) Trans Tech Publications, Switzerland
doi:10.4028/www.scientific.net/AMR.989-994.2693

Camshift Algorithm Based on Multi-features, and Its Further Improvement Study

Lin Jianhua[1, a], Fu Gang[1,a]

[1]China Satellite Maritime Tracking and Control Department, China

[a]348237548@sina.com

Keywords: Camshift algorithm; Object tracking; Multi-feature fusion; Texture feature; histogram

Abstract. Camshift is an efficient single-feature algorithm based on color-kernel for simple object tracking. However, it's easy to be interfered by sudden illumination variation or the similar color object in the background. Experiments show that the improved algorithm can track object accurately in dealing with sudden illumination variation and the similar color object in the background, and can meet the requirements of the actual task of object tracking.

0. Introduction

MeanShift and CamShift algorithm is the typical representatives of the mean shift algorithm in moving object tracking algorithm[1]. In these two methods, color histogram is used to indicate the target model, through iteration target centroid to track object. Look from the calculation, MeanShift algorithm[2] is slightly complicated, and the size of tracking template is fixed, cannot adapt to the object size scaling, therefore CamShift algorithm applies more widely, which is able to provide a template adaptive adjustment.

In view of the poor tracking quality of the characteristic of single color CamShift tracking algorithm under the condition of illumination change obviously or similar background interference , edge and texture information were fused with color information in this article, established the characteristics of target template, formed the CamShift tracking algorithm based on multiple features adaptive fusion[3], And further improvements have been proposed on these basis through modify feature-histogram and set a reasonable search region. Experimental results show that the improved CamShift algorithm can effectively deal with the interference.

1. Multi-feature adaptive fusion Camshift algorithm

Considering the problem that the tracking effect of the traditional single color features Camshift tracking algorithm is poor when illumination changes significantly, this article uses the color Hue component, Sobel edge gradient, and local three value mode (LTP) texture[4] to establish multi-feature model, and realize the adaptive fusion according to some fusion rules, thereby enhance algorithm robustness to illumination change.

LTP operator computation formula is as follows. In the formula, nc is the center pixel value (x, y), ni is the pixel value of p pixels which are interval distributed on the circle, its center is (x, y) and radius is R.

$$LTP_{P,R}(x,y)=\sum_{i=0}^{P-1}s(n_i-n_c)3^i$$

$$s(x)=\begin{cases}1, & x\geq T\\ 0 & -T<x<T\\ -1, & x\leq -T\end{cases} \tag{1}$$

On the basis of the above, this article also optimized feature weights on the attenuation mechanism, in order to ensure that when a certain features have been unable to achieve tracking its weights can be small enough. Set S_1, S_2, S_3 represent the value ofα,β,γrespectively, d_1, d_2, d_3, represent the similarity value under the color, edge, texture feature, which is obtained by the

formula (1) (the range is [0, 1], and the higher the value, the greater the similarity), T_1, T_2 and T_3 represent thresholds for judging α,β,γrespectively, e-ax is a index function (a=10), the feature weights can be adjusted according to the formula:

$$S_i = \begin{cases} S_i & d_i \le T_i \\ S_i e^{-a(d_i - T_i)} & d_i > T_i \end{cases} \quad (i = 1,2,3) \tag{2}$$

From the above, for some feature, when the similarity value *di* between search window histogram and background window histogram is less than the threshold value T_i, the feature weights S_i remain unchanged; On the other hand, the weights of S_i will be carried out in accordance with the exponential attenuation $e^{-a(d_i - T_i)}$. T_i changes with the change of feature and scene (T_i is 0.5 in this article).

2. The further improvement of the algorithm

Multi-feature adaptive fusion Camshift algorithm is improved on the robustness than traditional Camshift tracking algorithm, but there are still some defects. For example, in the scenarios with similar background (especially the three feature models are close to the background), the algorithm still cannot achieve stability tracking. For this problem, this paper made some further improvements based on the multi-feature adaptive fusion Camshift tracking algorithm. The improvement strategy is as follows.

3. Analysis of experimental results

In experiment 1, the paper respectively use the traditional Camshift tracking algorithm based on single color features and the Camshift tracking algorithm based on multiple features adaptive fusion for target tracking. In using video clips, target to orange and with a certain texture features of ellipse, the target has moved from the darker area to a light region.

Figure 1 shows the target tracking results of traditional Camshift algorithm, can be seen from the diagram, as the change of light intensity, The tracking window of Camshift algorithm which is sensitive to illumination change based on color feature expands unceasingly, the tracking effect is poor.

Figure 2 shows the target tracking results of the Hue component of color features and LBP texture feature fusion Camshift tracking algorithm, which is proposed in the literature [5], from the diagram, the ability of strain illumination change for the improved algorithm is still poor.

Figure 3 shows the target tracking results of Camshift tracking adaptive fusion algorithm based on the Hue component of color features, Sobel edge and LTP texture feature which are proposed in this paper, the algorithm has good tracking performance and strong robustness.

The changes of each feature weights (the initial weights of edge, color, texture feature are 1/3) in figure3 were recorded in Table 1. Can be seen from the table, on the 18th frame and 26th frame, the sum of the weight of three features is not 1, the reason is that feature weights of the attenuation according to formula (2).In the process of tracking, while the influence of the edge feature under illumination changes is not big, but because of its ability to rotate is poorer, and the target is rotating, so the ratio of edge feature in the table has been is not high, and the greater the degree of target rotational deformation, the smaller the edge feature weights. Also can be seen from table 1, in the 26th frames, weight of color feature is only 0.180342, the reason for this is that near the 26 frame, the target is in a transition from the dark area to a lighter area. Due to the color feature is sensitive to illumination change, the search window and background window in this area are hard to distinguish, so the weight of color feature is reduced. In addition, because the texture feature affected by illumination change and rotation is not big, so its weight has been higher.

Table 1 Analysis of feature weight changes

Frame number	edge	color	texture
8	0.323416	0.330171	0.346413
18	0.295449	0.346996	0.334443
26	0.229718	0.180342	0.351304
35	0.298807	0.364907	0.336268
45	0.225453	0.382281	0.392267

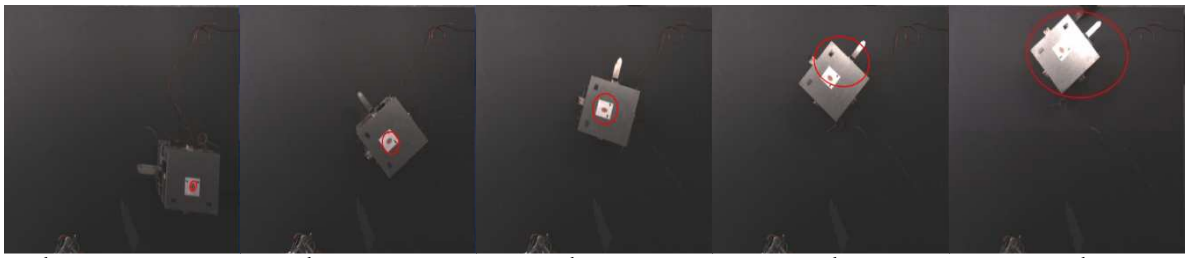

8th frame 18th frame 26th frame 35th frame 45th frame

Figure 1 Traditional Camshift tracking

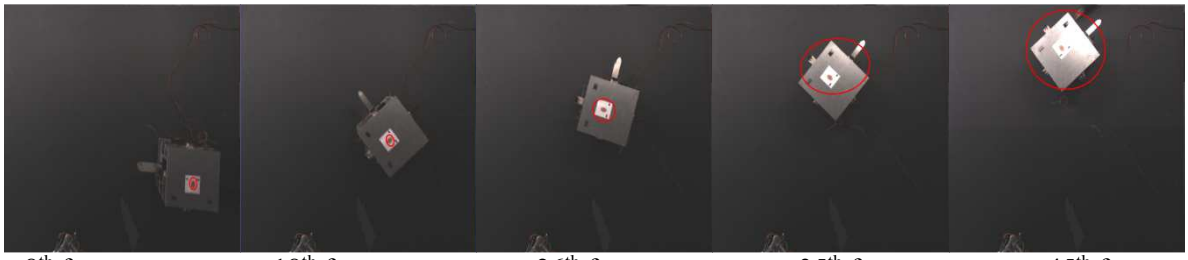

8th frame 18th frame 26th frame 35th frame 45th frame

Figure 2 Hue feature and LBP texture feature fusion Camshift tracking

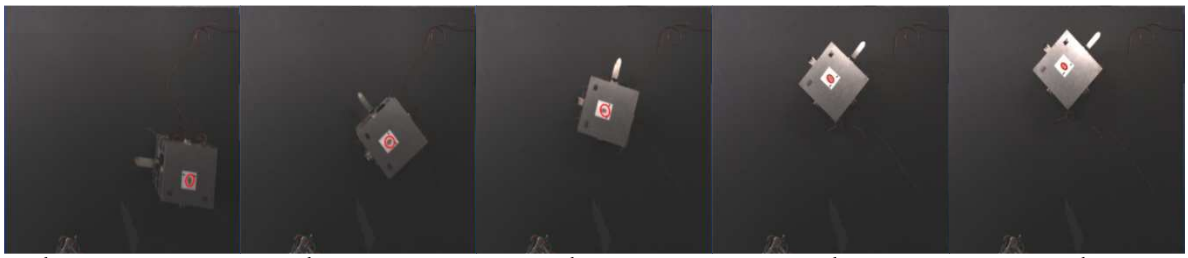

8th frame 18th frame 26th frame 35th frame 45th frame

Figure 3 Multi-feature adaptive fusion Camshift tracking

4. Conclusion

Camshift tracking algorithm based on single feature is often failure for the tracking because of the limitations of the features. In view of this, this article fused the multiple features, constitute a multi-feature fusion Camshift tracking algorithm, make full use of the complementarity between different features, to better adapt to the scene changes, and enhance the robustness of target tracking.

5. References

[1] Xiaoxiao Xu. Visual tracking algorithm based on feature-learning and feature-imagination[D]. Hefei: University of science and[1] technology of China, 2010.
[2] Fashing M, Tornasi C. Mean shift is a bound optimization[J]. IEEE Transactions on Pattern Analysis and Machine Intelligence, 2005, 27(3): 471-474.
[3] Bradski G R. Computer vision face tracking for use in a perceptual user interface[J]. Intel Technology Journal, 1998, 2(2): 1-15.
[4] Tengyue Zou, Xiaoqi Tang, Bao Song. Improved Camshift Tracking Algorithm Based on Silhouette Moving Detection[C] //2011 Third International Conference on Multimedia Information Networking and Security. Shanghai: Shanghai University, 2011: 11-15.
[5] Exner D. Fast and robust CAMShift tracking[C] //2010 IEEE Computer Society Conference on Computer Vision and Pattern Rocognition Workshops. San Francisco, CA: IEEE Computer Society, 2010: 9-16.

Advanced Materials Research Vols. 989-994 (2014) pp 2697-2701
© (2014) Trans Tech Publications, Switzerland
doi:10.4028/www.scientific.net/AMR.989-994.2697

Study of numerical simulation of RF wave in magnetized plasma

Jianfeng Jiang[1, 2, a], Zhonghe Jiang[1, 2, b], Xinfeng Sun[1, 2, c], Weixin Guo[1, 2]

[1]State Key laboratory of Advanced Electromagnetic Engineering and Technology, 430074, Wuhan, China

[2]School of Electrical and Electronic Engineering, Huazhong University of Science and Technology, Wuhan 430074, China

[a] jiangjf@hust.edu.cn, [b] zhhjiang@hust.edu.cn, [c] xinfenghappy@hust.edu.cn

Keywords: Plasma; RF wave heating; numerical simulation

Abstract. Wave heating is an important way to implement the controlled fusion. The propagation and absorbability of wave in the plasma are described by the two-fluid equations and Maxwell's equations. A numerical algorithm based on the FDTD method and the MacCormack scheme is designed. The numerical simulation based on parallel computing is carried out to verify the validity of the algorithm and simulation.

Introduction

A promising and possible way to develop and use fusion energy is magnetic confinement fusion [1]. The tokamak is a device using a large toroidal background magnetic field to confine the fusion plasma in the shape of a torus. In order to reach the high enough temperature and satisfy the fusion ignition condition, both of ohmic heating and auxiliary heating play an important role in the tokamak reactor. The toroidal current induced by the transformer in a tokamak reactor produces ohmic heating. The fact shows that the temperature provided by ohmic heating is limited; therefore, the other auxiliary heating methods are required to increase the fusion plasma temperature, such as the radio frequency (RF) wave heating [2]. If the launching frequency is given, the RF wave will resonate with one of eigenfrequencies of the electrons or ions in the plasma. The wave-particles resonance is the basic mechanism by which the plasma could absorb energy from incident RF wave. Thus, it is very important to research the propagation and absorbability of the RF wave in the plasma.

The propagation and absorbability of the RF wave are described by the two-fluid equations and Maxwell's equations. A numerical algorithm suitable for simulation is put forward to solve the equations. As a first step it is important to examine the validity of the algorithm and simulation. In this paper, only topics related to the algorithm design and numerical simulation of linear wave propagation in the cold plasma will be discussed. The simulation of nonlinear process in the hot plasma deserves to be discussed more comprehensively in the future. So this will not be proposed in this paper. The outline of this paper is as follows. In Section 2 a brief introduction of the simulation model is presented. The design method of the algorithm is described in Section 3. The numerical simulation results are presented in Section 4 and Section 5 is a short summary.

Simulation Model

In tokamak, the plasma is constrained in the shape of a torus. In the cross section which is perpendicular to the toroidal direction, the equilibrium density of plasma increases to a maximum N_0 in the core of the torus, and then decreases to a minimum value in the other edge. The direction of the background static magnetic field $\boldsymbol{B}_0$ is along the toroidal direction. The density of the background magnetic field increases monotonically. The value of the background static magnetic field in the center of plasma is B_0. In our model, the toroidal direction is assumed as z direction and the density gradient of the plasma is x direction. For simplicity, we assume that all the electric and magnetic fields exhibit no spatial variation in y direction. Thus, the simulation model has been converted into two-dimensional space [3].

Since the electrons and ions in the plasma are treated as fluids, the motion of electrons and ions are described by the two-fluid equations [4]. The temporal and spatial evolution of the electromagnetic field is described by Maxwell's equations. Consider the plasma with equilibrium density gradient in x direction $N_{e0}= N_0(x)$ and $N_{i0}= N_0(x)$, perturbed electron fluid and ion fluid densities N_{e1} and N_{i1}, unperturbed electric field $\boldsymbol{E}_0=0$, unperturbed electron fluid and ion fluid velocities $\boldsymbol{u}_{e0}=0$ and $\boldsymbol{u}_{i0}=0$, perturbed electron fluid and ion fluid velocities $\boldsymbol{u}_{e1}$ and $\boldsymbol{u}_{i1}$, perturbed electric field $\boldsymbol{E}$, and perturbed magnetic field $\boldsymbol{H}$. The basic equations are:

$$\frac{\partial N_e}{\partial t} + N_e \nabla \cdot \boldsymbol{u}_e + \boldsymbol{u}_e \cdot \nabla N_e = 0 \tag{1}$$

$$\frac{\partial N_i}{\partial t} + N_i \nabla \cdot \boldsymbol{u}_i + \boldsymbol{u}_i \cdot \nabla N_i = 0 \tag{2}$$

$$\frac{\partial \boldsymbol{u}_e}{\partial t} + \boldsymbol{u}_e \cdot \nabla \boldsymbol{u}_e + \frac{e}{m_e}\left[\boldsymbol{E} + \boldsymbol{u}_e \times (\boldsymbol{B}_0 + \mu_0 \boldsymbol{H})\right] = 0 \tag{3}$$

$$\frac{\partial \boldsymbol{u}_i}{\partial t} + \boldsymbol{u}_i \cdot \nabla \boldsymbol{u}_i - \frac{e}{m_i}\left[\boldsymbol{E} + \boldsymbol{u}_i \times (\boldsymbol{B}_0 + \mu_0 \boldsymbol{H})\right] = 0 \tag{4}$$

$$\nabla \times \boldsymbol{E} = -\mu_0 \frac{\partial \boldsymbol{H}}{\partial t} \tag{5}$$

$$\nabla \times \boldsymbol{H} = \varepsilon_0 \frac{\partial \boldsymbol{E}}{\partial t} + e(N_i \boldsymbol{u}_i - N_e \boldsymbol{u}_e) \tag{6}$$

where e and $m_e(m_i)$ are the charge and the mass of an electron(ion), respectively. $N_e(N_i)$ and $\boldsymbol{u}_e(\boldsymbol{u}_i)$ both contain unperturbed quantity and perturbed quantity. Here, the nonlinear terms are included into the equations just to ensure the integrity of equations. They are deferred for future studies.

Algorithm Design

It's obvious that partial differential terms are contained in the basic equations. In order to deal with these terms, the MacCormack scheme is used to solve the two-fluid equations. The Finite Difference Time Domain (FDTD) method is applied to solve Maxwell's equations. In addition, due to the large computational space all the simulations are based on parallel program with Message Passing Interface (MPI).

The FDTD method was first proposed by K.S. Yee in 1966 [5]. The partial differential equations are transformed to finite-difference equation from by the spatial and temporal discretization of the electromagnetic field vector. Having assumed the perturbed quantities with no spatial variation in y direction, we consider TE wave as the incident wave. The perturbed electric field $\boldsymbol{E}$ has two polarization components E_x and E_z. The perturbed magnetic field $\boldsymbol{H}$ has only one component H_y [6]. The two-dimensional Maxwell's equations are:

$$\frac{\partial H_y}{\partial t} = \frac{1}{\mu_0}\left(\frac{\partial E_z}{\partial x} - \frac{\partial E_x}{\partial z}\right) \tag{7}$$

$$\frac{\partial E_x}{\partial t} = -\frac{1}{\varepsilon_0}\frac{\partial H_y}{\partial z} + \frac{e}{\varepsilon_0}(N_e u_{ex} - N_i u_{ix}) \tag{8}$$

$$\frac{\partial E_z}{\partial t} = \frac{1}{\varepsilon_0}\frac{\partial H_y}{\partial x} + \frac{e}{\varepsilon_0}(N_e u_{ez} - N_i u_{iz}) \tag{9}$$

The numerical solution of E_x is selected to explain the process of discretization as an example. The difference form of the equation is:

$$E_x\Big|_{i+1,j}^{n+1} = E_x\Big|_{i+1,j}^{n} - \frac{\Delta t}{\varepsilon_0}\frac{H_y\Big|_{i,j+1}^{n} - H_y\Big|_{i,j}^{n}}{\Delta z} + \frac{e\Delta t}{\varepsilon_0}\frac{N_e\Big|_{i+1,j}^{n} + N_e\Big|_{i,j}^{n}}{2}\frac{u_{ex}\Big|_{i+1,j}^{n} + u_{ex}\Big|_{i,j}^{n} + u_{ex}\Big|_{i+1,j}^{n-1} + u_{ex}\Big|_{i+1,j}^{n-1}}{4} - \frac{e\Delta t}{\varepsilon_0}\frac{N_i\Big|_{i+1,j}^{n} + N_i\Big|_{i,j}^{n}}{2}\frac{u_{ix}\Big|_{i+1,j}^{n} + u_{ix}\Big|_{i,j}^{n} + u_{ix}\Big|_{i+1,j}^{n-1} + u_{ix}\Big|_{i+1,j}^{n-1}}{4} \tag{10}$$

Similarly, the numerical solutions of E_z and H_y can be obtained. In Eq. 10, subscripts i and j refer to the spatial position of a certain point in the x-z two-dimensional plane, respectively. The superscripts n and n+1 refer to a certain moment and the next moment, respectively. This result looks a little complex since semi-implicit form is applied to deal with the difference of $N_e(N_i)$, $u_{ex}(u_{ix})$ and $u_{ez}(u_{iz})$ [7]. The method can effectively improve the numerical stability.

To the two-fluid equations, numerical results had tested that MacCormack scheme was suitable for this model. It is based on explicit difference scheme and has second-order accuracy in time and space. In the fluid model, the density of electron fluid can be calculated by the following form:

$$N_e\Big|_{i,j}^{n+1} = N_e\Big|_{i,j}^{n} + (\frac{\partial N_e}{\partial t})_{av}\Delta t \tag{11}$$

where $(\partial N_e/\partial t)_{av}$ is a representative mean value of $\partial N_e/\partial t$ between times t and t+Δt. In MacCormack scheme, this average time derivative $(\partial N_e/\partial t)_{av}$ is obtained from a predictor-corrector philosophy.

Predictor step: In Eq. 1, the spatial derivative term is approximated by a forward difference. Thus, the predicted value of density is obtained as follows.

$$\frac{\partial N_e}{\partial t}\Big|_{i,j}^{n} = -(N_e\Big|_{i,j}^{n}\frac{u_{ex}\Big|_{i+1,j}^{n} - u_{ex}\Big|_{i,j}^{n}}{\Delta x} + u_{ex}\Big|_{i,j}^{n}\frac{N_e\Big|_{i+1,j}^{n} - N_e\Big|_{i,j}^{n}}{\Delta x} + N_e\Big|_{i,j}^{n}\frac{u_{ez}\Big|_{i,j+1}^{n} - u_{ez}\Big|_{i,j}^{n}}{\Delta z} + u_{ez}\Big|_{i,j}^{n}\frac{N_e\Big|_{i,j+1}^{n} - N_e\Big|_{i,j}^{n}}{\Delta z}) \tag{12}$$

$$\overline{N_e}\Big|_{i,j}^{n} = N_e\Big|_{i,j}^{n} + \frac{\partial N_e}{\partial t}\Big|_{i,j}^{n}\Delta t \tag{13}$$

Corrector step: The spatial derivative term is approximated by a backward difference. We first obtain the predicted value of the time derivative at t+Δt. Thus, the final corrected value is obtained.

$$\frac{\partial \overline{N_e}}{\partial t}\Big|_{i,j}^{n+1} = -(\overline{N_e}\Big|_{i,j}^{n+1}\frac{\overline{u_{ex}}\Big|_{i,j}^{n+1} - \overline{u_{ex}}\Big|_{i-1,j}^{n+1}}{\Delta x} + \overline{u_{ex}}\Big|_{i,j}^{n+1}\frac{\overline{N_e}\Big|_{i,j}^{n+1} - \overline{N_e}\Big|_{i-1,j}^{n+1}}{\Delta x} + \overline{N_e}\Big|_{i,j}^{n+1}\frac{\overline{u_{ez}}\Big|_{i,j}^{n+1} - \overline{u_{ez}}\Big|_{i,j-1}^{n+1}}{\Delta z} + \overline{u_{ez}}\Big|_{i,j}^{n+1}\frac{\overline{N_e}\Big|_{i,j}^{n+1} - \overline{N_e}\Big|_{i,j-1}^{n+1}}{\Delta z}) \tag{14}$$

$$N_e\Big|_{i,j}^{n+1} = N_e\Big|_{i,j}^{n} + (\frac{\partial N_e}{\partial t})_{av}\Delta t = N_e\Big|_{i,j}^{n} + \frac{1}{2}(\frac{\partial N_e}{\partial t}\Big|_{i,j}^{n} + \overline{\frac{\partial N_e}{\partial t}}\Big|_{i,j}^{n+1})\Delta t \tag{15}$$

Other quantities N_i, $\boldsymbol{u}_e$ and $\boldsymbol{u}_i$ in the two-fluid equations are obtained by the same method.

In computations, the whole simulation region is divided into several sub-regions in x direction. Every sub-region is assigned to certain cluster resource and storage resource. The data of the two adjacent sub-regions are exchanged by non-block communication functions, *MPI_Isend* and *MPI_Irecv*. The parallel simulation program is submitted to the server cluster with Linux OS and carried out on the MPICH2 environment.

Results and Discussion

Based on the algorithm above, we investigate the coupling effects between the lower hybrid wave (LHW) and the magnetized plasma in order to examine the validity of the algorithm and simulation. The parameters used in the numerical simulation are shown as Table 1. The linear theory of wave propagation has indicated that the coupling and propagation are strongly affected by the parallel wavenumber k_z, the same direction as $\boldsymbol{B}_0$, and k_0, k_0=ω/c, where ω is the frequency of the incident wave and c is the velocity of light [8]. If the parallel wavenumber k_z is less than k_0, the

wave couldn't propagate into the plasma from the vacuum. If the parallel wavenumber k_z is more than k_0 , the wave will evanesce in the outer layer of the edge plasma, where the density N_e is below the critical density N_c that given by $\omega_{pe}=\omega$, and propagate in the internal layer, where the density N_e is above the critical density N_c [9].

Table 1. Parameters used in the numerical simulation

Grid spacing Δx Δz	$0.02\pi c/\omega$
Time step Δt	$0.002\pi/\omega$
Number of grids in x-axis L_x	1440
Number of grids in z-axis L_z	120
Number of time steps	50000
Value of density N_0	2.79×10^{17}
Value of magnetic field B_0	1.5T

In x direction, the grids from 1 to 180 are in the vacuum and the grids from 181 to1440 are in the plasma. The position of the critical density N_c is at x=600. The background magnetic field only exits in plasma. In the simulation model, the distribution curves of the equilibrium density $N_0(x)$ and the background magnetic field $B_0(x)$ are shown as Fig. 1.

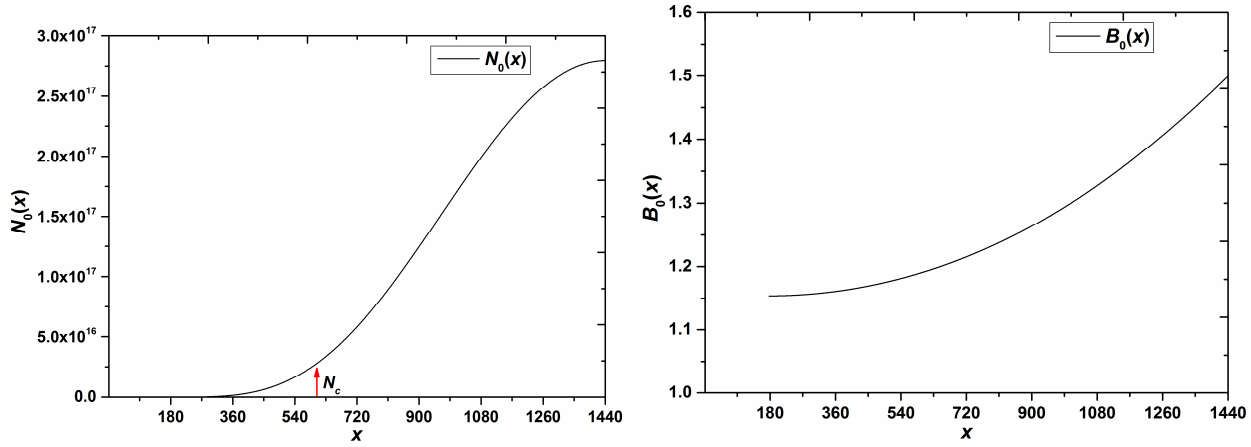

(a) distribution of $N_0(x)$ (b) distribution of $B_0(x)$

Fig.1 The distributions of $N_0(x)$ and $B_0(x)$

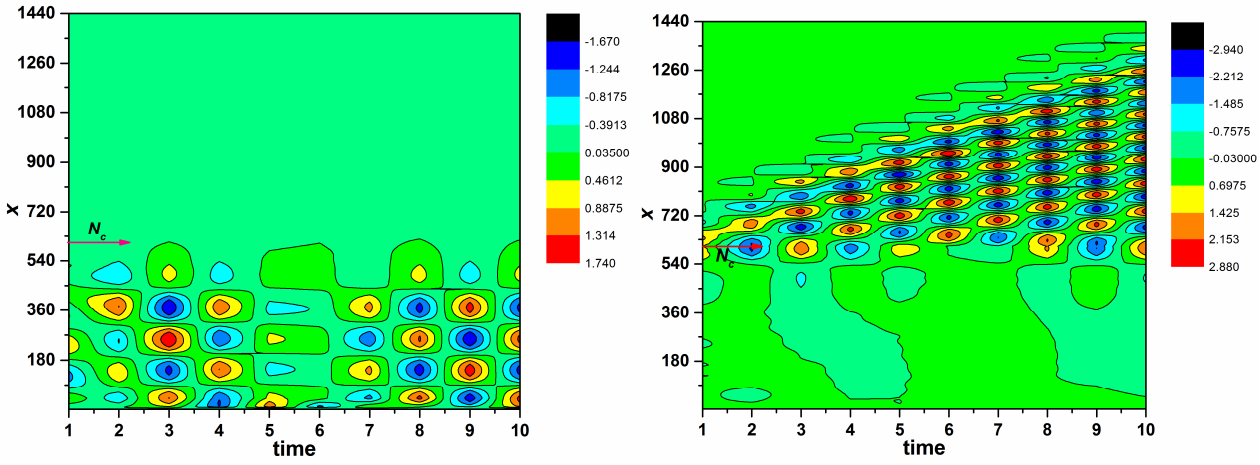

(a) k_z=0.8k_0 (b) k_z=1.2k_0

Fig.2 The numerical solution of H_y

Two different situations for k_z=0.8k_0 and k_z=1.2k_0 are simulated, respectively. Here, the spatial and temporal evolution of H_y from numerical solution is shown in Fig. 2.

Obviously, the wave can't propagate in the region, x>600Δx, where the density $N_0(x)$ is above the critical density N_c, for the first situation k_z=0.8k_0. When it comes to the other situation, k_z=1.2k_0, the value of H_y is zero in the region, x<600Δx and the waveform appears in the region, x>600Δx. These results mean that the incident wave can propagate into the internal layer of plasma which also shows that our simulation results are in accordance with the linear theory.

Summary

Based on the two-fluid equations and Maxwell's equations, the numerical algorithm is designed to study the propagation of the RF wave in the plasma. In present study, we treat a simple case that the background plasma to be a cold plasma medium and ignore the nonlinear effects. The numerical algorithm contains the FDTD method and the MacCormack scheme. On the basis of the simulation results, we can clarify that the numerical algorithm and numerical simulation are useful and convincing. For future studies, we will treat the plasma as a hot plasma and investigate the wave-particles interaction with nonlinear effects.

Acknowledgement

In this paper, the research was supported by National Natural Science Foundation of China (Grant No. 10990214 and No. 115450).

References

[1] D. Campbell, Magnetic confinement fusion. Europhysics news, 1999, 29(6): 196-201

[2] J. Sheffield. The physics of magnetic fusion reactors. Reviews of Modern Physics, 1994, 66(3): 1015

[3] Y. Katoh, M. Iizima. A computer simulation study on the mode conversion process from slow X-mode to fast X-mode by the tunneling effect. Earth Planets Space, 2006, 58(12): e53-e56

[4] M. Ishii, Thermo-fluid dynamic theory of two-phase flow. NASA STI/Recon Technical Report A, 1975, 75: 29657

[5] K.S. Yee, Numerical Solution of initial boundary value problems involving Maxwell's equations. IEEE Trans. Antennas Propag, 1966, 14(3): 302-307

[6] M. Brambilla. Slow-wave launching at the lower hybrid frequency using a phased waveguide array. Nuclear Fusion, 1976, 16(1): 47

[7] D.N. Smithe. Finite-difference time-domain simulation of fusion plasmas at radiofrequency time scales. Physics of Plasmas, 2007, 14(5): 056104

[8] A.C. England, O.C. Eldridge, S.F. Knowlton et al. Power transmission and coupling for radiofrequency heating of plasmas. Nuclear Fusion, 1989, 29(9): 1527-1633

[9] P. Bonoli, Linear Theory of Lower Hybrid Heating. IEEE Trans. On Plasma Science, 1984, 12(2): 95-107

Advanced Materials Research Vols. 989-994 (2014) pp 2702-2704
© (2014) Trans Tech Publications, Switzerland
doi:10.4028/www.scientific.net/AMR.989-994.2702

Research on Workpiece Deformation in Electromagnetic Forming Process with Finite Element Method

Chang Peng[1], Li Qiu[1, a,*], Keshen Gong[1], Dingjun Wang[1]

[1]College of Electrical Engineering and New Energy, China Three Gorges University, Yichang, 443002, China

[a]Corresponding author email: Doctor_QiuL@163.com

Keywords: Electromagnetic Forming; Workpiece Deformation; Finite Element Method

Abstract. Electromagnetic forming is a kind of processing technology that use lorentz force to make rapid prototyping of metal workpiece, which can significantly improve the metal forming performance,and it is expected to become an emerging technology that alternative to traditional machining to process light alloy materials. Based on the understanding the basic structure of the electromagnetic coupling on the basis of physical process of electromagnetic forming, this article adopt ANSYS sequential coupling method to simulate the electromagnetic coupling process of electromagnetic structure, and analysis of tube electromagnetic forming and plate of workpiece in the process of free bulging deformation behavior. The solenoid coil tubing have an axis of symmetry due to bulging, and it's electromagnetism load and constraint has symmetry, so its formability is uniform in hoop direction. When the plank free bulge, the distribution of the electromagnetic force caused by the flat spiral coil is not uniform,and the artifacts accelerate fastest in the part of the radius of coil 1/2, but the center area of the workpiece's forming height is highest.

Introduction

Electromagnetic forming is a kind of processing technology that use lorentz force to make rapid prototyping of metal workpiece, and the forming process rank millisecond, forming speed is generally more than 300 m/s [1][2], the schematic diagram as shown in Fig. 1. Through the capacitor power discharge to drive coil, there produce powerful pulse current in the drive coil, at the same time eddy current is producted in the metal artifacts. Electromagnetic force between excitation current and the induced current drive metal workpiece to accelerate and lead to plastic deformation. Electromagnetic pulse shaping is the use of magnetic force to sheet metal forming, which has the following characteristics:

In the pulsed electromagnetic force, the work obtain a large kinetic and energy to achieve the forming acceleration at the moment. The intensity of magnetic pulse can accurately control, easy to realize mechanization and automation. Electromagnetic forming load force to plate via the medium of magnetic field. There are no mechanical contact and forming surface have a high quality.

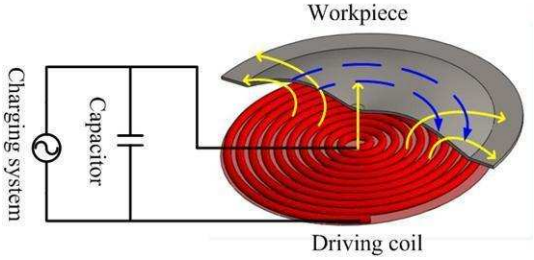

Fig. 1. Electromagnetci forming process.

AL-Hassani studied and analyzed the electromagnetic force distribution of different shapes coil on the sheet metal [3]; Takatsu studied the free bulging process of electromagnetic plank taking the flat spiral coil for example , and the simulation and experimental results are basically identical [4]. Scholars studied and simulated the electromagnetic tube bulging process and so on, with the method of electromagnetic and structural decoupling, namely, the loosely coupling method [5] [6].

Fenton and Daehn analyzed the Planar-Magnetic free bulging process by using the algorithm of 2 d arbitrary Lagrangian,and the simulation results matched with the experiment very well [7]. However, loosely coupling method did not consider the influence between the structure and the magnetic field , so the model is only applicable to the simulative electromagnetic forming process of small deformation workpiece.

Based on the understanding of basic electromagnetic structure coupling process of electromagnetic forming,this article adopts a sequence coupling method to simulate the electromagnetic coupling process of electromagnetic structure, and analyzes the deformation behavior of workpiece in the process of tube electromagnetic forming and plate workpiece's free bulging.

Basic principle of electromagnetic forming

Field forming process of pulse high magnetic field is a complicated physical field coupling issue, involving many other disciplines such as the electromagnetic field, structure field, temperature field and material science. In view of the main problems,the forming process can be considered as a coupling physical process of electromagnetic structure. the electromagnetic process of workpiece's inside can be calculated according to Faraday's law of electromagnetic induction:

$$\nabla \times E_{\varphi} = -\frac{\partial B_z}{\partial t} \quad (1)$$

The electromagnetic force of workpiece is:

$$F_z = J_{\varphi} \times B_r \quad (2)$$

In the forming process of pulse magnetic field, the workpiece speeds up and becomes distored under the action of pulse electromagnetic force . Bz and Br in equation (1) and (2) stand for the magnetic flux density inside the workpiece.Apart from its being associated with time, its value is related to the workpiece deformation caused by the displacement changes. At the same time, the magnetic flux density distribution also varies with the shape changing. Magnetic flux density and electromagnetic force, along with the change of displacement and shape workpiece are the workpiece structure field effect of electromagnetic field.

Sequential coupling method

Because of the development of computer technology and finite element software,finite element simulation study of pulsed magnetic field has become one of the main physical processes shaping the electromagnetic coupling structure.Sequential coupling method has achieved the analysis of electromagnetic coupling structure. The specific flow chart shown in Figure 1:Build geometric models;Clear structural loads and boundary setting, Set electromagnetic model unit type, load, borders, etc. Written electromagnetic physical environment;Clear electromagnetic load and boundary setting,Forming structural unit type field and boundary conditions.Written to structure physical environment; settings the simulation time and time step, the preparation of the electromagnetic coupling cycle program sequence structure:Read out electromagnetic physics model, solving electromagnetic model; read out structure physical model, loaded electromagnetic force load, solving the structure of the model;Updated according to the results of the workpiece and nearby structures air grid; determine whether the step is the last step, if not, continue to the next magnetic field and deformation analysis, and if so, stop the cycle, end coupling analysis.Generally, high pulsed magnetic field formed the discharge process as microseconds, milliseconds forming process; After the discharge, the movement and deformation of the workpiece can do a simple structural analysis. Therefore, in order pulsed magnetic field coupling loop ends after forming, usually set up a new simulation time and time step, the process used to analyze the deformation of the workpiece under the action of inertial force.

Analysis of deformation behavior

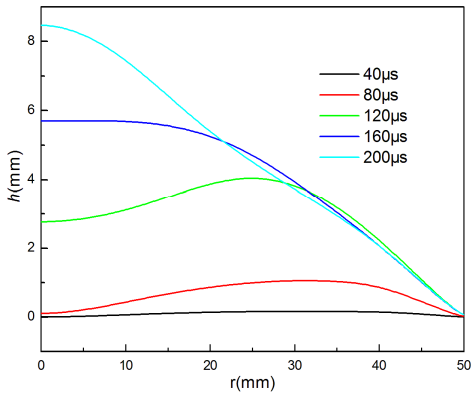

Fig. 2. Workpiece deformation behavior.

With flat spiral coil plate free bulging, circle constraints outside the workpiece must be fixed; Due to uneven distribution of flat spiral coil of electromagnetic force, the artifacts accelerate fastest in the part of the radius of coil 1/2(as shown in fig. 2); When the 1/2 of workpiece was accelerated to high speed, the central portion of the workpiece is drived to accelerated, eventually the center area formed the highest height due to the minimum binding. Figure 5 showed the free forming process of electromagnetic plate,which clearly reflects the free bulging's deformation process.

Conclusion

Electromagnetic forming process is a complicated physical field coupling problem, which involves the electromagnetic field, structure field, temperature field and material science, and other disciplines. In view of the main problems, pulse magnetic field forming can be considered as an physical process of electromagnetic structure's coupling.That adopt the electromagnetic structure coupling finite element method to analyze the electromagnetic forming process, can effectively response deformation behavior of work piece under different loading conditions, and also can provide powerful theory basis for parameters optimization design of electromagnetic forming.

Acknowledgement

This work is supported by Science and Technology Foundation of Hubei Provincial Department of Education (Q20141202) and State Key Laboratory of Advanced Electromagnetic Engineering and Technology (Huazhong University of Science and Technology).

References

[1] Glenn S. Daehn. High Velocity Metal Forming. ASM Handbook, Volume 14B, Metalworking: Sheet Forming, Published 2006, ASM International, pp. 405-418.
[2] AG Mamalis, DE Manolakos. Electromagnetic forming and powder processing: Trends and developments. Appl Mech Rev. 2004, 57(4): 299-324.
[3] Al-Hassani, S. T. S. Magnetic Pressure Distributions in Sheet Metal Forming. Electrical Methods of Machining, Forming and Coating. Inst. Electr. Eng. Conf. Publ., 1975, pp. 1–10.
[4] Takatsu N., Kato M., Sato K., et al. High-speed forming of metal sheets by electromagnetic force. The Japan Society of Mechanical Engineers, 1988, 31(1): 142–148.
[5] F. Azzouz, B. Bendjima, M. Feliachi. Application of Macro-Element and Finite Element Coupling for the Behavior Analysis of Magnetoforming Systems. IEEE Transaction on Magnetics, 1999, 35(3): 1845-1848.
[6] B. Bendijima, M. Feliachi. Finite element analysis of transient phenomena in electromagnetic forming system. Computation in Electromagnetics, IEE Conference Publication, 1996, pp. 113-116.
[7] Fenton G K, Daehn G S. Modeling of electromagnetically formed sheet metal. Journal of Materials Processing Technology, 1998, 75: 6-16.

Advanced Materials Research Vols. 989-994 (2014) pp 2705-2708
© (2014) Trans Tech Publications, Switzerland
doi:10.4028/www.scientific.net/AMR.989-994.2705

Research on Learning Algorithm of RBF Neural Network Based on Extended Kalman Filter

Xu-Sheng Gan[1,a], Hai-Long Gao[2,b]

[1]XiJing College, Xi'an, Shaanxi, 710123, China

[2]Unit 93132 of PLA, Qiqihar, Heilongjiang, 160072, China

[a]ganxusheng123@163.com, [b]ghlljyx@sina.com

Keywords: Radial Basis Function; Neural Network; Extended Kalman Filter; Learning Algorithm

Abstract. To improve the learning capability of Radial Basis Function (RBF) neural network, a RBF neural network algorithm based on Extended Kalman Filter (EKF) is proposed. First the basic idea of EKF algorithm and RBF neural network are introduced, and then EKF is used to optimize the parameters combination of RBF neural network to obtain the better model. The experiment proves its feasibility.

Introduction

RBF neural network has many advantages, and has been widely used such as image recognition, speech recognition, nonlinear system identification and so on. According to the characteristics of RBF neural network, a variety of RBF neural network algorithms have been proposed, but these algorithms has the shortcoming such as poor explanation, requirement of high quality data, theory depth and so on.

Based on this, a extended Kalman filter algorithm for RBF neural network training is proposed to optimize the parameters of the network from sample data. The experiments show its validity.

Extended Kalman filter algorithm

Kalman filter is a highly efficient recursive filter (autoregressive filter) that can estimate the state of dynamic system. be measured from a series of measurement without incompletely containing noise. This filter method was named by its inventor R. E. Kalman. However, the simply Kalman Filter need be applied in system following Gauss distribution, later scholars had made many improvements on it, one of which is Extended Kalman Filter (EKF) [1] that can be applied in the nonlinear dynamic system.

Filter theory initially proposed by Kalman is only suitable for linear systems, Bucy, Sunahara et al proposed and studied EKF, and it be further applied in the field of nonlinear filtering theory. The basic idea of EKF is that first the nonlinear system is linearized, and then Kalman flter is executed, so EKF is a suboptimal filter. In addition, the proposition and application of various second-order EKF methods further improve the estimation performance of Kalman filter for the nonlinear system. The second -order filter method considers the quadratic term of Taylor series expansion, thus it can reduce the estimation error caused by the linearization, but greatly increases the amount of computation, so campared to first-order EKF[2], it was not used widely in practice.

When the state equation and measurement equations are nonlinear, EKF usually is adopted. EKF conduct the first-order linearization truncation for Taylor expansions of nonlinear function, ignoring the rest of the high order item, thus the nonlinear problem is transformed into the linear problem, Kalman filter algorithm of can be applied in the nonlinear system, which solves the nonlinear problem.

For a nonlinear discrete systems

$$x_t = \Phi_{t,t-1} x_{t-1} + \Gamma_{t-1} w_{t-1} \tag{1}$$

$$z_t = H_t x_t + v_t \tag{2}$$

where t is the present moment, x_t is the system state vector, z_t is the observation vector, $\Phi_{t,t-1}$ is the state transition matrix, H_t is the observation matrix. Process noise w_t and measurement noise v_t is the series with unrelated zero mean white noise, its statistical characteristics is as follows:

$$E[w_t] = 0;\ E[w_t w_j^T] = Q_t \delta_{tj} \tag{3}$$

$$E[v_t] = 0;\ E[v_t v_j^T] = R_t \delta_{tj} \tag{4}$$

$$E[w_t v_j^T] = 0 \tag{5}$$

where $\delta_{tj} = \begin{cases} 1 & t = j \\ 0 & t \neq j \end{cases}$.

Suppose that the initial state of statistical characteristics is

$$E[x_0] = \mu_0;\quad E[(x_0 - \mu_0)(x_0 - \mu_0)^T] = P_0 \tag{6}$$

and x_0 is completely irrelevant to w_t, v_t, namely

$$Cov(x_0, w_t) = 0;\quad Cov(x_0, v_t) = 0 \tag{7}$$

The filtering process of the system is as follows:

$$\hat{x}_{t|t-1} = \Phi_{k|k-1} \hat{x}_{t-1} \tag{8}$$

$$\hat{x}_t = \hat{x}_{t|t-1} + K_t (z_t - H_t \hat{x}_{t|t-1}) \tag{9}$$

$$K_t = P_t H_t^T R_t^{-1} \tag{10}$$

$$P_{t|t-1} = \Phi_{t,t-1} P_{t-1} \Phi_{t,t-1}^T + \Gamma_{t-1} Q_{t-1} \Gamma_{t-1}^T \tag{11}$$

$$P_t = (I - K_t H_t) P_{t|t-1} \tag{12}$$

RBF neural network

Neural network has a strong ability of nonlinear fitting, and can execute the mapping for arbitrarily complex nonlinear relation with simple learning rules and easy computer realization. It has very strong robustness, memory capacity, nonlinear mapping ability and strong self-learning ability, so it has great application foreground[3].

RBF neural network is a feed-forward neural network with excellent performance. RBF network can approximate any nonlinear function through arbitrary precision, and has the ability of global approximation, solving the problem of local optimum BP neural network radically, and its topology structure is compact, its structure parameters can realize the separation learning with fast convergence speed[4]. The advantages of RBF neural network mainly include:

① It has a unique optimal approximation properties without local minimum.

② RBF neural network has strong mapping function for input and output, and it has be proved that, in feed-forward neural network, RBF neural network is the best network completing the mapping function.

③ The relationship between connection weights and output of network is linear.

④ It has a good classification ability.

⑤ The learning process has a rapid convergence speed.

In fact, RBF neural network generally has only one hidden layer with RBF activation function. For Fig.1 shows the structure of RBF neural network, the expression of RBF neural network is as follows:

$$z=\sum_{i=1}^{n}\omega_i f(\|x-C_i\|/\delta_i) \tag{13}$$

or if considering threshold value we have

$$z=\sum_{i=1}^{n}\omega_i f(\|x-C_i\|/\delta_i)+d \tag{14}$$

where ω_i is the connection weight of output layer, C_i is the center of radial basis function, $f(\cdot)$ is the RBF function, $x\in R^n$ is the input of neural network, δ_i is the sensitive domain of RBF, d is the threshold value of output layer, $\|\bullet\|$ is the distance operator, n is the number of hidden neurons.

Suppose that the training samples $S_m=\{X_i,Z_i\}$, $i=1,2,\cdots,m$, then the training process of RBF neural network is to hunt for $\Theta=\{C_i,\delta_i,\omega_i\}$ to acheive the minimization of following function

$$\min e_{RBF}(S_m,F_n(X,\Theta))=\frac{1}{m}\sum_{i=1}^{m}|Z_i-F_n(X,\Theta)|^2 \tag{15}$$

$$F_n(X,\Theta)=\sum_{i=1}^{n}\omega_i f(\|x-C_i\|/\delta_i) \tag{16}$$

Because the output layer of RBF neural network is the linear neurons, so as long as C_i and δ_i are determined, the parameters of output layer can be constructed by least square method. In learning algorithm of RBF neural network, the main task is to search the optimal vector $\Theta=\{c_i,\sigma_i,w_i\}$.

Learning process of RBF neural network based on extended Kalman filter

The state space model is a dynamic model in time domain in which the connotative time is regarded as the argument. Application of state space model in the analysis of time series are increasing rapidly. The state space model that is more commonly applicated is the canonical correlation method proposed by Akaike and further evolved by Mehra. The new method of state space model that can estimate the vector value proposed by Aoki et al can get the state space model with so-called internal balance, if only the corresponding element in the system matrix can be removed, any low order approximation model can be obtained without re-estimation, and as long as the original model is stable, low order approximation model obtained is also stable.

For RBF neural network shown in Fig.1, its network learning is optimal estimation for the network parameters Θ (including c_i,σ_i,w_i) so as to search the optimal network parameters. Therefore, Θ is taken as the state variables of the network system, the output as the measurement equation of the network, the state space model of RBF neural network can be expressed as

$$\Theta_{t+1}=\Theta_t+\eta_t \tag{17}$$

$$z_t=f(X_t,\Theta_t)+\mu_t \tag{18}$$

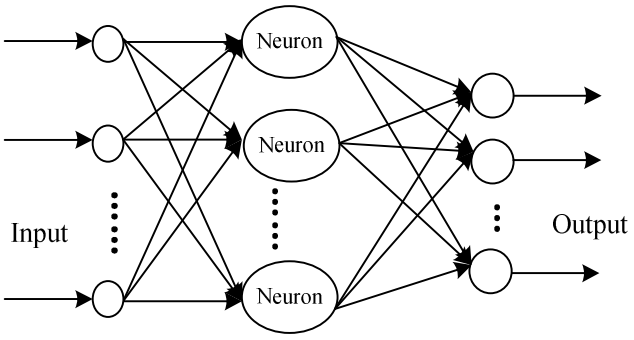

Fig.1 Topology Structure of RBF neural network

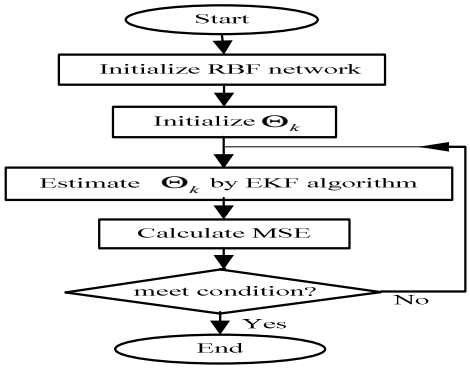

Fig.2 Flow of EKF-RBFNN

where X_t is the input of the network, z_t is the output of the network, $f(X_t, \Theta_t)$ is the nonlinear function parameterized. η_t is the process noise and in paper is taken as Gauss white noise with mean 0 and variance Q_t, η_t is the measurement noise and in paper is taken as Gauss white noise with mean 0 and variance R_t, noise.

Through EKF training RBF neural network, we can use EKF algorithm to obtain the optimal parameter vector $\Theta = \{c_i, \sigma_i, w_i\}$. The training flow of RBF neural network using EKF algorithm is shown in Fig. 2, where Mean Square Error (MSE) is taken as the error indicators of network training.

Simulation example

The simulation object is a function with multi-peak and dramatic changes as follows

$$y_i = \frac{\sin(9x_i)}{(x_i - 0.16)^2 + 0.1} \tag{19}$$

Suppose that the training set is 100 points following the uniform distribution in $[0,6]$, namely $\{(x_1, y_1), \cdots, (x_{100}, y_{100})\} \in R^1 \times R^1$. The training input is $x_1, x_2, \cdots, x_{100}$; the training output is $y_1, y_2, \cdots, y_{100}$. The input of the test set is 100 points that are randomly generated in $[0,6]$, the test output is the corresponding function values according to the formula (19).

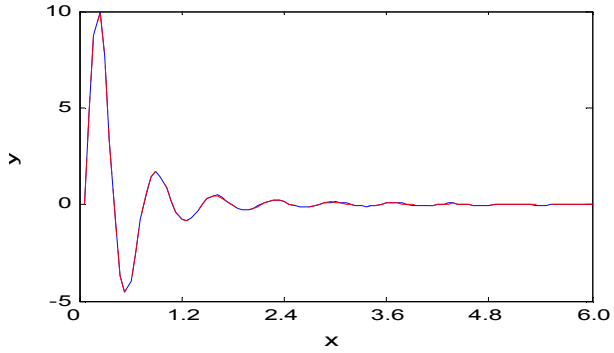

Fig.3 Approximation effect of function

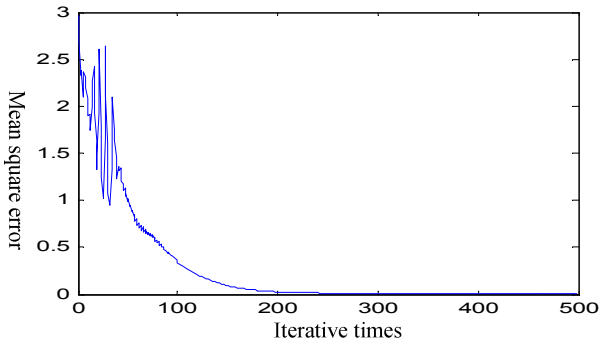

Fig.4 Training convergence curve

The experiment result as shown in Fig.3 and Fig.4 indicates that, the proposed learning algorithm of RBF neural network based on EKF has a good approximation ability with rapid convergence rate.

Conclusions

A learning algorithm of RBF neural network using EKF is proposed. In the algorithm, the traditional EKF algorithm is used to estimate the optimal parameters of RBF neural network for the network training . The simulation indicate that this learning algorithm can achieve a good modeling ability.

References

[1] K. J. Kim, J. B. Park, Y. H. Choi. The adaptive learning rates of extended Kalman filter based training algorithm for wavelet neural networks. MICAI, (2006), 327-337

[2] J. S. Oh, J. B. Park, Y. H. Choi. Path tracking control using a wavelet neural network for mobile robot with extended Kalman filter. International Conference on Control, Automation and Systems, (2003), 1283-1288

[3] S. Chert, P. M. Crant, C. F. N. Cown. Orthogonal least square algorithm for radial basis function networks. IEEE Transaction on Neural Networks, 2(2), (1991), 302-309

[4] S. Chert, S. A. Billings, P. M. Grant. Recursive hybrid algorithm for non-linear system identification using radial basis function networks. International Journal of Control, 55(5), (1992), 1051-1070

Advanced Materials Research Vols. 989-994 (2014) pp 2709-2712
© (2014) Trans Tech Publications, Switzerland
doi:10.4028/www.scientific.net/AMR.989-994.2709

Interpolation Algorithm Application of Zadoff-Chu Sequence Using Neural Networks

Jian Cao[a], Yanbin Li[b], Cong Yan[c]

Air Force Engineering University, Xi'an, Shaanxi Province 710051, P.R. China

[a]cao_jian1972@163.com, [b]Lyanbing@163.com, [c]yancong192@qq.com

Keywords: NN; CAZAC; Application; Interpolation

Abstract. In order to adapt the spectrum property of Zadoff-Chu sequence to the requirement of HF channel sounding transmitter-receiver, the Formula Direct Interpolation Algorithm (FDIA) is put forward by which the amplitude frequency characteristic of Zadoff-Chu sequence can be enhanced. Then the comparison of spectra of the sequences respectively interpolated by FDIA and commonly used interpolation algorithm is conducted, which affirms the superiority of FDIA. Finally, an effective method of achieving best decimation of the sequence interpolated by FDIA is provided. All these lay primary theory foundation for the application of Zadoff-Chu sequence to HF channel sounding.

Introduction

CAZAC sequence with a length of N^2 (N is an integer) which was used in the Zadoff-Abourezk patent of a synchronizing system was first proposed by Frank in 1950s. The CAZAC sequence proposed by Frank was described afresh by Frank and Zadoff in. Based on the work of Frank and Zadoff, D[1]. Chu proposed a sort of CAZAC sequence without restriction on its length, that is, Zadoff-Chu sequence. And he proved that certain linear phase shift of the form $\exp(j2\pi qk/N)$, when introduced into the sequence will not affect its correlation property, where q , k and N are integers, and k is relatively prime to L[2].

The spectrum of Zadoff-Chu sequence is flat in the full bandwidth, even though its periodic autocorrelation property is perfect, which indicates that the sequence cannot be transmitted directly by channel sounding transmitter because its energy is decentralized. Therefore, an interpolation algorithm is needed, by which the spectrum of Zadoff-Chu sequence can be compressed for the transmission in HF channel. Consequently, the paper proposes an interpolation algorithm which is suitable for Zadoff-Chu sequence, that is, the FDIA. Then the comparisons of the spectra, the real parts and the imaginary parts of the sequences respectively interpolated by FDIA and commonly used interpolation algorithm are carried out. The decimation method of the sequence interpolated by FDIA is investigated and an efficient method by which the optimal decimation position can be found is provided. The method makes use of the periodic auto-correlation property of Zadoff-Chu sequence. The simulation results show that the periodic auto-correlation property of Zadoff-Chu sequence is perfect[3]. The spectra of the sequence respectively interpolated by FDIA and commonly used interpolation algorithm have the same main-lobe width, but the spectrum of the sequence interpolated by FDIA has a faster roll-off and almost no big side-lobes. Besides, the optimal decimation position of the sequence interpolated by FDIA can be easily found out by the method provided[4].

The paper is organized as follows: Section II describes the periodic auto-correlation property of Zadoff-Chu sequence. In Section III, the FDIA is proposed. The comparisons of the spectra, the real parts and the imaginary parts of the sequences respectively interpolated by FDIA and commonly used interpolation algorithm are carried out in this section, too. Section IV provides the decimation method of the sequence interpolated by FDIA.

Correlation Property of ZADOFF-CHU Sequence

Fig.1 shows the PACF of Zadoff-Chu sequence with k=1 and L=1024. The PACF of m sequence with period of 1023 is also depicted in Fig.1 to clearly illustrate the perfect periodic autocorrelation property of Zadoff-Chu sequence. In addition, theoretical calculations show that the peak to side-lobe ratio of the PACF of Zadoff-Chu sequence ups to 280dB, and the peak to sidelobe ratio of the PACF of m sequence is only 60dB.

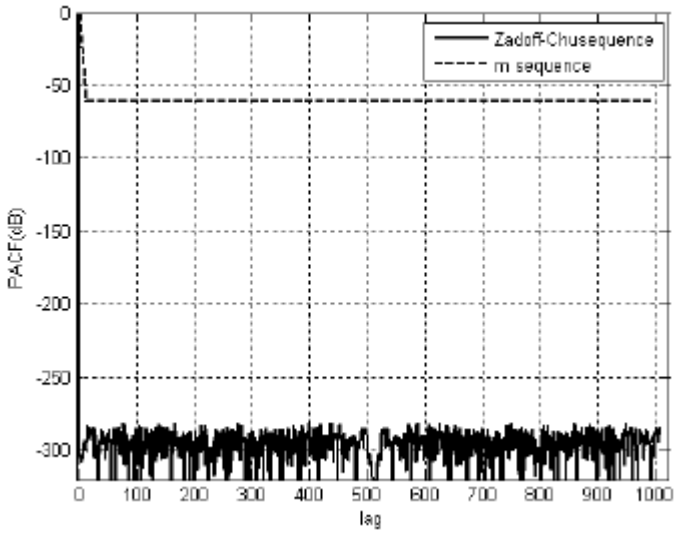

Fig.1 Normalized PACFs of Zadoff-Chu Sequence and m Sequence

Comparison of FDIA and the commonly used interpolation algorithm

Fig.2 shows the real parts and the imaginary parts of the original Zadoff-Chu sequence with L=32 and k=1 and of the sequences respectively 8 times interpolated by FDIA and commonly used interpolation algorithm. The real line represents the sequence interpolated by FDIA and the broken line represents the sequence interpolated by the commonly used interpolation algorithm.

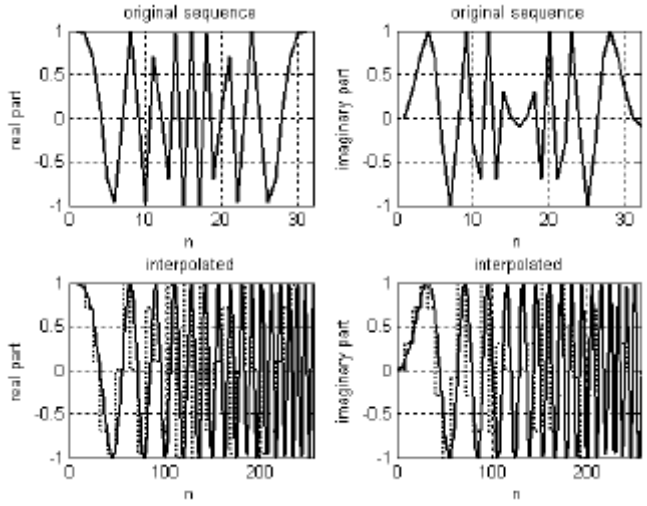

Fig.2 Waves of sequences respectively interpolated by FDIA (real line) and commonly used interpolation algorithm (broken line)

Motion Control Section

Motion control section can be divided into the control part and actuator, which is a classic servo closed loop position control, Motion control section diagram shown in Fig.3. Movement control card can receive PC control instruction, and the axes interface to be controlled send pulses to relevant servo controller to control motor rotation angle, and then ball-screw will convert rotation

angle to horizontal displacement, so as to carry the infrared supply horizontal or vertical movement. The control part mainly includes movement control card, servo controller and so on, motor control command is sent through the PC software to regular the movement control card to produce the corresponding output pulse. The whole movement process need two axes motor control respectively, it is adequate for us to use the movement control card supported four axes, and available for circular interpolation, continuous linear interpolation, so the card can meet the equipment requirements. Actuator is a key part of the whole system, which is designed three-rail plane, including two horizontal rails and one vertical rail, ball-screw inside, which can drive the slider with infrared light supply to move in the whole plane. There at the edge of rail separately installs limit switch and origin switch to determine the origin and the maximum boundary. The parts of actuators in detail designed as Fig.4 shows.

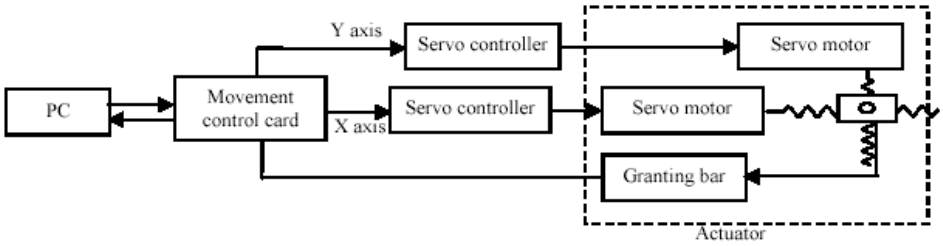

Fig.3 Motion control section

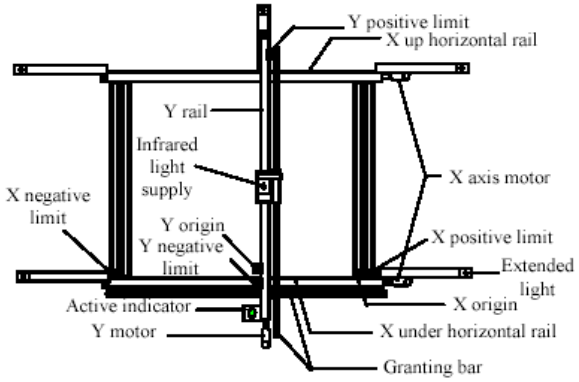

Fig.4 Part of actuator

Neural Network Augmented Model Inversion Architecture

This section details the architecture of the NN augmented model inversion as applied to the tiltrotor aircraft. Fig.5 contains a diagram of the architecture used for implementation of ACAH control in the pitch channel. The command filter serves both to limit the input rate, and as a model for desired response. This allows for straightforward implementation of ADS-33 handling qualities specifications. The presented architecture provides for excellent results in the longitudinal application, as is shown in following sections. Identical construction applies to the lateral channels.

The results in the lateral channels show similar performance.

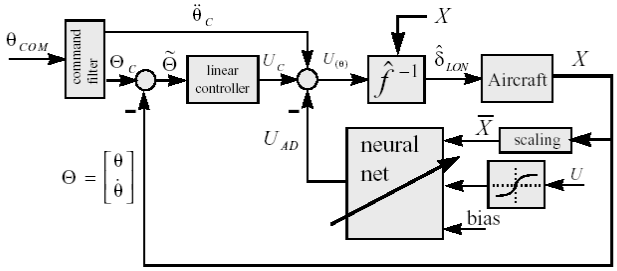

Fig.5 Adaptive NN augmented model inversion architecture in the longitudinal channel configured for ACAH

Conclusion

In HF channel oblique sounding, the selection or design of sounding sequences is a key technique. The paper investigates the periodic autocorrelation property of Zadoff-Chu sequence based on the introduction of the definition and properties of CAZAC sequences. Aiming at resolving the problem that the spectrum of Zadoff-Chu sequence is not band-limited which makes it be not suitable for transmission in HF channel, the FDIA is proposed in the paper by which the amplitude frequency characteristic of Zadoff-Chu sequence can be enhanced. The comparisons of the spectra, the real parts and the imaginary parts of the sequences respectively interpolated by FDIA and commonly used interpolation algorithm are carried out. At the same time, an effective method of achieving optimal decimation of the Zadoff-Chu sequence interpolated by FDIA is provided. The simulation results show that the periodic auto-correlation property of Zadoff-Chu sequence is perfect. The spectra of the sequence respectively interpolated by FDIA and commonly used interpolation algorithm have the same main-lobe width, but the spectrum of the sequence interpolated by FDIA has a faster roll-off and almost no big side-lobes, which means that it has a higher energy using ratio when transmission in narrow band HF channel. Hereby, this paper lays primary theory foundation for the application of Zadoff-Chu sequence to HF channel oblique sounding.

In the control process, it is convenient to process all necessary parameter setting and adjustment, and in the control process of the whole system the photovoltaic simulator shows superior performance and achieves the expected effect.

References

[1] J. B. John, D. Jeffrey, K. Ioannis and C. Shaw. “Zero autocorrelation waveforms: a Doppler statistic and multifunction problems,” Proc. of IEEE International Conference on Acoustics, Speech and Signal Processing.pp. 1117-1120, 2012.

[2] Li Chih-Peng, Huang Wei-Chieh. “A constructive representation for the Fourier dual of the Zadoff–Chu sequences,” IEEE Transactions on Information Theory, vol. 53, no.11, pp. 4221-4224,2007.

[3] The-Hanh Pham, Liang Ying-Chang, A. Nallanathan and H. K. Garg. “Optimal training sequences for channel estimation in bidirectional relay networks with multiple antennas,” IEEE Transactions on Communications, vol. 58, no. 2, pp.474-479, 2010.

[4] Fuqin Xiong. Digital Modulation Techniques, Artech House, INC, Boston, USA. pp. 129, 2010.

[5] R.L. Frank and S.A. Zadoff. “Phase shift pulse codes with good correlation properties,” IRE Transactions on Information Theory, vol. IT-8, pp. 381-382, Oct. 1962.

Advanced Materials Research Vols. 989-994 (2014) pp 2713-2718
© (2014) Trans Tech Publications, Switzerland
doi:10.4028/www.scientific.net/AMR.989-994.2713

Comparison on turnovers of agricultural products futures based on Hilbert-Huang transform

Qingbin Han[1, a],Haili Shi[2,b]

[1]University of Science and Technology Liaoning, Anshan, China

[2] Northeastern University, Shenyang, China

[a] hanneu@163.com, [b]421666182@qq.com

Keywords: Turnover amounts, Non-stationary signals, Hilbert-Huang transform, Empirical mode decomposition.

Abstract. In order to distinguish the different patterns and evolving trends on turnovers of agricultural products futures between Zhengzhou Commodity Exchange (Z-CE) and Dalian Commodity Exchange (D-CE), a novel time-frequency analysis approach, i.e. Hilbert-Huang transform (HHT), is investigated in this paper. Firstly, Hilbert-Huang transform is briefly introduced. Secondly, two different non-stationary signals of turnover of agricultural products futures from 2009 to 2013 coming from Z-CE and D-CE are described in Empirical Mode Decomposition (EMD). With these results, the two signals are distinctly different from each other. It is proved that the technique of HHT is effective for the purpose of distinction of turnover of agricultural products futures in commodity exchanges.

Introduction

Turnover of agricultural products futures of Zhengzhou Commodity Exchange (Z-CE) and Dalian Commodity Exchange (D-CE) includes so much information that it can be used to diagnose, treat or predict economic trends. The data turnover of agricultural products futures has one or more of the following problems, (a) the total data span is too short, (b) the data is non-stationary and (c) the data represents nonlinear process.

The time series of turnover of agricultural products futures is mainly regarded that, for the signal itself, there are stationary or non-stationary properties, while the linear or nonlinear properties should refer to its original system [1]. In economic community, most of the systems are regarded to be nonlinear; moreover, their signals are often non-stationary.

Historically, Fourier spectral analysis has provided a general method for examining the global energy-frequency distributions, but has some inherent restrictions, for example, the system must be linear and the data must be strictly periodic or stationary. So how to identify or at least to distinguish the non-stationary properties of the signals is of major concerned. In recent years, some time-frequency processing methods for nonlinear and non-stationary signals have been proposed, such as wavelet analysis, Wigner-Ville distribution, etc [2-5].

Recently, a new method based on Hilbert-Huang transform (HHT) for analyzing non-stationary signals has been proposed [6], in which the expansion bases are adaptive for signals from nonlinear and non-stationary processes. Based on this method, any complicated signals can be decomposed into a finite and often small number of 'Intrinsic Mode Functions' (IMFs) that admit well-behaved Hilbert transforms. And with the Hilbert transform, the IMFs yield instantaneous frequencies as functions of time that give sharp identifications of embedded structures. The final presentation of the results is an energy-frequency-time distribution, designated as the Hilbert spectrum.Compared to the Fourier-based linear and stationary spectral analysis and other time-frequency analysis methods, HHT is now considered a great breakthrough and used in non-stationary analyses and processing fields [7-9].

In this paper, we choose turnover of agricultural products futures between Zhengzhou commodity exchange and Dalian commodity exchange to analysis. From their time domain waveforms and their power spectrum densities, they are not easily to be distinguished. In using HHT, we obtain effective distinctions between them. The results demonstrate that HHT is effective

to identify the features of non-stationary signals of turnover of agricultural products futures between Zhengzhou commodity exchange and Dalian commodity exchange.

Basic algorithm procedure of HHT

HHT involves two aspects: empirical mode decomposition (EMD) and Hilbert spectral analysis (HAS) [6]. Firstly, a time-adaptive decomposing operation named EMD is applied to a signal, in which the signal are decomposed into a set of complete and almost orthogonal components named Intrinsic Mode Functions (IMFs). Secondly, with Hilbert transforming of those IMFs, a full energy-frequency-time distribution of the signal is obtained [10- 11].

The IMFs, which are regarded as both the amplitude modulation and the frequency modulation, satisfy the following requirements: 1) the number of extremes and the number of zero crossings in the IMF must either be equal or different at most by one; and 2) at any point the mean value of the envelopes defined by the local maxima and local minima must be zero. The process to find the IMFs of a signal $x(t)$ comprises the following steps:

1) Find the positions and amplitudes of all local maxima and minia in the input signal $x(t)$. Then create an upper envelope by cubic spline interpolation of the local maxima, and a lower envelope by cubic spline interpolation of the local minima.

2) Calculate the mean of the upper and lower envelopes; this is defined as $m_1(t)$.

3) Subtract the envelope mean from the original input signal,

$$h_1(t) = x(t) - m_1(t). \tag{1}$$

4) Check whether $h_1(t)$ meets the requirements to be an IMF. If the sifting result $h_1(t)$ is an IMF, stop the process. Otherwise, treat $h_1(t)$ as the new signal data and iterate on $h_1(t)$ through the previous step 1) ~ 4). That is, to set

$$h_{11}(t) = h_1(t) - m_{11}(t). \tag{2}$$

Repeat this sifting procedure k times until $h_{1k}(t)$ is an IMF. This is designated as the first IMF, shown below

$$c_1(t) = h_{1k}(t). \tag{3}$$

5) Subtract $c_1(t)$ from the input signal and define the remainder, $r_1(t)$, which is the first residue as following,

$$r_1(t) = x(t) - c_1(t). \tag{4}$$

6) Since the residue $r_1(t)$ still contains information related to longer period components, it is treated as a new data stream and the above-described sifting process is repeated until the last IMF. This procedure can be repeated n times to generate n residues, $r_n(t)$, and result in

$$r_2(t) = r_1(t) - c_2(t), \ldots, r_n(t) = r_{n-1}(t) - c_n(t). \tag{5}$$

The sifting process stops when either of two criteria are met: 1) the component $c_n(t)$, or the residue $r_n(t)$, becomes so small as to be considered inconsequential; or 2) the residue, $r_n(t)$, becomes a monotonic function from which an IMF can not be extracted. For example, the stopping condition for an IMF is

$$\sum_t \frac{[h_{k-1}(t) - h_k(t)]^2}{h_{k-1}^2(t)} < S. \tag{6}$$

where $h_k(t)$ is the sifting result in the kth iteration, and S is typically set between 0.2 and 0.3. Besides, in order to achieve the last IMF, a simple way can be used. The last IMF could be obtained when the cubic spline fitting stops due to the number of local maxima or minima of the residue is less than 2.

Finally, we obtain

$$x(t) = \sum_{j=1}^{n} c_j(t) + r_n(t). \tag{7}$$

In other words, the original signal can now be represented as the sum of a set of IMFs plus a residue.

Now apply Hilbert transform to all IMFs,

$$H\left[c_j(t)\right]=\frac{1}{\pi}\int_{-\infty}^{\infty}\frac{c_j(\tau)}{t-\tau}\mathrm{d}\tau . \tag{8}$$

After the Hilbert transform, $H\left[c_j(t)\right]$ and $c_j(t)$ form a complex signal. So, the envelope of every IMF $c_j(t)$,, is given by

$$a_j(t)=\sqrt{c_j^2(t)+(H[c_j(t)])^2} . \tag{9}$$

The phase functions are

$$\Phi_j(t)=\arctan\frac{H[c_j(t)]}{c_j(t)} . \tag{10}$$

And the instantaneous frequencies are obtained as

$$\omega_j(t)=\frac{\mathrm{d}\Phi_j(t)}{\mathrm{d}t} . \tag{11}$$

Having obtained the components of IMFs, we will have no difficulty to apply Hilbert transform to each component of them. With the Hilbert transform of each IMF component, we can express the signal in the following form,

$$X(t)=\sum_{j=1}^{n}a_j(t)\exp(i\int\omega_j(t)dt) . \tag{12}$$

Equation (12) also enables us to represent the amplitude and the instantaneous frequency as functions of time in a three-dimensional space, in which the amplitude can be contoured on the frequency-time plane. This frequency-time distribution of the amplitude is designated as the Hilbert amplitude spectrum, i.e. $H(\omega,t)$. With the Hilbert spectrum defined, we can also define the marginal spectrum, i.e. $h(\omega)$, as following

$$h(\omega)=\int_0^T H(\omega,t)dt . \tag{13}$$

The marginal spectrum offers a measurement of the total amplitude (or energy) contribution.

Results

We choose two time series of turnover of agricultural products futures between Zhengzhou commodity exchange and Dalian commodity exchange to be analyzed. These two time series are recorder as turnover of every day agricultural products futures of Zhengzhou commodity exchange and Dalian commodity exchange from the beginning of 2009 to the end of 2013.

There are two different non-stationary signals are shown in Fig 1, and there amplitude spectrum densities are shown in Fig 2 correspondingly. From Fig 1, the difference is obviously. But it is not easy to identify one from each other.

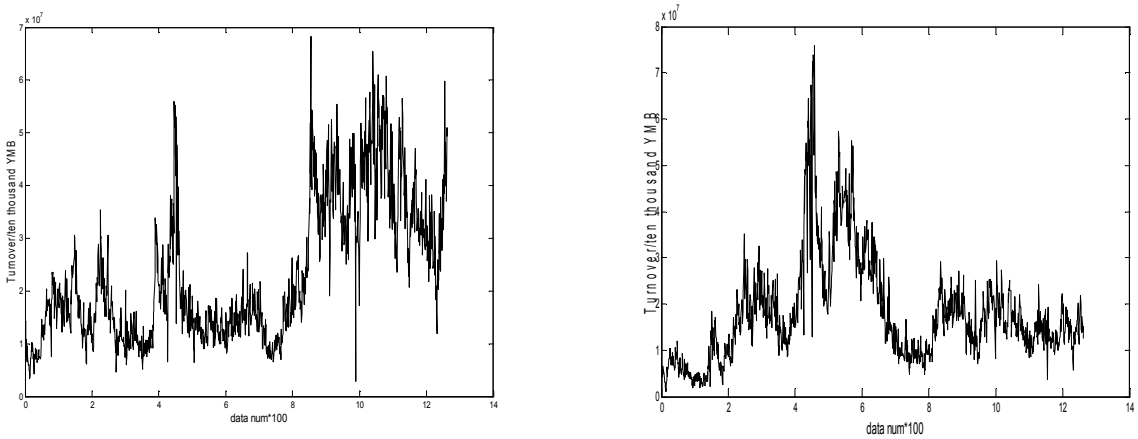

(a) (b)

Fig.1 Original signals of turnover of agricultural products futures
(a)Zhengzhou commodity exchange (b)Dalian commodity exchange

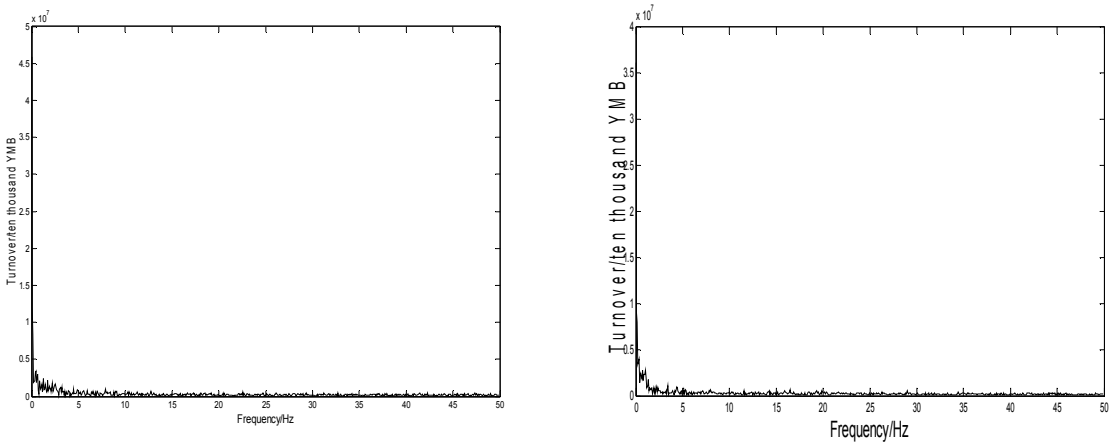

(a) (b)

Fig.2 Frequency spectra of original signals of turnover of agricultural products futures
(a) Zhengzhou commodity exchange (b)Dalian commodity exchange

Now apply HHT for the two signals. The calculated IMFs and instantaneous frequency (IFs) of turnover of agricultural products futures of Zhengzhou commodity exchange and turnover of agricultural products futures of Dalian commodity exchange are shown in Fig 3 and Fig 4.

From Fig.3 (a) and (b), we can see that there are both seven IMF components from signal of turnover of agricultural products futures of Zhengzhou commodity exchange and Dalian commodity exchange. So we can say that the signal of the two turnovers contain same frequency components which embody there same complexity in quantities way. The first IMF of turnover of agricultural products futures of Zhengzhou commodity exchange, c1, appears as amplitude modulation, is also completely different from that in turnover of agricultural products futures of Dalian commodity exchange. The second and third orders of the IMF of turnover of agricultural products futures of Zhengzhou commodity exchange, i.e. c2 and c3, appear frequency modulations, while turnover of agricultural products futures of Dalian commodity exchange is not. Correspondingly, IF of every IMF of the two time series are shown in Fig.4 (a) and (b), which are physically meaningful, and the differences between two time series are clearer.

(a)

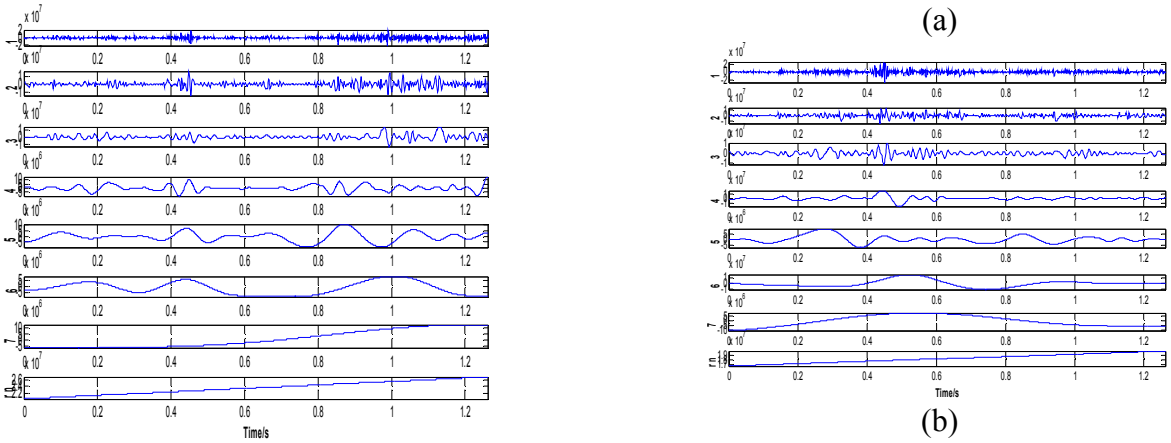

(b)

Fig. 3 IMFs and residual of turnover of agricultural products futures
(a) Zhengzhou commodity exchange (b)Dalian commodity exchange

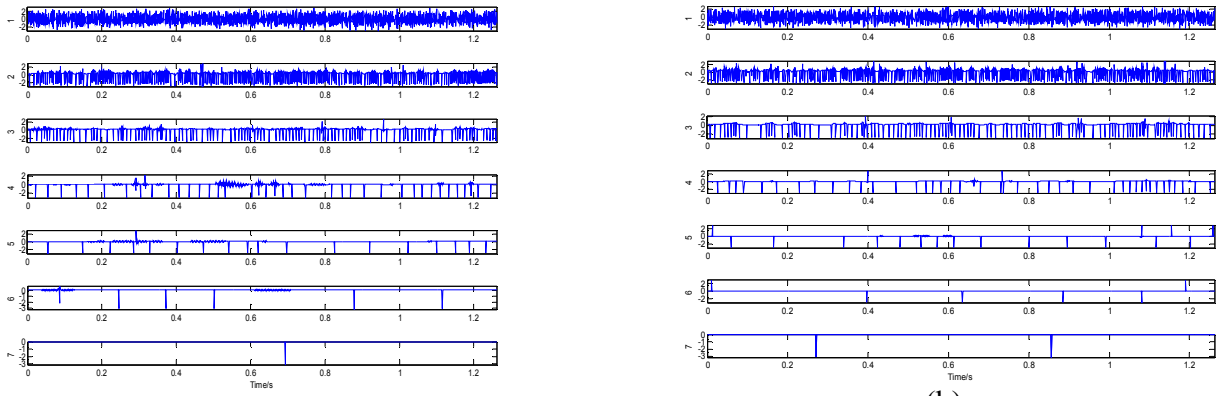

(a) (b)

Fig. 4 Instantaneous frequencies of turnover of agricultural products futures
(a) Zhengzhou commodity exchange (b)Dalian commodity exchange

Furthermore, their frequency spectra of Instantaneous frequencies are also obtained according to the results of IMFs. They are shown in Fig. 5. For the frequency spectra of Instantaneous frequencies of turnover of agricultural products futures of Zhengzhou commodity exchange and Dalian exchange, they offer the measurements of the total amplitude contributions from each frequency value. From Fig 5, we can find the values and their tendency of the total amplitude contributions of turnover of agricultural products futures are remarkable different of Zhengzhou commodity exchange and Dalian exchange. From the two frequency spectra of Instantaneous frequencies of turnover of agricultural products futures of Zhengzhou commodity exchange and Dalian exchange, we can distinguish the differences between them as well.

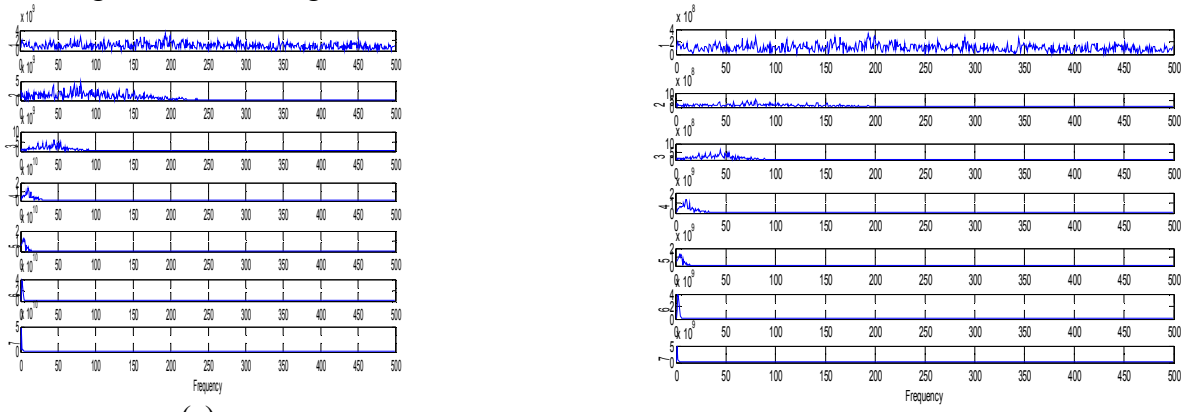

(a) (b)

Fig. 5 The frequency spectra of Instantaneous frequencies of turnover of agricultural products futures
(a) Zhengzhou commodity exchange (b) Dalian commodity exchange

Conclusions

Turnover of agricultural products futures of Zhengzhou commodity exchange and Dalian commodity exchange as two different non-stationary signals are used as examples to be described and distinguished in the time-frequency analyses of HHT in the paper. The technique of HHT is proved to be effective on processing and distinguishing the differences of the non-stationary signals.

For the original non-stationary signals of turnover of agricultural products futures of Zhengzhou commodity exchange and Dalian commodity exchange given here, the obtained IMFs with HHT are easily distinguished from each others. The frequency spectra are also different between them. These results demonstrate that the HHT can offer a new and more effective way for identifying the different features of turnover of agricultural products futures of Zhengzhou commodity exchange and Dalian commodity exchange.

References

[1] Holger, K. and Thomas, S.,in: Nonlinear Time Series Analysis, edited by Cambridge University Press, 1-20(1999).

[2] He,Z.J.,et al,in:Time-frequency(scale) analysis and diagnosis for nonstationary dynamic signal of machinery, edited by International Journal of Plant Engineering and Management,1(1),40-47(1996).

[3] Meltzer, G. S. and Ivanov ,Y. Y., in: Fault detection in gear drives with non-stationary rotational speed- Part I: the time-frequency approach, edited by Mechanical Systems and Signal Processing, 17(5),1033-1047(2003).

[4]Wang,W.Y., and Harrap,M. J., in:Condition monitoring of rolling element bearings by using cone kernel time-frequency distribution, edited by Processing of the SPIE Conference on Measurement Technology and Intelligent Instrument. Bellingham, WA, 290-298(1993).

[5]Katvonik ,V. and Stankovic, L., in:Instantaneous frequency estimation using the Wigner distribution with varying and data-driven widow length, edited by IEEE Transactions on Signal Processing, 46(9), 2315-2325(1998).

[6] Huang,N.E.,Shen,Z.,Long,S., Wu,M., Shih,H., Zheng,Q.,Yen,N.,Tung,C.,Liu,H., in:The empirical mode decomposition and the Hilbert spectrum for nonlinear and non-stationary time series analysis, edited by Proceeding of the Royal Society of London Series A, 454, 903–995(1998).

[7] Huang,N.E., Shen, Z., and Long, S. R., in:A new view of nonlinear water waves: the Hilbert Spectrum, edited by Annu.Rev.Fluid Mech. 31,417–457(1999).

[8] Cheng, S.J., Yu, D.J., Yang,Y., in:The application of the energy operator demodulation approach based on EMD in machinery fault diagnosis, edited by Mechanical Systems and Signal Processing, 21: 668-677(2007,).

[9] Peng, Z. K., Chu, F. L., in:A comparison study of improved Hilbert–Huang transform and wavelet transform: Application to fault diagnosis for rolling bearing, edited by Mechanical Systems and Signal Processing, 19,974–988(2005).

[10] Flandrin, P.,Rilling,G., Goncalves, P., in: On empirical mode decomposition as a filter bank, edited by IEEE Signal Processing Letters,11 (2)(2004).

Advanced Materials Research Vols. 989-994 (2014) pp 2719-2722
© (2014) Trans Tech Publications, Switzerland
doi:10.4028/www.scientific.net/AMR.989-994.2719

From Epanechnikov Mixture Model to Rule-centered Fuzzy Model And Its Application to Stock Index Prediction

ZHANG Qinli[1, a]

[1]China center for industrial security research, Beijing Jiaotong University, Beijing,100044, China

[a]zhangql1973@163.com

Keywords: Epanechnikov mixture model; Fuzzy model; Stock index.

Abstract. In this paper, the mathematical equivalence between the conditional mean of a Epanechnikov mixture model (EMM) and the defuzzified output of a rule-centered generalized fuzzy model (RCGFM) is derived theoretically. Our results provide a new perspective for fuzzy systems, i.e., interpreting them from a probabilistic viewpoint. Thus, instead of directly estimating the parameters of the fuzzy rules in a rule- centered generalized fuzzy model, we can first estimate the parameters of the corresponding EMM using any popular density estimation algorithm like the expectation maximization (EM) algorithm. Our experimental results clearly indicate that a rule-centered generalized fuzzy model trained in such a new way has higher approximation accuracy and generalization ability than other models.

Introduction

In [1], a novel technique regarding fuzzy modeling was proposed using a kind of probabilistic system, namely the Gaussian mixture model (GMM). Gan and Hanmandlu proved the mathematical equivalence between the condition mean of GMM , and the defuzzified output of generalized fuzzy model (GFM)[2]. They built a bridge between probability theory and fuzzy logic. The proposed modeling method lacks interpretability without taking into consideration the correlation among components of sample data, but is less time-consuming. A major advantage is that their results provide a study of the new perspective of fuzzy model by interpreting a fuzzy system from a probabilistic viewpoint.

In [3], Janos Abonyi et al. proposed a new fuzzy modeling algorithm which partitioned the input space more effectively than conventional fuzzy modeling algorithms by taking into consideration the correlation among components of sample data. The main advantage of the proposed method is that it yields compact and easily manageable fuzzy models. However, the algorithm is only suitable for the low dimensional case as a result of calculating the complicated eigenvalue of matrix.

In [4], M. Bikdash presented a new form of fuzzy inference systems (FIS) that was highly interpretable and easy to manipulate. The new form is based on a judicious choice of membership functions that have strong locality and differentiability properties and on a modification of the Sugeno and generalized Sugeno forms of the consequent polynomials as to make them rule-centered. Under these conditions, the coefficients in the consequent polynomials can be exactly interpreted as Taylor series coefficients. This increased interpretability bridges the gap between the linguistic and computational interpretations of fuzzy inference systems with great benefit to both. A major advantage, is that the rudiments of the calculus of fuzzy inference systems begin to emerge.

In [5], Dorin Comaniciu and Peter Meer proved the Epanechnikov kernel was the optimal kernel and yielded minimum mean integrated Square Error(MISE). This paper followed the example of GMM in establishing Epanechnikov mixture model (EMM) that repalced Gaussian kernel function with Epanechnikov kernel function.

In this paper, a new fuzzy modeling algorithm combining the advantages of [1], [3] and[4] is proposed: it is inspired by EMM, and avoids their disadvantages. The proposed model takes into consideration the correlation among components of sample data with a small number of fuzzy rules as well as Abonyi's model [3], is as easy to implement as Gan and Hanmandlu's[1] and highly

interpretable like Bikdash's[4]. The suggested model has the same structure as that of Azeem's model [2] and its identification mimics the simple identification procedure of Gan and Hanmandlu's one [1].

Rule-centered generalized fuzzy model with multidimensional and correlational membership functions(RCGFM-MCMF)

Generally speaking, fuzzy models are superior to linear models in capability to represent a given unknown system. In this chapter, RCGFM-MCMF is proposed based on the three models [2,3,4].

RCGFM-MCMF combines the merits and removes the demerits of the above three fuzzy models. RCGFM-MCMF rules and output can be represented as follows:

$$R_k: \text{If } x \text{ is } A_k(x), \text{ then } y \text{ is } B_k(f_k(x), v_k) \text{ and } y^o = \frac{\sum_{k=1}^{M} v_k \cdot A_k(x) \cdot f_k(x)}{\sum_{k'=1}^{M} A_{k'}(x) \cdot v_{k'}} \quad (1)$$

Where M is the number of rules, v_k is the index of fuzziness, $R_k(k=1,2,\cdots,M)$ denotes the k th fuzzy rule, $x=(x_1,x_2,\cdots,x_J)^T$ is the input vector and $A_k(x)$ is the multidimensional membership function defined on x. $f_k(x)$ is the varying centroid and has the following form:

$f_k(x)=b_0^k+b_1^k(x_1-r_1^k)+\cdots+b_J^k(x_J-r_J^k)$, where $r_k=(r_1^k,r_2^k,\cdots,r_J^k)$ is the k th rule center.

In the proposed framework, the partitioning of the input space is realized by means of multivariable fuzzy sets with taking into account the correlation among data components. Better accuracy was achieved than other models. The special form of $f_k(x)$ possesses a high degree of interpretability which follows from that of the coefficients of the consequent polynomials.

From EMM to RCGFM-MCMF

Let the input vector be x with dimensions $J(\mathrm{J}>1)$, and the output be y. The first J variables x form the input vector while the $(J+1)$ th variable is the output y. We can give the form of EMM according to GMM as follows:

$$G(x,y)=\sum_{k=1}^{C} p_k G_{(J+1)\mathrm{k}}\left(\begin{bmatrix}x\\y\end{bmatrix};\begin{bmatrix}\mu_{kx}\\\mu_{ky}\end{bmatrix},\Sigma_k\right) \quad (2)$$

where, $G_{(J+1)\mathrm{k}}\left(\begin{bmatrix}x\\y\end{bmatrix};\begin{bmatrix}\mu_{kx}\\\mu_{ky}\end{bmatrix},\Sigma_k\right)$ is the k-th component multivariate Epanechnikov kernel functions.

With $G(x,y)$, it is possible to estimate the expected value y_e. y_e is given

$$y_e=E(y|x)=\int_{-\infty}^{+\infty} yG(y/x)dy=\frac{\int_{-\infty}^{+\infty} yG(x,y)dy}{G(x)}=\frac{\int_{-\infty}^{+\infty} yG(x,y)dy}{\int_{-\infty}^{+\infty} G(x,y)dy} \quad (3)$$

The marginal probability density function (pdf) of the k th term of $G(x,y)$ is given by

$$G_{Jk}(x)=\begin{cases}\dfrac{4F^3}{3V_J(\sigma^{kyy})^2} & A^2-\sigma^{kyy}B+\sigma^{kyy}K^2\geq 0\\ 0 & otherwise\end{cases} \quad (4)$$

where $(x-\mu_{ky})^T\sigma^{kxy}=A$, $(x-\mu_{kx})^T\sigma^{kxx}(x-\mu_{kx})=B$ and $F=(\sigma^{kyy}K^2-\sigma^{kyy}B+A^2)^{\frac{1}{2}}$.

Hence, the marginal pdf of x is

$$G(x)=\int_R G(x,y)dy=\sum_{k=1}^{C} p_k G_{Jk}(x) \quad (5)$$

We can derive

$$\int_R yG_{(J+1)\mathrm{k}}\left(\begin{bmatrix}x\\y\end{bmatrix};\begin{bmatrix}\mu_{kx}\\\mu_{ky}\end{bmatrix},\Sigma_k\right)dy=\frac{4F^3}{3V_J(\sigma^{kyy})^2}\left(\mu_{ky}-\frac{(x-\mu_{kx})^T\sigma^{kxy}}{\sigma^{kyy}}\right) \quad (6)$$

By (2), (4) and (6), we have

$$\int_R yG(x,y)dy = \sum_{k=1}^{C} p_k G_{Jk}(x)(\mu_{ky} - \frac{(x-\mu_{kx})^T \sigma^{kxy}}{\sigma^{kyy}}) \tag{7}$$

Substituting (5) and (7) into (3), we obtain

$$y_e = \frac{\sum_{k=1}^{C} p_k G_{Jk}(x)(\mu_{ky} - \frac{(x-\mu_{kx})^T \sigma^{kxy}}{\sigma^{kyy}})}{\sum_{k'c=1}^{C} p_{k'} G_{Jk'}(x)} \tag{8}$$

Note that (8) is similar in form to (1), and both are equivalent if the following conditions are true.

Theorem 1: (8) and (1) are equivalent under the following conditions:

I. The number of rules, M , in the RCGFM rule base, equals the number of components, C , in the EMM, i.e., $\boxed{M = C}$.

II. he weight of each rule, υ_k , is given by the corresponding prior of the mixture model p_c, i.e., $\boxed{p_k = v_k}$

III. The regression function in the THEN-part of the RCGFM rules is linear, and is a function of all input variables, given by $\boxed{f_k(x) = \mu_{ky} - \frac{(x-\mu_{kx})^T \sigma^{kxy}}{\sigma^{kyy}}}$

IV. The membership function in the IF-part of the RCGFM rules, $A_k(x)$, is a generalized Epanechnikov function with mean μ_{cx} and variance σ_{cxx} , i.e., $\boxed{A_k(x) = G_{Jk}(x).}$

V. The fuzzy system is additive, with multiplicative conjunction and implication.

These are the conditions under which there is mathematical equivalence between the output of a RCGFM and the expected output of a EMM. What this means is that for any MISO system whose input-output joint probability distribution is known to be a Epanechnikov mixture, there exists, under the above five condisions, a fuzzy system which equivalently models its expected output. The new fuzzy system that is obtained from EMM is named as EMM-inspired RCGFM (EMM-I- RCGFM).

Applications

In this section, we validate the effectiveness and efficiency of the proposed EMM-I-RCGFM algorithm by comparison with GM Markov Model [6] on Shanghai composite index,.

To quantify the performance of the resulting EMM-I-RCGFM , we use the performance measure found in [7], which is a form of the mean squared error (MSE) function. The performance measure MSE is expressed by the formula: $MSE = \frac{\sum_{n=1}^{N} e^2(n)}{N \cdot y_r}$, where $N =$ total number of data; $e(n) = y_{target} - y_{forecast}$; $y_r = [\max(y_{target}) - \min(y_{target})]^2$.

We choose the Shanghai composite index (daily closing price) between January 5, 2009 and December 30, 2011 as historical data, and choose the Shanghai composite index between January 4, 2012 and March 29, 2013 as verification data. There is a total of 1025 observations.

Fig. 1 plots the target output (solid line) and the model output (dotted line), due to very small values of model error at each point, the dotted line has been almost completely hidden by the solid line.

Fig. 2 plots the target output and predicted output. As can be observed, even with the validation data, the proposed RCGFM has captured the characteristic and nuances of the Shanghai composite index. The shape of the predicted output plot follows the target output plot reaonably well.

Tabel 1 shows the experiment results of EMM-I-RCGFM and GM Markov Model. According to Tabel 1, the performance of EMM-I-RCGFM seems superior to GM Markov Model. Hence, it is clear that EMM-I-RCGFM works efftively in the forcast of Shanghai composite index.

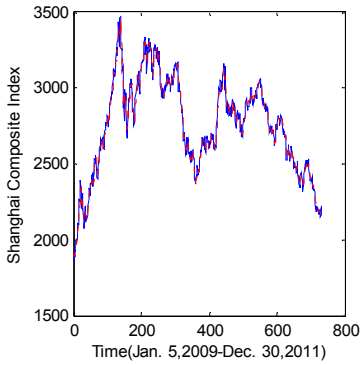

Fig. 1 Comparison of model outputs, original output data for the historical data of Shanghai composite index.

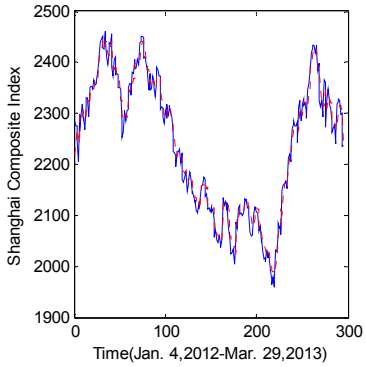

Fig. 2. Comparison of model outputs, original output data for the test data of Shanghai composite index

Table1 Performance comparison of different models for the test data of Shanghai composite index

Models	MSE
EMM-I-RCGFM	0.0019
GM Markov Model	0.0996

Conclusions

We have presented the theory and design of EMM-I-RCGFM. The parameters of RCGFM is computed using an efficient and simple probabilistic method. EMM-I- RCGFM provides a new viewpoint to design fuzzy system by probabilistic system. EMM-I-RCGFM has a markedly high interpretability stemmed from Epanechnikov kernel function and rule-centered consequent polynomials. The rule-centered consequent polynomials can be interpreted as the truncated Taylor series expansions of model output at rule center. EMM-I- RCGFM has taken into consideration the correlation among components , which resulted in an ineffective partition of the input space.Finally, the proposed fuzzy model has been used on stock applications: The results demonstrate the superiority of this model over other model in accuracy and generalization ability. Thus this paper makes an important contribution to the field of fuzzy modeling by introducing probabilistic and calculus theory into fuzzy model for dealing with real-life applications.

Acknowledgements

This work was financially supported by the Hebei Natural Science Foundation (F2011409007), China Postdoctoral Science Foundation(2014M550609) and Dr. Fund of NCIAE (ky-2009-05-B).

References

[1] Ming-Tao Gan and Madasu Hanmandlu: IEEE Transactions on Fuzzy System ,vol. 13(2005), p. 303.
[2] Y M. F. Azeem, M. Hanmandlu, and N. Ahmad: IEEE Trans. On Neural Networks, vol.11(2000), pp. 1332.
[3] Janos Abonyi, Robert Babuska and Ferenc Szeifert: IEEE Trans. on Systems, Man, and Cybernetics, vol.31(2001), p. 755.
[4] Marwan Bikdash: IEEE Trans. Fuzzy Systems , vol.7(1999), p. 686.
[5] Dorin Comaniciu and Peter Meer: IEEE Trans. On Pattern Analysis and Machine Intellegence, vol. 24(2002), pp. 603.
[6] Wan-cai Yang, Xin-qian Wu, Er-xin Zhang and Guang Zhu, in: *Proc. 19th international conference on industrial engineering and engineering management,* edited by Qi Ershi et. al./Springer, Changsha Hunan(2013).
[7] Benjamin Hartmann, Oliver Banfer, Oliver Nelles, Anton Sodja, Luka Teslic, and Igor Skrjanc, IEEE Transactions on Fuzzy ystems, vol. 19(2011), p. 1163.

Advanced Materials Research Vols. 989-994 (2014) pp 2723-2726
© (2014) Trans Tech Publications, Switzerland
doi:10.4028/www.scientific.net/AMR.989-994.2723

A Multifactor grey forecasting model of agriculture output value

Weizhen Chen[a], Lijuan Liang[b]
School of Electrical and Electronic Engineering，Wuhan Polytechnic University Wuhan 430023, China
[a]email: chenwz_2005@126.com, [b]email: 79108730@qq.com

Keywords: Multifactor; Grey forecasting model; Poor information; Agriculture output value.

Abstract. In this paper, a multifactor grey forecasting model of agriculture output value is proposed. Agriculture output value is very important in the country. It can help us to well know the situation of agriculture, and to modify the policy of agriculture. When the data change greatly, one-factor forecasting model may not be get good results. Grey forecasting model with multifactor would be better. From the simulation, this multifactor grey forecasting model with gross and total farm output value can get better effects.

Introduction

Agriculture output value is very important in the country. It can help us to well know the situation of agriculture, and to modify the policy of agriculture. As we all known, the perfect way to control the agriculture situation is to get forecasting value. That means, finding the appropriate forecasting model is a significant thing for agriculture planning. Agriculture output value can be gotten every year. How to use these values to construct the forecasting model is still a problem in this field. Although, agriculture output value can be gotten every year, it is difficult to describe the changes. The latest data should be more helpful to find the relevant between the past data and the future data. In this opinion, agriculture output forecasting value is still belong to poor information problem. Using grey system theory with multifactor may be expected to get good results.

Recently thirty years, grey system theory has been a quick development in china[1-6], and both the theory and practical applications of grey systems have achieved splendid results. This theory has been successfully applied in many scientific fields and various human endeavors. Relative to usual model, a grey system is a system with “poor” information. An excessively complex or complicated object, which generally shows a lack of completed model information, may be looked upon as a grey system.

In this paper, a multifactor grey forecasting model of agriculture output value is proposed. Based on multifactor to make grey forecasting model better. From the simulation, this multifactor grey forecasting model can get good effects.

A multifactor grey forecasting model

A grey system is a system with “poor” information. When analyzing grey problems, we try to see their own characteristics as a system through generating operation rather than finding their statistical features or probability distributions, and may find their latent laws through the integral generating transform(IGT for short) and Trend relational Analysis(TRA for short).When analyzing bridge-health forecast problem, we try to see it own characteristics as a system through generating operation rather than finding it statistical features or probability distributions, and may find it latent law through the IGT.

Based on mean-value, $SCGM_{mv}(1,h)$ has been propose several years before. In fact, $SCGM_{mv}(1,1)$ always has been used. That is to say, these forecasting model were built with one-factor[7-10] .

It is assumed that only a few of the discrete data observed from agriculture output values. such as $X_i^{(0)} = \{X_i^{(0)}(k) \mid X_i^{(0)}(k) \geq 0, k = 1,2,..., n\}$ $= (X_i^{(0)}(1), X_i^{(0)}(2), \dots, X_i^{(0)}(n)), i = 1,2,\dots,h$ which is called the original time series corresponding

to $X^{(0)}(t) \in X(\otimes,t)$. Now, it is required that a system model is established for agriculture output value forecasting. Taking the mean-value generating transform, we have the mean-value generating time series:

$$\overline{X}_i^{(0)} = (\overline{X}_i^{(0)}(2), \overline{X}_i^{(0)}(3), \ldots, \overline{X}_i^{(0)}(n))$$

$$\overline{X}_i^{(0)}(k) = 0.5[X_i^{(0)}(k) + X_i^{(0)}(k-1)], \qquad k = 2,3,...,n; i = 1,2,...,h.$$

According to the principle of grey dynamic modeling, if $\overline{X}_i^{(0)}$ tendency is satisfactorily related to the non-homogeneous exponential function with respect to discrete time, then the grey model of system cloud, denoted by $SCGM_{mv}(1,h)$ model of agriculture output value forecasting, can be constructed as

$$\dot{\hat{X}}^{(0)}(t) = \hat{A}\hat{X}^{(0)}(t) + \hat{U}, t \geq 0$$

and its solution (forecasting model) is

$$\hat{X}^{(0)}(t) = \underline{\hat{A}}^t \underline{\hat{B}} - \underline{\hat{C}}$$

or

$$\hat{X}^{(0)}(k) = \underline{\hat{A}}^{k-1} \underline{\hat{B}} - \underline{\hat{C}}$$

where

$$\underline{\hat{A}} = \underline{X}_{k+1}^T \underline{X}_k (\underline{X}_k^T \underline{X}_k)^{-1}$$

$$X_{k+1} = \begin{bmatrix} X_1^{(0)}(4) - X_1^{(0)}(2) & X_2^{(0)}(4) - X_2^{(0)}(2) & \cdots & X_h^{(0)}(4) - X_h^{(0)}(2) \\ X_1^{(0)}(5) - X_1^{(0)}(3) & X_2^{(0)}(5) - X_2^{(0)}(3) & \cdots & X_h^{(0)}(5) - X_h^{(0)}(3) \\ \vdots & \vdots & & \vdots \\ X_1^{(0)}(n) - X_1^{(0)}(n-2) & X_2^{(0)}(n) - X_2^{(0)}(n-2) & \cdots & X_h^{(0)}(n) - X_h^{(0)}(n-2) \end{bmatrix}$$

$$X_k = \begin{bmatrix} X_1^{(0)}(3) - X_1^{(0)}(1) & X_2^{(0)}(3) - X_2^{(0)}(1) & \cdots & X_h^{(0)}(3) - X_h^{(0)}(1) \\ X_1^{(0)}(4) - X_1^{(0)}(2) & X_2^{(0)}(4) - X_2^{(0)}(2) & \cdots & X_h^{(0)}(4) - X_h^{(0)}(2) \\ \vdots & \vdots & & \vdots \\ X_1^{(0)}(n-1) - X_1^{(0)}(n-3) & X_2^{(0)}(n-1) - X_2^{(0)}(n-3) & \cdots & X_h^{(0)}(n-1) - X_h^{(0)}(n-3) \end{bmatrix}$$

$$\underline{\hat{B}} = 2(I + \underline{\hat{A}}^{-1})^{-1} \underline{\hat{B}}$$

$$\underline{\hat{B}} = \left[(n-1) \sum_{k=2}^{n} \left(\underline{\hat{A}}^{k-1} \right)^T \underline{\hat{A}}^{k-1} - \left(\sum_{k=2}^{n} (\underline{\hat{A}}^{k-1})^T \right) \left(\sum_{k=2}^{n} \underline{\hat{A}}^{k-1} \right) \right]^{-1} \cdot$$

$$\left[(n-1) \sum_{k=2}^{n} \left(\underline{\hat{A}}^{k-1} \right)^T \overline{X}_{0.5}^{(0)}(k) - \left(\sum_{k=2}^{n} (\underline{\hat{A}}^{k-1})^T \right) \left(\sum_{k=2}^{n} \overline{X}_{0.5}^{(0)}(k) \right) \right] \quad \underline{\hat{C}} = \frac{1}{n-1} \left[\left(\sum_{k=2}^{n} \underline{\hat{A}}^{k-1} \right) \underline{\hat{B}} - \sum_{k=2}^{n} \overline{X}_{0.5}^{(0)}(k) \right]$$

$$\hat{A} = \ln \underline{\hat{A}}, \quad \hat{U} = \hat{A}\underline{\hat{C}}, \quad \hat{X}^{(0)}(1) = \underline{\hat{B}} - \underline{\hat{C}}$$

Demonstrating experiment

A. One-factor grey forecasting model

Agriculture output data can be gotten from Chinese Western statistical yearbook. Here we use the gross output value and total value of farm output in Nei Monggol province. From mass data(1991-1995) obtained, the approximate function will be found, and forecasting value in 1996 will be estimated. In the table 1, the test values are gross output from 1991 to 1995, and the forecasting value in 1996 is estimated.

Table 1. Results of gross output forecasting value(million yuan)

Year	Gross output value	Forecasting value	Error
1991	1065704	982342	-7.8%
1992	1194970	1177809	-1.4%
1993	1353978	1490980	10.1%
1994	2121949	1992732	-6.1%
1995	2694508	279.6621	3.8%
1996	3073205	4084584	33.0%

$SCGM_{mv}(1,1)$ forecasting model: $\hat{X}^{(0)}(k)=\hat{\underline{a}}^{k-1}\hat{\underline{b}}-\hat{\underline{c}}=(16022)^{k-1}\times(324608)-(-657733)$

In the table 2 the test values are total farm output from 1991 to 1995, and the forecasting value in 1996 is estimated.

Table 2. Results of total farm output forecasting value (million yuan)

Year	Total farm output value	Forecasting value	Error
1991	763191	704206	-7.7%
1992	871291	855948	-1.8%
1993	991439	1096595	10.6%
1994	1579087	1478233	6.4%
1995	2002403	2083468	4.0%
1996	2352458	3043300	29.3%

$SCGM_{mv}(1,1)$ forecasting model: $\hat{X}^{(0)}(k)=\hat{\underline{a}}^{k-1}\hat{\underline{b}}-\hat{\underline{c}}=(15859)^{k-1}\times(258998)-(-445208)$

Using one-factor grey forecasting model, the forecasting value is not satisfied. The result of test data maybe well, but the forecasting value in 1996 is not good. The reason is the test data changing greatly. In view of this situation one-factor grey forecasting model may not be used well.

B. Multifactor grey forecasting model

Based on relevant between multifactor, more information could be mined. Multifactor grey forecasting model is used here. In the table 3, the test values are gross output and total farm output from 1991 to 1995, and the forecasting value in 1996 is estimated.

Table 3. Results of gross and total farm output forecasting value(million yuan)

Year	Gross output forecasting value	Error of gross output forecasting value	Total farm forecasting value	Error of total farm forecasting value
1991	1139608	6.9%	821659	7.7%
1992	1121066	-6.2%	812823	-6.7%
1993	1427882	5.5%	1049907	5.9%
1994	2048045	-3.5%	1520619	-3.7%
1995	2768412	2.7%	2060871	2.9%
1996	3196688	4.0%	2373379	0.9%

From table 3, less error would be gotten. That means, using multifactor grey forecasting model with agriculture output value maybe achieved better results. The effects of two different grey forecasting models are be compared by errors. Obviously, the effects of multifactor grey forecasting model is better. The error value of gross output forecasting decreased for 33.0% to 4.0%. The error value of total farm output forecasting decreased for 29.3% to 0.9%.

$SCGM_{mv}(1,2)$ forecasting model:

$$\hat{X}^{(0)}(k)=\hat{\underline{A}}^{k-1}\hat{\underline{B}}-\hat{\underline{C}}$$

$$\hat{\underline{A}}=\begin{bmatrix}483534 & -358297\\ 626963 & -464257\end{bmatrix},\ \hat{\underline{B}}=\begin{bmatrix}-395052\\ -521864\end{bmatrix},\ \hat{\underline{C}}=\begin{bmatrix}-1216711\\ -1661472\end{bmatrix}$$

From the result, it can get better estimate value and less error.

Conclusions

Although agriculture output value can be gotten every year, the forecasting model still hard to be constructed in this situation. It is difficult or impossible to describe this complicated system. Generally, forecasting models always have been built up by one-factor. In this paper, multifactor have been used and a multifactor grey forecasting model has been proposed. Using relevant of multifactor, better result can be achieved. From the simulation, the effects of two different grey forecasting models are be compared by errors. Obviously, the effects of multifactor grey forecasting model is better.

Acknowledgments

The support of this research was by the national natural science foundation of China (No. 60773190，61075015,), Science Research Foundation of Education Department of Hubei Province (No.Q20121811) are gratefully acknowledged. The authors are grateful for the helpful suggestions and comments provided by the anonymous reviewers of this work.

References

[1]Y.Lin, M.Y.Chen and S.F.Liu. Theory of grey systems: capturing uncertainties of greyinformation.Kybernetes, Vol.33(2004), No.2, pp.196-218.

[2]M.Y.Chen, W.Z.Chen, Z.J.Chen. Grey state model and forecasting control of complicated systems. Proceedings of the 15th International Conference on Systems Science, Sept.7-10,2004, Wroclaw(Poland), pp.141-150.

[3]Z.J.Chen, W.Z.Chen, Q.L.Chen and M.Y.Chen. “Poor” signal processing and grey modeling technique. Proceedings of Eighteenth International Conference on Systems Engineering, August 16-18, 2005, Las Vegas, Nevada(USA), pp.251-256.

[4]Z.J.Chen, Q.L.Chen, W.Z.Chen and Y.N.Wang. Grey linear programming. Kybernetes, Vol.33(2004), No.2,pp.238-246.

[5]Weizhen Chen, Bingwen Wang, Hao Zhan, A Novel Grey Forecasting Model. Proceeding of the FSKD’09 Conferences,2009, August 14-16,571-575.

[6]W.Z.Chen, Z.J.Chen, Q.L.Chen and M.Y.Chen. Approaches to grey prediction and control of environmental systems. Processings of Eighteenth International Conference on Systems Engineering, August 16-18, 2005, Las Vegas, Nevada(USA), pp.152-157.

[7]W.Z.Chen, Z.J.Chen, Z.H.Xie, L.Zhou and M.Y.Chen. Multifactor process analysis and $SCGM_{mv}(1,h)$ forecasting model. Journal of Wuhan University of Technology(in Chinese), Vol.28(2004), No.2, pp.291-294.

[8]Weizhen Chen,Bingwen Wang and Xiaoya Hu. Grey Forecasting Model of Bridge-Health Condition. Proceeding of Computational Intelligence for Modeling, Control and Automation Conferences (CIMCA),2008 ,Dec.10-12:657-662.

[9]Weizhen Chen, Bingwen Wang, Xiaoya Hu.Vibration-based structural damage identification using grey forecasting model. Applied Mechanics and Materials, 2012, 128-129:1114-1117.

[10]Weizhen Chen. A novel method to estimate ARMA time-varying parameter using grey forecasting model. Advanced Materials Research,2012, 532-533,pp876-880.

Advanced Materials Research Vols. 989-994 (2014) pp 2727-2730
© (2014) Trans Tech Publications, Switzerland
doi:10.4028/www.scientific.net/AMR.989-994.2727

Research on Software Demodulation of PCM/FM Algorithm Based on MSD

Fu Gang[1,a], Wu Yanjun[1, a], Li Renlong[1,a] and Liping Wang[2,b]

[1]China Satellite Maritime Tracking and Control Department, China

[2]School of Computer Science, Engineering and Mathematics, Flinders University, South Australia 5042, Australia

[a]348237548@sina.com [b]wlp2005518@gmail.com

Keywords: Demodulation, PCM/FM, MSD

Abstract. Based on maximum likelihood, research a new based on Symbol Detection (Multi-Symbol Detection, MSD) soft demodulation method of PCM/FM telemetry signals. Introduced the basic principle of the demodulation method and the implementation process, analyzed the demodulation and synchronization factors and formulate the corresponding synchronization strategies.

Introduction

With the development of modern remote sensing system as well as to the requirement of signal post-processing is increasing, the demand for software to resolve tuning is becoming more and more urgent. Software signal demodulation greatly widened the signal receiving and processing system solutions, for software radio, signal processing provides an effective way. Of non-stationary random signal processing usually adopts the time-frequency analysis methods, such as proposed in the literature [1][2] FM signal demodulation method based on STFT and WD, although the noise resistance and resistance to fall excellent performance, but the computation is very big, takes a long time, is not conducive to real-time processing software.

1 Algorithms of MSD

Is not zero in PCM/FM (NRZ PCM/FM) is a kind of hybrid coding and modulation mode, used to send digital signal transmission line. This method is to use high frequency shift formula one Hertz carrier on behalf of the binary "1" state, low frequency shift f0 Hertz carrier on behalf of the binary "0" state.PCM/FM signal in the field of remote sensing is known as the continuous phase frequency shift keying (CPFSK) signals, and its mathematical expression is:

$$S(t) = A\cos\left[2\pi(f_c + f_d)t + K_m \int f(t)dt\right] \tag{1}$$

$$\phi(t;a) = \pi h \sum_{k=-\infty}^{n-l} a_k + 2\pi h a_n q(t - nT) \qquad (nT \le t \le (n+1)T) \tag{2}$$

This shows that the PCM/FM signal instantaneous phase is equal to the original on the basis of the instantaneous phase and the phase change from the current element.PCM/FM signal, therefore, is the symbol between before and after the phase of memory, and traditional demodulation methods did not use this information.MSD is based on the idea of maximum likelihood estimation, the use of symbols between before and after the memory, a multiple symbols for maximum likelihood detection. Its central idea is: the bit-rate received a signal that is not an immediate decision, but to continue to observe the following several yards after code, through the code of several code sequence estimation, on the whole sequence.

According to the core of the MSD, the MSD algorithm simulation concept description is as follows:

As a first step, according to the parameters of the signal, and observation of MSD length N, generating all possibility 2 N kind of local phase meter, and the corresponding modulation signal baseband sample, forming a series of related receiving channel, this paper will be off for observation length N = 5.

The second step, through telemetry channel receiving signals for digital quadrature down-conversion, it is advantageous to the carrier tracking, at the same time be able to get two I/Q signal component, which contains the signal phase information, and the I/Q phase two road rough adjustment in time domain, makes the frequency filter to the I/Q two-way signal shift effect to adjust to a symbol scope.

Third step, the next two road I/Q signal after frequency conversion merged into complex envelop form, the complex envelop are associated with the local sample signals of each channel operation, from the various channels selected related calculation is a maximum likelihood of the corresponding channel number.

The fourth step, find local code set of tables, the output channel number corresponding theory frame as the demodulation results.

According to the above derivation, MSD algorithm core operation flow, as shown in figure 1.

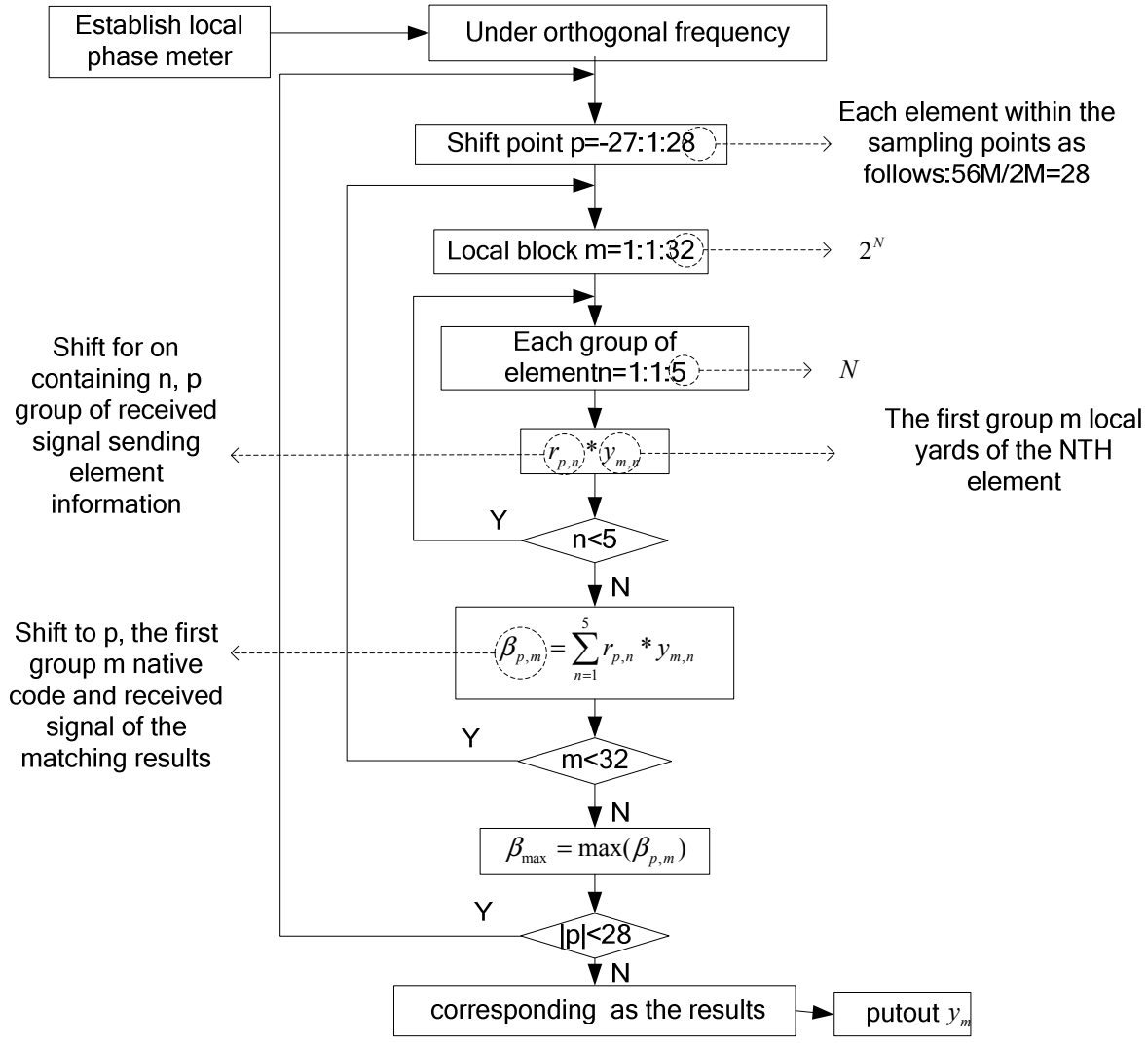

Fig 1 MSD algorithm simulation core operation flow.

2 Carrier synchronization

Received signal expression is:

$$r(t)=s(t)+n(t)=Ae^{j(\Delta wt+\theta+\pi h\sum_{k=-\infty}^{n-1}a_k+2\pi ha_n\frac{t-nT}{2T})}+n(t) \tag{3}$$

With deviation of received signal generation into the likelihood value expressions, eventually maximum likelihood values can be obtained and the relation between the frequency offset is as follows:

$$\beta_{\max}(\omega)=\frac{1}{N}\left|\int_{(n-N+1)T}^{(n-1)T}e^{\omega tj}dt\right| \tag{4}$$

The rise and fall of the final design frequency carrier synchronization block diagram is shown in figure 2.

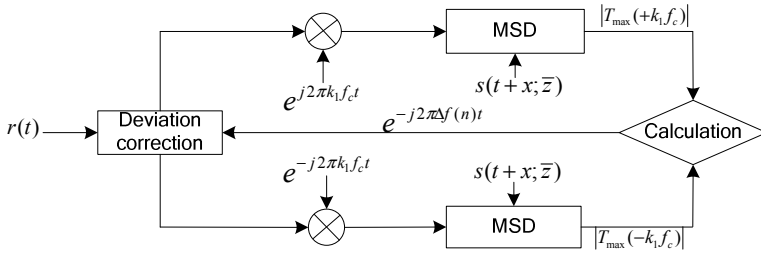

Fig 2 Based on the MSD deviation compensation principle diagram

Because of MSD is a kind of phase correlation algorithm, so the existence of time delay will also affect the phase, which affect the MSD. With similar carrier synchronization, by transforming the received signal with a delay expression generation into the likelihood value expressions can be eventually likelihood value and the relation between the time delay is as follows:

$$\left|\beta(\mathbf{a},r(t-T))\right|=\begin{cases}N\left|(\frac{1}{2}T-\frac{\Delta T}{4})\cos(\pi h\frac{\Delta T}{T})+\frac{T}{4\pi h}\sin(\pi h\frac{\Delta T}{T})\right|, 0\le\Delta T\le\frac{T}{2}\\ N\left|\frac{1}{4}(T+\Delta T)\cos(\pi h\frac{T-\Delta T}{T})+\frac{T}{4\pi h}\sin(\pi h\frac{T-\Delta T}{T})\right|, \frac{T}{2}\le\Delta T<T\end{cases} \tag{5}$$

Design a kind of time synchronization algorithm to synchronize time delay, similar to that in figure 2.

3 Algorithm performance.

The classical synchronization correction step is divided into fixed step length and step length. Cycle time deviation is 0.05 times the selected code, frequency deviation is 0.01 times the rate of synchronization precision as a threshold, when the synchronization error is lower than the threshold that enters the lock, bit error rate after enter lock area compared with the complete lock bit error rate of error is very small, the simulation results of fixed step length and variable step as shown in figure 3 and 4, respectively.

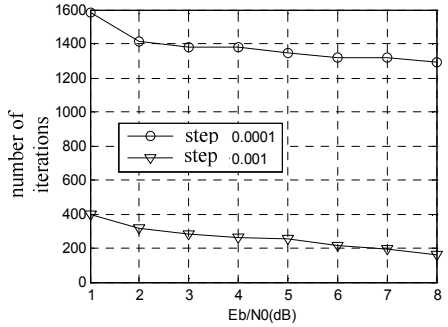

Fig 3 Fixed time step into the lock

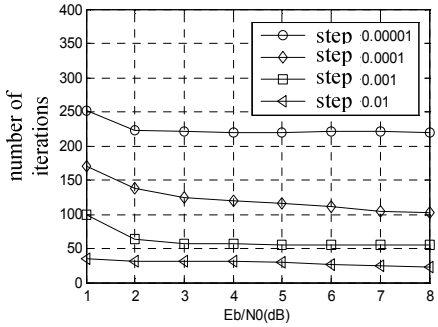

Fig 4 Variable time step into the lock

As shown in figure 3, the lock time and iterative step become inverse ratio, the iteration step length that synchronization of the required number of iterations increases, the iteration step length is 0.001 times the bit rate, the steps needed for synchronization iterative step is about 100; Iteration step length is 0.0001 times the bit rate, the steps needed for synchronization iterative step is about 1000, in the early time increase rapidly. To increase the capture speed, select the variable step parameter set, using smaller length L, smaller small scale fluctuation corresponding decision parameters k_1, smaller continuous motion corresponding decision parameters k_2, moreover the iteration step length increase rate should be greater than less.

Through the study of MSD algorithm and demodulation synchronization method, the following will be demodulation performance test of the entire software demodulation system. Signal intensity were 10.45 dB and 8.18 dB and 4.62 dB, then the MSD system software demodulation and the final error rate, and then with the hardware of MSD demodulation and STFT method and traditional method of frequency demodulation performance comparison, the article demodulation performance results in the diagram as shown in figure 5.

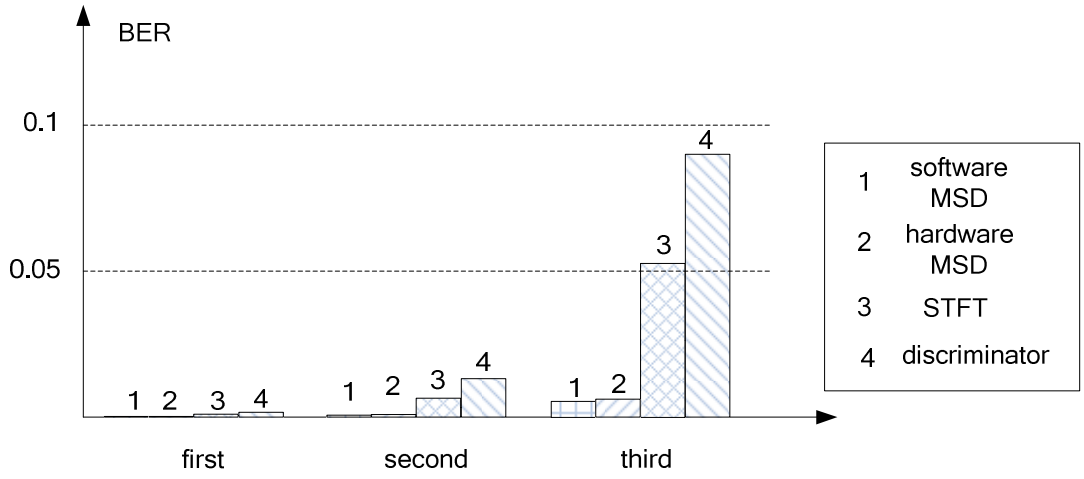

Fig 5 A comparison error rate

See from figure 5 can be more intuitive, MSD method of BER performance is far better than short time Fourier transform (STFT) [3]and the frequency discrimination laws, and get the bit error rate of MSD after demodulation software and hardware method (MSD) BER is after demodulation, consistent with the expected results of the test, software demodulation algorithm is practical and feasible, the demodulation results.

Summary

This article uses the symbol detection more demodulation method and the corresponding synchronization method to build the software demodulation system, verified by measured data was tested, the results show that the method of demodulation performance is very good, in line with expectations.

References

[1] Liu Donghua. Based on instantaneous frequency measurement of PCM/FM signal demodulation method research[J]. JOURNAL OF SYSTEM SIMULATION, 2005, 17(10): 2463-2466.
[2] Feng Xiaoping. Discrete STFT is used to implement FSK digital modulation signal demodulation method[J]. Journal of Xidian University, 2001, 28(6):812-815.
[3] Xu Xingyuan. Shipborne tt&c equipment based on MSD technology research rocket telemetry demodulation method[J]. Telemetry and Telecontrol, 2009, 30(5): 64-67.

Advanced Materials Research Vols. 989-994 (2014) pp 2731-2734
© (2014) Trans Tech Publications, Switzerland
doi:10.4028/www.scientific.net/AMR.989-994.2731

Mixed Features Based Improved Human Action Recognition Algorithm

Hailong Jia [1, a *], Kun Cao [2,b]

[1] Center of modern education technology Xinxiang University, 453003, China

[2] College of computer and information engineering Xinxiang University, 453003, China

[a]47160216@qq.com, [b]346856526@qq.com

Keywords: Action recognition, silhouette, optical flows, mixed characteristics, leave one out, improved algorithm.

Abstract. The choice of the motion features affects the result of the human action recognition method directly. Many factors often influence the single feature differently, such as appearance of human body, environment and video camera. So the accuracy of action recognition is limited. On the basis of studying the representation and recognition of human actions, and giving full consideration to the advantages and disadvantages of different features, this paper proposes a mixed feature which combines global silhouette feature and local optical flow feature. This combined representation is used for human action recognition.

Introduction

Human action recognition based on video is one of the important research directions in video analysis, which belongs to the low level of computer vision, having broad application prospects in the field of video surveillance, video retrieval, human-computer interaction, virtual reality, etc.

In the video sequence, motion information can usually use optical flow, silhouettes, points of interest and other features to describe. Document [1]proposed to use optical flow histogram to describe the motion information, and then using support vector machine classifier to identify players batting action. Optical flow representation can, without any prior knowledge of the background region, realize the detection and tracking of moving object; but the drawback is that it is not only greatly affected by noise and changes of light intensity, but also has a complex calculation method and large amount of calculation. Based on silhouette image, literature[2]divides moving target into vehicle, the human body and the crowd through extracting the distance feature from centroid to boundary points. Description method based on sketch is easy to realize and slightly affected by the illumination condition, but it is mainly dependent on the shape of the boundary information, cannot obtain the internal structure and easily affected by the background variation. In literature[3], standard body posture silhouette image is scaled into m*n sub block. By calculating the number of pixels in each sub block body of all sub pixels, it can count the maximum proportion to the analysis of human behavior. This method describes the silhouette of internal information and has simple calculation, too. But it is sensitive to the changes of angle and behavior.

Features Expression and Extraction

Image Preprocessing. Image processing can reduce the image area and process data of the study, which could reduce the amount of computation. Usually using background subtraction method to determine the approximate region of human body movement and the silhouette, as is shown in Figure 1 (b). Assuming that all action is performed in the static background, based on silhouette information, we can determine the region of interest is as shown in Figure 1 (c). After region of interest is determined, we can only process the information in region of interest.

Fig. 1. (a) Video in the Original Image; (b) The Human Body Silhouette; (c) Marked the Original Image (the green rectangular box is for region of interest)

Silhouette Feature Expression and Extraction. Single frame images of human silhouette can be used to describe the overall shape change information of human motion. The silhouette feature has following advantages: ① silhouette feature can provide simple and intuitive description of moving human shape; ②silhouette feature can be easily extracted; ③two-value silhouette is not sensitive to the image texture and color of foreground silhouette [4]. The purpose of this step is to convert motion information of original video into the associated morphological characteristics sequence which reflects the changes of the movement process.

Provided with a section of video T frame images such as I, $V = [I_1, I_2, \dots, I_T]$, moving silhouette sequence corresponding to $S = [S_1, S_2, \dots, S_T]$, S, have been obtained in the image preprocessing. For the sake of simplicity, we used the method of vector [5] to describe the overall shape of the contour information of human silhouettes. The detailed process is as follows:

Edge profile of each frame silhouette can be obtained by using canny operator, as is shown in Figure 2 (a). And the coordinate representation of edge profile can also be acquired, as is shown in Figure 2 (b). So the body contour can be expressed by n_t points, i.e.:

$\{(x_1, y_1), (x_2, y_2), \dots, (x_{n_t}, y_{n_t})\}, \quad t = 1,2,3, \dots, T$

The centroid of body contour can be obtained by formula (1).

$$(x_c, y_c) = \left[\frac{1}{n_t}\sum_{i=1}^{n_t} x_i, \frac{1}{n_t}\sum_{i=1}^{n_t} y_i\right] \quad (1)$$

Among which, (x_c, y_c) is the center, $(x_i, y_i)$is for edge point, n_t is the total number of edge profile in t image.

The distance from centroid to edge point can be obtained by formula (2):

$$d_i = \sqrt{(x_i - x_c)^2 + (y_i - y_c)^2}, i = 1,2, \dots, n_i \quad (2)$$

d_i is the distance of the corresponding centroid of the i edge point to edge point. Starting with the leftmost top point of contour record when doing the calculation, which should be the clockwise calculation, so we can get corresponding one-dimensional profile vector D_t from two-dimensional contour record of single frame image I_t.

$$D_t = [d_1, d_1, d_1, \dots, d_1, \dots, d_1,], i = 1,2, \dots, n_t \quad (3)$$

Feature Expression and Extraction of Optical Flow. Inaccurate silhouette image extraction may cause that the profile vector feature information could not accurately express action features. At this time, flow characteristics can accurately express the action information in video sequences. Extracting optical flow in movement region, and using local optical flow information of sub region to represent local features of human movement, can improve the anti-noise capability of optical flow. The specific process of optical flow extraction and expression is as follows:We can determine the position of the corresponding interest region of current frame image I_t, and shear the corresponding gray scale image region to the position of current frame and previous frame image to the region of interest, as is shown in Figure 3 (a1), (a2). Then we can use the method of Lucas -Kanade for optical flow detection in region of interest in current and previous frames. The optical flow field is shown in Figure 3 (b), the optical flow is decomposed into 2 components of vertical and horizontal, i.e. vertical flow, transverse flow.

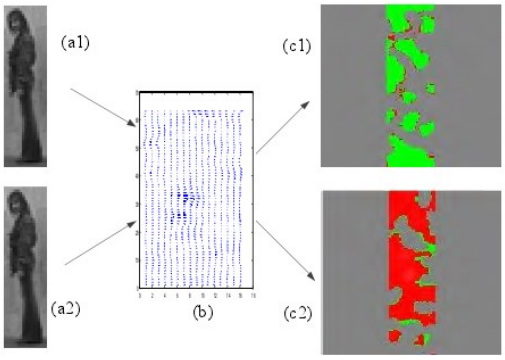

Fig. 3. (a1) Gray Level Image of t-1 Region of Interest Image;(a2) Gray Level Image of Interest Region at t Moment; (b) The Optical Flow Field at Time t（the optical flow field is divided into vertical and horizontal directions）; (c1) is for the longitudinal optical flow chart; (c2) is for the horizontal flow chart

In order to reduce the optical flow information dimension, find the identification ability of data expression, we can use the sub regional radial histogram method to count optical flow characteristics .

Firstly, according to the premise of the zoomed long side, the optical flow image will be standardized into the optical flow diagram in 120*120 dimensional unified sizes. As is shown in Figure 3 (c1), (c2).

The normalized optical flow diagram is divided into 2*2 sub frame S_1, S_2, S_3, S_4, which is in size of 60*60. The center points are respectively C_1, C_2, C_3, C_4, as is shown in Figure 4 (a). And then taking the center point of sub frames as the center, we can divide sub frame into 18 sub regions which are respectively $S_{i1}, S_{i2}, \dots, S_{i18}, i = 1,2,3,4$, as is shown in Figure 4 (b). Each central angle is of 20 degrees, so that 72 sub regions are forming[9].

The optical flow information of the whole image I_t can be expressed by the longitudinal and transverse flow O_L and H_L of 72 sub regions, such as is shown in type (4), (5), and (6).

$$O_L = [O_{L1,1}, \dots, O_{L1,18}, \dots, O_{L4,1}, \dots, O_{L4,11}] \quad (4)$$

$$O_H = [O_{H1,1}, \dots, O_{H1,18}, \dots, O_{H4,1}, \dots, O_{H4,11}] \quad (5)$$

$$O_t = [O_L, O_H] \quad (6)$$

Formula (4) is for longitudinal local optical flow vector O_L composed by the longitudinal optical flow of 72 sub regions, type (5) is for the transverse local optical flow vector O_H composed by transverse flow of 72 sub regions, in type (6), O_t is for the local optical flow vector.

By using the 2- norm to normalize O_t we can get the features expressed by radial histogram of local optical flow vector in current frame image I_t.

The Introduction of Recognition Method

There are many ways to solve the problem of statistical classification. This paper is mainly testing the identification ability of putting forward characteristics, so the most simple nearest neighbor classifier was chosen here[6]. The specific algorithm is as follows:

Firstly, the nearest neighbor of each frame in testing sequence ought to be found. Supposing that the feature vector of the t_{th} frame in testing sample sequences is M_Q^t, among which t=1, 2,… T, and the feature vector of the nth frame corresponding to the training sample is M_T^n. Then when using the Euclidean distance to test the similarity of M_Q^t and M_T^n, we can find that the training sample frame which keeps a minimum distance from M_Q^t is the nearest neighbor of the tth frame in testing sample sequence, as is shown in formula (7):

$$S_q=\min\|M_Q^t - M_T^n\|, \quad n=1, 2,...,N \quad (7)$$

Secondly, to assign the label of the action which is affiliated with the nearest neighbor training frame that is corresponding to the testing frame to the current testing frame, so that each frame in testing sequence will get an action label.

Finally, to do an action label statistic of each frame in the testing sequence, so that different testing sequence categories are classified, and each category is made of the actions which the same action labels are corresponding to. For example, there are 83 frames in diaria_bend sequence. Each frame is marked with the nearest action label, and the statistical results are [69,3,0,5,2,0,1,0,2,1], i.e. 69 frames are marked as No.1 action, 3 frames are marked as No.2 action, and so on. The largest number of votes is 69, and its action label is "1", the sequence will be identified as No.1 action.

Summary

This paper presents a human action recognition algorithm based on hybrid features. It combines the distance feature and contour flow characteristics of contour vector from contour centroid to the edge point, so as to get the mixed features to perform action recognition. From the recognition results of the third part, we can see that the mixed feature has been correctly identified 95% of the rate in Weizmann database and KTH database, fully demonstrating the effectiveness and feasibility of the algorithm.

References

[1]. ZHU G, XU C. Action recognition in broadcast tennis video[C] Proceedings of the 18th International Conference on Pattern Recognition, Hong Kong, China, NJ:IEEE, Press, 2006:251-254.

[2]. Yi yang, Jianguo Xing. Human Action Recognition Algorithm based on Minimum Spanning Tree of CPA Models [J]. Journal of Software, 2010, 7(7):1577−1584.

[3]. Ling Gan, Fu Chen. Human Action Recognition using APJ3D and Random Forests [J]. Journal of Software, 2013, 8(9):2238–2245.

[4]. WANG L, SUTER D. Recognizing human activities from silhouettes: motion subspace and factorial discriminative graphical model[C]Proceedings of the IEEE Conference on Computer Vision and Pattern Recognition, Minnesota, USA, NJ: IEEE,Press,2007:1−8.R. Nicole, “Title of paper with only first word capitalized”, *J. Name Stand. Abbrev.*, in press.

[5]. Dedeoğlu Y,A Silhouette-based method for object classification and human action recognition in video[C]Proceedings of the European Conference on Computer Vision, Graz, Austria,N J:IEEE,Press,2006: 64- 77.

[6]. GRITAI A,SHEIKH Y,SHAH M. On the use of anthropometry in the invariant analysis of human actions[C] Proceedings of the 17th International IEEE Conference on Pattern Recognition (ICPR) ,Cambridge ,UK,NJ:IEEE,Press,2004, Ⅱ:923－926.

Advanced Materials Research Vols. 989-994 (2014) pp 2735-2738
© (2014) Trans Tech Publications, Switzerland
doi:10.4028/www.scientific.net/AMR.989-994.2735

Knowledge-based fuzzy diagnostic model

Hongwei Lv [a], Xiaokai Li [b] and Kai Wang [c]

[1]Engineering University of CAPF, Xi'an Shanxi China

[a]940811752@qq.com, [b]1441826763@qq.com, [c]979466058@qq.com

Keyword: Diagnosis, Fuzzy set, Fault set, a sign set

Abstract: This paper discusses a diagnostic model based on the fuzzy relation equations in the diagnosis model, adding a time parameter, given the consistency between the fault symptom set and a set of observed signs of relevance, coverage, and equal quantitative indicators, these quantitative indicators can guarantee that the omission of a potential fault is neither in the case of incomplete knowledge, but also to get the best known symptom set matching solution. At the same time, diagnose problems in the knowledge of the adequacy and completeness of their relationships.

Introduction

Knowledge - based diagnosis of artificial intelligence branches. In practice , diagnose problems often related and time parameters , and diagnostic knowledge is often incomplete , reflected in two aspects : First , the observation of the signs of the system is not complete , for example , is limited by certain conditions , some the signs simply observe the less than or observation costly . Second, fault set and symptom set mapping relationship is not complete. How , in the case of incomplete knowledge , neither the omission of a potential failure , but also to get the best match solutions with existing observations , this paper investigates a stepwise refinement of diagnostic model , the model can be used with a deportation structure the various levels of the system .

Description of the problem

Diagnose problems p is defined as a seven- tupelo

$P = \langle\ D, M, R, M^+(\hat{D}, t+k), M^-(\hat{D}, t+k), M^+(t_0+i), M^-(t_0+i)\ \rangle$, among:

(1) $D = \{\ d_1, d_2 \cdots, d_q\ \}$ represents single - fault set of a given system, $A = \{\hat{D}_1, \hat{D}_2, \cdots, \hat{D}_p\ \}$ represents a set of failure modes of the system, then $D \subseteq A \subseteq \Gamma$, which Γ indicates the full combination of all single faults in the system. The base of the collection Γ and D is expressed as $|\Gamma|$ and $|D|$, respectively $|\Gamma| = 2^{|D|}$. Failure below represents the failure mode; failure set represents failure mode set.

(2) $M = \{m_1, m_2, \cdots, m_q\ \}$ represents a symptom set of a given system.

(3) $M^+(\hat{D}_j, t+k)$, $M^-(\hat{D}_j, t+k)$ $\hat{D}_j \in A$, $k = 0, \cdots, n$ respectively represents the sign sets that system inevitably appears and must not appear at the time of $t+k$ after system failure $\hat{D}_j$ at the time of t .

Definition 1: If $\forall \hat{D}_j \in A$, $k = 0, \cdots, n$ $M^+(\hat{D}_j, t+k) \bigcup M^-(\hat{D}_j, t+k) = M$, the system's diagnostic knowledge is sufficient. Otherwise, it is not sufficient.

If as $M^+(\hat{D}_j, t+k)$ and $M^-(\hat{D}_j, t+k)$ fuzzy subset, its membership functions are expressed as $\mu_{M^+(\hat{D}_j, t+k)}(m_f)$, $\mu_{M^-(\hat{D}_j, t+k)}(m_f)$. $\mu_{M^+(\hat{D}_j, t+k)}(m_f) = \mu_{M^-(\hat{D}_j, t+k)}(m_f) = 0$ represents nothing about the mapping relationship of $\hat{D}_j$ and m_f .

(4) $\mu_{t_0+i}(t+k)$, $k = 0, \cdots, n$ $i = 0, \cdots, m$ which indicates the degree of membership function or near at the time $t+k$ on the timeline moment t_0+i .

(5) $R \subseteq A \times M$ is the subset defined on the fuzzy relationship . The fuzzy set defined on $A \times M$, for each pair of $(\hat{D}_j, m_f)$, $\hat{D}_j \in A$, $m_f \in M$, $R(\hat{D}_j, m_f)$ is a set of $(\mu_{M^+(\hat{D}_j, t+k_1)}(m_f), t+k_1, \mu_{M^-(\hat{D}_j, t+k_2)}(m_f), t+k_2)$ .If $R_1 \subseteq D \times M$, apparently $R_1 \subseteq R$.

In fact, it is sufficient for a given system, the completion of the diagnostic problem solving knowledge does not need to be diagnosed. For either a failure mode, only require access to a subset of its symptom set premise is to ensure that the subsets of the signs can the corresponding failure modes and other failure modes to distinguish.

Definition 2:① in the accurate sets , $\forall \hat{D}_i, \forall \hat{D}_j \in A$, and $\hat{D}_i \neq \hat{D}_j$ so

$$DISCRIM(\hat{D}_i, \hat{D}_j) = \{ (M^+(\hat{D}_i, t+k) \cap M^-(\hat{D}_j, t+k)) \cup (M^-(\hat{D}_i, t+k) \cap M^+(\hat{D}_j, t+k)) \}$$

If $DISCRIM(\hat{D}_i, \hat{D}_j) \neq \varnothing$, the diagnostic knowledge of the system is complete.

②in the fuzzy sets, $\forall \hat{D}_i, \forall \hat{D}_j \in A$ and $\hat{D}_i \neq \hat{D}_j$

$$\mu_{DISCRIM(\hat{D}_i, \hat{D}_j)} = \max \{ \min(\mu_{M^+(\hat{D}_i, t+k)}(m_f), \mu_{M^-(\hat{D}_j, t+k)}(m_f)), \min(\mu_{M^-(\hat{D}_i, t+k)}(m_f), \mu_{M^+(\hat{D}_j, t+k)}(m_f)) \}$$

$\mu_{COMPLETE} = \min\{ \mu_{DISCRIM(\hat{D}_i, \hat{D}_j)} \}$, $\forall \hat{D}_i, \forall \hat{D}_j \in A$ and $\hat{D}_i \neq \hat{D}_j$ .When $\mu_{COMPLETE} > 0$, the system diagnostic knowledge is complete. In practice, given a threshold value, when $\mu_{COMPLETE}$ is greater than the threshold value, the diagnostic knowledge of the system is complete.

Proposition 1: If a system diagnostic knowledge is sufficient, the diagnostic knowledge of the system is complete. Otherwise may not be valid.

Proposition 2: If a system diagnostic knowledge is complete when the system fails, the diagnosis of the problem solving can be a unique interpretation.

3 Diagnostic models

3.1 Consistency diagnosis

Known $M^+(t_0 + i)$, $M^-(t_0 + i)$, $i = 0, \cdots, m$,consistent diagnostics is to find a fault set $\hat{D}_t$ .Any one of the failures of $\hat{D}_t$ is not contradictory with known symptom set, no contradiction in two aspects : First , the intersection between any failure of the corresponding necessarily occurred symptom set $M^+(\hat{D}_j, t+k)$, $k = 0, \cdots, n$ in $\hat{D}_t$ and known no signs of sets of $M^-(t_0 + i)$, $i = 0, \cdots, m$ is the empty set; The second, the intersection between the faults corresponding to the inevitable symptom set that does not appears $M^-(\hat{D}_j, t+k)$ $k = 0, \cdots, n$ and known to occur with the symptom set $M^+(t_0 + i)$, $i = 0, \cdots, m$ is the empty set, the precise collection represents as follows:

$$\hat{D}_{t_crisp} = \{ \hat{D}_j \subset A \quad \forall k = 0, \cdots, n \quad M^+(\hat{D}_j, t+k) \cap M^-(t_0 + i) = \varnothing \text{ and } M^-(\hat{D}_j, t+k) \cap M^+(t_0 + i) = \varnothing \} \tag{1}$$

For the accurate collection $F \cap G \neq \varnothing$ extending to fuzzy sets, the definition of an operator $cons(F, G) = \max(\min(\mu_F(u), \mu_G(u)))$

Definition 1: fuzzy subset $M^+(\hat{D}_j, t+k)$ and $M^-(t_0 + i)$ consistent degree of:

$$cons(M^+(\hat{D}_j, t+k), M^-(t_0 + i)) = \max (\min (\mu_{M^+(\hat{D}_j, t+k)}(m_j) * \mu_{t_0+i}(t+k) + \mu_{M^-(t_0+i)}(m_j))) \tag{2}$$

The degree of consistency of $M^+(\hat{D}_j, t+k)$ and $M^-(t_0+i)$ is higher, then the degree of inconsistency $\hat{D}_j$ and $M^-(t_0+i)$ is higher. Thus $cons(\ M^+(\hat{D}_j, t+k), M^-(t_0+i))$ is the degree of the conflict of $\hat{D}_j$ and $M^-(t_0+i)$.

Therefore, the degree of $M^+(\hat{D}_j, t+k) \bigcap M^-(t_0+i) = \varnothing$:

$$1 - cons(\ M^+(\hat{D}_j, t+k),\ \ M^-(t_0+i)) \tag{3}$$

Similarly, we can have the degree of $M^-(\hat{D}_j, t+k)$ and $M^+(t_0+i)$, $M^+(\hat{D}_j, t+k) \bigcap M^-(t_0+i) = \varnothing$. The membership function $\mu_{\hat{D}_t}(\hat{D}_j)$ of $\hat{D}_t$ is:

$$\begin{aligned}
\mu_{\hat{D}_t}(\hat{D}_j) &= \min(\ 1 - cons(\ M^+(\hat{D}_j, t+k),\ \ M^-(t_0+i)), \\
&\quad 1 - cons(\ M^-(\hat{D}_j, t+k), M^+(t_0+i))) \\
&= 1 - \max\ (cons(\ M^+(\hat{D}_j, t+k), M^-(t_0+i)), cons(\ M^-(\hat{D}_j, t+k), M^+(t_0+i))) \\
&= 1 - \max_{j=1,q} \max\ (\min\ (\mu_{M^+(\hat{D}_j, t+k)}(m_j) * \mu_{t_0+i}(t+k), \mu_{M^-(t_0+i)}(m_j)) \\
&\quad \min\ \ (\mu_{M^-(\hat{D}_j, t+k)}(m_j) * \mu_{t_0+i}(t+k), \mu_{M^+(t_0+i)}(m_j)))
\end{aligned} \tag{4}$$

For the known signs set $M^+(t_0+i)$ and no signs of sets $M^-(t_0+i)$, $\hat{D}_t$ includes all possible failure modes. If a failure mode $\mu_{\hat{D}_t}(\hat{D}_j) = 0$, you can rest assured that will give it up.

It should be noted here, because knowledge is not complete, some signs of the failure is not known, these failures and no known signs consistent diagnostic model, these failures are included in the explanation.

3.2 Diagnostic

Related diagnostic concern is the set of signs and known to occur , known to be no signs of failure, performance failure $\hat{D}_j$ occurs in the moment t, at the moment $t+k$ will inevitably be a sign of $M^+(\hat{D}_j, t+k)$ the moment t_0+i known symptom set $M^+(t_0+i)$ a certain degree of coverage, $\hat{D}_j$ necessarily does not occur at the timing $t+k$ the symptom set $M^-(\hat{D}_j, t+k)$ on a certain degree of time t_0+i is known not to occur symptom set $M^-(t_0+i)$ covering .

The precise collection is represented as:

$$\begin{aligned}
\hat{D}^*_{t_crisp} = \Big\{ & \hat{D}_j \in \hat{D}_{t-crisp}\ ,\ \ M^+(\hat{D}_j, t+k) \bigcap M^+(t_0+i) \neq \varnothing \\
& or \quad\ M^-(\hat{D}_j, t+k) \bigcap M^-(t_0+i) \neq \varnothing\ \Big\}
\end{aligned} \tag{5}$$

Extended to the fuzzy sets under expressed as:

$$\begin{aligned}
\mu_{\hat{D}^*_t}(\hat{D}_j) = \min(\mu_{\hat{D}_t}(\hat{D}_j),\ & \max(\ cons(\ M^+(\hat{D}_j, t+k),\ \ M^+(t_0+i)), \\
& cons(\ M^-(\hat{D}_j, t+k),\ \ M^-(t_0+i))))
\end{aligned} \tag{6}$$

3.3 coverage diagnosis

The accurate collection of the $\hat{D}^*_{t_crisp}$ further refinement can be obtained of the formula (7):

$$\begin{aligned}
\hat{D}^{**}_{t_crisp} = \Big\{ & \hat{D}_j \in \hat{D}^*_{t_crisp}\ ,\ \ M^+(t_0+i) \subseteq M^+(\hat{D}_j, t+k)\ \ or \\
& M^-(t_0+i) \subseteq M^-(\hat{D}_j, t+k)\ \ \exists k, \exists i, t+k = t_0+i,\ k = 0, \cdots, n \quad i = 0, \cdots, m\ \Big\}
\end{aligned} \tag{7}$$

Obviously there $\hat{D}^{**}_{t_crisp} \subseteq \hat{D}^*_{t_crisp}$,

E. Sanchez weak implication defined as

$$inc(F, G) = 1 \qquad \text{If}\ \ \mu_F \leq \mu_G \tag{8}$$

$$inc(F, G) = \mu_G \qquad \text{If}\ \ \mu_F > \mu_G \tag{9}$$

$$\text{For } k=0,\cdots,n \quad i=0,\cdots,m, \text{ if } \exists i, \exists m_f \in M^+(t_0+i),\ \exists k,$$
$$\mu_{M^+(t_0+i)}(m_f) \le \mu_{M^+(\hat{D}_j,t+k)}(m_f) * \mu_{t_0+i}(t+k),$$
$$\text{and } inc(\ M^+(t_0+i),\ M^+(\hat{D}_j,t+k)) = 1 \tag{10}$$

$$\text{For } k=0,\cdots,n \quad i=0,\cdots,m, \text{ if } \exists i, \exists m_f \in M^+(t_0+i),\ \exists k,$$
$$\mu_{M^+(t_0+i)}(m_f) > \mu_{M^+(\hat{D}_j,t+k)}(m_f) * \mu_{t_0+i}(t+k),$$
$$\text{And } inc(\ M^+(t_0+i),\ M^+(\hat{D},t+k)) = \mu_{M^+(\hat{D}_j,t+k)}(m_f) * \mu_{t_0+i}(t+k) \tag{11}$$

(10) Means that a sign belongs $M^+(t_0+i)$ the signs must belong to $M^+(\hat{D},t+k)$.This indicates that the coverage of the latter on the former, Therefore $\mu_{\hat{D}_t^{**}}(\hat{D})$=1. (11) Reflects the closeness of $\mu_{M^+(t_0+i)}(m_j)$ and $((\mu_{M^+(\hat{D},t+k)}(m_j),t+k)$.

Similarly defining $inc(\ M^-(t_0+i),\ M^-(\hat{D}_j,t+k))$.

In fuzzy sets:

$$\mu_{\hat{D}_t^{**}}(\hat{D}_j) = \min(\mu_{\hat{D}_t}(\hat{D}_j), inc(\ M^+(t_0+i),\ M^+(\hat{D}_j,t+k)),$$
$$inc(\ M^-(t_0+i),\ M^-(\hat{D}_j,t+k))) \tag{12}$$

3.4 Equality diagnostic

$$\text{In accurate collection, } \hat{D}_{t_crisp}^{***} = \{\hat{D}_j \in \hat{D}_{t_crisp}^{**},\ M^+(t_0+i) = M^+(\hat{D}_j,t+k) \ \ and$$
$$M^-(t_0+i) = M^-(\hat{D}_j,t+k) \ \ \exists k, \exists i, t+k=t_0+i,\ k=0,\cdots,n \quad i=0,\cdots,m \ \}$$

In fuzzy collection,

$$\mu_{\hat{D}_t^{***}}(\hat{D}_j) = 1 \quad \text{if } \min(\mu_{M^+(t_0+i)}(m_f), \mu_{M^+(\hat{D}_j,t+k)}(m_f) * \mu_{t_0+i}(t+k)) \ne 0 \ \ and$$
$$\min(\mu_{M^-(t_0+i)}(m_f), \mu_{M^-(\hat{D}_j,t+k)}(m_f) * \mu_{t_0+i}(t+k)) \ne 0 \tag{13}$$

4 Conclusions

This paper presents the stepwise refinement of diagnostic model to ensure that the omission of a potential failure, but also in the case of incomplete knowledge neither the solution with the best known symptom set match. Complexity of diagnostic problem solving, and to overcome the high price probability calculation based on the fuzzy relation equations, the model can be used to meet the real-time requirements. Text definition of 1 , 2 and Proposition 1,2 diagnose the problem solving knowledge completeness criterion also makes access to knowledge work with clear objectives , and avoid expending energy to get those redundant knowledge .

5 References

[1] J.A. Reggia, et al. A formal model of diagnosis inference-part Ⅰ : problem formulation and decomposition. Information Science, 1985, (37): 227 -256
[2] J. A. Reggia, et al. A formal model of diagnosis inference-part Ⅱ : algorithm solution and application. Information Science, 1985, (37): 257 - 285
[3] Y. Peng, et al: IEEE Trans. SMC, 1987, 17(2): 146-162
[4] Y. Peng, et al: IEEE Trans. SMC, 1987, 17(3): 395- 406
[5] D. Dubois, et al: Fuzzy sets and systems, 1995, (75): 119-134
[6] D. Cayrac, et al: IEEE Trans. Fuzzy Systems, 1996, 4(3): 251-268
[7] I. Mozetic: Int. J. Human - Computer Studies, 1991, 35(3): 329-362
[8] L. A. Zadeh: Machine intelligence, 1979, (9): 149-194.

CHAPTER 6:

Advanced Technologies in Mechanical Engineering, Mechatronics, Automation, Measuremant, Control and Manufacturing Technology

Advanced Materials Research Vols. 989-994 (2014) pp 2741-2744
© (2014) Trans Tech Publications, Switzerland
doi:10.4028/www.scientific.net/AMR.989-994.2741

Design and Simulation for New type Pulley Straightening Machine Based on Pro/E

Geng Jin-hua[1, a], Yu Bin[2,b], Fan Bin[3,c]

[1,2,3] Anhui University of Science & Technology, Huainan 232001, PR China

[a]174363363@qq.com

Keywords: pulley；straightening machine；automatic correction；motion simulation based on Pro/E

Abstract. Pro/Engineer(Pro/E) was applied to design a new kind of motorcycle belt pulley straightening machine, which was composed of electric cylinder and stepper motor in this paper. The effect of positioning and correcting were achieved by the straightening machine during operation. The motion simulation for correcting key parts was done under mechanical module of the software. The mechanism motion speed and the motion trails of the straightening machine were acquired under different positioning accuracy. Through analysis on the motion trails, the best range of the correcting parts′ rotational speed can be optimized.

Introduction

When a motor pulley has a deformation and bending and so on, it can affect the normal operation of the internal drive motorcycle. Even worse it will generate serious personal injury and property loss to motorcycle users. Existing motor pulley correction methods mostly make use of heavy manual equipment to correct, and the efficiency and accuracy of the correction methods are low. The common correction devices are roller plate straightening machine in sheet metal processing industry. The correction devices can automatically correct sheet, but it cannot be applied to the correction of a camber motorcycle pulley. In order to improve the correction efficiency and accuracy to the motor pulley, this paper designed a new type pulley straightening machine，which can greatly improve the low efficiency and low accuracy of the motor pulley[1].

Pro/E Software Introduction

Pro/Engineer is called for Pro/E, it has more powerful functions in product structure design and parametric modeling. Pro/E is the system adopt the entity modeling based on characteristics, it can random drawing and change the model parameters by means of parameter design. The Phenomenon any changes of the whole design project can reflected in the related links of the whole process of design can come true by Pro/E taking advantage of the unity of grassroots database. What's more, all modules of Pro/E are interconnected, for example, if a place be modified in the process of product development, Then the whole design content including engineering documents will automatically change. In the process design products by Pro/E, users can use familiar characteristics as the components of the product model, leading to the product design becoming easy. In terms of mechanical structure simulation, Pro/E is easy to find potential assembly conflicts and defects, and feedback the related information to the designer in time. Relatively speaking, Pro/E give a poor performance in surface modeling[2−3].

Straightening machine structure design

The main composition and working principle of structure. In this paper, when the motorcycle pulley straightening machine is working, the cylinder movement will fix the pulley on the fixed axis of the workbench. Following fixed pulley, the stepper motor drive the pulley rotating. When the motor drive the pulley rotating, the eddy current sensor collect data distance data, system set 5˚as a set of distance data, rotating a ring collect 72 sets of distance data used for detecting the deflection of the pulley. The distance data the eddy current sensor collected transfer to the single-chip microcomputer system, the position the highest point on the surface of the pulley can be calculated and located. The peak of the surface of the pulley can be located in underneath of the electric

cylinder head by controlling the stepper motor drive belt rotating. According to the difference of the highest point and the lowest point of the pulley measured by the device, the electric cylinder axis press, electric cylinder and the squeeze head can stamping pulley. If this operation has been completed, the above process repeat until the data measured up to the requirement of the pulley surface flatness[4].

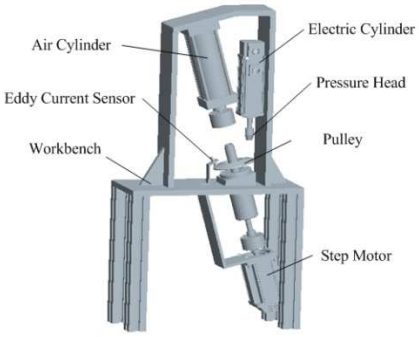

Fig.1 Pulley straightening machine structure chart

Selection and design of the key components. In the process of straightening machine working, the work on, the pulley can be fixed by the fixed shaft and the cylinder head, which on the worktable. In the process of eddy current sensor detecting surface deformation of the pulley, the stepper motor drive the pulley to rotate. When the electric cylinder and the squeeze head stamping to the peak of pulley, the position of the pulley is fixed. As a result, the rotation of the pulley is stop. Hence, it is necessary to design the cylinder head. In this paper, the cylinder head was used to fix pulley, which constitute a pair of tapered roller bearing, matching cups and bearing cower.

To improve the correction efficiency of the pulley for looms, the way of electric stepper motor can be corrected rapidly by shorting the cylinder's and electric cylinder's stroke and improving the speed of the cylinder, the cylinder and electric stepper motor. Comprehensive consideration the energy consumption of the straightening machine and pulley correction effect and the running speed of cylinder, electric cylinder and stepping motor can be controlled in a proper range. Eventually, the correction effect of the pulley for looms at different speeds is simulated by the Pro/E mechanism motion simulation module, which has obtained the best corrective running speed of the pulley for looms under that simulation.

Motion simulation analysis

Motion Simulation Setting. When the simulation is proceed by Pro/E，it can achieve the final assembly by setting various constraints, which consists of rigid constraints and user-defined constraints. Rigid constraint mainly aimed at the rigid assembly of fixed fittings. The assemblies ultimately are required limited at six degrees of freedom[5], the choose of assembly connection mode for rigid constraints including matching, insert and alignment, etc. User-defined constraints mainly aim at the assembly of the component, requesting guarantee freedom of moving parts is greater than 1 or equal to 1.What's more, the freedom constraint assembly connection mode including pin connection, sliding connection and slot connection and so on for the user to choose. The paper establishes the 3 d mode of motorcycle pulley straightening machine by Pro/E, setting the connection between the electric cylinder shaft and electric cylinder, the cylinder shaft and cylinder as sliding connection, setting the connection between the cylinder and the cylinder shaft, the fixed axis and the bearing as the pin connection, the rest constraints between the components and the workbench are rigid constraint.

When the assembly straightening machine model is input to the Pro/E motion simulation mechanism to simulate, three servo motor parameters is need to be defined on the basis of the actual work movement of the straightening machine[6]. According to the distance (L = 80 mm) between

the surface of the squeeze head and the pulley corrected, the speed of electric cylinder is set to 80*(t-2) mm/s, including 2s≤t≤3s. According to the movement condition of the cylinder and cylinder axis, the motor is set as slide servo motor, and the speed is set to t*75mm/s, including 0s≤t≤1s. According to the actual situation of step motor, the motor is set as rotary motor, and the speed is set to 360*(t-1)deg/s, including 1s≤t≤2s.When servo motor parameter setting is completed, mechanism analysis option need to be selected at the machinery analysis interface, which set a series of motion simulation operation parameters, including the begin time ,the end time, the total frame number and the time per frame. This paper set the begin time to 0s and set the end time to 10s, and set the rest parameters as the default parameters.Specific straightening machine motion simulation parameters setting as shown in table 1.

Table.1 Motion simulation parameters settings table

simulation mechanism	parameters of velocity	time parameters
electric cylinder	80*(t-2)mm/s	2s≤t≤3s
air cylinder	t*75mm/s	0s≤t≤1s
Stepper motor	360*(t-1)deg/s	1s≤t≤2s

The simulation result and analysis. After setting the parameters of corrective machine movement simulation, the mechanism motion simulation analysis can start. At the same time, the straightening machine model can simulate the actual corrective motion of the belt pulley. After the simulation enter the playback interface, the simulation results also can be watched from different angles, and the dynamics characters of straightening machine can be shown. In the process of motion playback, the working parts movement can be analyzed, which detect he interference phenomenon. The interference areas can be automatically highlighted and stop play when the interference phenomenon is detected. Now the interference part is changes until all the motion have no interference, which achieving the expected requirements. An example of the squeeze head, the position, the velocity and the acceleration curve are shown in figure 2 according the setting parameters of the electric cylinder servo motor[7].

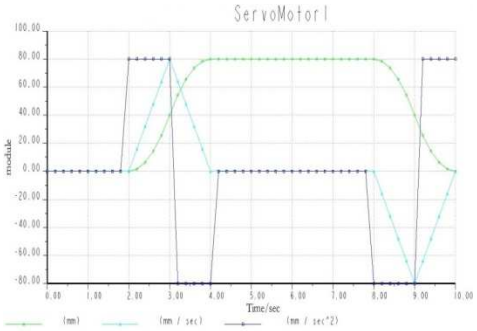

Fig.2 The simulation curve of the position of squeeze head, the velocity and the acceleration

From figure 2, press and return time of the squeeze head under the set speed is 2s.At the begin time and the end work time, the maximum acceleration of the squeeze head can reach ± 8 0mm/s2. But the numerical value is sudden change, which will have a certain impact on motive mechanisms. Considering the squeeze head's quality is small, the impact force will not affect the actual operation of the straightening machine.

Summary

In order to improve the motor pulley correction efficiency and quality of correction, this paper designs a new type pulley straightening machine based on Pro/E. Simulating the motion of the whole structure by mechanism simulation module of Pro/E, it can effectively discover design flaws and quickly achieve equipment operation and assembly requirements. And simulating the motion of

the component by mechanism simulation module of Pro/E, it can easily obtain running speed and acceleration. Above simulation data optimize the operation parameters of the electric cylinder and the stepping motor and other parts, providing reference data for confirming the final operation parameters of straightening machine.

Reference

[1]Zhang Rui-gang. The application of virtual assembly technology in modern design[J].Mechanical Management and Development, 2009,24(6);166-167.

[2]HashemianM.Design for adaptability [D].Canada: Galgary University, 2005.

[3]GuP, HashmianM, NeeAYC. Adaptable design[J]. CIRP Annals Manufacturing Technology, 2004,53(2).

[4]Wang Yue-jin. Mechanical principle[M].Beijing: Peking University Press, 2009:120-150.

[5]Zhu Run-hua, Zhang Jiang-hua. Pro/ENGINEER WILDFIRE mechanical design with the example explanation in Chinese[M].Beijing: Electron Industry Press.2007.

[6]Xue Mingzhai Computer education research.Example of Pro/E mechanism simulation movement[M].Posts & Telecom Press,2008.

Advanced Materials Research Vols. 989-994 (2014) pp 2745-2748
© (2014) Trans Tech Publications, Switzerland
doi:10.4028/www.scientific.net/AMR.989-994.2745

Based on the modeling and simulation analysis of the spray pump of Soildworks

Dandan Jiang[a], Zhebo Zhou[b], Jian Xu[c], Liang Chen[d], Ming Li[e]

School of Mechanical Engineering, Anhui University of Science and Technology, Huainan, China

[a]171597414@qq.com, [b]1930610174@qq.com, [c]472668600@qq.com, [d]782715743@qq.com, [e]562062603@qq.com

Keywords: The spray pump; Crankshaft; Soildworks; Simulation analysis

Abstract. For the research of the mine large displacement spray pump in structure characteristics, each part of the spray pump should make use of Solidworks 3 d modeling, then assembled to be assembly at the same time. During the process of assemble, the assembly must be checked for interference. And simulate the spray pump motion, operation parameters are obtained according to the basic parameters and theoretical analysis. It's of great significance to enhance the efficiency of the practical production in coal mine by bearing the main stress, testing and optimizing the performance of the crankshaft.

Introduction

With the rapid development of China's coal industry, there are higher and higher demands are proposed for the safety and the efficiency of fully mechanized equipment in coal reliability. The spray pump is the key equipment that high pressure spray pump station provides the required pressure water of spray system for large and medium-sized coal winning machine and heading machine. Whether its design is reasonable or not directly decides the safety and reliability of coal winning machine and heading machine during the working. With the constant progress of science and technology, spray pump are in a gradual increase in nominal flow rate and pressure, spray pump types are also increasing, in order to adapt to the working characteristic of various types of mining machinery. This makes the development and research that meet the requirements of the use of new emulsion pump has become the top priority in our country. In order to shorten the development cycle and reduce development costs, the use of Solidworks modeling and simulation analysis of course to be an ideal choice[4].

The main structure and working principle of the spray pump

Spray pump is a kind of device which can change mechanical energy of the motor's into the hydraulic energy of working medium. In the coal mine industry, spray pump are used mainly with spray pump body, explosion-proof motor, coupling, hydraulic system and the base together in working[2]. High pressure spray pump used in mine mainly relies on the power offered by the electrical machine, letting the rotation of the crankshaft movement into the straight line reciprocating movement of the spray pump column to realize the liquid of suction and ejection. The spray pump adopts horizontal three plunger structure which can shape increasing the nominal flow volume under the condition of guaranteed in minimize spray pump. Spray pump mainly include housing, crankshaft, connecting rod, connecting rod and the bush, etc[1,3]. Above all, the carrying capacity of crankshaft and connecting rod is the key to the normal operation of the spray pump as it is the main transmission part. The concrete structure diagram is shown in figure 1.

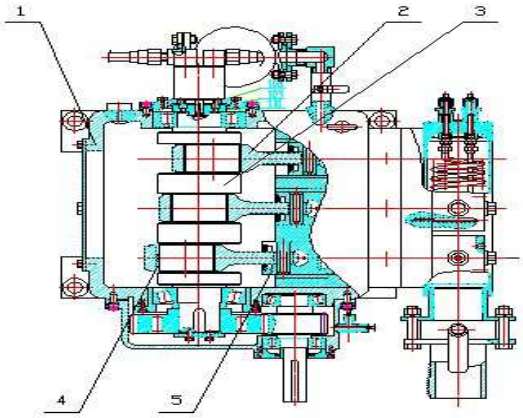

Fig. 1 Structure diagram of the new spray pump
1. The enclosure 2. Connecting rod 3.The crankshaft 4. Transport mechanism
5. The bush 6. The slider

Make use of Solidworks 3 d to model all the parts of the spray pump

Establishing the modeling of the spray pump modeling is the precondition of simulation analysis. In various parts of the spray pump, the crankshaft is the one of the core component. Its modeling is quite complicated. Now, in the case of the crankshaft, briefly describes the modeling process: first of all draw the outline of the crank on the sketch, stretching it into the crank entity, then use tensile entity command to create crank shaft neck. Similar to the above steps, gradually achieve the whole modeling of crankshaft. We can also finish other parts modeling of spray pump with the appropriate command[5].

The achievement of virtual assembly

Virtual assembly is to design and product 3 d model for preassembly by using the virtual technology in virtual environment. Solidworks virtual assembly modeling provides three effective way of assembly, including the top-down, bottom-up and more than the combination of the two ways. You can put the parts together as required just by a few simple steps. This paper chooses the assembly design approach which general engineering habit of top-down.

All the parts are assembled transfer into according to the reasonable when assembling and ordering. The part called first is often fixed default, then the others assembly parts are assembled with the requirements of assembly. The spray pump assembly model is shown in figure 2.

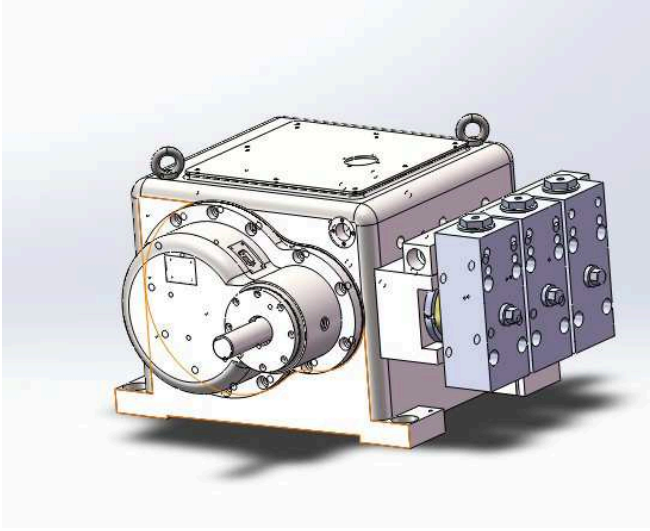

Fig. 2 The spray pump assembly model

After completion of assembly, interference check is needed. Several interference parts must be modified to be eliminated, some can be ignored completely, such as interference between threads and the bolts.

Based on the simulation analysis

SolidWorks simulation, not only can be used to simulate the mechanical movement of assembly and they produce force, but also can determine the related factors, such as the interference between parts, each parts pressure and energy consumption, etc. The designer can simulate the different motion state according to the given conditions and parameters of the product and inspection motion performance the correctness of the design and calculation[6]. At the same time can also determine the scheme of break time, failure time, parts and whether there is potential safety hazard or not, etc. The mechanical simplify are needed before the analysis, otherwise it is hard to calculate, even if the results are wrong. Therefore those which do not affect the results of the analysis of parts must be compressed or deleted. Simplified model is shown in figure 3.

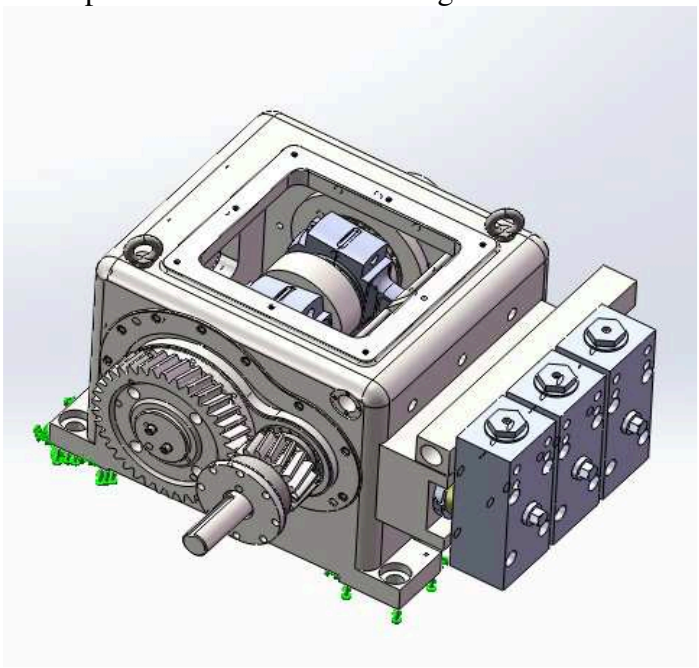

Fig. 3 The simplified assembly modeling

Set the parameters

Select material. The crankshaft as the main components of the spray pump, it choose 42CrMoA alloy steel in material;

Generate the static analysis example. Select the crankshaft initial state by generating the static analysis example;

Apply the fixed constraint and load pressure. Select power is 280 KW, rotational speed is 1480r / min motor as power source, so the input torque of 1806756 n, mm; Plunger cross section by the resistance of the emulsion, through the connecting rod is passed to the crankshaft. Each plug column resistance by about 2000 n through calculation;

Mesh. The parts mainly selecting the crankshaft as the grid, and grid for crankshaft by setting grid options;

Run the example. By running the example, the crankshaft stress, displacement and strain diagram can be received;

Evaluate the safety of the design. Through analysis of the force in maximize known crank of crankshaft stress, the dangerous section can be found, and then determine whether the design is reasonable or not.

Conclusion

(1) Through the simulation analysis of crankshaft, the data and the design value can be compared, then verify the validity of the design and calculation results, at the same time the deficiencies and defects in the design can be improved, which can make a design become more reasonable

(2) Which using the Solidworks 3 d modeling and simulation analysis are carried out on the products can improves the design efficiency and accuracy greatly, and also proposes more reliable and comprehensive analysis in product long life of the service and high reliability. Above all, it can be certainly seen that this method has practical application in production.

References

[1] Zhebo Zhou: Technical Study on Crankshaft Development for Large Displacement Emulsion Pump [J]. Journal of mechanical design and manufacturing, 2012 (7) : 45-147.

[2] Nannan Zhu: Design of Special Clamp for Process Large Crankshafe in Universal Equipment [J]. Journal of coal mine machinery, 2011 (12) : 133-134.

[3] Haizhen Liang: Method of Detecting Crankshaft's Key Geometric Relationship by Using General Gage [J]. Journal of coal mine machinery, 2012 (4) : 120-121.

[4] Baozhen Ge: Comprehensive mechanized coal mining technology [M]. Beijing: China labor social security publishing house, 2006.

[5] The second generation Long Zhen studio:Solidworks2011 high-level design [M]. Beijing: Qinghua university press, 2011.

[6] The second generation Long Zhen studio: Solidworks + Motion + Simulation modeling/organization/structure comprehensive training tutorial [M]. Beijing: Qinghua university press, 2011.

Advanced Materials Research Vols. 989-994 (2014) pp 2749-2752
© (2014) Trans Tech Publications, Switzerland
doi:10.4028/www.scientific.net/AMR.989-994.2749

Study on the Statics Analysis of Promoting the Drilling Efficiency of PDC Anchor Bit

Yan Li[a, 1], Yinfang Song[b, 2], Yilin Mao[c, 3]

[a ,b] School of Mining and Safety Engineering

Anhui University of Science and Technology, Huainan, China

Key Lab of Mining Coal Safety and Efficiently Constructed by Anhui Province and Ministry of Education, Huainan, China

[c] The Internet of Things Institute, CASC

[1]242716112@163.com, [2]236316257@qq.com,[3]843870367@qq.com

Keywords: PDC, Anchor bit, Tooth rake angle

Abstract. PDC anchor bit has the very good rock fragmentation abilities with high penetration rate and long drilling time,which makes the drilling efficiency highly improved and the economic benefit remarkably increased.Now PDC anchor bit has been widely used in drilling field.But for the reason that it is sensitive to the formation characteristics and working conditions,it doesn't achieve good performance in homogeneous formations such as conglomerate and interbeded sections.In order to reach the goal of enlarging the scope of PDC anchor bit application in oilfields,it is necessary to study the breakage mechanism in conglomerate formations and design the PDC anchor bit optimally.

Introduction

Drilling efficiency is the value of PDC anchor bit in the first study, this chapter through the establishment of the statics model of stress of the PDC anchor bit and drilling process chip fluid simulation model to study each bit geometric parameters of tooth rake angle α influence on the stress distribution.

Bit stress under different surrounding rock deformation

PDC anchor bit of finite element analysis combined with surrounding rock stress, in full consideration the factors that influence the PDC anchor bit stress change and the computer can spit out results, so the selection of PDC anchor bit F in the propulsion force and its speed v as the independent variable, the remaining factors as constants to simplify the mechanical model. PDC anchor bit by axial propulsive force F is provided by drill, drill the rated power of P unchanged, as a constant value. Bit by N increased with the increase of rotational speed to reduce torque and drilling mudstones high drilling time, drilling drilling time is low, therefore, by analyzing the change of the speed v to force under different surrounding rock stress, namely

$$P = dN \cdot v = const$$

When PDC anchor bit drilling litho logy according to the particle size and rotation of drilling obstructive divided into sandstone, sandy mudstone and shale, the corresponding stress changes following chart:

1. The mudstone of PDC anchor bit speed is about 750 rad/min

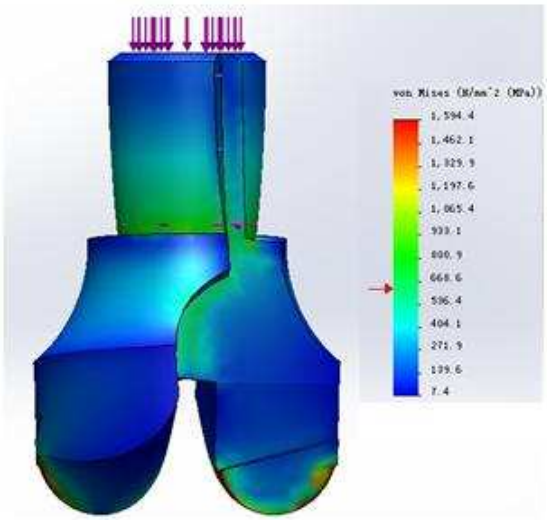

Fig. 1 Mudstone in bit stress nephogram

2. The shaly sand of PDC anchor bit speed is about 1100 rad/min

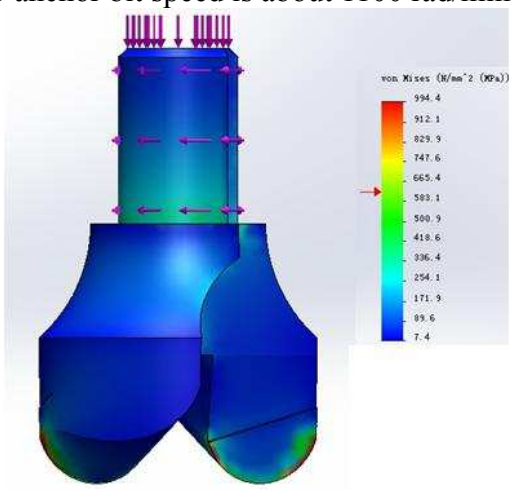

Fig. 2 Shaly sand in the bit stress nephogram

3. The sandstone of PDC anchor bit speed is about 1500 rad/min

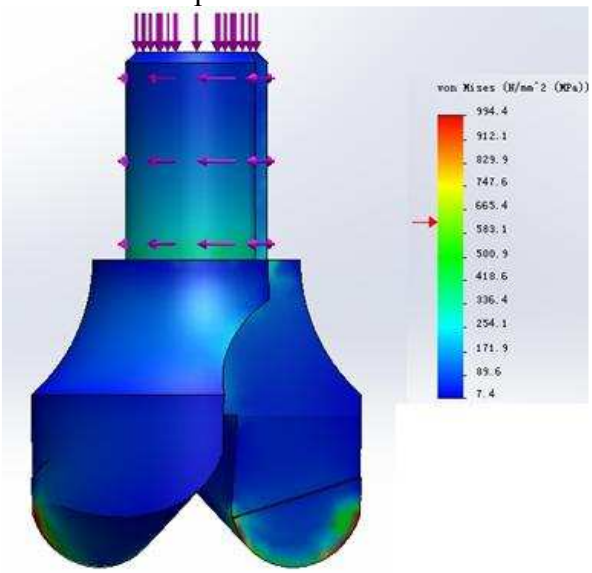

Fig. 3 Sandstone drilling stress nephogram

Under different litho logy of numerical statistics, tooth Angle alpha before the change on the dangerous point of maximum stress can be classified as the chart below:

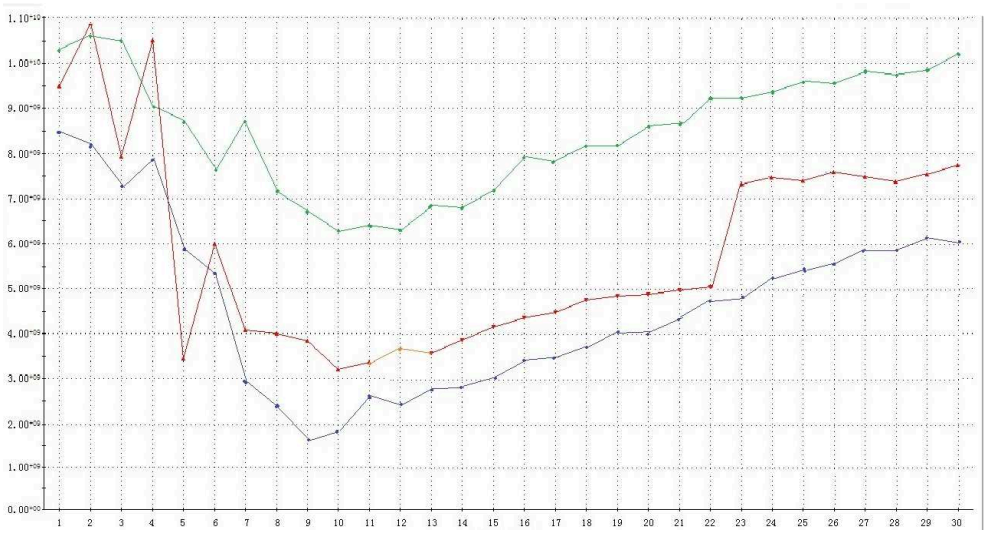

Fig. 4 The effects of the stress with tooth rake angle changing on

For PDC anchor bit, the accuracy of 1 degree is so large, but the actual calculations capability of the computer has to be considered. The way of superimposing two operations can improve the accuracy of tooth rake angle.

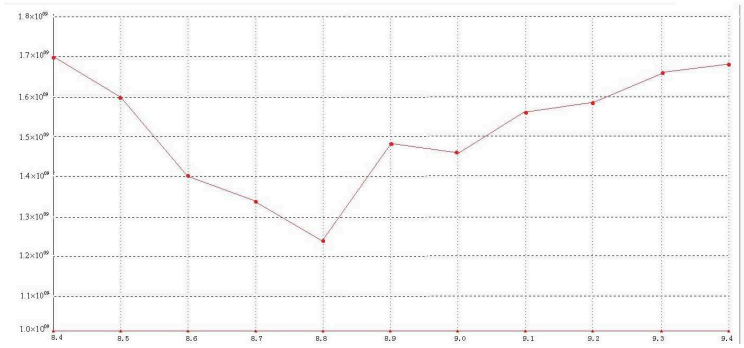

Fig. 5 The stress variation of tooth rake angle in mudstone

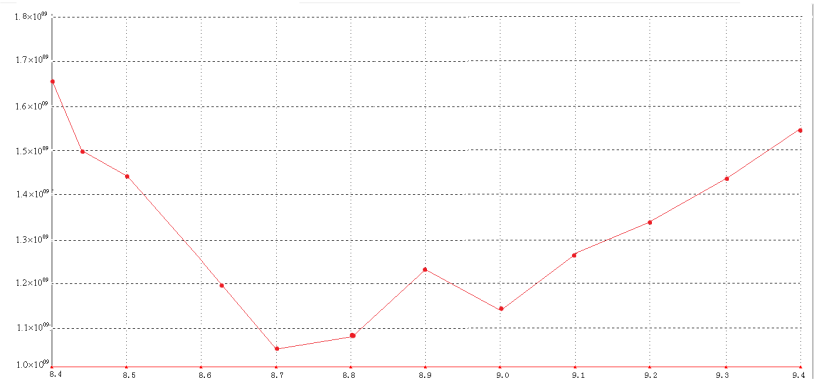

Fig. 6 The stress variation of tooth rake angle in shaly sand

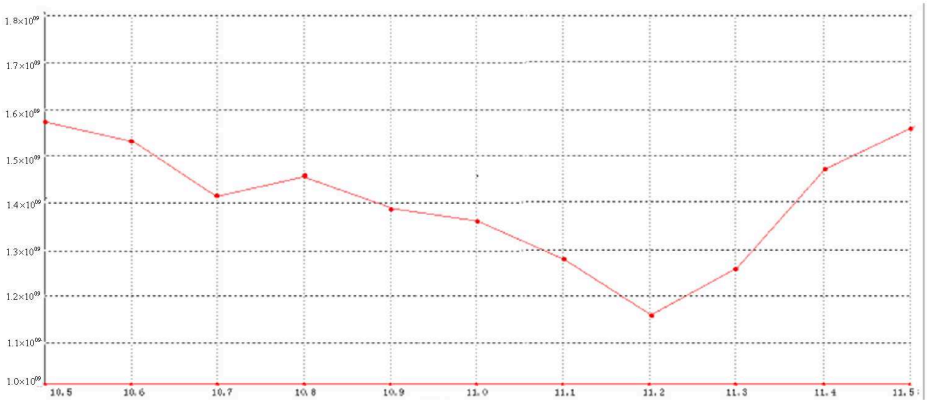

Fig. 7 The stress variation of tooth rake angle in sandstone

Conclusion

Established the statics model of PDC anchor bit, its stress and torque are simulated, and the geometric parameters of PDC anchor bit are classified and studied the Angle change on the tooth Angle alpha before the change of the maximum stress, contact the actual situation, under different surrounding rock is divided into sandstone, mudstone and argillaceous sandstone several ways to discuss, and try to under the condition of without increasing computer computation, two numerical simulation, in order to improve the calculated tooth Angle alpha before the best accuracy.

References

[1] Tetsuji.Ohno, etc. Cost reduction of polycrystalline diamond compact bits through improve durability. Geothermics, 31 (2002) 245-262

[2] Liu H. Y.,etc. Numerical simulation of the rock fragmentation Process induced by indenters[J]. Int. J. Rock Mech. Min. Sci.,2002,36:10-15

[3] H.Geoffroy; D.Nguyen Minh. Study on interaction between rocks and worn PDC'S cutter. Int.J. Rock Mech. & Min. Sci. Vol. 34,No. 3-4,1997

[4] D.Nguyen Minh, etc. Evaluation of Drilling Parameters of a PDC Bit. Int. J, Rock Mech. Min.S ci. Vol. 35,No. 4/5,pp. 578-580, Thesis No. 109, 1998

[5] John R.Smith, Jeffrey B. Lund, Robert K. Galloway. Friction on PDC Cutters at High Normal St ress.Journal of Energy Resources Technology.SEPTEMBER 2002,Vol.124:146-153

Advanced Materials Research Vols. 989-994 (2014) pp 2753-2757
© (2014) Trans Tech Publications, Switzerland
doi:10.4028/www.scientific.net/AMR.989-994.2753

Impact of Tooth Shape Parameters on Strength Safety Coefficient of Herringbone Planetary Train

Zengbao Zhu[a], Chaoqun Shu[b], Yingli Xu[c], Can Li[d], Min Yin[e]

School of Mechanical Engineering, Anhui University of Science and Technology, Huainan, China

[a]zbzhu@163.com, [b]455718369@qq.com, [c]1144317381@qq.com, [d]1326962149@qq.com, [e]578145038@qq.com

Keywords: Planetary train; Herringbone; Tooth profile parameter; strength safety coefficient

Abstract. The influence of tooth profile parameters on the strength safety coefficient can provides the basis for the design of high strength herringbone planetary train system. Through calculation of the three strength safety coefficients (contact strength, bending strength, bonding strength), curves of the relationships between the tooth shape parameters (addendum coefficient, tip clearance coefficient, spiral angle) and the strength safety coefficients have been obtained and the impact of tooth shape parameters on the three strength safety coefficients have been analyzed. The research results show that the bigger addendum coefficient can be selected for the design of high strength herringbone planetary train system. In order to satisfy bending strength, no-undercut and lubrication condition the smaller tip clearance coefficient should be taken. The strength safety coefficients are bigger with the increase of spiral angle, so a bigger spiral angle may be appropriately chosen.

Introduction

Herringbone has the advantages of strong bearing capacity, stable transmission, small vibration and noise etc. The herringbone planetary train system is widely used in the heavy mechanical train system of high speed and heavy load.

The strength safety coefficient of high speed and heavy load herringbone planetary train system is bigger. Variation of tooth profile parameter can change the strength safety coefficient. The influence of tooth profile parameters on the strength safety coefficient can provides the basis for the design of herringbone planetary train system. Domestic and foreign scholars on the impact of tooth profile parameters on the strength safety coefficients of the gear transmission system which conduct some theoretical and experimental research. Abroad, Doctor of Engineering Namigasenshou [1] researched in the influence of various important parameters of gear for surface contact strength, bending strength, bonding strength; Andrzej etc [2] by ISO and AGMA standard gear load is applied, come to different tooth profile parameters corresponding curves of root strength. China, Jinglong Hung etc [3] using the Hertz contact theory, analysis of impact of the tooth pressure angle on contact strength, the tooth strength with the variation regularity of pressure angle is obtained; Dongan Zhan etc [4] analyzes the influencing factors of helical gear spiral angle size and ranges in high speed gear transmission; Ying Wang etc [5] inspect impact of addendum coefficient, pressure angle, spiral angle, gear ratio and the modification coefficient on gear performance. These studies mainly on a single or a pair of meshing gears, but for the whole of herringbone planetary train system aspects little studied.

In this paper, by changing of the tooth profile parameters(addendum coefficient, tip clearance coefficient, spiral angle), calculation of strength safety coefficients, curves of the relationships between the tooth shape parameters and the strength safety coefficients have been obtained, and the impact regularity of tooth profile parameters on the strength safety coefficients have been analyzed.

Three strength safety coefficients

The strength safety coefficient of the gear transmission system including the contact strength safety coefficient, bending strength safety coefficient, scuffing load capacity safety coefficient.

Contact strength safety coefficient S_H expressed as:

$$S_H = \frac{\sigma_{H\lim} z_N}{\sigma_{HO}} \cdot \frac{z_L z_v z_R z_w z_x}{\sqrt{K_A K_v K_{H\beta} K_{H\alpha}}} \tag{1}$$

Bending strength safety coefficient S_F expressed as:

$$S_F = \frac{\sigma_{F\lim} y_{ST} y_{NT}}{\sigma_{FO}} \cdot \frac{y_{\sigma relT} y_{RrelT} y_x}{K_A K_v K_{F\beta} K_{F\alpha}} \tag{2}$$

Scuffing load capacity safety coefficient S_B expressed as:

$$S_B = \frac{\vartheta_{S\text{int}}}{\vartheta_{\text{int}}} \tag{3}$$

Eq. (1), (2) in symbol meaning see references [6], Eq. (3) in symbol meaning see references [7].

In the planetary gear transmission system, the gear contact strength safety coefficient including contact strength safety coefficient of sun gear, planetary gear and internal gear; the gear bending strength safety coefficient including bending strength safety coefficient of sun gear, planetary gear and internal gear; the gear scuffing load capacity safety coefficient including bonding strength safety coefficient of sun gear and planetary gear, bonding strength safety coefficient of planetary gear and internal gear.

Impact of tooth profile parameters on the strength safety coefficient. Herringbone planetary train system diagram see reference [8]， the main parameters of herringbone planetary train system: input power 85.5*kw*, spindle speed 6500*r/min*, life expectancy 24000*h*, transmission ratio 6.3, the number of planetary gear 3. Parameters of the gear transmission system shown in table 1.

Table 1 Parameters of the gear transmission system

parameter	value
modulus(mm)	4
sun gear teeth	19
planetary gear teeth	41
internal gear teeth	101
sun gear modification coefficient	0.229
planetary gear modification coefficient	-0.182
internal gear modification coefficient	-0.135
spiral angle(°)	24.399
tooth width coefficient	0.710

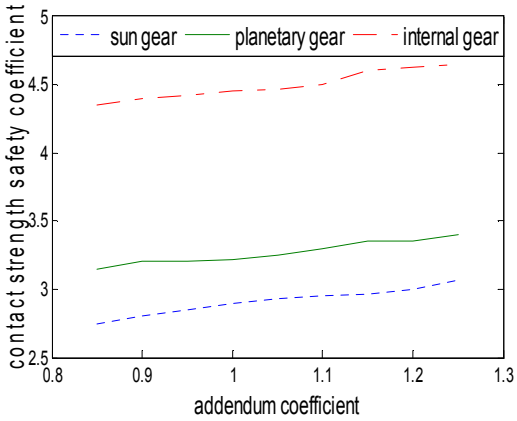

Fig.1 The addendum coefficient effect on the safety coefficient of contact strength

In this paper tooth profile parameters include the addendum coefficient h_a^*, tip clearance coefficient c^* and spiral angle β are studied. Due to the change of pressure angle α value, the actual center distance between sun gear and planetary gear and between planetary gear and internal gear will be changed, they may not equal, that does not meet the concentric condition, so do not

make the pressure angle α analysis of herringbone planetary train system strength safety coefficient impacts.

Impact of addendum coefficient on three strength safety coefficients. The other parameters unchanged, the three strength safety coefficients with addendum coefficients curve shown in figure 1 to figure 3. Figure 1, Figure 2 shows that contact strength and bending strength safety coefficient of sun gear, planetary gear and internal gear are bigger with the increase of the addendum coefficient. Figure 3 shows that scuffing load capacity safety coefficient has a decreasing trend with increases of the addendum coefficient, but not obvious.

Increase the contact ratio of gear transmission, to improve bearing capacity of gear transmission has important significance [9]. The contact ratio is bigger with the increase of addendum coefficient. Increase the addendum coefficient can improve the gear contact strength and bending strength. From figure 1, figure 2 and figure 3：The bigger addendum coefficient can be selected for the design of high strength herringbone planetary train system.

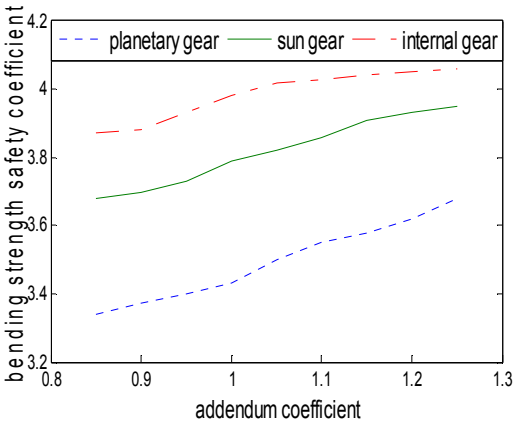

Fig.2 The addendum coefficient effect on the safety coefficient of bending strength

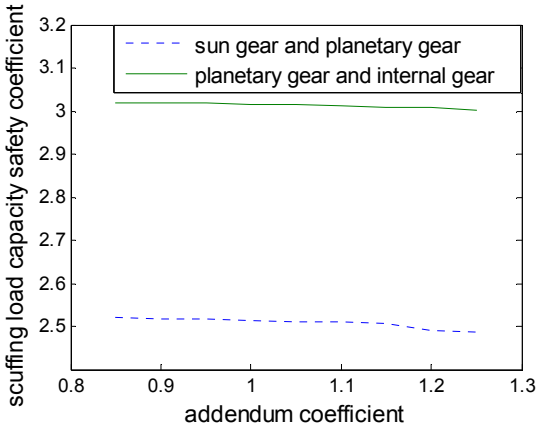

Fig.3 The addendum coefficient effect on the safety coefficient of scuffing load capacity

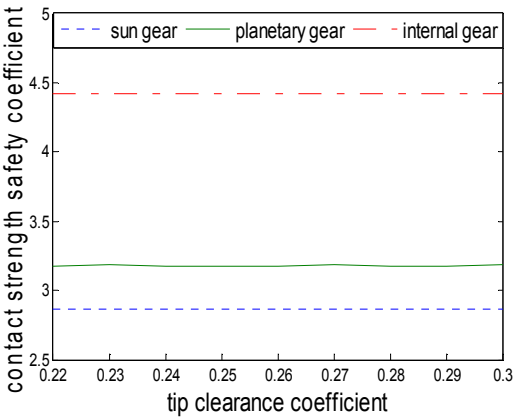

Fig.4 The tip clearance coefficient effect on the safety coefficient of contact strength

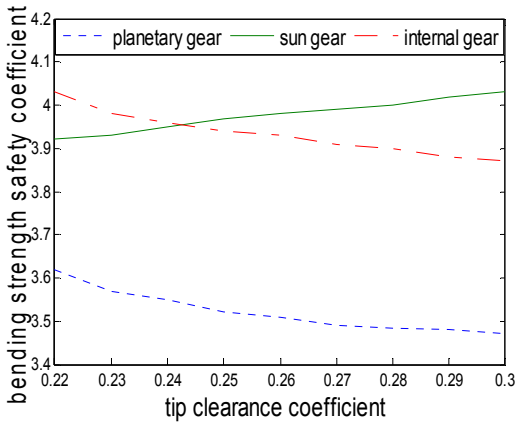

Fig.5 The tip clearance coefficient effect on the safety coefficient of bending strength

Impact of tip clearance coefficient on three strength safety coefficients. The other parameters unchanged, the three strength safety coefficients with tip clearance coefficient curve shown in figure 4 to figure 6 .Figure 4, Figure 6 shows that contact strength and scuffing load capacity safety coefficient of sun gear, planetary gear and internal gear altered little when the tip clearance coefficient increased. Contact strength and scuffing load capacity was mainly affected by the parameters of the tooth surface, so the tip clearance coefficient little effect on contact strength and scuffing load capacity.

Figure 2 show that contact strength safety coefficient of sun gear, planetary gear and internal gear are smaller with the increase of the tip clearance coefficient. Tip clearance coefficient increases,

single arm gear increases，reduced bending strength of the gear. For the design of high strength herringbone planetary train system，no-undercut and lubrication condition the smaller tip clearance coefficient should be taken.

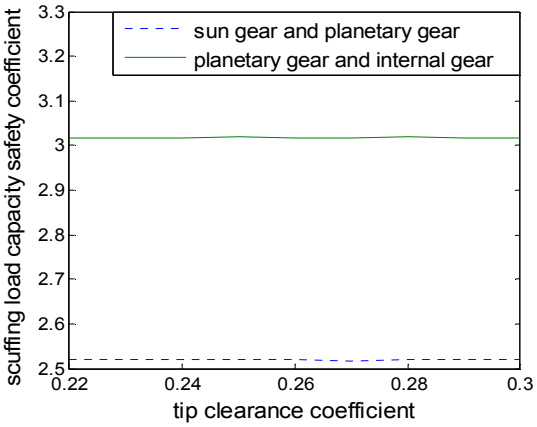

Fig.6 The tip clearance coefficient effect on the safety coefficient of scuffing load capacity

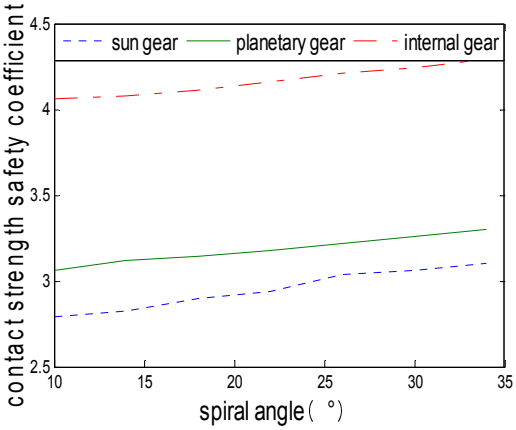

Fig.7 The spiral angle effect on the safety coefficient of contact strength

Impact of spiral angle on three strength safety coefficients . The other parameters unchanged, the three strength safety coefficients with spiral angle curve shown in figure 7 to figure 9. Visible, with the increases of spiral angle, three strength safety coefficients increase.

The contact ratio of herringbone is bigger with the increase of spiral angle [9]. Contact ratio increases and the number of meshing teeth increased. Single tooth to withstand the load becomes smaller, bearing capacity is stronger also. Scuffing damage not easy to be caused when single tooth to withstand the load becomes smaller .Increasing the spiral angle can improve the three strength safety coefficients.

Helical gear spiral angle is usually taken $\beta = 8^\circ \sim 15^\circ$, herringbone axial forces offset each other, β value up to 30°or more [1]. The bigger spiral angle can be selected for the design of high strength herringbone planetary train system under conditions permit.

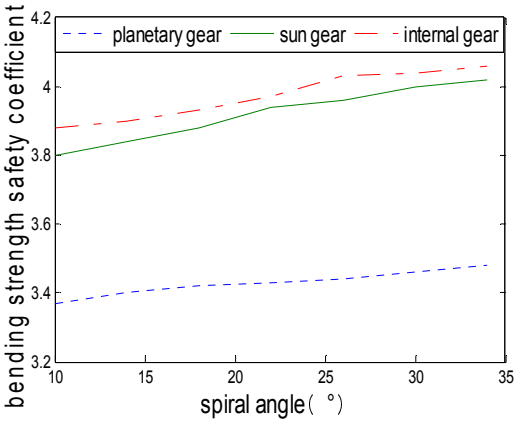

Fig.8 The spiral angle effect on the safety coefficient of bending strength

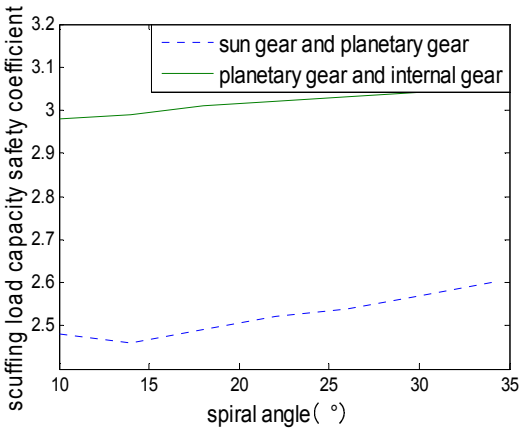

Fig.9 The spiral angle effect on the safety coefficient of scuffing load capacity

Conclusions

(1) Contact strength and bending strength safety coefficient of sun gear, planetary gear and internal gear are bigger with the increase of the addendum coefficient, the addendum coefficient little effect on safety coefficient of scuffing load capacity. The bigger addendum coefficient can be selected for the design of high strength herringbone planetary train system.

(2) Contact strength and scuffing load capacity was mainly affected by the parameters of the tooth surface, so the tip clearance coefficient little effect on contact strength and scuffing load capacity. Tip clearance coefficient increases, single arm gear increases，reduced bending strength of the gear. To meet no-undercut and lubrication condition the smaller tip clearance coefficient should be taken.

(3) The contact ratio of herringbone are bigger with the increase of spiral angle. Contact ratio is bigger，bearing capacity is stronger also，and scuffing damage not easy to be caused. Appropriate increase spiral angle can improve three strength safety coefficients.

Acknowledgments

This paper is supported by the Natural Science Researh Projecet of the Education Department of Anhui Province(No.KJ2013A093, No.KJ2013A083)

References

[1] (Japan) Namigasenshou: Gear design of high strength [M]. Machinery Industry Press,1981.

[2] Andrzej K,Jerzy W, Dariusz C. Comparative Analysis of Tooth-Root Strength Using ISO and AGMA Standards in Spur and Helical Gears With FEM-based Verification [J]. ASME J. Mech. Des , 2005, 128(5): 1141-1158.

[3] Jinglong Hung, Xiexing Miu, Shanming Luo, etc: Impact of teeth pressure angle on gear strength in analysis [J]. Machine Design and Research,2007,34(7):9-15. (In Chinese)

[4] Dongan Zhan, Yunxiao Fan, Junru Yan: Choice of lead angle and design of tooth direction high speed of helical gears [J]. Journal of Shandong University of Science and Technology, 2000,19(3):67-69. (In Chinese)

[5] Yin Wang, Sanmin Wang, Hui Wang: Impact of high-speed heavy helical gears transmission parameters on performance research [J]. Journal of Mechanical Transmission, 2012,36(7):21-26. (In Chinese)

[6] National Standards Institute. GB 3480—83 calculation methods of load capacity for in volute cylindrical gears [S]. Beijing: National Standards Institute, 1983. (In Chinese)

[7] National Standards Institute. GB 3480—86 calculation methods of scuffing load capacity for in volute cylindrical gears [S].Beijing: National Standards Institute, 1986. (In Chinese)

[8] Zengbao Zhu, Rupeng Zhu, Yingsheng Li, etc: Impact of mesh stiffness on dynamic load characteristics of herringbone planet train [J]. Acta Armamentarii,2013,34(6):732~738. (In Chinese)

[9] Wensheng Peng, Zhiming Li, Hualiang Huang: Design of machinery (second edition) [M]. Higher Education Press, 2008. (In Chinese)

Advanced Materials Research Vols. 989-994 (2014) pp 2758-2760
© (2014) Trans Tech Publications, Switzerland
doi:10.4028/www.scientific.net/AMR.989-994.2758

Design of Monitoring System for Hydraulic Support Based on LabVIEW

Shanshan Tang[1,a], Chaokun Wei[2,b]

[1,2]School of Mechanical Engineering, Anhui University of Science and Technology,Huainan, China
[a]1323823076@qq.com ,[b]weichaokun@126.com

Keyword: Hydraulic support, LabVIEW, Pressure monitoring

Abstract: Hydraulic support is widely used under the mine while the pressure is the most important factors of its safety.In view of the defects about present pressure monitor of mining hydraulic support ,designing a mining hydraulic support pressure monitoring system based on LabVIEW.This article mainly introducing the overall structure of the system, hydraulic system principle, the LabVIEW program, data communication and interface design.Using LabVIEW collection and storage support's real-time pressure information. On the basis of the single chip microcomputer and the LabVIEW for data processing and display, improving the real-time control of hydraulic support.

Introduction

Coal industry got a great development in recent years, but coal mine accidents still occurred frequently.For example, January this year in ZhuJi mine ,Huainan Mining Group, anhui province,happening a downhole caving accidents which many miners are trapped.As such cases occur frequently, the development of coal industry is greatly affected and restricted.

At present, the roof support in mostly adopts the hydraulic support while the factors such as strata movement and mining work, making the roof pressure constant change. So hydraulic support pressure's real-time monitoring is requirement.Most of the existing hydraulic support work, pressure is monitored by the recording instrument for monitoring which connected on the support column that required staff to go to working face to get the data so it is difficult to learn the current pressure on the hydraulic support[1].For this problem, this paper designed a mining hydraulic support pressure monitoring system based on LabVIEW, which can achieve real-time monitoring pressure of the hydraulic support.Therefore ,effective measure can be timely taken when a special circumstances happened.

System structure

The pressure of the hydraulic support can be read through the pressure sensor, then the pressure would be transmitted to the corresponding data collection which would preprocess the information.After that,the information would be show on the display.The information would be sent to the monitor host through center station,then the data in LAN can be compared with the collected pressure while center station would achieve real-time monitoring, fault alarm, key data record query and other functions[2].The overall block diagram is shown is Fig 1.

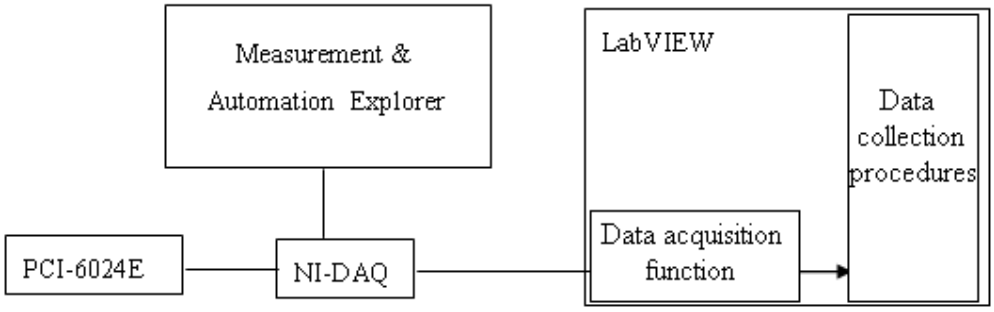

Fig 1 The overall block diagram

The hardware design

The microprocessor

AT89C51 microprocessor is chose(produced by ATMEL company)in this system , which belong to the MCS - 51 series micro-controller.System composed of C51 series single chip microcomputer and AT89C51 do not need without extension program, which make it widely used.

Data acquisition card

PCI - 6221 data acquisition card is a 16-bit resolution, 250 ks/s sampling rate, 2 road 12 analog input, eight digital I/O lines and two 24 bits counter which through USB interface power supply.It is suitable for mining work under the record and environmental testing, at the same time, can also meet the needs of the measurement of this system.

Pressure sensor

Pressure sensor selection: PTG501 strain type pressure sensor which electing high stability and high precision resistance strain gauge sensor chip as transmitter, SMT process including a complete set with zero and full range compensation which could convert the measured pressure into standards electrical signals,such as 4 ~ 20 mA, 0 ~ 5 VDC, 0 ~ 10 VDC, 0.5 ~ 4.5 VDC . The structure is whole sealing , which would make the product of the impact resistant ability, overload ability, such as sealing performance improved greatly, the product the highest pressure can be up to 150 MPa[3].

The choice of strain gauge and layout

BF 120 metal foil strain rosette is elected as the elastomer strain gauge which has good linearity, high fatigue life, small creeping and strong anti-jamming capability.The value is 120 Ω, sensitivity coefficient is 2.0.

Strain gauge is deployed in the maximum strain of the elastomer,which is the roof beam hydraulic support.In order to derivate the signal lines facilitated,a hole is opened on the elastomer.The elastomer should be patch nearly that could reduce the the signal output length[4].Therefore, four slices of strain elastomer are used ensuring the survey of mining hydraulic support, R1, R2, R3 and R4 are used to express the electricity resistance while R1 and R3 express tensile strain gauge and R2 and R4 express compressive strain gauge.In order to obtain larger output sensitivity, full bridge connection is adopted , which is shown in the Fig 2.The initial resistance strain gauge are the same, setting as R.

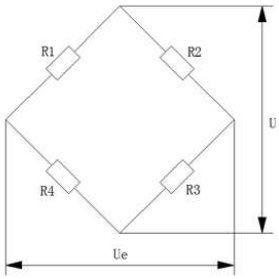

Fig 2 Full Bridge Connection

During the using process, strain gauges resistance is changed as the elastomer's deformation by the effect of load , resistance are supplied as $R_1+\Delta R_1$, $R_2-\Delta R_2$, $R_3+\Delta R_3$, $R_4-\Delta R_4$.As the patch location of strain gauge are symmetry, $\Delta R_1=-\Delta R_2=\Delta R_3=\Delta R_4=\Delta R$ is got.Resistance of strain gauge are as follows:

$$R_1=R_3=R+\Delta R$$

$$R_2=R_4=R-\Delta R$$

Analyze the bridge road, getting the output of the bridge is:

$$U_0=\frac{\Delta R}{R_0}U_e$$

The software design

According to the needs of the real-time monitoring of hydraulic support pressure, landing module, fault monitoring module, data acquisition module, data display module are designed in the

software system. graphical programming language LabVIEW developed by NI company is used in this design which is a general software development platform, not only can provide almost all of the classic analog signal, but also easy to be integrated with data acquisition card.It can improve efficiency at a lower cost[5].The front panel of software system is shown in Fig 3.

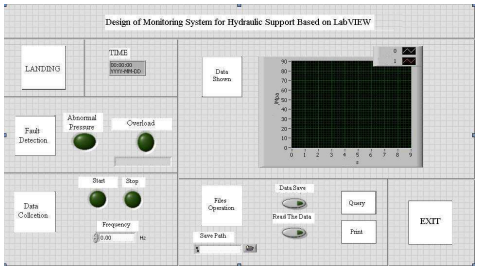

Fig 3 Front Panel

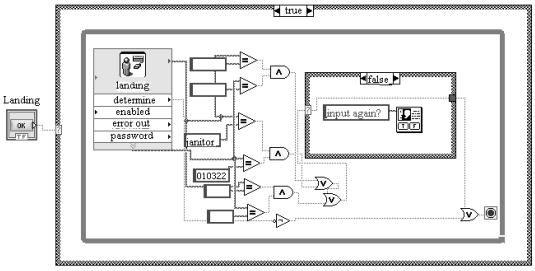

Fig 4 Login module

Login module

In order to prevent the non-working personnel do STH without authorization changes of detection system, a multi-level user management system program is setted in the system.The system only can be operated after a correct password.Administrator logged can add a regular user, thus can effectively avoid the improper operation.Login module's program block diagram is shown in Fig 4.

Pressure real-time display module

This monitoring system can simultaneously monitor ten hydraulic support's pressure ,while each holder's pressure can be displayed the in the beside oscilloscope over time.Pressure real-time display module's program block diagram is shown in Fig5.

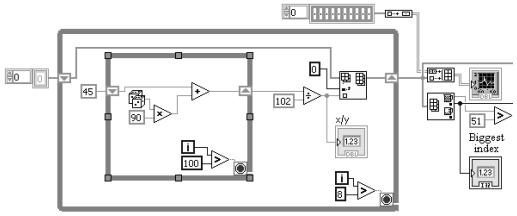

Fig5 Pressure real-time display module

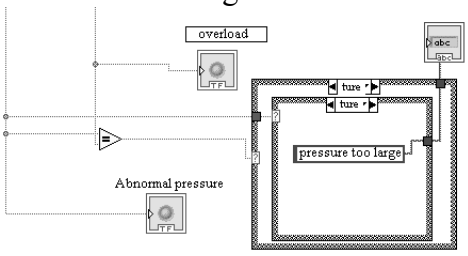

Fig6 Alarm module

Alarm module

Alarm module is an important part of hydraulic support pressure monitoring system.when the hydraulic support's pressure is abnormal or overload, abnormal pressure and overload indicator will light up that reminding the exception occurs to operators.Effective measures can be timely taken to avoid accidents.Alarm module's program block diagram is shown in Fig 6.

Conclusion

A mining hydraulic support pressure monitoring system has been developed based on LabVIEW in this paper which can vividly reflect the mining hydraulic support real-time working condition.In this way,the real-time pressure could be got that proposed an effective and feasible method for the area of fully mechanized working face's pressure monitoring .

References

[1] QIU Weidong,JING Xiaojun,Design of hydraulic support pressure monitoring system software. The Electronic World 2012(12):99-100.

[2] LI Rongsheng,LIAN Zisheng,MA Qinghu.Hydraulic support pressure sensor structure design analysis [J], Coal Mine Mechanical and Electrical.2008(6):47-48.

[3] WANG Chaohui. New technology and equipment hoisting system of the mine. Coal industry publishing house, 1999:99-101.

[4] Mitsubishi electric corporation, FX1N programming manual.2001:85-89.

[5] JIN Jiang,YUAN Xiaoming,LI Daming.Application of LabVIEW centralized control mine electrical switch test bench [J], mining machinery.2007(9):127-129.

Advanced Materials Research Vols. 989-994 (2014) pp 2761-2763
© (2014) Trans Tech Publications, Switzerland
doi:10.4028/www.scientific.net/AMR.989-994.2761

Research of laser induced fluorescence detection techniques based on microfluidic devices

Cheng Yongqiang[1, a], Guo Cuilian[1], Zhao Bin[1], Yang Li[1]

[1]Shandong Provincial Key Laboratory of Ocean Environment Monitoring Technology, Shandong Academy of Sciences Institute of Oceanographic Instrumentation, Qing Dao, 266001, China

[a]chengyongqiang6@163.com

Keywords: Laser induced fluorescence, Confocal arrangement, Nonconfocal arrangement

Abstract. Laser induced fluorescence (LIF) detection technique is one of the most sensitive detection method in micro total analytical systems (μTAS) as its good monochromaticity, strong collimation and high optical density. It is widely used in biochemical analysis systems and the detection limit could reach 10^{-9}-10^{-12} mol/L. Due to the important role in μTAS, different optical structure arrangements of LIF detection techniques were continuously developed. We reviewed the recent progress of the optical structure arrangement and the applications of the LIF detection techniques.

Introduction

Recently, μTAS has gained much interest for high-efficiency separation of biological samples such as DNA fragments, amino acids and proteins. μTAS currently mainly rely on one of the six major detection techniques: fluorescence, electrochemical (EC), chemiluminescence (CL), UV-Vis absorbance, massspectrum and Nuclear Magnetic Resonance (NMR). Because of the high sensitivity and selectivity, LIF is one of the most preferred detection techniques to μTAS, particularly in chip-based capillary electrophoresis (CE) systems. Currently, the LIF detection systems are homemade in many laboratories. They usually consist of a laser excitation source, a laser excitation optical arrangement, a fluorescence collecting optical arrangement and a photosensitive detector. When the laser excitation optical with the fluorescence collecting optical is coaxial, its termed as 'confocal arrangement ' and the vice versa is termed as 'nonconfocal arrangement '.

Traditional confocal LIF arrangement

The confocal LIF arrangement mainly consists of a dichroic mirror, microscope objective, lens groups, pinhole, etc[1-7]. The laser passed through an optional filter, a beam expander, then is reflected by a dichroic mirror and focused in the separation channel by a microscope objective. Meanwhile, the fluorescence is collected by the microscope objective, was passed through the dichroic mirror, then was focused by the lens groups onto a pinhole located at the focal point and was detected by a photomultiplier tube (PMT). Currently, the confocal LIF arrangement that can be used for some commercial instruments (such as the Agilent Bioanalyzer 2100) is available.

Mathies and their coworkers [8-10]firstly introduced the confocal LIF technique into μTAS using high-speed DNA sequencing in capillary array electrophoresis. Ocvirk et al.[2] demonstrated a series of biological assays on-chip by confocal LIF detection. 300 fM fluorescein (S/N=6.1) was measured in continuous-flow mode and 1 pM fluorescein (S/N=5.8) was detected in the capillary zone electrophoresis. Zhu et al.[11] obtained the limit of detection (LOD) of 66 fM (S/N=5.8) for sodium fluorescence by reducing the background noise of the confocal LIF detection. Since the excellent detection limits is obtained, the confocal LIF detection for microfluidic-based analysis systems is applied in single-molecule detection [1,3,12]. Schiro et al.[12]used two-beam line-confocal detection geometry for measuring the total mobility of individual molecules in continuous-flow CE separation.

Though the confocal LIF arrangement has the advantage of high sensitivity and wide suitability, the vast size and complex optical structure is a major challenge for the development of

the miniaturization and integration. For overcoming the shortcoming, the bulk conventional lasers[13,14] are replaced with the diode laser [4,15,16]under keeping high-sensitivity detection. In order to the further miniaturization of microfluidic systems, light-emitting diode (LED) should be an excitation source in replace of the diode laser. Dang et al.[17] used the LED confocal fluorescence detection in microfluidic chips. The LOD for APTS-labeled glucose was about 1.98×10^{-8} mol/L (S/N=5.8).

The nonconfocal LIF arrangement

Compared to the confocal LIF arrangement, the nonconfocal LIF arrangement is more simple and easy to build, which mainly consists of a microscope objective, lens groups, pinhole, etc. Some typical bevel incident laser optical arrangements for the microfluidic chip were reported[18-22] . The laser beam impinged upon the microchip at a 45° angle from the microchip surface and parallel to the separation channel. The fluorescence was collected in a direction perpendicular to the microchip surface. Xu et al.[23] reported a LIF detection system based on a line laser beam to assist the alignment with the micro-channel, which simplified the optical structure and reduced the difficulty of building and operating. The LOD of 1.284×10^{-10} M fluorescein isothiocyanate(S/N>12) was obtained.

In order to reduce the background interference generated from reflections and refraction, the layouts of the laser excitation and fluorescence collecting optical arrangements were continuously researched. Fu et al.[24] developed an orthogonal optical arrangement for microfluidic chips. Using a laser beam perpendicular to the chip, the fluorescence was collected from the microchannel through the sidewall of the chip, which effectively reduced the background noise level resulting from scattered excitation light. The LOD of 1.1 pM fluorescein (S/N=3) was obtained. Yang et al.[25] reported small-angle (20°) optical deflection system from the collinear configuration, which eliminated the interference from scattered excitation light, reflection and refraction light generated from the microfluidic chip. The LOD of FITC was estimated to be 2 pM (S/N = 3). Li et al.[26] reported a similar LIF detection system with a small-angle (18°) optical deflection from collinear configuration with silver mirror coating detection window, which greatly enhanced fluorescence intensity. The LOD of 0.5 pM FITC (S/N=3) was obtained.

Incorporating optical fibers into the μTAS is also a good approach used to simplify the optical system by minimizing the number of required optical components. Fang et al.[27] reported a simple nonconfocal LIF arrangement for the chip-based systems. The laser beam was reflected and focused to the separation channel by a 7-cm-focal length concave mirror from below the chip at an incident angle of 45°. The fluorescence was collected perpendicular to the surface of the glass chip by a 2-mm-diameter optical fiber positioned immediately below the chip. Li et al.[28,29] used a multimode optical fiber to transmit the laser beam to the detection point and the PMT to detect directly the fluorescence without the collimation, collection optics and mirrors.

Conclusion

As a traditional optical mode, the confocal arrangement has high sensitivity and wide suitability, which is often applied to single-molecule fluorescence detection. The nonconfocal arrangement has the advantage of simple structure and easy to miniaturization, also got the favour of the researchers. Unfortunately, the size of the LIF detection system is large relative to the size of the microfluidic chip，which is a major challenge for the development of the miniaturization and integration. To overcome this problem, the small and compact optical components, such as small light source (high-output LED) or micro-lens, should be further introduced to the μTAS. Integrating micro lens on the microfluidic through the means such as etching should greatly reduce the volume of the optical system. At the same time, some optical components were replaced by optical fibers, which benefits the integration of the μTAS.

Acknowledgements

Financial supports from Natural Science Foundation of China (No. 21207080), Natural Science Foundation of Shandong Province (No. ZR2011BQ021), Research Special Funds for Public Welfare Projects of State Oceanic Administration of China (201005025-4), National Key Technology R&D Program of the Ministry of Science and Technology (2012BAF14B04) are gratefully acknowledged.

Reference

[1] Fister, J. C., Jacobson, S. C., Davis, L. M., Ramsey, J. M., *Analytical Chemistry* 1998, *70*, 431-437.
[2] Ocvirk, G., Tang, T., Harrison, D. J., *Analyst* 1998, *123*, 1429-1434.
[3] Haab, B. B., Mathies, R. A., *Analytical Chemistry* 1999, *71*, 5137-5145.
[4] Jiang, G. F., Attiya, S., Ocvirk, G., Lee, W. E., Harrison, D. J., *Biosensors & Bioelectronics* 2000, *14*, 861-869.
[5] Shi, Y. N., Simpson, P. C., Scherer, J. R., Wexler, D., Skibola, C., Smith, M. T., Mathies, R. A., *Analytical Chemistry* 1999, *71*, 5354-5361.
[6] Emrich, C. A., Tian, H. J., Medintz, I. L., Mathies, R. A., *Analytical Chemistry* 2002, *74*, 5076-5083.
[7] Chen, J. F., Jin, Q. H., Zhao, J. L., Xu, Y. S., *Biosensors & Bioelectronics* 2002, *17*, 619-623.
[8] Huang, X. C., Quesada, M. A., Mathies, R. A., *Analytical chemistry* 1992, *64*, 2149-2154.
[9] Woolley, A. T., Mathies, R. A., *Proceedings of the National Academy of Sciences of the United States of America* 1994, *91*, 11348-11352.
[10] Woolley, A. T., Mathies, R. A., *Analytical chemistry* 1995, *67*, 3676-3680.
[11] Zhu, Y., Chen, N., Li, Q., Fang, Q., *Analyst* 2013, *138*, 4642-4648.
[12] Schiro, P. G., Kuyper, C. L., Chiu, D. T., *Electrophoresis* 2007, *28*, 2430-2438.
[13] Manz, A., Harrison, D. J., Verpoorte, E. M. J., Fettinger, J. C., Paulus, A., Ludi, H., Widmer, H. M., *Journal of Chromatography* 1992, *593*, 253-258.
[14] Flanagan, J. H., Legendre, B. L., Hammer, R. P., Soper, S. A., *Analytical Chemistry* 1995, *67*, 341-347.
[15] Jansson, M., Roeraade, J., Laurell, F., *Analytical Chemistry* 1993, *65*, 2766-2769.
[16] Mank, A. J. G., Yeung, E. S., *Journal of Chromatography A* 1995, *708*, 309-321.
[17] Dang, F., Zhang, L., Hagiwara, H., Mishina, Y., Baba, Y., *Electrophoresis* 2003, *24*, 714-721.
[18] Jacobson, S. C., Hergenroder, R., Koutny, L. B., Ramsey, J. M., *Analytical Chemistry* 1994, *66*, 2369-2373.
[19] Jacobson, S. C., Hergenroder, R., Koutny, L. B., Ramsey, J. M., *Analytical Chemistry* 1994, *66*, 1114-1118.
[20] Jacobson, S. C., Ramsey, J. M., *Analytical Chemistry* 1996, *68*, 720-723.
[21] Liang, Z. H., Chiem, N., Ocvirk, G., Tang, T., Fluri, K., Harrison, D. J., *Analytical Chemistry* 1996, *68*, 1040-1046.
[22] Roulet, J. C., Volkel, R., Herzig, H. P., Verpoorte, E., de Rooij, N. F., Dandliker, R., *Analytical Chemistry* 2002, *74*, 3400-3407.
[23] Xu, B. J., Yang, M., Wang, H., Zhang, H. L., Jin, Q. H., Zhao, J. L., Wang, H. M., *Sensors and Actuators a-Physical* 2009, *152*, 168-175.
[24] Fu, J.-L., Fang, Q., Zhang, T., Jin, X.-H., Fang, Z.-L., *Analytical Chemistry* 2006, *78*, 3827-3834.
[25] Yang, L., Li, X. T., Li, J., Yuan, H. Y., Zhao, S. L., Xiao, D., *Electrophoresis* 2012, *33*, 1996-2004.
[26] Li, M., Ji, H., Li, J., Yuan, H., Xiao, D., *Electrophoresis* 2013, *34*, 3163-3170.
[27] Fang, Q., Xu, G.-M., Fang, Z.-L., *Analytical Chemistry* 2002, *74*, 1223-1231.
[28] Li, H. F., Lin, J. M., Su, R. G., Uchiyama, K., Hobo, T., *Electrophoresis* 2004, *25*, 1907-1915.
[29] Li, H. F., Cai, Z. W., Lin, J. M., *Analytica Chimica Acta* 2006, *565*, 183-189.

Advanced Materials Research Vols. 989-994 (2014) pp 2764-2767
© (2014) Trans Tech Publications, Switzerland
doi:10.4028/www.scientific.net/AMR.989-994.2764

Detecting Ultra low Carbon and Sulfur Contents in Steel by Using Infrared Absorption Method

Bayati, M.R., Pengyi WEI

Department of Materials Science and Engineering,

North Carolina State University, Raleigh, NC 27695, United States
email: pengyiwei5101@sina.com

Keywords: Detecting, Ultra low Carbon and Sulfur, Steel, Infrared Absorption Method

Abstract. The detection of carbon with the contents ranging from 0. 000 5 % to 0.010%, and of sulfur with the contents ranging from 0.000 2% to 0.010%, has become an inevitable requirement for steelmaking process control. Due to the extreme low carbon and sulfur contents, using infrared carbon sulfur technical analysis has lower peak value than the background value of the instrument, and it is difficult to control the best analysis conditions of obtained valid signal; in addition, the small errors brought by crucible blank, sample weight, and uniformity of the samples may have great impact on the detection results. To solve this technical problem, this study gives up the single point calibration applied by infrared absorption method, but uses linear calibration method to detect ultra low carbon and sulfur contents in steel, which effectively meets the demand of manufacturers on the development of high-value-added products, and provides reliable data for production.

Introduction

Carbon and sulfur are the routine test items of steel products. Standards such as ASTM E 1019[1] and ISO 15350[2] are applicable for the detection of 0.005%～4.3% carbon contents (mass fraction, same as bellow) and 0. 000 5%～0. 33% sulfur contents. Along with the fast development of production and scientific research, the steel manufacturing today has shown a trend of diversified and lean production. Production scale of ultra low carbon and sulfur steel has been increasingly growing, which raises higher demand on the detection of ultra low carbon and sulfur. The detection of carbon with the contents ranging from 0. 000 5 % to 0.010%, and of sulfur with the contents ranging from 0.000 2% to 0.010%, has become an inevitable requirement for steelmaking process control. Due to the extreme low carbon and sulfur contents, using infrared carbon sulfur technical analysis has lower peak value than the background value of the instrument, and it is difficult to control the best analysis conditions of obtained valid signal; in addition, the small errors brought by crucible blank, sample weight, and uniformity of the samples may have great impact on the detection results. Although there are reports on detecting ultra low carbon by using spark source atomic emission spectrometry [4][5], but the requirements on the conditions for such detection is extremely high, also with high costs. Since a lot of factors may affect the detection of ultra low carbon and sulfur contents, this detection has long been taken as a challenge[6]. To solve this technical problem, this study gives up the single point calibration applied by infrared absorption method, but uses linear calibration method to detect ultra low carbon and sulfur contents in steel, which effectively meets the demand of manufacturers on the development of high-value-added products, and provides reliable data for production.

Test Methods

Put crucible with ultra low carbon and sulfur into a muffle furnace; after burning 2h under the temperature of 1 000℃; after cooling down, it is placed into a dryer for future use. Preheat the infrared carbon sulfur analyzer, make the analyzer in a normal operation state, and set the best analysis parameters. Clear the inlet and outlet of the combustion furnace, replace magnesium perchlorate and alkali asbestos, open the switch of carrier gas and power gas, and check the air tightness of combustion furnace.

The circular blank value measurement method is employed to measure the blank values [7][8] of carbon and sulfur. Take 2. 000 g of fluxing agent into crucible with ultra low carbon and sulfur, select the sample name of "Blank" and default input mass of 1. 000 g, and raise the crucible supporting to conduct the analysis. After two times of measurements, and over 3 times of analysis, at least 3 results with good repeatability are chosen; then the average total blank value is calculated, and it is entered into the analyzer. The analyzer will automatically deduct the blank value during the detection later.

Put the processed crucible with ultra low carbon and sulfur on a balance scale, take (0. 600±0. 025)g sample into the crucible, evenly spread 2. 0 g of tungsten granular on the sample, and conduct the analysis in infrared carbon sulfur analyzer.

Conclusion and discussion

1. Selection of Calibration Method

In the experiment, the single point calibration method with single standard sample is applied, but the accuracy of this method can not be guaranteed when the contents of the elements to be measured in the samples have large deviation with calibration standard value. To solve this technical problem, the linear calibration method is employed with multiple standard samples (at least 3 samples) to conduct the linear calibration based on the range of carbon content of 0. 000 5 %～0.010％ and the range of sulfur content of 0.000 2%~0.010% in the steel production,. By eliminating the analytical deviation caused by individual causal factors, the analytical range has been expanded notably, and this calibration can meet the requirement of quality monitoring during routine production.

2. Selection of sample weight

Sample weight test is conducted by taking different quantities of iron standard substance AR-673[C:0.0005%±0.0001,S:0.0011±0.0002%] according to test method. The result shows that, along with the increase of sample weight of cutting shape samples, the intensity value will become higher. However, the increase of sample weight may lead to incomplete combustion, decreased liquidity and an unmelted sample. Meanwhile, the splash occurs, which may increase pollution degree of the combustion furnace, and thus may affect the measurement result. Experiment result shows, the sample weight is controlled at (0.600±0.025)g.

3 Selection of fluxing agents and their dosage

The experiment investigates the effect of different fluxing agents such as tin and tungsten granular on the detection result [9]. The result shows that, different fluxing agents have small impact on the detection result, but have certain impact on the detection process. The pollution degree of various links, such as combustion furnace and gas routes is notably increased when adding tin granular. Tungsten granular is selected as fluxing agent, for tungsten can react with oxygen at the temperature of 400℃ to generate tungsten trioxide, and its oxidation process releases huge amount of heat, which can increase the calorific capacity of hot-melting substance. The generation of tungsten trioxide is conductive to the release of carbon dioxide and sulfur dioxide, and the volatilization of tungsten trioxide increases the diffusion rate of carbon and sulfur, which makes them sufficiently oxidized and increases their liquidity. It is concluded that, tungsten granular is conductive to the detection of carbon and sulfur.

Proper fluxing agent dosage can completely melt down sample without splash. In experiment, since the carbon and sulfur contents in the sample are low, the sample weight is increased. Properly increasing the tungsten granular dose can effectively promote the fluxing, but along with the increase of tungsten granular dose, the pollution degree of gas route also increases, and the trailing effect is also getting worse. The tungsten granular dose of this study is 2. 000 g.

4. Selection of minimum analysis time and comparator level

Sample analysis time is determined by minimum analysis time and comparator level. Too long duration of analysis leads to unnecessary analysis delay, but insufficient analysis time may lose effective signal. Comparator level of analyzer is a constant 5 plus a percentage of the peak value. A large number of experiments have been conducted on analysis of ultra low carbon and sulfur contents, and the experiment results show that, since detection signal is low and the fixed constant of the instrument is relatively high. Therefore, it is of no use to set up comparator level. The sample analysis time is determined by minimum analysis time.

Figure 1 is the peak shape of minimum analysis time 30s of carbon, and figure 2 is the peak shape of minimum analysis time 35s of sulfur. By analyzing the integral peak shape, it is found that, the integral completion time of detecting ultra low carbon and sulfur contents is above 25s.

Therefore, integral time of 25-40s is chosen for a series of experiments; see the table 1 for data.

Tab. 1 Influence of the minimal analytical time on analytical results

minimal analytical time	average w/%	
	C	S
25	0.002 63	0.001 23
28	0.002 91	0.001 55
31	0.002 92	0.001 80
34	0.002 99	0.001 92
37	0.002 99	0.001 90
40	0.003 00	0.001 88

Table 1 shows that, along with the increase of minimum analysis time, the analyzed value increases, and the measured values of carbon have no significant change when the minimum analysis time is between 28s and 30s; when time exceeds 34s, the measured value of sulfur has no significant change. The minimum analysis time of carbon is 30s and the minimum analysis time of sulfur is 35s.

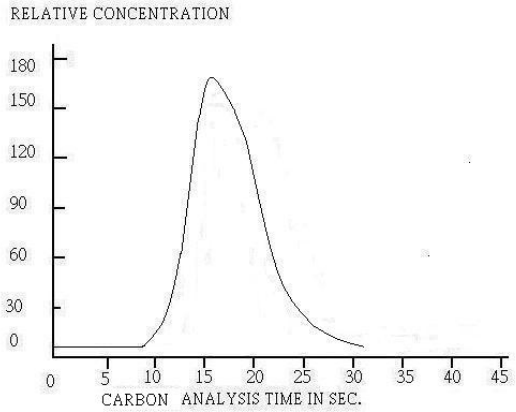

Fig. 1 Peak shape of minimum analysis time of carbon

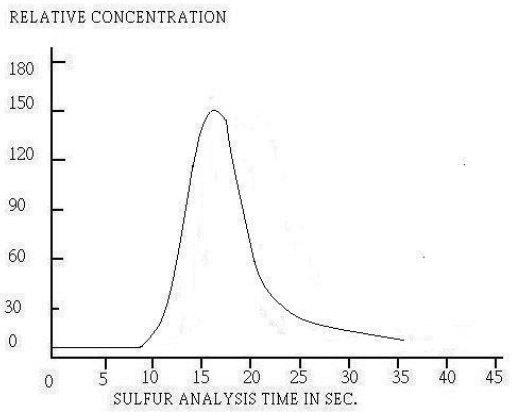

Fig. 2 Peak shape of minimum analysis time of sulfur

5. Working curve and detection limit

Take 0.600 g of standard substances to conduct the detection. Each item is measured over 3 times, and the linearity ranges of carbon and sulfur of 0.000 5%～0.003 5% and 0.000 8%～0.004 8% are calibrated respectively. Under experiment conditions, 11 times of parallel detections for the blank values are conducted. The detection limits of carbon and sulfur are calculated and they are 0.000 235% and 0.000 068 % respectively.

6. Precision test

A piece of ultra low carbon and sulfur sample is selected. Its surface is processed with milling machine, and drilling machine is used to get the drilling powder. The parallel detections of samples are conducted for 9 times with the selected analysis procedure. The average values of carbon and sulfur are calculated and they are 0. 001 82% and 0. 005 20% respectively; the relative standard deviations are 2. 9% and 3. 9% respectively.

7. Analysis of standard samples

According to the experiment method, 4 standard samples of ultra low carbon and sulfur are analyzed, and their results are illustrated in the Table 2.

Tab. 2 Analyt. results of standard samples %

samples	C		S	
	Standard value	Measured value	Standard value	Measured value
CRM No.C1a	0. 003 5	0. 003 4	0. 004 0	0. 003 9
LECO 502-402	0. 002 9	0. 002 7	0. 004 8	0. 004 7
LECO 502-348	0. 001 4	0. 001 5	0. 000 8	0. 000 9
AR-673	0. 000 5	0. 000 4	0. 001 1	0. 001 2

The experimental conditions of this detection method such as detection conditions, fluxing agents, sample weight, minimum analysis time, and comparator level are tested, and a simple,fast, accurate, and a reliable detection method for ultra low carbon and sulfur contents in steel is established by using linear calibration method. This detection method can meet the demand of production.

References

[1] ASTM E1019-11 Standard Test Methods for Determination of Carbon, Sulfur, Nitrogen, and Oxygen in Steel, Iron, Nickel, and Cobalt Alloys by Various Combustion and Fusion Techniques.

[2] ISO 15350-2000 Steel and iron - Determination of total carbon and sulfur content - Infrared absorption method after combustion in an induction furnace (routine method).

[3] KunioTakada, Tetsuya Ashino, Yukitoshi Morimoto, Hisao Yasuhara, Mayuko, Kurosaki, Kenji Abiko. Determination of trace amounts of sulfur in high-purity iron by infrared absorption after combustion: removal of sulfur blank, Materials Transactions ISSN:1345-9678, Vals. 41(2000), 1, 53-56.

[4] Zhang Xianghui, Tao Jing, Song Liwei, et al., Study on stability of analytical results for spark source atomic emission spectrometry[J]. Metallurgical Analysis, 2006,6（4）：62-65.

[5] Ma Aifang, Feng Shijuan, Zheng Lianjie et al., Online detection of ultra low carbon and sulfur contents in steel by using spark source atomic emission spectrometry method[J]. China Metallurgy, 2010,20 (9) : 30-33.

[6] L.M.Steckel. Determination of trace amounts of sulfur in graphite, UNION CARBIDE NUCLEAR COMPANY Division of Union Carbide Corporation, 1962.

[7] Jianhuan Wei, Huafeng Sun, Shengjie Yang, the cycle measurement of sulfur blank value with the CS-444 infrared ray carbon sulfur analyzer, Advanced Materials Research, Vals.399-401(2012).2173-2176.

[8] Lawrenz D. Ultra-low sulfur determination in high purity base metals and high temperature nickel base alloys, Physica Status Solidi.A, Applied Research. ISSN:0031-8965, Vals. 167(1998), 2, 373-281.

[9] Ashino T., Takada K.;Morimoto Y., Abiko K. Determination of trace amounts of sulfur in high-purity iron by infrared absorption after combustion: Selection and pre-treatment of reaction accelerators, Physica Status Solidi. A, Applied Research. 2002, 189, 1, 123-132.

Advanced Materials Research Vols. 989-994 (2014) pp 2768-2773
© (2014) Trans Tech Publications, Switzerland
doi:10.4028/www.scientific.net/AMR.989-994.2768

Research Progress of Detection Method of Sulfur in Iron-Base Alloys

Bayati, M.R., Pengyi WEI

Department of Materials Science and Engineering,

North Carolina State University, Raleigh, NC 27695, United States
email: pengyiwei5101@sina.com

Keywords: Sulfur; Iron-base alloys; Analytical method; Summary

Abstract. The paper summarizes the research progress of analytical method of sulfur element in iron-base alloys as of 2012. Major analytical methods for sulfur element in iron-base alloys include infrared absorption, photoelectric direct reading spectrometry, inductively coupled plasma atomic emission spectrometry, ion chromatography method, mass-spectrography, and electrochemical method. The paper also predicts the future trend of the analytical methods for sulfur element in iron-base alloys.

Introduction

Sulfur is a harmful element in iron-base alloys, and it can generate a “hot shortness” effect to iron-base alloys, namely, in case of thermal deformation, workpiece cracks. So it is very harmful. Surlfur may also undermine the mechanical property of iron-base alloys, and especially degrade their fatigue limit and abrasive resistance significantly, which affects the lifespan of iron-base alloys. High sulfur contents may cause such negative effects as welding difficulty and degradation of corrosion resistance.

However, addition of appropriate amount of sulfur into some iron-base alloys with specific specifications may improve the cutability, machinability, and magnetic property. The sulfur contents of free-cutting iron-base alloys can reach over 0.2%. Sulfur contents of ordinary steel are usually no more than 0. 05％; high-quality steel and tool steel no more than 0. 045％, 0. 03％; high-grade fine steel no more than 0. 02％. Solid solubility of sulfur in iron-base alloys is extremely small, but it may form various types of sulfide, such as FeS, MnS, VS, ZrS, TiS, CrS, NbS, etc. when there are large amount of manganese in iron-base alloys, the major form of its existence is MnS, and the secondary form is FeS. Sulfur is one of low content elements in iron-base alloys, and also the element that is listed as the important detection item in iron-base alloys.

The purpose of analysis of sulfur element in iron-base alloy is to meet the demand of new product development, and to improve the product quality of iron-base alloys. Therefore, control of each detection step, and reducing the facts which may cause errors during the detection of sulfur may has great significance for guiding production, developing new products of iron-base alloys, and controlling the quality of iron-base alloy products. In recent years, sulfur analyses, especially the analyses and reports of sulfur in metallurgical industry show an increasing trend. Along with the development of the research on high-performance alloy, and advancement of refining techniques, It requires to accurately detect the ultra low sulfur content in iron-base alloys(mass fraction less than 0.001％). However, limited by many factors such as blank, instrumental sensitivity, and lack of low sulfur standard samples, sulfur detection has long been the subject of the exploration for years. The paper mainly discusses the progress of the detection methods of sulfur element in iron-base alloys, including infrared absorption, photoelectric direct reading spectrometry, inductively coupled plasma atomic emission spectrometry, ion chromatography method, mass-spectrography, and electrochemical method.

Infrared Absorption Method

Currently, the most widely applied sulfur analysis of iron-base alloys in production is infrared absorption method. The experimental device for detecting surlfur in iron-base alloys by using this method is a special analyzer integrated with the units of infrared source, gas absorption pool, high temperature furnace (usually high frequency induction heating furnace), and detector. After heating and melting in high temperature, sulfur in the sample generates SO_2 in oxygen, and the contents of sulfur could be measured by using infrared absorption method. In recent years, the infrared gas analysis technique has shown a fast development, and various analyzers using high frequency induction heating combustion and infrared spectroscopy absorption principle have also been developed. Infrared absorption method has become the standard method of ASTM E1019-11[1] and ISO 15350--2000[2] to measure the sulfur in steel. Detection of sulfur by using high frequency combustion infrared absorption method usually should consider the factors of crucible (sample weight, aridity, and electromagnetic induction), fluxing agents (types, ratio, adding sequence, and adding amount) reagent for purifying gas (anhydrous magnesium perchlorate), setting of blank values, etc. Jiang Qicui [3] discussed the factors to affect the detection repeatability and accuracy, when conducting detection of trace sulfur in steel by using high frequency combustion infrared absorption method. In the experiment, a molecular sieve was connected to the gas inlet so as to remove the moisture in the gas, and an external mounting oxygen purification furnace was equipped to further eliminate the moisture in oxygen. 1.5 g of tungsten granular was added as fluxing agent each time. The result showed that the sulfur release curve was smooth, and the accuracy of the analysis result was high. Kunio Takada et al. [4] improved the conditions of detecting trace sulfur in pure iron by using infrared absorption through experiments with various conditions, and lowered and stabilized the sulfur blank values of crucible, fluxing agent, and gas. Then the sulfur blank value is deducted, so as to achieve the objective of detecting trace sulfur contents. Zhou Jun [5] detected the sulfur in cast iron by using CS-344 Infrared Carbon Sulfur Analyzer. Through experiment, the best analysis conditions for sulfur detection in cast iron, such as fluxing agents, sample weight, combustion analysis time, were identified. By applying LECO CS-444LS Carbon Sulfur Analyzer, Hong Zhian[6] conducted sulfur detection in ultra pure iron, high purity steel, and desulfurated silicon steel, and the capture method and regular approach were used for analysis. Capture method was to add a SO_2 trap with a special molecular sieve on original CS-444 Carbon Sulfur Analyzer. Molecular sieve could capture the sulfur released from the sample at normal temperature. It concentrated the contents of ultra low sulfur. When completing the capture, the molecular sieve was instantaneously heated to high temperature. By taking helium as a carrier gas, it can send the SO_2 captured in the molecular sieve to the detector for detection. The result showed that, the analysis result of capture method was relatively accurate, and this method has been used for detecting the sulfur contents of high-purity iron(mass fraction 0. 000 224%), high purity steel (mass fraction 0. 000 563%) and desulfurated silicon steel (mass fraction 0. 000 940%). Sun Ying et al.[7] also made the research on the conditions of using LECO CS-444LS Infrared Carbon Sulfur Analyzer for sulfur detection in steel（mass fraction less than $10\mu g \cdot g^{-1}$） and concluded that the system blanks of the analyzer mainly come from oxygen, laboratory environment, detector noise signal, and accumulation of tungsten dust of combustion system. Ashino T.[8] et al. made special processing to the fluxing agents used for detecting trace sulfur and achieved good effect. According to the method and procedure of uncertainty detection and evaluation of analytical test, Li Gang et al. [9], by introducing uncertainty components, evaluated the factors such as repeated measurements, standard substances, electronic scales, analytical instruments, working curve fitting, etc. According to the calculation, the composite uncertainty of sulfur was 0. 00146, effective degree of freedom 253. 0, and expanded uncertainty 0. 0024. The calculation of uncertainty provided guidance for the detection of sulfur contents in cast iron by using CS-902T Infrared Carbon Sulfur Analyzer in laboratory.

In detecting trace sulfur contents in iron, sometimes the system blank value is almost same with the analyzed value of a sample, even higher than analyzed value of a sample. Therefore, the

correct use of blank value method will directly affect the accuracy of the analytical result of trace sulfur contents in samples. The latest development of detecting blank values is The Cycle Detection of Sulfur Blank Value(CMSBV)[10] created by Jianhuan WEI et al.. Firstly, the blank value reduction and stabilization steps are carried out; then The Cycle Detection of Sulfur Blank Value (CMSBV) is employed to measure the total blank value; Finally, the measured total blank values are entered into the detector, and the detector will automatically deduct the blank values. The blank value impact analysis value can reach 0. 000 03%, and the impact of sulfur blank value to measured value of sample could be completely eliminated.

Photoelectric direct reading spectrometry method

Featured with high speed, high precision, low detection limit, high degree of automation and intelligence, and less interference, photoelectric direct reading spectrometry has become a basic means for modern metallurgical analysis. Currently, steel industry mainly applies photoelectric direct reading spectrometry for analysis of iron-base alloys, especially for analysis of the most important non-metallic element, sulfur. However, since its structure is not evenly distributed, the analysis result is not accurate. In recent years, the reports of the studies on detection of sulfur element by using photoelectric direct reading spectrometry have been mainly concentrated in the aspects of condition optimization and new method improvement. Cai Jijie et al.[11] used direct-reading spectrometer to optimize various analysis parameters, and it has achieved high precision and accuracy when making a fast analysis of the chemical components of stainless steel sheet and thin belt. The light source of modern direct-reading spectrometer usually uses spark light source with high-repetition-rate, which has high excitation frequency and high-energy pre-combustion function. By using direct reading spectrometry, Li Gang et al. [12] studied the impact of the relative intensity of standard sample to the accuracy of the result of detecting sulfur element in cast iron. The research adjusted the relative spectral line intensity of sulfur generated from two standard samples of both high and low sulfur contents, so that the system error of the standard value of the standard sample lower than the system value was eliminated, and thus the accuracy of sulfur element analysis in cast iron samples was effectively improved.

Inductively coupled plasma atomic emission spectrometry

With its advantages of high sensitivity, low detection limit, good stability, less interference, wide linear range, fast analysis, simultaneous and sequential detection of multiple elements, Inductively coupled plasma atomic emission spectrometry(ICP-AES) has become an indispensable important analytical method in the research field of metallurgical analysis. In analysis of iron-base alloys, it can detect over 50 kinds of elements, but few cases of using ICP-AES method to measure sulfur in iron-base alloys have been reported. The key for using ICP-AES method to detect sulfur is the pre-processing of samples. Sulfur exists in iron-base alloys in the forms of sulfides. When using reducing acid or hydrogen nitrate to dissolve samples, sulfur is easy to generate H_2S and to vaporize, causes serious loss of sulfur, and thus affects the detection results.

Combined with flow injection（FI）technology, Yamada[13] used ICP-AES method to detect the sulfur contents in high purity iron, which greatly improved the detection efficiency, with the detection limit of $0.3\mu g \cdot g^{-1}$. Li Jie et al. [14] studied influential factors of using ICP-AES method to detect the sulfur content in steel samples, such as pre-processing of samples to be detected, selection of analysis conditions of analyzer, matrix effect, etc. Potassium chlorate was added into oxidation sample with the mass ratio of 5:95, so that sulfur did not vaporize in the form of H_2S during pre-processing. After experiment, it is found that, iron matrix may affect the detection result. Matching between working curve with sample matrix is applied to eliminate the interference of iron matrix; finally a proper detection method of detecting sulfur in low alloy samples (mass fraction >0.001％) is identified. No only is this method easy to operate, but also solves the traceability problem of constant value analysis process of samples. Xu Jianping[15] used IRIS-Advantage ICP spectrograph to establish the method for detecting sulfur contents in steel, with

the detection limit of 0. 000 24%; He also discussed the loss of sulfur in various dissolving system and the deduction method for the blank values of low content sulfur (mass fraction<0.01%), identified Potassium chlorate--nitric acid--hydrochloric acid mixed acid dissolving sample, prevented the sulfur loss during the sample decomposition processes, and effectively improved the accuracy of the method; From the comparison, it is found that, by using standard substance to draw working curve, the accuracy of the method could reach the level of Barium sulphate gravimetric method, but the analysis speed could be improved over 10 times.

Ion chromatography

By virtue of speediness, sensitiveness, good selectivity, less interference, and simultaneous detection of multiple samples, Ion chromatography (IC), as an instrumental analysis techniques, shows a rapid development and is widely applied in analysis and detection fields. Currently, the Ion chromatography (IC) is widely applied in the detection of anions in liquid samples [16]. It is reported that the detection limit of SO_4^{2-} has reached to $ng \cdot L^{-1}$ level. However, when combustion method is applied to process steel sample, the sulfur release rate and conversion rate is not stable, with high blank value. Therefore, before applying Ion chromatography, the separation and purification with activated aluminium oxide is conducted, in order to eliminate the metal ion. By taking activated alumina column as preliminary separation column, Hu Jingyu [17] used acid soluble samples, to quickly separate the trace sulfur from matrix of steel sample and make a quantitative recovery. 2.25 $mmol \cdot L^{-1}$ of potassium hydrogen phthalate solution was used as mobile phase, and Shimadzu CLASS-LC10 ion chromatograph is applied to conduct the detection by using single column ion chromatography. By using sample pre-treatment technologies such as microwave digestion and activated alumina adsorption column separation, Lan Yuwei et al. [18] established microwave digestion--activated alumina adsorption column separation--ion chromatography method to detect trace sulfur in steel. The linear range of the method is 0. 2～100 $mg \cdot L^{-1}$, with detection limit of 0. 12 $mg \cdot L^{-1}$. The method is used to detect the sulfur contents in standard steel samples, and its relative standard deviation is 3. 3%～6. 7%. This method is suitable for the detection of a large number of samples.

Mass-spectrography

Mass-spectrography is an important instrument analytical method [19-20], but it is rarely applied in metallurgical analysis, especially the analysis of iron-base alloys. Early in 1979, Watanabe[21] has established isotopic dilution mass spectrometry (IDMS) to detect the sulfur contents in steel and high temperature alloys. Sample was processed by using nitric acid and hydrochloric acid solution samples, and then the bromine was used to oxidize the sulfur into SO_4^{2-} for detection. Finally the sulfur contents in the standard sample(mass fraction 0. 004%～0. 329%) was detected, and the relative standard deviation of measured value was less than 1.5%. Grégoire[22] made a in-depth research on the combined technology between Inductively Coupled Plasma Mass Spectrometry(ICP-MS) and electrothermal vaporization (EVT) such as micro waveguide--inductive coupling, and thus established a method for detecting sulfur element; and he further developed a detection method for trace sulfur in steel, called ETV-ICP-MS, with the detection limit of $0.05 \mu g \cdot g^{-1}$[23]. By applying Thermal ionization mass spectrometry (TI-MS) combined with isotope-dilution analysis, Kelly[24] established a method for detecting low sulfur contents in steel, with the detection range of 0. 000 6%～0. 011 9%. By using this method, Kelly successfully detected 6 kinds of standard substances of National Institute of Standards and Technology (NIST) of USA.

Electrochemical method

Analytical method of identifying substance contents by detecting the solution conductance is called conductometric analysis method. The principle of conductometric analysis method to detect

the sulfur element contents in iron-base alloys is as the following: Under high temperature of 1 250～1 350℃, iron-base alloy sample is burning in oxygen flow, and sulfur element is oxidized to generate O_2; then SO_2 is introduced into sulfur absorption pool with oxidant solution (usually potassium iodate). Then oxidation-reduction reaction occurs between SO_2 and potassium iodate, to generate SO_4^{2-}：

$$KIO_4 + SO_2 + H_2O = 2H^+ + SO_4^{2-} + KIO_3$$

The conductivity in the sulfur absorption pool changes after absorption, and its variables has functional relationship with the sulfur contents, so that the mass fraction of sulfur in steel sample could be calculated. Yang Jiahe [25] used a DFY-12 conductometer to establish a conductometric analysis method to detect the sulfur contents in alloy steel, high temperature alloys, stainless steel, ordinary steel, and spheroidal graphite cast iron. Li Yuangui et al., [26] took hydrogen peroxide as the absorbent solution of SO_2, to detect the sulfur (mass fraction 0. 021%) in carbon steel.

Electrochemical analytical methods for detecting the sulfur in iron-base alloys also include coulometry analytical method. Kurusu et al. [27] established coulometry method to detect sulfur element in iron-base alloys, with the detection range of 0. 000 07%～0. 010%. Jiang Xiumei et al. made research on the influential factors of coulometry method for detecting sulfur, and proposed corresponding optimization method.

Outlook

In recent years, research on analytical method for detecting sulfur in iron-base alloys has made significant progress. The analytical methods have shown the features of diversification, and the sensitivity and selectivity of these methods tends to be increasingly higher. In production sector, with its advantages of high accuracy, wide application range, and good stability and reliability, especially with its notable advantage in detecting ultra low sulfur contents, Infrared Absorption is the most widely applied method; by optimizing the detection conditions such as blank value measurement method, fluxing agents, oxygen purity, integral time, crucible, etc., Infrared Absorption method is further improved, and the research in this regard is also underway.

Studies on sulfur detection method were mainly focused on ICP-MS methods, on the detection of trace sulfur, and the application scope of the method is expanded by combining the new technologies such as flow injection, chromatographic separation, electrodissolution, etc. From the literature, it can be seen that, analysis of sulfur in iron-base alloys has been gradually converted from chemical methods and single element analysis to instrumental analysis and multiple elements simultaneous analysis. Looking into the future, the study on detection of sulfur contents in iron-base alloys will have breakthrough in the aspects of using fast, accurate, and highly automatic methods and instruments, as well as in realizing online detection of sulfur during the smelting process of iron-base alloys, so that the detection of sulfur in iron-base alloys will be upgraded into a higher level.

References

[1] ASTM E1019-11 Standard Test Methods for Determination of Carbon, Sulfur, Nitrogen, and Oxygen in Steel, Iron, Nickel, and Cobalt Alloys by Various Combustion and Fusion Techniques.

[2] ISO 15350-2000 Steel and iron - Determination of total carbon and sulfur content - Infrared absorption method after combustion in an induction furnace (routine method).

[3] Jiang Qicui．Metallurgical Analysis[J], 2005, 25(4)：95-96．

[4] Kunio Takada, Tetsuya Ashino, Yukitoshi Morimoto, Hisao Yasuhara, Mayuko Kurosaki and Kenji Abiko, Determination of Trace Amounts of Sulfur in High-Purity Iron by Infrared Absorption after Combustion： Removal of Sulfur Blank, Materials Transactions, JIM, Vol,41,No. 1(2000)pp. 53 to 56.

[5] Zhou Jun．Special Steel Technology[J], 2006, 14(3): 46—47.

[6]Hong Zhian. Research on Iron and Steel[J], 1997, 25(6): 36-38.

[7] Sun Ying, Song Weidi．Metallurgical Analysis[J], 2000, 20(2)：54-59．

[8] Ashino T.; Takada K.;Morimoto Y.;Abiko K. Determination of trace amounts of sulfur in high-purity iron by infrared absorption after combustion: Selection and pre-treatment of reaction accelerators, Physica Status Solidi. A, Applied Research. 2002, 189, 1, p123-132.

[9] Li Gang, Li Xusheng, Kong Yuan, et al., Shandong Metallurgy[J], 2006, 28(2)：63—65．

[10] Jianhuan Wei, Huafeng Sun, Shengjie Yang, the cycle measurement of sulfur blank value with the CS-444 infrared ray carbon sulfur analyzer, Advanced Materials Research, Vals.399-401(2012)pp2173-2176.

[11] Cai Jijie, Huang Zongping, Yang Lihui．Chinese Journal of Spectroscopy Laboratory[J], 2003, 20(2)：221—223．

[12] Li Gang, Wu Weiyan．Physical and Chemical Inspection--Chemical[J], 2008, 44(2)：125-130．

[13] YAMADA K, MCLEOD C W, KUJIRAI O, et al. J Anal Atom Spectrom[J], 1992, 7(4)：661-665．

[14] Li Jie, Zhang Suizhong．Wisco *Technology*[J], 2005, 43(3)：9-11．

[15] Xu Jianping．Metallurgical Analysis[J], 2004, 24(4)：31-33.

[16] Zhang Fang．Spectroscopy Laboratory[J], 1998, 15(2)：31-35．

[17] Hu Jingyu, Shao Guangdi, Hu Xiaoyan et al., Analytical Chemistry[J], 1999, 27(11)：1313-1316．

[18] Lan Yuwei, Lu Jianping, Zhang Zhangfa et al., Metallurgical Analysis[J], 2008, 28(1)：24-26．

[19] HOUK R S, FASSEL V A, FLESH G D, et a1．Anal Chem[J], 1980, 52(14)：2283-2289．

[20] HOUK R S Anal Chem[J], 1986, 58(1)：97A-105A

[21] WATANABE K. Talanta[J], 1979, 26(3)：251—253．

[22] Grégoire D C. J Anal Atom Spectrom[J], 1995, 10(10)：823—828．

[23] NAKA H, Grégoire D C. J Anal Atom Spectrom[J], 1996, 11(5)：359—363．

[24] KELLY W R, CHEN L T, GRAMLICH J W, et al. Analyst[J], 1990, 115(8)：1019—1024．

[25] Yang Jiahe．Journal of Sanming University[J], 1998, 15(1)：48-49．

[26] Li Yuangui, Liu Yuying, Zhang Ping．Shangdong Mechanical[J], 2000, 36(3)：37-38．

[27] KURUSU K, YAMAMOTO T．Anal Chim Acta[J], 1991, 244(1)：59-62．

[28] Jiang Xiumei, Yao Likun．North China Electric Power[J], 2007, 37(Suppl. (1)：136—137.

Advanced Materials Research Vols. 989-994 (2014) pp 2774-2777
© (2014) Trans Tech Publications, Switzerland
doi:10.4028/www.scientific.net/AMR.989-994.2774

Experimental Study on Active Vibration Control of Flexible Manipulator based on Improved PPF Algorithm

Du Fei[a] , Ma Tianbing[b]

Anhui University of Science & Technology, Huainan 232001, PR China

[a]dfmtb@163.com, [b]tbma@aust.edu.cn

Keywords: flexible manipulator; vibration control; positive position feedback; direct velocity negative feedback; piezoelectric

Abstract. The positioning accuracy and work efficiency of flexible manipulator is seriously affected by its vibration. Therefore, vibration control of single joint flexible manipulator is studied by using an improved PPF algorithm based on LabVIEW and piezoelectric technology. Firstly, the improved PPF algorithm principle is introduced. Then, the experiment process is discussed in detail. Experimental result shows that the improved PPF algorithm can effectively control the first two modal vibration of flexible manipulator. The control effect is close to 14 dB and improved nearly 4.5 dB compared with PPF algorithm.

Introduction

LQG, LQR, variable structure control, independent modal space control (IMSC), positive position feedback(PPF) and speed negative feedback (DVFB) and other methods are widely used in piezoelectric active vibration control of flexible structures. However, LQG, LQR algorithm depends on accurate mathematical model so that its application become complicated[1].Variable Structure Control usually shows high frequency fluttering in the vicinity of the slide plane origin point, so it affects its practical application. IMSC has the advantages of clear physical concept and easy to implement, but it needs multiple piezoelectric actuators in multi-modal control[2]. PPF algorithm has the advantages of simple and not sensitive to overflow, but there are dual character in the compensation damping ratio[3], contradictory effects between robustness and low order modal control modes[4].Direct velocity feedback method has the unconditional stability, but it is easy to control overflow[5].In order to overcome the shortcomings of traditional PPF algorithm, PPF and negative feedback velocity method are combined in this paper in order to further improve the system damping. Experimental results of active vibration control for piezoelectric flexible manipulator show that this method could have better stability and control effect.

Principle of PPF-DVFB algorithm[6]

The principle of PPF control based on position measurement and alignment control is that position coordinates of the controlled plant are positively fed back to the controller, then the controller voltage is acting on the actuator to suppress the vibration of the structure [3]. According to the report in the literature [6], PPF-DVFB algorithm theory containing a low pass filter is shown as Fig.1.

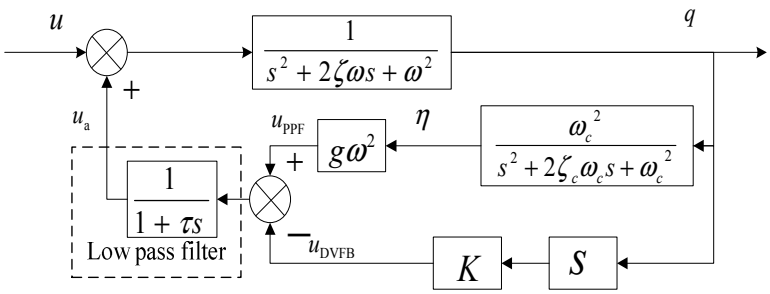

Fig.1 Principle of PPF-DVFB algorithm

In the above, q and η are the structure displacement and compensation coordinates. ζ and ζ_c are the structure and compensator damping ratio respectively. ω and ω_c are the structure and the natural frequency of the compensator. g is PPF algorithm for the feedback gain. u is the excitation signal. u_{PPF} is the input voltage of PPF controller to the actuator. u_{DVFB} is input voltage of DVFB controller to the actuator. K is feedback gain of DVFB algorithm. s is Laplace transform factor. τ is a positive number.

Determination of the structural parameters

Taking into account the vibration energy of systems focused on the previous order modal, two modal of manipulator was selected as the main control objective. When the stepping motor is rotating at a constant speed under the action of the driver, the manipulator vibration will be excited. Amplitude-frequency characteristic curve is obtained by Fourier transform for the response signal of the piezoelectric. Then, the frequency of first two modals can be observed as 15Hz and 81Hz. Then the first two modal damping ratios of system are calculated for 0.09 and 0.04 by the frequency response method as the literature[7].Finally, according to the literature [8] method, the first two modal compensation damping ratio is set to 0.4 and 0.2.

Experiment of active vibration control

Experimental system establishment. Experimental device shown as Fig.2 consists of computer, NI CRIO-9024 system, Nanjing Buddha company's HVP-300B-type amplifier, DT-2A type low pass filter, 300mm×52mm×1.5mm aluminum robotic arm, 50mm×30mm ×0.2mm piezoelectric and Changzhou Wan Tai company's 57BYG type stepper motor and its control system. The manipulator is driven by a stepper motor. Because the torsional stiffness of stepper motor is much larger than the stiffness of manipulator, boundary conditions approximate cantilever beam[3]. The position of the largest strain for first two vibration modal is the root of manipulator, so the piezoelectric ceramic (PZT) are pasted on this location symmetrically. Taking into account the continuity of stepper motor rotation and minimizing the volatility of step process, drive frequency of stepper motor is set to 128 (maximum frequency division), step angle is set to 1.8 degree, driving frequency of controller is set to 2500Hz.

A pair of piezoelectric is pasted symmetrically in the experiment, one is used as sensor and the other is used as actuator. NI 9229 AI DAQ card is used to acquire piezoelectric sensor signal. Then the signal is supplied to the CRIO system. After the signal processing of algorithm by LabVIEW software, the control voltage is sent to NI 9263 AO card, then the signal passes through a low pass filter (frequency be set to 100Hz) to the input of the power amplifier, and Finally, the output voltage of power amplifier drives the piezoelectric actuator to achieve manipulator vibration suppression.

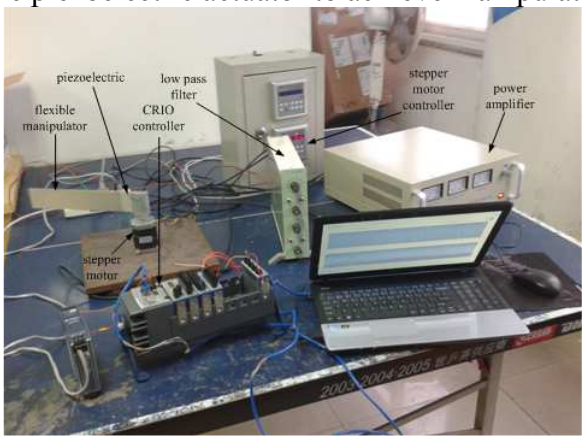

Fig.2 Experimental photo of flexible manipulator vibration control

Software Programming. The LabVIEW software based on CRIO works at scan interface mode, control cycle clock to be synchronized with the scanning engine, and sampling rate is set to 2KHz. Velocity negative feedback coefficient is set to 0.05 and PPF gain coefficient is set to 0.9 by many experiments, other modal parameters are set as described in Section 2.Considering the impact of

input and output Delay, the delay module is increased in the software program. According to calculating method in reference [9],the compensation time is 0.0005s. The output voltage limit of AO card is ± 10V, so the signal limiter is added.

Experimental results and analysis. Vibration suppression effect of flexible manipulator is shown as Fig.3 by two different control methods when it is driven at a constant speed. when the control voltage amplitude is increased to about 50V, for the first order modal, PPF-DVFB control effect reached 14 dB and PPF is 9.5 dB, meanwhile, for the second order modal, PPF-DVFB control effect is 13.7 dB and PPF is 9.3dB. It is shown that the control effect of PPF-DVFB algorithm could obviously be better than the PPF algorithm, especially in some other frequences. The main reason is that every compensator PPF controller is set up for a particular mode, so it has only effect on specific frequency, but DVFB has attenuation effects for every frequency components. There are other modal harmonic frequency in addition to modal frequency as shown in Fig.3(b), this phenomenon of harmonic vibration is caused mainly due to the stepper function to some extent, PPF algorithm effect is poor in these harmonic frequences, but PPF-DVFB method can still hold good effects.

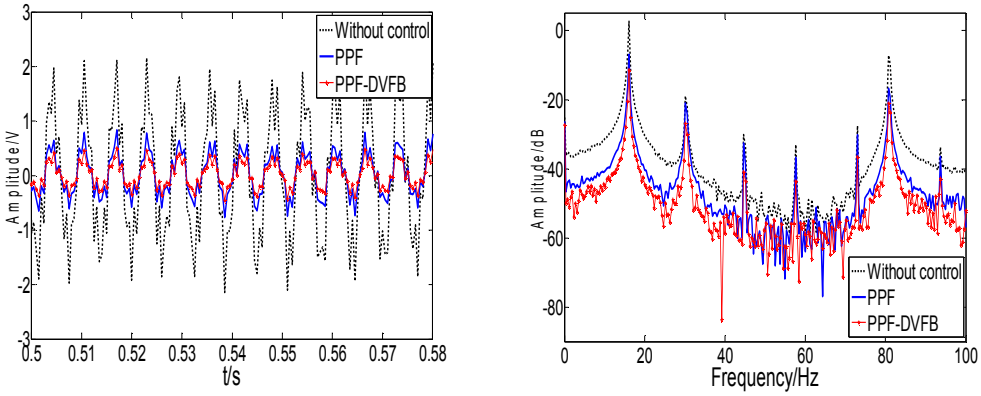

(a) Time Domain (b) Frequency Domain

Fig.3 Time domain and frequency domain response of flexible manipulator

Summary

In this paper, PPF and PPF-DVFB algorithms are used to achieve vibration control for first two modal of flexible manipulator. Experimental results show that PPF-DVFB algorithm either in modal frequency or in other modal harmonic frequencies has better control effect compared with the traditional PPF algorithm, Which can further enhance the working stability of the flexible manipulator.

Acknowledgement

This research is supported by the National Natural Science Foundation of China (No. 51305003) and the key Foundation of Anhui province of China for Outstanding
Young Teachers in University (No. 2012SQRL045ZD).

References

[1] Wang Zongli, Lin Qirong, Liu Zhengxing: State Dependent LQR Vibration Control for Piezoelectric Intelligent Beam [J]. Journal of Shanghai Jiaotong University, 2001,35(4):503-508.

[2] Qiu Zhicheng. Study on Variable Structure Vibration Control for Flexible Manipulator [J]. Journal of Dynamics and Control, 2007,5(1):62-67.

[3] QIU Zhicheng ,XIE Cunxi ,ZHANG Honghua ,WU Hong-xin. Active Vibration Control for Flexible Piezoelectric Manipulator [J]. Robot, 2004,26(1):45-48.

[4] Song G,Schmidt S P,Agrawal B N.Active Vibration Suppression of a Flexible Structure Using Smart Materialand a Modular Control Patch[J].Proceedings of the Institution of Mechanical Engineers, Part G,2000, 214(4):217-229.

[5] Wang Bo, Improvement Methods for Vibration Control of Piezoelectric Intelligent Structures[D].Chong Qing:Chongqing University,2004.
[6] Ma Tianbing,Qiu Jinhao, Ji Hongli,Yuan Ming.Local Strain Compensation and Improved PPF Algorithm for Vibration Control[J].Journal of South China University of Technology(Natural Scienca Edition),2012,40(5):41-45.
[7] Xiong Shibo,Huang Changyi. Mechanical engineering testing technology[M].Bei jing:CHINA MACHINE PRESS,2009.
[8] Rew KeunHo,Han JAEHung,Lee In.Multi-modal vibration control using adaptive positive position feedback[J]. Journal of Intelligent Material Systems and Structures,2002,13(1):13-22
[9] Wu Haoyi.Research of Active Control Method for Piezo-smart Cantilever Beam[D].Da Lian:Dalian University of Technology,2012.

Advanced Materials Research Vols. 989-994 (2014) pp 2778-2781
© (2014) Trans Tech Publications, Switzerland
doi:10.4028/www.scientific.net/AMR.989-994.2778

The Wind and Light Power Supply System Controller in the Mobile Base Stations

Hong Ma

Nanjing Institute of Industry Technology,Nanjing China

mh_purple@163.com

Keywords: wind,light, controller, power supply

Abstract: With the rapid development of economy, the consumption of energy increasing year by year, the conventional energy is facing increasingly draining.The wind and light power supply system controller in the mobile base stations is a kind of power supply management system,used the wind and light, which have the biggest and the most development potential renewable energy and new energy technology at present.That especially suitable for mobile communication base station,and remote sensing, remote control base station power supply and operation environment. The controller can reduce run maintenance cost, improving the quality of communication and system management level,and the efficiency of the whole.

I INTRODUCTION

With the rapid development of economy, the consumption of energy increasing year by year, the conventional energy is facing increasingly draining,urgently needs a new type of clean renewable energy. The wind and light, which have the biggest and the most development potential renewable energy and new energy technology at present,and they are an inexhaustible renewable energy.

In recent years, with the rapid development of mobile telecommunication in China, network scale has become the first status in the world, the communications industry has become a pillar industry to promote the development of Chinese economy. As the network scale expands unceasingly, the communications equipment quantity and energy consumption are increasing. Effective energy saving and emission reduction measures not only is contributing strength for the country, helping reduce operating costs for enterprises, improving operational efficiency,and enhancing competitiveness in the whole business competition environment.

According to the characteristics of the power supply technology used the wind and light, energy management technology is the actual researched and developed of the design,i.e.,improving energy efficiency and economy of power supply system. It is easy to causing the communication interrupt such as local area communication network,once the failure occured in the base station.The design can be implemented for remoting centralized monitoring for the base station power and environmental parameters, for grasping the real-time system information and failure information,particularly suitable for unattended base stations.

II POWER SUPPLY TECHNOLOGY USED THE WIND AND LIGHT

Due to the attention of the environment and energy, all countries carried out researching and developing of new energy. Europe is in the leading level in this field, especially in wind power and solar power technology has made a lot of achievement. Europe mainly has the following research in the field of new energy,such as large grid electric field and related technology. The difficulties of domestic research in the field of new energy is lack of funds,combined with the actual demand, mainly research focused on control algorithm of wind power and solar power and the small new energy system.The research on small power supply system used the wind and light are brought to the attention of the people,and limited to research aspect including system composition and control, the selection of equipment and system simulation, etc in the domestic.

Chinese renewable energy storage is very rich,especially in the solar and wind power. Wind and solar power has natural complementarity,as strong sunlight during the day, the solar energy is

rich, wind energy abundant in the evening, and wind and solar power also has the very good complementary effect in the summer and winter.The characteristics of complementary can be used to a stable power supply. As an independent power supply system, has considerable advantages,used in outdoor lighting. It not only achieving the purpose of energy saving,but also simplifing installation procedures, convenienting application and maintenance,because do not need to connect the grid and solve the problem of circuit laying, saving investment of equipment.

Power supply used the wind and light combined with the advantages of solar photovoltaic power and wind power generation system, solving the poor power supply problem by solar photovoltaic power at night or rainy weather, and improving the continuity, stability,reliability of the power supply system. The system mainly is suitable for the regions where wind energy, solar energy resources are relatively abundant.

The main characteristics of power supply technology used the wind and light as follows:

(1) using the complementary characteristics of wind energy and solar energy, and making full use of natural resources, realizing the power output day and night, can obtain relatively stable total output, improving the reliability of the power supply;

(2) the short construction period, installed flexible;

(3) Compare the independent wind power and photovoltaic power system, under the condition of the same power supply, can greatly reduce the capacity of the energy storage battery;

(4) Through the reasonable design and matching of power system, the power supply by the wind/light system can be implemented, can obtain good social and economic benefits, realizing very good energy saving effect.

III TECHNICAL DESIGN

The working environment of mobile communication base station power supply is more and more poor,making the power supply must be reliable operation under various temperature and humidity conditions,and withstanding the erosion of dust, insect and lightning. These requirements make the design of the key factors is rectifier equipment,standby power supply and power distribution circuit in environmental protection,safety,installation and maintenance and other aspects.

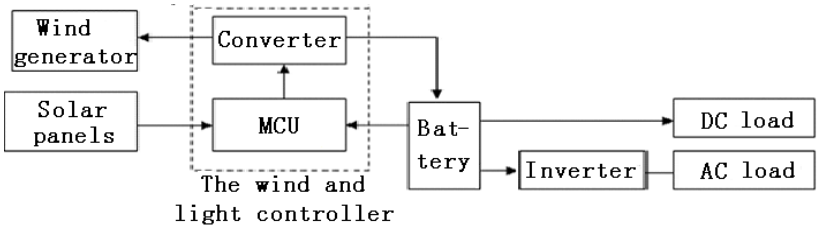

Figure 1 Structure diagram of the wind and light power supply system controller in the mobile base stations

The design plan of the wind and light power supply system controller is illustrate in figure 1, including wind generator, solar panels, the wind and light controller,battery and inverter. Control chip using PIC16F877A MCU, which is responsible for the control of the whole system,and is the core part.The peripheral circuit including voltage and current sampling circuit, power driving circuit, protect circuit, communication circuit, auxiliary power supply circuit, etc.

1 The main circuit

Main circuit is made up of two independent of buck circuit which parallel on the output side, one is photovoltaic power generation system, the other one is wind power system. As shown in figure 2.

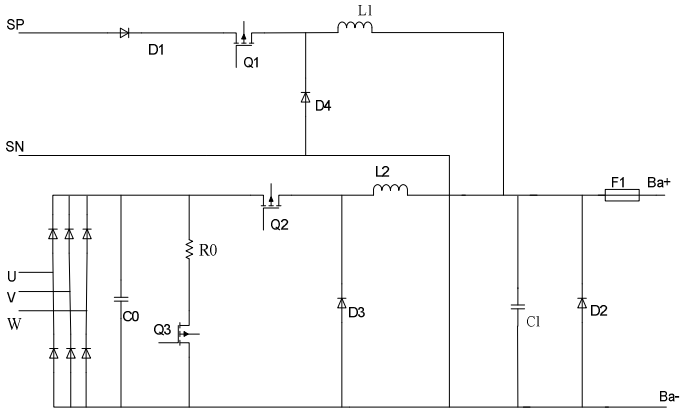

Figure 2 Hardware main circuit structure

(1) photovoltaic part

Solar photovoltaic panels is another Generate electricity part.It is responsible for converting sunlight into electricity.

maximum power point voltage of photovoltaic panels is 17.6 V, open circuit voltage is 21.6 V. Photovoltaic parts used four solar photovoltaic batteries, output voltage range is 60 ~ 90 V.

(2) Wind power generation part

The wind power generation part is the one of the parts of the wind and light power supply system controller in the mobile base stations, consisting of the wind turbine,transmission mechanism and generator, etc.

The role of generator in wind power generation systems is converting mechanical energy into electrical energy, that is converting wind energy into mechanical energy, transmission mechanism transfer mechanical energy, finally converting mechanical energy into electrical energy. Generator direct impact the performance, the efficiency and quality of power supply of the conversion process. Therefore, It is mportant task for wind power generation part that selecting high reliability, high efficiency, good control and power supply performance.The types of generator of the small wind and light power supply system has the following kinds,typically three-phase permanent magnet synchronous generator, DC generator, electromagnetic alternator, claw pole generator, reluctance generator and induction generator, etc.

2 Battery

The battery is the important auxiliary equipment of the wind and light power supply system controller in the mobile base stations. Three functions of the battery in the power generation systems such as: The first is the energy storage,as the natural wind and sunshine is unstable, the battery can store extra electricity after supply load under the wind, sunny conditions, in the case of poor wind, sunshine,only can output power to the load. Second is stable voltage, the speed of the wind decide rotational speed and output voltage of wind power generator,as the change of natural wind is great,strong randomicity,making voltage floating range is very large,through battery adjusting, power supply can be stabilized;Third is the wind and light power supply, wind power and photovoltaic power are two independent power system,and power strength of them some times are a big difference,thus using the battery can combine the two electricity, realizing complementary.The rationality of battery capacity configuration will impact technical and economic indicators of the small wind and light power supply, if choose the small capacity, the excess electricity system sends out will not be stored, and if choose the big capacity,one will increase investment,two will make the battery may be long in the condition of insufficient charging, directly affecting the efficiency and life of use. Commonly used batteries mainly such as lead-acid batteries, alkaline nickel battery and iron nickel battery.The lead-acid battery has advantages such as low cost, reliable performance, high safety, and the technical progressing and improving.

Over charge and discharge of battery will affect its life, when the battery discharge serious, the voltage is too low, also can damage the battery, thus the design using the method of disconnect the discharge circuit through the relay circuit,and opening the discharge loop again when voltage is

back. In order to keep the system stable work,the design also uses discharge voltage hysteresis control,preventing the battery excessive discharge.

IV. CONCLUSION

This design is based on the application of new energy technology, the research conclusion can adapt to the rapid development of mobile communication field, the research achievements in energy conservation and environmental protection,the new generation of information technology has extensive application value,and achievements diffusion has the good economic and social benefits.The design can remote check the status of the wind and light, and can automatic transformation according to the set of parameters, checking the battery state of the residual capacity and discharge protection mode of battery voltage. The design with features such as preventing the surge, preventing short circuit, preventing reverse, preventing overload, etc,and controlling fan braking through automatic and manual mode, temperature compensation, and the temperature probe automatic recognition,thus this design can avoid to cause too much compensation.

References

[1]Hongxing Y,L Lin,Z.Wei. A novel optimization sizing model for hybrid solar-wind power generation system .Solar Energy, 2007, 81 :p.76-84 .
[2]Chedid R. Unit sizing and control of hybrid wind-solar power system .IEEE Transactions on Energy Conversion, 1997, 12(1) :79-85 .
[3]ELHADIDY M A,SHAAHID S M. Parametric Study of Hybrid (Wind+Solar+Diesel) Power Generating Systems[J] .Renewable Energy, 2000, (21) :129-139 .
[4]Yang J M,Cheng K W E,Wu J,etal. The Study of the Energy Management System Based-On Fuzzy Control for Distributed Hybrid Wind-Solar Power System[J].2004,
:113-117 .
[5]Tae-Yeop Kim,Ho-Gyun Ahn,Seung Kyu Park,et al. A Novel Maximum Power Point Tracking Control for Photovoltaic Power System under Rapidly Changing Solar Radiation .IEEE International Symposium on Industrial Electronics,2001.Proceedings.ISIE. 2001, (2) :1011-1014 .

Advanced Materials Research Vols. 989-994 (2014) pp 2782-2786
© (2014) Trans Tech Publications, Switzerland
doi:10.4028/www.scientific.net/AMR.989-994.2782

Study on dynamic mechanism of LOGINK service innovation based on system dynamics

LingliLI[1, a], Shouwen JI[2,b], Linshuai Wang
[1]Center of Cooperative Innovation for Beijing Metropolitan Transportation, China
[2]Center of Cooperative Innovation for Beijing Metropolitan Transportation, China
[3]Center of Cooperative Innovation for Beijing Metropolitan Transportation, China
[a]lilinglijiayou@gmail.com,[b]jishouwen@126.com, [c]11120898@bjtu.edu.cn
[1] Corresponding author.Address: Room 0822, Building 8, Student Apartment, NO.18, Jiaotong university east road, Haidian district, Beijing, China.Tel.:+8615210577465.
Email adress: lilinglijiayou@gmail.com

Keywords: Service innovation; Dynamic mechanism; LOGINK; System dynamics; In-tree

Abstract. According to system dynamics and in-tree structure, we choose National Transport & Logistics Public Information Platform (LOGINK) as a research object. Then, considering new service concept, new customer interface and new delivery system, its dynamic mechanism of service innovation is studied. Finally, we establish the corresponding dynamic relationship model and deduce dynamic relationship equation.

Introduction

LOGINK stands for National Transport & Logistics Public Information Platform, which is mainly founded by China's Ministry of Transport. Having a nationwide and internationally switching network exchanging basic logistics information and portal web site, LOGINK achieves reliable, safe, efficient and smooth information exchange between related logistics information system and platform and unifies information exchange standards, which effectively promotes the ex-change of information and resource sharing between each link of logistics industry chain [1].

The generation of LOGINK service innovation is a complicated course, which can be analyzed through system dynamics and in-tree structure theory. Based on opinions that structure determines behavior, system dynamics establish models from the micro structure of internal system and analyze internal relations between dynamic behaviors and system structure and function using the method of numerical simulation in order to find a solution [2]. According to the core idea of system dynamics, LOGINK service innovation depends on the circulation of “flow” in system internals, and the flows forms feedback loops to connect key variables and other variables, which presents the system structure whose each other and mutually restrict each other [3].

Mechanism research of factors influencing LOGINK service innovation based on in-tree structure theory

Service concept monitor subsystem. The state variables of LOGINK service concept include basic data exchange, public information services and logistics software.

Basic data exchange can unifies information exchange standards between different kinds of logistics public information platform to avoid isolated island of information, low efficiency of information transfer and high cost.

Public information services can solve these problems such as logistics public information serviceresources in national level are scattered, the demand of logisticsinformation service can’t be met and so on.

The development of the logistics common software can avoid repeated development and construction ofsoftware, meanwhile can mesh with the standardization.

The in-tree structure of service concept is shown as Figure 1.

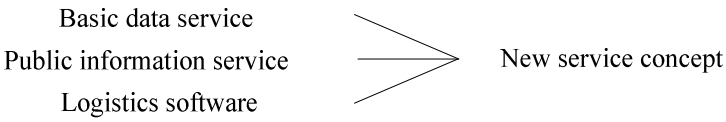

Fig.1 The in-tree structure of service concept

The in-tree structure of basic dataservice is shown as Figure 2.

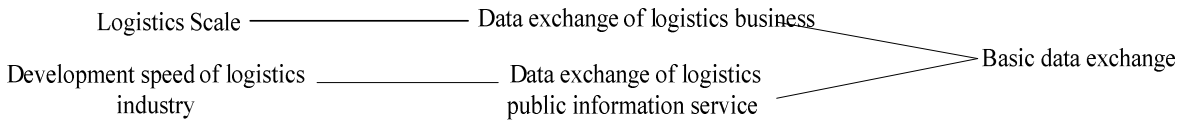

Fig.2 The in-tree structure of basic data service

The in-tree structure of public information service is shown as Figure 3.

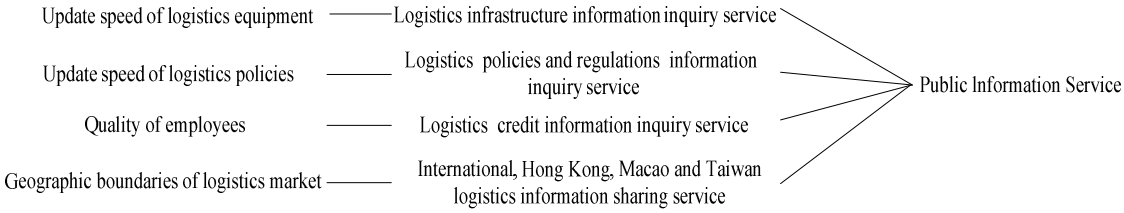

Fig.3 The in-tree structure of public information service

The in-tree structure of logistics software is shown as Figure 4.

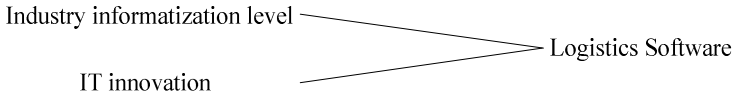

Fig.4 The in-tree structure of logistics software

Based on the above analysis, the dynamic relationship model of service concept can be shown in Figure 5.

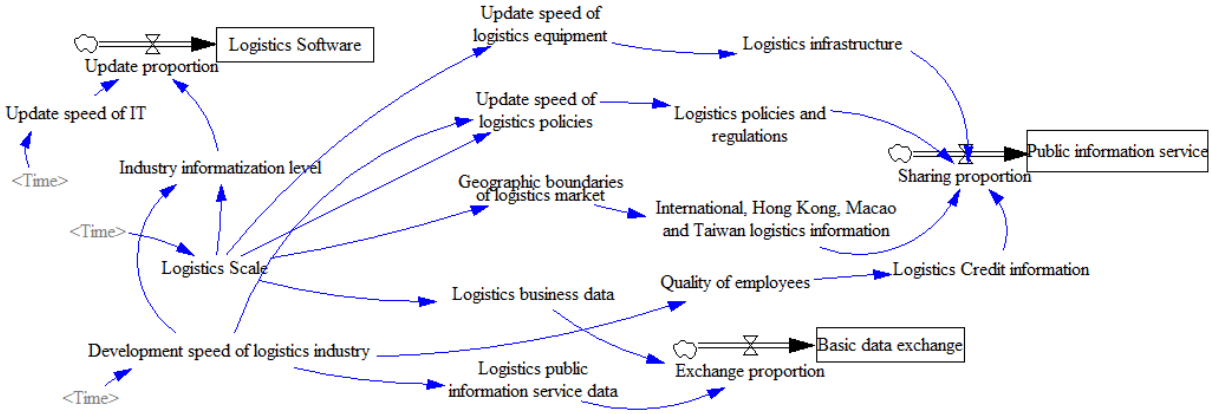

Fig.5 Dynamic relationship model of service concept

According to the dynamic relationship model of service concept, the dynamic relationship equations are listed as follows.

$$LSOFT=UP*IT+UP*IIL \quad (1)$$

$$TPIS=SR*（LII+LIPR+IHMT+LCI）= SR*（LERS+LPUS+LMGB+SQ） \quad (2)$$

$$BDE=ER*（LBD+LPISD）= ER*（LS+LIDP） \quad (3)$$

Customer interfacemonitor subsystem. The characteristics of LOGINKservice interface are public good, open and shared. The customer interface includes access interface and user interface. The in-tree structure of customer interface is shown as Figure 6.

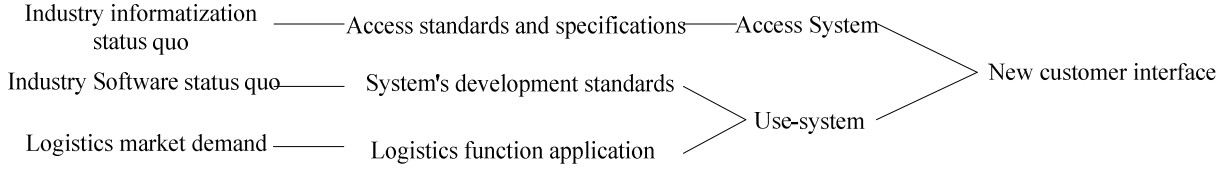

Fig.6 In-tree structure of customer interface

Based on the abovestructure, the dynamic relationship model of customer interface can be shown in Figure 7.

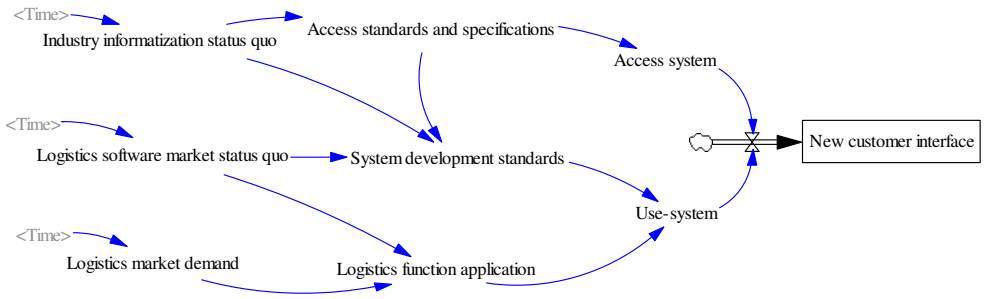

Fig.7 Dynamic relationship model of customer interface

According to the dynamic relationship model of customer interface, the dynamic relationship equation is listed as follows.

$$NCI=ITTS+UTS=ASS+SDS+LFA=IISQ+LSMSQ+LMD \quad (4)$$

Service delivery monitor system. The state variables concerned by service delivery monitor system of LOGINK are technical expert group, management center and joint conferencesystem.

The in-tree structure of technical expert group is shown in Figure 8.

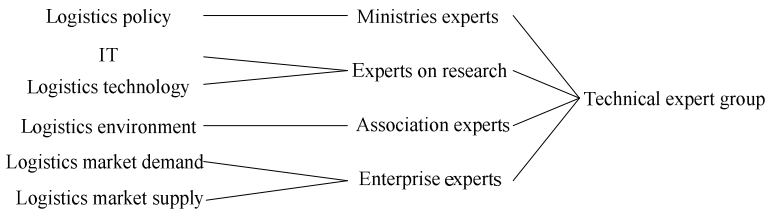

Fig.8 In-tree structure of technical expert group

The in-tree structure of management center is shown in Figure 9.

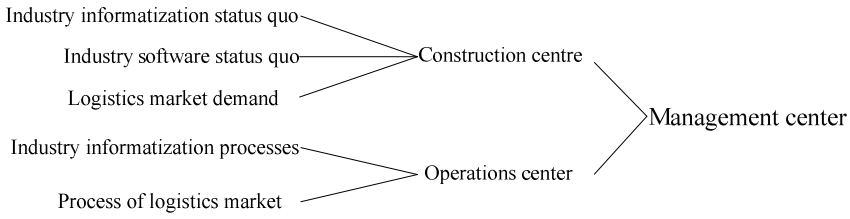

Fig.9 In-tree structure of management center

The in-tree structure of joint conferencesystem is shown in Figure 10.

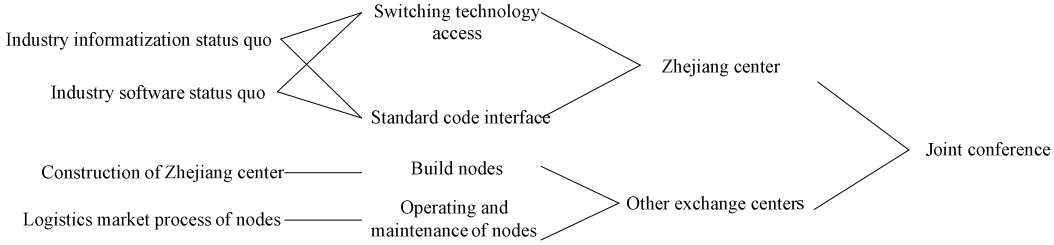

Fig.10 In-tree structure of joint conference system

Based on the abovestructure, the dynamic relationship model of service delivery monitor system can be shown in Figure 11.

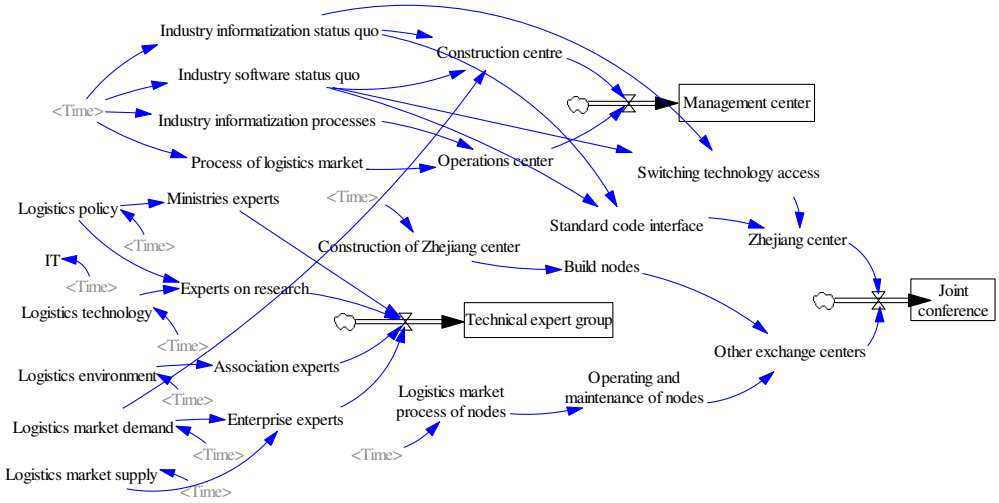

Fig.11 Dynamic relationship model of service delivery monitor system

According to the dynamic relationship model of service delivery monitor system, the dynamic relationship equations are listed as follows.

MC=TCC+OC=IISQ+SISQ+LMD+IIP+PLM (5)

TJCS=ZJC+OEC=STA+SCI+TNC+NOM= 2 *（IISQ+SISQ）+ZJCSC+NLMP (6)

TETG=GE+SE+AE+EE=LP+IT+LT+LE+LMD+LMS (7)

Mechanism research of factors influencing LOGINK service innovation

Combining above analysis about service concept, customer interface and service delivery system, we can get the dynamic relationship model of LOGINKserviceinnovation which is shown in Figure 12.

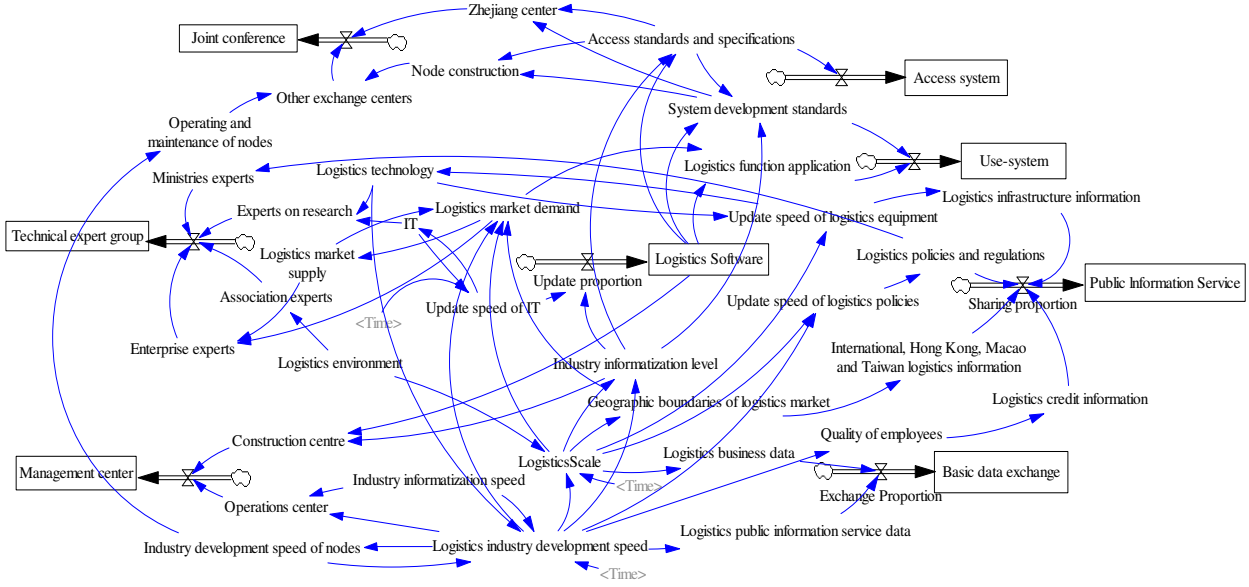

Fig.12 Dynamic relationship model of LOGINK service innovation

According to the dynamic relationship model, the dynamic relationship equations are listed as follows.

JC=OEC+ZJC=HRM+HC+IS+SDS (8)

ETP=MCE+SRE+AE+EE=LPRI+(IT+LT)+LE+(LMD+LMS) (9)

MC=CS+RMS=(IIL+LS)+(IIV+LID) (10)

LS=IIL+ITUV=(LIDV+LS)+IT (11)

BDE=LBD+LPISD=LS+LIDV (12)

CIS=LBSI+LPRI+IGATI+LCI=LEUV+LPUV+LMLB+SQ=(LT+LS)+(LS+LIDV)+LS+LIDV (13)

NUS=SDS+LFA=(IS+IIL)+2LS+LMD (14)

NIS=IS=LS+IIL (15)

Summary

Serviceinnovation of regional logistics information platforms can be generated by service concept, customer interface and service delivery system. Factors influencing LOGINKserviceinnovation include economic environment, policy environment, industry environment, platform strategy, IT, customer, developer, public sector and so on, which together push forward the generation of LOGINKserviceinnovation.

Foundation item: A research subject of state science and technology support program (2014BAH24F01)

References

[1] Wijnberg N M, Gemser G. Adding value to innovation: Impressionism and the transformation of the selection system in visual arts Vol. Organization Science 11(2000),p.323-329.

[2] Information on http://www.logink.org.

[3]ROBERTS E B, in: Managerial Applications of system Dynamics/ Productive Press Publishing, Cambridge, Mass(1978),in press.

Advanced Materials Research Vols. 989-994 (2014) pp 2787-2790
© (2014) Trans Tech Publications, Switzerland
doi:10.4028/www.scientific.net/AMR.989-994.2787

Numerical Simulation of the Kinetic Energy Projectile Deflected by Targets Moving Along Transverse Direction

Jun CHEN[1,a], Xiaojun YE[2,b]

[1]New Star Institute of Applied Technology, Hefei, 230031, China

[2] Nanchang Military Academy, Jiangxi, 310103, China

[a]email:358759332@qq.com, [b]email:tykfye@163.com

Keywords: numerical simulation; the kinetic energy projectile; moving targets transverse direction

Abstract: When the kinetic energy projectile into concrete target movement, angle of attack can affect the penetration process of ballistic performance, resulting deflection effect, thus affecting the penetration depth. For the analysis of kinetic energy projectile penetrating the lateral movement of the target deflection model, using the finite element simulation software for lateral movement of the target missile penetrates the process of numerical simulation. The results showed that: rigid lateral movement of the target missile and projectile kinetic energy projectile velocity has some deflection effect. Playing the role of the kinetic energy of the lateral movement of the target, the missile body yaw angular velocity increases and then decreases after the first, but not so obvious kinetic energy projectile yaw.

1 Introduction

When the kinetic energy projectile into concrete target movement , angle of attack can affect the penetration process of ballistic performance , resulting deflection effect , thus affecting the penetration depth . When the target projectile penetrates the lateral movement , so playing experience deflection , thus affecting the penetration ability of elastomers .

For the analysis of kinetic energy projectile penetrating deflection lateral movement of the target model , using the finite element simulation software ANSYS / LS-DYNA projectile penetrates the lateral movement of the target process simulation .

2 Projectile translational cause deflection model analysis

When the target projectile penetrates the lateral movement , mainly by two forces . First, because the target has a lateral movement after contact with projectile and target collision , playing the role of lateral impact by the pulling force , the role will generate kinetic energy projectile centroid of torque , the torque acting on the kinetic energy of the projectile , resulting in the occurrence of kinetic Bouncing body deflection ; second , due to the impact force acting on the projectile , playing experience to get lateral velocity , causing its speed direction deflected . As the high-speed impact of stress and strain in the process of the law is more complicated, so here doing the following assumptions: (1) the kinetic energy projectile is rigid ; (2) friction and gravity is negligible; (3) of the kinetic energy of the projectile motion of the target force is always perpendicular the axis of the rod , and the same size .

Kinetic energy projectile on target time after perforation force shown in Figure 1 (a). Target of the role of sport at the point of impact pressure . According to Theorem translational force , equivalent to the centroid of the lever , urging dipole moment , the equivalent force in Fig 1 (b) above.

Obtained by the theory of theoretical mechanics

$$M = Fd \tag{1}$$

$$J\frac{d^2\varphi}{dt^2} = M \tag{2}$$

Where: kinetic energy projectile equivalent vertical centroid distance between the front line of action; moment of inertia of the rod to confront the heart; deflection angle for the projectile.

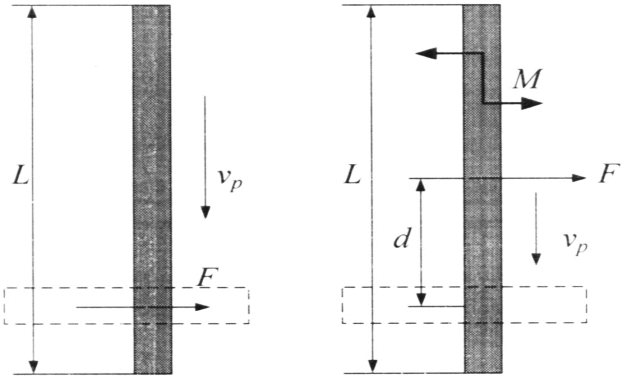

(A) prior to the equivalent force (b) the equivalent force

Fig.1 Kinetic energy projectile on single target time by trying

Assuming no change with time is a predetermined value, then

$$\omega_0 = \frac{d\varphi}{dt} = \frac{12F}{m_p L^2}\left(\frac{Lt}{2} - \frac{v_p t^2}{2}\right) \tag{3}$$

$$\varphi_0 = \frac{12F}{m_p L^2}\left(\frac{Lt^2}{2} - \frac{v_p t^3}{6}\right) \tag{4}$$

Where: piercing process and were shot in the body and yaw angular velocity deflection angle; into kinetic energy projectile length; was piercing time; mass elastomers; was projectile speed.

Were substituted into the formula (3), (4) have

$$\omega_1 = 0 \tag{5}$$

$$\varphi_1 = \frac{FL}{m_p v_p^{\ 2}} \tag{6}$$

Where: deflection angle and yaw angular velocity and were passing through the movement of the target projectile after; for the projectile through the movement of the target time.

F is a constant amount in the assumptions, there is a constant acceleration in the vertical axis of the rod kinetic energy projectile impact in the sports board. When the kinetic energy of the projectile through the tail, the transverse velocity kinetic energy of the projectile is

$$v_x = \frac{FL}{m_p v_p} \tag{7}$$

Assuming the initial kinetic energy projectile velocity constant direction, the direction of the final projectile velocity change the angle of the tangent is

$$\tan\phi = \frac{v_x}{v_p} = \frac{FL}{m_p v_p^2} \tag{8}$$

From Equation (6) shows that, $\tan\phi \approx \varphi_1$, while φ_1 and $\tan\phi$ are very small, and therefore $\phi \approx \varphi_1$.

Thus, the kinetic energy of the projectile into the lateral movement of plates in the process, not only the attitude of the deflection occurs, the direction and speed of change accordingly, both changing the angle of roughly the same, so the final kinetic energy of the projectile velocity direction remains its axial direction, does not produce significant yaw angle.

3 Simulation Study

3.1 model and boundary conditions. The use of ANSYS / LS-DYNA software diameter 10 mm, length to diameter ratio of 12, the speed of 1 500 m / s tungsten alloy vertical kinetic energy projectile penetrating single 5 mm, speed was 100 m / s and 200 m / s for lateral movement of the steel target for numerical calculations. In the theoretical model derivation process, the kinetic energy of the projectile is assumed to be rigid, so the choice of where the kinetic energy projectile rigid material model.

3.2 Process Analysis. projectile deflection due to numerical parameters of each node can only get the objects, the results can not be obtained directly kinetic energy projectile deflection, and the projectile deflection angle is very small, so the use of projectile head and tail nodes lateral distance and relative transverse velocity to the amount of deflection of the elastomer represents the deflection angular velocity. Numerical results of the processing to obtain a kinetic warhead craniocaudal and lateral end of the lateral distance relative speed versus time curve shown in Figure 2, Figure 3.

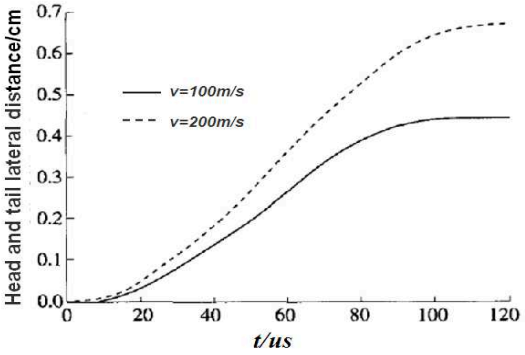

Fig.2 Projectile head and tail lateral distance versus time in Figure

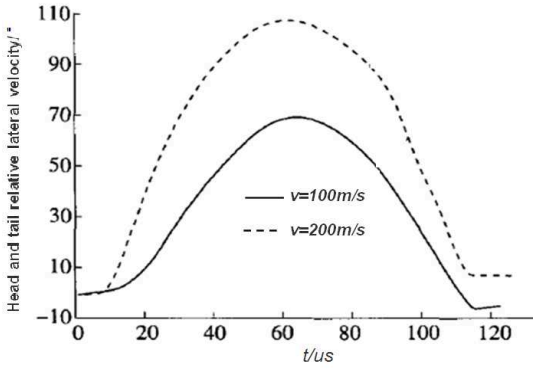

Fig.3 Projectile end to end relationship lateral velocity and time

In Figure 2 and Figure 3 , the target speed of 200 m / s at the top of the curve of the target speed 100 m / s curve can deduce the target speed of 200 m / s the kinetic energy of the projectile impact force is large, so that although a target of lateral forces kinetic energy projectile can be considered approximately constant , but its size and the speed of movement on the target .

Figure 3 represents the deflection trends indirect angular velocity kinetic energy projectile . Can be seen from Figure 3, the yaw angular velocity projectile is then decreased for . This is because the target for the kinetic energy projectile impact on the torque rod centroid positive work on the kinetic energy of the projectile to do first , after doing negative work . 60 is about half the kinetic energy of the projectile through the movement of the target projectile long time , so the two curves in the left and right portions of the approximate time symmetrical shape. Finally, the yaw angular velocity is reduced to about 0 rad / s, the deflection stopped the maximum deflection angle .

3.3 Effect of transverse velocity of the projectile deflection angle . Target effects of kinetic energy projectile kinetic energy projectile deflection not only , but also to obtain a lateral velocity kinetic energy projectile , causing it to deflect the direction of the actual speed . Speed equal to the tangent of the deflection angle of the transverse velocity of the longitudinal velocity ratio. Because time is proportional to the transverse velocity , vertical velocity change is small relative to the longitudinal velocity transverse velocity is small, so the speed of the deflection angle and time was approximately proportional relationship . Deal with the numerical results obtained two kinds of cases, and its speed projectile final deflection angle , shown in Figure 4 .

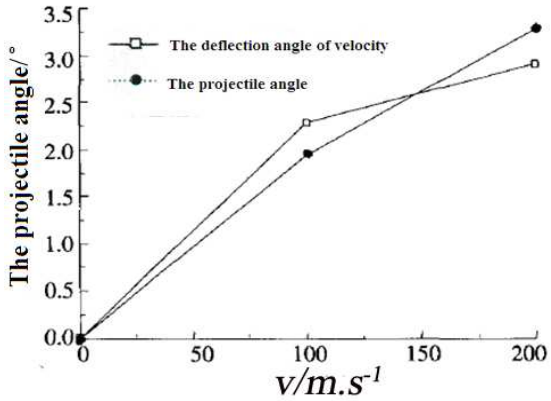

Fig.4 Bouncing body kinetic energy and speed of the deflection angle of the relationship between the target speed

As can be seen from Figure 4, when the certain conditions, the deflection angle of the final elastomer and an elastomer is very close to the speed of the deflection angle, which is more consistent with the deflection model; when the speed is increased, the deflection angle increases, but the two are not directly proportional relationships. Yaw angle difference between the two kinds is the deflection angle of the projectile, since both the size quite close, so very small projectile yaw angle, yaw obvious.

4 Summary

(1) rigid lateral movement of the target projectile and projectile kinetic energy projectile velocity has some deflection effect.

(2) the impact of the movement of the target model are the kinetic energy projectile deflection and numerical calculation process is basically the same, indicating that the theoretical model and numerical calculation with good consistency.

(3) under the action of kinetic energy projectile lateral movement of the target, the projectile body yaw angular velocity after the first increases and then decreases, and finally to 0 rad / s, this time projectile reaches its maximum deflection angle.

(4) The final projectile deflection angle and deflection angle is very close to the projectile velocity, projectile yaw angle is very small, indicating that lateral movement of the target can not make the obvious kinetic projectile yaw.

References

[1] Dai Qb, Yan L-h. Analysis on the Plugging Model of Concrete Targets struck by Rigid Projectiles, J. Journal of Ballistics. 19(2007)51-54.

[2] Wang M.y; ZHENG D. The scaling problems of penetration and perforation for projectile into concrete media, J. Explosion and Shock Waves．24(2004) 108-114.

[3] LSTC. LS DYNA keyword user's manual, version 970. Califomia, USA: LSTC, 2003.

[4] J Glucklich． Fracture of plain concrete．Journal of the Engineering Mechanics Division, ASCE 1963，89 (6) : 127— 138．

[5] Holmquist T J，Johnson G R，Cook W H．A computation alconstitutive model for concrete subjected to large strains，high strain rates，and high pressure，The 14th Inter-national Symposium on Ballistics，1993: 519 — 600．

Advanced Materials Research Vols. 989-994 (2014) pp 2791-2795
© (2014) Trans Tech Publications, Switzerland
doi:10.4028/www.scientific.net/AMR.989-994.2791

City sludge's differential scanning calorimetry analysis

Lu Yang[1, a] Shun Hong Lin[2, b]

[1] College of Mechanical and Dynamic Engineering, Chongqing University of Science and Technology, Chongqing 401331, China

[2] College of Mechanical and Dynamic Engineering, Chongqing University of Science and Technology, Chongqing 401331, China

[a]email:yyanglu36@163.com [b]email:Dim001@163.com

Keywords: DSC; power difference, municipal sewage sludge

Abstract. The differential scanning calorimetry is a thermal analysis. Under program controlled temperature, measure and input to the relationship between the the sample and the reference's power difference and temperature. The curve which the differential scanning calorimetry recorded called DSC curve. DSC curve in the sample's rate of endothermic or exothermic as ordinate and in temperature or time as abscissa, which can determine a variety of thermodynamic and dynamics parameters, such as specific heat capacity, the reaction heat, thermal changes, phase diagram, reaction rate, rate of crystallization, polymer crystallinity, purity of a sample,etc. The method has a wide temperature range -175 ~ 725 ℃, high resolution, less samples . This topic utilizes differential scanning calorimetry and had a pyrolysis experimental analysis for urban sludge. Due to the rapid development of technology and analyzer's constant improvement, and computer technology's speedy development, DSC plays an increasing role in the sludge treatment field.

Introduction

With the increase of urban sewage treatment capacity and the degree of deepening the water's treatment, sludge as wastewater treatment's secondary pollutant, its production also increased significantly, if handled improperly, or not timely, which will lead to serious secondary pollution. The final destination of the sludge increasingly attract people's attention: on the one hand, the sludge contains heavy metals, pathogens, toxic organic compounds which is difficult to be degraded, and improperly handling can endanger people's health ;on the other hand, the sludge is rich in organic matter and N , P, K and other nutrients, it is hoped to achieve sludge resource utilization.Thus sludge treatment and disposal has become an important environmental issue. The purpose of treating and utilizing sewage sludge is mainly to achieve reduction,stable,harmless and resources.Because it is completely harmless and reduction, sludge thermochemical treatment's status has gradually increased. This topic utilizes differential scanning calorimetry and had a pyrolysis experimental analysis for urban sludge , the type of the precision balance using in the experiment is BT224S.

The reaction mechanism

The sludge pyrolysis process analyzing from reaction process can be divided into three stages:
1)Dehydration stage (room temperature 100 ^{o}C).At this stage, biomass just has physical changes , mainly lose moisture.
2)Solid decomposition stage (100 ~ 380 ^{o}C).This is the main pyrolysis.At this stage, biomass thermal decomposition under anoxic conditions,with the increasing of temperature,various volatiles correspondingly separate out,most of the raw material occurs most mass loss.
3)Carbonization stage (> 400 ^{o}C).At this stage, decomposition occurs very slowly,the mass loss is much smaller than the second stage.At this stage,C-H, C-O bond in coke is further broken,but the volatilization is continuing,coke weight decreases with a slow rate and tend to be stabilized, which resulting in the enrichment of carbon in the residual solid.

Reaction conditions

Try to control the laboratory's room temperature at 15 °C -25 °C, the results of the experience has higher accuracy and repeatability under the constant temperature condition, at the same time, clean sample care and experimental area by ear-insufflating ball before the experiment start, to ensure the accuracy of the experimental results, heating the empty instrument about 30 minutes first when using it.Temperature can be setted to 600 °C, the rate can be setted to 5 °C / min, the thermostat can be setted to 0min. The amount of the sample should not be too much and generally around 20mg will be better. Powdered sample should be compacted. Heating rate generally be setted to 10-20 °C / min .If the heating rate is too high ,the curve will occur drift and resolution will be reduced.If the heating rate is too low,the time of measure will be too long. Before measuring the sample,regulating the instrument by using anhydrous copper. When regulating and measuring, the temperature can be setted to 600 ℃, the rate can be setted to 10 °C / min.

Reaction results and results description

1) The effect of experimental conditions

During the DSC , the heating rate has mainly effect on the curve's peak temperature and peak shape. Generally speaking, when the heating rate becomes faster, the DSC curve's peak temperature will be higher, the peak area will bigger and the peak shape will be more sharp. This effect is largely associated with the types of the sample and the types of thermal transition. High heating rates can cause uneven temperature distribution inside the sample. When it exceeds a certain heating rate, the mutative picture in the sample reaction can not be accurately recorded because the system can not quickly respond to changes , in addition, if the heating rate is too fast, it can result in overheating. Furthermore, in order to avoid some test substances occurring oxidation, deoxidation and other chemical reactions during the experience, so different substances should be tested in different atmosphere.

2)The effect of the sample's nature

During the DSC, generally the amount of sample is very small, which about dozens milligrams. If the amount is excessive, the sample's internal heat transfer will be reduced, and the temperature gradient will become larger, which causes the peak shape become larger and the resolution will be reduced.In addition, the granularity has certain effect on DSC, but it is a little complicated. Generally speaking, large particles has greater thermal resistance,which can decrease sample's melting temperature and melting enthalpy. When the crystal sample is ground into fine particles, due to the distorted crystal structure and the decreased grain size, which can also cause similar results. If the powdered sample with static electricity, it dues to the electrostatic attraction between the particles makes the powder agglomerate, which can lead to the melting enthalpy become larger.

3)The results description

1.1 DSC curves of pond sludge

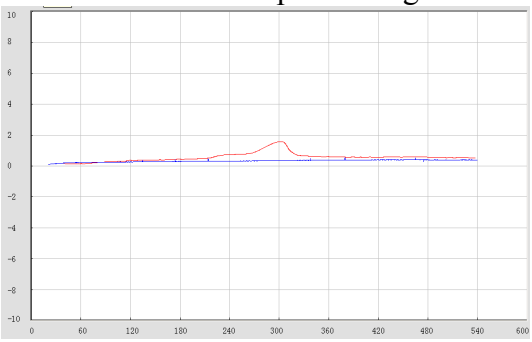

Sample Name: pond sludge
Sample Quality: 20.0mg
Heating rate: 10 ℃ / min
Gas Name: Air

1.2 pond sludge's unit enthalpy diagram

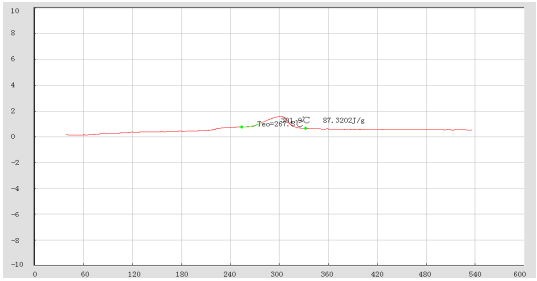

Results description and calculation : As can be seen from Figure 1.1: Overall baseline occurs drift within the allowable range. Sludge pyrolysis has an obvious exothermic peak. From Figure 1.2,it can be drawn that the exothermic peak occurs mainly at 254.8 ℃ -327.9 ℃. In this interval, sludge has thermal decomposition under the hypoxic conditions, with the increase of temperature, all volatiles corresponding separate out and the sludge occurs most mass loss . At this time,after releasing heat and heat air, sludge pyrolysis basically tends to be stable and has no-calorie variations.

$$Q_1 = 87.3202J/g * 0.02g = 1.746404J$$

1.3 The sludge added calcium oxide DSC map

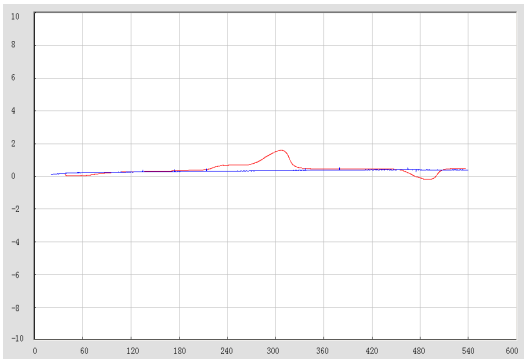

Sample Name:sludge plus calcium oxide
Sample Quality: 20.0mg
Calcium oxide Quality: 10.0mg
Heating rate: 10 ^{o}C / min
Gas Name: Air

1.4 The units enthalpy of sludge which is added calcium oxide

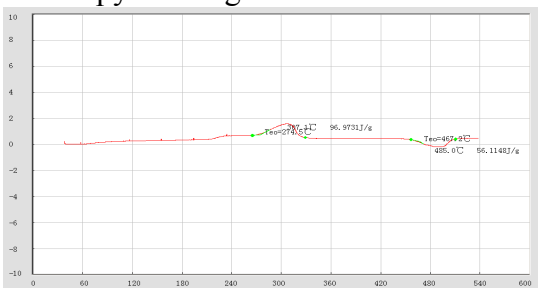

Results description and calculation

As can be seen from Figure 3.15: Overall， baseline occurs drift within the allowable range. Sludge pyrolysis has a significant exothermic peak and a endothermic peak. Exothermic peak occurs mainly in 266.3 ℃ -329.8 ℃. Because the sludge is dry sludge, so this figure is almost no change before the 266.3 ℃,

Heat release is:

$$Q_1 = 96.9731J/g * 0.02g = 1.939462J$$

Endothermic peak occurs mainly in 456.9 ℃ -508.9 ℃. And following, there is no heat generated. Heat absorption is:

$$Q_2 = 56.1148J/g * 0.02g = 1.122296J$$

1.5 Comparison of sludge with calcium oxide and without calcium oxide DSC atlas

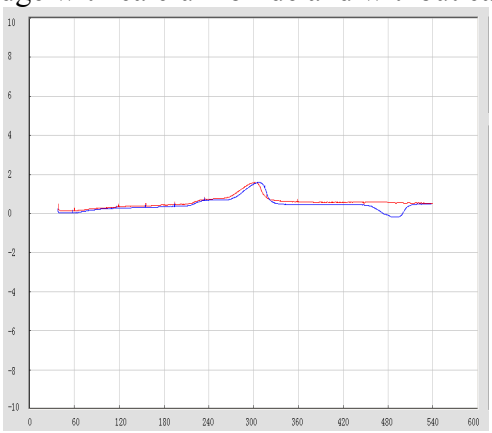

Comparative results description:

The red curve is the DSC map without calcium oxide .

The blue curve is the DSC map with calcium oxide

It can be seen from Figure 1.5: calcium oxide has no catalysis on sludge.Originally calcium oxide in the pyrolysis process,the chemical properties will not be changed and it means that there is no heat change, but in contrast, I found the experimental curve which added a small amount of calcium oxide began a trough at about 460 ^{o}C, which may be due to the addition of calcium oxide component is impure and it has become a calcium carbonate. According to statistics that the calcium carbonate would decompose at about 500 ℃,.In experimental heating process, the thermal, decomposition and endotherm of calcium carbonate resulting in an trough. Reaction equation:

$$CaCO_3 = CaO + CO_2$$

1.6DSC Atlas Summary

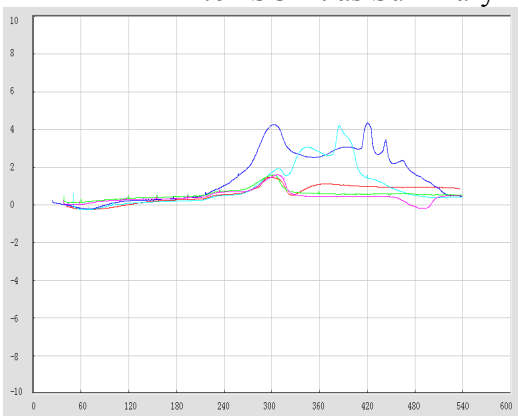

Comparative results description:

Figure 1.6 is a DSC atlas summary adds starch, tree bark, paper, sludge and the sludge which added Calcium oxide.Starch, tree bark, paper, sludge occur endotherm reaction at about 300 ^{o}C. Tree bark released heat most, probably due to the tree bark contains lignin, grease and other substances, the components is a little complex , when the lipid decompose and it inevitably releases a lot of heat. In the experiment, paper is used as the test sample and it also releases a lot of heat , Which may be associated with some of the chemical composition of the waste paper when producing it. Sludge curve and starch curve have little difference, which indicates that most of the ingredients contained in the sludge are starchy substances.

Conclusion

Differential scanning calorimetry is a method that can maintain the same heat flow rate and measure the temperature's difference between sample and reference, it can also quantitatively determine the thermodynamic parameters during the sludge pyrolysis process. This method has wide temperature range, high resolution, less samples, which will be widely used in municipal sludge treatment process.

Acknowledgement

In this paper, the research was sponsored by the key project of scientific and technological of Chongqing (Project No. cstc2012gg-yyjsB20002) .

References

[1] Joan J. Manyà, Jose L. Sanchez, Alberto Gonzalo, and Jesus Arauzo. Air Gasification of Dried Sewage Sludge in a Fluidized Bed: Effect of the Operating Conditions and In-Bed Use of Alumina [J]. Energy Fuels. 2005, 19 (2): 629–636.

[2] Joan J. Manya, Jose L. Sánchez, Javier Abrego, Alberto Gonzalo, Jesús Arauzo. Influence of gas residence time and air ratio on the air gasification of dried sewage sludge in a bubbling fluidised bed [J]. Fuel. 2006, 85(10): 2027-2033.

[3] María Aznar, Marta San Anselmo, Joan J. Manyà and M. Benita Murillo. Experimental Study Examining the Evolution of Nitrogen Compounds during the Gasification of Dried Sewage Sludge [J]. Energy Fuels, 2009, 23(6): 3236–3245.

[4] Thomas W. Marreroa, Brendan P. McAuleya, William R. Sutterlina, J. Steven Morrisb, Stanley E. Manahana. Fate of heavy metals and radioactive metals in gasification of sewage sludge [J]. Waste Management. 2004, 24(2): 193-198.

[5] Murat Dogruc, Adnan Midilli, Colin R Howarth. Gasification of sewage sludge using a throated downdraft gasifier and uncertainty analysis [J]. Fuel Processing Technology. 2002, 75(1): 55-82.

[6] Adnan Midillia, Murat Dogrub, Galip Akayb, Colin R Howarthb. Hydrogen production from sewage sludge via a fixed bed gasifier product gas [J]. International Journal of Hydrogen Energy. 2002. 27(10): 1035-1041.

[7] Pike E B Pathogen in sewage agricultural use of sewage sludge and the control Of disease. Water Pollution Control.1986,85:472.

[8] Yang Xiaowen, Du Yinghao. Sludge treatment and resource use options. the drainage of China .2002 (18): 31-32.

[9]Zhou Shaoqi. Municipal sludge treatment and disposal and resources. Guangzhou: South China University of Polytechnic Press, 2002: 29-33.

Advanced Materials Research Vols. 989-994 (2014) pp 2796-2801
© (2014) Trans Tech Publications, Switzerland
doi:10.4028/www.scientific.net/AMR.989-994.2796

Research on the Regionalism Air-Conditioning System Design of Car and Saving Energy

Li OUYANG[1, a], Die LI[1, a]

[1]School of Automobile Engineering, Wuhan University Technology, Wuhan, 430070, China

[a]email: ouyangli-002@163.com

Keywords: Car; Air-Conditioning System; Regionalism Design; Saving Energy

Abstract. The air-conditioning load is directly related to energy consumption of the car. Based on the characteristics and sources of the air-conditioning load of the car driven in four typical cities, this paper gives an analysis on the air-conditioning load using the steady-state heat transfer calculation method. The result indicates the regionalism design on the air-conditioning system for car is feasible and beneficial to save energy.

Introduction

As a moving object, the structure of car is very complicated, the moving direction of car is changed constantly, and the travelling environment of the car also changes, which result in more random influences on the air-conditioning load. So the car is special air conditioning object. Obviously, the air-conditioning load can be affected by different regional climate conditions, which leads in different energy consumption [1]. However, we note here that the lack of study or design on regionalism air-conditioning system [2] [3] [4] [5] [6]. For this reason the air-conditioning load of the car driven in four typical cities are calculated and analyzed by using steady-state heat transfer calculating method in this paper. We conclude the regionalism design on air conditioning system for car is available for saving energy.

Air-Conditioning Load Steady-State Heat Transfer Calculation

Heat Load Sources Analysis 1) In summer, the ambient temperature is higher than the indoor. Especially, based on the effects of solar radiation, the heat transfer through the car envelope into the indoor can lead to an increase in the indoor temperature. 2) The hot ambient air flows into the indoor through the door, window or floor of the car, which also lead to an increase in air-conditioning load. 3) The heat gain from human bodies is also the important contributor to load, which should be considered in air-conditioning load calculation. 4) The heat load of the engine room should be also considered.

Air-Conditioning System Design Parameters In accord with the design requirement of the air-conditioning system for car in China, the design parameters can be given as follows:

The outdoor air relative humidity is about 60%.The indoor air velocity should be less than 0.2m/s. The volume ventilation is about 11m^3 per man-hour. The indoor air relative humidity is about 55%, and the indoor air dry bulb temperature is 25℃. This car speed is 40 km/h, and the quantity of air leak is 18m^3/h. In this paper, June is considered as the computing date, and which can be assumed to be sunny. In addition, one driver and three passengers are considered for air conditioning load calculation. The Table 1 lists north latitudes and meteorologic parameters in four cities.

Pick Parameters of Materials Consisting of the Car Envelop Parameters of materials consisting of the car envelop are given in Table 2.

Mean Heat Transfer Coefficient Calculation

Car Envelope Heat Transfer Coefficient Calculation In this paper, the car envelope is simplified. That is, the car envelope consists of steel structure and glass window, in which the steel structure is complicated multilevel structure. And the material quality each layer of material is considered to be uniform. The heat transfer is also considered to be one-dimensional. Accordingly, the mean heat transfer coefficient of the car's side panel, front or back wall, dome, floor, window, etc., can be calculated by

$$k = \frac{1}{\frac{1}{\alpha_{in}} + \sum_{i=1}^{n} \frac{\delta_i}{\lambda_i} + \frac{1}{\alpha_{out}}} \quad \text{W/(m}^2\cdot\text{℃)} \tag{1}$$

where δ_i is the thickness of the i th material, m. λ_i is the thermal conductivity of the i th material, W/(m·℃). α_{in} and α_{out} denote, respectively, the inner and outer surface convection heat transfer of the indoor. Table 3 provides the thermal conductivity of the materials consisting of car envelope.

Table 1 North latitudes and meteorologic parameters in four cities

City	North latitude	Outdoor air dry bulb temperature (℃)
Kunming	25°01′	25.8
Wuhan	30°37′	35.2
Huhehaote	40°49′	29.9
Haerbin	45°41′	30.3

Table 2 Parameters of materials consisting of the car envelop

Envelop	Area (m^2)	Thickness (mm)	Material	Heat conductivity (W/(m·℃))
Total surface area	15.85			
Internal surface areas of the engine room	8.6			
Roof	1.51	0.7	Steel	48
Front wall	1.05	1	Steel	48
Back wall	0.52	1	Steel	48
Floor	3.17	0.7	Steel	48
Front windshield	1.1	4.8	Glass	0.754
Back windshield	0.93	3.2	Glass	0.754
Front glass doors & windows	0.54	3.5	Glass	0.754
Back glass doors & windows	0.54	3.2	Glass	0.754

Table 3 Thermal conductivity of materials consisting of the car envelope

Material	Glass	Wood	Fibreboard	Rubber	Foam plastics
Thermal conductivity (W/(m·℃))	0.754	0.14-0.29	0.23-0.34	0.16	0.04

On the basis of the value of air velocity in air conditioning zone, which is the one of the main design parameters, the convection heat transfer of the inner surface of indoor is small. The difference in temperature between the inner surface and air in indoor is denoted by Δt_b, and we get Δt_b=5℃.

Thus, $\alpha_{in} = 3.49 + 0.093\Delta t_b$ [2] $\text{W/(m}^2\cdot\text{℃)}$ (2)

Then, $\alpha_{in} = 3.49 + 0.093 \times 5 = 4$ $\text{W/(m}^2\cdot\text{℃)}$

But the convection heat transfer of the outside surface, α_{out}, varies with the running speed of the car, the air velocity and direction, etc. In this paper, the convection heat transfer of the outside surface, α_{out} is calculated from the empirical relationship, which is given by [2]

$$\alpha_{out} = 1.163\left(4 + 12\sqrt{v}\right) \quad \text{W/(m}^2\cdot\text{℃)} \tag{3}$$

in which we get v=40km/h, then, α_{out} is about 50 W/(m^2·℃).

1) For the car roof, we can give

$$\sum_{i=1}^{n}\frac{\delta_i}{\lambda_i} = \delta_{top}/\lambda_{top} + \delta_{hood}/\lambda_{hood} = 0.09\ (\text{m}^2\cdot\text{℃})/\text{W} \tag{4}$$

where we get $\delta_{top}=0.7\times10^{-3}$m, and $\delta_{hood}=6\times10^{-3}$m.

Then, k_{roof}=78W/(m^2·℃).

2) For the car's side panel, front or back wall, we can give

$$\sum_{i=1}^{n}\frac{\delta_i}{\lambda_i} = \delta_{iron}/\lambda_{iron} + \delta_{air}/\lambda_{air} + \delta_{iron}/\lambda_{iron} + \delta_{insulation}/\lambda_{insulation} = 2.7\ (\text{m}^2\cdot\text{℃})/\text{W} \tag{5}$$

where $\delta_{iron}=10^{-3}$m, and $\delta_{air}=3.2\times10^{-3}$m, which is considered as carpet

Then, k_{side}=W/(m^2·℃).

3) For the floor, we can give

$$\sum_{i=1}^{n}\frac{\delta_i}{\lambda_i} = \delta_{wood}/\lambda_{wood} + \delta_{plastics-carpet}/\lambda_{plastics-carpet} = 2.66\ (\text{m}^2\cdot\text{℃})/\text{W} \tag{6}$$

Then, k_{floor}=7W/(m^2·℃).

4) For the window

The heat transfer coefficient of window is related to the velocity of the ambient air and heat bridge dissipation from metal framework join. In this paper, based on the car can be assumed to be moving building, so we can get k_{glass}=6.38 W/(m^2·℃) from the Building Handbook.

Heat-Transfer Areas Calculation The heat-transfer areas can be determined with design drawings. In general, the heat-transfer areas can be calculated on the basis of geometric mean without respect to the influence of strengthening rib, which can be written as $A = \sqrt{A_H}\sqrt{A_B}$ m^2. And A_H and A_B denote, respectively, the total surface areas of the inside and outside of car envelope. Correspondingly, A is about 11.68m^2.

Average Heat-Transfer Coefficient Calculation The average heat-transfer coefficient can be expressed as

$$k_{cp} = \frac{\left(k_{side}A_{side} + k_{floor}A_{floor} + k_{roof}A_{roof} + k_{glass}A_{glass}\right)}{A} \quad \text{W/(m}^2\cdot\text{℃)} \tag{7}$$

Solving for k_{cp}, k_{cp} is about 3.83W/(m^2·℃)

Air Conditioning Load Calculation

The air conditioning load involves the heat transfer of the car body, the solar radiation through the glass, the fresh air load, the heat load for infiltration from the door and window of the car, and the human body heat dissipation. At steady state, the heat transfer can be given by

$$Q = kA\Delta t \quad \text{W} \tag{8}$$

where Δt is the temperature differences between the inner and outer surface of the car body, in℃. A is the surface areas of the car envelope, in m^2, and k is heat transfer coefficient, in W/(m^2·℃).

Heat Transfer of the Car Envelope Calculation The car envelope includes roof, side floor, engine room, whose heat transfer calculation is determined from

$$Q_{envelope} = k_{cp}A\left(t_{out} - t_{in}\right) \quad \text{W} \tag{9}$$

in which k_{cp} denotes the average heat transfer coefficient of the car body, and t_{out} is the outdoor air temperature. In accord with the specification in automobile air conditioning design, the indoor air conditioning design temperature t_{in} ranges from 24℃ to 28℃. In this paper, t_{in}=25℃. The symbol A

denotes the total surface areas of the car envelope, in m^2. The following Table 4 gives heat transfer of the body calculation results for the four typical cities.

Table 4 Heat transfer of the body calculation results

City		Kunming	Wuhan	Fuhehaote	Haerbin
Outdoor air dry bulb temperature	(℃)	25.8	35.2	29.9	30.3
Q_{body}	(W)	35.8	456.2	219.2	237.1

Solar Radiation through the Glass Calculation The solar radiation heat transfer through the glass is calculated

$$Q_{solar-radiation} = MA_{glass}C(\mu J_{c,\max}) \quad \text{W} \tag{10}$$

where A_{glass} is surface areas of the glass, in m^2. μ is multilayer glass correct coefficient (for standard glass, μ=1). C is the sunshade coefficient of the glass (The value of C is usually set to 1). M is areas coefficient of the glass (The value of M can be set to 0.8 for front windshield and back windshield, but for double-side glass surface, let M=0.5). And the results of the solar radiation heat transfer through the glass are listed in Table 5.

Table 5 Solar radiation heat transfer through the glass calculation results

	$J_{c,max}$ (W/m^2)				$Q_{solar-radiation}$ (W)			
City	South	East	North	West	South	East	North	West
Kunming	151	572	138	572	326.76	1237.8	298.6	1237.8
Wuhan	190	688	123	688	411.16	1488.8	266.2	1488.8
Fuhehaote	314	578	134	578	679.50	1250.8	290.0	1250.8
Haerbin	376	576	129	576	813.66	1246.5	279.2	1246.5

Fresh Air Load Calculation The fresh air load calculation can be evaluated according to the relation, as follows:

$$Q_{fresh-air} = l_o n\rho(h_o - h_i) \quad \text{W} \tag{11}$$

where n is passenger quantity(n=4). l_o is fresh air volume per man-hour. In this paper, l_o=11m^3 per man-hour, and the minimum fresh air requirement is at least 10m^3 per man-hour. ρ is the density of the air, and ρ =1.146kg/m^3. h_o is the outdoor air enthapy, in kJ/kg, which is obtained from psychrometric chart. But h_i denotes the indoor air design enthapy, and which can be also obtained via psychrometric chart. Locating the point on the psychrometric chart where the air dry temperature is 25℃, and the relative humidity is 55%, the corresponding value for h_i is about 52.5kJ/kg. The fresh air load calculation results for four typical cities are given in Table 6.

Table 6 Fresh air load calculation results for four typical regions

City		Kunming	Wuhan	Fuhehaote	Haerbin
Outdoor air dry temperature	(℃)	25.8	35.2	29.9	30.3
Outdoor air relative humidity	(%)	60	60	60	60
Outdoor air enthapy	(kJ/kg)	58	91	70	73
Fresh air load	(W)	277.3	1941.3	882.4	1033.7

Permeation Load from the Door and Window Slits of the Car Calculation The permeation load from the door and window slits of the car can be written as

$$Q_{permeation} = Ll_c\rho(t_{out} - t_{in}) \quad \text{W} \tag{12}$$

where t_{out} is the outdoor air temperature, in℃. ρ is the air density, ρ=1.146kg/m^3.The symbol l_c represents the length of the door and window silts of the car (about 12m for the door silts, and 8.5m for window silts).

The infiltration rate per meter opening joint in door and window L, m^3/h, varies with the air velocity, which can be given in accord with the dates used in civil building. In this paper, $L=4.0m^3/h$ for single steal window silts per meter, and $L=10.0m^3/h$ for door silts per meter, when the air velocity is 3m/s. The permeation load from the door and window slits of the car calculation is obtained using given data, and the calculation results for the four cities are also tabulated as

Table 7 Pereation load from the door and window silts of the car for the four cities

City	Kunming	Wuhan	Fuhehaote	Haerbin
Outdoor air dry temperature (℃)	25.8	35.2	29.9	30.3
$Q_{permeation}$ (W)	141.2	1800.3	864.9	935.5

Heat Gain From Human Bodies The heat gain from human bodies can be calculated from

$$Q_{human-body} = Q_s + qnn' \quad \text{W} \tag{13}$$

where Q_s is the heat gain from the driver (about 170W). n is the number of people (n=3). n' is clustering coefficient ($n' = 0.89$), and q is heat gain per hour from one people (q=108W).Thus the heat gain from human bodies $Q_{human-body}$ is about 458.4W.

Heat Load from Equipment and Illumination Calculation From reference[2], the heat load from equipment and illumination is

$$Q_{equipment} = (0.6 \sim 0.75)Q_1 \quad \text{W} \tag{14}$$

Thus, $Q_{equipment}$ is about 60W,when Q_1=100W from experience point.

Steady-State Total Air-Conditioning Load Calculation. At steady state, the total air conditioning load of the car can be computed from

$$Q_{total-load} = Q_{envelope} + Q_{solar-radition} + Q_{flesh-air} + Q_{permeation} + Q_{human-body} + Q_{equipment} \quad \text{W} \tag{15}$$

And the calculation results for the four cities are also shown in the following Table 8.

Table 8 Steady-state total air conditioning load of the car (W)

	Kunming	Wuhan	Fuhehaote	Haerbin
South	1299.46	5127.36	3164.4	3538.36
East	2210.5	6205	3735.7	3971.2
North	1271.3.2	4982.4	2774.9	3003.9
West	2210.5	6205	3735.7	3971.2

Analysis on the Energy-Saving

The results show that, the air-conditioning load of the car driven in Wuhan is largest, but the one in Kunming is smallest, so, which can be further compared using formula as follows:

$$\frac{Q_{total-\max} - Q_{total-\min}}{Q_{total-\min}} \quad \% \tag{16}$$

When the four directions, North, South, East and West, taken into account, the comparative results are

South: $\dfrac{5127.36 - 1299.46}{5127.36} = 74.66\%$

East: $\dfrac{6205 - 2210.5}{6205} = 64.38\%$

North: $\dfrac{4982.4 - 1271.3}{4982.4} = 74.48\%$

West: $\dfrac{6205 - 2210.5}{6205} = 64.38\%$

At last, based on above calculation results, the average of the decrease percentage of air conditioning load of car driven in Kunming can be calculated, which is about 69.48%.

Conclusion

The decrease of air conditioning load is up to 69.48%. The result shows that the regionalism design on the air-conditioning system of car has marked energy-saving effect.

Acknowledgement

In this paper, the research was sponsored by the Fundamental Research Funds for the Central Universities (Project No. 2011-IV-123).

References

[1] Kim Jaeheun, Park Jungseo, Bae Choongsik. Effect of the Air-conditioning System on the Fuel Economy in a Gasoline Engine Vehicle [J]. Proceedings of the Institution of Mechanical Engineers, Part D: Journal of Automobile Engineering, 2013, 227: 66-67.
[2] Xiangbo Xu, Yixiong Hu. Building and Automobile Air Conditioning Load [M]. Hefei: National University of Defense Technology Press, 1997.
[3] Baozhi Wu. Automobile Air Conditioning Load [M]. Beijing: Aerospace Press, 1991.
[4] Xiongcai Que, Jiangping Chen. Automotive Air Conditioning Technology [M]. Beijing: China Machine Press, 2003.
[5] Xubing Shen, Zixue Du.The influence of the Solar Radiation to the Temperature Field and Air Conditioner Heat Load Inside the Compartment of Mini Car [J]. Refrigeration & Air conditioning. 2002, 4: 51-59.
[6] Shuang Wu. Contrast and Analysis on the Calculation Methods of Air Conditioning Load in Automobile [J]. Refrigeration & Air Conditioning, 2002, 2(6): 20-27.

Advanced Materials Research Vols. 989-994 (2014) pp 2802-2806
© (2014) Trans Tech Publications, Switzerland
doi:10.4028/www.scientific.net/AMR.989-994.2802

Design of the hydraulic system for carrying manipulator with 6-DOF

WANG Min[1] ， WANG Caidong[2]，ZHENG Hui [2]，Fan Guofeng [2]

（[1.] Zhengzhou Aircraft Equipment Co. Ltd. of China Aviation Industry, Zhengzhou, 450005

[2.] Zhengzhou University of Light Industry, Zhengzhou, 450002）

Keywords： manipulator; six degrees of freedom; hydraulic system; optimization

Abstract. According to the requirements for wheel hub assembly line, the structure and hydraulic system of carrying manipulator with six degrees of freedom (DOF) is designed. The working principle of the hydraulic system is analyzed. To minimize the output force of the hydraulic cylinder, a mathematical model of hydraulic cylinder output force and structural parameters is established. And then the manipulator structure is optimized based on Matlab software. The key components of the hydraulic system are selected. This research provides reference for design of similar hydraulic system of industrial robot.

Introduction

As the rapid progress of industrial automation, the manipulator is more and more widely applied in industry, especially in the environment of high temperature, high pressure, dusty and radioactive pollution [1].Most domestic material handling industries still continue the manual operation mode of production, and the problems of high labor intensity, poor working conditions, low efficiency are seriously restrict the development of the companies[2].In a wheel hub assembly line, as the hanging operation of the washing line to the spray painting line were completed by manual, the process was limited by the rhythm of the whole production line , so the labor intensity of workers was high , and the labor conditions was bad in the painting environment. It will not only reduces the labor intensity of workers, but also improves the production automation level and productivity, and ensuring product quality and safety when adopt handling robot instead of human to repeated the operation of putting hub up and down. In this paper, a carrying manipulator with six degrees of freedom (DOF) is researched, the mechanical structure and hydraulic control system are designed.

The scheme of manipulator

In order to make the manipulator system has stronger function to complete complicated tasks, the degrees of freedom are set to 6. The 3D model of the carrying manipulator is shown in figure 1. The 6 joints are all rotational joints, which are shoulder revolute joint, shoulder pitch joint, elbow pitch joint, forearm revolute joint, wrist pitch joint, and wrist revolute joint respectively. According to the power source, the drive system of the manipulator can be classified as hydraulic, pneumatic and electric. These three types can also be combined to form a composite type of drive system as needed. The main advantage of hydraulic is the big power-to-weight ratio. It means that a small drive can export a larger driving force or torque[3-4].As the manipulator mainly completes the handling work of wheel hub, and the load capacity demand is bigger, so the hydraulic driving is chosen. The forearm revolute joint of manipulator adopts swing hydraulic cylinder to driving, the shoulder and wrist revolute joints are driven by hydraulic motors, the rest joints adopt hydraulic cylinder to driving. The end of the sixth joint is designed as universal tool interface, so it can meet different material handling requirements (such as gripper, electromagnetic sucking disc).

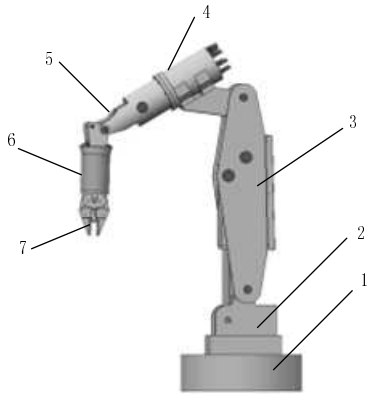

1 - Base 2 - Shoulder 3 - Forearm 4 - Elbow 5 - Forearm 6 - Wrist 7 - Gripper

Fig. 1 The three-dimensional model of the carrying manipulator

According to the material handling requirements of wheel hub assembly line, the technical parameters of the manipulator are formulated as follows:

Degrees of freedom: 6 The maximum working radius: 2m

The end-effecter: paw, electromagnetic sucker Rated load: 60kg

The motion range of the manipulator joint is shown in table 1.

Table 1 The motion range of the manipulator joint

Joint	Actuator type	Range of motion
Shoulder rotary	Cycloid motor	360°
Shoulder pitch	Single-rod hydraulic cylinder	-30°～90°
Elbow pitch	Single-rod hydraulic cylinders	-10°～120°
Forearm rotary	Swing cylinders	270°
Wrist pitch	Single-rod hydraulic cylinders	-60°～60°
Wrist rotary	Orbital motors	360°
Paw	Single-rod hydraulic cylinders	100mm

The reliability of the manipulator is decided by the reasonable layout of manipulator hydraulic piping. Most of the traditional oil pipeline are fixed on the outside of the manipulator joints, the oil supply line is easily intertwining with rotating parts, which will damage the pipelines and also looks complicated. Therefore, the connection part of the joint adopts cavity structure, and the pipeline of the mechanical wrist adopt interior layout. This can reduce the volume and weight of the swing cylinder effectively, and can improve the reliability of the manipulator.

Hydraulic system design of the manipulator

According to the operation realization of the manipulator hydraulic control loop, it includes shoulder joint rotary loop, elbow pitch control loop, wrist and paw control loop. The principle diagram of manipulator hydraulic control system is shown in figure 2. Because the velocity of all the manipulator joints should be precisely controlled, the servo valve is used to control the manipulator. The hydraulic cylinders of the joints(shoulder pitch joint , elbow pitch joint , wrist

pitch joint) which are bearing gravity load are equipped with a one-way liquid control valve with better sealing performance. When the system unload, the cylinder will be locked without moving, so that the joint realize the self-locking function. The paw joint adapts the two-way lock loop of the hydraulic one-way valve, so that the paw can lock the current location reliably. In order to meet the material grabbing requirements, a pressure reducing valve 15 is fixed on the hydraulic to adjust the clamping force. To ensure the stability of the wrist rotation joint movement, a back pressure valve 13 is installed on the oil return line of motor so as to reduce the starting impulse.

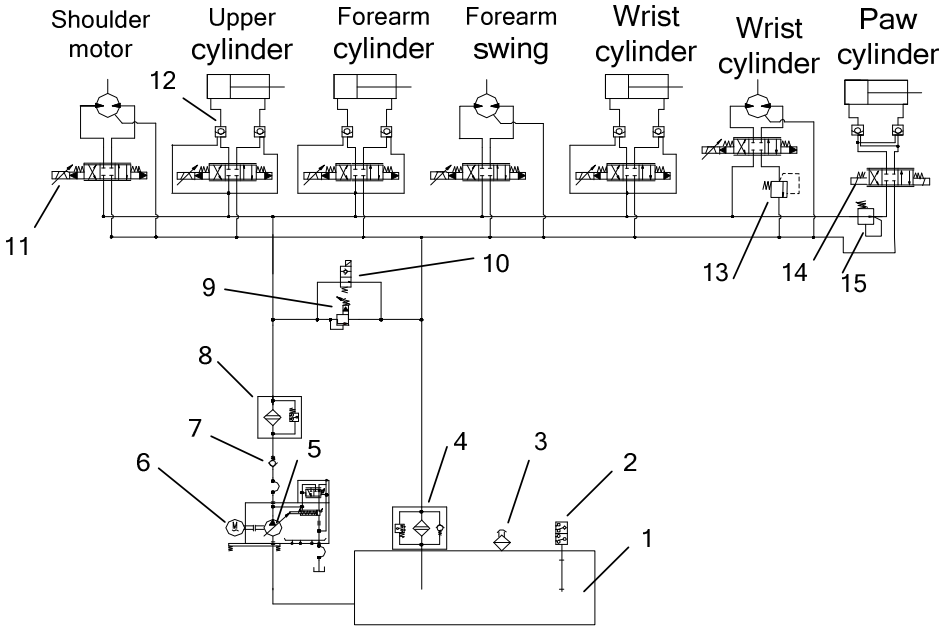

1 .Tank 2. Tevel relay 3. Air filter 4 . Return filter 5. Piston 6 . Motor
7. Check valve 8.High pressure oil filter 9 . Relief valve 10. Solenoid valve 11. Servo valve
12. Pilot operated check valve 13 . Backpressure valve 14. Solenoid valve 15. Valve
Fig. 2 The hydraulic system schematic of manipulator

In order to keep the system oil clean , a high pressure cleaner is fixed at the outlet of pump and an oil filter is fixed at the inlet of tank. When the oil circuit is clogged by impurities, the pressure relay of oil filter is working, the system stops running and alarms to ensure the work reliability.

Important components design of hydraulic system

Calculation design of hydraulic cylinder. Because of the limited space, the article take the wrist pitch joint hydraulic cylinder as an example to design and analysis, and the design method of the other hydraulic cylinders are in the same.

The force analysis of hydraulic cylinder. Wrist pitch joint is an oscillating guide bar mechanism and its force analysis is shown in figure 3. Point A is connection point of the pin and shaft at wrist joint, B is the fixed point of hydraulic cylinder, O is the fixed point of wrist rotating shaft, a is the length of the rocker, b is the length of the frame. Hydraulic cylinder is the active part and does reciprocating motion, the connecting rod OA is drove by hydraulic cylinder to complete the pitching motion of wrist joint. ϕ is the angle between the initial position of the bar($\theta = 0$)and the frame, the force of the hydraulic cylinder is related to a, b, ϕ . G=(60+21)×9.8 = 793.8N , $-60^\circ \le \theta \le 60^\circ$. In the traditional design process, the maximum output force of hydraulic cylinder is considered at the point that the manipulator is in horizontal straight state. This assumption ignored the force transfer performance among the connecting bars, the calculation did not conform the real stress state of the mechanism. In order to make the hydraulic cylinder has the smallest load(output force), the force equation of the mechanism is established and the parameters is also optimized.

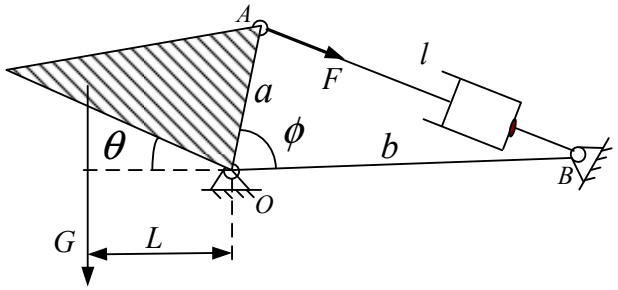

Fig. 3 The force diagram of wrist joint

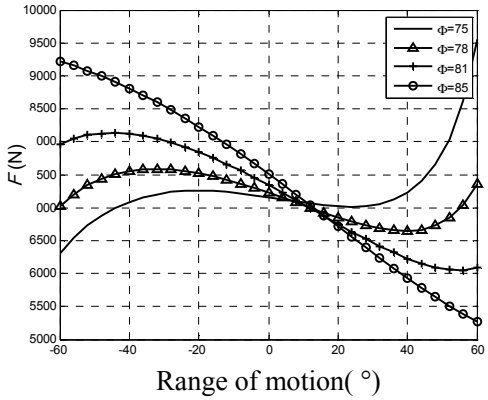

Fig. 4 The effect of the value ϕ on the load force

The force balance equation according to O point can be gotten as follows

$$\mathrm{G}\times L\times\cos\theta = F\times\frac{ab\sin(\phi-\theta)}{l} \tag{1}$$

Where : G - gravity equivalent load , N; L - the effectiveness lever of arms , L=0.461m;
θ - Wrist pitch angle , °; a, b - Rod length , m;

From equation (1) , the output force F expression of cylinder can be obtained:

$$F=\frac{G\times L\times\cos\theta\times l}{ab\sin(\phi-\theta)} \tag{2}$$

Obviously, the output force F is not only related with the structure parameters *a, b*, but also associated with the initial position. In order to minimize $F_{\max}$, different a, b, ϕ are chosen, the mechanical structure parameters are determined through optimizing design by Matlab software simulation. Considering the workspace requirements of the manipulator, set up the range of the parameter, then the driving force F can be calculated, as is shown in Figure 4, 5, 6.

(1) Setting a=55mm, b=170 mm, changing the value of ϕ. The relationship between F and the wrist pitch angle is shown in figure 4. From the figure, it can be seen that ϕ has a significant effect on F, which is nonlinear, when ϕ=78 °, the average value of output force is the smallest.

(2) Setting a=55mm, ϕ=78 °, changing the value of b . The relationship between the load capacity and the wrist pitch angle is shown in figure 5. From the figure, it can be seen that b has little effect on F, the curve of output force is symmetry about $\theta=0$, this means the force of hydraulic cylinder in the extended and retracted process are the same.

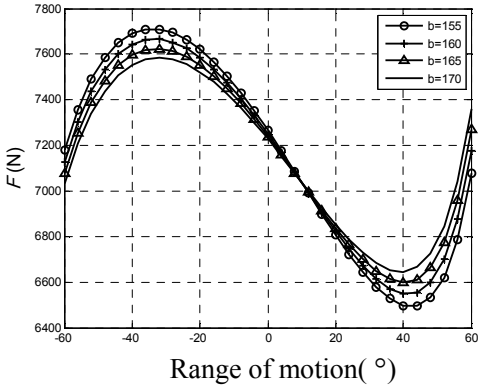

Fig. 5 The effect of the value *b* on the load force

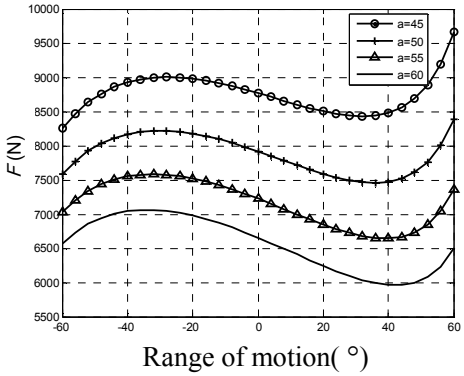

Fig. 6 The effect of the value *a* on the load force

(3) Setting b=170 mm, ϕ=78°, changing the value of a. The relationship between F and the wrist pitch angle is shown in figure 6. It can be seen that the effect of a to F is monotone increasing.

Combined with the calculation results and considering the overall size requirement of the manipulator, setting a=55mm, b=170mm, ϕ=78 °. With the parameters, the needed load force of the hydraulic cylinder is smaller, that is, the whole forced condition of the manipulator is good. According to the above, $F_{\max}$ =7530 N, taking it into the correlation formula, the structural parameters of hydraulic cylinder can be gotten: D=34mm, d=24mm.

The maximum output force checking of hydraulic cylinders. The maximum thrust of the Hydraulic cylinder is as follows

$$F_t = \frac{\pi}{4} D^2 P_1 = 16085\text{N} \quad (3)$$

Where, P_1 is the highest working pressure in the working process of hydraulic actuator, $P_1 = 16\text{MPa}$.

The maximum pulling force of hydraulic cylinder is as follows

$$F_t = \frac{\pi}{4}\left(D^2 - d^2\right) P_1 = 8482.3\text{N} \quad (4)$$

The above results can meet the load requirements.

The calculation of hydraulic cylinder stroke. The displacement formula of Hydraulic cylinder piston is as follows:

$$ll = l - l_0 = \sqrt{a^2 + b^2 - 2ab\cos(\phi + \theta)} - \sqrt{a^2 + b^2 - 2ab\cos(\phi)} \quad (5)$$

Where, l_0 is the length of hydraulic cylinder when it is in median.

$$l_{\max} = \sqrt{a^2 + b^2 - 2ab\cos 140} = 225\text{mm}$$

$$l_{\min} = \sqrt{a^2 + b^2 - 2ab\cos 20} = 130\text{mm}$$

The Stroke of Hydraulic cylinder can be gotten : $S = l_{\max} - l_{\min} = 95\text{mm}$.

Conclusion

The structure and hydraulic control system of carrying manipulator with 6-DOF has been designed in this paper. The hydraulic system has completed the servo control of the manipulator, and can meet the carrying requirements of automobile hub. Based on this research, the manipulator can be applied on material handling and stacking in the other industry, such as machinery manufacturing, metallurgy, building materials, with change of the end effector

References

[1] Yu Dianyong, Liu Xingyi, Application of a handling robot based on the control of PLC and touch-screen. Manufacturing automation, Vol.31 (2012) ,No.8,pp.121-127.

[2] Zhang Xiaoli, Lin Herong, Design of the hydraulic drive system for the aluminium-ingot stack-manipulator. Hydraulic and pneumatic, (2011), No.10,pp.44-46.

[3] Yang Jing, Tong Zhixue, Wang Ruipeng, Liu Tao, Exploring Fuzzy PID Control of electro-hydraulic proportional system of Hydraulic Manipulator. Mechanical science and technology, Vol.32 (2013), No.6,pp.834-839.

[4] Wang Guanglei, Tong Xuezhi, Zhang Zhanping, Simulation study on load sensing system of hydraulic manipulators based on AMESim. Mining Machinery, Vol.39(2011), No.12,pp.105-109.

[5] Cheng Daxian, Mechanical Design Manual. Hydraulic Transmission. BeiJing, Chemical Industry Press,(2004).

Advanced Materials Research Vols. 989-994 (2014) pp 2807-2810
© (2014) Trans Tech Publications, Switzerland
doi:10.4028/www.scientific.net/AMR.989-994.2807

Simulation and Study of SPWM Variable-Frequency Drives of Asynchronous Motors Based on Aerostatic Guide Way

Long Wei [1,a]，Liu Yan [2,b]，Zhang xiao-long[3,c]，Wang ting-you [4,d]

([1,2,3,4.]School of Electromechanical Engineering，Kunming University of Science and Technology，Kunming China 650000)

[a]daifor@163.com, [b]jizi0931@163.com, [c]km.zxlong@qq.com, [d]wtyhome@sina.com

Keywords: asynchronous motor, SPWM, aerostatic guideway, vector control

Abstract: The asynchronous motor is converted to a model similar to DC motor to control through coordinate transformation, and adopt SPWM inverter circuit, the motor runs with load implements ideal speed and steady operation, providing appropriate speed for aerostatic guide way. Realize simulation of asynchronous motor variable frequency speed regulation system by simulink.

0.Introduction

In recent years, domestic demand for precision and ultra-precision machining and measuring equipment is increasing, Ultra-precision machine tools is the fundamental condition to achieve primary ultra-precision machining, and rail component is critical among ultra-precision machine parts[1]. Since air has low viscosity, small vibration, thermal stability and does not pollute the environment etc. Small changes in load ultra-precision machine tools and measuring machines and other precision machinery usually adapt aerostatic guide way, which is widely used in ultra-precision machining[2], its movement accuracy reaches micron level. That motor provides a stable output speed is an important guarantee to achieve its precise movement.

Compared with DC motor, AC motor is more simple, rugged, reliable, low cost, easy maintenance etc, which is widely used in industrial areas. This paper adapts vector control method, and use SPWM to control induction motor speed in simulink. With given load, obtain ideal output speed. Additionally it has used a three-phase rectifier circuit to change AC into DC power supply.

1.Mathematical model of induction motor

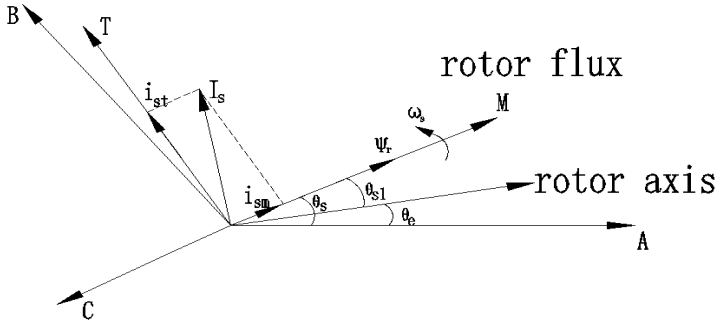

Fig1. Rotor field orientation M-T coordinate system and static *abc* coordinate system

The basic idea of vector control is to define i_m as current component, obtain two-phase AC control volume i_α， i_β by vector rotating coordinate transformation, obtain three-phase AC control volume i_a， i_b， i_c by two-phase to three-phase coordinate transformation external the motor[3].

In figure 1, i_{st} and i_{sm} are stator current components, ψ_r is Rotor flux, in M-T coordinates of Rotor magnetic oriented field, T-axis coincides with rotor flux Axis, thus flux component *m* equals rotor flux amplitude ,*t* component equals 0, mechanical speed ω_r is state variables, u_{st} on variable *t* and u_{sm} on variable *m* of Stator voltage vector are both controlled quantities.

Torque equation in M-T rotate axis and Equation of stator current component ψ_r in M-T axis:

$$T_e = n_p L_{md}(i_{st} i_{rm} - i_{sm} i_{rt}) \tag{1}$$

$$\Psi_{rt} = 0 = L_{md} i_{st} + L_{rd} i_{rt} \tag{2}$$

From (1) and (2): $$T_e = n_p \frac{L_m}{L_r} i_{sm} \psi_r \tag{3}$$

Obtain voltage equation from rotor-oriented three-phase asynchronous motor mathematical model:

$$\begin{bmatrix} u_{sm} \\ u_{st} \\ 0 \\ 0 \end{bmatrix} = \begin{bmatrix} R_S + PL_{sd} & -\omega_S L_{sd} & PL_{md} & -\omega_S L_{md} \\ \omega_S L_{sd} & R_S + PL_{sd} & \omega_S L_{md} & PL_{md} \\ PL_{md} & 0 & R_r + PL_{rd} & 0 \\ \Delta\omega L_{md} & 0 & \Delta\omega L_{rd} & R_r \end{bmatrix} \begin{bmatrix} i_{sm} \\ i_{st} \\ i_{rm} \\ i_{rt} \end{bmatrix} \tag{4}$$

It can be obtained by the third line of equation (4) as:

$$i_{rm} = -\frac{P\Psi_r}{R_r} \tag{5}$$

Besides, $$\Psi_r = L_{md} i_{sm} + L_{rd} i_{rm} \tag{6}$$

By equation (5) and (6),we have

$$\Psi_r = \frac{L_{md}}{T_r + 1} i_{sm} \text{ ; where } T_r = \frac{L_{rd}}{R_r} \tag{7}$$

Equation (8) and (4) show that flux determined by i_{sm}, torque determined by i_{st} respectively [4].which realize a decoupling of torque and flux.

2.Coordinate transformation

In the case of produce the same rotating magnetic field, three-phase symmetrical sinusoidal alternating current can be converted into two-phase symmetrical sinusoidal AC. Two- phase sinusoidal alternating current can be converted into a two-phase alternating current rotation. Expression is as follow[5]:

$$i_{MT} = C_{3/2} i_{abc} = \sqrt{\frac{2}{3}} \begin{bmatrix} \cos\varphi & \sin\varphi & 0 \\ -\sin\varphi & \cos\varphi & 0 \\ 0 & 0 & 1 \end{bmatrix} \begin{bmatrix} 1 & -\frac{1}{2} & -\frac{1}{2} \\ 0 & \frac{\sqrt{3}}{2} & -\frac{\sqrt{3}}{2} \\ \frac{1}{\sqrt{2}} & \frac{1}{\sqrt{2}} & \frac{1}{\sqrt{2}} \end{bmatrix} i_{abc} = \sqrt{\frac{2}{3}} \begin{bmatrix} \cos\varphi & \cos(\varphi - 120) & \cos(\varphi + 120) \\ -\sin\varphi & -\sin(\varphi - 120) & -\sin(\varphi + 120) \\ \frac{1}{\sqrt{2}} & \frac{1}{\sqrt{2}} & \frac{1}{\sqrt{2}} \end{bmatrix} i_{abc} \tag{8}$$

3 System Simulation

3.1 System Simulation Model

Motor parameters: rated power: 1.5kw, rated speed: 1600r/min, n_p=2, L_s=0.071H, L_r=0.071H, L_m=0.069H, J=0.02kgm^2, R_s=0.435Ω, R_r=0.816Ω, default speed: 1400r/min.

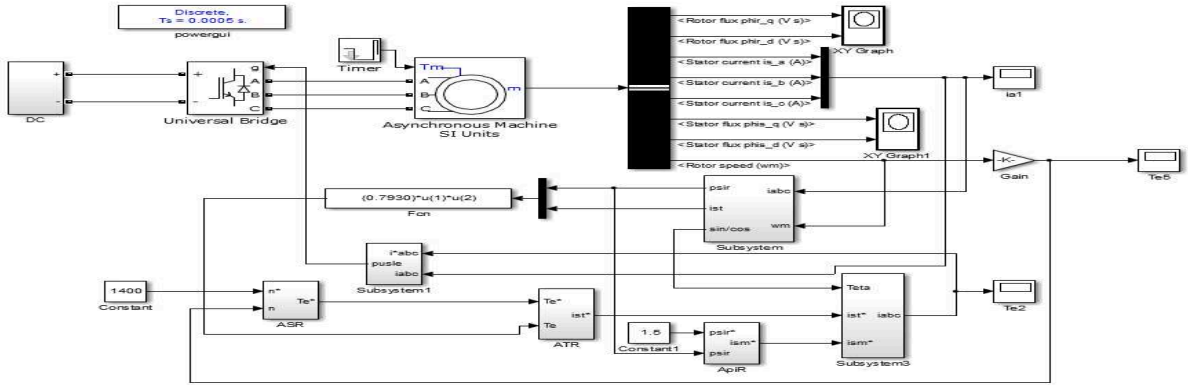

Fig2.System simulation

3.2 flux observer module

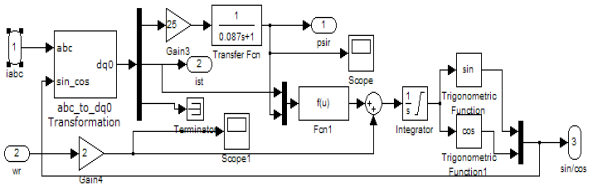

Fig3. Flux observe module

According to field-oriented equation, we have:

$$\Psi_r^*=\frac{L_{md}}{T_r n_p+1} i_{sm}^* \tag{9}$$

$$\Delta\omega^*=\frac{i_{st}^* L_{md}}{T_r \Psi_r^*} \tag{10}$$

$$\Delta\omega^* + \omega = \omega_S \tag{11}$$

$$\int (\Delta\omega^* + \omega)\mathrm{d}t = \varphi_S \tag{12}$$

3.3 Current hysteresis control module

The module is composed of three hysteresis controllers and three logical operators, its input quantities are three-phase current , actual measured values and its output quantities are 6-channel PWM inverter control signal, by controlling each bridge arm on-off time to regulate average current[6] to control motor speed. According to changes in input signal, relay hops between logic 0 and 1 to control on and off of diodes in full bridge, producing sinusoidal phase current.

Torque and flux modules adapt PI regulator, besides adapt PID regulator ways to control speed.

4 Simulation results and analysis

4.1 AC to DC circuit output voltage image

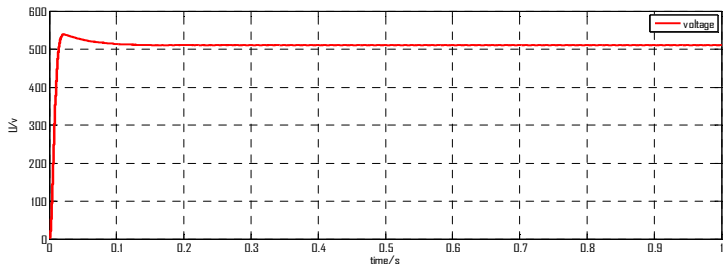

Fig. 4. Voltage curve

The figure shows voltage value stabilized at 510V at 0.05s after the start, meeting requirement.

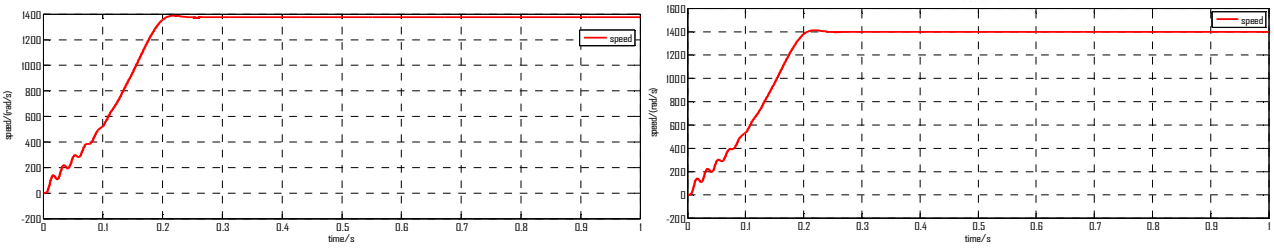

a) no-load speed curve b) load speed curve

Fig5. Asynchronous motor speed curve

4.2 motor speed curve

As Figure 5a) shows, from 0s to 0.1s, speed undulates because of unsteady current. It reaches 1400r/min quickly at 0.2s and runs stably afterwards. As figure 5b) shows, with 5Nm load, speed slows down only a little after steady. Because torque is combined with active torque caused by supply voltage, offset torque caused by sensor voltages and torque caused by load, they keep balance, once increase the load, it will reduce speed to keep balance. The design results of smooth running closes to 1400r/min after loaded, meeting requirements of aerostatic guideway running.

5. Conclusion

By simulation, we can get a fast speed response curve, which is easier to realize than M function. The system function is complete, which can simulate the actual system realistically. Meanwhile we can obtain the following conclusions:

1. A steady DC power can be obtained through three-phase power by rectifier to achieve an inverter to adjust the motor speed.
2. Induction motors can be converted into the similar DC motor to control by the coordinate transformation.
3. Rotor flux and torque can be achieved by calculating the corresponding decoupling, easy individually controlled and implement.

This simulation system provides a reference for the design of actual asynchronous motor speed and the accurate running of precision air hydrostatic guideway

Project funds: (1) Plane Project of Yunnan Provincial Science and Technology Department （KKSA201101049）, (2) National Natural Science Foundation of China（51305185）

References

[1] Dong Pengcheng. Static and dynamic characteristics of ultra-precision hydrostatic guides Analysis and Control Technology: Harbin Institute of Technology. (2013)

[2] Chen Wenzhe, Xu Xipeng, Dai Pinqiang, Chen Yonglu and Jiang Zhengyi. Analysis on the Individual Stiffness of the Aerostatic Guide Way and Error Sources of its Vibration: Advanced Materials Research February, Vols. 472-475 (2012), p.862-868

[3] Li Huade etc. AC Speed Control System: Electronic Industry Press.(2002)

[4] Zhang Xinghua. Modeling and Simulation of induction motor speed control system based on simulink / PSB: Journal of System Simulation. Vol. 17 No 9 (2005), p.2099-2103

[5] Chen Boshi. Electric drive automatic control system (Second Edition): Machinery Industry Press.(1997)

[6] Hu Yingzhan , Guo Suna. Asynchronous Motor Vector Control System Based on Space Vector Pulse Width Modulation: Mechatronics and Automatic Control Systems Lecture Notes in Electrical Engineering .Vol. 237(2014).p675-682

Advanced Materials Research Vols. 989-994 (2014) pp 2811-2814
© (2014) Trans Tech Publications, Switzerland
doi:10.4028/www.scientific.net/AMR.989-994.2811

Implementing Lean Techniques on the Shop Floor Improvement of a Delivery Company

Jason Shay[1, a] and Peter Iming Shieh[FIET,FIMechE,EurIng,CEng,PhD][2,b]

[1]Dept of Business Administration, National Chengchi University, Taipei, Taiwan

[2]Global Consulting, P O Box 6-12, Huwei, Yunlin, Taiwan

[a] lovercomplaint@g.mail.vt.edu, [b] pimshieh@gmail.com

Keywords: Lean management techniques, Value stream mapping, Current state map, Future state map, Waste, Packages flow, Hub centers, Automation process, Cellular layout

Abstract. CTC Express is the leading domestic company in delivery service and wants to improve their business efficiency by establishing lean management in the shop floor activities. Lean management is generally adopted by the manufacturing industries as a significant technique to reduce waste and operation costs. This paper investigates the continuous improvement through value stream mapping, begins with describing the current situation and proposes the future condition. Several improvements were implemented in the company such as the transformation of automation process, better result in visual control and standardization processes. The new proposed system has shown being able to reduce the works of loading/unloading and in the same time to increase the performance of material handling in each cycle time.

Introduction

Tight competition among delivering service companies forces the companies to rethink about the performance improvement in their business processes. In the process of improving the performance, companies attempt to construct new approaches to increase the quality of their business activities and to concurrently reduce the waste processes. In order to fulfill the improvement activities, lean management techniques are generally used as a central knowledge for many companies to develop their continuous improvement environment [1].

Lean manufacturing was first popularized by Toyota Company with the name of "Toyota Production System" [2]. It was then introduced to the academia under the new term of "Lean Manufacturing" or "Lean Thinking" [3]. The purpose of Lean Manufacturing is to eliminate waste, where waste means everything in the processes that will add cost without adding value.

This study explored the principles of lean manufacturing for improving the logistics process efficiency of the CTC Express, a leading delivery service company in Taiwan. This logistic process is focus on a central hub warehouse, where the package-flow could come from branch-warehouse and the customer at the central hub city.

Empirical follow up study shows that the overall performance after the implementation of the automation system improved the company's efficiency by 25% without the need for overtime labor hours.

Literature Review

The related literature review is made on the area of lean in the Logistics Industry. The benefits of lean ideology successfully breakthrough in several research areas [4], most researches tried to improve algorithms for developing alternative and efficient initial layout. A significant layout lean principle came from ALCAST Pte Ltd Manufacturing [5]. It mentioned the benefits of using the cellular layout to improve the manufacturing process with several additional lean principles, the result could detect the several non-value adding activities and considered as an important source for the improvement process.

Value Stream Mapping (VSM) is considered as an important tool on the implementation of lean principles. One example of the VSM use performed by SMC Company [6], the SMC Company uses the VSM and Kaizen tools to optimize the assembly line. Another good example of the VSM applied by ABS Company [7], the research found out the benefits of VSM combined with lean tools and justified it through statistical approach. The example of VSM implementation in the service area performed by health sector [8], it has proved that VSM could eliminate the non-value added waste in their procurement facility.

The automation process has been realized by researchers for period of time as an important part in the lean principles. In one of the research [9], the idea of automation process was investigated in the shop-floor data-capture to enable the automation in the manufacturing process. Automatic Identification and Data Capture (AIDC) was proposed to improve the inventory performance. Another automation process using belt conveyor in lean area performed in the manufacturing [10], the research design the optimal conveying system in order to implement the lean principles.

Shop Floor Improvement

Even as the largest B2B/B2B2C logistic provider in Taiwan, the CTC Company still operates solely based on manual power. Four main procedures that would have to be done before packages are delivered out of the hub center: unloading, barcodes scanning, verifying, and uploading.

The *current state map* and *future state map* were derived using the lean principles [11]. The two maps provide valuable criteria to find out the waste jobs and to re-arrange the package flow. Automated conveyor systems were introduced to improve the performance of package flow.

The conveyor would allow the sorting procedure and the verifying procedure be eliminated. The future value stream of the company would be flowing from unloading procedure directly to the palleting and uploading procedure. It has decreased the workers' workload to walking and in the same time eliminating the vulnerable condition of injury.

In addition, the system is designed to ensure that the information obtained at the work flow could be output to the computer which could then be integrated with the information system.

The intelligent weighting cells and barcode scanning equipment were integrated in the system so that every package would be weighed to increase the company's profitability without adding work load on the workers. The completed novel system shows being able to handle one truckload of packages in ten minutes, compared to the currently procedure, which needs sixteen minutes, indicating a 63% capacity increase.

Takt Time Analysis

To measure the effect of increasing performance, *Takt Time* analysis is performed in this study. Takt Time is a formulation in lean principles to define the rate of a process required to produce in order to fulfill the customer demand, the formula can be seen in the equation as follow,

$$TaktTime = \frac{Time\ Available\ during\ the\ Period}{Customer\ Demand\ in\ Period} \quad (1)$$

The Takt Time is used to know the rate in which a process needs to produce to fulfill the customer demand; if the product is done faster than Takt time then it will become *over production* and if it is lower than Takt Time then the outcome has *downstream shortages* that need overtime to fulfill the needs [12].

Two shifts working practice is normally employed in CTC which indicates 14 hours (50400 second) of work. The established package processed numbered at 198,000 every day. Therefore the standard Takt Time equals to 0.25second/package. However, the Takt Time generated in the current system is 0.28 second/package. An encouraging result of 0.21second/package was obtained from the trial-run of the proposed system.

Statistical T-Test Analysis

To measure the effect of increasing performance, T-Test analysis is performed in this study. Several parameter comparisons were used between Current State Map and Future State Map which comprise of Total Time; Value Added Time; performance of VSM; Performance of Savings; Performance of Gap Time.

The result of T-Test analysis by using Minitab Software is shown on Table 1. The result of T-Test analysis prove the significant different between the Future State Map and Current State Map with the T-Value of 1.53. Statistically, Future State Map has greater performance with the P-value of 0.093 in the confidence level of 90%. It is accepted that the proposed automated system is causing significant improvement.

Table 1. T-Test Result by Using Minitab Software

	n	Mean	StDev	SE Mean	T-Value
Future System	6	48.4	53.3	21.8	1.53
Current System	6	38.2	37.6	15.4	

Summary

Lean techniques are widely applied under manufacturing context; they are being applied to the delivering business successfully in this research. Improved efficiency with less labor hours is observed. However, takt time and labor hours are the only factors considered as performance indicators in this research. It is suggested to the future researches that more lean limitations and indicators to be used to evaluate the implementation of Lean techniques in the delivering industry for further in depth understanding of the effect of Lean.

References

[1]John F Krafcik, “Triumph of the Lean Production system”, Sloan Management Review, Vol 30, No 1, 1988

[2] Reichhart, Andreas, & Holweg, Matthias, Lean distribution: concepts, contributions, conflicts, International Journal of Production Research, 45(16), 2007

[3] Womack, J. P, Lean thinking: where have we been and where are we going? Manufacturing Engineering, 129(3), 2002

[4] Grajo, E. S, Strategic layout planning and simulation for lean manufacturing: a LayOPT tutorial, Simulation Conference Proceedings, 1995. Winter.

[5] Pattanaik, L. N., & Sharma, B. P, Implementing lean manufacturing with cellular layout: a case study, The International Journal of Advanced Manufacturing Technology, 42(7-8), 2009.

[6] Rahani, A. R., & al-Ashraf, Muhammad.Production Flow Analysis through Value Stream Mapping: A Lean Manufacturing Process Case Study. Procedia Engineering, 41(0), 2012.

[7] Abdulmalek, Fawaz A., & Rajgopal, Jayant, Analyzing the benefits of lean manufacturing and value stream mapping via simulation: A process sector case study. International Journal of Production Economics, 107(1), 223-236, 2007

[8] Teichgräber, Ulf K., & de Bucourt, Maximilian, Applying value stream mapping techniques to eliminate non-value-added waste for the procurement of endovascular stents. European Journal of Radiology, 81(1), 2012

[9] Campbell, S, Tracking lean (automated shop floor data-capture technologies for lean automotive manufacturing). Manufacturing Engineer, 83(1), 38-41, 2004

[10] Zamorano, S. P, Mean and lean—conveyor design for the 1990s Mining Latin America/ Minería Latinoamericana, Springer Netherlands. 1994, pp. 265-278

[11] Jason Soros Shay, Improving Goods Flows and Information Flow Process through Value Stream Mapping: Case Study of a Delivery Company, CTC Internal Report, June 2013.

[12] Allen, J., Robinson, C, & Stewart, D, Lean Manufacturing: A Plant Floor Guide: Society of Manufacturing Engineers, 2001

Advanced Materials Research Vols. 989-994 (2014) pp 2815-2819
© (2014) Trans Tech Publications, Switzerland
doi:10.4028/www.scientific.net/AMR.989-994.2815

Research on Direct Torque Control adaptive Fuzzy Neural Network Controller of Permanent Magnet Synchronous Motor

Chaofan Lu[1, a], Hongbin Yu[1,b]

[1]School of Mechanical Engineering, Tianjin Polytechnic University,Tianjin,300380, China

[a]luchaofan_lz@163.com, [b]hbyu@yahoo.cn

Keywords: permanent magnet synchronous motor (PMSM); direct torque control (DTC); fuzzy neural network (FNN)

Abstract. Has the advantages of quick response of PMSM using the method of DTC, but will make the high torque and big magnetic flux linkage ripples. In order to solve this problem, using the fuzzy neural network hybrid system to replace the traditional hysteresis controller, Strong learning ability and fuzzy logic in handling uncertain information has the adaptive ability of neural network, the fuzzy neural network hybrid system to produce the expected voltage vector, the speed of a smooth transition of permanent magnet synchronous motor. The proposed method is validated by simulation under external disturbances in motor is very effective to reduce the ripple of torque and flux, the speed of the fast response and smooth transition.

Introduction

PMSM is widely used and the key of PMSM is how control it. Direct torque control method is proposed in recent years, it can make the PMSM has fast response, but the flux and torque fluctuations are larger. In this thesis presents a method combined with control of permanent magnet synchronous motor direct torque fuzzy neural network hybrid system. This thesis introduces the principle of fuzzy neural network hybrid system and direct torque control, modeling and simulation by MATLAB/SIMULINK, the simulation verify the effectiveness of the theory.

The Principle of Fuzzy Neural Network Hybrid System

At present, the network structure and learning algorithm of fuzzy neural network inference based on Mamdani, it is the most widely used. It is based on Neural Network memory the fuzzy control rules. According to the operation steps of hierarchical structure of fuzzy logic system, then by using the neural network learning algorithm do not change the fuzzy logic system[6~9].

The input vector is $x=[x_1,x_2,\ldots,x_n]^{\mathrm{T}}$, for each component x_i is fuzzy language variables, set $\mathrm{T}(x_i)=\{A_i^1,A_i^2,\cdots,\mathrm{A}_i^m\},i=1,2,\cdots,n$,among them $A_i^j(j=1,2,\cdots,m_i)$ is x_i the first j language variable value, it is defined in the domain U_i of a fuzzy set, The membership function of the corresponding is $\mu_{A_i^j}(x_i)$, （ $i=1,2,\cdots,n;j=1,2,\cdots,m_i$ ） . Output y is Fuzzy linguistic variables $\mathrm{T}(y)=\{B^1,B^2,\cdots B^{m_y}\}$, among them $B^j(j=1,2,\cdots m_y)$ is y the first j language variable value, it is defined in the domain U_y of a fuzzy set, the membership function of the corresponding is $\mu_{B^j}(y)$.

A description of the relation between input and output of fuzzy rules： if x_1 is A_1^i and x_2 is A_2^i and $\cdots x_n$ is A_n^i, then y is B^i , among them $i=1,2,\cdots,m$, m express the total number of rules , $m\le m_1m_2\cdots m_n$.

According to the fuzzy model of fuzzy system constructed above, such as fuzzy neural hybrid system is shown in Figure 1.

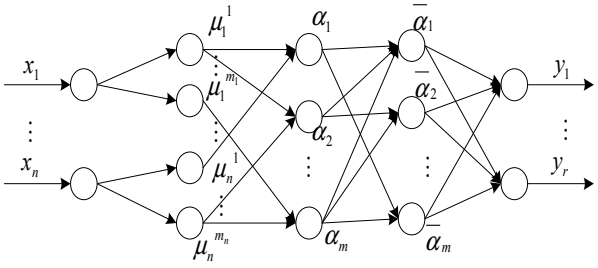

Fig.1 Structure fuzzy neural hybrid system

This structure is divided into five layers. Among them, the first layer is the input layer; the second layer of every node is the role of computing input component, representing a linguistic variable value. The formation of a fuzzy set, to construct the membership function μ_i^j , then $\mu_i^j = \mu_{A_i^j}(x_i)$, $i = 1,2,\cdots n; j = 1,2,\cdots m_1,$ among them m_1 is x_1 the fuzzy partition, n is The number of input variables; The third layer is used to match the premise part of fuzzy rules; each node represents a fuzzy rule, fitness degree of every rule, $\alpha_i = \min\{\mu_1^{i_1}, \mu_2^{i_2}, \cdots, \mu_n^{i_n}\}$ Among them $i_1 \in \{1,2,\cdots,m_1\}; i_2 \in \{1,2,\cdots m_2\}, \cdots, i_n \in \{1,2,\cdots,m_n\}, j = 1,2,\cdots,m, m = \sum_{i=1}^{n} m_i$ .Principle of the fourth layer and the third layer is the same.Objective is calculated to achieve normalization, $\overline{\alpha}_j = \dfrac{\alpha_j}{\sum_{j=1}^{m} \alpha_j}, j = 1,2,\cdots m$ .The right of the layer is the output layer, the purpose is clear to calculate fuzzy, $y_i = \sum_{I=1}^{M} w_{ij}\overline{\alpha_j} = \dfrac{\sum_{i=1}^{M} w_{ij}[\mu_{B^{ij}}(w_{ij})]}{\sum_{i=1}^{M}[\mu_{B^{IJ}}(w_{ij})]}, i = 1,2,\cdots r$,Among them w_{ij} is the j language value Membership function the center value, written in vector form: $y = W\overline{\alpha}$,

Among them, $y = \begin{bmatrix} y_1 \\ y_2 \\ \vdots \\ y_r \end{bmatrix}, W = \begin{bmatrix} w_{11} & w_{12} & \cdots & w_{1m} \\ w_{21} & w_{22} & \cdots & w_{2m} \\ \vdots & & \ddots & \vdots \\ w_{r1} & w_{r2} & \cdots & w_{rm} \end{bmatrix}, \overline{\alpha} = \begin{bmatrix} \overline{\alpha_1} \\ \overline{\alpha_2} \\ \vdots \\ \overline{\alpha_m} \end{bmatrix}$.

It is proved that fuzzy neural network has the ability of universal approximation property [6]. Fuzzy neural network has the universal approximation property and learning algorithm, Fuzzy neural network controller as shown in figure 2. $w_r(n)$ is the current moment motor actual speed, $w^*{}_r(n)$ is The current moment motor speed setting, $w_r(n-1)$ is the actual motor speed the former cycle, $w_r(n-2)$ is the actual speed of the motor of two former cycle , $i_q(n)$ is the present moment the stator current, $i_q(n-1)$ The stator current the former cycle, $\Delta i^*{}_q(n)$ is set value, $\Delta i_q(n)$ is the stator current domain value5%.

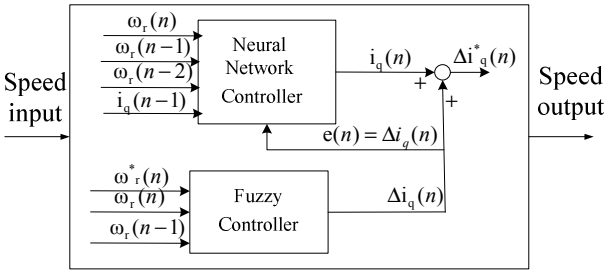

Fig.2 Fuzzy neural network controller

When motor running, the error value of each sampling period transmission to the fuzzy controller, if the actual speed of the motor is equal to the set value, fuzzy controller error value is zero, to calculate the network weights and threshold according to the neural network controller before sampling. If not equal to the set value, continue to adjust.

The Principle of Direct Torque Control

ψ_s is the stator magnetic flux linkage, ψ_r is the rotor magnetic flux linkage, PMSM rotor magnetic flux linkage is produced by permanent magnet, so ψ_r is constant. T is Electromagnetic torque, θ is ψ_s and ψ_r Angle [1]. Figure 3 is a permanent magnet synchronous motor M – T reference coordinate system.

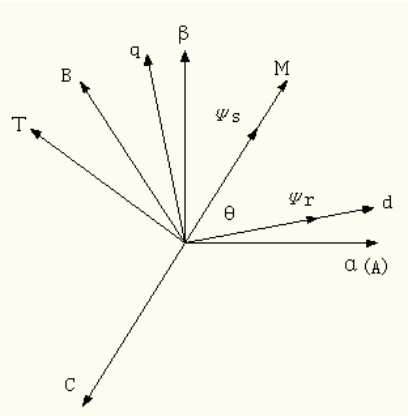

Fig. 3 M – T reference coordinate system

From Fig3 Can be drawn in permanent magnet synchronous motors M – T reference coordinate system Torque equation [1]:

$$T = \frac{3p|\psi_s|}{4L_dL_q}[2\psi_r L_q \sin(\theta) - |\psi_s|(L_q - L_d)\sin(2\theta)] \quad (1)$$

if ψ_s is constant, then T control θ [2].

Ignoring the effect of stator resistance R, According to the $\psi_s = \int (V_S - Ri_s)dt$ known, ψ_s to V_s applied in permanent magnet synchronous motor voltage vector direction adjustment. The switch tube has 8 working state combination, Inverter produce 8 voltage vector, including six non-zero voltage vector $V_1 - V_6$ and Two the zero vector V_0 and V_7. Voltage vector plane is divided into six areas, as shown in Figure 4 (a) shows, ψ_s in different regions, you can select different voltage vector. Because the choice of voltage vector relationship only with the ψ_s region, direct torque control the core is that According to the different voltage vector V_s adjustment ψ_s size come true θ change, in order to control T [2].

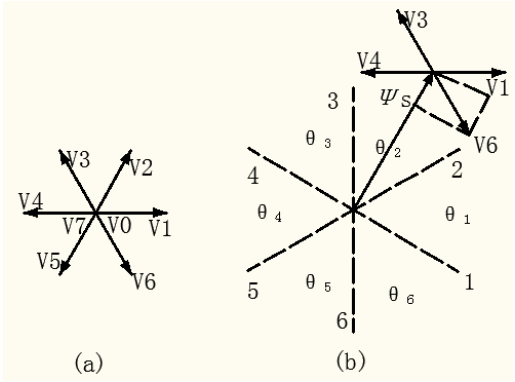

Fig. 4 Voltage space vector diagram

In order to realize Reduce The torque and magnetic flux linkage pulsation We must as soon as possible to change between the stator and rotor magnetic flux linkage θ, By selecting the appropriate space voltage vectors, ψ_s constantly advance and retreat, through the instantaneous change θ, control torque T, reducing pulsation of torque. The vertical and radial of space voltage vector decomposition of two directions in accordance with ψ_s, so the vertical component of the voltage vector can change the size of the electromagnetic torque, the radial component of the voltage vector can change the size of the stator magnetic flux linkage, Figure 4 (b) is the decomposition of with V_2 as example.

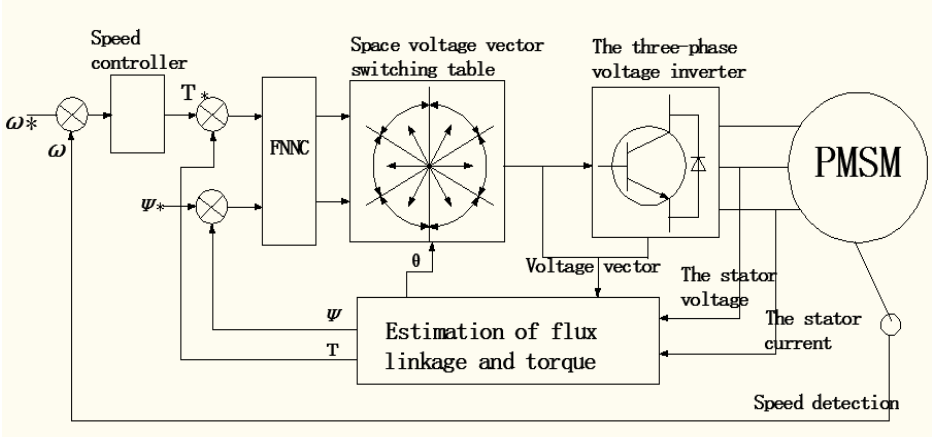

Fig. 5 The DTC system principle diagram of PMSM

The principle of PMSM of DTC is that compares between actual speed and the given speed of PMSM, the error between the two as input speed controller, speed controller output given torque. Three phase current and phase of the measured stator voltage delivery to the magnetic flux linkage and torque estimation process, The output torque value compared with the given torque speed controller output, the error input them into FNN control system. The flux values compared with the stator flux given value, error input to the FNN control system. The two output FNN control system and the stator flux linkage region judgment value as input of switching table, draw a set of control pulse, Control of three-phase voltage inverter switching, and control of PMSM.

Through FNN hybrid system generate the expected voltage vector, according to a sampling period of flux linkage and torque deviation determine voltage vector expected next sampling period. It is determined by the switching two adjacent non-zero voltage vector [3]. To achieve smooth flux trajectory and reduced torque pulsation [10~12]. Fig. 5 is the DTC system principle diagram of PMSM.

4. Simulation of DTC using FNN hybrid system

The PMSM parameter is: rated power $P_N = 3kW$, rated voltage $U_N = 380V$, magnetic pole $P = 2$, the stator resistance $R_S = 0.518\Omega$, direct axis inductance $L_d = 0.9(mH)$, quadrature axis inductance $L_q = 0.9(mH)$, $\psi_f = 0.1252(Wb)$, $\psi^* = 0.1252Wb$.

Input conditions: $T = 0N \cdot m \rightarrow 10N \cdot m \rightarrow 0N \cdot m \rightarrow 10N \cdot m$, $\omega^* = 1500r/\min$, the simulation results as shown in Fig. 6:

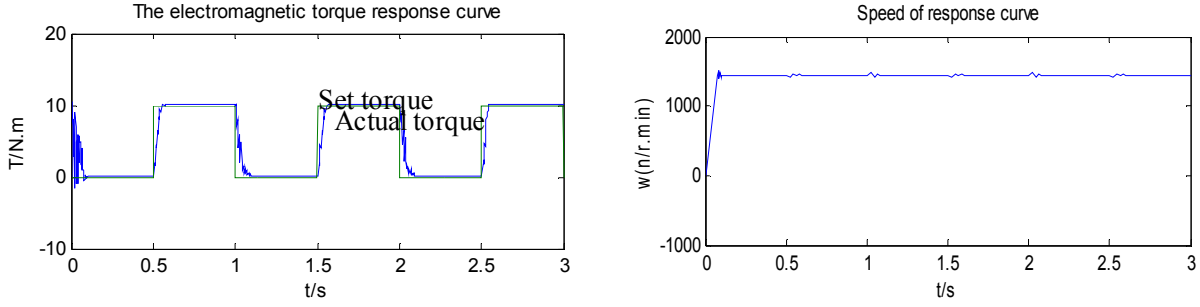

Fig. 6 The electromagnetic torque response curve and speed of response curve

From the Fig. 6 we know: The actual torque value well track torque setting and faster into a stable state to reduce torque ripple. Speed on the torque step jumping nodes only has small fluctuation, and soon the stability to the set speed. To demonstrate the effectiveness of DTC control of speed improvement of PMSM by use of FNN.

Acknowledgements

This thesis is supported by the Civil Aviation Joint Research Foundation (grant number U1333129).

References

[1] Xianqing Cao, Jianguang Zhu, Renyuan Tang. Simulation of Fuzzy Direct Torque Control System of Permanent Magnet Synchronous Motor [J].Proceedings of the CSU-EPSA, 18(4): p.76- 81(2006) (in Chinese).

[2] Lin Gui. The Research and Simulation of the Direct Torque Control for Permanent Magnet Synchronous Motor.Wuhan University of Technology (2012)(in Chinese).

[3] Yingjie Wei. The new cold storage door motion controller research and design [D]. Nanjing University of Science and Technology (2006)(in Chinese).

[4] Xianqing Cao, Jianguang Zhu, Renyuan Tang. Vector Controlled Permanent Magnet Synchronous Motor Drive with Adaptive Fuzzy Neural Network Controller [J].Proceedings of the CSEE (2006), 26(1):137-141 (in Chinese).

[5] Zhexue Ge, Zhiqiang Sun. Neural network theory and MATLAB R2007 Implementation. Beijing: Electronic Industry Press (2007) (in Chinese).

[6] Hairong Sun. The Research and Application of the Fuzzy Neural Network [D]. North China Electric Power University (2006) (in Chinese).

[7] Chunmei He. The performance and learning algorithm of Fuzzy Neural Network [D]. Nanjing University of Science and Technology (2010) (in Chinese).

[8] Jian Zhang. The model of fuzzy neural network algorithm research and Application [D]. Daqing Petroleum Institute (2002) (in Chinese).

[9] Fangju Ai. Study on Structural Optimization of Fuzzy Neural Network [D]. Graduate University of Chinese Academy of Sciences (2006) (in Chinese).

[10] Xianqing Cao. A Rapid Efficiency-optimization Control Scheme of PMSM System [J]. MICROMOTORS (2013), 46(10):69-73 (in Chinese).

[11] Dan Sun. High performance direct torque control for permanent magnet synchronous motors [D] . Zhejiang University (2004) (in Chinese).

[12] Bin Wang, Yue Wang, Zhaoen Wang. Direct torque control of permanent magnet synchronous motor drives using space vector modulation [J].Electric machine and control (2010), 14(6):45-50 (in Chinese).

Advanced Materials Research Vols. 989-994 (2014) pp 2820-2824
© (2014) Trans Tech Publications, Switzerland
doi:10.4028/www.scientific.net/AMR.989-994.2820

The Series and Parallel Energy Storage System based on Super Capacitors

Zhao Kuo[1, a], Zhang Yibin[1,b] and Yu Bo[1,c]

[1]Northeastern University, No. 3-11, Wenhua Road, Heping District, Shenyang, 110819, P.R.China

[a]zhaokuo13@126.com, [b]zhangyibinneu@163.com, [c]458119339@qq.com

Keywords: energy storage, super capacitor, series and parallel, power smoothing, power quality

Abstract. The series and parallel energy storage system based on super capacitors can quickly adjust a wide range of active and reactive power in two directions, which is a new way to improve the stability and power quality of new energy power generation system. In this paper, double converters structure is used to achieve the series and parallel compensation effect and their control strategies according to Instantaneous Power Theory. It is simulated in PSCAD that series and parallel energy storage system of super capacitor contribute to the impact on wind turbines power as environment conditions change. Simulation results show that the energy storage system can greatly improve the stability and power quality of grid-connected wind turbines.

Introduction

In recent years, it's a power industry hotspot to utilize energy storage systems for solving the problem of new energy generation system power fluctuations and power quality. With the excellent characteristics [1][2], super capacitors is gaining favor in many scholars. Currently, super capacitor energy storage devices are mostly connected to the grid in parallel [3]. If the double converters structure is adopted in the energy storage system to achieve series and parallel compensation active and reactive power can quickly adjust in two directions and a wide range. By this way, the series and parallel energy storage system of super capacitors is able to maintain the power stability and improve power quality of new energy power generation.

Principle of the series and parallel energy storage system

The energy storage system is installed in the point where the new energy generation system is connected to grid. The structure of the series and parallel energy storage system of super capacitors is shown in Figure 1.

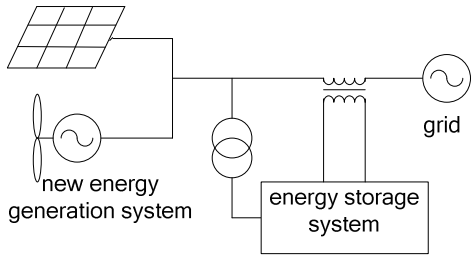

Fig.1 Structure of the series and parallel energy storage system of super capacitors

Parallel inverter of the energy storage system injects current to the system. Through the parallel compensation device, it's easily to injected or absorbed active and reactive power from the system. Therefore, parallel compensation can control the active and reactive power balance of power system. Series inverter of the energy storage system can inject a voltage component changing continuously and voltage fluctuation and voltage sag is easily offset through the series compensation from the energy storage system. Therefore, the series compensation can guarantee stability of the supply voltage [4-6].

Energy storage system of super capacitors

The energy storage system of super capacitors need for DC / DC converter and it control system helping super capacitor charging and discharging [7]. The circuit topology of super capacitor energy storage system is shown in Figure 2, which consists of bi-directional DC / DC converter and super capacitors.

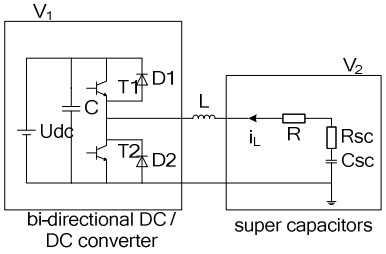

Fig.2 Super capacitor energy storage system circuit topology

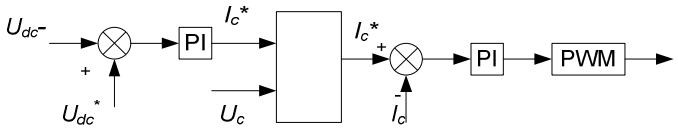

Fig.3 Converter control diagram

The control target of DC/DC converter [8] is not only to maintain a constant high DC voltage of energy storage system but also to meet the super capacitor power limit. Converter control diagram is shown in Figure 3.

In the diagram, U_{dc} stands for measurements value of the DC high voltage; U_{dc}* stands for DC high voltage reference value, determined by the charging and discharging state of super capacitors. According to U_c, the actual voltage of the super capacitor, the current reference value is limited in a certain range. Then based on the current reference value I_c* and the current flowing through super capacitor I_c , control signal can be obtained.

Control strategy of the parallel inverter

The circuit topology of parallel storage system is shown in Figure 4, the connected-grid voltage of new energy power is U_{wa}, U_{wb} and U_{wc}, connected-grid current is I_{wa}, I_{wb} and I_{wc}, and output power is P_w and Q_w. Filter capacitor in parallel storage systems is C_{pf}, the power flowing into the filter capacitor is P_b and Q_b, and current is I_{ba}, I_{bb} and I_{bc}. The parallel transformer is T_p, and the filter inductor is L_{pf}, the current flowing into filter inductor is I_{bpa}, I_{bpb} and I_{bpc}. The DC voltage rectified by converter is U_{dc}, and the capacitor of DC side is C_{dc}. DC side is connected to super capacitor energy storage module.

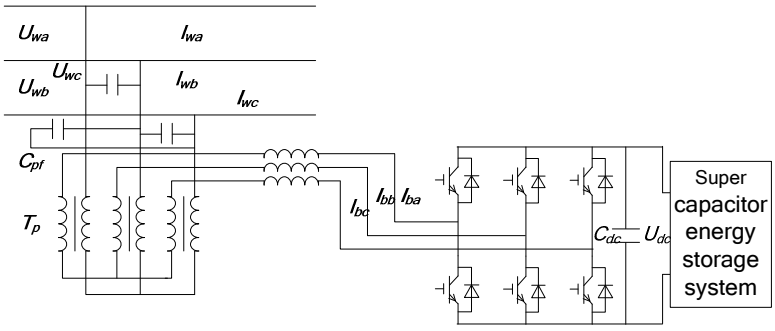

Fig.4 Circuit topology of parallel storage system

First, U_{wa}, U_{wb} and U_{wc} are transformed to U_{wd} and U_{wq} by DQ transformation. By the same way, I_{wa}, I_{wb} and I_{wc} are transformed to I_{wd} and I_{wq}, and I_{ba}, I_{bb} and I_{bc} are transformed to I_{bd} and I_{bq}. The parallel compensation is mainly used to smooth output power of new energy generation systems [9]. Therefore, active and reactive power is the control signal, and active and reactive power is respectively controlled in the steady-state conditions. Its inverter control diagram is shown in Figure 5.

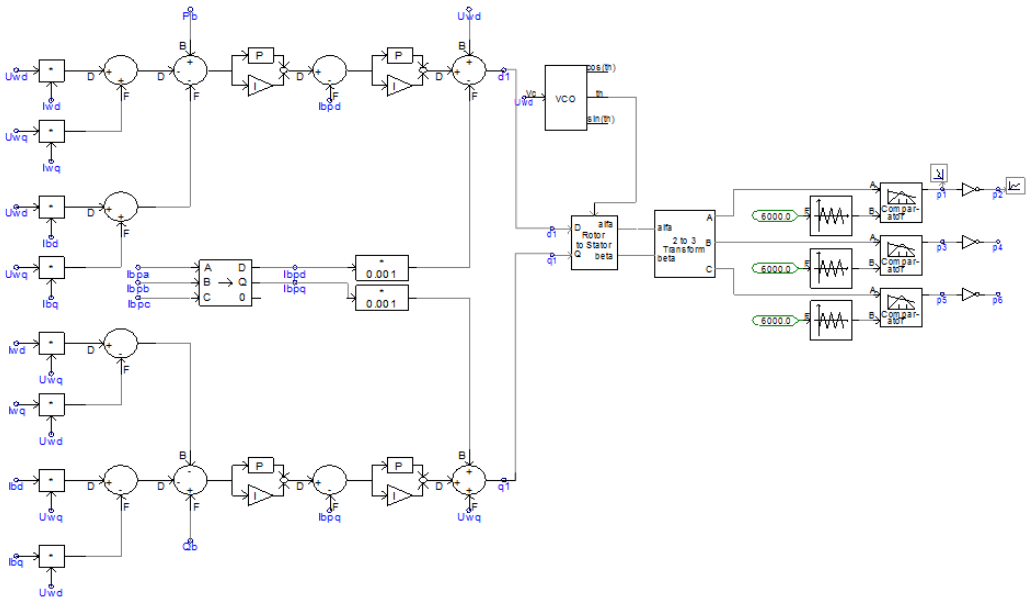

Fig.5 Parallel inverter control diagram

Control strategy of the series inverter

The circuit topology of series system is shown in Figure 6. It is connected to new energy power system through the transformer T_s. Phase voltage drop of transformer T_s is named as U_{ca}, U_{cb}, U_{cc}. The filtering capacitor is C_{sf}, current flowing into C_{sf} is I_{bsa}, I_{bsb}, I_{bsc}, and filter inductor is L_{sf}, voltage after L_{sf} is U_{bsa}, U_{bsb}, U_{bsc}. Through DC voltage converter rectified as U_{dcs}, DC capacitor is C_{dcs}. DC side is connected to super capacitor energy storage module.

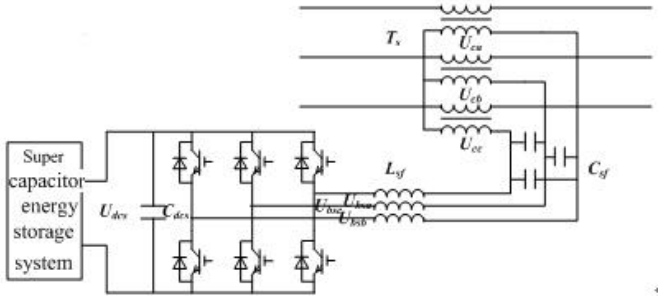

Fig.6 Circuit topology of parallel series system

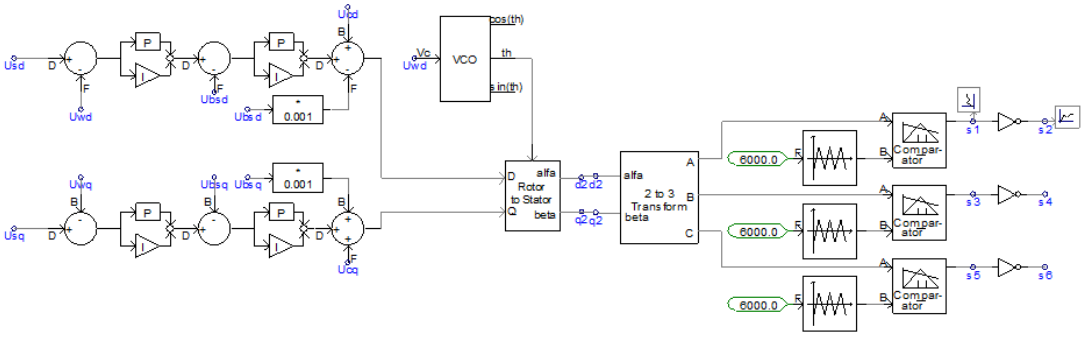

Fig.7 Series inverter control diagram

First U_{sa}, U_{sb}, U_{sc} are transformed to U_{sd}, U_{sq} by DQ transformation. By the same way, U_{bsa}, U_{bsb}, U_{bsc} are transformed to U_{bsd} and U_{bsq}; U_{ca}, U_{cb}, U_{cc} are transformed to U_{cd}, U_{cq}. Series compensation can change the characteristics of the natural distribution line voltage by inserting a voltage source [6]. The connected-grid voltage of new energy generation systems is the control signal for controller. The inverter control diagram is shown in Figure 7.

Simulation

The simulation model is established in PSCAD/EMTDC, with series and parallel energy storage system connected to double-fed wind power generation system. At 0.5s, active power has a short drop, and double-fed induction motor absorbs reactive. During 0.5s-4s, output active is about 0.5MW. At 4s, the average wind speed increases by 1m/s, active power increases to 0.8MW, double-fed induction motor does not output or absorb reactive power. Active and reactive waveforms are shown in Figure 8.

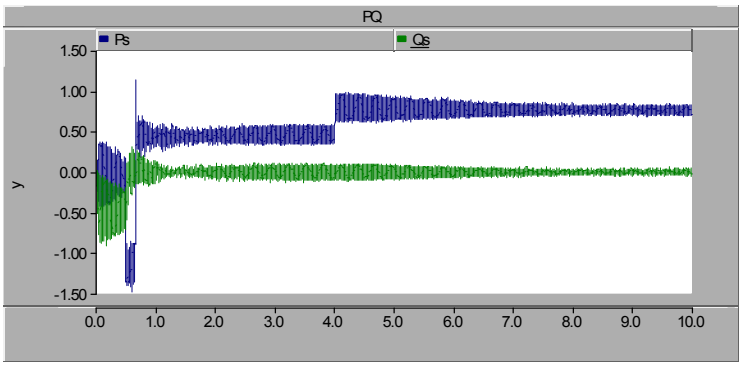

Fig.8 Active and reactive waveforms before utilizing the device

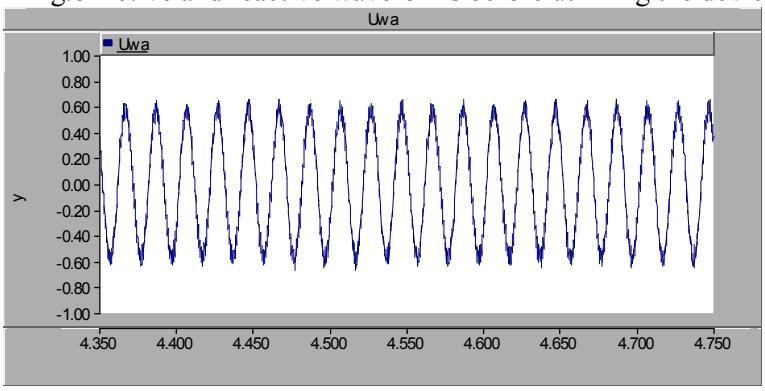

Fig.9 Connected- grid voltage before utilizing the device

It can be seen that active waveform fluctuations is in the wide range of about 0.2-0.3MW without super capacitor energy storage system. At the same time, connected-grid voltage amplitude of wind power generation system is about 0.6kV, and voltage harmonic is serious as shown in Figure 9.

After utilizing the series and parallel energy storage system of super capacitors, active and reactive power waveforms are shown in Figure 10. Compared with previous figure, active power and reactive power fluctuations are significantly reduced, achieved power smoothing.

After utilizing the series and parallel energy storage system of super capacitors, the voltage waveform of connected-grid side is shown in Figure 11. The voltage harmonic is reduced obviously.

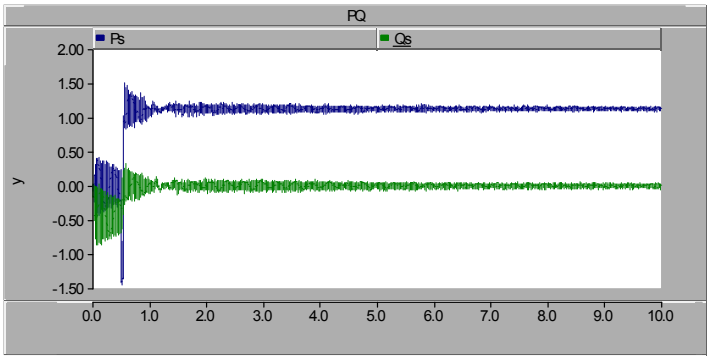

Fig.10 Active and reactive waveforms after utilizing the device

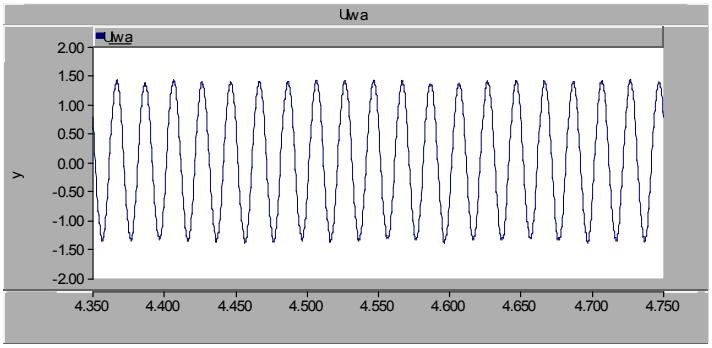

Fig.11 Connected- grid voltage before utilizing the device

Summary

In this paper, the series and parallel energy storage system based on super capacitor is designed, which achieves a wide range and fast regulation for active and reactive power in two directions and is able to improve power quality. Simulation results show the effectiveness of the above conclusion.

References

[1] Sikkabut S, Fuengwarodsakul N H, Sethakul P, et al. In: Power Electronics and Drive Systems (PEDS), 2013 IEEE 10th International Conference: 1213-1218 (2013).

[2] Toledo O M, Oliveira Filho D, Diniz A S A C: Renewable and Sustainable Energy Reviews. Vol. 14(1): 506-511 (2010).

[3] Brekken T K A, Yokochi A, Von Jouanne A, et al: Sustainable Energy, IEEE Transactions on. Vol. 2(1): 69-77 (2011).

[4] Zhang Z, Liu C, Zhang X: A Summary of Harmonic Detection in Electricity Distribution Based on the Instantaneous Power Theory (Mechatronics and Automatic Control Systems. Springer International Publishing, 2014).

[5] Guerrero J M, Loh P C, Lee T L: Industrial Electronics. Vol. 60(4): 1263-1270 (2013).

[6] Wasiak I, Pawelek R, Mienski R: Generation, Transmission & Distribution. Vol. 8(3): 463-472 (2014).

[7] Hu X, Tseng K J, Srinivasan M. In: Power Electronics and ECCE Asia (ICPE & ECCE), 2011 IEEE 8th International Conference: 1552-1557 (2011).

[8] Barton J P, Infield D G: IEEE Trans on Energy Conversion. Vol. 2: 44l-448 (2004).

[9] Silva P V, Pinheiro R F, Aguiar M V, et al. In: Power Electronics Conference (COBEP), 2011 Brazilian. IEEE: 782-787 (2011).

Advanced Materials Research Vols. 989-994 (2014) pp 2825-2828
© (2014) Trans Tech Publications, Switzerland
doi:10.4028/www.scientific.net/AMR.989-994.2825

Nonsmooth Bifurcations in a Cracked Rotor-Active Magnetic Bearings System

Fenghong Yang[1, a], Hongzhi Tong[2,b]

[1] School of Statistics and Mathematics, Central University of Finance and Economics, Beijing 100081, China

[2] School of Statistics, University of International Business and Economics, Beijing 100029, China

[a]fhyang@cufe.edu.cn, [b]tonghz@uibe.edu.cn

Keywords: nonsmooth bifurcation, chaos, cracked rotor-active magnetic bearings

Abstract. A cracked rotor-active magnetic bearings (AMB) system with the time-varying stiffness is modeled by a piecewise smooth system due to the breath of crack in a rotating shaft. The governing nonlinear equations of motion for the nonsmooth system are established and solved with the numerical method. The simulation results show that a grazing bifurcation, period-double bifurcation and chaotic motions exist in the response. These nonsmooth bifurcations can give rise to jumps between periodic motions, quasi-periodic motions and chaos.

Introduction

Active magnetic bearings (AMBs) present a technology that has many advantages compared to traditional bearing concepts and have been used in many engineering applications, for example, mechanical engineering, aeronautic engineering, astronautic engineering and many others. Research on the properties of the nonlinear dynamics and stability for the rotor-AMB system has received more attentions in the recent years [1,2].

Fatigue cracking of the rotor shaft is an important fault observed in the rotating machinery which can lead to catastrophic failure. So, detailed investigation into the dynamic response of a rotor with crack in the shaft is very important for diagnosing and preventing rotor cracks. For a cracked rotor, the crack opens and closes with rotation. When the crack is opening, the material shaft stiffness will decrease. When the crack is closed, the shaft stiffness will return to the value identical to that of the noncrack shaft. The rotating shaft has a discontinuous stiffness value, so the system is piecewise smooth. A great deal of research effort has been devoted to the study of the nonlinear responses and the transition to chaos of cracked rotors [3,4]. For piecewise smooth systems, there exist some nonconventional bifurcations, i.e., grazing bifurcation and sliding bifurcation. The nonconventional bifurcation, which was defined as nonsmooth bifurcation, may occur when a system solution collides one of the state-space boundaries, as the system parameters are varied [5].

In this paper, we investigate nonsmooth bifurcations in a cracked rotor-AMB system with time-varying stiffness. At first, the governing nonlinear equation of motion is established for the rotor-AMB system with the quadratic and cubic nonlinear terms. Then the effect of using controller parameters on the dynamics of the active cracked rotor is analyzed.

Model and Equations of Motion

Rotor Model. The rotor system to be studied, as in [3], is a massless flexible shaft with a central disc, which is supported on two identical rigid bearings as shown in Fig. 1a. In order to simplify the analysis, an AMB is located at the disc position as a damper in order to control the vibration of the disc. There is a transversal crack close to the middle disc. The stiffness of the uncracked rotor system is symmetric and the damping at the middle disc due to the air resistance effect is viscous.

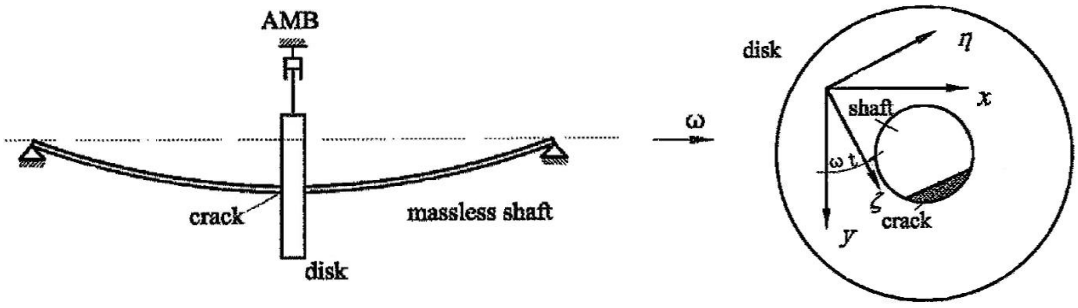

(a) (b)

Fig. 1. The cracked rotor model with an AMB.

Crack Model. The switching crack model (also known as hinge model) is often used to simulate the crack breathing in rotors, as shown in Fig. 1b. The typical behavior of the crack (the breathing of the crack under weight influence) is described by the very simple model of Gasch [6]. When crack is open, the local stiffness of shaft will have a decrease of stiffness, which depends on the crack's depth. When crack is closed, the stiffness will be identical with that of the noncracked shaft. The opening and closing of crack are dominated by the sign of ζ : If $\zeta > 0$, the crack bears the tension stress and opens; if $\zeta \le 0$, the crack bears compression stress and closes.

Let f is the switch function that represents the opening and closing of crack with rotation, and

$$f(\zeta) = \begin{cases} 1 & \zeta > 0 \\ 0 & \zeta \le 0 \end{cases}. \tag{1}$$

The transfer matrix between rotating coordinates and fixed coordinates is

$$\begin{bmatrix} \zeta \\ \eta \end{bmatrix} = \begin{bmatrix} \sin \omega t & \cos \omega t \\ \cos \omega t & -\sin \omega t \end{bmatrix} \begin{bmatrix} x \\ y \end{bmatrix}. \tag{2}$$

So $\zeta = x \sin \omega t + y \cos \omega t$. While the rotor is running, the ζ is varied with t. When ζ transverses the critical value 0, the stiffness will switch back and forth between two values. That makes the vector field piecewise smooth. And we call the line $\zeta = 0$ the switch line.

Equations of motion of the rotor system. The equations of motion of the rotor system in stationary Cartesian co-ordinates can be written as

$$\begin{bmatrix} m & 0 \\ 0 & m \end{bmatrix} \begin{bmatrix} \ddot{x} \\ \ddot{y} \end{bmatrix} + \begin{bmatrix} c & 0 \\ 0 & c \end{bmatrix} \begin{bmatrix} \dot{x} \\ \dot{y} \end{bmatrix} + K(t) \begin{bmatrix} x \\ y \end{bmatrix} = \begin{bmatrix} 0 \\ mg \end{bmatrix} + me\omega^2 \begin{bmatrix} \cos \omega t \\ \sin \omega t \end{bmatrix} + \begin{bmatrix} F_x \\ F_y \end{bmatrix} \tag{3}$$

where x and y are the displacements of the disc in the stationary co-ordinate system, $K(t)$ is the stiffness matrix of the cracked shaft in the disc position, and

$$K(t) = \begin{bmatrix} \overline{k}_0 - f\Delta k \sin^2 \omega t & -f\Delta k \sin \omega t \cos \omega t \\ -f\Delta k \sin \omega t \cos \omega t & \overline{k}_0 - f\Delta k \cos^2 \omega t \end{bmatrix}, \tag{4}$$

where $\overline{k}_0$ is the stiffness of the uncracked shaft, Δk is the decrease of stiffness in the ζ direction when crack is opening. m is the equivalent mass in the disc position, c is the viscous damping coefficient, e is the imbalance eccentricity between the centre of the gravity and the geometric centre of the disc, g is the acceleration due to gravity, ω is the rotational speed of the rotor system, F_x and F_y are the feedback control forces produced by the AMB in the x and y directions, respectively, see [1] in detail.

For the simplicity in computation, we transform the above motion equations into a dimensionless form. Dividing both sides by $m\omega^2\delta_{st}$, one obtains the non-dimensional equations of motion of the cracked rotor system with the AMB as

$$\ddot{X} + \frac{2\xi}{\Omega}\dot{X} + \frac{1+\alpha_1}{\Omega^2}X - \frac{f\Delta K}{\Omega^2}(X \sin^2 \tau + Y \sin \tau \cos \tau) = U \sin \tau + \frac{\overline{F}_x}{\Omega^2}, \tag{5a}$$

$$\ddot{Y}+\frac{2\xi}{\Omega}\dot{Y}+\frac{1+\beta_1}{\Omega^2}Y-\frac{f\ \Delta K}{\Omega^2}(X\sin\tau\cos\tau+Y\cos^2\tau)=U\cos\tau+\frac{\overline{F}_y}{\Omega^2}, \tag{5b}$$

where

$$\overline{F}_x=\left(3\mu_2X^2+3\mu_3X\dot{X}+\mu_2Y^2+2\mu_3Y\dot{Y}\right)\dot{X}+\left(2\mu_2XY+\mu_3X\dot{Y}\right)\dot{Y}+\mu_4X\dot{Y}+\mu_4\dot{X}Y$$
$$+\alpha_2X^3+\alpha_3XY^2+\alpha_4XY+(-2f_{11}X+f_{12}XY)\cos(w\tau),$$
$$\overline{F}_y=\left(3\mu_2Y^2+3\mu_3Y\dot{Y}+\mu_2X^2+2\mu_3X\dot{X}\right)\dot{Y}+\left(2\mu_2XY+\mu_3\dot{X}Y\right)\dot{X}+\mu_4X\dot{X}+\mu_5Y\dot{Y}$$
$$+\beta_2Y^3+\beta_3X^2Y+\beta_5X^2+\beta_6Y^2+(-2f_{21}Y+f_{22}Y^2+f_{23}Y^2)\cos(w\tau),$$

where $X=x/\delta_{st}$; $Y=y/\delta_{st}$; $U=e/\delta_{st}$ is the rotor imbalance parameter, $\xi=\overline{\mu}/2m\omega_{cr}$ is the viscous damping ratio, $\Omega=\omega/\omega_{cr}$ is the rotational speed ratio, δ_{st} is the corresponding deformation of the shaft due to the weight of the rotor, $\omega_{cr}=\sqrt{k_0/m}$ is the critical speed of the uncracked rotor, k_0 is the stiffness of the uncracked rotor, $w=\tilde{\omega}/\omega$ and $\tau=\omega t$ is non-dimensional time. The prime refers to differentiation with respect to τ. The other parameters are ignored here.

Simulations and Analysis.

In this section nonlinear behavior of the cracked rotor is examined. In order to investigate the bifurcation characteristics, we take rotational speed Ω as control parameter and its effect on nonlinear dynamic response has been undertaken in the present work. Using the following rotor configuration, the dynamic response is studied using bifurcation diagram, orbit plot and Poincare map. Selected parameters values: $\alpha_i=-0.1,0.5,0.2,-0.5,\ i=1,2,3,4;$ $\beta_i=-0.3,0.3,0.3,-0.25,0.6,\ i=1,$ $2,3,5,6;\ u_i=-0.5,-0.4,0.5,1.7,\ i=2,3,4,5;\ f_{12}=0.6;\ f_{21}=f_{11},\ f_{2i}=0.3,1.02, i=2,3$; $\xi=0.01,$ $w=2.5$. For the disc's position of cracked rotor, if ζ (ζ represents the displacement of the disc in the ζ direction) touches tangentially the switch line $\zeta=0$, a grazing bifurcation will take place.

Fig. 2 provides the bifurcation behavior of the cracked rotor ($\Delta K=0.6,\ f_{11}=0.19,\ U=0.1$). The rotating speed ratio Ω is taken as the control parameter, which is defined as the ratio of rotation speed to the natural frequency of the uncracked rotor. It can be seen from Fig. 2 that, as the speed increases, there are obviously four chaotic zones. the rotor motion experiences period-double bifurcation, grazing bifurcation ($\zeta=0$) and chaos.

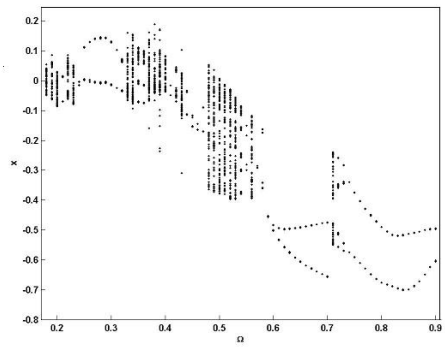

Fig. 2 Bifurcation diagram at $\Omega=0.18$ to 0.9.

(1) Period-double bifurcation. Fig. 2 shows that there are several period-double bifurcations. Near $\Omega=0.59$ and $\Omega=0.75$, period-double bifurcation and inverse period-double bifurcation occur.

(2) Gazing bifurcation. There are two grazing periodic-4 motions at $\Omega=0.729,0.726$. Fig. 3 shows phase portraits, the switch line and Poincare sections at $\Omega=0.729$. When Ω increases a little, $\Omega=0.731$, the responses turn to chaos as shown in Fig. 4. It is found that the grazing bifurcation can cause the response to turn to chaotic motion directly.

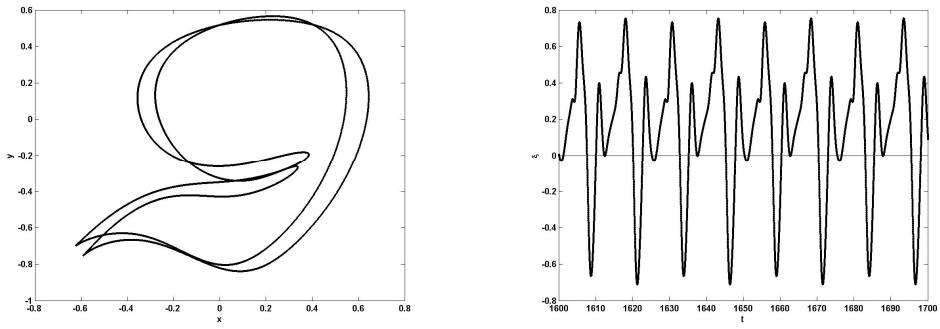

(a) Periodic-4 motion at $\Omega = 0.729$. (b) Grazing the switch line at $\Omega = 0.729$.

Fig. 3 Evolution of the response near at $\Omega = 0.729$.

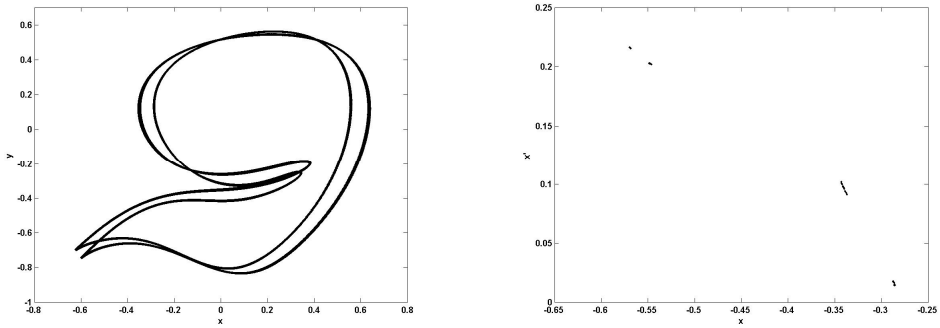

(a) Chaotic motion at $\Omega = 0.731$. (b) Poincare section at $\Omega = 0.731$.

Fig. 4 Evolution of the response near at $\Omega = 0.731$.

Conclusions

This paper focuses on a cracked rotor-AMB system with quadratic and cubic terms and time-varying stiffness. First, the governing nonlinear equation of motion is established for the rotor-AMB system with two-degree-of-freedom. Then, the nonsmooth bifurcations of the system are investigated using numerical method. From the results，the following conclusions can be drawn. For the nonsmooth cracked rotor-AMB system, there exists grazing bifurcation and periodic bifurcation in the response. The grazing bifurcation can cause the response to jump from one periodic motion to chaos directly.

Acknowledgements

This work was financially supported by the Natural Science Foundation of China.

References

[1] W. Zhang, X. P. Zhan, Periodic and chaotic motions of a rotor-active magnetic bearing with quadratic and cubic terms and time-varying stiffness. Nonlinear Dynamics, Vol. 419 (2005), p331

[2] M. Eissa, M. Kamel and H.S. Bauomy, Dynamics of an AMB-rotor with time varying stiffness and mixed excitations, Meccanica, Vol. 47 (2012), p585

[3] C.S. Zhu, D. A. Robb and D. J. Ewins, The dynamics of a cracked rotor with an active magnetic bearing. Journal of Sound and Vibration, Vol. 265 (2003), p469

[4] W. Qin, G. Meng, R. Xingmin, Grazing bifurcations in the response of cracked Jeffcott rotor, Nonlinear Dynamics, Vol. 35 (2004), p147

[5] M. D. Bernardo, C. Budd and A. Champney, Grazing, skipping and sliding: Analysis of non-smooth dynamics of the DC/DC buck converter, Nonlinearity, Vol. 11 (1998), P859

[6] R. Gasch, A survey of dynamic behaviour of a simple rotating shaft with a transverse crack, Journal of Sound and Vibration, Vol. 160 (1993), p313

Advanced Materials Research Vols. 989-994 (2014) pp 2829-2833
© (2014) Trans Tech Publications, Switzerland
doi:10.4028/www.scientific.net/AMR.989-994.2829

Modeling and Analysis of Arresting Property of EMAS

Hehuan Zhao[1, a], Hongbin Yu[2,b]

[1,2]School of Mechanical Engineering, Tianjin Polytechnic University, Tianjin, China, 300387

[a]892896238@qq.com, [b]hongbinyu@aliyun.com

Keywords: aircraft, EMAS, Arresting, static analysis, dynamic model

Abstract. The EMAS of aircraft-pavement is a dedicated device that used to block aircraft overrunning the runway. To protect the safety of aircraft and passengers, the EMAS can safely arrest the overrun aircraft in an allowed distance and inertial load without injuring aircraft passengers and damaging aircraft. Combining with actual situation, this paper made statics and dynamics analysis under the action of the wheel of EMAS， and provides effective theoretical support for further research of EMAS of aircraft-pavement.

Introduction

With the development of the society, the air traffic is increasing. Because of the meteorological factors, mechanical accident, the driver reason and so on. How to reduce the suffered harm the plane on the runway accident effectively, ensure the safety of life on further, reduce the damage of aircraft, has become an urgent problem need to solve for the world's largest airport. Now the hydraulic system is used more than others[1], but the system structure is complex and has many shortcomings. EMAS can arrest aircraft has different quality and different speed, make it stop within a safe distance from causing serious damage for passengers and aircraft[2].

Current Situation of EMAS

EMAS is a new kind arrestor system of aircraft, laid by the lightweight foam concrete that tire can be pressed into. It is important security measures and usually installed at the end of the runway of the airport. At present, the ESCO corporation and FAA of the United States developed engineered materials arresting system(EMAS) has become a special equipment to arrest the plane overrun the runway[3]. The key technology of EMAS such as material research[4] and development, the mathematical model[5] establishment and structure design applied has been more mature in the United States[6], and the system has been applied widely in the United States, played an important role in the actual use. By the end of the April 4, 2014, EMAS has 74 runway at the airport in the United States has carried on the installation, there have been nine incidents where EMAS has safely stopped nine overrunning aircraft with a total of 243 crew and passengers aboard those flights[7].

Due to various reasons, Aircraft may overrun the runway during takeoff and landing, the tire will crushed and sunk into EMAS. In this process, the plane's kinetic energy translate into the energy of the crushed material. With increasing the distance of the plane into the EMAS, the height of the EMAS will also increase gradually, Foamed concrete will provide the wheel greater resistance moment, and finally the aircraft stopped at a safe distance.

Mathematical Model of EMAS

Interaction mechanism of wheel and foamed concrete. In order to determine the arresting performance of foamed concrete, we established the interaction model of the wheel and foam concrete. The model is a dynamic model of aircraft arresting system, as the plane drown EMAS, it can calculate the dynamic load acting on the wheel of foam concrete. The wheel for a given direction of motion, F_D is the horizontal total drag force between the tires of an aircraft and the arrestor materials, F_C is the overall total reaction force applied by the foamed concrete on the wheel. the resistance is

composed of four parts, Including foam concrete dynamic Crushing resistance $F_{D1,}$ tearing force $F_{D2,}$ adhesive resistance F_{D3} and equivalent friction F_{D4}.

1) Dynamic Crushing resistance. When the plane crossed into foam concrete, it will produces a rut with certain depth and width. The section between the wheel and the foam concrete is divided into two parts, i.e. the arc segment and the wheel footprint segment, as shown in Fig. 1.

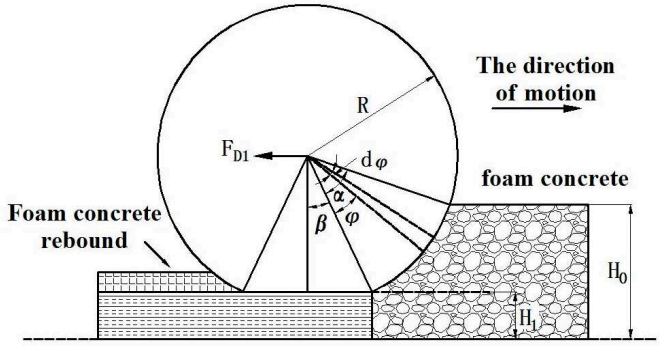

Fig.1. Schematic of the interaction between an aircraft tire and foamed concrete

H_0 is the initial height of the foam concrete and H_1 is compaction height in this diagram. R is the radius of wheel. The figure also defines the angleβ, calculated as follows:

$$\beta = arc\ \sin\ (\frac{Mg}{P_L B}) \tag{1}$$

Where M is the weight of aircraft, G is the acceleration of gravity, P_L is the tire pressure, t B is the effective width of wheel. According to the compression strength condition, the horizontal resistance under the incremental φ of angle dφ on wheels is

$$\mathrm{d}F_{H1} = \sigma_C BR\sin(\beta+\varphi)d\varphi \tag{2}$$

According to the mechanical properties of foam concrete, we assume that the stress-strain curve obeys a power law model[8]. The stress σ_C can be calculated as

$$\sigma_C = \sigma_0 + \mathrm{k}\varepsilon^{\mathrm{n}} \tag{3}$$

Where ε is compression strain of foam concrete, σ_0 is initial yield stress, k and n is the parameters associated with mechanical properties of the material. Based on the assumption that no relative sliding between tire and foam concrete, compression strain ε can be expressed as

$$\varepsilon = \frac{\sqrt{2}R}{H_0}\sqrt{1-\cos(\alpha-\varphi)} \tag{4}$$

Integrating between φ=0 and α gives the compressive resistance on one tire, get the horizontal compaction resistance

$$F_{D1} = BR\sigma_0[\cos\beta-\cos(\beta+\alpha)]+\frac{2^{\frac{n}{2}}kBR^{n+1}}{H_0^2}\int_0^{\alpha}\sin(\beta+\varphi)[1-\cos(\alpha-\varphi)]^{\frac{n}{2}}d\varphi \tag{5}$$

2) Tearing force. When the tire pressure through the foam concrete, it can tear on either side of the foam concrete, as shown in Fig. 1, tearing force F_{D2} can be expressed[9]

$$F_{D2} = 2\int_0^{\alpha}\gamma R\sin(\beta+\varphi)d\varphi = 2\gamma R[\cos\beta-\cos(\beta+\alpha)] \tag{6}$$

3) Adhesive resistance. When the tire rolling in the foam concrete, due to inertia effect, concrete under the tires move with the tyre tread in the tangent direction and produce resistance F_{D3}, as shown in Fig. 2

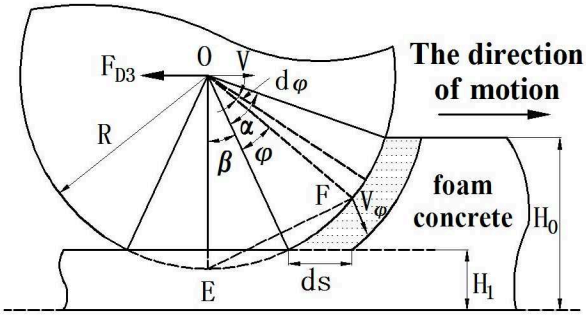

Fig.2. Adhesive resistance of tire Under pure rolling condition.

As the wheels speed in the horizontal direction is V, we can calculate the Vφ is

$$V_{\varphi} = 2V\cos(\frac{\beta+\varphi}{2}) \tag{7}$$

When the wheel moves forward a micro period ds, the kinetic energy dT of the micro section of foam concrete expressed as (1/2) • m • V_{φ}^2=F_{D3} • ds, eliminate ds and F_{D3} can be expressed

$$F_{D3} = \rho_0 BRV^2[\alpha + \sin\beta + \sin(\alpha+\beta)] \tag{8}$$

4) equivalent friction. In order to ensure that the aircraft can stop in a safe area of runway, the friction between the tire tread and runway should meet the document [10, 11]. After the wheel entering the EMAS, between the wheel and the concrete will produce two part friction, One part is the friction between the tire surface and the compressed foam concrete, another part is the friction between the wheel and the two side section of concrete. Because the side pressure is little, the side friction is negligible. equivalent friction F_{D4} can be expressed

$$F_{D4} = \mu F_C \tag{9}$$

Where μ is the equivalent friction coefficient. In conclusion, the total resistance of a single wheel by foam concrete is

$$F_D = F_{D1} + F_{D2} + F_{D3} + F_{D4} \tag{10}$$

Dynamic Equations of EMAS. The plane rush into the EMAS is a very complicated process, in order to get the system dynamics model, as shown in Fig. 3. We make the following assumptions and Simplification: The plane is the ideal rigid body, elastic deformation can be ignored; The plane motion only in the vertical plane; θ is a small inclination angle, less than $\pm 10^\circ$; To simplify the landing gear into the spring damper, the main gear elastic coefficient is K_M, damping coefficient is C_M, the nose gear elastic coefficient is K_N, damping coefficient is C_N.

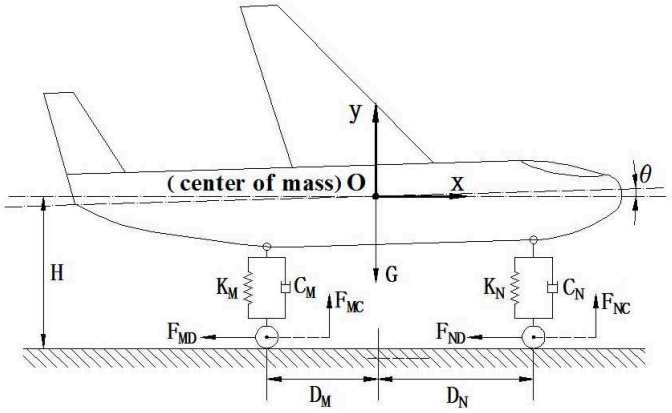

Fig.3. Aircraft dynamic model

The dynamic aircraft model has three degrees of freedom, which are aircraft horizontal traveling distance x, aircraft vertical displacement y, aircraft pitch angle θ,dynamic equations of the system are established by using the Lagrange equation.

1) kinetic energy of the system. The kinetic energy of the system including the plane translation and rotational kinetic energy as follows

$$E_K = \frac{1}{2}m(\dot{x}^2 + \dot{y}^2) + \frac{1}{2}J_0\dot{\theta}^2 \tag{11}$$

2) potential energy of the system. Potential energy of system consists of gravitational potential energy and elastic potential energy as follows

$$E_P = mgy + k_M y_M^2 + \frac{1}{2}k_N y_N^2 = mgy + k_M[\frac{D_N}{2(D_M + D_N)k_M}(G - C_L \bullet \frac{1}{2}\rho V^2 S) + H - (y - D_M\theta)]^2 +$$

$$\frac{1}{2}k_N[\frac{D_M}{(D_M + D_N)k_N}(G - C_L \bullet \frac{1}{2}\rho V^2 S) + H - (y + D_N\theta)]^2 \tag{12}$$

Where y_M is the amount of compression of main gear spring damper, y_N is the amount of compression of nose gear spring damper, G is gravity of the plane, F_L is lifting force, CL is coefficient of lifting force, ρ is air density, S is wing area, D_M is A is the distance of main landing gear to the center of gravity, D_N is A is the distance of nose landing gear to the center of gravity.

3) Rayleigh dissipation function of the system. The landing gear is simplified as elastic damper, then there must exist a viscous friction, the Rayleigh dissipation function as follows

$$\psi = C_M(\dot{y} + + D_M\dot{\theta}) + \frac{1}{2}C_N(\dot{y} + D_N\dot{\theta}) \tag{13}$$

4) Establish dynamic equations. The Lagrange equation[12] as follows

$$\frac{d}{dt}\frac{\partial L}{\partial \dot{q}_i} - \frac{\partial L}{\partial q_i} + \frac{\partial \psi}{\partial \dot{q}_i} = Q_i^{'} \tag{14}$$

Where $L=E_K+E_P$, q_i is generalized velocity, $Q_i^{'}$ is generalized dissipation force, substituting E_K and E_P into Eq. (14), the dynamic equations can be expressed as

$$\begin{cases} M\ddot{x} = -F_{ND} - 2F_{MD} \\ M\ddot{y} = (2C_M + C_N)\dot{y} - (2K_M + K_N)y + (C_N D_N + 2C_M D_M)\dot{\theta} + (2K_M D_M - K_N D_N)\theta + 2K_M \\ \quad + +2K_M[\frac{D_N}{2(D_M + D_N)k_M}(G - C_L \bullet \frac{1}{2}\rho V^2 S) + H] + K_N[\frac{D_M}{(D_M + D_N)k_N}(G - C_L \bullet \frac{1}{2}\rho V^2 S) + H] \\ J_0\ddot{\theta} = (2C_M D_M + C_N D_N)\dot{y} + (2K_M D_M - K_N D_N)y + (2C_M D_M^2 + C_N D_N^2)\dot{\theta} - (2K_M D_M^2 + K_N D_N^2)\theta \\ \quad - 2K_M D_M[\frac{D_N}{2(D_M + D_N)k_M}(G - C_L \bullet \frac{1}{2}\rho V^2 S) + H] + K_N D_N[\frac{D_M}{(D_M + D_N)k_N}(G - C_L \bullet \frac{1}{2}\rho V^2 S) + H] \\ \quad - (2F_{MD} + F_{ND})y - 2F_{MC} \bullet D_M + F_{NC} \bullet D_N \end{cases} \tag{15}$$

Conclusions

This paper established the static and dynamic analysis model of aircraft pavement engineering material arresting system, got the resistance and support force of the landing gear and the main landing gear by the plane. At the same time ,we also obtained the mathematical function of dynamic compaction resistance and the density of crushed the foam concrete material, they plays an important role in arresting the aircraft. In addition, we have reasonable assumptions and analysis for the collapse of transient. The aircraft model is reasonably simplified and established dynamic equations of the system. Later the dynamics simulation further verify the reliability of the model. In addition, this article can be for the material density, height and size or other factors determine and for the true test is a direct support of the theory. In this paper, research methods and strategies of aircraft also has reference significance for the further study of the pavement EMAS.

Acknowledgement

This thesis is supported by the Civil Aviation Joint Research Foundation (U1333129).

Then, I want to express my gratitude to all those who helped me during the writing of this thesis. My deepest gratitude goes first and foremost to Professor Yu Hongbin, my supervisor, for his constant encouragement and guidance. He has walked me through all the stages of the writing of this thesis. Without his consistent and illuminating instruction, this thesis could not have reached its present form.

I am also deeply indebted to all the other tutors and teachers in Translation Studies for their direct and indirect help to me. Special thanks should go to my friends who have put considerable time and effort into their comments on the draft.

Finally, I am indebted to my parents for their continuous support and encouragement.

References

[1] Gang Liu, Hong Nie. Dynamics analysis for aircraft arresting based on absorbing aircraft kinetic energy [J]. In Chinese. China Mechanical, 2009, 20(4):450- 454

[2] FAA.Order5200.9, Financial Feasibility and Equivalency of Runway Safety Area Improvements and Engineered Material Arresting Systems [G].FAA, 2004.

[3] Engineering, 2009, 20(4): 450- 454(in Chinese)ICAO．Status Engineered Material Arresting System Installations in the United States．A presentation by the North American，Central American and Caribbean Directors of Civil Aviation[G]．IGAO，2006.06.22

[4] Suits L David, sprinkle Michael M, et al. Control of cracking In concrete state of the art, E- C107 [R]. Transportation Research Board of the National Academies, 2006.

[5] Ragsdale W A. A generic landing gear dynamics model for LASRS + + [C]. AIAA Modeling and Simulation Technologies Conference. Denver CO: 2000, 1-9.

[6] Heymsfield E, Hale W M, Halsey T L. A parametric sensitivity analysis of soft ground arrestor systems [J], ASCE , 2007, 262(20) : 227-236.

[7] Fact Sheet Engineered Material Arresting System (EMAS) June 12, 2012 http://www.faa.gov/news/fact_sheets/news_story.cfm?newsid=13754

[8] Pattofatto S, Elnasri I, Zhao H, Tsitsirisa H, Hilda F, Girardb Y. Shock enhancement of cellular structures under impact loading: part II analysis.Journal of the Mechanics and Physics of Solids 2007;12(55):2672e86.

[9] Z.Q. Zhang, J.L. Yang. An analytical model of foamed concrete aircraft arresting system[J], International Journal of Impact Engineering 61 (2013) 1-12.

[10] Heymsfield E, Hale W M, Halsey T L. Aircraft response in an airfield arrestor system during an overrun. Journal of Transportation Engineering 2012;138(3):284e92.

[11] Heymsfield E. Performance prediction of the strong company's soft ground arrestor system using a numerical analysis. Technical report MBTC-2090. Mack Blackwell Rural Transportation Center; 2009.

[12] Ruisheng Fu. The form of Lagrange equation [J]. In Chinese. Journal of henan university, 1986(4)

Advanced Materials Research Vols. 989-994 (2014) pp 2834-2838
© (2014) Trans Tech Publications, Switzerland
doi:10.4028/www.scientific.net/AMR.989-994.2834

Comparison Research on Aerodynamic Drags and Pressure Coefficients of Reference Car Models in Automotive Wind Tunnel

Ying-chao Zhang[1,2], Wei Ding[1],Zhe Zhang[1,a],Jie Li[1]

[1]State Key Laboratory of Automotive Simulation and Control, Jilin University, Changchun, China
[2] Department of Mechanical Engineering, the Hong Kong Polytechnic University, Hung Hom, Kowloon, Hong Kong
[a]Corresponding author: zhangzhejlu@jlu.edu.cn

Keywords: automotive wind tunnel, contrast test, aerodynamics, reference car models

Abstract. The aerodynamic drags of different reference car models were investigated to calibrate the performance of the Automotive Wind Tunnel in Jilin University. The two kinds of reference models--MIRA and SAE reference car models were involved in this paper, considering the actual situation of the Automotive Wind Tunnel in Jilin University. The results of the research show that the Automotive Wind Tunnel in Jilin University can meet the demand for automotive wind tunnel tests and it can get the same performances as other wind tunnels have and reliable test data can be obtained in it.

Introduction of wind tunnel test

Road vehicle aerodynamics plays a critical role in car design and the road vehicle aerodynamics focuses on investigating the interaction between flow air and vehicles. Aerodynamic coefficients are one of the most important parameters. It has great effects on automotive dynamics, handling and stability.[1] Researches have been conducted mostly on scale reference models to investigate flow characteristics and aerodynamic forces and moments and to correct and compare results in different automotive wind tunnels.[2]

Recently under the increasing fuel problem and high-speed travel of vehicles, aerodynamic drag reduction of road vehicles, which affect their fuel economy, is being pay close attention to[3-4]. So many wind tunnels focusing on aerodynamics of road vehicle were built in different countries[5].

Now, there are many kinds of wind tunnels all around the world, but there are hardly any two wind tunnels are exactly same, so the test results in each wind tunnel vary more or less. According to the description of certain documents, contrast tests were conducted between automotive wind tunnel and aeronautic wind tunnel for testing vehicles such as the wind tunnel of NRCC(Network Routing Control Center), LOCKHEED Wind Tunnel and so on. The test results show that aerodynamic drag figures tested in different wind tunnels are different. According to the reports, those automotive wind tunnels of which the test results have great differences have been improved and now their test data are already very close. [5]

The Automotive Wind Tunnel in Jilin University

The Automotive Wind Tunnel in Jilin University began to be built in May, 2002 and was completed in 2008. This paper compares the Automotive Wind Tunnel in Jilin University with other automotive wind tunnels by testing the reference car models .

The Automotive Wind Tunnel in Jilin University is equipped with special six-component balance system, rolling road (or moving belt) system, aerodynamic pressure scanner system and other specialized measuring systems. The balance system consists of force sensors and model supporting structure. The overall accuracy of sensors and data acquisition system is under 0.05%F.S. (Full Scale).

The main technical parameters:The test section size: 8m(length)×4m(width)×2.2m(height); Maximum wind velocity: 60m/s; Contraction ratio: 5.17; Power of the main motor: 1000kw; Range of the rotating table: ±30°.

The Automotive Wind Tunnel in Jilin University is a closed circuit wind tunnel. It has an open test section as shown in Fig.1. For the existing of the moving belt system of the Automotive Wind Tunnel in Jilin University and the automobile wind tunnel assembles the balance, this paper adopts the wheel center supporting system as shown in Fig.2. The support position of this kind of supporting system is not the car tires but the car wheels. The car balance of this kind of supporting system lies at the bottom of the automotive wind tunnel test section and four supporting columns reach out from the balance to the wind tunnel test section. The supporting columns are connected to the axletree through a transversal horizontal rod to fix the automotive car models.

Fig. 1. The test section

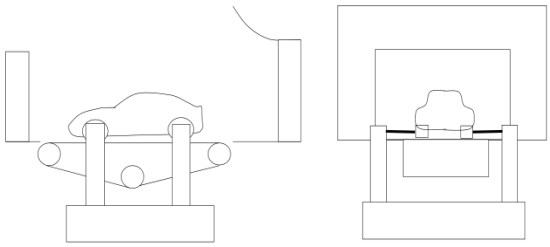

Fig. 2. The supporting system

The test section of the Automotive Wind Tunnel in Jilin University is open test section, and the mechanical balance is installed at the bottom of the test section. The automotive wind tunnel is equipped with the rolling road ground effects simulation system and it adopts wheel center supporting system to reduce the blocking effect, to take the advantages of the simulation system for the rolling road ground effects, to avoid transformation of the car and to obtain the aerodynamic force accurately. But the Automotive Wind Tunnel in Jilin University cannot get the original aerodynamic coefficients data directly because of the interference of the aerodynamic force of supporting columns. Considering these situation, this paper has deducted the interference of the supporting columns aerodynamic force before obtaining the final test results. So the test results obtained in this paper at last is accurate.

Introduction of the experiment

To arrive at an accurate experimental conclusion, this paper compares test results of the Automotive Wind Tunnel in Jilin University with test results of the other automotive wind tunnels with reference to certain automotive car models. The technical precept will be described following. Firstly, select standard car models for reference and design the supporting forms according to the actual situation of the Automotive Wind Tunnel in Jilin University. Secondly, manufacture the real object models according to the geometric dimensioning data of the car models. Thirdly, complete the wind tunnel test with the real object models and measure the aerodynamic force by ways of wind tunnel test. Finally, complete the data processing on the basis of the test results and compare the obtained data with test results of other automotive wind tunnels and then come to an accurate conclusion.

The reference models

To conduct the wind tunnel contrast test and come to an accurate conclusion, the car models selected for reference should be of geometric similarities, of high comparability, easy to meet the demands of the automobile standards. Besides, the car models should also posses test data of other automotive wind tunnels and must be representative, universal and have deferent forms.

Considering the construction demand of the Automotive Wind Tunnel in Jilin University and the actual situation of the paper, this paper selects the MIRA and SAE car models[6,7] as the standard models for reference. The test is conducted with the car models made at the rate of 1:2 to obtain more accurate data.

The MIRA car models are simplified vehicle car models which are very close to real vehicles. The MIRA car models have wheels but do not have wheel cavity. The bottom of the model is very smooth and the engine hood has certain angel of slope. The side windows of the car models incline and the tail of the model warps upward. There are totally four forms of the MIRA car models: the notchback, the fastback, the square back and the pickup[7,8].

The SAE car models are relatively simple body car models. Only certain planes and edges of the SAE car models are chamfered. The SAE car models do not have wheels or wheel cavities. But at the bottom, there are four small columnar legs to fix the car models. Besides, a diffuser is set at the end of the bottom. There are also four forms of the SAE car models in total: the notchback, the fastback, the squareback and the hatchback[7]

Both the MIRA and the SAE car models are in possession of abundant wind tunnel test data and these data provide good reference for the research in this paper. In terms of the need of the research, this paper has summarized the test data for contrast research of the two models on the basis of large quantities of reference and information[6-8] as shown in Table Cd in reference.1. In this paper, the contrast test is conducted based on the test results in Table1.

Test precepts based on standard model cars

Considering the actual situation of the Automotive Wind Tunnel in Jilin University, this paper designs four series of test precepts based on the two standard car models. Part of the MIRA and SAE car models' process are shown from Figure 3 to Figure 9. One of the test precepts of the MIRA car models is shown from Figure 3 to Figure 6 and they respectively show the test process of the notchback, the fastback, the pickup, and the square back of the MIRA car models. In this precept, because of the four wheels at the bottom of the car models, a Z-shape supporting rod is stuck beside the four wheels assisted by a certain amount of glue.

Fig. 3. MIRA model1

Fig. 4. MIRA model2

Fig. 5. MIRA model3

Fig. 6. MIRA model4

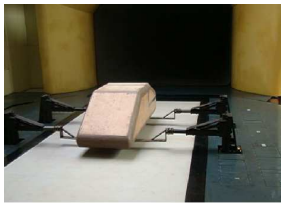

Fig. 7. SAE model1

Fig. 8. SAE model2

Fig. 9. SAE model3

One of the test precepts of the SAE car models is shown from Figure 7 to Figure 9 and they respectively show the test process of the fastback, the notchback, and the square back of the SAE car models. In this precept, because there are no wheels or other attachment to get stuck at the bottom of the model, some screws are installed at the bottom of the body to fix the SAE car models to ensure the stability of the model.

Contrast of the test results

The Figure 10 shows the contrast of the test results of the upbody surface aerodynamic force between Jilin University and the test data of IVK/FKFS Universität Stuttgart. The blue scatter points are made based on the upbody test data of IVK/FKFS Universität Stuttgart and the red scatter points is made based on the upbody test results of Jilin University. By contrast, it can be found that there exists errors between the upbody test results of Jilin University and IVK/FKFS Universität Stuttgart. But on the whole, the consistency is good. The Figure 10 doesn't show the contrast of the test results of the downbody surface aerodynamic force between Jilin University and IVK/FKFS Universität Stuttgart. In the contrast test, it is found that there's a larger error of the downbody. But the overall trend is still the same.

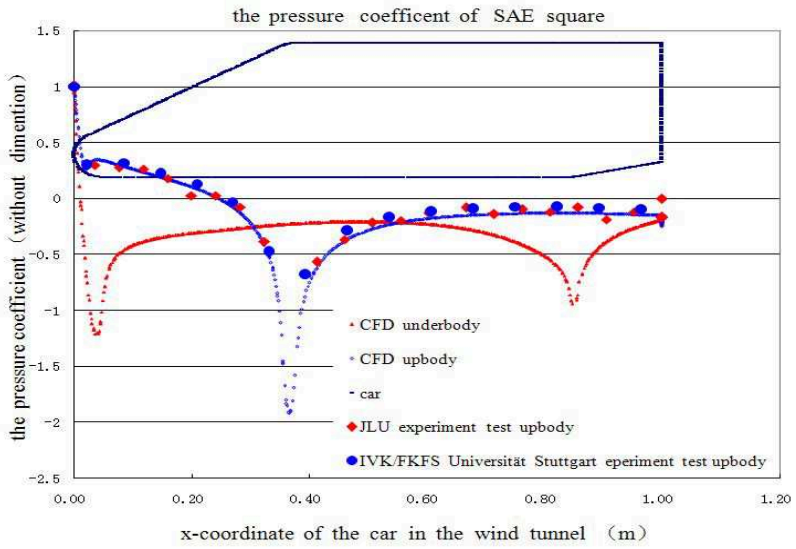

Fig. 10. The contrast of the body surface

The Table 1 shows the contrast results of test data between Jilin University and other wind tunnels. It can be found that there exist certain errors between the Automotive Wind Tunnel in Jilin University and other wind tunnels. The contrast error of the pickup of the MIRA automotive car models is the least, only 0.63%, while the contrast error of the square back of the MIRA automotive car models is the largest, to be 1.94%. The contrast errors of the other forms of the automotive car models are within this scope. On the whole, the contrast errors are all within 2%.

Table. 1. The contrast results between Jilin University and other wind tunnels

No.	The car models	Cd in reference	Cd in Jilin University	Error
1	Notchback of MIRA	0.30	0.303	0.83%
2	Fastback of MIRA	0.27	0.265	-1.70%
3	Square back of MIRA	0.35	0.357	1.94%
4	Pickup of MIRA	0.32	0.322	0.63%
5	Notchback of SAE	0.21	0.210	-0.14%
6	Fastback of SAE	0.23	0.226	-1.61%
7	Square back of SAE	0.29	0.294	1.28%

Through the contrast above, it can be found that there exist differences between the Automotive Wind Tunnel in Jilin University and other wind tunnels. There are certain errors between the test data, but on the whole, the error is very small. It indicates that the quality of the Automotive Wind Tunnel in Jilin University is high and it can meet the needs for automotive wind tunnel tests.

Conclusion

This paper analyzes the structure layout of the Automotive Wind Tunnel in Jilin University on the basis of summarizing the forms of test section and model supporting structure at home and abroad and then compare the test data of the Automotive Wind Tunnel in Jilin University with test data of other wind tunnels after determining the test precept and conducting the automotive wind tunnel test. The research results show that the precision can meet the needs and that the quality of the Automotive Wind Tunnel in Jilin University is high and it possesses the same performances as other wind tunnels have. Therefore, reliable test data can be obtained through automotive wind tunnel test conducted in it.

Acknowledgements

Thank the National Natural Science Funds (10802033), the Hong Kong Scholar Program and the project of State Key Laboratory of Automotive Simulation and Control in Jilin University for the financial aid.

Reference

[1] Geoffrey M.Le Good,Kevin P.Garry. On the Use of Reference Models in Automotive Aerodynamics, SAE Paper 2004-02-1308.

[2] Zhang Yingchao, Numerical simulation of road vehicle aerodynamics, edited by Peking University Press, 2011

[3] Kazuhiro Maeda,Kozo Kitoh and Hirotsugu Nozaki.Correlation Tests Between Japanese Full-Scale Automotive Wind Tunnels Using the Correction Methods for Drag Coefficient. SAE Paper 2005-01-1457.

[4] Geoffrey M.Le Good,Kevin P.garry. On the Use of Reference Models in Automotive Aerodynamics. SAE Paper 2004-01-1308.

[5] Gerhard Wickern. On the Application of Classical Wind Tunnel Corrections for Automotive Bodies. SAE Paper 2001-01-0633

[6] Antonello Cogotti. A Parametric Study on the Ground Effect of a Simplified Car Model. SAE Paper 980031.

[7] He Baoqin. Research On Automotive Aerodynamic Characteristics of Platoon. (2008): Jilin University. In Chinese

[8] Jeffrey Hoffman, Bill Martindale, Stephen Arnette, Jack Williams, Stan Wallis. Development of lift and drag corrections for open jet wind tunnel tests for an extended range of vehicle shapes. SAE Paper 2003-01-0934.

Advanced Materials Research Vols. 989-994 (2014) pp 2839-2844
© (2014) Trans Tech Publications, Switzerland
doi:10.4028/www.scientific.net/AMR.989-994.2839

Performance Analysis and Simulation Study of Boiler-Turbine Coordinated Control System

Jiang Yi-Yang [a], Wang Dong-Feng [b]

Department of Automation, North China Electric Power University,Baoding 071003, China
[a] jiangyiyang91@gmail.com, [b] wangdongfeng@ncepubd.edu.cn

Keywords：Coordinated control system, load control mode, signal constraint, simulation.

Abstract. The boiler-turbine coordinated system is a very important process of a power generation unit. This paper takes 300MW power plant as the controlled object and conducts simulation study on its different kinds of load control modes under the environment of the MATLAB. The parameters of PID controller are optimized using signal constraint (S-C) module in Simulink toolbox. By analyzing the results of the simulation and comparing both the advantages and disadvantages of them, we can provide references for the choices of load control mode of power unit.

Introduction

The thermal power unit is a nonlinear, inter-coupling, large inertia, large delay, multi-variables and time-varying complicated controlled object, which has many uncertain factors [1]. At present, the unit power plants with great power and big parameters have been widely used, which are operated in a load following mode due to the rapid development of power industry. As a key component of power network automatic generation control (AGC), the coordinated control system (CCS) of fossil-fueled generating units play a vital role in the safe and economic operation. It is required that the boiler-turbine-generator set reacts to the load demand change quickly. While, it must make sure that the set can perform safely, stably and economically. Consequently, it is crucial to choose the best control strategy according to different units to develop good control qualities [2].

Coordinated Control System Structure

When the coordinated control system receives the real power command N_0 from load command management center, the boiler-turbine coordinated controller will send the boiler firing rate (coal feeder speed) command B and opening degree of the steam turbine regulating value command μ to corresponding local control loop respectively based on some control method.

The load command management center and boiler-turbine coordinated controller have many realization forms. And the system might not be definitely divided into two parts either. For the purpose of discussions, the two parts will be discussed separately. As for boiler and turbine command local control loop, we can group them into generalized objects. Therefore, the block diagram of simplified coordinated control system is given as Figure1.

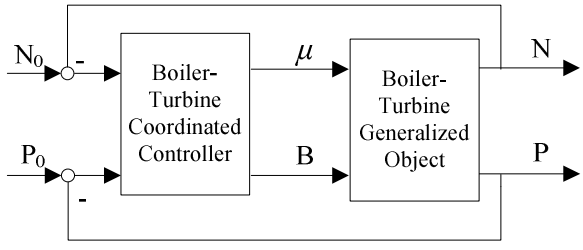

Fig.1 Simplified coordinated control system in unit plant

Controlled Object Model

The boiler-turbine coordinated control system can be simplified as a multiple-input multiple-output (MIMO) system. B and μ are input variables, N and P are output variables. B is the command variable about boiler firing rate (coal feeder speed) and μ is the command variable about the opening degree of the steam turbine regulating value. N is the real power that generating unit outputs and P is the main steam pressure.

In this paper, we take the 300MW coal-fired once-through power plant unit as the study object. The linearized mathematical model of this unit plant under the 100% load operation condition is described by [3]:

$$\begin{bmatrix} N \\ P \end{bmatrix} = \begin{bmatrix} W_{11}(s) & W_{12}(s) \\ W_{21}(s) & W_{22}(s) \end{bmatrix} \begin{bmatrix} \mu \\ B \end{bmatrix} \tag{1}$$

Where:

$$W_{11}(\mathrm{s}) = \frac{4.665s(1+99s)}{\left(1+50s+58^2 s^2\right)(1+4.1s)} \tag{2}$$

$$W_{12}(\mathrm{s}) = \frac{2.069(1+311s)}{(1+149s)^2(1+22.4s)} \tag{3}$$

$$W_{21}(\mathrm{s}) = -1.42\left(0.04+\frac{0.96}{1+70s}\right) \tag{4}$$

$$W_{22}(\mathrm{s}) = \frac{1.265(1+205s)}{(1+128s)^2(1+11.7s)} \tag{5}$$

Signal Constraint Optimization of PID Parameters

To compare the control qualities of different load control modes, we should eliminate the influence of the controller's parameters of each control method. In order to achieve the best control state of current method, Signal Constraint (S-C) module in Simulink toolbox is introduced to optimize the PID parameters [4].

First, we make constraint on the upper and lower boundary of expected curve and set up initial value of PID parameters. Then, we select the optimal parameters and optimization method. In this article, Gradient Descent is adopted for its faster rate of convergence than others. Finally, by constantly increasing constraint of the expected curve until, we can receive the best control effect.

Simulation and Comparative Analysis

To compare different kinds of load control modes' performance about rapid response to grid load and maintaining the pressure stability, each simulation process is conducted under the test of power setting value step disturbance and pressure setting value remaining unchanged. In the figures below, W_T is turbine PID controller and W_B is boiler PID controller. Red line represents N curve and blue line represents P curve.

A. Turbine and Boiler Separate Control Mode

The separate control mode means one controlled variable can be only controlled by one manipulated variable. There are two basic kinds of separate control mode: boiler following control and turbine following control mode [5].

a) Boiler Following (BF) Control Mode

The principle of boiler following control mode is that turbine controller regulates the unit power and boiler controller regulates the steam pressure.

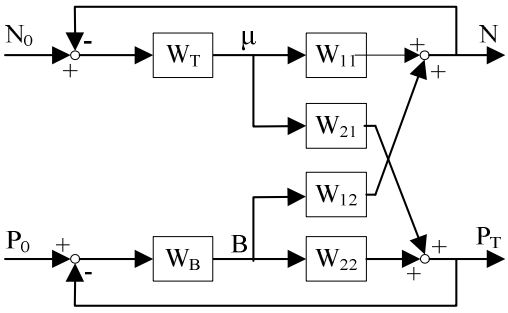

Fig.2 Structure of BF mode

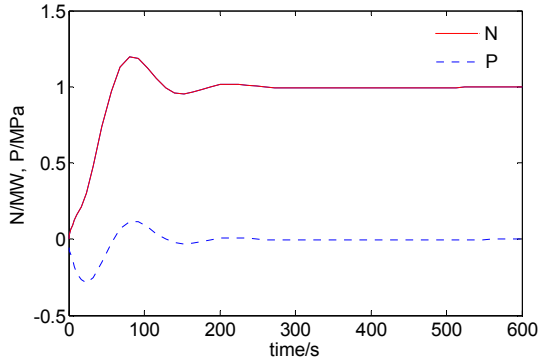

Fig.3 Simulation curves of BF mode

Using the methods mentioned above, we can get the best curve of output which is shown in Fig.2: the parameters of turbine PID controller: kp=1, ki=0.0159, kd=0; the parameters of boiler PID controller: kp=4, ki=0.097, kd=0.

The result shows that the unit power tracks the set value rapidly, but the main steam pressure has a great fluctuation. It also verifies that boiler following control mode has a great adaptability to the power and an unacceptable fluctuation in the main steam pressure, which uses boiler heat storage.

b) Turbine Following (TF) Control Mode

The principle of boiler following control mode is that turbine controller regulates the steam pressure and boiler controller regulates the unit power.

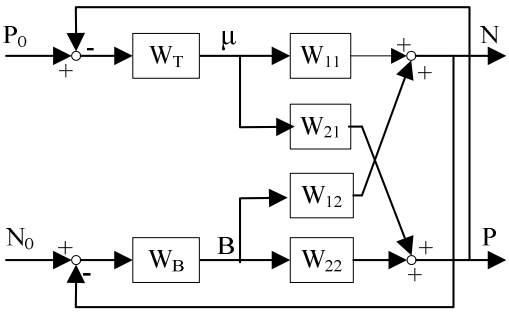

Fig.4 Structure of TF mode

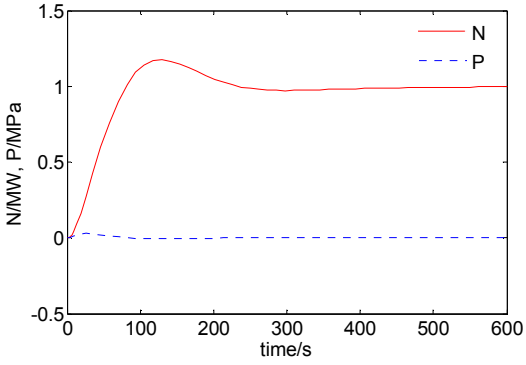

Fig.5 Simulation curves of TF mode

The parameters of turbine PID controller: kp=-11.4272, ki=-0.5, kd=-5.0501; The parameters of boiler PID controller: kp=0.7, ki=0.015, kd=0.7702.

Compared with boiler following control mode, the fluctuations of main steam pressure under this mode are maintained within a small range. However, the curve of power reaches the given value slowly after the first peak. That is to say, the unit power will begin to change only when the main steam pressure is changing after the boiler firing rate has been changed under this kind of control mode.

B. Coordinated Boiler-turbine Control Mode

Both turbine following control mode and boiler following control mode are extreme situations. They cannot balance the contradiction between unit power and main steam pressure. Coordinated boiler-turbine control system makes boiler and turbine as a whole and the control methods were introduced into the controller, such as feed-forward, compensation and so on [6]. There are many

forms of coordinated control mode; we choose three typical strategies to research their respective control qualities.

a) Unidirectional Decoupling Boiler Following (BF) Coordinated Control Mode

This kind of coordinated control mode is based on boiler following control mode and introduces the pressure deviation into boiler controller.

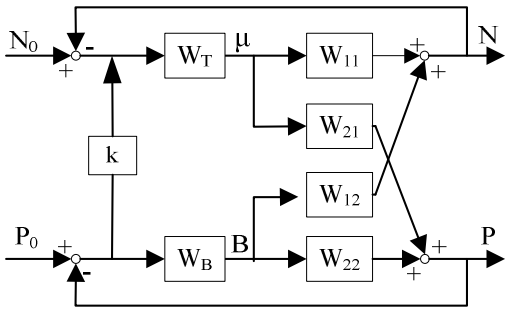

Fig.6 Structure of unidirectional decoupling BF mode

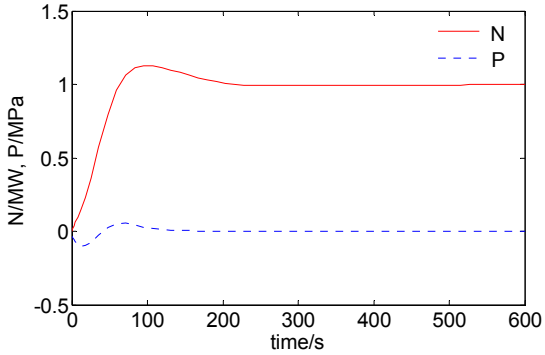

Fig.7 Simulation curves of unidirectional decoupling BF mode

The parameters of turbine PID controller: kp=0.5175, ki=0.0178, kd=0.0102; The parameters of boiler PID controller: kp=4.5168, ki=0.0628, kd=-0.0133; decoupled coefficient k=0.2.

When N_0 changed，turbine controller alter the opening degree of turbine valve to change the steam flow，so that N will rapidly approach to N_0. Changes in the heat storage lead to steam pressure changes, and then according to the pressure deviation signal, turbine and boiler controllers regulate the boiler firing rate and opening degree of turbine valve respectively at the same time. On the one hand, boiler heat storage is compensated by the change of boiler firing rate. On the other hand, turbine valve opening is restricted to prevent overusing of the heat storage, so that the pressure fluctuation cuts down and trends to steady. In short, unidirectional decoupling boiler following coordinated control mode, compared to pure boiler following control mode, has a better control quality.

b) Unidirectional Decoupling Turbine Following (TF) Coordinated Control Mode

This kind of coordinated control mode is based on boiler following control mode and introduces the unit power deviation into turbine controller.

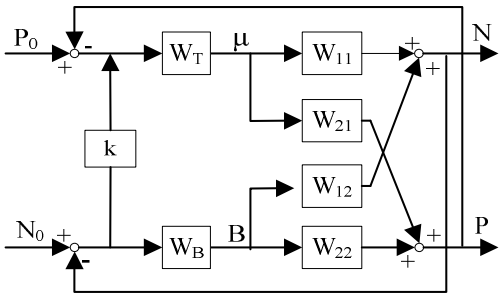

Fig.8 Structure of unidirectional decoupling TF mode

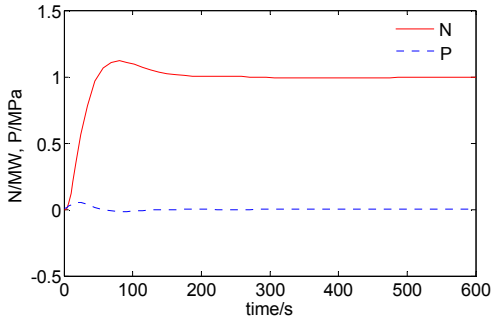

Fig.9 Simulation curves of unidirectional decoupling TF mode

The parameters of turbine PID controller: kp=-11.4264, ki=-0.4963, kd=-5.0507; the parameters of boiler PID controller: kp=1.3632, ki=-0.4963, kd=0.7607; decoupled coefficient: k=0.1.

When load command changed, boiler and turbine controllers both receive the signal to regulate the corresponding actuating mechanism. During the boiler combustion delay period, temporarily

using of boiler heat storage makes the output rapidly response to the unit power command. As Figure 9 shows, unit power reaches the steady value very quickly after first peak; regulation quality is much more improved though the pressure has a little instability.

c) Bidirectional Decoupling Boiler Following (BF) Coordinated Control Mode

The two coordinated control modes mentioned above only realize unidirectional coordinated control, which means that just one of the regulated variables is coordinated controlled by two regulating variables, while the other is still being adjusted by one，so it is relatively simple coordinated control scheme. Integrated coordinated control mode achieves bidirectional coordinated control to get better control effect.

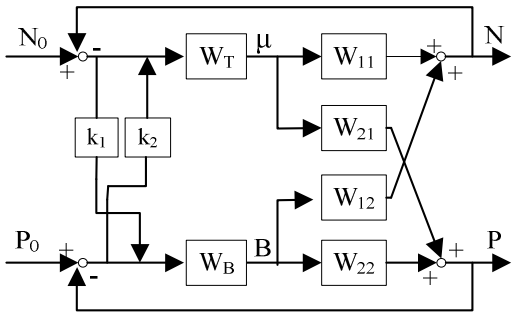

Fig.10 Structure of bidirectional decoupling BF mode

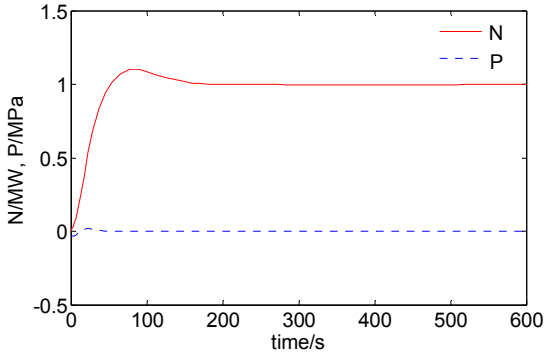

Fig.11 Simulation curves of bidirectional decoupling BF mode

The parameters of turbine PID controller: kp=4.487, ki=0.0578, kd=-0.0037; the parameters of boiler PID controller: kp=15.0545, ki=1.2987, kd=0.0196; decoupled coefficient: k1=0.3619, k2=-50.1625.

The simulation results indicate that the method has a good dynamic performance and curve of output power tracks the set value smoothly and rapidly with smaller overshoot and shorter adjusting time. At the same time, the main steam pressure has little fluctuations descending to the stable value soon.

Conclusions

This paper takes 300MW power plant as the research object, conducting simulation study on 5 kinds of load control mode which are classified as turbine and boiler separate control mode and coordinated boiler-turbine control mode. The simulation experiments show that, under pure boiler following control mode, the main steam pressure fluctuates wildly for power constant-disturbance, is likely to affect the safety of operation; under pure turbine following control mode, output power tracks the set value slowly which has a bad load adaptability[7]; coordinated boiler-turbine control mode combine the best of both, which can not only adapt to changes of the load in power network quickly, but also make the main steam pressure to maintain nearby the rating [8]. Further, the performance of bidirectional decoupling coordinated control mode is better than unidirectional ones. But it also increases the complexity of design and difficulty of regulation.

Acknowledgements

This research is supported by the Fundamental Research Funds for the Central Universities(Grant No. 2014MS139).

References

[1] G. Prasad, G.W. Irwin, E. Swidenbank, B.W. Hogg, "Plant-wide predictive control for a thermal power plant based on a physical plant model," IEE Proceedings-Control Theory and Applications, vol. 147, 2000, p. 523–537.

[2] D.H. Li, H.H. Zeng, Y.L. Xue, X.Z. Jiang, "Multivariable Nonlinear Control Design for Boiler-Turbine Units," Intelligent Control and Automation, 2006. WCICA 2006. The Sixth World Congress on, vol. 2, p. 7518–7522.

[3] Z.L. Liu, E.H. Zheng, J. Sun, and L. Chen, "Decoupling control based on support machines ath-order inversion for the boiler-turbine coordinate systems," Control and Decision Conference (CCDC), 2011 Chinese. The Sixth World Congress on, 2011, p. 2620 - 2623.

[4] N. Manafeddin, O. Basturk, "DC motor position control using fuzzy proportional-derivative controllers with different defuzzification methods," Turkish Journal of Fuzzy Systems.vol. 1, 2010, p.36-54.

[5] J.S. Heo, K.Y. Lee, R. Garduno-Ramirez, "Multi-objective control of power plants using particle swarm optimization techniques," IEEE Transactions on Energy Conversion, vol. 21, 2006, p. 552-561.

[6] J. Jiang, W. Pan, "Simulative study of the coordinated control system for 300MW unit generator," Journal of Changsha University of Science and Technology(Natural Science), vol. 2, 2005, p. 49-55.

[7] X. Guo, Y. Xi, Z. Wang, Z. Li, G. Hou, An improved generalized predictive control algorithm and its application in unit plant coordinated control system," Control and Decision Conference (CCDC), 2012 24th Chinese, 2012, p.1654-1658.

[8] D.G. Peng, H. Zhang, P. Yang, "The boiler-turbine coordinated control system based on immune feedback mechanism," Machine Learning and Cybernetics, 2007 International Conference on. IEEE, vol. 1, 2007, p.449-453.

Advanced Materials Research Vols. 989-994 (2014) pp 2845-2848
© (2014) Trans Tech Publications, Switzerland
doi:10.4028/www.scientific.net/AMR.989-994.2845

Exploration on the Dual spool design of rotary hydraulic valve

Lijun Qiu[a] ,Suying Xu[b]

Eaestern Liaoning University,Dandong, Liaoning118003,P.R.China

[a]Qlj7710@163.com

[b]Xusuying0002@163.com

Keywords: rotary valve, single- spool , double- spool , axial force, torque

Abstract: There is also a monomer leak valve body on the single spool, Leakage between the guide groove affected the layout of the form guide groove. Two end faces of the single spool work in the different fluid pressure in the chamber. When the working pressure of the hydraulic system is high, the pressure differential will cause the spool bearings subject to large axial force. It will increase the resistance torque of bearing rotation. Effects of axial force also limits the increase spool diameter. Double spool valve with two spool rotation series manner. Each spool in the same pressure in the working medium. Eliminating the axial force of the valve body due to fluid pressure differential generated, also reduces the resistance to rotation of the spool moment and the impact of guide groove arrangement by oil leak, and also the commutation frequency of the rotary valve can be improved by increasing the diameter of the spool.

Introduction

We can improve the conversion rate by increasing the rotational speed of the rotary valve or increasing the number of the guide groove to increase the operating frequency of the rotary valve. However, under the current conditions, improving the speed of the rotary valve is limited by speed of drive motor. The rotary valve shaft is increased to increase the number of its circumferential arrangement of the guide groove. And it is necessary to increase the diameter of the rotary valve to increase the number of lead tank. Increasing the diameter of the rotary valve to increase the speed of a method for easily implemented . Increasing the diameter of the rotary valve to increase the commutation speed is the method for easily implemented[1] .

The diameter of rotary valve spool shaft is increased,the axial force acting rotary valve shaft needs to be reduced . The diameter of the spool shaft can be increased to increase the number of the guide groove . While increasing the diameter of the spool shaft but also increases the pressure receiving area of the end face. For this reason we solve the question only from the pressure difference between the working chamber. Select the low viscosity hydraulic oil can reduce the drag torque of the rotary valve . Raise the operating temperature of the hydraulic oil can reduce the viscosity of the hydraulic oil. However, the use temperature of the hydraulic oil is limited . Viscous fluid drag torque calculation formula including the resistance torque of the valve body , thrust bearing rotation resistance torque of the rotary valve to withstand the viscous drag torque[2] :

$$M_2 = M_{21} + M_{22} = C_2 \mu \cdot n \tag{1}$$

Coefficient C only depends on the structure of the rotary valve. K is an additional factor
The total drag torque of the rotary valve is

$$M = M_1 + M_2 = C_1 P + C_2 \mu \cdot n \tag{2}$$

Formula： M_1 is the moment of resistance of the thrust bearing.

The drag torque of the rotary valve is composed of two resistance moment . One resistance torque is caused by the pressure difference, the resistance moment of the Bearing rotation; Another is the moment of resistance caused by fluid viscosity . From equation (2) we can see the resistance of the rotary valve depends on the following factors in three areas

a.The differential pressure of the working chamber of rotary valve spool p

b.speed of the rotary valve spool shaft n

c.Hydraulic oil viscosity.

These three factors determine the drag torque of the rotary valve. The problem of structure designed of the rotary valve is to reduce the pressure differential of working chamber to increase the diameter of the rotary valve and the control of the rotary valve spool drag torque .

Structure and stress analysis of the dual rotary valve spool

Figure 1 is the structure of the dual rotary valve spool .

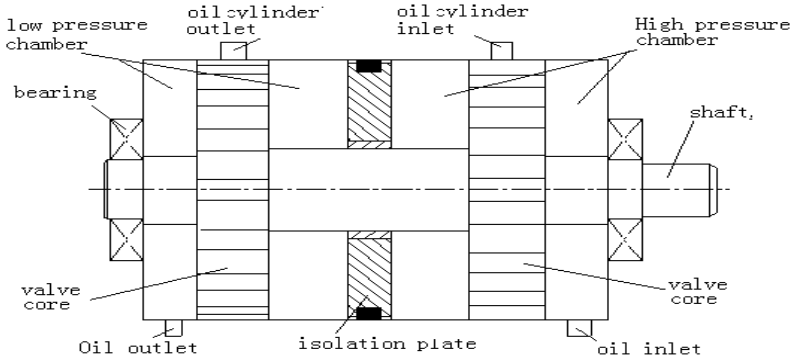

Figure 1.Schematic diagram of dual rotary valve spool

Dual rotary valve spool can be used in two structural forms . one is designed for a body double valve structure . This structure, the rotary valve spool mounted on a shaft. Rotary valve housing into two parts , high-pressure working chamber and low- pressure working chamber .Another structure is the series combination of two rotary valve[3] . Respectively, for the rotary valve and low pressure working chamber working chamber . respectively, for the high-pressure working chamber and a low pressure working chamber .If the two end faces of two pressure if the spool is the same area as the axial force generated by the valve body is equal to zero[4] .

Bearing resistance moment

$$M_1 = Gf_1 \frac{d_1}{2} + Ff_2 \frac{d_2}{2} \tag{3}$$

Formula:G—Weight bearing radial load, turn the valve(N);F—Axial load of the thrust bearing(N); f_1, f_2 —Radial, thrust bearing friction coefficient; d_1, d_2 —Radial, thrust bearing diameter(m)

Since G << F, so the formula (3) the first radial bearing drag torque is negligible.

For the same pressure of the working oil chamber , the pressure difference is zero. I.e., resistance force generated by the axial bearing moment $M_1 = 0$

Fluid viscous drag torque

Figure 2 is a schematic structural view of a valve switch . When the rotary valve work one end thrust bearing races and rolling element bearing ring follows the axis of rotation . Oil resistance consists of three parts moment. when rotating the rotary valve.

The oil resistance moment of gap between the rotary valve spool and housing .

$$M_{21} = 2\pi \cdot \mu \cdot \ell_0 \cdot \frac{R_0^3}{\delta} \cdot \omega \tag{4}$$

Formula： μ- Dynamic viscosity of the oil($N \cdot S / m^2$); ℓ_0 - Rotary valve width(m);

R_0 - The radius of the rotary valve(m); ω- Angular speed of rotation of the rotary valve(rad/s).

Thrust bearing drag torque preventde by the oil between the thrust bearing and valve.

$$M_{22} = 4\pi\mu \cdot \ell_1 \frac{R_1^2 R_2^2}{R_2^2 - R_1^2} \omega \tag{5}$$

Formula： ℓ_1 - Width of the rotating part of the thrust bearing(m).

R_1 - Thrust bearing outer radius(m); R_2 - The valve body bore radius(cm).

The remaining symbolic significance for formula(4).Spool valve body by double rotation suffered very little axial force , without using the thrust bearing , so $M_{22}=0$.

Moment of resistance actioned on the end face of the rotary valve by oil.

This part of the moment of resistance is difficult to quantitatively calculated using the expression represented in the form factor[5] .

Oil for rotary valve rotating moment of resistance.

$M_2 = K(M_{21}+M_{22}) = KM_{21}$

Here K is the coefficient of drag torque considering additional oil on the end face of the rotary valve . The (4) and (5) into too

$$M_2 = \frac{1}{15}\pi^2 \cdot \ell_0 \cdot \frac{R_0^3}{8} K \cdot \mu \cdot n = C_2 \mu \cdot n \tag{6}$$

Formula： C_2 is the amount of the transfer parameters related to the valve arrangement，for specific rotary valve is a constant。

Let: $R_0 = 6\times10^{-2}m$, $\ell_0 = 7\times10^{-2}m$, $\delta = 1\times10^{-4}m$ and $0.5\times10^{-4}m$,K=1.3 Calculated C_2

$\delta = 1\times10^{-4}m$, $C_2 = 1.295\times10^{-1}$. $\delta = 0.5\times10^{-4}m$, $C_2 = 2.588\times10^{-1}$

30 ℃, the dynamic viscosity of the oil

The 20th Oil， $\mu = 5.085\times10^{-2}N\cdot s/m^2$ .The 30th Oil， $\mu = 8.194\times10^{-2}N\cdot s/m^2$.

The rotation speed 300, 600, 1200, 1800 r/min. fluid resistance moment M_2 .

The rotation speed (rpm)			300	600	1200	1800
$M_2(N\cdot m)$	$\delta = 1\times10^{-4}m$ $C_2 = 1.295\times10^{-1}$	The 20th Oil	1.976	3.951	7.902	11.853
		The 30th Oil	3.183	6.367	12.733	19.100
	$\delta = 0.5\times10^{-4}m$ C_2=2.58	The 20th Oil	3.948	7.896	15.792	23.688
		The 30th Oil	6.362	12.724	25.447	38.171

By the formula (6),we can see that the rotation of the rotary valve oil on the oil viscosity and drag torque proportional to the speed of the rotary valve . A gap δ between the rotary valve and the valve body also has a great impact on M_2, the smaller δ and the larger M_2.

Conclusion

Rotary valve with dual valve structure, The two end faces of the valve body fluid pressure at the same area. Axial force in the same conditions spool end area of the hydraulic force generated by zero . Rotary valve spool shaft supporting structure can no longer install the thrust bearing . Drag torque thrust bearing axial force caused disappeared.

Dual rotary valve spool drag torque effects by the oil viscosity as the same as the single rotary valve spool. Oil viscosity is the same, the spool speed increased, the resistance of the rotary valve torque increases. Under conditions of constant temperature rotary valve speed is only proportional to the resistance moment

Each double valve body fluid pressure in the working chamber type , the guide groove may be slotted through the peripheral surface of the spool . High and low pressure working chamber lead tank will not leak between them.

Because the dual spool axial force of the rotary valve can be eliminated , and therefore the diameter of the valve body of the rotary valve can be designed to be larger. This can increase the number of the guide groove of the valve body , for the rotary valve to increase the frequency.

References

[1] Qiu Lijun, Yang Jia, Advanced Materials Research, V 322, p497-500.2012

[2] WANG Ji Wei, Zhang Wang A , Huang Yi hydraulic and pneumatic drive . Machinery Industry Press , 2012.6.p8-56

[3] Zhao Mingsheng, Mechanical engineer handbook, Second edition, Machinery Industry Press , 2001.3.p443-445

[4] YANG Nai Joe, hydraulic transmission oil situation and development [J] . Hydraulic and pneumatic seals , 2004, (5) .

[5] Zhang Deming . Hydraulic balancing circuit application examples analysis [J] . Hydraulic and pneumatic seals , 2007, (6).

Advanced Materials Research Vols. 989-994 (2014) pp 2849-2853
© (2014) Trans Tech Publications, Switzerland
doi:10.4028/www.scientific.net/AMR.989-994.2849

Computing Method of Auto-rotated Precision Index of Gun Barrel Based on Exterior Ballistic Computation

Yang Yadong[a], Ma Jisheng, Jia Changzhi
Ordnance Engineering College, Shijiazhuang 050003, China
422677012@qq.com

Keywords: Auto-rotated precision of gun barrel, Polynomial fit, External ballistics, Firing table

Abstract: Auto-rotated precision of gun barrel is a key operation of firing, and the research of its testing method should depend on its index computing. According to discrete value in the firing table and the exterior ballistic computation based on least square polynomial fit method, the mapping function between battle sight and range dispersion was confirmed. And by analyzing the effect of offset induced by auto-rotated precision of gun barrel, the index function which could offer a data origination for the verification of testing method of auto-rotated precision of gun barrel was provided.

Introduction

A self-propelled artillery functioned a gun barrel auto-rotated system has the preemption capability of firing by saving battery time. However, gun barrel auto-rotated system always consists of complicated electromechanical devices each operating error of which may induce the offset of sophisticated shooting. The most critical piece is whether the operation effect of gun barrel auto-rotating system match the data in the elevation table. Accordingly, it is indispensable to check the error of auto-rotating precision which decided the elevation prediction correction.

The gun barrel rotated precision was used to detecting by computing the difference of angular height and firing azimuth between fore-and-aft gun barrel rotated with the device theodolite or total station apparatus[1-4]. This technique take the advantage of theodolite and total station apparatus with high-accuracy measuring, high universality and low cost, but it is intricate to operate for the operation must be finished by team working of *3* to *5* manipulators. Also with the disposition request, this technique should be finished in the well geographical environment. The optical fiber gyroscope and laser gyroscope were mentioned in some papers to be used to detect the parametric detection of firing control system which may be a good idea to actualize the detection of gun barrel rotated precision[4,5]. However, for the inherent attribute of transducer, investigators have to remodeling and testing ceaselessly to solve the problem of measurement accuracy, zero drift, definition etc. And to all the detecting technique, the criterion of the determination data should be first confirmed.

This paper compute the exterior ballistic by fitting the discrete value in the firing table based on least square polynomial fit method. By studying the mapping relationship of gun battle sight and range of fire, the auto-rotated precision index function was put forward which could be used as the criterion of the determination data of auto-rotated precision of gun barrel.

Analysis of exterior ballistic computation method

Exterior ballistic computation can be divided into the approximate solution type and the exact solution type which include ballistic table computation method and numerical integration method. To the ballistic table computation method, computation of ballistic data is actualized by direct selection or calculus of interpolation based on the discrete value in the firing table. To the numerical integration method, computation of ballistic data is acquired from the trajectory equation computation, it is always actualized by step-by-step integration based on fourth-order Runge-Kutta method or Adams algorithm. Both of these two method take the disadvantage of cannot give the

descriptive mathematics model of firing data. The approximate solution type of exterior ballistic computation which could describe mathematics model of firing data whereas take the disadvantage of relative high accumulated error is computing the integral quantity of exterior ballistic directly in the restrictive conditions[6].

According to the advantage and disadvantage of above exterior ballistic computation method, this paper compute the exterior ballistic by fitting the discrete value in the firing table based on the least square polynomial fit method which could give the descriptive mathematics model of firing data and have a relative low computation error at the same time.

Used the battle sight and its correspondent discrete value in the firing table.Hypothesize the polynomial fitting function as:

$$X = a_0 + a_1\theta + ... + a_m\theta^m = \sum_{j=0}^{m} a_j\theta^j \qquad (m < n) \tag{1}$$

And construct the error sum of squares function as:

$$F(a_0, a_1, ..., a_m) = \sum_{i=1}^{n} \left(X - X_i \right)^2 \tag{2}$$

Compute the partial derivative of the multinomial coefficient a_0，a_1，…，a_m，and make a_0=a_1=…=a_m=0, then

$$\frac{\partial F}{\partial a_j} = 2\sum_{i=1}^{n} \left(X - X_i \right)\theta_i^j = 0 \qquad j = 0,1,...,m \tag{3}$$

It means

$$a_0\sum_{i=1}^{n}\theta_i^j + a_1\sum_{i=1}^{n}\theta_i^{j+1} + ... + a_m\sum_{i=1}^{n}\theta_i^{j+m} = \sum_{i=1}^{n} X_i\theta_i^j \qquad j=0，1，2，…，m \tag{4}$$

In this function, the coefficient is a positive definite symmetric matrix which means a_0，a_1，. . . ，a_m have a unique solution, and according to the solution, the least square polynomial by fitting the discrete data of θ_i and X_i can be actualized.

Polynomial evaluation

It is necessary to do segmented approximation in the exterior ballistic fit based on least square polynomial fit zconfirmed to use *4* degree polynomial and the high-angle firing trajectory was confirmed to use *5* degree polynomial to fit. And in the simulation, there comes the problem that when the degree was greater than *3*, the higher-degree polynomial coefficient was minor which may be regard as *0* in the computational process. And it is effective to use the normalization method to avoid this problem.

According to the results of least square polynomial fit, in this specified firing condition, the average error of the flat trajectory, the bending trajectory and the high-angle firing trajectory was separate *0.20m*, *1.40m* and *2.55m*. Obviously, the average error satisfied the precision request. Figure*1* ~ figure*4* showed the results of *3* separate trajectory and the exterior ballistic.

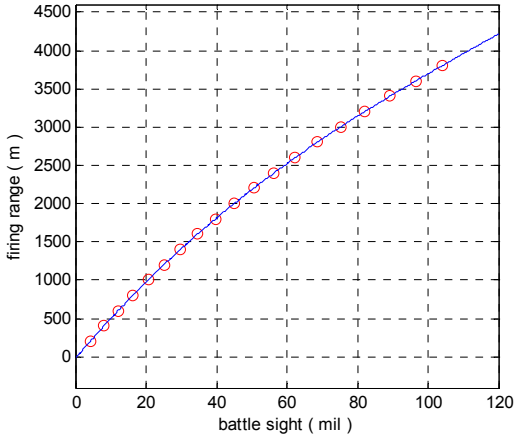

Figure1 Fitting result of flat trajectory

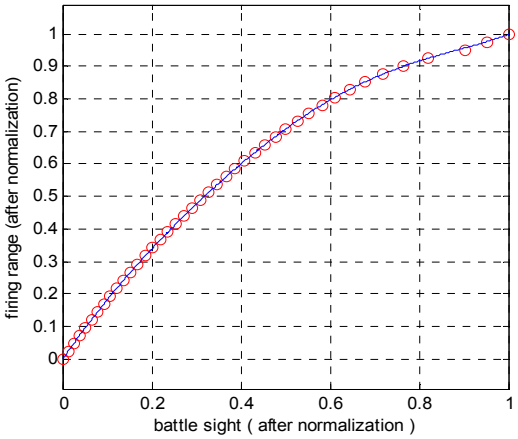

Figure2 Fitting result of bending trajectory

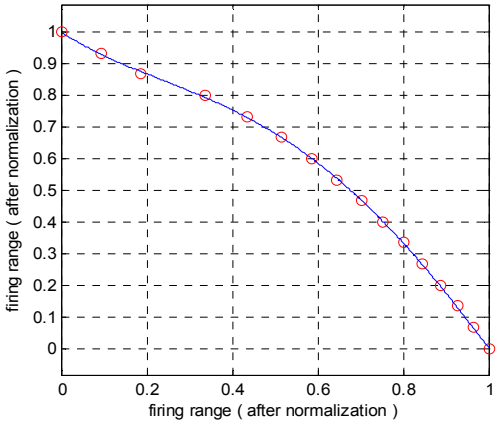

Figure3 Fitting result of high-angle firing trajectory

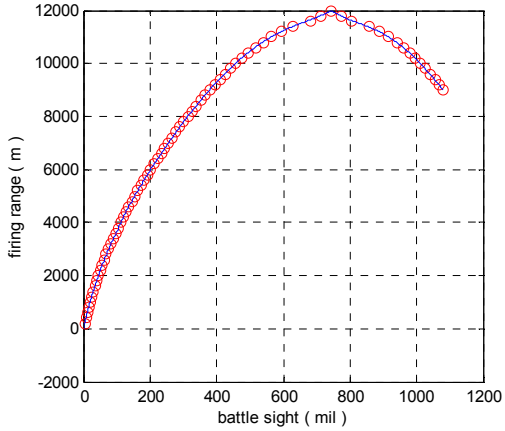

Figure4 Fitting result of exterior ballistic

Analysis of rotated precision index of gun barrel

Hypothesize θ as specified battle sight, $X(\theta)$ as the correspondent firing range and h as rotated precision, the dispersion error induced by rotated precision could be described as:

$$F(\theta,h)=X(\theta+h)-X(\theta) \qquad \theta+h\le 1080 \tag{5}$$

And

(1) To the flat trajectory:

$$F(\theta,h)=0.0018h\theta^2+\left(0.0018h^2-0.4678h\right)\theta+(0.0006h^3+54.1111h),\quad \theta+h\le 104.1 \tag{6}$$

The partial derivative to θ $\dfrac{\partial F(\theta,h)}{\partial\theta}<0$.

According to the fitting result, the dispersion error induced by rotated precision have the maximum error value in the starting point of curve. Therefore, to flat trajectory, when the rotated precision was h, the maximum error value of rotated precision was:

$$F(4.2,h)=0.0006h^3+0.00936h^2+52.1465h \tag{7}$$

(2) To the bending trajectory:

$$F(\theta,h)=8200\times\left\{2.0304\frac{h}{644.1}-2.2864\left[\left(\frac{\theta-104.1+h}{640}\right)^2-\left(\frac{\theta-104.1}{640}\right)^2\right]+3.9742\left[\left(\frac{\theta-104.1+h}{640}\right)^3-\left(\frac{\theta-104.1}{640}\right)^3\right]-4.7343\left[\left(\frac{\theta-104.1+h}{640}\right)^4-\left(\frac{\theta-104.1}{640}\right)^4\right]+2.0152\left[\left(\frac{\theta-104.1+h}{640}\right)^5-\left(\frac{\theta-104.1}{640}\right)^5\right]\right\} \quad 104.1<\theta+h\le 744.1 \tag{8}$$

The partial derivative to θ was also less than *0,* and of course its higher term could be neglected. Similarly as the flat trajectory, the dispersion error induced by rotated precision have the maximum error value in the starting point of curve. And after linearization, when the rotated precision was h,

the maximum error value of rotated precision was：

$$F(h) \approx 25.9h \tag{9}$$

(3) To the high-angle firing trajectory:

$$F(\theta,h)=3000\times\left\{-\frac{0.8753h}{335.9}+1.5860\left[\left(\frac{\theta-744.1+h}{335.9}\right)^2-\left(\frac{\theta-744.1}{335.9}\right)^2\right]-2.7504\left[\left(\frac{\theta-744.1+h}{335.9}\right)^3-\left(\frac{\theta-744.1}{335.9}\right)^3\right]\right.$$
$$\left.+1.0432\left[\left(\frac{\theta-744.1+h}{335.9}\right)^4-\left(\frac{\theta-744.1}{335.9}\right)^4\right]\right\} \quad 744.1<\theta+h\le 1080 \tag{10}$$

It means the dispersion error induced by rotated precision have the maximum error value when the firing range was the maximum. Also according to the linearization method, when the rotated precision was h, the maximum error value of rotated precision was:

$$F(h) \approx 16.0h \tag{11}$$

Consequently，in the condition of project the burst cartridge with normal charge in standard ballistic condition, the rotated precision index of gun barrel could be summarized as：

$$F(h)=\begin{cases}52.1h & 4.2<\theta\le 104.1\\ 25.9h & 104.1<\theta\le 744.1\\ 16.0h & 744.1<\theta\le 1080\end{cases} \tag{12}$$

According to the above function, it could be concluded that the least square polynomial fit method can be used to compute the rotated precision index of gun barrel after contrasting the result with the firing table (the maximum error of the flat trajectory, the bending trajectory and the high-angle firing trajectory induced by *00-01mil* firing range was separate *52.0m*, *26.0m* and *17.0m*[7]).

Therefore, based on least square polynomial fit method, the rotated precision index of gun barrel in the other conditions can also be computed. For example, the rotated precision index of gun barrel in conditions of 1500m altitude and project the burst cartridge with normal charge was:

$$F(h)=\begin{cases}53.4h & 4.1<\theta\le 100.0\\ 27.8h & 100.0<\theta\le 705.0\\ 18.1h & 705.0<\theta\le 1080\end{cases} \tag{13}$$

For contrasting the influence of difference of rotated precision index of gun barrel in the different conditions, this paper computed the rotated precision index of gun barrel in *1500m* altitude and *0m* altitude using normal charge which was shown in figure *5,* also the rotated precision index of gun barrel in conditions of project the burst cartridge with normal charge and *1#* zone charge in *0m* altitude was shown in figure*6*. In the two figures, the x axis was the rotated precision index of gun barrel, the y axis was the range sight, the z axis was the error value.

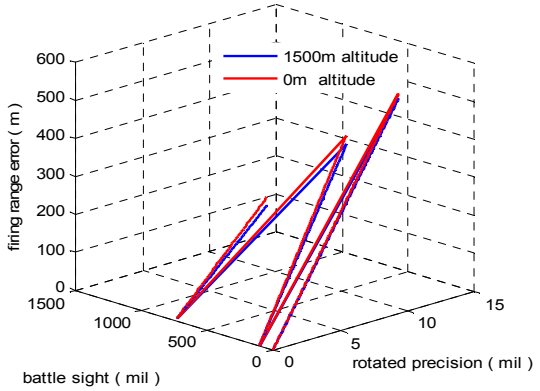

Figure5 Index function of rotated precision in different altitude

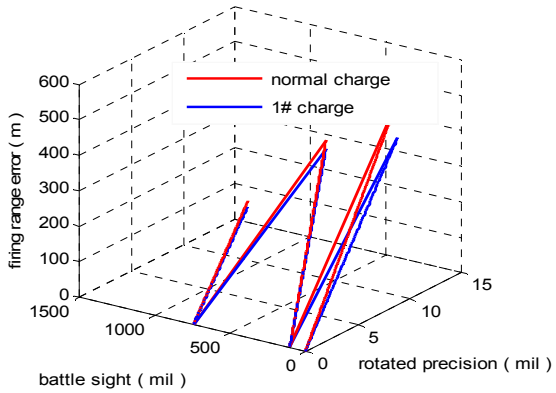

Figure6 Index function of rotated precision in different charge

There comes the result that along with the increase of charge and altitude, the coefficient of rotated precision index of gun barrel increased according to curves in figure *5* and figure *6*.

Therefore, in the firing table, the condition of maximum charge and *1500m* altitude was the extremal condition which can be used to compute the rotated precision index of gun barrel. And the maximum rotated precision index of gun barrel of the flat trajectory, the bending trajectory and the high-angle firing trajectory induced by *00-01mil* firing range was separate *53.4m*, *27.8m* and *18.1m*.

Conclusion

The mapping function of battle sight and firing range was computed based on least square polynomial fit method according to the data in the firing table in this paper, also it put forward these conclusions list next.

(1) The exterior ballistics should be divided into flat trajectory, bending trajectory and high-angle firing trajectory to be used to fit based on least polynomial fit method, and this piecewise fitting technique takes the advantage of high accuracy.

(2) Along with the increase of charge and altitude, the coefficient of rotated precision index of gun barrel increased, so it is necessary to select the high altitude and maximum charge condition to be used to compute the rotated precision index of gun barrel.

(3) The dispersion induced by rotated precision of gun barrel include the distance dispersion and direction dispersion, and the computed result put forward in this paper was based on distance dispersion that induced by rotated precision of gun barrel. So when used as the criterion of the determination data of auto-rotated precision of gun barrel, the direction dispersion induced by rotated precision of gun barrel should also be taken into account, and of course the least square polynomial fit method could be tried to accomplish the study.

References

[1] Wang Chunyan, Wang Zhijian. A Mesaurement System for Artillery Static Direction Angles[J]. ACTA ARMAENTARII, 2004, 25(6): 660-67

[2] ZHANG Guang, REN Guo-quan, ZHANG Ying-tang, et al. The Method of Gun Rotated Precision Detection based on Total Station Optima Disposition Apparatus[J]. Journal of Ordance Engneering College, 2010, 22(3): 44-47

[3] QIU Jin, MOU Shao-feng, YANG Jun. Data Analysis for Aiming Accuracy of Self-propelled Gun[J]. Fire Control and Command Control, 2007, 32(1): 105-107

[4] Yan Debin, Hu Chaogen, Chen Hongjun. Design of Gun Turntable System Based on Ring Laser Gyro Strap-on Inertial Navigation System[J]. Ship Electronic Engineering, 2011, 31(9): 57-59

[5] WANG Jian, ZHOU Li-hui, HE Ci, et al. Research of Measurement Precision of Gun Control System Induced by Direction of Barrel[J]. Armament Experiment, 2010(1): 4-10

[6] ZHAO Xin-sheng, SHU Jin-rong. The Theory and Application of Trajectory Calculation[M]. The Publishing House of Ordnance Industry, 2006

[7] PLA Central Staff. Firing Table of a Howitzer[S]. PLA Publishing House, 2001

Advanced Materials Research Vols. 989-994 (2014) pp 2854-2858
© (2014) Trans Tech Publications, Switzerland
doi:10.4028/www.scientific.net/AMR.989-994.2854

Parameter matching and Simulation Analysis on Power System of Plug-in hybrid vehicles

Duan Ji[1, a], Haifeng Zhang[1, b], Jun Yang[2, c]

[1]Liuzhou Vocational & Technical College, Liuzhou, Guangxi, China

[2]Liuzhou Wuling Automobile Industry Co.,Ltd

[a]chinajiduan@sina.com.cn, [b]151328718@qq.com.cn, [c]814717903@qq.com.cn

Keywords: Plug-in hybrid, Power system, Parameters design, Simulation analysis

Abstract. Based on design requirements of plug-in hybrid vehicle, using the method of theoretical analysis, the parameters matching design of drive motor, engine-generator set, battery, transmission and other subsystems is executed, and modeling and simulation are carried out using AVL-CRUISE software, simulation results show that the design is reasonable, laying a good foundation for the smooth development of the plug-in hybrid vehicle.

Introduction

Compared with hybrid vehicle of Energy conservation type, energy storage system of plug-in hybrid vehicle（PHEV）can be charged on running , and also charged via a power outlet, it can work longer in mode of battery power, for particular distance of daily commute, PHEV can work in mode of pure electromotion, The internal combustion engine provides additional power required by traveling of the long distance, PHEV possesses ability of better using alternative fuels and has wide development prospects in the field of new energy vehicles[1][2]. Compared with the traditional internal combustion engine vehicles, PHEV possesses motor, engine – generator set, battery and many other subsystems, in the early stage of development of PHEV, power, economy and reliability of vehicle can be improved greatly through the accurate design of power system parameters, coordination of subsystem performance and good match[3][4][5].

1. Vehicle parameters and the basic performance requirements

Table 1 Vehicle parameters

Parameter name		Value	Unit
Kerb mass		1200	kg
Gross Mass		1580	kg
Wheel base		2467	mm
Centroid height		500	mm
Frontal area		1.97	m^2
Drag coefficient		0.284	-
Rolling resistance coefficient		0.013	-
Wheel radius	Static radius	287	mm
	Dynamic radius	301	mm

With the continuous development of the drive motor, battery and transmission technology, power performance of electric vehicles ban be comparable to conventional car basically. Combining the

performance characteristic of electric vehicle, according to demand for vehicle performance, the basic parameter and vehicle performance index of PHEV vehicle are shown in Table 1 and Table 2.

Table 2 Performance index of vehicle

Performance requirement	Items	Index
Speed requirement	Maximum speed	≥120 km/h
Acceleration performance	0~50km/h	≤8s
	50~80km/h	≤10s
Climbing performance	Maximum speed when slop is 4%	≥70 km/h
	Maximum speed when slop is 12%	≥40 km/h
	Maximum gradeability	≥20%

2. Parameters design of power system for PHEV

Parameters design of drive motor. Power requirement of PHEV can be obtained by the formula (1), (2) and (3) on three states of maximum speed, acceleration and climbing.

$$P_{e1}=\frac{1}{\eta_T}\left(\frac{mgfu_a}{3600}+\frac{C_D A u_a^3}{21.15\times 3600}\right). \tag{1}$$

$$P_{e2}=\frac{1}{\eta_T}\left(\frac{mgfu_a}{3600}+\frac{C_D A u_a^3}{21.15}+\delta m u_a\frac{du}{dt}\right). \tag{2}$$

$$P_{e3}=\frac{1}{\eta_T}\left(mgf\cos\alpha u_a+\frac{C_D A u_a^3}{21.15}+\mathrm{mg}u_a\sin\alpha\right). \tag{3}$$

Where, η_T is driveline efficiency, m is full load quality, f is rolling resistance coefficient, C_D is air resistance coefficient, A is frontal area, u_a is maximum speed, v is speed, δ is moment of inertia conversion coefficient, α is climbing angle.

Table 3 Estimated data of motor peak power

Performance requirement	Motor power
Maximum speed v_{max} ≥120 km/h	20.88 kW
Acceleration performance 0~50km/h≤7s	49.3 kW
Acceleration performance 50~80km/h≤8s	38.6 kW
Max stable speed of slop of 4%≥70 km/h	19.85 kW
Max stable speed of slop of 12%≥40 m/h	24.93 kW
Maxi stable speed of slop of 20%≥5 km/h	4.83 kW

According to formula (1), (2) and (3), the maximum power demand estimated under kinds of conditions are shown in Table 3.

To meet the power performance, rated power of drive motor must satisfy the power needs of the maximum speed, peak power must meet the need of acceleration performance. From Table 3, the rated power is not less than 20.88kW, peak power of motor is not less than 49.3kW, and the rated power of motor is taken as 25kW, peak power of motor is 50kW.

Permanent magnet drive motor has advantages of high efficiency, high power density, Its working

voltage is 100 ~ 400V, maximum rotational speed is 4000-10000r/min, constant power factor is up to 2.25, drive motor adopts permanent magnet synchronous motor, parameters of drive motor in the design are shown in Table 4.

Table 4 Parameters of drive motor

Parameters	Value
Rated power	25kW
Overloading coefficient	2
Base speed	3000rpm
Motor voltage	324V
Peak power	50kW
Peak torque	160Nm
Peak speed	8000rpm

Parameters design of engine-generator set. In case of sufficient electric quantity PHEV switches off engine, uses electrical energy preferentially, when the electric quantity of power battery drops to a certain extent and power battery can not continue to supply or electrical power provided by battery can not meet the needs of motor, the engine-generator set start work to provide enough power satisfying the needs of vehicle.

To reduce the charge and discharge times of battery and ensure battery safety, in the design, when the state of charge of battery is below 40%, the generator begins work, and it meets the demand of peak power. Design of engine- generator set not only meet the needs of the motor peak power, but also meet engine and generator working located in each area efficient district. Based on the above analysis and match of work area, the parameters of engine and generator determined are shown in Table 5

Table 5 Parameters of engine-generator set

Engine		Generator	
Maximum rotational speed	6000rpm	Maximum rotational speed	6000rpm
Maximum torque / speed	115Nm/4500rpm	Voltage	324
Maximum power	62kW	Maximum power	50 kW
Displacement	1.5L	Peak torque	160Nm

Parameter design of battery pack. The Endurance mileage of pure electromotion has a great influence to cost and application performance of PHEV, here, the endurance mileage of pure electromotion is driving distance when the battery is fully charged and doesn't rely on the engine to recharge. Rated capacity of battery can be obtained by formula (4).

$$W_0 = \frac{P_v S}{0.7 v \eta_m}. \tag{4}$$

Where, W_0 is rated total energy of battery, P_v is motor power traveling with the velocity of v, S is distance traveling with the velocity of v. Rated capacity Q satisfies formula (5).

$$Q = \frac{W_0}{U_B}. \tag{5}$$

Where, Q is rated capacity of battery, U_B is battery voltage.

In the design, PHEV is required traveling 90km with the velocity of 40km/h using pure electric, According to formula (4), battery capacity is obtained as 10.39kwh. According to formula (5), the rated capacity of battery is obtain as 32.07Ah.

Transmission System Design. Speed ratio of transmission system needs follow the requirement of meeting the needs of maximum gradeability and ensuring the desired maximum speed. Gear ratio of transmission is required to satisfy the formula (6) and (7).

$$i_0 \geq \frac{mg(f\cos\alpha_{\max}+\sin\alpha_{\max})r}{T_{\max}\eta_t}. \tag{6}$$

$$i_0 \leq \frac{0.377 n_{\max} r}{v_{\max}}. \tag{7}$$

Where, i_0 is speed ratio of transmission, r is wheel rolling radius, $T_{\max}$ is peak torque of motor, $n_{\max}$ is maximum speed of drive motor. In the design, the value of i_0 is chosen as 7.05.

3. Simulation Analysis

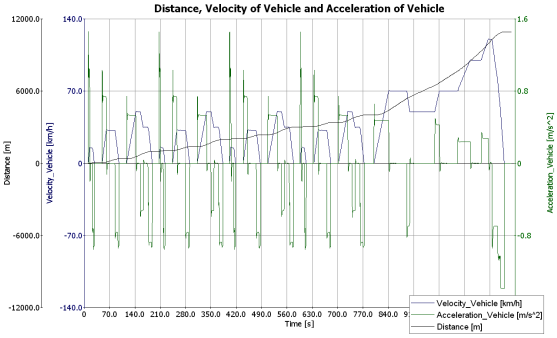

Fig. 1 NEDC condition

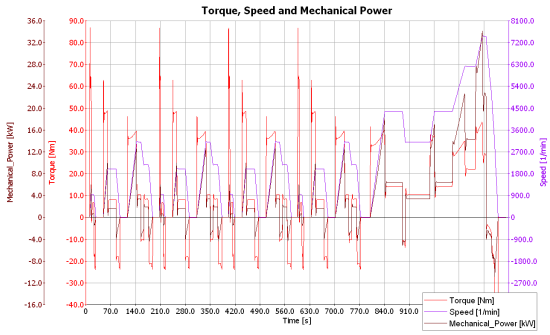

Fig. 2 Working curve of drive motor

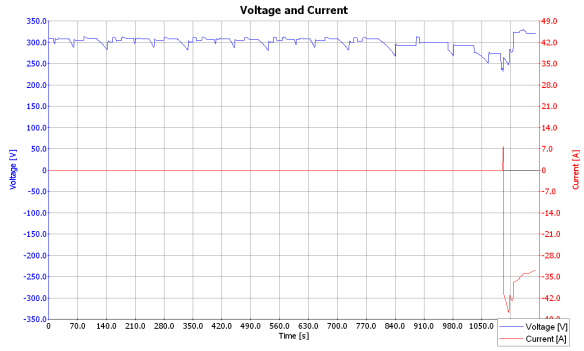

Fig. 3 Working curve engine

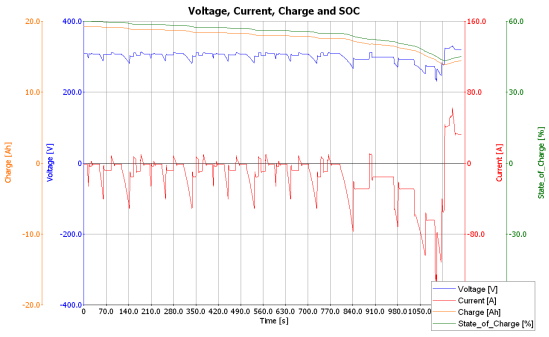

Fig. 4 Working curve of battery

To verify the reasonableness of design, power system of PHEV is simulated using AVL-CRUISE, simulation results under NEDC condition are shown in Fig. 1, Fig. 2 Fig. 3 and Fig. 4.

Table 7 Power performance simulation results

Performance requirement	Item	Simulation result	Reference index
Speed requirement	Maximum speed	128 km/h	≥120 km/h
Acceleration performance	0~50km/h	6.6s	≤7s
	50~80km/h	5.82s	≤8s
Climbing performance	Maximum speed when slop is 4%	128 km/h	≥70 km/h
	Maximum speed when slop is12%	83 km/h	≥40 km/h
	Maximum gradeability	23.8%	≥20%

It can be seen from Fig. 1 to Fig. 4, total mileage is 10.93km under NEDC cycle condition, and duration is 1179.8S, maximum speed is 120.5km/h, maximum acceleration is 1.46m/s^2, maximum deceleration is -0.953 m /s^2. Drive motor works in the range of 2000-7500rpm at most of the time, state of charge of battery is 60% in the beginning, from the beginning of 1100 seconds, the state of charge of battery is approaching 43%, engine–generator set starts automatically, providing power for the drive motor to maintain the normal running of the vehicle, at the same time charging the battery. It can be seen from Table 7, maximum speed of PHEV is 128km/h, acceleration time is 6.6s from 0 to 50 km/h, acceleration time is 5.82s from 50 to 80 km/h, Maximum gradeability is 23.8%, and the power indexes meet design requirements.

4. Conclusion

According to performance index of vehicle, basis on theoretical calculation, the parameter of drive motor, the engine-generator set, battery, transmission system and other subsystems were designed, the vehicle model is built using AVL-CRUISE software, vehicle performance and vehicle power performance under NEDC cycle condition are simulated. Simulation results show that the PHEV designed can meet operation requirements under the NEDC cycle condition, while the maximum speed, climbing performance, acceleration performance meet the design requirements, parameters design of drive motor, the engine–generator set, battery, transmission system and other subsystems is reasonable, it lays a good foundation for the smooth development of the PHEV.

Acknowledgements

The paper has been sponsored by 2013 Scientific Research Project of Educational Department in Guangxi Zhuang Autonomous Region for the project “Teaching Practice Platform Construction on New Energy Vehicle Technology in Vocational Colleges and Teaching Project Development”. Item Number: 2013JGA326.

Reference

[1] Chengliang Yin,Jianlong Zhang. New energy vehicles-typical type and structures (Shanghai science and Technology Press, China 2013).

[2] Iqbal Husain. Electric and Hybrid Vehicles: Design Fundamentals (China Machine Press. China 2012).

[3] Zhisheng Yu. The Theory of Automobile (China Machine Press, China 2009).

[4] Xue Nianwen, Ma Xianmeng, Pan Chaofeng, in: Study and Design of Power up and Power down Control Strategy of Plug-in Electric Vehicle, edited by volume 31of Journal OF ChongQing JiaoTong University(2012).

[5] Songlin Liu, Liqiang Gu, in: Simulation and Analysis of Hybrid Electric Vehicle Power Train Based on Cruise, edited by volume 22 of Drive System Technique(2008).

Advanced Materials Research Vols. 989-994 (2014) pp 2859-2864
© (2014) Trans Tech Publications, Switzerland
doi:10.4028/www.scientific.net/AMR.989-994.2859

Buckling Stability Analysis of Parallel Micro-spring

Jing Zhang[1,a], Li Sui[2,b], Xuhong Guo[3,c] and Guohua Liu[4,d]

[1,2,4]National Lab of Mechatronic Engineering and Control, Beijing Institute of Technology, China

[3]Huaihai Industry Group co., Ltd, China

[a]0181@bit.edu.cn, [b]bit_suili@bit.edu.cn, [c]guoxh.mems@gmail.com, [d]2120120171@ bit.edu.cn

Keywords: micro-spring; parallel spring; eigenvalue buckling analysis; stability

Abstract. Compression deformation will cause a micro-spring to buckle, and structural parameters, constraint conditions and structural forms of a micro-spring will affect its critical load and buckling mode. In order to study the influence on the micro-spring's stability caused by structural forms and find a structure to improve its critical load in the end, this paper designs a new kind of parallel micro-springs, which consists of two same-structured S-shaped planar micro-springs. We have carried on eigenvalue buckling analysis on the parallel micro-spring by software ANSYS, and have gotten its six orders' buckling mode. Because the critical load of the parallel micro-spring may change with the length of the beam connecting the two sub-springs, this paper studies the effect of the beam's length on the parallel micro-spring's critical loads and buckling mode. From comparing the analysis results between parallel micro-spring and single micro-spring with same stiffness, this paper concludes the stability's degree of improvement.

Introduction

Micro-spring is a very important and typical micro-mechanical element, and it is a key part for micro sensors, micro actuators and micro gyroscope. It can provide elastic force for these inertial devices, and transfer energy [1]. Due to differences of micro-mechanical processing technology and conventional processing technology, both structure, size and weight of micro-spring and conventional spring vary a lot. Compared with traditional spring, micro-spring has more kinds of structural forms. The structural form of planar micro-springs is completely different from traditional coil springs. In terms of material mechanics and structural mechanics, planar micro-spring can be seen as planar steel frame, which is connected to each other by elastic beams. Several researchers have studied structural forms, properties and detection methods of planar tensile micro-spring [2-4], however, few has researched properties and design methods of compression micro-spring. In addition, compression deformation will cause a micro-spring to buckle, for micro-springs are almost planar and with thickness of only a few hundred microns. Therefore, theoretical analysis and design method of the stability of micro compression spring should be improved.

U.S. Naval Air Warfare Center has developed an electromagnetic micro-mechanical security system to remove insurance for distributed missile in fuze. The security system is composed of three micro-springs [5]. In normal state, two springs are in a state of pretension to fix two locking pins in insurance position respectively, and sliding block is locked by two locking pins. When the projectile is launched, two locking pins successively leave insurance location, and the slider is moved to positive position. Meanwhile, electromagnet is powered off, and the locking pin clicks into the slider, so that insurance is removed. Paras Chawla in India Tapaer University has designed a RF micro-mechanical switch [6]. In this design, mechanical operation of RF switch mainly depends on stiffness coefficient of micro-spring K, which adopts the "bow" shape in order to reduce the stiffness coefficient. H. F. Lin and H. T. in the thirteenth Research Institute of China Electronic Technology Group Corporation have designed a kind of universal micro-mechanical collision switch [7]. The switch is composed of four symmetrically-distributed micro-springs, mass block, collision steps and collision step bottom. When the whole structure is impacted along any direction in XY plane, mass block contacts collision steps and signal is conducted; when the whole structure is impacted along Z direction, mass block contacts the bottom and signal is conducted.

Micro-springs in the switch have three modes of action, which is not only the pure tensile or compressive movement. From above micro-springs' applications in various fields, we can see that as an element of transferring force or energy, micro-spring not only produces tensile deformation, but also develops compression deformation in some applications. So it is necessary to study the stability and deformation characteristics of compression micro-spring.

Z. Wang in Beijing Institute of Technology has researched the influence of S-shaped micro-spring's structural parameters on buckling stability. By optimizing micro-spring's structural parameters on condition of satisfying spring stiffness, she concludes that the critical buckling pressure of optimized structural parameters' micro-spring is increased by 126.8% than that of primary micro-spring [8]. The authors have researched the influence of S-shaped micro-spring's constraint on buckling stability, and find that the critical buckling pressure of micro-spring is increased by 32.2% by adding constraints in X direction. The factors influencing micro-springs' structural stability contain structural parameters, constraints and structural forms. Therefore, we study the effect of parallel micro-spring satisfying stiffness conditions on critical load and buckling mode.

Stability Analysis of Micro-spring

Planar micro-spring has different kinds of structural shapes, such as S shape, W shape, Z shape, the Great Wall shape and L shape. This paper mainly studies the S-shaped planar micro-spring. Compression deformation will cause a micro-spring to buckle. Micro-spring stable failure generally can be divided into equilibrium bifurcation instability and extreme point buckling. In order to research the influence of S-shaped micro-spring's structural form on stability, we ignore the influence of internal defects, and adopt eigenvalue buckling analysis to evaluate the buckling stability of micro-spring.

Firstly, we determine the micro-spring's structural parameters, model and export the spring model's parasolid file by software UG. The spring model is shown in Fig. 1. Secondly, we import model file, carry out buckling analysis and get the critical buckling pressure by software ANSYS. The general process of ANSYS analysis is shown in Fig. 2.

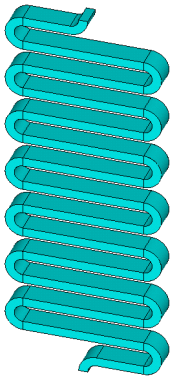

Fig. 1 The spring model

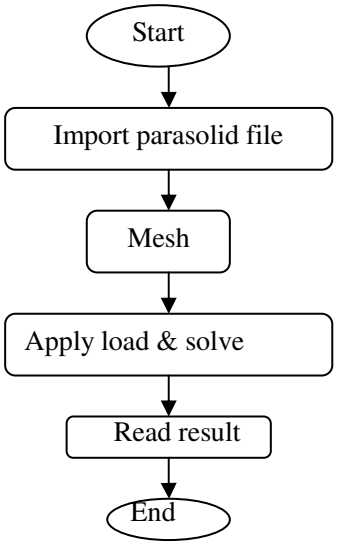

Fig. 2 General process of ANSYS analysis

Analysis Methods

In order to study the improvement level of parallel micro-spring on the stability, we conduct eigenvalue buckling analysis by software ANSYS. The parallel spring and S-shaped planar micro-spring, with the same spring stiffness, are analyzed.

Structural Parameters' Design. Structures of micro-springs are shown in Fig. 3, where a) is the structure of S-shaped plane micro-spring, and b) is the structure of the parallel spring. S-shaped

planar micro-spring can be described by five parameters: number of units *n*, thickness of micro-spring *h*, straight beam width *w,* width of section *b* and inside bend radius *r*, as shown in Fig. 4 a). The parallel spring can be described by the above five parameters and the distance between the two sub-springs *L*, as shown in Fig. 4 b). There are mainly three kinds of working modes: axial deformation, radial deformation and normal deformation. The relationship between S-shaped micro-spring's parameters and elastic stiffness in three working modes are worked out and calculation formula of spring stiffness is

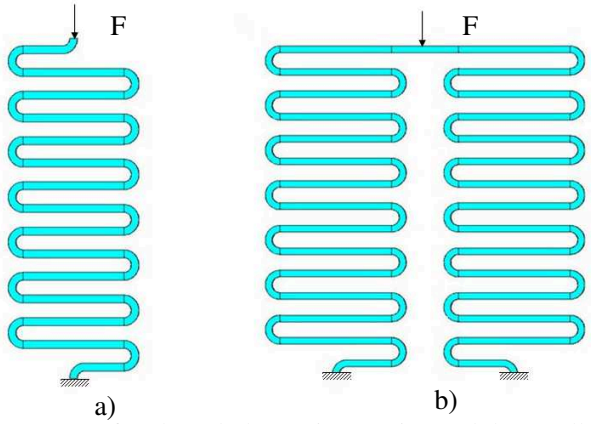

Fig. 3 Structures of S-shaped plane micro-spring and the parallel spring

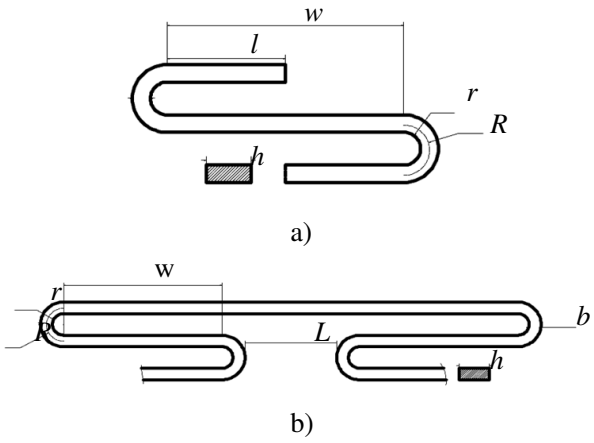

Fig. 4 Structure parameters of S-shaped plane micro-spring and the parallel spring

derived [9]. This paper mainly studies the influence of S-shaped micro-spring in the axial deformation mode on the stability. In the mode of axial deformation, stiffness coefficient of S-shaped micro-spring k is given by Eq. 1.

$$k = \frac{b^3 hE}{n\left[16l^3 + 12R\left(2l^2\pi + 8lR + R^2\pi\right)\right]} \tag{1}$$

where $l = \frac{w}{2}$, $R = r + \frac{b}{2}$, E is the young's modulus of elasticity, n is number of units, h is thickness of micro-spring, b is width of section, l is half of straight beam width w and R is arc radius. The values of S-shaped micro-spring parameters are shown in Table 1. According to Eq. 1, stiffness coefficient of the S-shaped micro-spring k_0 is 448.2534N/m.

Stiffness coefficient of the parallel springs is the sum of each spring stiffness coefficients. Therefore, to make the stiffness coefficients of the parallel spring and S-shaped planer micro-spring mentioned above equal , stiffness coefficient of the parallel spring is supposed to be half of stiffness

coefficient of the S-shaped micro-spring k_0, namely $k1 = ko / 2$.On condition of unchanging *r, w, h, n*, and *E*, only change *b* to fulfill the equation $k1 = ko / 2$.Through calculation, the width of section of parallel spring *b* should be 62μm, which can satisfy that stiffness coefficient of the parallel spring is equal to that of the S-shaped planar micro-spring. Parameter values of S-shaped planar micro-spring and parallel spring are shown in Table 1.

Table 1 Parameter values of S-shaped plane micro-spring and parallel spring

Parameters	Value	Value
Straight beam width *w* [μm]	1060	1060
Inside bend radius *r* [μm]	75	75
Width of section *b* [μm]	80	62
Thickness of micro-spring *h* [μm]	200	200
Number of units *n*	7	7
Young's modulus of elasticity *E* [GPa]	170	170
Poisson ratio *v*	0.3	0.3
Number of S-shaped micro-springs *m*	1	2

Eigenvalue Buckling Analysis. To study improvement level of parallel micro-spring on the stability, both load and constraint of S-shaped plane micro-spring and parallel spring should be the same in the buckling analysis. All degrees of freedom of the bottom of micro-spring are constrained and force F of 1N along the opposite Y axis is applied on the centre of micro-spring top surface, as shown in Fig. 3.

Although the distance between these two springs constituting the parallel spring *L* has no effect on spring stiffness, it does affect the spring buckling stability. Therefore, when *L* changes from 0.1mm to 2mm, eigenvalue buckling analysis of parallel spring is done, and buckling mode is expanded to six orders.

Results and Discussion

Six orders' buckling modal deformation diagrams are shown in Fig. 5, where a) is the deformation of S-shaped planar micro-spring, and b) is the deformation of parallel micro-spring. We can see that the buckling modes of these two kinds of springs have different deformation directions and sequences.

As shown in Fig. 6, the blue solid curve P1 and the green hollow curve P2 respectively show the first-order and second-order critical buckling pressure of the parallel micro-spring with the distance between the two sub-springs *L,* and the thick black line S1 and the thin red line S2 respectively show the first-order and second-order buckling pressure value of the S-shaped planar micro-spring. We can conclude that with the value of *L* increasing, the first-order critical buckling pressure of the parallel micro-spring decreases slowly, while the second-order buckling pressure of the parallel micro-spring increases greatly. The first-order and second-order critical buckling pressure of the parallel micro-spring are both significantly increased than the first-order and second-order buckling pressure of the S-shaped planar micro-spring.

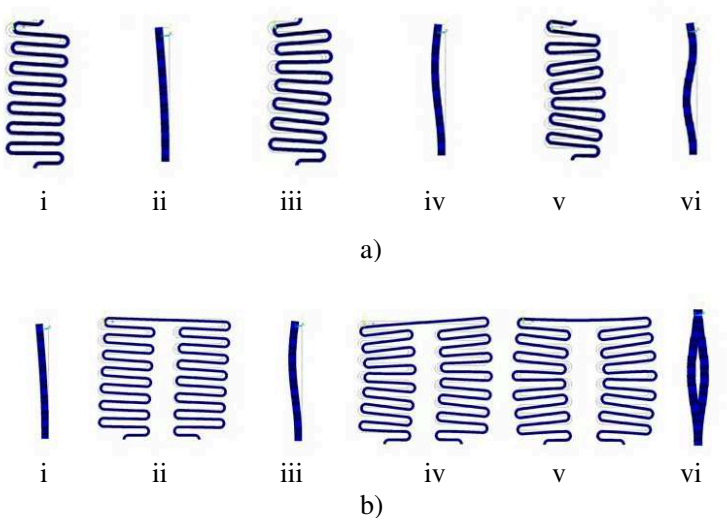

Fig. 5 Six-order buckling modes deformation diagram of S-shaped planar micro-spring and parallel micro-spring

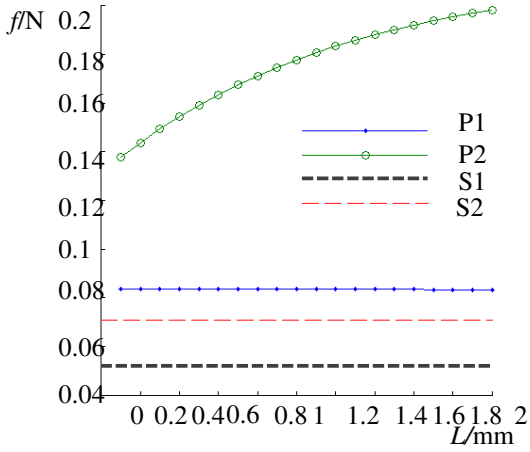

Fig. 6 The first-order and second-order buckling pressure curve of the parallel micro-spring and S-shaped planar micro-spring

Conclusions

This paper designs a parallel micro-spring based on two sub single S-shaped planar micro-springs. In order to research the stability's degree of improvement of the new type of micro-spring, this paper builds FEA model for the parallel spring and the single spring, and the two types of spring have same stiffness. From changing the length L of the beam connecting the two sub-springs, critical load and buckling mode will also change. This paper obtains two curves which respectively show the first-order critical load and second-order critical load with the length L. From comparing the analysis results between the parallel micro-spring and the single micro-spring with the same stiffness, we can conclude that the parallel micro-spring improves the stability significantly. When L is 0.1mm, the parallel spring's first-order critical load is increased by 60% than the single spring, and the second-order critical load is increased by 94.8%. With the increase of the length L, the first order critical load decreases slowly and the second order critical load increases quickly. In the future, another structural form which can improve spring's stability will be carried out.

References

[1] G.C. Shi and H. Li: Journal of Detection & Control. Vol. 30 No. 2(2008), p. 8-12 (In Chinese)

[2] H. Li, in *Research on Ubmunition Fuze Safety System Based on MEMS Technology*. Doctor's Degree Thesis of Beijing Institute of Technology, China (2006). (In Chinese)

[3] L.B. Zheng, in *Research on MEMS Elastic Element's Application in the Fuze*. Doctor's Degree Thesis of Beijing Institute of Technology, China (2006). (In Chinese)

[4] H. Zhang, in *Research on MEMS Safety System Problems*. Doctor's Degree Thesis of Nanjing Institute of Technology, China (2008). (In Chinese)
[5] Cope, Randall D. MEMS S-A Technology: Naval Air Warfare Centre, Weapon Division, China Lake,(1999)
[6] Paras Chawla and Rajesh Khanna: International Journal of Physical Sciences. Vol. 8 (2013), p. 1628-1638
[7] H.F. Lin, H.T. He and Y.M. Bian: Micro-nano Electric Technology. Vol. 46 (2009), p. 358-361
[8] Z. Wang, in *Stability Analysis and Optimization of Micro Compressed Spring*. Master's Degree Thesis of Beijing Institute of Technology, China (2014). (In Chinese)
[9] H. Li and G.C Shi: Piezoelectrics & Acoustooptics. Vol. 29 No. 2(2007), p. 237-139(In Chinese)

Advanced Materials Research Vols. 989-994 (2014) pp 2865-2868
© (2014) Trans Tech Publications, Switzerland
doi:10.4028/www.scientific.net/AMR.989-994.2865

Passivity-Based Control of Motor for Reaction Wheel

Renlong Yu[a], Jing Jin[b]

Department of control science and engineering in school of astronautics, HIT, China

[a]yurenlong@hotmail.com, [b]jinjinghit@hit.edu.cn

Keywords: Magnetically suspended reaction wheel, passivity-based control, permanent magnetic brushless DC motor, speed mode

Abstract: To achieve high-precision tracking control of motor speed for magnetically suspended reaction wheel, mathematical model combining BUCK converter with permanent magnet brushless DC motor system is established, and a MSRFW speed mode Passivity-based control method is presented. A passivity-based controller of speed tracking is designed in order to enhance the speed of tracking performance. Experiments on MSRW platform show that passivity-based control method can improve the speed of the dynamic response and tracking accuracy, from which the validity is verified.

Introduction

Brushless DC motor (BLDCM) has been widely used in aerospace inertial actuator because of its fast response, high power density, high reliability and maintenance-free. The complexity is evident in the development of a torque/speed regulator. Using d-q transformation to ease the complexity of analyzing three phase motor may serve to design an adequate controller. However, development of a controller based on the transformation of the a-b-c equations to the d-q variables is only advantage for permanent magnet motor with sinusoidal back EMF. Applying the d-q transformation to a trapezoidal back EMF motor can not eliminate the angle dependent phase inductance. The author in Ref.1 applied the d-q transformation to a BLDCM by fixing the synchronous reference frame to the instantaneous rotor flux linkage instead of the rotor geometric axis. However, this approach is cumbersome since the instantaneous rotor flux linkage must be found experimentally and programmed into a digital signal processor. Sliding mode control technique has been proved to be computational extensively when self-adaptive parameter estimation is used to estimate load parameters 2,3. Hysteresis current control and pulse-width modulation (PWM) control coupled with continuous control theory produce the most widely used BLDCM control techniques 4,5. Hysteresis current control is essential toward achieving adequate servo performance 6, namely instantaneously torque response yielding faster speed response compared with PWM control. For most applications, a proportional-integral current and speed compensators are sufficient to establish a well-regulated speed/torque controller. In other cases, a state feedback control is needed to achieve more precise control of the BLDC motor.

To achieve high-precision tracking control of motor speed for magnetically suspended reaction wheel(MSRW), a MSRW speed mode Passivity-based control method is presented based on the established BUCK converter and permanent magnet BLDCM system combining with mathematical model. Passivity-based controller of speed tracking is designed in order to enhance the speed of tracking performance targets. Experiments on MSRW platform show that passivity-based control method can improve the speed of the dynamic response and tracking accuracy, from which the validity is verified.

Mathematical model

Consider a permanent magnet BLDCM for MSRW with its armature circuit loaded into a buck type DC-DC converter, which is shown in Fig.1.

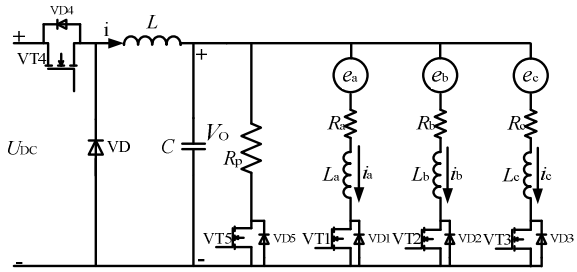

Fig.1 Schematic diagram of reaction wheel motor drive system

Assume that three phase of motor is symmetry, namely L_a-M_a=L_b-M_b= L_c-M_c=L_m , R_a=R_b=R_c=R_m, influence of commutation is omitted.Such a configuration constitutes a tetrad quadrant speed control for a BLDCM drive. The mathematical model of the composite system can be expressed by:

$$\begin{cases} L\dfrac{di}{dt} = -v + Eu \\ C\dfrac{dv}{dt} = i - i_a \\ L_m\dfrac{di_a}{dt} = v - R_m i_a - K_e\omega \\ J\dfrac{d\omega}{dt} = -B\omega + K_m i_a + T_p \end{cases} \tag{1}$$

where i is the input current of buck converter, v the output voltage of buck converter, i_a the BL DCM armature current, ω the speed of motor, T_p the torque perturbation which is assumed to be zer o. The control input is represented by the variable u, which represents a switch position taking value s 0 or 1. The system is controllable and flat because it is linear system with the typical form compos ed of four 1-order deferential equations.

Passivity based controller

A fundamental design idea for the feedback passivity based controller of reaction wheel motor is introduced. The control design method is known as the energy shaping and damping injection method [7,8].

Let the stored energy function of the system and its gradient vector be given as

$$H = \frac{1}{2}x\begin{pmatrix} L & 0 & 0 & 0 \\ 0 & C & 0 & 0 \\ 0 & 0 & L_m & 0 \\ 0 & 0 & 0 & J \end{pmatrix}x^T \tag{2}$$

$$H = \frac{1}{2}\left(Li^2 + L_m i_a^2 + Cv^2 + J\omega^2\right) \tag{3}$$

$$\frac{\partial H}{\partial x} = \begin{pmatrix} Li & Cv & L_m i_a & J\omega \end{pmatrix}^T \tag{4}$$

Then, consider the following Generalized Hamiltonian Canonical representation of the reaction wheel motor system[9,10]:

$$\begin{cases} \dot{x} = (M+N)\dfrac{\partial H(x)}{\partial x} + gu \\ y = h(x) = i \end{cases} \tag{5}$$

Where $M=\begin{pmatrix} 0 & -\frac{1}{CL} & 0 & 0 \\ \frac{1}{CL} & 0 & -\frac{1}{CL_m} & 0 \\ 0 & \frac{1}{CL_m} & 0 & -\frac{K_e}{JL_m} \\ 0 & 0 & \frac{K_m}{JL_m} & 0 \end{pmatrix}$, $N=\begin{pmatrix} 0 & 0 & 0 & 0 \\ 0 & 0 & 0 & 0 \\ 0 & 0 & -\frac{R_m}{L_m^2} & 0 \\ 0 & 0 & 0 & -\frac{B}{J^2} \end{pmatrix}$, $g=\begin{pmatrix} \frac{E}{L} \\ 0 \\ 0 \\ 0 \end{pmatrix}$, $M+M^T=0$, $N=N^T$

Using the energy shaping and damping injection method to design a dynamic output feedback controller. Consider the following energy function for the tracking error $e=x-x^*(t)$

$$H_e\left(x-x^*\right)=\frac{1}{2}\left(x-x^*\right)^T\begin{pmatrix} L & 0 & 0 & 0 \\ 0 & C & 0 & 0 \\ 0 & 0 & L_m & 0 \\ 0 & 0 & 0 & J \end{pmatrix}\left(x-x^*\right) \tag{6}$$

The function $H_e(x-x^*)$ is a positive definite function and $H_d(x-x^*)$ denotes the following time derivative:

$$\dot{H}_e\left(x-x^*\right)=\left(x-x^*\right)^T\begin{pmatrix} L & 0 & 0 & 0 \\ 0 & C & 0 & 0 \\ 0 & 0 & L_m & 0 \\ 0 & 0 & 0 & J \end{pmatrix}\left(\dot{x}-\dot{x}^*\right) \tag{7}$$

Letting the reference state trajectory be generated by the dynamic system:

$$x^*=M\frac{\partial H\left(x^*\right)}{\partial x^*}+N\frac{\partial H\left(x^*\right)}{\partial x^*}+gu-N_d\frac{\partial H\left(x-x^*\right)}{\partial\left(x-x^*\right)} \tag{8}$$

$$\dot{e}=M\frac{\partial H(e)}{\partial e}+\left(N+N_d\right)\frac{\partial H(e)}{\partial(e)} \tag{9}$$

Finally, equation(12) becomes

$$\dot{H}_e(e)=\frac{\partial H(e)}{\partial e^T}\dot{e}=\frac{\partial H(e)}{\partial e^T}M\frac{\partial H(e)}{\partial e}+\frac{\partial H(e)}{\partial e^T}(N+N_d)\frac{\partial H(e)}{\partial e}$$

Thus,

$$\dot{H}_e\left(e\right)=-R_mL_me_{i_a}^2-BJ\omega<0 \tag{10}$$

We can obtain the dynamical feedback controller expression for the average input using the exogenous system equations and solution for the average control input u which is denoted by u_{av}.

$$u_{av}=\frac{L}{E}\left[\frac{d}{dt}\left(i^*\right)+\frac{v^*}{L}\right] \tag{11}$$

Experimental results

The experimental results of passivity based control are shown in the following. The ratings of the motor are described in Table 1, and the controller is implemented on a TI DSP TMS320F2812 digital signal processor. TMS320F2812 is a high-performance micro-controller designed for high-speed calculation and is equipped with many on-chip peripherals for motor control applications. The ADC unit built-in on the DSP is used to read the feedback current signal. The on-chip general purpose I/O and the capture units on the DSP are applied to capture signals of Hall sensor to generate precise firing commands for the power stage and calculate the motor speed. The PWM unit of the DSP creates the corresponding PWM waveform to drive the wheel motor according to the control command specified by the passivity based controller. A power stage block is used to provide a variable voltage source in driving the wheel motor, and there is a current sensor in this block to measure the fed current of motor. There is also a protection circuit block to protect the DSP from the high voltage and current from the power block.

Table 1 Important parameters

Specifications	Units	Specifications	Units
Number of poles	8	Phase resistance, R_m	1.2Ω
Moment of inertia, J	0.0955Kg-m2	Operated Speed	±5000rpm
Torque constant, K_m	0.0191	Inductance of Buck DC-DC converter, L	760μH
Back-EMF constant, K_e	0.002	Capacitor of Buck DC-DC converter, C	47μF
Armature inductance, L_m	50μH	Rated current, I_N	2A

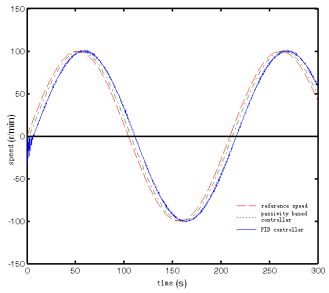

Fig.2 MSRW speed trace response of PID controller and passivity based controller

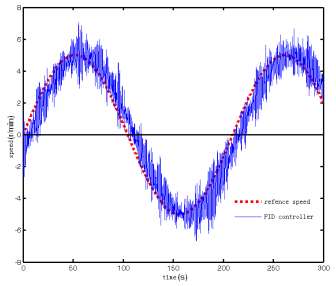

Fig.3 MSRW speed trace response of PID controller

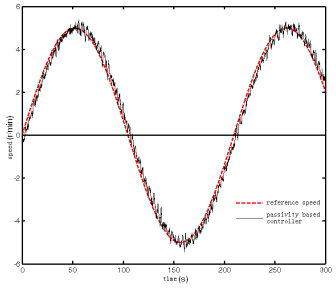

Fig.4 MSRW speed trace response of passivity based controller

Conclusions

The paper establishes mathematical model combining with BUCK converter and permanent magnet BLDCM and presents a passivity-based control method for MSRW speed mode. In order to enhance the speed of tracking performance targets, passivity-based controller of speed tracking is designed. Experiments on MSRW platform show that the proposed method can improve the speed of the dynamic response and tracking accuracy.

References

[1] C. W. Lu, Torque controller for brushless DC motors, IEEE Trans. Ind.Electron., vol. 46, no. 2, pp. 471-473, 1999.

[2] J. U. Lee, J. Y. Yoo, and G. T. Park, “Current control of a PWM inverter using sliding mode control and adaptive parameter estimation,” in Proc. IECON 20th Int. Conf., Sep. vol. 1, pp. 372-377, 1994.

[3] V. I. Utkin, “Sliding mode control design principles and applications to electric drives,” IEEE Trans. Ind. Electron., vol. 40, no. 1, pp. 23-36, Feb. 1993.

[4] M. A. El-Sharkawi, Fundamentals of Electric Drives. Pacific Grove, CA: Brooks/Cole, 2000, pp. 5–10.

[5] J. Chen and P.-C. Tang, “A sliding mode current control scheme for PWM brushless DC motor drives,” IEEE Trans. Power Electron., vol. 14, no. 3, pp. 541–551, May 1999.

[6] H. C. Chen, M. S. Huang, C. M. Liaw, Y. C. Chang, P. Y. Yu, and J. M. Huang, “Robust current control for brushless DC motors,” Proc. Inst. Electr. Eng. Electric Power Applications, vol. 147, no. 6, pp. 503–512,2000.

[7] R. T. Novotnak, J. Chiasson. Comments on Passivity-based control of saturated induction motors, J. IEEE Trans. on Industrial Electronics, pp: 820-821, 2003.

[8] L.U.Gökdere, M. A. Simaan, and C.W. Brice, Passivity-based control of saturated induction motors, J. IEEE Trans. on Industrial Electronics, pp: 870-872,2001.

[9] R.T.Novotnak, J.Chiasson, and M.Bodson, High-performance motion control of an induction motor with magnetic saturation, J.IEEE Trans. Control System Technology., pp: 315-327, 1999.

[10] L.U.Gökdere and M.A.Simaan, Response to comments on A passivity-based method for induction motor control, J. IEEE Trans. on Industrial Electronics, pp: 670-671, 1999.

Advanced Materials Research Vols. 989-994 (2014) pp 2869-2873
© (2014) Trans Tech Publications, Switzerland
doi:10.4028/www.scientific.net/AMR.989-994.2869

The study of Mine explosion-proof enclosure design and optimization

Qing-long Zhang[1, a], Su-jun Yang [2,b]

[1]School of Mechanical Engineering,Tianjin Polytechnic University ,, Tianjin 300387, China

(Grant from) The National Natural Science Funds(51274150),Modern mechanical and electrical equipment technology laboratory

[a]1079538908@qq.com,[b]yangsujun@tjpu.edu.cn

Keywords: the shell; elastic-plastic mechanics; ANSYS; APDL; The optimization design system.

Abstract. In this paper, the shell's strength and stiffness is calculated according to the theory of elastic mechanics and elastic-plastic mechanics theory.And the analysis of the ANSYS software verify the reliability of the theoretical calculation . Using ANSYS parameter design language (APDL)and the optimized design module of ANSYS,the author studies Material nonlinear static analysis ,and establish the parametric analysis program.

Introduction

With the rapid development of coal industry in our country,the design of the explosion-proof electrical equipment should be not only economic and reliable but also convenient .Therefore, it is necessary to conduct Elastic-plastic nonlinear finite element analysis In designing and calculating the shell， and establish the parametric analysis program[1].

The flame-proof principle of explosion-proof enclosure. According to the flame-proof enclosures "d" protection of the equipment in the explosive environment(GB_3836[1].2-2010 ）.Explosion-proof electrical equipment shell can withstand the internal explosive mixture explosion ,and don't be damaged .Don't cause external explosive gas environment lit[2].In other words,explosion-proof enclosure has a certain resistance to blast and flame-proof sex.the main reason of failure is the low material intensity or rigidity.

The following example illustrates Shell analysis optimization process.

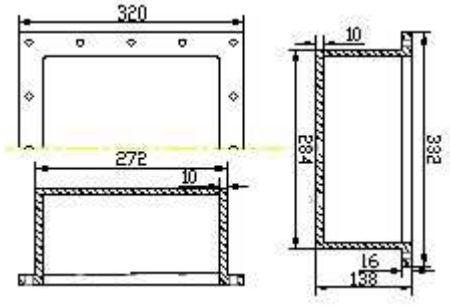

Fig1 The simplified graphic of the wall

Because the explosion-proof enclosure actual structure is complex,it is necessary to simplify off some accessories before calculating,and keep the basic shape and thickness of each panel[3].

The intensity and stiffness analysis of the shell

The theoretical calculation of the intensity and stiffness. The theoretical calculation of the structural strength and stiffness is divided into the elasticity and plasticity theory.The variables in the mechanics are mainly displacement, strain and stress [3].Based on elastic-plastic mechanics,when a material is subjected to a tensile or compressive load of sufficient magnitude, it will deform at first elastically and then plastically.

Based on the assumption of the small deflection of thin plates and the elastic-plastic mechanics theory[4]:

1）The large deflection of a four-sides-fixed rectangle plate:

$$w = 0.00126\frac{p_0 a^4}{D} . \tag{2.1}$$

a is the length of the short edge ; p_0 is the uniformly distributed load;D is the plate's bending strength.

$$D = \frac{Eh^3}{12(1-\mu^2)} . \tag{2.1}$$

E is the elastic modulus;h is the thickness ; μ is the Poisson ratio .

Maximum stress value occurs at the midpoint of the plate's fixed long side edge.When μ is 0.3,Maximal bending moment could be:

$$M_{center} = -0.0513 p_0 a^2 . \tag{2.3}$$

2）The large deflection of a simply supported rectangle plate：

$$w = 0.00406\frac{p_0 a^4}{D} . \tag{2.4}$$

Maximal bending moment occurs at the midpoint of the plate：

$$M_{\max} = \frac{9(1+\mu)}{256} p_0 a^2 \approx 0.0479 p_0 a^2 . \tag{2.5}$$

According to the relation between Stress and bending moment， the maximum stress was obtained：

$$(\sigma_x)_{z=\frac{h}{2}} = -(\sigma_x)_{z=\frac{h}{2}} = \frac{6M_x}{h^2} . \tag{2.6}$$

M_x is the bending moment around the Y-axis.

The concrete calculation result of the model. p_0 is based on the design requirement.the material is Carbon steel Q235-A， E is 2.06 GPa , μ is 0.3.Regarding the bottom and side plate as a simply supported rectangle plate;The cover plate is regarded as the four-sides-fixed rectangle plate .

Table 1 Shell's displacement and stress results under small deflection theory

The panel	Panel size mm	Thickness h/mm	Short edge a/mm	Maximum deflection w/mm	Maximum stress δs /MPa
Bottom plate	284×272×10	10	272	1.18	212.63
The left panel	272×112×10	10	112	0.04	36.05
The right panel	284×112×10	10	112	0.04	36.05
The cover plate	332×320×22	22	320	0.06	65.12

Table 1 is an Excel spreadsheet.We can easily get the initial thickness of the wall plate by Changing the parameter h or a.

The Linear elastic static analysis of ANSYS. Use spatial four nodes elastic shell element SHELL63 to Simulate the elastic plate[5].The analysis results are as follows.

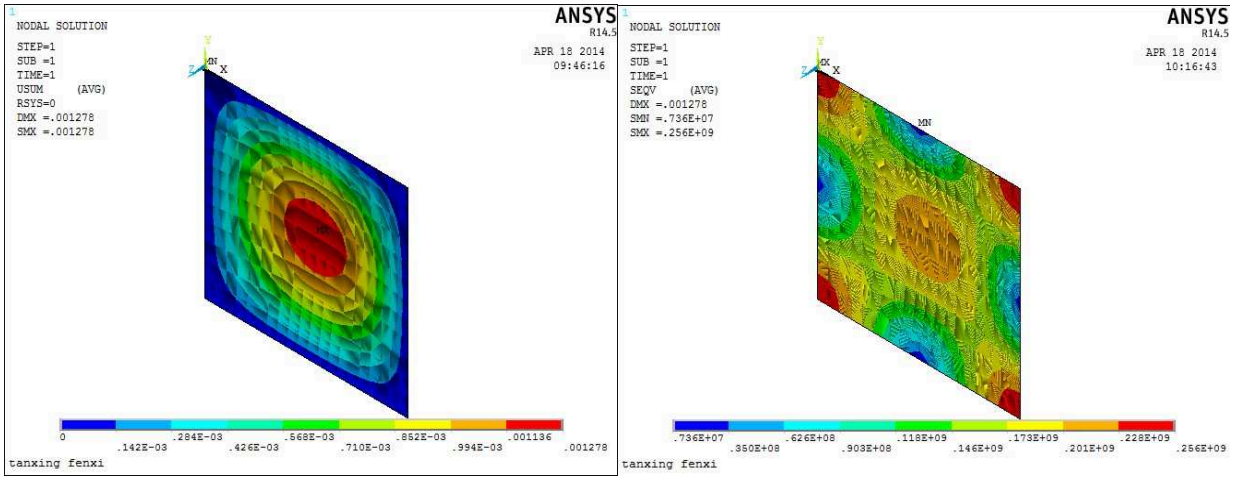

Fig2-1 The bottom board displacement in Z-axes,Fig2-2 The bottom board Mises stress nephogram
Analysis results are consistent with theoretical calculation results.

The plastic analysis and calculation of the wall. The plate's stress should be greater than the yield strength of the material,but smaller than Ultimate strength.Plastic deformation occurred.Therefore, it is needed to carried on preliminary structure optimization.

Table 2 The size and the stress value of the panel after preliminary improvement

The panel	Panel size mm	Thickness h/mm	Short edge a/mm	Maximum stress δs /M Pa
Bottom plate	284×272×9	9	272	393.76
The left panel	272×112×3.7	3.7	112	395.01
The right panel	284×112×3.7	3.7	112	395.01

Material work in the plastic zone at this time.Due to the theoretical calculation value can not reflect the real deformation and stress value， need to carry on elastic-plastic nonlinear analysis by using the ANSYS software.

Nonlinear finite element analysis. Use spatial four nodes Small plastic strain shell element SHELL143 to Simulate the plastic plate[5].The analysis results are as follows.

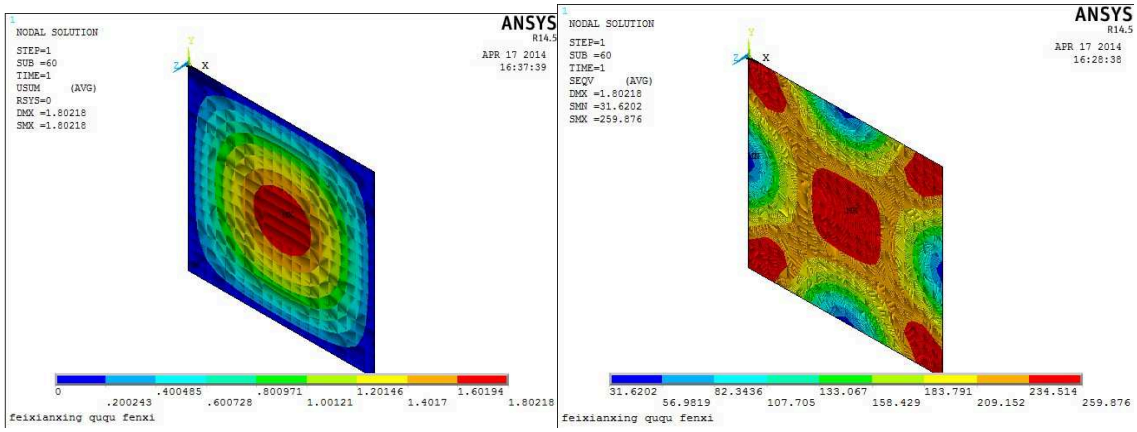

Fig2-1 The bottom board displacement in Z-axes,Fig2-2 The bottom board Mises stress nephogram
Analysis results show that the panel has enough strength,Its biggest deformation smaller than the plate's allowed permanent plastic deformation value.

$$w_{\max} = 1.6mm \le 2\% \times 284mm = 5.68mm \quad . \tag{2.7}$$

The design of the Mine explosion-proof enclosure is reasonable and reliable.

Stiffness analysis of the flange. Explosion pressure produces by the flammable gases's explosion inside of the shells Operates on the flame-proof joint surface ,which forms between the Cover plate and the box flange[2] .The flange must have enough stiffness and cannot occur large elastic deformation or plastic deformation,according to the criteria（GB_3836[1].2-2010）.Through analysis the boundary conditions of the box flange:the shorter edges is Simply supported;a long side is fixed;the other long edge is free .The general calculation formula of maximum deflection:

$$w_{\max} = \alpha \frac{p_0 L^4}{Eh^3} . \tag{3.1}$$

L is the bolt spacing; α is a given deflection coefficient.

The stiffness conditional is the sum of the maximum deflection less than the allowed deflection[2].

$$\sum w\max = w\max + w\max \le (W/2 - A)\psi / K = [f] . \tag{3.2}$$

W is the maximum clearance of flame-proof joint surface;A is the flatness tolerance; ψ is Weld coefficient;K is the safety factor and is set to 1.5.In conclusion ,the flange's theory Thickness can be calculated

$$T_a = a\{\alpha P_0 K / [E(0.5W - A)\psi]\}^{1/3} . \tag{3.3}$$

Explosion-proof surface will suffer certain mechanical damage during being used,such as scratches , pits,etc.Therefore, the designer of Mine Explosion-resistant Enclosure should not only consider the Wall thickness's additional amount of C but also consider retaining some machining allowance.Actual thickness of the flange is as follows

$$T_a = a\{\alpha P_0 K / [E(0.5W - A)\psi]^{1/3} + B + C . \tag{3.4}$$

B is the repair allowance of the flange,Plane flange generally take 15% of the flange thickness and is not less than 1.

$$C = C_1 + C_2 . \tag{3.5}$$

Table 3 Deflection coefficient α

Inspection requirements	Welding by both sides	The single side welding's Weld full length	
		Have backing plates	No backing plates
100%	1.00	0.90	0.75
Local inspection	0.90	0.80	0.70
No inspection	0.70	0.65	0.60

Table 4 Steel plate minus tolerance

Thickness	2	2.2	2.5	2.8 ~3.0	3.2 ~4.0	4.5 ~5.5	6 ~7	8 ~25
C_2	0.18	0.19	0.20	0.22	0.25 ~0.3	0.5	0.6	0.8

C1 is the Corrosion allowance,depends on the corrosion rate of materials in the environment.for carbon steel C1≥0.1mm.C_2 is steel plate minus tolerance.

Table 5 The corresponding data between the minimum joint surface width(L) and clearance(w)

junction surface width L (mm)	maximum clearance W (mm)corresponding to the shell's volume V (cm2)		allowable gap when S is 1.5(mm)
	V≤100	V>100	
6≤L<12.5	0.3	0.3	—
12.5≤L<12.5	0.4	0.4	0.133
25≤L	0.5	0.5	0.2

Developing the dedicated finite element analysis program.Parameterized design and sequencing analysis can effectively improve production efficiency.APDL as a program design language,can not only realize parameter modeling,but also develop the dedicated finite element analysis program procedure.

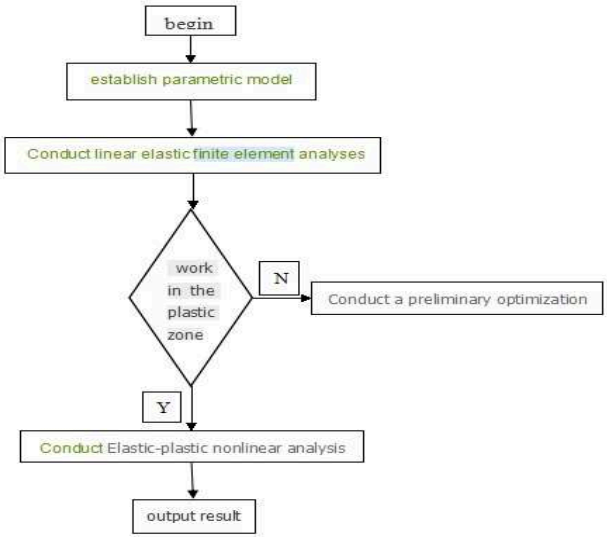

Fig4-1 The system flow chart ,

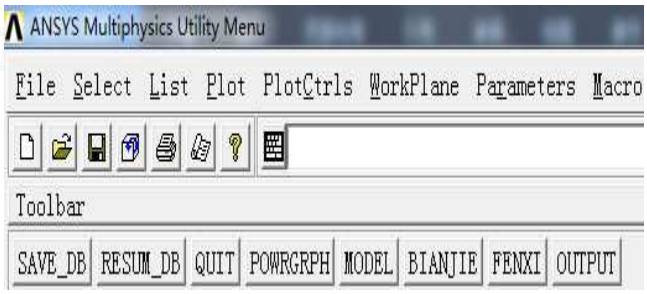

Fig4-2 User interface

Users click on MODEL button,input the geometric parameters of the explosion-proof enclosure pane that you want to analyze.The system automatically generated grids finite element model.Click on BIANJIE button and Select the corresponding boundary conditions ,then click FENXI button to set the solving process and analyze it.Click the OUTPUT button and output the result finally.

Summary

In this paper, the Mine explosion-proof enclosure has been carried on theoretical calculation and finite element analysis,and Developing the dedicated finite element analysis program.Not only save material but also improve the efficiency of design.

References

[1] Shao-chun Li, Status quo and prospect of China's explosion-proof electric apparatus manufacturing industry.[J]:market perspective. 18-20 (2008).
[2] GB_3836[1].2-2010,Explosive atmospheres-Part 2: Equipment protection by flameproof enclosures "d"[S]
[3] Xiao-e Guo,Design of Cuboid Flameproof Enclosure[J],Colliery Mechanical & Electrical Technology.7-9(2002).
[4] Yixuan Zhu,Application of elastic-plastic mechanics[M],zhengzhou,zhongzhou Ancient books Press. 177-182(1985).
[5]Zhao-hui zhang,ANSYS12.0 structure analysis engineering application examples analysis [M],beijing,China Machine PRESS. 345-352(2011).

Advanced Materials Research Vols. 989-994 (2014) pp 2874-2877
© (2014) Trans Tech Publications, Switzerland
doi:10.4028/www.scientific.net/AMR.989-994.2874

Research for guide groove configuration of rotary valve

Suying Xu

Eaestern Liaoning University,Dandong, Liaoning118003, P.R.China

Xusuying0002@163.com

Keywords: Rotary valve, Spool shaft, Guide groove, Coordinate gap, Leaks

Abstract. Rotary valve is a device to achieve fast commutation hydraulic transmission . Rotary valve is driven by a hydraulic motor drive and can achieve rapid conversion of the hydraulic circuit . Rotary valve spool by a rotating shaft , housing , shafts and bearings and other components. Guide grooves machined on the spool shaft is evenly distributed for hydraulic cylinder into the oil and return oil conversion. The coordinate gap between the spool shaft and valve chamber bore Because will affect the leakage in the leak. How to improve the guide groove structure? We can put the guide groove by high and low partition instead of overlapping arrangement. Reducing leakage within the valve chamber and Meet with the requirements of the spool shaft and valve chamber bore.

Introduction

The method to change the oil hydraulic system is to change the hydraulic oil flow path . The commutation circuit is generally intermittent and slow commutation. To achieve the required hydraulic circuit hydraulic vibration fast commutation, to meet the requirements of the desired frequency . The hydraulic circuit hydraulic vibration requires fast commutation, to meet the required frequency , we can use the rotary valve, rotary valve to meet the low-frequency hydraulic vibrator commutation request.

According to the design requirements of medium pressure hydraulic system. Design pressure of the rotary valve is 16Mpa. The shaft diameter of the rotary valve is 120mm. It can calculate the axial force effected on the rotary valve shaft is 166KN. The diameter of rotary valve shaft with this structure is not too large when the pressure of the hydraulic system is high. With the number of large diameter rotary valve tank can be set on the multi. Under conditions of constant speed rotary valve , the more frequency alternating the oil states , the frequency is high.

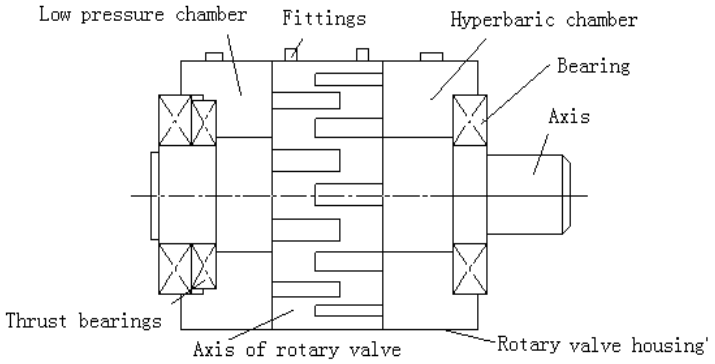

Fig 1 Schematic diagram of the rotary valve

Text Structure and parameters of the rotary valve

Fig 1 is a schematic structural view of the valve rotation .The rotary valve consists of spool shaft, enclosed housing body , bearings, sealing elements and Oil line connectors. Commutation by a plurality of guide groove in the circumferential direction of the rotary valve shaft[1]. The into the oil chamber of the rotary valve is connected with the front chamber of the piston. The front chamber of the piston is always connected with pressure oil. Into the oil circuit and oil return circuit are alternately connected by the with tank of the rotary valve shaft in the after chamber of the piston.

The selection of the coordinate gap of the rotary valve shaft and valve bore

The coordinate gap of the shaft and hole is decidede by two mainly factors. The first gap is that the temperature rise caused expansion by the rotary valve shaft. The second is the leakage what leak from the high pressure oil chamber to the low pressure oil chamber. These two factors determine the size of the clearance value[2].The volume expansion of the rotary valve diameter shaft caused by the temperature changed is :

$$\Delta d = \beta \Delta T d \tag{1}$$

Formula: β- thermal expansion coefficient , ΔT- oil relative to the temperature rise in degrees ℃, d- diameter of the rotary valve.

Chamber provided with a temperature difference between the temperature of the oil is 50 ℃. Rotary valve shaft diameter is 120mm. Diameter incremental of rotary valve shaft is 0.072mm. So control the range . Reduce the oil temperature can reduce the impact of oil changes with the gap .

Fig 2 shows the leakage when the rotary valve is working. Oil leak from the high pressure oil chamber to the low pressure oil chamber. The oil is flowing along the axial direction of the rotary valve and with the direction perpendicular to the tank. According to the structure of the rotary valve ,we can ignore the what is flowing along the axial direction of the rotary valve when we calculating the amount of leakage.It is considered that all the leakage is flowed from the high pressure chamber in the vertical direction of the low pressure sump tank . The leakage is:

$$Q = \frac{b\delta^3 \Delta p}{12\mu\ell} \pm \frac{vb\delta}{2} \tag{2}$$

Formula, The first is the amount of leakage caused by Pressure difference ΔP what is the difference from the high-pressure chamber and the pressure difference . The second is the amount of leakage caused by rotation of the rotary valve. Due to the rotation direction of the rotary valve is fixed, the movement of the rotary valve and side of the oil leak direction the same, the opposite on the other side,so the leakage caused by the rotation of the rotary valve can be cancel each other out. Leakage formula can be changed to :

$$Q = \frac{b\delta^3 \Delta p}{12\mu\ell} \tag{3}$$

Formula;b—Leak channel width m，ℓ—Leakage path length m，δ—Unidirectional gap of rotary valve shaft and valve borem，Δp—Pressure difference between the high and low pressure oil chamber of the rotary valve Pa，μ—Dynamic viscosity of the liquid Pa.s.

Given: b=9.6×10^{-1}m, δ=5×10^{-5}m, $\ell = 7.875\times10^{-3}$ m.

The 20th Oil, $\mu = 1.8\times10^{-2}\ Pa\cdot s$;The 30th Oil, $\mu = 2.7\times10^{-2}\ Pa\cdot s$. Two differential pressure valve chamber is 3Mpa.

Calculation of the rotary valve leakage are $2.126\times10^{-4}\ m^3/s$ and $1.416\times10^{-4}\ m^3/s$ The leakage is so large. By the formula (3), we can see that the amount of leakage is directly proportional to the width of leak channel, δ to the third power and the pressure difference between the two oil chambers, the amount of leakage is the amount of leakage is inversely proportional to the dynamic viscosity of the liquid and the length of the leakage path. We can effectively reduce the amount of leakage by reducing the gap.

The design of the tank matched rotary valve

The diameter of the rotary valve used in the test is 120mm.There are 24 tanks matdhed rotary valve uniformly arranged on the circumference of the shaft. The axial length of the rotary valve is 70mm, the room width of tank is equal to the groove width. The deepth of the groove is 18mm ,the length is 55mm. According to [1], the propagation speed of the hydraulic shock oil is 890-1270m / s.

Turn-on time with a tank is : $t = \frac{1}{n \times n_1}$ (4)

Formula： n —Speed of the rotary valve shaft， r/s; n_1—the number of one-way tank。When the motor speed 1800r/min, t = 1/360s.During this time interval, the opening of the tank with the zero - fully open - closed .When used full opening tank time is 1/720s. At this point the flow is maximum , the flow cross-section is $18 \times 7.85\,mm^2$.

The impact of hydraulic shock velocity： $\Delta P = \rho cv$ (5)

Formula： ρ —liquid densitometer Kg/m^3 v —The original flow rate in the tubing， m/s; c —Propagation velocity of shockwave， m/s.

Since the switching of the tank is in the commutation off state. Hydraulic shock produced additional impact pressure ΔP on the actuators. Hydraulic shocks can be reduced by increasing the width of the tank.That is the between width and groove width is not equal. The width is greater than the width between slots, so the switching with the oil is carried out continuously.

In Fig 1 we can see that the rotary valve leakage volume staggered overlapping tank matched rotary valve structure. The width of the leakage path is long , the length of the short leakage path is short . Therefore, the structural design of the rotary valve should give more consideration to the impact of leakage. Reasonable choice leakage channel width and length can effectively reduce the leakage of the rotary valve . In the condition of larger of difference pressure of two oil chambes , rotary valve leakage should be less than 20% of the main drive pump output volume .

Improved structural design of rotary valve

To further reduce the gap to reduce the leakage is already impossible. By the formula (2) we can seen that the amount of leakage is directly proportional to the width of leak channel,and inversely proortinal to the length of the leakage path. If b is reduced or ℓ is increased from the structure can be further reduced leakage[4].

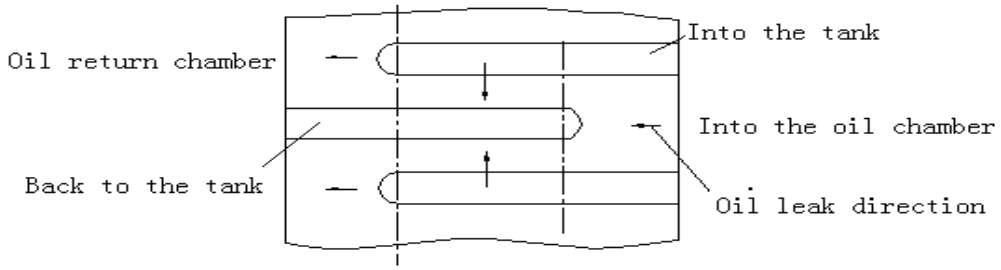

Fig 2 . Sump configuration diagram overlap

Leakage along the direction perpendicular to the sump. If the tank is configured in the form of non-overlapping. Tank configurations shown in Fig 3.

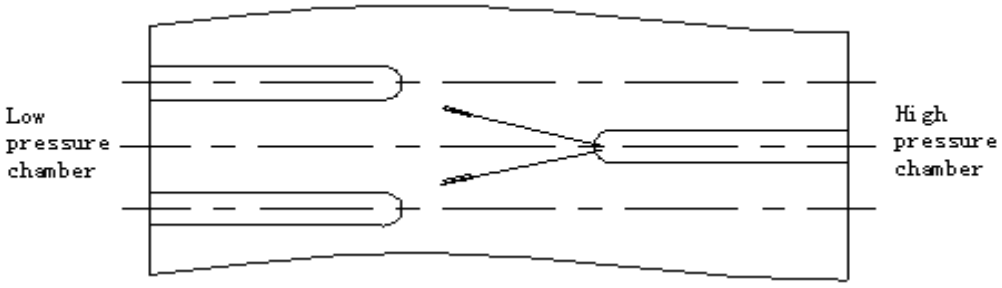

Fig 3 . Schematic diagram of non-overlapping configuration tank

In this configuration , the direction of the main flow of the oil leake is the axial flow [5].In this case the width of the drain passage b = 2πd .The length of the leakage path $\ell = \frac{1}{2}(\ell_{\min} + \ell_{\max})$ leakage flow throughthe annular gap .

$$\Delta Q = \frac{\pi d \delta^3 \Delta p}{12 \mu \ell}(1+1.5\varepsilon^2) \tag{6}$$

Formula： ε —Relative gap eccentricity.

Let's the structure size of the rotary valve : $d = 1.2\times10^{-1} m$ $\ell = 5.75\times10^{-2} m$, $\delta = 5\times10^{-5} m$. Pressure ： $\Delta p = 8MPa$ .Oil viscosity，t=50℃, $P = 8MPa$

The 20th Oil, $\mu = 1.5\times10^{-2} Pa\cdot s$ and the 30th Oil, $\mu = 2.7\times10^{-2} Pa\cdot s$.

When $\varepsilon = 0.5$ Leakage calculations are $4.5\times10^{-5} m^3/s$ and $2.70\times10^{-5} m^3/s$.

Such leakage relative to the pump output flow is allowed.If the allowable values [q] of the leakage was given, the gap value flowde through the annular gap can be calculated.

$$\delta = [\frac{12[q]\mu\ell}{\pi d \Delta p(1+1.5\varepsilon^2)}]^{\frac{1}{3}} \tag{7}$$

Let the allowable values $3.33\times10^{-5} m^3/s$ corresponds to the 20th Oil, $\delta = 5.6\times10^{-2} mm$ .30th Oil, $\delta = 6.4\times10^{-2} mm$. It can be seen that the amount of δ can put a gap wider than the tank get some of the overlapping structure.

Conclusion

The rotary valve consists of Spool shaft, transmission shaft, enclosed housing body, bearing, sealing elements and oil line connector. Rotary valve is a device to achieve fast commutation hydraulic transmission

The leakage of rotary valve is affected by the length of the drain channel and the gap between the spool shaft and the housing bore.The shorter distance is from the guide groove between the spool shaft to the drain oil passage of the r overlaped otary valve, the amount of leakage is greater. So the coordinate gap of the spool shaft and the hole must be smaller. Due to the increase of temperature , the gap is according to the temperature requirements, the guide groove of the rotary valve spool shaft must be overlapping set . The result is to reduce the pressure of the high pressure region.

Changing the arrangement of the axis of rotation of the guide groove of the spool, Change the original overlapping arrangement of high and low partition layout, meet with the requirements of the spool shaft and valve chamber bore

References

[1] Qiu Lijun . Research on new rotary valve hydraulic shaker . Graduate thesis . 1992.4

[2] Wang Jiwei, Zhang Hongjia , Huang Yi 《hydraulic and pneumatic drive》 . Machinery Industry Press , 2012.6.pp8-56

[3] Yang Naiqiao, hydraulic transmission oil situation and development [J] . Hydraulic and pneumatic seals , 2004, (5) .

[4] Yang Jia,Qiu Lijun,2011 2nd International Conference on Mechanic Automation and Control Engnieering,MACE2011-Proceedings,p325-328.

[5] Qiu Lijun,Yang Jia,Advanced Materials Research,V 322,p497-500.2012

Advanced Materials Research Vols. 989-994 (2014) pp 2878-2881
© (2014) Trans Tech Publications, Switzerland
doi:10.4028/www.scientific.net/AMR.989-994.2878

A Study of Influence of Shape Technique on Radar-Scattering Characteristic for Tank Turret

Yao Ma, Weidong Xu, Fangmo Shi, Jun Liu, Feng Lu, Liyan Zhu

College of Field Battle Engineering, PLA University of Science and Technology

No.1, Haifu Alley, NanJing, China

mayao_84@aliyun.com

Keywords: radar stealth technology, shape technique, radar-scattering characteristic, radar cross section (RCS), tank turret

Abstract. Radar-scattering characteristic which is an important aspect in stealth technology plays a key role in radar detection. Based on shape technique, this work studied the influence of geometric parameter on radar-scattering characteristic for a tank turret by establishing a scaled model as well as calculating the radar cross section (RCS) of this model. The results show that the tank turret can obtain better radar-scattering characteristic with much lower RCS by optimizing its shape and the dihedral angles between the tank turret and the tank body.

Introduction

Radar detects targets based on the difference of radar-scattering characteristic between the targets and the background. Therefore, radar-scattering characteristic plays an important role in radar detection and has also attracted much attention in stealth technology. Radar stealth technology is mainly used for reducing the probability of the targets detected by enemy radars, and is realized by reducing RCS of the targets through suppressing, absorbing and/or deviating radar echo signal [1]. Radar stealth technology has been intensively studied and widely used in military powers all around the world to degrade radar performance and improve battlefield survivability of weapon equipment.

Based on the interactive mechanism between radar wave and substance, main factors determining the radar-scattering characteristic of the target include surface materials of the target, target shape and incident direction of radar wave, etc. So far, absorbing materials and shape technique are two main ways to achieve radar stealth. Compared with the former, the shape technique suppresses echo signal and reduce RCS by changing target shape, thus resulting in the low possibility of the target being detected. This work studied the influence of shape technique on radar-scattering characteristic by establishing a scaled model as well as calculating the RCS of this model.

Radar-scattering characteristic of a scaled model for a tank turret

Tank faces serious threats from various high-efficiency anti-tank weapons in a battlefield. Among them, the threats related to radar mainly come from surveillance tracking radar and fire control radar, etc. The threat directions of radar against tanks are at the front and lateral sides with pitching angle ranging between 0°and 15° [2]. Among various components constituting a tank, the tank turret is especially easily to be detected by radar, because the RCS of a tank turret typically reaches up to tens of square meters at the front-side direction, and even increase with increasing pitching angle, which is harmful for tank survival in the battlefield.

Traditional tank turrets have a curved surface (e.g., cylindrical surface and cutting spherical surface), which leads to nearly omni-direction reflection of radar wave. To gain more insight into the radar-scattering characteristic for a traditional tank turret, we setup a scaled model based on a traditional tank turret with cutting spherical surface (shown in Fig. 1(a)) and calculate the corresponding RCS by using the software FEKO (shown in Fig. 1(b)).

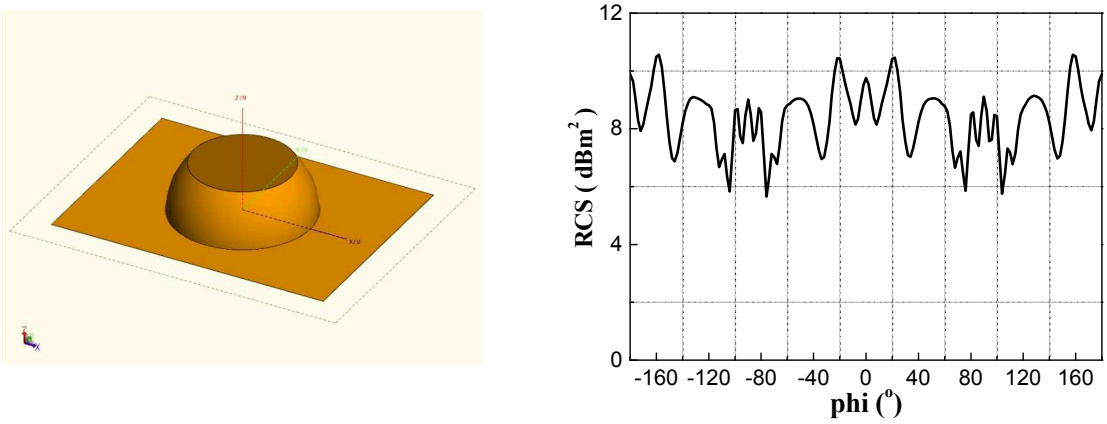

(a) (b)

Fig. 1 Traditional tank turret with curved surface. (a) The scaled model. (b) The RCS value.

From Fig. 1(b), the radar wave reflection for the traditional tank turret in Fig. 1(a) displays a uniform distribution in different azimuth angles. Furthermore, the calculated RCS can reach up to about 10 dB, which suggests that the scattering is intense, and therefore, the tank is easily detected by radar. Further efforts should be made to suppress the intense scattering.

Basic shape design for tank turret to improve the radar-scattering characteristic

To improve the radar-scattering characteristic, the French AMX-30B3 tank turret proposed an innovative polyhedron design [3]. Following this innovation, then most tank turrets have adopted flat surface by assembling pieces of large-area planes together, which is known as shape technique. It is noted that for the flat surface, although the side lobe intensity decays rapidly, the main lobe intensity is usually strong [4]. Therefore, it is believed that the flat surface can further improve the radar-scattering characteristic with remarkably low RCS if the main lobe of backscatter pattern is intentionally derived from the threat direction [5].

Therefore, the work need to do here is to appropriately select the inclined angle of flat surface. Fig. 2 shows the cross-sectional diagram as well as the key geometric parameters of the tank turret with flat surface, where γ represents the inclined angle of lateral surface for the tank turret, θ_c represents the range of radar threat angle, and $\Delta\theta$ is the angle between the surface normal direction n and the radar wave incident direction k.

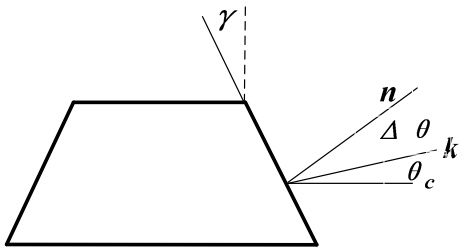

Fig. 2 RCS reduction principle of tank turret with flat surface.

From the geometrical relationship, γ can be expressed by

$$\gamma = \Delta\theta + \theta_c. \quad (1)$$

Note that θ_c as a variable is typically ranging between 0° and 15°. It is important to determine an optimal γ to make sure that not only the main lobe of backscatter pattern deviates from the threat direction, but also the RCS always keeps a low value as θ_c changes. Based on the above principle, a

series of simulation were performed by adjusting γ and then evaluating the RCS as θ_c changes under a given γ. Finally, we got the optimal model of the tank turret with flat surface shown in Fig. 3(a) as well as its calculated RCS shown in Fig. 3(b).

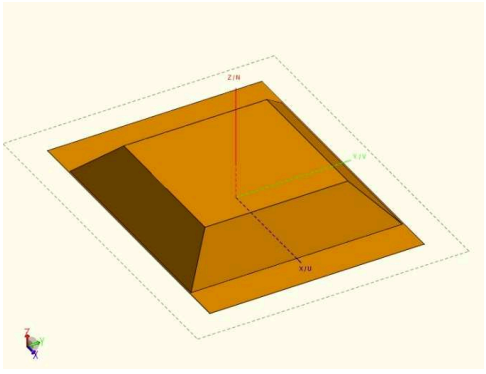

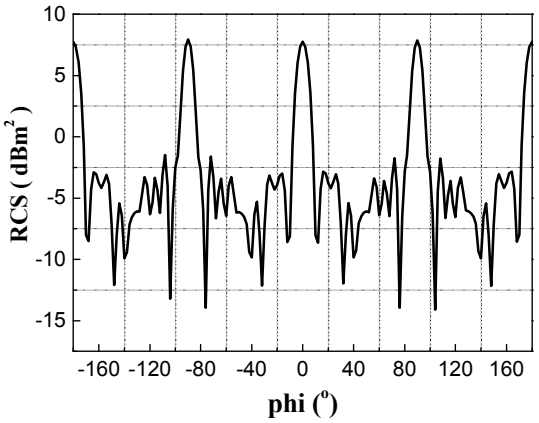

(a) (b)

Fig. 3 Optimal tank turret with flat surface using shape technique.
(a) The scaled model. (b) The RCS value.

As shown in Fig. 3(b), the optimal RCS by adjusting the geometrical parameters based on the shape technique is mainly below 0 dBm^2 and the minimum value is even as low as -14dBm^2, which is much smaller than the value for the traditional tank turret with curved surface in Fig. 1(b). Therefore, by optimizing the geometrical parameters, the shape technique is an effective way to suppress the RCS, and thus significantly reduces the probability of the tank being detected.

Further improvement of radar-scattering characteristic

In Fig. 3(a), the large-area planes used for constructing the tank turret form dihedral angles relative to the tank body. These parasitic dihedral angles are obtuse angles and usually lead to large back scattering in a wide range. In order to remove the adverse effect induced by these obtuse angles, we also propose a novel shape as shown in Fig. 4(a), where the formed dihedral angels turn to acute angles by optimizing the turret shape. The RCS based on this novel shape is also calculated and present in Fig. 4(b). Compare with the RCS for the turret with obtuse dihedral angles in Fig. 3(b), it can be seen that by using acute dihedral angles instead of obtuse dihedral angles, the RCS of the turret is obviously reduced, suggesting that the back scattering are significantly suppressed.

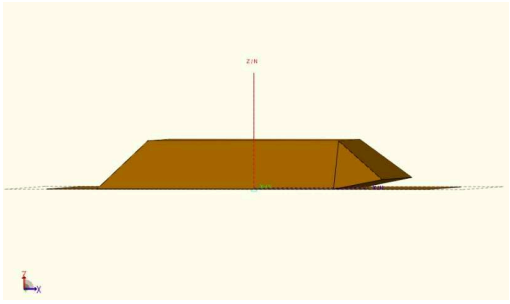

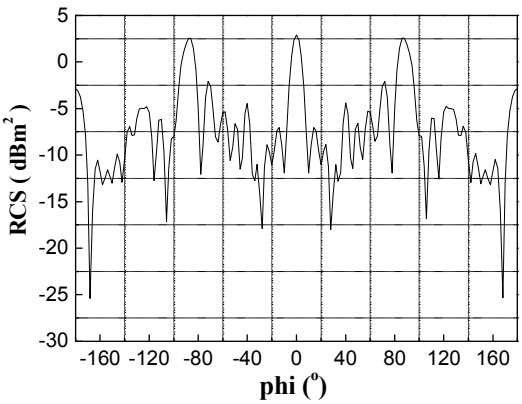

(a) (b)

Fig. 4 Tank turret model with acute dihedral angles between the tank turret and tank body.
(a) The scaled model. (b) The RCS value.

Summary

This work studied the influence of shape technique on radar-scattering characteristic of a tank turret by establishing a scaled model as well as calculating the RCS of this model. The results demonstrate that tank turret can obtain improved radar-scattering characteristic with low RCS by optimizing the geometric parameters of the turret itself and the dihedral angles between the turret and the tank body.

References

[1] Xiaoxuan Fan, Guotong Geng: Application on radar stealth technology on surface ships. Ship Science and Technology, vol. 4 (2012), pp. 140-143.

[2] Xiaofan Zhao: Research on active defense system of tanks and armed vehicles. Vehicle and Power Technology, vol. 3 (2002), pp. 53-57.

[3] Haoyuan Li: Stealth technology of tanks and armed vehicles. Journal of national defense science and technology, vol. 5 (2003), pp. 21-23.

[4] R A. Ross: Radar cross section of rectangular flat plates as a function of aspect angle. IEEE Transactions on Antennas and Propagation, vol. 3 of AP-14(1966), pp. 329-335.

[5] Zhiguo Tao, Dezhong Cai: A preliminary study on radar stealth shape technique of tank. Vehicle and Power Technology, vol. 3 (2004), pp.29-34.

Advanced Materials Research Vols. 989-994 (2014) pp 2882-2885
© (2014) Trans Tech Publications, Switzerland
doi:10.4028/www.scientific.net/AMR.989-994.2882

Feasibility Investigation for Visible-Laser Compatible Camouflage Thin Film

Zhu Liyan[a], Xu Weidong[b], Wan An, Zeng Zhaoyang and Ma Yao

PLA University of Science and Technology, Nanjing, 210007, China

[a]zhuliyan0522@163.coml, [b] xweibing1968@aliyun.com

Keywords: thin film. visible. laser. camouflage.

Abstract. Based on multi-layer film interference theory and optimization calculation, a film structure that can satisfy both visible and 1064nm laser camouflage requirements were put forward. The light transmission property of the structure was analyzed systematically and the thickness and refractivity of different layers were obtained.

Introduction

Wide application of modern electrooptical technology in surveillance and guidance results in expose of both sides in war, which means fatal threaten for military targets. As effective method to against surveillance and guidance, camouflage technology is off great importance. Technically the materials used in camouflage should be able to decrease the expose signs of target at all surveillance frequency. However, the camouflage materials presently available can't provide ideal compatibility, thus improvement in property is needed urgently. In optical band, the camouflage material should simulate the optical property of plant, which means high reflectivity in the 680~1200 nm band. As for laser camouflage, high reflectivity at 1064 nm wave length is unacceptable. Thus, new materials are necessary for visible-laser camouflage[1].

After many years of development, optical thin film has become very important part of optical technology. Complete analysis theory and design methods have been verified. Proper design for multi-layer film can enhance or weaken light transmission, thus structure design of film has potentiality in camouflage. The structure investigated in this paper was designed in such a way that it could remain high reflectivity while the reflectivity at 1064 nm was minimized. This property makes it possible to take infrared and laser camouflage into account simultaneously.

Basic theory for thin film

When a thin film is illuminated by a light beam, reflection and transmission rate is the result of multiple-beam interference (as shown in Fig. 1).

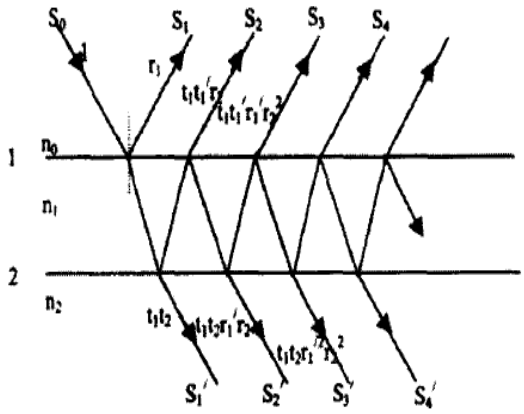

Fig. 1 Multiple-beam interference in thin film

For the purpose of convenience in light intensity calculation, the method of complex amplitude was used. In the following, r is the reflectance for light entering form medium with refractivity n_1 to medium with refractivity n_2, t is the transmittance. r′ is the reflectance for light entering form medium n_2 to medium n_1, t′ is the corresponding transmittance. If the refraction between medium n_1 and medium n_2 is neglected, then we have

$$r = -r' \tag{1}$$

$$r_2 + t_1 t' = 1 \tag{2}$$

If the absorption within the film is neglected and the amplitude of the incident light is supposed to be 1, then the amplitude of different beams in Fig. 1 is

$$\begin{cases} s_1 = r_1 \\ s_2 = t_1 t' r_2 \\ s_3 = t_1 t' r_1 r_2^{\,2} \\ \cdots\cdots\cdots\cdots \end{cases} \tag{3}$$

The subscription 1 and 2 in the above represent the upper surface and the lower surface, respectively. As for amplitude of the transmitted beams, it can be written as

$$\begin{cases} s_1' = t_1 t_2 \\ s_2' = t_1 t_2 r_1' r_2 \\ s_3' = t_1 t_2 \left(r_1' r_2\right)^2 \\ \cdots\cdots\cdots\cdots \end{cases} \tag{4}$$

The phase difference between adjacent beams is decided by

$$\delta = 2 n_1 d \cos\theta$$

where d is the film thickness, and θ is the incident angle.

Thus, the amplitude of the reflected beam from upper surface is

$$r = \left\{ r_1 + t_1 t_1' r_2 e^{-i2\delta} \left[1 + r_1' r_2 e^{-i2\delta} + \left(r_1' r_2\right)^2 e^{-i4\delta} + \ldots \right] \right\} \tag{5}$$

According to summation law of geometric sequence, the above equation can be reduced to

$$r = \left(r_1 + r_2 e^{-i2\delta}\right) \Big/ \left(1 + r_1 r_2 e^{-i2\delta}\right) \tag{6}$$

The phase change of the reflected beam is

$$\tan\varphi = \left[-r_2 \left(1 - r_1^{\,2}\right) \sin 2\delta \right] \Big/ \left[r_1 \left(1 + r_2^{\,2}\right) + r_2 \left(1 + r_1^{\,2}\right) \cos 2\delta \right] \tag{7}$$

Finally, the total reflectivity of the film is[1,4].

$$R = r \cdot r^* = \left(r_1^{\,2} + r_2^{\,2} + 2 r_1 r_2 \cos 2\delta\right) \Big/ \left(1 + r_1^{\,2} r_2^{\,2} + 2 r_1 r_2 \cos 2\delta\right) \tag{8}$$

Structure design for visible-laser compatible camouflage design

The system of visible thin film can always be represented by an effective interface, of which the reflection and transmission are determined by the conductance of the incident medium and the assemble conductance of the effective interface. The effect of every layer can be explained in term of its influence on the effective interface conductance. For multi-layer visible thin film, the feature matrix of the film is the product of the feature matrix of different layers,

$$\begin{bmatrix} B \\ C \end{bmatrix} = \prod_{j=1}^{k} \begin{bmatrix} \cos\delta_j & \frac{1}{\eta_j}\sin\delta_j \\ i\eta_j \sin\delta_i & \cos\delta_j \end{bmatrix} \begin{bmatrix} 1 \\ \eta_{k+1} \end{bmatrix} \tag{9}$$

The assemble conductance of the multi-layer film is Y=C/B, thus

$$B = \left(\frac{\eta_0 B - C}{\eta_0 B + C}\right)\left(\frac{\eta_0 B - C}{\eta_0 B + C}\right)^* \tag{10}$$

$$C = \frac{4\eta_0\eta_{k+1}}{(\eta_0 B + C)(\eta_0 B + C)^*} \tag{11}$$

$$\phi = arctg\left\{\frac{i\eta_0\left(CB^* - BC^*\right)}{\eta_0^{\,2}\left(BB^* - CC^*\right)}\right\} \tag{12}$$

The above equations consist of the foundation for property calculation for thin films[2-4].

A kind of A/0.025M10(HL)/S structure was analyzed in this paper, of which the reflection and transmission were calculated according to the equations mentioned above. In this structure, A represents air, S is the basement. M is the mental layer with refractivity 4.53 [5,6]. H is the TiO_2 layer with refractivity 2.15, whereas L is the MgF_2 layer with refractivity 1.38. The calculated results are shown in Fig. 2 to Fig. 4. The central wavelength is set to be 1064 nm. Obviously, the reflection rate within the 380~780nm band is about 70%, whereas the reflection rate at 1064 nm is only 25%. This kind of spectral reflectivity is just wanted by visible-layer compatible camouflage.

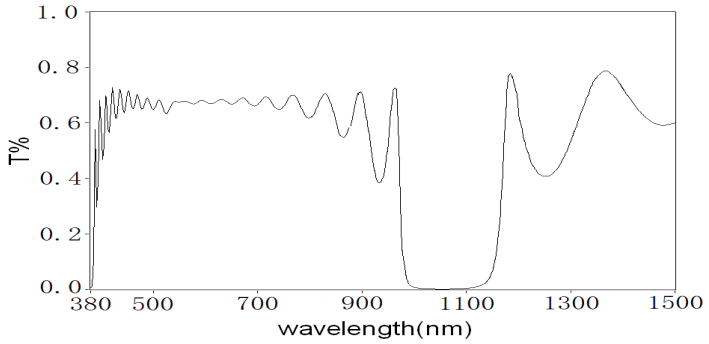

Fig. 2 The calculated transmission curve of the multi-layer system.

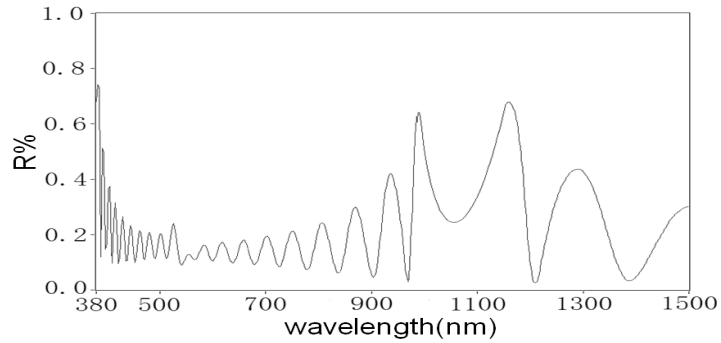

Fig. 3 The calculated reflection curve of the multi-layer system.

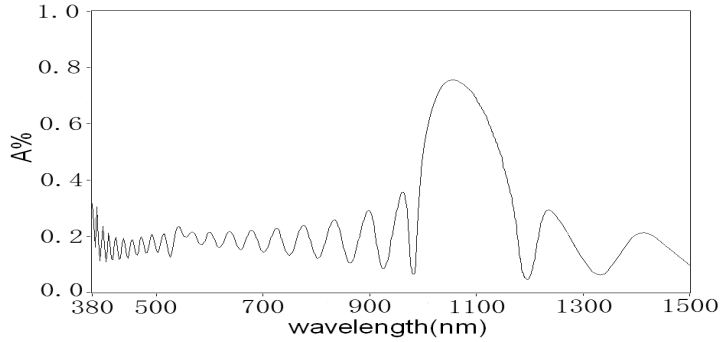

Fig. 4 The calculated absorption curve of the multi-layer system.

Conclusion

Spectral reflectivity of multi-layer system was calculated according to thin film theory. The results indicate that proper structure design can effectively reduce the reflection rate at 1064 nm wavelength, whereas the reflection within the visible band remains high. This film structure make it possible for visible-layer compatible camouflage.

References

[1] Wang Zirong,Sun Xiaoquan,Yu Dabin.Analysis of several contradiction problems in multi-band steath compatibility[J].Modern Defense Technology,2004,32(6):65～68.(in Chinses)

[2] Jinfa Tang,Optical Technology for Thin Film[M],Beijing,Mechanical Industry Press,1989, pp..297～300

[3] Fink Y,Winn J M,Fan S,et al. Adielelectric omnidirectional reflector[J]. Science,1998, 282: 1679～1681

[4] Tang Jinfa , Gu Peifu , Liu Xu et al . . Modern Optical Thin FilmTechnology[M] . Hangzhou : Zhejiang University Press , 2006.24～29

[5] Wang Jizhou,Xiong Yuqing,Wang Duoshu et al . Filtering characteristics and application of defect mode of one-dimensional photonic crystal [J] . Acta Optica Sinica , 2009 , 29 (10) :2914～2919

[6] Wiersma D S,Bartolini P,Lagendijk A D,et al.Localization of light in a disordered medium[J].Letters to Nature,1997,390:19～24

Advanced Materials Research Vols. 989-994 (2014) pp 2886-2889
© (2014) Trans Tech Publications, Switzerland
doi:10.4028/www.scientific.net/AMR.989-994.2886

PWM Control for Actively Clamped Resonant DC-Link Inverter on Soft-Switching

SHE Yan

Shunde Polytechnic, Foshan 528300, China

Shelley186@sohu.com

Keywords: soft-switching; active inverter; SVPWM; double CPU

Abstract. Due to the active inverter in industrial application, if use hard switching mode, not only may have the switch losses, but also may produce electromagnetic interference and harmonic, these power quality is affected. This paper presents the design of a soft-switching active inverter, that active clamped resonant DC-link inverter topology was used on the main circuit, the voltage space vector pulse width modulation (SVPWM) control mode was used on control circuit, using TMS320LF2407DSP programming, while the AT89C51 was responsible for liquid crystal display task, data exchanged and coordinated between double CPU. The experimental results show that, the device switching-losses can effectively reduce, the switching frequency can improve, input power quality can improve.

Introduction

Because the traditional inverter switching device exist high voltage and current stress, high du/dt and di/dt due to switching on and off form electromagnetic interference, and the influence of harmonic will reduce the power factor of the power grid, cause trouble to other electrical equipment in power grid. Generally the soft-switching PWM converter technique was used as a defensive measure[1]. This paper puts forward the effective design scheme for an active clamped resonant DC-link inverter topology, verify the feasibility and superiority of this scheme through the experimental study.

Soft Switching Inverter Main Circuit Design

The design adopts soft switching active clamp parallel resonant DC-link inverter main circuit as shown in Figure 1, through the control mode of SVPWM, make the resonant link and inverter main circuit matching, When the switching, first the DC bus voltage drop to zero through the resonance, then the switching device of inverter main circuit carry on soft switching, thereby reduce the voltage and current stress of the switching device, voltage stress clamp under the battery voltage Ud. Concrete analysis is as follows [2]:

State 1: Vs=on, Va~Vb=off, during T0 period, the flow of the load current is in Vs circuit, LrCr circuit is at rest.

State 2: Vs=on, Va~Vb=on, at a certain time, conducting Va and Vb , the action belongs to ZCS, inductor Lr current increases linearly from zero, until can maintain the needed energy to complete the process of the resonance, shutdown Vs, When the capacitor Cr voltage is kept Ud constant.

State 3: Vs=off, Va~Vb=on, shutdown Vs, the action belongs to ZVS. Then LrCr begin the resonance,

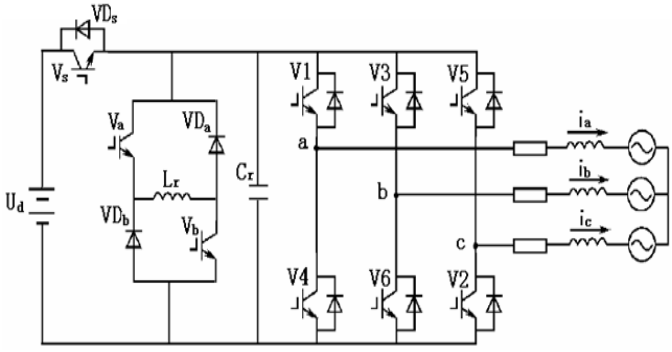

Fig.1 Inverter circuit topology structure

with resonant, capacitor voltage ucr drop to zero, the inductor iLr current increase to the maximum value ip, that provides ZVS conditions for the inverter switch tubes.

State 4: Vs=off, Va~Vb=on, capacitor ucr voltage remains zero, the inductor iLr current form loop circulation to continue along Va~VDa and Vb~VDb. During this mode, inverter switching devices with ZVS switch to the next state.

State 5: Vs=off, Va~Vb=off, After switching inverter, shutdown Va and Vb, the action belongs to ZVS. then the capacitor ucr voltage is slowly rising, the inductor iLr current form loop circulation to continue along VDa, VDb and Cr. due to LrCr resonance, ucr rise to Ud.

State 6: Vs=on, Va~Vb=off, when the capacitor voltage is slightly higher than Ud ,that with ZVS, diode VDs conduct with ZVS, capacitor voltage clamp on Ud, residual energy of Lr inductance feed to the power supply. The inductor iLr current drop to zero from I2, and the diode VDa, VDb, shutdown with ZCS.

So far, the resonant circuit complete a cycle. The waveform is shown in figure 2.

The resonant circuit can not only change the pulse width (DC-bus during non zero voltage), but also can change the pulse position, AC voltage waveform of inverter can control to has convenient, synchronizing with grid[2]. AC voltage waveform generated by the inverter can be real-time controlled to realize the synchronized with the power grid.

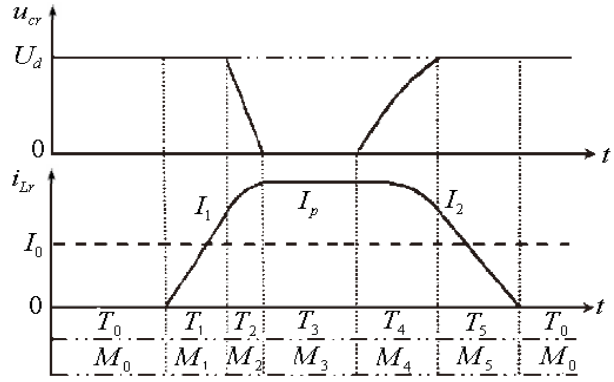

Fig.2 The waveform

The Design of Control Circuit

The design of control circuit plays a very important role in the inverter system, Here using two processors, TMS320LF2407 complete the main function of switch input and output, A/D converter, communication, SVPWM waveform output[3], AT89C51 is used to complete the liquid crystal display function.

The Measurement Circuit of A/D Conversion. The three-phase AC-side voltage and current amplitude, frequency, phase of the main circuit and DC-side voltage and current must accurately sampling in order to control the SVPWM waveform, make inverter generated AC waveform in accordance with the requirements of the grid. Three-phase AC-side select transformer to measure voltage and current, DC-side select Hall element to measure voltage and current, A/D converter provided by the LF2407 chip can complete these tasks, without the need for external A/D circuit. Figure 3 is the design of the AC voltage and current detection circuit, output amplitude < 3.3V with same frequency sine wave.

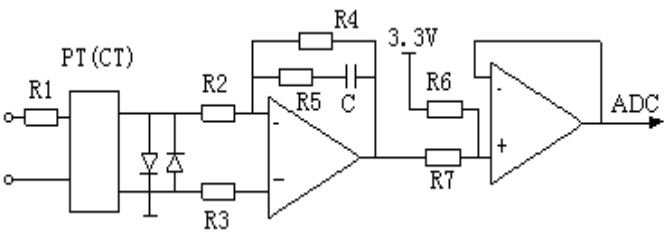

Fig.3 AC side voltage-current detection

The design of Communication Interface Circuit. As the need of the control system with PC communication, thus require communication circuit, TMS320LF2407 itself as a SCI interface, so you can easily achieve communicates with PC. Here the communication have two functions: one is to device parameter settings through the computer to download; two is that the device send the data monitored to a computer for further processing. The system design two kinds of commonly used serial communication interface standard RS232 and RS485 interface circuit, RS232

for local data transmission; RS485 for remote data transmission[4][5]. SCI serial communication circuit diagram is shown in figure 4 below.

SVPWM Output and Drive Isolation Circuit. Using SVPWM control algorithm and the DSP programming, produces 6-channel programmable dead and variable output polarity of the PWM waveform, drive IPM inverter module power device of the main circuit, through a drive circuit and a photoelectric isolation circuit, obtain sine waveform of a variable-voltage and variable-frequency effect, supply electrical power[4][6]. PWM isolation output circuit diagram as shown in Figure 5. The fault input signal can be sent to the main control board after the isolation.

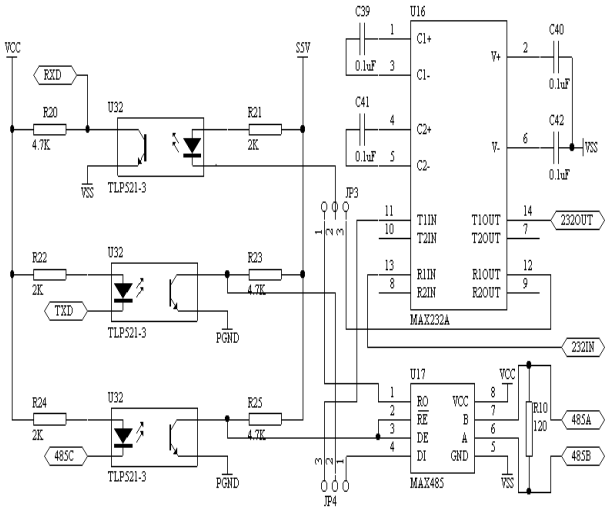

Fig.4 SCI serial communication circuit

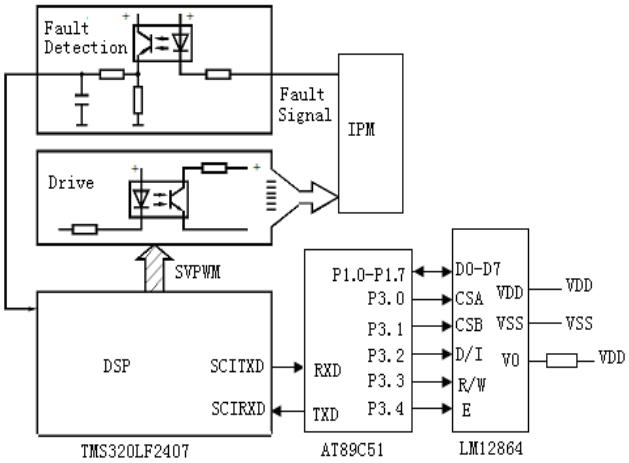

Fig.5 The SVPWM isolation output circuit and display interface circuit

Liquid Crystal Display Interface Circuit

Through send-receive data pins SCITXD, SCIRXD of the SCI module connected with AT89C51 serial input port RXD, TXD, the data will be sent to MCU to display. Because the TMS320F2407 is the device of TTL 3.3V level, and AT89C51 is the 5V device, the two are connected by two pieces of MAX3232 as DSP and MCU Interface, this method not only takes up DSP two I/O port, but also can extend the communication distance using RS232 interface, improve the anti-interference capability, and ealize the function of software[7]. using LM12864 in the liquid crystal display module, it is the LCD module with a built-in 128*64 Chinese characters dot matrix, can display letters, numbers, Chinese fonts and custom blocks, and the interface of MCU is flexible, the structure block diagram is shown in figure 5.

Conclusion

This paper analyzes the working principle of the active clamped resonant DC-link inverter on soft-switching, PWM control scheme for the active clamped resonant DC-link inverter is verified using double CPU, and effective waveform is obtained as shown in Figure 6 and figure 7[8][9]. Through the analysis of the experimental study showed that: 1) the inverter switches running on ZVS or ZCS, can reduce the switching losses and improve the switching frequency, and reduce the EMI; 2) the voltage stress of component is clamped at the DC voltage for device selection and circuit operation; 3) can output high precision waveform under SVPWM control mode , improve power quality, reduce the low order harmonic loss, is conducive to the application of the PWM active clamped resonant DC-link inverter to high performance and high power output.

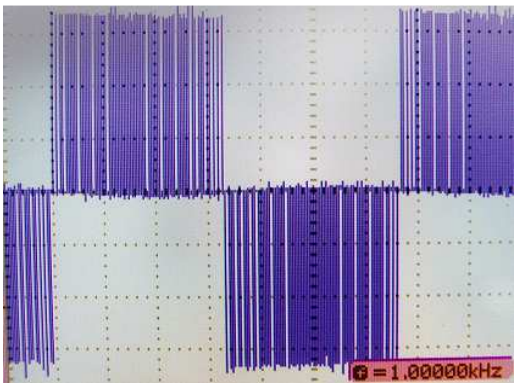

Fig.6 SVPWM switch driving waveform

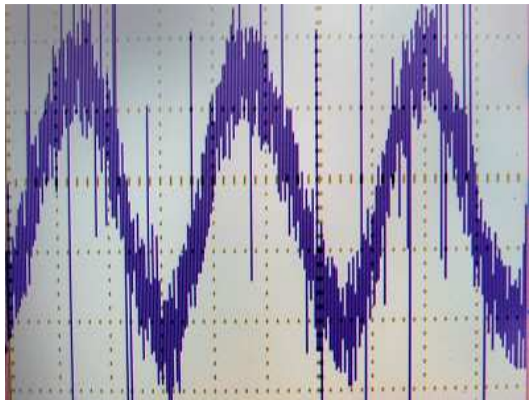

Fig.7 AC-side current waveform after inversion

References

[1]HE Hucheng, LIU Weiguo XIE En. A Novel Resonant Pole Inverter for Brushless DC Motor[J].Transactions of China Electrotechnical Society,2008,23（12）:99-107.

[2]LIN Weixun. Modern Power Electronic Circuit [M].Hangzhou:Zhejiang University Press, 2006.461-466.

[3]SHE Yan, LI Ling. Hardware Design of a Suit of Small Power Frequency-Variable Controlled Equipment[C].IEEE CS,CDCIEM2012:360-363.

[4]SHE Yan,SHE Yuanhua. Realization of digital vector controlled SVPWM frequency-variable speed-adjustable system[J].Electric Power Automation Equipment,2006,26(2) :76-79.

[5]TANG Lei. Research on High Power Factor Three-Phase Reversible Rectifier[D].Wuhan: Wuhan University, 2004. 6.

[6]PENG Qing. The PWM Control Scheme for Active Clamped Resonant DC link Inverter[D].Hangzhou: Zhejiang University, 2007.6.

[7]ZHENG Xiucong, XIE Yunxiang. Design of a system for the serial communication and LCD Between the Microcontroller and DSP[J]. Computer Engineering & Science,2011,33（6）: 173-177.

[8]ZHANG Shuangwen, ZHANG Dehua. An actively clamped resonant DC-link inverter of PWM type[J]. Mechanical & Electrical Engineering Magazine,2008,25（3）: 64-67.

[9]CHU Enhui, CHEN Chao, JIN Sheng, et al. Novel soft switching sine-wave PWM inverter[J]. Electric Machines and Control, 2009, 13(11) : 6-11.

Advanced Materials Research Vols. 989-994 (2014) pp 2890-2894
© (2014) Trans Tech Publications, Switzerland
doi:10.4028/www.scientific.net/AMR.989-994.2890

Design improvement on shipping container spraying production line

Okorie Sunday Onyedikachi[a], SHI Jing[b]

School of Mechanical Engineering and Automation, Liaoning University of Technology, Jinzhou 121001, Liaoning, China
[a]2243554142@qq.com, [b] 464408756@qq.com

Keywords: flip-frame, hydraulic cylinder clamping, chain drive, sprocket, mechanism

Abstract. This paper describes the design of a flip-frame mechanism for shipping container spray painting production line. The idea of the flip-frame mechanism is to reduce, to a large extent, paint wastage during spray painting of the quadrangular exterior surfaces of the shipping container. Clamping of the shipping container on the flip-frame is achieved by hydraulic cylinders. A roller chain and a sprocket is used to drive the flip-frame because of their simplicity, strength, ability to work under harsh condition and require little lubrication.

Introduction

In recent times, automatic spray-painting system for shipping containers has gone through several reform stages. These extensive reforms were borne out of global innovation in shipping-container industries, leading to constructive thinking in order to improve upon the existing state of the shipping container spray-painting production line. In the past, manual painting was applied to shipping containers while some cases involved the use of automatic spray guns operated manually by human labour; the results wasn't appealing enough due to even distribution of paints on the container walls were hardly achieved.

The introduction of automatic spray-painting booth system did not solve all the problems inherent to painting completely. Achieving even distribution of paint on the sprayed surfaces while spraying is still a major challenge. 'Painting requires that the spray gun deposit paint at each point on the target surface such that the variation of the resultant paint deposition is within acceptable limits; we term this the uniform coverage problem' [5].

Roland Bizolier in 1992 did some remarkable work in this area of research which he titled "Automatic painting machine particularly for painting the inside of a hollow body of quadrangular section and large size such as a shipping container" [4]. His work addressed the problem of spray painting the inside of the hollow body of a shipping container but did not address properly the problem of spray painting the external surfaces of the shipping container.

Current Situation

There are many fundamental challenges and issues that are still impeding and restraining reforms in the container production industries of which some would be solved by this research work. In this research, a close look is being given to some shipping container spray painting production lines within and outside China, in order to carry out this design improvement effectively.

From current findings, the following conditions are predominant in most shipping container spraying production line:

Paint wastage. Large amount of paints are being dropped during spray painting of shipping container walls, especially at the left and right sides of its quadrangular external surfaces. This continuous paint droppings constitute large portion of the paint wastage since they drop directly to the floor and recovery is most likely not possible.

Quality of spraying. The beauty of every finished product, no matter its proposed usage, is its appearance. Hence, the appearance of every product tells more about the finishing processes. The quality of sprayed shipping containers need to be improved. Even distribution of paint on the walls

of the shipping container while spray painting is a major challenge hindering the quality of the finished painted product, since manual labour is still required in large extent to operate the automatic spraying guns.

Human labour. Human labour is another major challenge being struggled with in most of these industries. The toxic nature of the paint pose great treat to the health of these workers, hence most workers don't retain their jobs at the spraying section of the production line; this leads to continuous loss of expatriates**.**

Safety on the Production Environment. Safety on the production environment is a major concern that cannot be overemphasized. It is as vital as the melting furnace to a Goldsmith. Inadequate control over (enforcement of) safety constraints, can occur either because hazards and their related constraints were not identified or because the control actions do not adequately enforce the constraints [3]. Also, the changes in work organizations and technologies without proper workers sensitization pose serious problem of workplace accidents. The employees are subjected to the known and unknown risk of occupational injuries and illnesses.

The Flip-frame Mechanism

Today, the concept of flipping (flip) can be found in many designs, ranging from clocks, maker boards, mobile phones, laptop computers, vehicles, etc. In this research work, the flip-frame mechanism is design to accommodate the shipping container in its hollow quadrangular section (see figure 1). A double-strand roller chain of ANSI No.240 is wound round the spherical center surface of the flip-frame. Attached to this double-strand roller chain is a sprocket. The sprocket is driven by an electric motor such that is allows a forward and reverse rotation of the flip-frame at a maximum angle of 180 degree (180°) from the starting point as demonstrated below in figure 2.

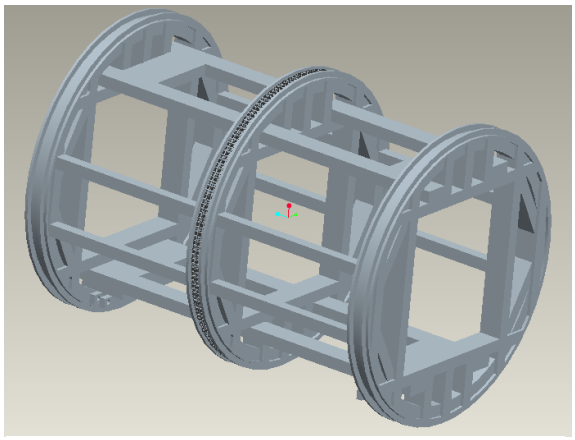

Figure 1: The flip-frame

The 6058mm (length) by 2591mm (height) by 2438mm (width) shipping container size is being used in designing this flip-frame mechanism, though larger shipping container sizes are applicable as far as the flip-frame is designed to accommodate such.

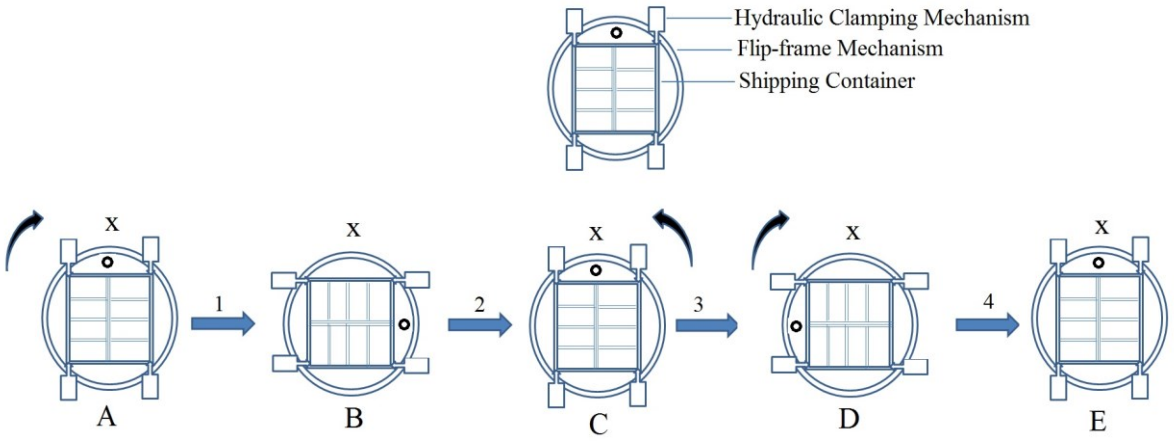

Figure 2: Rotations of the Flip-frame Mechanism

As the shipping container fits into the hollow quadrangular section of the flip-frame mechanism, the positional limit switch attached to the flip-frame switches-off the translational assembly line. Then the hydraulic cylinders attached to the flip-frame clamp the shipping container

on it corner posts. The exterior surfaces of the shipping container is made to be directly under the fixed automatic spraying guns, X, by the flipping of the frame (see figure 2).

After the clamping is done, the automatic spraying guns, X, are activated and spraying of the exterior surface directly under and parallel to the spraying guns, as seen in figure 2(A), is achieved. Following this, the flip-frame rotates at an angle of 90^o from A-B as seen at position "B" in the figure 2, after which the current surface is being sprayed. The same process occurs at point "D" after rotation to an angle of 180^o in the direction of B-C-D is achieved. The flip-frame is rotated at an angle of 90^o in the reverse direction from D-E so that position "E" is attained.

The flip-frame mechanism ensures that the exterior quadrangular surfaces of the shipping container are being sprayed only when they are directly beneath the automatic spraying guns "X". At this position, paint drops to the floor is almost zero since the surfaces are always horizontal and parallel to the spraying guns. Paint wastage occurs mostly when the external quadrangular surfaces of the shipping container are in vertical position parallel to the spraying guns during spray painting

Significance of this Design Improvement

Paint wastage during spray-painting will be drastically reduced. This research work aims at reducing paint wastage during spray painting of shipping containers to about 50%. Since the automatic spraying gun will only spray the exterior quadrangular surfaces of the shipping container when each side of the shipping container surface is rotated by the flip frame mechanism to be directly under and parallel to the automatic spray guns (see figure 2).

The plant production environment will be improved. Since the introduction of the flip-frame mechanism is a new innovation in the shipping container spraying production line, the production environment will definitely improve due to the new automation processes involving the flip-frame mechanism.

Increased safety on the production environment. Since the number of human labour in the spraying production line will be reduced by the implementation of the flip-frame mechanism, it is also expected that accidents in the production line will also be reduced since less human activities will now be require in the spraying production line. Hence, human accident will be reduced and safety increased.

Save labour. More labour force were required to handle and operate the automatic spraying guns while spraying the exterior quadrangular surfaces of the shipping container, but the introduction of the flip-frame mechanism will reduce this labour force since the automatic spraying guns will be fixed at an upper position above the flip-frame and the flip-frame is to rotate each side of the shipping container quadrangular surfaces to become parallel to the automatic spray guns for spraying process.

The Chain Drive

Chains normally have lesser weight as compared to their counterparts such as gear drives or belt drives [1]. Slip might occur on belt and rope drives but chains are used to prevent slipping. Many stiff links are used to make chain; these links are connected through pin joints to allow required

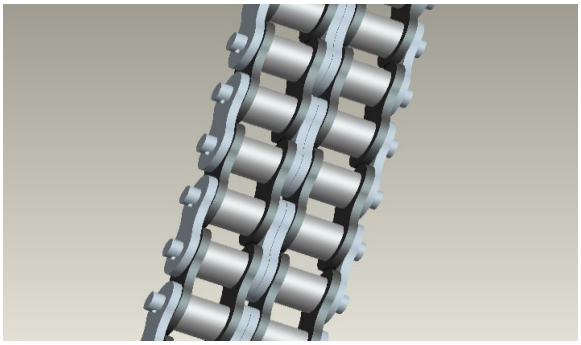

Figure 3: Double-strand roller chain

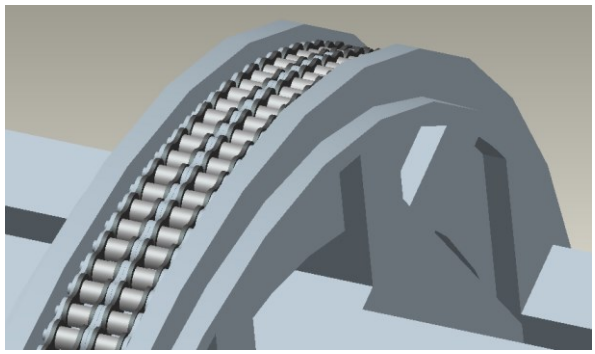

Figure 4: The double-strand roller chain wound round the flip-frame.

flexibility for rolling around the driving sprocket (see figure 3).Hence this design chooses to make use of roller chain drive system in order to maintain high tongue required to rotate the flip-frame mechanism and also to avoid slipping which is common with the belt drive system [2].The figure 4 below show the double-strand roller chain of ANSI No.240 wound round the flip-frame.

Chain drive design calculations

From the above figure 5, the base radius of the flip-frame is given as R, while the roller link radius of the chain drive is r.

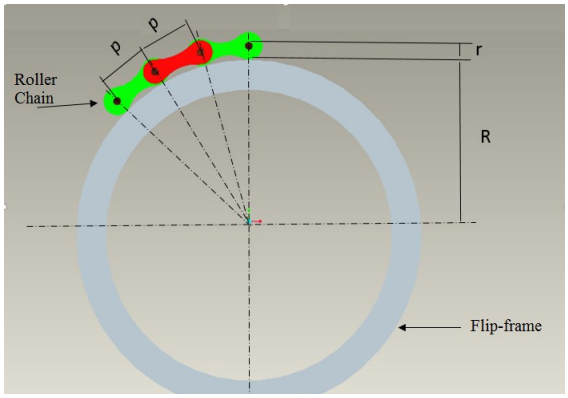

Figure 5: Front view of the flip-frame and the roller chain.

Pitch radius,R^*, of the flip-frame,

$$R^* = R + r \quad (1)$$

Using ANSI Chain No. 240,

Pitch, $p = 24 \times 3.175 = 76.2$ mm (2)

$$Roller\ link\ plate\ height, H_r$$

$$H_r = 0.95p \quad (3)$$

Substituting (2) into (3),

$$H_r = 0.82 \times 76.2 = 72.39mm$$

Roller link plate radius, r

$$r = \frac{1}{2}H_r = \frac{1}{2} \times 72.39 = 36.195mm$$

But Base radius of the flip-frame. R

$$R = 2370.5mm$$

Hence, pitch radius R^*

$$R^* = 2370.5 + 36.195 = 2406.695mm$$

$$Pitch\ Circumference, C_p = 2\pi R^*$$

$$C_p = 2 \times 3.142 \times 2406.695 = 15121.710mm$$

Number of pitches, P_n

$$P_n = \frac{Pitch\ Circumference}{Pitch\ length}$$

$$P_n \simeq 198\ pitches$$

Roller diameter, R_d

$$R_d = \frac{5}{8}p = \frac{5}{8} \times 76.2 = 47.625mm$$

Roller diameter, R_w

$$R_w = \frac{5}{8}p = \frac{5}{8} \times 76.2 = 47.625mm$$

Pin diameter, P_d

$$P_d = \frac{5}{16}p = \frac{5}{16} \times 76.2 = 23.8125mm$$

$$Thickness\ of\ inside\ and\ outside\ link\ plate, t$$

$$t = \frac{1}{8}p = \frac{1}{8} \times 76.2 = 9.525mm$$

$$Pin\ link\ plate\ height, x$$

$$x = 0.82p = 0.82 \times 76.2 = 62.484mm$$

Sprocket design

There were various factors such as, number of teeth on sprocket, chain pitch and roller diameter, which play important role in the designing of sprocket teeth. Tooth profile was designed according to ANSI Standards.

Since

Since Chain pitch =p, Number of teeth = N,

$$Roller\ diameter = R_d, and\ \ Seating\ curve\ diameter, Ds$$

$$Ds = 1.0005R_d + 0.003$$

$$Radius, R = Ds/2 = 0.5025R_d + 0.0015$$

Pitch diameter of Sprocket, $PD = \frac{P}{\sin\left[\frac{180^o}{N}\right]}$

References

[1] James C .Conwell and G.E Johnson. *Experimental Investigation of chain tension and roller sprocket impact forces in chain drives.*

[2] Sohail Anjum, Nabeel Kamal, Umar Shahbaz Khan, Javaid Iqbal, Umar Izhar, Nasir Rasheed, M.A. Khan.(2012). *Design of Non-Conventional Chain Drive Mechanism for a Mini-Robort.* National University of Sciences and Technology, College of Electrical & Mechanical Engineering, Peshawar Road, Rawalpindi

[3] Nancy G. Leveson, (2002). *System Safety Engineering: Back To The Future*. Aeronautics and Astronautics. Massachusetts Institute of Technology.

[4] Roland Bizolier, (1992), *Automatic painting machine particularly for painting the inside of a hollow body of quadrangular section and large size such as a shipping container*. Publication number: WO1992011951 A1, www.google.com/patents/WO1992011951A1 2013-8-17.

[5]Prasad N. Atkar, *Uniform Coverage of Simple Surfaces Embedded in R3 for Auto-Body Painting*, Carnegie Mellon University, Pittsburgh PA 15213, USA.

Advanced Materials Research Vols. 989-994 (2014) pp 2895-2898
© (2014) Trans Tech Publications, Switzerland
doi:10.4028/www.scientific.net/AMR.989-994.2895

Overview of the control methods for LTCC substrate shrinkage

Xiaodong Liu[a], Shaohong Wang[b], Zhaoxia Hou, Danzhou, Liqiong Yang

Liaoning Province Key Laboratory of New Functional Materials and Chemical Technology, Shenyang University, Shenyang 110044，China

[a]lxd860322@163.com, [b]Catelert@163.com

Keyword: LTCC technology; sintering; shrinkage; control methods；

Abstract: As a new integration and packing technology, the low temperature co-fired ceramic (LTCC) technology attracts close attention for its excellent advantages such as high speed transfer characteristics, high reliability, miniaturization, etc. However, the sintering shrinkage of LTCC substrate always affects the practical effect of it. In this paper, the material characteristics, methods to control the sintering shrinkage of LTCC substrate and the development trend for the control methods are mainly overviewed. It is contributed to the research and application of LTCC technology.

Introduction

LTCC technology is a new material technology which can co-fire ceramic dielectric materials with low melting point and high resistivity metal under low sintering temperature. It combines the advantages of High temperature co-fired ceramic technology and thick film technology [1] and has more obvious cost and integration advantage in the design of multilayer circuit modular [2]. It helps to the miniaturization, lightweight and multi-functionalization of electronic components and assembly module and has a very broad application prospect [3-4].

In LTCC technology, the co-firing of low melting metal and ceramic dielectric materials is very important and it directly affects the final quality of the products. To acquire good sintering effect, the co-fired materials are often required to have good co-firing compatibility. However, the shrinkage of LTCC substrates is always a problem in the practical application.

Shrinkage of LTCC substrate

Compared with other material packaging technology, LTCC technology is an ideal packaging scheme with obvious advantages and potential. But the shrinkage of LTCC substrate always occurs in the sintering process [5-8].

In the application of system with high integrated and performance, because of the small distance among the wirings on the low temperature co-fired ceramic substrates, it's very strict with the deformation of sintering. And the sintering shrinkage of ceramic substrates will affect the alignment of signal and ventilation holes. Moreover, the consistency of sintering shrinkage rate also has much effect on yield and properties of products.

Methods to control the sintering shrinkage of LTCC substrates

Till now, methods to control the sintering contraction are always reported. The methods are mainly done through the control of sintering process, without pressure assisted sintering, pressure assisted Sintering, self constrained sintering, sintering with sandwich structure are all belong to this style and feasible to the practical application[9-15].

(1) Without Pressure Assisted Sintering

This method was firstly developed by DuPont Company of America and the principle is shown in Figure 1. In the process of LTCC substrate lamination, it always has a certain thickness of porcelain as sacrificial layer in the bottom and top respectively and then sinter the whole component.

The sacrificial layer is always alumina raw tape, so it won't shrink during sintering and will leave enough space to discharge the binder in LTCC green tape. During the sintering process, the friction between LTCC substrate will restrict the shrinkage of LTCC substrate in the X-Y direction, so the shrinkage only occurs in the Z direction. The shrinkage rate of LTCC substrate with this method is less than 0.2% in the X-Y direction and the consistency error is less than 0.05%. After sintering, special process is used to remove the sacrificial layer [16].

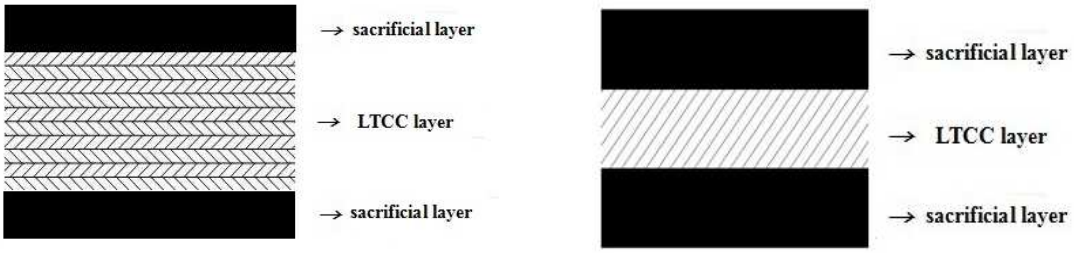

（Before the sintering） （After the sintering）

Fig1 Diagram of Without Pressure Assisted Sintering

(2) Pressure Assisted Sintering

This method overlies a layer of porous plate on each side after overlying sacrificial layers on both sides of LTCC substrate and then sent to a special sintering furnace for sintering. During sintering, uniaxial pressure will be given in the vertical direction of LTCC substrate (as shown in Fig.2) to increase static friction between LTCC substrate and sacrificial layer in the horizontal direction and the shrinkage of LTCC substrate in the X-Y direction is restricted. By using Pressure Assisted Sintering method, the sintering shrinkage can be reduced to less than 0.05% and the consistency error is less than 0.008%. The sintered LTCC substrate has high density and almost no defects. But the cost of production is much high.

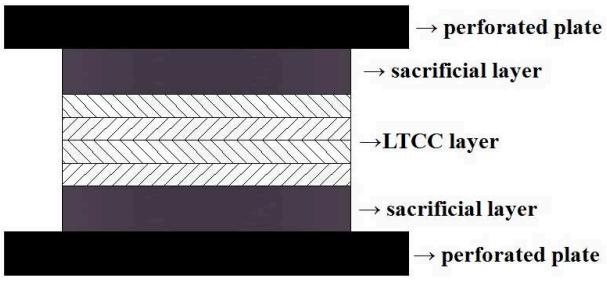

Fig 2 Diagram of Pressure Assisted Sintering

(3)Self Constrained Sintering

Self Constrained Sintering is the method which uses the characteristics of LTCC substrate to inhibit the shrinkage in plane direction. This method can present free sintering to realize the zero shrinkage of LTCC substrate in horizontal. And it is compatible with existing LTCC manufacturing process and equipments, even the conventional LTCC substrate or which with cavity can satisfy the requirements of substrate interconnection. According to the latest research results, the sintering shrinkage of Self Constrained Sintering can be reduced to less than 0.2% and the consistency error is less than 0.02%.

(4) Sintering with sandwich structure

Shrinkage LTCC substrate with sandwich structure is developed by Heraeus company of Germany. This structure is also divided into three layers. Up-down layers are mixed with glass and ceramic, the middle layer is oxidation porous medium (as shown in Fig 3). During sintering, porous

medium of middle layer is required sintered firstly, kept high mechanical strength in the heat and can resist the contraction stress of layers on both sides. As sintering, the glass of up-down layers and ceramic composites start to melt and has a series of chemical reaction with Al_2O_3. When the fluid viscosity of glass decreases to a certain value, it will penetrate into the porous structure of the middle layer. So it should leave enough space for glass fluid infiltration after the middle layer is sintered. Then we can get compact and zero shrinkage LTCC substrate. Study shows that the properties of this LTCC substrate material related to the invasion of the melted glass. So decreasing the melt viscosity of glass as far as possible and reducing the content of glass and choosing proper particle size of Al_2O_3 powder in middle layer can all enhance the invasive to improve the performance of LTCC substrate.

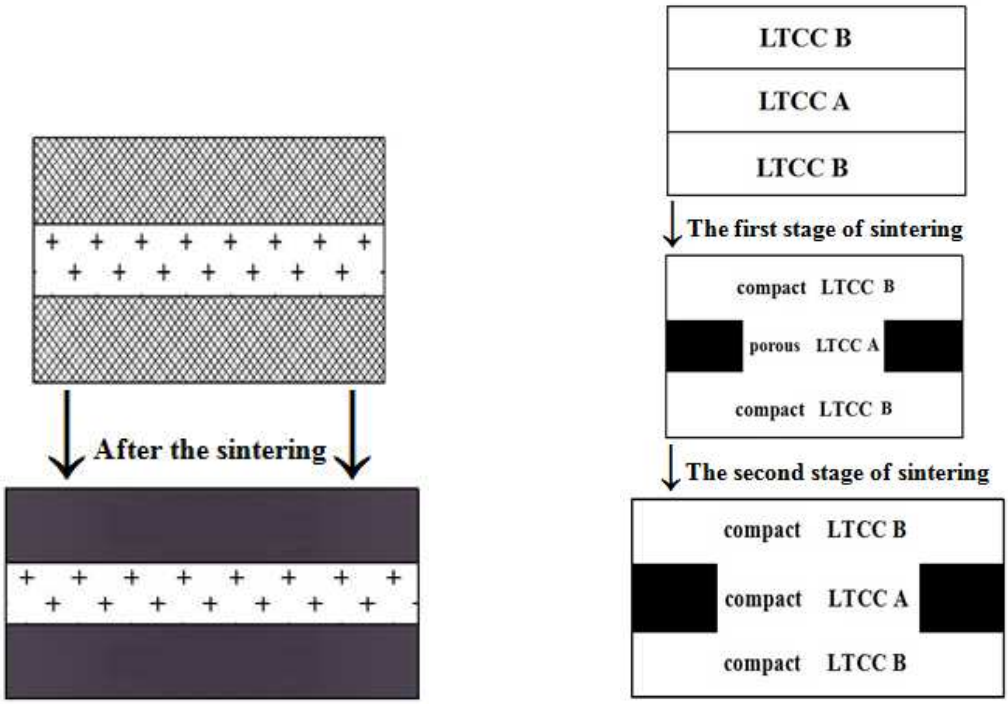

(a) Sandwich structure (b) Sandwich structure

Fig 3 Diagram of two different structure of LTCC sintering

Conclusion

LTCC is a key technology in the field of microelectronics with multilayer and ceramic packaging. The process is very difficult involving many theoretical problems and the substrate shrinkage is the important one for the research and application. The control methods for LTCC substrate shrinkage is in ceaseless development. In the future, more comprehensive methods contains the preparation of material itself is a feasible direction.

References

[1] S.Young: New York: Marcel Dekker, 1986

[2] A.Beiley, W.Foley, M. Hageman, et al: Microwave Symposium Digest-IEEE MTT-S International, Vol.2(1997), p.999-1002

[3] S. R .Winzer, N. Sharker, A. P. Ritter: J. Am. Ceram. Soc,72(1990),p.2246-2257

[4] B. Robert: Ceramic Industry, Vol.9(1997), p.28-29

[5] Zhong Yu, Zhongwen Lan, Jingmei Wang: Chinese Journal of Materials Research, Vol. 2(2004), p.176-180

[6] Ruzhang Ma:Beijing: Metallurgical Industry Press,1999

[7] A.D.P. Rao, B. Ramesh, P. R. M. Rao, et al: J. Alloys and Compds, Vol. 282(1999), p.268-273

[8] Zhiyi Zeng, Haoqin Wang, Xubo We: J. Magn. Mater. Device, Vol. 38(2007), p.7-10

[9] H. Nishikawa. Proceedings of the 1993 Japan International Electronic Manufacturing Technology Symposium, Kanazawa, 1993, p.238 -241

[10] K.R. Mikeska, D.T. Shaeffer, R.H Jensen: US: 5085710, 1992

[11] M. Itagaki, K. Miura, Y. Hakotani, et al. Proceedings of the 29th International Symposium on Microelectronics, Dallas, 2105(1993), p.221-225

[12] M. Nicak, B. Psota, P Kosina, et al: Electronics Technology (ISSE), 2012 35th International Spring Seminar on. 2012, p. 128-132.

[13] M.Hintz, H.Thust, E.Polzer: Proc IMAPS Nordic, Stockholm, Sweden, 2002

[14] K. Miura. Proceedings of the 8th International Microelectronics Conference, Omiya Sonic, 1994, p.220-224

[15]Torsten Rabe, Wolfgang A. Schiller, Thomas Hochheimer, et al: International Journal of Applied Ceramic Technology. 2(2005), p.374-382.

[16] Shin-Yu Tzeng, Jau-Ho Jean：J. Am. Ceram. Soc,Vol.85(2002), p.35-40

Advanced Materials Research Vols. 989-994 (2014) pp 2899-2903
© (2014) Trans Tech Publications, Switzerland
doi:10.4028/www.scientific.net/AMR.989-994.2899

Research on fault diagnosis method for crankshaft of drilling pump based on operational deflection analysis

Fengfeng BIE[1,a], Junfeng PEI [2,b], Fengxia LV [3,c]

[1] Mechanical Science and Engineering Institute, Northeast Petroleum University, Daqing, 163318, China

[2]School of Mechanical Engineering, Changzhou University, 213016, China

[3] Mechanical Science and Engineering Institute, Northeast Petroleum University, Daqing, 163318, China

[a]email: fengf721@sina.com, [b]email:13861085769@yeah.net, [c]email:fengxxxx@sina.com

Keywords: Drilling Pump; Drive System; Operational Deflection Shape; Fault Diagnosis

Abstract. Crankshaft is the critical component of the drive system of drilling pump. A new state feature extraction method for crankshaft based on operational deflection analysis is presented in this paper. The superiority, feasibility and validity of the system deflection analysis method are figured out with comparison of traditional methods. The vibration deflection technique can supplement with the time-frequency variation of key parts of the crankshaft for the normal measurement information on which the system fault diagnosis is processed. The process illustrates that the method of vibration defection analysis can extract the working state feature entirely and accurately, while provide the valid support for the corresponding fault mode recognition.

Introduction

Crankshaft is the critical component in the drive system whose working state directly affects the overall performance of drilling pump, which is a complex reciprocating mechanical system with a large number of unknown information, whose structural feature and the non-stationary and nonlinear feature of the vibration signal determine the conventional vibration monitoring and signal processing methods are difficult to achieve the anticipated target [1]. Research on fault diagnosis method of reciprocating machinery and equipment on vibration monitoring and analysis aims at two key domains [2, 3]: the accuracy acquisition of the vibration signal and the common character recognition of the reciprocating mechanical failure modes. The former is the basis and prerequisite for accurate fault diagnosis, limited by the actual working conditions or present monitoring tools, the vast majority of data information based on vibration information is only a finite number of vibration monitoring source, which fundamentally limits the accuracy and practicality of fault diagnosis. Hence, enriching vibration data acquisition means and improving the multi-directional vibration signal analysis means becomes particularly necessary. For the latter domain, the research that aiming at the single type of reciprocating machinery has begun, but the method of fault pattern matching is not equipped with effective universality and generality.

The analysis method of operational deflection shape with finite vibration monitoring data as input in monitoring and fault analysis for machinery and equipment system, by the establishment of the vibration model of the system, considering the actual shape of the device under test as a whole or its key components, providing the means and basis for the final precision fault diagnosis. Currently, the research and application of vibration deflection technology is limited in the structure or typical running equipment systems, such as the static and dynamic testing of a car, while general running equipment system is still for exploratory research [4, 5].

Vibration deflection analysis method is applied to the field of the crankshaft of reciprocating machinery fault diagnosis, in which the multi-channel vibration signal frequency information is made full use as input for system fault diagnosis, as the result, the accuracy and comprehensiveness of the information is ensured, while the precise monitoring of the reciprocating machinery vibration and the accurately find of the failure modes is achieved. The research may provide a new train of

thought for finding the common characteristic of reciprocating machinery vibration and fault diagnosis.

Basic principle of operational deflection shape

In ODS process, a series of the vibration measurement signal is input for analyzing the actual working vibration deformation of the system, and the output is the operational mode of the moving facility, by which the quantitative analysis for the working conditions of the system is achieved. The key technique is to carry on dynamic processing for the vibration conditions of the mechanical system [6, 7]. The advantage in the qualitative or quantitative vibration analysis when the system input cannot be determined and its output is the modes of the dynamic equipment system operation is highlighted, including the vibration of a machine, structural or where the excessive vibration level occurs. Fault source can be located through vibration deflection analysis and the transmission route can be judged for the correlation study between the various subsystems of the vibration excitation [8].

Excitation vector is replaced by a certain point response of vibration system in the ODS dynamic treatment, and the transfer function is a point of the response and the reference point response ratio of the vibration system [9]:

$$\{T_{ij}(j\omega)\} = \frac{\{x_i\}}{x_j} \tag{1}$$

where $T_{ij}(j\omega)$ is the relative value of the ODS; x_i is the response of a measuring point (ODS absolute value); x_j is the response of a reference point (ODS reference value).

Coherence function method is applied in quality inspection which is analyzed by ODS; the coherent function can be expressed as:

$$Y_{ij}^2(\omega) = \frac{|G_{ij}(\omega)|^2}{G_{ii}(\omega)G_{jj}(\omega)} \tag{2}$$

where $G_{ij}(\omega)$ is the cross power spectrum between $X_i(\omega)$ at reference point i and $X_j(\omega)$ at measuring point j, and $G_{jj}(\omega)$ is the power spectrum of $X_j(\omega)$ at the measuring point j.

The absolute value of ODS of every measuring point and simulating point can be obtained by Formula (1) and reference the effective value of the power spectrum [10].

$$\{X_i(\omega)\} = T_{ij}(j\omega)\sqrt{G_{jj}(\omega)} \tag{3}$$

Compared with the experimental modal analysis, ODS analysis have several superiorities. First of all, its foundation is from uncertain outside incentives. The result of the ODS analysis changes with the incentive which not only associates with the system itself, but also depends on the external excitation. Secondly the ODS dynamic treatment can obtain the measurement frequency under different working conditions, and build the corresponding relationship with the external excitation individually. Finally, the frequency component from sensor signal is set as the research object in the ODS analysis, while the target is the vibration characteristics in case of the unknown system excitation.

Vibration measurement and analysis

(1) Vibration measurement

The corresponding physical model of the drilling pump is established on which the vibration testing point is projected as shown in Fig.1 (a). The practical testing points mainly locate at crankshaft bearings, crankshaft outer layer, pistons and fluid end, from which the signal may use for supplement proof.

Fig.1 (b) shows that the radial vibration of the crankshaft cap end is measured. The practical vibration signal including normal in Fig.2 (a) and abnormal in Fig.2 (b) is preliminarily analyzed.

Compared with the former, the abnormal time-frequency signal is disordered with greater vibration amplitude from 2 to 10 G and more complex frequency distribution, in which the lower band is similar while the higher is obviously distinct. The initial analysis illustrates the fault of crankshaft system to certain extent which needs deeper analysis for accurate systematic diagnosis. The Local Wave Method is employed in time-frequency analysis as the base and supplement of systematic vibration deflection analysis.

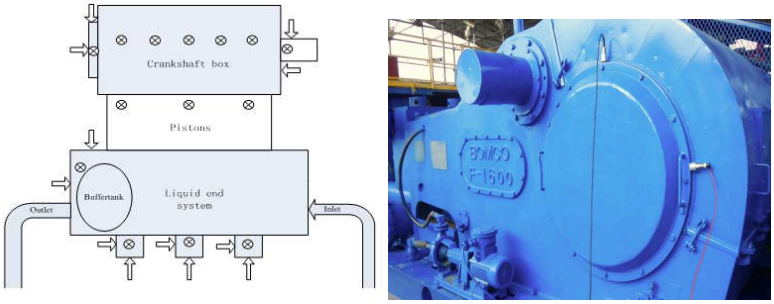

(a) (b)

Fig.1. Vibration testing point location and practical measurement on the crankshaft

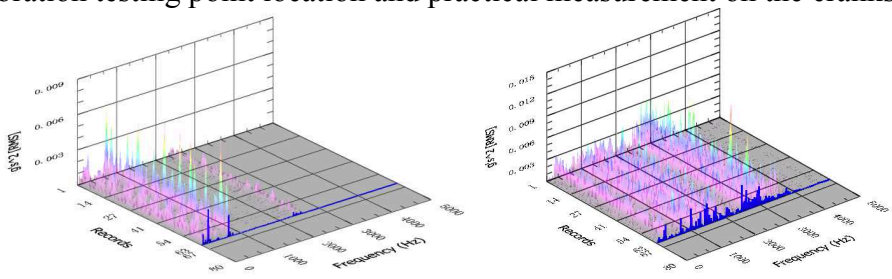

(a) (b)

Fig.2. Time-frequency analysis of vibration signal comparison

(2) Local wave time-frequency spectrum analysis

Local Wave Method is a self-adaptive analysis method for mechanical signal of non-stationary and non-linear which is established on the instantaneous frequency. By Local Wave Method, the vibration signal is decomposed into IMFs which can meet suitable conditions. These IMFs are analyzed through Hilbert transformation, as the result, the instantaneous frequency and time-frequency character of the vibration signal are extracted, as so-called local wave time-frequency analysis. By Local Wave Method, the original signal is decomposed into IMFs and residual component which is an average trend or a constant. After the Hilbert transformation for each IMF, the signal data can be expressed as Formula (4):

$$X(t) = \sum_{j=1}^{n} a_j(t) e^{i\omega_j(t)t} \tag{4}$$

where $a_j(t)$ is the instantaneous amplitude, $\omega_j(t)$ is instantaneous frequency. Virtually, the signal amplitude can be expressed as both the function of time and instantaneous frequency in 3-dimensional space and contour lines in time-frequency plane, while the amplitude distribution in time-frequency plane can be defined as local wave time-frequency spectrum.

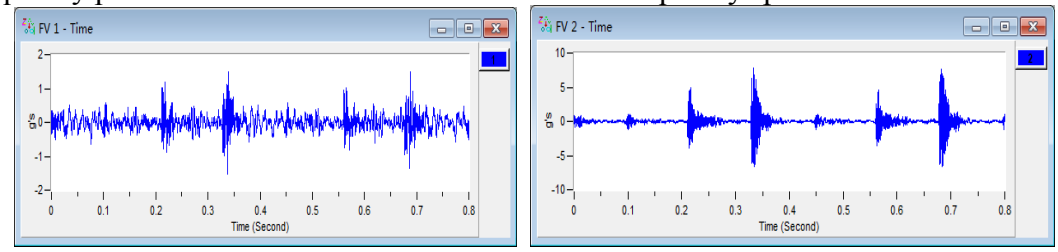

Fig.3. Practical measurement vibration signal of two edges of the crankshaft

The time-domain signal of the both crankshaft end is shown in Fig.3. By Local Wave Method the signal is decomposed and the time-frequency spectrum is obtained respectively as shown in Fig.4. The two signals contain apparent features, including time domain and frequency domain which can be quantitatively analyzed for accurate fault diagnosis.

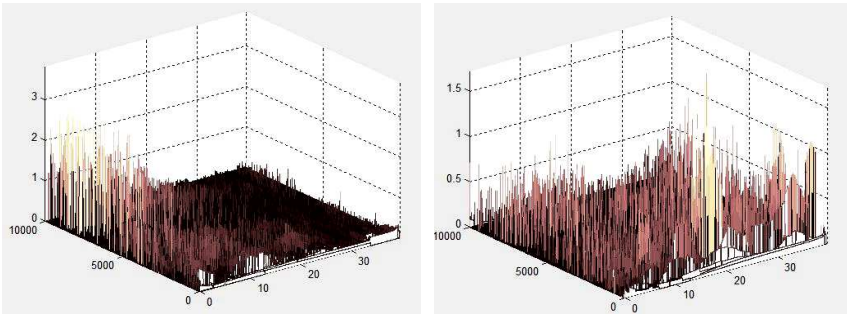

Fig.4. Local wave time-frequency spectrum of the two measurement points

(3) Overall ODS analysis

Set the real measured vibration signal as the input of the entire vibration deflection model, the ODS simulation is processed as shown in Fig.5. Thus the vibration information of the critical point is achieved, whether from the real or the analog. The local wave time-frequency analysis method is applied in revealing the energy gray level distribution of the characteristic frequency bands as list in Tab.1, while the corresponding frequency bands comes from reference [2] in which the author gives the entire experiment process and the final conclusion of the specified type drilling pump: band 1 is 0-200Hz for driven mechanism, especially for bearings, band 2 is around 1000Hz for crankshaft and bearing bush, band 3 is around 2000Hz for plunger system and band 4 is around 2500Hz for liquid end of the pump. The time domain signal and local wave time-frequency spectrum of the max vibration severity point in Fig.6 reveals the impact character of concentrated spectrum energy distribution.

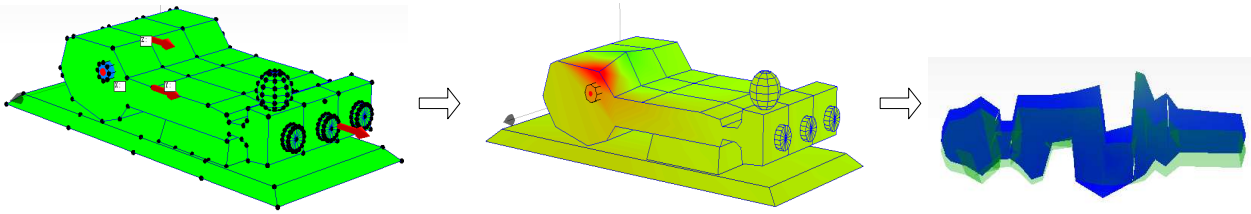

Fig.5. Drilling pump operation deflection when the crankshaft in abnormal load system

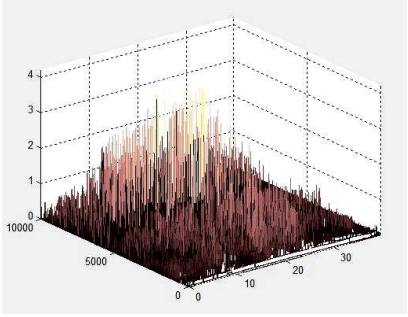

Fig.6. Local wave time-frequency spectrum of the max vibration severity point

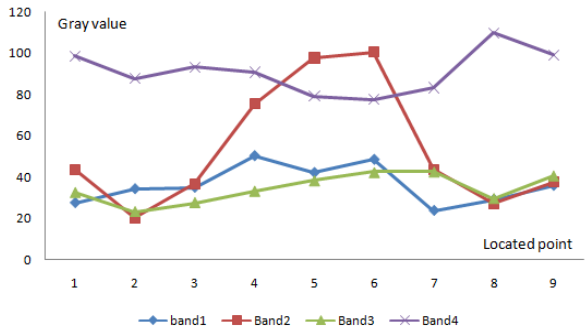

Fig.7. Energy gray value variation trend of the crankshaft located points

Fig.7 shows the variation trend of the characteristic frequency bands, while the variation of band 2 is obvious in the located point of the crankshaft. The entire energy gray level fluctuation illustrates the working state of the crankshaft system.

Tab.1. Energy gray value of the ODS analysis for part of crankshaft measured and analog points

Number	Measuring point	Type	Direction	Band1	Band2	Band3	Band4
1	Crankshaft end cap axial	Measured	1z	27.6	43.63	32.55	98.65
2	Crankshaft end cap vertical diameter	Measured	1y	34.36	20.17	23.22	87.83
3	Crankshaft end cap horizontal radial	ODS	1x	35.06	36.5	27.66	93.22
4	Crankshaft central axial	ODS	2z	50.44	75.48	33.18	90.71
5	Crankshaft central vertical diameter	ODS	2y	42.24	97.58	38.28	79.17
6	Crankshaft central horizontal radial	ODS	2x	48.63	100.38	42.3	77.55
7	Belt wheel end axial	ODS	3z	23.78	43.67	42.55	83.12
8	Belt wheel end vertical diameter	Measured	3y	29.2	27.22	29.58	109.83
9	Belt wheel end horizontal radial	ODS	3x	35.96	37.5	40.66	99.26

Note: testing direction x presents horizontal, y is vertical and z is axial.

Conclusion

With finite vibration information as the input of the vibration deflection analysis method, the result of the multichannel analog acquisition vibration signal analysis is achieved on which the vibration detection and feature extraction for the crankshaft of the drilling pump is completed with the intelligent recognition on the system fault source and mode. The dynamic analysis contributes to the solution of the full vibration analysis of the critical components in the moving equipment system. The required vibration information of key locations can be achieved from the information of several experimental measurement points, hence the problems such as inadequate information and inaccurate analysis of the fault diagnosis in the complicated mechanical system can be solved, by which the foundation of accurate fault diagnosis process is established. The experimental research process of the typical case testifies the feasibility of the method, which provides a reference for the visualization monitoring and sophisticated fault diagnosis for large reciprocating mechanical system.

Acknowledgement

The research was sponsored by the National Natural Science Foundation of China (Project No. 51175051) and Youth Fund Project of Northeast petroleum University (Project No. 2012QN119).

References

[1] Leclere Q. Multi-channel spectral analysis of multi-pass acquisition measurements [J]. Mechanical Systems and Signal Processing, 2008.

[2] Bie F. Research on fault diagnosis method for reciprocating machinery based on vibration visualization analysis [D]. Postdoctoral outbound report of Northeast Petroleum University. 2012.

[3] ZHANG C, LI Bing, YANG Z, XIAO W & HE Z. Crack location identification of rotating rotor systems using operating deflection shape data [J]. SCIENCE CHINA Technological Sciences, Vol.56, No.7, July 2013, p. 1723–1732.

[4] Xiang J W, Matsumoto T, Long J Q, et al. Identification of damage locations based on operating deflection shape [J]. J Nondestructive Eval, 2012.

[5] Chen J L, Zi Y Y, He Z J, et al. Construction of adaptive redundant multiwavelet packet and its application to compound faults detection of rotating machinery [J]. Sci China Tech Sci, 2012, 55, p. 2083–2090.

[6] Andrzej Piotr Koszewnik, Zdzisław Gosiewski. Frequency domain identification of the active 3D mechanical structure for the vibration control system [J]. Journal of Vibroengineering. Vol.14, 2012, p. 451-465.

[7] Ervin Sejdic, Igor Djurovic, Jin Jiang. Time–frequency feature representation using energy concentration: An overview of recent advances [J]. Digital Signal Processing, Vol.19, 2009, p. 153–183.

[8] S. Krishnan. A new approach for estimation of instantaneous mean frequency of a time-varying signal [J], EURASIP J. Appl. Signal Process.Vol.17, 2005, p. 2848–2855.

[9] L. Angrisani, M. D'Arco, R.S.L. Moriello, M. Vadursi. On the use of the warblet transform for instantaneous frequency estimation[J], IEEE Trans. Instrum. Measur. Vol.54 , issue 4, 2005, p. 1374–1380.

[10] Christopher Warren, Christopher Niezreckin, Peter Avitabile, Pawan Pingle. Comparison of FRF measurements and mode shapes determinedusing optically image based, laser, and accelerometer measurements[J]. Mechanical Systems and Signal Processing, Vol.25, 2011, p.2191–2202.

Advanced Materials Research Vols. 989-994 (2014) pp 2904-2907
© (2014) Trans Tech Publications, Switzerland
doi:10.4028/www.scientific.net/AMR.989-994.2904

Hydraulic vibration exciter and hydraulic circuit design research

Jia Yang

Eaestern Liaoning University,Dandong, Liaoning118003,P.R.China

onlyyangjia@163.com

Keywords: Vibration;Hydraulic Vibration Exciter; Displacement Response; Hydraulic System

Abstract. Pressure of the liquid is used as power source of hydraulic vibration exciter. Rotary directional control valve is the realization of oiling-way veversing components . The piston is reciprocated under the influence of the change of the hydraulic. The reciprocating movement of the piston is a result of fluid pressure.Working area of the piston multiplied by the pressure of the liquid is equal to the thrust of the piston.Displacement response of the vibration exciter can be simplified to the second-order vibration systems.Elastic beam is used as limit components of piston of vibration exciter,the piston vibration waveform is a sine wave .The volume of elastic beam is smaller than the volume of fluid elastic element . The hydraulic circuit is a dual pump fuel supply circuits.Pumps are used to supply rotary valve and hydraulic cylinder .Dual pumps fuel supply system is conducive to control fluid pressure and flow of the rotary valve and vibration piston.

Introduction

Vibration process is widely used in machinery manufacturing cold areas such as cutting, grinding , broaching and other aspects of the application in precision machining and processing vibration machining difficult materials have unique advantages. But drawing, trombone success in laboratory testing in the processing of plastic materials only . There are two characteristics of vibration processing :. A cutting speed v <2πfx. energy b. cutting needed is provided by the vibration exciter . cutting machining to provide a non-vibrating energy only for feeding speed

Ultrasonic vibration has been applied in cold areas , but the characteristics of plastic processing metallurgical enterprises is power, can not use ultrasonic vibrations. Hydraulic vibration exciter can produce high- vibration energy.

Constitutes a principle of hydraulic vibration exciter

Hydraulic vibration exciter constitution principle as shown. Vibration exciter mainly consists of three parts , cylinder, rotary valve and elastic beam 1. The rotary valve rotated by a hydraulic motor. Valve spool in the rotational direction of the circumference of the radial oil grooves . Realization of the oil tank is arranged alternately commutation purposes.

Right chamber of the piston by the oil pressure force F1 acts , leftward , when changing the oil pressure to the oil chamber with the port is turned on, and the piston into the left chamber of the high pressure oil passage on state, since the pressure receiving area of the piston about the type , the piston by right hydraulic force F2 , the piston moves to the right [1].

The elastic beam is an essential element to ensure continuous operation of the hydraulic exciter . Due to intermittent supply cylinder valve cavity left low and high pressure zones in changing . Eventually left cylinder piston reaches the surface caused by vibration dead . Elastic beam is maintained at a certain piston position . Rigid beam reach vibration requirements , elastic stiffness K is too small , it becomes flexible beam limit would not achieve the role . Therefore, the design of the elastic beam stiffness values according to the force of the hydraulic piston vibration exciter determined to achieve the purpose of the piston vibration .

The force on the piston shown in Figure 2.

F (t) periodic force can be decomposed into two components, namely the constant component and periodic component:

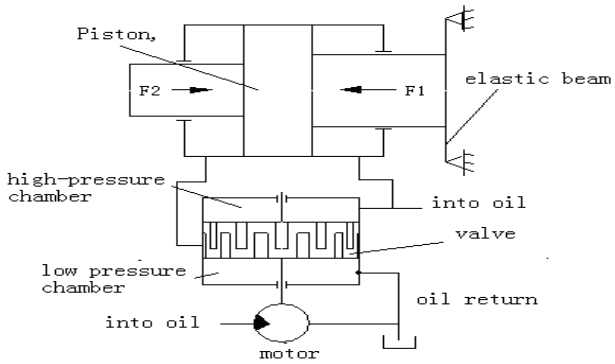

Fig. 1. Schematic of hydraulic vibration exciter constitute

Constant component: $F_0 = \frac{1}{2}(F_1 - F_2)$

Periodic component: f (t)

The same component can only make the piston produces the static displacement, cannot make the piston vibration, f (t) to make the piston vibration cycle components only, the Fourier series expansion cycle component[2]:

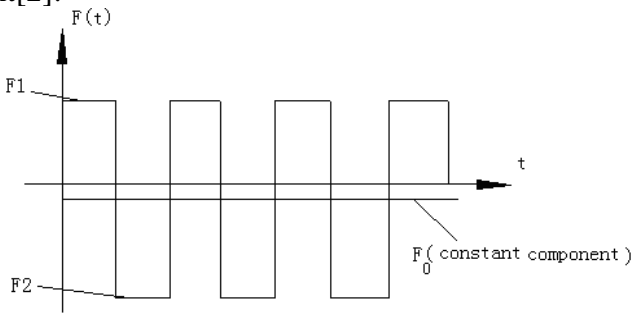

Fig 2. Pistons by trying

$$f(t) = \frac{4F}{\pi}\sum_{n+1}^{\infty}\frac{1}{2n-1}\sin(2n-1)\omega t = \sum_{2n-1}^{\infty}\frac{4F}{\pi i}\sin(i\omega t) \quad (1)$$

Because the system is linear, the piston in f (t) under the action of the displacement response of x (t) is equal to f (t) separate the components in the system response superposition, namely

$$x(t) = \frac{4F}{\pi}\sum_{i=2n-1}\frac{\beta_i}{i}\sin(i\omega t - \varphi_i) \quad (2)$$

Type: β i—i order harmonic component of vibration amplification factor

φ_i —i order harmonic component phase lag Angle

ω - vibration frequency

Due to the phase Angle of each harmonic component is different. The displacement response of x (t) waveform is different from the waveform of exciting force F (t).The displacement response waveforms of x (t) depends on the system the value of the parameter m, K and C each order harmonic response amplitude x_i.Easy to prove that: the $x_1 >> x_2 >> x_3 >>\cdots x_{n-1} >> x_n$, that is to say, the displacement response of x (t) more than three times harmonic component are small and can be left out, then

$$x(t) = \frac{4F}{\pi}\times\frac{1}{2\xi K}\sin(\omega t) \quad (3)$$

Type: ξ -damping ratio, K - elastic beam stiffness.

For frequency ratio r= $\omega / \omega_0 > 0.7$, the above conclusion is reasonable. So there are

$$x(t) = \frac{4F}{\pi}\beta \sin(\omega t - \varphi) \tag{4}$$

$$Type: \beta = \frac{\frac{1}{K}}{\sqrt{(1-r^2)^2 + (2\xi r)^2}}$$

$$\varphi = \arctan[-\frac{2\xi r}{1-r^2}]$$

Indicates that the vibration of the piston is sinusoidal vibration.

To two things: a. If not set elastic beam when the piston under the action of force of F1 and F2, overcome damping, soon arrived at one end of the cylinde.The directional control valve has not been reversing, the piston has reached the end. The oil cylinder end cover is the rigid body k=∞.Therefore the piston is not moving.

Setting elastic beam bearing, the piston force under the action of F1 and F2, overcome damping work, one side will be part of the work shift as the elastic deformation of beam power storage. When reversing the deformation of elastic beam work and released and the effect of hydraulic power superposition, accelerate the rate of movement of the piston.

Another function of the elastic beam is on the limit of piston. The piston vibration is always in a certain position. Meanwhile elastic beam should be set at the side that force is small,so that the elastic beam during the vibration exciter is always in force pressing the state to prevent it from loosening and useless.

b. The elastic beam compared with oil spring. If the oil spring as the elastic element, in order to obtain sufficient elasticity deformation, on both ends of the cylinder should be set up two large piston. And elastic beam is used as the elastic element structure of small dimension, small volume.

The hydraulic system design

Hydraulic vibration exciter hydraulic circuit design problem to consider is the hydraulic motor and speed control and stability of the oil cylinder. Under normal circumstances, the shear vibration or vibration frequency stability requirement when processing in a certain range, hydraulic motor rotation speed can be controlled, the vibration frequency of controllability.

Vibration process similar to the requirement of vibration amplitude is set in a certain range, the vibration amplitudes are not affected by the interference of mechanical feed speed, namely input cylinder liquid flow rate and velocity control requirements. Vibration amplitude with the rotary valve guide groove is proportional to the oil on time. Rotary valve low rotating speed of cylinder vibration amplitude. Rotary valve of high rotational speed is the vibration of the cylinder small amplitude.

Supply oil to the vibration piston hydraulic motor and oil pump, piston of hydraulic oil demand is related to the vibration amplitude and vibration frequency. Through the throttle valve and the adjustment of speed regulating valve under the condition of its vibration frequency determine to achieve more precise amplitude. So the piston vibration amplitude control requirements are within a small range. Amplitude control to conform to the requirements of machining accuracy.

According to the design requirements of the above design of hydraulic system are shown in figure 4, hydraulic motor oil supply loop[4]. The hydraulic oil filter through to arrive at the pump. Relief valve installed in the pump is used to control the export of oil pump oil supply pressure and pressure of the hydraulic system. Oil flows through the one-way valve, the two two-way valve, control valve to hydraulic motor. Pressure gauge installation position should be at the side of the overflow valve, adjust the pressure can be easily observed when the hydraulic pump output pressure. Pressure gauge is installed on the back of the check valve can be closer to the real working pressure of hydraulic system. At the same time can be indirectly detect the working state of the check valve.

The basic composition of the hydraulic cylinder oil supply loop is the same as the hydraulic motor oil circuit. Add an accumulator in hydraulic circuits. To meet the requirements of vibration oil cylinder of flow fluctuation. Graphical position has always been the oil chamber of hydraulic cylinder of high pressure oil chamber. Inferior vena is realized in conversion between high and low pressure piston to move up and down. Due to the same shape guide groove, so the piston displacement of moving the same amount[5].

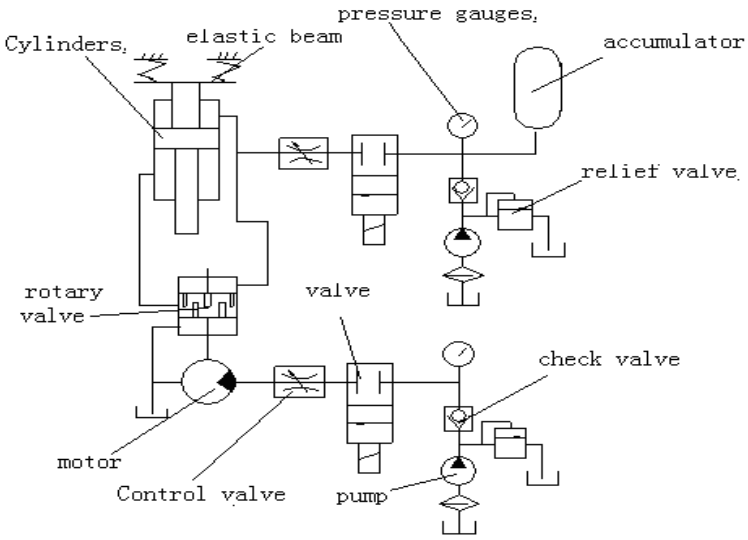

Fig 3.Hydraulic system

Conclusion

Hydraulic vibration exciter is hydraulic circuit by using the rotation type directional control valve, the direction of the transformation. According to the piston stress cycles using Fourier series expansion is derived by reasonable simplification of the vibration exciter displacement response expression. The hydraulic vibration exciter can be thought of as the second order vibration system. The vibration of the piston is a sine wave.

The piston of hydraulic vibration exciter adopted elastic beam as a limit switch. Compared with the oil elastic element elastic beam, the small size. Elastic beam in the application of the vibration exciter is piston vibration components is a must.

Oil supply loop hydraulic circuit with double pump, used for rotary valve and hydraulic cylinder oil supply. Double piston pump oil supply system is advantageous to the rotary valve and vibration of the regulation of the oil pressure and flow rate. Speed regulating valve of flow control accuracy is more advantageous to the working stability of vibration system.

References

[1] Yang Jia,Qiu Lijun,2011 2nd International Conference on Mechanic Automation and Control Engnieering,MACE2011-Proceedings,p325-328.

[2]Zuo Shusheng, Mechanical impedance method and application , Machinery Industry Press，p19-21.1987

[3] Qiu Lijun,Yang Jia,Advanced Materials Research,V 322,p497-500.2012

[4] Wang Jiwei,Zhang Hongjia,Huang Yi, Hydraulic and pneumatic drive . Machinery Industry Press.2012.6.p8-56

[5] Northeast University of Technology， Mechanical parts design manual， Second edition, Metallurgical Industry Press.1990

Advanced Materials Research Vols. 989-994 (2014) pp 2908-2912
© (2014) Trans Tech Publications, Switzerland
doi:10.4028/www.scientific.net/AMR.989-994.2908

Path Planning for Circular Cutter Envelop Milling of Steam Turbine Blade

Wang Jianjun[1,a], Wang Ke[1,b], Wu Qiong[2,c]

[1]Shenyang University of Technology, Shenyang 110023, China

[2]Zhejiang University of Water Resources and Electric Power, Hangzhou 310018, China

E-Mail: [a]wangjjyf@qq.com, [b]sunxingw@ 126.com,[c]385191263@qq.com

Keywords: Steam turbine blade, Circular cutter, Envelope machining, Cutter contact, Surface reconstruction, Residual height, Tool path

Abstract: In order to solve the problem of poor steam turbine blade processing efficiency, and on the basis of analyzing the turbine blade surface and the existing processing methods, a model of circular cutter turbine blade machining is built. By comparing the tool paths of horizontal and vertical section envelope machining, choosing quasi-vertical cross section envelope machining method and utilizing the original datum and NURBS surface matching mathematic methods, this paper provides an algorithm of residual height calculating, and based on this, the tool path can be planned. Datum show that, the tool path of circular cutter machining blades is much longer than the tool path of ball-end cutter envelop milling machining blades, and the machining efficiency is also highly enhanced.

1. Introduction

Steam turbine blade is the key part of a steam turbine, which can turn heat energy of the steam and gas into mechanical energy directly. Steam turbine blade is also an important and most widely used component in steam turbine. There are thousands of blades in one steam turbine. The processing requirements of blades is strict, the workload is heavy, the processing quality requirement is high, and the workload of blades machining accounts for one fourth to one third of the total steam turbine workload. Practice indicates that the design and manufacturing level of the blade is one of the important indicators to measure turbine technology. Blade manufacturing efficiency directly influences the turbine manufacturing cycle, and manufacturing quality directly affects the operating efficiency and the safety of the steam turbine unit, that is why improving the machining efficiency and machining precision of the blade becomes one of the important research among scholars and engineering technicians at home and abroad.

In order to obtain high efficiency of numerical control machining tool path, many scholars have carried out studies and put forward a variety of algorithms. Someone has put forward the method of using parallel machine tool to do the blade machining [2] , but because of the processing method which uses ball-end cutter to do machining on the four-axis or five-axis numerical control machine tool, the target of improving processing efficiency is limited. In this paper, based on the analysis on the surface of the blade, the method of circular cutter turbine blade machining is presented, and the mathematical model of blade surface reconstruction is established, and by controlling the residual height, turbine blade machining tool path is planned on this method.

2.Processing Object Analysis

2.1Blades Types

Steam turbine blades include constant chord blade and variable chord blade, the former can be achieved by molding or contour machining to meet the processing requirements because of the simple mechanism. Variable chord blades include variable cross-section straight blades and variable cross-section twisted blades. Variable cross-section straight blades, the blade section shape is changing along with the height, and there is no reverse between adjacent two sections, and forming milling cutter can be used for oblique milling; Variable cross-section twisted blade, Variable cross-section twisted blade, namely with the blade height changing, cross-section shapes are different, and adjacent two sections are twisted, and due to its high efficiency, this method is widely used [3].

2.2Blades Composition

The research object of this paper is the rotor blade on steam turbine rotor, whose structure contains blade body, blade root and blade shroud [4]. Blade body is the basic working part of blade, whose structure is complex. And most of blade bodies are torsion free surfaces. Blade body is composed of concave side, convex side, gas inlet side fillet, gas outlet side fillet, blade root fillet, blade shroud fillet and lacing wire. The function of blade root is to fasten rotor blade, in order to prevent it from dropping from the rim groove under the high pressure of driving force and rotating centrifugal force. The blade root types include fork shape, ladder shape, tenon tooth shape, T shape, mushroom and longitudinal tree shape. The blade shroud is the fixation of the outer side of blade, which usually equipped with shroud ring. The shroud ring can combine several blades together into a blade group.

2.3 Manufacturing of Blade Parts

Manufacturing methods of blade parts include copying method, special processing method and the numerical control milling method. Coping method is the most traditional method, and because of its low efficiency and less accuracy, this method has gradually been eliminated. Special processing method mainly refers to electrolysis processing, which cannot be limited by the hardness of the material, but the bottleneck of this method is its low accuracy and instability of machining process. Ball-end cutter is the most widely used method in modern society.

3.Research on Circular Milling Cutter

3.1 Envelop Machining Model

The model of blade machining with circular envelop milling cutter is shown in Fig. 1. Set up the workpiece coordinate system O-XYZ, while circular cutter moving along X to the opposite blade vertically, the front and back sides moving along Y, and upper and under sides moving along Z. If it is a twisted blade and moves associatively along A, in order to obtain an ideal disc diameter D and cutting state, cutting tool coordinate system can define two location parameters angle B and angle C. During the period of envelop milling, B and C do not take part in associative moving.

3.2 Quasi-Vertical Cross Section Envelop Milling

As it can be seen in the model of blade machining with circular envelop milling cutter, according to different cutting methods, horizontal and vertical cross section envelop milling can be achieved. Seeing from the horizontal cross section, the enveloping principle is shown in Fig. 2. These two methods can be simplified as the enveloping problems of sets of space curves. The difference is, the outline of horizontal cross section envelop milling is a plain curve, while the vertical one is space free curve.

Considering the different sizes of different blade parts, the original datum of blades surface reconstruction are several point coordinates on horizontal cross section. In order to simplify the calculation of tool path and consider the tool path twist state and the different widths of the two sides of the blade, vertical cross section envelop milling can be improved. After improvement, the cutting pattern can be named as “quasi-vertical cross section envelop milling”.

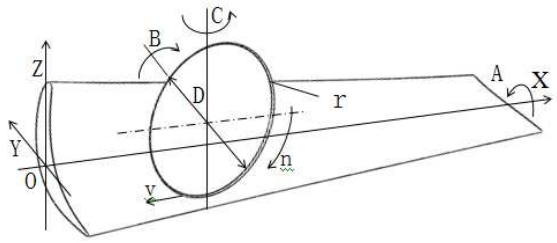

Fig. 1 Envelope machining model

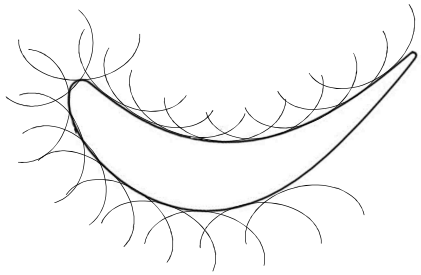

Fig.2 Circular cutter envelope machining sketch

3.3 Interference Discrimination

In the process of steam turbine blade surface machining, due to the complex structure of blade surface, cutter interference is easily happened. The most common situation is: global interference and part interference. Global interference, namely collision interference, means the moving parts of the machine tools or cutters intervene with blade workpiece or fixtures. The mostly happened part of global interference in circular cutter envelop blade milling is blade root, which can be prevented

by adjusting the location parameter of the cutter. But because of the cutter sizes or the unreasonable path planning in the part interference, which will cause overcut or undercut. As to the steam turbine blade, the part inference is mostly happened in the place of blade concave whose curvature is changeful or the part with small curvature radius. The part interference can be prevented by choosing reasonable cutter diameter D.

4.Steam Turbine Blades Surface Reconstruction

4.1Mathematic Model of Circular Cutter

Torus, refers to a ring-shaped surface generated by rotating a circle around an axis that does not intersect the circle**.** Circular cutter refers to the circular surface cutter which is formed in the process of cutting edge machining. As shown in Fig. 3, in the cutter coordinate system $s(o_t xyz)$, circular surface is generated by radius r rotating around an axis z. The path of the circle center o_r rotating around axis z in the plane $xo_t y$ is defined as lead circle. The radius of lead circle, suppose M is a point on the circular surface, the coordinate of M can be expresses as formula 1.

$$\begin{cases} x = (r\cos\alpha + R)\cos\beta \\ y = (r\cos\alpha + R)\sin\beta \\ z = r\sin\alpha \end{cases} \quad (1)$$

In the formula, r is the arc radius of cutter point, R is the radius of lead circle, α is the angle between the joint line of movable point M on circular surface and the circle center o_r and its projection line in plane $xo_t y$, β is the angle between movable point M in the plane $xo_t y$ and axis x.

4.2 Relation between Array Pitch and Residual Height

The array pitch is in co-relation with residual height, actual radius of cutting tool and the partial radius of curvature surface. As seen in Fig. 4, as to the circular envelop milling cutter blade surface, the direction of array pitch is parallel to the blade and perpendicular to the direction of tool path. Given the array pitch L, actual radius of cutting tool R_e, and partial radius of curvature surface R_b, the allowable value of residual height is h, the array pitch and residual height can be expressed as formula (2).

$$L = \sqrt{8hR_eR_b/(R_b \pm R_e)} \quad (2)$$

In the formula, blade concave is negative，the blade convex is positive.

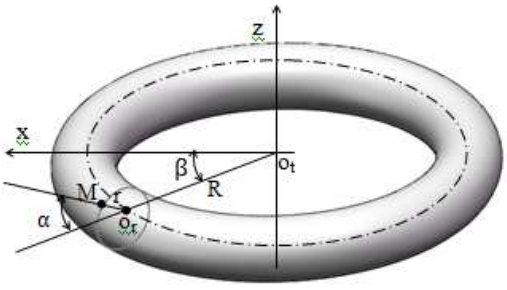

Fig.3 Circular Cutter Structure

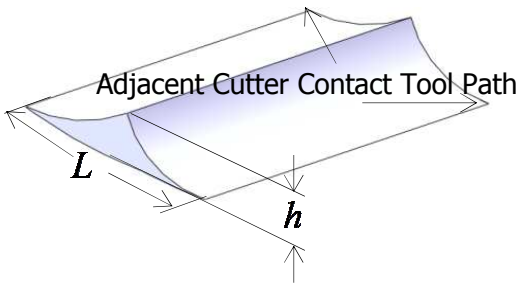

Fig.4 Residual Height

4.3Mathematical Model of Blade Surface Reconstruction

NURBS surface matrix can be seen as the promotion of surface matrix representation, this paper adopts bi-cubic NURBS surface matrix, which is similar to a space surface, $k \times l$ times NURBS surface can be represented as:

$$f(x,y)=\frac{\sum_{i=0}^{n}\sum_{j=0}^{m}\omega_{ij}r_{ij}N_{i,k}(x)N_{j,l}(y)}{\sum_{i=0}^{n}\sum_{j=0}^{m}\omega_{ij}N_{i,k}(x)N_{j,l}(y)} \quad (3)$$

r_{ij} is the control vertex, i,j are sequence numbers of control vertex respectively in x,y two directions. Obviously, the number of control vertices in x,y two directions are $n+1$ and $m+1$ respectively. $N_{j,l}(y)$ is the NURBS curve basis function of l timesin y direction. ω_{ij} is the weight factor of blade surface. Control vertex r_{ij} is the cross point of cutting lines in x,y two directions, namely the cross point of number i cutting line in x direction and number j cutting line in y direction. The corresponding weight factor ω_{ij} of control vertex r_{ij} is some constant greater than zero, when the weight factor grows, the surface will get close to control vertex r_{ij}, especially when weight factor tends to infinity, surface overpasses control vertex r_{ij}.

The rational fractional function of bi-cubic NURBS surface can be expressed(p,q are the substitutions of (i,j)). Through deducing, we can achieve rational fractional function of the number (i,j) surface patch of NURBS surface is Formula (4).

$$f_{i,j}(x,y)=\frac{\sum_{p=i-3}^{i}\sum_{q=j-3}^{j}\omega_{pq}r_{pq}N_{p,3}(x)N_{q,3}(y)}{\sum_{p=i-3}^{i}\sum_{q=j-3}^{j}\omega_{pq}N_{p,3}(x)N_{q,3}(y)}=\frac{N_{i,3}^{x}W_{pq}^{r}(N_{j,3}^{y})^{T}}{N_{i,3}^{x}W_{pq}(N_{j,3}^{y})^{T}} \quad (4)$$

In this formula: $N_{i,3}^{x}=(N_{i-3,3}(x)\quad N_{i-2,3}(x)\quad N_{i-1,3}(x)\quad N_{i,3}(x))$;

$$N_{j,3}^{y}=(N_{j-3,3}(y)\quad N_{j-2,3}(y)\quad N_{j-1,3}(y)\quad N_{j,3}(y));$$

$$W_{pq}^{r}=\begin{pmatrix}\omega_{11}r_{11} & \omega_{12}r_{12} & \omega_{13}r_{13} & \omega_{14}r_{14}\\ \omega_{21}r_{21} & \omega_{22}r_{22} & \omega_{23}r_{23} & \omega_{24}r_{24}\\ \omega_{31}r_{31} & \omega_{32}r_{32} & \omega_{33}r_{33} & \omega_{34}r_{34}\\ \omega_{41}r_{41} & \omega_{42}r_{42} & \omega_{43}r_{43} & \omega_{44}r_{44}\end{pmatrix} \quad W_{pq}^{r}=\begin{pmatrix}\omega_{11} & \omega_{12} & \omega_{13} & \omega_{14}\\ \omega_{21} & \omega_{22} & \omega_{23} & \omega_{24}\\ \omega_{31} & \omega_{32} & \omega_{33} & \omega_{34}\\ \omega_{41} & \omega_{42} & \omega_{43} & \omega_{44}\end{pmatrix}$$

5.Application Examples

Taking a domestic steam turbine low pressure rotor blade processing as an example, the length of the rotor blade is 440mm. The original datum are profiles of 23 horizontal cross sections as shown in Table 1, and the cross section distribution is shown in Fig.5. This paper does some researches on machining with circular milling cutter, utilizes the method of quasi-vertical cross section envelop milling, and discusses from the aspect of surface reconstruction, horizontal and vertical section line interpolation,deciding cutter contact tool path and calculating of cutter location point. As to the blade convex, the arc surface will not be interfered by machining surface, and to the blade concave,the radius of arc surface must be smaller than the radius of the smallest radius of surface.

Table1. The Original Data

Num	X=440		X=420		……		X=0	
	Y	Z	Y	Z	Y	Z	Y	Z
1	8.008	22.659	7.52	19.009	……	……	-2.657	-2.688
2	8.67	24.146	8.217	20.547	……	……	-1.27	-0.228
3	9.348	25.626	8.928	22.079	……	……	0.145	2.216
4	10.04	27.1	9.656	23.603	……	……	1.588	4.644
5	10.747	28.566	10.399	25.119	……	……	3.057	7.056
6	11.471	30.024	11.159	26.627	……	……	4.554	9.451
7	12.208	31.475	11.933	28.128	……	……	6.081	11.827
8	12.96	32.919	12.723	29.621	……	……	7.661	14.168
…	……	……	……	……	……	……	……	……

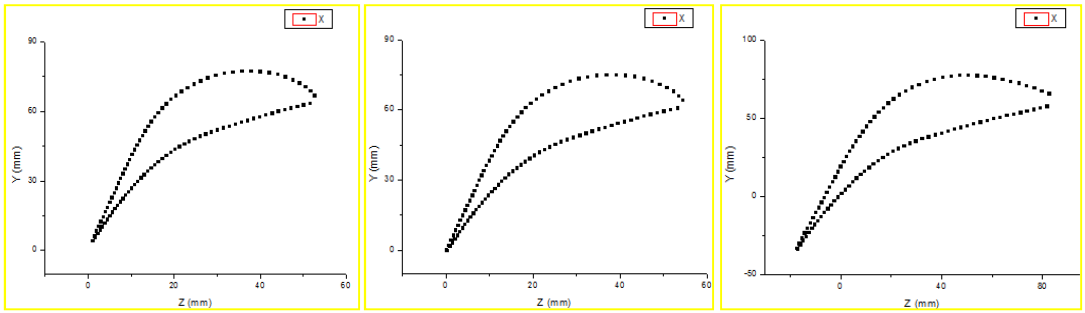

X=440mm X=420mm X=0

Fig.5 Part of Cross Section Scatter

6.Summary

In the process of steam turbine blades envelop milling machining with circular cutter, the curvature distribution of milling is variable and can fit curvature distributions of all processing surfaces, which shows “curvature match” and good cutting condition. This can help to keep a constant speed of ball-end cutter cutting and prevent the problem of the zero cutting speed of axis of rotation, narrow chip space and cutting angle differences. In the process of machining, the cutter contact point moves along the circular ring successively, which can use the parts wear of the full width cutting tools of circular disc cutter, so as to extend the life of the tools.

References

[1]Wu Yue, Chen Yongxiang and Zhong Chenming et.:T-turbine blade root processing Technology Based on Cimatron E[J]. Manufacturing Automation，2011,33 (10):40-43.

[2] Chen Guangming: Research on NC Machining Technology of Turbine Blade Based on Parallel Machine Tool[J]. MachineToolandHydraulics，2010,38(11)：26-30.

[3]Yue Ying. Cutter Paths Computation for NC Machining of Steam Blade [J]. Turbine Technology，2010, 52 (3)：235-237.

[4]Chen Guang-ming，Zhan Xuyang: Research on the structure features of turbine blade and NC machining technology[J]. Manufacturing Automation，2011,33(9):93-98.)

[5]Jin Junfeng, Zhou Laishui and An Luling, et. : On Toolpath Planning for NC Machining of a Free-form Blade Surface[J]. Mechanical Science and Technology for Aerospace Engineering,2008,27(5)：652-656.

Advanced Materials Research Vols. 989-994 (2014) pp 2913-2916
© (2014) Trans Tech Publications, Switzerland
doi:10.4028/www.scientific.net/AMR.989-994.2913

Improving Design of Cup Conveying Part for Sealing Machine Based on PLC

Liai Pan[1, a] ,Qiulei Du[2,b] and Yanli Wu[3,c,*]

[1,2]College of Mechanical and Vehicle Engineering Changchun University, Changchun, 130022, China
[3]Agriculture Product processing Centre, Jilin Agri-machinery Research Institute. Changchun, 130022, China.

[a]email:panli636@126.com, [b]email:apriljuan@hotmail.com, [c]email:wyljlnj@163.com

*Corresponding author

Keywords: Sealing machine. Conveying part. Control system. PLC; Design

Abstract. In order to improve the sealing quality and reduce the labor intensity of people, the stepping motors have been adopted in the salver mechanical transmission part and sealing part of the original sealing machine. In the paper, salver feeding and control system of sealing machine have been designed. The results have been obtained such as control principle diagram of the control system, equivalent circuit diagram and outer wiring diagram of PLC and PLC control program. It can realize the automatic control of the sealing machine. Improved sealing machine has the characteristic of simple mechanical transmission parts, advanced control system, small human error, low fault rate and easy operation.

Introduction

With the development of science and technology and people living standard rise, people is higher and higher requirement for the quality of food and health. Therefore, in order to make our products to seal save, keep the quality of our products and avoid loss of products, the packaging container needs to be sealed.We call it sealing machine that packing container for filling sealing machine. It is a product of The Times. At present there are many kinds of sealing machine. According to the mechanical properties of packaging materials, sealing machine is divided into a flexible container sealing device and rigid container sealing machine. According to the shape of the container, the sealing machine is divided into plastic bags and cup sealing machine. And cup sealing machine is mainly suitable for soybean milk, milk tea and other hot and cold drinks. Because of its simple structure, small volume, and easy to operate, it is widely used. [1]

In the paper, the cup sealing machine has been studied. On the basis of its working principle and structure of the sealing machine, the sealing machine has been improved design, especially for the cup conveying system. The design make it's from a cup of a seal, sealed into four cups can now be done automatically. The automatic control system has been designed to improve the degree of automation, more convenient to use, and make up for the lack of traditional cup sealing machine design.

Structure of Sealing Machine

(1) The structure of original sealing machine [2]: it is mainly by the motor, CAM transmission mechanism, pressure head, conveying mechanism and feeding mechanism through the frame of connection as shown in figure 1.

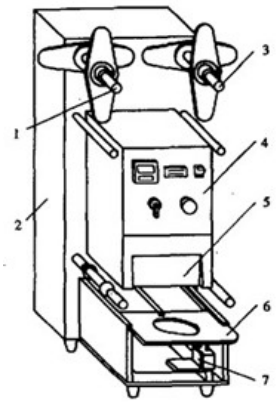

Fig1. Main structures and names

1.accept membrane shaft； 2.the case;3. put membrane shaft; 4.the electrical box; 5.security barrier ; 6. the film ;7. salver

(2) The improved structure

The main body structure of the improved sealing machine is the same as the original sealing machine. In order to improve the sealing efficiency and reduce labor intensity of workers, mainly for the sealing machine tray modification design sections and compressive bar. Part of the ptray is the original c plate, can only send into a cup, manual control; To adopt stepper motor control, can add four cups, automatic sealing processing in turn. Compressive bar part of the original sealing machine adopts lever, manual complete sealing and cutting, the improved using stepper motor, through the control system to realize automatic sealing and cutting.

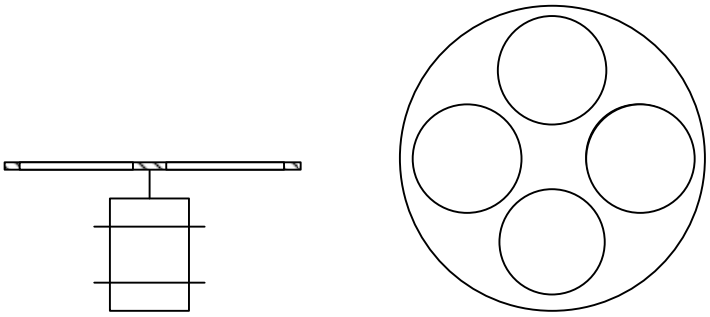

Fig2. Diagram of improved feeding structure

Design of the Control System

3.1 The control principle of sealing machine

Food was packed and into the tray with a piezoelectric sensor. Piezoelectric sensors work and send electrical signals. The electrical signal amplified by amplifying circuit, and the more meet the requirements, the signal is output. PLC input interface 2 received signal, the output interface 2 according to the programmed data output pulse signals. Stepper motor Ⅰ work, began to spin the tray to a fixed position. Detection sensor detects the tray to the specified location, signal. Signal amplifying circuit output signal. PLC 3 received signal input interface, it also control output interface 3 and 4 output interface. 3 according to the programmed output interface data output pulse signal, the stepper motor Ⅱ to complete various tasks (); 4 according to the programmed data output pulse signal output interface, indicating lamp is opened, at this time due to the stepper motor Ⅱ work, manual switch is prohibited to use; Closed detection sensor at the same time, when the stepper motor Ⅱ completion of tasks, light bulbs, open detection sensor. If only to complete a specified task, can be manually switch open stepper motor Ⅰ alone, take out the sealing good items.

Sealing machine control principle diagram is as shown in figure 3.

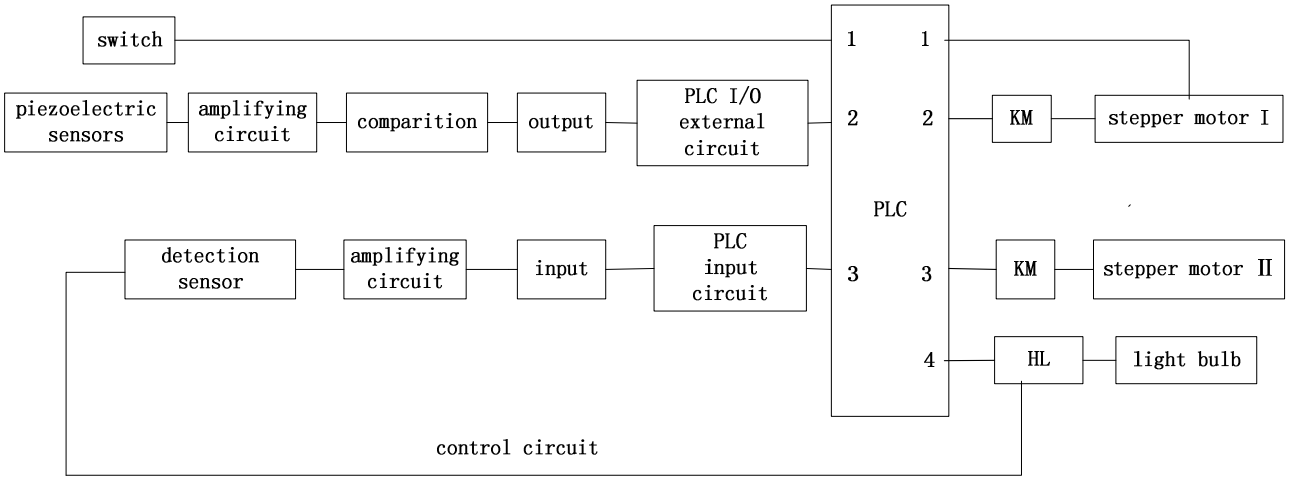

Fig3. Diagram of sealing machine control principle

3.2 The function of the control system

1) The self-check function. Each, the cup packed goods is into the tray, start work, detection sensor detects whether the cup to the sealing position, and a signal is output.

2) The alarm function. In the process of automatic operation, the light bulb can both guarantee the normal work of the system, and can detect sensor control switch.

3.3 The PLC control principle of sealing machine[3,4]

The equivalent circuit diagram of sealing machine PLC as shown in figure 4, outer wiring diagram of PLC is shown in figure 5.

The PLC control principle is: when according to pick up on the outside button SB, drive the first cascade X1 normally open contacts closed, with subsequent T1 by series. (T1 received signal immediately start the countdown, the end of the timing, open, normally closed joint motor (1) off work due to the contact closure, closed on Y1, X1, Y1 forming circuit, relay drive motor 1 works.

When open FR1 by external signal, through the series and subsequent T2. (T2 received signal immediately start the countdown, the end of the timing, open, normally closed joint motor (2) off work due to the contact closure, closed on Y2, X2, Y2 forming circuit, relay drive motor work 2.

When open FR3 by external signal, through series and subsequent T3 and T5. T3 and T5 received signal immediately start the countdown, due to the contact closure, closed through to Y3, X3, Y3 forming circuit, relay drive motor work 2. After the T3 timing, open, normally closed joint motor 2 stop working; After the T4 timing, closed, normally open joint motor 2 began to work again; After the T5 timing, open, normally closed joint motor 2 stop working.

When open FR3 by external signal, through the series and the subsequent T6. T6 received signal immediately start the countdown, due to the contact closure, Y4 closed connect, X3, Y4 forming circuit, relay drivers instructions bulbs work, any action has been prohibit at this time. After the T6 timing, normally closed joint is opened, the indicator bulb stopped working.

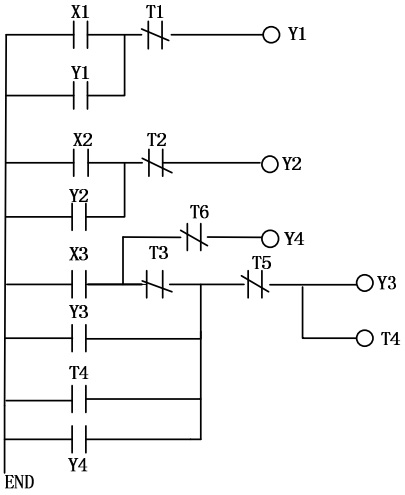

Fig4. The equivalent circuit diagram of the machine PLC

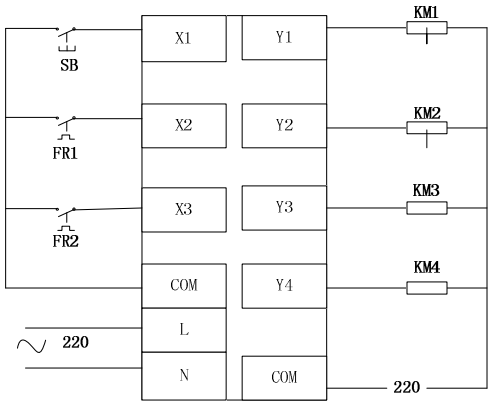

Fig5. PLC external wiring diagram

3.4 PLC introductions[5]

1 LD X1; 2 ANI T1; 3 ANI Y1; 4 OR Y1; 5 OUT Y1; 6 LD X2; 7 ANI T2; 8 ANI Y2; 9 OR Y2; 10 OUT Y2; 11 LD X3; 12 ANI X3; 13 ANI T3; 14 OR Y3; 15 OR T4; 16 OR Y4; 17 ANI T5; 18 ANI Y3; 19 OR T4; 20 OUT Y3; 21 LD X3; 22 ANI X3; 23 OR Y4; 24 ANI T6; 25 ANI Y4; 26 OUT Y4.

Conclusion

In the paper, the cup sealing machine has been studied. On the basis of its working principle and structure of the sealing machine, the sealing machine has been improved design, especially for the cup conveying system. The design make it's from a cup of a seal, sealed into four cups can now be done automatically. The automatic control system has been designed.

The PLC control principle of sealing machine is described in detail, the equivalent circuit and the external wiring diagram have been draw, and the PLC instructions have been written. The cup body movement and control system design of this sealing machine can not only improve the degree of automation, more convenient to use, but also make up for the lack of traditional cup sealing machine design.

References

[1] Jianfeng Sun. Design of the Desktop Automatic Sealing Machine of Plastic Cup. Packaging and food machine. 2001,18(6):7-9

[2] Lamei Du, Xiaohong Zeng, Youwei Yuan. Intelligent design of Vertical Bag-making Filling Packaging Machine Sealing Mechanism. China's packaging industry. 2001，（4）:16-18

[3] Xiaofeng Lin. The principle and application of programmable controller. Higher education press.1991.

[4] Hewei Guo. Three with PLC Control and Prevent the Short Circuit of the Motor and ReversingControl Circuit. Fuzhou: Woodworking Machine. 2003, (3) : 35~ 37.

[5] Xuelin Hu, Hong Sun. Electrical control and PLC. Beijing: metallurgical industry press, 1997.

Advanced Materials Research Vols. 989-994 (2014) pp 2917-2921
© (2014) Trans Tech Publications, Switzerland
doi:10.4028/www.scientific.net/AMR.989-994.2917

Research on the Optimal Design and Gear modification of Gearbox of a Wind turbine Based on the Virtual Prototype

Huibo HE[*1, 2, a], Huaying LI[1, b], Jun YANG[1], Guocheng LU[1] and Tao GU[1]

[1]College of Engineering and Technology, Southwest University, Chongqing, 400715, China,

[2]Department of Chem. and Mat. Eng., University of Alberta, Edmonton, AB, T6G 2V4, Canada,

[a]email: hehuibo@126.com, [b]email: lhyhhb@swu.edu.cn

Keywords: Optimal Design; Gear modification; Gearbox; Wind turbine

Abstract. This article describes a new mixed transmission system about the wind power gearbox. It is composed of one NGW planetary gear stage and two parallel gear stages. The modeling and optimization analysis of gearbox have been performed using Romax designer software. The load case of gear, gear modification, transmission error and Fast Fourier Transform Harmonics of wind gearbox have been carried out to investigate various performances of gearbox system. Results of the investigation show the maximum load per unit length of gear reduces about 7.2%, Transmission Error of gear reduces 74.3% and Fast Fourier Transform Harmonics decreases 77.4% after gear modification. This kind of design method has a remarkable effect on smooth running. And it provides a new research method for gear box of wind turbine.

Introduction

The worldwide demand for energy is steadily growing. At the same time, this trend is being accompanied by rising greenhouse gas emissions. So we urgently need to correct this course [1]. Wind power is sustainable and clean energy. Compared with conventional energy, generating electricity from the wind does not need fuel; hence there is no risk of a fuel price rise. There are no environmental costs, such as carbon emissions, in the generation process. Wind power has the added advantage that it is widely available worldwide [2].

With the development of modern industry, wind turbine has been taken into account in more and more countries. It is reported that the failure rate of gearbox is very high in the wind turbine [3]. Therefore, it is very important to design a wind gearbox reasonably. And thus many researchers have investigated the wind turbine gearbox transmission system for optimum design of gearbox [4-9].

In the current work, a model of 1.5MW wind gearbox was established with virtual prototype using Romax designer software. The duty cycle, load case of gear, gear modification, transmission error and fundamental frequency harmonic response of wind gearbox have been carried out to investigate various performances of gearbox system. And a lot of parameters of components have been optimized after analyzing and operating in virtual work environment.

Design of the Transmission Scheme

At present, there are many kinds of structures used in gearbox of a wind turbine. In general, multi-stages cylindrical gear transmissions are applied in small and medium-sized power system. While single-stage or multi-stages planetary and cylindrical gear transmissions are used in large power system. Planetary transmission types can be divided into NGW and NW models. In this paper, 1.5 MW wind turbine gearbox is composed of one NGW planetary gear stage and two parallel gear stages. Design requirements of the gearbox are given in table 1. The schematic diagram of wind turbine gearbox is shown in Fig. 1. Table 2 demonstrates the Geometric parameters of gear transmission at all stages after design and calculating according to the design requirements. The 3D model of wind turbine gearbox is shown in Fig. 2 using Romax designer software.

Tab.1 Design requirements of gear box

rated power	transmission ratio	output speed	input speed	pressure Angle	hours of service
1.5MW	94.527	1500~700r/min	14.8rpm	15°~25°	20 years

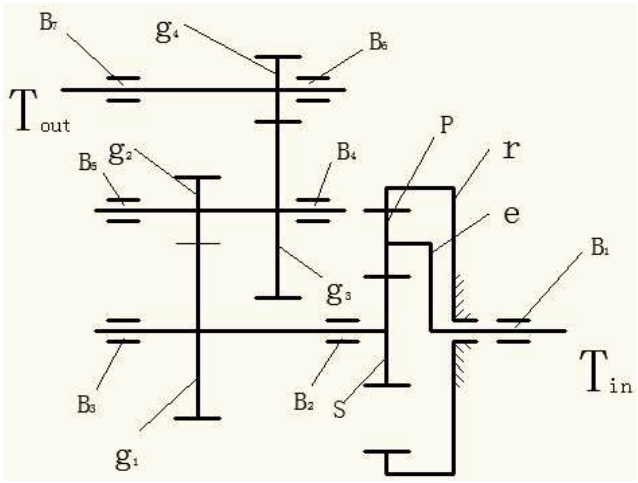

Fig. 1 Schematic diagram of wind turbine gearbox

P. planet gear; r. gear ring; S. sun gear; g_1. 1st driving helical gear; g_2. 1st driven helical gear; g_3. 2nd driving helical gear; g_4. 2nd helical gear; B. rolling bearings; e. planet carrier; i. Number of bearings, i=1, 2…, 8

Tab.2 Geometric parameters of gear transmission at all stages

planetary gear stage	Sun gear Z_a	Planet gear Z_c	Gear ring Z_b	Module Gear m	Face width b/mm	pressure angle α (°)	center distance a/mm
	27	54	135	13	265	20	526.5
1st stage	driving gear Z_{a1}	driven gear Z_{a2}	normal module m_n	helical angle β (°)	Face width b/mm	pressure angle α (°)	center distance a/mm
	100	20	10	14	210	20	619
2nd stage	driving gear Z_{a3}	driven gear Z_{a4}	normal module m_n	helical angle β (°)	Face width b/mm	pressure angle α (°)	center distance a/mm
	95	30	6.5	14	200	20	419

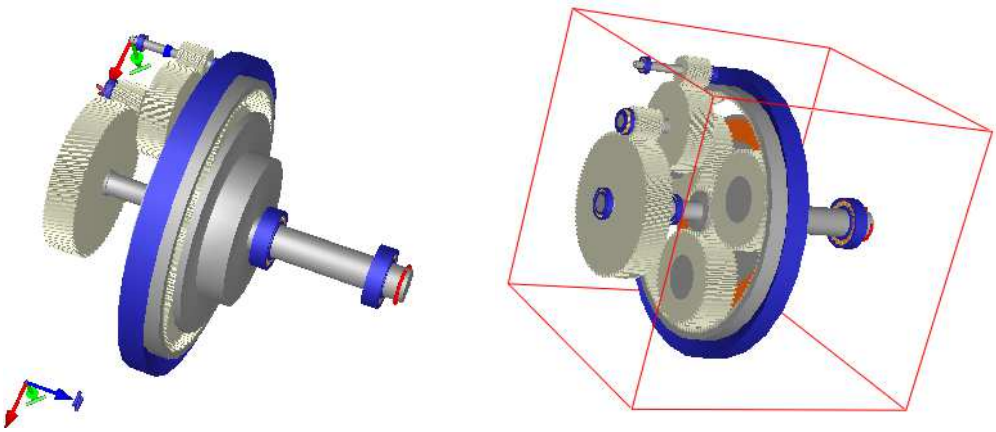

Fig.2 3D model of wind turbine gearbox

Defining Load Conditions

In current work, Tab. 3 shows the detailed load case.

Tab.3 The detailed load case

Load Case	Input speed（rpm）	Input power（Mw）	Time of duration（hrs）
1st Speed	14.8	1.5	24

Tooth profile optimization of gears

Fig.3 demonstrates that gear mesh deflects due to the elastic deformations of shaft, bearing and gear, and thus the load case in teeth direction is unbalanced. In order to make force balance in teeth width direction, teeth modification should be performed to meet its requirement. The implementation method is through the removal of material to conduct the modification of gear.

Fig. 4 shows load distribution for per unit length of gear. As seen in this figure, gear load in 1st stage presents serious uneven distribution in gear direction. And therefore, it is necessary to conduct gear modification in gear direction. Clicking “Micro Geometry” under “tool menu”, then, double-clicks “Right Flank the Target Form”, and last, clicking “Lead” optimization button, the optimal quantity can be set as “lead slope” in the gear direction. After optimization, the Optimum amount of modification is 5.3 μ m. Fig. 5 shows load distribution after lead modification of gear.

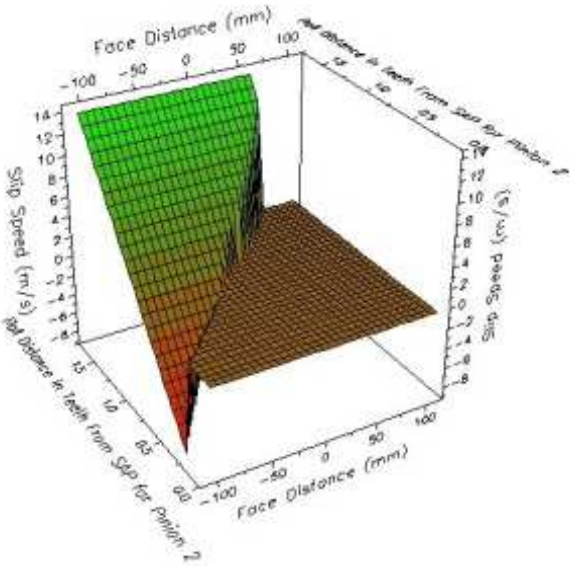

Fig.3 Load surface for gear mesh

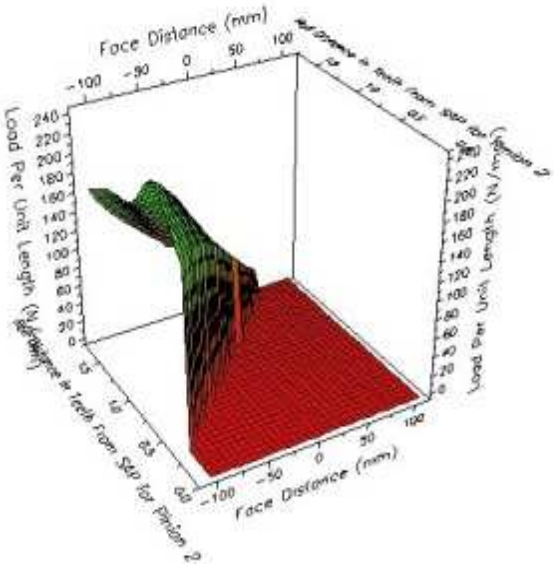

Fig.4 Load distribution for per unit length of gear

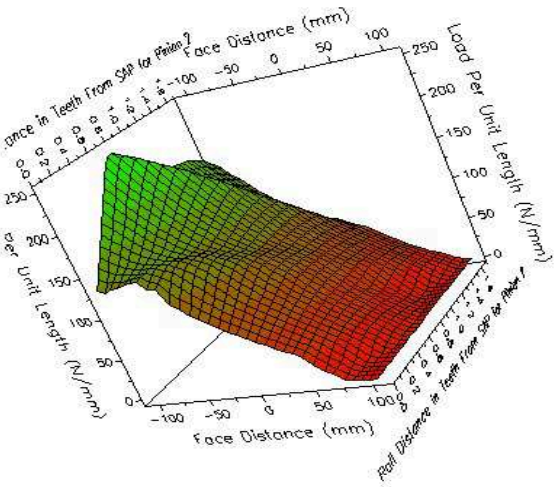

Fig.5 Load distribution after leap modification

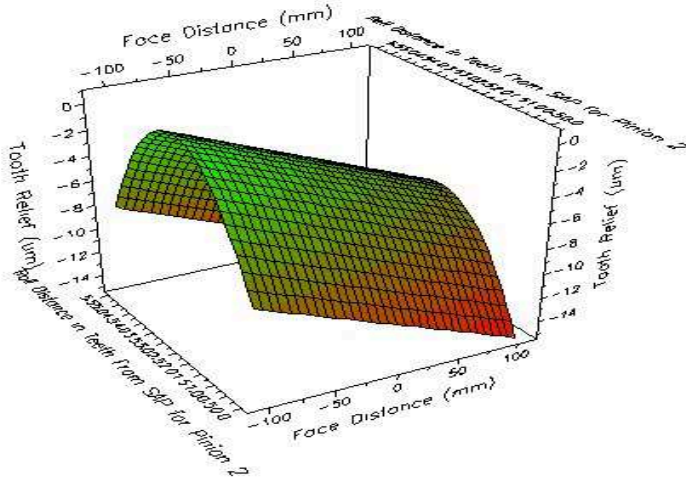

Fig.6 Conjugate mesh relief after gear modification

As seen in Fig.3, mutation of load is very obvious when gear teeth mesh each other. And thus gear involutes modification should be conducted to reduce the mutation of load. After optimization, the Optimum amount of modification is 9μm. Fig. 6 shows Conjugate mesh relief after gear modification. Gear mesh becomes very smoother transition after gear modification.

Comparison analysis of gear before and after optimization

As shown in Fig. 4, the maximum load per unit length of gear is 247 N/mm before gear modification. While the maximum load per unit length of gear is 229 N/mm after gear modification (as seen in Fig. 5). The tooth load decreases about 7.2%. There are load mutations in gear mesh before gear modification. But the gear mesh becomes smooth transition after gear modification.

Gear transmission error curve is an important index reflected the dynamic performance of the gear system. It is an evaluation index of meshing noise. Fig.7 and Fig.8 demonstrate gear transmission errors before and after modification are 0.74 and 0.19, respectively. The gear transmission error reduces approximately 74.3%. The comparison shows that fluctuation of transmission error has not eliminated after gear modification. But error range of gear transmission is significantly reduced.

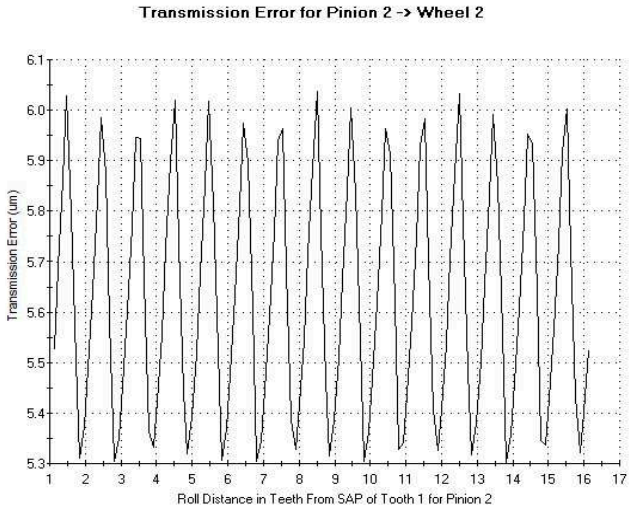

Fig.7 Transmission Errors before gear modification (6.04-5.30=0.74um）

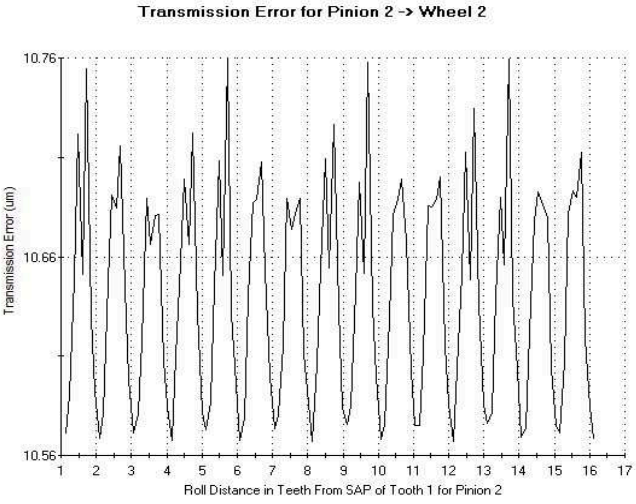

Fig.8 Transmission Error after gear modification（10.76-10.57=0.19um）

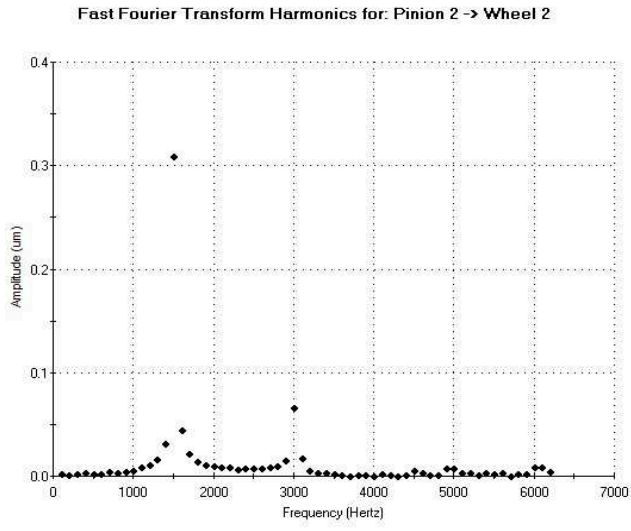

Fig.9 Fast Fourier Transform Harmonics before gear modification

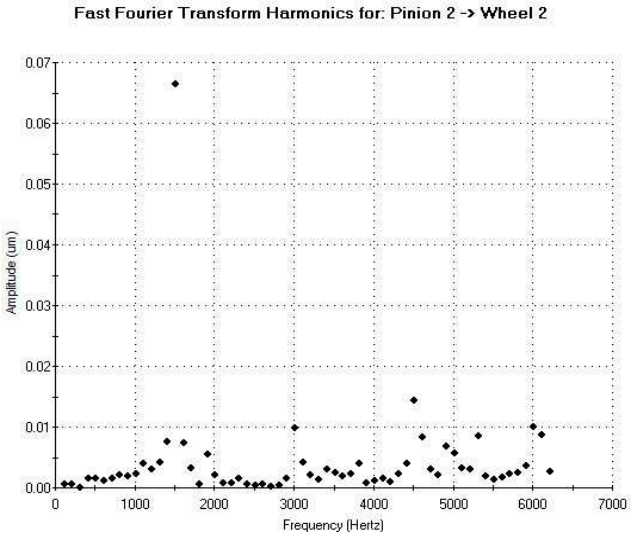

Fig.10 Fast Fourier Transform Harmonics after gear modification

The fast Fourier transform harmonics are present in Fig.9 and Fig.10 before and after gear modification. Through the observation, the Fast Fourier Transform Harmonics (i.e., evaluation index of radiation noise) are 0.31 um and 0.068 um, respectively. It decreases about 78.1%. And thus it plays an important role in improving the bearing capacity of the gear teeth and reducing the noise of gear mesh.

Conclusion

（1）The maximum load per unit length of gear reduces about 7.2% after gear modification. The load mutations in initial gear mesh can be decreased to make it become smooth transition after gear modification.

（2）After gear modification, Transmission Error of gear reduces 74.3%, and Fast Fourier Transform Harmonics decreases 77.4%. And thus it plays an important role in improving the bearing capacity of the gear teeth and reducing the noise of gear mesh.

（3）Romax Designer software can balance the load distribution of tooth surface, improve the quality of gear mesh and reduce the vibration noise of gear. It provides a new research method for gear box of wind turbine.

Acknowledgement

This work was supported by the Fundamental Research Funds for the Central Universities (Project No. XDJK2012C002, XDJK2013D015 and XDJK2011C066), the Natural Science Foundation Project of Chongqing (Project No. CSTC2011BB4013).

The first author gratefully acknowledges the financial support from the Chinese Scholarship Council (CSC).

References

[1] GWEC. Global Wind Report Annual Market Update 2013. Global Wind Energy Council. 2014.

[2] Li Junfeng Gao Hu Shi Pengfei Shi Jingli. China Wind Power Report 2007.

[3] Tugrul U. Daima, Elvan Bayraktaroglub. Optimizing the NW off-shore wind turbine design [J]. Mathematical and Computer Modelling. 2012 55(3-4) 396–404.

[4] Jing Wei, Cheng Lv, Wei Sun, Xiang Li, Yang Wang. A Study on Optimum Design Method of Gear Transmission System for Wind Turbine [J]. International Journal of Precision Engineering and Manufacturing, 2013 14(5) 767-778.

[5] Wei Sun, Tao Chen, Jing Wei. Dynamic reliability of gears in a wind turbine gearbox under the conditions of variable wind speed and small samples. Proceedings of the Institution of Mechanical Engineers, Engineers, Part C: Journal of Mechanical Engineering Science [C], 2012.

[6] Slim Soua, Paul Van Lieshout, Asanka Perera, Bryan Bridge. Determination of the combined vibrational and acoustic emission signature of a wind turbine gearbox and generator shaft in service as a pre-requisite for effective condition monitoring[J]. Renewable Energy, 2013 51 175-181.

[7] Tengjiao Lin, Runfang Li. A finite element method for 3D static and dynamic contact/ impact analysis of gear drives [J].Comp. Meth. Appl. Mech. Eng., 2007 196 (9) 1716-1728.

[8] Qin, D. T., Zhang, Z. Y., Wang, J. H. Optimization design of system parameters of the gear transmission of wind turbine based on dynamics and reliability [J]. Chinese Journal of Mechanical Engineering, 2008 44 (7) 24-31.

[9] Ambarisha, V. K., Parker, R. G. Nonlinear dynamics of planetary gears using analytical and finite element models[J]. Journal of Sound and Vibration, 2007 302 (3) 2577-595.

Advanced Materials Research Vols. 989-994 (2014) pp 2922-2925
© (2014) Trans Tech Publications, Switzerland
doi:10.4028/www.scientific.net/AMR.989-994.2922

Thermal structure coupling analysis of lathe built-in electric spindle under intermittent load

Wang Ke[1,a], Liu Jihang[1,b] , Wu Guokui[2,c] and Sun Xingwei[1,d]

[1]School of mechanical engineering, Shenyang University of Technology, Shenyang, 110870,China

[2]Liaoning Province Highway Management Bureau Kangping Office, Shenyang, 110500, China

[a]email: wk2222@sina.com, [b]email: liujihang029@sina.com, [c]email: ndcaizi@126.com, [d]email: sunxingw@126.com

Keywords: Built-In Electric Spindle; Intermittent Load; Thermal-Structure Coupling; Finite Element

Abstract. Built-in electric spindle has been the core component of machine tool, whose temperature problem is serious. Internal heat source are greatly influenced by load. Based on which has the function of automatic clipping chuck inversion type vertical lathe built-in electric spindle prototype as the research object, using the theory of thermal stress and finite element, established the intermittent load cases hot - structure coupling numerical analysis model of the electric spindle. After overall analyzing electric spindle within the transient temperature field under the action of the intermittent load, the winding temperature changing with time curve is given. On that basis, electric spindle thermal deformation has been carried on the analysis and calculation, gets the shaft extension end axial thermal deformation, provides theoretical basis for the thermal error compensation.

Introduction

With the advancement of CNC machine tools and frequency control technology, electric spindle unit has developed. Spindle performance directly affects the accuracy, stability and range of machining system and applications, thermal characteristics of which has a crucial role during processing. Electric spindle internal heating, thermal conductivity and thermal deformation mechanism doing detailed analysis and research is needed. Determine which method can be effective in calculating the temperature distribution and the spindle thermal deformation under the allowable error range, provides reference for the spindle structural design and thermal error compensation.

For spindle thermal properties of a number of scholars at home and abroad have carried out some research. Bernd Bossmanns and Jay F.Tu [1] established the overall thermal model of electric spindle from the perspective of power distribution for the first time to study the internal heat and cooling spindle forms. Bossmanns and Tu [2] further proposed the overall energy flow model of electric spindle, explaining the main heat sources of spindle system. Guo Jun et al [3] using the finite element method in thermal contact with the temperature field Electric spindle analyzed, and through experiments on the finite element analysis model was checked and verified. XU [4] have got the computational model which has been applied to a large gradient temperature field with combining of the contact thermal resistance model and finite element model. Zhang Minghua [5] conducted steady state, transient temperature field and thermal structure coupled field analysis, and used step-loaded the transient thermal analysis simulates the actual machine tool working one day, got the electric spindle temperature field changes. Holkup et al [6] established a thermal structure coupling model of electric spindle using the finite element method, the thermal structure coupling model can predict the state of the electric spindle under actual working temperature distribution, stiffness and thermal displacement and contacting load bearing through experimental verification. Stein and Tu [7] presented the dynamics digital simulation model of a spindle system from the laws of physics of heat transfer and thermal elasticity, which can be tested as part of the spindle bearing preload system. Jorgensen and Shin [8] analyzed the effect of temperature distribution on the spindle unit dynamics. Sun Min Kim [9] carried out a detailed study on thermal characteristics of

high-speed spindle bearings, got the effects of bearing preload, interference and other changes on the thermal characteristics of the electric spindle. Jenq Shyong Chen et al [10] combined the spindle bearing temperature with thermal displacement by studying the effects of thermal expansion of the spindle bearing friction heat on the spindle, and established a spindle temperature - thermal displacement models.

The calculation of those previous researching is conducted based on continuous operation spindle. The internal heat sources of continuous operation spindle is essentially constant, the temperature curve of which monotonically increasing trend. After reaching a stable temperature, all parts of the spindle thermal deformation also will be stabilized. While the internal heat source of intermittent operation lathe spindle active and passive cooling heat alternates with starting and stopping of the spindle. Internal temperature of electric spindle fluctuations wave ascend. In order to analyze the impact of its internal temperature fluctuations on the thermal deformation of the spindle structure, In this paper, after calculating whole temperature field on the spindle, the spindle thermal deformation under intermittent load conditions has been calculated using the finite element method, providing a theoretical basis for spindle temperature compensation.

Spindle structure and thermal process analysis

The typical structure of built-in spindle is showed in Fig1.

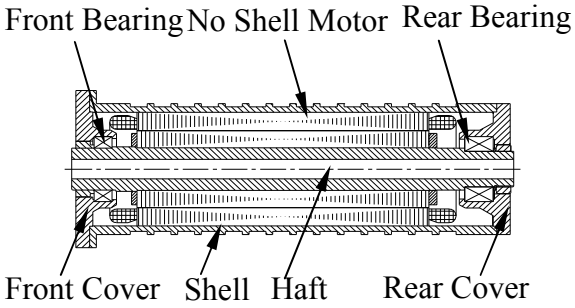

Fig. 1 Typical structure of built-in spindle

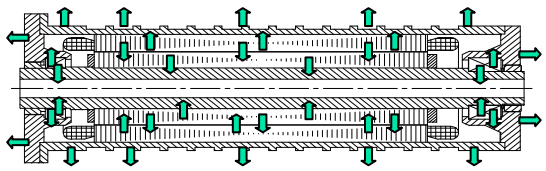

Fig.2 Thermal conduction analysis

For interior permanent magnet synchronous motor spindle systems, the most severe temperature rising of the main place are the stator and front and rear bearings three parts. Part of the heat generated in the stator heat by convection to the front and rear ends of gas passed, and the other housing part with the outside air through the stator heat convection away.There are two ways to heat the rotor: part of the cooling gas generation gap convective heat transfer; transfer to another part of the spindle. There are three ways bearing the heat: the inner part by conduction to the spindle; portion passed through the outer spindle front cover; There is another part of the gas is cooled lubricated away by convection heat transfer; Thus thermal conditions of the bearing is mainly affected the amount of oil flow and cooling gas. In addition, the spindle housing still exist with the surrounding air convection and radiation.

Heat source Analysis under intermittent load cases

Electric spindle move to the upper knife holder after gripping the work piece with power chuck and prepare for cutting. In this process, the rotor accelerated circularly and drive spindle, chuck and work piece from rest. So load of spindle is Traction coursed by Accelerated circular motion and friction of bearing. Rotor and spindle bearings to withstand gravity and preload

Axial spindle accelerates to the desired speed machining, Load only include rolling bearings friction. Screw drive spindle to do feed movement, and spindle start cutting. When cutting, spindle bearing reaction force to withstand the cutting forces, Built-in motors with increased cutting force proportional to the size of copper consumption, In this case the maximum heat for stator winding spindle. Bearing loss increased due to load bearing friction increases.

Finite element method calculations

Lathe spindle can be considered axis of symmetry from the structure and the temperature distribution. So take half spindle profiles to analyze. After simplifying the spindle thermal-structural coupled finite element analysis model was established.

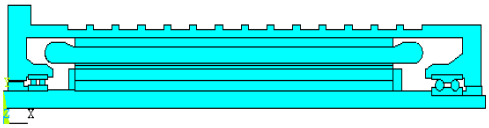

Fig. 3 Aaxial section geometry

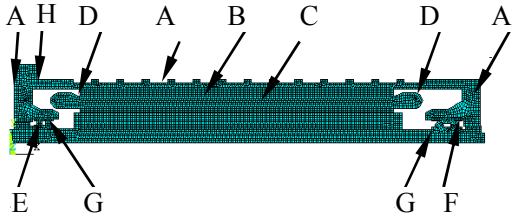

Fig. 4 Meshing and boundary conditions

The actual transfer process is simplified for the finite element model as shown in Figure 4, the winding and core spindle were imposed on copper consumption load B and iron consumption load C, Front and rear bearings apply friction heat generation E and F. Shell and convective heat transfer to the ambient air instead of A, Windings and internal air convection heat transfer to D, Bearings with internal air convection heat transfer to G. Structure boundaries, has been each part of its thermal boundary. Spindle and the base is a fixed location H, Displacement constraints imposed here.

Temperature calculation results shown in Fig. 5, 6.

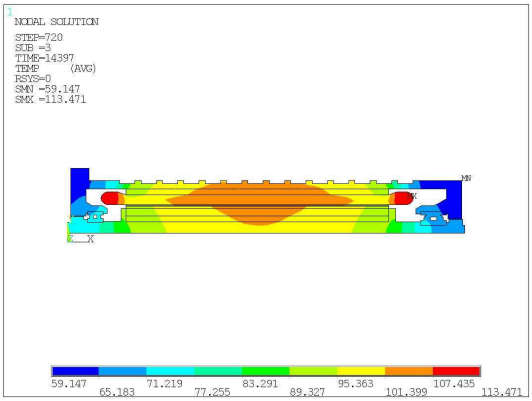

Fig. 5 Internal temperature distribution

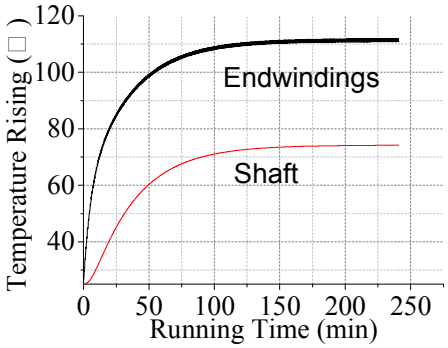

Figure 6 Temperature of winding and shaft end

The highest temperature occurs at where the shaft section end of winding, coursing poor heat transfer conditions of the end windings, External winding complex thermal insulation structure has seriously hindered the end windings. The highest part of the permanent magnet temperature is close to the outer end of the rotor, temperature reaches 110℃.

After running four hours the axial and radial displacement calculation results shown in Fig7, 8.

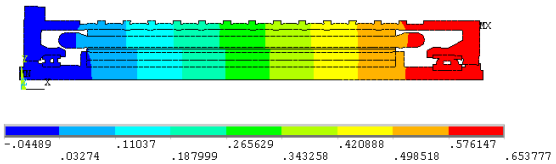

Fig. 7 Axial displacement distribution

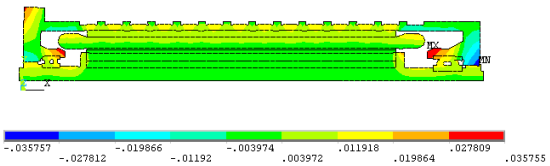

Fig. 8 Radial displacement distribution

Conclusion

Based on which has the function of automatic clipping chuck inversion type vertical lathe built-in electric spindle prototype as the research object, using the theory of thermal stress and finite element, established the intermittent load cases hot - structure coupling numerical analysis model of the electric spindle. After overall analyzing electric spindle within the transient temperature field under the action of the intermittent load, got the following conclusions：

(1) Intermittent load impact seriously on the temperature field spindle, The main factor is the intermittent heat load makes periodic changes in the state over time.

(2) Heat transfer process of active and passive heat alternate. Only the steady-state analysis of the situation when you can not meet the needs of continuous processing multiple parts spindle temperature calculation.

(3) Varying the processing temperature curve should be based compensation to reduce the error between the machine spindle multiple parts.

References

[1] Bernd Bossmanns, Jay F. Tu. A power flow model for high speed motorized spindles heat generation characterization. International Mechanical Engineering Congress and Exposition, Anaheim, CA, USA, 1998.

[2] Bernd Bossmanns, Jay F. Tu. A thermal model for high speed motorized spindles. International Journal of Machine Tools & Manufacture 1999(39): 1345-1366.

[3] GUO Jun, ZHANG Bolin, XIAO Shuhong, ZHAOHu. Research on motorized spindle's thermal properties based on thermal contact. Machine Tool & Hydraulics 2006(7)：26-30.

[4] Xu M, Jiang S Y, Ying C. An improved thermal model for machine tool bearings. International Journal of Machine Tools and Manufacture, 2007(47)：53-62.

[5] Zhang Minghua, Yuan Songmei, Liu qiang. Research on thermal characteristics for high speed motorized spindle based on finite element analysis. High Speed Mechining Technology. 2008(4)：29-32.

[6] Holkup T, Cao H, Kolar P. et al. Thermo-mechanical model of spindles. CIRP Annals Manufacturing Technology, 2010(59):365-368.

[7] J. L. Stein, J. F. Tu, A state-space model for monitoring thermally induced preload in antifriction spindle bearings of high-speed machine tools, Transactions of the ASME 1994(116):372-386.

[8] Jorgensen B R, Shin Y C. Dynamics of Machine Tool Spindle Bearing Systems Under Thermal Growth. Journal of Tribology,1997(119):875-882.

[9] Sun-min Kim, Kang-Jae Lee, Sunkyu Lee. Effect of bearing support structure on the high-speed spindle bearing compliance. International Journal of Machine Tools & Manufacture, 2002(42)365-373.

[10] Jenq Shyong Chen, Wei Yao Hsu. Characterizations and models for the thermal growth of a motorized high speed spindle. International Journal of Machine Tools & Manufacture 2003(43):1163-1170.

Advanced Materials Research Vols. 989-994 (2014) pp 2926-2930
© (2014) Trans Tech Publications, Switzerland
doi:10.4028/www.scientific.net/AMR.989-994.2926

Analysis of Impact of Driving Amplitude on Resonance Frequency of Silicon Microgyroscope

Shaodong JIANG[1, a], Yan SU[1, b], Qin SHI[1, c], Anping QIU[1, d]

[1]School of Mechanical Engineering, Nanjing University of Science and Technology, Nanjing, 210094, China

[a]email: shdjing_njust@163.com, [b]email:suyan@mail.njust.edu.cn,

[c]email:sqinhy@mail.njust.edu.cn, [d]email:apqiu@mail.njust.edu.cn

Keywords: Silicon Microgyroscope; Driving Amplitude; Resonance Frequency; Nonlinear

Abstract. Increasing the driving amplitude could improve the sensitivity of silicon microgyroscope, which is the effective way to enhance the performance of gyroscope. However the large driving amplitude leads to the nonlinear effect. As a result, the resonance frequency is dependent with the driving amplitude, which influences the frequency stability of gyroscope. The equivalent model of driving beam is established, and the stiffness formulas of driving beam are derivated according to the large deflection theory. The linear stiffness of driving beam is 270.1N/m and the nonlinear stiffness is 3.237×108N/m^3, which are 2.7% and 6.4% different from the simulative results. Harmonic balance method can be used to establish the relationship between driving amplitude and resonance frequency. The theoretical analysis results are carried out compared with the simulative analysis results. Also the impact of driving amplitude on resonance frequency is confirmed by experiment test. This paper is significant for improving the frequency stability, and provides a theoretical basis for optimizing the structure of gyroscope.

Introduction

The development of silicon micro-gyroscope offers improvement in cost, size, and ruggedness relative to traditional gyroscope. Thus the silicon micro-gyroscope has a large potential for different types of application, such as navigation, positioning, stabilization, and guidance[1]. Faced to the requirements of high precision applications, the development of high performance silicon microgyroscope is in urgent need. Increasing the driving amplitude is an effective way to improve the performance of gyroscope, which could improve the sensitivity of silicon gyroscope. However the large driving amplitude leads to the nonlinear effect. As a result, the resonance frequency is dependent with the driving amplitude, which influences the frequency stability of gyroscope[2]. The research on frequency stability mainly focused on the temperature characteristic of resonance frequency[3-4]. But the research on impact of driving amplitude on the resonance frequency is rarely reported.

Firstly, the equivalent model of driving beam is established, and the stiffness formulas of driving beam are derivated according to the large deflection theory. Secondly, harmonic balance method is used to establish the relationship between driving amplitude and resonance frequency. Lastly, the impact of driving amplitude on resonance frequency is confirmed by simulation and experiment test.

Theoretical Analysis

Equivalent model of driving beam. The shape of driving beam is U-beam, and a U-beam can be seen as two constrainted cantilevers in series[5]. The schematic of the constrainted cantilever beam is shown in Fig.1(a). A torque M_0 and a force F_x are applied at B, and C is the center of the beam. According to the energy theorem[6], the rotational angle at B is

$$\theta_B = \int_0^L \frac{F_x x + M_0}{EI} dx = \frac{F_x L^2/2 + M_0 L}{EI} \tag{1}$$

where E is the Young's modulus, $I=h^3b/12$ is the moment of inertia. L, h, b are the length, width, and thickness of the beam, respectively. According to the boundary condition, $\theta_B=0$. So the displacement and rotational angle at C are

$$\delta_c=\int_{L/2}^{L}\frac{(F_x x+M_0)(x-\frac{L}{2})}{EI}dx=\frac{F_x L^3}{24EI},\quad \theta_c=\int_{L/2}^{L}\frac{F_x x+M_0}{EI}dx=\frac{F_x L^2}{8EI} \tag{2}$$

Meanwhile, according to the moore integration, the displacement and rotational angle of the cantilever, as shown in Fig.1(b), are

$$\delta_{canti}=\int_0^{L/2}\frac{F_x x^2}{EI}dx=\frac{F_x L^3}{24EI},\quad \theta_{canti}=\int_0^{L/2}\frac{F_x x}{EI}dx=\frac{F_x L^2}{8EI} \tag{3}$$

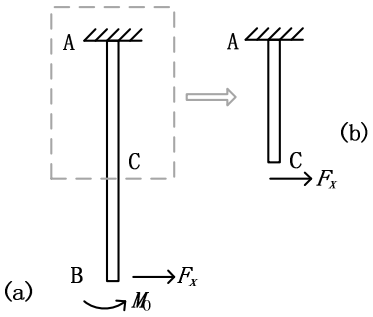

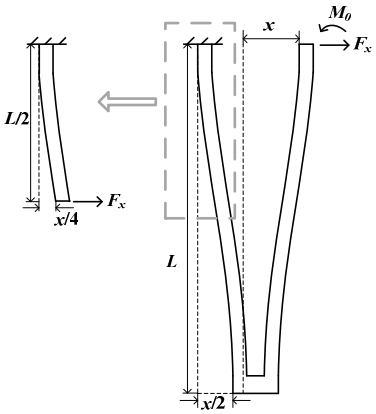

Fig.1 Schematic of constrainted cantilever beam Fig.2 Schematic of equivalent model of driving beam

Contrast Equ.(2) and Equ.(3), the rsults are the same. So four series of cantilevers can be used to take the place of a driving beam. The relationship of the displacement and force are shown in Fig.2.

Nonlinear stiffness of driving beam. The cantilever AC(as shown in Fig.1) is deflective largely under the force F_x. The end of cantilever moves from C to C′, as shown in Fig.3. θ_C is the rotational angle, and δ_h, δ_v are the horizontal and vertical displacement, respectively.

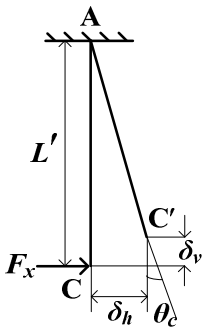

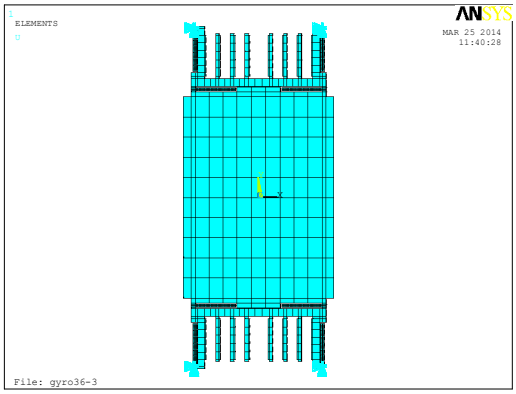

Fig.3 Large deflection of cantilever beam Fig.4 Meshed model of silicon microgyroscope

According to the large deflection theory of beam[7], θ_C, δ_h and δ_v are

$$F(k)-F(k,\phi)=\sqrt{\frac{F_x L'^2}{EI}},\quad \frac{\delta_h}{L'}=1-\sqrt{\frac{4EI}{F_x L'^2}}[E(k)-E(k,\phi)],\quad \frac{\delta_v}{L'}=1-\sqrt{\frac{2EI\sin\theta_b}{F_x L'^2}} \tag{4}$$

where $F(k)=\int_0^{\pi/2}\frac{dt}{\sqrt{1-k^2\sin^2 t}}$, $F(k,\phi)=\int_0^{\phi}\frac{dt}{\sqrt{1-k^2\sin^2 t}}$, $k=\sqrt{\frac{1+\sin\theta_b}{2}}$, $\phi=\arcsin\frac{1}{k\sqrt{2}}$. $F(k)$ and $F(k,\phi)$ are the elliptic integral of the first kind.

$E(k)=\int_0^{\pi/2}\sqrt{1-k^2\sin^2 t}\,dt$, $E(k,\phi)=\int_0^{\phi}\sqrt{1-k^2\sin^2 t}\,dt$. $F(k)$ and $F(k,\phi)$ are the elliptic integral of the second kind.

Because the transcendentality of Equ.(4), the iterative method is used to obtain the relationship between $F_x L'^2/EI$ and δ_h/L'. The specific precess is: 1. Set initial value to θ_c($0°<\theta_c<90°$); 2. Solve k; 3. Solve ϕ; 4. Solve $F(k)$ and $F(k,\phi)$; 5. Solve $F_x L'^2/EI$.

According to the solving program of elliptic integral[8], the program of obtaining the relationship between $F_x L'^2/EI$ and δ_h/L' is achieving by C++. One hundred sets of $F_x L'^2/EI$ and δ_h/L' are outputted by the program. Then the curve fitting is achieving by matlab.

$$\frac{F_x L'^2}{EI} = 3\frac{\delta_h}{L'} + 3.15\left(\frac{\delta_h}{L'}\right)^3 \tag{5}$$

Equ.(5) can be written as $F_x = k_{c1}\delta_h + k_{c3}\delta_h^3$, $k_{c1} = 3EI/L^3$ is the linear stiffness of the cantilever, $k_{c3} = 3.15EI/L'$ is the nonlinear stiffness. According to Fig.2, $\delta_h = x/4$, $L' = L/2$.

$$F_x = \frac{6EI}{L^3}x + \frac{1.575EI}{L^5}x^3 \tag{6}$$

where $k_{u1} = 6EI/L^3$ is the linear stiffness of the driving beam, $k_{u3} = 1.575EI/L^5$ is the nonlinear stiffness.

Impact of driving beam on resonance frequency. The motion equation of the mass under the harmonic driving force is

$$M\ddot{x} + C\dot{x} + K_1 x + K_3 x^3 = F_x \sin\omega t \tag{7}$$

where C is damping coefficient, ω is the frequency of driving, and K_1=4k_{u1}, K_3=4k_{u3}. Assuming the solution of Equ.(7) is $x(t) = X_m \sin(\omega t - \varphi)$. According to the harmonic balance method[9],

$$X_m = \frac{F_x / M}{\sqrt{\left(\omega_n^2 - \omega^2 + \frac{3}{4}\frac{K_3}{M}X_m^2\right)^2 + \left(\frac{C\omega_n}{M}\right)^2}} \tag{8}$$

So the resonance frequency when the amplitude is the largest is

$$\omega^2 = \omega_n^2\left(1 + \frac{3}{4}\frac{K_3}{K_1}X_m^2\right) \tag{9}$$

Taylor expansion can be used to obtain the approximate relationship between the amplitude and resonance frequency.

$$\omega \approx \omega_n\left(1 + \frac{3}{8}\frac{K_3}{K_1}X_m^2\right) \tag{10}$$

The resonance frequency shifts with the change in driving amplitude, and the shift value is approximate linear with the square of the amplitude. As the amplitude increases, the effect of nonlinearity on the resonant frequency can not be ignored.

Simulative Analysis

ANSYS is used to analyse the motion of the gyroscope. The meshed modal of the gyroscope is shown in Fig.4. All the degrees of freedom on the ends of driving beams are constrained. The different displacements along X axis are applied on the mass. And the displacements along Y axis and Z axis are set zero. The large deformation option is opened, and the reaction forces of one driving beam are extracted with FSUM command. The simulative result is shown in Fig.4. The simulative values of stiffness of the driving beam are obtained by matlab fitting. Both the theoretical values and the simulative values are listed in Tab.1

Tab.1 Theoretical and simulative results of stiffness of driving beam

Stiffness	Theoretical Value	Simulative Value	Error
k_{u1}(N/m)	270.1	263.1	2.7%
k_{u3}(N/m^3)	3.237×10^8	3.458×10^8	6.4%

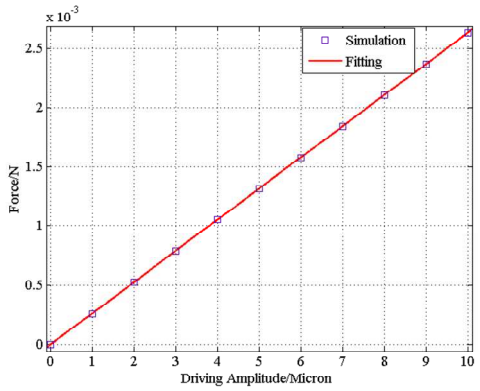

Fig.5 Simulative results of stiffness of driving beam

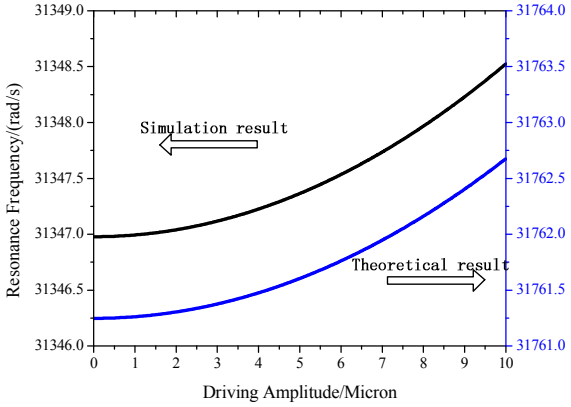

Fig.6 Theoretical and simulative results of impact of driving amplitude on resonance frequency

According to Equ.(10), the simulative result of the impact of driving amplitude on resonance frequency can be obtained, as shown in Fig.6. The theoretical result is validated by the simulation.

Experimental Analysis

The gyroscope is driven in open-loop mode. The driving DC bias voltage V_d is 15V, and set the amplitudes of driving AC voltage V_a are 20mV, 40mV and 60mV respectively. The signal source is used to sweep the frequency of V_a. Meanwhile, the driving-sensing voltage is recorded, as shown in Fig.7.

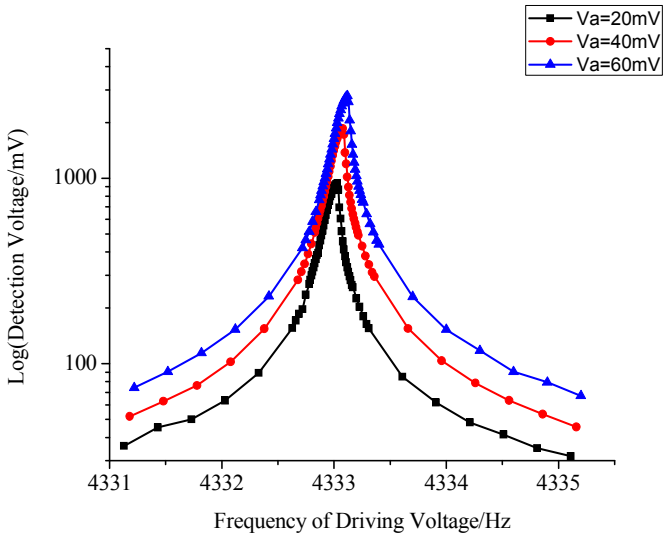

Fig.7 Amplitude-frequency characteristics of driving detection signal with different driving AC voltage

As seen in Fig.7, at the same frequency, the driving-sensing voltage increases when V_a is increased. The resonance frequencies of gyroscope increases with the increase of driving amplitude. The impact of driving amplitude on the resonance frequency is validated by the experiment.

Conclusion

The equivalent model of driving beam is established in this paper, and the stiffness formulas of driving beam are derivated according to the large deflection theory. The linear stiffness of driving beam is 270.1N/m and the nonlinear stiffness is $3.237\times108\text{N/m}^3$, which are 2.7% and 6.4% different from the simulative results. The theoretical formulas are verified by the simulation. Harmonic balance method is used to establish the relationship between driving amplitude and resonance frequency. The resonance frequency shifts with the change in driving amplitude, and the shift value

is approximate linear with the square of the amplitude. The theoretical and simulative reults of the impact of driving amplitude on the resonance frequency are given, and the impact is validated by the experiment. This paper is great significance for improving the frequency stability of the gyroscope, and can provide practical guidance and theoretical basis for design and optimization of the gyroscope.

Acknowledgments

This work was supported by the Jiangsu Research and Innovation Program (No. CXZZ13-0197).

References

[1] Alper S E, Temiz Y, Akin T, "A compact angular rate sensor system using a fully decoupled silicon-on-glass MEMS gyroscope," Microelectromechanical Systems, Journal of, vol. 17, pp. 1418-1429, 2008.

[2] Kaajakari V, Mattila T, Oja A, et al. Nonlinear limits for single-crystal silicon microresonators[J]. Microelectromechanical Systems, Journal of, 2004, 13(5): 715-724.

[3] Feng R, Qiu A P, Shi Q, et al.. Temperature characteristic of natural frequency of double-mass silicon micro-mechanical gyroscope[J]. Journal of Nanjing University of Science and Technology, 2013, 37(1): 94-100.

[4] Trusov A A, Schofield A R, Shkel A M. Performance characterization of a new temperature-robust gain-bandwidth improved MEMS gyroscope operated in air[J]. Sensors and Actuators A: Physical, 2009, 155(1): 16-22.

[5] Jiang S D, Qiu A P, Shi Q, et al.. Calculation and Verification of Quadrature Coupling Coefficient of Silicon Microgyroscope [J]. Opt. Precision Eng., 2013, 21(1): 87-93.

[6] Liu H W. Mechanics of Materials Ⅱ (Fourth Edition) [M]. Beijing: Higher Education Press, 2004.

[7] Gere J M, Timoshenko S P. Mechanics of materials [M]. CA: Cole Pacific Grove, 2001.

[8] Xu S L. C Algorithm Assembly(Second Edition) [M]. Beijing: Tsinghua University Press, 1996.

[9] Liu Y Z, CHEN L Q. Nonlinear Vibrations [M]. Beijing: Higher Education Press, 2001.

Advanced Materials Research Vols. 989-994 (2014) pp 2931-2934
© (2014) Trans Tech Publications, Switzerland
doi:10.4028/www.scientific.net/AMR.989-994.2931

Research on Credit Evaluation and Verification Model in Equipment Manufacture Industry

Lifeng ZHAO[1, a], Shenghan ZHOU[2, b]

[1]School of Economics and Management, Beihang University, Beijing, 100191, China

[2] School of Reliability and System Engineering, Beihang University, Beijing, 100191,China

Email:ZhouSH@buaa.edu.cn

Keywords: Credit Evaluation; Vague Set; Factor Analysis; Structural Equation Model

Abstract. The paper aims to develop the credit evaluation and verification model in equipment manufacture industry. The study defines the vague set of linguistic variable firstly. Then the calculation rules are defined with the vague set. The research uses the expert subjective judgment to build the initial evaluation model. And the relevant 128 data items are collected by survey. These items are used to make factor analysis to test the structure of the evaluation system and build the initial SEM. The result of SEM shows the possible modification. Finally, the empirical research is given to verify the developed approach.

1. Introduction

The equipment manufacture industry is the important part of national economy. In traditional, most of the Chinese equipment enterprises are state owned. And most of the equipment R&D projects are developed by investment of state. The target customers are often allocated by the authority sectors in advance. So the assets of project should be managed by State property management sectors. And the profit of the project should belong to the state. The Relationships among the enterprise, the management sector and the target customers have not the simple link of business transactions but the co-operational partners shared with common interests. However, the enterprises may have their own position and interest though it is state owned. The enterprises don't want to the target customers or state sectors know the details about their technology level, finance status and management method for their own benefit. In fact, it is difficult to the target customers to get hold of the real status of the enterprise [1]. The past research shows that many manufacture resource was wasted [2]. And the authority sectors lack detection methods to evaluation the equipment enterprises [3].

To analyze the real status of the manufacture industry for the management sectors, it is required to establish the credit evaluation system of the enterprises. The enterprise credit is used to describe the compliance capabilities and financial level. At first, the credit level mainly refers to the commercial credit. Then it became an important indictor to all of the investors. In manufacture industry, the credit level describes the debt affordability, service level and compliance capability of the enterprise.

The past researches often build the evaluation system with subjective method or objective method. Tian Fei believe each of methods presents advantages and disadvantages [4]. So he suggests that the different method should be applied to make a balance. The research builds the initial evaluation model with the fuzzy evaluation method firstly. This model is mainly developed by the experts' expertise and judgment. The evaluation index system and procedure are two core factors of credit evaluation standardization. Then the research verifies the system with the structural equation model. The structural equation model may suggest the Modification of the evaluation system [6]. Finally, the empirical research suggests it is an efficient method.

2. Basic Definitions

Definition 1: Set U is the universe of discourse, the element x belong to U, the vague set in U is a couple membership function $t_A(x)$, $f_A(x)$. The membership function meet the following requirements[5]:

1) $t_A(x) \to [0,1], f_A(x) \to [0,1]$; (1)

2) $0 \le t_A(x) + f_A(x) \le 1$ (2)

The $t_A(x)$ is called true membership function, the $f_A(x)$ is called false membership function, the $\pi_A(x) = 1 - t_A(x) - f_A(x)$ means the hesitate level.

Definition 2:Let Comparison linguistic variable P={xj}, xj=[ti, 1-fi], j is odd number and j>1, i=1,2,…,j. the Comparison linguistic variable follow the below rule:

1) If i≥k, then ti≥tk , it means that ti gets the higher degree of membership on xj than tk;
2) The comparison linguistic variable is transformed into triangular fuzzy number, and the interval number is defined as λ-cut sets of triangular fuzzy number.
3) Abstention part π_{ij} of linguistic variable rise from both ends to midrange, but it is zero in the midpoint. i.e., the interval number of 7 level linguistic variables is given by Table I(λ=0.5).
4) Set U is the universe of discourse, the linguistic variable x display a couple membership function t_{ij} , f_{ij} , let $a_{ij} = [t_{ij}, 1 - f_{ij}]$, $t_{ij} \to [0,1]$, $f_{ij} \to [0,1]$, $0 \le t_{ij} + f_{ij} \le 1$,then the vague set in U, the vague set of 7 level comparison linguistic variables is defined as Table II.
5) Abstention part π_{ij} of linguistic variable rise from both ends to midrange, but it is zero in the midpoint. Miller (1956) believes the human beings have a limited capacity to work simultaneously with more than nine categories [6]. So the most common used linguistic variable is defined no more than 9 levels.

3. Credit Evaluation and Verification

The research builds the initial credit evaluation model with fuzzy method. The mainly steps as below:

Step 1: Get the linguistic variable of evaluation index by the classic expert judgment;

Step 2: Transform the linguistic variable to the vague based on the former definition;

Step 3: Calculate fuzzy weight of evaluation index based on the complementary judgment matrix and it's calculate rules;

Step 4: Get the α cut set of the fuzzy weight set, and take it as the initial path coefficient of the credit evaluation model.

Then the study investigates relevant data of evaluation factors and makes the factor analysis. The factor analysis is used to test the structure of evaluation system. An initial structural equation model (SEM) was built based on the result of factor analysis. The structural equation model is used to explore the real relationship between the different variables. The SEM builds a $p \times p$ sample covariance matrix with the P observations of N samples to test the relationship between the different variables.The model can be solved with the below equation set[7]:

$$X = \Lambda_x \xi + \delta \quad (3)$$

$$y = \Lambda_y \eta + \varepsilon \quad (4)$$

$$\eta = B\eta + \Gamma\zeta + \zeta \quad (5)$$

The B and Γ are path coefficients, the B suggest the relationship between the endogenous latent variable, and Γ is the influence of exogenous latent variable to the endogenous latent variable. ζ is the error item. The test indictor may give the possible modification of the evaluation model.

4. Empirical Research

The authorities take moves to boost the national economy with a revitalization plan in 2008 global financial crisis. The authority sectors decided some equipment R&D projects to response to the crisis. The management sector tried to build evaluation system to analyze the status of these enterprises which take part in the plan. The credit evaluation and verification is the important part of this system. The authority sector wants to know the status of the compliance capabilities, product quality, after-sale services and financial level through the study.

They studied a random group of 31 enterprises from these equipment enterprises which take part in revitalization plan. The 25 experts give their personal evaluation based the way shown in basic definitions. The group calculates the final result with the method defined in former paragraph. The result of weight is in the table 1 and fig 2.

Table 1 Weight assigned by Experts

Index	*Fuzzy Weight*	*Classic Weight*
Customer Satisfaction	(0.44, 0.61, 0.79)	0.615
Qualification	(0.56, 0.74, 0.88)	0.733
Past Production Level	(0.73, 0.93, 1.00)	0.901

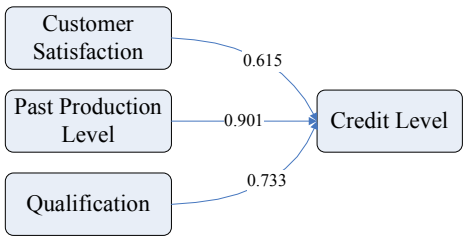

Fig. 2. Credit level Evaluation Model

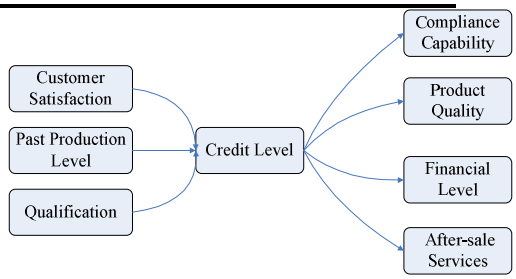

Fig. 3. Initial Credit level Model

Then the research investigated the data of 128 items. These items involved with past compliance capabilities, quality, customer service and financial level. And the study group developed an analysis model for credit level with factor analysis. The Kaiser-Meyer-Olkin，KMO value(0.805) suggests is fit for factor analysis[8][9]. The result of factor analysis show the 128 items belong to four factors. All Cronbach's Alpha of four factors are bigger than 0.90, it means acceptable reliability [10]. The research names the four factors as compliance capability, product quality, after-sale services and financial level factor. The initial model is given in fig 3.

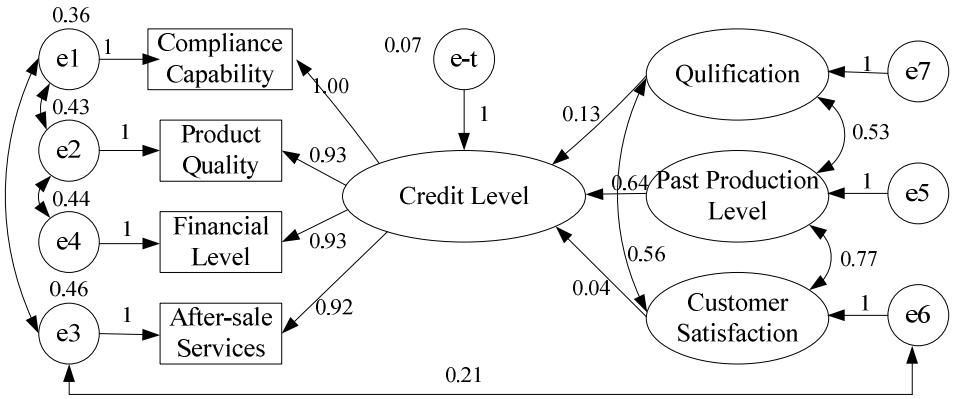

Fig. 4. Modification Credit Evaluation System

The study verifies the initial model with structural equation model. The structural equation model result suggests the possible modification of the evaluation system. The path coefficient is in the fig 4.

5.Conclusion

This paper investigates equipment enterprise credit evaluation problems with fuzzy expert judgment and survey information. We first define the vague set of linguistic variable and its calculation rules. Then the research makes the factor analysis to build the initial evaluation model. With the result of factor analysis, a structural equation model was built to test the path coefficients. The result of the SEM shows the possible modification. Finally, the empirical research is given to verify the developed approach.

Acknowledgement

The authors wish to thank Professor Wei Fajie. The paper is supported by the Fundamental Research Funds for the Central Universities and the Technical Research Foundation. The study is also sponsored by the National Natural Science Foundation of China (Grant No. 71271014).

References

[1] Wen Zi.The Research of purchaser and supplier's relationship management summary [D].Hefei: Hefei University of Technology, 2010.

[2] Xu Chunyu. Study on Supplier Management in equipment Acquisition [D].Changchun: Jilin University, 2006.

[3] Wu Hongtao. A Study on the Building of Trust Mechanism in China's Government Procurement [D].Soochow University, 2013

[4] Tian Fei. The Construction of Social Indicator System with Structure Equation Modeling Technology [J]. Journal of Anhui University(Philosophy & Social Sciences), 2007，31(6): 92-95

[5] Zhou Shenghan and Chang Wenbing. Extended linguistic variable based on the modified words [J]. Dalian, China: Trans Tech Publications, 2012.

[6] G.A.Miller. The magical number seven or minus two: some limits on our capacity of processing information [J]. Psychological Rev, No 63:81-87,1956

[7] Feng Xiuqin, et.al. The customer satisfaction evaluation of mobile industry based on multilevel structural equation model [J], Grey Systems and Intelligent Services, 2009. GSIS 2009: 947-951

[8] Y.L. Yi, Q. Z. and Q.D. Pan., "The Research of Custom Satisfactory Evaluation in Enterprise Based on the Artificial Neural Network" Value Engineering, No.10, pp. 89–91. Dec., 2006.

[9] J.H. Geng, et al, Community Satisfaction Evaluation System's Research Based on AHP and Factor Analysis[J], Journal of Systems & Management, vol. 16, No. 6, pp. 673–677. Dec., 2007.

[10] Victor A, et al, A Scenario Based Assessment Model: SBAM [J]. Technological Forecasting and Social Change, In Press, Corrected Proof, Available online 12 September 2006.

Advanced Materials Research Vols. 989-994 (2014) pp 2935-2938
© (2014) Trans Tech Publications, Switzerland
doi:10.4028/www.scientific.net/AMR.989-994.2935

The Improvement for the Stuctrue of the Coil Transporters and Its FEA

Qi WANG[1, a] ,Yan SUN*[1,b] , Zhe LI[1, c] , Xuanqian PENG[1,d] ,Bing HAN[1, e]
[1]School of Mechanical Engineering & Automation, University of Science and Technology Liaoning, Anshan, 114051, China
[a]email:1054076062@qq.com,[b]email:sunyan20000@163.com [c]email:413030438@qq.com,
[d]email:1915527827@qq.com, [e]email:hanb75@126.com

Key words: coil transporters; running mechanism; lifting device; guide pulley

Abstract. Coil transporters are widely used in rolling production line to transport coils among different positions. Aiming at the inaccurate parking space, low production efficiency, high requirement of working accuracy, inconveniency in repair and other problems during the working process, the running mechanism and lifting gear of the coil transporter have been improved, And the author analyze the structure of the improved body by FEA. The results of the analysis of car body show that strength and stiffness meet the requirements. The general property of the improved coil transporter has been, in a good condition, effectively bettered. It can meet the production requirement and enhance the economic benefits.

Introduction

The development of steel rolling production depends not only on the increasing speed of the main equipment of steel rolling and shortened rolling cycle, but also largely on the continuous improvement and enhancement of the auxiliary equipment of steel rolling production. As an important auxiliary equipment of steel rolling, coil transporter whose performance directly affects the quality of the coil and the production efficiency of the unit is widely used in steel rolling production line and used for different location between the transmission coil. Therefore, improving the structure of the coil transporter is particularly important. It aims at increasing the operation efficiency of the production, reducing the maintenance cost, and improving the iron and steel enterprise economic benefits.

The current situation of traditional coil transporter

Traditional coil transporter is composed by walking track, running mechanism, lifting gear, hydraulic system and the energy chain. Walking track is made by two stell tracks which is attached at the bottom of the fixed platform. It is also the support rails of the framework's horizontal motion. Framework is composed by lifting frame, car body, wheel assembly, and lifting hydraulic cylinder. lifting frame is welding structure with 4 guide pillars. Car body is also a welding structure equipped with 4 guide sleeve. Lifting hydraulic cylinder installed is in the central part of the framework. Four wheels are installed on the car body convenient for the car to walk on the orbit.

Running mechanism can promote the coil car do horizontal motion in orbit working with ac motor via a reducer, coupling two wheels. The distance is measured by the proximity switch trip. Due to the low power of the torque in the coil transporter and the walking system, the existing steel coil transporter is driven by concentrated form[1]. The travel mechanism of steel coil transporter is shown in figure 1.

Lifting device is driven by hydraulic cylinder. When hydraulic cylinder drives the lifting body up and down, 4 guide sleeve and 4 guide posts make relative movement in the vertical direction. In this way, the movement not only plays a guiding role, also controls the accuracy of vertical movement. The cooperation of guide sleeves and guide columns adopts automatic lubrication by concentrated dry oil. At the same time, movement distance is measured by the proximity switch. The lifting device of the steel coil transporter is shown in figure 1.

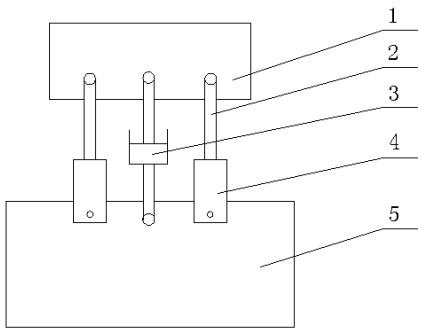

1- Motor 2-coupler 3 –Reducer
2- 4-Transmission 5-Active wheel

a. Running mechanism

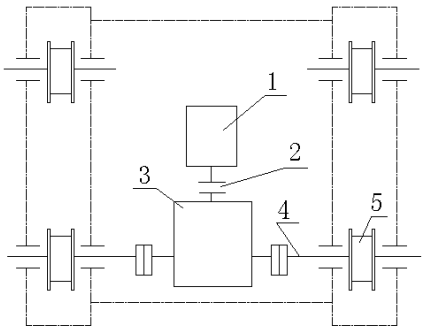

1-The lifting body 2-Guidepost 3-Hydraulic cylinder 4-Guide sleeve 5-Car body

b. Lifting device

Fig. 1 The schematic diagram of the original running mechanism and lifting device

Common problems and their causes in the coil transporter working process

Common problems and their reasons in the running mechanism working process

Problems often appear in the working process, like the wheel sliping, inaccurate parking position, and the strong impact when workers start and stop the machines. The reasons are: the traditional coil transporters are driven by the wheels, and the wheels are driven by motor and the gear reducer. Transporters walk and brake relying on the friction between the wheel and rail car. After a period of working, the wheels wear, and the surface become smooth, which lead to the reduction of the friction. Because of the relative sliding between rails and wheels in the braking process, wheels will slip on the surface of the rails, resulting in the inaccurate parking positions[2]. In addition, the transporters that are driven by a motor are easy to get strong impact when workers start and stop them. The traditional steel coil transporters are parked by the proximity switch to control positioning, so after a period of time, due to the deformation of the guide rails, the proximity switch can't be connected with signal part, which also leads to the same problem.

Common problems and their causes in the lifting device working process

The lifting device often have serious problems, like serious friction in the guide structure, high precision in manufacturing, inconvenient repair, high processing cost, and low productivity. The reasons are: The lifting frame driven by the hydraulic cylinder moves up and down, 4 guide sleeve and 4 guide columns relatively moves in the vertical direction[3], therefore the high manufacturing precision and the rigidity of the guide columns and guide sleeves are highly required. The guide columns will shake when rising. Imprecise-produced guide columns and guide sleeves or bad surface lubrication in the work process can cause serious friction loss on contact surface, can consume extra energy, and can influence the efficiency of rolling production. And, the guide columns and the guide sleeves need larger space. Once they are in trouble, it is not convenient to detect and repair. If bigger problems appear, artifacts are needed, which greatly increases the cost and reduces economic benefits.

The improvement of the structure and its effects

The improvement of the running mechanism

The original running mechanism is connected with the wheel by a motor, a reducer and a coupler, driving wheels and the car. After the improvement, the gear driven by the hydraulic motors, through the meshing of the gear and the walking track below the fixed rack, the gear shaft and the body rotate which can drive the carriage walk. In this process, wheels are passively driven. The accuracy of gear shaft position can make sure the right position of the transporters. At the same time, the gear is connected with the encoder, which means that parking position is controlled by the encoder, and that the car can be parked in the right position for a long time only after one adjustment in the process of operation. Precision is guaranteed. At the same time, the running mechanism is driven by a hydraulic motor, without any impact when working. The improved steel roll running mechanism of transporters is shown in figure 2.

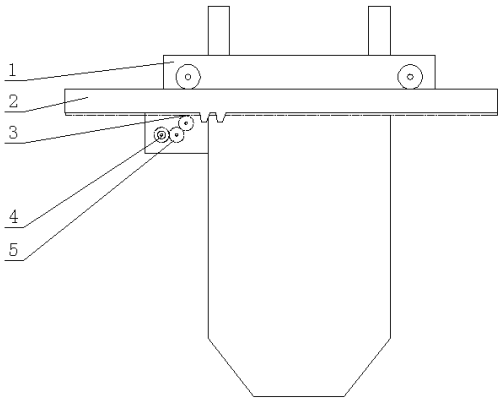

1-Car body 2-Rack 3-Gear rack transmission
4-Motor 5-Gear meshing transmission

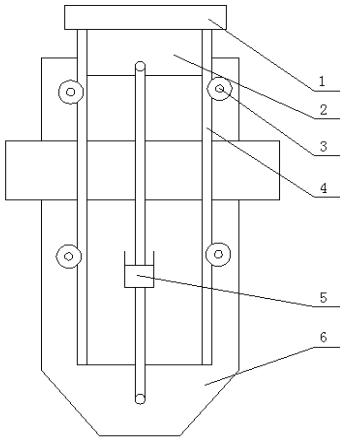

1-The saddle 2-Lifting frame body
3-Guide wheel 4-Steering column
5-Hydraulic cylinder 6-Car body

a. Running mechanism b. Lifting device

Fig 2 The schematic diagram of the improved running mechanism and lifting device

The improvement of the lifting device

The original lifting device is guided by guide posts and the guide sleeve, improved device is only guided by the guide wheel. They have simpler structure, low requirement for machining precision. The lifting frame works more stably, reduces the shaking, is easily repaired , and is conveniently removed and replaced, which save equipment maintenance time and improve the car online operation rate. At the same time, the proximity switch detecting the lifting frame position is changed to the encoder that can more accurately position. After the improvement, the steel coil lifting device of transporters is shown in figure 2.

The analysis of the coil transporter

After the improvement of the coil transporters, the running mechanism and the lifting device structure has changed greatly, leading to the structure of the car body' changes. When working, the car body bears the steel coils, lifting frame, the saddle. So it is necessary to analyze the strength of the structure of car body. In this paper, the model was established by Solid-Works software. The author simplifies the model, deleting the features which have no or few effects on the practical issues, such as some smaller hole thread structure. This way can reduce the number of features of model[4]. The Solid-Works model is imported into ANSYS software. The car body is analyzed and calculated by ANSYS software, so as to obtain the stress and deformation data when the car body bears the steel coils, and to test whether they meet the requirements.

The whole car body is made by Q235B carbon steel, whose elastic modulus is 210 gpa, poisson ratio is 0.3, the density of 7850 kg/m3, and the yield limit of 235 MPa[5]. The coil weighs 25 tons. The car body, the lifting parts, the saddle totally weighs 6000 kg. Using solid45 hexahedron unit in the ANSYS to proceed the free meshing the model.Impose all constraints on the surface of the four cylindrical holes' inner surface of the wheels in the car body. In the working process, the total weight of the steel coil, the transporter, the lifting parts, and the saddle loads on the lower surface of the hydraulic cylinder in the transporter. Through finite element analysis, the equivalent stress distribution chart is shown in picture 3. According to the picture, welded stress value is bigger on the position of the holes in the transporter and on the connected position of the horizontal plates and vertical plates, the maximum stress being 102 MPa. As we can see, the maximum stress of car-body is less than the material yield limit in the process of lifting steel coil, satisfying the requirement of static strength. Displacement nephogram is shown in picture 3. The picture shows that the maximal displacement deformation of the transporter occurs connected part between the body and the lift hydraulic cylinder, the maximum being 0.114 mm. The tiny deformation has no effect on the normal work of the steel coil transporter. Stiffness also meets the requirements.

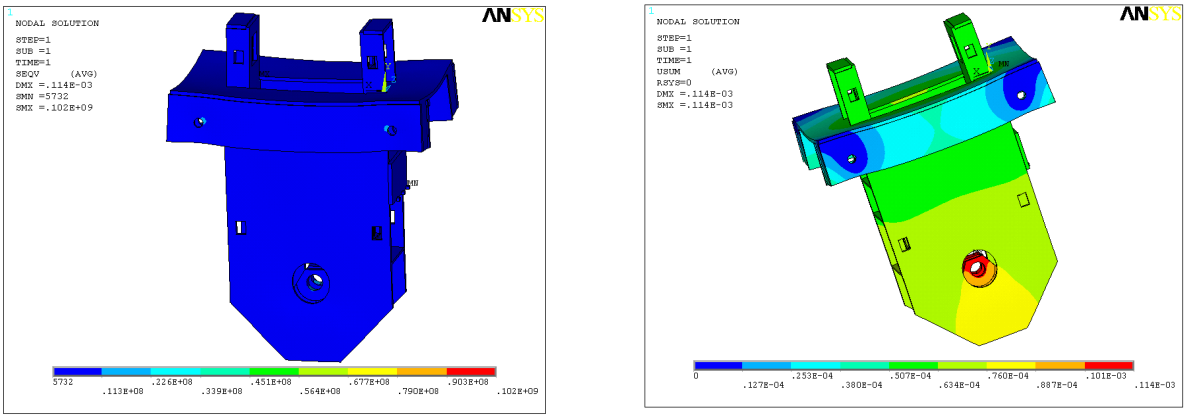

a. Equivalent stress distribution nephogram b. Displacement nephogram

Fig 3 Equivalent stress distribution nephogram and displacement nephogram of the car body

Conclusion

1) The improved steel coil transporter, proved by simulation use, can completely meet the needs of production. Compared with the old machine, the improved structure is simpler, has no impact on the brake, runs more smoothly, positions more accurately, maintain more conveniently. It can really achieve smoothness, accuracy, high efficiency, energy saving. The rate of the equipment failure is greatly reduced, and maintenance is easier and more convenient.

2) Through the study of the finite element analysis of car body, the results show that the improved structure has sufficient strength and rigidity, and can satisfy the demands for the normal work of the steel coil transporter.

References

[1] Lianggui Pu, Guoding Chen, Liyan Wu; Mechanical design[M]; Higher education press, 2005

[2] Heng Su, Zuomo Chen, Wenjie Ge;Mechanical principles[M];Advanced Education Press, 2013

[3] Bangchun Wen ;Machinerys Handbook[M] China Machine Press, 2010

[4] Yi Zhou, Fang Liu, Fei Li, Lan He;The finite element analysis of the maglev train suspension frame structure in Using SolidWorks and ANSYS[J].Modern manufacturing engineering, 2012,8:17-20

[5] Hongwen Liu, Mechanics of Materials[M]. Beijing: Advanced Education Press, 2007

Advanced Materials Research Vols. 989-994 (2014) pp 2939-2942
© (2014) Trans Tech Publications, Switzerland
doi:10.4028/www.scientific.net/AMR.989-994.2939

The Influence of Diamond Graver's Edge Radius in diffraction grating Scoring Process

Peng Sun[1, a],Hongwei Wang[1, b],Xianyu Zhan[1, c],Liming Qiao[1, c],Xiuling Wei[1, d]

[1] Aircraft and Dynamics Department, Aviation University of the Air Force,Changchun,130022, China

[a]email:rocy527@163.com, [b]email:whw1001@126.com

[c]email:Zczwhbbg@sina.com, [d]email: shisq104 @163.com

Keywords: Ruled Grating; Edge Radius; Finite Element

Abstract. Diffraction grating is a kind of very sophisticated optical element, It is usually used diamond ruled grating. Edge radius is one of the important parameters of diamond ruled grating, the effect of the edge radius to diffraction efficiency and ruled depth is analyzed by the theoretical calculation and finite element analysis in this paper. Get the influence law of diffraction efficiency, ruled depth and the ruling force, which has provided the theory basis for correctly precision edge radius.

Introduction

Along with the rapid development of spectral instruments and laser fusion technology, ruled grating has been more and more widely used in the economic, scientific research and the military field.The same attention to the development of grating manufacturing in China. The diffraction grating as the precision of the optical element[1].Among them, the sort is the use of diamond scribing iron grating in coated metal film layer on the base of extrusion, the polishing process. So to get high quality ruled grating, first must have a very sharp, accurate angle, excellent roughness, abrasive resistance is discussed [2].

The ruled grating graver is one of the ultra-precision diamond tool. No matter how fine production, can not be made into a sharp geometry line in production [3]. Within the cross section perpendicular to the main blade, The main cutting edge is actually a curve. Commonly used arc instead of the main blade edge shape. The circular arc of the edge radius to express the degree of the cutting tool edge sharp in order to adapt to a variety of processing requirements, edge radius range from 20nm-l μ m. In this paper, the study on edge radius on the grating diffraction efficiency, ruled depth and the ruling force [4].

The Influence of the grating diffraction efficiency

Diffraction efficiency of grating is one of the basic features, when choosing the cutting edge radius, the first thing to consider about the influence of diffraction efficiency.Grating trough theoretical contour shape is a triangle, as shown in figure 1 [5].

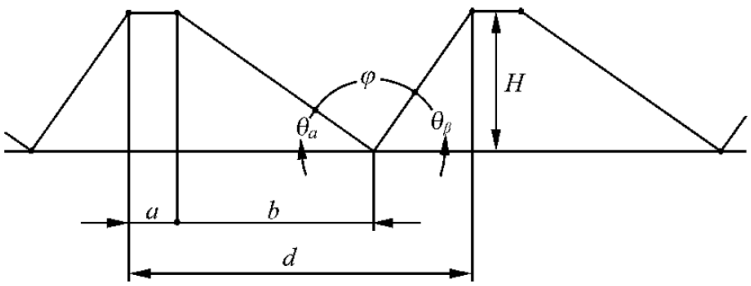

Fig.1. The theory outline of grating trough

In the figure 1, θ_a stands for blazed angle; θ_β stands for other blazed angle; φ stands for grooved angle; *a* stands for the zero-order surface width; *b* stands for transverse dimensions of effective blazed surface; *d* stands for grating constant ; *h* stands for the depth of the trough.

As a result of the existence of the edge radius, shining side with the shining side of intersect with a circular arc, this will reduce the effective glare grating surface transverse size *b*, thereby reduce the diffraction efficiency of grating.

We already know that the diffraction efficiency as follows :

$$\eta = a^2 \sin c^2[m\frac{a}{b}] + b^2 \sin c^2\{b[\frac{m}{d} - \xi]\} - 2ab \sin c[m\frac{a}{b}] \sin c\{b[\frac{m}{d} - \xi]\} \cos \pi \left[m\frac{a}{b} \right] \tag{1}$$

In the type, $\xi = \frac{1}{\lambda}[\cos\alpha + \cos\beta]\tan\theta_a$, *a* stands for angle of incidence, β stands for diffraction angle.

Don't consider the zero-order surface *a*=0, we can find:

$$\eta = b^2 \sin c^2 \left\{ b\left[\frac{m}{d} - \xi \right] \right\} \tag{2}$$

Considering edge radius, $b = \left[\frac{H}{\sin\theta_a} - r \right] \cos\theta_a$, In the type, we can find:

$$\eta_e = \left\{ \left[\frac{h}{\sin\theta_a} - r \right] \cos\theta_a \right\}^2 \sin c^2 \left\{ \left[\frac{h}{\sin\theta_a} \right] - r \right\} \cos\theta_a \left[\frac{m}{d} - \xi \right] \tag{3}$$

With the theory of diffraction efficiency ratio, we can find:

$$\frac{\eta_e}{\eta} \approx \left\{ \frac{\frac{h}{\sin\theta_a} - r}{\frac{h}{\sin\theta_a}} \right\}^2 = \left[1 - \frac{\sin\theta_a}{h} \cdot r \right] \tag{4}$$

Calculated by the formula 4,we find the table 1.

Table 1 Diffraction efficiency of different edge radius

Edge radius	*r* = 0. 1μm	*r* = 0. 2μm	*r* = 0. 5μm	*r*= 1μm
Efficiency ratio	96. 496%	93. 055%	83. 105%	67. 773%

The Influence of ruled depth

Mechanical characterization of grating, the precise characterization of ruled depth, guarantee the design outline of the correct contact, avoid excessive ruled[6].Actual ruled process, the use of diamond characterization of grating graver is usually asymmetric grating graver, so the center of the circular arc edge is not in circular arc edge and aluminum membrane directly above the contact point, the △X and △Y is a function of the edge radius.So when making the graver, position error compensation should be made for grating graver position error compensation formula can be made of geometric relationships as follows:

$$\Delta X = \sqrt{2} \sin\left[\theta_a - 45°\right] r \tag{5}$$

$$\Delta Y = \left\{ \sqrt{2} \cos\left[\theta_a - 45°\right] - 1 \right\} r \tag{6}$$

So we can get actual indented depth of grating graver ,

$$h = h_0 - \Delta Y = h_0 - \left\{ \sqrt{2} \cos\left[\theta_a - 45°\right] - 1 \right\} r \tag{7}$$

In this type, h_0 is the theory of indented depth. From what has been discussed above. With the increase of cutting edge radius, indented depth increased.

The Influence of ruling force

Despite its grating in the process of mechanical characterization can be divided into three: forward force, crossrange force, press force.Forward force along the grating graver ruled direction, provide the grating graver forward momentum; Lateral force vertical grating graver curve direction; Vertical grating surface under press force, control the indented depth [7].

By using the finite element software Deform-3d simulation of grating mechanical process, despite its research in the process of mechanical characterization.

Table 2 The Influence of the three force

Radius force /N	0.1μm	0.5μm	1.0μm
Forward force	0. 00489	0. 00506	0. 00512
Crossrange force	0. 0558	0. 0529	0. 052
Press force	0. 213	0. 221	0. 233

Deform is the Battelle colom bus laboratory development of large general finite element analysis software, mainly used for the analysis of all kinds of metal forming and its associated forming process and heat treatment process[8].By Deform -3d simulation of the process in which arc grating graver ruled diffraction grating, to reduce the number of grid, reduce the calculation time, the selection of aluminum film covers an area of 200μm x 120μm, the thickness of 3.5μm.

In the process of ruled, aluminium film plastic and elastic deformation occurs, thus it set as elastic-plastic body;For diamond tool material, its strength and hardness is much higher than the aluminum membrane materials, in the process of characterization of strain is very small, so it is set to the rigid body.Featured in the simulation process, the aluminum membrane fixed at the bottom, before and after the face said constraints;Indented depth under different cutting edge radius is selected according to table 2, the ruled rate is 50 mm/s[9].

Using Deform -3d finite element calculation, the ruling force in the process of characterization of measurement, measurement results as shown in figure 2.

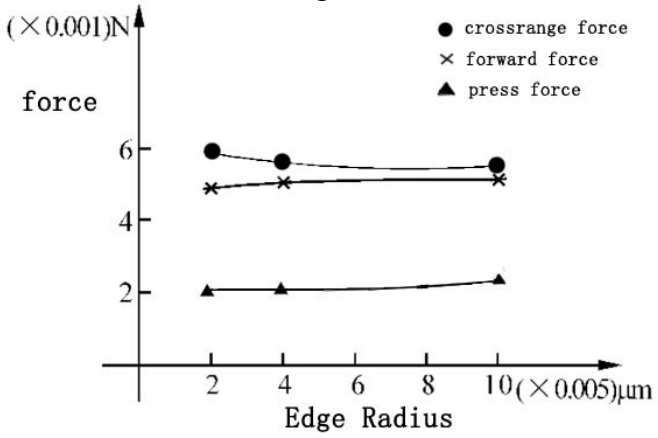

Fig.2. The change curve of ruling force

Respectively to make progress, crossrange force, press force change with arc nicking tool edge radius curve, as shown in figure 2.You can see from figure 2 progress, the pressure increases with cutting edge radius and bigger, this is because the knives on the direction of progress, under pressure to split of aluminium film, blade, cutting tool dull, need to force too big.Crossrange force increases with cutting edge radius and smaller, because the crossrange force main effect is to ironing grating groove surface polishing, increases as the edge radius, ironing area decreases, and thus less crossrange force also.

Conclusion

Ruled in the grating edge radius increases, shining surface transverse effective grating size b decreases, and the diffraction efficiency is lower.In the process of mechanical characterization of grating, affect the ruled of knife edge radius location and characterization of depth, and according to the position error compensation formula, ruled cutter location compensation, determine the actual

ruled depth, can avoid the occurrence of excessive ruled.Finite element simulation results show that edge radius, ruled knife is sharp, progress and smaller pressure, reduce the ruled consumed power;Crossrange force become larger, the enhancement of the grating groove surface polishing effect, improve the quality of the grating groove face.

References

[1] Li Yinghai,Ba Yinhexige,Qi Xiangdong. For the development of the diffraction grating score of ultra-precision diamond point[J] . Microfabrication technology, 2006(6) : 15- 17.

[2] Zhu Shaobo,Zhou Xinghai,Bao Xucheng.Diffraction grating [M].BeiJing: Mechanical industry press, 1986.

[3] Ba Yinhexige,Qi Xiangdong.10.6μm Laser level output high diffraction efficiency of the development of the blazed grating [J]. Photoelectron laser, 2004, 15(10) :1137- 1140.

[4] LI Haiying.Ultra precision diamond cutting tool-diffraction grating score knife. Optical precision engineering, 1996, 4(3) : 81- 84.

[5] Liu Zhiping,Dong Lihua, Han Yisong.Ultra-precision diamond tool grinding technology research [J] . Journal of artificial crystal, 2001, 30(4) : 413- 418.

[6] Xue Yongdong,Han Jingtao. Based on DEFORM the metal pressure processing of numerical simulation [J] . Metallurgical equipment, 2007(4) : 34- 37.

[7] Zhao Lei, Deng Yuanchao,wang jun. Based on DDFORM-3d finite element simulation of high-speed cutting [J] . Automation and control, 2007(5) : 69- 70.

[8] Zhou Chaohui, Cao Haiqiao JiWei, etc. Software DEFORM finite element analysis system and its application [J] . The hot working processes, 2003(4) : 51- 52.

[9]KIwata,KOsakada,YTerasaka. Proeess modeling of orthogonal cutting by therigid-Plastie finit eelement.J.Eng.Mater.Teehnol.,1984,106:132-138

Advanced Materials Research Vols. 989-994 (2014) pp 2943-2946
© (2014) Trans Tech Publications, Switzerland
doi:10.4028/www.scientific.net/AMR.989-994.2943

Stress Characterization and Mechanical Analysis for Supporting Leg of SiGe/Si MQWs based bolometer

Bo Jiang[1], Tao Dong[2, a], Yong He[1], Yan Su[1]

[1] School of Mechanical Engineering, Nanjing University of Science and Technology, Nanjing, China.

[2] Department of Micro and Nano Systems Technology, Faculty of Technology and Maritime Sciences, Høgskolen i Buskerud og Vestfold, Norway

[a]Corresponding Author, PhD Tao Dong, Email: tao.dong@hbv.no

Keywords: stress characterization; MEMS; mechanical analysis

Abstract. The paper presents an "L-type" leg applied in SiGe/Si Multi Quantum Wells (MQWs) based bolometer. Characterization structure has been designed to take measurement for α-SiNx:H film stress. The displacement of beam endpoint in the structure is 0.48 micron and the interior stress is about 87 MPa totally through generalized Hooke law. Furthermore, the mechanical analysis for SiGe/Si MQWs based bolometer has been taken and the largest stress is about 600 MPa in the calculation. The bolometer SEM photograph is shown at last.

Introduction

Bolometer plays a pivotal role in uncooled infrared detector [1-2]. Many researches have been reported in last two decades to improve the performance [3-4]. All of them are based on the 'bridge' structure published by Honeywell in 1992. Thermal performance analyses have been focused in researches because pixel is immobile in working state which means few mechanical supporting and large deformation issues should be taken into account in most case. Shorter width and longer length of supporting legs contribute to improve the thermal conductance which leads to higher static response [5]. The limited dimension in contact lithography is about one micron and the leg width less than two micron should be difficult with several alignments in MEMS process.

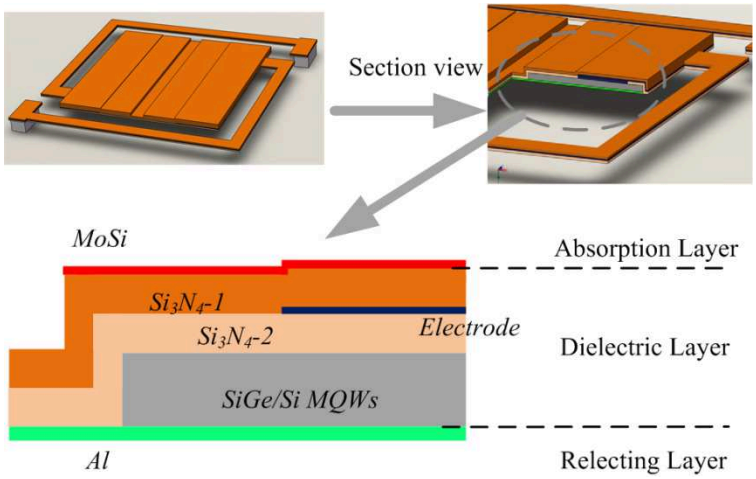

Fig.1. "L-type" supporting leg applied in SiGe/Si Multi Quantum Wells (MQWs) based bolometer

The bolometer with SiGe/Si Multi Quantum Wells as thermistor has higher temperature coefficient resistance (TCR) and lower noise due to mono-crystalline silicon and silicon-germanium [6]. The structure is difficult and more than nine steps of lithography alignments are needed in the process [7]. To maintain the equivalent thermal performance, L-type beam as supporting leg have been present in the paper as illustrated in Fig.1. The leg with L-type beam has lower thermal conductance compared with straight beam. However, longer beam also leads to larger stress and the

α-SiNx:H (amorphous silicon nitride containing hydrogen atom) layer, employed as supporting leg, induces interior stress in PECVD (Plasma Enhanced Chemical Vapor Deposition) process. As a result, mechanical analysis and α-SiNx:H layer stress characterization should be taken into account.

The paper presents the stress formation mechanism and characterization structure for α-SiNx:H film. Both simulation and experiment results have been given. The interior stress of α-SiNx:H on SiGe/Si MQWs is about 100 MPa as the calculations. In the third section, mechanical analysis have been present and the scanning electron microscope graph of bolometer have been shown at last.

Stress Characterization of α-SiNx:H layer

α-SiNx:H layer is employed as mechanical supporting layer in the structure. However α-SiNx:H layer manufactured by PECVD always have interior stress. The stress formation mechanism is always classified into intrinsic stress and thermal stress. Thermal stress induced due to the mismatch of coefficient of thermal expansion between α-SiNx:H and SiGe/Si MQWs. Intrinsic stress during PECVD are dependent with temperature, RF power frequency and reactive gas flow rate. The higher growth temperature has a positive influence on the structure of films [8]. However, the temperature should be less than 300℃ due to the limited temperature of read-out circuits in the substrate. The high frequency thin film residual stresses performance as tensile stress, yet the low frequency thin film residual stresses performance as compressive stress. In the experiment, the α-SiNx:H was deposited by high-low frequency alternation RF power to compromise the intrinsic stresses. The parameters are list as follow.

Table I α-SiNx:H deposition process parameters by PECVD

Flow rate (sccm)			Pressure	High RF Frequency		Low RF Frequency	
SiH4	NH3	N2	(mTorr)	Frequency(MHz)	Power(W)	Frequency(kHz)	Power(W)
13.5	10	1000	1700	13.56	67	380	53

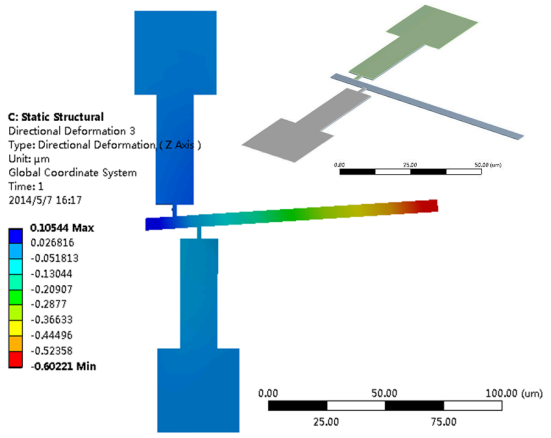

Fig.2. The beam displacements of α-SiNx:H film stress characterization structure in simulation

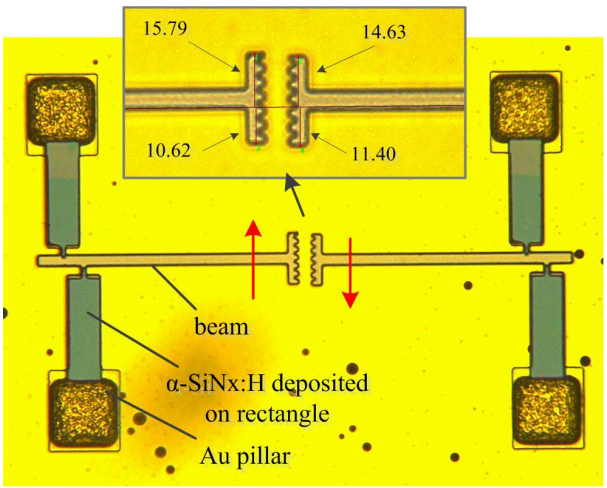

Fig.3. The photograph of film stress characterization structure after process.

The stress characterization structures are designed as shown in Fig.2. The α-SiNx:H film was deposited on rectangle substrate, SiGe/Si MQWs. The deformation of the rectangle was reflected on the displacements of long beam, on which there is no α-SiNx:H. All of the structures mentioned above are suspended and supported by Au pillar. The displacement amplification of beam endpoint is 0.48 micron by lever structure. The structure in simulation is 0.60 micron which is similar to experiment results. According to generalized Hooke law, three-dimensional stress-strain (σ-ε) relationship is expressed as Equ.(1).

$$\begin{pmatrix}\varepsilon_x\\ \varepsilon_y\\ \varepsilon_z\end{pmatrix}=\frac{1}{E}\begin{pmatrix}1 & -\mu & -\mu\\ -\mu & 1 & -\mu\\ -\mu & -\mu & 1\end{pmatrix}\begin{pmatrix}\sigma_x\\ \sigma_y\\ \sigma_z\end{pmatrix} \quad (1)$$

where E and μ is Young's modulus and Poisson's ratio of α-SiNx:H material. The interior stress is about 87 MPa in the calculation.

Mechanical Analysis for SiGe/Si MQWs based bolometer

L-type beam as supporting leg has lower thermal conductance compared with straight beam, which has lower demand of lithography alignments accuracy during process. However mechanical analysis is necessary for L-type supporting legs. Bolometer is immobile in working state and gravity has few influences on the structure. The interior stress of α-SiNx:H layer is about 87 MPa in stress characterization mentioned above. The simulations have been conduct and results are illustrated as shown in Fig.4 to Fig.6.

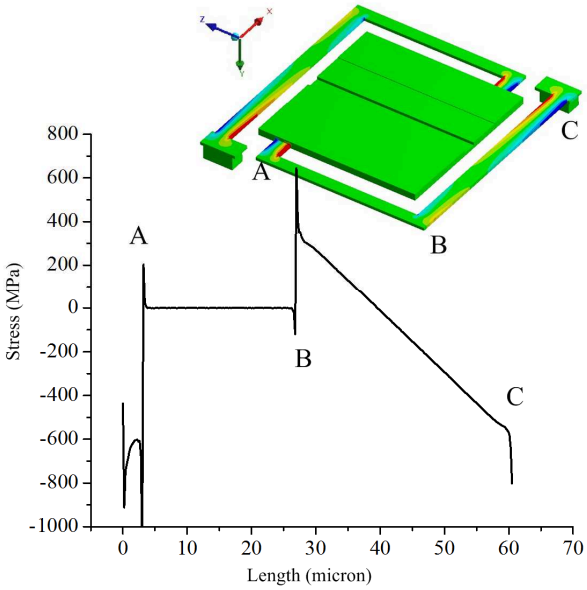

Fig.4. Stress distribution of supporting legs along x-axis

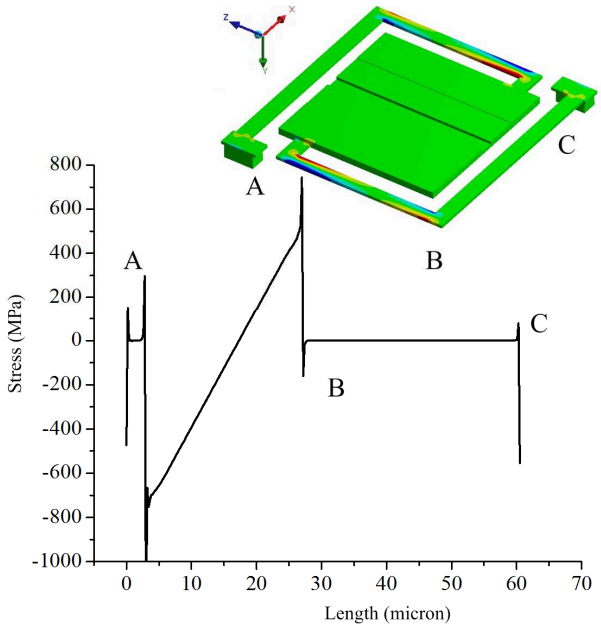

Fig.5. Stress distribution of supporting legs along z-axis

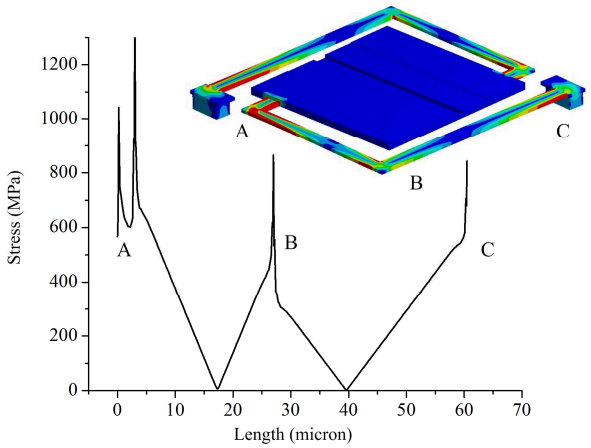

Fig.6. Stress intensity distribution of supporting legs

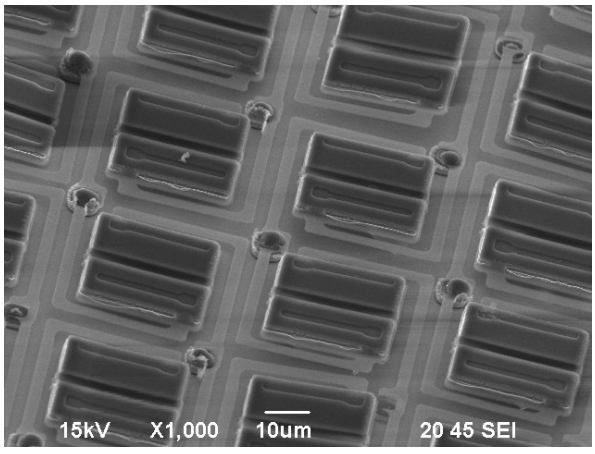

Fig.7. SEM photograph of bolometer

Stress distributions of supporting legs along x-axis and z-axis are illustrated in Fig.4 and Fig.5. Film stress valued with 87 MPa applied on the L-type legs. Stress along x-axis from B-C take a dominant position due to bending moment along y-axis. The same situation happened about the

stress along z-axis. Summarized, the stress intensity distribution is illustrated in Fig.6 and the point A, B, C is the place where maximum stress occurs. The maximum value is less than 600 MPa, which meets the requirement of mechanical supporting. There is no obvious deformation or distortion as shown in Fig.7.

Conclusion

The paper presents an “L-type” leg applied in SiGe/Si Multi Quantum Wells (MQWs) based bolometer. The stress measurement and analysis of “L-type” leg were conduct and the interior stress is about 87 MPa with the experiments and the calculation through generalized Hooke law. Stress distributions along two directions have been analyzed and the maximum value is less than 600 MPa which meets the requirement of mechanical supporting.

Acknowledgement

In this paper, the research was sponsored by t Scientific Research Project (No. A2620110012), China, Natural Science Foundation Project, (No.51375244), and Jiangsu Research and Innovation Program (No.CXZZ13-0197). This research work was also supported by Norsk regional kvalifiseringsstøtte fra Oslofjorfondet (Mikrofluidisk plattform integrert med lavkostnads fotodetektorer, proj. no: 229857).

References

[1] A. Rogalski. Infrared detectors: an overview [J]. Infrared Physics & Technology, vol. 43, pp. 187-210, 2002.
[2] T. Dong, Z. Yang, Q. Bi, et al. Freon R141b flow boiling in silicon microchannel heat sinks: experimental investigation [J]. Heat and Mass Transfer, vol. 44, pp. 315-324, 2008.
[3] S. Eminoglu, M. Y. Tanrikulu and T. Akin. A Low-Cost 128×128 Uncooled Infrared Detector Array in CMOS Process [J]. Journal of Microelectromechanical Systems, vol. 17, p. 20, 2008.
[4] L. Zhang and T. Dong. A Si/SiGe quantum well based biosensor for direct analysis of exothermic biochemical reaction [J]. Journal of Micromechanics and Microengineering, vol. 23, p. 045011, 2013.
[5] M. Kolahdouz, A. A. Farniya, M. Östling, et al. The performance improvement evaluation for SiGe-based IR detectors [J]. Solid-State Electronics, vol. 62, pp. 72-76, 2011.
[6] Jiang B, Dong T, Su Y, et al. Epitaxial Growth and Characterization of Self-Doping Si1-xGex/Si Multi-Quantum Well Materials [J]. Journal of Microelectromechanical Systems, vol. 23, pp. 213 - 219, 2014.
[7] Zhong F, Dong T, Yong H, et al. Void-free wafer-level adhesive bonding utilizing modified poly (diallyl phthalate)[J]. Journal of Micromechanics and Microengineering, 2013, 23(12): 125021.
[8] Duerinckx F, Szlufcik J. Defect passivation of industrial multicrystalline solar cells based on PECVD silicon nitride[J]. Solar Energy Materials and Solar Cells, 2002, 72(1): 231-246.

Advanced Materials Research Vols. 989-994 (2014) pp 2947-2950
© (2014) Trans Tech Publications, Switzerland
doi:10.4028/www.scientific.net/AMR.989-994.2947

Analysis of Aircraft Hydraulic System Failures

Wenguang ZHANG[1, a], GuoMin LIN[2, b]

[1]Department of graduate Xijing University, Xi'an, 710123, China

[2]Department of graduate Xijing University, Xi'an, 710123, China

[a]email: 935460009@qq.com, [b]email: bgmlin@21cn.com,

Keywords: Aircraft hydraulic systems; hydraulic pipe; failures; Oil Pollution

Abstract. The hydraulic system of Aircraft is an important power organization and plays an important role in the process of airplane operation. The failures of the airplane have the character of concealment, complexity and uncertainty. So if the hydraulic system ran out of order it not only cause huge casualties and economic losses, but also has a long and low efficiency maintenance cycle. This text analyzes the common causes of the failures and the failures that newly appeared of the aircraft hydraulic systems in detailed. Some of effective solutions have been proposed which quicken accelerate the speed of fault diagnosis and improve the efficiency of aircraft maintenance.

Introductions

The failure of the airplane characterize by its concealment, complexity and uncertainty. Therefore if the plane hydraulic systems go out of order, it will have a long and low efficiency maintenance cycle. With the development of the modern aircraft industry, the hydraulic structures of the plane are becoming more and more complex, it also increase the failure probability of the aircraft hydraulic system.

Recently a new kind of diagnostic technology has been emerged. The method of the technology is to giant information with the sensor and signal measurement technology. Using computer and a variety of testing instrument to establish the mathematical model and dealing with the data. But Mathematical model of the method is very complex in addition to its uncertainty and external disturbance. In some cases, the model even cannot be established. So knowing common failures of the aircraft and the corresponding solutions will significantly shorten the maintenance cycle, reduce the maintenance personnel technical level and improve the economic benefits.

Division of aircraft failures

The paper analyzes the failures of the aircraft from aspects of oil pollution, hydraulic pipe fracture, high oil temperature and leakage in detail. Some of the corresponding solutions have been put forward in order to improve the maintenance efficiency.

Oil pollution. The oil pollution means that oil mix with solid particles, water, gas, chemicals materials and some microbes etc. The most serious pollution is solid particle pollution. The foreign statistical data shows that 60% contaminants coming into the hydraulic system when the installation process. The pollutants draw into the system in the regular maintenance Accounted for 20% and the granules produced by parts natural wear accounted for 20%. The Airplane crashes that caused by hydraulic system failure be up to 90% [1].Therefore the solid particle pollution is the mainly responsible for the trouble of hydraulic system, and it is also the key of routing maintenance.

The first source of the particle contaminants come from outside of the system. In the process of assembly, disassembly and daily maintenance, some of the polyester fibers and solid particles will attach to the piston rod, or through the vent pipe mouth coming into the oil tank and caused oil pollution. The second kind of the pollution particle is cause by the parts wear. When the system working in high temperature for a long time the oil would be oxidized and produce colloidal sediment. The Third kind of Pollutant is residual pollutants. These contaminants have already

existed before the system assembled such as iron filings, welding slag and cotton fiber. It is difficult to completely eliminate and would throughout the hydraulic system when the aircraft working [2].

Aircraft hydraulic system Components must be cleaned before installation with silk cloth instead of cotton and linen material cloth. In order to avoid fiber stranded on the surface of the parts and then introduce into the hydraulic system.

Oil filter should be used properly. The hydraulic oil filter should be selected according to hydraulic system pollution level. Generally, there are three oil filters in the aircraft hydraulic system, 1 for supply pressure pipeline, 2 for oil return pipeline. In order to avoid pollutants entering the hydraulic system the oil should be infect into the system from filter whose absolute precision above 3um. New type of filter element has been widely used in aircraft for the purpose of improving the ability to filter out dust. Metal rubber is a new type of elastic and porous material and made up of metal wire via special preparation process. It has the advantage of high bearing capacity, anti-clogging ability and the pressure continuous adjustable performance of its throttling pore. The new material has been used oil filter making.

Tube fracture. From analysis of aircraft accidents caused by hydraulic tube broken recent years Aircraft maintenance engineer knows that the tube broken actually is a kind of fatigue fracture.

Fig. 1: Wrinkles in hydraulic pipe wall of airplane

Fig. 2: The micro cracks on the tube bell mouth

Most of the damaged places are the area where there have stress concentration such as unreasonable hydraulic pipeline designing, too much Bending or fold appear on the inside wall of the oil-pipe (refer with: Fig. 1).The main reason of the tube broken is that the aircraft hydraulic system working in the high pressure, big flow pulse, huge hydraulic impact and high-frequency pressure oscillation environment. For this reason the oil tube of the system will fatigue breakdown by suffering of radial vibration and bending vibration.

Firstly, the size and the material of the hydraulic tube must be chosen according to the pressure requirements. In normal conditions, high pressure system should choose stainless steel tube and aluminum tube. Rubber hose always used in low system and scavenge oil system. Much attention should be paid to when choosing a hydraulic pipe; the surface of the tube must not have the obvious machining tool, micro cracks and other defects. Fluorine plastic pipe can also be used in hydraulic section where Stainless steel tube difficult to install or the places with big pressure pulsation and vibration [3].

Secondly, in order to avoid the faction between the tubes, the proper gap should be keep between them. In the process of installation do not install forcefully when the tube are not aligned, in case of stress concentration and crack produced on the bell mouth and the surface of the bend(refer with: Fig. 2) [4].Thirdly, a support frame should be installed at the area where prone to come about resonance. It is the effective way to solve pipe resonance and avoid hydraulic pipe fatigue cracking.

Leakage. Aircraft hydraulic system is using liquid oil as the working medium, so it has been accompanied by the problem of oil leakage from the date of the birth. The reasons that cause hydraulic system leakage and corresponding solution showed as below.

Fig. 3: Connectors can't be totally matched

Fig. 4: The complex layout of aircraft hydraulic pipe

Firstly, untight seal of connection join would cause pipe leakage. Screw the pipe connection tightly when connect hydraulic pipe line. But screw too tight will destroy interface of the screw thread and lead to leakage. The tightening force usually ensured by the torque spanner in engineering. Unmatched thread of the connectors can also result in leakage in system. In the process of installation and maintenance of the airplane, different criteria thread cannot be matched and some threading connector with same size can't be matched together because of their different pitch and number (refer with: Fig. 3).

Secondly, sealing ring failure can also lead to leakage. This is mainly because the bad sealing environment. Hydraulic oil has the character of corrosive especially when system works for a long time in high temperature. The high temperature oil will accelerated the oxidation and corrosion loss of the rubber sealing ring. So in the aircraft daily maintenance the sealing ring should be checked out and replaces them when they have defects.

Thirdly, unqualified maintenance behavior can also give rise to leakage. During the pipe installation, tightening torque does not conform to the requirements and inappropriate tools using will cause causing hydraulic system leakage, therefore, in the process of daily maintenance must be carried out accordance with the manual strictly.

High oil temperature. In the hydraulic system, high oil temperature will also lead to the oxidation and decomposition of hydraulic oil. It is also the important source of oil pollution. The high oil temperature will aggravate aging failure of the sealing device. So high oil temperature is an important reason that causes hydraulic system failure. The reason of high oil temperature and the corresponding solution shown as blew.

Firstly, unreasonable layout designing of the attachment will rise system temperature. Because the hydraulic pump working through drive of the engine rotor rotation, many hydraulic accessories and tubes are installed around the engine compartment. The engine will generate lots of heat and rising the temperature around when it working. Secondly, the complexity of the tube line and too much turning will cause oil hit in the process of flow, a lot of kinetic energy is converted into heat, which is an important reason of high temperature of hydraulic system oil(refer with: Fig. 4).

In currently aviation industry, there are two solutions to control hydraulic system temperature. The first way is to increase heat dissipation and the other method is to reduce the energy loss. In general machinery, the tank capacity could be increased in order to accelerated heat dissipation. But the planes have a strict requirement of space. So the method of increasing the capacity of the tank is not feasible in the aircraft. At present, the most successful technology is to arrange the export

pipeline of the pump to the lower temperature area (the plan wings) and then go back to tank. Using AMESim simulation software to analyze the thermal characteristics of airplane hydraulic system, the result shows that the temperature of back pipe line which arrange at wing drop nearly 8 degree [5]. So some of the hydraulic accessories and pipeline should be arranged in the places where the environment temperature is lower. For the catheters that have to install in the high temperature environment, heat insulation measures should be taken to control the oil temperature. If the heat mainly comes from the radiation of engine, insulation board with lower black degree coefficient or multilayer insulation measures can be used to reduce the heat [6].

Conclusion

Solid particles pollution of oil, pipe fracture, oil leakage and high temperature can lead to aircraft failure and causing serious consequences. In order to avoid the occurrence of the above problems, effective measures is not confined to the daily maintenance but also embrace the process of aircraft designing, parts producing and assembling. Before the designing, some method should be prepared to deal with the failures with high probability. To the problems that have already happened the maintenance technicians should take measures according to the method proposed.

References

[1] Lailin DU. The particle pollution of plane hydraulic system and maintenance [J]. Hydraulics Pneumatics & Seals. 2010 (5) 12-15.

[2] Dong ZHENG. Particle pollution of airplane hydraulic system and maintenance [J]. Science and technology innovation and application. 2013 (3) 126.

[3] Lipeng DU. Hydraulic filters multiple-pass test technology present state and perspective [J]. Machine Tool & Hydraulics. 2013 (9) 176-178.

[4] Zhizhu ZHAO. analysis of Aircraft hydraulic system failure causes and countermeasures[J]. Equipment Manufacturing Technology. 2011 (4) 191-193.

[5] Yanyan LUO. Xinmin WANG, Analysis of influence of hydraulic line on the system heat load [J]. Hydraulics Pneumatics & Seals. 2013(9)36-39.

[6] Xiuxia WANG. Aircraft hydraulic system temperature control method [J].Fluid Power Transmission and Control. 2009 (1) 40-42.

Advanced Materials Research Vols. 989-994 (2014) pp 2951-2954
© (2014) Trans Tech Publications, Switzerland
doi:10.4028/www.scientific.net/AMR.989-994.2951

Design and Realization of Remote Control UAV's Flight Controller

TIAN Ye[1, a], DENG Hongde[2, b], Zhuang Haoyue[3,]

[1,2,3]National Key Laboratory of Science and Technology on UAV, Northwestern Polytechnical University, Xi'an 710065, China

[a]email: tiane-9@163.com, [b]email:denghongde@126.com, [c]email:zhuanghaoyue823@163.com

Keywords: Remote Control UAV; Flight controller; LabWindows/CVI; GL Studio

Abstract. To provide UAV's operator with flight information in real time, according to the property of remote control UAV and human-machine interface design, a flight controller has been implemented. The flight controller used LabWindows/CVI, GL Studio and UDP communication as the main developing platform. The system has been used in projection, and the test had showed that it could meet the need of the GCS(ground control station) of remote control UAV.

Introduction

The remote control UAV is one kind of UAV that can either fly remotely, and can also be controlled by the GCS(ground control station). The flight controller is the "nerve center" of the system, and the hub of human-computer interaction [1]. The controller is consist of background data processing and foreground data displaying. The former is remote telemetry data interacted with ground control system by UAV. The interactive data will be precisely, vividly and intuitively displayed on the human-computer interaction interface. The flight controller developed by LabWindows/CVI is embedded with the GL Studio controls, it uses UDP protocol for data communication. It provides the human-computer interaction platform for the ground controlling staff, conveniently control in real-time.

1. Development environment

LabWindows/CVI based on C language is a virtual instrument software development tool developed by the NI company. It has advantages of high efficiency, fast interface design, powerful language and flexible performance. It is well applied to the establishment of systems detection, automatically detecting environment and signal analysis processing, especially for the development of complex testing system. In addition, LabWindows /CVI also has a strong capacity of network communication data transmission, which provides the API function based on UDP communication protocol to realize the efficient, reliable, connection-oriented data communication network [2] .

GL Studio is developed by DISTI company for instrument simulation. It is used to develop real-time, two -dimensional or three-dimensional, photo-realistic and interactive graphical interface software [3]. GL Studio is consist of two parts: the graphical interface designer and the code generator. A graphical designer allows operator to draw the graphics system quickly and easily ,and use the intuitive way to complete the appearance and interaction design of graphic panels; the code generator draw the graphic look of object interaction to generate c + + / OpenGL source code, then become dynamic controls.

2. Functional analysis and the design of human-computer interactive interface

2.1 Functional Analysis

The flight controller plays an important role in UAV flight, real-time display is its main function. The controller save the information of flight attitude and flight parameters, send state monitoring, remote data regularly and control the flight status. Operators can effectively control the UAV through the platform to ensure the normal work of the UAV platform. According to the functional requirements, overall structure design of flight controller is shown in figure1:

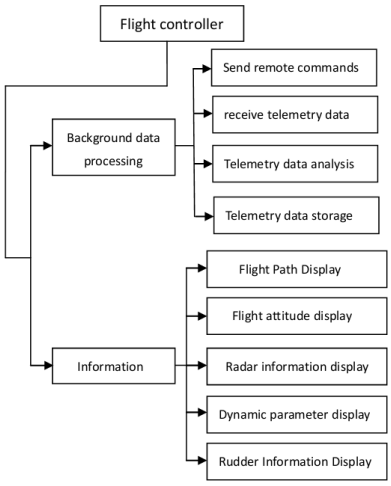

Figure1: Structure drawing of flight controller

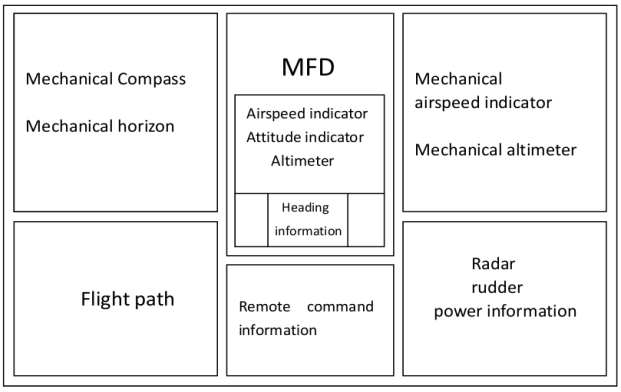

Figure 2: Interface layout of flight controller

2.2 Design of human-computer interactive interface

The flight controller provides important flight parameter, operator handle the UAV on the ground on the basis of the information. Therefore, the data display and the layout of panel are extremely important. The flight controller is modeled based on the U.S. military standard MIL-STD-1787C [4] and principles of human-computer interface design [5] of aviation.

The compass, horizon, airspeed indicator, altimeter and MFD (Multifunction Display) are developed by GL Studio. The 4 mechanical instruments provide a backup for the MFD, that is, if there are problems in the electronic instrument, mechanical instruments can still display flight attitude information, so that you can continue to manipulate the UAV. Flight path: It is used to display the track within a specified area. When the target appears, the radar display the distance and direction of the aircraft. Rudder, elevator and other parameters are displayed in the aileron control surface. Parameters such as engine speed, amount of remaining oil will be shown in dynamic information monitor.

3. Software design and implementation

The flight controller is mainly developed by LabWindows/CVI platform, embedded with the dynamic control developed by GL Studio [5]. The data communication is realized by using UDP. We initial the data-driven screen by using the main thread and only use the UDP event mechanism sequence control method. The software process is shown in Figure 3.

3.1 Communication between flight controller and the ground terminal

Because of the flying machine data transmitted between the flight controller and the ground terminal is relatively small, but the high demand of real-time data transmission (sending and receiving data processing must be completed in every 20ms), we chose the UDP protocol.

The UDP protocol was packaged by LabWindows / CVI. When the aircraft receive data from the ground terminal, an event has been triggered. Then the callback function was invoked automatically. Callback function process the telemetry data, control the drive of GL Studio and send the remote data. Finally, we realize the real-time communication between flight controller and ground terminal [6]. The format of telemetry data during the communication is shown in the figure 4.

Among them, area A is data frame header; phase 2,3,4-byte in area B are of the same content, all of them are telemetry data category; area C stores telemetry data, it will put the result (5 to 21 byte checksum) on the position of the 22th bytes; area D is the tail. Detailed instruction of frame header, data, categories, telemetry data storage format and frame tail are explained in the communication protocol. Remote data frame is defined similar to the telemetry data frame.

When the flight controller receives downlink telemetry data, it will first determine whether the frame header, data length and frame tail are consistent with the protocol, if so, the data frame can be received. Then it determines the data from area B: if the contents (2 to 4) are the same, they are considered as the same data type in area C, data from the area C are parsed according to the protocol; if the three bytes of data are not identical, the contents of two bytes are considered as the data type in area C, repeating the above steps; if the three bytes of data are completely different, the frame data should be discarded and the controller is ready to receive the next frame data. Key code:

```
datanumber=UDPRead(channel,buff,bufsize,timeout,sourcePort, sourceAddr);
if((datanumber==DATANUM)&&(buff[0]==0xxx)&&(buff[1]==0xxx))
{
……// Further judgment and data processing
}
```

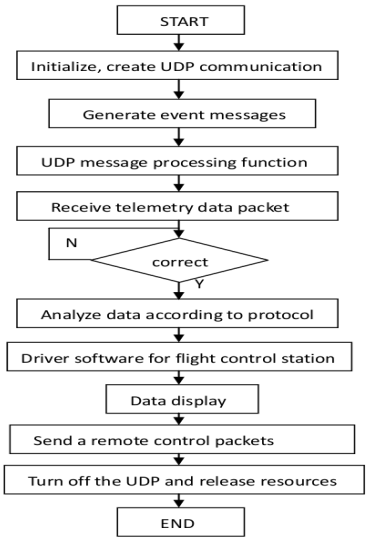

Figure 3: Flow chart

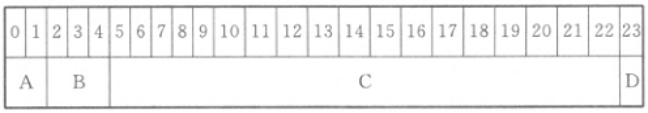

Figure 4

3.2 The development and encapsulation of GL Studio controls

When developing dynamic controls in GL Studio, you need to select "GL Studio Live Component" if you create the project (generate the dynamic component). After creating behavior code and adding external data interface for each section, the model need to be debugged, compiled and linked, then the *.dll dynamic file types are generated. Finally, encapsulate and generate control.

1) We can add an external data interface by creating a sub function with the property of "property" in the main control window, and the external data can drive the control through function calls by other software. External data interface function is as follows:

```
void rotateClass:: data_interface (const float& value)
{
…….; }
```

Data_interface is the name of the external data interface function and is the property created for controlling; float is the type that can drive control of external data. The above two can be created and set as needed.

2) Control encapsulation: control encapsulation is to make *.Cab file. The generated DLL file should be packaged by the written file (make_cab. Bat), the contents of the package include two:

1. The *. DLL files;

2. VC files provided by GL Studio. Version associated with GL Studio version and the version of VC + + should match each other.

Writing make_cab.bat program according to the file path and file name. Its main contents are as follows:

"%GLSTUDIO%\bin\cabdev\bin\cabarc.exe"-s6144N" (generate the name of control， for example: example.cab)" "(document storage path, for example: D:\example\debug\example.dll)" "%GLSTUDIO%\bin\glstudio3_2_1_vc60.dll".

Among them, cabarc.exe is the packaged application provided by GL Studio, the example.dll and glstudio3_2_1_vc60.dll are packaged to generate example.cab file when the program is automatically called, then the encapsulation of control has been done.

3.3 Embed GL Studio controls to CVI

The GL Studio controls are embedded in LabWindows / CVI, Specific steps are as follows:

1）Add an ActiveX control into CVI to load *.cab file;

2）Create GL Studio drive function and load it;

3）Filling in the control path location and adding controls ;

4）Edit properties of control;

5）Add the appropriate behavior code and driver controls in the "*. C" file.

The main code is as follows:

```
/ / Get the GL Studio control handle and driven by an external data
GetObjHandleFromActiveXCtrl(panelHandle, PANEL _GLSPLAYER, &objhandle);
/ / Data type conversion
CA_CStringToBSTR ("data_interface", & str);
/ / Conveying external data to the control
GLSPlayerLib__DGLSPlayerSetAttrib (objhandle, NULL, CA_VariantBSTR (str), CA_VariantFloat (rdata [0]));
```

Among them, the STR data type is BSTR. rdata [] stores the data which UDP received.

4. System verification

Detecting results show that the flight controller can receive, process and display the remote data correctly. Virtual instruments developed by GL Studio are also working properly; the controller can sent the remote control commands correctly, fast and timely to the ground terminal when clicking the takeoff, climb, level off buttons. The design of flight controller meet the functional requirements of ground station system.

5. Conclusion

The design and development of the remote control UAV flight controller has certain universality, it solves the problems in the complexity of data-driven scene and the real-time communication. The flight controller give full play to the advantages of LabWindows/CVI and GL Studio, improve the quality and speed of development. According to military specifications and human-computer interface design principles, we fully consider the visual information acquisition characteristics of the operator, implement the information classification, prioritize location layout, improve the efficiency of achieving information, reduce the fatigue. As a result, the flight controller improve the Operational efficiency of the UAV to a certain extent.

References

[1] Li Dajian, Jia Wei, Qi Min. Design and application of UAV Ground Control Station [J], Computer Measurement &Control, 2011，(6)，51—53.

[2] Wang Jianxin, Yang Shifeng, Sui Meili. LabWindows / CVI testing technology and engineering applications [M], Beijing ;Chemical industry press;2006

[3] Yu Hui, Zhao Jingcheng, Fu Zhanping. GL Studio virtual instrumentation technology application and system development [M], Beijing, National Defense Industry Press, 2010.

[4] United States military standard military instrument MIL-STD-1787C

[5] Distributed Simulation Technology Inc. GL studio User's Guide [M].Version 3.2,2006.

[6] Bryan E. Walter, Jared S. Knutzon, Adrian V. Sannier and James H. Oliver. Virtual UAV Ground Control Station [J]. AIAA 2004-6320.

Advanced Materials Research Vols. 989-994 (2014) pp 2955-2958
© (2014) Trans Tech Publications, Switzerland
doi:10.4028/www.scientific.net/AMR.989-994.2955

Study of AT based on the lever method

Jiangjiang Li , Jinghua Li

TianJin Vocational Institute,Tianjin,300410,China

Keywords: Design reasonableness of transmissions;Lever method;Improvement of design of transmissions;Drive scheme

Abstract. The rotation speed and shift process of automatic transmission were analyzed intuitively based on lever method in this paper, the design reasonableness of transmissions was verified as well; At the same time the measure of improvement of design of transmissions scheme was put forward.

Introduction

Lever method is a simple analytical method conducting to analyze planetary mechanism about their kinematics and dynamics . Based on the lever method analyze, the shift process of AT, especially its reasonable design of transmission scheme ,can get a comprehensive analysis.

The analysis with shift process of automatic transmission(example of WV 01M AT)

The related information about 01M AT. The related shift data about 01M AT shown in table 1 and figure 1:

Table 1 The movement of implementation components of each shift of different gears

Gear(trasmisson ratio)	B1	B2	K1	K2	K3	F0	K0
1H（2.714）			⊙			⊙	
1M（2.714）			⊙			⊙	⊙
2H（1.507）		⊙	⊙				
2M（1.507）		⊙	⊙				⊙
3H（1.000）			⊙		⊙		
3M（1.000）			⊙		⊙		⊙
4M（0.7037）		⊙			⊙		⊙
R（-2.375）	⊙			⊙			

Note: □Said work

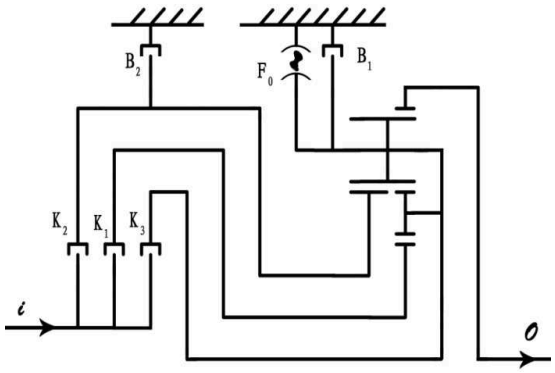

Fig.1: The transmission diagram of 01M AT

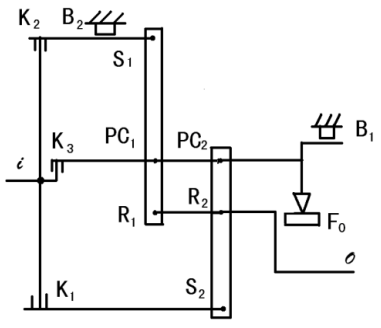

Fig.2:The lever figure of 01M AT

According to the information above, it is easy to make out lever diagram of 01M AT, as shown in figure2:

Figure 2 explanation: S1 is the sun gear of the front row, PC1 is planet carrier of front row, R1 is front row's ring gear, PC2 is rear planet carrier, R2 is rear ring gear, S2 is the rear sun gear; From the

lever figure we know that the front planetary row is planetary gear row, rear planetary row is double planetary gear row. The whole institution is the typical ravi type gear train institutions.

The analysis of rotate speed of each gear about 01MAT. According to the figure ,there has the drawing about equivalent lever speed figure of 01M AT ,as shown in fig.3:

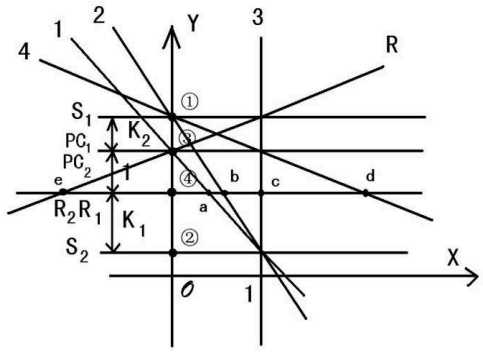

Fig.3: The equivalent lever rotate speed figure of 01M automatic transmission

Figure 3 explanation: the node ① represents S1 component, the node ② represents PC1PC2 component, the node ③ represents R1 and R2 component, the node ④ represents S2 component. The distance of 01 on the X axis represents the input shaft rotate speed to be 1. 1,2,3,4 respectively represents 1st, 2nd, 3rd and 4th gear.

$$K_2 = \frac{ZR_1}{ZS_1} \tag{1}$$

$$K_1 = \frac{ZPC_2}{ZS_2} \tag{2}$$

We have following conclusions according to the equivalent lever speed fig.3 about 01M automatic transmission:The output rotate speed of 1st divides the input rotate speed of 1st is the distance of oa in the X axis: $oa = \frac{1}{K_1+1}$; The output rotate speed of 2nd divides the input rotate speed of 2nd is the distance of ob in the X axis: $ob = \frac{K_2+1}{K_1+K_2+1}$; The output rotate speed of 3rd divides the input rotate speed of 3rd is 1; The output rotate speed of 4th divides the input rotate speed of 4th is the distance of od in the X axis: $od = \frac{1+K_2}{K_2}$;The output rotate speed of R gear divides the input rotate speed of R gear is the distance of oe in the X axis: $oe = -\frac{1}{K_2}$,direction is the opposite.

The analysis of rationality of transmission scheme about 01M AT.

The analysis of design's rationality of transmission scheme about 01M AT based on lever method:

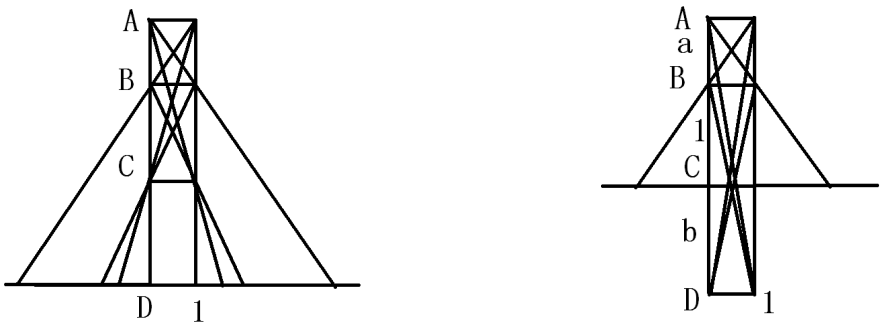

a) Endpoint output b) Intermediate point output

Fig.4: The analysis of equivalent lever of output point

01M AT belongs to three freedom of motion and the structure of double planetary row, from the perspective of output point, which has two kinds of possibility, as shown in fig.4:

Making end point A (A and D, 2 points are equivalent) as output point (as shown in aof fig 4); Through the analysis of lever transmission, it shows that there are 3 reverse, 3 overdrive, 1 directly gears, but no deceleration gear, so this kind of scheme of making endpoint as output point doesn't work obviously.

Making end point B(BC, two points are equivalent)as an output point(as shown in b of fig.4). Comprehensive form such as shown in table2, all kinds of transmission schemes: AB=a, BC=1, CD=b.

Table 2 The various states of transmission of making equivalent lever intermediate point B, C points as output point (except direct gear)

Serial numbers	Input points	Braking points	Transmission ratio	Remarks
①	A	D	(1+a+b)/b	deceleration shift
②	B	D	(1+b)/b	deceleration shift
③	D	B	1+b	deceleration shift
④	D	A	(1+a+b)/(1+a)	deceleration shift
⑤	B	A	a/(1+a)	overdrive shift
⑥	A	B	-a	reverse shift

Through the analysis of the table 2 and figure4, it shows that the transmission scheme of 01M AT adopts to be③④⑤⑥, when input points is changeless, only changing the braking points to realize the shift between deceleration gears. Rather than using ①②⑤⑥transmission scheme(by changing input points to shift between deceleration gears). Their transmission ratios are varies slightly between the adjacent deceleration gear as well, which is a reason that the shift smooth and manufacturing technology are greatly improved. From the above terms, undoubtedly ③④⑤⑥ transmission scheme is better than the①②⑤⑥transmission scheme. It could also be the designer's original intention of design of 01M AT. Other solutions are not comparable besides these two kinds of schemes of transmission design.

The inspection of rationality about the transmission scheme of 01N AT through the evaluation factors of transmission scheme. According to the literature 5 we know that: the evaluation factors of transmission scheme include: size parameters, process parameters, motion parameters and torque parameters etc.

The size parameters $K = \frac{Zr}{Zs}$, The value K directly affect the size of shape layout and weight of planet row, The value K scope is (1.4, 4.5), while the value K = 2.7, it is the best value; The process parameters $T = \frac{K\min}{K\max}$, The value T directly affect the manufacturing technology of gearbox and the scope is (0.33, 1), its value more close to 1, manufacturing technology will be better; The motion parameters $N = \frac{Ni(max)}{N_0}$, the size of the values of N is related to a bearing life, the value N scope is (0,3), the value N is bigger while the design requirement of bearing will be higher. The torque parameters $M_i = \frac{M_{max}}{M_0}$, The value Mi affect to be the required of strength and service life of the components, the value Mi should be as low as possible.

The value K of front planet row of 01N AT: K1=57/24=2.375, The value K of Rear planets row:

K2=36/21=1.714;T=K1/K2=0.722;N=2.714,which is transmission ratio of 1st gear; By the torque analysis we know that Mi=36/21+1=2.714.

Comprehensive three above aspects ,we can conclude that 01N AT which can realize 5 gears (include a reverse) possesses outstanding design in three dof double planetary gear mechanism.

Conclusion

Through the analysis above, it is clear that the leverage method is really more intuitive and convenient in the analysis of complex multiple rows of planetary gear in AT design and shift process performance than analytical method.

References

[1] Zhengsi Deng. Auto maintenance. Vol.10 (2007), p.30-35. (In Chinese).

[2] Chirs R, Ciesia M J. SAE paper. vol.2 (1995), p.238-246

[3] Zongyi Huang. Transmission technology. vol.2 (2003), p.18-25. (In Chinese)

[4] Liming Cao, Qinwu Geng etc. The maintenance essence of auto automatic transmission, edited by Mechanical industry Publications, (2006), p.448-450. (In Chinese)

[5] Guoqi He, Fangming Tan, Shaoliang Wang etc. Mechanical transmission. Vol.30 (2009), p.69-73. (In Chinese)

Advanced Materials Research Vols. 989-994 (2014) pp 2959-2961
© (2014) Trans Tech Publications, Switzerland
doi:10.4028/www.scientific.net/AMR.989-994.2959

Design and analysis of hydraulic piston structure exciter

Shijuan Wang, Kelong Yu

Eaestern Liaoning University,Dandong118003，Liaoning118003,P.R.China

yukelong1966@126.com

Keywords: vibration, the piston movement, leakage and sealing

Abstract: The movement characteristics of hydraulic exciting piston is a small displacement and high reversing frequency. The movement of the piston is to adapt to the requirement of quick reversing resistance. The mating surface seal uses to reduce the motion resistance to meet the requirements of the piston movement. Piston position should be in the oil chamber oil area to meet the requirements of the piston movement and oil circulation. Elastic beam with hydraulic cylinder is connected together . This structure is conducive to the piston and the connection of elastic beam and the installation of the oil cylinder. The causes of the different moving displacement of piston is leaking.

Introduction

Hydraulic vibrator vibration by piston movement. The vibration frequency of hydraulic vibrator is relatively low, but can produce larger output power value. Apply to the vibratory pile driver, vibration shear machine as well as the larger power works required. The vibration of hydraulic vibrator output form is based on the output of the piston displacement as its vibration amplitude, repeatedly mobile number per unit time is its vibration frequency. Thus to realize the two conditions of hydraulic vibrator vibration is entering piston hydraulic circuit quickly reversing and piston moving smoothly. In design and operation of the piston vibration encountered problems and solutions are put forward.

The piston vibration forming elements and analysis

Piston under certain frequency vibration should as far as possible to reduce the resistance of the piston motion. Design of a piston sealed often from the perspective of leakage. Piston seal on the set up multi-channel time. The seal under the action of the oil pressure, low tightly affixed to the hole wall and the large resistance. Reduce the resistance of the piston can remove seals, the use of mating surface seal form, or by a single sealing ring seal structure. In order to reduce power loss of the movement process of piston[1].

Piston elastic locating method is installed in one end of the piston stress smaller elastic element and elastic beam. Does not the installation of the oil cylinder fixed cylinder body, piston movement. The piston movement can put the elastic beam with fixed cylinder body is an organic whole repeatedly. So we can put the elastic and cylinder, piston of a unit.

As shown in figure 1 for the working principle of hydraulic vibrator. Hydraulic vibrator is by the hydraulic oil cylinder and the rotation type directional control valve.

The diameter of the connecting shaft at the ends of the piston is not the same. The right end shaft diameter greater than the diameter of the left end of the shaft. According to the change law of pressure at the ends of the piston hydraulic oil can be seen. Piston right cavity is high pressure oil workspace. The working chamber of the liquid pressure is not change. The left cavity of the piston working liquid pressure is changing. The oil pressure in the work place life is through the rotary valve constantly changing the inlet pressure, formation of a piston moving back and forth. In the process of the mobile, the work pressure of piston is equal. Leakage impact on the movement of the piston is not. The piston moves to the left, left cavity for the low pressure cavity of the piston. Right of piston chamber for the high pressure chamber. This is the influence of the leakage is the piston amplitude decrease. When the leakage of the vibration of the piston will be difficult to continue[2].

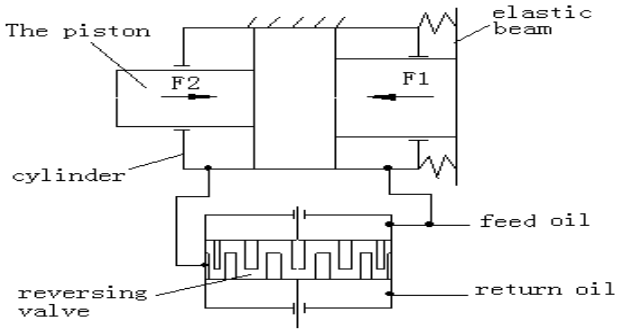

Figure 1. The working principle of hydraulic vibrator

According to the existing cylinder structure size. The diameter of the piston d=95mm, The sealing length $\ell = 5.75cm$,The piston and cylinder clearance $\delta = 0.7\times10^{-2}\,cm$

The oil of the severe : $\gamma = 0.9\times10^{-3}\,Kgf/cm^3$

The oil temperature 30°C，The oil pressure 3MPa. In 20 machine oil, for example. Kinematic viscosity of the oil ν=60 Li pool. According to the formula (1) calculate the leakage ΔQ[3]：

$$\Delta Q = \frac{\pi d\delta^3 \Delta p}{12\mu\ell}(1+1.5\varepsilon^2) \tag{1}$$

Type in the ： ε —The relative eccentricity gap

The structure of a rotary valve size: $d = 1.2\times10^{-1}$ m, $\ell = 5.75\times10^{-2}\,m$; $\delta = 7\times10^{-5}\,m$

The pressure difference：ΔP=3Mpa.The oil temperature t=30°C，The oil viscosity.

The dynamic viscosity of 20th hydraulic oil μ=1.8× $\mu = 1.8\times10^{-2}\,Pa\cdot s$

When the gap of relative eccentricity epsilon take 0.5 when calculating leakage are respectively $4.16\times10^{-5}\ m^3$ /s.This relative to the hydraulic pump output flow leakage is permitted. Piston leakage to the influence of vibration can be determined by the clearance between the piston and cylinder hole. The influence of the clearance is to leak to the influence of the piston displacement.

The piston is not the cause of the vibration piston end face contact with the cylinder face. Piston end face contact with the end of the cylinder rigid limit of piston displacement. Will be moved to the middle of the oil cylinder piston position, piston vibration. This phenomenon shows that the two content

One is the position of the piston to move. The piston vibration need a balanced position. The second is the piston itself cannot be rigidly. The piston can overcome force cannot be more than the most strongly from the piston. Otherwise the piston will lose excitation function.

Analyzing the piston to move right

If good seal piston in the process of vibration should shift to the left should not moves to the right. Can be showed by the following calculation:

The piston to the left movement of the thrust

$$F_1 = \frac{\pi}{4}(d^2 - d_1^2)p = 32.398\,p$$

Type in the: d —the piston diameter,95mm.

d_1 -- the left end diameter of piston rod,70mm。

The piston movement to the right of thrust

$$F_2 = \frac{\pi}{4}(d_1^2 - d_2^2)p = 25.918\,p$$

In the formula： d_2 -- the piston rod diameter，40mm.

Hydraulic system of the oil pressure under certain conditions, $F_1 > F_2$. So in the piston movement of a loop, mobile distance is greater than the distance to the right to the left. In fact in the process of the vibration of the piston piston moves to the right. Analysis of the cause of leakage is impact factor.

The piston moves to the right, the piston cavity pressure equal on both sides of the work. There is no leakage. Therefore, to the right total thrust F_2 is equal to the theoretical calculation values. On both sides of the piston cylinder volume change no leakage and the effect of the movement of the piston is associated with total thrust. The piston moves to the left, on both sides of the piston pressure difference exists. Working cavity leakage between the piston. Leakage is made by high pressure flow to the low pressure cavity. Due to leakage, high pressure cavity oil pressure ΔP, so the movement to the left when the total thrust F_1 is not equal to the theoretical calculation values. Due to the leakage at the same time, on both sides of the piston cylinder volume change affected by the spill. The piston of the actual displacement caused by the piston moves to the right[4].

In fact, the piston is working, inlet pressure fluctuations ΔP =1MPa. Assumes that the oil pressure of hydraulic system p =3MPa. Leakage caused by the piston working pressure =2MPa. The results is $F_1 < F_2$.

According to the structure of the piston can explain the reason of the piston moves to the right. In the piston movement of a cycle, the piston moves to the left, left the oil chamber of piston by flowing through the rotary valve oil distribution into the mouth rotary valve of low pressure cavity. Piston moves to the right of the rotary valve and pressure chamber high pressure oil by rotary valve oil distribution mouth to the left oil cavity of the piston[5].

In fact, when the piston moves left, on both sides of the piston pressure difference exists. The piston leakage between two working chamber. When the piston moves to the right, the pressure on both sides of the piston are equal, there is no leakage. When the piston moves left, the rotary valve oil distribution mouth oil discharge amount is quantitative. The piston right cavity left cavity leakage into the oil. So the piston left cavity clean oil discharge quantity decreased. When the piston moves to the right, the rotary valve oil distribution mouth feed and quantitative. The piston does not leak, so the piston moves to the right quantity is big, thus in the process of the vibration of the piston, the piston to the right.

Conclusion

Piston under certain frequency vibration should reduce the resistance of the piston motion. The piston rod with one sealing ring seal and the seal leakage of oil into the low pressure oil .

Using elastic beam is the necessary components to maintain the piston vibration. Elastic beam is connected to the cylinder body.The piston unit structure is compact.

Compared with ordinary mobile piston vibration,the displacement of a vibration piston is small and high frequency direction change. The piston in the reversing impact force is large. Should be used as much as possible with the face seal. The piston mating surface seals are used.

The influence of the leakage of piston on displacement should be controlled within the allowed number.

References

[1] Qiu Lijun, Yang Jia, Advanced Materials Research, V 322, p497-500.2012
[2] WANG Ji Wei, Zhang Wang A , Huang Yi hydraulic and pneumatic drive . Machinery Industry Press , 2012.6.p8-56
[3] Zhao Mingsheng, Mechanical engineer handbook, Second edition, Machinery Industry Press , 2001.3.p443-445
[4] Pu Lianggui, Mechanicaldesign, fifth edition, Higher education press . 1995.4.p8-62
[5] Zhang Deming . Hydraulic balancing circuit application examples analysis [J] . Hydraulic and pneumatic seals , 2007, (6) .

Advanced Materials Research Vols. 989-994 (2014) pp 2962-2964
© (2014) Trans Tech Publications, Switzerland
doi:10.4028/www.scientific.net/AMR.989-994.2962

Design of Underground Gas Concentration and Humidity Monitoring System Based on RS-485

Long Yuehong

College of Electrical and Information Engineering,Anhui University of Science and Technology ,Huainan 231001 China

Keywords: monitoring of gas concentration and humidity underground coal mine;MJC4/3.0L; HS1101; RS-485;RS-232;upper computer

Abstract: In order to achieve long distance monitoring of gas concentration and humidity underground coal mine,a new monitor of gas concentration and humidity,which contains upper computer,master station and a lot of monitoring points,is designed.Every monitoring point is consisted of gas concentration sensor MJC4/3.0L and humidity sensor HS1101,which is used to conveys the data to master station by RS-485,again by RS-485 transmitted to the upper computer and it realizes the real-time monitoring of gas concentration and humidity undereground coal mine.

Introduction: Recent years,gas accidents are happening with a high frequency,this has caused a certain number of casualties and economic losses and at the same time the environment underground the coal mine is the basic working conditions for miners and has a direct relationship with the miners's safety and the efficiency of the mine production.So to realize a real-time monitoring of the coal mine gas concentration and the humidity of the coal mine working face has a very important significance[1].Then a new type of detector composed of upper computer and multiple monitoring device has been designed.This design includes a main unit and multiple monitoring points.RS485 communication has been adopted between the main unit and the monitoring points.Distributed layout has been used in the process of actual installation.The main unit is mainly responsible for collecting the gas concentration and air humidity of the monitoring points ,and then transmit the collected data to the upper computer through the 485 bus.

If the upper computer uses the RS232 communication interface, a RS485 RS232 converter should be added to complete the protocol conversion. Each monitoring point is consisted of the gas concentration sensor MJC4/3.0 L and the humidity sensor HS1101. It's used to monitor the downhole gas concentration and the humidity of the air, and transmit data to the the master station via RS - 485 in order to realize the real-time monitoring of the gas concentration and the humidity underground coal mine.[2]

1.The overall design of the gas concentration and mine humidity detection system

The gas concentration and mine humidity detection system is mainly composed of upper computer, the main unit and multiple monitoring equipments. Each test equipment contains multiple monitoring points and the sensor of monitoring point is mainly composed of gas concentration sensor MJC4/3.0 L (catalytic combustion type gas sensitive element) and precision electric air humidity sensor HS1101. The two kinds of sensors of each monitoring point transmit the collected data values to the singlechip in the form of analog.The analog value the sensor transmits is 0-5 v voltage in this design. Design of the analog voltage reference should be paid attention when the simulation sampling circuit of the single chip microcomputer is designed.This design uses 5v dc voltage.To guarantee the quality of power supply in the process of actual use, too much interference shouldn't be used. So filter circuit should be added to filter the clutter in the power .After acquisition of the analog from the sensor,the single chip of the monitoring point transforms the collected analogue to the corresponding gas concentration and air humidity value by reading the number of the AD register, and then some corresponding formula transformation.Single chip then packs the collected data, waiting for the instruction of the main unit. Monitoring point will transmit the packed data to the master station after receiving the command of sending data.MCU of the testing point will process the received nformation from the sensor and then transmit it to the master station via RS - 485 .After receiving the data,the main unit transmits it to the upper computer via RS232 and displays it through the kingview software in the upper computer.[3]

The operating principle of the gas concentration sensor MJC4/3.0 L in the monitoring device is the catalytic combustion effect.[4]Detecting element and compensating element become two arms of a bridge. When faced with combustible gas,resistance of the detecting element increases, bridge circuit output voltage variation, and the variable voltage varies with gas concentration increases. workers should be on-site investigation, avoid the accident when see voltage exceed ratings .

The humidity sensor HS1101 of the test system is mainly used for the detection of underground air humidity. HS1101 is a capacity cell, its capacitance increases with the increase of the measured air humidity. [5]Workers should be on-site investigation when see the capacity increases to a certain degree.The overall system design is shown in figure 1.

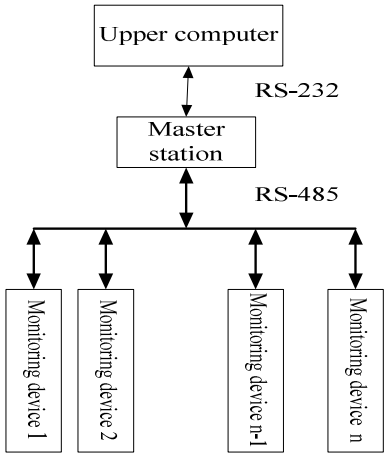

Figure 1: The system overall design

Table 1: Packet structure

start bit	A node	Humidity value	Calibration	check bit	stop bit

2. Sensor of the detection device

Sensors used in this system are the gas concentration sensor and the humidity sensor. They have good performance in measurement accuracy, corresponding speed, and pressure range.Here are the design of the sensor and the two chips were introduced.

1) **Gas concentration sensor**

The working principle of the catalytic element --MJC4/3.0 L is the catalytic combustion effect. Detecting element and the compensating element matching the two bridge arm of a bridge.

The detecting element resistance increases, when faced with gas combustible and the bridge circuit output voltage changes, the variable voltage varies with gas concentration increases. Its features are 1) bridge circuit output voltage is linear; 2) fast response; 3) has a good repeatability, selective; 4) components work stable and reliable; 5) resistance to H2S poisoning technical indicators.

2) **Humidity sensor**

Humidity sensor HS1101 has the following marked characteristics: 1) full interchangeability, does not need correction in a standard environment; 2) Long time fast dehumidifying under saturated 3) can be automated welding, including wave or water; 4) high reliability and stability for a long time; 5) patent solid polymer structure; 6) can be used in linear output voltage or frequency circuit; 7) rapid response time.

When the relative humidity is between 0% and 100% ,capacitance changed from 162 pF to 200 pF and the error is not greater than ±2% RH, response time is less than 5 s;temperature system is 0.04 pF /℃ . The accuracy of the humidity sensor is relatively high.

3. RS-485

RS-485 is a serial data communication, using two-way half-duplex communication protocols, its interface uses a combination of balance drive and the differential receiver ,it has a strong ability of common-mode interference, that is, good resistance to noise.

Software addressing is used in the RS - 485 . After the system is running, to make sure the RS-485 in each monitoring device has a unique address label,software addressing should be used.

When addressing for software, monitoring device can also save the host unit address, so monitoring device can communicate directly with the main unit point to point.

The main unit transmits data to the monitoring unit in the form of broadcast communication.Each monitoring device receives a packet.The monitoring will make some corresponding processing to the data when the received destination address matches its own. Packet structure is shown in table 1.

Due to this design contains multiple monitoring stations,if not controlled in actual use , there will be multiple monitoring points sending data at the same time , the correctness of the data transmission will be greatly reduced.

In order to solve this problem, this design uses the rotation machine to control the monitoring data transmission. For example, when the main unit need read the data of the monitoring stations 1, the main unit will send a read command to the whole network.

Each monitoring stations in the network will receive the read instructions, and then extract the address in it , if matching and the instruction is correct, then the corresponding monitoring will send the processed data to the main unit.

This mechanism has largely reduced the bit error rate in the process of communication, so as to improve the communication quality.

4. PC communication

The main unit receives data from various monitoring devices through RS485 bus and uses the single-chip microcomputer for data processing.

Data will be sent to the PC through the RS485 serial port after processing. The data will be displayed on the kingview software platform.

The software will number each monitoring point to make the display clear and intuitive.Even the monitoring point can check any historical record of the monitoring points.[6]

5. Summarize

The humidity of the gas concentration sensor designed in this paper adopts 1-wire bus specification, this makes the SCM read humidity and gas concentration signal via a data line. RS - 485 communication is used.To ensure safe and reliable in data transmission, no packet will be lost in the process of short distance communication.

6. References

[1] Feng Lei. Coal mine gas concentration monitoring and alarm system. [D] master's degree thesis, xi 'an university of electronic science and technology, xi 'an, 2010.

[2]Mao Deping,Lin Youzhu. A system of temperature and humidity measurement and control based on RS485.[J]The modern electronic technology2007(02)

[3] Wu Xingzhong OuQingLi. A design of PC and single chip machine RS232 serial port communication[J]. Journal of electronic measurement technology abroad. 2009 (01).

[4] Chen Liang. A design of a monitoring system of coal mine gas sensor hardware [J]. Journal of information science and technology. 2009 (16).

[5] Liu Pinzhen. Selection methods of humidity sensor[J]. Journal of monitoring instrumentation and analysis. 1990 (02).

[6] Hu Yuliang,Dong Guanjun. Design of PC software based on 51 single chip microcomputer .[J]. Journal of shanxi metallurgy, 2009 (01).

Advanced Materials Research Vols. 989-994 (2014) pp 2965-2969
© (2014) Trans Tech Publications, Switzerland
doi:10.4028/www.scientific.net/AMR.989-994.2965

Adaptive controller for ROV based on Hybrid theory

XIE Yehai
Kunming Shipborne Equipment Research & Test Center, Kunming 650051, China
E-mail: xieyehai@gmail.com

Keywords: ROV, adaptive, backsteeping, trajectory control

Abstract. In order to deal with the model uncertainties of ROV (remotely operated vehicles) caused by current disturbances, umbilical cable and robotic manipulators, an adaptive backstepping controller and an adaptive PD controller are applied to control the ROV. The adaptive backstepping controller is used to control the horizontal motion, and the adaptive PD controller is applied to control the Vertical motion. Finally, the method is verified effective by the computer simulation.

Introduction

There are various categories of unmanned underwater vehicles. The most often used underwater vehicle is a remotely operated vehicle (ROV) [1~8]. The ROV is usually connected to a surface ship by a tether, which all communication is wired through. Drag from the tether influences vehicle's motion and may represent significant disturbances and energy loss.

Some approaches have been studied to solve above challenges. In [1], the sliding variable structure control method is proposed to realize high precision trajectory control of ROV. An adaptive PID controller is designed to deal with the disturbances by ROV manipulators in [2]. The adaptive backstepping control was firstly developed to deal with model uncertainties of ROV [3].

The backstepping controller is designed to realize trajectory control for AUV under ocean current disturbance [11].

In this paper, in order to deal with the effect of ROV by environment disturbances, an adaptive backstepping controller and an adaptive PD controller are applied to control the ROV. The adaptive backstepping controller is used to control the horizontal motion of ROV, and the adaptive PD controller is applied to control the Vertical motion. Finally, the method is verified effective by the computer simulation.

ROV Model

The highly nonlinear, time-varying dynamic behavior of ROV continually changes the parameters of the system model [6~8]. The 6 DOF ROV equations of motion can be divided into the horizontal motion (surge, sway, yaw) and Vertical motion(pitch, heave).

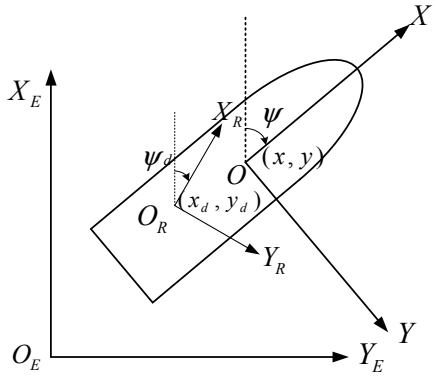

Fig. 1: Earth-fixed, reference-parallel and body-fixed frame

In ROV systems, the motions and state variables of the control system are defined and measured with respect to some reference frames or coordinate systems as shown in Figure. 1. The Earth-fixed reference frame is denoted as the $O_E - X_E Y_E Z_E$, the body frame is $O - XYZ$ see [1].

The horizontal model of ROV. The horizontal model of ROV in the frame can takes the form:

$$\begin{cases} \dot{\boldsymbol{\eta}}_1 = \boldsymbol{R}_1(\psi)\boldsymbol{v}_1 \\ \boldsymbol{M}_1\dot{\boldsymbol{v}}_1 + \boldsymbol{D}_1\boldsymbol{v}_1 = \boldsymbol{\tau}_1 + \boldsymbol{R}_1^{\mathrm{T}}(\psi)\boldsymbol{e}_1 \end{cases} \tag{1}$$

The state vector $\boldsymbol{\eta}_1 = [x, y, \psi]^{\mathrm{T}}$ is the position of the ship given in an inertial frame, $\boldsymbol{v}_1 = [u, v, r]^{\mathrm{T}}$ is the velocity vector in body frame $O-XYZ$.; $\boldsymbol{\tau}_1 = [\tau_{\mathrm{x}}, \tau_{\mathrm{y}}, \tau_{\psi}]^{\mathrm{T}}$ is the control vector consisting of forces and moments produced by the thruster system; $\boldsymbol{b}_1 \in \boldsymbol{R}^{3\times 1}$ is environmental disturbance. $\boldsymbol{M}_1$ is system inertia matrix including added mass; $\boldsymbol{D}_1$ is damping matrix:

$$\boldsymbol{M}_1 = \begin{bmatrix} m - X_{\dot{\mathrm{u}}} & 0 & 0 \\ 0 & m - Y_{\dot{\mathrm{v}}} & mx_G - Y_{\dot{\mathrm{r}}} \\ 0 & mx_G - N_{\dot{\mathrm{v}}} & I_z - N_{\dot{\mathrm{r}}} \end{bmatrix}, \quad \boldsymbol{D}_1 = \begin{bmatrix} -X_{\mathrm{u}} & 0 & 0 \\ 0 & -Y_{\mathrm{v}} & -Y_{\mathrm{r}} \\ 0 & -N_{\mathrm{v}} & -N_{\mathrm{r}} \end{bmatrix}$$

X_{u}, $X_{\dot{\mathrm{u}}}$, Y_{v}, $Y_{\dot{\mathrm{v}}}$, Y_{r}, $Y_{\dot{\mathrm{r}}}$, N_{v}, $N_{\dot{\mathrm{v}}}$, N_{r}, $N_{\dot{\mathrm{r}}}$, I_z is hydrodynamic coefficients, x_G is the surge coordinates to the center of gravity with respect to the point O in the body-fixed reference frame. $\boldsymbol{R}_1(\psi)$ is the transformation matrix:

$$\boldsymbol{R}_1(\psi) = \begin{bmatrix} \cos\psi & -\sin\psi & 0 \\ \sin\psi & \cos\psi & 0 \\ 0 & 0 & 1 \end{bmatrix}.$$

The Vertical model of ROV. If the rolling model is assumed to be negligible, this model reduces to the vertical model:

$$\begin{cases} \dot{\boldsymbol{\eta}}_2 = \boldsymbol{R}_2\boldsymbol{v}_2 \\ \boldsymbol{M}_2\dot{\boldsymbol{v}}_2 + \boldsymbol{D}_2\boldsymbol{v}_2 = \boldsymbol{\tau}_2 + \boldsymbol{R}_2^{\mathrm{T}}\boldsymbol{e}_2 \end{cases} \tag{2}$$

$\boldsymbol{\eta}_2 = [z, \theta]^{\mathrm{T}}$ is the depth and pitch angle of the ship given in an inertial frame; $\boldsymbol{v}_2 = [w, q]^{\mathrm{T}}$ is the heave vector and pitch angle vector in body frame $O-XYZ$; $\boldsymbol{\tau}_2$ is the control vector consisting of forces and moments produced by the thruster system; $\boldsymbol{b}_2 \in \boldsymbol{R}^{2\times 1}$ is environmental disturbance. $\boldsymbol{M}_2$ is system inertia matrix including added mass; $\boldsymbol{D}_2$ is damping matrix.:

$$\boldsymbol{M}_2 = \begin{bmatrix} m - Z_{\dot{w}} & -mx_G - Z_{\dot{q}} \\ -mx_G - M_{\dot{w}} & I_y - M_{\dot{q}} \end{bmatrix}, \quad \boldsymbol{D}_2 = \begin{bmatrix} Z_w & Z_q \\ M_w & M_q \end{bmatrix}$$

I_y is the moments of inertia about the; $Z_{\dot{w}}$, $Z_{\dot{q}}$, $M_{\dot{w}}$, $M_{\dot{q}}$ are add mass. The transformation matrix takes the form:

$$\boldsymbol{R}_2 = \begin{bmatrix} \cos(\theta) & 0 \\ 0 & 1 \end{bmatrix}.$$

The controller of ROV

In order to deal with the model uncertainties of ROV (remotely operated vehicles) caused by current disturbances, umbilical cable and robotic manipulators, an adaptive backstepping controller and an adaptive PD controller are applied to control the ROV.

The adaptive backstepping controller of horizontal motion. In the past decade, the backstepping control design procedures have been proposed in the literature [3, 10]. This control technique is a systematic and recursive design methodology for nonlinear systems, which offers a choice to accommodate the unmodeled nonlinear effects and parameter uncertainties. The idea of backstepping design is to select recursively some appropriate functions of state variables as pseudo-control inputs for lower dimension subsystems of the overall system. Each backstepping stage results in a new pseudo-control design, expressed in terms of the pseudo-control design from preceding design stages. The procedure terminates a feedback design for the true control input which achieves the original design objective by virtue of a final Lyapunov function which is formed by summing the Lyapunov functions associated with each individual design stage.

In this section, an adaptive backstepping controller is designed to controller surge, sway and yaw motion.

First, we defined the tracking error:

$$z_1 = \boldsymbol{\eta}_1 - \boldsymbol{\eta}_{1d} \tag{3}$$

$\boldsymbol{\eta}_{1d}$ is the desired state in an inertial frame.

A first Lyapunov function for the first error variable is defined as:

$$V_1 = \frac{1}{2} z_1^{\mathrm{T}} \boldsymbol{P}_1 z_1 \tag{4}$$

$\boldsymbol{P}_1 > 0$， $\boldsymbol{P}_1 = \mathrm{diag}\{p_{11}, p_{22}, p_{33}\}$ is a positive definite diagonal matrix.

The derivative of (4) is obtained as:

$$\dot{V}_1 = z_1^{\mathrm{T}} \boldsymbol{P}_1 \left(\boldsymbol{R}_1 \boldsymbol{v}_1 - \dot{\boldsymbol{\eta}}_{1d} \right) = -z_1^{\mathrm{T}} \boldsymbol{C}_1 z_1 + z_1^{\mathrm{T}} z_2 \tag{5}$$

With $\boldsymbol{C}_1 > 0$, $\boldsymbol{C}_1 = \mathrm{diag}\{c_{11}, c_{22}, c_{33}\}$ withis a positive definite diagonal matrix. The second error variable z_2 is given as:

$$z_2 = \boldsymbol{C}_1 z_1 + \boldsymbol{P}_1 \left(\boldsymbol{R}_1 \boldsymbol{v}_1 - \dot{\boldsymbol{\eta}}_{1d} \right) \tag{6}$$

The estimate of the vector $\hat{\boldsymbol{e}}_1$ is denoted, and the parameter estimation error is written.

$$\tilde{\boldsymbol{e}}_1 = \hat{\boldsymbol{e}}_1 - \boldsymbol{e}_1 \tag{7}$$

The candidate Lyapunov function in this case is defined as:

$$V_2 = V_1 + \frac{1}{2} z_2^{\mathrm{T}} \boldsymbol{P}_2 z_2 + \frac{1}{2} \tilde{\boldsymbol{e}}_1^{\mathrm{T}} \boldsymbol{\Gamma}^{-1} \tilde{\boldsymbol{e}}_1 > 0 \tag{8}$$

where $\boldsymbol{P}_2 > 0$, $\boldsymbol{P}_2 = \mathrm{diag}\{f_{11}, f_{22}, f_{33}\}$ and $\boldsymbol{\Gamma}_2 > 0$, $\boldsymbol{\Gamma} = \mathrm{diag}\{\gamma_{11}, \gamma_{22}, \gamma_{33}\}$ are a positive definite diagonal matrix.

The derivative of (8) is obtained as:

$$\dot{V}_2 = -z_1^{T} \boldsymbol{C}_1 z_1 + \frac{1}{2} \tilde{\boldsymbol{e}}_1^{\mathrm{T}} \boldsymbol{\Gamma}^{-1} \dot{\hat{\boldsymbol{e}}}_1 + z_2^{\mathrm{T}} \boldsymbol{P}_2 \boldsymbol{P}_1 \boldsymbol{R} \boldsymbol{M}_1^{-1} \left(\boldsymbol{\tau}_1 - \boldsymbol{D}_1 \boldsymbol{v}_1 + \boldsymbol{R}_1^{\mathrm{T}} \boldsymbol{e}_1 \right) + z_2^{\mathrm{T}} \left(z_1 + \boldsymbol{P}_2 \boldsymbol{C}_1 \dot{z}_1 + \boldsymbol{P}_2 \boldsymbol{P}_1 \left(\dot{\boldsymbol{R}}_1 \boldsymbol{v}_1 - \ddot{\boldsymbol{\eta}}_{1d} \right) \right) \tag{9}$$

Collecting terms in $\tilde{e}_1$, yields:

$$\begin{aligned} \dot{V}_2 &= \tilde{\boldsymbol{e}}_1^{\mathrm{T}} \boldsymbol{\Gamma}^{-1} \left(\dot{\hat{\boldsymbol{e}}}_1 - \boldsymbol{\Gamma} \boldsymbol{R}_1 \boldsymbol{M}_1^{-\mathrm{T}} \boldsymbol{R}_1^{\mathrm{T}} \boldsymbol{P}_1 \boldsymbol{P}_2 z_2 \right) + z_2^{\mathrm{T}} \left(z_1 + \boldsymbol{P}_2 \boldsymbol{C}_1 \dot{z}_1 + \boldsymbol{P}_2 \boldsymbol{P}_1 \left(\dot{\boldsymbol{R}}_1 \boldsymbol{v}_1 - \ddot{\boldsymbol{\eta}}_{1d} \right) \right) \\ &+ z_2^{\mathrm{T}} \boldsymbol{P}_2 \boldsymbol{P}_1 \boldsymbol{R}_1 \boldsymbol{M}_1^{-1} \left(\boldsymbol{\tau}_1 - \boldsymbol{D}_1 \boldsymbol{v}_1 + \boldsymbol{R}_1^{\mathrm{T}} \hat{\boldsymbol{e}}_1 \right) - z_1^{\mathrm{T}} \boldsymbol{C}_1 z_1 \end{aligned} \tag{10}$$

The parameter adaptation law:

$$\dot{\hat{\boldsymbol{e}}}_1 = \boldsymbol{\Gamma} \boldsymbol{R}_1 \boldsymbol{M}_1^{-\mathrm{T}} \boldsymbol{R}_1^{\mathrm{T}} \boldsymbol{P}_1 \boldsymbol{P}_2 z_2 \tag{11}$$

The control force

$$\boldsymbol{\tau}_1 = \boldsymbol{D}_1 \boldsymbol{v}_1 - \boldsymbol{R}_1^{\mathrm{T}} \hat{\boldsymbol{e}}_1 - \boldsymbol{M}_1 \boldsymbol{R}_1^{\mathrm{T}} \left(\dot{\boldsymbol{R}}_1 \boldsymbol{v}_1 - \ddot{\boldsymbol{\eta}}_{1d} \right) - \boldsymbol{M}_1 \boldsymbol{R}_1^{\mathrm{T}} \boldsymbol{P}_1^{-1} \left(\boldsymbol{C}_1 \dot{z}_1 + \boldsymbol{P}_2^{-1} \left(z_1 + \boldsymbol{C}_2 \boldsymbol{Z}_2 \right) \right) \tag{12}$$

$\boldsymbol{C}_2 > 0$, $\boldsymbol{C}_2 = \mathrm{diag}\{\lambda_{11}, \lambda_{22}, \lambda_{33}\}$ is a positive definite diagonal matrix.

Finally yields $\dot{V}_2$ non-positive by

$$\dot{V}_2 = -z_1^{\mathrm{T}} \boldsymbol{C}_1 z_1 - z_2^{\mathrm{T}} \boldsymbol{C}_2 \boldsymbol{Z}_2 \le 0 \tag{13}$$

Thus the system is globally asymptotically stable, that is to say that z_1 converge to 0.

The adaptive PD controller of Vertical motion. Vertical motion of ROV include the heave motion and the pitch motion.The robustness of the 6 DOF adaptive PD controller is illustrate by [2]. In this paper, a 6 DOF adaptive PD controller is paoposed:

$$\begin{cases} \dot{\hat{\boldsymbol{e}}}_2 = -\boldsymbol{\Gamma} \boldsymbol{\Phi}^{\mathrm{T}} (\boldsymbol{\eta}_2) \left(\dot{\boldsymbol{\eta}}_2 + \dfrac{\varepsilon_0}{1 + a \left\| \tilde{\boldsymbol{\eta}}_2 \right\|} \tilde{\boldsymbol{\eta}}_2 \right) \\ \boldsymbol{\tau}_2 = -\boldsymbol{R}_2^{\mathrm{T}} \boldsymbol{K}_P \tilde{\boldsymbol{\eta}}_2 - \boldsymbol{R}_2^{\mathrm{T}} \boldsymbol{K}_D \dot{\boldsymbol{\eta}}_2 + \boldsymbol{R}_2^{\mathrm{T}} \boldsymbol{\Phi} (\boldsymbol{\eta}_2) \hat{\boldsymbol{e}}_2 \end{cases} \tag{14}$$

$\tilde{\boldsymbol{\eta}}_2 = \boldsymbol{\eta}_2 - \boldsymbol{\eta}_{2d}$ is the position error, $\hat{\boldsymbol{e}}_2$ is the estimate environment force, $\boldsymbol{\eta}_{2d}$ is reference trajectory, $\boldsymbol{\Phi}^{\mathrm{T}} (\boldsymbol{\eta}_2)$ is the regression matrix, $\varepsilon_0 < 1$ and a are positive constants; $\boldsymbol{\Gamma} \in \boldsymbol{R}^{2\times 2}$， $\boldsymbol{K}_P \in \boldsymbol{R}^{2\times 2}$， $\boldsymbol{K}_D \in \boldsymbol{R}^{2\times 2}$ is a positive definite matrix.

Simulation Research

To demonstrate the performance of the proposed controller in this paper, the ROV called "Ukwiał" is used as case study, the ROV having 1.5 m long and having a propulsion system consisting of 6 thrusters. The following ROV model of dynamics has been used in the computer simulation:

$$\boldsymbol{M} = \mathrm{diag}\{\ 99.0,\ \ 108.5,\ \ 126.5,\ \ 8.2\ \ 32.9,\ \ 29.1\}$$

$$\boldsymbol{D}(\boldsymbol{v}) = \mathrm{diag}\{10.0,\ \ 0.0,\ \ 0.0,\ \ 0.223\ \ 1.918,\ \ 1.603\} + \mathrm{diag}\begin{Bmatrix} 227.18|u|, & 405.41|v|, & 478.03|w| \\ & 3.212|p|, & 14.002|q|, \quad 12.937|r| \end{Bmatrix}$$

$$\boldsymbol{C} = \begin{bmatrix} 0 & 0 & 0 & 0 & 26.0w & -28.0v \\ 0 & 0 & 0 & -26.0w & 0 & 18.5u \\ 0 & 0 & 0 & 28.0v & -18.5u & 0 \\ 0 & 26.0w & -28.0v & 0 & 5.9r & -6.8q \\ -26.0w & 0 & 18.5u & -5.9r & 0 & 1.3p \\ 28.0v & -18.5u & 0 & 6.8q & -1.3p & 0 \end{bmatrix} \quad \boldsymbol{g}(\boldsymbol{\eta}) = \begin{bmatrix} -17.0\sin(\theta) \\ 17.0\cos(\theta)\sin(\varphi) \\ 17.0\cos(\theta)\cos(\varphi) \\ -279.2\cos(\theta)\sin(\varphi) \\ -279.2\left(\sin(\theta)+\cos(\theta)\cos(\varphi)\right) \\ 0 \end{bmatrix}$$

Simulation experiments were made for tracking control under interaction of sea current disturbance (speed 0.5 m/s, direction 30^0). The matrix $[30,-70,30,0,0,0]$ is used as the by umbilical cable and robotic manipulators. The vehicle was assumed to follow the trajectory beginning from position and orientation:

$$\begin{cases} x = \dfrac{3}{500s+1} \\ y = \dfrac{10}{500s+1} \\ z = 10 \\ \theta = 0^\circ \\ \psi = 50^\circ \end{cases},$$

the vessel controller gains are shown in table 1 and table 2. The simulation curve shown in Figure 2 and Figure 3.

Table 1 The gains of adaptive backstepping controoler

Matrix	Diagonal element		
$\boldsymbol{\Gamma}$	2.6	2.0	2.4
$\boldsymbol{P}_1$	2.4	1.8	3.2
$\boldsymbol{P}_2$	2.9	1.5	4.9
$\boldsymbol{C}_1$	2.8	3.2	2.8
$\boldsymbol{C}_2$	2.4	3.3	4.3

Table 2 The gains of adaptive PD controller

Matrix	Diagonal element
$\boldsymbol{K}_p$	$\boldsymbol{M}\times 0.016$
$\boldsymbol{K}_d$	$\boldsymbol{M}\times 0.8$
$\boldsymbol{\Gamma}$	[2,0;0,1]
ε_0	0.6
a	2
$\boldsymbol{\Phi}$	[1,1;1,1]

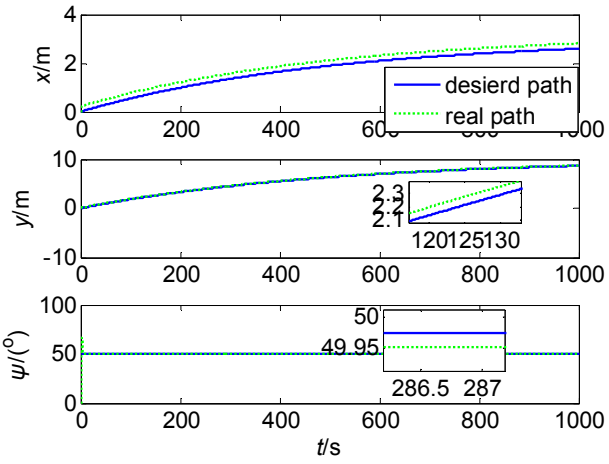

Figure 2 The simulation curve of adaptive backstepping controller

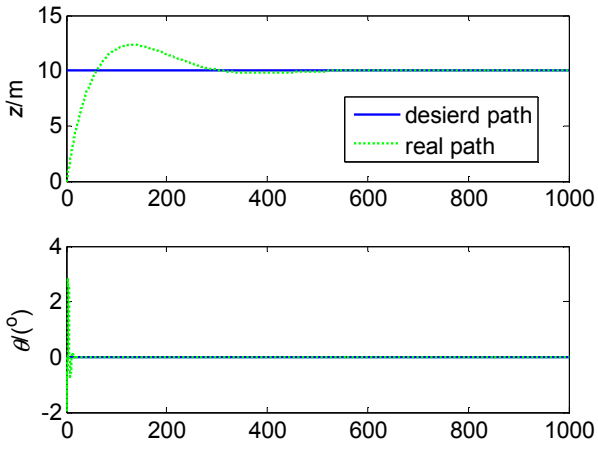

Figure 3 The simulation curve of adaptive PD controller

From Fig.2 and Fig.3, we can see that the adaptive backstepping controller and an adaptive PD controller output was smooth,meanwhile, the controller provid good dynamic response performance and small tracking error.

Conclusions

In this paper, the adaptive backstepping controller and an adaptive PD controller is proposed to deal with the model uncertainties of ROV, which is caused by current disturbances, umbilical cable and robotic manipulators.The simulation results show the proposed controller performs well with stability and robustness and can improve the accuracy of ROV.

References

[1] Rui M F Gomes, José B S, Fernando L P. Integrated maneuver and control design for ROV operations[C]// International conference on Oceans, San Diego, USA, 2003:703-710.

[2] Nguyen Q H, Edwin K. Adaptive PD-controller for positioning of a remotely operated vehicle close to an underwater structure: Theory and experiments [J]. Control Engineering Practice, 2007, 15(4): 411-419.

[3] Fossen T I, Sagatun S I. Adaptive control of nonlinear underwater robotic systems. International conference on Robotics and Automation, Sacramento ,1991:1687-1694.

[4] Sjoerd van der Z, José S V. Real-time Vision-based Station Keeping for Underwater Robots, IEEE Conference on OCEANS, 2001:1058-1065.

[5] Whitcomb L L. Underwater robotics: out of the research laboratory and into the field[C]// IEEE 2000 International conference on robotics and automation, San Francisco, 2008: 709-716.

[6] David S, Ralf B, Louis W. A New Remotely Operated Underwater Vehicle for Dynamics and Control Research[C]// In Proceedings of the 11th International Symposium on Unmanned Untethered Submersible Technology, Durham, NH, 1999: 370-377.

[7] Gomes R M F, Sousa J B, Pereira F L. Modeling and control of the IES project ROV

[8] Robert E P, Wayne A P, Greene H G, Don G. Conducting Visual Surveys with a Small ROV in Shallow Water. Marine Habitat Mapping Technology for Alaska, 2008: 109-128.

[9] Wang XL, Liu D, Shan X X. Study on the Three Dimensional Trajectory Control for Airship [J]. Journal of Shanghai Jiao tong University, 2006,40 (12) :2164-2168.

[10] Vladimir D, Dulan. Command filtered backstepping design in MOOS-IvP helm[C]// Proceedings of the2010 American Control Conference, ACC2010. Piscat-away United states: IEEE Computer Society. 2010: 5997-6003.

[11] Shi S W, Yan W S, Gao J. Path-following Control of an AUV in the Horizontal Plane with Constant Ocean Currents[J]. ACTA ARMAMENTARII, 2010, 31(3) :375-380.

Advanced Materials Research Vols. 989-994 (2014) pp 2970-2974
© (2014) Trans Tech Publications, Switzerland
doi:10.4028/www.scientific.net/AMR.989-994.2970

Data Storm Monitoring System of Large Power Industrial Control Network under Non uniform Format

Lang Liao[1,a], Yonghong Huang[2,a], Changjiang Zhao[3,a]

[1.]Department of Computer Science, Shenzhen Institute of Information Technology, ShenZhen GuangDong 518172, China;
[2.]Chongqing University of Posts and Telecommunications ChongQing 400065, China
[3.]Chongqing University of Posts and Telecommunications ChongQing 400065, China
[a]22900699@qq.com

Keywords: large power industrial control network; network security; data storm; data storm monitoring

Abstract. In the high power industrial control network, due to the large user base, the data traffic is plodding, the data formats are inconsistent, the network data storm is difficult to monitor. A kind of high power industrial control network data monitoring and control system is designed under non-uniform formats. The network node information collector is designed, the data is collected, and the data collection result is taken as the mathematical expectation, the mathematical expectation is trained. The problem of data flow storm statistics is solved. In the system, the format conversion function is added, data storm monitoring results is taken with the format conversion, and they are stored as text format. The monitoring program reads and displays the result, the difficulties brought by the format is not unified are solved. System test results show that the system can monitor the large power industrial control network data storm, the monitoring result is precise, and it can make the formatting process fast. A size of the generated result file is 18.1%, of the original file, and can fully reflect the network data storm characteristics, the effect is perfect.

Introduction

With the deepening development of network technology and digital technology, the large power industrial control network is getting more and more important in electric power plant, and the military system. The large power industrial control network is widely applied in different areas. The large power industrial control network application is developing rapidly, and the technology us upgrading constantly, because the user base is too large, the number of computers is large. The network data storm data is very complex, so the monitoring crisis is increasing gradually[1].

In the high power industrial control network, due to the large user base, the data traffic is plodding, the data formats are inconsistent, the network data storm is difficult to monitor. A kind of high power industrial control network data monitoring and control system is designed under non-uniform formats[2]. The network node information collector is designed, the data is collected, and the data collection result is taken as the mathematical expectation, the mathematical expectation is trained. The problem of data flow storm statistics is solved. In the system, the format conversion function is added[3], data storm monitoring results is taken with the format conversion, and they are stored as text format. The monitoring program reads and displays the result, the difficulties brought by the format is not unified are solved. System test results show that the system can monitor the large power industrial control network data storm, the monitoring result is precise, and it can make the formatting process fast. The simulation result shows that the new method has good performance in application.

System design principle

The design of system module mainly includes 2 parts: coordination monitoring module, and the system operation module, the system module structure is shown in Figure 1. The main functions of the system include:

Figure 1 System module structure

(1) Monitoring new data storm nodes continuously in real-time, each of the data information are collected with sub module, and it is allocated with the only identification code in gather module distribution.

(2) Waiting for the feedback data of storm nodes monitoring results, the self organization method is adopted to transmit each node monitoring module data, upload to the coordinator module storage unit.

(3) In the coordinator module, automatic centralized data collected by the storm monitoring system is transmitted to the control center, in the control center, the monitoring algorithm is used to analyze the data storm data in real time, the network can be used to monitor real-time network data storm and control the relevant data sending program[4].

The flow chart of network monitoring module is shown in Figure 2, the main functions include:

(1) Initialization module, the self-organization mode is taken for adding the nodes to the network storm monitoring area;

(2) Obtain sole identification code of data storm from the coordinator node, and monitoring network control information.

(3) Acquisition network data storm information data timing, and data storm monitoring algorithm is designed to analyze the data, the data is transmitted to the coordinator node.

(4) Executes operation step (3), until leaving the monitoring area network.

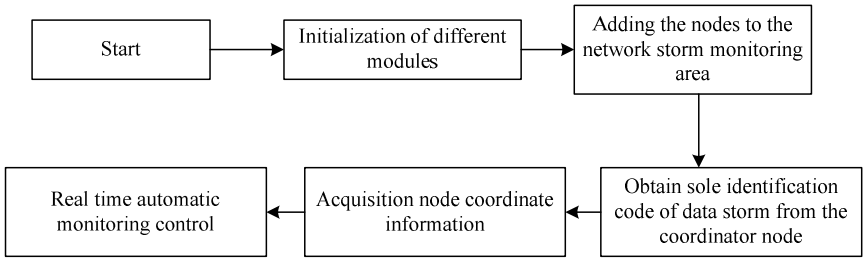

Figure 2 Flow chart of monitoring system design flow chart

Monitoring system design

A.Design of data acquisition module of network node data storm

This function module is affected by the underlying network greatly, and the large power industrial control network should be controlled[5], the network data storm should be managed, we must maintain the real-time monitoring of large power industrial control network data, to determine the statistical characteristics of the data storm, the statistical characteristics are calculated. The information collector is used to receive the data storm information, so the structure diagram of the module is shown in Figure 3.

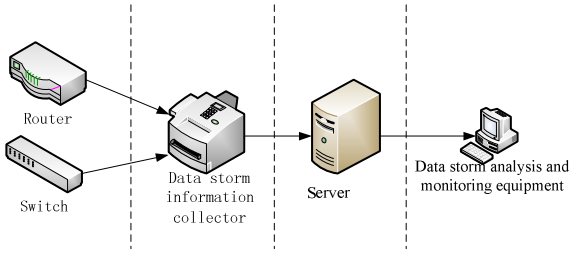

Figure 3 Structure diagram of data storm monitoring module

In the large power industrial control network system, the network switch and router are used to analyzed the statistics of storm data, the result is transmitted to the information collector, and the information collector is summarized to the server, and then passed to the data analysis and monitoring equipment to monitor the storm, this function is implemented on the Windows platform, data statistics calculation and storm display can be realized with this method, and according to the data statistics result, the monitoring can be realized, and the VC++6.0 is used for the program realization, including data processing module and data statistics module of the storm.

The information collector is the core module of monitoring nodes, the to complete the analysis of the network interface data acquisition, data statistics and storm monitoring function, in the data analysis process, the network intrusion feature can be detected, the process is shown in Figure 4.

The machine IP address is realized by the C++ function, gethostname function and gethostbyname function are designed, at the same time, the cache setting is obtained, the socket and a port number are created, and the thread is started. The AIP function of Microsoft is used to count the IP data, and the statistics information of network data storm can be calculated, according to monitoring changes in network performance, the network data storm trend can be predicted.

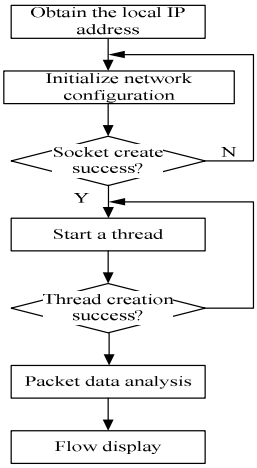

Figure 4 Monitoring module design process

B.Network data storm flow module design

In order to monitor the network data storm, the network flow should be flowed effectively, for any kind of shunt method, the basic functions of the network data storm is important, it is divided into stream files, and the process will include the source IP address, source port, destination IP address, destination port and protocol, etc. form a complete stream file. The mechanism of this process is relatively simple, but with the rapid development of P2P network, data network storm become extremely complex, data redundancy is increasing, and it should be removed. How to flow the massive data with several GB is difficult, and the process research is important. We should realize the rapid flow of network data the storm in the Windows environment.

In the large power industrial control network, the user most contains the engineers and workers at the grass-roots level, the data storm whereabouts is mainly plant room and staff accommodation, the user is divided in accordance with the regional division, in each area, the information collector is installed. The data is captured in three hour, the compressed data storm is crated with the file, and the size is 10GB. After the conversion trace, the original pcap file is more than 3 times with conversion, and the data packet task is huge. In the process of storm tracks, the data storm test and comprehensive are balanced in efficiency.

Before the bypass flow, the data storm trace files are extracted, based on network data storm, the network data storm will have the same elements which are similar to class files, and these elements are referred as source IP address, source port, destination IP address, destination port and protocol as above. For testing the network data storm in different period data, the protocol is analyzed, the results is expressed in table 1.

Table 1. Document classification of data collection protocol

	UDP	TCP	IPv6	Other	Total number
1	67.1%	30.1%	1.0%	1.8%	1814391
2	67.3%	30.1%	0.9%	1.7%	258315
3	67.1%	30.3%	0.3%	1.6%	539341

According to the statistics results, the TCP protocol and UDP protocol files are taken about more than 97%, and other data storm file types and the ratio is no more than 3%, there exists only a small amount of IP protocol and IPv6 protocol file. So the protocol type rare special data package is ignored, so as to accelerate the speed of flow analysis. Because the file of data trace is large, and it occupies more space in memory, the random sampling of the data file is captured in export mirror at the storm data, in different periods, the parallel and serial operations are taken, and the test time is five minutes and ten minutes. The process is shown in Figure 5.

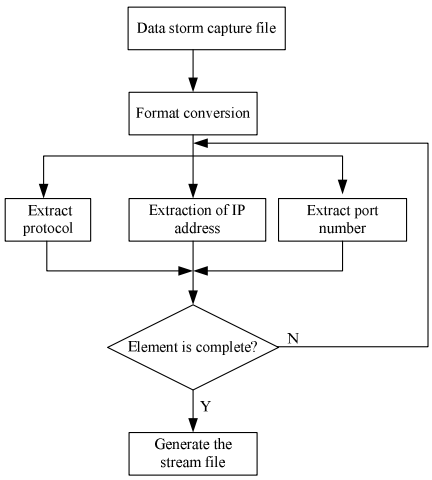

Figure 5 Network data distribution process

Test result and analysis

In the simulation, the local area network of a college is taken as the example, and modules are tested, the information collector is designed to collect all the storm of campus network in 60 seconds, and the captured data set is saved as pcap format, the format conversion is taken to generate the TXT text file. The data pretreatment is taken, and the GA-BP neural network with multi input multi output (MIMO) is used for training, the training expected value is provided by the stream file generated in advance. After generating the TXT text file, the result is shown in interface as display, by the use of data storm, the scheduling is obtained to facilitate the administrator. The system structure is shown in Figure 6.

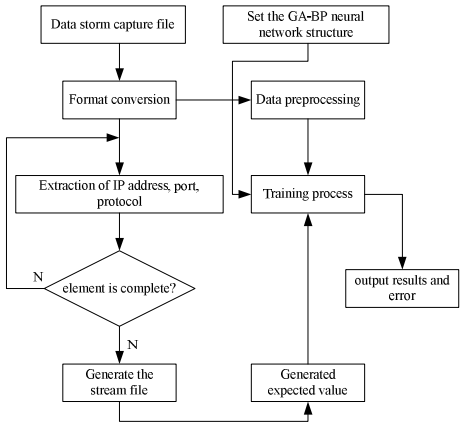

Figure 6. Structure of the overall system

The distribution results of network data storm is shown in Table 2, we can conclude that, in single threaded mode, just a few minutes of continuous time, it also needs 2 hours or more time for distribution, and it affect real time performance of storm monitoring system. The new BP neural network algorithm based on GA, the processing time is reduced.

Table 2. Storm distribution result record

	Data length	Distribution time	File size
1	60s	1459s	1.28GB
2	120s	3091s	2.11GB
3	300s	7851s	5.68GB

The BP neural network algorithm based on GA, the algorithm of the initial file is set, and the data pre-processing storm file, and set the BP neural network structure, the expected value according to the statistical results average worth, and the split files display division of the regional network evolution, to display the shunt factory of each room and staff accommodation data storm. The network storm data is monitored for 60 seconds, and the monitoring results are expressed as follows: Data length of data storm is 80s, and the training time is 24781s, the result display time is

143s, and the size of TXT file is 232MB, the success rate of abnormal data storm monitoring is 89%. It shows that the new method has better monitoring performance in application.

Conclusion

In this paper, a big power network data storm monitoring system is designed under non uniform format, the distribution time consumption is reduced, and the monitoring results are streamlined and display, the data duration reduced to 80 seconds, and the TXT format can be saved safely, the size is reduced to 232MB, and it is 18.1% of original TXT, the volume occupied effect is reduced effectively, and the data availability is good, the system has certain practical application in prospect.

Acknowledgement

Supported by the MOE（Ministry of Education in China）Project of Humanities and Social Sciences : “Rules of Electronic Evidence in Criminal Procedure"（Project No.13YJC820109）

References

[1] ZHANG Ren-shang. Network Intrusion Detection System Based on Expert System and Neural Network[J]. Computer Simulation. 2012; 29(9): 162-165.
[2] Ke Hua-mingl, Chen Chao-zhenl, etc. Application of BP neural network classification with optimization of genetic algorithm for remote sensing imagery based on Matlab[J]. Journal of Southwest University of Science and Technology, 2010, 3(2): 127-131.
[3] Zhu Hong. Fault Diagnosis for Analog Circuits Based on D-S Evidence Theory and PSO Neural Network[J]. Computer Measurement & Control. 2013; 21(4): 868-870.
[4] Zhao Juan, Zhao Qiang, Wu Fenxia. Self-organizing Map Neural Network Based Image Retrieval Algorithm[J]. Bulletin of Science and Technology. 2013; 29(2): 55-57.
[5] SHAN Dong-hong, ZHAO Wei-ting. Research on Intrusion Detection System Neural Networks and Principal Component Analysis[J]. Computer Simulation. 2011; 28(6): 153-156.

Advanced Materials Research Vols. 989-994 (2014) pp 2975-2979
© (2014) Trans Tech Publications, Switzerland
doi:10.4028/www.scientific.net/AMR.989-994.2975

Design and calculation of a new type of elastic gear coupling and finite element analysis

Chen Feng[1, a] , Li Zheng-feng[1, b], Liu Yuan-xiang[1, c]

[1]Wuxi Institute of Commerce，Wuxi，214153，China
[a]chenfeng790923@163.com,[b]lizhengfeng@edu.cn,[c]liuyuanxiang@edu.cn

Keywords: elastic, gear coupling, design, finite element analysis

Abstract： This paper introduces a new type of elastic gear coupling structure, and gives the calculating strength formula and related material of the parts, establishes the three-dimensional model, simulates the nonlinear elastic gear ring, gets the analysis of the distribution of strain and stress in the ANSYS software, verify the strength condition.

0 Introductions

Couplings are usually used to connect two axis and transfer movement and power. According to the difference of compensating the migration ability, couplings can be divided into two categories, named rigid coupling and flexible coupling. Flexible couplings are divided into non elastic element coupling and flexible coupling. Gear coupling is a kind of no elastic coupling which connect the two half parts using internal and external gear meshing. It can transfer large torque, high speed, with reliable work, low requirement on installation accuracy, but the structure is complicated, with difficult manufactory, high cost [1]. We design a new type of elastic gear coupling, try to keep the advantages of gear coupling that can transfer large torque, and has the feature of shock absorption.

1 The structure of elastic gear coupling

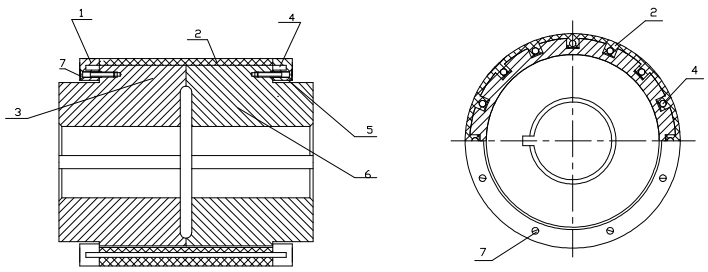

1 Left circlip
2 elastic gear ring
3 left half coupling
4 strengthen shaft
5 right circlip
6 right half coupling
7 screws

Fig. 1 The sketch of the elastic gear coupling

The elastic gear coupling's structure is shown in Figure 1, the two half couplings are connected through a elastic gear ring 2, each tooth of the ring embedded with strengthening shafts 4, which is inserted into the hole of left circlip 1 and right circlip 5 [2]. Aim at the following advantages: obtain the stability of transmission, without rigid impact and noise; can compensate the larger axial displacement, small radial and angular displacement; no need of lubrication.

2 The strength of elastic gear coupling

2.1 Working torque

According to Mechanical Design Manual, the working torque is: $Tc=K_wKK_zK_tT$ (1)

Where T is the nominal torque; K_w is the power coefficient; K is condition coefficient; K_z is starting condition coefficient; K_t is the temperature coefficient [3].

2.2 The size and material determination of strengthen shaft

According to the "mechanical design manual", referring to the elastic pin sleeve coupling size relationship, the distribution diameter of strengthen shaft is: $D=(15\sim16.5)\sqrt[3]{Tc}$ (2)

The shear force of each strengthening shafts Fs:

$$Fs = \frac{2Tc}{\mathrm{D}n} \times \varphi \quad (3)$$

Where Dn is the distribution diameter of strengthen shafts; n is strengthening shafts' number; φ is uneven coefficient of each tooth.

According to mechanics of materials, calculate the shear strength condition of strengthen shafts:

$$\tau_{\max} = \frac{4}{3} \frac{4Fs}{\pi \mathrm{D}^2} \le [\tau] \quad (4)$$

According to the "mechanical design manual", refer to the elastic pin sleeve coupling bending strength condition, calculate the bending strength condition of strengthen shafts:

$$\sigma_{\max} = \frac{10Tc(l+2c)}{0.8D\mathrm{n}d^3} \le [\sigma] \quad (5)$$

Where l is the width of the elastic ring; C is the clearance of two half couplings' ends; D is the distribution diameter of strengthen shafts; d is the diameter of strengthen shafts; $[\sigma]$ is the allowable bending stress of strengthen shafts , and generally $[\sigma]$=（0.4～0.5）σ_s.

2.3 Strength check of elastic ring

Calculate the tooth surface pressure:

$$\mathrm{P} = \frac{2Tc}{nhlD} \le [p_p] \quad (6)$$

Where h is height of tooth; l is width of tooth ring.

3 The design example of the elastic gear coupling

The couplings are used for the plate chain conveyor, the requirements are: working torque is 500N.m, transmission power is 3.5kW, and compensating capacity shall reach or better than the flange coupling and hydraulic coupling.

In order to reduce manufacturing difficulty and cost, consider using a standard synchronous toothed belt with the strengthening shafts. According to the synchronous toothed belt main dimensions and parameters in national standard, select XH type synchronous belt, as an example, carries on the design calculation. According to the formula (1), (2), (3), calculate the shear force of each strengthening shafts Fs:

$$\mathrm{Fs} = \frac{2Tc}{\mathrm{D}n} \times \varphi \frac{2 \times 600 \times 10^3}{130 \times 20 \times 0.7} = 659.25N$$

According to the formula (4), calculate the shear strength condition of strengthen shafts:

$$\tau = \frac{4}{3} \frac{4Fs}{\pi \mathrm{D}^2} = \frac{4}{3} \times \frac{4 \times 659.25}{3.14 \times 141.56^2} = 0.056\mathrm{Mpa}$$

It is found that the strengthening shaft shear capacity was enough, the shear stress is much less than the allowable stress of metallic material.

According to the formula (5), calculate the bending strength condition of strengthen shafts:

$$\sigma = \frac{10Tc(l+2c)}{0.8D\mathrm{n}d^3} = \frac{10 \times 600 \times 10^3 \times (101.6 + 2 \times 2)}{0.8 \times 130 \times 20 \times 7^3} = 888\mathrm{Mpa}$$

Check the "Material Handbook" to meet the requirements of the material, can select GCr15 bearing steel, or spring alloy steel. Geometry may refer to the material and size of needle for roller bearing.

According to the formula (6), calculate the surface pressure of elastic ring's teeth:

$$p = \frac{2Tc}{nhlD} = \frac{2 \times 600 \times 10^3}{20 \times 6.35 \times 101.5 \times 130} = 0.72\mathrm{M}pa$$

General rubber allowable pressure $[p_p]$ =2~2.5Mpa, so extrusion strength with the rubber ring's teeth was enough.

4 Modeling and analysis of elastic gear coupling

Establish the coupling model shown in figure 2 in the Pro/E software. And transfer the model to the finite element analysis software ANSYS to do mechanical analysis.

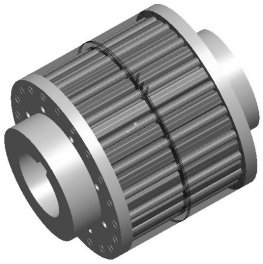

Fig.2 Elastic gear coupling model

The elastic gear coupling ring is composed by rubber layer and the strengthening layer etc, in this analysis, the elastic ring is simplified to a single rubber material. In order to simplify the problem, this paper does not consider the influence of parts' clearance and centrifugal force. And consider that in the work process, two half couplings and ring are not isolated; the pre-tightening force of screw extrusion pressure is negligible. Based on these simplifications, to do the finite element analysis of the coupling [4]。

4.1 Setting of material properties

Engineering Data provides sample material data categorized into several libraries. Setting the material properties of two half couplings and the strengthening shafts to structure steel as system default material selection in engineering data.

For the nonlinear material properties, ANSYS software provides Hyperelastic Materials, such as Mooney-Rivlin model, Yeoh model, the Mooney-Rivlin model. Elastic ring's deformation is small in the normal working range, choose Mooney-Rivlin model [5][6] [7], we stretch into the rubber experimental uniaxial stress-strain data, shear stress- strain data. Stress-strain data curves as shown in Figure 3 and figure 4.

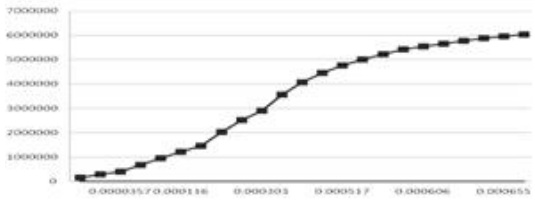

Fig.3 Uniaxial stress-strain curves

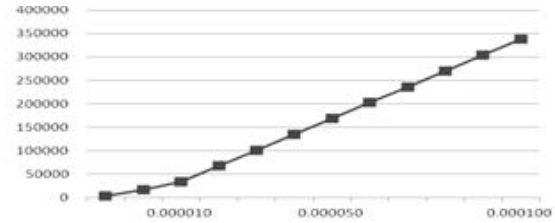

Fig.4 Shear stress-strain curves

4.2 Element type and mesh generation

Because the coupling is mainly solid element, SOLID185 Homogeneous Structural Solid Geometry with 8 nodes mesh the mode, the final element count is 62170, the node count is 312356.The finite element model of coupling is shown in figure 5.

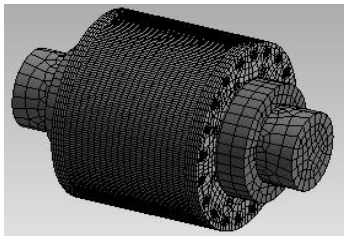

Fig. 5 The meshed finite element model in workbench

4.3 constraints and loadings

According to the actual stress of the coupling, creates constraints and loadings. Creates a fixed constraint on the left half shaft end; contact constraints on coupling shaft and key, two half couplings and shafts, two half couplings and ring etc.Add the torque of 500N.m on circumferential surface of the right half coupling, which is equivalent to the right coupling shaft as a driving shaft, the left as driven shaft [8].

4.4 Results and discussion

The model was calculated in ANSYS workbench, the total deformation, stress and strain distribution of model was shown in Figure 6; strain distribution of strengthening shafts which were key components was shown in Figure 7; stress distribution of strengthening shafts was shown in Figure 8; stress distribution of elastic ring was shown in Figure 9.

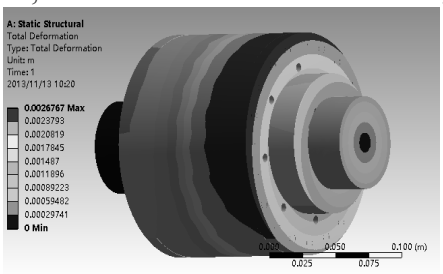

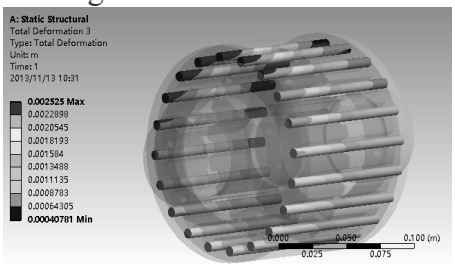

Fig. 6 The total deformation, stress and strain distribution of model

Fig. 7 Strain distribution of strengthening shafts

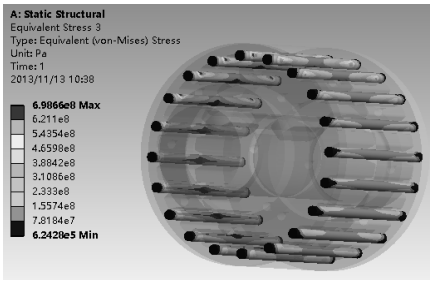

Fig. 8 Stress distribution of strengthening shafts **Fig. 9 Stress distribution of elastic ring**

5 Conclusions

Through the analysis, the maximum deformation occurs on the surface of elastic ring nearby the key connection, and on the strengthening shafts and the circlips. The maximum equivalent stress occurs on the key connection, and on the contact points of the strengthening shafts and the circlips, the maximum equivalent stress is 698.7Mpa. We come to conclusions that the strengthening shafts are

Key components for this elastic gear coupling in the simplified working environment, the stress of elastic gear ring mainly reduce the vibration affection on which of stress is less, the analysis results act in accordance with design results. According to the results of the analysis, design sizes of the model can be further optimized [9]

References

[1]Li Zhengfeng, Jiang Liqiang. Fundamentals of Mechanical Design [M]. Chemical Industry Press, 2011: 246-248.

[2]Li Zhengfeng, A Synchronous Belt Coupling, the utility model patent [P]. Patent No. 200910235346.9.

[3]Cheng Daxian, Handbook of Mechanical Design: Shaft and Connection [K].Chemical Industry Press, 2010:5-48.

[4] Zhang Zhan- li, LIU Xiao-han, Analysis New Type of Elastic Coupling for Coal Machinery Drive on ANSYS [J]. Coal Mine Machinery,2009（5）: 29-30.

[5] WANG Ying，GUO Yong-cun，Stress analysis of a serpentine spring coupling with ANSYS workbench software [J]. Machinery Design ＆ Manufacture，2011（1）90-91

[6] Zhang Zhenxiu, Nie Jun, Shen Mei, XinZhenxiang，Superelasticity model in ANASYS and its application in rubber engineering[J]. CHINA RUBBER/PLASTICS TECHNOLOGY AND EQUIPMENT, 2005(6):1-5.

[7] Yang Peng-jun，WU Ya-ming，Finite Element Analysis of Elastic Characteristics of Rubber Damper for Inertial Platform [J]. The fifth China CAE analysis technology journal, 491-497.
[8]Hu Qi，HYDRAULIC SERVO ACTUATOR O-RING TEST AND FINITE ELEMENT ANALYSIS. Harbin Institute of Technology, 2011.6,24-47.
[9] Shentu Liufang, Zhang Xiangyan, The Optimal Design of Structure of a Joint Flexible Laminated Membrane Coupling(JFLMC)[J]. CHINA MECHANICAL ENGINEERING Vol.14,No.19,2003, 1637-1640.

Advanced Materials Research Vols. 989-994 (2014) pp 2980-2984
© (2014) Trans Tech Publications, Switzerland
doi:10.4028/www.scientific.net/AMR.989-994.2980

Study of Sub-synchronous Control Interaction (SSCI) based on the test signal method

Benfeng Gao [a], Jin Liu [b] , Shuqiang Zhao[c],

Department of Electrical Engineering,North China Electric Power University,Baoding,Hebei,071000,China;

[a]gaobenfeng@126.com, [b]liujin19891217@126.com, [c]ZSQDL@163.com

Keywords: Sub-synchronous Control Interaction; DFIG; test signal method; equivalent model;

Abstract. Large-scale wind turbine generators with power electronic converters that operate near series compensated transmission lines are susceptible to un-damped sub-synchronous oscillations. This sub-synchronous oscillation is called Sub-synchronous Control Interaction (SSCI). Based on PSCAD / EMTDC simulation platform the establishment of Double Fed Induction Generator(DFIG) equivalent inverter controlled sources and network model, and verify the correctness of the equivalent model. Analysis the impact of series compensation and rotor -side converter PI parameters characteristic of the SSCI based on test signal method and time-domain simulation method. The results show that increasing the degree of series compensation , inner gain constant increases and inner integral time decreases will help increase SSCI, outer ring of PI parameters has little effect on the SSCI .

Introduction

In recent years , wind power at home and abroad has been rapidly developed , by 2020 , China's total installed capacity of wind power will be more than 200 million kilowatts , where offshore wind power capacity has reached 30 million kilowatts, wind power generating capacity will reach 390 billion kwh . Wind power generating capacity in power generation will be accounted for more than 5% [1-2] . Because wind farms are mostly located in remote areas , far from the centers , to address the problem of large-scale wind power deliveries , series compensation technology has been widely used. However, compensation may induce sub-synchronous oscillation problems , impact safety of wind farms as well as outgoing and stable operation of the system [3-8].

According to the interaction of different objects , sub-synchronous oscillation of wind turbines have three types of problems , which are sub-synchronous resonance (SSR), referring to the interaction between wind turbine shaft and the fixed series compensation ; Sub-synchronous Torsional (SSTI), mainly refers interaction to between the role of wind turbine controller or an adjacent FACTS device controller and wind turbine shafting ; Sub-synchronous Control Interaction(SSCI), such is defined by the interaction of wind turbine controller with fixed series compensation triggered the SSO .

This article creates a detailed DFIG equivalent inverter controlled sources and network model, and equivalent to verify the correctness of the model simulation . Based on PSCAD / EMTDC simulation platform, combined with the time-domain simulation of complex torque coefficient method-test signal method to analyze the impact of series compensation control parameters of the transmission line and the rotor-side converter of SSCI , but also time-domain simulation method analyze the impact of these parameters on the SSCI .

System Model

DFIG sent power via the fixed line infinite series compensation system is shown in figure 1 . Induction generator using a single rigid model does not consider the effect of torsional vibration interaction. Induction generator parameters according to the literature [9] settings, as shown in Table

1 ; self-induction generator impedance parameters in Table 1's reference value are its' rated power and voltage.

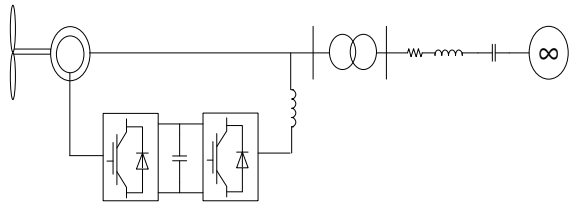

Fig.1 The schematic diagram of DFIG-based wind-power system

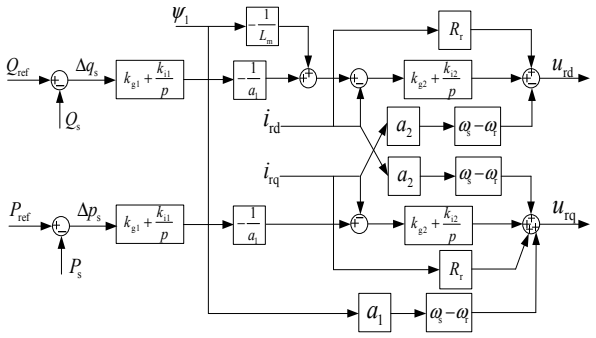

Fig.2 DFIG rotor -side converter control block

Tab.1 The parameters of the induction generator

parameters	Value
rated power	1.5MW
rated voltage	0.69kV
Grid frequency	50Hz
Stator leakage reactance	0.177p.u.
Rotor resistance	0.1p.u.
Rotor leakage reactance	0.116p.u.
Magnetizing reactance	4.68p.u.

Figure 2 is a DFIG rotor -side converter control system block diagram . Using dq decoupling double-loop control , d -axis fixed Qref reactive power control , q -axis wind turbine output to strike at a wind speed maximum power tracking mechanism based on the maximum wind energy , after removing the mechanical losses ,use it as DFIG output active power reference value.

Δp_s , Δq_s was DFIG output instantaneous active and reactive power variation ; k_{g2}, k_{i2}, k_{g1}, k_{i1} were inside the controller, outer PI parameters.

When using test signal analysis the original circuit model DFIG , due to the full-controlled inverter power high-frequency electronic devices turned on and off the course , electrical damping can not converge .

This paper established a model of DFIG equivalent inverter controlled source simulation , integrated VSC AC side and DC side controlled voltage source controlled current source characteristics , will be simulated controlled sources DFIG rotor side and the network side using VSC,as in Figure 3 . High-frequency inverter through controlled source model without taking into account the full-controlled power electronic devices , so a test signal analysis electrical damping convergence, simulation time is much shorter.

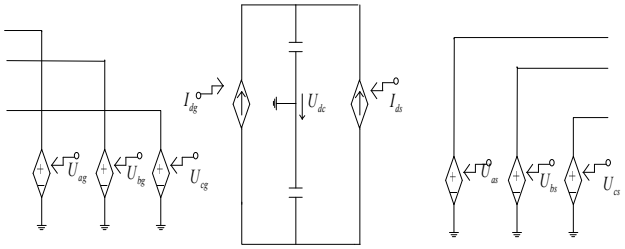

Fig.3 DFIG equivalent model of the controlled source converter

Verify the correctness of the equivalent model

Control input signal step change. After the wind turbine equivalent model is stable, the control input signal step change , the operation model shown in Figure 4 . When 10s the reactive power output of wind turbines from 0.04Mvar rises to 0.44Mvar. When 12s the wind turbine output active power increases from 0.66Mw to 0.96Mw.

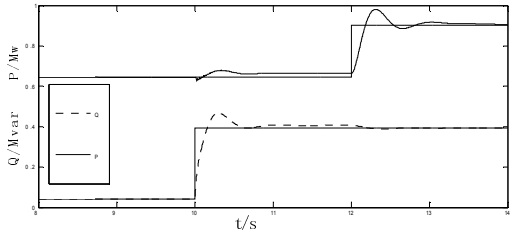

Fig.4 Command trace diagram of the control system in the equivalent controlled source model

As can be seen from Figure 4 , the input signal when changing settings , the equivalent model of the control system can quickly and accurately track settings. When the wind turbine output reactive setpoint changes , changes in reactive power output , active output basically unchanged ; when active setpoint changes , active output changes , reactive output basically unchanged. Active and reactive power output of the wind turbine can achieve decoupling control .

Test signal method analysis system SSCI characteristics

For the oscillation frequency λ of the system components , the electromagnetic torque increment can be expressed as:

$$\Delta\dot{T}_e = K_e(\lambda)\Delta\dot{\delta} + D_e(\lambda)\Delta\dot{\omega} \quad (1)$$

so:

$$\Delta\dot{T}_e / \Delta\dot{\omega} = D_e(\lambda) - jK_e(\lambda) / \lambda \quad (2)$$

$$D_e(\lambda) = \mathrm{Re}(\Delta\dot{T}_e / \Delta\dot{\omega}) \quad (3)$$

Steps to using the electrical test signal damping method is as following:

(1) in operating conditions , when the system enters the steady state , applying a small sinusoidal excitation generator rotor torque $\Delta T_m = \sum_a T_a \cos(a\omega_0 t + \Phi_a)$ bunch of sub-synchronous frequency $f = af_0$.

(2) When the system is re-entering the steady state , intercept the generator electromagnetic torque T_e and the generator speed ω on a common cycle .

(3) The amount of the two spectral decomposition to obtain the corresponding $\Delta\dot{T}_e$ and $\Delta\dot{\omega}$ of different frequency.

According to formula (3) can be calculated electrical damping torque coefficient.

Analysis SSCI Characteristics. The current study generally considered SSCI mainly affected by the rotor -side converter PI parameters and the degree of series compensation [8] . Therefore, the following article will be studied electrical damping computing systems , analyze the impact of these parameters on the SSCI . When the induction generator parameters set in Table 1 , the rotor -side converter in accordance with the PI parameters unchanged , according to the value shown in Table 2, the set wind speed is 10m / s.

Tab.2 The PI parameters of the rotor side converter

parameters	value
k_{g1}	0.01
k_{i1}	0.1
k_{g2}	0.1
k_{i2}	1.0

Set up the series was 20% , calculated on the electrical damping system . When setting the inner rotor -side converter proportional gain k_{g2} of 0.05, 0.1 and 0.2, respectively, in Figure 5 shows electrical damping coefficient curve with different inner loop gains.

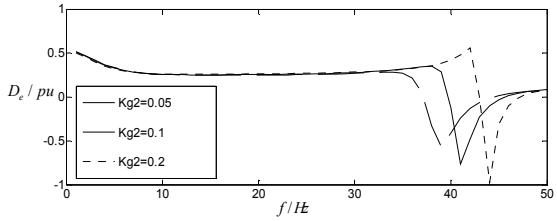

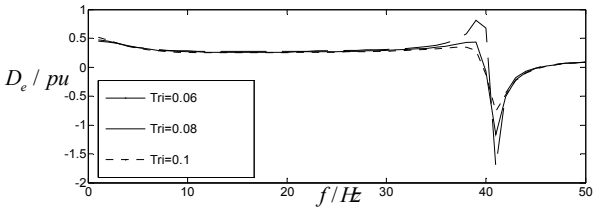

Fig.5 The electrical damping coefficient curve with different inner loop gains

Fig.6The electrical damping coefficient curve with different inner loop integration time constant

When electrical damping is negative, if the system damping of mechanical and electrical damping is negative , it may occur SSCI. As can be seen from Figure 5 , with the inner rotor side converter kg2 proportional gain is increased, the electrical frequency of the lowest point of the damper increases , the system gradually increases the frequency of the SSCI , electrical and negative damping system , the SSCI gradually increases. When setting the inner rotor -side converter integral time constant T ri = kg2 / ki2 were 0.06 and 0.08 and 0.1, respectively, The electrical damping coefficient curve with different inner loop integration time constant is shown in Figure 6 .

Conclusions

Based on PSCAD / EMTDC simulation platform for the establishment of a DFIG equivalent source inverter controlled grid model **,**then verify the correctness of the equivalent model , and pointed out higher simulation efficiency advantages of equivalent model. Analysis the impact of series compensation and rotor -side converter PI parameters characteristic of the SSCI based on test signal method and time-domain simulation method. The results show that increasing the degree of series compensation , inner gain constant increases and inner integral time decreases will help increase SSCI, outer ring of PI parameters has little effect on the SSCI .

Acknowledgements

Support by“the Fundamental Research Funds for the Central Universities”（12QN37）is gratefully acknowledged.

References

[1] Sahni M, Muthumuni D, Badrzadeh B, et al. Transmission and Distribution Conference and Exposition (T&D), 2012 IEEE PES. IEEE, 2012: 1-9.

[2] Garth Irwin. Subsynchronous Iteractions with Wind Turbines. Austin, 2010.

[3] Irwin G D, Isaacs A, Woodford D. Transmission and Distribution Conference and Exposition (T&D), 2012 IEEE PES. IEEE, 2012: 1-4.

[4] Gao Ben-feng, Zhao Cheng-yong, Xiao Xiang-ning, Guo Chun-lin, Zhao Yang. Transactions of China Electrotechnical Society, 2010, 11: 022.

[5] Gao Ben-feng, Zhao Cheng-yong, Xiao Xiang-ning, Zhao Yang, Guo Chun-lin..Power System Protection and Control, 2010 (023): 6-10.

[6] G. Irwin, A.K. Jindal, A.L .Issacs. 2011 IEEE Power and Energy Society General Meeting, pp 1-6.

[7] Wong W, Daniel J. ABB presentation on CREZ Reactive Study-ERCOT RPG Meeting[J]. 2010.

[8] Liu Qihui,Xie Mengli. Transactions of China Electrotechnical Society, 2012, 27(10): 60-67+78

[9] Zhang Jian,Xiao Xiangning,Gao Benfeng. Mechanism and Characteristic Study on Sub-Synchronous Control Interaction of a DFIG-Based Wind-Power Generator[J]. Transactions of China Electrotechnical Society, 2013, 28: 12.

Advanced Materials Research Vols. 989-994 (2014) pp 2985-2989
© (2014) Trans Tech Publications, Switzerland
doi:10.4028/www.scientific.net/AMR.989-994.2985

Estimation of A State Vector of An Inertial Unit

Zhang huiping[1] , Pei Peng[1], Roger Ceschi[2] ,Olivier Rabreau[2]

[1] Beijing institute of Petrochemical Technology Beijing 102617

[2] Graduate School of Engineering France

Keywords: Inertial unit; kalman filter; matlab

Abstract. An inertial unit includes many parameters, such as: position, speed, acceleration and so on. Now estimate the acceleration and angular velocity may seem simple, because an accelerometer can provide a measure of acceleration and a gyroscope can provide a measure of angular velocity. Nevertheless, we will see below that this apparent ease of hiding the very real difficulties.The aim of this paper is not to recreate an complex inertial unit, but try to estimate the inclination angle and the angular velocity of an object by using some math filters, This problem we will not only tap away the complexity of the implementation of an inertial, but more importantly to use a math filter to make the prediction information and data fusion multi -sensors.

Introduction

Now more and more people become disabled because of ill, accident and something else. And a part of them may cover in rehabilitation center, but most part of them may stay in the wheelchair to live their left life, the wheelchair has become a most important tool in their life. They should control the wheelchair very well. But how does the doctor or the invalid them want to know they have already control the wheelchair very well.[1]

Our project is to build a system which will install in the wheelchair to access the people who drive the wheelchair.

The structure diagram of the project

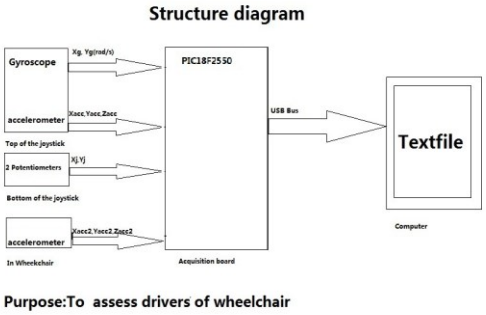

Fig. 1

We will use two kinds of sensors in this project:

Accelerometer:

• Detecting the proper acceleration of a movable. It brings us back accelerometer values of acceleration noise.

Gyroscope:

• Detecting the angular velocity of a movable. It returns values with gyroscope angular velocities noisy and biased.

Problems must be solved before the modeling

The difficulty of the problem is that the gyroscope has a bias that changes over time! And we do not know the shape of the drift.[2] But the bias of the gyroscope change very slowly, So, we can think that it does not move! And Before beginning a modeling system, we will make some assumptions about the mobile sensors.[3]

• First, we consider that the mobile does not undergo any acceleration
• Next, we consider the noise of the sensors as Gaussian
• It is considered that we should review the accelerometer values directly acceleration in meters per second
• It is considered that the gyroscope values we refer directly to angular velocities in radians per second
• Finally, we consider using the gyroscope in rehabilitation center (which is not too complicated to implement in practice).

Kalman Filter[4]

The Kalman filter model assumes the true state at time k is evolved from the state at (k − 1) according to

$$X_k = A_k \bullet X_{k-1} + B_k \bullet U_k + W_k$$

Where

- A_k is the state transition model which is applied to the previous state X_{k-1};
- B_k is the control-input model which is applied to the control vector U_k, And in our project, we don't use control system , So B_k is zero in our project;
- W_k is the process noise which is assumed to be drawn from a zero mean multivariate normal distribution with covariance Q_k.

$$W_k - N(0, Q_k)$$

At time k an observation (or measurement) Zk of the true state Xk is made according to

$$Z_k = H_k \bullet X_k + V_k$$

Where

- H_k is the observation model which maps the true state space into the observed space
- V_k is the observation noise which is assumed to be zero mean Gaussian white noise with covariance R_k.

$$V_k \sim N(0, R_k)$$

Note: The initial state, and the noise vectors at each step {x0, w1, ..., wk, v1 ... vk} are all assumed to be mutually independent.

A. Modeling of the object

To apply a Kalman filter, we must create the model of the project based on the parameters to be measured by the sensors.[5][6] Measuring the angular velocity of the inertial unit by the gyroscope (u) is obtained by adding the noise of the gyroscope (b_1) and the bias of the gyroscope (b) to the true value of the angular velocity of the inertial unit (a_1).

The measurement of the angle of inclination of the inertial unit by the accelerometer (a_M) is obtained by adding the noise of the accelerometer (b_2) to the true value of the angle of inclination of the inertial unit (a_2)

We deduce the following equations:

$u = a_1 + b + b_1$

$a_M = a_2 + b_2$

We can write these equations in matrix form Y = HX + B is called the measurement equation

- Y is called the measurement vector
- X is the state vector
- B, the noise vector
- H, the observation matrix

$$[a_M] = [0 \quad 1 \quad 0] \bullet \begin{bmatrix} a_1 \\ a_2 \\ b \end{bmatrix} + [b_2]$$

- we do not model the evolution of the angular velocity of the mobile. We will therefore also be considered to be fixed: $a_{1(k+1)} = a_{1(k)}$
- Finally, one can express the inclination of the movable as a function of the angular velocity at the preceding instant:

$a_{2(k+1)} = a_{2(k)} - a_{1(k)} \bullet \mathrm{T}_s$.

(Note: T_s is the sample period of the system).

Again, we can rewrite these equations in matrix form $X_{(k+1)} = A_{(k)} \bullet X_{(k)}$ called the equation of state

- $X_{(k+1)}$ is the new state vector
- $X_{(k)}$ is the former state vector
- $A_{(k)}$ Ak is the transition matrix

$$\begin{bmatrix} a_{1(k+1)} \\ a_{2(k+1)} \\ b \end{bmatrix} = \begin{bmatrix} 1 & -T_s & 0 \\ 0 & 1 & 0 \\ 0 & 0 & 1 \end{bmatrix} \bullet \begin{bmatrix} a_{1(k)} \\ a_{2(k)} \\ b \end{bmatrix}$$

To use the Kalman filter, we are missing two matrices appearing in the calculation: the covariance matrix of measurement noise and the covariance matrix of control noise.

Since we have two sensors with Gaussian noise, the covariance matrix of measurement noise is a matrix with one dimensional, the square of the standard type of sensor noise. (Indeed, the noises of the sensors are considered to be Gaussian and uncorrelated with each other)

$R = (\sigma_1^{\,2})$

- σ_1 is the noise standard deviation of the accelerometer

Finally, the covariance matrix of the control noise is the system modeling errors. It is through this matrix that the errors in modeling (here, it was estimated that the bias and angular velocity were

constant when in reality it is false) will be "erased". This matrix is a diagonal matrix of dimension three (it was a state vector of size 3). The terms on the diagonal correspond to the square of the standard deviations of the maximum error that we allow for each of the parameters to be estimated. This matrix is to be determined empirically based on the problem.

Please understand that if we set the error terms too small compared to reality, then the Kalman filter will not happen to rectify the errors of the model and make biased estimates. By constant, if the error terms are too large compared to reality, then the model will not be biased, but the estimates produced are of poor quality (the error covariance will be important)

The difficulty of the Kalman filter is to properly estimate the covariance matrix of control noise in order to have an estimate as accurately as possible without having bias.

$$Q = \begin{bmatrix} \varepsilon_{a_1} & 0 & 0 \\ 0 & \varepsilon_{a_2} & 0 \\ 0 & 0 & \varepsilon_b \end{bmatrix}$$

- ε_{a_1} is the variance of the maximum allowable error on the modeling of the angular velocity (equation of state)
- ε_{a_2} is the variance of the maximum allowable error on the modeling of the slope (equation of state). In our example, this value should be forced to 0. Indeed, the model for the slope was completely determined by the previous inclination and angular velocity before. There is no mistake.
- ε_b is the variance of the maximum allowable error on the modeling of the gyro bias (equation of state)[7,8]

B. Application of the Kalman filter

- **Predict**

Predicted state estimate	$\tilde{X}_{(k\|k-1)} = A \bullet \tilde{X}_{(k-1\|k-1)}$
Predicted estimate covariance	$P_{(k\|k-1)} = A \bullet P_{(k-1\|k-1)} \bullet A^T + Q_k$

- **Update**

Innovation or measurement residual	$\tilde{y}_k = z_k - H_k \tilde{X}_{k\|k-1}$
Innovation (or residual) covariance	$S_k = H_k P_{k\|k-1} H_k^T + R_k$
Optimal Kalman gain	$K_k = P_{k\|k-1} = P_{k\|k-1} H_k^T S_k^{-1}$
Updated (*a posteriori*) state estimate	$\tilde{X}_{k\|k} = \tilde{X}_{k\|k-1} + K_k \tilde{y}_k$
Updated (*a posteriori*) estimate covariance	$P_{k\|k} = (I - K_k H_k) P_{k\|k-1}$

Note: $X_{(k|k)}$ as the estimate of the new state vector and $P_{(k|k)}$ as the new covariance matrix of the estimated state. This matrix will tell you about the accuracy of the estimate of each parameter.

Simulation with MatLab

After making the model, we only need choose the suitable process-based error and suitable measurement error.

Here is the result of simulation of this example in Matlab.

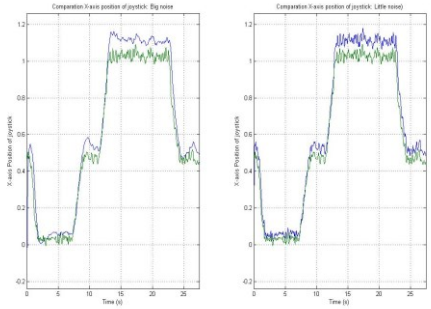

Conclusions

Kalman filter is suitable for our system the reason is that our system is a linear system. When kalman filter was used, creating a model of this system was very easy and it can minimize the variance of the estimation. And when the kalman filter was used in our system The matrix of the noise was the only thing we need get, it's an very easy task. So kalman filter is suitable for our system.

Reference

[1] John, Wiley. Discrete Stochastic Processes and Optimal Filtering[M]. 2rd Edition. Wiley-ISTE, 2010-02.
[2] White noise. http://en.wikipedia.org/wiki/White_noise
[3] Dan Simon. Kalman Filtering[J]. Embedded Systems Programming JUNE 2001
[4] Cane, Kalman filter vs Complementary filter[J]. http://robottini.altervista. org/kalman-filter-vs-complementary-filter
[5] starlino. A guide to using IMU(Accelerometer and Gyroscope Devices) in embedded applications. http://www.starlino.com/imu_guide.html
[6] Radar tracker. http://en.wikipedia.org/wiki/Radar_tracker
[7] Greg Welch and Gary Bishop. An Introduction to the Kalman Filter. Department of Computer Science University of North Carolina at Chapel Hill
[8] A. D. Young. Comparison of Orientation Filter Algorithms for Realtime Wireless Inertial Posture Tracking. Institute for Computing Systems Architecture School of Informatics, University of Edinburgh

Advanced Materials Research Vols. 989-994 (2014) pp 2990-2994
© (2014) Trans Tech Publications, Switzerland
doi:10.4028/www.scientific.net/AMR.989-994.2990

Study Of A Predictive Compensator For Internet-Based Remote Vehicle Steering Control

ZHONG Mingen[a], HONG Hanchi[b]

Department of Mechanical Engineering

Xiamen University of Technology Xiamen Fujian, China

[a]zhong1980me@gmail.com

[b]hchong@xmut.edu.cn

Keywords: List the keywords covered in your paper. These keywords will also be used by the publisher to produce a keyword index.

Abstract. Packet loss during network transmission through internet has negative influence on vehicle remote steering operation. Model of the remote steering system was built to analyze the steering quality. On basis of former study, a kind of packet loss compensator was designed from the aspect of predictive compensate control using hybrid pi-sigmoid fuzzy neural network. Simulation results showed that the compensator worked effectively. It was able to reduce the bad influence of packet loss during remote vehicle steering procedure.

Introduction

Statistics about the traffic accidents from year 2007 to 2009 [1,2,3] show that risky-driving-related traffic accidents account for from 54% to 90% of the total, such as fatigue driving, driving after drink, and so on. If the driver is in risky state, there will be a significant decline of capacity in vehicle steering control, decision making and implementation, which is one of the key reasons to raise both injury rates and death rates. From this point of view, remote vehicle steering shows its great practical significance.

Development and prevalence of internet has made it feasible and convenient for remote vehicle steering. There will be the phenomenon of time delay and packet loss when packets are transferred. Researches on reducing the affect of packet loss can be classified into two major areas so far. One focuses on developing and improving the User Datagram Protocol, such as TCP OVER UDP and UDT [4]. However, these methods are not applicable for public internet. The other one aims at a set of control theories and strategies. SOGLO has invented a compensate estimator to deal with delay and packet loss problem so as to improve control performance [5]. LONG has designed open-loop estimator and closed-loop estimator separately according the whether packet loss phenomenon occurred or not [6]. However, both of the theories make assumptions and requirements on delay and packet loss rate, which are impossible for real internet transfer.

This work is going to present a packet loss compensator constructed by the hybrid pi-sigmoid fuzzy neural network theory without any prerequisites for internet parameters.

Influence of Packet Loss on Internet Based Remote Vehicle Steering

Fig.1 shows a simplified schematic for internet-based remote vehicle steering control. Symbol r stands for the reference input steering angle. Go(z) is a simplified static discrete model of a certain vehicle steering system with a sampling period Ts as 10 milliseconds.

$$G_o(z)=\frac{A(z^{-1})}{1-B(z^{-1})}=\frac{a_1z^{-1}+a_2z^{-2}+\cdots+a_mz^{-m}}{1-b_1z^{-1}-b_2z^{-2}-\cdots-b_nz^{-n}}=\frac{0.025z^{-1}+0.178z^{-2}}{1-0.56z^{-1}-0.32z^{-2}-0.61z^{-3}} \quad (1)$$

As we can see, the controller and the object controlled are separated by internet. Internet is the communication channel for them. v(k) stands for control values from the remote controller. y(k) means steering angle of the front wheels.

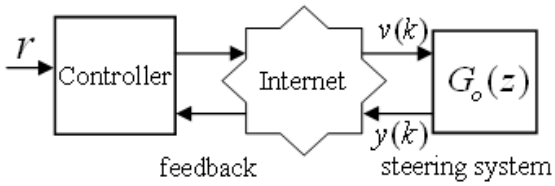

Fig.1 Schematic of the internet based remote vehicle steering

Suppose that l consistent packets are lost from the k0th sampling, then the input control values of the steering system will change to v(k0+i) = v(k0+i-1) = ⋯ = v(k0) where i=1,2,…,l. Considering of Eq.1, when $i \geq m$, we come to a result as

$$y(k_0+i) = v(k_0)\sum_{j=1}^{m} a_j + \sum_{h=1}^{n} b_h y(k_0+i-h) \quad . \tag{2}$$

Eq.5 tells us that when the number of the consistent lost packets is bigger than that of the model's zeros, pattern of the remote steering control process will turn from close-loop to open-loop. This probably results in the risk to traffic accidents.

Structure of The Hybrid Pi-sigmoid Fuzzy Neural Network

In previous study [8], we successfully developed a robust controller to kick off the effects of transfer delay. Here we will focus on the matter of packet loss, trying to work out a predictive compensate control strategy. Histories of the input control information will be used to predict the current lost one. Since packet loss phenomenon happens at random and is time-varying, the predict arithmetic must have both latest short-term control law parameters identification function and fast dynamic self-learning ability. Thus, we prefer to use both the fuzzy logic and neural network modeling, which are the basis of hybrid pi-sigmoid fuzzy neural network theory.

Tagaki-Sugeno fuzzy logic can be described as $R^i : if\ x_1\ is\ A_1^i\ ,\ x_2\ is\ A_2^i\ ,\cdots, x_m\ is\ A_m^i$, $then\ y^i = f^i(x_1, x_2, \cdots, x_m)$. R^i (i=1,2,…,n) means the ith rule. Parameter n means total number of the rules. yi means the conclusion of the ith rule. xj (j=1,2,…,m) are the premise input variables. m is the count of the input variables. A_j^i stand for the fuzzy sets. n_i means number of the domains xj.

Fig.2 shows the Tagaki-Sugeno fuzzy logic implemented by a pi-sigmoid neural network.

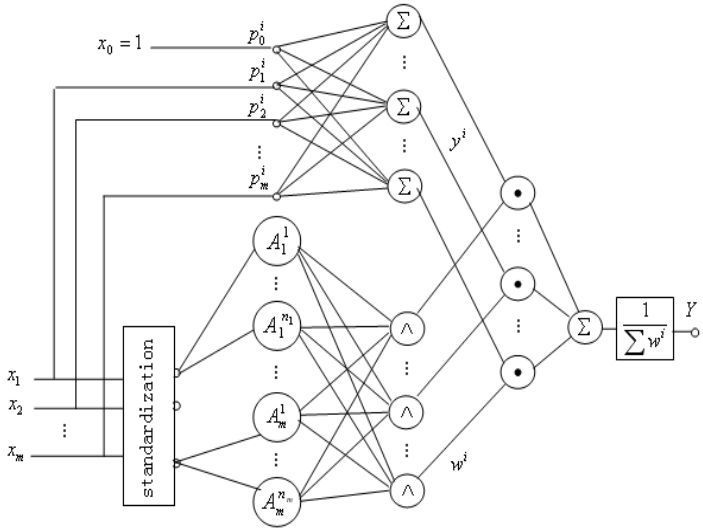

Fig.2 Structure chart of hybrid pi-sigmoid fuzzy neural network

In Fig.2, symbol Σ means addition operation. Symbol $\bullet$ means multiplication. Symbol $\wedge$ means taking the minimum. x0 takes value as 1 all the time. Thus, we get the output of the network as

$$Y = \sum_{i=1}^{n} w^i y^i \Big/ \sum_{i=1}^{n} w^i \quad , \tag{3}$$

where $y^i = \sum_{j=0}^{m} p_j^i x_j$, $\mu_{A_j^i} = \exp[-(x_j - a_j^i)^2 / b_j^i]$, and $w^i = \mu_{A_1^i}(x_1) \wedge \mu_{A_2^i}(x_2) \wedge \cdots \wedge \mu_{A_m^i}(x_m)$.

Training Algorithm of The Neural Network

Training of the hybrid pi-sigmoid fuzzy neural network aims at adjusting the consequent parameters p_j^i as well as the premise parameters a_j^i and b_j^i. If we mark the output of the network as Y^d and define the target deviation function as

$$E = \frac{1}{2}(Y^d - Y)^2, \tag{4}$$

then according to the gradient method, there will be

$$\frac{\partial E}{\partial p_j^i} = \frac{\partial E}{\partial Y} \cdot \frac{\partial Y}{\partial p_j^i} = -(Y^d - Y) \cdot \left[\frac{\sum_{i=1}^{n} w^i y^i}{\sum_{i=1}^{n} w^i} \right] \Big/ \partial p_j^i = -(Y^d - Y) \cdot \frac{w^i}{\sum_{i=1}^{n} w^i} \cdot \frac{\partial y^i}{\partial p_j^i}. \tag{5}$$

Then, we get

$$\Delta p_j^i = -\alpha (Y^d - Y) \cdot w^i \Big/ (\sum_{i=1}^{n} w^i) \cdot x_j, \tag{6}$$

, where α stands for the learning speed of the consequent parameters.

We must notice that gradient method is no longer applicable when we try to calculate the increments of a_j^i and b_j^i, since there exists such nonlinear operation as taking the minimum. We could not make certain about which component parameter has raised the deviation. In this case, we adopted a one-step-search method. Firstly, we assumed that it was the corresponding component parameter that had raised the deviation. Secondly, we calculated the deviation of the network's output, which was then used to update the network's nodes. Thirdly, we recalculated the output deviation of the updated network. Finally, we made a compare about the deviations to check out which update resulted in the best results. We recognized the best one to update its corresponding nodes and restored the other nodes. Following these rules, we have reached

$$\frac{\partial E}{\partial a_j^i} = \frac{\partial E}{\partial Y} \cdot \frac{\partial Y}{\partial a_j^i} = \frac{\partial E}{\partial Y} \cdot \frac{\partial Y}{\partial w^i} \cdot \frac{\partial w^i}{\partial a_j^i} = -2(Y^d - Y) \cdot \frac{y^i \sum_{i=1}^{n} w^i - \sum_{i=1}^{n} w^i y^i}{(\sum_{i=1}^{n} w^i)^2} \cdot (x_j - a_j^i) \cdot w^i / b_j^i \tag{7}$$

as well as

$$\Delta a_j^i = -2\beta (Y^d - Y) \cdot \left[y^i \sum_{i=1}^{n} w^i - \sum_{i=1}^{n} w^i y^i \right] \cdot (x_j - a_j^i) \cdot w^i \Big/ \left[b_j^i (\sum_{i=1}^{n} w^i)^2 \right], \tag{8}$$

where β stands for the learning speed of the premise parameters. Similarly, we obtained

$$\Delta b_j^i = -\beta (Y^d - Y) \cdot \left[y^i \sum_{i=1}^{n} w^i - \sum_{i=1}^{n} w^i y^i \right] \cdot (x_j - a_j^i)^2 \cdot w^i \Big/ (b_j^i \sum_{i=1}^{n} w^i)^2. \tag{9}$$

Principle of The Packet Loss Compensator

A novel packet loss compensator was designed as shown in Fig.3 with the help of hybrid pi-sigmoid fuzzy neural network theory showed above.

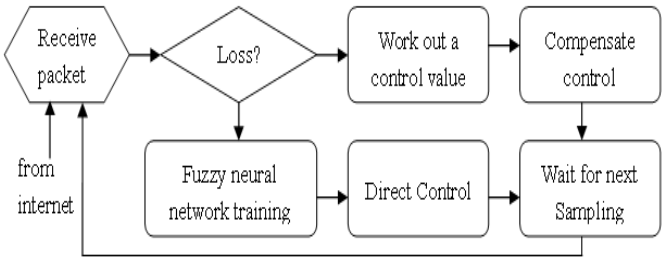

Fig.3 Procedure chart of packet loss compensator in remote vehicle steering system

There are two auto-switch procedure modes for the compensator. One is called as learning mode. This mode works when data packets that carry the control information are transferred successfully. Control information received are not only used to drive the vehicle steering system but also used to train the neural network and adjust p_j^i, a_j^i and b_j^i. As a result, transfer function of the neural network is consistent with the latest short-term control law of v(k).

The other mode is called predictive compensate control mode. This mode works when the packets are lost. In that case, the auto-trained neural network will work out a predicted control value to help drive the steering system so as to guarantee a complete steering process.

Simulation and Results

There were some specifications for the simulation.

1) We took control value v(k) and its first-order difference $\Delta v(k) = v(k) - v(k-1)$ as input training samples of the hybrid pi-sigmoid fuzzy neural network, and then made v(k+1) as its ideal output. Thus, m got the value as 2.

2) Fuzzy sets were divided as {NL, NM, NS, ZE, PS, PM, PL}, which correspondingly meant negative-large, negative-middle, negative-small, zero, positive-small, positive-middle and positive-large. As we could see, there were 49 rules, thus to say n equaled 49.

3) The consequent parameters were initialized as $p_j^i = 4$. Its learning speed α was defined as 0.01. While the premise parameters were initialized as $a_j^i = 0.95$ and $b_j^i = 0.8$, and its learning speed β was defined as 0.005.

4) Network transfer delays were set as a const value of 250 milliseconds. Besides, packet loss sampling intervals were defined as k∈ {15,25} ∪ {55,70} ∪ {125,135} ∪ {165,180} ∪ {220,235} ∪ {300,315} ∪ {400,425} ∪ {455,460} ∪ {480,490}.

5) Control arithmetic followed a delay-dependent robust control theory that we had already provided in [9].

Following the specifications, we sent a command for Go(z) to steer 45 degrees from the remote control terminal through the constructed internet environment. When regardless of the case of ground resistance, the steering angles of the front wheels measured were shown in Fig.4.

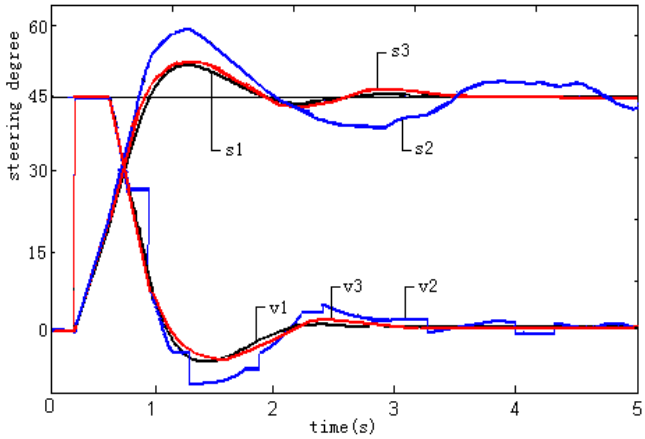

Fig.4 Steering angles measured when perform a 45 degree remote steering

In Fig.4, curve v1 and s1 stand for the input control value and steering angle respectively when there is no packet loss. v2 and s2 stand for the ones when there is packet loss but without help from the compensator provided above. v3 and s3 stand for the ones with the help of the compensator.

It is clear that packet loss will make remote steering lack of valid control input, which results in a heavy over-steering, steering fluctuations and instability. However, with the help of the compensator constructed by the hybrid pi-sigmoid fuzzy neural network, remote steering process is almost same as the one when no data packets are lost. It helps to decrease the over-steering angle and make the steering both fast and stable, and what's more, without a static deviation.

Conclusions

The compensator constructed by the hybrid pi-sigmoid fuzzy neural network is able to train automatically and dynamic adjust its parameter on line fast and effectively. It is capable of digging out the latest short-term control law from the control values received and providing an alternative compensate control value when data packet loss happens. Results of the simulation prove the effectiveness of the theory we have provided in this paper. It may be a solution to kinds of remote control and operation based on internet. We will put a further study on it.

References

[1] NHTSA, "Traffic safety facts 2007: a compilation of motor vehicle crash data from the fatality analysis reporting system and the general estimates system", Washington DC: National Highway Traffic Safety Administration, pp.32-43, 2007.

[2] Centre for Accident Research and Road Safety, "State of the road: A fact sheet of the centre for accident research and road safety Queensland [EB/OL]", http://www.carrsq.qut.edu.au/publications/drink_driving_fs.pdf, 2008-10/2009-12-31.

[3] ETSC, News release [EB/OL], http://www.etsc.eu/documents/copy_ of_Press release_Flash 15.pdf, 2009-12-11/2009-12-31.

[4] LI Guo-dong, ZHOU Hong, BI Yan-jun. "Video transmission in robot teleoperation system based on TCP OVER UDP technique". Journal of North China Electric Power University(Natural Science Edition), Vol.33, pp.47-50, July 2006.

[5] SOGLO Bienvenu, YANG Xian-hui. "Compensation for Network-induced Delays and Packet Dropout and System Stability Analysis". Control and Decision, Vol.21, pp.201-204, 2006.

[6] Long CN, Dai SF, Guan XP. "The Compensation Method of Networked Control System with Data-packet Dropout". Proc of the 5th World Congress on Intelligent Control and Automation, Hangzhou China, pp.1348-1351, 2004.

[7] ZHONG Ming-en, WU Ping-dong, HUANG Jie. "Delay-dependent robust control for internet based shared control system". Control and Decision, Vol.23, pp.883-887, 2007.

Advanced Materials Research Vols. 989-994 (2014) pp 2995-2998
© (2014) Trans Tech Publications, Switzerland
doi:10.4028/www.scientific.net/AMR.989-994.2995

Research on Auto-test System of Telescope Laser Indicator

Na Zhou, Yonghao Li, Xinyan Li

North Vehicle Research Institute of China, Beijing 100072

Beijing special vehicle Research Institute, Beijing 100072

Keywords: gantry cranes; theoretical calculations; finite element; structural strength

Abstract. Telescope laser pointer is generally used firearms and other light weapons systems, to ensure accurate light weapons capable of targeting, this paper presents a telescope system automatically detects a laser pointer, laser pointer can be the role of the distance, the laser divergence angle of the laser spot size of the laser optical axis adjustment range and the laser optical axis deviation and other parameters were measured. In this paper, the detection system structure, optical structure was designed; proposed laser pointer detection principle of the parameters; and software design. At last, to meet the requirements of this system has been experimentally derived by experimental verification, measurement accuracy.

Introduction

Telescope laser pointer is generally used firearms and other light weapons systems; light weapons can ensure accurate targeting and thus damage the target at the expected location. With small arms vigorously development, the telescope laser pointer parameter testing higher and higher demands are proposed. However, the majority of domestic research department no new weapons testing and calibration equipment laser pointer, not objective advantage product technical condition, difficult to ensure the quality of production. For these reasons, the laser pointer to the gun telescopic system design a multi-parameter testing system, the measurement system of the telescopic system in laser designator, laser divergence Angle, the role of distance laser spot size, laser optical axis adjustment range and measure the parameters of the laser optical axis deviation vector.

System Architecture Design

The measuring instrument is composed of parallel light tubes, CCD camera, partition plates and measuring system consists of a laser light source, by the computer and analysis software computing systems, and fastening systems as well as the composition of the sample holder which supports the protective effect of the mechanical system composed by a shield composed.

The detector works as follows: Parallel light pipe and coaxial telescopic system, the telescopic system provides limited far or infinity target, when a laser designator light coaxial with telescopic system, the laser beam and optical axis coincidence of parallel light pipe, put CCD camera, the focal plane of the objective by recording the movement of the spot on the CCD camera, calculate the corresponding parameters using the computer program.

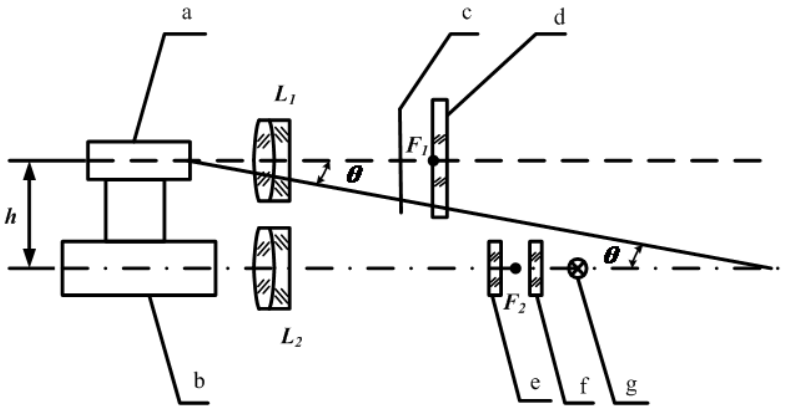

Fig. 1 Schematic diagram of the optical test system

(a) the measured laser pointer (b) telescope system (c) attenuator

(d) CCD Camera (e) reticle (f) Feather Glass (g) laser light source

As shown in Figure 1, will have instruction function of telescopic system frame fixed on the sample, the telescope system(b） with a laser pointer(a） and the distance parallel to the axis of the theoretical *h*, so that the collimator (b) coaxial with the telescope system, by laser light source (g), the reticle (e), MAO glass (f), object collimator lens L_2 telescope system to provide limited or unlimited far away targets. When the laser light source and telescopic system coaxial, the laser beam with parallel light pipe (a) optical axis coincidence, Placed at the focal plane of the objective CCD camera (d), by recording the CCD camera (d) on the spot of mobile.

Indicator parameter detection principle

Indicator measuring principle of the parameters as follows:

1) Laser divergence angle measurement: the laser beam through the collimator lens L_1, attenuators (c) image on the CCD, collimator focal length by $f^{'}$, Measured on the spot by CCD image height y ', by type (a) calculating the laser divergence Angle.

$$\theta = \arctan\frac{y'}{f'} \tag{1}$$

2) range measurements: measured distance l and calibration distance measured $l^{'}$ place, the intensity of illumination in the CCD for E and E', Spot diameter respectively $D = D_0 + 2l\tan\theta$ and $D' = D_0 + 2l'\tan\theta$, θ as the divergence Angle, D_0 as the starting point in a laser designator (a) the diameter of the output beam, flare area represented by A and A' respectively, by the formula (2) below.

$$\begin{cases} A = \pi\left(\dfrac{D}{2}\right)^2 = \pi\left(\dfrac{D_0}{2} + l\tan\theta\right)^2 \\ \quad = \pi\left(\dfrac{D^2{}_0}{4} + D_0 l\tan\theta + l^2\tan^2\theta\right) \\ A' = \pi\left(\dfrac{D}{2}\right)^2 = \pi\left(\dfrac{D_0}{2} + l'\tan\theta\right)^2 \\ \quad = \pi\left(\dfrac{D^2{}_0}{4} + D_0 l'\tan\theta + l'^2\tan^2\theta\right) \end{cases} \tag{2}$$

By the light intensity and the spot size is inversely proportional to the formula (3)

$$\frac{E}{E'} = \frac{A'}{A} = \frac{\dfrac{D^2{}_0}{4} + D_0 l'\tan\theta + l'^2\tan^2\theta}{\dfrac{D^2{}_0}{4} + D_0 l\tan\theta + l^2\tan^2\theta} \tag{3}$$

By calculating the type, can solve the measured distance *l*.

3) laser optical axis deviation measurement: first of all, according to a predetermined working distance, the optical axis offset and the focal length of the parallel light pipe calculated under normal circumstances indicating light spot on the focal plane off center distance (CCD optical axis). Comparing the actual and the ideal offset of the offset difference between the optical axis of the laser to obtain the amount of deviation.

4) divergence angle of the laser beam, the laser spot size measurements: laser CCD optical axis parallel incident, according to the CCD lens focal length and light spot on the CCD pixel number, of using computing software can calculate the Angle of laser beam are scattered and spot size.

5) laser optical axis adjustment range of measurement: the laser pointer laser summicron-m is parallel to the CCD, when the laser pointer along a certain direction, according to the amount of light spot on the CCD jitter flare adjusting range can be calculated.

Software Interface Design

The software consists of image pre-processing, and file manipulation functions to measure three modules, the following will introduce based on interface design part of the three modules, interface is shown in Figure 2.

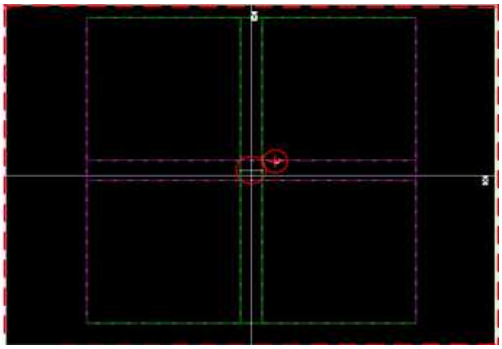

Fig. 2 Software interface Figure

Experiment

In order to test the effectiveness of the system, qualified for a certain type of telescope to detect laser pointer experiment. This laser pointer is known technical indicators are as follows:

(1) divergence angle of the laser beam:

$$\theta \le 1mrad$$

(2) the amount of spot move: 60 meters distance of laser speckle is 1.5 mrad;

(3) the laser optical axis adjustment range and deviation: along the horizontal (vertical) direction to adjust the optical axis, the adjustment range in the horizontal (vertical) direction within $\pm 15mil$ walk, move in the vertical deviation amount (horizontal) direction within $\pm 1mil$;

(4) the role of distance: emitted from the laser pointer in the 60 meters at a distance, can clearly see the laser spot, the background illumination $\le 50LX$ this system is used for detecting the experimental data shown in Table 1.

Table 1 Measured Data Sheet

	Spot radius (mm)	Beam angle (mrad)	The amount of walking (mrad)	The adjustment range (mil)	Deviation (mil)
the first group	0.034	0.242	0.172	(up and down) -12.712,10.828 (Left and right) -10.692,13.592	(Left and right) -0.235,0.369 (up and down) -0.398,0.632
the second group	0.030	0.218	0.559	(up and down) -12.365,14.852 (Left and right) -12.582,11.226	(Left and right) -0.352,0.563 (up and down) -0.523,0.365
the third group	0.038	0.276	0.395	(up and down) -13.635,10.358 (Left and right) -10.582,12.368	(Left and right) -0.254,0.357 (up and down) -0.329,0.368

Conclusions

Telescope system automatically detects the laser pointer realized the automatic acquisition and automatic processing of data, the role of the laser pointer can be the distance, the divergence angle of the laser, the laser spot size, and the adjustment range of the optical axis of the laser optical axis of the laser parameters such as the amount of deviation is measured. Through this system to a certain type of qualified laser pointer detection experiments shows that this system is effective for a laser pointer quantitative assessment of performance parameters.

References

[1] Hui Wang, Huiping Gu. Research dual probe laser divergence angle measurement system. Harbin Institute of Technology. 2006.6.
[2] Shanshan Gong, Yuegang Fu. Laser beam divergence angle measurement. Changchun University of Technology. 2009.3.
[3] Guanqun Tang. Comparison of several laser spot center location algorithm. Beijing Institute of Machinery. 2009.3,24 (1) :61-64.
[4] Bing Shun, Zhao Wang, Yushan Tan. Based circle fitting laser spot detection algorithm. Infrared and Laser Engineering. 2002.6,31 (3) :275-279.

Advanced Materials Research Vols. 989-994 (2014) pp 2999-3002
© (2014) Trans Tech Publications, Switzerland
doi:10.4028/www.scientific.net/AMR.989-994.2999

The Development of Underground Personnel Data Terminal Based on RSSI Location

Hongyi Li, Chuanzhong Chen

Xinxiang Vocational and Technical College, Henan, Xinxiang, 453006

KeyWords: RSSI; CC2431; Underground; Location

Abstract: Based on the emerging ZigBee wireless RF communication technology, this paper presents the design of a miner information collection terminal. The entire system is designed around the CC2431 SoC hardware circuit, through ZigBee networking, to achieve the location of underground environment and miner vital signs data acquisition, so that it can provide effective help to quickly carry out rescue work.

Introduction

Currently, most major mine safety monitoring system applies the wired way for data transmission, once the mine disaster, equipment and cables tend to be compromised and cannot provide useful information for searching and rescue work after the mine disaster, due to ground monitoring persons cannot master the underground operations and the distribution of personnel, so the rescue of persons in distress, safety ambulance is inefficient, rescue result is poor. This paper designs a personal data mobile terminal equipment, worn on a miner's helmet, which can simultaneously capture miner's body temperature, heart rate and other vital signs and the surrounding environment's oxygen gas concentration. Through ZigBee network, parameters will be collected and terminal address information will be sent to the ground command center by wireless transmission. In the center of the monitor screen, the exact location of each miner can be seen, even mine resulting roadway collapsed, causing interruption of wireless communications, the distribution of the moment by the former mine personnel can also provide the basis for drilling. By drilling, the oxygen can be sent to miners for the rescue to gain time, and a new ZigBee gateway can be sent to the distress area by drilling. ZigBee network will automatically find and establish new contacts to terminal for the ground command center miners for more information.

1 The overall structure of the data terminal

The system structure block diagram is shown in Figure 1, here, ME2-O2 is an oxygen concentration sensor, for acquiring down-hole oxygen concentration data, and which outputs a current signal proportional to the concentration of oxygen, MH-440V/D is the methane concentration sensor for detecting underground gas concentrations, DS1631 is a digital temperature sensor for miner temperature acquisition, HK2000A pulse sensor is used to capture the heart of miners. CC2431 is a ZigBee wireless location chips, during 2.4G ISM band wireless achieving data transmission function, which integrates a 51-core chip microcontroller with a 14bit A /D. The framework structure of the data terminal, CC2431 as to the core components, is shown in Figure 1.

In Figure 1, oxygen concentration and gas concentration measurement devices, mainly detect for underground miners usually work environment the oxygen concentration and gas concentration. When the gas exceeds safe limits, sound and light alarm, when faced with mine disaster, real-time environmental parameters in which the trapped miners timely deliveries to the command center, easy to carry out rescue work.

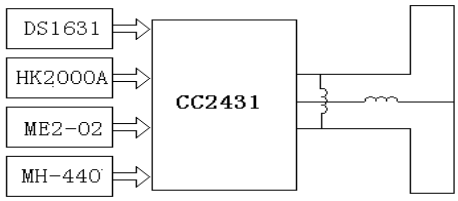

Figure 1 The system structure block diagram

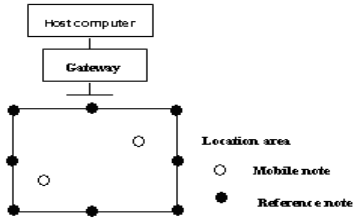

Figure2 Positioning system block diagram

2 Environmental information acquisition circuit

2.1 Oxygen concentration sensor

Employing electrochemical oxygen sensor ME2-O2, the working mechanism is electrochemical primary batteries: Cathodic oxygen reduction reaction occurs in the sensor, an oxidation reaction at the anode. Oxidation and reduction reactions to produce a current proportional to the oxygen concentration, follow Farada's law.

Its main technical parameters:

Range: 0～25%vol

Maximum measurement limit: 30%vol

Response time: （T90） ≤15S

Temperature range: －20℃～+50℃

2.2 Low- density gas sensor

Used to detect the ambient gas in the coal mine gas concentration, the main component of the gas is methane, gas concentration measurements uses the MH-440V/D infrared gas sensor. The sensors use non-dispersive infrared (NDIR) principle to detect CH4 present in the air, with good selectivity, without oxygen dependence, stable performance, long life, built-in temperature sensor for temperature compensation. Working voltage 3～5V, the measurement range 0～5%vol.

The output of oxygen concentration and gas concentration sensor is a voltage signal, through the filter circuit to filter out interference, evacuation 14bit A / D channel of CC2431 for analog / digital conversion.

2.3 Measurement of vital signs

The data terminal collection is miners' pulse and temperature data in distress, which are relatively easy to be acquired, in the case of cross-referenced to reflect the basic vital signs of the miners. Since the terminal is placed on the outside of the miners' helmets, body temperature and the pulse collection depend on the nearest principle. Temperature acquisition with a DS1631integrated temperature sensor, which connects CC2431 through the I2C bus and can directly output the measured temperature digital, without going through A / D conversion, the resolution can be adjusted. At 12-bit resolution, it may be up to 0.0625 ℃, after correction accuracy in near 37 ℃ measurement accuracy up to ± 0.1 ℃. Pulse acquisition using HK-2000A integrated pulse sensor , PVDF piezoelectric film, temperature compensation, signal conditioning circuitry are integrated within the HK-2000A integrated pulse sensor, the output pulse is in synchronization of pulse signal fluctuations . The PVDF is placed inside the helmet, close to the temple, used to feel the vibration of the temporal artery, the output pulse signal to the CC2431 counting unit measuring the vibration frequency of temporal artery, converted into pulse data.

Since temperature and output pulse signal are all digital, it no longer requires signal conditioning and analog / digital conversion, simplifying the circuit design.

3 ZigBee-wireless location network based CC2431

3.1 Construction of wireless location network

TI produces location engine CC2431 with hardware, based on RSSI (Received Signal Strength Indicator) technology, the location of the own node can be accurately calculated based on the received signal strength and the known reference point, and its location information is transmitted to the receiving end, achieving 3 ~ 5m positioning accuracy and resolution of 0.25m . It operates in the 2.4GHz ISM band, on-chip integration of ZigBee frequency (RF) front-end , memory, and 8051 controllers. Wireless Location System is composed of two kinds of nodes: a plurality of reference nodes and mobile nodes. The reference node is a fixed node, its position is known. This node can send data packets to each other information on each location through the Internet. The mobile node receives the data from the respective reference nodes, by measuring the received signal strength and the position information obtained from the reference node to calculate the own position by location engine. Figure 2 is a block diagram of the RSSI positioning system.

The role of each part is as follows:

(1) Host computer: a host connects to the reference node through a gateway, to manage the reference node such as setting coordinates of the reference node, and receives the data from the reference node via a gateway, on the screen can observe the location of each mobile node and various information collected by the mobile node.

(2) Gateway: the gateway is placed in the roadway, whose core is a CC2340, acting as a bridge between the reference node and the host, through fiber optic and CC2340 long-distance communications, ZigBee network is composed of CC2340 and reference node, the mobile node collected to transmit to the host.

(3) The reference node: fixed coordinate specified by the user, and supplies the coordinates and the average RSSI value for the mobile node.

(4) The mobile node: having internal positioning engine, the coordinates of its own can be calculated based on a fixed coordinates value of the reference RSSI node, and sends the coordinates , ID number to the gateway .

To ensure accuracy, multiple reference nodes are arranged on both sides of the roadway, forming a wireless network. Miners nodes computes their position in the located network, and their position, ID, environmental information and miners vital signs and other information, real-time wireless upload to the host computer. On a large screen in the center of the ground control room, computer images clearly indicate precise location of each miner, accuracy 2.5m^2.

3.2 Location algorithm based on RSSI

CC2431 positioning algorithm is based on the received RSSI (received signal strength indication) value. RSSI value will decrease with increasing distance:

$$RSSI = -(10n\log_{10}d + A) \tag{1}$$

Where, n is signal propagation constant, d is the distance between the sender, A is signal strength a meter far from the sender.

For mobile node M (x, y), the distance equation between two points in the plane, the equation can be obtained:

$$\begin{pmatrix} (X_1 - x)^2 + (Y_1 - y)^2 \\ M \\ (X_n - x)^2 + (Y_n - y)^2 \end{pmatrix} = \begin{pmatrix} d_1^2 \\ M \\ d_n^2 \end{pmatrix} \tag{2}$$

A linear transformation represented by the formula (2):

$$2A\begin{pmatrix} x \\ y \end{pmatrix} = B \tag{3}$$

$$A = \begin{pmatrix} X_1 - X_n & Y_1 - Y_n \\ M & M \\ X_{n-1} - Xn & Y_{n-1} - Y_n \end{pmatrix}$$

$$B = \begin{pmatrix} d_n^2 - d_1^2 - X_n^2 + X_1^2 - Y_n^2 + Y_1^2 \\ d_n^2 - d_{n-1}^2 - X_n^2 + X_{n-1}^2 - Y_n^2 + Y_{n-1}^2 \end{pmatrix}$$

Using the least squares method to get the coordinates of the mobile node:

$$\begin{pmatrix} x \\ y \end{pmatrix} = \frac{1}{2}(A^T A)^{-1} A^T B \tag{4}$$

3.3 The experimental results

In order to verify the effect of the positioning of the system, we do field tests in an office building's underground car park, having been completed but not put into use. Selecting length of 100 meters and wide of 6 meters as experimental zone, place 10 reference nodes evenly every25 meters around the spaced, the computer is placed in approximately 60 meters of 20 floors. Communications between gateway and computer test area using the RS485 level way, the dialogue between the two communicate using walkie-talkies, and upload data update once per second. Testing personnel wear data terminal during the test zone to run fast moving , uploading data to located information significantly lag; when less than 5Km / h speed mobile, data upload timely, no lag, positioning error <10m; when stationary, positioning error <5m, In the three cases, environmental parameters and vital signs are stable and reliable. After testing, the design meets the requirements in the whole.

4 Conclusion

RSSI-based location data terminal Underground staff is successfully developed, resolving the miners accurate positioning issues in time when the mine disaster. More importantly, real-time vital signs every miner and its surrounding environment information can be able to be got for rescue work smoothly to provide effective help. With this system, the ground control personnel can grasp the operation and distribution of underground personnel to improve safety ambulance efficiency with some promotional value.

Reference

[1] Liu Yang, Yang Jieming. Study on position method for underpit operators based on CC2431[J]. Coal Mine Machinery, 31(6): 49-51
[2] Xu Zhijing, Hu Bo. Wireless positioning technology research based on CC2431[J]. Electronic Design Engineering, 2009(10): 10-12
[3] Lizhi, Liu Jianhui. Research of mine rescue robots' communication based on the ZigBee technology[J]. Science Technology and Engineering, 2008(7): 34-36
[4] Guo Jian. RFID technology in coal mine personnel positioning system[J]. Fujian Quality Management, 2008(9): 62-63
[5] Song Baoye, Liu Yanzhao. CC2431-based wireless sensor networks[J]. Ordnance Industry Automation, 2008(4): 47-50
[6] Hu Qingxin, Cheng Zhen. The design of wireless sentor network platform positioning system based on ZigBee. Embedded Technology, 2009(11): 26-29
[7] Song Baoye. Wireless orientation engine and application improvement of CC2431[J]. Microcontrollers & Embedded Systems, 2008(2): 22-24

Advanced Materials Research Vols. 989-994 (2014) pp 3003-3006
© (2014) Trans Tech Publications, Switzerland
doi:10.4028/www.scientific.net/AMR.989-994.3003

The design of embedded video monitoring system based on DSP processor

Wenbin Hu

Engeneering department ,Xijing University,xi'an,china

Keyword: Video monitoring, Linux operating system, Video losing

Abstract: This paper designs a embedded video monitoring system based on ARM processor Ep9315 and TMS320DM642, and using embedded Linux operating system. In the system, video capturing module uses the video decoder TW2814. In order to capture better data, the control of TW2814 is needed. Through the imitation of I2C bus, the driver provide the application with the function of the setting of capturing parameters such as hue, color saturation, contrast and brightness, and the check of video losing.

Introduction

With the development of technology and the advancement of people's living standard, video monitoring system is widely used in the industry, security field and daily life. Video monitoring technology, combining the technology of computer, multimedia, telecommunication and network, is one of the focuses that are being researched and it has extensive future and practical value. With development of the embedded system and the degree of the integration of the chips, embedded video monitoring technology is getting more and more attention and being applied in many occasions[1]. Monitoring system can be used to campus safety monitoring, test monitoring, urban traffic monitoring, etc, and bring people good living environment.

1 Embedded video monitoring system overview

Embedded video monitoring system is composed of the collection part, coding part, transmission part, the controlling and display section. In the acquisition part, it needs to provide a full range of video monitor for completing analog video capture, while video loss detection function needs to be provided. When encoding, the image information acquisition should be encoded. In the transfer section, the image needs to be transmitted in real time after encoding, achieving the transmission in a variety of ways to meet the needs of different users, and is transmitted with low loss and requires a reliable transmission quality. In the display portion, the system needs to achieve real-time decompression of the video data playback, the video data stored in the video, the playback of history video recording, setting the alarm of video-interest part, the alarm time analysis and management. In the control section, you need to control the focal length of the camera aperture, image brightness, contrast, hue, saturation adjustment, image compression quality, frame rate control, PTZ control and external device control.

Because of the continuous powerful function, the application of embedded video monitoring system is also more extensive. Now, it can be used in security, access to information and command scheduling, providing a variety of services for production process control, security in large public facilities, medical care, distance education[2].

2 Hardware structure of embedded video monitoring system

The embedded system based on ARM processor, with its own rich resources, low power, low cost, is supported by many vendors, more and more applications in a variety of embedded systems requiring complex control and communication functions. As a dedicated digital processing circuit, DSP digital signal processing capability is very powerful, but more difficult to achieve task management, communications, human-computer interaction and other functions. If combining these two processors together, that is, the DSP combines the acquisition circuit sampling and processing signals, the ARM processor, as a platform, sends the results after DSP to the user for further

processing, and provides a graphical friendly interactive environment, completion of data analysis and network transmission and other functions, which will maximize the function of both directors[3].

The embedded video monitoring system is composed of the ARM and DSP dual-processor, ARM processor uses a Cirrus Logic's EP9315, DSP is TI's TM320DM642. In this way, we can take full advantage of the powerful DSP data processing capability, and the advantages of ARM processors in control. EP9315 processor is a highly integrated system on chip processor, and has opened a new road for next-generation consumer and industrial electronic products. EP9315 features an advanced 200 MHz ARM920T processor, and supports Linux, Windows CE and many other memory management unit of embedded operating system. TI's TMS320DM642 is the launch of a new fixed-point programmable DSP suitable for multimedia applications, TMS320C64x nuclear, using the same architecture of TMS320C6000 and a high-performance, advanced long instruction kernel.

Taking advantage of the characteristic of a dual-processor, some functionality of the video monitoring system is divided into modules, equitable distribution on two processors running, thus effectively improving system performance. To this end, the design takes a certain division of labor policy, running embedded Linux operating system and some applications software on EP9315. TM320DM642 is responsible for video data encoding, video capture and display. Between two processors, a host interface HPI of DM642 is used for data communication, coordinating the various operations, so as to achieve the purpose of making better use two chips operating in parallel. Concrete realization of the principle of the design is shown in Figure 1.

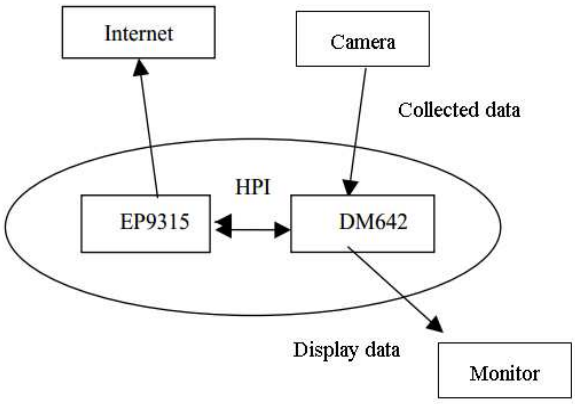

Figure 1 Video monitoring system schematic

Video capture terminal uses a decoder chip TW2814, the video chip provides the external I2C bus control interface. Due to EP9315 chip without I2C controller, the system is connected to the video chip TW2814 by EP9315 GPIO pin, then using these two GPIO port to simulate the I2C controller, and sending a control signal to the video chip. Through access to EP9315 interrupt pin, TW2814 makes the system achieve video loss detection function.

3 The software architecture of embedded video monitoring system

As the embedded video monitoring system requires a strong network transmission and many other sophisticated features, in this paper, the system chooses Linux as the operating system on the ARM processor EP9315. Linux opened kernel source, combining with ARM architecture processor, can play Linux systems' advantages of supporting a variety of network protocols and existing multi-process scheduling mechanism, so that shorten the development cycle, scalability enhancements[4].

The DM642 uses DSP / BIOS, simple embedded operating system provided by TI, which itself occupies only minimal CPU resources. DSP / BIOS provides the underlying application program interface, which can be achieved mainly by invoking a series of DSP / BIOS real-time database API functions. From a functional perspective, the system consists of the following modules: video capture module, video encoding module, data transmission module, network transmission module, the video display module. The relationship between the various modules:

DM642 video data acquisition module runs and collects data into the memory of a good address space by encoding module out of the data collected and packed into the other one for encoding the specified address space. In the data transmission module, EP9315 reads encoded data interface via HPI, and then stores data on the hard drive by the storage module or sends video data to the network by the network. So users can monitor real-time images through a Web browser. The video display module is a separate module from other modules for displaying monitoring video. The relationship between the various modules is shown in Figure 2.

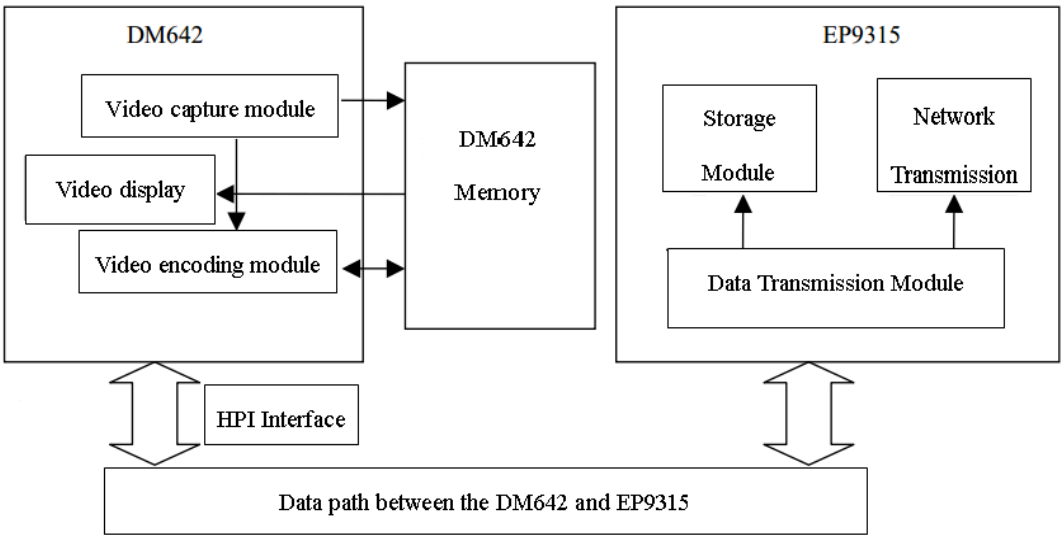

Figure 2 Software module diagram

Video capture of the system is done by video chip TW2814. TW2814 converts the input analog signal into a digital signal. The DSP digital signal acquisition module is responsible for reading TW2814 conversion. After reading the data from the acquisition memory, the encoding module encodes the data, packing it into the designated memory region for reading. Before coding, the video sequence must first be analyzed, each video object divided from the original image, and then encoded separately for each video object, respectively. Each object has its own shape information, motion information and texture information. The encoded video object is these three kinds of information. Since our entire video sequence is rectangular, there is not the arbitrary shape coding, only the motion information is related to coding and texture information encoded, we use the encoding algorithms associated with the motion compensation and discrete cosine transform associated with texture coding, and quantization, Zig-Zag scanning, variable-length coding algorithms. Data transmission module consists of the driver on EP9315 and applications together. Storage module is running on the EP9315 application, and then reads the data packaged by DM642, analyzing data packets, extracting the video data, and the data stored on the hard disk. Network transmission module, borne by EP9315 applications, is responsible for submitting programmed stream to TCP / IP protocol for network transmission. Video display module running on DM642, sends video data to the D / A converter chip ADV7179, and displays the video on the video monitor.

4 Conclusion

In the system that consists of two processors, data transfer in the two processors is indispensable. Through the HPI port provided by DM642, the read and write operation can easily be implemented. In order to achieve the transfer, HPI driver is programmed. Also, the performance of different interfaces in the driver is analyzed and how to start DSP by using HPI driver is discussed. The system needs the support of graphic system to make users control it conveniently. Therefore, display driver is devised and implemented through extending HPI driver. In this way, users can configure and manage the system through graphic system, increasing the degree of convenience of users' interacting with the system.

References

[1] Cui Guangzuo, Li Zhaolin. MT ARM: multithreading implementation in Arm7 architecture. In: Ting-Ao T, Huihua Y, Wang A, et al. ASICON 2001. 2001 4th International Conference on ASIC Proceedings. Shanghai, China. 2001. Piscataway, NJ, USA: IEEE, 2001:793~796

[2] Segars S. The ARM9 family-high performance microprocessors for embedded applications. In: Proceedings International Conference on Computer Design. VLSI in Computers and Processors. Austin, Texas, US. 1998. Los Alamitos, CA, USA: IEEE Comput. Soc, 1998:230~235

[3] Li-Hsun Chen, Teng-Yi Wang, Chi-Lung Wang. An adaptive DSP processor for high-efficiency computing MPEG-4 video encoder. Circuits and Systems, 2004, 2(23):57~60

[4] Pascal Meunier, Sofie Nystrom, Seny Kamara, et al. ActiveSync, TCP/IP and 802.11b Wireless Vulnerabilitiesof WinCE-Based PDAs. In： Proceedings of the 11th IEEE International Workshops on enabling technologies. Pittsburgh, Pennsytvania, USA. 2002. US：IEEE computer society, 2002:145~152

Advanced Materials Research Vols. 989-994 (2014) pp 3007-3010
© (2014) Trans Tech Publications, Switzerland
doi:10.4028/www.scientific.net/AMR.989-994.3007

A Calibration Method of Binocular Stereo Vision System Based on Halcon

Zhixian Zhang[a], Zhende Zhu[b]
[1]School of Shenyang Aerospace University, Shenyang 110135,China;
[a]zzx_syiae@tom.com, [b]114345098@qq.com

Keywords: Camera Model, binocular stereo vision system, calibration, Halcon.

Abstract. This paper describes the pinhole camera model combined with an area sensor and a regular lens and the imaging model of the binocular stereo vision system. Also a method to determine the internal and external parameters of a camera by transferring the coordinates three times is described. Then a calibration experiment is carried out with the Halcon calibration board which proved the method works. The method mentioned in this paper has laid a good foundation for measuring the size of objects with the binocular stereo vision system.

Introduction

Lately, the machine vision is much more frequently used in the area of industrial measurement because of the influences such as the measuring environment and measuring accuracy. However, in the machine vision, the internal and external parameters can be easily changed. Hence, it is necessary to calibrate the cameras in order to get the 3D information of an object. The calibration refers to set up the correspondence between the pixels in the image and the points in the real world. The way is calculating the parameters by the known point's image coordination and world coordination based on the camera model [1].

Currently, the camera calibration methods can be divided into three categories: traditional calibration, self-calibration and the calibration based on active vision. The traditional calibration works by photographing an object in exactly known size and get the camera's internal and external parameters in a series of calculating. Self-calibration works by the relationship between multiple images instead of a known object as the reference. The calibration based on active vision works by moving the camera in exact moving parameters to get multiple images and calibrate with the moving parameters and the images [2-5].

Camera Model. To calibrate a camera, a model for the mapping of the 3Dpoints of the world to the 2D image generated by the camera and lens is necessary. Two different types of lenses are relevant for machine vision: regular and telecentric lenses. Regular lenses perform a perspective projection and telecentric lenses perform a parallel projection. Furthermore, two types of sensors need to be considered: line sensors and area sensors. This paper established a pinhole camera model consisted of area sensors and regular lens, as shown in Fig.1. Four coordinate systems are shown in the figure: the world coordinate system (WCS)(x_w,y_w,z_w), the camera coordinate system (CCS)(x_c,y_c,z_c), the pixel coordinate system (PCS)(r,c) and the image coordinate system (ICS)(u,v). Here, s_x and s_y are scaling factors, and they represent the horizontal and vertical pixel pitch on the sensor. The point P_w in the WCS is projected to the point p in the image plane by the projection center. If there were no lens distortions present, p would lit on a straight line from P_w through the projection center, indicated by the dotted line. Lens distortions cause the point p to lie at a different position. The image plane is located at a distance of f behind the projection center. The f is the principal distance here. It is easier to pretend that the image plane lies at a distance of f in front of the projection center, which simplifies many calculations.

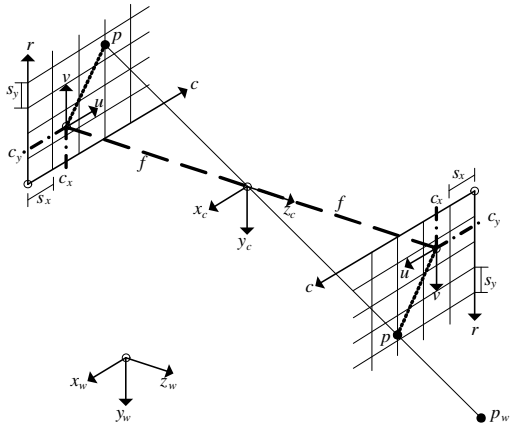

Fig.1 Pinhole camera model

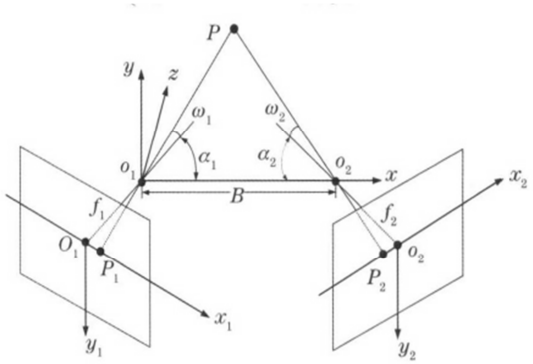

Fig.2 The principle of binocular stereo vision system.

In order to project the point P_w into the point p, three transformations of the coordinate systems are needed:

1. Transform from the WCS to the CCS. The point $P_c = (x_c, y_c, z_c)^T$ in the WCS is given by the point $P_c = (x_c, y_c, z_c)^T$ in the CCS, where $P_c = RP_w + T$. Here, $T = (t_x, t_y, t_z)^T$ is a translation vector and $R = R(\alpha, \beta, \gamma)$ is a rotation matrix, which is determined by the three rotation angles α (around the x axis of the CCS), β (around the y axis of the CCS), γ (around the z axis of the CCS). The six parameters (t_x, t_y, t_z, α, β,γ) of R and T are called the external camera parameters, cause they determine the position of the camera with respect to the world.

2. Transform from the CCS to the PCS. For the pinhole camera model, the projection is a perspective projection, which is given by:

$$(u, v)^T = \frac{f}{z}(x_c, y_c)^T \tag{1}$$

Considering the lens distortions, the coordinates $(u, v)^T$ will be modified. For most lenses, the distortion can be approximated sufficiently well by a radial distortion, given by:

$$(u', v')^T = \frac{2}{1 + \sqrt{1 - 4k(u^2 + v^2)}}(u, v)^T \tag{2}$$

The parameter k models the magnitude of the radial distortions. If k<0, the distortion is barrel-shaped; while k>0, it is pincushion-shaped. This model has a great advantage that the distortion correction can be calculated analytically by:

$$(u, v)^T = \frac{1}{1 + k(u'^2 + v'^2)}(u', v')^T \tag{3}$$

3. Transform from the PCS to the ICS. This process is given by:

$$(r, c)^T = \left(\frac{v'}{s_y} + c_y, \frac{u'}{s_x} + c_x\right)^T \tag{4}$$

Here, the point $(C_x, C_y)^T$ is the principal point of the image. The six parameters (f, k, S_x, S_y, C_x, C_y) are called the internal camera parameters, cause they determine the projection from 3D to 2D performed by the camera.

The principle of binocular stereo vision system. As shown in Fig.2, the binocular stereo vision system is based on the principle of parallax, and get the 3D information of the observing object by two cameras. Here, we pretend the ICS of the two cameras are $O_1 - x_1y_1$ and $O_2 - x_2y_2$, and the point p is projected into p_1 (x_1, y_1) and p_2 (x_2, y_2), with the points o_1 and o_2 being the principle points. We set up a measuring coordinate system (MCS) $O - xyz$ with the point o_1 as the origin and the point p located in the plane $O - xz$. The line o_1o_2 is named the base line, with the length B. If the focuses of the cameras are f_1 and f_2, the angles between the axis x and light axis O_1o_1, O_2o_2 are

α_1 and α_2, and angles between the lines through the principle points and the point p and the light axis are ω_1 and ω_2, then we can get the coordinates of the point p in the MCS:

$$\begin{cases} x = \dfrac{B\cot(\omega_1+\alpha_1)}{\cot(\omega_1+\alpha_1)+\cot(\omega_2+\alpha_2)} \\ y = Y_1\dfrac{z\sin\omega_1}{f_1\sin(\omega_1+\alpha_1)} = Y_2\dfrac{z\sin\omega_2}{f_2\sin(\omega_2+\alpha_2)} \\ z = \dfrac{B}{\cot(\omega_1+\alpha_1)+\cot(\omega_2+\alpha_2)} \end{cases} \tag{5}$$

Where ω_1 and ω_2 can be get by:

$$\begin{cases} \omega 1 = \arctan(X_1 / f_1) \\ \omega 2 = \arctan(X_2 / f_2) \end{cases} \tag{6}$$

The experiment of the binocular stereo vision system.

The calibration board. The calibration needs enough coordinates of the points in the WCS, so in here we can use a calibration board which is exactly measured and movable. There are 49 points in the board and a black triangle located in one of the corners in order to determine the direction.

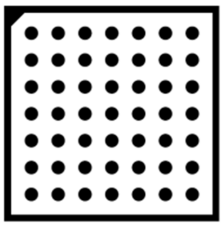

Fig.3 The calibration board

Fig.4 The experiment platform

Set up the experiment platform. We use two cameras MER-130-30UM-L, with the port USB 2.0, and the parameters is provided in the Table 1:

Table 1 The parameters of the cameras

Type	MER-130-30UM-L
Resolution	1280x1024
Pixel size/μm	5.2 x5.2
Spectrum	Grayscale

The experiment platform is shown in the Fig.4:

The experiment results. We need the two cameras shoot images of the calibration board at the same time, and the board is required to be complete in all of the images. In every experiment, we got 30 groups of images, 5 of them is shown in Fig.5:

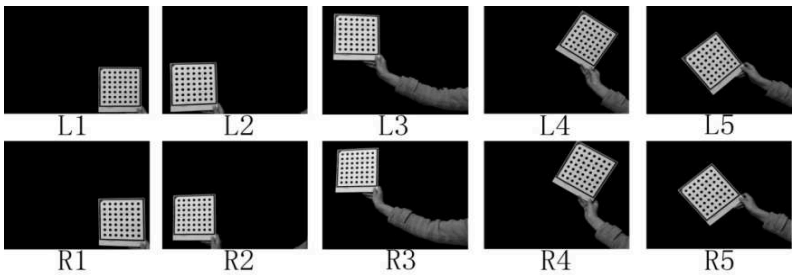

Fig.5 Several images for calibration

The experiment results are provided in Table 2 and Table 3:

Table 2 The results of internal parameters

	$f(mm)$	$k(1/m_2)$	$S_x(\mu m)$	$S_y(\mu m)$	$C_x(pixels)$	$C_y(pixels)$
Left camera	11.66	-320.296	5.23	5.20	685.48	554.01
Right camera	12.41	-254.741	5.17	5.20	653.58	497.27

Table 3 The results of external parameters

	$R(\alpha,\beta,\gamma)(degree)$	$T(tx,ty,tz)(mm)$
Left camera	(357.965,355.124,358.316)	(101.975,-104.856,1058.49)
Right camera	(357.746,15.6635,357.211)	(9.91253,-11.1875,176.568)
The pose of the Right camera to the Left camera	(0.755279,340.852,1.57459)	(410.069,47.9801,6.19998)

Summary

This paper introduces the principles of the calibration and the binocular stereo vision system, and operated the experiment with the error in 3mm, which proved that the method is feasible. The method mentioned in this paper has laid a good foundation for measuring the size of objects with the binocular stereo vision system.

References

[1] Guangjun Zhang. Machine Vision[M]. Beijing：Science Press, 2005

[2] Song L M, Wang M P, Lu L, et al. High precision camera calibration in vision measurement [J]. Optics & Laser Technology, 2007, 39(7)：1413-1420.

[3] Triggs Bill. Autocalibration from Planar Scenes [C]// Proceedings of the 5th European Conference on Computer Vision. London, UK：Springer-Verlag, 1998, 1：89-105.

[4] Zhang Y, Zhang Z, Zhang J. Camera calibration technique with planar scenes [C]// Machine Vision Applications in Industrial Inspection XI. Santa Clara, CA, USA：SPIE, 2003：291-296.

[5] Tsai R. A versatile camera calibration technique for high-accuracy 3D machine vision metrology using off-the-shelf TV cameras and lenses [J]. IEEE J. Robotics and Automation, 1987, 3(4)：323-344.

Advanced Materials Research Vols. 989-994 (2014) pp 3011-3014
© (2014) Trans Tech Publications, Switzerland
doi:10.4028/www.scientific.net/AMR.989-994.3011

The brief introduction of several common subway shock absorber fasteners in china

Huapeng Luo[a], Dunjin Cai[b], Mingliang Liu[c] and Ping Wang[d]

MOE Key Laboratory of Highspeed Railway Engineering, Southwest Jiaotong University, China

[a]756468322@qq.com,[b]1198876623@qq.com,[c] 1282135564@qq.com,[d]wping@home.swjtu.edu.cn

Keywords: subway shock, shock absorber, fasteners

Abstract. Due to the large and medium-sized cities in our country is more; the urban rail speed is low and the environmental protection high capacity requirements. Each city urban rail structures more or less differences. Especially fastener system is various, even in the same line also exist different deduction system; Because the subway in China fastener system is various and not a fixed is widely used fastener system; The paper gives a simple summary of subway common shock absorber fasteners in China. I hope it can give a reference to researchers on fasteners.

Introduction

The fastener system is a connection of rail and sleeper . The fastener system has its important role in the track. Urban rail transit in China has been vigorously developed in decades. The urban rail transit has the characteristics of the short circuit, the low speed, the high demand in noise reduction and environmental protection, etc. But, on the whole, all kinds of new fasteners are based on the research and development of several typical fasteners. The paper gives a simple introduction of common shock absorber fasteners system in our nation.

LORD damping fasteners

The main structure of fastener which is designed by LORD Company is sandwich-type cementation and metal plate. As is shown in figure 2.Its main characteristics are vulcanizing supporting rail plate, perforated rubber and base plate to achieve a whole, making use of the deformation of rubber hole to achieve vibration reduction. LORD fastener directly supports rail track, sets up the plate which adjusts the height . LORD fastener has been used in 4th subway routes line of Guangzhou.

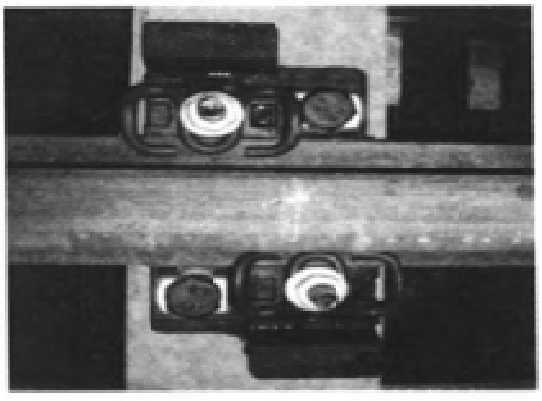

Fig.1 LORD Vibration fasteners

LORD damping fastener has characteristics of integrated design, perfect integrity, the appropriate structural height which consistent with the existing line, the track vertical subsidence which is less than 1.5 mm, meeting requirements for the technology of linear motor, etc.

2 Shock absorber fasteners (cologne egg)

With reference to foreign information on track shock absorber and other domestic shock absorber and characteristic of subway track structure, the shock absorber is usually designed as elliptic cone to avoid stress concentration. As is shown in figure 2, it can effectively reduce vibration energy of track to achieve the effect of damping and buffering. Damper fastener is a separated shoulder fastener which is designed as elliptic cone. The elliptic cone bonds inner ring and outer ring with rubber vulcanizates. Its vibration reduction effect is remarkable. Shock absorber buckle has a large deflection under wheel-load, reducing the mechanical impedance of the upper buildings and vibration excitation. It uses rubber shearing deformation to attain high elastic vibration reduction.

Rail vibration absorber fasteners are a widely used transit damping products in urban rail. Beijing, Shanghai, Guangzhou and other cities have been successfully used it in subway lines.

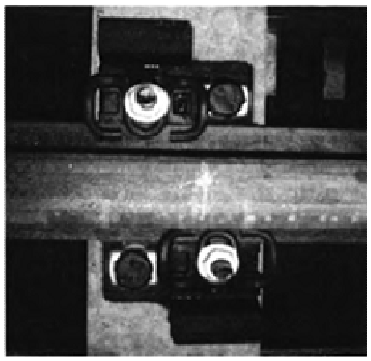

Fig.2 Absorber fastener

3Ⅰ type shock absorber on the rail fastener

Beijing urban construction design & research institute researched and designed the Ⅰ type shock absorber on the rail fastener as early as 1988, then it applied for patent (figure 3). Its structural characteristics is using rubber ring which vulcanizes sleeper rail supporting iron plate and the iron plate under the base of rail in a body to withstand shear effect [2]. Because its shear elasticity is better than that of the compressive elastic rubber, rail damper fastener has very low vertical static stiffness, generally in 10 ~ 18 KN/mm.

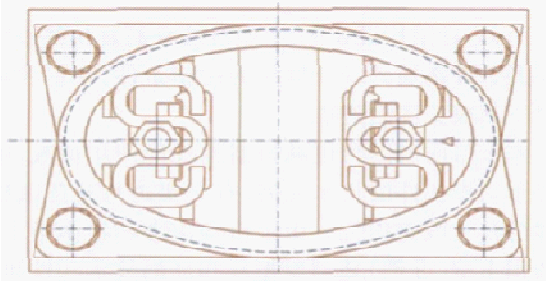

Fig.3 Ⅰtype rail absorber fastener

Ⅰ Type shock absorber on the rail fastener which is applicable to 60 kg/m rails based on the design concept of "egg" cologne in Germany, which is a rectangular base plate, Its connection of rail plate supporting and the base is oval. It is an open fastener without retaining shoulder has a

lower vertical static stiffness (generally in the 10 to 18 KN/mm). The product passed the scientific and technical appraisal of Shanghai in 1990 laid in Shanghai metro line 1, 2. The rubber ring which is made from domestic neoprene attains material formula from product manufacturer .According to the research report of Ⅰ type shock absorber on the rail fastener, the laboratorial detection performance of first generation rail shock absorber is good. It has a good damping effect, its fastener vibration acceleration level decreases by 10-20 dB compared with DT Ⅲ type. In the use of Shanghai metro line 1, its early damping effect is obvious, playing an important role .It fills in the blank of no shear fastener the our country that only has compression type fastener.

4 Ⅱ type orbital damper fastener

Ⅱ type shock absorber on the rail fastener develops from Ⅰ, mainly adjusted withhold rail parts, apply to 50 kg/m rails. it is without retaining shoulder open elastic fasteners.

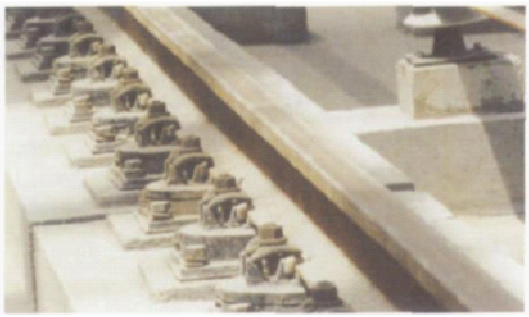

Fig.4 Ⅱ type orbital damper fastener

5 double stiffness Ⅲ orbital damper fastener

Double stiffness Ⅲ orbital damper fastener is a new type of subway track damper fastener which develops from Ⅰ(Ⅱ). The gauge for adjustment amount is: + 8 ~ -12 mm; Rail horizontal adjustment quantity as follows: under the rail allows up to 10 mm, vibration isolator allows up to 20 mm. The rail dynamic subsidence limit take 3 mm; Static stiffness is 8 ~ 12 KN/m, output ratio of Q-switching to free running control in the range of 1.2 ~ 1.25, Stiffness design for double stiffness, the first stage stiffness is also known as stiffness, damping significantly improve the effect of the vibration, static stiffness for 8 ~ 12 KN/mm. Stiffness is also known as the second order safety stiffness, static stiffness control the order in 25 ~ 40 KN/mm, guarantee the necessary support stiffness of which the change of rail geometry in the safety of the allowable range. Withhold with no bolt elastic condition, no bolt e shaped article, facilitate the subway all play in the form of a unified, improve the adaptability of fasteners. Double stiffness Ⅲ orbit damper fastener as shown in figure 5. The vertical load of 15 ~ 35 KN, horizontal lateral load is 10 ~ 20 KN, within the scope of the load vibration and exert effective.

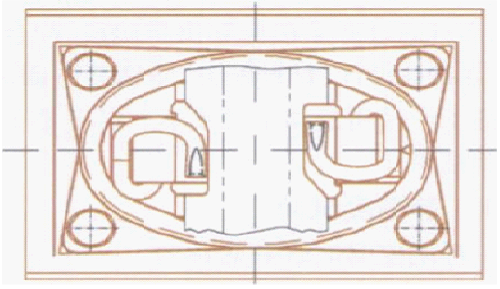

Fig.5 Ⅲ type track vibration isolator fasteners

6 GJ - Ⅲ damping fasteners

GJ - Ⅲ double nonlinear damping fasteners is no block separated shoulder type elastic fasteners, mainly used in Guangzhou metro. The fastener for compression damping fasteners, its static stiffness is 10.94 KN/mm, dynamic and static stiffness than < 1.3. GJ - Ⅲ type double nonlinear damping fasteners develops from the bottom plate type fastener system , on the basis of the design of double nonlinear elastic plate system, reduce the system stiffness, improve the damping of structure, and effectively reduce the secondary noise and vibration. As is shown in figure 6, it constitutes rubber mat under the rail, fen plate and rubber pad in the middle, the iron plate and self-locking mechanism. Low stiffness system reduces the vibration transmission of its supporting system, so as to reduce the spread of the ground vibration. The unique "self-locking structure" is a big window. It can be very convenient to connect the component, greatly reduces the maintenance cost. On the whole, GJ - Ⅲ fastener is compact size, relatively light, height 60 mm, using polyethylene as the material of high plate, adjust static stiffness of plate greater than1000 kN/mm, which has no effect on the system stiffness.

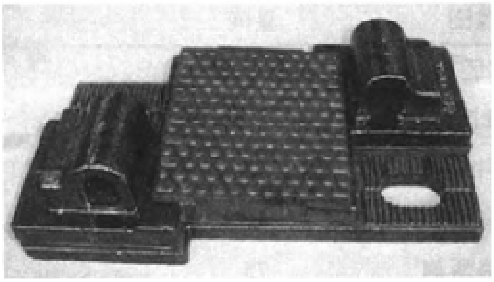

Fig.6 GJ - Ⅲ double nonlinear damping fasteners

Conclusion

In this paper, several common fasteners of the subway are made a brief introduction and it give a reference to researchers. Our metro fastening system complicated, since there is no uniform standard, mostly do part research on existing fastening systems; various research units of their research are relatively conservative and cannot brainstorming developed a widely accepted fastening systems. I hope the relevant departments to organize our research unit jointly develop suited to China's national conditions, with our own intellectual property, can be widely used the subway damping fastening systems.

References

[1] Wang yujie. Scheme comparison of north of Guangzhou metro line 4 delay period project of rail vibration reduction[J]. Railway standard design.2012(11), In Chinese

[2] Ren jing. Ⅲ type double track vibration isolator stiffness fastener design[J]. Civil engineering technology,2007. In Chinese

[3]Yang hongwei. New type damping Vanguard fastener short sleeper rail project construction technology[J].Rail/road,2006. In Chinese

Advanced Materials Research Vols. 989-994 (2014) pp 3015-3018
© (2014) Trans Tech Publications, Switzerland
doi:10.4028/www.scientific.net/AMR.989-994.3015

Design of the Improved Accompanying Temperature Logger

Juan GUO[1,a], Shiying Liang[1,b] and Zongtao Yin[1,c]

Shijiazhuang Vocational Technology Institute, Shijiazhuang 050081, China;
[a]juanguoluck@126.com, [b]liangshy@mail.sjzpt.edu.cn, [c]yinzt@ mail.sjzpt.edu.cn

Keywords: Power consumption; Temperature measure; Logger; Low power

Abstract: This paper describes research on some methods of reducing power consumption to reduce the volume accompanying logger. For the requirement of ultra-low power consumption and miniature, the design is described separately from the hardware and software, mainly including temperature detecting module, interface of communication, low current circuit hardware, energy conservation ,arouse from power down state, communication protocol, etc. The experimental tests for device prove that the research can achieve low power requirements.

Introduction

In the course of the different stages of production, transportation and storage of chemical, food, medical and other products, in order to ensure the best quality products, continuous tracking temperature is critical. Currently accompanying logger and power consumption are large volume, high cost, which limits its extensive use. Therefore, a small volume of low-cost and long-time continuous measurement of micro-recorder, compact and easy to carry, is needed.

Therefore, the paper starts two studies of the volume miniaturization and micro-power and designs a micro recorder whose volume equivalent to only several coins stacked together, and the recorder can be attached to the surface of the object, along with objects placed inside the bag.

Since October 2012, the recorder has been formally put into production, Asia Brewery Xinxiang, Hunan Seven Swords Beer Company and other units have used the product to record the pasteurization temperature with favorable results and some promotional value.

1 The working principle of the temperature recorder

Temperature sensor measures the ambient temperature and transfers to the microprocessor for temperature signal processing, and the compressed data stored in the internal RAM, the data read out by the computer[1].

A temperature sensor is placed in a stainless steel shell and has good heat conductivity with the inner wall, which can be sensitive to the temperature of inner wall. The shell is made of stainless steel, communication by the housing, and without communication interfaces, long-term work in a variety of harsh environments where liquids or acid, communication with a computer, controlling the recorder, through the interface circuit.

The recorder's temperature range of -40 ℃ ~ + 85 ℃, temperature resolution of 0.0625 ℃, measurement accuracy of ± 0.2 ℃, it can record 4K data, and recording interval can be set discretionarily, inside lithium battery life> 5 years.

2 The miniaturized design of logger circuit

2.1 Temperature measurement and conversion mechanism

The miniaturized design not only reduces circuit board area, but also reduces the power consumption and ensures the accuracy of the measurement, not the traditional temperature

measurement and conversion circuit. The digital temperature sensor DS620 by Maxim can 1.7V-3.5V voltage, -55℃-+125 ℃ working temperature down to 10 to 13 precision output temperature values at 0℃-+70 ℃, maximum error ≤ ± 0.5℃, corrected measurement accuracy can be improved to ≤ ± 0.2 ℃. Small, its μSOP package only 5 × 3mm, very consistent miniaturization requirements[2].

According the error statistics graph of DS620 in the range of 0-70 ℃, making its Mean polynomial curve to get the formula between error Δ t ' and the measured value t:

$$\Delta t' = 0.0002(t/10)^3 + 0.0148(t/10)^2 - 0.1566t/10 + 0.3479℃$$

In the formula, t is the measured temperature, Δt' is t Mean deviation of the curve. The actual offset calibration error Δt", the total error correction Δt = Δt' + Δt", to improve the measurement accuracy of the DS620 ≤ ± 0.2℃.

2.2 Based Mega328P recorder core circuit

In the miniature, the core circuit is only a 5 × 5 × 1.0mm QFN package and small resistive and capacitive components of Mega328P, DS620 and several pieces of 0420, using micro SMD 32.768KHz crystal. Use FPC circuit board, circuit board logger overall thickness not exceeding 1.8mm. Circuit diagram is shown in Figure 1.

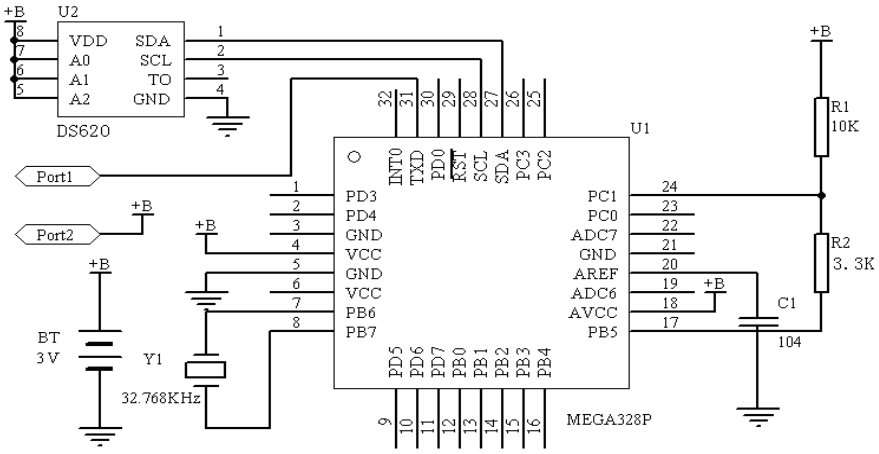

Fig.1 Logger core schematic

Here, DS620 converts the measured temperature to 10-13digital bits transmitted through the I2C bus to Mega328P[3], the data compressed is stored in 2K bytes of RAM, the resistors R1 and R2 are the battery voltage measurement circuit, PB5 low usually, R2 to ground, the battery voltage is obtained by the ADC; PB5 output high, reducing the current consumption of R1 and R2. Chips waked and communications are done via TXD pin, in order to adapt to work in a conductive liquid, the battery positive as ground, so even if the electrode of communication and the shell are shorted , which will not have impact on Mega328P.

3 Logger software energy-saving design

3.1 Logger Software Process

Temperature logger software adopts modular design, including single-chip power-on initialization, system timing, command parsing, temperature measurement and recording, communication, etc.

System after power-up, power-down state to enter (turned off). Only Mega328P external interrupt can wake it up from power-down state. Use of certain external interrupt consisting of command sequence: If you receive a boot command, the system self-test, self-test by entering records state. Sleep when not sampling, only the timer work. When the sampling time, to exit hibernation, temperature sampling, data recording, and then re-enter hibernation; If you receive a

communication command, then stop recording, the recorded data is transmitted to the computer via the interface circuit. Communication over, enter the power-down state again.

3.2 Serial software simulation

Given Mega328P not working in a power-down state, only the external interrupt can wake it up, so take advantage of MCU pin interrupt function to simulate a receiver serial port. Via 328P hardware serial communications to send large amounts of data, TXD pin also receives external commands. TXD pin is usually set as input, active low enable external interrupt. TXD pin by pulling 100ms, wake Mega328P. After the wake 328P, the TXD falling edge interrupt mode is set to trigger at the same time start the timer T0 interrupt interval timer for TXD. Command, nine consecutive falling edge pulse, is sent to the 328P, the first pulse T0 timing synchronization , following 8 pulses are the communication of information , low on going 1ms to "0", 2ms to "1"[5]. TXD pin waveform is shown in Figure 3.

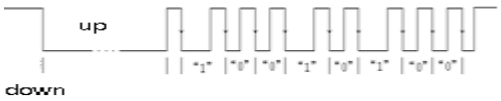

Fig.3 TXD Pin wave chart

When the logger outside communication, the TXD pin is set to output to enable hardware serial communications and close its external interrupts. After the communication, TXD low level triggers external interrupt, waiting to receive another frame command.

3.3 Software micro-power design

Recorder energy devices primarily are MCU Mega328P and DS620. Mega328P operating current has a great relationship with its operating mode, when IDLE, the operating current is only about 15% of ACTIVE current, full use of IDLE can reduce the operating current. The main factors affecting the Mega328P operating current is the clock frequency, reducing the clock frequency can greatly reduce the operating current[4]. Due to the speed of AVR MCU 1MIPS/MHz, using low frequency 32.768 KHz crystal can meet the computing speed. Such Mega328P at 3V ACTIVE state current consumption is 60μA, IDLE state current of 10μA, the power-down state current is less than 1μA. DS620 temperature conversion work when current is 0.8mA, when not converting less than 1μA, conversion time and is proportional to conversion accuracy, the resolution of 0.5 ℃ conversion time is 25ms, 0.0625 ℃ time is 200ms. Current Logger is calculated by the formula (2).

$$I = \Sigma I_i T_i / \Sigma T_i \quad (2)$$

Here， under certain state operating current Ii, μA; the state duration Ti, ms. At a resolution of 13, a temperature of the collected per minute.

Working state	Duration (s)	Operating current (μA)
IDLE	59.97	10
ACTIVE	0.01	60
Sample	0.02	800

The average current

$$I=\Sigma I_i T_i/\Sigma T=(10*59.97+60*0.01+800*0.02)/60=10.27\ (\mu A)$$

4 The experimental results

Experimental tests were carried out for the design of low -power and accuracy. In 0℃ice-water mixture, carrying out at a temperature above 10 ℃ oil bath at test temperature. The measurement results are shown in Table 1.

Tab.1 Error experimental data

No.	Standard Temperature	Original error	Correction error
1	0.0℃	-0.3℃	-0.1℃
2	20.0℃	- 0.2℃	0.0℃
3	40.0℃	-0.2℃	0.0℃
4	60.0℃	-0.1℃	0.0℃
5	80.0℃	-0.2℃	0.1℃

By contrast, it is found that the temperature error after correction ≤ ± 0.1 ℃, reaching ≤ ± 0.2 ℃ design requirements. As the overall power consumption is closely related to the sampling and recording interval accuracy, precision experiments at 13 intervals of one minute recording conditions, with Agilent34401A logger to measure the operating current. Since the operating current cyclical and jump, use the capture function 34401A peak and measure overall maximum current 856.3μA, minimum current of 9.6μA, the average current is 11.5μA, and theoretical calculations are consistent. Such a capacity of 450mAh battery records once per minute, continuous measurement time 54 months, about 4.5 years , power consumption meets the design requirements.

5 Conclusion

The miniature and low-power design of accompanied temperature logger reduces the volume, power consumption, enabling miniature recorder to work longer. While using unique stainless steel shell structure, the recorder can work reliably under complex situations in a variety of fields. And its miniaturization and energy efficient design also provides a reference for designing other similar electronic devices.

References

[1] Wu Taihu, Zheng Jiewen, ZhaoPeng, etc. Development of a mini temperature logger with ultra low-power based on C8051F320 MCU [J]. China Association for Medical Devices Industry. 2009, 15(6): 30-33

[2] DS620 Low-Voltage, ±0.5°C Accuracy Digital Thermometer and Thermostat [Z].

[3] 8-bit AVR Microcontroller with 32K Bytes In-System Programmable FlashAtmega328P [Z].

[4] AVR4100: Selecting and testing 32KHz crystal oscillators for Atmel AVR microcontrollers[Z].

[5] Zhang Jun. Practice and Thinking of a microcontroller worker[M]. Beihang University Press, 2008, 185-188.

Advanced Materials Research Vols. 989-994 (2014) pp 3019-3024
© (2014) Trans Tech Publications, Switzerland
doi:10.4028/www.scientific.net/AMR.989-994.3019

Coiling Tension Control System of PID Simulation

Zhongchu Wang[a], Yuan Ding[b],Hongyang Zhao[c] and Xiaodong Hu[d]

University of Science and Technology Liaoning, Anshan 114051, China

[a]wangzhongchu01@126.com, [b]ding00yuan@163.com,[c]zhy@ustl.edu.cn,[d]hulinas@sohu.com

Key words: coiler; tension control; traditional PID; simulation

Abstract. Coiling tension control system is the main control means to ensure the quality of the rolling process. According to the characteristics of coiling tension control characteristics and the requirements of actual engineering, establish the mathematical model of the double closed loop control system and use the traditional PID to tuning the model parameters. It is proved by Matlab simulation experiments that traditional PID can effectively improve the response process of coiling tension control system and greatly enhance the dynamic and steady-state performance.

Introduction

The coiling is an important process of cold rolling production process, can realize the rolling with tension. Its control accuracy directly determines the quality of the final product. Tension control system is one of the widely used in modern industrial control systems[1].In the process of rolling, the stability of coiling tension has great effect on adjusting the shape, thickness control and the quality of the products, also can prevent the work piece deviation phenomenon. Therefore, the tension control is a very important link in the control system of cold rolling mill.

The PID control is integrated control method based on the deviation of proportional, integral and differential. It has many advantages of simple principle, easy realization, robustness, wide applicability and also can improve dynamic and steady-state characteristics of the system. As long as the correct setting its parameters can realize its control function, so it is widely used as a controller applied to the tension control system[2].In this study, six roller cold rolling machine used is based on indirect constant tension control of torque control and compensation control. We establish the main mathematical models, tune parameters and use traditional PID control algorithm to simulate of the model. It improves the control precision and provide a strong guarantee for obtaining good shape and gauge control results.

Tension control principle and system structure

The system used is based on indirect constant tension control mode of constant linear velocity without tension detection feedback you can get more stable tension control effect，and also use speed loop and current loop of double closed loop cascade speed regulation system.In the process of speed control, the speed loop finally finishes speed regulation by adjusting the torque to control the current.In the process of tension control, the speed regulator is saturated,and adjusts the output torque of the motor by controlling the current limit value to achieve the constant tension control[3].

According to the literature[5],Coil winding characteristic of motor is:

$$M_D \cdot n = \frac{v_2 i}{2\pi} \cdot T = K \cdot T \tag{1}$$

In the process of coiling, the size of the tension is generated by the motor output torque, and is represented by the armature current I_a of the motor.Motor torque is:

$$M_D = C_m \phi I_a = M_T + M_O \pm M_d = \frac{TD}{2i} + M_O \pm M_d \tag{2}$$

Formula, M_D is the output torque of the motor, $N \cdot m$; M_T is the establishment of

tension torque tension required, $N \cdot m$; M_O is no-load torque, $N \cdot m$; M_d is dynamic torque required for acceleration and deceleration, $N \cdot m$; T is tension, N; n is coiling motor speed, $r/\min$; v_2 is reel line speed, $m/\min$; K is constant; D is reel diameter, m; i is reduction ratio; ϕ is motor flux, $\times 10^{-8} Wb$; I_a is armature current of motor, A; C_m is structure constant of motor.

When coiling machine stably works, in order to ensure the constant tension, it needs to maintain a constant speed winding. $M_d = 0$,ignore the no-load torque.So the tension is:

$$T = 2C_m i \frac{\phi I_a}{D} = K_m \frac{\phi I_a}{D} \tag{3}$$

It is seen from formula(3),as long as the guarantee of I_a is proportional to $\frac{D}{\phi}$,it can keep constant tension and make full use of motor power and to obtain the maximum output torque,namely maximum torque method.

Real-time volume diameter is calculated using the indirect method of calculation and usually uses the speed ratio, the basic formula is:

$$D = \frac{v_1}{\pi n} \tag{4}$$

Formula, v_1 is strip line speed, $m/\min$; n is coiling motor speed, $r/\min$; D is reel diameter, m According to the principle of the indirect tension control,tension control system is actually the process given its conversion into a motor torque current value,to control the coil current for limiting, is to control the current of the motor winding machine.Indirect coiler constant tension control system structure is shown in figure 1.

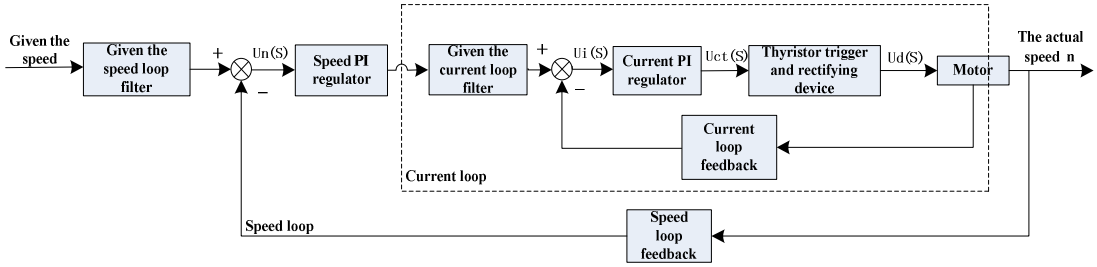

Fig. 1 Structure block diagram of double closed loop speed control system

Mathematical models

Tension dynamic mathematical model. In the actual rolling process, the reason why there is tension rolling effect is due to the presence of a speed difference in the longitudinal direction of the rolling member so that the relative displacement in the rolling of metal to produce the different parts of the tension[4].According to Hooke's law, the strip coiling tension is:

$$T = \frac{\delta E}{l} \int_0^{t_1} (v_2 - v_1) dt \tag{5}$$

Formula, δ is strip section area, m^2; E is the elastic modulus of strip; l is the distance between the reel and the work roll, m; t_1 is time to build tension winding mechanism, $\min$.

In the actual production, v_1 is constant,and to maintain a constant tension, it should ensure $v_2 - v_1$ constant.Namely reel line speed is constant and coiling motor speed increases with the volume but inversely proportional to the diameter decreases linearly.According to the literature[5],through the relationship between tension T and speed v, after calculation, the transfer function is obtained:

$$G(s) = \frac{T(s)}{\Delta v(s)} = \frac{K_t}{T_t \cdot s + 1} \tag{6}$$

Formula, T is tension, N ; Δv is reel and work roll on the surface of the linear velocity difference, $m/\min$; T_t is the time of establishment tension, $\min$.

The mathematical model of the coil motor. The motor is used in DC separately excited motor, through the derivation of the relation between input and output that voltage and current,torque and speed of winding motor,according to the literature[5],we can get the transfer function of the motor:

$$W(s)=\frac{n(s)}{U_d(s)}=\frac{1/C_e}{T_m T_l s^2+T_m s+1} \tag{7}$$

Formula, C_e is DC motor EMF constant; T_m is electrical and mechanical time constant of electric drive system; $T_l=\frac{L}{R}$ is the armature circuit of electromagnetic time constant.

Thyristor trigger and rectifying device model. Rectifier link system consists of a thyristor trigger and rectifying device[6],in the project it can generally be considered to be a first-order inertia link.The input is the control voltage trigger circuit U_{ct} , the output is the output voltage transmission device U_d ,from the literature[5],we can get its transfer function:

$$\frac{U_d(s)}{U_{ct}(s)}=\frac{K_s}{T_s+1} \tag{8}$$

Formula, K_s is rectifier links magnification; T_s is thyristor maximum time out of control,thyristor rectifier lag time constant takes 0.0017s.

The traditional PID control

PID algorithm. PID control is a controller that is based on the system error,and use proportional, integral, differential controller to calculate a control amount for control.In engineering practice, the traditional PID control is the most widely used control algorithm, which has the advantages of simple structure, good stability, easy parameter adjustment.In practice,there are PI control and PD control[7].The conventional PID control system block diagram is shown in figure 2.

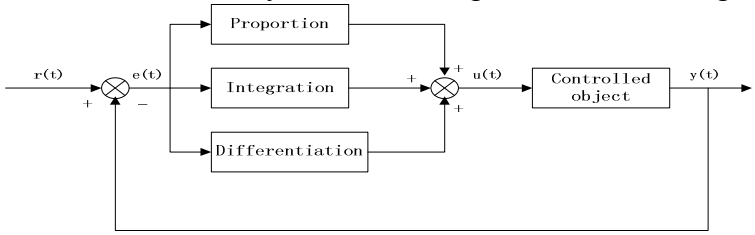

Fig.2 Block diagram of the PID control system

The differential equation of PID regulator is:

$$u(t)=K_p\left[e(t)+\frac{1}{T_i}\int_0^t e(t)dt+T_d\frac{de(t)}{dt}\right] \tag{8}$$

The transfer function can be represented as:

$$G(s)=\frac{U(s)}{E(s)}=K_p\left(1+\frac{1}{T_i s}+T_d s\right) \tag{9}$$

Formula, $u(t)$ is the output of the controller; $e(t)=r(t)-y(t)$ is the deviation input of the controller; K_p is proportional coefficient; T_i is integral time constant; T_d is differential time constant.

The parameter setting based on the conventional PID regulator. In the winding process, in order to ensure a constant tension, the system has two controllers.The one is the current controller the role of which is in the roll diameter increases the moment of inertia by dynamically compensated control current to perform dynamic compensation system to ensure constant tension;the other is the speed controller that is to control the speed v_2 of motor winding and makes v_2-v_1 constant to ensure

constant tension.In parameter tuning process of both regulators, we assume that parameters of the system is unchanged, according to the state when an empty roll winder design speed control system.

The static characteristics of PI regulator is:when the saturated output reaches the limit, the output is constant and the output is not affected by the impact of the input;when the regulator is unsaturated, the role of PI is to make the input offset voltage in the steady state be always zero.Therefore,the final fluctuations when the steady state of tension is zero.The controller design is achieved according to the PID control mode.According to the actual requirements of the system, the current loop in sudden control hopes no overshoot amount or as small as possible.Therefore,current loop should be corrected into a typical type Ⅰ system, while the control object is a double inertia type.Consequently,current loop uses PI regulator and its transfer function is:

$$W_{LT}(s) = K_i \cdot \frac{\tau_i s + 1}{\tau_i s} \tag{10}$$

In order to make the regulator of the zeros and the controlled object with large time constant pole cancellation, choose the time constant is $\tau_i = T_l = 0.025s$ .The scaling factor K_i depends on the desired current loop cut-off frequency ω_{ci} and dynamic performance index $(\sigma_i\% \le 5\%)$,chooses $K_p T_{\Sigma i} = 0.5$,and gets that:

$$K_i = \frac{T_l \cdot R}{2K_s \cdot \beta \cdot T_{\Sigma i}} = \frac{T_l \cdot R}{2K_s \cdot \beta \cdot (T_I + T_s)} = 1.25 \tag{11}$$

Formula, β is current loop feedback factor, gets 0.0095; T_I is current feedback filter time constant,gets 0.002s;Similarly, in order to maintain constant tension, the system should be no static error, and therefore,it should be corrected speed loop into a typical type Ⅱ system, has a strong anti-jamming ability.Speed loop also uses PI regulator and the transfer function is written:

$$W_{ST}(s) = K_n \cdot \frac{\tau_n s + 1}{\tau_n s} \tag{12}$$

A typical system parameters according to type Ⅱ selection methods are:
$\tau_n = h \cdot T_{\Sigma n} = h \cdot [T_N + 2 \cdot (T_I + T_s)] = 0.087s$ （$h = 5$) .According to the open-loop gain of the speed loop,we obtain proportional coefficient K_n is:

$$K_n = \frac{(h+1)\beta C_e T_m}{2h\partial R T_{\Sigma n}} = 60.98 \tag{13}$$

Formula, α is speed loop feedback factor,gets 0.01; T_N is speed feedback filter time constant,gets 0.01s.

Simulation

The conventional PID coiling tension control system is simulated with Matlab/Simulink software.Since the detection current signals often contain AC component, on the need to increase the low pass filter, but in order to balance the signal delay effect, need to join the inertial filter in the signal given, so as to meet the requirements of design and control.Enter the given value U_n^* of the rotational speed of the set is the step response.Stable speed is $100r/\min$ .The sampling time of the control object is 1s.Mechanical and electrical time constant of the motor is 0.148s.The response curves of the reel drum in empty volume simulation are shown in figure 4 and figure 5.

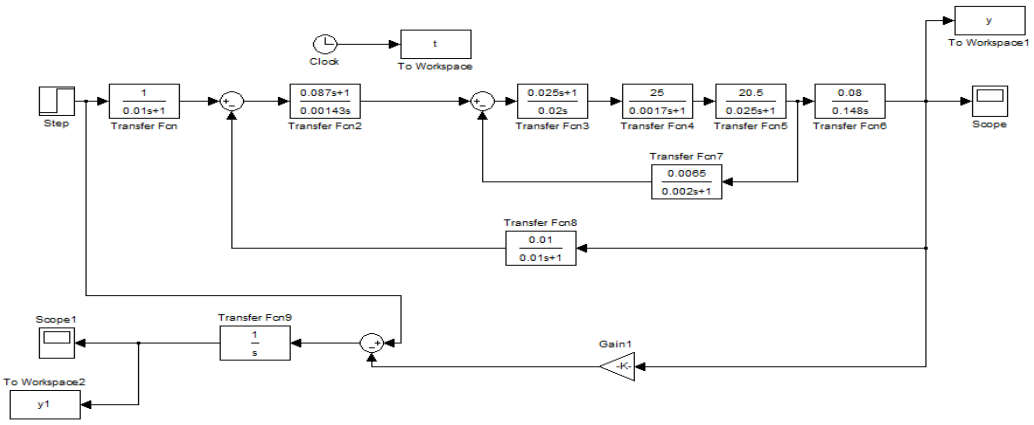

Fig. 3 The system simulation diagram of drum air volume

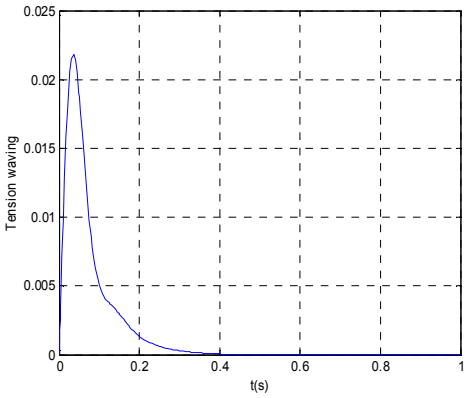

Fig.4 Speed response curve of no-load roll

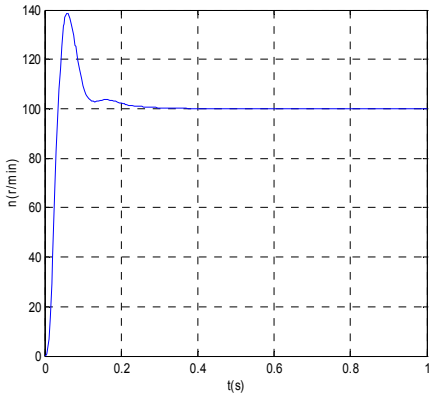

Fig.5 Tension fluctuation figure of no-load roll

Figure 4 shows, according to the typical Ⅰ type system design of current loop has good performance , fast system response and speed stability time t_s is only 0.5s.Speed ring is designed by typical type Ⅱ system , the overshoot of system is 38.7%.The simulation results are in conformity with design setting conditions.According to formula(4), the tension of the strip is produced by $v_2 - v_1$,and when the drive motor speed follow performance is very good, also the corresponding tension fluctuation is small.As can be seen from the figure 5, tension fluctuation amplitude is associated with the speed overshoot and wave time is also consistent with speed settling time at the same time, about 0.5s.After that the speed difference is kept constant, and therefore tension is constant and fluctuation is zero.

As the strip is wound to the drum, electromechanical time constant of the motor is increased.The electromechanical time constant T_m in figure 3 is selected 0.6s,at the same time,the reel is in the coiling process.The control object sampling time is 3s, the response curves of simulation are shown in figure 6 and figure 7.

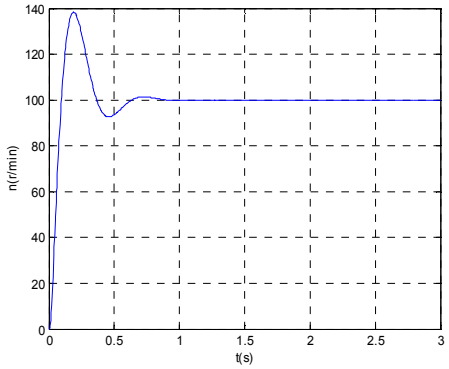

Fig.6 Speed response curve during coiling

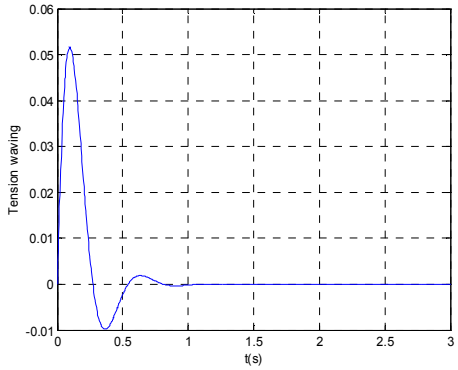

Fig.7 Tension fluctuation figure during coiling

Figure 6 shows,in the process of coiling, speed stability time is 1.4s, the overshoot of the system is 38.3%, the simulation results also meet the design index.Figure 7 shows,tension fluctuation amplitude is only empty volume doubled. Wave time is also consistent with speed settling time at the same time, about 1.4s. Finally, tension is kept constant and fluctuation is zero.Thus, the simulation results demonstrate the traditional PID control in winding tension control can basically achieve good results.

Conclusions

Through the experimental simulation of the coiling tension control system model, it is proved that the traditional PID control has the advantages of fast convergence, small overshoot and good stability.Application in the coiling tension control system improves the control precision, reduces the tension fluctuation and provides the theoretical basis for the production of fine material in practice.

References:

[1]Z.Q Yin and J.Zhu: Adaptive Tension Control,(2001)No.6,p.67.
[2]T.G Tang.The Research and Application of Cold Rolling Tension Control System for Single Stand Four High Aluminum Strip(Ph.D.,Northeastern University,China 2008),p.2.
[3]P.Xu and D.W Wang:MSB-6C-900A Six Roller Reversible Cold Rolling Mill Tension Control System,Vol.24(2007),No.5,p.122.
[4]C.Cai and W.Zhu:Discussion on Uncoiler Tension Control Method:(2006),No.19,p.52.
[5]Q.Z Su .The Research of Cold Rolling Coiling Tension Control System(Ph.D.,Northeastern University,China 2010),p.5.
[6]J.H Liu:AC and DC Speed Control Applications(Shanghai Science and Technology Press,China 2007.
[7]J.K Liu:Advanced PID Control and Matlab Simulation(Electronic Industry Press,China 2011).

Advanced Materials Research Vols. 989-994 (2014) pp 3025-3028
© (2014) Trans Tech Publications, Switzerland
doi:10.4028/www.scientific.net/AMR.989-994.3025

Structure principle and measurement index of new energy reclaiming suspension

Jing Bai[1, a], Yanzhao Guo[1, b], Ming Peng[2, c]

[1] Beijing Modern Vocational and Technical College, Beijing 101300, China

[2] Hubei Key Laboratory of Advanced Technology of Automotive Parts, School of Automotive Engineering, Wuhan University of Technology, Wuhan 430070, China;

[2.] Tech. Center, Wanxiang Group, Hangzhou 311200, China

[a] jing_bai@yeah.net, [b]guoyanzhao126@126.com, [c] pengming422@qq.com

Keywords: Energy recycling, damping force, vibration, efficiency

Abstract. The traditional hydraulic shock absorber suspension converts the vibration energy between the sprung mass and unsprung mass into heat energy. The realization of vibration energy recycling can reduce vehicle's energy consumption, developing ideals for the research of the active suspension/ semi-active suspension. Four kinds of energy reclaiming suspension's structure principle is introduced in detail and the development restricting factors of the suspension at present are worked out through the unified measure, indicating the technology breakthrough points.

Introduction

Suspension system is an important assembly parts of vehicles, and is the transmission and connection device between the vehicle body and wheels. The effect of the suspension system is to moderate and attenuate the impact passed from road to the body, and to ensure the normal running of the vehicle and passenger's comfort. Traditional hydraulic shock absorber suspension transforms the mechanical energy of relative linear motion between sprung and unsprung mass into heat dissipated [1]. If this part of the vibration energy can be recycled and stored in the form of hydraulic or electrical energy to supply the hydraulic energy dissipation device or the electrical equipment of the vehicle, it is possible to reduce the energy consumption of the vehicle. The research of regenerative suspension not only can reduce the energy consumption of the vehicle, but also be substantively meaningful to the exploration of active suspension or semi-active suspension.

Structure scheme of existing regenerative suspension

Rack-and-pinion suspension. The motor and rack pinion mechanism is used to replace the traditional hydraulic shock absorbers in rack and pinion suspension [2,3], and the rack connects the unsprung mass, gear connects the sprung mass, and motor rotor is connected to the gear. When the wheels jump up and down, the gear and rack move relatively to drive the motor rotation, converting the vibration energy of the frame and body into electrical energy through the generator. The structural principle of rack and pinion suspension is shown in figure 1.

The gap between the stator and the rotor is not affected by changes in suspension travel, and electromagnetic induction force is proportional to the speed of the motor, and the adjusting range of damping force is extensive. Weihua Wang, Changmiao Yu and others of Jilin University's proposed a electromagnetic energy regenerative suspension actuator solutions [4] combined the rack and pinion mechanism with DC servo motor .

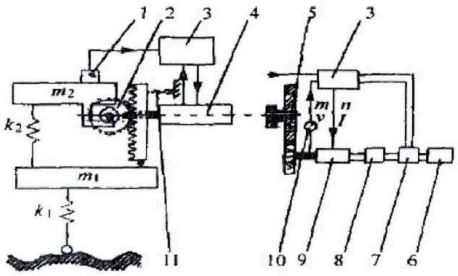

1-Acceleration sensor, 2-Rack and pinion structure can be fed, 3-The control unit, 4-Controllable AC generators, 5-High Speed gear group, 6-Electrical load, 7-Battery, 8-Rectifiers, 9-Generator, 10-Speed sensor, 11-Compression spring

Fig. 1 Structure principle of a rack and pinion suspension

Ball-screw suspension. The ball-screw mechanism is used to replace the traditional hydraulic shock absorbers in ball screw suspension [5,6], and the linear motion of the sprung and unsprung mass is transformed into rotary motion of the motor. The motor and ball screw mechanism consist of feeding components, recovering the vibration energy between the body and wheels into electrical energy. The structural principle of ball suspension is shown in figure 2.

Ball screw suspension alternately compressed and expanded in stroke in the moving process of vehicle, namely the ball nut moves up and down along the axial direction driving the ball screw and motor rotor to rotate. Fan Yu, Xuechun Zheng and others of Shanghai Jiao Tong University designed a suspension combined the ball-screw mechanism with a permanent magnet brushless DC motor according to the domestic and foreign patents[7].

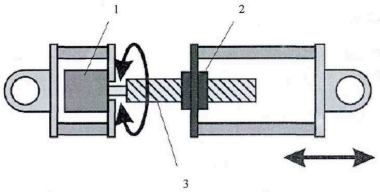

1-Electric motor, 2-Ball nut, 3-Screw

Fig. 2 Structure principle of ball screw suspension

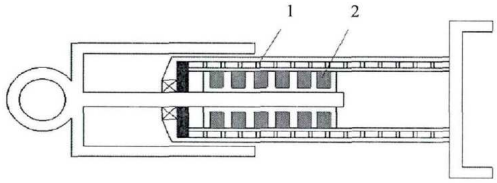

1-Magnet, 2-Coil

Fig. 3 Structure principle of linear motor suspension

Linear motor suspension. A linear motor is used to replace the traditional hydraulic shock absorber in linear motor suspension [8], and the mechanical energy of the linear motion between the body and the frame is converted directly to electric energy, or in turn. The motor is in the electric or braking state according to control instruction, so as to initiatively ease and attenuate the impact caused by the uneven pavement. The structural principle of linear motor suspension is shown in Figure 3.

When the motor generates electricity, the counter electromotive force generated by the motor works as the damping force of the suspension system to attenuate vibration. Bose Company adopts the scheme in initial loading test, and the results show that the scheme can realize the vibration energy recovery.

Fluid power regenerative suspension. Fluid power regenerative suspension [9, 10, 11] is to transform the linear motion of the vehicle sprung and unsprung mass into invariable direction rotational motion of hydraulic motor through hydraulic rectifier bridge, driving the generator connected generating electricity, and transforming the vibration energy between the body and the wheel into electrical energy. Use the damping effect of counter electromotive force in generator to simulate the role of traditional hydraulic shock absorber damping. Structural principle of fluid power regenerative suspension is shown in Figure 4.

Xuexun Guo, Lin Xu and others of Wuhan University of Technology proposed an energy recovery scheme, and then had simulation analysis and bench tests have test, and both of which verified the feasibility of energy recovery principles and the effectiveness of the scheme.

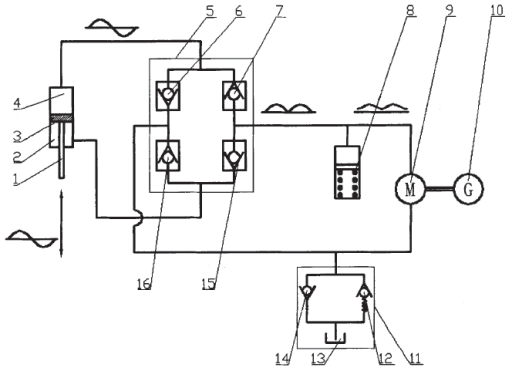

1-Rod, 2-Rod chamber, 3-Piston, 4-Rod chamber, 5-Hydraulic rectifier bridge, 6-Check valve B, 7-Check valve D, 8-Accumulator, 9-Hydraulic motor, 10-Generator, 11-Changes in unit volume, 12-Check valve E, 13-Tank, 14-Check valve F, 15-Check valve A, 16-Check valve C

Fig. 4 Structure principle of fluid power regenerative suspension

Measurement index

The existing structural schemes of feed-suspension are complex and diverse. In order to be able to reasonably evaluate various types of feed-suspension and be easy to carry out further research on the feed-suspension, it is necessary to establish a unified measure.

Basic characteristics of the suspension. The basic characteristic of the feed-suspension is the basic condition to realize the vibrational energy recycling dissipated in the form of heat transformed in traditional hydraulic shock absorber suspension, that's the three indicators in suspension system associated with ride comfort and handling stability - body acceleration, suspension dynamic deflections and wheel dynamic load. The three indicators should be quite the same with that of the traditional hydraulic shock absorber suspension.

The characteristics of feeding energy. The feeding energy characteristics of the feed-suspension are the stored form of energy that recycled from vibrational energy between the body and the wheels, and the feed-energy efficiency. Feed-energy efficiency can reflect the size of the recycling energy, which is the efficiency transformed to electricity from vibration energy in feed-suspension.

Linear motor suspension can transform excitation energy into electric energy directly, which has less energy transfer [8], so high efficiency. Compared with the liner motor suspension, rack and pinion suspension has smaller copper loss and relatively high feed-energy efficiency. Ball screw suspension generally has no mechanical rectifier bridge, and the motor rotor is in a process of continuous reversing, so it has lower energy efficiency. The design and performance of hydraulic rectifier bridge in fluid power regenerative suspension is easier than the mechanical rectifier bridge. The hydraulic rectifier bridge rectifier not only can implement effective rectification, the rectifying effect can also be realized by matching the appropriate check valve in the high-frequency excitation, so this scheme has a more efficient generator [11].

Structural Reliability. Structural reliability of the feed-agency is one of the important aspects considered in the design of energy regenerative suspension, which reflects the organization's work processes and determines the comprehensive performance of the feed-suspension. Meanwhile, the manufacturing cost of the suspension and installability cannot be ignored.

When the pavement impact is too large, it is easy to cause tooth fracture of rack and pinion mechanism in the work process of rack and pinion feed-suspension. And it is easy to cause fatigue failure under the long time use of harsh conditions, so this suspension has lower structural reliability [3]. Ball-type feed-suspension has a strong ability of anti-interference for bad environment, and it has a high structural reliability. It has a longer working life than that of rack and pinion suspension, and small size of installation. The volume of linear motor feed-suspension is small, but the structural reliability is general. Since the liner motor itself is expensive, the manufacturing cost is relatively high. The accumulator can greatly weaken the impact of the shock when the fluid power regenerative suspension suffers significant road shocks and it will be able to gradually release the impact energy after the impact, so the structural reliability of this scheme is much better.

Conclusion

Through the detailed introduction of structure principles of four kinds of main feed-suspension, the measurement index of feed-suspension is summarized. It is not difficult to find that the ball screw suspension and fluid power regenerative suspension are structure schemes with strong research, but due to the complexity of the suspension's structural parameters matching and damping force's adjustment, these schemes have not yet entered the final stage of real vehicle performance testing, and they are still in the stage of theoretical analysis and simulating adjustment. It's the developing direction of feed-suspension to achieve the control of damping force and the improvement of feed-efficiency under the premise of guaranteed basic characteristics of the feed-suspension; it is also the technology breakthrough for the future development of the active suspension/semi-active suspension.

References

[1] D.F. Yu, X.L. Li, M. Biao: Vehicle Suspension Damper Theory and Practice (Weapon Industry Press, China 1988).
[2] Z.C. Li: Structure Selection and Performance Simulation of Energy Regenerative Suspension (Ph.D., Jilin University, China 2009).
[3] C.M. Yu, W.H. Li, Q.N. Wang: Engineering Science of Jilin University, Vol. 39 (2009) No.4, p.841.
[4] C.M. Yu: The Research on Hybrid Vehicles Regenerative Suspension (Ph.D., Jilin University, China 2008).p.104.
[5] X.C. Zheng, F. Yu: Society of Automotive Engineers, Vol. 13 (2005) No.5, p.64.
[6] F. Yu, M. Cao, X.C. Zheng: Vibration and Shock, Vol. 24 (2005) No.4, p27.
[7] Y.C. Zhang, K. Huang: *Vehicular Electronics and Safety* (Beijing, Dec., 2007).Vol. 2. p. 32.
[8] W. Jones: Vehicle Technology, Vol. 42 (2005), No.5, p.12.
[9] L. Xu: SAE Technical Paper, Vol. 1 (201l) No.7, p.60.
[10] L. Xu: Study on Hydraulic Transmission Energy-regenerative Shock Absorber (Ph.D. Wuhan University of Technology, China 2011).
[11] Z.G. Fang: Energy Recovery Theory and Damping Characteristic Research of Vehicle Hydraulic Electromagnetic Shock Absorber (Ph.D. Wuhan University of Technology, China 2013).

Advanced Materials Research Vols. 989-994 (2014) pp 3029-3032
© (2014) Trans Tech Publications, Switzerland
doi:10.4028/www.scientific.net/AMR.989-994.3029

Method Research on Bending Fatigue Test of Vehicle Steering Wheel

Xunjiong Xu [1, a], Liang Tian [2, b]

School of Automotive Engineering, Wuhan University of Technology, Wuhan 430070, China
School of Naval Architecture and Ocean Engineering, Wuhan Technical College of Communications, Wuhan 430065, China

Keywords: Steering-wheel, actuator, counter, pressure sensor, displacement sensor

Abstract. Through researches a new method of bending fatigue test of vehicle steering wheel was raised in this paper. The new method is closer to the actual using condition of vehicle steering wheel, which enhances the reliability of the test.

Bending Fatigue Test of Vehicle Steering Wheel

Steering wheel is a vital part of automobile steering system, which influents the safety of the automobile directly. In order to bearing the steering force from the driver, reliability is very important for a steering wheel. Therefore, the durability test is necessary to checkout if it conforms to the technical requirements or not. With axial force, the steering wheel generates free deformation. The bigger the force, the less the radial distance between the force bearing point and the central plane of the steering wheel. However, the weakest part of the steering wheel was connected rigidly to the actuator with a fastener in the bending fatigue test of vehicle steering wheel at present. Because of the rigid connection between the steering wheel and the actuator, rectilinear motion of actuator adds a lateral force to the deformed steering wheel, which impedes the free deformation of the steering wheel; moreover, in the return stroke of the actuator the speed of the actuator affects the resilience speed of the elastic deformation of the steering wheel, which impedes the elastic recovery of the steering wheel. Therefore, previous method of test can't simulate the actual using condition sufficiently, which influences the accuracy of the test result.

Through researches a durability test bed was proposed in this paper, on which the steering wheel was put on force at both side without any clamp device on the force bearing point of the wheel. Pressure sensor and displacement sensor were used to measure values. On this test bed, the axial loading condition was simulated at the time when the steering wheel sheers off. In this way, the testing condition is closer to the actual using condition.

Description of problem analysis

(1) Unilateral reciprocating actuator is commonly used in present fatigue test bed. In the return stroke, this kind of actuator will impede the free resilience of the steering wheel after the force. In the actual use of steering wheel, man's hand won't impede free resilience of the steering wheel.

(2) Rigid Fasteners bound is used on the force bearing point of the steering wheel present fatigue test bed. Because the connection between the actuator and the steering wheel is rigid, the actuator will apply a outward radial force, which speed up the fatigue fracture of the steering wheel. In the actual use of steering wheel, the force from human hand will change along the displacement orientation, so the radial force won't occur.

(3) At moment, the check method of durability break of the steering wheel is observing crack. There are some disadvantages. Before the crack occurred, the strength of the steering wheel may decline a lot, even disabled. But we can't watch it out. So this method can't meet our requirement.

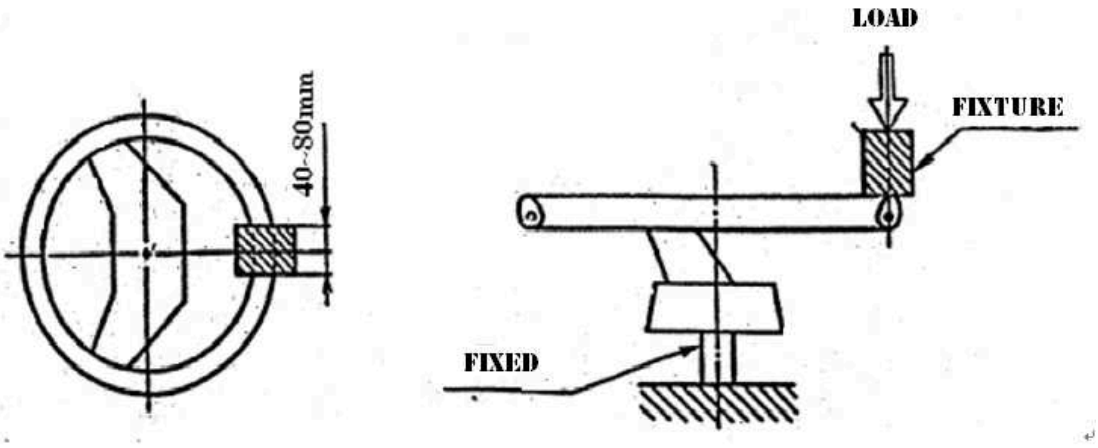

Fig.1 Sketch map of present test bed

Technical proposal of problem solving

(1) On the both sides of the force bearing point of the steering wheel, bidirectional actuator will apply cyclic load on the force bearing point. When the actuator on one side left the steering wheel after finish loading, the actuator on the other side will apply cyclic load.

(2) None constraint construction was used on the actuator, which applied force on the force bearing point. According to the national standard, rigid briquetting was used to guarantee its free deformation.

(3) Form the pressure sensors and the displacement sensors; the force-displacement curve was obtained. So the state of fatigue can be conformed, and the performance of the steering wheel can be tested.

Implementation of the technique proposal

The platform 1 with T slot fixed two square boxes 2 with T slot (fig.2). The distance between the two boxes is adjustable. Two bidirectional actuators were fixed on the boxes respectively. They are in the same horizontal plane. The actuator 3 with 2 guide bars moves up and down along the box 2. Fix the steering wheel on one of the box 2, the steering wheel can move up and down along the box 2 with T slot. In this way, the steering wheel can be fixed on proper position. Two pressure sensors were installed on the cylinder rod of the actuator 3 with guide bar. Two briquetting 7 were put on the pressure sensor 4. On one side of the box, an actuator 5 is fixed, connected with the pressure sensor 4 rigidly.

At the same time, the movement of box 2 with T slot, actuator 3 and the steering wheel 6, makes the briquetting 7 pointing on the both side of weakest part of the steering wheel 6. Then the actuator 3 with guide bar applied load on the weakest part of the steering wheel 6. Adjust the actuating time of the actuator 3 with guide bar, to realize the alternate loading of the two actuators, on the weakest part of the steering wheel 6. Pressure sensor 4 was used to monitor the force applied to the steering wheel 6. According to the data measured by pressure sensor 4 and displacement 8, the force-displacement curve was obtained. To judge the wheel fatigue state through counter 5 can read actuators on the steering wheel 6 times the force applied, counting functions.

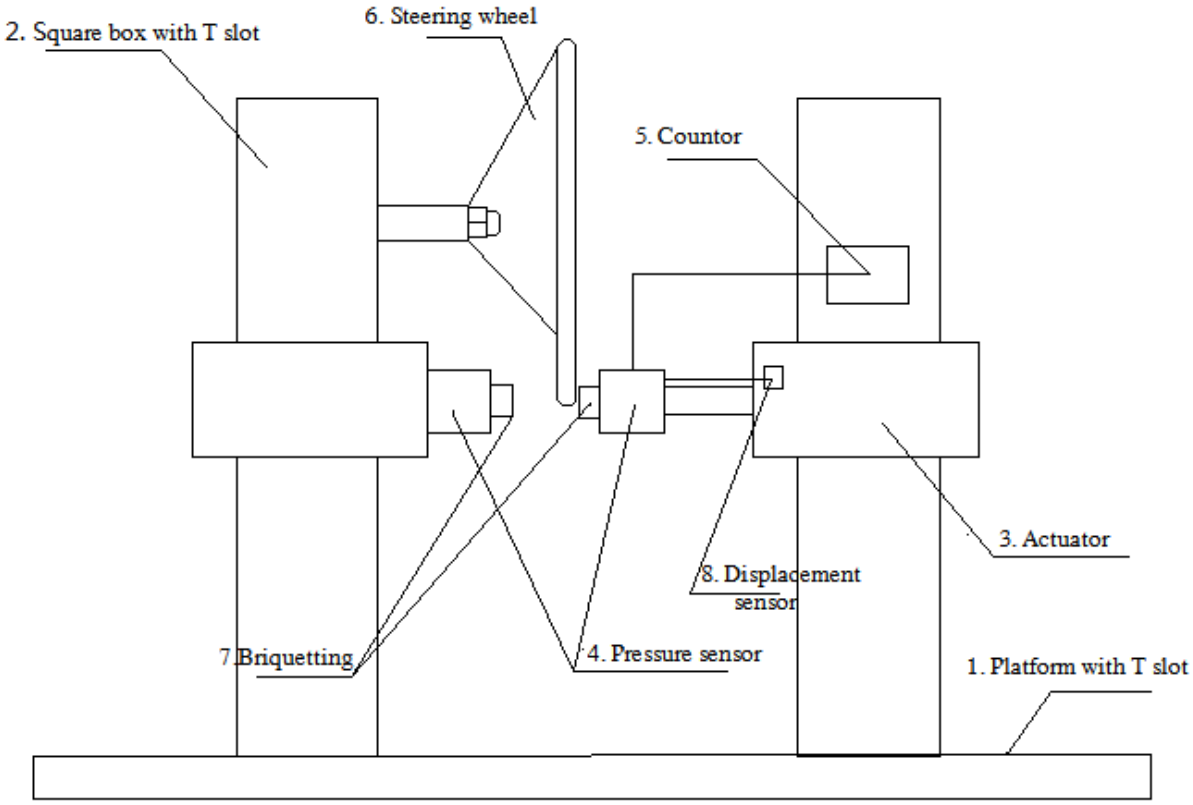

Fig.2 Bed structure of new proposal

Characteristics of the technique proposal

(1) Bidirectional actuators were used to apply load on the both sides of the weakest part of the steering wheel.

(2) The force bearing point of the steering wheel is free of clamp device. According to the national standard, Size of rules of extruded rigid blocks was used.

(3) The use of platform with T slot and boxes is convenient for the movement of steering wheel up and down, and finding the best force bearing point.

(4) Through the data measured by pressure sensors and displacement sensors, it is easy to conform the state of fatigue of steering wheel and to go on performance of the steering wheel.

(5) The counter can read the times that the actuator applied force on the steering wheel.

Conclusion

Through the alternate load that the two actuators applied on the steering wheel, the test process simulated the actual use condition that human hand handling the steering wheel sufficiently, which increased the reliability of the test result greatly. The pressure sensors and the displacement sensors can monitor the force that the actuator applied on the steering wheel in real time. So we can obtain the force-displacement curve, which can show the state of fatigue and the performance of the steering wheel. Force applying times of actuator that recorded by the counter is used for the verification durability of the steering wheel.

References

[1] The People's Republic of China machinery industry ministry standards, QC/T 563-1999. Steering wheel of automobile, test method.

[2] Baixue Fu, Auto test technology. Beijing, Beijing Institute Technology Press. 2007.8

Advanced Materials Research Vols. 989-994 (2014) pp 3033-3036
© (2014) Trans Tech Publications, Switzerland
doi:10.4028/www.scientific.net/AMR.989-994.3033

The Method of the Abnormal Sound Detection for Final Drive Based on DSP Technology

Xunjiong Xu [a], Zhigang Fang [b, *]

School of Automotive Engineering, Wuhan University of Technology, Wuhan 430070, China

[a] 314117748@qq.com, [b] Zhigang_Fang@whut.edu.cn

Keywords: Abnormal sound detection; DSP; Final drive.

Abstract. According to the mechanism of the main reducer abnormal sound signal is different from the interfering noise, a detection method based on the digital signal processing technology was proposed. With the qualified main reducer noise signal as the reduction sample, the detected main reducer noise signal is de-noising by means of spectrum analysis, and then be estimated whether the detected main reducer is qualified based on certain threshold values. Finally, the detection method is validated, which provided a new thought on the final drive abnormal sound on-line detection.

Introduction

The final drive abnormal sound is generated because of the defects of components or assembly (such as the tooth surface bump, tooth root interference, poor contact area, bearing indentation, etc.), resulting in an abnormal sound when it driving. The abnormal sound not only makes the vehicle not meet the noise standard and regulation and prone to early failure, but also it has some security risks. Therefore, it is necessary to do abnormal sound detection to prevent substandard product flowing out of production line in the main reduction assembly process.

Although the automotive NVH test technology has been greatly developed, but the automated detection technology for the final drive abnormal sound is not universal because of the cost, versatility and reliability of equipment, etc. The existing detection technology is still based on human listening with noise and vibration detection supplemented，which is that the result of human ears is as the primary judgments. Experienced listener is hard to be trained and tend to make wrong judgments when tired and not concentrated after long hour works. Therefore, the research on automated detection method of the final drive abnormal sound has great practical significance.

In the abnormal sound detection processing, with the ambient noise and normal noise interfering when testing equipment and main reducer working and the intensity of abnormal sound usually lower than the interference noise, it's unable to judge directly whether the final drive abnormal sound exists by the noise signal intensity. Because the mechanism of the main reducer abnormal sound signal is different from the interfering noise, its spectrum information and interfering noise have great difference. For the abnormal sound, a detection method based on the digital signal processing technology was proposed, which is simple, practical and benefit for the automatic online detection of abnormal sound for final drive.

Digital Signal Processing Introduction

Digital Signal Processing (DSP) is a technical discipline on signal analysis, conversion, filtering, detection, modulation, demodulation and fast algorithm by digital method. This method captures target signal by dealing with original signal to make signals easy to be captured and utilized. Since its birth in the 1960s, with the development of digital circuits, system technology and computer technology, the theory and technology of DSP is becoming more and more sophisticated. DSP has been gradually replaced by analog signal processing, which has been widely used in various fields like multimedia communications, wireless applications, robot control, audio signal processing, biomedical science and physical geography, etc [1]. Signal spectrum analysis is an important tool for

digital signal processing technology. It's easy to get an in-depth understanding of the characteristics of the signal by analyzing and processing signals from frequency domain. Traditional spectrum analyzers are expensive, bulky and not convenient to be carried by engineering technicians. But with the development of computer technology, the virtual spectrum analyzers have changed the overall design concept of original spectrum analyzer by using software instead of hardware and made the engineering and technical personnel can easily complete the acquisition, processing and frequency signal spectrum analysis just with a laptop computer carried to the site [2].

Method of the Abnormal Sound Detection for Final Drive Based on DSP Technology

In the main reducer abnormal sound detection, with the ambient noise and normal noise interfering when the main reducer working, if the traditional control technology of noise is applied to reduce noise, through isolating the noise source, using muffler and different sound absorbing materials and improving system structure to reduce resonance mode, it is much pricy and hard to achieve the desired results. The main reducer noise detection method based on the concept of active noise reduction, use the incoherence characteristic of noise spectrum of different system to do spectrum analysis to identify and suppress the noise signal, which can achieve the elimination of noise interference and keep the abnormal sound signal [3-4].

Detection Thinking. Due to the different part production batches and abnormal sound modes, the final drive abnormal sound regularity is too complicated to do statistical calculation, while the thinking of this detection is based on the high volume of qualified noise samples(normal signals) formed after collection, analysis, counting and authentication through human judgment and then removing the "normal signal" section of the spectral analysis of noise signal to be detected and the rest deviates from the "normal signals ".So without statistical regularity, it can identify the abnormal noise reducer only through setting the threshold the "normal signals" allowed to be deviated from.

Firstly, with the qualified representative sample by human judgment being a standard and the operating noise being a sample, the signals of the ambient noise, equipment idling noise and the operating noise in the actual detection process are simultaneously recorded. Then noise reduction is performed on the operating noise signal by spectral analysis. At last, the threshold judgment is performed on the post-processing waveform to be tested whether the final drive is qualified. For the compatibility and identification of different types of final drives, library of sample noises of various final drives should be built by sample noise signals of standard final drives of various types and car models.

Detection Processing. Fast Fourier Transformation (FFT) algorithm, which is commonly used nowadays ， is utilized to reduce noise in the detection process, and the process can be divided into three steps [5-6]:

(1)Perform FFT on the sampled signals;

(2)Suppress the spectrum of target signal noise;

(3)Perform Fourier reverse transform on the processed signals;

Presume that collected signal is $f(t)$, the signal after noise reduction is $g(t)$, its Fourier Transformation result is $F(\omega)$ and $G(\omega)$, signal used by filter to suppress noise is $H(\omega)$ and the whole process can be showed as below:

$$G(\omega) = H(\omega) \cdot F(\omega)$$

The whole online detection process of abnormal sound for final drive is showed in Fig.1.

Effectiveness Verification. Each 10 of the qualified，tooth surface roughness，tooth scraping sound and tooth surface bump is picked by human ears, this detection method is used to detect and recognize abnormal sound. All the 40 main reducers can be identified correctly once after the empirical parameters are set.

The figures below from 2 to 5 indicate the contrasts of the waves before and after the process of noise reduction of one of the four final drives. The abscissa of each figure is time(s) and the ordinate is norm.

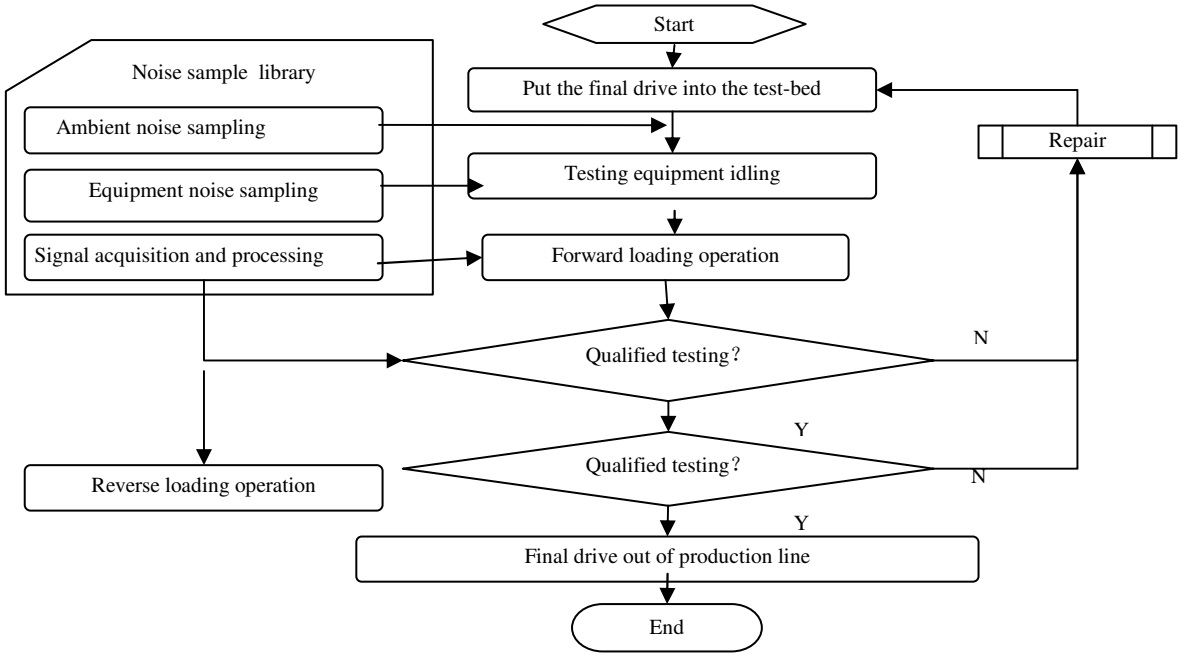

Fig.1 Detection processing of abnormal sound for final drive

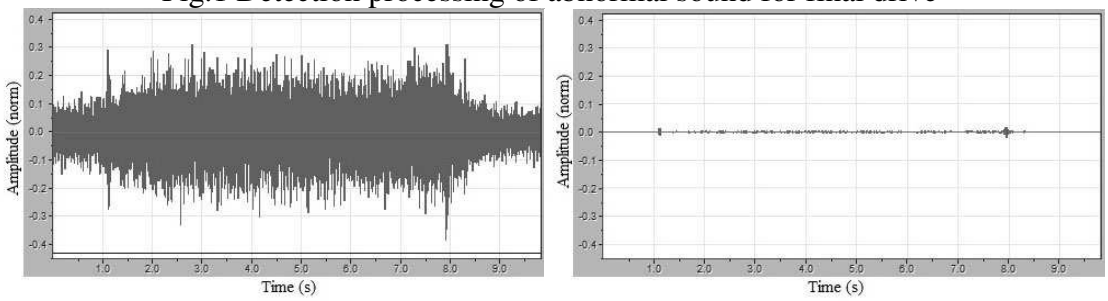

(a) before noise reduction processing (b) after noise reduction processin

Fig.2 Waveform of qualified final drive

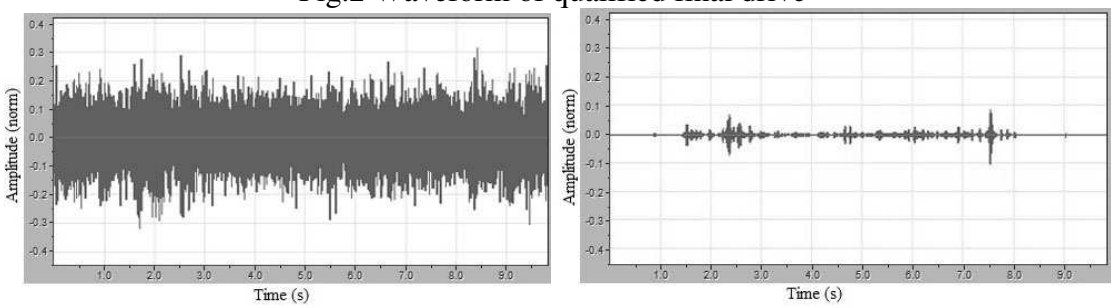

(a) before noise reduction processing (b) after noise reduction processin

Fig.3 Waveform of tooth surface roughness final drive

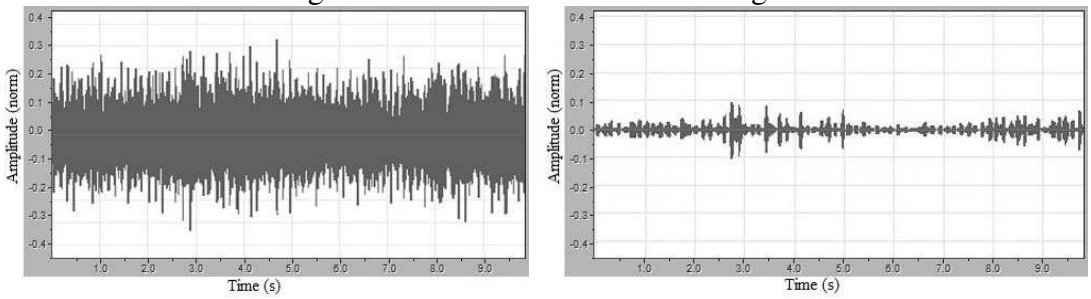

(a) before noise reduction processing (b) after noise reduction processin

Fig.4 Waveform of tooth scraping sound final drive

(1). Samples of qualified final drive: it is indicated in Fig.2 (b) that the final drive waveform with the noise interference excluded has only a small amount of residual abnormal sound signals and its

intensity is below a pre-set empirical threshold, so such final drives can be identified as qualified products.

(2). Samples of tooth surface roughness: because the gear tooth surface roughness is unqualified after gears pairing and grinding, it results in abnormal noise when the gear meshing. The waveform of these final drive noise signals after noise reduction processing is shown in Fig.3 (b). Such substandard parts are usually repaired by the way that the gears are re-ground.

(3). Samples of tooth scraping sound: they are usually generated due to the great processing errors or the unreasonable choice of the installation gaskets, resulting in the abnormal noise because of the gear teeth top or root interference when the gears meshing. The waveform of these final drive noise signals after noise reduction processing has obvious abnormal sound，shown in Fig.4 (b). The abnormal sound of such substandard parts is usually eliminated by the way that these installation gaskets are adjusted or the sides of the gears are swept.

(4). Samples of tooth surface bumping: they are usually generated due to the projections or recesses left since the tooth surface contact area bumps into small hard objects when the gears meshing, resulting in the abnormal noise when the gears meshing and the abnormal sound period is significantly inversely proportional to the input speed of the final drive. The waveform of these final drive noise signals after noise reduction processing is shown in Fig. 5 (b). The abnormal sound of such substandard parts is usually eliminated by the way that these bumping points are grinding and removed.

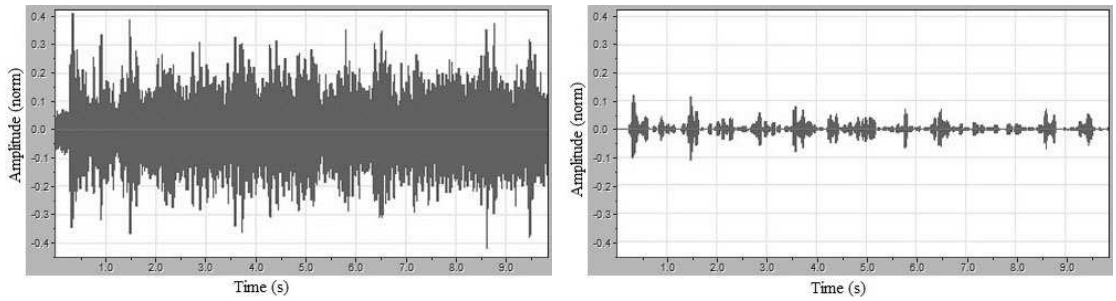

(a) before noise reduction processing (b) after noise reduction processing

Fig.5 Waveform of tooth surface bumping final drive

Conclusion

According to the effectiveness verification above, the method of the abnormal sound detection for final drive based on DSP technology meets the requirements of online detection. Compared with other detection methods, the method is simple and convenient, easy to be implemented and applicable for detecting specific target signals under the other needs.

Acknowledgements

Supported by 'the Fundamental Research Funds for the Central Universities (WUT: 2014-IV-036)'.

References

[1] Meng Han, Sheng Liu: Technology Information, 2009, (24):148-148.
[2] Guolin Liu, Guanxi Yin. Electronic Measurement (China Machine Press, China 2003)
[3] Yonglin Zho, et al. Automotive Noise Theory, Detection and Control (Environmental Science Press, China 1992)
[4] Sen M Kuo, Mor Gan: proc. IEEE, 1999, 87:943-973.
[5] A.V. Oppenheim. Discrete-time Signal Processing (Xi'an Jiaotong University Press, China 2001)
[6] Qingjie Liu, Guiming Chen, et al: Data Acquisition and Processing 2009,(24):58-60.
[7] Zhijun Zhao. Study on On-line Quality Inspect of the Main Reducer Based on Order Analysis and Vibration Velocity Method (PhD., Hefei University of Technology, China 2009).

Advanced Materials Research Vols. 989-994 (2014) pp 3037-3040
© (2014) Trans Tech Publications, Switzerland
doi:10.4028/www.scientific.net/AMR.989-994.3037

The multi-body dynamics contact simulation on transmission gears

Xiaohe Deng[1, 2, *]

[1] School of Wuhan University of Technology, Wuhan 430070, China;

[2] Hubei Key Laboratory of Advanced Technology of Automotive Parts, Wuhan 430070, China

*xiaohe_d@163.com

Keywords: Transmission gear, multi-body contact dynamics, gear meshing force

Abstract. Based on the theory of gear dynamics and contact, the paper uses multi-rigid-body dynamics software ADAMS to build transmission simulation model. The model takes the highest shift gears of a transmission as objects to finish gear meshing simulation analysis. The corresponding meshing force and its Fourier transform results are acquired based on the analysis to get the transmission gears meshing properties.

Introduction

Transmission is mainly used to change the torque and rotational speed from the engine to the drive wheels. Mechanical transmission of power transmission is accomplished through a gear system. In the process of meshing gear, single and double gear engaging period alternate with shocks when engaging-in and out. The shock will cause load change and rotation speed fluctuation, and then vibration problems. As the main part of load bearing and power transferring, the gear transmission may come up with multiple problems such as fatigue, fracture，abrasion, noise vibration, etc. Therefore, it is necessary to analyze the characteristics of the gear meshing process, provide the basis for design and assessment of the gear system. In view of the gear system dynamics simulation, many scholars and experts have carried on thorough analysis with some achievements [1-7]. Their researches are mainly concentrated in the meshing gear pair alone or empirical formula. The idea of taking the whole gear system as the object for analysis will be a good direction. But the using the numerical methods such as finite element method requires the precision calculation of the simulation model and the high equipment of computer hardware. So it is necessary to adopt a more rapid and efficient method to obtain more credible data. Based on a variety of algorithms and the evaluation of software, in this paper the ADAMS software is chosen for the analysis of the gear transmission system, contact algorithm is adopted to build multi-body dynamics model, and then the related results are obtained.

Establishment of the transmission gear system

Mathematical model. In the transmission process of gear system, the shaft and gear can be assumed to be rigid if our main concern is the effect of gear contact. But in the process of gear contact, we need to consider the tooth surface contact because it is a nonlinear contact condition.

In the ADAMS model, we adopt contact collision algorithm, the calculation formula of collision force is

$$F=\begin{cases}\max\left(0,k(x_1-x)^e-STEP(x,x_1-d,C_{\max},x_1,0)\times\dot{x}\right) & x<x_1\\ 0 & x\geq x_1\end{cases} \quad (1)$$

There, x is the distance variable in the collision function. $\dot{x}$ is collision speed, and x_1 represents the displacement.In the model, the contact stiffness of the gear can be simplified according to Hertz contact theory.The calculating formula for the contact stiffness is

$$K=\frac{4}{3}ER^{\frac{1}{2}} \quad (2)$$

There, $R=\frac{R_1R_2}{R_1+R_2}$ represents the synthetical radius of curvature at the meshing point in the tooth profile surface. $E=\frac{E_1+E_2}{(E_1+E_2)(1-\mu^2)}$ is the synthetical elastic modulus. μ is poisson ratio.

The dynamics equationof gear system considering contact can be expressed as

$$\begin{cases} M\ddot{q}+Kq+f_q^T\lambda=Q+F \\ f(q,t)=0 \end{cases} \quad (3)$$

There, F is the contact force, Q is generalized matrix. M and K is generalized mass matrix and generalized stiffness matrix respectively. $f(q,t)$ is constraint equation. f_q^T is the jacobian matix of constraint equation. λ is the Lagrangian multiplier.

The numerical calculation was processed under the ADAMS software. In order to simplify the calculation, we proposed several hypotheses below in mathematical modeling:

A. The geometry models only consider the gear pairs and shafts, ignoring the gearbox and other components.
B. Regarding gear pairs and shafts as ideal rigid body, the gear and shaft connection relationships adopt solid or empty set according to the calculated working condition.
C. Simplifying transfer power gear pairs with contact relationship.

Determination of physical property parameter. The physical property parameter was determined by a chosen transmission used in a car. The materials of gears and shaft are $20CrMnTi$ .The Density is $7800kg/m^3$ .The elastic modulus is $2.06+E11N/m^2$ .The Poisson's ratio is 0.3.The parameters of gear pairs are in the table.1 below. The 4th gear pairs are

Table.1 The parameters of gear pairs

	1st	2nd	3rd	4th	5th
Driving gear teeth	14	22	32	22	41
Driven gear teeth	44	39	37	27	27
Transmission ratio				1.227	0.658
modulus	1.95	1.75	1.5	2.25	1.5

Simulation model. Choosing the 5th forward constant speed as the working condition, both the 5th gear pairs and the 4th gear pairs are engaging to transfer motion and force. The input speed was applied on the input shaft with $3000r/\min$, the resistant torque was applied on the output shaft with $88N\bullet m$ .In order to avoid sudden changes of speed and load, the step function was used to make the load process smooth within0.002s. According to the parameters in Table.1， we can calculate the speeds of intermediate shaft and output shaft as follows

$$n_{lay}=n_{in}i_5=3000\times1.227=4556r/\min \quad (4)$$

$$n_{out}=n_{in}i_5i_4=3000\times1.227\times0.658=3711r/\min \quad (5)$$

Based on the mathematical model and hypotheses above, the simulation model is established, as is shown in Fig.1.The speeds of each shaft are shown in Fig.2.the whole simulation time is 0.06s, and the steps are 1000.At 0~0.002s,the speed of input shaft increased from 0 to $3000r/\min$. After that the gear transmission reaches the constant speed period. In the constant speed process, the speed of output shaft and the layshaft fluctuated up and down in their respective theoretical average value.

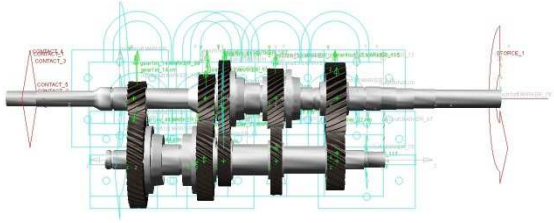

Fig.1 The gear transmission system

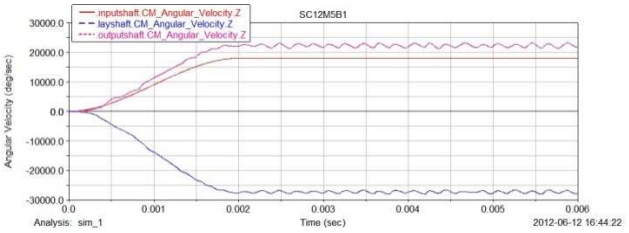

Fig.2 The shaft speed

Simulation results

Gear tooth meshing force. Since the gear models are the ideal models, periodic fluctuations are mainly caused by stiffness excitation and impact excitation. Based on mechanical theory, the involute helical gear circumferential force, radial force and axial force can be calculated as follows:

$$F_t = 2T / d$$
$$F_r = F_t \tan\alpha / \cos\beta \quad (6)$$
$$F_a = T \tan\beta$$

There, T is the torque. d is the reference radius. α is the pressure angle of reference circle. β is the helix angle.

At 5th speed, power flow is transferred by 5th gears and constant meshing gears. The contact forces of the 5th gear pair in the collision process are shown in Fig 3.Before 0.002s, meshing gears rotate from static state to engaging state, undergoing tremendous impact force from each other. So there are large fluctuations in the gear meshing force curves. After 0.002 s, gears turned to uniform motion of the stationary phase. The gear meshing force changes periodic fluctuation near the theoretic average value. Three directions of meshing force extracting from the smooth process and the corresponding theoretical results are shown in Table 2.

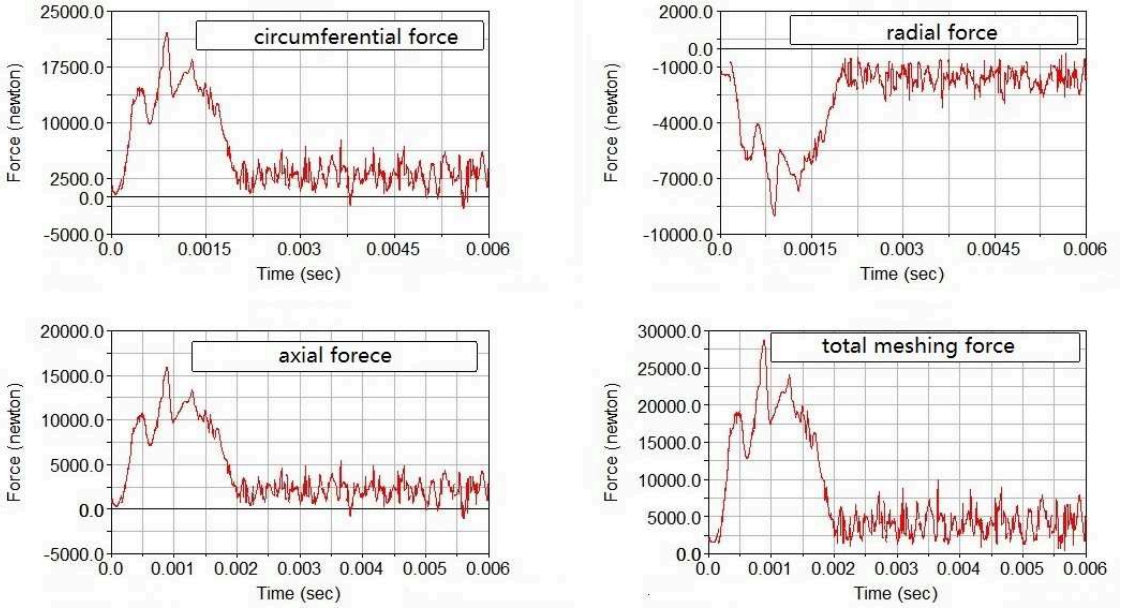

Fig3 The meshing force at 5th gear pairs speed

Table.2 The comparison between the theoretical and simulation meshing forces

Meshing forces (N)	circumferential force	radial force	axial force	total meshing force
Theoretical values	2885	1117	2058	3715
Simulation values	2924	1563	2107	3928

The Fourier transform of meshing force. In order to get periodic data, the simulation time increased to 0.5 s, The corresponding total meshing force is shown in Fig. 4.The Fourier transform of meshing force data is shown in Fig.5.

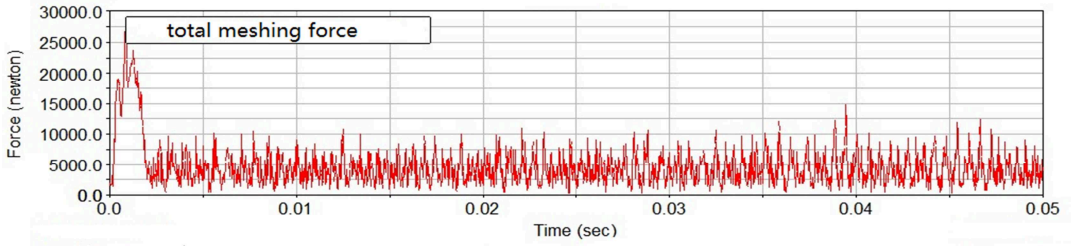

Fig.4 The total meshing force

The theoretical mesh frequency is

$$f = zn / 60 \quad (7)$$

There，z is the number of gear tooth, n is the rotation speed of gear tooth.The comparision of mesh frequency between the theoretical value and simulation value are show in Table.3. The simulation results is consistent from the datas.

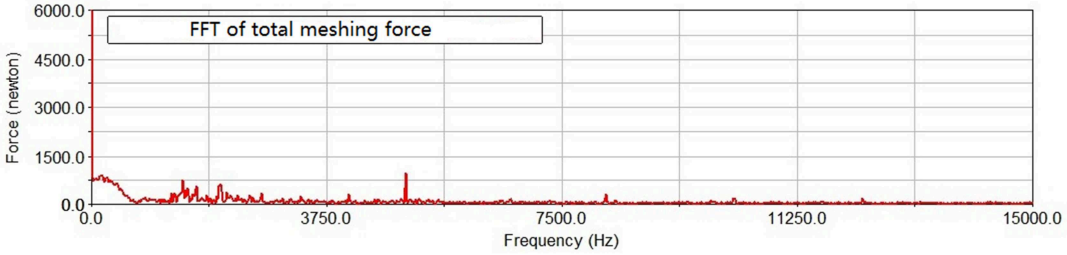

Fig.5 The Fourier transform of total meshing forces

Table.3 The mesh frequency of each shift

Mesh frequency (Hz)	1st	2nd	3rd	4th	5th
Theoretical value	700	1100	1600	1670.4	2050
Simulation value	696	1099	1673	1673.6	2051

Conclusion

This paper built the multi-body dynamics contact simulation model of the transmission gear system. Simulation results can reflect the changes of the system in the gear meshing process. The meshing frequency by using Fourier transform of gear meshing force was agree with the theoretical value Since the computation time is short, the results are reliable, this method can provide a new way of thinking to establish the gear dynamic model. It will help to do the in-deep research on influence of the parameters of the gear dynamic motivation.

References

[1] Tamarozzi, T.; Ziegler, P.; Eberhard, P., Static modes switching in gear contact simulation, Mechanism and machine theory, vol. 63 (2013), p. 89-106.

[2] Chen, Zaigang; Shao, Yimin; Su, Daizhong. Dynamic simulation of planetary gear set with flexible spur ring gear. Journal of Sound and Vibration, vol. 332 (2013) no. 26, p. 7191-7204.

[3] Palermo, A.; Mundo, D.; Hadjit, R,.Multibody element for spur and helical gear meshing based on detailed three-dimensional contact calculations, Mechanism and machine theory, vol. 62 (2013), p. 13-30.

[4] Shao, Yimin; Chen, Zaigang. Dynamic features of planetary gear set with tooth plastic inclination deformation due to tooth root crack. Nonlinear Dynamics, vol. 74 (2014) no. 4, p. 1253-1266.

[5] Chen, Siyu; Tang, Jinyuan; Chen, Weitao. Nonlinear dynamic characteristic of a face gear drive with effect of modification. Mechnica, vol. 49 (2014) no. 5, p. 1023-1037.

[6] Wu, James Shih-Shyn; Xu, Shu-Ling; Lin, Yi-Tsung. 3D contact analysis of conjugate spur gears by a complete mating process, vol. 27 (2013) no. 12, p. 3787-3795.

[7] Li Xiufeng; Wang Yabin. Analysis of Mixed Model in Gear Transmission Based on ADAMS. Chinese Journal of Mechanical Engineering, vol. 25 (2012) no. 5, p. 968-973.

Advanced Materials Research Vols. 989-994 (2014) pp 3041-3044
© (2014) Trans Tech Publications, Switzerland
doi:10.4028/www.scientific.net/AMR.989-994.3041

Analog Circuit Parameters Measurement System Based on Multiplier

Yongxi Wang [1, a],Mei Hu [1, b]

[1]School of Electronic and Information Engineering, Lanzhou Institute of Technology, Lanzhou 730050,China.

[a]wyx831@126.com, [b]humei-2006@163.com

Keywords: analog circuit parameters, multiplier, measurement system, high accuracy.

Abstract. For the more complicated principles and the lower accuracy for the existing methods of the measurement of the analog circuit parameters, the paper constructs a measurement system for the analog circuits parameters based on the multiplier. The signal source generates two orthogonal sinusoidal analog signals with same frequency, and then one of the signals goes through the analog circuits. Then the multiplication and filtering are completed with the two DC signals. At last the phase and amplitude of the analog circuit are obtained through the DAQ and LabVIEW software. The amplitude and phase errors are less than 3%. The results show that the system has simple circuit, fast speed and high accuracy. So it is a feasible plan for the measurement system of the analog circuit parameters at present.

1. Introduction

Practical application of analog circuits has been a research focus, but its amplitude and phase parameters of the measuring methods are often neglected [1]. The existing measuring methods of analog circuits parameters mainly use simulation software (such as Pspice, Multism), measurement instrument(frequency sweep meter, distortion analyzer, spectrum analyzer, etc.[2]) and some indirect measuring methods such as based on the phase - time transformation, FFT spectrum analysis, correlation function of phase [3]-[7]. Due to the complexity of these principles, the lower accuracy and the methods can't measure the amplitude and phase of the analog circuits at the same time, so these methods are not widely applied. The paper constructs a measurement system for the analog circuits parameters based on the multiplier. The system consists of signal source, the tested analog circuits, the signal processing circuits, ADC and the processing circuits of the DC signals with the LabVIEW software.

The hardware of the system is given in detail. The results show that the system has many advantages of simple circuit, fast speed and high accuracy.

2. Principle of Measurement

There are two orthogonal sinusoidal signals($A_1 \sin \omega t$, $A_1 \cos \omega t$) with same frequency. The $A_1 \sin \omega t$ signal becomes $A_2 \sin(\omega t + \varphi_1)$ after the tested analog circuits are gone by. And then the signal $A_2 \sin(\omega t + \varphi_1)$ multiplies by $A_1 \sin \omega t$ and $A_1 \cos \omega t$ respectively. The second and the more than second harmonic signals ($\frac{A_1 A_2}{2} \cos(2\omega t + \varphi_1)$, $\frac{A_1 A_2}{2} \sin(2\omega t + \varphi_1)$) of the product are filtered by the low-pass filter. Only the rest of the DC signal is $\frac{A_1 A_2}{2} \cos \varphi_1$ and $\frac{A_1 A_2}{2} \sin \varphi_1$. At last the phase φ_1 and amplitude A_2 of the tested analog circuits can be get by mathematical calculations, as shown in formulas 1 ~ 6.

$$A_1 \cos \omega t \times A_2 \sin(\omega t + \varphi_1) = \frac{A_1 A_2}{2} \left[\sin(2\omega t + \varphi_1) + \sin \varphi_1 \right] \tag{1}$$

$$A_1 \sin \omega t \times A_2 \sin(\omega t + \varphi_1) = \frac{A_1 A_2}{2} \left[\cos(2\omega t + \varphi_1) - \cos \varphi_1 \right] \tag{2}$$

$$\frac{A_1 A_2}{2}\cos\varphi_1 = m \tag{3}$$

$$\frac{A_1 A_2}{2}\sin\varphi_1 = n \tag{4}$$

$$\begin{cases} \varphi_1 = arctg\dfrac{nA_1}{mA_2} & (5) \\ A_2 = \dfrac{2\sqrt{m^2+n^2}}{A_1} & (6) \end{cases}$$

3. Measurement System

3.1 System Block Diagram

On the basis of the above principles the measurement system for the analog circuits parameters based on the multiplier is build. The system is composed of the signal source, the tested analog circuits, the multiplication circuit, the filters, ADC and the processing circuits of the DC signals with the LabVIEW software. The phase shift circuit as a signal source to produce two orthogonal sinusoidal signals with the same frequency. After one of the above signals goes through the tested analog circuit multiplies by the two orthogonal signals respectively, then the signals are filtered. The two dc signals are dealt with the DAQ data acquisition card and the LabVIEW software by collecting and calculating signals to get phase and amplitude of analog circuit. The principle block diagram of the measurement system is shown in fig.1.

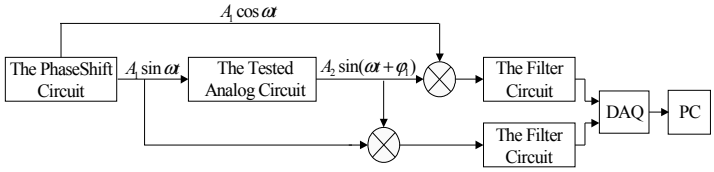

Fig.1 Analog circuit parameters measurement system principle block diagram

3.2 Signal Source

The active phase shift circuit as a signal source produces two orthogonal sinusoidal signals with the same frequency, as shown in fig.2. The input and output signal become the orthogonal signals by means of choosing potentiometer resistance in simulation experiments.

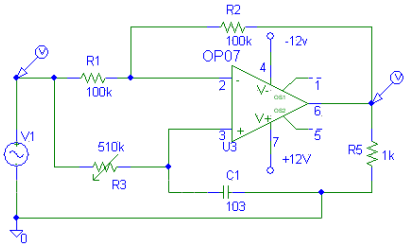

Fig.2 Active phase shift circuit

3.3 Signal Processing Circuit

The signal source generates two sinusoidal orthogonal signals with same frequency, which multiply by $A_2\sin(\omega t+\varphi_1)$. The MLT04 chip integrating four independent multipliers in Analog Devices Inc is used in the multiplication circuit. Its input and output are voltage. Calculation formula of the output voltage is as follows $W = X\times Y/2.5V$ [8].

The products go through the filter to generate two dc signals by filtering the second and the more than second harmonic signals. The resistance of 500kΩ and 100kΩ are connected respectively with two 500kΩ potentiometer in parallel to emerges the low-pass filter with different cutoff frequency, which filters the harmonic signals in different frequencies. The output of the filter is connected to the voltage follower in order to improve the input impedance and the stability of the output signal.

3.4 ADC

The ADC module uses the NI PCI-6024E, which is driven by NI-DAQ software, supporting the LabVIEW and many application development environment. The NI PCI-6024E contains 12 bit A/D converter with the highest sampling rate of 200 kbit/s [9].

3.5 DC Signals Processing with LabVIEW

The dc signal is dealt with by the LabVIEW software, which is collected by PCI – 6024E. The sampling points, acquisition channels, sample rate, the amplitude of sine and cosine are set in the software. The LabVIEW software uses the Function template→the subtemplate of All Functions→the subtemplate of NI Measurement→ the subtemplate of Data Acquisition→AI Acquire Waveform.vi's node in the subtemplate of Analog Input. Finally the phase and amplitude are got on the front panel as shown in fig.3.

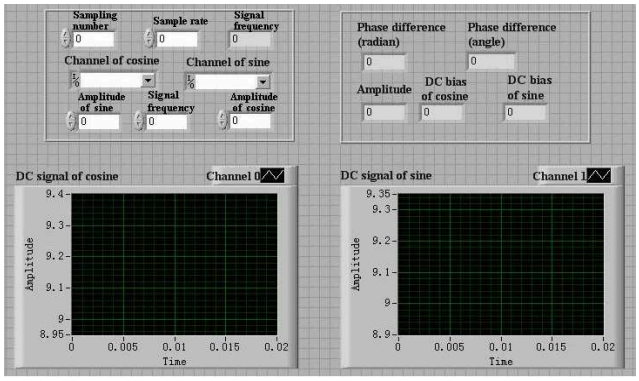

Fig.3 The front panel

4. Experimental Results and Analysis

The first-order RC low-pass filter is the tested circuit. The amplitude-frequency curve, the phase-frequency and curve error curve are shown in fig. 4 and 5. The error curve of phase-frequency is relatively flat in the entire spectrum and the error is less than 2%. While the error curve of amplitude-frequency has sharp fluctuations but the error is within 3%.

Because two multiplied signals reduce the intermediate process and effectively suppress the interference signals. The dc signal which is collected by the data acquisition card reduces the requirement for the performance of the front-end hardware circuit, avoiding the distortion of sampling. Thus the amplitude and phase errors are less than 3%.

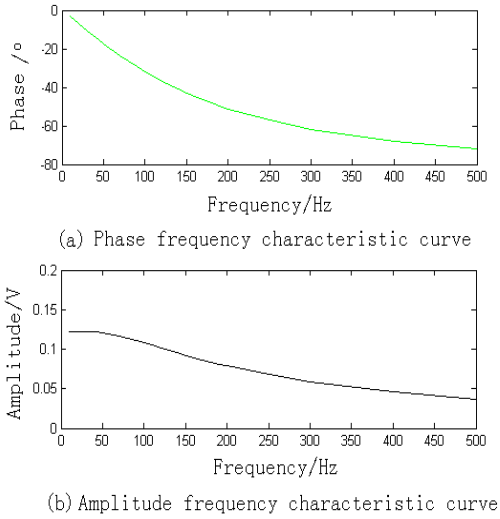

Fig.4 First-order RC low-pass filter phase frequency and amplitude frequency characteristic curve

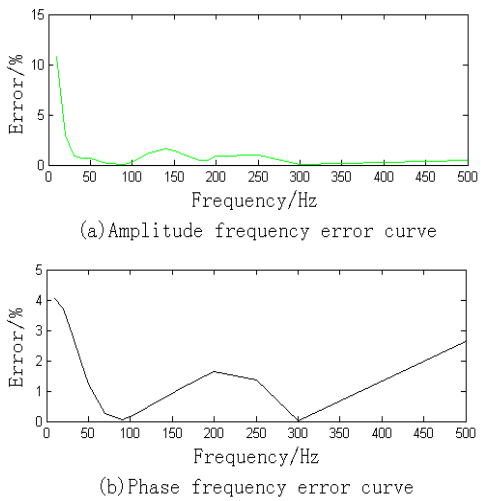

Fig.5 First order RC low-pass filter amplitude frequency and phase frequency error curve

5. Conclusions

On the basis of the above principles the measurement system for the analog circuits parameters based on the multiplier is build. This paper details the system structure, each function module and the experimental results. Results show that the system has some advantages such as simple circuit, easy implementation, the higher accuracy and faster speed. So it is a practical plan for the measurement system of the analog circuit parameters at present.

References

[1] Zhenhua Li, Jiabin Chen and Tao Ma: "Unsupervised FIR adaptive filtering and its frequency domain analysis," Journal of Beijing Institute of Technology, Vol. 21 (2012) No.2, p.234–239.

[2] Jeffrey D.Klein: "Fast algorithms for single frequency estimation," IEEE Trans. Signal Processing, Vol. 54 (2006) No.1, p. 1268–1278.

[3] Aminian M, Aminian F: "A modular fault-diagnostic system for analog electronic circuits using neural networks with wavelet transform as a preprocessor," IEEE Trans. Instrumentation and Measurement, Vol. 56 (2007) No.5, p. 1546–1554.

[4] Y. He, Y. Tan and Y. Sun: "Wavelet neural network approach for fault diagnosis of analogue circuits," IEE Proceedings of Circuits, Devices and Systems, Vol. 151(2004) No.4, p. 379–384.

[5] Yue Hao, Runqin Guo: "Method of parameter statistical analysis for bipolar integrated circuit design," Journal of Electronics, Vol. 8(2007) No.4, p. 373–377.

[6] Bo Liu,Yan Wang and Francisco V. Fernández: "Integration," the VLSI Journal, Vol. 42(2008) No.2, p.137–148.

[7] Yanjun Li, Houjun Wang and Ruey-Wen Liu: " A Method on Analog Circuit Fault Diagnosis with Tolerance,"Journal of Electronic Science and Technology of China, Vol. 7(2009) No.4, p.297–302.

[8] Yangcan Xiao, Ping Wei: "Further result in the fast and accurate estimation of single frequency," Journal of Systems Engineering and Electronics, Vol. 18(2007) No.3, p.646–649.

[9] Hui Zhang, Yang Zhao and Alex Doboli: "A scalable σ-space based methodology for modeling process parameter variations in analog circuits," Microelectronics Journal, Vol. 39(2008) No.12, p.1785–1796.

Advanced Materials Research Vols. 989-994 (2014) pp 3045-3049
© (2014) Trans Tech Publications, Switzerland
doi:10.4028/www.scientific.net/AMR.989-994.3045

Numerical simulation of skid steer loader steering characteristic

Feng Ren[1,2, a], Xinhui Liu[1,2, a], Jinshi Chen[1,3,a], Ping Zeng[1,a], Xuefeng Jia[1,a], Qinmeng Wang[1,a]

[1]School of Mechanical Science and Engineering,Jilin University,Changchun 130022, China.

[2] State Key Laboratory of Automobile Simulation and Control,Jilin University,Changchun 130022, China.

[3] compact product R&D, Jiangsu Liugong Machinery Co.Ltd., Zhenjiang 212005, China.

[a]renfeng12@mails.jlu.edu.cn

Corresponding Author: Jinshi Chen

Keywords: skid steering, dynamic characteristic, co-simulation.

Abstract. In order to analyze the steering dynamic characteristic of the skid steer loader, refer to the theory of tracked vehicle, established the steering Kinematic and dynamic models. use AMESim software platform and Motion software platform to establish a Co-Simulation model of steering system based on theoretical analysis of skid steer loader steering travel. The results show that: the model can predict the dynamic characteristics of the skid steer loader skid steering process.

Introduction

Skid steer loader adopts hydrostatic driving technology and the traveling system adopts double closed-loop systems and the variable pump drive traveling motor which transmit power to the wheel via chains to rotate the tires. Since there is no differential device, when the vehicle is steering, it rely on the speed difference of both sides of the tire. Due to the current published relevant results which research for skid steering load characteristics of skid steer loader are rare and the research results in other fields can be used .Therefore, this paper conduct the research from two aspects. The first one is skid theory of tracked vehicle, the main research results in this area include that Bruce Maclaurin and others who use magic formula to study skid characteristics of tracked vehicles get good results, which proves that the magic formula for rubber tires can also apply to the vehicle skid theory[2,3]. This can help establish the skid steering theory of wheeled skid steer loader. The other one is the load characteristics theory of the tire and the ground .Michael and others who have researched on control method of wheeled skid robot steering process developed a corresponding control system which achieved good control accuracy[1]. Jesus morales and others have researched the energy loss of tracked vehicle skid process[5]. Jingang yi and others have analyzed the kinematics and dynamics characteristics of wheeled skid robot and designed the control system by using kalman filter[4].YangLei and others have simulated and analyzed the armored tracked vehicle steering characteristics by using matlab/simulink and analyzed the influence in the hydraulic system pressure of the vehicle speed change[6]. Bekker and others have analyzed the effect relationship between tire and the ground by using test and analysis methods. Karafiath have analyzed the characteristics of the tire steering and skidding in soft ground[7-9]. This can help establish the kinetic model of the tire and the ground. In addition, there are many related researches for matching the engine and hydraulic system, have accumulated a large number of research results which provides a reference for establishing the hydraulic system model in this paper.

The load characteristic of skid steer loader is very complex, especially the load characteristic of tire and the ground in steering process which directly affect the dynamics and stability of the machine. So it is very important to research the load characteristic of tire and the ground in steering process. Traditional research methods mainly base on simple theoretical calculation or using dynamics software to do simulation analysis. This method does not combine the transmission system analysis

and dynamic analysis of the vehicle and ignores a number of key parameters so that it cannot accurately analyze the real steering characteristics of vehicle and the overall performance. So this paper conducts the co-simulation analysis by using multi-body dynamics software Motion and hydraulic system simulation software AMESim. By this way the analysis of vehicle steering characteristics can be more realistic and it is of great significance on the whole vehicle system matching and performance prediction.

1.Kinematic and dynamic models

The kinematics equation in the process of steering is[9]:

$$R = \frac{B}{2}\frac{(r\omega_r + r\omega_l)}{(r\omega_r - r\omega_l)} = \frac{B(K_s+1)}{2(K_s-1)} \tag{1}$$

$$\Omega_z = \frac{r\omega_r + r\omega_l}{2R} = \frac{r\omega_l(K_s-1)}{B} \tag{2}$$

Where, R is the turning radius, Ω_z is the yaw velocity of the vehicle, ω_r is the angular speed of right wheels, ω_l is the angular speed of left wheels, r is the radius of the wheel, K_s is the angular speed ratio ω_r / ω_l.

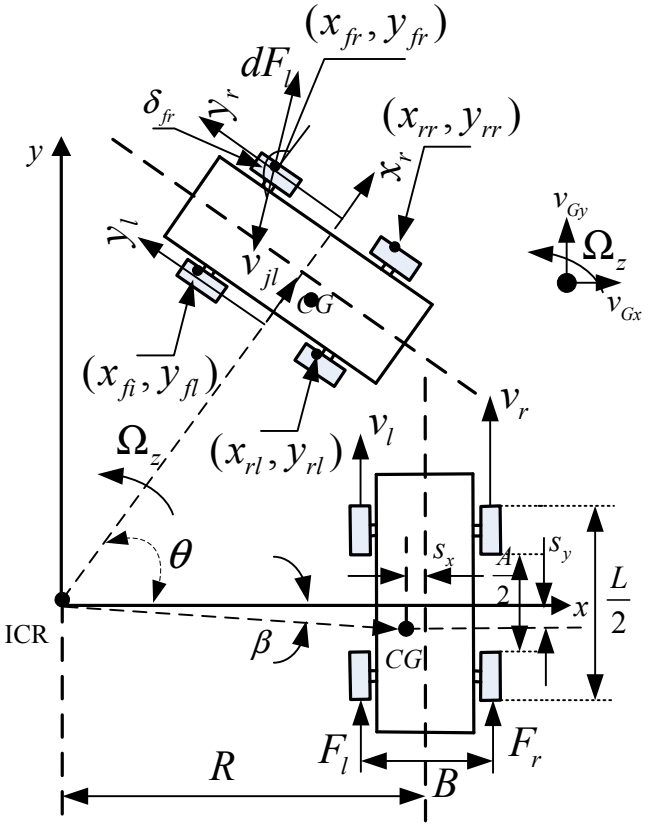

Fig 1 Schematic diagram of the steering of vehicles

When model takes into account the longitudinal slip ratios i_l and i_r of the left and right wheels, the turning radius R' and yaw velocity Ω_z' are given by.

$$R' = \frac{B[K_s(1-i_r)+(1-i_l)]}{2[K_s(1-i_r)-(1-i_l)]} \tag{3}$$

$$\Omega_z' = \frac{r\omega_l[K_s(1-i_r)-(1-i_l)]}{B} \tag{4}$$

Based on theory in [9] assumed the shear stress τ and shear displacement j relationship can be described as follows:

$$\tau = \sigma\mu(1-e^{-j/K}) \tag{5}$$

where σ is the normal pressure, μ is the coefficient of friction between the wheel and the ground, K is the shear deformation modulus, is a terrain-dependent parameter, like the rolling resistance and coefficient of friction, j is the shear displacement.

On the right wheels:

$$dF_r = \tau_r dA = \sigma_r \mu(1-e^{-j_r/K})dA \tag{6}$$

On the left wheels:

$$dF_l = \tau_l dA = \sigma_l \mu(1-e^{-j_r/K})dA \tag{7}$$

Where τ_r and τ_l are the shear stress, σ_r and σ_l are normal pressures, and j_r and j_l are shear displacements of the elements of the right and left wheels, respectively.

The longitudinal forces F_{yr} and F_{yl} can be expressed as follows:

$$F_{yr} = -\int_{A/2}^{L/2}\int_{-b/2}^{b/2}\sigma_r\mu(1-e^{-j_r/K})\sin\delta_{fr}dx_{fr}dy_{fr} - \int_{-A/2}^{-L/2}\int_{-b/2}^{b/2}\sigma_r\mu(1-e^{-j_r/K})\sin\delta_{rr}dx_{rr}dy_{rr} \tag{8}$$

$$F_{yl} = -\int_{A/2}^{L/2}\int_{-b/2}^{b/2}\sigma_{fl}\mu(1-e^{-j_l/K})\sin\delta_{fl}dx_{fl}dy_{fl} - \int_{-A/2}^{-L/2}\int_{-b/2}^{b/2}\sigma_{rl}\mu(1-e^{-j_l/K})\sin\delta_{rl}dx_{rl}dy_{rl} \tag{9}$$

Turning resistance of right wheels and left wheels can be expressed respectively by.

$$M_r = \frac{B}{2}F_{yr} \tag{10}$$

$$M_l = \frac{B}{2}F_{yl} \tag{11}$$

2.Dynamic characteristics simulation analysis of skid steering

In order to establish a more accurate dynamics model of vehicle steering process, this paper use multi-body dynamics software Motion to establish a model of the vehicle and the ground, shown in Figure 2.

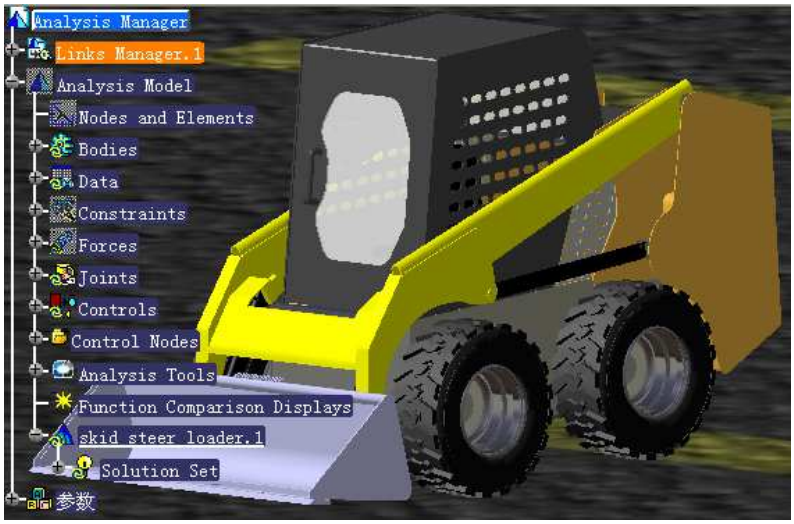

Fig 1 Multi-body dynamics model of vehicle

Take unilateral right steering with rated speed and fully load as an example, left traveling pump is main working pump which drives left traveling motor to output torque for driving the left side tires to overcome friction to move. The right traveling pump is in the neutral position and the right traveling motor is in braking condition, so there is speed difference between left and right side and the vehicle

steers around the slow side. Figure 3 is traveling hydraulic system pressure simulation curve of unilateral right steering, figure 4 is right wheel torque simulation curve of unilateral right steering, and figure 5 is left wheel torque simulation curve of unilateral right steering. Table 1 shows the traveling hydraulic system pressure dynamic response indicators of unilateral steering.

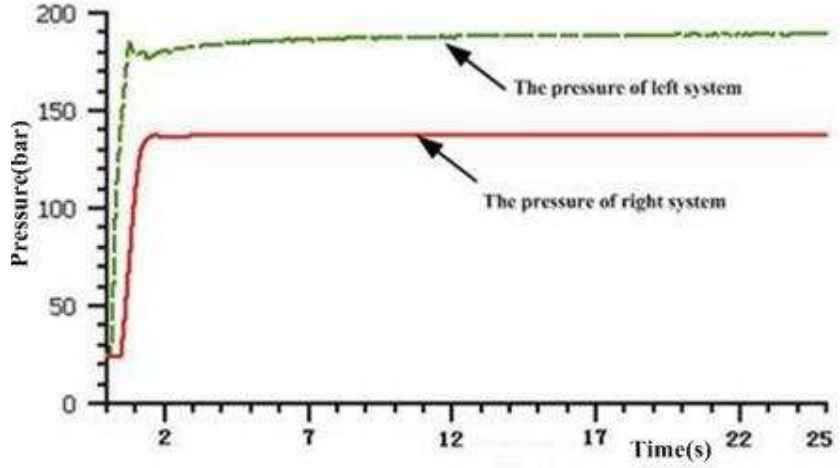

Fig 3 Traveling hydraulic system pressure of unilateral right steering

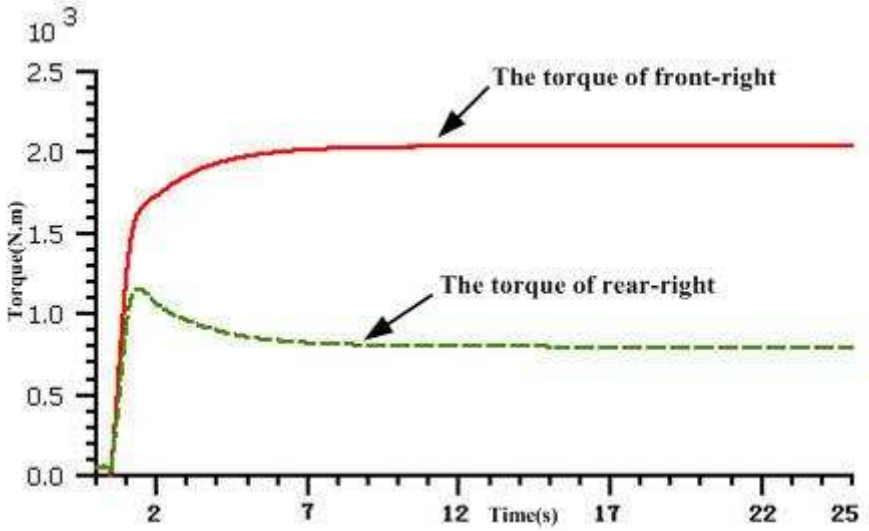

Fig 4 Right wheel torque of unilateral right steering

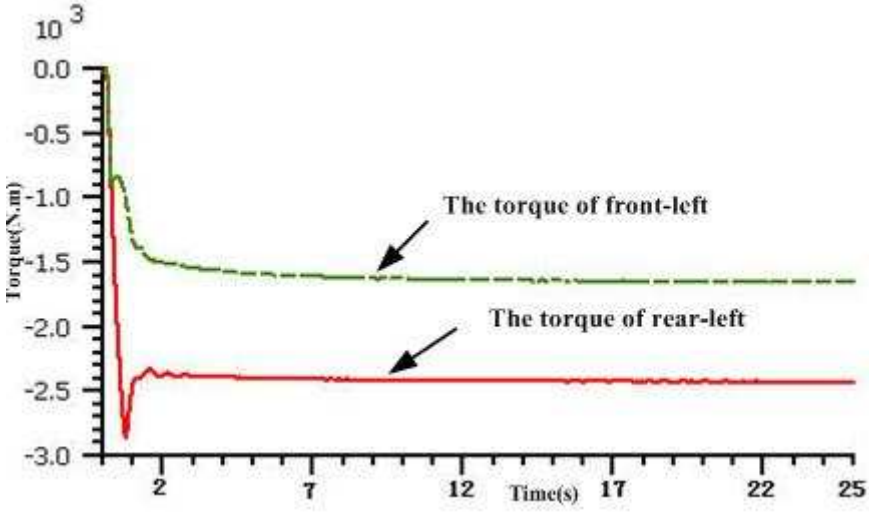

Fig 5 Right wheel torque of unilateral right steering

Table 1 Traveling hydraulic system pressure dynamic response indicators of unilateral steering

unilateral steering	delay s	regulation time s	max pressure MPa	steady pressure MPa	overshoot %
left side pressure	0.64	1.4	18.6	18.2	2.2
right side pressure	0.86	2.1	13.7	13.6	0.7

By figure 3, figure5 and table 1，the motor pressure of high pressure side can reach to 18.6MPa at the beginning of steering. In the unilateral steering stabilization phase, the mean value of left motor pressure is 18.2MPa and the mean value of right motor pressure is 13.6MPa. In this condition, vehicle steering radius is larger than bilateral steering. That means the left motor equivalent moment of inertia is less and so does the system overshoot. Therefore, the pressure of the steering system is relatively stable.

Conclusion

(1) Analyze the steering characteristics of skid-steer loader; establish the kinematics and dynamics model of the vehicle by using the slip theory of tracked vehicle and magic formulas, which provides a theoretical guidance to establish the simulation model.

(2) The test results indicate that, the co-simulation model and test results are relatively close either from the values or trend, which verifies that the method is feasible and the model is accurate. And the model can predict and evaluate the steering performance of the vehicle.

References

[1] Clarke, M. and Blanchard, T. Development of a Control System for a Skid-Steer Amphibious Vehicle 2010; Proceedings of TAROS.9(2010)41-46.

[2] Bruce maclaurin. A skid steering model using the magic formula. Journal of terramechanics.48(2011)247-263.

[3] Bruce maclaurin. A skid steering model with track pad flexibility. Journal of terramechanics. 44(2007)95-110.

[4] Jingang Yi, Hongpeng Wang, Junjie Zhang, Dezhen Song, Suhada Jayasuriya, Jingtai Liu. Kinematic modeling and analysis of skid-steered mobile robots with applications to low-cost inertial-measurement-unit-based motion estimation, IEEE Transactions on Robotics. 25(2009)1087-1097.

[5] Jesus Morales, Jorge L. Martinez, Alfonso J.Garcia-Cerezo, Salvador Pedraza. Power consumption modeling of skid-steer tracked mobile robots on rigid terrain. IEEETransactions on Robotics. 25(2009)1098-1108.

[6] YANG Lei, MA Biao, LIHe-yan, CHEN Bao-rui. Simulation of steering characteristic for hydrostatic drive tracked vehicle. 31(2010)663-668.

[7] E.Mohammadpour, M.Naraghi. Posture stabilization of skid steer wheeled mobile robots. 2010IEEE conference on robotics, Automation and Mechatronics, 2010163-169;

[8] W.Merhof, *FAHRMECHANIK DER KETTENFAHRZEUGE*, 1985

[9] J.Y.Wong. *The theory of ground vehicles*. John Wiley &Sons; 1981.

Advanced Materials Research Vols. 989-994 (2014) pp 3050-3053
© (2014) Trans Tech Publications, Switzerland
doi:10.4028/www.scientific.net/AMR.989-994.3050

A improvement of the Keep-Right-Except-To-Pass Rule in the model of Modified CA(cellular automata)

Yue Ma

School of North China Electric Power University, Baoding, 07100, China

mayuehuabeidianli@126.com

Keyword: Cellular automata, Variable speed limit , the New Principle.

Abstract. We build the model of Modified CA(cellular automata) to analyze the right-hand drive principle, at the same time we put forward the New Principle(In the principle, right lane is the high-speed lane and vehicles driving on it normally. This paper divides the whole principle process into four stages. The overtaking vehicle(A) send signals to the overtaked one(B),B moves to the low-speed lane to let A pass, A moves straight to finish overtaking and B returns.) and its creation is optimized by the model. At last, we use the model to analyze the traffic conditions in different principles or vehicle density or speed limit.

Introduction

In countries where driving automobiles on the right is the rule, multi-lane freeways often employ a rule that requires drivers to drive in the right-most lane unless they are passing another vehicle, in which case they move one lane to the left, pass, and return to their former travel lane.

There, we face the challenge that we need a mathematical model to analyze the performance of this rule in light and heavy traffic. And we must stress on tradeoffs between traffic flow and safety, the role of under- or over-posted speed limits, and other factors that may not be explicitly called out in this problem statement. We also need to judge whether this rule effective in promoting better traffic flow. If not, we need to create a better one.

Method

·Overtaking parametric analysis:

Two parallel lanes which directions are opposite, one-dimensional chain of discrete points we put each channel is defined as equidistant grid points consisting of "L". The spacing between the grids is 7.5m. Possible states for each grid point are: empty (no cars) or occupied by a vehicle with a speed of V =0,1,2…And the vehicle's maximum speed is $V_{\max}$. Normally the vehicle was traveling along the right lane, only in the process of overtaking can travel on the left direction.

Fig.1 is overtaking situation Schematic, black grids represent vehicles and white grids mean there doesn't have a vehicle. Assume at time "t", when the former vehicle "i" want to transcend the motorcade which length is n before. The spacing between the first vehicle of the motorcade and the closest vehicle in the same direction of it is "u". When overtaking starts, the overtaking sight is "s" ,and the spacing between the former vehicle and the nearest vehicle "j" on the neighbor road is "l".

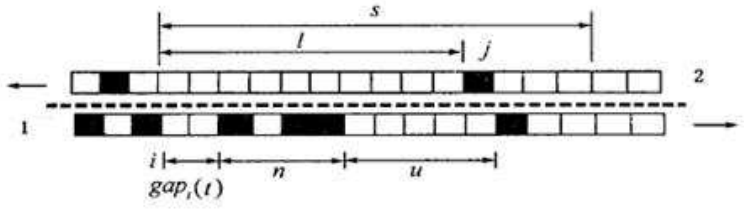

Fig.1 Overtaking analysis schematic diagram

·The analysis of the principle:

·Firstly, we define a new concept"Safety Factor"and we use a"S"to represent it.

$$S = \frac{sd \times \alpha_1}{v \times \alpha_2}$$

Besides, "sd" means the safe distance when overtaking," v" means the maximum limited speed. And"α_1",,"α_2" respectively represent the two factors' weighted calculation.

·The overtaking process contains three stages: lane changing, overtaking and lane returning.

(1) Lane changing condition:

- $v < \overline{V_f}$
- $\int_0^{t_c} (V_{Y_1}^0 + a_{Y_1}^a t) d_t - \int_0^{t_c} (V_{Y_0}^0 + a_{Y_0}^a t) d_t \geq d_s$
- $\int_0^{t_c} (V_{C_1}^0 + a_{C_1}^a t) d_t - \int_0^{t_c} (V_{Y_0}^0 + a_{Y_0}^a t) d_t \geq d_d$

(2)Overtaking condition:

- $v < \overline{V_j}$
- $\int_{t_c}^{t_c+t_0} (V_{C_1}^{t_c} + a_{C_1}^a t) d_t - \int_{t_c}^{t_c+t_0} (V_{Y_0}^{t_c} + a_{Y_0}^a t) d_t \geq d_s$
- $\int_{t_c}^{t_c+t_0} (V_{Y_0}^{t_c} + a_{Y_0}^a t) d_t < \max\{S_{Y_i} + (i+1) + \sum_{i=1}^{n} L_{c_i}\}$

(3)Returning condition:

- $v < \overline{V_j}$
- $\int_{t_{c+t0}}^{t_c+t_0+t_a} (V_{C_1}^{t_c+t_0} + a_{C_1}^a t) d_t - \int_{t_{c+t0}}^{t_c+t_0+t_a} (V_{Y_0}^{t_c+t_0} + a_{Y_0}^a t) d_t \geq d_s$
- $\int_{t_{c+t0}}^{t_c+t_0+t_a} (V_{Y_{(i+1)}}^{t_c+t_0} + a_{Y_{(i+1)}}^a t) d_t - \int_{t_{c+t0}}^{t_c+t_0+t_a} (V_{Y_0}^{t_c+t_0} + a_{Y_0}^a t) d_t \geq d_d$

Above all, under different limited speed conditions, the overtaking model can be described as:

$$\min Z = \max\{0, S_{Y_0} - \max[S_{Y_i} + (i+1) d_s + \sum_{i=1}^{n} L_{c_i}]\}$$

Besides, S_{Y_0} represents the overtaking vehicle's driving distance.

- According to the formulas above, we make out the simulation.

Table 1 Safe distance of following vehicle(A)

Vehicle	Limit at a speed of 60km/h	Limit at a speed of 80km/h	Limit at a speed of 100km/h
Overtaked vehicle	50	60	80
Overtaking vehicle	55	80	95
Following distance	16.73	34.82	50.35

Table 2 Safe distance when the vehicle lane changing(B)

Vehicle	Limit at a speed of 60km/h	Limit at a speed of 80km/h	Limit at a speed of 100km/h
Overtaked vehicle	50	60	80
Overtaking vehicle	55	80	95
Following distance	16.77	24.20	38.96

Table 3 Safe distance when the vehicle overtaking(C)

Vehicle	Limit at a speed of 60km/h	Limit at a speed of 80km/h	Limit at a speed of 100km/h
Overtaked vehicle	50	60	80
Overtaking vehicle	55	80	95
Following distance	13.82	27.80	44.32

To processing this data, we use the expert scoring method and get the weight of each distance. The scale factor of a, b, c is 0.5,0.3,0.2.Then we can get “Safety Factor” in the light or heavy traffic.

Table 4

Limited speed	Safe factor
60	0.457
80	0.375
100	0.267

We can learn from this table that the safe factor moves inversely to the limited speed.

·The right rule, left rule and the new rule’s traffic flow changing diagram is:

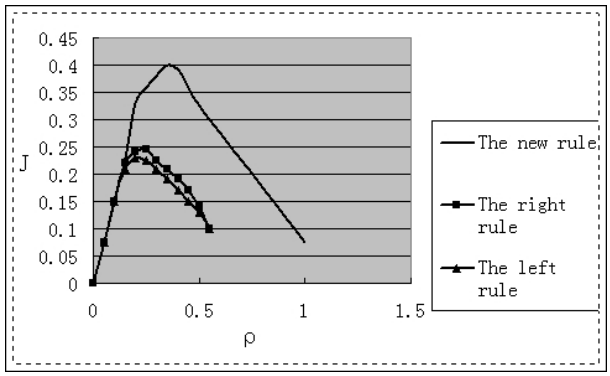

Fig.2 Diagram of different rule

Discussion

We can conclude from the diagram above that the right rule’s impact on the traffic is close to the left rule’s. But when the vehicles obey the new rule, it can improve the traffic flow to a large extent.

In countries where driving automobiles on the left is the norm, the left lane is high-speed lane, when one automobile wants to overtake, whistling and the automobile in front of it(driving in a lower-speed) moves to the right lane. The lower-speed automobile returns to the left lane as soon as the overtaking has been done safely.

Conclusion

In order to analyze traffic performance in different traffic rules, using the software “Matlab”and programming, we creatively establishes a one-way two lane Modified CA traffic flow model. Effect of vehicle density model on traffic flow are studied by numerical simulation. According to the results of our program, we can know that the traffic flow first increases and then decreases as the traffic load’s increasing. At the same condition, the security’s reducing speed increases.

We use the Modified CA model to simulated the New Principle. Learning from the calculation result, we find that our New Principle makes full use of the high-speed lane and the traffic flow increase at a degree of 32%.

Strengths:

·Cleverly use the cellular automata model to simulate the flowing of vehicles.

·Define a new concept“Safety Factor”to analyze the safety issues, quantify the abstract problem and make the calculation clearly.

·The new rule we make can take full advantage of the fast lane to improve the traffic flow on a certain degree.

References

[1] K. Nagel and M. Schrekenberg:*A Cellular Automaton Model for Freeway Traffic[J]*.J. Phys. I France,1992,2:2221-2229.

[2] Wren A, Fores S and Kwan A S K, et al:*A Flexible System for Scheduling Drivers[J]*.Journal of Scheduling,2003,6(5) : 437-55.

[3]Yindong Shen:*Two Neighbourhood Search Approaches: 2-opt Heuristics and Tabu Search for Bus and Train Driver Scheduling[M]*.Beijing: Science Pres,2003.

[4] MA Jun:*A Study on Safe Distance between the Vehicles in Freeway[J]*.Journal of Xi,an Highway University,1998,18(4) : 90-94.

[5]Shen Y and Xia J:*Integrated Bus Transit Scheduling for the Beijing Bus Group based on a Unified Mode of Operation[J]*.International Transactions in Operational Research,2009,16(2) : 227-242.

Advanced Materials Research Vols. 989-994 (2014) pp 3054-3057
© (2014) Trans Tech Publications, Switzerland
doi:10.4028/www.scientific.net/AMR.989-994.3054

Design and implementation of remote control system Based on embedded mobile network

Jingxin Wei

NCIST Teaching Affairs Department，Bejing East, Yanjiao 101601

Keywords: SMS, AT instruct.

Abstract: On employing GSM network as the way for data wareless transmission, this thesis puts emphasis on introducing operating principle of TC35i module and AT89C51 as well as the perpheral interface circuit. Meanwhile, it designs the system hardware circuit, computer control solfware and SCM system solfware with offering the application program for TC35i module and AT89C51 interface partially. After the debugging and practising, it comes to the data transmission terminal with GSM module.

1 Introduction

With the development of computer communication technology, computer network monitoring has become an important site monitoring of various technical means necessary for remote monitoring, and using wireless remote monitoring has become the development trend of the control field. GSM network enjoys wide coverage , stable signal, no co-channel interference , confidentiality , massive short messages handling, data and fax transmission and other business functions, and GSM short message is characterized of online without dialing, cheap, wide-range covering, particularly suitable for small flow applications for transmitting data , and is widely used in oil fields , weather, port inspector , water network , hydrology, environmental monitoring, vehicles, ships , mobile operations, and other places.

Simple remote control system consists of two parts-host and remote . Host computer is used to monitor the operation of computers that are connected to a network, while the remote receives the data for the analysis, interpretation and execution. Design and implementation of the design focuses on the host , and a whole host of information to get the design and implementation of the module , the host MCU control via mobile phone module to achieve data transmission system that uses the short message data transmission mode , the system with the use of flexible , reliable operation.

2 Hardware Design

System hardware consists of a computer control center , data transceiver GSM module , single-chip control panels and other parts. Control Center computer using a normal computer, connected to the data transceiver GSM module is the result of conversion chip MAX3238, will be converted into TTL level RS-232 level [1] , and then directly connected to the computer serial port ; For microcomputer control system , GSM data transceiver module connection is through conversion chip MAX232, will be converted into TTL level RS-232 level , and then directly connected to the microcontroller development board serial port.

2.1 GSM data transceiver module

Data transceiver module is mainly composed of TC35i GSM module, SIM cards, interface circuits , antennas and other components , and the core is Siemens TC35i module, with the main function of remote data transmission through the mobile communication network.

Design uses Siemens TC35 Series TC35i. TC35i data interface (CMOS level) is a serial of asynchronous transceiver which meets ITU-TRS232 standard, with 8 data bits and 1 stop bit , no parity. AT command can be bi-directional transfer instructions and data to support Text and PDU format of SMS (Short Message Service, SMS) , available through AT commands or restart and shutdown signal to achieve fault recovery . Because it is relatively simple for Text mode to send and receive the short message, the design is based on AT commands using the Text mode.

2.1.1 Send and delete messages.

Before sending the message , the information must be set to send the transmission format , use the "AT + CMGF = 1" command to send the format to Text mode, the write command "AT + CMGS = other phone numbers " and other GSM module reply " > " symbol can be written to the content to be sent after using the shortcut key " Ctrl + Z " to send text messages , if the messages is issued by the GSM module, it will reply + CMGR: digital , OK; if the error happens, it will reply ERROR.

Filling in the blanks is used to store newly received short message in TC35i, and it will always put the received short message in the smallest ordinal position. When all the stores are filled, it will no longer receive new short message. So after a short message to be processed promptly removed. Delete short message AT command : AT + CMGD = n, where n represents the number of short messages to be deleted.

2.1.2 The short message receiving and storing

Because of the short message's delay in transmission , the short message's arrival time is uncertain . Therefore, you must set the short message arriving prompts command and regular testing [2] , so you can power up when TC35i be initialized achieved. Set short messages arriving automatically prompts the AT command AT + CNMI = 1,1,0,0,1. When you receive a short message arrives + CMTI: "SM", n prompt message, where + CMTI: Prompt header information , "SM ' is short message storage area for the SIM card memory , n is new short message to the specified storage area in the storage number , you can send "AT + CMGR = n" to the specified storage area to read out a short message . After this command is issued, if the GSM module has received a short message, then from the UART interface returns the following information:

+ CMGR: "REC UNREAD", " sender phone number " , "Send Time"

xxxxxxxxxxxxxxxxx (Receive short text message)

2.2 MCU control board

AT89S51 microcontroller control board is mainly composed of microcontroller, digital tube display , eight light-emitting diodes and other components [3] . Its main function is to receive commands and data from the control center , and to control the device (light emitting diode analog). Minimum system design AT89S51 clock signal is generated by the clock signal which is generated by the circuit capacitor C5, C7 and crystal Y1, power-on reset circuit consists of C6, R13 constitute , manual reset circuit consists of S1, R12 composition. In the system C5, C7, we take 22PF, which can stabilize the system clock oscillation stability . In order to ensure a sufficiently wide differential circuit generates a pulse , RC time constant should be more than two machine cycles , here we take 10uF capacitor , 8.2K resistor , AT89S51 minimum system circuit shown in Figure 1.

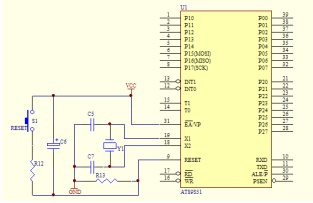

Figure 1 AT89S51 system

3 Software System Design

Mobile communication network remote control system software design includes computer control software, microcontroller control panel software design

3.1 Computer Control Software Design

Computer control interface uses a VB 6.0, and the control interface is very easy to use, and powerful. Control interface shown in Figure 2.

Computer as a control terminal to overcome the microcontroller can not store large amounts of data , no real-time updates of data, and other shortcomings. Computer control terminal is used to initialize the serial device, to send information (communication of information and control

commands) , to receive the information returned by the receiving terminal , to carry out real-time information processing, to store, storage, delete, view information.

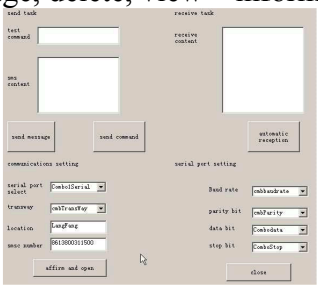

Figure 2 Computer control terminal interface

MSComm control serial events provided by Vb [4] [5] [6]is used for computer communication module TC35i control information processing . Vb program is done through the queries of serial communication control MSComm Oncomm event. After the program starts, it initializes the modem and the serial port.

3.2 SCM system software design

SCM system uses an external microcontroller directly TC35i module to receive information , uses the query method to detect information soon. And receive text messages and read the contents , determine the end of a remote control device , a light emitting diode used here to indicate the state.

4 System debugging

4.1 Computer terminal debugging

After the program 's interface and the code is written , run the application and select End communication configuration after clicking "Confirm configuration and open the serial port " in the back of the test command input after the "AT" clicking "Send Command" , finds that the received content appears "AT OK" behind words , indicating GSM module can communicate with a computer[7] [8] [9] . Now once the process to send and receive text messages , first enter "AT + CMGF = 1" command to set the text in the test format , to receive content appears "AT + CMGF = 1 OK" behind the words ; After the test command input "AT + CMGS = other phone number " to receive content behind a" > "character, the content of the message in the message you want to send the contents of the input click" Send SMS " , if sent successfully , you will receive the content in the event of " + CMGS,, *** OK " words , indicating that the information has been issued , if there is " OK " or " ERROR " word then the information is not given; After the test command input "AT + CNMI = 1,1,0,0,1" Set SMS prompt arrival , when a new message arrives there will be "+ CNMI:" After receiving the contents of the word ME ", <index>", which indicates the position of <index> just received text messages stored , you can read the messages based on this parameter to write programs ; according to the location to get the message , and after the test command input "AT + CMGR = <index>", at the reception content will appear after "+ CMGR:" REC UNREAD "," sender phone number " , " message received time " message content " OK "; To delete a message long after the test command input "AT + CMGD = <index>" can be. Meanwhile module has closed echo function , for close echo enter the word "ATE0" in the test command, appears the word "OK" after receiving the content only after the above test , the function can achieve , computer terminal debugging success.

4.2 SCM side debugging

After you have written SCM test program , you should first burn the program into the microcontroller , double tick Easy 51Pro.exe programmer icon. When the program starts , after automatic hardware detection and connection, in status box will display the word " Ready ", which means that the programmer connections and settings are normal. After repeated testing , the system is working properly.

5 Conclusion

The design, with the use of VB, develops successfully a set of message system to receive and send messages. And receiving and sending text messages via a PC is used to achieve the desired results. In addition , the remote host, the single-chip control panel, sends text messages to the remote end user via the serial port, and single-chip GSM engine module is capable of receiving a signal sent from the right , analyzing the signal, and controlling the object.

References

[1]Y.G. L V,The design of interactive network platform integrated with GSM short message,Journal of the Hebei academy of sciences ,Mar.2012.
[2]W.J. S U,Design and implementation of a Fault Real-time Alarm Control System Based on GSM ,computer measurement & control, Vol.20，No.08,2009.
[3] D.Y.DONG，Design of Wireless Data Transmission Module Based on GSM Technology，Automation & Instrumentation，No.11,2010.
[4]P.Z.Gong，Concise Guide to Visual Basic Programming (Second ed.)，Higher Education Press ,Beijing, 2003.
[5]E.Z.Liang，Visual Basic 6.0 programming with examples of analytic，Science Press, Beijing, 2000.
[6]Y.Z.Fan，Visual Basic with RS232 serial communication control，Tsinghua University Press, Beijing, 2002.
[7]GSM Reference Manual
[8]J.Q.Li，Visual Basic serial communication technology and combat Detailed monitoring and control applications， People's Posts and Telecommunications Press , Beijing ,2007.
[9]W.Q.Cao，SMS using GSM remote control，radio Engineering Vol.32，No.10,2002

Advanced Materials Research Vols. 989-994 (2014) pp 3058-3061
© (2014) Trans Tech Publications, Switzerland
doi:10.4028/www.scientific.net/AMR.989-994.3058

Vibration Analysis of Cable Suspended Parallel Mechanisms with Dynamic Base Platforms

Yongpan Hu[a], Limin Tao[b]

National University of Defense Technology, Changsha 410073, China;

[a]huyongpan1986@163.com, [b]tlm1964@sina.com

Keywords: Cable suspended parallel mechanism, offshore cargo handling, vibration analysis

Abstract. Cable suspended parallel mechanisms have potential applications in offshore cargo handling. Due to the flexibilities of the cables, the cargo will vibrate under the excitation of wave-induced ship motion. This paper analyzes the vibration of cable suspended parallel mechanisms with dynamic base platforms. Based on the linearization of the dynamic model about a nominal trajectory, the vibration equation is given. The natural frequencies, sensitivities and frequency responses of the mechanism are derived from the vibration equation. Numerical results of an example are discussed, which validate the analysis given by this paper.

Introduction

Cable suspended parallel mechanisms (CSPMs) are a class of cable-driven parallel mechanisms with suspended configurations. One important potential application of CSPMs is offshore cargo handling. Because of the elasticity of the cables, the payload platform inevitably vibrates due to the wave-induced ship motion. Some researchers have studied the vibration characteristics of cable-driven parallel mechanisms with fixed base platforms. For example, Diao and Ma analyzed the vibration caused by cable flexibilities in both axial and transversal directions [1]. Liu et al. determined the natural frequencies and analyzed the sensitivities of the fundamental frequency to structure parameters[2]. However, as far as we know, the vibration characteristics of CSPMs with dynamic base platforms have not been studied yet, which motivates the research in this paper.

Vibration Equation

A general model of a CSPM with m cables is shown in Fig. 1, where $i=1,\cdots,m$. Three coordinate frames F_P, F_B and F_N are fixed to the base platform, the payload platform and the inertial space, respectively. $\mathbf{l}_i \in R^3$ $(i=1,2,\cdots,m)$ is the vector along the ith cable and has the same length as the cable, which is represented by scalar l_i. $\mathbf{e}_i$ is the unit vector along the ith cable.

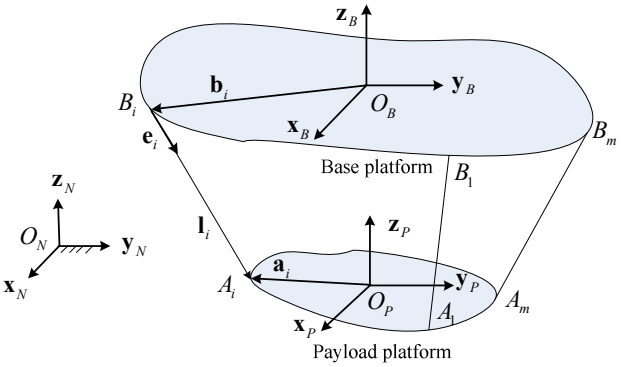

Fig. 1 General model of a CSPR with m cables

Let $\mathbf{t}=(\dot{x},\dot{y},\dot{z},\omega_x,\omega_y,\omega_z)^T$ denote the velocity vector of the payload platform, where $(\dot{x},\dot{y},\dot{z})^T$ is the velocity of O_P and $\boldsymbol{\omega}=(\omega_x,\omega_y,\omega_z)^T$ is the angular velocity of F_P, both represented in F_N. According to the rigid body kinematics [3], we have $\mathbf{t}=\mathbf{H}\dot{\mathbf{x}}$, where

$$\mathbf{H}=\begin{bmatrix}\mathbf{E}_{3\times3} & \mathbf{0}_{3\times3}\\ \mathbf{0}_{3\times3} & \mathbf{h}\end{bmatrix},\ \mathbf{h}=\begin{bmatrix}C\phi C\theta & -S\phi & 0\\ S\phi C\theta & C\phi & 0\\ -S\theta & 0 & 1\end{bmatrix}$$

ϕ and θ are yaw and pitch angles of F_P, $\mathbf{E}$ and $\mathbf{0}$ stand for identity matrix and zero matrix respectively.

On defining $\mathbf{L}=\left(l_1,l_2,\cdots,l_m\right)^T$, the Jacobian matrix can be calculated by $\mathbf{J}=\partial\dot{\mathbf{L}}/\partial\mathbf{t}$. Using Newton-Euler's laws, the dynamic model of the payload platform is formulated as

$$\mathbf{M}\dot{\mathbf{t}}+\mathbf{C}\mathbf{t}-\mathbf{G}=-\mathbf{J}^T\mathbf{u} \tag{1}$$

where

$$\mathbf{M}=\begin{bmatrix}m\mathbf{E}_{3\times3} & \mathbf{0}_{3\times3}\\ \mathbf{0}_{3\times3} & \mathbf{R}_P^N\mathbf{I}\mathbf{R}_N^P\end{bmatrix},\quad \mathbf{C}=\begin{bmatrix}\mathbf{0}_{3\times3} & \mathbf{0}_{3\times3}\\ \mathbf{0}_{3\times3} & [\boldsymbol{\omega}\times]\mathbf{R}_P^N\mathbf{I}\mathbf{R}_N^P\end{bmatrix},\quad \mathbf{G}=\left(0,0,-mg,0,0,0\right)^T$$

m is the mass of the payload platform (including the payload), $\mathbf{I}$ is the 3×3 inertial matrix of the payload platform about O_P, and $\mathbf{u}=\left(u_1,u_2,\cdots,u_m\right)^T$ denotes the cable tensions.

The vibration equation can be obtained from the linearization of (1) about a nominal trajectory. Let $\mathbf{t}_n$ denote the velocity vector of the payload platform on the nominal trajectory. The cables are supposed to be taut all the time and can be modelled as linear springs. We define a function $\mathbf{g}(\ddot{\mathbf{x}},\dot{\mathbf{x}},\mathbf{x})$ as

$$\mathbf{g}(\ddot{\mathbf{x}},\dot{\mathbf{x}},\mathbf{x})=\mathbf{M}\dot{\mathbf{t}}+\mathbf{C}\mathbf{t}-\mathbf{G}+\mathbf{J}^T\mathbf{k}(\mathbf{L}-\mathbf{L}_0)=\mathbf{0} \tag{2}$$

where $\mathbf{L}_0$ means the cable lengths without tension and $\mathbf{k}$ is the stiffness matrix of the cables.

Substituting $\mathbf{x}=\mathbf{x}_n+\delta\mathbf{x}$ into (2) and performing Taylor series expansion about $\mathbf{x}_n$, the vibration equation of the CSPR is derived as

$$\bar{\mathbf{M}}\delta\ddot{\mathbf{x}}+\bar{\mathbf{C}}\delta\dot{\mathbf{x}}+\bar{\mathbf{K}}\delta\mathbf{x}=\bar{\mathbf{f}} \tag{3}$$

where

$$\bar{\mathbf{M}}=\mathbf{M}_n\mathbf{H}_n,\ \bar{\mathbf{C}}=\mathbf{M}_n\dot{\mathbf{H}}_n+\begin{bmatrix}\mathbf{0}_{3\times3} & \mathbf{0}_{3\times3}\\ \mathbf{0}_{3\times3} & [\boldsymbol{\omega}\times]\mathbf{R}_P^N\mathbf{I}\mathbf{R}_N^P-[\mathbf{R}_P^N\mathbf{I}\mathbf{R}_N^P\boldsymbol{\omega}\times]\end{bmatrix}_n\mathbf{H}_n,\ \bar{\mathbf{K}}=\mathbf{J}_n^T\mathbf{k}\mathbf{J}_n\mathbf{H}_n$$

are the 6×6 mass, damping, and stiffness matrices, respectively. $\bar{\mathbf{f}}=-\mathbf{M}_n\dot{\mathbf{t}}_n-\mathbf{C}_n\mathbf{t}_n+\mathbf{G}-\mathbf{S}_n\mathbf{G}$ denotes the equivalent applied force vector. The expressions with the subscript *n* stand for the corresponding variables and formulas on the nominal trajectory.

Vibration Characteristics

The dominating vibration characteristics of CSPMs include natural frequencies, sensitivities and frequency responses. The natural frequencies ω_i and the corresponding modal vectors $\boldsymbol{\varphi}_i$ of the CSPR can be calculated from [2]

$$(\bar{\mathbf{K}}-\omega_i^2\bar{\mathbf{M}})\boldsymbol{\varphi}_i=0 \tag{4}$$

where $i=1,2,\cdots,6$.

Sensitivities reflect the influences of system parameters on natural frequencies, which can be derived from equation (4) as

$$\frac{\partial \omega_i}{\partial p}=\frac{1}{2\omega_i}\frac{(\mathbf{H}_n\boldsymbol{\varphi}_i)^T\dfrac{\partial(\mathbf{J}_n{}^T\mathbf{k}\mathbf{J}_n)}{\partial p}(\mathbf{H}_n\boldsymbol{\varphi}_i)}{(\mathbf{H}_n\boldsymbol{\varphi}_i)^T\mathbf{M}_n(\mathbf{H}_n\boldsymbol{\varphi}_i)}-\frac{\omega_i}{2}\frac{(\mathbf{H}_n\boldsymbol{\varphi}_i)^T\left(\dfrac{\partial\mathbf{M}_n}{\partial p}\right)(\mathbf{H}_n\boldsymbol{\varphi}_i)}{(\mathbf{H}_n\boldsymbol{\varphi}_i)^T\mathbf{M}_n(\mathbf{H}_n\boldsymbol{\varphi}_i)} \tag{5}$$

where p is the symbol that represents any parameter.

Based on the fact that the rotation angles of wave-induced ship motion are small, the equivalent applied force $\bar{\mathbf{f}}$ can be rewritten as

$$\bar{\mathbf{f}}=\tilde{\mathbf{M}}\ddot{\mathbf{x}}'+\tilde{\mathbf{C}}\dot{\mathbf{x}}'+\tilde{\mathbf{K}}\mathbf{x}' \tag{6}$$

where $\tilde{\mathbf{M}}=-\mathbf{M}_n\mathbf{H}_n'$, $\tilde{\mathbf{C}}=-\mathbf{M}_n\dot{\mathbf{H}}_n'-\mathbf{C}_n\mathbf{H}_n'$. It can be seen from equation (6) that the equivalent applied force depends on the mass property of the payload platform, the motion of the base platform and the orientations of the two platforms.

By substituting equation (6) into equation (3) and performing Laplace transform, we have

$$(s^2\bar{\mathbf{M}}+s\bar{\mathbf{C}}+\bar{\mathbf{K}})\delta\mathbf{X}(s)=(s^2\tilde{\mathbf{M}}+s\tilde{\mathbf{C}}+\tilde{\mathbf{K}})\mathbf{X}'(s) \tag{7}$$

Therefore the frequency responses of the cable deformations corresponding to the motions of the base platforms are

$$\mathbf{H}(\omega)=\mathbf{J}_n\mathbf{H}_n(-\omega^2\bar{\mathbf{M}}+j\omega\bar{\mathbf{C}}+\bar{\mathbf{K}})^{-1}(-\omega^2\tilde{\mathbf{M}}+j\omega\tilde{\mathbf{C}}+\tilde{\mathbf{K}}) \tag{8}$$

Numerical Discussion

Vibration characteristics of an example CSPM is analyzed, whose top view is shown in Fig. 2. The base platform and the payload platform of the robot are circular plates with the radii of 0.3m and 0.1m respectively. The distribution parameters of the attachment points are $\alpha=\beta=30^\circ$. Moreover, the mass properties of the payload platform are $m=11.3\,\text{kg}$, $\mathbf{I}=\text{diag}(0.0636, 0.0636, 0.1272)\text{kg}\cdot\text{m}^2$.

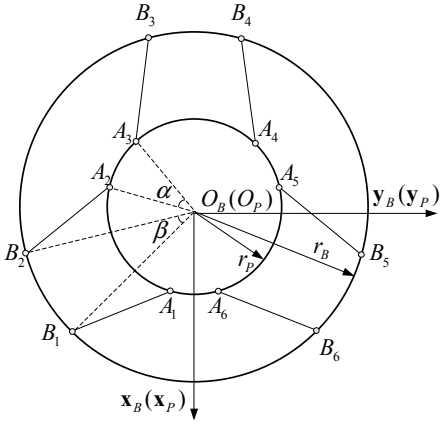

Fig. 2 Top view of the example CSPM

Based on equation (4), the natural frequencies of the example are computed using MATLAB and listed in Table 1. In order to validate the results, a model with the same configuration is built in MSC ADAMS and the natural frequencies are calculated from ADAMS/Vibration, which are also listed in Table 1. It is obvious that the natural frequencies computed from MATLAB and from ADAMS match very well.

Table 1 Natural frequencies of the example CSPM

	Natural frequencies (Hz)					
by MATLAB	3.5172	3.5172	4.7852	19.5508	19.5508	20.3222
by ADAMS	3.5172	3.5173	4.7854	19.5509	19.5510	20.3224

The sensitivities of the fundamental frequency of the example are calculated from equations (5) and listed in table 2. As a reference, small changes are made to the parameters of the model in ADAMS and corresponding variations of the fundamental frequency are recorded, which are used to generate the reference values of the sensitivities. By comparison, the conclusion can be drawn that the results of Table 2 and 3 are identical, which indicates equation (5) is correct.

Table 2 Sensitivities of the fundamental frequency

	$\frac{\partial \omega_1}{\partial \alpha}$ (rad/rad)	$\frac{\partial \omega_1}{\partial \beta}$ (rad/rad)	$\frac{\partial \omega_1}{\partial r_B}$ (rad/m)	$\frac{\partial \omega_1}{\partial r_P}$ (rad/m)	$\frac{\partial \omega_1}{\partial z''}$ (rad/m)	$\frac{\partial \omega_1}{\partial d}$ (rad/m)	$\frac{\partial \omega_1}{\partial m}$ (rad/kg)
by MATLAB	-19.0564	-19.0564	51.8700	27.7796	-47.5234	22262	-1.0002
by ADAMS	-19	-19	52	28	47	22260	-1

The frequency responses of the example are obtained using ADAMS/Vibration and shown in Fig. 3. It is obvious that every line has an extreme point at 3.5172 Hz, which is the fundamental frequency of the CSPM. When the motion frequency is lower than 3.5172Hz, the magnitude responses positively depend on the motion frequency. Therefore, in order to suppress the vibration, the fundamental frequency must be adjusted to be much higher than the motion frequency of the base platform.

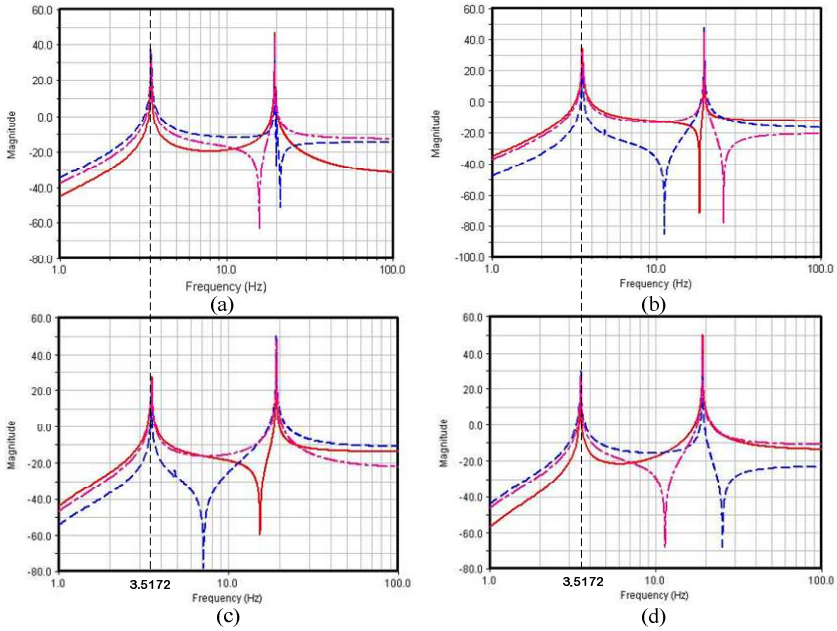

Fig. 3 Magnitude responses of cable deformations relative to (a) the translation along $\mathbf{x}_N$, (b) the translation along $\mathbf{y}_N$, (c) the rotation about $\mathbf{x}_N$, (d) the rotation about $\mathbf{y}_N$, dashed: cable 1 and 6, dashdotted: cable 2 and 5, solid: cable 3 and 4 .

Summary

In this paper, we address the vibration equation and vibration characteristics of CSPMs with dynamic base platforms. The study shows that the vibration induced by the motion of the base platform can be expressed by a vibration equation excited by a equivalent applied force that depends on the motion of the base platform. The vibration characteristics, including natural frequencies, sensitivities and frequency responses are derived from the vibration equation.

References

[1] X. Diao, O. Ma, Vibration analysis of cable-driven parallel manipulators, Multibody system Dynamics, 21(2009) 347-360.

[2] Z. Liu, X. Tang, Z. Shao, et al, Vibration characteristic of 6-DOF cable-driven parallel manipulator, Journal of mechanical Engineering, 49(2013) 49-55.

[3] S. R. Oh, J. C. Ryu , S. K. Agrawal, Dynamics and control of a helicopter carrying a payload using a cable-suspended robot, Journal of Mechanical Design, 128(2006) 1113-1121.

Advanced Materials Research Vols. 989-994 (2014) pp 3062-3069
© (2014) Trans Tech Publications, Switzerland
doi:10.4028/www.scientific.net/AMR.989-994.3062

The design of monitoring system in large hydraulic press aiming at the precise closed-loop control

Heng Du[1,3,a], Bin Huang[1, b], Lin Wang[2, c] and Shumei Chen[1, d]

[1]School of Mechanical Engineering and Automation, Fuzhou University, Fuzhou, China;

[2]Fujian Haiyuan Automatic Equipments Co., Ltd, Fuzhou, China;

[3]Post-doctoral Research Center of Chemical Engineering and Technology, Fuzhou University, Fuzhou, China.

[a]duheng@fzu.edu.cn, [b]binhuang.eh@gmail.com, [c]wanglin@haiyuan-group.com, [d]smchen@fzu.edu.cn

Keywords: Hydraulic press, closed-loop control, monitor, LabVIEW, test.

Abstract. In the research and development of the precise closed-loop control system in large hydraulic press, the touch screen and PLC are frequently applied to design, debug and test for the system. Though a better closed-loop control characteristic can be acquired after repeated testing by this way, the comprehensive state data of hydraulic press are unable to get, which leads to a long research cycle and also restricts the maintenance and upgrade with the equipment in the later period. In order to obtain the whole state information of hydraulic press easily and effectively, a monitor system of precise closed-loop control in large hydraulic press is designed. Based on reasonable cooperation of sensors and high-speed data-acquisition card, high-speed and precise signal acquisition is realized. In addition, data-acquisition software program is designed base on LabVIEW, it can achieve the functions of collecting, storing, displaying and analyzing data. Through the real measuring and analyzing on a certain large ceramic hydraulic press, the status of key parameters can be acquired effectively during the whole pressing process. So the monitoring system supplies the significant data basis to the precise closed-loop control, accelerates the design and development of high characteristic precise closed-loop control and also strongly supports to the maintenance and upgrade with the equipments in the later period.

Introduction

The large hydraulic press is important equipment in mechanical industry, which usually improves the mechanical property and rate of finished products by means of multi-stage compressions during pressing process [1]. Every pressing process concludes the position closed-loop control, velocity closed-loop control or pressure closed-loop control and so on. The measurement and control system is generally the teamwork of touch screen and PLC, the precise closed-loop control is realized through repeated testing of control parameters and modes in the touch screen. Although the precise control can be achieved in some extent, some problems still exist in rapid debugging and the highly precise control in closed-loop system.

Aiming at the teamwork of PLC and touch screen, on the basis of the above mentioned the realization of accurate and efficient closed-loop control testing and analysis are facing two technological difficulties. Firstly, the large hydraulic press needs multi-stage compressions and the working condition of pressing process is complex, measurement and control system of conventional large hydraulic press can't be visualized and observed with the core parameters directly. Depend on these, it is not clear of the comprehensive characteristic of hydraulic press, and it cannot be conduct contrastive analysis, which leads to a long cycle and low efficiency of design, development and testing. Secondly, the large hydraulic press proposes extremely demand on the signal quality during precise closed-loop control, especially the feedback signals of sensors. Millivolt voltage fluctuation or noise disturbance could cause the control precision reducing. Nowadays, the display method relies

on touch screen that cannot get the accurate data of signal, so that the signal processing and higher precision control are restricted. Due to the above two technological difficulties, the system of conventional hydraulic press is hard to realize efficient and accurate closed-loop control. Therefore the design of monitoring system, reflecting hydraulic press comprehensive characteristic, is especially important.

This paper takes the certain large ceramic hydraulic press as an example, on the basis of analyzing its operating principle and every key parameter, the monitoring system based on LabVIEW is designed [2]. The precision characteristics and model selection of sensors and data acquisition equipment are analyzed to meet monitoring system, and the software system based on LabVIEW is designed, which realize the collecting, storing, real-time displaying and analyzing the key parameters of hydraulic press, it provides the data support for realizing the efficient and accurate closed-loop control of hydraulic press [3].

Working Principle

Take a certain model of hydraulic press for example, the electro-hydraulic control technology is applied to achieve the accurate press of master cylinder and promise the precise shaping of ceramic product. The whole press process mainly includes three stages: fall of master cylinder, press stage and return stage. The press stage is the key process of compression moulding, it can divide into first press and exhaust, second press and exhaust and third press stage shown in Fig. 1. In order to realize the rapid, accurate and steady press during the compression moulding, electro-hydraulic proportional/servo closed-loop control method is adopted, and the closed-loop control method generally contains position closed-loop, like fall of master cylinder, pressure closed-loop, like first press and position-pressure compound closed-loop control and so on.

Hydraulic press closed-loop control method is the feedback control system based on feedback single acquired by position sensors and pressure sensors. The monitoring system established by LabVIEW can ensure the precise measurement and control of hydraulic press in each state. Closed-loop control in hydraulic press operation concludes following stages. Firstly, in fall of master cylinder stage, the pressure in master cylinder is so low that it is unnecessary to build pressure measure system. For rapidly falling down and steady touching powder, the position closed-loop of tracking deceleration curve is applied, and the position monitoring is extremely important at this time. Then, in order to improve the product mechanical property and rate of finished products, the pressure closed-loop control method is employed in the press process, especially the first press. The pressure in master cylinder is monitored by the high precision pressure sensor and precise closed-loop control is realized, which can avoid the poor compression moulding quality caused by too high or low pressure. Meanwhile, considering that the plane pressed by hydraulic press is large, uneven forcing leads to uneven product thickness in the press process. The plane absolute position is monitored via the position sensors beside the both side of master cylinder, so the high precision plane press of master cylinder is achieved. Finally, in the phase of master cylinder raising depended on hydraulic pressure, the request of position precision is lower at this stage, only needs the position sensor monitor the detail position for next cycle.

By above hydraulic press working process, precise closed-loop control of large hydraulic press must have a mass of pressure, position and velocity data as the support. Therefore, a monitoring system of whole state data base on LabVIEW is significant for condition monitoring, fault diagnosis and precise closed-loop control of hydraulic press [4].

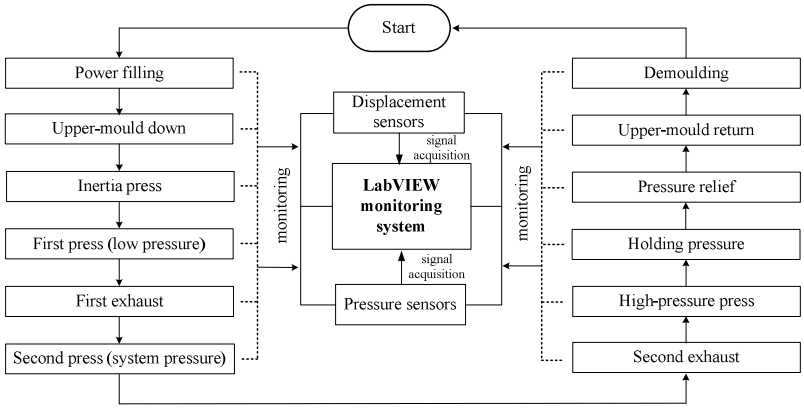

Fig. 1 The working principle of large hydraulic press

The Design of Overall Program of Monitoring System Based on LabVIEW

The overall program of monitoring system based on LabVIEW for large press is shown in Fig. 2. By analyzing the working principle, it shows that the master cylinder of hydraulic press, boosting cylinders, control valves and other components are involved in precise closed-loop control. The pressure and displacement sensors are installed to detect the key parameters of status signals in each component. Combining with hardware filtering, the data is acquired by acquisition card via signal shielded cable, then LabVIEW test software systems are installed in the industrial personal computer for testing, analysis and displaying. So we can operate the monitoring and control system with the man-machine interface in the display terminal.

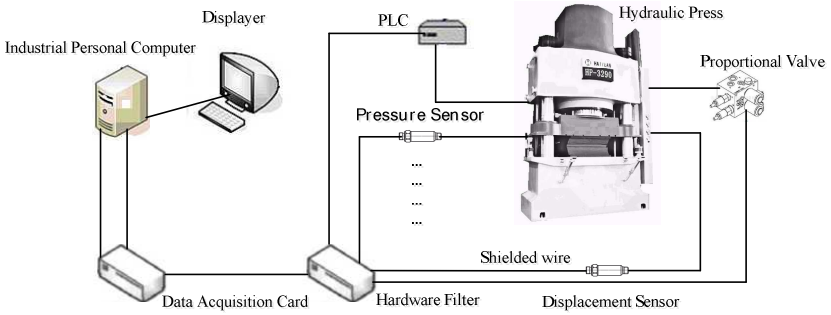

Fig. 2 The overall program of monitoring system based on LabVIEW for large hydraulic press

Hardware Design. According to the working principle and the overall program as shown in Fig. 2, the data monitoring system needed to test mainly involves the system pressure, the left displacement of upper mould, the right displacement of upper mould, the pressure in master cylinder rodless chamber (under chamber), displacement of master cylinder, proportional valve spool displacement in rod chamber(upper chamber), the proportional valve spool displacement in under chamber, command signal and other system status signals. Measured signals are mainly displacement and pressure signals, so pressure or displacement sensors can be selected. Each signal and sensor parameter is shown in Table 1. The USB high-speed data acquisition card of Advantech 4711A can be applied to data collection. Appropriate equipments are shown in Fig. 3.

Table 1 The key signals and parameters of sensors

Measured target	Measuring range in sensor	Output Signal	Measured target	Measuring range in sensor	Output Signal
system pressure	0~250bar	0~10V	displacement of boosting cylinder	0~450mm	0~10V
left displacement of upper mould	0~300mm	4~20mA	displacement of upper proportional valve spool	0~5mm (two-direct)	0~10V
right displacement of upper mould	0~300mm	4~20mA	displacement of under proportional valve spool	-5~5mm (three-direct)	-10~10V
pressure in boosting cylinder	0~400bar	0~10V	command signal	-10~10V (PLC)	-10~10V

Fig. 3 The data acquisition hardware of hydraulic press monitoring system

In the monitoring and control system of the large hydraulic press, the displacement signal of proportional valve spool in the upper chamber and under chamber is transmitted to PLC by 7 pin terminal in proportional valve amplifier. So the data acquisition card could acquire data directly via analog inputs of the PLC. The command signal of the closed-loop control system can also be transmitted from the PLC analog output terminals to data acquisition card. The selected Advantech 4711A card has 16 analog input channels, and it can achieve 8 differential voltage inputs. The left displacement of upper mould and the right displacement of upper mould signal are current signals, which can be converted to voltage signals collection through a 250Ω precision resistance. Therefore, the corresponding key parameters and data can be transmitted in a unified way of differential voltage input to the AI ports of the data acquisition card. For achieving high-quality signal acquisition, it connects sensors, PLC and data acquisition card through shielded cable and adds low-pass filters with cut-off frequency of 200Hz to each channel to eliminate noise interference. The IPC and data acquisition card could realize data acquisition, storage, display, analysis and other functions via connecting USB port [5].

The Design of Software System. Software system contains configuration management software and application development software. Configuration management software is mainly used for hardware identification and information interaction with all data acquisition cards. Application development software exploits the software base on graphical programming platform [6]. After configuring and debugging the testing system hardwares, data acquisition modes will be set through configuration management software. In this paper, we set all the channels as differential input mode, and then develop the required application software based on LabVIEW.

The software system structure and flow base on LabVIEW is shown in Fig. 4, and its primary functions include data acquisition, data saving, data analysis, real-time display and so on [7]. Firstly, all acquisition channel parameters are configured on the LabVIEW system plane of IPC base on the data in Table 1. Secondly, data acquisition begins and the data acquisition card sends the single measured by the sensor to the LabVIEW system. Then, single processing function is applied to display the data in real-time as required on the IPC, and if saving is needed, click on the save button to store data. Finally, to further detail analysis, storing data can be paged out for more precise and comprehensive analysis. The above methods can be efficiently used to realize data acquisition, storing, real-time displaying and analyzing all state data of large hydraulic press.

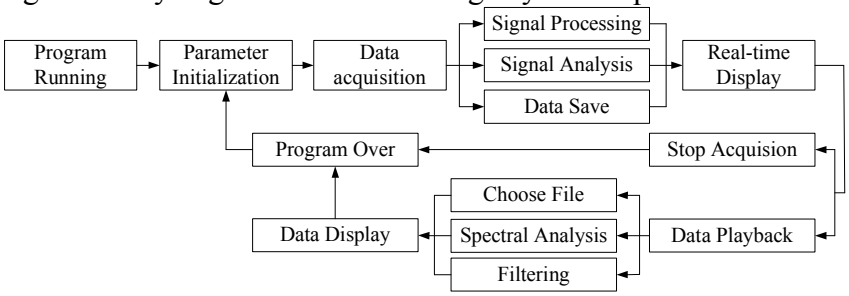

Fig. 4 The software system structure and process base on LabVIEW

In order to realize all state monitoring, the main program of software system base on LabVIEW is designed, and the front panel is shown in Fig. 5. It mainly includes setting parameters, starting acquisition, stopping acquisition, saving data, displaying data, stop and so on. Based on LabVIEW, the overall framework of main program is that the While loop structure is used to achieve the function of data acquisition and the Event structure is used to achieve the functions of setting parameters, saving data, displaying data and so on [8].

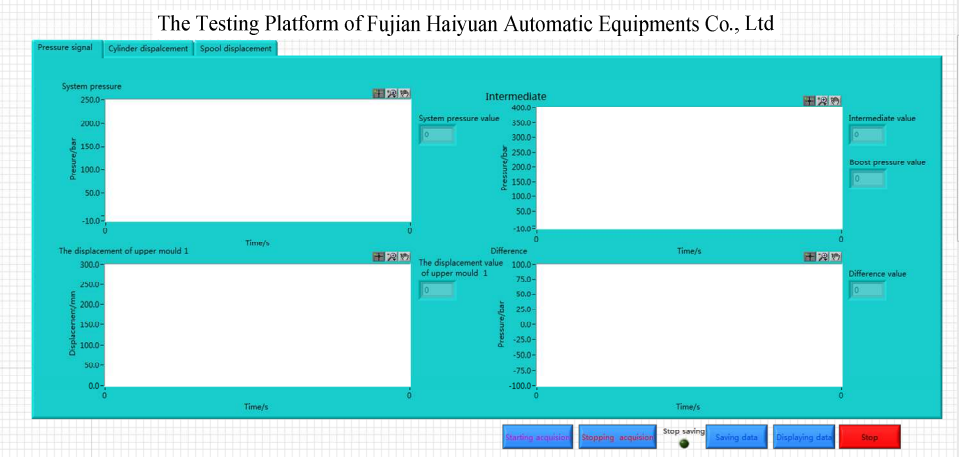

Fig. 5 The main program interface of status monitoring

A. Parameters setting. Before data acquisition, the channel parameters of acquisition card need to be firstly configured, and the front panel of subprogram used to set system parameters is shown in Fig. 6. The sampling rate in the front panel is the sum of each channel sampling rate, and the system sample rate is set to 8 kS/s. The sum of all channels is 8, from channel 0 to channel 8, and the sampling rate of each channel is set 1 kS/s, which ensures that the sum of the sampling rate in all channels is no more than 150 kS/s. The maximum count can be set up to the half of Advantech 4711A acquisition card FIFO (First in, first out), which is 512. BufferSize is the cache that user creates on the computer's memory, and it should be set the integer times of the product between the count and channel number, that is to say 4096=1×512×8. The input voltage range can be identified by each analog input channel, which is set by the code in gain list. The gain codes in all channels are set 4 in this paper, so all the input voltage ranges are ±10V.

Fig. 6 The front panel of parameters setting

B. Starting acquisition. When user chick on the button of ‘starting acquisition’ in the front panel, the program goes into the acquisition cycle and begins to read voltage value from each channel. In order to ensure that the data display and storage process will not affect the speed of reading data and avoid data loss, the producer-consumer structure is applied by the overall structure of acquisition program, whose program chart is shown in Fig. 7. After the producer cycle reads voltage value through subprogram from each channel, the data will be written into the queue. After the consumer cycle reads the data from the queue and converted them to the corresponding parameter values, the date will be displayed on front panel, and the data is stored in a temporary file by the TDMS format at the same time.

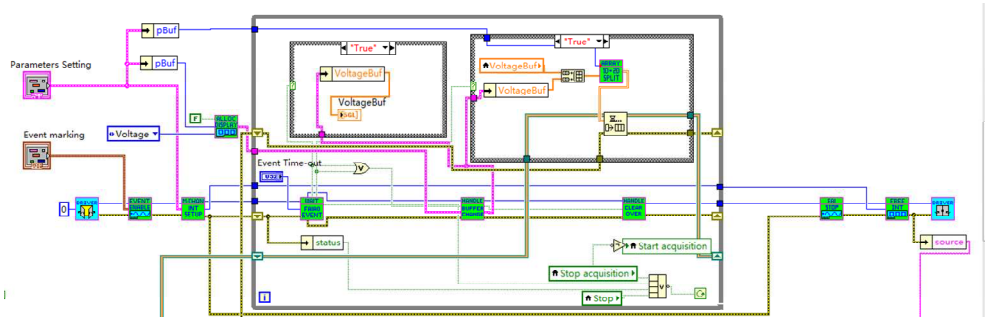

Fig. 7 The producer–consumer cycle of real-time monitoring program

C. Stopping acquisition. When user click on the button of ‘stopping acquisition’, acquisition cycle will be stopped and idle loop begins to execute.

D. Saving data. At the same time of data acquisition, data has been saved to a temporary file. If users need to save the current data, click 'Save' button on the front panel, then program executes corresponding event structure. Then the data is saved under the folder which has the same name with principal program path. Data file name is constituted with the name input by user on the front panel and current system time, and the program chart is shown in Fig. 8. If you do not need to save the current data, data in a temporary file will be overwritten when executing data acquisition next time.

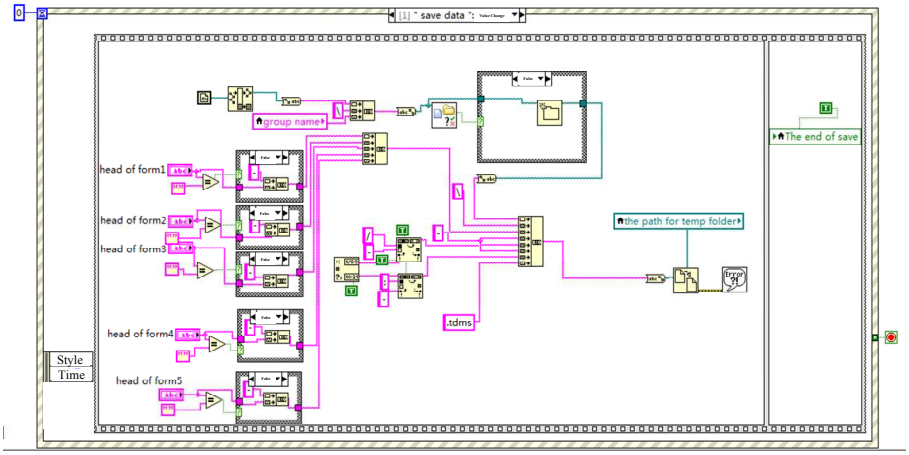

Fig. 8 The program of saving data

E. Displaying data. When the user clicks on the 'Data Display' button on the front panel, the program will execute the corresponding event and the popping subroutine front panel that displays the data is shown in Fig. 9. In the default circumstance, this subroutine has always scanned the file in the 'Test Data' folder and all the data files with suffix of '.tdms' are added to the 'Choose File' combo box for users to choose and observe. After the user selects the data file, user can check the options on the left of waveform diagram to show the corresponding curves, and similarly the name of curves on the right of waveforms diagram will be updated. In addition, users can also filter the curves, and the filtering frequency can be input by the user in the subroutine front panel. When you click 'Stop' button, the subroutine exits and the front panel is off automatically.

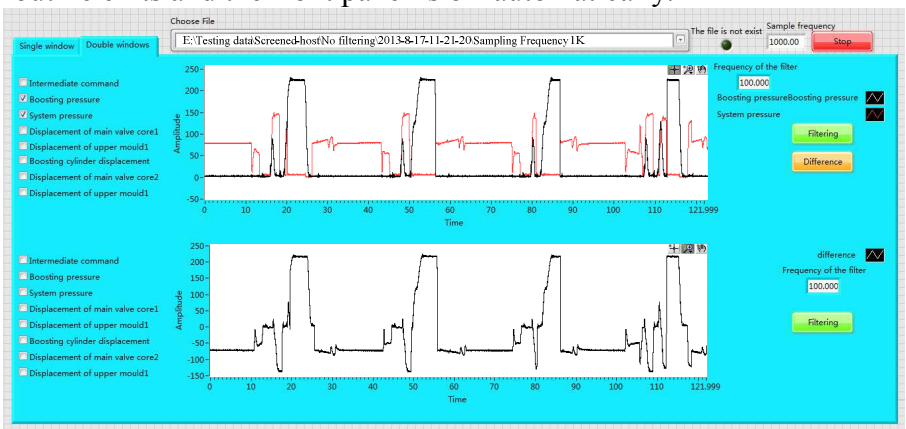

Fig. 9 The program of displaying data

F. Stop. When user click on the button of 'Stop', all applications will stop running no matter what the current operation state is.

Experiment and analyze of key parameters in large hydraulic press

The above data acquisition system based on LabVIEW is applied to monitor the working conditions in a large ceramic hydraulic press, and the data acquisition, real-time display and analysis of key parameters can be realized effectively [9]. This monitoring system can effectively acquire the status of system pressure, the pressure in master cylinder under chamber, displacement of master cylinder, proportional valve spool displacement in upper chamber, the proportional valve spool displacement in under chamber, command signal and so on. Fig. 10 and Fig. 11 respectively indicate the pressure in

master cylinder under chamber and proportional valve spool displacement in upper chamber with a certain type of ceramic hydraulic press, and all the curves contain only a single cycle.

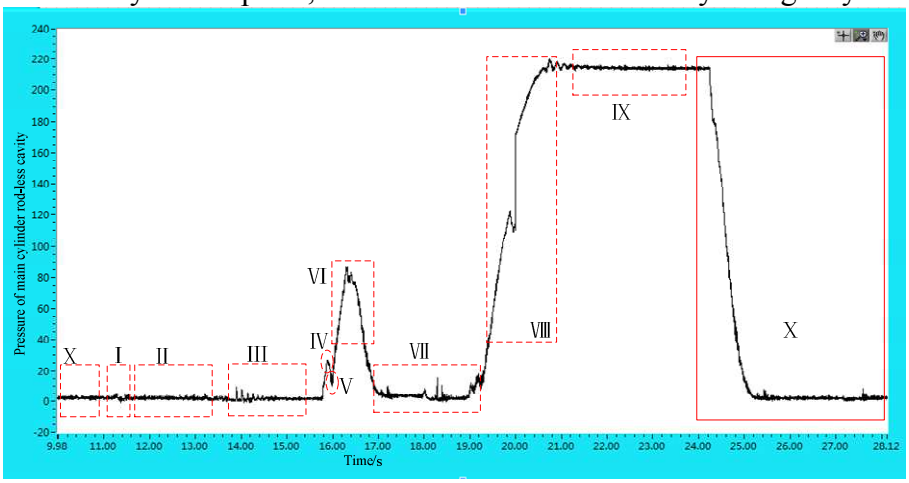

Fig. 10 The pressure curve of master cylinder in under chamber

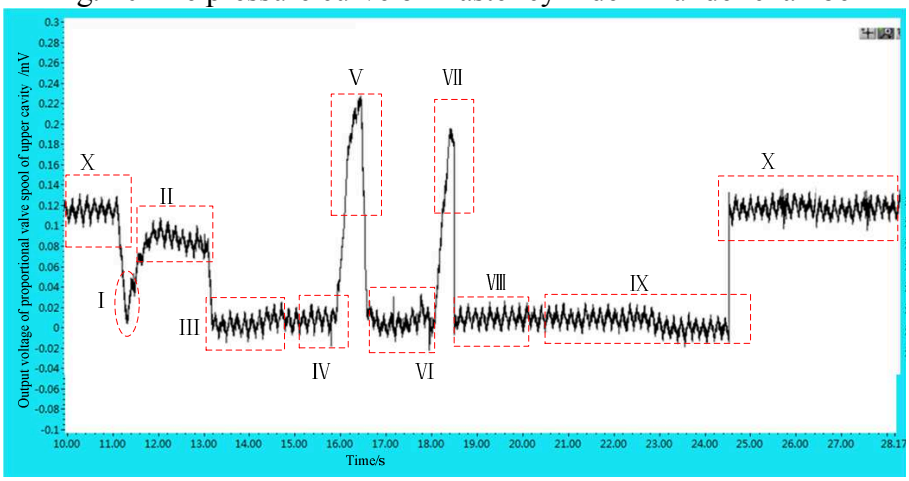

Fig. 11 The proportional valve spool displacement curve in upper chamber

The curves in Fig. 10 and Fig. 11 respectively show that the pressure of master cylinder in under chamber and the proportional valve spool displacement in upper chamber. The voltage value 0.12V in Fig. 11 represents that the three-way proportional valve is in neutral position. If the voltage value increases, the master cylinder will move up because the upper chamber of the master cylinder is imported high pressure oil. On the contrary, when the voltage value is decreased, the master cylinder will fall down because the oil in upper chamber of the master cylinder returns back to tank. So the voltage value indicates the size of the valve opening.

Firstly, the stage of the master cylinder falling down includes the fast falling stage Ⅰ and the slow falling stage Ⅱ, and at this moment the pressure in under chamber of master cylinder was low. Due to three-direct proportional controlled valve controlling oil in upper chamber to return to tank, the larger of the proportional valve spool opening, and the faster of master cylinder falling. Secondly, the press began inertial pressing stage Ⅲ and the master cylinder relayed on its dead weight for pressing. Similarly pressure of the under chamber was also low, and oil in upper chamber continues returning back to tank. Thirdly, it was the first press stage Ⅳ, and the pressure in under chamber was raised to about 25 bar. After that it would turn to the first exhaust stage Ⅴ, and in this moment the upper chamber linked with the high pressure oil would cause the main cylinder lifting a little for the first exhaust and the pressure in under chamber would reduce. Fourthly, when the first exhaust was finished, the press came into the second press stage Ⅵ, and that moment the pressure in under chamber was consistent with the system pressure, so the master cylinder was pressurized by the system pressure directly. And then the pressing process was transferred to the second exhaust stage Ⅶ, the pressure in under chamber will relief to 0 bar, and the main cylinder raised through connecting

high pressure oil with the upper chamber. Finally, booster stage Ⅷ indicates the booster cylinder pressurized the cylinder rodless chamber to the highest pressure. After the maintaining pressure stage Ⅸ and the pressure relief stage Ⅹ, the highest pressure dropped to 0bar.

Obviously, we can observe every running state of the press clearly according the above curves, and we also can deeply check the changing relationship between the states simultaneously to the pressing characteristics during the pressing process. The maintenance, upgrade and diagnosis of the large hydraulic press can be effectively achieved based on the measured data.

Conclusions

The monitoring system based on LabVIEW was designed for precise closed-loop control of large hydraulic press, and it is a method to acquire full state data of the press simply and effectively. The functions of the system include data acquisition, data saving, real-time display and process analysis and so on. The process data of the hydraulic press can be effectively recorded and saved, to lay the foundation for the establishment of a database system of the large hydraulic press.

The monitoring system can obtain the key parameters data of the pressing process and curves effectively, which can be used to analyze and correct the control system based on the data. It will improve the precision and efficiency of designed closed-loop control system and short the development cycle. The system has achieved good test and analysis results that applied in a certain type of large ceramic press, which can provide strong support for the subsequent equipment maintenance, fault diagnosis and the system upgrade.

References

[1]F. Gao, Z. W. Guo, Y. Q. Song, et al, Current development of heavy-duty manufacturing equipments, Journal of Mechanical Engineering. 19 (2010) 92-107.

[2]M. B. Jensen, D. E. Tallman, A LabVIEW-based virtual instrument for simulation and analysis of SECM approach curves, Journal of Solid State Electrochemistry. 17(2013) 2999-3003.

[3]S.M. Xiong, D.B. Bogy, Hard disk drive servo system based on field-programmable gate arrays, IEEE Transactions on Industrial Electronics. 61(2014) 4878-4884.

[4]Y. L. Zhang, B. G. Wang, H. W. Zhao, The application of LabVIEW in fault diagnosis in electro-hydraulic servo system, Chinese Journal of Scientific Instrument. S2 (2003) 256-257.

[5]Y. Tang, Z. P. Huang, L. D. Tang, et al, Experiment of constant pressure control characteristics for centrifugal pump, Transactions of the Chinese Society for Agricultural Machinery. 03 (2013) 59-63.

[6]H. F. Kong, B. B. Jiang, AMT data acquisition and analyzing system based on LabVIEW, Chinese Journal of Scientific Instrument. S1 (2006) 442-443.

[7]X. Wang, B. H. Zhang, Development of the measuring and controlling system of heat exchanger performance testing equipment based on LabVIEW, Chinese Journal of Mechanical Engineering. 04 (2009) 309-312.

[8]S. Wang, S. L. Huang, W. Zhao, Data acquisition and analysis system for a magnetic flux leakage tank floor corrosion scanner, Journal of Tsinghua University(Science and Technology). 1 (2008) 20-23.

[9]Babita, D. K. Sharma, Satish, et al, A versatile automation program using LabVIEW for low de current measurement, Journal of Scientific & Industrial Research. 73(2014) 91-94.

Advanced Materials Research Vols. 989-994 (2014) pp 3070-3074
© (2014) Trans Tech Publications, Switzerland
doi:10.4028/www.scientific.net/AMR.989-994.3070

Based on the geostress to research slope stability in the deep open pit

Qingwen Li[a], Lan qiao[b] , Lu Chen[c]

State Key laboratory of High-Efficient Mining and Safety of Metal Mines, University of Science and Technology Beijing, Beijing, 100083, China;

[a]qingwenli1118@gmail.com, [b]lanqiao612@gmail.com, [c]826686302@qq.com

Keywords: Geostress, Excavation, Numerical Simulation, Slope Stability, Deep Open Pit.

Abstract. Further excavation is extraordinary significant to the sustainable development of mine. For the rock slope, three-dimensional geostress in the deep mining area are presented complex and high, which were caused by previous excavation. Also, it is important to obtain the accurate geostress in mining area, which is the necessary precondition for determining the remaining ore mining scheme and the slope stability. In this paper, based on the in-situ geostress monitoring date, a 3D numerical model alongside the physical dimensions was built in finite element software FLAC3D, to accept the constitutive parameter and monitoring data, to predict the 3D stress and displacement distributions and detail failure information, to estimate stability of mining area.

Introduction

With the fast development of the mining technique, also, further excavation is extraordinary significant to the sustainable development of mine. In china, there are a huge number of mines adopted the Open-pit mining method [1]. And as long as the enlarging production scale and the mining excavation depth, the high and steep slope, whose stability is important and difficult manageable, must be increasing continually [2]. According to the statistics, in china, from 15% to 20% high and steep slopes are the unstable slopes or potential unstable slopes [3]. Hence, it is extremely urgent problem to be researched on the slope stability in the deep open pit. Although, many scholars have done huge efforts on the excavation and slope stability all the world. Lilly and Li (2000) estimated the excavation reliability by using the displacement modeling [4]; Sheng et.al., (2002) estimated the excavation disturbed zone in the permanent shiplock slopes [5]; Li et.al., (2007) used a Face-to-Face discrete element method to analyze the critical excavation depth for a jointed rock slope [6]; Cheng et.al., (2012) adopted the CFS theory to analyze the steep excavation slope failure [7]; Guo and Cheng (2013) had a consideration on group excavation engineering [8]; Guo et.al., (2013) did the research on the deformation stability of soft rock slope under excavation based on FLAC3D [9]; Hsieh et.al., (2013) used the three-dimensional numerical analysis of deep excavations with cross walls [10]; Wang et.al., (2014) did the research on the loess landslide induced by excavation and rainfall[11]. For the deep and steep rock slope in the metal mine, as the increasing of depth, the geostress are becoming huge and complex, which will generate a remarkable impact on the slope stability. In this paper, based on the in-situ geostress monitoring date, a 3D numerical modeling was built in finite element software FLAC3D alongside the real size of open air slope, to accept the constitutive parameter and monitoring data, to predict the 3D stress and displacement distributions, to determine the sequence of excavation and estimate the stability of mining area.

Engineering Background and In-situ Geostress

Engineering Background. In this paper, Shuichang open pit iron mine was chosen as the engineering background, it is a large typical magnet ore deposit with metamorphic rock, and locate in Qianan city, Heibei province. Now, the mining scale is the 11 million tons per year. And the elevation of stope bottom is -136.38m at present, and it will be excavated to the level of -440m in further. Based

on the real engineering situation, the particular models were built in software FLAC3D as shown in figure 1 and 2.

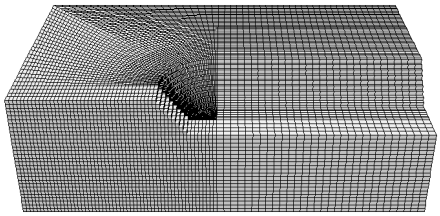

Fig. 1 The elevation of bottom with -136m

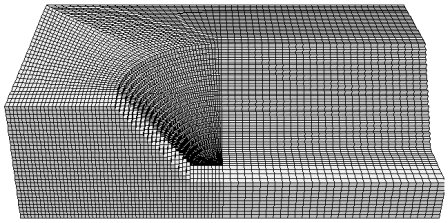

Fig. 2 The elevation of bottom with -440m

In the model, X axis was the horizontal direction along the long edge, and along the short edge direction, the horizontal direction was Y axis, The Z axis was vertical direction. And the length, width and height are respectively2900m, 1400m and 900m by according to the real size of the open pit. The finite element mesh consists of 14541 nodes and 138000 elements.

Constitutive parameter. Form the top to the bottom, there are 5 layers, which are artificial miscellaneous filled soil, sandstone, mudstone, magnetite and mixed granite, whose constitutive parameters were obtained from the lab test, as shown in table 1.

Table 1 Particular constitutive parameters of rock

Layer	Density （kg/m3）	E(MPa)	υ	bulk modulus (Mpa)	shear modulus (Mpa)	friction angle （°）	cohesion (Mpa)
Filled soil	2000	20	0.300	16.7	7.69	18	0.13
Sandstone	2570	9512	0.26	6605	3774	39	0.485
Mudstone	2510	1650	0.36	1964	610	30	0.31
Magnetite	3200	12500	0.23	7720	5080	40	0.917
Granite	2604	7130	0.24	4570	2880	49	0.646

In-stiu geostress. Based on the in-situ monitoring geostress data, after analysis and calculation, the relationship between the geostress and depth was shown from formula (1) to (3).

(a) The maximum horizontal geostress,

$$\sigma_{h.\max} = 0.93 + 0.0438H \quad (MPa) \tag{1}$$

(b) The minimum horizontal geostress,

$$\sigma_{h.\min} = 0.61 + 0.0269H \quad (MPa) \tag{2}$$

(c) The vertical geostress,

$$\sigma_v = 0.12 + 0.0259H \quad (MPa) \tag{3}$$

Where, H is the depth (m).

Numerical Simulation

Constitutive Model. According to the characteristics of each rock layer, in this simulation, the Mohr-Coulomb failure criterion with tension cut off were employed as constitutive model. It was expressed as the well-known formula below [12],

$$\sigma_1 \geq \sigma_2 \geq \sigma_3 \tag{4}$$

where, $\sigma_1, \sigma_2, \sigma_3$ respectively are the major principal stress of the elements, And the Mohr-Coulomb criterion can be represented in the plane (σ_1, σ_3), the failure envelope $f(\sigma_1, \sigma_3) = 0$, so $f^s = 0$ with

$$f^s = \sigma_3 - \sigma_1 N_\phi + 2c\sqrt{N_\phi} \tag{5}$$

A tension failure criterion of from $f^t = 0$ with

$$f^t = \sigma_1 - \sigma^t \tag{6}$$

Where ϕ is the friction angle, c is the cohesion, σ^t is the tensile strength, and

$$N_\phi = \frac{1+\sin\phi}{1-\sin\phi} \tag{7}$$

So the potential function is described by means of two functions, Q^s is the shear potential function, is

$$Q^s = \sigma_3 - \sigma_1 N_\psi \tag{8}$$

Where ψ is dilation angle, and $N_\psi = \frac{1+\sin\psi}{1-\sin\psi}$.

Q^t is the tensile potential function, is

$$Q^t = -\sigma_1 \tag{9}$$

Excavation Scheme. In order to simulate the real excavating form, in this model, the excavation with 10 steps was carried out. The height of each step was 60m, the particular form of excavating steps as depicted in figure 3

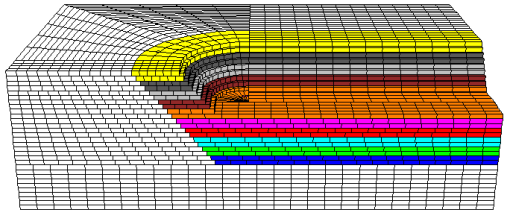

Fig. 3 Particular form of excavating steps

Simulation Results. After simulation, the results of the X, Y, Z displacement were illustrated in figure from 4 to 6, and the typical profile of displacement as depicted in figure 7

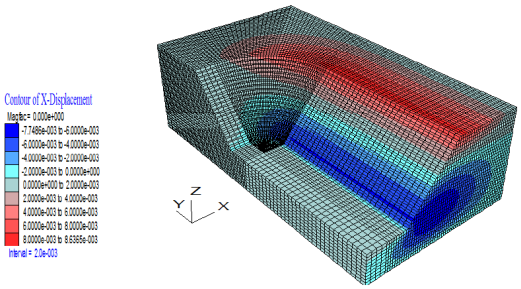

Fig. 4 3D X-displacement contour

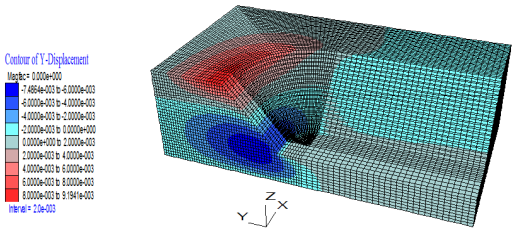

Fig. 5 3D Y-displacement contour

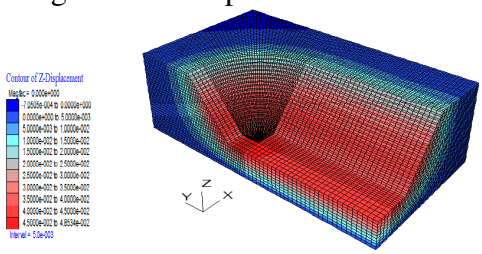

Fig. 6 3D Y- displacement contour

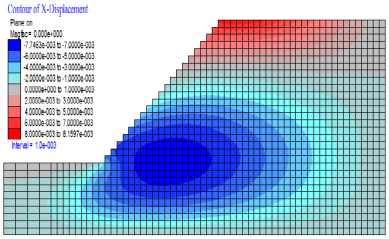

Fig. 7 Y=-800m typical profile contour

From the figure 4 to 6, the maximum positive (direction of pointing to the stope) horizontal displacement after excavation, which was caused by excavating to lead the stress springback and redistribution, appeared at the foot of slope. And the negative (reverse direction of pointing to the stope) horizontal displacement, due to weak strength of miscellaneous filled soil, occurred at the top of slope. And the vertical displacements had relationship with cover depth, due to the weight of the covered rock mass.

For the principal stress, the particular contour and typical profile contour were indicated in figure 8 to 9.

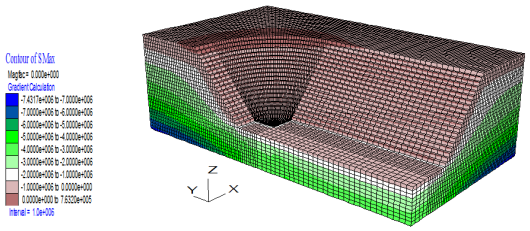

Fig. 8 The maximum principal stress contour

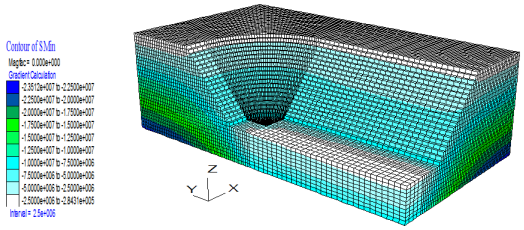

Fig. 9 The minimum principal stress contour

As shown in figure 8, the maximum principal stress was following the basic law, which was increasing from top to bottom with gradient. The maximum principal stress on the surface of slope was zero, due to the free boundary. Also, there was a small tensile stress zone with the 100m width and 50m depth on the top of slope at the corner of model, the value was 0.36 Mpa, other part was compressive stress zone. For the minimum principal stress as shown in figure 9, it also had the same law with the maximum principal stress, except, there is not tensile stress zone all over the slope model.

In order to obtain the detail information of the damage, typical profiles of plastic failure zone were necessary, which were extracted from the simulation model, as shown in figure 14 and 15.

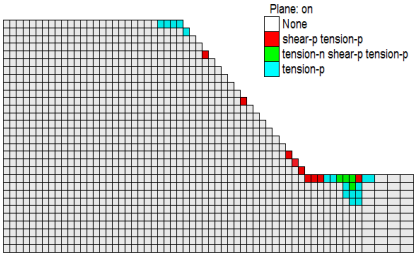

Fig. 14 Typical profile at the corner

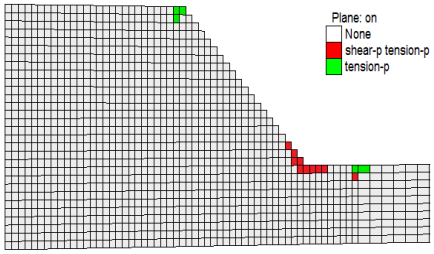

Fig. 15 Typical profile at X=-150m

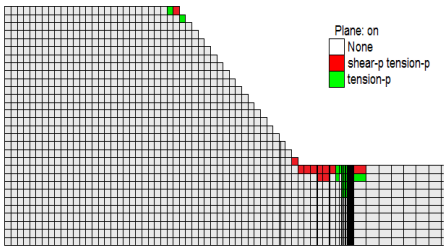

Fig. 14 Typical profile at X=-110m

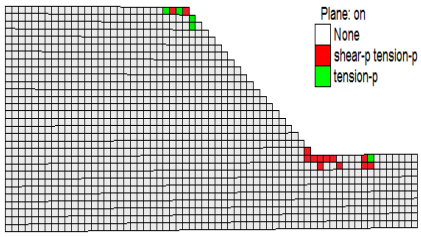

Fig. 15 Typical profile at X=-70m

As shown in the above typical profile, because, the larger tensile stress and weaker strength of the soil, there was a tension failure zone with 50m to100m width on the top of the slope closing to slope surface. And there was a shear damage zone at the foot of slope, due to the excavation, to lead the geostress was redistributed, the range was about 200m width and 50m depth.

Summary

(1) In order to analyze the stabilty of slope, it is important to monitor the accurate geostress in mining area, which are the necessary precondition for determining the remaining ore mining scheme and the slope stability.

(2) Based on the displacement analysis, the miscellaneous filled soil and the sandstone at the location of top slope closing to slope surface, should be support by a reinforcement measure. And at the foot of slope, there also had some rock falls off phenomenon, which was caused by the stress redistribution and springback.

(3) As shown in foregoing contour of stress, the maximum principal stress and the minimum principal stress both were following the basic law, which was diminishing form bottom to top. The stress on the surface of slope was zero, due to the free boundary. And there was a small tensile stress zone in the superficial layer of slope, which would lead to some partial tensile failure, the force would be easy to cause the rock falling off, hence, it is necessary to pay attention to fallen stones which would threaten

the safety of people and equipment working under this area but this tensile could not produce enough impact on the stability of the whole slope.
(4) Based on the foregoing analysis of typical profile of plastic failure zone, in detail, there also was a tension failure zone with the width 100m scope on the top of the slope in every figure. And there was a shear damage zone at the foot of slope with 200m width, which given a detailed analysis of the slope stability.

References

[1] Y.K., Sun, ZH.F., Yang, E.B., Ding, The stability of slope in China open pit [M], China Science and Technology Press, Beijing, 1999.
[2] J.P., Chai, L.Q., Zhu, D.W., Zhang, The analysis on the stability of slope in Heishan iron mine [J], Express Information of Mining Industry, 2008, 8, 74-76.
[3] T.A., Yu, X.G., Dai, The analysis of safety factors on the stability of slope in open pit [J], Mining Safety & Environmental Protection, 2008, 35(1), 73-76.
[4] P.A., Lilly, J., Li, Estimating excavation reliability from displacement modelling [J], International Journal of Rock Mechanics & Mining Sciences 37 (2000) 1261-1265.
[5] Q., Sheng, Z.Q., Yue, C.F., Lee, L.G., Tham, H., Zhou. Estimating the excavation disturbed zone in the permanent shiplock slopes of the Three Gorges Project, China [J]. International Journal of Rock Mechanics & Mining Sciences 39 (2002) 165–184.
[6] S.H., Li, J.G., Wang, B.S., Liu, D.P., Dong, Analysis of Critical Excavation Depth for a Jointed Rock Slope Using a Face-to-Face Discrete Element Method [J]. Rock Mech. Rock Engng. (2007) 40 (4), 331–348.
[7] H.H., Cheng, H., Zhang, B.J., Zhu, Y.L., Shi, Finite element analysis of steep excavation slope failure by CFS theory [J], Earthq Sci (2012)25: 177–185.
[8] L.Q., Guo, Y.G., Cheng, Consideration on Group Excavation Engineering [J]. Applied Mechanics and Materials Vols. 256-259 (2013) pp 315-319.
[9] F., Guo, W., Gu, J.J., Tang, M.H., Murong, Research on Deformation Stability of Soft Rock Slope under Excavation Based on FLAC3D [J], Applied Mechanics and Materials Vols. 275-277 (2013) pp 290-294.
[10] P.G., Hsieh, CH.Y., Ou, Y.L., Lin, Three-dimensional numerical analysis of deep excavations with cross walls [J], Acta Geotechnica (2013) 8:33–48.
[11] J.J., Wang, Y., Liang, H.P., Zhang, Y., Wu, X., Lin, A loess landslide induced by excavation and rainfall [J]. Landslides (2014) 11:141–152.
[12] Itasca, 2009, FLAC3D V4.0, Fast Lagrangian Analysis of Continua in 3 Dimensions, User's Guide. Itasca Consulting Group, Minneapolis, Minnesota 438pp.

Advanced Materials Research Vols. 989-994 (2014) pp 3075-3078
© (2014) Trans Tech Publications, Switzerland
doi:10.4028/www.scientific.net/AMR.989-994.3075

Improvements on structural static pushover analysis method in High-rise building structure

Miao Yu [1, a], Zhihong Dai[2, b] and Guijuan Hu[2, c]

[1,2] Guangxi University of Finance & Economics, Nanning 530003, China;

[3] Guangxi Polytechnic of Construction, Nanning 530003, China.

[a] yumiao-211@163.com, [b]snowgx@qq.com, [c]hgj1973@sina.com

Keywords: high-rise building, static pushover, improved capacity spectrum method.

Abstract. In this paper, a new analysis model to assess the structure seismic capability is established, using improved capacity spectrum method. The model can solve the problem of many unknown and big computation workload in the process of conventional Pushover analysis. Conventional Pushover is very complex when use in the analysis of structure dynamic problem and nonlinear problem, the new model can solve these problem.

Introduction

Static elasto-plastic seismic analysis of Pushover method to evaluation of the structure of the anti-seismic ability, mainly have the following steps: Firstly make the base shear-top floor displacement curve and translated into power spectrum; then determine the demand spectrum under the action of earthquake, according to the seismic intensity, site classification, structure period and damping ratio; the capacity spectrum and demand spectrum will be drawing in the same coordinate system, and get the intersection point, which called performance point; at last the displacement of performance point is transfer into the target displacement of structure, and comparing with the permissible value. So we can evaluate aseismic deformation capacity of structure.

Basic principles

Spline discretization. Discrete the plane projection of the structure under the bidirectional spline node, using spline basis function and the orthogonal polynomial linear combination structure to product the overall displacement field, the displacement function is:

$$
\begin{aligned}
u &= \sum_{m=1}^{R}\sum_{i=0}^{N}\sum_{j=0}^{M}\phi_i(x)\psi_j(y)a_{ijm}X_m(z) = \sum_{m=1}^{R}\left[\phi(x)\right]\otimes\left[\psi(y)\right]\left\{a\right\}_m X_m(z)\\
v &= \sum_{m=1}^{R}\sum_{i=0}^{N}\sum_{j=0}^{M}\phi_i(x)\psi_j(y)b_{ijm}Y_m(z) = \sum_{m=1}^{R}\left[\phi(x)\right]\otimes\left[\psi(y)\right]\left\{b\right\}_m Y_m(z)\\
w &= \sum_{m=1}^{R}\sum_{i=0}^{N}\sum_{j=0}^{M}\phi_i(x)\psi_j(y)c_{ijm}H_m(z) = \sum_{m=1}^{R}\left[\phi(x)\right]\otimes\left[\psi(y)\right]\left\{c\right\}_m H_m(z)\\
\theta_x &= \sum_{m=1}^{R}\sum_{i=0}^{N}\sum_{j=0}^{M}\phi_i(x)\psi_j(y)d_{ijm}\Theta_m(z) = \sum_{m=1}^{R}\left[\phi(x)\right]\otimes\left[\psi(y)\right]\left\{d\right\}_m \Theta_m(z)\\
\theta_y &= \sum_{m=1}^{R}\sum_{i=0}^{N}\sum_{j=0}^{M}\phi_i(x)\psi_j(y)e_{ijm}S_m(z) = \sum_{m=1}^{R}\left[\phi(x)\right]\otimes\left[\psi(y)\right]\left\{e\right\}_m S_m(z)\\
\theta_z &= \sum_{m=1}^{R}\sum_{i=0}^{N}\sum_{j=0}^{M}\phi_i(x)\psi_j(y)f_{ijm}T_m(z) = \sum_{m=1}^{R}\left[\phi(x)\right]\otimes\left[\psi(y)\right]\left\{f\right\}_m T_m(z)
\end{aligned}
\tag{1}
$$

$\phi_i(x)$, $\psi_j(y)$ is the discrete spline function of x,y direction respectively, $X_m(z)$, $Y_m(z)$, $H_m(z)$, $\Theta_m(z)$, $S_m(z)$ and $T_m(z)$ is the orthogonal polynomial of structure along the height.

$$X_m(z) = \sum_{n=1}^{m} (-1)^{n-1} \frac{(m+n)!}{(m-n)!(n+1)!(n-1)!} \left(\frac{z}{H}\right)^n$$
$$Y_m(z) = H_m(z) = \Theta_m(z) = S_m(z) = T_m(z) = X_m(z) \tag{2}$$

Type (1) written in matrix :

$$\{V\} = [N]\{\delta\} \tag{3}$$

The dynamic equations of structures. The whole structure is divided into p unit, total potential energy functional for the structure is:

$$\Pi = \sum_{e=1}^{p} \Pi_e = \sum_{e=1}^{p} \frac{1}{2} \{V\}^{eT} [k]^e \{V\}^e - \{V\}^{eT} \{f\}^e - [\mathrm{c}]^e \{\dot{V}\}^e - [\mathrm{m}]^e \{\ddot{V}\}^e \tag{4}$$

Formula(3) into (4):

$$\Pi = \frac{1}{2} \{\delta\}^T [K] \{\delta\} - \{\delta\}^T \{F\} - [C] \{\dot{\delta}\} - [M] \{\ddot{\delta}\} \tag{5}$$

$[K]$ is the total stiffness matrix, $[M]$ is the total mass matrix, $[C]$ is the total damping matrix, $\{F\}$ is The total load vector:

$$[K] = \sum_{e=1}^{p} [K]^e \quad \{F\} = \sum_{e=1}^{p} \{F\}^e \quad [M] = \sum_{e=1}^{p} [M]^e \quad [C] = \sum_{e=1}^{p} [C]^e$$
$$[K]^e = [N]_e^T [T]^{eT} [k]^e [T]^e [N]_e \quad [M]^e = [N]_e^T [T]^{eT} [m]^e [T]^e [N]_e \tag{6}$$
$$[C]^e = [N]_e^T [T]^{eT} [c]^e [T]^e [N]_e \quad \{F\}^e = [N]_e^T [T]^{eT} \{f\}^e$$

Using the Hamilton variational principle, The variation of the total potential energy functional (5) , and have the spline discretization dynamic equation of high-rise hybrid building structure system:

$$\mathbf{M}\ddot{\mathbf{X}} + \mathbf{C}\dot{\mathbf{X}} + \mathbf{K}\mathbf{X} = F(t) \tag{8}$$

Improved capacity spectrum method. Using general capacity spectrum method [1, 2] to calculate the target displacement needs to calculate and adjusted demand spectrum according to different equivalent damping values. The convergence performance is poor. Improved capacity spectrum method use elastic-plastic response spectrum as the earthquake demand spectrum. Take superposition calculation for different ductility coefficient of elastic-plastic response spectrum and the structure of power spectrum, and determine the structure of the target displacement. The results have good precision. Principle see paper [3,4].

Examples

As shown in Fig. 1, a steel frame - shear wall hybrid structure, story height 5m, 5 layers. Size of the rectangle steel tube columns is 400mm×400mm, size of beam is 450 mm×200 mm×8 mm×14 mm, thickness of shear wall is 200mm, floor is 100mm concrete slab. Each beam is under vertical load by 10kN/m. Design seismic intensity of 7 degrees, site for the class II, classification of design earthquake1. Analyzed the seismic performance of structures, and compared with the results of finite element analysis software MIDAS/GEN.

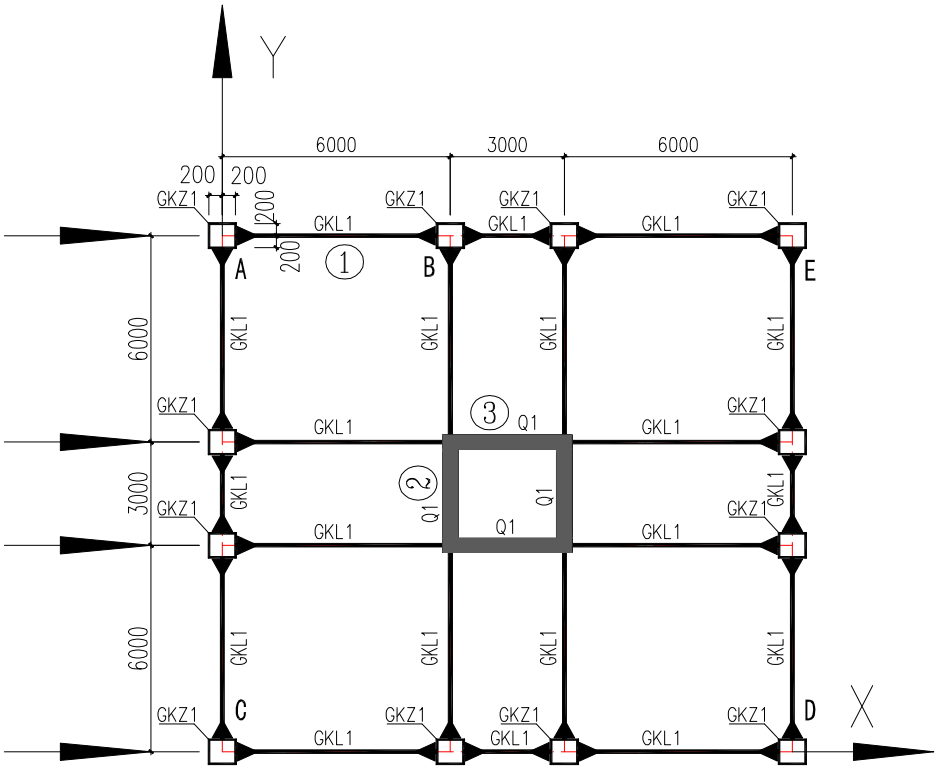

Fig. 1 The layout plane of spatial frame-shear wall structure

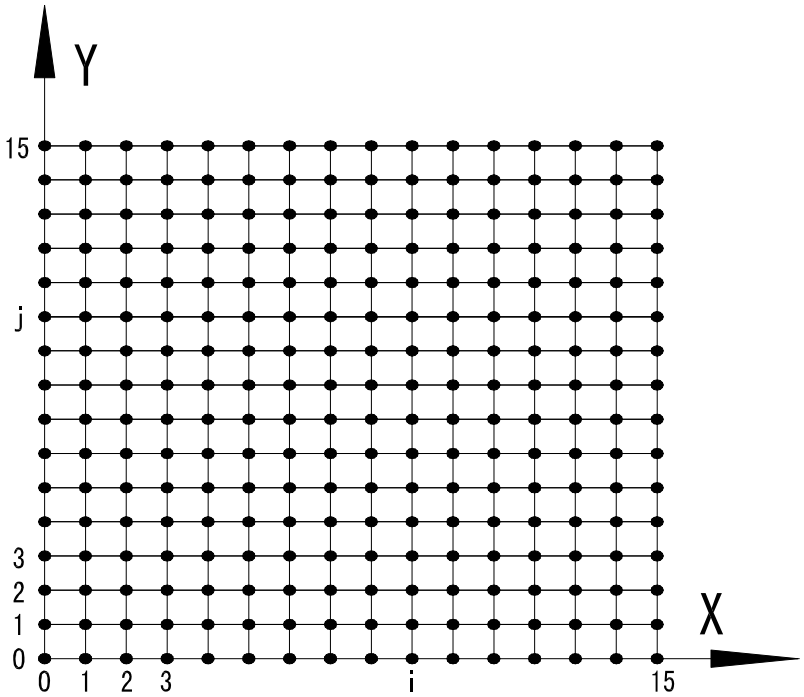

Fig. 2 Spline discrete planar graph

In this paper, discrete the structure by 1m finite element mesh (FIG.2), convergent series R = 5. Based on the first level of vibration mode loading method [5,6], The direction of vibration mode is according to the horizontal force loading direction, using inverted triangle loading mode. Get the displacement and shear force of structure(Table.1).

Table 1 Displacement and shear force of the first vibration mode

Observation Point	The first vibration mode	
	MIDAS	New method
Displacement（mm）	48.21	47.84
shear force（KN）	1663	1785

Conclusion

The improved pushover analysis method introduced in this paper considered the influence of high modes when choose the load mode and target displacement. When structure into elastic-plastic state, number of unknown quantity given no increase, do not need to enlarge stiffness matrix, and the total stiffness matrix form is uncomplicated. Using the overall displacement field function can reflect the whole failure process of the structure better. It can be seen from the results the example that the new method is feasible.

Acknowledgements

Project supported by Guangxi Education Department Science Research Subject (Grant No.2013LX137), and Guangxi University of Finance & Economics Subject (Grant No: 2012C04) for this work are gratefully acknowledged, and Project supported by Guangxi Education Department (No.2013YB312).

References

[1] Zhao Zhenwei, Application of pushover analysis on the actual engineering structure [D].XiAn: Xi'an University of Architecture and Technology,2010.
[2] Wang Tangrui. Design and pushover application on the structure [D] WuHan: Wuhan University of Technology, 2011.
[3] Chopra A, P Goel. Capacity-Demand-Diagram Method for Estimating Seismic Deformation of Inelastic Structures [R].University of California, Berkeley.in Report No. PEER -1999 /02.1999:
[4] Men Jinjie. Theory and methods of performance based seismic design for irregular reinforced concerte frame structure [D]. XiAn: Xi'an University of Architecture and Technology,2007.
[5] Zhu Minna, Wang Sheliang, Hu Zicheng. Review of lateral load pattern used in pushover analysis[J]. Shanxi architecture, 2007:33(33)11-12.
[6] Hou Shuang, Ou Jinping. A study of load pattern selection of pushover analysis and influence of higher modes [J]. Earthquake engineering and engineering vibration, 2004:24(3)89-97.

Advanced Materials Research Vols. 989-994 (2014) pp 3079-3083
© (2014) Trans Tech Publications, Switzerland
doi:10.4028/www.scientific.net/AMR.989-994.3079

Dynamics Analysis of Manipulator in the Hot Line

Dandan Zhang

College of Mechanical Engineering, Inner Mongolia University for the Nationalities, TongLiao 028000, China

Wangzai8402@163.com

Keywords: high-voltage transmission line, manipulator, dynamics analysis

Abstract. The high voltage transmission lines exposed for a long time are often broken down, thus, The manipulator arm of robot in the hot line was designed, The design is reasonable through kinematical analysis. First, make sure of the connecting rod coordinates and the connecting rod's D-H parameters. Matlab was used to draw 3D model of manipulator. Use functions in the Robotics Toolbox to solve kinematics analysis.

Introduction

Currently the length of EHV line is more than 230,000 kilometers. For the power sector high-voltage transmission lines, towers and its dependencies require regular maintenance, to ensure safe and efficient operation of high voltage transmission lines. Research on inspection robot starts later in our country than abroad.[1] [2] There are mainly Shenyang Institute of Automation, Wuhan University, Inner Mongolia University and other national research units in the field to carry out the research. The high-voltage transmission line maintenance robot which Robotics Institute, Inner Mongolia University for Nationalities developed can solve the problem of high-voltage transmission line maintenance well.

Based on the above, we proposed the studies of high-voltage special operations robot [3]. 500KV six-split transmission lines are usually using six LGJ-240.30 ACSR per phase with tower spanning between 400 ~ 1300m and wire slope <45 °. The robot not only can walk along the EHV transmission lines autonomously with a certain speed, but also intelligently stride across obstacles, which can detect towers, wires, etc by portable detection equipment and sent back the signal to the base station. High-pressure special operations manipulator plays an important role in the patrol line repair process for high-pressure special operations robot [4]. It is focused on the study of dynamic analysis for high-pressure special operations manipulator in the paper.

Analysis on the kinematics modeling of high-voltage transmission line maintenance manipulator

In the program high-pressure special operations manipulator is a more complex multi-drive space mechanism and a multi-variable nonlinear system. The kinematic equations used to describe them is necessarily complex and large. To derive these equations needs heavy workload and it can be error prone. Mathematical models which are created using a computer can be easily to solve these problems. When the constituting of mechanism make some changes, you just need to change some parameters. All the joints are rotational joints. The structural parameters and parameters of joint movement between the lever in manipulator model are shown in Figure 1.

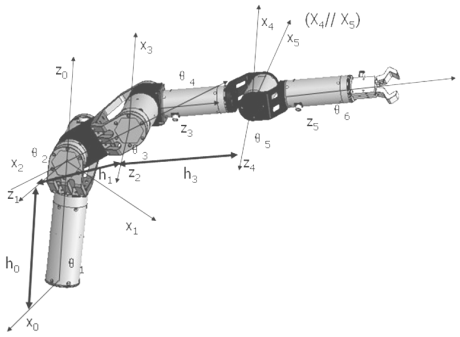

Fig.1 Arm structure mechanical model

1.1 link parameters of maintenance manipulator with D-H transformation

A coordinate system is established. The relationship between the two coordinate systems can be determined by four parameters hi, di, αi, θi from Figure 1.

hi — Along xi axis, the public perpendicular length from zi axis to zi+1 axis, which is called the link length.

αi — Around xi-1 axis, the angle form zi axis to zi+1 axis, which is called the twist angle.

di — Along zi axis，the length form xi-1 axis to xi axis, which is called offset distance or joint displacement.

θi — Around zi-1 axis, the angle from xi-1 axis to xi axis, which is called joint angle or deflection angle.

All the joints of robotic arm are rotated joints which are rotated around the Z axis. The joint angle θi is variable, while hi, di, αi are constant. structure parameters d, h, and the joint variables of the robotic arm are shown in Table

1.2 kinematics equation of high-voltage transmission line maintenance manipulator

Relative position and attitude between the coordinate system of each link is described with the D-H method. The homogeneous transformation to describe a relative relationship with a link to next link is called matrix A. In fact, a matrix A is the homogeneous transformation to describe the relative translational and rotational between coordinates of link. If A1 represents position and attitude from the first link to the base line and A2 represents relative position and the attitude from the second link to the first link. Then the position and posture of the second link in the base system is given by the multiplication of following matrices: $T_2 = A_1 A_2$. Similarly, if A3 represents relative position and the attitude from the third link to the second link, there are $T_3 = A_1 A_2 A_3$. The multiplication of these matrices is known as T matrix. For six degrees of freedom manipulator, there is the following matrix $T_6 = A_1 A_2 A_3 A_4 A_5 A_6$. expresses the kinematic equations between posture and joint variables of the end of link.

1.3 kinematic analysis of manipulator with Robotics Toolbox

Using Matlab Robotics Toolbox modules build a model of three-dimensional manipulator movement. we need to build motion parameters of each joint, and then build the entire manipulator object through a combination of joints [5] [6]. Building a complete manipulator objects means that binding DH parameters, kinematics, joint quality, Coulomb friction, viscous friction and gear ratio, using Matlab Robotic toolbox to build a three-dimensional model of manipulator motion. It needs to use the commands such as link, robot, plot in the Robotic toolbox. For example, we define a base coordinate origin of six degrees of freedom manipulator model, named "Robot-v1".

In practice, the key to control mechanical arm is the inverse position equation, geometric parameters of mechanical arm rod is known, given a specific gesture at the end point, the values of the variables of joint. The inverse kinematics problem can also use the Matlab toolbox in robotics toolbox q = ikine (robot, T) solution. T for the end effector poses matrix, mechanical arm for the 3D model of robot, Q as the variable parameters of each joint values.

The mechanical arm is in a reset state, the definition of each joint variable parameters for the q=[0 0 0 0 0 0], T=fkine (robot, q) positive solution, can get the end effector T at this time.

```
T =
1.0000         0         0    3.0000
     0    0.0000   -1.0000         0
     0    1.0000    0.0000         0
     0         0         0    1.0000
```

The end effector position in space coordinates is (3, 0, 0 for). Then the manipulator inverse solution, Q =ikine (robot, T), each joint parameter q:

q = 0 0 0 0 0 0.

The forward kinematics analysis:

Displacement given by bar and the geometrical parameters of the joints, solving the end effect coordinates relative to the base coordinate position. The forward kinematics problem can use the matlab function T = fkine (robot, q) solution, robot manipulator D-H model. Q is homogeneous transformation matrix pose of the end effecter given, if q is a vector, homogeneous transformation matrix fkine returns the tail end of the connecting rod, and if the q is a matrix will be used as the state vector of a joint, then fkine returns a matrix. For example: set the joint coordinate q = [-pi/4 00 -pi/4 0 0]; it can be used to solve by forward kinematics of fkine. With the trajectory of end joint as an example, Figure 2 is its trajectory.

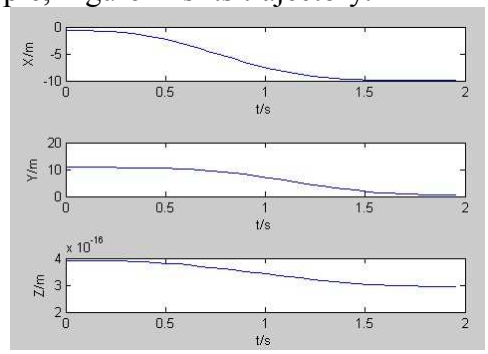

Fig.2 The track of the end joint

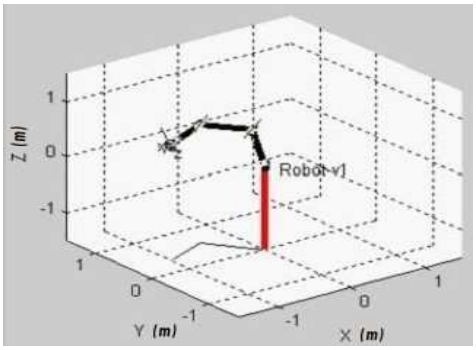

Fig.3 End joint simulation diagram

Inverse kinematics analysis:

Similarly, high pressure special robot manipulator inverse kinematics problem can also use the Matlab toolbox of robotics function in the toolbox q = ikine (robot, T) solution. T given above is 18.1362 1.0607 -0.6113 18.8496 18.9216 -32.2013.

Thus by homogeneous transformation matrix for each joint variable to get the value of . Figure 3 is the end joint simulation diagram.

Through the kinematics of manipulator is analyzed, fully demonstrated the high pressure special robot arm movement can meet the usual free telescopic movement, which verifies the rationality of design parameters of the mechanical arm, and the arm after the three joint motion can make the end joints with different attitude.

2 motion control analysis of maintenance manipulator

2.1 introduce of remote control interface

Combined with Robotics Toolbox in MATLAB plug, Simulink, GUIDE, a visual interface man-machine interface is produced. It mainly consists of three parts: a control operation area, workspace diagram, 3D operating status of manipulator .

Manipulator moves in a trajectory of a straight line. Control operating area can set the sampling interval time. The size of the interval time determines the linear distance of manipulator operation. The current space state parameter of the manipulator can be stored in order to restore the manipulator gesture when it runs next time. The data of each sampling time interval points of each joint can be stored in a document which is self-named to help user call in the controller. Serial operating area can set the parameters of the control interface and controller communication. And

then through downloading computer serial port emulation parameters of the six joints to the controller, it controls manipulator to make corresponding action.

During operation manipulator, by way of video detection, we can artificially predict the position of the target point and input the spatial position where the end of the manipulator will reach in the window, and then it moves to the target position by the manipulator trajectory.

2.2 trajectory control of high-voltage transmission line maintenance manipulator

Using Robotics Toolbox of MATLAB plugin a motion analysis on manipulator is made to build a manipulator motion trajectory control chart.

From Figure 4, we can see that by solving equations of motion with the three manually input position information in1, in2, in3 to the motion controller,, the value of the rotational angle of each joint is obtained. The variables are stored in the six angles which can be used for external manipulator to create a three-dimensional model of manipulator Robot-v1. The value of the joint angle in each of the time interval sample point changes until the desired position, and then the model outputs the manipulator motion trajectory which is drawn in the three-dimensional coordinates. This track is the whole process of the movement from the initial position of manipulator to the target position. The spatial coordinates of the target position point is (0.55, 0,2).

2.3 achievement of motion track

The motion trajectory of maintenance manipulator is always a straight line. The length of straight line is the distance from the expected target point to the current position point, and then the trajectory is divided into aliquots of the time interval sample point which is 0.02s. Each manipulator walking distance is one of aliquot times. Each section of the track must solve the equation of arm reverse movement to calculate the amount of a series of joints. Then the joint is driven by the controller to reach the next target point. Until finishing all of the lines, it reaches a desired point in space. In a given time all the joints and the joint variable parameters under different sampling time points (/ joint angle, unit: radian) are depicted which is shown in Figure 4.

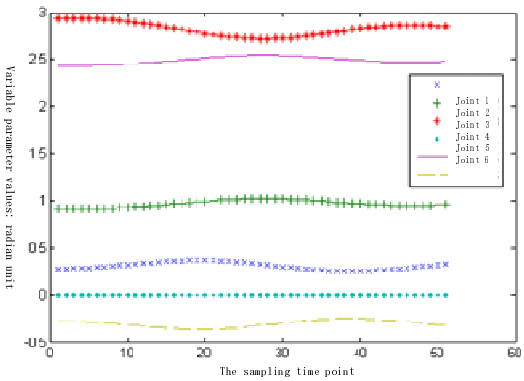

Fig. 4 The joint variables parameter variation chart

3 Conclusions

Denavit-Hartenberg (DH) method is used to establish a kinematic model of the robot manipulator which is used for maintenance of high-voltage transmission lines, and then the manipulator system simulation is achieved by using Robotics Toolbox and GUIDE programming in the MATLAB plugin. Based on analysis of kinematics direct and inverse problems and trajectory planning and the analysis on manipulator motion components and end position of each relationship in the space, an analytical method is provided to control the movement of the robot arm and manipulator kinematics simulation is made to ensure that the robotic arm controllers achieve intended function. Also, through interactive way and program, we make this module software to achieve the motion control of the manipulator track.

Through the analysis of the project shows that the movement of high-pressure special operations robot manipulator joint meet the requirements of the free expansion movement, which further validates the design of geometric parameters of the high-pressure special robot manipulator operations is reasonable.

Reference

[1] Wu Dawei. Auto control system of robot research and development of high voltage transmission line [J]. Shanghai Univer, 2008

[2] Zhu Anxi. The patrol robot technology development and application prospect of [J]. Yunnan electric power, 2011.6

[3] Zixing CAI.The robotics [M]. Beijing: Tsinghua University press, 2000:11-82

[4] Hu Yonghua, Luo Qingsheng, et al. A kinematic multipurpose manipulator with 8 degree of freedom [J]. analysis of mechanical and electronic, 2006.07

[5] Luo Jiajia, Hu Guoqing. The robot motion simulation of [J] based on MATLAB. Journal of Xiamen University (NATURAL SCIENCE EDITION), 2005.9

[6] Zhang Zhiyong, Yang Zuying. MATLAB tutorial [M]. Beijing: Beihang University press, 2010:82-167

Advanced Materials Research Vols. 989-994 (2014) pp 3084-3087
© (2014) Trans Tech Publications, Switzerland
doi:10.4028/www.scientific.net/AMR.989-994.3084

Design and Implementation of Driving Mechanism on Software Aerospace Measurement and Control System

Fu Gang[1,a], Kou Mingxin[1,a], Li Renlong[1,a]
[1]China Satellite Maritime Tracking and Control Department, China
[a]348237548@sina.com

Keywords: Software, Data stream, Parallel processing

Abstract. According to the signal processing unit in aerospace measurement and control system between the flow of water features, this paper proposes a software suitable for aerospace measurement and control system of driving mechanism. This paper first introduces the basic structure of aerospace measurement and control system software, having studied the static and dynamic data stream driving mechanism on the basis of detailed discusses the design and implementation process of this kind of driving mechanism of data stream. It adopts the method of message control, according to the dynamic data flow driven mechanism, realize the process of the signal processing unit and each signal processing unit between the data flow between the internal thread. Compared the same sort of dynamic data stream driving mechanism, the drive mechanism possesses the advantages of flexibility and easy to implement.

Introduction

With the continuous development of digital signal processing technology and the rapid improvement in general computer performance, the signal processing method in aerospace measurement and control system in has experienced from traditional hardware processing of the analog signal to digital processing based on software radio platform shift, pure software is beginning to change the direction of development. Abroad has been software radar (software radar) and software GPS receiver (GPS software receiver).The software here is different from the software radio, it is out of the programmable DSP and FPGA in software radio platform mainly dedicated hardware platform, the signal after A/D directly with general computer cluster as A platform to build, to complete signal real-time processing software processing way.[1][2] In recent years, computer cluster has been used in the field of large-scale complex data calculation (such as seismic data processing, the forecast calculation).As general, therefore, the continuous improvement of computer performance and network transmission speed, can use computer cluster as a control signal processing hardware platform, software processing way to complete the measurement and control signal of the real-time processing, the realization of software measurement and control system, and make future aerospace measurement and control system by the antenna + general computer cluster signal processing software system structure, software and generalization to measurement and control equipment.

1 System overview

Software is the essence of the aerospace measurement and control system using computer cluster of high-speed data processing ability of measurement and control signal real-time processing, the system structure are shown in figure 1 below. Are connected by a high-speed network and the whole system in high-speed network on the various processing units (including the system master control unit, signal input unit, signal processing unit and terminal processing unit).

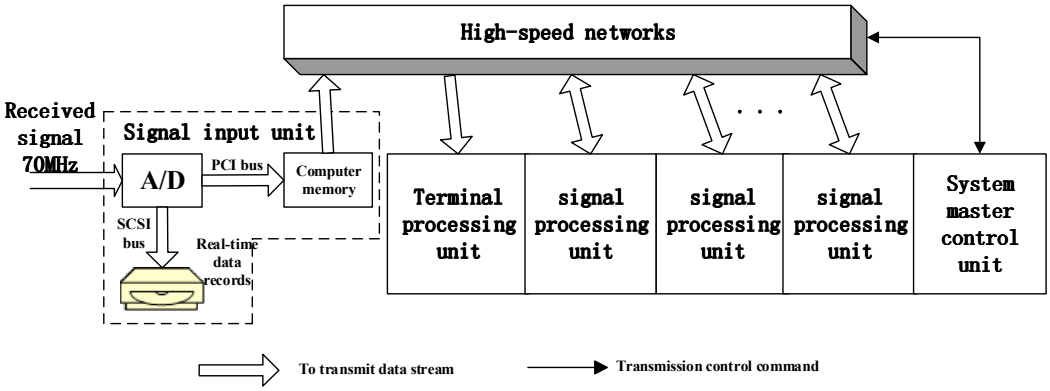

Fig1 System structure

High-speed network used to implement the interconnection between the various processing units. Currently used high-speed network construction of computer cluster has a Gigabit Ethernet, Gigabit Ethernet), high performance parallel interface (HiPPI) and scalable parallel interface (SCI), etc. In terms of network transmission performance, gigabit Ethernet is not the best, but compared with other high-speed network, it has good compatibility, the equipment system the characteristics of easy maintenance and low cost. At present, based on Windows NT operating system and TCP/IP protocol, gigabit Ethernet bandwidth effectively to 85 MB/S (680 MB/S).For USB measurement and control system, transmission code rate is low (maximum 2 MBPS), is BPSK and QPSK modulation way, so the intermediate frequency information is less than 5 MHZ bandwidth. Using bandpass sample solution (sampling frequency 20 installed base, 14 bit quantization) the intermediate frequency signal A/D transformation, get 40 MB/S data flow per second. So using gigabit Ethernet as computer cluster interconnection network can meet the requirements of data transmission. In order to improve the network transmission rate, based on the port must be used together switchboard star network topology structure, make the system work in full duplex mode, send and receive data at the same time.[3] For multiple input multiple output signal processing unit, by installing multiple network card connected to the switch, improve the rate of data exchange.

Each signal processing unit is a high-performance general-purpose computer. In order to improve the system capacity, should choose high frequency, double CPU, large memory capacity of computer as a signal processing nodes. Distribution of each signal processing unit independent of the input and output data buffer, adopted the structure of the table tennis, speaking, reading and writing. Input and output data buffer is divided into two equal, when one piece of data input operation, another piece of data read operations. To receive instruction message with the method of the water treatment, the processor to perform the current instruction at the next higher level to send and receive instruction, and open a thread, distribution computing resources (for input and output buffering), perform new operations, multithreading implementation instructions water treatment.

2 Data flow driven concept

Traditional Von Neumann computer adopts control flow drive mechanism, is through the program counter to determine the program of instruction execution sequence, the program counter sequencing by instructions flowing water. Because is essentially a sequential machine, at the same time, with the method of Shared memory, instructions and data between various correlation and operation control of complicated work may limit the flow of control mode in the development of computational parallelism. Data flow driven mechanism allows any instruction to be driven by data availability. In a data stream driving mode, the data directly in the form of data token passing between the instructions, once all the operands of a operating instructions here, will perform the operation, the operating results have token and then send to wait for these data the operation of the token. According to different tokens for data handling, data stream driving mode can be divided into: static data and dynamic data flows.

Driving mechanism of static data flow is: only when all input data and output the token here token is no output data, the operation can be performed. Token no tags, its main characteristic is data at the given moment when the input or output colleagues appear two or more data token, node will not be able to distinguish between them, which belong to the same data in control must be established in which the token to identify data token from one node to another node. So the static data stream processing efficiency is not high.

Dynamic data flow mechanism is the most important characteristics of the token with an ability to identify the token time successively relationship tag, as long as when the token of the same tag on each input, this operation can be performed. It overcame the shortcoming of static data flow driving mechanism, is currently the most in the world is often driven by the flow of data for data flow machine. However, due to mark the use of token, require specialized hardware to complete additional tags and tags for matching work.

3 Data flow based on message drive mechanism

Software signal processing software in aerospace measurement and control system is based on computer operating system, software system on the current computer operating system is widely adopted message mechanism, by the user to trigger messages, send messages and processing management and control, the realization of the convenient capture and recognition of various kinds of information. Measurement and control signal processing is the feature of the process of water type, a complete process of signal processing is divided into several functional modules, including the output of one or several function modules as the input of one or several function modules. When a module of the input data are in a state of mood, the data processing module began. Therefore, messages can be combination of mechanism and dynamic data flow driven mechanism, using the data in the sending messages as dynamic data flow mechanism tokens, the message in the message queue discharge sequence as to distinguish the token has the identity of the time, so you can according to the dynamic data flow mechanism drive software of aerospace measurement and control system run efficiently.

Processing unit is a software for signal processing in the measurement and control system of the core, in each processing unit contains a separate process, implement a feature in the process of signal processing. Through the process flow of data between drive, realize the measurement and control system of all functions. The data flow between the processing unit to drive the process is as follows:

First step, in the process of signal processing, the output of the signal processing unit at the next higher level after the data preparation, to send the data of the message to the signal processing unit. If the current signal processing unit of input data buffer is available, depending on the received message contained in the data area reads the input data, and send a confirmation message at the next higher level of the signal processing unit, the output data buffer is available at the next higher level. If the current processing unit of the input buffer is unavailable (i.e., cannot write data), at this time will decide whether is the number of data processing threads has reached optimal value (1.2 ~ 1.5 times of cpus). If not reached, then open a new data processing threads, the distribution of input and output data buffer, then according to the received message contained in the data area address complete data read, and at the next higher level node sends a confirmation message. If the current processing unit of data processing threads has reached the maximum value, will receive the message to join to the current processing unit of the message queue, waiting to be processed.

The second step, the current processing unit after completion of the required input data read, if the output data area is available (output data is be read from a lower level), the processing unit for data processing.If the current output data buffer is unavailable (namely cannot write operation data, the main reason is caused by the next level of data processing speed is lower than the speed of data processing), the current processing unit is in the ready state, until the output data buffer is available, the running state of the processor converts the ready state, for data processing.

Third step, the current processing unit will output the result written to the output data buffer, read the data message sent to the next level of processing units, by the lower level circulation in turn perform all operation of the process, data flow between processing units.

Within each signal processing unit consists of a signal processing process, each process includes input control, signal processing and output control three threads. Input control thread receives at the next higher level processing unit to read data sent messages, and will at the next higher level data is read in the input buffer to the current processing unit; Signal processing thread to handle the data in the input buffer, and the data processing results stored in the output buffer, Output control thread data updated in the output buffer, reading messages sent down primary treatment unit. In order to improve the operation efficiency of each signal processing unit, the unit adopts water structure of the data processing method, within each thread given a ping-pong structure of input and output buffering. Through the way of sending a message to achieve input data read, signal processing and data output work in parallel mode.

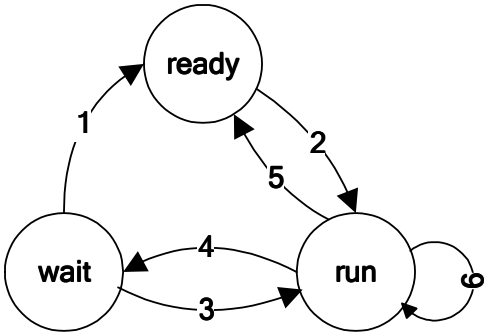

Fig2 Work process state transitions

When input control thread receives the processing unit at the next higher level after reading data from the news, will be done according to the information contained in the data area identification of input data to read. If the output data buffer is unavailable at this time state (that is, the output buffering any a cached data in the table structure was not at the next lower level processing unit finished reading), then this process by "wait" state transition for the "ready" state (1) in figure 2 curve, signal processing threads wait for output control thread sends the message. Output data in the buffer after the data is read by a next level node, the output control thread sends a message to the signal processing thread, in the "ready" state of the process into a state of "run", started the data processing (curve 2 in figure 2).For the process of "waiting" status, if the input the data in the buffer zone is updated, all at the same time in this thread output data buffer data read by the next level processing unit has been finished, the process of converting "waiting" status "running" state (curve 3 in figure 2).When signal processing thread processing has been completed, the input control thread state of data buffer is not available, the process for "waiting" by "running" state transition curve (FIG. 2 (4).If the data has been updated in the input buffer, and the data in the output data buffer is not the primary treatment unit reads (state) is not available, the process by "running" state transition for the "ready" (curve in figure 2. 5).If the input data buffer and output data buffer is available at the same time, the process to continue in a state of "run" (6) curve in figure 2.

Through the message transfer between three threads, control signal processing unit conversion process in working state. Ideally, the signal processing process should be in a state of continuous "run" (6) curve in figure 2.But in the actual cases, due to the different processing units before and after the operation load and processing time delay will be different. So, a signal processing process working condition will be in three different status (i.e., waiting, ready and running) conversion between.

Summary

Proposed in this paper, based on the message control data flow driven mechanism, give full consideration to the characteristics of the current computer operating system platform and stream processing structure of measurement and control signal itself, is suitable for the aerospace measurement and control system software design and implementation, to improve the parallel performance of the system. Compared to the same sort of data flow driving mechanism, the drive mechanism possesses the advantages of flexibility and easy to implement, and by dynamically adjusting the number of data processing threads and processes of work status, make full use of computer resources.

Reference

[1] T. Grydeland，F. D. Lind，P. J. Erickson，J. M. Holt. Software Radar Signal Processing[J]. European Geosciences Union 2004.

[2] John J. Schamus, Veridian Engineering, Dayton, OH. Real-Time Software GPS Receiver[J].ION GPS 2002,24-27.

[3] Mitchell L. Loeb, Andrew J. Rindos, William G. Holland, Steven P. Woolet. Gigabit Ethernet PCI Adapter Performance[J]. IEEE NetWork 2001.Apr.

Advanced Materials Research Vols. 989-994 (2014) pp 3088-3091
© (2014) Trans Tech Publications, Switzerland
doi:10.4028/www.scientific.net/AMR.989-994.3088

Research on workshop layout based on SLP and Witness

Qiang Cheng[1, 2],Tianmin Guan[1] ,Li Sun[1, a]and Fengbin Jing [1, b]

[1]School of Dalian Jiao tong University, Dalian 116028, China;

[2] Dalian Locomotive & Rolling Stock Co., Ltd. CNR Group, Dalian 116028, China.

[a] sunli@djtu.edu.cn, [b]353017373@qq.com

Keywords: SLP algorithm, workshop layout, Witness simulation, logistics optimization

Abstract. In the paper, the connecting rod production line in one workshop is taken as the research object. The workshop layout is designed by SLP algorithm. The specific work includes dividing the operating units, quantifying logistics relations and non-logistics relations, determining the importance of proportion and the integrated relationship of activities that based on the actual situation of the workshop, and then getting the plan finally. The Witness simulation is applied to simulate the theoretical analysis results and imitate the production logistics situation of the factory. Finally, the optimization scheme is determined by the comparison of several schemes in the aspects of logistics and the number of back flow.

Introduction

According to the research, the real time of materials being processed which from raw materials into the plant to the finished products accounts for 5%～10% of the production cycle, however the time of warehouse and transport state accounts for 90%～95% [1]. So production logistics is a key part of corporate logistics. Therefore, only reasonable layout of the production plant, optimized production and logistics systems can enhance the competitiveness of enterprises. The most representative method of the factory layout—System Layout Planning (SLP) which proposed by Richard Muther is applied to the workshop facilities planning [2].Then created a system model with computer simulation technology and simulated the real running. At last, the overall layout of the workshop is improved. So an excellent selection program is presented.

Overview of Layout Methods

The first step of application of SLP method is conducting material flow analysis and activity relationship analysis. Secondly, the space relationship diagram is set up. According to the actual area which each activity needed to decide each area of activities and the actual area instead of relational graph nodes, forming the space relationship diagram. Thirdly, several layout schemes are established based on the actually usable areas, then they are evaluated and preferred. This article set up an improved plant layout design method by combining SLP method with Witness (system simulation software), so that the planning and management personnel can understand the workshop layout scheme intuitively by the Witness. It contributes to the testing, analysis and evaluation of system, so as to achieve the goal of low cost and high efficiency. It can reduce unnecessary materials transport, improve logistics efficiency and cut down logistics cost [3].

Instance

According to the demand of the market, some measures are taken in order to make the construction of workshop meeting the requirements of lean production. For example, solving the exiting problems of the workshop, reducing production cost, maximizing space utilization and optimizing logistics processes. Connecting rod production line is taken as the research object. The workshop mainly

products the models of 265, 240 and 280.The model of 265 of engine connecting bar production line is taken as an example to carry on the analysis.

Division of activity. First of all, we need to divide the activities, the Z represents the set of activity :

Z = （Z1，Z2，…，Zi，…，Zj，…，Zn）

Where n is the number of activity. The logistics quantity of raw materials, accessories and finished products in the manufacturing plant is huge, so the logistics relations and non-logistics relations of the activity all can be evaluated and analyzed by the activity relationship chart. We divide the production line into 24 activities based on the production process of the connecting bar, sort as follows, parts turnover zone, polishing zone , inspection zone, coupling zone, layout block, planer-type milling machine, CNC boring machine, sawing machine, horizontal milling machine, vertical milling machine, CNC rough boring machine, CNC machine center, CNC grinding machine, ABA connecting bar grinding machine, connecting bar grinding machine, horizontal machine center, numerical control vertical milling, radial drill. Draw the initial layout of the workshop and the path of the logistics, as shown in figure 1.

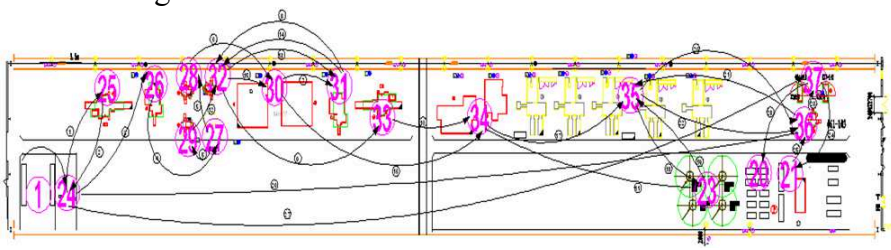

Fig. 1 Workshop initial logistics path graph

Activity's Integrated Relationships Analysis. The placement of the activity Z_j in the workshop is determined by the calculation in the workshop. First, the logistics strength levels of each activity are analyzed. The logistics strength can be converted into five levels which are A, E, I, O and U. Their logistics strength is gradually reduced. These grades are ultra-high, particularly high, higher, general and negligible logistics strength correspondingly. According to the actual situation, the logistics strength level is converted into five levels based on equivalent flow capacity. So the logistics volume in the range of 890-1870 is designated as A level, 210-890 as E, 170~210 as I, 40-170 as O.

As to the analysis of non-logistics relations of activity, 8 main factors is selected which are frequent mergers of materials handing, adapting to requirements of the Tatk Time, operation similarity, common public facilities, the same model of processing equipments, coordination environment of the activity, work safety, urgent degree of service as the main reference factors of the non-logistics. The levels of A,E,I,O,U are determined in the same form of logistics relationship diagram. Then the relationship diagram of activity's non-logistics is set up, as shown in figure 2.

Then the activity's integrated relationships are analyzed. The steps are as follows：

1) It can determine the weighted ratio of relative importance between logistics and non-logistics of the production line as 1:1 in accordance with the production processes of connecting bar and the similar influence between the logistics and other factors.

2) After quantifying the logistics strength grade and the non-logistics close degree level, A is equivalent to4（A=4），E is equivalent to 3，I is equivalent to 2，O is equivalent to 1,U is equivalent to 0,X is equivalent to -1. Then the comprehensive relationship of all the activities that have been quantified is calculated. The total number of activity pair is determined by the formula which is P=N（N-1）/2.In this article, the N is 18, so the P is equivalent to 153(The following lists only list A,E,I,O) .We default the others which are not listed as grade U. So there are 127 pairs of activities of U.

3) Classification of the integrated relationship grade. When merging the correlation table of the logistics and the non-logistics, we should pay attention to the processing of X level because the result of the merging between any level of logistics relationship with the X level of non-logistics relationship should not exceed O level. After the adjustment, we establish the integrated relationship diagram [4], as shown in figure 3.

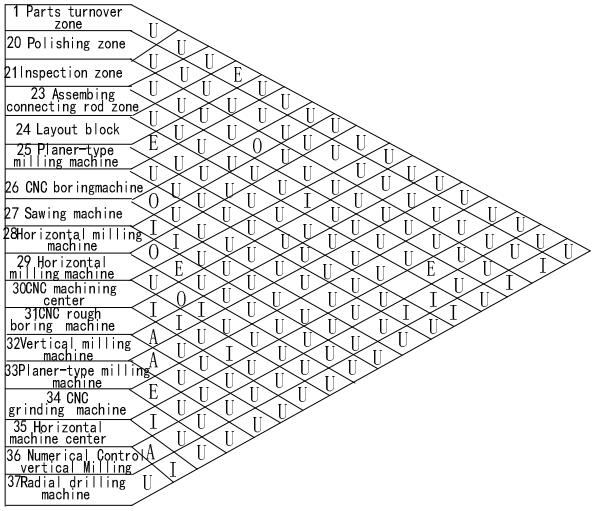

Fig. 2 Non-logistics relationship diagram

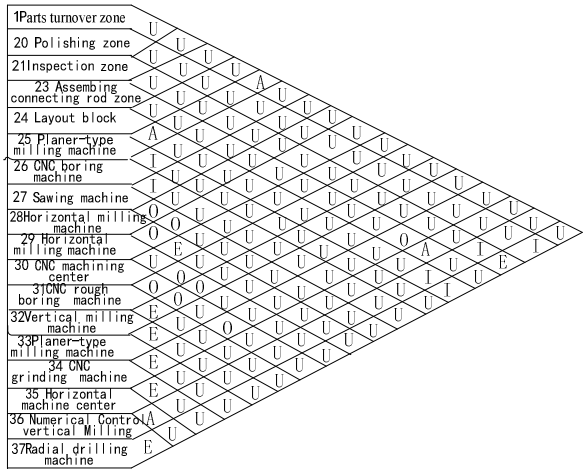

Fig. 3 Integrated relationship diagram

4) The locations of activities are adjusted by area related chart, as shown in figure 4. It can form several layout programs by considering the limitation and effective of all the factors. Then 2-3 feasible schemes can be chose after removing the unrealistic program. At last, the feasible schemes are simulated by the Witness software.

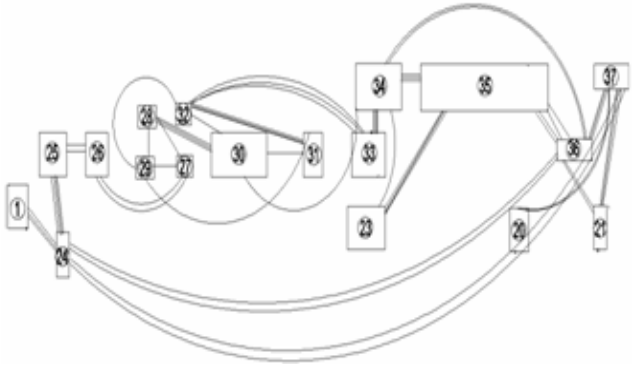

Fig. 4 Area related chart

Simulation

In the paper, the workshop layout is simulated by the software of the Witness. At present, the number of the processes of the model of 265 which is the study object is up to 50 and the entire production line appears that the connecting bar body and cover are placed respectively in different coupling zone. In the workshop, it is easy to emerge a lot of repeated processes and the cross logistics [5].

The first step, the workshop layout is imported into the simulation software of the Witness. Then the entity element's properties of each activity are defined. Through the visual setting of the elements that adjusting the properties of the Text, Icon, Rectangle in the Display box, it can realize flow conditions of the materials between the pairs of the activities in the workshop. So the scheme A and B of the workshop layout simulation modeling are shown in figure 5 and 6. We do some statistics of the size of the workshop logistics by setting the parameters of variable. Specific analysis is shown in table 1.

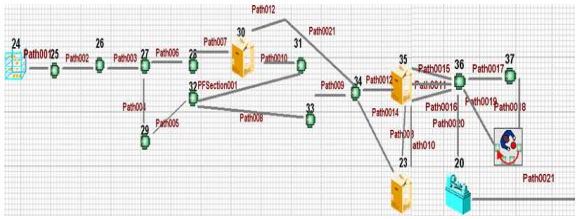

Fig.5 Scheme A

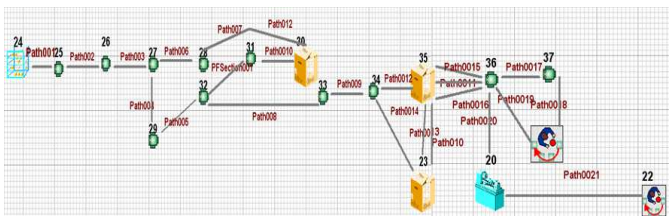

Fig.6 Scheme B

The cost variance that generates from different materials of per unit transportation in different routes is ignored. The cost of material handing is proportional to the distance of handing, that is to say the total cost of material handing is proportional to general distance of handing. The total cost of material handing C is recorded as(1):

$$C = \mathrm{w}\sum_{i=1}^{n} w_i \qquad (1)$$

W—total flow distance

Wi—flow distance between the pair of the i activity

The comparison of the layout of the scheme A, B and the original scheme is shown in table1.

Table 1 Comparison

Layout Scheme	Handing Distance	Flow Distance	Cross Path	Back Flow
Original Scheme	9153.09	4424039	16	7
Scheme A	9311.34	3905807	12	3
Scheme B	8259.55	3908379	12	4

After comparison, the distance, the cost, the number of cross path and backflow of materials handing of scheme B is reduced by 9.76%, 11.66%, 42.86%, 25% compared with original scheme. Above all, scheme B is better than scheme A because the blocking rate of logistics path, the distance, the cost of materials handing and the number of cross path of scheme B get a great improvement while scheme A appeared a phenomenon that the physical distance increases and the total cost reduces. Because the distance of the route which has a large quantity of logistics is reduced .And the distance of the route which has a small quantity of logistics is increased slightly. Then the flow distance of scheme A is less than original scheme. Although the total flow distance is decreased, it is not much more desirable than scheme B. But in manufacturing, 20%～50% of the total operation cost is used by materials handing, so the saving of the cost of materials handing considered preferentially in the layout optimization design. Compared scheme A with scheme B, it can be concluded that B is much better than A.

Summary

In view of the character of bulk production of workshop within the mechanical processing workshop, the system simulation software of Witness combined with the SLP method, it can make up for the shortcomings that SLP method application in the production line is lack of dynamic flexibility and mobility analysis. Through the simulation of the production logistics system with Witness, the layout can be evaluated intuitively and quantitatively. At last, the accuracy and rationality of the workshop layout design can be improved.

References

[1] F Q Guan, W Zhuan, Modern logistics facilities and planning. Beijing: Mechanical industry press, 2009.

[2] W Y Chao, M H Wu, Production logistics system modeling and simulation. Beijing: science press, 2006.

[3] L Qin, L Z Rong, A production workshop logistics facilities layout analysis and design. journal of modern manufacturing engineering, 2011(8):67-70.

[4] M H Wu, Facilities planning and logistics system design. Beijing: Higher education press, 2005.

[5] R Muther, System layout design. Beijing: Mechanical industry press, 1986.

Advanced Materials Research Vols. 989-994 (2014) pp 3092-3095
© (2014) Trans Tech Publications, Switzerland
doi:10.4028/www.scientific.net/AMR.989-994.3092

Study on the Voltage Measurement in a Battery Manage System Based on LTC6802

ZHU Yu-wei[1,a], Shi Bing[1,b]

[1]Engineering College, Ocean University of China, Qingdao 266100, China.

[a]zhuyuwei2002@163.com, [b]bings@ouc.edu.cn

Keywords: Battery Manage System, Lithium-ion Battery, Electric Vehicle, Battery.

Abstract. This paper presents an implementation of voltage measuring system in a battery manage system, which is based on micro-controller AT90CAN32 and LTC6802 integrated circuit chips. The design for hardware and software is mentioned in the first, and then an experiment platform is set up for the function test. The test is successful and the result shows that the implementation is valuable and practicable.

Introduction

Many applications, such as plug-in hybrid electric vehicles (PHEV) and fully electric vehicles (EV), have a need for substantially battery pack used as its primary energy storage device [1, 2]. Since one cell voltage is low, a lithium-ion battery usually comprises several cells that are connected in series and/or in parallel to provide the high voltage, current and capacity [3]. It is the weakest cell that determines the performance for the battery that the lowest capacity cell will cause the battery conditions to trip [4]. Therefore, it's essential to have a battery management system (BMS) to monitor the voltages [5, 6].

However, in a BMS of battery stack, cell monitoring and balancing is critical. The voltages of the individual cells will start to drift away from each other throughout the operation of the pack, which will result in a lower efficiency for the operation of the pack. Moreover, when the number of cells grows, its high common mode voltage may be up to several hundreds of volts in modern EV applications, which makes the measurement harder. A possible solution is to use optical isolation between the cells and the measuring unit. Initially, the circuits of measurement for voltage are made from discrete components or special-driving integrated circuits(IC). A multi-winded transformer method is discussed in [7], which requires a transformer for each cell and a set of switches to choose a cell to measure. A differential amplifiers concept is presented in [8], where, high common mode voltage is not a problem since each module has its own ground reference. There're some ICs launched by chip makers, as shown in Table1.

Table 1 List of integrated circuit chips for cell measurement.

Chip maker	Elithion	Linear	AD	TI	Maxim	Atmel
Part number	EL01 EL02	LTC®6802-2	AD7280	BQ77PL900	MAX11068	ATA6870
Best pack scale	Large packs, 48 V to 1 kV	Any size pack, 24 V to 800 V	Any size pack, 8 V to > 1.1 kV	Small packs, 12 V to 1 kV,	Any size pack, 8 V to 1.4 kV	Medium pack, 10 V to 355 V
Topology	Distributed cell boards +1BMS	Modular: 12cells/board	Modular: 6 cells /board	Modular: 4cells//board	Modular: 12 cells /board	Modular: 6 cells /board
Max bank	~16	1: 192	~16	1: 192	1: 192	1: 192

This combination made it difficult to find a suitable IC, but the task finally fell on LTC6802-2. The chip is a complete battery monitoring IC, which includes a 12-bit digital to analogue converter (ADC), a precision voltage reference, and each chip can measure up to 12 series connected battery cells, with a total voltage up to 60V. Each LTC6802-2 has an individually addressable serial interface, which allows up to 16 LTC6802-2 devices interface to one control processor and operate simultaneously [9].

The purpose of this work is to find an efficient, simple and cheap way to keep cells in a battery stack monitored. Since this is one task of the battery management system, the BMS should be mention in this paper. While the field of BMS is quite big, therefore, there are some limits in the thesis.

1. Topology of Voltage Measurement System

The Voltage Measurement System is a component of a BMS, in which a master control chip unit is essential as well as the Voltage Measurement circuit. The master control IC in this paper is AVR AT90CAN32, while LTC®6802 is used as the slave for monitoring the cells in stack. A high-speed serial peripheral interface (SPI) communication links both the terminals together in the topology based on the iCoupler technology, which is shown as Fig.1.

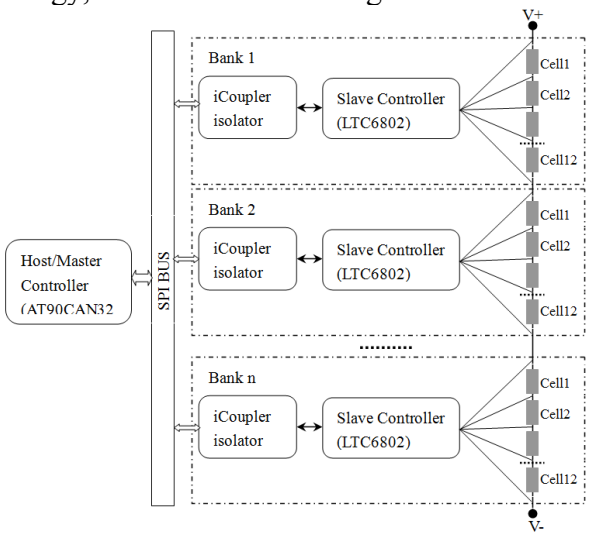

Fig. 1 Topology of voltage measurement system

2. Design of Hardware

The logic of the LTC®6802-2 is generated by its interior circuit, the logic level for the chip are taken out by the Pin VREG and V–. In a Multiple LTC®6802-2 devices application, each of the chips can monitor 12 cells in a bank. To address the proper bank, LTC®6802-2 chip supply its A0, A1, A2, A3 inputs. Although Linear Technology Corporation supplies a daisy-chain topology for applications, there are some drawbacks for this mode [10]. Since all modules have different ground potentials, there some kind of digital isolation between the master and the slave is needed. An Analog Devices has come up with a digital isolator called ADUM1411, which uses the iCoupler® technology. Its block diagram is shown in Fig.2, and Fig.3 is the schematic diagram for measurement circuit.

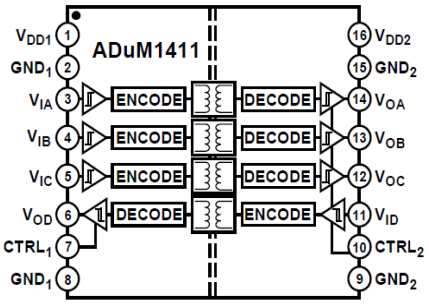

Fig.2 Functional block diagram of ADuM1411

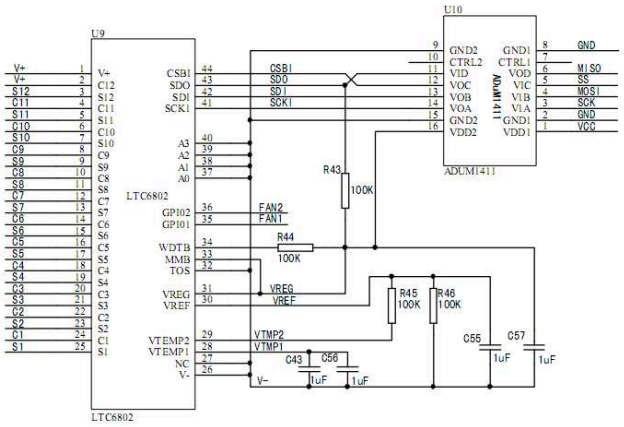

Fig.3 Schematic diagram for measurement circuit

The schematic diagram and Topology are embedded in the BMS printed circuit board (PCB), the layout of the PCB is shown in Fig.4. The voltage measuring circuit is just in the centre of the PCB, where, a car icon is printed, and a LTC®6802-2 is routed. On the right of the board, there are plug-in sockets for linking the cells in the bank, while on the left there are 15 SPI interfaces for other banks. Based on the PCB, an Assembly is finished; the photograph of the BMS is shown in Fig.5.

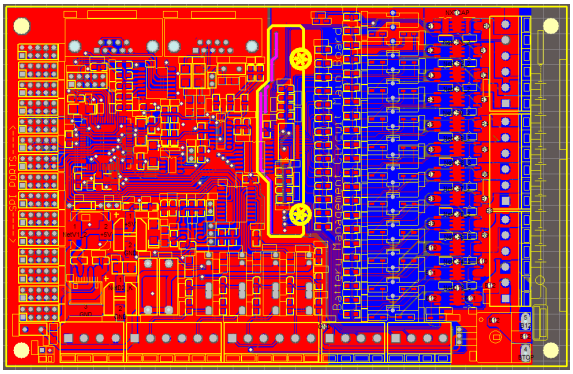

Fig.4 The final version layout of the PCB

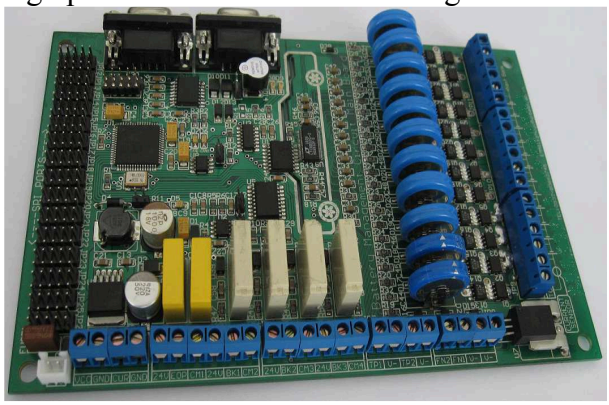

Fig.5 The photograph of the BMS

3. Design of Software

The master must accommodate itself to the slave in the communication. Both of them prepare the data to be sent in their respective shift registers, and the Master generates the clock pulses for SCK. Data are shifted from the master to the slave on MOSI, while from the slave to the master on the MISO. After data are packed, the AT90CAN32 will synchronize the LTC6802 by pulling the CSBI down. When exchanging data, the most significant bit (MSB) of the word is transferred first. Where an external oscillator is used as the system clock input, its frequency is $f_{cklio} = 8$ MHZ, so $f_{sck} = f_{cklio}/8 = 1$ MHz. The program flow chart is shown in Fig.6. Fig.6 (a) is the main program chart for the BMS, at first which initializes the BMS, and then enters an endless loop to acquire the voltages from the slave. Fig.6 (b) is the interrupt routine. When the start command reaches LTC6802, it starts an ADC for cell voltage measurement. If the conversion is finished, the slave may feedback data to the master by SPI communication. The arrival of the data in master buffers will trigger the interrupt routine as Fig.6 (b). Thus, an interaction loop mechanism is made, and it goes well in the test platform.

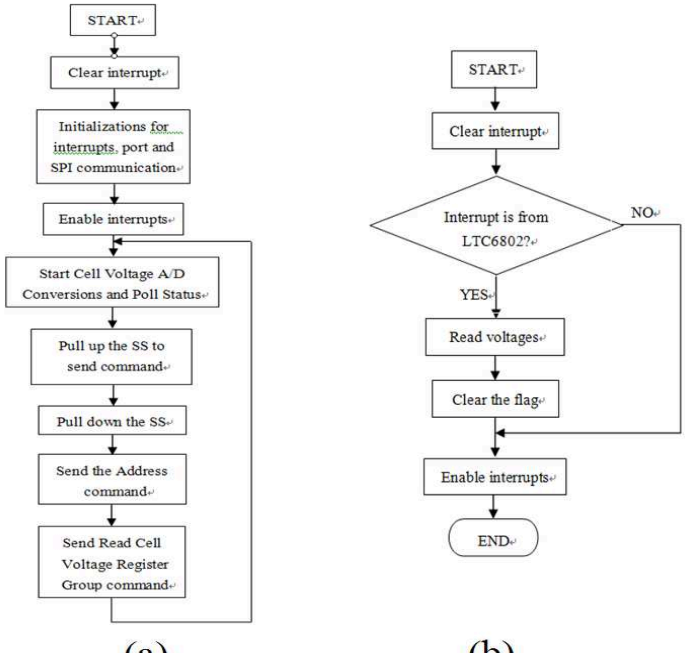

(a) (b)

Fig.6 The program flow chart

4. Test and results

A test platform is set up in this work, which includes a 12-cell-in-stack battery and some voltmeters linked to each of them. The battery voltage measuring system works with the platform. The result is shown in the Table2.

Table 2 Result comparison between the data measured by LTC6802 and detected by voltmeters.

Number for Cell	1	2	3	4	5	6	7	8	9	10	11	12
Measure Data(V)	3.54	3.81	3.97	3.62	3.99	3.56	3.34	3.39	3.94	3.57	3.67	3.33
Detected Data(V)	3.52	3.80	3.94	3.60	3.98	3.56	3.32	3.46	3.91	3.56	3.70	3.32
Absolute Error(V)	0.02	0.01	0.03	0.02	0.01	0	0.02	-0.07	0.03	0.01	-0.03	0.01

5. Conclusions

This paper presents an implementation of a voltage measuring system based on LTC6802 in a BMS. As one of the most important part in the BMS, the demonstration of voltage measuring is carried out on the latest BMS PCB assembly which includes the circuit in this paper. The experimental results indicated that the voltage measurement is achieved with a very accurate circuit as well as it provides up to 12 measurements per module to reduce the cost. Moreover, the topology of the voltage measurement system is stackable and expandable for monitoring large Li-Ion battery packs, with its voltage up to 800 V. Although it is only the first step for a perfect BMS construction, there is some significative work for the further study.

6. Acknowledgements

This study was funded by National Natural Science Foundation of China(Grant No. 51279189; 50879084). The writers are grateful for the comments provided by the Editors and the reviewers, which have significantly improved the quality of the paper.

References

[1] A. Affanni, A. Bellini, G. Franceschini, et, al. Battery Choice and Management for New Generation Electric Vehicles[C]. IEEE Transactions on Industrial Electronics, vol. 52, October 2005.

[2] XIONG Wei-wei, ZHANG Yong, YIN Cheng-liang. Configuration Design, Energy Management and Experimental Validation of a Novel Series-parallel Hybrid Electric Transit bus [J]. Journal of Zhejiang University SCIENCE A, 2009 10(9):1269-1276.

[3] Daniel Abraham. Advances in Lithium-Ion Battery Research and Technology[J]. JOM, March, 2002:18-19.

[4] WANG Zhen-po, SUN Feng-chun. Study of the EV Battery Pack Attended Mode[J]. Journal of Asian Electric Vehicles, 2004(2), 1:517-520.

[5] B. Yurkovich and Y. Guezennec. Lithium Ion Battery Pack Model and Simulation for Automotive Applications[C], ASME Dynamic Systems and Controls Conference, 2009.

[6] WANG Xiao-peng, Cyrus Ashtiani, Ahmad Pesaran. A Modular Battery Management System for HEVs[D]. The University of Toledo, May 2001.

[7] Jan Williams, Mark Thoren. Developments in Battery Stack voltage Measurement[R]. Linear technology Corporation, 2007, Application Note 112.

[8] Olov Ershag. A Balancing and Monitoring System for Battery Cell Stacks in Electrical Vehicles [D]. Luleå University of Technology, 2008.

[9] Linear Technology Corporation. LTC®6802-2 Datasheet[M]. Milpitas, CA, Linear Technology Corporation, 2011.

[10] An Shi-qi, Qi An-ning, Zhu Yu-wei. Design and Realization of SPI Interface in Lithium-ion Battery Voltage Measuring System[C].The 6th International Conference on Computer Science & Education (ICCSE 2011).

Advanced Materials Research Vols. 989-994 (2014) pp 3096-3099
© (2014) Trans Tech Publications, Switzerland
doi:10.4028/www.scientific.net/AMR.989-994.3096

Research on multistage horizontal well fracturing in the east of Sulige gas field

Xue Yafei[1,2] , Li Da[1,2], Zhu Zhiying[3,a]

[1]PetroChina Changqing Oilfield Company Sulige Research Centre, Xian, 710018, China

[2]National Engineering Laboratory of Exploration and Development in Low Permeability Oil and Gas Field, Xian, 710018, China

[3]China University of Petroleum Institute of Petroleum Engineering, Beijing, 102249, China

[a]email:zhiying_2008@hotmail.com

Keywords: horizontal well, low damage fracturing fluid, multistage.

Abstract. Sulige gas field had been developed for a long term, but the yield is hard to keep a high value. How to improve the daily production is a key problem. In the past, we usually fracture horizontal well in single section. In this paper, we talk about horizontal well fracturing in multistage. And meanwhile, introduce some low damage fracturing fluids. Finally, fracturing evaluation shows horizontal well multistage fracturing can improve the yield effectively. This experience can be popularized in similar gas field.

Gas reservoir characteristics

Sulige gas field is located in the Ordos basin in the west of YiShan slope, is a Large lithologic trap gas reservoir develop from Carboniferous - Permian coal measures. The main gas-bearing section is dyas sandstone reservoir of Shihezi formation He8 section and Shanxi formation Shan1 section[1]. Shihezi formation thickness is between 260m and 340m, and better than Shanxi formation in terms of size and connectivity. It is the most favorable reservoir in this area. Shanxi formation stickness is between 70m and 80m, according to the sedimentary sequence, from bottom to top, is Shan1 section and Shan2 section respectively. Shan2 section is the main hydrocarbon source rocks of Sulige gas field He8 section, and Shan1 section is the important auxiliary reservoir of He8 section [2].

The reservoir porosity of He8 section ranges from 4.0% to 13.0%, and mean value is 8.9%; permeability is $(0.03\sim2.0)\times10^{-3}$ μm^2, and mean value is 0.5425×10^{-3} μm^2. The reservoir porosity of Shan1 section ranges from 4.0% to 13.0%, and mean value is 8.5314%; permeability is $(0.04\sim1.0)\times10^{-3}\mu m^2$, and mean value is 0.3566×10^{-3} μm^2. It can be viewed as low porosity low permeability sandstone reservoir. It is hard to develop the gas field based on poor pore structure characteristics. Hence, fracturing is necessary if wish a high yield.

Fracturing technical analysis

Principle. Hydrofracturing is a mining technique in which a liquid (in most cases water) is mixed with sand and chemicals and the resultant mixture injected at high pressure into a wellbore. This creates small fractures in the deep rock formations, typically less than 1mm wide, along which gas, petroleum and brine may migrate to the well. Hydraulic pressure is removed from the well, and then small grains of proppant hold these fractures open once the rock achieves equilibrium [3].

Multistage horizontal well fracturing technology. To Sulige gas field, yield-increasing effect is not obvious after normal fracturing. Therefore, this method is not suitable to Sulige gas field.

Sedimentary system, temperature, pressure and reservoir physical properties of He1 section are similar with Shan1 section. Exploiting reservoirs together are recommended because of thin gas reservoirs and low reserves. Horizontal section length is becoming longer and longer, in order to increase the yield, we should try to increase the number of crack.

Stress characteristics. Sandstone stress is 50.43MPa. Stress difference of sand shale and mudstone is 4.47MPa, and the stress difference of mudstone and sandstone is 6.19MPa. In Sulige gas field the stress difference of He8 up section and down section is 3-10MPa, Physical property difference and heterogeneity are strong. The stress difference of Shan1 section is 6-12MPa, the stress shielding is better.

Matching technology. Depending on reservoir characteristics, to decrease formation damage, we test three kinds of low damage fracturing fluid. They are carboxymethyl, anion and low concentrations of guanidine gum. And we test 300 wells.

Table 1 Compare three kinds of fracturing fluids system with general fracturing fluid system

System types	Surface tension （mN/m）	Sludge content （mg/L）	Gel breaking liquid viscosity （mP.s ）		Ratio of core sample permeability，%	System characteristics
			Lab tests	Theater tests		
General	33.82	510	＜10	7.6	27.06	High thickner concentration, Good theologic property, High residue content
carboxymethyl	31.53	88	＜5	3.3	19.1	Break easily, Flowback easily
anion	28.21	0	＜5	3.2	18.3	No residue, Flowback easily
low concentrations	26.70	290	＜5	3.6	20.0	Low thickner concentration, Gel breaking completely, Flowback easily

Table 1 shows that compare with general fracturing fluid, the advantages of three kinds of fracturing fluids system are low surface tension, low residue content, low ratio of core sample permeability, break easily and flowback easily.

Instance analysis

With the development of horizontal well fracturing technology, the chance of drilling to effective reservoir is becoming higher and higher. During gas testing, the average open-flow capacity improved significantly.

Figure1 shows horizontal well fracturing message from 2010 to 2012. For each year there are three information, they are well number, section number and open-flow capacity from left to right. We can know that the fracturing well number and fracturing section number are becoming more and more, and at the same time open-flow capacity is increasing. These mean multistage fracturing can increase yield effectively.

From table 2 we know that we test 19 wells by low damage fracturing fluids, including 15 wells by low concentration fracturing fluid, average open-flow capacity is 29.3875×104m3/d,4 wells by carboxymethyl fracturing fluid, average open-flow capacity is 17.6011×104m3/d. Compare with general guanidine gum fracturing fluid, Single well output has increased by 4.6 times, Implementation effect is better.

At the same time, we test different kinds of fracturing fluid. The production information is shown in Table 3. From Table 3, we know that the effect of 0.35% carboxymethyl is the best in 3 testing

fracturing fluids. The cumulative production for 100 days is 413.4×104m3. Meanwhile, the cumulative production is 102.4×104m3when using 0.4% carboxymethyl.

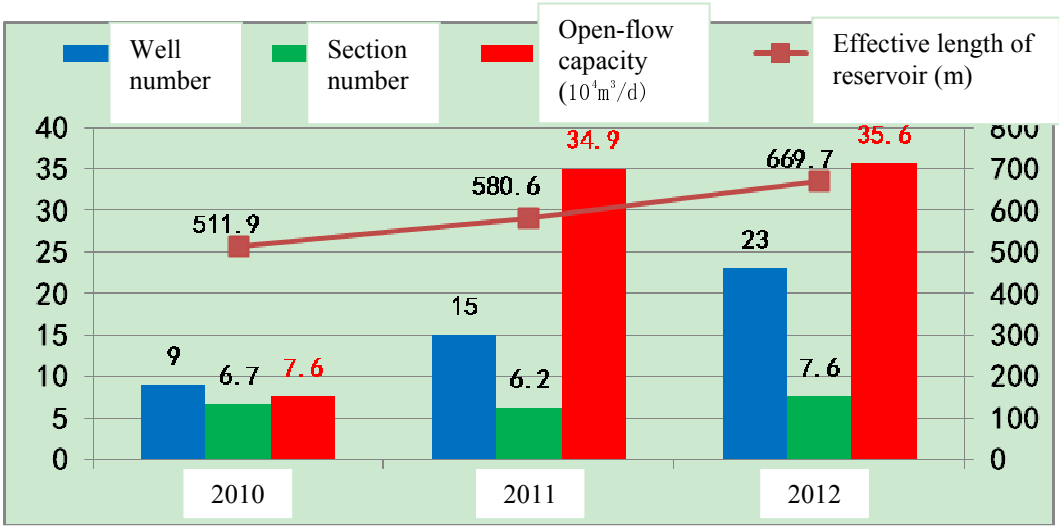

Fig. 1 Horizontal well fracturing statistics from 2010 to 2012

Table 2 Correlation table on gas testing effect

(V1 is well number, V2 is horizontal section length, V3 is sandstone length, V4 is sand ratio drilled, V5 is effective thickness of reservoir, V6 is effective reservoir ratio drilled, V7 is fracturing stage number, V8 is amount of sand, V9 is flowback rate, V10 is open-flow capacity)

Fracturing fluid type	V1	V2 (m)	V3 (m)	V4 (%)	V5 (m)	V6 (%)	V7	V8 (m^3)	V9 (%)	V10 (10^4m^3)
0.4%low concentrations	15	964.8	793.3	81.9	574.0	59.3	5.9	42.24	77.80	29.3875
0.35% carboxymethyl	2	654.1	546.2	68.9	385.1	50.8	5.0	32.0	84.30	29.7855
0.4% carboxymethyl	2	1079.6	952.1	88.3	534.6	49.5	4.5	28.5	62.0	5.4167
0.50%-0.55%general guanidine gum	9	999.0	871.1	86.1	555.2	54.6	6.7	30.54	77.00	5.7787

Table 3 Correlation table on production data by different fracturing fluids
(V1 is well number, V2 is fracturing stage number, V3 is casing pressure before production, V4 is initial capacity, V5 is the 100th day casing pressure, V6 is the 100th day production, V7 is 100 days cumulative production, V8 is the unit pressure drop of gas production, V9 is the unit pressure drop of gas production for single crack)

Fluid type	V1	V2	V3 (Mpa)	V4 (10^4m^3/d)	V5 (Mpa)	V6 (10^4m^3/d)	V7 (10^4m^3)	V8 (10^4m^3/Mpa)	V9 (10^4m^3/Mpa)
0.50-0.55% guanidine gum	6	6	18.2	1.57	9.6	1.2	113.4	13.2	18.9
0.4% guanidine gum	7	6	21.1	4.78	17.1	3.1	228.6	56.3	38.1
0.35% carboxymethyl	2	5	22.1	4.83	15.8	4.7	413.4	65.9	82.7
0.4% carboxymethyl	2	6.5	19.9	1.55	17.1	0.6	102.4	36.1	15.7

Summary

Three kinds of low damage fracturing fluid can meet multisections of a tight sandstone gas reservoir fracturing needs. Average open-flow capacity can be improved to above 20%. And carboxymethyl and low concentration guanidine gum fracturing fluid have advantage in price and implementation.

Multistage fracturing can raise the yield of gas field, should be extended in other areas and further tests.

In the future, we should try to carry out after fracturing effect evaluation and long-term production of dynamic tracking. To fracturing effect, evaluation method is relatively single. Recommend that increasing crack monitoring, zonal testing, well testing and so on. These works can provide strong support for fracturing effect evaluation.

References

[1] Kang Yili, Luo Pingya, Present situation and prospect on china tight sandstone gas reservoir exploration and development key engineering technology, J. Petroleum Exploration and Development, 2007, 34(2): 239-245. (in chinese)

[2] Zhuang Hua. Research on gas productivity predictionbased onlogs for post-frac yight sandstone reservoirs in Sulige area. Master thesis, Jilin University, 2013. (in chinese)

[3] Information on http://en.wikipedia.org

[4] Chen Li, Wang Anpei, Wang Guoqing. Horizontal well multistage gracturing technology in unconventional oil-gas reservoir. Technology Supervision in Petroleum Industry, 2013, 6: 51-53. (in chinese)

[5] He Hongmei, Huang Yuzhong, Ren Shan, Multi-stage fracturing technology and its application in horizontal well of tight gas reservoir, Drilling and Production Technology, 2012, 35(4): 62-65. (in chinese)

Advanced Materials Research Vols. 989-994 (2014) pp 3100-3104
© (2014) Trans Tech Publications, Switzerland
doi:10.4028/www.scientific.net/AMR.989-994.3100

Numerical Analysis of Heat and Mass Transfer Performance of the Packed-type Parallel Flow Dehumidifier

Zhang Ruihang Wang Ziye Niu runping [a, *]

School of Environment and Energy Engineering, Beijing University of Civil Engineering and Architecture, Beijing 100044, China

[a] niurunping@bucea.edu.cn

Keywords: Heat and mass transfer, dehumidifier; parallel flow

Abstract. TA mathematical model describing heat and mass transfer performance of packed-type parallel flow dehumidifier was set up. The numerical solution of differential equations was derived. Taking the heat and mass transfer coefficients obtained by experiments as the input parameters of the model, the impact of solution inlet parameters on outlet parameter of air was described. The simulation results indicated that the mathematical model could be used to predict the performance of liquid dehumidification. The results showed that the mathematical model can be of great value in the design and improvement of dehumidifier.

Introduction

Solution dehumidifier is a device which the desiccant directly contacts with moistair.It's a device of air dewetting. It's a vital unit of liquid desiccantsystem. Toagreatextent, the whole property of desiccant system depends on desiccant property of dehumidifier. As a result, the research of desiccant property of dehumidifier is particularly important. Wenzhong Gao etc al. [1] devote to improving dehumidifying effect of desiccant solution. They advised adding nano-Cu in the solution to enhancing its heat transfer performance. Zhijia Huang [2] reached a conclusion .That is the bigger padding of specificarea is ,the better dehumidifying effect is in the solutiondesiccant process by using industrial waste heat as heatsource of actified solution. Yaodong Hu, etc al. [3] built model of solution desiccant air-conditioner and applied it into dehumidificationsystem in order to numerical simulation. The deviation of reckoning and experimental results is very small from that model. When liquid desiccant applies into comfortable AC system, author is studying the impact of inlet air and solution parameter on outlet air temperature and humidity. Then draw the influence curve.

The establishment and solving of dehumidifier mathematical model

Establishment of model. In this paper, the parallel adiabatic dehumidifier is adopted, and the stuff we choose to use is metallic padding. The desiccant solution (LiCl) is sprayed from the top of the dehumidifier vertically. On the surface of the filler, an electrolyte film comes into being. There is a saturated air film between air and liquid membrane, and the temperature of it is identified as the same as the one on the solution surface of the saturated air layer. The passing of substances and energy between gas and liquid is through the saturated air layer. Now the mathematical model of the desiccant solution and the forward flow of air are set up, and then we make the following assumptions:

1) Air and solution is an ideal parallel flow, and the flow is stable;

2) There is no heat and moisture exchange between the internal and external environment of the dehumidifier, and the process is adiabatic;

3) The mass transfer resistance is mainly on the side of the air, and the mass transfer resistance on the surface of the solution absorbing the water vapor is neglected;

4) The surface of the stuffing is fully wet, and the interface of heat and mass transfer are the same;

5) The heat and mass transfer only exist in the Z direction ignoring the transfer in the X and Y direction.

According the assumptions below, there is no heat and mass transfer along the length and width direction of the dehumidifier only existing in the direction of height (Z direction). It becomes a one-dimensional heat and mass transfer problem. An infinitesimal body is chosen from the entire dehumidifier to analyze the exchange process between the solution and air. The exchange process of air and liquid complies by the conservation of mass and energy. Analyze an infinitesimal body in the length of dz from figure 2.2 and establish the mathematical model of downstream flow in the following:

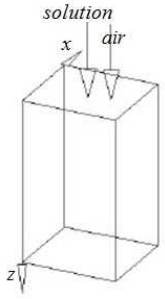

Figure2.1 Physical model of dehumidifier

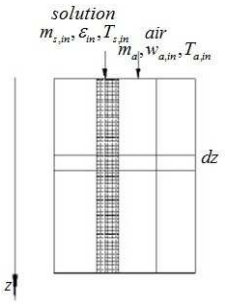

Figure2.2 Schematic plot of downstream

According to conservation of mass, the increment of air humidity equals to the quality change of solution, and that is the mass balanced equation of water vapor in the control volume:

$$m_a \frac{\partial w_a}{\partial z} + \frac{\partial m_{sol}}{\partial z} = 0 \tag{2-1}$$

Where m_a is mass air flow, kg/s ; m_{sol} is mass flow rate of solution, kg/s; w_a is air humidity , g/kg .

According to conservation of energy, the changing of liquid film heat equals to the change of heat-absorption of air, and that is the energy balanced equation in the control volume:

$$\frac{m_{sol}}{DY} dy \cdot \frac{\partial h_{sol}}{\partial z} dz = -\frac{m_a}{DY} dy \cdot \frac{\partial h_a}{\partial z} dz \tag{2-2}$$

Where DZ is the height of padding, mm; DY is the length of padding, mm; h_{sol} is specific enthalpy of solution, kJ/kg ; h_a is specific enthalpy of air, kJ/kg.

Eq. (2-2) can be arranged and simplified:

$$\frac{\partial (h_{sol} \cdot m_{sol})}{\partial z} = -m_a \frac{\partial h_a}{\partial z}$$

Mass transfer equation of air and solution in the control volume:

$$\frac{m_a}{DY} dy \cdot \frac{\partial w_a}{\partial z} dz = -\frac{\alpha_{ad} F_a}{DY \cdot DZ} (w_a - w_{sols}) dydz \tag{2-3}$$

Where F_a is the gas-liquid interfacial area of mass transfer, m^2; α_{ad} is the mass transfer coefficient , kg/m^2s ; w_{sols} is the humidity of solution surface , g/kg.

Make $NTU_{am} = \frac{\alpha_{ad} F_a}{m_a}$, then Eq.(2-3) is simplify:

$$\frac{\partial w_a}{\partial z} = \frac{NTU_{am}}{DZ} (w_a - w_{sols}) \tag{2-4}$$

The change of solution:

$$\frac{\partial m_{sol}}{\partial z} = \frac{m_a NTU_{am}}{DZ} (w_a - w_{sols}) \tag{2-5}$$

Heat transfer equation of air and solution in the control volume:

$$\frac{m_a}{DY} dy \cdot \frac{\partial h_a}{\partial z} dz = -\frac{\alpha_{ac} F_a}{DY \cdot DZ} (t_{sols} - t_a) dydz - \frac{r \alpha_{ad} F_a}{DY \cdot DZ} (w_{sols} - w_a) dydz \tag{2-6}$$

Simplify:

$$\frac{\partial h_a}{\partial z}=-\frac{\alpha_{ac}F_a}{m_a DZ c_{pm}}\left[c_{pm}\left(t_{sols}-t_a\right)+r\left(w_{sols}-w_a\right)c_{pm}\frac{\alpha_{ad}F_a}{m_a DZ}\cdot\frac{m_a DZ}{\alpha_{ac}F_a}\right] \tag{2-7}$$

$$\frac{\partial h_a}{\partial z}=-\frac{NTU_a}{DZ}\left[\left(h_{sols}-h_a\right)+\left(\frac{1}{Le}-1\right)r\left(w_{sols}-w_a\right)\right] \tag{2-8}$$

$$\text{where: } Le=\frac{\alpha_{ac}c_{pm}}{\alpha_{ad}}\ ,\ NTU_a=\frac{\alpha_{ac}F_a}{m_a c_{pm}} \tag{2-9}$$

Heat transfer equation of air and solution:

$$\frac{m_{sol}}{DY}dy\cdot\frac{\partial h_{sol}}{\partial z}dz=-\frac{\alpha_{ac}F_a}{DY\cdot DZ}\left(t_{sols}-t_a\right)dydz-\frac{r\alpha_{ad}F_a}{DY\cdot DZ}\left(w_{sols}-w_a\right)dydz \tag{2-10}$$

Simplify:

$$\frac{\partial h_{sol}}{\partial z}=-\frac{m_a NTU_a}{m_{sol}DZ}\left[\left(h_{sols}-h_a\right)+\left(\frac{1}{Le}-1\right)r\left(w_{sols}-w_a\right)\right] \tag{2-11}$$

Boundary condition:

$$z=0\ ,\ t_a=t_{a,in}\ ,\ h_a=h_{a,in}\ ,\ t_{sol}=t_{sol,in}\ ,\ w_{sols}=w_{sols,in} \tag{2-12}$$

Mass transfer coefficient: adopt the empirical formula [7] in the document.

Formula (2-4),the discrete equation of air humidity can be reached because of using difference equation instead of differential equation:

$$w_a\left(i+1\right)=\frac{NTU_{am}}{DZ}\left(w_a\left(i\right)-w_{sols}\left(i\right)+w_a\left(i\right)\right) \tag{2-13}$$

The change of solution flow rate can be obtained because of the discretization ofdifferential equation (2-5):

$$m_{sol}\left(i+1\right)=m_{sol}\left(i\right)-m_a\left(w_a\left(i+1\right)-w_a\left(i\right)\right) \tag{2-14}$$

The discrete equation of air enthalpy comes from differential equation(2-8):

$$h_a\left(i+1\right)=-\frac{NTU_a}{DZ}\left(h_{sols}\left(i\right)-h_a\left(i\right)\right)+\left(\frac{1}{Le}-1\right)r\left(w_a\left(i\right)-w_{sols}\left(i\right)\right)+h_a\left(i\right) \tag{2-15}$$

The change of solution enthalpy the discretization of differential equation(2-12):

$$h_{sol}\left(i+1\right)=-\frac{m_a NTU_a}{m_{sol}\left(i\right)DZ}\left(h_{sol}\left(i\right)-h_a\left(i\right)+\left(\frac{1}{Le}-1\right)r\left(w_{sols}\left(i\right)-w_a\left(i\right)\right)\right)+h_{sol}\left(i\right) \tag{2-16}$$

According to the equations(2-13)～(2-16)below, easy solved discrete equations are made up.

Solution of Model. The parallel adiabatic dehumidifier is selected, and the form we choose to use is packed tower whose size is 0.4m×0.4m×0.4m,.Metallic perforated &corrugated plate padding is adopted, whose specific surface is 500m^2/m^3.

Table 1 Range of entrance parameter

Inlet parameter Range of LiCl solution			Inlet parameter Range of air		
Concentration	Temperature	Flow rate	Humidity	Temperature	Flow rate
25-35%	25-35˚C	0.3-0.9 kg/s	16-24 g/kg	26-36˚C	0.2-0.9 kg/s

The inlet moist air enthalpy can be received through looking up the enthalpy-humidity diagram by using inlet air temperature and inlet air humidity or from the formula below:

$$h=C_{pg}\cdot t_{sol,in}+(2500+C_{pq}\cdot t)\frac{w}{1000} \tag{2-17}$$

C_{pg} is specific heat at constant pressure of dry air, 1.005kJ/kg·˚C; C_{pq} is specific heat at constant pressure of water vapor, 1.84 kJ/kg·˚C. Mass specific heat of water is 4.19 kJ/kg·˚C

The vapor pressure value of the solution surface can be reached though looking up vapor pressure diagram [6] of LiCl solution by using solution concentration and inlet temperature of solution.

The humidity of solution surface comes from $w = 0.622\dfrac{P_q}{B - P_q}$.

Where B is overall pressure of air; P_q is saturated vapor pressure of wet light bulb temperature.

The air humidity h_{sols} of the solution surface can be reached from (2-17) though looking up specific enthalpy data table of LiCl.

Regarding the parameters below as the initial value, it means that we can receive the value of the first node. The value of the second node can be received by using differential equations(2-14)——(2-16).Each parameter which contains the value of every node in the dehumidifier can be got by operating the MATLAB program written before. As a result, the last value of node is outlet parameter of the dehumidifier.

Analysis and discussion

Our research discusses the impact of inlet parameter on the outlet parameter through making use of numerical simulation method and control variable method. Firstly, choose a standard operating condition.

Table 2 Standard operating condition

Inlet parameter Range of LiCl solution			Inlet parameter Range of air		
Concentration	Temperature	Flow rate	Humidity	Temperature	Flow rate
30%	28˚C	0.6kg/s	20g/kg	34˚C	0.3kg/s

The impact of inlet solution concentration on the outlet parameter of air. When the solution concentration ranges from 25% to 35% and other parameters remain the same, the outlet humidity of air ranges from 14.5g/kg to 12.5g/kg. It means that the humidity removal is increasing because of the rising of concentration of desiccant solution, but the effect is not obvious.

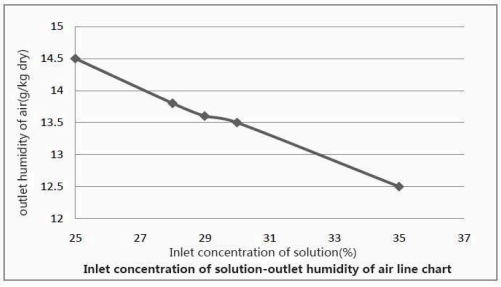

Figure3.1 The impact of inlet solution

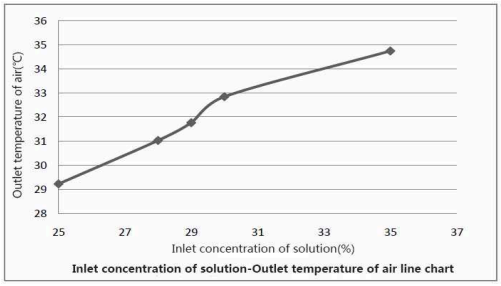

Figure3.2 The impact of solution temperature

It can be seen from figure3.2, the air temperature at the outlet is increasing. Because of the rise of entrance concentration of solution, partial pressure of water vapor on the surface is decreasing. That means the increasing partial pressure of water vapor makes dehumidification improve. So there is more condensed water vapor in the air. Water vapor gives out more latent heat of phase change due to condensing.

The impact of solution temperature on outlet parameter of air. As seen from Figure3.3,air moisture content at the outlet greatly ranges from 11 g/kg to 16g/kg. Air moisture content at the outlet is increasing by the rise of inlet solution temperature. This is due to the increasing solution temperature at the inlet making surface vapor pressure increase. That means partial pressure difference of water vapor is decreasing. It's bad for solution absorbing moisture in the air.

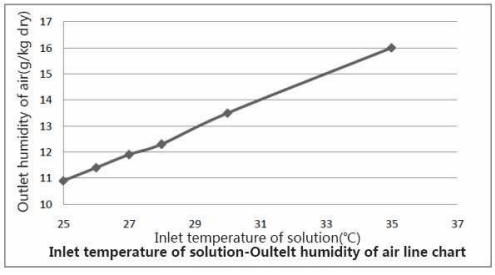

Figure3.3

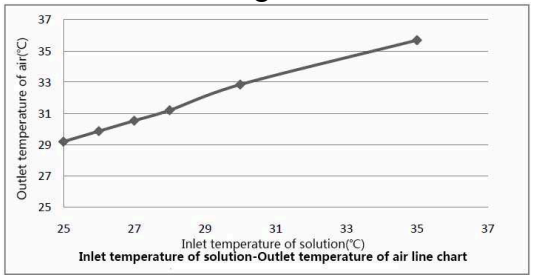

Figure3.4 Air temperature at the outlet rises

Figure3.4 shows that air temperature at the outlet rises from 29℃to 35 ℃. There are the same trend of Figure3.3 and Figure3.4. This is due to the decreasing heat transfer difference between air and solution. And then the outlet air temperature is increasing.

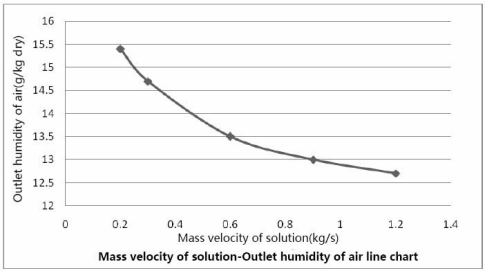

Figure3.5 The temperature of air

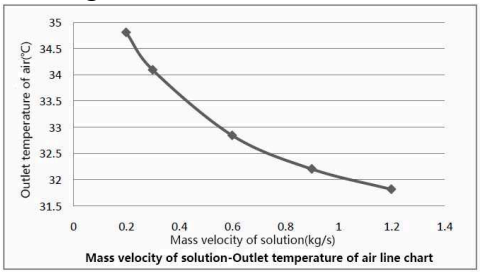

Figure3.6 The temperature of air

The impact of solution mass flow rate on outlet parameter of air. It can be seen from the Figure3.5 that the solution mass flow rate increases 1.0kg/s, and the air moisture content reduces to 12.7g/kg. The air moisture content at the outlet reduces as the solution mass flow rate increases. All of this is because that the increase of solution mass flow rate can promote the mass transfer between solution and air.

As seen from figure 3.6, the temperature of air at the outlet reduces from 34.8℃ to 31.8℃ . This temperature reduces with the increase of solution mass flow rate at the inlet. Because with the increase of solution mass flow rate, heat transfer coefficient increases , which then increases the heat transferring between air and solution.

4 Conclusions

Based on the simulation results, the following conclusions are concluded.

1)Referring to the energy balance and mass balance equation, A mathematical model describing heat and mass transfer performance of packed-type parallel flow dehumidifier was developed.

2)The effects of air flow rate, solution flow rate and inlet parameters of air and solution on the outlet parameters were also investigated.The outlet air moisture content is increasing with inlet air mass velocity, however it is decreasing with increasing of solution mass velocity. The outlet air moisture content is decreasing with increasing of inlet solution concentration.

Acknowledgments

The research described in this paper was supported by the National Natural Science Foundation of China (Grant No. 51106007) and Beijing Municipal Commission of Education (Grant No. 201210016018) and Beijing Nova Programm (No. XX2013011). These supports are gratefully acknowledged.

References

[1] Zhijia Huang, Luyue Hong, Fu Lei, The experimental research on liquid dehumidifier [D]. Ma'anshan in Anhui. Technology Engineering and Architecture institute of Anhui University, 2012

[2]Wenzhong Gao, Huajian Liu, Zhimin Wu, Qing Zhang, The study of strengthening heat transfer in the liquid desiccant of air conditioning system [J]. Refrigeration and Air-conditioning, 2010, 31(3)

[3]Yaodong Hu, Shiming Xu, Numerical simulation of the process of adiabatic and desiccant in solution [J]. Building Energy & Environment, 2012, 31(3)

[4]Weirong Zhang, Xiaohua Liu, Zhen Li, etc, The research of property of salt solution in liquid desiccant air conditioning system[C] National abstract book of heating ventilation air conditioning and refrigeration in annual academic conference(1), 2004

[5]Longzhou Tian, Absorption dehumidification in technological research [D]. Beijing: Beijing University of Chemical Technology, 2009

[6]Xiaoqin Yi, Study on character of desiccant solution in common use[D]. Beijing:Qsting Hua University,2011.

Advanced Materials Research Vols. 989-994 (2014) pp 3105-3109
© (2014) Trans Tech Publications, Switzerland
doi:10.4028/www.scientific.net/AMR.989-994.3105

A Novel Vertical Lift Machine and Its Precise Pose Control

Xiaobo Liu[1/2, a], Xiaofeng Wei[2, b], Xiaodong Yuan[2, c], Wei Ni[* 2, d]

[1]School of Mechanical and Electrical, Chongqing College of Electronic Engineering, Chongqing 401331, China;

[2] Research Center of Laser Fusion, China Academy of Engineering Physics, Sichuan 621000, China.

[a]lianhaopo@126.com, [b]xfwei@caep.cn, [c]xdyuan@caep.cn, [d]daweiym@126.com

* Corresponding author

Keywords: Vertical Lift Machine; 4-SHS Parallel robot; Inverse Kinematic analysis; Precise Pose Control.

Abstract. This paper deals with the design and theoretical analysis on a novel vertical lift machine which can vertically lift above 700 kg load up to 3.2 meters above the floor and located the load with high accuracy of position and orientation. Firstly the design model based on the installment demands of line-replaceable units (LRUs) is constructed. Then theoretical analysis including the number of degree of freedom of the lift machine, the inverse kinematic, the control principle, the lift platform pose error and the precise pose control method are conducted in the article. The validity of the design model and the effectiveness of the precise pose control system are confirmed by experiments using a prototype lift machine.

1. Introduction

Our laser facility which use over 2000 large optics of 26 different types to focus up to 48 laser beams on a dime-size target, currently under design and construction, will be the China's largest laser facility when completed [1]. As shown in Fig.1 the optics are held in large optic-mechanical assemblies called line-replaceable units (LRU) supported by a frame assembly unit (FAU) which is suspended 3.2 meters above the floor. The assembled LRUs which weigh up to 700 kilograms, and are about the size of a phone booth have strict specifications with respect to cleanliness, alignment, vibration, and wave-front so that once activated, each beam which must be enclosed in a stringently controlled environment will meet their performance requirements [2].Due to precision alignment requirements of the LRUs, LRUs in canister which mainly supports clean environment itself must be precisely located in 0.1mm position accuracy and 0.1° orientation accuracy relative to the FAU. Some traditional lift equipments such as the scissors lift platform [3], the forklift [4] can meet lifting demands of LRUs installment, but scissors lift platform is always unsteady and the forklift brings a lot errors. This paper deals with the design and theoretical analysis on a novel vertical lift machine which is capable to fulfill the tasks of LRUs installment. The machine primarily adopts 4-*SHS*-1*H* mechanism and a pose error compensation system, Herein, *S* and *H* represent spherical joint and helical joint respectively.

2. Vertical Lift Machine Description

As shown in Fig.1, the vertical lift machine is composed of four primary components: cleanness canister, four jacks leveling mechanism, vertical lift mechanism and electrical control system. Herein the four jacks and lift mechanism are extracted to construct a mechanical transmission model of vertical lift machine as shown in Fig.2. The four jacks leveling mechanism is composed of a fixed base, a moving platform and four identical *SHS* motion chains, which will be used to derive inverse kinematic equations. The 1-*H* mechanism is composed of a fixed base, a moving platform and only one *H* motion chain. The fixed base of leveling mechanism is attached to the earth, but the fixed base of the latter is the moving platform of leveling mechanism. The moving platform of the latter will be

used to lift LRUs as vertical lift machine's end manipulator. Theoretically the LRUs which are aligned with the entrance of FAU can install into the FAU easily when the lift platform and the FAU are paralleled with the same floor. But actually the mission is hardly realized because a lot of error such as fabrication error, measure error and installation error are concurrent. In order to install the LRUs quickly and precisely, the lift platform must be keep level during lifting in case of FAU paralleled with the same floor. The kinematic analysis of the lift machine is conducted in order to realize how to keep the platform level.

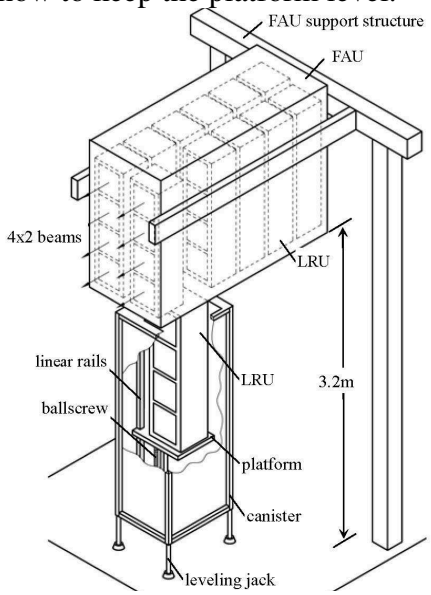

Fig. 1 Arrangement of LRUs in laser facility

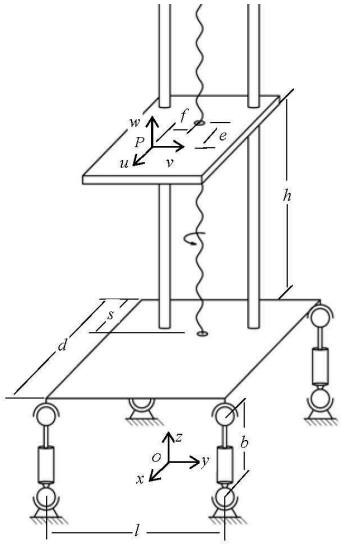

Fig. 2 Mechanical transmission model

The degree of freedom of the 4-*SHS* mechanisms can be solved through the traditional *G-K* formula [5] as follows easily:

$$M = 6(n-g-1)+\sum_{i=1}^{g} f_i + \nu - \varsigma = 6\times(8-9-1)+21-6 = 3$$

Where n is the number of the bar of mechanism, g is the number of kinematic joints of mechanism, f_i is degrees of freedom of i kinematic joints, v is the number of the virtual constraint of mechanism, ζ is the partial freedom of mechanism. It is well known that leveling the platform can be realized by three jacks but one chain of 4-SHS is a redundant motion chain, like door hinges, which is merely designed to reinforce structure rigidity and stability. So the 4-SHS mechanism has three degrees of freedom, which are a rotation about x axis, a rotation about y axis and a translation along z axis.

3. Inverse kinematic analysis

In this section, kinematics of the simplified model is derived and used for the output of precise pose control system. The pose of the load supporting place (LSP) of the lift platform in the machine is represented by the 4x4 matrix operator

$$\begin{bmatrix} {}^{O}S_{\mathrm{i}}{}^{\mathrm{u}} \\ 1 \end{bmatrix} = \begin{bmatrix} {}^{O}_{P}R & {}^{O}P \\ 0 & 1 \end{bmatrix} \begin{bmatrix} {}^{P}S_{\mathrm{i}}{}^{\mathrm{u}} \\ 1 \end{bmatrix} \text{ (i=1}\sim\text{4)} \quad (1)$$

Where ${}^{O}S_{\mathrm{i}}{}^{\mathrm{U}}$ and ${}^{P}S_{\mathrm{i}}{}^{\mathrm{U}}$ are respectively position vector of the upper spherical joint in floor frame $\{O\}$ and platform frame $\{P\}$. ${}^{o}_{P}R$ is the rotation matrix of frame $\{P\}$ related to frame $\{O\}$, and so on. The definition about matrix ${}^{o}_{P}R$ as follows [6]: Start with the frame coincident with a known frame $\{O\}$. Rotate $\{P\}$ first about x-$\{O\}$ by an angle γ, then about y-$\{O\}$ by an angle β, and finally, about z-$\{O\}$ by an angle α. The rotation matrix is

$$ {}^{o}_{p}R = \begin{pmatrix} c\alpha c\beta & c\alpha s\beta s\gamma - s\alpha c\gamma & c\alpha s\beta c\gamma + s\alpha s\gamma \\ s\alpha c\beta & s\alpha s\beta s\gamma + c\alpha c\gamma & s\alpha s\beta c\gamma - c\alpha s\gamma \\ -s\beta & c\beta s\gamma & c\beta c\gamma \end{pmatrix} \tag{2} $$

Where $c\alpha = \cos\alpha$, $s\alpha = \sin\alpha$, α, β, γ are the *X-Y-Z* fixed angles and so on. The inverse displacement problem of this machine can be stated as follows: given the pose (position and orientation) of moving platform and structural parameters, determine four strokes of helical input joints. Suppose the pose of moving platform is given, the rotation matrix as shown in Eq. (2) and ${}^{O}S_{\mathrm{i}}{}^{\mathrm{U}}$ as shown in Eq. (1) are determined When

$$ {}^{O}P = [s+e-d/2,\ f-l/2,\ h+b]^{\mathrm{T}};{}^{o}S_{1}^{U} = [d/2,\ -l/2,\ b]^{\mathrm{T}};{}^{O}o = [0,\ 0,\ 0]^{\mathrm{T}} $$

There are the solutions about ${}^{O}S_{\mathrm{i}}{}^{\mathrm{U}}$ as follows:

$$ \begin{cases} {}^{O}S_{1\mathrm{x}}{}^{\mathrm{U}} = d/2 + h(\sin\alpha\sin\gamma + \cos\alpha\sin\beta\cos\gamma) + (f-l/2)(\sin\alpha\cos\gamma - \cos\alpha\sin\beta\sin\gamma) + (e-d+s)\cos\alpha\cos\beta; \\ {}^{O}S_{1\mathrm{y}}{}^{\mathrm{U}} = (\mathrm{e}-d+s)\sin\alpha\cos\beta - \mathrm{h}(\cos\alpha\sin\gamma - \sin\alpha\sin\beta\cos\gamma) - (f-l/2)(\cos\alpha\cos\gamma + \sin\alpha\sin\beta\sin\gamma) - 1/2; \\ {}^{O}S_{1\mathrm{z}}{}^{\mathrm{U}} = b - (f-l/2)\cos\beta\sin\gamma - (e-d+s)\sin\beta + h\cos\beta\cos\gamma. \end{cases} \tag{3} $$

Suppose α, β and γ equal zero, namely the load platform is absolutely parallel with the floor. According to mechanism theory, ${}^{O}S_{1\mathrm{x}}{}^{\mathrm{U}*}$, ${}^{O}S_{1\mathrm{y}}{}^{\mathrm{U}*}$ and ${}^{O}S_{1\mathrm{x}}{}^{\mathrm{U}*}$ which are coordinate of theoretical level point must be existed in Eq. (2). Thus the stroke of the first helical input joint is obtained as follows:

$$ \Delta H_1 = \sqrt{({}^{O}S_{1\mathrm{x}}{}^{\mathrm{U}} - {}^{O}S_{1\mathrm{x}}{}^{\mathrm{U}*})^2 + ({}^{O}S_{1\mathrm{y}}{}^{\mathrm{U}} - {}^{O}S_{1\mathrm{y}}{}^{\mathrm{U}*})^2 + ({}^{O}S_{1\mathrm{x}}{}^{\mathrm{U}})^2} \tag{4} $$

ΔH_2, ΔH_3 and ΔH_4 are obtained easily in this way.

4. Control Principle

It is well konwn that the cantilever structure which is bearing the load always exists the bench deformation. So these LRUs which are put in the load platform are impossible to be lifted at the required height without any help due to these deformations existed. The offset of pose of the lift platform detected by a level sensor which is located in the platform is then fed to the vertical lift machine's pose error compensation system which drives the four helical legs to determine their respective strokes in Eq. (4). The pose of LRU during Its installment will be real-timely corrected until gaining designed lift position and orientation. The control principle diagram of the lift machine is constructed as shown in Fig.3. β and γ which are the misalignment of the platform from its intended docking orientation are detected by the 2-axis orientation sensor whose precision is superior to fractions of a degree. The mass of LRU is detected by three load sensors, and the lift height is detected by the lift actuator's encoder once the pitch of ball screws and gear speed is given. Of course these parameters have been calibrated with the aid of level instrument, scale, calipers and gravity platform before the lift machine is put to use.

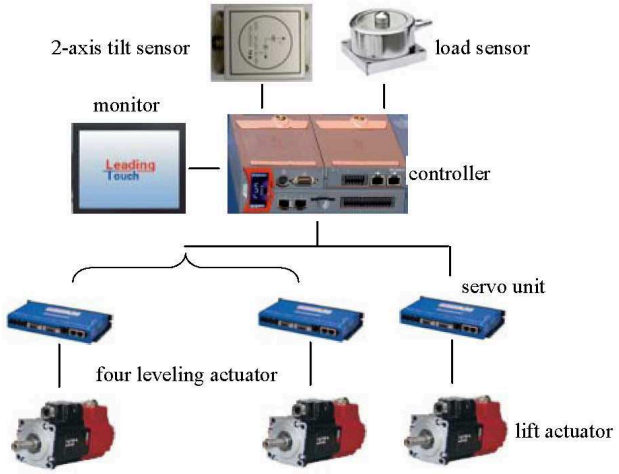

Figure.3 Control principle diagram of lift machine

5. Experiments

In this section, some experiments, such as load capacity, positioning accuracy, orientation accuracy, velocity test were provided to justify validity of the design model and the effectiveness of the precise pose control system. The model parameters of experiment are given in Table 1. The prototype of the vertical lift machine has been fabricated as shown in Fig 4.

Table 1 Parameters of the lift machine

F (Kg)	l (m)	d(m)	b(m)	h(m)	s(m)	e(m)	f(m)
750	1.15	1.1	0.25 ~ 0.58	0.35 ~ 2.80	0.2	0.1	0.1

At last the vertical lift machine obtains a 750Kg LRU positioning accuracy of 0.1 mm and orientation accuracy of 0.1 degree detected by Leica TCA1800 laser ranging equipment (made in Switzerland) at the place where is designed to locate the LRU in FAU. Experimental results state the vertical lift machine meets the demand of the LRUs installment.

(a) outside view

(b) LRU lift test

Figure.4 Prototype and test process of the lift machine

6. Conclusion

A novel vertical lift machine which is primarily composed of the 4-SHS-1Hmechanism and pose error compensation system to precisely vertical lift heavy load at large stroke is proposed in this article. At last the linear error less-than 0.1mm and angular error less-than 0.1^{o} are received with the aid of the vertical lift machine. The analysis including the number of degree of freedom of the lift machine, inverse displacement, control principle and the lift platform pose error caused by gravity of load merely during lifting are conducted in the article. The contributions of this study are proposing a kind of vertical lift machines that meets these demands such as heavy load, large stroke, high precision and cleanness. Above all the lift platform pose offset can be compensated real-timely by the kind of vertical lift machine during load-lifting.

References

[1] H.S. Peng, X.M. Zhang and X.F. Wei: Status of the SG-III Solid-State Laser Project, SPIE[C],1998,3492:25-33.

[2] Yu Haiwu, Jing Feng, Wei Xiaofeng and Zheng Wanguo**:** Status of Prototype of SG-III High-Power Solid-State Laser, SPIE[C], 2009, 7131: 713112-1-713112-6.

[3] Tian Hongyu and Zhang Ziyi: Design and Simulation Based on Pro/E for a Hydraulic Lift Platform in Scissors Type, Procedia Engineering. 16 (2011),772-781.

[4] Tim Horberry, Tore J Larsson, Ian Johnston and JohnLambert: Forklift safety, traffic engineering and intelligent transport systems: a case study, Applied Ergonomics. 35 (2004), 575-581.
[5] Huang Zhen, Zhao Yongsheng, Zhao Tieshi: *Advanced Spatial Mechanism kinematics*(Higher Education Press, China, 2006).p.115-135.
[6] HONG Jiazhen, YANG Changjun: *Theoretical Mechanics*(Higher Eduacation Press, Beijing, 2008).p.158-178.

Advanced Materials Research Vols. 989-994 (2014) pp 3110-3113
© (2014) Trans Tech Publications, Switzerland
doi:10.4028/www.scientific.net/AMR.989-994.3110

Investigation on Flat Wheel In-Suit Measuring System and Errors Compensation for Wheel Radius under Aspheric Grinding Process

Fengming Nie [1,2, a], Zhanguo Li [1,3, b] Qingtang Wu [3, c]

[1] Changchun University Of Science And Technology, ChangChun 130022, China;

[2] Changchun Institute of Process Equipment, ChangChun 130022, China;

[3] Changchun University, ChangChun 130022, China;

[a]nfm2006@sina.com, [b]250793721@qq.com, [c] wqtwj@sohu.com,

Keywords: Flat Wheel, Aspheric Grinding Process, Errors Compensation.

Abstract. The paper mainly studied flat wheel's surface precision, through envelope method, the wheel is used for grinding large aperture axial symmetry aspherical surface. With non-contact measuring method, designed and developed measuring system for wheel in-suit inspection. Aimed at wheel radius errors, proposed the compensation method, so it has certain value to enhance the surface precision.

Introduction

Aspheric method is used for grinding large aperture aspherical surface ,in the process of precision grinding, the diamond plat wheel occured wear, it would influence shape precision. in order to ensure the aspheric surface precision. Lan Shan-chao studied the influence law of the grain size for grinding wheel wear. using the DEFORM, analyzed the wear regularity of single CBN grain. Liu Jia studied the influence law of the processing parameters for corrected surface roughness and grinding force, under the process that diamond roller dressed cup CBN wheel. Got the best corrected parameter[1]~[5].

The paper aimed at plat wheel used for grinding aspherical surface, designed the measuring equipment for wheel in-suit inspection. It could detect the wheel shape error. Build the mathematical model. It was used to analyze the wheel's surface precision. measured the wheel radial error and carried out the compensation grinding test for 330~330mm square axial symmetry aspheric surface.

Envelope grinding theory for aspheric surface

When the generation line rotates about its rotational axis, the surface of revolution will form. This is structural feature of the axial symmetry aspheric surface. The aspheric surface meridional transversal is the rotational generation, the mathematical expression of curvilinear equation is:

$$Z(x)=\frac{cx^2}{1+\sqrt{1-c^2(k+1)x^2}}+dx^4+fx^6+gx^8+..... \quad (1)$$

c---------- surface vertex curvature, $c=1/R_0$;

R_0----------surface vertex curvature radius;

k----------quadric surface eccentricity function;

d,f,g--------higher term coefficientof the equation;

z---------- rotational axis of the axial symmetry aspheric surface.

When k<-1,the shape is hyperbola; when k=-1,the shape is ellipse;when -1<k<0,the shape is circle; when k>0,the shape is oblate ellipsoid. When the rotational generation rotates about Z axis, secondary rotational surface will take shape.

The envelope grinding theory for aspheric surface was shown in the Fig.1.In grinding processing, along the aspheric surface optical element meridian,the X,Y,C axis achieved interpolation motion. It

ensured that grinding point was always tangent to the aspheric optical elementsurface.Through the work piece rotary motion,wheel feed movement and rotational motion of wheel spindle turntable, the aspheric optical could be grinded out. According to the envelope grinding theory, Each axis equations of motion are:

$$X = x_i - R_w \times Sin(\arctan(f'(x_i)))$$
$$Z = f(x_i) + R_w \times Cos(\arctan(f'(x_i))) \quad (2)$$
$$C = \arctan(f'(x_i))$$

X, Z, C ——control center coordinatesof the machine tool;

x_i ——interpolate Point x position of the axial symmetry aspheric surface generation;

$f(x_i)$ ——the axial symmetry aspheric surface generation function;

R_w ——plat wheel radius;

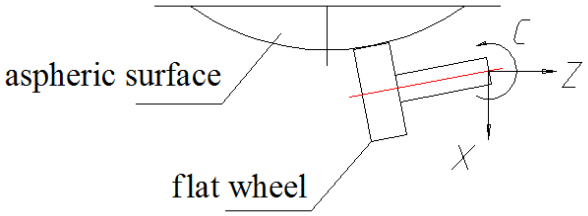

Fig.1. The theory of the plat wheel grinding the aspheric surface

Design of the wheel measuring system

The diamond particles form diamond wheel by cementation. So the wheel is a kind of porous object. According to different shapes, the diamond wheel includes plat wheel ,arc wheel and Spherical wheel. The plat wheel is often used to grind convex aspheric surface, as shown in the Fig.2;But the wear caused by long-term use will change the surface shape accuracy, then influence grinding performance and profile accuracy, therefore, before grinding the aspheric surface, must measure the wheel profile error, choose appropriate wheel radius, and achieve surface error compensation during grinding.

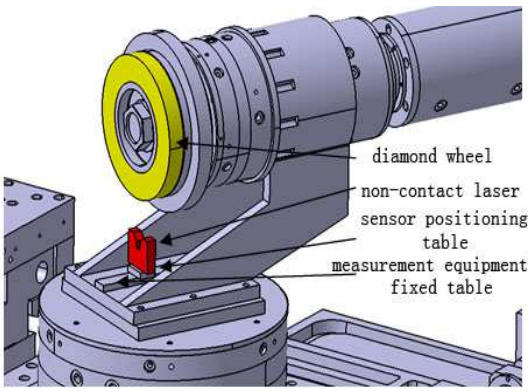

Fig.2. Measuring system for flat wheel in-suit inspection

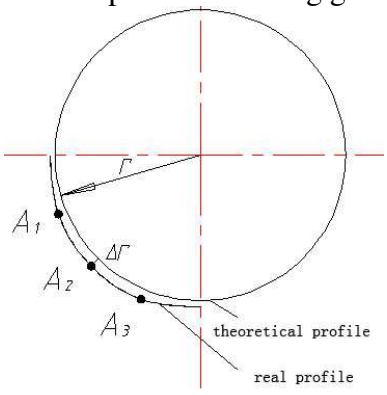

Fig.3. Plat wheel measuring point

In this paper,designed and developed measuring system for wheel profile in-suit inspection,the system included non-contact laser displacement measurement sensor,sensor positioning table,measurement equipment fixed table and measurement software.The measurement range was ±1mm,beam diameter was 1mm×20μm,resolution ratio was 0.02μm,measurement accuracy was ±0.1μm,and sampling period is 110μs.As shown in the figure 3,when measuring,the non-contact laser pointed at width midpoint of the plat wheel,when the wheel rotated a circle,the shape precision of circular cross section could be measured,then figured out the wheel radius, profile accuracy and radial error.

Wheel shape error compensation method

As shown in the figure 3, the wheel surface existed non-collinear three points:A_1 (x_1, y_1), A_2 (x_2, y_2), A_3 (x_3, y_3).the outer circle equation was:

$$x^2 + y^2 + Dx + Ey + F = 0 \tag{3}$$

plugged A_1 , A_2 , A_3 into equation(3):

$$\begin{cases} x_1 D + y_1 E + F = -(x_1^{\,2} + y_1^{\,2}) \\ x_2 D + y_2 E + F = -(x_2^{\,2} + y_2^{\,2}) \\ x_3 D + y_3 E + F = -(x_3^{\,2} + y_3^{\,2}) \end{cases} \tag{4}$$

according to Cramer's rule:

$$D = \frac{\begin{vmatrix} -(x_1^{\,2}+y_1^{\,2}) & y_1 & 1 \\ -(x_2^{\,2}+y_2^{\,2}) & y_2 & 1 \\ -(x_3^{\,2}+y_3^{\,2}) & y_3 & 1 \end{vmatrix}}{\begin{vmatrix} x_1 & y_1 & 1 \\ x_2 & y_2 & 1 \\ x_3 & y_3 & 1 \end{vmatrix}} = \frac{\begin{vmatrix} -(x_1^{\,2}+y_1^{\,2}) & y_1 & 1 \\ (x_1^{\,2}+y_1^{\,2})-(x_2^{\,2}+y_2^{\,2}) & y_2-y_1 & 0 \\ (x_1^{\,2}+y_1^{\,2})-(x_3^{\,2}+y_3^{\,2}) & y_3-y_1 & 0 \end{vmatrix}}{\begin{vmatrix} x_1 & y_1 & 1 \\ x_2-x_1 & y_2-y_1 & 0 \\ x_3-x_1 & y_3-y_1 & 0 \end{vmatrix}}$$

$$E = \frac{\begin{vmatrix} x_1 & -(x_1^{\,2}+y_1^{\,2}) & 1 \\ x_2 & -(x_2^{\,2}+y_2^{\,2}) & 1 \\ x_3 & -(x_3^{\,2}+y_3^{\,2}) & 1 \end{vmatrix}}{\begin{vmatrix} x_1 & y_1 & 1 \\ x_2 & y_2 & 1 \\ x_3 & y_3 & 1 \end{vmatrix}} = \frac{\begin{vmatrix} x_1 & -(x_1^{\,2}+y_1^{\,2}) & 1 \\ x_2-x_1 & (x_1^{\,2}+y_1^{\,2})-(x_2^{\,2}+y_2^{\,2}) & 0 \\ x_3-x_1 & (x_1^{\,2}+y_1^{\,2})-(x_3^{\,2}+y_3^{\,2}) & 0 \end{vmatrix}}{\begin{vmatrix} x_1 & y_1 & 1 \\ x_2-x_1 & y_2-y_1 & 0 \\ x_3-x_1 & y_3-y_1 & 0 \end{vmatrix}}$$

plugged D, E into original equation,got the $O(x_0, y_0)$ expression：

$$\begin{aligned} x_0 &= -\frac{D}{2} = -\frac{1}{2}\frac{(y_3-y_1)(x_1^{\,2}+y_1^{\,2}-x_2^{\,2}-y_2^{\,2})-(y_2-y_1)(x_1^{\,2}+y_1^{\,2}-x_3^{\,2}-y_3^{\,2})}{(x_2-x_1)(y_3-y_1)-(x_3-x_1)(y_2-y_1)} \\ y_0 &= -\frac{E}{2} = -\frac{1}{2}\cdot\frac{(x_2-x_1)(x_1^{\,2}+y_1^{\,2}-x_3^{\,2}-y_3^{\,2})-(x_3-x_1)(x_1^{\,2}+y_1^{\,2}-x_2^{\,2}-y_2^{\,2})}{(x_2-x_1)(y_3-y_1)-(x_3-x_1)(y_2-y_1)} \end{aligned} \tag{5}$$

Actual measurement wheel radial error was:

$$\Delta r = r - R_w = \sqrt{(x_1-x_0)^2+(y_1-y_0)^2} - R_w \tag{6}$$

Considering the actual measurement wheel radial error,the actual grinding control equation was:

$$\begin{aligned} X &= x_i - (R_w + \Delta r)\times Sin\left(\arctan(f'(x_i))\right) \\ Z &= f(x_i) + (R_w + \Delta r)\times Cos\left(\arctan(f'(x_i))\right) \\ C &= \arctan(f'(x_i)) \end{aligned} \tag{7}$$

Compensation grinding test

The aspheric surface accurate grinding tool adopted linear interpolation method and could achieve the grinding test.The wheel revolving speed was 1100rpm,workpiece rotational speed was 81rpm,the grinding feed was 0.5μm, the feed speed was 10mm/min.The tool could grind 330~330mm square axial symmetry aspheric surface, the inductance type micrometer with 0.01μm resolution could

measure the first grinding aspheric surface and measured surface error was 12μm,the result was shown in figure 4.

After measuring ,should compensated the wheel radius.When compensation grind completed with the same parameter,the measurement aspheric surfaceerror PV was less than 3μm,the result was shown in figure 5.

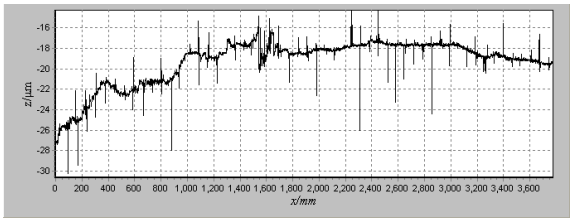

Fig.4. The initial grinding diagonal error

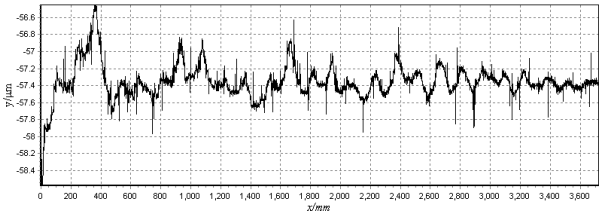

Fig.5. The compensation grinding diagonal error

Conclusion

The paper mainly studied flat wheel's wear problem,through envelope method,the wheel is used for grinding large aperture axial symmetry aspherical surface.With non-contact measuring method,designed and developed measuring system for wheel in-suit inspection. Proposed the wheel radius errors compensation method and carried out the compensation grinding test for 330~330mm square axial symmetry aspheric surface.It was observed that developed wheel measurement device could achieve the wheel on-machine measurement request,its measurement accuracy was ±0.1μm and speed was very fast.The compensation grinding test showed that the wheel radial compensation method could satisfy the aspheric surface grinding request,the accuracy was improved by 9μm,So it has certain value to grind the aspheric surface.

References

[1] S.H.Yin, H.F.Li, Y.F.Fan, etal. Development of ultra-Precision grinding Proeess for aspheric surface based on feed rate controlling and error Compensation methods. Advanced Materials Researeh, 2010, 97-101: 2192-2196.

[2] H.B.Cheng, Z.J.Feng, K.Cheng, etal. Design of a six-axis high Precision maehine tool and its application in machining aspherical optical mirrors. International Journal of Maehine Tools and Manufaeture, 2005, 45(9): 1085-1094.

[3] T.Suzuki,K.Syoji, T.Kuriyagawa,et al.Machining Non-axisymmetric Aspheric Surfaces with Parallel Grinding Technology. Proc.of JSPE, Tokyo Japan, 2001,(3):236～241

[4] W. Ling, H. Omori, T. Yamada, et al. Studies on Manufacture of Long Dimension X Radial Mirror. Proc. of JSPE, 2006, (10):296～300.

[5] T. Suzuki, K. Syoji, T. Kuriyagawa, et al. Machining Non-axiymmetric Aspheric Surface with Parallel Grinding Technology. Proc. of JSPE, 2008, (3):236～241

Advanced Materials Research Vols. 989-994 (2014) pp 3114-3116
© (2014) Trans Tech Publications, Switzerland
doi:10.4028/www.scientific.net/AMR.989-994.3114

An Intelligent Fault Monitoring System for Hydraulic Excavator

Lin Ni[1a], Xiusheng Chen[2b], Anlin Wang[3c], Shukun Cao[2d]

[1]Shanzhong Construction Machinery co,Ltd, Linyi 276024, China
[2]School of Mechanical Engineering, University of Jinan, Jinan 250022, China
[3]School of Mechanical Engineering, Tongji University, Shanghai 200092, China

[a]nilin@ strongest.cn,[b]chenxiusheng@aliyun.com, [c] wanganlin@tongji.edu.cn ,
[d]me_caosk@ujn.edu.cn

Keywords: monitoring system; inspection controller; traveling controller.

Abstract. In this paper, functions of intelligent fault monitoring system of hydraulic excavator are analyzed. Architecture of the fault monitoring system is presented. Key technologies of the monitoring system are discussed detailed. Key parts of the fault monitoring system such as inspection controller, travel controller and programmable monitor, remote monitoring system is developed. As a result, the intelligent monitoring system is of great useful for monitoring the faults of hydraulic excavator.

Introduction

Fault is one of the main factures which affect the hydraulic excavators' working efficiency. Two methods can be used to decrease the faults. One is improving the reliability the machine's design and manufacturing process. The other is to detect and eliminate the fault in time. Due to the severe working condition, faults of hydraulic excavator cannot be eliminated completely through the design and manufacturing process. Using the fault monitoring system, fault of the construction machines can be detected and eliminated rapidly. In the monitoring system, faults are detected by the sensors set on the fault parts. Fault monitoring system is seen as one of the key parts of modern construction machines by the construction machine manufactures such as Caterpillar, Kamatsu, Volvo, Hitachi , Xugong, Shantui[1-4], etc. Caterpillar's monitoring system named as EMS and Advisor. Kamatsu's monitoring system is KOMTRAX. Both of the monitoring systems of caterpillar and Kamatsu have the following functions[1,2]: monitoring the temperature of motor cooling water, oil temperature of hydraulic system, transmission system, oil pressure, fuel level, air piper temperature, cooling water flux, electric system's working condition, etc. The application of the monitoring system greatly improved the constructions' quality.

Obvious progress have made in the area of monitoring systems' research and development, however, most of domestic hydraulic excavator manufacturer have not developed a useful fault monitoring system for hydraulic excavators. Therefore, this paper proposed a hydraulic excavator's fault monitoring system. The system can meet the requirements of fault monitoring and intelligent diagnostics of modern hydraulic excavator.

Architecture of the Fault Monitoring System

To execute the monitoring function, the monitoring system is designed to be composed of sensors, system controller, motor electrical control unit, traveling controller, detection controller, GPS terminal device, data base server and user interface, etc. System controller is used to receive and display the inspection data. The controller can be divided into programmable controller, programmable monitor and CAN bus. Traveling controller is used to control the machine's movement. Functions of the detection controller are dealing with detection data. Sensors are used to monitoring the parts' status and collecting state data. GPS terminal device is used to send the monitoring data to the remote monitoring system (center) and receive the orders from the monitoring system. The remote monitoring system is applied to remote monitoring the machining working status and displays the monitoring data on its screen. When necessary, the monitoring center can send out instructions to control the hydraulic excavator. Construction of the system is shown in Fig.1.

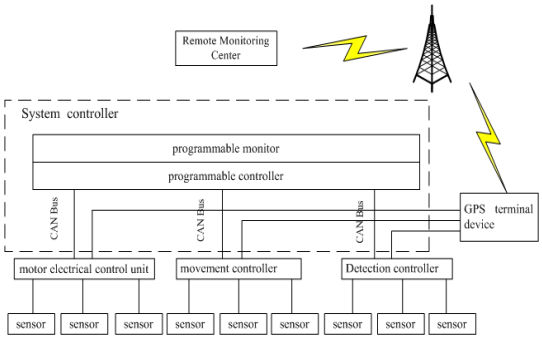

Figure 1. Construction of the Fault Monitoring System

Key parts of the Fault Monitoring System

1. Detection controller

Detection controller is connected with air cleaner sensor, working oil cleaner sensor, traveling oil cleaner sensor, fuel level sensor, hydraulic oil temperature sensor, travel brake solenoid valve, start the system battery relay, start battery relay, safety battery relay, and start motor. The controller real time detects the sensors and analysis the collected data. Using the CAN bus, the analyzed data is transferred to the monitor. The data is further analyzed by the monitor. If the abnormal signal is found, the fault message will be informed to the hydraulic excavator diver through the words displayed on the monitor's screen. The displayed message contains air cleaner clogging, movement oil cleaner clogging, movement brake magnetic valve fault, hydraulic oil temperature, etc.

2. Traveling controller

Traveling controller is connected with traveling systems handle, solenoid valves, travel motor and motor speed sensors. Using the data transferred from the sensors, the controller can make the judgments of the handle potentiometer's working status, CAN bus's communication status, solenoid valve's working status, travel motor's working status, etc. The judgments accompanied with handle resistance value and motor speed values are transferred to the monitor. The received signals classified and processed by the monitor, and then informed to the driver.

3. Programmable monitor

The programmable monitor is composed of ARM series CPU, 2M memories FLASH, real-time clock chip, memories for the parameters storage, monitor control chip, LED light control chip, etc. The whole system runs under the control of the ARM CPU. The monitor communicate with engine and controllers through CAN bus. Monitor received the monitoring information through the CAN bus, judge and displays the analogs (such as engine cooling water temperature, oil pressure, fuel quantity, and so on), switch information and alarm messages.

4. Remote monitoring system

Remote monitoring system is composed of GPS device, computer hardware and software.GPS device contains GPS module, communication module, control module. Main function of the control module is processing the received information. GPS module is used to positioning the hydraulic excavator. Communication module is used to send and receive the wireless signal. A user interface is developed to display the monitoring information of hydraulic excavators. Using the interface, information of the hydraulic excavator (Fig.2) working status (Fig.3), and monitoring parameters (Fig.4) can be displayed.

Excavator Information					
No.	Excavator Serial	Excavator type	Sailing status	Business agent	Current location
1	18264	913D	In warehouse		Shandong Linyi
2	401966	913D	Sailed	Anhui Shanzhong co,Ltd	Anhui Hefei
3	400440	921C	On sailing		Shandong Linyi
4	400902	921C	Sailed	Yunnan Shanzhong co,Ltd	Yunnan Kunming
5	400130	808D	In warehouse		Shandong Linyi
6	400900	913D	Sailed	Yunnan Shanzhong co,Ltd	Yunnan Dali

Figure 2 Information of the hydraulic excavator

Excavator Information					
No.	GPS manufacture	GPS mode	Lock	Working time	Working Status
1	Nanjing Jimeisi	Nomal	Unlock	20.6H	no working
2	Nanjing Jimeisi	Nomal	Unlock	109.5h	working
3	Nanjing Jimeisi	Nomal	Unlock	19.3H	no working
4	Nanjing Jimeisi	Nomal	Unlock	201.9H	working
5	Nanjing Jimeisi	Nomal	Unlock	10.5H	no working
6	Nanjing Jimeisi	Nomal	Unlock	77.3H	working

Figure 3 Hydraulic excavator working status

GPS serial	401966	GPS type	CAN	Star number	14	Latest time	2012-10-10 12:42:13	User information
Current location	Binhe Road, Linyi, Shandong, China							
GPS alarming				Device alarming				
Warehousing date	2012-10-09	The delivery date		Sails date		GPS beginning date		
Speed	1577rpm	Water temperature	100	Fuel level	99%	GPS ending date		

Figure 4 Monitoring parameters displayed on the user interface

Conclusions

The monitoring system presented (proposed) in this paper has been applied on the hydraulic excavators of Shanzhong Construction Machinery co,Ltd. The application shown that the fault monitoring system is great useful to aid in time finding and dealing with the hydraulic excavators' faults.

Acknowledgement

The authors gratefully acknowledge the support of this research by Postdoctoral innovative projects fund of Shandong Province (Grant no.201002006) and Doctoral Research Foundation (Granted by University of Jinan, XBS0831).

References

[1] http://china.cat.com/equipment/track-type-tractors http://china.cat.com/, [EB/OL]. 2010.10.
[2] http://www.bjhengri.com/News/ShowInfo.aspx?ID=54[EB/OL]. 2010.10
[3] http://www.hitachi-c-m.com/cn/products/excavator/medium/index.html,[EB/OL].2010.10
[4] http://www.volvo.com/constructionequipment/asia/zh-cn/BAHome_ILF.htm, [EB/OL].2010.10

Advanced Materials Research Vols. 989-994 (2014) pp 3117-3121
© (2014) Trans Tech Publications, Switzerland
doi:10.4028/www.scientific.net/AMR.989-994.3117

Modeling and Simulation of Feed Drive System Vibrations Based on Dual Inertia System

Liang Luo[a], Weimin Zhang[b] and Yuelei Zhang[c]

School of Mechanical Engineering, Tongji University, Shanghai 201804, China.

[a]luoliang0909@126.com, [b]iamt@tongji.edu.cn, [c]zyl741862@qq.com

Keywords: Machine Tool, Feed Drive Vibration, Trajectory Profiles

Abstract. The motion commands to feed drives constitute a major source for excitation of the vibrations. In this paper the vibration of feed drive caused by the motion commands is simulated by using a mathematic method. The mechanical transmission system is modeled as a dual inertia system. Three typical trajectories are used to analyze the effect of motion profiles on feed drive vibration by using a simulation model of feed drive controller.

Introduction

The motion commands to feed drives constitute a major source for excitation of the vibrations [1]. In order to push the speed and accuracy boundaries of present systems further, current research focus on the vibration reduction and avoidance of the feed drives. Additional damping modules or structures are integrated in the control loops to achieve this goal, such as semi-active damping system and set point filtering etc. Active damping system reacts only when a vibration is present and set point filtering can lead to path deformation [2, 3, 4]. Another way to solve this problem is generate a smoother trajectory. For this purpose, numbers of trajectory algorithms are found out and the frequency contents of the trajectory orders are discussed and compared [5, 6]. The vibration caused by the trajectory is difficult to analyze on hardware because of the coupling factor of various excitation sources.

In this paper the vibration of feed drive caused by the motion commands is simulated by using a mathematic method. The mechanical transmission system is modeled as a dual inertia system. Three typical trajectories are used to analyze the effect of motion profiles on feed drive vibration by using a simulation model of feed drive controller.

Structural dynamic model of feed drive

The typical structure of ball screw drive system consists of servo-motor, lead screw coupling, ball screw with nut and table, as shown in Fig. 1. Ball screw drives exhibit torsional flexibilities at the motor shaft-screw coupling, screw itself, and nut. Currently the structural flexibility of the machine tool reflected to the drive is not explicitly considered in rigid body based controllers. Rigid body transfer function can't describe the vibrations of the ball screw feed drive. Thus the flexible body model of the feed drive is needed to illustrate the vibrations of the ball screw feed drive.

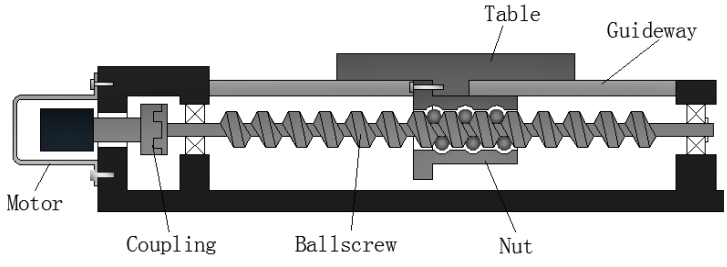

Fig. 1 Typical structure of ball screw drive system

A simple structural dynamic model of the ball screw drive system can be approximated by the reflected inertias at the motor (JM) and lead screw (JL) connected by a torsional spring (k) and damping (c) elements as shown in Fig. 2. The relative vibration of the dual inertia system can be denoted as $\theta_M - \theta_L$.

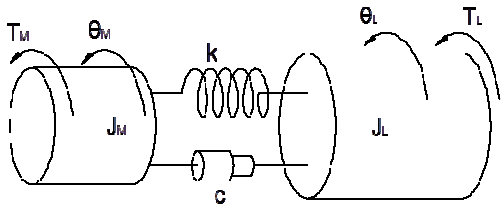

Fig. 2 Dual inertia system model of feed drive

According to D' Alember's principle we have:

$$\left.\begin{aligned} J_M\ddot{\theta}_M + c(\dot{\theta}_M - \dot{\theta}_L) + k(\theta_M - \theta_L) = T_M \\ J_L\ddot{\theta}_L + c(\dot{\theta}_L - \dot{\theta}_M) + k(\theta_L - \theta_M) = T_L \end{aligned}\right\} \tag{1}$$

Where θ_M, T_M are the angle motion and torque of the motor shaft. θ_L and T_L are the angle motion and torque of the lead screw. The structural dynamics of the ball-screw system can be expressed by:

$$\left(s^2\begin{bmatrix} J_M & 0 \\ 0 & J_L \end{bmatrix} + s\begin{bmatrix} c & -c \\ -c & c \end{bmatrix} + \begin{bmatrix} k & -k \\ -k & k \end{bmatrix}\right)\begin{Bmatrix} \theta_M \\ \theta_L \end{Bmatrix} = \begin{Bmatrix} T_M \\ T_L \end{Bmatrix} \tag{2}$$

The transfer function of the system can be leaded as:

$$[G(s)] = \frac{\begin{bmatrix} J_L s^2 + cs + k & cs + k \\ cs + k & J_M s^2 + cs + k \end{bmatrix}}{s^2\left[J_M J_L s^2 + c(J_M + J_L)s + k\left(J_M + J_L\right)\right]} \tag{3}$$

The system has the torsional natural frequency:

$$w_n = \sqrt{\frac{k(J_M + J_L)}{J_M J_L}} \tag{4}$$

The block diagram of the dual inertia system is as Fig. 3:

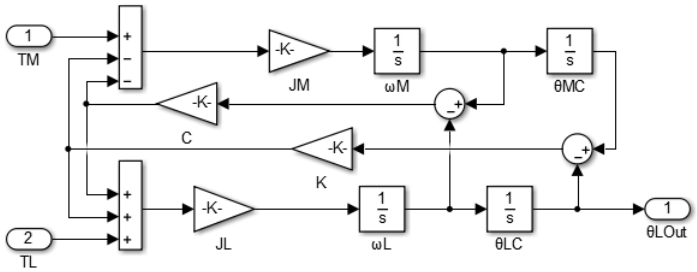

Fig. 3 Block diagram of transmission mechanisms

Dual inertia system based simulation of the feed drive system

Trajectory generation. The present CNC systems use linear acceleration motion profiles, trapezoidal acceleration motion profiles and sine-squared acceleration motion profiles. The acceleration functions are as function (5), (6), (7). Where $A_{L(t)}$, $A_{T(t)}$ and $A_{S(t)}$ are the acceleration profiles of linear acceleration profiles, trapezoidal acceleration profiles and sine-squared acceleration profiles. V_m, A_m and J_m are the maximum velocity, the maximum acceleration and the maximum jerk of the trajectory profiles.

$$A_{L(t)}=\begin{cases} A_m,(t\in[0,t_1)) \\ 0,(t\in[t_1,t_2)) \\ -A_m,(t\in[t_2,t_3)) \end{cases} \tag{5}$$

$$A_{T(t)}=\begin{cases} J_m t,(t\in[0,t_1)) \\ A_m,(t\in[t_1,t_2)) \\ -J_m(t-t_2),(t\in[t_2,t_3)) \\ 0,(t\in[t_3,t_4)) \\ -J_m(t-t_4),(t\in[t_4,t_5)) \\ -A_m,(t\in[t_5,t_6)) \\ J_m(t-t_6)),(t\in[t_6,t_7]) \end{cases} \tag{6}$$

$$A_{S(t)}=\begin{cases} A_m\sin^2(kt),(t\in[0,t_1)) \\ A_m,(t\in[t_1,t_2)) \\ A_m\cos^2(k(t-t_2)),(t\in[t_2,t_3)) \\ 0,(t\in[t_3,t_4)) \\ -A_m\sin^2(k(t-t_4),(t\in[t_4,t_5)) \\ A_m,(t\in[t_5,t_6)) \\ -A_m\cos^2(k(t-t_6)),(t\in[t_6,t_7]) \end{cases},k=\frac{J_m}{A_m} \tag{7}$$

Typically feed drive has a physical limitation on torque and velocity. And the parameter J_m should be given to generate trapezoidal acceleration motion profiles and sine-squared acceleration motion profiles. Here the three typical trajectory algorithms are used to generate a 50-rad-motion profiles with the parameters as follows：

$$V_m=120rad/s;A_m=2000rad/s^2;J_m=55000rad/s^3 \tag{8}$$

The position, velocity, and acceleration profiles and the frequency contents of the acceleration profiles are compared in Fig. 4. In trapezoidal and sine-squared acceleration profiles the high frequency contents are significantly reduced.

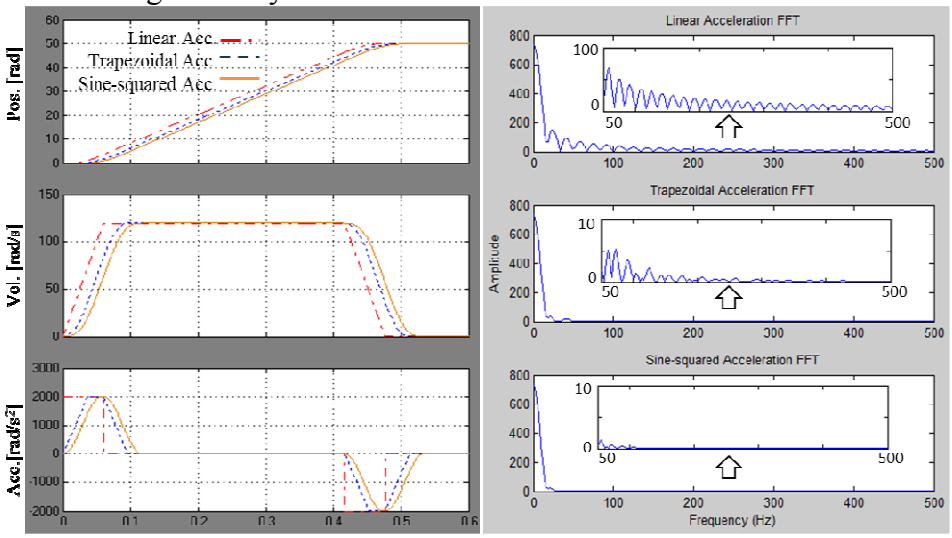

Fig. 4 Comparison of the three trajectories

Modeling and simulation of the feed drive system. Fig. 5 illustrates a Simulink model built according to the typical architecture of most feed drive control systems. Where K_{pp}, K_{vp}, k_{vi} and T_{rg} are the positional proportional gain, the velocity proportional gain, the velocity integral gain and torque command gain [7].The mechanical transmission system is set up as a dual inertia system as in fig.3. The nature frequency of the mechanical system can be calculated through Equation (4). T_L is set

as constant 0 to eliminate the effect of load on the system vibrations. The trajectory profiles in fig. 4 are added to the Simulink model with a nature frequency of 150 Hz of the mechanical system as motion command. The Comparison of the vibration and error of the simulation result are as Fig.6.

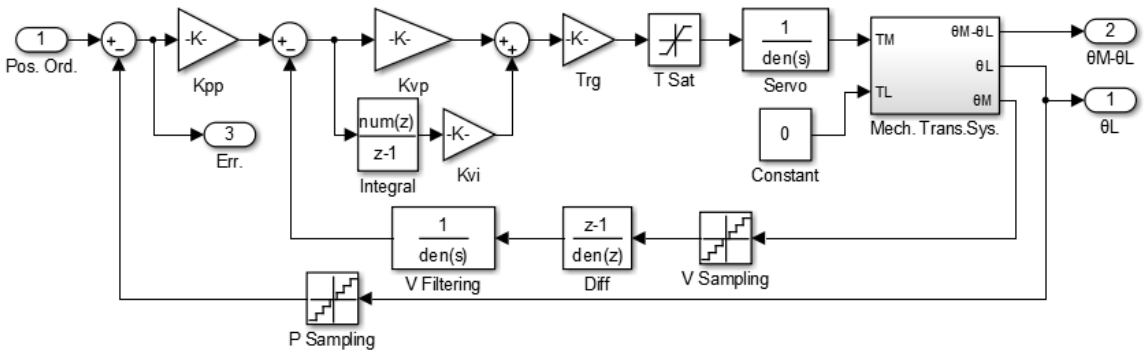

Fig. 5 Simulink model of the feed drive system

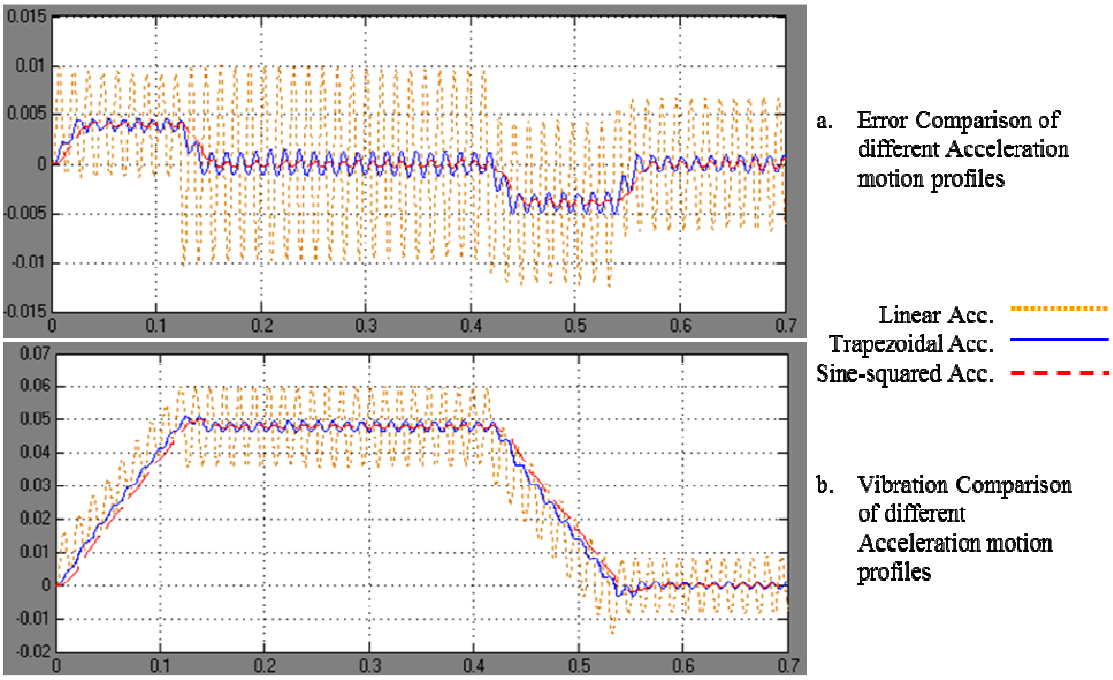

Fig. 6 Comparison of the vibration and error

Vibrations exist in all typical trajectories motions, but the motion of trapezoidal acceleration profiles and sine-squared acceleration profiles have much smaller vibration amplitude, and therefore the control error is significantly reduced.

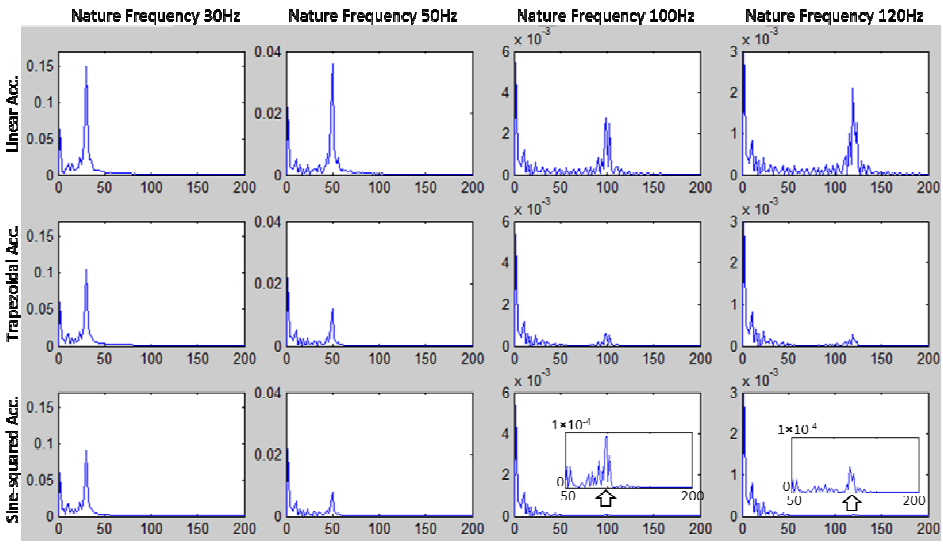

Fig. 7 Response spectrum analysis

Response spectrum analysis. The three typical trajectory motion profiles are given to the mechanical transmission system with nature frequency 30 Hz, 50 Hz, 100 Hz and 120 Hz as position orders. Fig .7 illustrates the frequency contents of the vibration $\theta_M - \theta_L$.

It's easy to find out that, vibrations of mechanical transmission system with nature frequency 30 Hz is excited by all the trajectory motion profiles but the vibrations are difficult to be excited when mechanical system has higher nature frequency and trajectory has smoother profiles. This means low nature frequencies of mechanical transmission systems must be avoided in order to keep the feed drive stable. The vibrations of mechanical system with high nature frequency can be avoided by using smoother trajectory profiles.

Summary

In this paper the vibration of feed drive is simulated by using a mathematic method. The mechanical transmission system is modeled as a dual inertia system. Three typical trajectories are used to analyze the effect of motion profiles on feed drive vibrations by using a simulation model of feed drive controller. Come to the conclusion that lower nature frequencies of mechanical transmission systems are easy to be excited to vibrations and must be avoided to keep the feed drive stable. The vibration of mechanical system with high nature frequency can be avoided by using smoother trajectory profiles.

Acknowledgments

Fund Project: "high-end CNC machine tools and basic manufacturing equipment" science and technology major project (2012ZX04005031).

References

[1] Y. Altintas, A. Verl, C. Brecher, L. Uriarte and G. Pritschow: CIRP Annals - Manufacturing Technology, Vol. 60 (2011), p.779.
[2] A. Verl and S. Frey: CIRP Annals - Manufacturing Technology, Vol. 61 (2012), p.351.
[3] A. Dietmair and A.Verl: Science Journal, 2009, October, 130-134.
[4] M. Yang, H. Hu and D.G. Xu: Electric Machines and Control, Vol. 16 (2012) No.1, p.79.
[5] J.R. Sun: *Research on ACC/DEC Control and Contour Error of CNC System* (Ph.D., Lanzhou University of Technology, China 2012), p.31.
[6] K. Erkorkmaz and Y. Altintas: International Journal of Machine Tools and Manufacture, Vol. 41 (2001) No.9, P.1323.
[7] R. Sato: Key Engineering Materials, Vol. 516 (2012), p. 154.

Advanced Materials Research Vols. 989-994 (2014) pp 3122-3126
© (2014) Trans Tech Publications, Switzerland
doi:10.4028/www.scientific.net/AMR.989-994.3122

Comparative Study of Moving Target Analysis System

Min Feng[1, a], Huaichang Du[1, b]

[1]Information Engineering Institute, Communication University of China, Beijing 100024, China.

[a]xiai117@163.com, [b]cucudu@163.com

Keywords: Moving target detection, moving target tracking.

Abstract. This paper compares two kinds of moving target analysis systems, which are the motion history image system and the moving object tracking system. Each system includes two parts which are moving target detection and tracking, achieving respectively detection of the direction of moving targets or representation of motion trajectory. Through experiment analysis of moving human and vehicles, each system is determined which situation it is suitable for.

Introduction

Target detection and tracking in image sequences has been a very popular issue in computer vision, image processing, pattern recognition and other fields. Target detection and tracking in image sequences means to detect every independent moving target in each frame image, or the area that users are interested in, and to locate these moving targets or area in the subsequent frames. It organically combines image processing, automatic control and information science. Besides it becomes a kind of technology that can automatically identify target from the image signal in real-time, extract target position information, and track the target movement. It can not only display motion direction and trajectory of the surveilled target, but also provide reliable data source for motion analysis of moving targets in the scene, and scene analysis[1].

Moving target detection is the basis for advanced applications such as target tracking, target classification, target behavior understanding. Its main purpose is to extract moving targets from video images and obtain feature information of moving objects, such as color, shape and contour. The process of moving object extraction is actually a kind of image segmentation. Since only in the continuous image sequences (such as video image sequences) the moving object can be seen, the process of moving object extraction is to find differences in the consecutive image sequences, and to extract the differences showed through object motion.

The subsequent step of target detection is target tracking[2]. Target tracking means while we do not know about the target motion information in advance, we estimate the target motion state in real time by the data from information source, so as to judge the position and movement of target. Moving target tracking is a complex estimation problem. At first it is mainly used for military research, because it is the key technology of precise weapon guidance. At present, with further study of image tracking technology, application of image tracking has penetrated into more and more fields such as visual surveillance and medical diagnosis. Studying a kind of target tracking method with good robustness, high precision, stable performance and powerful applicability is still faced with great challenges, and has important theoretical significance and practical value.

This paper compares two kinds of moving target analysis system, which are the motion history image and the moving object tracking. Each system includes two parts that are moving target detection and tracking. The motion history image system chooses frame difference method[3] as the method of moving target detection and algorithm based on motion template as the tracking algorithm. While the moving object tracking system selects background difference method[4] as the method of moving target detection and algorithm based on blob as the tracking algorithm[5]. Through detection of the motion direction or representation of motion trajectory of human and vehicles, each system is determined which situation it is suitable for.

The Motion History Image System

Frame Difference Method. The frame difference method is a motion detection method based on pixels. The difference operation of two or three adjacent images in a sequence of video images is performed to obtain the contours of the moving objects. From a theoretical point of view, the frame difference algorithm is actually a kind of dynamic edge extraction operation, while from a practical point of view, it can detect parts of contour information of moving objects. The frame difference method is adaptive to the dynamic environment, but in test results, it can not obtain all the feature pixels of moving objects. Besides the moving objects inside can easily cause holes, which is very bad for the subsequent operation.

First of all, use formula (2-1) to calculate the difference between the k image and the k-1 image, then get difference image Dk, and then use image segmentation algorithm formula (2-2) to binarize the difference image Dk. If a pixel value in the difference image is more than the threshold value, the pixel is foreground pixel, otherwise considered the background pixel. After that we can filter the binary image using mathematical morphology, and then get the image Rk. Finally analyze the regional connectivity of image Rk. When a connected area is greater than a given threshold, it is the target and that area of the region is the target minimum outside, so that we can determine the target rectangle.

$$D_k(x,y) = |f_k(x,y) - f_{k-1}(x,y)| \tag{2-1}$$

fk (x, y) and fk-1 (x, y) are the two consecutive frame images; Dk (x, y) is the frame difference image.

$$R_k(x,y) = \begin{cases} 0 & D_k(x,y > T) \\ 1 & D_k(x,y \le T) \end{cases} \tag{2-2}$$

T is the value of the image binaryzation threshold.

Tracking Algorithm Based on Motion Template. Tracking algorithm based on motion template, is on the condition that there is intersection between two adjacent frames of moving target in the screen. Targets in marine radar images and vehicles in crossroads both match the condition. This algorithm can clearly display the trajectory, velocity and direction of the target without extrapolation, correlation analysis and trajectory post-processing. The algorithm is based on moving target foreground image from moving target detection of the previous section. Specific process is described as follows:

1. Save detected foreground image and decrease the gray level of previous frames;
2. Add time stamp to the current frame and save it into historical image;
3. Form gradient image;
4. Segment gradient image to get the position of the target, calculate the gradient to obtain the velocity and direction of the target and add marker.

This algorithm simplifies the target correlation operation, can stably track targets without understanding target movement trend in the initial state, and also has better real-time performance.

Experiment Results.

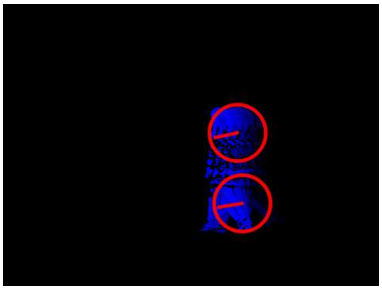

Fig. 1 Result of human tracking based on motion template

As we can see from fig.1, when detecting moving human in video images, tracking algorithm based on motion template has the problem that head and body are separately detected. And in the experiment results, the detected motion direction in most cases is correct, but in the several starting and ending frames of the video the direction is wrong.

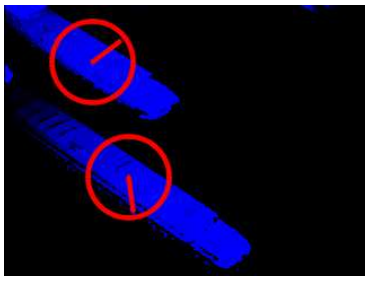

Fig. 2 Result of vehicle tracking based on motion template

As can be seen from fig.2, the detected direction of moving vehicles in video image is wrong in most cases by using tracking algorithm based on motion template. That means tracking algorithm based on motion template is not suitable for detection of targets that move too fast.

The Moving Object Tracking System

Background Difference Method. Background difference method compares the input image and the background image to detect moving targets. Since the background difference method is simple, fast, and can completely detect targets in most cases, it has become the most widely used motion detection method.

In order to solve problems of frame difference method and improve detection effect, the background difference method has been developed.

The principle of background difference method is very simple. Firstly use the formula (3-1) to calculate subtraction of the background image fbk and current frame image, then according to the formula (3-2) binarize the difference image Dk and filter it using mathematical morphology, and analyze regional connectivity of the result Rk. When a connected region area is greater than a given threshold, it is the target and that region is the target area, so we can determine the minimum enclosing rectangle of the target.

$$D_k(x,y) = | f_k(x,y) - f_{bk}(x,y) | \tag{3-1}$$

Fk (x, y) is two consecutive frames, and Dk (x, y) is the frame difference image.

$$R_k(x,y) = \begin{cases} 0 & D_k(x,y > T) \\ 1 & D_k(x,y \le T) \end{cases} \tag{3-2}$$

T is the value of the image binaryzation threshold.

Tracking Algorithm Based on Blob. The basic principle of tracking algorithm based on blob is to segment the candidate pixel, judging whether the pixel belongs to the target, the background or other areas. Tracking algorithm based on blob can also be called tracking method based on image segmentation, because it has the same way with image segmentation, which is to optimize pixel selection, combination and separation according to the given clues, and to gather the pixels with the same feature into a region. It has difference with the traditional image segmentation. Visual object tracking is to locate the target in image sequences. It can be not accurate in pixel classification on a certain degree, because it only needs to segment results to distinguish target from background, while the traditional image segmentation algorithm needs to accurately display the target contour. Segmentation cues generally include target movement characteristics, texture features and image depth information.

In many applications, we hope to detect the moving objects, number them and track them, finally get the motion trajectory. In order to achieve the aforementioned function, based on the knowledge we discussed before, we can subdivide the whole process into the following modules, which are foreground detection module, new blob detection module, blob tracking module, trajectory generation module and trajectory post-processing module.

The foreground detection module of moving objects is to judge whether a pixel is foreground or background. Input data is the current frame image, while output is foreground mask of the current frame. OpenCV can detect completely stationary background. In practical application background is possible translated or rotated, in order to meet the background changes, we need to use the camera calibration. The foreground detection module divides the pixels of current frame into foreground and

background. A moving object is considered as the foreground, while unchanged parts in the video as the background region.

The blob feature detection module of moving objects is to detect blob, a collection of pixels of motion objects in a scene using results of foreground detection. Input data is the mask of current frame and existing blobs, while output data is the blob newly detected. In order to meet the application in radar system, graphic features and motion correlation analysis of blob should be taken into consideration, in addition the operation after fusion among blobs and between blob and background pixels should be considered. This module can detect new blobs according to the current foreground mask, like the objects newly coming into the scene.

The blob tracking module of moving objects includes blob list and a single blob tracking. It uses the results of new blob detection. The input data are the current frame, the mask of current frame and the new blobs, while output data is the blob information of current frame, including ID, position, speed and direction of movement.

The trajectory generation module is to collect position information of all the blobs, establish the trajectory list and deal with the correlation processing. The purpose of this module is to save the whole trajectory into a specified file, and also to calculate some data of each blob (using the original image and the foreground mask) and save them. Input data of trajectory generation module is all the blobs in the current frame, while output data is the trajectory list we have saved.

The trajectory post-processing module is to remove the jitter of position and motion trend when marking moving objects, and smooth the trajectory. Input data of trajectory post-processing module is all the blobs in the current frame, as well as the output data.

This module can be used as glue, because it can bind other sub-modules into a complete process.

Experiment Results. Target tracking algorithm based on blob is aimed at detecting and tracking multiple moving targets in video image. Compared with the tracking algorithm based on motion template it is more complex, and widely used.

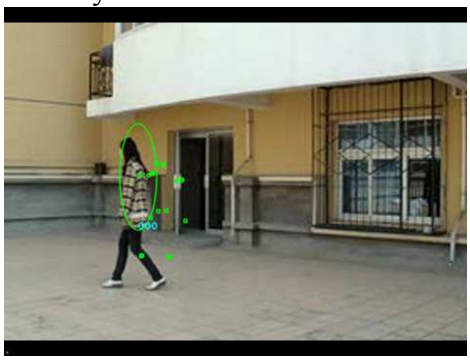

Fig. 3 Result of human tracking based on blob

Fig.3 is the result of human motion tracking by using tracking algorithm based on blob. It is observed that this algorithm on detecting and tracking moving body is basically right, but still has the problem that head and body are separately detected. Small rectangles in picture show the center of detected motion target in several video frames. Due to the above-mentioned problems, tracking algorithm based on blob can not accurately display the motion direction and trajectory of moving body.

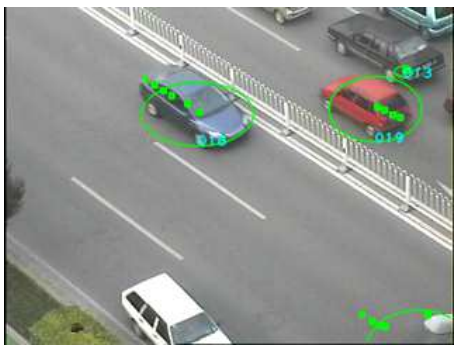

Fig. 4 Result of vehicle tracking based on blob

Fig.4 is the result of vehicle motion tracking by using tracking algorithm based on blob. As can be seen from the picture, the detection and tracking of moving vehicles in video image is correct in most cases, and the algorithm can mark the moving targets. But sometimes the vehicles newly coming into the picture can not be detected and tracked. For the rigidity and integrity of vehicle target, tracking algorithm based on blob can correctly display the motion direction of target and present part of the trajectory in video frame.

Conclusion

With the above discussion of algorithms and experiment results, we can reach the conclusions:

When it comes to the motion history image system, tracking algorithm based on motion template applies to detect and track simple single moving target. Comparing the results of human motion tracking and vehicle motion tracking, the motion history image system is more suitable for detecting and tracking human that moves slowly, and it can correctly display motion direction.

When referring to the moving object tracking system, tracking algorithm based on blob is a little complex and it is suitable for detecting and tracking multiple moving targets in video image sequences. We have introduced each module of tracking algorithm based on blob, realized the detection and tracking of multiple moving objects in video, and shown the motion direction of each moving target, as well as part of the trajectory. This algorithm has some problems on tracking moving body. It can not detect the complete human body, therefore the moving object tracking system is not suitable for detection and tracking of human motion.

Moving target detection and tracking usually is used as a pre-treatment technology of visual object behavior understanding and description, and other advanced processing technologies. In recent years, although scholars have done lots of researches, but due to the complexity of target surroundings, as well as the target itself possible transformation, and the influence of weather, illumination, shadow and other natural conditions and human disturbance, the target detection and tracking technology is still a complex process, and a difficult issue needed further researches.

References

[1] T. Yuan, T.T. Niu and S.H. Zan. A novel robustalgorithm for realtime object tracking. Acta Automatica Sinica, Vol. 28 (2002) No.5, p.851.

[2] Comanniciu D, Ramesh V and Meer P. Kernel-based object tracking. *IEEE Transactions on Pattern Analysis and Machine Intelligence*(2003). Vol. 25, p.564.

[3] R. Cucchiara, C. Grana, M. Piccardi and A. Prati. Detecting Motion Targets, Ghosts, and Shadows in Video Streams. *IEEE Trans, Pattern Anal and Machine Intell*(2003). Vol. 25, p.1337.

[4] Haritaoglu, L.S. Davis and D.Harwood. w4: who? when? where? what? A real time system for detecting and tracking people. *International Conference on Face and Gesture Recognition*(Japan, 1998).

[5] M. Taj, E. Maggio and A. Cavallaro. *Multi-feature Graph-Based Target Tracking* (Springer-Verlag Berlin Heidelberg, 2007). p.190.

Advanced Materials Research Vols. 989-994 (2014) pp 3127-3131
© (2014) Trans Tech Publications, Switzerland
doi:10.4028/www.scientific.net/AMR.989-994.3127

The injection mold design of clamshell phone upper cover

GuoDong Liang[1, a], JunHui Liu[1, b]

[1] Heyuan Polytechnic, Heyuan 517000, China.

[a]50331264@qq.com, [b]34060604i@qq.com

Keywords: Upper cover of clamshell phone; dual-mode; side gate; inner slider; inclined pushing rod.

Abstract. The design of injection die on the upper cover of clamshell phone is introduced. The dual-plate die has side gate for opposite glue injection, the parts are ejected by ejector pin, the side reversed buckle contains three blocks, the reversed buckle at flip shaft consists of two inner sliders, and all the eight inner reversed buckles are made up of inclined pushing rods, and the cooling system embraces "U" shaped cooling waterway. Its application in practice has proved the reasonable die structure, smooth remolding, and qualified plastic part design.

1. Analysis of plastic part process

The upper cover of clamshell phone is shown in Fig. 1. It is made of polycarbonate PC .This medium-and small plastic part's size: 78.02 mm × 43.22 mm × 8.04 mm (L*W*H). The two outer reversed buckles on the head of plastic part (Fig. 2) consist of sliders; the inner reversed buckle at the shaft of the head (Fig. 3) is made up of inner sliders; the inner reversed buckle on the head (Fig. 4) is composed by inclined pushing rod; the product's two side edges respectively wear two outer reversed buckles (Fig. 5) formed by side sliders and two inner reversed buckles (Fig. 6) formed by inclined pushing rods, and the tail wears two inner reversed buckles (Fig. 7) composed by inclined pushing rods.

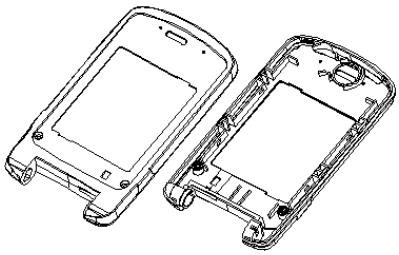

Fig. 1 Part

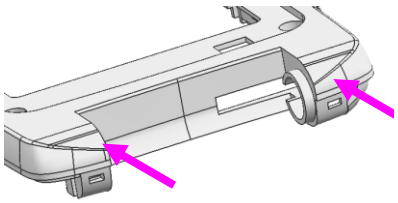

Fig. 2 Outer reversed buckles on the head

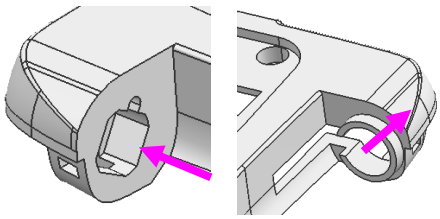

Fig. 3 Inner reversed buckle at the shaft

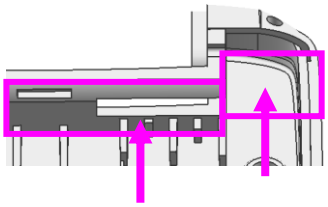

Fig. 4 Inner reversed buckle on the head

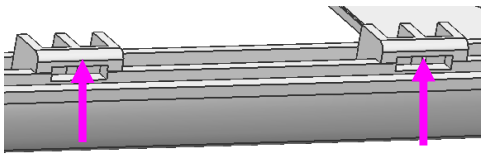

Fig. 5 Outer reversed buckles at the side

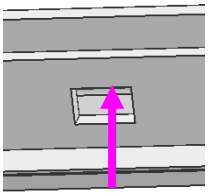

Fig. 6 Inner reversed buckle at the side

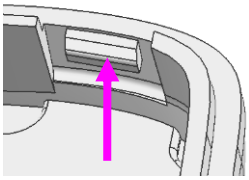

Fig. 7 Inner reversed buckle on the tail

2 Design of the die structure

2.1 Design of gating system and parting surface

The overall structure of the die is shown in Fig. 8. This dual-plate die with 1 cavity has side gate for glue injection, the parts are ejected by ejector pin. When the parts are well modeled, the gate will be sheared. In order to not hinder the assembly by the shearing of gate, a shallow groove is needed for glue injection. The maximum parting line is the maximum contour line; since the product maximum contour is also the product's bottom boundary line, so the maximum parting surface is the bottom surface of the product

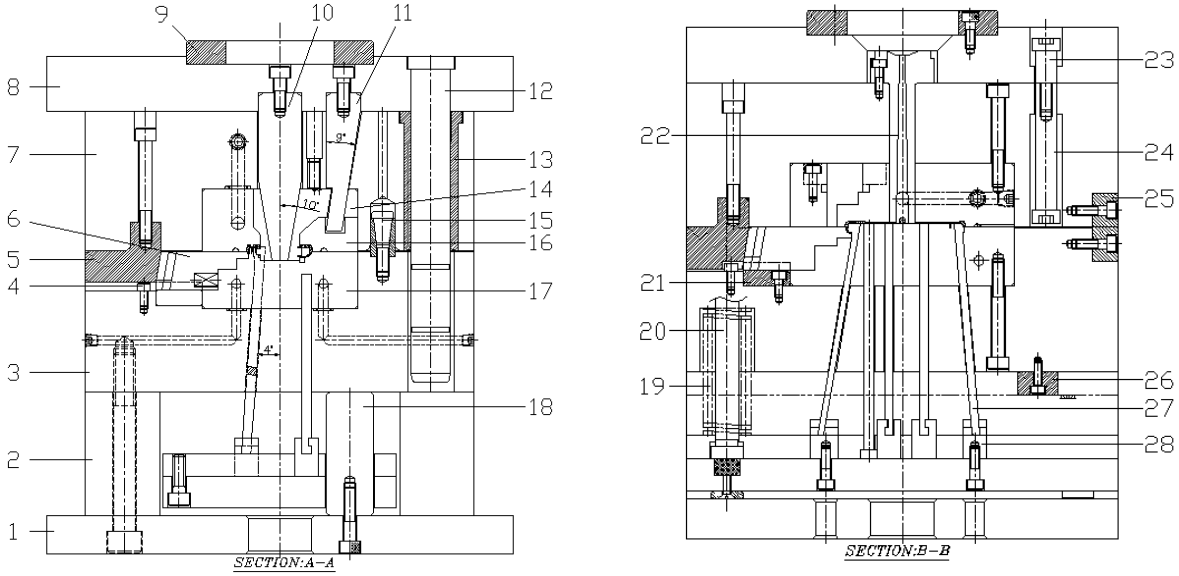

Fig. 8 Die structure

1 Movable mode's seat plate 2. Cushion block 3 Movable mode's template 4 Slider's spacing screw 5. Wedge block of sliders 6. Side slider 7 Fixed mode's template 8 Fixed mode's seat plate 9 Positioning ring 10 Wedge block of inner slider 11 Pin of block of inner slider 12 Guiding pillar 13 Guiding sleeve 14 Inner slider 15 Nylon buckle 16. Cavity 17 Core 18 Supporting columns 19 Resetting spring 20 Resetting rod 21 Wear-resistant plate 22 Sprue bushing 23 Screws of the same height 24 Travel rod 25 Side lock 26 Limit block of ejection 27 Inclined pushing rod 28 Slanted ejector's seat

2.2 Design of main parts

The main parts of the die include cavity (No. 16), core (No. 17), three side sliders, eight inclined pushing rods and two inner sliders. The cavity (No. 16) is embedded in the cavity plate (No. 7), and the core (No. 17) is inlaid in the core plate (No. 3) This design allows easy processing and die repair, and low cost. The three side slider's glue injection gates and the sliders are relatively small, so integral design is preferred. Due to limited space, the strength of the inner slider's head is weak (Fig. 9), so iron is added at the head's non adhesive position to improve the slider head's strength (Fig. 10). The part's material depends on the amount of products. Large amount of products should be made of good materials, and heat treatment is required; while the medium or small amount of products can be made of cheaper materials. The cavity should be made of harder material than the core, so that the cavity won't be destroyed by the product's surface.

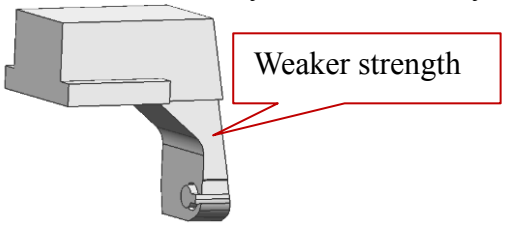

Fig. 9 Inner slider

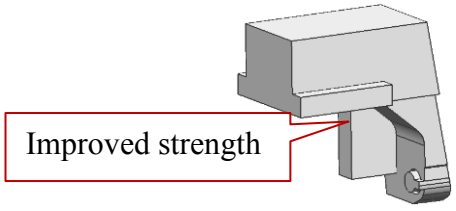

Fig.10 Slider (with improved strengthen)

2.3 Design of inner slider's structure

The design of inner slider's structure is the difficult and key part of the die. The inner slider's structure is shown in Fig. 11.

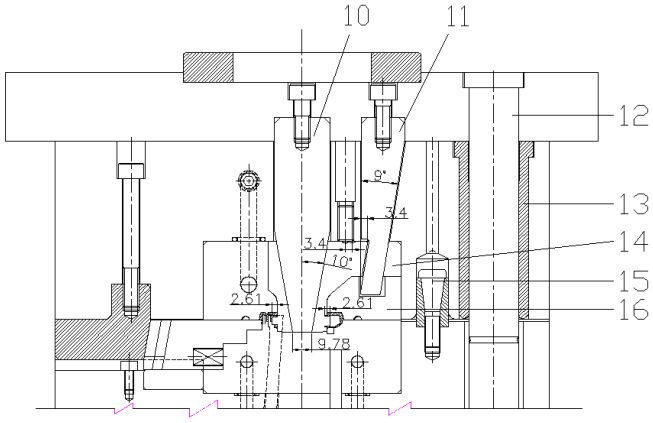

Fig. 11 Inner slider's structure

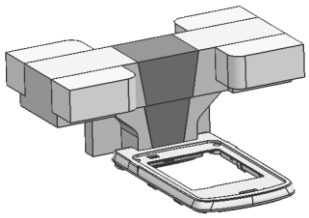

Fig. 12 3D structure of inner slider

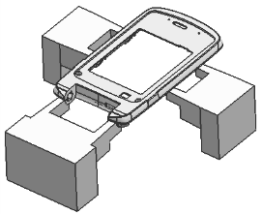

Fig. 13 3D structure of side slider

The size of two reversed buckles of inner slider is 2.61mm. Usually, the slider's backward distance = reversed buckle's size + safety value for 1 ~ 2mm; if the safety value is 2mm, then the inner slide's backward distance should be: 2.61+2=4.61mm, which means the minimum distance between two inner sliders is 9.22mm. In order to avoid the interference between the two inner sliders after demoulding, safe distance should be designed. The thickness of inner slider's weakest part should be 5mm or above, then the two sliders' total backward distance is only 9.78mm, the safe distance between two inner sliders is only: 9.78-9.22=0.5mm. This is not safe or reasonable, so the sliders' backward distance should be properly reduced. When the safe value is 0.8mm, the sliders' backward distance is: 2.6+0.8=3.4mm, the distance between the two inner sliders is: 9.78-3.4*2=2.98mm. This is relatively reasonable. The wedge block's angle (at single side) should be larger than the inner slider's pin's by 1 ~ 2 °. According to the inner slider's height and backward travel, the inner slider's pin's angle is 9 °, the inner slide's wedge block's angle at single side is 10 °. The slider travel is limited by Tsai screw. The 3D structure of inner slider is shown in Fig. 12 (excluding the pin and positioning screw).

2.4Design of side slider's structure

Product head's two outer reversed buckles are respectively formed by a side slider, its two side outer reversed buckles are also respectively formed by a side slider whose 3D structure is shown in Fig. 13 (excluding the side slider seat, pin and inclined guiding pillar).

Design of side slider's structure: (1) The three side sliders contain two reversed buckles, and the slider's backward travel= reversed buckle's size + safety value for 1 ~ 2mm. (2) The side slider's driving mechanism can be inclined guiding pillar or "T" shaped block, and here the latter is adopted. The wedge block is directly processed as "T" shaped block, and slider's seat is processed into "T" slot, with inclined guiding pillar eliminated. This process is complicated. The calculation of parameters of side slider is shown in Fig. 14. $\alpha \leq 25$, S1=S3+1 ~ 2mm, S2=h*tg α =S1, α (Note: α is the inclination angle of "T" slot, S1 is the distance between limited screw and slider, S2 means the slider's backward travel, S3 is the size of reversed buckle, h refers to the height of "T" slot). In order to ensure correct resetting of sliders, S1 =S2. Since the maximum size of all the side sliders' reversed buckle is 1.02mm, so S3=1.02mm, S2 = 3mm, α =10 ° is preferred according to the height of the slider, h=18mm, so as to meet the design requirements. (3) The sliders should be installed with limiting spring, to ensure the correct position of sliders influenced by limiting spring and limiting screw as well as smooth opening and closing demoulding.

2.5 Design of inclined pushing rod

All of the 8 inclined pushing rods' inner reversed buckles can mode the buckles and eject the products. The plane structure of inclined pushing rod is shown in Fig. 15.

Design of inclined pushing rod: (1) If reinforced bar leis behind inclined pushing rod, the inclined pushing rod should be ensured with enough space for backward movement without interference with the reinforced bar, namely S2>S3. (2) The calculation of parameters of inclined pushing rod: S3=S1+1 ~ 1.5mm (safety value), S3=h* tgα, wherein S3 is the backward travel of inclined pushing

rod, S1 is the size of reversed buckles, α is the angle of inclined pushing rod, h is the ejection height of inclined pushing rod. The eight inclined pushing rods allow different inverted values but the same ejection height, thus the design should enable the inclined pushing rod to safely exit from the reversed buckles and ensure normal use.

2.6 Design of exhaust system

Mobile phone shell requires high accurate surface. In order to ensure good surface quality, exhaust system is usually required. The exhaust system of cavity is usually designed into the following forms: (1) In case of the die's plane parting surface, deep exhaust groove can be milled at the position 5-8mm away from the molding position, and then the plane grinding machine grinds the shallow exhaust groove lying between the molding region and the exhaust groove; the grinding depth is less than 0.03mm, the width is less than 10mm (Fig. 16). (2) The gap between inserts can be used for exhaust (3) The gap between the pushing rod and the core can be used for exhaust.

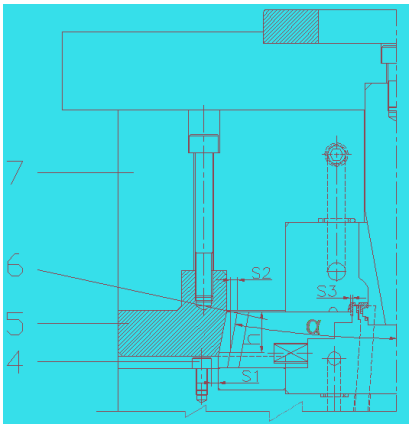

Fig. 14 Plane structure of side slider

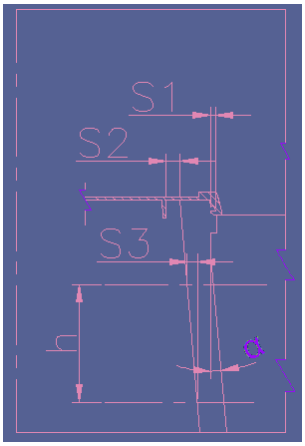

Fig. 15 Inclined pushing rod

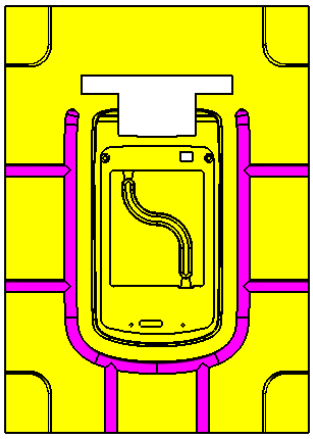

Fig. 16 Exhaust system

2.7 Design of cooling system

In the process of injection for molding, the temperature of melt in the cavity is generally 200 ~ 300 ℃. In order to enable rapid cooling and molding of the melt, the die's temperature shall be cooled to 60 ℃ before the products are taken out. In order to shorten the molding cycle, the die should be cooled.

As is demonstrated by the experiments, of all the heat transferred from plastic parts to the die, about 5% is diffused to the air by radiation and convection, 95% is taken away by cooling medium. The cooling time, pipe's diameter and length of pipe in cooling system can be calculated.

The parameters of cooling system are usually not determined by calculation, but by empirical value. Plastic phone housing requires high quality surface, so cavity and core both require cooling water channels. Since the product is not big, and one die contains only one cavity, the cooling water channel is designed into single "U" shape, and the channel diameter is 8mm. In order to ensure good cooling effect, usually the die's temperature is controlled at around 60℃ by the system of injection molding machine, and the temperature gap between inlet and the outlet should be less than 5℃.

2.8 Design of ejection system

The plastic product is shallow, with many low bars, so ejection rods are preferred for ejection. The main principles for location of pushing rods: (1) They should be placed at the position with thick glue; (2) They should be placed at the high position with more bars and greater holding force; (3) They should be placed in balanced manner, for balanced ejection force; (4) Round pushing rods are preferred, and only flat ones with simple specifications are preferred only at high bar position.

2.9 Design of guide positioning system and resetting mechanism

Guiding and positioning system guarantee the accuracy and life span of the die. The guide components comprise guiding pillar (No.12), guiding sleeve (No.13), side lock (No.25), cavity (No.

14), core's (No.17) positioning mouth. The resetting mechanism consists of resetting spring (No.19) and resetting rod (No.20). These positioning parts and resetting mechanism ensure the precision of die, the quality of products and the service life of die.

3 Opening and closing process of die

The plastic melt is injected into the die's cavity via the nozzle; after the injection, pressure holding, cooling and solidification, the die is opened. In the opening process, under the influence of nylon buckle, the fixed template is firstly separated from the fixed mode's seat plate for the first parting, then the inner slider's wedge block (No.10) is separated from inner slider (No. 14), and the fixing mode's seat plate (No.8) drives the inner slider's pin (No. 11) and the inner slide (No. 14) to demould the reversed buckle; then continue to open the die, under the influence of travel rod (No.24) and screws of the same height (No.23), the fixed template is separated from the movable one, for the second parting; finally, the pushing rod ejects the products. In the closing process, firstly the fixed mode's template (No.7) and fixed mode's seat plate (No.8) are closed, followed by the fixed template and the movable one.

4 Conclusions

The dual-plate die has side gate for opposite glue injection; the two inner sliders' shaft for moulding wear reversed buckles. The outer reversed buckles at the three sides are made up of sliding blocks. The 8 inclined pushing rods wear inverted buckles, and the parts are ejected by pushing rods. The real application has demonstrated the reasonable structure of die, stable production, and qualified plastic part design.

Acknowledgements

The Project for College High Level Talents of Guangdong Province (2013-221).

References

[1]w.g. Wang, B.S. Tian and Y.C. Tian: Plastic Injection Mold Design Techniques and Examples (Chemical Industry Press, China 2004) , p.194-198.
[2]Plastic Mold Technology Handbook Editorial Board: Plastic Mold Technology Handbook(Machinery Industry Press, China 1997) , p.176-180.
[3]Q.X. Li: Plastic Mold Design (Northwestern Polytechnical University Press, China 1995) , p. 156-157.
[4] W.H. Zhang, Mold Industry, Vol. 37 (2011) No.5,p.50-52.
[5] X.Q. DU. Mold Industry, Vol. 37 (2011) No.1,p.50-52.

Advanced Materials Research Vols. 989-994 (2014) pp 3132-3135
© (2014) Trans Tech Publications, Switzerland
doi:10.4028/www.scientific.net/AMR.989-994.3132

Based on PMAC control 4-DOF manipulator

Jinwei Fan [a], Yijia Liu [b], Ling Chen [c] and Chao Liu [d]

College of Mechanical Engineering and Applied Electronics Technology, Beijing University of Technology, Beijing100124, China

[a] jwfan@bjut.edu.cn, [b] 413087669@qq.com, [c] 510023302@qq.com, [d] 807268900@qq.com

Keywords: 4-DOF manipulator; PMAC; openness

Abstract. To complete the step of pacing bolts more accurate and efficient in factory, This article design the 4-DOF manipulator Based on PMAC motion controller, including hardware architecture, software architecture. This control system combines the IPC strong management and real-time control of PMAC to achieve a 4-axis robot, smooth fast-precision, high efficiency, high reliability, cost-saving design goals.

Introduction

In currently, Placing bolts in the domestic mechanical assembly process step used mainly done manually or three degrees of freedom manipulator controlled by PLC completed. Manual processing could ensure various types of boltscan be placed in any positionin three-dimensional space, but it has low efficiency and high cost. When using three degrees of freedom manipulator processing controlled by PLC, we will get higherefficiency,but lower scrap rates and costs.Due to structural limitations of three degrees of freedom manipulator, boltsinstalled only in the two-dimensional plane limited locations. This design basing on PMAC programmable multi-axis motion control card controls to achieve a 4-DOF manipulator completes bolts placed in anywhere of three-dimensional space, and higher efficiency, lower cost

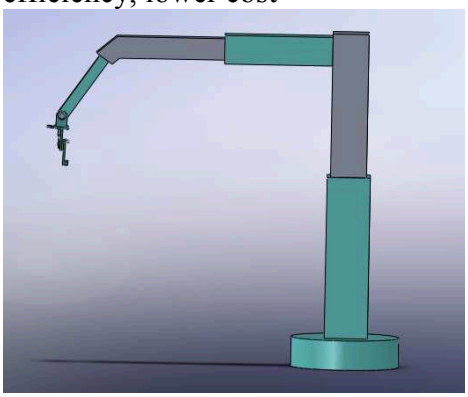

Fig. 1 Manipulator simulation diagram

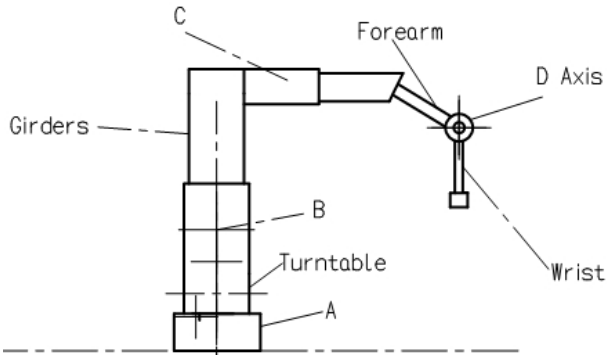

Fig. 2 Manipulator organization chart

4 DOF manipulator mechanical structures

4-DOF manipulator including industrial control computer, PMAC programmable multi-axis motion control card, servo drives, AC servo motor, single-stage small hydraulic cylinders, hydraulic cylinder drives and encoders, rotary devices and other components bearing hardware platform. Manipulators mechanism shown in Figure 2.

Themanipulator and the clamping mechanism are drived by hydraulic cylinder to drive the joints to complete trajectory. The mechanical arm islong, generating larger torque, so we choose a large area of circular base, enhancing the stability of the structure and design the turntable, girders, forearm, wrist and rack and pinion mechanism to achieve a good manipulator work. Throughout themanipulator are installed at the bearing rotary table, slewing achieves 360-degree rotation around the axis A drive by a servo motor through the inner gear .the manipulator equipped with encoder to feedback rotational

speed, angle. The frame, arm and wrist, all driven by hydraulic cylinders, to achieve the B C D three degree of freedom motion, so as to ensure adequate operating range and the accuracy of the movement. Manipulator gripping mechanism shown in Figure3.

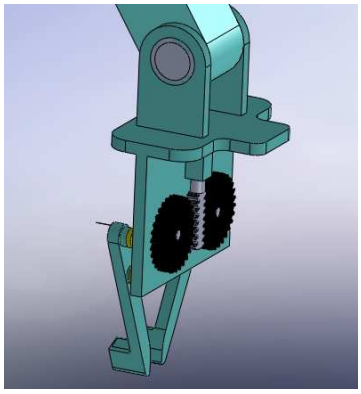

Fig. 3 Rack and pinion clamping mechanism

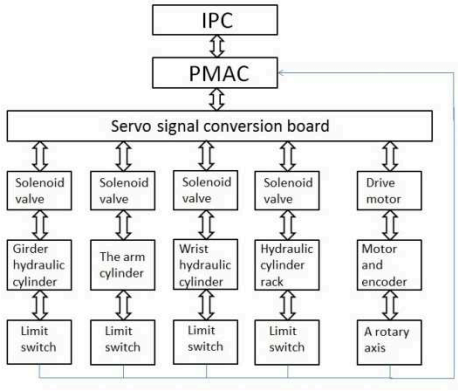

Fig. 4 Control system structure

The clamping mechanism of manipulator use rack and pinion to keep the clamp arm opening or closing .instead of the direct driving by motor available in the market. A double-sided rack rigidly connected to the cylinder, double-sided rack driven by a hydraulic cylinder for reciprocal motion, double-sided rack mesh with two gears respectively, keeping the clamp arm opening or closing. When the cylinder moves to the Bottom, the clamp arm closes to the minimum angle, completing gripping action. When the cylinder block extends to the longest position, two clip arms open to the maximum angle, completing release action.

Manipulator available on the market usually use motor-driven, but the vibration caused by the motor is large, leading the system unstable. Hydraulic cylinder 's vibration is smaller than the motor's , the system also be more stable, In order to reduce the vibration caused by the motor and improve the accuracy of the Manipulator, the Manipulator is driven primarily by hydraulic cylinders driven , keeping smooth the Manipulator operation, quickly. Compared with the motor driving, cylinder driving omitted gear mechanism, getting the simpduce the weight of the body and the required stiffness of the Manipulator. Save manufacturing costs asle mechanism and high reliability of the Manipulator. Omitting the gear unit can re well.

Control system hardware design

The control system uses the upper and lower two control devices, IPC and PMAC programmable multi-axis motion control card. IPC has the computing capacity, stable operation and fast response; while PMAC has the strong ability to handle real-time tasks, controlling motion directly. IPC connects PMAC via a data bus [1]. Upper and lower levels, the control device designed in this paper, can make good use of the advantages of IPC and PMAC to achieve 4-axis joint movement, meet the high precision, fast movement requirements. The system selects Mitsubishi synchronous AC servo motor, and equips with encoder providing speed and position feedback. Small hydraulic cylinder drive beams, arm, adapter. On the same time the gripping arm has a small hydraulic cylinder, driving a rack to achieve the gear operation, so that the clamp arm works smoothly. The structure of the control system shown in Figure 4.

Software designs of control systems

Software system structure. System software can be divided into two categories, the one is IPC as the core management software, the other one is PMAC as the core of motion controlling software, they consist of the host computer and the next crew hierarchical control framework. IPC has these responsibilities for managing system, setting initialization parameter of system, communicating between the PMAC and IPC, monitoring system status, and controlling by man-machine interface to achieve the function of automatic controlling, manual controlling and real-time showing of the state

of motion. PMAC has these responsibilities for the real-time motion controlling system, including the trajectory controlling, speed controlling, servo-loop real-time updating, security procedures. The main function of the Manipulator software system is completing motion controlling tasks to ensure the normal operation of the 4-DOF manipulator grip, through management and real-time control of digital machines PMAC host computer.

IPC software. 4-DOF manipulator IPC software is developed by VC Windows platform + + Prepared, Stored in the IPC (IPC). The IPC calls Pcomm32 achieve system initialization function achieves, real-time monitoring system status, system communication and manual control functions

(1) System initialization module. System initialization module download via dynamic connection Pcomm32 program functions provided from Delta. System initialization files in the IPC hard drive are stored directly to the downloaded to PMAC, initializing the PMAC, and activating the next crew program. We also can set PMAC parameters directly [2].

(2) System monitoring module. This system monitoring module can samples the various parameters of the Manipulator in real time, and reflects in the interface, these parameters include the position of each cylinder, stretching speed, pressure, motor position, speed and Alarm information. The monitoring module is also charged with the task of system communication bus. PMAC communicates with the host computer through dynamic link library PComm32.PComm32 contains all methods of communication with the PMAC, including PMAC.dll, PMAC.says, PMAC.vxd. it also contains more than 250 function. [3.], but we only need grasp the following functions which can achieve most of the communication function, shown in Table 1.

Table 1 PMAC Program function figure

	Function code	Function
1	BOOL OpenPmacDevice(DWORD dw De-vice)	Open communication channel for the program using PMAC
2	BOOL ClosePmacDevice(DWORD dw De-vice)	After the program ran, this function closes the open channel
3	BOOL PmacSetMotor (HWND hwnd,DWORDdw Device)	This function can set PMAC communication with the host computer:buscommunication or serial communication
4	Void PmacSendCommandA(DWORD dw Device, PCHAR command)	This function may send a command to the specified PMAC directly, the parameters of the command are strings

(3) Manual control module. Manual control module function like a conventional manual CNC system control panel, so as to established a human interactive interface. Users can send commands directly to the manipulator module to achieve jogging, precise positioning, reset, suspend sports function. precise positioning means input pinpoint the exact coordinates in the coordinate system,so that the hydraulic cylinders can reach the specified location, while using a feedback signal to the comparator to ensure the positioning accuracy. By changing these PMAC I variables to control the speed.

Manual function achieve its function by calling PComm32 PmacGetResponseA (DeviceNumber, response, 255, "string") to achieve, changing the string to the PMAC. Among them, jog's string is "# n j +" or "# n j-"; precise positioning's string is "# n 172 -> L: $ 082B" [4].

PMAC Control module. PMAC motion programs can be interpreted by the G code interpreter, M code interpreter or T code interpreter,it also can be edited by PEWIN32 software. This design of the manipulator is edited via a PMAC program for editing text editor and a PEWIN32 PMAC serial terminal interface oriented interface. PMAC motion control program is developped and debugged by PEWIN32 executing software, including position control, speed control, servo loop update, security and other real-time tasks.

PMAC can support up to 256 motion programs, arbitrary coordinates can execute at any time any such a program. you first define the coordinate system and the shaft, One or a group of synchronous motors for the same purpose of organizing consisted of the PMAC coordinate system. By definition statement for the motor shaft axis to create a coordinate system assigned. Secondly, according to the requiredmotion, PMAC selects the appropriatemotion commands, and then follows thesyntax for writingPMACmotion programs,downloads toPMACmemory, the last run

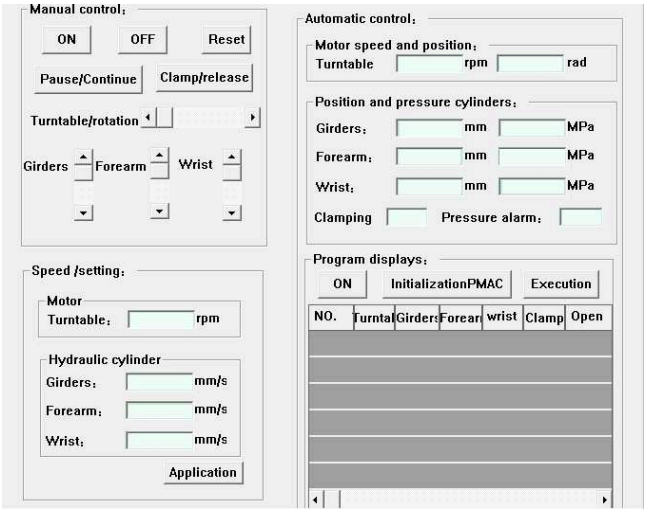

Fig. 5 Interface

Summary

This paper presents a 4-DOF manipulator based on PMAC controller. The Manipulator is driven primarily by hydraulic cylinders driven rather than motor driven, keeping smooth the Manipulator operation, quickly. Cylinder driving omitted gear mechanism, getting the simple mechanism and high reliability of the Manipulator. Omitting the gear unit can reduce the weight of the body and the required stiffness of the Manipulator, save manufacturing costs as well. Control system hardware and software has been designed .The IPC (IPC) as the core of management to manage the host computer system software; The PMAC as the core of components of lower machine to control the real-time motion. They constitute the host computer and the next crew hierarchical management framework so as to combine the dual advantages of IPC and PMAC. Compared with the conventional PLC controlling Manipulator, it improves the response speed, shortens the response time, enhances multi-tasking capabilities. We also design the PMAC interface, write software. After the simulation, the system is running well

References

[1] YueQiu-qin, TaoGui-bao, YuHua. Based on open multi-axis CNC system research and application of PMAC [J]. Manufacturing information, 2012,(4):60-62.

[2] Fan Jin-wei, TanFu-tao, WangZhi-yuan. Design and Research of image acquisition system in the inner wall based on the PMAC motion controller. Mechanical design and manufacturing2013,(5):36-38.

[3] Li Yan-dong, WangZong-yi, LiuTao, ChaiXiao-hui, The designing of three-axis turntable servo system Based on PMAC. Applied Science and Technology, 2007,34(7): 50-53

[4] Liu Qin, Sun Zhi-yong. NC fault monitoring system based on PMAC. Mechanical design and manufacturing, 2008,9(9): 92-93.

Advanced Materials Research Vols. 989-994 (2014) pp 3136-3139
© (2014) Trans Tech Publications, Switzerland
doi:10.4028/www.scientific.net/AMR.989-994.3136

Development of a Rotary Drilling Mechanism for Impregnated Diamond Bits

Zhantao Li[1, a], Yongzheng Ma[2, b] and Ken-ichi Itakura[3, c]

[1] School of Mechanical Engineering, Ningbo University of Technology, Ningbo 315016, China;

[2] School of Architecture and Civil Engineering, Ningbo University of Technology, Ningbo 315016, China;

[3] Department of Civil Engineering and Architecture, Muroran Institute of Technology, Muroran 050-8585, Japan.

[a] lzt2002@gmail.com, [b] xyz_kent@163.com, [c] itakura@mmm.muroran-it.ac.jp

Keywords: impregnated diamond bits, specific energy, uniaxial compressive strength, drilling mechanism.

Abstract. Impregnated diamond core bits are often used in core drilling for geological surveys. A tri-state theory is proposed to describe the three states in drilling processes for a diamond particle or a bit. These states are contacting state, cutting state, and ploughing state. Furthermore, the relations among thrust and other mechanical parameters are also summarized. The optimal value of the specific energy is in the cutting state. Several experiment results verified the proposed model. This mechanism is useful for selecting operation parameters in core drilling using impregnated diamond core bits.

Introduction

Geological surveys are important for the purpose of creating a geological map or model in petroleum fields, coal mines, and civil engineering constructions. Although various methods have been proposed for geological surveys in the past decades, core drilling is still the most intuitive and reliable advanced geological forecast technology. For core drilling, impregnated diamond core bits are often used. Therefore, it is important to elucidate drilling mechanism for the selection and design of diamond impregnated bits. In particular, quantitative knowledge related to drilling processes such as penetration rate and resistance forces are indispensible.

Nishimatsu discussed the relations between the penetration speed and operational parameters of the drilling for several types of bits [1]. And, the relation for impregnated diamond bits was summarized as the following:

$$F_t=\mu F_N \tag{1}$$

Herein, F_t is the circumferential force, F_N is the thrust force, *and* μ is the friction coefficient in a broad sense. Meanwhile, we have

$$F_N=\sigma_c u \Delta r, \tag{2}$$

where σ_c is uniaxial compressive strength (UCS), u is penetration per revolution, and Δr is the width of the bit blade.

Eq.(1) shows that a drilling process of an impregnated diamond bit can be regarded as a friction process between the bit and the rock, and the principal force (torque/radius) is proportional to the thrust force. Eq.(2) shows that the thrust force is proportional to the product of UCS and penetration per revolution. These two equations are succinct, and can be applicable to a certain extent. But they cannot describe the complex relations among mechanical parameters and rock strengths precisely. Several studies reported that the proportional relations as shown in Eq.(1) and Eq.(2) are valid only in a limit range of trust forces [2-4], but the bit-rock interaction mechanism for impragnated diamond bits was not illustrated.

Mechanism of Impregnated Diamond Bits

Three States in the Cutting Process of a Diamond Particle. Using small-diameter impregnated diamond bits, several drilling experiments were conducted, and the drilling processes were observed. Based on the results, a bit–rock interaction model for impregnated diamond bits was proposed. According to this model, a cutting motion of a diamond particle is divided into 3 states by the penetration depth as shown in Fig.1. In this figure, *h* is the pop-out height, and *d* is the penetration depth into the rock.

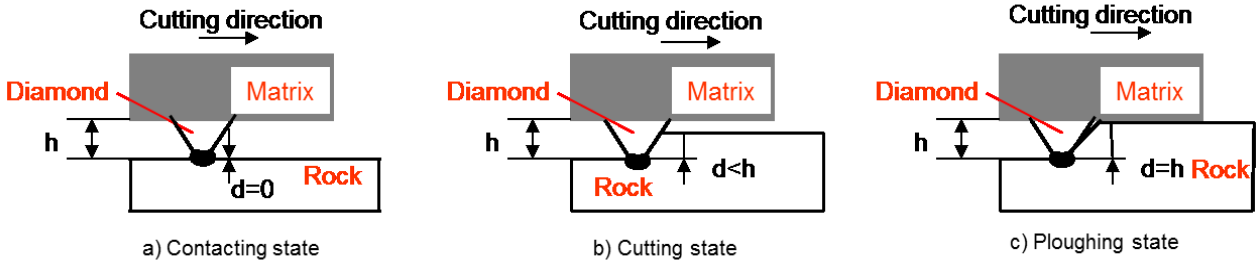

Fig.1 3 states in cutting process of a diamond particle

Contacting state (*d=0*)

In this state, the diamond particle is contacting to the rock lightly. The matrix is separated from the rock. Friction is the main bit-rock interaction pattern while cutting action can be ignored.

Cutting state (*d<h*)

The diamond particle penetrates into the rock. Friction still exists, but cutting becomes the main action. The matrix is separated from the rock.

Ploughing state (*d=h*)

The exposed portion of the diamond particle penetrates into the rock entirely, and the bottom of the matrix around the particle contacts the rock completely. There is ferocious friction between the matrix bottom and the rock. Cutting and friction occur at the same time.

Three states in the cutting process of an impregnated diamond bit. The model is shown as Fig.2.

Contacting state (*d=0*)

Some diamond particles are contacting to the rock lightly while others not. The matrix is separated from the rock completely. Friction is the main bit-rock interaction pattern while cutting action can be ignored.

Cutting state (*d<h*)

Some diamond particles penetrates into the rock while others not. Friction still exists, but cutting is the main action. The mmatrix is separated from the rock.

Ploughing state (*d=h*)

Exposed portion of all diamond particles penetrates into the rock entirely, and the bottom of the matrix around the particle contacts the rock completely. There is ferocious friction between the matrix bottom and the rock. Cutting and friction occur at the same time.

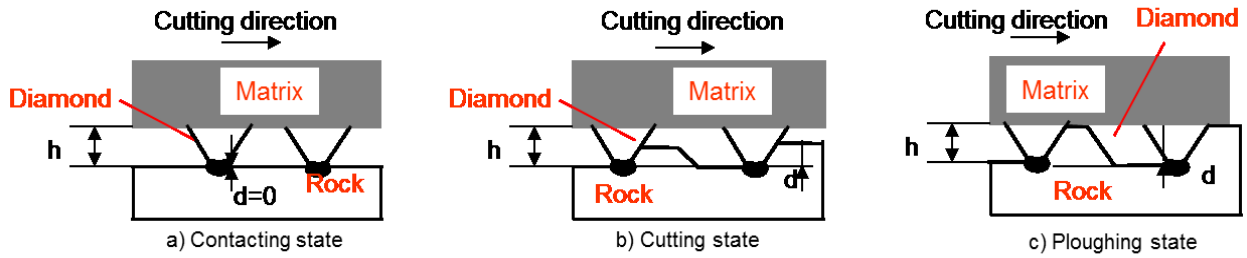

Fig.2 3 states in cutting process of impregnated diamond bit

Relations among Mechanical Parameters in Each State

In above chapter, the definition of the tri-state theory was proposed. For actual processes of drilling, each state may occur depending on the thrust. The exposure degrees of particles vary, hole-bottom surface is irregular, and the states of the particles are different with each other. Therefore, it is impossible to precisely describe the state for each particle. Nevertheless, basic behavior of each state of the bit can be described.

In this paper, drilling parameters discussed are explained as follows.

P: Principal component force, or conferential resistant force, torque / radius (N).

Q: trust, the resistant force in the penetration direction. (N).

u: penetration speed. (mm/s).

d: penetration rate, or penetration depth per revolution. (mm).

SE: specific energy. It is defined as the amount of work necessary for removal of a unit volume of rock. The specific energy can be expressed as shown below [5]. （MPa）

$$SE = \frac{Q}{A} + \frac{2\pi NT}{Au} \tag{3}$$

Therein, *T* is the torque, and *A* is the effective cross-sectional area of the hole. Here, effective cross-sectional area means the area of the circular loop formed by the outer and inner radii of a bit.

Relation Between the Principal Force and Thrust. We propose an equation to express the relation between the principal force and thrust in drilling processes using diamond bits as the following:

$$P = fQ \tag{4}$$

Herein, f is friction coefficient in a broad sense. This equation is the same in shape as Nishimatsu's equation. Meanwhile, we have

$$P = P_c + P_f = P_c + P_{df} + P_{mf} \tag{5}$$

The principal force P consists of cutting force P_c and friction force P_f. The latter includes two parts: the friction force between the bottom of the particle and the rock P_{df}, and that between the matrix and the rock P_{mf}. Furthermore, about friction coefficients, we have

$$f = f(f_c, f_{df}, f_{mf}), \tag{6}$$

Herein, f_{df} is the friction coefficient between particles and rock, f_{mf} is between matrix and rock, and f_c is the ratio of the cutting force and trust. This equation shows that general friction coefficient f is the function of f_c, f_{df}, f_{mf}.

For a contacting state, $P_c=0$, $P_{mf}=0$, the principal force is

$$P = P = P_c + P_f = P_c + P_{df} + P_{mf} = P_{df}$$

Theoretically, there is no cutting action in this state, and the bit removes rock mainly by grinding and friction of diamond particles. Depth of drilling per revolution is near zero. Thus the specific energy is significant.

In a cutting state, with the increasing of thrust, torque and penetration rate also increases proportionally. According to Eq. (3), the specific energy keeps constant.

In a ploughing state, penetration rate reaches its maximum value even though that thrust continues to increase. Torque from friction is increasing while penetration rate is constant, thus the specific energy increases significantly.

Indoor Experiment Results

Experimental devices. To measure mechanical data, several drilling experiments were conducted using a bench drilling machine (HITACHI B13RH) equipped with a displacement sensor, a torque sensor, a tachometer, a load meter, and an electricity meter. Four types of impregnated diamond bits, 5mm, 10mm, 20mm and 30mm in diameter respectively, by Asahi Diamond Industrial Co., Ltd., were used. Rock specimens were taken from sulfide minerals. UCS is in the range of 10-22MPa, the porosity is 20-30%.

Experiment method and process. The rotary speed was set to 580r/min. Thrust was changed from 0 N to 600 N. The hole depths were greater than 80 mm. Water was used as cutting fluid. Signals of these sensors were amplified through an amplifier circuit. They were shown and recorded in a computer with sampling time of 100 ms.

Experimental results. We report the results of verification of the proposed model, by taking the result of 10mm bits as an example. The changing trends of torque, penetration rate, friction coefficient, and the specific energy with the increasing of thrust, are shown in Fig.3

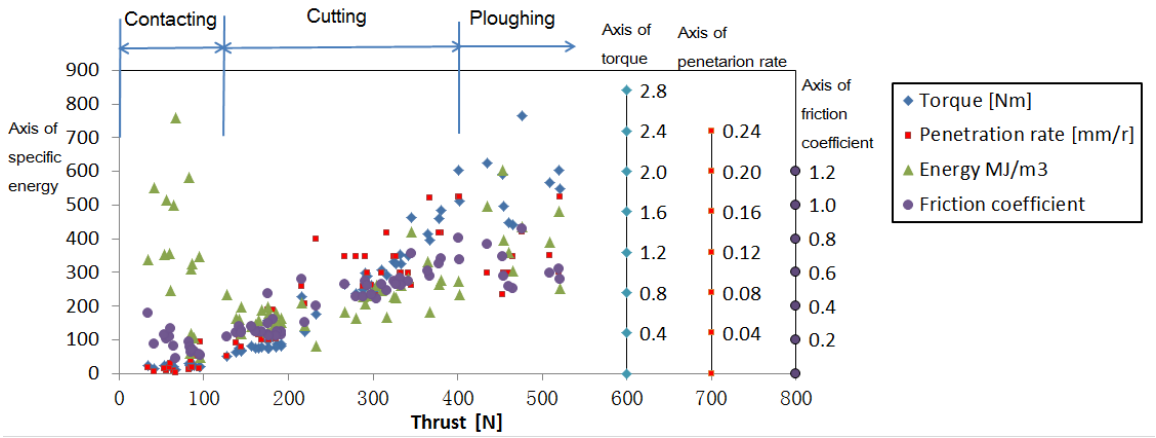

Fig.3 Changing Tendency of the mechanical parameters when the thrust increases

When the thrust changes from 0N to 500N, the torque increases from 0.02Nm to 2Nm. However, the wide-sense friction coefficient is not constant, and it changes in a range of 0.1-0.7. The penetration rate increases with the increasing of the thrust when the thrust is lesser than 400N. When it exceeds 400N, the penetration rate does not increase any more. This penetration thrust is the limit for the drill, bits, and the drilling conditions. The specific energy changes in a low-high-low trend. Above results verified and validated the proposed model.

Conclusions

In this paper, a tri-state theory for drilling processes using diamond impregnated bits was proposed. The relations among some drilling parameters were analyzed. Experiment results verified the correctness of the proposed model and theory.

Acknowledgments

Ther authors gratefully acknowledge the support of Ningbo Natural Science Foundation (Grant No. 2013A610195) and Zhejiang Provincial Natural Science Foundation of China (Grant No. Y1111133).

References

[1] Y. Nishimatsu: The Drilling Rate as the Mathematical Function of Operational Parameters of Drilling Machine [in Japanese], Shigen-to-Sozai, Vol. 121(2005) No. 3, p.1-10.

[2] T. Richard: DET-CRC Internal Report, Australian Resource Research Centre, CSIRO Perth. (2011)

[3] K.U.M. Rao, A. Bhatnagar, and B. Misra: Laboratory Investigations on Rotary Diamond Drilling, Geotechnical and Geological Engineering, Vol. 20(2002), No. 1, p.1-16.

[4] Z. Li and K. Itakura: An analytical drilling model of drag bits for evaluation rock strength. Soils and Foundations, Vol. 52(2012), No.2, p.216-227.

[5] R. Teale: The Concept of Specific Energy in Rock Drilling, Int. J. Rock. Mech. Min. Sci. Vol. 2(1965), p.57–73.

Advanced Materials Research Vols. 989-994 (2014) pp 3140-3144
© (2014) Trans Tech Publications, Switzerland
doi:10.4028/www.scientific.net/AMR.989-994.3140

Studies on Backward Median Current Waveform Control Research in Pulsed MIG Welding

Qiang ZHU[1,2,a], Jiaxiang XUE[1], Xiaoli ZHANG[1], Changwen DONG[1], Zhensheng CHEN[1], Zhihui LI[1], Ping YAO[3]

[1]School of Mechanical and Automotive Engineering, South China University of Technology, Guangzhou, 510640, China

[2]School of Electronic and Information Engineering, Guangdong Communication Polytechnic, Guangzhou, 510800, China

[3]School of Electrical and Mechanical, Guangdong Polytechnic Normal University, Guangzhou, 510635, China

[a]Email: zhuscut@163.com

Keywords: pulsed MIG welding; current waveform control; droplet transfer control

Abstract. The one-droplet-per-pulse transfer is widely considered to ensure the stability of the welding process in pulsed MIG welding; a peak pulse followed by a median pulse in a square wave pulse can effectively enhance droplet transfer controllability and improve weld appearance. The instantaneous current and voltage waveforms, the probability density distributions of current and voltage, and U-I graphs collected by the waveform wavelet analyzer were used to assess the welding quality and weld bead appearance. The 1.2-mm carbon steel welding wire experiments showed that under the same conditions, using a median waveform could significantly improve the welding quality. If the median current was too small or too large, the influence on the welding process was not obvious, and was only representing an increase of the base current or peak current phase. If the median time was too short, the energy accumulated was not enough to control the droplet transfer; conversely, too much median time led to globular droplet transfer. With a backward median current range of 180A-225A and duration range of 8ms-12ms, all experiments resulted in a nice weld effect.

Introduction

The rapid development of electronic and computer technology is making modern welding inverters increasingly intelligent; welding processes using expert systems, neural networks, and fuzzy control methods have achieved some success. For pulsed metal inert gas welding (PMIG), one-droplet-per-pulse transfer is widely considered the best welding process, providing a stable arc voltage, infrequent spatter, and a nice weld. Making a quantitative analysis of droplet transfer is difficult, however, because the process is affected by liquid surface tension, ion current force, gravity, spot pressure, electromagnetic force, as well as welding speed and shielding gas composition and other factors.[1-4] The authors wrote a program to control the output welding current of a self-developed soft switching pulsed MIG welding inverter power based on the DSP2808. Through backward median waveforms experiments, the authors were able to conduct significant research on how current waveform parameters influence droplet transfer.

Characteristics of a Backward Median Waveform

Current strength has an important influence on droplet transfer when the droplet size is small. From the idea of current waveform-controlling droplet transfer, welding researchers have proposed a backward median waveform control method,[5] which is shown in Fig.1. Compared to a single pulse square waveform, a backward waveform adds two parameters: median current, I_m, and median time, t_m. The median phase is designed to enhance droplet transfer controllability. During the welding process, the peak current phase plays the role of droplet growth, the base current phase maintains the stability of the arc burning, and the median phase controls the droplet transfer.

The quality of the welding can be reflected in the stability of the welding process, the amount of splash, arc sound and weld bead appearance, et cetera. Instantaneous current and voltage waveforms can reflect the stability of the welding process; the arc voltage probability density can reflect welding process stability and droplet transfer regularity; the current and UI drawing probability density can show peak energy stability. From the aforementioned methods, we were able to capture the instantaneous current and voltage signals using a Hall sensor and could remove high-frequency interference using wavelet filtering. Then, we studied the optimal parameters of backward median waveform procedure by analyzing the collected data.

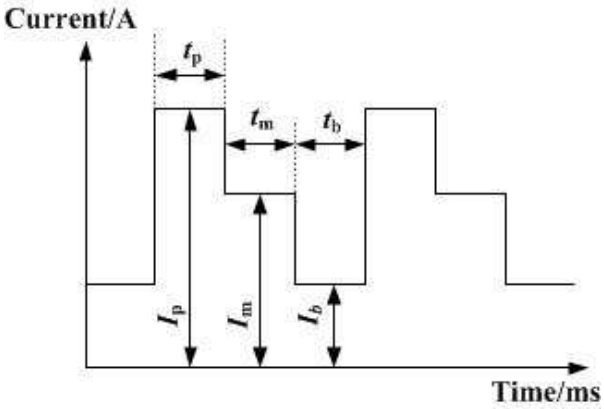

Fig. 1. The backward median waveform

Table 1. Welding experimental data

NO.	Peak current/A	Base current/A	Median current/A	Median time/ms
1	355	82	0	0
2	300	65	0	0
3	355	82	210	8
4	300	65	225	8
5	355	82	210	3
6	355	82	210	12
7	355	82	210	18
8	300	65	180	8
9	300	65	140	8

Experimental Data and Platform

The experimental platform includes the Advantech IPC 610, Advantech PCL1800 signal acquisition card, automatic moving devices, arc dynamic waveform wavelet analyzer, pulsed MIG welding soft switching inverter, and wire feed machine. The experimental conditions are 1.2-mm carbon steel wire, model ER50-6, surface welding on 8mm plate low-carbon steel. The protective gas is 99.99% argon gas with a flowing rate of 17L/min, the wire extension is 18mm, speed of automatic moving devices is 0.35m/min with a constant wire feed speed. Experimental data used as shown in Table 1; the peak current time is 7ms, the base current time is 8ms, and this remained unchanged during the experiment.

Experimental Results Analysis

Effect of the median phase on welding quality. Experiment No. 1 and Experiment No. 2 have no backward median waveform. From comparing these with Experiment No. 3 and Experiment No. 4, we can see a significant difference, as shown in Fig. 2.

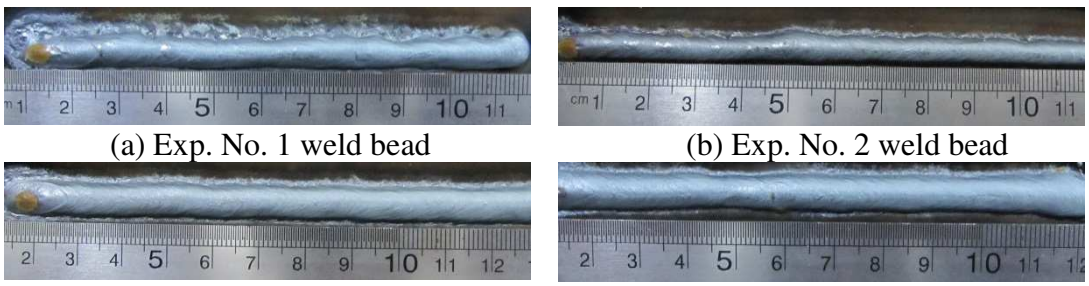

(a) Exp. No. 1 weld bead (b) Exp. No. 2 weld bead

(c) Exp. No. 3 weld bead (d) Exp. No. 4 weld bead

Fig. 2. Weld appearance contrast with and without backward median phase

From Fig. 2, we found that Experiments No. 1 and No. 2's weld beads had uneven widths and their welding processes produced "cracking" noises with obvious splashes; Fig.2 (a) had some undercutting. Experiment No.3 and No.4 had nice weld appearances with even, uniform surface ripples, their welding processes were stable, there were no short circuits or breaking arcs, the arcs produced a soft sound, and no splashing occurred.

While analyzing the current and voltage signal acquired, as shown in Fig. 3 and Fig. 4, the arc length was not stable in experiment No. 1; the voltage increased suddenly between 11148ms-11194ms with slight arc breaking. This indicates that the droplet transfer was inconsistent and there was globular transfer behavior. Experiment No. 3's voltage and current waveforms were regular, with a clear droplet transition phase. The process was reproducible and had no short circuits or arc breaking.

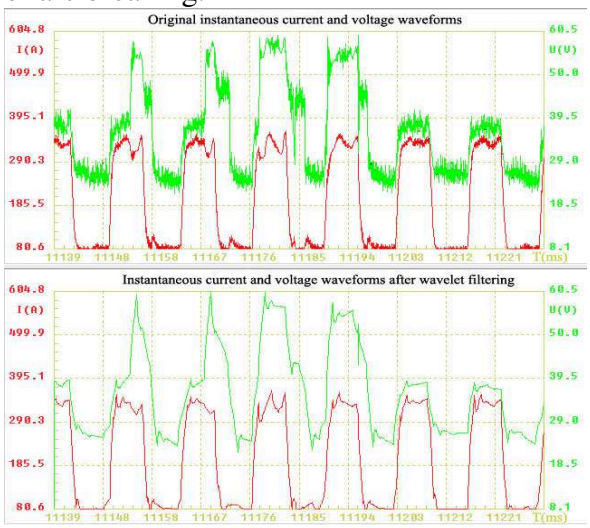

Fig. 3. Exp. No. 1 current and voltage waveforms

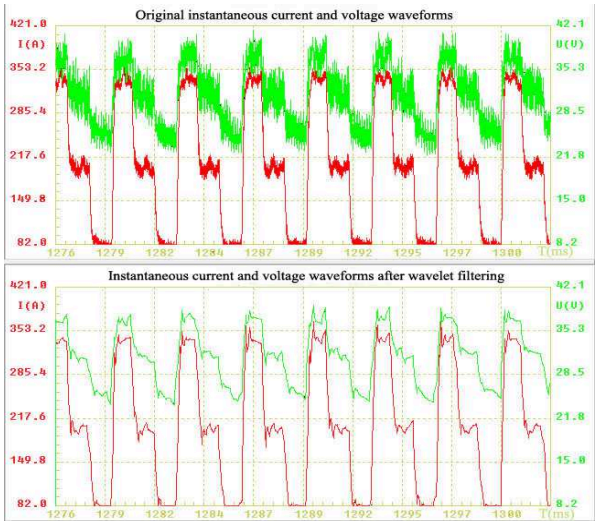

Fig. 4. Exp. No. 3 current and voltage waveforms

As shown in Fig. 5, Experiment No. 1's voltage signals' probability distribution and U-I graph were more scattered than those found in Experiment No. 3, which indicated that Experiment No. 3's welding process was more stable. In experiment No. 3, droplets were growing during the peak phase; when the current was switched to the median phase, the electromagnetic force made the droplets transfer into a molten pool，so that one-droplet-per-pulse occurred. The droplet transfer process could be controlled by adjusting the parameters of the median current. The experiments detailed above show that backward median currents can effectively control droplet transfer and improved weld bead appearance.

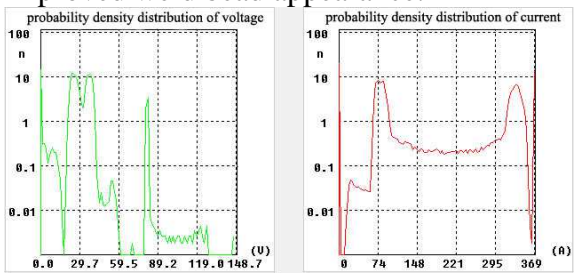

(a) Exp. No. 1 probability density distribution of voltage and current

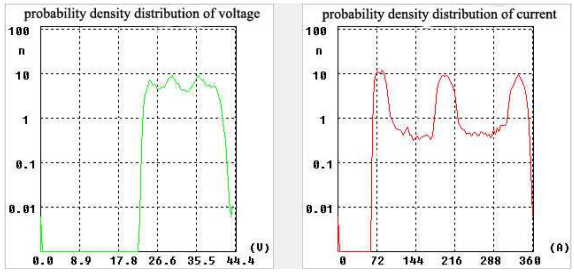

(b) Exp. No. 3 probability density distribution of voltage and current

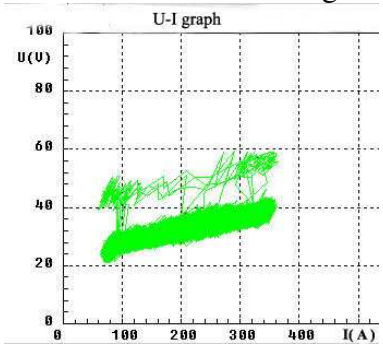

(c)Exp. No. 1 U-I graph

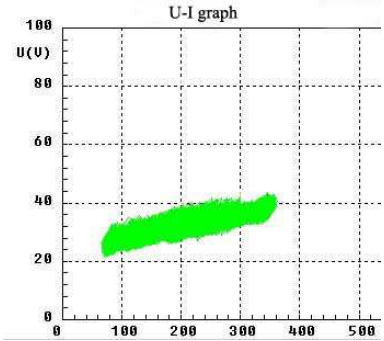

(d) Exp. No. 3 U-I graph

Fig. 5. Signal contrasts with and without backward median phase

Effects of median time on welding quality. As seen in the experiment results shown above, No. 3 had a good weld and a stable welding process. Thus, we set I_m=210A, made t_m different while

keeping other parameters unchanged, and studied the effect of welding when the median time varied.

Fig. 6 showed the weld appearance of different median time, appearance of Fig.6(b) was the best, the weld surface was smooth , surface ripple even and uniform. When t_m was 3ms and t_m was 18ms, the welding process could only be maintained, but the arc sound harsh, splash obvious with short circuit transition behavior, weld width were uneven.

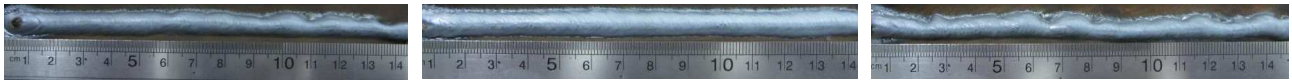

(a) Exp No.5 weld (t_m=3ms) (b) Exp No.6 weld (t_m=12ms) (c) Exp No.7 weld (t_m=18ms)

Fig.6. Weld appearance contrast of different backward median time

Analyzed weld appearance contrast of different backward median time, when the time was too short, the energy accumulated in median phase was not enough to make droplet transfer, during the next pulse droplet became larger, this led to short circuiting transfer or globular transfer of one-droplet-multi-pulse. In the case of constant wire feed speed, droplet transfer was not regular, so weld width was uneven and welding process was unstable with bad weld bead.

When the median time was appropriate, in the peak phase droplet began to grow up, in the median phase droplet grew up continually with sufficient energy and the electromagnetic force made droplet transfer into molten pool. The welding process was stable and reproducible, arc sound soft, current and voltage waveforms regular, welding quality nice.

When the median time was too long, the median phase energy was large enough to make more than one droplet transferred and grow up, which resulted in droplet transfer irregularities. Droplet transfer happened in peak phase, median phase and base phase, each pulse had varying amounts and sizes of droplets transferred into the molten pool, at this time, arc breaking and short circuit were easy to happen, weld bead as shown in Fig.6 (c).

Effect of the median current on welding quality. Based on experiment No.4, we made I_m different while kept other parameters unchanged, studied the effect of welding when median current varied.

From the view of data acquired in experiment No.4, No.8 and No.9, the welding processes were stable when the median current varied from large to small, current and voltage waveforms were regular, no broken arc and short circuit occurred, the arc voice sound soft. As Fig.2(d) and Fig. 7(a) shown, there were smooth weld bead appearance, suitable weld width and penetration and seldom splash when I_m was 225A and I_m was 180A. The welding process was stable but weld appearance began to uneven when I_m was 140A, if it continued to reduce the current, weld effect significantly became worse.

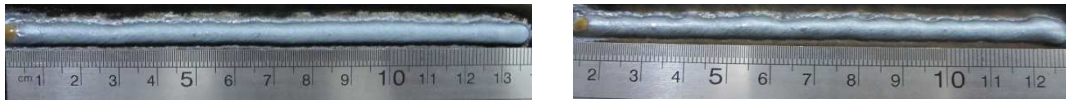

(a) Exp No.8 weld (I_m=180A) (a) Exp No.9 weld (I_m=140A)

Fig.7. Weld appearance contrast of different backward median current

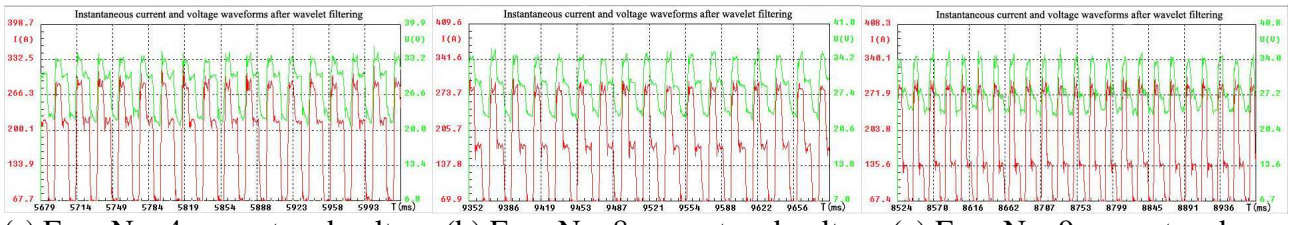

(a) Exp. No. 4 current and voltage waveforms (I_m=225) (b) Exp. No. 8 current and voltage waveforms(I_m=180) (c) Exp. No. 9 current and voltage waveforms(I_m=140)

Fig. 8. Different backward median current and voltage graphs

After analyzing the experimental results, it was found that when the median current was appropriate, droplets were transferred into a molten pool in the median phase, which made the

one-droplet-per-pulse transfer occur. When the median current was small, the accumulated energy was less than the threshold value of the spray transfer. The droplet transfer was not performed at this phase, and the median phase did nothing but allow droplets to grow; the transfer behavior happened at the next pulse through electromagnetic force. If the median current continued to decrease, the median phase would lose effect equivalent to an increase of the base time; this led to a globular transfer multi-pulse with inappropriate peak parameters. The experimental results showed that the value of the median current range was relatively wide, and that welds were better when the median current was more than 140A.

Conclusions

A single pulse followed by a median current waveform could effectively control the droplet transfer process and significantly improve welding quality. The instantaneous current and voltage data acquired from the waveform wavelet analyzer, the U-I graph obtained by analyzing signals, and the voltage and current probability density distribution were effective in the evaluation of the welding process.

The experiments illustrated that the effect of the backwards median time was greater than the current. The welding process was stable and weld bead was better when using 1.2-mm carbon steel welding wire, with the time around 8-12ms and the current between 180A-225A.

Acknowledgements

In this paper, the research was sponsored by Huangpu District Science and Technology Project (Project No. 201341), Foshan Science and Technology Planning Project (Project No. 2011AAl00175), Guangdong Province Commissioner Workstation (Project No. 2010B090500008). Foundation for Distinguished Young Teachers' Training of Guangdong under Grant Nos (Project No. Yq2013106).

References

[1] Ghosh, P.K., L. Dorn, et al. Journal of Materials Processing Technology, Vol. 209(2009) No. 3, p. 1262.

[2] Jittavisuttiwong, P. and B. Poopat: *The 7th International Conference on Materials Science and Technology* (Bangkok, Thailand, June 7-8, 2012). Vol.545,p.219.

[3] Kozakov, R., G. Gott, et al. Journal of Physics D: Applied Physics, Vol. 46(2013) No. 22, p.1.

[4] Wu Chuansong, Chen Maoai, and Li Shikai. Chinese Journal of Mechanical Engineering, Vol. 42(2006) No.02, p. 76.

[5] Kaiyuan Wu: *Study on DSP-based Digital Intelligent Control System for GMAW-P Inverter* (Ph.D., South China University of Technology, China 2005) ,p.82.

Advanced Materials Research Vols. 989-994 (2014) pp 3145-3148
© (2014) Trans Tech Publications, Switzerland
doi:10.4028/www.scientific.net/AMR.989-994.3145

Soil moisture monitoring system based on RS485 bus

Lei Wang*

School of Jianqiao University, Shanghai 201319, China

*gench_wl009@126.com

Keywords: Oscillation clock, RS 485, MODBUS, PC.

Abstract. In order to greenhouse plants for automatic irrigation operation, was designed based on the soil moisture monitoring system of RS 485 bus system, the oscillation frequency of the clock oscillation circuit, and a main chip count, frequency signal PC software will be the main chip records show, form curve, thus providing the basis of the data for the automatic irrigation, experimentally tested for a long time, the system performance is stable and reliable.

Introduction

In order to be precise on greenhouse soil automatic irrigation operation, monitoring on the need for soil moisture, when monitoring soil moisture did not reach the design threshold start irrigation system requires spray irrigation operation. Soil moisture or humidity is called soil moisture[1], soil moisture is dry and wet soil, the soil water content, available soil moisture percentage of dry soil weight representation. The traditional irrigation mode is the farmer's experience to judge, the artificial irrigation, which will produce the occurrence of irrigation is not timely, irrigation amount of too much or too little, thus affecting the growth of crops. In order to solve this problem, the system research and development of FSD100 soil moisture sensor, and realizes the real-time monitoring of soil moisture with PC software.

The system mainly use RS485 bus to realize the data monitoring soil humidity in the greenhouse, can long distance multi node in soil moisture monitoring greenhouse, and through the monitoring data of graph data, thus for the following automatic soil irrigation to provide information support, through the calibration to perform initial equipment, monitoring tasks can be very good to complete soil humidity, and can be combined with sprinkler irrigation equipment to complete the automatic irrigation operation in the greenhouse. The system mainly includes three parts, one is for the 485 transmission chip for information transmission, the second is the main chip ATTINY13A-SSU, mainly used for frequency counts, the third is the clock oscillation circuit NE555, mainly used for monitoring soil moisture.

The hardware design

The clock oscillator circuit design： Clock oscillation circuit chip is used in this system is NE555, a model in which the chip belongs to the timing of IC 555 series, 555 series IC, pin functions and application are compatible, but the models of different because of the different prices of the oscillation frequency stability, power saving, can produce rate is not the same and the 555 time IC; is a very versatile and widespread, only a few of the resistance and capacitance, can produce a variety of different frequency needed for digital circuit. The system circuit diagram is shown in figure 1.

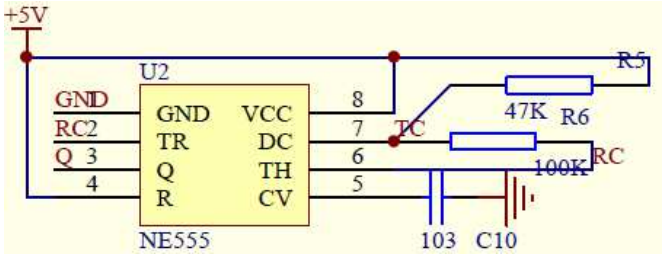

Figure 1. Clock oscillation circuit diagram

Through the combination of NE555 chip resistors and capacitors which clock oscillation circuit simple, by changing the resistance value in the capacitor rated conditions at different oscillating frequencies. The resistance variation of resistance will be accompanied by the change of the soil moisture change.

RS 485 circuit design： In greenhouse humidity monitoring requires a multi node monitoring, namely, a plurality of soil moisture monitoring at the same time, it can be the whole automatic irrigation operation according to the soil moisture in overall greenhouse, multi node communication distance is far, then the signal data using the RS 485 bus for moisture transmission, circuit diagram as shown in Figure 2, the RS 485 is an electrical interface standard, communication interface belongs to the physical layer, there is no uniform communication protocol, but now widely used is the MODBUS protocol, the MODBUS protocol is introduced for.

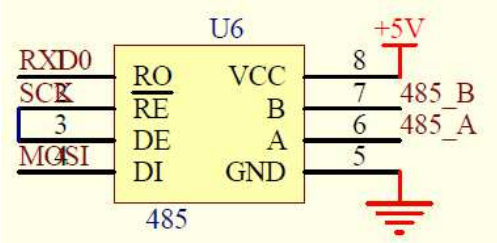

Figure 2. RS 485 circuit diagram

MODBUS was invented in 1979 by Modicon, is the world's first true for bus protocol in industrial field. MODBUS protocol is a common language used in the electronic controller of. Through this agreement, each controller, the controller through the network (such as Ethernet) and other communication devices can be. It has become the industry standard. This protocol defines a controller can use the information to understand the structure, regardless of what they are after the network communication. It describes the process controller requests access to other equipment, how to respond to the request from other equipment, and how to detect errors and records. A common format it set a pattern of information and content domain. When the communication on the MODBUS network, the agreement determines each controller needs to know the device address, recognize the address sent the message, and decide what action. If you need to respond, the controller will generate feedback and issued by the MODBUS protocol. In other networks, including the MODBUS protocol messages into frames or packets used on this network structure. This transformation is extended according to the specific network address, solution section routing path and error detection. The protocol supports the RS-232, RS-422, RS-485 and Ethernet equipment. Many industrial equipment, including PLC, DCS, intelligent instruments are in the use of the MODBUS protocol as the communication standard between them[2].

MODBUS has the following characteristics:

(1) open standard, users can freely, use the MODBUS protocol to safely, do not need to pay a licence fee, does not violate intellectual property rights. At present, support MODBUS manufacturers more than 400, more than 600 kinds of products that support MODBUS.

(2) the MODBUS can support a variety of electrical interfaces, such as RS-232, RS-485 etc, also can be transmitted in a variety of media, such as twisted pair, fiber, wireless.

(3) the MODBUS frame format is simple, compact, easy to understand. The user is easy to use, manufacturers to develop simple.

MODBUS can use RTU or ASCII communication mode, communication in the standard MODBUS. In the configuration of each controller, the user must select the communication of serial port communication mode and parameters. On the MODBUS bus all equipment should adopt the mode of communication and serial communication with the same parameter. Select RTU or ASCII for the MODBUS bus standard, it defines the serial transmission information bus on the meaning of the decision information, packaging and decoding method. The transmission mode used in the project to RTU mode, the following briefly introduced the basic situation of RTU model. The controller in RTU mode on the MODBUS bus communication, information in each of the 8 bits into 2 4 16 hexadecimal characters, the main advantage of this model is its transmission character density is higher than that of ASCII mode in the same baud rate, each information must be continuous transmission.

MODBUS information transmission in frames, each frame has a starting point and end point determination, the receiving device in the beginning of the read address information, and determine to addressing device (broadcast on all equipment, clockwise) and the transmission of information over time, can detect the partial information, false information can also be set as a results. When the communication command is sent to the instrument, with the communication command corresponding address code equipment, and remove the address code, read the information, if there is no error, is to perform their tasks; and then the execution results back to the sender. Send back information including address code, action code, execute the action result data and error checking code. If the error will not send any information.

Address code is the first byte of the information frame (8), from 0 to 255. The byte that host placed in information frame from the machine address code area, and from the machine address. In response, his address in the response information of the address code area, let the host recognition has a response from the machine.

Function code is the information frame to second bytes, 1-225 is a valid code range, when the host to send information from the machine, the function code that should be executed actions to Cong machine. Such as reading a set of register data, read the cluster diagnostic state, when the slave response host, the function code can be explained from the machine normal response or abnormal response, normal, the machine will simply return to the original function of the code, is not normal, returns a code phase equivalent with the original code from the machine, and the most significant bit is set to "1".

The data area includes the need from the machine to execute what action or by the return of information collected from machine. This information can be numerical, reference address etc.. For example, the function code tells the register values from the machine, the data must include the start address register to read and read length. For different from the machine, the address and data information are not the same[3].

MODBUS transmission under RTU mode using parity CRC cyclic code check is redundant, the check code contains 2 bytes, or 16 bits. CRC code from the sending device, tail placed in transmitting information. Receiving information equipment re computing the information received by the CRC code, comparing the calculated CRC code is consistent with the received, if they do not match, then that error. The calculation method of CRC code is, first preset 16 bit register all 1. Then gradually the processing each 8 bit data information. Only in the CRC code for calculating 8 data bits, the start bit and stop bit, such as the parity bit word also comprises the parity bit, do not participate in the calculation of CRC code. In the calculation of CRC code, 8 bit data and register data dissimilarity or, obtained results to the low shift a byte, fill the highest with 0. Check the most low, if the lowest is 1, the register contents and preset number dissimilarity or, if the low of 0, not for xor. This process is repeated 8 times. The eighth shift, the next 8 then and now the contents of register different or, this process is repeated 8 times above. When all the data after the information processing, and finally the contents of register is the CRC code value. Data transmission, CRC codes in the receiving low byte at the front[4].

The main chip circuit design： The main chip used in the design of system is ATTINY13A, the chip is a ATTINY chip produced by ATMEL company integrated with ATMEL's AVR micro controller

and flash memory, including 1KB and 4KB, with 32 KB to 256 KB SRAM. These devices support SPI and TWI communication, provides the high flexibility and the working voltage of 1.8V to 5.5V. ATTINY AVR using ATMEL's patented PicoPower technology, low power consumption. Circuit diagram is shown in Figure 3, the frequency signal in this system is mainly the use of the chip to collect the clock oscillation circuit for counting, and to cooperate with the PC software, generate soil moisture curve, so as to ensure that when soil moisture is lower than a certain value for automatic irrigation operation. Circuit diagram is shown in figure 3.

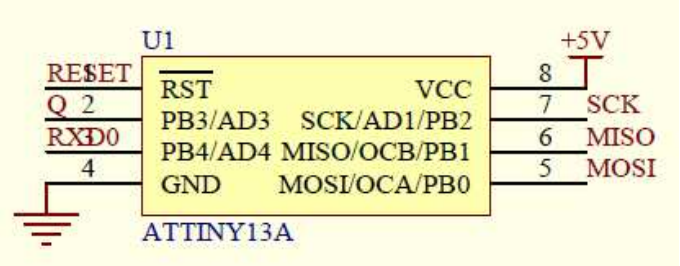

Figure 3. The circuit diagram of the main chip

The PC software design

The sampling system using the oscillating circuit to soil moisture, and the sampling frequency results delivered to the main chip count, the PC has been the main chip to communicate the soil moisture information displayed on the screen, allowing the simultaneous real-time display of the 10 monitoring points in the system design, the test system can monitor 10 use soil moisture conditions, the overall operating normally, curve display effect is obvious, the effect shown in Figure 4 as shown in fig..

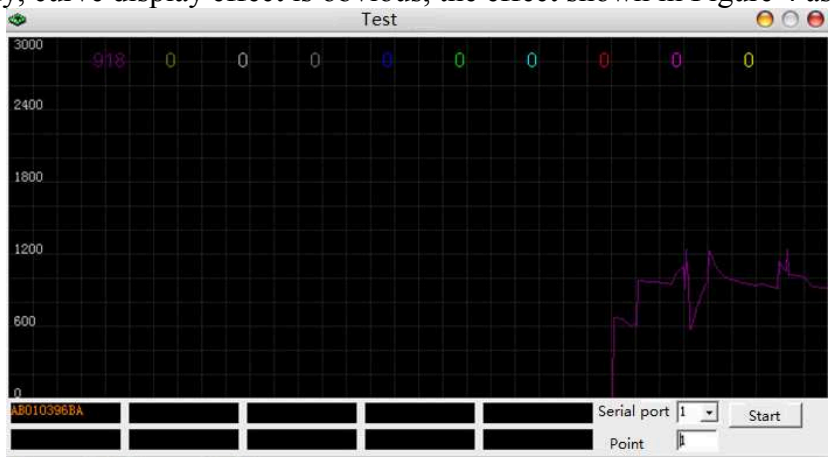

Figure 4. PC software interface

Conclusion

System uses a resistance detection methods of monitoring soil moisture, and the data transmission distance by RS 485 bus interface with PC software, forming the curves of the variation of humidity, automatic irrigation and ultimately for the greenhouse provides data information, through a large number of experiments, the whole system runs normally, for real-time monitoring of soil environmental change, and has a good application prospect and popularization value.

Reference

[1] Deng Xiaolei: The Chinese society of Agricultural Engineering, Vol.28(2012)No.9,p.30
[2] Zhu Mutian: Micro computer information, Vol.1(2004)No.6,p.9
[3] Pan Yue: *The design of Modbus protocol research and experiment system* (Master's degree, Harbin Institute of Technology, 2007),p.20.
[4] Hou Lili: Chinese instrument,Vol.10(2009)No.10,p.47

Advanced Materials Research Vols. 989-994 (2014) pp 3149-3152
© (2014) Trans Tech Publications, Switzerland
doi:10.4028/www.scientific.net/AMR.989-994.3149

The Finite Element Analysis of the Large-Diameter Composite Slurry Valve Gate

Jie Wu [1, a], Zhaomeng Yang[1, b] and DongZheng Wang [2, c]

[1]School of Mechanical Engineering, Shenyang University, Liaoning 110044, China;

[2] Faculty of Electronic information and Electrical Engineering, Dalian University of Technology, Liaoning 116024, China.

[a]wujied85@163.com, [b] 1852609778@qq.com, [c]418731866@qq.com

Keywords: Composite Slurry Valve Gate, Large-Diameter, Finite Element Analysis.

Abstract. In a long distance slurry pipeline transport system, pulp valve plays a vital role, which combined the pulp valve application is more, ram is one of the important components of composite slurry valve. This article mainly aims at gate has carried on the design and analysis, finite element modeling, and study the corresponding constraints, in the process of loading method, large diameter combination valve gate stress and strain distribution are obtained, combined with the optimization method and finite element analysis software for its structure optimization research, realize the lightweight of the gate. To reduces the manufacturing cost of the gate, as to provide theoretical basis for design.

Introduction

The slurry valve is one of the important equipment of long distance slurry pipeline transportation. The reliability is an important part of whether the safe operation of the long distance slurry pipeline transport system .Composite slurry valve is used higher on the market now .The valve is a kind of parallel plate type valve [1]. Due to its simple structure, convenient maintenance and disassembly, low cost, long service life, has good abrasion resistance, compression performance. It can realize remote hydraulic control and installation where the operator is not easy to reach. So they are widely used in mines, power plants, metallurgy, chemical industry and other departments of granular material slurry transportation, especially on high pressure slurry in pipeline, is the ideal replacement valve.For a long time, because the problems of bending stiffness caused by valve disc in the elastic deformation are failed to properly solve. To make the problems of valves jammed in the valve gate existing during the work.

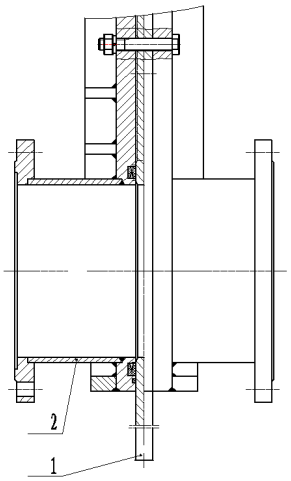

1- gate 2- composed of valve body

Fig. 1 Diagrammatic Sketch of Composite Slurry Valve

Gate is still lack of detailed theoretical analysis on the design, some formulas and coefficients of reference which have used are not accurate enough or hard to search, resulting in widely use in the design of flexible disc analogy method and the inheritance law, and then the accuracy and repeatability of the calculated value is lost relatively[2] .This article makes a deep research and analysis on the problem, the stress calculation, found out the theories of solutions to gate elastic deformation , put forward the feasible measures to solve this problem.

The large diameter combination slurry valve structure

Composite slurry valve is a kind of parallel plate gate valve (Fig. 1). When the valve opens, gate rise to match it's holes to a seat hole, equal to the outer pipe diameter, constitute a spool valve. When the valve is closed, gate fell and brake channel to death. Between gate and seat placed polyurethane seals and support ring, support ring also plays a role of sealing, so it is double seal. So no matter open or close the valve, sealing performance is good.

Due to the combined pulp valve is the off-standard valve gate, no molding formula can be drawn lessons from the process of gate design. The design of the blindness still exists, conventional design methods led to too thick gate problem. Aimed at the problem this article chooses the following two sets of formula design of comparison, the selected gate size 600 mm, nominal pressure of 4Mpa, The structure of gate is shown in Figure 2.

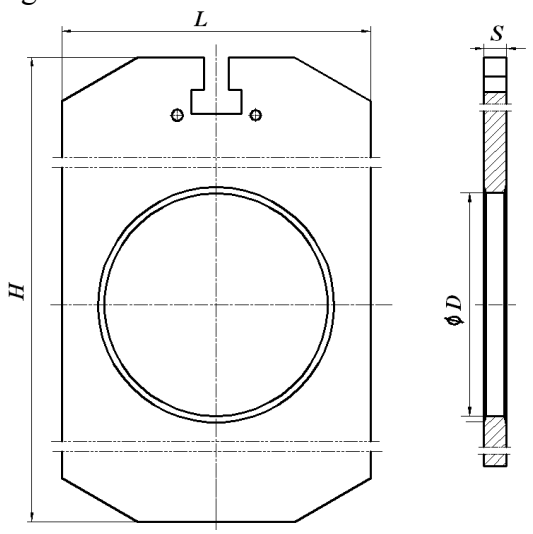

Fig. 2 The Structure of Gate

The traditional gate thickness design formula is:

$$S = 0.55 D_{MP} \sqrt{\frac{P}{[\sigma]}} + C \tag{1}$$

Where，S is thickness of the gate, unit: mm.

D_{MP} is the average diameter of sealing surface , unit: mm.

P is the pressure, the unit: Mpa.

$[\sigma]$ is allowable bending stress of material, unit: Mpa.

C is the design margin, unit: mm.

According to the actual engineering situation, this design gate choose materials for 45 # steel.The allowable bending stress is 135 Mpa. The nominal pressure is 4 Mpa. The design margin is 2 ～ 3 mm, The average diameter of sealing surface is 740 mm.Above the known parameters in formula (1) was calculated and the gate thickness for 75 mm.

The finite element analysis of gate

There are many finite element analysis software now .Such as ANSYS, DYNA3D, NASTRAN, ABAQUS, ADINA, and AFEMS. In this article ANSYS finite element software is used. Because gate

model structure is simple, first of all, used Sold Works software modeling, and then passed to the ANSYS finite element software to make a proper modification analysis, generated finite element model, in ANSYS static analysis. Gate materials are stainless steel 45 # steel, gate main dimensions and material properties such as table 1.

Table 1 The main dimensions and material properties of gate

Projects	Value	Unit
Thickness of the gate(S)	75	mm
Total Length of the gate (L)	820	mm
Total Height of the gate(H)	2140	mm
Hole diameter in the gate(D)	600	mm
Gate total weight(Wg)	812	kg
allowable bending stress of material ($[\sigma]$)	135	Mpa
Density	7850	Kg/m^3
The Elastic Modulus (E)	2.06×10^5	Mpa
Poisson's Ratio (u)	0.3	

Gate simplified for ax symmetric structures from the geometric shapes, gate force has the following three states.

1) When the valve is in open state, gate in a double sealed a medium in the pipe.

2) When the valve is closed, the gate in a single seal, valve side have medium.

3) The valve is in a state of half closed, gate double medium, gate in a state of balance.

In the three states stress, gate in the first kind of circumstance condition, namely single seal were the biggest load. Therefore load on the finite element analysis.

According to the actual working status of the valve, and its constraints mainly through the gate between the sealing plate and support for fixed, therefore, carried out on the contact surface between gate and seal plate displacement constraints. The load and supports of analysis setting is as shown in figure 3.

Because gate model structure is simple, the whole structure with eight nodes hexahedron element meshing.The meshing model is as shown in figure 4 .

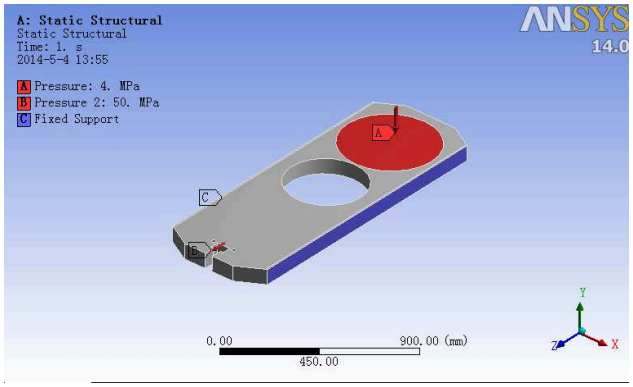

Fig. 3 Load and Supports of the Gate

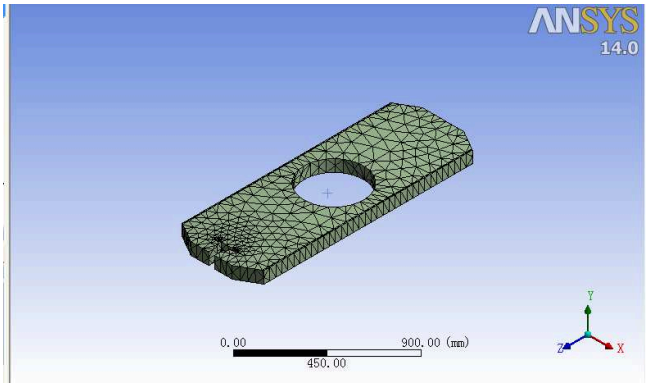

Fig.4 Finite Element Model of the Gate

The purpose of finite element analysis is obtained the response of the mechanics basic variables under a certain load, such as stress, displacement and elastic strain. Discussed the deformation, stress and elastic strain condition after the gate under external force action .According to the actual working status of the valve, and its constraints, mainly through the gate between the sealing plates and support for fixed, therefore, carried out on the contact surface between disc and seal plate displacement.

Due to the main load bearing of gate is the sealing surface of slurry nominal pressure, therefore, this article on the damper applied load: Role in the seal surface of 4 MPa nominal pressure. After the calculated by finite element analysis, get the contour plot of gate stress distribution (figure 5), the contour plot of gate displacement distribution (figure 6), and the contour plot of gate strain

distribution (figure 7).To see from the picture, the area of gate stress concentration distribution in the pipeline on both sides of the seal plate support, gate maximum bending deformation occurred in the location of the contact with the pipe size, this result in conformity with the actual.

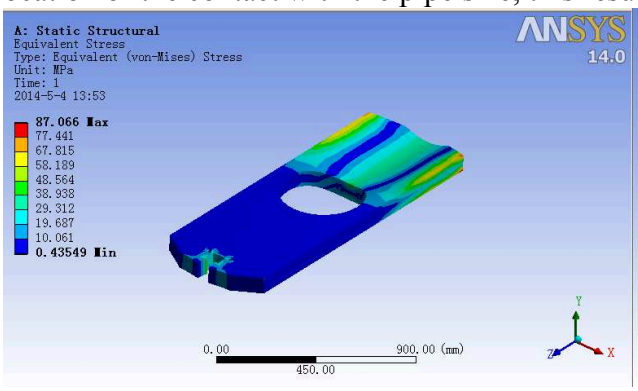

Fig. 5 The Contour Plot of Stress Distribution of Gate

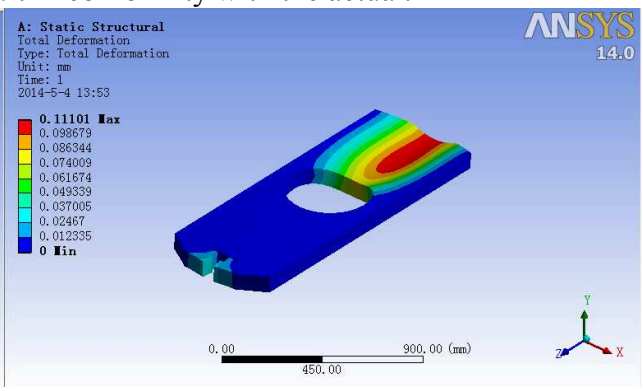

Fig. 6 The Contour Plot of the Gate Displacement Distribution

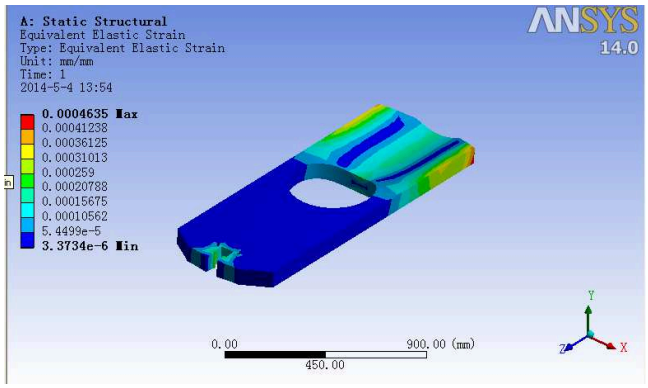

Fig. 7 The Contour Plot of the Gate Strain Distribution

Conclusion

This article introduced the structure design of gate, and Sold Works software for 3D entity modeling, and then conducted on the physical model of reasonable simplification, select the unit type finite element analysis, meshing, set up the finite element model of the gate, after applying constraints and loads, the static model, according to the result of model calculation, to analyze the structural strength and stiffness of the gate is verified. Finite element analysis show that the stress concentration area of composite slurry valve gate distribution in the sealing plate on both sides of the support of the contact with the pipe, gate maximum bending deformation occurred in contact with the pipe size of the circle domain.

References

[1] H.p. Xie，S. Zhang and Y. Yang: Annals of the PR, Vol. 30 (2008) No.1, p.87.
[2] M.F. Spotts: Design of Machune Elements (China machine press, China2002).
[3] ChristoPh M: Constraint-BasedComPuter-AidedDesig,Journal of Computing and InformationSeienceinEngineering,2005,Volumes,Issue3,P182.
[4] S.J. Lee: Capitation detection of butterfly valve using support vector machines ,Journal of sound and Vibration, 2005,P25.

Advanced Materials Research Vols. 989-994 (2014) pp 3153-3156
© (2014) Trans Tech Publications, Switzerland
doi:10.4028/www.scientific.net/AMR.989-994.3153

Fit Degree Calculation of an Aircraft Part Manufacturing Process

Xiongfei Huang [1, a], Fang Zhu [2, b] and Na Wei [2, c]

[1]Department of Marines, Naval Marine Academy, Guangzhou 510430, China;

[2] Department of Aircraft Maintenance and Engineering, Guangzhou Civil Aviation College, Guangzhou 510403, China.

[a]xiongfeifang@sohu.com, [b]zhufang@caac.net, [c]weina@caac.net

Key words: Fit degree, Aircraft part, Assembly process, Economical manufacturing.

Abstract: Aircraft manufacturing process normally requires very high precision assembly parts which are achieved in practice by a high-precision machining parts followed by a high coordination degree assembly process. The current practice in aircraft parts manufacturing process is that the manufacturing cycle is long, the rework rate is high and the manufacturing precision is difficult to improve. This can be sometimes infeasible or very costly. In this paper, we consider a fit degree calculation method to achieve precision aircraft parts with economical manufacturing processes. We consider an analytical approach to establish a physical process model to guide the design and machining process of assembly parts, which can assume the fit degree. The results show that the approach can obtain the nearly optimal process parameters at designated fit degree. At last, a case is developed to verify the proposed methods.

Introduction

An aircraft is known as a kind of transportation which has complex product composition, complex product technologies, complex manufacturing processes, and complex project management, complex mechantronics equipment, micro-sensors etc. In the process of design and manufacture of an aircraft, it is very important that part tolerance is practically designed to meet the requirements of aircraft's quality, performance, machining, assembly, manufacture, cost, and so on [1]. Currently practice for the manufacturing process of the aircraft parts is to control each part machining process of the assembly parts respectively. Although this independent control method could be an effective selection of improving aircraft manufacturing precision and fit degree of final product assembly process, its cost will be considerably high to achieve a desired fit degree. Therefore, this paper will develop an effective fit degree calculation method with fully utilizing the quality information of the overall aircraft parts manufacturing process and the relationship between the two assembly parts. In the past study, Kannan and Jayabalan [2] proposed a grouping method for a complex assembly with three mating parts. Kumar and Kannan [3] proposed a method using a genetic algorithm for obtaining optimum manufacturing tolerance to reduce the number of surplus components and manufacturing cost. Asha et al. [4] proposed a method for finding the best combination of components with multiple quality characteristics to minimize clearance variation. Matsuura and Shinozaki [5] derived an optimal manufacturing mean design that minimizes the number of surplus mating parts. Kannan et al. [6] proposed a method for obtaining the best combination of components under Taguchi's loss function.

Manufacture parameters of aircraft parts for Fit degree calculation

The manufacturing parameters of aircraft parts for fit degree calculation have been provided. In this framework, each key phase parameters of manufacturing process is embodied by a functional component. Fig. 1 shows an overview of the fit degree calculation method proposed in this paper.

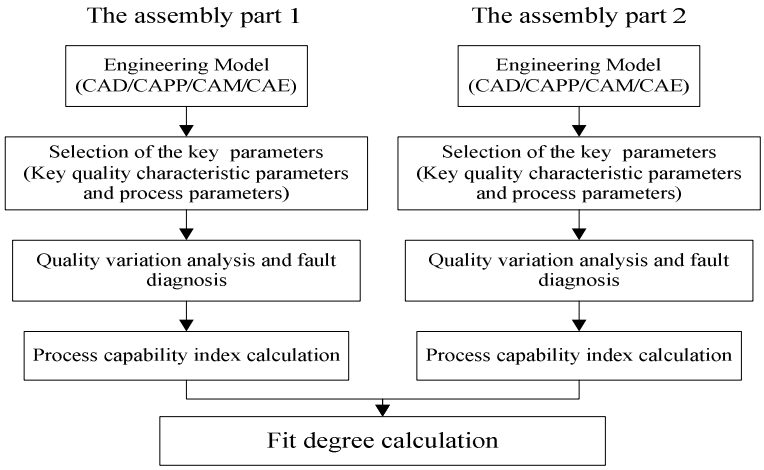

Fig.1. Fit degree calculation framework of aircraft parts manufacturing process

In this fit degree calculation method, each component has its specific functionality. The manufacturing parameters of aircraft parts are provided by each key manufacturing process. After the required manufacturing information is obtained, we can calculate the fit degree of two mating aircraft parts. The fit degree in aircraft parts assembly is defined as the ratio of suitable mating parts assembled to those manufactured including defective parts, which means the percentage of two matched parts that can be paired off. Fit degree can be calculated through the PCI of two mating parts, which indicates how well the predicted result fits within the specification limits. This component is able to support the evaluation and improvement of the aircraft parts manufacturing process. If the quantitative fit degree value of mating parts can be calculated, certain precautions or quantitative quality feedback on how to adjust manufacturing process or parameters can be taken to reduce surplus parts, thus, guarantying the desired fit between mating parts and increasing the effectiveness of the aircraft parts manufacturing process.

Fit degree calculation

In an aircraft part manufacturing process, the machining process is a controllable and adjustable multistage process, so the quality data often fit the curves represented by a mathematically derived normal distribution curve. Therefore, the normal distribution is adopted in the analysis although the fit degree calculation method.

From aircraft parts manufacturing process, we can get the overall process capability index C_{pm}:

$$C_{pm} = \frac{USL - LSL}{6\sqrt{E(X-T)^2}} = \frac{USL - LSL}{6\sqrt{E(X-\mu+\mu-T)^2}} = \frac{USL - LSL}{6\sqrt{E[(X-\mu)^2 + (\mu-T)^2 - 2(X-\mu)(\mu-T)]}}$$

$$= \frac{USL-LSL}{6\sqrt{E(X-\mu)^2+(\mu-T)^2-2E(X-\mu)(\mu-T)}} = \frac{USL-LSL}{6\sqrt{\sigma^2+(\mu-T)^2-2(\mu-T)(\mu-\mu)}} = \frac{USL-LSL}{6\sqrt{\sigma^2+(\mu-T)^2}} \quad (1)$$

Let P_d represent the percent defective of process output, P_y and P_d are all the functions of two variables C_{pm} and k, where k is defined as the ratio of the bias of process mean to its target (Kane[7]). The two process quality indexes in terms of C_{pm} and k are shown as follows:

$$P_y = \Phi\left[3\frac{C_{pm}}{\sqrt{1-9k^2C_{pm}^2}}(1-k)\right] - \Phi\left[-3\frac{C_{pm}}{\sqrt{1-9k^2C_{pm}^2}}(1+k)\right] \quad (2)$$

$$P_d = 1 - \Phi\left[3\frac{C_{pm}}{\sqrt{1-9k^2C_{pm}^2}}(1-k)\right] + \Phi\left[-3\frac{C_{pm}}{\sqrt{1-9k^2C_{pm}^2}}(1+k)\right] \quad (3)$$

The estimated percentage of dimensions falling into each selective group *i* can be expressed as:

$$\begin{aligned} P_i &= P\left[\left(USL - i\frac{USL-LSL}{t}\right) < x \le \left(USL - (i-1)\frac{USL-LSL}{t}\right)\right] \\ &= P\left[3\frac{C_{pm}}{\sqrt{1-9k^2C_{pm}^2}}\left(1-k-2\frac{i}{t}\right) < Z \le 3\frac{C_{pm}}{\sqrt{1-9k^2C_{pm}^2}}\left(1-k-2\frac{i-1}{t}\right)\right] \\ &= \Phi\left[3\frac{C_{pm}}{\sqrt{1-9k^2C_{pm}^2}}\left(1-k-2\frac{i-1}{t}\right)\right] - \Phi\left[3\frac{C_{pm}}{\sqrt{1-9k^2C_{pm}^2}}\left(1-k-2\frac{i}{t}\right)\right] \end{aligned}$$

i=1,2,…,t (4)

The fit degree in the aircraft parts assembly process is defined as the ratio of mating parts assembled to those manufactured parts. The fit degree of two mating parts P_{md}, which is,

$$P_{md} = \sum_{i=1}^{t} \min[P_{fi}, P_{mi}] \quad (5)$$

$$P_{md} = \sum_{i=1}^{t} \min\left\{\begin{array}{l}\left\{\Phi\left[3\frac{C_{pmf}}{\sqrt{1-9k_f^2C_{pmf}^2}}\left(1-k_f-2\frac{i-1}{t}\right)\right] - \Phi\left[3\frac{C_{pmf}}{\sqrt{1-9k_f^2C_{pmf}^2}}\left(1-k_f-2\frac{i}{t}\right)\right]\right\}, \\ \left\{\Phi\left[3\frac{C_{pmm}}{\sqrt{1-9k_m^2C_{pmm}^2}}\left(1-k_m-2\frac{i-1}{t}\right)\right] - \Phi\left[3\frac{C_{pmm}}{\sqrt{1-9k_m^2C_{pmm}^2}}\left(1-k_m-2\frac{i}{t}\right)\right]\right\}\end{array}\right\} \quad (6)$$

Equation (6) means that, we can get C_{pmf}, C_{pmm}, and k_f and k_m from the aircraft parts manufacturing process, the fit degree P_{md} in the aircraft parts manufacturing process can be calculated.

Example

The following example is presented to illustrate the performance of the developed fit degree calculation method of aircraft parts manufacturing process. The process of a cylinder and piston (as shown in Fig. 2) assembly, which is used in a kind of aircraft engine, provides an example of high precision pair of mating parts. The fit of cylinder and piston is a clearance fit in this case study and high accuracy of this pair of assembly parts is essential, because there is a target value for the clearance. High precision machining and match assembly are usually adopted for these aircraft parts manufacturing process, the allowable minimum clearance is 0.01 mm, and the allowable maximum clearance is 0.02mm. The manufacturing specifications for the mating parts are as the follows.

Table 1 Quality specification and machining process of cylinder

Stage No	Stage name	Content of stage and its quality characteristic (mm)
1	Milling	Mill locating surface---the bottom side of cylinder block and the flatness of it is less than 0.01mm, need to ensure the distance between this surface and machining datum surface.
2	Clamping	Clamp the machined locating surface and the flatness of the surface is less than 0.02.
3	Boring	Bore the inner diameter of cylinder to $\emptyset 150.12_{0}^{+0.034}$
4	Grinding	Grind the inner diameter of cylinder to $\emptyset 150_{0}^{+0.018}$

Table 2 Quality specification and machining process of piston

Stage No	Stage name	Content of stage and its quality characteristic (mm)
1	Milling	Mill locating surface---the bottom side of piston and the flatness of it is less than 0.01mm
2	Rough turning	Mill the external diameter of piston to $\emptyset 150.2_{-0.01}^{+0.024}$
3	Finish turning	Mill the external diameter of piston to $\emptyset 150_{-0.009}^{+0.009}$

By Tables 1 and 2, the machining process of the two mating parts includes three stages respectively, in which the inner diameter dimension of cylinder and external diameter dimension of piston are the key quality attributes to be satisfied.

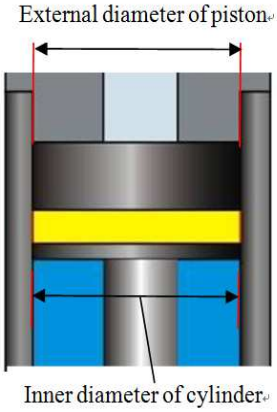

Fig. 2 A cylinder and piston assembly

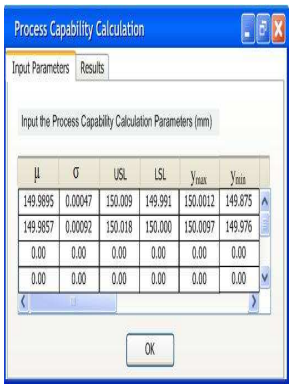

Fig. 3 Process capability calculation parameters inputting

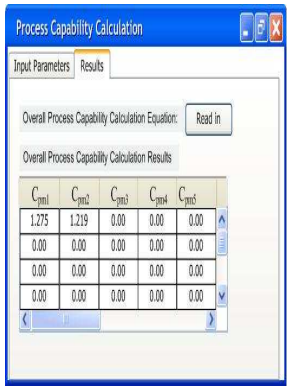

Fig. 4 Process capability calculation results

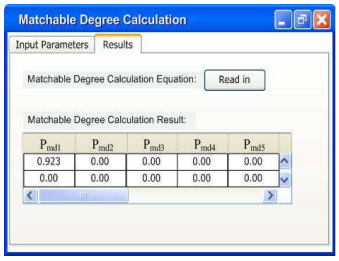

Fig. 5 Fit degree calculation results

After the overall process capability indexes C_{pm} of the two mating parts were obtained (as shown in Fig. 3 and 4), the results were sent to the fit degree calculation. The calculation output is shown in Fig. 5. This aircraft part manufacturing process is acceptable, as its P_{md} is 0.923.

Conclusion

As the fit degree of an aircraft part manufacturing process can be calculated, the complex product design and manufacturing processes could be adjusted in time to reduce the cost. In this sense, the fit degree calculation method as presented in this paper can be adopted to reduce the unnecessary loss of manufacturing cost and time.

References

[1] J. B. Wang. Research on aircraft sheet metal digital manufacturing system and it s key technology. Xi'an Northwestern Polytechnical University ,2004.

[2] S. M. Kannan and V. Jayabalan . A new grouping method to minimize surplus parts in selective assembly for complex assemblies. International Journal of Production Research, Vol.39 (2001) No. 9, p.1851-1864

[3] M.S. Kumar , S.M. Kannan and V. Jayabalan.. A new algorithm for minimizing surplus parts in selective assembly by using genetic algorithm. International Journal of Production Research, Vol.45 (2007) No. 20,p.4793-4822

[4] A. Asha, S.M. Kannan and V. Jayabalan. Optimization of clearance variation in selective assembly for components with multiple quality characteristics. International Journal of Advanced Manufacturing Technology, Vol.38 (2008)No. 9-10,p. 1026-1044

[5] S. Matsuura and N. Shinozaki. Optimal process design in selective assembly when components with smaller variance are manufactured at three shifted means. International Journal of Production Research, Vol.49(2011)No.3,p.869-882

[6] S.M. Kannan, A.K.Jeevanantham and V.Jayabalan. Modelling and analysis of selective assembly using Taguchi's loss function. International Journal of Production Research, Vol.46(2008)No. 15,p. 4309-4330

[7] V.E.Kane. Process capability indices. Journal of Quality Technology, Vol.18(1986).No. 1,p. 41-45.

Advanced Materials Research Vols. 989-994 (2014) pp 3157-3160
© (2014) Trans Tech Publications, Switzerland
doi:10.4028/www.scientific.net/AMR.989-994.3157

Fuzzy adaptive PID controller optimization design in temperature control system

Xiaopeng Li[a], Lanzhen Chen[b, *]

Information engineering institute of Gannan Medical University，Ganzhou 341000，China

[a]happyday-007@163.com, [b]danrou_2006@qq.com

Keywords：fuzzy control；PID control；Smith predictor

Abstract：A new self-adjusting PID controller based fuzzy inferences is proposed. Using fuzzy inferences method, the PID parameters can be adjusted adaptively online for the varying state of the system. This approach has more significant performance and robustness than conventional PID contorllers in any conditions. Traditional fuzzy control systems have difficulties for plants with great delay．A fuzzy PID system based on the Smith compensation theorem is proposed in the paper．It allows to change the transfer function of the plant．Simulation results are also given．

1.Introduction

In the study of Biomedical Engineering, the requirements on temperature are very strict. The traditional temperature control system generally adopts PID control algorithm. However, in the temperature control process which using this algorithm, often encounter delay, and the existence of time delay affects the stability of the system seriously, cause the system overshoot becoming big, the adjusting time becomes longer, even oscillation, divergence, which makes the dynamic quality of the system greatly decreased. If you still use the conventional PID controller, it is hard to tune the PID parameters. Aiming at this problem, this paper designs an improved self-adaptive fuzzy PID controller, which has the advantages of fuzzy control is flexible, adaptable, and has high precision of PID control, self-tuning function online and can realize the PID parameter and reduce the impact of time delay.

2.The traditional PID control

The control algorithm of the conventional PID controller is as follow:

$$u(t) = K_P e(t) + K_I \int_0^t e(t)dt + K_D de(t)/dt$$

Consider of the stability of the system, the speed of response, overshoot and steady-state accuracy into account, the roles of KP, KI, KD are as follows:

(1)The role of proportional coefficient (KP) of is to accelerate the response speed of the system, improve the system control accuracy.

(2)The function of integral action coefficient (KI) is to eliminate the steady-state error of the system.

(3)The role of differential coefficient (KD) is to improve the system dynamic characteristics, its main function is to change in response to inhibition of deviation in any direction, the deviation changes were predicted in advance.

3. The optimal design of the fuzzy adaptive PID control

Based on the traditional fuzzy adaptive PID controller, the optimized fuzzy adaptive controller added a Smith predictor; the controller error E and error rate of change of EC as input, which can meet the different moments of E and EC on PID parameters self-tuning requirements. The structure of the controller as shown in Figure 1:

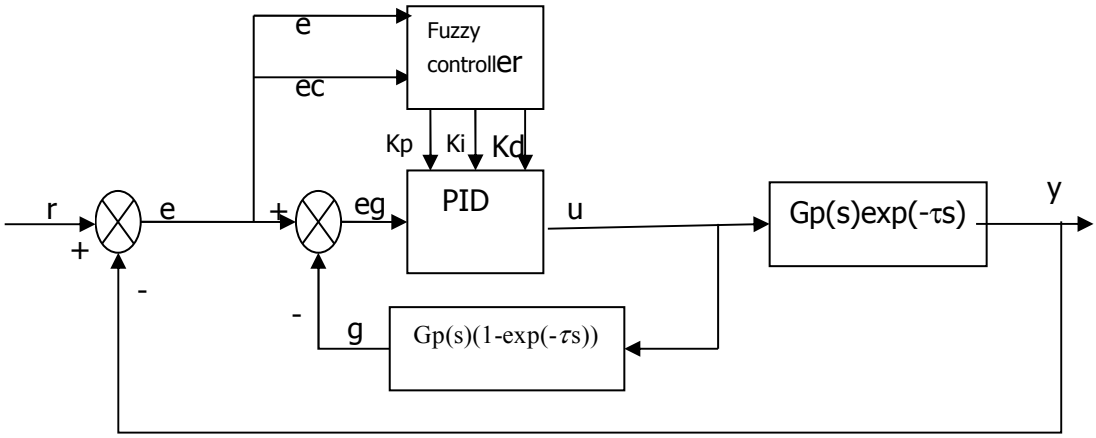

Fig. 1 Fuzzy adaptive PID controller schematic

The key of PID parameters fuzzy self setting is to find the three PID parameters KP, KI, fuzzy relation between KD and E and EC, through the continuous detection of E and EC in the operation, according to the fuzzy control principle to achieve the KP, KI, modify the KD online, which meet the needs of different e and EC to control parameters of the request, the object has good dynamic and static performance.

3.1 The fuzzy language variables and the determination of their membership functions

Set the input temperature fuzzy controller E and temperature change rate of EC, the fuzzy treatment to obtain the fuzzy linguistic variables E and EC, the fuzzy subset of E and EC are {NL, NM, NS, ZO, PS, PM, PL}, the same output KP, KI, fuzzy subset of KD were {NL, NM, NS, ZO, PS, PM, PL}, selection of fuzzy language variables E and EC as well as KP, KI, domain KD were {-6, -5, -4, -3, -2, -1, 0, 1, 2, 3, 4, 5, 6}, and let E and EC obey the triangle membership function curve, KP, KI, KD obey Gauss membership function curve, in order to obtain good steady-state performance, the input variable of E were irregular division, at the temperature E is zero in the vicinity of a high sensitivity, guarantee the steady state system to achieve higher control precision.

3.2 Establish control rule table

Fuzzy adaptive PID is performed by calculating the fuzzy inference system error E and error change rate of EC, using the fuzzy rules for the fuzzy reasoning, and inquiring fuzzy matrix table to parameter adjustment. The core of fuzzy control design is the use of technology to support engineering staff knowledge and practical experience, taking into account the role of the relationship between the three parameters at different times and with each other, through repeated experiment adjustment to get the fuzzy control rule table which according to three parameters self-tuning:

Parameters 1

ΔK_p ec / e	NL	NM	NS	ZO	PS	PM	PL
NL	PL	PL	PM	PM	PS	ZO	ZO
NM	PL	PL	PM	PS	PS	ZO	NS
NS	PM	PM	PM	PS	ZO	NS	NS
ZO	PM	PM	PS	ZO	NS	NM	NM
PS	PS	PS	ZO	NS	NS	NM	NM
PM	PS	ZO	NS	NM	NM	NM	NL
PL	ZO	ZO	NM	NM	NM	NL	NL

Parameters 2

ΔK_I ec / e	NL	NM	NS	ZO	PS	PM	PL
NL	NL	NL	NM	NM	NS	ZO	ZO
NM	NL	NL	NM	NS	NS	ZO	ZO
NS	NL	NM	NS	NS	ZO	PS	PS
ZO	NM	NM	NS	ZO	PS	PS	PS
PS	NM	NS	ZO	PS	PS	PM	PL
PM	ZO	ZO	PS	PS	PM	PM	PL
PL	ZO	ZO	PS	PM	PM	PL	PL

Parameters 3

ΔK_D ec / e	NL	NM	NS	ZO	PS	PM	PL
NL	PS	NS	NL	NL	NL	NM	PS
NM	PS	NS	NL	NM	NM	NS	ZO
NS	ZO	NS	NM	NM	NS	NS	ZO
ZO	ZO	NS	NS	NS	NS	NS	ZO
PS	ZO	ZO	ZO	ZO	ZO	ZO	ZO
PM	PL	NS	PS	PS	PS	PS	PL
PL	PL	PM	PM	PM	PS	PS	PL

3.3 The fuzzy reasoning which based on the fuzzy rule table

According to the fuzzy control rules table 1 ~ 3, 49 control rules can be obtained:

(1) If (e is NL) and (ec is NL) then (K_P is PL) (K_I is NL) (K_D is PS)

(2) If (e is NL) and (ec is NM) then (K_P is PL) (K_I is NL) (K_D is NS)

……

(49) If (e is PL) and (ec is PL) then (K_P is NL) (K_I is PL) (K_D is PL)

According to the fuzzy membership function of the fuzzy subset assignment table and the parameters of the control model, the application of fuzzy reasoning of fuzzy matrix synthesis of the design parameters of PID, the online correction of PID parameters, the calculation formula is as follows:

$K_P=K_P'+\Delta K_P$

$K_I=K_I'+\Delta K_I$

$K_D=K_D'+\Delta K_D$

4.The results of simulation

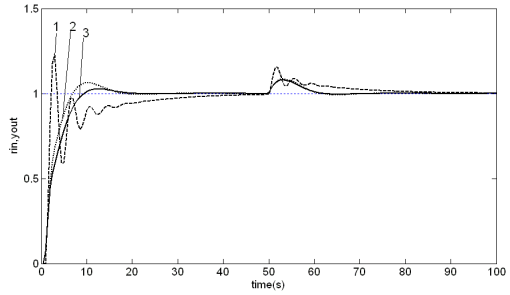

From the above step response curve can be seen, with the traditional PID control and fuzzy adaptive PID control is compared, the optimized fuzzy PID response curve of the most superiority, its fast response, small overshoot, and robustness is high, which is combined with the traditional PID control and fuzzy adaptive PID control's advantages at the same time, by adding a Smith predictor, eliminates the detrimental effect of time delay in temperature control system.

5. Acknowledgements

This work was financially supported by the natural science foundation of Jiangxi province of China(No. 20122BAB215002), Education department of Jiangxi province science and technology of China(No. GJJ1255) , Industry-University-Research Cooperation of the Higher Education Institutions of Jiangxi Province of China (No. KJLD13082)

6. References

[1] S.S.Hu: Principle of Automatic Control(National Defence Industry Press,China2007).

[2] Y.B.Zhang,J.H.Zhao andH.Xian: Computer control technology (National Defence Industry Press,China2008).

Advanced Materials Research Vols. 989-994 (2014) pp 3161-3164
© (2014) Trans Tech Publications, Switzerland
doi:10.4028/www.scientific.net/AMR.989-994.3161

Research on the correction of regeneration opportunity of DPF using GW4D20 engine

Shijie Qiao[a], Yu Liu[b]

College of Automotive Engineering, Jilin University, Changchun 130025, China

[a]qiaosj2013@163.com, [b]26288380@qq.com

Keywords: Particle filter; Regeneration opportunity; Pressure drop

Abstract. The accurate diagnose of the timing of regeneration is the key factor of solving the problem that the filter body is damaged and the process of regeneration is uncomplete. The timing of regeneration judged by the exhaust back pressure is a type of widely accepted control method, the essence of which means to estimate whether the quantity of particle in the filter can fulfil the demand of regeneration or not. In the process of practical application, this kind of method is influenced by the engine conditions, therefore, we must monitor the engine at any moment by speed and load of signal acquisition.In this article,it summarizes two dimensional pulse spectrum" exhaust flow--pressure drop" through universal characteristics test. Meanwhile it conducts the temperature correction in order to simplify the complexity of the judge-ment of regeneration opportunity.

Introduction

The Diesel engines has been developed and introduced in the transportation and other fields,with the benefits of better fuel economy and higher thermal efficiency.However,with the deteriotation of global environment and the strictness of emission regulations,the emission of diesel engines has drawn widely attention from the world.The mainly harmful emissions of the diesel engines are NO_X and particulate. The amount of particulates released by the diesel engines is about 30-80 times of the amount of the gasoline engine[2].Diesel particulate filter is the one of the major aftertreatment technologies to meet airpollution environment regulation,because of higher capture efficiency,up to 90%.Two major points,namely capture and regeneration,have been repeatedly taken into consideration.The accurate diagnose of the timing of regeneration is determined by the amount of the particle which are deposited on the filter.Not only can the deposition of the particulate lead to the rising of the back pressure but affect the ability of the engine and the regeneration process[3].Nowdays,the determination of the regeneration opportunity is based the three priciples:(1)the rising of back pressure caused by the deposition of the particulate in the filter;(2)the effect of the amount of the deposition in the filter for the regeneration process;(3)the relation between regeneration energy consumption and regeneration effieciency[4].The regeneration opportunity judged by the exhaust back pressure is a type of widely accepted control method,this method is not only influenced by the engine conditions but the amount of deposition. There are still relatively larger errors ,including the change complexity of the engine load and dramatic change in the flow rate of the exhaust[5].In this article,it summarize two dimensional pulse spectrum"exhaust flow--pressure drop"through universal characteristics and the temperature correction to simplify the control method ,depending on the control strategy of back pressure and giving up traditional three dimensional pulse spectrum"speed-load-pressure drop".

Experiment equipment

Test engine is a 4-cylinder diesel engine to meet stage V emission regulation, and its related technical parameters are listed in Table 1.

Table 1 The basic parameters of engine GW4D20-V

Displacement (L)	2.0
Rating power/speed kW/ (r/min))	110/4000
Maximum power/speed (N·m/(r/min))	320/1800-2800
Low fuel consumption (g/kW·h)	205
Emission standard	stage V emission regulation
Fuel systerm	electronically controlled high-pressure common rail
Aftertreatment system	DOC＋DPF

Engine universal characteristics test

In order to obtain the original datas,including the original engine exhaust soot, DOC outlet temperature and the exhaust flow ,the experiment system contains the aftertreatment only with the installation DPC and without the installation of DPF, and operats on this woking conditions that speed ranges from 1000 ~ 4000r/min, rising in the order of 200r/min, each of which corresponds to six different throttle opening, including the engine idling condition.the universal characteristic tests can be achieved by these engine operating conditions. Using EEPS-3090 measures levels of particulate matter in the exhaust;and thermocouple temperature sensors were installed in the DOC inlet and outlet to do temperature measurements.

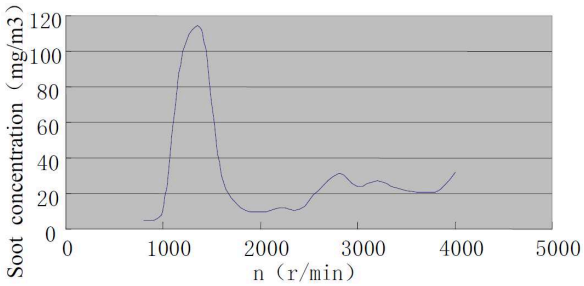

Fig. 1 The soot distribution of engine universal characristics

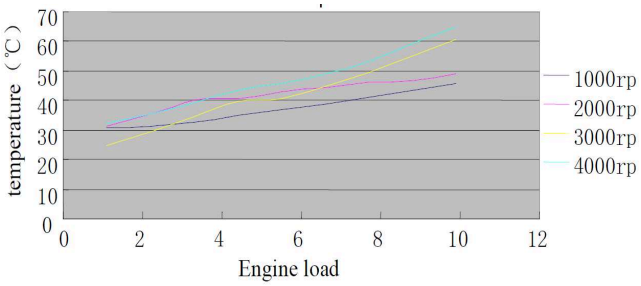

Fig. 2 DOC inlet temperature of the universal characteristics

As shown in Figure 1, the distribution of soot concentration of the engine at the full load. It can be observed from the figure that as the the engine speed ranges from 1000r/min to 1800r/min , soot concentration rised first and then declined ,in the process ,the soot concentration get to the peak,about 110mg/m3, at the full load and the speed of 1400r/min. In the range from 1800r/min to 2400r/min , soot emission concentration is relatively lower overall average concentration about 11.2mg / m3. After 2400r/min, the concentration of soot emissions is more than 20 mg/m3, but overall remain lower. In summary, the engine has a large amount of soot emissions when at low speed and full load; It is relatively lower concentrations of soot emission at high-speed and large load. Figure 1 shows the general characteristics of this engine soot emission at the full load, but also provide a reference for choice to the working conditions of the following pressure drop characteristics and soot load test.

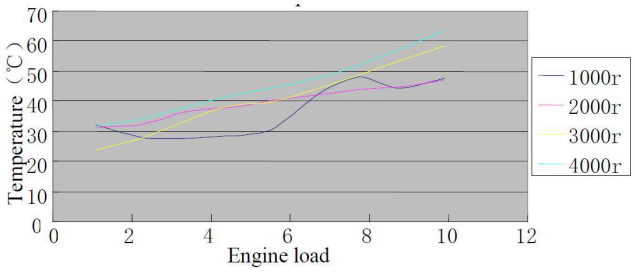

Fig. 3 DPF inlet temperature of the universal characteristics

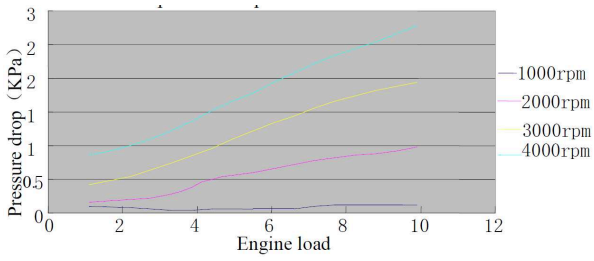

Fig. 4 The pressure drop of DPF in universal characteristic conditions

Figures 2 and 3 are respectively the change of the DOC inlet temperature and the DPF inlet temperature at the full load. From the figure we can clearly see the DOC and DPF inlet temperature distribution under different conditions. Exhaust temperature of diesel cars are overall lower and as seen from the figure, there is rarely working conditions that exhaust temperature can exceed 600 ℃ and almost in full speed and full load . To ensure a smooth DPF regeneration, DPF inlet temperature needs to be maintained at about 600 ℃, but it's difficult for the vehicle in the normal condition to meet this requirement, which requires additional measurements to address this problem. Figures 2 and 3 help choose the working conditions for the following pressure drop test and regeneration.

DPF pressure drop test

The universal characteristics of fresh DPF. For the fresh DPF,when the DPF carrier has certain physical parameters without any soot loading, pressure drop depends only on the engine exhaust. In the detailed testing process of this part,ensure that the DPF soot loading is below 5%. During the test,block EGR tube so that EGR does not work to restrict high soot emissions at certain conditions. Figure 4 shows fresh DPF pre-ssure drop distribution at a universal characteristic condition . Because when DPF pressure drop depends on the volume flow of the exhaust gas, the higher the gas temperature, mass flow rate will increase, the greater the volume flow rate . As showed from the figure, the higer engine speed and the greater the load, the greater DPF exhaust pressure drop.

The pressure drop of fresh DPF. Figure 5 shows the exhaust flow conditions at the full load. As seen from the figure,the engine's exhaust flow rate range is from 0.015 to 0.157kg / s. According to the engine's universal characte-ristic test, the exhaust flow for all the engine's working conditions is consistent with exhaust flow at the full load,and not listed separately here.

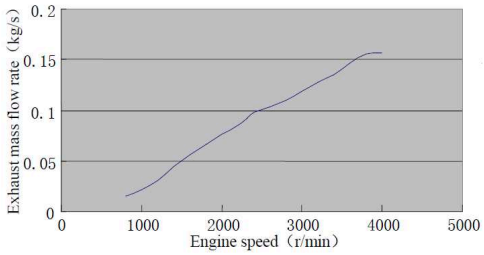

Fig. 5 The range of engine exhaust flow

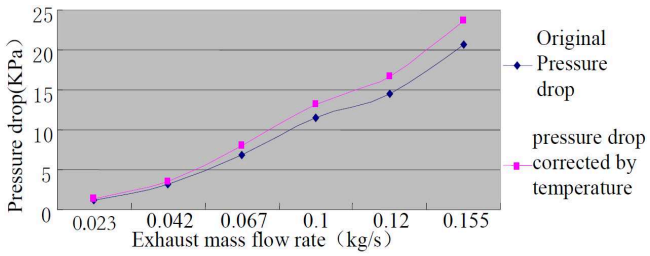

Fig. 6 The pressure drop characteristics of the fresh DPF

The experiment process needs to maintain a constant engine load and is tested at several speeds, during the entire testing process avoid that DPF is loaded more than 10%.The measurement interval covers the engine exhaust flow. According to preliminary experimental data select 6 wo-rking conditions as shown in Table 2 a, b, c, d, e, f to do pressure drop characteristics test of fresh DPF. Exhaust flow is obtained by adding the engine intake air flow and fuel consumption, which is ,for steady-state conditions, very accurate, and more close to the actual engine exhaust flow. As seen from the table, six exhaust flow conditions increase from 0.023kg/ to 0.155kg/s, covering almost the entire engine exhaust flow range.

Table 2 The working conditions of pressure drop

Working conditions	Exhaust temperature (℃)	Exhaust Flow (kg/s)	Pressure Drop (KPa)	Corrected pressure drop (KPa)
a	249.6	0.023	1.12	1.29
b	396.6	0.042	3.1	3.56
c	414.5	0.067	6.9	7.93
d	519.5	0.1	11.5	13.22
e	580.3	0.12	14.5	16.67
f	604	0.155	20.6	23.67

For the fresh DPF pressure drop measured at various conditions as shown in the table,is corresponding to the original pressure drop curve in the Figure 6. As seen from the figure, with the increase of the exhaust mass flow rate, DPF pressure drop increases, and at almost linear growth. However, we notice that, in Table 3, the exhaust gas temperature are different at a variety of conditions. This paper introduces a temperature correction for pressure drop of the DPF, you can make a three-dimensional pulse spectrum"speed - load - drop" into a two-dimensional pulse spectrum "exhaust flow - Pressure Drop,". And we have done this part to serve this idea. For DPF, its formula for exhaust pressure drop can be summarized as follows:

$$\Delta \mathrm{P} = \mathrm{c}q^2 \tag{1}$$

Wherein: Δ P is the pressure drop of DPF; q is the volume flow rate of gas; c is a const-ant. G enerally, the exhaust gas volume flow rate is substantially proportional to the exhaust gas temperatu re, therefore the exhaust gas temperature has a great influence on the DPF pressure drop.

Here, we introduce two states, state a and state b. Wherein, a represents the standard state, the s tate b indicates the detected actual engine operation state. According to the formula (1) and the gas equation of state, it is not difficult to come:

$$\frac{\Delta \mathrm{P_b}}{\Delta P_a} = \left|\frac{q_b}{q_a}\right|^2 = \left|\frac{T_b}{T_a} \bullet \frac{1+\Delta P_a}{1+\Delta P_b}\right|^2 = \left|\frac{T_b}{T_a}\right| \bullet \left|\frac{1+\Delta P_a}{1+\Delta P_b}\right| \tag{2}$$

In practical applications, the solution (2) is complicated and simplified to:

$$\Delta \mathrm{P_b} = \frac{8.57\times 10^4}{273.15+T} \bullet \Delta P_a \tag{3}$$

According to the formula (3), do the temperature correction for the measured pressure drop of the DPF,and the result is shown in Figure 6,and that is the pressure drop curve shown in the temperature correction. The corrected pressure drop curves is more universal, which is crucial to determine the DPF regeneration timing.

Summary

1. Build a test bench and do the external characteristics test of the engine. The emission of soot is large when Engine at low speed of external characteristics;while engine at high-speed and large load,soot concentration is relatively low which provides a preliminary test basis for pressure drop characteristics and regeneration characteristics

2. At the working conditions of the universal characteristics , the DOC inlet temperature and DPF inlet temperature are low on the whole .

3. Investigate the pressure drop for the fresh DPF and the DPF with different soot load amount and get the two dimensional pulse spectrum”exhaust flow -- pressure drop”by introducing temperature correction method to provide the basis for determining the timing of subsequent regeneration to lead to over-temperature.

References

[1] Jiang Dahai. Diesel exhaust particulate trap regeneration reverse jet technology. Tianjin: Academy of Military Transportation, 2002.

[2] Wahiduzzaman S, et al. Modeling of Integrated Aftertreatment Systems. SAE Paper 2007-01-4127.

[3] He Xinyun,Ning ZHI. Research Status of diesel particulate traps and application prospects.

[4] Lai Tiangui, Liu Mengxiang. Diesel Particulate Filter Materials and Methods and Research regeneration. Chongqing: internal combustion engine, 2004(6): 83-88.

[5] Masoudi M,Heibel A, Then P M. PredictingPressure Drop of Wall- Flow Diesel ParticulatenFilters Theory and Experiment. SAE, 2000, 2000-01-0184.

[6] Yang Desheng,Gao Xiyan. Research ceramic diesel particulate filter regeneration timing of electrical heating. Internal Combustion Engine Engineering, 2003, 24(4):42-44.

Advanced Materials Research Vols. 989-994 (2014) pp 3165-3168
© (2014) Trans Tech Publications, Switzerland
doi:10.4028/www.scientific.net/AMR.989-994.3165

Dynamic Characteristics of Arch Steel Tower in Construction Stages

Yu Li[1,a], Che Yanyang[1], Wang Sen[1], Zhao Guohui[1]

[1] Key Laboratory of Ministry of Communications for Bridge Detection & Reinforcement Technology, School of Highway, Chang'an University, Xi'an, 710064, China

[a]liyu@chd.edu.cn

Keywords: cable-stayed bridge; arch steel tower; dynamic characteristics; bridge in construction; completed bridge

Abstract. Based on Hangzhou Zhijiang Bridge, FEA models of arch steel tower in construction and completed stages are established by using ANSYS software. Before closed and completed are considered to compute the dynamic characteristics of different structural system for arch steel tower. The results show that the wind-reduced vibration can be generated easily. It can cause some bad effect on the construction, equipments and the safety of staff. So, some proper measures should be adopted to decrease the wind-induced vibration of arch steel tower in construction and completed stages. So, some meaningful references are provided for the further research on control of wind-Induced vibration for arch steel tower.

Introduction

Arch tower cable-stayed bridge[1-15] is a kind of new bridge in recent years. The bridge has a great innovation in some aspects of structure, technology and bridge model, but its structure is complex. Main arch is also the cable tower on modeling. The space geometric composition of the cable, the arch and girder makes structure stereo sense stronger, adapting to the surrounding environment and can be used as a landmark. At present, the domestic bridge for this type of arch tower cable-stayed bridge is less, and 246 m of Zhijiang Bridge is the longest span in arch tower cable-stayed bridges.

Zhijiang Bridge is a two-tower cable-stayed bridge with the span arrangement of 129+258+258+129 m. The main girder is steel box girder with the width of 40.5 m. Tower adopts the 97.5 m high door tower with the upper tower of rectangular steel box structure and the lower tower of concrete rectangular solid structure. The height of steel combined section to pile caps is 22.5 m. As shown in figure 1.

Fig.1 Zhijiang Bridge

Because of the unique shape and small damping of steel arch bridge, the reaction is more sensitive to the wind .As the current research is mainly concentrated in the conventional bridge tower[1-15], so there is no literature to mention the wind vibration control of steel arch tower.

Based on Hangzhou Zhijiang Bridge, this paper carried out dynamic characteristics research of the steel arch tower construction state and completed state, and provides a scientific reference for the research of wind induced vibration of arch bridge tower.

Dynamic Performance of 1/2 Completed

As shown in figure 2, the FEA model uses Beam4 unit to simulate the pile caps, concrete arch tower (T0), the arch steel tower section (T1 ~ T7), steel crossbeam, the support (column, horizontal and horizontal), main girder section and the next bracket (column, horizontal and diagonal). And MASS21 unit is used to simulate the crossbeam and the additional mass on the steel tower.

The first 10 order frequency and period of Zhijiang steel arch bridge tower of 1/2 completed are shown in table 1, the first two order models are shown in figure 4.

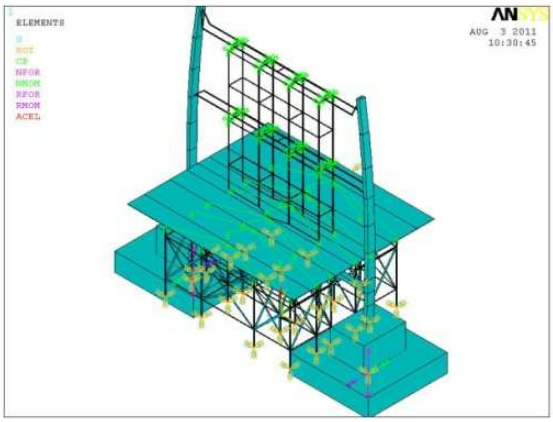

Fig.2 FEA model of 1/2 completed

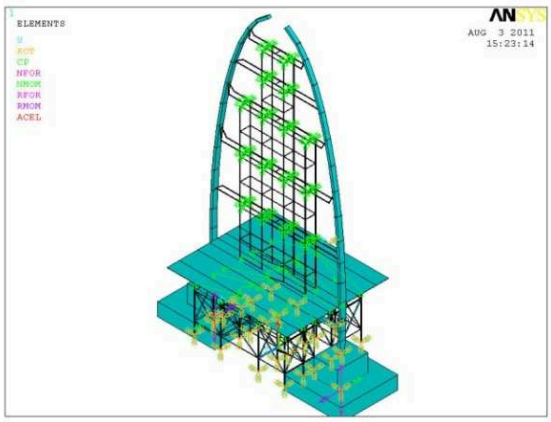

Fig.3 FEA model of before closed

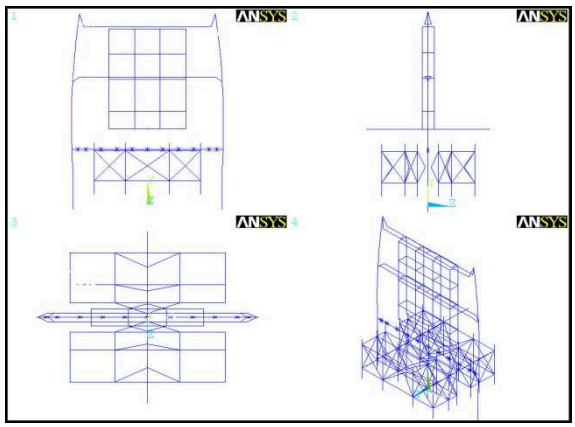

Fig. 4(a) Model one

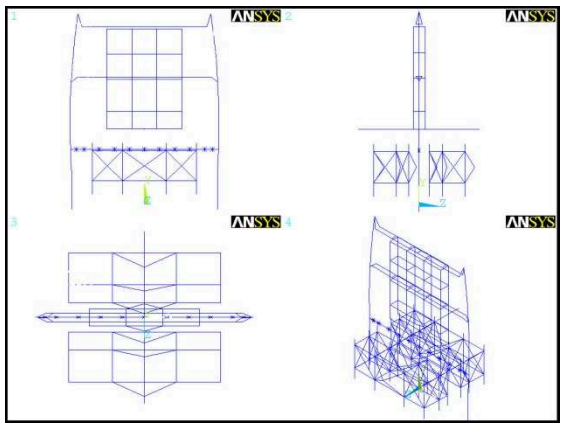

Fig. 4(b) Model two

The dynamic characteristics before close

Fig.3 shows the model use Beam4 unit to simulate cap, arch concrete tower segment (T0), steel arch tower segments (T1 ~ T14), steel cross beams, the bracket (column, flat-linking and cross brace), main beam segment and lower bracket (column, Ping Luen bracing); using MASS21 unit to simulate the additional mass on the beams and steel tower.

The first ten natural frequencies and periods of complete steel arches tower of Zhijiang Bridge shown in Table 2, the first two vibration modes shown in Figure 5

Table.1 Result for previous ten models

No.	frequency (Hz)	period(S)	No.	frequency (Hz)	period (S)
1	1.5942	0.627274	16	2.4428	0.409366
2	1.5942	0.627274	17	2.4428	0.409366
3	1.5949	0.626999	18	2.4429	0.40935
4	1.5949	0.626999	19	2.4429	0.40935
5	1.5949	0.626999	20	2.443	0.409333
6	1.5949	0.626999	21	2.443	0.409333
7	1.6306	0.613271	22	2.6626	0.375573
8	2.0695	0.483209	23	4.0896	0.244523
9	2.3726	0.421479	24	5.0747	0.197056
10	2.4402	0.409802	25	7.1441	0.139976

Table.2 Result for previous ten models

NO	frequency(Hz)	period(s)	NO	frequency(Hz)	period(s)
1	0.623	1.606	16	2.443	0.409
2	0.689	1.452	17	2.443	0.409
3	0.994	1.006	18	2.443	0.409
4	1.594	0.627	19	2.443	0.409
5	1.594	0.627	20	2.443	0.409
6	1.595	0.627	21	2.443	0.409
7	1.595	0.627	22	2.443	0.409
8	1.595	0.627	23	2.639	0.379
9	1.595	0.627	24	3.287	0.304
10	2.320	0.431	25	3.331	0.300

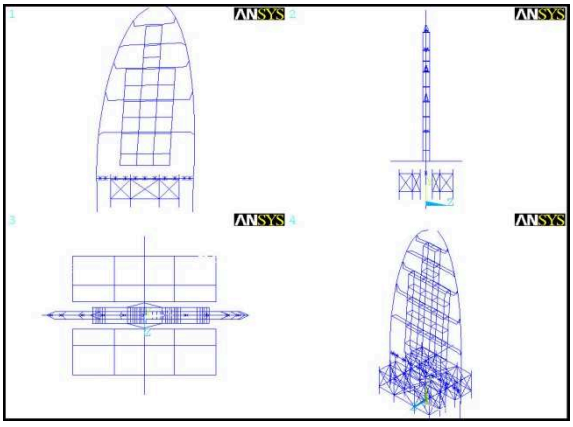

Fig. 5(a) Model one

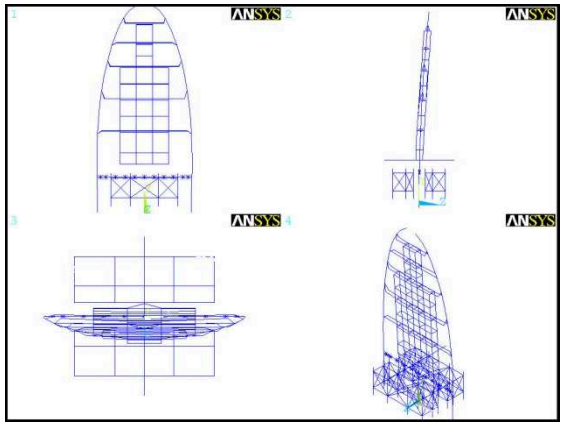

Fig. 5(b) Model two

Conclusion

We use ANSYS to calculate the dynamic characteristics of arched steel towers under five states (considering construction equipment), including: completion of the concrete section of the steel tower, steel tower built in 1/2, steel tower built in 2/3, before steel tower, after closure of steel tower, Figure 6 shows the effect of different arch-shaped steel tower construction states on the first six natural frequencies, we conclude:

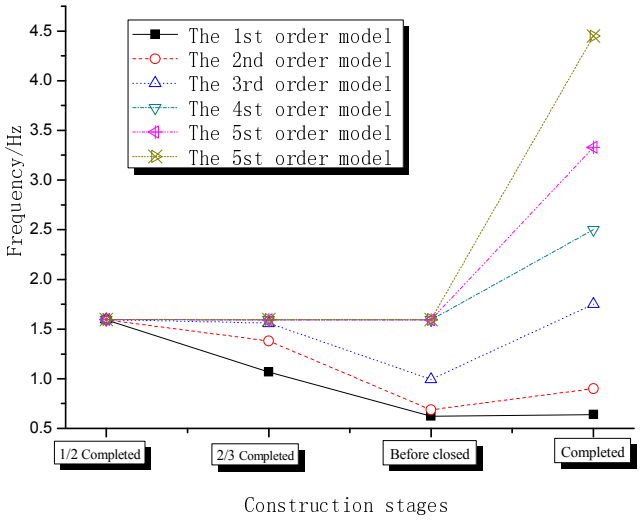

Fig.6 Effect of construction stage on frequency

(1) As the arch steel bridge tower construction, bridge tower constantly grow, the first and second-order frequency of the structure continue to decrease, this is because the arch steel tower become lack of horizontal linkages during construction, after the closure, its structural stiffness become larger , and vibration mode also change.

(2) Before arched steel bridge tower closed, 3 to 6 order frequency of structure also diminishes with the progress of construction, after the bridge tower closed, the third to six order frequencies substantially increase.

(3) We can see, the arch steel tower is lack of horizontal linkages during the construction, after the closure of arch steel tower, its structural stiffness become larger, and vibration mode also change. In other words: the state of construction and completion arch steel tower will be very sensitive to the wind, it is easy to cause the wind-induced vibration, and thus have a greater impact on the quality of the steel arch tower construction and the safe of construction equipment and people. Therefore, we need to take appropriate measures to reduce the wind-induced vibration of arch steel tower construction and completion.

Acknowledgements

This work was financially supported by the Fundamental Research Funds for the Central Universities (2013G1211006) and natural science foundation of Shaanxi Province (2014JQ7253).

References

[1] Larose G L, Falco M, Cigada A . Aero elastic Response of the Towers for the Proposed Bridge over Stretto di Messina[J]. Journal of Wind Engineering and Industrial Aerodynamics, 1995, 57:363-373.

[2] Stoyan Stoyanoff. A Unified Approach for 3D Stability and Time Domain Response Analysis with Application of Quasi-Steady Theory[J]. Journal of Wind Engineering and Industrial Aerodynamics, 2001, 89: 1591-1606.

[3] Francesco Ricciardelli. Prediction of the Response of Sustension and Cable-Stayed Bridge Towers to Wind Loading[J]. Journal of Wind Engineering and Industrial Aerodynamics, 1996, 64: 145-159.

[4] Ingham T J, Rodriguez S, Nader M. Nonlinear Analysis of the Vincent Thomas Bridge for Seismic Retrofit[J]. Computers& Structures, 1997, 64(3):1221-1238.

[5] Igusa T, Xu K. Wide band-response characteristics of multiple subsystems with high modal density [C]//Proceedings of the Second International Conference on Stochastic Structural Dynamics. USA, 1990.

Advanced Materials Research Vols. 989-994 (2014) pp 3169-3171
© (2014) Trans Tech Publications, Switzerland
doi:10.4028/www.scientific.net/AMR.989-994.3169

Inhibition of Return Effect Reversed by Perceptual Load

Xingjuan LIU[1], Zhihao FAN[2], Jianzhong ZHOU[3*]

Department of Psychology, College of Humanities Jilin Agriculture University Changchun,130118, China

[1]email: xingzi1980@126.com, [*]email: xyzjz@163.com

Keywords: Inhibition of return (IOR), cue and target integration, Perceptual load.

Abstract. Perceptual load theory was considered to resolve the conflict between early and late selection models. We investigated whether perceptual load work well using IOR paradigm. The results showed that IOR disappeared in different level of perceptual load. The results indicated the onset time of IOR was influenced by perceptual load, indicating that perceptual load hinder the spatiotemporal correspondence between the cue and target integration.

Introduction

Perceptual load theory was considered to resolve the conflict between early and late selection models[1-2].According to this theory, to what extent the task-irrelevant stimuli are processed is determined by whether there are spare attentional resources left when they are used to process the task-relevant stimuli. If the current task has high perceptual load fill attentional capacity, irrelevant stimuli will be excluded before they interfere with task performance, but if perceptual load is lower the spare capacity will be directed automatically to the irrelevant information, which will then interfere with task performance [3-4]. Liu, Zhang and Zhou(2013) investigated whether the effect of distractors in IOR in discrimination tasks was changed by the location and number. The results showed that the trend of the general IOR effect was approximately the opposite in the two experiments. Different manner of cue target integration was adopted by participants when location and number of distractors were taken into account[5].

In present experiment, perceptual load was mad using IOR experiment paradigm(cue-target paradigm) participants responded to a letter (M) present in the peripheral box, which appeared simultaneously with high or low perceptual load. We measure the inter effect of perceptual load and IOR.

Experiment

Participants

Seventeen participants (12 females) participated in the present experiment (age20~23). All the participants had corrected-to-normal or normal vision. They were naïve to the purpose of the experiment and were paid after the experiment.

Apparatus and Stimuli

Stimuli were presented on a Dell/PC-compatible computer, and responses were recorded via the computer mouse using E-prime software. The target on each trial appeared in the central of one of two boxes, displayed to the upper or the down of fixation point (a plus sign "+"), which remained on the central of screen throughout the whole trial and only disappeared between trials. The distance between the center fixation and one of the peripheral boxes was 3.5° of visual angle. The target stimulus were white letter "M" (0.5°×0.5°).

Procedure

Fig 1 depicted the sequence of events on each trial. A fixation point was displayed together with the four boxes for 500ms, and then one of the boxes became white for 100ms, participants were required to gaze at the fixation point and not scan. Following the cue, the fixation point was

displayed together with the two boxes for 50ms. Then the central fixation cued for 100ms. The target was displayed at any of peripheral position for 2000ms or until response. If no response was obtained within 2,000 ms after target offset, then the next trial began.

All possible combinations of the cue location and target location variables were presented randomly within a block of trials. The experiment was interrupted every 96 trials to allow the participants to rest. Participants were instructed to press right key of mouse to letter "M" and participants also were reminded to maintain central fixation throughout the trials. They were instructed to discriminate targets and respond quickly while avoiding errors.

Design

The experiment had a 2×2×2 within-subjects variables, cue validity (valid, invalid), SOA (400ms and 1000ms), perceptual load (low, high). A total of 64 practice trials were run before the 512 experimental trials. Participants sit about 50cm from the screen in a dimly lit, quiet room.

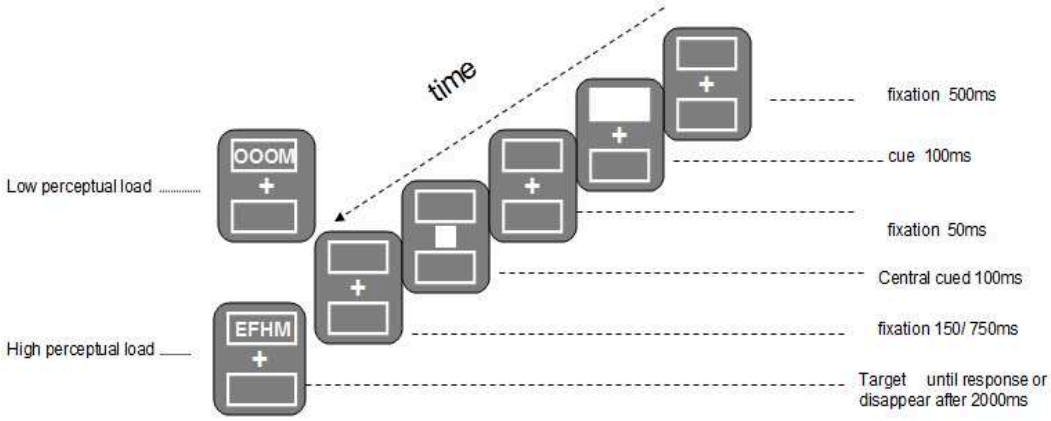

Fig.1 Illustration of Sequence and timing of a trial in Experiment

Results

Trials with RTs smaller than 342ms (anticipations) or larger than 1125ms (misses) outliers were defined as the saccade latencies. Fig. 2 illustrates the results of experiment.

RT of correct trials was submitted into a repeated variance analysis (ANOVA). The main effect of cue validity was significant, $F(1, 16) = 16.02$, $p<0.001$, RT was faster to targets at the valid location (754ms) than at the invalid location (782ms), which was the typical facilitation effect. The main effect of perceptual load was significant, $F(1, 16) = 9.30$, $p<0.01$, RT was faster to targets when perceptual load was high than when perceptual load was low. The main effect of SOA was significant, $F(1, 16) = 10.02$, $p<0.001$, RT was faster to targets at 400ms than at 1000ms. The interaction between cue validity and perceptual load was not significant, $F(1, 17) = .767$, $p>0.05$.

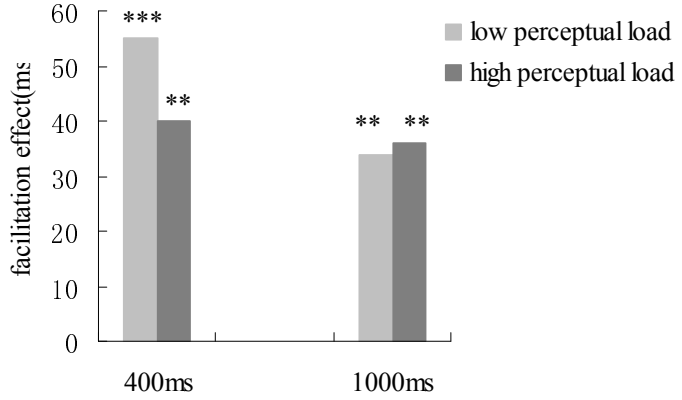

Fig. 2 Facilitation effect IOR effect in the peripheral target detection task as a function of cue validity, SOA and in the condition of low perceptual load.

Discussion

Lupiáñez, et al. (2007, 2010) propose a "three hypothetical effect" theory [6-7], which suggests that the time course of IOR is influenced by spatial orienting benefit, onset detection cost and spatial selection benefit. Peripheral cues trigger a short-lived exogenous spatial orienting of attention, thus improving target perception and/or responses to it, which is called "spatial orienting benefit". The cue-target integration process would facilitate processing by helping to select the target location in advance, an effect that is represented as the "spatial selection benefit". However, the integration of the target within the cue representation would produce a cost in detecting the onset of the target, which is "onset detection cost". The facilitation or inhibition of responses to peripherally cued targets would result from the sum of the detection cost, spatial benefit, and spatial orienting benefit [8]. The results showed that facilitation effect was significant when perceptual load was low and high. IOR magnitude was different with previous research when an interference letter was present together with the target [9].

In present experiment, the disappearance of IOR when perceptual load was conducted indicated that the perceptual load is critical for onset of IOR, indicating that there has no spare attentional resources to process other stimuli and they will be excluded before they interfere with task performance in the current task. The perceptual load distractors hinder the spatiotemporal correspondence between the cue and target integration. Another prediction that can be drawn from Lupiáñez et al.'s view is that in our experiment, cue and target integration was more harmful than in the common cuing tasks where adding perceptual load. This suggestion would surely predict later onset of IOR in those experiment conditions.

Acknowledgement

The research reported here was supported by general planning project of Ministry of Education Humanities and Social Sciences (12YJAZH211) and the innovative undertaking training program of University Students in Jilin Agriculture University (The Construction of Beyond Curriculum) and Humanities and Social Sciences in the Twelfth Five-Year Plan project of Education Office in Jilin Province (201226). We thank Jing Li and Jin Dan for help with data acquisition.

References

[1] Lavie, N. Perceptual load as a necessary condition for selective attention [J]. Journal of Experimental Psychology, 1995,21(3), 451-468

[2] Lavie, N. Distracted and confused Selective attention under load [J]. Trends in Cognitive Sciences, 2005,9(2), 75-82

[3] Lavie, N., Hirst, A., Fockert, J. W. et al. Load theory of selective attention and cognitive control [J]. Journal of Experimental Psychology, 2004,133(3), 339-354

[4] Lavie, N., & Tsal, Y. (1994). Perceptual load as a major determinant of the locus of selection in visual attention. Perception & Psychophysics, 56(2), 183-197

[5] Liu, X.J., Zhang, M., Zhou, J.Z. Distractors Processing Modulate the Onset of Inhibition of Return in Discrimination tasks. ICME International Confenence on Complex Medial Engineering, 2013

[6] Lupiáñez, J. Inhibition of return. In: Nobre K, Coull J (Eds). Attention and time[C]. New York:Oxford University Press, 2010,17–33

[7] Lupiáñez, J., Ruz, M., Funes, M., & Milliken, B. The manifestation of attentional capture: Facilitation or independing on task demands [J]. Psychology Research, 2007,71 (1), 77–91.

[8] Liu, X.J., Zhang,Y., Wang, H.Y., Zhang, M. Three Factors Theory of the Time Course of Inhibition of Return and Its Development [J]. Journal of Psychological Science, 2014,37(01), 31-36.

[9] Liu, X.J., Tang, X., Zhou, J.Z. The Influence of Flanker Interference on Inhibition of Return. IEEE .International Confenence on Mechatronics and Automation,2013

Advanced Materials Research Vols. 989-994 (2014) pp 3172-3176
© (2014) Trans Tech Publications, Switzerland
doi:10.4028/www.scientific.net/AMR.989-994.3172

Brushless DC Motor Speed Control System Based on Fuzzy PID Control

Yihui Zhang[1,a], Lepeng Song[1,b]

[1] Chongqing University of science and technology, Chongqing, China

[a]zhangyihui1@163.com, [b]slphq@163.com

Keywords: brushless DC motor; fuzzy PID control; Matlab/Simulink simulation; fuzzy control

Abstract. Brushless DC mo tor speed control system is a multivariate, strong coupling, non linear, time-varying complex system, but adopting traditional PID control method to carry ou t control is difficult to achieve good control effect A kind of PID controller with fuzzy algorithm setting on-line PID parameters automatically was designed and applied in brush less DC motor speed control system, using the voltage , speed and torque equation of brush less DC motor, according to the parameters of the mo tor, the controler adopts fuzzy theory to adjust the PID parameters, in order to obtain high-precision speed control Results of simulation experiment show that the fuzzy PID control method compared with normal PID control is with better control performance, non overshoot quick velocity response, higher control precision and good rubustness, which is insensitive to the parameter chattering and many disturbances.

Introduction

Brushless DC motor is a permanent magnet motor, its change is realized by electronic circuit outside the. Permanent magnet brushless DC motor speed control system is a nonlinear, multivariable, time-varying system[1-2], parameters tuning difficult, a set of tuning the parameters can only be a good control effect in a smaller range, when the parameters change more than a certain range, the system control effect is poor, resulting in conventional PID control is difficult to to meet the requirements of the system[3-4].

Although the modern control theory. Some new results include linear regulator based on pole assignment and optimal control, the exact feedback linearization, model reference adaptive control into the motor control technology, effectively improves the running performance of Brushless DC motor, but the modern control theory still rely on mathematical model of motor accurately, the performance of the system influenced by the variation of istics imotor parameters and various uncertain factors[5-6]. Since 1965 USA University of California cybernetics expert Zadeh fuzzy mathematics, the theory and method of improving, short decades, fuzzy control (Fuzzy Control) is widely used in natural science and social science and engineering control field[2-4].

This paper presents a speed control system of Brushless DC motor based on adaptive fuzzy PID model. The model input parameters deviation and deviation change between the given speed and actual speed rate as fuzzy control inference machine, fuzzy theory, adaptively adjust the PID parameter, and the simulation of control system in MATLAB. The simulation results show that, the control system of quick response, small overshoot, and strong robustness, dynamic characters obviously better than that of traditional PID control and the fuzzy control.

1 mathematical model of the brushless DC motor

Brushless DC motor with a rectangular current wave, trapezoidal back emf. Mutual inductance of stator and rotor is nonlinear. Therefore, in the analysis and Simulation of BLDCM control system, in order to establish the simplified simulation model, make the following assumptions: the complete symmetrical three-phase winding, the air gap magnetic field for Fang Bo, stator current, rotor magnetic field distribution is symmetric; ignore the cogging, commutation process and armature reaction effects; circuit is not saturated, regardless of eddy current and hysteresis loss.

Voltage balance equation BLDCM:

$$\begin{bmatrix} u_a \\ u_b \\ uc \end{bmatrix} = \begin{bmatrix} R & 0 & 0 \\ 0 & R & 0 \\ 0 & 0 & R \end{bmatrix} \begin{bmatrix} i_a \\ i_b \\ i_c \end{bmatrix} + \frac{d}{dt} \begin{bmatrix} L-M & 0 & 0 \\ 0 & L-M & 0 \\ 0 & 0 & L-M \end{bmatrix} \begin{bmatrix} i_a \\ i_b \\ i_c \end{bmatrix} + \begin{bmatrix} e_a \\ e_b \\ e_c \end{bmatrix} \quad (1)$$

Type u_a, u_b, u_c as the phase windings of the motor phase voltage; i_a, i_b, i_c as the phase windings of the motor phase current; e_a, e_b, e_c opposite electromotive force of the phase windings of the motor; R, L, M three-phase winding phase resistance, self inductance and mutual inductance between phases.

Electromagnetic torque equation BLDCM:

$$T_{em} = \frac{p_n(e_a + e_b + e_c)}{\omega_n} \quad (2)$$

As the electrical machinery velocity in type, as the pole number, electromagnetic torque.

The motion equations of the motor:

$$T_e - T_L - B_\omega = J\left(\frac{d\omega}{dt}\right) \quad (3)$$

For the electromagnetic torque of type, as the load torque, B damping coefficient, J for the moment of inertia, the motor mechanical angular velocity.

Fuzzy adaptive control system design

Brushless DC motor fuzzy PID control system structure diagram as shown in figure 1. First calculate the deviation of the actual speed of the motor and the speed of n given NR E and deviation change rate of EC, then they are fuzzy, fuzzy E and EC by the fuzzy control rule reasoning, fuzzy solution to obtain Kp, Ki and kd. In the control process, parameter online real-time modification of conventional PID controller, the conventional PID controller of Brushless DC motor speed regulation.

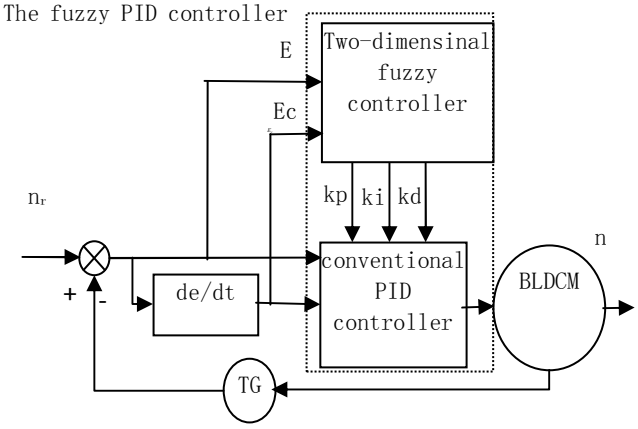

Figure 1 BLDCM fuzzy PID control system structure diagram

The design steps of fuzzy adaptive PID control system are as follows: the controller input variables and the actual speed and the given speed error E and error rate of change of EC, the output variables through the PID parameter KP, Ki, KD adjusted. Domain domain are set to [-6,6] set the input language variables and the output variables of the fuzzy, fuzzy language variable selection 7: NB, NM, NS, ZO, PS, PM, PB. The ambiguity solution method using center of gravity method, the weighted average method.

Membership function using triangular distribution function. On KP, Ki, KD were tuning, fuzzy control rule of the three as shown in Table 1, 2, 3 show.

Table 1 Fuzzy control rules of Kp

	NB	NM	NS	ZO	PS	PM	PB
NB	PB	PB	PM	PS	PS	ZO	ZO
NM	PB	PB	PM	PS	PS	ZO	NS
NS	PM	PM	PM	PS	ZO	NS	NS
ZO	PM	PM	PS	ZO	NS	NM	NM
PS	PS	PS	ZO	NS	NS	NM	NM
PM	NS	ZO	NS	NM	NM	NM	NB
PB	ZO	ZO	NM	NM	NM	NB	NB

Table 2 Fuzzy control rules of Ki

	NB	NM	NS	ZO	PS	PM	PB
NB	NB	NB	NM	NM	NS	ZO	ZO
NM	NB	NB	NM	NM	NS	ZO	ZO
NS	NB	NM	NM	NS	ZO	PS	PS
ZO	NM	NM	NS	ZO	PS	PM	PM
PS	NM	NS	ZO	PS	PS	PM	PB
PM	ZO	ZO	PS	PS	PM	PB	PB
PB	ZO	ZO	PS	PM	PM	PB	PB

Table 3 Fuzzy control rules of Kd

	NB	NM	NS	ZO	PS	PM	PB
NB	PS	NS	NB	NB	NB	NM	PS
NM	PS	NS	NB	NM	NM	NS	NS
NS	ZO	NS	NM	NM	NS	NS	ZO
ZO	ZO	NS	NS	NS	NS	NS	ZO
PS	ZO	ZO	ZO	ZO	ZO	ZO	ZO
PM	PB	NS	PS	PS	PM	PS	PB
PB	PB	PM	PM	PM	PM	PS	PB

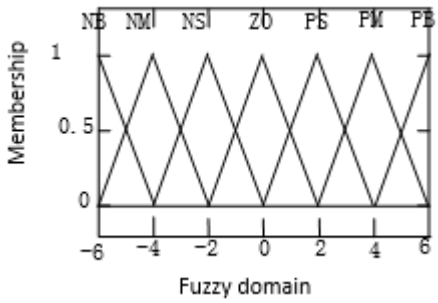

Figure 2 The input and output membership function curve

Taking into account the coverage degree and the sensitivity of the domain, robustness and stability principle, selection of input and output fuzzy membership function uses triangle membership function in fuzzy membership function of fuzzy logic toolbox in the editor. As shown in figure 2.

According to the control characteristics of the rotated speed of Brushless DC motor, induction of Kp, Ki and Kd fuzzy control rules, the fuzzy inference to derive the fuzzy relation, according to the reasoning of fuzzy relation and the input variables E, EC synthesis, Ki and Kd Kp are output linguistic variables, and then converted into precise speed actuator can accept the value after defuzzification operation.

Fuzzy reasoning using CRI (CRI) max-min synthesis of Mandan I reasoning method, reasoning, according to the relationship between fuzzy implication operator, fuzzy min and Max, select / maximum and minimum 0 operations as the synthetic operation, the fuzzy output value [5]. Fuzzy solution by using the weighted average method. In order to realize the real-time control, the system to meet the rapid control requirements, the off-line calculation form, namely fuzzy control rules to control query table, the reasoning process is simplified to a lookup table operation, it is easy to realize the real-time control of fuzzy controller through the look-up table, to improve the response speed of the system.

Simulation results

To establish the system simulation in the Matlab/Simulink software platform, system parameters: rated power of 3 kW 220V; rated voltage; rated current is 13164A; rated torque Rated speed is 22N*m; 1460r/min; moment of inertia for 0157kg*m2; each phase resistor of 0.21 per phase inductance is 0.21mH. Simulation of control as shown in figure 3. Through the above methods, the design parameters of fuzzy PID control in the parameter perturbation and disturbance simulation test input, simulation experiments with traditional PID control in the same parameters were compared. The simulation curve 5 as shown in Figure 3, figure 4, figure.

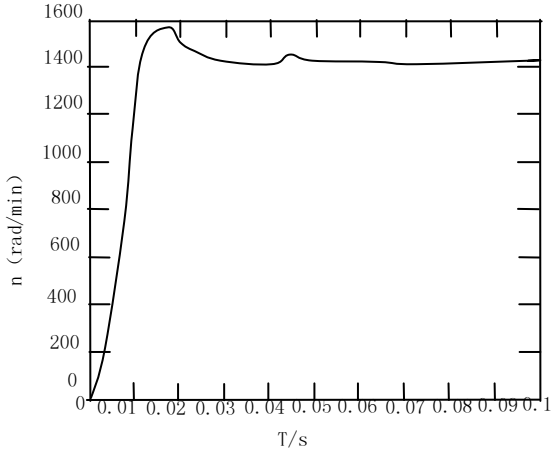

Fig. 3 Block diagram offuzzy PIDcontrol system simulation

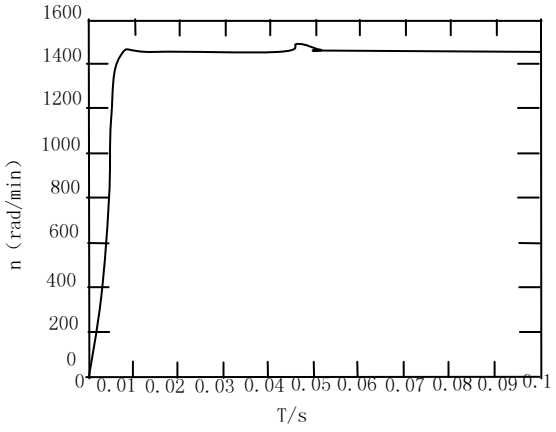

Fig. 4 Conventional PID controller speed simulation curve

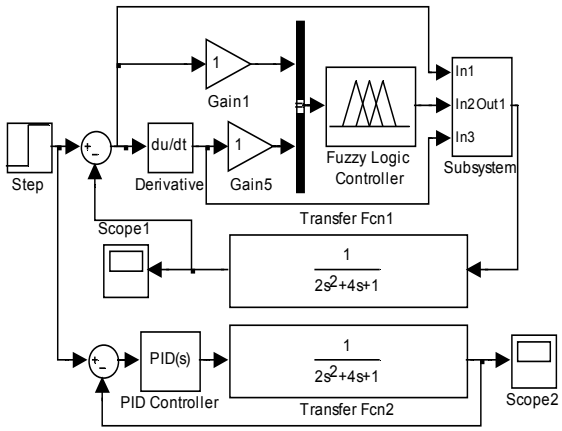

Fig. 5 Fuzzy PID controller speed simulation curve

Two kinds of controller performance data from the simulation curve and table 4 summarizes the apparent: using brush DC motor without speed fast response, no overshoot fuzzy adaptive PID control; in the t= 0.04 s, response curves fluctuation system load when the mutation rate, and quickly return to the rated speed, short adjusting time and strong anti-interference ability, a good dynamic characteristic, greatly improving the robustness of Brushless DC motor system.

Table 4 Performance parameters of two controller

The two controller	Overshoot δ/%	Regulation time ts/s
The conventional PID controller	9.85	0.029
The fuzzy PID controller	0	0.011

Conclusion

This paper describes the design of a non brush DC motor double closed loop speed regulation system based on fuzzy PID controller, PID controller is adopted in the current loop, speed loop adopts fuzzy PID control. Changes of input parameters based on. Using the principle of fuzzy on-line self adjustment of PID parameters, the motor during start-up and operation load case, on MATLAB, a simulation experiment is carried out. The simulation results show that, the fuzzy PID control scheme is proposed in this paper can improve the response speed of Brushless DC motor system, restrain the overshoot, and improve the control accuracy, robustness and dynamic and static performance, its control performance is superior to the conventional PID control.

Reference

[1] LI Bin，TANG Yong-zhe．Appl ication of Fuzzy PID Algorithms in Brushless DC Motor system[J] ．Micromotors，2006，(2)：14-15．

[2] QU Yi，NING Duo，LIU Fei-hang，GUO Fei-fei．Design of Fuzzy-PID Controller Its Simulation[J].Computer Simulation，2009，26(12)：133-132．

[3] WANG Ling，LIU Wei-guo．Simulation of BLDCM Speed Control System Based on Fuzzy-PI Control Method[J]．Computer Simulation，2009，26(10)：186-189．

[4] LI Jun-hong，LI Lan-jun，YANG Wu-jiao．Neural Adaptive Sliding Model Variable Structure Control for Brushless DC motor Speed Systems[J]．Microcomputer Information，2010(2)：68-70．

[5] LI Guo-yong．Intelligent Control and its MATLAB Implementation[J]．Beijing Publishing House of electronics industry，2005，27(4)：252-260．

[6] FENG Tian-lin，TANG Xiao-qun，TIAN Song．Study on Proportional Control Valve for Air Flow[J]．Petro-Chemical Equipment，2008，37(2)：20-22

Advanced Materials Research Vols. 989-994 (2014) pp 3177-3180
© (2014) Trans Tech Publications, Switzerland
doi:10.4028/www.scientific.net/AMR.989-994.3177

Research on Algorithm to improve performance of Multi-wheel Steering Control System

Shaosong Wan[1,a], Jian Cao[2,b], Qunsong Zhu[2,c], Cong Yan[2,c]

[1]XiJing University, Xi'an, Shaanxi Province 710123, P.R. China

[2]Air Force Engineering University, Xi'an, Shaanxi Province 710051, P.R. China

[a]12156555@qq.com, [b]cao_jian1972@163.com, [c]yancong192@qq.com

Keywords: Control System; Improving; Experiment; Algorithm

Abstract. There are many factors that can affect network performance, such as delay, packet loss and capacity utilization. Vehicle handling directional stability has been more and more important, experiments for steering wheel corner step input response, steering oil tank response property, steady state turning and steering angle of all steering wheels were conducted in this paper, the experimental results show that multi-wheel steering system can fulfill its function very well and reach target angle, it provides a new method for researching for the vehicle handling directional stability.

Introduction

Structure of the multi-wheel steering electrohydraulic proportional control system can be divided into the electronic control unit (ECU) and the actuators[1][2][3]. The core of the whole control system is the electronic control unit (ECU), which completes the acquisition of the input feedback signal and the action of actuators. The actuator which is the hydraulic valve system includes oil source, electro-hydraulic proportional valve and hydraulic cylinder. According to PWM wave control signal of ECU output, the ratio solenoid coil of electro-hydraulic proportional valve gains a certain current, therefore controls the size of its force or displacement control valve proportional size of the opening. Extensional structure of the multi-wheel steering vehicle is shown in Fig.1.

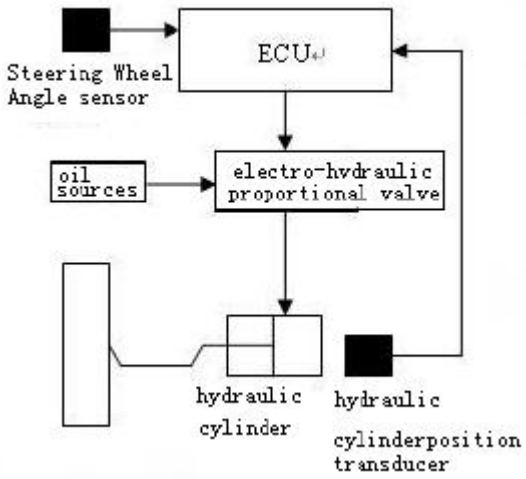

Fig.1 Diagram of multi-wheel steering vehicle control system

Most of modern cars use the front wheel steering to meet steering movements in the case of the general road condition and speed, with the development of the modern road transportation system and the advanced automobile technology, vehicle speed becomes faster and faster, so the motor vehicle handling directional stability has been concerned more than ever, one of the primary means to improve the motor vehicle handling directional stability is multi-wheel steering technology, which can better meet the Ackerman theorem and reduce tire wear. In this paper, an 8 × 8 wheel

vehicle steering mechanism has been transformed, developed a multi-wheeled vehicle steering wheel and its control system, and conducted bench and road tests[4][5].

Experimental Setup

Multi-wheel steering is a very important and effective way to improve vehicle maneuverability and handling stability. In order to get control parameters, verify electronic control unit of the control law and working performance, we turned to experiments carried out several rounds of bench and road test the car[6].

The device of the multi-wheel steering system's bench test

To verify the law of the control and test the working performance, a series of bench experiments were performed under the condition of the electronic control unit installed in the body after transformation, multi-car wheel steering.

The contents include the step input response of the steering wheel angle, and bench test bench test validation control law, steering cylinder response experiments, steady-state experiments and the rotary steering wheel steering angle measurement experiments. Car steering wheel like the overall layout of the control mechanism is shown in Fig.2.

Fig.2 General overall layout of multi-wheel sterling's control mechanism

The bench test of steering wheel angle step input response

The electro-hydraulic proportional control system is mainly actuators in multi-wheel steering control system; it is composed of the oil sources, electro-hydraulic proportional directional control valve and asymmetric hydraulic cylinder. Oil sources include tanks, pumps, filters, etc. Electro-hydraulic proportional valves are symmetrical, and hydraulic cylinder is asymmetric cylinders, forms a system that symmetric electro-hydraulic proportional valve controls asymmetric hydraulic cylinder. Under the control of the ECU, the system which makes use of hydraulic oil provides the oil sources to complete the actions required steering wheel.

Experimental purpose: to test electro-hydraulic proportional valve on the steering wheel input signal response performance in the multi-wheel steering system. Experimental methods: The steering wheel angle input is set to step excitation signal .The spool opening step response is measured in this case. And then by adjusting the electro-hydraulic proportional valve PID control proportional, integral and differential parameters of the optimal response. The experiment condition to do the steering wheel is 0-150 angle input step stimulus and 0-150 spool opening under the more response-order experiments. Experimental results are shown in Fig.3.

Waveform can be obtained from the above, the more order average response time is 0.14s, a positive step response is faster than the negative. To stabilize the target in a certain overshoot before the oscillation, the maximum overshoot of 3.3% (normal range within 10%), which is within the normal range.

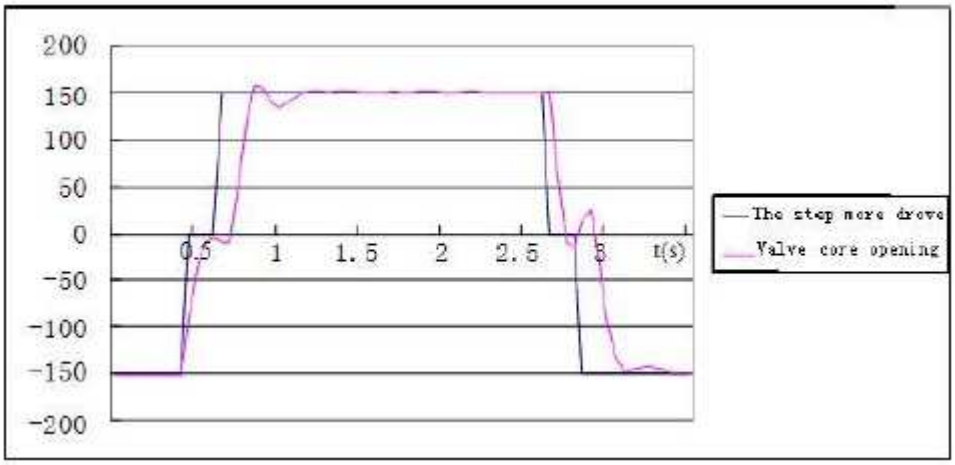

Fig.3 Steering wheel corner inputs response characteristic

The response experiment of steering cylinder

Experimental purpose is to test the steering cylinder on the steering wheel input signal response performance in the multi-wheel steering system. Experimental method is to use the steering wheel to rotate at different speeds in both directions around the maximum point, record the experimental data, analysis of response characteristics of the fuel tank. The results are shown in Fig.4 and Fig.5.

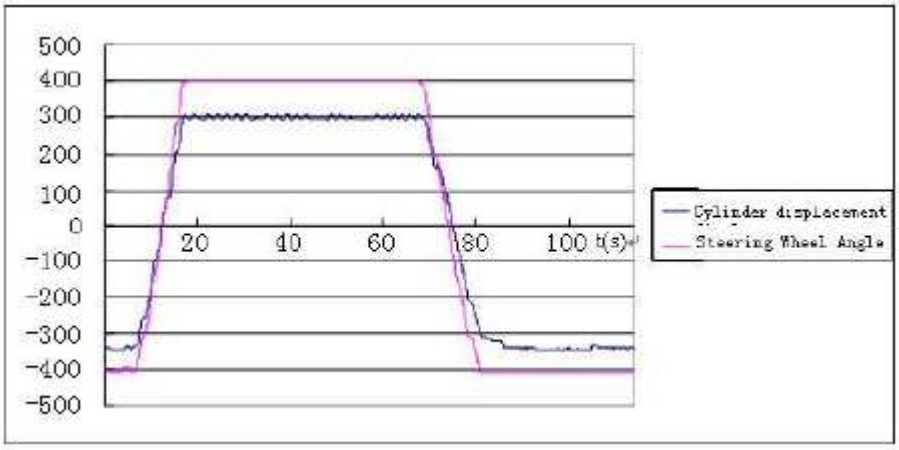

Fig.4 Hydraulic cylinder's response characteristic when steering wheel corner change is quick

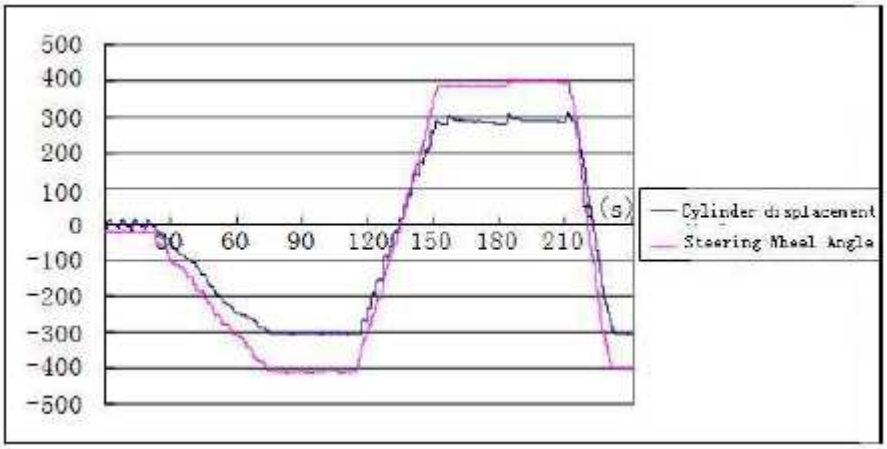

Fig.5 Hydraulic cylinder's response characteristic when steering wheel corner change is slow

Conclusion

The bench test of steering wheel angle step input response verified the second bridge turn rotation angle of the input control signal transient response characteristics. Experimental results show good dynamic characteristics. The reaction time is shorter, a smooth transition process. The steering implementation body that is the hydraulic cylinder in terms of response time or response for the accuracy of the results has been good. Multi-wheel steering system can achieve its function well and its target angle. The multi-wheel steering system has greatly enhanced the mobility of wheeled vehicles, to achieve the desired function. Through using proper control policies and control parameters, steering the mismatch occurred during sync basically resolved the problem. It achieved good control effect.

References

[1] Suman Sarkar, Hong-Hsu Yen, Sudhir Dixit, Biswanath Mukherjee, “A novel delay-aware routing algorithm (DARA) for a hybrid wireless-optical broadband access network (WOBAN)”, IEEE International Conference on Communications (ICC) 2009

[2] Abu (Sayeem) Reaz, Vishwanath Ramamurthi, Suman Sarkar,Dipak Ghosal, Sudhir Dixit, Biswanath Mukherjee, “CaDAR: an efficient routing algorithm for wireless-optical broadband access network”, ICC, Beijing, China, May. 2010.

[3] Abu (Sayeem) Reaz, Vishwanath Ramamurthi and Suman Sarkar, “Flow-aware channel assignment for multi-radio wireless optical broadband access network”, IEEE ANTS, Bombay, India, Dec. 2012.

[4] Abu (Sayeem) Reaz, Vishwanath Ramamurthi, Suman Sarkar, Dipak Ghosal and Biswanath Mukherjee, “Hybrid wireless optical broadband access network (WOBAN): capacity enhancement for wireless access”, IEEE Globecom, New Orleans, LA, USA, Nov-Dec. 2009

[5] J. Li, X. Ba, S. Anjum and J. Chen, “Adaptive PLL Based Carrier Tracking Algorithm for GPS Signals IN High Dynamic Environment,” Chinese Journal Of Electron Devices, vol. 30, no. 4, pp.1440-1443, August 2007.

[6] S. K. Shanmugam, “New Enhanced Sensitivity Detection Techniques for GPS L1 C/A and Modernized Signal Acquisition,” Ph. D. Thesis of University of Calgary, Calgary, Alberta, 2010.

Advanced Materials Research Vols. 989-994 (2014) pp 3181-3184
© (2014) Trans Tech Publications, Switzerland
doi:10.4028/www.scientific.net/AMR.989-994.3181

Research on Image Vectorization Based on Dual-Thumb Pneumatic Flexible Robot Hand

Shaosong Wan[1,a], Jian Cao[2,b], Qunsong Zhu[2,c], Cong Yan[2,c]

[1]XiJing University, Xi'an, Shaanxi Province 710123, P.R. China

[2]Air Force Engineering University, Xi'an, Shaanxi Province 710051, P.R. China

[a]12156555@qq.com, [b]cao_jian1972@163.com, [c]yancong192@qq.com

Keywords: Grasp; Image; Robot Hand; Expert System

Abstract. Because the traditional linear vectorization methods have some shortcomings including processing data slowly, being sensitive to noises and being easy to be distorted. Fuzzy rules and its inference mechanism are the assurance of achieving feature fusion. This paper has a design and analysis on the dual thumb pneumatic flexible robot hand base on the active flexible bending joints we have developed. The flexible joint is composed of four elongation artificial muscles with parallel arrangement. The robot hand has five multi-actuated fingers each with three flexible joints. To improve the flexibility and stability of grasp, the other four fingers are orthogonal and symmetrical except the middle finger, which forms the dual thumb oriented grasp model. Furthermore, we study on the position and posture of fingers applying the parameterized homogeneous transformation to the large deformation and nonlinear problems of flexible joint.

Introduction

Genetic algorithm (GA) is an effective probability searching algorithm based on the natural selection and the genetics principle, and it carries on the search and the optimization through the simulation organic evolution, and it automatically gains and accumulates the related knowledge of searching space in the searching process, and it controls the searching process to obtain the optimal solution of the question.

The simulation and experiments verifies the model and the grasp capability of robot hand. The robot hand we developed has good flexibility and compliance, and easy to soft control, which provide a new way to solve the entire flexibility of robot hand[1][2]. This algorithm has many characteristics such as automatic identification of antigen, feature extraction, the diversity of immune body, distributional examination, learn and memory, self-plan etc, and it is also parallel distributional self-adaptive system which has the great potential in the application of intelligent computation. In recent years the immunity genetic algorithm has obtained the widespread application in many domains because it can effectively maintain the diversity of population and eliminate not mature astringency and the oscillatory occurrences. The reference presented an immunity genetic algorithm which extracts vaccine from the system knowledge and vaccinates to the evolution process, thus, it can fully use the system message, but the algorithm has not considered the diversity of population which influences the evolution process[3][4][5].

Structure and Principle of Flexible Robot Hand

Flexibility and universality are two characteristics of robot hand we developed. All joints of robot hand are pneumatic and flexible which improve the flexibility of robot hand; the universality is implemented by the amount and arrangement of fingers.

Structure of Bidirectional Active Flexible Bending Joints

In Fig.1, the flexible joint we developed is mainly composed of four elongation artificial muscles and flanges, with two ends fixed on the flanges. It can axial elongate and bend two-dimensional two-way control in space simultaneously, and it has three degrees of freedom. Through controlling the air pressure of the four artificial muscles, the joint can bend anti-stretch, abduct and adduct.

For example, ensuring the air pressure of muscle is equal to muscle and more than muscle and muscle simultaneously, the joint can bend about Y-axis. The degree of bending is determined by the pressure differential controlled by the proportion valve. The bending of joint behaves like the nonlinear beam with large deformation which is characterized by the elongation of axis and the bending angle of the end.

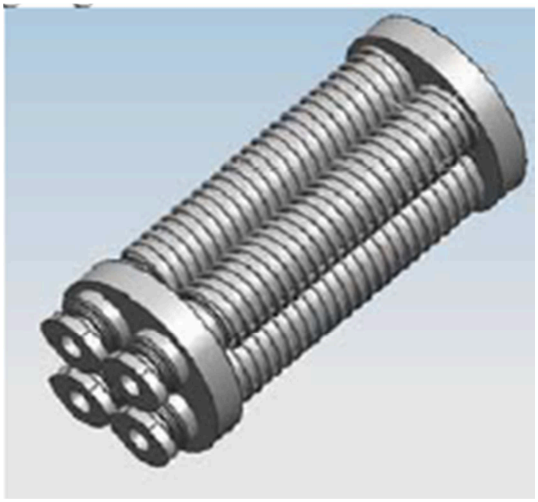

Fig.1 Structure of joint

For ease of comparison and visualization, the discriminator gains were normalized. The discriminating performance curves of the three algorithms with the correlator placing d = 0.25 (chip) and d = 0.5 (chip) are presented respectively in Fig.2.

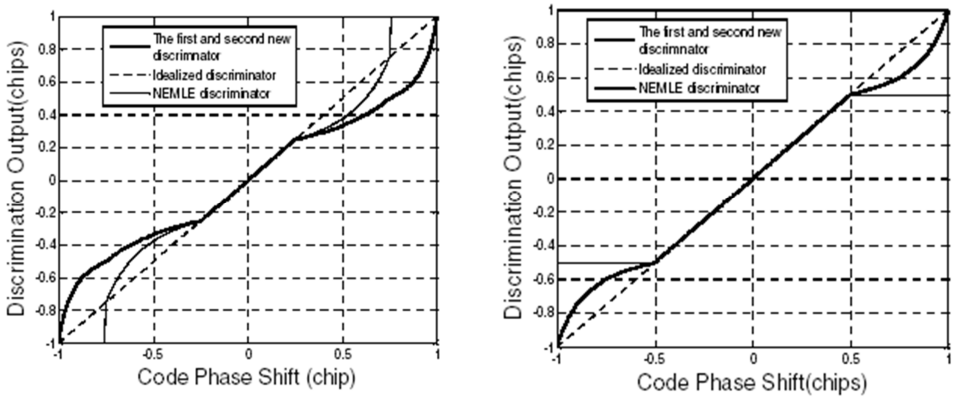

Fig.2 Discriminating performance curves with the correlator placing *d=0.25*(*chip*) and *d=0.5*(*chip*)

The analysis of the comparison obtained from Fig.2 is that, discriminator is better when d=0.25(chip), and the two new discriminators are better when d=0.5(chip).

Structural Design on Finger of Robot Hand

In Fig.3, The flexible finger is made of three pneumatic flexible joints connected in series, with the two ends of joint fixed on the wedge plate. One finger has one degree of freedom and two degrees of maneuvering. Thanks to the wedge angle of wedge plate, the bending angle about the orthogonal directions will increase to 3 ±120° at the maximum working pressure, which greatly improve the flexibility and grasp range of robot hand.

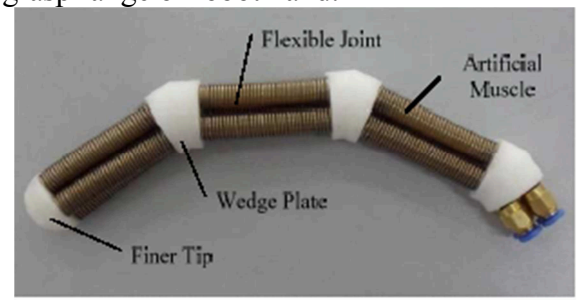

Fig.3 Structure of finger

Structural Design of Five-Fingered Flexible Robot Hand

The multi-fingered robot hand is composed of five fingers, and each finger is made of three bidirectional active flexible bending joints in series. The other four fingers are orthogonal and symmetrical except the middle finger, and the palm is axial symmetry along the middle finger. This distribution of fingers has good adaptability with the variety of object to grasp and it is easy to achieve the geometry- closed and force-closed.

For convenience and computational efficiency, five fingers are just the same to each other. The geometry characteristic forms the dual-thumb oriented grasp model in which four fingers predominate, or the thumb oriented and the others to cooperate it.

Simulations and Grasp Experimental Analyses on Position and Posture of Finger

We obtain the coordinates of typical control points and related points using Matlab. Fig.4 shows the trajectory and the pose of the finger. According the coordinates of each finger within palm coordinate system, as shown in Fig.5, we get the limits of posture of finger when the air pressure is 0.35MPa. It illustrates that the simulation results is consistent with the theoretical model. Bending grasp can manipulate the sphere, box, triangle object and other arbitrary shape objects effectively using one to five fingers. It is obvious that the bending grasping is the main effective work mode of the robot hand.

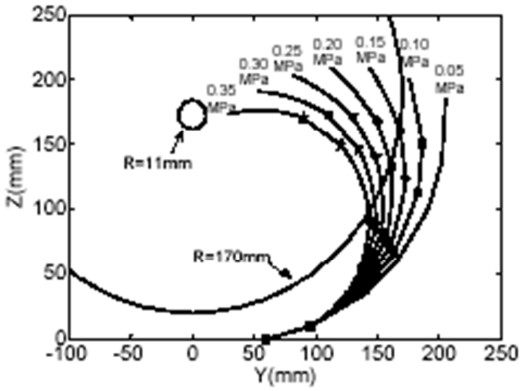

Fig.4 Finger trajectory when bending

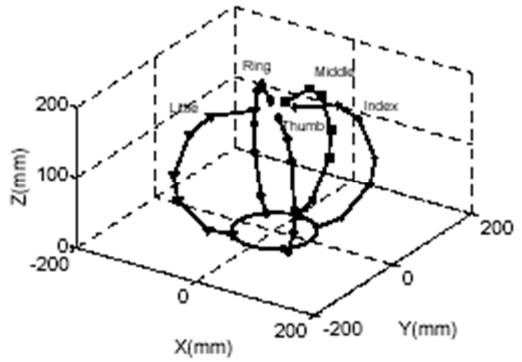

Fig.5 Pose of robot hand when bending grasp

Conclusion

This paper proposed a dual-thumb pneumatic flexible robot hand. It focuses on the pose and posture of the flexible joints, fingers and robot hand on the basis of analysis of their structures and performances. Improved algorithm brings the question space and the corresponding solution space into correspondence with the antigen and the immune body, and it controls the reproduction of the partial optimal solution through the density. The algorithm can improve the search speed because chaos is introduced in the initial population and diversity adjustment. The algorithm can carry on the local optimization and increase precision nearby the optimal solution. The result of experiment shows the algorithm validity. We can draw a conclusion from experiment comparison, the paper's algorithm makes average movement algebra small, and the algorithm overcomes the shortcoming of slow convergent speed which generic algorithm has, and the algorithm is superior to convergent speed of immune genetic algorithm. The simulation results and the experiments prove the validity of the theoretical model. It shows that the robot hand has good flexibility and compliance, and easy to soft control. It has strong and continuous adaptability, and can perfectly do the actions of grasp, clamp, flip and fiddle etc. It is agile and tightly to grasp the small object within 1 kg, and possesses good practical value.

References

[1] Olfa Nasaroui, Fabio Gonzdez, Dipankar Dasgupta .The Fuzzv Artificial Immune Svstem: Motivations, basic Concepts and Application to Clustering and Web Profiling [J].Fuzzy Systerm 2012, 1(2):711-716.

[2] LEANDRO N, CASTRO DE TIMMIS J Artificial immune system: a novel computational intelligence approach [M]. Springe–Verlag 2010.

[3] S. Wang, D. Yang, Z. Liu and D. LUO, "Simulation Study on High Dynamic GPS Software Receiver," The international journal for computation and mathematics in electrical and electronic engineering, vol. 28,iss. 6, pp.1386- 1401, 2009.

[4] J. Li, X. Ba, S. Anjum and J. Chen, "Adaptive PLL Based Carrier Tracking Algorithm for GPS Signals IN High Dynamic Environment," Chinese Journal Of Electron Devices, vol. 30, no. 4, pp.1440-1443, August 2007.

[5] Q.Y. Wu, "Convergence properties of pairwise NQD random sequences," Acta Math.Sin.vol.45, pp. 617–624, June 2012.

Advanced Materials Research Vols. 989-994 (2014) pp 3185-3188
© (2014) Trans Tech Publications, Switzerland
doi:10.4028/www.scientific.net/AMR.989-994.3185

Based on ANASYS with finite element analysis and calculation of cracked pipeline

Xiumei Zhu[1,a], Yuping lv[2,b]

[1]Yantai Engineering & Technology College, Yantai, 264006,China

[2]Yantai Engineering & Technology College, Yantai, 264006,China

[a]zhuxiumei@tom.com, [b]408599905@qq.com

Keywords: finite element; pipe; crack

Abstract. Pipeline in the entire oil and gas transportation industry play an important role and in the soil is corroded in order to produce the stress corrosion crack. The topic analyzes and calculates cracked pipeline with finite element method by use of ANSYS software mainly, and provides the theory basis for safety evaluation of pipeline.

Introduction

The engineering system can be converted to the finite element system by finite element method, and it makes up of node and element in order to Replace the Original engineering system, and it can transform into the mathematical model, that get the solution of the finite element system with the nodes and elements. Complete finite element model in addition to the node and the element, include the boundary conditions of the engineering system personally, the constraint conditions, and the negative force load etc [1].

Before Processing

Create a geometric modeling

Using good graphic user interface (GUI) of the ANSYS software establishes directly geometric model. As shown in fig.1.

Mesh generation

Model that has been created can be meshed, and the division of grid needs set up grid cell type, material properties, etc.

Selection of unit type：The model is three dimension unit, that selects 20 nodes hexahedron elements the of the Lagrange type, that the interpolation function is comparatively easy. As two-dimensional rectangular L shape function, the three dimensional regular hexahedron L shape functions is respectively "three linear", "three second", "three three times" and so on.

"Quadratic element" has 20 nodes, as shown in fig.2.

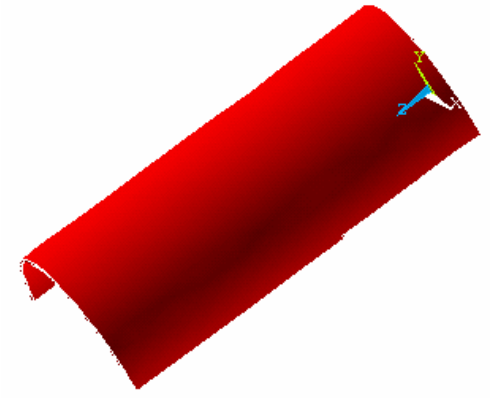

Fig.1. Geometric model

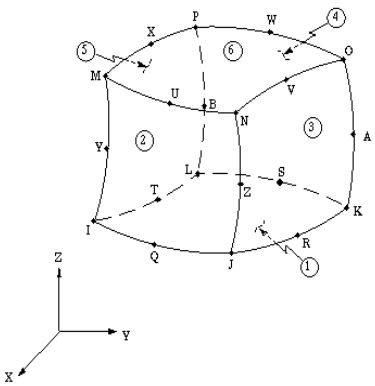

Fig.2. SOLID95 3-D 20-Node Structural solid

About any argument is secondary, its shape function as the vertices

$$\Psi_i^{(0)}(\xi,\eta,\zeta)=\frac{1}{8}(1+\xi_i\xi)(1+\eta_i\eta)(1+\zeta_i\zeta)(\xi_i\xi+\eta_i\eta+\zeta_i\zeta) \quad (1)$$

Among them （ξ_i,η_i,ζ_i) for the itch the vertices of the natural coordinates

$$\xi_i=\pm1,\eta_i=\pm1,\zeta_i=\pm1, \quad (2)$$

Among them （ξ_i,η_i,ζ_i) for the itch the vertices of the natural coordinates

For the surface nodes: $\xi_i=0,\eta_i=\pm1,\zeta_i=\pm1$ (3)

$$\Psi_8^{(0)}(\xi,\eta,\zeta)=\frac{1}{4}(1-\xi)^2(1+\eta_i\eta)(1+\zeta_i\zeta) \quad (4)$$

For the surface nodes: $\xi_i=\pm1,\xi_i=\pm1,\zeta_i=0$ (5)

$$\psi_i^{(0)}(\xi,\eta,\zeta)=\frac{1}{4}(1-\zeta^2)(1+\eta_i\eta)(1+\xi_i\xi) \quad (6)$$

For the surface nodes: $\eta_i=0,\xi_i=\pm1,\zeta_i=\pm1$ (7)

$$\psi_i^{(0)}(\xi,\eta,\zeta)=\frac{1}{4}(1-\eta^2)(1+\xi_i\xi)(1+\zeta_i\zeta) \quad (8)$$

Another type is MATRIX50 as shown in fig. 3.

Define the material properties

Material properties is the physical properties, can define a variety of material properties as unit. Different properties show different material number. Pipeline that is rigid material select 60 s.

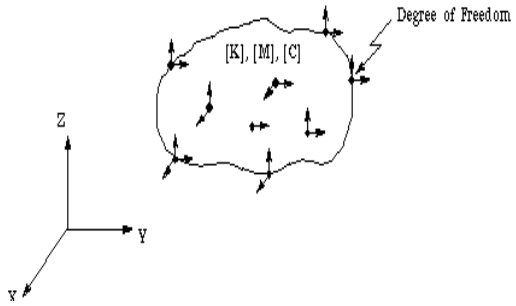

Fig. 3. MATRIX50 Super element

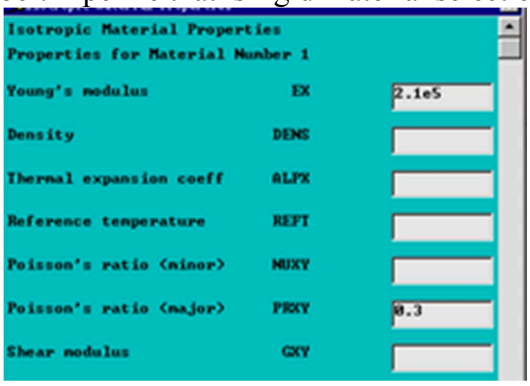

Fig. 4. Linear material properties

Linear material properties includes elastic modulus (EX, EY, EZ), poisson's ratio (PRXY, PRYZ, PRXZ), shear modulus (GXY, GYZ, GXZ), thermal expansion coefficient (ALPX, ALPY, ALPZ), etc. But some properties of analysis are irrelevant. In the analysis, the thermal conductivity of materials is no meaning to analysis [2]. Input material in warehouse can also define your own material attribute. Depending on the type of rigid material selection as shown in fig. 4.

Net and control

Grid control can control unit in shape, mesh density, node location, local grid, etc., In the accuracy of the models and moderate cost on computer resources properly the grid density is important. it that is too thick not want accuracy and that is too thin is likely to waste a lot of computing resources, that includes unnecessary stand of time and space. For meshing grid, I chooses the precision of the part of the grid of 8, another part of the precision of the grid is 5, the default precision is 6, 1 is the fine grid, 10 is the coarse grid. [3]

After defining the element properties and the grid control, can point network entity model, it is a solid model into finite element model of step.

Solid Modeling can be meshed after defining the element properties and parameters as shown in fig. 5.

The Problem Solving Process

DOF constraints are constraining the node degrees of freedom. The basic variables of the node degrees of freedom are to solve the equation, you can also specify a node degrees of freedom value,

once the value is specified, the solution will remain the same. Set the DOF is set its degrees of freedom value [4]. Constraint degree of freedom can be added in the online, on the surface, key point and nodes. Constraints are on surface crack of pipes. As shown in fig.6.

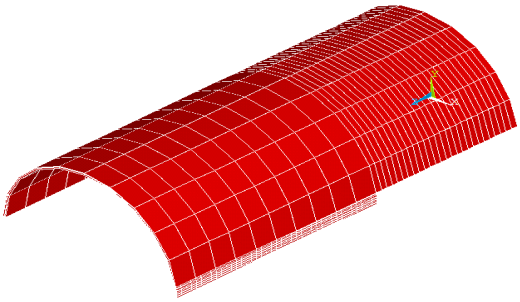

Fig. 5. Model grid

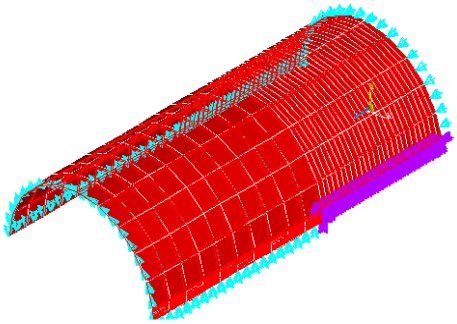

Fig.6.Constraints with crack pipe

I put crack pipes into unit strength, as a beam element, the pressure load on both ends of the side of the beam and that can be used to pressure and pressure gradient. For the lateral pressure, the size of the force per unit length, along the tangential and normal respectively, set up JOFFST to 1, can be simplified as the any place of the force on the beam element [5].

With pipeline analysis of crack is linear problem; it is ok to use the program default, namely a new analysis of static problems, using the current load step to solve.

The default form of analysis is a static analysis, ANSYS procedure for linear static analysis, the structure of the balance equation is: $[K]\vec{u} = \vec{F}$ (9)

Among them, called the overall stiffness matrix, for the node displacement vector of load vector, including applied to load on the structure and the structure of reaction load. That is: $[K]\vec{u} = \vec{F}^{r} + \vec{F}^{nd} + \vec{F}^{e}$ (10)

The above equation is the first reaction load on the right, the second is applied to the load of nodes, and the third is applied to unit load.

Any model, through the finite element discrete equation has the same form:

$[K]\vec{u} = F^{a}$ (11)

Among them, the coefficient matrix; for the location of the DOF freedom vector, load is applied. So, the problem is to solve the above equation. If it has nothing to do with equations for linear; otherwise, is nonlinear. Solution of the static analysis is the simplest form, but it is also the foundation of other forms of solving. The pipe selection result diagram is as follows: (unit) Fig. 7.

Post Processing

Post-processing is to check the analysis results. Read the data： ANSYS is not the result data into database automatically, so you need to take the results into the database.

Deformation shows： Deformation shows is mainly used for graphic structure deformation influence of external load, by which the direction and size of structure deformation can be obtained. Deformation is small, so the figure is a sign for the nature of the deformation, but not completely the size of the deformation is on the diagram. Deformations enlarge fig. 8.

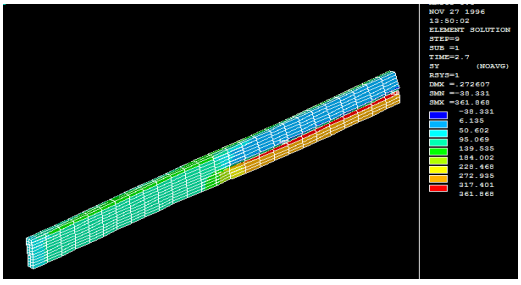

Fig. 7. Pipeline analysis diagram

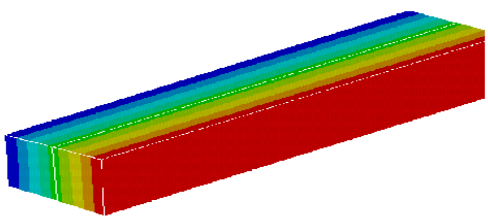

Fig. 8. Deformations Show

Conclusion

The values of the maximum stress of crack pipe cracks are in the corners fig.8. in red mark from the above results. it perfectly match with theory calculation, so the design completely meets the requirements.

References

[1] Public Inquiry Concerning The Stress Corrosion Cracking of Cancadian Oil and Gas Pipelines. MH-2-95. National Energy Board, Calgary, November 2006.

[2] Rice JR，Levy N.The pulic through surface crack in an elastics plate. J.Appl.mech,2012.

[3] ASTM Standard E 112-88, standard Test Methods for Determining Average Grain Size, American Society for Testing and Materials, Philadelphia, 2010.

[4] Z. Li, X. Yan, Y. Jiang, L. Qin and J. Wu: Mechanika, Vol. 18 (2012), p. 29-34.

[5] T. Patel, M. Zuo and A. Darpe: Proc. Inst. Mech. Eng. Part C J. Mech. Eng. Sci., Vol. 225 (2011), p. 700-713.

Advanced Materials Research Vols. 989-994 (2014) pp 3189-3194
© (2014) Trans Tech Publications, Switzerland
doi:10.4028/www.scientific.net/AMR.989-994.3189

Simulation Study of Magnetic Memory Signal Correlation Effect of Dual Defects by ANSYS

Xiaowen XI[1, a], Shangkun REN[1, b], Yafan ZHANG[1, c], Yin HUANG[1, d]

[1]Key Laboratory of Nondestructive Testing of Ministry of Education, Nanchang Hangkong University, Nanchang 330063, China

[a]email:xixiaowen_nchk@163.com, [b]email:renshangkun@yeah.net, [c]email:zhangyanfan2328@163.com, [d]email:huangyin_0828@126.com

Keywords: Magnetic Memory Testing; ANSYS Simulation; Correlation Effect; Stress Concentration

Abstract. To study the correlation effect of multiple defects of metal magnetic memory (MMM) testing technology, the stress-magnetization effect on 20# steel specimen with dual defects under exercise of the geomagnetic field and tensile load is simulated by using the finite element analysis (FEA) software ANSYS. With the stimulation, the magnetic flux leakage (MFL) distribution with different measured paths and different lift-off values of the surface specimen is given. The results showed that the correlation effect of dual defects produce more severe stress concentration phenomenon on the associated region of ferromagnetic specimen, and had no obvious effect on the edge of ferromagnetic materials; Gradient value K of the normal component H(z) of leakage magnetic field in the specimen, as a parameter evaluation of stress concentration in the specimen, has high reliability in areas without correlation effect, but it has no credibility in areas under dual defect correlation effect. Moreover, this article also discusses the influence of measured path and the lift-off value on magnetic memory signals.

Introductions

Magnetic memory testing method as a new nondestructive testing technology has received the attention of scholars both at home and abroad [1-2]. The method, based on the principle of stress-magnetization effect on ferromagnetic components, that is, under the action of working load and geomagnetic field, the magnetic domain organization will orientate in a irreversible way, thus forming magnetic flux leakage in stress concentration zone, is used to locate early injured parts with the main characteristics of stress concentration of the ferromagnetic components by examining the magnetic flux leakage [3]. The essence of stress magnetization effect law is the magnetization law of component caused by stress. It mainly studies the magnetic flux leakage distribution caused by the tensile stress and other stress load under the action of magnetic field [4-5]. At present, the technology research mainly focuses on the basic experiments of testing mechanism. However, little is explored on the numerical simulation study of the testing mechanism.

Based on the principle of stress-magnetization effect of ferromagnetic components [6], with force-magnetic coupling finite element analysis of the 20# steel under external stress and ground magnetic field conditions by using the finite element simulation software (ANSYS). The distribution law of magnetic memory signals of the surface air layer and the distribution law of internal stress of dual defects specimens are given. The credibility of normal component gradient K value of the magnetic flux leakage as stress concentration evaluation parameters is examined. And the influence of measured path and lift-off value on magnetic memory signals is also discussed.

Coupled field principles

Coupled field analysis considers interaction and coupling of two or more disciplines in the process of the finite element analysis [7]. Sequential coupling method consists of two or more analysis carried out by a certain sequence, every kind of analysis carried out in different physical environments. By applying the previous results as the load to the following analysis, the coupling of two different physical fields is realized.

Numerical simulation analysis metal magnetic memory testing technology mainly considers the influence of stress on magnetic flux leakage of ferromagnetic components, while the magnetic field effect on the stress is very small, even negligible. So the ANSYS simulation analysis adopts sequential coupling numerical simulation analysis that combines structure static analysis and static magnetic analysis.

Numerical simulations

To contain the V-shaped and semicircle notch for the dual prefabricated defects of 20# steel as the research object, specimen sizes and main technical parameters are shown in Fig.1. Respectively, to extract the magnetic flux leakage form the specimen surface in path A, B, C, D and E, where is apart from the notch tip of 0mm, 2mm, 4mm, 6mm and 8mm, and the specimen thickness is 3mm.

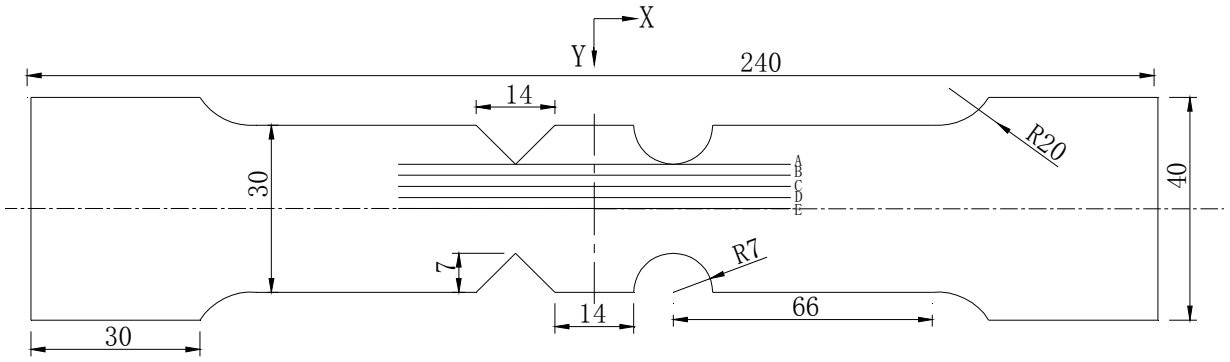

Fig.1 Specimen sizes of dual defects

Table 1 Main technical parameters of 20# steel

Parameters	E(GPa)	Poisson's ratio	σ_S(MPa)	μ_t
Value	203	0.28	235	285

Given the sample is symmetrical, in order to save computing time, computer hardware resources and to ensure the accuracy of the condition, a 1/2 modeling under test conditions is adopted. Due to the magnetic flux leakage of the external air layer need to extract, and analyzed the influence of the lift-off value, so thicker air layer model around the specimen is built. When dividing grid unit, method of manual control unit size and freedom divide is adopted, making the grid of ferromagnetic material area and the air layer area near prefabricated defects relatively dense and grid away from the prefabricated defects relatively sparse [8-9]. Specimen and air layer finite element mesh model as shown in fig.2 and 3, respectively.

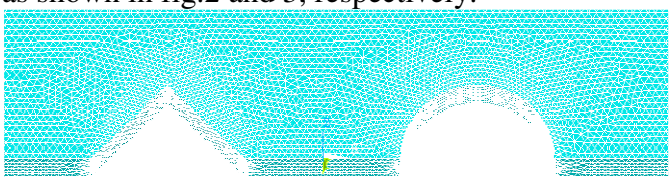

Fig.2 Finite element models of specimen

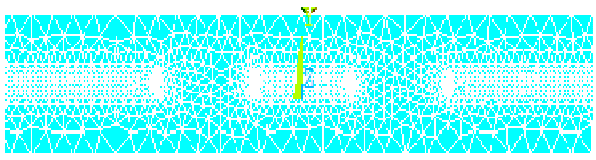

Fig.3 Finite element models of air layer

The simulation analysis is divided into static analysis and static magnetic analysis. In static analysis, displacement constraints and tensile load are respectively imposed on symmetric plane and about face of the model. These two different tensile loads are then written to load step, making it possible to carry out nonlinear static analysis under the condition close to real experiment. In static magnetic analysis, by applying a 39.8 A/m size of external environment magnetic field, the size of the earth's magnetic field on average, direction along the specimen with the X axis (see Fig.1). The magnetic flux leakage values of the path A, B, C, D, E, and different lift-off values is extracted by using APDL parametric program of ANSYS. As a result of the magnetic scalar potential method simulation, so the magnetic flux parallel boundary automatically satisfied, without human input.

Results

Stress distribution

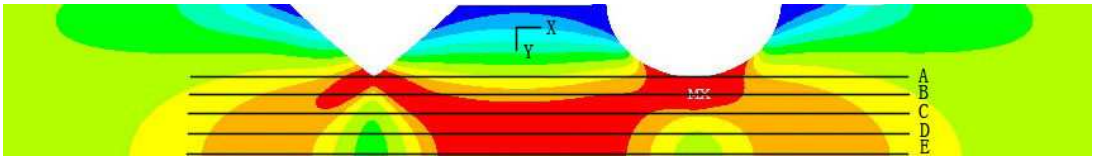

Fig.4 Contours of the internal stress distribution at F=150MPa

Nonlinear static analysis in ANSYS post-processing stage, contours of the stress distribution inside the specimen is obtained, which showed in fig.4. The simulation results show that: near the notch tip and corresponding position, V-notch and semicircle notch all show that the stress concentration phenomenon, which is the red area in the contours of the internal stress distribution. As can be seen from the contours, the width of the semicircle notch is slightly larger than the width of V-shaped notch; Along the Y axis from notch tip position, the stress concentration at the tip of V-shaped and semicircle notch significantly lower. In the specimen center along the Y axis, stress concentration significantly increased, appeared similar near the notch tip stress concentration phenomenon, and the range is bigger than the notch tip. Accordingly, gap shape also affects degree of the stress concentration and distribution. As a conclusion, with correlation effect of dual defects, the stress concentration is more obvious in the central of specimen than in the notch tip, leading to the specimen fracture more easily, with greater potential danger.

Magnetic flux leakage distribution

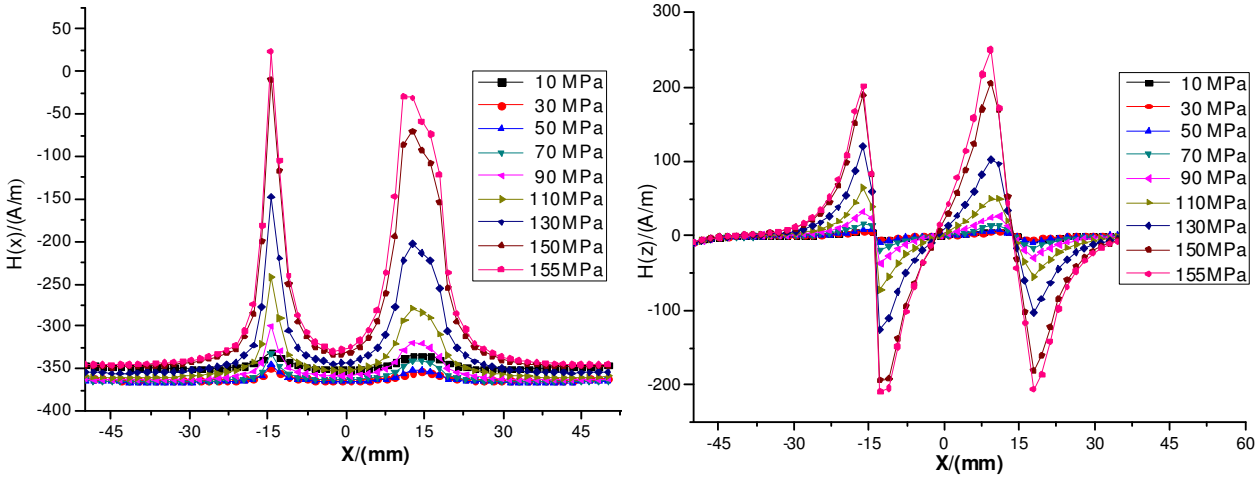

(a) Tangential component H(x) (b) Normal component H(z)

Fig.5 Size of magnetic flux leakage changing with tensile stress at h=1mm, path A

Figure 5 is the distribution curve of tangential component H(x) and normal component H(z) with the average stress by 20MPa ladder loaded, where is lift-off h=1mm from the surface of the specimen and path A (close to the edge of the specimen). Simulation results well accord with metal magnetic memory testing technology of detecting characteristics, namely in the stress concentration area, the tangential component H(x) of magnetic flux leakage has a maximum value, and the normal component H(z) of leakage magnetic field shows to change sign and a zero value. The figure shows that different notch, the peak-peak height and width of the magnetic memory signals have different values. The tangential component H(x) of V-shaped notch is higher, but the narrow; the tangential component H(x) of semicircle notch is weaker, but wide. The normal component H(z) of V-shaped notch is weak and semicircle notch is wide. The simulation results show that the stress concentration degree of different notch is different; also, there isn't any stress concentration in the area between two gaps. As shown in the leakage magnetic field value of path A, multi-defects correlation effect doesn't produce any stress concentration at the edge of the specimen, hence basically no effect on the edge.

In the actual detection, due to various factors such as interference of outside magnetic field, the use of the tangential component of the magnetic field and the normal component to determine the stress concentration is limited, prone to misjudgment and false negatives. Therefore, GB/T

26641-2011 "General NDT magnetic memory testing" puts forward it is recommended to use normal component of the magnetic field intensity gradient K value as a characteristic judgment.

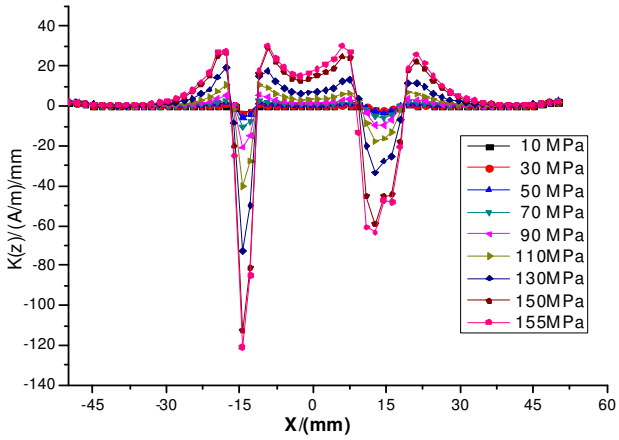

Fig.6 Normal component H(z)

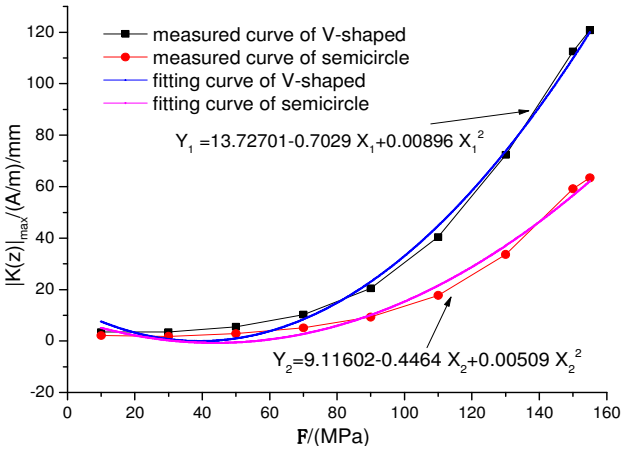

Fig.7 Maximum gradient of absolute value

Figure 6 is the distribution curve of normal component gradient K on the edge of the specimen change with tensile stress. The figure shows that the gradient K peak-peak amplitude increases in reverse with the increase of stress on the stress concentration area. Also, it more clearly reflects the stress concentration degree and width. Figure 7 is the curve of maximum gradient of absolute value $|K(z)|_{max}$ change with tensile stress. From the fitting curve, the gradient K first increased slowly, and then increased obviously; |K(z)|max of V-shaped notch specimen increases rapidly than that of the semicircular notch specimen. V-shaped notch specimen is more sensible to stress and easier to be detected. The simulation results show that gradient K changes obviously with stress, and is free from interference of outside magnetic field and other factors. It can be concluded that gradient K of the normal component of leakage magnetic field in the specimen has high reliability in evaluation of stress concentration at the edge of dual defect correlation specimen or the non-associated region.

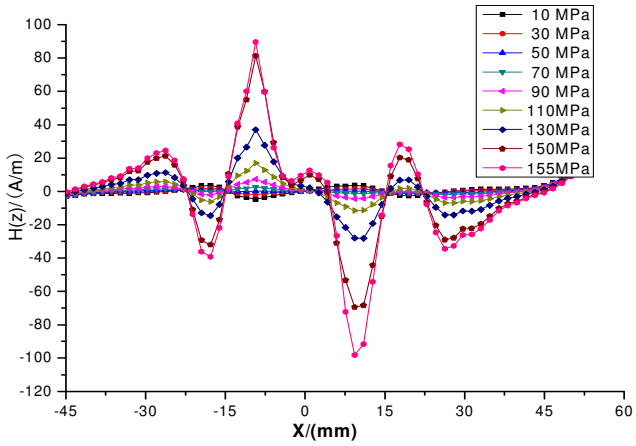

(a) Normal component H(z)

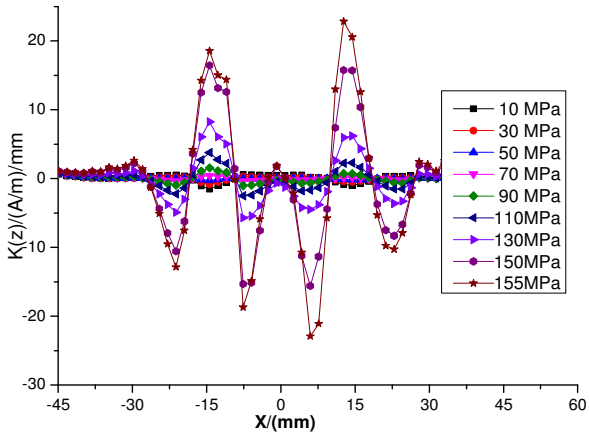

(b)Gradient K (Normal component)

Fig.8 Size of magnetic flux leakage changing with tensile stress at h=1mm, path E

To study the correlation effects of dual defects and the evaluation credibility of gradient K, obtained distribution curve of normal component H(z) and gradient K with tensile stress changes, where is lift-off value h=1mm from the surface of the specimen and path A (the centre of the specimen), shown in Fig.8. The figure shows that, with the increase of tensile stress, the normal component H(z) and its gradient K are increased gradually. As shown in the normal component H(z) of the specimen, along the X axis direction appears three different levels stress concentration areas with the characteristics of changing positive-negative symbols and having a zero in the maximum stress concentration zone. The degree of stress concentration at the centre of specimen is significantly greater than that of areas near notch top of the specimen. There appears displacement for the stress concentration on the X direction. Stress concentration at the center of the specimen significantly greater than V-shaped, semicircular notch near the tip, and the stress concentration area in the X direction to generate a displacement. However, in Fig.8 (b), the curve of gradient K

can be drawn from four stress concentration areas through the judgment characteristics of gradient K increasing reverse. Compare with the internal stress contours of the specimen (Fig.4), the results showed that: the correlation effect of dual defects produce more severe stress concentration phenomenon on the associated region of ferromagnetic specimen, and has important influence on specimen life; Gradient value K of the normal component H(z) of leakage magnetic field in the specimen, as a parameter evaluation of stress concentration in the specimen, has high reliability in areas without correlation effect, but it has no credibility in areas under dual defect correlation effect.

Influence of measured path and lift-off value

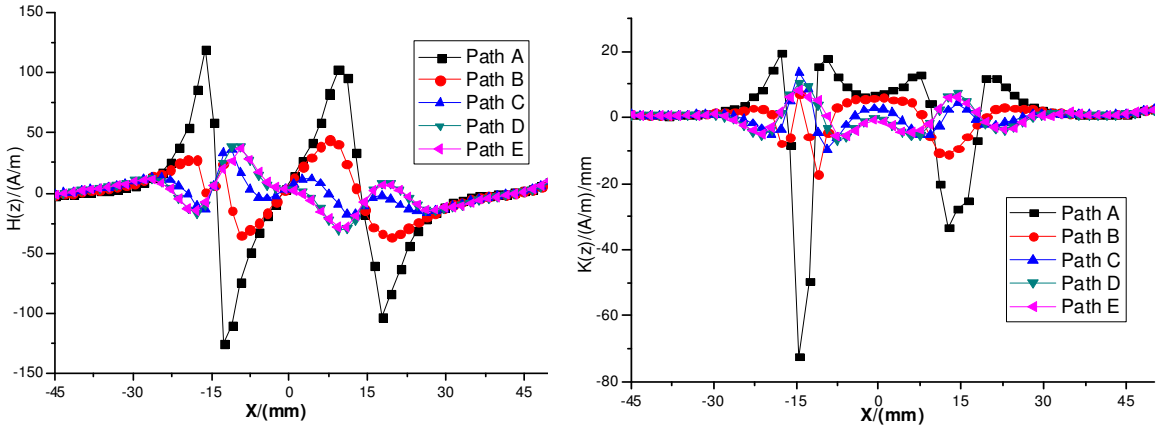

(a) Normal component H(z) (b)Gradient K (Normal component)

Fig.9 Size of magnetic flux leakage on different measuring path at h=1mm, F=130MPa

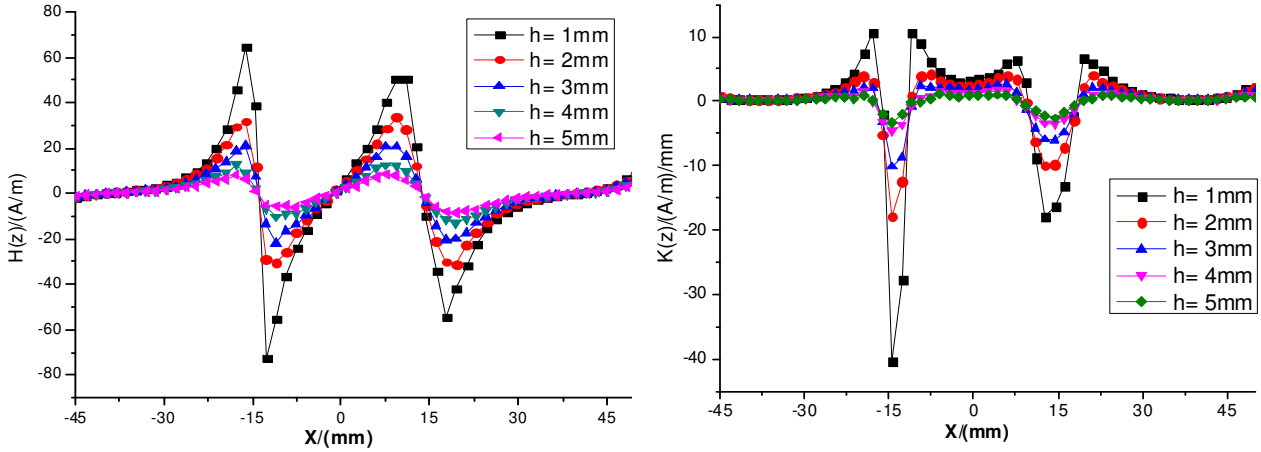

(a) Normal component H(z) (b)Gradient K (Normal component)

Fig.10 Size of magnetic flux leakage on different lift-off value at Path A, F=130MPa

Due to the magnetic memory signal is weak, and vulnerable to the interference of outside factors. In order to study the influence factors of metal magnetic memory testing signals and extract the normal component H(z) and the gradient K in the different measured path and the difference lift-off value on the surface of specimen, as shown in fig.9 and 10. From fig.9 shows that far from notch tip along the Y axis, the normal component H(z) peak-peak amplitude began to smaller in terms of exponential law and appear reverse changes in the path B. The magnetic field gradient K distribution can be seen from the more obvious results. The results show that different measured path, magnetic memory signal is not the same size and distribution, and further proved the validity of the gradient K evaluation characteristics. From fig.10 shows that with the increase of lift-off value, the normal component H(z) peak-peak amplitude began to smaller in terms of exponential law, and the gradient K is also more obvious. Simulation results show that: different lift-off value, the magnetic memory signal changes in the larger, has greater influence on the determination of stress concentration.

To sum up, the measured path and the lift-off value for the magnetic memory signals have a more significant effect. Therefore, in the use of metal magnetic memory testing technology practice

operation, should fully consider the measured path and the lift-off effect on the signal of metal magnetic memory.

Conclusions

(1) The correlation effect of dual defects produces more severe stress concentration phenomenon on the associated region of ferromagnetic specimen, and had no obvious effect on the edge of ferromagnetic specimen. It can be seen that the correlation effect of dual defects mainly affects specimen center area, making it more likely to rupture, thus shorten the service life of the specimen.

(2) Gradient value K of the normal component H(z) of leakage magnetic field in the specimen, as a parameter evaluation of stress concentration in the specimen, has high reliability in areas without correlation effect, but it has no credibility in areas under dual defect correlation effect.

(3) With the change of measured path and lift-off value, the normal component H(z) peak-peak amplitude began to smaller in terms of exponential law, and its gradient K is more obvious. Therefore, in the use of metal magnetic memory testing technology practice operation, should fully consider the measured path and the lift-off effect on the signal of metal magnetic memory.

Acknowledgements

In this paper, the research was sponsored by the Nature Science Foundation of China (Project No. 51261023).

References

[1] Doubov A. Diagnostics of metal items and equipment by means of metal magnetic memory [J]. NDT'99 and UK Corrosion'99, 1999: 287-293.

[2] Dubov A A. Development of a metal magnetic memory method [J]. Chemical and Petroleum Engineering, 2012, 47(11-12): 837-839.

[3] Jilin Ren, Junming Lin. Metal magnetic memory testing technology [M].Beijing: China Electric Power Press, 2000.

[4] Weimin Zhang, Hongguang Liu, Haitao Sun. Magnetic memory effect of low and medium carbon steel under static tension conditions [J]. Transactions of Beijing Institute of Technology, 2004, 24(7): 571-574.

[5] Yao K, Wang Z D, Deng B, et al. Experimental research on metal magnetic memory method[J]. Experimental mechanics, 2012, 52(3): 305-314.

[6] Ying Zhang, Kai Song, and so on. Application of software ANSYS in metal magnetic memory testing[J]. Nondestructive Testing, 2004, 26(5): 217-220.

[7] Shuguang Gong, Guilan Xie. ANSYS commands and parametric programming [M]. Beijing: China Machine Press, 2004.

[8] Yao K, Deng B, Wang Z D. Numerical studies to signal characteristics with the metal magnetic memory-effect in plastically deformed samples[J]. NDT & E International, 2012, 47: 7-17.

[9] Jilin Ren, Minghang Shu, and so on. Simulation of stress-magnetization effect on 18CrNi4A steel by ANSYS[J]. Journal of Material Engineering, 2009, 11: 009.

Advanced Materials Research Vols. 989-994 (2014) pp 3195-3198
© (2014) Trans Tech Publications, Switzerland
doi:10.4028/www.scientific.net/AMR.989-994.3195

Temperature Control Features and Simulation Research on High and Low Gimbals

Zuojiang XIAO[1], Xiaoxue GUO[1,a], Haibin ZHU[2], Zhigang XU[2], Zhiyong AN[1]

[1]Changchun University of Science and Technology, Changchun 130022, China

[2]JiLin Dongguang Precision Machinery Factory, Changchun 130022, China

[a]email: 821956304@qq.com

Keywords: High and Low Gimbals; Temperature Control; Dahlin Algorithm; Smith Predictive Control Algorithm; Simulink

Abstract. In view of characteristics owned by high and low gimbals, for instance pure lag, large inertia, strongly nonlinear and so on, which was employed in low light level (LLL) weapon sight reliability detection system. The basic working principle and mathematical model of Dahlin and Smith predictive control algorithm were mainly researched. And ideal control curves were obtained by software emulation. The simulated results showed that the two algorithms each have their advantages, shortcomings and the proper situations, but as to improve the control efficiency of system, the Dahlin is superior.

Introduction

High and low temperature environmental simulation system is widely used in many fields, which plays an extremely important role in light weapon sight reliability test. Many algorithms are commonly used in the field of temperature control, but they are applied to different control systems considering of their advantages and disadvantages. Delay is inherent in industrial process, control issues of large inertia, pure time delay objects during industrial control process are universal existence. It is prone to encounter bigger overshoot, longer settling time and other problems, production process control quality will be affected to a great extent. For large time-delay system, a variety of combined algorithms are derived from conventional control algorithm, such as fuzzy control based on combined Smith predictor, fuzzy proportional integral derivative control (PID), adaptive compensation control and so on[1-6]. And during the course of the pure lag control system, Dahlin and Smith predictive control algorithm also be widely employed.

Establishment of Temperature Control Model

Temperature object suffers from big time constant, serious time-delay, flexible and complex influencing factors. In general case, temperature shows an exponential relationship with time. An analysis of main causes of time delay has been made as follows. Because heat transfer is a slow process and temperature element has a certain inertia, controlled temperature change is lag behind controller output[7]. Moreover, correlated analysis shows that the temperature control system has the following traits: weak adaptive ability, heating and heat preservation by means of power supply, using air cooling, so its temperature curve has characteristics of high peak overshoot and long stability time.

The results show that temperature control features of high and low gimbals are pure time delay, large inertia and nonlinear. Dahlin and Smith predictive control algorithm are both effective in controlling of the pure delay system. However, differences exist in the Dahlin and Smith predictive control algorithm. So it has important meanings to select better one to control the system by analysing of their advantages and disadvantages. According to the principles of thermodynamics, mathematical model of the controlled object as following shows:

$$G_0(s) = \frac{Ke^{-\tau s}}{TS+1} = G_P(S)e^{-\tau s} \tag{1}$$

Where K is the magnification, τ is pure delay time, T is process time, $G_p(S)$ is the part without pure delay in the controlled object. Close-loop transfer function can be expressed as:

$$G(S)=\frac{G_C(S)G_P(S)e^{-\tau s}}{1+G_C(S)G_P(S)e^{-\tau s}} \tag{2}$$

$e^{-\tau s}$ respects to lag link which would influence the stability of the system. The greater the $e^{-\tau s}$ is, the more unstable the system.

Research of Temperature Control Algorithms

There are many algorithms are applied to control temperature, among them Dahlin and Smith predictive control show great inhibitory effects on pure lag control system.

(1) Dahlin algorithm

The Dahlin algorithm was put forward in 1968. Its principle is: anticipant closed-loop response is designed as one step inertia adds delays, and then conversely obtains controller satisfied the closed-loop response. Control system block diagram as the Figure 1 below:

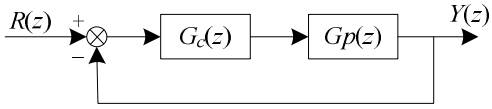

Fig.1. Single loop control system diagram

Where $G_C(z)$ is digital controller, $G_P(z)$ is controlled object.

Transfer function is given by:

$$\phi(s)=\frac{Y(s)}{R(s)}=\frac{e^{-\tau s}}{T_\varphi s+1} \tag{3}$$

Where T_φ is the time constant of the closed-loop system.

Dahlin algorithm has good control effect on pure delay system.

(2) Smith predictive control algorithm

Smith predictive control system structure diagram as shown in Figure 2:

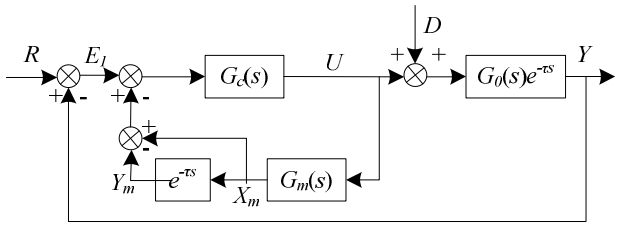

Fig.2. The equivalent figure of Smith predictive control system

The transfer function of system with delay time as shown in Formula 2, and the characteristic equation can be represented as:

$$1+G_C(s)G_0(s)e^{-\tau s}=0 \tag{4}$$

Smith compensation controller is added to overcome the instability of the system caused by the pure delay time (τ) , the closed loop transfer function of the system can be expressed as:

$$1+G_C(s)G_0(s)=0 \tag{5}$$

The influence of pure time delay on system stability can be well controlled.

Simulation based on Simulink

According to the transfer function (Formula 2), we can take on the value K=1.5, τ =80, T=2000, so reference model for the control system can be written as:

$$G_m(s)e^{-\tau s}=\frac{1.5}{2000s+1}e^{-80s} \tag{6}$$

A. Buildup of simulating model for the system

The maximum output temperature desired in the experiment is 70 ℃. Then simulation to the system was carried when the input was a step function. Corresponding principle block diagrams established in the Simulink as shown in Figure 3 and 4:

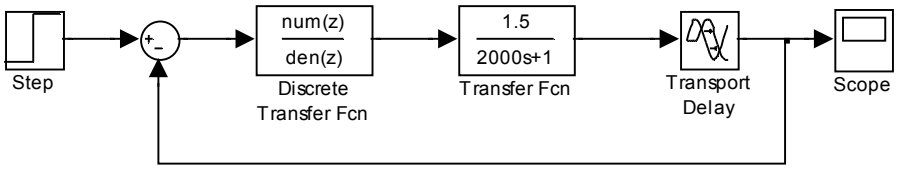

Fig.3. The simulating schematic diagram based on Dahlin algorithm

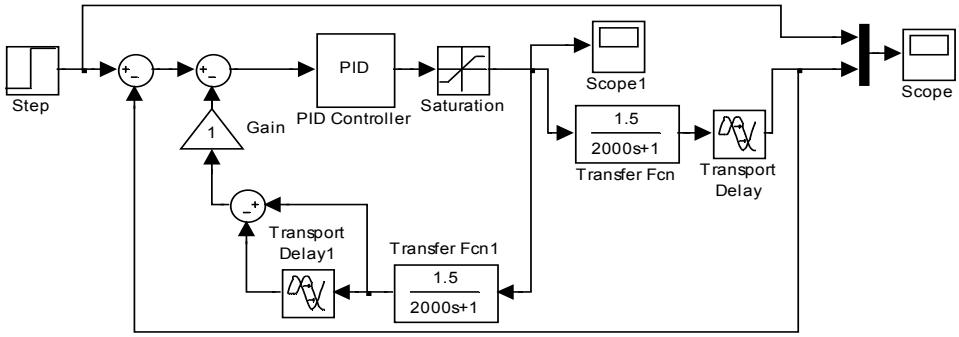

Fig.4. The simulating schematic diagram based on Smith predictive control algorithm

B. Results and discussion

The algorithm was proposed, through analyzing the simulation curves of the two algorithms in different condition, which was more suitable for the temperature control system. The Smith predictive control involves a proportional integral control (PI), where the proportional factor $k_p = 4$, integral coefficient $k_i = 0.007$. (Abscissa is time: s; Ordinate is temperature: ℃)

(1) When two control models are optimally matching with system model, simulation curves are illustrated in Figure 5.

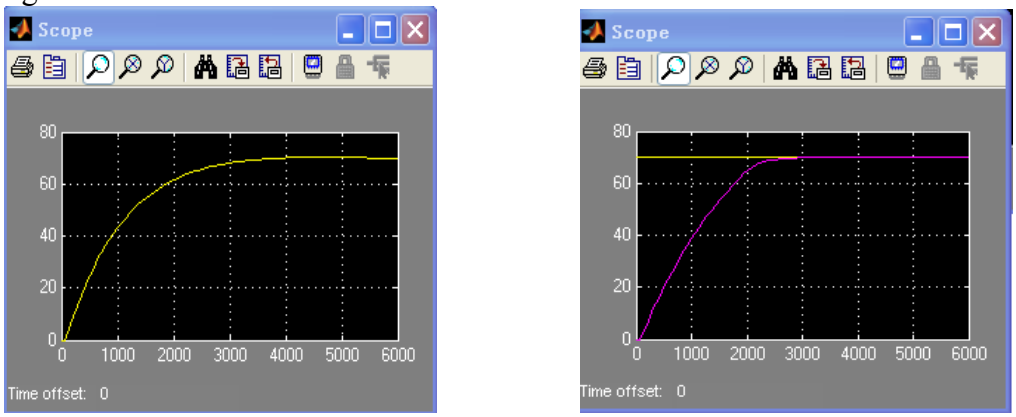

(a) Dahlin algorithm (b) Smith predictive control algorithm

Fig.5. Step response curves based on the two algorithms

As seen from above simulation results, both of them have no steady state error, but Smith predictive control algorithm is relatively ideal, which has fast response to the setting with compare to Dahlin.

(2) When two control models and system model are mismatching, simulation results are shown in Figure 6. Let K=2, τ =110, T=1600, reference model of the control system is given by:

$$G_m(s)e^{-\tau s} = \frac{2}{1600s+1}e^{-110s} \tag{7}$$

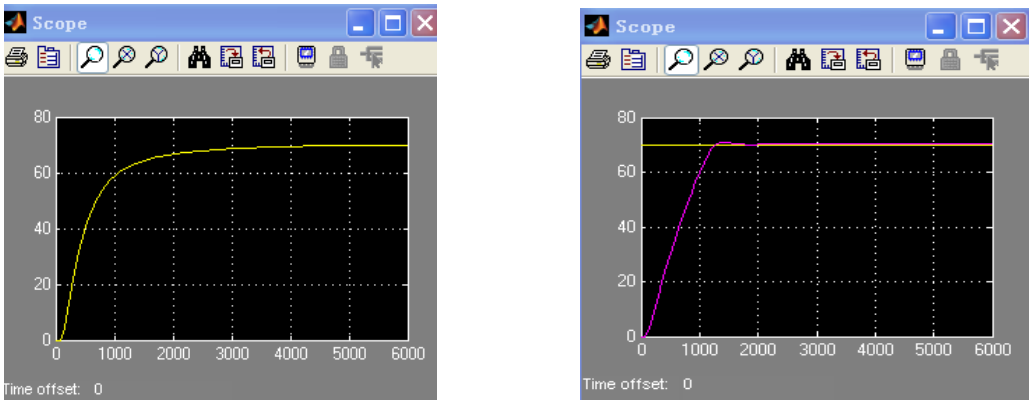

(a) Dahlin algorithm (b) Smith predictive control algorithm

Fig.6. Step response curves based on the two algorithms

The Figures illustrate the difference behavior of two controllers under the same situation for the specific set points:

Response time: Smith predictive control algorithm appears to have fast response for setting value in comparison with Dahlin algorithm.

Overshoot: Due to the fast response, the Smith predictive control algorithm has positive overshoot. In contrary, overshooting is hardly observed in the experiments of the Dahlin algorithm. Oscillation can be eliminated using Dahlin arithmetic, which is caused by model error. And it makes the system have better stability, adaptability and control precision. The Figures reflect that both of algorithms are suitable for the pure delay system. But compared with the Smith, the Dahlin is more stable and has better effect.

Conclusion

On the basis of analysis of temperature control features of high and low gimbals, this paper mainly studied the control effect of Dahlin and Smith predictive control algorithm which are common algorithms for pure lag control system. It can be concluded that the Dahlin algorithm is more stable, despite its slow response speed. This algorithm suitable for the system which have no or less super adjusting and do not require high rapidity demands. Smith predictive control algorithm has unique advantages in temperature control system. However, it still need to be improved furtherly. Certainly, there are many more effective and advanced algorithms exist in many practical applications of the pure delay system. This article mainly discussed the general characteristics and differences of the two algorithms.

References

[1] Zhenping Ji, Jinqi Fan. Application of Fuzzy-PID control in temperature control system[J]. Transactions of Shenyang Ligong University. 2013 (3) 40-43.

[2] Mohanmmed Elnour A/ Alla. Walleed Ibrahim Mohammed Taha. PID and fuzzy logic in temperature control system[C]. ICCEEE.2013.

[3] Jianping Sun, Ying Qu, Zhuang Shi. Fuzzy-Smith control of the time-delay system and optimization of the parameters[J]. Chinese Journal of Scientific Instrument. 2006 (4) 427-429.

[4] Srismrita Basu, Realization of fuzzy logic temperature controller[J]. International Journal of Emerging Technology and Advanced Engineering. 2012 (2) 151-155.

[5] Aritra De, Water temperature controller using microcontroller and correction using fuzzy logic[J]. International Journal of Emerging Technology and Advanced Engineering. 2012 (2) 310-314.

[6] G. S. Nhivekar, S. S. Nirmale, R. R. Mudholker, Implementation of fuzzy logic control algorithm in embedded microcomputers for dedicated application[J]. International Journal of Engineering, Science and Technology. 2011(3) 276-283.

[7] Jiangxia Duan. Application study on fuzzy PID controller in temperature control system with large inertia and time delay[D]. Lan Zhou: Lan Zhou University. 2013.

Advanced Materials Research Vols. 989-994 (2014) pp 3199-3203
© (2014) Trans Tech Publications, Switzerland
doi:10.4028/www.scientific.net/AMR.989-994.3199

Prediction System Design on Noise Airworthiness Compliance

Yan Guohua[1,a], Liu Shiqi[1,b] and Song Wenqian[1,c]

[1] Civil Aviation University of China, Tianjin, 300300, China

[a]ghyan@cauc.edu.cn , [b]lsq0421@hotmail.com ,[c]song_wenqian@126.com

Keywords: Noise; NPD Database; Static Prediction

Abstract. According to the method described in Technical Manual of Aircraft Noise Evaluation Procedures, this system can predict the EPNL (Effective Perceived Noise Level) of aircraft take-off, approaching and side boundary. The system also contains the function of managing andcalling NPD database, and can assess the predictive value basing on the noise stringency curve. This saves a number of cost for the airworthiness certification of aircraft noise, and is a new engineering practice which has a good application value.

Introduction

The technology of aircraft noise predictions is already mature in Europe and America. Completed aircraft noise prediction systems have been built, and the measurement criterions, methods, steps and procedures have been included in the corresponding technical manuals. But the results of research have been always in a state of blockade to China, and the training costs are too expensive. The domestic standards or guidelines about the flight noise prediction according to the static test data are not completed, researches on aero-engine noise airworthiness are still in the infancy.

The static prediction, as an alternative method for airworthiness certification of aircraft noise, is to predict aircraft noise level by using aero-engine static far-field noise measurement data. This paper shows a particular algorithm which outputs the noise value for the flight state by measuring the engine noise data under static conditions. The results can be compared with the NPD data of the corresponding aircraft, the algorithm is available if the error is within the acceptable range [1].

Prediction principles and procedures

The prediction procedure includes：build NPD database；select the appropriate methods to correct for static data according to the main correction factor，acquire static test data mapping to third-octave 24 center frequency corresponding sound pressure level in flight; calculate the effective perceived noise level under certain conditions according to CCAR36; compare the results to the NPD data.

The construction of NPD database

After a sufficient number of noise measurement，the noise-power curves of lateral and fly-over noise for certain distances can be made. Expand these curves in a certain distance by calculating or using additional flight test data, to form a generalized noise database. This database which is used for "flight data" and noise certification of derivative models, commonly referred to the NPD[2]。

During the airworthiness certification process of a certain type of aircraft noise, NPD noise test is conducted. Select the appropriate noise measurement points according to the circumstances of the airport runway of flight test and environmental climate. When the test site, test instruments and equipment as well as test day atmospheric conditions meet the requirements of the flight noise, the test of aircraft noise begin, to obtain NPD data. Aircraft noise certification procedures specified that for the noise certification, the measurements of noise level of approach, lateral and take-off are mandatory. And there are strict requirements about the locations of the measurement points. As is shown in figure 1,the noise measurement reference point for approach is located in the extended

runway center line at 2000m from the runway threshold, the noise measurement reference point for take-off is located in extended runway center line at 6500m from the start point of take-off, the lateral noise measurement reference point is located in the sideline which is parallel to and 450 meters from the extended runway center line, where the maximum noise level is measured after take-off.

In each case of takeoff thrust(power) including a full thrust and reduced thrust (power), the aircraft flies over the lateral and fly-over sensor according to the program. The figure 2 shows the programmed flight path of take-off measurement, in which the point C is the equivalent entry point. The aircraft maintains a constant height from point A to point B, continues to climb from the beginning of point B, climbs at a constant angle from the point C, intersects the takeoff reference flight path intersection continues until the end of the reference trajectory takeoff noise assessment. The point D is the theoretical take off launch point, to establish referencetrack, and it will be the point E with reducedthrust. The point F is the end point of takeoff flight path for noise assessment. When approaching, the aircraft normally covers the planned flight path and maintains a stable configuration and power until the PNLTM 10dB reduction. The aircraft then continues to circle without landing.

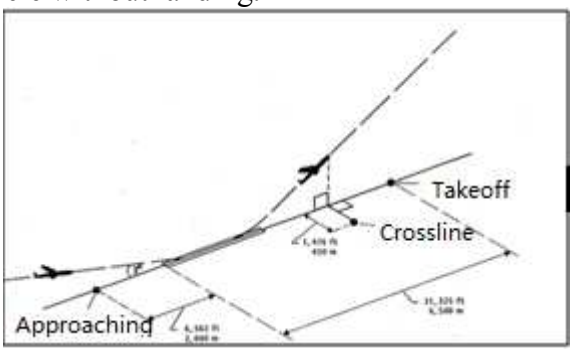

Fig.1 Reference Track Procedure

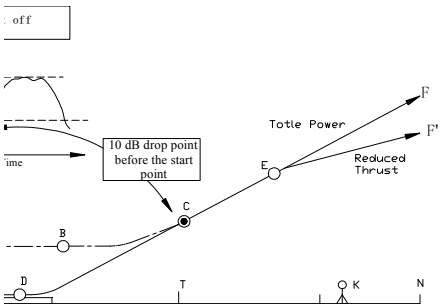

Fig.2 Cut-in Flight Procedure

Then we fit the data into the NPD curve with Matlab, the noise level calculated with NPD data interpolation method is the reference noise level, it is available only for infinitely long flight path with constant power under the ideal conditions. The corrections of influence factors in the actual environment are necessary aiming at the finite length path which is concerned in the noise certification, such as non reference velocity, engine mounting influence (lateral), the sideline attenuation. Furthermore, the noise NPD database is established.

The correction of static data and the calculation of effective perceived noise level

Map the static testing data to the sound pressure level which is corresponded to twenty-four a third octave center frequency. There are many factors to be modified while mapping these data from static to flight status. Here we mainly considerated are as followed: the correction of mobile noise resource, the correction of outside airplane structure, the correction of noise influenced by wind speed and the sound attenuation.

The appendix 16 in ICAO mentions that the essential element of noise qualified approval criteria is the measurement standard of noise assessment which is called effective perceived noise level and is unit of dB. EPNL is a numerical evaluation of the human subjective influence of airplane noise, which is composed of instantaneous perceived noise level which has been modified by the frequency spectrum irregular correction and sustaining time correction. In order to determine the value of EPNL, it is required to calculate the instantaneous sound pressure level in twenty-four a third octave every 0.5 second in the process of airplane noise testing. Then induce the effective perceived noise level (i.e. EPNL) to evaluate human's subjective reaction with all the noise physical quantities. There are five following steps [3]:

a) Convert the sound pressure level of twenty-four a third octave into the perceive noise values referring to the sonar table and combine these noise values into instantaneous perceived noise level named as PNL(k);

b) Calculate the pure tone correction named as C (k) for every frequency spectrum;

c) Add the pure tone correction to the perceived noise level and will gain the pure tone perceived noise level named as PNLT (k) in every half a second increment.

$$\mathrm{PNLT}(k) = \mathrm{PNL}(K) + \mathrm{C}(k)$$

Then induce the instantaneous value of pure tone correction perceive noise level and determine the maximum value named as PNLTM.

d) Through integrating of pure tone correction perceive noise level and time relation curve we can compute the sustaining time correction called D;

e) Algebra add the maximum pure tone perceived noise level to the sustaining time correction and gain the effective perceived noise level named as EPNL, namely

$$\mathrm{EPNL} = \mathrm{PNLTM} + \mathrm{D}$$

The Verification of Computing Result

Compared the computing effective perceived noise level with the NPD database in corresponding airplane's type, compute the error and portray the noise stringent curve and finally verify its accuracy.

The System of Noise Prediction

Introduction to Prediction System

The system of noise prediction is based on the software platform of SQL Server2008 and visual C++2010 in visual C++2010 compiling environment where the routine at the front desk is compiled with Frame MFC and the backend database is built with SQL Server 2008. The system consists of user management module, data management module, core calculation module, airworthiness assessment module and evaluation result output module and so on.

The exploit steps of the static testing prediction system are as follow:

1) Establishing the NPD database and the static testing database with the SQL platform;
2) Compiling the main structure of the software with visual C++2010 language;
3) Establishing the interface to input the initial condition data of static testing and compiling the procedure code of modifying factors algorithm;
4) Establishing the link with the static testing database and compiling the procedure code of calculation and display;
5) Deriving the modified data;

Read-in data through the software of calculating EPNL and you will get the corresponding EPNL value. Comparing the value with the original database and there is a difference value named Δ. Add the obtained value to the difference value is the NPD value of the derived airplane.

Static prediction calculation example

This example is based on static data engine test data obtained from measurement and aircraft company to predict aircraft approach noise level. Use of the noise prediction system described in this paper is demonstrated as follows:

Enter the user name and password, login noise prediction system.

NPD database calls and static data correction.

First of all, import previous NPD data into NPD database. For example, the 3JT8D engine EPNL is 100.7dB under the condition of distance 630 and the thrust of 3000.

Input Maher number, engine number, the aircraft flight data approved, reference wind speed, temperature, humidity, maximum take-off weight parameters into the reference parameter input interface. The system will correct the parameters of the static test data and the reference data mainly considering the correction of noise source mobile, correction of the shape and structure of aircraft, correction of noise with the wind speed and noise attenuation. It can respectively get the modified value of noise source mobile is 25.739dB, airframe noise correction value is -30.103dB, shape correction is 4.771dB, geometric divergence attenuation calculated is -8.519dB, also can calculate the attenuation caused by atmospheric absorption.

Fig.3 Reference Parameters Input

3) Calculation the EPNL by the revised data.

Prediction software can calculate the effective perceived noise values in different stages of the aircraft take-off, approach, lateral, and intuitively output the parameters in the calculate process, such as instantaneous perceived noise level PNL (k), the maximum value of PNLTM, as shown in Figure 5, figure 6. The predicted value is finally evaluated according to the noise strictly curve, as shown in figure 7.

The calculated EPNL of prototype airplane is 96.990dB, EPNL of derivative aircraft is 97.758dB. According to the formula:

$$\mathrm{NPD}_{\mathrm{Modification}} = \Delta\mathrm{EPNL}_{\mathrm{Prototype}} + \mathrm{EPNL}_{\mathrm{Modification}}$$

Substituting the data available:

$$NPD_{Modification} = (100.7\mathrm{dB}-96.990\mathrm{dB})+97.758\mathrm{dB}=101.468\mathrm{dB}$$

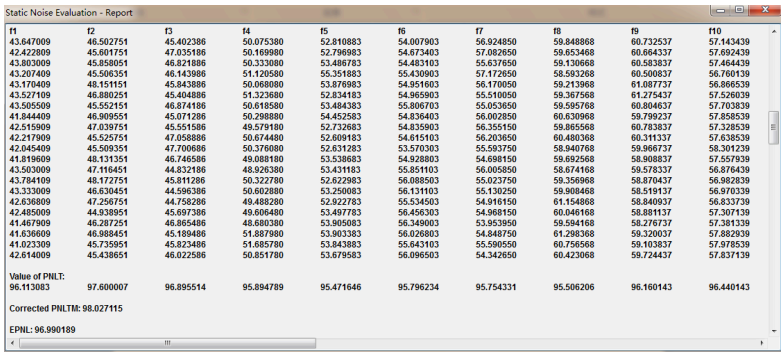

Fig.4 Prototype Engine Three Octave Sound Pressure Level after Correction

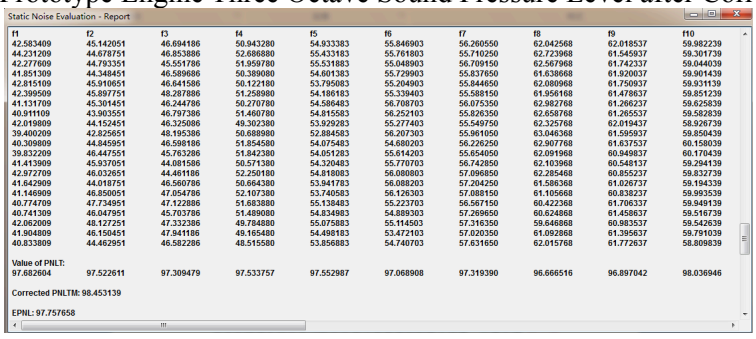

Fig.5 Derivative Engine Three Octave Sound Pressure Level after Correction

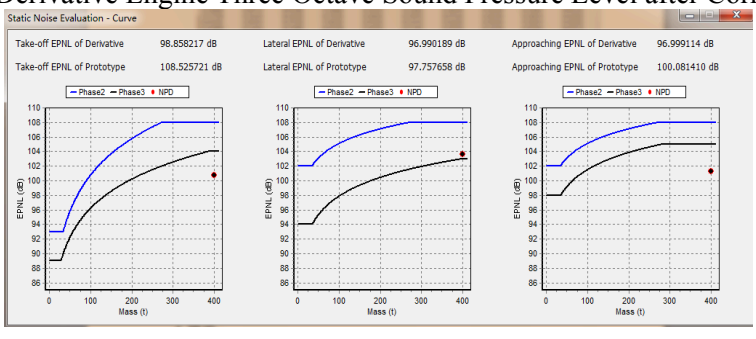

Fig.6 Prototype and Derivative Flight Effective Perceived Noise Level EPNL

There is a slight error between the real value 98.7dB and the calculation value, because the correction factors are not considered in the prediction system development process. But it's less than 3 dB and in the standard allowable range [4]. According to prototype the NPD data extrapolation noise to the examination and approval of qualified stipulated in the distance, under the thrust of feeling noise effectively, and according to the requirements of aircraft noise certification assessment, so as to provide a basis for validation of aircraft noise airworthiness.

Conclusions

Static prediction system introduced in this paper is of high speed, large capacity, saving features high accuracy, which can effectively reduce the redundant computation in the noise airworthiness certification process, improve accuracy and reduce the error, simplify noise airworthiness certification program and greatly reduce the derived type machine's noise certification costs. At present, the development of China civil aviation industry is in the key period. As well as a pioneering attempt in the domestic and the results also show that the attempt is successful.

References

[1] ICAO Environmental Technical Manual on the Use of Procedures in the Noise Certification of Aircraft[S], 2000.

[2] Decree No.182nd of the General Administration of civil aviation, aircraft airworthiness certification model and noise regulations[S]. Beijing: the Civil Aviation Administration of China, 2007.

[3] ICAO. Environmental Protection Annex 16 Volume 1[S]. 1993.

[4] ICAO. Environmental Technical Manual On The Use Of Procedures In The Noise Certification Of Aircraft[S]. Third Edition, 2004

Advanced Materials Research Vols. 989-994 (2014) pp 3204-3207
© (2014) Trans Tech Publications, Switzerland
doi:10.4028/www.scientific.net/AMR.989-994.3204

Separating the Time Field Signal of Rotor Unbalance Vibration Based on EMD Method

Shihai Zhang[1, a], Xiongwen Guo[2, b], Zimiao Zhang[1, c]

[1]College of Mechanical Engineering, Tianjin University of Technology and Education, Tianjin 300222, China

[2]Han Steel of Hebei Iron and Steel Group, Hebei, 056015, China

email: [a]4haizhang@163.com, [b]hmhl89@163.com, [c]zzm19850126@yahoo.com.cn

Keywords: Unbalance Vibration; EMD; Time Field; Signal Separation

Abstract. It is the premise conditions of dynamic balance monitoring and control technology that the unbalance vibration signal is separated accurately. Based on the theory analysis of EMD (Empirical Mode Decomposition), the time field method of unbalance vibration signal separation is proposed. The basic principle is that the reference signal and radial vibration of rotor must be simultaneously measured, and then the IMF(Intrinsic Mode Function) components are separated based on the EMD method. The time field signal of unbalance vibration can be identified by comparing the IMF's frequency with rotational frequency. The method effectiveness has been proved by experimental data analysis.

Introduction

The unbalance is one of the key problems which limit the machinery industry development. In order to solve the unbalance problems, the unbalance vibration signal must be separated accurately. Usually, many harmonic components are hidden in the rotor vibration signal, and some special reasons are directly related with those harmonic components, however the unbalance vibration component is only related with rotating frequency. Based on the principle, the relative studies are concentrated on signal filtering and noise reduction based on FFT method. The practice shows that the frequency and phase error of the separated signal are large based on frequency field analysis method. The EMD is driven by data itself and belongs to the time field method. The advantage of EMD is obvious when it applied to analyze the nonlinear and nonstationary signal [2]. The unbalance vibration signal separation method based on EMD is discussed in the paper.

The theory of EMD

The EMD method was firstly proposed by Norden E. Huang in 1998 [3], and the essence of EMD is to decompose adaptively signal. A series of IMF are supposed at first, and the IMF must meet two basic conditions: (1) On whole data series, the difference between extreme points and zero-crossing points must be zero or one point. (2) The mean of envelope curve, which formed by local maxima and local minimum, is zero at any time points. Based on the assumption, any signal can be decomposed to many IMF components, and the decomposition steps of EMD are as follows [3]:

(1) All the maximum points of signal X (T) must be found firstly, and then the upper envelope curve of original data sequence can be interpolated by spline function and denoted as $m_u(t)$.

(2) All the minimum points of signal X (T) are found secondly, and then the lower envelope curve of original data sequence can be interpolated by spline function and denoted as $m_u(t)$.

(3) The average envelope curve can be obtained by the mean of upper and lower envelope curve and denoted as $m_1(t)$. The equation can be expressed as follow:

$$m_1(t) = \sum_{i=1}^{n} [m_u(i) + m_d(i)] / 2 \qquad (1)$$

In the equation 1, n is the data length. The new data series $h_1(t)$ can be obtained by subtracting the average envelope curve $m_1(t)$ from original data series X(t). The equation is expressed as follow:

$$h_1(t) = X(t) - m_1(t) \quad (2)$$

The data series $h_1(t)$ is the first IMF component if it satisfies the IMF conditions.

(4) Otherwise, we can take $h_1(t)$ as the initial data and calculate the new average curve $m_{11}(t)$ by repeating step1~3, and then the new data series $h_{11}(t)$ can be calculated by $h_{11}(t)=h_1(t)-m_{11}(t)$. If $h_{11}(t)$ doesn't satisfy IMF conditions, we can repeat the above steps for k times until the data series $h_{1k}(t)$ satisfies IMF conditions, and the $h_{1k}(t)$ is calculated by $h_{1k}(t)=h_{1k}(t)-m_{1k}(t)$. Now we record $h_{1k}(t)$ as $C_1(t)$ and take $C_1(t)$ as the first IMF component of X(t).

The whole disposition process is just like a sieve, and the finest IMF component can be decomposed through this sieve step by step. In order to make sure the amplitudes and frequencies of these IMF components have some definite physical meanings. The appropriate stopping criterion is essential to limit screening time. The criterion of simulating Cauchy convergence was provided by Huang etc in which the standard deviation (SD) of mode component $h_{lk}(t)$ and $h_{l(k+1)}(t)$ could be calculated and the definition of SD is as following [3]:

$$SD = \sum_{t=0}^{T} \left[\frac{\left| h_{1k}(t) - h_{1(k+1)}(t) \right|^2}{h_{1k}^2} \right] \angle \varepsilon \quad (3)$$

In the equation 3, T is the signal length. The screening process will stop when SD is less than ε, and the value of ε ranges from 0.2 to 0.3.

(5) The new data series $R_1(t)$ can be gained by subtracting $C_1(t)$ from X(t) .

$$R_1(t) = X(t) - C_1(t) \quad (4)$$

The IMF component $C_2(t)$ will be decomposed by taking $R_1(t)$ as the initial data and repeating steps 1~4. Repeat the above steps p times until no IMF component can be separated. The p components and remains E_p of the initial signal X(t) will be discomposed, and then signal X(t) can be showed as:

$$X(t) = \sum_{i=1}^{p} C_i(t) + E_m \quad (5)$$

It can be seen from above dispose progress, the nonlinear and nonstationary signal can be decomposed to linear and stationary data series based on EMD method. The IMF component, including only one frequency component, can be applied to identify the unbalance vibration signal.

The unbalance vibration signal separation for rotor based on EMD method

In theory, the unbalance vibration frequency equal to rotating frequency. The EMD principle indicates that it is driven by data itself and the most refined component can be separated. Therefore, the unbalance vibration signal of rotor can be separated by combining EMD method with the rotating frequency. In addition, in order to obtain the phase of unbalance vibration signal, the reference signal and radial vibration signal of rotor must be collected synchronously. The application step of the method is as follows:

Firstly, the original vibration signal should be decomposed by EMD method, and all the IMF components of the signal are separated.

Secondly, the frequency feature of each IMF components is analyzed, and then the unbalance vibration component is identified by comparing with rotating frequency.

Thirdly, considering of end effect，the middle and no contamination part of the IMF data series are intercepted as the effective data[4].

In order to test the validity of method, the monitoring signal from rotor vibration experiment is analyzed in the paper. The vibration signal and reference signal are shown as figure 1. The testing speed is 1800 r/min, the sampling frequency is 10 kHz, the sampling length is 9000 points.

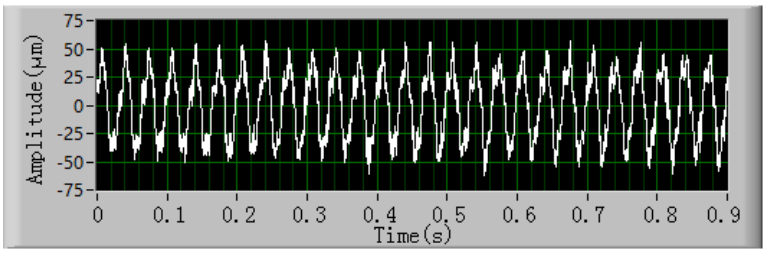

(a) the vibration signal of rotor

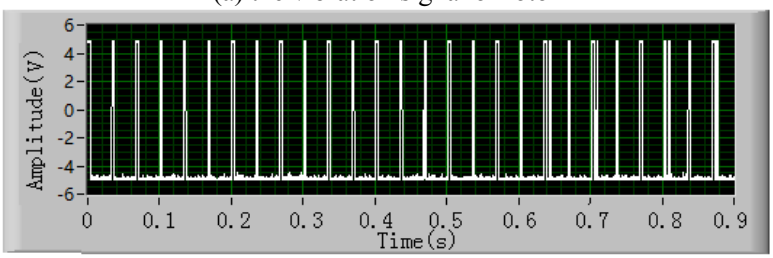

(b) the reference signal of rotor

Figure 1. The monitoring signal of rotor

The IMF components of vibration signal in figure 1(a) can be decomposed based EMD method, and then the power spectrum of each IMF component is estimated. For example, the IMF5 to IMF8 and their power spectrums are shown as figure 2. In figure 2, the data series from 1000 to 5000 of IMF component is displayed.

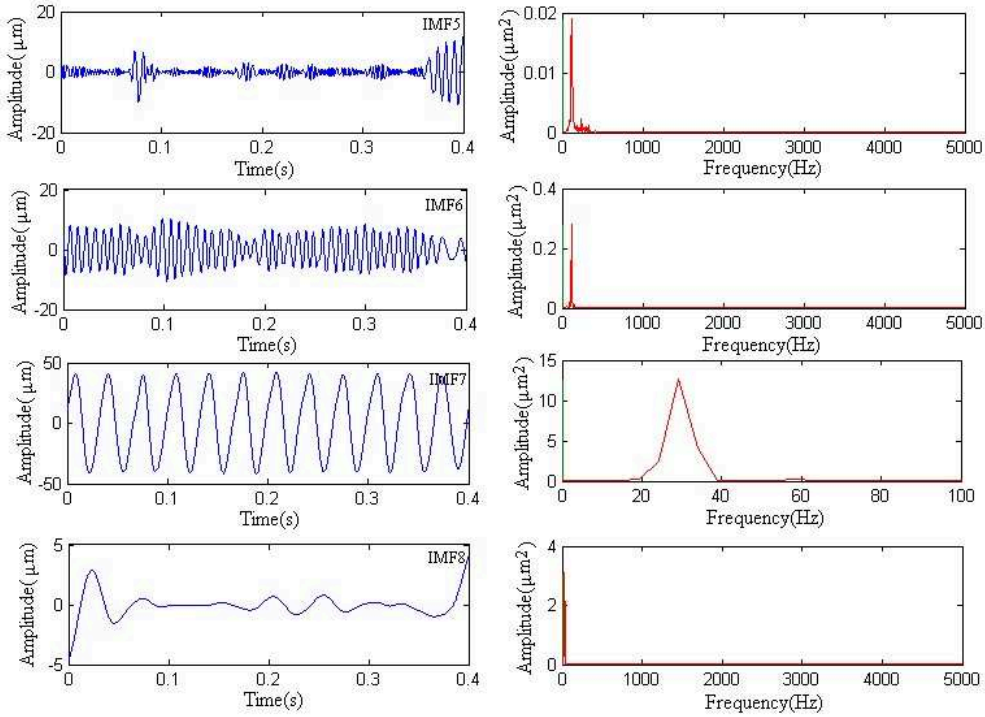

Figure 2. The IMF components and their power spectrum

It can be seen from figure 2, the frequency of IMF7 is about 30Hz (equal to rotating frequency). So the IMF7 can be taken as the time field signal of rotor unbalance vibration. The IMF7 and corresponding reference signal are shown as figure 3.

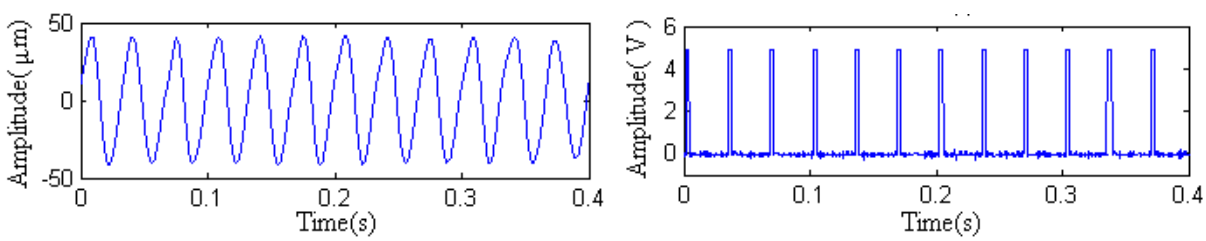

(a) The unbalance vibration signal (b) The reference signal

Figure 3. The unbalance vibration and its reference signal

The amplitude of unbalance vibration signal can be obtained from figure 3(a) as 41.62μm. Meanwhile, the phase of unbalance vibration signal can be obtained by analyzing the discrete data series of figure 3. The method is as: the position corresponding to the first positive peak value in figure 3(a) is found as N1 (=97), and then the position corresponding to the first pulse rising time figure 3(b) is found as N2(=5). Combined with sampling frequency (denoted by sf) and rotating frequency (denoted by sf) message, the phase of unbalance vibration signal can be calculated as follow equation.

$$\alpha = \frac{N2 - N1}{sf / rf} \times 360^o = \frac{5 - 97}{1000/3} \times 360^o = -99.36^o$$

In order to test the accuracy of the separated signal, the sine function is constructed by the rotating frequency (30 Hz) and unbalance vibration vector($41.60\angle -99.36^o$), and then the residual signal can be obtained as figure 4 shows by subtracting the sine function from the original signal in figure 1(a).

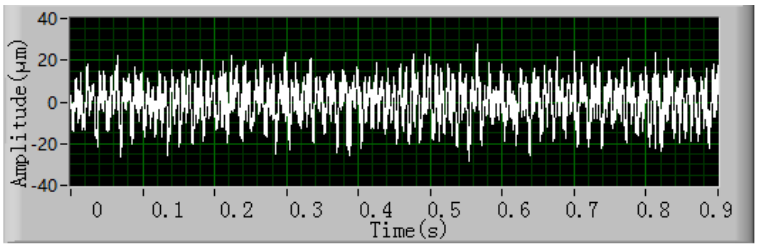

Figure 4. The residual vibration signal

It can be seen from figure 4, the amplitude of the residual vibration signal is decreased obviously, and the periodicity of the signal is not obvious. It proves that the unbalance vibration component in rotor original vibration signal has been eliminated, and the EMD method is effective for the rotor unbalance vibration signal separating.

Conclusion

Based on EMD principle, the method for rotor unbalance vibration signal separating is proposed in the paper. The experimental data analysis indicates the separating accuracy is high, and the amplitude and phase message can be obtained based on the time field signal analysis. The method can be applied in the rotor unbalance vibration condition monitor and the dynamic balance field.

Acknowledgement

The paper supported by the science foundation of Tianjin University of Technology and Education (NO. KYQD12018).

References

[1] Li Xin, Luo Xueke, Zhang Chaoying. Development of an Expert System Based on Fault Diagnosis of Rota ting Machinery Experiment. Equipment Manufacturing Technology. 2009(2):108-111

[2] ShiPeiming, LiGeng, HanDongying.Study on Coupling Faults of Rotary Machinery Diagnosis Method Based on Improved EMD. China Mechanical Engineering. 2013(24):2367-2372

[3] Huang N.E, etal. The empirical mode decomposition and the Hilbert spectrum for nonlinear and non-stationary time series analysis. Proc.R.Soc.Lond.A.1998(454):903-995

[4] Qi Keyu, Shi Kunlin, Huo Pengfei, He Zhengjia. EMD Boundary Processing Method and Its Application to Friction Fault Diagnosis of Rotor System. Journal of Vibration, Measurement &Diagnosis. 2010(30): 492-592

Advanced Materials Research Vols. 989-994 (2014) pp 3208-3211
© (2014) Trans Tech Publications, Switzerland
doi:10.4028/www.scientific.net/AMR.989-994.3208

Application of Rapid Prototyping Technology in Product Design

Dantong LI[a], Zheng ZHANG, Jiawen Deng, Mingyu HUANG[b],
Xiaofeng Wan, Hongjun NI

School of Mechanical Engineering, Nantong University, Nantong 226019, China

[a]ldthh@163.com, [b]huang.my@ntu.edu.cn

Keywords: Rapid prototyping; Product development; Optimization design

Abstract. The rapid prototyping technology was introduced, including its definition, principle and characteristics. The advantages of rapid prototyping technology in new product development were analyzed. Application of rapid prototyping technology in design of mechanical parts, industrial model, medical model, ceramic products, automobile model and products based on ergonomics was discussed. The feasibility of rapid prototyping technology in product design and the optimization direction was prospected.

Introduction

Rapid Prototyping (RP) technology is developing in recent years as a new manufacturing technique. It is a major breakthrough in the field of manufacturing technology in recent years. Rapid Prototyping technology can meet the needs of the modern manufacturing technology development, because of its fast developed in the manufacturing industry, biological engineering, etc[1]. At present, RP technology has got the attention of the industry, especially in household appliances, automobiles, toys, light industrial products, building models, medical devices and artificial organs, spacecrafts, military equipments, archaeology, industrial manufacturing, sculptures, film production, and engaged in CAD department, and many good application cases have been made [2,3].

In product design, test analysis and performance evaluation of the product design were carried out based on rapid prototyping, which can shorten product development cycle and reduce design cost. After years of development, Rapid Prototyping technology is not limited to the original sense of the concept "prototype", it has fast developing toward rapid parts, rapid tools, etc. The research in product optimization design based on Rapid Prototyping, however, has not developed yet. In this paper, application of rapid prototyping in the product design was discussed, and research direction of Rapid Prototyping technology in product optimization design was prospected.

Rapid prototyping technology

Rapid prototyping technology involves the CAD, CAM, CNC, precision servo drive, optoelectronics, and new materials technology, etc. According to the structure of product 3D CAD model, layered slices and outline of each section was obtained. According to the outline, selective laser jets, solidifying liquid resin (or cutting layers of paper, or sintering powder material layers), or the injection source selectively spraying layers of binder or hot melt material, form the cross section, gradually accumulating into a 3D product.

Compared with the traditional processing methods (removing material and deformation method), the processing method of rapid prototyping technology is the material accumulation method, rapid prototyping processing principle is shown in fig. 1.

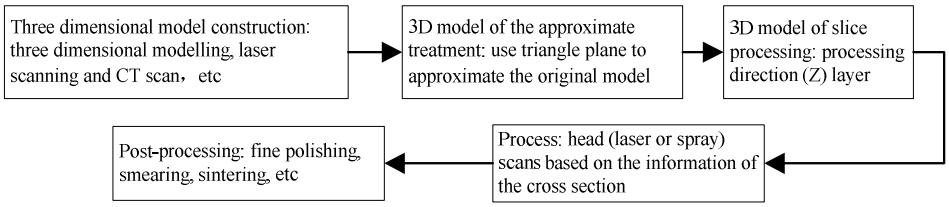

Fig.1 Rapid prototyping processing principle

The advantages of rapid prototyping in product design

Rapid prototyping processing principle and the traditional processing principle are different. The differences are shown in table 1.

Table 1 Difference between rapid prototyping processing and traditional processing

	Traditional processing	Rapid prototyping processing
material	Most metal, less metal plate and plastic	ABS, PMMA, wood, gypsum, etc
production cycle	2-4 months, sometimes even six months	only 2 to 7 days from the CAD model to the entity
Processing cost	High cost, mass production cost will reduce accordingly	Processing cost has nothing to do with bulk
Parts shape	Not too complex	Can produce complex parts

Product design method using rapid prototyping technology has following advantages [4]:

1）Functional test and evaluation

Although the assembly problem can be solved in the design software and analysis software, such as ANSYS, but it still can't meet the function verification and design requirements. Therefore, it needs rapid prototyping manufacturing samples to do functional test.

2）Eliminate the problem before manufacture mould

Samples are made by rapid prototyping technology first, the errors can be found, avoiding unnecessary loss.

3) Shorten product design time

Design and manufacture can be synchronized. Designers can design and modify the design at the same time, so the design can be completed soon.

Application of rapid prototyping technology in product design

Mechanical parts design

Parts manufactured by rapid prototyping technology can be assembled with other parts, in this way assembly validation and function test were done, which can examine the rationality of the design. Liu W D [5] made clamp by rapid prototyping technology and assembly, the final result satisfies the requirement of enterprise.

Medical model and prosthetic design

Rapid prototyping is applied to the teeth planting technology, product model was completed in CAD software, then the product entity was obtained by rapid prototyping for functional verification [6,7].

The innovation design of product design based on ergonomics

Rapid prototyping technology was used to validate the rationality and comfortable degree of product. As shown in fig.2 is product innovation design process based on rapid prototyping technology. ZHANG T H[8] innovation design of the atomizer box considering the ergonomics about the human body characteristics. With the rapid prototype samples, the design cycle was shortened, and the speed of spray products innovation design was accelerated.

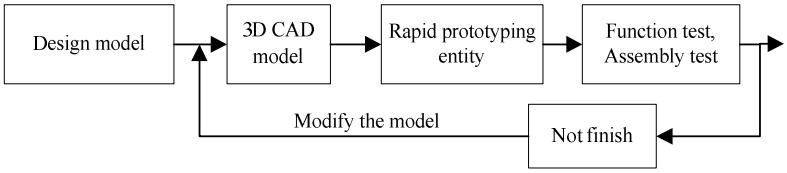

Fig.2 Product innovation design process based on rapid prototyping technology

The design of industrial design model

At present in China, industrial design model making teaching mainly is based on manual models, there are some limitations, such as the production cycle is long, it is difficult to achieve the complex appearance, etc[9].Using rapid prototyping technology can fast and truly show three-dimensional shape of model , shortening the cycle of model making, reflect the feasibility of the design idea , find problems as early as possible. A wheel model based on RP technology is shown in fig.3.

Fig.3 A wheel model based on RP technology

Fig.4 Cellular ceramics produced by rapid prototyping

Ceramic products design

Xu L Q [10] scanned purple clay teapots by using laser scanning technology. and handled data by using Geomagic software. Entity was manufactured by 3D printing technology and the design was optimized, Alberto Ortona[11] use selective laser curing to product honeycomb structure ceramic, he applied the method of 3D design combined with rapid prototyping technology, overcoming the limit of surface finish. Cellular ceramics produced by rapid prototyping is shown in fig.4.

Automobile modeling design

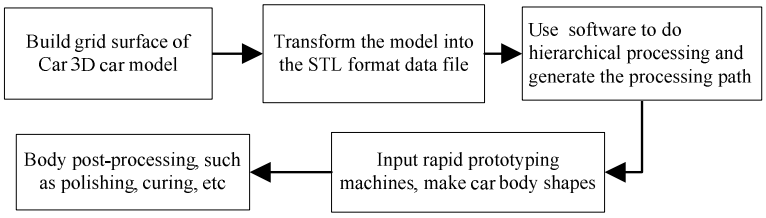

Fig.5 Rapid prototyping process of model car

For car body design process, the design method based on rapid prototyping technology can become a fast design method is suitable for China's national conditions. For the design of the automobile modeling, physical model is indispensable, because any car modeling approver could not only according to the pictures and the screen to examine and approval of modeling, They must see 1:1 entity model, domestic use the clay model, but the clay model is expensive. Rapid prototyping process of model car is shown in fig.5.

Conclusions

Rapid prototyping technology provides designers with intuitive, reliable reference model, ensuring the rationality of the design. Design method based on rapid prototyping technology will be a new design method, and it has obvious advantages and provids new ideas and new method for the product development and optimization.

Acknowledgements

This work was supported by Jiangsu province Science and Technology Plan Project (BK20130391),(BY2013042-04),Nantong Science and Technology Plan Project (BK2013029) and Project Funded by the Graduate Workstation of Jiangsu Enterprises. Corresponding author: Tel: +8613813720032; E-mail address: huang.my@ntu.edu.cn (Mingyu Huang).

References

[1] YAN Y, LI SH J,ZHANG R J, etc. Rapid prototyping and manufacturing technology: principle, representative, technics, application, and development trends[J].Tsinghua Science and Technology, 2009,14:1-12.

[2] JIN J, ZHANG An Y. Rapid prototyping technologies and their application[J].Journal of Zhejiang University of Technology,2005,33(5):592-595.

[3] Thomas B, Mieke V, Jorg S,etc. A review of trends and limitations in hydrogel-rapid prototyping for tissue engineering[J]. Biomaterials, 2012(33):6020-6041.

[4] LIU X H. Development of Rapid Prototyping Technology[J].Agricultural Equipment & Vehicle Engineering,2008(2):10-13.

[5] LIU W D,LIU J X,LIU M ZH. The Application of Rapid Prototyping to Exploit of Clincher[J]. Informatization of Manufacturing Industry,2005(3):65-67.

[6] G Q Jin, W D Li, L Gao. An adaptive process planning approach of rapid prototyping and manufacturing[J]. Robotics and Computer-Integrated Manufacturing, 2013(29):23–38.

[7] Vaibhav B, Shirish D, Darshana D, etc. Use of rapid prototyping and three-dimensional reconstruction modeling in the management of complex fractures[J]. European Journal of Radiology,2011(80):814– 820.

[8] ZHANG T H, ZHANG X,XU R P,etc. Innovative Design of atomizer box based on rapid prototyping[J].Development & Innovation of Machinery & Electrical Products, 2007,20(6): 16-17.

[9] QIAN S L,WAN F C. Exploration Application of Rapid prototyping technology in modern industrial design model performance[J].Guangxi Journal of Light Industry,2011(5):50-52.

[10] Xu L Q. Application of Rapid Prototyping Technology in Ceramic Industry[J]. Jiangsu Ceramics, 2009,42(5):23-24.

[11] Alberto O, Claudio D, Sandro G, etc.Cellular ceramics produced by rapid prototyping and replication[J]. Materials Letters 80 (2012) 95–98.

Advanced Materials Research Vols. 989-994 (2014) pp 3212-3215
© (2014) Trans Tech Publications, Switzerland
doi:10.4028/www.scientific.net/AMR.989-994.3212

AHP Effectiveness Evaluation of Electronic Warfare Command And Control System Under Complex Electromagnetic Environment

Guo-sheng Wang[1, 2, a] and Zong-feng QI [1,b]

[1]The State Key Laboratory of Complex Electromagnetic Environment Effects on Electronics and Information System (CEMEE), Luoyang, 471003, China

[2] Department of Control Engineering, Academy of Armored Forces Engineering, Beijing 100072, China

[a] gswang@126.com, [b] xanadu_0402@163.com

Keywords: Electronic warfare command and control system, Complex electromagnetic environment, Effectiveness evaluation, AHP

Abstract. The effectiveness evaluation problem of electronic warfare command and control system (EWCCS) under complex electromagnetic environment is investigated by using the analytic hierarchy process (AHP) method. First, the evaluation hierarchy structures of EWCCS under complex electromagnetic environment are put forward and can be classified into target hierarchy, rule hierarchy and scheme hierarchy. Then, the AHP Algorithm is given as a preliminary knowledge to evaluate the effectiveness evaluation of EWCCS under complex electromagnetic environment. Finally, an effectiveness evaluation example of EWCCS under complex electromagnetic environment is considered by using AHP Algorithm.

Introduction

The electronic warfare equipments are important in modern information battles. With the development of the computer technology, the electronic warfare equipments become more and more complex, pregnable and damageable such that it is difficult to evaluate the performance and effectiveness of the electronic warfare equipments. Fuzzy-AHP in evaluation of ECM command effectiveness is investigated to calculate the influence degree of each ingredient and evaluate the ECM command effectiveness in [1]. According to its characteristics of insufficient information and uncertainty, the EW system operation effectiveness is evaluated by using the method of grey hierarchy evaluation in [2]. The effectiveness of instructed EW system is calculated by using analytic hierarchy process, the weighted coefficient of each guideline is defined, and the effectiveness of instructed EW system is calculated in [3]. An effectiveness evaluation index system of airborne ECM system is built, which can reflect the airborne ECM system capacity generally and impersonally in [4]. With the adoption of the grey system theory and the analytic hierarchy process (AHP), the evaluation model of the reconnaissance capabilities of the ECM reconnaissance troops based on the multilevel grey theory is created in [5].

Evaluation Hierarchy Structures of EWCCS Under Complex Electromagnetic Environment

According to the features of EWCCS under complex electromagnetic environment, many factors which are related with the performances of EWCCS under complex electromagnetic environment can be found out and can be classified into target hierarchy, rule hierarchy and scheme hierarchy.

The target hierarchy or the first hierarchy for effectiveness evaluation of EWCCS under complex electromagnetic environment can be denoted by A. The rule hierarchy of EWCCS under complex electromagnetic environment includes scouting and detecting ability B1, command and control ability B2, communicating and safeguarding ability B3, and battlefield electromagnetism environment B4. The hierarchy structure between the target hierarchy and the rule hierarchy can be shown in Figure 1.

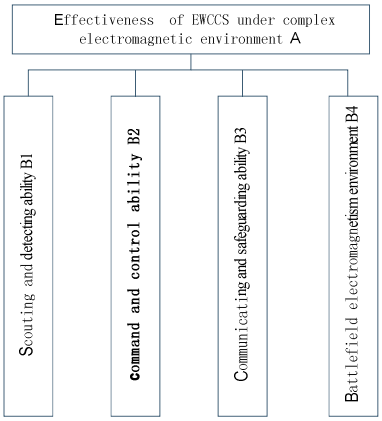

Fig. 1 The hierarchy structure between the target hierarchy and the rule hierarchy

The secondary hierarchy or rule hierarchy of B1 includes scouting and detecting method C11, scouting and detecting range C12, target density C13, probability of detecting target C14, alerting probability of C15, false-alarm probability of C16 and ability of identifying target C17. The hierarchy structure between the target hierarchy B1 and its scheme hierarchy can be shown in Figure 2.

The scheme hierarchy of B2 include ability of auxiliary decision C21, decision delay C22, ability of scientific decision C23, ability of threat judgment C24, campaign range C25, command scale C26, commanders' capability C27, and ability of weapon control C28. The hierarchy structure between the target hierarchy B2 and its scheme hierarchy can be shown in Figure 3.

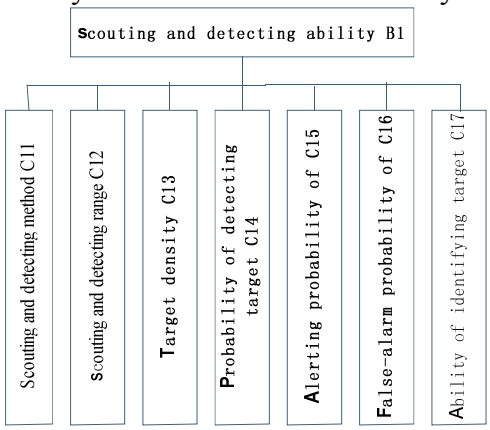

Fig. 2 The target hierarchy structure of B1

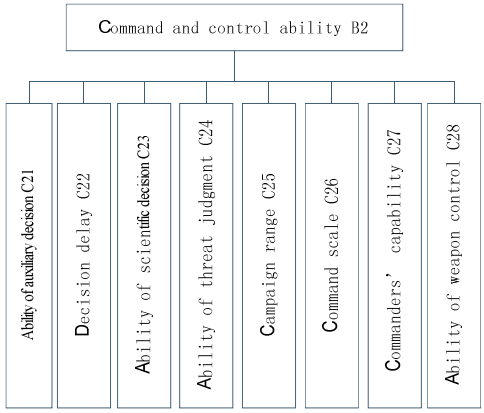

Fig. 3 The target hierarchy structure of B2

The scheme hierarchy of B3 include covering range C31, communicating capacity C32, operation types C33, miscode rate C34, communicating delay time C35, secrecy ability C36 and interlinkage ability C37. The hierarchy structure between the target hierarchy B3 and its scheme hierarchy can be shown in Figure 4.

The hierarchy structure of B4 includes quality of electromagnetism radiant point C41,density of electromagnetism signal C42,intensity of geomagnetism signal C43,parameters of geomagnetism signal C44. The hierarchy structure between the target hierarchy B4 and its scheme hierarchy can be shown in Figure 5.

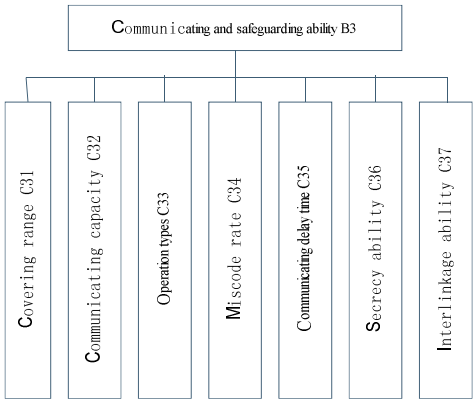

Fig. 4 The target hierarchy structure of B3

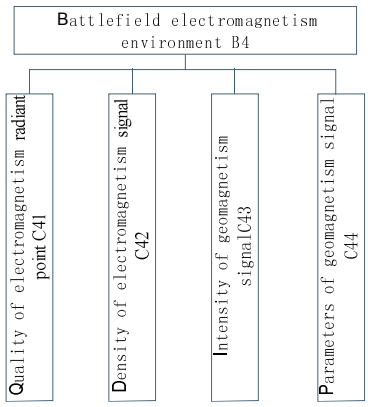

Fig. 5 The target hierarchy structure of B4

A Numerical Example for Effectiveness Evaluation of EWCCS under Complex Electromagnetic Environment

Based on the AHP method, many generalized AHP methods and their applications are studied in [6, 7]. Assume that the experts give the relative importance of the criteria in the pair-wise judgment matrices of the EWS under complex electromagnetic environment. The corresponding pair-wise judgment matrix among complex electromagnetic environment include B1, B2, B3 and B4 can be given by the following table 1.

Table 1. The pair-wise judgment matrix among B1, B2, B3 and B4

A	B1	B2	B3	B4	W
B1	1	5	3	7	0.553
B2	0.2	1	0.3333	5	0.1313
B3	0.3333	3	1	6	0.2704
B4	0.1429	0.2	0.1667	1	0.0454
$\lambda_{max} = 4.2359$		$C.I. = 0.0786$		$C.R. = 0.0883 < 0.1$	

The corresponding pair-wise judgment matrix between C11, C12, C13, C14, C15, C16 and C17 in scouting and detecting ability B1 can be given by Table 2.

Table 2. The pair-wise judgment matrix among C11, C12, …, and C17

B1	C11	C12	C13	C14	C15	C16	C17	W
C11	1	0.5	0.5	1	6	3	4	0.1601
C12	2	1	1	2	9	4	3	0.252
C13	2	1	1	3	9	6	7	0.3194
C14	1	0.5	0.3333	1	5	2	2	0.1258
C15	0.1667	0.1111	0.1111	0.2	1	0.5	3	0.0369
C16	0.3333	0.25	0.1667	0.5	2	1	4	0.0701
C17	0.25	0.3333	0.1429	0.5	0.3333	0.25	1	0.0357
$\lambda_{max} = 7.5238$			$C.I. = 0.0873$			$C.R. = 0.0642 < 0.1$		

The corresponding pair-wise judgment matrix between C21, C22, C23, C24, C25, C26, C27, and C28 in command and control ability B2 can be given by can be given by Table3.

Table 3. The pair-wise judgment matrix among C21, C22, …, and C28

B2	C21	C22	C23	C24	C25	C26	C27	C28	W
C21	1	0.3333	1	3	1	4	4	4	0.1596
C22	3	1	3	5	3	6	6	6	0.343
C23	1	0.3333	1	3	1	4	4	4	0.1596
C24	0.3333	0.2	0.3333	1	0.3333	2	2	2	0.0666
C25	1	0.3333	1	3	1	4	2	3	0.1412
C26	0.25	0.1667	0.25	0.5	0.25	1	1	5	0.0506
C27	0.25	0.1667	0.25	0.5	0.5	1	1	0.3333	0.0393
C28	0.25	0.1667	0.25	0.5	0.3333	0.2	3	1	0.0402
$\lambda_{max} = 8.654$			$C.I. = 0.0934$				$C.R. = 0.0663 < 0.1$		

The corresponding pair-wise judgment matrix between C31, C32, C33, C34, C35, C36 and C37 in communicating and safeguarding ability B3 can be given by Table 4.

Table 4. The pair-wise judgment matrix among C31, C32, …, and C37

B3	C31	C32	C33	C34	C35	C36	C37	W
C31	1	2	3	4	7	5	2	0.326
C32	0.5	1	3	2	5	7	4	0.2674
C33	0.3333	0.3333	1	0.5	1	3	2	0.0964
C34	0.25	0.5	2	1	1	3	2	0.1196
C35	0.1429	0.2	1	1	1	2	3	0.0877
C36	0.2	0.1429	0.3333	0.3333	0.5	1	2	0.0496
C37	0.5	0.25	0.5	0.5	0.3333	0.5	1	0.0532
$\lambda_{max} = 7.6113$			$C.I. = 0.1019$			$C.R. = 0.0749 < 0.1$		

The corresponding pair-wise judgment matrix between C41, C42,C43 and C44 in battlefield electromagnetism environment B4 can be given by Table 5.

Table 5. The pair-wise judgment matrix among C41, C42, C43 and C44

B4	C41	C42	C43	C44	W
C41	1	1	6	2	0.3769
C42	1	1	3	5	0.3985
C43	0.1667	0.3333	1	0.3333	0.0747
C44	0.5	0.2	3	1	0.1449
$\lambda_{max} = 4.2507$		$C.I. = 0.0833$		$C.R. = 0.0939 < 0.1$	

From Table 1, we can know that the weight vector of B1, B2, B3 and B4 $[0.553 \quad 0.1313 \quad 0.2704 \quad 0.0454]^T$ can be shown by Figure 1. From Figure 1, we can directly find that the sort order of the relative importance among B1, B2, B3 and B4 is "B1»B3»B2»B4", where "»" implies that the former is more important than the later. We can obtain the weight vector of the components in the scheme hierarchy as

$$W = [0.0885 \quad 0.1394 \quad 0.1766 \quad 0.0696 \quad 0.0204 \quad 0.0388 \quad 0.0198 \quad 0.0209 \quad 0.045 \quad 0.209$$
$$0.0087 \quad 0.0185 \quad 0.0066 \quad 0.0052 \quad 0.0053 \quad 0.0881 \quad 0.0723 \quad 0.0261 \quad 0.0323 \quad 0.0237$$
$$0.0134 \quad 0.0144 \quad 0.0251 \quad 0.006 \quad 0.0123 \quad 0.0021 \quad]^T$$

which is shown in Figure 7. From Figure 7, we can directly know that the sort order of the relative importance among the components in the scheme hierarchy as "C13»C12»C11»C31»C32»C14 »C22»C16»C34»C33»C41»C35»C23=C21»C15»C17»C25»C37»C36»C43»C24»C26»C42»C28»C2 7»C44".

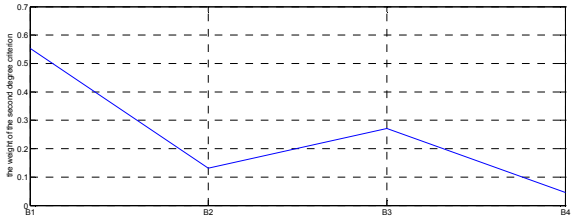

Fig. 6 Relative importance of the rule hierarchy

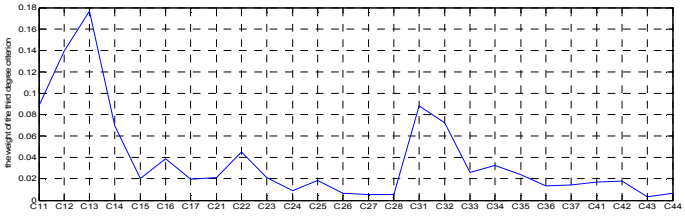

Fig. 7 Relative importance of the scheme hierarchy

Assume that the satisfactory degrees of components C13, C12, C11, C31, C32, C14, C22, C16, C34, C33, C41, C35, C23, C21, C15, C17, C25, C37, C36, C43, C24, C26, C42, C28, C27 and C44 in the scheme hierarchy are

$$R = [8 \quad 9 \quad 6 \quad 5 \quad 6 \quad 7 \quad 8 \quad 5 \quad 4 \quad 7 \quad 8 \quad 8 \quad 5 \quad 5 \quad 6 \quad 7 \quad 6 \quad 5 \quad 7 \quad 6 \quad 9 \quad 6 \quad 7 \quad 8 \quad 5 \quad 8 \quad]^T$$

Based on the above data, the effectiveness of EWCCS under complex electromagnetic environment is obtained as $U = 6.7201$ .Thus the effectiveness of the EWCCS under complex electromagnetic environment is satisfactory and distinct.

Conclusions

By using the AHP method, an effectiveness evaluation example of EWCCS under complex electromagnetic environment is considered, and the relative importance among the components in the scheme hierarchy of EWCCS under complex electromagnetic environment is proposed. In the next research, we will investigate the grey AHP method and the fuzzy AHP method to evaluate the effectiveness evaluation problem of EWCCS under complex electromagnetic environment.

Acknowledgements

This work was financially supported by the Open Project Foundation in the State Key Laboratory of CEMEE (CEMEE2014K0305B).

References

[1] R. Shi, C. J. Han and J. Huang: Fuzzy-AHP in Evaluation of ECM Command Efficiency, Command Control & Simulation, Vol. 28 (2006), p. 59

[2] H. Yu, G. X. Lu, Y. Chen and L. Zhou: Grey Hierarchy Evaluation of Operation Effectiveness of EW System, Radio Engineering, Vol. 39 (2009), p. 61

[3] G. Z. Chen, Y. F. Xue: Effectiveness Evaluation of Instructed EW System Based on AHP, Electronic Warfare, Vol. 106 (2006), P. 26

[4] Z. Y. Liu, D. F. Ping and L. Wang: Effectiveness Evaluation of Airborne ECM System Based on Grey Arrangement Model, Ship Electronic Engineering, Vol. 32 (2012), p. 68

[5] X. L. Zhu, Q. Cai and H. Z. Zhu: The Evaluation of Reconnaissance Capabilities of ECM Reconnaissance Troops Based on Multilevel Grey Theory, Radar and ECM, Vol. 32(2012), 3p.15

[6] K, C. Hing, X. J. Wang, G. R. White and N. Yip: An Extended Fuzzy-AHP Approach for the Evaluation of Green Product Designs, IEEE Transactions on Engineering Management, Vol. 60 (2013), p. 327

[7] H. Y. Tsai and Y. L. Huang: An Analytic Hierarchy Process-Based Risk Assessment Method for Wireless Networks, IEEE Transactions on Reliability, Vol. 60(2011), p. 801

Advanced Materials Research Vols. 989-994 (2014) pp 3216-3219
© (2014) Trans Tech Publications, Switzerland
doi:10.4028/www.scientific.net/AMR.989-994.3216

Design of Quadrotor's Control System Based on DSP

Qiang Lv, Pei-pei Ni, Guo-sheng Wang, Feng Liu

Department of Control Engineerin, Academy of Armored Force Engineering, Beijing 100072, China

answer9@126.com

Keywords: quadrotor; DSP; inertial measurement unit (IMU); optical flow sensor; attitude control;

Abstract. A problem of quadrotor's control system based on DSP is investigated in this paper. STMS320F28335 is used as the main processer, due to its advantages of high-speed processing capability and powerful floating point processing capability. The inertial measurement unit is selected for inner-loop attitude control, while the optical flow sensor is adopted for outer-loop attitude compensation. Infrared range finder is choosed for altitude control with PID method. Quadrotor uses XBee-Pro wireless module to contact with ground station and sends statement information in accordance with the Mavlink protocol. Test results show that the control system is reliable and can meet the requirement of the attitude control system.

Introduction

Unmanned air vehicles (UAVs) are self-propelled aerial robots. They can be equipped with various instruments and payloads, making them capable of performing various civilian or military tasks. Quadrotors are Vertical Take-Off and Landing (VTOL) four rotor helicopters with small size, light weight. Due to these characteristics, the quadrotor can operate in numerous robotic applications, for instance, search& rescue, inspection and exploration. Many scholars studied on it, proposed PID, LQR and other control algorithms according to its mathematical model, and made experimental verification in [1,2] . Cortex-M4 is adopted as the main processer and GPS is used to realize outdoor position control in [3]. A hardware system of quadrotor based on an embedded system of DSP/FPGA is designed in [4].

Texas Instruments (TI)'s DSP uses a modified Harvard architecture. It has strong data processing capabilities, rich peripherals, low power consumption, small size and cheaper than the processor which has the same performance.

Design of quadrotor's control system hardware

TMS320F28335 has 150MHz high-speed processing capability, 32-bit floating point processing unit, six DMA channels which support ADC, McBSP and EMIF, up to 18-way PWM output which has 6 unique way of higher precision PWM output, and 12-bit 16-channel ADC. Thanks to its floating-point unit, the user can quickly write control algorithms without spending too much time and effort in dealing with the fractional operation. The main processor is responsible for collecting attitude information from MTI-G high accuracy IMU, translational velocity from PX4FLOW []optical flow sensor and altitude from SHARP GP2Y0A02YK0F infrared range finder, and figuring out PWM to drive the 4 brushless motors according to the control algorithms. The control system hardware construction shows as Fig.1.

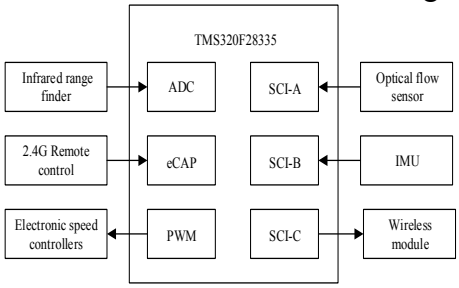

Fig. 1 Control system hardware construction

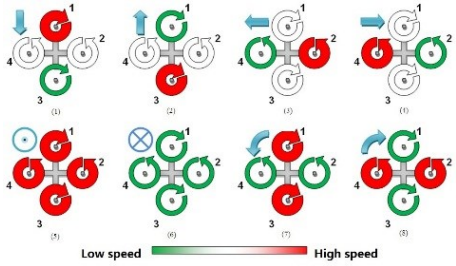

Fig. 2 Description of quadrotor motion

Attitude control's dynamic model

Quadrotor is controlled simply by changing the rotation speed of the four rotors (Fig. 2). The front and rear rotors (2, 4) rotate in a clockwise direction while the left and right rotors (1, 3) rotate in a counter-clockwise direction to balance the torque created by the spinning rotors. The up/down motion is achieved by increasing/decreasing the rotors speed while maintaining an equal individual speed. The forward/backward, left/right motions are achieved through a differential control strategy of rotors speed.

The control system can divide into attitude control and altitude control. According to attitude control's dynamic model, its state equation can be drawn as equation (1):

$$f(X,U)=\begin{pmatrix} x_2 \\ x_4x_6a_1+b_1U_2 \\ x_4 \\ x_2x_6a_2+b_2U_3 \\ x_6 \\ x_4x_2a_3+b_3U_4 \end{pmatrix} \tag{1}$$

$x_\alpha=[\varphi\ \dot{\varphi}\ \theta\ \dot{\theta}\ \psi\ \dot{\psi}]$ is state variable, $U=[U_1\ U_2\ U_3\ U_4]^T$ is input vector as equation (2). Equation (1) can be divided into pitch channel, roll channel and yaw channel from up to down.

$$\begin{cases} U_1=b(\Omega_1^2+\Omega_2^2+\Omega_3^2+\Omega_4^2) \\ U_2=b(-\Omega_2^2+\Omega_4^2) \\ U_3=b(\Omega_1^2-\Omega_3^2) \\ U_4=d(-\Omega_1^2+\Omega_2^2-\Omega_3^2+\Omega_4^2) \end{cases} \tag{2}$$

where Ω_α^2 is motor speed.

Design of hovering control algorithm

Attitude estimation based on the Inertial Measurement Unit usually makes certain errors, besides, GPS has disadvantages in low accuracy and environment limitation, so the quadrotor drifts a lot while hovering. A method based on optical flow sensor for hovering calibration is provided. The optical flow sensor is mounted in the bottom of the quadrotor aircraft. Attitude estimation is compensated to correct hovering with the horizontal velocity detected by the optical flow information. A cascaded (inner-outer loop) structure is often adopted. Fig. 3 is controller structure for hovering control of the quadrotor with the controller parameters roughly tuned in the experiments.

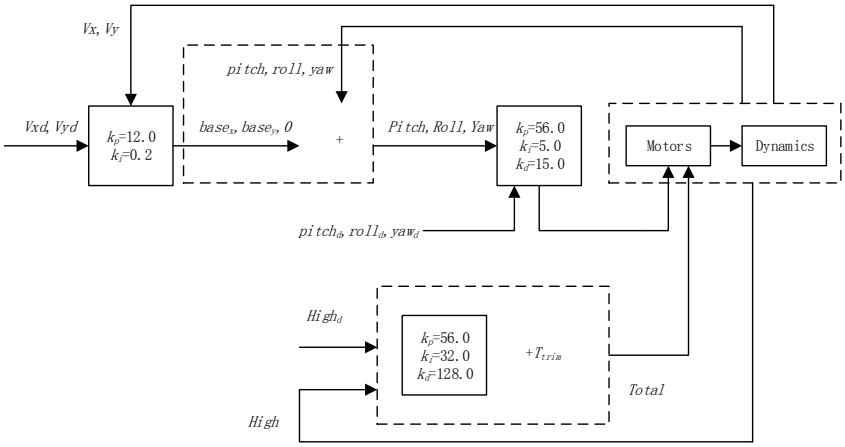

Fig. 3. Controller structure for hovering control

v_x and v_y are horizontal velocity in x-direction and y-direction, respectively, measured by optical flow sensor. v_x is proportional to pitch error $base_x$ and v_y to roll error $base_y$, besides, $v_x, v_y \in (-1.0,1.0)m/s$. The expected horizontal velocity is $0m/s$. PI controller is chose as the

out loop controller. v_x and v_y are control input , $base_x$ and $base_y$ are control output, then the real attitude angular are

$$\begin{cases} Pitch = pitch + base_x \\ Roll = roll + base_y \\ Yaw = yaw + 0 \end{cases} \quad (3)$$

where $pitch$, $roll$ and yaw are measured by magnetometer。

Due to the expected attitude angular are all 0°, we take the calibrated Pitch, Roll and Yaw as control input and use PID controller as the inner loop controller. The control output can be drawn as

$$\begin{cases} u_x = kp_x \cdot Pitch + ki_x \cdot \sum_0^n Pitch + kd_x \cdot v_p \\ u_y = kp_y \cdot Roll + ki_y \cdot \sum_0^n Roll + kd_y \cdot v_R \\ u_z = kp_z \cdot Yaw + ki_z \cdot \sum_0^n Yaw + kd_z \cdot v_Y \end{cases} \quad (4)$$

where v_p , v_R and v_Y are the angular rate measured by MTI-G.

Altitude control also uses PID controller, the altitude control output is

$$u_h = kp_h \cdot High + ki_h \cdot \sum_0^n High + kd_h \cdot (High_n - High_{n-1}) \quad (5)$$

where $High$ is the altitude measured by infrared range finder. Then the four duty cycles are

$$\begin{cases} CMPA1 = 4000 + u_x - u_z + u_h \\ CMPA2 = 4000 + u_y + u_z + u_h \\ CMPA3 = 4000 - u_x - u_z + u_h \\ CMPA4 = 4000 - u_y + u_z + u_h \end{cases} \quad (6)$$

where 4000 is the trim value T_{trim} during hovering.

Hovering control test

Fig. 4 is the description of quadrotor's hovering track. We can conclude that quadrotor can hovering within a circular area with a radius of 12cm. From Fig. 4. Fig. 5 to Fig. 7 are pitch, roll and yaw control effect respectively. We can draw that attitude can be stable within $\pm 5°$ and quadrotor can hover stably. Fig. 8 is altitude curve. In the take-off stage, about 8cm overshoot happened when it reach the maximum altitude; altitude stables at 50cm or so, the maximum error is less than 10cm; from takeoff to landing, the altitude control had a good performance.

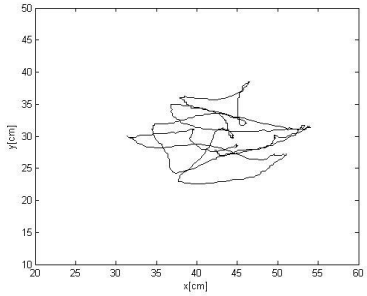

Fig.4. Description of quadrotor's hovering track

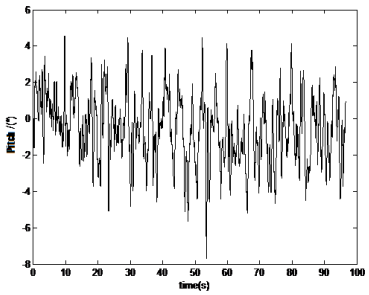

Fig.5. Pitch control curve

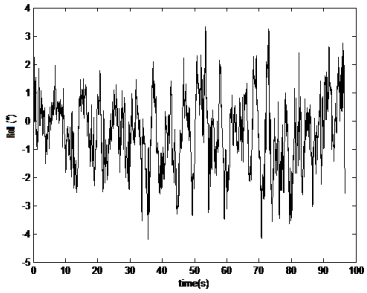

Fig.6. Roll control curve

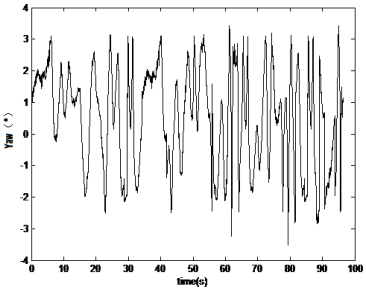

Fig.7. Yaw control curve

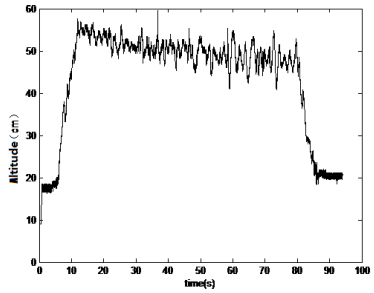

Fig.8.Altitude control curve

Conclusion

In this paper, we take advantage of STMS320F28335, and select MTI-G IMU, PX4FLOW optical flow sensor and SHARP GP2Y0A02YK0F infrared range finder to design quadrotors' control system. The hovering calibration idea with optical flow sensor is proven to be very effective in eliminating the long-term drift. Indoor experiments show that the control system has stable performance to meet the requirements of attitude control.

References

[1] Q Lv, D L Wang, F Liu and H R Bai: Discrete-time Mode Variable Structure Control Based on Nonlinear Exponential Reaching Law. Journal of Projectiles, Rockets, Missiles and Guidance. Vol.32, No.5 (2012), p: 50-54: 25-28.

[2] F Guo. Localization for Quadrotor Unmaned Aerial Vehicle in Complex Environment . Master thesis. Tianjin: Tianjin University, 2012.

[3] M Ji, J T Lu. Design of quadcopter's control system based on Cortex-M4. Computer & Control, Vol.21, No.7 (2013), p: 1816-1821.

[4] L Wang. Research on control technology of quadrotor unmanned aerial vehicle. Master thesis. Harbin: Harbin Engineering University, 2012.

Advanced Materials Research Vols. 989-994 (2014) pp 3220-3223
© (2014) Trans Tech Publications, Switzerland
doi:10.4028/www.scientific.net/AMR.989-994.3220

Fault Diagnosis of Rolling Bearing based on MED and Morphological Filtering[1]

Shangkun Liu[a], Guiji Tang[b], Bin Pang[c]

Department of Mechanical Engineering, North China Electric Power University, Baoding, Hebei, 071003, China

[a]lsk1213@163.com, [b]tanggjlk@ncepubd.edu.cn, [c]huadianpb@126.com

Keywords: minimum entropy deconvolution, morphological filtering, rolling bearing, fault diagnosis.

Abstract. One rolling bearing fault diagnosis method based on minimum entropy deconvolution (MED) and morphological filtering is proposed. Firstly, the strong background noise of rolling bearings is decreased by the MED method, then the morphological filtering which have different length of structure elements is designed and applied to the de-noised signal. Subsequently, bearing's fault characteristic frequency is extracted by the amplitude spectrum analysis to the best morphological filtering component which have the maximum kurtosis. This method is used to analyze both a simulated bearing signal and an experimental inner ring fault signal, and the good result validated the effectiveness of this method.

Introduction

The rolling bearing is an important and vulnerable part in rotating machinery, about 30% mechanical failure is caused by the local damage of the bearings. How to extract the weak impact features and repetition frequency from the strong background noise is the key to the fault diagnosis of rolling bearing. Morphological filter which bases on mathematical morphology transform is a nonlinear filtering method, Hu Aijun [1] used combined morphological filter to remove the random noise and impulse interference in vibration signal of rotating machinery for demodulation. Zhang Lijun [2] extracted the gearbox fault feature using mathematical morphological filtering. Because the difference morphological filtering demodulation involves only addition and subtraction, it avoids the window effect and mixing effect, so it can be used well in the field of fault diagnosis of rotating machinery. In this paper, the noise of fault rolling bearing vibration signal is decreased by the MED firstly, then the bearing's fault characteristic frequency is extracted by the difference morphological filter. In the morphological filtering and demodulation process, the difference morphological filter which has different length of structuring elements is designed and applied to analyze tentatively. At last, the best morphological filtering component is selected by the kurtosis criterion for the next demodulation.

MED principle

Local failure of rolling bearing can lead to periodic impact signal. Because of the influence of transfer path, the entropy becomes bigger after the convolution of the impact signal and transfer function. The core idea of MED is to remove the prominent sharp pulse process and to get the "certainty" in the signal through the deconvolution, and it usually uses maximum kurtosis value as the stop condition.

Actual collected rolling bearing fault vibration signal can be expressed as Eq. 1:

$$y(n) = h(n) * x(n) + s(n) \tag{1}$$

Here, $x(n)$ is the impact of the fault signal, $h(n)$is the transfer function, $s(n)$is the noise. To facilitate the analysis, $s(n)$ can be ignored firstly. The purpose of MED is to find a optimal deconvolution transfer function $w(n)$to calculate input signal $x(n)$ from the output signal $y(n)$ through Eq. 2.

$$x(n) = w(n) * y(n) \tag{2}$$

Assumed $\hat{w}(n)$ is the estimate value of $w(n)$, an estimated value $\hat{x}(n)$ of $x(n)$ would be obtained after deconvolution. The smaller the sequence entropy value is, the simpler the shape of $\hat{x}(n)$ is, and the stronger the impact of the signal is, also $\hat{w}(n)$ tends to optimal. Wiggins defined entropy function:

$$E[\hat{x}(n)] = [\sum_{n=1}^{N} \hat{x}^2(n)]^2 / \sum_{n=1}^{N} \hat{x}^4(n) \tag{3}$$

Therefore, MED essentially makes the recovered signal have the minimum entropy by constructing an "optimal" filter, Lee [3] seeks the optimal MED filter by the target function method. The detailed process can reference the reference [4].

Morphological Filtering

Principle of morphological filtering. Mathematical morphology has two kinds of basic form function: dilation and erosion. If *f(n)* is one-dimensional signal and its' domain is F={0,1,2,···,N-1}, *g(n)* is one-dimensional structure elements sequence and is defined in G={0,1,2,···,M-1}, and N≥M, then the dilation and erosion calculation is defined as:

$$(f \oplus g)(n) = \max[f(n-m) + g(m)], m \in G \tag{4}$$

$$(f \Theta g)(n) = \min[f(n+m) - g(m)], m \in G \tag{5}$$

Based on the dilation and erosion calculation, the open and close operation can be constructed respectively, the expression is:

$$(f \circ g)(n) = (f \Theta g \oplus g)(n) \tag{6}$$

$$(f \bullet g)(n) = (f \oplus g \Theta g)(n) \tag{7}$$

Mathematical morphology open operation can smooth the positive impact of the signal and the close operation can smooth the negative impact of the signal. For the purpose of demodulation, the positive and negative impact can be extracted by constructing a close-open margin calculation. The expressions is:

$$dif(f) = f \bullet g - f \circ g \tag{8}$$

The selection strategies of the structural elements based on kurtosis criterion. In the morphological filtering process, only the signal element which matches the structural element size and shape is reserved. So it is the decisive factor to select the shape, amplitude, and the length of the structural elements. Some structural elements are commonly used, such as flat, triangular, semicircular etc.. Although the more complex of the structure element shape is, and the stronger its filtering ability is, it consumes more calculating time. Reference [5] points out that the structure of element shape has little effect on the filtering effect, considering the signal characteristic and the calculation complexity, the flat structure element is selected in this paper. In order to determine the appropriate structure elements length, Nikolaou and Antoniadis [6] proposed that structure element length should be 0.6 times to the fault pulse period (T).It becomes the experience formula of choosing the length of structural elements. The paper set the length of structural elements to 0.1T, 0.2T, 0.3T···T separately, then analyzes the signal using difference filter to generate 10 morphological filtering components, and selects the maximum kurtosis component to analyze the fault spectrum.

Analysis of simulation signal

Literature [7] gives the rolling bearing fault model with inner race fault. It is:

$$\begin{cases} x(t) = s(t) + n(t) = \sum_i A_i h(t - iT - \tau_i) + n(t) \\ A_i = A_0 \cos(2\pi f_r t + \varphi_A) + C_A \\ h(t) = e^{-Bt} \cos(2\pi f_n t + \varphi_m) \end{cases} \tag{9}$$

Set the sample frequency f_s=20kHz, the rotation frequency f_r=20Hz, the natural frequency of the system f_n=3kHz, the inner fault characteristic frequency f_i=120Hz, the noise component is added and the SNR of $x(t)$ is -9dB, amping radio β=0.04.The time-domain waveform and envelope spectrum of simulated signal $x(t)$ is shown in Fig. 1 and Fig. 2.

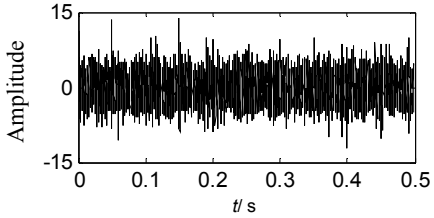

Fig. 1 Waveform of simulation signal

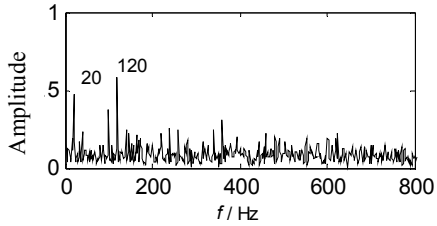

Fig. 2 Envelope spectrum of simulation signal

Because of the noise, the impact fault characteristic of waveform is not obvious in Fig.1. Although the peak is corresponding to the inner ring fault characteristic frequency in Fig.2, other frequency components of the fault are not easy to find. The result analyzed by MED is shown in Fig.3. We can see that the impact characteristic of the signal is obvious. Then the paper constructs the difference morphological filtering according to the construction method of the structure element, and gets the 10 morphological filtering components. The kurtosis values of each morphological filtering component are calculated in Table1. We can find that the L=T morphological filter component's kurtosis value is maximum. Fig.4 shows its amplitude spectrum. The peak is obvious at the inner race fault frequency and its multiplication frequency, and it is clear that the inner ring fault frequency and rotating frequency modulation characteristic.

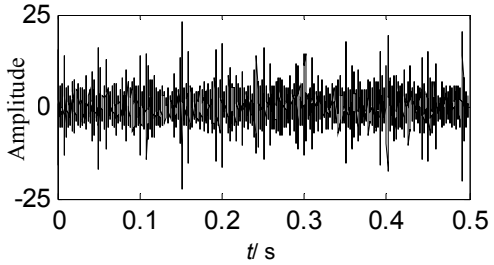

Fig.3 Time domain Waveform after MED

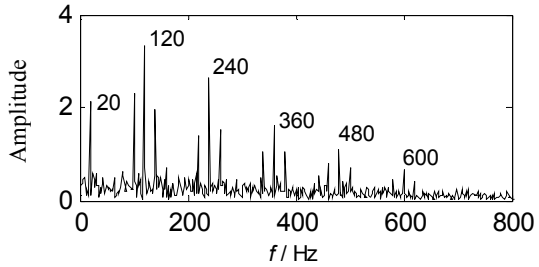

Fig.4 Spectrum of max kurtosis value component

Table1. Kurtosis values of simulation signal's each morphological filtering component

0.1T	0.2T	0.3T	0.4T	0.5T	0.6T	0.7T	0.8T	0.9T	1T
1.139	1.287	1.380	1.664	1.665	2.162	2.192	3.175	3.819	6.240

Fault diagnosis example

The paper selects the data of American Case Western Reserve University bearing data center for the inner ring fault diagnosis. The bearing type is 6205-2RS JEM SKF in the experiment. The pitch circle diameter D=39.04mm, diameter of steel ball d=7.94mm, rolling number n=9, pressure angle α =0 °, rotating frequency f_r=28.7Hz. The inner ring fault characteristic frequency of bearing is :

$$f_i = \frac{n}{2}(1+\frac{d}{D}\cos\alpha) f_r = 155.4Hz \tag{8}$$

Fig.5 is the time domain waveform and Fig.6 is the amplitude spectrum of the inner ring fault signal. Fig.5 reflects the impact and the noise are obvious. There is a small peak at 155.3Hz in Fig.6, corresponding to the inner ring fault characteristic frequency of bearing, it showes that it may be the inner fault. The MED de-noise method is applied to the fault signal, and we regards the inner fault impact cycle as the standard cycle T of structure elements to morphology filtering. 10 morphological filtering components are generated. The kurtosis value of each component is shown in Table 2.

When the length of structural elements is L=0.1T, the kurtosis value of morphological filtering component is maximum, so the paper does the spectral analysis to this component, the result is shown in Fig.7. The frequency and frequency doubling of fault is in the graph, the order as high as 6. Fig.8 is

the inner ring fault signal's envelope spectrum, although there is inner fault frequency of bearing, but only 2 times frequency component is obvious. So the paper's method can more effectively in extracting the impact characteristic of rolling bearing fault and frequency doubling.

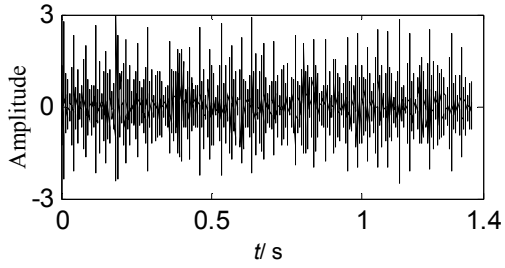

Fig.5 Inner ring fault signal

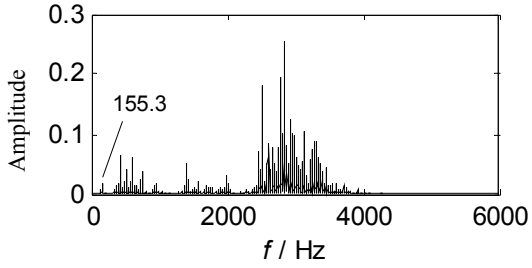

Fig.6 Envelope spectrum of inner ring fault signal

Table2. Kurtosis values of example signal's each morphological filtering component

0.1T	0.2T	0.3T	0.4T	0.5T	0.6T	0.7T	0.8T	0.9T	1T
13.516	9.260	6.794	6.780	5.239	4.406	3.664	3.128	2.670	2.345

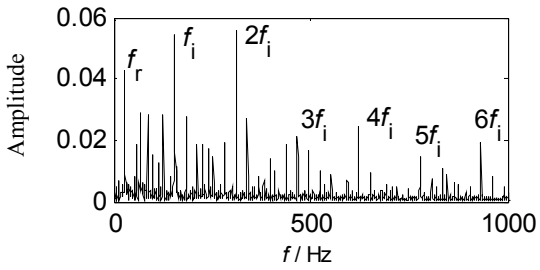

Fig.7 Analysis result of fault signal

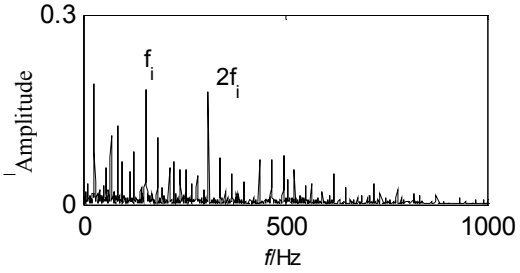

Fig.8 Envelope spectrum of fault signal

Conclusion

The paper proposes one rolling bearing fault diagnosis method based on MED and morphological filter. The MED has good ability of de-noise and difference morphological filtering can extract impact characteristic in the signal. The result of simulated signal and example signal showes that this method can extract the rolling bearing impact characteristic and frequency doubling effectively, and the result is better than traditional envelope spectrum.

The Fundamental Research Funds for the Central Universities(2014MS156)

References

[1] Hu Aijun,Tang Guiji,An Liansuo. De-nosing technology for vibration signals of rotating machinery based on morphology filter[J]. Chinese Journal of Mechanical Engineering, 2006, 42(4): 127-130.

[2] Zhang Lijun,Yang Debin,etc.. Approach to extracting gear fault feature based on mathematical morphological filtering [J]. Chinese Journal of Mechanical Engineering, 2007, 43(2): 71-75.

[3] Lee J Y, Nandi A K. Extraction of impacting signals using blind decomposition [J]. Journal of Sound and Vibration1999,232(5):945-962.

[4] Wang Hongchao, Chen Jin, Dong Guangming. Fault Diagnosis Method for Rolling Bearing's Weak Fault Based on Minimum Entropy Deconvolution and Sparse Decomposition [J]. Chinese Journal of Mechanical Engineering, 2013, 49(1)：88-94.

[5] Y. Dong,M. Liao,X. Zhang, F. Wang, Fault diagnosis of rolling element bearings based on modified morphological method,Mech. Syst. Signal Process., vol.25, no.4,1276–1286,May 2011.

[6] N. G. Nikolaou and I. A. Antoniadis, Application of morphological operators as envelope extractors for impulsive-type periodic signals, Mech. Syst. Signal Process, vol. 17, no. 6, pp. 1147–1162, Nov. 2003.

[7] Ho D, Randall R B. Optimization of bearing diagnostic technique using simulated and actual bearing fault signals [J].Mechanical system and Signal Processing,2000,14 (5) :763- 788.

Advanced Materials Research Vols. 989-994 (2014) pp 3224-3227
© (2014) Trans Tech Publications, Switzerland
doi:10.4028/www.scientific.net/AMR.989-994.3224

Transform a mechanical testing machine into high-temperature disk spring stress relaxation test equipment

Xiaoyu ZHOU[1, 2, 3, a], Yizhong YU*[4,b]

[1]School of Materials Science & Engineering, Tianjin University of Technology, Tianjin 300384, China.

[2]Tianjin Enterprise Key Laboratory of Cooper Wires for Electrical Purposes

[3]Tianjin Engineering Research Center of Manufacturing Technology For Precise Die & Mold

[4]School of Electronic Engineering, Tianjin University of Technology and Education, Dagu Road 1310, Hexi district, Tianjin 300222, China

[a]zxy1680@sina.com, [b]yizhongyu@sina.com

* Corresponding Author: Yizhong Yu, School of Electronic Engineering, Tianjin University of Technology and Education, Dagu Road 1310, Hexi district, Tianjin 300222, China.
Email: yizhongyu@sina.com

Keywords: Disk Spring, Stress Relaxation, Failure, Life Time.

Abstract. Prediction of disk spring failure life due to stress relaxation is necessary for users; the problem was not solved before. According to special test requirement, we modified a 100N mechanical testing machine into high temperature testing equipment which can be used for different types of disk spring. With a test for 36 days on a group of 45×22.5×3.5×2.5 mm disk springs, a result of prediction of 3.38% load loss ratio after 12 years relaxation is obtained, these disk springs are qualified. Our modified equipment has the advantages of real time, heavy loading, high sensitivity and good generality.

Introduction

Disk spring has the characteristics of super high elasticity, compact axial size, variable stiffness etc, it is widely used in the area of mechanism of preloading, seal, mechanism reset, security protection etc. Disk spring acts as very important role; once it is installed, it is to be used for a long period up to 10 years [1].

Stress relaxation is a common phenomenon in metal material or element. The stress under constant strain would be decreased with the lapse of time. It is the main form of elastic element failure [2,3].

There was no disk spring stress relaxation testing method and equipment for a long time, and there was no special requirement for it in national standard GB/T1972-2005. However, with the production and use of high temperature disk spring, the higher the temperature, the greater the influence. It is eager to design and manufacture disk spring relaxation testing equipment [4].

Equipment requirements

Due to the characteristics of disk spring, the equipment should satisfy following requirements:

Real time ability. To predict the load loss ratio after some years, the stress relaxation curve is needed to extrapolate the life time. To obtain the stress relaxation curve, the real time load changes should be measured at high temperature.

Heavy loading. Disk spring can be used for heavy loading. 40×20.4×2.25×3.15 mm disk spring can be loaded on 6540N, 100×51×6×8.2 mm for 48000N and 200×102×8×13.6 mm for 76400N.

High sensitivity. Load change caused by stress relaxation of disk spring is very small for a short period of time, the sensitivity requirements for the test system is very high.

Generality. Standard disk spring is divided into 3 series, each series is divided in to 3 classes, each class has 29 types. Coupled with non standard disk spring, the specifications is very complex. Testing system should have good generality.

Heating device. For simulation of the actual environment at different temperature, testing equipment should have a thermal isolation furnace.

Test Principle

There are two methods for testing [5]:

Screw or bolt method. The disk spring string is put in a bolt and the amount of compression of each disk spring is calculated. We firstly made a mark on the bolt as initial hight of the string and measured the corresponding load, then locked the string by a nut until next measurement. We remeasured the load on the same mark after a certain time, then we obtained the stress relaxation curve.

The results could not be accurate, although this method is simple. This is because of huge elastic coefficient and small stress relaxtion of disk spring. Obviously, this method is not feasible.

Real time testing method. Prof. Su, De Sheng from Material Institute of Tianjin University, China, proposed a method for helical spring [6]. In this method, the spring is preloaded and the reduction of force is recorded by computer using A/D conversion. This method can reflect the real stress relaxation more accurately.

Equipment Modification

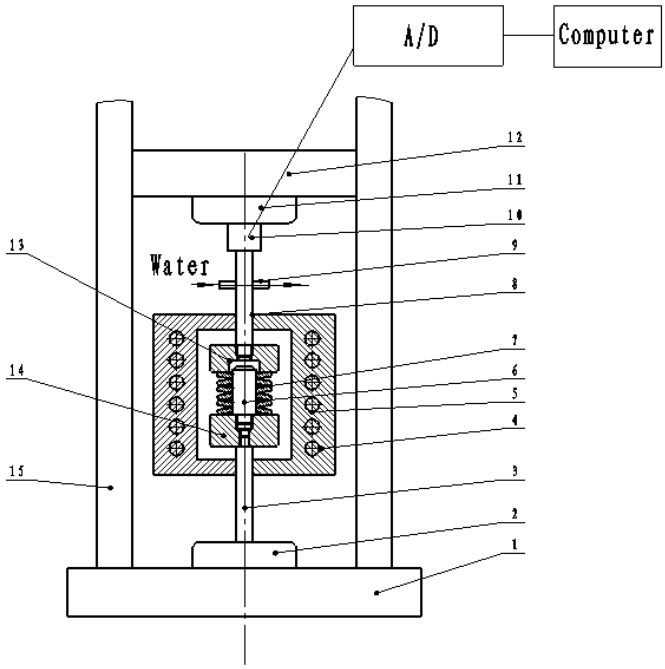

1-the base of electric universal mechanical testing machine 2-lower flange 3-lower support connecting link 4-electric furnace 5-electric heating wire 6-inner rod 7-disk spring 8-upper support connecting link 9-cooling water pipe 10-senser 11-upper flange 12-beam of electric universal mechanical testing machine 13-upper platen 14-lower platen 15- portal rigid frame of electric universal mechanical testing machine

Fig. 1 Diagram of real time testing equipment

Due to heavier load of disk spring and smaller deformation, the stress relaxation numerical value is extremely small. Required real time testing equipment should provide sufficient force and precise range of measurement. A 100N mechanical testing machine meets the requirements for the experiment, and the modification diagrammatic sketch is shown in Fig. 1. A Photo of the equipment is shown in Fig. 2.

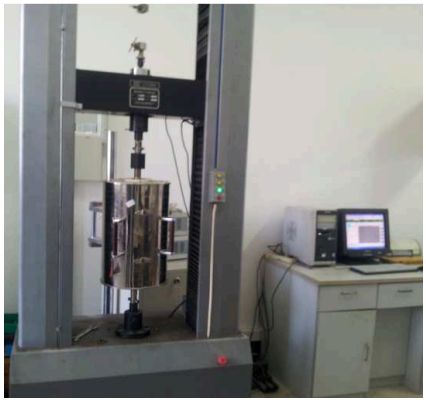

Fig. 2 Photograph of high temperature stress relaxation testing equipment

The support link is Lengthened, and the disk springs are placed in electric heating furnace. All the disk springs are put on inner rod. The force is transffered through upper and lower platen. The upper link rod is cooled by flowing water to prevent senser from being heated. Different disk spring can be measured by replacing inner rod, and the generality is achived easily.

Measurement Example

Disk spring, material: 60Si2MnA; specification: 45×22.5×3.5×2.5 mm; 40 disk springs are cascaded by pairs, each pair has 2 double disks face to face; rated load: 15.4 kN. Results measured at room temperature are shown in Table 1.

Table 1 Results of real time testing of stress relaxation of disk spring

Time [min]	Ln(time)	P [kN]
0		15.4
1	0	15.35
3	1.0986	15.3
5	1.6094	15.26
10	2.3025	15.23
30	3.4012	15.2
1020	6.9276	15.11
1200	7.09007	15.1
2640	7.8785	15.09
2690	7.8972	15.08
4070	8.3114	15.07
6510	8.7811	15.06
9390	9.1474	15.05
10830	9.29	15.05
13710	9.5259	15.05
19470	9.8766	15.02
32430	10.3868	15.01
36750	10.81189	15.01
45390	10.723	15
52590	10.8703	15

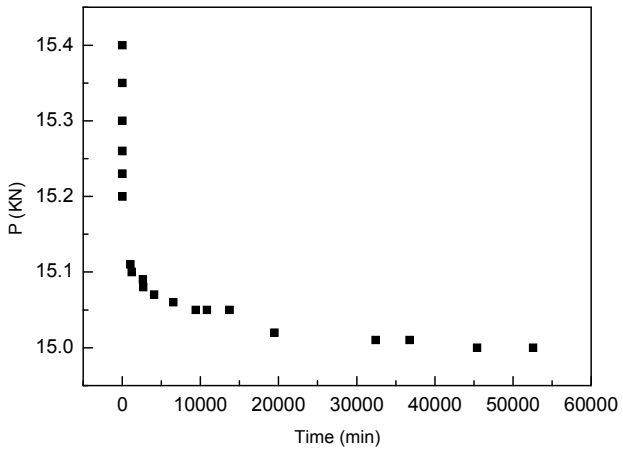

Fig. 3 Curve of load vs. time

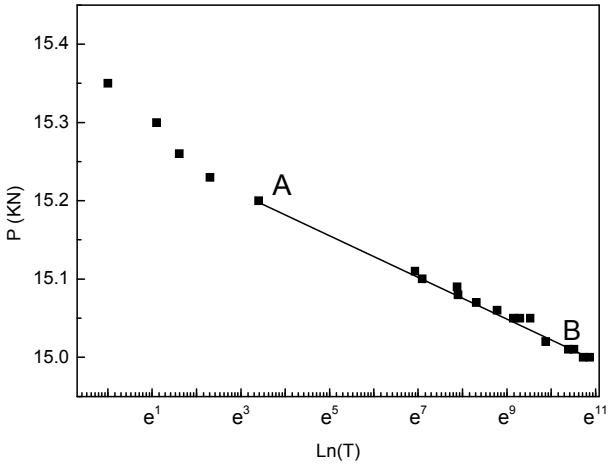

Fig. 4 Ln curve of load vs. time

Analysis

Fast and Slow Stages. In Fig. 3, it shows two stages of stress relaxation. One is fast stage (0~1000 min), another is slow stage (>1000 min).

Load loss ratio.

$$V = \frac{\Delta P}{P_0} \times 100\% = \frac{15.4 - 15}{15.4} \times 100\% = 2.60\% \quad (1)$$

Life time. The first stage is considered as permanent plastic deformation induced at the corner of disk spring, and the second stage is real stress relaxation. The relationship between load loss ratio and logarithm of time is linear. A linear equition is obtained from Fig. 4 [7]

$$y = a_0 - b \ln t \quad (2)$$

in which a_0 is initial load, b is the second stage line slope.

In the period from 1000 min to 60 days, a_0 =15.306 and b =0.028278 can be calculated from two selected points A (6.93, 15.11) and B (10.82, 15.00).

$$y = 15.306 - 0.028278 \ln t \quad (3)$$

The predicted life time of disk spring is 12 years. Use Eq. 3, load at that time can be calculated:

$$y = 15.306 - 0.028278 \ln t = 15.306 - 0.028278 \ln 12 \times 365 \times 12 \times 60 = 14.88 KN \quad (4)$$

Load loss ratio is

$$V = \frac{15.4 - 14.88}{15.4} \times 100\% = 3.38\% \quad (5)$$

Conclusion

Due to small stress relaxation and huge load of disk spring, the testing for stress relaxation is difficult to achieve. Using an electric mechanic testing machine modified with adding device, the testing measurement is successfully achieved. Not only the problem is solved, but also the precision and the reliability is ensured. The equipment development cost and time are greatly saved. By testing the stress relaxation, long time load loss ratio of disk spring can be calculated. By replacing mechanical fixture, disk spring with different specifications can be tested. The equipment has capability of high temperature testing with electric heating furnace.

References

[1] Junfang CHEN: Hebei Chem. Industry Vol. 32 No. 4 (2009), p. 50.

[2] Dade SU: Metal Products Vol. 26 No. 5 (2000), p.1.

[3] Hai NI，Zhirui WANG: Mat. Sci. Eng. A Vol. 314 No. 1 (2001), p. 12

[4] Xiaoyu ZHOU: Advanced Materials Research Vol. 6 (2010), p. 22.

[5] Xinlong CHANG, Bingji LIU and Liang WANG: J. of Propulsion Tech Vol. 20 No. 1 (1999), p.99.

[6] Deda SU: Spring Eng. Vol. 2 (1998), p. 11.

[7] Xinming ZHANG, Xinping MAO and Zhiqian DENG: Trans. of Nonferrous Metals Soc. of China Vol. 11 No. 6 (2001), p. 988.

Advanced Materials Research Vols. 989-994 (2014) pp 3228-3230
© (2014) Trans Tech Publications, Switzerland
doi:10.4028/www.scientific.net/AMR.989-994.3228

Vista of Silt Brick Cutting Machine Development Situation

Zhuo Zhou[1,2,a], Yi Lv[1,b], Hong Jun Ni[1,c], Cheng Qun Wu[1,d]

[1] School of Mechanical Engineering, Nantong University, Nantong, Jiangsu China, 226019

[2] Office of Nantong Wall Material Innovation, Nantong, Jiangsu, 226001, China

[a]1449756043@qq.com,[b]260443169@qq.com,[c]hjni910@aliyun.com,[d]1163780057@qq.com

Corresponding author: Tel: +86 13338061306;Email address: hjni910@aliyun.com (Hongjun Ni)

Keywords: silt brick-making; brick cutting machine; automatic control

Abstract. Brick cutting machine is the important device during the process of making bricks. The automatic control system, device of power and the pattern of cutting machine have been developing well. The new ideas, new technology and achievement of the brick cutting machine are taken out. The important achievement and application of the cutting machines are introduced, as well as the development tendency.

Foreword

As the rapid development of national economy, urban and rural construction, brick industry advocates saving land resources and energy, protecting environment and utilizing resources adequately. Making bricks with slit[1] can effectively protect the land resources and solve the problem of rivers blocked.

Slit brick cutter, an important part of the brick making machine, mainly consists of cutting platform, steel wire, steel wire hook, power plant and automatic control system. Brick-cutting machine has developed rapidly, the power system has developed from electrical machine to the hydraulic system. In terms of control system, relay control has been instead of Programmable Logic Controller(PLC). A good design of cutting machine can improve the production efficiency and quality, and it can save much silt resource. Therefore the design of cutter is valued by brick-making researchers.

Theory of silt brick-making and cutter

The main raw materials of mud sintered porous bricks are silt, coal gangue and something used to make micropores, they are mixed at a certain proportion, stirred, extruded, cut to prepare for making silt-bricks.

Currently the advanced cutter has basically realized intelligence and automation. When the cutter detects the slugs put out, it begins to cut mud strips constantly with steel wire under the control of PLC. In order to keep cross section neat, the cutting plane and mud should be synchronously moved. When the cutting machine finish cutting slugs, the accelerate belt quickly sends briquets to the next workbench. The whole cutter device is equipped with alarm system, once the steel wire is broken or equipment stops running, the device will buzz to alarm.

Development of brick cutting machine

Cutter power system

At present many enterprises use linkage to cut slugs, the working process is that motor drives the clutch, then drives the connecting rod to make the wire rack cut the mud constantly. The connecting rod cutter has many disadvantages [2]: (1) The working noise is loud, which will cause vibration and working process is not smooth. (2)The structure is complex, there are always a lot of faults, and it is not easy to maintain and repair. (3)The automation degree is low, labor force consumption is too large. (4)It is difficult to calculate the part size in detail and process accurately.

The domestic researchers have developed the hydraulic cutter with low noise, small energy consumption and high productivity [3]. This kind of cutter adopts hydraulic system as the power to cut mud, the largest stroke is 260 mm - 800 mm, and the maximum working pressure is 25Mpa. Shenzhen WoPeng limited company [4] in 2011 applied hydraulic cutting technology to concrete nondestructive cutting, and successfully developed the hydraulic concrete wall sawing machine and hydraulic rope saw machine and any other products. These products can be applied to cut any kind of clay bar. Hydraulic cutter has more prominent advantages: (1) Low energy consumption, energy is used more reasonably. (2)Working noise is low, operation is smooth, and guidance precision is better. (3)Hydraulic push rod system is simple, it's more convenient to control the cutting system. (4)Hydraulic push rod system uses the technology of two-stage pressure regulation, when the working pressure is higher than the safety system, it will relieve pressure automatically to ensure the security of machine. The disadvantage is that once the tubing is aged, it will leak easily, it is hard to maintain and the cost is high.

Cutter control system

Nowadays some brick enterprises still use the traditional relay to control the cutter. Relay consists of the middle relay, counter, time relay and on-off contacts. It achieves the goal of automatic cutting through the logic combination of contacts. Although the cutter with relay control is easy to manufacture and the cost is low, the number of contacts is large[5], the wire is complex, equipment is easy to age, control accuracy is not high, a loosen contact will affect the entire cutting system control and it is more difficult to find faults. Therefore, authorities stated that relay control must convert to PLC soon.

There has been great development in the automatic control technology because of PLC, the production efficiency is also greatly increased. The working process of the cutter controlled by PLC is that when the mud is detected by signal detector, the belt begins to turn to carry the mud from the vacuum extruder extrusion into the cutting device, all the information is transmitted to the control center, then the motor rotates to drive the cutting plane and conveyor synchronously. At the same time, the slug will be cut by the steel wire into certain shape neatly.

Wei Xiaolin[6] has used PLC to control the cutter, the automation of whole process can be implemented, such as sending board, feeding, demolding and cutting bricks. All the actions in cutting process are controlled by PLC, the operation is stable and reliable. Compared with the traditional relay control, the cutter controlled by PLC is higher reliability, stronger anti-interference ability, wider range, and easily programmed. It's proved that the qualification rate of products have reached 98% above, the brick-making number is more than 1200 per hour and various performance indicators of cutter meet the national standard.

Cutting patterns

At present the models and types are various, the cutting quantity and quality also need higher requirements, so various models of cutter are required to cut all kinds of bricks. Cutting pattern can be designed according to product model, transverse section and cutting quantity. Some commonly used cutting systems are illustrated below.

Vertical cutting. Vertical cutting refers to that the cutting wire, strained horizontally, cuts the mud vertically when the mud is transferred below the steel frame. After cutting, the cutting wire returns to top from the bottom, happening to separate the cut bricks. The vertical cutter invented by Liu Yunwu can make the cutting section smooth, make the size accurate, and it can also control the length at random. Either the hard or soft slug can be cut.

Combined cutting. The sizes of some productions are irregular, if cutting just once, it can't meet the requirement. Then the machine should repeatedly cut in order to produce various shapes of brick-products.

Model 4142 General Cutter invented by German Keller Company, adopts the combination of vertical and horizontal integration cutting system [7]. Combined cutting makes the cutting action at the same time or in turns. For example: the vertical cutting + chamfer + transverse cutting.

Vibrating cutting. Many producers add some combustible materials such as waste paper, waste wood chips, packaging rubbish and straw to the adobe, and then sintering bricks can form tiny holes

in order to achieve the purpose of heat preservation and heat insulation. But these additives may cause the cutting cross section deformation during cutting process, also can jam the inner hole of adobe, and the dry air cannot bring out the water vapor.

Making the steel wire reverberate under the action of magnet to prevent or reduce the occurrence of this situation, which is called vibration cutting[8].A good vibration cutting can increase the rate of hole, and the cutting deformation is reduced to minimum. The wire needs highly elastic so that the wire will avoid broken under the influence of resonance frequency.

Vista

The development trend of cutter is intelligent and systematic. The researchers of cutter pay more attention to the reliability, security, economy and environment. At present although domestic tile production equipments have developed quickly and the brick-making technology has made great progress, there is still a large gap compared with abroad in many ways. It is necessary to improve the structure property, research technology, productions quality and efficiency to meet the requirements of the brick market.

(1) Steel wire fracture is almost inevitable because of the alternate bending and tension. When the steel wire is cutting the slush mud, the resistance and friction loss will cause the wire fatigue and fracture. The quality of wire is critical to the production efficiency, so how to improve the quality of steel wire is still the researching focus in the future.

(2) The cross section of brick is not neat or cutting incompletely because of the impurity in sludge. In the future the mud material must be mixed fully before cutting, making sure the impurities particle size is less than 3 mm. In the aspect of cutting system, vibration cutting can be used to improve the cutting quality.

(3) Currently many brick enterprises equipments are relatively backward in the country. The researching focus is how the vacuum brick-making machine extrude more slugs than before. There are various bricks on the market, if each kind of brick only can be produced by one special cutter, it will obviously waste time. In the future, the procedure of each kind of production will be programmed into the cutter control system, when producing one kind of brick, the related program will be called. The cutting efficiency is greatly improved.

Peroration

Cutting machines play an important role in the brick industry, the development of cutters directly affect the production quality and efficiency. At present, the cutter structure is complete increasingly, production efficiency and degree of automation are very high. The rapid development of the national economy and housing industry modernization create a wide market for block production equipments. Strengthening technology innovation, developing advanced, practical and reliable products are the top priority. The development of the cutter for bricks has brought positive impact on the brick industry.

Acknowledgments

This work is supported by the Natural Science Research Project of Nantong University of Jiangsu and the application Research Project of Nantong ([2013]742-1) ([2013]742-2).

References

[1] He. H, Yue Q. Journal of Hazardous Materials.Vol.203(2011),p.53-61.
[2] Zhang Jin. World of Brick.Vol.6(2011),p.30.(In Chinese)
[3] Zong Xiufu. Brick.Vol.1(2010),p.33.(In Chinese)
[4] Yu Jie. Manufacturing Technology & Machine Tool.Vol.2(2013)p.14.(In Chinese)
[5] Zhao Jingjiang. Coal Mine Machinery.Vol.30(2009),p.166-167.(In Chinese)
[6] Wei Xiaoling. Chemical Engineering Abstracts.Vol.2(2010),p.48-49. (In Chinese)
[7] Xu Ming, Wang Yajuan. World of Brick.Vol.3(2010),p.43-54. (In Chinese)
[8] Zhang Liaoyuan, Wang Shuo. Applied Mechanics and Materials. Vol. 395(2013),p.1044-1048.

Advanced Materials Research Vols. 989-994 (2014) pp 3231-3235
© (2014) Trans Tech Publications, Switzerland
doi:10.4028/www.scientific.net/AMR.989-994.3231

The design of the single-phase inverter based on DSP (TMS320F2812)

Zhaoxia Zhou[1,a], Jiaen Huang[2,b]

[1.2]School of Information Science & Technology, Xiamen University Tan Kah Kee College

[a]xia1108@126.com, [b]531462635@qq.com

Keywords: DC-DC, DC-AC, Single-phase, full-bridge inverter, SPWM, DSP

Abstract. This paper designs a single-phase inverter.Battery as a 12V DC input, and output for the 24V,50 HZ standard AC wave. The load is resistive.The power supply adopts the Boost booster and two full-bridge inverter transform. For the control circuit, the preceding Boost converter using tl494 chip control closed-loop feedback and for the inverter part, adopting the 6N137 to finish the optical coupling isolation.Then,through the DSP (TMS320F2812) to complete the output of SPWM modulation.And the modulated SPWM signal can drive chip IR211 conducting the full bridge inverter. Finally, through a low-pass filter output the standard sine AC inverter power.

Introduction

In the electronic technology,Inverter technology is the most major and cored one. it combines modern power transformation, the analog and digital electronic technology, PWM technology, frequency meter, phase modulation technology, switching power supply technology and control technology, etc.At present, the digital AC power has gained rapid development, and the DSP is widely applied to the power supply .For using DSP chip as the core control chip, the SPWM wave signal produced by DSP can help the inverter power supply offer more perfect sine wave to its continuity [1], and it can be got low noise and high efficiency advantage through using of DSP.

Design index and design scheme

Design index: Design a single-phase inverter power supply.The input voltage is 12 V DC.The output RMS voltage is 24 V AC sinusoidal alternating current.The load is resistive.Specific indicators :

① the rated input voltage: $U_i = 12V$
output voltage: $U_{ORMS} = 24 \pm 0.5V$,frequency: f_O=50±0.5Hz

②Full rated output power:11.52W（$R_L = 100\Omega$）;Output sine wave voltage, $THD \le 3\%$

③Tunable output frequency:40HZ~60HZ

Structure diagram is shown in figure 1:

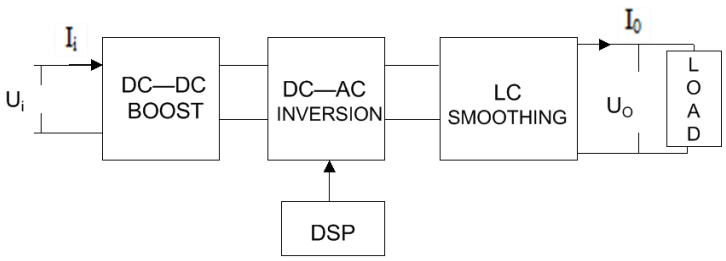

Figure 1:The hardware design block diagram

The overall design scheme: System has two power supply, the input of the 12 v DC voltage supply the DC - DC converter and the DC-AC converter,and these two converters respectively drive the chip TL494 and chip IR2111 work normally. By 7805 chip, the input voltage DC 12 v can be changed to an output with 5 v linear regulated power supply.It can drive 6N137, 74LS06, DSP(TMS320F2812) work normally.

System design block diagram is shown in figure 2

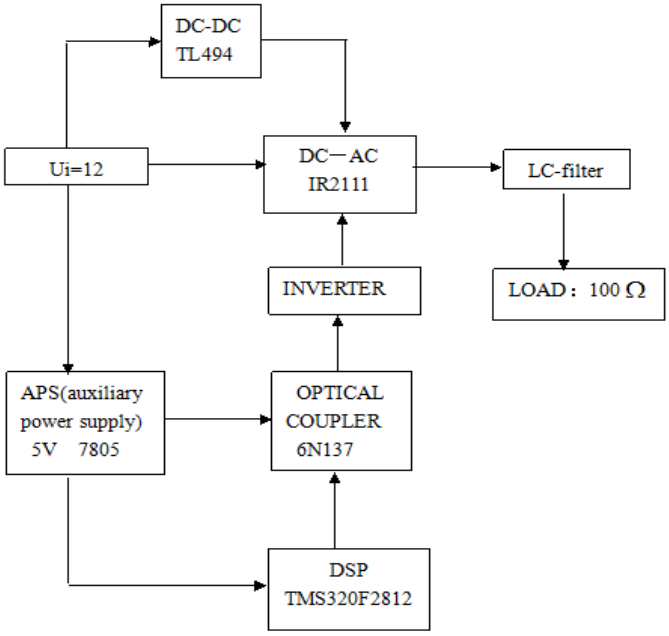

Figure 2 System design diagram

The design principle of each module

Boost DC - DC boosted circuit: Boost DC - DC converter.when the MOS tube opened , inductance L will store energy by V_{in} ,making the current increasing [2]. At the same time, the corresponding polarity of the electromotive force will change.Left is positive, negative right.The load's power supply provided by the capacitance C.When the MOS tube is cut-off,the current which through the inductive L will decrease constantly.And,the corresponding polarity of the electromotive force will change again.At this moment, the polarity is the same as V_{in} .After voltage's superposition and a part of power consumption on the diode, all the rest voltage was applied to the load.Meanwhile,the capacitor is recharged.So the DC voltage finishes the transformation from low to high.The principle diagram is shown in figure 3:

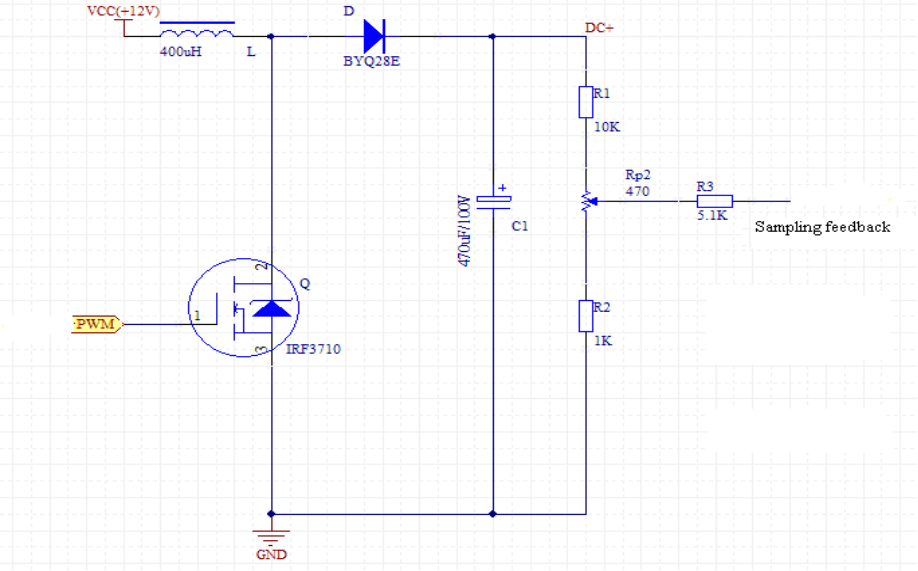

Figure 3 The principle diagram of the DC - DC boost converter

DC - DC transform drive circuit: DC - DC converter drive circuit composed of TL494 PWM pulse[3]. Modulate PWM pulse's frequency to 50KHZ ,choosing oscillation capacitance CT of 1000 PFand the resistance RT is 22 k Ω . The working principle diagram as shown in figure 4:

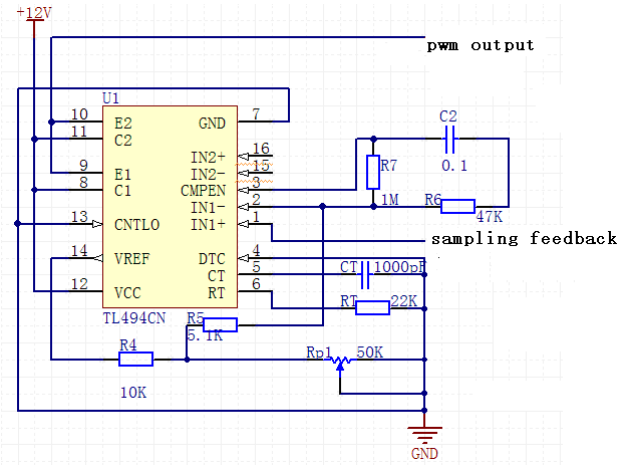

Figure 4 The principle diagram of the DC - DC converter controller

DC-ACinverter circuit: DC/AC adopts single-phase full bridge inverter circuit [4].It is made up of four IRF3710 bridge inverter circuit.In order to power the load, it uses the half bridge driver IR2111 which provide the drive signal to change the DC into 50 HZ AC .The working principle diagram as shown in figure 5:

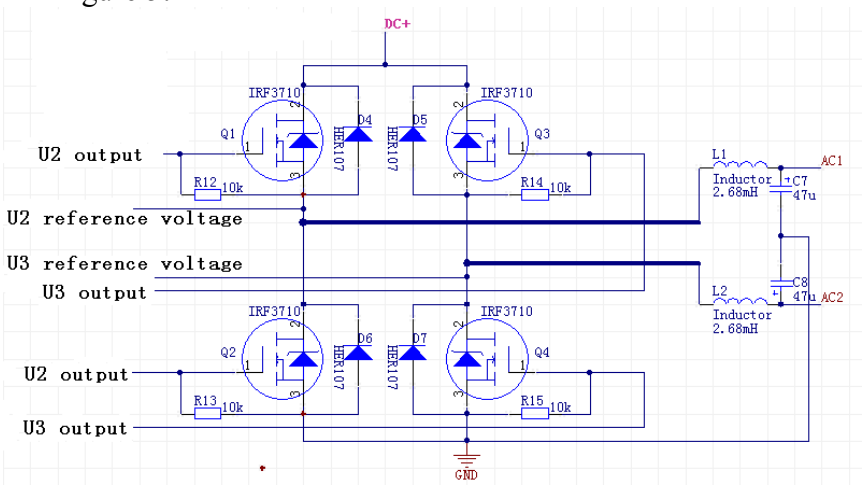

Figure 5 The principle diagram of the DC - AC inverter circuit

DC - AC converter drive circuit: The design of DC-AC inverter circuit adopts IR2111 half bridge driver chip.Single polarity SPWM signal generated by the DSP goes through the optical coupling isolation and the inverting step-up by74 LS06 inverter,the single output as an input conveies to the IR2111 half bridge driver chip.As long as controlling these two pieces of IR2111 half bridge driver chip can complete the drive of single phase full bridge inverter circuit.The working principle diagram is shown in figure 6:

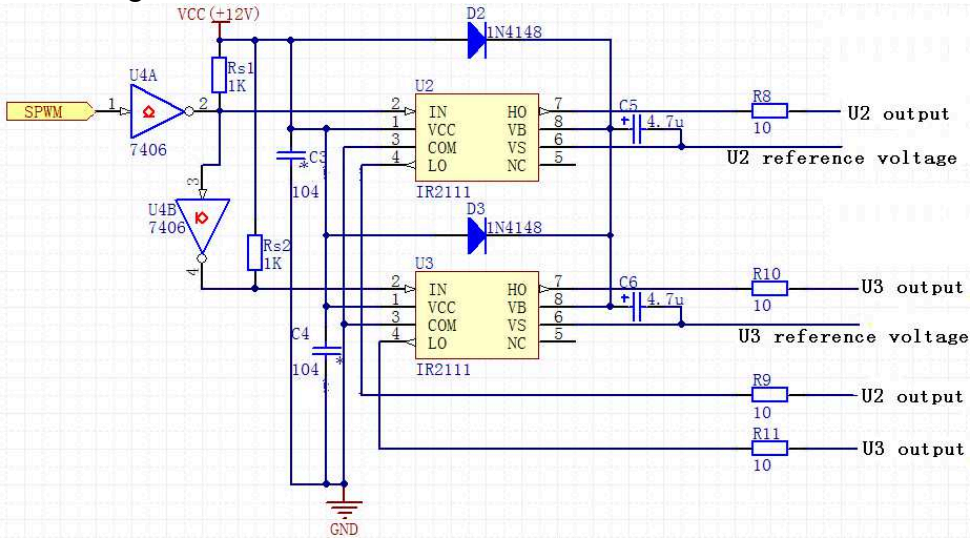

Figure 6 The principle diagram of the DC - AC converter drive circuit

Optical coupling isolation circuit: Optical coupling isolation circuit hardware as show in figure 7.SPWN wave signal generated by DSP processed Optical coupling isolation is outputed.The 6 N137 optical coupler is a high-speed optocoupler for single channel [5].

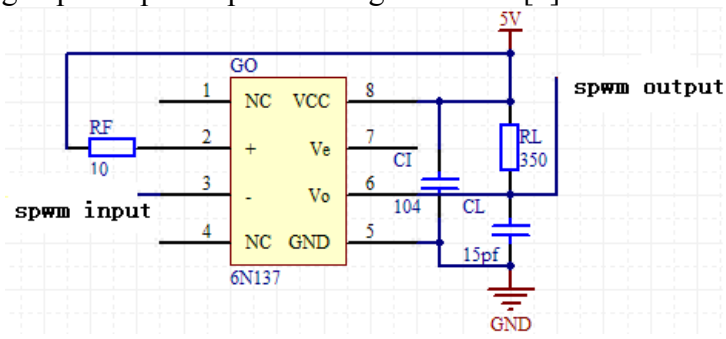

Figure 7 The principle diagram of the Optical coupling isolation circuit

The design of auxiliary power supply: The hardware circuit diagram of auxiliary power supply as shown in figure 8.Using a 7805 regulating circuit can obtain input + 12 v ,output+ 5 v ,and it is the power source of the DSP, optical coupling 6 N137 and 74 LS06 inverter.

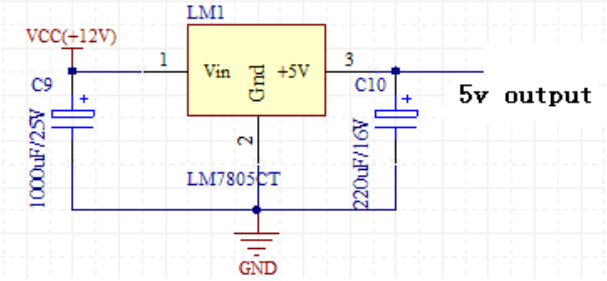

Figure 8 The principle diagram of the design of auxiliary power supply

System joint debugging

When in the test, debugging the situation without load first,the author adjust RP2 to make the output sampling voltage of DC - DC converter become 2.4 V.At this point, through the voltmeter measurement,we can see the DC - DC converter's output voltage is 34 v.Then the author adjusts the SPWM signal's modulation degree to1 as the input, and the output true RMS voltage of whole hardware and software system reachs 24 v. After finishing the no load debugging, the author disconnects the input power.In the output side,the author puts a 1 100 Ω resistance (load), making the whole system into a state of on-load.Opening the power supply,the Author adjusts RP2 again to make output sampling voltage of DC - DC converter become 2.4 V.Then,the author adjust the Rp1, to make the internal reference voltage of TL494 reach 2.4 V.Eventually, make DC - DC converter's output voltage reach 34 V.Meanwhile, the author adjust the SPWM signal modulation degree to 1, making the output true RMS voltage of whole hardware and software system reach 24V, and the output current is 0.25A.At this time, the whole hardware and software system debugging has completed.Physical test waveform which is the result of running on-load as shown in figure 9:

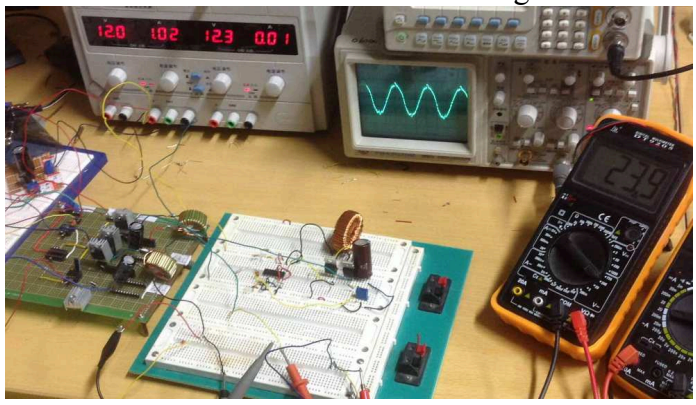

Figure 9 Waveform figure with on-load

Conclusion

Based on TMS320F2812 DSP chip can realize the drive digital control for inverter power supply. In the process of control, it should be point out that the reliability of hardware and software system is high, the precision affected by environment is weak, and it has strong programming. So it is superior to the traditional analog circuit. The result of experimental test obtained good sine waveform.

References

[1] GuanQing, Peng Qizong. DSP integrated development environment [M]. Beijing: electronic industry press, 2004.

[2] Liu Qiuju. BoostDC/DC converter circuit analysis and simulation [J]. Science and technology innovation herald, 2009, 5) : 99.

[3] Mao Xingwu Liu Fuyi. Secondary intelligent switch power supply voltage type PWM control chip KA3511 [J]. Power technology applications, 2001, 11:578-578.

[4] Wang Yunliang. Variable speed constant frequency motor system design and control [D]. Nanjing: southeast university, 2006.

[5] Yang Fangfang. Sensorless brushless DC motor based on DSP control system research and design [D]. Suzhou: suzhou university, 2010.

Advanced Materials Research Vols. 989-994 (2014) pp 3236-3239
© (2014) Trans Tech Publications, Switzerland
doi:10.4028/www.scientific.net/AMR.989-994.3236

LDO of High Power Supply Rejection with Two-Stage Error Amplifiers and Buffer Compensation

Yi-Tsung Chang[1, a*], Yu-Da Shiau[2, b], Po-Chun Wu[3, c], Ren-Hao Xue[4, d] and Po-Yu Cheng[5,e]

[1-5]Department of Electrical Engineering University of National Sun Yat-Sen Kaohsiung, 804, Taiwan, R.O.C.

[a*]ytchang@mail.ee.nsysu.edu.tw, [b]s5100687@yahoo.com.tw, [c]pettitte100@hotmail.com, [d]tfkc1744990@gmail.com, [e] schumi1031@gmail.com

Keywords: LDO, power supply rejection ratio, ultra-low output buffer, compensation, error amplifier

Abstract. This study develops a low dropout regulator linear regulator, characterized by a high power supply rejection ratio using ultra-low output resistance buffer and two-stage error amplifiers. The high power supply rejection is based on a closed-loop LDO regulator. The ultra-low output resistance buffer achieves ultra-low output impedance with dual shunt feedback loops, subsequently improving load and line regulations, as well as the transient response for low voltage applications. The proposed LDO regulator linear regulator functions under an input voltage of 1.8~3V, and the output voltage can be maintained at around 1.27V. Moreover, its output voltage is independent of input voltage. The proposed regulator is applicable to light-emitting diode driver integrated circuits. The layout chip area of the LDO linear regulator is 21.5μm × 42.6μm.

Introduction

With the widespread use of battery-powered portable devices such as mobile phones, laptops, and various handheld devices, power management should be one of priority concern when attempting to maximize the battery lifetime and provide energy to multiple on-chip blocks. In LDO regulator design, a linear LDO regulator is characterized by its ability to remain stable under various operating situations. This regulator can also provide regulated low-noise and precision supply voltage. Capable of providing a precise output voltage and regulating the output noise, the linear LDO regulator is increasingly applied. In linear LDO regulator design, stability in various operating conditions should be of priority concern. Many frequency compensation schemes have been developed to ensure the stability of the regulator. The conventional approach forms the left half plane zero frequency by using the equivalent series resistance of the output capacitor. However, this approach is limited by its insufficient transient responses, owing to inaccuracy of the value of equivalent series resistance for different operating conditions. Pole-splitting by a nested-miller capacitor can also increase the stability of circuit operations. However, this approach requires a large area, owing to internal compensation and large quiescent current of the regulator as the load current is increased. This work attempts to improve the power supply rejection ratio (PSRR) by using a buffer of ultra-low output impedance with and two stage EAs.

LDO Linear Regulator

The circuit schematic of the conventional linear LDO regulator with the internal buffer is shown in Fig. 1. EA generates an error signal by comparing the reference voltage and feedback signal from a resistive divided output voltage. Several performance issues of the linear LDO regulator must be addressed in terms of line and load regulations, PSRR, load current and dropout voltage. A large voltage gain of the error amplifier is necessary to increase the loop gain for high regulation and PSRR performance [1], which can be achieved by using a large output resistance of the amplifier. According to our results, poles generated by the EA output resistance and parasitic capacitance of a pass transistor might cause system instability and, correspondingly, a large value of output capacitor with proper equivalent series resistance, which deteriorates the bandwidth of the regulator.

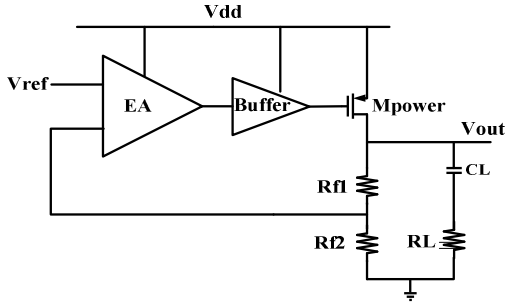

Fig. 1 Conventional linear LDO regulator using buffer compensation. (EA: Error amplifier)

The buffer circuit is added of the EA output it is shown in Fig. 1 [3]. By using two pairs of a parallel circuit, low output impedance can be achieved for frequency compensation, subsequently allowing the transient response to enhance low voltage applications, as shown in Fig. 2 (a). The small signal circuit is shown in Fig. 2 (b). This buffer contains two shunt feedback loops: on composed of M1 and M2, and other composed of M1-M2-M3. The output resistance of the proposed buffer $r_{o,Buf}$ is show as ,

$$r_{o,Buf} \approx \frac{1}{g_{m1}g_{m2}r_{o1} + g_{m1}g_{m3}g_{m4}r_{o1}r_{o3}} \tag{1}$$

The buffer prevents the circuit from operating in such an unstable condition by using its low input capacitance and output resistance characteristics. A dominant pole P_1 consists of output load capacitor C_L and equivalent output resistance R, which can be obtained as [$r_{o,mp} \parallel (R_{fb1} + R_{fb2}) \parallel R_{load}$], where $r_{o,mp}$ is the output resistance of the error amplifier. The second pole P_2 is generated from output resistance of the error amplifier $r_{o,ea}$ and capacitance, which results mainly from input capacitance $C_{i,buf}$ of the buffer. The third pole P_3 is generated from buffer output resistance $r_{o,buf}$ and parasitic capacitance C_p of the large size pass transistor. These three poles can be obtained as,

$$P_1 = \frac{1}{2\pi R_{out} C_L} \qquad P_2 = \frac{1}{2\pi r_{o,ea} C_{i,buf}} \qquad P_3 = \frac{1}{2\pi r_{o,buf} C_p} \tag{2}$$

The non-dominant pole need to very large, which let phase margin can be steady state operation. The gain of the error amplifier is shown in Fig. 3 (a). From the transient analysis to observe, when Vdd from 1.8V to 3.0V, rise time (R) and fall time (F) are both 10ps. The output voltage difference will not exceed 0.03V. The Vdd change with transient (R, F = 10ps) is shown in Fig. 3 (b). The Vout change with transient (R, F = 10ps) is shown in Fig. 3 (c). If the R and F are both 4μs, its output voltage difference will not exceed 0.06V, either. The Vdd change with transient (R, F = 4μs) is shown in Fig. 3 (d). The Vout change with transient (R, F = 4μs) is shown in Fig. 3 (e). Therefore, two EAs of added buffer circuit can improve PSRR. Then LDO circuit diagram is shown in Fig. 4.

(a)

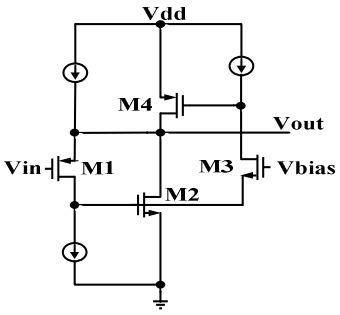

(b)

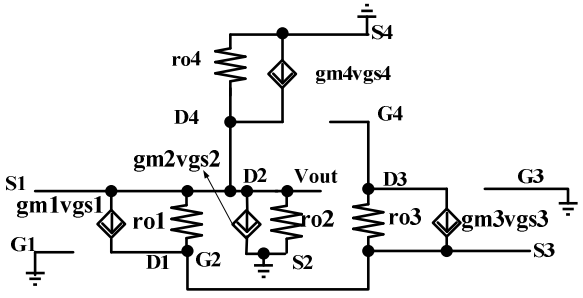

Fig. 2 (a) Circuit schematic of ultra-low output resistance buffer. (b) Small signal circuit of ultra-low output resistance buffer.

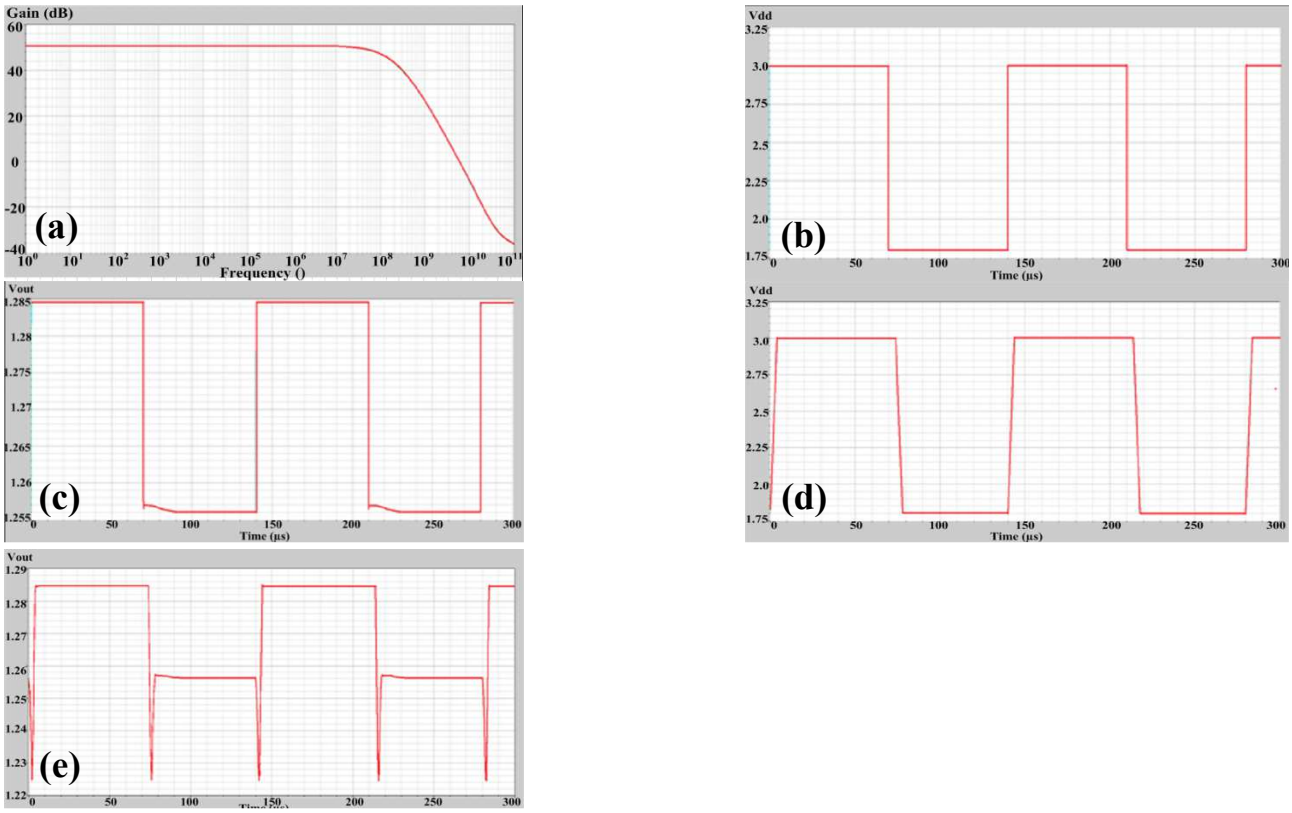

Fig. 3 (a) The gain of the EA. (b) The Vdd change with transient (R, F = 10ps). (c) The Vout change with transient (R, F = 10ps). (d) The Vdd change with transient (R, F = 4μs). (e) The Vout change with transient (R, F= 4μs)

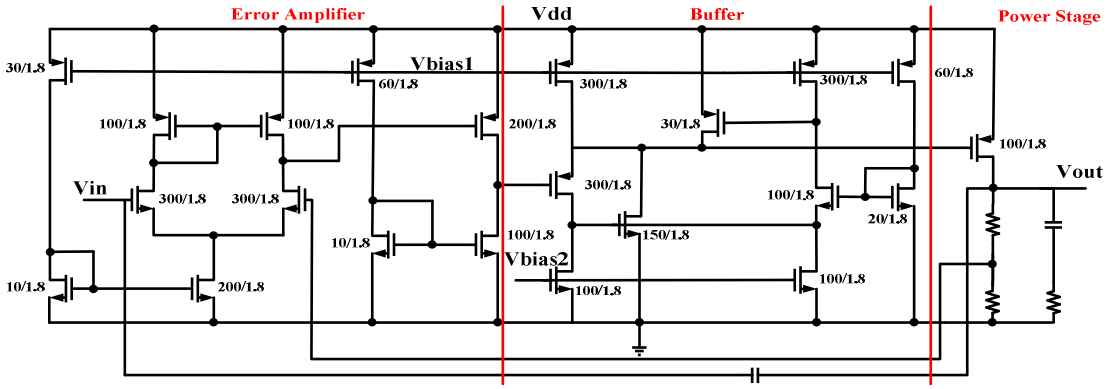

Fig. 4 Schematic circuit of the LDO using two stage error amplifiers and ultra-low output resistance.

Table 1 (a) Summary of this study performance. (b) Summary of existing LDO and this study.

(a) Process	TSMC 0.18μm CMOS
Vdd voltage	1.8V~3.0V
Output voltage	1.27V
Gain of EA	About 50dB
PSR	-60dB
PSRR	>60dB

(b) Paper	[2]	[3]	[4]	[5]	This work
Input voltage(V)	2.5~4	2.5~5.5	NA	1.8~4.5	**1.8~3**
Output voltage(V)	NA	0.6~3.3	NA	1.6V	**1.27**
PSRR(dB)	NA	>45	>45	40	**>60**
Dropout voltage(V)	0.15	0.12	0.2	0.2	**0.53**

NA: Not applicable

Simulation results

Above experiments are list in Table 1(a) and 1(b). Simulation results indicate that, when the supply voltage ranges from 1.8V to 3V, the output voltage can be held at 1.27V, as shown in Fig. 5 (a). Consequently, the output voltage is stable and independent of supply voltage. By the

definition PSR=$V_{dd}=\frac{V_{out}}{V_{dd}}$, PSRR=$\frac{A_d}{A_{dd}}$, this circuit of PSR = -60dB is shown in Fig. 5 (b), and PSRR is more than 60dB which that is better than [3] and [4] is obtained. The LDO linear regulator is implemented in a 0.18-μm double-poly five-metal CMOS process. The layout chip area of LDO linear regulator is 21.5 μm× 42.6 μm as shown in Fig. 6.

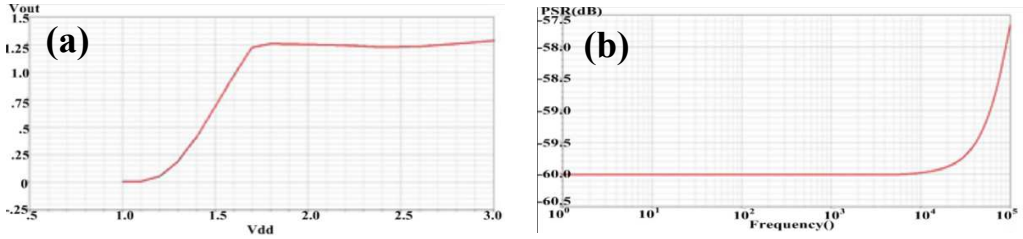

Fig. 5 (a) The output voltage at supply voltage 0V to 3V. (b) Measurement results of PSR.

Conclusions

In summary, this work demonstrates the feasibility of combining ultra-low output resistance buffer and two-stage amplifiers for LDO applications. Simulation results indicate that the high PSRR, stable output voltage and the circuit's PSRR is higher than 60dB, which is better than [3] and [4] obtained in this study. In addition to reducing the layout area, the proposed low dropout regulator linear regulator can add capacitors, which are needed based on the bandwidth. The circuit is designed and fabricated in a TSMC 0.18μm CMOS technology.

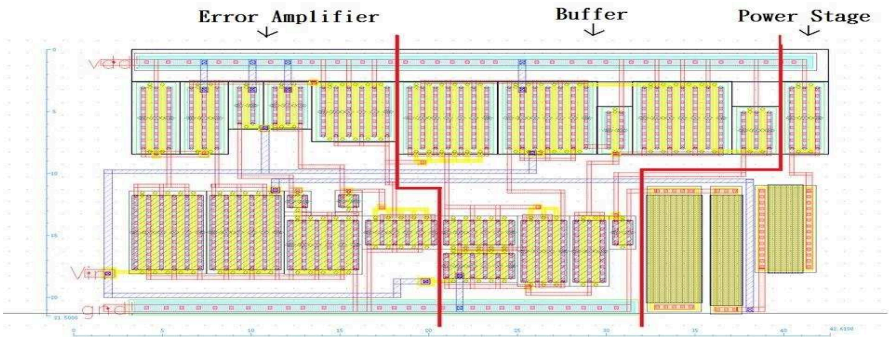

Fig 6 Layout of the LDO linear regulator. The layout chip area is 21.5μm × 42.6μm.

References

[1] Yali Shao, Yi Wang, Zhihua Ning, and Lenian He : Analysis and design of high power supply rejection LDO (IEEE 8th Interna-tional Conference, vol. 20-23, pp.324-327, Oct. 2009.)

[2] Xin Ming, Ze-kun Zhou, Bo Zhang: A low-power ultra-fast capacitor-less LDO with advanced dynamic push-pull techniques (IEEE/IFIP 19th International Conference, vol. 3-5, pp.54.59.3-5, Oct. 2011.)

[3] Jungsu Choi, Jungeui Park, Wooju Jeong, Junsang Lee, Seok Lee, Jayang Yoon, Jaehoon Kim, and Joongho Choi : Design of LDO linear regulator with ultra-low-output impedance buffer (International SoC Design Conference 2009).

[4] Al-Shyoukh, M. Hoi Lee, and Perez R.: A Transient-Enhanced Low-Quiescent Current Low-Dropout Regulator With Buffer Impedance Attenuation, IEEE Journal OF Solid-Sate Circuits, vol. 42 (2007) pp.1732-1742.

[5] Ho. E.N.Y., and Mok. P.K.T.: A Capacitor-Less CMOS Active Feedback Low-Dropout Regulator With Slew-Rate Enhancement for Portable On-Chip App-lication, IEEE Circuits and Systems, vol. 57 (2010) pp.80-84.

Advanced Materials Research Vols. 989-994 (2014) pp 3240-3243
© (2014) Trans Tech Publications, Switzerland
doi:10.4028/www.scientific.net/AMR.989-994.3240

The Research of Numerical Control Transformation Based on Turbo PMAC

Sun Hongchang[1, a], Li Lina[2, b], Deng San-peng[1, c]

[1]TianJin University of Technology and Education, Tianjin, China, 300222,

[2]TianJin Transportation Vocational College, Tianjin, China, 300110

[a]sunhog@126.com, [b]lilina_edu@126.com, [c]dengsanpeng@qq.com,

Keywords: Numerical Control Transformation; System Development; Turbo PMAC;

Abstract. A numerical control transformation （NCT）system for a conventional lathe machine is introduced in this paper. The NCT system is considered as the key equipment to the manufacture of the transmission shaft. According to the construction feature and technological requirements, both the hardware and software construction are analyzed, as well as the implementation method of the NCT system. By practical operation, the experiment test result is given at the end of the paper to support the usefulness and practicality of the NCT system.

Introduction

The transmission shaft is one of the key parts of engineering vehicle, by which the power transmission is completed from engine to wheel hub, bearing larger twisting and rolling load [1]. Therefore, the improvement of the transmission shaft hardness is crucial to improve the surface mass density and surface finishing [2]. Although the rolling and strengthening process processes have a long history and laggard implementation of conventional and ordinary lathe machines. This situation lead to high labor intensity, low machining efficiency and long measurement cycle, so a numerical control transformation from conventional lathe to highly automated rolling machine is under badly need[3].

Description of the control objective

The construction of the rolling machine tool is shown in fig.1. The rolling machine is transformed from a conventional lathe machine. The transmission shaft 2, to be rolled, is stuck within the spindle 1 and goes through the center for the rolling head. By using the operating panel 3, the carriage 7 carries the rolling head 5 moving along the horizontal direction while the hydraulic pressure is engaged to the rolling head by hydraulic system. At the same time, the laser displacement sensor 4 in rolling process will carry out a measurement of the part size both before and after the rolling process.

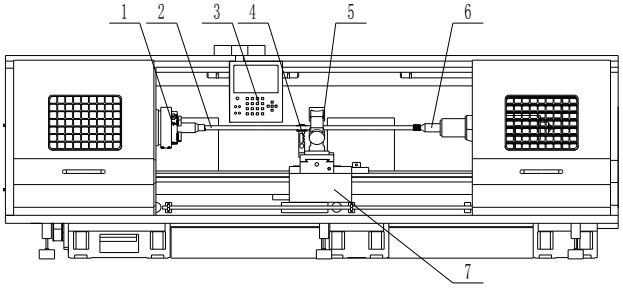

1-Spindle C） 2-Transmission shaft 3-Operating panel 4-Laser range sensor
5-Rolling head 6- Hydraulic tailstock 7- Carriage
Fig.1 Construction of the Rolling Machine Tool

The process parameters of the rolling will be preserved and analyzed through the process database system. According to the reinforcement processing characteristics and manufacture feature of the rolling transmission shaft, there are two kinds of rolling head 5, the rod rolling head and the gear rolling head, which are used differently according to the rolling position of the transmission shaft.

The transmission shaft has a centrosymmetric structure and each end of the transmission shaft is the transitional arc from the rod to the gear. By crossing the rod, the rolling head goes from the gear at left to another at right. According to the process demand, the hydraulic pressure is dynamic-adaptive changed according to the dimensional size of the transmission shaft, which rises up a high precision and swift response control demand both on hydraulic servo control and the displacement measurement, as well as the motion control.

Hardware technique scheme

The NCT system is based on Turbo PMAC (Programmable Multi-Axis Controller), which is the product of Delta Tau Data System Inc. It is and the key part of the whole control system and the representative for open CNC system .The NCT system consists of embedded PLC control system, hydraulic control system ,measurement and data acquisition system, process database system; The Machine tool carriage goes along the X axis direction, spindle rotation is around the C shaft, hydraulic control system outputs accurate pressure value according to the demand of rolling process, control and measurement system of acquisition of transmission shaft parts will get surface size parameters, by detecting the diameter deviation of the transmission shaft before and after the rolling. At last, the rolling process of each parts of various process parameters will be transmitted to the remote process database server.

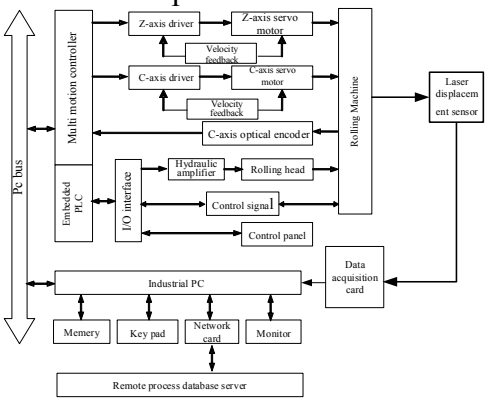

Fig. 3 The hardware principal of the NCT system

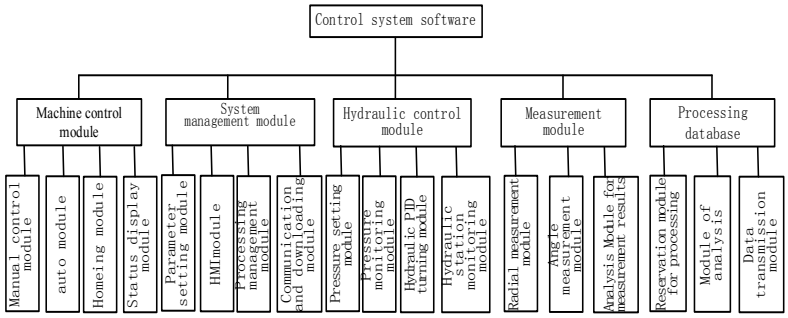

Fig.4 Schematic software construction

Motion control system consists of multi motion controller, I/O interface, servo motor, optical encoder, travel switches and other parts. It is the core of the rolling machine tool, which is responsible for the motion control, the interpolation between Z and C axis, encoder signal input and output, tooth rolling dividing control etc...

Embedded PLC control system is the core of the logical control of the rolling machine tool including digital I/O, A/D, D/A conversion function and the processing of the feedback signal, electromagnetic valve, hydraulic tailstock etc...

The hydraulic control system is composed of PID control algorithm, analog input and output card, servo amplifier, hydraulic servo module, hydraulic pipeline, hydraulic pump station, and rolling head[3]. It provides constant oil pressure within certain process section, and the pressure will also change swiftly from one dimension to another. To realize this swift and constant hydraulic pressure adjustment a pressure sensor is installed within the rolling, and giving the pressure feedback to the hydraulic control system. Under the precise pressure control, the rolling head generates corresponding force upon the transmission shaft, leading to a better surface density.

The diameter and the rotation angle of the transmission shaft, which are measured by the laser displacement sensor and optical encoder respectively [4-5], is considered to form a real-time section of the transmission shaft, which is shown in Fig.5-(a).The final process data can be determined, considering the section as well as the transmission shaft part size and location characteristics, by the remote process database system. Under the construction of the process data, the start point of the rolling, the specific pressure of each section and the rotation speed are all confirmed and applied intelligently [6-7].

Software of the NCT system

Object-oriented and modular programming technology are adopted during the control system software development which is based on Windows XP operating system. The application program is supported by Delphi 7. The structure of the system software is shown in figure 4. The software system includes five main modules: machine control module, system management module, hydraulic control module, measurement module, processing database.

Machine control module is responsible for all precise motion control functions, such as axis interpolation, acceleration and deceleration, etc... Status of servo system and hydraulic system can be monitored in this module in real-time.

System management module is mainly responsible for parameter settings of rolling pressure, velocity of the linear motion as well as the program file management, such as establishing, deleting, loading and store a program. Some communication functions among control system, multi motion controller and processing database are also integrated within this module.

By reading the output of the laser displacement sensor, the detection of the diameter changes can be obtained according to the angle that measured by optical encoder [8-10]. Also by this way, the cross section feature of the transmission shaft will be transferred into the industrial computer, which is shown in fig.5 (a). Under the help of the processing database, the processing parameters, such as the start point, endpoint, and adjustment of the rolling pressure will be calculated and confirmed by the control system software.

The hydraulic module makes a real-time controlling and monitoring to the rolling pressure. It is deigned to be every sensitive to maintain the continuation and stability by the PID turning algorithm embed within the multi motion controller. When the process data is changed, the rolling pressure will be changed intelligently and quickly according to the process data.

ACCESS format is applied in the database development, in which the part number, part dimension (before and after processing), processing capacity, processing date information are included. All the information to be analyzed and reserved will be uploaded to the remote database by TCP/IP protocol, every time the rolling is finished.

Rolling test

With the diameter of 45.84mm, the number of teeth is 44, a transmission shaft is rolled by the rolling machine tool with the control system. The sampling frequency is 10 kHz, 12450 coordinate points are gathered every rotation by the measurement module with time-consuming 1.25s. The measurement result of the rolling is shown in Fig.5 (1)， and the program data generated is shown in Fig.5 (b)

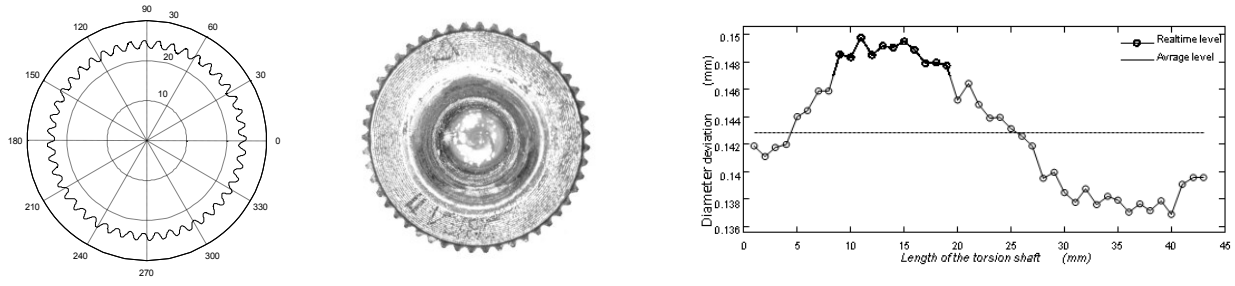

(a) Cross section of the transmission shaft (b) the diameter change after rolling

Fig.5 Experience result of the rolling

Summary

The NCT system is the combination of the numerical control technology, servo hydraulic technology, laser detection technology, database programming technology. The rolling of transmission shaft is implemented the by interpolation of C axis and Z axis, servo control and adjustment of the hydraulic pressure is carried out by PID auto turning algorithm.

The reconfigurable rolling module is used to meet the demand of rolling to different parts of a transmission, the surface of the rod, the transitional arc between the rod and the gear and the teeth of the gear. The whole control system is with high degree of automation, extension and easy system. By using the control system, the intelligent transmission shaft rolling is realized, the system is easy to extend, the efficiency of rolling process is also improved dramatically.

Acknowledgements

This work is supported by China National Funds for Young Scientists (61301040), the Tianjin Science and Technology Key Research Program (13ZCZDGX01500;14ZCZDSF00022).

References

[1] Yang Tao, Sun Wei, Wang Hongyan. *Fatigue Intensity Analysis of the Transmission Bar of a Tank Based on Virtual Prototyping Technique*[J]. Journal of Academy of Armored Force Engineering, 2006, 20(3):1. (in Chinese)

[2] Li hui, Wang Baichao, Zhang Dashun, et al. *Analysis on influence factors of fatigue life of transmission shaft*[J]. Manufacturing Automation, 2010, 32(1): 3. (in Chinese)

[3] Wang Chunxing. *Hydraulic Control System* [M].Beijing: Machinery Industry Press, 1999. (in Chinese)

[4] LI Xiaotian, ZHANG Tieqiang, ZHANG Shengyong, et al. *Small object's dimension measure and three-dimension reconstruction system based on laser triangulation* [J]. Optical Instruments, 2008, 30(6):21-26. (in Chinese)

[5] Y. KONDO, K. HASEGAWA, H. KAWAMATA,et al. *On-machine non-contact dimension-measurement system with laser displacement sensor for vane-tip machining of RFQs*[J]. Nuclear Instruments and Methods in Physics Research A,2012, 667:5-10.

[6] FUMIN ZHANG, XINGHUA QU, JIANFEI OUYANG. *An Automated Inner Dimensional Measurement System Based on a Laser Displacement Sensor for Long-Stepped Pipes*[J]. Sensors,2012, 12: 5824-5834.

[7] CEFU HONG, SOICHI IBARAKI. *Non-contact R-test with laser displacement sensors for error calibration of five-axis machine tools*[J]. Precision Engineering, 2013, 37:159-171.

[8] K. PRASHANTH ANANDAN, O. BURAK OZDOGANLAR. *An LDV-based methodology for measuring axial and radial error motions when using miniature ultra-high-speed (UHS) micromachining spindles*[J]. Precision Engineering, 2013, 37: 172-186.

[9] Y.C. TAN, Z.M. RIPIN. *Technique of Measuring Piston Secondary Motion Using Laser Displacement Sensors*[J]. Experimental Mechanics, 2012, 52:1447-1459.

[10] FEILONG LIN, STUART T. SMITH, GHAZANFAR HUSSAIN. *Optical fiber displacement sensor and its application to tuning fork response measurement*[J]. Precision Engineering, 2012, 36: 620-628.

Advanced Materials Research Vols. 989-994 (2014) pp 3244-3247
© (2014) Trans Tech Publications, Switzerland
doi:10.4028/www.scientific.net/AMR.989-994.3244

Rotor Local Rubbing Fault Feature Analysis based on Teager-Huang Transform[1]

Shangkun Liu[a], Guiji Tang[b], Bin Pang[c]

Department of Mechanical Engineering, North China Electric Power University, Baoding, Hebei, 071003, China

[a]lsk1213@163.com, [b]tanggjlk@ncepubd.edu.cn, [c]huadianpb@126.com

Keywords: rotor system; local rubbing fault; Teager-Huang transform; fault diagnosis

Abstract. An analysis method based on Teager-Huang transform for rotor local rubbing fault diagnosis is introduced. Firstly, the original vibration signal is decomposed into some Intrinsic Mode Function (IMF) components by using Empirical Mode Decomposition (EMD) approach, secondly, Teager energy operator is applied to estimate the instantaneous amplitude and instantaneous frequency of each IMF component, so the time-frequency distribution of the signal is obtained. The rotor local rubbing fault is simulated on a rotor test rig. The analysis results show that this method compared with Hilbert- Huang transform (HHT) can track the occurrence of rotor local rubbing fault better and can extract the characteristics of rotor local rubbing fault effectively. It provides a reliable method for timely and accurate diagnostic to the rotor local rubbing fault.

Introduction

With the requirement of high speed and efficient to rotating machinery, space between the rotor and stator is smaller and smaller. It often happens rubbing accidents between the rotor and stator, therefore, it is important to extract the fault feature of early local rubbing rapidly and to diagnose the rotor rubbing early. It is significant to diagnose the rotor local rubbing which occurs before the full rubbing.

Rotor rub impact signal is nonlinear, non-stationary. Some non-stationary signal processing methods such as: wavelet analysis [1], Hilbert-Huang transform [2], singular value decomposition [3] are widely applied in extracting the rubbing fault feature. The Hilbert-Huang method is a common rub impact fault characteristics time-frequency analysis method. It is composed of two parts EMD and Hilbert transform. EMD can decompose the signal into some IMF and Hilbert transform can solve the instantaneous amplitude and instantaneous frequency of each IMF component, but the Hilbert transform itself has endpoint effect, and can produce meaningless negative frequency [4].

Teager-Huang transform bases on Hilbert-Huang transformation. It combines the EMD and Teager energy operator to analyze the vibration signal. EMD can decompose the signal into several IMF components adaptively, then the Teager energy operator gets the instantaneous amplitude and instantaneous frequency of each IMF component [5]. Teager energy operator can reveal the change of instantaneous frequency better from the energy trace point of view, so it is an effective means to monitor the rotor rubbing occurrence and to extract the local rubbing feature.

Fundamental of Teager-Huang transform

The EMD method. This method of Huang et al.[6] to extract such IMFs is a pure algorithmic method. Candidates for an IMF are extracted by first computing the upper $u(t)$, and lower $v(t)$, envelopes via a cubic spline interpolation from the maxima and minima of $x(t)$. Then the mean envelope is obtained by computing $m(t)=[u(t)+v(t)]/2$ and finally the candidate by $r_1(t)= x(t)-m(t)$. Generally, r_1 does not fulfill the properties of an IMF. A good candidate can be reached by iterating the same process to r_1 and the subsequent r_k. The final retained IMF is $x_1(t)= r_n(t)$. Then the next IMF is obtained by the same algorithm applied on $x(t)- x_1(t)$. The remaining IMFs can be computed by repeating this algorithm on the successive residues.

Teager Energy Operator(TEO). Because TEO is high demodulation precision and high speed, in recent years, it is widely used in the instantaneous frequency and instantaneous amplitude analysis [7], the definition of TEO for continuous signal:

$$\psi[x(t)] = [\dot{x}(t)]^2 - x(t)\,\ddot{x}(t) \tag{1}$$

$x(t)$ is the original signal, $\dot{x}(t)$ and $\ddot{x}(t)$ are the first derivative and the two order derivative.

To discrete signal, TEO can be defined as

$$\psi[x(n)] = x^2(n) - x(n+1)x(n-1) \tag{2}$$

From the calculation of Eq.2, TEO requires only three sampling points every time, literature [7] analyzed the singe AM-FM signal by TEO. The instantaneous amplitude and instantaneous frequency:

$$f(n) = \frac{1}{2}\arccos[1 - \frac{\psi[x(n+1) - x(n-1)]}{2\psi[x(n)]}] \tag{3}$$

$$a(n) = \frac{2\psi\,[x(n)]}{\sqrt{\psi[x(n+1) - x[n-1]]}} \tag{4}$$

TEO compared with Hilbert transform has no complex number calculation, so its calculation amount is very small. It can quickly track the change of the amplitude and frequency of signals, and can reveal the instantaneous frequency mutation better.

Teager-Huang transform. The original signal can be decomposed into a series of IMF components through the EMD method, then calculate the instantaneous amplitude and instantaneous frequency of each IMF by Eq. 3 and Eq.4, so the time-frequency expression of the original signal is:

$$T(w,t) = Re\sum_{i=1}^{n} a_i(t)\exp^{j\int w_j(t)dt} \tag{5}$$

According to Eq.5, the time-frequency diagram and time-frequency-amplitude three-dimensional diagram can be constructed to reveal the signal time-frequency characteristic.

Rotor Local Rubbing Fault Analysis

When the rotor local rubbing occurs, the speed is unstable. The time frequency distribution characteristics assume the regular fluctuation along the base frequency. The mutation moment of instantaneous frequency is corresponding to the deformation point time in the time domain waveform, also this is the moment of the local rubbing occurrence. As the continuous rubbing process, the base frequency component changes acutely in the time frequency diagram at the late rubbing stage, at the same time the low frequency and high frequency appears.

The local rubbing simulation experiment is done at 3300r/min speed by Bently RK-4 rotor test rig. Two electrical vortex sensors are set up at the single plant's two sides to get the radial direction displacement vibration signal. The copper rubbing thimble is fixed in a place which has a small separation from the shaft. Sampling Frequency is 5120Hz. The analysis time is 60.4s.

Because the gathering data is large, the paper re-samples every 10 point to analyze, so the analysis frequency is 512 Hz. For tracking the whole process of rotor local rubbing, the time course is divided into three stages: the occurence stage, the early stage and the late stage.

The occurrence stage of rotor local rubbing impact. Analysis the 0-16s' data, the time domain waveform is shown in Fig. 1(a), it shows the signal amplitude distortion at the 9 second. Fig. 1(b) shows Teager-Huang transform analysis, it indicates the instantaneous frequency mutation at about the 9 second too, the low frequency and high frequency appears. Fig.1(c) is the time-frequency-amplitude three-diagram which shows the same result. Fig.2 is the analysis result by HHT, it doesn't show the instantaneous frequency mutation clearly when the rotor rubbing occurs. So

Teager-Huang transform can track the instantaneous frequency mutation better then HHT, and it can be used in the online rotor monitor and diagnosis.

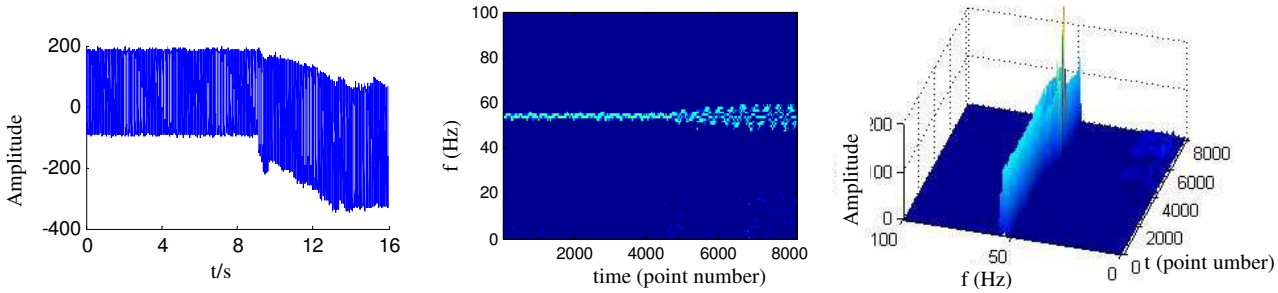

(a)time domain waveform (b)time-frequency diagram (c)time-frequency-amplitude dimensional

Fig.1 The occurence stage analysis by Teager-Huang transformation

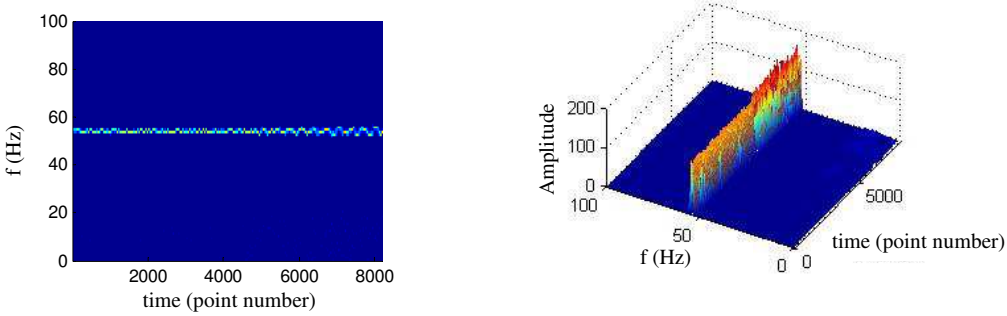

(a)time-frequency diagram (b)time-frequency-amplitude dimensional

Fig.2 The occurrence stage analysis by Hilbert -Huang transform

The early stage of rotor local rubbing impact. The paper analyzes the rubbing data of 17-19.9s by Teager-Huang transform. Fig. 3(a) shows the time frequency distribution. Fig. 3(b) shows the time-frequency-amplitude distribution. They show that the rubbing signal characteristic appears evident regular fluctuation, and the 1/2, 1/3 frequency components appear, all of this reflect the characteristics of early local rubbing.

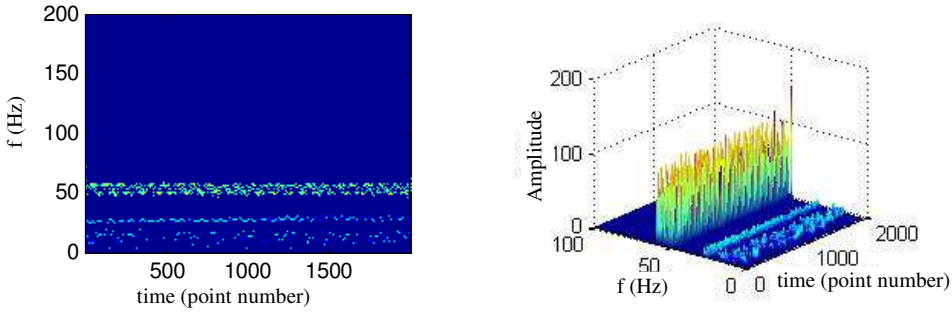

(a)time-frequency diagram (b)time-frequency-amplitude dimensional

Fig.3 The early stage analysis by Teager -Huang transform

The late stage of rotor local rubbing impact. The paper analyzes the late stage rubbing data of 56-59.9s by Teager-Huang transform. Fig. 4(a) shows the time frequency distribution. Fig.4(b) shows the time-frequency-amplitude three-diagram. They show the frequency components of this stage is more complex and the rubbing signal characteristic appears more high frequency besides the 1/2, 1/3 frequency components . The amplitude increases compared with the early stage, it assumes rotor vibration is more complex and acutely.

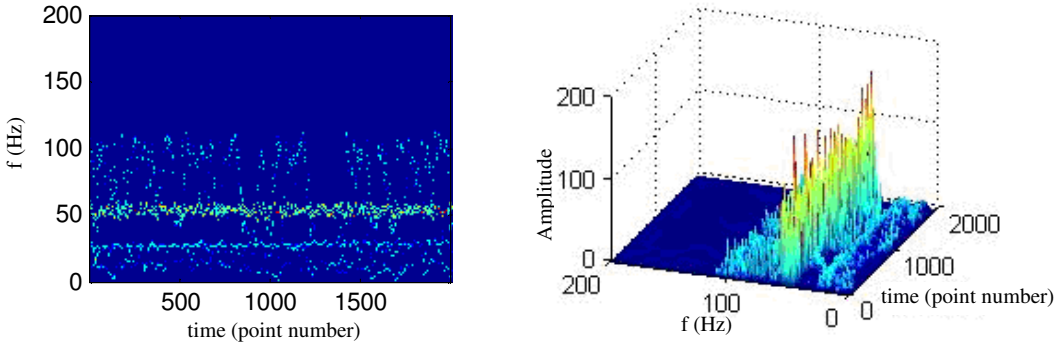

(a) time-frequency diagram (b) time-frequency-amplitude dimensional

Fig.4 The late stage analysis by Teager -Huang transform

Conclusion

The paper introduces the fundamental of Teager-Huang transform firstly, also simulates the rotor local rubbing fault at the constant speed condition through the Bently RK-4 rotor test rig, then analyzes the local rubbing process data by Teager-Huang transform. The results show this method can track the rotor local rubbing occurrence, development better, and can extract the rotor local rubbing fault feature effectively. It provides important method for the rotor local rubbing fault diagnosis.

The Fundamental Research Funds for the Central Universities(2014MS156

References

[1] Chen Xiangmin, Yu Dejie,Li Rong. The rotor signal resonance sparse decomposition and reassigned wavelet scalogram of rub impact fault diagnosis methods and the impact of vibration based on [J]., 2013, 32 (13): 26-29.

[2] Xiang Ling, Zhu Yongli, Tang Guiji.HHT method is applied in the vibration fault diagnosis of rotor in [J]. Chinese. Proceedings of the CSEE, 2007, 27 (35):83-88.

[3] Liu Xiandong, Yang Shaopu, Shen Yongjun, etc.. Singular value decomposition mutation journal, information detection method and its application in mechanical engineering based on [J]. 2002, 38 (6): 102 -105.

[4] Zhang Dexiang, Wang Ping, Wu Xiaobei, et al. The empirical mode decomposition and Teager energy spectrum of gearbox fault diagnosis [J]. Journal of vibration and shock, based on 2010, 29 (7):109-111.

[5] Li Hui, Zheng Haiqi, Tang Liwei.Teager-Huang transform in the fault diagnosis of gear crack applications [J]. Journal of vibration, measurement and diagnosis, 2010, 30 (1):1-5.

[6] HUANG N E, SHEN Z, LONG S R. The empirical mode decomposition and the Hilbert spectrum for nonlinear and nonstationary time series analysis [J]. Proc. R. Soc. Lond. A, 1998, 454：903-995.

[7] Marago s P, Kaiser J F, Quatieri T F. Energy separation in signal modulations with applications to speech analysis [J] .IEEE Transactions on Signal Processing, 1993, 41 (10) :3024- 3051.

Advanced Materials Research Vols. 989-994 (2014) pp 3248-3251
© (2014) Trans Tech Publications, Switzerland
doi:10.4028/www.scientific.net/AMR.989-994.3248

Coupled FE-SPH Simulation of a High-speed Grinding Process Using a Multiple-grain Model

Ruidong Shen[1, a], Xiumei Wang[1, b], Chunhui Yang[2, 3 c]

[1]School of Mechatronics Engineering and Automation, Shanghai University, Shanghai, 200072, China

[2]School of Computing, Engineering and Mathematics, University of Western Sydney, Penrith, NSW 2751, Australia

[3]Institute of Infrastructure Engineering, University of Western Sydney, Penrith, NSW 2751, Australia

[a]379739419@qq.com, [b]wangxm@shu.edu.cn, [c]r.yang@uws.edu.au

Keywords: Grinding; Multiple-grain cutting; Finite element method (FEM); Smooth particle hydrodynamics (SPH); Cutting Force.

Abstract. A multiple-grain cutting model is developed to simulate the grinding process for rolled homogeneous armor steel (RHA) 4043 using a coupled three-dimensional (3-D) finite element (FE) - smoothed-particle hydrodynamics (SPH) approach in the research. The proposed numerical model is then employed to investigate interactions and interferences among the grains at high speed cutting. The numerical results show the cutting forces and pile-ups of chips are greatly influenced by these interactions and interferences during the cutting process.

Introduction

Grinding is a commonly-used material removal processes using grinding wheel as cutting tool and employed as a finishing process in machining for shaping workpieces with high precision. The grinding wheel is an expendable wheel and composed of an abrasive compound used for various grinding and abrasive machining operations. These particles are termed as abrasive grains at a large number and their size and distribution are very random and therefore it makes the grinding process a very complex machining process to be studied. For simplicity, the cutting process of a single grain has attracted research interests using both numerical and experimental means, which becomes a precursor to understand the entire grinding process. However in reality, the single-grain cutting process is not easy to be studied using traditional experimental approaches because the grain is too tiny at micro scale. Therefore, numerical modelling and simulation techniques have been widely used for simulating the single-grain cutting process, including kinematic approaches, finite element analysis and molecular dynamics, etc.[1] and among them, the finite element method (FEM) is the most powerful tool for simulating cutting processes [2][3]. The smooth particle hydrodynamics (SPH) method is also used, which was originally developed for problems in astrophysics and now it is used in fluid and continuum mechanics.

Doman et al. [3] developed an experimentally validated finite element model with the Lagrangian method for the rubbing and ploughing phases as precursors to the cutting phase in scratch tests. Also using the Lagrangian method, Öpöz and Chen[4] conducted a 3-D simulation of single grain grinding with the adaptive remeshing technique for the rubbing and ploughing phases. Su et al. [2] conducted a simulation of single grain cutting based on fluid-solid interaction method, in which the grain was modeled by Lagrangian meshes while the workpiece was modeled by Euler meshes. In the work of Anderson et al.[5], a finite element model combined the Euler and Lagrangian methods was developed in which Euler meshes were implemented in large deformation zones while Lagrangian meshes were used in others. Villumsen et al.[6] introduced a simulation approach on metal cutting using the SPH method and Niklaus et al.[7] conducted a simulation of single grain cutting using the SPH method to investigate influences of grain geometry, grain orientation and grain placement on cutting forces, burr

generation and chip removal rates. Recently a coupled 3D FE-SPH model of a single-grain cutting process for the grinding on RHA 4043 was developed by authors [8], focusing on influences of grain negative rake angle as well as high and super-high cutting speeds from 100 m/s to 260 m/s.

In this study, based on authors' previous work on single-grain model, a three-dimensional (3-D) numerical model of the multiple-grain cutting, using the coupled Lagrangian finite element (FE)-smoothed particle hydrodynamics (SPH) approach, is developed for the high speed grinding of RHA 4043 workpiece. The multiple cutting grains are modelled as several truncated pyramids, which can be made with cubic boron nitride (CBN) abrasive materials. The developed numerical model is employed to investigate the interactions and interferences of grains during the grinding process. The results extracted from the proposed model mainly include the cutting force and chip formation.

Coupled FE-SPH Model for Multiple-grain Cutting

In the current study, the multiple-grain cutting model was idealised as a RHA 4043 workpiece (160 μm in length, 200 μm in width and 40 μm in height) and three CBN cutting grains as shown in Fig. 1 (a). The single grain was treated as a truncated rectangular pyramid which is made of cubic boron nitride (CBN) abrasive materials.

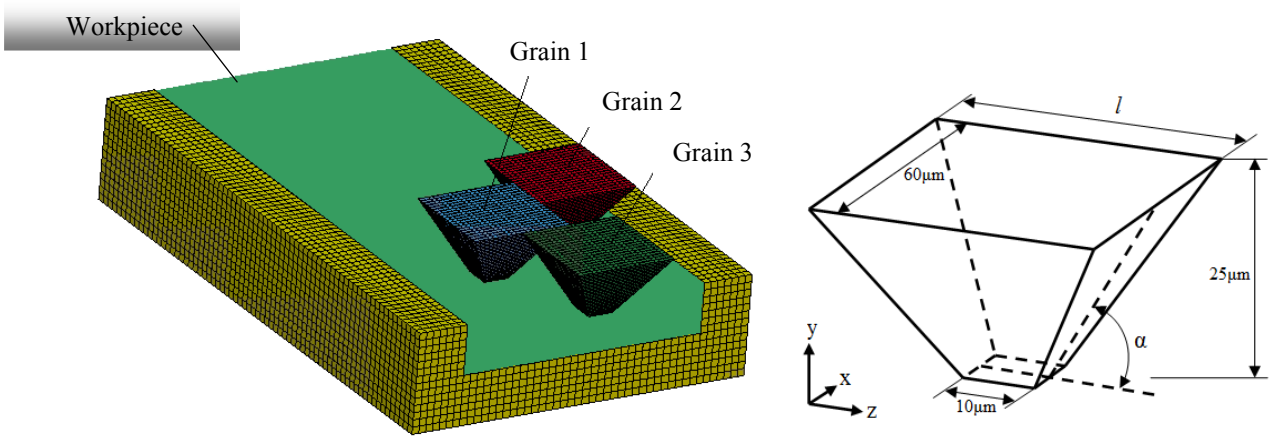

(a) (b)

Fig. 1 The multiple-grain cutting model

In high deformation zones close to contact zone between the workpiece and the grains, the SPH method was implemented in the central part of the workpiece as a cuboid of 160 μm × 120 μm × 20 μm with fully taking advantage of this method. The benefits employing the SPH method include a fracture criterion is not required to initiate chip formation since the workpiece material defined by SPH particles will naturally flow around these cutting grains and also adaptive meshing which is usually implemented in cutting process using the Lagrangian method is avoided. In the regions relatively far from the contact zone, since the deformations are relatively small, the Lagrangian finite element method was implemented for the rest zones in the workpiece and the grains using 8-node solid hexahedral Lagrangian elements. The coupling between Lagrangian elements and SPH particles was achieved using "automatic nodes_to_surface" contact type where the slave part was defined with SPH particles and the master part was defined with the Lagrangian elements [10]. Also considering the symmetry of the model, only a ½ model was used to reduce the computational costs. The SPH zone has a mesh density of 512×10^6 nodes/mm^3.

The geometry of the CBN abrasive was captured under the scanning electron microscope (SEM) in literature [8] and the mathematical model of a single grain is the truncated pyramid and its dimensions are shown in Fig. 1 (b), which can be treated as elastic. The single grain model has an adjusted dimension – its length l, which can be varied to get different values of negative rake angle α of interest. In the numerical simulation, the grain was moved along the positive direction of the z-axis in a defined moving path depicted in Fig. 2.

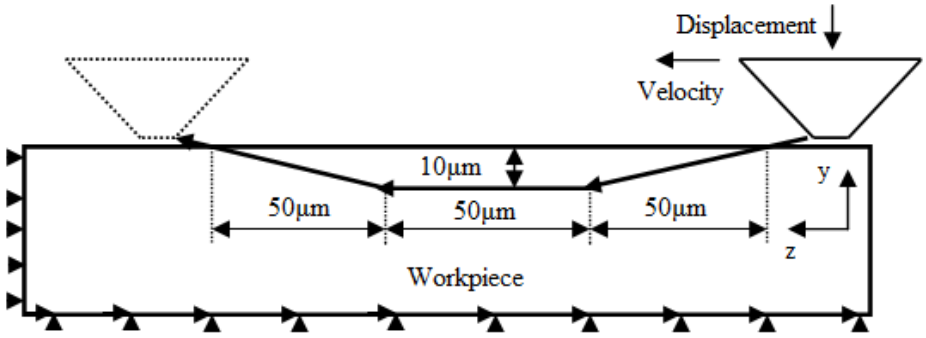

Fig. 2 Grain cutting path and boundary conditions in the numerical model

To model the mechanical behaviours of RHA 4043 steel at high strain rates and material softening caused by plastic heating, the Johnson-Cook material model was chosen for the workpiece and its general form is given as

$$\sigma_y = \left[A + B\left(\varepsilon_p\right)^n\right]\left(1 + C\ln\frac{\dot{\varepsilon}_p}{\dot{\varepsilon}_{p0}}\right)\left[1 - \left(\frac{T - T_0}{T_m - T_0}\right)^m\right] \quad (1)$$

where σ_y is the material yield stress, ε_p is the effective plastic strain, $\dot{\varepsilon}_p$ and $\dot{\varepsilon}_{p0}$ are the effective plastic and reference strain rates, and T, T_0, T_m are the current, ambient, and melting temperatures, respectively. A, B, n, C and m are materials constants. The main parameters in this model were adopted from literature[10].

Results and Discussion

A series of simulations were conducted to investigate the interactions and interferences among the cutting grains. The grains were set with a same negative rake angle of -31° and moving at the same cutting speed of 200 m/s. The total simulation time was set as 0.8 μs. Total forces of all three grains during the cutting process were obtained and shown in Fig. 3 (a).

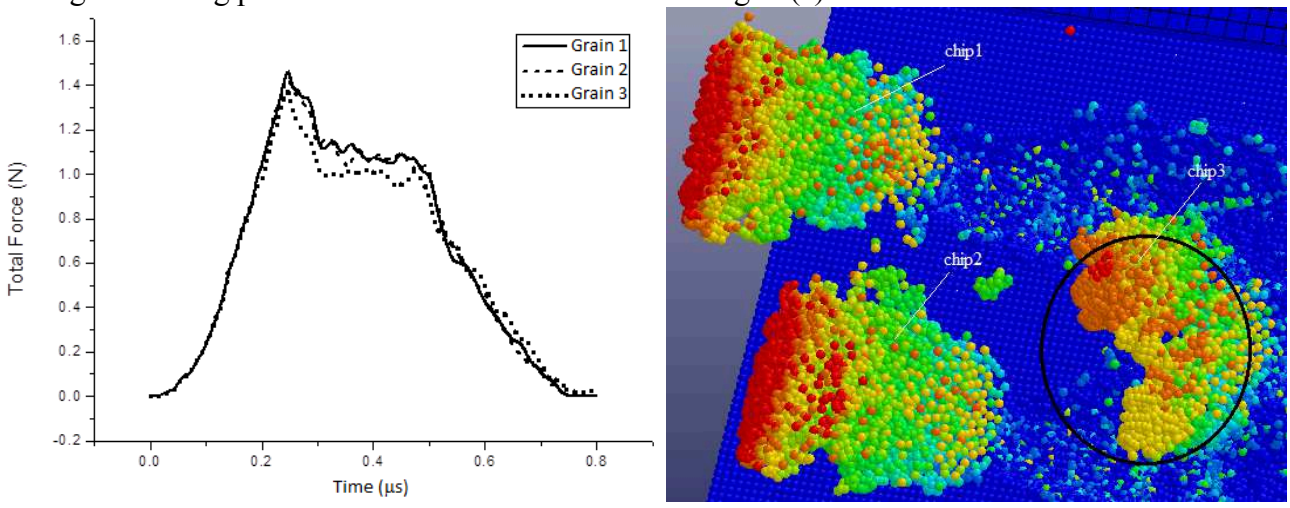

(a) (b)

Fig. 3 Total force and chip formation at each grain from 3-D simulations

In the model, Grain 2 was arranged right to Grain 1 while Grain 3 was just behind these other two. Grains 1 and 2 have much closer results during the cutting process compared to Grain 3 since these two grains are located in the upstream. These two grains influence each other almost at the same level. However the comparisons between Grain 3 with other two are more interesting and there are three stages identified: 1) $0 < t < 0.18$ μs, total forces have no difference with each other as Grain3 was not influenced by other two and still out of the affected region; 2) $0.18 < t < 0.55$ μs, Grain3 began to

reach the heat-affected zone where the workpiece material was softened by a large amount of heat generated by Grains 1 and 2. The material became much easier for Grain 3 to cut and thus the cutting force from Grain 3 was much lower than the other two; and 3) $t > 0.55$ μs, in this last stage, all grains finished the cutting on the workpiece and cutting forces were all dropped dramatically meanwhile the generated heat undergone a rapid decrease too.

The chip generation was also checked during this multiple-grain cutting process as shown in Fig. 3 (b). Pile-ups generated by Grains 1 and 2 were found ahead of Grain 1 while the softening was decreased, thus the cutting force of grain1 became larger than those from Grains 2 and 3. In addition, the interferences on chip generation have been found in the cutting process. Chips generated by Grain 3 were squeezed to fracture.

Summary

In this study, a 3-D multiple-grain model has been devised for modelling a high speed grinding using the coupled FE-SPH approach to investigate the interaction and interferences among the grains during the cutting process. Numerical results show that cutting force variation of these grains can be divided into three stages to show such interactions and interferences. When the subsequent grain is in the heat-affected zone and the workpiece material is softened by heat, the cutting force of the subsequent grain becomes much lower than those of the forward ones.

Acknowledgements

Shen and Wang would like to show their gratitude to Shanghai University's funding on the research project - Genetic Engineering of Materials. Yang would like to acknowledge the financial support on his research of advanced materials and smart structures from University of Western Sydney.

References

[1] E. Brinksmeier, J.C. Aurich, E. Govekar, C. Heinzel, H.-W. Hoffmeister, J. Peters, R. Rentsch, D.J. Stephenson, E. Uhlmann, K. Weinert and M. Wittmann: CIRP Annals-Manufacturing Technology 55(2) (2006), p.667-696.

[2] C. Su, J. Hou, L. Zhu, W. Wang: Journal of System Simulation 19 (2008): 045, p.5250-5253.

[3] D.A. Doman, R. Bauer, A. Warkentin: Proceedings of the Institution of Mechanical Engineers, Part B: Journal of Engineering Manufacture 223(12) (2009), p.1519-1527.

[4] T.T. Öpöz, X. Chen: Proceedings of Advances in Materials and Processing Technologies AMPT2010 International Conference, 1315 (1), p.1467-1472.

[5] D. Anderson, A. Warkentin, and R. Bauer: Int. J. of Machine Tools and Manufacture 51(12) (2011), p.898-910.

[6] M.F. Villumsen, T.G. Fauerholdt: LS-DYNA. Anwenderforum, Bamberg (2008), p.17-36.

[7] Ruttimann, Niklaus, Sebastian Buhl, and Konrad Wegener: J Mach Eng 10 (2010), p.17-29.

[8] R. Shen, X. Wang and C. Yang: Applied Mechanics and Materials 483 (2014), p.3-8

[9] J.O. Hallquist: *LS-DYNAs Theoretical Manual*, LSTC, Livermore, 2006.

[10] M. Jutras: Dissertation, Université Laval, 2008.

Advanced Materials Research Vols. 989-994 (2014) pp 3252-3257
© (2014) Trans Tech Publications, Switzerland
doi:10.4028/www.scientific.net/AMR.989-994.3252

Sensorless Control of Switched Reluctance Motors Based on Pulse Injection, Position Sectors Divided and Variable Thresholds

Zifei Jia[1,a], Dean Zhao[1,b] and Yuyan Zhao[2,c]

[1]School of Electrical and Information Engineering ,Jiangsu University, Zhenjiang, 212013, China

[2]Changzhou College of Information Technology, Changzhou, 213000, China

[a]307561694@qq.com, [b]dazhao@ujs.edu.cn, [c]56869043@qq.com

Keywords: switched reluctance motor, sensorless control, variable thresholds, position estimation error

Abstract. To realize starting operation and reduce position estimation error of switched reluctance motor(SRM) without position sensor, a novel control method based on pulse injection, divided angle section and variable threshold is presented. The starting operation of SRM can be accomplished by injecting high frequency pulse and judging position sectors. Variable threshold is used to reduce position estimation error. The value of threshold is obtained by looking up table prestored in controller. The method avoids complicated mathematical model and is suitable for starting operation with two phases. Besides, rotor position estimation error of this method is analyzed and the method which can decreased the error is proposed. At last, the experiment has been done to verify the performance of the control method.

Introduction

Switched reluctance motor (SRM) has received widespread attentions on account of its good speed performance and fault tolerance. The using of position sensor, however, increases the system cost, reduces the reliability of the system and limits the range of application of SRM. Therefore, the development of reliable and low cost sensorless control method is quite necessary. To realize the sensorless control of SRM, a method based on pulse injection, position sectors divided and variable thresholds is proposed. The way of pulse injection is suitable for SRM at starting and low speed[1]. Divided sector simplifies the estimation of position[2-3]. The estimation error can be decreased by means of variable thresholds. Experimental results testify the advantage and feasibility of the method.

The Principle Analysis of Position Estimation Method

The Base Principle of Pulse Injection and Position Sectors Divided. The position of traditional SRM is detected by means of using a number of photoelectric tube installed on motor stator and a toothed plate installed on the rotor. The photoelectric tube outputs the logic value accordingly as long as the motor rotates. The controller receives the logic value and judges which position sectors the motor is located at. Thus, the electrical degrees of position is divided into several sectors. The controller receives the logic value of position sensor to judge the position sectors of the motor. The motoring phase changes according to the change of position sector.

the phase voltage equation of SRM can be expressed as

$$U_{dc} = Ri + L\frac{\mathrm{d}i}{\mathrm{d}t} + i\frac{\mathrm{d}L}{\mathrm{d}\theta}\omega \quad (1)$$

Here, U_{dc} is the bus voltage, $dL/d\theta$ is the change rate of phase inductance, ω is the angular speed.

With three-phase motor, for example, when the SRM is still, the high frequency voltage pulse is injected into three phase winding. Because the motor is static and the frequency of voltage pulse is very high, the amplitude of responding current is small. SRM does not rotate. The counter

electromotive force(EMF) and voltage drop of phase resistance can be neglected. the phase voltage equation can be simplified as

$$U_{dc} = L\frac{\mathrm{d}i}{\mathrm{d}t}. \tag{2}$$

From Eq. 2, the responding current value can be derived as

$$di = U_{dc}dt / L(\theta). \tag{3}$$

For discretization Eq. 3, the magnitude of current can be expressed as

$$\Delta i = U_{dc}\Delta t / L(\theta_0). \tag{4}$$

Here, Δi is the magnitude of responding current, $L(\theta_0)$ is the value of inductance at initial position θ_0, Δt is the pulse duration.

From Eq. 4, it can be found that the amplitude of responding current is inversely proportional to the value of phase inductance[4]. So the phase inductance can be determined according to the responding current amplitude. The phase inductance value of motor is in accordance with the electrical position. These are shown in Fig. 1.

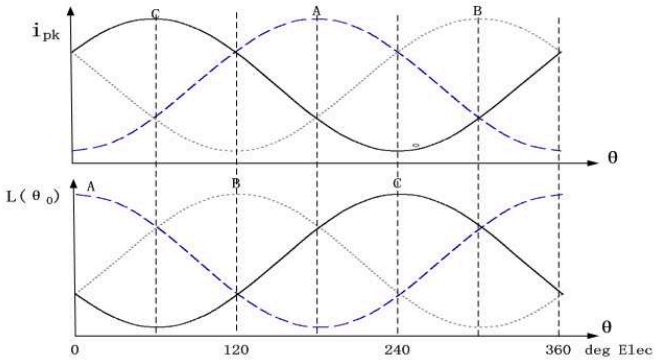

Fig.1 The value of responding current and phase inductance.

So, the position sectors of SRM can be determined by comparing the value of responding current with the thresholds which are used to distinguish the rotor position of SRM.

Rotor Position Estimation at Starting and Low Speed. The starting algorithm for the sensorless operation has to be able to run the machine from any initial condition. To do so, the power converter is used to inject current pulses simultaneously on all three phases of the SRM. The rotor position can be obtained based on a comparison of the pulse amplitudes and the two thresholds[5]. Table 1 summarizes the comparison algorithm. For example, if the initial position of SRM is located at the sector 3, the pulses are injected into all three phases of the SRM simultaneously to detect the position, the relative amplitude of the three phase pulses will be that: the pulse amplitude of phase A is lower than The Low Threshold, the pulse amplitude of phase B is also lower than The Low Threshold and at the same time the pulse amplitude of phase C is higher than The High Threshold. By looking up Table 1, it can be judged that the position is located at sector 3. The operation in sector 3 is phase B motoring and phase A sensing. After that, the starting of SRM will be realized.

Table 1: Sector in function of pulses amplitudes

sector		Phase A pulse amplitude	Phase B pulse amplitude	Phase C pulse amplitude
3	Phase B Motoring Phase A Sensing	$I_A<TL$	$I_B<TL$	$I_C>TH$
1	Phase C Motoring Phase A Sensing	$TL<I_A<TH$	$I_B<TL$	$TL<I_C<TH$
5	Phase C Motoring Phase B Sensing	$I_A>TH$	$I_B<TL$	$I_C<TL$
4	Phase A Motoring Phase B Sensing	$TL<I_A<TH$	$TL<I_B<TH$	$I_C<TL$
6	Phase A Motoring Phase C Sensing	$I_A<TL$	$I_B>TH$	$I_C<TL$
2	Phase B Motoring Phase C Sensing	$I_A<TL$	$TL<I_B<TH$	$TL<I_C<TH$

The algorithm is suitable for any repetition of three-phase machines. For machines with high number of phases, a suitable sector arrangement can be made similar to the three-phase implementation. The value of thresholds will depend on the inductance profile of the machine. After the starting of SRM, the suitable motoring and sensing phases in terms of the sectors are shown in Fig.2. Here, R, Q and P represent the logical value of position sensor in traditional SRM. The bold line represents the responding current which is given by injecting high frequency pulse after starting. The Low Threshold is used to determine when the phase used for motoring has to change. The High Threshold is used to determine when the phase used for sensing has to change.

A summary of the phase selection for motoring and position sensing as functions of the sectors related to the Table 1 sensing and motoring phases rotor position is shown in Fig.2. Fig.3 is the flowchart describing the SRM motoring operation. This algorithm directly depends on the sector information[6]. This information is first generated by the initialization algorithm, and then maintained with the phase selection algorithm.

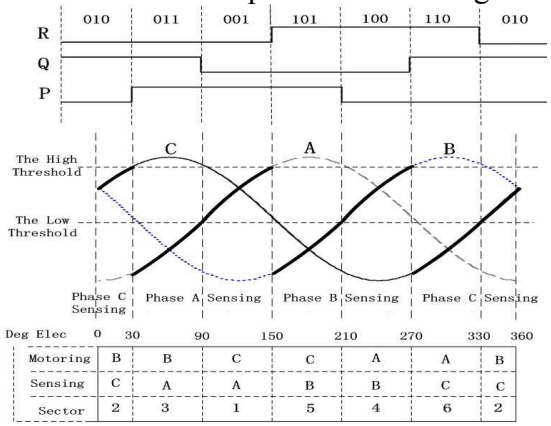

Motoring	B	B	C	C	A	A	B
Sensing	C	A	A	B	B	C	C
Sector	2	3	1	5	4	6	2

Fig.2 Position sectors and responding currents.

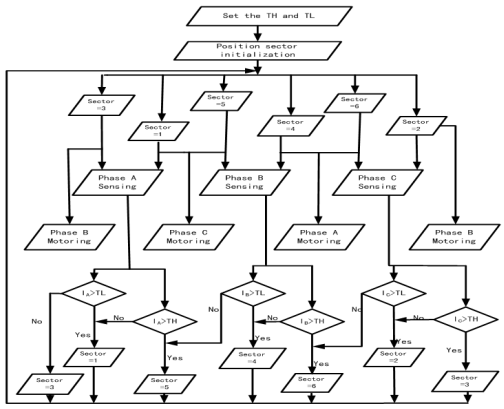

Fig.3 Flowchart of SRM sensorless operation.

The Variable Threshold under the Condition of Different Speed. It can be seen from equation (1) that the pressure drop of the winding and counter EMF are neglected when estimating the position of SRM. Solving the differential Eq. (1), the value of responding current can be derived as

$$i = \frac{U_{dc}}{A}(1 - e^{-\frac{A}{L}t}) \quad . \tag{5}$$

Where, $A = R + \frac{dL}{d\theta}\omega$.

When the SRM starts, the value of back EMF increases with the speed increasing. So the amplitude of responding current will decrease. The position estimation on certain point will have great error if still using the threshold which is setted before. It is illustrated in Fig. 4: ω1, ω2 and ω3 represents the curves of responding current amplitude when the SRM speed are respectively 0rpm, 200rpm, 500rpm. When the speed of SRM is 0rpm, the value of responding current is biggest because of the back EMF is zero. When the speed is 200rpm, the value of responding current decreases. When the speed becomes 500rpm, the value of responding current is smaller than its of 200rpm. The Threshold 1 is assured as The Low Threshold which is used to compare with responding current. Take the speed 0rpm and 500rpm for example, the phase commutation point is $A_1$when the SRM is still. This point can be detected as the 90 deg electrical. But when the speed increases to 500rpm, the phase commutation point will be A'_1 if still using The Threshold 1 as The Low Threshold. At the same time, the controller will take A'_1 as the 90 deg electrical. Actually, A_2 is the phase commutation point which should be obtained by comparing the responding current with The Threshold 2. So it needs to change threshold according to different speed.

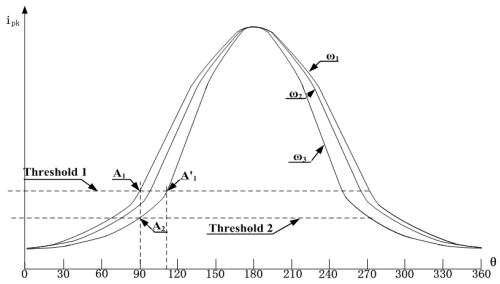

Fig.4 The variable thresholds under different speed.

To decrease the position estimation error caused by speed, a variable threshold method is proposed. The detail procedure is that testing The Low Threshold and High Threshold at different speed and then storing it in a table for controller to look up. The controller chooses different thresholds according to different speed to decrease the position estimation error.

Position Estimation Error Analysis

The machine structure, especially the number of rotor poles, and the inverter switching frequency limit the position resolution and fix the rotor position error. The resolution varies with the operating speed gradually worsening as the speed increases. For an SRM operating at a speed of n rpm and with a pulse injection frequency of pulse, the resolution in mechanical degrees is

$$\theta_{\delta} = \frac{n}{60} \times 360 \times \frac{1}{f_{pulse}} \quad (6)$$

The resolution in electrical degrees for an SRM with N number of rotor poles is

$$\theta_{e\delta} = \frac{n}{60} \times 360 \times \frac{1}{f_{pulse}} \times N \quad (7)$$

It can be inferred from Eq. (7) that with the senseless operation, the maximum position error occurs at the maximum speed of the machine, and the number of poles repetition directly affects the speed range of the senseless method. If the number of pole repetition is low, the senseless method will be able to reach higher speeds. For a pulse injection frequency of 3kHz, a SRM with 6/4 structure, the position resolution is 1.6 deg electrical at the speed of 200rpm and 4 deg electrical under condition of 500rpm. While if the SRM is 12-8 structure, the position resolution will be 3.2 deg electrical and 8 deg electrical. The frequency of pulse injection can be increased to decrease the position error under the allowance of switch devices and Signals to Noise Ratio(SNR).

Experimental Verification

To verify the performance of the control method, the experiments are implemented at a three-phase, 1KW, 6-4, low speed SRM. The base speed of the machine is 1000 rpm with a DC bus voltage 30V. The SRM drive used in this experiment is a classical bridge power converter with the phase winding between the two switches of the same phase. High capability price ratio DSP chip of TMS320F28335 of TI cooperation and CPLD chip of EPM3032 of ALTERA Company are chosen as the digital controllers. The phase current signals are obtained by the hall current sensor ACS750 timely. An absolute encoder is fixed on the shaft of motor to detect the position of SRM. A DC motor is fixed on the output of SRM to drive the SRM with a certain speed. The digital controller stores The Low Threshold and High Threshold under different speed. Hardware of the experimental system is shown in Fig. 5 and Fig. 6.

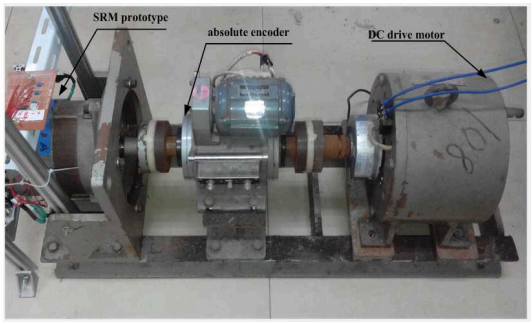

Fig.5 Hardware of the SRM.

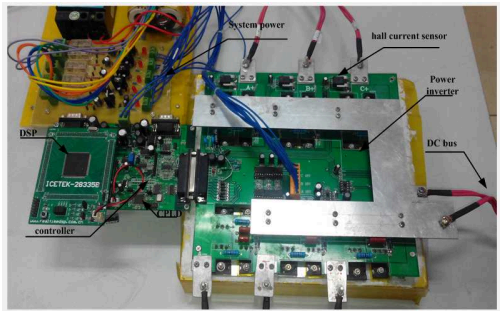

Fig.6 Hardware of control system.

The SRM is motioned by DC motor with a certain speed. At the same time, a high frequency pulse is injected into three phases and the phases give the responding current. The DSP will receive the signal of responding current which has been amplified and filtered. The DSP stores The Low Threshold and High Threshold at 22.5 deg mechanical and 37.5 deg mechanical which can be obtain by absolute encoder. Fig. 7 is a scope screen shot of one phase responding currents and position waveforms of SRM under the speed of 100rpm, Fig. 8 is under the condition of 500rpm. The High Threshold and Low Threshold under different speed is shown in Table2.

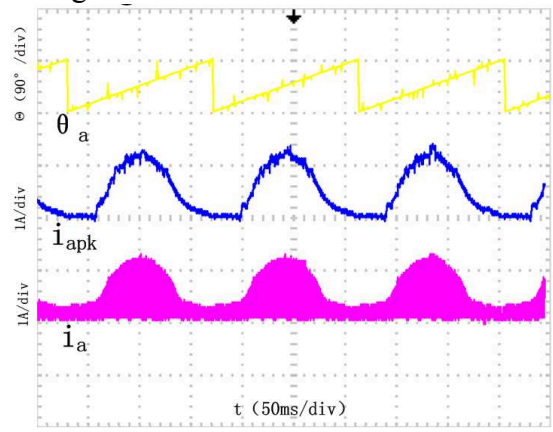

Fig.7 Wave under 100rpm.

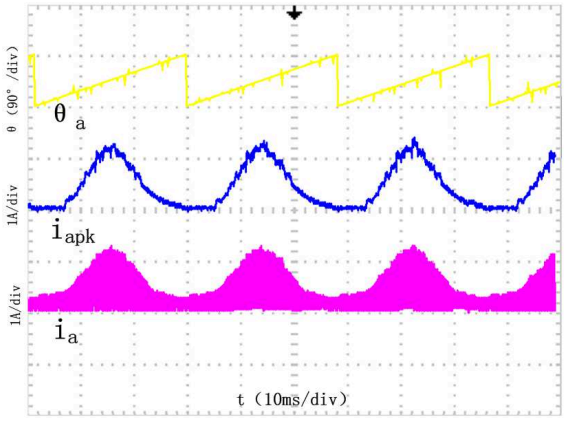

Fig.8 Wave under 500rpm

Table 2 The Low Threshold and High Threshold under different speed

Speed (rpm) / θ_c (deg)	0	100	200	300	400	500	600	700	800	900	1000
22.5°	0.454	0.45	0.448	0.445	0.441	0.439	0.436	0.431	0.427	0.421	0.41
37.5°	1.231	1.229	1.226	1.224	1.221	1.217	1.212	1.205	1.198	1.191	1.182

The position estimation errors under different speed are shown in Fig. 10. It can be seen from the Fig. 9 that the position estimation errors become bigger with the increasing speed of SRM. With the increasing of speed, the number of pulses in one sector becomes less. The resolution of responding current becomes low and the position estimation errors become big.

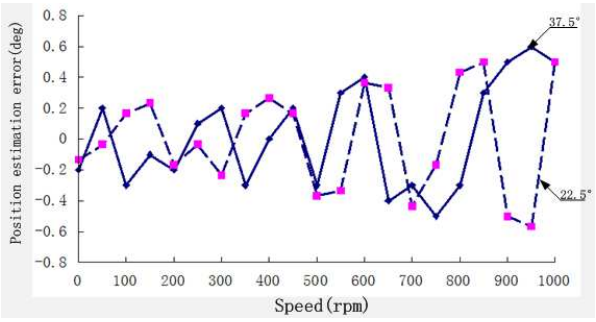

Fig.9 The position estimation errors under different speed

Conclusion

To overcome the starting and position estimation error problems of the SRM without position sensor, a algorithm based on pulse injection, position sectors and variable thresholds is proposed. By using this method, the position estimation error can be decreased and this method needs only the sector of the position instead of the precise position of SRM. The value of High Threshold and Low Threshold is changeable with different speed by looking up the table which is restored in controller and avoids complicated mathematical model. The high frequency pulse is injected in one phase only when SRM runs. It means that the SRM can work in condition with two phase motoring. The experimental results fully verify the proposed senseless scheme and demonstrate its advantages.

Acknowledgements

The key projects of the Jiangsu Provincial Science and Technology Support Program (Industry): Nuclear Power Plant uses High Reliable Switched Reluctance Speed Regulation Electric Actuator of Valves to develop (BE2012136); the projects supported by Advantage Discipline Construction Engineering of Jiangsu universities (PAPD).

References

[1] Qiu Yihui, Ma Zhiyuan and Zhan Qionghua, in: Start exploration of position sensorless SRM without rotor reversing[J]. Transactions of China Electro technical Society ,2001,16(2):18-22

[2] Zhou Jingcheng, Wang Xiaolin, and Deng Zhiquan, in: The Position Sensorless Technolo gy of Switched Reluctance Motor Based on the Regional Comparison of Three-Phase Inductance[J]. Transactions of China Electro technical Society ,2012,27(7):34-40

[3] L. Shen, J. H. Wu, and S. Y. Yang, in: Initial position estimation in SRM using bootstrap circuit without predefined inductance parameters. IEEE Trans. Power Electron., vol. 26, no. 9, pp. 2449–2456, Sep. 2011.

[4] Cai Jun and Deng Zhiquan Sensorless control of switched reluctance motor based on phase inductance model in linear regions[J] .Proceedings of the CSEE,2012,32(15) :114-123.

[5] Gao Hongwei, Salmasi F R and Ehsani M, in: Inductance model-based sensorless control of the switched reluctance motor drive at low speed[J]. IEEE Transactions on Power Electronics, 2004, 19(6): 1568-1573

[6] Pasquesoone G, Mikail R and Husain I, in: Position estimation at starting and lower speed in three-phase switched reluctance machine using pulse injection and two thresholds[J]. IEEE Transactions on Industry Applications,2011,47(4):1724-1731.

Advanced Materials Research Vols. 989-994 (2014) pp 3258-3261
© (2014) Trans Tech Publications, Switzerland
doi:10.4028/www.scientific.net/AMR.989-994.3258

Research on the Static Cushioning Property of Folding Corrugated Cushions

Qi Yuming[1, 2, a], Gao Wenhua[3, b,*]

[1]School of Mechanical Engineering, Tianjin University, Tianjin, 300222, China

[2]College of Mechanical Engineering, Tianjin University of Technology & Education, Tianjin, China, 300222

[3]College of Packaging & Printing Engineering, Tianjin University of Science &Technology, Tianjin, China, 300222

[a]chigym@163.com, [b]gaowenhua@tust.edu.cn

*Author for correspondence: Gao Wenhua, gaowenhua@tust.edu.cn.

Keywords: Corrugated cushion, Static cushioning property, Corrugated paperboard

Abstract. 0940 type cushion of E-flute corrugated paperboard is selected as the research object. By changing the load area, side breadth and the height of the cushions separately, static compression tests were done. The effects of structural parameter to cushioning property were analyzed through energy absorption method. It is useful to promote the application of corrugated board cushion.

Introduction

Since the requirements of "green packaging", when choosing cushion, they takes into account not only rationality of cushion structure and economy of cost, but also the importance of environmental protection of materials. So Compared with the traditional foam packaging materials, paper materials are valued more and more. Due to the light weight, good absorption of impact energy, extending the acting time of shock pulses, easy recycling and low recycling cost, corrugated paperboard gain growing popularity.

There have been many research on cushion property of corrugated paperboard structure. Some scholars in China or abroad have researched on the mechanical properties of different corrugated structures. Bending test of corrugated cushions for both horizontal and vertical on five different structural forms have been done by Myung Hoon Lee [1] . Sek tested the cushioning property of on stacked type corrugated board through dynamic shock [2]. Xu Wencai only tested the dynamic property of two cushioning structural forms of corrugated board [3, 4]. Wang Dongmei researched the static and dynamic properties of corrugated composites on four different structures [5]. In this paper, the author selects 0940 type cushion of E-flute corrugated paperboard as the research object. By changing the load area, side breadth of the cushions separately, static compression tests were done. And The effects of structural parameter to cushioning property were analyzed through energy absorption method. Gain the energy value E of the maximum compressive load by integrating to force-displacement curve getting in the static compression process. Further, its unit volume energy absorption E' is obtained. E' not only considers the effects of all parameters, also meets its cushioning mechanism. Then defines cushion efficiency $\rho = E/F$, and ρ can compare cushioning property under different parameter changes more comprehensively [6].

Experiments

Material and Equipment. Experimental materials: Materials used in the experiment were E-flute corrugated paperboard purchased from SCA (Tianjin) Packaging Products Limited Company, the thickness is 1.8mm, the basis weight is 475 g/m^2. The material surface is clean, no paper defects. The top of test sample is square, the smallest size 100mmx100mm, Max 160mmx160mm, the range of height and breadth both range from30mm to 60mm, and there are 4 parallel samples in each group.

Experimental equipment: Packaging prototype (PRODUCER1317) from Beijing State technology development limited, electronic universal material testing machine (model 3300) from Instron Company of the United States.

Experimental method. In order to study the effects of every parameter on the structure energy-absorbing, the cushioning structure were divided into two groups. The first group, load area(s) is the only variable. The second group, breadth is the unique variable. Height is 35mm constantly. All the parameters are showed as Figure 1. All size of the samples in three groups are showed in Table 1. Every group of the samples includes seven size.

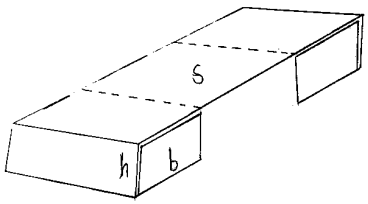

Fig.1 Diagram of 0940 type cushion

Table 1 Sample parameters of the three groups

b=40mm, s(mm^2)	100×100	110×110	120×120	130×130	140×140	150×150	160×160
s=150mm×150mm, b(mm)	30	35	40	45	50	55	60

The experiment was done according to GB 8168 "Testing methods of static compression for package cushioning materials". The test temperature is 23 ℃, relative humidity is 50%. In order to increase the friction to prevent the sliding during the experiment, two pieces of wooden board were fixed to the upper and lower pressing plates separately.

Results and analysis

Effect of load area on cushioning property. The relationships of load area and unit volume of energy absorption, cushioning efficiency, maximum compression loads in first group are shown in the Tables 2 below.

Table 2 Cushioning parameters under different load area

Load area（mm^2）	100×100	110×110	120×120	130×130	140×140	150×150	160×160
Load（N）	1683.83	2004.46	2122.82	2503.48	2301.51	2457.54	2811.50
E（KJ/m^3）	26.5	17.6	23.2	30.9	19.2	14.5	14.1
ρ	7.4	10.6	7.2	11	3.5	3.4	10.6

In order to see the trends of maximum load and energy absorption visually, fit the discrete points in the table 2, the results as shown in Fig.2.

From Fig.2 we can see, as load area increasing, maximum compression load increased, but the energy absorption of unit volume changes irregularly. When area that surrounded by the load and load area increasing, the energy absorption increasing. That is when the sample's deformation appears platform and the maximum compression load appeared at large deformation, the sample cushioning property is the best. So combining data and figure analysis, the energy absorption of unit volume is best while the load area to be 130mm×130mm. The cushioning efficiency of the structure is shown as Fig.3.

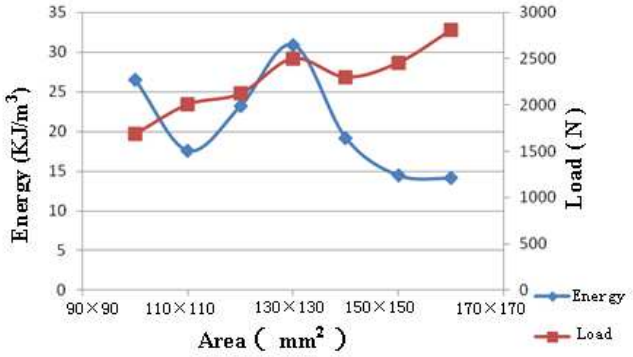

Fig. 2 Energy absorption of unit volume and maximum load curve

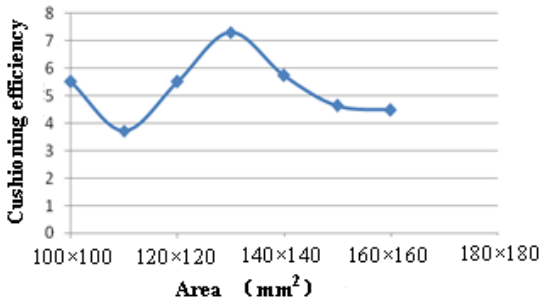

Fig. 3 Cushioning efficiency-area curve

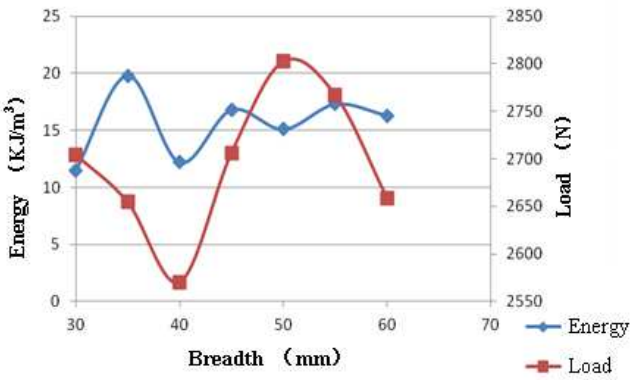

Fig. 4 Energy absorption of unit volume and maximum load curve

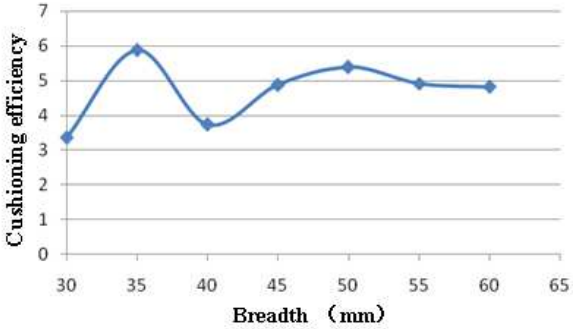

Fig. 5 Cushioning efficiency-breadth curve

Combining table 2 and figure 3, the maximum cushioning efficiency also appears at s=130mm×130mm, namely the cushioning effect is best.

Effect of breadth on the cushioning property. The relationships of breadth and energy absorption of unit volume, and unit volume of energy absorption, cushioning efficiency, maximum compression load are shown in the tables 3.

Table 3 Cushioning parameters under different breadth

Breadth（mm）	30	35	40	45	50	55	60
Load（N）	2704.51	2654.52	2570.08	2706.35	2802.85	2767.33	2658.32
E（KJ/m³）	11.5	19.8	12.2	16.8	15.1	17.3	16.3
ρ	3.36	5.88	3.73	4.88	5.39	4.91	4.82

In order to see the changing trends of maximum load and energy absorption of unit volume following load area visually , the discrete points are fitted. The results is as shown in Fig.4.

With the increase of breadth, energy absorption of unit volume and maximum load have no fixed changing trends, but within the breadth of the experiment, there is an extreme point, which the corresponding breadth is 35mm. Maximum load appears at b=50mm.

The cushioning efficiency of the structure is shown as Fig.5 .

Combining tables 3 and figure 5, the largest cushioning efficiency appears at b=35mm, so the cushioning effect is best.

Summary

In this paper, through the static compression cushion test for 0940 type cushion, came with the increase of load area and side panel breadth, maximum load, the energy absorption of unit volume and cushioning efficiency and best value. Results show that in all tests of the paper, when the load area is 130mm×130mm, side breadth is 35mm, the cushioning efficiency is highest, the cushioning property is best.

Acknowledgments

In this paper, the research is supported by The National Youth Science Fund Project(61301040); Tianjin Science and Technology Planning Project (13ZCZDGX01500) and (14ZCZDSF00022).

References

[1] Lee Myung Hoon, Park Jong Min. Flexural Stiffness of Selected Corrugated Structures [J].Packaging Technology and Science. 2004, 17(5): 275-286.

[2] SEKM, ROUILLARDV, TARASHH. Enhancement of Cushioning Performance with Paperboard Crumple Inserts. Journal of Packaging Technology and Science, 2005, 5(18): 273-278.

[3] Xu Wencai. Research on the cushion property of corrugated board. Packaging Engineering, 1997, 18(2): 78-79.

[4] Xiang Ming, Xu Wenca.The dynamic property of corrugated board cushion. Packaging Engineering, 1997, 18(5): 23-25.

[5] Wang Dongmei. Static Com pression and Energy Absorption Properties of Corrugated Composites. Packaging Engineerin, 2007, 28(12): 71-73.

[6] Li Zhaoyuan. Research on cushioning property and stimulation of typical corrugated board structure [D]. Jiangnan University, 2008.

Advanced Materials Research Vols. 989-994 (2014) pp 3262-3265
© (2014) Trans Tech Publications, Switzerland
doi:10.4028/www.scientific.net/AMR.989-994.3262

Interesting Packaging Structure Design of Children's Biscuits

Qi Yuming[1, 2, a], Gao Wenhua[3, b,*]

[1]School of Mechanical Engineering, Tianjin University, Tianjin, 300222, China

[2]College of Mechanical Engineering, Tianjin University of Technology & Education, Tianjin, China, 300222

[3]College of Packaging & Printing Engineering, Tianjin University of Science &Technology, Tianjin, China, 300222

[a]chigym@163.com, [b]gaowenhua@tust.edu.cn

*Author for correspondence: Gao Wenhua, gaowenhua@tust.edu.cn.

Keywords: Children's food, Packaging design, Fun packaging, Food packaging

Abstract. Biscuit, as a common snack, in order to attract the children's attention, besides its taste and shape, packaging design is equally important. The beautifully decorated surface of the box can be divided into a number of blocks (4 or 9) by setting the punch lines. After the biscuits are eaten up, tear the box along the punch lines, then it becomes a simple jigsaw puzzle. Inside the box except the biscuits bag, a cute clamp like scissors added. So the children can gripping biscuits by the clamp rather than by hand directly.

Introduction

Food industry and food market develop rapidly in China. The total output of food industry has risen to the first one in the country. A survey shows that food is the first one in China's urban residents' consumption structure, where children's consumption in the proportion of total household occupying more than 33% in more than 90% of families. The sixth Chinese population census in 2010 shows that the number of children in our country accounts for about 16.60% of the population, We can see children's food market is a considerable market [1].

In recent years, world food consumption grows constantly, and biscuits consumption topped the list in most countries. Although the types of children's food had become more and more, biscuits are always one of most favorite food for kids. Because biscuit can not only satisfy one's hunger, but also can be eaten as a snack. And compared with bread, pastries, biscuit can be stored and carried easier, so it is also liked by the parents [2].

Children are a special consumer group. They are curious and like to explore. Because the children's recognizing of products begin from the overpacks. The colorful pattern and the lively graphics of the overpack can impress children's mind very much. Most of children's biscuits have possessed that basically. Therefore, the entry point of this article is the packaging structure. The aim is to increase interest of the biscuits.

Children's biscuits purchase decision analysis

With the development of market economy and people's changes of consumption, biscuit that is used to allay our hungers or as gift for others before, is moving to leisure, health-based direction. And so are children's biscuits [3]. Children's food market is a special market. Although the target consumer group is children, but parents are the participants during the consumption process, and sometimes parents are the decision-makers. A survey shows children that are under 6 years old, 80% of purchase decisions are made by parents; 70% of children that are 6 years old to 12 years old have the decision-making power. So there are two decision-makers whether or not the product is purchased: children and parents. In consume concept, children and parents are quite different. Children's consumption is a typical emotional consumption, while parents are rational consumption. Whether to buy the biscuit or not, consumers can only determine through the packaging before purchase it. So

packaging is an important factor that attracts their purchase decision. If you want to attract the children's and parents' eyes through packaging, to master their consumer psychology is necessary during the packaging design stage.

Analysis of children's and parents' consumer psychology

Curiosity. Children are curious about everything. Something new and interesting can be a strong temptation for children. Therefore packaging with novel shape, distinctive appearance and full of changes can attract children's attention. Before making purchase decision children judge the biscuit only from packaging styles firstly, and then determine whether to buy it or not. So children's consumer behavior has obvious novelty, odd psychological characteristics, for them the interesting packaging is very important [4].

Fickleness. Children's consumer behavior is purely emotional in nature. They are interested in one thing quickly, and lose interest fast. The unique shape or bright colors of a commodity may attract the attention of children temporarily, but over time will slowly in the cold. Because they find that something else is more interesting. Therefore, in order to keep a kind of biscuit for a long freshness in children's heart the packaging must have sufficient "playable."

Health and safety. When parents are shopping for their children, the first consideration is health and safety. Particularly, food safety issues appeared frequently in modern society, which adds to parents' anxiety while buy food for children. And thus they are more cautious to it. After all, there is only one child per family, it is important than anything else that children grow up healthily. Food safety problems caused by many reasons, in addition to the food itself, the packaging is also the main reason. Even though both of these have no problems, it is bad for children's health while they taking food with unclean hands.

Versatility. For the average family, the children's consumption holds a big proportion of the total household expenditure. If buying one thing can meet children's various needs, which is helpful to reduce the family burden. With the growing awareness of environmental protection, considering the packaging to be versatile at the design stage, and it is popular that do not let them become "disposable" consumables.

So, to be able to attract children's attention, the biscuit packaging had to be novel, rich interesting; to attract the attention of parents, the biscuit packaging must be hygienic and versatile.

Packaging status of children biscuit

Paperboard carton. Now children biscuits mostly chose paper cartons as their sales packaging. And the inner packaging is composite plastics. Because paper materials are more environmentally friendly, recycling convenient and lower production costs, to be printed easier by variety of printing methods and to be decorated by rich colors. Structurally speaking, children biscuit cartons are rectangular mostly, And always decorated by bright colors, cartoon patterns looked lively. This packaging is stronger, and can protect the biscuits well. Once it's squeezed, biscuits will not be crushed easily.

Composite plastic bags. Another big category of children biscuit packaging is composite plastic bags. The characteristics of such packaging are easier processing, lower cost, but weaker protection to the product. Generally, biscuits are crisp, when transported or stored, they are easy broken. Nobody wants to buy a bag of crushed biscuits.

Other packaging forms. There is also a small proportion of children biscuit packaged by metal can or corrugated packaging boxes. Biscuits in metal can are often as gift. This packaging is stronger than others, and can protect the biscuits well. But it is deformed easily while impacted by others. The packaging cost is higher. Corrugated packaging is less cost. But it's more suitable for family pack, and is difficult to attract children's attention.

Interesting packaging design of children biscuits

Biscuit carton design. Packaging is a rapidly growing, high eliminating industry. 70% of packaging output will become waste after single-use. So how to recycle use packaging waste is an extremely meaningful thing.

There are already many food companies are sought to develop multifunctional or recycled biscuit packaging, such as Glico clamshell packaging cartons, Kraft plastic sealed cans biscuits packaging . In order to increase the attractiveness of biscuits and increase the fun of eating biscuits for children, and to avoid the packaging becoming waste immediately after the biscuits were eaten out, children's biscuit carton structure are made the following improvements in this paper. But the decorating style is not changed [5].

Biscuit carton is still the original rectangular structure, and the decoration is also cartoon-based style. On the front side are brand logo, biscuits taste and other information. For the bottom side, cartoon image or beautiful situation that children familiar with are used. And this side can be divided into 4, 6 or 9 pieces with punch lines. According to the increasing ages of the consumer group, the number of pieces can be increased. After the biscuits were eaten out, the packaging carton would become a fun toy – a jigsaw puzzle. The divided bottom side is shown in Fig.1.

Fig.1 The divided bottom side

The benefits of this design are the package's reuse after emptied, and it can also cultivate children's attention and develop their intelligence. The versatile packaging can stimulate the purchase desires of both parents and children. Moreover, these can also be designed as a series of jigsaw puzzles. Children will be curious about collecting all of puzzles, and then they will also enjoy this kind of biscuits.

Biscuit clip design. Now most of the children biscuits require grabbing with hands directly. It is neither hygienic nor interesting, and lack of challenging and fun. It is easy to cause disease if the children just come back outside, do not wash their hands and ate biscuits directly. It is a core objective of children product packaging that making learn more interesting. If we design a lovely "clip" for biscuit, it would be more interesting for eating. Younger children are at the stage of exercise capacity in all aspects. This cute little "clip" not only avoids children's hand contacting with food directly, but also to inspire their desires of learning to grab something with tools. At the same time, their muscles of hands and hand-eye coordination being exercised. So parents will be more confidence when children eating biscuits. In order to attract children, the head of the clip can be designed into a variety of animal heads, for example, bear head. It is shown as Fig.2.

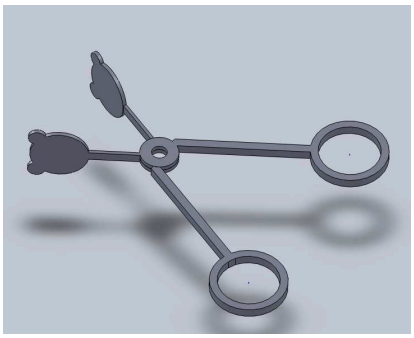

Fig.2 Biscuit clip

Summary

With the social development, the improvement of consumer demand, packaging sustainability is concerned more and more. packaging in line with the requirements of green packaging will be more and more. Child is a special consumer groups. Children's food packaging need constant improving to capture children's interests. Children's food packaging must meet the psychological needs of the consumer group. Besides basic functions, hygiene and interests of packaging are important for children's growth, which is a new challenge presented by age.

Acknowledgments

In this paper, the research is supported by The National Youth Science Fund Project (61301040); Tianjin Science and Technology Planning Project (13ZCZDGX01500) and (14ZCZDSF00022).

References

[1] Huang Wei, Li Baojiang. Children Biscuits Packaging Design. China Packaging Newspaper, 2005 -8-19 (3).

[2] Meng Qinghong. Analysis of the Essential of children's Article Packaging Design Based on children'ss Consumption Psychology. Packaging Engineering, 2009.04, p165-167.

[3] Ni Qian, Liu Qing, Wang Anxia. Research on Packaging reuse design. Packaging Engineering, 2010.03, p126 -128.

[4] Mark Hampshire (England), Keith Stephenson (England). Demographics Packaging. Beijing: China Youth Publishing Group, 2009:16 -17.

[5] Zhu Lingyu, Huang Liang. The humanistic requirements for children food packaging. CAIDCD2010 Vol.1. p601 - 603.

Advanced Materials Research Vols. 989-994 (2014) pp 3266-3269
© (2014) Trans Tech Publications, Switzerland
doi:10.4028/www.scientific.net/AMR.989-994.3266

Study on Axis Calibration Method of the Coordinate Measurement System Based on Binocular Vision

Zhang Zimiao[a], Zhang Shihai[b], Yanan Yu[c]

College of Mechanical Engineering, Tianjin University of Technology and Education, Tianjin 300222, China

[a]zzm19850126@aliyun.com,[b]4haizhang@163.com, [c]jesuisyyn@126.com

Keywords: Coordinate Measurement. Binocular Vision. Axis Calibration of Rotation Stage. Measurement Range

Abstract. For a coordinate measurement system based on binocular vision, system calibration is an important factor for measurement accuracy. In this paper we present a flexible calibration method for the axis calibration of rotation stage which is installed in front of the binocular vision system to increase the system measurement range. By putting a standard ball in front of the binocular vision system, a sequence of pictures is taken by the two cameras with a few different rotation angles of the rotation stage. With the method of space intersection of two straight lines, the reference points(the ball centers at each rotation angles) for axis calibration are figured out. The trail of standard ball is a circle. Since all ball centers of rotation are on a plane perpendicular to the axis, the center of circle is on the axis of rotation stage. The rotation axis of stage is then calibrated according to the calibration model.

Introduction

A basic problem in binocular stereo system is recovering the 3D construction of a world scene or object from a pair of images[1]. The main method to solve the problem is to find a binocular vision calibration method, which has a key effect on the measurement accuracy. To increase the measurement range of the system, a rotation stage is installed in front of the binocular vision system [2, 3], as shown in Fig.1.To reduce effect for the measurement accuracy of the turntable rotation, the rotation axis of stage needs to be calibrated before measurement.

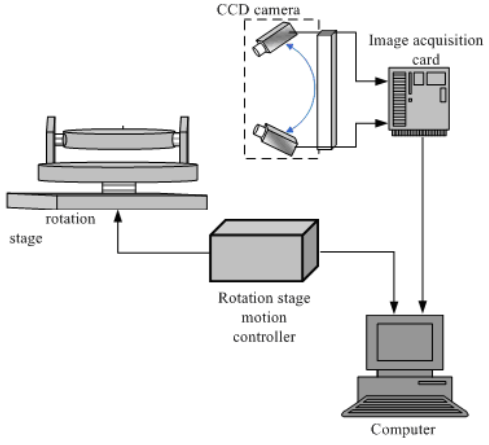

Fig. 1 The system structure

The measurement principle of system

The measurement model is shown in Fig.2[4, 5]. To increase the measurement range of the system, a two-axis rotation stage is installed in front of the binocular vision system.

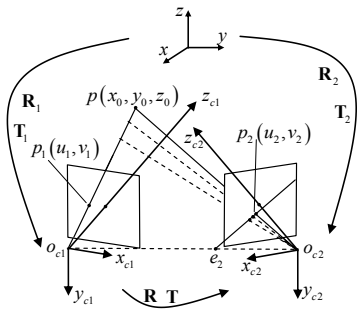

Fig. 2 The measurement model

Since the two axes usually do not intersect at one point, the measurement model should be constructed for this situation as shown in Fig.3: Firstly, the three axes are calibrated using a standard ball with the calibration method. Secondly, $O_{Ay}(x_{Ay}, y_{Ay}, z_{Ay})$ of azimuth axis is set as the origin and the upward direction of azimuth axis is set as the $O_{Ay}Y_{Ay.}$ In this way, the coordinate system Ay is established and the rotation and translation matrix M_{Ay} is determined. Based on the calibration information of pitch axis, two points s_1, s_2 are obtained and these two points can be converted into the representation in the coordinate system Ay. The rotation and translation matrix of pitch axis is M_{Ax}. Finally, given rotation matrix R (x) and R (y) which donate a object rotate around a fixed axis, the measurement model is built as shown in formula (1) according to the rotation order: azimuth (rotation angle a)→pitch (rotation angle b).

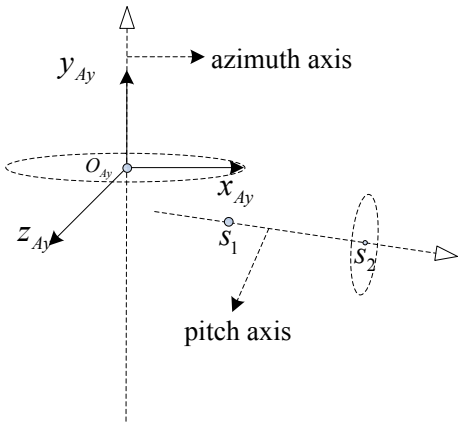

Fig. 3 The measurement model of two-axis rotation stage

$$\begin{bmatrix} \cos a & 0 & \sin a & 0 \\ 0 & 1 & 0 & 0 \\ -\sin a & 0 & \cos a & 0 \\ 0 & 0 & 0 & 1 \end{bmatrix} \mathrm{M}_{\mathrm{Ax}}(b)\mathrm{M}_{\mathrm{Ay}} \begin{bmatrix} x_{wi}^1 \\ y_{wi}^1 \\ z_{wi}^1 \\ 1 \end{bmatrix}^T = \mathrm{M}_{\mathrm{Ay}} \begin{bmatrix} x_{wi}^2 \\ y_{wi}^2 \\ z_{wi}^2 \\ 1 \end{bmatrix}^T \tag{1}$$

The calibration method of rotation stage axis

The basic principle of rotation axis calibration is to locate a line which represents the rotation axis and this line is donated by a vector and a point on the line.

In the process of calibration, after the images of a standard ball are acquired by the two cameras with different rotation angles of stage, the calibration of rotation axis is carried out. With the binocular vision system calibrated, the world coordinate of the standard ball center at each rotated position can be worked out considering the intersection of the ball center projecting line in the two cameras respectively. Because of the rotation of the stage, the trail of the ball center is a circle, whose center is on the rotation axis. All ball centers rotated are on a plane perpendicular to the axis.

The rotation axis of stage is expressed with a point on the axis and its vector. The calibration process is shown in Fig.4:

1) Rotate the stage and the coordinates of standard ball center in N positions are measured. So N groups of standard ball centers′ coordinates $O_n(x_n, y_n, z_n)$ are obtained.

2) Using the N groups of standard ball centers′ coordinates obtained in step 1, the least squares method is used to fit a plane. The plane can be considered as the rotation trail of ball center and the normal vector of the plane is the direction vector of the rotation axis, as shown in formula (2).

$$\begin{cases} A x_n + B y_n + C z_n + D = 0 \quad (n = 1, \cdots) \\ \mathbf{u} = [r_1 \quad r_2 \quad r_3]^{\Gamma} = \left[\dfrac{A}{\sqrt{A^2 + B^2 + C^2}} \quad \dfrac{B}{\sqrt{A^2 + B^2 + C^2}} \quad \dfrac{C}{\sqrt{A^2 + B^2 + C^2}} \right]^{\Gamma} \end{cases} \tag{2}$$

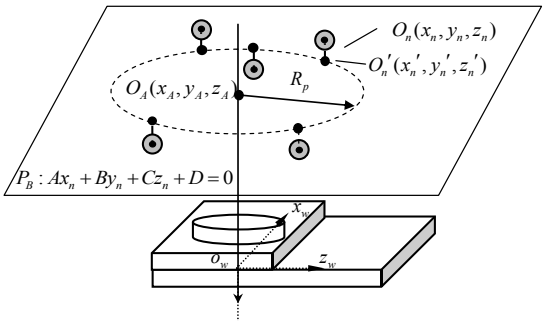

Fig. 4 The calibration of rotation axis

3) The N groups of standard ball centers′ coordinates $O_n(x_n, y_n, z_n)$ obtained in step 1 are projected to the plane obtained in step 2 and N groups of corresponding projection coordinates $O_n'(x_n', y_n', z_n')$ are obtained. The point that has the minimum distance to these projection points is searched in the trail plane by the objective function in formula (3). In this way, the point $O_A(x_A, y_A, z_A)$ is obtained which is the intersection point of the rotation axis and the trail plane of ball centers.

$$f(x_n', y_n', z_n') = \sum_{i=1}^{N} \left(\sqrt{(x_n' - x_A)^2 + (y_n' - y_A)^2 + (z_n' - z_A)^2} - R_p \right) = \min \tag{3}$$

Experiment Results

The following method is used to verify the accuracy of rotation calibration: the standard ball is placed on the two-axis rotation stage. The coordinates of ball centers are measured in 12 different locations through the rotation of stage and the mean value of coordinates are calculated according to formula (4).

$$\bar{x} = \frac{\sum_{i=1}^{12} x_i}{12}, \bar{y} = \frac{\sum_{i=1}^{12} y_i}{12}, \bar{z} = \frac{\sum_{i=1}^{12} z_i}{12} \tag{4}$$

The error of measurement results is calculated according to formula (5).

$$e_i = \sqrt{(x_i - \bar{x})^2 + (y_i - \bar{y})^2 + (z_i - \bar{z})^2} \tag{5}$$

The RMS of measurement results is finally calculated and is shown in table 1.

Conclusion

In summary, this paper presents a flexible calibration method for binocular stereo vision. A new calibration pattern with four big circles is designed, whose spatial coordinates system is built by the position of the four big circles. With several views of the plane pattern in different orientations, the parameters of the binocular stereo vision system, including the intrinsic parameters of each camera as well as the relative position translation matrix of two cameras, is calibrated using Zhang

plane-based calibration algorithm. The exterior orientation of the turntable axis is figured out by a sequence of images of a standard ball with different rotating angles. In the experiment, the diameter of a column bearing, whose diameter is 50.181mm measured by CMM, is measured using the calibrated binocular stereo vision system. With the least square method, the precision of the final measurement result is better than 0.025mm.

Table 1 Experiment results

Serial	Angle	Error(mm)	RMS
1	0°	0.066	0.0236mm
2	30°	0.052	
3	60°	0.071	
4	90°	0.090	
5	120°	0.017	
6	150°	0.062	
7	180°	0.061	
8	210°	0.047	
9	240°	0.042	
10	270°	0.010	
11	300°	0.045	
12	330°	0.032	

Acknowledgement

The paper supported by the science foundation of Tianjin University of Technology and Education (NO.KYQD14010).

References

[1] Chen H and Xu Z, "3D map building based on stereo vision," Proc ICNSC, Networking, sensing and Control, 969-973 (2006).

[2] Xie ZX, Zhan QM and Zhang GX, "Modeling and calibration of a structured-light-sensor-based five-axis scanning system," Measurement, Vol36, 185-194, 2004.

[3] Yan Y, Zhu Q, Lin Z, and Chen Q, "Camera calibration in binocular stereo vision of moving robot," Proc. WCICA 06, Intelligent Control and Automation, Vol2, 9257-9261, 2006.

[4] Tao Jin, Hongzhi Jia, Wenmei Hou, etc, Evaluating 3D position and velocity of subject in parabolic flight experiment by use of the binocular stereo vision measurement, Chinese Optics Letters, 2010, 8(6): 601-605.

[5] Xie Z.X, Zhang Q.M and Zhang G.X, "Modeling and calibration of a structured-light-sensor-based-five-axis scanning system", Measurement, Vol.36, 185-194 (2004).

Advanced Materials Research Vols. 989-994 (2014) pp 3270-3273
© (2014) Trans Tech Publications, Switzerland
doi:10.4028/www.scientific.net/AMR.989-994.3270

Research on Cantilever Used for Thermal Flow Meter as Switch

Zhang Zhili[1,a], Wu Yuanqing[2,b], Liu Chunmei[2,c]

[1]Tianjin Sino-German Vocational Technical College,Tianjin,300350,China

[2]College of New Energy, Bohai University, Jinzhou 100032, China

[a]tjzhangzhili@126.com, [b]wuyuanqing123@163.com, [c]liuchunmei1130@163.com

Keywords: Cantilever. Low consumption. Flow meter

Abstract. In order to reduce consumption of thermal flow meter and prolong its working life, this article makes a research on cantilever switch, which control the circuit and save its energy. A cantilever was added into flow meter and was put into the air flow aisle in front of sensors. Process was designed and nano-imprint method was used to realize cantilever. The device was simulated and the effect on reducing consumption was certified, which has great significance on thermal flow meter.

Introduction

MEMS (Micro Electro Mechanical Systems) thermal mass flow meter response quickly, has large detection range, has perfect sensitivity and good stability for low flow, with excellent applicability in industrial and civil. However, the device has energy problems due to the use of DC battery power, and the circuit needs to be designed to improve energy efficiency. It is a good way to decrease power consumption by turning off the circuit when no gas passes through, but when the gas passes again, we need to open the circuit.

Under these circumstances, this article designed a kind of switch by use of cantilever. There are so many other applications in fluid measurement about cantilever, most of which take advantage of its dynamic characteristics to readout the velocity of flow, there are many restrictions and high demands on the circuits. In this paper, the static characteristic of the cantilever was used to open the circuit when gas flowed, and then the flow meter worked to read the flow rate and cumulate the count. The circuit switched off when there is no airflow, which greatly reduces power consumption, and the complexity of circuit.

Technical principle

Structure of cantilever was shown in Fig.1, there are two state positions about the cantilever, the position 1 of the cantilever in a stress-free state, and the position 2 of the cantilever was deformed to connect the lower electrode by external pressure.

When the cantilever is affected by a uniform distribution of stress q, we can get the deflection ω [1]:

$$\omega(x)=(x^2-4Lx+6L^2)qx^2/24EI \quad (1)$$

X is the distance from measured point to the fixed point, L is the length of the cantilever, E is Young's modulus, I is the moment of inertia.

If X = L, the maximum deflection of the cantilever end is:

$$\omega(L)= qx2/8EI \quad (2)$$

Fig.2 show us the structure of flow meter in aisle, from which we can find the switch is consists of two parts, metal cantilever and metal contacts. Put the cantilever in the aisle whose bending direction is parallel to the gas flow channel. Pressure of flow passed will make the cantilever bending downward to touch the metal contacts, then the circuit turns on, and switch is in "ON" state; if no ambient fluid, the cantilever will restored to initial state, the circuit is disconnected, then the switch is in "OFF "state. In "ON" state, the switch insertion loss is mainly determined by cantilever resistance and contact resistance; in "OFF" state, the main switch isolation is determined by the capacitor

between cantilever and micro strip line. From Fig.2 we can found, the switch structure can be equivalent to a micro strip gap in series of a cantilever, which can illuminate its equivalent circuit.

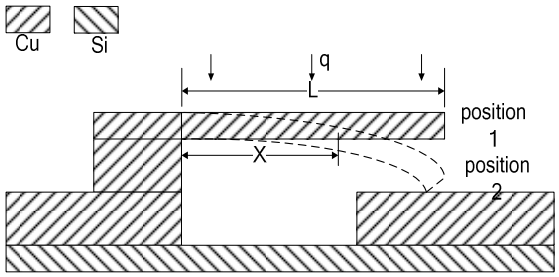

Fig.1 Mold of cantilever changed with force

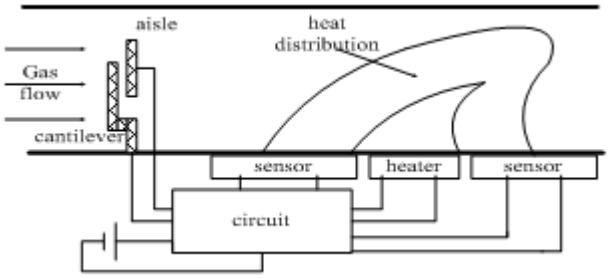

Fig.2 Structure of flow meter in aisle

Process of Cantilever

Nano imprint technology subject to top-down manufacturing technology, and has great advantages of simple operation, high resolution, low cost and high production efficiency. It can be used in high repetitive manufacturing of micro/nano graphical structure, which can decrease cost and process compare to lithography [2-3]. We designed the cantilever by use of nano-imprint technology combined with microelectronics process, and the specific process is shown as follows (Fig.3):

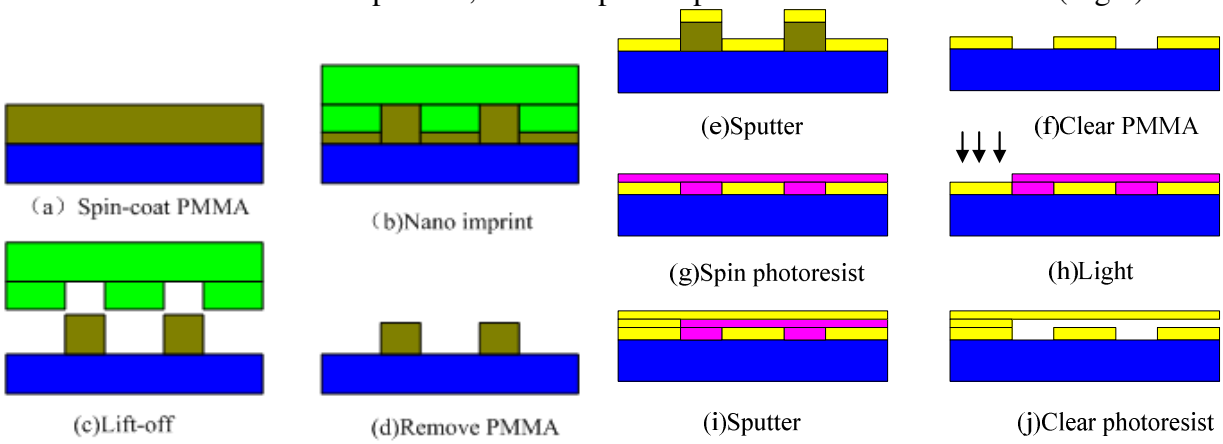

Fig.3 Process of MEMS switch

Preparation of cantilever is the key of our design. The bottom layer of cantilever in this article is Silicon, mainly plays a role of insulation and supporting; the middle layer and the top layer are metal, which consist of the cantilever switch. There are two key factors which can influence the cantilever: lithography and temperature. Lithography determines the graph of cantilever, and temperature is another important factor, the sacrificial layer here is photo resist, which is difficult to be removed if temperature upper to 120 ℃ in whole process [4-6].

Simulations

Using IntelliSuite software, we modeled and simulated the cantilever beam. Impose simulation conditions on the device, and add airflow onto cantilever, then the micro-cantilever deformed and connected to metal contacts, the circuit turned on. Cantilever in the gas path is perpendicular to the channel, and gravity can be ignored.

Applying pressure onto the upper surface of the cantilever, the beam will bend downward. There are many different results by changing the material of metal layer at same conditions as Fig.4, the material parameters are shown in Table 1. Thickness of cantilever is 0.1μm, length is 20μm, and width is 10μm.Simulation pressure is 2e-3 Mpa.

The simulation results is shown in Fig.4, we can found the degree of bending is different for each material under same conditions, copper material is deformed about 3.58μm, the aluminum material is about 6.29μm, aurum material is about 5.5μm, and platinum material is about 2.97μm. By analysis of

the results, we found the Young's modulus of the material is closely related to the curvature. To verify this idea, a series of simulations were done by only changing Young's modulus on copper. The simulation result of different young's modulus shown in Table 2 below.

Table 1 Setting and result of simulation

material/parameter	Young's modulus（GPa）	Poisson ratio	density(g/cm3)	deformation（μm）
copper	122.5	0.34	8.9	3.58
aluminum	68.85	0.36	2.7	6.29
aurum	74.48	0.42	19.28	5.50
platinum	146.9	0.35	21.45	2.96

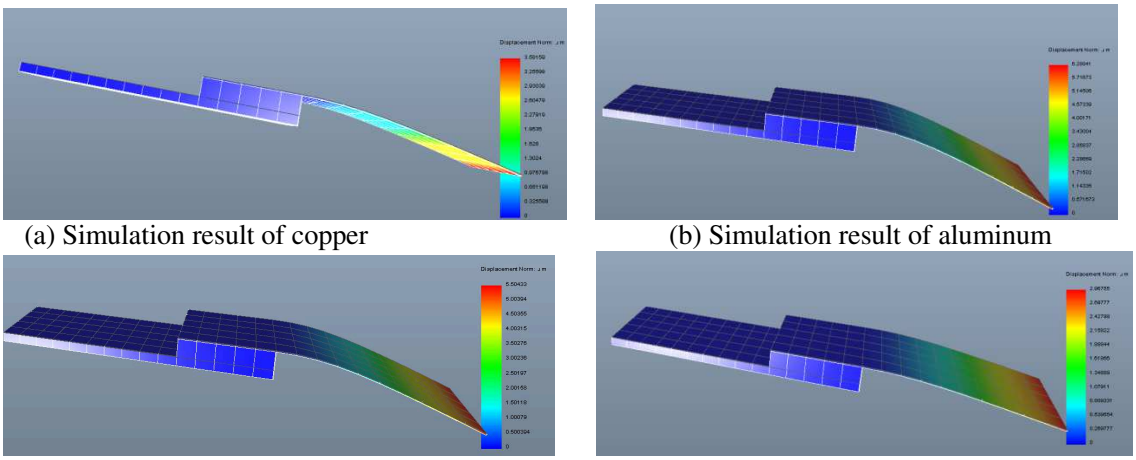

(a) Simulation result of copper (b) Simulation result of aluminum

(c) Simulation result of aurum (d) Simulation result of platinum

Fig.4 Result of simulation for materials

Table2 Simulation result of different young's modulus

Young's modulus (Gpa)	122.5	100	80	68.85
Bending displacement(μm)	3.58	4.39	5.48	6.29

The result tells us, bending degree of the device is increased with the decline of Young's modulus. When the Young's modulus decreases to the size of aluminum, the bending displacement is the same of aluminum. Then the results can be drawn, bending degree of one structure is only correlated with Young's modulus, and bending degree is inversely proportional to the Young's modulus of material.

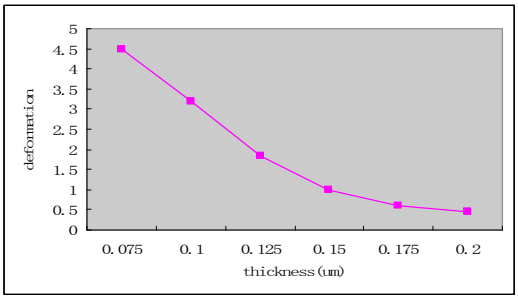

Fig.5 (a) influence of thickness

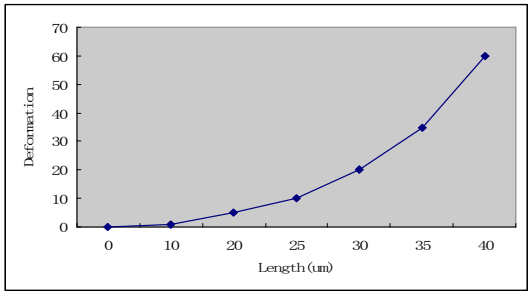

Fig.5 (b) influence of length

Fig.5 shows the effect of the Cantilever size. In Fig.5a, with the increases of cantilever thickness the bending is exponentially decline. Fig.5b shows the effect of the length of cantilever. It can be seen that bending of cantilever is exponentially increased with the increasing length. Thus shows that cantilever scales have a decisive impact on switch. Fig.6 shows the examples of curved cantilevers which is deformed under same condition.

Experiments

MEMS process was used to fabricate switch, combined with nano-imprint lithography process. PMMA was used as imprint glue, and Cu film was sputtered as electrode after making proper

graphics. By using photolithography technique, the sacrificial layer is made of photo resist. Then Cu film was used to make the cantilever. We also found that, with the increase thickness of Cu film, there are many holes on the film, which indicate that there is large stress of Cu film deposited. So the thickness of cantilever should be considered, we chose 2μm in this article, and Fig.6 is the picture of cantilevers.

From the test result of our experiment, the switch can work in the isle, but there are also some other problems need to be solved in next work.

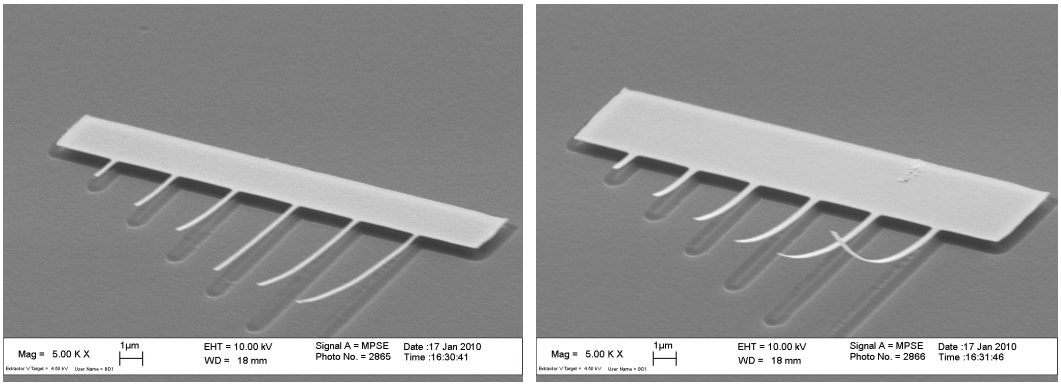

Fig.6 Deformation of cantilevers

Summary

From the simulations of the device in terms of pressure, this article verified the cantilever deflection is inversely proportional to Young's modulus. By adjusting the film thickness and length, we can find the curvature of the cantilever is different, degree of bending is proportional to the length, and inversely proportional to the thickness. But a quite long cantilever has a poor resistance to fatigue, so the size of cantilever should be determined by actual.

The usage time of gas is far below its idle time, put the Cantilever switch into a fluid channel can greatly reduce power consumption and save energy.

References

[1] Wang Zhe Yao, micro-systems design and manufacturing. Tsinghua University Press, 2008:53-61.

[2] Paolo Bruschi, Michele Dei, et al "Low-Power 2-D Wind Sensor Based on Integrated Flow Meters", IEEE SENSORS JOURNAL, VOL. 9, NO. 12, DECEMBER 2009. 1688-1696.

[3] Yu-Hsiang Wang, Chang-Pen Chen.et al "MEMS-based gas flow sensors", Microfluid Nanofluid (2009) 6:333–346.

[4] Shuo Huang, Xin Fu, et al " A numerical investigation of conjugate forced heat transfer for a micro thermal flow sensor," 2009 IEEE/ASME International Conference on Advanced Intelligent Mechatronics Suntec Convention and Exhibition Center ,Singapore, July 14-17, 2009.1510-1514.

[5] Minako Terao, Tomomi Akutsu and Yoshiaki Tanaka " Non-wetted thermal micro flow sensor," SICE Annual Conference 2007 Sept. 17-20, 2007, Kagawa University, Japan.2084-2088.

[6] Joost W. van Honschoten, et al "Optimization of a Thermal Flow Sensor for Acoustic Particle Velocity Measurements," JOURNAL OF MICROELECTROMECHANICAL SYSTEMS, VOL. 14, NO. 3, JUNE 2005.436-443.

Advanced Materials Research Vols. 989-994 (2014) pp 3274-3277
© (2014) Trans Tech Publications, Switzerland
doi:10.4028/www.scientific.net/AMR.989-994.3274

The Design of Multichannel Marine Seismic Acquisition Unit Based on ADS1282

Zhang Zhili[a], Zhang Ying[b] , Chen Peng[c]

Tianjin Sino-German Vocational Technical College,Tianjin 300350,China

[a]tjzhangzhili@126.com, [b]21223863@qq.com, [c]zdchenpeng@126.com

Keywords: ADS1282;FPGA.Multichannel. Marine seismic exploration

Abstract. For marine seismic data acquisition needs,a multichannel marine seismic data acquisition unit was designed,which used the 32-bit analog-to-digital ADS1282 as a core and Field programmable gate array(FPGA) as the acquisition controller.The unit can achieve multichannel seismic data sampling and transmission functions.The design fully used with the design ADS1282 chip integration,with the corresponding anti-jamming measures,not only simplified the circuit design,but also ensured the quality of signal acquisition and system stability.the design used FPGA to realize a multichannel hydrophone signal synchronization sampling.

Introduction

Data Acquisition Systems Acquisition in signal quality depends largely on the analog-to-digital converter and Application.To meet the high accuracy and multichannel requirements of Marine seismic data acquisition, this paper design a high level of integration of multichannel seismic data acquisition system,it can achieve 12 channel marine seismic signal acquisition and data transfer capability.Using the new-style analog-to-digital converter ADS1282 to realize the data conversion, it is not only could obtain high fidelity, high-resolution data signal, but also could use gain and offset calibration registers to realize self-test and system calibration. So it is assured the sampling data quality won't be changed with the time,location,environment and condition.Using FPGA as controller of the system,can achieve a multichannels data synchronous acquisition and transmission.The unit has a low-power,small-footprint, high-precision and high-resolution features. It is very suitable for high precision marine seismic exploration area.

Introduction of ADS1282

The ADS1282 provided by Texas instrument company is an extremely high-performance, delta-sigma($\Delta\sum$) analog-to-digital converter(ADC).The converter provides 24-bit or 32-bit output data in data rates from 250SPS to 4000SPS. It is composed of multiplexer,programmable gain amplifier,delta-sigma ($\Delta\sum$) modulator,gain and offset calibration register,over-range detection circuit, control logic,SPI serial interface and so on.The ADS1282 is available in a compact TSSOP-28 package and is fully specified from –40°C to +85°C, with a maximum operating range to +125. It is well applied in industry fields such as energy exploration, seismic monitoring and other exacting applications. The ADS1282 has following features[1].

Data Acquisition System Design

System composition. Multichannel marine seismic data acquisition unit design is based on a distributed design philosophy of marine seismic data acquisition system,the data acquisition unit can achieve multiple channel marine seismic data acquisition and data transmission capabilities, can effectively remove the interference signal in the analog signal transmission, improving the quality of seismic signal acquisition, seismic signal processing and waveform display and logging features, done by a control host.

Multichannel seismic data acquisition hardware is mainly composed of piezoelectric hydrophone, A/D converters, FPGA, power supply management module and transmission interface.For

low-power, small-footprint design purposes using the FPGA realization data gathering and the data multiple transmission. For high precision and high resolution,analog to digital conversion using the ADS1282.Distributed marine seismic exploration data acquisition system for each collection interval up to 300 meters, the system dedicated transfer chips for high-speed data in long-distance transport.Fig.1 is the block diagram of data acquisition unit.

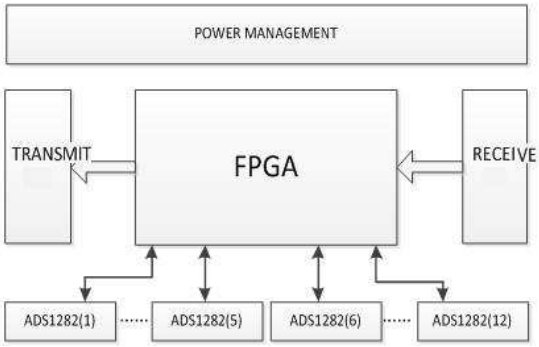

Fig. 1 Hardware Compose of Digital Geophone

Interface of Hydrophone with ADS1282.The data acquisition unit is mainly used for marine seismic exploration , the sensor(hydrophone) gets a seismic wave signals are converted to digital signals and then pass through the transport interface to control host. In order to enhance the quality of sampling signal and effectively reduce noise created by environment, the output signal of hydrophone is sent to analog inputs of ads1282 through front-end filter network with differential mode.

Fig.2 is the interface circuit of hydrophone and ADS1282.In this application,ADS1282 is provided by ±2.5 V power.High-frequency normal mode components from the input signal is removed by the filter network which consists of R1, R2 and C1,C2,C3.To maintain good common-mode performance, R1,R2 should be matched to 0.1%. Capacitor C3 in parallel with C1 can effectively reduce the common-mode errors caused by C1,C2 not matching. If C3 is 10 times larger than C1, the common-mode error will be reduced 20 times[2].

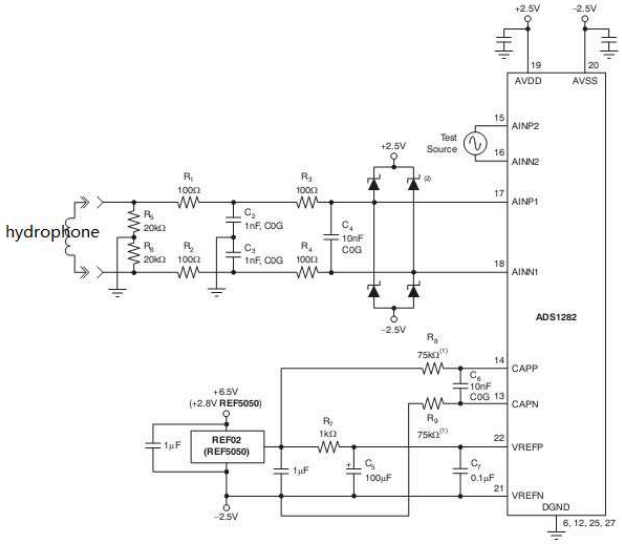

Fig. 2 Hydrophone Interface Application

Clamping diodes are used to protect the ADS1282 inputs from voltage overloads. REF5025 provide the voltage reference for the ADS1282.The output of filter through R5, C7,C8 provide high frequency bypass for input signals reference.C8 should be placed close to pins of the ADS1282.R3,R4 and internal resistance form the divider voltage circuit to provide offset voltage for the ADS1282.The offset can remove low level useless tones from pass-band. To maintain good common mode rejection, R3 and R4 should be matched to 0.1%[1,2].

Interface of ADS1282 with FPGA. ADS1282 accessed through the serial interface to read data and set register,ADS1282 provide 32-bit binary complement format data.The serial interface is 3-wire SPI interface,which includes three basic signals:SCLK,DIN and DOUT.ADS1282 also has synchronized signal, clock signal, reset signal.When converting data ready for reading, DRDY signal can be used to mark the judgment, when it changes into a low level indicates a new conversion data is prepared,the data will be captured at the next rising edge of SCLK by FPGA.

Total of 12 channels ADS1282 in the acquisition unit,they take parallel connection mode, and 12 channel ADS1282 with a CLK,SCLK ,DRDY and reset signals.each ads1282 has a DOUT signal and DIN signal connect with FPGA,so that ensures all ADS1282 synchronization of acquisition[3,4].Fig.3 is the data transmission and control interface of ADS1282 with FPGA.

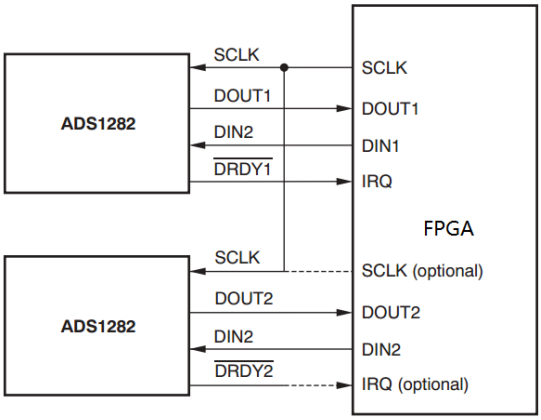

Fig. 3 Interface of ADS1282 with FPGA

Experiment

According to national standards for marine seismic data acquisition system,We tested the performance of acquisition unit,include equivalent input noise,Harmonic distortion,Common Mode Rejection Ratio and Channel crosstalk[4,5].In the sampling frequency is 1000SPS, the preamplifier gain of 0dB,the input signal frequency is 31.25, scope is 2V test condition, carries on 5 tests respectively to 10 gathering units, finally averages the value.the result of compare test results with national standards is shown in table 1.From the test results show that this acquisition unit to meet national standards A-index of petroleum seismic data acquisition system requirements.

Table 1 The compare of test results with national standards

Test Items	Test Results	National Standard
Equivalent input noise level	1.26	≤1.6uV
Harmonic distortion	0.00021%	≤0.0005%
Common mode rejection ratio	113dB	≥90dB
crosstalk	118dB	≥100dB

Summary

Take ADS1282 as the A/D chip,FPGA as the controller is a new pathway of multichannel marine seismic exploration acquisition unit,it simplifying the circuit design,reduces power consumption while increasing the stability of the system,is ideal for high-accuracy data acquisition system.The acquisition unit has been applied to distributed marine seismic data acquisition systems,performance is good.The sampling unit can also apply to other situations that require high-accuracy data acquisition,has broad application prospects.

Acknowledgments

This work was financially supported by Tianjin Higher Education Science and Technology Development Fund(No.2013032).

References

[1] Texas Instruments. High-Resolution Analog-to-Digital Converter ADS1282[EB/OL]. (2009-03-23) [2010-04-05].http://focus.ti.com.cn/cn/lit/ds/symlink/ads1282.pdf.

[2] WANG H.X,LIU H.M,ZHU G.W. Development of New Essential Safety Distributed Mine 3-component Seismograph[J].Journal of Electronic Measurement and Instrument, 2008(S2): 247-252.

[3] GAO G.T. Application Techniques for Sensor and Signal Conditioning[M].Beijing: Science Press.2002.

[4] The National Development and Reform Commission.SY/T5391-2007. The Oil and Gas Industry Standard of China-The Oil Seismic Data Acquisition System[s]. Beijing: Petroleum Industry Press,2008.

[5] PENG Z,DENG Y,MA CH. Improvement and Implementation of FPGA Based Seismic Data Acquisition Unit[j]. Journal of Computer Measurement & Control,2013(1):282-284.

Advanced Materials Research Vols. 989-994 (2014) pp 3278-3281
© (2014) Trans Tech Publications, Switzerland
doi:10.4028/www.scientific.net/AMR.989-994.3278

Complicated Manufacturing System Dynamic Measure-Control and Intelligence Diagnosis

Ma Jun[1,a], Li Weiwei[1,b], Liu Pengting[1,c]

[1]College of Mechanical Engineering, Tianjin University of Technology and Education, Tianjin 300222, China

[a]969265760@qq.com, [b]liww@163.com, [c]liupt@163.com

Keywords: Weak signal extraction. Multi information fusion. Hybrid intelligent diagnosis. Embedded online monitoring unit

Abstract. As an important mean to ensure machining accuracy, the dynamic measurement and intelligent fault diagnosis technology can be used in aviation manufacturing machine. In recent years, several theoretical results are gotten on weak signal feature extraction, multiple sensor information fusion of early fault identification as well as the set up of embedded online monitoring units. This article is the summary of those results, the existing problems is analyzed, and the trend of the development in this field is also discussed.

Introduction

As the requirements of improving machining quality in advanced manufacturing technology, the technology innovation and breakthroughs of high-end multi-axis NC machine represented by high speed, high precision have the important significance and engineering application value. Because of the complexity structure, many factors lead to poor machining quality, if the error sources can not timely and accurate diagnosis, the machining quality and accuracy will not be able to guarantee and even cause other major losses such as machine scrap. It is necessary to study dynamic monitoring and intelligent diagnosis technology, especially in abnormal processing state recognition and intelligent maintenance theory, the dynamic measurement and intelligent diagnosis software is also need to develop in order to display machining state, diagnose fault and predict performance [1-5].

Analysis of the current situation and trend of development

The fault of high-end CNC machine tools includes electrical fault and mechanical fault. the electrical system fault can be diagnosed by means of NC system self-check such as drive current, Angle, torque motor, etc. The commercial monitoring system, such as Siemens EPS and FANUC 18I series monitoring system have already developed. Although single functional monitoring and diagnosis system is developed, such as Kistler cutting force monitoring system and ARTIS tool monitoring system, those monitoring systems mentioned above can diagnosis specific fault based on monitoring information. But according to the characteristics of high signal-to-noise ratio and complexity signal modulation of fault signal, further study in early failure of weak signal detection and fault signal extraction technology is still need to research. The effective hybrid intelligent fault diagnosis model should be set up to improve the accuracy of fault prediction.

The manufacturing quality in precision machining is easily influenced by the CNC equipment organic fault. Fault once appear, will immediately change the machining accuracy. However, the early fault characteristic signal, such as the amplitude of vibration, current, acoustic emission is relatively small, further more, by the influence of noise, data acquisition device noise, signal transmission coupled noise, signal to noise ratio often low. The primary task of weak signal noise monitoring and feature extraction is signal noise reduction, which requires the use of electronics, information theory, computer and physics methods. According to the statistical characteristics of the measured signal and noise and their differences, find useful signal from the background noise. In addition, due to the rapid and real-time needs in fault diagnosis, the data length often limited. Therefore, the development of the weak signal detection technology should be attributed to two

aspects: one is to improve the detection capability, reduce the noise of the signal and get an accessible signal to noise ratio; another is to improve the detection speed, meet the real-time monitoring and diagnosis requirements.

At present, the main methods of weak signal detecting is in time domain and frequency domain, the time domain method including sampling integral, digital average, correlation detection, adaptive noise cancellation, frequency domain method including FFT, power spectrum density, filter etc.. However, for short data point, low signal to noise ratio, when the noise frequency and signal frequency is close or coincident, the weak signal detection method has some defects, such as short data lead to low resolution when the FFT is used, the noise can not be average out. When the noise is suppressed, the useful signal is also filtered. These problems affected the common detection methods mentioned above. In recent years, some new methods of weak signal detection is studied, such as: differential oscillator, wavelet transform, cyclic statistics theory and high order statistics, independent component analysis, empirical mode decomposition, stochastic resonance and integrated applications of various methods.

Due to the one sensor can only get signal information, for the complex information of CNC machine fault, a variety of sensors should be acquired to get different information. Multi sensor information fusion is a multi information detection system from the aspects of various sensors and the integrated use of their respective advantages, to achieve accurate, timely operation condition judgment of mechanical system. In this method, the multi sensor information fusion system can effectively use the sensor resources. Compared with the single sensor system, the prominent advantage of multi-sensor information fusion is that information redundancy, fault tolerance, complementary, real-time and low cost.

The machine features are always complex, as the multi signal modulation and the diversity characteristics of monitoring signal, dynamic monitoring and intelligent diagnosis of machine has such characteristics like : a large amount of signal should be measured, the variability of diagnostic process, randomness, fuzziness and other issues, a single fault diagnosis method is difficult to make accurate prediction. Therefore, using the method of multi information fusion and intelligent hybrid fault diagnosis strategy is the development trend of intelligent fault identification.

In recent years, researchers use the fault diagnosis expert system, fuzzy theory, neural networks, evolutionary algorithm analysis, and artificial intelligence methods in NC machine fault diagnosis. Neural network is widely adopted method applied in recent years. But this method has some problems such as diagnosis information is not complete, lack of training samples. There are some other methods like expert system structure based on Web, radial basis function neural network, intelligent diagnosis model empirical mode decomposition and least square support vector machine.

The setup of CNC machine dynamic monitoring platform

The ultimate goal for theoretical study on dynamic monitoring and intelligent diagnosis technology is to build these algorithms in NC machine online detection platform, real-time detect and diagnose machining operation state. From the existing online detection equipment, due to volume constraints lead to complexity of installation, and special embedded monitoring module always has a long development cycle, it is difficult to adapt to the development needs of open architecture and function module of reconfigurable CNC system. The following describes the construction method of online detection unit modular with reconfigurable features, this online monitoring framework include network technology, database technology and artificial intelligence technology, which is on behalf of the dynamic monitoring and intelligent diagnosis's direction of NC machine.

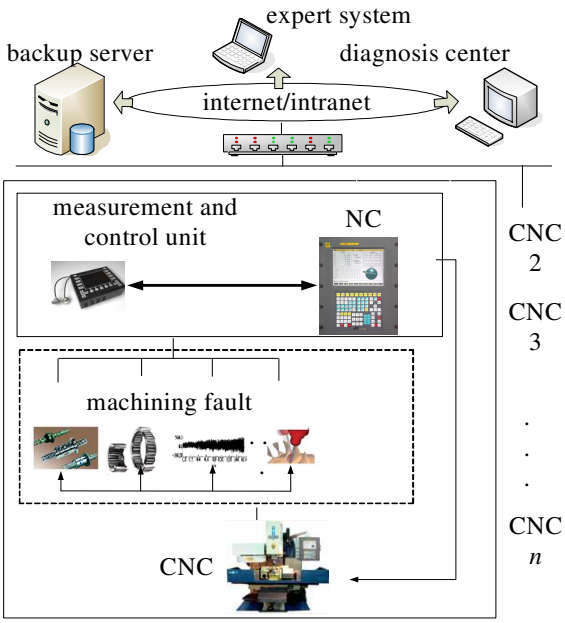

Fig. 1 Integrated monitoring embedded measurement unit on the open architecture CNC system

Fig.1 shows integrated monitoring embedded measurement unit on the open architecture CNC system, this embedded measurement unit has the independent central processor to ensure the real time implementation of NC instructions and online monitoring function. Construction of online monitoring unit includes PC104 PLUS architecture bus, signal conditioning module, the data acquisition card, XPE embedded operating system installed in the CF card and online monitoring software.

The monitoring data acquired by embedded condition monitoring unit can be upload and fault diagnosis code in remote monitoring system can be download by internet when those information has not real time requirement. The network structure use hybrid architecture of C/S and B/S structures, the system provides a variety of commonly used network database options (such as Sql Server, Oracle), the whole system can be divided into three layer network, including C/ S model of fault monitoring system and B/S model equipment management information network, and finally constructs in ERP system in the enterprise.

Data transmission protocol of fault information is used by the information description method of "factory - monitoring unit - point - monitoring quantity". The data transmission protocol mainly includes the following 4 parts: (1) The initial data segment: including initial identification monitoring data, monitoring, monitoring time and date. (2) Monitoring global data section: provide status acquisition parameter setting information, such as the parameter analysis of frequency, gain, sampling points, the total channel number, channel settings. (3) Monitoring data: the machine monitoring signal, waveform information. (4) End of data identification segment: including the identification of the data packet end.

Summary and Prospect

Several methods have used in complex manufacturing system fault diagnosis, such as multi sensor information fusion, hybrid intelligent fault diagnosis modeling and on line monitoring platform for weak signal. But it should be noted that, dynamic monitoring and intelligent diagnosis are still false forecast, especially for real time intelligent control needed further studies. Carry out the study of dynamic monitoring and intelligent diagnosis theory and engineering application is important to the promotion of Chinese industry level of manufacturing, which has important significance and engineering application value.

Foundation: Tianjin application foundation and frontier technology research program (12JCQNJC02500)

Reference

[1] D.A. Tobon-Mejia, K. Medjaher, N. Zerhouni, CNC machine tool's wear diagnostic and prognostic by using dynamic Bayesian networks, Mechanical Systems and Signal Processing, Volume 28, April 2012, Pages 167-182

[2] Roberto Augusto Gómez Loenzo, Pedro Daniel Alaniz Lumbreras, René de Jesús Romero Troncoso, Gilberto Herrera Ruiz, An object-oriented architecture for sensorless cutting force feedback for CNC milling process monitoring and control, Advances in Engineering Software, Volume 41, Issue 5, May 2010, Pages 754-761

[3] E. García-Plaza, P.J. Núñez, D.R. Salgado, I. Cambero, J.M. Herrera Olivenza, J. García Sanz-Calcedo, Surface Finish Monitoring in Taper Turning CNC Using Artificial Neural Network and Multiple Regression Methods, Procedia Engineering, Volume 63, 2013, Pages 599-607

[4] M. Mori, M. Fujishima, Remote Monitoring and Maintenance System for CNC Machine Tools, Procedia CIRP, Volume 12, 2013, Pages 7-12

[5] Huang Wei, Li Baojiang. Children Biscuits Packaging Design [N]. China Packaging Newspaper, 2005 -8-19 (3).

Advanced Materials Research Vols. 989-994 (2014) pp 3282-3285
© (2014) Trans Tech Publications, Switzerland
doi:10.4028/www.scientific.net/AMR.989-994.3282

Communication Module Design of Offshore Drilling Platform Cleaning Robot

Jiang Yongxiang[1,a], Liu Jingfang[2,b], Zhang Xinghui[3,c], Zhao Yuling[1,d]

[1]College of Mechanical Engineering, Tianjin University of Technology and Education, Tianjin 300222, China

[2] Luohe Technician College, Henan,462000; [3] Tianjin Sino-German Vocational Technical College,Tianjin,300222, China

[a]jyx1212@qq.com, [b]821529487@qq.com, [c]xhzhang@163.com, [d]ylzhao@126.com

Keywords: Offshore drilling platform cleaning robot. Communication module. Multi-sensor. Control strategy

Abstract. Communication module design is one of the key technologies in offshore drilling platform cleaning robot, through overall design and analysis of communication systems, the communication module is selected and technology roadmap is analyzed. thus communication module hardware architecture (PC, PLC and multi-sensor) is designed, multi-sensor (Sonar, infrared, camera, SINS, pressure sensors and fiber optic gyrocompass) underwater monitor is designed and selected, the system software is programmed (PC configuration software, PLC software and communication protocol software); Finally, control structure and running track is designed. The research ensures the operation accurately and improves the cleaning efficiency.

Introduction

Offshore drilling platform is the structure used for drilling, the research of attachments cleaning robot for offshore drilling platform is used for replacing manual operation, and get high efficiency and safety work environment for attachments cleaning[1]. Because of the complexity of the underwater environment, offshore drilling platform cleaning robot is operated under the complicated condition, such as deep water depth[2], water quality turbidity, currents and other restrictions, thus, the communication module should be designed to ensure accurate delivery of operating instructions to robots, and meanwhile, the real-time state should be feedback to the operators and improve the cleaning efficiency[3-4].

In view of the above problems, the communication module of offshore drilling platform cleaning robot is studied. Based on the overall design and analysis, each communication system module is selected and research technical route is designed. the communication module (include PC, PLC and sensors) hardware structure is designed, multi sensors (include sonar, infrared, camera, inertial navigation, optical fiber and the pressure sensor) is selected, under water monitoring software is programmed (include PLC software and communication protocol, the PC configuration software); Finally , the cleaning robot mechanical structure and control method is studied. The research ensure the operation precision of the offshore drilling platform cleaning robot, and improve the cleaning efficiency[5].

The general design of communication module

The hardware of offshore drilling platform cleaning robot communication module is mainly composed of PC, console, display, PLC and sensor module. The main content of communication is to control the monitoring data of underwater upload and control date download. The overall design structure diagram is shown in Figure 1.

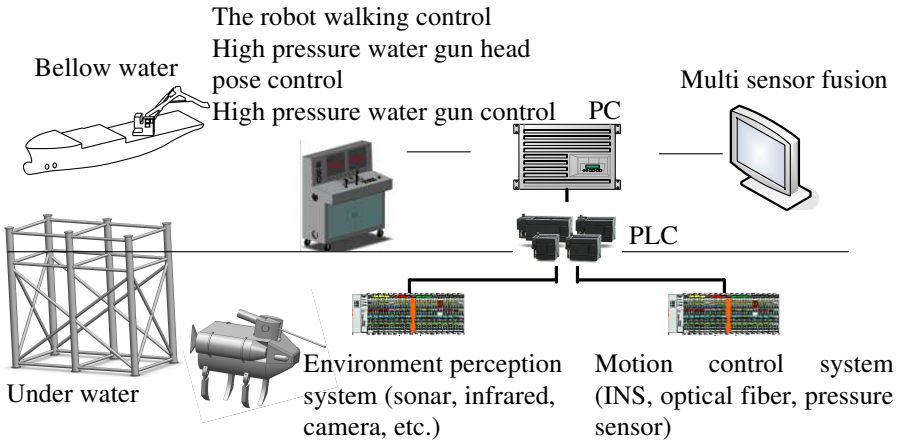

Fig. 1 The overall design of communication module structure diagram

In Figure 1, the control data transmission refers to the robot operator using the ship console, PC and display system sending instructions to PLC, after switching input, output, analog input, output module, the logic arithmetic, A/D, D/A conversion as well as the input signal, feedback signal processing, electromagnetic valve, motor actuators is under control. The upload of underwater monitoring data refers to all types of sensors of the robot with access to the underwater environment and cleaning state data, via PLC upload to the computer, and the software can display it real-time.

The hardware structure design of communication module

The communication between host computer and PLC as shown in Figure 2, the computer is composed of industrial control computer, host computer mainly process two part of the data, the data receiving and display. The Siemens S7－200 is selected. The communication between PC and PLC use PC/PPI cable to implementation and communication.

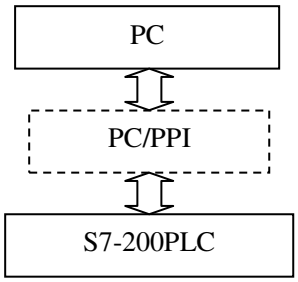

Fig. 2 The communication between host computer and PLC

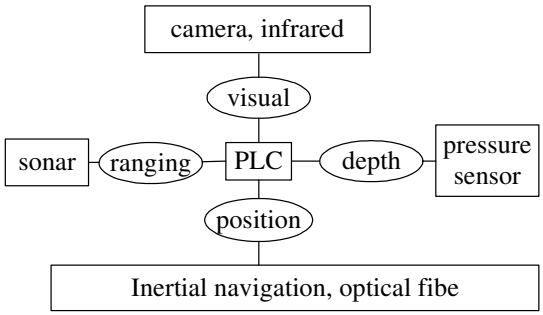

Fig. 3 Multi sensor information flow chart

PPI communication protocol, the computer and PLC chose master-slave mode of communication interface, the master equipment is the computer, slave equipment is PLC. In the process of communication, computer and PLC send handshake protocol to make and receive signal instructions. The PLC instructions signal is received and checked, if without any error, PLC will feedback checked and correct information to the computer, after the computer receives the feedback signal, the confirm order is send back to the PLC and began to implement the operation response.

The multi-sensor structure design of Communication module

The multi-sensor system of offshore drilling platform cleaning robot include environmental perception system module (sonar, infrared, camera) and the movement control system module (inertial navigation, optical fiber gyro, pressure sensor), inertial navigation and optical fiber gyro,

which are used for positioning the cleaning robot when offshore drilling and production platform diving operations; The camera and the infrared sensor is used to read the image of the seafloor environment, sonar is used for measure the distance between offshore drilling platform cleaning robot and the jacket; Pressure sensor used in cleaning robot to obtain depth information. The multi-sensor information flow chart is shown in figure 3.

In communication design of multi sensors, the core idea is the multi sensor information fusion technology, establishes the integrated navigation system based on multi sensor fusion technology (a combination of strap down inertial navigation system, pressure sensor, optical fiber compass). Take strap down inertial technique as the main navigation system, optical fiber and pressure sensor as the aided navigation system, compensation and correction of the error of strap down system. The final construction of navigation system model shown in Figure 4, achieve multi-sensor fusion integrated navigation and ultimately achieve control of posture and movement.

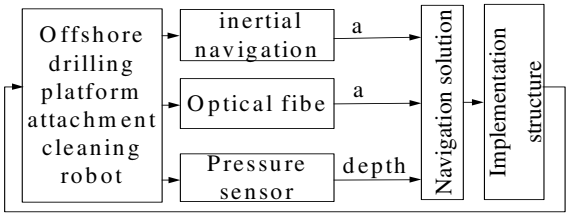

Fig. 4 Multi-sensor integrated navigation model

Fig. 5 PC monitor screen

The structure design of communication module software

The communications of pressure sensor information go through PLC EM231 analog expansion module and converted to digital signals to PLC. PLC EM231 analog input port is AIW0, Pressure sensor range choose 0~16MPa, current range 0~20mA, in the internal of S7-200 CPU, 0~20mA corresponding to the numerical range 0~32000. So that the sea level pressure is 0.1MPa, Seawater depth 0~1000 meter corresponds to0.1MPa~16MPa. The program can get based on the principle of the above analysis,

As shown in Figure 5, the PC monitor screen can display real-time propeller work, depth information and video surveillance footage, the software can also control the related operation of cleaning robot in the other interface.

The control strategy design of communication module

From the first step when robot work, the work path optimization should not only makes the cleaning efficiency, but also reduces the probability of unnecessary fault. Robot motion path is shown in figure 6. At the appropriate position of the cleaned water institutions(tower), the start point is seledted, Then design an unrepeated pathway until back to the starting point .The advantages of this path design is difficulty homogeneity robot task, no duplication of work and the total workload can be optimized.

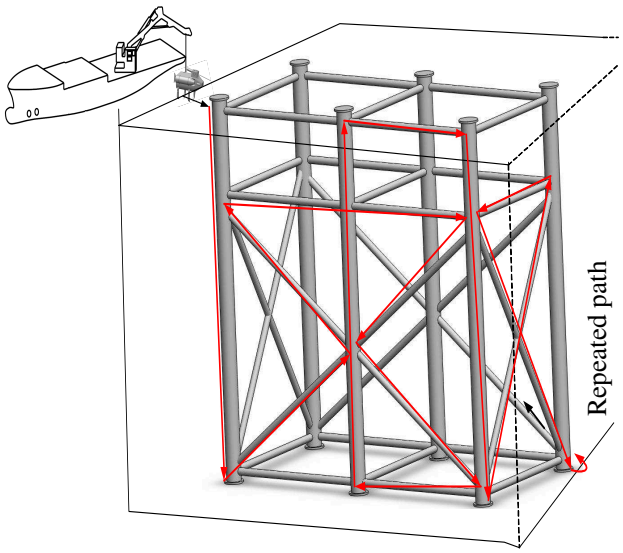

Fig. 6 The robot path planning under water

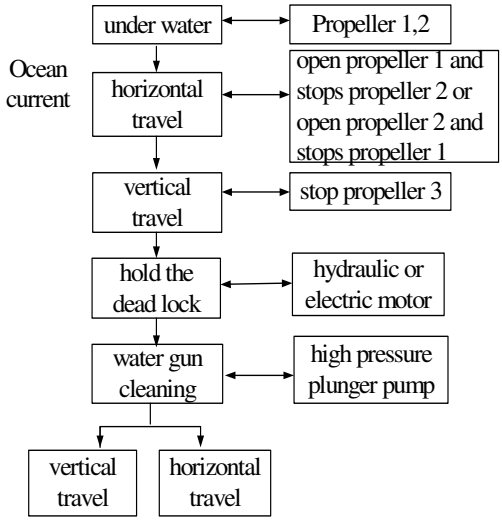

Fig. 7 Mechanical control flow chart

Figure 7 shows the mechanical control flow chart reference figure 6. When the robot into the water, the first step is float to dive location, to maintain balance in the water, propeller 1 and 2 on the back of robot should be opened at the same time, considering the current factors, the method such as open propeller 1 and stops propeller 2 is needed to achieve turning motion. When the robot gets the top of a specified target, the floating propeller 3 is closed to enable the robot dive. The locking motor is designed to make robot arms and fixed for the next step, high-pressure plunger pump is used to drive water hydraulic clean the jacket. After cleaning, the robot swim to other target as mentioned above and gradually completed all cleaning work. The recovery process of robot is shown as follow, clean off the pressure water gun, loose the robot from jacket, open up propeller 3 to make the robot above the surface of the water, open propeller 1 or 2 to make robot back to the initial position. Then, the whole mechanical control process ends.

Foundation: Tianjin Municipal Science and technology support program (13ZCZDGX01500)

Reference

[1] Tang Zhiguo. Research on Control System of Intelligent Cleaning Robot[D]. Hunan University, 2012.

[2] Dong Dasheng Liu Haifeng, zhang guohua, Zhang Shuwe. A New Type of Long-term Ocean Environment Monitoring System and Its Antifouling Device[J]. Journal of Marine technology, 2012,01:27 -30.

[3] ZHENG Jun-jie, LIU Zhi-hua, Study on the Key technology of Marine environment Monitoring System ased on Underwater Three-dimensional Sensor Networks[J]. Journal of Marine technology, 2012, 2012:1-4.

[4] Gao Rui, zhang. Digitization Control and Monitoring System Based on Simatic PLC[J]. Industrial control computer, 2013, 11:100-101.

[5] Xu X-R, Su M-Z . Luminescence and luminescent materials. Beijing: Chemical Industry Press, 2004 (in Chinese).

Advanced Materials Research Vols. 989-994 (2014) pp 3286-3289
© (2014) Trans Tech Publications, Switzerland
doi:10.4028/www.scientific.net/AMR.989-994.3286

Design of Pneumatic Parachute-Packing Machine

Wang Yingfei[1,a], Deng Sanpeng[1,b,*], Chen Bo[1], Zhang Linling[2]

[1]Insitute of Mechatronics Engineering,Tianjin University of Technology and Education, Tianjin,300222, China

[2]Hangyu Life Saving Equipment Co., Ltd, Xiangyang, 441600. China

[a]wangying_fei@126.com, [b]sanpeng@yeah.net

*Author for correspondence: DENG Sanpeng, sanpeng@yeah.net

Keywords: Aircraft drag parachute. Drag parachute pneumatic packing machine. The finite element analysis. The pneumatic control system

Abstract. As ground support equipment, drag parachute packing machine is used for packaging aircraft drag parachute. It is driven by high-pressure inert gas. Drag parachute will be compacted in the cylinder loading institution by high pressure. The overall structure of drag parachute packing machine is designed. The finite element analysis and structure optimization of drag parachute packing manipulator is completed. The pneumatic control system is designed. It provides an approach for drag parachute packing technology.

Introduction

By a drag parachute machine is meant a set of ground equipment used for packing the drag parachutes, so that the collection, storage and reuse of umbrella resistance could be made conveniently[1-3]. The current drag parachute machines mainly employ ball-screw and hydraulic type, both of which are large in volume, heavy in quality and not convenient to move. In order to overcome these problems, a new type of pneumatic umbrella packing machine is necessary.

Overall Structure of Drag Parachute Machine

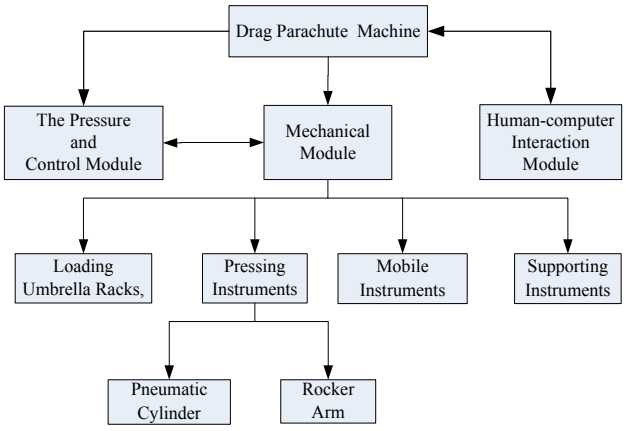

Fig. 1 Structure Diagram of Drag Parachute Machine

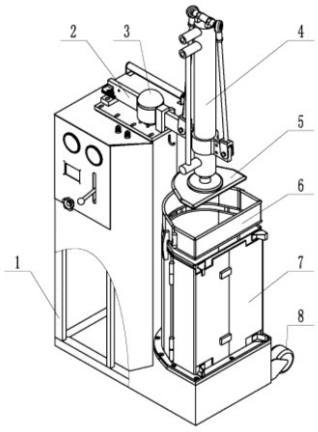

1. Body frame 2. Rocker arm 3.Axis of rotation 4. Pneumatic cylinder 5.Pressure plate 6.The auxiliary umbrella cylinder 7. The main umbrella cylinder 8.Moving wheel

Fig. 2 Mechanic Diagram of Packing Machine

Based on modular design, the pneumatic drag parachute machine adopts a simple structure, benefiting the daily maintenance and repairing of equipment. As shown in figure 1, three modules comprise the whole equipment, that is, mechanical module, the pressure and control module and human-computer interaction module[4-5].

As is shown in figure 2, the mechanical module is composed of loading umbrella racks, pressing instruments, mobile instruments and supporting instruments. By support institutions 1, we mean is the system used to support the supporting instrument, mount the loading umbrella racks, fix the mobile instrument and carry air pressure drive system, as well as to overcome the structural distortion from the pressure of work and turning torque. The pressing instrument, which is composed of the rocker arm 2, the air cylinder 4, and the compression plate 5, is responsible for compact the drag parachute, which is otherwise loose, tightly in the loading umbrella rack according to the requirement, in order to facilitate the transport and use. Large in size, the parachute, in order to be packed into the parachute bag, requires not only

A large pressure but also a strict sequence according to which the professional personnel pack the parachutes. For the convenience of packing the drag parachute in the racket, the pressing instrument is designed to rotate for 90 degrees horizontally with axis 3 as the center of rotation. In order to facilitate the job of worker, the air cylinder and pressing plate will rotate back to the position right upon the parachute racket when packing the parachutes. The compression parachute racket comprises a main and an auxiliary racket, with the former responsible for accommodating the inner racket when working. In order to facilitate the loading (or deloading) of the inner racket, an outward sliding door should be set outside the main racket. In this way, in order to load (deload) the inner racket, all we need to do is pull out (push in) the main racket. The mobile instrument 8 is designed as a mobile wheel. Driven by high-pressure gas, the new parachute machine, compared with the existing ones, is lighter, smaller and more convenient to operate. When the machine is required to be moved, what the worker needs to do is slant the whole packing machine by a certain degree with the clench of the handle and drag the packing machine to the destination.

Static Stress Analysis of Rocker Arm

The air cylinder works at the pressure of 4×10^{6}Pa. The cavity of the cylinder without rods boasts an effective area of $3.85\times10^{-3}m^{2}$, while the gas in the cylinder with rods emits in to the atmosphere directly. As a result, the counter pressure of the cylinder turns out null. Based on the settings above, it is easy to calculate that the working thrust of the cylinder is 15.4KN, a number signifying that the pressing instrument undertakes a giant deformation force when working. In order to ensure that the racket arm can sustain the deformation, it is desirable to perform an finite-element analysis upon the pressing instrument with SolidWorks Simulation and optimize the whole part structurally with the data obtained.

Topic of studies. By topic of studies is meant to decide which aspects of the pressing instrument to study. In this paper, we would perform static stress analysis upon the pressing instrument.

Material. The axis and the whole of the racket arm employs structural alloy steel while other parts apply ordinary steel.

Constraint. Constraint in the study includes fixture constraint and joint constraint.

Load. When the parachute is packed, it would exert upon the surface of pressing plate a reaction, of magnitude 15.4KN and upward in direction.

Calculate. Based on the settings above, the static stress analysis of the pressing instrument can be carried out.

Results analysis. Analyze the stress, deformation and displacement of the pressing instruments with SolidWorks Simulation. Fig. 3 illustrates the results, based on which we can tell the max stress σ of the racker arm is 292MPa and the yield limit of structural alloy steel equals 710MPa, that is, $\sigma = 292$MPa$<[\sigma_s] = 710$MPa. It could be easily seen that the stress runs behind the yield limit by far[4,5].

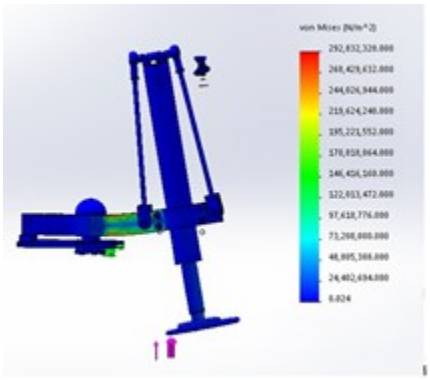

Fig. 3 Screenshot of Stress Analysis in Racker Arm

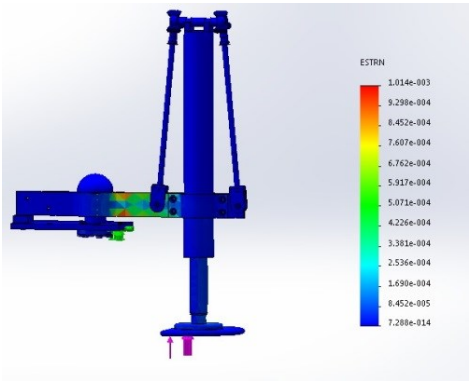

Fig. 4 Screenshot of Deformation Analysis in Racker Arm

Fig.4 illustrates the deformation of racket arm. Based on the data, the deformation ε equals1.01×10^{-3}, a magnitude small enough to be omitted.Fig. 5 illustrates the displacement of the air cylinder. Based on the data, the max displacement of the pressing instrument, of magnitude 3.28mm, occurs at the top the air cylinder, with the displacement of the pointed racket arm around 1.3mm.

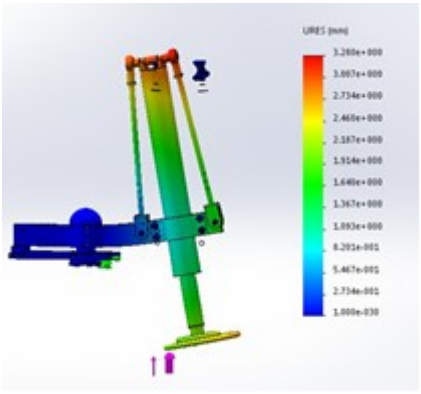

Fig. 5 Screenshot of Displacement Analysis in Air Cylinder

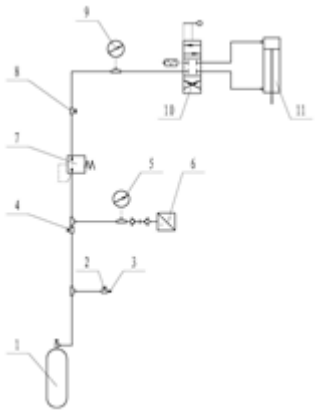

1. Accumulator 2.Throttle valves 3.Muffler 4. Throttle valves 5.Gas cylinder piezometer 6. Pressure transmitter 7. Pressure reducing valves 8. Throttle valves 9.Working piezometer 10. Hand-operated direction valves 11. Pneumatic cylinder

Fig. 6 Pneumatic Schematic Diagram

Considering the high price of structural alloy steel, it is advisable substitute it with 45# normalized steel at 870°C in order to save money while meet the demand of pressing instruments. In order to test its feasibility, the data of the steel is listed in Table 1, with the comparison of those from structural alloy steel.

Table 1 Material parameter between before with after

Parameter / Material	Stress (MPa)	Deformation (10^{-003})	Displacement (mm)
alloy constructional steel	292	1.01	3.28
45#	292	0.99	3.28

Table 1 indicates an invisible change emerges after the material is altered. Though the safety factor and the yield limit surpass what is necessary by far when structural alloy steel is applied, it could, in another perspective, perceived as a waste of material and increase the expenditure. The analysis made by SolidWorks Simulation justifies the conclusion that the application of 45# normalize steel not only meets the demand but also lowers the cost.

Air-pressure Drive and Control System

With high-pressure inactive gas as working medium, the packing machine works at 4MPa. Safe yet causing no pollution, inactive gas could be emitted into the atmosphere directly after used, which make collecting devices unnecessary. Prior to work, the inactive gas should be stored in the energy accumulator, thus the parachute could be packed even without power. Fig.6 shows the pneumatic schematic diagram.

Conclusion

The following merits are found when the new parachute packing machine driven by high-pressure inactive gas is applied in a certain airport.

1) The modular design in the new machine facilitates daily maintenance and repairmen.

2) The pressing instrument could revolve around the axis of rotation, benefiting the loading of drag parachutes into the racket.

3) The application of high-pressure gas as working medium makes pneumatic motors and fuel tanks unnecessary, which renders the machine small in size, light in weight and cheap to manufacture.

Acknowledgements

In this paper, the research is supported by The National Youth Science Fund Project(61301040); Tianjin science and technology planning project (13ZCZDGX01500) and (14ZCZDSF00022).

References

[1] Tang You-cai,Wang Zhan-yong. The Design of Power System of the BSJ-I ComprehensiveBand Resistance Umbrella [J].Chinese Hydraulics&Pneumatics,2001（4）11-12.

[2] Liu Zhikuo,Du Junling. Packing Methods for UAV Recovery Parachute [N], Journal of Nanjing University of Aeronautics &Astronautics,2009,(41)79-83.

[3] Wang Ji-fang,Zhang huai-cun. Comparison and analysis of the new parachute-packing machine[J],Machinery Design&Manufacture,2005,(5)60-61.

[4] Qi Yuming, Zhu Xianzhu, Deng Sanpeng, Wang Zhongmin. An Approach of Spindle Bearing Pre-tightening Based on Spacer Sleeve Adjustment[C]. Applied Mechanics and Materials, Vols. 488 (2014):1087-1090.

[5] Deng Sanpeng, Xu Xiaoli, Li Chongning, etc. Research on the oil tank sludge cleaning robot systemSource[C]. MACE2010, p 5938-5942.

Advanced Materials Research Vols. 989-994 (2014) pp 3290-3293
© (2014) Trans Tech Publications, Switzerland
doi:10.4028/www.scientific.net/AMR.989-994.3290

Development of G-code Based on PMAC in CNC Machining Center

Cao Chuanchuan[1], Sun Qihan[1], Deng Sanpeng[1,a,*], Zhou Yu[2]

[1]Institute of Mechatronics Engineering, Tianjin University of Technology and Education, Tianjin, 300222,China

[2]Powerise CNC Technology Co., Ltd. of Tianjin, Tianjin, 300222, China

[a]sanpeng@yeah.net

* Author for correspondence: Deng Sanpeng, Email: sanpeng@yeah.net

Keywords: PMAC Motion Controller. FANUC. G-code.

Abstract. PMAC motion controllers serve not only as a receiver of the orders from CNC systems of many kinds, but also as a controller of the motion of machine tools' axles. With G83 as an example, a code commonly seen in the processing cycle of deep holes in CNC machining centers, it is advisable to come up with a method to write a special set of subprograms to invoke PMAC motion controllers with the application of G-code. Based on the method, case programing and machining simulation can be launched. Experiments justify that the method obtained can realize the compiling of fixed cycles with the use of G-code and, in turn, boast substantial significance in the development of open CNC processing machine tools.

Introduction

By a CNC machine is meant the device which can perform automatic and efficient procession according to the machining programs compiled in advance. As a general-purpose machining language, G-code is applied to carry out NC programs, so as to realize the precise motion of all feed shafts. The Turbo PMAC2-Eth-Lite controller is a low-cost PMAC designed by Delta Tau cooperation, which enjoy the merits of integration and extraordinary control performance. Introducing the Turbo PMAC2 CPU, the controller is equipped with 4-axis servo or step controls and 32 general digital I/O points. Moreover, the application of Ethernet and serial COM ports, based on the standard, offers a convenient method for the users to connect the controllers and upper computers and to decide whether to active the expansion function of the channel servo and I/O ports in the expansion cards of the shaft [1]. The probe into open CNC machining tools would be of great practical significance with the cyclic code for deep hole working as example which is commonly employed in the CNC system in the processing center.

Analysis of G83 in Procession Center

In the processing center, particular cycles of processing operation have been typified, for instance, drilling or boring a hole, which is realized by positioning the hole, fast forwarding, machining, fast back warding, etc. Typical machining actions have already programmed in advance and stored in the internal storage. When some action is required, the corresponding G-code would be invoked directly from the internal storage, which simplifies the process of programming.

The fixed cyclic G-code usually found in the CNC system in the processing center primarily takes on as the following program format: data type, reentry-point plane, type of hole machining, data of the hole position, data of hole machining, cycle index [2]. Considering, data types (G90 or G91) have been determined when the program works, it is unnecessary to mention them in the format of the fixed cyclic programs [3]. With the cyclic code (G83) for deep hole working as example, the code writes in the format as follows:

G98（G99）G83 X_Y_Z_R_ P_Q_ F _ K _

In the format, the first G-code (G98 or G99) stands for that for the reentry-point plane, among which G98 represents the initial reentry plane and G99 does the initial plane for R-point. With X and Y indicating the position of holes, Z is the coordinate value of Z, the bottom of the hole, and R is the coordinate vale of R, when the program is written absolutely. However, Z equals the distance from Z, the bottom of hole, to R stands for the distance from R to the initial point, and when the program is written inclemently. P means the pause time, during which the chopper stays at the bottom of the hole, Q does amount of feed every time, F does the speed of drilling, and K does cycle index. The fixed cyclic processing program, or G83, works as is illustrated in Fig. 1.

The tool will be quickly positioned to the places X and Y stands for respectively, and then positioned quickly to R. After drilling downward by the distance represented by Q (Q should dwarf zero, emerging as increment) at the feed rate equal to F, the tool is to return R quickly. Then, after quick position to the place, with the distance of d (determined by the internal parameters of the system) above the lowest point in the proceeding procedure, the tool shall drill downward by Q+d, and quickly return to R. The procedures above shall be performed repeatedly until the bottom point represented by Z is reached. When “d” symbolizing the creep feed of tools, it is by the internal parameters of the system that the distance is set between the point at which the descent of tools is switched from the mode of fast to cutting feed and the other one at which the proceeding mode of cutting feed takes place[3].

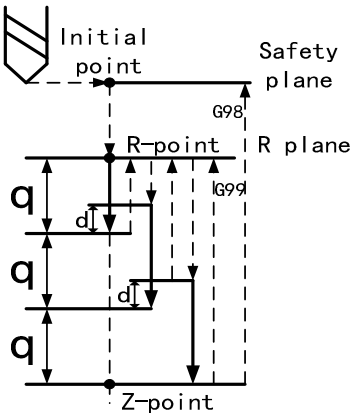

Fig. 1 Processing Fixed Recycle of G83

Development of G-83 Program

Turbo PMAC Clippe is able to compile RS-274 programs and operate G-code programs directly. Working according to its standards, users will get a flexible access to the creation and operation of various programs [5]. The value can be a constant or an expression in the programs, which emerge as a computing and logistic structure and resemble operating languages of the machine when figuring out problems of complex structure [4]. DeltaTau cooperation provides a small number of simple operation G-codes. Employing G-code as subprograms, PMAC, when coming across an operation program with the letter of definite value, would take it for granted that the program employs the orders of “1000.nn000”, and the values (say, X1000) following the line where “nn000” appears would be viewed as parameters, a phenomenon commonly found when dealing with a fixed cyclic program or a executable subprogram without any variables. In the case of meeting a return statement halfway, PMAC would return to operate the program employing the subprogram and carry out the rest orders as it would when dealing with a static G-code [4]. The codes representing subprograms can be omitted and be considered standard G-codes of the equipment when applied by the users. To write the G-codes with more fixed recursion instructions, what the manufacturers need to do is come out with the procedures according to which the subprograms is to be conducted. Fig.2 illustrate the procedures required to write G-83, the deep-hole processing recursion code usually employed in the CNC system of the processing center.

The key code is as follows:

```
undefine all
&1
#1->2000x
#2->2000y
#3->200z
#define farg       Q106
.....
.....

peck_clearance=1
open prog 1000 clear
N0   rapid     return
.....
.....
N83000
read(x,y,z,r,q,p,f,k)
jarg=qarg
gosub 1
gosub 0
x(x_pos)y(y_pos)
while (repeats>0 )
repeats=repeats-1
z(z_rplane)
z_depth=z_rplane-first_peck
while(z_depth-z_pos!<qarg)
gosub 1000
 z(z_depth)
gosub 0
z(z_rplane)
z(z_depth+peck_clearance)
next_peck=jarg+peck
z_depth=z_depth-next_peck
endwhile
gosub 1000
  z(z_pos)
dwell(q116*1000)
gosub 0
endwhile
z(z_cplane)
return
close
```

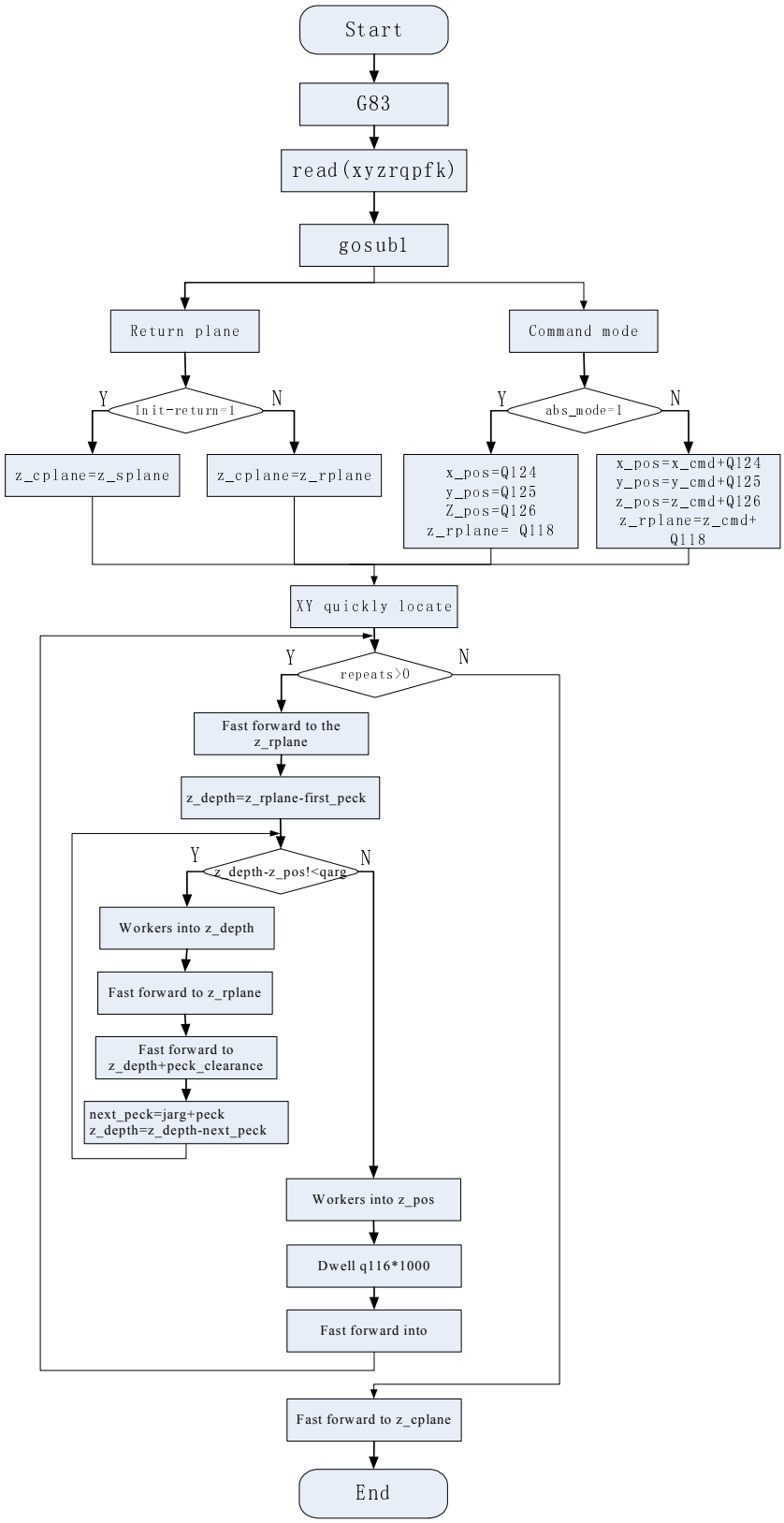

Fig. 2 Flow Chart of Writing G83 Codes

Verification through Experiment

We are to carry out analog simulation of the written programs with G83 with PEWIN32PRO2 and PMAC Plot Pro2. After downloading Prog 53, the written program upon the PMAC card, we see a satisfying result. Fig. 3 show the trajectory data collected.

```
open prog 53  clear
g00 g90 x 0 y 0  z 0
g99 g83 x 20 y 10 z -50 r 2 q 5 f 100
g00    x 0  y 0
close
```

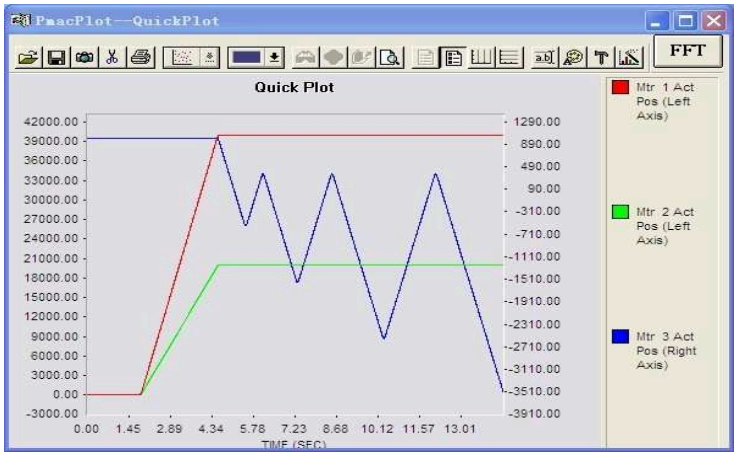

Fig. 3 Show the trajectory data collected.

Summary

The paper tries to develop an open CNC system based on PMAC motion controller. With as example G83, a deep-hole procession recursion code usually employed in the CNC in the processing center, the author probes into the code itself and combines precise algorithms with G-codes necessary to employ the peculiar subprograms of the PMAC motion controller. Experiments show that G-codes can be compiled to realize the fixed recursion instruction and enjoy high practical significance in developing the open CNC machining tools.

Acknowledgements

This work is supported by China National Funds for Young Scientists (61301040), the Tianjin Science and Technology Key Research Program (13ZCZDGX01500;14ZCZDSF00022).

References

[1] Delta Tau clipper Motion Control Card（OL）(2009).

[2] FANUC 0i-MB Operating Instructions. Beijing FANUC company(2008).

[3] Chen Xi Ling: Using a macro program optimization CNC milling of deep drilling, urban construction Industry Press(2011).

[4] Rockets three axis simulator-based study of PMAC (D) Harbin: Harbin Engineering University(2008).

[5] Turbo PMAC (PMAC2) Software Reference Manual (Chinese version) (2011).

Advanced Materials Research Vols. 989-994 (2014) pp 3294-3297
© (2014) Trans Tech Publications, Switzerland
doi:10.4028/www.scientific.net/AMR.989-994.3294

Research on Automatic Changing Film Mechanism of $PM_{2.5}$ Sampler

Mei Yang[1, a], Deng Sanpeng[1, b]*, Yang Kai[2], Zhou Wangfa[1], Wu Jintao[1]

[1]Insitute of Mechatronics Engineering, Tianjin University of Technology and Education, Tianjin, 300222, China

[2]China National Environmental Monitoring Center, 100012, China

[a]wzmin86@163.com, sanpeng@yeah.net

[1] *Author for correspondence: Deng Sanpeng, associate professor, sanpeng@yeah.net.

Keywords: $PM_{2.5}$; Automatic film-changing mechanism; Sampler

Abstract. The problem of air pollution is very serious now, so it is important for developing a monitoring mechanism of $PM_{2.5}$. An automatic changing film mechanism is designed and manufactured in the paper. Then static stress, vibration analysis and structural optimization are carried out by Solidworks software. Experiments show that the mechanism of $PM_{2.5}$ is reasonable and reliable.

Introduction

Environmental problem is common throughout the world. Since the quality of the air has a direct link to the health of human beings, air pollution draws our supreme attention. Among all the pollutants, $PM_{2.5}$ affects our health most, which grants the monitoring of the $PM_{2.5}$ top concern from China [1]. At present, China mainly relies on imported devices to implement the monitoring and analysis of $PM_{2.5}$ [2].

On the international level, the federal methods of equals and of reference is commonly used to monitor $PM_{2.5}$, with the former made up of spectrometry of light scattering, Beta ray method, light turbidity method of Beta rays and oscillating balance method. Relatively speaking, the latter method renders a more accurate description of $PM_{2.5}$ concentration in the air [3]. Based on the method of reference, the $PM_{2.5}$ automatic sampler is designed to collect the fine particles of $PM_{2.5}$ in the air. The automatic film-changing mechanism in the sampler can automatically, rapidly and accurately replace filter membrane holders in the place where to collect the particles, a feature presenting the difficulty as well as the key of the whole device [4][5].

$PM_{2.5}$ Automatic Changing-film Sampler

A $PM_{2.5}$ automatic changing-film sampler is meant a device that can precisely collect $PM_{2.5}$ particles floating in the air, which can be applied to the unmanned monitoring over an extended period. With the help of the PM_{10} inertial impact cutter and $PM_{2.5}$ whirlwind cutter in the device, $PM_{2.5}$ particles can be screen out and transported upon the quartz films at a constant rate of flow. When the film is used up, a second one would be employed to serve the collection. Once the whole collecting process is completed, the obtained particles shall be weighed and the dense of $PM_{2.5}$ would be acquired based on the data. Fig.1 illustrates the $PM_{2.5}$ automatic changing-film sampler.

Composition of Automatic Film-changing Mechanism

Automatic changing film involves a relatively complicated series of movement. That is to say, each movement has a chance of impacting the film changing and in turn influence the dense of $PM_{2.5}$ obtained. Therefore, all the movements should be implemented precisely so as to guarantee the quality of film-changing and accuracy of samples. Fig.2 shows the detailed composition of the automatic film-changing mechanism.

Fig.1 $PM_{2.5}$ Automatic film-changing sampler

The automatic film-changing mechanism should be installed at the center of the sampler. The whole mechanism is composed of the loading buckets, storing buckets, working cylinders, pushing cylinders, rodless cylinders, grippers, enclosure of aluminum foil and relevant accessories. A manipulator consists of the rodless cylinders and grippers. With rubber tail margins attached downward to lessen the pressure, the aluminum trunk envelops the majority of the mechanism. The loading bucket and storing bucket, to accommodate the box of filtering films to collect particles and having collected particles respectively, resides at the bottom of the trunk. Powered by the air from the air pump, the plungers residing in the buckets could drag the box of films downward and upward. Considering the complex composition of particles in the air, including some corrosive substances, say, nitrates and sulfates, the seal ring of the plunger should be made from silicon rubber, which has a good corrosion protection, covered by tetrafluoroethylene.

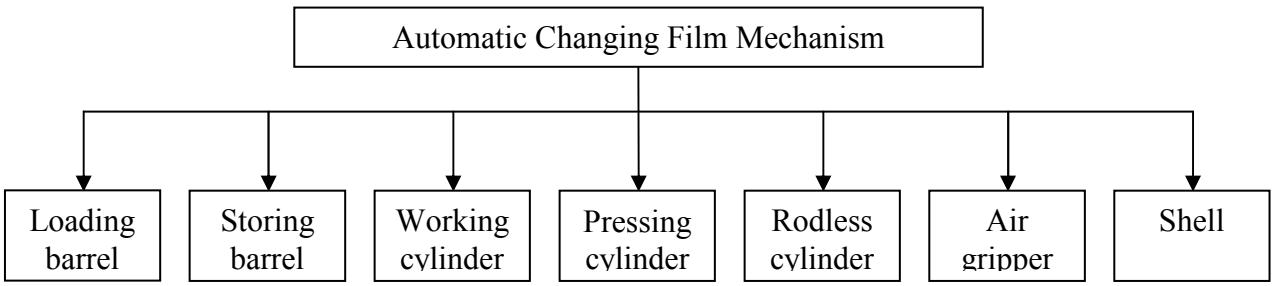

Fig.2 Composition of automatic film-changing mechanism

When the mechanism is started, the manipulator will move to the loading position, making preparation for the loading of film boxes. Once the magnet switch detects the manipulator has reached the targeted position, the two position three way solenoid valve, controlling the loading bucket, would be switched on and the plunger in the loading bucket will drag the box of films upwards until it reaches the loading position sensed by the switch. Then the manipulator will clamp the box to working position. When the box reaches, the manipulator gets loose and the working cylinder pushes upwardly, leaving 2 V-shaped seal rings clamping tightly the box. Then the collecting process can be launched. When the process ends, the working cylinder pushes downwardly, leaving the 2 V-shaped seal rings downward. The manipulator, afterwards, drags the box of collected films to the storing position. Pushed downwardly by the pushing cylinder, the box arrives in the storing bucket, waiting to be analyzed.

Optimum Structural Design

While working, the automatic film-changing mechanism is primarily influence by the gravity and vibration. Based on the analysis of static stress and vibrational frequency upon the mechanism with Solidworks simulation, we can optimize the structure and material of the mechanism. The process of optimizing runs as follows:

Create diffsets. Employ the plug-in of simulation in Solidworks to create diffsets. Make use of the analysis of static stresses.

Choose materials. Define the material characteristics of each accessory respectively. If no restriction exists, define the coordinating settings of the accessories in the modeling.

Choose clamps. Based on the working condition of the mechanism, define the restriction of clamps so as to ensure the applicability of the clamps in the mechanism.

Adding external loads. Since the mechanism merely works under the influence of gravity, the load added should equals the gravity ($9.81 m/s^2$) , and the temperature should be set as the average working temperature (20 ℃).

Construct grid models. Based on the complexity of the mechanism, define the parameters of the grid as follows: as for grids based on curvature, the unit falls into the range from 0.2mm to 5mm. The number of minimum units in the cycle is 8, with the rise ratio over a unit equal to 1.6 and Jacobian point set to 4.

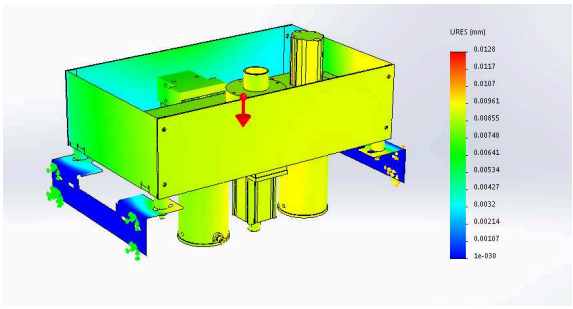

Fig.3 Displacement analysis of static stresses

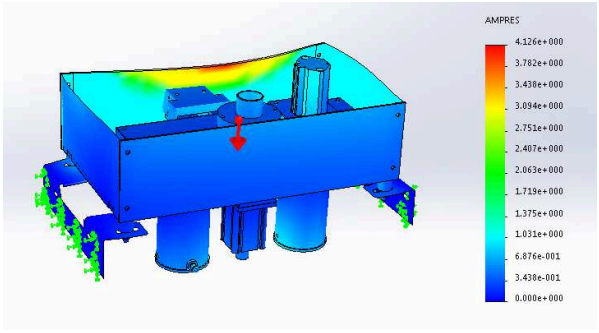

Fig.4 Analysis of frequency

The analysis the static stresses indicates that the maximum static stress upon the mechanism is about 2Mpa, strain about 0.00002747, and maximum displacement of static stress about 0.01mm. In effect, the aluminum product employed in the mechanism boasts a yield strength of about 80 Mpa and the mechanic precision of the whole mechanism reaches about 0.01mm. The simulation proves that the structure of and material adopted in the mechanism meets the requirements of static stresses.The analysis of frequency resembles that of static stresses. Please refer to analysis of static stresses to land the process of setting. Fig.4 shows the outcome of the analysis.

The vibration of the mechanism originates mainly from the air pump. The analysis demonstrates the point with the greatest amplitude lies at the back of the aluminum trunk, with the head cover out of concern. The existence of the head cover can lessen the vibration of the trunk and decrease the amplitude significantly.

Based on the analysis of static stresses and frequency, under the influence of gravity and vibration, the chosen material and structure could ideally satisfy the working requirements.

Experimental Analysis

Table 1 gives a contrast of data observed by 3 devices located in the top building of the monitoring center of Tianjin environmental protection agency (with a height of some 20 meters, E: 117°09′04″, N: 39°05′49″). One is the $PM_{2.5}$ automatic film-changing sampler, another is the Partisol 2025i-D sampler, and the other is β-ray $PM_{2.5}$ online monitor.

Seen from Table 1, the 1st two devices employ the federal method of reference and the last device makes use of light turbidity method of Beta rays. The data obtained shows that the error rate of the 1st and 3rd devices reaches about 0.03, while the 2nd falls in the order of 0.03, a much better figure over those of the other two devices. The difference can be traced back to the fact that, with the federal method of reference, the dense of $PM_{2.5}$ worked out bases on the factual data while the method of Beta rays figures out the dense of $PM_{2.5}$ based on the degree of attenuation of rays. Thus, the federal method of reference renders a more accurate outcome. A relatively small difference exists between the data of the sampler and the Partisol 2025i-D sampler, a fact justifying that the automatic film-changing sampler is designed reasonably and satisfies the working requirements.

Table 1 Contrast of experimental data

Devices \ Date	2014.4.14-15	2014.4.15-16	2014.4.16-17
$PM_{2.5}$ automatic film-changing sampler	0.076873916	0.060727725	0.127249365
Partisol 2025i-D sampler	0.076682028	0.061124732	0.126909091
β-ray $PM_{2.5}$ online monitor	0.072456467	0.059521739	0.125391304
The error rate of the Comparison with partisol 2025i-D sampler	0.002502385	-0.006495034	0.002681242
The error rate of the Comparison with β-ray $PM_{2.5}$ online monitor	0.061061638	0.020261263	0.014818101

Conclusion

The paper gives a detailed description of the principle of the pneumatic automatic film-changing sampler of $PM_{2.5}$, renders a finite element analysis of setting processes and data, and finally implements a contrast with other devices recognized by the country through an experiment. The test indicates the outcome lies the accepted range. Basically meeting the national standards, the sampler can play a competent role in monitoring the dense of $PM_{2.5}$.

Acknowledgements

This work is supported by National key Scientific Instrument and Equipment Development Projects (2012YQ06014704), the Tianjin Science and Technology Key Research Program (13ZCZDGX01500; 14ZCZDSF00022).

References

[1] Wang Wei. Development and application of model TSP-PM10-PM2.5-2 medium volume sampl ing system[J]. Environmental Monitoring in China,2003, Vol.19, p.35-38.

[2] Yang Xinxing. Air Particulate Matter PM2.5 in Beijing and Its Harm. Frontier Science, 2012, 6(21).22-31.

[3] Hao Ming-tu. Current Pollution Status and Pollution Characteristics of PM2.5 in China[J]. ENVIRONMENTAL SCIENCE AND MANAGEMENT.2006, Vol.32, p.58-61.

[4] Vladutescu, V. ; Diaz, J. ; Charles, L. ; Gross, B. ; Moshary, F. ; Ahmed, S. Aerosol Layer Properties and their Effect on Optical Depth Relations to PM2.5 Concentrations. Geoscience and Remote Sensing Symposium, 2008,Vol.4, p.589-592.

[5] H.S. Lim, M.Z. MatJafri, K. Abdullah, etc. Algorithm for PM2.5 mapping over Penang Island, Malaysia, Computer Graphics, Imaging and Visualization, 2008, p. 385-388.

Advanced Materials Research Vols. 989-994 (2014) pp 3298-3301
© (2014) Trans Tech Publications, Switzerland
doi:10.4028/www.scientific.net/AMR.989-994.3298

Design of Shock-absorbing System for Disaster Rescue Robot

Xie Lei[1, a], Qi Yuming[2, 1, a,*]

[1]Institute of Mechatronics Engineering, Tianjin University of Technology and Education, Tianjin, 300222, China

[2]School of Mechanical Engineering, Tianjin University, Tianjin, 300222, China

[a]tzsd001@126.com

* Author for correspondence：Qi Yuming. E-mail: chigym@163.com

Keywords: Disaster Rescue Robot. Shock-absorbing System. Geometry design. Performance analysis

Abstract. Disaster Rescue Robot is a small caterpillar robot used for carrying first aid articles, reasonable shock-absorbing system is an indispensable part to reduce the rush of the ground because it has to plummet from a certain level to the ground when it works. We use the method of modular design in this article and design the landing gear based on the performance of conical spring in order to absorb some of the forces during a fall. Then the three-dimensional modeling software is used to establish the parametric model of the robot shock-absorbing system to provide an effective way for the design of the Disaster Rescue Robot.

Introduction

More than 70 percent of Chinese cities and more than 50 percent of the Chinese population are located in areas vulnerable to serious earthquakes, or meteorological, geological or marine disasters [1]. Chinese people's lives and properties and economic and social development suffered very heavy losses during major natural disasters happened over the years. Disaster Rescue Robot is a small caterpillar robot used for carrying first aid articles, and it integrates many advanced multidisciplinary fields such as mechanical engineering, electronic technology, intelligent control and computer science research. In the military field it can be used for battlefield reconnaissance, break the barrier and tracking target designation or entering into the nuclear, chemical and biological pollution area to carry out combat mission, connect the signal or provide precision strike against the enemy. In the field of public safety it can be used in security monitoring, explosion-proof, anti-terrorism, emergency rescue, disaster relief, and acts as an intelligent transportation [2].

Disaster rescue robot mainly completes the information acquisition of the disaster environment. In this article, we use the method of modular design which has the advantage of convenient disassembly and maintenance, adapt complex pavement, and by the rotation of the swing arm before control module to adjust the robot's posture change to auxiliary climbing obstacle and across the ditch [3]. Robot will have perfect environmental adaptability, motor skills and resist impact from the drop of a certain height after reasonable structural layout and design. We conduct the detailed engineering design of the robot not only on the aspects such as the principle, performance and organization of the movement and anti-throw structure and so on several aspects of research, but also combined technology with the modern theory of mechanical design, optimization method, new materials.

Performance analysis and design of the Disaster Rescue Robot

A lot of critical questions include precise and safe landing, remote wireless communication, flexible mobile in ruins, anti-seismic waterproof and fireproof need to be solved to design a special robot system that can be dropped into the disaster areas by the plane to get information of the disaster and carry out emergency rescue. According to the function, the robot system can be divided into landing control system umbrella, soft landing machine, remote wireless communication, intelligent control

and robot ontology modules, etc. The design of the detection robot which can walk on the ground includes the flexible mobile design to travel on the ruins; the reliable design of anti-seismic waterproof and fireproof in the disaster environment; the ability to carry sensors, communications equipment and emergency supplies [4].

In condition, general design requirements for robots act as the followings:

1). The total weight of the robot is less than 50kg, the movement speed is more than 10m/min, the working time can last more than 1 hour, and the remote control design to travel on the ruins flexibly. The robot can also load all kinds of detection devices and emergency supplies.

2). The wireless communication distance of remote control should be more than 10km to make sure the reliable transmission of the image, noise and various sensors and control signal.

3). The robot has to have the characteristic of anti-seismic waterproof and fireproof, etc.

4). The robot should have good capability of riding over obstacles obstacle, be suitable for all kinds of disaster

The argument about the robot's shock-absorbing scheme

The design of the shock-absorbing system mainly adopts the spring suspension method which can produce large elastic deformation under the load [5]. According to the differences of the load, spring can be divided into tension spring, compression spring, torsion spring and bending spring. According to the shape of the spring, spring can also be divided into helical spring, ring spring, belleville spring, flat leaf spring, coil spring and so on.

The basic formula of spring:

1) The formula of strength calculation

$$d = 1.6\sqrt{\frac{KFC}{[\tau]}} \tag{1}$$

K stands for curvature correction factor， $K = \frac{0.615}{C} + \frac{4C-1}{4C-4}$；

F stands for load；**C** stands for spring index，**C=D2/d**；**[τ]** stands for the allowable twisting stress of the spring material. Then the diameter of the spring wire ***d*** can be computed.

2) The formula of stiffness

$$n = \frac{Gd^4}{8FD_2^3} = \frac{Gd\lambda}{8FC^3} \tag{2}$$

n stands for the effective coil number of the spring; **G** stands for the shear modulus of the spring; **λ** stands for the deflection of the spring; $\mathbf{D_2}$ stands for the medium diameter of the spring ring; the other symbolic significance has the same meaning as previous.

3) In order to limit the spring load, the stability formula **F** is less than the instability of critical load **Fcr** in the stability formula. We generally take F=Fcr/(2 ～ 2.5) and the critical load $F_{cr} = CB \cdot k \cdot H_0$,CB stands for instability index.

After the demonstration, the conical spring is adopted as the mainly spring suspension of the Disaster Rescue Robot as Fig. 1 shows.

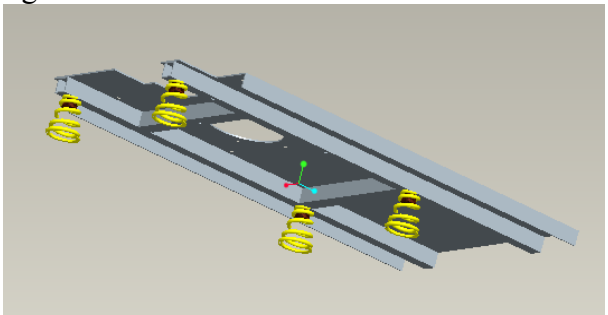

Fig. 1 Spring suspension system

Geometry design of the spring suspension

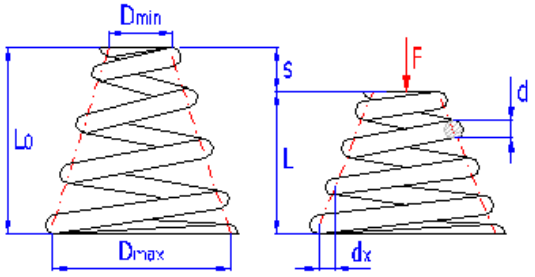

Fig. 2 The dimensions of the conical spring.

Fig. 2 shows the conical spring used in the shock-absorbing system of the robot. Four conical springs made of the materials of 65Mn are used. The small diameter $D_{\min}$ takes 20mm, big diameter $D_{\max}$ takes 60mm, L_0 takes 60mm, M takes 30kg.

$$F_c = \frac{L_0 - L_s \cdot G \cdot d^4}{8 \cdot n \cdot D_{\max}^3} \tag{3}$$

The conical spring is made of spiral coil, and the gap between the work coils is constant to absorb the axial external forces. The coil spring whose wire diameter is about 6mm is cold forming. The thermal forming spring must be used for high load of products whose wire diameter is greater than 10mm.The conical spring is used in the condition that the spring coefficient changed along with the compression quantity. Increased along with the conical spring compression, the adjacent working coil contact gradually (The first coil diameter is the largest). Then the compression deformation of the coil is no longer involved in deformation resulting in spring coefficient increase gradually. The work characteristics can be divided into two areas [6].

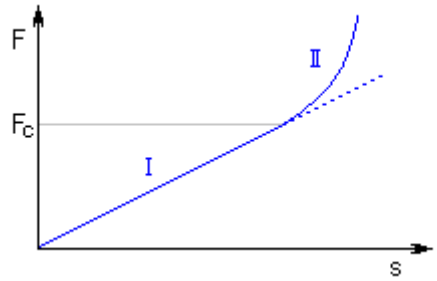

Fig. 3 Basic relations of the conical spring calculation

1) The linear work area (the spring constant is constant) F<FC
2) Incremental feature work area- After contacting with the first largest coil F>FC

The decisive factor of the limiting force FC is the space between the coils p that also means the size of the length of free spring. The limiting force FC has a positive relationship with the length of spring and the linear spring coefficient.

Coil bending causes additional coil bending stress, therefore the correction coefficient is used to correct the pressure. The correction coefficient of the coil springs with circular section is determined by Formula (4).

$$K_s = 1 + \frac{0.5}{c} \tag{4}$$

The correction coefficient of springs with square section is determined by the given proper nomogram of spring diameter ratio b/h. Coefficient of the status quo has been included in the correction calculation.

Considering the several different design closure of compression spring, closing coil is the end coil of the spring and has the same axle with working coil. Its angle and the spacing won't change when the spring works. Closing coil is usually used as the braced and stayed surface of spring and finish on

both ends is the most often used in compression spring. The grinding flat coil is the end of the coil, and it is processed to a plane perpendicular to the axis. It lasts from the three quarters of half edge processing coil to the open end. The diameter of the spring used in the grinding flat coil is usually more than 1mm.

The shock-absorbing system of the disaster rescue robot has four supporting points and each point fixed with a taper spring (The tolerance of the taper spring is 5Kg.). The taper springs are the most important part of the shock-absorbing system. The size of the conical spring showed in Table 1 is calculated by formula (3) and (4).

Table 1 The size of the conical spring

Spring diameter ratio $\mathbf{C_{min}}$	min.3
Spring diameter ratio $\mathbf{C_{max}}$	max.20
Diameter $\mathbf{D_{max}}$	max.40mm
Ratio $\mathbf{D_{max}/D_{min}}$	min.2
Number of working coil **n**	min.2
Ratio **b/h**	5:2
slenderness ratio $\mathbf{L_0/D}$	2/5

Summary

Through the design of the robot body, we discussed several forms of the shock-absorbing system, designed and selected the shock-absorb system and the spring suspension system was found. We also discussed the relationship of the two working areas and the design and calculation is on the basic of it. The function of anti-seismic has proved by experimental research.

Acknowledgements

In this paper, the research is supported by The National Youth Science Fund Project(61301040); Tianjin science and technology planning project (13ZCZDGX01500) and (14ZCZDSF00022) and Xiqing District special scientific and technological innovation project (XQCXZX2012-003).

References

[1] Deng Sanpeng, Xu Xiaoli, Li Chongning, etc. Research on the oil tank sludge cleaning robot systemSource[C]. MACE2010, p 5938-5942.

[2] Hydrovac industrial & petroleum serv.(oil storage).Tank cleaning made easy with quick assembly unit[J] Chem.Eng(Rugby), 1986,431(12):34.

[3] Qi Y. M., Wang Z. M., Deng S. P., Meng Z. X., c, Wang C.G., Research on Concrete Hydraulic Crushing Based on Five-plunger Pump[C]. Advanced Materials Research, Vols. 756-759 (2013): 257-260.

[4] Petroleum Ferment.Cleaning sludeg from oil storage tank-using entirely hydraulic vehicle to fluideze sludge and jet resultant mix[P]. US 880913 4770611,1988.

[5] Qi Yuming, Zhu Xianzhu, Deng Sanpeng, Wang Zhongmin. An Approach of Spindle Bearing Pre-tightening Based on Spacer Sleeve Adjustment[C]. Applied Mechanics and Materials, Vols. 488 (2014):1087-1090.

[6] Tan, Gui Ling, Qi Yu Ming, Deng San Peng, etc. Research of pure tone detection for faulted on-vehicle loudspeakers based on image fractal[C]. Applied Mechanics and Materials, Vols. 494-495 (2014):171-174.

Advanced Materials Research Vols. 989-994 (2014) pp 3302-3305
© (2014) Trans Tech Publications, Switzerland
doi:10.4028/www.scientific.net/AMR.989-994.3302

Failure Analysis and Preventive Measures of Cooling Tower Fan Gearbox

Chen Jianping[1, a], Wang Yali[1, b], Zhao Chunxiao[1,c], Li Xing[1,d]

[1]College of Mechanical Engineering, Tianjin University of Science & Technology, Tianjin 300222, China

[a]chjp@tust.edu.cn, [b]yali3305@126.com, [c]yali3305@126.com, [d]lixingfamily@126.com

Keywords: Cooling Tower Fan Gearbox. Failure Analysis. Preventive Measures

Abstract. To avoid fatal accidents caused by premature gear failure of cooling tower fan, research and analysis of gear tooth surface pitting and tooth breakage which are the two main failure forms of cooling tower fan gear are conducted in this article, the specific reasons of the fan gear failure are got, and corresponding suggestions of improvements and preventive measures are put forward, this can be taken as reference to the gear design and fault analysis.

Introduction

Cooling tower fan widely used in petroleum, chemical, electric power industry, carries industrial water circulating cooling function and its operational status directly affects the industrial production. The fan reducer deliveries rotary rotation from the motor to the fan impeller by a pair of spiral bevel gears and a pair of helical cylindrical gears, level input and vertical output as showed in figure 1.

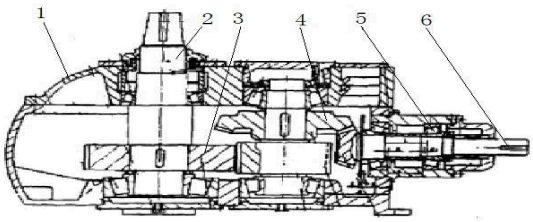

1. Box 2. Output shaft 3. Cylindrical helical gear 4. Spiral bevel gear
5. Bearing 6. Input shaft

Fig. 1 Cooling tower fan drive structure

The premature gear failures directly affect the fan working reliability and efficiency; In engineering applications, some domestic cooling tower fan reducer gear appear tooth surface premature failure and frequent teeth broken conditions after only working three to five months, especially more severe in high temperature area and summer. The failure analysis was aimed at identifying the root cause of the gear damage in order to prevent their recurrence[1-3].

Cooling Tower Fan Gear Failure Form and The Reason Analysis

Gear Tooth Surface Pitting Analysis. In a overhaul of cooling tower fan gearbox in a petrochemical plant, it is found that different degrees of pitting exist on gear, Fig. 2-1 and 2-2 show helical gears tooth pitting, high density of tiny pits distribute uniformly on the low tooth surface near the pitch line, and numerous micropittings will be seen after magnifying the damage surface[4-5].

Fig. 2-1 Active helical gear tooth pitting

Fig. 2-2 Passive helical gear tooth pitting

Focus on the helical gears pitting situation, failure judgment on gear pitting is made, then we declare that the gear is failure and should be discarded. Through examination and final analysis, we get the root reasons of pitting are as follows.

1) During cooling tower fan gear operation, cyclic contact stress will generate on meshing surface of helical gears ,because the additional load and gear partial load caused by unbalanced moment of inertia of the blade, the load that gear bearing will increase, After certain cycles, the tooth surface contact stress exceeds the fatigue limit of the material, which will make the gear surface and sub-surface crack under the effect of fatigue, the cracks expand and extend, eventually metal bits shed from tooth surface.

2) The transmission power of cooling tower fan gear is large while the meshing contact surface of helical gears and spiral bevel gears both are wide that the oil temperature likely to rise easily so the oil prone to failure due to oxidation, poor lubrication is liable to happen and effective lubricating film is difficult to form, which finally cause gear pitting.

Gear Tooth Breakage Analysis

Analyzing gear tooth broken failure of the cooling tower fan reducer, it is found that most of the gear tooth broken of helical gear and bevel gear are usually local broken. In a recent cooling tower fan speed troubleshooting, we found severe tooth broken on active bevel gear upon input shaft and rough fracture morphology,1/3consecutive face cutting on driven spiral bevel gear, as shown3-1 and 3-2 figures.

Fig. 3-1 Active spiral bevel gear tooth broken

Fig. 3-2 Driven spiral bevel gear tooth broken

Figure 3-1 shows the active spiral bevel gear tooth end breakage, through macroscopic examination, it is found that active tooth cracked from bottom and fractured to the concave of root, which is evidently due to strength insufficient of the tooth root. The obvious destructive pitting and spalling in the fractured tooth indicate the presence of partial load condition which cause partial overload of gear and make the tooth surface contact stress much higher, this is the main reason of gear tooth broken. Figure 3-2 displays the driven spiral bevel gear teeth broken; the driven gear

failure mainly appears in gear meshing area above the pitch circle, which should be caused by a huge impact the moment driving gear broken in meshing area.

Due to assembly errors, the misalignment error of two bevel gears cone top is too large and work cone distance is inconsistent to the design, so the meshing bevel gears contact on gear small end. And because the input shaft connected to the active bevel gear shaft is longer, linear deviation is easily produced, which caused unbalanced gear running.

Measures To Prevent Premature Gear Failure:

General Measures. 1) Choose the larger module gear within the scope of the permission to improve the gear tooth root bending strength. Choose larger diameter gear with the smaller curvature of involute for reducing the contact pressure .Considering the larger vibration and impact of cooling tower fan gear, the selected safety coefficient should be greater than the critical value.

2) Reduce surface roughness through tooth surface gear lapping; improve the heat treatment and chemical heat treatment, ensure enough hardness of surface layer and core.

3) Use appropriate adjustment sheet adjust installation distance in spiral bevel gear assembly to get good lateral clearance and contact area; Because of the speed reducer input shaft is longer, the balance of shaft and gear should be proofread after right installation.

Lubrication and Lubrication Management

Gear pitting and tooth fracture of cooling tower fan are closely related to the lubrication. In gear using, reasonable lubrication can prevent the occurrence of early pitting, suppress and mitigate the development of pitting. Proper gear lubrication management is essential to ensure gear to achieve the desired working life.

1) Lubricating oil viscosity changes with external conditions (pressure and temperature), in order to ensure the viscosity stability of lubricating oil ,we suggest operators observe the change of the viscosity of gear lubrication oil regularly and replace lubricating oil when viscosity rise or fall 15%.

2) Cooling tower fan gear works in continuous operation at full load in summer, which cause serious fever, while works in intermittent operation and light load conditions in winter. So different specifications of the lubricating oil should be changed according to different seasons, we recommend use low viscosity oil in winter, high viscosity in summer.

3) Pay attention to the oil cleaning and change gear lubrication oil according to the maintenance cycle. If impurities entering the gear work surface, it is not only can destroy the film, but can also cause abrasive wear, so operators must pay attention to the cleaning of lubricating oil.

Other Gear Failure Preventive Measures

1) Take regular care and maintenance of gearbox, including wheel surface, bearings, housing, fasteners, oil seals, etc.

2) Monitor cooling tower fan gearbox running status, such as temperature, pressure, noise, vibration, etc. When abnormal phenomena occur, stop the device promptly to avoid major accidents.

Summary

Through analyzing gear tooth surface pitting and tooth breakage, two main failure forms of cooling tower fan reducer gear, corresponding preventive measures and correct repair process are put forward. Proposal of lubrication, lubrication management and other auxiliary measures to prevent premature gear failures are given. The above schemes are important for the cooling tower fan frequent failure status caused by faulty gear.

References

[1] Zhan Zhang: Gear failure and Countermeasures (China Machine Press, Beijing 2011).

[2] Weiming Liu, Yanqiu Xia, Xingguo Fu: Gear lubricating material (Chemical Industry Press, Beijing 2005).

[3] Xiaolu Zhu: Handbook of Gear Design (Chemical Industry Press, Beijing 2004).

[4] Chen Baoqing, Zhang Guosheng, Zhang Jinxin, Research on Remanufacture for Construction Machinery[J], Equipment Management and Maintaining. 2011,12(7):41-42.

[5] Zhou min, Study of NC Milling Machine Cylinder Repairing Accuracy Based on Remanufacturing Technology[J], Hydraulic Pressure and Pneumatic. 2011,12(12): 84-87.

Advanced Materials Research Vols. 989-994 (2014) pp 3306-3309
© (2014) Trans Tech Publications, Switzerland
doi:10.4028/www.scientific.net/AMR.989-994.3306

Application of Viscous Pressure Forming in Aeronautics and Astronautics

Li Jiguang[1], Zhang Jiegang[2], Liu Jingping[2], Zhao Ruifeng[1], Li Yang[1], Li Yuchen[1], Yu Shixiang[1], Wang Zhongjin[2]

[1]Tianjin Long March Launch Vehicle Manufacturing Co. Ltd, Tianjin 300462, China

[2]Capital Aerospace Machinery Company, Beijing 100076, China

[3] School of Materials Science and Engineering, Harbin Institute of Technology, Harbin 150001, China

Keywords: Viscous pressure forming(VPF). Super-alloy. Thin-walled part with variable diameters. Corrugated thin-walled part. Asymmetrical thin-wall part with variable diameter

Abstract. Viscous pressure forming(VPF) is a new developed sheet soft-punch forming process in 1900s. The basic principle and characteristics of VPF are described. The applications of VPF technologies of nickel-based super-alloy corrugated thin-walled part, asymmetrical thin-wall part with variable diameter, super-alloy thin-walled part with variable diameters, corrugated thin-walled part with larger diameter and small section are presented. The results show that VPF is suitable for the forming of parts with high strength, low plasticity, super thin-wall and complex shaped.

Introduction

Development with the modern industry, more sheet metal parts with very complex three-dimensional shape are made with high strength, difficult-to-deform and super thin-sheet materials in the industry of present aeronautics, astronautics, automobile, chemical and other high-tech industries. The requirement to these parts in dimensional accuracy and surface quality, especially wall-thickness uniformity, becomes higher and higher. So the more advanced the forming technology is needed. The usually flexible-die forming technology and conventional stamping method has its own application range. But because of its good characteristics, viscous pressure forming(VPF), which makes use of a kind of viscous material as pressure carrying medium, has good perspective[1-3].

Principle and characteristic of VPF

VPF was invented by M. L. Rhoades and L. J. Rhoades in 1992[4], and is different from conventional flexible sheet technology, in that it uses a kind of semi-solid, flowable and viscous materials as the pressure-carrying medium. In VPF, the viscous medium is used as a soft punch when it is applied on one side of the sheet metal and used as a soft punch and back-pressure when it is applied on both sides of the sheet metal. Through the injecting of viscous medium, the pressure distribution is applied in the die-container and the sheet is formed under the pressure of the viscous medium. A schematic diagram of VPF is shown in Fig.1. Compared with the conventional sheet metal forming process, the viscous medium can fill a complex-shaped surface very well. The parts formed by VPF have good surface quality and high dimensional accuracy[5].

The tangential adhesive stress of the viscous medium has a key effect on the sheet metal in VPF. The sheet metal is subjected to the tangential adhesive stress of the viscous medium during the whole forming process. The value of tangential adhesive stress is affected by the viscous medium pressure, viscosity and forming time. However, the punch gradually makes contact with the sheet metal and the friction force is then related only to the surface quality of sheet metal and the rigid punch. Comparing the thickness of parts formed by VPF, rigid punch forming and hydro-forming with the numerical simulation method, the thickness of parts obtained by VPF is more uniform than that by rigid punch forming and hydro-forming[6-9].

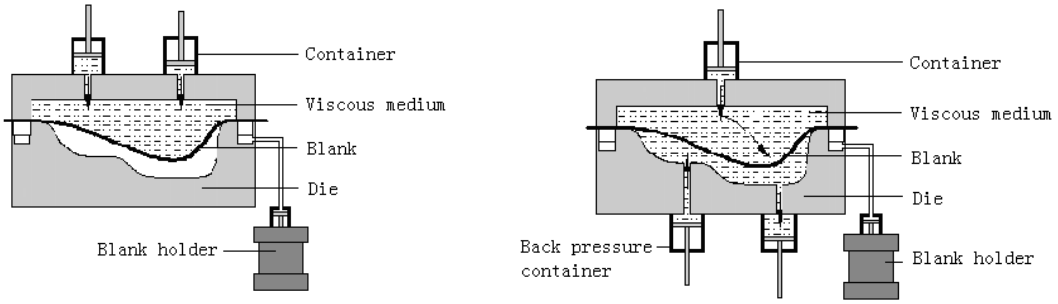

a) Single surface loaded b) Double surfaces loaded

Fig. 1 Principle of viscous pressure forming

Applications of VPF

Application of VPF was developed by Leonid B Shulkin firstly. The geometry for the VPF test part "sub-inner panel" was developed based on a nozzle inner panel component currently produced by Pratt & Whitney (Fig. 2). And it was explained through finite element analysis method (Fig. 3) by PAM-STAMP. The FEM results are compared with experimental VPF results. The viscous medium "blow through" phenomenon between the blank holder and the sheet during VPF is described and quantified.

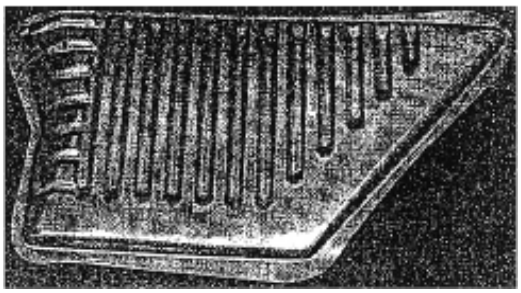

Fig. 2 Pratt and Whitney nozzle inner panel

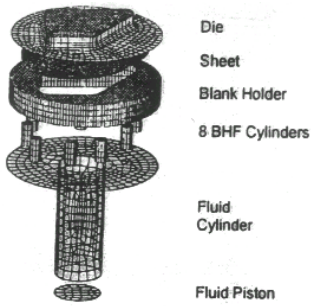

Fig. 3 FEM model for VPF simulations

VPF is used in the areas of aeronautics and astronautics successfully by Harbin institute of technology. A nickel-based super-alloy corrugated thin-walled part (Fig.4)[11], asymmetrical thin-wall part with a variable diameter (Fig.5)[12],thin-wall parts with variable diameter (Fig.6)[13] and thin-wall parts with larger diameter to thickness ratio and complex small section (Fig.7) were produced successfully. The nickel-based super-alloy corrugated thin-walled part is a typical large-dimension, thin-walled and complex-shaped part formed by VPF. The shape and the main dimensions of the corrugated thin-walled sheet part with small radius are shown in Fig.4. where the wall-thickness is 0.3 mm, the width is 81 mm, and the radius of all ripples with non-uniform depth is 2.3 mm. With rigid punch forming, the wall-thickness of parts would thin severely and the parts could even fracture at corrugated surfaces during forming. With rubber or polyurethane flexible punch forming, corrugated surfaces could not be formed to meet the requirements of dimensional accuracy due to this being beyond the deformation limits of rubber or polyurethane. With VPF, the dimensions of small radius corrugated surface can meet the requirements of dimensional accuracy.

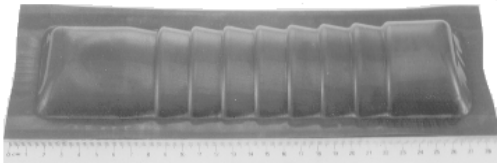

Fig. 4 A nickel-based super-alloy corrugated thin-walled part

The asymmetrical thin-wall part with a variable diameter is one of the typical lightweight complex construction components in aeronautics, astronautics and automobile industry. The traditional method to form this kind of part is by the way of forming each part separately and then assembling together by welding. Because of too many working procedure, it is difficult to control the forming quality, this method can't satisfy the increasing requirement of improving the properties

of forming parts. Aiming at the problems, a new no-seal tube-blanks forming technique is proposed, which pressure provided by the viscous medium. Because of the free in the circumferential direction of the no-seal tube-blank, sheet blank flow in the circumferential direction can compensate the deformation of the local forming area. This new technique increases the forming limit and provides a new way to form the asymmetrical thin-wall part with a variable diameter.

Fig. 5 The asymmetrical thin-wall part with a variable diameter

Tube-compression is one of the most typical forming methods for variable diameter parts. Because of compression instability, buckling and wrinkling easily come into being in tube-compression process, especially for the thin-wall parts, which restricts the applications of tube-compression. In order to solve problems in tube-compression of thin-wall parts with complex shape, by applying the viscous pressure forming (VPF) method in tube-compression, a new forming method, local tube-compression by VPF, is developed. Taking advantage of the mechanical property and easily loading mode of viscous medium, the occurrence of tube buckling can be delayed and the wrinkling can even be removed in a certain extent during local tube-compression process by VPF, which increase the diameter reduction limit. The new tube-compression method can be used in tube-compression of high strength materials and the precise plastic forming of thin-wall parts with larger variable diameter.

a) Preformed tube-blank b) The specimen of tube-compression c) Cross section of the specimen

Fig. 6 Thin-wall parts with variable diameter

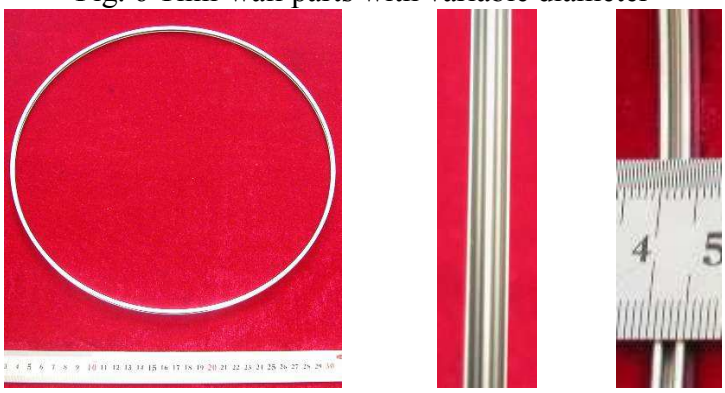

Fig. 7 Thin-wall parts with larger diameter to thickness ratio and complex small section

Thin-wall parts with variable diameter which have the characteristics of larger unit variable diamerer ratio (3.5~7.2), larger diameter to thickness ratio (500~1750) and ultra thin wall-thickness (0.2~0.3mm) are the important functional parts of new-type aerospace and power machineries. Meanwhile dimensional precision of the parts is higher and materials are heat-resistant alloy. During to the characteristics such as structure, wall-thickness and precision and so on, the cricital

techniques in the forming process is control of wall-thickness uniformity and dimensional precision, material flow, plastic deformation and stress distribution. For these problems, viscous adhesive stress between the interfaces and non-uniform viscous pressure has been taken full advantage; viscous quasi-bulk pressure forming was raised. In this method, the material flow has better been controlled, which can restrain the wall-thickness reduction and has the better stress distribution.

Conclusion

Compared with conventional sheet metal forming technology, VPF can improve the formability of sheet metal and the parts obtained by VPF have high surface quality and high dimensional accuracy. And the viscous medium can fill a complex-shaped surface very well. VPF is suitable for manufacturing high strength, low plasticity and difficult-to-form materials and complex-shaped parts. Meanwhile, VPF is suitable for forming multi-kinds, small quantity and promptly update products in the areas of aeronautics and astronautics. Viscous medium outer pressure necking uses semisolid, flowable, highly viscous and certain rate sensitivity super-polymer as pressure carrying medium which can solve wrinkling problem during necking forming effectively and increase necking limit of specimen.

References

[1] Wang Zhongren, Teng Bugang, Tang Zejun. New Development of Plasticity Process Technology[J]. Chinese Journal of Mechanical Engineering, 2009, 20(1): 108-112

[2] W. Singer, H. Kaiser, X. Singer, G. Weichert. Hydroforming of Super-conducting Tesla Cavities[J]. Journal of Metal Processing Technology, 2000, 87: 102-108

[3] Fang Li, Richard Patton, Khurram Moghal. The relationship between weight reduction and force distribution for thin wall structures[J]. Thin-Walled Structures, 2005, 43: 591-616

[4] M. L. Roades, L. J. Roades. Method and Apparatus for Die Forming Sheet Material[P], United States Patent No.5085058, Feb4, 1992

[5] J. Liu, B. Westhoff, M. A. Ahmetoglu, T. Altan. Application of Viscous Pressure Forming (VPF) to Low Volume Stamping of Difficult-to-form Alloys Results of Preliminary FEM Simulations[J]. Journal of Materials Processing Technology, 1996, 59: 49-58

[6] J. Liu, M. A. Ahmetoglu, T. Altan. Evaluation of Sheet Metal Formability Viscous Pressure Forming (VPF) Dome Test[J]. Journal of Materials Processing Technology, 2000, 98: 1-6

[7] Wang Zhongjin, Wang Zhongren. Analysis of Strain Rate Variations during Viscous Pressure Bulging of Sheet Metal[J]. Journal of Plasticity Engineering, 1999, 6(3): 46-48

[8] Liu Jianguang, Wang Zhongjin, Gao Tiejun. Experimental Study on Effect Factors of Viscous Adhesive Stress in Viscous Pressure Forming[J]. Chinese Journal of Mechanical Engineering, 2006, 42(10): 146-150

[9] Song hui. Experimental Research of Mechanical Property of Viscous Medium[D]. Harbin: Dissertation for the Master Degree in Engineering of Harbin Institute of Technology, 2004, 44-58

[10] L B Shulkin, R A Posteraro, Mustafa A Ahmetoglu et a1. Blank Holder Force(BHF) Control in Viscous Pressure Forming (VPF) of Sheet Meta1[J]. Journal of Materials Processing Technology, 2000, (98): 7-l6

[11] Z. J. Wang, J. G. Liu, X. Y. Wang, Z. Y. Hu, B. Guo. Viscous Pressure Forming (VPF): State-of-the-Art and Future Trends[J]. Journal of Materials Processing Technology. 2004, 151: 80-87

[12] Wu Weibiao. Forming Process Depending on Sheet Blank Flow in the Circumferential Direction for Asymmetrical Thin-wall Parts with a Variable Diameter[D]. Harbin: Dissertation for the Master Degree in Engineering of Harbin Institute of Technology, 2009: 22-36.

[13] WANG Zhong-jin, GAO Tie-jun. Inner and outer pressure forming of the nickel based super-alloy thin-walled part with variable diameter sections[J]. Transactions of Nonferrous Metals Society of China. 2008, 18: 285-290

Advanced Materials Research Vols. 989-994 (2014) pp 3310-3313
© (2014) Trans Tech Publications, Switzerland
doi:10.4028/www.scientific.net/AMR.989-994.3310

Methods of Metal Parts Unfolding

LI Yang[1,a], ZHANG Jiegang[2], LI Jiguang[1], LI Yuchen[1]

[1]Tianjin Long March Launch Vehicle Manufacturing Co.Ltd, Tianjin 300462, China

[2]Capital Aerospace Machinery Company, Beijing 100076, China

[a]liyang408874329@163.com

Keywords: Sheet metal unfolding. Neutral plane. Pro/E

Abstract. There are a variety of sheet metal parts in rocket body structure. The exact length calculation of sheet metal structure work is the key to ensure better quality of product. This paper describes two methods of sheet metal part unfolding which are method of formula and method of software. Two quick unfolding ways using AUTOCAD and EXCEL are described aim at method of formula. Summarize the notes of using Pro/E to unfold aim at method of software.

Introduction

Sheet metal parts cover a large proportion of rocket body structure, and there are many species and different structure of sheet metal parts, and their production process will take bending forming method. Before forming sheet metal parts developed length should be calculated. With the rapid development of computer technology, widely used in automated processing methods, and urgent demand of rocket model development mission, sheet metal parts process method has greatly changed. Method of formula has low sheet metal parts unfolding accuracy and large computation, so this method is suitable to calculate parts which have low accuracy requirements and simple structures. Method of software has high sheet metal parts unfolding accuracy, can save raw materials and reduce the workload of manual trimming, so this method is suitable to calculate parts which have high accuracy requirements and complex structures, and commonly used software is 3-dimensional graphics software Pro/E.

Theoretical analysis of bending process

Length of neutral plane does not change in the bending process, so neutral plane is the standard of calculating developed length. But neutral plane does not coincide with geometric center plane of material thickness. When inner radius is large and bending angle is small, neutral plane is close to geometric center plane. When inner radius is small and bending angle is large, neutral plane moves inward [1-4]. In the actual production process, the position coefficient of neutral plane K is used to calculate curvature radius of neutral plane ρ:

$$\rho = R + Kt \tag{1}$$

ρ——curvature radius of neutral plane;

R——inner radius;

K——the position coefficient of neutral plane;

t——material thickness.

Method of formula

According to the principle that developed length is equal to length of neutral plane, just get the position of neutral plane, developed length can be got.

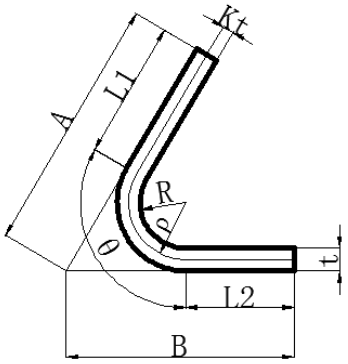

Fig.1 Schematic diagram of calculating developed length

Fig.1 is schematic diagram of calculating developed length.

Because the position of neutral plane is related to mechanical properties of the material, material thickness, bending angle, and inner radius, so it's difficult to get an accurate value of the position coefficient of neutral plane K. In the actual production process, empirical data is cited in calculating. Commonly used the position coefficient of neutral plane K is shown in Table 1.

Table 1 Common position coefficient of neutral plane K

R/t	K	R/t	K
1.0	0.32	3.0	0.40
1.2	0.33	4.0	0.42
1.3	0.34	5.0	0.44
1.5	0.36	6.0	0.46
2.0	0.38	7.0	0.48
2.5	0.39	≧8.0	0.5

After the appropriate value of the position coefficient of neutral plane K is selected, there are two quick unfolding ways in order to save computation. (1) Using AUTOCAD to draw sectional view of sheet metal parts, using the Shift function to make all inside edge of parts shift Kt to outside, and using the Polyline function to link all lines which are obtained by shifting. The linked line is neutral plane, so developed length can be measured quickly. (2) Using programming and computing functions of Excel, formula of calculating developed length can be programmed into the software, and let parts sizes be input parameters and developed length be output parameter. The interface for the calculation in Excel is shown in Figure 2.

Calculation in Excel					
parts sizes do not cover length of bend curve			parts sizes cover length of bend curve		
length:	L1=	4	length:	A=	10
length:	L2=	4	length:	B=	10
inner radius:	R=	4	inner radius:	R=	4
the position coefficient of neutral plane:	K=	0.5	the position coefficient of neutral plane:	K=	0.5
material thickness:	t=	2	material thickness:	t=	2
bending angle:	θ=	90	bending angle:	θ=	90
developed length:	L=	15.85	developed length:	L=	15.85

Fig. 2 The interface for the calculation in Excel

Method of software

Sheet metal module of Pro/E has powerful capabilities to unfold. Dimensional model of sheet metal parts should be built first, and using the Unbend function unfolding model of sheet metal parts can be got. There is essential difference between method of Pro/E and method of formula. Method of Pro/E is parametric and intelligent, and it is based on the simulation of sheet metal bending process to unfold. Through the unfolding model of sheet metal parts, Pro/E can direct output 2-dimensional drawings in various formats which can be directly applied to CNC cutting and punching devices[5-6]. Dimensional model and unfolding model of sheet metal parts in Pro/E are shown in Figure 3.

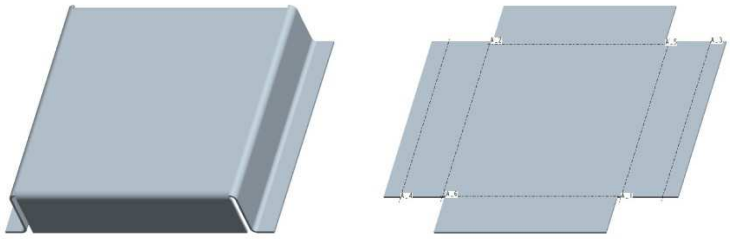

Fig. 3 Dimensional model and unfolding model of sheet metal parts in Pro/E

Before using the Unbend function to unfold, K-factor in Bend allow should be set up. It is worth noting that K-factor is equal to the position coefficient of neutral plane K, so K-factor is also an empirical data. Generally, in order to obtain the most accurate developed length, several sample parts are made firstly, and through measuring those pasts size, K-factor can be corrected.

Using Pro/E to unfold sheet metal parts, the following points should be noted:

1) Setting model environment: In order to make system of unit and view standard in Pro/E consistent with those used in CNC sheet metal equipments, model environment should be set before building dimensional model. Editing Config file or using Setup menu can change model environment.

2) Examine the dimensional model: Unfolding model is generated by dimensional model, so correctness of dimensional model should be ensured. Using Measure function or Model analysis function in Analysis menu can measure all key elements sizes. In addition process of sheet metal parts should be reasonable, otherwise Pro/E will refuse to unfold.

As can be seen that method of Pro/E has a lot of advantages, such as parametric, intelligent, quickly, high accuracy and paperless processing etc. So method of Pro/E adapt to the trend that sheet metal manufacturing develops toward CAD/CAE/CAM.

Summary

Through the introduction of this paper, both method of formula and method of software have advantages and disadvantages. Method of formula has low sheet metal parts unfolding accuracy and large computation, but it is easy to use. Method of software has high sheet metal parts unfolding accuracy, can save raw materials and reduce the workload of manual trimming, but it needs to skillfully use Pro/E. In addition, no matter which method is chosen, the position coefficient of neutral plane K is a key factor affecting sheet metal parts unfolding accuracy. So processors should correct K based on the actual sizes of sheet metal parts, and accumulate empirical data which is suitable to materials and equipments commonly used.

References

[1] LI Yingjie. Sheet Mental Bending Technology[M]. Beijing: China machine Press.

[2] HAN Zhongmin. YIN Haijun, etal. The Sheet Metal Part's Development Generation Research [J]. Machinery Design & Manufacture, 2007, 1:98-99.

[3] CAO Wei, GAN Zhong. Automated Flat Pattern Development System for Aircraft Sheet Metal Components [J]. Aeronautical Manufacturing Technology, 2008, 1:84-87.

[4] LI Suli, LIU Wei. Research on Size of Curving Semi-finished Materials Launching [J]. New Technology & New Process, 2012, 2:36-37.

[5] XIAO Liming. PRO/ENGINEER Sheet Metal Structural Design and Process Analysis [M]. Beijing: China machine Press.

[6] HU Zhiwei. Application of Pro/E in Sheet Metal Expanding Size and Confirm Factor Y [J]. Manufacturing Information, 2010:98-99.

Advanced Materials Research Vols. 989-994 (2014) pp 3314-3318
© (2014) Trans Tech Publications, Switzerland
doi:10.4028/www.scientific.net/AMR.989-994.3314

Equipments of Pulsed Welding System and its Application

Lou Liyan[1,a], Gao Ying[1,b]

[1]Tianjin Key Laboratory of High Speed Cutting & Precision Machining, Tianjin University of Technology and Education, Tianjin 300222, P. R. China

[a]louly88@126.com, [b]gaoying@tju.edu.cn

Keywords: Pulse. Welding. Microcontroller

Abstract. With the development of welding power control technology, pulsed welding technology was becoming more and more popular, for it could control the droplet transfer process by pulse current. In this paper the characteristic of pulsed welding technology was analyzed, and the equipment—welding pulse controller was introduced, which could upgrade the existing welding system to pulsed welding system without too much changes. This paper introduced pulsed MIG welding system and double wire pulsed welding system constructed by welding pulse controller, and the development prospect in the welding field is described.

Introduction

The generation of pulsed welding process was a big leap in the developing history of welding technology in the 60s'. This technology provided a new way to establish welding process, and fundamentally broke the block thought of obtaining stable welding process through constant welding current (voltage). Then the development and application of welding technology moved into a new enormous field.

Since the 1990s', with the updating of welding power control technology, pulsed welding technology got improved gradually and its application range was more extensive. Pulsed MIG/MAG/SAW and other related pulsed welding technology was gradually formed then. Those technology improved the quality and efficiency of welding production greatly, and had great practical value[1].

Characteristics of pulsed welding technology

Wider adjustment range of welding current. With the increasing of alloy element content and strength level, **t**he adjustment range of welding current for the base metal becomes narrow in the welding process. And the production efficiency can be reduced greatly if the welding current is below the lower limit of adjustment range. And weld appearance and welding joint quality can not be good if the welding current is higher than adjustment range limit. Pulsed welding technology can expand the adjustment range of welding current, which is beneficial for production.

Well control heat input and quality of welding joint get improved. In the welding process of high grade steel, the heat input of base metal is limited for its high heat sensitive. If ordinary welding method is adopted, since the selected welding current is small within the adjustment range, the penetration will be shallow and the welding root can have defects such as defective fusion easily. But if pulsed welding method is adopted, the penetration will be deep (penetration depends on the amplitude of pulse current) and the average welding current can be controlled within a lower level. The ductility and toughness of welding joint will be good because the superheated degree of heat-affected zone and weld beam get decreased.

Easy to achieve all position welding. In pulsed welding process, the welding pool is small since the average welding current is decreased. At the same time, the flowing of welding pool is not easy to happen, because the droplet transfer process and the heating of the welding pool is intermittent.

Get refined grains. The stirring of the welding pool by pulse welding current could refine the grain size since the normal growth of grains gets interfered. Common welding defects such as welding porosity and slag inclusion can be decreased at the same time[2].

Pulsed-MIG welding system based on welding pulse controller

The existing traditional welding power source can realize impulse output with the aid of welding pulse controller. The technical solution can be realized by low investment without replacing welding source power in a large scale. And the principle of welding pulse controller is shown in figure 1.

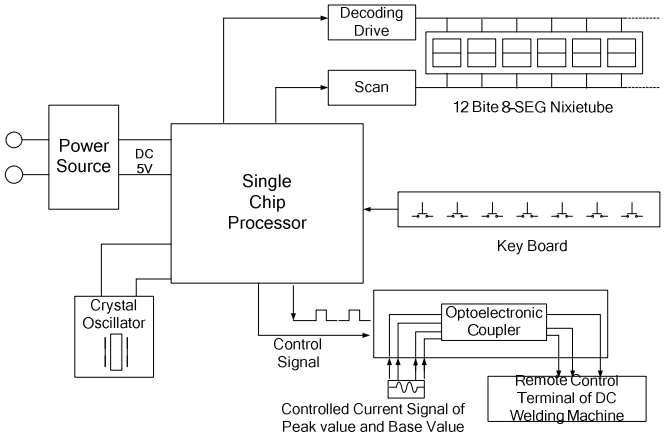

Fig. 1 The principle of welding pulse controller

Under the control of single chip processor, pulse signal is generated, while the frequency and duty cycle can be adjusted according to the requirements of DC pulsed welding. And through the optoelectronic coupler, the given pulsed welding signal is sent to the external remote control terminal of DC welding machine. The output current can be controlled in the form of controlling the given current. And the output peak value and base value can be adjusted independently. In addition, keyboard and nixietube are set on the welding pulse controller to enhance the operation convenience and visualization[3].

Pulsed welding system is composed of pulse welding controller and V300 Lincoln welding machine, shown as figure 2.

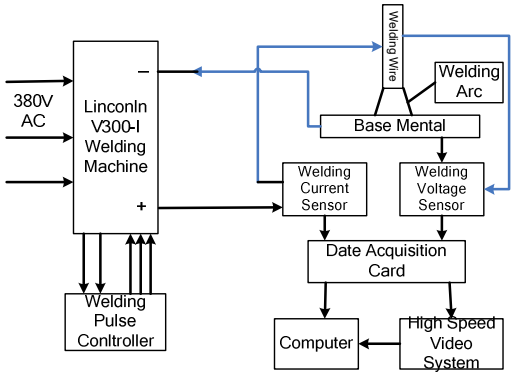

Fig. 2 Pulsed welding system

Welding electric signal waveform within 0.5s of pulsed welding system is shown in figure 3.

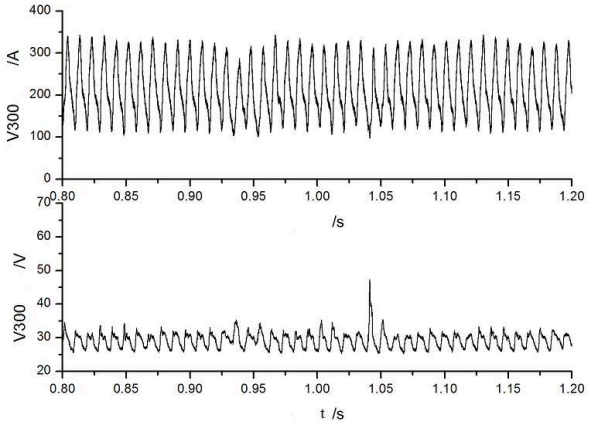

Fig. 3 Welding electric signal waveform of pulsed welding system

The droplet transfer process of one cycle in pulsed welding process is shown in figure 4, and metal transfer mode is one droplet pure pulse.

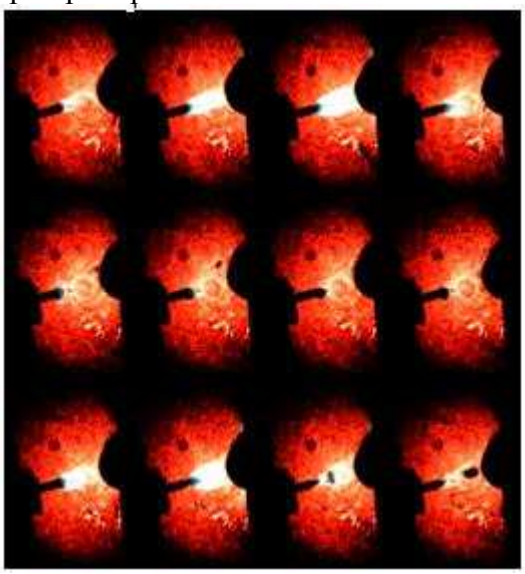

Fig. 4 Droplet transfer process in one cycle(one droplet pure pulse)

Double-wire MIG welding system

Double-wire welding technology developed on the basis of traditional GMAW welding process. In double-wire welding system, two troches are combined in one nozzle, and two completely independent pulse welding sources of the same type are adopted while two conduct tips insulate to each other. Welding parameters of two arcs can be the same or different, the requirement is that the wire feeding must be reliable and the maximum wire feeding speed can reach 15m/min. Two wires melt at the same time, the deposition rate is significantly higher than twice the deposition rate of signal wire welding process, and the welding speed also get increased significantly, which could reach 1m/mim. Double-wire welding system is shown in figure 5, pulse welding current is generated in a push-pull way. In double-wire welding process, in order to obtain welding joint of high quality, the droplet transfer process should be controlled appropriately, or the arc will influence each other, and perturbations will appear[4].

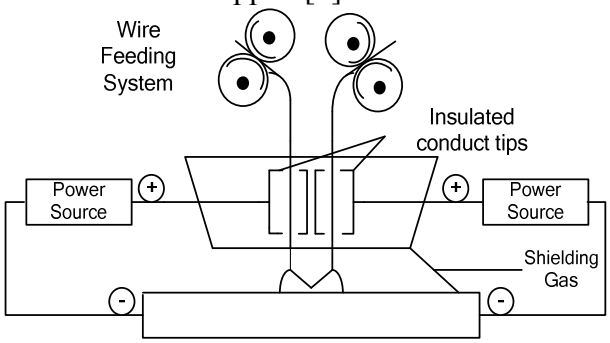

Fig. 5 Double-wire(Tandem)welding system

Double-wire welding system can be formed by adding a V300 Lincoln welding machine and a wire feeding mechanism on the basis of the system shown in figure 2, and the welding electric signal waveform of double-wire pulsed welding process is shown in figure 6.

Two arcs are in push-pull output mode, so the forces between two arcs can be well controlled and the stability of welding process can get ensured.

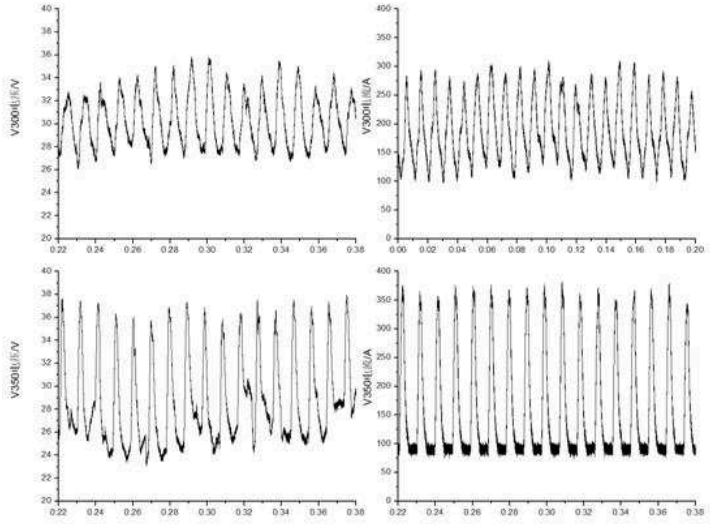

Fig. 6 Welding electric signal waveform of double-wire pulsed welding process

High speed video pictures of double-wire welding process is shown in figure 7, it's obvious that one arc is at peak value state and the other arc in at base value state.

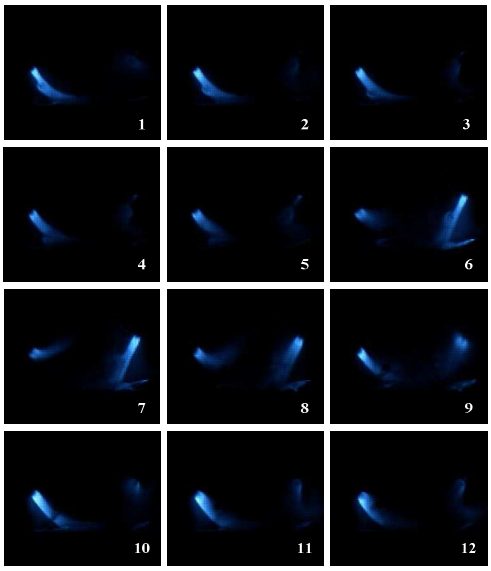

Fig. 7 High speed video pictures of double-wire welding process

Application of pulsed welding technology

In the welding production of X80 steel pip, in order to increase the welding efficiency, the welding current in SAW must be increased, which will lead to grain growth and related performance degradation. While in pulsed SAW process, the property of welding joint is improved since the heating mode is changed and grain size of welding beam is refined by electromagnetic vibration.

Based on DC1500 Lincoln welding power source and welding pulse controller, pulsed SAW system is constituted. Through the analysis of comparative experiment, the grain of welding joint with pulse current is smaller. And it shows that pulsed SAW technology has a good application prospects and certain advantages in welded pipe production.

Through comparing the welding seam under pulsed welding process and non-pulsed welding process at the same current level, it can be seen that the grain of pro-eutectoid ferrite is coarse in non-pulsed welding process. As X80 is fine grain steel, such coarse grains could affect its properties seriously. The appearance of coarse grain means that in grain growth process, the superheated degree and dwell time in the over-heating stage in non-pulsed welding process are much higher. And it proves that the heating mode between pulsed and non-pulsed welding process is different, and pulsed SAW welding process has advantage in grain refinement than ordinary SAW welding process[5].

Conclusion

1) Pulsed-MIG welding system and double wire MIG welding system were constructed with welding pulse controller, so the exiting welding system got upgrade without too much change.

2) In the experiment, the metal transfer process and corresponding wave-form of welding current, arc voltage were recorded which showed the welding pulse controller can realized pulsed output.

3) The welding pulse controller has great application value for production.

References

[1] Yang Chunli: *Foundations of arc welding technology* (Harbin Institute of Technology Press, China 2003)

[2] P.Praveen, P.K.D.V.Yarlagadda, M.J.Kang, in: *Advancements in pulse gas mental arc welding,* edited by Journal of Materials Processing Technology (2005), in press

[3] Li Huan, Cui Jia, Niu Yong, in: *Research and engineering application of the arc welding pulsed controller technology*, edited by China Welding(2005), in press

[4] Li Yang, Huang Shisheng, Lu Peitao, in: *microproeesso r syn ch ronic controller for twin —wire pulsed GMAW* ,edited by Journal of South China University(2006), in press

[5] Zhang Zhanzhan: *Studies on the welding property of X80steel pipes* (Zhengzhou University, 2013)

Advanced Materials Research Vols. 989-994 (2014) pp 3319-3322
© (2014) Trans Tech Publications, Switzerland
doi:10.4028/www.scientific.net/AMR.989-994.3319

Reviews on Automobile Abnormal Sound Fault Diagnosis

Tan Guiling[1, a], Miao Dehua[1,b]*,,Qi Yuming[1, c], Deng Sanpeng[1, d]

[1]School of Mechanical Engineering, Tianjin University of Technology and Education, Tianjin, 300222, China

[a]tanguiling@sina.cn, [b]miaodh@126.com, [c]qiyuming1221@gmail.com, [d]sanpeng@yeah.net

*Author for correspondence: Miao Dehua(1957-), Male ,
Dr. Research direction: Monitoring detection and vehicle safety

Keywords: Abnormal sound on-vehicle, Fault diagnosis, Warning system, ECU

Abstract. Automotive abnormal sound is an important manifestation of the automotive system components early malfunction. It can effectively improve safety and reliability of the vehicle system by characteristics extraction of abnormal vehicle sound and prediction of the development trend of fault. What's more, it can solve the problem that ECU can't identify tire failure and other problems. As a result, it will reduce the number of traffic accidents, protect human safety and property.

Introduction

Car abnormal noise is the most obvious manifestation of the early fault of vehicle. For example, the abnormal noise of " zhi, zhi, zhi" when braking indicates that the wear of automotive brake friction Lining is beyond the limit; If you hear a harsh abnormal noise of "qiu, qiu, qiu" that comes from the engine, it indicates the excessive wear or slack of the v-belt; If you hear abnormal noise of metal collision that comes from the tire's internal, it is probably caused by broken damper and bearing [1-2]. Automotive abnormal sound will not affect the car's driving immediately, but it will seriously affect the ride comfort, causing the passenger irritability, decreasing the attention of the driver or other adverse symptoms. Given no timely maintain, it will cause other automotive fault. The faults that can be indicated by abnormal sound include engine noise, transmission noise, braking noise and tire abnormal sound. For the early stage of abnormal noise, it is mainly judged by experienced garage men or drivers. But for the widespread use of cars, drivers are increasingly diversified and young, and most of them don't have ability of correct judgment. So developing a method for fault diagnosis through automatic abnormal noises is more and more urgent.

At present, research for car fault diagnosis system is limited to typical faults or single fault mostly .Most fault diagnosis systems use the contact vibration test for on-line fault monitoring, or use the method for separating parts for Offline detection [3]. But the fault in car when moving is complicated and coupling, so the fault signal is also coupling, and the components of signal are complicated, current method of contact vibration can't detect assembly fault source and early stage of fault completely, and it's also difficult to test car's assembly operation state and fault accurately by the method of traditional time domain or frequency domain analysis, especially the incipient fault after mechanical system's long wear [4].How to develop a fault diagnosis technology of vehicle system that is efficient, accurate and multi-source information integrated has been the concern of people and a new research focus.

Engine noise

There are multiple causes that can lead to engine noise. The belt howling relatively harsh, it is generally caused by belt slippage. If the external metal parts emit dry friction sound when the engine is running, it suggests that the generator bearing has been damaged.

Ming-Long Zhou, from Anhui University of Engineering, has proposed an automobile engine fault diagnosis method of genetic algorithm, wavelet and neural network [5]. Wen-Ping Yang, from Northwestern Polytechnical University has studied the nonlinear characteristics of automotive

engine systems by solving the system of the largest Lyapunov exponent to diagnosis and monitors the engine fault [6]. Yu-Xiu Xu from Tianjin Polytechnic University has studied that using support vector machine method to realize the diagnosis and identification of engine failure in the case of car engine without disassembly [7]. Huan Li, from Zhoukou Normal University, has made a car engine sensor fault detection method based on fuzzy energy self-learning [8].

Currently, there are many ways to study the automobile engine fault diagnosis, mainly focus on the engine compartment offline measurement and static in on-line measurement. The methods are mainly neural networks supporting vector machines, or the application engine fault identification of abnormal sound signals. They are feasible, however, these diagnostic methods are studied and validated based the known faults, it has not yet had a way to diagnose the online fault of engine. Meanwhile, there is no way to separate the abnormal sound of the engine from the vehicle information system in the whole different sound information.

Gearbox Abnormal Sound

When driving, if all the crosspieces, except the direct crosspiece, make some abnormal noise, it indicates that the noise is from the second front axle of the transmission; if there is a "rustling" sound in the gearbox when driving, and when depressing the clutch, it disappears, this is caused by the gearbox bearing or gear wears, bearing spots. Nissan CVT, Volkswagen DSG gearbox problem still exist, Fault diagnosis can provide more protection for it.

Lu Jianwei etc, from College of Mechanical and Automotive Engineering of Hefei University of Technology, analyzed the transmission gear abnormal sound failure from the perspective of nonlinear dynamics [9]. Wu Xiaobing, from Beijing Institute of Technology, found the optimal parameters for each failure through gray cognate analysis combined with rough set theory [10]. Tongji University ’Wan De’an etc use the time domain synchronous averaging method in auto gearbox fault diagnosis system of the fault to diagnose [11]. Liu Ze etc. in Changchun University of Technology use improved ID3 algorithm to the automobile gearbox fault diagnosis [12].

Vibration detection and diagnosis is currently the most widely method for Gearbox fault diagnosis, as abnormal sound information is easily mixed with ambient noise, so abnormal sound detection and diagnosis has not been well developed and applied. With the development of technology, the techniques of dealing with noise and the ability of hardware and software is also rising, online fault diagnosis method for different sound will be the main developing direction of the gearbox fault diagnosis.

Brake abnormal sound

The abnormal noise, made by the automobiles when breaking, is probably arose by these factors, such as the improper use of the material or big distortion of Brake Disc or the hardness, the Porosity, Friction Characteristics and squeezing properties of Brake Friction Lining are unqualified. If there was no timely treatment of these faults, especially under high speed driving, the drivers may have dangerous.

LI Rong from Shantou University designed the information extraction and Data Processing for the Monitoring System, by using the technology and theory of sensor array and Multi-sensor Data Fusion [13]. Through quality monitoring system of DSP brake disc’s internal defect, by using computer control technology, DSP technology and Sensing Technology to collect the key characteristic variable, based on Bayes’s stepwise discriminant analysis, Zhou Guanxiong, from zhejiang university, established the discriminant function of diagnosing the Brake Disc’s Internal Defect[14].

The fault diagnosis method of Brake System’s running state is not that popular at present. The existing diagnosis method is almost based on the detection according to brake disc itself. There is no On-line detection of the abnormal noise of the brake disc at present.

Tire abnormal sound

The noise of tire must be rhythmic, and the frequency rises with the driving speed. If the noise is like “PA PA”, it is probably caused by big distortion, bulging deformation, wear or Shortage of tire air pressure; If the noise is like “DA DA”, it is probably caused by the little stones in tire tread; if the noise is like “HU HU”, and car body shakes intensely even runs deviation, it is probably caused by tire burst.

At present Tire Pressure Monitoring System is used during driving. It measures the internal pressure and temperature by the detecting sensor installed in the tire. These measured values are shown on the Panel directly. If the values exceed the safety range, it will send out warning signal. Fangwei and some of his colleagues, from Wuhan Digital Engineering Research Institute, have established a Distributed Condition Monitoring and Fault Diagnosis System for tire, by using sensor technology, microelectronics, embedded technology and Radio Frequency Communication Technology[15]. Wang Chengrui and his colleagues, from Dalian University of Technology, have designed a direct Condition Monitoring and Fault Diagnosis Active Forewarning System for tire, by using ZigBee technology to forewarn the tire fault actively [16].

The existing Diagnosis Methods for tire fault are all based on the internal pressure and temperature measured by sensors. But even when these values are normal, if the abnormal noise made by foreign body in the tire or the tires’ not being fixed well are not judged correctly by the drivers, the continuing driving may cause problems or even traffic accidents. Temporarily there isn’t an On-line detection of the abnormal noise of the foreign body in the tire.

Automotive ECU self-diagnostic function

ECU with self-diagnostic and protection functions ，When a system failure, it automatically records the fault code through the use of protective measures RAM and read from the alternative procedures inherent in the program to maintain the engine running . While these faults are displayed on the instrument panel and keep immortal, make the driver to detect problems.

Recently, ECU applies not only in engines, but also in anti-lock brake system, 4 wheel drive system, Auto Manual Transmission and active suspension system and so on.

Conclusion

Fault diagnosis method of the part of automotive is mostly applied in off-line fault detection, and it has a higher requirement in Computer Aided inspection and diagnosis system, so it can’t be used as the early fault diagnosis in automobiles which are traveling. Through the above analysis, abnormal noise can describe the early fault diagnosis in automobiles which are traveling, and realize real time monitoring and early-warning. The existing fault diagnosis technology has some problems, such as:

1) Can’t do analysis of the whole automobile failure diagnosis.
2) Have not a way to do early fault diagnosis.
3) The engine diagnosis method is researched based on all known failure.
4) The automobile brake system diagnosis method is based on brake pad.
5) The present tire fault diagnosis method is based on tire pressure and temperature diagnosis.

In conclusion, the comprehensive fault diagnosis method based on abnormal noise can diagnose and warn the early fault diagnosis and abnormal noise of each part, and it offers the field of automobile safety a practical way. The method also can improve the driving stability and security and achieve better economy benefit and social benefit by monitoring the development trend for automobile early fault. It fills a gap in automobile abnormal noise diagnosis field, and has a immeasurable value and meaning in automobile reliability research.

Acknowledgements

In this paper, the research is supported by The National Youth Science Fund Project (61301040); Tianjin science and technology planning project (13ZCZDGX01500) and (14ZCZDSF00022). Tianjin University of Technology and Education graduate student innovation fund (YC13-07).

References

[1] Li Gang, Ma Peigen. Investigation and Fault Diagnosis Method of Diesel Engine Abnormal Voices[J]. Journal of Lanzhou Jiaotong University, 2010，29（6）：64-66.

[2] Chaoming Huang, Hongliang Yu, Delin Guan, Guobin Li, Qili Wu. Feature extraction of frictional vibration based on CWT time-frequency image[C]. Intelligent Control and Information Processing (ICICIP), 2010: 192-196

[3] Ito A, Aiba A, Ito M, Makino S. Detection of Abnormal Sound Using Multi-stage GMM for Surveillance Microphone[C]. Information Assurance and Security, 2009. IAS '09. Fifth. 2009(1): 733-736.

[4] Antoni J, Daniere J, Guillet F. Effective vibration analysis of IC engines using cyclostationarity: par tⅡ-new result s on the reconstruction of the cylinder pressures [J]. Journal of Sound and Vibration, 2002, 257(5): 839-856.

[5] Yu Bingrong, Zhou Minglong, Li Lingchun. The analysis of fault diagnosis for automotive engine based on genetic algorithm, wavelet transform and neural Network[J].Journal of Anhui Polytechnic University, 2011，26（1）：55-57.

[6] Yang Wenping, Chen Guoding, Shi Boqiang, etc. Application of Lyapunov Exponents to Fault Diagnosis of Diesel Engines[J].Journal of Vibration Engineering, 2002，15（4）：476-478.

[7] Xu Yuxiu, Yang Wenping, Lv Xuan,etc. Fault diagnosis for a car engine based on support vector machine[J].Journal of Vibration and Shock, 2013，32（8）：143-146 .

[8] Li Huan, Liao Li. Car Engine Sensor Network Fault Diagnosis Methods Research Based on the Fuzzy Energy Self Learning[J]. Bulletin of Science and Technology, 2013，29（6）：86-88.

[9] Lu Jianwei, Shen Bo, Qian Lijun. An Analysis on the Abnormal Noise of Gearbox Based on Gear Nonlinear Dynamics[J]. Automotive Engineering, 2007，29（6）：533-536.

[10] Wu Xiaobing. The Fault Diagnosis of Vehicle Gear-Box Based on Gray-Rough Set Mode[J]. Journal of Beijing Institute of Technology，2000，20（5）：576-580.

[11] Wan Dean, Sun Dongji, Zhao Yongjie. Synchronous Revolution Order Analysis Application in Fault Diagnosis of Auto Gearbox[J]. Computer Measurement & Control，2006，14（3）：299-330(332).

[12] Liu Ze, Pan Hui. Automotive gearbox fault diagnosis system based on ID3 a lgorithm[J]. Journal of Changchun University of Technology(Natural Science Edition), 2011，32(6)：534-537.

[13] Li Rong.The application and research on the dynamic monitoring of the brake linings with multisensory integration theory[D]. Shantou University, 2001.

[14] Zhou Guanxiong. Research of Car Brake Pad Internal Defects Detection Svstem Based on DSP Svstem[D]. Zhejiang University,2012.

[15] Fang Wei, Ou Zhonghong, Yang Chunchang. Design and realization of distributed tire fault diagnosis system[J]. Computer Engineering and Design, 2007，28（21）: 5186-5189.

[16] Wang Chenrui, Duan Fuhai, Zhao Kuibing,etc. Design of tire pressure monitoring system based on CC2530 and MPXY8020A[J]. Modern Electronics Technique, 2012，35（21）: 105-108.

Advanced Materials Research Vols. 989-994 (2014) pp 3323-3327
© (2014) Trans Tech Publications, Switzerland
doi:10.4028/www.scientific.net/AMR.989-994.3323

Research on Disassembling Equipment for Construction Machinery Hydraulic Cylinder

Zhang Xinghui[a], Zhang Jianxin[b]

Tianjin Sino-German Vocational Technical College,Tianjin 300350,China

[a]xhzhang@tute.edu.cn, [b]zjx_tj@189.cn

Keywords: Construction machinery; Hydraulic cylinder; Disassembly and assembly equipment; hydraulic system;

Abstract. Construction machinery hydraulic cylinder is usually discarded after service cycle. The residual value of discarded products can be recycled greatly by remanufacturing. Disassembly and assembly is the key process in hydraulic cylinder remanufacturing. The construction machinery hydraulic cylinder disassembly and assembly equipment is developed. Hydraulic power is adopted in this equipment. The clamping, positioning of cylinder tube is realized by hydraulic clamping mechanism automatically. The piston component pulling out or into cylinder tube is realized by hydraulic working mechanism automatically. This equipment has been applied successfully in the project of "key technology and equipment for construction machinery parts remanufacturing" in a research institute. The results indicate that the application of this equipment will not only increase the automaticity and efficiency remarkably, but also reduce the damage to hydraulic cylinder key part greatly.

Introduction

After serve cycle, the volume efficiency and working pressure of construction machinery hydraulic cylinder will decline remarkably [1]- [2]. There is little damage occurs in key parts, such as piston rod, piston and cylinder tube dismantled from discarded construction machinery hydraulic cylinder. The failure parts of discarded hydraulic cylinder tend to occur only in sealing elements [2]. The performance of discarded hydraulic cylinder will improve remarkably, even measure up to new products by disassembling, cleaning, replacing sealing elements and reassembling. Thus, the residual value of discarded construction machinery hydraulic cylinder can be recycled greatly [3].

Cylinder rod component must be pulled out from cylinder tube in disassembling process. This process is very difficult because of the serious damage, deformation, tearing and aging in sealing elements of piston and guide sleeve [4]. Mounting piston rod component in cylinder tube is also a difficult process in assembling hydraulic cylinder. Unnecessary damage to key parts usually occurs during assembling and disassembling process without specialized equipment [4]. The disassembly and assembly equipment for construction machinery hydraulic cylinder is developed in this paper.

Mechanism Designing

The functions of disassembly and assembly equipment for construction machinery hydraulic cylinder are described as follow. The clamping, positioning of cylinder tube is realized by hydraulic clamping mechanism automatically during assembling and disassembling process. After cylinder head fixing parts (e.g. flange bolt or clasp) are dismounted, piston rod component and guide sleeve of disassembled hydraulic cylinder can be pulled out from cylinder tube by hydraulic device in disassembling process. Piston rod component and guide sleeve of assembled hydraulic cylinder can be mounted in cylinder tube by hydraulic device in assembling process.

Structure of Equipment

The disassembly and assembly equipment for construction machinery hydraulic cylinder is shown in Fig 1. The main components of the equipment installed on the cylinder clamping base frame 11 and

the slide rail base 9, these two base frames are connected each other by bolts. The hydraulic cylinder to be repaired can be clamped on the cylinder clamping base frame 11. Two V blocks of cylinder tube bracket are installed on two screw rods separately, so the height of V block is adjustable. The cylinder tube can be lifted to the appropriate height so as to clamping. There are two sets clamping device, which is composed of positioning V block 10 and clamping V block 3. Positioning V block 10 is drove by screw rod and clamping V block is drove by Hydraulic cylinder. Adjusting the position of V block 10 by screw rod, the position of the cylinder tube axis can be ensured on the medium position, in order to connect the piston rod mounting hole of hydraulic cylinder to be repaired to connecting flange 8. If the hydraulic cylinder to be repaired has a mounting hole on the rear of cylinder tube, the mounting hole on the rear of cylinder tube can be connected to mounting hole of the bracket 1 directly. Adjusting all these devices and placing the cylinder tube on V block 2, then the cylinder tube can be positioned and clamped by hydraulic devices.

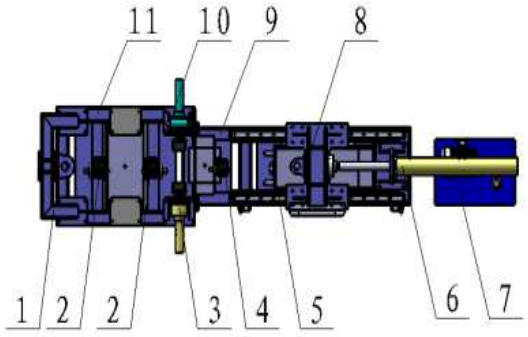

Fig.1: Disassembling/assembling equipment for hydraulic cylinder

The working mechanism of this equipment is composed of linear guide rail 5, fluid cylinder 6 and slider block bracket 8. Linear guide rail 5 mounted on guide rail base frame 9. The slider block bracket 8 is drove by hydraulic cylinder 6 and reciprocate on linear guide rail 5. The piston component of hydraulic cylinder to be repaired can be pulled out o inserted into cylinder tube by retracting and stretching of hydraulic cylinder 6. The V block with rubber sheet mounted on piston rod carrier 4 can move up and down. During disassembling process, piston rod will fall onto the V block after pull out of cylinder tube, so as to avoid the damage to piston rod. During assembling process, the function of the V block is vertical positioning for piston rod. 7 shown in this figure is hydraulic power unit.

Working principle

Disassembling Process of Hydraulic Cylinder

1) Adjusting the position of V block on cylinder tube carrier 2, screw rod centering device 10 and piston rod carrier 4 according to the diameter of cylinder tube to be disassembled. Attention: the height of V block on cylinder tube carrier should lower 0 - 5mm than theoretical height and the height of V block on piston rod carrier shouldn't higher than theoretical height. Then place the cylinder tube on V block 2;

2) Stretching the piston rod of clamping device hydraulic cylinder 3, clamping the cylinder tube of hydraulic cylinder to be disassembled by a pair V blocks on clamping hydraulic cylinder 3 and screw rod centering device 10;

3) Dismounting and removing fasteners on hydraulic cylinder head to be disassembled;

4) Starting working device hydraulic cylinder 6, moving slider block bracket 8 to the appropriate position, mounting piston rod mounting hole of hydraulic cylinder to be disassembled on connecting flange of slider block bracket 8;

5) Retracting piston rod of working device hydraulic cylinder, the cylinder lid, guide sleeve and piston component will separate from cylinder tube;

6) Retracting piston rod of clamping device hydraulic cylinder and unclamping clamping device, removing cylinder tube and piston rod component of hydraulic cylinder to be disassembled from this equipment[3-4].

Assembling Process of Hydraulic Cylinder

1) Adjusting the position of V block on cylinder tube carrier 2, screw rod centering device 10 and piston rod carrier 4 according to the diameter of cylinder tube to be disassembled. Attention: the height of V block on cylinder tube carrier should lower 0-5mm than theoretical height and the height

of V block on piston rod carrier should lower 0-1mm than theoretical height. Then place the cylinder tube on V block 2;

2) Stretching the piston rod of clamping device hydraulic cylinder 3, clamping the cylinder tube of hydraulic cylinder to be assembled by a pair V blocks on clamping hydraulic cylinder 3 and screw rod centering device 10;

3) Fitting the cylinder lid, guide sleeve component on piston rod and fixing piston on piston rod;

4) Starting working device hydraulic cylinder 6, moving slider block bracket 8 to the appropriate position, mounting piston rod mounting hole of hydraulic cylinder to be assembled on connecting flange of slider block bracket 8;

5) Stretching piston rod of working device hydraulic cylinder, the piston component to be assembled will be inserted into the cylinder tube;

6) Fixing guide sleeve and cylinder lid on hydraulic cylinder head to be assembled;

7) Retracting piston rod of clamping device hydraulic cylinder and unclamping clamping device, removing hydraulic cylinder disassembled from this equipment.

Main Design Parameter

In order to meet the requirement of most construction machinery hydraulic cylinder disassembling/assembling process, according to the mainstream hydraulic cylinder used in loader and grader, which have large quantity and are widely used the main parameter of the construction machinery hydraulic cylinder disassembling/assembling equipment are designing as follows:

Table 1: Main design parameter

item		parameter
hydraulic cylinder to be repaired	min. outside diameter of cylinder tube	90mm
	max. outside diameter of cylinder tube	300mm
	max. stroke	1800mm
clamping device	max. clamp force	2.5t
	stroke	160mm
working device	max. pulling force	0.9t
	max. thrust force	1.8t
	stroke	950mm
rhythm of production	clamping	5s
	pulling out piston component	≤25s
	inserting piston component	≤25s

Designing of Hydraulic System

The hydraulic principle diagram for this equipment is shown in Fig 2: there are two actuator units and one power unit in this hydraulic system, which are working hydraulic cylinder 15, clamping hydraulic cylinder 21 and hydraulic pump 6.

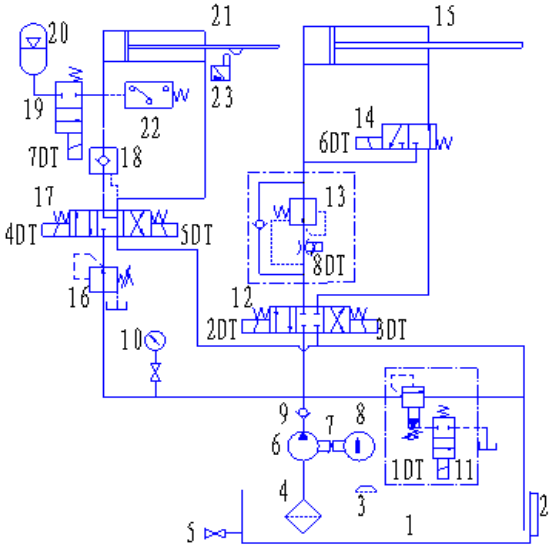

Fig. 2: Hydraulic principle diagram

Clamp Cylinder Tube of Hydraulic Cylinder to be Disassembled/Assembled

Solenoid 7DT switch on, after 0.5 second, solenoid 4DT switch on, power system supply oil for rodless cavity of clamping cylinder 21 and accumulator 20, the piston rod of 21 stretches out and clamps the cylinder tube. While the clamping force increasing to the force setup prior, pressure relay 22 switch off the

solenoid 4DT. The pressure in rodless cavity of clamping cylinder 21 will sustain by accumulator 20 and one-way valve 18, so that the cylinder tube remain clamping status while the piston component is being pull out or inserted into cylinder tube. The clamping force is setup by pressure relay 22. The maxima clamping force is setup by reducer valve 16, so as to avoid damage to cylinder tube while there is fault in pressure relay.

Slider Block Bracket Adjusting and Positioning

Adjusting and positioning slider block bracket is realized by stretching and retracting of piston rod of working hydraulic cylinder 15.Switching on Solenoid 2DT, the piston rod of working hydraulic cylinder will stretch. Switching on Solenoid 3DT, the piston rod of working hydraulic cylinder will retract. Taking work condition and efficiency into consideration, if the piston rod must stretch a long distance, the solenoid 6DT switch on, thus the differential connection is realized.

Pulling Out and Inserting of Piston Modula

Solenoid 2 switching on, working cylinder 15 will stretch and hydraulic cylinder piston rod component will assembly in cylinder tube. Solenoid 3 switching on, working cylinder 15 will retract and hydraulic cylinder piston rod component will pull out of cylinder tube. Valve 13 is an electromagnet proportionality speed regulating valve. While the hydraulic cylinder piston approaching the cylinder head, the speed should reduce by valve 13 for safety. After this stage, the speed may increase to normal level. The speed is controlled by electromagnet proportionality speed regulating valve and adapt remote operation mode, so the flexibility and convenience is improved remarkably.

Unclamping Cylinder Tube of Hydraulic Cylinder to be Disassembled/Assembled

Solenoid 5DT switching on, piston rod of clamping cylinder 21 retract. Solenoid 7DT switching off to avoid unnecessary release of accumulator pressure energy. While approaching end, position switch SQ1 switch off solenoid 5DT.

Off-loading and Overload Protection

The maximal working pressure of this system is setup by electromagnetic relief valve 11, which used as overload protection and off-loading. While the work status of electromagnetic valve 17 and 12 is neutral (i.e. 2DT, 3DT, 4DT, 5DT switch off), this system is on off-loading status by valve 11. If the equipment is out of service for a long time, pressure energy stored in accumulator can be released by switching on solenoid 5.

Applicationg

This equipment has been applied successfully in the project of "key technology and equipment for construction machinery parts remanufacturing" in a research institute. The steering hydraulic cylinder of ZL50 loader is being disassembled on this equipment as shown in fig.3. Disassembling this hydraulic cylinder require 3 minutes and assembling require 5 minutes. The results indicate that the application of this equipment will not only increase the automaticity and efficiency remarkably, but also reduce the damage to hydraulic cylinder key part greatly.

Fig.3:Application of This Equipment

Acknowledgements

This work is supported by China National Funds for Young Scientists (61301040), the Tianjin Science and Technology Key Research Program (13ZCZDGX01500)and(14ZCZDSF00022).

References

[1] Chen Baoqing, Zhang Guosheng, Zhang Jinxin, Research on Remanufacture for Construction Machinery[J], Equipment Management and Maintaining. 2011,12(7):41-42.

[2] Zhou min, Study of NC Milling Machine Cylinder Repairing Accuracy Based on Remanufacturing Technology[J], Hydraulic Pressure and Pneumatic. 2011,12(12): 84-87.

[3] Liu Guokai, Zhu Weihong, Application of Green Manufacturing Technology in Machine Manufacturing[J], Weekly Grand Sight. 2012,52(37):125.

[4] Wu zishan, Xu shubing, Dismantling Device for Construction Machinery Hydraulic Cylinder[J],Construction machinery. 2010,12(11):63-64.

[5] Jiang Zhiqin, The Development and Design of Device for Disassembly of Hydraulic Cylinder[J],Machinery, 2009,12(5):68-70.

[6] Liao Mihe, Liu Guangwen, Hydraulic Element Parameter of Disassembling/Assembling Machine [J], Mining Science Technology, 2001,12(3):38-39.

Advanced Materials Research Vols. 989-994 (2014) pp 3328-3330
© (2014) Trans Tech Publications, Switzerland
doi:10.4028/www.scientific.net/AMR.989-994.3328

Stiffness Modeling andSensitivity Analysis for Worm Geared Transmission

Lin Han[1,a], Houjun Qi[1,b]

[1]Tianjin Key Laboratory of High Speed Cutting & Precision Machining, Tianjin University of Technology and Education, Tianjin 300222, China

[a]hanlin147@163.com, [b]qihoujuntj@163.com

Keywords: Worm geared transmission, Static stiffness, Sensitivity analysis

Abstract. The worm geared transmission chain is widely employed in rotary feeding table of machine tools. This article proposes a static stiffness model and conducts sensitivity analysis of the transmission chain. Firstly, a unified static stiffness model is established, considering meshing stiffness, torsional stiffness and pre-load related axial stiffness of worm shaft. Then sensitivity with respect to individual stiffness element is derived based on partially differentiating method. Simulation results show that the closer to the end gear pair or shaft is, the more sensitive meshing stiffness or torsional stiffness is.

Introduction

As a key component of multi-axis machine tool, the performance of rotary feeding table has an important influence on that of the whole machine tool.The dynamic stiffness depends on static stiffness, inertia or mass of components, damping etc [1,2]. Feng investigated the axial stiffness of rotary table by proposing a new type of rotary table with a comprehensive performance of high stiffness and low cost, then a multi-objectives optimum design was conducted [3]. Huang investigated the dynamic characteristics of the axial and circumferential directions of a large and heavy NC rotary table [4]. The positioning accuracy of the rotary feed system without load mainly depends on the geometric error (e.g., free play between meshing teeth); however, when torque load is applied, rotating angular deviation from the desired mainly comes from the stiffness of the transmission chain. However, few researches could have been found [5].

Figure 1 shows a typical transmission chain employed in rotary table for rotary feeding, where there're both cylindrical gear pairs and worm gear pair.

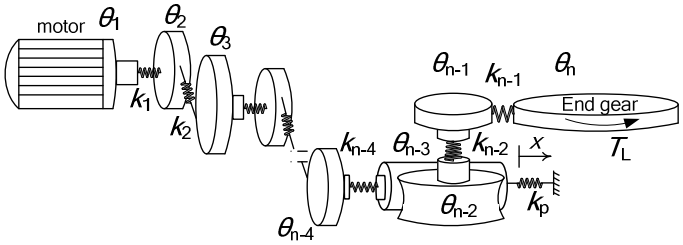

Figure 1 Schematic of general worm geared transmission chain

As shown in the figure, the rotating angles from the input motor to the end gear of the transmission chain are denoted as $\theta_1 \ldots \theta_n$, respectively. Similarly, the stiffness of each elastic element is represented by $k_1 \ldots k_{n-1}$, respectively, where n=odd means the torsional stiffness of shaft and n=even stands for the meshing stiffness of gear teeth. In addition, k_p stands for the axial stiffness of worm shaft, mainly depending on the supporting bearings on both ends of worm shaft.

Based on static equilibrium equations, the torsional stiffness of the chain could be obtained,

$$k_s = k_{n-1} r_{bn}^2 - k_{n-1} r_{b(n-1)} r_{bn} A_{(n-1)n} \tag{1}$$

where A_{12}=0, and $A_{i(i+1)}$ ($2 \leqslant i \leqslant n-4$) takes following form

$$A_{i(i+1)}=\begin{cases}\dfrac{k_i}{k_i+r_{bi}^2k_{(i-1)}-r_{b(i-1)}r_{bi}k_{(i-1)}A_{(i-1)i}} & i=odd\\ \dfrac{k_ir_{bi}r_{b(i+1)}}{k_{(i-1)}+r_{bi}^2k_i-k_{(i-1)}A_{(i-1)i}} & i=even\end{cases} \tag{2}$$

According to the Eq.(1) &continuous differentiating method, the analytical sensitivity models for each component's stiffness are derived as

$$\frac{\partial k_s}{\partial k_i}=\begin{cases}\dfrac{\tilde{r}_{bn-2}\overline{r}_{bn-3}}{\overline{r}_{bn-2}\tilde{r}_{bn-3}}(A_{i(i+1)}-1)^2\prod_{j=i+1}^{n-1}A^2{}_{j(j+1)} & i=odd\\ \dfrac{\tilde{r}_{bn-2}\overline{r}_{bn-3}}{\overline{r}_{bn-2}\tilde{r}_{bn-3}}(r_{bi}A_{i(i+1)}-r_{bi+1})^2\prod_{j=i+1}^{n-1}A^2{}_{j(j+1)} & i=even\end{cases} \tag{3}$$

Simulation results discussions. The schematic of a transmission chain with worm gear pair is shown in figure 2. Obviously, the index n=7 in this example, and the angle of end gear is denoted as θ_w.

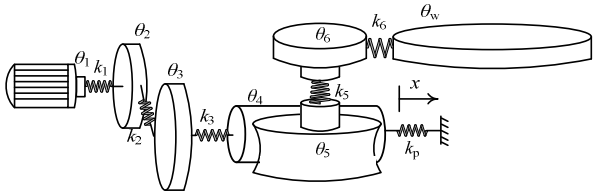

Figure 2 Transmission chain used in simulation

To verify the proposed static stiffness model, a comparison between the result obtained from finite element method and these from the analytical model is made. The parameters of the chain are shown in Table 1.

Table 1 Parameters of the transmission

	Z_2	Z_3	Z_4	Z_5	Z_6	Z_w
teeth number	21	67	1	31	17	71
module (mm)	4		4		5	
width (mm)	56				70	
pressure angle	20°					
r_1 (mm)	20	r_3 (mm)	15	r_5 (mm)		20
L_1 (mm)	70	L_3 (mm)	80	L_5 (mm)		75

The results from both FEM and analytical model are given in Table 2.

Table 2 Comparison between FEM and analytical model

(mm)	Torsional static stiffness (Nm/rad)		(N/m)	Torsional static stiffness (Nm/rad)	
r_5	FEM	Analytical model	k_p	FEM	Analytical model
30	2.3801×10^6	2.4002×10^6	1.4×10^8	2.0213×10^6	2.0392×10^6
25	2.1277×10^6	2.1708×10^6	1.2×10^8	1.8768×10^6	1.8901×10^6
20	1.7119×10^6	1.7146×10^6	1.0×10^8	1.6819×10^6	1.7094×10^6
15	9.6614×10^5	9.6918×10^5	0.80×10^8	1.4885×10^6	1.5038×10^6

As could be seen from the table, there're little differences between the results from two models and the stiffness obtained from finite element model is a little lower than those from the analytical model. These differences may be introduced by the non-rigid worm shaft and gear bodies.

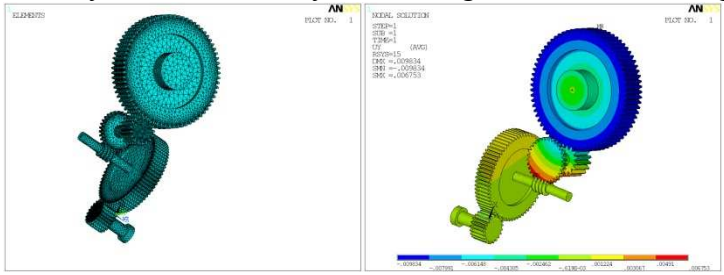

Figure 3 FEM model

Sensitivity to stiffness component. Two methods are employed in sensitivity analysis: analytical method presented in above sections and the difference method. The simulation results from two methods are shown in the following figure.

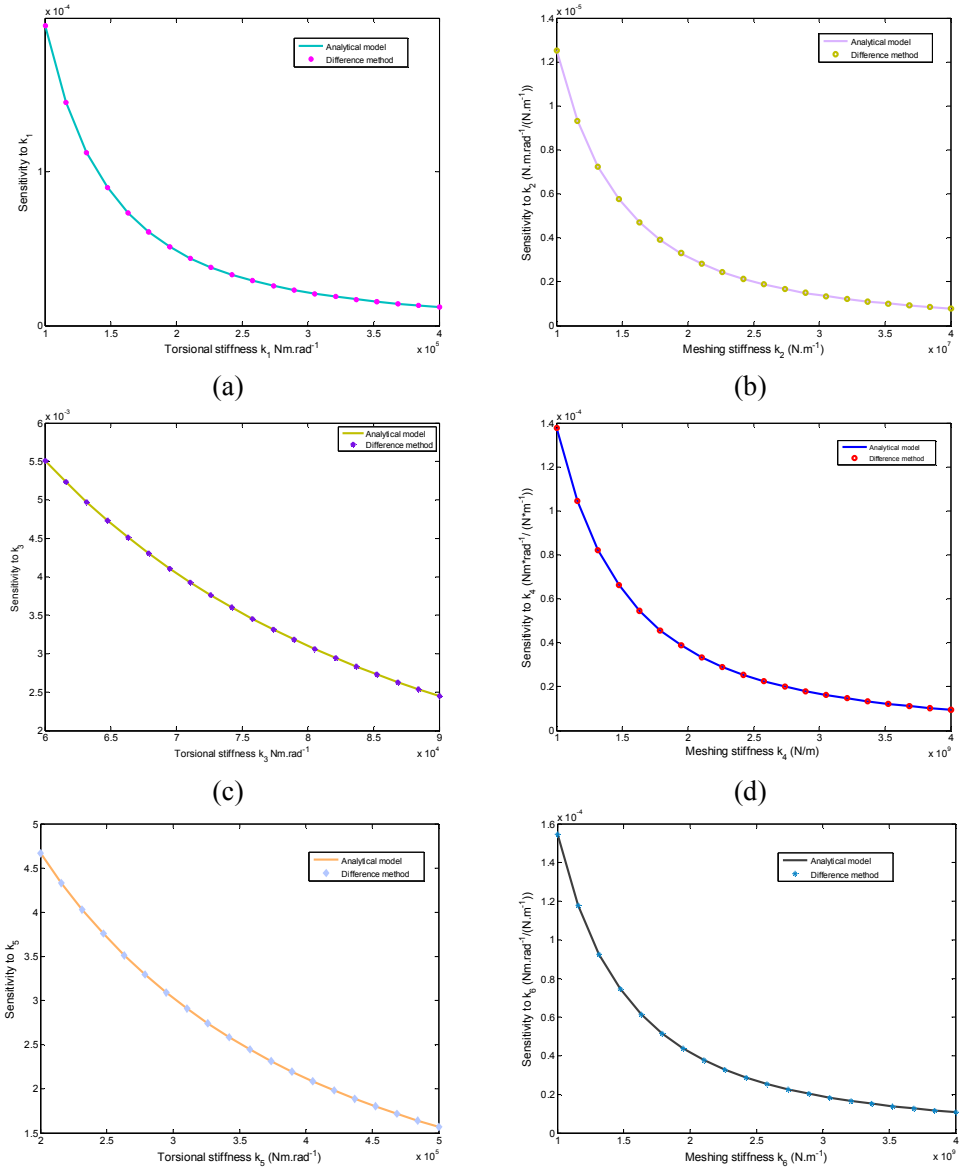

Figure 4 Verification of analytical sensitivity model

Compared to the meshing stiffness of gear pairs, the torsional stiffness of shaft is more sensitive to the static stiffness of the whole transmission chain; the closer to the end gear pair or shaft is, the more sensitive meshing stiffness or torsional stiffness is. And in this case, the axial stiffness of bearing supporting worm shaft is relatively lower than others except k_5, as could be seen from Fig.4.

Acknowledgements

This work was financially supported by the project funded by Tianjin University of Technology and Education (No. KYQD14008).

References

[1]. R. Ramesh, M.A. Mannan, A.N. Poo: Int. J Mach. Tools. Manu.Vol.40, (2000), p.1235.
[2]. R. Ramesh, M.A. Mannan, A.N. Poo: Int. J Mach. Tools. Manu.Vol.40, (2000), p.1257.
[3]. Feng, H. and Jiang, S.:Proc.IMechE. Part J: J Eng. Tri.2013; doi: 10.1177/1350650113483053.
[4]. Yu, C., Huang, X. and Fang, C.:J Mech. Sci. Technol. Vol.27(4),(2013), p.1081.
[5]. Han L, Zhang D W, Tian Y L, Wang F J and Xiao H.: Proc.IMechE. Part C: J Mech. Eng. Sci., Vol.228(8), (2014), p.1431.

Advanced Materials Research Vols. 989-994 (2014) pp 3331-3334
© (2014) Trans Tech Publications, Switzerland
doi:10.4028/www.scientific.net/AMR.989-994.3331

Theoretical Surface Roughness Model in High Speed Face Milling

Tao Zhang[1,2,a], Guohe Li[1,2,b], Lin Han[1,2,c]

[1]Tianjin Key Laboratory of High Speed Cutting & Precision Machining, Tianjin University of Technology and Education, Tianjin 300222, China

[2]School of Mechanical Engineering, Tianjin University of Technology and Education, Tianjin 300222, China

[a]Goldsound@163.com, [b]lgh790723@163.com, [c]hanlin147@163.com

Keywords: Theoretical model, High speed milling, Surface roughness, Cutting parameters.

Abstract. High speed milling is a newly developed advanced manufacturing technology. Surface integrity is an important object of machined parts. Surface roughness is mostly used to evaluate to the surface integrity. A theoretical surface roughness model for high face milling was established. The influence of cutting parameters on the surface roughness is analyzed. The surface roughness decreases when the cutter radius increases, total number of tooth and rotation angular speed, while it increases with the feeding velocity. The high speed face milling can get a smooth surface and it can replace the grinding with higher efficiency.

Introduction

High speed machining is a newly developed advanced manufacturing, and it improves the manufacturing efficiency [1], lowers the manufacturing cost, lowers the cutting energy. The high surface integrity of workpiece can be obtained after high speed machining [2]. High speed machining has been widely used in the world due to the great many advantages. Surface integrity is a most obvious character of high speed machining. To obtain the higher quality of surface roughness is a challenging work for high speed machining.

Ozcelik[3] once developed a statistical model for surface roughness estimation in a high-speed flat end milling process including spindle speed, feed rate, depth of cut, and step over, Ozcelik found the order of depth of cut, step over, spindle speed and feed rate on the surface roughness. Lee [4] established a surface roughness model considering the cutting tool deflection in end milling. Colak [5] have predicted the surface roughness with the gene expression programming. Dweiri [6] optimized the cutting parameters with adaptive neuro fuzzy inference system (ANFIS) in down milling of Alumic-97, and concluded that the better surface roughness can be obtained with four flutes.

The paper aims at the goal of modeling the surface roughness in high speed face milling. The influence of cutter radius, total number of tooth, feeding velocity and rotation angular velocity on surface roughness were analyzed.

Modeling the surface roughness

The trajectory of cutting edge is shown in Eq. (1).

$$\begin{cases} ox_i = vt + r_c \cos(\omega t + \alpha - \dfrac{2\pi i}{N}) \\ oy_i = r_c \sin(\omega t + \alpha - \dfrac{2\pi i}{N}) \end{cases} \tag{1}$$

where v is the feeding velocity in the ox direction, r_c is the radius of face milling cutter, ω is the rotation speed of face milling cutter, α is the initial angle of the first cutter in the face milling cutter, i is the No. of the tooth, N is the total number of tooth.

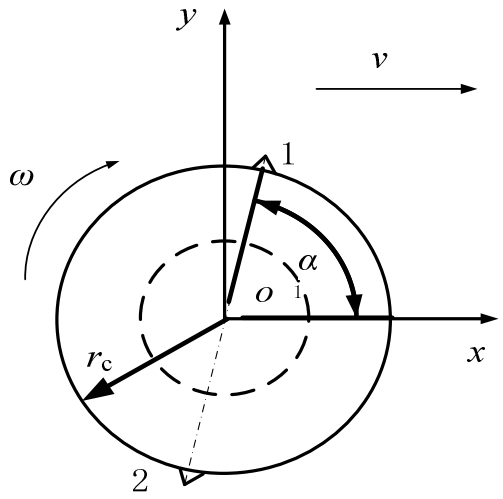

Fig. 1 Sketch of face milling cutter

Fig. 2 shows the scallop height h after the face milling cutter passes. As shown in fig. 2, h can represent the surface roughness in face end milling. To obtain the value of h is a challenging problem to optimize the cutting parameters.

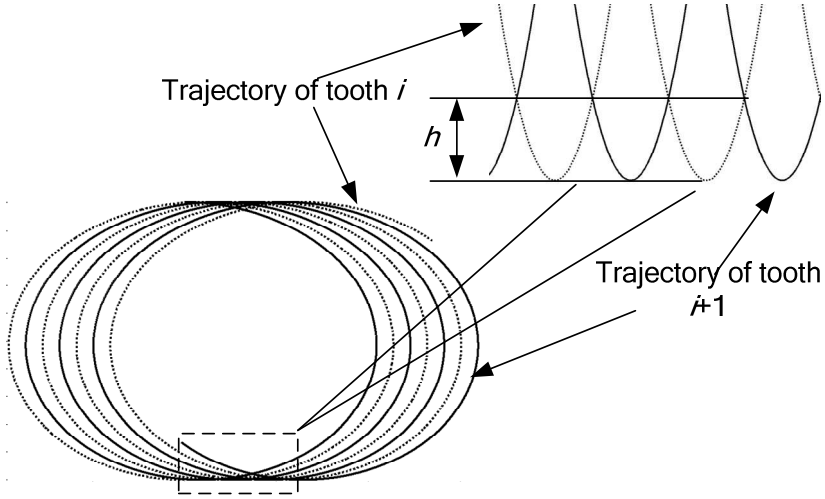

Fig. 2 Diagram of scallop height in high speed face milling

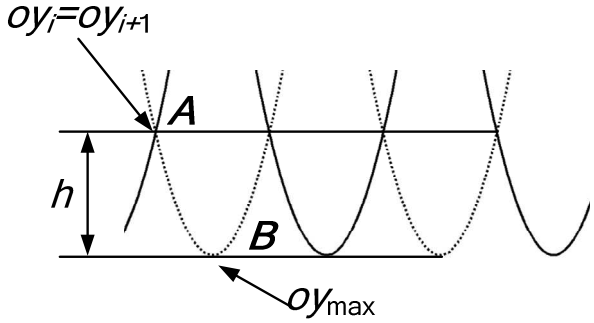

Fig. 3 Diagram of scallop height in high speed face milling

$$h = \left| oy_{i+1} - oy_{\max} \right| \tag{2}$$

$oy_{\max}$ is the maximum trajectory in the oy direction, oy_1 is the interaction point of trajectory of the tooth i and i+1 as shown in Fig. 3. The $i$tooth reaches point A when the milling time go to t, and the (i+1)th will pass point A later. in the feed direction, the position ox can be calculated with Eq. (3).

$$ox_i = ox_{i+1} \tag{3}$$

then an equation of time t can be got with Eq. (4).

$$f(t) = r_c \sin\left(\omega(t + \Delta t) + \alpha - \frac{2\pi(i+1)}{N} \right) - r_c \sin\left(\omega t + \alpha - \frac{2\pi i}{N} \right) - f_z \tag{4}$$

where f_z is the feed per tooth, Δt is the increment time between ith and (i+1)th, it can be calculated with Eq. (5).

$$\Delta t = \frac{\omega}{2\pi N} \tag{5}$$

The Eq. (5) is a complex and difficult to solve, Eq. (6) gives a Newton-Rapson method to solve the milling time.

$$t_{i+1} = t_i - \frac{f(t)}{f'(t)} \tag{6}$$

Results and discussion

Table 1 shows the cutting conditions in detail. Fig. 4 shows the surface roughness variation with the parameters shown in Eq. (1). It can be seen that the surface roughness decreases with the cutter radius, total number of tooth and rotation angular speed decreasing, while it increases when the feeding velocity increases. The surface roughness even can be smaller than 0.01 μm. It can be seen that the high speed face milling has a promising future to replace the grinding.

Table1 Cutting conditions

Total number of tooth	Feeding velocity (m/min)	Rotation angular speed(rad/s)	Radius of cutter(mm)
2-4	0.1-0.3	52.4-261.8	40-65

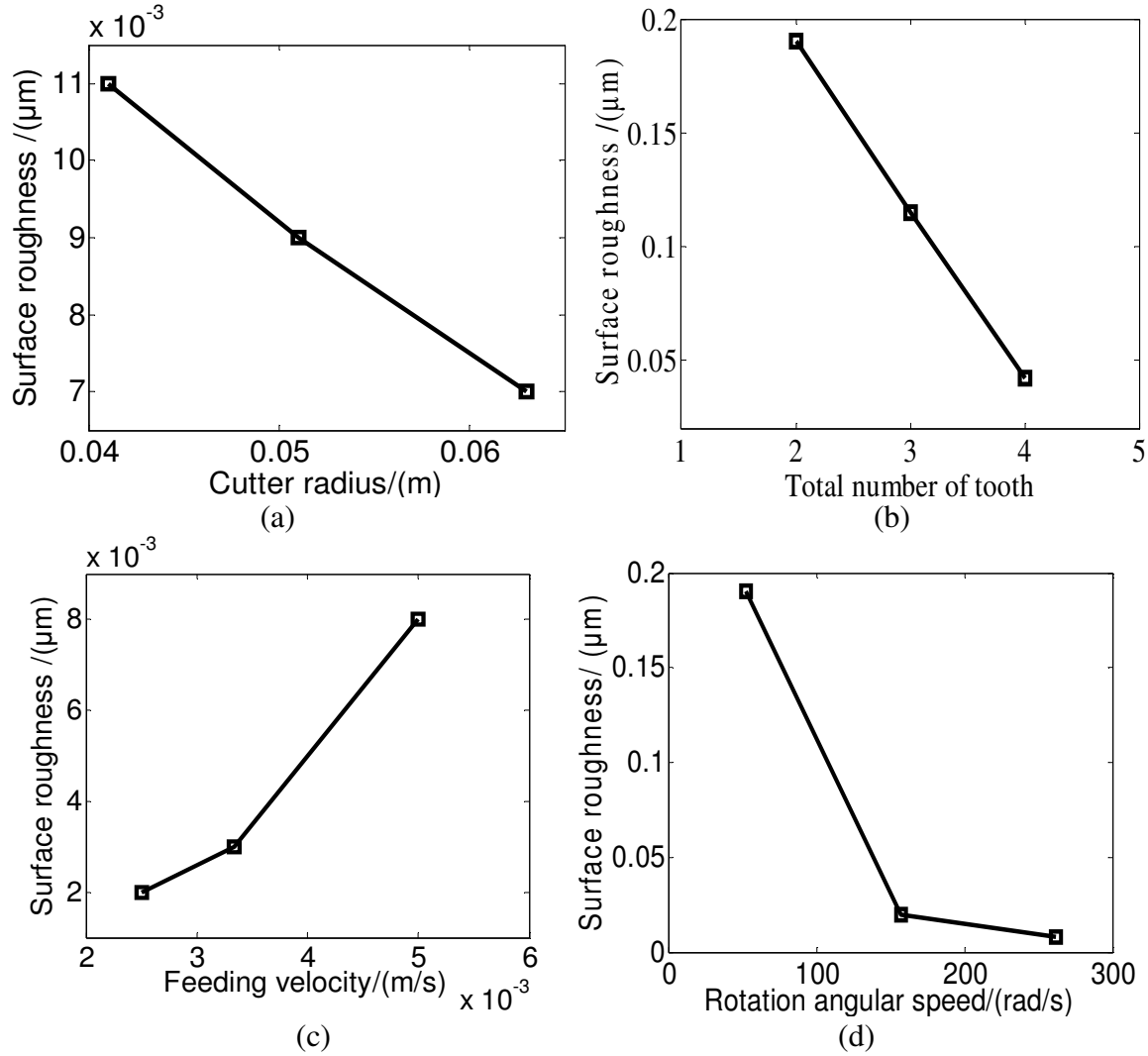

Fig. 4 Surface roughness variation with cutting parameters

Conclusions

Surface roughness is an important parameter of surface quality. The milling parameters have great influences on the surface roughness in high speed face milling. A theoretical model is established to investigate on the surface roughness in high speed face milling. The model can be used to optimize the surface roughness in the expected range. The following conclusions can be drawn:

1) The surface roughness decreases with the cutter radius increasing.
2) The surface roughness decreases with the total number of tooth increasing.
3) The surface roughness increases with the feeding velocity increasing.
4) The surface roughness decreases with the rotation angular speed increasing.

Acknowledgements

The authors would like to acknowledgement the financial support of Tianjin University of Technology and Education (No. KYQD14013).

References

[1] H. Schulz, T. Moriwaki: CIRP Ann-Manuf Techn Vol. 41 (1992), p. 637

[2] P. Fallböhmer, C.A. Rodríguez, T. Özel, T. Altan: J Mater Process Tech, Vol. 98 (2000), p. 104

[3] B. Ozcelik, M. Bayramoglu: Int J Mach Tool Manu Vol. 46, (2006) p. 1395

[4] K.Y. Lee, M.C. Kang, Y.H. Jeong et al. : J Mater Process Tech Vol. 113 (2001), p. 410

[5] O. Colak, C. Kurbanoğlu, M.C. Kayacan: Mater Design Vol. 28 (2007), p. 657

[6] F. Dweiri, M. Al-Jarrah, H. Al-Wedyan: J Mater Process Tech Vol. 133 (2003), p. 266

Advanced Materials Research Vols. 989-994 (2014) pp 3335-3339
© (2014) Trans Tech Publications, Switzerland
doi:10.4028/www.scientific.net/AMR.989-994.3335

An Analysis of Electric Inertia Simulation Method On The Test Platform of Electric Bicycle Brake Force

Zhaoxu Yu[1,a], Hongbin Yu[2,b]

[1,2]School of Mechanical Engineering, Tianjin Polytechnic University, Tianjin, China, 300387

[a]836665408@qq.com, [b]hongbinyu@aliyun.com

Keywords: Electric bicycle brake force; Electric inertia simulation; Test platform

Abstract. This paper analyzes the electric inertia simulation method deeply. By analyzing the brake torgue in the braking process, this paper makes a conclusion about the relationship between the moter's torgue in the braking process and the simulation of inertia. The test uses the method of combining the mechanical simulation and electrical simulation. In this method, it invites the test platform of electric bicycle brake force, and realizes the inertia simulation. On the test platform, the results showed: by using the electric inertia simulation, the performance of the system is obviously better than the one on the test platform which using flywheel groups. This method improves the degree of automation on the test platform.

Introduction

As the call of low carbon and environmental protection, National restrictions on private cars, the utilization rate of Electric bicycle is higher and higher. Safety requirements for electric bicycles will be too high as well. Therefore the braking performance requirements are very high. Brake manufacturer needs to perform various quality inspection and comprehensive evaluation of performance of the brake [1]. The ways to evaluate braking performance of electric bicycle are usually divided into three categories:

(l)Obtaining data of Electric bicycle in the practical road test to evaluate the electric bicycle brake performance. This can truly reflect the braking performance of electric bicycle.

(2)Set the electric bicycle brake force test platform of electric bicycle brake function of various parameters related. In the process of test, Take the different experimental methods according to the different test items test platform. To simulate a variety of road conditions of various parameter data and the electric bicycle brake performance assessment.

(3)Mathematical models are established according to the various test parameters. Simulation of dynamic process of electric bicycle braking simulation method by use of computer, then evaluating electric bicycle braking performance through the simulation data.

At present, brake bench test platform is commonly used as the traditional mechanical method. Through the rotary inertia large inertia wheel to simulate the mechanical inertia electric bicycle in motion process. But the torgue of inertia can hardly be continuously adjusted in the large inertia, and manufacturing cost is higher and not convenient to install. In view of the problems, with the design idea to develop an electric inertia simulation of mechanical inertia of the electric bicycle brake performance testing platform. According to certain control algorithm by motor output torque and rotational speed to simulate the mechanical inertia. Such devices occupy less space and money, and it can be continuously adjusted and convenient debugging.

Firstly, the traditional mechanical inertia simulation methods are briefly introduced. Then according to the principle of electric bicycle mechanical inertia of the electric simulation technology to make up the expression of the dynamic wheel in detail. Finally design the dynamic test platform and test platform for electric simulation system.

Traditional Mechanical Inertia Simulation Method

The use of mechanical inertia flywheel group to simulate is widely used traditionally. Using the test platform to simulate the electric bicycle mechanical inertia fly wheel. The fly wheel is made up of

multiple sizes of the flywheel. The test device combines with the main rolling chassis dynamometer through the clutch [2]. By controlling the number, size of the flywheel to simulate different inertia. The method has the advantages of simple operation, but the defects are showed as follows：its quality fixed once flywheel finished, This means that a testing platform once assembled, the simulation of quality fixed, unless the flywheel replaced, otherwise it cannot realize the diversification of demand; The flywheel mass is greater, the higher requirements of design and manufacturing, This will increase the cost of the whole system; Flywheels will produce large noise and vibration in the operation process. Once a mechanical fault, it may pose a threat to the surrounding the safety of equipment and personnel; The inertia of the flywheel equipment system is huge normally, and needs higher installation accuracy, thus the installation and replacement of the flywheel will take a long time.

Analyze The Technical Principle of Simulating A Electric Bicycle's Electric Inertia Instead of Mechanical Inertia

The core content determination of mechanical inertia use electrical simulation technology of electric has 2 points. First, to determine the mechanical inertia of bicycle. Second, electric simulation technology need to adopt electric drive system and make precise control of output torque, because different bicycle have difference inertia. Through the different tests results of a same t bicycle o adjust the speed and acceleration of the electric bicycle in the deceleration process. The above parameters can be measured by the torque, so the core problem of electric simulation technology of mechanical inertia is the control of torque [3].

The mechanical inertia simulation is the use of inertial rotation of the flywheel stored energy, in the test bed frame simulating various models of electric bicycle of equivalent quality on the road. Torgue $J\ (kg\cdot m^2)$ of inertia simulation test bench calculated as follows:

$$J = \frac{\eta}{1+\eta}(m_1 + 0.071m)r_k^2 \tag{1}$$

Where η is Electric bicycle wheel braking force distribution ratio before and after, m1 is the rated quality of electric bicycle, m is electric bicycle vehicle quality, rk is the wheel diameter of electric bicycle.

The spindle speed of inertia test platform by the following formula

$$n = 2.645v / r_k \tag{2}$$

Where v is the initial velocity of electric bicycle test.

The brake is loaded in pure flywheel inertia test platform, the relationship between its braking torque and inertia fly wheel and the rotational speed is as follows:

$$\alpha_j = \frac{d\omega}{dt} = \frac{M}{J} \tag{3}$$

Where α_j is the test platform frame spindle angular speed reduction. M is braking torque. ω is test platform frame spindle angular velocity.

By Eqs. (3), When the torgue of inertia J unchanged, braking deceleration is only related to braking torque. So the essence of the inertia brake test is to test the deceleration of the inertial system features, and then simulate the process of electric bicycle brake to slow down. Among them, torgue of inertia J is only for storing kinetic energy. If replace fly wheel stored kinetic energy with motor output energy, and keep the relationship between braking torque and speed reduction, can be used for simulating the mechanical inertia, called electrical inertia simulation. Electric inertia simulation process can be expressed as

$$M = M_1 + J_0 \frac{d\omega}{dt} \tag{4}$$

Where M_1 is the output torque in the process of motor brake. J_0 is the mechanical inertia of test platform that Including servo motor rotor, shaft coupling, main shaft and a fixed wheel inertia. M is a measured values, and can be used as a control volume.

By Eqs. (3), Substituting (dω/dt)=(M/J) into Eq. (4) and we can get the equation

$$M_1 = (\frac{J - J_0}{J})\,\mathrm{M} \tag{5}$$

J and J_0 are known in Eqs. (4). Therefore, the so-called electric simulation is through control the output torque of motor M_1 and make the tested brake have the same deceleration (dω/dt) with purely mechanical simulation system.

In known braking deceleration (dω/dt), the relationship between the brake on the brake torque M and the output torque of the motor M_1 the total inertia J and the basic inertia J_0 as follows:

When $J=J_0$, the mechanical inertia simulation of inertia is equal to the system, is the mechanical simulation system, the output torque of the motor is zero.

When $J<J_0$, M_1 is negative, the motor output brake torque, the direction of torque and rotate is opposite.

When $J>J_0$, M_1 is positive, the motor output Driving torque, the direction of torque and rotate is uniform.

Electrical analog control steps are as follows. First, measure the braking torque M. Second, calculate the output torque M_1 of the motor in the brake according to Eqs.(5). Third, By D/A conversion output electric inertia means the output torque M_1 of the motor in the brake. The sampling interval from the measurement to the output is short, it depends on the calculation speed of the computer and generally no more than 50ms.

A Structure Design For Braking Test Platform

In order to give full play to the function of electric bicycle testing existing test platform, electric inertia test platform on the basis of existing test bench can classify the function and design. Brake test system consists of test machine and computer control system. Test system Schematic diagram of the host structure is shown in Fig. 1, it can describe electric inertia test platform of the whole machine structure. Control system structure is shown in Fig. 2.

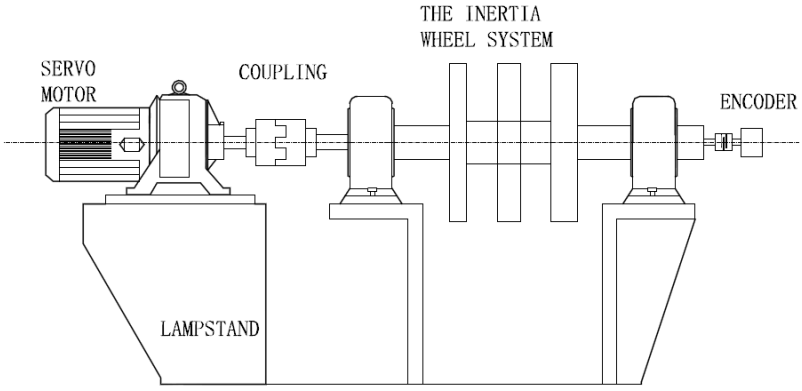

Fig. 1.Test system Schematic diagram of the host structure

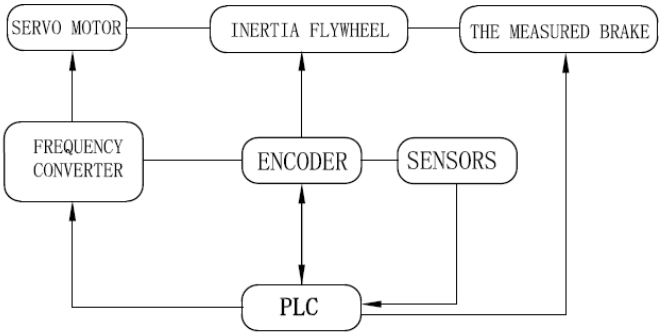

Fig. 2.Control system structure

The test system comprises a servo motor, inertia flywheel, transducer, encoder, sensor, PLC etc. In the development of the electric bicycle brake test-bed design combined with mechanical and electrical simulation method. During the test, the measured brake clamp on the test bed according to the installation as the electric bicycle. Motor drive shaft rotates, when it reaches to the speed of simulated electric bicycle. The control force is applied to the brake control force, making brake braking torque, forcing spindle stop [5]. DC speed regulating device to control the rotation of the DC motor. The encoder will dynamic speed feedback to the device and computer DC speed regulation, form a closed-loop control system. Applying pressure to the brake of the brake control force for a given organization is the pneumatic servo system controlled by computer, it can accurately simulate the brake operating force in actual driving. Test to measure the brake shoe temperature using thermocouple, thermocouple installed in the brake disc or drum brake shoe of the specified location. Brake temperature rise, and flooding after all can produce braking efficiency of the recession, it makes a strong impact on the safety performance in actual driving. So required by the test of brake blowing wind speed is accurately controlled by computer. In the water recession test, water spray for the brake can also be accurately controlled by computer. QC/T654-2005 Standard specified the test initial conditions, the braking original speed and braking deceleration, initial temperature, etc, which can be set whether the different models of the brake.

A Design for Electrical Simulation System of The Test Platform

When designing electric bicycle brake test bench, the first to determine the types and specifications of motor, its torque characteristics can be found from the product manual or the samples. Fig. 3 is the torque characteristic curve of the 30 kW DC motor. As can be seen from the Fig. 3 , the motor base speed is 600 r/min, the maximum speed is 1500 r/min. In the base speed zone, the maximum torque that motor can output is constant, the output power linearly increase gradually, so the base speed area is known as the constant torque area;When the motor speed exceeds the base speed, the maximum output power of the motor is constant, the maximum output torque curve gradually decline, so this area is called the constant power area. And the maximum torque corresponding to a speed point is the velocity and the corresponding power point torque value, can be calculated by the formula $M_1 = \frac{9550P}{n}$. (6)

Substituting it into equation (5) can take:

$$M = 9550\frac{P}{n}(\frac{I}{I - I_0}) \quad . \tag{7}$$

Practice proves that the combined system consisting of several additional inertia flywheel (as shown in Fig. 1), can expand the inertia simulation scope of platform. A combination of both can eliminate the differential, and reduce the test volume, improve simulation accuracy. Electric bicycle inertia of Brake test bench simulated by flywheel system. The inertia wheel system is consist of 3 inertial wheel and 2electromagnetic clutch that mounted on the spindle, the quantity of combination flywheels is one, the activity flywheels is two. The inertia wheel is selected by the computer according to the parameters of set brake and electric bicycles, at the start of the experiment through the electromagnetic clutch automatic select inertia wheel [6]. The inertia wheel simulated inertia difference by electric inertia simulation compensation. The inertia wheel simulated inertia difference shall be compensated by the differential electrical inertia simulation.

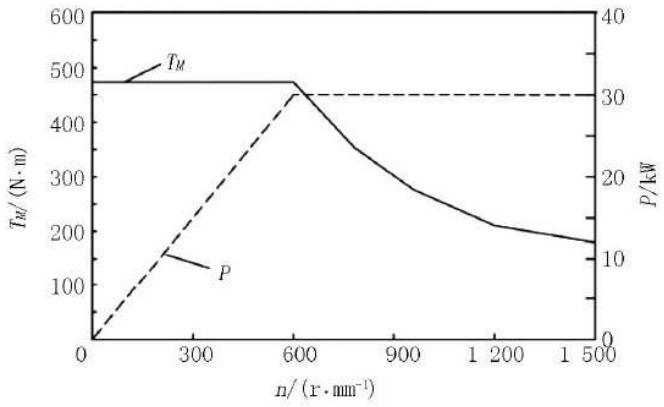

Fig. 3.The torque characteristic curve of the DC motor

The test uses the method of combining the mechanical simulation and electrical simulation. Precision of pure electric inertia simulation precision is low, and it uses Large capacity motor , Motor speed control device is of great capacity, These all will increase the cost. Simple mechanical inertia simulation requires many different inertia wheel in different combinations, and always exist analog differential, at the same time this makes the test bed volume very large. The combination of the two can eliminate the differential, reduces volume, improves the accuracy of the simulation and Save the cost. The testing system can simulate electric bicycle driving inertia in the series of 50 to 250.

Conclusion

The relationship between braking torque, the motor in the brake output torque and inertia simulation is given in this article through the analysis of the braking process of braking torque. The proposed method can effectively identify and optimize the mechanical inertia of the flywheel hybrid simulation system and driving motor matching relationship. Electric bicycle brake test platform that has been designed realized the simulation of inertia with the Methods of mechanical simulation and electrical simulation combined.

References

[1] GIULIANO A, MICHELE C. Microarray image gridding with stochastic search based approaches[J]. Image and Vision Computing, 2007, 25(2):155-163.

[2] Sahoo P K, So ltani S, Wong A K C, eta. l A survey of thresholding techniques[J]. Computer Vision Graphics Image Processing, 1988, 41:233-260.

[3] CHEN Jian-jun, Control to electric simulation of mechanical inertia of brake testing system[J], Hoisting and Conveying Machinery, 2007, 12, P27-30(Ch).

[4] James K, A M. Inertia Simulation in Brake Dynamometer Testing, SAE Technical Paper Series, 2002. 01. 2601.

[5] Michael A. , Sartori and Panos J. Anteaklis，Implementation of learning control system using neural networks[J], IEEE CSM，1992

[6] James K, ThomPson, Aaron Marks, Denis Rhode. Inertia Simulation in Brake Dynamometer Testing[J]. SAE International, 2002. 10.

Advanced Materials Research Vols. 989-994 (2014) pp 3340-3343
© (2014) Trans Tech Publications, Switzerland
doi:10.4028/www.scientific.net/AMR.989-994.3340

A Simple Criterion for Robust Stabilization Design of Interval Time-Delay Systems

Chien-Hua Lee[1,a] and Ping-Sung Liao[1,b]

[1]Department of Electrical Engineering, Cheng-Shiu University, Kaohsiung 833, Taiwan, R.O.C.

[a]chienhua@csu.edu.tw, [b]bsliao@csu.edu.tw

Keywords: robust stabilization; time-delay; interval system; Riccati equation approach; stabilizability criterion; decaying rate.

Abstract. This paper addresses the robust stabilization problem of interval time-delay systems. By applying an upper bound to the Riccati equation approach, a stabilizability condition and a controller are proposed. It is easy to test the presented condition and to implement the controller.

Introduction

In real-life systems, time delay and uncertainty exist naturally. Since both of them can lead to variations of eigenvalues and the loss of a certain amount of system accuracy, they hence are always sources of instability for controlled systems. Therefore, the robust controller design problem such that one can keep the inaccuracy to within an allowable bound becomes an attractive research topic. In literature, a number of works have adopted the LMI approach to solve the robust stabilization problem for uncertain systems with time-varying or time-invariant delay(s) [3-6]. In addition to the LMI approach, the Riccati equation approach has often been applied to solve the same problem for the aforementioned systems [1, 2, 7, 8]. However, most of those criteria and controllers obtained by this approach involve some modified Riccati equations which may be troublesome or even unsolvable. Among those works that use the Riccati equation approach, [8] applied an upper eigenvalue bound of the solution of the standard Riccati equation to the mentioned approach to develop a stabilizability condition and construct two stabilization control laws for uncertain time-delay systems. The obtained results can avoid the mentioned drawback. Therefore, the method presented in [8] can be considered as an improvement of the Riccati equation approach. In this paper, we extend the method proposed in [8] to solve the same problem of interval time-delay systems. However, we use a matrix bound to replace the eigenvalue bound that has been used in [8]. Then, a new stabilizability criterion and the corresponding control law can be obtained. When the interval system model is simplified to that presented in [8], comparison between the proposed stabilizability criterion and that of [8] will be made. It will be shown that the obtained result is sharper.

Main results

Consider the time-delay systems with parametric uncertainties

$$\dot{x}(t) = A_I x(t) + A_{dI} x(t-d) + B_I u(t). \tag{1}$$

where $x \in \Re^n$, $u \in \Re^m$, $d > 0$, respectively, denote the state, the input, and the delay, A_I, A_{Id}, and B_I represent interval matrices with appropriate dimensions and have the following properties:

$$A_I = [a_{Ipq}],\ u_{Ipq} \le a_{Ipq} \le v_{Ipq},\ p,q = 1,2,\ldots,n\ , \tag{1}$$

$$A_{dI} = [a_{dIpq}], u_{dIpq} \le a_{dIpq} \le v_{dIpq},\ p,q = 1,2,\ldots,n. \tag{2}$$

$$B_I = [b_{Ipq}], e_{Ipq} \le b_{Ipq} \le f_{Ipq},\ p,q = 1,2,\ldots,n. \tag{3}$$

For the above properties, we define the following matrices:

$$U = [u_{Ipq}], V = [v_{Ipq}], U_d = [u_{dIpq}], V_d = [v_{dIpq}], E = [e_{Ipq}] \text{ and } F = [f_{Ipq}]. \tag{4}$$

Define matrices A_i, A_{ij}, and, B_{ij}, respectively, as

$$A = 0.5(U+V),\ A_d = 0.5(U_d + V_d), \text{ and } B = 0.5(E+F). \tag{5}$$

Then, system (1) can also be represented as follows.

$$\dot{x}(t) = (A + \Delta A)x(t) + (A_d + \Delta A_d)x(t-d) + (B + \Delta B)u(t) \tag{6}$$

where (A, B) is assumed to be a controllable pair and ΔA, ΔA_d, and ΔB now denote the parametric uncertainties with the following properties:

$$\left[|\Delta A|\right] \le R, \left[|\Delta A_d|\right] \le S, \text{ and } \left[|\Delta B|\right] \le T \tag{7}$$

where $\left[|A|\right] = \left[|a_{ij}|\right]_{n\times n}$ means the modulus matrix of matrix A and R, S, and T are defined as

$$R = 0.5(V - U),\ S = 0.5(V_d - U_d) \text{ and } T = 0.5(F - E). \tag{8}$$

Once again, the application of the fact $\|A\| \le \left\|\left[|A|\right]\right\|$ results in

$$\|\Delta A\| \le \left\|\left[|\Delta A|\right]\right\| \le \|R\| \equiv \beta,\ \|\Delta A_d\| \le \left\|\left[|\Delta A_d|\right]\right\| \le \|S\| \equiv \gamma, \text{ and } \|\Delta B\| \le \left\|\left[|\Delta B|\right]\right\| \le \|T\| \equiv \eta. \tag{9}$$

It is assumed that the pair (A, B) is completely controllable. Then, the objective of this paper is to design a memoryless state feedback controller in the form of

$$u(t) = -Fx(t) \tag{10}$$

where F is the gain matrix such that the resulting closed-loop system is asymptotically stable.

By using linear algebraic techniques, a robust stabilization design for system Eq. 1 is given as follows.

Theorem 1. If there exists a positive constant η such that

$$A^T + A - \alpha BB^T + 2[\mu(R) + \gamma + \frac{\|A_d\|}{2}]I + \frac{A_d^T A_d}{\|A_d\|} + \alpha\eta\|B\| I < 0 \tag{11}$$

then the system (1) can be stabilized by a state feedback controller in the form of (11) with

$$F = 0.5B^T P \tag{12}$$

where the positive definite matrix P satisfies the Riccati equation

$$A^T P + PA - 0.5\alpha PBB^T P = -Q \tag{13}$$

where the $n\times n$ real positive definite matrix Q is given as

$$Q = \frac{\alpha}{2}\eta^2 q^2 I + q\left[(2\mu(R) + 2\gamma + \|A_d\|)I + \frac{A_d^T A_d}{\|A_d\|}\right] \tag{14}$$

and constant $q > 0$ is defined as

$$q = \frac{-\lambda_1(M)}{\alpha\eta^2} \quad \text{with} \quad M \equiv A^T + A - \alpha BB^T + \frac{A_d^T A_d}{\|A_d\|} + [2\mu(R) + 2\gamma + \|A_d\|]I. \tag{15}$$

Proof. Let a positive semi-definite matrix W is defined by

$$W \equiv 0.5\alpha(P - I)BB^T(P - I). \tag{16}$$

Then, we can rewrite the Riccati equation (14) as

$$(A - \frac{\alpha}{2}BB^T)^T(qI - P) + (qI - P)(A - \frac{\alpha}{2}BB^T) = -W + Q + \frac{\alpha}{2}BB^T + q(A^T + A - \alpha BB^T). \tag{17}$$

In light of (15), w have

$$Q + \frac{\alpha}{2}BB^T + q(A^T + A - \alpha BB^T)$$

$$= \frac{\alpha}{2}\eta^2 q^2 I + q\left[A^T + A - \alpha BB^T + (2\mu(R) + 2\gamma + \|A_d\|)I + \frac{A_d^T A_d}{\|A_d\|}\right] + \frac{\alpha}{2}BB^T. \tag{18}$$

From (19), (16) and using the fact that $K \le \lambda_1(K)I$ where K is a real symmetric matrix, we have

$$Q + \frac{\alpha}{2}BB^T + q(A^T + A - \alpha BB^T) \le \frac{1}{2}\left[\alpha\eta^2 q^2 + 2\lambda_1(M)q + \alpha\|B\|^2\right]I. \tag{19}$$

Condition (12) implies that $\lambda_1(M) < 0$. Applying (16) to (20) results in

$$Q + \frac{\alpha}{2}BB^T + q(A^T + A - \alpha BB^T) \le \frac{1}{2\alpha\eta^2}\left[-\lambda_1^2(M) + \alpha^2\eta^2\|B\|^2\right]I. \tag{20}$$

Obviously condition (12) can guarantee that the right-hand side of (21) is a negative definite matrix. Furthermore, it also infers that $(A^T + A - \alpha BB^T) < 0$ and then one can conclude that the matrix $A - 0.5\alpha BB^T$ is stable. Therefore, equation (18) is a Lyapunov equation and then the solution $(qI - P)$ of this Lyapunov equation is positive. That is, the solution of the Riccati equation (18) has

$$P < qI . \tag{21}$$

Using the controller (11) with (13), then system (1) becomes

$$\dot{x}(t) = [A + \Delta A - \frac{\alpha}{2}(B + \Delta B)B^T P]x(t) + (A_d + \Delta A_d)x(t-d) . \tag{22}$$

For this system, we construct a Lyapunov function as

$$V(x(t),t) = x^T(t)Px(t) + q\int_{t-d}^{t} x^T(\tau)(\frac{A_d^T P A_d}{\|A_d\|} + \frac{\Delta A_d^T P \Delta A_d}{\gamma})x(\tau)d\tau \tag{23}$$

where $P > 0$ satisfies (14). We also use symbols V, x, and x_d to replace $V(x(t),t), x(t)$, and $x(t-d)$, respectively. Now, taking the derivative along the trajectories of (1) gives

$$\dot{V} = x^T[(A + \Delta A)^T P + P(A + \Delta A) - \alpha PBB^T P + \frac{A_d^T P A_d}{\|A_d\|} + \frac{\Delta A_d^T P \Delta A_d}{\gamma}]x - \frac{\alpha}{2}P(\Delta BB^T + B\Delta B^T)P$$

$$- x_d^T(\frac{A_d^T P A_d}{\|A_d\|} + \frac{\Delta A_d^T P \Delta A_d}{\gamma})x_d + x_d^T(A_d + \Delta A_d)^T Px + x^T P(A_d + \Delta A_d)x_d . \tag{24}$$

Since

$$-P\Delta BB^T P - PB\Delta B^T P \le PBB^T P + P\Delta B\Delta B^T P , \tag{25}$$

$$x_d^T A_d^T Px + x^T PA_d x_d \le \frac{1}{\|A_d\|}x_d^T A_d^T PA_d x_d + \|A_d\| x^T Px , \tag{26}$$

$$x_d^T \Delta A_d^T Px + x^T P\Delta A_d x_d \le \frac{1}{\gamma}x_d^T \Delta A_d^T P\Delta A_d x_d + \gamma x^T Px , \tag{27}$$

then

$$\dot{V} < x^T[A^T P + PA - \alpha PBB^T P + \Delta A^T P + P\Delta A + \frac{A_d^T PA_d}{\|A_d\|} + \|A_d\| P + \frac{1}{\gamma}\Delta A_d^T P\Delta A_d + \gamma P$$

$$+ \frac{\alpha}{2}PBB^T P + \frac{\alpha}{2}P\Delta B\Delta B^T P]x \tag{28}$$

If condition (12) is satisfied, then the upper bound (22) exists and (25) becomes

$$\dot{V} < x^T[-Q + q(\Delta A^T + \Delta A + \frac{A_d^T A_d}{\|A_d\|} + \|A_d\| I + \frac{1}{\gamma}\Delta A_d^T \Delta A_d + \gamma I + \frac{\alpha}{2}q\eta^2 I)]x$$

$$\le x^T[-Q + q(2\mu(R) + \|A_d\| + 2\gamma)I + q\frac{A_d^T A_d}{\|A_d\|} + \frac{\alpha}{2}\eta^2 q^2 I]x = 0 . \tag{29}$$

Where relation (15) and the following inequality are used.

$$\Delta A^T + \Delta A \le 2\mu(\Delta A)I \le 2\mu(|\Delta A|)I \le 2\mu(R)I \tag{30}$$

Therefore, the resulting closed-loop system (23) is robustly stable. Thus, the proof is completed.

In the literature, [8] has discussed the following uncertain time-delay system

$$\dot{x}(t) = (A + \Delta A(k(t)))x(t) + (A_d + \Delta A_d(r(t)))x(t-d) + Bu(t) . \tag{31}$$

Then, a stabilizability criterion for system (32) has been derived as

$$\lambda_1(A^T + A - \alpha BB^T) + 2(\beta + \bar{\gamma} + \|A_d\|) < 0 \tag{32}$$

where positive constants β and $\bar{\gamma}$, respectively, are defined by

$$\beta \equiv \sup_{t\in\mathbb{R}^+}\|\Delta A(k(t))\| \text{ and } \bar{\gamma} \equiv \sup_{t\in\mathbb{R}^+}\|\Delta A_d(r(t))\| .$$

Let $\Delta A = \Delta A(k(t)), \Delta A_d = \Delta A_d(r(t))$ and $\Delta B = 0$. Then system (7) becomes system (32). Besides, using the relation $\mu(\Delta A(r(t))) \le \|\Delta A(r(t))\| \le \beta$, condition (12) now becomes

$$A^T + A - \alpha BB^T + 2[\beta + \overline{\gamma} + \frac{\|A_d\|}{2}]I + \frac{A_d^T A_d}{\|A_d\|} < 0 . \quad (33)$$

In light of the relation $A_d^T A_d \le \lambda_1(A_d^T A_d)I = \|A_d\|^2 I$ and the inequality $\lambda_1(A+B) \le \lambda_1(A) + \lambda_1(B)$ for $A^T = A$ and $B^T = B$, we have

$$A^T + A - \alpha BB^T + 2(\beta + \overline{\gamma} + \frac{\|A_d\|}{2})I + \frac{A_d^T A_d}{\|A_d\|} \le \lambda_1[A^T + A - \alpha BB^T + 2(\beta + \overline{\gamma} + \frac{\|A_d\|}{2})I + \frac{A_d^T A_d}{\|A_d\|}]I$$

$$\le \lambda_1(A^T + A - \alpha BB^T)I + 2(\beta + \overline{\gamma} + \|A_d\|)I . \quad (34)$$

Therefore, it is obvious that condition (34) is sharper than (33).

Conclusion

In this paper, the robust stabilization problem for interval time-delay systems has been addressed. By applying an upper matrix bound and linear algebraic techniques to the Riccati equation approach, the mentioned problem is solved. A simple criterion and the corresponding memoryless state feedback controller have been presented to guarantee the asymptotic stability of the resulting closed-loop systems. It is shown that they are easy to be tested and implemented. From a comparison, it is shown that the obtaining condition is sharper than that proposed in [8] for systems without input uncertainty.

Acknowledgement

The author would like to thank the National Science Council, the Republic of China, for financial support of this research under the grant NSC 102-2221-E-230-014.

References

[1] W. Chen, S. Chang, and W. Zhang. Linear matrix inequality-based repetitive controller design for linear systems with time-varying input delay, IET Control Theory & Applications, 2010 (4) 1071-1078.

[2] M. R. Hsu, W. H. Ho, and J. H. Chou. Stable and quadratic optimal control for TS fuzzy-model-based time-delay control systems, IEEE Transactions on Systems, Man and Cybernetics, Part A: Systems and Humans, 2008 (38) 933-944.

[3] G. Wei, G. Feng, and Z. Wang. Robust H_∞ control for discrete-time fuzzy systems with infinite-distributed delays, IEEE Transactions on Fuzzy Systems, 2009 (17) 224-232.

[4] L. Wu, X. Su, P. Shi, and J. Qiu. A new approach to stability analysis and stabilization of discrete-time T-S fuzzy time-varying delay systems, IEEE Transactions on Systems, Man and Cybernetics, Part A: Systems and Humans, 2011 (41) 273-286.

[5] J. Zhang, Y. Xia, and P. Shi, and M. S. Mahmound. New results on stability and stabilization of systems with interval time-varying delay, IET Control Theory & Applications, 2011 (5) 429-436.

[6] H. Zhao, H. Zhang, and P. Cui. Steady-state optimal filtering for continuous systems with time-delay, IEEE Signal Processing Letters, 2009 (16) 628-631.

[7] C. Y. Chen and C. H. Lee. Delay-independent stabilization of linear systems with time-varying delayed state and uncertainties, J. Franklin Institute, 2009 (346) 378-390.

[8] C. H. Lee. Simple stabilizability criteria and memoryless state feedback control design for time-delay systems with time-varying perturbations, IEEE Trans. Circuits and Systems-I, 1998 (45) 1121-1125.

Advanced Materials Research Vols. 989-994 (2014) pp 3344-3348
© (2014) Trans Tech Publications, Switzerland
doi:10.4028/www.scientific.net/AMR.989-994.3344

Optimization of operation frequency in the evaluation of TBCs using microwave technique

Yu'e YANG[1 a] ， Gaimei Zhang[2 b]

[1.]School of Mechanical Engineering, University of Jinan，Jinan, Shandong 250022, China
[2.] Beijing Institute of Graphic Communication, Beijing, 102600, China

[a]email: yangyve@163.com, [b]email: zhanggaimei@bigc.edu.cn

Keywords: Thermal barrier coatings, Microwave NDE, Optimization, Operation frequency

Abstract: Thermal barrier coatings (TBCs) were developed to increase the operating temperatures of turbine blades in gas turbine engines. Non-contact inspection and the ability to penetrate into dielectric materials are two of the most important attributes of microwave non-destructive evaluation (NDE) and make it suitable for the non-destructive inspection of TBCs. In order to improve the detection sensitivity, it is important to optimize operation frequency. Computer simulation technology-microwave studio (CST-MWS) was used to optimize operation frequency in the evaluation of the top coating (TC) porosity and the metal substrate surface defects using microwave NDE. The results showed that the sensitive frequency is different when the TC thickness of under detection changes. So, it is necessary to choose appropriate operation frequency according to TC thickness to evaluate TBCs using microwave NDE.

1．Introduction

Thermal barrier coatings (TBCs) are used to achieve higher overall efficiency for aircraft engines and land-based gas turbine systems. However, the characteristics of TBCs are influenced of the spraying parameters and the work environment. Despite the considerable progress that has been made in the last few years, non-destructive evaluation (NDE) techniques of characterizing coatings, such as piezospectroscopy, eddy current, electrochemical impedance, etc., are still unable to provide a sufficiently precise description of a multilayer system [1]. Non-contact inspection and the ability to penetrate into dielectric materials are two of the most important attributes of microwave NDE and make it suitable for the non-destructive inspection of TBCs. The thickness of TBCs, defects on substrate interface, cracks and pores of TC can be easily visualized using microwave scanning probe [2]. The phase and magnitude of the microwave reflection coefficient can evaluate the TBCs delamination induced by acute angle laser drilling using microwave NDE [3]. The phase difference of microwave reflection coefficient can be used to evaluate the thickness of TC and TGO in TBCs using microwave NDE operating over K- and W-band frequency range [4]. A good resolution of 1º change in phase for 8μm TC thickness was obtained when the TC thickness was evaluated using microwave NDE [5]. Reflection coefficient is a function of various parameters such as, dielectric layer's thickness, standoff distance, dielectric properties, operation frequency, etc. Therefore, by measuring the reflection coefficient under certain conditions, it is possible to evaluate the above parameters. When an in-contact inspection technique was applied for detecting and evaluating the characters of TBCs, the operation frequency is one of the major factors to affect the reflection coefficient. In order to improve the detection sensitivity, it is important to optimize operation frequency.

In this paper, Computer simulation technology-microwave studio (CST-MWS) was used to optimize operation frequency in the evaluation of the top coating (TC) porosity and the metal substrate surface defects using microwave NDE. The results revealed that the U-band frequency should be used to detect TBCs when the TC thickness was from 300μm to 350μm and the Ka-band frequency should be used to detect TBCs when the TC thickness was from 400μm to 500μm.

2. Theoretical bases

The problem of transmission and reflection of uniform plane waves from a multilayer dielectric medium has been investigated by many investigators. This microwave NDE is based on wave reflection from a dielectric media interface. Metallic BC thickness does not affect microwave signals, so, in this case, TC was deposited directly onto the metal substrate. Uniform waves were normally incident into the TC system and then reflected by the metal surface (good conductor layer). These forward- and backward- traveling waves inside the TC layer were formulated by enforcing the appropriate boundary conditions at the air-TC and TC-conductor boundaries. Finally, the reflection coefficient was set as the ratio of the reflected and incident waves [6]. Figure 1 shows the incident and reflected electric fields traveling in TC systems: the incident electric fields of the probe, E_0^i(Vm^{-1}), that incident into TC system, E_{TC}^+, and that reflected by the metal surface, E_{TC}^-. After being completely reflected by the TC and substrate, the field emerged as a reflected electric field in the probe, E_0^r. The reflection coefficient is the ratio of E_0^r and E_0^i. The reflection coefficient Γ and its phase ϕ at the sensor aperture can be written as follows:

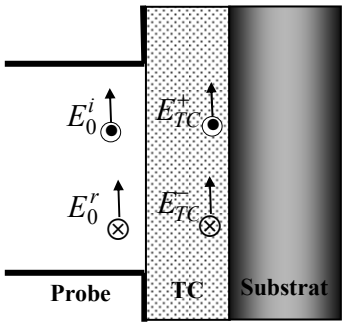

Fig. 1 Incident and reflected electric fields traveling in TC systems consisting of a rectangular waveguide probe and TC backed by a conducting metallic substrate

$$\Gamma = \frac{E_0^r}{E_o^i}$$
$$\phi = \tan^{-1}\left[\frac{\mathrm{Im}(\Gamma)}{\mathrm{Re}(\Gamma)}\right] \quad (1)$$

When microwave signals travel within TC systems, the permittivity of the TC affect the electric field, thereby affecting the reflection coefficient. In this study, TC porosity associated with TC permittivity can be informed by the reflection coefficient. Besides, the surface conditions of the metal substrate influence the reflection coefficient. So, the reflection coefficient was used to characterize the metal substrate defects.

3 CST model

CST-MWS is a specialized tool for the 3D electromagnetism (EM) simulation of high-frequency components. CST MWS' unparalleled performance often makes it the

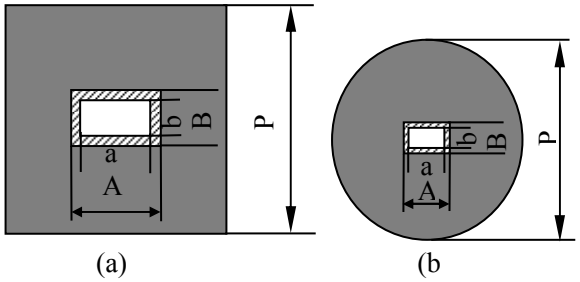

Fig. 2 The structures of rectangular waveguide probes (a) WR28, (b) WR18

first-choice technology in research and development departments. CST MWS enables fast and accurate analysis of high-frequency (HF) devices such as antennas, filters, couplers, planar and multi-layer structures. Exceptionally user friendly, CST MWS quickly gives researchers insight into the EM performance at high frequency. CST-MWS is seen as a standard industry development tool. M.T. Ghasr et al. simulated the reflection coefficient at the aperture of a probing open-ended waveguide using CST-MWS [7]. Ghasr's experimental results [8] were similar to [7] calculated results. Contact evaluation was used to evaluate TBCs using a rectangular waveguide probe. Two probes WR28 and WR18 were used. Figure 2 shows the structures of WR28 and WR18. Table 1 shows the size of the probes.

Table 1 Type and size of rectangular waveguide

Waveguide probe	a (mm)	A (mm)	b (mm)	B (mm)	P (mm)
WR28	7.112	9.14	3.556	5.59	19.1
WR18	4.775	6.81	2.338	4.42	28

4 Results and discussions

4.1 Detection of TC Porosity

The phase difference was calculated for TC of 10% relative to 3% porosity when TC thickness was kept constant within one group to limit its influence. Figure 3 shows the phase difference vs. frequency using two probes, WR18 and WR28. Figure 3 shows that the maximum phase difference in each phase difference curve and that TC thickness was equal to one quarter of the wavelength of the microwave when the microwave operated at the frequency corresponding to the maximum phase difference, which is called the sensitive frequency. Thus, under actual testing conditions, TC porosity was able to be determined using this microwave technique by selecting the appropriate frequency, which was estimated according to TC thickness. Once this was known, the appropriate waveguide probe was selected. The phase difference of the microwave reflection coefficient indicated TC porosity using probe WR18 when TC thickness was 300 to 350 μm, and probe WR28 when TC thickness was 400 to 500 μm.

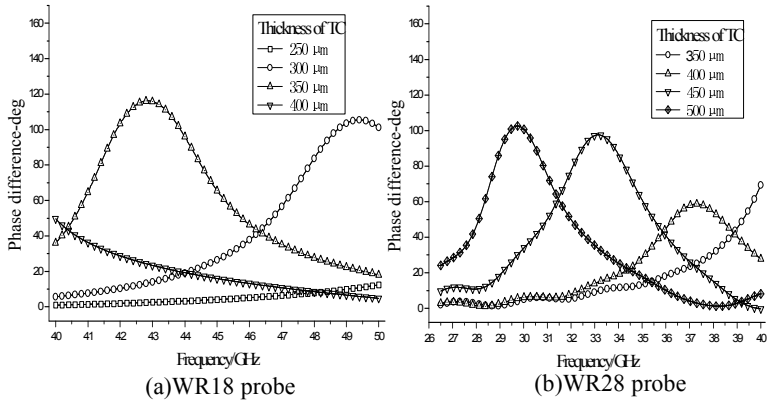

(a)WR18 probe (b)WR28 probe

Fig. 3 Phase differences of 10% and 3% TC detected by (a) WR18 and (b) WR28 for TC of different thicknesses

4.2 Detection of Substrate Defects

When the subtract defect was detected using microwave technique, the characteristic of TBCs influence the evaluation results, because that microwave signals transmit in TBCs. The effect of the TBCs thickness was studied to optimize the operation frequency. Figure 4 showed that the phase

difference of TC between with defect and without defect vs. operation frequency. Figure 4(a) showed the phase difference detected by WR18 for different thickness TC. The results indicated that the phase difference curses have maximum evaluating 300μm and 350μm thickness TC. The frequency corresponding to the maximum phase difference is called the sensitive frequency. Figure 4(b) showed the phase difference detected by WR28 for different thickness TC. The results indicated that the phase difference curses have maximum evaluating 400μm, 450μm and 500μm thickness TC. The sensitive frequencies are relevant to the thickness of TC when the substrate defects are detected using microwave NDE.

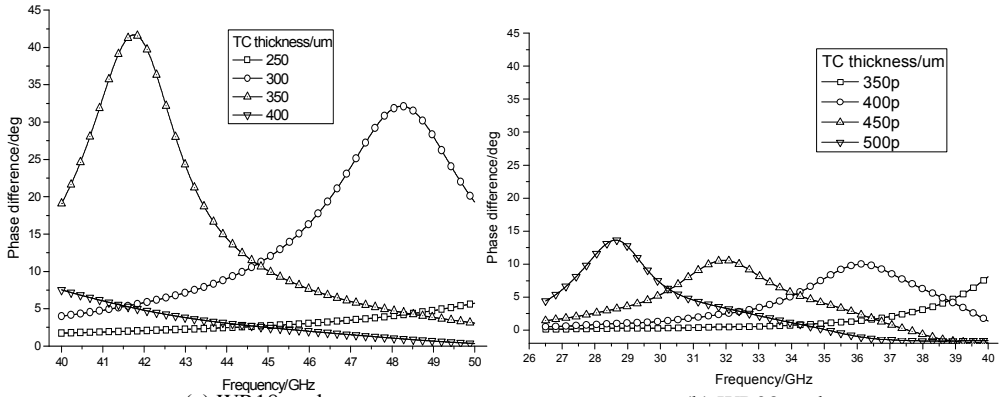

(a) WR18 probe (b) WR28 probe

Fig. 4 Phase differences of TC with and without defects detected by (a) WR18 and (b) WR28 for TC of different thicknesses

5 Conclusions

Based on microwave communication and reflection theory in thermal barrier coatings on metal substrates, the optimization of operation frequency was presented in the evaluation of the top coating (TC) porosity and the metal substrate surface defects using microwave NDE. The results showed that the sensitive frequency is different when the TC thickness changes and that the greater the TC thickness, the higher the sensitive operation frequency. When the TC thickness was between 300μm and 350μm, U-band rectangular waveguide (WR28) was used to detect the TC porosity or the metal substrate defects. When the TC thickness was between 400μm and 500μm, Ka-band rectangular waveguide (WR18) was used to detect the TC porosity or the metal substrate defects. Special study is needed to distinguish the TC porosity and the substrate defects.

6 Acknowledgments

The authors would like to express their gratitude to the National Natural Science Foundation of China (Project No: 51305038), the Scientific research foundation of the university of Jinan (Project No: xky1311) and the Dr Foundation of the university of Jinan (Project No: xbs1411).

7 References

[1] Newaz, Golam and Chen, Xiaoqun. Progressive damage assessment in thermal barrier coatings using thermal wave imaging technique. Surface and Coatings technology, 2005,190(1):7-14

[2] A.M. Grishin, V.P. Denysenkov. Broad band microwave probe for nondestructive test of dielectric coatings. IEEE International Symposium on Applications of Ferroelectrics, 2002: 91-93.

[3] H K Sezer, Lin Li, Z Wu, B Anderson, P Williams. Non-destructive microwave evaluation of TBC delamination induced by acute angle laser drilling. Measurement Science and Technology,2007, 18(1):167-175

[4] M. Sayar, D. Seo, K. Ogawa. Non-destructive microwave detection of layer thickness in degraded thermal barrier coatings using K- and W-band frequency range. NDT&E International, 2009, 42 (5) :398–403

[5] He Cunfu, Yang Yu'e and Wu Bin. Experimental study on thickness detection of thermal barrier coatings using microwave. Chinese Journal of Scientific Instrument,2011,32(11): 2590-2595

[6]J. Edwards and R. Zoughi. 1993 Microwave sensitivity maximization of disbond characterization in conductor backed dielectric composites. Journal of Nondestructive Evaluation.v12,n3,p193-198

[7] M. T. Ghasr, Devin Simms and R. Zoughi. 2009, IEEE transactions on instrumentation and measurement.v58,n5,p1505-1513

[8] Karl J. Bois, Aaron D. Benally and R. Zoughi. 1999, IEEE transactions on instrumentation and measurement.v48,n6,p1131-1140

Advanced Materials Research Vols. 989-994 (2014) pp 3349-3353
© (2014) Trans Tech Publications, Switzerland
doi:10.4028/www.scientific.net/AMR.989-994.3349

Damage Detection of the Honeycomb Sandwich Panel Based on frequency dactylogram

LI Guo-chen[1, a], LI Yong-qiang[2, b], HE Yong-liang[2, c]

[1]Dongguan Polytechnic, Dongguan 523808, China;

[2]School of Sciences, Northeastern University, Shenyang 110819, China.

[a]Guochen_li@163.com, [b]lyq_neu@126.com, [c]807272349@qq.com

Keywords: honeycomb sandwich panel, damage detection, frequency dactylogram.

Abstract. An aluminous honeycomb sandwich panel with some structural damages was selected as the objective in this study. The panel was simply supported along four edges and its natural frequency data was collected through modal experiment with a hammering method. Application of frequency dactylogram method for honeycomb sandwich panel damage is identified. The detection results show that the frequency dactylogram method can be constructed using the frequency data of honeycomb sandwich panel, which is only related with the positions of damage and not the degree of damage.

Introduction

Currently, most of the study about the honeycomb sandwich structure damage is focused on the damage mechanism and repair [1, 2]. Engineering often use visual method, hammer percussion method and acoustic resistance meter detection method, X-ray method to check out whether there is any damage. However, the literatures which do research about honeycomb sandwich structure damage detection based on the dynamic characteristics were rare. The technology of structure damage detection which based on dynamic test is a global damage detection technology. The basic idea is that the structure damage is bound to cause the changes of some structure parameters, such as weight, the stiffness and damping. Then resulting in the changes of structural of dynamic characteristic (modal parameters and frequency response function, etc.), while the structure dynamic characteristics is the intrinsic characteristics of the structure, only the structure changes (components damage), the condition of its dynamic characteristics will change, so we can determine the structure damage by studying the change of parameters of the structure dynamic characteristics. Damage diagnosis method based on structural dynamic characteristics is now under the attention of scholars at home and abroad, and will become the focus of the study.

By using the frequency data of the structure, we can only construct frequency dactylogram related with the damage location and not the degree of damage [3-8]. Frequency dactylogram can be used to locate the structural damage. Whether the structure damage exists or not can be determined by the comparison between the frequency which is observed currently and the former one. Therefore, it is an effective way to detect the structure damage only by using the data of frequency [9].

Basic principle of frequency dactylogram

If the structure with multiple degrees of freedom is in good condition, then the motion equation of free vibration is

$$(K-\lambda M)\phi=0 \tag{1}$$

While the damage exists, the rigidity of structure K and weight M will have little changes ΔK and ΔM, according to perturbation theory, equation (1) can be

$$((K+\Delta K)-(\lambda+\Delta\lambda)(M+\Delta M))(\phi+\Delta\phi)=0 \tag{2}$$

In this paper, most of the study of the damage of honeycomb sandwich panel is minor damage. So, ΔM=0. Launch equation (2) and omit the second order, it will be

$$\Delta\lambda = \phi^T \Delta K \phi \Big/ \left(\phi^T M \phi\right) \tag{3}$$

Therefore, the changes of eigenvalue in modal at In-order can be written as

$$\Delta\lambda_i = \phi_i^T \Delta K \phi_i \Big/ \left(\phi_i^T M \phi_i\right) = \sum_n \phi_i^T \Delta K_{nl} \phi_i \Big/ \left(\phi_i^T M \phi_i\right) \tag{4}$$

Among the equation: ΔK_{nl} is the rigidity changes of the element *(n, l)*.

Only the element (*n, l*) damaged, the equation should be changed as

$$\Delta\lambda_i = \phi_i^T \Delta K_{nl} \phi_i \Big/ \left(\phi_i^T M \phi_i\right) \tag{5}$$

Consider the damage factor of element (*n, l*) is α, then $\Delta K_{nl}=\alpha K_{nl}$, the equation (5) will be

$$\Delta\lambda_i = \alpha \phi_i^T K_{nl} \phi_i \Big/ \left(\phi_i^T M \phi_i\right) \tag{6}$$

Equation (6) is the change of the eigenvalue in structure at In-order. Take any two eigenvalue of modal in structure $\Delta\lambda_i$ and $\Delta\lambda_j$, their rate is

$$\frac{\Delta\lambda_i}{\Delta\lambda_j} = \left(\frac{\phi_i^T K_{nl} \phi_i}{\phi_i^T M \phi_i}\right) / \left(\frac{\phi_j^T K_{nl} \phi_j}{\phi_j^T M \phi_j}\right) \tag{7}$$

Combined with (2), it can be deduced that $\Delta\lambda=(\omega+\Delta\omega)^2-\omega^2$, omit the second order, then $\Delta\lambda=2\omega\Delta\omega$, substitute $\Delta\lambda=2\omega\Delta\omega$ into equation (7) and we can sort out that:

With and without the structure damage, the rate of any two orders of frequency changes is

$$RCF_{ij}^{nl} = \frac{\Delta\omega_i}{\Delta\omega_j} = \frac{\left(\frac{\phi_i^T K_{nl} \phi_i}{\phi_i^T M \phi_i}\right) / \omega_i}{\left(\frac{\phi_j^T K_{nl} \phi_j}{\phi_j^T M \phi_j}\right) / \omega_j} \tag{8}$$

With and without the structure damage, the rate of any regularized frequency at the first order is

$$NRF_i^{nl} = \frac{\Delta\omega_i / \omega_i}{\sum_{j=1}^{q} \Delta\omega_j / \omega_j} = \frac{\left(\frac{\phi_i^T K_{nl} \phi_i}{\phi_i^T M \phi_i}\right) / \omega_i^2}{\sum_{j=1}^{q} \left[\left(\frac{\phi_j^T K_{nl} \phi_j}{\phi_j^T M \phi_j}\right) / \omega_j^2\right]} \tag{9}$$

Among this: q is the order of the vibration mode and the frequency; the vibration mode Φ, frequency ω, rigidity K and weight M .These parameters are from nondestructive structure; K_{nl} is the structure rigidity when element (*n, l*) was damaged.

Equation (8) and (9) shows that, with and without the structure damage, any two orders of the frequency changes' ratio, the rate of any regularized frequency at the first order do nothing with the degree of the structure damage, and is connected with the location of the damage. Therefore, these two parameters can be used to construct the location of structure damage.

Numerical examples validate of frequency dactylogram damage detection

Because of the complexity of the panel structure and boundary conditions, we use the beam structure to analyze feasibility of the frequency dactylogram at first in this paper. The structure of composites beam is 350mm×25mm×25mm, the length of fixed support is 50mm, as Fig. 1. Among all the same size of composite beam specimen with damage, the distance of the damage location and free end is 125mm.

Use the finite element analysis method to calculate out the first three order natural frequency of composites beam with and without damage as Table 1.

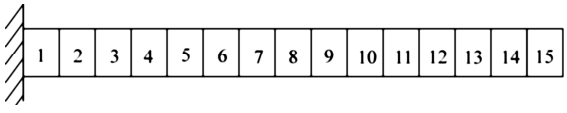

Fig. 1 Mesh and element number of composite beam

We can get the frequency of composite structure without damage and with each damaged element after calculation, as Table 2.

Table 1 Natural frequency of composites beam with and without damage

	Natural frequency /Hz		Rate of change of frequency for damage and without damage)/ %
	without damage	with damage	
First modal	33.69	33.45	-0.712
Second modal	207.72	205.57	-1.035
Third modal	574.74	570.99	-0.653

Table 2 Frequency of composite structure without damage with each damage element

		Natural frequency /Hz		
		first modal	second modal	third modal
Without damage		33.550	207.05	573.22
Number of element for damage	1	32.730	202.48	561.41
	2	32.790	203.70	565.59
	3	32.880	204.46	565.88
	4	32.940	204.60	563.93
	5	32.990	204.32	562.62
	6	33.040	203.84	563.35
	7	33.080	203.37	565.25
	8	33.107	203.09	566.25
	9	33.129	203.10	565.14
	10	33.144	203.36	562.86
	11	33.154	203.76	561.46
	12	33.159	204.16	562.09
	13	33.162	204.45	564.09
	14	33.163	204.58	565.73
	15	33.163	204.61	566.28

According to the result of calculate the vibration of beams, the rate of frequency changes is: Δf_1=-0.712%, Δf_2=-1.035%, Δf_3=-0.653% and the rate is: $\Delta f_2/\Delta f_1$=1.453, $\Delta f_3/\Delta f_1$=0.916.

Based on the finite element analysis, with the regularized coordinate of length in structure χ as abscissa, with frequency change ratio δ as the ordinate drawing a curve line of the location of damage-the frequency change ratio, then use the frequency change ratio which calculated through the results of experimental test, $\Delta f_2/\Delta f_1$=1.453, $\Delta f_3/\Delta f_1$=0.916, drawing two horizontal lines, and supersede it to the damage position-frequency change ratio curve, we can get 6 crossing points among the observation and the result calculated, as Fig. 2, two of the crossing points, the abscissa of point 3and point 4 are very close, the coordinate is the location the damage exists, the regularized coordinate is 0.56, transform it into physical coordinates is 168 mm, while the real location is 175 mm, considering the error of the experiment, it shows that the method is feasible.

It should be pointed out that, the premise of Eq. 8,9 are the structure of damage is minor, so minor data above the second order can be omit while carrying out the structure perturbation analysis. Thus,the conclusion we got is a approximate conclusion actually, the dactylogram of this conclusion largely depends on the damage location, meanwhile on the structure damage degree to some extent.

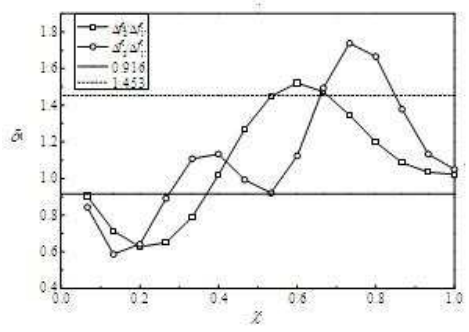

Fig. 2 Results of position finding of the damage

Frequency dactyllogram used for damaging location for honeycomb sandwich panel detection

The method carried out to collect the vibration modal data of the honeycomb sandwich panel is hammering method, the laboratory equipment contains force-hammer, piezoelectric accelerometer, DLF-3 four unification amplifier with double channel, INV3018C intelligently acquit and analyze signal instrumentand Coinv DASP MAS modal and dynamic analysis software. The materials chose in this experiment are aluminum cementing honeycomb sandwich panel. The size of its length and width is 200×200mm and the thickness of its is10mm. A fixturewith simply supported on four sidesis used in experiment. The structure data of honeycomb sandwich panel: the thickness of skin is 1mm, the thickness of honeycomb cell is 0.05mm, and the length of honeycomb cell is 6mm, as Fig. 3.

Fig. 3 Honeycomb sandwich panel and fixture with simply supported boundary in experiment

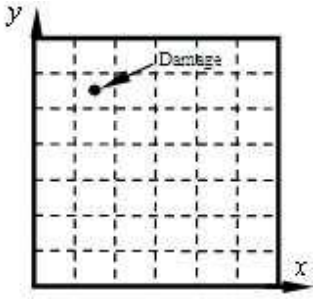

Fig. 4 Schematic diagram of the damage location for honeycomb sandwich panel

Divided the honeycomb into 7 elements along both the length and width direction, we got 7×7 elements. Because the method is only used to detect the honeycomb damage location, it has a tiny damage at the central of a quarter of honeycomb sandwich panel (the second element at x axis, the sixth element at y axis), as Fig.4.

Use finite element analysis to calculate the first four order modal of each damage skin in the honeycomb sandwich panel, then collect the frequency dactylogram data of damage skin location in the honeycomb sandwich panel. The frequency dactylogram can be calculated through equation (8) and (9). The certain guiding principle can be followed while collecting the damage location dactylogram:

(a) Firstly, the accuracy of frequency dactylogram must be considered, generally speaking, the lower the frequency rate order is, and the better it will be;

(b) The dactylogram with better monotonicity should be selected while using just one of the frequency dactylogram to detect the damage location;

(c) While using two or more frequency dactylogram to locate the damage, each one should be ensured and present reverse monotonic trend, meanwhile, pay attention to ensuring that there is enough distance among the dactylogram data of the same damage location.

According to the principles above, selecting the results of calculated dactylogram in this paper is: the rate of frequency changes at the fourth order to the first order is δ_{41}, as Fig.5； the rate of the third order regularized natural frequency δ_{31}, as Fig.6.

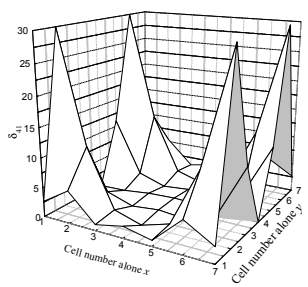

(a) calculation results for along the *x* axis and *y* axis

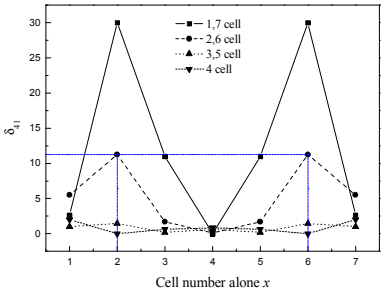

(b) calculation results for along the *x* axis

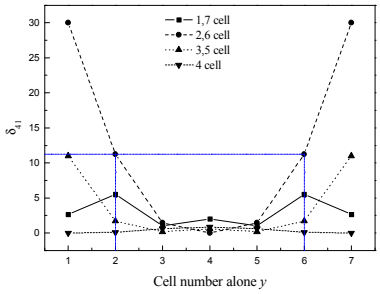

(c) calculation results for along the *y* axis

Fig. 5 δ_{41} of honeycomb panel frequency

The actual damage conditions dactylogram data of honeycomb sandwich panel which calculated through equation (8) and (9): frequency change ratio δ_{41}=11.82, regularized frequency change ratio δ_{31}=0.136. With the data of the honeycomb sandwich panel frequency change ratio δ_{41} and regularized frequency change ratio δ_{31}, draw a horizontal line at graph (b) and graph (c) in Fig.5 and Fig.6. The x-coordinate of crossing points on the horizontal and curve is the damage element.

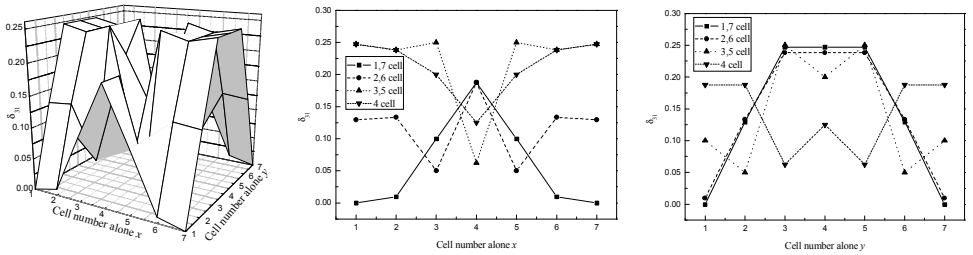

(a) calculation results for along the x axis and y axis

(b) calculation results for along the x axis

(c) calculation results for along the y axis

Fig. 6 δ_{31} of honeycomb panel frequency

In graph (b) and graph(c) at Fig.5, while using the frequency change ratio δ_{41} to locate the damage, 4 damage elements can be determined: the two elements at intersection of second columns and second rows and intersection of second columns and sixth rows, the two elements at intersection of sixth columns and second rows and intersection of sixth columns and sixth rows. These location results not only determined that the element (2, 6) is the damage element correctly, but also determined another three elements which are symmetric with the element (2, 6).To locate the damage with regularized frequency change ratio δ_{31}, as the curve (b) and (c) in Fig.6 shows, the same results were determined. The reason: the three elements in the panel and element (2, 6) are symmetric, it is unable to distinguish the structure symmetric damage only based on frequency, and this is the shortcoming of frequency dactylogram. However, this positioning work is greatly convenient while using other ways to do the final confirmation of the damage location.

Summary

In this paper, we use frequency dactylogram to determine the minor damage of honeycomb sandwich panel, the position of damage can be determined more accurately by using the method which test the structure's natural frequency and combines the results calculated by finite element analysis, As for the symmetrical structure, such as the honeycomb sandwich panel with simply supported boundary , the damage detection results symmetrical with the real damage, it cannot shows the real position of damage intuitively, it contains the other three positions which is can help us narrow the range of damage detection.

Acknowledgement

The research work was supported by programming foundation research of Dong'guan polytechnic (2013a02).

References

[1] Foo C C, Seah L K and Chai G B: Composite Structure, (2008) No. 85, p.20–28.
[2] Dear JP, Lee H, Brown SA: INT J ENG SCI, (2005) No.32, p.130-154.
[3] Adams R D, Cawley P, et al: P I MECH ENG C-J MEC, Vol.20 (1978) No.2, p.93-100.
[4] Cawley P and Adams R D: Journal of Strain Analysis, Vol.14 (1979) No.2, p.49-57.
[5] Cawley P and Adams R D: Composite Materials, (1979) No.13, p.161-175.
[6] Hearn G and Testa R B: J J STRUCT ENG-ASCE, Vol.117 (1991) No.10, p.3042-3061.
[7] Kaminski P C: Journal of Process Mechanical Engineering, (1995) No.209, p.117-123.
[8] Li Guo-qiang, Liang Yuan-sen and Chen Su-wen: Journal of Vibration, Measurement &Diagnosis, Vol.25 (2005) No.1, p.8-12.
[9] MO Shuhua and Wang Chun-yuan: Acta Material Compositae Sinica, Vol.26 (2009) No.1, p.96-99.

Advanced Materials Research Vols. 989-994 (2014) pp 3354-3358
© (2014) Trans Tech Publications, Switzerland
doi:10.4028/www.scientific.net/AMR.989-994.3354

The Research of Fluid in the Cross Micro-channel

Li Jianyi[1,a], Zhou Wei[1,b], Zhang Xu[1,c], Jiang Yunfeng[1,d], Yang Li[1,e], Zhang Sixiang[1,f*]

[1]Modern Control Technology Institute of Hebei University of Technology, Tianjin, China.

[a]email lijianyi@hebut.edu.cn, [b]email zhouwei@hebut.edu.cn, [c]email zhangxu@hebut.edu.cn, [d]email jyf@hebut.edu.cn, [e]email yangli5781@126.com, [f*]email zhangsixiang@hebut.edu.cn,

Keywords: micro-channel, surface tension, droplets, laminar flow

Abstract. The phenomenon of laminar flow in the micro-channel is demonstrated by the software simulation. It shows different velocity produces different flow layer. Water-in-oil droplets are obtained by the experiments. These experiments take water as the dispersed phase and take the oil as the continuous phase. Analyze forming process and forming factors of the droplets and the column flow. The main factors of forming droplets are surface tension, viscosity shear force and the liquid velocity. The size of droplet is associated with the flow and channel width of two liquids. Changing the pressure of the inlet can obtain droplets in different size.

Introduction

Due to the particularity of micro-fluidic chip under the microscopic, using micro-fluidic chip which analyses and tests a cell and micro liquid drop, has received more and more attention. Therefore, another kind of droplet chip operation has appeared. It uses two incompatible liquid to form the micro droplets in the micro-channel. Digital micro-fluidic has wide application prospects in many fields, such as cell analysis, biomedical, clinical detection and so on.

According to the recent micro-droplet preparations, two kinds of micro-channel (T- slot and cross- slot) are widely used. Both channels can create droplet which can control the size and can create the laminar flow with phase flow also. Laminar flow can be used for the screening of cell and organic matter particles[1]. Droplets can be used in medical biological research, including the analysis of human mitochondrial DNA, the research of protein and the research of the separation and analysis amino acid[2,3]. In the micro scale, multiphase flow problem is the main research area[4]. Thorsen[5] is the first person who used T-shaped micro-channel to form droplets successfully. Shear force and surface tension are the main factors for the formation of droplets. By means of the study of T-slot, Garstecki[6] thinks that the shear stress is not the main factor for the formation of droplets. The main reason is that the dispersed phase blocking micro-channel leads to continuous phase pressure increased and reacts with interface tension, and then droplets form. Hua[7] thinks that droplet generation process is controlled by the viscous drag force and surface tension. High capillary number, continuous phase and dispersed phase under different flow rate, Amit Gupta[8]had studied flow mechanism for the two incompatible liquid with the interaction. In microscale multiphase flow channel, because there are crushing, shearing, jet and many other decentralized modes, can be obtained droplets flow, columnar flow, stratified flow and etc[9,10]. Regulated flow and material characteristics can let the fluid shape change come true[11,12].

Cross type structure is also called double T type structure. It can produce continuous mini droplets. Compared with T type structure, the cross structure can produce monodisperse micro droplets, and generate volume less than 1 liter micro-droplet.

Design micro-channel

Using of COMSOL geometry model tools can build two-dimensional model which corresponds to three-dimensional structure. Here sets entryway initial pressure values to 2 pa, 4 pa, 8 pa, 16 pa, in order to do the test. Setting the height of the channel cross section is High, the width of the channel cross section is Width, and the ratio of height and width is Ratio. The study shows that the

flow velocity will change correspondingly in the case of different pressure and different ratio of height and width, as shown in figure 1. When the depth-width ratio of the channel is 1:1, the slope of the fitting curve is the biggest and the velocity is the fastest. According to the results of the experiments, it can acquire the biggest velocity when the depth-width ratio of the channel is 1:1.

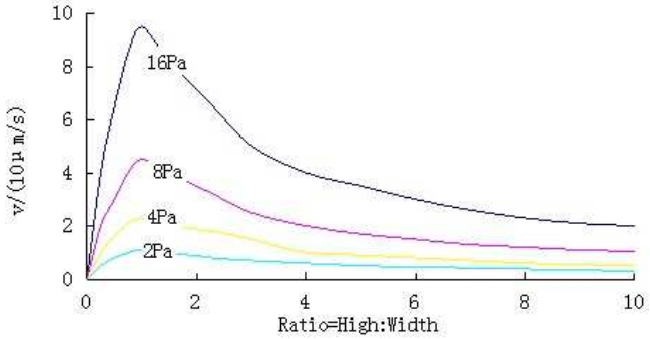

Fig.1 The different aspect ratio of the flow rate change in the microchannels

Same phase flow simulation

Laminar flow is hard to see in the experiment, so the effect can acquire clearly through the simulation. And the effect is as same as the experiment. To imitate three entrances and put the same fluid into these three channels, it can create three layers of non-interference. As shown in figure 2, the three channels have the same pressure.

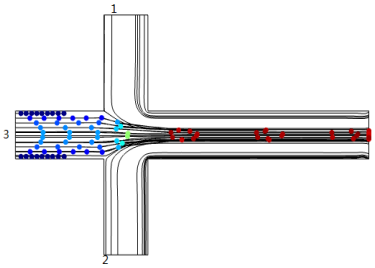

Fig.2 Three inlets have the same pressure

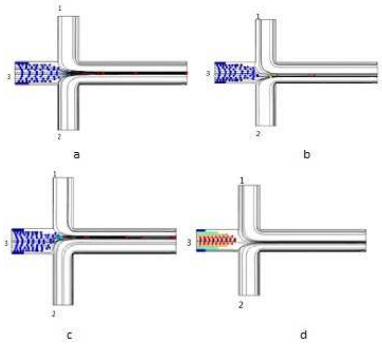

Fig.3 Change the pressure of channel inlet

Changing the pressure of three channels, only change the width and position of laminar flow, but the effect of laminar flow does not change. Figure 3a the up and down entrances pressures have increased, the middle entrance pressure does not change, it can be seen the middle laminar flow becomes thin. Figure 3b changing the up entrance pressure and other entrances pressure do not change, the middle laminar flow is biased below. On the contrary, is biased upward side. As shown in figure 3c.When the up and down pressures are far greater than the middle one, the middle fluid will be blocked. As shown in figure 3d.

Different phase flow experiments in cross-shaped microfluidic channel

When different liquids enter into the micro-channel, according to the theory of laminar flow, they are also the laminar flow. However, the test shows that the oil and water cannot produce laminar flow in some of the pressure and will create drops, because they have different viscosity and incompatible surface tension. Furthermore, when the water pressure is too large and far more than the oil pressure, it will appear the phenomenon of laminar flow.

Droplet formation process

Droplet formation process: When the cross channel is filled with oil, the two oil-way and reservoir are interlinked. The oil pressure has decreased, the water pressure won't change. Compared with the oil pressure, the water pressure are bigger than the oil pressure, the water will pour in the cross channel. As shown in figure 4a. Because the existence of the surface tension, the

front of the water column shrinks likes a water ball. The water pour into the cross channel again, the structure likes a ball will be increased. As shown in figure 4b. When the water sphere has increased to a certain degree, as shown in figure 4c, the water sphere has filled with the cross channel and jammed the two oil entrance. Then the oil pressure is larger than water pressure, the oil column began to squeeze water column. The water sphere has been flattened. As shown in the figure 4d. Under the shear of the oil, the water column has appeared to the bottleneck. As shown in the figure 4e. Water bottleneck is oppressed, and becomes very thin almost broken. As shown in the figure 4f. Finally, the water sphere will be cut and form a water column and pour into the reservoir. As shown in the figure 4g.

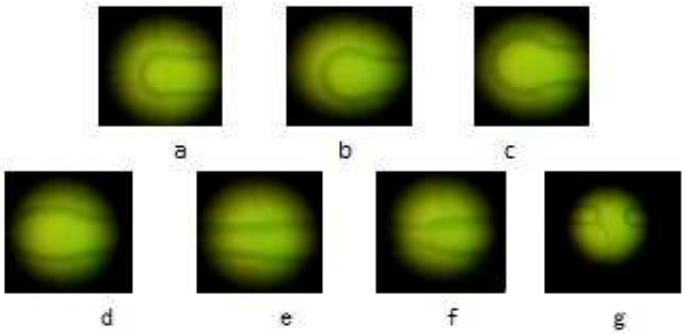

Fig.4 The process of droplet formation

The principle of droplet forming

Experiments show that the surface tension of the water and oil is the reason for the formation of droplets, in other way the pressure of the water and oil are alternating. Owing to water sphere jam the oil-way, it will form the pressure difference between the water and oil. Under the action of oil viscosity, cutting the water-way and forming the droplets.

When generating small droplets, they cannot be completely blocked the micro-channel cross structure and only rely on the flow shear stress. When the micro droplet is bigger, it can be completely blocked interleaving structure of cross channel, makes stress accumulates rapidly. Only smaller flow velocity can be free of surface tension and burst. If the oil and water flow rate ratio is too large, in other means the water pressure is bigger than the oil. The oil can't cut off the water.

As shown in the figure 8. The water is not cut off. The main reason is the water pressure is too big and the velocity ratio is too big. To solve this problem, it can increase the oil pressure and reduce the water pressure.

The formation of the laminar flow

During the experiment, it forms the laminar flow with some pressure. That is a water column wrapped in a layer film. As shown in the figure 5. The main cause of the laminar flow formation is water - oil pressure ratio is relatively large. The width of the laminar flow is different with the different of water - oil pressure ratio. With the increase of oil pressure, water laminar narrows, until the oil can cut off water laminar, form a small water column.

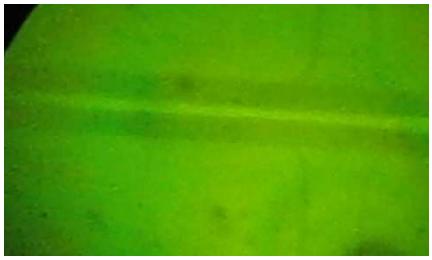

Fig.5 The formation of laminar flow

Factors affect droplet formation

The flow rate of the fluids impacts droplets size. Changing inlet pressure, liquids flow rate can be changed. In this paper, we do some experiments. The results of the experiment are similar as the literature[13].

Water-oil pressure ratio is 0.8, as shown the figure 6. It has small droplets. Water-oil pressure ratio is 1, as shown the figure 7. It has large droplets. When water-oil pressure ratio is 1.4, the liquid column is very long. When the water pressure is too big, it can hardly form the droplets and it will form the laminar flow. When the oil pressure is too big, the water won't flow. Take reasonable pressure ratio, the oil pressure is larger than the water pressure, in proportion to increase oil pressure and water pressure and it can quickly get uniform liquid droplets.

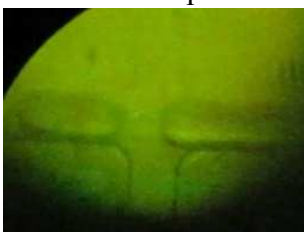

Fig. 6 The pressure ratio of water and oil is 0.8, L/W of the droplet is 1.8

Fig. 7 The pressure ratio of water and oil is 1, L/W of the droplet is 2

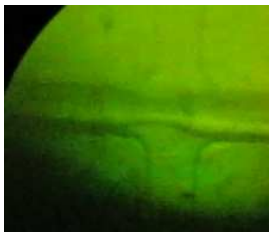

Fig. 8 The water pressure is too large, the flow is not cut off, droplets do not form

The figure 9, the oil pressure is constant, increasing the water pressure. The figure 10, the water pressure is constant, increasing the oil pressure. Fwater for water pressure, Foil for the oil pressure, L for the length of the droplets, W for the width of the channel. When the oil pressure is not change, with increasing of the water pressure, the length of the fluid column has increased. With decreasing of the water pressure, the length of the fluid column has decreased. When the water pressure is not change, with increasing of the oil pressure, the length of the fluid column has decreased. With decreasing of the oil pressure, the length of the fluid column has increased.

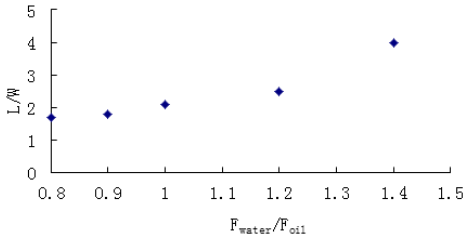

Fig.9 Oil pressure constant, increases the pressure of the water

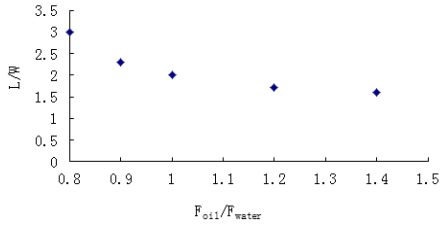

Fig.10 Water pressure constant, increases the pressure of the oil

The experiment shows that droplet formation is related to liquids viscosity, surface tension and liquids flow rate. The size of droplets is associated with channel and liquids flow rate. For the selected two kinds of liquids, as long as changing their feed pressure and then can get the required droplet. When generated the same size droplet, different viscosity of oil required for different feed pressure.

Conclusion

Using the cross slot can generate laminar flow and nanoliter droplets. For same kind fluid, controlling import flow velocity, it can control the width of the middle part. Laminar flow can be used to separate particles, such as cells, organic matter, etc. For multiple fluids, we can control the fluids pressure in order to generate controlled size of the droplets. The choice of the reasonable fluid, the reasonable velocity ratio and the reasonable channel, can obtain the droplets.

Acknowledgements

This work was financially supported by the Hebei University of Technology Innovation Fund for Outstanding Youth (2012008)

References

[1] Bhagat A A S, Kuntaegowdanahalli S S, Papautsky I. Inertial microfluidics for continuous particle filtration and extraction, Microfluid Nanofluid, (2009), 7:217–226

[2] Kersaudy-Kerhoas M, Dhariwal R, Desmulliez M P Y, et al. Hydrodynamic blood plasma separation in microfluidic channels.MicrofluidNanofluid,(2010),8:105–114

[3] Rodriguez-Villarreal A I, Arundell M ,Carmona M, et al. High flow rate microfluidic device for blood plasma separation using a range of temperatures , Lab Chip, (2010),10: 211–219

[4] Zhao C X, Middelberg A. Tow-phase microfluidic flows[J]. Chem. Eng. Sci., (2011), 66(7): 1394-1411

[5] Thorsen T, Roberts R W, Arnold F H, et al. Dynamic pattern formation in a vesicle-generating microfluidic device [J]. Phys Rev Lett, (2001),86(18)4163-4166

[6] Garstecki P, Fuerstman M J, Stone H A, et al. Formation of droplets and bubbles in a microfluidic T-junction-scaling and mechanism of break-up [J]. Appl Phys Lett, (2003), 82 (3): 364-366

[7] Hua J, Zhang B, Lou J. Numerical simulation of microdroplet formation in coflowing immiscible liquids [J].AIChE Journal, (2007),53(10): 2534-2548

[8] Amit G,S M Sohel M, Ranganathan K. Droplet formation and stability of flows in a microfluidic T-junction. Applied Physics Letters, (2009),94(16): 164107-3

[9] Baroud C N, Gallaire F, Dangla R. Dynamics of microfluidic droplets[J]. Lab Chip, (2010), 10(16): 2032-2045

[10] Gunther A, Jensen K F.Multiphase microfluidics: From flow characteristics to chemical and materials synthesis[J]. Lab Chip, (2006), 6(12): 1487-1503

[11] Utada A S, Fernandez-Nieves A, Stone H A, Weitz D A. Dripping to jetting transitions in coflowion liquid streams[J]. Phys. Rev. Lett., (2007), 99: 0945029

[12] Tostado C P, Xu J H, Luo G S. The effects of hydrophilic surfactant concentration and flow ratio on dynamic wetting in a T-junction microfluidic device[J]. Chem. Eng. J., (2011), 171(3): 1340-1347

[13] Piotr G, Michael J F, Howard A S, George M W. Formation of droplets and bubbles in a microfluidic T-junction—scaling and mechanism of break-up[J]. Lab Chip, (2006), 6, 437-446

Advanced Materials Research Vols. 989-994 (2014) pp 3359-3362
© (2014) Trans Tech Publications, Switzerland
doi:10.4028/www.scientific.net/AMR.989-994.3359

Research to the Model Design of Real Platform Based on the Simulating Network

LIU Guanqun[1, a]

[1]HuNan Radio&TV University, Changsha 410004,China

[a]LIUGuanqun05@yeah.net

Key words: Networked control systems; simulation; MATLAB; Winsock; networked control systems;

Abstract. One of the research works of network control systems is the effect of network upon control systems. A simulation platform of networked control systems is designed for this purpose. Matlab is used to build models of real systems. Communication between controller and process is fulfilled with Winsock. The simulation platform supports many control algorithms and gives good environment for the analysis and gives good environment for the analysis and design of networked control systems.

1. Introduction

With the development of society and the interesting competition, better result of control for process industry are required, including high profit, low cost, rapid feedback and so on. Industrial enterprises are required to apply more advanced control. It's significant to affirm the security and profit of advanced control. [3]Aim at the request of process industry, this paper put forward building an experimental platform for advanced control based on simulation training system. In order to affirm the security of advanced control and lower expenses of research, the experiment control should be done on the experimental platform before practical application. Thus it can accelerate the transformation of advanced control from theory to application. this paper gives an integrative introduction of process control, including the mission, request, development, actuality and the trend of process control, then it explains the necessity and feasibility of building the experimental platform for advanced control.

In the distributed control system, if the control loop sensor, actuator, and the controller are connected through a communication network, and control the controlled variable and the control variables in the system by the digital form is transmitted in the network, this system call control system for the network (NCS, networked control system). [1] Its typical structure is showed in figure 1. Because the control system is the exchange of information through the communication network, which can reduce the number of system connection, enhances the reliability and scalability of the system. With the falling price of related products in NCS network, compared with the traditional DCS, greatly reduces the cost of system. But on the other hand, because the network is introduced into the control loop, will inevitably increase the complexity of the system, most notably in real-time situations, the benefits of reducing the network control system simulation platform NCSS. [5] The structure highlights the actual network for control system analysis and design, and it is very helpful to NCS. On this basis, using some simple objects (such as motor) instead of simulation object, it can constitute a network control system.

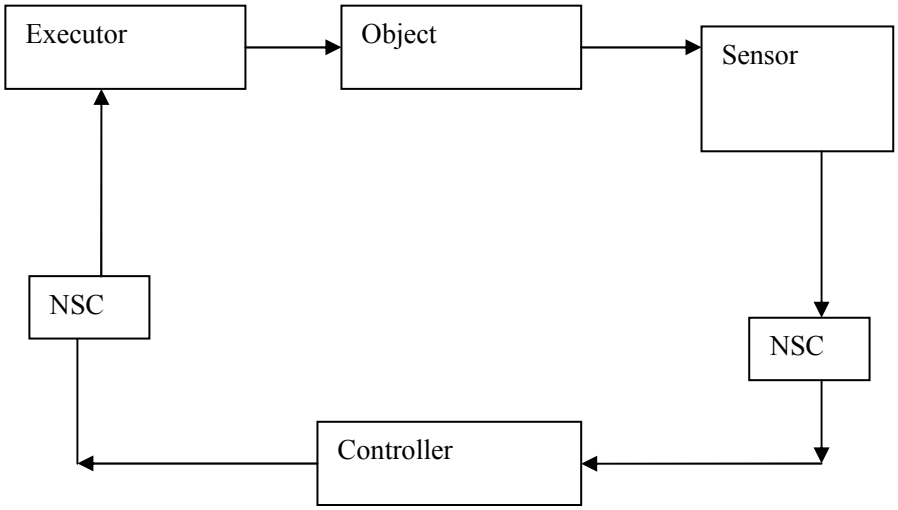

Figure 1 Network control system structure diagram [4]

Network control system simulation platform based on NCSS TCP/IP protocol, which can realize the software simulation of physical network all support TCP/IP protocol, analysis and design, and can directly use the Matlab and Simulink environment for network control system. By using the DSP control card, can also realize the remote control of the servo motor.

2. Scheme

Network with star structure, with the Cisco3550 switch as the central switchboard, using optical fiber jumper and Cisco2950G switch is connected with a uplink port, 100m extraoral even a server, the server through a broadband connection. Cisco 2950 switch and 3550 fast port connected, but also even under a TPLINK hub. As the PC network nodes can be connected to any port switches and hubs. PC machine is equipped with PCI-7841CAN bus card, you can use the CAN bus and F2407A DSP control card communication, and then realize control motor and stepper motor function. As shown in figure 2. [2]

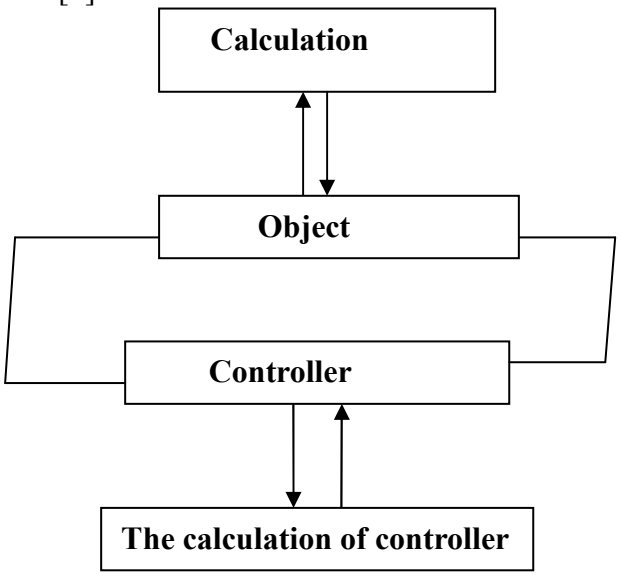

Figure 2 Network control system hardware structure

3. Network control system simulation platform

Based on the characteristics of NCS, we can study network combined with the simulation software of NCS, using PC as the network nodes, the simulation object and using software control method, simulation in the real network.

4. To construct the simulation platform

As the simulation software is currently the most popular, MATLAB plays an important role in control system analysis and design. Building on the foundation of MATLAB Simulink, can easily construct the control system model of complex; MATLAB toolbox and powerful computing ability, can achieve a variety of complex algorithms. But MATLAB itself does not provide communication interface, other methods must be used to achieve data exchange between nodes on the network. Windows socket (Winsock) defines the network programming interface of windows, and Microsoft MFC complex Winsock API package to the CAsynesocket class, which makes the preparation of web applications more easily. [1]Therefore, we can use the MATLAB structure of the actual object, used to simulate the actual object operation, and then through the MATLAB structure of the actual object, used to simulate the actual object, then the objects are transmitted to the Visual data by MATLAB C++ engine (VC) application program, VC program and then use Winsock to pass data to the remote controller operation, then use the same method to control the amount of applied to the object.

Simulation platform is constructed using this method, by using the powerful functions of MATLAB, the dynamic characteristics of the actual object to be as much as possible for real simulation, improved algorithm further research and provide a convenient. Simple controllers such as PID algorithm can be directly implemented in VC, the control complex algorithm can M files or Simulink model, called MATLAB therefore, software architecture is very flexible.[3]

5. Communication and simulation object and controller

The client or server communication mode is adopted between the object and the controller, the object for the server side, the controller as a client. In the control of the actual object, sensor, controller, actuator signal asynchronous, so CAsyncsocket needs to be placed in a non blocking mode, through the appropriate callback notification function call socket (such as OnReceive) to complete the asynchronous call. The Winsock API function with very rich, can also achieve some scheduling functions by calling the API function, such as Try-Once-Discard scheduling method. Communication between the object and the controller classes C pseudo code as shown in Table 1, where OnReceive the Winsock receives a message, and Ontimer timer message. [5]

Table 1 The controller classes C pseudo code

Controller	Objective

CreateListenSocket;
CreateCornerSocket;
 	
Do(ReceiveManage)
{
If(Message= =OnReceive)
{
ReceiveProcessOutput;
CallController;
SendProcessInput;
}
}while（End Program）
	CreateListenSocket;
	CreateCornerSocket;
	Start Timer;
	SendInitialState;
	Do(ReceiveManage)
	{
	If(Message= =OnReceive)
	{
	ReceiveProcessIntput;
	UpdateprocessInput;;
	SendProcessOutput;
	}

6. Conclusion

Simulation of the actual object and controller based on MATLAB, to realize the communication between the network through the VC and Winsock, which formed a network control system simulation platform NCSS. The simulation platform structure is flexible, can simulate the real object and calls the various control algorithms based on MATLAB and C in a variety of physical network environment on the basis, analysis and design is very beneficial to network control system.

7. Acknowledgements

The Research Is Supported By Education and Teaching Reform Project of Professional Colleges in Department of Education Hunan Province (ZJC2012029)

References

[1] W. Zhang, M.S.Branicky, S. M. Philips. Stability of Network Control Systems, IEEE Control Systems Megazine, 2011, 85-99.
[2] G.C.Walsh, H, Ye. Scheduling of Networked Control Systems, IEEE Control Systems Magazine, 2011, 21.
[3] J.W. Overstreet, An Internet-based Real-time Control Engineering Laboratory, IEEE Trans, On Communication, 2009, 19.
[4] MATLAB Manuals, The Math Works, Inc, 2012.
[5] Simulink Reference, The Math Works, Inc, 2012.

Advanced Materials Research Vols. 989-994 (2014) pp 3363-3366
© (2014) Trans Tech Publications, Switzerland
doi:10.4028/www.scientific.net/AMR.989-994.3363

Fatigue Loads Prediction Based on a Hybrid Road Approach

Yihe Mei[1, a], Qingsen Xie[1, a]

[1] School of Mechanical Engineering, Tianjin University, Tianjin 30072, China

[a]meiyihe1221@126.com

Keywords: Hybrid road approach, fatigue, road profile, TWR.

Abstract. Based on a hybrid road approach, a reliable process of fatigue load prediction is proposed. This approach known as Time Waveform Replication (TWR) relies on test data and multi-body model. The test data is used to back-calculate the hybrid road profile that will cause the same forces on the multi-body model. The road load is measured on the proving ground, and simulation of the multi-body model is ran by TWR to back-calculate the hybrid road profile. The simulation signals are verified by the experimental signals collected by wheel force transducers (WFT) and acceleration sensors.

Introduction

The durability of the automotive body is paid much more attention among the vehicle performance due to increasing demand of lightweight. In the early design stage, this is a key factor to reduce development time and cost. The fatigue loads that can accurately represent the field durability tests have an important role in the CAE analysis.

The hybrid approach known as TWR relies on test data and multi-body model [1]. The data collected on the proving ground is used to back-calculate the hybrid road profile (the equivalent spindle or vertical tire contact patch displacements) that will cause the same forces on the multi-body model. The approach is a Semi-Analytical method. It has several beneficial aspects with respect to the methods of Direct Measurement and Fully Analytical Road Load Data [2]. No dedicated prototype is needed, such as the tire model. Moreover it is well known that if the forces measured by WFT are applied directly to the unconstrained multi-body model, it will result in an un desired drift because of a mismatch in the mass and inertial properties between the real vehicle and its model.

In this study, a development process is proposed to accurately predict the fatigue loads for a commercial vehicle.

1. Full vehicle road test and virtual model

A vehicle test is conducted to collected load data on a proving ground. The wheel force transducers (WFT) are utilized to measure the wheel loading and acceleration sensors are also used to obtain the interesting signals. Fig. 1 shows the apparatus in the test. Signal processing should be done before applied to the virtual prototype, such as TimeEdit, Spike Filter, and Drift Correction.

Fig. 1 Wheel force transducer

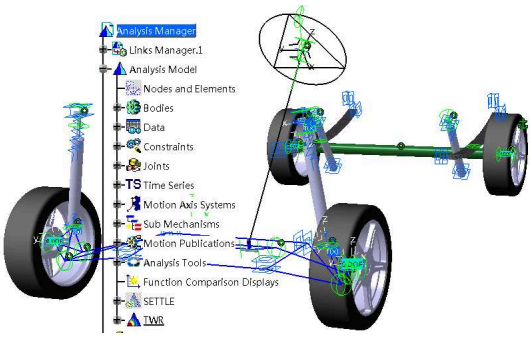

Fig. 2 LMS model for simulation

Considering hard point, mass parameters and nonlinear characteristic of bushing, the multi-body dynamics model of the vehicle is developed in the LMS environment (Fig. 2). The model mainly consists of a McPherson front suspension and a Hotchkiss LeafSpring rear suspension. In order to validate the model, a comparison of the axle weights between the model and real vehicle is conducted.

2. The hybrid road approach: Time Waveform Replication

The approach presented is similar to the set-up on a durability test rig. In fact, the hybrid road method is iterative back- calculate problem for a nonlinear system. TWR is the core technology that enables to compute a set of inputs (hybrid road profile) that will result in the response outputs at the relevant location on the model by multi-body simulation (MBS). A flowchart of the procedure with System Identification and Target Simulation [3] is provided in Fig. 3.

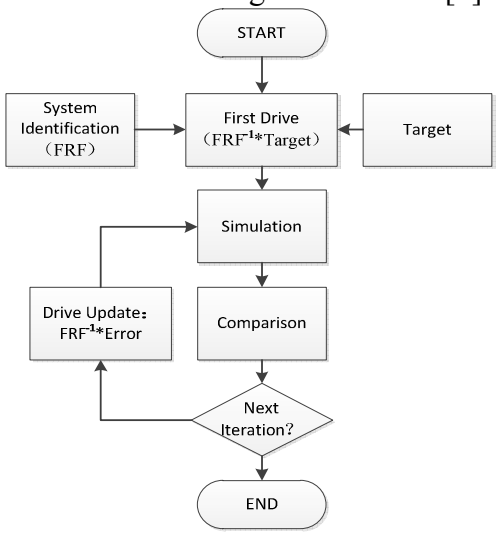

Fig. 3 Flowchart of the hybrid road method

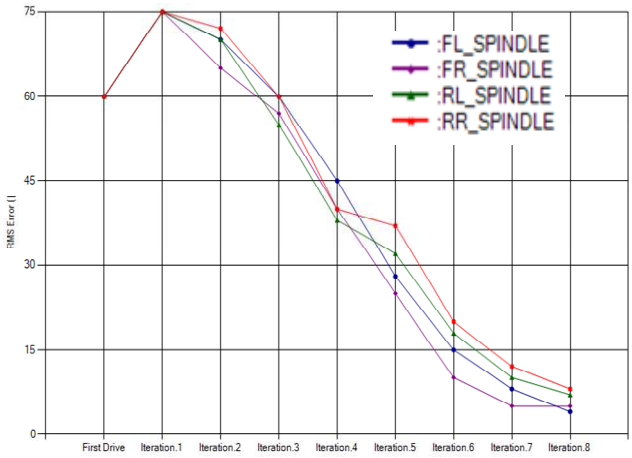

Fig. 4 Targets RMS

2.1 System Identification

The model is identified as a linear system by TWR. It's necessary to acquire a high quality Frequency Response Function (FRF) for the convergence of the result. Firstly, a reasonable White Pink Noise (WPN) is generated. The signal is defined by standard deviation, border frequency and power in the frequency domain. Secondly, the response output signal is obtained at the target location while the multi-body model is driven by WPN at the actuator location. The FRF is estimated from the time historied of the WPN and the responses according to equation [4] (1):

$$H(f)=\frac{G_{xy}(f)}{G_{xx}(f)} \tag{1}$$

Where $G_{xy}(f)$ is called cross-spectral density and $G_{xx}(f)$ is the input auto-spectrum.

2.2 Target Simulation

The target is a signal that has been measured in the road tests [5]. In general the real vehicle is nonlinear system due to the bushing and damper. And then the response from the System Identification differs from the test target. To cope with this problem, the Target Simulation is set up iteratively until the criterion is met. Firstly, the target signal multiplied by the inverse FRF is used to estimate the first drive signal followed equation (2).

$$u(t)=F^{-1}(d\bullet H(f)^{-1}\bullet g\bullet T(f)) \tag{2}$$

Where F is the Fourier transform, d is the Drive Gain, g is the Target Level, $T(f)$ is the target signal, $u(t)$ is the estimation of the first drive.

Secondly, the multi-body model is driven by the first drive to get the response signal, and then the error can be calculated between the response and the target.

$$e(f)=F(g\bullet T(t)-y(t)) \tag{3}$$

Where $T(t)$ is the target signal in time domain, $y(t)$ is the response signal and $e(f)$ is the error in frequency domain.

Lastly, error is used to update the drive signal until it is below an acceptable threshold followed equation (4).

$$u(t)_{i+1} = u(t)_i + F^{-1}(d \bullet H(f)^{-1} \bullet k \bullet e(f)) \tag{4}$$

Where the index i is the iteration, k is the error gain， this is a constant value between 0 and 1, like d and g， which can control the convergence[3].

Some indexes that we pay more attention are calculated to evaluate the quality of the every iteration. In particular the time histories/PSDs of the responses and the targets can be overlapped, and the RMS of the error for each channel is evaluated according to equation (5) [6]. Generally the iteration can be accepted while ε <10%.

$$\varepsilon = \frac{RMS(e(t))}{RMS(T(t))} \tag{5}$$

2.3 Application

The fatigue loads prediction process has been carried on a light vehicle. The spindle vertical accelerations are regarded as the target signal that we want to reproduce and that has been measured experimentally. Also, the WFT vertical forces and the vertical accelerations at the body interface are the monitors. Take Belgian road as example, we can get the results after several iterations have been completed. Fig. 4 is the targets RMS at the every iteration.

At the last iteration, we can obtain the comparison between the experimental signals and the responses in time or frequency domain, as shown in Fig. 5, Fig. 6 and Fig. 7.

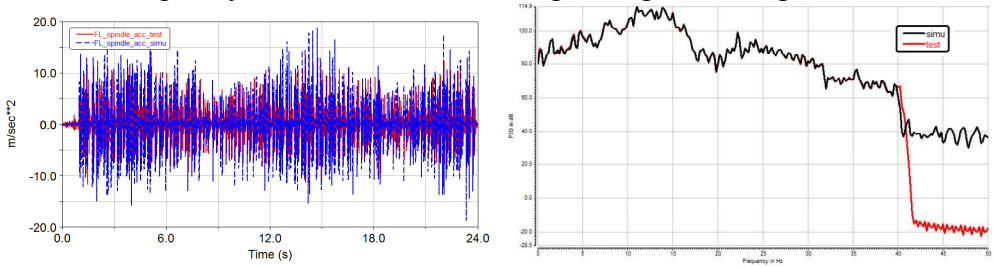

a) time domain b)frequency domain

Fig. 5 Comparison of vertical acceleration at front spindle

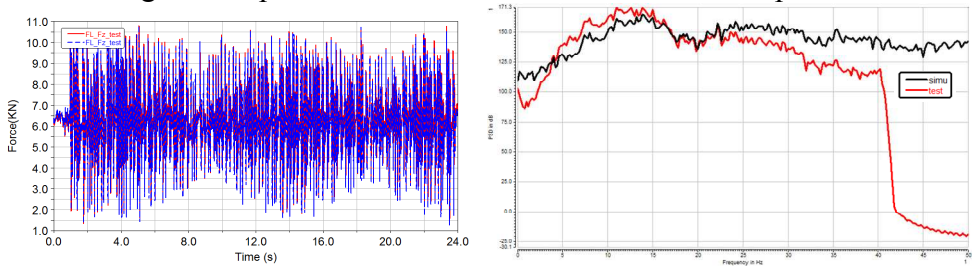

a) time domain b)frequency domain

Fig. 6 Comparison of vertical force at front spindle

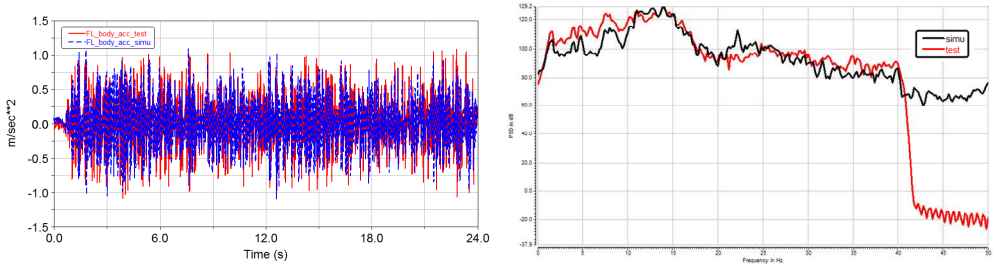

a) time domain b)frequency domain

Fig. 7 Comparison of vertical acceleration at body interface point

As shown in the above figures, the RMS value is acceptable. The response signals is in consistent with the experimental signals both in time and frequency domain. In particular, the vertical forces at

the spindle that is the responses of the model at the last iteration is same as the signals measured from the WFT. As a result, the experimental signals are replicated in high quality, which ensure the loads prediction accuracy.

The hybrid road profiles back-calculated at the last iteration, also called the last drive signals, is used to drive the model to predict the fatigue loads at the interface points. The vertical load spectrums at some interface points are shown in Fig. 8.

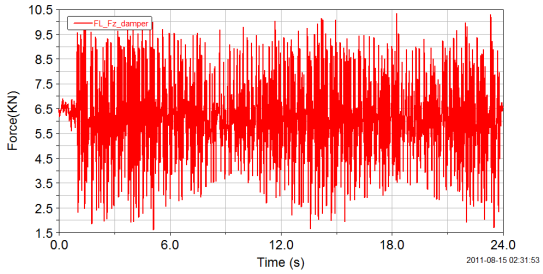

a) left-front damper point

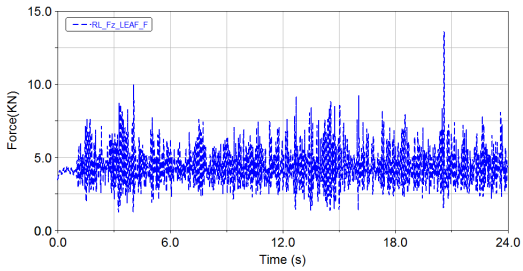

b) leafspring front point

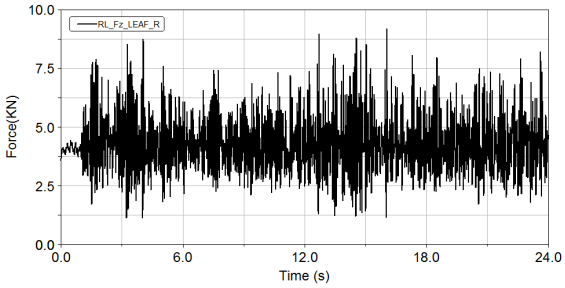

c) leafspring rear point

Fig. 8 Vertical force signals

Summary

A procedure for fatigue loads prediction has been implemented successfully. The road test data on the proving ground multiplied by the MBS is used to back-calculate the hybrid road profile through the proposed method. The hybrid profile applied on the model can replicate the experiment targets accurately, which is validated by the comparison between the response and the target. More, the hybrid road profile that can transfer to a new vehicle for its invariability is applied to the multi-body model to obtain the body interface load.

References

[1] A. Toso, Integration of time waveform replication process in a multi-body software for reverse load identification, J. Proceedings of the ASME Design Engineering Technical Conference. 8(2011)903-909.

[2] J.M. da Cruz, A semi-analytical method to generate load cases for CAE durability using virtual vehicle prototypes, J. SAE. 2003-01-3667.

[3] M. Backer, The hybrid road approach for durability loads prediction J. SAE. 2005-01-0628.

[4] S. Ryu, A study on obtaining excitation load of virtual test lab using virtual iteration method. J. SAE. 2010-01-0011.

[5] Z.X. Hong, Road simulation test of DCT key parts based on RPC. J. China Mechanical Engineering. 11(2013).

[6] R. Moller, Component load determination for a case based fatigue life prediction of a new bus type. J. Fraunhofer Publica MP Materials Testing. 51(2009)309-316.

Advanced Materials Research Vols. 989-994 (2014) pp 3367-3370
© (2014) Trans Tech Publications, Switzerland
doi:10.4028/www.scientific.net/AMR.989-994.3367

Assessing the Harmonic Emission Level Based on Partial Least-squares Regression with Data Envelopment Analysis

Xiang Li[1,a], Minyou Chen[1,b] and Yongwei Zheng[2,c]

[1]State Key Laboratory of Power Transmission Equipment & System Security and New Technology,Chongqing University, Chongqing, China

[2]Neijiang Electric Power Bureau of Sichuan Electric Power Corporation,Neijiang, Sichuan Province,China

[a]liandheqc@163.com, [b]mchencqu@126.com, [c]aoyun200888pm8@126.com

Keywords: Data envelopment analysis; Partial least-squares regression; Outliers; Utility harmonic impedance; harmonic emission level

Abstract. A novel method is used for assessing the harmonic emission level, which is based on the partial least-squares(PLS) regression with data envelopment analysis(DEA). Based on measuring the harmonic voltage and current at the point of common coupling(PCC) and removing the inefficiency data with DEA, regression coefficients are worked out through partial least-squares algorithm. Consequently the harmonic emission level of customer is calculated.The proposed approach removes the effect of outlying data points and gets accurate estimation results. The simulation results prove that the proposed method is more effective than PLS.

Introduction

In recent years harmonic problems in power systems have been considerable increasing due to the widespread use of power electronic loads. In order to ensure good power quality, incentive-based schemes[1] were proposed to encourage the utility and the customer side to retain harmonic distortion between the limits. And the scheme must be based on determining the contribution of both sides to harmonic distortion accurately and effectively.

Various techniques have already been presented to quantify customer and utility share of harmonics at PCC. According to the IEC 61000-3-6 Technical Report, the existing approaches are mostly based on calculation of the utility harmonic impedance including invasive methods and non-invasive methods. The invasive methods[2] accurately estimate utilities and customers parameters by injecting the harmonic (or interharmonic) current to utilities or switching on (or off) any loads. These methods may be harmful to utilities. The non-invasive methods compute the utility harmonic impedance by measuring harmonic voltage and current at PCC, which mainly include the utility harmonic impedance linear regression method[3,4,5] and the fluctuation method[6]. The fluctuation method may induce big errors for evaluation results because of the harmonic parameters variation of the utility side and measurement noise. The latest linear regression method-PLS regression can model to obtain accurate results under the condition of independent variables with serious correlation.

However, the modeling data may contain some outliers in practical project. Although PLS regression has high estimation precision, the estimated results are severely affected by the presence of outliers. PLS with DEA[7] is proposed to overcome the defect. The simulation results prove that PLS with DEA is accurate and has engineering application value.

DEA model and PLS with DEA

Assume that there are n decision making units(*DMUs*)—DMU_1, DMU_2…DUM_n, each *DMU* has m types of inputs and s types of outputs

Assume $x_j=(x_{1j}, x_{2j},\ldots, x_{mj})^T$, $y_j=(y_{1j}, y_{2j}, \ldots, y_{sj})^T$, x_{ij}=the amount of the ith input to DMU_{-j}, y_{rj}=the amount of the rth output of DMU_{-j}, for $j=1, 2,\ldots,n$, $i=1, 2,\ldots, m$, and $r=1, 2,\ldots,s$. For convenience,

denote the inputs and outputs of DMU_{j0} by $x_0=x_{j0}$, $y_0=y_{j0}$, respectively. the DEA model(C^2R model) for evaluating DMU_{j0} is given by

$$\begin{cases} \max \dfrac{u^T y_0}{v^T x_0}, \\ \dfrac{u^T y_j}{v^T x_j} \le 1, \quad j = 1, 2, \cdots, \quad n, \\ v \ge 0, u \ge 0, \quad v \ne 0, u \ne 0. \end{cases} \tag{1}$$

In this model, $v=(v_1, v_2,\ldots, v_m)^T$, $u=(u_1, u_2,\ldots, u_s)^T$ are the weighting parameters for m inputs and s outputs respectively. Using Chames-Cooper transformation, the fractional programming is transferred into a linear programming problem. Let $t = \dfrac{1}{v^T x_0}, \omega = tu, \mu = tv.$ The corresponding linear rogramming problem of C^2R model and its dual programming are

$$\left(P_{C^2R}\right)\begin{cases} \max \mu^T y_0 = h_0, \\ \omega^T x_j - \mu^T y_j \ge 0, j = 1,2,...,n, \\ \omega^T x_0 = 1, \\ \omega \ge 0, \mu \ge 0. \end{cases} \tag{2}$$

$$\left(D_{C^2R}\right)\begin{cases} \min \theta. \\ \sum_{j=1}^{n} x_j \lambda_j \le \theta x_0, \\ \sum_{j=1}^{n} x_j \lambda_j \ge y_0, \\ \lambda_j \ge 0, j = 1,2,...,n. \end{cases} \tag{3}$$

Definition 1. If $\left(P_{C^2R}\right)$ has optimal objective value $h^0=1$, then DMU_{j0} is called weak DEA efficient h^0 is called efficiency index.

Definition 2. If $\left(P_{C^2R}\right)$ has an optimal solution $\left(\omega^0, \mu^0\right)$ such that $\omega^0>0$, $\mu^0>0$ and $\mu^0 y_0 = 1$, then DMU_{j0} is called DEA efficient.

The optimized PLS with DEA can detect the disturbed data and obtain accurate estimation results with right model. Analysis and modeling steps are as follows:

1) According to the theory of DEA and the C^2R model, it is convenient to evaluate the measured harmonic voltage and current information and remove the inefficiency data. Regression coefficients are worked out through PLS algorithm with the remained data.

2) Extract principal component t_1, $t_2,\ldots,t_r$ on the basis of independent and dependent variable matrix E_0 and F_0(centered and normalize). Determine the number of principal components with cross validation analysis.

3) Obtain the regression equation. According to Eq. (4) and the relationship between the principal component and independent variable, the regression equation of y and x are calculated.

$$\begin{cases} E_0 = t_1 \alpha_1^T + \cdots + t_r \alpha_r^T + E_r \\ F_0 = t_1 \beta_1^T + \cdots t_r \beta_r^T + F_r. \end{cases} \tag{4}$$

Harmonic Source detection Principle

In the IEC Techical Report 61000-3-6, the harmonic emission level is defined as the magnitude of the harmonic voltage vector at each harmonic frequency, which is caused by the considered installation at the point of evaluation.

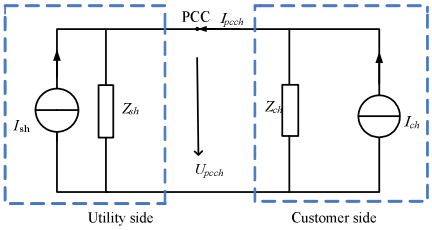

Fig.1 Harmonic source detection model

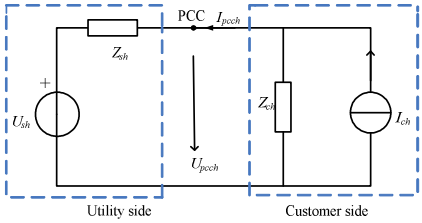

Fig.2 Thevenin-Norton model

In Fig.1, the disturbance sources are the customer harmonic source I_{ch} and the utility harmonic source I_{sh}; Z_{ch} and Z_{sh} are the harmonic impedances of the respective systems. The current phasor I_{pcch} and voltage phasor U_{pcch} are measured at PCC. According to Fig.1, Eq.5 and Eq.6 are obtained, where $U_{pcch\text{-}pre}$ and $U_{pcch\text{-}post}$ present the harmonic voltage at PCC before and after the customer is connected to the network.

$$U_{pcch\text{-}pre} = I_{sh} Z_{sh} \tag{5}$$

$$U_{pcch\text{-}post} = I_{sh} Z_{sh} + I_{pcch} Z_{sh} \tag{6}$$

The custom harmonic emission level E_{ch} can be calculated by subtracting Eq.5 from Eq.6.

$$E_{ch} = I_{pcch} Z_{sh} \tag{7}$$

According to Eq.7, system harmonic impedance calculation is the key to the harmonic emission responsibilities of utility and customer. PLS regression with DEA is presented to estimate the system harmonic impedance in this paper. Thevenin-Norton model is presented in Fig.2 to establish the regression model and Eq.8 and Eq.9 are obtained.

$$U_{shx} = U_{pccx} - I_{pccx} Z_{shx} + I_{pccy} Z_{shy} \tag{8}$$

$$U_{shy} = U_{pccy} - I_{pccx} Z_{shy} - I_{pccy} Z_{shx} \tag{9}$$

Regression coefficients U_{shx}, U_{shy}, Z_{shx}, Z_{shy} are worked out through PLS regression with DEA. Then the customer harmonic emission levels can be obtained by Eq.7.

Computer Simulation

The computer simulation based on the harmonic source detection model evaluates the *h*th harmonic voltage emission level using the software Matlab/Simulink, where $\dot{U}_{sh} = 50\angle 51^\circ$ V, $\dot{I}_{ch} = 6.36\angle 45^\circ$ A, the mean value of Z_{sh} and Z_{ch} are 15+j30 Ω and 25+j300 Ω respectively.

The harmonic voltage and current data measured at PCC are shown in Fig.3, which has 500 sample points.

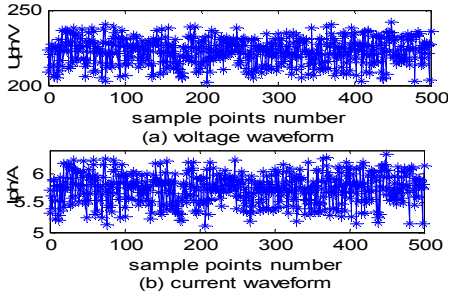

Fig.3 Magnitude waveforms of *h*-th current at PCC

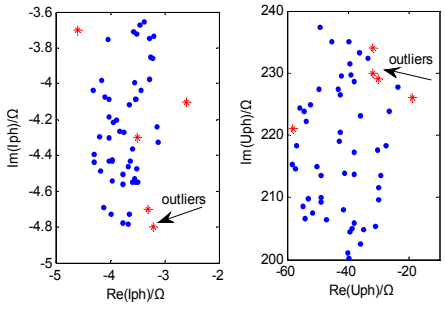

Fig.4 50 sample points of voltage and current at PCC and five outliers

The results of the Z_{sh} are estimated in three different cases(50 sample points as a subinterval). In case 1, the estimation results are computed based on PLS regression. In case 2 and 3, five outliers are

added in every 50 sample voltage and current points artificially. As shown in Fig.4, it is difficult to remove the outliers directly. The results of the Z_{sh} are estimated based on PLS and PLS with DEA, respectively. The results in three cases are shown in Table 1.

Tab.1 Comparison of errors of Z_{sh} in three cases

	Reference Value	Case 1	Case 2	Case 3
Error of Z_{shx}/%	15	0.847	19.98	1.133
Error of Z_{shy}/%	30	0.458	10.8	1.177

The relative errors of Z_{shx} and Z_{shy} estimated in case1,case2 and case 3 are shown in Table 1. From Table 1, we can see the estimation errors in case 2 are about ten times in case 1 and case 3. Estimation errors in case 1 and case 3 are both small. In comparison with the errors of the Z_{sh}, it demonstrates that PLS with DEA can get more precise results than PLS when modeling data contain outliers.

According to Eq.7, the customer harmonic emission level is 193.24V, about 87.01% of the harmonic voltage at PCC. The assessment result agreed in the theoretical calculation result indicates that the proposed method is valid.

Conclusion

This paper presents a new approach to evaluate the harmonic emission level of the utility and customer side, which is based on partial least-squares regression with data envelopment analysis. Due to the power system fluctuation or measurement error, the modeling data may contain some outliers. And PLS regression is very sensitive to abnormal data. This method retains the advantages of PLS and avoids the effect of erroneous data. The laboratory results indicate that the proposed method is effective and accurate.

References

[1] Tomaž Pfajfar, Boštjan Blažič, Igor Papič. *Harmonic Contributions Evalution With the Harmonic current vector method*. IEEE Transactions on Power Delivery. 2008; 23(1):425-433

[2]Xiuling Liu, Hongrui Wang. *Measurement and Correction of Network Harmonic Impedances*. Proceedings of the CSU-EPSA. 2007; 19(2):55-59

[3] Wei Zhang, Honggeng Yang. *A Method for Assessing Harmonic Emission Level Based on Binary Linear Regression*. Proceedings of the CSEE. 2004; 24(6):50–54

[4] Xu Yonghai, Huang Shun, Liu Yingying. *Partial Least-Squares Regression based harmonic emission level assessing at the point of common coupling*. International Conference on Power System Technology. Chongqing. 2006; 1-5

[5] LI Li, MA Hongzhong, JIANG Ning, WANG Chunning, LI Jun. *Assessing harmonic impedance and the harmonic emission level based on improved partial least-squares regression method*. Power System Protection and Control. 2011;39(1):92-95

[6]Yang. H, P. Pirotte, A. Robert. *Harmonic Emission Levels of Industrial Loads Statistical Assessment*, CIGRE 1996; 36-306

[7] Wei Quanling. *Data Envolepment Anlysis*, Beijing, Science Press,2003; 1-317

Advanced Materials Research Vols. 989-994 (2014) pp 3371-3374
© (2014) Trans Tech Publications, Switzerland
doi:10.4028/www.scientific.net/AMR.989-994.3371

Software design of micromouse dash motion

Zhang Haoming[1, a], PEH lian Soon[2,b], Wang Yinghai [3,c]

[1] Department of Electrical and Information Engineering, Tongling University, Anhui Province, China

[2]SHINING SUNSHINES GLOBAL PTE LTD, Singapore

[3] School of Electrical and Information Engineering, SIPIVT, Jiangsu Province, China

[a]zhm20060616@163.com, [b] bai_ls@yahoo.com, [c] yin287362@163.com

Keywords: Micromouse Maze dash motion command

Abstract. Micromouse is a small autonomous robot, which must navigate itself through an unknown maze from the start to the destination, the main challenge for micromouse is to solve the maze and find the optimum path. Detailed design of best-path finder was given. According to the different dash mode combination, dash path of micromouse in complex maze was analyzed. Motion command generator is developed to generate list of the motion commands in order to guide the robot dash from the start to its destination.

Introduction

For micromouse system, it is mainly controlled by a microcontroller (MCU) and a field-programmable gate array (FPGA). All of the calculations and decision makings will be executed by the MCU and the FPGA will handle the pulse-width modulation (PWM) and I/Os address mapping. Besides that, the system also has 6 pairs of infrared sensors for the obstacle detection[1-4].

Micromouse is able to navigate through an unknown maze in search for a faster path from the start to the finish point[5-8].The maze is configured by placing walls along the grid-points formed by multiples of 18cm square, the squares are arranged in a 16 x 16 row-column matrix, as shown in figure 1.

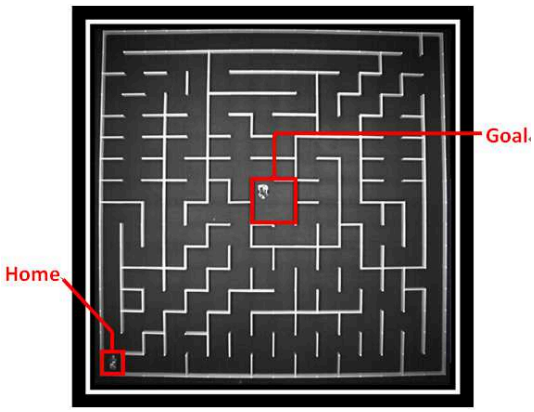

Fig.1 Mouse and maze

The main funciton for micromouse travelling in the maze under the help of sensors, then find the whole information of the maze, then the robot has to solve the maze and find the best path from home to desitnation, then micromouse dashes to destination according the best path in the shortest possible time.

Best-path finder (BPF)

After searching the maze, a best-path dinder is developed to determine the shortest path for the robot to run from the current position to the nearest goal.

Best-path finder will analysis the 4 cells of goal and mark the one with the smallest solving step number as the final destination for the future routing purpose. Then the best-path finder will start the checking from that goal back to the ‘current’ position. The finder will store the position of the cells in

the ‘best’ route into a special memory list. The finder will determine which the next suitable cell is by checking the solving step number in its surrounding cells. If there are few surrounding cells containing the same number, it will choose the cell in the same direction from the previous cell.

Fig.2 Maze solve

The graph shows that there are three surrounding cells containing the solving step number of 21, so the Best-Path finder will have to choose which one is the most suitable cell for it to form the most optimal route. Since the previous cell of 23 is on the ‘north’ side of the cell, so the finder should choose the cell of 21 on the ‘south’ side in order to form a straight path to save the travelling time as running a straight path will spend less time than making few turns.

Figure 3 shows the flowchart of best-path finder.

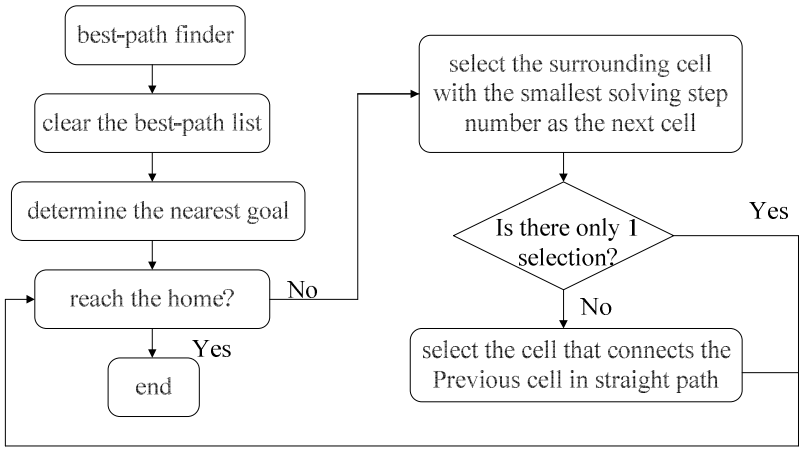

Fig.3 The flowchart of best-path finder

Dash mode

In general, micromouse dashes along the straight dash, or make a 90 degree left or right turn, but in special circumstances, the mouse will dash into below maze as shwon in , in order to save time, the best way is dahing along diagonal path, as shown in fiugue 4.

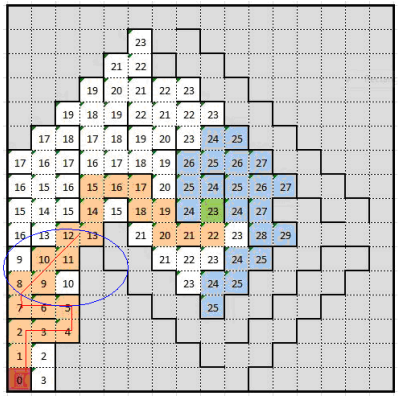

Fig.4 Maze for dash in diagonal

According to the different dash combination, dash mode of micromouse in complex maze as shown in figure 5.

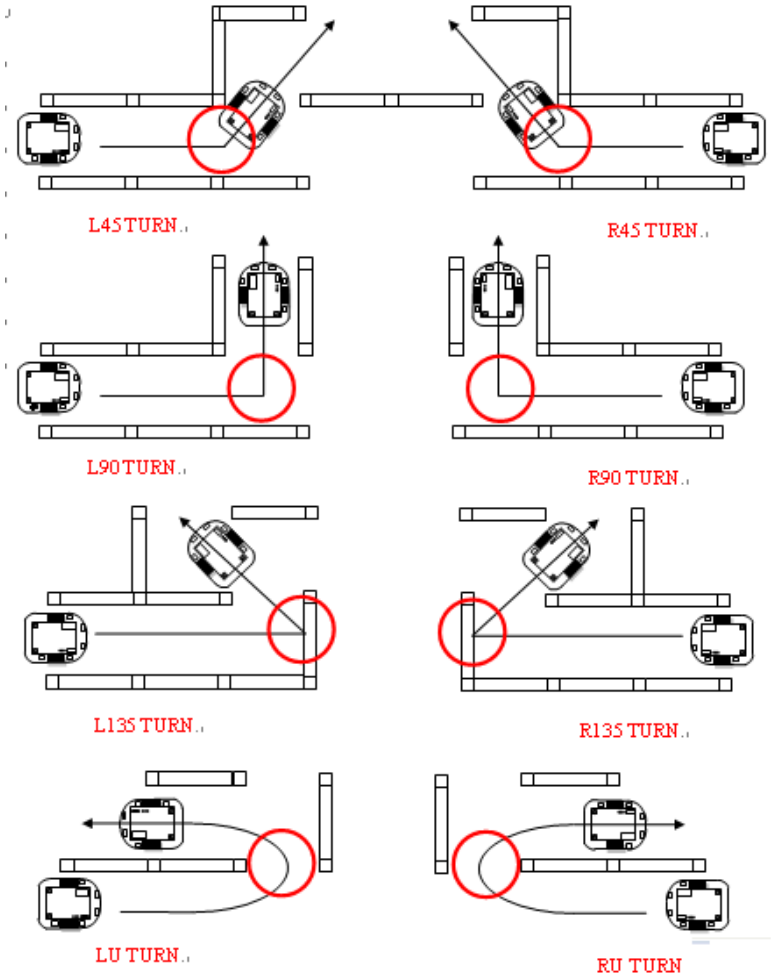

Fig.5 Normal dtraight-diagonal dash

Motion command generator (MCG)

After analysis the possible dash path of micromouse , a motion command generator is developed to generate another list of the motion commands in order to guide the robot dash from the start to its destination.

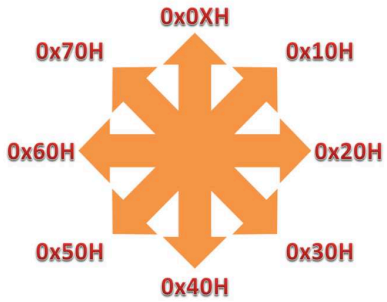

Fig.6 The Star chart of motion direction

The graph above shows the relation between robot's directions and motion commands. The robot will move forward or turn left or right according to the motion command. A motion command is an 8-bit data and can be represented as two digits in hexadecimal format which can be from 0x00 to 0xFF.

The first digit is used to represent the moving direction while the second digit represents the number of blocks that the robot is going to move for. So if the robot is going to move forward for X blocks, then the command will be 0X in hexadecimal format. If the command is 0x60H, then the robot will try to perform a left turn.

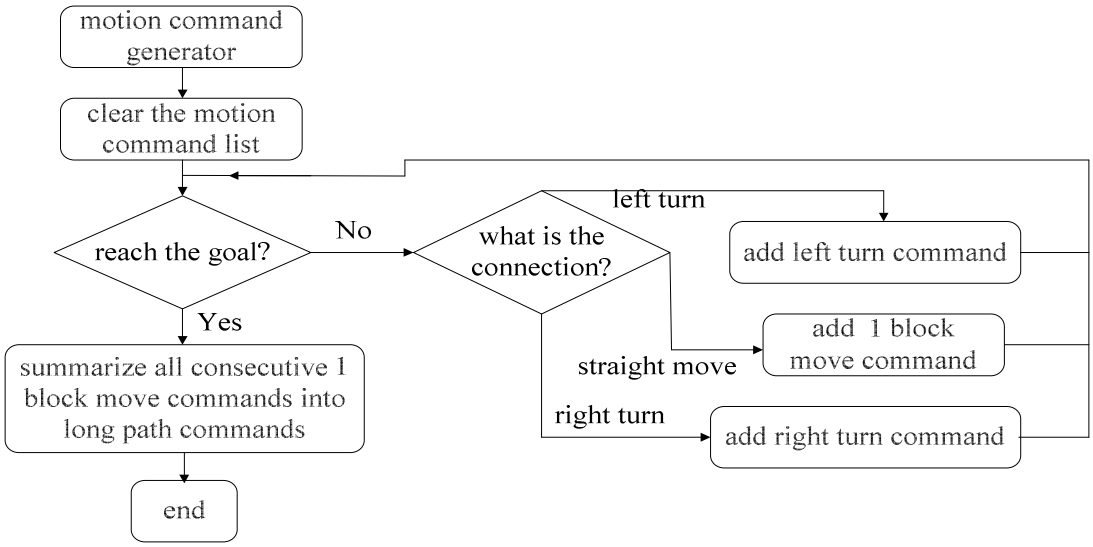

Fig.7 The flowchart of Motion Command Generator for dash

Summary

One of main challenges for micromouse is to solve the maze after searching and find the optimum path. Detailed design of best-path finder based on flood-fill was given. According to the different dash mode combination, dash path of micromouse in complex maze was analyzed. Motion command generator is developed to generate list of the motion commands.

Acknowledgement

It is a project supported by basic research programs of Suzhou science and Technology Department - industrial application part (SYG201327) and 2012 Innovation Project of JiangSu Province.

References

[1] Su,Juing-Huei; Lee, Chyi-Shyong; Huang, Hsin-Hsiung, etc. A micromouse kit for teaching autonomous mobile robots[J], International Journal of Electrical Engineering Education, 2011,Vol.48(2):188-201

[2] Mishra Swati, Bande Pankaj. Maze Solving Algorithms for Micro Mouse[C]. Proceedings of the 2008 IEEE International Conference on Signal Image Technology and Internet Based Systems.2008,11.

[3] Kiblcr S G,Ilauer A E, Giesscl D S, etc. IEEE Micromouse for mechatronics research and education[C],Mechalronics (1CM), 2011 IEEE International Conference: 887-892.

[4] Po-Jen Cheng,Chin-Hsing Cheng,Chun-Cheng Tung. Design of DC motor's torque control using DSP[J]. Journal of Information and Optimization Sciences,2009,Vol.30(6):1197-1207

[5] Zhang Haoming, PEH lian Soon,Wang Yinghai. Two axes micromouse PWM generator based on FPGA[J].Applied Mechanics and Materials Vols. 496-500:1674-1680.

[6] Zhang Haoming, PEH lian Soon,Wang Yinghai. Design of a Edubot--Micromouse based on MCU+FPGA[J].Applied Mechanics and Materials Vols. 496-500:1664-1669.

[7] Jiang Xiong,Ren Hua-long,Ma Zhong-li. Research on How ARM-based Micromouse Gets Out of Maze[J], Modern Electronics Technique , 2011(08):14-16.

[8] TONDR A D, HALL Drew. The inception of chedda: a detailed design and analysis of micromouse [D] . Las Vegas: University o f Nevada, 2004.

Advanced Materials Research Vols. 989-994 (2014) pp 3375-3378
© (2014) Trans Tech Publications, Switzerland
doi:10.4028/www.scientific.net/AMR.989-994.3375

Double DSP communication based on CAN Bus Interface

Hongde DENG [1, a], Zhian YAN [2, b]

[1,2]Science and Technology on UAV Laboratory, Northwestern Polytechnical University, Xi'an 710065, China

[a]email: denghongde@126.com, [b]email:zhian.yan@163.com

Keywords: DSP communication; CAN bus; double buffer

Abstract: In view of the problems on communication in double DSP systems, various communication methods are compared and advantages of CAN bus are also presented. This paper introduces hardware and software of communication using with CAN bus in DSP systems. The registers configuration of CAN is described in particular. Data are received by interrupt and stored double buffer. The scheme has been applied in a UAV flight control system which performs very

Introduction

Digital signal processor（DSP）plays an important role in industrial control because of its ample command systems, high-speed and high-precision computing ability, as well as its various peripherals. The C2000 serial DSPs of TI are widely used. With the increasing computing complexity and real time requirement, the single DSP can't provide the required peripheral interfaces and computing capacity, so multiple DSPs system is needed [1].

This scheme is designed to complete the communication between the double DPSs of a small UAV flight control system. In this system, one TMS320F28335(28335)DSP（DSP A）is in charge of attitude and navigation computations through collecting data from sensors including the angular rate gyroscopes, accelerometers, magnetometers and GPS; the other DSP（DSP B）is in charge of flight control and missions execution. These two DSPs should transfer 80 bytes to each other in 5ms, this requires the reliable and real time communication between these two DSPs.

1. DSP communication schemes compare

Generally, there are three interlink architectures among DSPs: parallel, serial and integrated operations. In parallel operation, CPU should support the parallel operation or public memory which is not included in C2000 serial DSPs [2]. In serial operation, the CPUs can communicate through DSP serial port, DMA channel, dual-port RAM, FIFO, or public memory. Using DSP serial port and DMA channel is convenient because they are integrated in DSP chip. But using dual-port RAM, FIFO or public memory is not so easy because they usually need to be expanded by operator and need extra hardware support.

The following serial peripherals can be used for DSP communication: SCI, SPI，I2C，CAN and McBSp. As TMS320F28335 for example, table 1 compared the performance among these peripherals, and shadow part s mean the highest performance.

The primary difficulties when using these peripherals: SPI interface could receive pseudo data; SCI data length is 8-bit, but DSP is a 16-bit system, so the high 8-bit data received are invalid. McBSP is the peripheral with highest speed, but the interfaces and software used are too complex. Through comparing, CAN module has the following advantages: 32 mailboxes of 32-bit data length for storing data; transferring data with strong anti-jamming capability and the biggest rate 1Mb/s only using 2 data wires. Most important, two CAN module interfaces can transmit or receive data simultaneously without considering the conflicts, and the program used is simple. So choosing CAN module is the most ideal communication scheme for small data exchange.

Table 1 Performance compare of peripherals

	SPI	SCI	I^2C	CAN	McBSP
Rate b/s	SYS[1]/4	SYS/16	400k	1M	>50M
FIFO level	16	16	16	32 mail-boxes	16
Data length	16	8	16	32	32
Interface number	1	3	1	2	1
Wire number	4	3	2	2	6
Anti-jamming	medium	medium	medium	strong	medium
Complex degree	medium	medium	simple	simple	complex

Note: 1. SYS means the system low-speed peripheral clock frequency

2. Hardware design of CAN communication interface

The CAN controller integrated in TMS320F28335 is a 32-bit peripheral module. This module is compatible with CAN2.0B agreement and provides 32 message mailboxes of 8−byte data length, a 29−bit identifier, and several control bits. The module also has the following features: programmable wake-up on bus activity, automatic reply to a remote request message, automatic retransmission of a frame in case of loss or error and self-test functions [3] [4].

Although CAN controller is integrated in DSP, the serial communication signal of DSP is not compatible with the standard CAN bus agreement, and after testing, simply connecting the TX and RX between two DSP CAN modules is not working. The signal must be converted to the standard CAN bus data through driver chip, then the two CAN modules can communicate properly.

The hardware design of CAN communication interface is shown in figure 1 (at the end of this paper). In this design, the driver chip SN65HVD230 from TI company is used. In order to match bus impedance, the resistances of 120Ω （R1 and R4）are added to the both ends of bus to improve the anti-jamming and reliability of data communication.

Although the mailbox of DSP eCAN module can be configured as a receive or send mailbox, and using the advantage of two eCAN modules in each DSP, this scheme configures one eCAN module as the receive module responsible for receiving data only and the other as the send module responsible for sending data only. This design can guarantee reliability and real time performance of the flight control system as well as support follow-up big data transfer.

3.Software design of CAN communication interface

The software design includes four parts: initialization module, mailbox configuration module, transmitting data module and receiving data module. Only 32-bit accesses are allowed to the eCAN module registers and these registers must be configured through defining shadow registers. As the mailbox enable register for example, the shadow register must be defined first before enabling some mailbox. For example, we can set Struct ECAN_REGS ECanaShadow as following:

```
ECanaShadow.CANME.all=ECanaRegs.CANME.all;
  ECanaShadow.CANME.bit.ME0 = 1;//enable mailbox 0
ECanaRegs.CANME.all=ECanaShadow.CANME.all;
```

Only through the above method, can the values of bits in the ECanRegs be setted properly. To be simple, in the following text, this step is omitted in all eCAN register setting.

3.1 Initialization module

Initialization must be done before using CAN module, including setting bit timing configuration register and communication baud rate, resetting mailbox control register and state register. The initialization process is shown in figure 2.

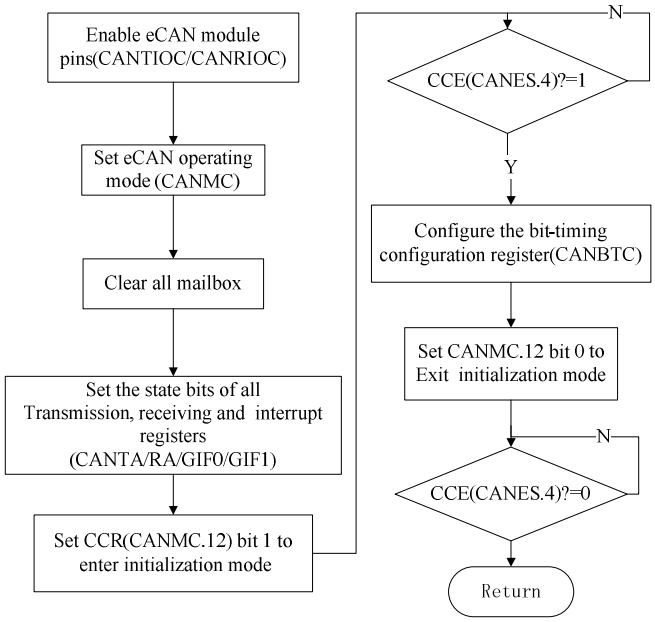

Figure 2 eCAN module initialization

Every step in the above process lists the name of register which should be configured. This process can refer to the TI document DSP2833x_ECan.c. This system sets CAN module operating in eCAN mode, mailboxes 16 to 31 can be used and the communication baud rate is 1Mbps.

3.2 Mailbox configuration module

This module is used primarily to set the mailbox function (transmitting or receiving), mailbox identifier and interrupts. Mailbox function is defined by the register CANMD: the value 0 means that this mailbox is defined as a transmit mailbox, the value 1 as a receive mailbox. For example, this setting CANMD.bit.MD0=0 means that mailbox 0 is defined as a transmit mailbox. 40 bytes should be transferred in 5 ms and each mailbox can store 4 bytes, so 10 mailboxes are needed for each transmitting and receiving module.

We configure the mailboxes eCANA0~9 as transmitting mailboxes and eCANB0~9 as receiving mailboxes. Registers MSGID and MSGCTRL determine the mailbox parameters [5]. To insure the real time performance in receiving data, the receive mailbox receives data in interrupt mode.

3.3 Receiving data module

The data is received in interrupt mode. In order to generate interrupt again, ISR needs to save the data received and clear the interrupt flag bit. This scheme uses double-buffer to make sure the data is received and saved correctly. The two buffers are uint64 cell array with 20 bytes data length. Each buffer can store 40 bytes data from mailboxes 0~9. The cycle of the interrupt received is determined by the transmitting cycle, and the cycle 5ms is defined in this design.

3.4 Transmitting data module

To start a transmission is simple. Just write the message data into the mailbox data field MDH and MDL, then set the corresponding flag in the transmit request register to start the transmission of the message. If the message is sent successfully, transmit-acknowledge flag of the corresponding

mailbox is set to 1. Generally, before next step, we should wait transmit-acknowledge flag is set. But if the data can't be transmitted successfully, the program will fall into infinite loop. To avoid this, we wait a little while after transmit-acknowledge flag is set. This design waits for 640us after transmitting 80 bytes with baud rate 1Mbps.

4. Conclusion

The scheme has been applied in a UAV double DSP flight control system for exchanging data and commands. After testing, this system performs very well. The CAN bus communication method between two DSPs introduced in this paper can also be used for communication between DSP and other system.

References

[1] Liu Wei, LEI Yingjie, Ni Ming, Chai Xiaoli. Application of Software FIFO in Communication of Multi-DSP [J], Computer Engineering, 2005, No.16, 228-230

[2] ZHANG Wei, LIU Wen, LIU Zhao-hui. HighSpeed Communication of Dual DSP Based on McBSP, Micro Computer Information[J], 2008, No. 7-2, 192-193

[3] TMS320F28332/4/5, 28232/4/5, Data Manual, Texas Instruments Co., Ltd , 2010

[4] TMS320x28xx, 28xxx Enhanced Controller Area Network (eCAN) Reference Guide (Rev.E), Texas Instruments Co., Ltd, 2006

[5] CPU and peripherals of S320C28x serial DSP, Texas Instruments Incorporated, 2005

Advanced Materials Research Vols. 989-994 (2014) pp 3379-3381
© (2014) Trans Tech Publications, Switzerland
doi:10.4028/www.scientific.net/AMR.989-994.3379

Aerospace Test and Launch Process Dynamic Management System Based on the Network Diagram Method

WANG YAN[1,a], WANG HUA[2], and LI YAN[2]

[1]Company of Postgraduate Management, the Academy of Equipment, Beijing 101416, China

[2]Department of Space Equipment, the Academy of Equipment, Beijing 101416, China

[a]08wy@163.com

Keywords: Aerospace Test and Launch Process; Dynamic Management System; Network Di agram Method; Optimization.

Abstract. To manage and optimize aerospace test and launch process in real time and dynamically, the aerospace test and launch process dynamic management system based on network diagram method has been designed in this paper. Firstly, we summarize the research status of test process optimization in references to find the shortages in optimization and management. Secondly, we design the system from three aspects including the process design, data management and indexes evaluation, respectively. Subsequently, the software is introduced briefly. Finally, the deficiencies of the system and improvement goal are put forwarded.

0 Introduction

In order to guarantee the normal function, the good performance, safety, and on-time launch, comprehensive and integrated test and evaluation of the rockets before launch is necessary. At present, the optimization of the test process mainly finished by the department of aerospace industry and engineering, technical personnel in launching site. Because of their long-term engineering practice accumulated, they concentrate on quality assurance and technical feasibility to simplify test project or compress test process. In addition, the systemic theory and method has not been formed.

Therefore, increasing the test's effectiveness, optimizing test process fundamentally, and shortening the test time really effectively can adapt China's space launch to distance test and control, and high density launch mission.

1 Demand Analysis

1.1 Research Status of Test Process Optimization and the Enlightenment

Aiming at the insufficiencies of test process, there are a lot of references optimize it. For instance, reference [2] analyzed that the constraints to shorten the test time are the reliability of the components, single, system and the rockets' bus structure problems. Reference [3] presents two kinds of ideas of spacecraft test process reengineering. The first one is the optimization and improvement for the current model and the second one is the process reengineering pattern. Reference [4] is in the light of the problem of launch site test process reengineering, some basic conceptions were put forwarded. Reference [5] optimizes the test process using the process optimization matrix.

In space launch task, it is necessary to establish task flow chart. While using computer software system instead of artificial hand is a wise choice. Not only because it can save a lot of manpower, material and financial resources, but also to facilitate partial adjustment for flow chart in real-time without affecting the whole process, so as to achieve the purpose of optimizing the process. Therefore, it is necessary to design and develop a software system which is dedicated to draw flow chart of aerospace test and launch. This paper tries to build a software system, manage the establishment and optimization of process in a real-time dynamic way.

1.2 Research Ideas and Methods

This article plans to study from the following three aspects. First one is the design of the process. We choose network diagram method to design the test and launch process. Second one is the data management. We use SQL SERVER 2005 database system as data support. Besides, we use Microsoft Visual Studio as the programming environment to develop the software. The third one is the process index evaluation. There are many evaluation methods. Improved analytic hierarchy process which is the combination of qualitative and quantitative analysis is used to evaluate the process scheme.

2 Integrated Technical Program

2.1 System Functions and Composition

Aerospace Test and Launch Process Dynamic Management System can make optimization design for the different test and launch processes of the Aerospace task. Moreover, it can take effective management of each project node in the test launch processes. According to the input and constraints, use the process configuration and evaluation algorithms, it can make comprehensive evaluation of the implementation effect of the various stages of the mission. In this way it can provide related business personnel training support for the task processes design, optimization and dynamic configuration. The main functions are as follows.

Table 1 Functions of the Process Dynamic Management System

System functions	Details
1. Design and display of the Process	multiple process designs in once test mission, display each process, task node and the relationship of them graphically
2. Management of the task nodes	display and edit various input conditions and constraint information of each node, including task name, node name, key equipment information and ,etc.
3. Dynamic configuration of task nodes	dynamically configure the input and output parameters and constraints which can synchronized with the actual work tasks
4. Assess of the process and task node	Real-time assessment of the current task node is allowed in the task implementation process to provide guidance for the next phase of task orientation.
5. Data and Information Management	To store tasks, equipments, processes, task nodes, etc. Application software can read the previous task processes information and do graphical reduction

Aerospace Test and Launch Process Dynamic Management System is made of the following four parts:

(1) Application Files: HTCPM；

(2) Application Extension Files: KERNEL32.DLL, MFC42D.DLL, MFCO42D.DLL, MSVCRTD.DLL；

(3) Access Database File: HTCPMDB；

(4) Custom Document Library Files.

3 The System Software

To make the development of the Aerospace testing and launching Process Dynamic Management System(A), we first to consider about the implementation and integration of software functions, then optimize the interactive and practicality of the interface. We use Microsoft Visual Studio as the programming environment, and the SQL SERVER 2005 database system as data support. System software includes three modules, named Process Design and Configuration, Process Database Management and Evaluation of the Process indexes, respectively.

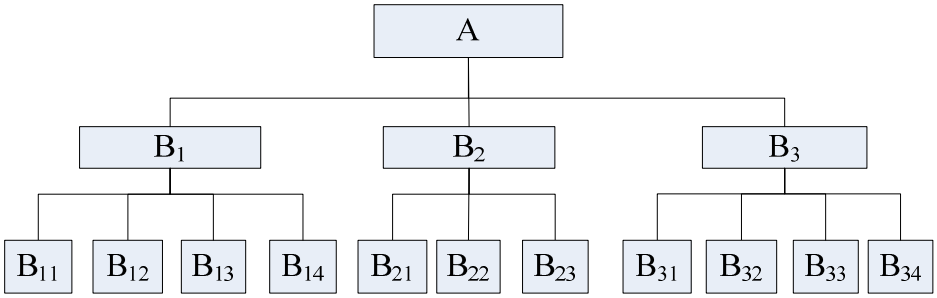

Figure 1 System Software Composition

Process Design and Configuration (B_1): Display and edit various input conditions and constraint information of each task node in the process, including the task model, the task name, job name, job content, time consumption, energy resource consumption, reliability, the device key information, the priority, importance, and operating direction and so on. Nodes can be combined edit to complete multiple process designs in once test mission. The multiple processes including four modules, which are the Flowchart Element Editing Module (B_{11}), the Process Document Management Module (B_{12}), the Process Parameter Calculation Module (B_{13}) and the Process Output Module (B_{14}), respectively.

Process Database Management (B_2): Relational database table format are included to store and manage tasks, equipment, project node and other information. Process file format is formulated and file storage of the process information is achieved. Reading the previous stored process files to restore files and graphical reduction is supported, which is ease of analysis, comparison and printing output. Good interactively method can be considered and utilized to graphically edit and display each process, task node and the relationship of them which help to the comparative analysis. Include the Process Import and Export Modules(B_{21}), the Process Query Module (B_{22}) and the Process Relations Display Module (B_{23}).

Evaluation of the Process Indexes (B_3): Main to complete the evaluation of the node or the whole process in one project, provide guidance for the next phase of task orientation. Four modules named the Evaluation Index Management Module (B_{31}), the Expert Information Management Module (B_{32}), the Assess Event Management Module (B_{33}) and the Assessment Calculation Module (B_{34}) are included.

4 Conclusion

Design of aerospace test and launch process dynamic management system not only improves the efficiency of the flow chart drawing and facilitate adjustment and improvement, but also provides important technical means for process optimization. However, the system we proposed still exist some shortcomings. In the future system operation interface can be enriched to make the operation easier. In addition, in the future real time optimization based on personnel, equipment, the weather element can be increased for key nodes, so that the optimization of the process is not only limited to the optimization based on time.

References

[1] Xia Kehan, Mou Jianhua, Bao Feihu, et al. Design and Implementation for Missile Testing Process Optimization System [J]. Missiles and Space Vehicles, 2012,(2):43-46.

[2] Cai Yuanwen, Wang Hua, Sang Aiqun, et al. Research on Rocket Test and Optimization Method[J]. Equipment command institute of technology.

[3] Zhu Liangping, Tao Huanmei, Huang Zhoulei. Idea for Spacecraft Test and Launch Process Reengineering[J]. Xichang Satellite Launch Center.

[4] Chang Jijun. Preliminary Studies for Spacecraft Test and Launch Process Reengineering[J]. China Academy of Space Technology Overall Department.

[5] Zhuang Ke, Chen Zibei. BPR Theory And Matrix Method to Optimize the Application of The Space Launch Process[J].Launching Site Experiment and Management. 2011,(4):20-22,33.

Advanced Materials Research Vols. 989-994 (2014) pp 3382-3385
© (2014) Trans Tech Publications, Switzerland
doi:10.4028/www.scientific.net/AMR.989-994.3382

Research to the Development of Network-anticipated Controlled System based on Arbitrary Bounded Packet Loss

LIU Guanqun[1, a]

[1]HuNan Radio&TV University, Changsha 410004,China

[a]LIUGuanqun05@yeah.net

Keywords: Networked Control Systems; Packet Loss；Linear Matrix; BP Neural Network

Abstract. In recent years, due to the rapid development of computer technology and the expanding of its controlling scale, people pay more and more attention to the study of network control system. Network control system is closed loop control system connecting the communication network connect sensor, controller, actuator etc. At the same time, the introduction of the communication network control system brings a lot of problems, such as data transmission delay, network packet loss and so on, which make the analysis of the network control system become very complicated. This paper analyzes background of the topic, significance and research status, and review the network control system.

1. Description of the network control system

Normally we does not consider network, thinking actuators, controlled object and sensors are together. The three objects can be seen as discrete time system. Between sensor and controller, the controller and actuators it is the network connection, which form a closed loop control. Sometimes in order to study it conveniently, we consider only one of the networks. [1]The traditional control problem considers system itself has a disturbance, parameter uncertainty and so on. After network's join the state can not reach to or can not completely reach to the controller. In the case of this kind of random, we have to study other control problem including the stability of the system and its performance. Network control system structure diagram is shown in figure 1.

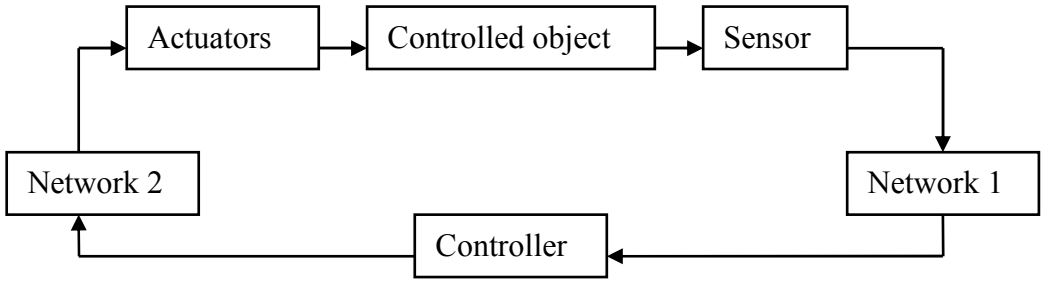

Fig1. The Configuration of the Networked Control System

1.1 Network structure

Topology structure of control network must be able to make each network node in networked control systems (such as sensors, controllers and actuators, etc.) easy to interconnect, and save connection as much as possible and easy to maintain. [2] This structure must be able to assign the system processing function and calculate load to as many smaller computational network unit as possible. In the central control system, once a single controller node fails, the system will be paralyzed; in contrast, network control system of the control network must be able to implement multiple distributed controls, the controller node so as to enhance the system robustness.

1.2 Network communication protocol

According to the different levels of network application, currently a variety of communication protocols has been put forward; these protocols are mostly follow seven layer open system interface of ISO standards issued by the OSI.

Considering the particularity of control network, the communication protocol used in the control network is not necessarily in accordance with the standard of the seven layer model.

1.3 Network performance

Performance indicators of a network system about evaluation of whether to meet the demand of real-time control mainly include: Access latency, Transmission Time, Response Time, Message Collision, Message Throughput, Packet Size, network utilization, and some other certain industry, etc. For control system, the ideal control network must satisfy at least the following two principles: bounded delay and guaranteed transmission. [3]That is to say, in the control of network information there have to achieve success in bounded time of transmission. Unsuccessful information transmission or too-long transmission delay may degrade the performance of the network control system, and even destroy its stability.

2. Packet loss characteristic of network control system

There are always many data transmits at the same time, it may lead to collision between different data transmission, or an individual node failure in competition, as a result, packet loss born. In order to avoid the happening of this kind of situation, a lot of network has set retransmission mechanism, but due to being influenced by time, retransmission may fail, resulting in the loss of packets. However, not network packet loss will cause the loss of system stability, instead as long as in a certain range, the system remains stable. Therefore, the effect of data packet loss on the stability of the system is still an issue.

2.1 Analysis of packet loss in NCS

In national communicative system, the packet loss mainly includes the passive and active packet loss. Active packet loss refers to the measures network control system take in order to achieve a certain purpose. [4] Passive packet loss is caused by data communication mechanism and network bandwidth restrictions. In this case, the packet loss is harmful for the performance of networked control systems.

At present, three methods are commonly used to describe the data packets lost. The first one is statistical method, as well as the probability distribution of the data packet; the second one is the total amount of packet loss, the last one is to see it as the connection channel. It will have a packet loss of replication as dynamic switch system.

2.2 Impact of packet loss on the stability of the system

Usually, in the process of study, we separately consider the network induced delay and packet loss. Due to the unreliability of the network transmission path, in the process of transmission, it may lead to transmission delay, even the packet loss.

An asynchronous dynamic system structure is shown in figure 2.

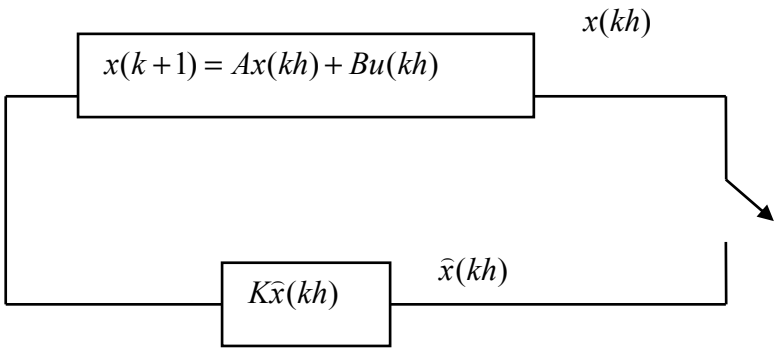

Fig.2 Structure of asynchronous dynamical system

A dynamic characteristic of system is as follows:

$$\begin{cases} S_1 = \hat{x}(kT) = x(kT) \\ S_2 = \hat{x}(kT) = x((k-1)T) \end{cases} \tag{1}$$

If the system's augmented matrix is $z(kT) = \left[x^T(kT), \hat{x}^T(kT)\right]^T$, then closed loop system of the network with the existence of packet loss can be expressed as the following type:

$$z((k+1)T) = A_i z(kT), i = 1,2 \tag{2}$$

When the switch is in position 1, $A_1 = \begin{bmatrix} A & BK \\ 0 & BK \end{bmatrix}$, when the switch is in position 2, $A_2 = \begin{bmatrix} A & BK \\ 0 & I \end{bmatrix}$.

Usually, in the case of a certain packet loss the network control system still can guarantee the stability of the system. In this case, the inferences were as follows:

Corollary 3.1: suppose closure rate of system switch r. If exists Lyapunov function $v(x(kT)) = x^T(kT)Px(kT)$ and scalar factor α_1 and α_2 alpha in the system that satisfy the following conditions: $\alpha_1^r \alpha_2^{1-r} > 1$, $A_1^T P A_1 \le \alpha_1^{-2}$, $A_2^T P A_2 \le \alpha_2^{-2} P$, then the index of the closed-loop system is asymptotically stable.

Theorem 3.1: if the open-loop system is critical stable, so for $0 < r \le 1$, the index of the closed-loop system is asymptotically stable. If open loop system is not stable, then for $r_x < r \le 1$, the index of the closed-loop system is asymptotically stable.

$$r_x = \frac{1}{1 - r_1 / r_2} r_1 = \log[\lambda_{\max}^2 (A + BK)], \lambda_2 = \log[\lambda_{\max}^2 (A)] \tag{3}$$

3. Generalized prediction principle

With the development and application of MAC and DMC, Clarke and some others put forward Generalized Predictive Control (GPC) based on the parameter model of in 1984. This algorithm's controlled object model uses CARIMA model introduces the multi-step optimization performance index on the basis of generalized minimum variance Control, which can effectively overcome the influence of random disturbance and random noise.

3.1 Object model

Different from MAC, the GPC adopted minimized model. [5]It takes discrete difference equation with step non-stationary random noise disturbance to describe the generalized predictive control of the controlled object:

$$A(z^{-1}) y(k) = B(z^{-1}) u(k-1) + C(z^{-1}) \xi(k) / \Delta \tag{4}$$

Multiply both sides respectively by the difference operator Δ:

$$\overline{A}(z^{-1}) y(k) = B(z^{-1}) \Delta u(k-1) + C(z^{-1}) \xi(k) \tag{5}$$

In the type, $\overline{A}(z^{-1}) = A(z^{-1})\Delta = 1 + \sum_{i=1}^{n_\alpha + 1} \overline{a}_i z^{-i}$

By the two types, we can see that through mathematical processing, the mathematical model of controlled object has become the system with control increment and integral action and stationary random noise. Unlike previous CARMA model, this model is called the Controlled Auto-Regressive Integrated Moving-Average), namely the CARIMA model.

Summary

Aiming at the networked control systems with arbitrary bounded lost package, this paper proposes a feasible guarantee, network predictive controller design method of a smaller amount of calculation. Extended state space model is used to describe the network control system; the condition of using state feedback controller of the system stability was obtained. Through endless time domain control parameters into a free control function and a state feedback control law, satisfied the system state constraints and input constraint network predictive controller.

Acknowledgements

The Research Is Supported By Education and Teaching Reform Project of Professional Colleges in Department of Education Hunan Province (ZJC2012029)

References

[1] Walsh G C, Beldiman O, Bushnell L. Scheduling of networked control systems. IEEE Control Systems MagaZine. 2002, 21(l): 57-65.
[2] Rabello A, Bhaya A. Stability of asynchronous dynamical systems with rate constraints and application. IEEE Proceedings: Control Theory Application[C]. 2003, 150(5): 545-550.
[3] F.L.Lian, Analysis, design, modeling and control of networked control systems: [Ph.D.dissertation]. Dept. echanical Engineering University of Michigan, U.S.A, 2001.
[4] Wei Zhang, M.S.Branicky, and S.M.Phillips, Stability of networked control systems. IEEE Control Systems Magazine, 2001, 21(1):84-99.
[5] Vijay Gupta, Babak Hassibi, Richard M.Murray, Optimal LQG control across packet-dropping links, Systems & Control Letters, 2007，56(6):439–446.

Advanced Materials Research Vols. 989-994 (2014) pp 3386-3389
© (2014) Trans Tech Publications, Switzerland
doi:10.4028/www.scientific.net/AMR.989-994.3386

Flatness Feed-forward Control Model Based on Neural Networks

Zhuwen Yan[a], Henan Bu[b], Dianhua Zhang[c] and Jie Sun[d]

State Key Laboratory of Rolling and Automation, Northeastern University, Liaoning, China

[a]zhuwen19880301@163.com, [b]bhn_neu@126.com, [c]zdhua@mail.neu.edu.cn, [d]sunthird@163.com

Keywords: feed-forward control, rolling force fluctuations, feed-forward adjustment amount, regulatory agencies, neural networks

Abstract. The influence on the shape of the strip from rolling force fluctuations has been analyzed. The combination of intermediate roll bending and work roll bending has been adopted. The principle of rolling force feed-forward control has been analyzed. The feed-forward control model has been established on the basis of neural networks. The model has been successfully applied to a rolling mill and a good effect has been achieved.

Introduction

Plate-shaped automatic detection and automatic control board is the only way to improve the quality level of the strip shape[1]. Theoretical research and production have proved that incoming steel crown with volatility is one of the largest factors affecting the quality of the finished strip shape, especially in the lead with the tail section[2]. In tandem cold mill flatness control, rack control to achieve zero bias alone is difficult. The steel profiles according to the principle of equal proportions of crown should be adopted to control flatness. If the front of the rack plate shape can be controlled, finished rack can be easier to good quality control strip shape. In the study of cold tandem rolling unit, cold rolling mill plate-shaped feed-forward control method has been developed on the basis of neural networks. Existing automatic flatness control model has been improved and feed-forward control strip between the plate-shaped rack has been achieved in the front plate-shaped feed-forward control link. The disadvantage of the closed-loop feedback control has been remedied. The shape control accuracy has been increased further. In cold rolling process, rolling force fluctuations shapes a deep impact on flatness. The combination of work roll bending and intermediate roll bending is adopted in feed-forward control.

Impact on flatness from rolling force fluctuation

Rolling force is affected by many factors, such as the geometric characteristics of the strip[3], the deformation resistance, friction coefficient, the roller diameter reduction, rolling speed, the tensile stress distribution and so on. In the rolling process, not only incoming thickness and hardness of the crown will change, but also friction coefficient, the rolling speed and the tension will change, which can lead to rolling force constantly changing during the rolling process. The rolling force variation caused elastic deformation of the roll change. Load roll gap shape changes, and ultimately the strip shape is affected.

Regulatory agencies of feed-forward control

The impact of hydraulic bending on exports strip thickness is small[4]. Since the control response time of hydraulic bending roller and hydraulic pressure are similar, the bending force is adopted to compensate for changes in the rolling force. The shape feed-forward control strategy is essentially to compensate rolling force. Compared with closed loop control system, there is no hysteretic problem. So it is called feed-forward control. According to shape control efficiency coefficient, influence on the shape of the rolling force is similar with bending control. The bending rolling force control is adopted to offset the impact of fluctuations on the plate-shaped.

Principle of feed-forward control

The front plate-shaped overall compensation principle feed-forward control is to compensate impact on flatness from rolling force changes. The rolling force per unit width change amount is adopted to solve corresponding bending force compensation amount:

$$\Delta F_{\mathrm{W}} = \zeta \cdot \frac{\Delta P}{W} \tag{1}$$

$$\zeta = -\frac{K_{\mathrm{PB}}}{K_{\mathrm{FW}}} \tag{2}$$

Where, ζ is impact on strip crown from rolling force per unit width and unit bending force. K_{PB} is rolling force per unit width of the impact on the strip crown ratio. K_{FW} is roll bending force of the impact on the strip crown ratio.

When the roll diameter is constants, increasing the rolling force can lead to increase deflection roll and strip crown. Influence on the rolling force of the strip crown is:

$$K_{\mathrm{PB}} = \frac{\Delta C}{\Delta p} = \frac{C - C_0}{p - p_0} \tag{3}$$

Where, Δp is the rolling force per unit width change amount.

In order to avoid appearing adjusting the oscillation, rolling force fluctuation compensation dead zone is set up. When rolling force fluctuation is in compensation dead zone, feed-forward control is closed. When rolling force fluctuation exceeds compensation dead zone, feed-forward control is open.

Feed-forward adjustment amount model

The change of rolling force can lead to change in the distribution of the pressure of the roll gap. Elastic deformation of the roll is changed[5]. The extensional deformation is inconsistent along the width direction. The cont trol of work roll bending and intermediate roll bending on the shape is to change the load distribution within the seam roller pressure.

$$J = \sum_{i=1}^{\mathrm{N}} \left[\Delta P_i - \alpha_{\mathrm{W}} f_{\mathrm{W}i} - \alpha_{\mathrm{I}} f_{\mathrm{I}i} \right]^2 \tag{4}$$

Where, J is objective function. α_{W} is feed-forward correction work roll bending force. α_{I} is feed-forward correction intermediate roll bending force. $f_{\mathrm{W}i}$ is work roll bending force on the load factor in the regulation of the seam roller pressure distribution. $f_{\mathrm{I}i}$ is intermediate roll bending force on the load factor in the regulation of the seam roller pressure distribution. ΔP_i is measured rolling force variation.

In neural networks[6], there are N neurons in network input layer, Q neurons in competitive layer and M neurons in network output layer. The connection weight vector from network input layer to competitive layer is W_J. The connection weight vector from competitive layer to network output layer is V_l

(1) Initialize W_J and V_l. Choose value from 0 to 1. Normalize A_k as follows:

$$a_i^k - \frac{a_i^k}{\left\| A_k \right\|} \tag{5}$$

$$\left\| A_k \right\| = \sqrt{\sum_{i=1}^{N} a_i^k} \tag{6}$$

(2) Give k-th input pattern to the input layer of the network.

(3) Normalize W_J as follows:

$$w_p = \frac{w_i}{\|W\|} \tag{7}$$

$$\|w_p\| - \sqrt{\sum_{i=1}^{N} w_i^2} \tag{8}$$

(4) Sum each neurons in competitive layer as follows:

$$S_j - \sum_{i=\tau}^{N} a_i^k w_j \tag{9}$$

(5) Solve W_R as follows:

$$W_R = \max_{i=1}^{Q} \sum_{i=1}^{N} a_t^2 w = \max_{i=1}^{Q} s_i \tag{10}$$

(6) Adjust as follows:

$$w_R(t+1) = w_{R'}(t) + \alpha[a_t^2 - w_R(t)] \tag{11}$$

(7) Solve weighted input in network input layer as follows:

$$c_t' = \sum_{j=1}^{Q} b_j v_{ij} \tag{12}$$

(8) Return (2) until all input mode is given to the network.

(9) Set $t = t+1$. Assign value again.

Application results

The proposed flatness feed-forward control mathematical model has been successfully applied to a 1450mm five-stand cold rolling process control system. In order to verify its application results, the application results with flatness feed-forward control mathematical model is compared to the application results without flatness feed-forward control mathematical model. When the flatness feed-forward control mathematical model is not adopted, the deviation of strip flatness control is large. When the flatness feed-forward control mathematical model is adopted, the deviation of strip flatness control is decreased. Therefore, flatness feed-forward control mathematical model can increase flatness control accuracy.

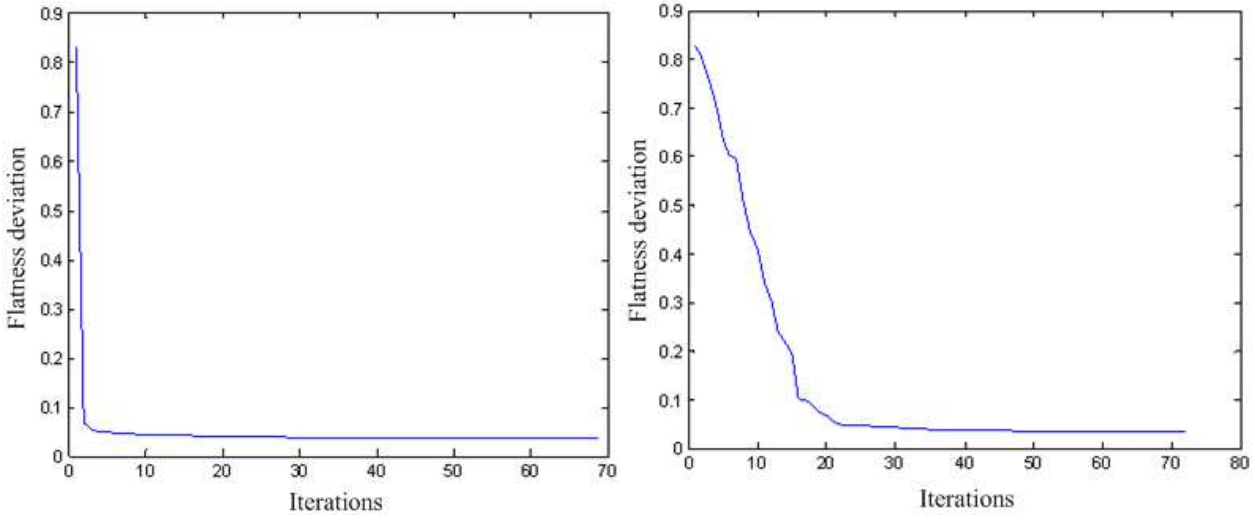

a) with flatness feed-forward control model b) without flatness feed-forward control model

Fig.1 Variation of deviation of flatness

In fig.1, when the flatness feed-forward control mathematical model is adopted, we can see that the flatness is good in strip. When the flatness feed-forward control mathematical model is adopted, we can see that it appears flatness defection.

Conclusions

(1) The impact of roll temperature to flatness is analyzed and the roll temperature field model is established.

(2) The flatness feed-forward control mathematical model is established. The neural networks is adopted by the model to solve the feed-forward adjustment amount and the feed-forward adjustment amount of model can decrease deviation of strip flatness control, and the flatness quality has been increased greatly.

Acknowledgements

This research was financially supported by National Natural Science Foundation of China (51074051).

References

[1] WangY. Q， Sun F，Liu J，ea al. Chinese Journal of Mechanical Engineering，2009，22(2)：282-286．

[2] L.Wang，Y. K. Sun. Computer Simulation, 2003, 20(2): 82-85．

[3] Yuanxiang Zhang. Advanced Materials Research, 2012,538(541):1208-1212.

[4] Jingqi Zhang. Journal of Materials Science, 2012,47:4000-4011

[5] TIAN Yong, SCIENCE CHINA Technological Sciences, 2012,55(6):1566-1571

[6] Huifang Lan. steel research international, 2012,83(2):139-145.

Advanced Materials Research Vols. 989-994 (2014) pp 3390-3393
© (2014) Trans Tech Publications, Switzerland
doi:10.4028/www.scientific.net/AMR.989-994.3390

The Design of Greenhouse Environment Monitoring System Based on ZigBee

Chen Guoshao，Wang Zhongsheng ，Shang Xiao

Department of Computer Science & Engineering, Xi'an Technological University, Xi'an 710021, P.R.China,

Keywords: ZigBee; Serial communication; Wireless sensor network; Real-time monitoring

Abstract. The internet is widely used in daily life, of course, also be applied in agriculture. This paper is focus on the technology of ZigBee and serial communication. The ZigBee communication module transfers the data from greenhouse to the monitoring system. Growers can get the data timely, and according to the received data to control greenhouse environment. The monitor computer program is based on VB.NET. ZigBee module gets the data from sensor, through serial ports the information is transferred to the monitor computer. The monitoring software stores the data and displays it on the user interface. If the data beyond the threshold value, the system will give an alarm sounds.

Introduction

Greenhouse environment monitoring system detects greenhouse temperature, humidity and other environmental parameters, reducing workload of plant personnel. Records the data on time, convenient growers to control greenhouse environment, facilitate to the growth of crops. At present, the signal propagation mode in most of the greenhouse control systems are wire transmission, a large number of wiring is inevitable. It has many disadvantages, such as high cost, routing is complex, maintaining is difficult. However, the wireless transmission method can effectively solve the above problems.

The system designed in this paper, the data acquisition node is consists of single-chip computer, temperature sensor and humidity sensor, applies radio frequency technology for data transmission. The wireless node is to collect information and monitor computer displays it to the system interface.

ZigBee Technology Introduction

ZigBee is a low-power, cheap and short-range wireless network communication technology, it is used in almost all industries of low rate and short-range wireless communication, such as home furnishing, traffic, and building etc. Significant features of it are the low rate, low power, low cost, self configuration and flexible network topology structure. Due to in non working mode, the ZigBee node is in a dormant state. Because the ZigBee protocol stack is much simpler than others, reduces requirements of the controller, so we can use single-chip computer and a small amount of memory, to reduce the cost greatly. In the communication distance, it through the network coordinator setting network automatically, using the CSMA-CA methods for channel access; and the node device is free to join and leave, is a self-organizing network configuration.

System Structure Design

The system is composed of terminal node, coordinator (also known as the ZigBee gateway) and database management system. As shown in Fig 1, the terminal node is consist of temperature sensor and humidity sensor, collects data in real-time, the data through the C51 single-chip computer uploaded to the ZigBee wireless network. Each ZigBee module also has relay function, so as to avoid too far distance to transfer. The module is responsible for wireless transmission. Database management system applies VB.NET develop human machine interface. The terminal node is to collect and send data, database management system is to analysis and storage data. The coordinator

is responsible for collecting information through RS232 transmit to the host computer, and the system is responsible for realizing real-time display data, and to realize data storage, query, delete and other functions.

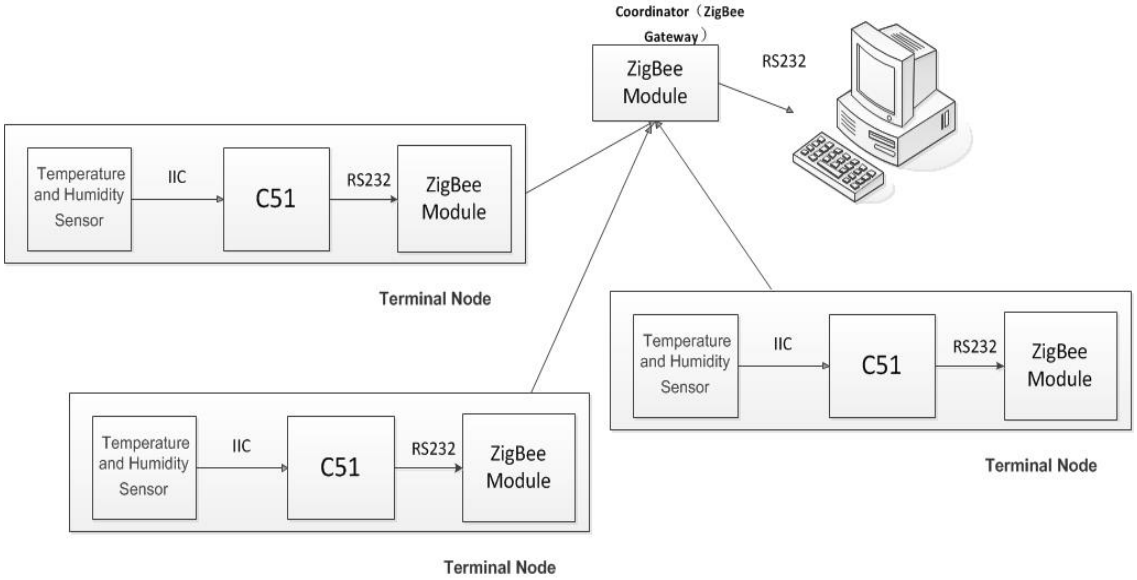

Fig.1 Structure diagram of system

System Hardware Designing

Environmental monitoring system hardware device is composed of terminal node and coordinator, as shown in fig 2. coordinator, it mainly includes microcontroller, RF sending-receiving unit, wireless node and power module and interface unit. From the system hardware, we should mainly consider the accuracy of the temperature and humidity, the detecting range and economic aspects. In this paper, the ZigBee module includes the integrated temperature and humidity sensor and CC2530.

The terminal node includes the temperature sensor and the humidity sensor, MCU and ZigBee module. The terminal nodes are placed in the greenhouse, the temperature sensor and the humidity sensor gets the information. Through the IIC bus MCU transfers the data to ZigBee network, then the coordinator transfer the information to database management system through the RS232 serial port. When distance the terminal node to coordinator is too long to transfer information directly, the data can be transfer to other terminal node, and then transfer to the coordinator.

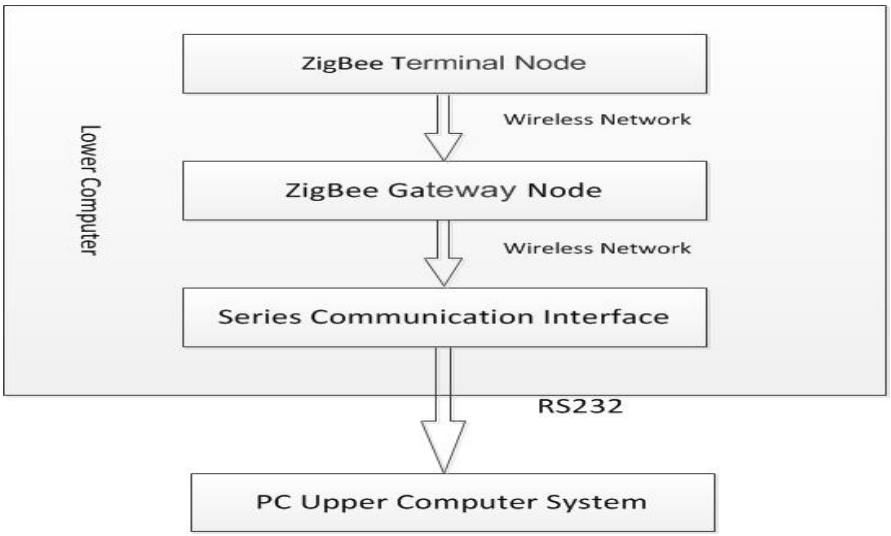

Fig.2 Structure diagram of lower computer system

System Software Design

The monitoring software is developed in Microsoft Visual Studio 2008 environment, the system transfers the data which is collected by terminal node to access database. Growers can through computer monitoring software query the history data, through monitoring interface monitor the data changes in real time, and can set the alarm threshold and the matching parameters etc.

Data Receiving Module

To transfers the data to database management system. The software is programmed In Microsoft Visual 2008, generally, we uses communication control of Microsoft Communication Control (MSComm).

Step follows:

(1) open the serial port connection (2) determine whether the terminal node parameters are correctly chosen (3) set the serial parameters according to the machine parameters (4) establish serial port communication events (5) receive data information.

Section code follows:

```
Private Sub SerialPort1_DataReceived(ByVal sender As System.Object, ByVal e As
System.IO.Ports.SerialDataReceivedEventArgs) Handles SerialPort1.DataReceived
        'introduce SerialPort class, receive data HOneData（the humidity of first node）three
group of six data
  Dim byteToRead As Int16 = SerialPort1.BytesToRead( )
        If byte To Read = 21 Then
            Dim ch(byte To Read) As Byte
            Dim bytesRead As Int16 = 0
            bytesRead = SerialPort1.Read(ch, 0, byteToRead)    'store the received data
  If ch(0) = 170 And ch(1) = 85 Then    ' judge whether the length of data is effective
              HOneData = CLng("&H" & Hex(ch(2) & ch(3))) / 10
              ……' transform hexadecimal into decimal（front），decimal point moves
single bit to the left(divided by 10）.
```

Data Processing Module

When the computer receives the data, the data be decomposed into three parts, the node number, values of temperature and humidity data, then the data will be transform hexadecimal data into decimal data, at last save to the database. Flow chart of data processing module is as shown in fig 4.

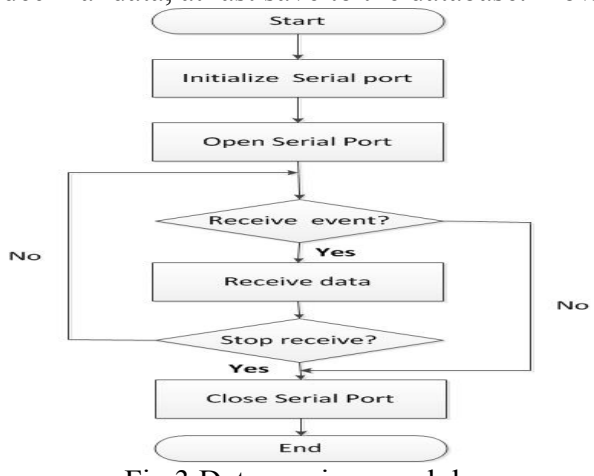

Fig.3 Data receiver module

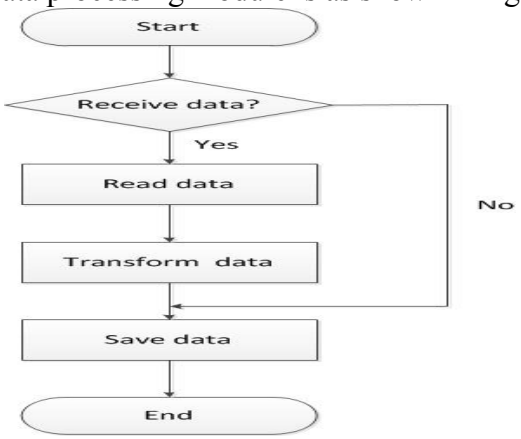

Fig.4 Data processing module

Section code follows：

```
Imports System.Data.OleDb 'apply access control
Public LHGconn As New OleDb.OleDbConnection("provider=microsoft.jet.oledb.4.0;" & "data source=" & My.Application.Info.DirectoryPath & "\NewData.mdb;") 'open database，relative path
    Public Sub LHconnopen( )
        Try
            If LHGconn.State < > ConnectionState.Closed Then LHGconn.Close( )
            LHGconn.Open( )
            Call RAlarm( )'database connection，alarm if error
```

Data Display Module

The data display module is the most important module in the system, GDI+ which is provided by.NET Framework converts the data to a picture, and displays it to growers. The system interface has two axes which are used to display the temperature and humidity data, through mathematical calculation to determine the coordinate value of the data on the axis. Connect adjacent coordinate points together to form a real time display curve. Use the Bitmap class to package GDI+ bitmap. Bitmap is used for processing image which is defined by the pixel data. The Graphics.FromImage can create a new Graphics from specified Image, at last using the PictureBox control to display the graphics and images.

Conclusion

The system detects temperature and humidity data based on ZigBee, it has many advantages, such as reliable, simple, flexible, low cost etc. The system can collect real-time data and transfer it to the user, the user can timely grasp the greenhouse environment, so as to adjust and control the environment, and there are values of application.

References

[1]QU Lei, HU Xianbin etc. ZigBee Technology&Application.Beijing: BEIHANG UNIVERSITY PRESS, 2007.

[2] GAO Shouwei, WU Canyang etc. ZigBee Technology Practice Guide .Beijing: BEIHANG UNIVERSITY PRESS, 2009.

[3] ZHANG Yigang. Single-chip Microcomputer Principle and Interface Technology, 2011.

[4] ZigBee Alliance, ZigBee Specification Version 2.0,De-cember 2006, http://www.zigbee.org

[5] China Communications Standards Association, ZigBee Technique and its Applications, 2007.(in Chinese)

Advanced Materials Research Vols. 989-994 (2014) pp 3394-3398
© (2014) Trans Tech Publications, Switzerland
doi:10.4028/www.scientific.net/AMR.989-994.3394

The design of portable granary thermometer

Gang Qin[a], Dequan Cui[b]

Xi'an Technological University, Electronic-Information Engineering College Xi'an, China

[a]494524028@qq.com; [b]Cdq061002@163.com

Keywords: msp430f149; temperature collection; portable; low power consumption

Abstract. This article designed a portable granary thermometer to solve the shortcomings of present similar products ,such as complex structures , high performance price ratio and lack of flexibility , this thermometer used ultra-low power microcontroller MSP430F149 and programmable temperature sensor DS18B20 as the main components, it can collect, display and store the temperature on a real-time basis . Based on actual use, this apparatus possess the advantage of complete function, low power consumption, easy to operate, low price, portable and wide occasions of application etc.

Introduction

Granary thermometer an instrument of detecting grain temperature in the granary. With the development in science and technology, our domestic granary temperature measurement system develops greatly. In ordinary, the system adopts classification structure made of measuring host machine and slave machine. Main machines are placed in the side of the computer to collect and store the data, and then transmit the temperature data to the computer through serial ports; Measuring extension machines are installed in the warehouses of the granary, the extension number is corresponded with warehouse number. Therefore, the temperature signal processor is indispensable in the granary which also should be supplied power by utility power. The temperature measuring cable generally made of several connecting wires which connected to signal processor, the complicated structure with many signal cables and power cables, so that it is hard to install, maintain and with high cost. Some small granaries are not suitable to install the equipment said above for the sake of technology and funds. According to above problems, one kind of portable granary thermometer was designed which is convenient to measure the temperature, so that granary keepers could be more intuitive to know the change of the temperature in the granary. It has following features high measurement accuracy, small volume, low price, portability etc. It is mainly applied in small and medium granaries to realize the monitor of granaries through measuring and storing temperature.

System Hardware Composition

Portable thermometers mainly consist of microcontroller modules, data acquisition modules, data storage modules, display modules, clock modules and power modules. Hardware structure is shown in figure 1.

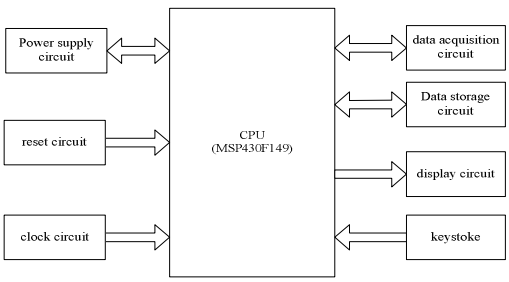

Fig.1 Hardware block diagram

A. Microcontroller Modules

Low power consumption is most important in the design of portable equipments. On promise of the design, Microcontroller should not only work in low voltage but also has lowest power consumption for power. Supplying with battery reason. In addition the anti-interference ability should be also considered in system design, especially for portable system design, so choosing the suitable system core devices is the key to finish the design successfully, and microcontroller is the most important as the core of acquisition system. This text is to study a portable granary temperature measuring system which is convenient to detect in the field, display and store the data, and then send the data to upper computer terminal for analyzing when needed. Considering hardware resources, development tools, and power of microcontroller, ultra-low power consumption microcontroller MSP430F149 of TI is applied in this design as the core controller of the portable thermometer.

B. Data Acquisition Module

Using sensors to collect temperature data of the grain. Early temperature sensors usually use copper resistance, thermal resistance or thermocouple as sensor elements, which reflect the changes of grain temperature through examining the variation of resistance value, but it is inefficient, inaccurate, and insensitive to carry out the work bit by bit by manual operation. Considering measuring accuracy, range, economy efficiency and other factors, DALLAS DSl8B20 is chosen as the thermometric element which is the unibus digital temperature sensor made by DALLAS with the features of simple structure, operation flexibility, and no need of external circuit. DSl8B20 interface is shown in figure 2.

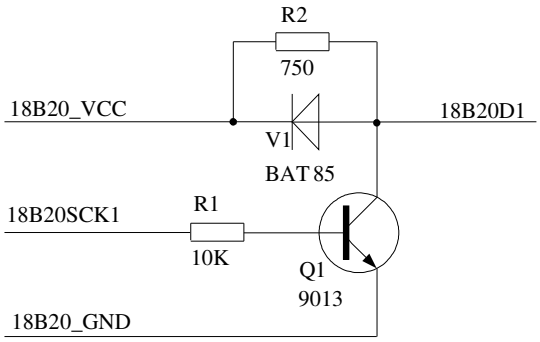

Fig.2 DS18B20 interface circuit

C. Data Storage Module

The main advantages of this kind of thermometer are portability and convenience so that the data measured is easy to store and transfer. Therefore we should consider the portability and dismountable performance of the data storage medium. Because the system does not belong to fixed real-time measurement, when there is a need to measure the temperature of the granary, the system will collect the data, after finishing the measurement, workmen could take the data away for further research and analysis. Since SD memory card could meet the above requirements, we choose SD memory card as data storage.

SD cards mainly store the measured temperature and humidity data. When the SD card works, it needs to be drived and managed by a control chip CH376, which is used to connect SD card with the microcontroller, and manages the data transmission between them. SD card interface circuit is shown in the figure 3 :

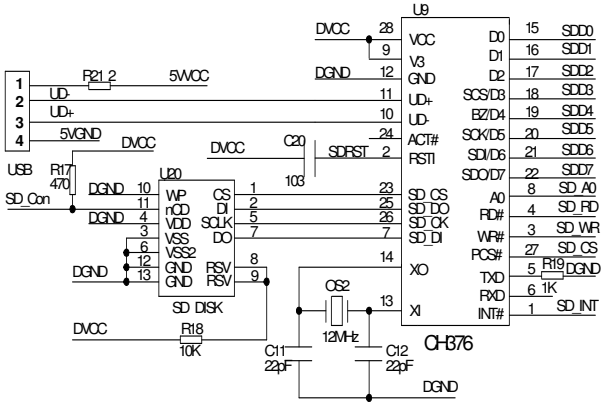

Fig.3 SD card interface circuit

It adopts directcurrent supply 3.3Vas the power supply source, so V3 terminal and VCC should be connected to DVCC together. UD- and UD+ are used to be the data input and output for the spare U Disk socket. Two 22pF in 12MHz crystal oscillator are used for oscillation starting and frequency stabilization. The pin SD_CS, SD_CK, SD_DO, SD_DI connect with SD card slots as chip selection, clock, data input and output terminal

D. Display Module

Common used LCD module mainly has physic and dot-matrix types. The design uses dot-matrix LCD module YM12864C. It mainly drives by adopting the dynamic driving principle -- controller and segment driver make a 128 (column) x 64 (lines) full dot-matrix LCD display. The display monitor adopts COB soft packaging mode, to connect LCD through conductive rubber and pressure box connection which makes its long life and reliable connection.

Due to the low data and control signal voltage outputted from microcontroller parallel ports, display module needs to increase drive chip to enlarge signals, enhance load capacity, which could make YM12864C work normally. Drive chip adopts TTL 74LS245 chip. The microcontroller could enhance the load capacity through this chip to control the LCD module data. Interface circuit is shown in figure 4.

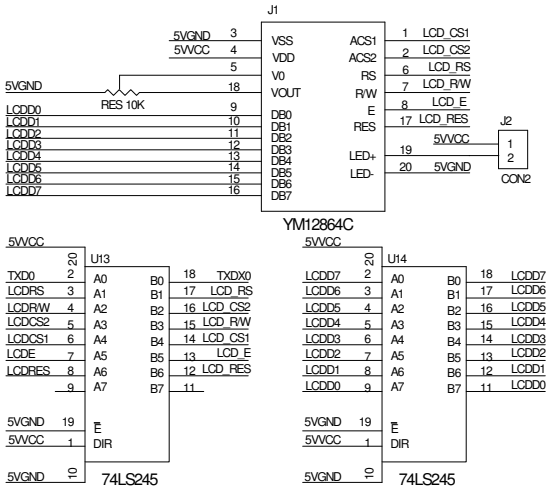

Fig.4. LCD interface circuit

E. Clock Module

The clock modules in granary temperature measuring system are to provide workmen with the time and data. The microcontroller configures the chosen chip to finish the display and data remark after measuring data. The clock chip is PCF8653 which is a low power consumption CMOS made by PHILIPS. It provides a programmable clock output, interrupt output and power down detector.

F. Power Module

Power supply is the system dynamics in the granary temperature measuring system. The reliable power is the guarantee of the normal work of the system. The thermometer adapts 3 V button batteries which doesn't need utility electric. This also shows portable features. Since various elements may need different working voltage, power supply should be regulated. Using stabilivolt L6920 and SP6201 and relative external circuit could get 5V and 3.3V voltage.

3.3V voltage is mainly used for 430 microcontroller, I^2C storage, SD card, four-key keyboard, JTAG programming interface power. These parts need much reliable voltage, or the core of the system could not work normally.

5V voltage is mainly used for temperature sensors, LCD display module, clock chip, external benchmark source power supply. These parts also need reliable voltage or the system time will disorder, sensors and LCD screen doesn't work normally.

System Function and technical indexes

System function is shown in the figure 5.

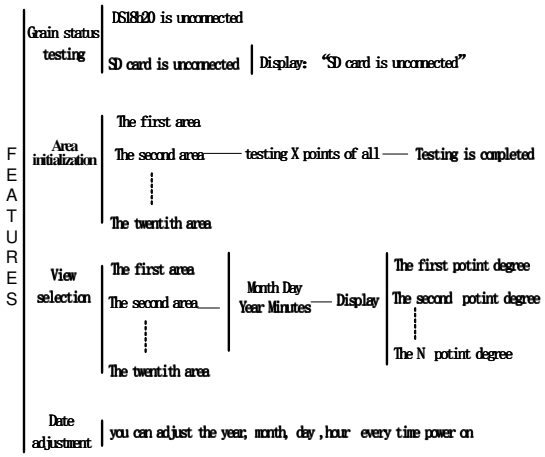

Fig.5. System function diagram

- Grain status testing function : First display area, scroll by up/down keys, choose area by clicking "ok" to collect real-time data of grain temperature, warehouse temperature, and warehouse humidity. It shows "spare" at the time of no value, and shows "finish detection"if nomal（automatic storage）.
- initialization function：First display area, scroll by up/down keys, choose area by clicking "ok ",then initialize to recognise the code with DS18B20, then click "ok", Don't need to initialize after a period of fixation.
- View function selection：First display area, scroll by up/down keys, choose area by clicking "ok" to show the time. croll by up/down keys, choose date by clicking "ok". Display according to DS18B20 sequence,four points（N, N+1, N+2, N+3）are a screen. Scroll by up/down keys to check by every screen and area.
- Date adjustment function：Show the latest year firt, scroll by up/down keys to choose year by clicking "ok". It is the same way to choose month, day, hour, sectond, and hour is responded with 24 hours.

Technical indexes Thermometer could achieve 0.1℃ resolution, less than ±0.1℃ measurement error. Working temperature is -40℃~ +85℃, 2.4V button battery power supply it could work more than 2 years with not changing the battery.

System Software Design

The main function of portable granary thermometer is to measure the temperature of grain in warehouse. The system uses microcontroller to program storage extension procedure and read or write extension chip, to finish the temperature measurement, LCD display and data storage.

Integral software flow chart of the system as shown in figure 6

Conclusion

The portable granary thermometer introduced in this text has many advantages such as small volume, simple operation, high accuracy and convenient detection. It could detect any granaries flexibly, the detected data is easy to store and transfer which could be taken away by workmen for further research and analysis. This system is much suitable for the small and medium granary. It has a great practical value and application prospect.

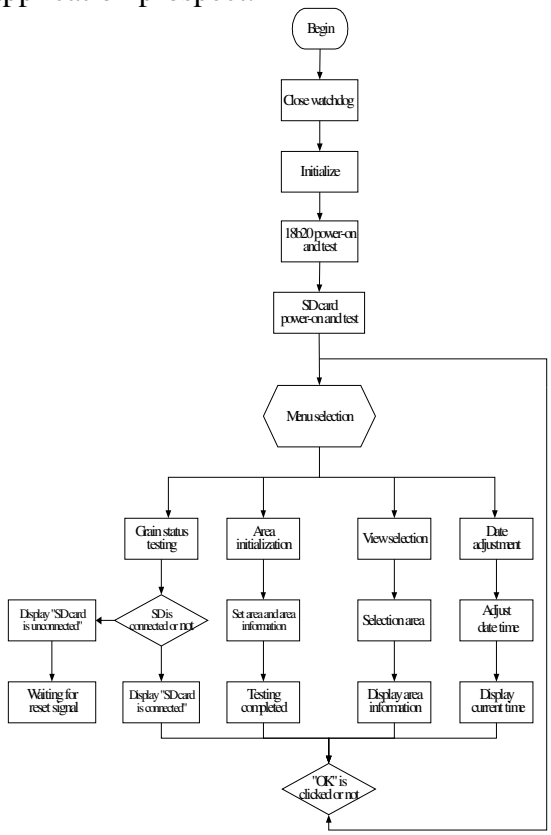

Fig.6. Integral software flow chart of the system

References

[1] Shen Jian-hua et al write. MSP430 series 16-bit ultra low power microcontroller Principles and Applications [M].Beijing: Tsinghua University Press, 2004.

[2] Mo shao;DENG Peng .MSP430-based low-power portable thermometer design [J].Electronics Engineers, 2008 (3) :34-38.

[3] Lu jun-Fang. Sensor interface circuit and testing equipment [M].Beijing Aerospace University Press, 1995.10.

[4] Qin Long.MSP430 microcontroller 16-bit ultra-low power practice and system design .Tsinghua University Press, 2005.4.

Advanced Materials Research Vols. 989-994 (2014) pp 3399-3406
© (2014) Trans Tech Publications, Switzerland
doi:10.4028/www.scientific.net/AMR.989-994.3399

Research and design of light moisture tester

Yaping TANG

Hunan Railway Professional Technology College, Zhuzhou, 412001
398741983@qq.com

Keywords: Light moisture meter; The coal quality analysis; Through nitrogen drying; The heating rate

Abstract: This paper introduces the research and design of a light moisture tester. In the coal quality analysis field, moisture test most of the use of infrared heating pipe heating or drying box to measure, low heating rates, nitrogen through a single mode, before heating furnace uniform nitrogen filled with test conditions and have the test conditions, the same way caused by nitrogen, nitrogen waste. Based on this study, the heating pipe comprises an infrared tube into a light tube, the heating rate is improved; the general nitrogen control size flow switching mode using 2.5min before the experiment, large flow quick heating furnace filled with nitrogen, achieved through experimental conditions drying nitrogen, open a small flow, keep the atmosphere. The improved design of a light moisture meter analysis of water air drying method precision test, analysis of water air drying method accuracy experiments, 6 water - air drying method of precision experiment, 6 water - air drying method accuracy experiments, analysis of water through nitrogen drying method precision experiment, analysis of water. Nitrogen drying method accuracy experiments, ¢ 6 full water through nitrogen drying method precision experiment, ¢ 6 full water through nitrogen drying method accuracy experiments, results in line with national standard test, repeatability.

Introduction

Water is an important indicator of coal, which have an important role in the basic research of coal utilization and processing. Coal processing and utilization of its water, trade and storage and transportation has a significant impact. Generally high water is not a good thing. Combustion in the boiler, the water will affect the combustion stability and high thermal conductivity; in the coking industry, high moisture will reduce the coke yield, and because a lot of evaporation of moisture and heat away to extend the coking cycle; in coal trading, coal moisture is an important measure of the quality and count. In the coal analysis, coal moisture coal analysis is the basis of the results of different data base conversion. In the field of coal quality analysis, water testing most of the infrared heating tube to measure the blast oven or using a heating rate of low nitrogen-way single, uniform heating furnace filled with nitrogen test conditions before and after the test conditions have, through nitrogen same way, wasteful of nitrogen. In this paper, based on this study, infrared heating tube light tube to tube, increasing the heating rate; nitrogen is controlled by the size of the air flow through the switching mode, before the experiment 2.5min open large furnace filled with nitrogen flow so fast, to pass nitrogen drying experimental conditions, and then open a small flow, keeping the experimental atmosphere.

The principle of the test system

A certain amount of coal samples, placed in a furnace, coal water molecules under the action of heat, moisture evaporates quickly calculate total moisture or water based on mass loss analysis based coal samples after drying.

Instruments hardware system design

Overall block diagram of the hardware design. Entire hardware system includes the following main modules: SCM control module, light heating pipe heating module, thermocouple module, AD sampling module, over-temperature, burnout hardware protection module, nitrogen module, power module. The hardware block diagram shown in Fig. 1.

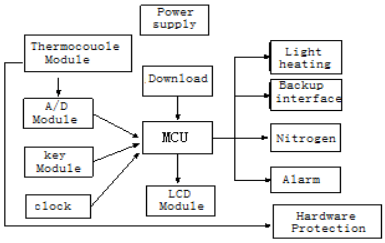

Fig. 1 Instrument calibration flow chart

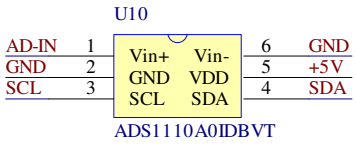

Fig. 3 AD sampling module

The main hardware circuit module design. Thermocouple Module: K-type thermocouple (consider the effect of a good loss prevention sheathed thermocouple), pre-amplifier AD620 op amp, amplifier taken magnification 50.4 times. Cold junction temperature measured by the temperature measurement chip LM75A. The design principle shown in Fig. 2.

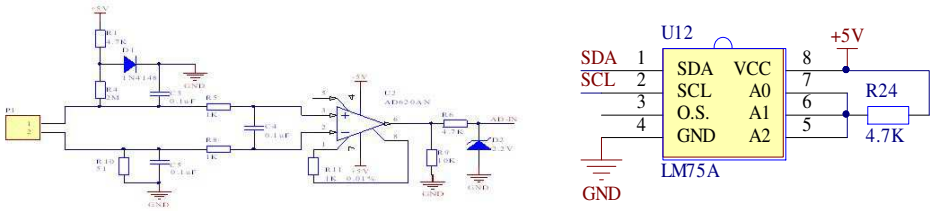

Fig. 2 Thermocouple module principle diagram

A-D sampling module: AD sampling chip ADS1110A0IDBVT, this lower chip prices, small size, fewer external components, high-precision (16-bit). The principle shown in Fig.3。

Light control circuit heating pipe: Using two heat pipes, each heat pipe 1.25KW. Modulated wave to the microcontroller output thyristor power regulator for heating pipes. 2 after heating tubes in parallel with the thyristor connected in series, while the over-temperature, Burnout series hardware protection relays, and then through the switch and fuse access AC220V grid (where a heating tube is connected in series with a relay, can disconnect the power supply itself alone). Using the heating tube 2 may be beneficial to fine temperature control, if the heat pipe 1 2.5KW same effect can be achieved, will consider only A heating pipe.

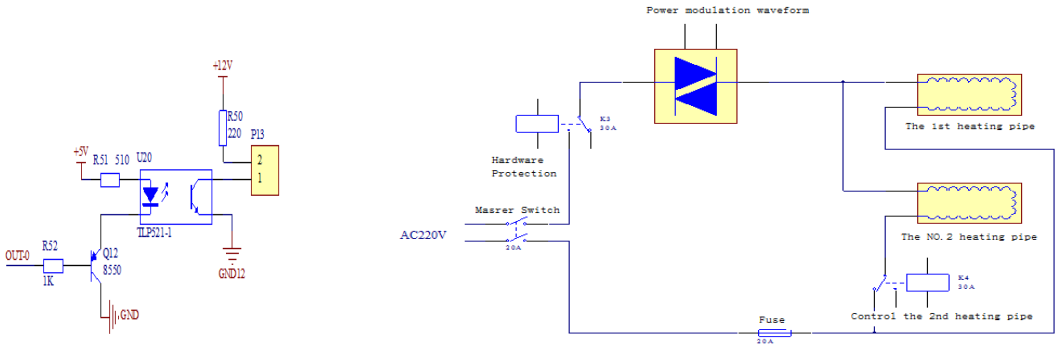

Fig.4 Heating pipe connection diagram

Instrument System Software

Instrument software system designed by CAN communication, laboratory module, Temperature module, AD converter, the abnormality detection of several parts. CAN communication is completed with the upper and lower bit machine data exchange, independent of the experimental module to complete the data acquisition components and related need to perform the entire experiment, monitoring, temperature module is mainly calculated by table look-up and calibration temperature, while the PID algorithm achieve temperature control. AD converter module is handled automatically by the SCM process, the software only on the relevant registers corresponding configuration; anomaly detection module is the main program loop timed to judge the state of the system-related, such as abnormal then upload exception message while locking the corresponding action parts until the fault is removed。

Test

Through hardware and software design of the light moisture tester meter air-drying method for analysis of water precision test, analysis of water and air dried Law accuracy of the experiment, ¢ 6 all-water air-drying method precision experiments, ¢ 6 all-water air-drying method accuracy experimental analysis of water through nitrogen drying method precision experiments, analysis of water through nitrogen drying accuracy experiment, ¢ 6 full water through nitrogen drying method precision experiments, ¢ 6 full water through nitrogen drying method to verify the accuracy of the experiment, the test data as follows.

Analysis of water drying method precision experiments									
Experimental conditions: heating time: First 480s, Second 360, Third 360s, 360s thermostat incremental point: 107 ℃									
Sample Code	Sample weight (g)	Mad (%)	Test time (min)	Level error (%)	Mean (%)	Oven value (%)	Indication error (%)	Meets GB requirement	Remark
Users like the 1st	0.9491	4.92	14:33	0.12	4.93	4.86	0.07	√	
	0.9660	4.87	14:57						
	1.0162	4.89	15:21						
	1.0049	4.90	15:45						
	1.0034	4.98	16:07						
	1.0026	4.96	16:31						
	0.9940	4.99	16:55						
	0.9498	4.90	17:19						

Sample Code	Sample weight（g）	Mad (%)	Test time (min)	Level error (%)	Mean (%)	Oven value (%)	Indication error (%)	Meets GB requirement	Remarks
Users like the 1st	1.0068	4.91	14:37	0.14	4.92	4.86	0.06	√	
	0.9609	4.90	15:01						
	0.9761	4.84	15:23						
	0.9785	4.95	15:47						
	1.0278	4.98	16:11						
	0.9595	4.96	16:35						
	1.0274	4.92	17:03						
	0.9650	4.92	17:27						
Analysis of Water Air-drying experiment accuracy									
Experimental conditions: heating time: First 480s, Second 360, Third 360s, 360s thermostat incremental point: 107 ℃									
Sample Code	Sample weight（g）	Mad (%)	Test time (min)	Level error (%)	Mean (%)	Oven value (%)	Indication error (%)	Meets GB requirement	Remarks
Users like the 1st	0.9887	1.26	8:27	0.01	1.26	1.27	0.01	√	
	0.9619	1.27	8:49						
Users like the 2st	0.9905	4.97	14:34	0.07	4.94	4.86	0.08	√	
	0.9818	4.90	14:59						
Users like the 3st	0.9683	9.47	20:46	0.04	9.49	9.55	0.06	√	
	0.9712	9.51	21:10						
Users like the 4st	0.9759	7.16	16:06	0.02	7.17	7.12	0.05	√	
	1.0173	7.18	16:30						
Sample Code	Sample weight（g）	Mad (%)	Test time (min)	Level error (%)	Mean (%)	Oven value (%)	Indication error (%)	Meets GB requirement	Remarks
Users like the 1st	1.0012	1.27	8:25	0.01	1.28	1.27	0.01	√	
	0.9642	1.28	8:45						
Users like the 2st	1.0357	4.84	14:43	0.12	4.90	4.86	0.04	√	
	0.9974	4.96	15:05						
Users like the 3st	1.0089	9.43	20:37	0.00	9.43	9.55	0.12	√	
	0.9856	9.43	21:01						
Users like the 4st	0.9900	7.17	16:17	0.02	7.18	7.12	0.06	√	
	0.9911	7.19	16:41						
¢ 6 all-water air-drying method precision experiments									
Experimental conditions: heating time: First 1800s,Second 900,Third 600s, 600s thermostat incremental point: 107 ℃									
Sample Code	Sample weight（g）	Mad (%)	Test time (min)	Level error (%)	Mean (%)	Oven value (%)	Indication error (%)	Meets GB requirement	Remarks
all water No. 5	10.9580	7.99	45:27	0.31	8.11	8.19	0.08	√	
	10.6171	8.09	45:52						
	11.3827	8.13	46:19						
	11.3776	7.99	46:42						
	10.8424	8.07	47:05						
	11.1596	8.07	47:39						
	10.5220	8.30	48:07						
	10.5168	8.25	48:30						

Sample Code	Sample weight（g）	Mad (%)	Test time (min)	Level error (%)	Mean (%)	Oven value (%)	Indication error (%)	Meets GB requirement	Remarks
all water No. 5	10.6630	8.23	45:43	0.28	8.07	8.19	0.12	√	
	11.0332	8.09	46:05						
	11.4550	7.95	46:29						
	10.6953	8.14	46:53						
	11.1617	8.11	47:17						
	11.2446	7.95	47:43						
	10.5658	7.95	48:07						
	10.5306	8.16	48:33						
¢ 6 all-water air-drying experiment accuracy									
Experimental conditions: heating time: First 1800s, Second 900,Third 600s, 600s thermostat incremental point: 107 ℃									
Sample Code	Sample weight（g）	Mad (%)	Test time (min)	Level error (%)	Mean (%)	Oven value (%)	Indication error (%)	Meets GB requirement	Remarks
all water No. 1	10.8015	1.93	30:24	0.04	1.91	1.93	0.02	√	
	10.8185	1.89	30:51						
all water No. 2	11.2687	10.54	55:28	0.01	10.54	10.44	0.10	√	
	11.3503	10.55	55:50						
all water No. 3	10.8949	7.33	47:10	0.03	7.32	7.44	0.12	√	
	11.3940	7.30	47:36						
Sample Code	Sample weight（g）	Mad (%)	Test time (min)	Level error (%)	Mean (%)	Oven value (%)	Indication error (%)	Meets GB requirement	Remarks
all water No. 1	11.2048	1.87	30:23	0.02	1.86	1.93	0.07	√	
	11.2425	1.85	30:47						
all water No. 2	10.5850	10.41	55:32	0.16	10.33	10.44	0.11	√	
	10.5392	10.25	55:56						
all water No. 3	10.7238	7.20	47:17	0.08	7.24	7.44	0.20	√	
	10.6977	7.28	47:40						
Analysis of water through nitrogen drying method precision experiments									
Experimental conditions: nitrogen flow: 6L thermostat before 2.5min10L after point: 107 ℃ Heating time: the first 600s, second 300, third 480s, 480s increments									
Sample Code	Sample weight（g）	Mad (%)	Test time (min)	Level error (%)	Mean (%)	Oven value (%)	Indication error (%)	Meets GB requirement	Remarks
lignite No. 2	0.9642	15.95	31:22	0.11	15.93	15.97	0.04	√	
	1.0406	15.98	31:46						
	0.9719	15.95	32:09						
	0.9987	15.89	32:28						
	0.9838	15.95	32:50						
	0.9794	15.94	33:13						
	0.9913	15.92	33:33						
	0.9961	15.87	33:54						
Sample Code	Sample weight（g）	Mad (%)	Test time (min)	Level error (%)	Mean (%)	Oven value (%)	Indication error (%)	Meets GB requirement	Remarks
lignite No. 2	0.9775	15.95	31:23	0.18	15.93	15.97	0.04	√	
	1.0187	15.96	31:47						

	1.0169	15.97	32:10						
	0.9550	16.02	32:32						
	0.9819	15.91	32:56						
	1.0446	15.84	33:18						
	1.0246	15.93	33:40						
	1.0179	15.85	34:02						
Analysis of water through nitrogen drying accuracy of the experiment									
Experimental conditions: nitrogen flow: 6L thermostat before 2.5min10L after point: 107 ℃ Heating time: the first 600s, second 300s, third 480s, 480s increments									
Sample Code	Sample weight（g）	Mad (%)	Test time (min)	Level error (%)	Mean (%)	Oven value (%)	Indication error (%)	Meets GB requirement	Remarks
lignite	0.9661	16.09	31:31	0.05	16.06	15.97	0.09	√	
No. 2	0.9742	16.04	31:55						
bituminous	0.9759	7.49	16:05	0.01	7.48	7.22	0.26	√	
No.4	0.9862	7.48	16:29						
lignite	0.9776	11.44	24:03	0.00	11.44	11.43	0.01	√	
No.4	0.9985	11.44	24:25						
lignite	1.0143	11.22	24:45	0.02	11.23	11.31	0.08	√	
No. 7	0.9545	11.24	25:07						
Sample Code	Sample weight（g）	Mad (%)	Test time (min)	Level error (%)	Mean (%)	Oven value (%)	Indication error (%)	Meets GB requirement	Remarks
lignite	1.0496	16.02	31:31	0.01	16.02	15.97	0.05	√	
No. 2	0.9430	16.01	31:55						
bituminous	0.9564	7.35	16:09	0.09	7.40	7.22	0.18	√	
No.4	0.9828	7.44	16:29						
lignite	1.0231	11.35	24:23	0.00	11.35	11.43	0.08	√	
No.4	0.9768	11.35	24:45						
lignite	0.9353	11.08	25:07	0.02	11.07	11.31	0.24	√	
No. 7	0.9932	11.06	25:29						
¢ 6 full water through nitrogen drying method precision experiments									
Experimental conditions: nitrogen flow: 6L thermostat before 2.5min10L after point: 107 ℃ Heating time: the first 1800s, the second 900, the third 600s, 300s increments									
Sample Code	Sample weight（g）	Mad (%)	Test time (min)	Level error (%)	Mean (%)	Oven value (%)	Indication error (%)	Meets GB requirement	Remarks
	11.2908	2.72	30:34						
	10.6903	2.73	30:56						
	11.0982	2.70	31:16						
	11.3883	2.67	31:38						
	10.9104	2.77	32:00						
all water No. 1	11.1944	2.73	32:22	0.10	2.73	2.74	0.01	√	
	10.8441	2.77	32:42						
	10.9641	2.72	33:06						

Sample Code	Sample weight（g）	Mad (%)	Test time (min)	Level error (%)	Mean (%)	Oven value (%)	Indication error (%)	Meets GB requirement	Remarks
all water No. 1	11.7605	2.66	30:26	0.23	2.67	2.74	0.07	√	
	11.3901	2.77	30:48						
	11.1516	2.71	31:11						
	11.0281	2.68	31:32						
	11.3666	2.54	31:54						
	10.8619	2.65	32:14						
	11.3372	2.78	32:36						
	11.5683	2.57	32:56						
¢ 6 full water through nitrogen drying accuracy of the experiment									
Experimental conditions: nitrogen flow: 6L thermostat before 2.5min10L after point: 107 ℃ Heating time: the first 1800s, the second 900, the third 600s, 300s increments									
Sample Code	Sample weight（g）	Mad (%)	Test time (min)	Level error (%)	Mean (%)	Oven value (%)	Indication error (%)	Meets GB requirement	Remarks
all water No. 1	11.1129	2.71	30:36	0.05	2.74	2.74	0.00	√	
	10.8324	2.76	30:56						
all water No. 2	10.9826	8.91	45:33	0.14	8.98	8.98	0.00	√	
	10.8855	9.05	47:34						
all water No. 3	10.7683	20.47	60:33	0.17	20.38	20.36	0.02	√	
	10.9860	20.3	60:55						
Sample Code	Sample weight（g）	Mad (%)	Test time (min)	Level error (%)	Mean (%)	Oven value (%)	Indication error (%)	Meets GB requirement	Remarks
all water No. 1	11.1994	2.66	30:18	0.00	2.66	2.74	0.08	√	
	11.4992	2.66	30:42						
all water No. 2	11.5963	8.14	46:13	0.14	8.21	8.12	0.09	√	
	11.0496	8.28	46:35						
all water No. 3	11.0405	20.39	60:33	0.13	20.32	20.36	0.04	√	

Summarizes the data analysis and experiments

This design light moisture tester entire disk with precision seed samples meet the national, standard requirements, no systematic bias. Selected for high, medium and low moisture coal sample experiment, the light moisture tester moisture analysis, experimental results ¢ 6 total moisture with infrared heating tube heating water meter, compared with higher efficiency characteristics, the test results we meet the national standard.

References

[1] Chen Dixiang, Tang Ying, Pan Mengchun. Design of high precision intelligent sulfur determination instrument[J] Chinese
Journal of scientific instrument2008 29(06)：1307-1309.

[2] Guard beam Hui, Chen. Design of intelligent sulfur determination instrument[J] Instrument technology 2005 (04):41-42.

[3]Chen Dongmei. Treatment method of measurement signal of infrared sulphur meter[J] Instrument technology.2004 (03):39-40.

[4]Li Hongsheng, The design of the intelligent P89C668 system based on MCUsulfur tester[J] Micro computer and information 2012 28(04)：38-41
[5]Zhang Mingrong. Liu Fayou. Wang Delong et l. Researcha and application of infrared sulfur analyzer[J] Shandong metallurgy. 2002 21(10):8-10
[6] Li Hong Sheng. Rapid intelligent constant of sulfur analyzer system[J] Chinese instrument.2004. (11):25-27.
[7] Mao Wen. A method of automatic sulfur tester[J]. Chinese measurement. 2002 10(06):50-51.
[8] Wang Yu leaves Jiawei. Xie Zhendong. Traffic flow system design and application of simulation software[J]. Computer and communications. 2006 24(04)：5-8.

Advanced Materials Research Vols. 989-994 (2014) pp 3407-3410
© (2014) Trans Tech Publications, Switzerland
doi:10.4028/www.scientific.net/AMR.989-994.3407

Software System for Unmanned Surface Vehicle Using PCI8602

Xiang Shi[1] , Shiming Wang[1, a] , Zhe Xu[1], Qingyi He[1]

[1]College of Engineering Science and Technology, Shanghai Ocean University, Shanghai 201306, China;

[a]smwang@shou.edu.cn

Keywords: USV, Software System, PCI8602, VB

Abstract. The design of software system for unmanned surface vehicle using PCI8602 is introduced. The software system includes the drive program of PCI8602, wireless transmission program and master controller program. Visual Basic is used to write programs, which doesn't write complicated communication protocols between each layers and integrating subsystem is easy. At last, the experiment results demonstrate that the control system for USV has a way to real-time acquisition data, sending data and accomplishing remote control.

Introduction

Unmanned Surface Vehicle (USV) is an intelligent and unmanned surface platform, which can navigate autonomously in the marine environment and complete various tasks such as environmental perception, target detection. At present, many countries have carried out relevant research in the unmanned vehicle, and U.S. and Israel stand at the forefront of study and application in USV fields. In civilian, it mainly includes USV[1] of Massachusetts Institute of Technology in USA, SESAMO USV[2] of National Antarctic program in Italy, DELFIM USV[3]of the Portuguese system and robotics institute, edredon USV[4] in Poland, Measuring Dolphin[5] in Germany and so on. In military, it is represented by Spartan USV[6] in USV and Protector USV in Israel. In China, USV technology is still in the conceptual starting phase.

USV has become new hot spot area of robotics research, to which extensive attention are paid from scholars at home and abroad. State oceanic administration subsidizes Shanghai ocean university, and Shanghai ocean university is studying the control system of USV, and draws some conclusions after many experiments. In the paper some phased objectives are presented as follows.

Introduction to Control System

The control system of USV in the project is divided into USV carrier, shore-based monitoring system and wireless transmission system. The way it works is that shore-based monitoring system is keeping the data, correcting the position of USV carrier and controlling the speed of USV carrier according to the way of comparing the data with expect data, and the data mainly includes longitude and latitude which comes from differential global positioning system which is installed on USC carrier while USV carrier is sending the data to shore-based monitoring system through wireless transmission system.

Fig. 1 The hardware system of the prototype

The hardware system of the prototype is shown as Fig. 1. USV carrier mainly includes: IPC, PCI8602 data acquisition card, differential global positioning system, propellers, battery and other

sensors. The master controller is an IPC and PCI8602 data acquisition card. IPC connects with debugging interface by TCP protocol and connects with differential global positioning system by serial ports of RS232. PCI8602 data acquisition card controls DC motor installed in propellers and collects the data which comes from other sensors. Shore-based monitoring system mainly includes PC computers, and it communicates with USV carrier by wireless transmission system.

So the work pattern of the control system is IPC of the bottom layer in USV carrier and PC computer of the top Layer in shore-based monitoring system. The manipulation is remote control and autonomous operation. The drive mode is two propellers, and two propellers produce speed difference to achieve swerve.

Software System of USV

The Drive Program of PCI8602. The advantage of PCI8602 data acquisition card is that the users do not care of hardware of control in detail but sampling frequency and so on. Then it collects and outputs the signal according to some simple functions in the software package of relevant drive program.

Table1 The explan of functions of drive

Name of function	Explain of function
CreateDevice	Create PCI device object (logical unit numbers)
CreateDeviceEx	Create PCI device object (physical device numbers)
ReleaseDevice	Close the device, and release the PCI bus device object
InitDeviceProAD	Initialize the device of AD，and be ready to transmit
SetDevFrequencyAD	Dynamically change the sampling frequency of AD
StartDeviceProAD	Start the device of AD，and begin to switch
ReleaseDeviceProAD	Release the device of AD
InitDevProDA	Set the output range of the assigned channel of DA
WriteDevProDA	Write the data of DA
GetDeviceDI	Switch the input function
SetDeviceDO	Switch the output function
RetDeviceDo	Backward read the state of data output

In the project, VB is written to control the drive program of PCI8602. Because the drive program is object-oriented programming, a hDevice of object handles is created by a function of CreateDevice before all objects are used. If getting the hDevice, absolute control of the object will be got. Then the hDevice which is taken as the parameter transmits to some relevant drive program. At last, it is released by the function of ReleaseDevice. Table1 lists the main function of drive in the software package of relevant drive program.

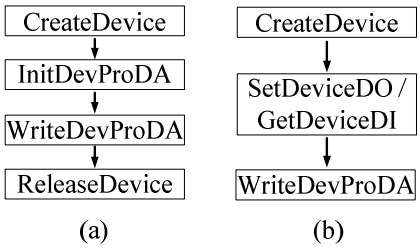

Fig. 2 The calling sequence of function

The master controller mainly uses the function of input and output of DA analog quantity and the function of input and output of DIO digital quantity in PCI8602 data acquisition card, and their calling sequence of function are shown as fig. 2(a) and fig. 2(b). According to figure 2 and the service regulations of PCI8602 drive program, the input and output of DA analog quantity and the input and output of DIO digital quantity are achieved.

Wireless Transmission Program. A pair of wireless transmit units connect with IPC on USV carrier and PC computer on the shore-based monitoring system by serial ports of RS232, and at the same time MSComm in VB reads and sends the data at RS232, so the data enters into serial ports of RS232 of IPC and PC computer, after determining series rate, transmitted power, radio frequency rate and so on, and then MSComm reads and sends the data of serial ports of RS232. At last achieve the wireless transmission.

As mentioned, the wireless technology has been mature and they are immediately applied to the project, so the key to the wireless transmission program lies reading from and sending to serial ports of RS232 in real time. Calling MSComm controls is more convenient than calling API function in practice, and it use less code to achieve the same function.

According to the under steps which call MSComm controls can read and send the data of serial ports of RS232.

(1) Add communication units that is MAComm project.

(2) Set numbers of communication port that is CommPort property.

(3) Set communications protocol that is HandShaking property.

(4) Set parameters such as speed of transmission and so on that is Setting property.

(5) Set other parameters, and add other properties in necessity.

(6) Open ports of communication, and set PortOpen to be true.

(7) Send or read character string, and use input and output property.

(8) Close ports of communication, and set PortOpen to be false.

Follow the steps above, which establishes the transmission system of serial data. Notice that step(2) to (5) is set in properties window of design environment and set in programs, and step(6) to (8) only set in VB.

Master Controller Program. After calling MSComm controls to read and send the data of serial ports of RS232, the VB function editors of character string are used, for instance, Instr function which cut out commands of data and then the master system responses according to commands. The relevant commands in the system are shown as table 2.

Table2 Commands of system and system responses

Command	Response
Start	Begin the command
Over	End the command
Right	USV turns right
Left	USV turns left
Forward	USV goes forward
Back	USV goes backward
Stop	USV stops
H_Sc_	Govern the speed of USV
H_Ch_	Govern the speed of USV
Value	The speed value of USV

Every command in the data starts with ‘ Start’, and ends with ‘Over’, so the system begins to cut out commands, when the system detect ‘Start’, and the commands end, when the system detect ‘ Over’. As above, on the basis of wireless transmission program, master controller program mainly consists of the VB function editors of character string which detect and response commands of data, and the system responses is mainly according to the drive program of PCI8602.

Water Experiments

The control system of USV in the project has made some experiments on the water, and the results of Z tests and rotary experiments have introduced as follows. The results of water experiments are shown as Fig. 3.

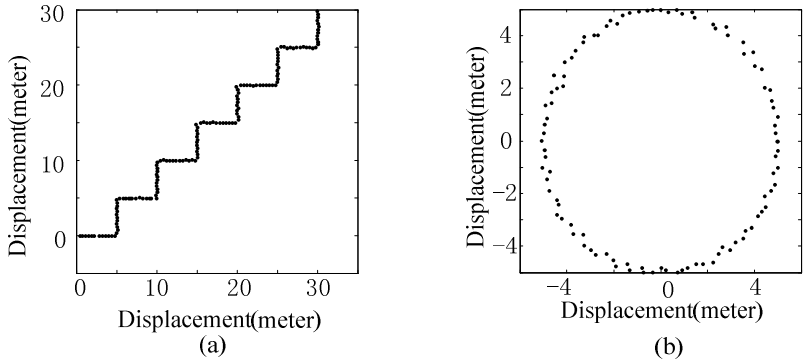

Fig. 3 Results of Water Experiments

USV carrier was remotely controlled to reach the center of lake, and the course was 0° at original state, and the rated speed of motors were 1370 (r/min). After the Z test began, the left motor turned positive direction of rotation at the rated speed and the right motor turned negative direction of rotation at the rated speed. Then, after USV carrier turned to the other side, the rated speed did not change, the left motor turned negative direction of rotation and the right motor turned right direction of rotation. Later, repeat the first step after USV carrier turned to the other side, and cycle all over again until the experiment ended. After the rotary experiment began, the left motor turned positive direction of rotation at the rated speed and the right motor stopped, until the rotary experiment ended. At last, the experiment results show that each systems were in good conditions, and the control system for USV has a way to real-time acquisition data, sending data and accomplishing remote control.

Conclusions

The key to the control system of USV in the project lies PCI8602 data acquisition card, and its advantage is described as follows. It does not need to write complex communication protocols among each layers, which reduces the difficulty of programme and it is easy to integrate each subsystems. At last the results of experiments demonstrate that the control of USV meets expectations, and the way of design is feasible.

References

[1] J. Manley, A. Marsh, W. Cornforth, et al. Evolution of the Autonomous Surface Craft AutoCat[C]//Proc. Oceans 2000 MTS/IEEE Conference and Exhibition (Oceans'2000), Sept. 2000.

[2] M. Caccia, R. Bono, Ga. Bruzzone, et al. Sampling sea surfaces with SESAMO [J]. Robotics and Automation Magazine, 2005, 12(3): 95-105.

[3] J. Alves, P. Oliveira, A. Pascoal, et al. Vehicle and Mission Control of the DELFIM Autonomous Surface Craft [C]//Proc. 14th IEEE Mediterranean Conference on Control and Automation (MED 2006), June 2006.

[4] Piotr Szymak. Course Control of Unmanned Surface Vehicle. Solid State Phenomena. Vol.196(2013): 117-123.

[5] J. Majohr, & T. Buch, Modelling. Simulation and control of an autonomous surface marine vehicle for surveying applications: Measuring Dolphin MESSIN[J]. Advances in unmanned marine vehicles, IEEE Control Series, 2006: 329-352.

[6] Maguer A, Gourmelon D, Adatte M, et al. Flash and /or Flashs Dipping Sonars on Spartan Unmanned Surface Vehicle (USV): A New Asset for Littoral Waters [M]. Turky: Turkish International Conference Acoustics, Istanbul, 2005

Advanced Materials Research Vols. 989-994 (2014) pp 3411-3414
© (2014) Trans Tech Publications, Switzerland
doi:10.4028/www.scientific.net/AMR.989-994.3411

Research on Integrated Application of Multi-display Technology in the Mobile Terminal

Xiaomeng Mao[1,a] Jingao Liu*[1,b]

[1.] Shanghai JianQiao University

[a.] maomxm@163.com, [b.] jgl0000@126.com

Keywords: Multi-display, Mobile Terminal, Instrument

Abstract: Nowadays, the mobile display devices have become the most significant section of the mobile terminal. During nearly a decade development, lots of display technologies have been maturely applied in the mobile terminal instrument. This paper analysis the integrated application of several display technology utilized in mobile devices according to their characteristics, and predict the tendency of their development in the rapidly development stage of 3D display. Mobile terminal has become the mainstream of IT equipment, including intelligent mobile phone, pad computer and so on which is at a rapidly developing stage. On the other hand, currently technology on human machine interaction is concentrated in display devices, touch screen for instance.

Mobile Terminal Technology and Its Development

Multi-display technology has become the concentrated reflection of novel display technology, and the consisted technologies of this are:

Liquid Crystal Display (LCD) Technology

Since the LCD technology firstly emerged in the 1990s, with many technical evolution, as the result of different developing stage, many different products came out and each of them appeared various characteristics, shown in.

Table.1 Selected LCD Technology and Their Characteristics

STN	TFT	TFD	UFB
● Low energy consumption ● Mainly display light green and orange	● Short response delay ● Wider visual angle	● Less energy consumption than TFT ● Higher display quality	● Contrast radio is twice than STN

In terms of manufacturing methodology, two main processes are present below:

Low Temperature Poly Silicon (LTPS): Low temperature poly silicon (LTPS) enjoyed a significant statue in the development of LCD display technology. From the view of technical, LTPS could enhance the transmission capacity of panel so that some complex electric element could connect to the screen directly, which could realizing the function without being depended on the high cost individual parts and complex interfaces.

Continuous Grain Silicon (CGS): By contrast, Sharp's continuous granular crystalline silicon, by contrast, patent technology enables the company to develop than regular LTPS smaller screen size, higher resolution of the display screen, due to CGS could perform better than LTPS in Electron transfer properties.

Organic Light-Emitting Diode (OLED): OLED compared to the LCD manufacturing process is simpler, it only USES two thin film and glass or plastic substrate. Electricity enabled, layers of organic molecular materials will emit light, the display effect than LCD brighter and more exquisite, can also be very obviously save power consumption. Because of the OLED can our own light shine, so there is no used for LCD back light etc.

The laser projection

Using high power laser projection of red, green, blue (three primary colors) monochrome laser as the light source, there are many methods to realize scanning line and field, when the scanning speed

is larger than the critical flicker frequency imaging, can satisfy the requirement of human visual residue, the human eye can be observed clearly. Critical flicker frequency is observed periodic goal just can't feel the blinking frequency.

Due to the laser possesses the characteristics of high brightness, good directivity and the laser projection of long distance, large screen display advantage is unmatched by any other method:

(1) projection can be surface can also be a plane surface, can be a fog (smoke and steam fog), water, also can be metopic, curtain, or flat ground glass, so long as is light scattering material;

(2) By the three primary colors mixed into a rich color hue saturation;

(3) NO afterglow phosphor, background clean, high contrast;

(4) Owing to no need of big heavy screen, the whole system is small and light, easy to carry.

Integrated application of multi-display technology in mobile terminals

In the smartphone or tablet, mobile computing, to achieve different functions, the need to adopt different display technology integration application. In the future, a variety of display technologies to mobile terminals are the carrier play their role. Especially in the area of 3 d display related technology, mobile terminal has its unique advantages, such as can integrate all kinds of sensors, video collection equipment and the new type of display device miniaturization. Under the integrated application of many kinds of display technology, can create a lot of new applications.

The display and lighting related aspects

Mobile terminals such as smart phones in addition to the main display, also need to match other semaphores, message light, signal lights or rechargeable lights and flashing light. Part of the mobile computer keyboard backlighting is needed.

The attached show generally using LED light source, its advantage is that energy consumption is small, can play a prominent role at the same time.

3D Augmented Reality Network Game

3D game refers to give a person with a 3D game feeling. Conceptually, 3D game is using 3D model to make the characters in the game, such as the scene, allowing players to experience in the game three high three dimensions, from different angles for the game. This will greatly increase the degrees of freedom, fun and authenticity of the game. The current 3D game has become the market mainstream type of game.

Combined with the real scene shooting 3D online games can use the 4G era of large bandwidth, bring brand-new feeling, can largely reduce the distance of the people at the same time. Make the game is not only a man and machine communication, more become the carrier of communication between people.

3D Augmented Reality Electronic Commerce

At present, e-commerce site, product distribution and display are mostly based on hypertext links and two-dimensional image, the limitations of the technology more or less restricting the development of electronic commerce.3D with 3D technology as the core of e-commerce, shopping environment and shopping behavior simulation of reality, and through the merchants "face to face" communication interaction with customers, to create a consistent with the reality of the virtual network commercial shopping environment. It not only can show the appearance of the product, quality, comprehensive features, automatic demonstration function and operation method, under certain circumstances may even be able to open the shell to check the internal information. For one commodity, consumers can use their own virtual model fitting; In addition, you can actively match product components, customize their favorite style. 3D augmented reality reflects the e-commerce network economic characteristics of the consumer demand oriented.

Mobile Internet 3D video

Network video is a popular application of the Internet in recent years, the birth of many listed companies such as Youtube and youku potatoes. At home, the network video industry relative good momentum of development, is China's netizens after instant messaging, search, music, news of the fifth largest applications. With the development of the market, users of network video content and

quality also put forward higher requirements; with the rapid development of 3D film and television works, network video industry is gradually introduced into 3 d content.

3D Augmented Reality Mobile Navigation Service

The popularization and application of intelligent terminal, APP development market, make the development of mobile Internet business of 3 d and augmented reality also ushered in the opportunity. Enterprise can with the aid of augmented reality, and make full use of the advantages of apps, on the basis of 3 d display, overlay virtual information, achieve the enhancement purpose to the field of vision, present a more comprehensive navigation information to users, to make up for the current most of the two-dimensional information is not comprehensive.

Mobile terminal display technology development direction

Can a new type of three dimensional display applications on mobile devices at present main direction are based on the plane of 3 d display technology. Based on the plane of 3 d display technology has the following several main developing direction.

Double viewpoint double LCD system

Sharp, one of the design of a single light source by the beam splitter can be divided into two beams, respectively, after both sides mirror reflection as two sides of the LCD background light, to illuminate two LCD, again through the beam splitter can be divided into two beams of light. If the two sides about a pair of 3 d image of LCD, is in the figure shows the eye will see stereo images. This method has the advantages of high brightness, high resolution, but can only be seen in a specific location stereo effect

Double viewpoint single LCD system

Barrier Gate System: In the barrier gate stereo display system, barrier gate can be placed in front or rear of the observer LCD, studies have shown that front grating can be made to observe the visual areas achieve good observation of light intensity uniformity and observe the effective width, and then set about grating can make the image of interference is smaller. Usually adopt the front barrier gate to achieve stereo display.

Micro Lens Array Design: Micro lens array is similar to barrier gate, also have a stagger around view sequences were projected to the left and right eyes visual function. Besides have the characteristics of principle of barrier gate, Polaroid stereo display can also adjust the Polaroid polarization direction of the transition of 2 d and 3 d display mode, which is one of the advantage of its application prospect is good.

Multi-view System: In order to realize many different angles to watch different image at the same time closer to reality. The PHILIPS Company of stereo display technology research is based on the traditional method of micro cylindrical lens. The company auto stereoscopic LCD monitor is in front of the LCD screen, add a layer of micro cylindrical lens make LCD screen like plane on the focal plane of the lens. Under each column lens are divided into several sub pixel, pixels of the image that can be in a different direction projection lens each pixel, eyes watch display, from different angles to see different sub pixel.

Four perspective stereo display device

Japanese Sanyo in 2004 put forward a four Angle of stereo display device, this method is similar to PHILIPS method on the basis of the principle of micro lens. Through four cameras placed side by side, 4 parallax image of target is obtained through format conversion, the four picture pixel level and horizontal staggered to flat display device, which can be seen in the three visual areas target different perspective of the three-dimensional images. It draws on multi-view stereo display method of the PHILIPS company could realize in the barrier gate, this method also has the same border stripe down and image deformation reduced proportion.

NEC LCD Technology HDDP Three-Dimensional Display

Announced in October 2008, NEC LCD technology, successfully developed the naked eye can see the three-dimensional image 31 cm (1211) in amorphous silicon TFT LCD screen, 800 @ 600 pixels (SVGA), mainly used for movies and games and other entertainment, Digital Signage

(Digital Signage), and industrial use CAD and resolution of images for medical use of industrial equipment and so on.

The integration of a variety of display technology in the Pudong new area

A variety of display technology in the Pudong new area has been part of relevant enterprises, how to promote the enterprise application and technology integration development, the relation between the whole display industry and mobile Internet industry is very important. With the advantages in the Pudong new area, existing relevant enterprises and economic development, the integration of a variety of display technology development is in the following aspects worthy of attention.

3D display technology is to be active and to the naked eye 3D. From a technical point of view, glasses-free 3D technology is the trend of the development of the 3D; And from the perspective of the consumer need to wear special glasses in order to appreciate the elegant demeanor of 3 d technology, there is the inconvenience of use. And 3D content is also the important driving force of the 3 d technology, the advance of the Pudong new area, including science and technology museum, the exhibition group such as exhibition could combine related 3 d content, the popular science activities, should be able to promote the promotion of new display.

As the 4G mobile communication standards and the development of the three-dimensional Internet business, mobile terminal hardware platform put forward higher request to the user. Pudong new area of the application of various IT leading enterprise for a variety of display technology even more consideration to the new hardware and software combination of the audience.

Facing the challenges of the battery, introduction and use of all kinds of new business need durable high capacity battery, 3G, the big screen, data interaction and the future of open 3D technology puts forward higher demands on batteries. Now is still the mainstream of the market, lithium-ion batteries in the battery itself under the condition of performance is not strong, mobile phones more and more thin, more and more light, the battery will only become more and more small room to play. With the development of battery technology, in addition to lithium batteries, lithium polymer battery, fuel cells, biological cells, solar cells, such as technology also in development, but do not have it in mobile terminal to realize the commercial scale. How to provide more sufficient power for mobile phones, so as to prolong the life time of the mobile phone, will be a worth studying for a long time.

References

[1] He Fengtao, Jia Qiongyao, Sun Linjun. Liquid Crystal Laser Projection Display System Design [J], Infrared and Laser Engineering. 2010.10

[2] Sun Lingsheng, Nan jinshi, Xun Xianchao. The Current Research Status of 3-D display technology [J]. China Optics and Applied Optics. 2009.4

[3] Tan Ran, Xiong Xiong. Efficient Display Strategy Research based on Mobile Terminals [J]. Application Research of Computers. 2008.2

[4] Guo Jing. Mobile terminal oriented pseudo three-dimensional image processing technology research [J]. Shanghai: Shanghai Jiaotong University, 2011

Advanced Materials Research Vols. 989-994 (2014) pp 3415-3418
© (2014) Trans Tech Publications, Switzerland
doi:10.4028/www.scientific.net/AMR.989-994.3415

Design of remote monitoring system of temperature and humidity based on Internet of things technology

Lei Wang*

School of Jianqiao University, Shanghai 201319, China

*gench_wl009@126.com

Keywords: The Internet of things, Sensor, The AVR kernel, RS485 bus.

Abstract. Design a things related technology based on remote monitoring system of temperature and humidity, sampling using SHT10 digital temperature and humidity sensors, temperature and humidity variables, and data transmission through the RS485 serial bus interface, using AVR kernel 8 bit chip for processing, resulting in a host computer display temperature and humidity changes, the indoor multi node the environment through the test, system has stable function, good display data change, relatively low cost advantages.

Introduction

Temperature and humidity monitoring production industry in the people's home life,, has great application prospect in agricultural planting and other aspects, the traditional application in the monitoring of temperature and humidity is mainly depend on the mercury thermometer and hygrometer for observing and recording, the disadvantage is the interpretation of data are inaccurate, can not be real-time monitoring, and the data cannot be automatic electronic processing. Through the use of Internet technology, the system integrates the embedded technology, sensor technology and remote transmission technology, to achieve the larger space humidity automatic monitoring, real-time display of curves, and corresponding control functions.

The sensor system design for digital temperature and humidity sensor [1], type SHT10, this kind of digital temperature and humidity sensor can be directly detected data is output using the digital quantity, check on the sensor before they leave the factory, the user does not need to check operation.

System composition

This system mainly consists of four parts, one is the information collecting part, use SHT10 digital temperature and humidity sensor of indoor temperature and humidity data acquisition, and data processing unit, used by the Atmel Corp's ATMEGA48PA as the main chip, the data transmission part, uses the RS485 serial bus standard, the fourth is the result of display unit, display and graphical display using the PC software for temperature and humidity. The system according to the environmental space size selection of node set series network structure, to realize the automatic monitoring of operating temperature and humidity multi node.

The hardware design

The main chip. In this system the main chip selected 8 bit AVR processor produced by Atmel Corp, this processor is the AVR enhanced RICS structure for low power 8 bit micro controller based on CMOS, AVR kernel has a rich instruction set with 32 general-purpose working registers, all registers are directly connected to the arithmetic logic unit, so that an instruction can be two independent registers to be accessed in one clock cycle, the system circuit diagram is shown in figure 1.

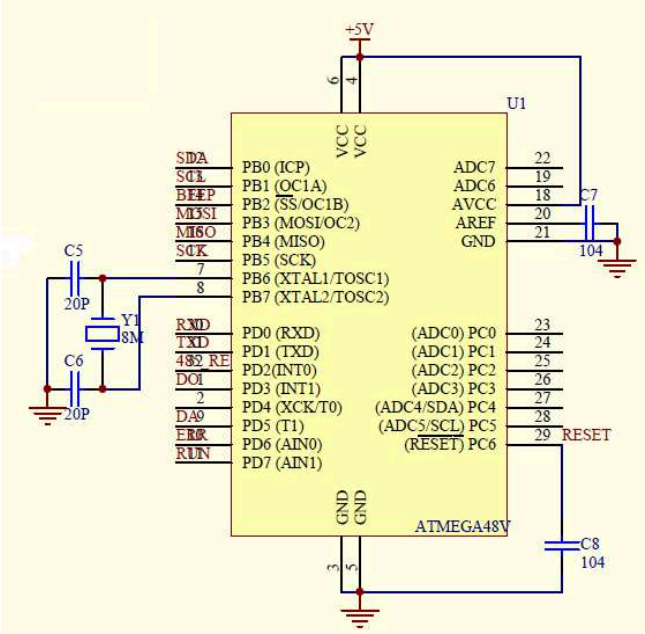

Fig. 1 The circuit diagram of the main chip

Temperature and humidity sensor. This system adopts the SHT10 digital temperature and humidity sensor as signal acquisition unit, the sensor has a free debugging, calibration free, the measurement resolution can be programmed, the ultra small package size etc.. The sensor and integrated temperature and humidity sensors, humidity measurement operation can be used for temperature compensation, and can provide high quality of dew point calculation function, high measuring accuracy, is a preferred equipment [2] a variety of temperature and humidity testing applications. The typical application circuit diagram is shown in figure 2.

The power supply voltage of the sensor is 2.4 to 5.5V. Sensor after power on, wait for the 11ms to cross the dormant state. No need to send during any instruction. Power supply pins (VDD, GND) can increase the capacitance of a 100nF, for decoupling.

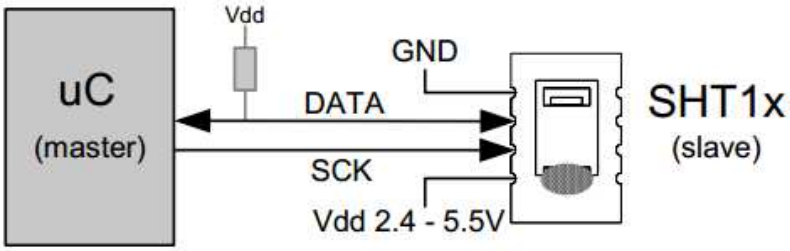

Fig. 2 Typical application circuit diagram

RS485 serial bus. Because the system needs to carry on the real-time monitoring of each node in a large space, the communication distance is long, therefore the RS485 bus mode for data transmission, RS485 a balance to send and receive difference, therefore has the ability to reject the common mode interference. RS485 uses half duplex mode, any time there can be only one point in the sending state, therefore, sending circuit required by the enable control signal. And RS485 can network constitutes a distributed system, the theory allows up to 32 parallel drive and 32 receiver, to ensure the reliability of data transmission, generally only connect the 8-16 node [3]. For temperature and humidity monitoring system of multi node, the node number is enough, circuit diagram is shown in figure 3.

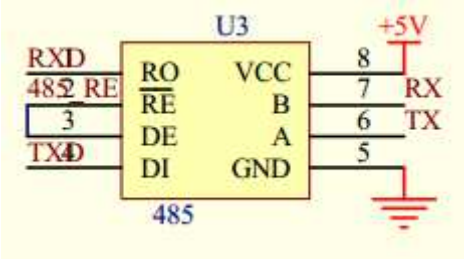

Fig. 3 RS485 circuit

Software design

Software design of temperature and humidity monitoring system mainly refers to the design of PC, the PC software for RS485 bus address settings, real-time changes and to monitor the indoor temperature and humidity through the graph, showing the effect of Figure 4 is shown in figure.

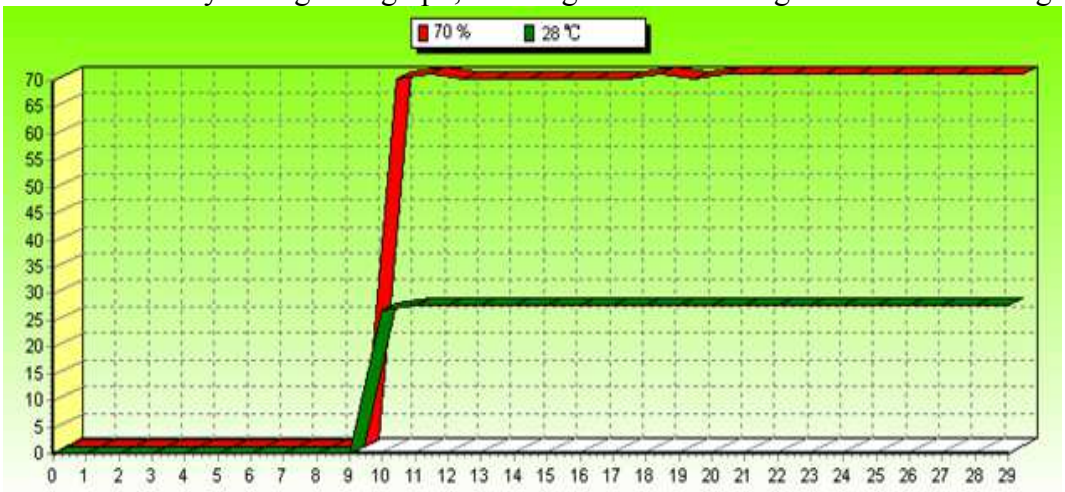

Fig. 4 Temperature and humidity state curve

The actual test result values in the software design program needs, by formula conversion mode is converted into real values, and displayed in the graph, the conversion code is as follows:

```
void SHT10_Cal(void)
{
   float RH_Lin;
   float RH_True;
   float Temp_C;
   Temp_C = -40.1 + 0.01 * temp;
   RH_Lin = -2.0468 +0.0367* duty + -0.0000015955 * duty *duty;
   RH_True = (Temp_C - 25) * (0.01 + 0.00008 * duty) + RH_Lin;
   if( RH_True > 100 ) RH_True = 100;
   if( RH_True < 0.01) RH_True = 0.01;
   temp = 10*Temp_C;
   duty = 10*RH_True;

}
```

Conclusion

This system after several tests, the operation performance of normal and stable, can view real-time temperature and humidity information of different nodes through the PC software, the humidity range from 20% to 90%, the precision is 0.3%, the temperature range of - 55 ° C to +125 ° C, precision is 0.1 ° C, system features such as:

(1) through the use of RS485 serial bus mode monitoring distance increases, can set the number of monitoring nodes in different regional indoor, so as to ensure the full monitoring of the environment.

(2) the system more flexible, only need according to the actual demand of new monitoring nodes, and the nodes can be connected in series by mode of access system.

(3) the system uses digital temperature and humidity sensor, improves the temperature and humidity monitoring accuracy, and can accurately display real-time curve.

(4) the PC software has the advantages of simple operation, the changes of temperature and humidity conditions can each node real-time monitoring, and display it in the most intuitive diagrams.

(5) the AVR kernel chip, 8 bit, low cost, system scalability.

Reference

[1] Liu Ximing. Chinese Journal of scientific instrument, Vol.28(2007).No.4,p53
[2] Wu Yukang. automation panorama,Vol.4(2010).No.4,p99
[3] Ma Dong. China agricultural chemical daily,Vol.34(2013).No.2,p121

Advanced Materials Research Vols. 989-994 (2014) pp 3419-3422
© (2014) Trans Tech Publications, Switzerland
doi:10.4028/www.scientific.net/AMR.989-994.3419

The design of intelligent Home Furnishing system of Internet of things

Lei Wang*

School of Jianqiao University, Shanghai 201319, China

*gench_wl009@126.com

Keywords: The Internet of things, intelligent Home Furnishing, CC2530 chip, GPRS, ZigBee.

Abstract. Through the market investigation was designed based on the environmental monitoring system, intelligent control system and simulation system of security system, intelligent Home Furnishing system, this system uses CC2530 and sensors to build a ZigBee network, and realizes the remote monitoring through GPRS module, configuration of the PC software for the system, realized the function of intelligent furniture system through the actual test, that, the system is stable and reliable, practical.

Introduction

The Internet of things is called following the computer, the Internet, the third wave of global information industry. At present, many countries have spent vast sums of in-depth study, the Internet of things is a new technology system is composed of the fusion of several information technology into.

The so-called Internet by means of radio frequency identification (RFID), infrared sensors, GPS, laser scanners and other information sensing device, as agreed in the agreement, any objects connected to the Internet, the exchange of information and communication, to realize intelligent identification of objects in a network positioning, tracking, monitoring, don't and management [1] .

The key technology of things including RFID technology, sensor technology, wireless sensor network technology, intelligent technology and network communication technology etc.. RFID technology, also known as electronic tags, radio frequency identification, is a kind of communication technology, through the specific target radio signal recognition and to read and write data, between without recognition system with specific target to establish mechanical or optical contact. Commonly used with low frequency, high frequency, ultra high frequency, passive technology, RFID reader is divided into fixed and portable, the application of RFID technology is very broad, such as: library, access control system, food safety traceability [2].

Sensor technology is one of the basic technology of the Internet of things, perception layer in the IOT architecture [3]. As the basic unit of IOT, sensors in the network information collection level, can complete the data acquisition, has become the key to the success or failure of the physical network. Sensor is one kind of the signal measured specific, according to certain rules to convert a signal output device or devices available, to meet the information transmission, processing, recording, display and control requirements. The types of sensors and expansion, there is a common temperature sensor, humidity sensor, a pressure sensor, a light sensor, displacement sensor, ultrasonic sensor, gas sensor etc..

System architecture

Intelligent Home Furnishing called wisdom Home Furnishing or intelligent residential, said Smart Home in foreign countries. Approximate and intelligent Home Furnishing meaning of home automation (Home Automation), electronic family (Electronic Home, E-home), digital home (Digital Family), the home network (Networks for Home), intelligent home/building (Intelligent Home/Building), in China Hongkong and Taiwan areas, and digital home, digital Home Furnishing known method .

Generally speaking, intelligent Home Furnishing or intelligent residential (Smart Home), is based on the family home as a platform, the use of advanced computer technology, Internet technology, wireless communication technology, sensor technology and modern control technology, will be associated with Home Furnishing life of household electronic equipment (such as lighting, security, network appliances, information exchange) and other organic combined together, and the control and management of centralized on it, so as to create efficient, comfortable, safe, convenient, environmentally friendly living environment [4].

This system through the variety of the intelligent products and systems available on the market are analyzed, combined with the relevant systems have advantages and disadvantages, puts forward a solution of intelligent Home Furnishing system, the program will focus on four major subsystems, and the modular approach to the design and production of the whole, consists of four subsystems specific (1) environmental monitoring system; (2) the intelligent control system; (3) intelligent security system; (4) subsystem scene simulation. The so-called modular approach refers to the scheme will be intelligent Home Furnishing system as a pineapple, each intelligent Home Furnishing equipment as one of the pieces, the backbone of the four subsystem modules can be installed in accordance with the requirements based on the random selection of users, so you can Home Furnishing flexible intelligent system design according to the different needs of different users, in order to improve the system of intelligent Home Furnishing audience and user acceptance.

Four subsystems of intelligent Home Furnishing system is at the core of the program, the content of the relevant environmental monitoring system is introduced, based mainly is carries on the real-time monitoring of the home environment, the monitoring content can include temperature, humidity, light monitoring, dust monitoring, voice monitoring, and related monitoring may include single point monitoring and multi-point monitoring, can use a single sensor or multiple sensors for environmental monitoring data real-time statistics, and ultimately can conduct real-time broadcast by voice.

Intelligent security system is security, mainly refers to the use of the Internet of things technology security configuration on the family, to prevent theft, fire and other incidents, the specific prevention include fingerprint access control, door sensor, vibration sensor alarm, gas, fire, smoke alarm, infrared sensor, a human body induction, infrared curtain alarm, surveillance camera, voice control etc..

Intelligent control system mainly refers to the use of various control of all kinds of household appliances in Home Furnishing, specific control mode can include a universal remote control, Webpage mode control, mobile phone text messages and voice control etc..

Scene simulation system mainly refers to the joint operation of multiple functions, to realize the simulation of the scene, such as home mode, automatic turn off all lights, close the curtains when the user home; home mode, when the user back home, automatically open the curtains opened, lighting, background music etc..

Through the matching of the four subsystems, combined with pineapple Modular Intelligent Home Furnishing system model, the Internet of things technology applied to the intelligent Home Furnishing system, which provides a convenient, comfortable, intelligent living environment for users.

The hardware design

The main chip selection : This system takes into account the actual demand and cost when designing, we select STM32F103VCT6 as the micro controller, the chip is STM32F103 enhanced series, the use of high performance ARM Cortex-M3 32 bit RISC kernel, the frequency of 72MHz, built-in 256K cache, enhanced I/O port and connected to the two APB bus. Rich. STM32F103VCT6 can be connected with the two oscillator provides clock source for internal system, one is the external clock frequency for high speed, provide accurate for the system, because the chip of STM32F103 enhanced series, so the clock frequency is 72MHZ, the most typical of 8MHZ crystal, the frequency of the mode reached 9 the frequency of the requirements; second is the low external clock, the frequency of quartz crystal 32.768MHZ, used to provide precise calendar clock function for the system, and in the design

of the crystal is equipped with a battery, even if the accuracy of power down still can ensure the system clock. In addition, when designing the pin on the chip part was redefined.Chip design installation of reset circuit, the circuit design of the 14 pins of the chip is connected to a 10K resistor and a 104 capacitor complete reset circuit mainly by.

ZigBee wireless transmission module : ZigBee wireless transmission module in the intelligent Home Furnishing application widely, due to its advantages of flexibility, low power consumption and is widely used in the ZigBee chip, the CC2530 chip, the chip uses a system of the new generation SOC 2.4GHz, and also with the TI TI yellow gold unit ZigBee protocol stack and the Remo TI, you can supports the IEEE 802.15.4 standard, can provide a powerful and complete solutions in the ZigBee and ZigBee RF4CE remote control applications.

The GPRS module： The system requires the use of Short Message mode in the design of real-time information query and Short Message alarm, so the design increases the GPRS module, then chose Shenzhen Fangyuan company production of GU900D models, the model contains the DTU (data terminal equipment) function, and use the AT command to control, send for example use the AT+CMGS command can be Short Message. Circuit diagram is shown in figure1.

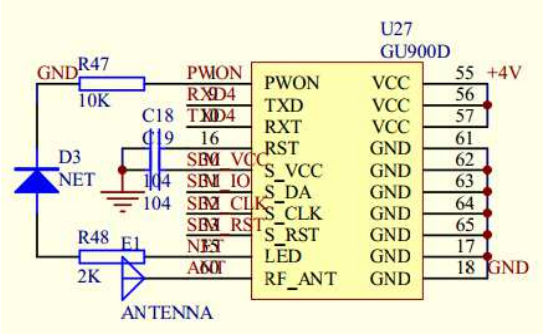

Figure 1. GPRS circuit

RS-485 bus module circuit design: This system when designing, system requirements of communication distance, so give up the traditional RS-232 bus interface and the RS-485 bus interface, the interface a balance to send and receive difference, therefore has the ability to reject the common mode interference. Bus transceiver coupled with high sensitivity, can detect voltage as low as 200mV, so the transmission signal can be recovered in kilometers. The RS-485 bus interface using half duplex mode, any time there can be only one point in the sending state, therefore, sending circuit shall be determined by the enable signal to control. RS-485 is used for the multipoint interconnections is very convenient, can save a lot of signal lines. The system uses the MAX3485 chip in RS-485 bus circuit design, the chip is required to power the 3.3V, transmission bandwidth is 10Mbps. Circuit diagram is shown in figure2.

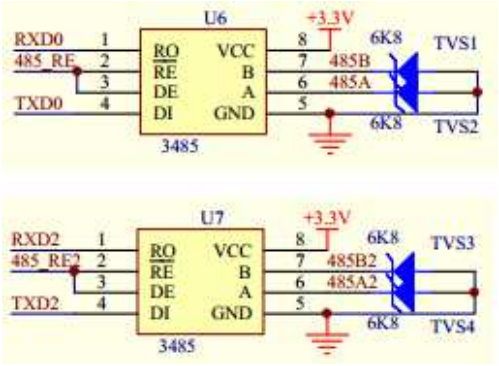

Figure 2. RS-485 bus module circuit diagram

Software design

The design of the control software of GPRS : Remote control in this system using the GPRS module of the system, through the use of Shenzhen GU900D model GPRS module and a radius of the

company production to complete the send and receive Short Message, first set the GPRS to Short Message mode must be in Short Message query, then the mobile phone SIM card into the GPRS module supporting the card slot, card send a message to the SIM through Short Message, specific code is as follows:

```
void send_sms(char * dh,char * smstxt) {
if (sms_from[0]==0) return;
      sprintf(send_buf5,"AT+CMGS=\"%s\"\r",dh);
      send_len5=strlen(send_buf5);
      mysend5();
   Delay(300000);
      sprintf(send_buf5,"%s\x1A",smstxt);
      send_len5=strlen(send_buf5);
      mysend5();
   Delay(300000);
}
```

The design of PC： The PC software mainly realizes the functions including real-time intelligent query Home Furnishing environmental information, including indoor temperature, humidity, brightness, and can change curve view environment, such as the opening and closing of the curtain by the control of the relay, the light open and close, and all kinds of home appliance control operation, and also can realize personalized customization by PC software, simulated operation of different users to achieve a different scene, the test results show that, the system can meet the demand of real-time monitoring and remote control of intelligent Home Furnishing system, realize the perfect combination of GPRS and ZigBee technology.

Conclusion

Through the analysis and Research on the networking intelligence Home Furnishing system, puts forward a set of intelligent Home Furnishing system based on four basic subsystem, the main control board, ZigBee module, GPRS module, various types of sensors as a basic hardware and software system design, PC, perfect control function of intelligent Home Furnishing system, after the completion of system development, through the long time experiment show that the system is running stable, easy operation, strong practicability, has higher application value.

Reference

[1] Wen Jiabao.*2010 years the government work report* [EB/ OL]. (2010.03.15)
[2] Kang Dong:*Radio Frequency Identification (RFID) Core Technology And Typical Application Development Case*(Beijing 2008).
[3] Wang Zhi Liang: *Network Engineering* (Beijing 2011).
[4] Gao XiaoPing: low voltage electrical apparatus. Vol.4 (2005),No.4,p.18

Advanced Materials Research Vols. 989-994 (2014) pp 3423-3426
© (2014) Trans Tech Publications, Switzerland
doi:10.4028/www.scientific.net/AMR.989-994.3423

Transmission Delay Monitoring Method in Intelligent Substation

Xiaohui Song[1, a], Zhizhong Guo[1] and Guobin Li[2, b]

[1] Department of Electrical Engineering, Harbin Institute of Technology, Haerbin 150001, China

[2] XJ Electric Corporation Limited, Xu Chang 461000 , China

[a]xiaohuis@xjgc.com, [b]guobinl@xjgc.com

Keywords: Delay Monitoring, Transmission, Intelligent substation

Abstract. In view of the current situation of the development of smart substation, this paper analyses the standing domain information sharing, information network transmission delay effects on substation protection system. Based on above, advances the information transmission time delay of the solution. This paper uses the accurate computing information packet switches reside within the delay ΔT and into the sampling value (SV) message, giving to protection device. Protection device dependent on local time benchmark, the use of MU inherent latency and link to reside the total delay ΔT reduction received multiple interval sampling data of the moment, on the basis of implementing protection control function.

Introduction

In Intelligent substation, the protection and control equipment are in need of the amount of multiple communication collected information, to complete the accident analysis, monitoring, control, data analysis, etc. Therefore, MU, protection and control equipment in substation requires accurate clock synchronization and accurate absolute time scale. MU output data synchronization in intelligent substation quality mainly depends on the following link: (1) master clock satellite signal; (2) the clock signal extension equipment; (3) MU synchronous signal connection; (4) to protect the sync signal connection

Ethernet communication technology due to its low cost, good openness, easy interface etc, obtained the rapid development in the field of network communication, more and more business data transmission based on Ethernet communication technology load. Based on Ethernet communications network layer adopts Ethernet switches as a general network transmission equipment, but as a result of general Ethernet switch based on store and forward exchange principle, theoretical analysis, the transmission delay of precise monitoring more difficult. So for the application of intelligent substation difficult.

Transmission delay in intelligent substation

The intelligent substation relay protection adopts the model of "network mining network jump" the biggest obstacle lies in the fact that span intervals protection must rely on external clock, to ensure the synchronization of sampling data, when loss of external clock or external clock malfunction, across space protection will run out. So have to delay uncertainty analysis.

Analog samples values cooperation unit and phase compensation and synchronous sampling, to the process bus transmission through Ethernet frame format SV, message transmission time delay in the transmission process of Td, namely the sending node application sends a message to the receiving node application receives the packet interval, involving different physical devices (such as Ethernet switches) communication processor working time delay and network transmission delay, packet delay t1 and t2 processing. Delay of message handling, mainly including the sending node communication processor protocol package delay t1 and receiving node communication processor to unpack the delay t2, associated with the software and hardware design and performance of communication processor, use appropriate microprocessor, real-time operating systems and protocols for efficient

encoding/decoding algorithm ensures the t1 / t2 values of certainty. Switches, for example, the delay of message handling, t1, fixed size depends on the switch chip processing media access control address table, virtual local area network (LAN), priority functions such as speed, general industrial Ethernet switch message processing delay no more than 10 mu s.

2）Delay the TSM message sent. Switches use a store-and-forward mechanism, after receive the complete data packet to forward data packets, and to support different rates port between the exchange of data message, keep high speed between the port and low-speed port work together. Store and forward the data packet delay caused by the TSM related to data packet length, data rate r L, can be said for the TSM = L/r.

3）Message transmission delay of tp. Physical device between the data message to close to the speed of light propagation in optical fiber links the time required for the tp, WAN (wide area network, WAN) cosco distance propagation delay of ms, and LAN (local area network, LAN) in the propagation delay, generally only several or dozens of mu mu s s, the proportion of the whole communication delay is small. Tp physical properties depend on the size of the link and the propagation distance, has nothing to do with the transmission of information, assuming that the physical distance between source port and destination port for D, the speed of light is c, transmission medium correction coefficient for k (about 0.65 k) in the coaxial cable, propagation delay can be represented as tp = D/(kc).

Delay calculation

"Network mining network jump" mode, the sampling data packet transmission depend on the switch, and the message transmission delay is uncertain in the switch, so when the external clock loses, protective device cannot judge whether the sampling data synchronization.

Through exchange report transmission time delay method can solve this problem, principle is the precise resides within the message on the switch delay Δ T and into the SV message, protection device dependent on local time benchmark, use MU inherent latency and link to reside the total delay Δ T reduction received multiple interval sampling data of the time, complete the sampling values of synchronous processing.

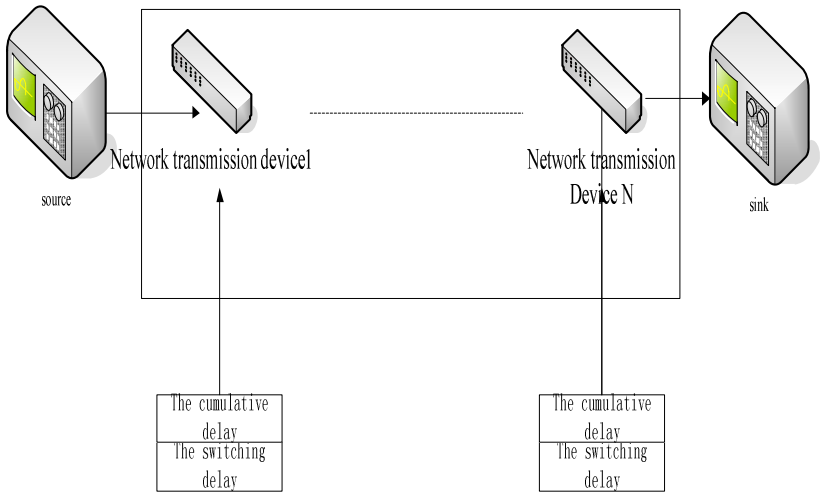

Fig. 1 Transmission system

Based on switched Ethernet network technology, application of the link layer communication mode, and there is higher demand for real-time data transmission of business data transmission system, as shown in figure 1, including source equipment, among a number of network transmission equipment and obtaining-information equipment, from the source device from the carrier Ethernet data frame message through all levels of the middle layer network transmission equipment, network transmission carrier equipment using Ethernet data frame packet link layer reserved bytes of storage

when extension store-and-forward delay at all levels, and obtaining-information end equipment through to get the information from the source to the obtaining-information accurate delay, so as to realize switched Ethernet in the link layer communication of accurate delay monitoring.

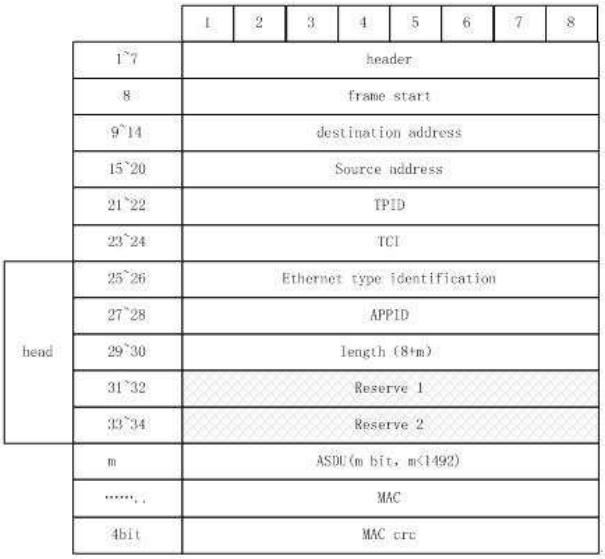

Fig. 2 Frame format

Ethernet link layer communication data frame format shown in figure 2, the 31 ~ 32 bytes and 33 ~ 34 for the Ethernet packet header reserved four bytes, in specific business applications, in do not break general definition, compatible with ordinary Ethernet, on the basis of data frame format, message to achieve accurate monitoring of transmission delay information, can be the proprietary defines four bytes, this is also one of the key points of this invention.

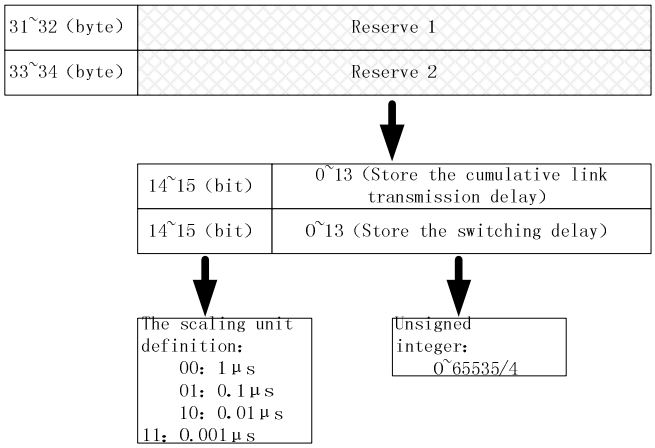

Fig. 3 Cumulative link transmission delay

Four bytes can be divided into two groups, respectively for MouJi/jump to store intermediate network transmission equipment of the cumulative link transmission delay (from the source to the level/jump all transmission delay between the transmission equipment accumulation) and dance at the corresponding level/transmission equipment switching delay (this value depends on the transmission equipment's data exchange mechanism, such as store and forward, or address passthrough, etc.), a detailed description is shown in figure 3.

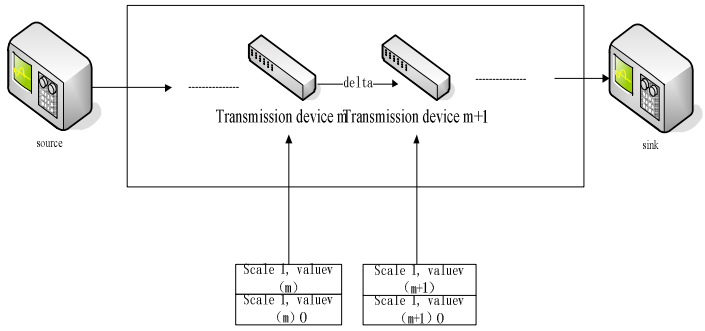

Fig. 4 Application system

In order to ensure the accuracy of transmission delay of storage, the invention adopts scale mode of two time delay of the deposit, concrete is: double byte high two type definition for scale, is divided into four kinds, representing 1 microsecond, 0.1 microseconds, 0.01 microseconds, 0.001 microseconds. After the double byte 14 for deposit after the scale of values, use unsigned integer way, value range of 0 ~ 65535/4.

Conclusion

In this paper, the information delay solution. This paper uses the accurate computing information packet switches reside within the delay Δ T and into the SV message, giving to protection device. Protection device dependent on local time benchmark, the use of MU inherent latency and link to reside the total delay Δ T reduction received multiple interval sampling data of the moment, on the basis of implementing protection control function.

Based on the information described in this article, therefore, delay the solution can be in a new generation of intelligent substation system application. According to station domain sharing information, realizes the fault points of fast, accurate and reliable isolation. Improve the performance of relay protection, in order to meet the requirement of large complex power grid safe and stable operation.

References

[1] WANG Bin, DONG Xinzhou, XU Fei, Analysis of Data Sharing for Protection and Control System in Smart Distribution Substation[J]. Proceedings of the CSEE 2011.31: 1-6.

[2] MA Jing, ZENG Hui-min, LIN Xiao-hua. A novel wide area backup protection for multi-terminal transmission lines system Power System Protection and Control. 2012, 40(11): 61-69.

[3] Li Zhenxing, Yin Xianggen, A Study of Wide-Area Protection Algorithm Based on Integrated Impedance Comparison, [J].TRANSACTIONS OF CHINA ELECTROTECHNICAL SOCIETY, 2012, 27(8) : 179-186.

[4] Jiang Xianguo, Wang Zengping, Zoning Scheme of Regional Autonomy Backup Protection, [J].TRANSACTIONS OF CHINA ELECTROTECHNICAL SOCIETY, 2013, 23(1) : 234-241.

[5] CHEN Zhao-hui, ZHAO Man-yong, ZHOU Hong-yang, Research and implementation of network protection system based on integrated and wide area information[J]. Power System Protection and Control. 2009, 37(24):106-108,113

[6] LI Zhen-xing, YIN Xiang-gen, ZHANG Zhe, WANG Yu-xue Hierarchy of wide area protection system based on multi-Agent[J]. Power System Protection and Control. 2012, 40(4):71-75

Advanced Materials Research Vols. 989-994 (2014) pp 3427-3432
© (2014) Trans Tech Publications, Switzerland
doi:10.4028/www.scientific.net/AMR.989-994.3427

Study of maximum power point tracking control based on GRNN neural network

Liu Kun[1,a], Ji Tongzhou[1,b], Li Xianyun[2,c], He Xiongfeng[1,d], Zhang Mei[1,e]

[1]School of Electrical & Automation Engineering, Nanjing Normal University, Nanjing 210042, China

[2]School of Electric Power Engineering, Nanjing Institute of Technology, Nanjing 211167, China

[a]liukunstyle@gmail.com, [b]61035@ninu.edu.cn,[c]alixy@sohu.com,[d]he_xiongfeng@163.com, [e]sunymei2014@163.com

Keywords: Maximum power point tracking, Neural network, Photovoltaic cells

Abstract. detailed analysis of mathematical model, expounded maximum power point tracking (MPPT) control principle, then a improved constant voltage tracking of maximum power point tracking control based on GRNN neural network is proposed, this control strategy uses predicted voltage of GRNN neural network to instead of constant voltage, has be simulated in Matlab /Simulink, and result is this MPPT method can be more accurate compared to traditional control strategy.

Preface

Energy is a shield of our Social stability and economic development, and improves the quality of our lives. With the rapid population growth and urban modernization, meeting the energy demands of a big city becomes a formidable task. The world relies on oil, coal and gas for about 80 percent of its energy, but these non-renewable energy resources produce considerable pollution in process of using. More and more people are concerned about Solar energy due to its vast and easily accessible reserves, Study of MPPT control has become research hotspots in order to achieved higher conversion rate for turning light into electricity.

Analysis of Solar cell output characteristics

Photovoltaic cell is core research content of photovoltaic power generation system, the output characteristic of photovoltaic cells is nonlinear, this is because photovoltaic cell is greatly affected by the external factors such as strength of illumination and temperature, the following is the equivalent circuit diagram of photovoltaic cells[2].

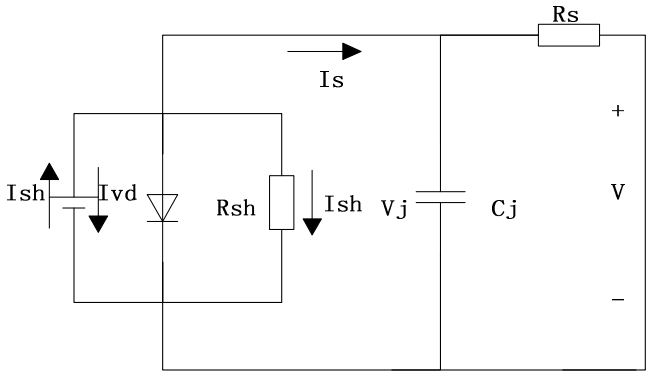

Fig. 1 PV equivalent circuit

In this figure, Rs is series resistor of circuit, its resistance is less than 1Ω, Rsh is parallel resistance of thyristor, it has bigger resistance value, Cj is junction capacitance, resistance of Rsh and Rs can be ignored in the simplified circuit. The simulation model is built in Matlab /Simulink and get output curve of photovoltaic cells through the simulation[1].

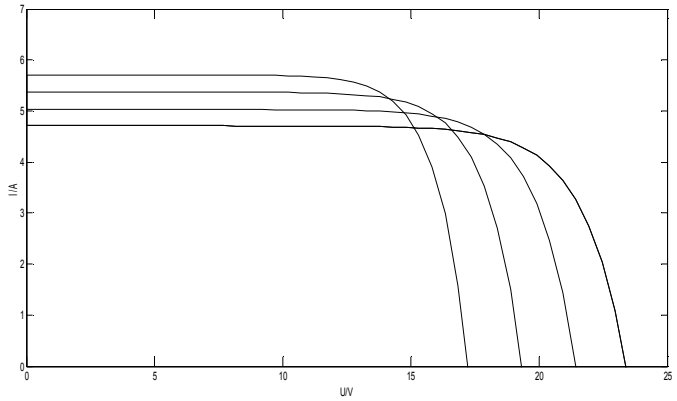

Fig. 2 I-V characteristic curve

I-V characteristic curve as shown in Fig.2, the working current of photovoltaic cells is stable at first, when the output voltage increases, output current is decreased and become zero eventually.

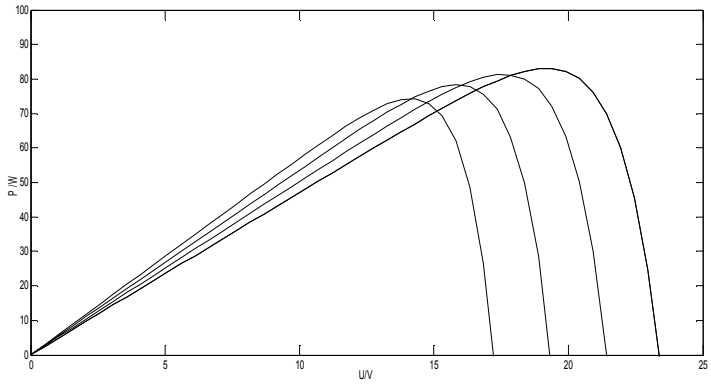

Fig. 3 P-V characteristic curve

P-V characteristic curve as shown in Fig.3, the output power increases as the voltage increases, and reaches a maximum value at a fixed voltage value, then output power is reduced when voltage increases continuously.

Based on the analysis above, we can conclude that the maximum power point of photovoltaic cells exists. In order to improve the efficiency of photovoltaic power generation, photovoltaic power generation always working at maximum power point is important[3].

Principle of MPPT

The output characteristic of photovoltaic cells is nonlinear, short-circuit current and open-circuit voltage are significantly affected by strength of illumination and temperature, the output power of photovoltaic system is unstable due to this reason. As is known to all, the external environment of photovoltaic cells changes quickly, in order to reduce the power loss and improve energy conversion rate, making adjustments according to this change is necessary. Even if strength of illumination and temperature remain unchanged, the output power will change as well due to variation in load, for this reason, to ensure photovoltaic power generation works at maximum power point, photovoltaic system and load cannot be directly connected.

According to relevant conclusion of circuit, when the output resistance of photovoltaic cells is equal to equivalent resistance, photovoltaic cells output maximum power. In real terms, equivalent resistance of household appliances is random, and internal resistance of inverter and storage battery will change in the process of using, these reasons account for load change of photovoltaic cells, so the principle of MPPT as follows:

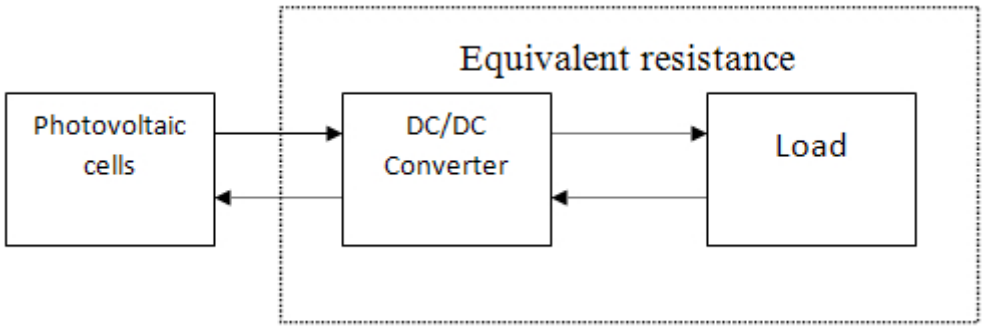

Fig. 4 PV system structure diagram

In Fig. 4, if DC/DC converter and load of photovoltaic cells is equivalent to resistance, according to theory of power electronics, output impedance can be changed by adjusting DC/DC converter duty ratio. The key of MPPT is adjusting DC/DC converter duty ratio by control strategy, when output impedance of photovoltaic cells and equivalent impedance are equal, photovoltaic power generation system works at maximum power point

MPPT control based on GRNN neural network

With the development of artificial intelligence, learning ability and predictive ability of artificial neuron was found, inputs and outputs of nonlinear system can be simulated by artificial neuron. So this paper presents MPPT control algorithm based on GRNN neural network, utilizes GRNN neural network to predict working voltage of the maximum power point. Using this predicted value to instead of the fixed voltage of constant Voltage Tracking will improve control accuracy.

Principle of GRNN neural network. GRNN is shorted for General Regression Neural Network, it is a new neuron structure proposed by Donald • F • Specht and based on nonlinear regression theory. GRNN neural network has fast learning speed and better predictive ability compared with BP Neural Network and RBF Neural Network. This neural network has only one adjustable parameter and less thresholds, and learns relying on sample in the whole learning process, so the influence of human factors is slight.

GRNN neural network and RBF neural network are similar in network structure, includes input layer, pattern layer, summation layer and output layer.

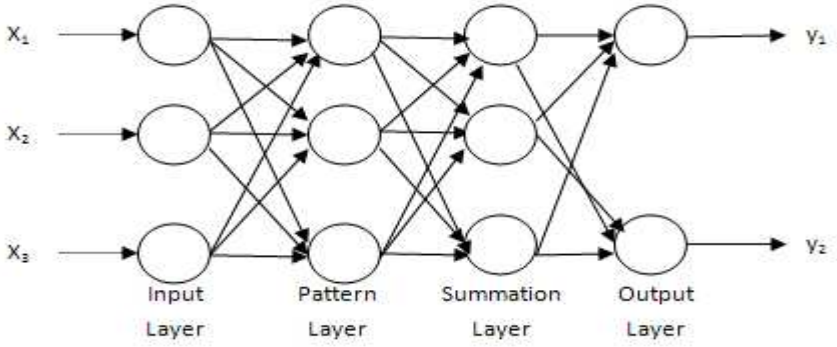

Fig. 4 Structure of generalized regression neural network

The number of input units is equal to the number of input variables, the control strategy mentioned in this paper has two input variables, one is temperature and the other is strength of illumination.

The number of pattern layer units is step with the number of learning samples, transfer function of pattern layer is as follow:

$$p_i = \exp[-\frac{(x-x_i)^T(x-x_i)}{2\sigma^2}] \quad (1)$$

In this formula, i=1,2,3……, x is input quantity, xi are learning samples of neural network.

There are two neurons in the summation layer, one is the sum of the output variable of pattern layer, and the formula is as follow:

$$S_1 = \sum_{i=1}^{n} p_i \quad (2)$$

The second neuron in the summation layer is the weighted sum of the output variable of pattern layer, and the formula is as follow:

$$S_2 = \sum_{i=1}^{n} p_i y_{ij} \quad (3)$$

The number of output units is equal to the number of output variables, there are only one output variable that working voltage of the maximum power point in this paper, transfer function of output layer is as follow:

$$y_j = \frac{S_2}{S_1} \quad (4)$$

Principle of MPPT control based on GRNN neural network. Here are several key steps to MPPT control based on GRNN neural network:1, Finding out the output voltage corresponds to different temperature and strength of illumination by the simulation waveform;2, Training GRNN neural network with the data obtained in step 1; 3, To replace the fixed voltage of constant voltage tracking with the trained neurons. This method uses neural network to forecast the optimum operating voltage, in order to change the output voltage , takes the difference between predictive voltage and the actual output voltage of DC/DC conversion circuit as the signal to drive PWM device, this PV system keep the maximum power output finally. In this paper, DC/DC conversion circuit is BOOST circuit, because BOOST circuit conversion is more stable and less energy loss than BUCK circuit.

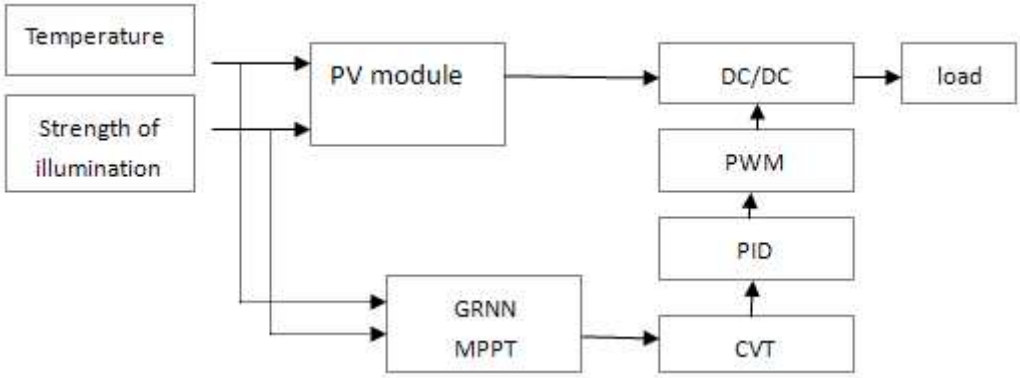

Fig. 6 Boost control principle with MPPT

Simulation analysis

Simulation research on MPPT control based on GRNN neural network, a simulation model was established in Matlab/Simulink, the simulation parameters are as follows: step is 0.01;the energy-storage capacitor is 0.005F; resistance R is 10Ω; inductance values of BOOST circuit are 6mH and 3mH ; spread value of GRNN module is 0.7.

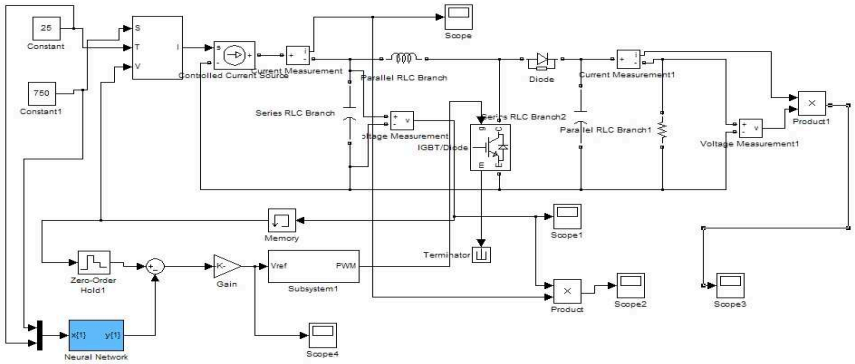

Fig. 7 Simulation model of MPPT based on GRNN

Ambient temperature is set to 20℃, simulation time is 2S; the input strength of illumination are 1000W/㎡ and 500W/㎡respectively, the output power curve of P&O is as follow:

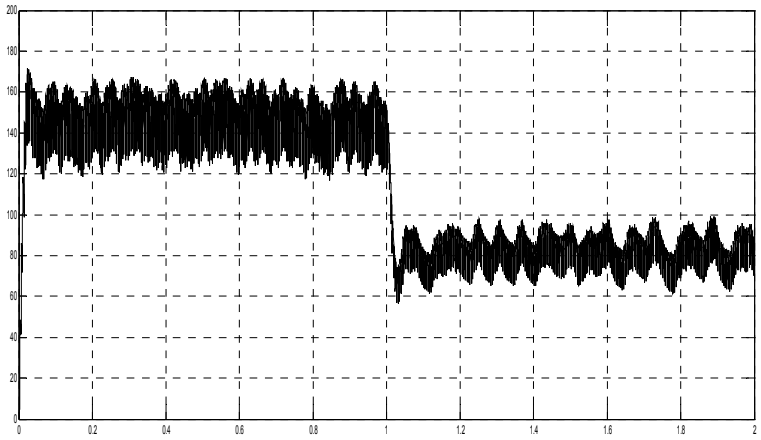

Fig. 8 Output power curve of P&O

Perturb & observe algorithm acts quickly, the time this control strategy spent on acting is less than 0.1s, but its shortcomings are obvious, the first one is waveform fluctuations in the whole control process, even action was completed. Fluctuations of output power waste a lot of energy and increases the burden of the hardware. Secondly, when external conditions change dramatically, MPPT cannot be finished quickly, as can be seen from the table, tracking performance of Perturb & observe algorithm is lower than the proposed control strategy.

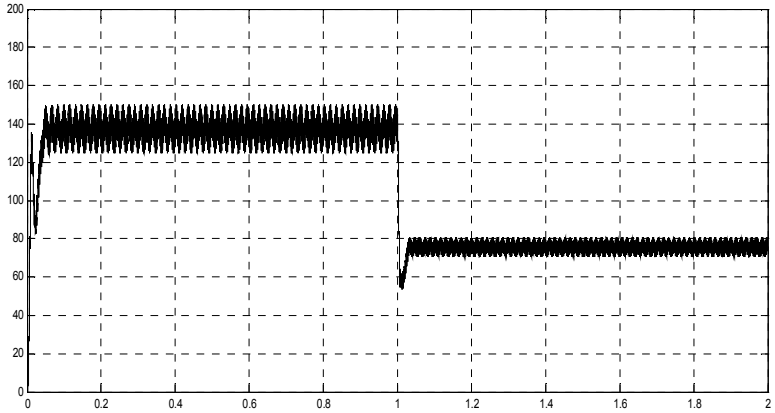

Fig. 9 Output power curve of MPPT based on GRNN

The above picture is the power output waveform of MPPT tracking control based on GRNN neural network, the power output waveform is more stable than Perturb & observe algorithm, and the efficiency of energy utilization is improved. When time is 1s, the strength of illumination changes, MPPT tracking control based on GRNN neural network can be fast-tracking, so the proposed control strategy is better than conventional MPPT control algorithm.

Conclusion

PV Simulation model was established in this paper, analysed output characteristic curve of PV cells, illustrated the principle of MPPT, proposed MPPT control based on GRNN neural network. At last through the simulation analysis, effectiveness of this Control strategy is proved. The proposed control algorithm has higher accuracy and stability, tracks quickly even the external conditions change.

References

[1] Zainal Salam,Jubaer Ahmed,Benny S. Merugu. The application of soft computing methods for MPPT of PV system: A technological and status review[J]. *Applied Energ*y,2013,107:.

[2] Nuri Gokmen,Engin Karatepe,Faruk Ugranli,Santiago Silvestre. Voltage band based global MPPT controller for photovoltaic systems[J]. *Solar Energy*,2013,98:.

[3] S. Zahra Mirbagheri,Saad Mekhilef,S. Mohsen Mirhassani. MPPT with Inc.Cond Method using Conventional Interleaved Boost Converter[J]. *Energy Procedia*,2013,42:.

[4] Ali Murtaza,Marcello Chiaberge,Mirko De Giuseppe,Diego Boero. A duty cycle optimization based hybrid maximum power point tracking technique for photovoltaic systems[J]. *International Journal of Electrical Power and Energy Systems*,2014,59:.

[5] Jubaer Ahmed,Zainal Salam. A Maximum Power Point Tracking (MPPT) for PV system using Cuckoo Search with partial shading capability[J]. *Applied Energy*,2014,119:.

Advanced Materials Research Vols. 989-994 (2014) pp 3433-3436
© (2014) Trans Tech Publications, Switzerland
doi:10.4028/www.scientific.net/AMR.989-994.3433

Arrangement of sensor nodes for wireless sensor network in aquatic products breeding

Shi Bing, Xu Shoukun, Jiang Jianming

School of city rail transportation, Changzhou University, Changzhou, 213164, China

email: shibings@163.com

Keywords: sensor node; Data Analysis; Optimal arrangement

Abstract. In order to overcome the disadvantages of ccomplexity of monitoring systems, inconvenience of installation for equipment and wiring, high error rate of data transmission, the technology of wireless sensor network is adopted. Through analysis of pond water testing results on the space distribution of water environmental factors, and the number and location of the sensor nodes is determined based on the distribution law of key factors. Experiments show that the system has higher accuracy and stability.

Introduction

The scale aquaculture has become a major commercial aquaculture farming methods, and in aquaculture, accurate measure and control of dissolved oxygen, pH, salinity, temperature and other environmental factors are very important. Currently monitoring systems adopted in aquaculture mostly based on cable, all sensors are connected to the cable. The traditional way to build such a system will face many problems. While increasing the number of sensors, change of system parameters will be resulted in, and modifications of the upper application may even be brought. It will also lead to a large number of on-site connecting cable lines, increasing cost of installation and maintenance. The technology of wireless sensor network is introduced to replace traditional wired systems.The monitoring system is based on a new wireless multi-parameter sensor networks, the parameters data collecting by sensor nodes are sent to the sink node via wireless communication, and then the sink node share the data via a internet network. The arrangement of sensor nodes is the key to collecting the comprehensive and correct data. Study on the arrangement of sensor nodes will be valuable significantly.

System Structure

The system consists three parts: real-time monitoring unit, control and execution unit and wireless sensor network unit, system architecture is shown in Figure 1.

Real-time monitoring unit includes two grades: site monitoring center and remote monitoring center. There are three basic functions of site monitoring center: receiving transmission data from WSN sink nodes, processing data and controlling the work of execution unit, uploading data to remote monitoring center through GPRS. And there are also three basic functions of remote monitoring center: accepting data from site monitoring center through GPRS network, database support, providing WEB services. The upper and lower computers can both complete data inquire, data analysis and other work. And the unit can also provide messages to mobile phone users.

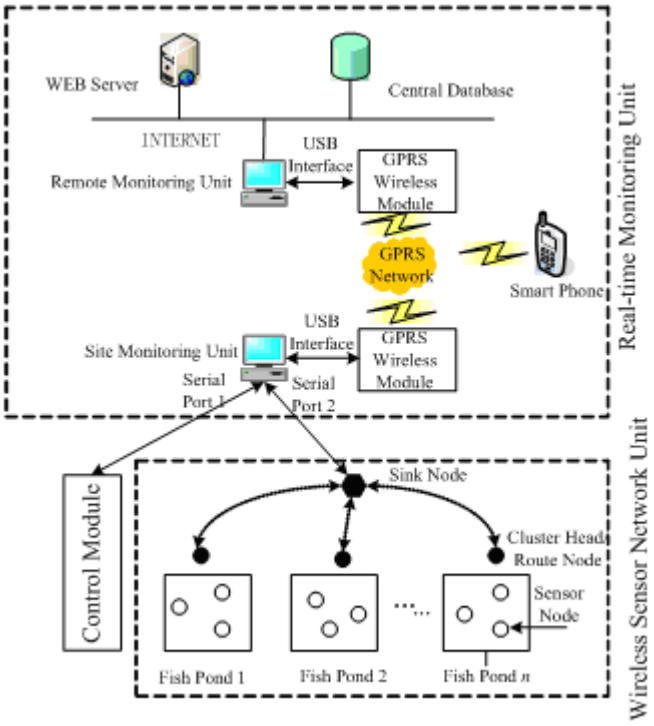

Fig.1. System structure

The upper computer of monitoring center can achieve functions such as data management, intelligent decision-making, statistical analysis of historical data, fault diagnosis, display, printing and output; and through image acquisition system, using computer image processing technology, the growth of fish in site aquaculture can be monitored real-timely, and beep in time when the fish die or in bad condition.

The control and execution unit is composed by actual hardware equipment, such as solenoid valves, transducers, relays and electrical switchgear. According to farmed fish species, growing season and other factors, the site monitoring computer determine the given values of optimal environmental factors through expert system, and send the values to the control unit processor via the serial port; the microprocessor will compare the values of environmental factors from site central computer with the given values, then give the corresponding control signals through appropriate treatment of control algorithm; control the execution unit such as frequency converters, solenoid valves, pump, pH pump; and complete the regulation tasks related to environmental factors; in order to achieve precise control of water quality parameters of the breeding pond.

Wireless sensor network unit is the basis of data transmission in this system, it is composed of a large number of sensor nodes, routing nodes and a cluster node. Sensor nodes are used to monitor the water environmental factors in each fish pond real-timely, and then convert the values collected by sensors to digital signals, and transmit these parameters to sink nodes in appropriate route traffic through wireless sending module, the values are such as temperature, dissolved oxygen content, pH, water level, and turbidity. At last, the data are transmitted to site monitoring computer by sink nodes through the serial port, and the uploading work is completed.

Sensor node arrangement

The arrangement for sensor node in crab pond has to take account of the actual size of the pond, water depth and construction materials. Therefore, spatial distribution of dissolved oxygen, temperature, and pH must be determined firstly at different location, and different depth. And then the arrangement for network nodes can be determined order to effectively achieve the purpose of optimization.

Environmental conditions:
Standard atmospheric pressure, ambient temperature 22 ~ 24 ℃, southeast wind 3 to 4;

Test Object:
Length of Pond: 150m, width of pond: 50m, depth of pond:1.5m;

Acquisition parameters:
Dissolved oxygen, temperature and pH value;

Sampling point:
Sampling points are shown in Figure 2.14, and each collection point away from the surface of the pond 0.3m, 0.6m, 0.9m, 1.2m and 1.5m at the sampling. The positions of sampling points are shown in Figure 2.

Test method:
Manually standard instruments are adopted.

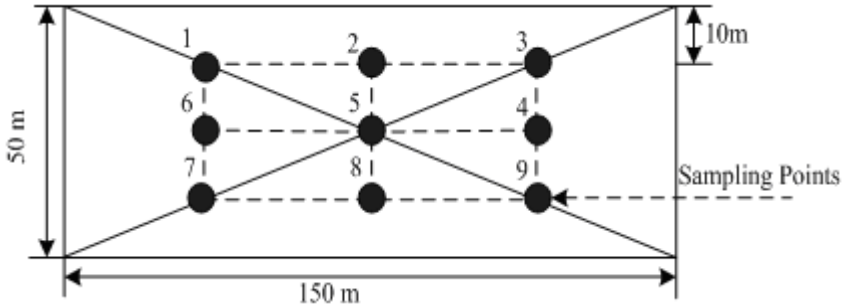

Fig.2. Distribution of sampling points

The data analysis from sampling points shows that: value changes of dissolved oxygen and temperature are little; however, in the horizontal direction the value changes are large. The value change of pH is significant both in the horizontal and vertical direction.

The curve of dissolved oxygen, temperature, pH and depth of water are show in figure 3.

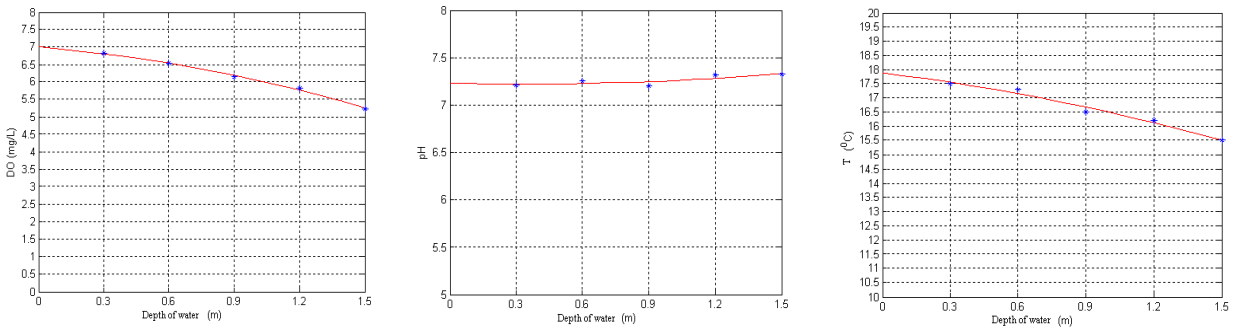

(a) Curve of DO and depth (b) Cure of pH and depth (c) Cure of temperature and depth

Fig.3. Sampling curve

Test results

The test three ponds are three adjacent outdoor ponds with size of 150m × 50 m, and water depth of 1.5 m, standard atmospheric pressure, and ambient temperature 22 ~ 24 ℃. The sensor nodes work for collecting temperature data and sending then to the sink node, the sink node can display the data through its own extended LCD, and simultaneously upload the data to the control center computer via the RS232/RS485 circuit.

Table 2 Temperature testing data unit: ℃

Test Times	Standard Equipment Data	Sink Node		Computer On-site	Computer Remote	Error
		Data	Error	Data	Data	
1	21.0	20.8	-0.20	20.8	20.8	-0.20
2	23.5	23.4	-0.10	23.4	23.4	-0.10
3	27.0	27.1	+0.10	27.1	27.1	+0.10
4	30.0	30.3	+0.30	30.3	30.3	+0.30
5	33.0	32.8	-0.20	32.8	32.8	-0.20
Absolute Error			0.18			0.18

Table 2 shows that the data from node data center, on-site monitoring data and remote monitoring center are the same, and the error between data and data from standard equipment is within ± 0.3 ℃. The security and reliability of communications in the wireless sensor network are satisfied.

Conclusion

Through a lot of experimental results, the parameters characteristic of distribution in the horizontal direction and the vertical direction is determined and the sensor nodes are arranged appropriately based on the physical location.Experiments show that the system has higher accuracy and stability.

References

[1] Zhao De'an, Liu Xingqiao, Pan Tianhong. Application of fault tree analysis(FTA) in reliability design of monitoring and controlling system for aquatic products breeding [J]. Transactions of The Chinese Society of Agricultural Engineering, 2003, 19 (4) :249~253.

[2] Timmons M .B. A Mathematical Model of Low-head Oxygenators[J]. Aquacultural Engineering,2001, 24: 257-277.

[3] Wyban J. A. Current and future use of instrumentation in U.s qauiculture, would aquaculture [J]. The Ocean nstitute. Honolulu, 1990, 84~101.

[4] Jerschewski P. A flow system for calibration of dissolved oxygen sensors. Fresenius J AnalChenm, 1997(6):667-682.

[5] Mariolakos,I.,et al.,2007.Real-time monitoring on Evrotas River (Laconia, Greece):dissolved oxygen as a critical parameter for environmental status classification and warning.Desalination 213,72–80.

[6] Jian-yu Xu,Shao-rong Cui.Behavioral Responses of Tilapia to Acute Fluctuations in Dissolved Oxygen Levels as Monitored by Computer Vision[J].Aquacultural Engineering , 2006, 35 :207-217.

[7] Tai, Haijiang, I.,et al., Design of an intelligent PH sensor for aquaculture industry. Computer and Computing Technologies in Agriculture IV 347,642–649.

Advanced Materials Research Vols. 989-994 (2014) pp 3437-3442
© (2014) Trans Tech Publications, Switzerland
doi:10.4028/www.scientific.net/AMR.989-994.3437

A platform of lightning protection business based on tablet-PC

ZHANG Yanhua[1], ZHOU Junchi[1], JIAO Xue[1], ZHOU Jing[2], ZENG Qingfeng[3]

[1]Jiangsu Lightning Protection Center,Nanjing,210009,P.R.China

[2]Jiangsu Meteorological Society, Nanjing,210009,P.R.China

[3]Shenzhen Meteorological Agency, Shenzhen,518000,P.R.China

Keywords: Lightning protection business, Lightning protection devices(LPD) inspection, On-site data process, Mobile GIS technology

Abstract. As a most grievous meteorological disaster in the world, lighting calamity is destructive and could be inducement of fire explosion accidents. Lightning protection business mainly consists of lightning protection devices (LPD) inspection, lightning disasters authentication and lightning risk evaluation, for which on-site data gathering is indispensible, and the status in quo has common defects. Based on tablet-PC and mobile information technology, we developed a platform including such seven modules as system configuration, LPD inspection of existing buildings, LPD inspection of under-construction buildings, identification of lightning disasters, lightning risk assessment, location of inspected clients and location of inspectors. Mobil GIS technology and fast-developing method of forms were taken into use as key technologies. With its help, an promotion of facilitation, standardization and intellectualization of lightning protection business is achieved.

Introduction

As a most grievous meteorological disaster in the world, lighting calamity is destructive and could be inducement of fire explosion accidents. Society and the authority is laying higher attention on lightning protection and disaster reduction.

Inspection of lightning protection devices is indispensable especially for petroleum and chemical industry and places with high density of people. Evaluation of lightning-disaster risks is a growing business of lightning protection by assessing lightning risk of such places as major projects and hazardous areas, and by proposing rectification measures based on systematical analysis of lightning caused damages and casualty. Identification and investigation of lightning disasters is part of social management and important for settlement of insurance claim [1].

Maturity of tablet PC and WIFI make integrity, intelligence and standardization of business process above possible. As a result, utilization of intelligent terminal will improve lightning protection technical services quality and enhance authority supervision [2].

Status in Quo of Lightning Protection Business

Lightning protection business mainly consists of lightning protection devices(LPD) detection, lightning disasters authentication and lightning risk evaluation, for which on-site data gathering is indispensible, and the status in quo has common defects. Let's take SPD detection for example. It is undertaking growing responsibility and venture in attention of the society, and the problems are obvious as below. Firstly, randomness of detection items and technical process lead to lack of standardization, which is to say, an inspector may use different methods at different spots and even come to a converse conclusion for the same one inspected unit because of disparity of personal and subjective factors. Secondly, manual manipulation leads to lack of accuracy and quality control. For instance, the grounding resistance is usually the only value a detection report carries, while location, material and corrosion is not considered. In case of a lightning disaster, it is impossible to judge accurately the lightning protection devices are qualified or not, leading to a potential responsibility risk of SPD detection business. Finally, low efficiency of on-site inspections and inconvenience of documentary management come as a result of manual data input. On one hand, inspection data

inputting takes much time and repetitive hand work, on the other hand, carrying, handling and storage of massive paper documents is also a problem for quality control. Risk assessment and authentication of lightning disasters are facing the same dilemma. Unstandardization and randomness of business process comes up as an obstacle for efficiency improvement. Uniformity and automation of lightning business is in urgent need, and tablet-PC based system could solve the problem to a large extent.

Advantages of Tablet-PC

Application of tablet PC has exploded in recent years. Not just for casual use, tablets are also superbly powerful business tools, which is why more and more businesses are turning to tablets for their everyday IT needs. You can go places that normal computers can't, because they're as portable and accessible as clipboards, with integrated wireless networking. They're almost as light as clipboards too. Tablet PC could be well applied in lightning business for such reasons as below.

Firstly, lighter Than Laptops. The extremely lightweight and handy characteristics of tablet PCs as compared to laptops are definitely the biggest advantage. Tablet PCs can be easily tucked under the arm and moved from place to place even by teenagers [3]. Secondly, input personlization. As tablet PCs are functional with the help of the special digital pen or stylus like gadget, the handwriting of a person becomes the input [4]. This enables better personalization and value-addition to work-based input than possible with a touchpad or mouse. Thirdly, flat Working Surface. The form factor and convertible design characteristic of a tablet PC enables it to be laid flat on any working surface [3]. This facilitates better presentations, personalized interactions with people or ability to showcase work to others in any work setting.

Besides, multiple professional software and platforms are indispensible in lighting business. Tablet PC is competitive with ARCGIS(a professional geographic information system) , MATLAB(a professional scientific computation software) and alike in the environment of iOS, Windows or Android [5]. So that technical process could be smoothly carried out on-site.

Development of the platform and its key technology

System Structure

Data collecting & processing system based on tablet PC takes use of intelligent terminals for on-site data collection and process, and data collected is sent to lightning integrated business platform for further handling. Lightning protection technical service product is finally achieved and is distributed to regarding users in terms of internet or paper documents. Integration of mobile data collecting system and business platform is shown as Fig.1. Business tasks are downloaded from the platform by LAN or WIFI and technical and data support is guaranteed. After that, data collection, input and process is carried out via mobile terminal, which is sent back to the platform and filed in the database of lightning protection center. The database is stored in the demilitarized zone(DMZ) [6] [7], which builds a security area to protect the intranet. Intranet users could get access to such business as LPD inspection, risks assessment and lightning disasters analysis. Inspected users could also register and refer to business progress and technical support.

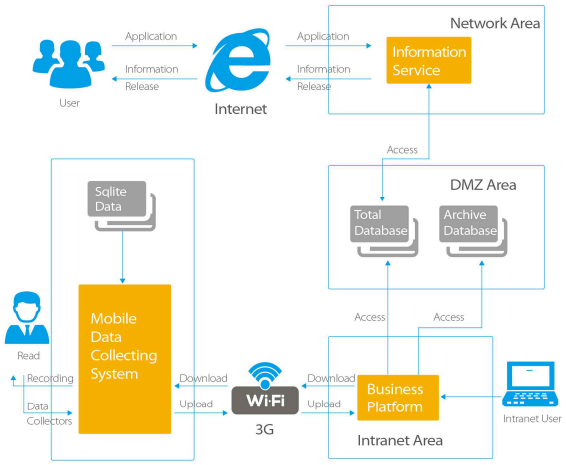

Figure 1. System structure

Key Technology

1) Mobil GIS technology: On-site inspection requires fast positioning and geographic information. Based on mobile internet and smart cellphones, mobile geographic information system(GIS) realizes offline maps, mobile positioning, mobile cartography and mobile office. It enjoys advantages as below.

a) Mobility: Installed on mobile terminals, mobile GIS could offer space information service by means of interaction with the server via WIFI communication anytime and anywhere.

b)Diversity of client terminals: Users have a wide range of terminals to choose, from laptops with strong calculation ability to PDA or smart phones of satisfying portability, which guarantee mobile GIS an open and Scalable platform.

c)Timeliness: Information could be processed and sent to clients without delay by help of positioning devices and internet [8].

2) Fast-developing method of forms: There are massive forms to handle in lightning business. Efficiency will be relatively low by use of traditional forms developing methods. However, based on the fast-developing method, different kinds of forms and menus could be generated automatically and visibly [9]. Patterns could also be deployed flexibly. Structure of the fast-developing method is shown as Fig.2.

The form designing module consists of the following four submodules: visual programming, forms mappings, XML release and Engine access interfaces. The form engine module includes such submodules as forms management, data process, O-RMapping and reports management. Reports output module is for forms inquiry, data statistics and forms display.

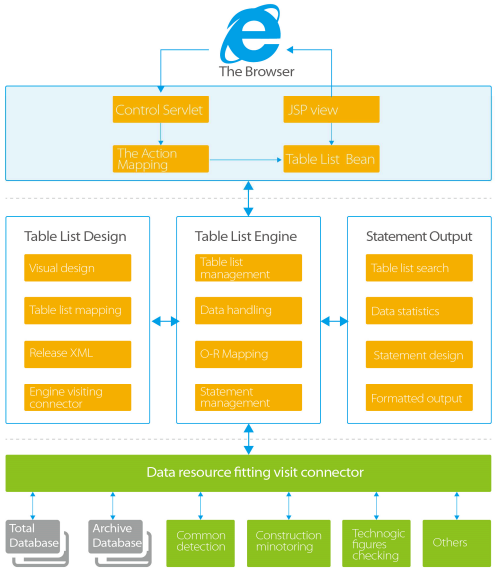

Figure 2. Structure of forms fast-developing method

Functional modules

Mobile LPD inspection system consists of the following seven modules: system configuration, LPD inspection of existing buildings, LPD inspection of under-construction buildings, identification of lightning disasters, lightning risk assessment, location of inspected clients and location of inspectors. Its functional structure is shown as Fig.3.

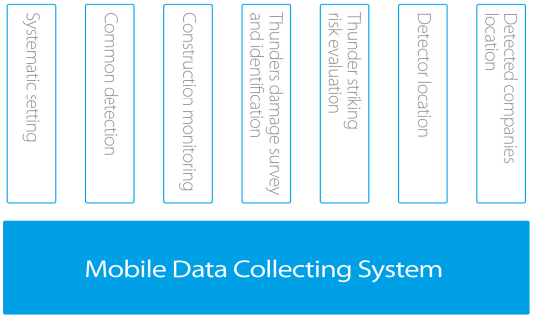

Figure 3. Functional modules of the platform

1) System configuration

System management is the main function of system configuration module, including parameters settings, personal management, authority settings, instruments management, standards documentation, clients' information and accessories, with which lightning protection rank, protection domain of a lightning rod, power resistance, impulse resistance, security distance, distribution of electro-magnetic field could be calculated.

2) On-site LPD inspection of existing buildings

According to the standard GB-50057(2010), lightning protection devices of existing buildings should be inspected annually, and semi-annually for explosion-hazard environment [10]. Meanwhile, surge protection devices (SPD) of low-voltage distribution system and signal system should also be inspected to avoid damage of electronic devices caused by lightning impulse and inductive surge.

This module includes such submodules as tasks download, current tasks, input of clients' information and on-site inspection data, auxiliary drawing, hand signature and inspection results upload. The process structure is shown as Fig.4.

First of all, an inspection task is downloaded via tablet PC, including inspection forms, clients' information and inspection history. Secondly, inspection information is completed in case of defective preliminary information. Thirdly, complete the inspection form and sketch map, marking location of the inspection spot, inspection value and further information alike. After that, lightning protection rank, protection domain of a lightning rod and electro-magnetic field intensity could be calculated based on data process and analysis. Then, the inspector will communicate with the client who will sign the report to guarantee validity of the inspection result. Finally, inspection forms and results will be uploaded to the server of lightning protection center.

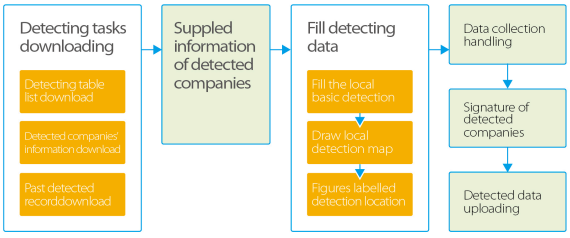

Figure 4. Process of On-site LPD inspection of existing buildings

3) On-site LPD inspection of under-construction buildings

LPD inspection of under-construction buildings is an approach of quality control of direct and inductive lightning-hit protection devices by inspecting each step during construction.

This module includes the following five submodules: tasks download, current tasks, input of clients' information and on-site inspection data, auxiliary drawing, hand signature and inspection results upload, which is similar to that of LPD inspection of existing buildings.

4) On-site inspection of lightning disasters authentication

The main function of On-site inspection of lightning disasters authentication is to analyze the reason of suffering lightning, conclude the main feature of lighting disaster and put forward effective protection instructions through the survey of lightning disaster site, lightning disaster monitoring analysis and late data reduction. The function of on-site inspection of lightning disasters authentication includes detection task downloading, detection information record, assistant drawing, detection recording uploading.

5) On-site inspection of Lightning Risk Assessment Site

The main function of lightning risk assessment business is a aggregate risk calculation in extent of casualties, property loss and injury according the analysis of lightning and disaster feature. At the same time, it is a evaluation methodology that offering constructive opinions for site selection of construction project, distribution of function division and determine of lightning category and protection measure.

The function of lightning risk assessment site detection includes detection task downloading, detection information record, assistant drawing, and record uploading. Lightning risk assessment site detection is mainly completing data gathering of lightning risk assessment site by using tablet PC.

6) Mobile positioning

Mobile positioning system consists of both inspectors positioning and clients positioning. The former one could be used to supervise inspectors' presence and the other one could be used for driving route guidance.

Functional modules

Let's take gas station as example of the application of lightning protection detection using mobile data collection system in tablet PC.Testers should download work tasks through a tablet computer first and query the current task. All of current tasks in the tablet PC should be shown in the calendar. Click on the calendar date, the detailed task for the day will be shown at the bottom of the screen in a table format. Click on a particular detection task inside the table, a detailed content will be shown. Detailed contents have three modules: the basic information about inspection unit, detection of basic information, detection of image information. Lastly, fill the detailed content in the corresponding module based on the situation.

As is shown in Fig.5, the sketch map is drawn according to the practical conditions. Detail abstracts and inspection values are added to the platform, and photos could also be taken on-site. Inspectors and administrators could have a comprehensive view of the inspection condition. Meanwhile, visualization input of inspection data offers an easy access to inspection value and other information.

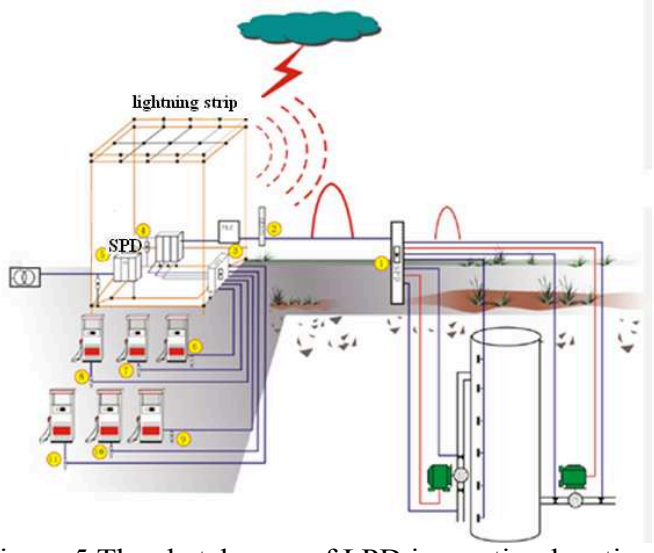

Figure 5.The sketch map of LPD inspection location

Conclusions

Based on tablet-PC and mobile information technology, we developed a platform including such seven modules as system configuration, LPD inspection of existing buildings, LPD inspection of under-construction buildings, identification of lightning disasters, lightning risk assessment, location of inspected clients and location of inspectors. Mobil GIS technology and fast-developing method of forms were taken into use as key technologies.

Mobile data collecting system contributes to standardization of LPD inspection business, avoiding massive repetitive input of original data. Besides, better efficiency could be achieved by promoting calculation and data process ability with help of tablet PC. Image manipulation and photographing function contributes to recapitulation of on-site inspection work, which could help monitoring service quality for administrators, and the sketch map generation module offers a much more convenient method to draw a sketch map on-site. Combination of LPD inspection business and information technology gives an promotion of its facilitation, standardization and intellectualization.

Acknowledgement

In this paper, the research was sponsored by the Jiangsu meteorological scientific research fund （KM201214）.

References

[1] Ding Weijie, Yan Lvxuan, Huang Zhicong; Design and implementation of lightning protection archives management system[J]; Guangdong Meteorology, 2007, 29 (1) : 53-55

[2] Lightning protection design specification of building (GB 50057-2010); China Planning Press, 2011.

[3] Li Wei; Brief introduction to integration of measurement information inside and outside the industry [J]; Coal Technology, 2004, (8)

[4] Zhong Yu, Jia Jia, Zhang Sheng; Planning and construction of business management system of Shanghai lightning protection detection; The tenth forum of lightning protection and disaster alleviation, 2012.

[5] Zhao Xiong, Guo Da; Industry research based on the tablet[J]; Focused on the international communication show in 2011, 36-38

[6] Wang Hua, Li Dan, Wang Wei; Business management system of lightning protection [J]; Journal of Meteorology and Environment. 2009, 121-137

[7] Xu Ying, Wei Fengyuan; Discussion on Key technology of moving GIS and development mode[J]. Geomatics & Spatial Information Technology, 2008, 4 (31) : 74-79

[8] Deng Shiyin; Research of 3D graphics engine technology in terminal equipment of mobile communication; Chengdu, Sichuan Province: University of Electronic Science and Technology of China; 2006

[9] Zhou Hui, Yin Jianwei, Chen Gang, Dong Jinxiang; Rapid Application Development Platform for Web Form Based on Struts Framework; Application Research of Computers, 2004, 8: 183-191

[10] Wang Zhigang, Tang Yao, Zeng Xianghong, etc; Research and Development of Visualized Analysis System of Lightning Disaster Data, Meteorological Monthly, 2009, 35(5),98-104

Advanced Materials Research Vols. 989-994 (2014) pp 3443-3446
© (2014) Trans Tech Publications, Switzerland
doi:10.4028/www.scientific.net/AMR.989-994.3443

Prediction and analysis of safety production accident in mining based on the GM(1,1)

Chenfang Jiang[1,a], Kepeng Hou[1,b*], Huafen Sun[1,c]

[1]Faculty of Land Resource Engineering, Kunming University of Science and Technology, Kunming 650093, China

[a]jiang.chenfang@163.com,[b]gasihou@sina.com,[c]sunhuafen@126.com

Keywords: GM (1, 1); accident; prediction; mining safety; MATLAB

Abstract. According to the grey theory, in order to predict and prevent accident effectively, the paper built a grey model and forecast the mine accidents in china in 2013 based on the statistics of mine accidents happened in China during period from 2007 to 2012. MATLAB was used to write procedure code of GM (1, 1) and empirical verification follows. The prediction results show that if high accuracy goes with the precision of the calculable model, which could be used to provide the basis for decision making to the safety production management practices in China. This case study indicates that GM (1, 1) plays an important role in mine safety management.

Introduction

Due to the high-risk of mining industries, the safety accident is easily to happen with serious consequences. Prediction and analysis of accidents will play a warning role on accident prevention work to improve energy industry. The GM (1, 1) model [1] was established on the grey system theory, which can be used to make a short period forecast line by a part clearly, part unclear with uncertainty sample. According to statistical data mining safety production accidents in China from 2007 to 2012, the total number of safety production accidents in mining industry is predicted by using the GM (1, 1) model and MATLAB software. It confirms that the GM (1, 1) model can be used to predict safety production accidents. And this provides a scientific theory basis for government, enterprises or relevant department to make a safe production management and decision.

The establish principle and method of the Grey GM (1, 1) model

The grey prediction theory. The grey system theory was created by Professor Deng Julong in China in 1982[1]. It has become a new cross discipline. In general, it is called the grey prediction which was predicted by the GM (1, 1) model. In particular, it must be predicted using the grey theory after the related test. The grey prediction test[2] includes: a. data inspection. b. The model test. c. Prediction test. The extrapolated reliability would be studied on the models.

Data feasibility test. The feasibility must be tested on the level of the original sequence by using data preprocessing method, including the translation method, the sqrt method, the logarithm method, the strengthening and weakening operator method.

A. Time series data consist of known accident data are represented by the formula. $x^{(0)}(\mathrm{n})$ is the accidents data in the annual year n.

$$\mathrm{x}^{(0)} = \left(x^{(0)}(1), x^{(0)}(2), \cdots, x^{(0)}(\mathrm{n})\right) \tag{1}$$

B. The accident number columns, $\sigma_x^{(0)}(k)$, is a accidents number ratio of between the previous year and the next year. as follows:

$$\sigma_x^{(0)}(k) = \frac{x^{(0)}(\mathrm{k}-1)}{x^{(0)}(k)}, \quad k = 2,3,\cdots, \quad n \tag{2}$$

$\sigma_x^{(0)}(k)$ is a level of the original accident sequence $\mathrm{x}^{(0)}$ in the annual year k.

The level sequence of the accident sequence was calculated by (1) (2):

$$\sigma^{(0)} = \left(\sigma^{(0)}(2), \sigma^{(0)}(3), \cdots, \sigma^{(0)}(n)\right) \tag{3}$$

C. It was tested whether all levels were belonging in the admissible covering area. If all levels were belonging to the admissible covering area, the accident sequence could be predicted by GM (1, 1) model. Otherwise, it needs a transform process to make the accident sequence belonging in.

$$\sigma_x^{(0)}(k) \in \left(e^{-\frac{2}{n+1}}, e^{\frac{2}{n+2}}\right) \tag{4}$$

D. Translation transformation: $y^{(0)}(k)$ is the accident data after transformation for the annual year k. c is a selected constant. $\sigma_y^{(0)}(k)$ would also be got. It should be satisfied to the requires of equation (4).

$$y^{(0)}(k) = x^{(0)}(k) + c, \quad k = 1,2,\cdots, \quad n \tag{5}$$

$$\sigma_y^{(0)}(k) = \frac{y^{(0)}(\mathrm{k}-1)}{y^{(0)}(k)}, \quad k = 2,3,\cdots, \quad n \tag{6}$$

The establish of the GM (1, 1) model [3]

A. $y^{(0)}$ was the initial sequence of the accident data.

$$\mathrm{y}^{(0)} = \left(y^{(0)}(1), y^{(0)}(2), \cdots, y^{(0)}(n)\right) \tag{7}$$

B. $y^{(1)}$ would be got by making one cumulative process on $y^{(0)}$.

$$\mathrm{y}^{(1)} = \left(y^{(1)}(1), y^{(1)}(2), \cdots, y^{(1)}(n)\right) \tag{8}$$

Above, $y^{(1)}(1) = y^{(0)}(1)$; $y^{(1)}(k) = \sum_{j=1}^{\mathrm{k}} y^{(0)}(j), k = 2,3,\cdots,n$.

C. $\mathrm{z}^{(1)}$ would be got by making a mean on $y^{(1)}$.

$$\mathrm{z}^{(1)} = \left(z^{(1)}(1), z^{(1)}(2), \cdots, z^{(1)}(n)\right) \tag{9}$$

Above, $z^{(1)}(k) = 0.5y^{(1)}(k) + 0.5y^{(1)}(k-1), k = 2,3,\cdots,n$, $y^{(1)}(1) = y^{(0)}(1)$.

D. The grey differential equation of the grey prediction model would be got. If the variable k is considered as a continuous time variable t, $y^{(1)}$ can be regarded as a function of the time t, as $y^{(1)} = y^{(1)}(t)$. Then the white differential equation of the grey GM (1, 1) also can be got.

$$y^{(0)}(k) + az^{(1)}(k) = b \tag{10}$$

$$\frac{dy^{(1)}}{dt} + ay^{(1)}(t) = b \tag{11}$$

E. The least square solution can be obtained by using the least square method. B is a data matrix. Y is a data vector.

$$u = (a,b)^T = \left(B^T B\right)^{-1} B^T Y \tag{12}$$

Above, $B = \begin{bmatrix} -z^{(1)}(2) & 1 \\ -z^{(1)}(3) & 1 \\ \vdots & \vdots \\ -z^{(1)}(n) & 1 \end{bmatrix}$ $\mathrm{Y} = \left(y^{(0)}(2), y^{(0)}(3), \cdots, y^{(0)}(n)\right)^T$.

F. The value of a and b could be obtained by using the solver of the grey differential equation (10). Then the prediction model equation would also be obtained.

$$\hat{y}^{(1)}(k+1)=\left(y^{(0)}(1)-\frac{b}{a}\right)e^{-ak}+\frac{b}{a};k=1,2,\cdots,n,\cdots \tag{13}$$

G. The estimate restore value of the original data, $\hat{y}^{(0)}(k+1)$, would be got by making a lago on $\hat{y}^{(1)}$. Finally, the simulation sequence can be obtained.

$$\hat{y}^{(0)}(k+1)=\hat{y}^{(1)}(k+1)-\hat{y}^{(1)}(k),k=1,2,\cdots,n,\cdots \tag{14}$$

Test on the accuracy of the model

The prediction model can be used, only if it passed the accuracy test. The quality of the model can be evaluated by using the model accuracy grade. It shows in table.1.

Table.1 The accuracy grade

Critical value	A	B	C	D
Relative error/ $\Delta 0$	0.01	0.05	0.10	0.20
Correlation degree/R0	0.90	0.80	0.70	0.60
The mean variance ratio/C0	0.35	0.50	0.65	0.80
Small error probability/P0	0.95	0.80	0.70	0.60
The evaluation result	Excellent	Qualified	Reluctantly qualified	Unqualified

Forecast applications

According to the state administration of work safety dispatch center statistics 2007-2012 domestic mine production safety accidents month distribution, distribution of accident year results is got and is shown in table.2. The number of domestic mine production safety accident for 2013 was forecasted.

Table.2 The annual distribution of domestic mine production safety accident in 2007-2012

Year	2007	2008	2009	2010	2011	2012
Accident	294	233	194	153	130	106

The predicted results were calculated by mathematics MATLAB programming and prediction model run data in table.3.

Table.3 The results of actual cases of GM (1, 1)

Year	$\mathbf{y^{(0)}}$	$\hat{y}^{(0)}$	ε	Δ	$\overline{\Delta}$	R	C	P
2007	294	294	0	0	0.0096	0.9985	0.0313	1
2008	233	232.7	0.3	0.0012				
2009	194	191	3	0.0155				
2010	153	156.6	-3.6	0.0235				
2011	130	128.5	1.5	0.0115				
2012	106	105.4	0.6	0.0057				
2013	—	86.5	—	—	—	—	—	—

Comparison with table.1, the model was tested, the relative error is less than 0.01, correlation is greater than 0.90, the mean square error is less than 0.35, a small error probability is greater than 0.95, the model determines the accuracy of grade level, excellent performance prediction, forecasting results with higher reliability. And the domestic mining production safety accidents predictive number is 86.5 in 2013, the actual number will be close to this data. The domestic mining production safety accidents decreasing trend, but the number of accidents is still at a high level.

Conclusion

The quantity of Safety production accidents reflects the level of safety operation. The total accidents were obtained by statistics. It is a typical Gray features. The accidents quantity could be highly predictive with less data by using the grey GM (1, 1) model.

The results show that security in our country is getting better; the safety production accident only is about 87 in mining industry in 2013. It has a great significance to the safety management work by using a scientific and reliable method to make an accurate prediction.

References

[1]J.L. Deng: *The grey system theory* (Huazhong University of science and Technology Press, China1990).

[2]X.P. Zheng, M.T. Liu, W. Li: Study on accident prediction methods [J], Journal of safety and environment, (2008) No.8, p162-169.

[3]S.F. Liu, Y.G. Guo, Z.G. Fang, et al: *Grey system theory and its application* (Science Press, China 2010).

Advanced Materials Research Vols. 989-994 (2014) pp 3447-3451
© (2014) Trans Tech Publications, Switzerland
doi:10.4028/www.scientific.net/AMR.989-994.3447

A production planning and scheduling process study based on dynamic information feedback

Qing Yang, Yanhua Ni

Industrial engineering and logistics engineering of Shanghai Jiaotong University, Shanghai 200240

[a]xuanbin3019@163.com , [b]Yanhuani84@163.com

Keywords: dynamic information feedback, multi-objective decision, scheduling rule, high resolution management

Abstract. Many factories usually can't use the production scheduling plan generated by some software directly, such as ERP and MES. Two main reasons are founded, one is the fixed parameter and data used in the planning and scheduling process; the other one is lack of Ability to respond to the dynamic production environment. This paper tries to improve the plan by using the dynamic information feedback and experience from workers, and a test states it is helpful in the daily work.

Introduction

Among all the production activities in the factories, making a good production plan is a critical step, because a good plan can not only satisfy the clients' requirement, but also ensure the production smoothly [1,2]. Nowadays most factories are using some software to make the production plan, such as ERP and MES. However, there are some shortages in the above two main software, the ERP system weaken the production scheduling module and the data monitoring and tracking module function in the shop floors[3], the MES system has made up the above two shortages of ERP systems, but the two software always can't work cooperatively[4,5].

This paper has done some research in some process industrial firms, two main typical problems are founded in their production plan. Firstly, some parameters in the software is relatively fixed (such as lead time, economic lot size and process route), which can't reflect the real dynamic production environment, the production plan generated by the software needs to be adjusted by experienced workers before used. Secondly, the actual production planning and scheduling process is a process of multi-objective constraint negotiation process, as the production environment changes, the objective and constraints of production plan is changing. The existing system can't adjust the objective and constraints according to the dynamic information. Finally, the result is that the workers have to collect the dynamic information they need from the shop floor, and adjust the production plan.

In order to make a good production plan, it is necessary to study how to improve the parameters and the production plan by using the dynamic information. In the latest researches, Professor Huang is doing the comprehensive research about using the RFID technology to improve the production, not only the material management, but also the production process in the shop floor [6,7,8,9]. By using this advanced technology, it is easy to obtain sufficient dynamic information. However few papers pay attention to improve the existing production planning methods by using the dynamic information feedback, Peter Cowling develop a general framework for using real time information to improve scheduling decisions [10]. So, Based on the situation of a real firm, this paper makes a further research to improve the parameters and the production plan by using the dynamic information. The following articles comes as five parts: part 1 illustrates the real problems founded in the firms; part 2 presents the new planning and scheduling framework; part 3 studies the method of dealing with the dynamic information; part 4 is a case study; finally the conclusions are presented in part 5.

Problem description

This paper makes an extensive investigation in a firm, which is producing the special lubrication oil. The existing planning and scheduling process are divided into three steps (Fig.1). Firstly, the ERP software generate monthly production plan by using some data, such as product demand, and economic production lot. Secondly, dealing with the monthly production plan and some fixed data, the MES software makes the weekly scheduling plan. Finally, the experienced workers adjust the plan according to the dynamic information and their experience, which is the most important.

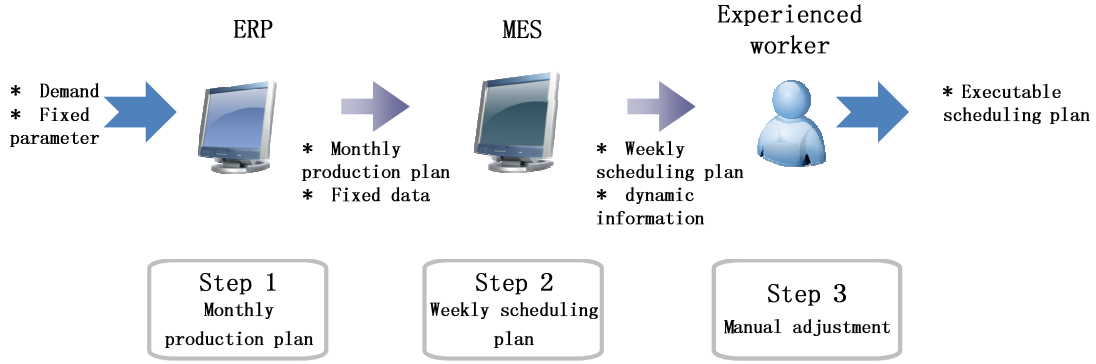

Fig.1 The existing production planning and scheduling process

The main problems in the existing process could be concluded into three aspects: Firstly, because of the fixed parameters (such as economic production lot), the monthly production plan generated by the ERP can't reflect the real production situation, and misleading production; Secondly, the fixed data (such as the processing time) may easily make the weekly scheduling plan fail in the execution phase; Thirdly, although experienced workers could adjust the plan, but they can't ensure that all the adjustment is the best.

Planning and scheduling framework

Given the above three main problems, A new planning and scheduling framework is proposed (Fig.2). As described in figure, the main Characteristics of the new framework are followed:

On the one hand, real time data are used to optimize the fixed parameters and data in the ERP and MES. For example, in the process of planning, the economic production lot (EPL) and processing time are the key factor for this firm. So, real time data should be used to optimize these two factors primarily. But different period of real time data is for different use. The EPL is used in the monthly production planning, and the relative long-time accumulation of real time data is more useful, however the processing time is varied according to the environment, workers, and other factors, the relative short-time accumulation of real time data is more useful. Part 3 study the key method in the real time information processing.

On the other hand, real time information could also help worker to handle the failed plan. In the real operation, different information could be processed with different rules, and these rules always can't be programmed into the software. So it is very necessary to build the clear or fuzzy connection between the real time information and the rules, when a certain activity is carried out, a relative responded rule could be picked immediately. Part4 presents the rules-based the scheduling process.

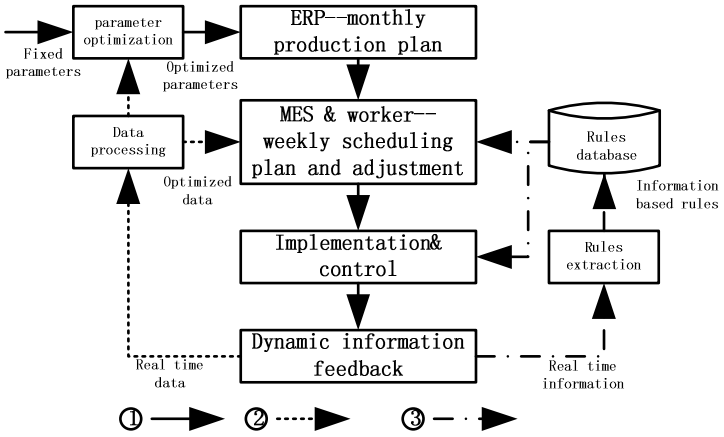

Fig.2 The new planning and scheduling framework

Dynamic information handling

For the best use of the real time information, different time-period of information should be processing with different method. Because the statistical methods are extensively used [11], so it is relatively easy to find the changing rules for the long-time accumulation of data, and the certain affecting factors in the short-time accumulation of data. This paper would not present the basic methods to process the data, and pay the main attention into how to use the processed data.

Building the connection between the data and rule is the key, a quadruple form $\langle S, A_t, V, R \rangle$ is proposed[12], $S = \{s_1, s_2, \ldots, s_n,\}$ is the finite set of production factors which can be collected data in the shop floor; $A_t = \{a_1, a_2, \ldots, a_m,\}$ is the finite set of attributes of production factors; $V = \{v_1, v_2, \ldots v_m,\}$ is the range of attributes, and v_i could be described by $\left[\underline{v}, \overline{v}\right]$; $R = \{r_1, r_2, \ldots r_l,\}$ is the corresponding rules according to varied attribute values.

According to the above definition, the attribute value could be presented by $U = (S, A_t, V)$, and the corresponding connection between R could be presented as:

$$U_1 \wedge U_2 \wedge U_3 \wedge \ldots U_m >= R(r_1 \wedge r_2 \wedge r_3 \wedge \ldots r_n) \quad (m \geq 1, n \geq 1) \tag{1}$$

For example, the processing time a_5 of the reaction kettle s_4 is extended to $\left[\underline{v_2}, \overline{v_2}\right]$ (which is also presented by $U_1 = \left(s_4, a_5, v_2 = \left[\underline{v_2}, \overline{v_2}\right]\right)$, and then the corresponding rules are r_1 (adjust the preparing activity of the follow-up process) and r_2 (raise the process priority). In a word, the final expression form is $U_1 = \left(s_4, a_5, v_2 = \left[\underline{v_2}, \overline{v_2}\right]\right) >= R(r_1 \wedge r_2)$.

This method is easy

Rule-based scheduling process

From the extensive study of the firms, a fact should be admitted that the scheduling process heavily rely on the experience worker. The software can't replace the worker, especially for the multi-objective scheduling and varied production environment. So, in order to make the scheduling plan more effective, experienced rules should be paid more attention.

For this firm, three main objectives are considered during the scheduling process: delivery date, capacity utilization rate and kettle cleaning frequency. And "production order" could be presented as $J = (v, d)$, $v = (v_1, v_2, v_3, \ldots, v_N)^T$ is the total number of the consumer order v_i, the delivery date of the consumer order is $d = (d_1, d_2, d_3, \ldots, d_N)^T$.

The main work of the scheduling is to sequence the production order $J=(v,d)$, and make sure that all the above three objective can get a relatively satisfied value. This paper tries to make a new scheduling process that not only can be easily used in the real production, but also consider the rules extracted from the experienced workers. The steps of the process are as followed:

Step one: export the weekly production order $J_j=(v_j,d_j)$ from the ERP;

Step two: export the optimized data (processing time, machine capacity), and information based rules.

Step three: sequence the production order $J_j=(v_j,d_j)$ under each of the above three objectives, and note three different result as $Q_{1,j}\left(\frac{D_j-t}{t_j}\right)$(delivery date), $Q_{2,j}\left(\min\{C_j\}\right)$(capacity utilization rate) and $Q_{3,j}\left(\min\{T_{clean}\}\right)$(kettle cleaning frequency).

Step four: coordinate the weekly changed weight $w_m(d)$ of the three objectives according to dynamic information feedback and information-based rules weekly, and determine the final sequence of the production orders $Q_j=\sum_{m=1,2,3}\left(w_m(d)\cdot Q_{m,j}\right)$ [13];

Step five: adjust the scheduling plan daily according to the daily information feedback. Two main rules are used, rule one is to split the production order according to the daily production situation; rule two is to increase the utilization rate of some automation machines.

Rule 1: IF ($C_j>d_i\{d_i\in J_j\}$) THEN ($reduce(V(J_j))$ AND ($split(J_j\rightarrow J_{j,l}+J_{j,k})$ (2)

Rule 2: IF ($(T_{D-finish}-T_{D-end})\geq T_{J_{j+1},d+1}\pm t_0$) THEN ($J_{j+1,D+1}\rightarrow J_{j+1,D}$) (3)

Case study

To examine the method proposed in this paper, a test has been done in the firms, three Index are compared between the methods used before and after. Just depicted in the table1, the on-time delivery rate and utilization rate of automation machines has been improved, but the kettle cleaning frequency is increased slightly, the true reason is that rule1 increases both on-time delivery rate and the kettle cleaning frequency.

Table1 Index comparison

Index	before	after
On-time delivery rate	85.5%	90.5%
kettle cleaning frequency	11.2/week	12.1/week
utilization rate of automation machines	55%	65%

What' more, this method makes it more effective for the production planner to cope with daily work and dynamic production environment.

Summary

This paper tries to use the dynamic information and experience from workers, to improve the existing planning and scheduling process, a test states that the method proposed in this paper is helpful in the production, but several parts are still needed to study, such as optimize the algorithm and establish perfect expert knowledge base.

References

[1] J. Váncza, T. Kis: CIRP Annals-Manufacturing Technology, 2004, 53(1): 377-380.
[2] X. D. Zhang, H. S. Yan: Chinese Journal of Mechanical Engineering, 2005, 41(9): 98-105.
[3] E. Shehab, M. Sharp: Business Process Management Journal, 2004, 10(4): 359-386.
[4] B. Saenz de Ugarte, A. Artiba: Production planning and control, 2009, 20(6): 525-539.
[5] L. Monostori, J. Váncza: Information Control Problems in Manufacturing, 2006, 1: 561-566.
[6] G. Q. Huang, Y. Zhang: Robotics and Computer-Integrated Manufacturing, 2007, 23(4): 469-477.
[7] R. Y. Zhong, Q. Dai: Robotics and Computer-Integrated Manufacturing, 2013, 29(2): 283-292.
[8] T. Qu, H. Yang: Journal of Intelligent Manufacturing, 2012, 23(6): 2343-2356.
[9] R. Y. Zhong, Z. Li: International Journal of Computer Integrated Manufacturing, 2013, 26(7): 649-662.
[10] P. Cowling, M. Johansson: European Journal of Operational Research, 2002, 139(2): 230-244.
[11] R. Miao: *Engineering Statistics* (China Machine PRESS, 2010).
[12] Y. Chai, J. Li, L. Q. He: High Technology Letters, 2001, 11(11): 2-5.
[13] Y. F. Lee, Z. B. Jiang: Journal of Shanghai Jiaotong University, 2008, 42(2):209-213.

Advanced Materials Research Vols. 989-994 (2014) pp 3452-3455
© (2014) Trans Tech Publications, Switzerland
doi:10.4028/www.scientific.net/AMR.989-994.3452

The Key Technology Research on Information Acquisition about Tropical Crop Production Environment

Lingling Wang[1, 2,a], Kun Lu[1,2,b], Hongxia Luo[1,2,c], Jihua Fang[1,2,d]

[1]Institute of Information and Technology, Chinese Academy of Tropical Agricultural Sciences, Danzhou,China;

[2]Key Laboratory of practical research on tropical crops information technology in Hainan, Danzhou, China.

[a]zishi-010@163.com, [b]xxskyb@126.com, [c]120081008@163.com, [d]fangdil@163.com

Keywords: information acquisition, sensors, production environment, tropical crop

Abstract. The information of tropical crop production environment includes the wind velocity and direction data, light intensity, air humidity, air temperatures, soil moisture, concentration of carbon dioxide, rainfall and so on. These data will be of great reference value to environmental control and scientific field management. As the characteristics of tropical crop growth and tropical climate conditions, information acquisition and tracking about the environment of crop growth are quite behind the time. This research is precisely centers on this core question to launch, carrying on analysis on the key technology of intelligent sensor and monitoring about tropical crop production environment. We build a system on a tiny210 chip using android operating system. Sensors that will be linked include air humidity & temperature sensor, illumination sensor, soil moisture sensor, wind-direction sensor and wind power sensor. This research focuses on field information dynamic acquisition and management. This study can offer references for in field environmental control and further research work.

Introduction

Now the studies of intelligent sensor and monitoring technology on tropical crop production environment include mainly the following several aspects: (1) data acquired portable terminal device[1-3], (2) the data collection and processing techniques include GPS, GIS, RS, RFID, sensor, wireless network, crop production model and infrared radiation spectroscopy technologies[4-9], etc, (3) information gathering and monitoring system[10-11]. The research emphatically analyzes the information of soil nutrients and moisture[12], intelligent management of water and fertilizer[13], information acquisition including field geographical information, moisture, soil, light, facility agriculture[14,15], etc.

Tropical crops require an appropriate growth environment for successful germination and establishment, because environment will directly affect the quantities and quality of the products. This study focuses on the field environment requirements for information technology in tropical crop production.The paper studies the key technique of intelligent sensor and monitoring, using sensor technology, monolithic integrated circuit, database and control technology, to explore an information collection system with the advantages of strong practicability, simple and convenient operation and low cost. The system can realize the dynamic monitor of the field environment, improve the field management and offer reference data for manipulation of field environment.

Key Technology

Overall Design. We will build a system of intelligent sensor and monitoring technology about tropical crop production environment, using sensor technology, monolithic integrated circuit, database and control technology. Android development environment and JAVA programming language are used in the software design of the controlling system. The hardware of the system includes TINY210 development board and sensors. Data acquired from the system includes wind

velocity and direction, light intensity, air humidity, air temperatures and soil moisture. The functions of the system include data collection, field production and management, and environmental control. The overall design of the system is as shown in Figure 1.

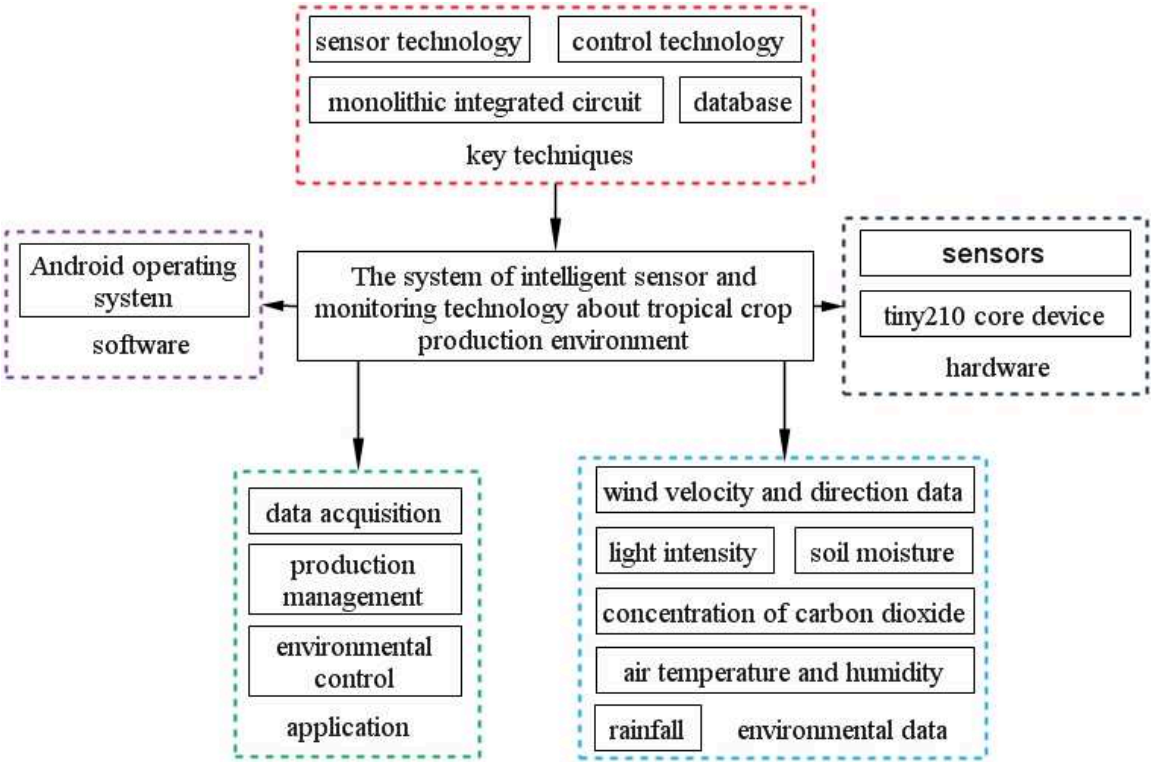

Fig.1 The overall design of the system

Software Design. Software Design uses eclipse programming tools, which is specialized for embedded systems based on android. The information acquisition system uses JAVA. The system design includes function require, datasheet design and interface code design. Background applications of the system operating interface is as shown in Figure 2.

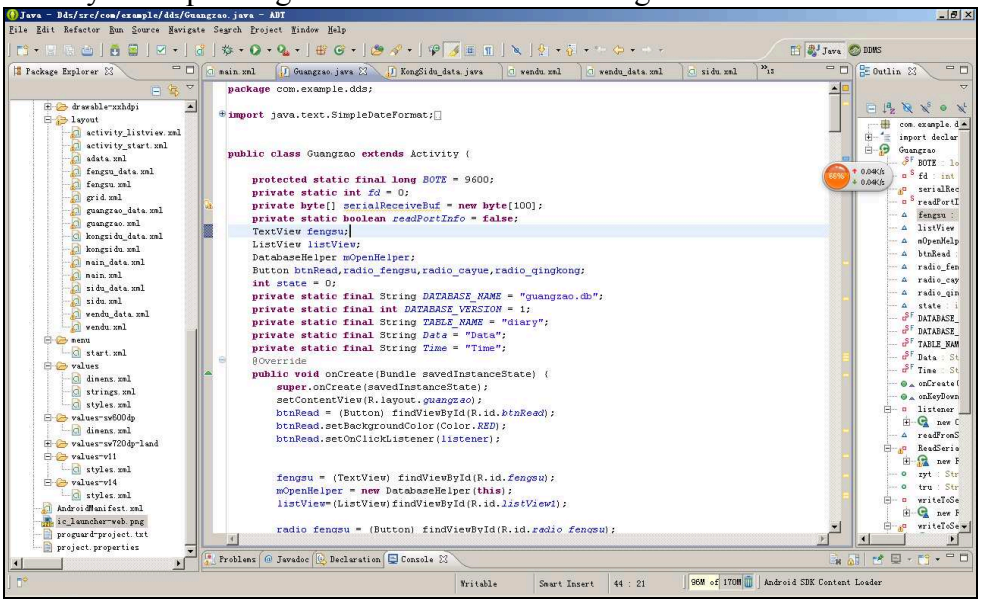

Fig.2 Background applications of the system operating interface

Main Interface of the System. Functions of the wind velocity and direction data, light intensity, air humidity, air temperatures, soil moisture, concentration of carbon dioxide, rainfall are designed in main interface in the system. The design of main interface of the system is as shown in Figure 3.

Fig.3 The design of main interface of the system

System Test. Precision test and dynamic application test have been done for the whole system experiment. Experiments showed that the system is feasible and practical. The test data of the system is as shown in Figure 4.

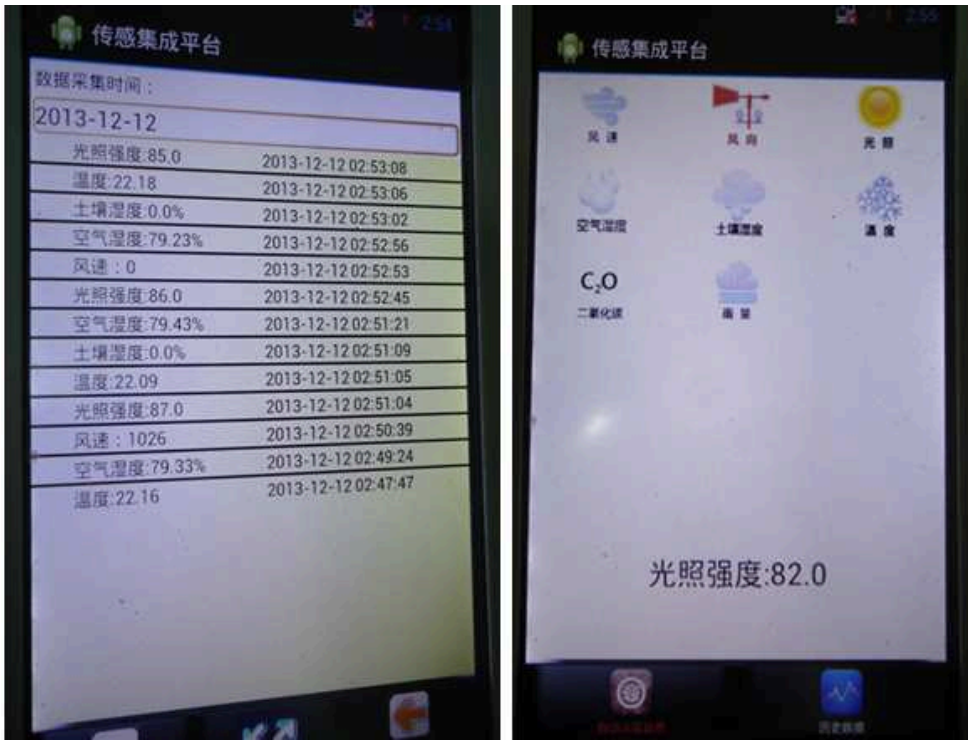

Fig.4 The test data of the system

Summary

With the development of information technology, it will realize intelligent and scientific management for tropical fields manegement. modern agricultural will be modernized and agricultural productivity will be raised.

Acknowledgements

Supported by State Spark-Program(2012GA8000022), State Science and Technology Support Program(2012BAD35B04), Hainan Natural Science Fund Project(613172) and Basic Research Fund of State Level Research Institutes(Chinese Academy of Tropical Agricultural Sciences) (1630022012018).

References

[1] Li Zhiwei. Study and Exploitation on Farmland Information Acquisition Based on 3S Technology[D]. Nanjing Agricultural University(2005) . (in Chinese with English abstract)

[2] Qiu Zhengjun. Study on the technology of field information acquisition and process in precision agriculture based on GPS, GIS and virtual instrument[D]. Zhejiang University(2003). (in Chinese with English abstract)

[3] Ye Tao. Research and Development of Information Acquisition System in Precision Agricuture[D]. Chinese Academy of Agricultural Sciences(2006) . (in Chinese with English abstract)

[4] Huang Liyan. Xiao Jiang. Ecological environment monitors of Flower Base used the technology of wireless sensor network[J]. Science and Technology Innovation Herald. 2005, No.05: 15-16. (in Chinese with English abstract)

[5] Li Nan, Liu Chengliang, Li Yanming, et al. Development of remote monitoring system for soil moisture based on 3S technology alliance[J]. Transactions of the CSAE, 2010, 26(4): 169－174. (in Chinese with English abstract)

[6] Haiqing Yang. Modelling and Instrumentation of Soil and Plant Selected Properties Based on Visible-near-infrared Spectroscopy[D]. Zhejiang University(2011). (in Chinese with English abstract)

[7] Fang Hui. The research on field information on collection system based Palm-sized PC[D]. Zhejiang University(2013). (in Chinese with English abstract)

[8] Xu Fuan, Xin Xiuli. Wireless Monitoring System for Environmental Parameters in Field and Its Application [J]. 8-10,14.

[9] Sharma S, Gifford S. Using RFID to evaluate evacuation behavior models[J].Fuzzy Information Processing Society,2005.NAFIPS2005.Annual Meeting of the North American,26-28June2005: 804-808.

[10] Wang Lingling, Huang Jiajian, Weng Shaojie, et al. Field information collection system for characteristic and tropical farming based on RFID [J]. Transactions of the CSAE, 2010, 26(Supp.2): 98-102. (in Chinese with English abstract)

[11] Liu Honggang. Modern Agricultural Production Environmental Monitoring Configuration and integration of Technology Research and Demonstration Application[D]. South China University of Technology(2011). (in Chinese with English abstract)

[12] Zhao Yandong1, Bai Chenxiang1, Kuang Qiuming. Performance of three types of soil moisture sensors:SWR,TDR and FD. JournalofBeijingForestryUniversity(2006)Vol.28(3):158--160. (in Chinese with English abstract)

[13] Kuang Yingchun. Studies on the Automatic Regulating System for Rice Water-Saving Irrigation in South Hilly Region[D]. Hunan Agricultural University(2011). (in Chinese with English abstract)

[14] Sun Yanghong. Configuration of Wireless Sensor Network on Collection Data of Field Information[D]. Henan Agricultural University(2010). (in Chinese with English abstract)

[15] Zhang Shujuan. The study of the collection and process of field information of Precision Agriculture based on the GPS and GIS[D]. Zhejiang University(2003). (in Chinese with English abstract)

Advanced Materials Research Vols. 989-994 (2014) pp 3456-3459
© (2014) Trans Tech Publications, Switzerland
doi:10.4028/www.scientific.net/AMR.989-994.3456

Flow field Simulation in Water Washing Tank of Explosion-Proof diesel

LONG Risheng[1, 2,4,a], LIAN Zisheng [1,2,b] ,SUN Shaoni [3,c] and WANG Qiliang[1]

[1]College of Mechanical Engineering, Taiyuan University of Technology, Shanxi, Taiyuan 030024, China;

[2]Shanxi Key Laboratory of Fully Mechanized Coal Mining Equipment, Taiyuan University of Technology, Shanxi, Taiyuan 030024, China;

[3] School of Mechanical Engineering and Automation, Northeastern University, Liaoning, Shenyang 110004, China;

[4] Shenyang Puyue Group, Liaoning, Shenyang, 110127, China

[a]etomi@163.com, [b]lianzis@vip.sina.com.cn, [c]shnisun@me.neu.edu.cn

Keywords: Explosion-Proof Diesel; exhaust purification; water-washing tank; numerical simulation; flow field

Abstract. In order to improve the cooling & purifying effect of exhaust, reducing the water-jetting phenomenon during working time, the waste-gas flow field simulation in water-washing tank of Explosion-Proof Diesel (*EPD*) was conducted through *ANSYS CFX*/*Fluent*. The results revealed the inner flow condition and outlet temperature of emissions in water-washing tank. It provided a reference for the future design and optimization of the water-washing tank of *EPD*.

Introduction

According to the Chinese Coal-mine industry safety standard, the waste gas of Explosion - Proof Diesel (*EPD*) must be cooled to the final exhaust temperature which is no higher than 70 ℃[1]. At present, from the perspective of safety and reliability, water-washing is the main cooling for the emissions of *EPD*. Taking the difference of output power and flame arrester grid layout into account, there are large variations in the shape and internal structure of the water-washing tanks. Through the washing process, the most carbon particles and NO_x from insufficient combustion will be coerced by water. For the obstruction of the stainless steel tank-walls, it is impossible to observe the gas-liquid flowing movement in tanks. It is also impossible to obtain the flow image even open an observation mouth on the tank-walls, because the observation mouth will soon be contaminated after the starting of diesel engine. Therefore, through the *ANSYS CFX/Fluent* module, the simulation of gas flowing in the exhaust water washing tank of *EPD* was conducted [2-9]. It is the only means to grasp the gas-liquid flowing condition inside the water-washing tank, and it will provide a reference for the future optimized design of water-washing tanks.

Simplifying and Setting of CFD Model for EPD

The water-washing tank consists of exhaust flame arrester, intake pipe, tank, partition board, diffuser, exhaust pipe and water-adding valve. All of them have great impact on the gas-liquid disturbing behavior during water-washing process. So it is necessary to take an interview to affect mechanism. In order to reduce the computing time, the un-important components, such as intake pipe, exhaust pipe, stiffener plates, flame arrester and float-ball valve chamber etc., were simplified away. Meanwhile, taking into account the symmetry of the model, as shown as in Figure 1, to further reduce the computational workload, the final analysis model is only 1/4 of the real water-washing tank. The model was meshed with free mesh method, and the model after meshing was shown in Figure 2.

In actually, the discharging velocity and flow capacity of *EPD* exhaust varied in a wide range. For the absence of exhaust data, this paper just provides a research method for the flow field interview of water-washing tank. So, in this simulation, the initial temperature of the gas-liquid two-phase flow equals 20 ℃, the surface tension coefficient equals 0.072 *N/m*, convection conduction heat transfer

coefficient equals 100 $W/m_2/K$. It is through the VOF method to track the interface and achieve the two-phase flow simulation field of water-washing tank. Taking one-way coupling method, the calculation time t equals 3 s, the time step $DELTA$ equals 0.01 s. Create a model with two non-buoyant fluid, air and water, and turn on Mesh Motion function, Thermal Conduction option set to Thermal Energy options. In the initial setup, it is required to set initial distribution and static pressure distribution with air and water VOF expressions. Meanwhile, set the inlet velocity Vinlet of 35.57 m/s, inlet temperature of 320 ℃, the exhaust pressure of 1 Atm.

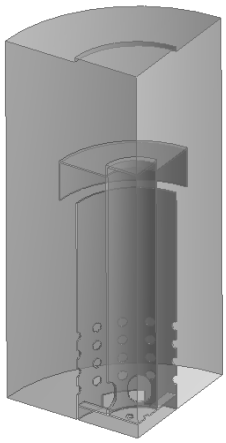

Fig.1 CFD model after simplification

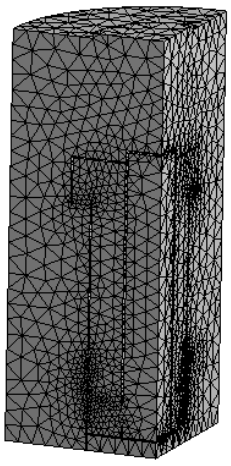

Fig.2 Mesh model of water-washing tank

Results of Simulation

Fig.3 is the serial photos of water volume fraction in water-washing tank at different time. From those photos, the changing processing of water volume fraction can be revealed, and the variation characteristics of water volume fraction can also be concluded. Before the 0.06 S, the interface between water and gas is clear. The 0.12 S was critical time, the water start to be coerced by exhaust and escaped finally. At 3.6 S, almost all of the water in water-washing tank had been taken away with the exhaust of EPDs.

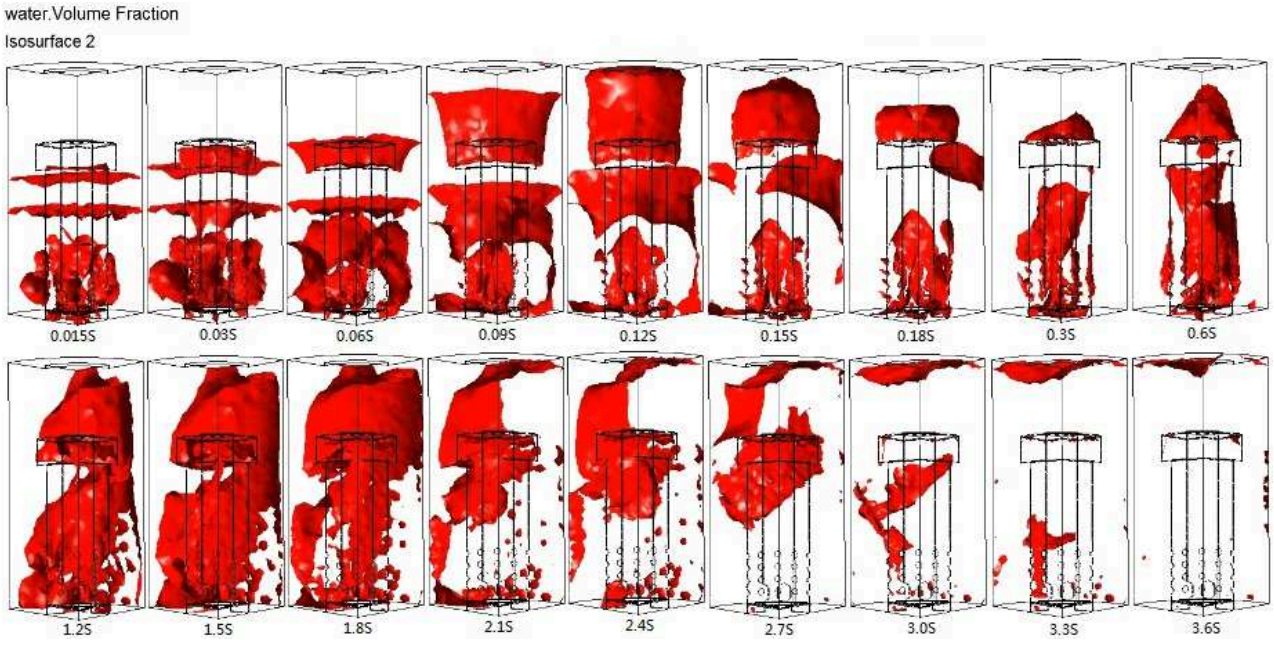

Fig.3 Water volume fraction photos inside of the water-washing tank at different time

Fig.4 is the serial photos of velocity flow field in water-washing tank at different time. From the simulation, the flow velocity vector & value of water-washing fluid inside of the water-washing tank

can be obtained. The following rules can be concluded: (a) the fluid velocity at the inlet and large holes of cavity is faster than other regions; (b) the fluid velocity gradually slowed down after flowing through the lumen to the outer chamber. The maximum fluid speed inside the water-washing tank is 80.37 *m/s*, around the large holes between the washing chamber and the inside of the outer chamber.

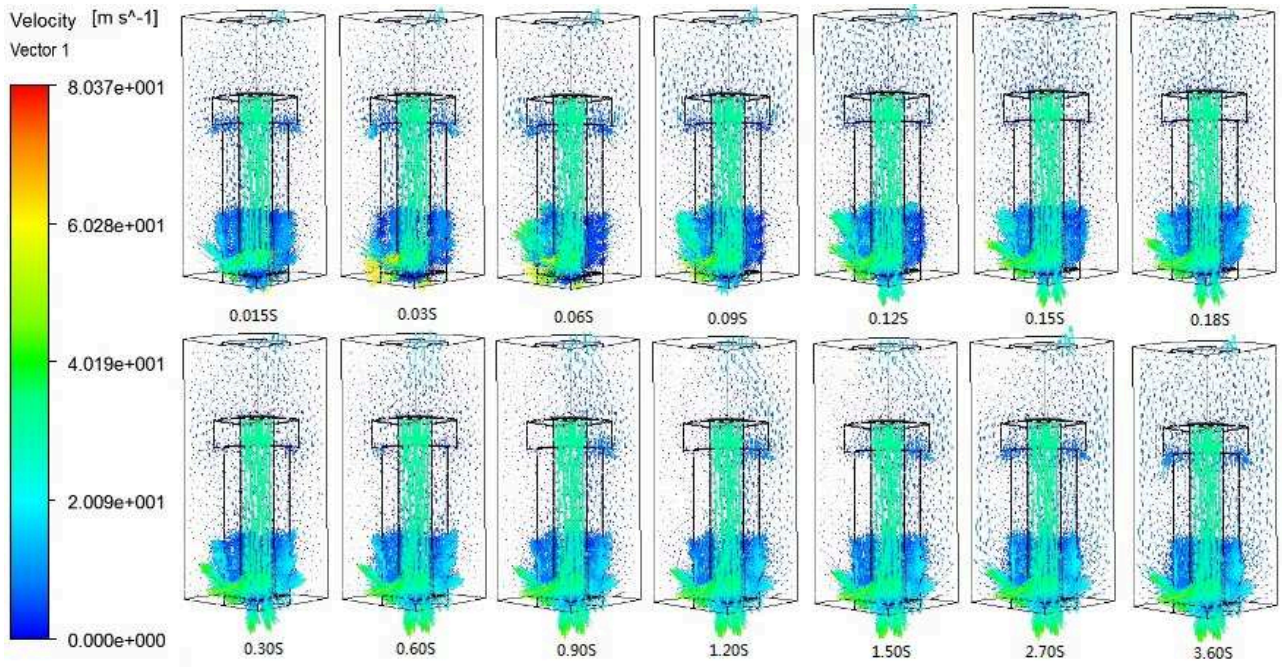

Fig.4 Velocity flow field photos inside of the water-washing tank at different time

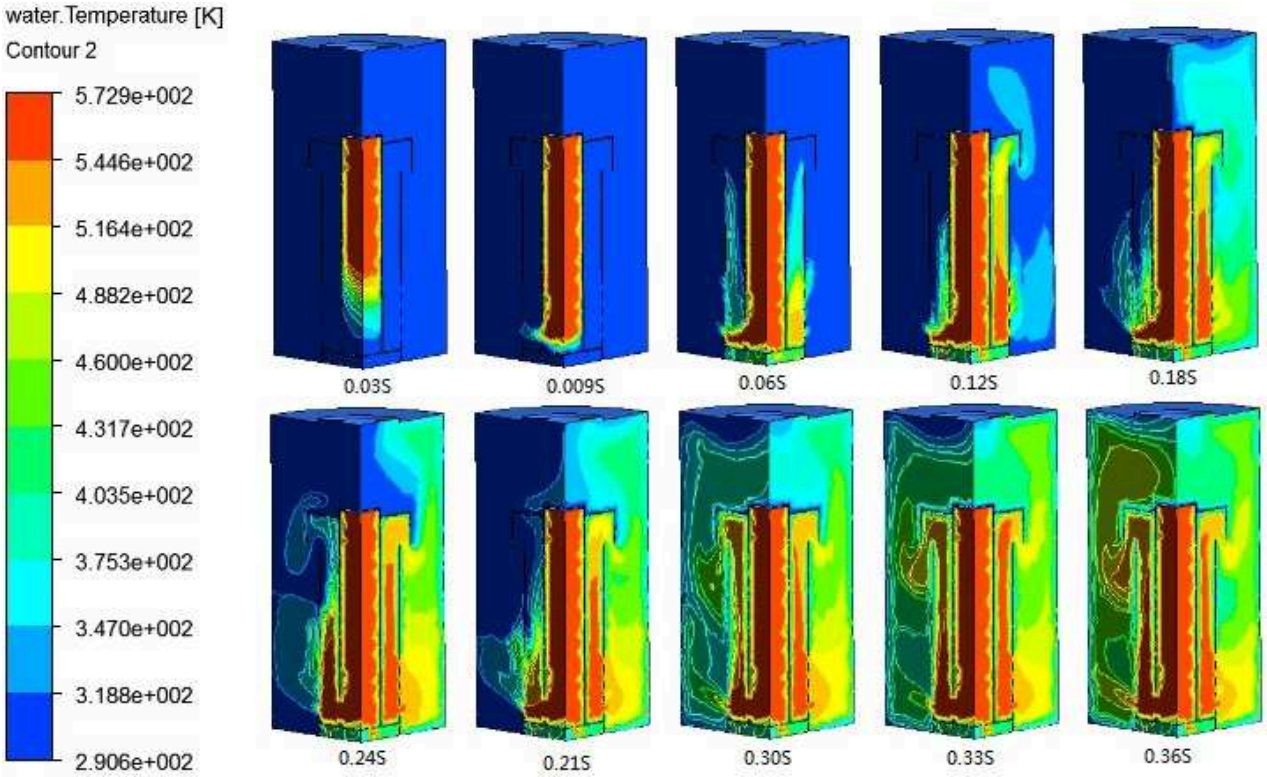

Fig.5 Distribution of the fluid temperature photos inside of the water-washing tank at different time

Fig.5 revealed the dynastic changing process of water-washing fluid temperature distribution inside of the water-washing tank from 1 *s* to 6 *s*. With the time increasing, the temperature of the water-washing fluid is gradually increasing. At the 2.1 *s*, the outlet temperature of water-washing tank equals 70 ℃(343 *K*); At the 6s, the outlet temperature of water-washing tank reaches 253 ℃ (526 *K*). This is because the simulation of water-washing process didn't take the water real-time

adding factor into accounting. So, at the 4S, it is almost all of the water had been taken away from the tank.

Conclusion

Through the simulation of the gas-liquid flow in water-washing tank of the *EPD*s, we could obtain the fluid velocity vector and temperature distribution inside of the water-washing tank. It provided a reliable method to study the complex flow condition inside of the water –washing tank of *EPD*s, and it also provided a reference for the future design and optimization of the water-washing tank of *EPD*. From the above results, the following conclusions can be gotten:.

1)The maximum speed of the fluid reached 80.37 *m/s* at the large hole between the chamber and the outer chamber inside water-washing tank.

2)With increasing time, fluid temperature in water-washing tank gradually increased. At 2.1 *s*, the outlet temperature of water-washing tank equaled 70 ℃; and it reached 253 ℃ at 6 *s*. This is because the simulation did not consider the real-time water replenishment of the water-washing tank. Therefore, in order to prevent the water-washing tank outlet temperature from increasing too high, we should always pay attention to the water replenishing during the operation of the equipment.

In the future, when considering the real-time replenishment water and exhaust flame arrester, we will do in-depth study the curve of temperature distribution, replenishment water rate, water level and exhaust temperature inside water-washing tank.

Acknowledgement

Supported by : Science and Technology Major Project of Shanxi province, P.R. China. "Research and development of electro-hydraulic control valve for Hydraulic roof supporters", 20111101025

References

[1] MT/T989-2006, Mine Explosion-Proof Diesel trackless rubber tire vehicle general technical conditions, Chinese mine standard. (In Chinese)

[2] S. Aita. Numerical simulation of swirling Port-Valve-Cylinder flow in diesel engines. SAE Paper, 1991-02-63

[3]R. D. Reitz, C. J. Rutland. Development and Testing of Diesel Engine CFD Models. Prog. Energy Combust Sci, 1995, 21: 173-196.

[4]Mobasheri Raouf, Peng Zhijun, Mirsalim Mostafa Seyed. Analysis the Effect of Advanced Injection Stragies on Engine Performance and Pollutant Emissions in a Heavy Duty DI-Diesel Engine by CFD modeling. International Journal of Heat and Fluid Flow, 2012, 33:59-69.

[5]F. Payri, J. Benajes, X. Margot et al. CFD Modelling of the In-Cylinder Flow in Direct-Injection Diesel Engines. Computers & Fluids, 2004, 33: 995-1021.

[6]Amin Maghbouli, Rahim Khoshbakhti Saray, Sina Shafee, et al. Numerical Study of Combustion and Emission Characteristics of Dual-Fuel Engines Using 3D-CFD Coupled with Chemical Kinetics. Fuel, 2013, 106: 98-105.

[7]Jiang Shuisheng, Zhu Siwei, Wen Hua, et al. Parameter Analysis of Diesel Helical Intake Port Numerical Design. Energy Procedia, 2012, 16:558-563.

[8]Wang Haigang, Chen Shi, Liu Shi. Simulation of air flows in intake-port and cylinder of internal combustion engines with moving valves. Journal of Engineering Thermophysics, 2002, 23(03): 312-314.(in Chinese)

[9]Liu Botang, Gan Xianshan. Full three-dimension flow calculation in the inlet channel of disel engine. Journal of Huazhong University of Science and Technology, 1999, 27(11): 42-44. (in Chinese)

Advanced Materials Research Vols. 989-994 (2014) pp 3460-3463
© (2014) Trans Tech Publications, Switzerland
doi:10.4028/www.scientific.net/AMR.989-994.3460

Research on Jet Current Field Characteristic under Waves by Numerical Modelling in Flowing Ambient Fluid

LI Ming-chang[1,2,3,a], SI Qi[1] and WANG Ying[1]

[1]Laboratory of Environmental Protection in Water Transport Engineering, Tianjin Research Institute of Water Transport Engineering, Tanggu, Tianjin, 300456, China;

[2]State Key Laboratory of Coastal and Offshore Engineering, Dalian University of Technology, Dalian 116024, China;

[3]School of Environmental Science and Engineering, Tianjin University, Nankai, Tianjin, 300072, China

[a]lmcsq1997@163.com

Keywords: jet, current field, wave, numerical modelling, flowing

Abstract. A variable density anisotropic turbulent buoyant jet model is applied for simulating the current field under waves. The numerical simulation results show the present model is efficient to describe the construction characteristic of current field. This model could be an efficient tool for sewage treatment by deep sea discharge.

Introduction

The sewage treatment by deep sea discharge has been become the major means in the nearshore district owing to the lower cost and environmental pollution. The sewage is mixed with environmental waters by jet means. So the jet characteristic of current field is key factor for the sewage deep sea discharge.

Jet's characteristic researched by the experiment and numerical simulation has been implemented for the sewage treatment by deep sea discharge. Many methods have been presented, such as dimensional analysis method [1], momentum integral method [2], differential equation method [3] and experimental method [4].

In this paper, a variable density anisotropic turbulent buoyant jet model is applied for simulating the current field under waves.

Anisotropic turbulent buoyant jet model

The jet's characteristics in flowing ambient fluid is studied by using the anisotropic turbulent buoyant jet model [5]. The governing equation is as follows:

Continuity equation:

$$\frac{\partial U_i}{\partial x_i}=0 \qquad (1)$$

Momentum equation:

$$\frac{\partial U_i}{\partial t}+U_j\frac{\partial U_i}{\partial x_j}=-\frac{1}{\rho_a}\frac{\partial P}{\partial x_i}+\nu\frac{\partial^2 U_i}{\partial x_j^2}-\frac{\partial \overline{u_i u_j}}{\partial x_j}+g_i\frac{\rho-\rho_a}{\rho_a} \qquad (2)$$

Concentration equation:

$$\frac{\partial C}{\partial t}+U_i\frac{\partial C}{\partial x_i}=\frac{\partial}{\partial x_i}(\lambda\frac{\partial C}{\partial x_i}-\overline{u_i c})+S_c \qquad (3)$$

An anisotropic algebraic stress model is applied to close the basic governing equation, as follows:

Turbulent kinetic energy equation:

$$\frac{\partial(\rho k)}{\partial t}+\frac{\partial}{\partial x_k}(\rho U_k k)=\frac{\partial}{\partial x_k}[c_k\rho\frac{k}{\varepsilon}\overline{u_k u_l}\frac{\partial k}{\partial x_l}+\mu\frac{\partial k}{\partial x_k})]+P_k+P_b-\rho\varepsilon \qquad (4)$$

Dissipation rate of turbulent kinetic energy equation:

$$\frac{\partial(\rho\varepsilon)}{\partial t}+\frac{\partial}{\partial x_k}(\rho U_k\varepsilon)=\frac{\partial}{\partial x_k}(c_\varepsilon\rho\frac{k}{\varepsilon}\overline{u_k u_l}\frac{\partial\varepsilon}{\partial x_l})+c_{\varepsilon1}\frac{\varepsilon}{k}P_k+c_{\varepsilon3}\frac{\varepsilon}{k}P_b-c_{\varepsilon2}\rho\frac{\varepsilon^2}{k} \quad (5)$$

Algebraic stress equation:

$$-\overline{u_i u_j}=\frac{k}{c_1\varepsilon}\frac{1}{\rho}\{(c_2-1)P_{ij}+(c_3-1)P_{ij,b}-\frac{2}{3}\delta_{ij}[c_2P_k+c_3P_b+\rho(c_1-1)\varepsilon]\} \quad (6)$$

Turbulent concentration propagation equation:

$$-\overline{u_i c}=\frac{k}{c_{T1}\varepsilon}\frac{1}{\rho}[(-P_{i,T}+\rho(1-c_{T3})\beta g_i\overline{cc}-\rho c_{T2}\overline{u_m c}\frac{\partial U_i}{\partial x_m} \quad (7)$$

Pulsating concentration squared equation:

$$\overline{cc}=-\frac{1}{c_{\theta1}}\frac{k}{\varepsilon}\overline{u_k c}\frac{\partial C}{\partial x_k} \quad (8)$$

The turbulent equations (2)-(9) is closed as the initial and boundary conditions are determined. In this paper, the variable density turbulent buoyant jet is considered by introducing the density state equation.

$$\rho=\frac{(C-C_a)\rho_0-(C-C_0)\rho_a}{C_0-C_a} \quad (9)$$

To study the influence of jet water's density, this paper introduces a buoyancy coefficient. It expresses the changing rate of water's density as the concentration of pollutant changes.

$$\beta=\frac{1}{\rho_a}\frac{\partial\rho}{\partial C}=\frac{1}{\rho_a}\frac{\rho_0-\rho_a}{C_0-C_a} \quad (10)$$

Boundary conditions:

Inlet section: $u=u_{in}$, $v_{in}=0$, $w=w_{in}=0$, $k=k_{in}=0.058(u_{in}^2+v_{in}^2+w_{in}^2)$, $\varepsilon=\varepsilon_{in}=k_{in}^{3/2}/(0.4h)$, $c=c_{in}$

Outlet section: $w=0$, $\frac{\partial}{\partial x}[u,k,\varepsilon,c]=0$

Free surface: rigid-lid hypothesis is used. $w=0,\frac{\partial}{\partial z}[u,k,\varepsilon,c]=0$

Side: $\frac{\partial}{\partial y}[u,v,w,k,\varepsilon,c]=0$

Wall [6]: $u=v=w=k=\varepsilon=0$, $\frac{\partial c}{\partial y}=0$, $\frac{\partial c}{\partial z}=0$

Jet inlet section: $u=u_0=w_j\cos\theta$, $v=v_0=0$, $w=w_0=w_j\sin\theta$, $c=c_0$, $k=k_0=0.058w_j^2$, $\varepsilon=\varepsilon_0=k_0^{3/2}/(0.4D)$, where, w_j is the initial velocity of jet; θ is the jet angle, D is the diameter of jet spout.

Case study

Set of the model parameters and mesh. In this paper, a case study is used to describe the current field characteristic. In this case, the model parameters are set as the values which are shown in the Table 1. In this table, T is the period of wave; L is the length of wave; H is the height of wave; U_w is the characteristic velocity of wave; R_j is the jet ratio. The computational region is divided into many pieces as shown in the Figure 1. The size of mesh is from 0.2cm to 2cm.

Table 1 Model parameters set

D（cm）	w_j（cm/s）	h（cm）	T（s）	L（cm）	H（cm）	U_w（cm/s）	R_j
2	50	50	1.18	200	4.5	7.60	6.58

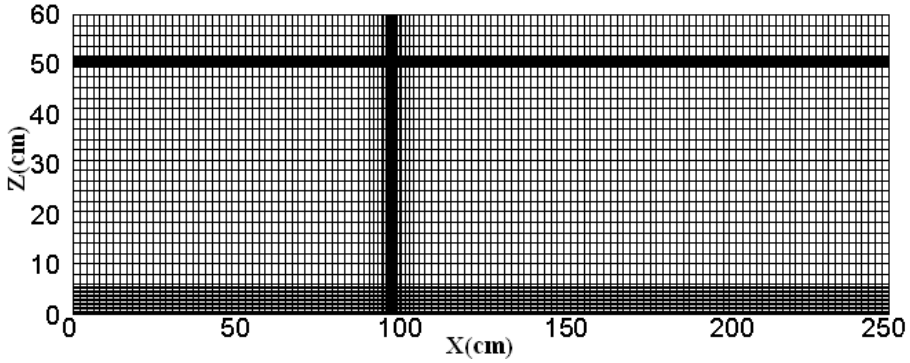

Fig.1 Diagram of computational mesh

Results of numerical modelling. Input the model parameters into the jet model, the results are obtained. The instant current field is shown in the Figure 2.

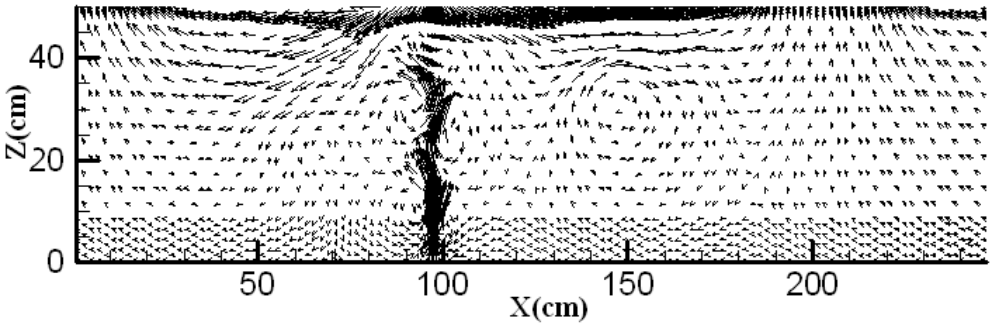

（a）t=11.80s

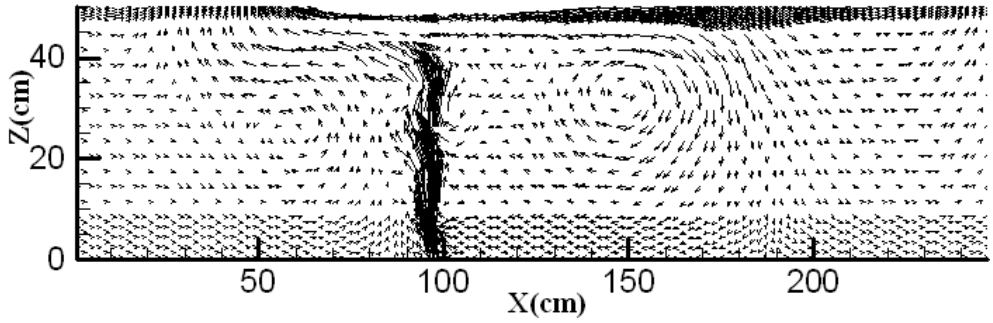

（b）t=12.09s

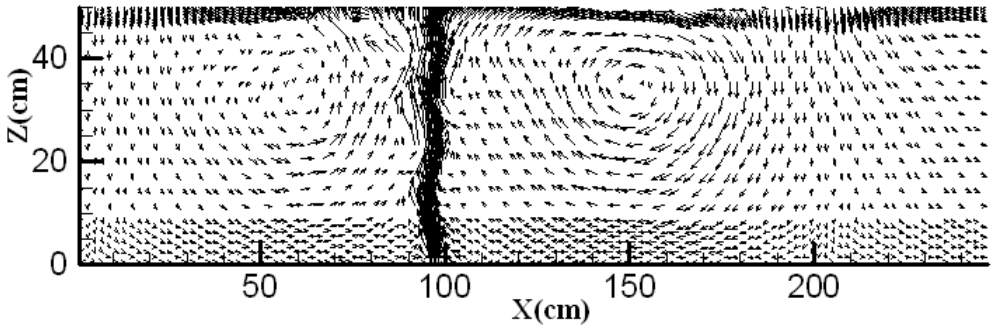

（c）t=12.39s

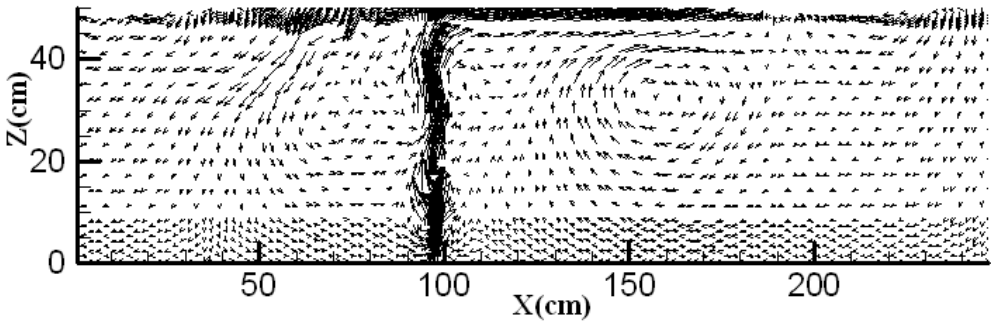

（d）*t*=12.68s

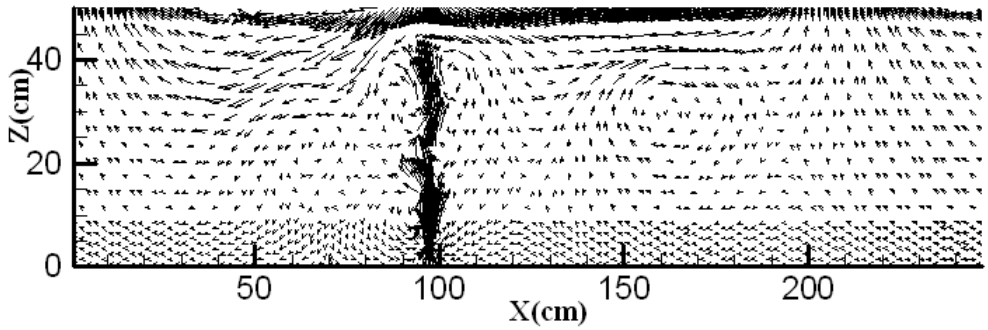

（e）*t*=12.98s

Fig.2 Instant current field

Fig. 2 shows the instant current field of simulation results. The numerical simulation results show the jet construction of current field under waves. The whole current field is very complicated. Small vertexes exist near the jet nozzle and the big vertexes occur far from the jet nozzle.

Conclusions

In this paper, a variable density anisotropic turbulent buoyant jet model is used for modeling the jet under waves. The numerical simulation results show the present model is efficient to describe the construction characteristic of current field. This model could be an efficient tool for sewage treatment by deep sea discharge.

Acknowledgements

This work was supported by the National Natural Science Foundation of China (No.51209110), the project of Science and Technology for Development of Ocean in Tianjin (KJXH2011-17) and the National Nonprofit Institute Research Grants of TIWTE (TKS130215 and KJFZJJ2011-01).

References

[1] R.B. Wallace and S.J. Wright: Journal of Hydraulic Engineering Vol. 110(1984), p. 813

[2] S.K.B. Cheung, D.Y.L. Leung and W. Wang: Proceedings of Computer Graphics International Conference, (2000), p. 75

[3] Y.R. Chang and K. S. Chen: International Journal Heat and Mass Transfer, Vol. 37(1994), p. 2935

[4] B.A. Haven and M. Kurosaka: Journal of Fluid Mechanics, Vol. 352(1997), p. 27

[5] H.Q. Ni, N.J. Wang and L.X. Zhou: Numerical simulation of nonisotropic turbulent buoyant recirculating flows by an algebraic stress model. ACTA Mechanica Sinica, Vol. 21(1989), p. 26 (in Chinese)

[6] B.E. Launder and D.B. Splanding: Computer Methods in Applied Mechanics and Engineering, Vol. 3(1974), p. 269

Advanced Materials Research Vols. 989-994 (2014) pp 3464-3467
© (2014) Trans Tech Publications, Switzerland
doi:10.4028/www.scientific.net/AMR.989-994.3464

Feedforward Improved PID algorithm to control the smart car

Yinghui Xie[1, a], Xiaoqiu Liu [1, a]

[1] School of Information Science & Engineering, Hunan International Economics University,Changsha, China

[a] e-mail:matlab_wjf@126.com

Keywords: Feedforward, improved PID algorithm, fuzzy, smart car.

Abstract. In the self-designed smart car, to control the speed and direction is the control core of the intelligent vehicle system . Due to hardware limitations, there is a delay in the smart car speed and direction control, which is adversely affected for the control of the smart car . For the above problems, the intelligent vehicle control will be applied by the feedforward and feedback control methods, the disturbance which is caused by the deviation will be treated in advance, Digital PID algorithm is improved , the incomplete differential and differential current algorithm is introduced to the PID algorithm to improve the dynamic performance of the system. Aftet this new algorithm is adopted, the dynamic performance of the intelligent vehicle system has been greatly improved.

INTRODUCTION

Smart car system is a time-varying and nonlinear systems using conventional PID feedback control algorithm for a single system will overshoot varying degrees of oscillation, can not get the desired control effect. This article will feedforward control is introduced to control the smart car system, effectively improve the real-time system, improve the response speed of the system [1]; and according to the characteristics of intelligent vehicle systems, digital PID algorithm has been improved by introducing the differential forward and incomplete differential links, improve the dynamic characteristics of the system; same time, the use of fuzzy control has not sensitive to parameter variations and robustness characteristics [2], this paper, fuzzy algorithm and PID algorithm combined effectively improve the smart car's adaptability and robustness, improved control system performance.

IMPROVED PID ALGORITHM

Smart car control is done by Freescale S12 chip, so the smart car control to computer control methods. In this paper, the particularity of intelligent vehicle control, the traditional digital PID algorithm made some improvements, so you can better meet the needs of intelligent vehicle control. Improved PID algorithm.

A. Incomplete differential PID

The direction and speed of the differential control aspects of the introduction of the smart car, obviously improves the dynamic performance of the system, but the error is particularly sensitive to disturbance mutations, stability of the system has some adverse effects. To overcome these shortcomings, the order inertia are incomplete differential PID algorithm are added in a PID algorithm[3].

The first-order inertia link directly applied to the differential link, the system transfer function can be obtained as follows:

$$U(s)=(K_p+\frac{K_I}{s}+\frac{K_D\cdot s}{1+T_f\cdot s})=U_p(s)+U_I(s)+U_D(s) \quad (1)$$

The term is derived differential equation (1) and finishing, get the following equation:

$$u_D(k)=K_D(1-\alpha)[e(k)-e(k-1)]+\alpha\cdot u_D(k-1) \quad (2)$$

Where, by the time constant of the system is a constant and a time constant of order inertia decision. To facilitate programming, can be written as (2) type:

$$\begin{aligned} u_D(k)&=K_D(1-\alpha)e(k)+\alpha u_D(k-1)-K_D(1-\alpha)e(k-1)\\ &=K_D(1-\alpha)e(k)+H(k-1) \end{aligned} \quad (3)$$

Where, $H(k-1)=\alpha\Delta u_d(k-1)-K_d(1-\alpha)e(k-1)$.

Analysis of formula (3) shows that after the introduction of incomplete differential, differential output in the first sampling period is reduced, then they follow a certain percentage of attenuation [3] [4]. Experiments show incomplete differential effectively overcome the bias of intelligent vehicle speed control interference to the adverse effects of having better control effect. Figure 1 is incomplete differential PID algorithm program flow.

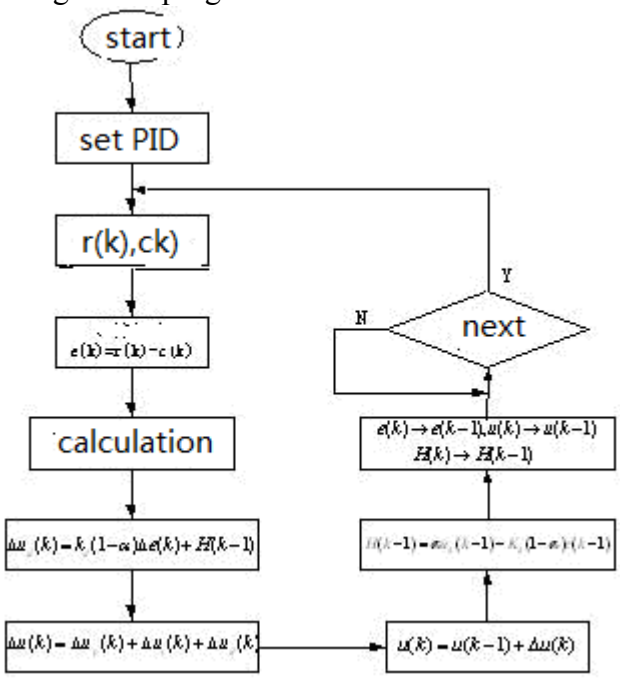

Figure 1. Incomplete differential PID algorithm program flowchart

B. Differential forward PID

As the Smart car driving on the track, turning often encounter the situation, so intelligent vehicle speed setting and direction setting changes frequently occur, resulting in an oscillating system. To solve the adverse effects of frequent changes to the system settings to bring this article on the smart vehicle speed and direction of advance of differential PID control algorithm is introduced, which is characterized by only the output of the differential amount, i.e., only the speed and the measured value differentiating the steering deflection amount, speed and direction without setting the differential value. Thus, when the setpoint changes, output does not change, but the relative change in the amount charged is more relaxed, which nicely avoids oscillation frequent changes to the system settings caused, apparently improves the dynamic performance of the system.

Differential first incremental control formula below.

$$\Delta u(k)=K_p[e(k)-e(k-1)]+K_i\cdot e(k)-K_d[c(k)-2c(k-1)+c(k-2)] \\ -K_d[c(k)-c(k-1)] \quad (4)$$

FEEDFORWARD CONTROL APPLICATIONS

Because smart car track width is limited, so after a sharp turn when, if the speed and direction control is not timely, intelligent vehicles could runway. Since the feedforward control is the open loop control, feedforward control response speed quickly. The feedforward control is introduced into the smart car control, to improve the response speed servo and servo motors, improving dynamic performance of intelligent vehicle systems.

*C. **Intelligent vehicle control system architecture***

Smart car control is mainly reflected in two aspects: one is to control the direction, that is, control of the steering gear; the other is for speed control, that is, the servo motor control. Servos relatively simple mathematical model has good linearity characteristics, using only feedforward control; intelligent vehicle speed control is relatively complex, the velocity model can not be

accurately established, feedforward - Improved PID control algorithm. Smart car control system architecture is shown in Figure 2.

This figure is a mathematical model of the servo motor and servo. As can be seen from the drawing, the intelligent control of the vehicle direction and speed are controlled independently of each other, and they are determined by the route deviation. Correspondence between the steering angle and route deviation between the mathematical model is based on the resulting steering, speed control loop, both feedback loop also includes the amount of feed forward control, servo motor is based on feedforward compensation then calculated by the incremental PID algorithm.

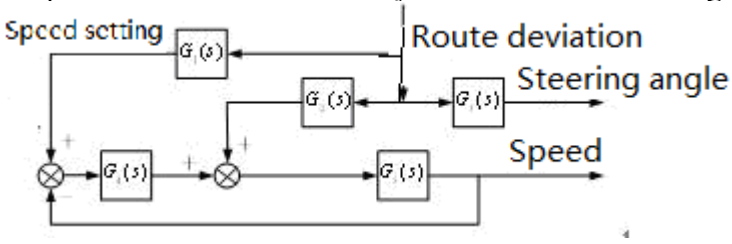

Figure 2. Smart car control system architecture

D. *Application In the directional control*

Control of the direction of the smart car has two requirements: on the straights, the direction remains stable; in the corner, you need to change direction quickly and accurately. The only way to ensure that the smart car speed, stable operation on the runway. In order to improve the robustness of directional control, the paper also carried a route deviation fuzzy processing. Figure 3 is a block diagram of fuzzy intelligent vehicle direction feedforward control, block diagrams $G_Z(s)$ and $G_W(s)$ are two cases before the straights and corners under feedforward control functions.

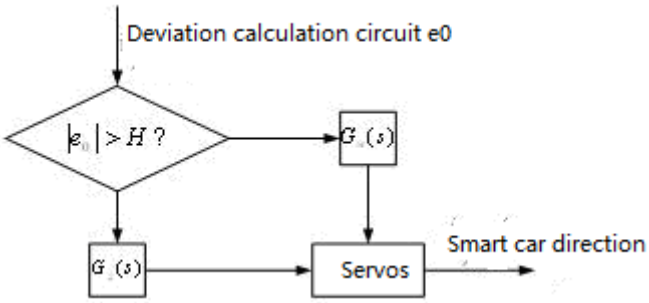

Figure 3. Intelligent vehicle directional control system structure

E. *Application In the speed control*

In order to make the smart car on the straight run at a faster speed, in turn, prevents the smart car skidded off the runway, you must reduce the speed of the smart car, which requires intelligent vehicle speed control system has good acceleration and deceleration performance. When the Smart car through continuous turning track, the frequent changes in the route deviation will result in frequent changes in speed setting, which may cause oscillation speed control systems, and differential interference links for error is very sensitive mutations, likely to cause system instability. In order to solve the above problems, this paper digital PID algorithm has been improved, will not be fully differential and differential first introduced to the PID algorithm, which greatly improves the dynamic performance of the speed control system.

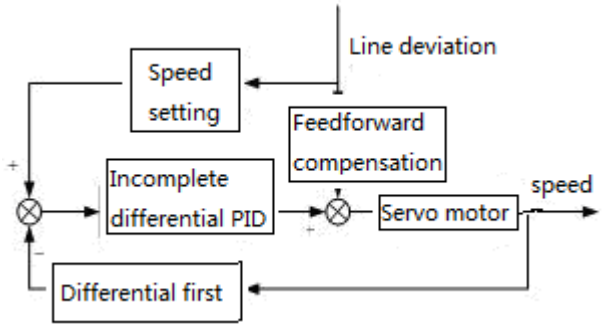

Figure 4. Intelligent Vehicle speed control system structure

Figure 4 is an intelligent vehicle speed control system structure. Due to road conditions and the smart car track attitude will often change, so the speed control system model is also uncertain, in order to improve the adaptability of the system, speed control system, this paper uses a fuzzy PID algorithm. The speed and the actual speed of the fuzzy set of files [5] [6], obtained under different conditions relative to the optimal PID parameters through commissioning, to ensure that the speed control system in different circumstances have good control effect.

CONCLUSIONS AND OUTLOOK

The proposed feedforward - Improved PID algorithm is an effective way to control the smart car, the algorithm makes intelligent vehicle system[7-11] not only has a good dynamic performance and reaction speed, and improve the adaptability and robustness of the system, make the smart car can run on different runways at a faster rate. Experimental results show that: the proposed control algorithm effectively improve the smart car's performance, running on the same runway, using a new algorithm for intelligent vehicle than traditional PID feedback control algorithm for intelligent vehicle speed has increased, running a reduce the average lap time of 3.2 seconds, and the proposed algorithm makes intelligent vehicle running stability improvements, improved adaptability smart car on the runway. This method has a good prospect.

References

[1] TANG Gong, high Dexin nonlinear systems with persistent disturbances feedforward - feedback optimal control [J] Control and Decision, 2005 04.
[2]. PK Dash, AC Liew. Anticipatory fuzzy control of power systems [J]. IEE Proc.-Cener. Transm. Distrib., Vol. 142, No. 2, March 1995:211-218
[3] Tao Yonghua New PID control and its application [M] Beijing: Mechanical Industry Press, 2002.3
[4] Rong Gang, Wang Shuqing fuzzy frequency domain based on a new type of PID controller design and parameter tuning [J] Journal of Zhejiang University: Natural Science Edition, 2000 Volume 34 No. 2
[5] Jiang Ying, Ye Bicheng. Control based on TS fuzzy neural network model [J]. Control Engineering .2006 November Volume 13, Issue 6
[6] Frank Klawonn, Jorg Gebhardt, Rudolf Kruse Fuzzy Control on the Basis of Equality Relations with an Example from Idle Speed Control [J] IEEE TRANSACTIONS ON FUZZY SYSTEMS, VOL 3, NO 3, AUGUST 1995:336 – 350
[7] Ding Fang, Gu Xiangyu, Like Wei, Yang Ming. Fuzzy algorithm in the intelligent vehicle control [J]. Journal of Civil Aviation University of China in 2009 (01)
[8] Zhang Shuqian Kingdom right. Recognition algorithms and intelligent vehicle control strategy black line [J]. Electronic technology 2009 (03)
[9] high Yuet Wah Design [J]. Semiconductor optoelectronic infrared photoelectric sensor based on smart car automatic tracking system in 2009 (01)
[10] B. Eyring, Qushao Cheng, Liu Dong, Zhu Lijia Xu Bin. CCD camera based on intelligent vehicle path identification and tracking [J]. Electronic Measurement Technology 2009 (08)
[11] Wubin Hua, Huang Weihua, Cheng Lei, Yang Ming Design [J]. Electronic technology path identification based on smart car system. 2007 (03)

Advanced Materials Research Vols. 989-994 (2014) pp 3468-3472
© (2014) Trans Tech Publications, Switzerland
doi:10.4028/www.scientific.net/AMR.989-994.3468

Evaluation of Various Turbulence Models in Predicting Airflow and Turbulence around a Generic Vehicle Model

Cheng Wu[1,a], Yiping Wang[1*,b], Xue Yang[2,c]

[1] Hubei Key Laboratory of Advanced Technology of Automotive Components, Wuhan University of Technology, Wuhan 430070, China

[2] Wuhan Ordnance Noncommissioned officers School, Wuhan 430075, China

[a]email: wucheng@whut.edu.cn, [b]email:wangyiping@whut.edu.cn, [c]email:157035890@ qq.com

Keywords: Ahmed model; External flow filed; Turbulence model; RANS

Abstract. For vehicle external aerodynamic computation, the selection of the turbulence model is very important. In current research, ten RANS turbulence models were introduced to compute the time-averaged flow field around the Ahmed model with 25° backlight angle. In order to evaluate the feasibility of the turbulence model, the results were compared with the related published experimental data. The results showed that the two equations RANS turbulence models were more favorable to compute the vehicle external flow field, but parts of the two equations turbulence model just could predict the aerodynamic drag coefficient or lift coefficient effectively. However, the results further revealed that the realizable k-ε could obtain the more accurate drag coefficient and lift coefficient simultaneously, and simulate the complex separation flow in the wake.

Introduction

The external aerodynamics is concerned with many relevant aspects of a ground vehicle such as handling stability, comfort and fuel consumption [1]. Flow field around road vehicles is highly three-dimensional, unsteady, separated and turbulent. The main contributions to aerodynamic drag for a bluff body type vehicle are the flow separation in the rear, causing pressure recovery losses and vorticity in the wake. With the rapid development of computer power, the computational fluid dynamic (CFD) was introduced as a new technological solution for the design and testing. It is unquestioned that the numerical simulations could perform in-depth analysis to the complex phenomena without resorting to expensive prototypes and difficult experimental measurements. This trend, to bring CFD to bear on vehicle aerodynamics design issue, is appropriate and timely in view of the increasing competitive and regulative pressure being faced by the automotive industry [2]. For the application of CFD in vehicle aerodynamic simulation and its significant, Hucho [1] had performed a comprehensive review. Since the first researchers [3, 4, 5] applied CFD to vehicle external aerodynamic prediction, applications of CFD for airflow predictions around the vehicle have become widespread. However, since the turbulence models in CFD used approximations, the simulation results may contain uncertainties. Therefore, it is very important to evaluate the generality and robustness of the turbulence model for predicting airflow around a vehicle.

In order to investigate the performance of turbulence models for complex geometry cases, a simplified car model, known as the Ahmed body [6] was often employed as a benchmark in vehicle aerodynamic. The Ahmed body is a generic car type bluff body shape which is enough simple for accurate flow simulation but retains some important practical relevant features of automobile bodies [7], as shown in figure 1. More detailed measurements using LDA for the backlight angle 25° have been performed by Lienhart and Becker [8]. With the availability of published experimental data and the advantage of simple surface geometry, the Ahmed body became a popular test case to validate the computational accuracy, meshing strategy, turbulence modeling and so on.

In the literature, a certain number of researches are now available for the angle 25°of the backlight angle using different turbulence modeling approaches. At first, the RANS or unsteady RANS (URANS) approaches were employed to compute the external flow field and the turbulence models employed varied from standard k-ε model, k-ω model, Explicit Algebraic Reynolds Stress

Model to Reynolds Stress Model. However, The flow computed for the slant angle 25° does not match the experimental results, and Krajnović[9] argued that the possible reasons of the failures may be that the shear due to the partial detachment of the flow on the upper part of the slant related to a Kelvin-Helmholtz instability, which significantly increase the momentum transfer across the mean streamlines and enhance the three-dimensionality as well as the unsteadiness of the flow.

Many RANS turbulence model had been employed to investigate the flow field around the Ahmed model, and the performance of the different turbulence model were also compared partly. It can be concluded that, for the simulation of vehicle external flow filed, each turbulence model has its own advantages. However, there are no systematic analyses and comparisons for the different turbulence model in the vehicle aerodynamic simulation. Therefore, in current research, in order to investigate the performance of the different turbulence model in the vehicle aerodynamic simulation comprehensively, the different RANS models were employed to compute the exterior flow filed around the Ahmed model.

Geometry and computational parameters

The Ahmed model is shown in Fig. 1. Here, only the 25° backlight angle is investigated. The length of the model is L =1044 mm, the width is W =389 mm, the height is H =288 mm. The ground clearance is G =50 mm, and the diameter of the four feet, which are used to fix the model to the floor of the wind tunnel, is Φ = 30 mm. The reference axis (X, Y, Z) is linked to the model. The origin of these axes is related to the point O located on the floor of the wind tunnel at the base of the model and in the symmetry plane of the model.

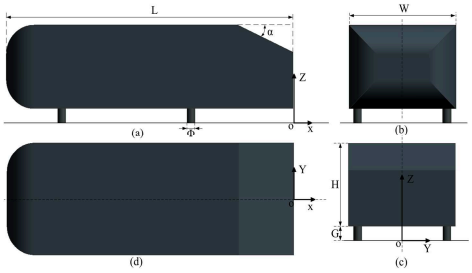

Fig.1 Side, rear, front and top view of the Ahmed body and the coordinate system

The upstream velocity is V_0=40 m/s. The computational domain starts 2L in front the model and extends to 5L behind the model. The cross-section of the computational domain is 1.87 m and its height is 1.4 m, which gives a blockage ratio of 4.3%, is identical to the open test section of the wind tunnel used in the experiments [8]. The boundary conditions are no slip walls for the Ahmed body geometry and the floor of the computational domain, while the roof and the side walls of the computational domain are treated as slip walls. At the inlet, the uniform velocity V_0 is imposed while at the outlet, the pressure is imposed.

Numerical method

In current research, Spalart-Allmaras model, standard k-ε, RNG k-ε model, realizable k-ε, standard k-ω, Shear-Stress Transport (SST) k-ω, the k-kl-ω transition, Explicit Algebraic Reynolds Stress, v2f model, Reynolds stress model were employed to compute the flow field around the Ahmed body, and the performance of the turbulence models was evaluated and compared.

All these turbulence model equations mentioned above can be written in a general form as:

$$\rho\frac{\partial\bar{\phi}}{\partial t}+\rho\frac{\partial\overline{u_j}\bar{\phi}}{\partial x_j}-\frac{\partial}{\partial x_j}\left[\Gamma_{\phi,eff}\frac{\partial\bar{\phi}}{\partial x_j}\right]=S_\phi \tag{1}$$

Where ϕ is variables, $\Gamma_{\phi,\,eff}$ is the effective diffusion coefficient, and S_ϕ is the source term. Due to the space limit of the paper, a more detailed description of these models is not possible. Since many of the models are available in some commercial software, one could also refer to the user manual.

This study used commercial CFD software, FLUENT to conduct all the numerical investigations. The RANS models used the second order upwind scheme for all the variables except pressure. The discretization of pressure is based on a staggered scheme, PRESTO! The SIMPLE algorithm was adopted to couple the pressure and momentum equations. If the sum of absolute normalized residuals for all the cells in flow domain became less than 10^{-3} for all variables, the solution was considered converged. Grid dependence of each case was checked using two different grids to ensure that grid resolution would not have a notable impact on the results.

Results and Discussion

According to the drag force coefficient showed in table 1, most of the turbulence models were over-predicted, and the Realizable *k-ε*, SST *k-ω*, RSM and Transition SST whose error were within 5% may be considered more accurate, especially for the SST *k-ω*, the error was -1.75%. However, for the lift force coefficient, all the turbulence models were under-predicted relative to the experimental data, and the results revealed that Realizable *k-ε*, Standard *k-ε* and *k-kl-ω* whose errors were within 5% may be considered more accurate, especially for the Realizable *k-ε* the error was about -1.75%. Based on the comprehensive analysis of the drag coefficient and lift coefficient, it could be concluded that although parts of the turbulence models could predicted the drag coefficient, the error of the lift coefficient was unreasonable, such as SST *k-ω*. In other words, these turbulence models cannot predict the aerodynamic force fully. However, not only for the drag coefficient, but also for the lift coefficient, the Realizable *k-ε* could obtain more accurate results. Therefore, the Realizable *k-ε* was better for the prediction of aerodynamic force.

Table 1 Drag and Lift force coefficient

	Cd			Cl		
Turbulence model	CFD	Experiment	Error (%)	CFD	Experiment	Error (%)
Realizable *k-ε*	0.294	0.285	3.16%	0.393	0.400	-1.75%
RNG *k-ε*	0.308		8.07%	0.377		-5.750%
Standard *k-ε*	0.479		68.07%	0.388		-3%
SST *k-ω*	0.280		-1.75%	0.263		-34.25%
Standard *k-ω*	0.851		198.60%	0.365		-8.75%
RSM	0.275		-3.51%	0.255		-36.25%
S-A	0.348		22.11%	0.379		-5.25%
k-kl-ω	0.364		27.72%	0.385		-3.75%
Transition SST	0.291		2.11%	0.355		-11.25%
v2f	0.327		14.74%	0.242		-39.5%

In order to evaluate the predication ability of the turbulence model for the aerodynamic characteristic further, the mean velocity profiles of the tail were extracted to compare with the experimental data (see Fig.2, the square legend is the experimental data). The experimental data is provided by the Prof. Becker [8] at the Universitaet Erlangen-Nuernberg in Germany. The results revealed that the airflow attached on the surface, and did not separate except for the standard k-ω at X/L=0.80. Perhaps this was the reason why the error of the drag coefficient predicted by the standard k-ω reached to 198.6%. At X/L=0.89, the airflow began to separate, and the separation became stronger and stronger as the distance increase. For the wake, especially for the center of the wake, the results obtained by the Realizable *k-ε* were closer to the experimental data. Therefore, the results of the mean velocity profile of the wake could further explain why the Realizable *k-ε* could predict the external flow field fully and accurately.

Conclusion

In current research, ten RANS turbulence models were introduced to compute the time-averaged external flow field of the Ahmed model with 25° backlight angle, and the accuracy of the turbulence model in the vehicle external flow field were evaluated by comparing the result with the related published experimental data.

Results indicate that the scale of the wake vortex obtained by numerical is smaller than that of the experimental result. The two equations RANS models were more favorable for the computation of vehicle external flow field. The realizable k-ε could obtain more accurate drag coefficient and lift coefficient simultaneously, and simulate the complex separation flow in the wake.

Compared with the Ahmed model in current research, the external aerodynamics of a ground vehicle is more complex. Therefore, the future investigation should include the vehicle wheel and the accessories of the vehicle and so on. And the vehicle aerodynamic simulation also should be computed by coupling the flow field of the internal with external aerodynamics. Moreover, flow field at the rear end of road vehicles is highly unsteady, so DES (detached eddy simulation) or LES (large-eddy simulations) model should be taken to investigate the transient characteristics of the wake vortex in the future.

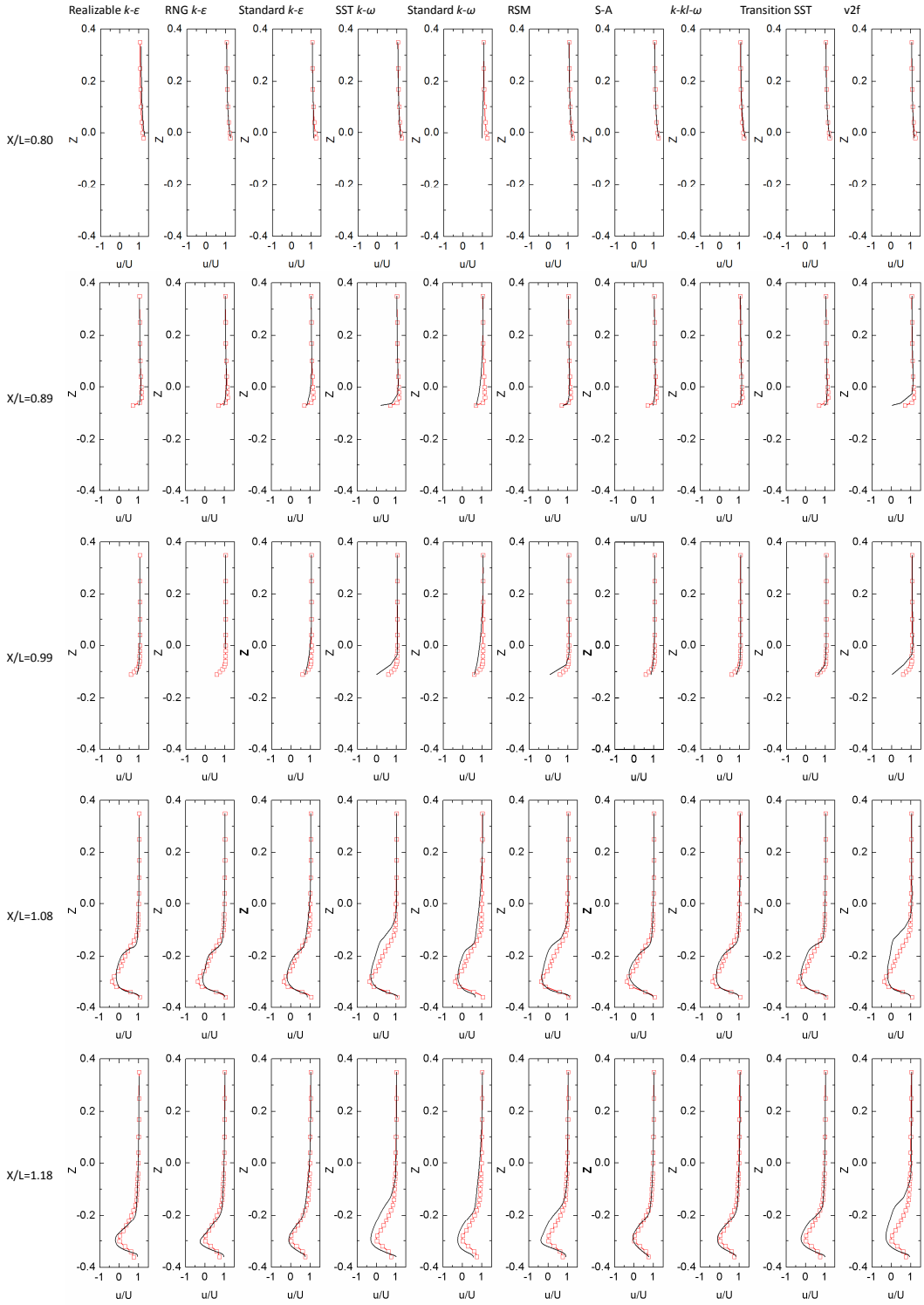

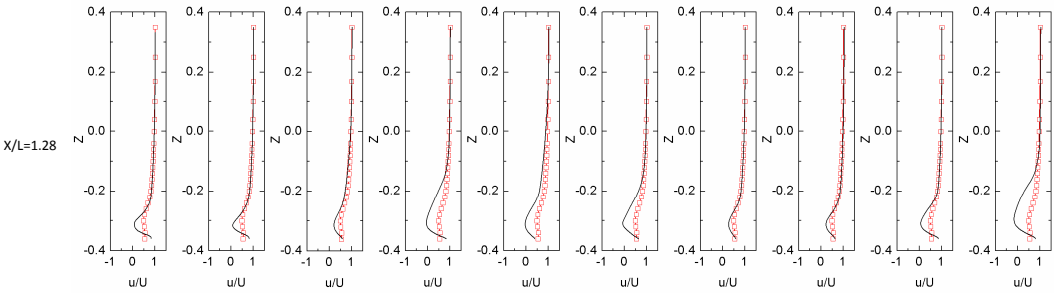

Fig. 2 Velocity profile along the symmetry

Acknowledgement

The research was supported by National Natural Science Foundation of China (51305312), Wuhan Youth Chenguang Program of Science and Technology (2013070104010001), Hubei Key Laboratory of Advanced Technology of Automotive Components (2012-07).

Reference

[1] Hucho W. H., Aerodynamics of Road Vehicles, SAE International, Warrendale, PA (1998).

[2] Khalighi, B., Jindal, S., Johnson, J.P., Chen, K.H., Iaccarino, G., Validation of the Immersed Boundary CFD Approach for Complex Aerodynamic Flows The Aerodynamics of Heavy Vehicles II: Trucks, Buses, and Trains Lecture Notes in Applied and Computational Mechanics Volume 41, pp 21-38, 2009.

[3] Nishikawa, S., Watanabe, Y., Fujitani, K., Himeno, R. et al., "Numerical Simulation of Flow around a Heavy-Duty Truck Body," SAE Technical Paper 890599, 1989.

[4] Kawaguchi, K., Hashiguchi, M., Yamasaki, R., and Kuwahara, K., "Computational Study of the Aerodynamic Behavior of a Three-Dimensional Car Configuration," SAE Technical Paper 890598, 1989.

[5] Hashiguchi, M., Kawaguchi, K., Yamasaki, R., and Kuwahara, K., "Computational Study of the Wake Structure of a Simplified Ground-vehicle Shape with Base Slant," SAE Technical Paper 890597, 1989.

[6] Ahmed S. R., Ramm G. and Faltin G., Some Salient Features of the time-Averaged Ground Vehicle, SAE Paper 840300 (1984).

[7] RodrigoR. Paz, Norberto M. Nigro and MarioA. Storti. On the efficiency and quality of numerical solutions in CFD problems using the Interface Strip Preconditioner for domain decomposition methods, International journal for numerical methods in fluids, 52(1):89-118 2006.

[8] Lienhart H, Becker S. Flow and turbulence structure in the wake of a simplified car model. SAE paper 2003-01-0656, 2003.

[9] Krajnovic S, Davidson L. Flow around a simplified car. Journal of Fluids Engineering 127:907–28, 2005.

Advanced Materials Research Vols. 989-994 (2014) pp 3473-3476
© (2014) Trans Tech Publications, Switzerland
doi:10.4028/www.scientific.net/AMR.989-994.3473

Ground simulation method for envelope performance of airship in near space

Longbin LIU[1, a], Panpan MI[1, b], Shuai CAO[1, c], Mingyun LV[1, d]

[1]Aeronautical Science and Engineering, Beihang University, Beijing, 100191, China

[a]email:longbuaa@sina.com, [b]email:blucemi@163.com, [c]email:caofan1024@126.com, [d]email:lv503@buaa.edu.cn

Keywords: Near Space Airship; Performing Environment, The Envelope Material, Ground Simulation Test, Weathering Performance

Abstract. Performing characteristics on envelope composite of near space airship (NSA) are quite different from that of the low altitude airship essentially. The NSA envelope material should meet excellent applicative characteristics including light weight, high strength, anti-aging, anti-ultraviolet radiation, gas-tightness, weather resistance. Ground simulation test is critical for the envelope design and development process of NSA, and the environmental features of near space is analyzed for NSA, then corresponding ground simulation test methods are proposed to involve mechanical strength of the ground test methods among the changing weather temperature and over pressure changes, materials weather resistance and air tightness test. Finally the coupling relationship between various mechanical test and environmental test methods is also investigated.

Introduction

With the development of high strength envelope material and cycle solar energy technology, the near space airship attract more and more interest of researchers [1]. As near space airship plays critical roles in various areas involving long-term floating in space, high detection, fixed floating, operational effectiveness evaluation, missile defense, ECM (electronic countermeasures) and others [2].However, it is a quite long way to realize engineering application of high altitude long-term floating airship in near space [3]. And with the severe influence of wind, thermo, UV (ultraviolet) and other stratospheric environmental factors, the mechanics and reliability of flexible envelope composite material degenerate gradually. Consequently, Micro cracks or micro holes go expansion and the envelope material become failure [4].

Single mechanism or multiple coupling mechanisms influence of near space environmental factors further accelerated the performance degradation. Consequently the mechanics of material, physical and chemical properties decreased badly [5]. The performance of airship envelope material has two aspects together including the mechanical properties of both fabric yarn bundles and composite laminated or coated properties. Currently the related available studies mainly focus on macro-mechanical properties and material fatigue life of airship envelope under single environment affecting factors [6], and usually combined with the flight test or ground simulation environment measurement to test the mechanical characteristics of the airship envelope under the influence of complex space environment [7]. Because the current commercialization envelope material on the domestic market mainly relied on foreign imports. So this results in the lack of intellectual property rights of self- development performing materials of near space airship, and the scientific test standard and testing methods of NSA envelope have not formed.

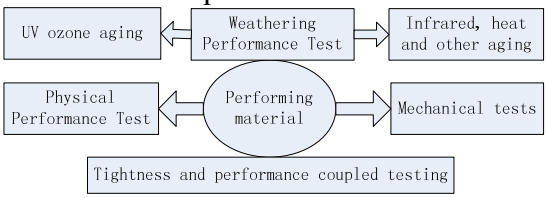

Fig.1. A integrated schematic diagram for ground simulation test methods of performing material

Based on the previous studies, the ground simulation test methods are analyzed under multiply near space environment factors shown in Fig. 1. The physical properties and mechanical strength simulation tests of long time performing envelope are investigated and summarized including temperature changing and over pressure changing in near space environment. Then coupling relationship is further analyzed between the various test methods, and major factors are also noted for selecting long-endurance performing envelope composite.

Test methods for the physical properties of the envelope material

Spacecraft can work for a long time and it requires envelope material has a high efficiency of weight. That is to say that weight of envelope material will be small and we usually use specific gravity (weight) to measure its size. So the per surface density should be below 135g/m2 and the envelope material requires uniform texture. Thickness of material are tested by GB/T 3916-1997 standard shown in Fig. 2. Thickness of the envelope material is generally less than 0.35mm.

Fig.2. Envelope material laminated fabric thickness tester

In recent years, more and more researchers are also concerned about the flexible airship envelope material components, as well as skin material components in space under the influence of environmental factors in the fiber bearing layer, blocking helium layer, layer aging resistance micromechanics characterization, and forecast stratosphere envelope material in real-fatigue life. Airship envelope material is a multilayer film laminate; using high strength polyethylene filament a aliphatic Veteran fiber reinforced TPU film laminated synthetic material in Fig 3 (a). The film thickness is 0.16mm and the inner layer is formed by 10 feature films adhesive bonding together, as shown in Fig 3 (b). Fibers are the plain weave braid and physical geometric parameters are shown in Table 1, which are measured by standard test equipment.

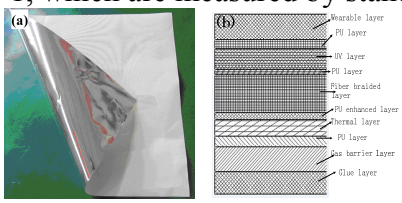

Fig.3. Envelope specimens

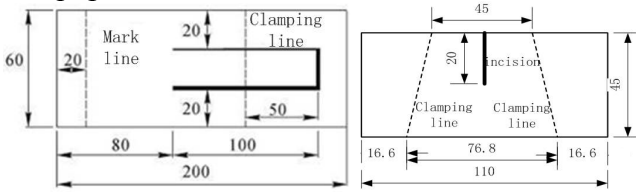

Fig.4. Parameters of test specimen (mm)

Table 1 The mechanical parameters of specimens

Thickness	Fiber bundle density	Yarn density	The areal density of the material
0.16mm	10*10 root/cm	220tex	130g/m^2

Ground simulation methods for the mechanical strength of the envelope material

Mechanical strength contains strength index and elasticity parameters. A method to simulate the mechanical properties is uniaxial and biaxial tensile test. The former can be used to determine the tensile strength of unidirectional performance, elongation at break and tear strength. Tensile test specimens generally are rectangular sample which can be divided into radial test specimen and the weft pieces by the direction of the filaments. Size detection plane are often used in the industry standard test material shown in Fig. 4. According to the results of a flexible material woven fiber Vectran, composite test data based on found trapezoidal method test data error is smaller, mainly because with using the trapezoidal method during the test, the sample is less disturbing factors affecting the tensile mechanical strength testing.

The more important factor is the shear strength. Adhesive layer strength in different space environment between the coating layers plays a decisive role. Thus the ground simulation tests need to consider the mechanical strength of the adhesive layer under different conditions of temperature and radiation. Here mainly test method for linear expansion characteristics of the test method according to standard GB1036-89. The quartz tube tester can be chosen and its test accuracy is 0.002mm. In accordance with the adhesive properties, then:

$$\overline{\alpha} = \frac{L_2 - L_1}{l(t_2 - t_1)} \tag{1}$$

Where t_1 represents the temperature of the material at low temperature, ℃; t_2 represents the temperature of the material at high temperature, ℃; l_1 represents a length of the material at low temperatures, mm; l_1 represents a length of the material at high temperature, mm; l of raw material length, mm. If the envelope deformation is too large, the adhesive layer is likely to produce deformation or separation degumming, resulting in the destruction of the whole structure of the envelope material. Mechanical shear strength can be measured by the tensile test method and we also need to control the tensile test carried out in a high temperature environment and the test environment conditions approaching space vehicle condition consistent.

For flexible performance materials generally include ground simulation test method T-peel method, 90 ℃ peel method, 180 ℃ peeling method, Bell peel (floating roller peel) method, and the like climbing drum peel method, etc. A relatively common and easy to operate method is T-peel test method that never ends glued start peeling force, making the laminate along the gum line and gradually stripped under load. According to the national standard GB-2791-81 and draw contour method, the principle of laminated peel strength test can be obtained:

$$\sigma_T = \frac{F}{B} \tag{2}$$

Where the T-peel strength, KN / m; F is the average peel force, the unit is N, B is the width of the sample separation unit m. Peel test methods whereby the shear strength of the material in performance. As the large temperature difference between daytime and night in near space. Ground environment simulation requires high temperature humidity environmental chambers conducted. Near space temperature usually ranges from -65℃~55℃ and atmospheric pressure is in the range of 4500Pa~1atm. If it requires simulating the real material conditions of service under the alternating load, high and low temperature test material is applied. Also it need to require to control the cycle of alternating high and low due to the real conditions of the cycle is 24 hours, even skin material withstand high and low temperature load, performing to analyze the mechanical properties of the long voyage skin material changes.

Weather resistance and air tightness of ground simulation test method

The ground simulation of natural weathering cost a long time, a high testing cost, and the choice of the natural environment need to be close to the climate characteristics of the space environment near space. While taking it into account that the long-endurance service material characteristics, excellent weathering properties of the material is required, therefore weathering test must be carried out in service of the material. Usually under laboratory conditions, a single artificial ground simulation test were tested by UV aging characteristics, effects of ozone aging characteristics, infrared light and other radiation on the mechanical properties of the material. Such as ozone aging test selection model BH-OZ2000 testing machine, testing requirements in line with the national standard GB/T 7762-2003, etc. The test machines can observer status at any time inside the box of the test material. Its technical parameters tested in the following table. Due to the special nature of the airship envelope material commonly used in the stratosphere and extremely complex environment, the envelope material is in mechanical load, while inevitably be in stratospheric environment of multiple factors.

Table 2 Parameter range of environmental simulation test

Temperature Range	0℃～70℃	Ozone density	0~500pphm，0～100ppm or more（1ppm=100pphm）
Temperature Fluctuation	±0.5℃	Airflow velocity	12-16mm/s
Humidity Range	≤65% R.H	Fixture category	Suitable for static stretching; dynamic tensile

And ultra-low temperature , thermal radiation , thermal stress fatigue , light aging , ozone, ultraviolet radiation aging , plasma impact, etc.) coupled synergy of tearing skin material damage and failure also has accelerated the impact effect, but a single mechanism and a variety of environments effect mechanism features investigation is little. At present, there are some relevant test methods including reinforcing fibers for thermal aging skin material and mechanical properties, the Australian Defense Science and Technology Organization using differential scanning calorimeters(DSC) and thermo-mechanical mechanical analysis (TMA) study Kevlar49 high temperature properties of fiber bundles and Nomad fiber bundles, concurrent happens now when the high temperature 440 ℃ thermal degradation phenomena, and studied the fiber bundle under ultraviolet light and heat and the bending fatigue mechanical properties.

Conclusion

(1) This paper studies the environmental characteristics of the long-time flying near space airship, and the ground simulation test methods are summaried up for physical geometry measurement of the airship envelope material, including the test methods under weathering characteristics of mechanical strength and single / multiple coupling mechanisms. The envelope tests under multi-mechanism coupled environmental factors could truly reflect actual working conditions in the stratospheric space.

(2) The envelope material testing methods under the true conditions are analyzed involving high and low temperature, ozone, thermal stress fatigue in near space environment. And the prospects for various types of test problems and further research is discussed. For lack of multi-mechanism coupled tests, the airship envelope material is usually designed and used with a very high factor of safety, to avoid the influence of various environmental factors on performance of the NSA envelope, and the coressponding relationship between the different coupling test methods is obtained.

References

[1] Anthony. High-Altitude, Long-endurance airships for coastal surveillance: NASA: TM, 2005.

[2] Liu L B, Liu D X, Lv M Y. A new design of inflatable and lightweight device for planetary exploration[J]. Advanced Materials Research, 2011, 217: 158-162.

[3] Liu L B, Gu Y C, Cao S, et al. The research on oblique crack tip deformationfield of airship envelope composites based on the digital speckle correlation method[J]. Applied Mechanics and Materials, 2014, 477: 34-38.

[4] Bai Jiangbo, Xiong Junjiang, Cheng Xu. Tear resistance of orthogonal Kevlar PWF-reinforced TPU film [J].Chinese Journal of Aeronautics 2011;24:113-118.

[5] Dever J A, Pietromica A J, Stueber T J, et al. Simulated space vacuum ultraviolet (VUV) exposure testing for polymer films [J]. AIAA Paper, 2002; 01(54): 638-95.

[6] Tan Huifeng, Liu Yuxi, Liu Yuyan, et al. Research progress and requirement analysis of envelope materials for near space airship [J]. Acta Materiae Compositae Sinica, 2012; 29(6): 1-8.

[7] Han J H, Kim C G. Low earth orbit space environment simulation and its effects on graphite/epoxy composites [J]. Composite structures, 2006; 72(2): 218-226.

Advanced Materials Research Vols. 989-994 (2014) pp 3477-3479
© (2014) Trans Tech Publications, Switzerland
doi:10.4028/www.scientific.net/AMR.989-994.3477

Based on 3-D modeling and value simulation of the intake system in CNG

LI Jing-hua, Li Jiang-jiang
TianJin Vocational Institute,Tianjin,300410,China

Keywords: intake air system;GAMBIT modeling; FLUENT simulation;analysis of fluid flowing quality

Abstract. The structure of the air intake system directly affect the combustion and heat load in each cylinder. In this paper, using the CFD experience can look the intake pipe gas flow as a 3-D compressed steady flow. It is easy to built a 3-D model grids with the help of GAMBIT software .Using the FLUENT soft software ,it is reasonable to get the the fluid velocity distribution in flow field , and calculate the fluid flowing quality at the exit of manifold, as well as analyze the inhomogeneity of the inlet air.

Introduction

CNG gas engine is an improved engine ,which is increased gas mixing injector device between the intake manifold and the cylinder head to achieve mixing outside the cylinder. Based on the main intake manifold air ,ECM will calculate the average allocation air for each cylinder. According to the intake air of each intake manifold ,the propel fuel will be injectd into the corresponding maniford to form a pre-combustion mixture. On the contrary ,If the distribution of the mixed gas for each cylinder is not be uniform , then causing the difference combustion for cylinder which will lead to the combustion heat load .

Calculation model

Model building and meshing

Using the pre-processing software GAMBIT ,it is easy to build a three-dimensional flow model of the intake system based on CAD .We can consider the internal cavity of intake system as the outer boundary of the computational model, including the construction of the intake manifold, intake manifold and cylinder cover, also including inlet air flow throughout the channel. Entrance model is the inlet of main intake manifold and the outlet is the inlet terminal. With the applying of GAMBIT software ,the three-dimensional model can be meshed as unstructured tetrahedral meshes. The front surface of the inlet could be set as mass flow inlet boundary,and the outlet face is set as pressure outlet boundary, others are wall boundary. Calculation model shown in Figure 1.1, the outlet 1-6 correspond to the 1-6 intake of cylinder.

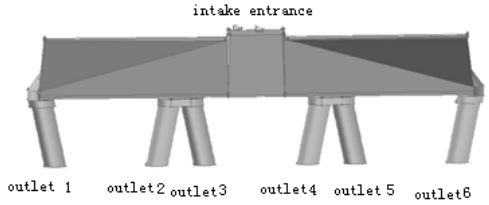

Fig1.1 The calculated model of the air inlet system

The selection of calculation model and boundary conditions

The flow of gas in the intake system can be regarded as a three-dimensional compressible unsteady flow, conditions of turbulent flow. The Calculation mainly solve the continuity

equation, momentum equation, energy equation and turbulence equations. Because of variable of the compressible fluid density , we have to treat the gas as an ideal gas ,at the same time add the state of ideal gas equation that solving the problem. Turbulence model is still used the common standard $k-\varepsilon$ equations, the constant coefficients in the model is showed in Table 1.

Table 1 The coefficient of the standard $k-\varepsilon$ model

C_μ	$C_{\varepsilon 1}$	$C_{\varepsilon 2}$	$C_{\varepsilon 3}$	$C_{\varepsilon 4}$	σ_k	σ_ε
0.09	1.44	1.92	0.8	-0.33	1.0	1.3

Area boundary model includes outlet boundary wall and solid wall. Import using mass flow boundary conditions ,the estimation which is obtained according to the normal engine operating condition is that:the total mass flow of imported face is $0.28^{kg/s}$, turbulence parameters is $k=0.046m^2/s^2$, $\varepsilon=0.451m^2/s^3$,setting temperature is 300K, pressure is 101325^{Pa}. Export can use the boundary of outlet pressure, the pressure is set to 100^{KPa}, the temperature is set to 320K, turbulence parameters is $k=0.046m^2/s^2$, $\varepsilon=0.451m^2/s^3$ .Solid wall boundary is set to a constant temperature 320K , the velocity is use of no-slipping boundary condition.

The results of simulation and analysis

With the using of the FLUENT software , it is easy to get the result of calculating model based on three-dimensional numerical simulation. Meanwhile, results of the uniformity of induction system were analyzed.

The simulation results of air flow field and analysis

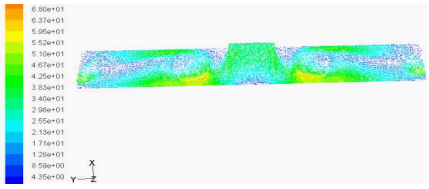

Fig1.2 Velocity vector of underside of the inlet

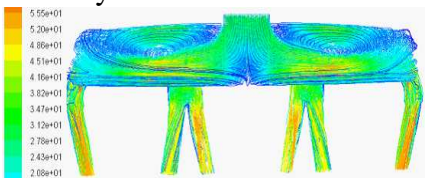

Fig1.3 The streamline of the air inlet system

Analysis of the figures 1.2 and 1.3, we can draw the characteristics of entire intake system: the flow of movement is symmetrical, symmetry plane is the central axis of the intake manifold inlet face. The velocity vectors of inlet pipe bottom shows that the flow velocity in the intake pipe is uneven.The right side of first cylinder intake manifold and the left side of the sixth cylinder intake manifold appear the larger low velocity zone at the same time,and the entrance of the third, fouth, fifth intake manifold show the some low velocity zone. It is not difficult to find these low flow areas exist reflow phenomenon,which caused increase of flow resistance and reduce of flow velocity. Figure1.3 shows that the low velocity zone have the backflow phenomenon,and in these regions due to reflow generate swirl. It can be seen from Figure 1.3 that flow rate of the first and sixth cylinder is the maximum. The third,four cylinder followed and the second, fifth cylinder is minimum. In order to more clearly show the entrance of each cylinder flow field, we made a enlarge figure of velocity vector of each cylinder intake entrance, Figure 1.4 and Figure 1.5.

Fig1.4 Velocity vector of intake manifold of 1-3 cylinder

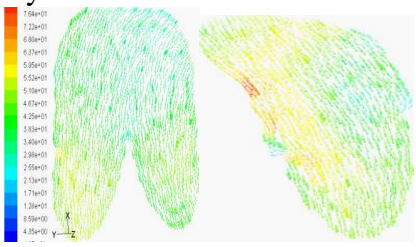

Fig1.5 Velocity vector of intake manifold of 4-6 cylinder

As can be seen from the enlarged views, the air speed of the first cylinder and sixth cylinder have greater speed with the same direction of velocity and outlet. The second cylinder and the third cylinder use the same intake manifold. The vector diagram shows that velocity vector in the tube is closer to the outlet direction of the third cylinder, the flow of the second cylinder actually change a direction. For this reason, the flow resistance of the second cylinder is slightly larger than the third cylinder. The flow relationship of the fourth and the fifth cylinder are the same as the second and the third cylinder.The flow direction of the fourth cylinder is closer to inlet flow, more smooth flow and flow rate greater. The outlet face of the mass flow rate calculated as shown in Table 2.

Table 2 Mass flow rate of each exit of the air inlet system

intake number	1	2	3	4	5	6
mass flow rate (kg/s)	0.050	0.044	0.046	0.046	0.044	0.050

Conclusion

This article analyses and simulates the CNG engine intake uniformity.What's more,established engine air intake system model containing intake pipe and inlet of the, using the FLUENT software study the intake inhomogeneity base on 3-d numerical simulation and getting the results of inlet mass flow rate of each cylinder.On the other hand, with analysis of intake inhomogeneity of the engine cylinder found that the problem about uniformity of engine air intake system is obvious,which caused the second and the fifth cylinder mixture abnormal, remains to be further improved.

References

[1] B. Peters,A. D. Gosman. Numerical Simulation of Unsteady Flow in Engine Intake Manifolds. SAE Paper No. 930609.1993

[2] Li JiangJiang, You Mingfu. Hydraulic system design of the automatic transmission Based on the logical analysis [J]. Machine Tool & Hydraulics, 2011.(chinese) M. G. Lisbona，C. Vafidis. Adoption of CFD in the engine design process:present and future. SAE paper 97AO08

[3] W. Bauer，H. Ehrenreich，H. Reister. Design of cooling systems with computer simulation and underhood flow analysis using CFD. SAE paper 954061

[4] Gerhard Meister，Simon Grilc，etal. CFD application in compact engine development. SAE paper 982016

[5] Permart Deist，Eiaon Lrilch. CFD application in SI engine. SAE paper 983002

Advanced Materials Research Vols. 989-994 (2014) pp 3480-3484
© (2014) Trans Tech Publications, Switzerland
doi:10.4028/www.scientific.net/AMR.989-994.3480

The metabolic GM (1,1) prediction of the absolute gas emission quantity in a certain mine

Xiangyun Meng [a], Rihui Chen [b], Shibin Wang [c]

Faculty of Land Resource Engineering, Kunming University of Science and Technology, Kunming 650093, China

[a]yan761415498@163.com,[b]chenrihui555@126.com, [c]wsb18288667554@163.com.

Keywords: the gas emission quantity, GM (1, 1), the GM (1, 1) metabolism model

Abstract: the paper briefly discusses the gas emission prediction method, puts forward the grey model prediction method combined with domestic actual, and according to the material of the absolute gas emission quantity of the mine in the past decade, sets up the GM (1, 1) metabolism model. By solving the model, predictions are given, and the results are tested. The paper draws the predicted value of the absolute gas emission quantity over the next five years, analyzes the overall trends and gives general advice.

Introduction

Gas disaster is the head of "five natural disaster" in the coal mine production, often leads to major malignant accidents, has an impact on mine sustainable healthy development, and results in a very bad consequence on the society and national economy. In recent years, with a surge in demand of coal resources and the degree of mechanization of mining industry to be improved continually, the mine gas emission quantity has a sharp rise to threaten the coal production safety seriously. Therefore, it is particularly important to strengthen the pre-mining and pre-pumping of gas in the coal mine, the forecast of gas emission quantity, and the management of gas.

The application status of the prediction of gas emission quantity at home

For a long time, the coal mine in China utilizes mainly the mine statistical method to predict the mine gas emission quantity [2], but the mine statistical method requires a huge enough sample space, a similarity between the predicting regional and the reference area in mining technical conditions and geological conditions, while its forecast range is very restricted. But the mine production is a extremely complicated system engineering, and with the extension of mining, geological conditions and technical conditions of each seam, development methods, and mining method are always changing to lead to a dynamic change of the mine gas emission quantity, which seriously influence the application range and prediction accuracy of the mine statistical method.

In this case, to explore a new path which is able to accurately predict the gas emission quantity is imperative. By chance, the grey system theory is a subject that lays particular emphasis on the connotation and excludes external uncertain factors to find out the actual rule, so it can be well applied to the mine gas emission quantity prediction. In addition, the development coefficient of the gray model reflects the development trend of the corresponding sequence (the absolute gas emission quantity) accordingly to solve the dynamic change problem of the mine gas emission quantity. And the gray system requires only a few data sample size, only with the mine gas identification data over the years, can predict the gas emission quantity in the future several years, which makes it more practical operability.

The establishment of the GM(1,1) model

The grey system theory is an emerging discipline which was founded by a famous scholar Professor Deng Julong in China in 1982, which takes "partial information known, some information unknown" "uncertain system" as the research object, and through the generation and development of the "part" of the known information, achieves the precise description and understanding of the world[3]. Among above, the GM (1, 1) model is the core of grey prediction and it is a first-order differential equation, in which a single variable is predicted and whose discrete time response function presents exponential law.

The data processing.

A. Let the original time data sequence $X^{(0)} = \left(x^{(0)}(1), x^{(0)}(2), \cdots x^{(0)}(n)\right)$;

B.To $X^{(0)}$, do 1-AGO, in which $x^{(1)}(k) = \sum_{i=1}^{k} x^{(0)}(i), k = 1, 2\cdots, n$,

So $X^{(1)} = \left(x^{(1)}(1), x^{(1)}(2), \cdots x^{(1)}(n)\right)$

C. The mean generation with consecutive neighbors of $X^{(1)}$, in which $z^{(1)}(k) = 0.5x^{(1)}(k) + 0.5x^{(1)}(k-1)$, so $Z^{(1)} = \left(z^{(1)}(1), z^{(1)}(2), \cdots z^{(1)}(n)\right)$;

The establishment of the model.

A. The establishment of differential equation. What the albino differential equation of the dynamic model $GM(1,1)$ of first-order differential equations with a variable is: $\frac{dx^{(1)}}{dt} + ax^{(1)} = b$

In which, a, b are parameters to be identified, and -a is the development coefficient that reflects the development trend of $\hat{x}^{(1)}$ and $\hat{x}^{(0)}$; b is the grey action quantity that reflects the change relationship between data.

So what its time response function is: $\hat{x}(k+1) = (x^{(0)}(1) - \frac{b}{a})e^{-ak} + \frac{b}{a}$

B. The calculation of parameters. What the least square estimation of the parameter column $\hat{a} = \left(a, b\right)^T$ is: $\hat{a} = (B^T B)^{-1} B^T Y = (a, b)^T$, In which, what "B, Y" respectively is:

$$B = \begin{bmatrix} -z^{(1)}(2) & 1 \\ \vdots & \vdots \\ -z^{(1)}(n) & 1 \end{bmatrix} \qquad Y = \begin{bmatrix} x^{(0)}(2) \\ \vdots \\ x^{(0)}(n) \end{bmatrix}$$

C. The calculation of the simulating value. We can work out the simulation value $\hat{X}^{(1)}$ of $X^{(1)}$ by using the time response type of model. To $\hat{X}^{(1)}$, do IAGO to get $\hat{X}^{(0)}$, in which: $\hat{x}^{(0)}(k) = \hat{x}^{(1)}(k) - \hat{x}^{(1)}(k-1)$

D. The accuracy test. Whether he gray prediction model GM (1, 1) established above meets the accuracy requirements remains to be tested. With the grey theory model, we usually have three kinds of methods [4]: the method of test for the residual size, the method of test for the correlation, the method of test for the posterior error reification. The paper adopts the method of test for the residual size used frequently to test the model.

Let the residual $\varepsilon(k) = x^{(0)}(k) - \hat{x}^{(0)}(k)$;

Let the relative error $\Delta_k = \left|\varepsilon(k)\right| \Big/ x^{(0)}(k)$;

Let the average relative error $\overline{\Delta} = \frac{1}{n}\sum_{i=1}^{n} \Delta_i$.

According to Δ_n and $\overline{\Delta}$, we calculate the accuracy grade with the table 1. The larger value in Δ_n and $\overline{\Delta}$ is usually used to determine the accuracy grade by being compared with the table 1. The accuracy grade seen in the table 1[3] below:

Table 1 The accuracy grade in testing

The accuracy grade	first	second	third	fourth
The relative error	<0.01	0.01-0.05	0.05-0.10	>0.10

The metabolic GM (1, 1)

The general GM (1, 1) model requires less data, which will to some extent its practical operability and yet will also has some influence on the accuracy of the GM (1, 1) model making the long-term prediction. And the paper is planned to make predictions about the gas emission quantity in the next five years, which has a longer length, so we need optimize the general GM (1, 1) and then we raise the metabolic GM (1,1).

The metabolic GM (1, 1): we let the original data sequence $X^{(0)}$ =($x^{(0)}$(1), $x^{(0)}$(2),…, $x^{(0)}$(n)), introduce new information $x^{(0)}$(n+1)/ $\hat{x}^{(0)}(n+1)$, clear away old information $x^{(0)}$(1), declare that the GM (1, 1) established by $X^{(0)}=\left(x^{(0)}(1),x^{(0)}(2),\cdots x^{(0)}(n+1)\right)$ / $\hat{x}^{(0)}(n+1)$) is the so-called metabolic GM (1, 1).

From the perspective of the predicted, the metabolic GM (1, 1) is a better model. As the system evolves, the significance of the old data will be being reduce, and when the new information is constantly added, we get rid of old information in time to make the sequence better reflect the characteristics of the system in the present[4].

The prediction analysis of a certain mine gas emission quantity based on the metabolic GM (1, 1)

The measured data f a certain mine gas emission quantity in nearly a decade is shown in table 2:

Table 2 Statistics of a certain mine absolute gas emission quantity

years	2003	2004	2005	2006	2007	2008	2009	2010	2011	2012
The absolute gas emission quantity (m^3/min)	40.09	43.47	41.66	32.86	44.06	38.74	49.67	46.38	49.67	46.15

The establishment of the GM (1,1)

A. Let the original time data sequence $X^{(0)}$ come from the table 2, so

$$X^{(0)}=\left(x^{(0)}(1),x^{(0)}(2),\cdots x^{(0)}(10)\right)=(40.09,\ 43.47\ldots\ 46.15)$$

To $X^{(0)}$, do 1-AGO,so $X^{(1)}=\left(x^{(1)}(1),x^{(1)}(2),\cdots x^{(1)}(10)\right)$=(40.09,83.56,…,432.75)

The mean generation with consecutive neighbors of $X^{(1)}$, so

$$Z^{(1)}=\left(z^{(1)}(1),z^{(1)}(2),\cdots z^{(1)}(n)\right)=\left(61.83,\ \ldots\ ,409.68\right)$$

B. To figure out the parameter column $\hat{a}=(a,b)^T$ by the least square estimation.

$$\hat{a}=(B^TB)^{-1}B^TY=(a,b)^T=(-0.0262,\ 37.637)^{\mathrm{T}}$$

What its time response function is:

$$\hat{x}(k+1)=(x^{(0)}(1)-\frac{b}{a})e^{-ak}+\frac{b}{a}=1478.0774\exp\ (0.0262k)-1437.987$$

C. To figure out $\hat{X}^{(1)}$, and then do IAGO to obtain $\hat{X}^{(0)}$, so

number	1	2	3	4	5	6	7	8	9	10
the simulating value	40.09	39.20	40.24	41.30	42.40	43.52	44.68	45.86	47.08	48.33

D. The accuracy test. We can work out "Δ_{10}= 0.0471， $\overline{\Delta}$=0.0846", comparing it with the table 1, to know that its accuracy is level 3. Even so, the paper only forecast the next data, so the model can be used.

The prediction of the metabolic GM (1, 1)

A. To predict the absolute gas emission quantity in 2013 by the model in "(1)",

So $\hat{x}^{(0)}(11)$=49.61

B.To $X^{(0)}=\left(x^{(0)}(1),x^{(0)}(2),\cdots x^{(0)}(10)\right)$, we introduce new information $\hat{x}^{(0)}(11)$, clear away old information $x^{(0)}(1)$, to get new original data sequence:

$$X^{(0)}=\left(x^{(0)}(2),x^{(0)}(3),\cdots x^{(0)}(11)\right)=(43.47,\ 41.66\ldots\ 49.61)$$

Putting $X^{(0)}$ into (1), we can predict the absolute gas emission quantity $\hat{x}^{(0)}(12)$=52.23 in 2014, meanwhile Δ_{11}= 0.0180， $\overline{\Delta}$=0.0784,comparing it with the table 1, know that its accuracy is level 3.

C. To repeat B. we are able to get respectively the prediction of the absolute gas emission quantity in 2015, 2016, 2017, so $\hat{x}^{(0)}(13)$=54.92， $\hat{x}^{(0)}(14)$=55.30， $\hat{x}^{(0)}(14)$=57.40

To analyze the absolute gas emission quantity predicted in the next five years.

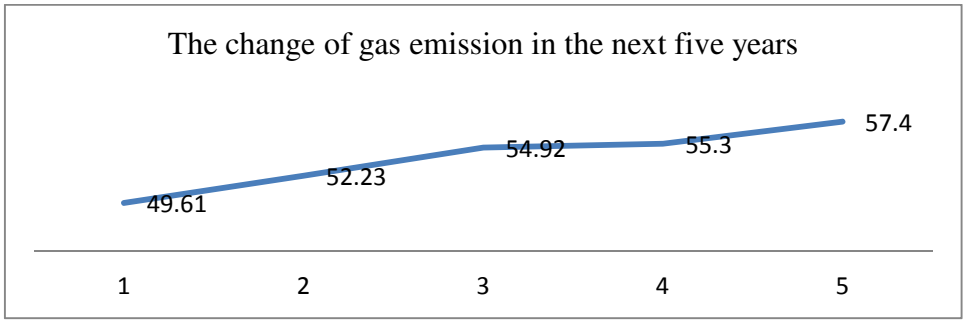

From the figure, we obtain that the absolute gas emission quantity in the next five years remains increased by years. Therefore, formulating the mine ventilation system improvement program, arranging the pre-mining and pre-pumping of gas and choosing the coal mining method, the mine should take into account the needs of gas drainage, with the permission of economic and technical conditions, prefers to set aside the operational space of gas drainage.

Conclusion

With the metabolic GM (1, 1) to predict, while at first the accuracy of Δ_k and $\overline{\Delta}$ is level 3, the accuracy presents both a declining trend in metabolism, especially Δ_k reaching level 1 later, which shows that the metabolic GM (1,1) predicting the absolute gas emission quantity in a period of time is able to obtain a more reliable result.

With the deepening of mining level, expansion of mining area and mining mechanization degree increasing, and the growth of coal output, the absolute gas emission quantity is increasing year by year. Therefore, when the mine makes gas control measures for a period of time, it is applicable to take the metabolic GM (1, 1) model as the mine absolute gas emission quantity prediction model, which is able to reflect the changing dynamics and the general trend of the mine gas emission quantity, so its prediction results has an important reference value for the gas management.

Reference

[1] WU Aiyou, XIAO Hongfei, WANG Conglu. Establishment and application of weights and association based on coal and gas outburst controlled assessment: Journal of China coal society, vol.30 (2005) no.1, p.58-62.
[2] XIE Wanxing, SUN Huimin. The gray prediction of mine gas emission quantity: Journal of China coal society, vol.33 (2002) no. 4, p.32-33.
[3] LIU Sifeng, XIE Naiming. The grey system theory and its application. Beijing: Science press, 2008 (in Chinese).
[4] DENG Julong. The grey system theory tutorial. Wuhan: East China University of science and technology Press, 1999 (in Chinese).
[5] ZHANG Chunhua, LIU Jingong. Multivariable grey model and its application to predicting gas flow from boreholes: China safety science journal, vol.16 (2006) no.6, 50-54.

Advanced Materials Research Vols. 989-994 (2014) pp 3485-3488
© (2014) Trans Tech Publications, Switzerland
doi:10.4028/www.scientific.net/AMR.989-994.3485

Numerical analysis of the wind tunnel effect on the Chinese kang in the northern China

Zhong-liang Lu[1], Ya-hui Xu [1, a] and Hong-li Wang Dada Xi[2]

[1]School of Safety Science & Engineering, Henan Polytechnic University, Jiaozuo 454000, China;

[2] School of Mathematics & Information Science, Henan Polytechnic University, Jiaozuo 454000, China.

[a]a493147307@126.com

Key words: Chinese kang, Ventilation, Heating, Chimney, Wind tunnel, Numerical simulation.

Abstract. In the northern part of China, the heating system of the Chinese *kang* occupies a significant proportion of usage, particularly during the winter. To achieve better heating effect, this article explored the wind tunnel (commonly known as the "dog hole") of the Chinese *kang* in the Northern area. The paper conducted three experiments, established a two-dimensional mathematical model on the flow of high temperature gas in the chimney, utilized the FLUENT software to simulate the flow, and analyzed the inlet flow of the chimney flue and effect of wind tunnel on the heating system of Chinese *kang*. Wind tunnel was found to prevent natural reversed wind effectively and reduce the influence of outside wind.

Introduction

Chinese *kang* is a typical furnishings in northern China. In previous years, it was used by people to withstand the cold temperature during winter. According to the local custom, different local people have built different *kang* structures, and constantly innovated the original foundation. With an optimized flue, the *Zaotang*, *kang* wall, and other parameters enhanced thermal efficiency and reduced fuel consumption[1-2]. Generally, the Chinese *kang* is composed of a stove, *kang*, and chimney. The stove transmits hot gas to *kang* by fuel burning. Then, the *kang* transmits the gas to the room to increase the temperature indoor, and the chimney finally emits the gas outdoor[].The specific structure of Chinese *kang* is shown in Fig. 1.

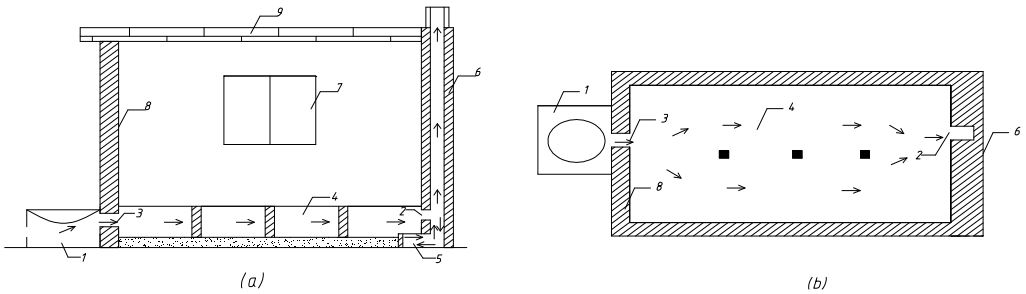

1 Stove 2 Import of chimney 3 Import of *kang* 4 *Kang* 5 Wind tunnel 6 Chimney 7 Window 8 Wall 9 Roof

Fig. 1. Structure of Chinese *kang*

The wind tunnel (commonly known as the "dog hole") mainly alleviates the reversal of air in the chimney. When reverse airflow enters the chimney, the wind tunnel avoids the fuel gas from turning to the *kang* and stove, as such phenomenon causes insufficient burning of fuel and causes the gas to flow to the room, which may have adverse health effects [3-4]. This article uses the FLUENT software to simulate the flow inside the chimney, and analyzes the effects of wind tunnel on ventilation and heating.

Experiment

We selected a residential building in northern China to obtain data.

The size of the house was 4 m × 3.5 m × 3 m. The size of the *kang* was 3.3 m × 2 m × 0.6 m. The size of the wind tunnel was 0.3 m × 0.5 m × 0.2 m. The size of the adobe was 0.3 m × 0.5 m × 0.1 m.

The wall was made up of approximately 200 mm concrete bricks.

The equipment used in this experiment included a drilling rig (CF-166), stopwatch, electronic thermometer (KT-300), anemograph (475AV), and pitot tube.

To study the effects of different forms of chimneys on the ventilation and heating, we divided the study into three experiments to determine the initial velocity and temperature of the gas. Through the hole drilled in the inlet of the chimney, the velocity and the temperature were measured by using electronic thermometer, stopwatch, anemograph and pitot tube per minute. First, we measured both under condition of cooking in stove-fire，the velocity and temperature at point 2 in Figure 1 (outlet of *kang*) was measured per minute. Second, we measured velocity and temperature in the foundation of the first group, in which the amount of constant wind enters from the chimney outlet (set to 2.6 m^3/s), thereby determining the data of point 2. The third measurement was based on the first and second groups, conducted by blocking the wind tunnel with adobe, and carrying on to point 2 on temperature and velocity.

Experimental data allowed the plotting of the figures on the outlet velocity. The temperature of *kang* was calculated with Matlab (Figures 2 and 3). Figure 3 shows that the velocity of point 2 initially increases quickly, reaching a peak after 15 min, then gradually decreases. The velocity of normal ventilation was higher than when in air drums. The velocity with wind tunnel was higher than without it. Figure 2 is to study the effect of wind tunnel on the temperature of *kang* and indoor, and it shows a positive correlation between the trend of temperature and velocity with time.

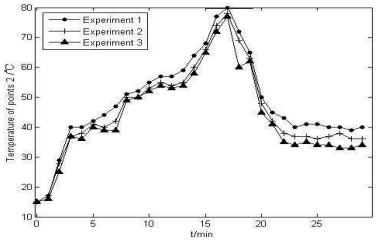

Fig. 2. Temperature of chimney inlet (2 points)

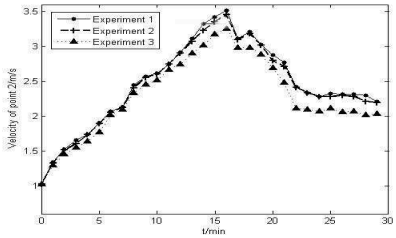

Fig. 3. Velocity of chimney inlet (2 points)

Combined with the measured experimental data, the experiment provided reference data for the inlet boundary condition of mathematical modeling.

Mathematical modeling

Based on the selected data, we established three 2-D mathematical models with GAMBIT, and then divided the mesh and exported the files to FLUENT. In this experiment, the high temperature gas was a viscous incompressible fluid. The *kang* was confined sufficiently. We used K-epsilon turbulence model to study fluid movement [5]. Finally, the boundary condition of inlet velocity, along the horizontal direction, was determined, with 3.1 m/s size, and 338.15 K (65 °C) temperature. (The high temperature gas density is ρ =1.39 kg/m^3, and the air density is ρ_0=1.2 kg/m^3).

We designed the model to cover conservation equations of mass, momentum, and energy equations [6].

The equation for the conservation of mass is as follows:

$$\rho \frac{\partial v_i}{\partial x_i} = 0 \tag{1}$$

For an incompressible fluid, $\frac{\partial \rho}{\partial t} = 0$.

Conservation of momentum equation:

$$\rho\frac{\partial v_i}{\partial t}+\frac{\partial}{\partial x_j}\left(\rho v_i v_j\right)=-\frac{\partial p}{\partial x_i}+\mu\frac{\partial^2 v_i}{\partial x_j^2}+\rho g_i \tag{2}$$

p is the static pressure; μ is the dynamic viscosity; g_i is the volume force of gravity.

Conservation of energy equation

$$\rho\frac{\partial E}{\partial t}+\frac{\partial}{\partial x_j}[\mu_j(\rho E+P)]=\frac{\partial}{\partial x_j}(\eta_{eff}\frac{\partial T}{\partial x_j})-\sum_j h_j J_j+u_j(\tau_{ij})_{eff}+S_h \tag{3}$$

E is the thermodynamic energy per unit mass of the fluid;

$\eta_{eff}=\eta_t+\eta$ is an effective thermal conductivity，η_t is the viscosity of turbulent，η is the dynamic viscosity caused by molecular diffusion;

τ_{ij} is stress tensor; $J_{j'}$ is the diffusion of j'; S_h is the chemical reaction of heat and other volumetric heat sources.

Results and discussion

We imported the figure of the chimney's flow model from FLUENT into TECPLOT for post-processing. We obtained the following figures：

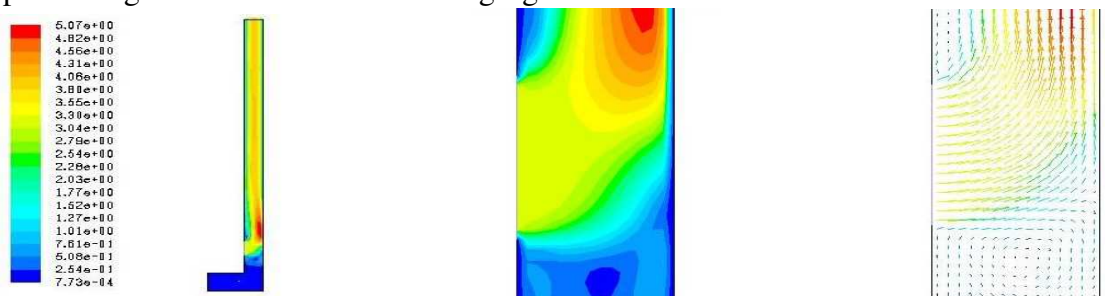

(a) Model of overall chimney velocity (b) Velocity distribution of inlet (c) Velocity vector of inlet

Fig. 4. Flow model of normal ventilation in the chimney with wind tunnel

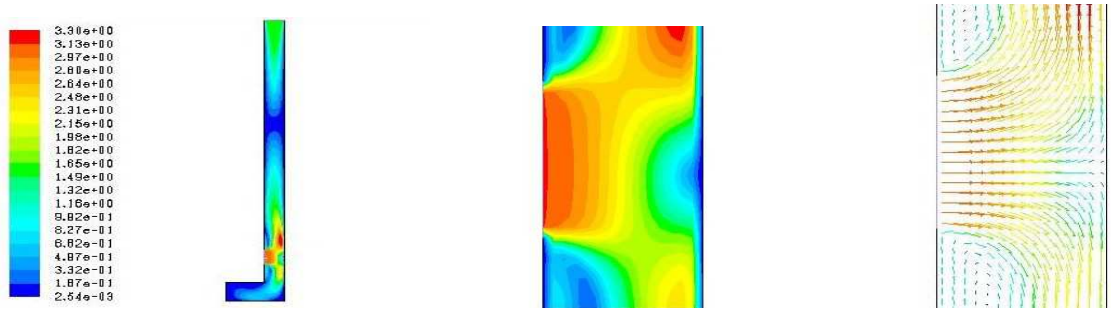

(a) Model of overall chimney velocity (b) Velocity distribution of inlet (c) Velocity vector of inlet

Fig. 5. Flow model of reverse ventilation in the chimney with wind tunnel

Figure 4 shows the flow model of normal ventilation in the chimney with wind tunnel. Figures 4 (b) and (c) reflect the motion of the gas at the inlet. High temperature gas by pressure moved upward from the inlet of the chimney, and a small part of the gas moved downward to the wind tunnel. Given the potential change, the speed initially increased, then decreased gradually, until and the trend stabilized. Shear forces were also in between the wall and flow gas in the process. Thus, the velocity of the gas close to the wall was less than that in the central chimney. The gas flowed outside from the outlet of the chimney.

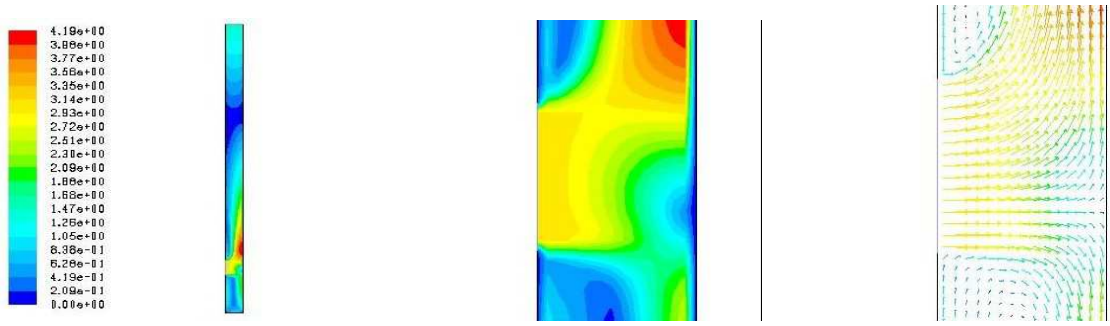

(a) Model of overall chimney velocity (b) Velocity distribution of inlet (c) Velocity vector of inlet

Fig. 6. Flow model of reverse ventilation in the chimney without wind tunne

Figure 5 shows the flow model of reverse ventilation in the chimney with wind tunnel. According to the principle of conservation of energy, air flow was almost 2.6 m^3/s in the chimney inlet drums. After hot gas entered the chimney, part of the gas slowly went upward, which then sped up toward zero at a certain height. Another part of the gas moved downward to the wind tunnel, where the velocity reduced gradually. Thus, the wind tunnel prevented natural reversed wind and reduced the function of the outside wind.

Figure 6 shows the flow model of the reverse ventilation in the chimney without a wind tunnel. When using adobe block, the tunnel and drums enabled air flow of about 2.6 m^3/s (Figure 6). Then, the gas flowed downward to the bottom chimney, and after reaching the bottom, it moved up to the inlet of the chimney again. This kind of structure did not reduce the effect of the outside natural airflow, instead creating a part of gas backflow to the *kang*.

Conclusions

When the reverse wind flows into the chimney, on the one hand, the wind tunnel can decelerate the flow of the gas, thus weakening the reverse airflow at the outlet of *kang*. On the other hand, it can accelerate the burning of fuel, keep the *kang* in higher temperature, and maintain an ideal indoor environment. If the *kang* does not have a wind tunnel, with reverse airflow into the *kang*, the fuel of the stove is not fully burned, thereby transferring less energy from the stove to the *kang*. Hence, the temperature of the *kang* cannot reach the ideal level, thus reducing the quality of air indoor. Therefore, when constructing the *kang*, a wind tunnel should be built at the bottom of the chimney using bricks and adobe to prevent reverse wind.

References:

[1] L. DuanMu, Y. Zhao and Z.SH. Wang: Building Science, Vol. 25 (2009) No.12, p.30.
[2] Z. Zhuang: *Smoke Flow and Thermal Performance of Chinese Kangs* (Ph.D., Dalian University of Technology, China 2009), p.18.
[3] Z. Zhuang, Y.G. Li, B. Chen, et al: Energy and Buildings, Vol.41 (2009) No.1, p. 111.
[4] P.H. Zhang, F.L. Xia and J.Y. Fu: Journal of Shenyang Jianzhu University(Natural Science), Vol.25 (2009) No.2, p, 342.
[5] X.P. Wang: Architecture Technology of Low Temperature, Vol.32 (2010) No.1, p.112.
[6] S.L. Wang: *Advanced Engineering Fluid Mechanics* (China Power Press, China 2001), p.20.

Advanced Materials Research Vols. 989-994 (2014) pp 3489-3492
© (2014) Trans Tech Publications, Switzerland
doi:10.4028/www.scientific.net/AMR.989-994.3489

Photometric Data Procession of the Swift/UVOT Instrument

Xiaopan Li [1, a], Cheng Yang[2, b], Li Zhou[1, c] and Haitao Yang[1, d]

[1]College of Physics and Electronic Engineering, Zhaotong University, Zhaotong 657000, China;

[2] College of Optoelectronic Engineering, Yunnan Open University, Kunming 650223, China.

[a]lxpzrc@163.com, [b] prc_yc@163.com, [c] zhouli7506@126.com, [d] 540252720@qq.com

Keywords: Swift satellite, Ultraviolet/Optical Telescope, HEASoft software, PKS 0537-441.

Abstract. The Ultraviolet/Optical Telescope (UVOT) which is one of three scientific instruments onboard the NASA-led Swift satellite provides simultaneous ultraviolet and optical photometric data. We present the installing procedures of HEASoft software and the detailed method for using the HEASoft in UVOT photometric data processions. We focus on the application of photometry processes, and present the photometry of Quasar PKS 0537-441. The analysis of the photometric data shows that this source has extreme variations in optical and ultraviolet bands and the shape of photometric flux curves in each band is excellently in agreement with each other.

Introduction

Over the last few decades, space instruments such as the Hubble Space Telescope, the Fermi Telescope and Swift Gamma-Ray Burst (GRB) satellite have created an infusion of scientific discovery, particularly in high energy environments. The Swift satellite rocketed into space in 2004 on a mission to study GRB and other transient or variable phenomena. As a multi-wavelength space observatory, Swift carries three instruments, the Burst Alert Telescope (BAT) [1], the X-ray Telescope (XRT) [2] and the Ultraviolet/Optical Telescope (UVOT) [3]. The primary research of the Swift is rapidly locates new GRB and then brings XRT and UVOT to bear on that location.

The UVOT instrument onboard Swift is a 0.3m aperture Ritchey-Chrétien reflector using a fast readout CCD detector capable of detecting low signal levels. These are photon counting devices which have a resulting image field of 2048×2048 pixels, covering a field of view of 17 × 17 arcmin^2. UVOT obtains the photometric data in ultraviolet and optical bands in parallel after the BAT trigger. Thereafter, the instrument executed cycled exposures through each of six color filters housed in a filter wheel, u, v and b in optical band together with uvw1, uvm2 and uvw2 in ultraviolet band [4]. The characteristics of these filters are shown in Table 1. The standard software suite, HEASoft, could provide excellent processing platform for the photometric data procession of GRBs. However, the official software installation and data analysis guide concentrate more emphases on generality and completeness but pay less attention to usability and pertinence. In this paper, we first present the installing procedures of software and provide methods for the procession of UVOT images. Then, we describe the photometric observations of Quasar PKS 0537-441 and present our conclusions.

Table 1 UVOT filter characteristics.

Filter	$\lambda_{central}$(Å)	FWHM(Å)	Filter	$\lambda_{central}$(Å)	FWHM(Å)
uvw2	1928	657	u	3465	785
uvm2	2242	498	b	4392	975
uvw1	2600	693	v	5468	769

Installing HEASoft Software

HEASoft is designed for the analysis of scientific astronomical observations at extreme ultraviolet, X-ray and Gamma-ray wavelengths. HEASoft 6.15.1 is the current version of HEASoft, which resolved some known issues and provides a more powerful data processing platform. The

corresponding source code distribution and individual Swift mission package must be downloaded from the website [5] before installing. The following are a description of the steps we took to install HEAsoft software on Fedora 20.

Step 1: Build environment and configure the software. Use the package manager ("yum") to install "gcc" , "gcc gcc-c++", "gcc gcc-gfortran", "ncurses-devel", "libXt-devel", "compat-gcc-34-g77" and "perl-ExtUtils-MakeMake" with root or administrator permissions. Unpack the downloaded file to create a directory named heasoft-6.15. Then go to the BUILD_DIR directory and set the relevant environment variable by executing "export CC=/usr/bin/gcc", "export CXX=/usr/bin/g++" and "export FC=/usr/bin/gfortran" and "export PERL=/usr/bin/perl".

Step 2: Install HEAsoft and set the environment variable. Starts the build process by executing "./configure >& config.out &", "make >& build.log &" and "make install >& install.log &" in order. These processions finally create an appropriately-named system-dependent directory i686-pc-linux-gnu-libc2.18 under heasoft-6.15.1/.

Step 3: Build the Swift Calibration Database (CALDB). The HEASARC'S Swift CALDB system which stores and indexes datasets associated with the calibration of the Swift instrument is essential for data reduction and analysis. Create a directory where the calibration data will be located and define the $CALDB environment variable with "export CALDB=/usr/local/caldb". Then, download the CALDB file from the website [6] and unpack the file in $CALDB directory..

Step 4: Install SAOImage DS9. DS9 is the terrific image viewer application for the fits, binary tables, multiple frame buffers, region manipulation, and many scale algorithms and colormaps ubiquitous in astronomy. Download the tar files and unpack in /usr/local directory by executing "tar -zxf ds9.linux.7.2.tar.gz". After this, type the command ds9 in a terminal window to start ds9.

Photometric Data Procession Method

The UVOT data can be described using three basic modes: Image, Event and Image & Event. Here, we consider the analysis of image mode data; in the further article, we consider how to deal with the Event mode data. The publicly available data can be downloaded from the HEASARC archive [7].

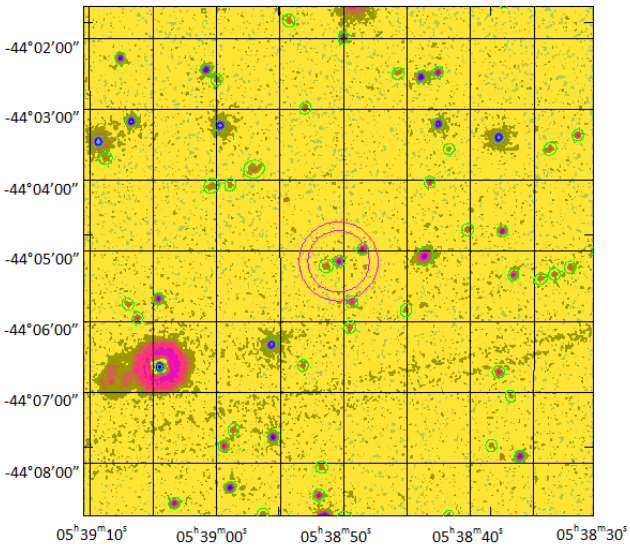

Fig. 1 UVOT image on November 24, 2005.The central target is Quasar PKS 0537-441.

Based on the Level 2 data contained in the HEASARC archive, we first make a general processing for position determination. Because of the extractors' capability to detect and measure extended sources, the source detection routine uvotdetect was designed to detect all sources in an UVOT image. Uvotdetect requires one mandatory input file containing one or more sky coordinates images and one optional one containing an array of weights for each pixel in the input image. To run uvotdetect the user provides a detection threshold which is measured in standard deviations above the noise. Uvotdetect has a single output file which contains a table of detected source positions, count rates and

1-sigma errors for each parameter. Run uvotdetect prompting for mandatory arguments for an u-filter sky image of Quasar PKS 0537-441 might be: "uvotdetect infile=0537.fits outfile=source.fits expfile=none threshold=3". Fig. 1 shows the UVOT image with all the detected sources marked on November 24, 2005. A description of Quasar PKS 0537-441 will be provided in the next section.

After finishing the general position determination, a tool named uvotsource returns information about the count rate from the source, the source's magnitude, and flux density information should be used to perform aperture photometry on a single source in a sky image. Loads the UVOT image in DS9 and specify the source extraction region and background region using region files. The source position returned by uvotdetect should be adopted, and the region files must be done with the fk5 coordinate system. That is recommendable to define a source aperture of radius 5 arcseconds to use for photometry. Run uvotsource for an u-filter sky image of Quasar PKS 0537-441 as: "uvotsource image=0537.gz srcreg=src.reg bkgreg=bkg.reg sigma=5 syserr=yes outfile=sources.fits". It is necessary to point out that uvotsource returns detection significance and coincidence-corrected count rate, magnitude and flux density in erg cm^{-2} s^{-1} A^{-1} with 1-sigma error. However, if the source is faint or the signal-to-noise is low, the uvotimsum tool should be used to sum extensions within an image.

Photometry of Quasar PKS 0537-441

We search for the publicly Swift data of Quasar PKS 0537-441 from the HEASARC interface [7]. Quasar PKS 0537-441, at redshift z=0.896, is a typical BL Lac object and has been observed for decades of years [8]. Many researchers have observed and studied this source and have found significant achievements. Recently, D'Ammando reported strong Gamma-ray variability and a harder-when-brighter behavior during multi-wavelength observations [9]. Based on the Swift data of Quasar PKS 0537-441, we follow the processing steps to do photometry. First, sum of all the slices using the uvotimsum tool. Second, extract the source position and then do target photometry using uvotdetect and uvotsource tool successively. Finally, use the E(B-V) value to correct magnitudes.

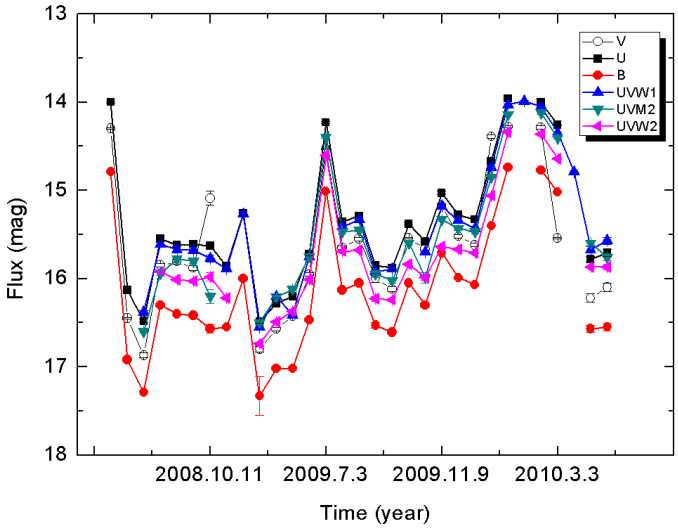

Fig. 2 Photometric flux curve of Quasar PKS 0537-441 in u, v, b, uvw1, uvm2 and uvw2 bands.

We carried out photometric observations of Quasar PKS 0537-441 from 2005 July to 2011 September in optical and ultraviolet bands. We performed photometric observations in Fig. 2. It is important to point out that all the photometric data are corrected for foreground Galactic interstellar reddening using the E(B-V) value at the query position [10]. As can be seen from Fig. 2, Quasar PKS 0537-441 has extreme variability in flux in optical and ultraviolet bands. More than 3 significant flux peaks appeared in the light curve during 6 years. These peaks correspond to large flare. Because of the lack of photometric data in the whole observation period, it is hard to carry out the periodicity just from the variation trend of the flux curve. Therefore, the particular method of signal processions, such as DCF, DFT and Wavelet analysis should be used to search for the periodicity in extra work.

Comparisons of the photometric flux curves, we can find that the shapes of photometric flux curves are similar and almost overlapping. Furthermore, the minimum optical variability time-scale of the BL Lac objects is longer than one more hour, and most are longer than 2 or 3 hours [11]. Hence, the quasi-simultaneous observations can be used to calculate the spectral index from a linear-square fit for spectral variation studying. Preliminary optical spectral variability analysis of Quasar PKS 0537-441 suggests that when the long-term flux variations increase, the optical spectra becomes bluer. The variation could be interpreted as changing of the jet viewing angle.

Conclusions

In this work, we take Fedora 20 Linux operating system as the platform to install HEASoft. First, build environment and configure the software, and then install HEASoft and set the environment variable. After the completion of the Swift CALDB building, install DS9 software finally. The detailed process and method of photometry are also presented. Specifically, the uvotimsum tool sums extension, the uvotdetect tool extracts the source position; the uvotsource tool does the photometry. Based on the photometric process and method, we present the optical and ultraviolet photometric data of Quasar PKS 0537-441 from 2005 to 2011. In our photometric data analysis, Quasar PKS 0537-441 has extreme variability, and the shapes of photometric flux curves are similar. What is more interesting is that whether there is an obvious time lags exist in optical and ultraviolet photometric flux curve. Once the time lag is determined, the more valuable information can be gotten for understanding the physical radiation mechanism.

Acknowledgements

This work is supported by the Youth Program of the Natural Science Foundation of Yunnan Province, China (2013FD056). We are grateful to the entire Swift team and the UK Swift Science Data Centre.

References

[1] Barthelmy S. D. et al., The Burst Alert Telescope (BAT) on the SWIFT Midex Mission, Space Sci. Rev, 120 (2005) 143-164.
[2] Burrows D. N. et al., The Swift X-Ray Telescope, Space Sci. Rev, 120 (2005) 165-195.
[3] Roming P. et al., The Swift Ultra-Violet/Optical Telescope, Space Sci. Rev, 120 (2005) 95-142.
[4] Poole T. S., Photometric calibration of the Swift ultraviolet/optical telescope, Monthly Notices of the Royal Astronomical Society, 383 (2008) 627-645.
[5] Information on http://heasarc.gsfc.nasa.gov/docs/software/lheasoft/download.html
[6] Information on http://heasarc.gsfc.nasa.gov/FTP/caldb/software/tools/caldb_setup_files.tar.Z
[7] Information on http://heasarc.gsfc.nasa.gov/docs/archive.html
[8] Pian, E., Falomo R., Hartman R. C., et al., Broad-band continuum and line emission of the gamma-ray blazar PKS 0537-441, Astronomy and Astrophysics, 392 (2002) 407-415.
[9] D'Ammando F., Antolini E., Tosti G., et al. Long-term monitoring of PKS 0537-441 with Fermi-LAT, Monthly Notices of the Royal Astronomical Society, 431 (2013) 2481-2492.
[10] Schlegel D. J. et al. Maps of Dust Infrared Emission for Use in Estimation of Reddening and Cosmic Microwave Background Radiation Foregrounds, Astrophysical Journal, 500 (1998) 525-553.
[11] Xie G. Z., Chen L. E., Li H. Z. Mao L. S., Estimates of AGN Black Hole Mass and Minimum Variability Timescale, Chinese Journal of Astronomy and Astrophysics, 5 (2005) 463-470.

Advanced Materials Research Vols. 989-994 (2014) pp 3493-3496
© (2014) Trans Tech Publications, Switzerland
doi:10.4028/www.scientific.net/AMR.989-994.3493

Process Simulation and Parametric Analysis of Gas Fractionation Unit

Qingrui Li[1], Ping Li[2], Peng Zhang[3]

[1.]School of Automation, Northwestern Polytechnical University, Xi'an 710000
Email: liqingrui0317@163.com

[2.]School of Information and Control Engineering, Liaoning Shihua University, Fushun 113001
Email: liping@lnpu.edu.cn

[3.] School of Automation, Northwestern Polytechnical University, Xi'an 710000
Email: strawberry7890@163.com

Key Words: Gas Fractionation Unit, Process Simulation, PROII

Abstract: Considering the problem of the energy consumption in the gas fractionation unit, PROII process simulation software is used to calculate the gas fractionation unit and to analyze the effect of process parameters. On the premise of ensuring product quality, these parameters can reduce energy consumption, improve economic benefit.

1 INTRODUCTION

Gas fractionation unit [1] is a device, which can separate liquefied petroleum gas in fluidized catalytic cracking unit into various fractions. Gas fractionation unit is mostly distillation column, the most energy has been consumed by the distillation process in the petroleum refining and chemical enterprises [2-3]. Therefore, the biggest problem in the control optimization is to select the best operating conditions and improve plant economic efficiency [4].

300 thousand tons per year of depropanizer column is the object in this paper. According to the problem of large energy consumption, PROII [5] process simulation software which was developed by SIMSCI company of American is used to simulate the depropanizer column. On the premise of ensuring product quality, various parameters is used to analyze the effect of column, and production device for energy conservation is achieved finally.

2 DEPROPANIZER COLUMN

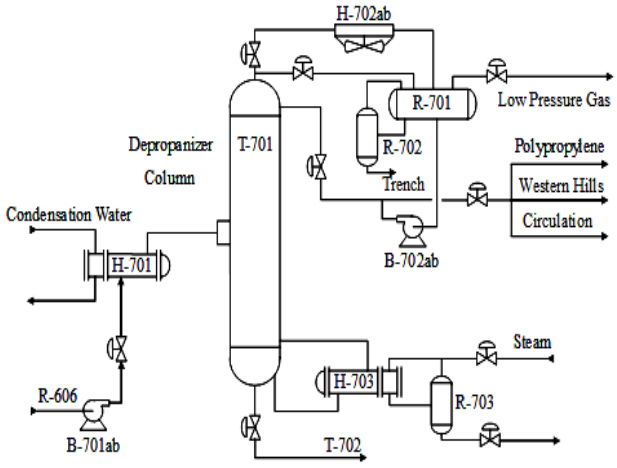

Fig. 1 Process flow diagram of depropanizer column

Liquefied petroleum gas(R-606) by a feed pump (B-701ab) is fed into the feed preheater (H-701), and sent to the depropanizer column (T-701) after heating. The reboiler (H-703) is heated by 1.3MPa (Gauge) steam. Carbon three fractions which are outflowed from the top of column are entered into the condenser (H-702ab), and then sent into reflux tank (R-701). By the reflux pump (B-702ab), part of the condensate is flowed back into column, part of it is sent to storage device or polypropylene unit as finished produce. The bottom of the column of the materials is fed into isobutene column (T-702), as in figure 1.

3 PROCESS SIMULATION

In PROII, equation of state of Soave-Redlich-Kwong is used to calculate the thermodynamic model. Lee-Kesler is used to calculate the liquid density. Pumparound is used for the top of the column. The iterative algorithm chooses Enhanced I/O. Actual measured values are compared with simulated values, as in table 1.

Table1. Actual Measured Values and Simulated Values of Operating Parameters

Operating Parameters	Control Targets	Measured Values	Simulated Values
Feed Temperature/℃	—	40.63	40.63
Top Temperature/℃	31-46	40.37	38.9
BottomTemperature/℃	75-115	96.9	95.3
Top Temperature/MPa	1.40-1.80	1.60	1.60
Content of C4 inTop/%	≤2	0	0.01
Content of C3 in Bottom/%	≤2	0	0.01

Table 1 shows that the simulated values of operating parameters and product quality are basically consistent with the actual values. It illustrates that the calculation of using the thermodynamic equation and the establishment of simulation processes have higher credibility.

4 SIMULATION ANALYSIS

4.1 Feed Temperature

In the case of the reflux rate unchanged, the feed temperature has an effect on the energy consumption in the entire process, as in table 2.

Table2. Feed Temperature and Energy Consumption

Cycle Number	Temperature ℃	C-Duty GJ/Hr.	H-Duty GJ/Hr.	Liquid Fraction
1	40.6300	-12.3227	15.0431	1.000
2	65.0380	-13.5141	14.1361	0.9999
3	66.1858	-14.0647	13.7938	0.9004
4	67.3336	-14.6542	13.4979	0.8027
5	68.4814	-15.2726	13.2316	0.7059
6	69.6292	-15.9185	12.9887	0.6092
7	70.7770	-16.5924	12.7647	0.5120
8	71.9248	-17.2970	12.5571	0.4136
9	73.0726	-18.0340	12.3630	0.3133
10	74.2204	-18.8.44	12.1808	0.2110
11	75.3682	-19.6075	12.0092	0.1064
12	76.5160	-20.4395	11.8481	8.8008E-05
13	77.6638	-20.4826	11.8215	0.0000

According to the table of data, actual working, bubble point and dew point conditions of energy consumption and cost data are calculated, as in table 3.

From the table3, the operating cost has reduced from 1240.31 Yuan per hr. to 1053.98 Yuan per hr. if the feed temperature can be raised to dew point. 15.02% of the saving extent can be reached, the effect is very obvious.

Table3. Energy Consumption and Cost

Feed Temperature（℃）		40.630	65.0380	76.5160
C-Duty	(GJ/Hr.)	-12.3227	-13.5141	-20.4395
Water/Cost	(T/.,Yuan/Hr.)	147.19/88.31	161.42/96.85	244.14/146.48
H-Duty	(GJ/Hr.)	15.0431	14.1361	11.8481
Steam/Cost	(T/,Yuan/Hr.)	7.68/1152	7.22/1083	6.05/907.5
Total Cost	(Yuan/Hr.)	1240.31	1179.85	1053.98

4.2 Feed Location

For multi-component distillation column, feed location is also a critical operating parameter. Reflux ratio,condenser duty and reboiler duty has been changed along with the feed location, as in figure 2 and figure 3.

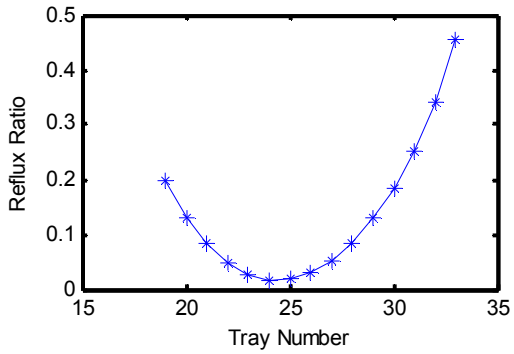

Fig.2 Change of reflux ratio

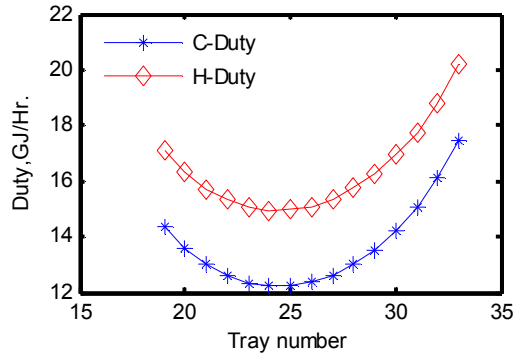

Fig.3 Change of duty

From the above figures, when the feed location in the twenty-fourth tray, reflux ratio, condenser duty and reboiler duty has reached minimum value. Condenser duty has reduced from12.3227 GJ/Hr. to 12.2128 GJ/Hr.. Reboiler duty has reduced from15.0431 GJ/Hr. to 14.9347 GJ/Hr..

4.3 Product Output of The Top

According to the material balance, the product quality has been changed by the product output of the top, in figure 4.

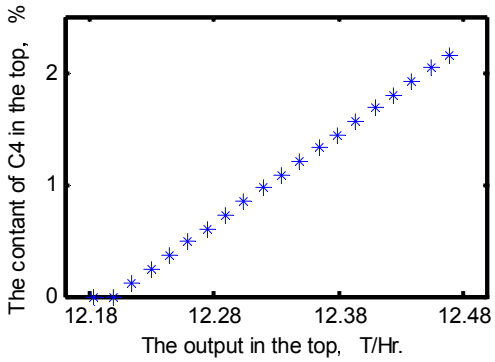

Fig.4 Changes of carbon four contents in the top

Figure 4 shows the relationship between product output and carbon four content in the top of the depropanizer column. With the increase of product output, the purity of propane has declined, the content of carbon four has obviously increased, and the problem of the high purity of propane has been solved. But continued to increase the output, it will lead to a substandard product. Therefore, the product quality is just standard by adjusting of product output, the unnecessary economic losses can be reduced.

5 CONCLUSION

According to the depropanizer column's technical characteristics, PROII software is used to simulate the column, the simulation values are basically consistent with the measured values. Through the analysis of the feed temperature, the feed location and the product output of the top, the column of the total energy consumption has been reduced, the industrial economic benefit has been improved.

This work is supported by Liaoning Province Natural Science Foundation Project (20102127), The Liaoning Province University Innovation Team Support Program (2009T062, LT2010058).

REFERENCES

[1] Lin Shixiong. Petroleum Refinery Engineering. Petroleum Industry Press, Bei Jing,2000.

[2] Wang Zheng, Lv Xianghong, Lu Enxi, etc..The optimization of the process conditions of gas fractionation process. Journal of Qingdao University of Science and Technology, Vol.25,No.4,311-313,2004.

[3] Xu Ying, Ye Qiliang, Li Yu'an, etc.. Simulation and optimization of gas fractionation unit. Anhui Chemical Industry, Vol.36,No.1,49-54,2010.

[4] Marcelo F A, Marcelo C. Modeling and simulation of reactive distillation columns using computer algebra. Computers and Chemica Engineering,Vol.29,No.9,1878-1884,2005.

[5] Simsci. Hydrocarbon Distillation. PROII Workbook, 1996.

Advanced Materials Research Vols. 989-994 (2014) pp 3497-3500
© (2014) Trans Tech Publications, Switzerland
doi:10.4028/www.scientific.net/AMR.989-994.3497

Design and simulation of airborne circular omni-directional slot antenna

Luo REN[1,a], Yongzhong ZHU[1,b],Dan SU[1,c],Xin DENG[1,d]

[1] Department of Information Engineering, Engineering University of CAPF, Xi'an 710086, China

[a]1587904030@qq.com, [b]bsbs1980@sina.com, [c]sudan19901021@126.com, [d]1558125018@qq.com

Keywords: airborne, circular slot antenna, gain, frequency.

Abstract. The airborne omni-directional antenna must not only satisfy the indicators of omni-directional horizontal requirements, but also have conformal shape with the surface of airplane. The common monopole antenna and microstrip antenna can not meet the above requirements. Under the background of the airborne antenna miniaturization and conformal demand, this article designs a kind of airborne circular slot antenna. The structure of the antenna is simple, which meets pattern VSWR < 1.4 bandwidth of 350 MHz to 376 MHz and meets pattern VSWR < 2 bandwidth of 338 MHz to 438 MHz .Its maximum gain within the operating frequency range can be 4.205 dB .

Introduction

In aircraft applications, there are very strict requirements for airborne antenna: airborne antenna should not only meet all kinds of electrical indicators requirements and environmental requirements, but also meet the conformal design with the aircraft[1]. With the continuous development of technology, the microstrip antenna, the slot antenna and the monopole antenna become the main three types of airborne antenna[2]. For common microstrip antenna,though it can achieve the conformal design with the body,it can't form a bearing surface to the direction of the diagram.For monopole antenna,though it can achieve omni-directional pattern, it is hard to realize the conformal design[3]. Based on the research of this problem,this article designs an airborne ring slot antenna model, and the model by HFSS software simulation optimization finally obtains the ideal result. When the slot antenna is used on the surface of fast flying object ,it cannot introduce additional air resistance and it can hide the antenna itself[4]. Especially it can fully fit in the conformal installation of carrier and surface[5], realize the carrier surface smooth with no bump, and well meet the requirements of the airborne antenna.

Antenna Design

A. The theoretical analysis. The main advantage of the ring slot antenna lies in its good directed pattern. In order to better play its excellent properties, many scholars has carried out the comprehensive and in-depth research and analysis. So the ring slot antenna in the present and in the future research or application has a broad development space[6]. Figure 1 depicts the geometry which is digged a circular groove and the coordinate system in an ideal conductive plate. The magnetic fluid distribution equivalent circuit diagram is shown in figure 1:

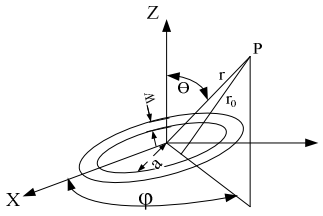

Fig1 Annular gap and coordinate system

$$\bar{M}(\rho,\varphi') = \bar{E}_a(\rho,\varphi') \times \hat{n} \tag{1}$$

The mouth surface electric field in formula(1) is shown by $\bar{E}_a$; the unit vector $\hat{n}$ is perpendicular to the mouth. Electric vector formula (2) ought to be used in calculating the far field radiation pattern of the ring slot antenna .

$$\bar{H}(r) = -j\omega\bar{F}, \bar{E}(r) = \eta_0\bar{H}(r) \tag{2}$$

Distant district Θ and φ of radiation electric field component needs to plug in the corresponding electric vector for calculation:

$$E_\theta = \frac{-jk_0}{4\pi}\frac{e^{-jk_0r}}{r}\int_0^{2\pi}\int_a^{a+W_s}\{M(\rho)\sin(\varphi'-\varphi) - M(\varphi')\cos(\varphi'-\varphi)\}\cdot$$
$$e^{-j\rho k_0\sin\theta\cos(\varphi'-\varphi)}\rho d\rho d\varphi'$$
$$E_\varphi = \frac{jk_0}{4\pi}\frac{e^{-jk_0r}}{r}\cos\theta\int_0^{2\pi}\int_a^{a+W_s}\{M(\rho)\cos(\varphi'-\varphi) - M(\varphi')\sin(\varphi'-\varphi)\}\cdot$$
$$e^{-j\rho k_0\sin\theta\cos(\varphi'-\varphi)}\rho d\rho d\varphi'$$

Besides the annular gap in radius is "a",and

$$\bar{M}(\rho,\varphi') = M(\rho)\hat{\rho} + M(\varphi')\hat{\varphi}' = -E_{\varphi'}\hat{\rho} + E_\rho\hat{\varphi}'$$

the Ws is far less than λ_0 ,and $E_{\varphi'} = 0$, $E_\rho = E_0$ is a constant.

$$E_\theta = \frac{-jk_0W_s}{4\pi}\frac{E_0ae^{-jk_0r}}{r}\int_0^{2\pi}\cos(\varphi'-\varphi)e^{jak_0\sin\theta\cos(\varphi'-\varphi)}d\varphi'$$
$$E_\varphi = \frac{-jk_0W_s}{4\pi}\frac{E_0ae^{-jk_0r}}{r}\cos\theta\int_0^{2\pi}\sin(\varphi'-\varphi)e^{jak_0\sin\theta\cos(\varphi'-\varphi)}d\varphi'$$

Integral φ' can be launched

$$E_\theta = \frac{k_0W_s}{2}\frac{E_0ae^{-jk_0r}}{r}J_1(ak_0\sin\theta),\ E_\varphi = 0,\ E_\theta = \frac{-jk_0W_s}{4\pi}\frac{E_0ae^{-jk_0r}}{r}\int_0^{2\pi}\cos n\varphi'\cos(\varphi'-\varphi)e^{jak_0\sin\theta\cos(\varphi'-\varphi)}d\varphi'$$
$$E_\varphi = \frac{-jk_0W_s}{4\pi}\frac{E_0ae^{-jk_0r}}{r}\cos\theta\int_0^{2\pi}\cos n\varphi'\sin(\varphi'-\varphi)e^{jak_0\sin\theta\cos(\varphi'-\varphi)}d\varphi'$$

Integral φ' can also be launched

$$E_\theta = \frac{-j^nk_0E_0aW_s}{2}\frac{e^{-jk_0r}}{r}\cos n\varphi J_n'(ak_0\sin\theta)\quad E_\varphi = \frac{j^nnE_0W_s}{2}\frac{e^{-jk_0r}}{r}\sin n\varphi\cot\theta J_n(ak_0\sin\theta)$$

Because the annular slot antenna can produce linear polarization field, and other methods of radiation characteristics and application of microstrip antenna are essentially the same,we can make sure according to the formula of field.

B .Antenna structure. Ring slot antenna is a circular aperture slot digged on the floor of the antenna dielectric substrate without any doubt[7].As is shown in Fig 2 a, A_5 is a good conductive plane. Make inward a rectangular cavity with a side length of D * D, height of H, and material being qualitative with good conductors. Open a circular radiating slot A_1 whose width is S on the A_5, and use the inner conductor column A_4 of the coaxial line to connect A_5 and the conductor cavity and feed the antenna. There are two impedance matching metal rings A_2 and A_3 in the conductor cavity. When the antenna loaded on the helicopter, you can put a layer of non-conductive material on the surface of the antenna to make the surface of the helicopter more smooth.

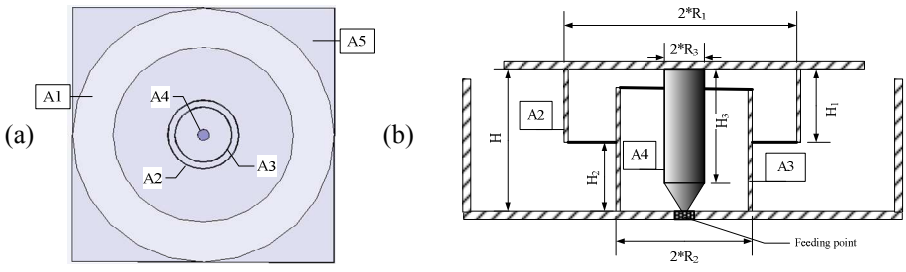

Fig 2 The structure diagram of annular slot antenna.(a) Antenna top view. (b) Antenna section

From fig 2 b antenna section to be seen, the inner conductor A_4 is kind of vertebral body which is connected by two halves .The first half is a cylindrical conductor and the second half is a vertebral body with radius of diminishing. The end of the conductor is connected to the feed point.In order to match impedance with conductor column A_4,we load a metal ring A_2 and A_3 on the surface of the metal cavity up and down respectively. As is shown in fig 2 b, the height of the outer ring A_2 is H_1,and the radius is R_1.The height of the inner ring A_3 is H_2 ,and the radius is R_2.The cone height of the inner conductor A_4 is H_3,and the radius is R_3.

Results and Analysis

A.The Antenna Performance. According to the simulation optimization of the HFSS Ansoft, the specific body size of the antenna can be determined in the following table:

Table 1 Structure size parameters of the ring slot antenna(unit: mm)

Part name	The numerical	Part name	The numerical
Slot depth (H)	80	Slot width (D)	500
The metal ring height (H1, H2)	79	Metal ring radius of A2 (R1)	118
Annular gap width (N)	50	Metal ring radius of A3 (R2)	40
Conductive cylinder height (H3)	68	Conductive cylinder radius (R3)	9

B .The Antenna Bandwidth.

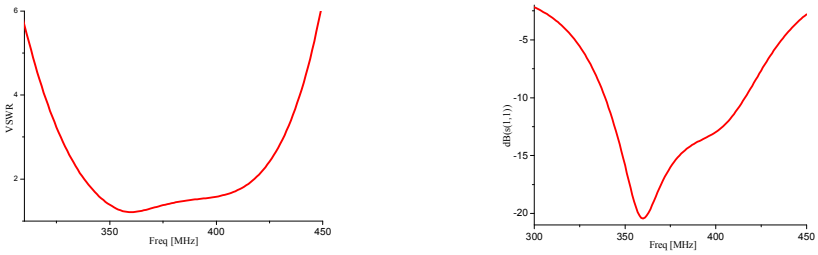

Fig 3 Standing wave and return loss of annular slot antenna

As the Fig 3 shown, on the 300MHz to 450MHz band, the band width of antenna pattern which meets VSWR<2 is 338MHz～438MHz and relative bandwidth is 22.22%. When the band width is 350MHz～376MHz,its VSWR<1.4 which achieves 26MHz completely covering the relevant ultra short wave communication frequency band.In the 350MHz, VSWR is 1.384 and S_{11} is -15.859dB. In the 370MHz, VSWR is 1.309 and S11 is -17.462dB. In the 350MHz to 370MHz frequency range, S11 is less than -14.6dB. They meet the requirements of the relevant communication equipment to the antenna.

C.Radiation Characteristics

By observation of Fig 4a) and Fig 5a), antenna pattern can get the biggest gain in the θ value around 45° and 315°. Due to the reflection of electromagnetic wave, between the θ value of 90° and 180°, radiation intensity has the phenomenon of attenuation. According to the requirements of practical application of airborne antenna, the basic characteristics of the antenna's radiation conform to the requirements of the airborne antenna radiation.

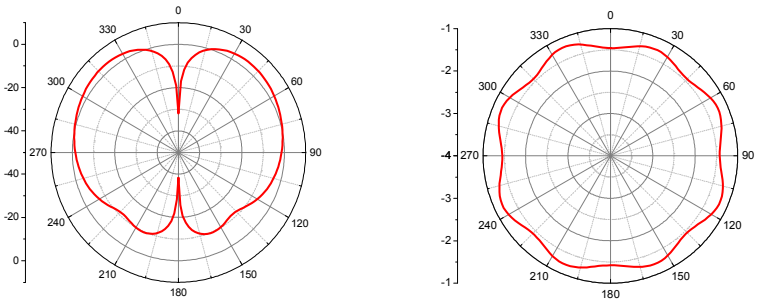

a) x-z plane b) x-y plane

Fig 4 Annular slot antenna pattern at 350MHz

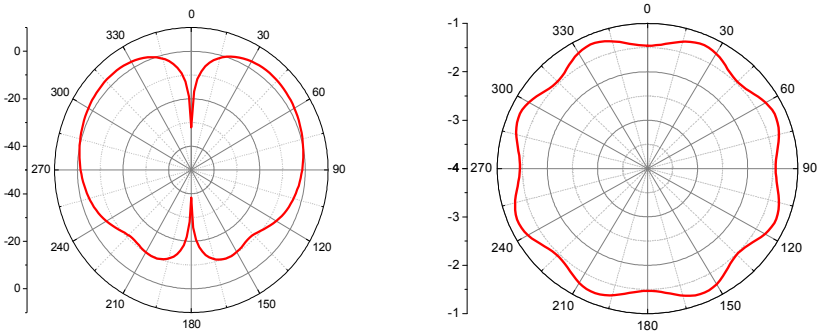

a) x-z plane b) x-y plane

Fig 5 Annular slot antenna pattern at 370MHz

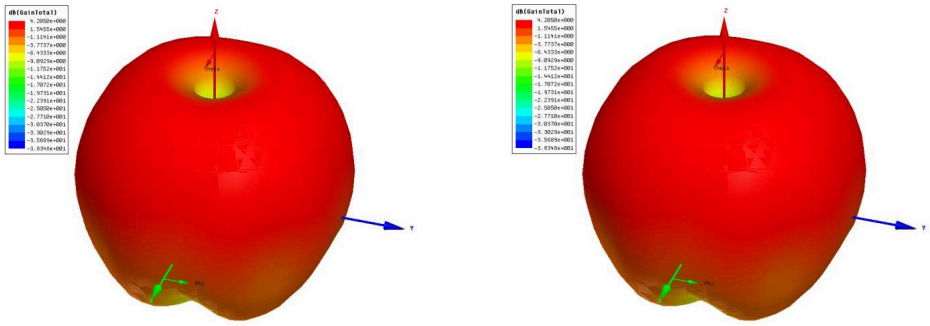

(a)350MHz Gain pattern (b)370MHz Gain pattern

Fig 6 Gain pattern of annular slot antenna

Conclusion

Based on the slot antenna as the breakthrough point, combined with relevant station technical index requirements of communication antenna, the paper designs out the annular slot antenna. The antenna can be well with the aircraft carrier conformal, to achieve reducing resistance and hiding antenna itself. The antenna pattern meet VSWR<2 and relative bandwidth is 22.22%. Within the working frequency band, antenna standing wave is greater than 3dB. Through careful simulation to compare the circular seam width with radius and height when impedance matching metal ring, the optimal size values can be determined. The antenna pattern simulation results meet that when the VSWR<1.4, the band width is 350MHz～376MHz; when the VSWR<2, the band width is 338MHz～438MHz and the biggest gain in the operating frequency range is 4.205dB. It successfully meets the design requirements for miniaturization and conformal of the airborne antenna.

Foundation item:The National Natural Science Foundation of China(61302051),The Natural science Research Program Foundation of Shanxi Province(2012JQ8026),The Basic Foundation of the CAPF Engineering University(WJY201309)

References

[1] X.S.Jin:*Re-entry Aircraft Antenna[M]*(National Defense Industry Press,BeiJing 2000)
[2] Y.K Wang, Y.Q. Li:*Line Antenna's Bandwidth Technology*(Xidian University Press,China 1995).
[3] J.H.Chu,*Research of VHF Airborne Broadband Antenna's Miniaturization*(MS.,Xidian University,China 2009).
[4] Y.Z.Zhu, J.D.Xu: Journal of Soochow University, Vol. 27(2011) No.4, p.34.
[5] Behdad N, Sarabandi K: Electronics Letters, Vol.40(2001) No.7,p.408.
[6] B.Zhao, H.Y.Li: Scientific Technology and Engineering, Vol. 12 (2012) No.16, p.3865.
[7] T.J.Yuan, L.Y.Zhou, Ouslimani H H,et al: *Proceedings of the 40th European Microwave Conference*(Paris,France,2010)Vol:3,p. 1481.

Advanced Materials Research Vols. 989-994 (2014) pp 3501-3504
© (2014) Trans Tech Publications, Switzerland
doi:10.4028/www.scientific.net/AMR.989-994.3501

Based on small current grounding fault analysis and testing

Huailian lv

Yantai Engineering & Technology College, Yantai, China

lhl1313@163.com

Keywords: Small Current Grounding Fault; FTU; Zero Sequence Current

Abstract. distribution network line usually adopt neutral point grounding way of three-phase three-wire power supply, improve the power supply reliability, reduce the line loss, increase the margin level of the distribution line, reduce the rate of tripping. But using three-phase three-wire power supply line in the actual operation of distribution network, the single-phase earth fault happens often, seriously affected the substation equipment and the safe and economic operation of the distribution network. Based on such fault is analyzed, and puts forward new on feeder terminal for such fault detection scheme.

Introduction

Distribution network medium and small current grounding generally refers to 10 kv and 6 kv single-phase grounding happening somewhere on the feeder. A neutral point is usually not grounded in our distribution network system, and basic for three-phase three-wire system running(the main transformer connection group to Y/Δ,Y/Y0 for distribution transformer connection group), Although certain changes in single-phase grounding running characteristics, but quite a small fault current value(Less than the normal load current) Damage is not obvious. But if long time grounding, grounding phase voltage will be reduced, the grounding phase voltage to rise to the line voltage, pose a threat to electric equipment insulation. Single-phase earth fault occurs after the system can't run for a long time. Therefore, the operational procedures of distribution network in China make clear a regulation, when the single-phase grounding distribution network system is allowed to run for two hours. This period of time can be used to find out the cause of the problem and troubleshooting.

The small current grounding fault analysis

Now the brief analysis of operational characteristics of the small current grounding as follows. In figure 1 as an example, the normal load can ignore its load characteristic constant impedance model instead of:

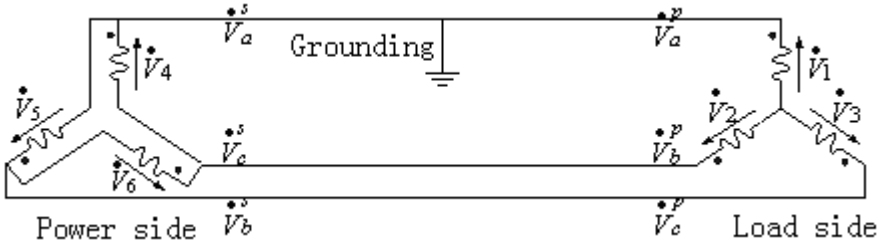

Fig. 1. No earth neutral system occur ground fault

Power supply side of main transformer secondary side for Δ connection form; Lateral load equivalent to a constant impedance, expressed as a Y wiring (wiring can also, analyze the conclusion). First assumed load asymmetric three-phase equilibrium and ignore electrical equipment parameters, when the normal operation of the voltage vector is symmetrical, as shown in figure 2:

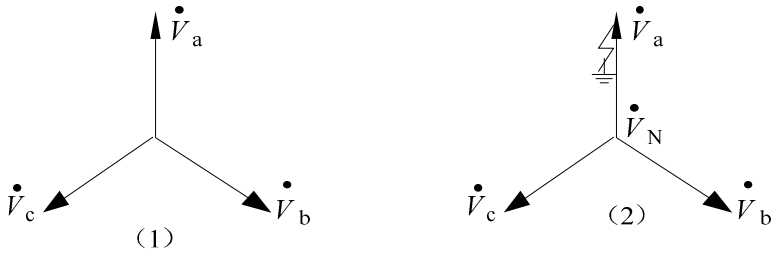

Fig. 2. Current ground fault phasor diagram

The line voltage vector $\dot{U}_{ab}$, $\dot{U}_{bc}$ and $\dot{U}_{ca}$ Is completely symmetrical，the neutral point voltage is only 0.

1. Ignore the line charging capacitance, assume that a phase of single-phase grounding, a phase voltage is equal to the voltage (zero value), the figure 2: the neutral point voltage is zero, no longer a phase voltage rise but negative; But no matter how the neutral point voltage changes, because is not grounded system, there is no zero sequence circuit, line voltage is kept constant, the line voltage vector, and still completely symmetrical. Therefore, at this time of single-phase grounding had no effect on the normal operation of the system.

2. Meter and the line charging capacitance, the capacitance through the ground to form current loop. But as a result of general distribution circuit charging capacitance is very small (especially the overhead line), the capacitance current is small on numerical (below 10 ~ 20), is far less than the normal load current (200 ~ 300). At this time of the line voltage vector due to the existence of the capacitive current and slightly affected, but basically is still in a symmetrical running state.

3. Considering the influence of the distribution of three-phase load characteristics. 400 v power distribution lines except some straight for industrial lines generally USES three phase four wire system running, three-phase load under normal circumstances there is asymmetry. This asymmetry makes the load current flows through a certain value in the neutral line, resulting in three phase line voltage to produce a certain degree of asymmetry. The line voltage due to asymmetric load asymmetric effect than effect of capacitive current lead to often, so the asymmetric characteristics caused by single-phase grounding is likely to have been load off the asymmetry of oblivion, is difficult to distinguish whether there is a single phase grounding.

4. Current transformer in our country mostly adopts the standard model, 500/5, 600/5, and so on. Because of the single phase grounding capacitive current is quite small, line current value is basically a superimposed on the load current is relatively small current, this small change in the CT secondary side is basically not to come out. In addition, if consider adopting zero sequence current transformer is measured, tend to see the asymmetry of current when single-phase grounding than the normal run time asymmetry caused by the asymmetric load current is small, so it is difficult to tell whether there is a single phase grounding.

5. 35 kv neutral point is usually used in distribution system via arc suppression coil grounding, although the capacitive current is 10 kv line is big, but due to the effect of compensation of the arc suppression coil largely offset the impact of capacitive current, show the running characteristics of basically similar to 10 kv system.

Based on the analysis, the small current grounding had little effect on characteristics of three-phase power distribution system, the conventional fault detection method is difficult to accurately locate the fault point, is one of the difficult problem of the current international.

FTU for small current grounding fault detection scheme

For such failure, we more reliable detection scheme is obtained through practice. Through acquisition of zero sequence current value and the event of a failure experience of zero sequence values compared to determine the small current grounding fault. Is the key technology of how to gather the zero sequence current. Here is to collect the zero sequence current based on our practice and figure out a practical method.

Used to measure the zero sequence current is used 100/1 of the special current transformer (figure 3), because of the zero sequence current transformer using plugin installation caused the inconvenience of use, then changed to remove the zero sequence current transformer, directly in the FTU collected by means of modified wiring zero sequence current. Now use scheme, switch the original A, B, C three-phase CT B phase CT is short of, the zero sequence CT secondary outlet connected to the original used to pick up the position of the B phase CT secondary outlet, so mining by FTU B phase current is, in fact, zero sequence current. Wiring principle as shown in figure 3:

After transforming: still use FTU B phase CT to measuring the zero sequence current, principle as shown in figure 4:

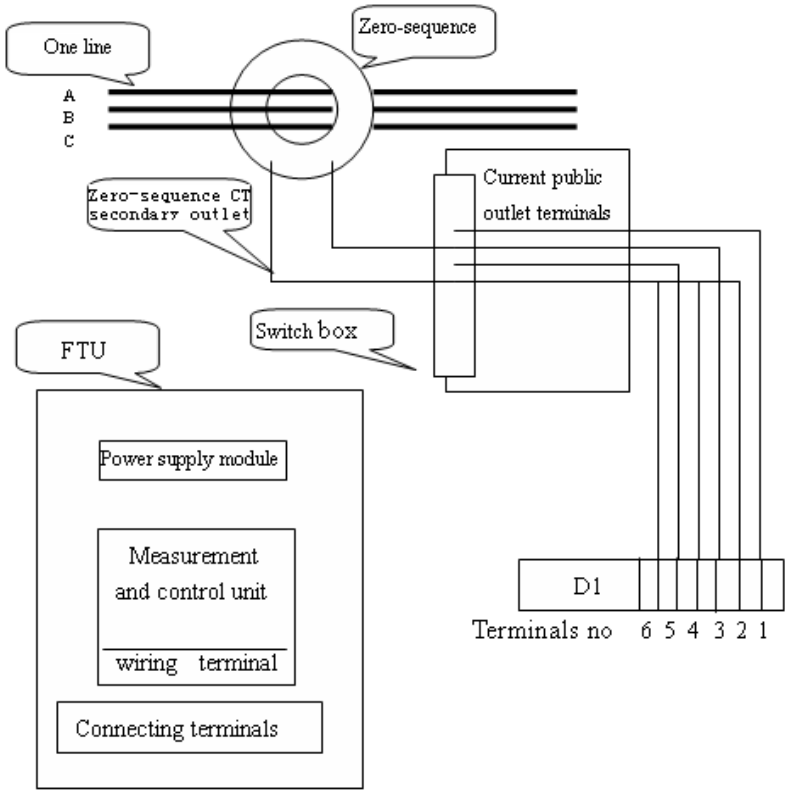

Fig. 3. Wiring diagram zero-sequence current ground fault

The switch side: From two lines of the zero sequence CT secondary side and from the terminal to connect the two wires short, the original short meet together from B phase CT secondary side of the two wires connected to the two vacant terminal.

FTU side: the original in the FTU terminals on the terminal 2 and 6 of D1 line connected to terminal 4, with two short wires respectively 2— 3, 3—6 short answer.

Such three phase current through the FTU B phase CT outflow, so at this time of FTU B phase CT measured is actually zero sequence current.

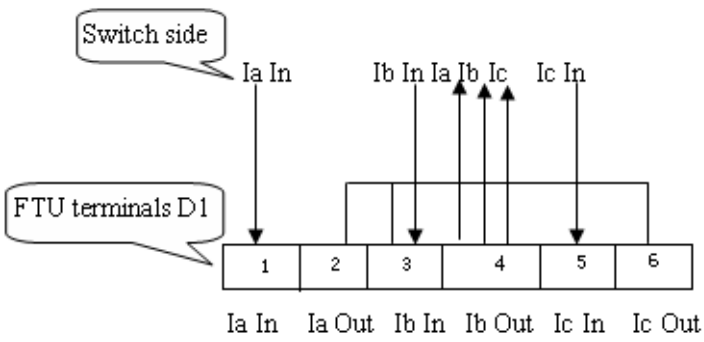

Fig. 4. Wiring diagram zero-sequence current changed ground fault

Conclusion

In this article, through the analysis of the small current grounding fault, put forward a good detection scheme, the fault in the actual played an important role in the operation of the system, save a lot of manpower and material resources, greater economic and social benefits were obtained.

References

[1] Zhang Yansheng,Du Zhaohui . The single-phase earth fault problem analyses the small current grounding system, Technology & Business,2012(20).

[2] Lin Gongping and so on. Technology strategy of distribution feeders automation solutions [J]. Automation of electric power systems,2001,25(7):52-55.

[3] Sui Bo, Based on the transient field, a new method of small current grounding fault location, The Enterprise of Science and Technology,2012(20).

[4] Zhou Yusheng, Zhou Youqing, Dai Zhengzhi. Power fault section judgement algorithm based on FTU [J]. Electric power automation equipment,2003,20(4):25-27.

[5] XiaoBai, Shu HongChun, GaoFeng. Current grounding system of single-phase grounding fault line selection methods were reviewed [J]. relay,2001,29(4):17-20.

[6] Ceng Xiangjun, root, yoon Chen Deshu. To adapt to the power distribution automation feeder grounding protection and research［J］.Automation of electric power systems，2000，24(15):37-41.

[7] Yuan Qincheng Wu Chuanhong. Distribution overhead line automation solution. China institute of electrical engineering distribution automation points designed annual conference 2004 [Conference papers,2004.

[8] Li Zhongyuan,Yin Shiyou, The small current grounding system analysis and comparison of various kinds of fault location principle, Entrepreneurs World.2011(10).

Advanced Materials Research Vols. 989-994 (2014) pp 3505-3508
© (2014) Trans Tech Publications, Switzerland
doi:10.4028/www.scientific.net/AMR.989-994.3505

Prediction Model of Silicon Content in Blast Furnace Hot Metal Based on Artificial Neural Network and Genetic Algorithm

Cheng Yonghua[1, a], Niu Caiwen[2,b] and Zhang Yuxin[3,c]

[1] Tangshan Industrial Vocational Technical College, Tangshan City, Hebei Province,China 063020

[2] Tangshan Industrial Vocational Technical College, Tangshan City, Hebei Province,China 063020

[3] Tangshan Industrial Vocational Technical College, Tangshan City, Hebei Province,China 063020

[a]chengyonghua1014@163.com, [b]niucaiwen@126.com, [c]yuxin200212@163.com

Keywords: Artificial neural network, Genetic algorithm, Blast furnace, Hot metal, Silicon content

Abstract. In this paper, a predicting model of silicon content in blast furnace hot metal is built based on artificial neural network and genetic algorithm, which optimizes the initialization weight values of neural network with genetic algorithm. This model can effectively improve the prediction accuracy and reduce the calculating time. Online application shows that the predicting model can effectively predict the silicon content in blast furnace hot metal and play an important role in production. when required absolute error was within ±0.03, the accuracy of model can reach 81.4%, and when absolute error was within ±0.04, the accuracy can reach 91.4%.

Introduction

Silicon content is an important index to describe hot metal quality, and silicon in blast furnace comes from the reduction of raw materials[1].

In actual production, there are many factors affect the silicon content in hot metal, such as coal rate, coke rate, air pressure, top pressure, iron ore grade and so on. As the complexity of the reactions in blast furnace, the factors involves many aspects in blast furnace, and the relationship between the silicon content in hot metal and the affect factors is not a linear, so traditional model is difficult to accurately predict the silicon content in hot metal.

The development of artificial neural network has provided conditions to solving such nonlinear problems[2,3]. So some researchers established artificial neural network prediction model to predict the silicon content in hot metal[4]. But neural network have some disadvantages, the prediction accuracy is not very ideal. Genetic algorithm has very powerful search capabilities. Combining neural network and genetic algorithm to search optimization is a new trend of numerical simulation[5,6]. In this paper, a predicting model of silicon content in hot metal is built based on artificial neural network and genetic algorithm, which optimizes the initialization weight values of neural network with genetic algorithm. This model aims to improve the prediction accuracy and reduce the calculating time.

Artificial Neural Network and Genetic Algorithm

Artificial Neural Network. Artificial Neural Network (short for ANN) is a nonlinear, adaptive, self-organizing system that composed of a large number of simple processing units, which is based on modern neuroscience research, trying to simulate the human nervous system to perform information processing, memory and processing methods, and designed an information processing system as human brain style. Artificial neural network has lots of characteristics, such as distributed memory, parallel processing, fault-tolerant ability, any complex nonlinear systems, self-learning, adaptive ability and so on, it has a unique advantage on resolving the production process problems with many parameters and inconspicuous regularity. In the artificial neural network algorithm, BP algorithm (error back propagation algorithm) is the most widely used training algorithm for multi-level network. BP neural network is compose of input layer, hidden layer and output layer.

Genetic Algorithm. Genetic algorithm (short for GA) is an adaptive heuristic global search algorithm based on natural selection and population genetics mechanism, which proposed by Professor J. H. Holland from the University of Michigan in early 1960's, and described in "natural and artificial adaptive system" published in 1975. Genetic algorithms start as a group of randomly generated candidate solutions (each solution are expressed as a string), through the use of genetic operators to combine these strings, so that these candidate solutions gradually evolve toward the direction of the optimal solution. These genetic operators (including the choice of reproduction, crossover and mutation) are simulation of natural reproduction, crossover and mutation phenomenon that occurred in natural selection and genetic processes. For a given problem, the group of P(t) that maintains a constant number of each generation is evaluated by calculating fitness value F (that the ability to adapt to the environment) of each individual in the group. The copy opportunities of individual are distributed according to the fitness value, and the individuals with high fitness value get more chance to reproduce in the next generation and produce more offspring, while individuals with low fitness value produced less offspring and even replaced by some better offspring. The selected individuals carry crossover and mutation operation through crossover probability Pc and mutation probability Pm to produce a new generation. The search ability of genetic algorithm is mainly given by the replication and cross, while the mutation operator guarantees the ability of searching every points of the solution space, which makes it has a global convergence.

Combination of genetic algorithms and BP neural network. Neural networks and genetic algorithms are theories imitating biological treatment mode to get intelligent information processing. Neural networks focuses on the brain's neural network micro-structure, through complicated connection of a large number of neurons, and using the method from the bottom to the top, though the parallel distributed arithmetic formed from self-learning, self-organizations and non-linear dynamics to deal with pattern information which is difficult to be verbalized, and it has a strong self-learning and associative memory function. Genetic algorithm is a search method depending on the simulation of the biological evolution phenomenon (natural selection, crossover and mutation, etc.), and using natural evolution mechanism to represent a complex phenomenon, with the purpose of solving various difficult problems effectively, which has irreplaceable advantages in the global search and self-adaptation.

From the own characteristics of BP algorithm neural networks and genetic algorithms, BP algorithm training is based on the weight modification principle of the error gradient descent, which inevitably exists the problem that falling into the local minima. Genetic algorithms are good at global searching, but lack of capacity for the exactly local search. The combination of genetic algorithms and BP algorithm achieves the mutual advantages result, to the benefit of better solving the problem of blast parameters prediction.

Though the genetic algorithm optimizes initial weights of BP neural network can make a wide range of values, and also introduce the information of peak error modification into initial weights, which improves the peak mapping accuracy. The flow chart of the model that genetic algorithm optimizes initial weights of BP neural network is shown in Figure 1.

Model Calculations

Model structure. (1) Input layer. In this model, based on the correlation of actual production conditions and the silicon content in hot metal, selected 11 closely related with the hot metal silicon content parameters as input variables, such as coal ratio, coke ratio, air pressure, top pressure, sulfur load, iron ore grade, blast capacity, air temperature, ventilating index, slag basicity and Si content. (2) Hidden layer. In this study, hidden layer is one layer. The number of hidden neurons expresses the nonlinearity degree of the input and output in the network, which has an important impact on the network model training speed and forecasting capabilities. Based on a large number of calculation tests, select the number of hidden layer neurons is 14. (3) Output layer. The number of neurons in the output layer depends on the system requirements of network function, in order to achieve the

prediction of silicon content in hot metal; the output variable in this model is the silicon content in hot metal, so the number of neurons in output layer is 1.

Samples normalized processing. Because of the different input variables units and the difference of absolute value, in order to avoid the influence of neural network model, the normalized processing of input parameters and output parameters is necessary. In this model, BP network uses Sigmoid function as the excitation function, requiring the input and the output value of each node should be in [0,1]. Therefore, the parameter values needed to be converted in [0, 1], the input layer parameter values use the following linear conversion:

$$x(p,i) = \frac{x_{act}(p,i) - x_{min}(i) \times 0.9}{x_{max}(p,i) \times 1.1 - x_{min}(i) \times 0.9}$$

Where: $x\ (p,\ i)$ - sample values of parameters in the sample; $x_{act}\ (p,\ i)$ - the actual value of parameters in the sample; $x_{min}\ (i)$ - the minimum sample set parameters; $x_{max}\ (i)$ - and maximum sample set parameters.

Selection of the main operational parameters. The main parameters in the calculation are: (1) Genetic algorithms: population size is 20, selection probability is 0.08, the crossover probability is 0.1, mutation probability is 0.055, the initial weight value space is [- 5,5], evolution generation is 200. (2) BP neural network: momentum coefficient is 0.7, learning rate is 0.9, excitation function is S-type function, and system error is 0.0022.

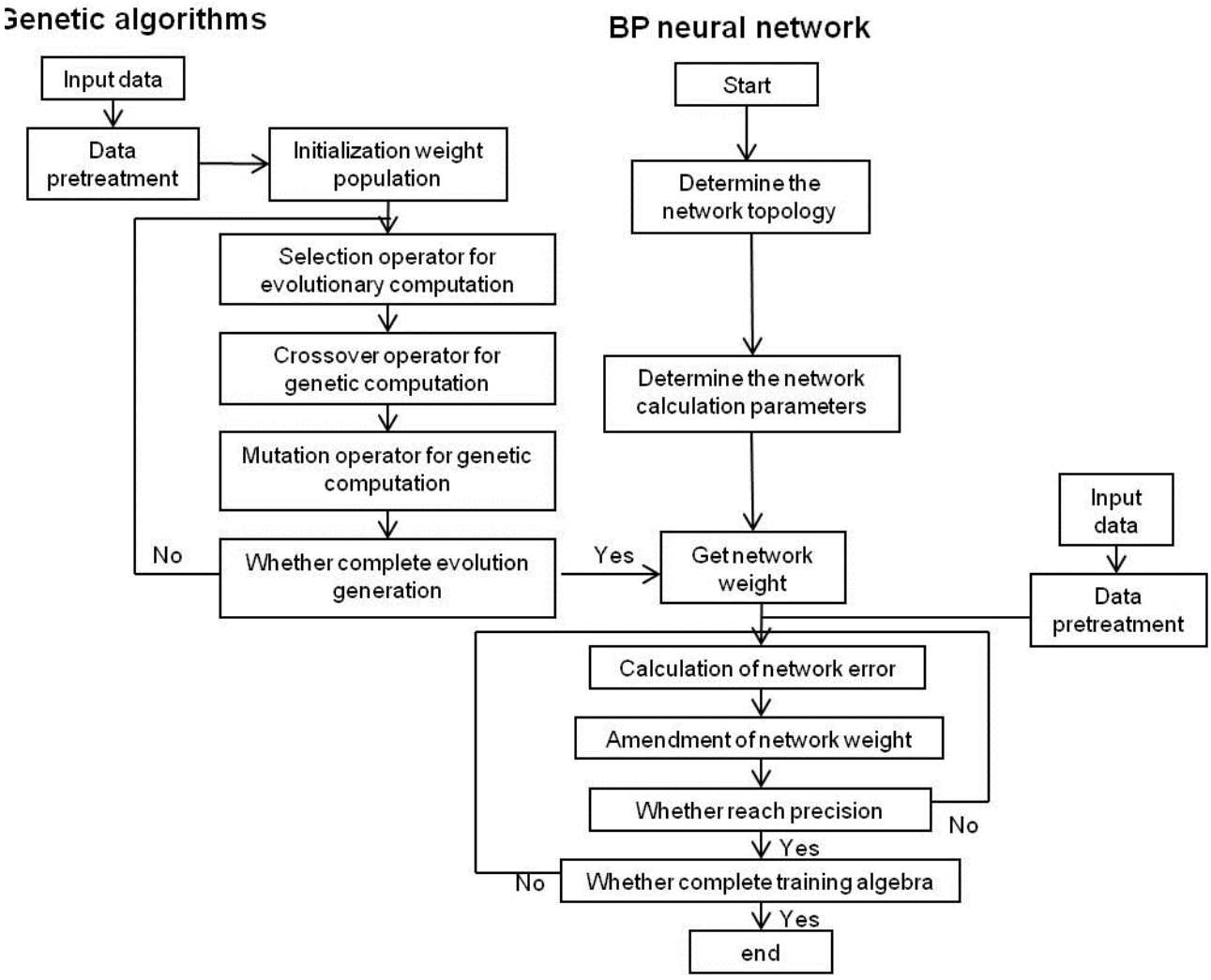

Fig. 3. Flow chart of genetic algorithm optimizes BP neural network initial weights model

Comparison of Calculation and Application

A 220 h continuous production data (220 groups) was used in calculation, including 150 sets of data used for training the network, another 70 sets of data for off-line prediction. First, the silicon content in hot metal was predicted by a neural network model. On this basis, adding genetic algorithm to optimize the model of neural network initial weights. The calculation training times of the former was 20,000, and the latter's training times was 10,000. The comparison of off-line prediction results of the two calculation methods were shown in Table 1. The comparison between the actual values and model calculation value after adding the genetic algorithm were shown in Figure 4.

Table 1. The comparation of calculation result of the two method

Error range/%	Neural network		Genetic network optimizes neural network	
	Hit sample number	Hit rate/%	Hit sample number	Hit rate/%
<0.03	55	78.6	57	81.4
<0.04	62	88.6	64	91.4
<0.05	65	92.9	67	95.7

From Table 1, it can be seen that the prediction precision of the combination model of genetic algorithm and BP neural network was superior to BP neural network prediction model. And the number of training times was reduced effectively.

Based on the modified prediction ideas, an online prediction function was designed to test silicon content in hot metal. With the blast furnace production running, the required real-time production data of each hour was imported into the system and the model did training again. At the same time, the first set of data in the group of samples was out according to the FIFO principle. Thus, with the production running, the network was learned and corrected momentarily, the model will adapt to the new production conditions better, so does the forecast results. Currently, the model has been tested and applied in actual production. Application results show the model was stable and reliable; and the hit rate of the model was higher. It provides a good guidance for the actual production of blast furnace.

Conclusion

This paper uses two methods of BP neural network, genetic algorithm and BP neural networks combination to establish a prediction model of hot metal silicon content. Two kinds of model were trained by 150 sets of data and finished off-line prediction through 70 sets of data. Prediction results indicate that the combinative model of genetic algorithm and BP neural network is better than BP neural network model in the aspects of precision rate and training times. Online application shows that the model can predict the silicon content in hot metal effectively; it plays a well directive role in the actual production of blast furnace.

References

[1] X.L. Wang, in: Iron and Steel metallurgy (Iron Making Part), Metallurgical Industry Press(2000).

[2] Y. Otsuka, M. Konishi and K. Hanaoka: ISIJ International, Vol.39(1999), p1047.

[3] G.Y. Zhang, in: Hot Metal Silicon Content Prediction System of Blast Furnace Based on the Stove Heat-index and BP Network, Chongqing University(2008).

[4] G.Q. Zuo, J.T. Ma and B. Bo: Ironmaking Conference Proceedings, 1996, p211.

[5] S. Kumar, M.P. Singh: Computers & Mathematics with Applications, Vol.60(2010), p1049.

[6] C.J. Wang, W.D. Yu and Z.Q. Chen: Journal of Nanjing University, Vol.39(2003), p459.

Advanced Materials Research Vols. 989-994 (2014) pp 3509-3512
© (2014) Trans Tech Publications, Switzerland
doi:10.4028/www.scientific.net/AMR.989-994.3509

Comparison of Two Computing Method on Thermal Conductivity of Aluminum Nitride

Xuemei Cai[1, a *], Qianneng Zhou[1, a], Jingmei Wang[1, a]

[1]College of Electronic Engineering, Chongqing University of Posts and Telecommunications, Chongqing 400065, China

[a]email: caixm@cqupt.edu.cn

Keywords: Aluminum nitride, Debye temperature, Thermal conductivity, Heat capacity

Abstract. Thermal conductivity of aluminum nitride (AlN) has been calculated by density functional perturbation theory (DFPT) and quasi-harmonic approximation (QHA) combined with Debye theory in the paper. Debye temperature is evaluated respectively from sound velocity and heat capacity. From 300K up to 1000K, the predicted thermal properties in pure crystal AlN based on these two Debye temperatures are compared with each other and the latter shows excellent agreement with Slack's experimental data. The relative difference based on Debye temperature from heat capacity is within the limits of ±5.5%. This agreement with experiment is due to the Debye temperature derived from capacity contains the temperature effect while describe the three phonon process.

Introduction

The thermal conductivity of materials is very important in a great variety of device applications where heat flow plays a role such as thermoelectric energy conversion, memories, or heat sinks [1-2]. AlN is an attractive substrate material for these applications due to its high thermal conductivity, low expansion coefficient, low dielectric constant and high electrical resistivity, as well as the good compatibility with complementary metal-oxide semiconductor technology [3]. In the case of high power light emitting diodes (LEDs), the heat dispersion has significant influence on its optical properties One of the effective thermal solutions for high power LEDs is using high conductivity AlN as heat sinks.

Thermal properties are determined by the diffusion of phonons through the solid in the case of AlN. In this paper, thermal conductivity of phonons in pure crystal AlN has been theoretically studied using the functional perturbation theory and quasi-harmonic approximation combined with Debye theory. Thermal conductivity is considered from temperature 300K up to 1000K. Two Debye temperatures evaluated respectively from sound velocity and heat capacity are used in the model. The results are compared with experimental data and good agreements in the latter one are achieved.

Theoretical Method

Heat transport is due to the energy excitations which are mobile, principally electrons and phonons. As the electronic thermal conductivity in insulators can be neglected, the total thermal conductivity is dominated by phonons, which can be calculated by using the standard Debye expression:

$$\lambda(T) = \frac{1}{3}\int_0^{\omega_D} v_m C_v(\omega,T) l(\omega,T) d\omega \tag{1}$$

In this model, the average sound velocity v_m of the material is a constant number and is assumed to be independent of the modes and wave vectors, thus can be taken out of the integral. $C_v(\omega,T)$ is the specific heat capacity at constant volume, ω_D is the Debye frequency, $l(\omega,T)$ the total phonon mean free path at different frequencies and temperatures. These parameters will be computed using the density functional perturbation theory, combined with quasi-harmonic approximation later.

The average sound velocity v_m is determined by the longitudinal wave speeds v_l and transverse wave speeds v_t:

$$v_m = [\frac{1}{3}(\frac{2}{v_t^3} + \frac{1}{v_l^3})]^{-\frac{1}{3}} \tag{2}$$

The relation of Debye temperature θ_D and average sound velocity v_m is:

$$\theta_D = \frac{\hbar}{K_B}(6\pi^2 \frac{N}{V})^{\frac{1}{3}} v_m \tag{3}$$

where N is the number of atoms in the unit cell, V is the cell volume. K_B is Boltzmann's constant and $\hbar$ Planck's constant.

The dependence of the frequency on the wave vector can be calculated through Hessian matrix. The Hessian matrix is:

$$D_{\mu\nu}(R - R') = \frac{\partial^2 E}{\partial u_\mu(R)\partial u_\nu(R)}\Big|_{u=0} \tag{4}$$

Here u refers to the displacement of a given atom and E is the total energy in the harmonic approximation. Phonon density of states (DOS) can be achieved from the phonon spectra.

The value of the Debye temperature at a given temperature can also be obtained by calculating the actual specific heat capacity at constant volume (Eq.6) and then inverting the Debye specific heat capacity (Eq.5) to obtain Θ_D.

$$c_v^D(T) = 9NK_B(\frac{T}{\theta_D})^3 \int_0^{\frac{\theta_D}{T}} \frac{x^4 e^x}{(e^x - 1)^2} dx \tag{5}$$

$$c_v(T) = K_B \int \frac{x^2 e^x}{(e^x - 1)^2} F(\omega) d(\omega) \tag{6}$$

where x is $\hbar\omega/K_BT$ and $F(\omega)$ is the phonon density of states. The DFPT is employed to determine the phonon density of states by using the norm-conserving pseudo-potential method. Based on the QHA theory, the actual heat capacity of AlN is calculated using the phonon density of states.

Results and Discussion

Before computation, the structure of wurtzite AlN is geometrically optimized. The experimental velocities of the longitudinal wave vl, transverse wave vt and the calculated average sound velocity vm are shown in Table 1. Debye temperature predicted from Eq.3 is also given in Table 1. The computed values are all in good agreement with experimental data.

Table 1 Sound velocities and Debye temperature in wurtzite AlN

Method	v_l [m·s^{-1}]	v_t [m·s^{-1}]	v_m [m·s^{-1}]	Θ_{DS} [K]
This work			6975.9	967.7
Experiments	10127*	6333*	6980**	950***

*Ref. [4] ** Ref. [5] *** Ref. [6]

The computed phonon DOS of wurtzite AlN is provided in Fig.1. A strong peak value about 0.42 of the optical phonon modes in the DOS appears at 19.97THz in this structure. The cut-off frequency of acoustical phonon modes is 17.72THz.

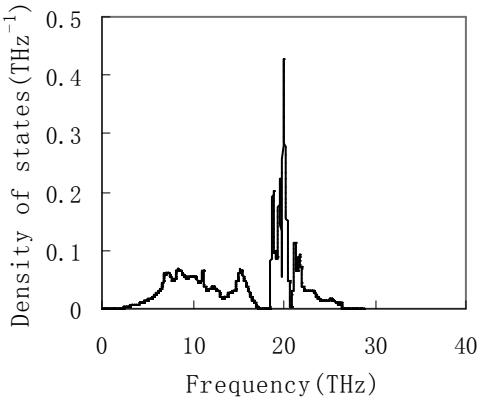

Fig.1 Phonon DOS in wurtzite AlN

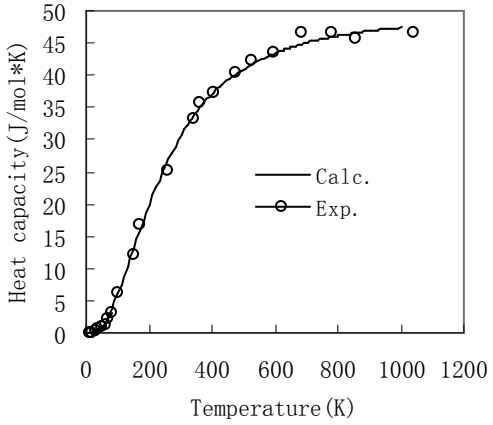

Fig.2 Heat capacity in wurtzite AlN

Fig.2 shows the calculated heat capacity and experimental values reported by Koshchenko et al [7]. The agreement is excellent below 600K, which shows the quasi-harmonic approximation gives correct results in this temperature region. The difference for higher temperature comes from the fact that the an-harmonic effects, which become important for high temperature, are not considered in the calculations. At high temperature，the specific heat capacity approaches to the Petit-Dulong limit. At low temperature, the heat capacity depends only on the characters of the long acoustic wave and the value is small.

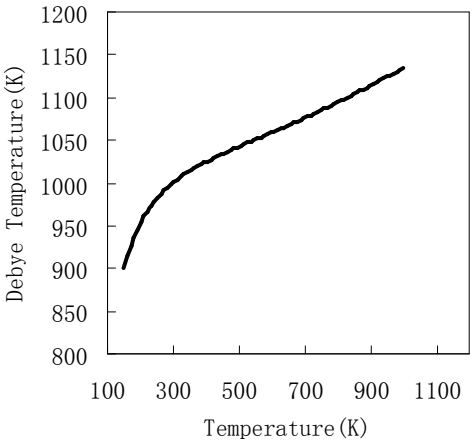

Fig.3 Debye temperature in wurtzite AlN

Debye temperature is not only related to sound velocity, but also to the specific heat capacity. Based on the calculated heat capacity, the Debye temperature can be predicted. The obtained Debye temperatures Θ_{DH} at various temperatures are shown in Fig.3. The Debye temperature increases more quickly at low temperature than that at high temperature.

Table 2 Theoretical and experimental thermal conductivity of pure wurtzite AlN

Temperature[K]	*300*	*350*	*400*	*500*	*600*	**1000**
λ from experiments* [W/m•K]	319	253	195	137	100	49
λ_{DH} from Θ_{DH} [W/m•K]	301.7	248.5	204.4	142.8	105.5	47.7
Δ_{DH} [%]	-5.4	-1.9	4.8	3.9	5.5	-2.6
λ_{DS} from Θ_{DS} [W/m•K]	355.3	297.4	251.3	180.5	137.2	70.8
Δ_{DS} [%]	11.4	17.5	28.8	31.7	37.2	44.4

* Ref. [6]

Table 2 shows the thermal conductivity λ of pure wurtzite AlN single crystal calculated from Eq.1. The Debye temperatures Θ_{DS} and Θ_{DH} used in the integration are derived from sound velocity and heat capacity respectively. The values from experiments are also shown in Table 2. The thermal conductivity computed from Θ_{DH} agrees better with the experimental data than that from Θ_{DS}. The calculated relative difference Δ_{DH} is within the limits of ±5.5%. As it was pointed out in Ref. [8] that the measurement error was ±10% beyond 300K, our theoretical results based on Θ_{DH} can be regarded as reliable. In the intermediate and high-temperature ranges, the intrinsic thermal conductivity of the sample is dominated by three-phonon scattering processes. The good agreement of theoretical values with experiments shows that the model we used describes the three-phonon scattering process correctly. The Debye temperature derived from capacity can describe the process more accurately because it contains the temperature effect.

Conclusion

Thermal conductivity of AlN has been theoretically studied in this paper based on density functional perturbation theory (DFPT) and quasi-harmonic approximation (QHA) theory combined with Debye theory. From 300K up to 1000K, thermal conductivities of pure crystal AlN are calculated respectively from Debye temperature evaluated from sound velocity and heat capacity. The comparison with Slack's results shows that Debye temperature evaluated from heat capacity gives a more reasonable thermal conductivity. These agreements suggest that the theoretical method we used in our study is an effective approach to calculate the thermal conductivity in pure crystal AlN. The one short coming of the methodology in this paper is that the grain sizes, the defects and the thickness of grain boundaries and Al vacancies generated by oxygen content in AlN are not taken into account.

Acknowledgments

This work was supported by the Scientific and Technological Research Program of Chongqing Municipal Education Commission（No. KJ120533 and KJ120503）and Natural Science Foundation of Chongqing Science and Technology Commission （No. 2012jjA50033 and jjA40011）

References

[1] G. W. Burr, M. J. Breitwisch, M. Franceschini, D. Garetto, K. Gopalakrishnan, B. Jackson, B. Kurdi, C. Lam, L. A. Lastras, and A. Padilla, J. Vac. Sci. Technol. B 28 (2010) 223.

[2] G. J. Snyder, and E. S. Toberer, Nature Mater. 7 (2008) 105.

[3] X. M. Cai, and Y. Luo: Sci. China Technol. Sci. 54[1] (2011) 1.

[4] D. Gerlich, S. L. Dole, and G.A. Slack, J. Phys. Chem. Solids 47[5] (1986) 437.

[5] G. A. Slack, R. A. Tanzilli, R. O. Pohl, and J. W. Vandersande, J. Phys. Chem. Solids 48[7] (1987) 6416.

[6] W. Gotz, Appl. Phys. Lett. 68 (1996) 3144.

[7] V. I. Koshchenko, Y. K. Grinberg, and A. F. Demidenko, Inora. Mater. 20[11] (1984) 1550.

[8] K. Watari, H. Nakano, K. Urabe, K. Ishizaki, S. Cao, and K. Mori, J. Mater. Res. 17[11] (2002) 2940.

Advanced Materials Research Vols. 989-994 (2014) pp 3513-3517
© (2014) Trans Tech Publications, Switzerland
doi:10.4028/www.scientific.net/AMR.989-994.3513

Numerical Simulation and Experimental Study on Thawing Time of Cylindrical Frozen Food

Amin JI[1, a], Xinchao NIU[1, b], Boning Tang[2, c], Fuliang Li[1, d]

[1]Energy and Civil Engineering, Harbin University of Commerce, Harbin 150028, China

[2]Harbin KeLi Refrigeration and Air-conditioning Installation Project Co. Ltd., Harbin 150028, China

[a]email: 13091439330@163.com, [b]email:xiaoniu881211@126.com

[c]email: Ladoruso@163.com, [d]email:lifuliangll@126.com

Keywords: food thawing; numerical simulation; cylindrical food; thawing time

Abstract. It is very meaningful to predict the temperature and thawing time during the thawing process of frozen food in production and life, this paper proposes a physical model of cylindrical frozen food during the thawing process, combine the finite difference method with element balance method to solve the thawing time and the temperature at regional center R/2 and boundary nodes. Take the beef as an example for the experimental verification. Through numerical calculation and experimental verification, the maximum error between the theory thawing time and experiment is 8.4%. The results show that: it is highly consistent with the experimental results that using numerical method to predict the thawing time and temperature change curve, at the same time, the temperature maximum error in center area is 1.2℃, the temperature maximum error of R/2 is 0.8℃, the temperature maximum error of the boundary node is 1.5℃, so the numerical simulation in studying thawing of freezing food is fairly reliable.

Introduction

Frozen food industry is one of the fastest growing food industries in the world, the development is also very rapid in China. In the first half of 2013, our country's frozen food trade volume trend is rising, the value of import and export is $13,290,000,000, it rose by 14.3% to over the previous year. At the same time, people have been concerned about the food freezing and thawing theory, because it is directly related to food safety and quality problems. Theoretically, thawing is the inverse process of freezing; they are different not only in phase change direction, cooling and heating process, but also in food freezing time and internal temperature variations [1]. The thawing process is to make the freezing ice melts into water inside the food, and absorbed by the food then restored to the fresh state before frozen. The degree of cells in the thawing recovery determines the thawing quality of frozen products [2]. Therefore the thawing process is much more complex than the freezing process.

Requirements in the process of thawing meat [3]: a. Homogeneous half thawed state is the best; b. The outflow of meat tissue in the thawing process to the less as far as possible; c. Inhibit the reproduction and generation of microorganisms; d. Thawing medium temperature is low, less than 20℃; e. The temperature can't be too high during the thawing process in order to avoid the destruction of tissue structure; f. Thawing as quickly as possible, so as to shorten the time when food stays in the higher temperature. Frozen vegetables, bread, pastries and so on are suitable for quick thawing; but to fish and meat, using slow thawing the effect is better [4].

This paper studies the thawing time of cylindrical food, taking frozen beef roll with a radius of R=32mm as the object of study. In order to research conveniently in the process of solving, putting forward several assumptions for the object of study and the environment: The thermal conductivity coefficient and specific heat of beef is only relevant to temperature ignoring other factors; Beef density is constant; deeming the surrounding environment is infinite space, so the temperature of the surrounding medium does not change with time; Considering the beef roll in the thawing process is big length to diameter ratio, so in the thawing process heat transfer occurs mainly in the

radial direction, while the heat transfer along the axial direction is weak and negligible, namely heat transfer is one-dimensional heat conduction; temperature field distribution is uniform.

Removed beef roll from the freezer, measured the initial temperature is -20℃, and the thawing end temperature requires that center temperature achieves 0.5℃, do research and experiment on the premise of the temperature.

Research methods

Physical model

The physical model of cylindrical beef roll in the thawing process of heat transfer shown in Figure 1, establish unsteady numerical model of cylindrical food [6]:

$$\rho c_p \frac{\partial T}{\partial \tau} = K\left(\frac{\partial^2 T}{\partial r^2} + \frac{1}{r}\frac{\partial T}{\partial r}\right) \tag{1}$$

The initial conditions: $\tau = 0 \quad T = T_0 \ (0 <= r <= R)$;

Boundary conditions: $\begin{cases} r = 0 & \dfrac{dT}{dr} = 0 \ (heat\ isolution) \\ r = R & -K\dfrac{dT}{dr} = h(T_R - T_f) \end{cases}$;

Numerical analysis

According to the shape of the beef roll, it can be regarded as a cylindrical, Placing the beef roll with the initial temperature of T=-20℃, radius R=32mm in the environment which temperature is 20℃and in 12℃ water thaw respectively under the natural state, the natural convection coefficient between beef roll and surrounding air is h_1 and the natural convection heat transfer coefficient between beef roll and water is h_2. Heat exchange between beef roll's surface and the surrounding air is in accordance with Newton's law of cooling and the heat of each point of the cylinder's outer surface is the same, so the cylindrical food temperature distribution along the diameter direction is symmetric [5]. In order to study the process conveniently, coordinate origin at the center of the circle, only study the parameters variation along the radius direction, its physical model is shown in figure 1. Figure 2 is the center node grid. Using finite difference method establishes the equation.

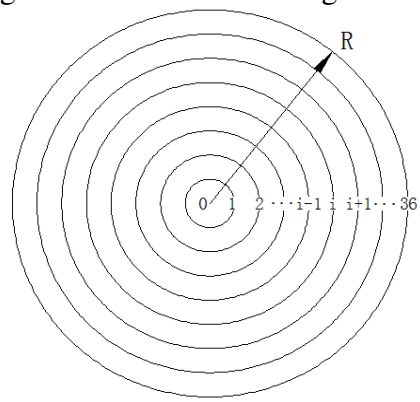

Fig.1. Heat transfer physical model

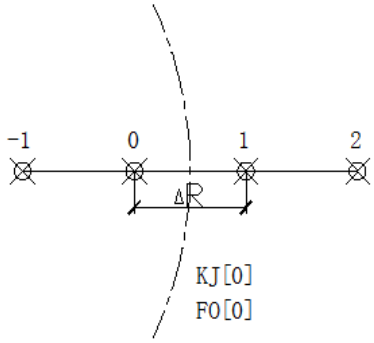

Fig.2.The center node grid of cylindrical food

As shown in Figure 1, using external node method to divide n-1 internal unit and two semi-unit (located in the center and the surface boundary) along the radius direction, in the figure solid line is the position line where the control node locates, there are n+1 nodes, $\Delta r = R/n$ is the spatial location step; $\Delta\tau$ is time step; In each unit take temperature as a lumped parameter approximation rather than the distribution function [5]. At the same time, in order to make the results convergence, control equation uses the implicit. In this way the results can be guaranteed unconditional convergence. When the central node temperature T<=0.5℃, the iteration process is over.

Establish difference equation

Shown in Figure 2, with the Taylor series expansion of the central node number 0 to establish the equation:

$$\rho c_p \frac{T_0^1 - T_0^0}{\Delta\tau} = 2KJ_0 \frac{T_{-1}^1 - 2T_0^1 + T_1^1}{\Delta r^2} = 4KJ_0 \frac{T_1^1 - T_0^1}{\Delta r^2} \quad (2)$$

$$\Rightarrow (1+4Fo_0)T_o^1 = 4Fo_0 T_1^1 + T_0^0$$

Figure 3 for the internal nodes meshing diagram, with element balance method for an internal node i establishment node equations:

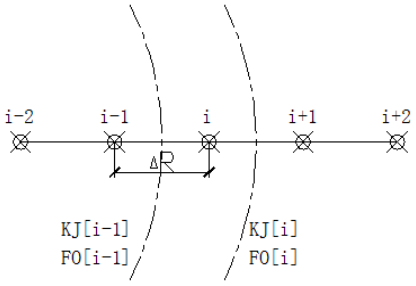

Fig.3.Internal nodes meshing diagram

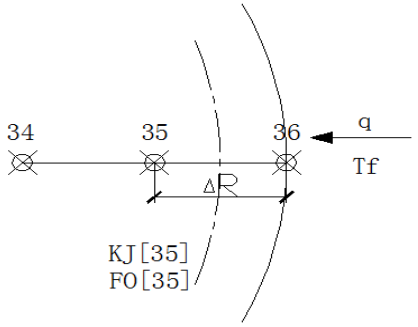

Fig.4.Boundary nodes meshing diagram

$$\rho c_p V_i \frac{T_0^1 - T_0^0}{\Delta\tau} = KJ_{i-1} \frac{T_{i-1}^1 - T_i^1}{\Delta r} F_w + KJ_i \frac{T_{i+1}^1 - T_i^1}{\Delta r} F_e \quad (3)$$

$$\Rightarrow (1+Fo_{i-1}+Fo_i)T_i^1 = (1+\frac{1}{2i})Fo_i T_{i+1}^1 + (1-\frac{1}{2i})Fo_{i-1}T_{i-1}^1 + T_i^0$$

Figure 4 for the boundary nodes meshing diagram, using Taylor series expansion method for boundary nodes 36 establishes node equation:

$$-KJ_{35} \frac{T_N^1 - T_{N-1}^1}{\Delta r} = h(T_N^1 - T_f) \quad (4)$$

$$\Rightarrow (1+Bi)T_N^1 = T_{N-1}^1 - BiT_f$$

Where: Δr for the space step, the value is 0.001m; $\Delta\tau$ is the time step, the value is 20s; T_i^1 is the temperature of n+1 moment; T_i^0 is the temperature of n moment, KJ_i is the thermal conductivity of the i number of the control body on the right interface, $KJ_i=2K_iK_{i+1}/(K_i+K_{i+1})$; K_i is the thermal conductivity of i node, According to the known thermal conductivity of frozen beef, it obtained by fitting equation about the relationship between the thermal conductivity and temperature, $K=-0.0001T^3-0.0062T^2-0.1407T+0.4848$(-30<=$T$<=0); T>0 K=0.48W/(m·℃); ρ is the density of beef, The values is 1050Kg/m³; C_p is the specific heat of beef, according beef freezing temperatures -2℃ to define Cp values, When T <=-2 Cp=3230J/(kg·℃); When T>-2℃ Cp=1720 J/（kg·℃）; Fo_i is the i number of Fourier number right boundary of the control volume, the formula is $Fo_i=KJ_i\Delta\tau/(\rho c_p\Delta r^2)$; Bi is the biot number.

Equation solving

Based on the TDMA method for physical model solving process, where *T[i]* represents the temperature of node i, when the temperature of the center node is not less than 0.5℃ iteration ended; M represents the number of iterations.

Results and discussion

With experimental and theoretical solved, the results obtained will be drawn into the thawing temperature change with time curve in the air and the thawing temperature change with time curve in the water, as shown in Figure5, 6. Due to space limitations, the figure shows only part of important nodes in temperature, such as the central nodes, *R/2* nodes, the boundary nodes. In addition, the theory of air and water thawing time compared with the experimental value is shown in Figure 7, 8.

From the curve in the figure, theoretical and experimental results are basically consistent, but inevitably there are errors, the numerical calculation shows that the error between the theoretical and experimental air thaw thawing time is 7.8% and water thaw thawing time is 8.4%.

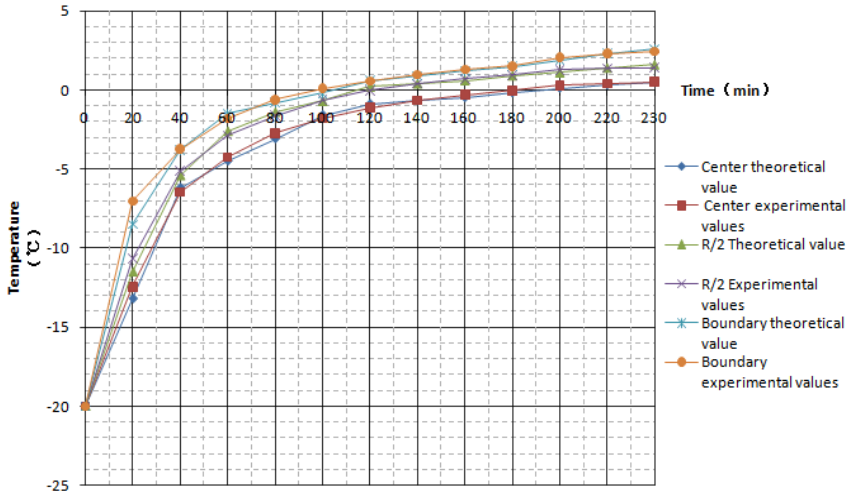

Fig.5.Thawing temperature by hourly value curve in the air

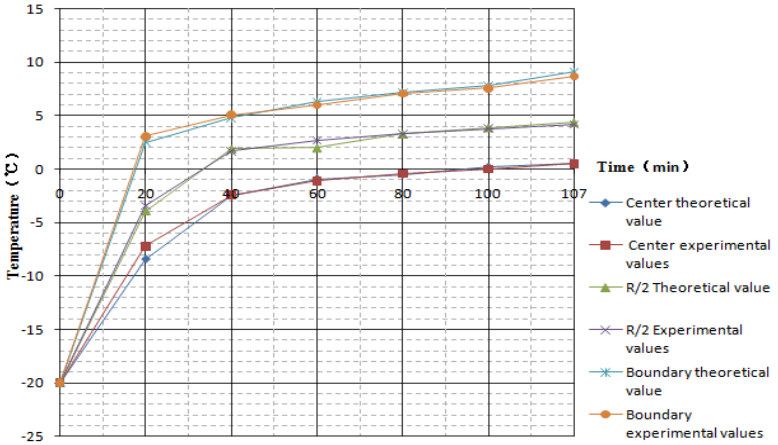

Fig.6.Thawing temperature by hourly value curve in the water

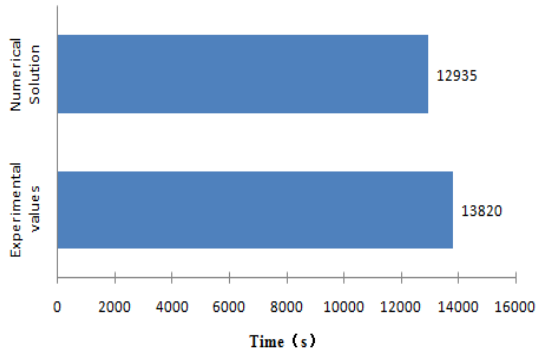

Fig.7.Air thawing time experimental and numerical value contrast

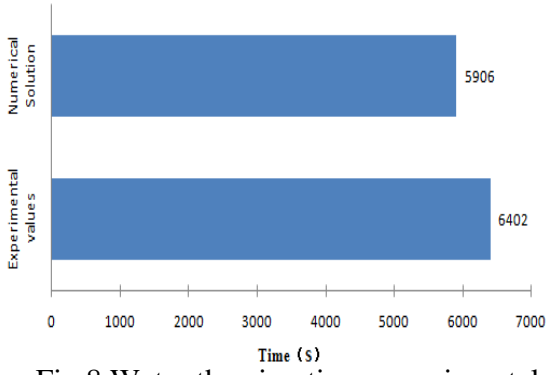

Fig.8.Water thawing time experimental and numerical value contrast

Meanwhile, Comparison of the two thawing ways the maximum error in the central region temperature is 1.2℃, the maximum error of temperature of *R/2* is 0.8℃, and the maximum error of the temperature of the boundary nodes is 1.5℃. The main reasons for generating the errors are:

a. Physical model established ignores the radiation heat transfer effects on the whole process.

b. Experimental instrument error due to the precision problems.

c. Be measured beef roll with a plastic film packaging make surface thermal resistance increase and weaken the heat transfer process, on the other hand, due to the moisture migration in the process of thawing will make its physical parameters change, which will make the experimental and theoretical results generate errors.

d. In the thawing process surrounding partial environment is not stable conditions.
e. The thawing ignores the axial heat conduction process.
f. Errors caused by human action, such as thermocouple probe buried point bias position.

Conclusion

(1) The solution that freezes thawed time and temperature distribution has important guiding significance and practical significance for the logistics process in the cold chain system. For example, in the condition of environmental temperature known, internal temperature of the frozen food is obtained by numerical calculation will change with time, this will play an important role in guiding when open the refrigeration unit of refrigerated truck. In the case of freezing temperatures to ensure the cold chain logistics process makes refrigeration units to reduce working hours in order to reduce energy consumption to achieve the energy saving effect.

(2) Through the numerical and experimental for thawing time which include water thaw and air thaw, more accurately predict the thawing time can be obtained, it has a certain guiding significance for the catering industry.

(3) If considering the axial heat and radiation heat transfer, calculation results with the experimental results will be more satisfactory.

Acknowledgement

In this paper, the research was sponsored by the Graduate Student Innovation Research Projects of Harbin Commercial University. (Project No. YJSCX2012-223HSD)

References

[1] Yu Min. Frozen food thawing technology [J]. Food Science, 2001, 22 (8): 87-90

[2] Ji Amin. Hemispherical thawing time numerical simulation and experimental study [J]. Chinese Food Science, 2006, 6 (3): 79-83

[3] Feng Wanping, Hu Juan. A new method of thawing of frozen pork comparative tests [J]. Agricultural products processing. Journal, 2011 (9): 33-36

[4] Li zhixin, Hu songqing, Chen ling. Advances in theory and technology of frozen food [J]. Food Science and Technology, 2007, 28(6): 223-225.

[5] Guan Zhiqiang, Dai Wuzi. Numerical calculation [J]. Journal of Zhanjiang Ocean University, time to thaw frozen food 1999, 19 (4): 45-48

[6] Tao Wenquan. Numerical heat transfer [M]. Xi'an Jiao Tong University Press, 2001

CHAPTER 7:

Communication, Signal and Image Processing, Data Acquisition and Recognation Technologies

Advanced Materials Research Vols. 989-994 (2014) pp 3521-3525
© (2014) Trans Tech Publications, Switzerland
doi:10.4028/www.scientific.net/AMR.989-994.3521

A Modified DFT-Based Channel Estimation method for OFDM-RoF System

Liqun Huang[1, a], Peng Zhang[2,b] and Guang Yang[1,c]

[1] School of Computer and Communications Engineering, Northeastern University at Qinhuangdao

[2] Beijing Research Institute, Huawei Technology Co. Ltd., Beijing, China

[a] persistent_hlq@sina.com, [b] zhangpeng3214@126.com, [c] yangguangneuq@163.com

Keywords: OFDM-RoF; channel estimation; DFT; the changing rate of energy.

Abstract. In this paper, we present a modified discrete Fourier transform (DFT)-based channel estimation method. The conventional DFT-based method will produce additional high frequency component in the channel impulse response, and degrade the accuracy of channel estimation. The modified algorithm can eliminate additional high frequency components by extending the LS estimate in frequency domain with a symmetric signal of its own, and selects the useful paths by calculating the changing rate of energy. Thus, the proposed algorithm become more accurate. The simulation results show the new algorithm can reduce the influence of noise on channel estimation efficiently, and the performance of the improved method is better than the LS and conventional DFT algorithm.

Introduction

OFDM can not only effectively enhance the transmission rate and capacity, but also combat multipath fading and inter-symbol interference (ISI) effectively [1]. RoF (Radio over Fiber) is a technique which uses the fiber to transport the high frequency microwave, millimeter wave or millimeter wave that carry information [2-3]. Combine OFDM with RoF, this system has the feature of high spectrum utilization, anti-electromagnetic interference and anti-dispersion. The receiver needs to know the channel information. So channel estimation is directly related to the performance of OFDM-RoF.

Many channel estimation algorithms have been presented. Least Square (LS) algorithm [4] has a low complexity. However, it is very sensitive to the noise, and has a larger mean square error. The conven- tional DFT-based channel estimation is an improved LS algorithm [5], which can reduces the noise in time domain. But the algorithm also has disadvantage, it will generate additional high frequency component when dealing with the discontinuous frequency response by FFT. If the component which is mistaken for noise is removed, the performance of the algorithm will decrease. In this paper, we propose an improved DFT algorithm, this algorithm use symmetry principle before IFFT to eliminate the impact of high frequency component. And then we will select useful paths effectively by calculating the changing rate of the energy. The channel estimation becomes more accuracy by above process.

OFDM-RoF System Model

Fig. 1 shows typical diagram of OFDM. The upper part of the channel is the transmitter, and the lower part of the channel is receiver. At the transmitter, incoming high-speed binary data is first converted into N parallel low-speed data streams and mapped according to a pre-specified modulation. After pilot insertion, the data $X(k)$ is sent to an IFFT block and transformed into time domain signal $x(n)$. In order to prevent inter-symbol interference (ISI), the cyclic prefix which contains a copy of the last part of an OFDM symbol is used. At the receiver, the binary will be obtained by the opposite processing.

Fig. 2 is a diagram of an OFDM-RoF system. The laser which is modulated by Mach-Zehnder Modulator (MZM) becomes an optical signal that has two different frequencies. After that, the optical becomes two beams of different frequencies of optical signal through different center frequency optical band pass filter. One of the two optical signal modulated by baseband OFDM symbol, then

coupling two optical signals into Single Mode Fiber (SMF). In order to ensure the quality of the optical signal, the optical amplifier is added to the system [6].At the receiver, we can use the optoelectronic detector to obtain the millimeter-wave electrical signal, and the frequency is the difference between frequencies of the optical signals. Then baseband OFDM symbol will be got by mixing and filtering.

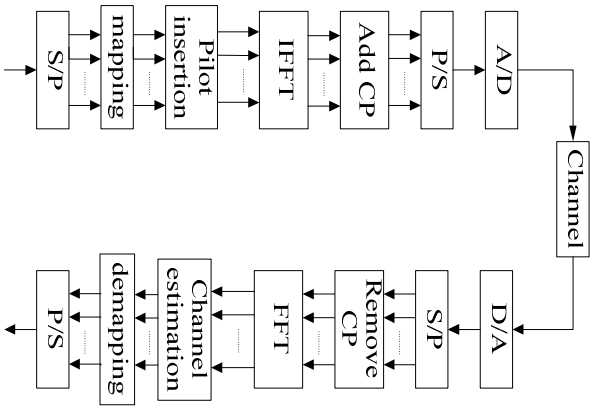

Fig. 1. The diagram of OFDM systems

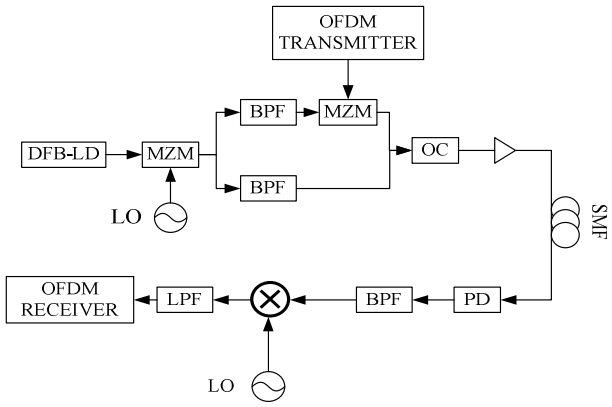

Fig. 2. The diagram of OFDM-RoF systems

A Modified Channel Estimation Metheod

LS algorithm is the simplest channel estimation. Assuming all subcarriers of the OFDM symbols are transmitted pilots, we can obtain the frequency response of the channel:

$$\hat{H}_{ls} = \frac{Y(k)}{X(k)} = H(k) + \frac{W(k)}{X(k)} \quad 0 < k < N-1 \tag{1}$$

LS algorithm is sensitive to noise, so it has a large MSE. In OFDM system, the length of the channel impulse response L is usually less than the length of the cyclic prefix L_g . Hence, conventional DFT channel estimation algorithm just takes advantage of this feature. It transforms the frequency response in frequency domain into impulse response in time domain, considers the part which is larger than L_g as noise, and then treats that part as zero in order to eliminate the noise of the impulse response.

If the original sequence is not continuous, DFT will generate additional high frequency component. In order to minimize the influence of high frequency component, we can preprocess the discontinuous sequence before IFFT. We use symmetry principle to make the sequence continuous. Moreover, we will select paths effectively by calculating the changing rate of the energy. The steps are as follows:

Step 1: Get the frequency response $\hat{H}_{ls}$ by LS algorithm;

Step 2: Extend $\hat{H}_{ls}$ with a symmetric signal of its own, so the original sequence becomes continuous, and the high frequency component can be eliminated effectively.

$$\hat{H}_{symmetric}(k) = \begin{cases} \hat{H}_{ls}(k) & 0 \le k \le N-1 \\ \hat{H}_{ls}(2N-1-k) & N \le k \le 2N-1 \end{cases} \tag{2}$$

Step 3: Transform $\hat{H}_{sym}(k)$ into time domain by IFFT:

$$\hat{h}_{symmetric}(n) = IDFT_{2N}\left[\hat{H}_{symmetric}(k)\right] \quad 0 \le n \le 2N-1 \tag{3}$$

Step 4: Select useful paths by calculating the changing rate of energy, useful paths will be reserved and other paths are set to zero. The energy of the channel impulse response can be expressed as:

$$E = \sum_{n=0}^{2N-1} \left|\hat{h}_{symmetric}(n)\right|^2 \tag{4}$$

the energy concentrates at the two ends of the sequences, So (7) can be written as:

$$E=\sum_{n=0}^{N-1}\left|\hat{h}_{symmetric}(n)\right|^{2}+\sum_{n=0}^{N-1}\left|\hat{h}_{symmetric}(2N-1-n)\right|^{2}=\sum_{n=0}^{N-1}E(n) \tag{5}$$

Where $E(n)$ is the sum of the energy of n-th and ($2N-1-n$)-th sampling points. The energy of front l paths can be expressed as:

$$E'(l)=\sum_{n=0}^{l}E(n)\ ,\quad 0\le l\le N-1 \tag{6}$$

$P(l)$ is defined as the changing rate of the energy. It represents the ratio of the energy of l-th path and the sum energy of front l paths.

$$P(l)=\frac{E'(l)-E'(l-1)}{E'(l)}\ ,\qquad 1\le l\le N-1 \tag{7}$$

We set an initial changing rate of the energy P'. If $P(l)\ge P'$, it shows that the energy of l-th path and ($2N$-1-l)-th path is large, these paths are useful and preserved. If $P(l)<P'$, this path is useless and superfluous. It will set to zero to eliminate noise. Then the channel response can be expressed as:

$$\tilde{h}_{DFT}(n)=\begin{cases}0 & l_{end}\le n\le 2N-1-l_{end}\\ \hat{h}_{symmetric}(n) & others\end{cases} \tag{8}$$

Where l_{end} is the last path which $P(l)$ is larger than P'. If l_{end} is larger than the length of CP, $l_{end}=L_g$.

Step 5: After padding with zeros, transform $\tilde{h}_{DFT}(n)$ to frequency domain by FFT:

$$\tilde{H}_{DFT}(k)=DFT_{2N}\left[\tilde{h}_{DFT}(n)\right]\ ,\qquad 0\le k\le 2N-1 \tag{9}$$

Step 6: According to the symmetric property, the corresponding frequency response is expressed as:

$$\hat{H}_{DFT}(k)=\frac{\tilde{H}_{DFT}(k)+\tilde{H}_{DFT}(2N-1-k)}{2}\ ,\quad 0\le k\le N-1 \tag{10}$$

Simulation Results

In this simulation, we use Optisystem and Matlab to build OFDM-RoF system. The baseband OFDM signal generated by Matlab. The rate of bit is 2.5Gb/s, the number of subcarriers is 512, the length of CP is 64. The parameters are shown in Table 1

Table 1 Simulation Parameters

The rate of bit	Mapping mode	Number of subcarriers	Fiber type	Fiber dispersion at 1550nm	The frequency of laser	Frequency of local oscillator
2.5Gb/s	16-QAM	512	SMF	17 ps/km-nm	193.13THz	30GHz and 60GHz

Fig. 3 shows the output constellation map without channel estimation. Due to the fiber dispersion effects, the constellation map is rotated, which will lead to incorrect judgments of transmitted signals.

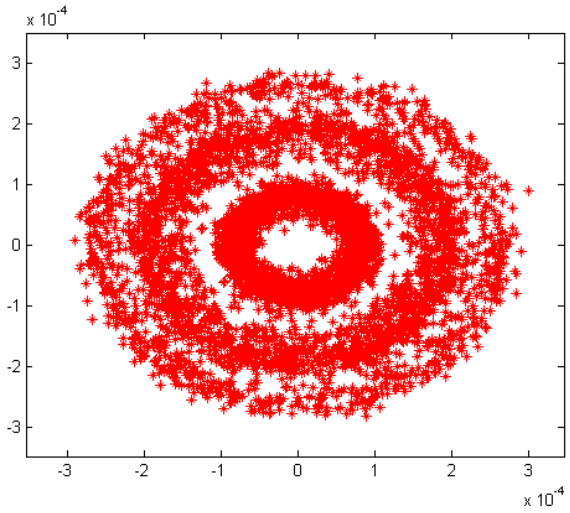

Fig.3. The output constellation map without channel estimation

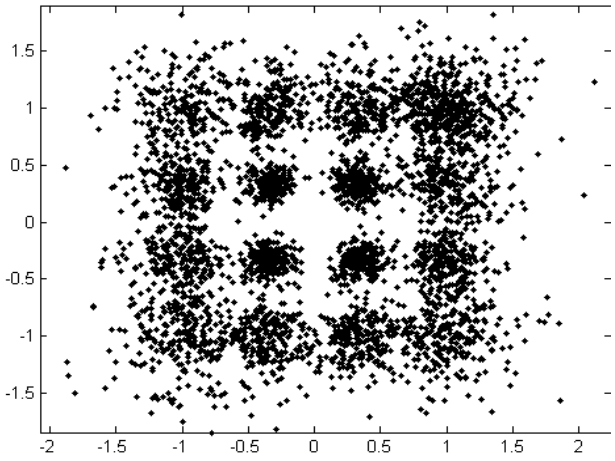

Fig.4. The output constellation map with the LS channel estimation

Fig. 4 is the output constellation map with the LS channel estimation algorithm. Obviously, this algorithm overcomes the impact of fiber chromatic dispersion, however, the noise influence still causes strong constellation dispersion, which degrades the BER performance of OFDM-RoF system.

Fig. 5 shows the output constellation map with the improved DFT channel estimation algorithm, and the constellation dispersion has been mitigated. Fig.6 demonstrates the BER performance of the improved algorithm, which adopts the symmetry principle and the energy changing rate of 0.19%, and limits the number of the selected paths less than the length of cyclic prefix. Because we accurately select the useful paths by calculating the changing rate of energy, the imroved algorithm is better than the LS and the conventional DFT channel estimation methods. The symmetry principle is helpful to eliminate the additional high frequency component.

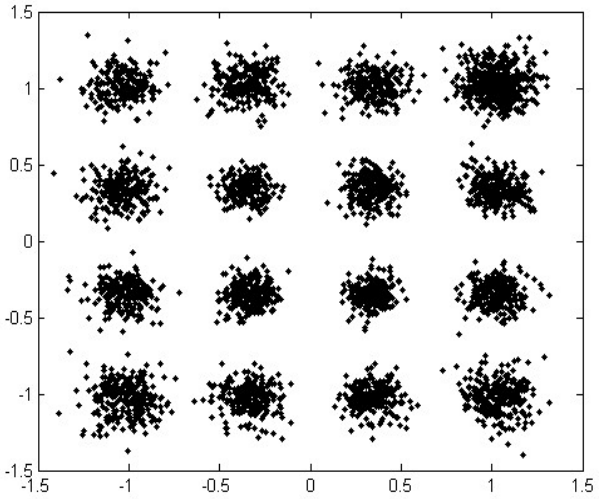

Fig. 5. The output constellation map with the improved DFT channel estimation algorithm estimation

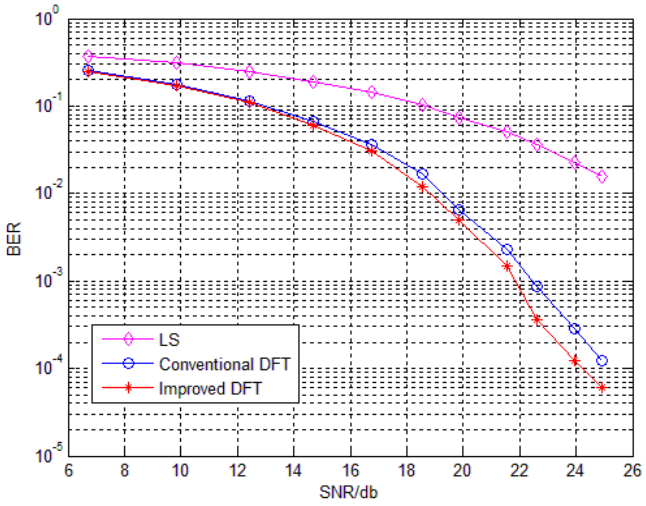

Fig. 6. BER comparison between the conventional and improved channel estimation algorithms

Summary

In this paper, an improved DFT channel estimation algorithm for OFDM-RoF is proposed. The improved algorithm uses the principle of symmetry and calculates the changing rate of energy to select useful paths efficiently and accurately. Simulation results show that BER performance of the improved method is better than LS estimation and conventional DFT channel estimation method. The improved method achieves a satisfying tradeoff between complexity and performance.

References

[1] J. Lowery and J. Armstrong, "Orthogonal frequency division multiplexing for dispersion compensation of long-haul optical system". *Optics Express*, vol.14, pp. 2079-2084, 2006.

[2] J. Yu, Z. Jia, and L. Yi, , "Optical millimeter-wave generation or up-conversion using external modulators", *IEEE Photon . Technol. Lett.*, vol. 18, no. 1, pp. 265-267, Jan. 2006

[3] C. T. Lin, J. Chen, P. –T. Shih, W. J. Jiang and S. Chi, "Ultra-high data-rate 60 GHz radio-over-fiber systems employing optical frequency multiplication and OFDM formats", *J. Lightw. Technol.*, vol. 28, no. 16, pp. 2296-2306, Aug. 2010.

[4] B.song, L.Gui, and W.Zhang, "Comb type pilot aided channel estimation in OFDM system with transmit diversity," *IEEE Trans. Broadcast*, vol.52, pp. 50-57, March. 2006.

[5] O. Edfors, M. Sandell, J.-J. van de Beek, and S. K. Wilson, "Analysis of DFT-based channel estimators for OFDM", *Wireless Personal Commun*, vol. 12, pp. 55-70, Jan. 2000.

[6] L. Chen, H. Wen and S. C. Wen, "A Radio-Over-Fiber system With a Novel Scheme for Millimeter-Wave Generation and Wavelength Reuse for Up-Link Connection", *IEEE Photon . Technol. Lett.*, vol. 18, no. 19, Oct. 2006.

Advanced Materials Research Vols. 989-994 (2014) pp 3526-3529
© (2014) Trans Tech Publications, Switzerland
doi:10.4028/www.scientific.net/AMR.989-994.3526

Dual station based bearings-only tracking using unscented filter

Hongwei Quan[1, a], Junhua Li [b], Mingshu Chen [c]

[1]Department of Mechanical and Electrical Engineering, Xijing University, Xi'an, 710123, China

[a]quanhw@126.com, [b]lijunhua@xijing.edu.cn, [c]chenmingshu@xijing.edu.cn

Keywords: bearings-only tracking, unscented filter, measurement model, data fusion

Abstract. This paper investigated the bearings-only tracking approach based on dual station detection. In order to solve the problem of strong nonlinearity in bearings –only measurement system, we introduced the unscented filter which is based on the idea of unscented transformation. Compared with traditional extended Kalman filter, unscented filter has shown better convergence and stabiltiy, especially in stabiltiy of tracking waveform. Matlab simulation scenario is taken for illustrating the effectiveness and validity of the unscented filtering algorithm.

Introduction

Bearings-only target tracking is a typical nonlinear estimation and filtering problem in signal processing [1-3]. In order to solve this problem, the most commonly used method is the extended Kalman filter (EKF) [4]. For bearings-only tracking, EKF behaves poor convergence because of the strong nonlinearity of the bearings-only measurement system. Even in many cases, the EKF is not convergent. This is because in EKF algorithm the measurement equation is approximated by linear transformation of the observation function.

Aiming at the problem of biased transformation in EKF algorithm, Julier S. J. proposed the unscented transformation (UT) [5]. Unscented transformation greatly reduced the biasness and computational complexity. Based on the idea of unscented transformation, an algorithm called unscented filter (UF) or unscented Kalman filter (UKF) is developed for dealing with nonlinear estimation [6-8]. In bearings-only target tracking, UF has shown better convergence and stability, especially in stability of tracking waveform compared with EKF.

Bearings-only measurement system model

For dual station based bearings-only target tracking system, we can acquire two measurement data in one observation cycle which are detected by two mutually independent observer stations. Compared with single observer platform, the system information has greatly increased. Obviously, the filtering convergence and stability in dual station-based system will get huge improvement. At the same time, the measurement data is acquired from two different stations, in order to obtain better target tracking trajectories, we need to consider how to fusion the measurement information in the filtering algorithms. In theory, this problem belongs to the multi-sensor data fusion. The observer-to-target geometry in dual station based bearings-only measurement system is shown in Figure 1.

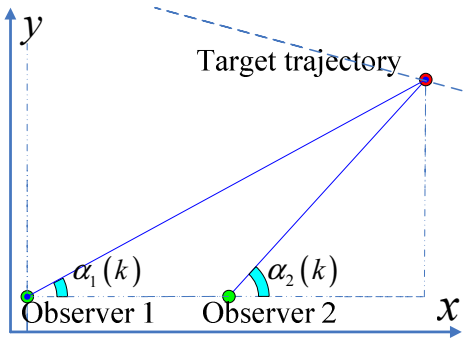

Fig. 1 The observer-to-target geometry

The position coordinates of observer 1 and observer 2 are known, designated by $\xi_1 = [S_{O1x}, S_{O1y}]^T$ and $\xi_2 = [S_{O2x}, S_{O2y}]^T$. The target state vector in time instant k is represented as

$$\eta(k) = [S_{Tx}(k), S_{Ty}(k), V_{Tx}(k), V_{Ty}(k)]^T \tag{1}$$

Target velocities are affected by random Gaussian noises defined as $v_1(k)$ and $v_2(k)$, which also can be interpreted as accelerations. The target state equation is

$$\eta(k+1) = A \cdot \eta(k) + v(k) \tag{2}$$

where $v(k) = [0, 0, v_1(k), v_2(k)]^T$ is process noise vector at time instant k,

$$A = \begin{bmatrix} 1 & 0 & T & 0 \\ 0 & 1 & 0 & T \\ 0 & 0 & 1 & 0 \\ 0 & 0 & 0 & 1 \end{bmatrix} \tag{3}$$

is target state transition matrix. Define $z(k) = [z_1(k), z_2(k)]^T$ as the measurement data of two observer stations at time instant k, $w(k) = [w_1(k), w_2(k)]^T$ as random Gaussian measurement noise which is mutually independent, the measurement equation is

$$z(k) = h[\eta(k), k] + w(k) \tag{4}$$

where

$$h[\eta(k), k] = \begin{bmatrix} h_1[\eta(k), k] \\ h_2[\eta(k), k] \end{bmatrix} = \begin{bmatrix} \alpha_1(k) \\ \alpha_2(k) \end{bmatrix} \tag{5}$$

$\alpha_1(k)$ and $\alpha_2(k)$ are the target bearings with regard to observer station 1 and observer station 2 which can be computed by following expression,

$$\begin{cases} \alpha_1(k) = \arctan \dfrac{\Delta y_1(k)}{\Delta x_1(k)} = \arctan \dfrac{S_{Ty}(k) - S_{O1y}}{S_{Tx}(k) - S_{O1x}} \\ \alpha_2(k) = \arctan \dfrac{\Delta y_2(k)}{\Delta x_2(k)} = \arctan \dfrac{S_{Ty}(k) - S_{O2y}}{S_{Tx}(k) - S_{O2x}} \end{cases} \tag{6}$$

In Formula (6), $\Delta x_1(k)$, $\Delta x_1(k)$, $\Delta x_2(k)$ and $\Delta y_2(k)$ are the relative distances between target and two observer stations in x and y coordinates. $\Delta r_1(k)$ and $\Delta r_2(k)$ are the range between target and observer stations which can be computed by following equation,

$$\begin{cases} \Delta r_1(k) = \sqrt{\Delta x_1(k)^2 + \Delta y_1(k)^2} \\ \Delta r_2(k) = \sqrt{\Delta x_2(k)^2 + \Delta y_2(k)^2} \end{cases} \tag{7}$$

The unscented filtering algorithm

The unscented filter can be derived by substituting the mean and covariance updating equations in EKF with the unscented transform. The unscented filtering algorithm consists of the following steps:

1. Computing one-step prediction of the means and covariance for system state variables at time instant k. Firstly we choose $2n$ samples:

$$\hat{x}_{k|k}^{(i)} = \hat{x}^{+}(k \mid k) + \tilde{x}^{(i)} \quad i = 1, \cdots, 2n \tag{8}$$

2. Using nonlinear function f in target state equation to transform $2n$ samples:

$$\hat{x}_{k}^{(i)} = f[\hat{x}_{k|k}^{(i)}, u(k), k] \quad i = 1, \cdots, 2n \tag{9}$$

3. Calculating one-step predictive mean and covariance of target state at time instant k:

$$\hat{x}^{+}(k+1 \mid k) = \frac{1}{2n} \sum_{i=1}^{2n} \hat{x}_{k}^{(i)} \tag{10}$$

$$P_x(k+1 \mid k) = \frac{1}{2n} \sum_{i=1}^{2n} \left[\hat{x}_{k}^{(i)} - \hat{x}^{+}(k+1 \mid k) \right] \left[\hat{x}_{k}^{(i)} - \hat{x}^{+}(k+1 \mid k) \right]^{T} + Q(k) \tag{11}$$

4. Calculating one-step predictive mean and covariance of measurement:

$$x_{k+1|k}^{(i)} = \hat{x}^{+}(k+1 \mid k) + \tilde{x}^{(i)} \quad i = 1, \cdots, 2n \tag{12}$$

5. Using nonlinear function h in measurement equation to transform $2n$ samples:

$$\hat{y}_{k}^{(i)} = h[\hat{x}_{k+1|k}^{(i)}, k] \quad i = 1, \cdots, 2n \tag{13}$$

6. Calculating one-step predictive mean and covariance of state:

$$\hat{y}^{+}(k+1 \mid k) = \frac{1}{2n} \sum_{i=1}^{2n} \hat{y}_{k}^{(i)} \tag{14}$$

$$P_y(k+1 \mid k) = \frac{1}{2n} \sum_{i=1}^{2n} \left[\hat{y}_{k}^{(i)} - \hat{y}^{+}(k+1 \mid k) \right] \left[\hat{y}_{k}^{(i)} - \hat{y}^{+}(k+1 \mid k) \right]^{T} + R(k+1) \tag{15}$$

7. State and covariance updating:

$$\begin{cases} W(k+1) = P_{xy} \cdot P_{y}^{-1} \\ \hat{x}^{+}(k+1 \mid k+1) = \hat{x}^{+}(k+1 \mid k) + W(k+1) \cdot [y(k+1) - \hat{y}^{+}(k+1 \mid k)] \\ P^{+}(k+1 \mid k+1) = P_x(k+1 \mid k) - W(k+1) P_y(k+1 \mid k) W(k+1)^{T} \end{cases} \tag{16}$$

Simulation and result analysis

Table 1 gives the parameters configuration for Matlab simulation scenario. The observation period is 1 simulation second. The initial state estimates and covariance are chosen as follows.

$$\eta(0) = \begin{bmatrix} 4050 & 5050 & 0 & 0 \end{bmatrix}^{T} \tag{17}$$

$$P(0) = \begin{bmatrix} 10 & 0 & 0 & 0 \\ 0 & 10 & 0 & 0 \\ 0 & 0 & 1 & 0 \\ 0 & 0 & 0 & 1 \end{bmatrix} \tag{18}$$

Table 1 Parameters configuration for simulation scenario

Number of observations	Target position	Observer positions	Measurement noise
150	(4000m,5000m)	(-2000m,0m), (2000m,0m)	**1°**

Figure 2 shows the target tracking trajectory and true trajectory with unscented filter.

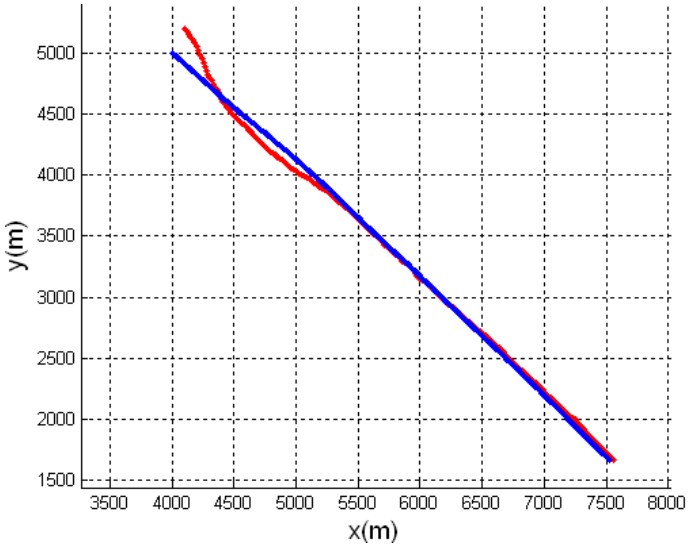

Fig. 2 Target tracking trajectory

Summary

This paper discussed the target tracking problem in dual station based bearings-only measurement system. The unscented filter is used in virtue of the strong linearity. First, the system model is given with target motion equation and observer measurement equation. Second, we introduced the unscented filtering algorithm which is based on unscented transformation. Finally, the Matlab simulation scenario is taken for illustrating the effectiveness and validity of the algorithm. From the simulation result, we can see that the unscented filter greatly reduced the biasness and computational complexity. Especially in bearings-only target tracking, the unscented filter has better convergence and stability compared with EKF.

References

[1] Kirubarajan, T., Bar-Shalom, Y., Lerro, D. Bearings-only tracking of maneuvering targets using a batch-recursive estimator. IEEE Trans. on AES, 2001, 37(3): 770-780.

[2] Nardone, S. C., Graham, M. L. A closed-form solution to bearings- only target motion analysis. IEEE Journal of Oceanic Engineering, 1997, 22(1): 168-178.

[3] Ferdowsi, M. H. Observability conditions for target states with bearing- only measurements in three-dimensional case. IEEE Intern. Conf. on Control Applications, 2006, 1444-1449.

[4] Rao, S. K. Modified gain extended Kalman filter with application to bearings-only passive maneuvering target tracking. IEE Proc.-Radar Sonar Navig, 2005, 152(4): 239-244.

[5] Julier, S. J. The scaled unscented transformation. Proceedings of the American Control Conference, 2002, Vol.6: 4555-4559.

[6] Julier, S. J., Uhlmann J. K., Durrant-Whyte, H. F. A new approach for filtering nonlinear systems. Proceedings of the American Control Conference, 1995, Vol.3: 1628-1632.

[7] Julier, S. J., Uhlmann, J. K. Unscented filtering and nonlinear estimation. Proceedings of the IEEE, 2004, 92(3): 401-422.

[8] LaViola, J. J. A Compcn of unscented and extended Kalman filtering for estimating quaternion motion. Proceedings of the American Control Conference, 2003, Vol.3: 2435-2440.

Advanced Materials Research Vols. 989-994 (2014) pp 3530-3533
© (2014) Trans Tech Publications, Switzerland
doi:10.4028/www.scientific.net/AMR.989-994.3530

Mobile Wireless Communications Device With Buffered Cock Distribution Network

Jia Jingpu[1, a], Wu Chuansheng[2,b], Chen Jianwei[3,c], Shi Yunqiu[4,d]

[1,3] Shijiazhuang Information Engineering Vocational College, China

[2,4]University of Science and Technology Liaoning, China

[a , c]51931057@qq.com, [b,d]gykwcs@163.com

Keywords: Mobile, Wireless communications, Buffered clock, Network

Abstract. The microprocessor generates many digital noises that find their way back from the clock reference input of the microprocessor to the reference clock lines with which the RF circuits are sharing. These digital noises are conductively coupled to the RF circuits, including any RF transceiver, Bluetooth module and other RF circuits, such as a local oscillator and phase locked loop circuits, to cause spurious signals and jitters in the circuits, which in turn, degrade the RF performance or cause a radio to fail certain specifications.

Introduction

Mobile wireless communications devices, such as cellular telephones and similar communications devices, include a housing and circuit board carried by the housing. A microprocessor, radio frequency (RF) transceiver and RF circuitry can be carried by the circuit board and operative with each other. An antenna could be located external or within the housing. A clock, such as a crystal oscillator, could be positioned external to the components and off the circuit board or mounted on the circuit board, and provide a clocking signal to the microprocessor[1], RF transceiver and other RF circuitry, including any Bluetooth modules, phase locked loop circuits, and local oscillator (LO) circuits. Typically, spurious signals and jitters caused by digital noise from a microprocessor creates problems because it shares the same clock with the RF circuits, such as the reference clock input to the phase locked loop. The clock from the crystal oscillator provides the reference clock input signal to both the RF circuits, such as the phased locked loop circuit, RF circuits and digital circuits, such as the microprocessor, but without buffering[2].

Mobile wireless communications device design mechanism

This is aiming at solving the aforementioned defects, providing an IoT intelligent gas meter and its control system based on the transmission of IoT, and adopting supporting network management system. Many different forms can be set forth and described embodiments should not be construed as limited to the embodiments set forth herein. Rather, these embodiments are provided so that this disclosure will be thorough and complete, and will fully convey the scope to those skilled in the art. Like numbers refer to like elements throughout, and prime notation is used to indicate similar elements in alternative embodiments.

A mobile wireless communications device includes a housing and a circuit board carried by the housing. A microprocessor, a radio frequency (RF) transceiver and RF circuitry are carried by the circuit board and operative with each other. Clock buffer circuitry is carried by the circuit board and connected to the RF transceiver, RF circuitry and microprocessor for isolating a clock signal from the noise of the microprocessor and allowing greater isolation for the RF transceiver from RF circuitry[3].

The RF circuitry includes a Bluetooth module and the clock buffer circuitry is connected to the Bluetooth module for isolating a clock signal after the RF transceiver. The RF circuitry could also include a phase locked loop circuit and the clock buffer circuitry is connected to the phase locked looped circuit for isolating a clock signal after the RF transceiver and Bluetooth module.

The RF transceiver is formed as a GSM/GPRS (Global System for Mobile communications/General Packet Radio Service) system. The clock buffer circuitry could be formed as a plurality of serially connected buffers each having an output connected to a predetermined one of the RF circuitry and microprocessor. Each buffer could provide about to about 80 decibels of reversed isolation from its output to its input in a non-limiting example. The plurality of serially connected buffers could also be formed as transistors connected as emitter followers. The housing can be configured for handheld operation and the RF transceiver, RF circuitry and microprocessor can be operative as a cellular communications device. An antenna could be carried by the housing and operative with the RF transceiver[4].

The implementation of an example of mobile wireless communication

Different embodiments show that different clock signals can be isolated from the noise of the microprocessor. More sensitive RF circuits, for example, the GSM/GPRS chip set, could be connected to the crystal oscillator output first with proper impedance matching. The output of a first buffer circuit could be connected to a less sensitive RF circuit, for example, a Bluetooth module or chip. The buffer circuit could provide about to about 80 decibel reversed isolation from its output to the input. Other buffer circuits could be included with separate isolation.

A brief description will now proceed relative to FIGS. 1- which disclose an example of a mobile wireless communications device, for example, a handheld portable cellular radio, which can incorporate the non-limiting examples of the various buffering circuits and clock distribution network. FIGS. 1-are representative non-limiting examples of the many different types of functional circuit components and their interconnection, and operative for use with the clock distribution network and buffering circuits as described.

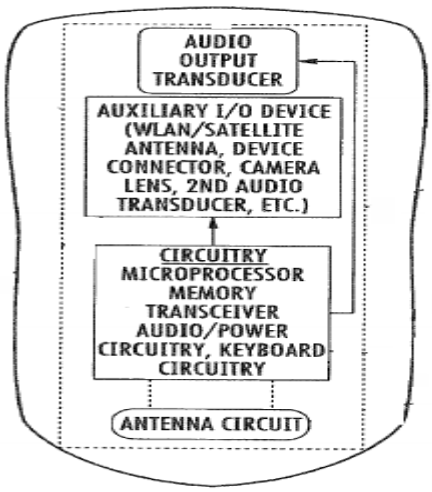

FIG. 1

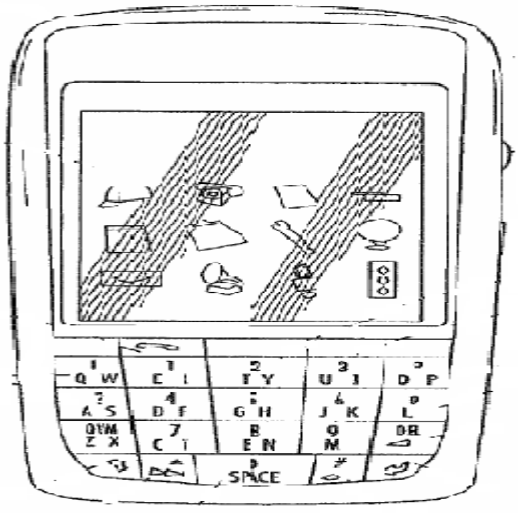

FIG. 2

Referring initially to FIGS. 1 and an example of a mobile wireless communications device , such as a handheld portable cellular radio, which can be used with the present invention is first described. This device illustratively includes a housing having an upper portion and a lower portion , and a dielectric substrate (i.e., circuit board) , such as a conventional printed circuit board (PCB) substrate, for example, carried by the housing. A housing cover (not shown in detail) would typically cover the front portion of the housing. The term circuit board as used hereinafter can refer to any dielectric substrate, PCB, ceramic substrate or other circuit carrying structure for carrying signal circuits and electronic components within the mobile wireless communications device . The illustrated housing is a static housing, for example, as opposed to a flip or sliding housing which are used in many cellular telephones. However, these and other housing configurations may also be used[5].

Circuitry is carried by the circuit board , such as a microprocessor, memory, one or more wireless transceivers (e.g., cellular, WLAN, etc.), which includes RF circuitry, including audio and power circuitry, including any keyboard circuitry. It should be understood that keyboard circuitry could be on a separate keyboard, etc., as will be appreciated by those skilled in the art. A battery (not shown) is also preferably carried by the housing for supplying power to the circuitry . The term RF circuitry could encompass the interoperable RF transceiver circuitry, power circuitry and audio circuitry.

Furthermore, an audio output transducer (e.g., a speaker) is carried by an upper portion of the housing and connected to the circuitry . One or more user input interface devices, such as a keypad (keyboard) FIG. , is also preferably carried by the housing and connected to the circuitry . The term keypad as used herein also refers to the term keyboard, indicating the user input devices having lettered and/or numbered keys commonly known and other embodiments, including multi-top or predictive entry modes. Other examples of user input interface devices include a scroll wheel and a back button . Of course, it will be appreciated that other user input interface devices (e.g., a stylus or touch screen interface) may be used in other embodiments.

An antenna is preferably positioned at the lower portion in the housing and can be formed as a pattern of conductive traces that make an antenna circuit, which physically forms the antenna. It is connected to the circuitry on the main circuit board . In one non-limiting example, the antenna could be formed on an antenna circuit board section that extends from the circuit board at the lower portion of the housing. By placing the antenna adjacent the lower portion of the housing , the distance is advantageously increased between the antenna and the user's head when the phone is in use to aid in complying with applicable SAR requirements. Also, a separate keyboard circuit board could be used.

More particularly, a user will typically hold the upper portion of the housing very close to his head so that the audio output transducer is directly next to his ear. Yet, the lower portion of the housing where an audio input transducer (i.e., microphone) is located need not be placed directly next to a user's mouth, and can be held away from the user's mouth. That is, holding the audio input transducer close to the user's mouth may not only be uncomfortable for the user, but it may also distort the user's voice in some circumstances. In addition, the placement of the antenna adjacent the lower portion of the housing also advantageously spaces the antenna farther away from the user's brain.

Another important benefit of placing the antenna adjacent the lower portion of the housing is that this may allow for less impact on antenna performance due to blockage by a user's hand. That is, users typically hold cellular phones toward the middle to upper portion of the phone housing, and are therefore more likely to put their hands over such an antenna than they are an antenna mounted adjacent the lower portion of the housing . Accordingly, more reliable performance may be achieved from placing the antenna adjacent the lower portion of the housing .

Still another benefit of this configuration is that it provides more room for one or more auxiliary input/output (I/O) devices to be carried at the upper portion of the housing. Furthermore, by separating the antenna from the auxiliary I/O device(s) , this may allow for reduced interference therebetween.

Some examples of auxiliary I/O devices include a WLAN (e.g., Bluetooth, IEEE 8011) antenna for providing WLAN communication capabilities, and/or a satellite positioning system (e.g., GPS, Galileo, etc.) antenna for providing position location capabilities, as will be appreciated by those skilled in the art. Other examples of auxiliary I/O devices include a second audio output transducer (e.g., a speaker for speaker phone operation), and a camera lens for providing digital camera capabilities, an electrical device connector (e.g., USB, headphone, secure digital (SD) or memory card, etc.).

Summary

Accordingly, the mobile wireless communications device as described may advantageously be used not only as a traditional cellular phone, but it may also be conveniently used for sending and/or receiving data over a cellular or other network, such as Internet and email data, for example. Of course, other keypad configurations may also be used in other embodiments. Multi-tap or predictive entry modes may be used for typing e-mails, etc. as will be appreciated by those skilled in the art.

Reference

[1] A Design of CAN-bus Based Collector for Automatic Meter ReadingSystem[A].Proceedings of 2010 Second International Computational and Natural Computing (CINC 2010) Volume 2[C]. 2010

[2] Intelligent fuzzy controller design of pressure ball drying system[A]. Proceedings of 2011 IEEE International Conference on Computer Science (CSAE 2011) VOL01[C]. 2011

[3] The Dairy Cattle Data Acquisition System Based on PDA[A]. Computer and Computing Technologies in Agriculture- I --Proceedings of the Third IFIP International Conference [C]. 2009

[4] The Research of Distributed Power Quality on-line Monitoring System Based on GRPS[A]. Proceedings 2010 IEEE International Conference on Software Service Sciences[C]. 2010

[5] The remote video monitor system design based on the FLASH technology[A]. Computer, Electrical, and Systems Sciences, and Engineering--Proceedings of 2011 International Conference on Computer (CESSE 2011)[C]. 2011

Advanced Materials Research Vols. 989-994 (2014) pp 3534-3539
© (2014) Trans Tech Publications, Switzerland
doi:10.4028/www.scientific.net/AMR.989-994.3534

POS Supported ADS40/80 Imagery Direct Geo-positioning and Positioning Accuracy Optimization

ZHANG Yan[1, a], WANG Tao[1,b] , FENG Wufa[1] ,FAN Yonghong[1] , RUI Jie[1]

[1] Institute of Geospatial Information, Information Engineering University, Zhengzhou 450052, China

[a]zhangyanxz7806@163.com, [b]wangtaoynl@163.com

Keywords: Airborne three-line array CCD Sensor, Direct Geo-positioning, Self-Calibration，Block Adjustment, ADS40/80

Abstract. On the basis of establishing direct geo-positioning model for three-line array sensor ADS40/80 images, in order to optimize the positioning accuracy, the self-calibration technology was used to update the ADS40/80 sensor imaging parameters. Moreover, the ADS40/80 camera error model and self-calibration bundle adjustment model were set up. Multi-groups of ADS40 data over the Songshan experimental field were used for direct geo-positioning and parameter updating experiments. Experimental results proved that the self-calibration adjustment technique can effectively update sensor imaging parameters and significantly improve image direct positioning accuracy.

Introduction

For a long time, it is a goal been pursued by photogrammetry community of realizing direct remote sensing image geopositioning from space to ground by measuring spatial positions and attitudes of cameras at imaging moments and obtaining exterior orientation elements of projection beam (photograph) directly[1]. If the direct-geopositioning mode does not rely on ground control, the outdoor work strength can be greatly released and aerial mapping cycles can be significantly shortened. Undoubtedly, it has important application value especially for disaster-prone and harsh natural conditions areas, borders and other disputed areas that are difficult to carry out ground control survey work.

With the development of sensor devices and related technology, direct remote sensing image geopositioning without ground control is becoming a reality. In the aerial remote sensing field, an important feature of ADS40/80 representative airborne linear CCD sensor is the sensor integration technology, which constitutes the direct positioning and orientation system (Postioning and Orientaiton System-POS) through integrating GPS and inertial measurement unit IMU (Inertial Measurement Unit)[2]. The POS system can obtain exterior orientation elements at imaging moments in real time. In theory, direct geospotioning can be achieved for remote sensing images using POS data without ground control. However, the actual application showed that although direct geopostioning can be achieved for ADS40/80 images using POS data, but the accuracy indicators is still unable to meet the large scale mapping and precise targeting requirements. Now it is an important research direction to effectively optimize direct positioning accuracy upon the current research basis.

Based upon the analysis about ADS40/80 sensor, the direct geopositioning model is built to realize direct image geopositioning firstly. And then the self-calibration technology is introduced to update sensor imaging parameters and optimize the direct positioning accuracy. Finally, the full set of ADS40 aerial flight data over Songshan remote sensing testfield is used to validate and evaluate the direct geopositioning accuracy and the optimization effect.

1. ADS40/80 Airborne Digital Sensor

ADS40/80 is a multi-line CCD digital aerial camera launched by Leica Ltd. in 2000, after wards upgrading to ADS80. It takes the three-line array push-broom imaging mode, which can image the

ground target from three different angles (ie, front, nadir and backward) synchronously and obtain three viewing angle panchromatic and four multispectral (R, G, B, NIR) images simultaneously. For ADS40/80 camera, single lens is used and different band image is separated by three colors splitter. All bands of linear array CCD detector areplaced in the same focal plane plate and the arrangement of all CCD linear array shown is in Figure 1. Each group of panchromatic CCD imaging line is composed of two CCD linear arrays arranged in half-pixel displacement, and for four multi-spectral bands each band corresponds to one CCD line. Each CCD linear array contains 12,000 pixels and each pixel size is 6.25mm.

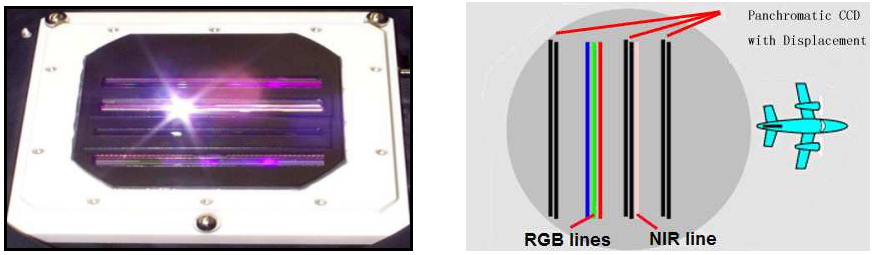

Fig. 1 Focal Plane Plate of ADS40/80 and Arrangement of CCD Linear Arrays

The main components of ADS40/80 camera include a sensor probe SH40, the control unit CU40, large capacity memory MM40, the operation display system OI40, navigation display system PI40 and gyro stabilized platform PAV30. Among them SH40 is the main optical imaging components, integrating optical lens system and IMU equipment. CU40 integrates GPS receiver and Applanix's POS / AV (Positioning and Orientation System for Airborne Vehicles) equipment and is mainly used to record synchronous photographic camera position and attitude data during flight. MM40 is primarily used to store video and GPS / IMU data, OI40 and PI40 is primarily used to provide a human-computer interactive interface.

2. The Direct Positioning Model of ADS40/80 Imagery

The ADS40/80 is a linear array CCD sensor and takes the pushbroom imaging mode. The scanning line acquired at each imaging moment has strict central projection relation with the ground imaged target and fulfills the line central projection relationship. Each scanning line has its own corresponding set of exterior orientation elements. If the instantaneous image plane coordinate system is established by taking the flight direction as x axis and the scanning direction as y axis, the instantaneous imaging equation is set up as.

$$\begin{bmatrix} x \\ y \\ -f \end{bmatrix} = \frac{1}{\lambda} R^{T} \begin{bmatrix} X - X_{Si} \\ Y - Y_{Si} \\ Z - Z_{Si} \end{bmatrix} \tag{1}$$

Dividing the former two equations in formula (1) by equation 3 and eliminating the scaling factor λ, the below formula can be gotten.

$$\begin{cases} x = -f \dfrac{a_1(X - X_{Si}) + b_1(Y - Y_{Si}) + c_1(Z - Z_{Si})}{a_3(X - X_{Si}) + b_3(Y - Y_{Si}) + c_3(Z - Z_{Si})} \\ y = -f \dfrac{a_2(X - X_{Si}) + b_2(Y - Y_{Si}) + c_2(Z - Z_{Si})}{a_3(X - X_{Si}) + b_3(Y - Y_{Si}) + c_3(Z - Z_{Si})} \end{cases} \tag{2}$$

In where (x, y) is coordinates of image point at instantaneous image plane coordinate system. For linear array image acquired by the same CCD, the x coordinates are all the same, and x always 0 for nadir image. For ADS40/80 images, the attached camera file recorded the coordinates of each CCD pixel center in the focal plane for all CCD linear arrays, and (x, y) can be queried from the camera file directly. (X,Y,Z) is the ground space coordinates of the corresponding ground point P. $(X_{Si}, Y_{Si}, Z_{Si}, \omega_i, \varphi_i, K_i)$ is the exterior orientation elements of the i-th scan line, R is the rotation

matrix formed by angle values (ω,φ,K),and $a_i,b_i,c_i(i=1,2,3)$ are elements in the rotation matrix $\boldsymbol{R}$. In this paper, the ω,φ,K angle system is taken.

Applying linearization on formula (2), we can obtain the linearized equation as follows,

$$\begin{cases} v_x = a_{11}\Delta X_S + a_{12}\Delta Y_S + a_{13}\Delta Z_S + a_{14}\Delta\omega + a_{15}\Delta\varphi + a_{16}\Delta\kappa - a_{11}\Delta X - a_{12}\Delta Y - a_{13}\Delta Z - l_x \\ v_y = a_{21}\Delta X_S + a_{22}\Delta Y_S + a_{23}\Delta Z_S + a_{24}\Delta\omega + a_{25}\Delta\varphi + a_{26}\Delta\kappa - a_{21}\Delta X - a_{22}\Delta Y - a_{23}\Delta Z - l_y \end{cases} \quad (3)$$

Where,

$$l_x = x + f\frac{\bar{X}}{\bar{Z}},\quad l_y = y + f\frac{\bar{Y}}{\bar{Z}},\quad \begin{cases} \bar{X} = a_1(X - X_{Si}) + b_1(Y - Y_{Si}) + c_1(Z - Z_{Si}) \\ \bar{Y} = a_2(X - X_{Si}) + b_2(Y - Y_{Si}) + c_2(Z - Z_{Si}) \\ \bar{X} = a_3(X - X_{Si}) + b_3(Y - Y_{Si}) + c_3(Z - Z_{Si}) \end{cases} \quad (4)$$

Obviously, if the interior and exterior orientation elements of the camera are known, formual (3) can be simplified as.

$$\begin{cases} v_x = -a_{11}\Delta X - a_{12}\Delta Y - a_{13}\Delta Z - l_x \\ v_y = -a_{21}\Delta X - a_{22}\Delta Y - a_{23}\Delta Z - l_y \end{cases} \quad (5)$$

Formula (5) is the error equation for the least-squares adjustment of multi-photo forward intersection. After the initial values are given out, ground coordinates (X,Y,Z)can be obtained by iterative computation. This is the direct ADS40/80 images positioning model adhpoted in this paper.

3. The Imaging Parameters Updating for ADS40/80 Based Self-calibration Technique

The self-calibration technique is based on the traditional photogrammetry theory and it is the most effective system error compensation method in analytical photogrammetry [5]. It basic idea is to treat the underlying systematic errors as undetermined parameters and absorb them into the overall adjustment for aerial block triangulation, which carries the optimal estimation on the main parameters and system error parameters simultaneously and assess accuracy. The final purpose is to eliminate or reduce system errors. Among various adjustment methods, the bundle block adjustment is most suitable for the introduction of additional parameters.

Considering the geometrical and physical factors in sensor imaging, if the self-calibration additional parameters can accurately reflect the systematic errors in sensor interior and exterior orientation elements and photographic lens optical distortions, the sensor geometric self-calibration can be successfully realized by the exact solution to the additional parameters through block adjustment[6]. This is the theoretical basis, for updating the ADS40/80 imaging parameters .

3.1 Fundamental Adjustment Equations

The basic formula of the self-calibration bundle block adjustment based on additional parameters is:

$$\left.\begin{aligned} x + \Delta x &= -f\frac{a_1(X - X_s) + b_1(Y - Y_s) + c_1(Z - Z_s)}{a_3(X - X_s) + b_3(Y - Y_s) + c_3(Z - Z_s)} \\ y + \Delta y &= -f\frac{a_2(X - X_s) + b_2(Y - Y_s) + c_2(Z - Z_s)}{a_3(X - X_s) + b_3(Y - Y_s) + c_3(Z - Z_s)} \end{aligned}\right\} \quad (6)$$

Where Δx and Δy represents the additional parameters function at the image point. If the control points are treated as the weighted observations, then the basic adjustment equations are listed as.

$$\begin{cases} V_X = A\Delta + C\Delta_S + B\dot{\Delta} - L_X & P_X \\ V_C = E\Delta_S - L_S & P_C \\ V_G = E\dot{\Delta} - L_G & P_G \end{cases} \quad (7)$$

Where V_X, V_G, V_C are the increment vectors of the image point, the ground control point and the self-calibration parameters observations respectively. $\dot{\Delta}$ is the increment vector of the unknown

ground coordinates, Δ is the increment vector of the unknown exterior orientation elements, Δ_S is the unknown self additional parameters; A, B, C are the coefficient matrixes corresponding to the unknowns; E are the identity matrixes, L_X is the constant observation vector for image point, L_S is observation value for self calibration parameters, L_G is observation value for for ground point; and the P_X, P_C, P_G are the corresponding weight matrixes.

3.2 Camera Error Model of ADS40/80

In order to compensate system errors effectively, a reasonable and effective self-calibration additional parameter model (ie camera error model) is particularly critical. Home and abroad scholars have carried out numerous investigation and put forward various parameter models, which can mainly be summarized into two types, namely polynomial type parameter model and the physical parameter model considering imaging aberration. Starting from the pure mathematics perspective, the former type does not consider the specific factors causing the point systematic error and does not emphasize the physical meaning of the additional parameters. It treats the combined effects of errors as a whole and uses a general form of polynomials as additional parameters. But the latter type starts from the physical factors causing the systematic errors for analyzing and designing the parameter model.

In the latter scenario, the 29-parameter model designed by Brown DC[7] has been widely used. Although the Brown model was originally designed for the film analog cameras, but applications demonstrate that it still applies for CCD digital sensor. In the ADS40/80 ORIMA adjustment software provided Leica, the used self-calibration module is modified form of Brown model, using a total of 18 additional parameters[8]. Its expression is as follows:

$$\begin{cases} dx = x_0 + a_1(r^2 - r_0^2)x + a_2(r^4 - r_0^4)x + a_3(r^6 - r_0^6)x + b_1x + b_2y \\ \quad + \dfrac{x}{f}\left[c_1(x^2 - y^2) + c_2x^2y^2 + c_3(x^4 - y^4)\right] + d_1xy + d_2y^2 + d_3x^2y + d_4xy^2 + d_5x^2y^2 \\ dy = y_0 + a_1(r^2 - r_0^2)y + a_2(r^4 - r_0^4)y + a_3(r^6 - r_0^6)y \\ \quad + \dfrac{x}{f}\left[c_1(x^2 - y^2) + c_2x^2y^2 + c_3(x^4 - y^4)\right] + d_6xy + d_7x^2 + d_8x^2y + d_9xy^2 + d_{10}x^2y^2 \end{cases} \quad (8)$$

In where (x_0, y_0) is coordinates of the principal point, f is the principal distance, a_1, a_2, a_3 are lens radial distortion parameters, b_1, b_2 are affine transform parameters, c_1, c_2, c_3 are photograph flatten parameters, $d_1 \ldots d_{10}$ are film deformation and lens non-radial distortion parameters, r_0 is principal point radial distance, r is the radial distance of image point, $r_0^2 = x_0^2 + y_0^2$, $r^2 = (x - x_0)^2 + (y - y_0)^2$.

4. Test and Analysis

4.1 Experimental Data

The used experimental data were ADS40 aerial remote sensing data s acquired over Songshan experimental field in August 2009. Through groups of data with the flying height being 600 m, 1000 m and 3000 m were selected for test and recorded as DataA, DataB and DataC. For DataA, the average flying height is about 600m and the average ground resolution is of 6cm. It includes two east-west routes and two north-south frame routes, and a total of 30 ground control points are selected from the coverage area. For DataB, the average flying height is approximately 1000m and the average ground resolution is 10cm. It comprises two east-west routes and a north-south frame route and 28 control points are picked out from the coverage area. For DataC, the average flying height is about 2900m and the corresponding ground resolution is 30cm, including two east-west routes and two north-south cross-routes and 35 chosen control points.

4.2 Experimental Methods and Results

1) Firstly, direct positioning experiments were carried out for three sets of data. Residuals on check points were statistically computed and the results were shown in Table 1, which calculated the maximum residual errors and the root mean squares (RMS) errors of check points. To facilitate the subsequent comparison, the RMS errors were computed in two standards meter and pixel resolution GSD.

2) Better quality data DataA and DataB were selected for self-calibration adjustment. The ORIMA software self-calibration module was used for self-calibration adjustment and to generate and extract the updated camera self-calibration file, denoted CamA and CamB (The raw camera file was denoted as Cam0).

3) The direct positioning test was carried out on three sets of data again using the new camera files CamA and CamB. Residuals on check points were statistically calculated and the results were shown in Table 2. The residual results were also converted into GSD standard. And comparison were made among direct positioning accuracy using Cam0 file, CamA file and CamB file respectively and the accuracy optimization results was evaluated and shown in Table 3.

Table 1. Direct Positioning Result of ADS40 data

Data	Maximum Error/m			RMS/m			RMS/GSD		
	X	Y	Z	X	Y	Z	X	Y	Z
DataA	0.395	-0.423	-0.815	0.235	0.200	0.408	3.917	3.333	6.800
DataB	-0.518	0.732	-1.261	0.290	0.309	0.527	2.901	3.090	5.274
DataC	-1.463	1.910	-4.331	0.814	0.764	1.258	2.714	2.545	4.194

Table 2. Direct Positioning Results for ADS40 DataUsing Updated Camera Files

camera file	DataA（RMS/m）			DataB（RMS/m）			DataC（RMS/m）		
	X	Y	Z	X	Y	Z	X	Y	Z
Cam0	0.235	0.200	0.408	0.290	0.309	0.527	0.814	0.764	1.258
CamA	0.169	0.126	0.135	0.164	0.246	0.212	0.253	0.360	0.719
CamB	0.164	0.112	0.140	0.153	0.249	0.199	0.261	0.333	0.690

Table 3. Comparison on Direct Positioning Accutacy Using Different Camera Files

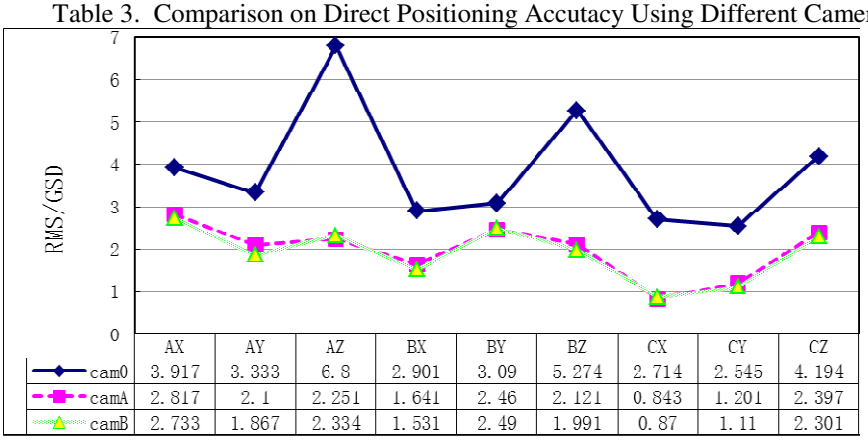

	AX	AY	AZ	BX	BY	BZ	CX	CY	CZ
cam0	3.917	3.333	6.8	2.901	3.09	5.274	2.714	2.545	4.194
camA	2.817	2.1	2.251	1.641	2.46	2.121	0.843	1.201	2.397
camB	2.733	1.867	2.334	1.531	2.49	1.991	0.87	1.11	2.301

4.3 Analysis on Experimental Results

1) It can be seen from Table 1,that although the direct positioning based on POS data can reach certain precision level for ADS40 image, but there still exists from a wide gap towards pixel-level accuracy. If evaluated in absolute accuracy, the accuracy of DataA was the best, the RMS errors on checkpoints were 0.235m, 0.200m and 0.408m respectively in X, Y and Z directions, followed by DataB and DataC in descending order. It shows that under normal circumstances, the direct positioning accuracy of ADS40 images positioning accuracy declined with the ground resolution. But if the evaluation standard was changed to GSD, the situation was opposite. DataC in the worst absolute accuracy was the highest, with 2.714, 2.545 and 4.194 GSD accuracy in X, Y, and Z direction. And DataA had the lowest accuracy in three-axis direction, respectively 3.917, 3.333 and 6.800 GSD.

2) From Table 1, it can be overall seen that the direct positioning accuracy for ADS40 images was relatively close in planar X, Y direction, ranging between about 2 to 4 GSD. It was much better than that in the Z direction from 4 to 7 GSD. Three groups of data had roughly the same changing trend in the three-axis directions and it presented the obvious system errors in direct positioning.

3) It can be seen from Table 2 that for three sets of test data, the accuracy of direct positioning using camA and camB was far superior to that using cam0, which validated that the updated camera file can

significantly improve the positioning accuracy. As it was seen from Table 3, better optimization results were achieved using CamA and CamB, and the enhanced extent were roughly equal. For both situations, the accuracy improvements were closer in the planar X, Y direction, at 1.3 GSD averagely, while the accuracy improvements were most obvious in Z direction with maximum value of 4.5 GSD and a minimum of 1.8 GSD. Accuracy curve corresponding to Cam0 undulated greatly, while those of CamA and CamB were relatively flat. And the two latter curves were very similar and relatively smooth, indicating that the direct positioning of ADS40 image has been basically stable.

5. Conclusions

Three sets of ADS40 data over Songshan field were taken to conduct onboard POS assisted three-line CCD image direct positioning test and precision optimization experiments. Experimental results show that when using the original camera files, direct positioning accuracy for ADS40 data can achieve 2 to 4 GSD in planar direction and 4 to 7 GSD in height direction without ground control, which lies a certain gap with the expected accuracy. Two sets of ADS40 data were selected for self-calibration bundle block adjustment through a reasonable set of camera error model. After self-calibration, the new camera files are updated. Using the newly generated camera files, the direct positioning accuracy were significantly improved for three groups of data, the accuracy enhancement in planar direction was 1.3 GSD averagely, and that in the elevation direction was about 3.1 GSD. The optimization effect is very obvious. Experimental results demonstrates the proposed method is feasible and effective, and has significantly implications for aerial work production.

Acknowledgements

The work was supported National Natural Science Foundation of China (No.41101396, 41001262); National High Technology Research and Development Program of China(863 program)(No.2012AA12A302-5); State Key Laboratory of Geo-information Engineering(No.SKLGIF2013-M-3-4).

Reference

[1] Li Deren. G*PS for Photogrammetry and Remote Sensing*, Beijin: Surveying and Mapping Press(1996).

[2] M.Cramer, *Digital Airborne Cameras – Status and Future*, Proceedings ISPRS Workshop "High Resolution Earth Imaging for Geospatial Information",University of Hannover, Hannover/Germany, May 17-20(2005)

[3] L.Hinsken. S.Miller. U.Tempelmann. R.Uebbing. T*riangulation of LH Systems' ADS40 imagery using ORIMA GPS/IMU*. International Archives of the Photogrammetry, Remote Sensing and Spatial Information Sciences,(2002),34 (Part 3A): 156–162.

[4] Sandual, *Design Principles of the LH Systems ADS40 Airborne Digital Sensor*. Int .Arch. of Photogrammetry and Remote Sensing,(2000), Vol.33 Part B2:258-265.

[5] WANG Zhizhuo. *PhotoGrammetry Principle*. Wuhan: Wuhan University Press(2007)

[6] WANG Tao, *Study on Theories and Methods of Linear CCD Sensor Geometric Calibration Based on Field* ,Zhengzhou: Information Engineering University Doctor Thesis(2012)

[7] Brown, D.C. *The Bundle Adjustment – Process and Prospects.* Invited paper, Commission III, Proc. of XIIIth ISP Congress, Helsinki, Finland, International Archives of Photogrammetry 21(3), p.33(1976)

[8] TU Xinru, XU Miaozhong, LIU Li. *The Geometric Calibration of Airborne Three-line-scanner ADS40*. Acta Geodaetica et Cartographica Sinica, 2011,40(1):78-83.

Advanced Materials Research Vols. 989-994 (2014) pp 3540-3543
© (2014) Trans Tech Publications, Switzerland
doi:10.4028/www.scientific.net/AMR.989-994.3540

The CDMA Spread-Spectrum Cell Mobile Communication Uplink System With Cooperative Diversity

Hancheng Liao

School of Software and Communication Engineering

Jiangxi University of Finance and Economics

Nanchang, China, 330013

Liaoemail@163.com

Keywords: Cooperative Diversity, CDMA, Uplink

Abstract. In this paper, physical layer cooperative communication of code division multiple access system is explored. Many mobile terminals relay signals for each other so as to achieve spatial diversity. The cooperative scheme of the mobile terminal is well designed. The uplink system model, as well as the receiving structure is given. The performance advantage of such system is clearly indicated through simulation.

Introduction

Code division multiple access (CDMA) system is famous for combating multipath fading in wireless communication [1-2]. Large-area-synchronized (LAS) codes are very suitable to act as the multiple access codes (MACs) due to their good auto-correlation property and cross-correlation property [3-4]. Cooperative diversity is a cooperative multiple antenna technique for improving performance or channel capacities which exploits user diversity by decoding the combined signal of the relayed signal and the direct signal in wireless networks [5]. A conventional single hop system uses direct transmission where a receiver decodes the information only based on the direct signal while regarding the relayed signal as interference, whereas the cooperative diversity considers the other signal as contribution. Hence, it can be seen that cooperative diversity is an antenna diversity that uses distributed antennas belonging to each node in a wireless network. In the discussion behind, cooperative diversity is applied to uplink CDMA system.

System Model

Usually, there are many antennas which can be installed on the base station (BS) for a practical CDMA mobile communication system, while only one antenna can be installed on each mobile terminal (MT) in view of the size. For simplicity, we suppose that the number of antenna in the mobile terminal and in the base station is both only one. Although both transmitting operation and receiving operation can make use of the same antenna by time-division duplex (TDD), we can assume that two antennas are mounted—one is focusing on transmitting data and the other is focusing on receiving data. Considering that all of the constellation points are in the unit circle, phase-shift-keying (PSK) is chosen as the modulation scheme. Furthermore, we take it for grant that perfect power control technology is implemented to completely eliminate the near-far effect in all cells. As for the multiple access codes, LAS codes are employed. In addition, it is a relay technology in nature when we refer to cooperative diversity. Hereafter, the uplink CDMA system model of LAS spread-spectrum cell mobile communication system applying cooperative diversity technology is studied, as well as some simplified cooperative protocol.

In this paper, we only talk about a single cell. Naturally, there are many active mobile terminals in each cell for such mobile system. Suppose that the base station has chosen K mobile terminals as a group for some short period by a given rule—being in near area, having similar angle-of-arrival (AOA), indicating the same distance to the base station. During such period, they are cooperators, that is to say, every one of them is be in duty bound to relay the data from the others. We only discuss the

situation that the relay number of times is one and the links with twice relays are not taken into consideration. Such cooperative CDMA cell is illustrated in Fig. 1. In this situation, one base station is placed in the center and one omnidirectional antenna is installed on it.

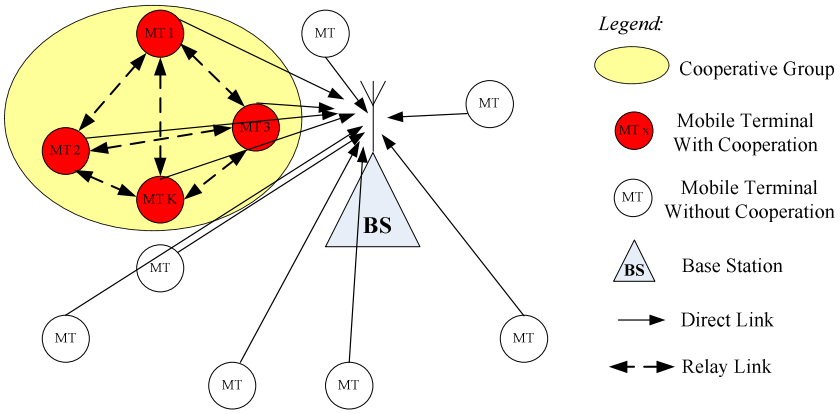

Figure 1. A cooperative CDMA cell with one base station and many mobile terminals

As we know, every each mobile terminal can acquire the spread-spectrum sequence or MAC for each other from the base station. Here, we begin with only one group consisting of K members and each member has stored K MACs from the beginning of cooperation. Other cases of many groups in a cell with either equal or different number of members in a group can be studied in further work. Also, we don't take such situation into account that any cooperative mobile terminal is working irregularly, no matter because of power cutting, interrupt or breakdown. The allocation scheme of time slots (TSs) in such cooperative uplink system is shown in Fig. 2. During the first K time slots, each mobile terminal transmits its data successively, e.g., No. k mobile terminal (named MT k) sends at No. k time slot (named TS k). Meanwhile, the other K-1 mobile terminals and the base station are receiving such data. Then it is followed by K-1 relay time slots, in which each one mobile terminal transmit data of the others by a given order. As shown in Fig. 2, the data of the first mobile terminal is transmitted by MT K in TS K+1, by MT K-1 in TS K+2, up to by MT 2 in TS 2K-1. Although there are more time slots than systems without cooperation, the communication efficiency is not reduced obviously in general according to the fact that a lot of mobile terminals have spare time in many kinds of business or even they are in standby mode.

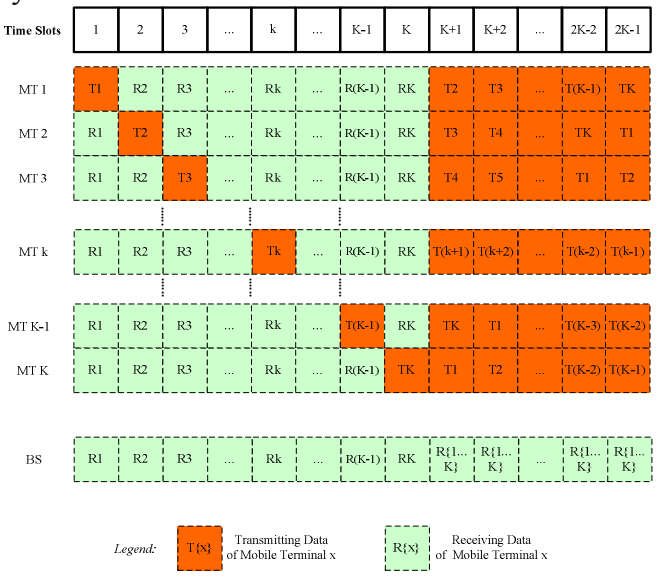

Figure 2. The allocation scheme of time slots in uplink system for K cooperative mobile terminals and one base station

Then we go on to the system model of any mobile terminal. Without loss of generality, we can only research the first mobile terminal. Its model is given in Fig. 3, where only baseband signals and

operations are mentioned. The transmitting and receiving signal of MT x is notated as $s_x(t)$ and $r_x(t)$. During the first time slot (named TS 1), MT 1 transmits its data. During the next K-1 time slots, MT 1 receives data from MT 2 to MT K in turn. In the figure, $\hat{s}_p^n$ represents the despread symbol of MT n received by MT p using MAC c_n, it is an estimate of symbol s_n^n for MT n and should be transmitted by MT p hereafter. The amplifying coefficient can be simplified as $a_p^n = 1/\left\|\hat{s}_p^n\right\|$ when PSK is employed. During the last K-1 time slots, the relay signals $a_p^n \hat{s}_p^n$ is spread with c_p and transmitted by MT p separately.

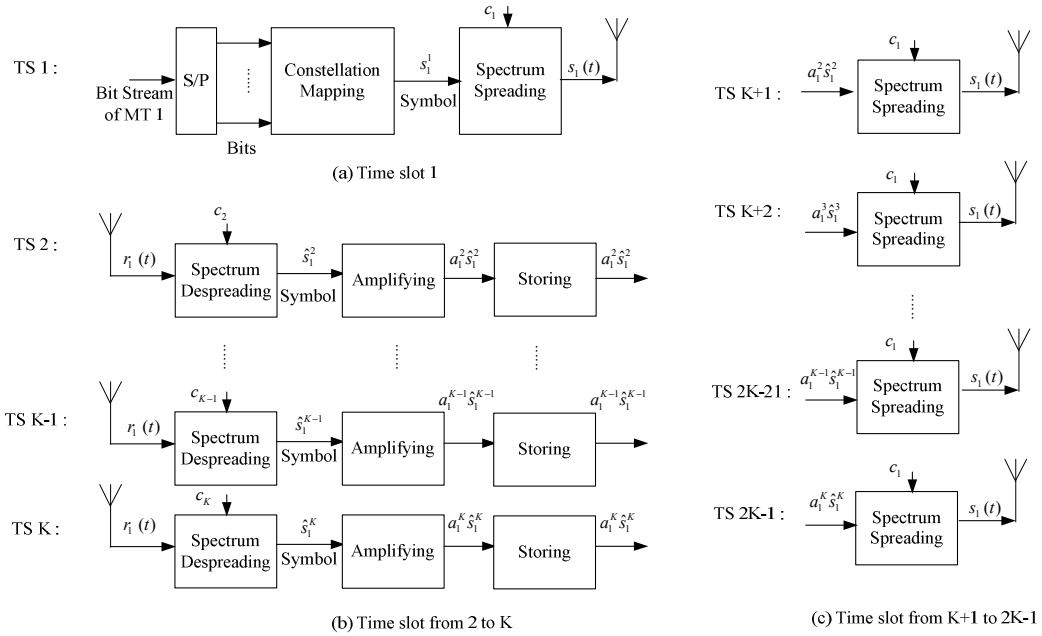

Figure 3. The uplink system model for the first cooperative mobile terminal (MT 1)

The corresponding uplink system model of base station is given in Fig. 4, where $r(t)$ is the received signal and r_j^n is the despread symbol for MT n using MAC c_n during TS j. r_{K+1}^1, r_{K+2}^1, …, r_{2K-1}^1 and r_1^1 are prepared for the next diversity combining operation. As the modulation type is PSK, we can choose equal gain combining (EGC) method and let $r^1 = \overline{r}/\left\|\overline{r}\right\|$, where $\overline{r} = (r_1^1 + r_{K+1}^1 + \cdots + r_{2K-1}^1)/K$.

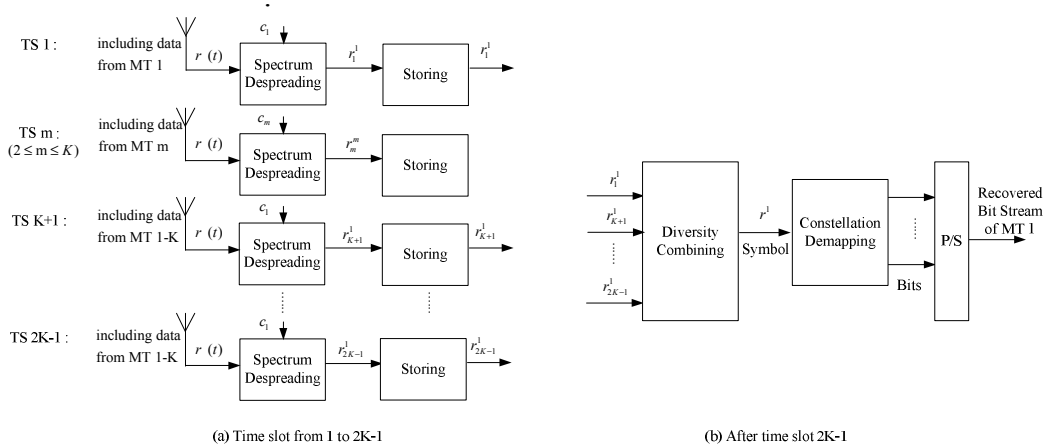

Figure 4. The uplink system model for the base station (only showing the operation concerning MT 1)

Performance Simulation

In the simulation, both system with cooperation (K>1) and system without cooperation (K=1) are considered. The spread factor is 16 and modulation type is QPSK. The channel model is ITU-VA 120 km/h. The base station knows the channel state information (CSI) but the mobile terminals don't. The bit error rate (BER) performance is simulated by MT 1 and is shown in Fig. 5. The diversity gain is obvious and almost linear to K.

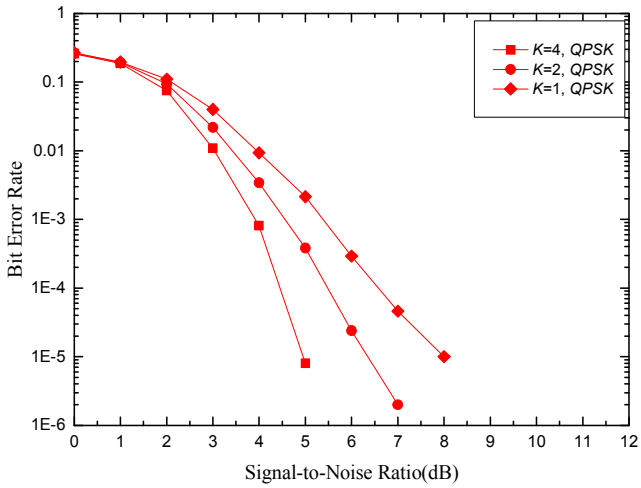

Figure 5. The BER performance of cooperative CDMA system

Summary

By applying cooperative diversity technology to existing CDMA spread-spectrum system, the system performance and capacity can be much better. As the number of cooperative users increases, the diversity gain augments. Our numerical simulation reveals that the cooperative scheme is able to extract the full distributed spatial diversity in the uplink. Of course, there is trade-off between the diversity gain and the loss of other wireless resource such as time and power resources because they are wasted to relay the signal from the source node to the destination node. Therefore, it is noteworthy that the number of cooperative users is limited.

Acknowledgement

In this paper, the research was sponsored by the Nature Science Foundation of Jiangxi Province (Project No. 20122BAB201036).

References

[1] A. Viterbi: *CDMA: Principles of Spread Spectrum Communication*, Addison Wesley, New York (1995)

[2] L. Hanzo, L. L. Yang, E. L. Kuan and K. Yen, *Single and Multicarrier DS-CDMA*, IEEE Press (2003)

[3] Hancheng Liao, Daoben Li and Qingrong Zhang: An example of LS codes, 16th International Conference on Computer Communication, Beijing, China (2003), p. 918

[4] Daoben Li: A spread spectrum coding method possessing interference free window, Chinese Patent PCT/CN00/0028.(1999)

[5] J. N. Laneman, D. Tse and G. W. Wornell:Cooperative Diversity in Wireless Networks: Efficient Protocols and Outage Behavior, IEEE Transactions on Information Theory, Vol. 50, No. 12(2004), p.3062

Advanced Materials Research Vols. 989-994 (2014) pp 3544-3547
© (2014) Trans Tech Publications, Switzerland
doi:10.4028/www.scientific.net/AMR.989-994.3544

3D Facial Shape Reconstruction From A Single Frontal Image

Qian Ma

Wuhan University of Science and Technology City College, Wuhan, China

icey_mq@163.com

Keywords: Shape from shading; Improved Fast Marching Method; Shape reconstruction

Abstract. In this paper, we propose an improved method for reconstruct 3D facial shape from a single frontal image. We use improved fast marching method to solve the Eikonal equation which can obtained from the method of shape from shading (SFS). In order to overcome the concave-convex ambiguity problems inherent to SFS, we find out the concave region and recover concave into the convex keeping the relative shape invariant to reconstruct the accuracy facial shape.

Introduction

The 3D shape recovery is a classical problem in computer vision. It recovers the relative height of each point to gets the 3D model through one or more gray images. Horn put forward the shape from shading (SFS) in the 70's [1]. He used a first order nonlinear partial differential equations (PDE) to express this problem. This equation is called the image irradiance equation. As we all know, the unique solution cannot be solved in the classical sense by SFS method. Actually, one gray image cannot avoid convex-concave ambiguities, because the singularity may correspond to the maximum value point (convex point) or the minimum point (concave point) or saddle point on the surface of the object. Thus how to avoid convex-concave ambiguities is the focus of current research.

Along with the rapid development of computer image technology, 3D face modeling and animation is applied so widely, that it has become a research focus of many scholars at home and abroad. Due to the less condition of the single view modeling, there is a great prospect of application. In this paper, we used a single frontal face image to reconstruct 3D facial shape. We transformed the image irradiance equation into the corresponding static Hamilton-Jacobi equation through the SFS method, then used the improved fast marching method to obtain the viscosity solution and it is a unique solution [2-3]. But it could only eliminate the ambiguity of saddle point [4], so we searched the concave areas which are convex actually, and recovered the accuracy facial shape by reflection.

Shape from Shading

We suppose the reflection model is a Lambert reflection model [5], in which the illuminant is located far enough from the surface, the imaging is the orthogonal projection and the albedo is constant and equal to 1. So the brightness of the image points on an object surface only decided by the cosine of the angle of incident light. The camera coordinate system is used as the reference system, and the surface is expressed as a function of $z=z(x, y)$. I is the normalized image brightness, $N = (N_x, N_y, N_z)$ is the unit normal vector of the surface, and $L = (L_x, L_y, L_z)$ is the illuminant direction. Thus we can have

$$I = N \cdot L \tag{1}$$

Consider the light source is vertical incidence, so $L= (0, 0, 1)$, and we can obtain the unit normal vector from the surface function as $n=(z_x, z_y, z_z)$, where $z_x = \frac{\partial z(x,y)}{\partial x}$ $z_y = \frac{\partial z(x,y)}{\partial y}$, $z_z = 1$. Then Eq.1 can be rewritten as

$$I = \frac{1}{\sqrt{z_x^2 + z_y^2 + 1}} \tag{2}$$

because $\nabla z(x,y)=(z_x,z_y)$, then

$$\left\|\nabla z(x,y)\right\|=\sqrt{\frac{1}{I(x,y)^2}-1} \tag{3}$$

This is a static Hamilton-Jacobi equation, also known as Eikonal equation.

Improved Fast Marching Method

The level set method was first proposed by Sethian and Osher in 1988[6], which is an efficient numerical algorithm to solve the partial differential equations. Eq.3 could be rewritten as:

$$\left\|\nabla z(x,y)\right\|=f(x,y) \tag{4}$$

Then the numerical algorithm of the level set arrival time method is:

$$\{[\max(D_x^- z_{ij},-D_x^+ z_{ij},0)]^2+[\max(D_y^- z_{ij},-D_y^+ z_{ij},0)]^2\}^{1/2}=f_{ij} \qquad i=1,...,N,\ j=1,...M \tag{5}$$

Its computational complexity is $O(N^3)$, in order to reduce the complexity, a fast algorithm has bee n developed, called "Fast Marching Method(FMM)". The basic idea of FMM is used the unidirectio nal movement of the curve in the arrival time method, creating an activated narrow-band around the transmission boundary. The arrival time of the inner points of the narrow-band is unknown, and the t ransmission boundary is one-way spread outward, like the spread of the water. When the point has b een spread, we froze the time of arrival in before, then created a new narrow-band with the recent wa ve. So we can gain the arrival time of each point finally. The computational complexity of the FMM is $O(N^2\log N)$.

The FMM used the first difference to approximately calculate the gradient ∇T. In order to improve the accuracy, we used the second order difference to approximately calculate the gradient whenever points are available, and reverted to a first-order approximation in the other cases. If we want to calculate the arrival time of the point (i,j), we need its neighbors as following: $(i\text{-}2,j)$, $(i\text{-}1,j)$, $(i,j\text{-}1)$, $(i,j\text{-}2)$.

The improved fast marching method used the second order difference to calculate the gradient if it meets one of the following two cases:

(1)The arrival time of the points which are two points away from (i,j) in each direction is known. For example, $z_{i-2,j}$ and $z_{i+2,j}$ must be known in the direction of x;

(2) The points which are two points away from (i,j) in each direction must have less arrival time than those points at one point away from (i,j). For example, in the direction of x, we must have $z_{i-2,j}\le z_{i-1,j}$ and $z_{i+2,j}\le z_{i+1,j}$.

Two order forward difference and the backward difference formula are as follows:

$$\begin{aligned} D_x^- z_{ij}&=\frac{3z_{i,j}-4z_{i-1,j}+z_{i-2,j}}{2\Delta x}, D_y^- z_{ij}=\frac{3z_{i,j}-4z_{i,j-1}+z_{i,j-2}}{2\Delta y}\\ D_x^+ z_{ij}&=-\frac{3z_{i,j}-4z_{i+1,j}+z_{i+2,j}}{2\Delta x}, D_y^+ z_{ij}=-\frac{3z_{i,j}-4z_{i,j+1}+z_{i,j+2}}{2\Delta y}\end{aligned} \tag{5}$$

By substituting the above formula into Eq.4, we can have

$$\begin{aligned}&[\max(\frac{3z_{i,j}-4z_{i-1,j}+z_{i-2,j}}{2\Delta x},\frac{3z_{i,j}-4z_{i+1,j}+z_{i+2,j}}{2\Delta x},0)]^2+\\ &[\max(\frac{3z_{i,j}-4z_{i,j-1}+z_{i,j-2}}{2\Delta y},\frac{3z_{i,j}-4z_{i,j+1}+z_{i,j+2}}{2\Delta y},0)]^2=f_{ij}^2\end{aligned} \tag{6}$$

It can be rewritten as:

$$\begin{aligned}&[\max(\frac{3z_{i,j}-\min(4z_{i-1,j}-z_{i-2,j},4z_{i+1,j}-z_{i+2,j})}{2\Delta x},0)]^2+\\ &[\max(\frac{3z_{i,j}-\min(4z_{i,j-1}-z_{i.j-2},4z_{i,j+1}-z_{i,j+2})}{2\Delta y},0)]^2=f_{ij}^2\end{aligned} \tag{7}$$

Let

$$Z = z_{i,j}, Z_1 = \min(4z_{i-1,j} - z_{i-2,j}, 4z_{i+1,j} - z_{i+2,j}), Z_2 = \min(4z_{i,j-1} - z_{i,j-2}, 4z_{i,j+1} - z_{i,j+2})$$

Then

$$[\max(\frac{3Z - Z_1}{2\Delta x}, 0)]^2 + [\max(\frac{3Z - Z_2}{2\Delta y}, 0)]^2 = f_{ij}^2 \tag{8}$$

Because the improved fast marching method guarantees the Z is larger than its neighbors Z_1 and Z_2. So we get

$$(\frac{3Z - Z_1}{2\Delta x})^2 + (\frac{3Z - Z_2}{2\Delta y})^2 = f_{ij}^2 \tag{9}$$

This equation can be simplified as follow:

$$aZ^2 + bZ + c = 0 \tag{10}$$

The coefficients are given as follow:

$$a = \frac{9}{4}(\frac{1}{\Delta^2 x} + \frac{1}{\Delta^2 y}), b = -\frac{3}{2}(\frac{Z_1}{\Delta^2 x} + \frac{Z_2}{\Delta^2 y}), c = \frac{1}{4}(\frac{Z_1^2}{\Delta^2 x} + \frac{Z_2^2}{\Delta^2 y}) - f_{ij}^2$$

The solution of equation is given as follow:

(1) If $Z<min(Z_1, Z_2)$, then the gradient component z_x and z_y are zero, so $Z^{(n+1)}=Z^{(n)}$;

(2) If $Z_1>Z>Z_2$, then $z_x \approx 0$, $z_y \approx Z^{(n+1)} - Z_2$, so $Z^{(n+1)}= Z_2+f_{ij}$;

(3) If $Z_2>Z>Z_1$, then $z_y \approx 0$, $z_x \approx Z^{(n+1)} - Z_1$, so $Z^{(n+1)}= Z_1+f_{ij}$;

(4) If $Z>\max(Z_1, Z_2)$, then solve equation: $(\frac{3Z - Z_1}{2})^2 + (\frac{3Z - Z_2}{2})^2 = f_{ij}^2$, so

$Z^{(n+1)}=\frac{Z_1 + Z_2 + \sqrt{8f_{ij}^2 - (Z_1 - Z_2)^2}}{6}$.

The experimental results are shown in Fig.1

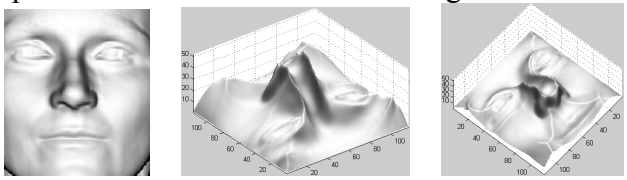

Fig.1

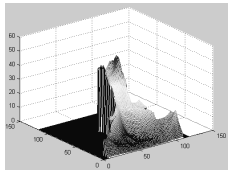

Fig.2

3D Facial Shape Reconstruction

As we can see in the experimental result, the integrity of the face shape is relatively good, but it cannot avoid convex-concave ambiguities. So we need the subsequent processing in order to get an accurate 3D face model.

We found out the recessed region firstly. Because the highest point of the nose is the lowest one in the recessed region at present, we got the initial curve which has the highest point of the nose in the vertical direction. According to the symmetry of the face, we extended each point to the horizontal direction on the curve. Then we putted the points into the concave point set which have the higher value of the height than the initial points, and updated the points and kept extend until the height decrease. The result of the recessed region which we found through the above steps is shown in Fig.2.

Then we reconstructed the recessed region keeping the relative shape invariant. Based on the boundary of the recessed region as a benchmark, we used mirroring to create convex surface so it can keep the relative shape invariant. The result is shown in Fig.3.

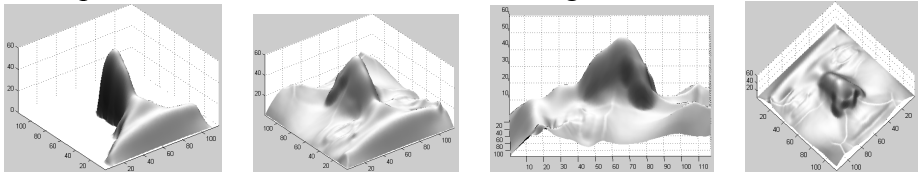

Fig.3

Experiments and Conclusions

We have performed extensive experiments on several facial images, and show a part of our results in Fig.1, Fig.2, Fig.3 and Fig.4. When the improved fast marching method to solve the SFS is used, it can recover the 3D model with integrity, but it cannot avoid convex-concave ambiguities. We can see this result from Fig.1. Then we used the proposed method in previous section to extracted concave region, we can see that the depression areas extraction are ideal from the experimental results from Fig.2. Based on the boundary of the recessed region which we found, we got the 3D face reconstruction which is shown in the Fig.3 and Fig.4. It can be seen from the results that the concave recovered into the convex keeping the relative shape invariant.

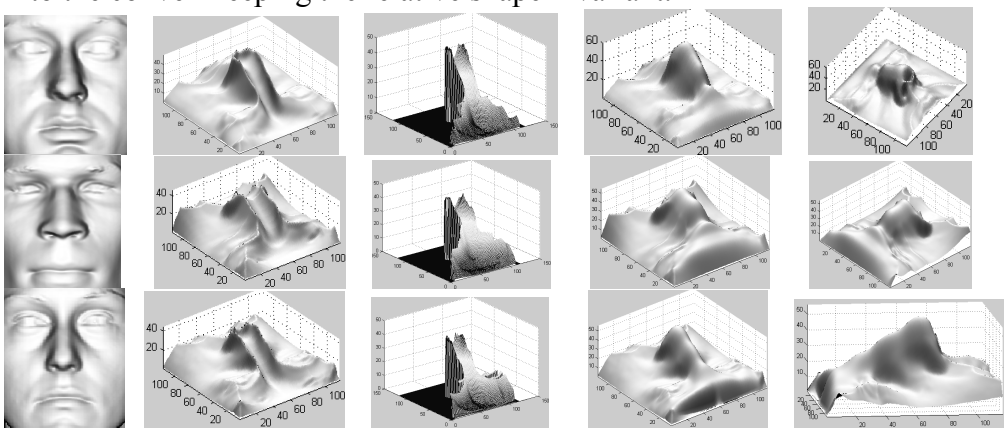

Fig.4

In this paper, we have introduced a framework to recover the 3D facial shape from a single image. We used the improved fast marching method to solve image irradiation equation based on the evolutionary algorithm, and reconstructed the concave into the convex. Experimental results have shown that our method is feasible and effective, and we can get a 3D face model which has high similarity with the original 2D image. However, much more work remains to be done in the future, for example, to consider if the light environment is more complex, and if the 2D facial image is not frontal.

Acknowledgements

This work was financially supported by the Hubei Provincial Department of Education Science and Technology Research Project (B20129101).

References

[1] Horn B. K. P. Obtaining shape from shading information. Chapter 4 in The Psychology of Computer Vision, P.H.Winston(ed.), McGraw Hill, New York, 1975, p. 115-155.

[2] G. A. Sor, V. K. Dhir, “Numerical Method in Fluid Dynamic,” Cambridge University Press, 1985.

[3] PRADOS E, FAUGERAS O. Shape from shading: a well-posed problem? [C]. IEEE Conference on Computer Vision and Pattern Recognition. Los Alamitos, CA, USA: IEEE Computer Society, 2005, p. 870-877.

[4] O. J. Liensis, “Uniqueness in shape from shading,” International Journal of Computer Vision. 1991, 6 (2), p. 75-104.

[5] H. Gouraud, “Computer Display of Curved Surfaees,” IEEE Conf. on Computer Graphics, Pattern Recognition, and Data Structure, Los Angeles, California, 1975, 5, p. 11-17.

[6] Osher S., Fedkiw R. Level Set Methods and Dynamic Implicit Surfaces[M]. Springer-Verlag, 2002.

Advanced Materials Research Vols. 989-994 (2014) pp 3548-3551
© (2014) Trans Tech Publications, Switzerland
doi:10.4028/www.scientific.net/AMR.989-994.3548

Processing and Mosaicing System of Civil Unmanned Aerial Vehicle Remote Sensing Image

Ying Yang[1, a], Lijun Wang[1, b], Lei Yang[1,2,c]

[1]College of Computer and Electronic Information, University of Guangxi, Guangxi, China

[2]Institute of Applied Physics, Guangxi Academy of Sciences, Guangxi, China

[a]yingy2004@126.com, [b]wlj250237@126.com, [c]Leiy2004@126.com

Keywords: Civil Unmanned Aerial Vehicle; Remote Sensing; Image processing; mosaicing

Abstract. With combining Unmanned Aerial Vehicle (UAV) and the high-precision of the low altitude Remote Sensing (RS) technology, UAV RS technology has become an important complement for satellite and manned aircraft RS, so it has drawn great attention of people at home and abroad. Most of UAV RS image technologies use small digital cameras to shoot so that it causes some problems such as lower magnitude, more and larger morphing image. The image processing and mosaicing system of UAV RS implements the function of image identifying, selection of image group control points, geometric correction, mosaicing, seam lines eliminating automatically and rapidly with Interactive Data Language (IDL), and is targeted to solve the practical application problems such as preprocessing, mosaicing, seam-lines removing of civil UAV RS image.

Introduction

At present, the study on UAV RS applications has become a craze at home and abroad, many scholars and scientific research institutes have done many beneficial explorations in this area [1,2], but most of UAV RS image mosaicing technology use the traditional processing method such as ERDAS, ENVI which are targeted to process images of satellite and manned aircraft RS [3]. Therefore, there is no system that processes and mosaic civil UAV RS image because of their characteristics. Most of UAV RS image technologies use small digital cameras to shoot so that it causes some problems, for example, lower magnitude, more and larger morphing image, etc. It needs longer time to process images and the efficiency has become a bottleneck leading to restrict the development and the application of civil UAV RS field. As a result, in geometric correction of image it should take into account these factors such as characteristics of RS images, parameters of camera calibration, attitude parameter when shooting and relative geometric model. In addition, a corresponding system needs to be developed to implement interactive processing with functions of image identifying automatically and mosaicing rapidly, meanwhile, to meet the request of real-time and rapidity in image processing of civil UAV [4].

Our system focuses on solving the problems such as image preprocessing, image mosaicing and seam-line eliminating automatically and rapidly, to satisfy the needs of present practical applications.

System Research and Design

According to the need of civil UAV RS image processing, our system has the following functions: (1) Image import, including import the description of image such as name, storage path and size. (2) Extract the feature points of a single image and match the feature points of two adjacent images. (3) Mosaic images automatically with obtaining feature points. (4) Selecting group control points for geometric correction of image. (5) Mosaic image interactively after geometric correction.

As to original data of UAV RS image, synchronizing and correcting camera interior error and exterior orientation attitude parameters of images in data reception department, the corrected images do further corrective processing by selecting character points and geometric precision correction.

Then, after mosaicing images, systematic eliminating seam-lines between two adjacent images, crop images and does other processes. The system processing procedure is shown as Fig. 1.

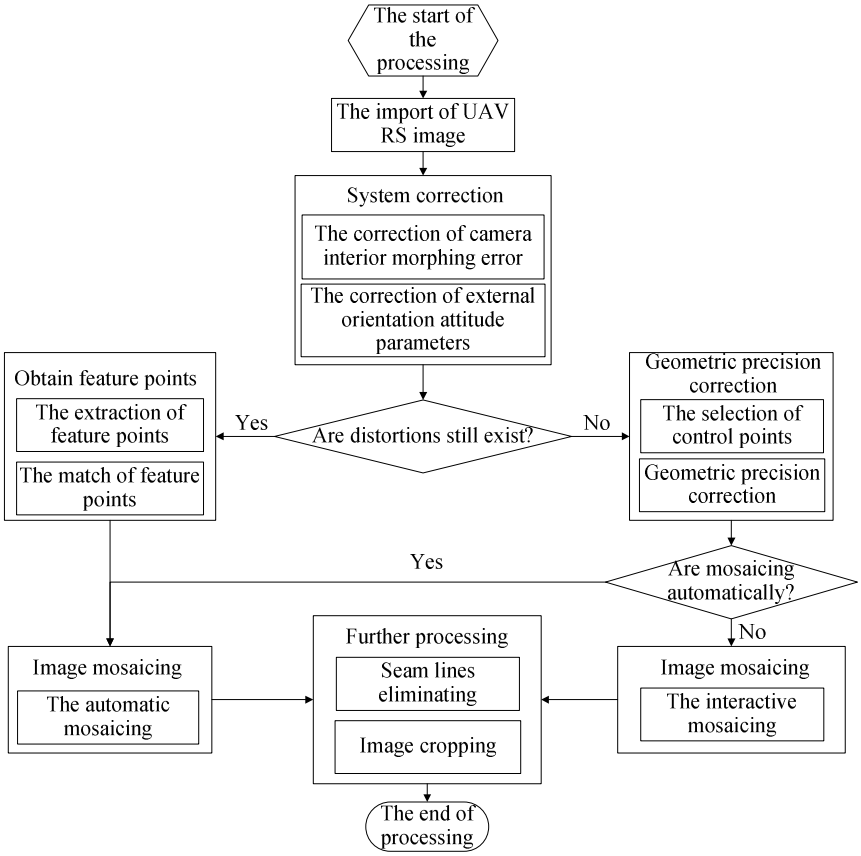

Fig.1 The system processing procedure.

Selecting control points is the first step for interactive correction and mosaicing of image. Its' quantity and quality affect corrective accuracy of image directly, as well as the geometric accuracy of mosaicing finally. The selecting procedure of control points is shown as Fig. 2: At first, the system display images with callout window; then enlarge the part of image at zoom window through clicking any area of callout window; at last locate control point accurately in zoom window.

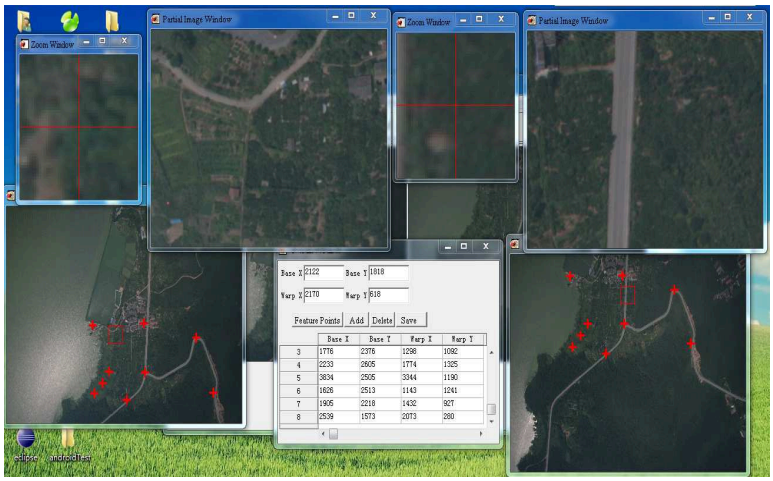

Fig.2 The window of control point selection.

After selecting a couple of control points, their coordinates are added into the control point list of the main window and are marked in the corresponding location of the marking window. The locations marked by the red crosses in Fig. 2 are control points selected. Click the preserving button of the main

window to preserve them when more enough and evenly distributed control points are selected. As The file format of preserving control points' coordinates can be saved by TXT text format as Fig. 3.

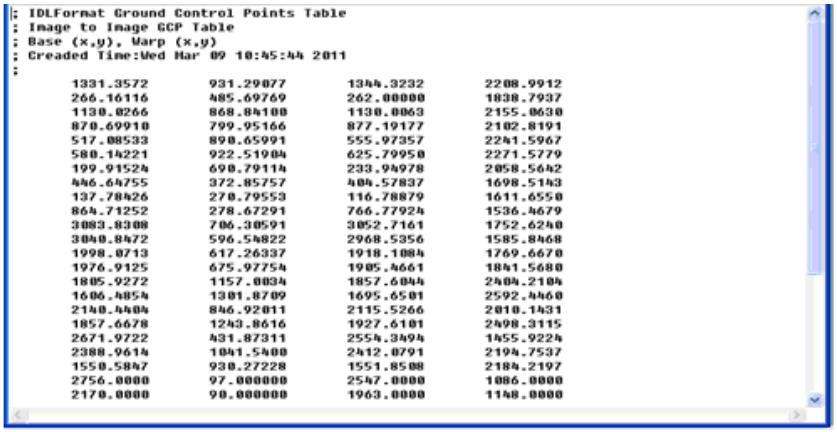

```
; IDLFormat Ground Control Points Table
; Image to Image GCP Table
; Base (x,y), Warp (x,y)
; Creaded Time:Wed Mar 09 10:45:44 2011
;
      1331.3572       931.29877       1344.3232       2208.9912
      266.16116       485.69769       262.00000       1838.7937
      1130.0266       868.84100       1130.0063       2155.0630
      870.69910       799.95166       877.19177       2102.8191
      517.08533       890.65991       555.97357       2241.5967
      580.14221       922.51904       625.79950       2271.5779
      199.91524       698.79114       233.94978       2058.5642
      446.64755       372.85757       484.57837       1698.5143
      137.78426       278.79553       116.78879       1611.6550
      864.71252       278.67291       766.77924       1536.4679
      3083.8308       706.30591       3052.7161       1752.6240
      3040.8472       596.54822       2968.5356       1585.8468
      1998.0713       617.26337       1918.1084       1769.6670
      1976.9125       675.97754       1905.4661       1841.5680
      1805.9272       1157.0834       1857.6044       2404.2104
      1606.4854       1301.8709       1695.6501       2592.4460
      2140.4404       846.92011       2115.5266       2010.1431
      1857.6678       1243.8616       1927.6101       2498.3115
      2671.9722       431.87311       2554.3494       1455.9224
      2388.9614       1041.5408       2412.0791       2194.7537
      1550.5847       930.27228       1551.8508       2184.2197
      2756.0000       97.000000       2547.0000       1086.0000
      2170.0000       90.000000       1963.0000       1148.0000
```

Fig. 3 The preserving file of control points.

Before correcting the two images interactively, select the control point file and then set the corresponding correction parameters, which include correction, polynomial and resampling methods, as shown in Fig. 4.

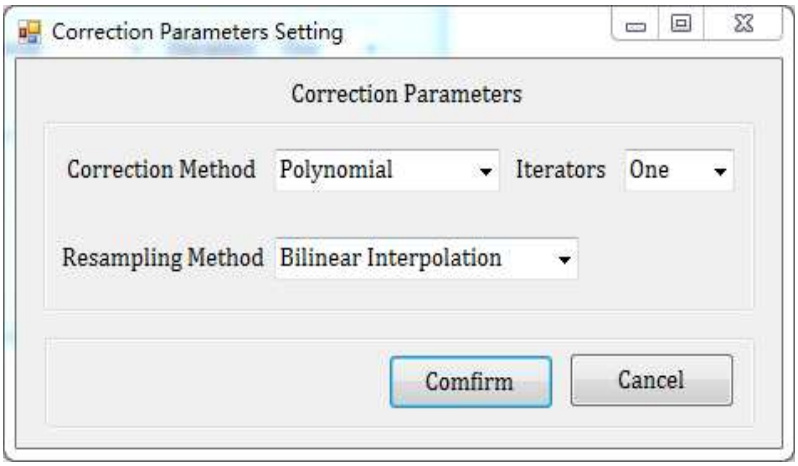

Fig. 4 The window of setting correction parameters.

The interactive mosaic of image is based on the mosaic of image pixels, is like that find the best mosaic location of the two images by moving them. And then according to the location of the image, construct a new array and assign values to finally preserve it [5]. The image with geometric precision correction can mosaic directly with the reference image. Our system adopted the strategy to mosaic the feature points automatically as follow: obtaining the corresponding relationship of the two images by using the polynomial model and then correct the reference image.

First of all, according to the corrected image, obtain the corresponding coordinates of its image pixels which are in its four angles. Then, obtain a region of covering the reference image and a minimal rectangle of the corresponding correction region as a new image to save. Next, ascertain the gray value of each image pixel in the new image.

The image pixels of the mosaic image are divided into four regions: the first kind of pixel point is belong to neither the reference image nor the correction image, called the background point; the second kind of pixel point is only belong to the reference image, called the reference image point; the third kind of pixel point is not only the reference image but also belong to the correction image, called the overlapping point; the forth kind of pixel point is only belong to the correction point, called the correction image point. The characteristics of these four regions' pixel points are different, so adopt different strategy to set gray value. For the background point, its pixel value is assigned to black. For

the reference image point, its pixel value is unchanged. For the overlapping point, its pixel value is replaced with pixel value of the reference image because of the geometric errors may be existed in the two image. For the correction image point, its pixel value is assigned to gray value of the correction image. Ensure the best mosaic location of the two images by moving their locations. At last, according to its location, select the start point and the end point of the seam-line and feather width. And then mosaic and feather the given area with compulsory improved algorithm provided by us [5]. Fig. 5 shows the effects after image mosaicing and feathering.

Fig.5 The effects after image mosaicing and feathering.

Summary

This system implements selection of image group control points, geometric correction, mosaicing, se- am lines eliminating and other functions with Interactive Data Language (IDL). It has been applied in Nanjing Meteorological Administration in China, and has already got the software copyright certific- ate authorized by Copyright Protection Center of China. It is targeted to solve the practical application problems such as preprocessing, mosaicing, seam-lines removing of civil UAV RS image.

Acknowledgments

This work was supported by the Fund of Guangxi Natural Science (2013GXNSFAA019344), Gui Financial Education Number [2013]19. It was also supported by the Plan of Science Research and Technology Development for Nanning (20121043), and for Nanning Qingxiu District (2013ZH19)

References

[1] H. Lu, Y.S. Li and J. He, in: An Automatic Mosaic Method in Unmanned Aerial Vehicle Images Based on Feature Points. Geography and Geo-In-formation Science. 2010. vol. 5, p. 16-19.
[2] R.S. Ma, H. Sun and Z.G. Lin, in: Geometric Correction and Registration of Optical Remote Sensing Image from Miniature Unmanned Aerial Vehicle. Journal of Nanjing Institute of Meteorology. 2012. vol. 5, p. 632-639.
[3] http://www.ittvis.com/language/en-US/Support/ENVIBooks.aspx. 2011.
[4] Y.C. Wan, D.L. Wang, J.H. Xiao, X.D. Lai, & J.Z. Xu, in: Automatic determination of seamlines for aerial image mosaicking based on vector roads alone. ISPRS Journal of Photogrammetry and Remote Sensing. 2013,p. 1-10.
[5] T.X. Huang, Y. Yang and L. Yang, in: Research on Geometric Precision Correction of Unmaned Aerial Vehicle Remote Sensing Image. Application Research of Computer. 2012. p. 76-79.

Advanced Materials Research Vols. 989-994 (2014) pp 3552-3555
© (2014) Trans Tech Publications, Switzerland
doi:10.4028/www.scientific.net/AMR.989-994.3552

Image Retrieval Based on Color Histogram of Saliency Map

Junfeng Wu[1, 2, a], Xianqiang Lv[1,] Wenlian Yang[1] ,Ye Tao[1], ,Jing Zhang[1], Song Yang[1]

[1] Educational Technology and Computing Center, Dalian Ocean University, Dalian, China, 116023

[2] School of Information Science and Technology, Dalian Maritime University, Dalian, China, 116023

[a]wujunfeng0411@gmail.com,

Keywords: Image Retrieval, Saliency Map, Color Histogram

Abstract. With the development of the internet, more and more images appear in the internet. How to effectively retrieve the desired image is still an important problem. In the past, traditional color histogram is used image retrieval system, but color histograms lack spatial information and are sensitive to intensity variation, color distortion and cropping. As a result, images with similar histograms may have totally different semantics. So the spatial information should be included in color histogram. The color histogram based on saliency map approach is introduced to overcome the above limitations. In this paper, we present a robust image retrieval based on color histogram of saliency map. Firstly, in order to extract useful spatial information of each pixel, the steady saliency map of the images is extracted. Then, color histogram based on saliency map is introduced, and the similarity between color images is computed by using the color histogram of saliency map. Experimental results show that the proposed color image retrieval is more accurate and efficient in retrieving the user-interested images.

Introduction

With the development of Internet, there is an explosive growth of color image databases. How to search through such a large scale collection effectively and efficiently is still a challenging task in computer vision [1] [2] [3]. The increasing number of images has opened the need for developing powerful tools for searching through such image databases. Automatic retrieval of an image from a whole data set using representative text-annotation comes from the early 1970s.However; manual indexing and annotation can be highly subjective, inefficient and tedious. Content based image retrieval (CBIR) techniques overcome these difficulties by making use of image-based features and attributes.So CBIR gets more and more attentions in nowadays [4].CBIR system relies on visual feature-based representations, such as color, texture, shape, etc., which can be extracted from images automatically. In these features, the most important feature is color because color is the most intuitionistic feature of a image, and it is robust to background complication and is independent of image size and orientation. Considerable research has been carried out on the basis of color content. The most popular representation of color information is global histogram. Statistically, it denotes the joint probability of intensities of the three-color channels, thus describing the global color distribution in an image. In general, the color histogram provides useful clues for the subsequent expression of similarity between images, due to its robustness to background complications and object distortion. Moreover, it is translation, scale, and rotation invariant, very simple to implement and systems encountering histograms exhibit a fast retrieval response that makes real-time implementation easier.

There are two main weaknesses in traditional color histogram. First, traditional color histogram doesn't take into account the spatial distribution of color across different areas of the image. The second, traditional color histogram cannot retrieve images with noise effectively [5].

To deal with the problems, a number of methods have been developed for integrating color and spatial information for content-based queries. Eauqueur [6, 7] make use of segmentation technology to obtain image's main areas in image retrieval, and then extract each area's color and spatial

information as image's features. But the image segmentation is still an open problem in computer vision so far. So these systems cannot generate extremely good performance. Wang [8] uses image's color area's spatial information and shape feature to calculate shape-matrix based histograms, but the model for similarity calculating has difference with human visual system. Ediz [9] suggests an image retrieval algorithm based on distance-orientation histogram, which calculates histograms in special distance and orientation. Jeong[10] uses Gaussian vector quantization technology to extract color histogram, but Gaussian quantization not only costs too much time but also the calculation is too complex. Wang [11] develops a method for making use of significant bit –plane, which could cut down time complexity and spatial complexity due to the low histogram's dimension.

In this paper, we propose a new color histogram based on saliency map. The saliency map, which can extract the important regions in the image, and can also separate the background and foreground. The color histogram based on saliency map is considered in the image retrieval system. The simulation experiment results have shown a significant improvement over the traditional methods.

The remainder of this paper is organized as follows: the calculation of saliency map is described in next section. And we will describe how to construct color histogram based on saliency map in Section 3. Extensive experiments results on benchmark datasets will be discussed in Section 4.We then make concluding remarks in Section 5.

The calculation of saliency map

In order to construct a novel histogram which contains spatial location information, a saliency map is combined with traditional scheme. So we should calculate the saliency map of the image [12].

2.1 Pattern distinctness

It's a common method to measure pattern distinctness based on comparing each image patch to all other image patches. If the patch is salient, it should be different from other patches. We also find the color image's non-distinct patches are mostly concentrated in the high-dimensional space, while distinct are mostly scattered. So all 9*9 patches are extracted and the average patch is computed. And then we compute the distance between each patch and the average patch and normalize by maximum distance. The average is shown as follows:

$$P_A = \frac{1}{N}\sum_{x=1}^{N} P_x \tag{1}$$

Where PA is image's average patch, p_x is image's 9*9 patch, if p_x is dissimilar to the average patch, this patch is considered salient.

In order to further improve the accuracy of measuring pattern distinctness, PCA coordinate is utilized. Thus, pattern distinctness $P(p_x)$ is defined as:

$$P(p_x) = \| \tilde{p}_x \|_1 \tag{2}$$

Where $\tilde{p}_x$ is p_x's PCA coordinate.

2.2 Color distinctness

Pattern distinctness is not sufficient for all images. So color distinctness should be used to further strengthen the extraction of salient objects. There are two steps for detecting regions of distinct color.

The first step, we utilize the SLIC superpixels to segment the image into regions. And then, we define the color distinctness of region in CIELAB color space as follows:

$$C(r_x) = \sum_{i=1}^{M} \| r_x - r_i \|_2 \tag{3}$$

Where M is the numbers of regions, r_x is the region we want to calculate and the r_i is the i-th region of M regions.

2.3The combination of pattern distinctness and color distinctness

After the steps above, we could get each patch's pattern distinctness and color distinctness. If the patch is distinct, the patch should salient both in color and pattern. So we could combine color and pattern as follows:

$$D(p_X) = P(p_x) \cdot C(p_x) \quad (4)$$

This map is normalized to the range [0, 1].

Generally speaking, the center of the image is more important than the surrounding. Because the salient object is generally located in the center of the image. So a weight map $G(p_x)$ that is weighted sum of all the Gaussians is generated. So the finally saliency map is shown as follows:

$$S(p_X) = G(p_x) \cdot D(p_x) \quad (5)$$

The calculation of color histogram based on saliency map

The traditional color histogram tells the global distribution of colors in the images. But color histogram doesn't take into account the spatial information. Adopting the saliency map could solve the problems. We don't calculate each color's distributing in the whole images any more, but in saliency map. We can eliminate useless information in the image but hold useful information. Because saliency map is important area in the image, so we could avoid the distribution of useless information. We now detail the different steps of scheme:

Step 1: calculating each color's saliency score in the image as section 2

Step 2: calculating the summation of each color's pixels' saliency score in the image

$$H(i) = \sum s(p_x) \quad (6)$$

Step 3: normalizing the vector $H(i)$ and calculating color histogram

Experiment results

To prove the capability of this paper, we give out the experimental results of our system, and compare the results with global histogram. During the experiment, we choose testing set which is used by system *SIMPLIcity* as image database. The images database are chosen form *Corel* image database, which includes 10 sorts (table 1) and which each sort has 100 images.

Table 1: Ten sorts of the image database

Class NO.	1	2	3	4	5	6	7	8	9	10
Semantic	Bus	Horse	Flower	Dinosaur	Building	Elephant	People	Beach	Scenery	Dish

To prove the validity of this paper, we choose 5 images in each sort randomly to calculate the precision and recall.

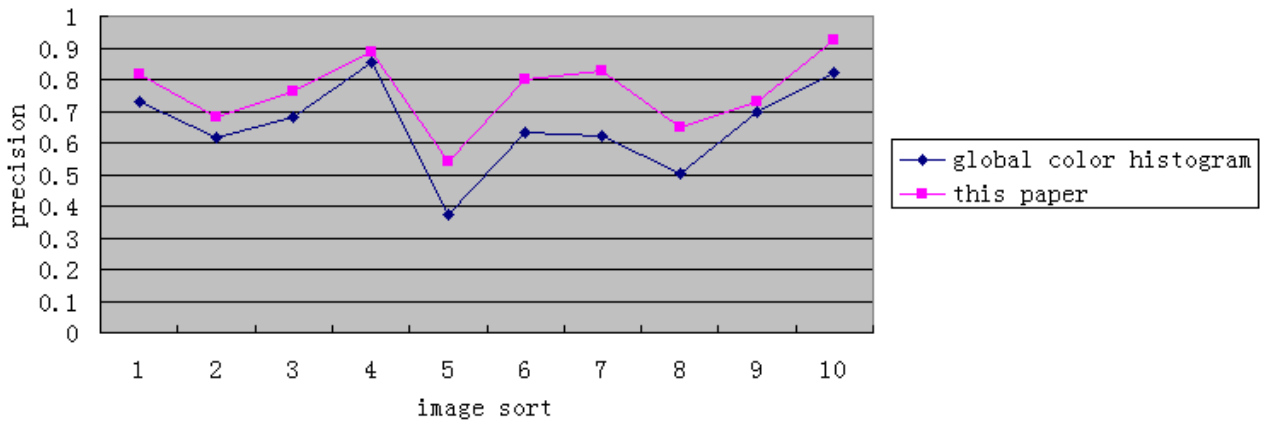

Fig1: Precision of global color histogram and this paper

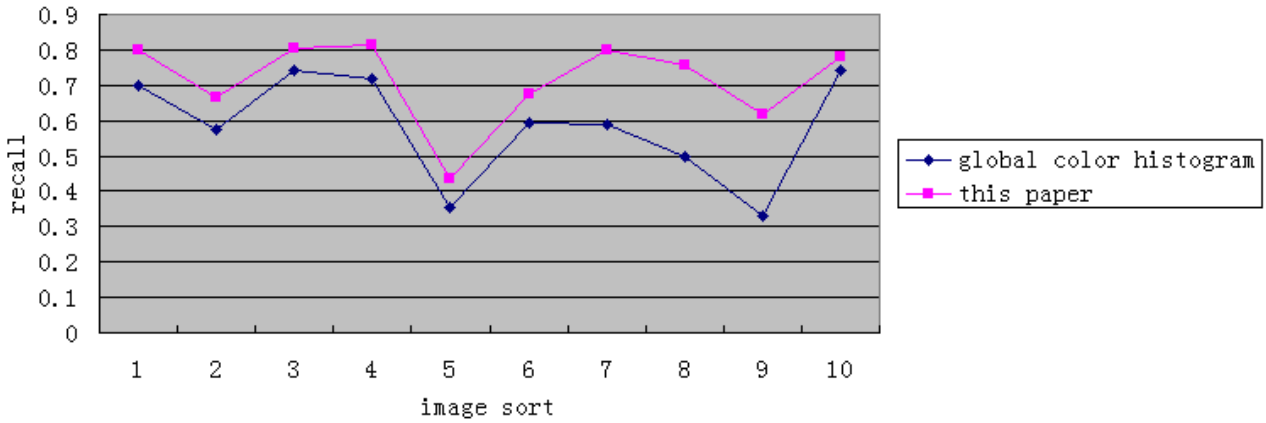

Fig2: Recall of global color histogram and this paper

Conclusion

In this paper, we propose a novel color histogram based on saliency map for image retrieval, saliency score of image is utilized to construct color histogram. In our new scheme, spatial location is contained in histogram, which can improve retrieval result. The simulation experiments show the effectiveness of our method.

References

[1] Xiaohui Shen, Zhe Lin, Jonathan Brandt, Ying Wu, "Detecting and Aligning Faces by Image Retrieval", In CVPR,2013

[2] R. Arandjelovic and A. Zisserman," Three things everyone should know to improve object retrieval",In CVPR,2012

[3] Datta R, Joshi D, Li J, Wang JZ," Image retrieval: ideas, influences, and trends of the new age", ACM Computing Surveys 40(2):1-60

[4] A.W.M.Smeulders, M.Worring, S.Santini, A.Gupta,and R.Jain. Content-based image retrieval at the end of the early years. IEEE Trans.on Pattern Analysis and Machine Intelligence, 2000, 22(12):1349-1380.

[5] Ritendra Datta, Jia Li, James Z. Wang . Content-based image retrieval-approaches and trends of the new Age. MIR'05, November 11-12, Singapore, 2005.

[6] Eauqueur J, Boujemaa N. Region-based image retrieval: Fast coarse segmentation and fine color description. Journal of Vision Languages and Computing (JVLC), Special Issue on Vision Information System, 2004, 15(1):69-95.

[7] Y. Deng, B. S. Manjunath, C. Kenney, M. S. Moore, and H. Shin. An efficient color representation for image retrieval. IEEE Trans. Image Processing, 2001, 10(1):140-147.

[8] Yongqing Sun, Shinji Ozawa. A hierarchical approach for region-based image retrieval. Systems, Man and Cybernetics, 2004 IEEE International Conference. 2004: 1117～1124

[9] Ruey-Feng Chang, Chii-Jen Chen, and Chen-Hao Liao. Region-based image retriveal using egeflow segmentation and region adjacency graph. Multimedia and Expo, 2004. ICME '04. 2004 IEEE International Conference,June 2004, 2004: 1883～1886

[10] HE X F,KING O,MA W Y,et al,Learning a semantic space form user's relevalce feedback for image retrieval[J]. IEEE Tracsaction On Circuit and System for Video Technology,2004,13(1):39-48

[11] Ediz Saykol, Ugur Güdükbay, Ozgür Ulusoy. A histogram-based approach for object-based query-by-shape-and-color in image and video databases. Image and Vision Computing, 2005, 23, 1170-1180.

[12] Ran Margolin, Ayellet Tal, Lihi Zelnik-Manor,"what makes a patch distinct",In 2013,CVPR

Advanced Materials Research Vols. 989-994 (2014) pp 3556-3560
© (2014) Trans Tech Publications, Switzerland
doi:10.4028/www.scientific.net/AMR.989-994.3556

Beamforming with Kerdock Codes in LTE System for High-speed Railway

YANG Zhi-hua[1, 2, a], WANG Lei-jun[1, b], FANG Ze-kai[1, c]

[1]School of Information Engineering, Wuyi University, Jiangmen 529020, Guangdong, China.

[2]Department of ECE, Sun Yat-senUniversity, Guangzhou 510275, China

[a]yhe9816@163.com, [b]leijun983@163.com, [c]1181479390@qq.com

Key words: Beamforming. High-speed Railway. Kerdock Codes. LTE

Abstract. Beamforming technique based the reciprocity of LTE communication system for high-speed railway is a practical way to improve the system performance in this paper. Kerdock codes, which facilitate efficient codebook and codeword search, are implemented in the LTE system for high-speed railway as the beamforming precoding codebook. The analysis of complexity and simulation results about the communication system of the beamforming with Kerdock codes (KBF) show that the proposed KBF can eliminate complex multiplications and improve the Bit Error Rate (BER) performance at large SNR compared with the existing beamfoming communication system for high-speed railway.

Introduction

With the rapid development of high-speed railway, the reliability and efficiency of wireless communication systems are facing serious challenges. The high speed mobility of onboard mobile stations brings serious Doppler Effect which reduces the performance of the existing communication systems. Recently, some of the advanced and innovative technologies of LTE can be applied to high-speed railway communication systems such as beamforming technique in [1,2]. Based on the linear topology of the high-speed communication systems base stations (eNodeBs) and the characteristic which the users and eNodeBs share the train running velocity information. Opportunistic Beamforming (OBF) [1] technology and Location information-assisted Opportunistic Beamforming (L-OBF) [2] for high-speed railway LTE system are proposed, and the L-OBF can obtain better achievable rate compared with the OBF.

In this paper, we apply Kerdock codes, whose codebook is generated by the transmitting antennas $M_t = 2^B (B \in \{1,2,\})$, as the beamforming precoding code in high-speed railway LTE system. We not only compare the storage and the search complexity between KBF and L-OBF, but also the BER performance and the achievable rate among KBF, L-OBF and OBF.

Channel Model for High Speed Railway

Linear network for high-speed railway communication is the same as in [2], each eNodeB has M_t antennas, the cell radius is R and the vertical distance from eNodeB to the track is d_{min}, the distance between the adjacent eNodeBs is L_e. Assume that there are U onboard transceivers on the train whose length is L, and then the equal space between the transceivers will be $L/(U-1)$. Every onboard transceiver, which can be viewed as a user u, is equipped with a signal antenna for communication with the eNodeBs. The distance gone through by user u is denoted by d_m, and as shown in Fig. 1, the angle of the direct path to user u's moving direction is Θ_u. Eq. 1 is the calculation of Θ_u.

$$\Theta_u = \begin{cases} arc\cot\left(\dfrac{\sqrt{R^2 - d_{\min}^2} - d_m}{d_{\min}}\right), & for \quad 0 \le d_m \le \sqrt{R^2 - d_{\min}^2} \\ \pi - arc\cot\left(\dfrac{d_m - \sqrt{R^2 - d_{\min}^2}}{d_{\min}}\right), & for \sqrt{R^2 - d_{\min}^2} < d_m \le 2\sqrt{R^2 - d_{\min}^2} \end{cases} . \quad (1)$$

Compared to the distance between the eNodeB and the user, the transmit antennas are at close proximity, and then the fading gains of the antennas are correlated [1]. The correlated Rician channel between the user u and the eNodeB's antenna n can be expressed as [3]:

$$h_{un}(t) = \sqrt{\frac{K_u}{1+K_u}} \exp(j\theta_{un}) + \sqrt{\frac{1}{1+K_u}} b_{un}(t) . \quad (2)$$

where K_u denotes the Rician factor of the physical channel from eNodeB to user u, and $b_{un}(t)$ is an independent complex Gaussian random variable with zero mean and variance one: $b_{un}(t) \sim CN(0,1)$. The angle θ_{un} is calculated as follows:

$$\theta_{un} = \frac{2\pi n d f_c \cos\Theta_u}{c} . \quad (3)$$

where the space d between two antennas is not larger than half wavelength, f_c denotes the carrier frequency, c represents the velocity of light.

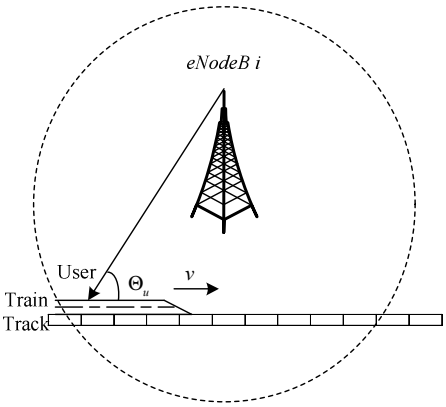

Figure 1: User *u*'s direction of arrival Θ_u

The Construction of Kerdock Codes

A brief illustration of constructing mutually unbiased bases (MUBs) for Kerdock codes was introduced in [4] and [5]. The Kerdock codes are used to generate the precoded LTE System for high-speed railway. The generated M_t+1 MUBs are $D, D^2, \ldots, D^{Mt+1} = I$. The general construction of Kerdock codebook is as follows.

1) Construct the $M_t \times M_t$ Sylveste-Hadamard matrix $H_{Mt} = H_2 \otimes H_2 \ldots (B\ times)$ by the Kronecker product of B Sylveste-Hadamard matrix $H_2 = \begin{bmatrix} 1 & 1 \\ 1 & -1 \end{bmatrix}$.

2) Generate a $M_t \times M_t$ diagonal matrix by $\{1, -1, j, -j\}$. Then get the matrix D by the product of the diagonal generator matrix and H_{Mt}. The generated M_t+1 MUBs are $D, D^2, \ldots, D^{Mt+1} = I$.

3) Take the columns of each basis to construct the beamforming codebook $F = \{f_1 = [D]_1, f_2 = [D]_2, \cdots, f_{(M_t+1)\times M_t} = [D^{M_t+1}]_{M_t}\}$.

Beamforming Communication System with Kerdock Codes for High-speed Railway

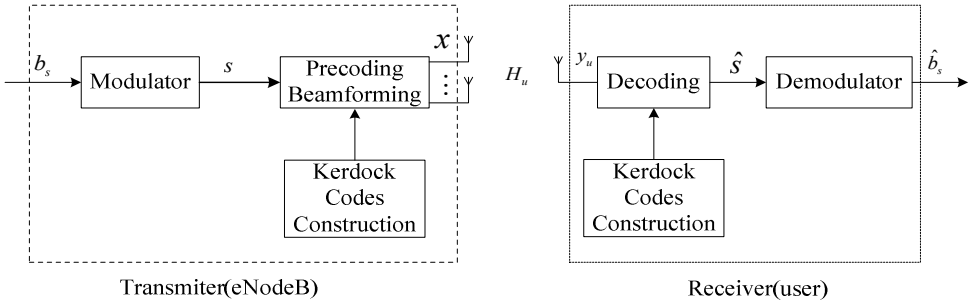

Figure 2：Beamforming with Kerdock codes communication system for high-speed railway

In the beamforming with Kerdock codes communication system for high-speed railway, let each eNodeB and user construct the beamforming Kerdock codebook $F=\{f_1,f_2,\ldots,f_N\}$. At time slot t, the eNodeBs select the user and the codewords according to the maximum ratio combining criterion such as

$$[u^*, F_u^*] = \arg \max_{\substack{u\in\{1,\cdots,U\} \\ F_i\in F}} \left| H_u F_i \right|. \tag{4}$$

The communication system model between eNodeB and the selected user is shown in Fig. 2. The i.i.d.(independent identity distributed) bit stream b_s is modulated to get $s(t)$ by MQAM modulation. The $s(t)$ is precoded to obtain the transmit signal vector $x=F_u^* s(t)$. The received signal vector of the user u is

$$y_u(t) = H_u(t)x + n_u(t). \tag{5}$$

where $H_u=[h_{u1},h_{u2},\ldots,h_{uMt}]$, and $n_u(t)$ is additive white Gaussian noise: $n_u(t)\sim CN(0,\sigma^2)$.

Then the user u get the signal by ML detection such as

$$\hat{s}(t) = \arg \min_{s(k)\in Q} \left| y_n(t) - H_u(t) F_u^* s(t) \right|. \tag{6}$$

Storage and Search Complexity

Table 1: The storage of eNodeB when M_t and U changes (N_b=8bits)

M_t	2		4	
U	8	24	8	24
KBF (bit)	64	64	96	96
L-OBF (bit)	256	768	512	1536

Storage. Assume that both the the eNodeB and the user need N_b bits to store a real number, and there are U users in the system. In [1] and [2], OBF and L-OBF need $2N_bUM_t$ bits for both the eNodeB and the user. However, KBF only needs $(4+2\times M_t)\times N_b$ bits. Compared to OBF and L-OBF, the storage of the KBF system has no relation with the number of the users.

For example, N_b = 8bits, the storage of the eNodeBs of the KBF and L-OBF system is shown in Table 1. It can be seen that the storage of the KBF is less than L-OBF.

Search Complexity. The search complexity is concerned about: I. the search of the user u by eNodeB; II. the search of the codeword F_u^* by eNodeB; III. the detection of the signal by the user u. Let the number of the users be U, the transmit antennas of the eNodeB be M_t, M-ary modulation be implemented. Multiplication and addition of complex numbers are considered in this section.

In the L-OBF system, the operation of I and II requires $M_t \times k \times U$ complex multiplications and $(M_t-1) \times k \times U$ complex additions. And for KBF system, the same operation of I and II in Eq. 4 need $UN \times (M_t-1)$ complex additions. For both L-OBF and KBF, the operation III in Eq. 5 requires the same M_t+M-1 complex additions, $M_t + M$ and M complex multiplications, respectively.

From the above comparison of KBF and L-OBF, the KBF system needs a small storage and the complexity is low at both the transmitter and the receiver.

Simulation Results

In this section, the results demonstrated below are based on Monte Carlo simulation over the channel for high speed railway. The simulation parameter settings are as follows: the antenna is omni-directional, f_c = 2GHz, K_u = 6, d_{min} = 30, R = 3km, L_e = 4.8km, transmission time interval Δt = 500ms, and the speed of the train is 360km/h. The Kerdock codebook for M_t = 4 and M_t = 2 are constructed by section 2(see in [4]).

The BER of 16QAM with Mt = 2 and Mt = 4 when U=16 is depicted in Fig. 3 and Fig. 4. It is observe that the performance of KBF system is better than L-OBF system when SNR > 12dB and SNR > 8.2dB, respectively.

$$R = E[\log_2(1+\rho F^H H^H HF)]. \tag{9}$$

The ergodic achievable rate of Mt = 2 and Mt = 4 with different number of users based on Eq. 9(ρ is the average SNR) is depicted in Fig. 5 and Fig. 6. We can see that the achievable rate of KBF system are lower than the L-OBF system, but higher than OBF system.

Conclusion

In this paper, Kerdock codes are applied as the beamforming precoding code in high-speed railway LTE system. In KBF system, the signal processing at eNodeB only needs addition operations. Although the signal detection at the user requires the same number of complex additions, the numbers of complex multiplications are less than L-OBF and OBF system. Therefore, the KBF system complexity is low, and can reduce implementation costs for signal processing. The simulation results show that the BER performance of KBF system is better than L-OBF system and OBF system at large SNR. The achievable rate of KBF system is lower than the L-OBF system, but higher than OBF system. So the beamforming with Kerdock Codes in LTE system for high-speed railway can get a tradeoff between the performance and complexity.

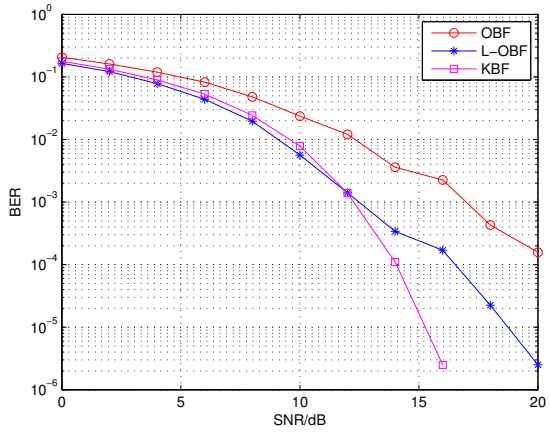

Figure 3：BER for M_t = 2

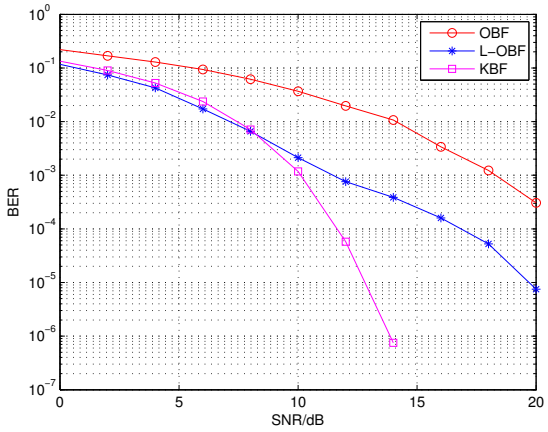

Figure 4：BER for M_t = 4

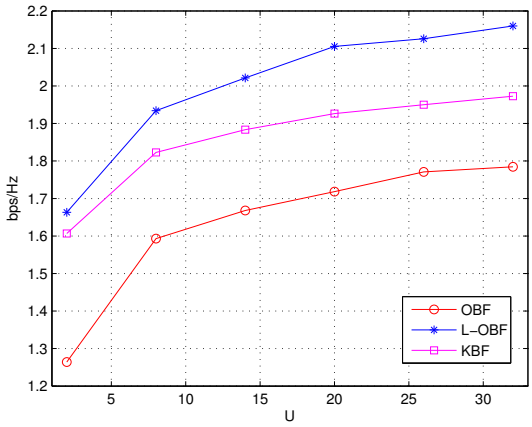

Figure 5：Achievable rate for $M_t = 2$

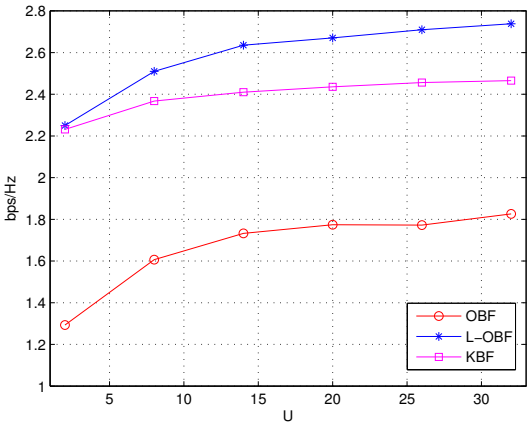

Figure 6：Achievable rate for $M_t = 4$

Acknowledgement

This work was supported by 973 Program (No.2012CB316100), NSF (No.61172082), NSF (No.61372193), NSF (No.61072127) and the finance and special funds of Jiangmen, Guangdong ([2010]201) of China.

References

[1] Viswanath P, Tse D N C, Laroia R: Opportunistic beamforming using dumb antennas. IEEE Transactions on Information Theory. 2002, 48(6): 1277-1294.

[2] Cheng M, Fang X: Location information-assisted opportunistic beamforming in LTE system for high-speed railway. EURASIP Journal on Wireless Communications and Networking, 2012, 2012(1): 1-7.

[3] Kim I M, Yi Z, Kim D, et al: Improved opportunistic beamforming in Ricean channels. IEEE Transactions on Communications. 2006, 54(12): 2199-2211.

[4] Inoue T, Heath R W: Kerdock codes for limited feedback precoded MIMO systems. IEEE Transactions on Signal Processing. 2009, 57(9): 3711-3716.

[5] Heath R W, Strohmer T, Paulraj A J: On quasi-orthogonal signatures for CDMA stems. IEEE Transactions on Information Theory. 2006, 52(3): 1217-1226.

Advanced Materials Research Vols. 989-994 (2014) pp 3561-3566
© (2014) Trans Tech Publications, Switzerland
doi:10.4028/www.scientific.net/AMR.989-994.3561

A chaotic image encryption algorithm based on a dynamical feedback operation

Guosheng GU[1, a], Jie Ling[1,b], Guobo Xie[1,c], Yuyi Ou[1,d]

[1]Faculty of Computer, Guangdong University of Technology, Guangzhou, China

[a]gsgu@foxmail.com, [b]jling@gdut.edu.cn, [c]guoboxie@163.com, [d]ouyuyi@163.com

Keywords: image encryption, chaotic map, dynamical diffusion

Abstract. This paper designs an image encryption algorithm with a dynamical feedback operation based on sensitive chaotic system. In the proposed algorithm, the piece wise linear chaotic map is selected to construct pseudo-random keystream sequences. The pseudorandom keystream sequences are used to permute and substitute the plain image data. To enhance the complexity and security of the algorithm, each pixel is dynamically confused by its two previous adjacent encrypted pixels which are specified by a quantized binary tuple derived from a chaotic element. Both theoretical analysis and experimental tests show that the proposed algorithm is secure and efficient.

Introduction

Securing of digital image has become an important research topic in recent years. Image data have particular properties such as bulk capacity, high redundancy and high correlation among image pixels. Traditional encryption technologies regard digital image data as common data without considering their special properties, so they are not suited in protecting digital image data.

The chaotic system has interesting and close relationship with cryptography. Besides, the chaotic system has a lot significant properties which are favorable to the digital image security, such as ergodicity, aperiodicity, nonconvergency and sensitivity to initial conditions [1]. Therefore a lot of chaotic encryption methods [2-12] are investigated and employed in securing digital image data. In the literature, most of the algorithms are composed of the permutation and substitution procedures to satisfy the Shanon's confusion and diffusion criteria. In a substitution procedure, feedback operation is always adopted to resist chosen-plaintext attacks. Generally, each pixel is confused by its previous adjacent encrypted pixel, such that feedback operation has a fixed mod.

In this paper, an image encryption algorithm based on sensitive chaotic system is proposed. First the original image is permuted by an effective matrix multiplexing transform. Second, each pixel of the image is dynamically confused by a chaotic element and the two previous adjacent encrypted pixels which are specified by a quantized binary tuple derived from a chaotic element. Such a dynamically feedback operation provides high complexity. Computer simulation results and analysis are provided to demonstrate the algorithm's high level performance of security and efficiency.

PWLCM

One dimensional chaotic function, Logistic map, is widely used in cryptography applications as its high level efficiency and low computational complexity. However, it is pointed out insecure to statistical attacks. To overcome the security weakness of Logistic map, piece wise linear chaotic map (PWLCM) is adopted to generate chaotic numbers in this paper. The PWLCM is described by:

$$x(n)=F(x(n-1))=\begin{cases} x(n-1)\times\dfrac{1}{r}, & \text{if} \quad 0\le x(n-1)<r \\ (x(n-1)-r)\times\dfrac{1}{0.5-r}, & if \quad r\le x(n-1)<0.5 \\ F(1-x(n-1)), & if \quad 0.5\le x(n-1)<1 \end{cases} \tag{1}$$

where r is a control parameter of PWLCM and $x(n) \in (0,1)$ is the iteration trajectory value. When $r \in (0,0.5)$, PWLCM evolves into chaotic state. PWLCM can produce excellent pseudo-random sequences as it has uniform invariant distribution and good ergodicity. The produced pseudo-random sequences are fit to digital image cryptographic application.

The Proposed Image Encryption Algorithm

The proposed algorithm is described in this section. The algorithm includes two parts: permutation procedure and substitution procedure. They are stated in the following subsections.

3.1 Permutation Procedure

For any size ($M \times N$) of a grayscale image $I(m,n)$, The permutation procedure is described as follows:

1. Use Eq. (1) to generate two groups of pseudo-random sequences $\{x_1(i)\}_{i=0}^{M-1}$ and $\{x_2(j)\}_{j=0}^{N-1}$, with the different initial values and parameters of $(x_1(0), r_1)$ and $(x_2(0), r_2)$ respectively.

2. Sort the sequences $\{x_1(i)\}_{i=0}^{M-1}$ and $\{x_2(j)\}_{j=0}^{N-1}$ in ascending order and get two ordered sequences $\{\overline{x_1}(i)\}_{i=0}^{M-1}$ and $\{\overline{x_2}(j)\}_{j=0}^{N-1}$.

3. Find the index values of $\{\overline{x_1}(i)\}_{i=0}^{M-1}$ in $\{x_1(i)\}_{i=0}^{M-1}$ and get the index transform sequence $\{T_1(i)\}_{i=0}^{M-1}$. Get another index transform sequence $\{T_2(j)\}_{j=0}^{N-1}$ from $\{x_2(j)\}_{j=0}^{N-1}$ and $\{\overline{x_2}(j)\}_{j=0}^{N-1}$ in the same way.

4. Define permutation matrices by

$$P_1(i,j)_{M\times M} = \begin{cases} 1 & for \quad (T_1(i), i) \\ 0 & others \end{cases}, \quad P_2(i,j)_{N\times N} = \begin{cases} 1 & for \quad (j, T_2(j)) \\ 0 & others \end{cases} \tag{2}$$

Then the permutation procedure is described as an effective matrix multiplexing transform

$$P = P_1 I P_2 \tag{3}$$

The inverse transform of permutation for decryption is described by

$$I = P_1^{-1} P P_2^{-1} \tag{4}$$

3.2 Substitution Procedure

The substitution procedure is described as follows:

1. Get the permuted image $P_{M\times N}$ from the permutation procedure of Section 3.1. We treat $P_{M\times N}$ as a linear sequence in the substitution procedure.

2. Iterate the PWLCM k times with initial value and parameter $(x_3(0), r_3)$ to get rid of the harmful effect of initial value.

3. For $i = 0$ to $M \times N - 1$ perform the following steps:

(a) Compute a chaotic state value x from PWLCM.

(b) Calculate an 8-bit random value

$$d_i = \mathrm{mod}(floor(x \times 2^{16}), 256) \tag{5}$$

and a binary tuple

$$q_i = (q_i(0), q_i(1)) = \begin{cases} (0,1) & if \quad 0 \le x < s \\ (1,0) & if \quad s \le x < 2s \\ (1,1) & if \quad 2s \le x \le 1 \end{cases} \tag{6}$$

where $s \in (0,0.5)$ is a control parameter which can be served as a part of the key.

(c) Compute the current value of the cipher image by the following formula

$$C_i = P_i \oplus \mathrm{mod}(q_i(0)\times C_{i-2} + q_i(1)\times C_{i-1} + d_i, 256) \quad (7)$$

where $\oplus$ is the bit-wise exclusive OR operator. The initial constant value C_{-2} and C_{-1} are served as a part of the key too. The inverse transform of diffusion for decryption is described by

$$P_i = C_i \oplus \mathrm{mod}(q_i(0)\times C_{i-2} + q_i(1)\times C_{i-1} + d_i, 256) \quad (8)$$

The permutation procedure and substitution procedures are to satisfy the Shanon's confusion and diffusion properties respectively. In order to enhance the security, these procedures will be repeated t ($t \geq 2$) times and the final encrypted image is obtained.

3.3 Discussion

The proposed encryption algorithm has a simple structure that combines two primitive procedures. This structure provides high efficiency and simplicity for implementation.

The proposed algorithm shows high sensitivity and feedback properties. Depending on the quantized binary tuples of PLWCM, any output value C_i of the substitution procedure is a dynamical confusion obtained from its two respective previous adjacent encrypted pixels C_{i-2} and C_{i-1}. Specified by the quantized binary tuple $(q_i(0), q_i(1))$, C_{i-2} and C_{i-1} are dynamically adopted to participate in confusing the plain pixel P_i, which greatly enhances the sensitivity and security of the algorithm.

Experiment Result

For validating the proposed algorithm, original and encrypted images of Barbara and Peppers are shown in Fig. 1. The results are achieved by setting $r = 0.3$, $s = 0.4$, $k = 1000$, and $t = 2$. From the figure, no visual relationship can be found between the original and encrypted images.

(a) Lena (b) Encrypted Lena (c) Peppers (d) Encrypted Peppers

Fig. 1 The original images and the encryption results

Performance Analysis

Several tests and analysis are made in this section to validate the security of the proposed algorithm.

5.1 Key Space

To provide the proposed algorithm with high security, the key space should be large enough to make any brute force attack infeasible [13]. The encryption algorithm consists of nine key parameters in this paper, they are $x_1(0)$, $x_2(0)$, $x_3(0)$, r_1, r_2, r_3, s, C_{-2} and C_{-1}, where the real numbers $x_1(0)$, $x_2(0)$, $x_3(0) \in (0,1)$, r_1, r_2, r_3, $s \in (0,0.5)$ and the integer parameters C_{-2}, $C_{-1} \in [0,255]$. If the calculation precision is 10^{-14}, the secret key space is $(10^{14})^7 (2^8)^2 \approx 2^{341}$. Clearly the key space is large enough to resist the brute force attacks.

5.2 Histogram Analysis

The histogram indicates the pixels distribution of an image. An encryption scheme is more robust against statistical attack and differential attack when the histogram of an encrypted image has a uniform distribution. Fig. 2(a) and (b) represent the histogram of plain Barbara and encrypted Barbara respectively. From the figure it is clear that the histogram of the encrypted image is completely uniform and significantly different from that of the plain image. Hence, it is not feasible to employ statistical attack or differential attack on the proposed algorithm.

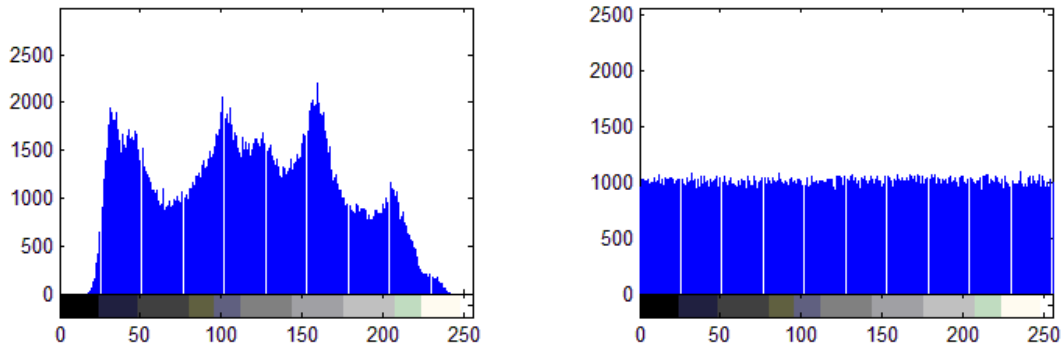

(a) Histogram of plain Barbara (b) Histogram of encrypted Barbara

Fig. 2 The histogram distribution of plain image and cipher image

5.3 Sensitivity Analysis

Sensitivity includes encrypted key sensitivity and plain image sensitivity.

First, we encrypt the original Barbara with a slightly change encrypted key (changing $x_1(0)$ with a precision of 10^{-14} compared to the encrypted key used in Fig. 1(b)). Fig. 3(a) shows the encrypted image with the changed key. Fig. 3(b) shows the absolute differential image between Fig. 1(b) and Fig. 3(a). With a simple computation, the difference between Fig. 1(b) and Fig. 3(a) is 99.59%, which means the encryption process is quite sensitive to the encrypted key. Tests on other secret parameters have similar results, so they are omitted from illustration.

Second, we encrypt a modified Barbara with a slightly change pixel (changing the last bit of the first pixel) using the same key that used in Fig. 1(b). Fig. 3(c) shows the encrypted image. Fig. 3(d) shows the absolute differential image between Fig. 1(b) and Fig. 3(c). The difference between Fig. 1(b) and Fig. 3(c) is 99.65%, which means the encryption process is quite sensitive to the plain image too.

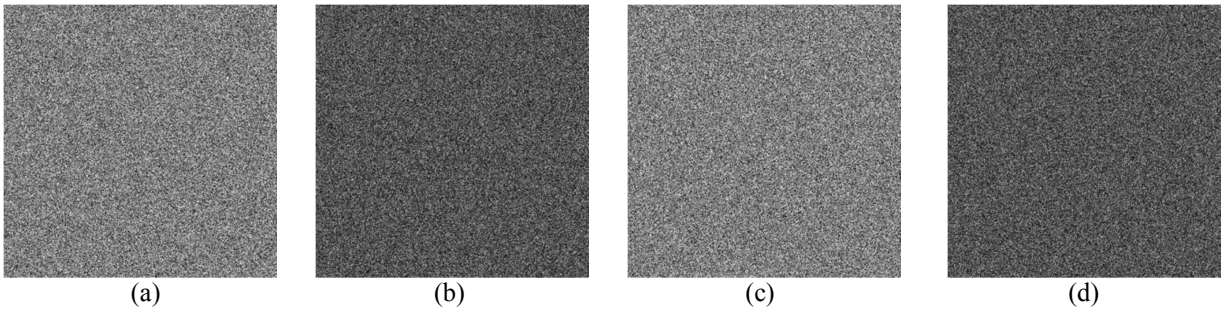

(a) (b) (c) (d)

Fig. 3 Sensitivity Analysis: (a) Encrypted image with only wrong initial value $x_1(0)$; (b) Differential image between Fig. 1(b) and Fig. 3(a); (c) Encrypted image with modified Barbara; (d) Differential image between Fig. 1(b) and Fig. 3(c)

On the other hand, two indicators, *NPCR* and *UACI*, are computed to measure the difference between the encrypted images when the respective original images have only one bit difference. *NPCR* indicates the number of pixels change rate between two encrypted images, $E(m,n)$ and $E'(m,n)$, while only one pixel of the plain image changed. *UACI* shows the average intensity of differences between two encrypted images. They are calculated by:

$$UACI = \frac{1}{M \times N} \sum_{m,n} \frac{|E(m,n) - E'(m,n)|}{255} \times 100\%, \qquad NPCR = \frac{\sum_{m,n} D(m,n)}{M \times N} \times 100\% \tag{10}$$

where $$D(m,n) = \begin{cases} 1 & if \quad E(m,n) \neq E'(m,n) \\ 0 & if \quad E(m,n) = E'(m,n) \end{cases} \tag{11}$$

Generally, an encryption scheme is robust against differential attack when the NPCR value is over 99.6% and the UACI value is over 33.3%. The result of the proposed algorithm is showed in Tab. 1.

Tab. 1 The *NPCR* and *UACI* performance

Encrypted image	NPCR	UACI
Barbara	99.6317	33.4387
Peppers	99.6195	33.3815

Tab. 2 Coefficients of the original image and the encrypted image

Correlations	Original image	Encrypted image
Horizontal	0.9814	0.0156
Vertical	0.9632	0.0108
Diagonal	0.9127	0.0113

5.4 Correlation Analysis

Commonly plain image has strong correlations among adjacent pixels which makes statistical attack possible. To investigate the correlations of adjacent pixels of the proposed algorithm, 1000 pairs of two adjacent pixels (in horizontal, vertical, and diagonal direction) are randomly selected from the plain Barbara and the respective encrypted image, and the correlation coefficient is calculated by the following formula:

$$r_{xy} = \frac{E(x - E(x)E(y - E(y))}{\sqrt{D(x)D(y)}} \tag{12}$$

where $E(x)$ and $D(x)$ are the expectation and variance of variable x, respectively. The average results are given in Tab. 2. It is clearly that all kinds of the correlation coefficients are extremely near zero which denotes low correlations.

5.5 Information Entropy Analysis

Information entropy is an important indicator of randomness in information theory. The information entropy is calculated by:

$$H(m) = \sum_{i=0}^{2^N - 1} p(m_i) \log_2 \frac{1}{p(m_i)} \tag{13}$$

where $p(m_i)$ represents the probability of symbol m. In the gray scale image processing case, there are totally 256 possible outcomes of the signal with equal probability. Thus, the information entropy should ideally be $H(m) = 8$ for an encrypted image. The test results of information entropy for encrypted image are listed in Tab. 3.

Tab. 3 The information entropy performance

Encrypted image	Information entropy
Barbara	7.9981
Peppers	7.9963

Tab. 4 Comparison of speed performance

Image size	Encryption speed of proposed algorithm(ms)	Encryption speed of DES(ms)
256*256	15	46
512*512	48	181
1024*1024	190	683

5.6 Speed Analysis

In practical image transmission, expecially in real-time internet applications, the encryption time must also be considered. Measurements of encryption speed of images with various sizes by using the

proposed algorithm and the well-known DES algorithm are listed in Tab. 4. The runing envirenment in the test is: Windows 7, Matlab 7.8, 2.6 GHz Intel Core2 Duo with 4GB memory. From Tab. 4 we can see the proposed algorithm is advantaged and it is fast enough for practical applications.

Conclusions

This paper proposes an image encryption algorithm with a dynamical feedback operation based on sensitive chaotic maps. The proposed algorithm has a simple structure that combines two primitive procedures: permutation and substitution. Each encrypted pixel is dynamically confused by its two respective previous adjacent encrypted pixels which greatly enhances the complexity and security of the algorithm. Several security and performance analysis are carried out to illustrate that the proposed algorithm has good encryption performance.

Acknowledgement

This work is supported by the Key Project of Natural Science Foundation of Guangdong, China (No. S2012020011071), Project on the Integration of Industry, Education and Research of Guangdong Province (No. 2012B091000037, No. 2012B091000041), Guangdong Provincial Key Laboratory of construction projects (2011A091000046), Guangdong-Hongkong Breakthrough Key Project (2012A080107007), Guangdong Province university discipline construction special funds for scientific and technological innovation projects (No. 2013KJCX0064) and Key Project of Guangdong Ministry of Science and Technology (No. 2012A080103010).

References

[1] J. Fridrich. Symmetric ciphers based on two-dimensional chaotic maps. Int. J. Bifurcation and Chaos, vol. 8, no. 6, 1998: 1259-1284.
[2] G. R. Chen, Y. B. Mao, K. C. Charles. A symmetric image encryption scheme based on 3D chaotic cat maps. Chaos, Solutions & Fractals, 2004, 21(3): 749-761.
[3] A. N. Pisarchik, M. Zanin. Image encryption with chaotically coupled chaotic maps. Physica D: Nonlinear Phenomena, 2008, 237(20): 2638-2648.
[4] X. Tong, M. Cui, Image encryption scheme based on 3D baker with dynamical compound chaotic sequence cipher generator. Signal Processing, 2009, 89(4): 480-491.
[5] R. S. Ye. A novel chaos-based image encryption scheme with an efficient permutation-diffusion mechanism. Optics Communications. 2011, 284: 5290-5298.
[6] W. Yong, W. W. Kwok, X. F. Liao, et al. A new chaos-based fast image encryption algorithm. Applied Soft Computing. 2011, 11(1): 514-522.
[7] X. Y. Wang, X. Qin. A new pseudo-random number generator based on CML and chaotic iteration. Nonlinear Dynamics. 2012, 70: 1589-1592.
[8] S. M. Seyedzadeh, S. Mirzakuchaki. A fast color image encryption algorithm based on coupled two-dimensional piecewise chaotic map. Signal Processing. 2012, 92(5):1202-1215.
[9] N. Bigdeli, Y. Farid, K. Afshar. A novel image encryption/decryption scheme based on chaotic neural networks. Engineering Applications of Artificial Intelligence, 2012, 25(4): 753-765.
[10] C. Y. Song, Y. L Qiao, X. Z. Zhang. An image encryption scheme based on new spatiotemporal chaos. Optik - Int. J. Light Electron Opt. 2012, http://dx.doi.org/10.1016/j.ijleo.2012.11.002
[11] X. L. Huang. Image encryption algorithm using chaotic Chebyshev generator. Nonlinear Dynamics. 2012, 67: 2411–2417.
[12] Q. Zhang, L. Guo, X. P. Wei. A novel image fusion encryption algorithm based on DNA sequence operation and hyper-chaotic system. Optik - Int. J. Light Electron Opt. 2013, http://dx.doi.org/10.1016/j.ijleo.2012.11.018
[13] D. R. Stinson, Cryptography: Theory and Practice. CRC press, 2007.

Advanced Materials Research Vols. 989-994 (2014) pp 3567-3570
© (2014) Trans Tech Publications, Switzerland
doi:10.4028/www.scientific.net/AMR.989-994.3567

The Application of the Movement Video Analysis Technology in the Sports Area

Xiao Xiao

Physical Education Department of Nanyang Institute of Technology Nanyang 473000

Keywords: Movement Video; Analysis Software; Network Technology; Multi-Media Technology

Abstract. In this paper, the author starts from the literature reviews and the development and application of the video analysis technology software in the sports area, discussing the movement video collection, the processed and transformed digits from the computer software. Through the application of the first-line coaches and teachers in the sports teaching course, the athletes or students can see the technical action and tactical implementation effects, get the timely and accurate analysis information of which it will be beneficial to put the language style into the intuitive image, make the exchange for the coach or the students at the spot. In this way, the sports training and the teaching results will be greatly improved.

At present, the visualization technology of the multi-media computers and the Internet in the motion analysis is setting off a revolution in the action skill improvement. It is long-standing to guide the athlete with the motion video analysis techniques. in the 1980s, the sports video analysis technology is widely used to the sports programs in the European countries. In the sports teaching process, students are able to see their technical movements and immediate tactical effects after the training, and get the quick and accurate analysis, change the language style into the visual images, make the live exchange for the teachers and students. In this way, the technology will be greatly applied to the increasing effectiveness of the sports teaching and training levels.

The Application of Video Analysis Technology in Physical Education Teaching

1.1 The Collection and Organization of Video Analysis Materials

Firstly, it is necessary to confirm the technical analysis action requirements in a project. you can download the information via the Internet or make a record by yourself. Generally, you can use an ordinary video equipment or a high-speed video equipment to record the video. according to the characteristics of each project, it needs to install a video capture device of which the capturing steps are divided into the following steps:

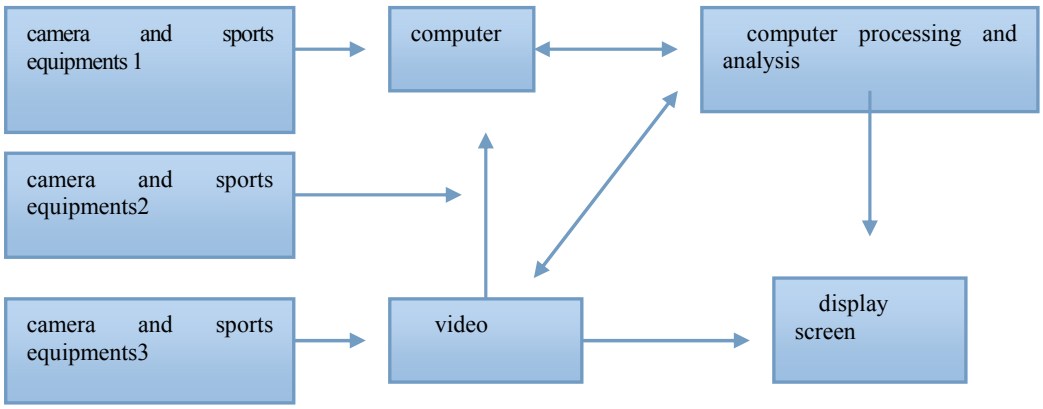

Figure 1 The major steps of video captures

Then entire collection equipments consist of two parts: one part is to complete the shooting, storage, and playback, delay and other requirements in terms of motion video; another part is the processing and analysis works in sending the commands to the computer, collecting the interesting

action video for the teacher or student. The images and related data processing results can be displayed in the big screen TVs and the computer display. In the computer, it is able to enter and store the collected video materials from the IEEE -1394 high-speed input interface or the video capture card.

Currently, the major domestic and international analysis system software are three-dimensional analysis software like dart-fish4.09 (Germany), sinimotion 3D7.2 (Switzerland), USA Ari-el, the gold medal coach DVCoach system. In the computer, the shooting films or images will be stored. The above mentioned software is used to organize and classify the interesting action videos for the teachers or the students.

1.2 Video Analysis

Through the collected digital video or the comparison methods, The main function of the sports video analysis technology is to improve the teachers' teaching level and the sports training level so that there is a higher level for the school sports training, competition and sports teaching process. For example: the sports video analysis software can offer the visual feedback in a direct, convenient and fast way of which the effective platform allows the students and teachers to make the technical communication and exchange; After the training, the sports video analysis software can also provide the in-depth analysis in comparing the completion situation of the technical action. The existing video analysis software has the following functions: video broadcast, manual drawing of video analysis, action video panorama synthesis, action video superposition contrast, the parameter acquisition of the human body motion , motion curve display and analysis. In sports training field, the quick feedback functions of the technical movement image is accessible to repeatedly play the students' immediate technical training. At the same time, it is able to take the technical video about the excellent students in the hard disk so as to make a comparison and analysis. As well, the freezing effects of the action video panorama is used to analyze the changing process and trajectory in a statical way so as to make an analysis about the understanding and completion of the action. It is able to overlay and compare the students' action with the video of the excellent athletes' action in the analysis software of which a seamless video is produced. In this way, the difference of the two actions can be clearly discovered for the athletes to master the essentials and improve the physical training performance in a faster way. With the powerful analysis and drawing tool (Figure 2) , it is able to calculate its speed, angle, height and length. The data table will be automatically generated so as to automatically track and calculate the changing data size, and then display and output the data in a generic data sheet. The teachers' training and scientific researches will be greatly improved.

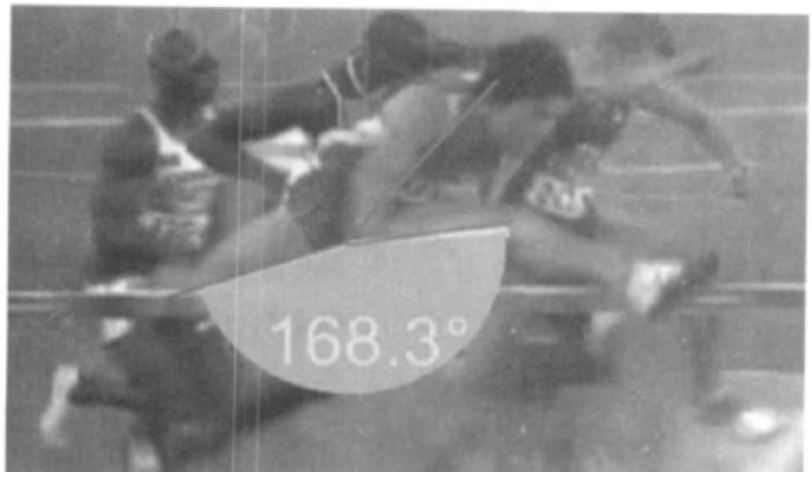

Figure 2

In the whole process, the teachers can extract all the technical parameters of the students (such as joint position, angle and angular velocity, etc) through the analysis software. with these analysis information, the teachers can provide the guidance and advices for the students in the training of which it is conducive for the improvement of the students' training level. These data are compiled

into a database so as to simulate the action. In the analysis software, it needs to enter the three-dimensional structure of the athletes. After that, the action will be converted into a standard level. In the process of training and teaching, the contrasting results will be sent to the students through the big screen or other media. For example, the human body motion parameters in the gold coach DVCoach system is based on the tracking technology of the human body movements in the video, acquiring the movement trajectory of the major human body parts and the joint angle. In figure 3 and figure 4, it shows the athlete's chest motion curve in a springboard game.

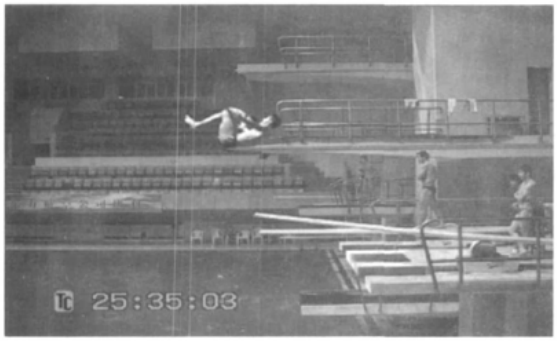

Figure 3

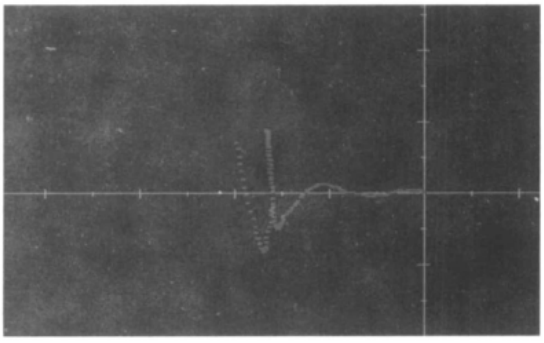

Figure 4

In the SimiMotion system, the technology parameters is used to construct the three-dimensional simulation model of the human body as well as the virtual movements under the background as stated in Figure 5 and Figure 6.

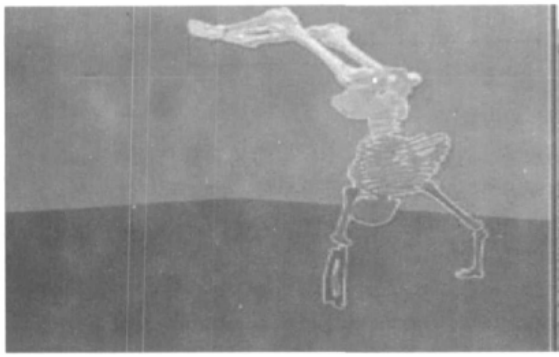

Figure 5

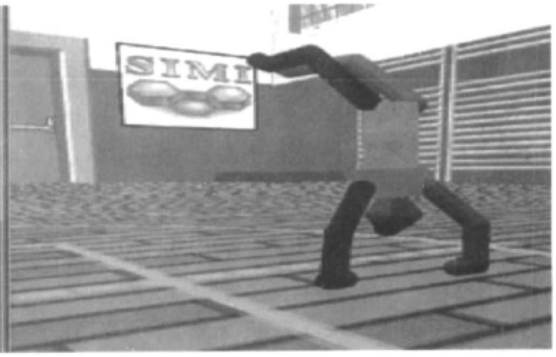

Figure 6

2 The unsolved issue of the sports video analysis technology in the sports teaching and training

With the rapid development of the computer and network technology, the training place or school takes form of the single unit. It is short of the connection for the multiple units. Without a network and data system, it will seriously affect the efficiency and sharing of the video analysis results. In this condition, it needs to firstly establish a huge sports video analysis database with the WEB2.0 technology (including blogs, RSS, peer-to-peer, instant messaging TM). In this way, the scattered units will be quickly assembled into a huge database while the it is able to make the exchange and information sharing in the network platform.

As a new technology, the sports video analysis has been widely used in the sports circles. Due to the equipments and the high cost to use, the rich data content has limited the development of the technology. According to the current situation in the domestic, the national team and a few of the provincial team is equipped with this device. There are less than 15 devices in the sports colleges in all. The high cost and the technology of the self-developed software is also undesirable. The professional video processing software (e.g., corel video studio pro multilingual10.0, Flash) is not professional while the obtained data is not quite accurate so that the data is difficult to be applied in the actual situation. In addition, the computer training for the physical education teachers is relatively lagging of which it has limited the use of the software. The computer level for most of the sports teachers shall be improved.

In the current sports circles, the application of the sports video analysis in the sports teaching and training is still relying on the teachers' naked eye observation, and undertake the action correction for the student in oral language. The students are difficult to form a definite concept of image in terms of their actions of which it will affect the correction of the action. Due to many technical actions are completed in an instant moment in the teaching, the fine point is difficult to be distinguished with the naked eye. Since the sports video analysis technology is applied in the communication of the teachers and students, the action analysis will be helpful for the students to speed up the comprehension of the action requirements and quickly improve the understanding of the correct action. With an intuitive understanding of their actions, they can quickly correct their wrong actions of which it accelerates the physical training courses study and physical exercise performance. For the students, the training can change, consolidate and improve the students' competitive ability of students in getting the good grades in the game. The competitive sports will go after the faster, higher, and stronger development. In a strict sense, the training process is to constantly find and solve the problems. Sports video analysis technology is not only applied in the communication of the teachers and students, not only becomes the platform for the Chinese and foreign teachers. The contrastive video analysis in the training and actual combating process help the students to better understand the teachers' demand on the actions and rapidly improve the performance. Through the contrastive action video analysis of the outstanding students, the advanced technology are understood in the world for the students's simulation and learning. Through the contrastive action analysis of the training and the match, the students' practical ability is strengthened. In particular, the action deformation and others are perceived with the changes of the psychology and endurance. With the help of the Dartfish software, the researchers of Beijing Institute Of Sports Science make our hockey ball defender Ma Yibo become one of the athletes who can master the skill action in the world.

The emergence of the sports video analysis software has greatly raised the level of sports training. In the future, the training process will certainly combine with the coaches, students, sports video analysis system software and network. The establishment of the sports video database will promote the development of the physical education teaching for the development of the national fitness campaigns. The traditional training pattern will disappear instead the training and teaching mode will be covered with the advanced technology and science and the reasonable training and teaching.

References

[1] Zheng Shaoyi. Foreign Computer Aided Teaching Development and Trend Study[J]. Journal of Foreign Education Information, 1996, (01) : 68-72.

[2] Wu Shujiang. Computer and Sports Education [J]. Journal of Juvenile Sports Training, 2005, (4) : 15 to 16.

[3] Tian Maijiu. Sports Training [M]. Beijing: People's Sports Publishing House, 2000.

[4] Mei Leifang. A Brief Introduction of the Application of Video Technology in the Swimming Teaching & Training [J]. Journal of Swimming, 2003, (5) : 10-12.

[5] Xie Lu, Liao Qingmin. The Design and Application of the Diving Training Video Analysis and Fast Feedback System [J]. Journal of Chinese Sports Science and Technology, 2005, (5) : 104-107.

Advanced Materials Research Vols. 989-994 (2014) pp 3571-3574
© (2014) Trans Tech Publications, Switzerland
doi:10.4028/www.scientific.net/AMR.989-994.3571

Anti-counterfeiting Technologies for Digital Halftone Images Based on Moire Methods

GE Jinghuan[a], PAN Jie[b], LI Mengxiao[c]

Shanghai Publishing and Printing College, Shanghai, China

[a]sytuprint@126.com, [b]jie-pan@sohu.com, [c]lmx_2011sppc@126.com

Keywords: Anti-counterfeiting technology, Information encryption, Halftone screening technology, Moire effect

Abstract. Moire effect is a special optical phenomenon caused by the interference of light. In the printing industry, it is also called Moire phenomenon which is caused by superposition of the multicolor printing dots for halftone images. Now it is widely used in the anti-counterfeiting areas. In this paper, we firstly introduce the basic principle of Moire effect. Then we describe several main applications of the Moire effect in the field of halftone image security. We review the main types of Moire-based anti-counterfeiting methods, compare them, and explain how they can be used for such security applications. It will provide the necessary technical information for the persons that in anti-counterfeiting area.

Introduction

Moire effect is a visual perception that occurs when viewing a set of lines or dots that is superimposed on another set of lines or dots, where the sets differ in relative size, angle, or spacing. In the printing industry, the Moire pattern is an artifact that occurs in the print reproduction process when any two, or more, repeating patterns overlap each other. Usually it is a harmful optical phenomenon when we print the multicolor halftone images. Many technicians are trying to find the method to avoid this problem in order to achieve better printing quality. However, it was found that the Moire patterns in the halftone images can be used in the anti-counterfeiting areas through special design or screening methods. To be specific, the Moire patterns are embedded in the halftone image by the peculiar screening technology invisibly. If the image is reproduced by scanning or photocopying simply, the latent image will be appeared. So the halftone prints with the anti-counterfeiting technology are difficult to copy. Moreover, the greatest advantage of this technology is that the security cost is low. In order to acquire good security effect, the designers can screen the image by the specific software when they make the printing plate. There is no other material cost during this simple process[1]. Therefore, it is an important anti-counterfeiting technology which is increasingly accepted by the printing industry.

The Principle of the Anti-counterfeiting Technologies

Normally, the Moire patterns can be avoided in this new technology, and we can only find them with special tools. Firstly, the image should be divided into two parts, the hidden figure area and graphic display area. Then these two parts are screened with different screen angles. If we print this image, you cannot find the hidden information. However, if someone should see the embedded information, he must use a decoding tool.

The specific process is as follows. The original image and the embedded information (image or characters) are inputted into the computer respectively. Then the encrypted methods which are also known as special screening technologies are used to obtain a new halftone image. Meanwhile, a decoding image showed with specific screened dots is generated by the corresponding algorithm, and we can output it onto a transparent film. If we put this film onto the printed image in the right place, the hidden information can be seen clearly. The screening algorithm for decoding information into the image is unique, and the counterfeiters are difficult to crack it. Also, we do not need any other materials in the whole process, so it is a cost-effective anti-counterfeiting technology[2].

The Main Methods for Anti-counterfeiting Technologies based on Moire effect

Phase Modulation Methods. This is a very simple method for hiding and extracting latent image. This method is based on the physical presence on the document of a latent image, which is generated using a technique known as "phase modulation". In this technology, we firstly print a fine, uniform line grating or screen of dots on the substrate, but the same line grating or dot screen is printed in a different phase within the predefined borders of the latent image. Because of the high frequency of the lines or dots, the latent image which printed on the substrate is hard to distinguish from its background. But when a reference transparency comprising an identical but unmodulated line grating or dot screen is superposed on the substrate, thereby generating a Moire effect, the latent image predesigned on the substrate becomes clearly visible[3].

As shown in Figure 1, let A and B be two identical line gratings with a small period. Assume that within the borders of a given shape, the parallel lines of grating A are shifted by half a period (see Figure 1(a)). Because the period is too small, the whole image seems uniform, and the latent image cannot be seen. If we print the line grating B on a transparent film by the same period with no latent images (see Figure 1(b)), and then superposed it on top of grating A at the same angle, there will be two results. It is showed in Figure 1(c) that the two gratings are superposed in-phase, and Figure 1(d) shows the superposition when grating B is shifted by half a period. Therefore, grating B can be seen as a decoding tool which can find the latent image hidden in grating A. The normal reproducing equipment cannot copy the gratings totally because of the high frequency, and we can obtain a uniform gray-level image after reproducing. If you put the decoding latent image on the same area, the original latent image is invisible.

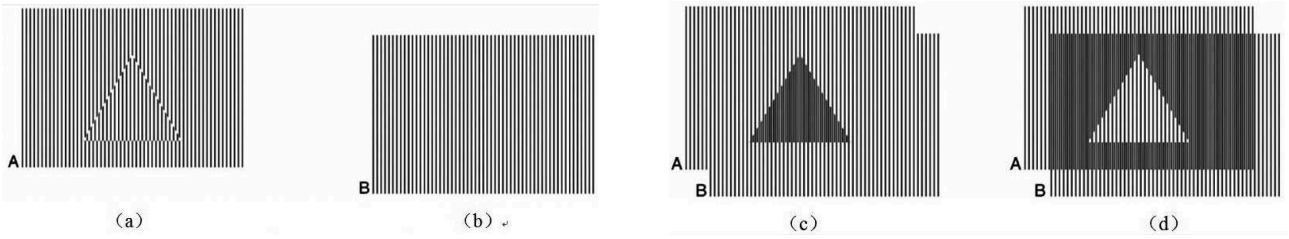

Fig.1 The basic principle of phase modulation methods

Grating Extract Methods. This is a way combined with the halftone image screening technology and optical reflection characteristics of the grating materials. When the grating sheet superposed on the prints, lenticular grating lines are interference with the printed dots based on Moire effect. It is occurred only in the situation that the lenticular grating lines and the dot lines are in the same direction. Then the embedded dots will be displayed. Therefore, we embed the information by processing the screened dots, and then detect it with the lenticular gratings. It is called as the grating extract method for anti-counterfeiting[4].

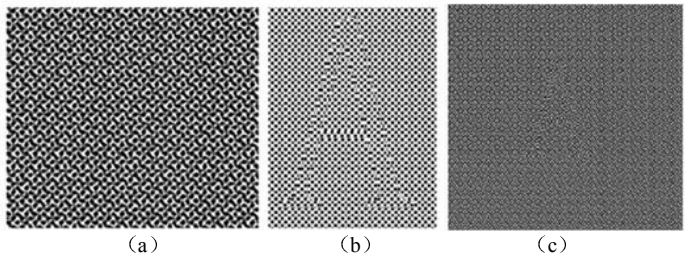

Fig. 2 （a）Original halftone image
（b）The channel of hidden information
（c）Overlaid halftone image

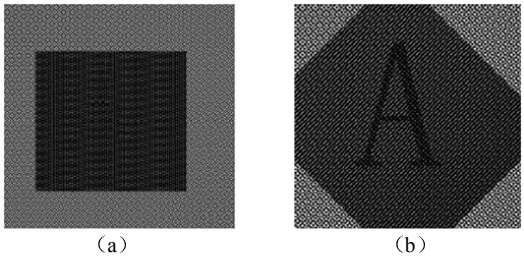

Fig. 3 （a）View in angle 0°
（b）View in angle 45°

During the process of this method, we firstly superimpose the four channels of the primary color; the result is showed in Fig 2 (a). Secondly, choosing a channel for hiding the special information, usually, we make use of the black channel. There is an A shaped area which is selected as the hidden area showed in Fig 2 (b). Then we move the dots in the specific area and hide the information in the

black channel. After that, the processed channel can be combined with the other three halftone channels. And the overlaid halftone image is obtained which is showed in Fig 2(c). If you want to detect the hidden information, a special lenticular grating should be put on overlaid halftone image. We can observe the different effects by changing the angle of the grating changes. Fig 3(a) shows the result of the image with an angle of 0 degrees of the grating, and Fig 3(b) shows the result of the image with an angle of 45 degrees of the grating. Because the screening angle of the black channel is 45 degrees, so we can see the hidden letters with this angle.

The 2D Moire Methods Based on the Microstructure Screening Technologies. Both two methods mentioned before are relatively simple, they are widely used in the printing industry. With the development of high-precision scanning technologies, the reproducibility of them is a problem recently. The 2D Moire methods based on the microstructure screening technology is put forwarded by Amidror from EPFL, Switzerland. The image must be microstructure screened firstly, and then choose decoding tools. There are two different points between the new method and the phase modulation methods. One is a way that we embed the hidden information with the microstructure dots in the screening process instead of the method of phase shift for inputting the latent image, and in the screening process using different shaped microstructures directly outlets directly into the implicit information; the other one is that the hidden information is decoded with a 2-fold periodic pinhole array rather than a 1-fold periodic grating made of linear slits. Three parameters in the new method must be strictly controlled, namely, the line screen, screen angle and dot shape. The theoretical basis is more complex, detailed explanation can be found in the reference[5].

Although the technical principle is slightly different from the other methods, the process is similar. We firstly screening images with the microstructure dots with the art "D" shape showed in Figure 4.

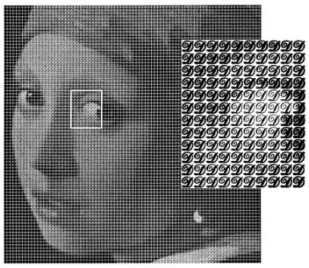

Fig. 4 The image screened by microstructure with local amplifier

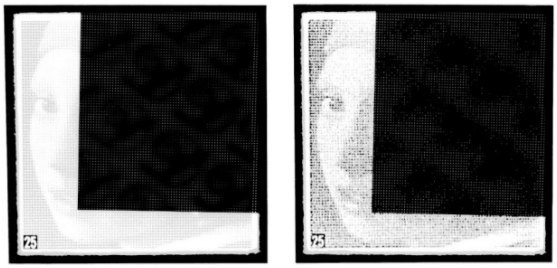

(a) (b)

Fig. 5 The diagram for the decoding image superposed on the origin and the copy

Due to the higher screening rulings, we cannot find any difference between the obtained halftone and the image screened by the traditional technology. But the hidden information is embedded into specific contour of the dots. The role of decoding tool is that it can amplify the tiny dot contour information in order to obtain the hidden information directly through the naked eye. The decoding tool is a 2-fold periodic pinhole array in the black background. We should superpose the decoding tool on the prints in the right position. If the hidden information can be seen just like the image showed in Fig 5(a), we can decide the authentication of the image. Otherwise, the destroyed image can be seen as it shows in Fig 5(b) which may be copied by duplication.

A specific function can be used for distortion of the microstructure screened image in order to increase the strength of security, and the distorted image is showed in Fig 6(a). The corresponding pinhole array in the decoding film should be distorted (Fig 6(b)). Then, the original contour information can be restored by the two images superimposed together (Fig 6(c)). It is difficult for counterfeiters to obtain the information directly from the image because of the uniqueness of the deformation function. Figure 7 is obtained with this method, and it can achieve better anti-counterfeit effect[6].

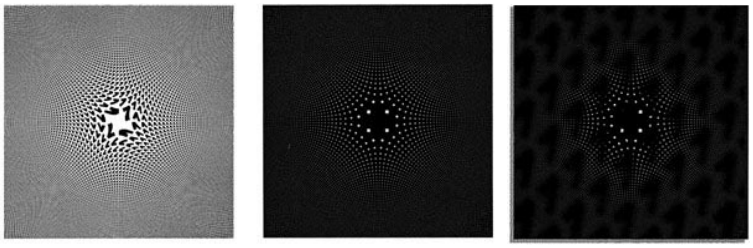

（a） （b） （c）

Fig. 6 （a）Image transformed with the specific function （b）The same transform with the decoding image （c）Decoding result

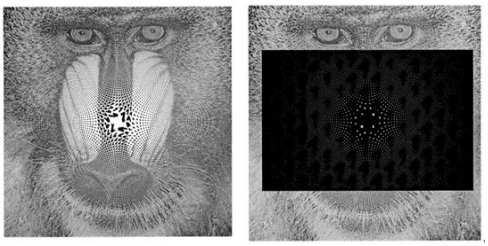

（a） （b）

Fig. 7 The diagram for the anti-co counterfeit effect by the method of Fig 7

In addition, the pseudo-random screening algorithms can be used in this method. In these variants, pseudo-random dot screens are used rather than periodic ones, and as a result the Moire effect which is obtained in the superposition is no longer periodic. It further improves the difficulty of counterfeiting[7].

Conclusions

The above studies proved that the anti-counterfeiting technology for halftone image based on Moire effect can achieve better security effect. We can widely use this method in document protection because there is no other material cost during the whole process. Also, with the rapid development of technology, a single security technology cannot meet the growing demand for anti-counterfeiting marketing. Further research will be focused on the combination of multiple anti-counterfeit techniques which is the trend of security domain.

Acknowledgments

This research is financial supported by “Chen Guang” project supported by Shanghai Municipal Education Commission and Shanghai Education Development Foundation. We gratefully acknowledge them and all the people who give the help to us.

References

[1] Y. Q. Liu, "The moire based printing technology for anti-counterfeiting," *Screen Printing,* vol. 6, no. 4, pp. 15-18, 2010.

[2] J. Wu, "A improved method for moire based printing technology," *Printing Quality & Standardization,* no. 1, pp. 11-12, 2012.

[3] I. Amidror, S. Chosson, and R. Hersch, "Moire methods for the protection of documents and products: A short survey," *ICSXII Journal of Physics: Conference Series,* vol. 77, pp. 43-52, 2007.

[4] S. S. Wen, "Research on the anti-counterfeiting technology based on digital screening," Master dissertation, School of Light Industry and Food Science, South China University of Technology, Guangzhou, China, 2012.

[5] I. Amidror, "A generalized Fourier-based method for the analysis of 2D Moire envelope-forms in screen superpositions," *Journal of Modern Optics,* vol. 41, no. 9, pp. 1837-1862, 1994.

[6] V. Ostromoukhov and R. D. Hersch, "Multi-color and artistic dithering," *in Proceedings of the 26th annual conference on Computer graphics and interactive techniques,* 1999, pp. 425-432.

[7] I. Amidror, "Authentication with built-in encryption by using moire intensity profiles between random layers," US Patent No. 7,058,202, 2006.

Advanced Materials Research Vols. 989-994 (2014) pp 3575-3578
© (2014) Trans Tech Publications, Switzerland
doi:10.4028/www.scientific.net/AMR.989-994.3575

Method Research on Based-Static Motion Image Retrieval

Siyu Sun[1, a], Chuansheng Wu[2,b]

[12] University of Science and Technology Liaoning Software College

[12] Anshan City,Liaoning province China Qianshan Road No. 185

[a]email:598645452@qq.com; [b]email: gykwcs@163.com

Keywords: Motion Image Retrieval;Based-Static Image Retrieval;object segmentation;image index

Abstract. In the face of mass movement of image data storage management and retrieval applications, traditional search techniques and methods have been completely incompetent. The emergence of the technology on Based-Static Motion Image Retrieval, points out a specific direction for the development of the field of information retrieval. First of all, the thesis analyze the basic principles of the Based-Static Image Retrieval technology and Based-Static Motion Image Retrieval technology. And the thesis discuss mainly the relevant key technologies and development situations whose based on the static motion image retrieval technology. Secondly, the thesis Introduce and analyze, briefly, the characteristics and application background of several motion image retrieval prototype system, which developed by the domestic and foreign research institutes.

Introduction

With the rapid development of electronic information technology and the progress of motion image acquisition equipment and the means of acquisition, the digital motion images have a very wide range of applications in the field of industrial, commercial, transportation management, military, etc. With the development and progress of the image analysis and motion image processing technology, the application of digital motion images, from the original motion image recording and motion image monitoring, is developing to the application of the Intellectualization motion image.

Facing the storage management of massive motion image data and retrieval applications, especially in the static-based analysis and retrieval application requirement, the Based-Static Motion Image Retrieval (BSMIR) emerge as the times require. Static-based image retrieval technology , a kind of fuzzy query technology , find out the closest image [1] to the query requirements in the feature space, through extracting the visual features of the image (color, texture, shape, spatial relationships, etc.) and semantic features (feature semantics, object semantics and abstract semantics) .

It based on the static of the motion image and context, extracts and descripts the feature and the static of the motion image automatically, in the case of no human involvement, so as to realize the technology and method of motion image data retrieval from the large-scale motion image database. Organization of the Text.

The feature of BSMIR

BSMIR is different from the traditional keyword-based retrieval and its main features embodies in [1]: it is based on the knowledge as image processing, pattern recognition, computer vision and image understanding.

It can, drawing on the knowledge and the data presentation as cognitive science, artificial intelligence, database management and human-computer interaction and information retrieval, Achieve Based-Static Motion Image Retrieval function by introducing a new media data, data mode, as well as effective retrieval algorithm and friendly man-machine interface. BSMIR which is relative to the method of the traditional text-based retrieval has two prominent characteristics: It breaks through the limitations of traditional retrieved based on the expression, And Analyzes Directly on the static of motion image. The process that the computer extract features and semantic automatically Avoids the subjectivity of artificial described.

It achieves Based-Static Retrieval by making use of these static to build aspect indexing and adopts the method of similarity matching to Query.

BSR technology and its Research status

Since the existence of the inevitable contact between the motion image and the image— The motion image is a sequence of the moving image.

The image is a frame of still motion image. In the research of Based-Static Image Retrieval, there are many technical issues of common concern in the BSMIR. Therefore, below is a brief introduction about Based-Static Image Retrieval techniques.

2.1 BSIR technology and its development situations

It is a hot topic in the image database study that BSIR technology, which starts with characteristic analysis and comprehension of the image mainly, take the advantage of vision features (color, texture, shape, spatial relationship, etc.) and semantic features (semantic characteristics, object semantics and abstract semantics) of the image to Retrieval In recent years.

Color is an important visual information. It has the features such as simple computation and stability, and has a strong robustness to rotation, translation transformation and the various deformation. It has become one of the characteristics of the most widely used in the existing retrieval system [1].

The common methods of color features include: histogram method, the cumulative histogram method, Color histogram method, color layout method, central moment method, etc. and the histogram method is one of the most commonly used method.

There is no formal definition for texture currently. it Is generally believed that the texture is the regular permutation and combination of the texture elements .but people regard the regional of Repetitive, simple shape and consistent strength as the texture elements. According to the psychology study of human towards the visual perception of texture, Tamura [1] put forward the expression of texture features, mainly including Roughness, directional Directionality, Contrast, Line-Likeness Regularity and Coarseness. After decades of research, the texture feature extraction methods have been proposed many methods [2], for example:Gray Level Difference Statistics method, Gray Run Length method, Spatial Domain Energy method, Regional Texture Primitive Parameter method, Co-occurrence Matrix method, the features extraction based on the texture spectrum , the texture features extraction based on mathematical morphology ,etc.

2.2 BSMIR technology and its development situations

(1) The motion image feature extraction

The motion image features including the underlying visual features and high-level semantic features. The extraction of the underlying visual features such as color, texture, shape, spatial relationship are basically the same as the method of the image feature extraction .The following main about motion feature of motion image is discussed. The motion is a unique feature of the motion image data, it shows that the development and changes of the motion image static in the timeline, and has a very important role for the description and understanding of motion image static [1].

Motion in the motion image is mainly divided into two types: motion of background and foreground. Background Motion is the overall movement of all pixels within the lens caused by the movement of the camera, also known as Global Motion or Camera Motion; But the Foreground Motion refers to the motion that the object being photographed in the scene, also known as Local Motion.

The methods that express and descript the motion information of the motion image mainly include: using the parametric motion model to describe the global motion , describing the local motion ,with the help of image segmentation and target tracking, describing The motion activity attribute of the motion image' static activity intensity level.

From the above three description methods, MPEG-7 recommended a descriptor respectively. There are two main kinds of methods for motion feature extraction and calculated / estimated: One is based on gray element time changes, thereby calculating a dense optical flow of the respective pixels. Under reasonable limitative conditions, two unknown components of the optical flow field can be obtained by solving a set of nonlinear equations.

The other is a group sparse features based on the first extracting the target, and track them in subsequent frames. Once the corresponding relationship is established among frames, and certain restriction is established according to the feature of target, motion component also can be obtained by solving a set of nonlinear equations.

The parameters of global motion estimation methods mainly include [3]: improved hybrid least squares estimation method, least square estimation method, iterative least squares estimation method, etc. Two main kinds of study on the feature extraction of the local motion in the motion image [4]:

Local motion vector field and motion image object motion trajectory.

Trajectory describes the object of the motion image during the movement, and the motion image feature is extracted by extracting motion information and its trajectory from the motion image sequence.

The trajectory can be usually directly obtained by the MPEG compressed stream α channel.

However, the effect is usually not very ideal that relying solely on the motion information retrieves the motion image data. In most cases, it needs to combine with others visual information features in order to achieve a satisfactory retrieval result.

(2) Motion image object segmentation

MPEG-4 introduces the concept of a motion image object to support object-based functions. It allows users to apply and study the specific algorithms according to the concrete applications, rather than obtaining the concrete methods of the motion image object from the motion image sequence.

Many domestic and foreign scholars have proposed a variety of motion image object segmentation algorithms can be roughly divided into two categories: motion segmentation based on time-domain information and segmentation method combined with temporal spatial domain information.

The earliest object segmentation based on time-domain information method is segmentation method based on optical flow field.

Based-motion-similarity Time-space object segmentation algorithm, which based on region segmentation, calculates the features of region motion and combines with image regions to form the motion object segmentation, according to the similarity of the regional motion .It can also realize object segmentation by clustering algorithm Based on region segmentation. Bayesian space-time object segmentation algorithm implemented at the regional level is a kind of motion object segmentation technology. Because of the image area with color, texture, shape and other characteristics, and the region motion features calculated by estimating region motion, the space-time Bayesian object segmentation algorithm separates object integrating the features of image and motion. The region tracking provides consistency clues of region motion in the timeline, in a period of time. Through the analysis of the spatial relationships in the area, you can take advantage of the regional time consistency to separate the segmentation motion image object.

(3) Motion image indexing technology

For the motion image data, you can build two indexes; one is based on visual features that can be extracted from the key frames; the other is the semantic primitive index based on the target or motion, which is usually more complex and needs further comment after the extraction.

The index based on visual features is to index the meaning that the visual primitives carry [3].According to Symbol linguistic analysis here, the meaning that visual primitives carry can be regarded as the meaning that symbols combination transmit, so it can be automatically extracted by checking the low-level visual features and combinations.

The visual nature can be modeled as a multi-dimensional feature points, such as color, texture and shape, so the index structure can use point access method. The performance of point access method depends on the number and the distance metric used by expression of the nature in the actual. For most point access method, its performance will decline in the number of features over 10 [1].Therefore, the high-dimensional data is often mapped to low-dimensional space before the index. Because the characteristics of visual features and field have a minor relevancy, the index based on visual features is more applicable to a variety of different motion images, and visual features automatically extracted from the motion image using image processing and analysis technology. The index based on semantic features is to index some semantic primitives around the target or visual elements which carry the meanings.

Some of the target elements can be extracted from the key frames, and compared with that from the query graph.

The motion image static is very complex, covering a broad field, so the motion index extraction is quite complex.

The motion image retrieval system technology and Its Research situation at home and abroad

At present, domestic and foreign have developed a number of the prototype system Based-Static Motion Image Retrieval [3], among them, the more famous are IBM's QBIC system, VisualSeek system that the joint research of the Columbia University, Department of Electronic Engineering and Telecommunications Research Center Image and Advanced Television Laboratory,

IDVL researched by Carnegie Mellon University, VideoQ system developed by Columbia University, TV-FI (Tsinghua Video Find It) motion image program management system developed by Tsinghua University, Webscope-BSMIR developed by Zhejiang University, etc. Although they, in terms of performance, cannot fully meet the needs of the business, but still has a higher theoretical reference value. QBIC system allows to use the example images, user-constructed sketches and drawings with their chosen color , texture patterns, and the lens and target motion graphics information, to query the large image and moving image database. VisualSeek is a based-static retrieval system on the Internet, collecting images and motion images through a automatic network engine in the network. it can automatically analyze and build indexes with images and motion images, which can be placed in a certain topic categories. IDVL developed by the Carnegie Mellon University specifically includes: the motion image segmentation, the motion image character recognition, the pronunciation analysis and recognition, the natural language processing, the face detection and so on, to retrieve and summarize the motion image data. VideoQ extends the traditional query method based on keywords and themes, allowing the users to retrieve image motion with the visual features and temporal and spatial relationship.

Concluding Remark

The motion image retrieval is no only one of the important research topics in the field of multimedia, but also the most extensive and difficult topics involving the subjects, which has made some achievements after years of research.

But there are still many technical issues to be further in-depth study and exploration for motion image retrieval.

For example, how to combine motion image low-level features with high-level semantics organically, how to design effective motion image similarity measures for multiple types of features, how to meet the comprehension of motion image similarity foe human .

Reference

[1] Zhang Yujin. Based-static visual information retrieval [M]. Science Press, 2013

[2] Wan Hualin, Chowdhury M, Hu Hong, et al. Image texture feature and application in.CBIR [J], Aided Design and Computer Graphics, 2013, 15 (2): 195～199

[3] Zhuo tongru .Introduction to motion image database management system [M]. Beijing: Introduction to motion image database management system, 2012

[4] Wang Jia, Wang Haifeng, Liu Qingshan, et al. Rapid global movement based on the three-parameter model estimation [J]. Journal of Computers, 2008, 29 (6): 920~927.

[5] Deng Li, Jin lizuo, Fei Shumin. Motion image retrieval Based on combination of the similarities [J]. Electronics & Information Technology,2011, 29 (5): 1023~1026.

Advanced Materials Research Vols. 989-994 (2014) pp 3579-3582
© (2014) Trans Tech Publications, Switzerland
doi:10.4028/www.scientific.net/AMR.989-994.3579

Relevance Feedback Based on Particle Swarm Optimize Weight-Vector for Image Retrieval

Feiya LV, Xiaohui YANG, Dengfeng LI

Institute of Applied Mathematics, School of Mathematics and Information Sciences, Henan University, Kaifeng, Henan, 475000, China

email: xhyang@henu.edu.cn.

Keywords: Image Retrieval; Weight-Vector; Particle Swarm Optimization; Relevance Feedback

Abstract. As the physical meaning of components are different in feature vector, this paper presents a weight query vector based on QPM to represent the user's true intention more properly, and then proposes two RF frameworks to learn the weights for positives and negatives in the feedback process of CBIR by PSO. Experiments were conducted to validate the proposed frameworks based on color histogram weight-vector. The proposed frameworks were compared and outperformed four other relevance feedback methods regarding their efficiency and effectiveness, thanks to the fact that they can make full use of the features' different importance.

Introduction

Relevance feedback (RF) technology has been shown to provide significant performance for reduce the semantic gaps in CBIR [1] [2]. QPM is an RF method used in CBIR, however there are three parameters need to be fixed. What's more, it does not consider the different importance of feedback images [3]. Therefore, improving the query vector may express the user's real query intentions better and raise the accuracy of retrieval. Image retrieval problems can be seen as a problem of optimizing query vector. Nowadays, many studies about image retrieval have done with particle swarm optimization (PSO) algorithm [3] [5] [7] [8]. Optimize query vector by PSO is to weight distribution of features through learning users' intention and adjust the weights dynamically and find the optimal solution by iteration.

On the basis of Rocchio formula, Jing proposed the weight QPM algorithm [5]. However it does not take the query vector obtained previously into the feedback iterative process, which can make the query information loss. PSO-CBIR [6] is a preliminary version first introduced through its effective space exploration mechanism to find the most similar images by iterative between particles. Evolutionary PSO-RF [7] redistributes the weight of feature vector dynamically. However, it has not consider the effect of former retrieval results directly, then a PSO-based interactive image retrieval [4] is proposed, it use particles' movement to adjust the weights of positive and negative cases in relevance feedback dynamically, finally optimize the query vector.

For the methods mentioned above all put forward based on the query vector, PSO is useful in learning the weights of positive images and negatives while weight-QPM is also meaningful. As we know the physical meaning of the various components' in feature vector may be different, we propose a weight query vector by improving the Rocchio equation with weight-vector. And then we put forward a PSO-based weight-vector techniques to optimize the query vector by PSO.

PSO-based weight-vector RF algorithm

As an index of visual features, we change it into weight-feature first, and then determine the initial weight query vector by QPM function, if the user is not satisfied with the initial result, adjust the weight query vector according to users' feedback information to let it closer to the positives, far from the negatives. On this basis, we use PSO for optimization, propose a PSO-based weight-vector framework,.

PSO-based weight-vector algorithm constructs weight query vector by taking use of $TF \times IDF$ model [7] to calculate weight-vectors and reconstructs it by PSO, finally outputs results by similarity matching.

2.1 Weight-Vector

In this paper, the composition of weight-vector is based on $ci \times ici$ technique [8]. The component importance (ci) is reflecting the relative importance of a feature component in feature internal, and the inverse collection importance (ici) is reflecting the difference of this feature component with component of other images.

Assume the feature vector of $i\text{-}th$ image is $F_i = [f_{i1}, \ldots, f_{ik} \ldots, f_{im}]$, we define,

$$ci_i = [\frac{f_{i1}}{mean_1}, \ldots, \frac{f_{ik}}{mean_k}, \ldots, \frac{f_{im}}{mean_m}], \quad (1)$$

$$ici_i = [\log_2(\sigma_1 + 2), \ldots, \log_2(\sigma_k + 2), \ldots, \log_2(\sigma_m + 2)], \quad (2)$$

where $mean_k$ is the mean value of component feature f_{ik} in all the features, σ_k is the standard deviation of the $k\text{-}th$ component of ci in all the features. Then the weight-vector is $w_i = ci_i \times ici_i$. While ci is a normalized representation for every component of feature that can reduce the different range of values, ici_i can use standard variance to weaken the effect of non-relevant component in features.

2.2 Weight Query Vector

In general, different descriptors are combined statically in retrieval process [8], if they can be combined more complex, users' visual perceptions can be characterized better. Allocating same weights to positive images in QPM, the distinctive importance of feedback images does not take into account, neither of the negative ones, that is, the query vector is not the optimum, it need to be improved. We changed it as,

$$Q_{i+1} = \alpha Q_i + \frac{1}{rel} \sum_{I \in REL} \beta_I w_I - \frac{1}{irr} \sum_{J \in IRR} \gamma_J w_J, \quad (3)$$

where Q_{h+1} is the updated retrieval vector while Q_h is the primary one. REL is a set of positive images indicated by user, and rel is the number of this set, similarly, IRR is a set of negative ones annotated and irr is its number. β_I, γ_J are different weights for different positive images and negative ones correspondingly that can be learned according to the feedback information.

PSO is starting with a group of initial solutions that randomly generated, and changing the velocity and location toward its pbest and gbest. We can get the optimal weight through learning the different importance of positives and negatives by PSO to construct the optimal weight query vector.

Experiment and Analysis

This paper conducted experiments based on color histogram and use Euclidean distance for similarity matching on Corel 1000 image database, an image library with 10 categories：Africa, Beaches, Monuments, Buses, Dinosaurs, Elephants, Flowers, Horses, Mountain, Food, each category of 100 images. Experimentally, the population size is selected as 60, five times of iterations, and the training set is 35, 0.95 for the inertia factor w, two acceleration factors set as $c_1 = 2, c_2 = 2$. N is assigned as 20.

First we give an effective instruction for the 10 categories. (1) For the categories have single background and outstanding theme, such as Dinosaurs, Flowers, only using 3 times positive feedback or even just 1 time positive and negative feedback can we get a relatively satisfaction results, which basically show our method is more efficient to this kind of image retrieval. (2) For the categories have simple outline and outstanding theme, such as Buildings, Buses, good results can we get after 3 times feedback. Less time is taken as the users are more willing to accept. (3) Then for the categories have complex structure or confused semantic those are difficult to retrieval, such as Elephants, Beaches, Food, 5 times of feedback can be taken to ensure a satisfying results from the perspective of user, for which time is relatively acceptable.

Second, we compare with other intelligence methods on the condition that top N similar images are retrieved, such as PSO-based algorithm, Evolutionary PSO-RF and QPM algorithm. $AP(20)$ is (a) and MAP is (b) in Figure 1. Then we compared the Recall and Precision of retrieval, as (c) in Figure 1. As $P \times R$ curve shows, the algorithm achieved higher precision when recall is fixed in most cases. Also the algorithm achieved better recall when precision is fixed. That means, the proposed algorithm detects more related images with better sorts. With the increase of feedback number, our algorithm may some extent lower than the previous algorithm, because of the image feature itself, based on this, a further study can be done by choosing fusion weight characteristics.

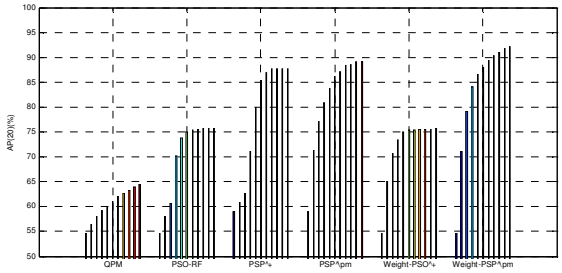

(a) AP(20) (%)

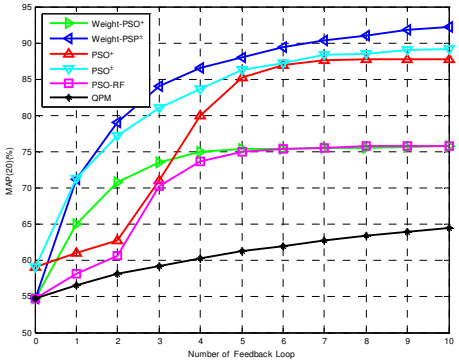

(b) MAP(20) (%)

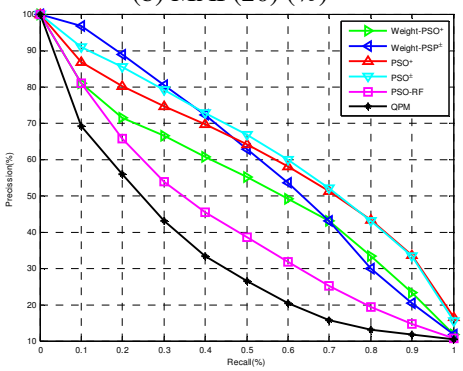

(c) $P \times R$

Fig. 1. Different objective measurement of 6 approaches after 10 times feedback

Intuitively, we give a set of results for PSO-based weight-vector interactive technology and PSO-based interactive technology after 10 times feedback as evidence. Figure 2 shows that our method is more effective.

(a) Query image

(b) The initial retrieval results

(c) PSO^{+} -based algorithm

(d) $PSO^{\pm}$ -based algorithm

(e) PSO^{+} -based weight-vector algorithm

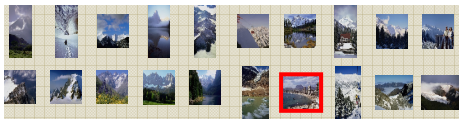

(f) $PSO^{\pm}$ -based weight-vector algorithm

Fig. 2. Retrieval results for different interactive technology

Conclusions

Two effective content-based relevance feedback frameworks, PSO^{+} -based weight-vector algorithm and $PSO^{\pm}$ -based weight-vector algorithm, are proposed in this paper based on particle swarm optimization and weight-vector. They all strengthen positive images and weaken negative ones by learning weights in feedback loop, and proved to be efficiency and effectiveness thanks to the fact that they can make full use of the features' different importance. We believe the retrieval accuracy will be further improved by considering the fusion features.

References

[1] Rui Y, Huang T S, Ortega M, Mehrotra S. Relevance Feedback: A Power Tool for Interactive Content-Based Image Retrieval [J]. IEEE Transactions Circuits Systems Video Technology, 1998,8(5):644–655.

[2] Liu R, Wang Y, Baba T, Masumoto D, Nagata S. SVM-Based Active Feedback in Image Retrieval Using Clustering and Unlabeled Data [J]. Pattern Recognition, 2008, 41(8):2645–2655.

[3] Cai L J, Yang X H, Li S C, Li D F. Relevance Feedback Based on Particle Swarm Optimization for Image Retrieval [C]. 2012 International Conference on Information Technology and Software Engineering Lecture Notes in Electrical Engineering, 2013 (212):749-756.

[4] Xu X L, Zhang L B, Yu Z Z, Zhou C G. The Application of Particle-Swarm Optimization in Relevance Feedback [C]. BioMedical Information Engineering. International Conference on Future, 2009: 156–159.

[5] Wei K P, Lu T W, Bi W, Sheng H H. A Kind of Feedback Image Retrieval Algorithm Based on PSO, Wavelet and Sub-block Sorting Thought [C]. Future Computer and Communication (ICFCC), International Conference, 2010: 796- 801.

[6] Ferreira C D, Asntos J A, Torres R S, Goncalves M A, Rezende R C, Fan W. Relevance Feedback Based on Genetic Programming for Image Retrieval [J]. Pattern Recognition, 2011 (32): 27-37.

[7] Salton G, McGill M J, Introduction to Modern Information Retrieval [M]. McGraw-Hill Book Company, 1983.

[8] Rui Y, Huang T S, Mehrotra S. Content-based Image Retrieval with Relevance Feedback in MARS [C]. International Conference on Image Processing, 1997, 2: 815-818.

Advanced Materials Research Vols. 989-994 (2014) pp 3583-3586
© (2014) Trans Tech Publications, Switzerland
doi:10.4028/www.scientific.net/AMR.989-994.3583

Design of Optical Fiber Transmission System based on Absolute Polar Duty Cycle Division Multiplexing(APDCDM)

Xinqiao CHEN [1,a], Lin TANG[2,b]

[1]College of Information Engineering, Communication University of China, Beijing, 100024, China

[2]College of Information Engineering, Communication University of China, Beijing, 100024, China

[a]email:chenxinqiao9999@163.com,[b]email:tanglin0@sina.com

Keywords: Multiplexing Technique, Bipolar, APDCDM

Abstract. This paper propose a new multiplexing technique which use the bipolar RZ signal to realize duty cycle division multiplexing(DCDM) ,we call it Absolute Polar Duty Cycle Division Multiplexing(APDCDM).Multiplexing and demultiplexing principle of APDCDM are analyzed. Here we have designed a optical fiber transmission system based on APDCDM of three users by Joint simulation with Optisystem and Matlab. Simulation result shows the feasibility of this system. By the analysis of signal energy, explain APDCDM can carry more users than DCDM.

Introduction

Multiplexing is a technique amis at solving the problem of how to use one channel transmit multiple signals simultaneously .The mature research currently are Time division multiplexing(TDM) , wavelength division multiplexing(WDM) and Code Division Multiplexing(CDM).

The main issue of TDM is clock recovery. In WDM system, a user can only transmit data on a single carrier. Duty Cycle Division Multiplexing(DCDM)[1] We proposed before solved these problems. However, with the number of users increasing, The multiplexed signal energy increasing rapidly. For MZ modulator, the nonlinear effects of lightwave output will be very obvious when the signal voltage is larger.. In order to solve this problem, we propose a new multiplexing technique which use the bipolar RZ signal to realize duty cycle division multiplexing(DCDM) named Absolute Polar Duty Cycle Division Multiplexing(APDCDM).This technique significantly reduce the energy of the multiplexed signal so that the system allows more users thus improve the bandwidth utilization.

Working Principle

APDCDM is the improvement of DCDM. A APDCDM system with three users below is used for an example to describe the principle of multiplexing and demultiplexing. Figure 1-(a),1-(b) and 1-(c) show the duty cycle distribution of three users system, where 0.25,0.5,0.75 duty cycle are used to represent user 1,user 2 and user 3 .Noting that user 2 has opposite polarity to user 1 and user 3 .Use the Periodic signal 10101010,11001100,00001111 represent these three users' signal respectively. Amplitude superimposed on the timeline when the three signals multiplexed. The multiplexed signal shows in figure 1-(d) and the absolute polar multiplexed signal shows in figure 1-(e).The system can be extended to n number of users, for the system of n users, each user is set to the duty cycle of 1 / (n +1), 2 / (n +1), 3 / (n +1) ..... n / (n +1),the odd user's polarity is positive and the even user's polarity is negative. Multiplexing the same principle.

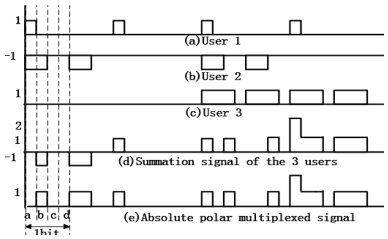

Fig.1 The multiplexing principle of APDCDM

Table1 The principle of demultiplexing

output1	output 2	output 3	a	b	c	d
0	0	0	0	0	0	0
0	0	1	1	1	1	0
0	1	0	1	1	0	0
0	1	1	0	0	1	0
1	0	0	1	0	0	0
1	0	1	2	1	1	0
1	1	0	0	1	0	0
1	1	1	1	0	1	0

In this paper, we designed a demultiplexer based on APDCDM with Matlab. The principle is shown below: divide every bit of the sampled signal on average into four segments as a, b, c, d. For three users, there are eight kinds of combinations, each case produces a unique waveform as shown in Table 1, we do demultiplexing just according to these 8 kinds of combinations. A de-multiplexing system of n users will be relatively complicated, the principle is similar to the former one. There are 2^n kinds of combinations and we do demultiplexing just according to them.

Simulation Experiment

a. The Design of Demultiplexer

In this paper, A demultiplexer based on APDCDM is designed by matlab, The design process diagram shows in Figure 2.

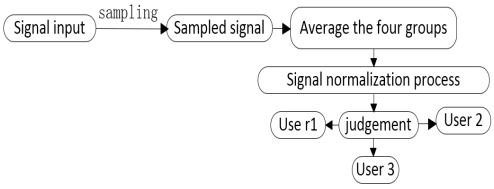

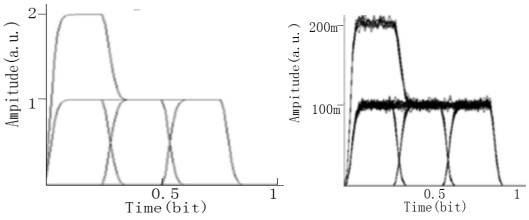

Fig.2. The design process diagram Fig.3- (a) Eye diagram of signal input Fig.3-(b)Eye diagram of the signal after transformed by optical fiber

The simulation setup three users' signal is periodic signal 10101010,11001100,00001111 respectively. Sampling a total of 8192 times, 64 bits per sample, sampling 128 bits and bit rate is 2.5 Gb/s. Put the number of sampled per bit divided into four groups, each group has 16 sampling points, considering the transmission distortion factor, get rid of the first four points and the last four points. Average the rest eight values, then every bit signals has only four values. In actual situation, the normalized processing should be done because the amplitude of signal receiving terminal receives will attenuation. The eye diagram of multiplied signal input and the signal after transformed by optical fiber shown in figure 3- (a) and 3- (b) respectively, two eye diagram just distortion on the amplitude and the range of eye diagram reflects the actual signal amplitude.Therefore, the signals' values whose energy fluctuate near 0,0.118m,0.229m and fluctuation amplitude is less than or equal to 0.03m are assigned to 0,1,2 respectively. The normalized value are four values of each bit, which corresponds to the values above of the group a, b, c, d in each bit. We do the judgment according to table 1 after the normalization ,and the signals which are binary can be separated out, then we can obtain the original signals by the zeroing signal generator. In table 2 we make a comparison of the separated signal of each user with the original one, and get a result that the two kinds of signals are coincident, which indicates that the this method of de-multiplex is feasible.

Table 2 The comparison of the signal before multiplexing and after multiplexing

	signal before multiplexing	signal after multiplexing
Use1	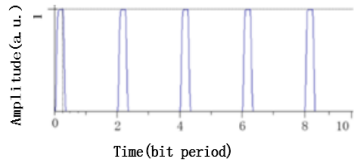	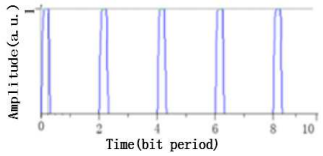
User 2	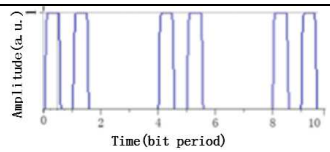	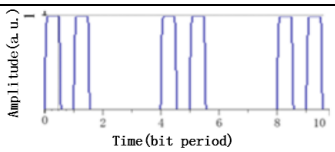
User 3	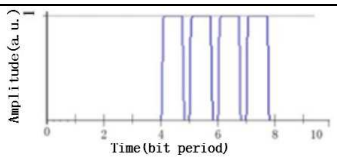	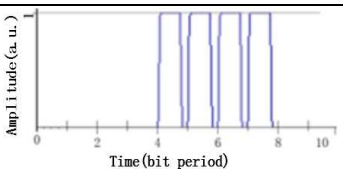

b. Simulation Setup

The simulation settings are shown in Figure 4. The three signals are multiplexed through adders, get the absolute value through a absolute signal generator. We use MZM to modulate the electronic signal to a continuous optical wave emitted from the laser whose wavelength is 1550nm, and photoelectrically converted by the optical detector to obtain the multiplexed electrical signal after the transmission through a 50Km optical fiber. Then input this signal to APDCDM demultiplexer, as a result the multiplexed electrical signal is separated into three binary signals, and finally recover the three users' original data by using the zero pulse generator.

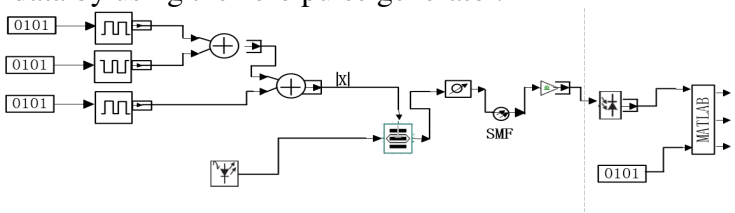

Fig.4 The simulation settings of APDCDM with three users

Result and Discussion

a. Average energy per symbol

The average signal energy per bit can be obtained from the signal waveform by calculating.We work out the signal energy of eight kinds of combinations and and show it in Figure 5.The energy of the signal is calculated as: $E_i = \begin{cases} \frac{n+1}{8n} \times A^2 T_i & n = odd \\ \frac{n+2}{8(n+1)} \times A^2 T_i & n = even \end{cases}$

Where, i = 1,2,3 ... 2^n, n is the number of users, A is the signal amplitude in volt, T_i is duration of the signal. Obtained signal average energy per bit of 8 kinds of combination $E_{everage} = \sum_{i=1}^{8} Ei \div 8 = \frac{2}{24} A^2 Ts$, T_s is the duration of each bit signal.

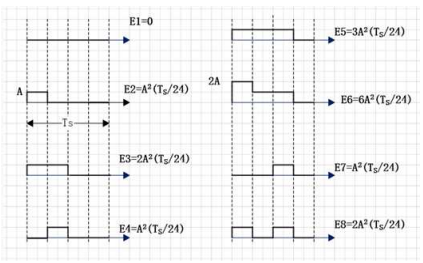

Fig.5 Energy for 8 cases of APDCDM with three users

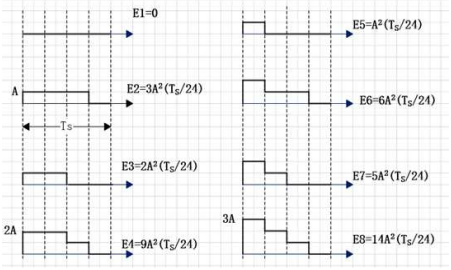

Fig.6 Energy for 8 cases of DCDM with three users

b. Comparison of APDCDM with DCDM

We use the same method to calculate the DCDM energy, and show it in Figure 6 . The average signal energy per bit of the eight kinds of combinations is: $E_{everage} = \sum_{i=1}^{8} Ei \div 8 = \frac{5}{24} A^2 Ts$,Comparing the average energy value DCDM with APDCDM , APDCDM reduce the transmission energy significantly. This solves the problem of DCDM that multiplexed signal energy increases rapidly with the number of users increases. It's obvious that APDCDM can carry more users than DCDM.

Conclusion

This paper propose a multiplex technology which use the bipolar RZ signal to realize duty cycle division multiplexing on the basis of DCDM, that is Absolute Polar Duty Cycle Division Multiplexing(APDCDM). We do the co-simulation by using OptiSystem and Matlab, design a APDCDM optical fiber transmission system of three users, and in the stimulation get a result that the separated signal of each user is consistent with the original one before multiplexing which verifies the viability of apply APDCDM to fiber-optic communication systems. Of course , we have confirmed that because of the introduction of the absolute polar, APDCDM can carry more users than DCDM and has higher utilization of bandwidth. The practical use of this technology still requires further research .

References

[1]Amin.Malekmohammadi,G.A.Mahdiraji,A.F.Abas,M.Mokhtar.30Gb/s Absolute Polar Duty Cycle Division Multiplexing In Dispersion Uncompensated Optical System[R].Proceedings of IEEE 6th National Conference on Telecommunication Technologies and IEEE 2008 2nd Malaysia Conference on Photonics, 26-27 August2008,Putrajaya,Malaysia.

[2]M.K.Abdullah,Amin.Malekmohammadi,G.A.Mahdiraji,A.F.Abas,M.Mokhtar.Absolute Polar Duty Cycle Division Multiplexing :An Economical and Spectral Efficient Multiplexing Technique[R].Wireless and Optical Communications Networks, 2008. WOCN '08. 5th IFIP International Conference on Date 5-7 May 2008.

[3]Amin. Malekmohammadi, G.A.Mahdiraji, A.F.Abas, M.K.Abdullah, M.Fadlee.Performance Analysis on Transmission of Multilevel Optical Pulses Using Absolute Polar Duty Cycle Division Multiplexing[R].2008 International Conference on Electronic Design on Date 1-3 December 2008.

Advanced Materials Research Vols. 989-994 (2014) pp 3587-3590
© (2014) Trans Tech Publications, Switzerland
doi:10.4028/www.scientific.net/AMR.989-994.3587

Target tracking based on improved Camshift and Kalman filter

Liying Ban[1, a], Yuehua Han[1, b], Yanhai Wu[1, c]

[1]Xi'an University of Science and Technology, Xi'an Shaanxi, 710054, China

[a]email: banliying@xust.edu.cn, [b]email:hanyuehua314@163.com, [c]email:wyh7388 @163.com

Keywords: target tracking; Camshift; Kalman filter; data fusion; Kim algorithm

Abstract. A tracking algorithm based on improved Camshift and Kalman filter is proposed in this paper to deal with the problems in traditional Camshift algorithm, such as tracking failure under color interference or occlusion. Firstly, the proposed algorithm improves the single color target model and presents a novel target model, which fuses color and motion cues, to enhance the robustness and accuracy of target tracking. And in order to increase the tracking efficiency, the algorithm combines Kalman filter with the improved Camshift algorithm by using Kalman filter to predict the position of the tracking target under color noises and occlusion. The experiment results demonstrate that the proposed algorithm can track the target object accurately and has better robustness.

Introduction

Visual tracking technique is a hot research topic in computer vision and has been widely applied in electronic monitoring system, intelligent traffic management, medicine and military fields. The Meanshift algorithm proposed by the Comaniciu D et al. [1][2] is widely recognized and it has the trait of non-parameters and fast pattern matching. However, the algorithm is not an adaptive mechanism, can not automatically adjust the size of tracking box. Meanwhile, the algorithm does not use the information of moving targets' direction and speed in the process of tracking, the tracking accuracy is low under the complex background and occlusion. Bradski[3] proposed a tracking algorithm based on color histogram--Continuously Adaptive Mean Shift algorithm. This algorithm can automatically adjust the size of the window, accurately track the target, but as with Meanshift algorithm it falls to track the target under color interference or occlusion. Kalman filter is extensively used for tracking in many areas of control theory, signal processing, computer vision and so on. The Kalman filter estimates the state of a dynamic system, even if the precise form of the system is unknown [4].

The Kalman filter theory

Kalman filter is an algorithm of estimating the linear minimum variance of state sequence of a dynamic system, using the state equation and observation equation to describe a dynamic system. In target tracking, the Kalman filter is used for the estimation of an object's location in the current frame, in accordance with the object's locations in the previous frames.

The state equation and observation equation of the system are:

$$X_k = AX_{k-1} + Bu_{k-1} + W_{k-1} \tag{1}$$

$$Z_k = HX_k + V_k \tag{2}$$

Where, X_k and X_{k-1} are state vectors of time k and $k-1$, A is state transition matrix, Bu_{k-1} is external input control, Z_k is the observation vector, the matrix W and V represent the state and the measurement noise with covariances Q and R, respectively.

The process of Kalman filter is divided into two stages: Prediction: includes the state prediction and error covariance prediction; Correction: includes calculating Kalman filter gain coefficients and using the gain coefficients to modify observations and error covariance, for making the correction values are more close to the target's real information.

The improved Camshift algorithm

The color feature is widely used in the process of tracking, for this is easily extracted. Moreover, the variation and complexity of tracking scene may easily lose the target, such as backgrounds with similar color or sudden light changes. If integrating multiple features the algorithm can improve the performance of tracking. Therefore, this paper adopts an improved target model of fusing color and motion information.

The extraction of motion information. This paper uses Kim algorithm to get the target motion information[6], namely, combining frame differential with background subtraction method to effectively extract the target. Supposing $f_{k-1}(x,y)$ and $f_k(x,y)$ are two adjacent frames, $f_b(x,y)$ is background image, calculate the difference between two frames, calculate the difference between current frame and the background image:

$$T_b(x,y)=\begin{cases}1, \left|f_k(x,y)-f_b(x,y)\right|>t_2\\ 0, \left|f_k(x,y)-f_b(x,y)\right|\le t_2\end{cases},\quad T_t(x,y)=\begin{cases}1, \left|f_k(x,y)-f_{k-1}(x,y)\right|>t_1\\ 0, \left|f_k(x,y)-f_{k-1}(x,y)\right|\le t_1\end{cases} \tag{3}$$

Then, calculating target motion template after binarization:

$$M(x,y)=\begin{cases}1, \left|T_k(x,y)\cap T_b(x,y)\right|=1\\ 0, \left|T_k(x,y)\cap T_b(x,y)\right|=0\end{cases} \tag{4}$$

Finally, the images obtained by formula (4) use morphological filter and connectivity analysis, then get motion probability distribution diagram I_m.

The fusion of color and motion information. Assuming that the candidate target is a rectangular area, (x,y) is the coordinates of the area of the pixel in the current frame, the color and motion information are:

$$M_c=\sum_x\sum_y I_c(x,y)\ ,\ M_m=\sum_x\sum_y I_m(x,y) \tag{5}$$

Where $I_c(x,y)$ and $I_m(x,y)$ are position (x,y) pixel values in color and motion probability distribution diagram.

The method of the fusion of color and motion information:

$$M=(1-\beta)M_c+\beta M_m=\sum_{x,y}((1-\beta)I_c(x,y)+\beta I_m(x,y)) \tag{6}$$

Here, M is joint zero moment, $\beta\in[0,1]$ is the weight of motion information, usually take 0.7. This kind of combining color with motion information to establish the target model is more stable and reliable than traditional algorithm which adopted single feature.

Improved Camshift algorithm. The specific process is as follows:

Ⅰ.Firstly, compute zero-order moment and first-order moment:

$$M_{00}=M=\sum_x\sum_y((1-\beta)I_c(x,y)+\beta I_m(x,y)),$$

$$M_{10}=\sum_x\sum_y x((1-\beta)I_c(x,y)+\beta I_m(x,y)),\quad M_{01}=\sum_x\sum_y y((1-\beta)I_c(x,y)+\beta I_m(x,y)) \tag{7}$$

Ⅱ.Calculate the centroid position of the search window:

$$x_1=\frac{M_{10}}{M_{00}}\ ,\ y_1=\frac{M_{01}}{M_{00}} \tag{8}$$

Then, locate the center of the rectangular area $C(x_1,y_1)$, and change the number of iterations $n=n_1+1$.

Ⅲ.If $\|C_1-C_0\|<\varepsilon$ or $n_1>n_0$ stop iteration, update the target position C_1; otherwise, take $C_0=C_1$, return to step Ⅰ.

Combining Kalman filter with improved Camshift algorithm

The Camshift algorithm is vulnerable to full occlusion in successive frames, because the iteration is initialized by using the results obtained in the previous iteration. Therefore, the Kalman filter can be used for full occlusion detection. If the desired object, during overlapping, then its location and speed can be predicted using the Kalman filter. The specific algorithm steps are as follows:

Ⅰ.Read the first frame, extract target manually, obtain the initial state of target, get the target model according to section 2.1;

Ⅱ.Initialize the parameters of Kalman filter, and calculate the predicted position of the object;

Ⅲ.Calculate the optimal target location under Camshift algorithm;

Ⅳ.Determine whether color interference or severe occlusion: if not, using Camshift algorithm optimal location as observed value to update Kalman filter; if yes, using Kalman filter predicted location as observed value to update Kalman filter;

Ⅴ.Read the next frame, return to step Ⅱ.

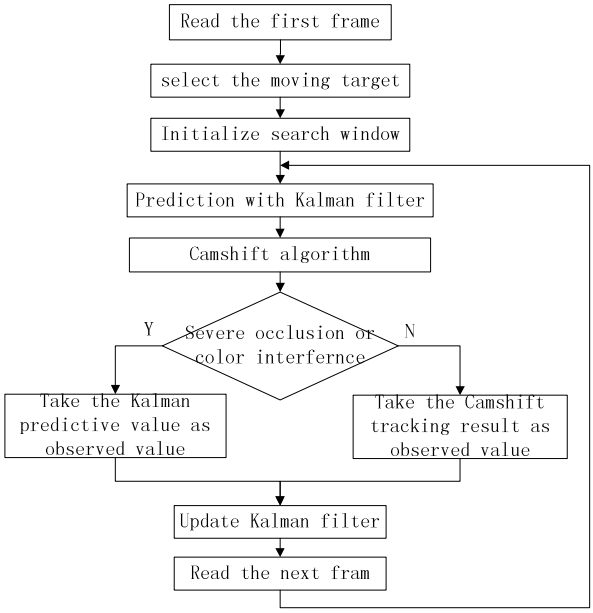

Fig.1 Flowchart of combining Kalman filter with improved Camshift

Experimental results

In order to verify the performance of the algorithm, we did the experiments respectively under the condition of the similar color interference and occlusion. Fig.2 shows the tracking results under similarly colored backgrounds. The traditional Camshift algorithm will gradually lose target, the search window stays on the road, while the proposed algorithm can track the target very well.

(a) Traditional Camshift algorithm

(b) Improved algorithm

Fig.2 Tracking results in the interference of similar color

Fig.3 shows the tracking results under the condition of server occlusion. When the moving people is totally occluded by the tree, the traditional Camshift algorithm fails to track the people and the search window will stay at a local region, however the proposed algorithm can track the people accurately.

(a) Traditional Camshift algorithm

(b) Improved algorithm

Fig. 3 Tracking results in the server occlusion

Conclusion

This paper presents a tracking algorithm based on improved Camshift and Kalman filter. Firstly, the algorithm improves the traditional target model and presents a novel target model, which fuses color and motion cues. Then, the algorithm combines Kalman filter with improved Camshift algorithm and uses Kalman filter to predict the position of the target when color noises and occlusion. The new approach can remove the interference of similar color and overcome the occlusion problem in the process of tracking. The experiment results demonstrate the proposed algorithm can track the target accurately and has a better robustness to occlusion.

Acknowledgements

This work is supported by Scientific and technological Research project of Science and Technology Department of Shaanxi Province (#2009K08-32)&(#2012K06-16) and Special project of Education Department of Shaanxi Province (#12JK0528).

References

[1]. Comaniciu D, Ramesh V, Meer P. Real-time tracking of non-rigid objects using mean shift[C]//Proc. IEEE Conference on Computer Vision and Pattern Recognition. [S. 1.]: IEEE Press, 2000,142-149.

[2]. Comamociu D, Ramesh V, Meer P. Kernel-based object tracking[J]. IEEE Trans. Pattern Analysis and Machine Intelligence, 2003, 25(5)564-577.

[3]. Bradski G R. Computer vision face tracking for use in a perceptual user inferface[J]. Inter Technology Journal. 1998, 2(2)1-15.

[4]. Zhou Hongren, Jing Zhongliang, Wang Peide, etc. Maneuvering Target Tracking[M]. Beijing: National Defence Industry Press, 1991.

[5]. Wang Xin, Tang Zhenmin. An improved camshaft-based particle filter algorithm for real-time target tracking[J]. Journal of Image and Graphics, 2010, 15(10)1507-1514.

[6]. Zhao Chunhui, Bao Yugang, Yao Bing. Moving objects tracking algorithm based on Camshift and Kim algorithms[J]. Journal of Natural Science of Heilongjiang University, 2010, 27(1)126-130.

[7]. Liu Ming, Zhao Xiaolei. Target tracking based on improved Camshift algorithm[J]. Journal of Nanjing University of Science and Technology, 2012, 37(5)755-760.

Advanced Materials Research Vols. 989-994 (2014) pp 3591-3594
© (2014) Trans Tech Publications, Switzerland
doi:10.4028/www.scientific.net/AMR.989-994.3591

Sensing matrix setting in cognitive Radio Networks

Xingzhi chen[1, a], Baidi chen[2, b]

[1]Faculty of information Engineering and Automation Kunming University of Science and Technology .Kunming 650504.PRC

[2]Science School Jiujiang University. Jiujiang 332005 .PRC

[a] Email: applelemmon@163.com , [b] Email:chenslide@163.com

Keywords: Cognitive radio; sequential spectrum sensing; sensing sequence.

Abstract. In this paper, the problem of maximizing the average throughput of a CRN through setting proper sensing sequences is investigated. In order to find the optimal sensing matrix, we obtain the spectrum sensing sequence. The structure of the proposed scheme is discussed in detail.

Introduction

Emerging new wireless applications and higher data rates rate have incredibly increased the demand for accessing to spectrum in the past ten years. Though the existing spectrum resources seem to not meet the ever-growing demand, many investigations reveal that the spectrum is grossly under-utilized in time, space, and other dimensions [1]. In order to alleviate the shortage of spectrum, cognitive radio (CR) concept, as a potential communication paradigm, has been introduced to improve spectrum efficiency by allowing low-priority secondary users (SUs) to opportunistically exploit the unused licensed spectrums of high-priority primary users (PUs), called white spaces, in a somewhat intelligent manner [2]. To protect primary users (PUs) from the harmful interference, CRs have to be capable of sensing the radio spectrum, learning and adapting to the wireless environment.

The rest of this paper is organized as follows. In Section II, we describe the system model. In Section III, the example and analysis are then presented. Finally, the paper is concluded in Section IV.

System Model

We assume a time-slotted CRN with N_s SUs, which attempt to opportunistically transmit on the channels dedicated to the N_p PUs. The SU exploits narrow-band spectrum sensing that is, it senses only one spectrum at a time. The SUs are synchronous in time-slots with other SUs as well as the PUs. The PUs start their transmissions only at the beginning of the slot whenever they have data for transmissions [3]. Therefore, in order to find the transmission opportunities appropriately and to protect the PUs from a harmful interference, the SUs sense the channels at the beginning of each time-slot, by which the channels can be established as occupied or vacant. We assume that the SU always has packets to transmit, that means, the SU starts its transmission when an opportunity is found. Each SU senses the channels according to its SS sequentially, i.e., the SU senses the channel from the top of the sensing sequence, and then starts sensing the second channel if and only if the first channel is sensed occupied. This procedure will be continued until a transmission opportunity is found.

In order to switch to a new channel, a secondary device needs a specific and constant time duration τ_{ho} to prepare its sensing circuitry. After sensing $K-1$ occupied channels, if the SU finds the K th channel free, the user will transmit data on that channel until the end of the slot. In this case, the wasted time length, i.e., the time spent on the sensing and handover, is equal to $(\tau+\tau_{ho})(K-1)+\tau$. The SUs do not have the adaptive modulation and coding capability; hence they transmit with a constant rate, R during the transmission section.

Then, we have [3]

$$B_k = Re_k = R[1-\frac{(\tau+\tau_{ho})(K-1)+\tau}{T}] \quad (1)$$

where B_k is the average throughput of the SU if the k th channel of its SS is chosen for the transmission. Apparenttly, we can see $B_k > B_j$, if $j > k$ .The objective of every SU is to find a good sensing sequence, which can make the transmission faster.

Here we define a coordinate matrix M with the dimensions of $N_p \times N_s$, where the i th row contains the SS dedicated to the i th SU [4]. The coordinate matrix M contains N_s rows because of N_s SUs. Every row contains N_p elements.

$$M = \begin{bmatrix} SS_1 \\ \vdots \\ SS_{Ns} \end{bmatrix} = [S_{i,j}] = \begin{bmatrix} S_{1,1} & \cdots & S_{1,j-1} & S_{1,j} \cdots S_{1,N_p} \\ & & & \\ S_{N_s,1} & & S_{N_s,j-1} & S_{N_s,j} \cdots S_{N_s,N_p} \end{bmatrix}$$

For the network throughput evaluation, we note that for each spectrum $S_{i,j}$ two possible cases might occur. First, the $S_{i,j}$ th spectrum has been sensed by some SUs in their previous mini-slots (the mini-slots before j th mini-slot). In this case, regardless of the presence or the absence of the PU, the spectrum is occupied (as we assumed error-free sensing in this section). That is, the SU which senses this channel at the first time will transmit if the spectrum is idle. The second case is that the spectrum is sensed at the j th mini-slot by i th SU at the first time. Hence, the occupation probability of this channel only depends on the PU activity. From the above discussion, the repetition of a spectrum in the M when assuming error-free case does not offer any benefit to the CRN throughput.

By the above discussion, the available probability [5] of i th SU for the $S_{i,j}$ th spectrum is expressed by,

$$P_{i,j}^{*} = \begin{cases} 0 \\ P_{0,S_{i,j}} \end{cases} \quad (2)$$

Where $P_{0,S_{i,j}}$ is he absence probability of the $S_{i,j}$ th PU.

However, we can see that the i th SU transmits at the $S_{i,j}$ th spectrum when the spectrums in their previous mini-slots have already occupied.

According to the conditional probability, we have

$$P_{i,j} = P_{i,j}^{*} \prod_{l=1}^{j} \left(1 - P_{0,S_{i,l}}\right) \quad (3)$$

Then, the final available probability is expressed by,

$$P_{i,j} = \begin{cases} 0 \\ P_{0,S_{i,j}} \prod_{l=1}^{j} \left(1 - P_{0,S_{i,l}}\right) \end{cases} \quad (4)$$

By the above discussion, the average throughput of the CRN is easily computed as,

$$Q = \sum_{j=1}^{N_p} \left(\sum_{i=1}^{N_s} P_{0,S_{i,j}} \prod_{l=1}^{j} \left(1 - P_{0,S_{i,l}}\right) \right) B_j \quad (5)$$

Where B_j is defined in (1)

Now, the optimal M is found by solving the following:

$$M^* = \arg\max Q \tag{6}$$

Example and Analysis

In this section, the performances of the proposed schemes are evaluated and compared by the analytical results and simulations considering the effects of different parameters introduced throughout the paper. The values of parameters used for the numerical evaluation are given in Table 1.

Table 1. Simulations Parameters

Parameters	Description	Value
T	Time-slot duration	200ms
τ_{ho}	Requires time for handover	0.1ms
N_p	Number of PUs	5
N_s	Number of SUs	3

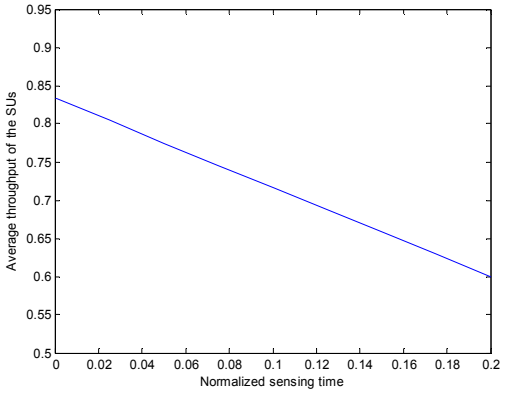

Figure 1 Average throughput against the normalized sensing time

Figure 1 validates our analysis and depicts the average throughput of the SUs against the normalized sensing time for an error-free sensing scheme. For the optimal M , the simulation result is provided. As realized, the average throughput linearly decreases by the normalized sensing time. This is owing to the fact that for the error-free case, there exists no error in the detection scheme and thus while the increase of sensing time does not have any positive effect on the correct detection, it linearly reduces the transmission time.

Conclusion

In this paper, a novel intelligent sensing matrix setting scheme has been proposed, which maximizes the average secondary users' throughput. As a future work, we aim to extend the proposed system by modeling the impact of error and latency on the throughput estimator block.

Acknowledgement

This work is supported by project of Jiangxi Natural science foundation of Jiangxi Province (Project No. 20132BAB201012) and Science and Technology of Jiangxi Education Bureau, (Project. No GJJ13714)

References

[1] I. F. Akyildiz, W. Y. Lee, M. C. Vuran, and S. Mohanty, “Next generation / dynamic spectrum access / cognitive radio wireless networks: a survey,” Comput. Netw. J., vol. 50, pp. 2127–2159, Sept. 2006.

[2] A. He, K. K. Bae, T. R. Newman, J. Gaeddert, K. Kim, R. Menon, L. Morales, J. Neel, Y. Zhao, J. H. Reed, and W. H. Tranter, “A survey of artificial intelligence for cognitive radios,” IEEE Trans. Veh. Technol., vol. 59, no. 4, pp. 1578–1592, May 2010.

[3] H. Shokri-Ghadikolaei and M. Nasiri-Kenari, “Sensing matrix setting schemes for cognitive networks and their performance analysis,” accepted in IET Commun. Available: http://arxiv.org/pdf/1111.4624v2, July 2012.

[4] Hossein Shokri-Ghadikolaei and Rajab Fallahi: ‘Intelligent sensing matrix setting in cognitive radio networks’. IEEE Communication Letters, November 2012

[5] Haykin S. Cognitive Radio: Brain-empowered Wireless Communications [J]. IEEE Journal on Selected Areas in Communications, 2005, 23(2): 201-220.

Advanced Materials Research Vols. 989-994 (2014) pp 3595-3598
© (2014) Trans Tech Publications, Switzerland
doi:10.4028/www.scientific.net/AMR.989-994.3595

Wavelet de-noising based on genetic adaptive threshold algorithm

Guangwen WU[1,2,a], Changming WANG[1,b]

[1]School of Mechanical Engineering, Nanjing University of Science and Technology, Nanjing 210094,China

[2] Department of Electronic Engineering, East China Institute of Technology, Fuzhou 344000, China

[a]email: wu_gw@163.com, [b]email:wu_gw@163.com

Keywords: wavelet; de-noising; genetic algorithm; threshold

Abstract. The central step of de-noising in wavelet domain is the threshold selection. To get the best de-noising result, the threshold should be selected according to the noisy observation. This paper presents a genetic adaptive threshold method, which gets the optimum threshold in the sense of least MSE by using an estimation function of the signals' MSE function. The simulation results with standard wavelet test signals shows that the operation speed of the proposed method four times the traditional continuous searching algorithm, moreover, the optimum threshold calculated is more accurate and reasonable.

Introduction

Wavelet transform could decompose noisy signal into several scales. Since signal and noise have different features on different scales, such a property can be used for separating the signal from noise. According to this theory, wavelet transform has been used in many fields for de-noising process [1-8].

The wavelet transform has primary properties such as compression or sparse which means that wavelet transforms of noisy signals tend to be sparse. Due to the fact that the wavelet transform of a noisy signal is a linear combination of the wavelet transform of the noise and the original signal, the noise energy can be suppressed significantly with a suitable threshold while the main signal features can be preserved. The functionality of the de-noising process is due to the threshold value and the thresholding rule. Hard thresholding function is a basic ones introduced by Donoho[8]. The coefficients less than the threshold value are set to zero and others remain unchanged. Therefore, the optimum threshold value selection plays an important role in de-noising process. Reference [1] presented a thresholding function, $t=\sigma\sqrt{2\log N}$, By using this equation, it is easy to get the threshold value of the coefficients of the orthogonal wavelet, however the method has limitation because the optimum threshold value varies with the total number of samples (for example, $N=4096$, $t\approx 4.079\sigma$; $N=1024$, $t\approx 3.723\sigma$). It is obvious that the threshold value get from the previous function is not optimum, and the best result of de-noising can not attained as well. For the noisy signal which contain Gaussian white noise, 99.74% noise are reduction if the threshold value is set as the next formula: $t=3\sigma$, where t is the threshold value and σ is Gaussian white noise standard deviation, furthermore, a suitable constant multiplied by σ could be the best threshold. Reference [7] proposed an approximation value of the mean square function, and the optimum threshold value can be achieved by choosing suitable parameter c, which was used in many applications. However, it is needed too large amount computation for the approximation value so that the process is useless in practice and almost all the practical application choose a random value between [2,3] instead.

Since it is difficult to get the optimum threshold value proposed in reference [7] by using the normal method used for optimum searching, this paper presents a genetic adaptive algorithm which could quickly find the best threshold value according to the objective observed noisy signal.

Wavelet hard thresholding

The signal's singular structures can be represented with the wavelet coefficients. The coefficients of signal and noise have different characters on different decomposition scales. The hard thresholding de-noising in the wavelet domain can be summarized as follows. (1) The noisy signal is decomposed in the wavelet domain; (2) The coefficients which below threshold are set to zero and others remain unchanged; (3) Applying inverse wavelet transform on modified coefficients to reconstruct the signal.

MSE(mean square error) function presents the difference between the real signal and the estimation data. Otherwise, in practical application, the real signal is always unknown. Therefore, the estimation of MSE is needed, and the minimum of the estimation can be used as the criterion for optimum threshold value searching. Reference [8] proposed a MSE approximation function,

$$F(c) \approx Error(c) = 2[\sigma^2 - \frac{k}{2erf(c)N}\int_{-c\sigma}^{c\sigma} x^2 \frac{e^{-x^2/(2\sigma^2)}}{\sqrt{2\pi}\sigma}dx] - E[\hat{W}_f^2] \tag{1}$$

$x \sim N(0,\sigma^2)$, $erf(c) = \frac{1}{\sqrt{2\pi}}\int_0^c e^{-y^2/2}dy$,Obviously, $2erf(c) \approx k/N$, $E[\hat{W}_f^2]$ in equation (1) is the residual wavelet coefficients after de-noising with the threshold $c\sigma$, and k wavelet coefficients are set to zero after de-noising, N is the quantity of samples. It is obvious that the integration process can not expressed by basic functions. Therefore, it is difficult to find optimum threshold value using normal algorithms. The minimum of the MSE correspond with the threshold parameter c which is a approximation of the optimum threshold value parameter. The algorithm above must calculate all the function value correspond with every discrete point in an interval of $c \in [1,6]$. Because of the integrate process need too large amount computations, a random number often be selected at interval [2,3] instead. Therefore, advanced algorithm must be found for searching the optimum threshold value.

Genetic algorithm can be applied for the formula (1) calculation procession which first selecting suitable population and generation, then using bound searching for optimal threshold value instead of continuous searching. In order to reduce the computation complexity and speed up searching process, this paper improves the traditional genetic algorithm. The procedure of new algorithm can be divided into the following steps.

Step 1: Deciding the encoding and decoding method. In this paper, L bits of binary strings are used for encoding and decoding. The bit of the binary is called gene, with a value of 1 or 0. The string of the binary is called chromosome. Suppose the minimum and maximum of c are $c_{\min}$ and $c_{\max}$, respectively, which are calculated according to Equation (1). The accuracy δ can be calculated by formula :

$$\delta = \frac{c_{\max} - c_{\min}}{2^L - 1} \tag{2}$$

in which $c_{\max} = 6, c_{\min} = 1$, suppose $L = 13$, then the accuracy $\delta = 0.00061$. Encode c into a binary code with bits of L, and c can be decoded from the binary code into a decimal number by equation (3):

$$c = c_{\min} + (\sum_{i=1}^{L} b_i 2^{i-1})\delta \tag{3}$$

in which b_i is the value of the i th bit of c in the binary style.

Step 2: Calculating the fitness of every individual of the population. Based on equation (1),

$$F(c) \approx Error(c) = 2\sigma^2 - (\frac{2k}{N\sigma}\frac{\int_0^{c\sigma} x^2 e^{-x^2/(2\sigma^2)}dx}{\int_0^c e^{-y^2/2}dy} + E[(W_f(c))^2]) \tag{4}$$

with $E[(W_f(c))^2] = E[(W_f .* |W_f > c\sigma|)^2]$. The fitness function of the genetic algorithm is defined as follows:

$$f=\frac{2k}{N\sigma}\frac{\int_0^{c\sigma}x^2e^{-x^2/(2\sigma^2)}dx}{\int_0^{c}e^{-y^2/2}dy}+E[(W_f(c))^2] \tag{5}$$

When the MSE Error(c) is at minimum, the fitness function (5) achieves the maximum. Then c is considered as the optimum threshold parameter and the optimum threshold value: $t=c\sigma$.

Step 3: Selecting the individuals in the current generation. Based on Equation (6) the selection probability p_i of the i th individual is determined. Dominant individuals are selected for genetic operation according to the selection strategy. In this paper, the roulette wheel selection scheme is used for selecting the individuals as parents.

$$p_i=\frac{f_i}{\sum f_i} \tag{6}$$

Step 4: selecting p_r percent elite chromosome to directly copied, and each chromosome copies n times, then the quantity of individual after reproduce is : $M_N=M*p_r*n$ (7)

in which M is the quantity of individual in current population. The next process is mutation. The probability P_m of mutation is showing as follows:

$$P_m=p_m*\frac{N-k}{N} \tag{8}$$

in which N is the length of a chromosome and $k=round(\log(10(c_{\max}-c_{\min})))$.

Step 5: updating the population. Replace $M*p_r$ chromosome by optimum chromosome in order to remain the quantity of population unchanged.

Parameters of the binary coding genetic algorithm are determined as follows: the population size N_s=40, the length of chromosome L=13, the copy times n=10, probability of mutation p_m=0.1, the update percent fat=0.2.

It is obvious that large computation concentrate on the calculating the chromosome's fitness functions. This process needs N_s times computation and each chromosome in every generation also need computation their fitness function which computation times is N_s*p_m*n. Therefore, all the operation times can be calculated as follows:

$$N=(N_s+N_s*p_m*n)*G \tag{9}$$

Test results

In order to prove the effect of the proposed algorithm, we designed MATLAB codes to carry out the hard threshold de-noising computation. By testing on the noisy signals which including wavelet noise test data, we can prove the accuracy and effective of the genetic adaptive algorithm. All computation in this paper is carried on by MATLAB codes in Microsoft Windows 7, 64-bits. The processor in the computer is an Intel Core i3 with max speed of 2GHz and 4 GB memory.

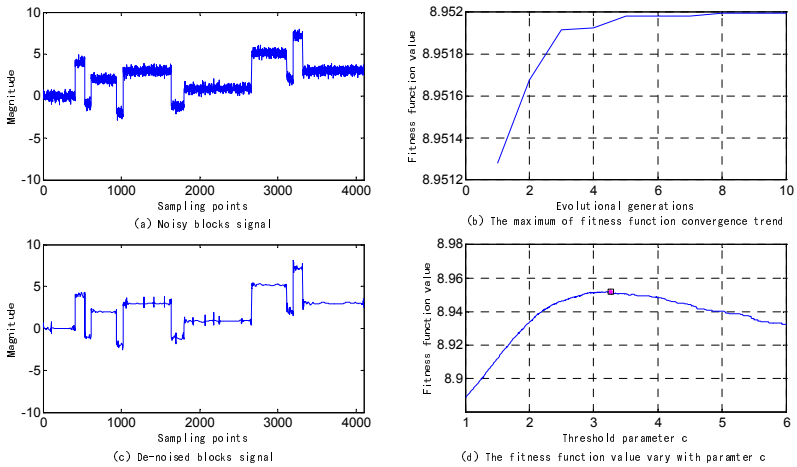

Figure 1. Experiment used blocks signal

The first experiment used 'blocks' signal, figure 1(a) shows the noisy signal which is a linear combination of 'blocks' and Gaussian white noise; Figure 1(b) shows the maximum of fitness function convergence trend with evolutional generations, from this figure it can be seen that the fitness is convergent when the evolutional generation $g > 8$, and the maximum of the fitness is 8.9520, the optimum parameter $c = 3.2628$; Figure 1(c) shows the result of genetic adaptive hard thresholding de-noising; Figure 1(d) shows the chart of fitness function's value using continuous searching algorithm, the searching step is 0.001, interval is [1,6], the maximum of fitness is 8.9520, and the optimum threshold value c=3.262. In this figure, the maximum of fitness calculated by genetic adaptive algorithm is marked with "□" and by continuous algorithm is marked with "*". The two marks almost overlapped at the same point, but the value calculated with genetic adaptive algorithm is more accurate. Furthermore, the time cost of continuous searching is t=14.76s and genetic algorithm time cost is t= 3.58s.

The test data of experiment 2 is 'bumps'; the experiment 3 using 'heavy sine' signal. The compare of traditional continuous searching algorithm and genetic one of each experiment are showing as tables 1.

Table 1. Comparison of two methods

Methods	blocks			bumps			heavy sine		
	Maximum	parameter c	Time (s)	Maximum	parameter c	Time (s)	Maximum	parameter c	Time (s)
Continuous	8.9520	3.262	14.76	3.4323	3.427	14.78	9.6879	3.720	14.84
Genetic adaptive	8.9520	3.2628	3.58	3.4323	3.4264	3.62	9.6879	3.7201	3.67

Conclusion

The paper proposed a fast calculation algorithm of the optimum threshold parameter at the means of least MSE, and the theory and practice proved it can be improve the calculation speed more than 4 times without loss accuracy. The traditional algorithm is random selecting a value between [3,4], the algorithm proposed in this paper solve the problem which can be adaptive selecting the optimum threshold parameter c according practical conditions.

Acknowledgement

This work is supported by Research Fund for Doctoral Program of Higher Education of China (No. 20133219110027) and National Nature Science Foundation of China (No. 61161010，11265001).

References

[1] D. Donoho. De-noising by Soft-thresholding [J]. IEEE Trans. on IT. , 1995, 41(3): 613-627.
[2] Jian Li, Changkui Cheng, Tianyan Jiang. Wavelet De-noising of Partial Discharge Signals Based on Genetic Adaptive Threshold Estimation [J]. IEEE Transactions on Dielectrics and Electrical Insulation, 2012, 19: 543-549.
[3] Tahsina Farah Sanam, Celia Shahnaz. Noisy speech enhancement based on an adaptive threshold and a modified hard thresholding function in wavelet packet domain [J]. Digital Signal Processing, 2013 ,23: 941-951.
[4] Mehdi Nasri, Hossein Nezamabai-pour. Image denoising in the wavelet domain using a new adaptive thresholding function [J]. Neurocomputing , 2009, 72: 1012-1025.
[5] W.Y.Liu, J.G. Han. The optimal Mexican hat wavelet filter de-noising method based on cross-validation method [J].Neurocomputing, 2013 ,108: 31-35.
[6] M. Beenamol, S. Prabavathy, J. Mohanalin. Wavelet based seismic signal de-noising using Shannon and Tsallis entropy [J].Computers and Mathematics with Applications, 2012 ,64: 3580-3593.
[7] Zhang L, Pan Q, Zhang H C, etc. On the determination of threshold in threshold-based de-noising by wavelet transform [J]. ACTA ELECTRONICA SINICA, 2001, 29(3):400-402.
[8] D.L. Donoho, I.M. Johnstone, Ideal spatial adaption by wavelet shrinkage, Biometrika 81 (3) (1994) 425-455.

Advanced Materials Research Vols. 989-994 (2014) pp 3599-3604
© (2014) Trans Tech Publications, Switzerland
doi:10.4028/www.scientific.net/AMR.989-994.3599

3D Graphical Representation of Protein Sequences Based on Conformational Parameters of Amino Acids

Qianjun XIAO[1, a], Zonggang DENG[1, b]

[1]Hunan Vocational Institute of Technology, Xiangtan, 411104, China

[a]email: xqjxt@126.com, [b]email: dengzonggangc-s@163.com

Keywords: ND5 protein Sequences; Similarity; Graphical Representation; L/L matrix; Leading Eigenvalue.

Abstract. Based on the helix and β-sheet and the β-turn conformational parameters, P_α and P_β and P_t, of the 20 amino acids, we propose a new 3D graphical representation of protein sequence without circuit or degeneracy, which may reflect the innate structure of the protein sequence. Then the numerical characterizations of protein graphs, the leading eigenvalues of the L/L matrices associated with the graphical curves for protein sequences, was utilized as descriptors to analyze the similarity/dissimilarity of the nine ND5 protein sequences.

Introduction

In recent years, some researchers proposed many methods to analyze the huge amounts of gene data. The graphical representation method initiated in 1983 by Hamori[1] is one of those methods. From Hamori, Graphical techniques became a very powerful tool for the visualization and analysis of DNA sequences[2-16]. However the graphical representation of protein sequence emerges only recently, and some representations are outlined[17-32].The emergence of graphical representations of proteins was delayed because it is more perplexed to deal with biological strings built on a 20-letter alphabet (representing the 20 natural amino acids) than to deal with biological strings built from only four letters (representing DNA or RNA). Moreover, Most of existing 2D and 3D graphical representations of proteins involve the arbitrary assignment of amino acids to vertices of graphs or geometrical objects considered. Following previous work, Yao et al.[27] outlined a 2D graphical representation for proteins based on the physicochemical properties of amino acids. But there exists circuit or degeneracy in Yao's 2D graphical representation for proteins which lead to losing much biological information due to overlapping and crossing of the curve with itself. In order to avoid deficiency in Yao's work, Wen et al.[28] proposed another 2D graphical representation for proteins based on the physicochemical properties of amino acids. But until now, just few 3D graphical representation of protein sequences was proposed[24,29-31].

In this letter, a 3D graphical representation of protein sequence was outlined utilizing the helix and β-sheet and the β-turn conformational parameters, P_α and P_β [33,34] and P_t [35], of the 20 amino acids, which may reflect the innate structure of the protein sequences. Significantly, our graphical representation avoids the degeneracy of graphical curve. With this graphical representation, we consider the numerical characterization of mutations and analyze the similarities among sequences belonging to nine ND5 (NADH dehydrogenase sub unit 5) proteins: human (Homo sapiens, YP 003024036), gorilla(Gorilla gorilla, NP 008222), common chimpanzee (Pan troglodytes, NP 008196), pigmy chimpanzee(Pan paniscus, NP 008209), fin whale(Balenoptera physalus, NP 006899), blue whale(Balenoptera musculus, NP 007066), rat(Rattus norvegicus, AP 004902), mouse(Musmusculus, NP 904338), and opossum(Didelphis virginiana, NP 007105).

3D graphical representation of protein sequence

The helix and β-sheet conformational parameters, P_α and P_β, of the 20 amino acids have been quantitatively determined from a statistical analysis of 15 proteins with known conformation[33,34].

Later, the β-turn conformational parameters, P_t, of the 20 amino acids was quantitatively determined from a statistical analysis of 12 proteins with known conformation[35]. In this paper, these three protein conformational parameters, P_α and P_β and P_t, of the 20 amino acids was selected as the basic to construct protein map. P_α and P_β and P_t values we have adopted listed in Table 1. From Table 1, we can find that the average of P_α and P_β and P_t values, $<P_\alpha>$and$<P_\beta>$and$<P_t>$, of 20 amino acids is 1.0005 and 1.0405 and 0.9655 respectively. If the point (1.0005,1.0405,0) is taken as the origin, there is 20 special vectors respecting the 20 amino acids in 3D Cartesian coordinates. The numerical values in the last three columns of Table 2 are the *x* and the *y* and the *z* coordinates for 20 amino acids along the *x*-axis with respect to P_α and along the *y*-axis with respect to P_β and along the *z*-axis with respect to P_t. From Table 1, each amino acid can be numerically characterized by a unique special vector. The points in the 3D graphical representation are obtained by the sum of vectors representing amino acids in the sequence. For example, given a protein sequence with *N* amino acids $S = s_1, s_2, \cdots, s_N$, inspect it by stepping one amino acid at a time. For the step *i* (i = 1, 2,… , N), the point $P_i(x_i, y_i, z_i)$ can be constructed as follow:

$$x_i = \sum_{k=1}^{i} S_k^1, y_i = \sum_{k=1}^{i} S_k^2, z_i = \sum_{k=1}^{i} S_k^3$$

where $S_k^j \left(j = 1,2,3\right)$ represents the *j*-th component of the vector corresponding to S_k. When i from 1 to N, we have points $P_1, P_2, \cdots, P_N$. Connecting the adjacent points, we can obtain the protein curve. Our graphical representation has no circuit or degeneracy. We can easily find that

Table 1: The helix and β-sheet and the β-turn conformational parameters, P_α and P_β [33,34] and P_t [35], of the 20 amino acids

Amino Acid (Abbreviation)	Pa	Pb	Pt
Gly	0.53	0.81	1.68
Asn	0.73	0.65	1.68
Ser	0.79	0.72	1.56
Pro	0.59	0.62	1.54
Asp	0.98	0.8	1.26
Tyr	0.61	1.29	1.25
Cys	0.77	1.3	1.17
Trp	1.14	1.19	1.11
Lys	1.07	0.74	1.01
Arg	0.79	0.9	1
Thr	0.82	1.2	1
Phe	1.12	1.28	0.71
His	1.24	0.71	0.69
Met	1.2	1.67	0.67
Ile	1	1.6	0.58
Ala	1.45	0.97	0.57
Gln	1.17	1.23	0.56
Leu	1.34	1.22	0.53
Glu	1.53	0.26	0.44
Val	1.14	1.65	0.3
	$<P_\alpha>$= 1.0005	$<P_\beta>$= 1.0405	$<P_t>$= 0.9655

Table 2: The 20 amino acids and their coordinates in 3D Cartesian coordinates for P_t-curve

Amino Acid	P_t-curve		
	x-Coord	y-Coord	z-Coord
Gly	-0.4705	-0.2305	1.68
Asn	-0.2705	-0.3905	1.68
Ser	-0.2105	-0.3205	1.56
Pro	-0.4105	-0.4205	1.54
Asp	-0.0205	-0.2405	1.26
Tyr	-0.3905	0.2495	1.25
Cys	-0.2305	0.2595	1.17
Trp	0.1395	0.1495	1.11
Lys	0.0695	-0.3005	1.01
Arg	-0.2105	-0.1405	1
Thr	-0.1805	0.1595	1
Phe	0.1195	0.2395	0.71
His	0.2395	-0.3305	0.69
Met	0.1995	0.6295	0.67
Ile	-0.0005	0.5595	0.58
Ala	0.4495	-0.0705	0.57
Gln	0.1695	0.1895	0.56
Leu	0.3395	0.1795	0.53
Glu	0.5295	-0.7805	0.44
Val	0.1395	0.6095	0.3

there is no circuit or degeneracy in our model. That's to say, no circuit exist in the graphical representation. The graphical curve and protein sequence follow a one-to-one correspondence, and sequence alignment can be done by simply identifying similar segments of the graph from our method. In addition, the protein sequence can be recovered from its graph mathematically without loss of biological information. If the point (1.0005,0,0.9655) and if the point (0,1.0405,0.9655) is taken as the origin, following the method mentioned above, we can get another two graphical curves for the same protein sequence. We called these three graphical curve as P_t-curve and P_β-curve and P_α-curve, respectively.

In Figure 1, we illustrate the dynamic 3D graphical representations of ND5 proteins for nine different species. Comparing the curves, we can find that the curves of the ND5 proteins of human, gorilla, common chimpanzee, and pigmy chimpanzee are more similar although gorilla is somewhat different, and the ND5 protein graphs are more similar for (fin whale, blue whale) and (rat, mouse) too. In addition, we find ND5 protein graph of opossum is obviously different from the other species. And their similarities/dissimilarities are consistent with the known fact of evolution. [27,28,36-38]

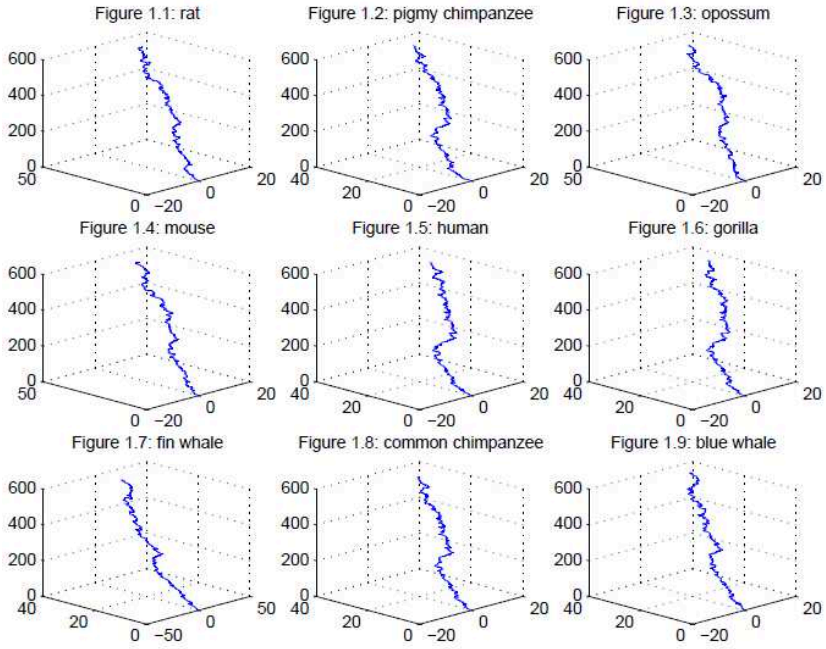

Fig. 1. The P_t-curve of nine ND5 proteins

Numerical characterization of protein sequence

In this section, we will illustrate the numerical characterization of graphical curve which facilitates quantitative comparisons of sequences. Mathematical invariants can be used to characterize the graphical curve. First we transform the graphical curve into a matrix to represent a sequence, then we use some of matrix invariants[6-7,9-16] as descriptors of protein sequence, such as the eigenvalue of constructed matrices. Especially, the leading eigenvalue of matrices is widely used in the comparison of sequences. In this report, the numerical characterization of the graphical curve is given by the matrix: L/L matrix.

The L/L matrix is the symmetric matrix whose off-diagonal elements are defined as a quotient of the Euclidean distance between two vertices of the zigzag curve and the sum of geometrical lengths of edges between the two vertices. By definition all diagonal entries are zero. In other words

$$l_{i,j} = \begin{cases} d_{i,j} / \sum_{k=i}^{j-1} d_{k,k+1} & if\ i \neq j \\ 0 & if\ i = j \end{cases}$$

We will characterize the protein sequences belonging to nine ND5 proteins by means of the leading eigenvalue of the L/L matrix. We list the leading eigenvalues of the L/L matrices associated

with three graphical curves, P_t-curve and P_β-curve and P_α-curve, representing each of the protein sequences in Table 3. The smallest magnitude of the leading eigenvalues is found for Opossum except for the P_β-curve.

Table 3: The leading eigenvalues of the L/L matrices associated with three graphical curves, P_t-curve and P_β-curve and P_α-curve

Species	λ for P_α-curve	λ for P_β-curve	λ for P_t-curve
human	527.618009	534.640631	536.241321
common chimpanzee	527.216431	535.674423	536.68723
pigmy chimpanzee	526.747668	535.455882	535.870302
gorilla	527.394065	534.894326	535.282623
fin whale	530.589867	539.041219	536.535591
blue whale	530.522835	539.519108	537.854552
mouse	528.001379	541.115469	538.310286
rat	530.359992	543.240098	541.283399
opossum	524.089115	536.40529	532.712324

Similarities/dissimilarities of protein sequences

Comparison of similarities/dissimilarities is the essential motivation of graphical representation. Here we also illustrate the use of our quantitative characterization of the protein sequences with an examination of similarities/dissimilarities among nine ND5 proteins. We represent the sequences with the corresponding 3-component vectors. Moreover, the leading eigenvalues can be normalized as mentioned above. The analysis of similarity among protein sequences represented by the 3-component vectors is based on the assumption that two protein sequences are similar if the corresponding 3-component vectors point to a similar direction in the 3D space and have similar magnitudes. The similarity/dissimilarity between these two vectors can be measured by calculating the Euclidean distance between their end points. Clearly, the smaller is the Euclidean distance the more similar are the two protein sequences.

Now we construct a 3-component vector consisting of the normalized leading eigenvalues $(\lambda_1 / N, \lambda_2 / N, \lambda_3 / N)$ of the L/L matrices associated with three essentially different graphical curves for protein sequences, where N represents the length of the protein sequence . In Table 4, we list the similarity/dissimilarity matrix for the protein sequences among nine ND5 proteins based on the Euclidean distances between the end points of the 3-component vectors. Observing from Table 4, we find that the proteins of human, gorilla, common chimpanzee, and pigmy chimpanzee are more similar with each other, and the proteins of fin whale-blue whale and rat-mouse are very similar. On the other hand, the opossum(the most remote species from the remaining mammals) is dissimilar to others among the six species except rat and mouse. So we think that the results of Table 4 about the similarity are consistent to the known fact of evolution[27,28,36-38].

Conclusion

On the basis of the helix and β-sheet and the β-turn conformational parameters, P_α and P_β and P_t, of the 20 amino acids, a new 3D graphical representation of protein sequence was outlined. The advantage of our method is that it allows visual inspection of data, helping in recognizing major similarities among different proteins, but also avoids the some loss of information of proteins. Then we get the numerical characterization of graphical curve, which facilitates the similarity analysis of protein sequence. The method we proposed is more simple, convenient, visible and the result based on our method well coincide with the real evolutionary relationship among these nine species.

Table 4: The similarity/dissimilarity matrix for the nine ND5 proteins based on the Euclidean distances between the end points of the 3-component vectors which consists with the normalized leading eigenvalues of the L/L matrices associated with three graphical curves, P_t-curve and P_β-curve and P_α-curve.

	c.chim.	f.whale	gorilla	human	mouse	opossum	p.chim.	rat	b.whale
c.chim	0	0.00496	**0.00268**	**0.00198**	0.00631	0.00689	**0.0016**	0.00599	0.00335
f.whale		0	0.00351	0.00489	0.00621	0.00523	0.00416	0.00652	**0.00232**
gorilla			0	**0.00169**	0.00654	0.00632	**0.00172**	0.00626	0.00335
human				0	0.00746	0.00762	**0.00207**	0.00706	0.00408
mouse					0	0.00211	0.00539	**0.00112**	0.00576
opossum						0	0.00569	0.00274	0.00559
p.chim							0	0.00502	0.0032
rat								0	0.00602
b.whale									0

Acknowledgement

In this paper, the research was sponsored by the Scientific Research Fund of Hunan Provincial Education Department (Project No. 10C0185) .

References

[1] E. Hamori, J. Ruskin, A novel method of representation of nucleotide series especially suited for long DNA sequences, J. Biol. Chem., 258:1318-1327,1983.
[2] E. Hamori, Novel DNA sequence representations, Nature, 314:585-586,1985.
[3] M.A. Gates, A simple way to look at DNA, J. Theor. Biol., 119:319-328,1986.
[4] A. Nandy, A new graphical representation and analysis of DNA sequence structure: I. Methodology and application to globin genes, Curr. Sci., 66:309-314,1994.
[5] A. Nandy, P. Nandy, Graphical analysis of DNA sequence structure: II. Relative abundances of nucleotides in DNAs, gene evolution and duplication, Curr. Sci., 68:75-85,1995.
[6] M. Randic, M. Vra_cko, A. Nandy, S.C. Basak, On 3-D graphical representation of DNA primary sequences and their numerical characterization, J. Chem. Inf. Comput. Sci., 40:1235-1244,2000.
[7] M. Randic, J. Zupan, M. Novic, On 3-D graphical representation of proteomics maps and their numerical characterization, J. Chem. Inf. Comput. Sci., 41:1339-1344,2001.
[8] X.F. Guo, A. Nandy, Numerical characterization of DNA sequences in a 2-D graphical representation scheme of low degeneracy, Chem. Phys. Lett., 369:361-366,2003.
[9] B. Liao, T.M. Wang, New 2D graphical representation of DNA sequences, J. Comput. Chem., 25:1364-1368,2004.
[10] B. Liao, A 2D graphical representation of DNA sequence, Chem. Phys. Lett., 401:196-199,2005.
[11] Y.H. Yao, X.Y. Nan, T.M. Wang, A new 2D graphical representationł Classification curve and the analysis of similarity/dissimilarity of DNA sequences, J. Mol. Struct.: Theochem, 764:101-108,2006.
[12] Z.H. Qi, T.R. Fan, PN-curve: A 3D graphical representation of DNA sequences and their numerical characterization, Chem. Phys. Lett., 442:434-440,2007.
[13] Z.H. Qi, X.Q. Qi, Numerical characterization of DNA sequences based on digital signal method, Comput. Biol. Medic, 39:388-391,2009.
[14] J.F. Yu, X. Sun, J.H. Wang, TN curve: A novel 3D graphical representation of DNA sequence based on trinucleotides and its applications, J. Theor. Biol., 261:459-468,2009.

[15] G.S. Xie, Z.X. Mo, Three 3D graphical representations of DNA primary sequences based on the classifications of DNA bases and their applications, J. Theor. Biol., 269:123–130, 2011.
[16] L.P. Yang, X.D. Zhang, H.G. Zhu, Alignment free comparison: Similarity distribution between the DNA primary sequences based on the shortest absent word, J. Theor. Biol., 295: 125-131,2012.
[17] M. Randic, 2-D Graphical representation of proteins based on virtual genetic code, SAR QSAR Environ. Res., 15:147-157,2004.
[18] M. Randic, J. Zupan, Highly compact 2-D graphical representation of DNA sequences, SAR QSAR Environ. Res., 15:191-205,2004.
[19] M. Randic, J. Zupan, A.T. Balaban, Unique graphical representation of protein sequences based on nucleotide triplet codons, Chem. Phys. Lett., 397:247-252,2004.
[20] M. Randic, D. Butina, J. Zupan, Novel 2-D graphical representation of proteins, Chem. Phys. Lett., 419:528-532,2006.
[21] M. Randic, A.T. Balaban, M. Novic, A. Zaloznik, T. Pisanski, A novel graphical representation of proteins, Period. Biolog., 107:403-414,2005.
[22] M. Randic, M. Novic, D. Vikic-Topic, D. Plavsic, Novel numerical and graphical representation of DNA sequences and proteins, SAR QSAR Environ. Res., 17:583-595,2006.
[23] M. Randic, J. Zupan, D. Vikic-Topic, On representation of proteins by star-like graphs, J. Mol. Graph. Model., 26:290-305,2007.
[24] F.L. Bai, T.M. Wang, On graphical and numerical representation of protein sequences, J. Biomol. Str. Dyn., 23:537-545,2006.
[25] B. Liao, J.W. Luo, R.F. Li, W. Zhu, Novel method for analyzing proteome, Int. J. Quant. Chem., 107:1295-1300,2007.
[26] W. Zhu, B. Liao, J.W. Luo, R.F. Li, Numerical characterization and similarity analysis of neurocan gene, MATCH Commun. Math. Comput. Chem., 57:143-155,2007.
[27] Y.H. Yao, Q. Dai, C. Li, P.A. He, X.Y. Nan, Y.Z. Zhang, Analysis of similarity/dissimilarity of protein sequences, Proteins, 73:864-871,2008.
[28] J. Wen, Y.Y. Zhang, A 2D graphical representation of protein sequence and its numerical characterization, Chem. Phys. Lett., 476:281-286,2009.
[29] H.H. Bai, C. Li, H. Agula, Jirimutu, J. Wang, L.L. Xing, Cp-curve, a Novel 3-D Graphical Representation of Proteins, ICCMSE2007, 963:57-60,2007.
[30] C. Li, X.Q. Yu, L. Yang, X.Q. Zheng, Z.F. Wang, 3-D maps and coupling numbers for protein sequences, Physica A, 388:1967-1972,2009.
[31] P.A. He, J.Z. Wei, Y.H. Yao, Z.X. Tie, A novel graphical representation of proteins and its application, Physica A, 391:93-99,2012.
[32] H.J. Yu, D.H. Huang, Novel 20-D descriptors of protein sequences and it's applications in similarity analysis, Chem. Phys. Lett., 531:261-266,2012.
[33] P. Y. Chou, G. D. Fasman, Structural and functional role of leucine residues in proteins, J. Mol. Biol., 74:263-281,1973.
[34] P. Y. Chou, G. D. Fasman, Conformational parameters for amino acids in helical, β-sheet, and random coil regions calculated from proteins, Biochemistry, 13:211-222,1974.
[35] P. Y. Chou, G. D. Fasman, Prediction of Protein Conformation, Biochemistry, 13:222-245,1974.
[36] M. Li, J.H. Badger, X. Chen, S. Kwong, P. Kearney, H. Zhang, An information- based sequence distance and its application to whole mitochondrial genome phylogeny, Bioinformatics, 17:149-154,2001.
[37] H.H. Otu, K. Sayood, A new sequence distance measure for phylogenetic tree construction, Bioinformatics, 19:2122-2130,2003.
[38] V. Makarenkov, F. Lapointe, A weighted least-squares approach for inferring phylogenies from incomplete distance matrices, Bioinformatics, 20:2113-2121,2004.

Advanced Materials Research Vols. 989-994 (2014) pp 3605-3608
© (2014) Trans Tech Publications, Switzerland
doi:10.4028/www.scientific.net/AMR.989-994.3605

Adaptive Image Feature Reduction for Object Tracking

Cong Lin[1, a], and Chi-Man Pun[1, b]

[1]Faculty of Science and Technology,

University of Macau, Macau SAR, China

[a]yb17403@umac.mo, [b]cmpun@umac.mo

Keywords: Feature refining, object tracking, texture feature, adaptive learning rate.

Abstract. A novel adaptive image feature reduction approach for object tracking using vectorized texture feature is proposed in this paper. Our contributions are three-fold: 1) a statistical discriminative appearance model using texture feature was proposed. 2) Majority of dimensions of the features are removed by judging their errors of the chosen distribution model. The remaining dimensions are most discriminative ones for classification task. The dimension reduction has advantages of reducing the computational cost in classification stage. 3) An adaptive learning rate was proposed to handle drifts caused by long term occlusion. Preliminary experimental results are satisfactory and compared to state-of-the-art object tracking methods.

Introduction

Nowadays, as cameras with video recording capability are so widely used, object tracking draws much attention from researchers. Object tracking locates object position in each frame and output its trajectory for further analysis. [1] Despite many methods have been proposed, the topic remains challenging since the target object keeps changing its appearance in some degree. Occlusion, Scaling and changes of illumination/intensity may lead to the appearance variation which causes a target drift during long term tracking. Moreover, as for mobile cameras, using background subtraction to find out the moving object is almost impossible. Based on the classification models, most tracking methods are categorized into either generative or discriminative. The discriminative tracking methods mathematically model the boundary and distance between target object and backgrounds in feature space. The problem is generally formulated as a binary classification which separates the target object from the background in each frame, which is also called "tracking by detection". The generative tracking models, on the other hand, build up the model of the object class merely using object patches (positive samples). The tracker tries to find out the patch in current frame that has highest similarity to the appearance model. Features along with metric/similarity measure are defined according to specific settings and applications.

In this paper, we adopted general discriminative tracking framework and proposed a simple yet feasible tracking method based on naïve Bayesian classifier. Our main contribution is that we proposed dimension reduction algorithm for vectorized features during training stage which enlarge inter-class distance and reduce influence of large variance in each dimension. An adaptive learning rate was proposed to handle drifts caused by long term occlusion.

Tracking Using Dimension-Reduced Vectorized Feature

Our tracking method shares similar framework with multiple instance learning (MIL)[2]. A general tracking methods consists with three main components: 1) appearance model. 2) motion model and 3)tracking model. The focus of this paper is on improving the appearance model which describes the target object and correctly adapts its changes in long term tracking. For the reasons that object in tracking task is usually dominated by one to three textures. Hence, we employ texture feature instead of haar-like features in MIL which has advantages in detecting contrast of bulks.

In order to reduce the influence of less distinguishing dimension, dimensions of features should be reduced by discarding indiscriminative dimensions and assigned with different weights. The

advantages of this process are obvious: 1) the computational cost in classification stage significantly reduced. 2) not only variance of samples within same class is reduced, but also boundaries between classes become clear. When dimension of feature vector is become low, the numbers of samples provided for training an appearance model decreases exponentially leading to a significant reduction of computational cost. Thus, we defined weights for remaining dimensions with inverse proportion of errors and discard the trivial dimensions. The definition is given as follows:

$$w_j = \begin{cases} b * e^{-c \bullet Err_j} & if \ \ c \bullet Err_j \le T \\ 0 \text{ and } j \text{ dimension discarded} & if \ \ c \bullet Err_j > T \end{cases} \tag{1}$$

where

$$Err_j = \sum_{i=1}^{2N} \left| y^i - p(x_j^i \mid \vec{\alpha}_j) \right|^2$$

$$j \in \{1, 2, ..., M\}$$

The $\overrightarrow{Err}$ is given by least square loss which measures how much the training data is different from an assumed distribution. The ***c*** and ***b*** are normalization factors for $\overrightarrow{Err}$ and $\vec{w}$ respectively. ***T*** is the predefined threshold for filtering dimensions. The empirical value for ***T*** is 0.08 throughout our experiments, which keeps around 15% of the dimensions and discarded other.(Fig.1 shows how the dimension reduction affects the image quality) y^i is the labeled sign denoting which class the $\vec{x}^i$ belongs to. In our case, object patches and backgrounds patches are defined into two classes which assigned 1 and 0 respective. Parameters $\vec{\alpha}$ characterize the chosen statistical model $p(\bullet \mid \vec{\alpha}_j)$. The function $p(\bullet \mid \vec{\alpha}_j)$ outputs a quantitative value, which is within a range of $[0,1]$, rather than a qualitative value. It provides us more flexibility in defining similarity. After this preprocess, ***M***, the number of dimension of feature, is reduced to $M' = \dim(\vec{w})$.

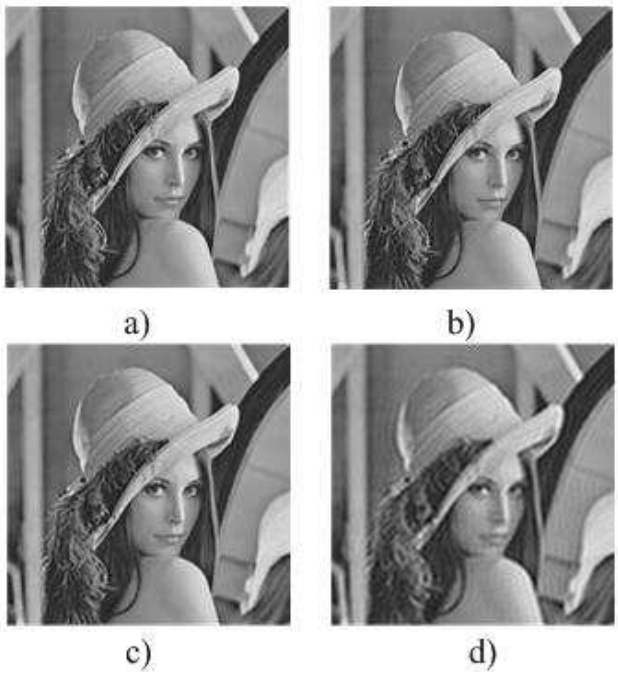

Figure 1. Reconstruction of image with percentage of dimensions shows how the dimension reduction affects the image quality: a) original image, b) reconstructed from remaining 16% dimension, c) reconstructed from remaining 6.25% dimension, d) reconstructed from remaining 2.25% dimension.

Experimental Results

The proposed method was tested on some common testing video clips from Babenko's dataset [4] and CAVIAR dataset. Target objects in these video clips experienced various non-rigid appearance changes including intensity variations, occlusions, rotations and cluttering. These non-rigid changes are considered challenging for object tracking. The dimension of feature vectors is reduced to around 15% of the original size for all the experiments. The 15% reduction rate is almost the highest that we could restore the image without noticeable visual quality loss.

Fig.2 shows the tracking results on 'sylv' video clip from Babenko's dataset. The target in 'sylv' experienced scaling and rotations. Moreover, the video clip contains more than 1300 frames, which is very long for an experiment. Test on this clip is very satisfactory. Tracker is able to track the target steadily and closely follow the ground truth locations.

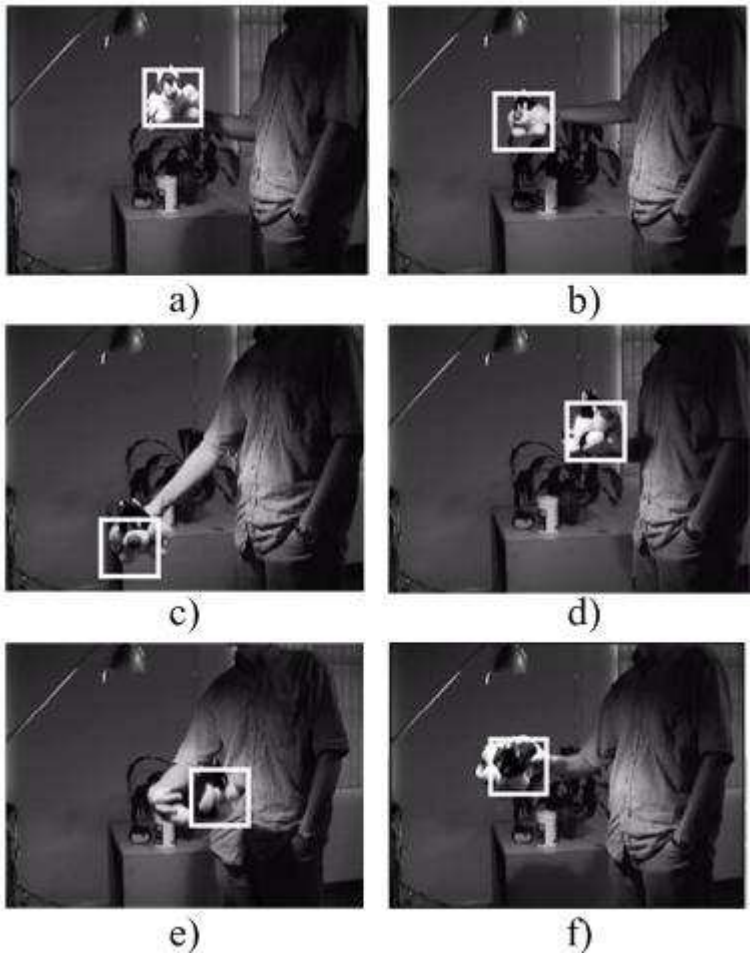

Figure 2. Snapshots of results on 'sylv' video clip. From a) to f) are frame #1 #222 #447 #535 # 1075 and #1165.

Conclusion

In this paper, we proposed a novel technique to refine vectorized texture features and an adaptive learning rate for appearance model in object tracking. Dimensions of feature vectors are selected and assigned with different weights according to the training errors. The challenge of long term occlusion in tracking problem is addressed by the proposed adaptive learning rate. The proposed method was tested on commonly used datasets with typical challenges in the field of object tracking. The results are presented in form of snapshots. Meanwhile, results are quantitatively compared to other state-of-the-art methods and showed that the proposed method outperforms others in several video clips.

Acknowledgement

The authors would like to thank the referees for their valuable comments. This research was supported in part by Research Committee of the University of Macau (MYRG181-FST11-PCM) and the Science and Technology Development Fund of Macau SAR (Project No. 008/2013/A1).

References

[1] A. Yilmaz, O. Javed, and M. Shah, "Object tracking: A survey," *ACM Comput. Surv.,* vol. 38, p. 13, 2006.

[2] B. Babenko, Y. Ming-Hsuan, and S. Belongie, "Robust Object Tracking with Online Multiple Instance Learning," *Pattern Analysis and Machine Intelligence, IEEE Transactions on,* vol. 33, pp. 1619-1632, 2011.

[3] K. Zhang, L. Zhang, and M.-H. Yang, "Real-time compressive tracking," presented at the Proceedings of the 12th European conference on Computer Vision - Volume Part III, Florence, Italy.

[4] "Boris Babenko's dataset," *http://vision.ucsd.edu/~bbabenko/project_miltrack.shtml*.

[5] H. Grabner, M. Grabner, and H. Bischof, "Real-Time Tracking via On-line Boosting," in *Proc. Conf. British Machine Vision*, 2006, pp. 47-56.

[6] H. Grabner, C. Leistner, and H. Bischof, "Semi-supervised On-Line Boosting for Robust Tracking." vol. 5302, ed: Springer Berlin / Heidelberg, 2008, pp. 234-247.

[7] A. Adam, E. Rivlin, and I. Shimshoni, "Robust Fragments-based Tracking using the Integral Histogram," in *Computer Vision and Pattern Recognition, 2006 IEEE Computer Society Conference on*, 2006, pp. 798-805.

Advanced Materials Research Vols. 989-994 (2014) pp 3609-3612
© (2014) Trans Tech Publications, Switzerland
doi:10.4028/www.scientific.net/AMR.989-994.3609

Research on Blind Signal Extraction based on Normalized Kurtosis

Yongjian Zhao

School of Information Engineering, Shandong University (Weihai), Weihai, 264209, China

email: zhaoyj@sdu.edu.cn

Keywords: Kurtosis; Information; Independence; Source; Signal

Abstract. Blind source extraction (BSE) is a promising technique to solve signal mixture problems while only one or a few source signals are desired. In biomedical applications, one often knows certain prior information about a desired source signal in advance. In this paper, we explore specific prior information as a constrained condition so as to develop a flexible BSE algorithm. One can extract a desired source signal while its normalized kurtosis range is known in advance. Computer simulations on biomedical signals confirm the validity of the proposed algorithm.

Introduction

Separating original sources from their mixture is an active research field that has attracted great interest in the field of biomedical signal analysis and processing, geophysical data processing, data mining, speech analysis and image recognition, etc. [1] [2]. Blind source separation (BSS) is a powerful statistical technique in blind signal processing, which considers the simultaneous recovery of all independent components from their mixture using some statistical properties of original sources. In practice, extracting all source signals from a large number of observed sensor signals may output hundreds of recordings, which can take a long time. In most cases, only one or a few sources are desired [3]. For example, in electrocardiogram (ECG) or electroencephalogram (EEG), more than 20 sensor signals can be observed where only a few are interesting and the rest can be regarded as interfering noise [4]. Therefore it is necessary to develop a flexible method to extract only one or a few desired signals that contain useful information.

Extracting a desired source signal from its mixture can be considered a particular BSS problem, blind source extraction (BSE), where the interest is focused on extraction of a specific source signal mixed with other ancillary ones [5]. In general, both BSS and BSE are unsupervised neural network techniques to transform a multivariate random mixture into components that are mutually independent in complete statistical sense. Traditional BSS method aims to separate all source signals simultaneously, whereas BSE is to extract only one or a few desired sources with some statistical properties instead of all sources [6]. In contrast to BSS, BSE provides more flexibility and has some potential advantages in terms of computational complexity especially when the spatial dimension of observed mixtures is large and the number of desired signals is small [5].

In many applications especially in biomedical signal processing, one may know certain prior information about a desired source signal in advance [4]. It is desirable to incorporate such prior information into the BSS/BSE model by using minor modifications of the estimation process, essentially imposing constraints on the model, thus making the output is the desired one. To achieve this goal, we introduce specific prior information about a desired source signal to a classical cost function so as to develop a flexible BSE algorithm. One can extract a desired source signal exclusively while its normalized kurtosis range is known in advance.

The Proposed Algorithm

Suppose n uncorrelated zero-mean sources $s(t) = [s_1(t), \cdots, s_n(t)]^T$ are mixed through an $n \times n$ nonsingular mixing matrix $A = [A_1, \cdots, A_n]$ to get the mixture $x(t) = [x_1(t), \cdots, x_n(t)]^T$ as

$$x(t) = As(t), \tag{1}$$

where superscript T denotes the transpose of vectors or matrices and t is the discrete time index. The crucial assumption at the core of BSS/BSE problem is that the original source signals are mutually statistical independent. Fundamentally, BSE is to find a specific vector w and then apply a process to the observed mixture, thus making $y(t) = w^T x(t)$ is a good approximation to the desired source signal.

To formulate the BSS/BSE problem, one must develop an appropriate cost function that depends on the parameters of the neural network model in (1) [3]. To extract an independent source signal, a flexible cost function is the one on the basis of negentropy [1], defined by

$$J(y) = \rho[E\{G(y)\} - E\{G(v)\}]^2, \tag{2}$$

where $y = w^T x$ is the algorithm output, ρ is a positive constant, v is a Gaussian variable with zero mean and unit variance, $E\{\cdot\}$ denotes the statistical expectation operator, and $G(\cdot)$ can be any non-quadratic function. The following practical functions are suggested for $G(\cdot)$ [1] [3]:

$$G_1(y) = \log coash(a_1 y)/a_1, \tag{3}$$

$$G_2(y) = \exp(-\frac{1}{2}a_2 y^2)/a_2, \tag{4}$$

$$G_3(y) = y^4/4, \tag{5}$$

where $1 \le a_1 \le 2$ and $a_2 \approx 1$. G_1 is a good general purpose function; G_2 may be better when the independent components are highly super-Gaussian, or when robustness is very important; G_3 is justified on statistical grounds only for estimating sub-Gaussian signals when there are no outliers. The cost function in (2) is robust to outliers and spiky noise. Maximizing this function can derive the famous one-unit FastICA algorithm [1]. As an algorithm on the basis of negentropy, FastICA will theoretically converge to an independent component, which has the maximum negentropy of all underlying components [1] [3]. That is to say, when one wants to extract a specific source signal, the FastICA algorithm is of little use. In BSS/BSE problem, one often knows prior information about the desired signal in advance. Therefore we use specific prior information to improve the FastICA algorithm, thus ensuring the output is necessarily the desired one [4].

In this paper, we assume that we have prior information about the desired source signal y as follows:

$$kurt4(y) \in [a, b], \tag{6}$$

where $kurt4(y)$ is the normalized kurtosis value of signal y, defined by

$$kurt(y) = E\{y^4\} - 3(E\{y^2\})^2, \tag{7}$$

and a and b are given scalars with $a<b$. The assumption denotes that the normalized kurtosis value of the desired source signal lies in a specific range whereas other undesired signals do not belong to this range. That is to say, the scope in (6) is correlated with the desired source signal exclusively. Maximizing the cost function in (2) and take into account the constraint in (6), we obtain the following constrained optimization problem:

$$\begin{cases} \max \quad J(w) = \rho[E\{G(w^T x)\} - E\{G(v)\}]^2 \\ s.t. \quad a \le kurt4(y) \le b \quad and \quad w^T w = 1 \end{cases}. \tag{8}$$

The Lagrange multipliers method may avoid the ill conditioning and numerical problems for limitable values of the penalty parameter in the penalty function method [2]. Therefore we explore the Lagrange multipliers method to get the optimal solution for the problem in (8). The augmented Lagrange multipliers is defined as

$$L(w, \lambda) = J(w) + \lambda\{[\max\{0, -(kurt4(w^T x) - a)\}]^2 + [\max\{0, -(b - kurt4(w^T x))\}]^2\} \tag{9}$$

where λ is the non-negative Lagrange multiplier corresponding to the inequality constraints in (6). The maximum point of this Lagrange function, where its gradient is zero with respect to w and λ, gives the solution to the constrained optimization problem in (8). The gradient of $L(w, \lambda)$ with respect to w can be calculated as follows:

if $kurt4(y) \le a$ then

$$\frac{\partial L(w,\lambda)}{\partial w} = \frac{\partial J(w)}{\partial w} - 2\lambda[a - kurt4(w^T x)]\frac{\partial kurt4(w^T x)}{\partial w}; \tag{10}$$

if $a \le kurt4(y) \le b$ then

$$\frac{\partial L(w,\lambda)}{\partial w} = \frac{\partial J(w)}{\partial w}; \tag{11}$$

if $kurt4(y) \ge b$ then

$$\frac{\partial L(w,\lambda)}{\partial w} = \frac{\partial J(w)}{\partial w} + 2\lambda[kurt4(w^T x) - b]\frac{\partial kurt4(w^T x)}{\partial w}. \tag{12}$$

Applying the gradient maximize learning rule [1] [2] to Eq.(9), we further derive a learning algorithm:

$$w \leftarrow w + \mu\frac{\partial L(w,\lambda)}{\partial w}, \tag{13}$$

$$w \leftarrow w/\|w\|, \tag{14}$$

where μ is the learning rate that controls the size of each step and is usually fixed during the iterative process.

Computer Simulations

The ABio7 data set proposed by Allan Barros [7] is a benchmark, which contains seven typical biomedical source signals. Each signal has 5000 samples with zero means and unit variances. This data set has been used by many BSS/BSE algorithms [3] [4]. Due to space constraints, here we only adopted three source signals, denoted by s1, s2, s3 in Figure 1. Their normalized kurtosis values are 37, -0.5 and -1.05, respectively.

A 3×3 mixed matrix A was randomly generated with rows $A1$=[0.149 0.219 0.561], $A2$=[0.113 0.872 0.258] and $A3$=[0.489 0.229 0.709]. The adopted three source signals were mixed by matrix A. The mixed results are shown in Figure 2.

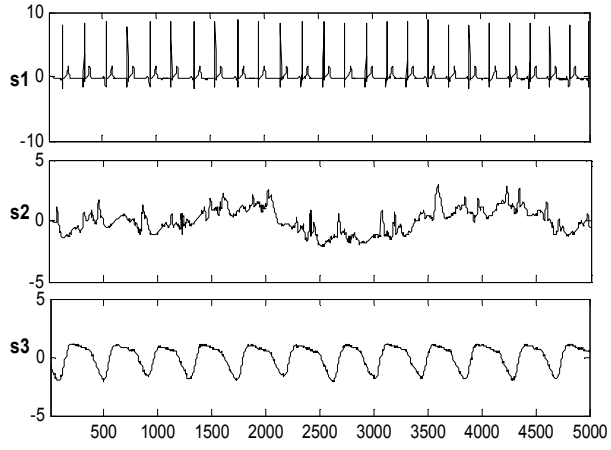

Fig.1. Original biomedical signals

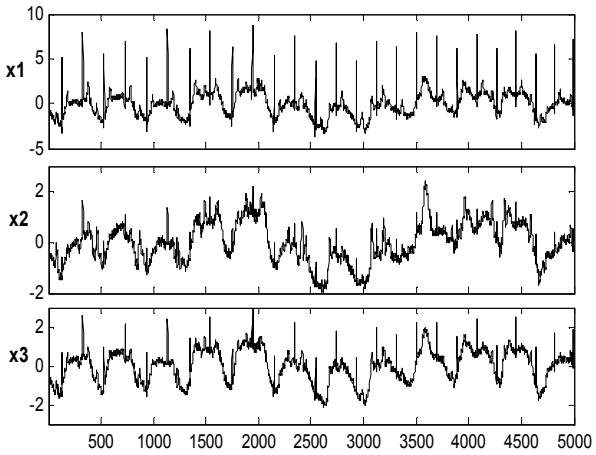

Fig.2. Signal mixture

Our objective is to extract source signals from their mixture shown in Figure 2. First, we set a=35 and b=38 to extract the ECG signal s1. With the learning rate μ, we can control the size of each step. In these simulations, μ was experientially set to 0.004; the Lagrange multiplier λ was initially set to 3 and gradually increased as the algorithm progressed by $\lambda = \lambda(1+1/k)$ where k is the iterative number. In the same way, we set a=-0.6 and b=0.2 to extract the second source signal s2, set a=-1.8 and b=-0.7 to extract the last one. Simulation results are shown in Figure 3 in turn.

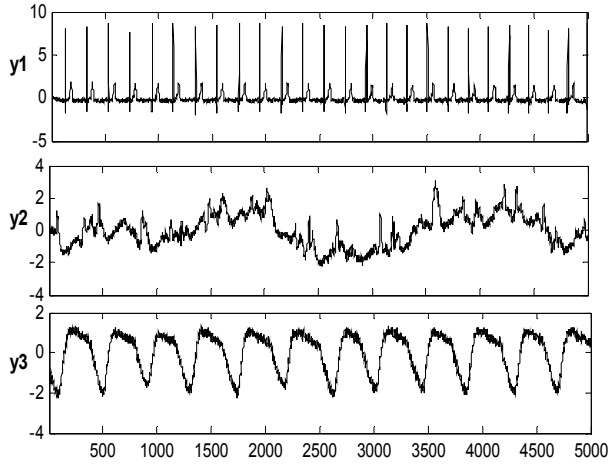

Fig.3. Signals extracted by the proposed algorithm

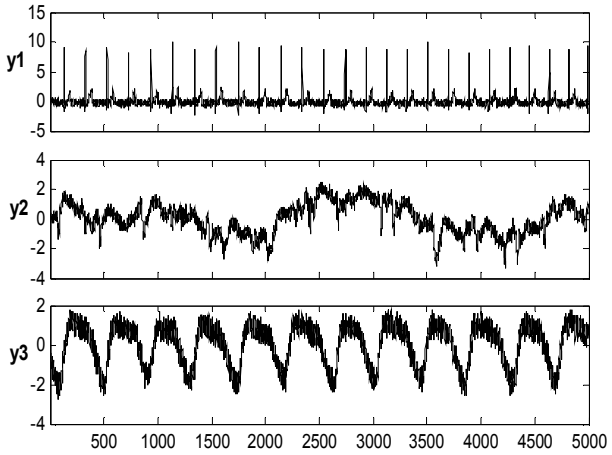

Fig.4. Signals extracted by the FastICA algorithm

Conclusion

This paper proposes a flexible BSE algorithm on the basis of normalized kurtosis. It can extract a desired signal as the first output while its normalized kurtosis value range is known in advance, regardless whether the corresponding value is the largest or not in the observed mixture. It is computationally simple, efficient, and provides more flexibility than traditional BSS algorithms. Computer simulations on biomedical data validates its good performance.

References

[1] A. Cichocki and S. Amari. Adaptive Blind Signal and Image Processing. New York: Wiley, 2003.

[2] A. Hyvärinen, J. Karhunen and E. Oja. Independent Component Analysis. New York: Wiley, 2001.

[3] Y. J. Zhao, H. He and J. X. Mi. Noisy component extraction with reference, Frontiers of Computer Science. 2013, 7.

[4] Y. J. Zhao, B. Q. Liu and S. Wang. A robust extraction algorithm for biomedical signals from noisy mixtures, Frontiers of Computer Science. 2011, 5.

[5] W. Y. Leong, D. P. Mandic. Noisy component extraction (NoiCE), IEEE Transactions on Circuits and System I. 2010, 57.

[6] C. J. James, C. W. Hesse. Independent component analysis for biomedical signals, Physiological Measurements. 2005, 26.

[7] Available online at: http://www.bsp.brain.riken.jp/ICALAB.

Advanced Materials Research Vols. 989-994 (2014) pp 3613-3616
© (2014) Trans Tech Publications, Switzerland
doi:10.4028/www.scientific.net/AMR.989-994.3613

Extraction of Signals with Reference

Yongjian Zhao[1, a], Haining Jiang[2, b]

[1]School of Information Engineering, Shandong University (Weihai), Weihai, 264209, China

[2]School of Information Engineering, Shandong University (Weihai), Weihai, 264209, China

[a]email: zhaoyj@sdu.edu.cn , [b]email:jian123cn@sina.com

Keywords: Extraction; Signal; Reference; Separation; Measure

Abstract. As a famous one-unit algorithm, FastICA can extract source signals one by one. In many applications, someone is only interested in a specific source signal. Through incorporating reference about the desired signal into a negentropy based contrast function, a constrained optimization problem is formed. Then an improved method is proposed which can extract the desired source signal exclusively. Computer simulations demonstrate its good performance.

Introduction

Independent component analysis (ICA) is a statistical and computational technique for revealing hidden factors that underlie sets of random variables, measurements, or signals [1]. As an extension to principal component analysis and factor analysis, ICA has become a powerful method for signal processing in the last few years, principally due to its ability to solve the problem of blind source separation (BSS) successfully [2].

The basic ICA model can be described as follows

$$X = AS \tag{1}$$

where $S = (S_1, \cdots, S_m)^T$ denotes the original independent sources and $X = (X_1, \cdots, X_n)^T$ denotes mixtures of original sources, and A is the unknown m×n constant mixing matrix. Here the term blind refers to the fact that neither the original sources nor the system are known in advance. The only assumptions about the model are that the original sources are statistically independent and that some general model is followed by the system [3]. The objective of ICA is to estimate independent components from observed mixtures. In many applications, the number of original sources is large and only one or a few are desired. In such cases, extracting all independent signals may output hundreds of recordings, thus causing heavily computation burden. It is necessary to develop a robust method to extract a desired original source exclusively.

To formulate the ICA problem, one must form an appropriate contrast function, which is greatly dependent on the parameters of the specified neural network model in (1). Maximization/Minimization of such a contrast function should enable the output of the model to satisfy the statistical conditions of stochastic independence and other inherent properties, depending on the specific problem [4] [5]. According to the Central Limit Theorem, sums of non-Gaussian independent random variables are closer to Gaussian than the original sources [6]. Therefore, a very intuitive and important principle of component estimation is to maximize/minimize non-Gaussianity. To extract an independent source signal, a reliable contrast function is given on the basis of negentropy [1], defined by

$$J(y) = \rho[E\{G(y)\} - E\{G(v)\}]^2, \tag{2}$$

where $y = w^T x$ is the algorithm output, ρ is a positive constant, and v is a Gaussian variable with zero mean and unit variance, $E\{\cdot\}$ denotes the statistical expectation operator, and $G(\cdot)$ can be any non-quadratic function. The following practical functions are suggested for $G(\cdot)$ [1] [3]:

$$G_1(y) = \log coash(a_1 y)/a_1, \tag{3}$$

$$G_2(y) = \exp(-\frac{1}{2}a_2 y^2)/a_2, \tag{4}$$

$$G_3(y) = y^4/4, \tag{5}$$

where $1 \le a_1 \le 2$ and $a_2 \approx 1$. G_1 is a good general purpose function; G_2 may be better when the independent components are highly super-Gaussian, or when robustness is very important; G_3 is justified on statistical grounds only for estimating sub-Gaussian signals when there are no outliers.

Maximizing function (2) can derive the famous one-unit FastICA algorithm [1], which will theoretically converge to an independent component having the maximum negentropy of all underlying components. In other words, when one wants to extract a specific source signal, the FastICA algorithm is of little use. In many applications especially in biomedical signal processing, one often knows specific prior information about the desired signal in advance. In the following we use specific prior information as reference to improve the FastICA algorithm, thus ensuring the output is necessarily the desired one [4].

The Extraction Algorithm with Reference

Denote the recovered signal y and its corresponding reference signal r. The closeness measure between y and r can be described as $\varepsilon(y,r)$. It is important to select a suitable distance, depending on the specific problem, as the closeness measure. In this paper, we select $\varepsilon(y,r) = E\{(y-r)^2\}$ and $\varepsilon(y,r) = 1/(E\{yr\})^2$. Suppose that the contrast function (2) has m local or global solutions w_i $(\mathrm{i} = 1,\cdots,m)$, which can give m estimations of the m source signals. From the selected closeness measure, one can deduce that $\varepsilon(w^{*T}\tilde{x}, r)$ is the minimum of $\varepsilon(w_i^T\tilde{x}, r),\ i = 1,\cdots,m$, i.e.,

$$\varepsilon(w^{*T}\tilde{x}, r) \le \varepsilon(w_1^T\tilde{x}, r) \le \cdots \le \varepsilon(w_m^T\tilde{x}, r) \tag{6}$$

where the optimum vector w^* corresponds to the desired output. Thus an appropriate threshold can be utilized to distinguish the desired source signal y^* from other ones, which means that the extracted signal $w^{*T}\tilde{x}$ is equal to y^* if and only if the following inequality relationship is satisfied:

$$h(w) = \varepsilon(w^T\tilde{x}, r) - \xi \le 0 \tag{7}$$

where $\xi \in [\varepsilon(w^{*T}\tilde{x}, r), \varepsilon(w_1^T\tilde{x}, r))$ is a threshold parameter.

By considering $h(w)$ a constraint incorporated into the contrast function (2), we develop the following constrained optimization problem for extraction of a desired source signal:

$$\begin{cases} \max & J(y) = \rho[E\{G(y)\} - E\{G(v)\}]^2 \\ s.t. & h(w) \le 0, \|w\| = 1 \end{cases} \tag{8}$$

As an additional constraint, $h(w)$ is introduced to guide the signal extraction process, ensuring that the resultant solution is a global maximum. Such a constrained optimization problem efficiently considers prior information about the desired source signal. Therefore one can extract the desired original source exclusively concerned with the corresponding reference.

Through maximizing the negentropy based contrast function for FastICA defined in (2), one can expect to adjust w in the direction of any local optimum of $J(y)$ such that one can get any estimation of the original sources; through maximizing the closeness measure function defined in (5), one can expect to adjust w in the direction of the demixing vector whose corresponding output is closest to the reference signal r such that one can get the desired original source exclusively. Generally speaking, the former can be considered a coarse pre-processing while the latter is an elaborate processing, thus the desired signals can be successfully extracted through alternately performing these two processes. Moreover, the latter can greatly accelerate the

convergence speed. In contrast, the proposed method can achieve good flexibility and relatively low computation load compared with the earlier ones.

Simulation Results

We tested the proposed algorithm in this paper with a synthetic data set of four known source signals, which was also used for testing the previous ICA methods in [7] [9]. The four original sources were depicted in Figure 1. They were sinusoid, funny curve, saw-tooth and impulsive noise, respectively. These sources were linearly mixed by a randomly generated mixing matrix. The mixed signals were depicted in Figure 2. Obviously, the waveform of any source signal was invisible in the mixed signals.

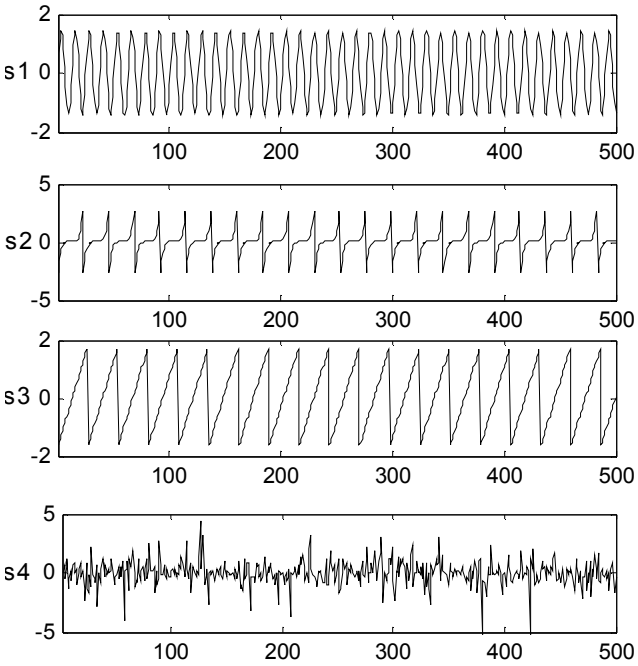

Fg.1 Four synthetic original sources

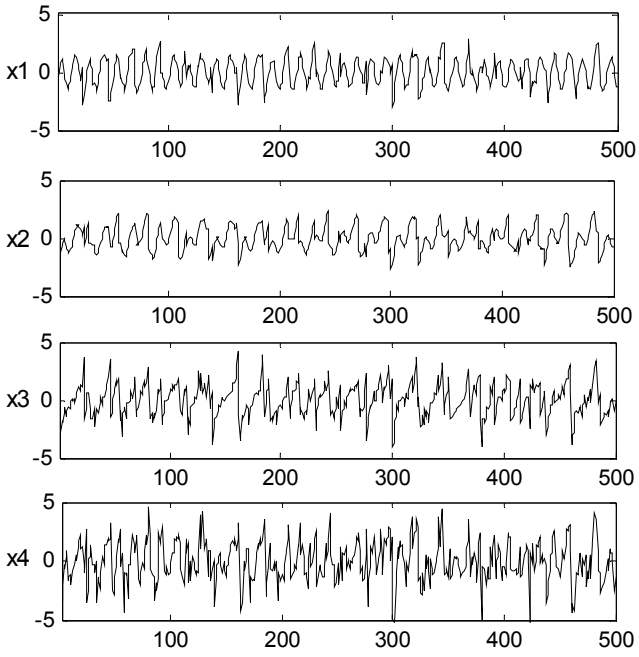

Fig.2 Signals mixed by a random matrix

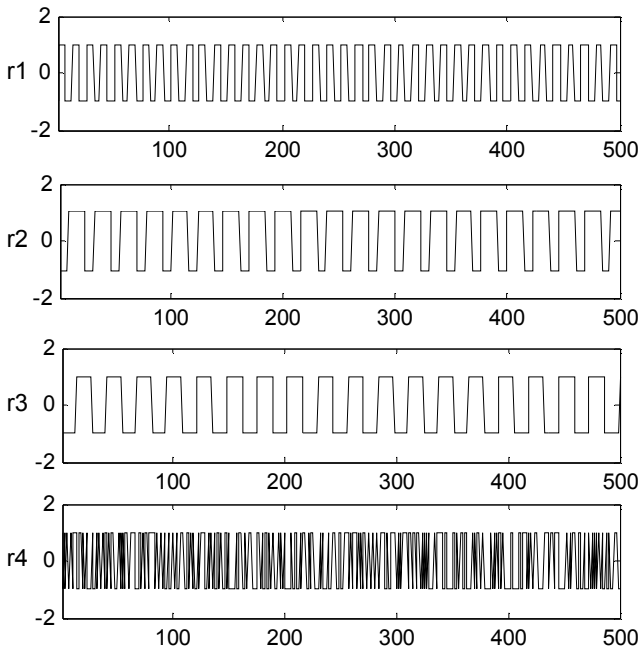

Fig.3 Four reference signals

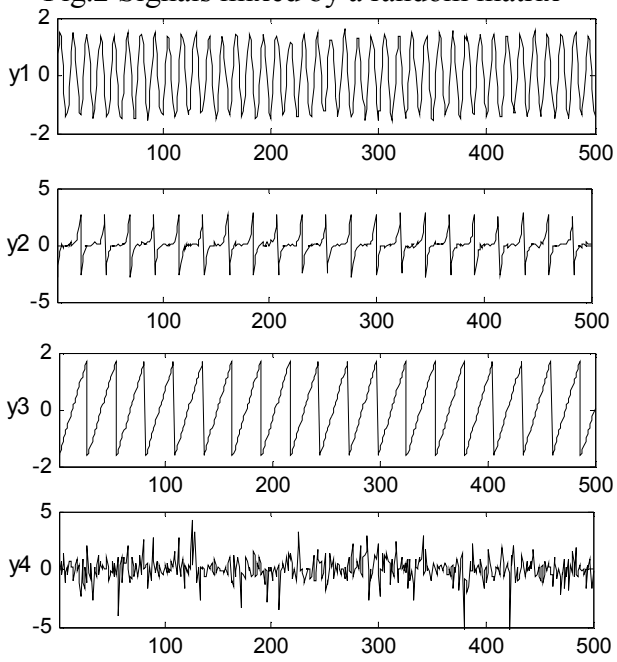

Fg.4 The extracted signals

An appropriate reference signal is important for the ICA algorithm with reference to extract a desired source signal. We intentionally formed reference signals as coarse representations of the

original sources except that the morphology of the underlying sources was precisely known. Four reference signals in Figure 3 were constructed with sign operation to roughly give the signs of the four original sources. In fact, these reference signals only carried the same frequency and phase as the corresponding original sources.

Our objective was to extract the four source signals from the signal mixtures shown in Figure 2. In these simulations, we adopted the four reference signals shown in Figure 3 in turn and performed the proposed algorithm in this paper on these signal mixtures. Typical simulation results were shown in Figure 4. The selection of the closeness measure is greatly dependent on the form of reference signal and the function G in (5). Indeed, it is important to select a suitable distance, depending on the specific problem, as the closeness measure. Here we selected $\varepsilon(y,r) = E\{(y-r)^2\}$. From these simulation results, one can find that the proposed algorithm may successfully extract the corresponding source signals although each reference signal is not a perfect match to the corresponding original source. At the same time, it can achieve good flexibility and relatively low computation load compared with the earlier methods.

Conclusion

Recently, ICA technique has received much research attention in the domain of applied mathematics, neural networks and statistical signal processing. Through incorporating specific prior information about a desired signal into the negentropy contrast function for FastICA, a constrained optimization problem is formed whose inequality constraint term is a closeness measure between the desired signal and its corresponding reference. By alternately optimizing the negentropy contrast function for FastICA and the closeness measure proposed in this paper, an improved method for signal extraction is introduced. It can achieve good flexibility and relatively low computation load compared with the earlier methods. Computer simulations demonstrate its good performance. Due to space constraints, we do not discuss the selection of threshold value in detail. How to design a suitable threshold is our future works.

References

[1] A. Cichocki and S. Amari. Adaptive Blind Signal and Image Processing. New York: Wiley, 2003.

[2] A. Hyvärinen, J. Karhunen and E. Oja. Independent Component Analysis. New York: Wiley, 2001.

[3] Y. J. Zhao, H. He and J. X. Mi. Noisy component extraction with reference, Frontiers of Computer Science. 2013, 7.

[4] Y. J. Zhao, B. Q. Liu and S. Wang. A robust extraction algorithm for biomedical signals from noisy mixtures, Frontiers of Computer Science. 2011, 5.

[5] W. Y. Leong, D. P. Mandic. Noisy component extraction (NoiCE), IEEE Transactions on Circuits and System I. 2010, 57.

[6] C. J. James, C. W. Hesse. Independent component analysis for biomedical signals, Physiological Measurements. 2005, 26.

[7] W. Lu, J. C. Rajapakse. ICA with reference. Neurocomputing, 2006, 69

[8] W. Lu, J. C. Rajapakse. Approach and applications of constrained ICA. IEEE Transactions on Neural Networks, 2005, 16

[9] D. S. Huang, J. X. Mi. A new constrained independent component analysis method. IEEE Transactions on Neural Networks, 2007, 18(5).

Advanced Materials Research Vols. 989-994 (2014) pp 3617-3620
© (2014) Trans Tech Publications, Switzerland
doi:10.4028/www.scientific.net/AMR.989-994.3617

Research on the Optimal Classification Method for Remote Sensing Image based on the Gabor-PCA Analysis

Jinghui YANG [1, a], Liguo WANG [1, b], Jinxi QIAN [2,3, a]

[1]College of Information and Communications Engineering, Harbin Engineering University, Harbin, 150001, China

[2]Institute of Telecommunication Satellites, China Academy of Space Technology, Beijing, 100094, China

[3]School of Electronic Engineering, Beijing University of Posts and Telecommunications, Beijing, 100876, China

[a]email: yang06081102@163.com, [b]email: wangliguo@hrbeu.edu.cn

Keywords: Remote Sensing Image; Classification; PCA; Spatial-Spectra Features

Abstract. According to the problem that the traditional remote sensing image classification methods focus only on analyzing the spectral features and have low utilization of the spatial information, a new spatial-spectral classification method is proposed in this paper, its core idea is to combine the spectral features base on the Principal Component Analysis (PCA) algorithm with the spatial features extracted by the Gabor filter. Experiments show that, compared with the traditional classification methods, the proposed method can improve the classification accuracy and the Kappa coefficient, which means to bring better classification and visual effects.

Introduction

Remote sensing image is widely used in a lot of fields, such as agricultural production, mineral mapping, target identification and detection, disaster warning, military reconnaissance, urban planning and so on [1]. The main feature of remote sensing image is that they have a very high spectral resolution, so they can obtain very narrow band ranges and get a large number of spectral bands, which could result in a continuous spectrum image data that containing a wealth of information [2].

In image processing, spatial information plays a critical role. Researches show that, the Gabor features have the ability to represent useful spatial information, showing good application value in the texture segmentation [3]. Literature [4] applied it into the face image representation and recognition. In literature [5], spatial feature extraction models for remote sensing image were discussed.

It needs to be emphasized that the remote sensing data should be treated as images instead of a mere collection of independent and identically distributed pixels [6]. Therefore, in order to improve the classification effects of remote sensing image, this paper proposes a remote sensing classification method by means of using the sparse representation, meanwhile, considering the spatial-spectral features in the image. Through the establishment of classification simulation model, the effectiveness of the method is analyzed and verified.

The Proposed Gabor-PCA based Spatial-Spectral Classification method

Better classification performance could not be achieved by just using spectral features while ignoring spatial features. In order to improve the classification accuracy of the image, the paper proposes the spatial-spectral method for the remote sensing image classification, while in the spectral feature extraction, the Principal Component Analysis (PCA) algorithm is used and the Gabor filter is applied in the spatial aspect. The proposed method first extracts the spatial-spectral features of the image, and then classifies the remote sensing image based on sparse representation classification (SRC) method, which improves the classification performance.

The implementation procedure of the proposed method is as follows:

First of all, extracting the image features from the original remote sensing data. Extract the spatial texture features using equation (1) [3]:

$$G(x,y,\theta,\lambda,\sigma,\gamma)=\exp(-\frac{x'^2+\gamma'^2y'^2}{2\sigma^2})\cos(2\pi\frac{x'}{\lambda}+\varphi) \tag{1}$$

where, $x'=x\cos\theta+y\sin\theta$, $y'=-x\cos\theta+y\sin\theta$, λ represents the wavelength of the cosine factor, θ represents the orientation of the normal to the parallel stripes of a Gabor function, φ is the phase offset, σ is the standard deviation of the Gaussian envelope, and γ is the spatial aspect ratio. In fact, the Gabor function is a special expression of the sinusoidal wave. However, a Gaussian function will be formed to make the Gabor filter.

Meanwhile, extract the spectral features using the PCA algorithm, which is a widely used dimensionality reduction technology in data analysis [1].Also, it computes the low-dimensional representation of a high-dimensional data set, and the algorithm can most faithfully preserve its covariance structure [7]. One needs to solve the eigenvalues and eigenvectors of the covariance matrix. The outputs of PCA are simply the coordinates of the input patterns in this subspace, and through using the directions specified by these eigenvectors to construct the principal axes. In PCA, the first few principal components contain the most information, and the remaining principal components contain much less information [8].

Then, combine the spatial and spectral features. Suppose the remote sensing image contains k different classes of samples, and the entire spatial-spectral features training set is A, $A=[A_1,\cdots,A_i,\cdots,A_k]$, where A_i is the training set of the ith $(1\le i\le k)$ class. Then, the linear representation of x can be rewritten as: $x=A\hat{s}$, where $\hat{s}$ is a coefficient vector.

In order to obtain $\hat{s}$, the following equation needs to be solved [9]:

$$\hat{s}=\min_s\frac{1}{2}\|x-As\|_2^2+\lambda\|s\|_1 \tag{2}$$

where λ is a compromise fact between data reconstruction and the sparsity, satisfying $\lambda>0$.

The redundancy reconstruct of the remote sensing image for the i th class is as follows [10]:

$$r_i(x)=\|x-A_i\hat{s}_i\|_2, i=1,2,\cdots,k \tag{3}$$

where $\hat{s}_i$ is the coefficient vector associated with the i th class.

Then the class label can be finally determined by the equation (4) [11]:

$$Class(x)=\min_{i=1,\cdots,k} r_i(x) \tag{4}$$

Experimental Results and Analysis

Hardware environment for the simulation is Intel (R) Xeon (R) CPU ES-16200, and the memory is 8 GB. Software environment for the simulation is Microsoft Windows 7, MATLAB 2010b.

Use a remote sensing image of the Indian Pine in Indiana State with a spatial resolution of 20 m for the simulation. In the original image, it has a size of 145×145 pixels. After eliminating the water absorption and low SNR bands in the original 220 bands, 200 bands are selected for simulation.

The paper selects all 16 typical land-cover classes which marked as the class 1-class 16 to do the simulation. All the above samples are used as the test set, and around 10% samples of each class are extracted uniformly as the training set. Figure 1 shows the information of the reference map.

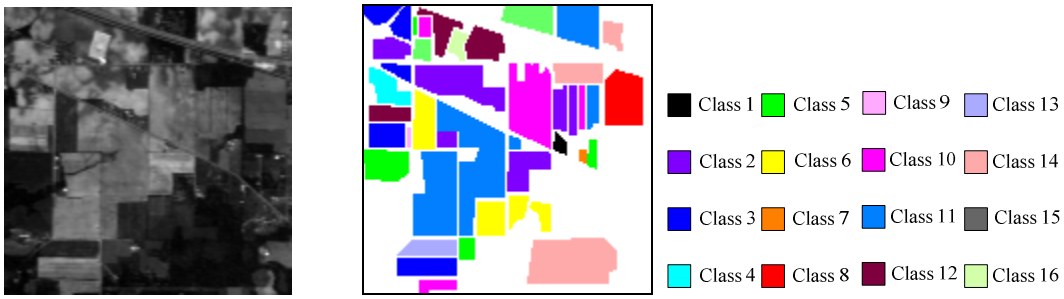

(*a*) Original Image. (*b*) Ground truth map.

Fig.1. Remote sensing image of Indian Pine.

The paper compares and analyzes the proposed method with Support Vector Machine (SVM)[2] [12]. The classification results of different methods are shown in figure 2. Here, the classification results are evaluated by overall accuracy (OA) and Kappa coefficient. Depend on the criteria, the evaluation results are shown in table 1. SVM method based on the original spectral information is represented by SVM, SVM method based on the PCA based spatial-spectral features is represented by S-PCASVM, SRC method based on the original spectral information is represented by SRC.

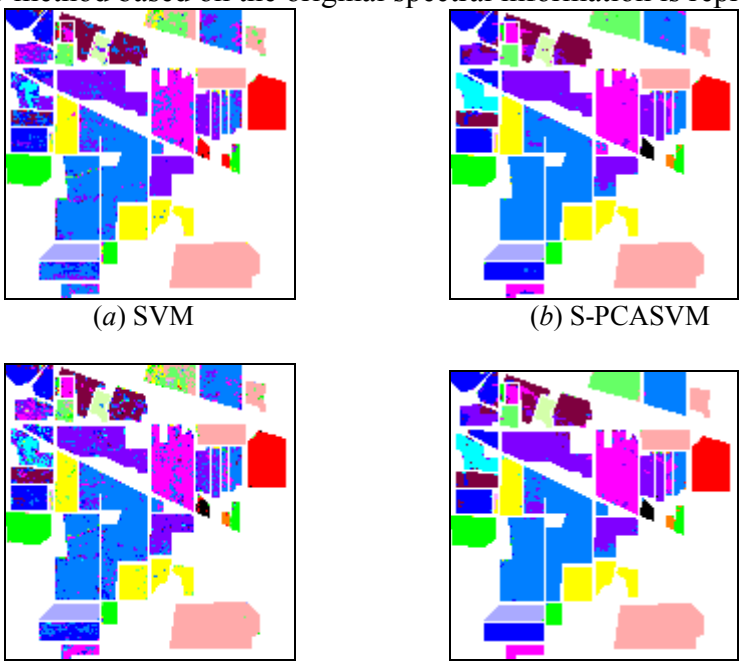

(*a*) SVM (*b*) S-PCASVM

(*c*) SRC (*d*) Proposed method.

Fig.2. Classification results.

Table 1 Quantitative assessment of different methods

Criteria	SVM	S-PCASVM	SRC	Proposed method
OA (%)	81.98	94.05	84.15	95.24
Kappa (%)	79.27	93.21	81.85	94.58

It is very intuitive to see from the figure 2 and table 1 that, the classification performances based on the spatial-spectral features, which can describe the remote sensing image more comprehensively from both aspects of spatial and spectral, are better than the classification performances only based on the original spectral information. It can be seen, out of the four methods, the proposed method obtains the optimal visual effects and the best classification criteria.

Conclusion

A new spatial-spectral classification method for remote sensing image is proposed in this paper. The method first extracts the spatial-spectral features of the image separately by the Gabor filter and the PCA algorithm, then solves the sparse representation of the remote sensing image, and finally, determines the class label by calculating the corresponding redundancy of the reconstructed image

for each class. The simulation results show that, the proposed method has better classification performance than the classification methods, which only consider the spectral information, in terms of either subjective or object evaluation criteria.

Acknowledgement

The research is supported by the National Natural Science Foundation of China (Grant No. 61275010, and Grant No.61077079), Ph.D. Programs Foundation of Ministry of Education of China (Grant No. 20132304110007).

References

[1] Rosa Maria Cavalli, Giorgio Antonino Licciardi, Jocelyn Chanussot, Archaeological Structures Using Nonlinear Principal Component Analysis Applied to Airborne Hyperspectral Image [J]. IEEE Journal of Selected Topics in Applied Earth Observations and Remote Sensing, 2013 6(2) 659-669.

[2] Wang Liguo, Liu Danfeng, Wang Qunming. Spectral Unmixing Model Based on Least Squares Support Vector Machine with Unmixing Residue Constraints [J]. IEEE Geoscience and Remote Sensing Letters .2013 10(6) 1592-1596.

[3] Anil K. Jain, Farshid Farrokhnia, Unsupervised texture segmentation using Gabor filters [J]. Pattern Recognition, 1991 24(12) 1167-1186.

[4] Chuan-Xian Ren, Dao-Qing Dai, Xiao-Xin Li, Band-Reweighed Gabor Kernel Embedding for Face Image Representation and Recognition [J]. IEEE Transactions on Image Processing, 2014 23(2) 725-740.

[5] Linlin Shen, Zexuan Zhu, Sen Jia, Discriminative Gabor Feature Selection for Hyperspectral Image Classification [J]. IEEE Geoscience and Remote Sensing Letters, 2013 10(1) 29-33.

[6] Antonio Plaza, Jon Atli Benediktsson, Joseph W. Boardman, Recent advances in techniques for hyperspectral image processing [J]. Remote Sensing of Environment, 2009 113 s110-s122.

[7] Guangyi Chen, Shen-En Qian, Denoising of Hyperspectral Imagery Using Principal Component Analysis and Wavelet Shrinkage [J]. IEEE Transactions on Geoscience and Remote Sensing, 2011 49(3) 973-980.

[8] Qian Du, James E. Fowler, Hyperspectral Image Compression Using JPEG2000 and Principal Component Analysis [J]. IEEE Transactions on Geoscience and Remote Sensing, 2007 4 (2) 201-205.

[9] John Wright, Allen Y. Yang, Arvind Ganesh, Robust Face Recognition via Sparse Representation [J]. IEEE Transactions on Pattern Analysis and Machine Intelligence, 2009 31(2) 210-227.

[10] Yi Chen, Nasser M. Nasrabadi, Trac D. Tran, Sparse Representation for Target Detection in Hyperspectral Imagery [J]. IEEE Journal of Selected Topics in Signal Processing, 2011 5(3) 629-640.

[11] Benqin Song, Jun Li, Mauro Dalla Mura, Remotely Sensed Image Classification Using Sparse Representations of Morphological Attribute Profiles [J]. IEEE Transactions on Geoscience and Remote Sensing, 2014 52(8) 5122-5136.

[12] Yanfeng Gu, Kai Feng. Optimized Laplacian SVM With Distance Metric Learning for Hyperspectral Image Classification [J]. Selected Topics in Applied Earth Observations and Remote Sensing, 2013 6(3) 1109-1117.

Advanced Materials Research Vols. 989-994 (2014) pp 3621-3624
© (2014) Trans Tech Publications, Switzerland
doi:10.4028/www.scientific.net/AMR.989-994.3621

Orthogonal Discrete Frequency -Phase Waveform Design based on Hybrid Chaos for MIMO Radar

Yanan XIE[1, a], Jiajia WANG [2, b]

[1]School of Communication and Information Engineering, Shanghai University, Shanghai, 200072, China

[2] School of Communication and Information Engineering, Shanghai University, Shanghai, 200072, China

[a]email: yxie@shu.edu.cn, [b]email:823702063@qq.com

Keywords: MIMO Radar; Hybrid Chaos; Orthogonal Discrete Frequency-Poly Phase Coded; Waveform Design

Abstract. Based on the good correlation and randomness of chaos, this paper uses hybrid Bernouli and Logistic chaotic maps to increase the complexity of chaos, at the same time, we do a combination of discrete frequency coded of non full code sets and poly phase coded, and then hybrid modulation waveforms base on hybrid chaos is proposed for MIMO radar. On the basis of the expression of average ambiguity function is derived, the average fuzzy characteristics of signal waveforms and orthogonality are analyzed in theory. Finally, numerical simulation results validate the correctness of the analysis and the reliability of the signal model.

Introduction

MIMO system is that a system has multiple-input and multiple-output, we apply this concept to on radar, so the MIMO radar which is a novel class of radar system and attracts extensive attention, is formed. Orthogonal radar waveform design is important to the performance of the radar, can make the whole radar system are very difficult to be cross positioned by enemy spy plane, so as to improve the battlefield survivability of the radar system. Commonly signals have orthogonal phase coded signal [1], orthogonal discrete frequency coded signal [2] and multi-carrier signals.

Poly phase coded signals and discrete coded signals are commonly used in MIMO radar waveforms. For the first time Deng [3] introduced modern computational methods to optimize waveform design, and then designed orthogonal discrete frequency coded associated with excellent characteristics by simulated annealing algorithm. Genetic Optimization algorithm is used to design phase coded signals for MIMO radar in [4]. Although the genetic algorithm can get some good waveform sets, but time-consuming, low efficiency of the algorithm.

To overcome those drawbacks, chaos has a sensitivity to initial values, and good autocorrelation and cross correlation properties [2][5]. In this paper, hybrid chaotic maps are applied on the modulated waveforms. In order to obtain both the advantages of discrete orthogonal frequency modulated and phase modulated signals, which are combined, and supplement mutual deficiencies. Compared with the single modulation signals, this paper retains Broadband spectral characteristics of phase modulated signals and anti-jamming advantage of orthogonal discrete frequency, greatly reduce the probability of being intercepted by enemy.

Hybrid Coded Model

Assuming MIMO radars have L independent transmitting unit, namely that waveform sets consist of L signals with each signal containing N sub-pulses of time duration T. The expression of MIMO radar orthogonal discrete frequency- phase hybrid coded waveform is shown as:

$$S_i^l(t) = e^{j2\pi f_i^l t} \otimes 1/\sqrt{N} \sum_{n=0}^{N-1} C_n V_1(t-nT) = 1/\sqrt{N} \sum_{n=0}^{N-1} C_n e^{j2\pi f_i^l (t-nT)} \quad ,0 < t < NT \qquad (1)$$

Where $V_1(t) = 1/\sqrt{T}$, $0<t<T$, C_n is the coefficients of coded sequences, they can be selected from $e^{j\cdot n\cdot 2\pi/M}$, $n \in \{0, 1, 2, \dots, M\text{-}1\}$. f_i^l is the frequency of sub-pulse i of signal l in the signal sets .where $\Delta f = 1/T$, frequency coded of the signal l can be expressed as $\{f_i\} = \{b_1\Delta f, b_2\Delta f, \dots, b_N\Delta f\}$. Not all will be transmitted for the frequency coded, but they don't repeat, it is a non-full code. The coefficients $\{b_1, b_2, \dots, b_N\}$ from $b_i \in \{1,2,3,\dots,P\}$, $N<P$. Namely , N non-repetitive discrete frequency coded are selected from b_i. In this paper the sub-pulse width of phase coded and discrete frequency coded are same.

The analysis of waveforms correlation properties

(1)Average Ambiguity Properties

Due to the randomness and sensitivity of chaotic map, single pulse can not accurately reflect the fuzzy characteristics of the whole. So we select the statistical average ambiguity function in time NT. where τ is delay, f_d is Doppler shift. The expression is defined as follows:

$$A(\tau, f_d) = 1/NT \int_0^{NT} S^*(t) S(t-\tau) \exp(j2\pi f_d t)\, dt \tag{2}$$

Make (1) into (2), the expression is simplified to obtain as：

$$\begin{aligned} A(\tau, f_d) &= 1/N^2T^2 \sum_{n=0}^{N-1} C_n{}^2 e^{-j2\pi b_n \frac{\tau}{T}} \int_a^b e^{j2\pi f_d t} dt + 1/N^2T^2 \sum_{n=0}^{N-1} \sum_{m=0, m\neq n}^{N-1} C_n C_m \cdot \\ &\exp\left(j2\pi \left(nb_n - mb_m - b_m \frac{\tau}{T} \right) \right) \cdot \int_c^d e^{-j2\pi b_n \frac{t}{T}} e^{j2\pi b_m \frac{t}{T}} e^{j2\pi f_d t} dt \end{aligned} \tag{3}$$

For (a, b),(c, d): when $0<\tau<T$, $n=m+1$,$a=n\,T+\tau$, $b=(n+1)T$, $c=n\,T$, $d=n\,T+\tau$, take these into (3) can be shown：

$$\begin{aligned} A(\tau, f_d) &= \frac{1}{N^2T^2} \sum_{n=0}^{N-1} C_n{}^2 e^{-j2\pi b_n \frac{\tau}{T}} e^{j2\pi fd(nT+\tau)} \frac{e^{j2\pi fd(T-\tau)} - 1}{j2\pi f_d} + 1/N^2T^2 \sum_{n=0}^{N-1} \sum_{m=0, m\neq n}^{N-1} C_n C_{n-1} \\ &\cdot e^{j2\pi\left(nTfd + b_{n-1} - b_{n-1}\frac{\tau}{T} \right)} \cdot \left(\exp j2\pi \left(fd + \frac{b_{n-1}}{T} - \frac{b_n}{T} \right) \tau - 1 \right) \Big/ j2\pi \left(fd + \frac{b_{n-1}}{T} - \frac{b_n}{T} \right) \end{aligned} \tag{4}$$

When $\tau>T$, in order to facilitate the calculation of expression, set $q\,T< \tau < (q+1)\,T$, $q=1,2\dots N\text{-}2$, now $c=n\,T$, $d=(n\text{-}q)T+\tau$, $n=1+m+q$, we get：

$$\begin{aligned} A(\tau, f_d) &= \frac{1}{N^2T^2} \sum_{n=0}^{N-1} C_n C_{n-q-1} \exp\left(j2\pi \left(\left(q+1-\frac{\tau}{T} \right) b_{n-q-1} + nTf_d \right) \right) \\ &\left(\exp\left(j2\pi \left(f_d + \frac{b_{n-q-1}}{T} - \frac{b_n}{T} \right) (\tau - qT) \right) - 1 \right) \Big/ \left(j2\pi \left(f_d + \frac{b_{n-q-1}}{T} - \frac{b_n}{T} \right) \right) \end{aligned} \tag{5}$$

Ambiguity function is symmetric, $|A(\tau, f_d)| = |A(-\tau, -f_d)|$. Thus the complete expression of the statistical average ambiguity function $A(\tau, f_d)$ can be obtained.

(2) Orthogonal Characteristic

For the aperiodic signals, Orthogonal signals required cross-correlation side lobe peak (CP) as small as possible, while autocorrelation side lobe peak (ASP) as low as possible, namely, the following condition is need as:

$$AA(S_l, \tau) = 1/(NT) \int_0^{NT} S_l(t) S_l^*(t+\tau)\, dt = 1\ , \quad l = 1, 2, \cdots, L \tag{6}$$

$$CC(S_p, S_q, \tau) = 1/(NT) \int_0^{NT} S_p(t) S_q^*(t+\tau)\, dt \approx 0 \quad , \ p \neq q,\ \ p, q = 1, 2, \cdots, L \tag{7}$$

Design Method of Hybrid Waveforms

Modified form of the expression of Bernoulli chaotic function is obtained as follows: $x_{n+1}=r(x_n + w\,g\,n\,(1, 1, h))$ (mod 1) (Where $x_n \in [0, 1]$). In the type: r is an integer ($r\geq 2$), $w\,g\,n\,(1, 1, h)$ is Gaussian white noise, h is noise intensity. Modified form of Bernoulli map within a certain range is unpredictable, so that the system can be regarded as a true random bit source. Logistic function is defined as: $x_{n+1}=\beta x_n(1+x_n)$, $\beta \in [0, 4]$, $x_n \in [0, 1]$.

Design method steps are gotten as follows:

(a) Randomly selected L initial values in [0, 1]. firstly, the length of the sequences which both Logistic and Bernoulli maps with L different initial values generate , is $N/2$, and then the sequences with L different initial values do hybrid cross processed, thus consist of L hybrid chaotic sequences of length N; And then chaotic sequences obtained do uniform and four phase quantization. (b) Where select the same initial values and the same method as phase coded, but the length of the sequences which both Logistic and Bernoulli maps with L different initial values generate , is $P\times k/2$, so consist of the length of $P\times k$. Finally, chaotic sequences obtained with L different initial values are conducted by sampling interval k. Due to the sequences of hybrid chaos generated are between [0, 1] decimals, before they would be encoded as orthogonal discrete frequency, they must be an integer. Use sort function "sort" to sort the hybrid chaotic sequences, the P index values for non-full code orthogonal frequency will be returned as frequency coded, but they are selected N index values which contains all the frequency values. (c) Combination with (a) and (b)

Simulation and results

Assuming L=4, N=1024, M=4, P=1100, sub-pulse time duration is T=4us, the sampling interval is set to k=10. The parameters of Bernouli chaotic map are h=20dBw and r=2. The parameter of Logistic chaotic map is β=2. The initial values are selected from [0.1, 0.2, 0.3, 0.4]. From Fig.1, only a single peak which is concentrated in the vicinity of the center position (0, 0) can be shown, the average ambiguity function is very close to the ideal "thumbtack" in Fig.1. As can be seen from Fig.2 and 3，the waveform of autocorrelation function is similar to an impulse function, the waveform of cross-correlation is close to zero, indicating the hybrid signal waveforms have good orthogonality. When the number of the waveforms and coded length are same, in this paper average ASP and CP are respectively -32.1334dB and -33.1155dB. Compared with literature [5], it present about 10dB improvement in ASP and 13dB improvement in CP.

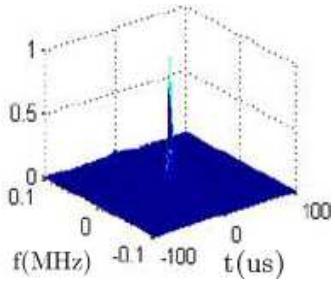

Fig.1 3D Average ambiguity

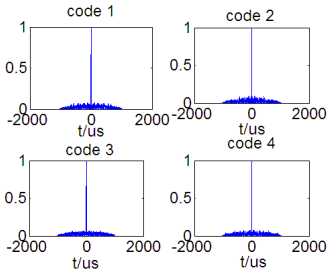

Fig.2 Autocorrelation

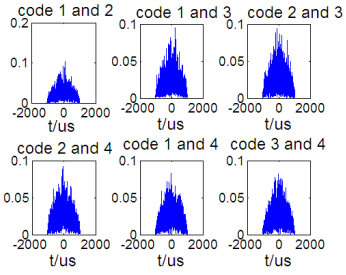

Fig.3 Cross-correlation

Conclusions

Hybrid coded waveforms based on hybrid chaos is proposed for MIMO radar application in this paper. The simulation results show that much better pulse compression performance, average ambiguity properties and less mutual interference were obtained by using good statistical properties of the hybrid chaos, compared with literature [5], ASP and CP are also greatly improved. At the same time, the optimization design of the waveforms remain to be further considered.

Acknowledgement

In this paper, the research was sponsored by Research Project of Shanghai Municipal Science and Technology Commission (Project No.11511501902).

References

[1] Sun C Y, et al. "MIMO radar chaos phase coded signal design and analysis." telecommunications technology 52.9 (2012) : 1497-1502.

[2] Li J J, Jiang Y H, Dan B. Orthogonal discrete frequency coding waveform design in the MIMO radar [J]. Journal of signal processing, 2013, 29(9).

[3] Deng H. Discrete frequency-coding waveform design for netted radar systems[J]. Signal Processing Letters, IEEE, 2004, 11(2): 179-182.

[4] Zishu L B H. Genetic Algorithm based MIMO Radar Polyphase Code Design [J][J]. Journal of Electronic Measurement and Instrument, 2008, 2: 017.

[5] Niu Z Y, Li X B. Design of Orthogonal Waveforms Set for MIMO Radar Based on Chaos Frequency Modulation[J]. Journal of Signal Processing (Xinhao Chuli), 2013, 29(3): 394-399.

Advanced Materials Research Vols. 989-994 (2014) pp 3625-3628
© (2014) Trans Tech Publications, Switzerland
doi:10.4028/www.scientific.net/AMR.989-994.3625

The Communication Capability of Shipboard Radio based on Path Loss

Xiaogang HUANG[1,a], Aimin ZHU[1,b], Senjie YAO[1,c]

[1]Zhenjiang Watercraft College, Zhenjiang, 212003, China

[a]email:jianhan131420@126.com,[b]email:zhuaimin001@qq.com, [c]email:plaperson@tom.com

Keywords: Communication; Path Loss; Simulation; Model; Shipboard Radio

Abstract. According to the communication demand between warship and ChongFeng Boat or between ChongFeng Boats, this paper researched the communication capability of shipboard radio boat when sailing and islanding. It analyzed the propagation characteristics of radio, the relation between path loss and distance/path loss and frequency, discussed the influence of path loss on the capability of radio based on simulation and made a conclusion.

Introduction

Sea Battlefield is an important part of modern information war, reliable communication in sea battlefield is important foundation to win the war. Select right communication frequency is very important in complicated war electromagnetism. As the particularity of sea surface, the radio propagation on sea is different from on land, so as the influence on communication capability. According to the communication demand between warship and ChongFeng Boat or between ChongFeng Boats, when sailing and islanding, this article analyzes the propagation path loss and the communication capability about the wireless radio propagating on sea, offers the general theory of communication capability.

System Model

A. Path Loss

When communication on sea, with the changing distance and frequency, path loss maybe tens or hundreds of dB. Based on "two-path model"[1][5], this paper applied Ludiw[2] formula to calculate pass loss on sea and rivised it according to the characteristics of the distance among warships or warships and Chongfeng Boat is short, the height of antenna is low.

Smooth earth plane radio propagation formula:

$$P_r = P_t\left(\frac{\lambda}{4\pi d}\right)^2 G_T G_R \bullet \left[1 + \mathrm{Re}^{j\Delta a} + (1-R)Ae^{j\Delta a} + \ldots\right] \quad (1)$$

According to "two-path model", Received power can be deduced and simplied as follows:

$$P_r = P_t G_T G_R \frac{h_t^{\,2} h_r^{\,2}}{d^4} \quad (2)$$

Convert to be propagation loss as follows:

$$L_{bg} = 120 + 40\log d\text{-}20\log h_r h_t \qquad (dB) \quad (3)$$

The problem analyzed above is simple, however, the influence of terrain environment along the radio propagation passway should be considered in practical application.

According to Grosskopf[2] empirical formula, Median field:

$$E = \frac{12 h_t' h_r'}{d^2}\sqrt{P_t} \quad (4)$$

Thus ,the receiving power is as follows:

$$P_r = 2.5\left(\frac{h_t' h_r'}{d^2}\right)^2\left(\frac{40}{f}\right)^2 P_t \quad (5)$$

The propagation loss is as follows:

$$L_m = 40\lg d + 20\lg f - 20\lg h_t' h_r' - 36 \qquad (dB) \tag{6}$$

The above deduction considers the antenna as half wave length, whenλ/4wave length is adopted, the gain reduces 3dB, altogether, the propagation loss raises 6dB.

Radio antenna on sea is close to ground, for convenience, the influence of ground is calculated to the height of antenna, the revised height of antenna is as follows:

$$|h'| = \left| h - j\frac{\lambda\sqrt{\varepsilon}}{2\pi} \right| \tag{7}$$

On the sea, the actual measured values of VHF and UHF radio waves are close to theoretically assessed one that propagate on the smooth earth plane or spherical surface. The rapid decline caused by ships navigation is ±3dB, the slow one is about1dB. Thus, the predictive value of median path loss can be tackled as propagation along smooth ground or spherical ground.

B. Simulation model

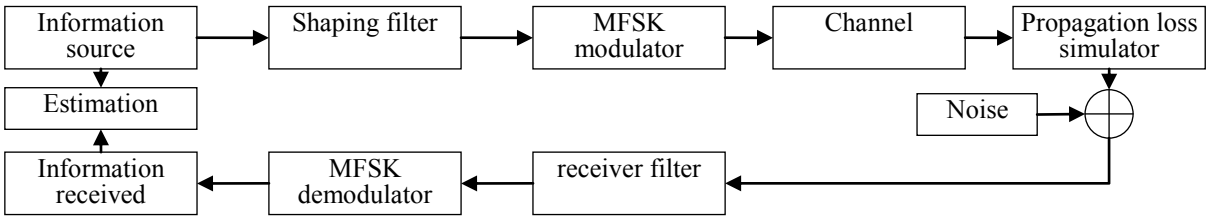

Fig.1 Base-band simulation of the influence of propagation loss to radio communication

Base-band digital transmission model is adopted in simulation, source information gets through shaping filter, modified by base-band and goes to information channel, add both practical communication path loss on sea, which simulated by propagation loss simulator, and background noise. The receiving terminal receives filter and demodulates signal. The estimation of the influence of propagation loss caused by distance and frequency to systematic bit error rate (BER). The physical model shows in Fig.1.

- **Channel parameter**. In simulation, Nonselective Rice Fading Channel [3] is adopted, when the fading factor k=0.08, the longest multipath delay Tm=10^{-6}, the greatest Doppler frequency-shift Fd=20Hz.
- **Propagation loss**. In simulation, the propagation loss depends on formula (6), the frequency range is 40-1500MHz, and the communication distance is within 5 kilometers.
- **Data rate**. For calculation convenient, data rate Rb=16K bit/s.
- **Modulate parameter**. The BFSK BER in noncoherent demodulation is $P_b = \frac{1}{2}e^{-\frac{E_s}{2N_0}}$ [3], Es is the energy of unit code element, Es=Ps/Rb, Ps is the input signal power of receiver, N_0 is the density of noise power spectrum, N_0=Pn/ B, Pn is noise power of receiver.
- **Background noise parameter**[4]. According to NBS, the background noise power P_n can be calculated by coefficient factor F_a. Pn = Fa +B-204 (dB), B is band width of receiver, B=16KHz.

Performance Analysis and Discussion

A. Propagation loss

According to the communication characteristics between warship and ChongFeng Boat or between ChongFeng Boats, this paper concentrates on the communication among radios. The radios of transmitting terminals and receiving terminals are the same type. The height of antenna in the ChongFeng Boats is about to people's eyes, which is 1.5m, the one in the warship is about 7m; the communication distance is short, usually no more than 5 kilometers; the range of frequency is 40-1500MHz; the dielectric constant of sea water is ε=80; the influence of weather, islands and other obstacles are not considered.

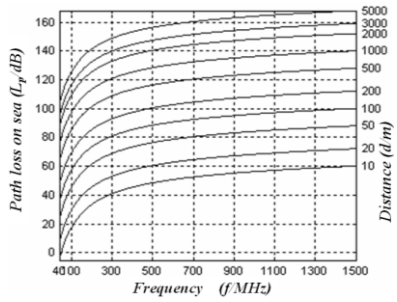

Fig.2 Path loss between ChongFeng Boats

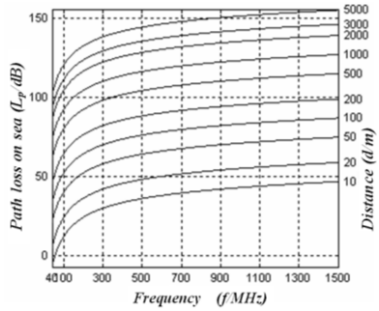

Fig.3 Path loss between warship and ChongFeng Boat

When the height of transmitting and receiving antenna are all 1.5m, the relation of path loss to frequency and distance can be obtained by simulation as in Fig.2 shows.

As the figures shows, when the communications distance increase, the propagation loss of wave grows gradually. When the communication distance is 1 kilometer, the frequency is above 100MHz, the path loss is more than 100dB, as the distance continues to increase, the increase range is getting small; in VHF frequency range, when the path loss is small, the changing range is big, in UHF frequency range, the path loss is big, however, the changing range is small.

When the height of transmitting and receiving are 1.5m and 1.7m , separately, the curves of path loss is showed in Fig.3. Compared with the above figure, the propagation loss is about 10dB decrease. The height of antenna is profoundly influence path loss, when the height of antenna increases, the communication distance is far more long, the higher frequency range can be selected.

In radio communication, the increase of distance and frequency will result in the increasing of propagation loss, which will decrease the receiving power in the receiving terminal, the input noise signal ratio of receiving terminal decreases, directly lead to the increase of systematic BER. When the loss reaches to some extent, it will influence the quality of communication heavily, even interrupt the communication. According to the derivation result of radio communication propagation loss prediction, we built a simulation model to analyze the influence of propagation loss to radio communication systematic BER. To be general, other anti-interference techniques adopted in radio communication system are not considered.

B. Coummunication capacity analysis

The definition of signal noise ratio (SNR): the ratio of input power that transmitting power reaches receiver after path loss to the input power of environment noise. By simulation, the four conditions are showed in Fig.4 as follows:

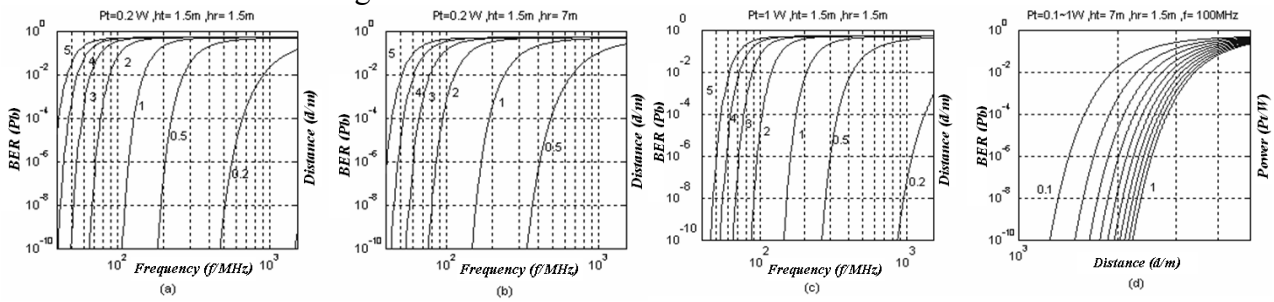

Fig.4 Simulation results

In Fig.4, when the transmitter power is 0.2W, the height of antenna is 1.5m, to ensure10^{-5} BER; the VHF band can provide long communication distance. Compared Fig.4 (a) to（c）,when the transmitter power increases five times to 1W, in the same frequency and communication distance, the signal noise rate improves about 45dB, the higher of the frequency, the lower the signal noise rate improves. In Fig.4 (b), considering that when the communication is between warship and ChongFeng Boat, the height of antennas are 7 meter and 1.5 meter separately, in the same frequency and BER, the communication distance increase 0.5 kilometer; in Fig.4 (d), the increase of transmitter power does not improve the communication distance much, 1 kilometer communication distance increase needs 6 times transmitter power increase.

Conclusion

By analysis above, when communication distance is long, VHF frequency band ranges between 20MHz-100MHz is good. If soldiers in a section below camp are close to each other, that is within 1 kilometer, the high frequency band of VHF and low frequency band of UHF could be considered. As the increase of frequency band, the environmental noise coefficient decreases, however, the path loss increases and the communication distance cuts. When the communication capacity is satisfied, the transmitter power of radio below 1W is suitable considering the portability and low energy consumption of the radio on the ChongFeng Boat.

In the practical sea environment, conditions are more complicated, especially when the weather is terrible, environmental noise, clouds and mist will influence the capacity of radio a lot. Higher demand is requested for the communication of hand-hold radio when the radios of adjacent troops and the interference of enemies add.

References

[1] Henry L. Bertoni. Radio Propagation for Modern Wireless Systems(English Edition). Electronic Industry Press, Beijing, 2002.

[2] Theodor S. Rappaport. Wireless Communications Principles&Practice: Prentice-Hall, NJ, 1996.

[3] William H. Tranter, K. Sam Shanmugan, Principles of Communication System Simulation with Wireless Applications, Pearson Education Asia Limited and China Machine Press,2004

[4] CCIR Reports 1990,Annex to volume V1.Section 6B,Radio noise,(Reports 258-5, 1151, 342-6,254-7),CCIR Report 322-3(1986)

[5]Dacheng YANG, Mobile communication environment, China Machine Press, Beijing, 2003

Advanced Materials Research Vols. 989-994 (2014) pp 3629-3632
© (2014) Trans Tech Publications, Switzerland
doi:10.4028/www.scientific.net/AMR.989-994.3629

Study of Synchronization Strategy Based on Timestamp

Li XU

Computer College, Beijing Information Science and Technology University, Beijing 100101, China

email:xuli_lh@139.com

Keywords: Virtual Reality; 3D Rendering; Synchronization Strategy; Multichannel System

Abstract. Aiming at the characteristics of the traditional multichannel rendering synchronization strategy and the existing problems, the paper proposes a new multichannel rendering synchronization strategy based on timestamp and makes a horizontal comparison between the experimental results and the traditional strategies, as well as verifies the advantages on systematic stability and fault tolerance of network transmission. The strategy will be suitable for using in a clustered, massive and high reliable multichannel system.

Introduction

In the field of modern virtual reality, the large-scale 3D scene rendering and immersive virtual reality experience are inseparable from the multichannel display auxiliary. Using multichannel display technology can break resolution limit of single display terminal, and realize the scene representation of interaction with ultrahigh resolution.One of the crucial problems in multichannel display system is synchronization problems,it is highly important to make sure the different channels displaying the scene simultaneously and promote the performance of the scene to display.

In this paper, a multichannel synchronization technology for rendering 3D scenes are targeted research, proposes a new synchronization strategy based on timestamp, and compares with the traditional synchronization strategy. The new synchronization strategy has great advantages in flexibility and system reliability, and it has the practical value in engineering practice, and has been applied in the digital city related to some projects.

Traditional Synchronization Strategy

The basic principle of the multichannel scene rendering, one is to ensure that the dynamic display of the content of each channel to keep smooth, namely not less than 30fps frame rate, the second is to ensure that the content of the same frame in the display of the time difference value between the two channels is not higher than a specified error value, its mathematical expression is:

$$F_n - F_{n-1} \leq \frac{1}{30} \tag{1}$$

$$F_n - G_n \leq \varepsilon \tag{2}$$

F_n is execution scene rendering time channel in A, G_n is the execution scene rendering time channel in B. ε is maximum time difference between two channel in synchronous.

The Synchronization strategies of multichannel 3D scene rendering has had some research, including Genlock, the frame sync (*FrameSync*) and the swap buffer sync (*SwapBufferSync*).

Genlock is the most traditional, but also the most restrictive multichannel synchronous strategy, this method is the most accurate synchronization, but not be implemented in software, need to buy expensive professional equipment.

FrameSync strategy is a common multichannel synchronous method. It requires that each node send to the serve a ready signal when each frame of each node began real-time rendering, after the server receive ready signals of all nodes, allowing all nodes at the same time start the current frame rendering. This strategy is easy to understand, and easy to be realized from the software, but because the different node rendering pressure is different, each frame completion time is uncertain, this may cause deviation of final display results.

SwapBufferSync is an upgraded version of *FramSync*. It has been by far the most widely used. The advantage of this approach for similar types of computer equipment, the buffer swapping almost at the same time as always, thus ensures the integrality of the picture. However, the biggest problem of *SwapBufferSync* is that if a node in multichannel system occur problems (e.g. software or hardware failure) or a frame rendering pressure is very great, will cause synchronization signal to cannot be issued, then the whole system will therefore have a serious hysteresis, even deadlock may occur.

Synchronization Strategy Based on Timestamp

The comprehensive analysis on characteristics of the above sync strategy and the existing problems, we propose a new synchronization strategy based on timestamp. This strategy does not cause the entire system of hysteresis or deadlock because of the abnormal situation, therefore effectively enhance the multichannel system stability and practical value.

In our strategy, after the user interaction events are transmitted to the sync server, calculate the current position and posture of the observer on the scene, encapsulate the position and posture information of each frame to a timestamp, and transmits the frame ID of the current rendering and the position and posture (it can be expressed in a 4x4 matrix) to each child node. Synchronous server can not consider the transmission time, as long as the guarantee in accordance with sufficiently high frequency (e.g. 60Hz) issue the latest timestamp objects.

The implementation process is each client node use an independent thread to keep on reading and recording the timestamp object come from the server, and save it to a list. Independent and continuous thread is used, so this process and the nodes of the current render states were not related. In the network delay is small, it can be considered that an timestamp object on the server-side can always arrive on each node computer at the first time. When the client node began to render a new frame, it will check the timestamp list to find the Nth timestamp object which distance the end of list, access to its contents as the scene's current position and posture.

Where N is a parameter variable, it determines the ability in synchronization adaptive, because the end of the list save the latest data come from the server , in the timestamp list of the different nodes, the Nth timestamp object from the end of list can be considered to be the same.If the N value is greater, then it means the node rendering content than the server actual state with a certain delay. this delay is holistic, not a certain node behavior. Therefore the reasonable N value is set, the actual observation on the scene and interaction not to produce too much influence. Mathematical description of this process is as follows:

$$N = \frac{F_L - F_{avg}}{\Delta t} \tag{3}$$

Where F_L is the server-side latest moment, F_{avg} is multichannel optimum synchronization time, Δt is the timestamp sending interval.

The biggest characteristic of synchronization strategy based on timestamp is for abnormal node processing, when abnormal nodes appear , the strategy can ensure that the whole system is not affected at the same time, to adaptively adjust abnormal node status, and allows it to keep as much as possible with other nodes synchronization.If the server sends a timestamp object frequency is S, the client node rendering a frame time is T, the timestamp of object is F_0, then when the frame is completed, it will select the next timestamp is F_1.

$$F_1 = F_0 + T * S \tag{4}$$

We assume the server sending frequency is 60Hz, there are three rendering node in the system, they render one frame time respectively for 1/20s,1/10s and 1/5s, then according to the above formula, in every moment, each node rendering timestamp of object are shown in table 1.

Table.1. Timestamp lists of each node

moment(S)	node1	node2	node3
0.0	F0 = 1	F0 = 1	F0 = 1
0.05	F1 = 4	-	-
0.1	F2 = 7	F1 = 7	-
0.15	F3= 10	-	-
0.2	F4 = 13	F2 = 13	F1 = 13

All nodes can be seen from table 1, the rendering frame rate have significant difference, but rendering object's timestamp is always aligned. If a client node lose response, then just itself no longer receive timestamp signals from the server, will not affect the operation of the whole system.

Test Run Results

We use 3D rendering engine *OpenSceneGraph* as development environment, and use the synchronous strategy based on timestamp achieved interactive real-time rendering on any channel. A six channels LCD TV wall display effect as shown in figure 1, the load of the digital city scene for more than 20GB.

Fig.1. Multichannel LCD TV wall

Transverse comparison *SwapBufferSync* ,*FrameSync*, and the synchronization strategy based on timestamp, the results are shown in table 2

.

Table2. Three types of synchronization strategies comparison

Event	FrameSync	SwapBufferSync	BasedOnTimestamp
sync accuracy	middle	high	middle
communication mode	reply	transfer: notice; sync: reply	notice
poor network	easy to deadlock	easy to deadlock	not deadlock
client lost	temporarily delay	temporarily delay	not affected.
client delay	temporarily delay	temporarily delay	rest is normal
client failure	temporarily delay	temporarily delay	rest is normal
long running	low reliability	low reliability	high reliability

Communication mode, "reply" show client need feedback information to the server, if the network or the client failure,client may not reply ; "Notice" show client does not need feedback, so the client's fault will not affect the system itself. From the comparison results can be seen, the Synchronization strategy based on timestamp, although a little less in accuracy compare with *SwapBufferSync*, the high stability of the system , a high degree of fault-tolerant in network transmission, a single client node missing or faulty for the entire system is not affected, so it is suitable used in a clustered, massive and high reliable multichannel system.

Conclusion

The new strategy has some advantages compared with existing solutions, such as high reliability, good fault tolerance, high performance, wide usage and easy implementation. Client node failure does not cause "short-board effect" of the entire system hysteresis, meanwhile the client node has

the adaptive ability, to ignore the rendering stress problem, always in sync with the overall progress. This strategy can be used not only in real-time rendering of 3D large-scene, but also for high definition video playback, or immersion system composed of multiple special-shaped display terminal.

Acknowledgements

In this paper, the research was sponsored by the Innovation Team Building of Beijing Municipal Institutions of Higher Learning and Teachers' Professional Development Program (Project No.IDHT20130519).

References

[1] S. Eilemann, M. Makhinya, and R. Pajarola. Equalizer: A Scalable Parallel Rendering Framework[J]. Visualization and Computer Graphics, 2009:15,(3):436-452.
[2] R. Ball, and C. North. Analysis of User Behavior on High-Resolution Tiled Displays[J]. Human-Computer Interaction, 2005:10(6):350-363.
[3] QIAO CaiLi, DAI ShuLing. Study of Synchronization Technique for Multi-tiled Display System[J] .Journal of System Simulation, 2007:19(15):3437–3440.
[4] XIAO Chao, YANG GongYu. Study of Synchronization Algorithm for Multi-channel Projection Display System [J]. Journal of SiChuan University (engineering science edit), 2012, 96:96-102.
[5] Choi SH,Yang XB,Yuen KK. An Intuitive 3D Interface Infrastructure for Virtual Reality Applications[M]. New York: Nova Science Publishers, 2012.

Advanced Materials Research Vols. 989-994 (2014) pp 3633-3638
© (2014) Trans Tech Publications, Switzerland
doi:10.4028/www.scientific.net/AMR.989-994.3633

Research on Multi-sensor Data Aggregation Based on Clustering Analysis and Correlation

Xiaochao DANG[1,2,a], Qi GAO[1,b], *Zhanjun HAO[1,2,c](Corresponding author)

[1]College of Computer Science and Engineering, Northwest Normal University, Lanzhou 730070, P.R. China

[2]Gansu IOT Research Center, Lanzhou 730070, P.R. China

[a]dangxc@nwnu.edu.cn,[b]gaoqi198@163.com,[c]zhanjunhao@126.com

Keywords: WSN, data aggregation, correlation, cluster analysis

Abstract. Multi-sensor is deployed for the target-monitoring in complex environment. However, the distribution of sensory data is irregular and inconsistent and the data is also highly redundant. For the purpose of obtaining accurate information, this article proposes a method for data aggregation of multi-sensor based on clustering analysis and correlation. By computing the correlation of the sensory data and the clustering analysis, the overall distribution of the data is analyzed. Finally, the method integrates sensory data by the correlation and uses the joint probability density function to compute the best integrated point. Simulated results show that the method is more effective in data aggregation than traditional methods.

Introduction

Wireless sensor networks [1][2] are applied to many aspects in our society in resent years and obtain well economical and social effects. However, the sensory data of targets collected from the multi-sensor is of large quantity and redundant, it is necessary to deal with the problems mentioned above during the data analysis and process so that the value of the target is closer to the value of target in the actual monitoring environment. The redundant information of sensory data is reduced by the correlation and we use data aggregation technology to fuse the sensory data. So it is fairly important to improve the networks' accuracy and robustness and prolong the lifetime of the entire network system.

In the wireless sensor networks, it is necessary to distribute a large number of homogeneous sensor nodes to monitor the targets. So it's obvious that the value of sensory data is in a large scale and its distribution is redundant. Additionally, some data is singular point. It is not an effective way to fuse the data by the simple weighted average method. Unlike the static environment, the sensor nodes are always disseminated in the areas that are usually inaccessible and large scale and changing regions. More importantly, the data of monitored target is also in the varying status. So the fusing methods such as principal component analysis and variance analysis can not acquire very good results. According to the current measurement theory, the purpose of multi-sensor data aggregation [3][4][5] is that when the data is superimposed, the noise in data will disappear and the fused data will be closely related with the actual value of the targets. However, many documents just assign the weight to the different properties, which causes that the noise will not disappear completely and it will have an influence on the final fusion results.

Based on analyzing the related research about the data fusion at home and abroad in recent years, this article will propose a data fusion method based on the non-weight assignment.

Related Works

In the related documents, there are many methods that are used to describe the difference of sensory data and the data differences are generally divided into the absolute difference and the relative difference. In other words, the relationship between data is judged by the linear and nonlinear function. If the two data sets are the same, the result of data comparison is 1, or the result is 0. The key problem in this method is that the normal difference of data sets. Under the condition

that the difference of sensory data sets is very small, the two data sets are also the same and the result of comparison is also 1. If the difference is large, that is, the similarity of the two data sets is low and the two data sets are different, so the result of data comparison is 0. Therefore, the similarity of data sets can not be described simply as the linear relationship. With the difference increases, the similarity will decrease slowly. When the difference reaches a threshold, the similarity will go down quickly until it drops to 0.In some documents the truncation method [6] is adopted to deal with the problems mentioned above. Here a threshold is set to verify the data sets whether they are same or different. If the difference is beyond the threshold, the result is 0, or the result is 1. The problems with this method are that the threshold is set randomly and empirically. So it can not reflect the overall distribution of sensory data. The *arccot* function [7] is used to measure the consistency of data and shows good continuity, but the simulated figure by the function can not effectively describe the actual physical meanings of sensory data.

All the articles introduce the weight [8] concept to deal with the redundant information of data, that is, the data has different meanings. The more important the meaning is, the bigger the value of weight is. However, this method does not take the many sets of data in consideration. In other words, the correlation of data in a set is high, but the correlation is low between the sets. The data under this condition can not be fused simply by setting the different weights for different sets. Of course, in the real environment, some reasons such as the irrational sensor nodes location and environmental mutations may cause serious data inconsistency. Analysis on the data inconsistency is very important for the system faults detection. The model of multi-sensor data aggregation based on correlation and the clustering analysis computes the correlation of data sets first and then uses the clustering algorithms to display the overall distribution of data sets and proves the feasibility and efficiency of data aggregation. Finally, the model fuses the sensory data.

Correlation Computing

Definition 1: The relative data distance is defined below referring to the article [6].

$$dist_{i,j}(k)=\begin{cases}\dfrac{Min\{x_i(k),x_j(k)\}}{Max\{x_i(k),x_j(k)\}}\end{cases} \tag{1}$$

Among the formula 3.1, $dist_{i,j}(k)$ represents the distance between node i and node j at the moment k. The domain of $dist_{i,j}(k)$ is $(0,1]$.

Supposed that the data collected from the sensor nodes are all computable, the improved distance definition take the distance d_a, d_b between target and sensor nodes and the distance d_{ab} between nodes into consideration. It is obvious that the correlation is inversely related with the d_{ab} and the d_a / d_b.The schematic diagram is shown in figure 1.

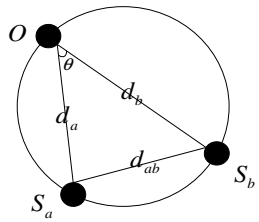

Fig. 1 Multi-sensor

Therefore, the data distance is defined as follows.

$$Sim=\begin{cases}1-dist\times\dfrac{d_a}{d_b}\dfrac{\varepsilon}{d_{ab}} & d_a\geq d_b, d_{ab}\leq d_0\\ 1-dist\times\dfrac{d_b}{d_a}\dfrac{\varepsilon}{d_{ab}} & d_a< d_b, d_{ab}> d_0\\ 0 & d_{ab}\to\infty\end{cases} \tag{2}$$

Definition 2: Data correlation is defined to measure the similarity of different sensory data sets. It is obvious that the correlation is proportionally related with the similarity, that is, if the similarity is high, the correlation is also high, or the two data sets are not related and the correlation is low and they can not be fused straightly and simply. The detailed idea is below, $LinD(X,Y)$ symbolizes the correlation. X,Y are the location of the sensor nodes. The correlation $LinD(X,Y)$ is right under the following conditions.

(1) Monotony. The overall tendency of the $LinD(X,Y)$ is falling.

(2) Exchangeability. $LinD(X,Y)=LinD(Y,X)$.

(3) The domain of the $LinD(X,Y)$ is $[0,1]$.

The closer the distance between sensor nodes, the bigger the value of the $LinD(X,Y)$ is. According to the limit concept, the value of $LinD(X,Y)$ is 0 when the distance is infinite and the value is 1 when the distance is infinitely small. The function curve is shown in figure 2.

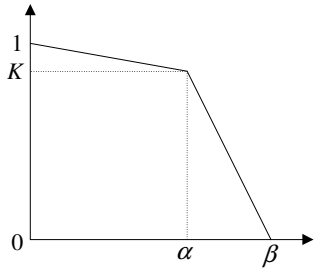

Fig.2 Data Correlation Function

As is shown is figure 2, the function curve is divided into three status. α and β are the critical points. When the data distance is smaller than the α, the correlation drops slowly. When the data distance reaches the α point, the correlation drops quickly before reaching the β point. When the data distance is beyond the β point, the value of correlation is zero. The correlation function formula is in the following section.

$$LinD=\begin{cases}1-\dfrac{1-K}{\alpha}\times Sim & Sim\le\alpha\\ \dfrac{K\times(\beta-Sim)}{\beta-\alpha} & \alpha\le Sim\le\beta\\ 0 & Sim\ge\beta\end{cases} \tag{3}$$

Among the formula 3.3, $LinD$ is the correlation function identifier. Sim is the data distance identifier. α and β are separately the critical points for correlation. K is the value of critical threshold for effective data aggregation in the function.

Clustering Analysis

Correlation computing is applied for the next clustering analysis. The clustering analysis [9][10][11] is used to cluster the data sets in order to get some sets in which contain data with close correlation. Therefore, the data in different sets has some common attributes so as to get the discrete degree of data. After computing the correlation, then clustering algorithms are applied to analyze the sensory data. Obviously, the correlation of data is stored in a matrix. $LinD_{i,j}$ represents the correlation of node i and node j. So the correlation of each sensor node $TLinD$ is computed as follows.

$$TLinD_i=\sum_{j=1}^{n}LinD_{i,j} \tag{4}$$

The bigger is the $TLinD$, the larger is the number of the nodes in the area. The smaller is the $TLinD$, the less is the number of the nodes or there are some isolated sensor nodes.

The detail procedure of the clustering analysis is in this section. Supposed that there are n sets $G_1, G_2, ..., G_n$ and they all empty at the beginning. Then the algorithm sorts the $TLinD$ by the sequence from big to small and forms the set $Degree$ .The tag of sets is $flag$.

(1) Set the $flag$ =1;

(2) Take out of first element from the set $Degree$ and put it in the set G_{flag}. Pop the data from set $Degree$ Continually and judge whether the element is beyond the threshold λ or not ant then determine whether put it in the set G_{flag} or not.

(3) Delete the elements that have been put in the set G_{flag}, and judge whether the set $Degree$ is empty or not. If it is empty, the algorithm is over, or goes to step (4).

(4) The $flag$ increases by one, the algorithm goes to step (2) until the set $Degree$ is empty.

λ is the threshold we set for the clustering radius and its value had better set referring to the value of K . That is because the correlation and difference of data sets is determined by the value of K .

The results of clustering analysis maybe contain several different statuses. Firstly, all elements in set $Degree$ are in one set such as G_i, which means the sensory data sets have the best correlation and they can be fused directly without any change. Secondly, most elements in set $Degree$ are in one set such as G_j, which means the sensory data sets have good correlation and the algorithm fuses the most elements in set $Degree$ with abandoning the a few data sets of bad correlation. Thirdly, each set $G_1, G_2, ..., G_n$ has some elements of set $Degree$, which means the elements in set $Degree$ don't have good correlation and they can't be fused directly. Clustering analysis diagrams are shown in figure 3.

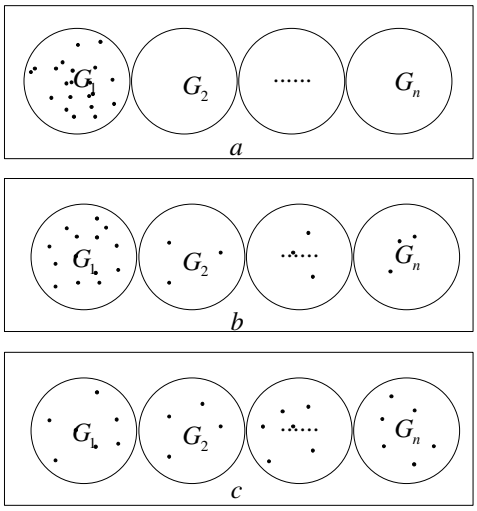

Fig. 3 Clustering Analysis Diagrams

Many reasons will cause the poor correlation of sensory data such as outside disturbances and unreasonable location of sensor nodes. If there are some non-artificial reasons that cause the bad data, the algorithm can use preprocessing mechanism to correct the sensory data. For instance, the data from node A is always higher than that from node B by 2, the algorithm will add 2 to the data from node B so that it can conveniently compute the correlation and fuse the data.

The algorithm also applies the joint probability density function to compute the best point for data aggregation. Supposed that the data from sensor node i obeys the Gaussian distribution $\rho_i(x) = (\mu_i, \sigma_i)$ and the function gets the biggest value at point μ_i for each node. The probability function is $\rho_i(x)$.

$$\rho_i(x)=\frac{1}{\sqrt{2\pi}\sigma_i}e^{-\frac{(x-\mu_i)^2}{2\sigma_i^2}} \tag{5}$$

Therefore the joint probability function is $L(x)$.

$$L(x)=\prod_{i=1}^{n}\rho_i(x)=\left(\frac{1}{\sqrt{2\pi}}\right)^n\frac{1}{\prod_{i=1}^{n}\sigma_i}e^{-\left(\sum_{i=1}^{n}\frac{(x-\mu_i)^2}{2\sigma_i^2}\right)} \tag{6}$$

It is obvious that $L(x)$ has the biggest value at point $\sum_{i=1}^{n}\frac{\alpha_i}{\sigma_i^2}\Big/\sum_{i=1}^{n}\frac{1}{\sigma_i^2}$.

Finally, here analyzes the time complexity of the algorithm and it mainly focus on two aspects. On one hand, the time complexity is the sort on $Degree$, on the other hand, the time complexity is the clustering analysis on sensory data. Here the algorithm adopts the best Quicksort algorithm to sort the elements in $Degree$, so the time complexity is $O(n\log(n))$. In the clustering analysis, the algorithm must scan the sets $G_1,G_2,...,G_n$ whether the set contains elements or not, so the time complexity is $O(n)$. In summary, the time complexity of this algorithm is $O(n\log(n))$. Thus, the complexity is just related with the number of sensor nodes.

Simulations

The simulated data comes from the article [12], as is presented in table 1.

Table 1. The sensory temperature

Sensor Node	Time					
	1	2	3	4	5	6
1	899.5	905.3	904.9	900.6	889.9	899.4
2	898.3	875.9	888.1	886.2	907.5	904.4
3	896.7	906.8	898.2	904.0	896.4	891.6

The real value of temperature is 900°C. Generally speaking, the precision of sensory data is one thousandth. If the sensory data is different from the real value by two thousandth, it's also regarded as normal. If the difference is beyond five hundredth, it's abnormal. The detailed parameters are set in table 2.

Table 2. Parameter

parameter	value
α	0.002
β	0.05
K	0.95
λ	0.9
d_a	10
d_b	10
d_{ab}	5

The simulated results of fusion are presented in table 3. According to the fusion results, the absolute difference is 13.3, which is better than the results of algorithms mentioned in the article [12]. The table 3 shows the fused nodes and the last fused results for six times. However, some parameters set is artificial, if the values of parameters are adjusted, the fused results will be better, but the values of parameters can not easily changed after set.

Table 3. Simulated results

Sensor Node	1	2	3	4	5	6
	$s_1+s_2+s_3$	s_1+s_3	s_1+s_3	s_1+s_3	s_3	s_1
1	899.5	905.3	904.9	900.6	889.9	899.4
2	898.3	875.9	888.1	886.2	907.5	904.4
3	896.7	906.8	898.2	904.0	896.4	891.6
Result	898.8	906.0	900.1	902.0	896.6	899.4

Conclusion

This article proposed an algorithm for data aggregation based on the correlation and clustering analysis, in which contains the correlation's definition and computing and the clustering analysis. The clustering analysis is responsible for judging the overall distribution of sensory data. At last, the algorithm uses the joint probability function to find the best point for data aggregation. Simulations results show that the method is better at fusing performance than other algorithms.

Acknowledgement

This paper is partially supported by Natural Science Foundation of China（the project Numbers: 61363059, Science and technology support project of Gansu province (the project Numbers: 010DKB021).

References

[1] Li Jian-zhong, Gao Hong. Survey on Sensor Network Research [J]. Journal of Computer Research and Development, 2008, 45(1):1-15.
[2] Lindsey S, Raghavendra C, Sivalingam KM. Data gathering algorithms in sensor networks using energy metrics. IEEE Trans. On Parallel and Distributed Systems, 2002, 13(9):924-935.
[3] HUANG Man-guo, FAN Shang-chun. Research progress of multi-sensor data fusion technology [J]. Transducer and Microsystem Technologies, 2010, 29(3):5-8+12.
[4] Lu Tiejun, Liu Chuanzhou,Wang Liujian. A target classification algorithm based on multi-sensor data fusion [J].Aerospace Electronic Warfare, 2013, 39(4):41-44.
[5] YANG Geng, LI Sen, CHEN Zheng-Yu,et al. High-Accuracy and Privacy-Preserving Oriented Data Aggregation Algorithm in Sensor Networks[J].CHINESE JOURNAL OF COMPUTERS,2013, 36(1): 189-200.
[6] JIAO Zhu-qing, XIONG Wei-li. Study on Multi-sensor Data Fusion Based on Approach Degree [J]. PIEZOELECTRICS & ACOUSTOOPTCS, 2009, 31(5):771-774.
[7] ZHANG Jian-ye, WANG Zhan-lei. Independent online fusion algorithm for multi-sensor data [J]. Journal of Computer Application, 2011, 31(10): 2869-2871.
[8] TAO Zhi-yong, WANG Xue. A Data Aggregation Algorithm for WSN Based on Clustering and Weighing-estimation [J].MICROELECTRONICS & COMPUTER, 2013, 30(11):136-138 +142.
[9] Yu S, Tranchevent L C. Optimized Data Fusion for Kernel K-means Clustering [J]. IEEE Trans. On Pattern Analysis and Machine Intelligence, 2012, 34(5):1031-1039.
[10] SHU Hong-ping, WANG Yun-feng, Xu Zhen-ming,et al. Research on multirada data fusion algorithm based on K-mean clustering[J]. Computer Engineering and Application, 2007, 43(16):183-185.
[11] WANG Ying-jie. A Study of Fuzzy Clustering Analysis in Data Mining [J].JOURNAL OF DALIAN UNIVERSITY, 2011, 32(3):1-4.
[12] DONG Jiu-ying. Study on principle component method for multi-sensor data fusion [J]. Computer Engineering and Application, 2009, 45(33):111-113.

Advanced Materials Research Vols. 989-994 (2014) pp 3639-3643
© (2014) Trans Tech Publications, Switzerland
doi:10.4028/www.scientific.net/AMR.989-994.3639

Automatic registration between high resolution SAR image and GIS road network based on pairwise constraint and ICM optimization

Haigang Sui[1, a], Feng Hua[1, b], Guang Chen[1, c], Chuan Xu[1, d]

[1] State Key Laboratory of Information Engineering in Surveying, Mapping and Remote Sensing, Wuhan University, Wuhan, 430079, China

[a]email: haigang_sui@263.net, [b]email:huafeng731@gmail.com

Keywords: SAR; GIS road network; registration; optimization;

Abstract. Synthetic aperture radar (SAR) technique has been widely applied in disaster monitoring and evaluation, because of its all-weather and all-time capability. In particular, the integration of high resolution SAR image and GIS data has been proved to be an effective solution to change detection for rapid disaster response. However, accurate registration of SAR image and GIS data remains a challenging task. On the one hand, SAR image and GIS data are two different representation levels of the real world. GIS data lacks of grey value and texture information, thus traditional use of grey-based and texture-based feature descriptors for feature matching in GIS data is impossible. On the other hand, the extraction of matching primitives is difficult in the SAR image due to the speckle noise. Moreover, though features can be extracted in the SAR image, the matching can be difficult since features may be fractured and missing. In this paper, we propose a new method for vector-to-SAR image registration which utilizes conjugate line-pair intersections as matching primitives. The core idea consists in two aspects: 1) Different from traditional road intersection based registration methods, conjugate line-pair intersections are employed as matching primitive in the proposed method. 2) To find out the optimal set of matching features, a matching technique that using pairwise constraint and the iterative conditional mode (ICM) optimization algorithm is introduced. Experiment results proved the reliability and feasibility of the proposed method.

Introduction

In recent years, the fast development of SAR systems such as TerraSAR-X, Cosmo-Skymed and Radarsat-2 have provided effective means for disaster monitoring and evaluation [1]. Especially, the fusion of SAR image and GIS data has great potentiality and advantage for road damage detection and flood monitoring etc. For example, road objects, especially important roads, are more likely to be static with slow change, thus the existing GIS road network can be employed to identify damaged road quickly and accurately [2]. However, the precise registration of SAR image and GIS data is a significant and essential step. In fact, remote sensing image and GIS data are two different ways to represent the surface objects, where images provide a continuous representation of geographic area and vector data represents objects as discrete entities. In addition, the SAR image suffers inherent speckle noise, which makes it more difficult to extract accurate features from the SAR image. Furthermore, even if features are extracted in the SAR image, the matching procedure tends to be an error-prone process, since many features are short and broken. Thus, accurate registration of SAR image and GIS data remains a challenging task.

The aligning of image and GIS road network requires identifying an appropriate set of conjugate features on the two data sources. Most widely used features are road intersection points, road line segment and road polyline. Song [3] presented an automated geospatial conflation method based on road intersections and terminations. Extracted points were matched by a relaxation labeling algorithm and a refinement algorithm was further applied to obtain better accuracy. However, road intersections were difficult to be identified in the SAR image due to the complexity of remotely sensed images and speckle noise. Liu [4] proposed an automatic registration approach using line segments and a modified Hough Transform. The drawback of the method is the Hough-like voting

strategy makes the algorithm time consuming and noise sensitive. Wang [5] introduced a novel approach to the registration problem based on polyline features and point networks. Topology and geometry of a network was utilized to establish correspondence. However, the process needed user interference to determine the index range of nodes in template construction.

Considering the state-of-the-art in image-to-vector registration, a new method based on conjugate line-pair intersection is proposed in this paper. Firstly, different from traditional road intersection based registration methods, conjugate line-pair intersections are employed as matching primitives in the proposed method. Then, a robust matching technique which using pairwise constraint and the iterative conditional mode (ICM) optimization is introduced to obtain accurate matching result. Pairwise constraint aims to obtain potential corresponding line-pair intersection. The ICM optimization aims to obtain the optimal set of corresponding features. Matched line-pair intersections are regarded as control points to perform transformation between the SAR image and GIS road data.

Methodology

For feature-based methods, one of the key problems is to establish a reliable correspondence between the matching primitives in the reference data and those in the floating data. Since there is no grey value or texture information in the GIS data, affine-invariant line matching [6] and mean-standard deviation line descriptor (MLSD) [7] are no longer suitable for our situation. Thus, in this paper, we investigate the line matching problem only based on the geometric relationship between line-pairs. The proposed method mainly consists in two aspects: 1) searching potential conjugate line-pair using pairwise constraint; 2) locating maximum matching cliques using the ICM optimization.

A) searching potential conjugate line-pair using pairwise constraints

Line-pair intersection is regarded as matching primitive in the proposed method. In order to obtain robust matching primitives, a line-pair must satisfy:

1) The length of each line segment is no lesser than t_l;

2) The angle between the two line segments is no lesser than t_a.

The first restriction limits the participation of non-robust line segments for generating matching primitive. The second restriction limits the generation of erroneous matching primitive from line segments with similar slope. The angle between the two line segments θ is considered as the angle of the current line-pair.

Considering two correspondingly matched line-pairs, it is necessary that the angle difference between two line-pairs is close. Thus, the angle difference can be used to guide pairwise constraint, which is illustrated in

$$\varepsilon_\theta = |\theta_i - \theta_j|, \qquad 0 < \varepsilon_\theta < t_\theta \tag{1}$$

θ_i and θ_j are the i^{th} SAR line-pair and the j^{th} GIS line-pair, respectively. t_θ is the user defined angle threshold.

B) locating maximum matching cliques using the ICM optimization

After using the pairwise constraint, all potential matching line-pairs are obtained. However, due to the angle ambiguity, many-to-many matching line-pairs may exist. Thus, in order to realize the efficient one-to-one correspondence, we should find out the maximum cliques from potential line-pairs to ensure the minimum matching error. Let us assume that the m pairs of potential line-pairs are obtained using the pairwise constraint. Then we have

$$C = \{c_i = (l_{i1}^b, l_{i2}^b, l_{i1}^w, l_{i2}^w, p_i, q_i) \mid i = 1, ..., m\} \tag{2}$$

l_{i1}^b and l_{i2}^b are line-pairs from the SAR image and l_{i1}^w and l_{i2}^w are line-pairs from the GIS data. p_i and q_i are the corresponding line-pair intersection.

In fact, one line-pair in the SAR image may have several potential matching line-pairs in the GIS data. Thus, four matrixes MB, MB_{loc} and MW, MW_{loc} are created to record each line-pair in the potential line-pairs. Assume that there are $N1$ different line-pairs in C from SAR image and $N2$ different line-pairs from GIS data, the matrixes can be defined as

$$MB = [mb_1, mb_2, ..., mb_m], \quad MB_{loc} = [\{loc1\}, \{loc2\}, ..., \{locN1\}]$$
$$MW = [mw_1, mw_2, ..., mw_m], \quad MW_{loc} = [\{loc1\}, \{loc2\}, ..., \{locN2\}] \tag{3}$$

Where $mb_i \in \{1, ..., N1\}$ and $mw_i \in \{1, ..., N2\}$ denote the order of i^{th} line-pair element in C for SAR image and GIS data, respectively. MB_{loc} and MW_{loc} are used to record the exactly locations of i in mb_i and mw_i. Then, we introduce a match matrix M of size $m \times 1$ to describe the match condition of potential matching line-pairs

$$M_i = \begin{cases} 1, & if\ the\ i^{th}\ element\ in\ C\ is\ a\ correctly\ matched\ one \\ 0, & otherwise \end{cases} \tag{4}$$

M should satisfy two-way constraints to ensure one-to-one correspondence,

$$\sum_{i=1}^{m} M_i f(mb_i == j) \le 1, \quad j = 1, 2, ..., N1$$
$$\sum_{i=1}^{m} M_i f(mw_i == k) \le 1, \quad k = 1, 2, ..., N2 \tag{5}$$

where $f(\ )$ is a Boolean function. All possible M can be obtained from the MB_{loc} and MW_{loc}. Firstly, $N1$ pairs of different line-pair from MB_{loc} and $N2$ pairs of different line-pair from MW_{loc} are selected. Then, the same values in $N1$ and $N2$ are considered as a match choice for M, which represents c_i in the same values are correctly matched. All match choices for M form a potential match set called M-set.

From the above definition, the problem of locating the maximum matching cliques can be solved by minimizing the following energy function,

$$[\hat{M}, \hat{T}] = \arg\min_{M,T} E(M, T),$$
$$E(M, T) = \sum_{i=1}^{m} M_i \| p_i - Tq_i \|^2 / \sum_{i=1}^{m} M_i \tag{6}$$

To solve the optimization problem, the ICM (Iterative Conditional Modes) algorithm is applied. In fact, the goal of the minimization of (6) is to simultaneously find the optimal transformation T model and the optimal match matrix M. Once the match matrix M is found in advance, the transformation matrix T will be determined using the least square method. Finally, weighted graph transformation matching (WGTM) [8] is used to check wrong pairs in the final matching primitives. The remaining corresponding points are used to produce the final registered data.
The pseudo-code of the ICM optimization algorithm is listed below.

Algorithm 1: The ICM algorithm

Initialize the match matrix M by selecting the first component in M-set.
$k=0$; $E_0 = E(M_0, T_0)$;
Begin A: (Do A until all components in M-set are checked)
1 Select the next component in M-set, and calculate the energy $E_{k+1}(M_{k+1}, T_{k+1})$;
2 Update the minimum energy $E_{min} = min\ (E_k, E_{k+1})$;
3 $k=k+1$;
End A.
$E=E_{min}$;
WGTM algorithm is applied.
End Algorithm 1.

Experiment and Analysis

In this section, we illustrate the proposed method on real SAR image and GIS data to demonstrate the effect of the proposed registration method. The reference image is a TerraSAR-X image (spatial resolution: 1m), which is captured on 2012 with a size of 3850×3169 pixels. The GIS data is downloaded from http://www.openstreetmap.org/ with a free charge. In the experiment, road line segments are detected using the Snake method [9], which has been widely used for road detection in SAR images. However, a well-known problem of active contour model is that it requires very good initialization. Thus, in order to provide a good initial estimation of the road location for SAR image, the GIS data is approximately aligned with the SAR image using a single manually selected tie point.

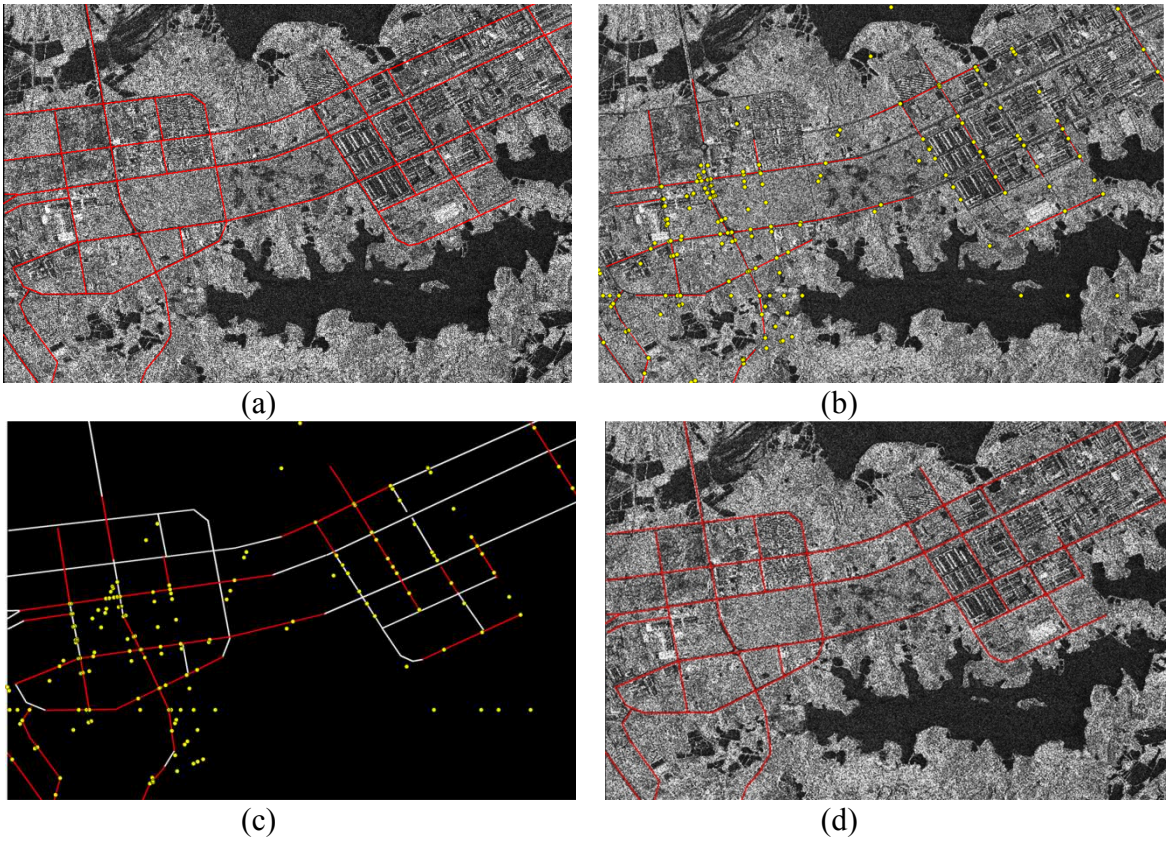

Fig.1. The experimental results. (a) Initial alignment using a single tie point; (b) Matched line-pair road segments and intersections in the SAR image; (c) Matched line-pair road segments and intersections in GIS data; (d) Final alignment using the proposed method.

From the above Figure 1(a), we can see that the SAR image and GIS data are approximately aligned; however, there is an obvious displacement in the right part of the image. (b) and (c) shows the matched road line segments and the corresponding points. 162 pairs of corresponding points are obtained using the proposed method. (d) shows a desired alignment between the SAR image and GIS data using the proposed method.

To evaluate the proposed matching method, the proposed method is compared with two line segment matching algorithms: Modified Hough Transform (MHT) [4], Gaussian Mixture Models and Expectation-Maximization (GMM-EM) [10]. The comparison results are given in Table I. 20 pairs of corresponding tie points are manually selected as a reference for RMSE assessment.

Table I: Comparison of the proposed method with other line segment matching algorithms

Algorithm	*Total matching primitives*	*RMSE*
Our	162	1.56m
MHT	30	11.32m
GMM-EM	32	2.12m

Conclusion

In this paper, we presented a novel high-resolution SAR image and GIS data registration method based on pairwise constraint and the ICM optimization. This technique uses the pairwise constraints to obtain potential matching line-pairs. Then, the ICM optimization is applied to obtain the optimal matching line-pairs for robust registration. Experiment shows that the proposed method is feasible and could achieve high accuracy.

Acknowledgement

In this paper, the research was sponsored by National Key Fundamental Research Plan of China (973) [Project NO. 2012CB719906], National High Technology Research and Development Programme of China (863 Programme) [Project NO. 2013AA122301] and National Natural Fund of China (NSFC) [Project NO. 41101414].

References

[1] Li Xin-wu and so on. A new approach to collapsed building extraction using Radarsat-2 polarimetric SAR imagery [J]. IEEE Transactions and Remote Sensing Letters, 2012, 9(4): 677-681.

[2] Li De-ren. Remotely sensed images and GIS data fusion for automatic change detection [J]. International Journal of Image and Data Fusion, 2010, 1(1): 99-108.

[3] Song Wen-bo and so on. Automated geospatial conflation of vector road maps to high resolution imagery [J]. IEEE Transactions on Image Processing, 2009, 18(2): 388-400.

[4] Liu Zhi-qing and so on. Automatic registration between remote sensing image and vector data based on line features [J]. 19th International Conference on Geoinformatics, 2011: 1-5.

[5] Wang Cai-xia and so on. Image-to-X registration using linear features [J]. IEEE International Fuzzy Systems Conference, 2007: 1-7.

[6] Chen Min and so on. Robust affine-invariant line matching for high resolution remote sensing images [J]. Photogrammetric Engineering & Remote Sensing, 2013, 79(8): 753-760.

[7] Wang Zhi-heng and so on. MSLD: a robust descriptor for line matching [J]. Pattern Recognition, 2009 (42): 941-953.

[8] Izadi M. and Saeedi P. Robust weighted graph transformation matching for rigid and nonrigid image registration [J]. IEEE Transactions on Image Processing, 2012, 21(10): 4369-4382.

[9] Liu Junyi and so on. Road extraction from SAR imagery based on an improved particle filtering and snake model [J]. International Journal of Remote Sensing, 2013, 34(22): 8199-8214.

[10] Long Teng-fei and so on. Automatic line segment registration using Gaussian Mixture Model and Expectation-Maximization algorithm [J]. IEEE Journal of Selected Topics In Applied Earth Observation and Remote Sensing, 2013: 1-12.

Advanced Materials Research Vols. 989-994 (2014) pp 3644-3648
© (2014) Trans Tech Publications, Switzerland
doi:10.4028/www.scientific.net/AMR.989-994.3644

Semi-Automatic Extraction Method for Low Contrast Road based on Gabor Filter and Simulated Annealing

Guang Chen[1, a], Haigang Sui[1, b*], Liang Dong[1, c], Hua Sun[1, d],

[1]State Key Laboratory of Information Engineering in Surveying, Mapping and Remote Sensing, Wuhan University, Wuhan, 430079, China

[a]email: teddycg0214@gmail.com, [b]email: haigang_sui@263.net, [c]email: 395475212@qq.com, [d]email: 113387449@qq.com

Keywords: Low Contrast Road; Remote Sensing; Road Extraction; Gabor Filter; Phase Grouping; Simulated Annealing

Abstract. High-resolution satellite remote sensing image are mostly used for accurate updating of GIS data. As the primary GIS data, urban roads on the image show the rich geometric features and radiation characteristics, that edge detection and grouping becoming an important way to solve the road extraction. However, edge elements obtained from images are always discontinuous for interference of noise and weak contrast between road and background. What more, vehicles, plant, buildings and shadow blocking results in weak grouping relation of elements. In processing, insignificant candidate road may be weeded out as noise and lead to failure road extraction. This paper presents a semi-automated extraction method for low contrast road basing on statistical grouping of orientation texture feature. Multi-direction and multi-scale Gabor filters are employed to detect directions of road texture. Then same direction pixels are grouped under constraining of rectangle template and generate road base elements. Finally, simulated annealing algorithm is used to optimize elements connection. Experiment results show that proposed method was effective in accurate extraction of low contrast road.

Introduction

Road extraction in urban areas is an important task for updating geographic information. Especially in recent years, the rapid development of urban areas makes it urgent to provide up-to-date road maps. Due to high spatial resolution (1 to 4 m), fast orbit repeatability, rich multi-spectrum information and stable, affordable acquisition cost, remote sensed images have been taken as the main data source for road extraction.

Via the research and development of several decades, various methods or models were proposed. In general, most methods of roads extraction are divided into three levels that are base features extraction in low level, characteristic analysis and selection in middle level, objects understanding and identifying in high level due to computer vision theory of Marr [1]. Rule or knowledge-based methods [2] is so called 'high level' processing in order to group and link line features detected in 'low-level' or 'intermediate level' processing. Whereas, well performed lines detection is the key of successful road extraction. As the basis for extraction method, it is assumed that spectral properties of roads are limited to a fixed range [3] and roads have good contrast with its adjacent areas [4]. However, in high-resolution images, roads may be hidden or not visible, and their surrounding environments are very complex [5], especially in urban areas, where objects like zebra crossings, vehicles, trees, building and shadows cause noises and reduction of contrast between roads and background. As a result, road extraction methods based on edge features are confronted with great difficulties.

Gradient is most considered in edges detection methods. Typically, phase grouping [6] is taken as an effective method for extraction of low contrast edges and it was used to extract roads with no clear and continuous boundaries in RS images in [7]. However, dramatic change of pixel value, complex noise of background, and density of edge features in high resolution images make it difficult to generate effective line support region. Therefore, it is hard to achieve better edge detection results under complex scene with methods basing spatial domain characteristics. As one

of the characteristics of material energy, spectrum in frequency domain has the unique advantages in description of edge [8] and texture [9] feature. Wu [8] proposed a method of edge feature detection from high-resolution remote sensing images based on frequency spectrum zone energy. In [10], Gabor filter was used for road lane marking extraction. Considering obvious directivity of texture feature of pavement, Moghadam [11] employed Gabor filters to detect vanishing-points in unstructured roads.

In this paper, the major problem to be overcome is center line detection of low-contrast urban roads in high resolution images. Fully considering the advantage of phase grouping in edge detection, and Gabor filter in road texture direction analysis, we propose a center line detection method of low-contrast urban roads based on statistical grouping of orientation texture feature. Firstly, road image is filtered using six-directional Gabor filter at multi-scale. Then, pixels directions are determined according to the response in each direction-filter. Line support regions are constructed basing on co-directional pixels. Considering geometric feature of urban roads, line support regions are constrained as rectangle with large ratio of length to width. These line support regions are taken as road base elements. Finally, assuming that road center line is consisted of polylines, and optimizing road center line using simulated annealing algorithm.

Methodology

The conceptual workflow of the proposed method consisted of four steps: direction feature detection; road base element extraction; optimization of road center lines. They are described in details below.

Directional Feature Detection with Gabor Filter. The 2D Gabor filter [9] has been successfully applied to a variety of image processing and pattern recognition problems, such as texture analysis [12], object detection [13] and image segmentation [14].

In this paper, Gabor filter is used to detect the direction feature of road texture. Considering the variance of road width, multi-scale texture response is needed to be considered. In the processing of texture extraction, multi-scale and multi-orientation Gabor filters is taken convolution with image by sliding window.

The Gabor filter function is shown as formula (1).

$$g(x,y;\omega,\varphi)=\frac{\omega}{\sqrt{2\pi}c}e^{\frac{-\omega^2(4a^2+b^2)}{8c^2}}\left(e^{ia\omega}-e^{\frac{-c^2}{2}}\right) \quad (1)$$

Where, φ denotes direction of texture, ω represents scales, a is equal to $x\cos\varphi+y\sin\varphi$, b is equal to $-x\sin\varphi+y\cos\varphi$, c is equal to $\frac{\pi}{2}$.

To determine texture direction, the conventional approach is choosing the maximum energy response as amplitude of corresponding pixel texture feature, and corresponding filter direction as the direction of pixel texture. However, there some opinions show that texture response detected by Gabor filter is not stable in some cases, i.e. the image pixel differences may lead to relatively large phase differences.

In order to obtain stable and reliable direction information of texture, it is calculated by weighted average according to each direction. Corresponding weights are determined by normalized texture amplitude of each direction.

Extraction of Road Base Elements. In complex scenes, pixels direction features are shown inconsistent within local areas that it is impossible to obtained significant linear road elements directly. Using the orientation grouping method, pixels are classified into eight groups according to predetermined directions that dividing the circle into eight equal parts. Then line support regions are detected from grouped pixels and it makes a great reduction of the interference coming from background.

In the process of semi-automatic extraction, several seed points are needed by manually selection. It is required that seed points are located in significant road corners. The general direction of road can be obtained based on input seed points. So there is no need to group pixels into

8 directions like phase grouping method. Our processing focuses on grouping pixels which have approximate directions with known direction. The difference of direction should be kept in specify angle threshold. Removing pixels with weak response that their amplitudes are less than given threshold, it generates original support regions consisted of co-directional pixels which are mutually connected.

Considering the geometrical characteristic, urban roads are mostly shown as long rectangular in images. Even if in the non-straight roads, local segments can be regarded as rectangular approximately. Here, rectangular template is used to detect line support regions from the original support regions under shape constraint. Each line support region is a candidate for a road base element.

Optimization of Road Center Line. It is a route optimization problem to detect road center line from base element. We suppose the seed points at both ends of the path as the starting and ending points. Route is consisted of base elements and joint lines. Target function is defined according to geometric and spectral characteristics of road. Simulated annealing algorithm is employed to search the optimal route which has the minimal target function value.

The definition of target function should take into account of the following factors: length of the path; variance of pixel value in route; direction variance of base elements and joint lines. The definition is shown as formula (2).

$$T_r(i) = a(l_i - l_{min})/l_{min} + b\sigma_{gray}/256 + c\sigma_{direct}/180 \quad (2)$$

Where, l_i denote length of the i-th route; σ_{gray} and σ_{direct} denote the Standard Deviation of pixel values and elements direction respectively. a, b, b represent corresponding weight coefficient respectively.

Acceptance principle of new route is according to Metropolis principle [15]. While target function value of new route is less than that of current optimal route, it is accepted as new optimal route. Otherwise, new path is accepted with probability of state transition. Finally, global optimal route is obtained by the model convergence. To remove rags, smoothing is carried out on route and the result is the final extraction results of road centerline.

Experiments

This section highlights the experiments performed based on the proposed algorithm. The image considered for experiment comes from QuickBird and it consisted of R, G, B bands (see Fig.1 (a)). Considering the average width of road, the scale of Gabor filter is set to be 0 and 1, while the direction parameters are set to be 0, 30, 60, 90, 120, and 150 respectively.

The road feature extraction result for experiment is shown in Fig.1 (b)-(c). Test image is used in contexts of urban, that roads are relatively straight, and with more obstructions from shadows, trees and vehicles. The proposed method does not consider the contextual information explicitly. From the filtered image, it is obviously that road in specify direction are prominent and backgrounds are well suppressed. Extraction results of base elements also show the robustness of proposed method.

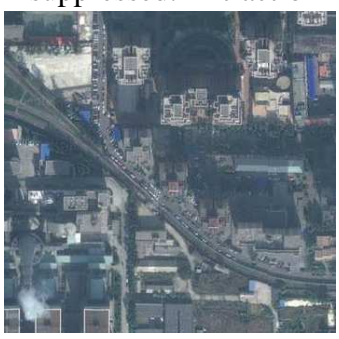

(a)

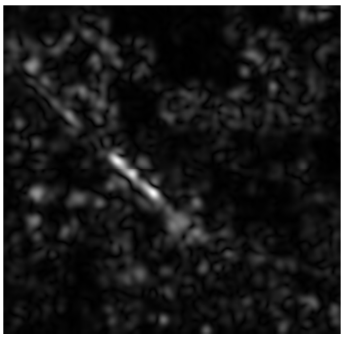

(b)

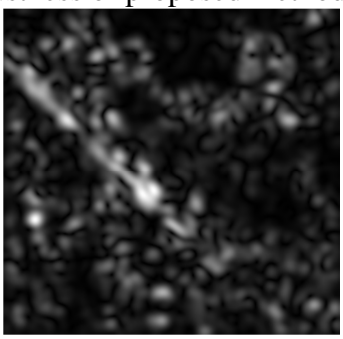

(c)

(d) (e) (f)

Fig.1. (a) Original image. (b)-(c) Filtered image with direction 120 and scale 0 to 1. (d) Extracted road base elements. (e) Extraction results of proposed method. (f) Hand-drawn reference road map

Fig.1 (e) shows the final extraction results. The proposed method has been evaluated based on comparing with hand-drawn reference road map (Fig.1 (f)). In general, main roads in image were extracted. Whenever roads are affected by minor anomalies (e.g., tree, shadows), the road centerlines are correctly extracted.

Conclusions

In this paper, we have presented a new approach to extract center lines of low contrast road in high-resolution aerial images over urban areas, based on multi-scale Gabor filtering and direction grouping. The direction of texture properties of road are effectively taken into account. The image is first filtered in different scale and direction. Then adjacent pixels with certain direction homogeneity and linearity in the structure are marked as line support regions. Regions which can surely be judged as non-road areas are eliminated by statistic distribution. Road base elements are generated from remaining support regions. In the post-processing step, optimal route of base elements connection is obtained using simulated annealing algorithm. The method is simple and not sensitive to noise and scene objects. It is specific for low contrast or strong interference roads in high resolution images. The future perspective is to make the processing more automatic without inputting seeds. Considering the variance of roads width, filter scale has to be adaptive for extracting salient direction features of roads.

Acknowledgement

In this paper, the research was sponsored by National Key Fundamental Research Plan of China (973) [Project NO. 2012CB719906], National High Technology Research and Development Programme of China (863 Programme) [Project NO. 2013AA122301] and the National Natural Fund of China (NSFC) [Project NO. 41101414].

References

[1] M. David, "Vision: a computational investigation into the human representation and processing of visual information," *WH Freeman,* vol. 1, p. 3, 1982.

[2] R. T O Njes and S. Growe, "Knowledge Based Road Extraction from Multisenor Imagery," *International Archives of Photogrammetry and Remote Sensing,* vol. 32, pp. 387-393, 1998.

[3] H. Long and Z. Zhao, "Urban road extraction from high-resolution optical satellite images," *International Journal of Remote Sensing,* vol. 26, pp. 4907-4921, 2005.

[4] S. Jing, L. Xiangguo, Y. Shi, and C. Wong, "Knowledge-Based Road Extraction from High Resolution Remotely Sensed Imagery," in *Image and Signal Processing, 2008. CISP '08. Congress on*, Sanya, China, 2008, pp. 608-612.

[5] P. Gamba, F. Dell'Acqua and G. Lisini, "Improving urban road extraction in high-resolution images exploiting directional filtering, perceptual grouping, and simple topological concepts," *Geoscience and Remote Sensing Letters, IEEE,* vol. 3, pp. 387-391, 2006.

[6] J. B. Burns, A. R. Hanson and E. M. Riseman, "Extracting Straight Lines," *Pattern Analysis and Machine Intelligence, IEEE Transactions on,* vol. PAMI-8, pp. 425-455, 1986.
[7] Z. Shao-guang and X. U. Yong, "To Extract Roads with No Clear and Continuous Boundaries in RS Images," *ACTA GEODAETICA ET CARTOGRAPHICA SINICA,* vol. 37, pp. 301-307, 2008.
[8] W. Guiping, X. Pengfeng, F. Xuezhi, W. Ke, and H. Qiuyan, "A Method of Edge Feature Detection from High-resolution Remote Sensing Images Based on Frequency Spectrum Zone Energy," *Acta Geodaetica et Cartographica Sinica,* vol. 40, pp. 587-591,609, 2011.
[9] J. G. Daugman, "Uncertainty relation for resolution in space, spatial frequency, and orientation optimized by two-dimensional visual cortical filters," *JOSA A,* vol. 2, pp. 1160-1169, 1985.
[10] H. Jin, Y. Feng and M. Li, "Towards an automatic system for road lane marking extraction in large-scale aerial images acquired over rural areas by hierarchical image analysis and Gabor filter," *International Journal of Remote Sensing,* vol. 33, pp. 2747-2769, 2012.
[11] P. Moghadam, J. A. Starzyk and W. S. Wijesoma, "Fast Vanishing-Point Detection in Unstructured Environments," *Image Processing, IEEE Transactions on,* vol. 21, pp. 425-430, 2012.
[12] A. C. Bovik, M. Clark and W. S. Geisler, "Multichannel texture analysis using localized spatial filters," *Pattern Analysis and Machine Intelligence, IEEE Transactions on,* vol. 12, pp. 55-73, 1990.
[13] D. M. Weber and D. P. Casasent, "Quadratic Gabor filters for object detection," *Image Processing, IEEE Transactions on,* vol. 10, pp. 218-230, 2001.
[14] J. V. B. Soares, J. J. G. Leandro, R. M. Cesar, H. F. Jelinek, and M. J. Cree, "Retinal vessel segmentation using the 2-D Gabor wavelet and supervised classification," *Medical Imaging, IEEE Transactions on,* vol. 25, pp. 1214-1222, 2006.
[15] N. Metropolis, A. Rosenbluth, M. Rosenbluth, A. Teller, and E. Teller, "Combinatorial minimization," *J. Chem. Phys,* vol. 21, pp. 1087-1092, 1953.

Advanced Materials Research Vols. 989-994 (2014) pp 3649-3653
© (2014) Trans Tech Publications, Switzerland
doi:10.4028/www.scientific.net/AMR.989-994.3649

Multi-threshold image segmentation based on improved particle swarm optimization and maximum entropy method

Yati Lu[1,a], Wenli Zhao[2,b] and Xiaobo Mao[3,c]

[1]School of Electrical Engineering, Zhengzhou University, Zhengzhou City, Henan Province, China

[2]Dept. of Mech. and Electr. Eng., Light Ind. Vocational Univ. of Henan Province, China

[3]School of Electrical Engineering, Zhengzhou University, Zhengzhou City, Henan Province, China

[a]1037607193@qq.com, [b]zwli2006@163.com, [c]mail-mxb@zzu.edu.cn

Keywords: PSO; expansion model; multi-threshold; image segmentation

Abstract. Both maximum entropy method and Particle swarm optimization (PSO) are common threshold segmentation methods which have been used not only in image segmentation, but also in multi-threshold segmentation. Maximum entropy method is time-consuming, PSO may easily get trapped in a local optimum. In view of this concerning issue, we propose the PSO and maximum entropy are combined to make improvements on the PSO introduced in expansion model and opposition-based module. The objective functions of the maximum entropy as well as the PSO are obtained, which have improved to optimize them and search the optimal threshold combination, to achieve multi-threshold image segmentation. The results demonstrate that the new algorithm improved the segmentation speed and enhanced the robustness. And the optimizing results are stable.

Introduction

Segmentation is a critical task in image processing. Image segmentation refers to dividing images into several meaningful areas according to some image features and making the features show similarity in one area and differentia in other areas. Threshold segmentation method is applied wildly in image segmentation and this method assumes that different objects in an image could be distinguished by gray value. So the key to this method is how to determine the threshold. Threshold method can be subdivided into the maximum entropy method, Otsu method and minimum error threshold method. However, these methods are initially only based on one-dimensional histogram and affected by the noise evidently. The maximum entropy method is little influenced by the target size, it can produce good segmentation results for images with different size and noise ratio of signal.

The maximum entropy threshold method proposed by Kapur that has been proved as an efficient method in image segmentation for single threshold. However, The calculation speed becomes greatly slow, which is difficult to meet the requirements of practical application of. Therefore its application is restricted. Recently, a new variant of esophageal atresia (EA), known as particle swarm optimization (PSO) [1], which is inspired by the emergent motion of flock birds searching for food, has been developed, mainly due to its simplicity, superior convergence characteristics and high solution-quality. PSO has become one of the most popular optimization techniques for solving optimization problems in systems, such as artificial neural network training, fuzzy system control, system optimization, control field and others. Particle swarm optimization algorithm has many advantages, but it declines rapidly in the late convergence. A characteristic of falling into local optimum easily makes the particle swarm algorithm often unable converge to the global optimal [2].

Document [3] illustrate the threshold segmentation based on particle swarm optimization, in the literature [4] describe the optimization object function by maximum entropy or Otsu method. The objective function is optimized by particle swarm optimization algorithm to achieve the optimal threshold segmentation. Taking advantage of the high efficiency of the particle swarm optimization algorithm, the literature [5] presents a method to solve multi-objective optimization problems using particle swarm optimization. The literature [6] respectively proposes a modified PSO for the global optimization of multimodal functions. But it is not fully solve the local optima, precocious and multi dimension problems.

In this paper, based on the advantages and disadvantages of the maximum entropy algorithm and particle swarm algorithm, a new algorithm is presented to improve the particle swarm algorithm and maximum entropy methods. An optimized objective function is obtained by the maximum entropy method. To obtain the initial candidate optimal solutions in the process of initializing population, opposition-based learning theory has been used. Introduction an expansion algorithm to restrain premature and to avoid local optimum, making up for the shortcomings of particle swarm algorithm and solving the problem of slow speed calculation of maximum entropy threshold. The algorithm achieves good segmentation results.

Related algorithms

Multi threshold segmentation based on maximum entropy. In this section, the maximum entropy based on threshold technique is introduced. Let the gray levels of a given image of N pixels range over [0, l-1]. The image with threshold is divided into two forms: target (A) and background (B). Let $P_t = \sum p_i$ ($0 \leqslant i \leqslant t$) Where p_i is the probability of gray appearance. Therefore maximize entropy is:

$$H_{(t)} = H_A + H_B = -\sum_{i=0}^{t} \frac{p_i}{P_t} \ln \frac{p_i}{P_t} - \sum_{i=t+1}^{l-1} \frac{p_i}{1-P_t} \ln \frac{p_i}{1-P_t} \tag{1}$$

The optimal threshold t^* can be obtained by maximizing $H_{(t)}$: $t^* = \text{argmax } H_{(t)}$ (2)

It can be extended to the multilevel threshold case with k thresholds as follows:

$$H(t_1, t_2, \ldots, t_k) = -\sum_{i=0}^{t_1} \frac{p_i}{P_{t_0}} \ln \frac{p_i}{P_{t_0}} - \sum_{i=t_1+1}^{t_2} \frac{p_i}{P_{t_1}} \ln \frac{p_i}{P_{t_1}} - \ldots - \sum_{i=t_k+1}^{l-1} \frac{p_i}{P_{t_k}} \ln \frac{p_i}{P_{t_k}} \tag{3}$$

The optimal thresholds (t_1^*, $t2^*$,..., tk^*) by maximizing $H(t_1, t_2,..., t_k)$: $t_1^*, t_2^*, \ldots, t_k^* = \text{argmax } \{H(t_1, t_2,..., t_k)\}$. Where, $0 \leq t_1 \leq t_2 \leq \ldots \leq t_k$. So, using the maximum entropy threshold method, multi threshold image segmentation problem can be summed up as the best threshold value of the optimization problem, where, $t^* = \{t_1^*, t_2^*, \ldots, t_k^*\}$.

In bi-level threshold, Kapur method can be utilized to find the optimal threshold efficiently. However, for the multilevel threshold problem, Kapur method has a disadvantage that the computational time will be very expensive due to the exhaustive search. In order to search the best threshold combination quickly and accurately, and make the image segmentation result more accurate, the improved particle swarm algorithm is applied to image segmentation. Such algorithm is used to find the optimal threshold combination and make the segmentation results accurate.

The basic principle of particle swarm algorithm. PSO is an algorithm inspired by bird-flocking and fish-schooling. Let x_i denote the particle's position and v_i is the corresponding velocity. In N-Dimensional search space, at iteration k, each particle i has its position and velocity defined by: $X_i^k = [X_{i,1}, X_{i,2}, \ldots, X_{i,N}]$, and $V_i^k = [V_{i,1}, V_{i,2}, \ldots, V_{i,N}]$

Velocity and particle updating are done using the following equations:

$$V_{i,n}^{k+1} = w \times V_{i,n}^k + c1 \times Rand()(pbest[i] - X_{i,n}^k) + c2 \times rand()(gbest - X_{i,n}^k) \tag{4}$$

$$\begin{aligned} X_{i,n}^{k+1} &= X_{i,n}^k + V_{i,n}^{k+1}, \quad \text{if } X_{min} \leqslant X_{i,n}^{k+1} \leqslant X_{max} \\ &= X_{min}, \quad \text{if } X_{i,n}^{k+1} < X_{min} \\ &= X_{max}, \quad \text{if } X_{i,n}^{k+1} > X_{max} \end{aligned} \tag{5}$$

Where, $i = 1,2,\ldots..$, M (M is the swarm size) ; $n = 1,2,\ldots..$, N;

In equation (4), *rand*() is a random number, *pbest* represents best position of a particle & *gbest* represents best of all *pbest* values. *c1* is cognitive parameter and *c2* is social parameter.In equation (5), X_{min} and X_{max} represent minimum and maximum values of particle positions respectively. Inertia weight w, which is an important parameter for PSO's convergence, is varied as:

$$w = w_{max} - \{(w_{max} - w_{min}) \ / iter_{max}\} \times iter \tag{6}$$

Where, w_{max} and w_{min} are the initial and final weight respectivel*ter* is the current iteration and $iter_{max}$ is the maximum number of iterations. This ensures that at the start of the algorithm, each particle further detects the good seed in the global scope; Later, the smaller value of w ensures that the particles

perform fine search in around the pole, the algorithm has a certain probability to converge to the global optimal value.

The initialization of the particle space: A good choice in selecting particle's spatial initialization will greatly reduce the convergence time. Random generation of particle group of a certain size sets the particle's initial position and velocity.

In the iterative process, the particle is closing to the optimal direction continuously. When meeting the local optimum, all particles' velocity quickly is reduced to zero, the particle becomes stagnant, and the emergence of the phenomenon of premature converges.

The improved particle swarm algorithm.

The introduction to opposition-based learning and expansion model. PSO is a relatively new optimization algorithm that has been applied to a variety of problems. However, it may easily get trapped in the local optima when solving complex multimodalproblems. In addition, to enhance the global convergence, when producing the initial population, opposition-based learning method is employed. Since 2005, opposition-based learning is a fast growing research field in which a variety of new theoretical models and technical methods have been studied for dealing with complex and significant problems. When evaluating a solution x to a given problem, simultaneously computing its opposite solution will provide another chance for finding a candidate solution which is closer to the global optimum.

Opposite number: let $x \in [a,b]$be a real number. The opposite of x is defined by: $x^* = a+b-x$ (7)

Similarly, the definition is generalized to higher dimensions as follows:

Opposite point: let $X=(x_1,x_2,\ldots,x_N)$ be a point in a N-dimensional space, where $x_1,x_2,\ldots,x_N \in R$ and $x_j \in [a_j,b_j]$, $j \in 1,2,\ldots,N$. The opposite point $X^*=(x_1^*,x_2^*,\ldots,x_N^*)$ is defined by: $X_j^* = a_j+b_j-x_j$ (8)

By applying the definition of opposite point, the opposition-based optimization can be defined as follows.

Opposition-based optimization: let $X=(x_1,x_2,\ldots,x_N)$ be a point in a N-dimensional space (i.e., a candidate solution). Assume $f(x)$ is a fitness function which is used to evaluate the candidate's fitness. According to the definition of the opposite point, $X^*=(x_1^*,x_2^*,\ldots,x_N^*)$ is the opposite of $X=(x_1,x_2,\ldots,x_N)$. If $f(X^*)$ is better than $f(X)$, then update X with X^*; otherwise keep the current point X. Hence, the current point and its opposite point are evaluated simultaneously in order to continue with the fitter one. Opposition based initialization reduces the time of particle swarm optimization in a certain extent and improves the precision and efficiency of the particle swarm search.

Expansion model refers to the particle goes forward and keep the direction of motion, but the motion of a particle changed expansionary in space. For example, A particle from the point A (1,1,1) to B (2,2,2) in 3D space with mandatory expansion. The corresponding formulas of changing the position was: $x(i+1)=x(i)+x(i)$, $x(i+1)=x(i)+a*x(i)$ is used in this paper, where a is the expansion factor.

Multi threshold segmentation based on improved particle swarm optimization.

In this paper, the maximum entropy threshold method is introduced into the improved PSO algorithm. Concrete steps of the algorithm are as follows:

a)The first, all the particles are opposition based initialization, and then in the range of [0，255] random sets the initial velocity, the initial position, *pbest* and *gbest* of the particle.

b)Make the position of the integer, evaluate the fitness value of each particle, According to the principle of multi threshold segmentation based on maximum entropy, the formula (3) objective function is calculated for each particle. On the basis, if it is better than *pbest*, the current position replaced *pbest*, if at all the particles *pbest* is superior to *gbest*, *pbest* will be set in the new *gbest*.

c)Change the particle's velocity and position according to the formula (4) and (5), they are used to check the position and velocity whether they are within the allowed range. There is another situation, when the optimal solution is constant, which has a need for expansion on the location, using the expansion model presented in this paper.

d)According to the termination condition, if reaching the maximum number, the iterations stops; if not, then it returns to step 2 to iterative optimization.

Experimental results and analysis.

Using this algorithm to Lena image (256 × 256) segmentation, and compared to the maximum entropy segmentation, maximum between class segmentation, 2D maximum entropy threshold segmentation, and multi-threshold image segmentation based on the particle swarm of maximum between class method, As shown in figure 1. Figure 2, 3 are for the simulation results of the improved algorithm for high SNR and low SNR image segmentation and the additive noise segmentation. Table 1 is the comparison of several algorithms for the segmentation performance.

(a)The original image Lena (b)Maximum entropy image segmentation (c)Otsu segmentation.(d)The 2-D maximum entropy threshold segmentation (e) Multi threshold segmentation based on Particle swarm and maximum between class (f) This algorithm

Figure 1 The simulation results of several image segmentation algorithm

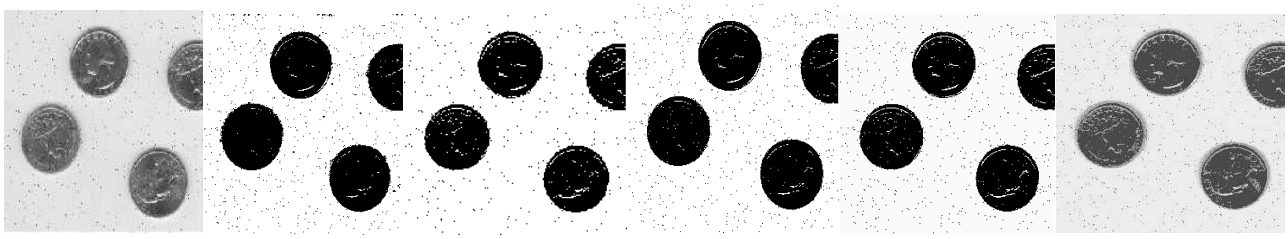

(a)The original image (b)Maximum entropy image segmentation (c)Ostu segmentatio(d)The 2-D maximum entropy threshold segmentation (e) Multi threshold segmentation based on Particle swarm and maximum between class (f) This algorithm

Figure 2 Several algorithms for high SNR image segmentation results

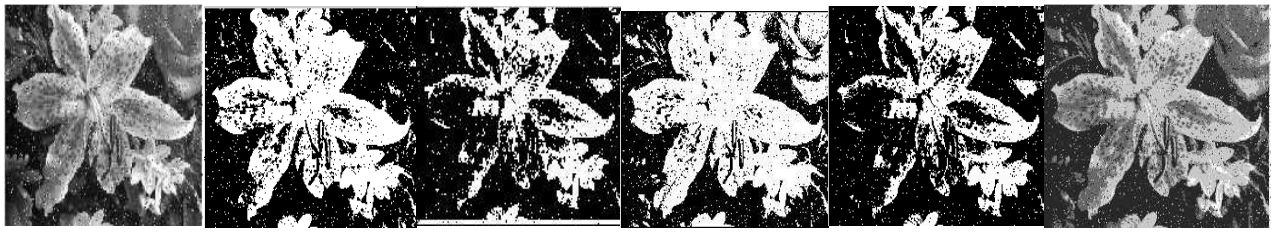

(a)The original image(b)Maximum entropy image segmentation(c)Ostu segmentation(d)The 2-D maximum entropy threshold segmentation (e) Multi threshold segmentation based on Particle swarm and maximum between class (f) This algorithm

Figure 3 Several algorithms in low SNR image segmentation results

Table 1 Comparison of several algorithms of segmentation performance

Figure (1)	The algorithm	The threshold	time (s)
Figure (b)	The maximum entropy threshold segmentation	137	0.991
Figure (d)	The 2-D maximum entropy threshold segmentation	94,100	103.812
Figure (e)	Multi threshold segmentation based on Particle swarm and maximum between class	116	2.203
Figure (f)	Multi-threshold image segmentation based on improved particle swarm optimization and maximum entropy method	3,95,120,164,263	1.490

It has been seen from the experimental results and table 1, Fig. 1 (b) in maximum entropy image segmentation by histogram to select the threshold value, although it has obtained the better effect of segmentation, but it tends to get high threshold. the segmentation effect is not good; Comparing Figure 2 and figure 3 Results, the traditional maximum between class segmentation graph (c) is the optimal threshold method a basis of uniformity measurement. This method of image for high SNR has greatly good segmentation effect, but for the low SNR is not ideal; Fig. (d) the image threshold segmentation of 2-D maximum entropy method is too long, it is difficult to meet the needs of real-time [7]; Graph (e) combining the maximum between class variance method with particle swarm optimization; for graph (c), maximum between class method have significant effects on the single threshold value segmentation. But for the multi-threshold segmentation, which is complexity and time-consuming; Map (f) represents 5 threshold segmentation, Figure (f) segmentation is more subtle than figure (e) segmentation, good robustness, and the particle swarm optimization, the speed of segmentation is improved, and the algorithm for the image (Fig. 2,3) of different signal to noise ratio have better segmentation effect, it has a wide application range.

Conclusions

Based on improved particle swarm multi-threshold segmentation, the characteristics of the particle swarm algorithm can be taken full advantages. The introduction of opposition-based learning, which is a better solution to excessive computing multi-threshold segmentation problem. Avoid the particle swarm falling into local minimum, the algorithm of this article introduced expansion model and combined with the maximum entropy algorithm. Avoid the maximum entropy threshold is too high, and make the split failure. Experimental results show that the proposed method is simple, fast, good robustness and easy to fall into local minima, etc. It is suitable for multi-threshold image segmentation.

Acknowledgements

The research is partially supported by Specialized Research Fund for the Doctoral Program of Higher Education, China (SRFDP) (No.20114101110005), and Science and Technology Research Key Projects of the Education Department, Henan Province, China (No.14A410001).

References

[1] Hui Zhang, Shengrong Gong, etc. Computer Science, 2012,9 (39) :1-4 In Chinese

[2] Frank Jiang, Michael R. Frater, Mark Pickering. School of Engineering and IT, The Univeristy of New South Wales.2012, IEEE978-1-4673-2181-5/12

[3] Huifeng Zhang, Weiping Wu, etc. Investigation Science and Technology, 2012, In Chinese

[4] Junna Zhang, Yunzhi Feng. LASER & INFRARED, 2013,5(43), In Chinese

[5] Ronghai Wang, Xuntao Xu. Ordnance Industry Automation, 2013,01(32), In Chinese

[6] Wei-feng Gao , San-yang Liu. Commun Nonlinear Sci Numer Simulat 17 (2012) 4316–4327

[7] Liping Zheng, Guangyao Li, Yun Bao. Improvement of grayscsle image 2D maximum entropy threshold segmentation method [C]//Logistics System and Intelligent Management 2010 IEEE International Conference, 3:324-328.

Advanced Materials Research Vols. 989-994 (2014) pp 3654-3657
© (2014) Trans Tech Publications, Switzerland
doi:10.4028/www.scientific.net/AMR.989-994.3654

Speech Enhancement Based on EMD and Wavelet Threshold in Noisy Environments

Ziqin Chen [2, a], Dexiang Zhang [1, 2, b], Daling Yuan [2, c]

[1] Key Lab. of Intelligent Computing and Signal Processing, Anhui University, Hefei 230039, China

[2] The School of Electrical Engineering and Automation, Anhui University, Hefei 230601, China

[a] 494993061@qq.com, [b] zdxdzxy@126.com (corresponding author), [c] dalingyuan@126.com

Keywords: Speech Enhancement, EMD, Wavelet Threshold, Noisy Environments

Abstract. Speech enhancement is crucial for speech recognition accuracy. How to eliminate the effect of the noise constitutes a challenging problem in speech processing. This paper presents a new technique for speech enhancement in a noisy environment based on the empirical mode decomposition (EMD) algorithm and wavelet threshold. With the EMD, the noise speech signals can be decomposed into a sum of the band-limited function called intrinsic mode functions (IMFs), which is a zero-mean AM-FM component. Then wavelet threshold of the IMF components can be used to eliminate the effect of the noise for speech enhancement. Experimental results show that the proposed speech enhancement by de-noising algorithm is possible to achieve an excellent balance between suppresses noise effectively and preserves as many target characteristics of original signal as possible.

Introduction

Reliable speech enhancement is a crucial preprocessing step in many speech recognition technologies and is essential in most analysis and synthesis system. The goal of speech enhancement is to identify the important voice of an audio segment for further processing, such as speech recognition, speech coding and communication [1].

Commonly the frequency band of noise is wide that of original signal is limited and mainly lies in low frequency bands. How to eliminate the effect of the noise constitutes a challenging problem in speech processing. Speech enhancement algorithms have been developing considerably. Many algorithms have been reported for solving the speech enhancement problem. In early speech-enhancement algorithms, Spectral subtraction (SS) method is to suppress the additive noise which has been the most widely used for the speech enhancement. However, the performance of speech enhancement by SS-based algorithms is not very satisfactory under noisy environments [2].

In this paper, we use a new technique called the empirical mode decomposition (EMD) has recently been introduced by Norden E. Huang et al. in 1998. This technique adaptively decomposes a non-stationary signal into sums of zero-mean amplitude modulation frequency modulation components. This method has quite good characters to analyze non-stationary signal and nonlinear signal. In most of the existing algorithms the Fourier transform or wavelet transform are used in signal decomposition. The speech decomposition is performed by fitting some predefined bases without satisfying its non-stationary nature. The idea behind EMD method is to decompose non-stationary signal into a number of basis function termed intrinsic mode functions. The speech signal is decomposed using EMD into the data adaptive bases up to the level of fundamental oscillations [3].

In this paper, a new speech enhancement method based on the empirical mode decomposition (EMD) algorithm and wavelet threshold is proposed. The basic principle of wavelet de-noising is to identify and zero out wavelet coefficients of the speech signal, which are likely to contain mostly noise. By identifying and preserving significant coefficients, wavelet thresholding preserves important high-pass features of the speech signal. We also compare this method with other traditional de-noising method, namely SS method, to validate the enhanced characteristics of this method to speech processing.

Empirical Mode Decomposition

The EMD methods will generate a collection of intrinsic mode functions. Given a signal $x(t)$, identify local maxima and minima, Then generate the upper envelope $x_u(t)$ and the lower envelops $x_l(t)$ by connecting the maxima and minima separately with cubic spline interpolation. Then the mean of the two envelops is denoted as:

$$m_1(t) = (x_u(t) + x_l(t))/2 \tag{1}$$

Thus, the first IMF $h_1(t)$ is obtained as:

$$h_1(t) = x(t) - m_1(t) \tag{2}$$

We can repeat this sifting procedure k times, until h_{1k} is an IMF, that is

$$h_{1k} = h_{1(k-1)} - m_{1k} \tag{3}$$

Then, designate h_{1k} as c_1

$$c_1 = h_{1k} \tag{4}$$

where c_1 is the first IMF of the original signal. We can separate $c_1(t)$ from the rest of the data by:

$$r_1(t) = x(t) - c_1(t) \tag{5}$$

Note that the residue $r_1(t)$ still contains some useful information. We can therefore treat the residue as a new signal and apply the above procedure to obtain:

$$r_N(t) = r_{N-1}(t) - c_N(t) \tag{6}$$

The sifting process will be continued until the final residue $r_N(t)$ is a constant, a monotonic function, or a function with only one maxima and one minima from which no more IMF can be derived. Combining the equations in (5) and (6) yields the EMD of the original signal:

$$x(t) = \sum_{i=1}^{N} c_i(t) + r_N(t) \tag{7}$$

The result of the EMD produces N IMF and a residue signal. It is observed that higher order IMFs contain lower frequency oscillations than that of lower order IMFs. If we interpret the EMD as a time-scale analysis method, each IMF reflects the characteristic of each scale, which shows the intrinsic mode characteristic of non-stationary and nonlinear signal.

Choice of Thresholding

In wavelet de-noising, it is common practice to use a soft thresholding function, where the coefficient is slightly reduced even when it is not set to zero. Under certain statistical assumptions, soft thresholding can result in slightly greater noise reduction [4]. The general soft-thresholding function is defined by

$$W_{out} = \begin{cases} \left(\dfrac{W_{in} - T_1}{\max(W_{in}) - T_1}\right)^P W_{in} & W_{in} > T_1 \\ 0 & |W_{in}| \le T_1 \\ \left(\dfrac{W_{in} + T_1}{\min(W_{in}) + T_1}\right)^P W_{in} & W_{in} < -T_1 \end{cases} \tag{8}$$

Its function is also illustrated in Fig. 1.

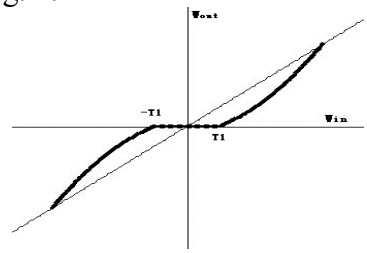

Fig. 1 Soft-thresholding function $0 \le p \le 1$, when p=0, function is corresponding to hard threshold.

The best thresholding in a wavelet basis is achieved when the threshold is adapted spatially and with scale. Here, we use a scale-adapted threshold that is proportional to an estimate of the noise standard deviation. The proportionality factor is explored experimentally. The threshold level in each sub-band is selected as $\sigma_j \sqrt{2\log N_i}$, where σ_j is the median absolute value of the coefficients in the sub-band and N_i is the length of the coefficients. As to white noise, its power is mainly concentrated in first level detail coefficient, and the noise level decreases with the increase of j , so the mean square white noise can be estimated with the each level coefficient $\sigma_j = \beta \cdot median(|D_{j,k}|)$, where β is a constant.

Experiments and Results

The experiment signal is a pure speech signal is shown in Fig.2. The sampling frequency is set to 10 kHz with 16-bit amplitude resolution. The noised experiment data is the pure speech signal in Figure 1 corrupted by white noise and SNR=7.5dB. The noised speech signal is shown in Fig. 3.

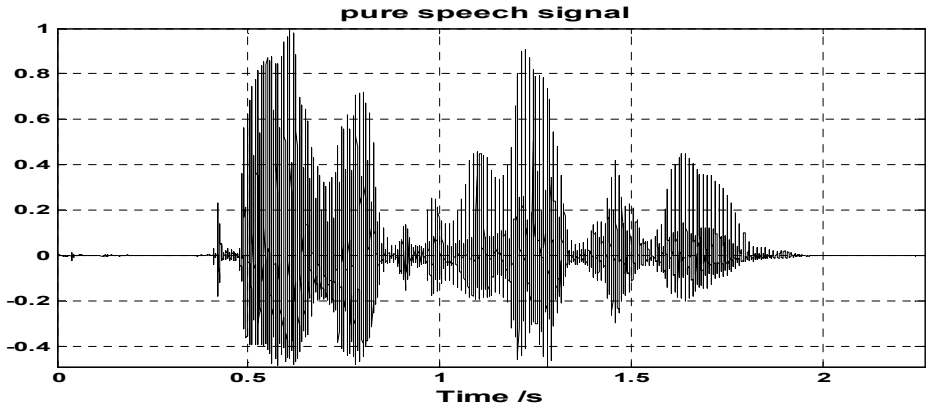

Fig. 2 The pure speech signal

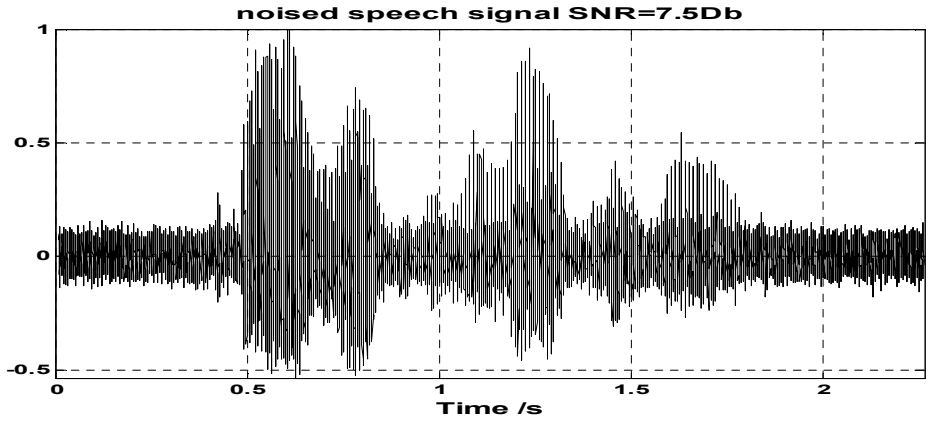

Fig. 3 The noised speech signal corrupted by white noise and SNR=7.5dB.

The noise removal procedures are as follows: (1) Decompose the noised original signal to IMFs by the EMD method; (2) Remove the IMFs whose content belongs to the noise on the base of the sudden increase of its amplitudes; (3) Reconstruct the signal with the rest of IMFs.

Figure 4 shows the result using the spectral subtraction speech enhancement method. Figure 5 shows the result using the proposed speech enhancement method. The experimental results illustrate the newly proposed speech enhancement method is effective.

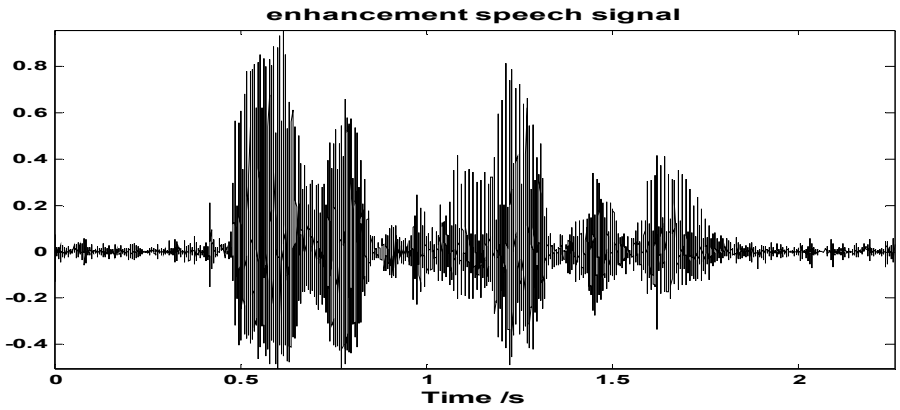

Fig.4. The result using the spectral subtraction speech enhancement method

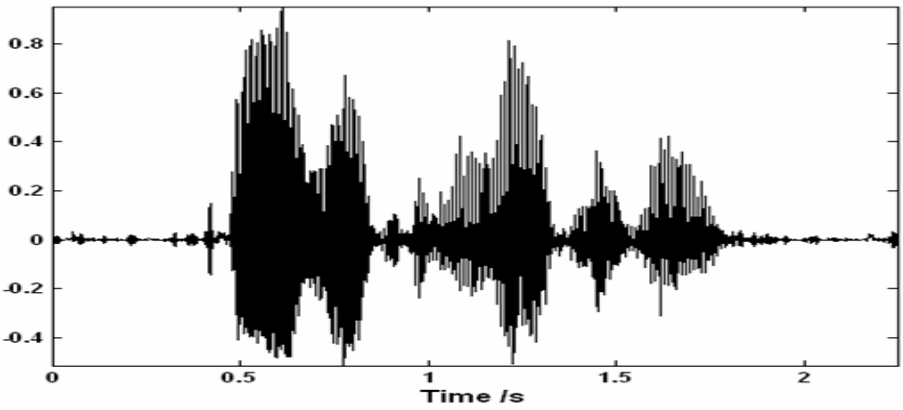

Fig.5. The result using the proposed speech enhancement method

Conclusion

In this paper, a method based on the empirical mode decomposition (EMD) algorithm and wavelet threshold is proposed to speech enhancement of a speech signal embedded in noise. The EMD is well adapted to non-stationary signals and has an excellent time resolution. The EMD and wavelet threshold gives good speech enhancement of a speech signal corrupted with noise. Our experiments show the proposed method can accurately extract the speech signals in differently background noises.

Acknowledgment

The support from the Chinese National Science Foundation Grant (No.61272025) for this research is gratefully acknowledged.

References

[1] G. Tanyer, H. Ozer, IEEE Trans. Speech Audio Processing, Vol. 8 (2000), p. 478
[2] Y.ephfsim, D. Malah, IEEE Transactions on Acoustics, Speech, and Signal Processing, Vol. 32(1984), p. 1109.
[3] N. E. Huang, Z. Shen and S. R. Long, Proceedings of the Royal Society London A, Vol. 454 (1998), p. 903
[4] S. Mallat, IEEE Trans. Pattern Anal. Machine Intell. Vol. 11 (1989), p. 674.
[5] Zhang dexiang, Gao Qingwei, Chen Jun-ning. Journal of Electronic Science and Technology of China, Vol. 4 (2006), p. 39-42

Advanced Materials Research Vols. 989-994 (2014) pp 3658-3662
© (2014) Trans Tech Publications, Switzerland
doi:10.4028/www.scientific.net/AMR.989-994.3658

Study of SC-FDMA reduce PAPR based on the power line carrier communication

Gangjun, Gong [1, a], Dangke Hao[2,b], Ye, Zhang[3,c], Jun, Lu [4 d], Gang ,Xu[5,e]

[1,2,4,5] School of Electrical and Electronics Engineering, North China Electric Power University, Beijing102206, China

[3] Sichuan province electric power company , Chengdu610041, China

[a] gonggangjun@126.com, [b]hdk613@163.com,[c]zhangye@126.com, [d]269380393@qq.com, [e]xugang@ncepu.edu.cn

Keywords: peak to mean ratio; OFDMA; SC-FDMA; uplink; emission efficiency

Abstract: In order to reduce peak to average power ratio (PAPR) higher of OFDMA problems, this paper proposes a power line communication system based on SC-FDMA model, compared this model and OFDMA system on peak to average, the same power with the throughput, the same throughput required simulation sub carrier number of needed power and power rate users; The results show that: when introduced the SC-FDMA into the power line communication, can effectively reduce the system PAPR, the terminal can obtain better emission efficiency.

Introduction

Orthogonal frequency division multiplexing access (OFDMA) as the current mainstream technology of power line communication system, Frequency selective fading caused by insufficient to overcome effectively in communication system, making full use of the spectrum, favored by more and more people. But the high PAPR makes the transmission efficiency of the system is limited. In the downlink power line communication system, transmitting the downlink signal collector, a multi-carrier technology, can greatly improve the system spectrum utilization rate and the data rate, which can make up for the high cost brought by PAPR power amplifier; In the uplink, the terminal as the sender, and the State Bureau of quality and technical supervision stipulates the power terminal power consumption standard, namely the acquisition terminal under normal power consumption should be less than 1W[1]; This requires the terminal to ensure transmit power at the same time to reduce the power consumption of the terminal as far as possible, However, high PAPR make this requirement becomes more difficult, At the same time, power requirements increase, also increase the cost and difficulty of realization of terminal equipment. In order to reduce the high PAPR value of this problem, many scholars put forward different solutions: The Article [2] put the shear and compression and expansion to reduce the PAPR value, but the distortion caused by the nonlinear signal; Document [3] proposed to reduce the PAPR value by signal encoding, but there are a lot of redundancy in the encoding process, which makes the communication rate lower; The Article [4] put the partial transmit sequences (PTS) to reduce the PAPR value, this sequence with minimal PAPR to send, it is easy to cause information loss. The reducing PAPR method based on the problems, according to LTE uplink communication technology schemes, the SC-FDMA technology is introduced to the PLC uplink.

At last, in order to show the efficiency of both SC-FDMA and OFDMA for uplink system in a power line communication system, In this paper, I simulated include: the characteristics of the PAPR, the terminal sends the same power resulting throughput, eNodeB need to achieve the same throughput required power and the same power are simulated with throughput .

Low voltage PLC communication system

Low PLC topological structure

Low voltage PLC communication network is to set up the communication network between concentrator and communication terminal, this will make the communication link between concentrator and communication terminal to maintain smooth. In the low-pressure side of the power line carrier communication, a transformer station in the region, and sometimes requires some communication terminal concentrator acts as a relay node can communicate with all communication between the terminals within the network. Topology shown in Fig 1, it is the most common single relative communication terminal network structure. The user through the PLC Modem connected to the indoor power socket[5], through the PLC connection with the building distribution transformer terminal PLC master device gateway, complete access to the last one hundred meters. Users only need to install a PLC-Modem, do not dial, receive and send Internet messages can be online.

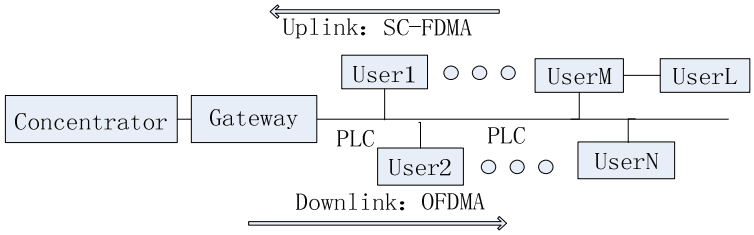

Fig 1 Connection diagram of user system

The PLC uplink and downlink communication technology

At low PLC topology, if multiple users at the same time to send the command of concentrator, the concentrator will need to provide a lot of information to the user in the circumstances allow, which requires the downlink data transmission rate of the massive. Due to the PLC communication system in the future and to satisfy users and concentrator information interaction, complete daily internet service business, it's for uplink data transmission ability put forward higher requirements. OFDMA technology scheme can realize the characteristic of orthogonal between users and the bandwidth strong extensibility, resistance to the decline, and can improve the multiuser diversity gain. But the existence of high PAPR value makes the system power utilization limited. For the downlink communication, concentrator as the transmitter, can tolerate higher cost and power amplifier. But in the uplink communication, terminal capacity is limited, especially the transmit power constraint, which makes the selectivity in the uplink transmission technology in the presence of great influence. The higher PAPR, the transmitting end to increase the ADC and DAC complexity, reduce the efficiency of RF power amplifier to meet the communication requirements, which eventually led to the transmitter power amplifier cost and power consumption increase. For the majority of end-users, this is intolerable. In LTE communication system, SC-FDMA system as the wireless uplink technology is feasible, then compared to the power line carrier technology of cable system also can be applied to technology. Therefore, this article will be to overcome the SC-FDMA technology as power line communications technology solutions downlink high PAPR problem, this program can effectively reduce the cost and power consumption of the transmitter power amplifier.

Principles reduce peak to average ratio

Peak to average ratio is defined

PAPR mainly characterize the magnitude of the peak and the average ratio between the transmitted signals. The mean PAPR calculation formula is as follows:

$$PAPR(\mathrm{dB}) = 10\log_{10}\frac{\max\limits_{0\le n\le N-1}\{|x_n|^2\}}{E\{|x_n|^2\}} \quad (0 \le n \le N-1) \tag{1}$$

In the uplink, SC-FDMA system is a frequency domain generated by the method, i.e., by the DFT-spread OFDMA system. DFT extension OFDM technology is the essence of IFFT in processing before to the discrete Fourier transform of expanding the system, the adoption of DFT processing, signal from time domain to frequency domain, and then through IFFT module from frequency domain to time domain. Since each user signal waveform is similar to single carrier, thus being regarded as single carrier technology. Because each user sends a signal waveform is similar to that of single carrier, thus being treated as a single carrier technology. The single carrier technology makes Max $\{|x_n|^2\}$ values of the formula (1) in the low formula, so that the peak to average relatively low.

In downlink link, the OFDMA signal in the OFDMA system is composed of multiple independent after addition of subcarrier signal modulation, and the synthesis of such signals is likely to have larger peak power, namely the relative formula 1 has a larger Max $\{| x_n|^2 \}$item, therefore OFDMA system has a larger average peak ratio.

Design and Simulation of the system model

Simulation design

Equipped with four users, their rate is Vp=[150, 150, 200, 200], which the top two real users, two for non real time users. In this paper, I am using MATLAB simulation both OFDMA and SC-FDMA in the system. Parameters are set as follows: Power is 10mW; the subcarrier number is 512; BER: real-time user of 10-4, non-real-time user 10-6; SNR: real-time user 5.4827, non-real-time user of 8.4213; Using equal power allocation algorithm; The DFT points to 16; choose QPSK modulation; For SC-FDMA centralized mapping, simulation performed 100 consecutive times.

Research and analysis of simulation results

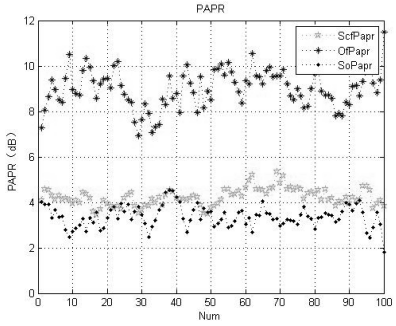

Fig 2 PAPR Compare

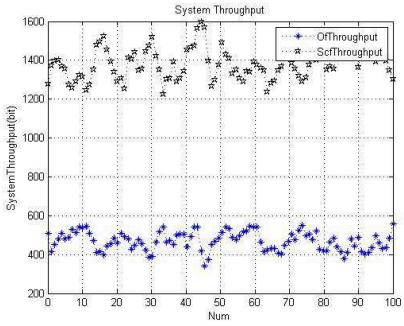

Fig 3 System Throughput Compare

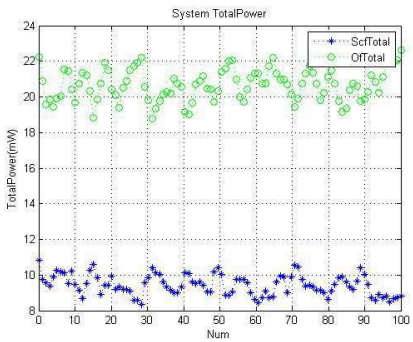

Fig 4 System Total Power Compare

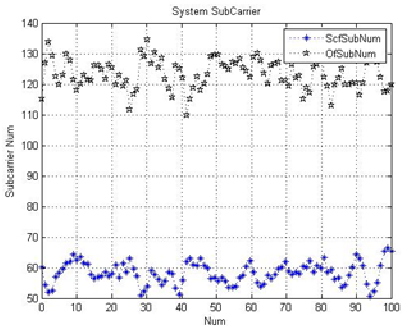

Fig 5 32 bits required subcarrier number

The OFDMA and SC-FDMA two PAPR value of the system are compared, the results as shown in Fig 2; The PAPR value of SC-FDMA is 4.2dB significantly less than the mean value of OFDMA system9dB, and compare with the baseband signal PAPR is relatively close, the value is slightly more than the value of PAPR baseband signal. Therefore, the SC-FDMA system can effectively improve the utilization rate of power communication system. Compared with SC-FDMA, the

baseband signal values of PAPR, OFDMA higher than about 4.8dB, this is mainly because the OFDMA is directly through the IDFT transform, achieve multiple sub carrier modulation, sub carrier super imposed parallel output; while the SC-FDMA is through a DFT-IDFT transformation, the two transformation, each point on the power change can be considered to be offset, this is because the transformed output as the input symbol or as a weighted superposition of input symbols, making SC-FDMA with low PAPR characteristics of single carrier unique.

The simulation with power under the system throughput

With the same power how throughput is in system as shown in Fig 3. Based on the equal power allocation algorithm, the 10mW resource is allocated to the 512 sub carrier, then according to the needs of users, the subcarrier allocation. The simulation results show that: in the premise of transmit power and subcarriers is certain, SC-FDMA per second throughput for 1400bit, while the OFDMA system per second throughput for 500bit, the total throughput of SC-FDMA system was significantly higher than that of OFDMA system throughput. Therefore, the power system using SC-FDMA was higher than that of the OFDMA system, the transmit power, the obtained throughput.

The simulation system under the same throughput of transmission power

When 100 bits as the output of the same throughput, and SC-FDMA on the power required to send the OFDMA system simulation, the simulation results shown in Fig 4. The results showed in Fig 4: 1500 bits per second to complete a certain need for SC-FDMA systems around 9.8087mW, while the OFDMA system requires about 20.1358mW; These results indicate that the same throughput requirements, SC-FDMA system requires far less than OFDMA transmission power system, further demonstrates the comparison with OFDMA systems, SC-FDMA uplink power communication system, the more efficient power utilization, low power consumption characteristics of the terminal.

The same rate under the same power required by the user subcarrier simulation

Set power source provided for the 10mW, the system in accordance with the equal power allocation algorithm to assign each user rate, the rate of each user to achieve 150bit/s, the simulation results are shown in Fig 5. It shows: the SC-FDMA system to provide users with sub carrier to about 58 to meet the needs of its rate, while the OFDMA system needs to provide sub carrier to about 128 to meet its rate to the user, the number of subcarriers for each user of the former than the latter reduces 70 subcarriers. Therefore, the SC-FDMA system compared to the OFDMA system so that the system resource utilization rate higher.

Conclusions

In this paper, the simulation of different power required for the PAPR OFDMA and SC-FDMA these two kinds of the value of the system, under the same power system with different throughput, throughput and power system with the same rate of case the user required a subcarrier number. The simulation results show that: compared with OFDMA, the SC-FDMA system has a number of sub carriers lower PAPR, under the same power, high throughput with low power and throughput under analogous rate less can meet the needs of users, the same rate etc..According to the characteristics of power line communication, further demonstrates the SC-FDMA system into the necessity and superiority of power line communication.

Acknowledgements

The work was supported by a general program from the Basic Science Research Fund of Central Un iversities (No.JB2014048).

Reference

[1] Power carrier meter reading system standard (ver2.0 repair).2003.3
[2] Han Seung Hee and Lee Jae Hong. An overview of peak-to-average power ratio reduction techniques for multicarrier transmission. IEEE Wireless Communication, 2005, 12(2): 56–65
[3] Davis J A and Jedwab J. Peak-to-mean power control and error correction for OFDM transmission using Golay sequences and Reed-Muller codes. Electronics Letters, 1997, 33(4): 267–268
[4] Kim Kang S G and Joo E K. A novel sub block partition scheme for partial transmit sequence OFDM. IEEE Trans. on Broadcasting, 1999, 45(3): 333–338
[5] Lai Zhengtian. Channel characteristics Analysis and Simulation of Power Line Carrier Communication System [J]. Power system communication.2010,31（216）：39-42.

Advanced Materials Research Vols. 989-994 (2014) pp 3663-3666
© (2014) Trans Tech Publications, Switzerland
doi:10.4028/www.scientific.net/AMR.989-994.3663

An Improved Image Stitching Algorithm

LI Dan[1,2,a]

[1]Xuzhou Institute of Technology, Xuzhou, China

[2] Xuzhou Machine Vision Application Engineering Technology Research Center, Xuzhou, China

[a]lidanonline@163.com

Keywords: stitching; phase correlation; SIFT; feature vector

Abstract: Proposed a new stitching algorithm to suit for coal mine. Cross-power spectrum phase information is used to coarse matching fast and overlapping regions can be found. Invariant features are extracted by using the dimensional reduced SIFT algorithm- sample principal component analysis. RANSAC combined with iterative L-M nonlinear optimization algorithm can improve projection matrix. New algorithm can improve the matching efficiency, and it's suit for coal mine environment.

1 Introduction

Image stitching technology is a hot research in computer vision. At present, to get the bigger perspective picture, most use the annular panoramic lens, fisheye camera and image mosaic methods [1, 2]. The annular panoramic lens and the fish eye camera will produce distortion, and has a low resolution, high cost. Image stitching takes many pictures photoed by ordinary machine according to features, you can get the big picture perspective and it has good market prospects. For coal and other low-light, high noise and blur complex environment, direct mosaic effect is not ideal, in order to adapt to the complex environment, it need an anti-light, noise, high speed, high precision stitching algorithm.

In this paper, First, using phase correlation algorithm reduced the image feature points overlapping ranges. Next, the sample principal component analysis [3] method reduced the dimensions of SIFT(Scale-invariant feature transform)[4] algorithm with 128 vector and improved the computing efficiency. Last, corresponding matching points of two images selected by SIFT combined with RANSAC (Random sample consensus) [5] and L-M (Levenberg-Marquardt) [6]to establish projection model for stitching.

2 Phase coarse matching

Phase correlation algorithm can quickly rough estimate overlap regions of image. Since the signal's characteristics in Fourier transform, using phase correlation algorithm cross power phase information can achieve image registration. This method is less dependent on the gray scale information, illumination changes well and noise robustness. Algorithm is as follows:

Let two images are $p_1(x,y)$, $p_2(x,y)$, its translational motion model is $p_1(x,y)=p_2(x-\Delta x,y-\Delta y)$, Δx, Δy are translation variables. After Fourier transform, getting $P_1(u,v), P_2(u,v)$. According to the shift characteristics:

$$P_2(u,v)=e^{-j2\pi(u\Delta x+u\Delta y)}\cdot P_1(u,v) \tag{1}$$

Image cross power spectrum is:

$$\frac{P_1^*(u,v)P_2(u,v)}{|P_1^*(u,v)P_2(u,v)|}=e^{-j2\pi(u\Delta x+u\Delta y)} \tag{2}$$

P_1^* represents a conjugate of P_1. Impulse function can be obtained after inverse Fourier transform:

$$F^{-1}[e^{-j2\pi(u\Delta x+u\Delta y)}]=\delta(x-\Delta x,y-\Delta y) \tag{3}$$

Wherein the peak size of impulse function represents a number of correlation between P_1 and P_2. Peak represents range of [0,1].

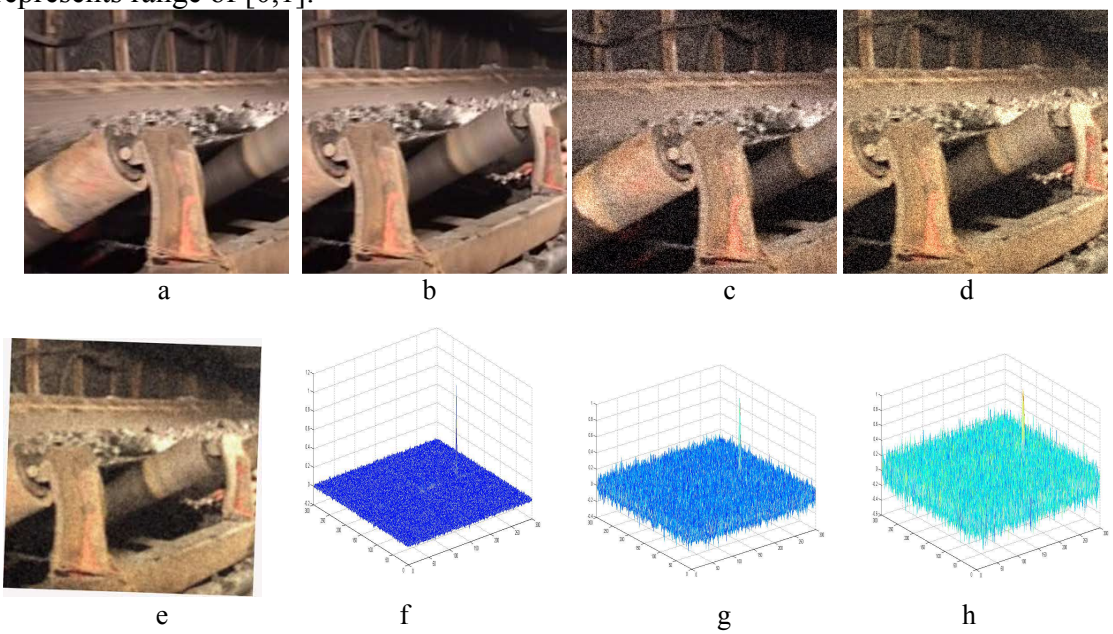

Fig.1 Phase correlation matching

In Fig.1, a and b are original images, f is the distribution of the impulse energy function after a and b normalized. The number of the overlapping area size determines the size of the peak. Image position determines the translational motion parameters. C is a plus Gaussian noise with variance 10. D is b plus noise and light meanwhile. G is impulse function energy distribution of c and d. Single peak of impulse function turns into scattered small peaks, and peak value remains stable. On the basis of d, e increased Gaussian blur, rotation effects. H is impulse function energy distribution of c and d. As can be seen, the peak is still very robust.

Phase correlation algorithm has high efficiency, but not high accuracy when estimating parameters. Therefore, as an initial registration, then we need to further take advantage of the feature points to establish accurate matching.

3 Invariant Feature Extraction

For the occlusion, blur, scale and lighting change and other issues in the environment, currently, there is no a detection operator can solve all problems.

3.1 SIFT dimension reduction

SIFT algorithm uses multi-scale transform to find the extreme points in the scale space by extracting the feature point position and direction to make eigenvector keep unchanged to accommodate various affine transformation. SIFT algorithm has 128-dimensional feature vector affecting the real-time monitoring system. This paper will combine SPCA (sample principal component analyse) and SIFT algorithm to reduce the dimensions.

N represents the number of feature points， p represents vectors for each feature point. Through following sample principal component analysis, it can reduce the dimensions for the vectors interrelated.

S1： $x_i=(x_{i1},x_{i2},...,x_{ip})^T, i=1,2,...n.$ is a sample of $X=(X_1,X_2,...,X_n)^T$， capacity is n， sample covariance matrix is expressed as:

$$\Sigma=\frac{1}{n-1}\sum_{k=1}^{n}(x_k-\bar{x})(x_k-\bar{x})^T \tag{4}$$

Where $\bar{x}=(\bar{x}_1,\bar{x}_2,...,\bar{x}_p)^T$， $x_j=\frac{1}{n}\sum_{i=1}^{n}x_{ij}, i=1,2,...p$.

S2：Eigenvalue of the covariance matrix is $\hat{\lambda}_1\geq\hat{\lambda}_2\geq...\geq\hat{\lambda}_p\geq 0$, orthogonal unit eigenvector is

$\hat{e}_1, \hat{e}_2, ..., \hat{e}_p$, $\hat{e}_i = (\hat{e}_{i1}, \hat{e}_{i2}, ..., \hat{e}_{ip})$, $\hat{e}_i \hat{e}_i^T = 1$, $i = 1, 2, ...p$. (5)

S3：The i-th sample main component is：

$$y_i = \hat{e}_{i1} x_1 + \hat{e}_{i2} x_2 + ... + \hat{e}_{ip} x_p \quad (6)$$

$i = 1, 2, ...p$, substituting observations i， $x_k = (x_{k1}, x_{k2}, ..., x_{kp})^T, k = 1, 2, ...n$, get the i-th principal component scores $y_{ki} (k = 1, 2, ...n)$ of y_i .

S4：Sample covariance of y_i and y_j is 0, where i is not equal to j， $\sum_{i=1}^{p} \hat{\lambda}_i$ is the total variance of the sample， $\hat{\lambda}_i / \sum_{i=1}^{p} \hat{\lambda}_k (i = 1, 2, ...p)$ is the i-th sample principal component contribution rate of x , $\sum_{i=1}^{m} \hat{\lambda}_i / \sum_{k=1}^{p} \hat{\lambda}_k$ is cumulative m sample principal component contribution rate.

As Fig.2 shows, experiment selected an locomotive image of 300 * 300 underground. Feature points extracted by the SIFT algorithm. Select the area surrounding the feature points with 12 * 12 to describe them. Sample characterization vectors are gray values of pixels within the region to analyze the principal component of samples.

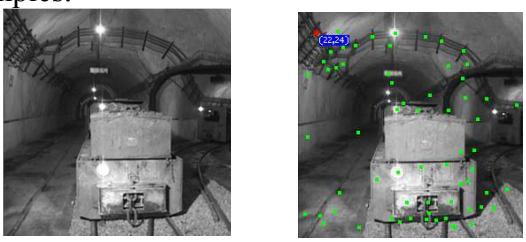

a. Locomotive b. Feature points

Fig.2 Feature points generated

Table 1 12 * 12-dimensional feature vector principal components contribute

Principal component	Eigenvalues	Difference between Eigenvalues	Principal component contribution rate (%)	Cumulative contribution rate (%)
1	4.41439183	2.36945738	0.4013	0.4013
2	2.04493446	0.80303153	0.1859	0.5872
3	1.24190293	0.29798645	0.1129	0.7001
4	0.94391647	0.22911305	0.0858	0.7859
5	0.71480343	0.29822424	0.065	0.8509
6	0.41657919	0.01050982	0.0379	0.8888
7	0.40606937	0.10042222	0.0369	0.9257
8	0.30564715	0.06445848	0.0278	0.9535

Fig.2 contains feature points generated by locomotive. As can be seen from Table 1, even though dimensions of feature vectors up to 144, but most information of feature vectors can be described by the above eight principal components. So it's no less to use the unrelated first few principal components to describe original image.

3.2 Accurate extraction and matching

To further eliminate error matched pairs and use exact matched pairs to establish image transformation matrix, the paper combined RANSAC algorithm of the angle, the length filter for exact match. Select the initial matching features, using the internal points which errors are less than the threshold point. Repeat random sampling within a set of internal points, when the number of the two set of points nearly identical, recalculate the estimate the model parameters. Using L-M algorithm to iterative and minimize the error function, then get the exact match pairs.

As Fig.3 below, a, b are original images of locomotive, the number of initial SIFT matching points are 128. Through the image transformation relations between a and b , transformation matrix H is obtained.

$$H = \begin{bmatrix} 0.9889 & 0.4865 & 30.9451 \\ 0.4167 & 0.9975 & 5.6196 \\ 0.0001 & 0.0001 & 1 \end{bmatrix}$$

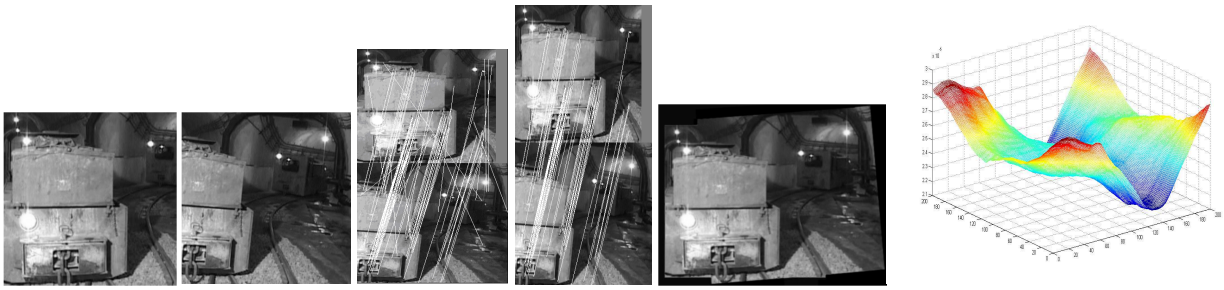

a b c d e f

Fig.3 Stitching trellis

Seen from the transformation matrix H, comparing to the first image, the size of the second image has a slight change, and exist the situation of displacement and rotation. Exact match contrast as shown in Fig.3.

Table 3 Match results

Dimension	Stitching Time	Match Points	Correctly matching points	Matching rate
9	0.83s	64	61	95.31%

In Fig.3, c, d are the initial and exact matching results. Can be seen, many error points removed by exact match. E is the stitching result of using sample principal component 9-dimensional exact match, f is the mesh representation. Because 9-dimensional feature vector rarely occupy storage space, matching efficiency has been greatly improved. Fig.3 shows that while enhancing systems real-time performance, it does not affect the matching accuracy.

4 Conclusion

Proposed a new stitching algorithm for the widespread existence of low resolution, blur, large noise, lighting changes characteristics in complex underground environment. Cross-power spectrum phase information is used to coarse matching fast and overlapping regions can be found. Invariant features are extracted by using the dimensional reduced SIFT algorithm- sample principal component analysis. RANSAC combined with iterative L-M nonlinear optimization algorithm can improve projection matrix. Experiments show that the new algorithm has a robust characteristic and stitch accurately and smoothly, it is better to grasp the overall message.

References

[1] Zhu Haijiang, Li Shigang. 2D pattern vs.surrounding 3D pattern for fisheye camera calibration [J]. Chinese Journal of Scientific Instrument, 2008, 29(7).

[2] Li Dan, Research on Object Detection and Tracking Technology in Coal Mine Video,[D]. Doctoral Dissertation of China University of Mining and Technology, 2011.

[3] Wang Kejun, Zou Guofeng, Zhang Jie. Analysis of the influence of SPCA parameters on the recognition of a single sample face [J]. CAAI Transactions on Intelligent Systems, 2011,6(6).

[4] Lowe D G. Distinctive Image Features from Scale invariant Key points[J]. International Journal of Computer Vision, 2004, 60(2).

[5] Zhou Jun, Chen Leiting, Li Yanmei. Optimize preview model parameters evaluation of RANSAC [J]. International Journal of Advancements in Computing Technology, 2012, 4(16).

[6] He Xiang. L-M neural network for data mining of oil saturation[C]. International Conference on Machine Learning and Cybernetics, 2009.

Advanced Materials Research Vols. 989-994 (2014) pp 3667-3670
© (2014) Trans Tech Publications, Switzerland
doi:10.4028/www.scientific.net/AMR.989-994.3667

Speech airflow and air-pressure signal editing platform

Shiliang Lv[1, a], Yasheng Jin [2, b]

[1] Key Lab of China's National Linguistic Information Technology, Northwest University for Nationalities, Lanzhou, China

[2] Key Lab of China's National Linguistic Information Technology, Northwest University for Nationalities, Lanzhou, China

[a]shilianglv@126.com, [b]jinysh550808@sohu.com,

Keywords: The speech signal; Airflow and air pressure signal; MATLAB; Analysis platform.

Abstract. Experimental phonetics development to today has undergone a long and complicated process. The field of study from the acoustic analysis of expansion to the physiological and perceptual field. Speech aerodynamics signal is one of the most important physiological signal language research, plays an important role in human phonation process. Air pressure signal as an important physiological signal, which has great significance to the study of speech physiology, mainly through speech aerodynamics equipment acquisition. In this paper, according to the need of research, established by MATLAB program analysis platform, can be edited on the speech, the airflow and pressure signal is better, which is more suitable for speech research.

Introduction

Experimental phonetics through long-term development has undergone a long and complicated process, from previous research in the field of acoustic parameters and characteristics are analyzed to study the physiological and perceptual voice multi-modal and gradually extended to the field of multi-modal speech research as the main content. By using various experimental instruments, acquisition and analysis of physiological signals to various speech. Study of speech from speaking to listen to the entire mechanism and principle, and properties of physiological, physical and psychological aspects of speech signals. And how to use these attributes to explain linguistic problems is the main objective of speech and voice multimodal study[1].

With the development of science and technology, voice multimodal research methods are constantly updated, more and more instruments are introduced into this area, from the early laryngoscopy, oscilloscopes, acoustic spectroscopy and X-ray, and now Airflow equipment (PAS6600), Electropalatography (EPG), Electronic glottis instrument (EGG), electromyography (EMG), electroencephalogram (EEG), respiration, nuclear magnetic resonance (MRI), etc. [2]. These various physiological signal acquisition instrument air pressures as the air flow signal, the voice signal and the EPG signal, also reveal more speech production mechanism is extremely characteristic. In the speech production process flow plays a vital role in generating speech without the participation of lung airflow, and airflow from the lungs, is bound to generate pressure. With the development of experimental phonetics, air flow and air-pressure parameters is also used in acoustics, speech recognition, speech synthesis, voice typology and other aspects of the progress to provide a great help[3].

At present, air pressure collection equipment produced for the U.S. KAY audible speech aerodynamics system, the signal analysis and processing are the main device supporting a series of software. Physiological research is mainly used for the series of software, but cannot meet the current needs of phonetics. And the software of KAY company to save the file as a NSP file, the existing speech analysis software cannot operate on the file format. Therefore, for the development of a set of speech multimodal analysis of airflow and pressure signal platform is necessary. This paper analyzes the NSP files and WAV file formats, combining voice multi-modal studies are needed to achieve NSP file and convert WAV files. Also can be used for signal processing method of analysis and research

the airflow and pressure signal, for the future research and provide the technical foundation for the development of analysis platform [4].

The Nsp Signal Acquisition and Analysis

2.1 Acquisition Equipment

The phonetic study widely adopted by America KAY company production of the sounds of speech air dynamic system (Phonatory Aerodynamic System 6600). The system external hardware module comprises a handheld device with both hands handle (handheld by speakers in the process of data collection), airflow mask, pressure sensor, test tube and a microphone to ergonomic criteria together. The signal conditioning, filtering and data sampling are in line with the strict standards of sound and aerodynamic data acquisition [5].

Before the signal acquisition, signal conditioning and data sampling equipment, in strict accordance with the standards of debugging, to calibrate microphone fixed position. In the acquisition process in order to ensure the accuracy of the pressure signal, entrance pipe is arranged in the pronunciation of population, and keep the mask and facial mask tightly to ensure no leakage, and then the signal acquisition after simple pronunciation training.

2.2 The NSP format file

Because there are few readily available information on the NSP file format specific introduction, we adopted UltraEdit software to open files to search matching to determine the file header and the data part. Figure 1 is the code above the input signal, shown below is the code without input signal. By contrasting the code file, the code of two signal file, the first eight lines of roughly the same. The ninth line began to have input file assumes the regular data are airflow and pressure signal. Without input signal data file because it is no empty file, then the code is 0. To exclude the impact time and file size and other parameters, we can draw the conclusion: airflow pressure signal NSP file header for the first eight rows. That is the first eight rows of data is the NSP file header information, ninth row start to finish for the signal data of NSP file.

0	1	2	3	4	5	6	7	8	9	a	b	c	d	e	f
46	4F	52	4D	44	53	31	36	12	E0	0C	00	48	44	52	38
2C	00	00	00	44	65	63	20	30	35	20	31	36	3A	33	31
3A	34	30	20	32	30	30	39	22	56	00	00	42	25	02	00
EC	0E	FF	FF	21	02	01	02	FF	FF	FF	FF	FF	FF	FF	FF
50	41	53	5F	28	00	00	00	01	0B	38	7C	FF	FF	FF	FF
33	33	33	33	33	33	3A	40	4E	6F	20	50	61	74	69	65
6E	74	00	00	30	EB	3D	00	01	00	00	00	03	00	00	00
4E	4F	54	45	01	00	00	00	00	00	53	44	41	5F	84	4A
04	00	03	00	03	00	03	00	04	00	04	00	03	00	03	00
03	00	03	00	03	00	03	00	03	00	02	00	03	00	03	00
04	00	03	00	03	00	03	00	03	00	03	00	04	00	04	00
04	00	04	00	04	00	04	00	04	00	03	00	03	00	03	00
0	1	2	3	4	5	6	7	8	9	a	b	c	d	e	f
46	4F	52	4D	44	53	31	36	12	E4	05	00	48	44	52	38
2C	00	00	00	53	65	70	20	32	34	20	31	30	3A	32	38
3A	33	34	20	32	30	31	30	22	56	00	00	42	FB	00	00
4F	00	FF	FF	02	00	03	00	FF	FF	FF	FF	FF	FF	FF	FF
50	41	53	5F	28	00	00	00	01	0B	38	7C	FF	FF	FF	FF
33	33	33	33	33	33	3A	40	4E	6F	20	50	61	74	69	65
6E	74	00	00	48	3E	F6	00	01	00	00	00	03	00	00	00
4E	4F	54	45	01	00	00	00	00	00	53	44	41	5F	84	F6
00	00	00	00	00	00	00	00	00	00	00	00	00	00	00	00
00	00	00	00	00	00	00	00	00	00	00	00	00	00	00	00
00	00	00	00	00	00	00	00	00	00	00	00	00	00	00	00

Figure 1. The NSP file format data

By comparing empty files and files containing the signal, we found that the first eight rows of data to a file paramount additional information, data files are stored is to start from the ninth row. We conclude that the data is divided into three parts, the front part of speech signal, the middle part of the airflow signal data, the last part is the air-pressure signal data. The three part data according to the time points are arranged, and each accounted for one-third of one. We use fread (fid, 'int16') function of MATLAB, the NSP files in hexadecimal readout on three columns of a matrix in which multiple rows. Among them, each row of the matrix corresponds to a point in time sampling frequency. The row of the matrix corresponds to the data in each part, wherein the first column data for speech, second column for airflow, third column for air-pressure. In the later need the data used, remove the corresponding columns from the matrix.

The NSP format into WAV format

3.1 The WAV format

WAV file as the acoustic format multimedia use, it is based on RIFF format as a standard. RIFF Resource Interchange File Format is the English abbreviation of the first four bytes of each WAV file is "RIFF". WAV file consists of two parts, the header and body composition data. Where the file header is divided into RIFF or WAV files and audio data segment identifier format segment two parts. WAV file content and format of each part as shown in Table1.

Table 1 The file header of WAV file

Offset address	Byte	Data type	Content
00H~03H	4	char	"RIFF" symbol
04H~07H	4	long int	The length of the file
08H~0BH	4	char	"WAVE" symbol
0CH~0FH	4	char	"fmt" symbol
10H~13H	4		Transition byte (indefinite)
14H~15H	2	int	Format categories (10H said sound data in form of PCM)
16H~17H	2	int	The number of channels
18H~1BH	2	int	The sampling rate (the number of samples per second), said the playback speed of each channel
1CH~1FH	4	long int	Waveform audio data transfer rate
20H~21H	2	int	Adjust the data block number (in terms of bytes)
22H~23H	2		All samples of each channel of the data bits
24H~27H	4	char	Data tag " data "
28H~2BH	4	long int	The sound data length

3.2 The NSP saved as WAV format

The entire program flow as shown below:

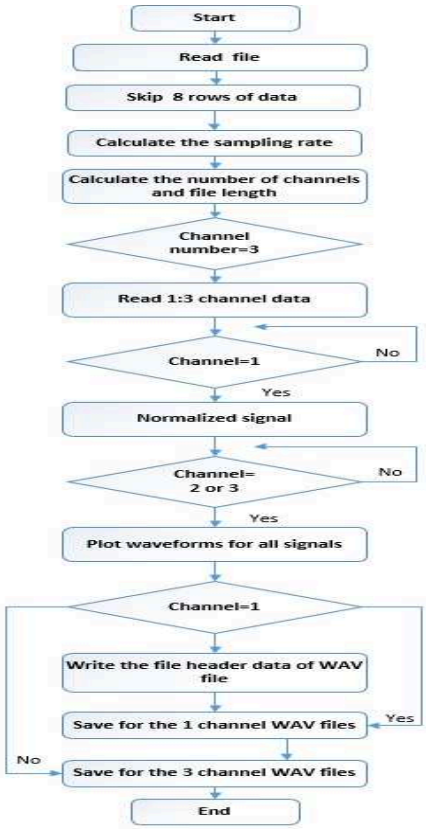

Figure 2. The analysis platform frame diagram

In order to facilitate the analysis separately for each channel signal, we make analysis platform in the MATLAB environment, combining the speech signal, airflow and air-pressure signal. By reading

the signal, NSP format will be saved as WAV format, for each channel data analysis. The platform should first read in Nsp format, and then through the GUI programming display waveform. In the waveform display, according to the signals required for data storage, unified format for the WAV.

First, read the NSP format files, remove header files first eight rows of data, the effective use of the data file fread (fid, 'int16') function, the NSP document read in hexadecimal. Then calculate the sample rate, number of channels, and file size. Then the normalized, normalized to the signal, only the first channel speech signal, the airflow and air-pressure signal is not normalized. Then the separation channel according to the needs of the study. If you only study the speech signal, then save the data of the first channel. If study the airflow and air-pressure signal, then save the data of all channel. Data storage formats are WAV files, is helpful to the study of late by the speech software.

When you save the format, first in the GUI display waveform, according to the quality of the signal at the different channels to be saved. If only the analysis of speech signal, save only the signal of the first channel. The program will automatically determine, if not only one channel, save the signals of all channels. Signal data are stored in WAV files, to facilitate the later analysis and research.

Conclusions

The platform can be realized on the NSP format file data of custom analysis, more conducive to the analysis of each channel signal data. Platform menu includes five main menus: File, Edit, View, Play, and Help. The menu File, including 7 sub menus are open NSP file, save the file as WAV, open the saved wav file, save file as, channel separation, save selected file, exit. Edit menu includes cut, trim reverse. In the View menu, including view all, view selected, zoom in, and zoom out. Play menu includes play all, play selected. The last one is MATLAB Help file. In the process of work later, will be further on the platform for perfection, while the realization of the basic functions, to achieve the parameters of the signal analysis and processing.

Acknowledgements

This research was financially supported by the National Natural Science Foundation of China (Grant NO. 61202187), the Northwest University for Nationalities graduate innovation project (Grant NO.ycx13017), and the laboratory open project of the Key Lab of China's National Linguistic Information Technology (Grant NO. 2012KF011).

References

[1] Peter Ladefoged, A Course in Phonetics, Thomson Wadsworth, 2006.

[2] Ladefoged, P. Aerodynamic Investigations. Phonetic Data Analysis, Oxford: Blackwell Publishing, 2003

[3] Kelso, J. A. S.,Saltzman. E. L. & Tuller, B., The dynamical perspective on speech production; data and theory. Journal of Phonetics 14, 1986

[4] Information on http://www.kaypentax.com

[5] Lv Shiliang, A Study of Phonation Air Flow and Pressure in Mandarin Plosives and Affricates, Northwest University for Nationalities, 2012

Advanced Materials Research Vols. 989-994 (2014) pp 3671-3674
© (2014) Trans Tech Publications, Switzerland
doi:10.4028/www.scientific.net/AMR.989-994.3671

Modeling Difficult-to-measure Process Parameters based on Intrinsic Mode Functions Frequency Spectral Features of Mechanical Vibration and Acoustical Signals

Jian Tang[1, a], Zhuo Liu[2,b], Yongjian Wu[2, c] and Lijie Zhao[3,c]

[1]Unit 92941, PLA, Huludao, Liaoning, China

[2] Research Center of Automation, Northeastern University, ShenYang, China

[3] Shenyang University of Chemical Technology, Shenyang,China

[a]powernature@126.com, [b]liuzhuo@mail.neu.edu.cnl, [c]lunlunzlj@163.coml

Keywords: Ensemble empirical mode decomposition (EEMD), Intrinsic mode function (IMF), Frequency spectral features, Mutual information (MI), Kernel partial least squares (KPLS)

Abstract. Heavy mechanical devices of complex industrial process produce soundly mechanical vibration and acoustical signals. Some difficult-to-measure key process parameters have direct relationship with these signals. A newly ensemble empirical mode decomposition (EEMD), Fast Fourier Transform (FFT), Mutual information (MI), and Kernel partial least squares (KPLS) based modeling approach is proposed to measure these process parameters. At first, different scale intrinsic mode functions (IMFs) of mechanical vibration and acoustical signals are obtained using EEMD technology. Then, FFT transforms these multi-scale IMFs into frequency domain, and MI based feature selection method selects interesting frequency spectral features. Finally, KPLS constructs the final soft sensor models using the selected features. Experimental results based on vibration and acoustical signals of ball mill demonstrate this approach is more effective than other exist multi-scale decomposition based methods.

Introduction

There are lots of heavy mechanical devices in complex industrial process such as mineral grinding process. These devices are always key important equipments of the whole product process. However, some important process parameters inside these devices cannot be accurate detected directly or in first principal. Thus, it is very difficult to realize the operational optimization control of such complex industrial process [1]. Normally, these devices produce soundly mechanical vibration and acoustical signals. Studies show that frequency spectra of these signals contain information relative to these difficult-to-measure key process parameters. For examples, frequency spectra of shell vibration and acoustical signals of ball mill in grinding process contain useful information for measuring load parameters (mineral to ball volume ratio (MBVR), pulp density (PD) and charge volume ratio (CVR)) inside the ball mill [2]. Many single-scale frequency spectrum based soft sensor models have been constructed using shell vibration and acoustical signals [3,4]. However, these models are difficult to understand and interpretation.

Studies show grinding mechanism inside ball mill is very difficult to explain. Moreover, shell vibration signal of ball mill is caused by different impact forces with different amplitudes and frequencies. Therefore, the shell vibration signal consists of different sub-signals. Moreover, shell vibration is the source of acoustical signal. Thus, how to decompose these multi-scale signals to different sub-signals with different physical meaning has become a new focus recently. Empirical mode decomposition (EMD) technology is one effective adaptively decompose method based on partial characteristic of the signal [5], which was first used in our former studies [6,7,8]. However, no satisfied modeling performance was obtained. What is the reason?

Reliable frequency spectrum is foundation to construct an effective mechanical vibration and acoustical signals based process parameter soft sensor model. Recently, many shortcomings of EMD

technology has been found, such as lacking a theoretical foundation, end effects, sifting stop criterion, extremum interpolation etc. One of the outstanding disadvantages is mode-mixing phenomenon. However, the newly proposed ensemble EMD (EEMD) can overcome the mode-mixing problem [9], which calculates the mean of an ensemble of decompositions that have different instances of noise added to the signal. Aims at the high dimensional problem of frequency spectrum, mutual information (MI) based feature extraction method are used widely. The MI is more comprehensive than the other normal feature selection method [10], which has been used in gene selection [11].

Therefore, a newly EEMD, Fast Fourier Transform (FFT), MI and Kernel partial least squares (KPLS) based modeling approach is proposed to measure these difficulty-to-measure key process parameters. At first, the original mechanical vibration and acoustical signals are decomposed into IMFs with different time scales. Then, these multi-scale IMFs are transformed into multi-scale frequency spectra. And these valued frequency spectral features relative to different key process parameters are selected based on MI based feature selection method. Finally, these selected features are serial combined and fed into KPLS based soft sensor models. The experimental results shows this approach is effective compared with the other exist multi-scale decomposition based methods.

Strategy of Intrinsic Mode Functions Features based Modeling approach

Based on the former analysis, a new intrinsic mode functions frequency spectral features based modeling approach is proposed. This approach consists of multi-scale mechanical vibration and acoustical signals decomposition module, multi-scale frequency spectrum transform module, frequency spectral features extraction module and difficulty-to-measure key process parameters modeling module, whose structural is shown as Fig. 1.

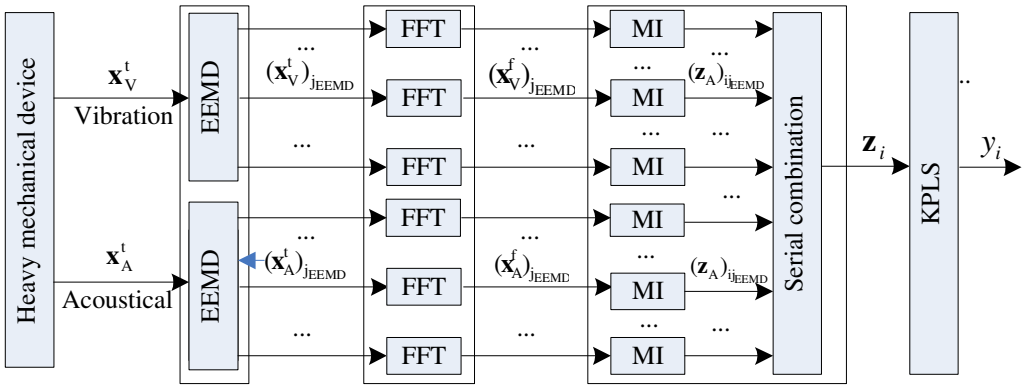

Fig.1 Strategy of intrinsic mode functions features based modeling approach

In Fig. 1, the superscript t and f represent time and frequency-domain signals; the subscript V and A represent mechenical vibration and acoustical signals; $\mathbf{x}_V^t$ and $\mathbf{x}_A^t$ are the original time-domain signals; $(\mathbf{x}_V^t)_{jEEMD}$ and $(\mathbf{x}_A^t)_{jEEMD}$ represent the j_{EEMD}th IMF sub-signals; $(\mathbf{x}_V^f)_{jEEMD}$ and $(\mathbf{x}_A^f)_{jEEMD}$ represent the j_{EEMD}th IMF frequency spectrum; $(\mathbf{z}_A)_{ijEEMD}$ and $(\mathbf{z}_A)_{ijEEMD}$ represent the j_{EEMD}th selected IMF frequency spectral features from $(\mathbf{x}_V^f)_{jEEMD}$ and $(\mathbf{x}_A^f)_{jEEMD}$ for the ith process parameters; $\mathbf{z}_i$ represent the combined frequency spectral features for the ith process parameters.

Multi-scale vibration and acoustical signals decomposition module: Based on EEMD technolegy, the original mechanical vibration and acoustical signals are decomposed into IMFs with different time scale. The relationships among them can be represented as:

$$\mathbf{x}_V^t = \sum_{j_V=1}^{J_{VEEMD}} (\mathbf{x}_V^t)_{jEEMD} + (r_{J_V})_{EEMD} \tag{1}$$

$$\mathbf{x}_A^t = \sum_{j_A=1}^{J_{AEEMD}} (\mathbf{x}_A^t)_{jEEMD} + (r_{J_A})_{EEMD} \tag{2}$$

where, $(r_{J_V})_{EEMD}$ and $(r_{J_A})_{EEMD}$ represent residual signals; J_{VEEMD} and J_{AEEMD} represent the number of vibration and acoustical IMFs respectively.

Multi-scale frequency spectrum transform module: Based on FFT, different time domain IMFs are transformed into frequency spectrum. Take the j_{EEMD}th IMF as example, this process can be reprented:

$$(\mathbf{x}_{\mathrm{V}}^{\mathrm{t}})_{\mathrm{jEEMD}} \xrightarrow{\mathrm{FFT}} (\mathbf{x}_{\mathrm{V}}^{\mathrm{f}})_{\mathrm{jEEMD}} \tag{3}$$

$$(\mathbf{x}_{\mathrm{A}}^{\mathrm{t}})_{\mathrm{jEEMD}} \xrightarrow{\mathrm{FFT}} (\mathbf{x}_{\mathrm{A}}^{\mathrm{f}})_{\mathrm{jEEMD}} \tag{4}$$

Frequency spectral features extraction module: Based on MI feature selection algorithm, MI values of different IMFs freqeuncy spectral features are calculated. These features with MI values higher than a threshold value are selected. Take the j_{EEMD}th IMF as example, this frequency spectrum feature selection process can be reprented as:

$$(\mathbf{x}_{\mathrm{V}}^{\mathrm{f}})_{\mathrm{jEEMD}} \xrightarrow{\mathrm{MI}\left((\mathbf{x}_{\mathrm{V}}^{\mathrm{f}})_{\mathrm{jEEMD}}\right)_{ip} > \theta_{threshold}} (\mathbf{z}_{\mathrm{V}})_{\mathrm{ij_{EEMD}}} \tag{5}$$

$$(\mathbf{x}_{\mathrm{A}}^{\mathrm{f}})_{\mathrm{jEEMD}} \xrightarrow{\mathrm{MI}\left((\mathbf{x}_{\mathrm{A}}^{\mathrm{f}})_{\mathrm{jEEMD}}\right)_{ip} > \theta_{threshold}} (\mathbf{z}_{\mathrm{A}})_{\mathrm{ij_{EEMD}}} \tag{6}$$

where, $\mathrm{MI}\left((\mathbf{x}_{\mathrm{V}}^{\mathrm{f}})_{\mathrm{jEEMD}}\right)_{ip}$ represent MI value of the pth frequency spectral features for the ith key process parameters; $\theta_{threshold}$ represent threshold value. All the selected features using MI method for the ith process parameters can be represented as:

$$\mathbf{z}_i = [(\mathbf{z}_{\mathrm{V}})_{i1_{\mathrm{EEMD}}},\ldots,(\mathbf{z}_{\mathrm{V}})_{ij_{\mathrm{EEMD}}},\ldots,(\mathbf{z}_{\mathrm{V}})_{iJ_{V\,\mathrm{EEMD}}},(\mathbf{z}_{\mathrm{A}})_{i1_{\mathrm{EEMD}}},\ldots,(\mathbf{z}_{\mathrm{A}})_{ij_{\mathrm{EEMD}}},\ldots,(\mathbf{z}_{\mathrm{A}})_{iJ_{A\mathrm{EEMD}}}] \tag{7}$$

Difficulty-to-measure key process parameters modeling module: Based on KPLS algorithm, construct soft sensor model for the ith process parameters using features $\mathbf{z}_i$.

Results and discussion

Mechanical vibration and acoustical signals of a laboratory scale ball mill (XMQL-420×450) of grinding process are picked up by accelerometer located on the mill shell and microphone near the abrasion zone of wet ball mill. Load parameters inside the mill (MBVR, PD and CVR) are modeling using the proposed modeling approach. EEMD with ensemble number 10 and white noise amplitude 0.1 is used to decompose shell vibration and acoustical signals into IMF sub-signals. The Same FFT parameters as literature [2] are used to obtain IMF frequency spectra. Maximum and minimum MI values between IMF frequency spectral features and mill load parameters are shown in Fig. 2.

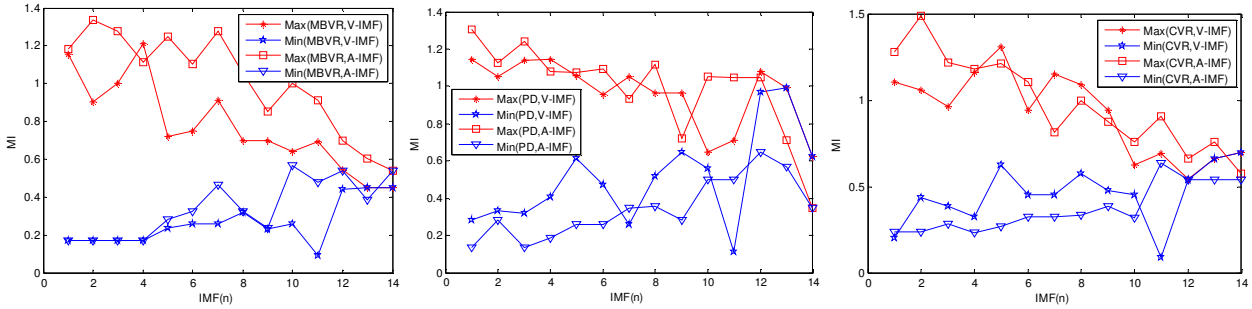

Fig. 2 Maximum and minimum MI values between IMF features and process parameters

Fig. 2 shows that the mapping relationships between IMF frequency spectral features and mill load parameters are different. According the maximum and minimum MI values, threshold values for MBVR, PD and CVR are selected as 0.4, 0.6 and 0.5 respectively. Numbers of the selected vibration and acoustical frequency spectral features for different mill load parameters are shown in Fig.3.

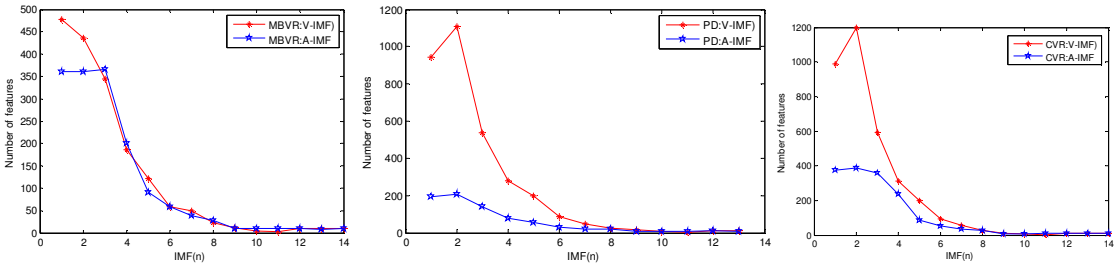

Fig. 3 Numbers of the selected vibration and acoustical features for different process parameters

Fig. 3 shows that feature numbers of MBVR is lower than that of PD and CVR. Using same RBF kernel, with kernel radius 0.4, 50 and 0.5 for MBVR, PD and CVR to construct KPLS based mill load parameters soft sensor models. Prediction results are shown in Fig. 4.

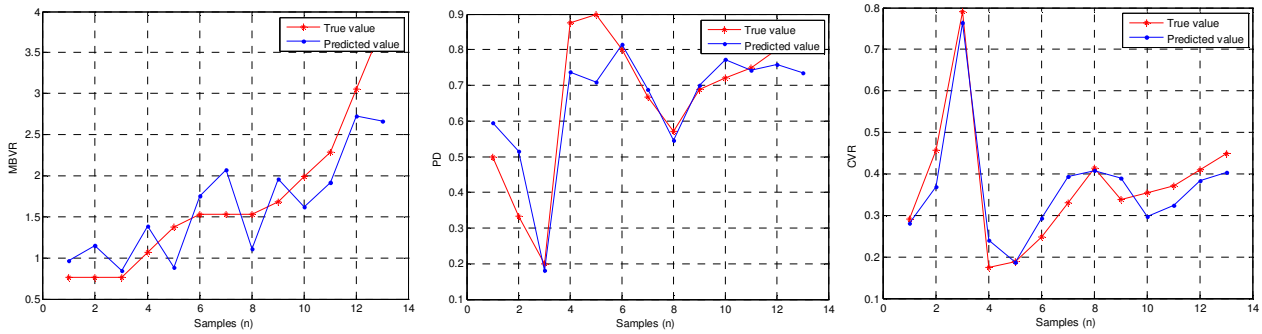

Fig. 4 Prediction curves of different mill load parameters

Fig.4 shows that MBVR model has the biggest prediction errors among three mill load parameters. The root mean square relative errors (RMSSEs) of MBVR, PD and CVR models are 0.2723, 0.1834 and 0.1610 respectively, which is lower than that of the former EMD based modeling methods. All these results show the proposed method is effective to modeling load parameters of ball mill.

Summary

This paper presents a novel modeling approach for difficult-to-measure key process parameters based on mechanical vibration and acoustical signals. Ensemble empirical mode decomposition, fast Fourier transform and mutual information technologies are used to select multi-scale frequency spectral features of these signals for different key process parameters. The selected features are fed into kernel partial least squares algorithm to construct final soft sensor model. Experimental results based on shell vibration and acoustical singles of ball mill show the proposed method has better prediction performance than former multi-scale based methods.

References

[1] T.Y. Chai: Acta Automatica Sinica, Vol. 39 (2013), p. 1744.

[2] J. Tang, L.J. Zhao, J.W. Zhou and T.Y. Chai: Minerals Engineering, Vol. 23 (2010), p. 720.

[3] J. Tang, T.Y. Chai, Y. Wen and L.J. Zhao: Control Engineer Practice, Vol. 20 (2012), p. 991.

[4] J. Tang, T.Y. Chai, W. Yu and L.J. Zhao: IEEE Transactions on Automation Science and Engineering, Vol. 10 (2013), p. 726.

[5] N.E. Huang, Z. Shen and S.R. Long: Proc. Royal Soc,Vol. 454 (1998), p. 903.

[6] J. Tang, L.J. Zhao, H. Yue, W. Yu and T.Y. Chai: Procedia Engineering, Vol. 16 (2011), p. 646.

[7] L.J. Zhao, J. Tang and W.R. Zheng: Journal of Theoretical and Applied Information Technology, Vol. 45 (2012), p. 179.

[8] J. Tang, L.J. Zhao, J. Jia, T.Y. Chai and W. Yu: Lecture Notes in Computer Science, Vol. 7367 (2012), p. 489.

[9] Y.G. Lei, J. Lin, Z.J. He and M.J. Zuo: Mechanical System and Signal Processing, Vol. 35 (2013), p. 108.

[10] H.W. Liu, J.G. Sun, L. Liu and H.J. Zhang: Vol. 42 (2009), p. 1330.

[11] R.C.Cai, Z.F. Hao, X.W. Yang and W. Wen: Neurocomputing, Vol. 72 (2009), p. 991.

Advanced Materials Research Vols. 989-994 (2014) pp 3675-3678
© (2014) Trans Tech Publications, Switzerland
doi:10.4028/www.scientific.net/AMR.989-994.3675

Image Retrieval of Self-Adapt Distance Measure Based on SLLE

Xiaofen Wang, Haina Zhang, Xiurong Qiu, Jiangping Song, Kexin Zhang

Shang Qiu Institute of Technology, HeNan Shangqiu China

Email:huangdi564@163.com

Key words: self-Adapt distance measure; identification information; manifold learning

Abstract. Self-adapt distance measure supervised locally linear embedding solves the problem that Euclidean distance measure can not apart from samples in content-based image retrieval. This method uses discriminative distance measure to construct k-NN and effectively keeps its topological structure in high dimension space, meanwhile it broadens interval of samples and strengthens the ability of classifying. Experiment results show the ADM-SLLE date-reducing-dimension method speeds up the image retrieval and acquires high accurate rate in retrieval.

1. Introduction

Manifold learning has risen in recent years specializing in nonlinear distribution data dimension reduction method, mainly includes isometric feature mapping (Isomer)[1] and the local linear embedded (LLE)[2] method. Compared with linear dimension reduction method, manifold learning dimension reduction method has many advantages. This paper in the local linear embedded (LLE) method, and on the basis of using the information has identified distance measure to replace the Euclidean distance measure, will identify information into the LLE algorithm. Which proposed learning methods of self-Adapt distance measure supervised locally linear embedding.

2. The algorithm of Self-Adapt distance measure

Support vector machine (SVM) is the most practical statistical learning theory, for its part, the core idea of it is to use the minimization principle into the classification of the structural risk minimization principle [3] into the classification. Its essence is to find out the training sample structure optimization classification hyperplane support vector. In mathematics sums up for a solution with inequality constraints of secondary rules. The plane can explicitly to write for:

$$w = \sum_{i \in SV} a_i y_i \Phi(x_i) \quad . \tag{1}$$

Among them, the $\Phi(x_i)$ is nonlinear from R^D to R^d projection, the a_i is Lagrange coefficient, The SV is support vector.

Assume that constraint Θ and characteristics of corresponding axis $\Theta \in \{e_1, e_2, \cdots, e_D\}$. Among them, the k feature for corresponding unit vector is e_k.The $|w \cdot \Theta|$ is Provide the kind of information to identify the characteristics of the measure of correlation. As $r_k = |w \cdot \Theta|$ in the nearest scale and the weight of each Θ d related weight. The big value of $|w \cdot \Theta|$ will make the nearest shape Θ along the contraction, And the little value of $|w \cdot \Theta|$ will stretch the nearest area along Θ the direction.

Our purpose is to use w the calculated point $r_k(x)$. Below type:

$$r_k(x) = |w \cdot \Theta| \quad . \tag{2}$$

The most attractive performance is w to capture the correlation between r_k the information, and the correlation to the index weight through the following methods of obtaining:

$$w_k(x) = \frac{\exp(Tr_k(x))}{\sum_{k=1}^{D} \exp(Tr_k(x))} . \tag{3}$$

Among them, T is a parameter, can choose the maximum r_k effect through. At the time of $T = 0$ and $w_k = 1/n$, thus ignore any difference between r_k. When T in a big change of r_k, w_k is exponentially influence. The weighted index is very sensitive to local features correlation changes, and can therefore better improve performance [4]. In addition, the index weight more stable, because it can prevent neighborhood in any direction enlarged unlimitedly.

Therefore, we hope parameters of T in the index weighted (3) with border the decrease of the distance with q increased. Using support vector in the border near the surface of the knowledge, we can through the calculation inquires the of nearest point with support vector distance estimating it is apart from the boundary of the distance.

$$B_q = \min_{s_i} \|q - s_i\| . \tag{4}$$

In this, the minimize is alternative no constraints ($0 < a_i < C$) support vector s_i. In the border around the spatial resolution by expanding support vector neighborhood of local volume unit and increase [5]. So, we can use the type to achieve our objective:

$$T = H - B_q . \tag{5}$$

In this, H is a parameter, equal to the training x and the boundary of the approximate average point distance.

$$H = \frac{1}{l} \sum_{x} \min_{s_i} \|x - s_i\| . \tag{6}$$

To do so, according to the value of the border to the relative position very well to adapt to each inquires the point. By the analysis on, adaptive local distance can use type says:

$$D(x_i, x_j) = \sqrt{\sum_{k=1}^{D} w_k (x_{ik} - x_{jk})^2} . \tag{7}$$

From this distance measure, can compute the neighbors k, and can be structure matrix of W.

3. Self-Adapt distance measure supervised locally linear embedding

For the purpose of dimension reduction is not only to the known sample points of dimension reduction, more important is to be able to find the unknown sample points inner manifold, and made the sample points to the classification of the interface distance increases as far as possible to improve generalization performance. Therefore, the use of the information has identified distance measure to replace the Euclidean distance measure construction-neighbors, put forward the measure of adaptive distance supervised learning method LLE manifold. Algorithms are described below:

Input: High dimensional data $X = (x_1, x_2, \cdots, x_n)$, $x_i \in R^D$, And every sample belong to the category of the Numbers.

Output: Low dimensional data $Y = \{y_1, y_2, \cdots y_n\}$, $y_i \in R^d$, ($d \ll D$).

4. FADM-SLLE feedback self-Adapt distance measure supervised locally linear embedding

The specific steps of Algorithm of FADM-SLLE [6] as follows:

Step1: Use LLE algorithm dimension reduction, by Euclidean distance measure similarity search method. In the initial in retrieval choose n image to give users, the user mark and retrieval of the relevant target image, get used to the feedback is an right example set I_p^0 and a error example set I_p^0. Update set I_p and I_n: $I_p = I_p \bigcup I_p^0$, $I_n = I_n \bigcup I_n^0$.And when the initial $I_p = 0$ and $I_n = 0$.

Step2: The I_p and I_n Will known as label information image point of (x_i, y_i), $x_i \in I_p \bigcup I_n$, $y_i = \begin{cases} +1, x_i \in I_p \\ -1, x_i \in I_n \end{cases}$.By SVM calculated surface classification $w = \sum_{i \in SV} a_i y_i \Phi(x_i)$.

Step3: Calculation adaptive local distance $D(x_i, x_j)$, $D(x_i, x_j) = \sqrt{\sum_{k=1}^{D} w_k (x_{ik} - x_{jk})^2}$.

From this distance measurement, high dimensional space to each of the sample points of x_i, the calculation of k neighbors, and then to build W.

Step4: The user on the feedback image to for labeling. Get used to the feedback is an right example set I_p^1 and error example set I_n^1. With this then to set I_p and I_n updated. $I_p = I_p \bigcup I_p^1$.

5. The experiment and application analysis

This paper put forward to evaluate theperformance of the algorithm is used for image retrieval, design the following experiment. The database of core image database, the selection of the 1000 images, divided into 10 categories, each containing 100 pictures. As shown in table 1 400 d image low-level features as an original features vector.

Table1. Used image feature in the experiments

Characteristic name	Dimension
Color histogram [12]	256
Color moment [13]	9
Edge histogram [12]	5
contourlet [14]	62
orientation histograms [15]	68
total	400

To remove dimension effects, in data analysis of data before pretreatment is indispensable. Were statistically speaking, regularization transform can make the poor of spacing increases, in reducing of distance, which is beneficial to the object classification expression. Therefore, this paper using this method features of pretreatment. Specific as follows:

$$x_{ij}^* = \frac{x_{ij} - \min\limits_{1 \le i \le n} x_{ij}}{R_j} \quad (8)$$

Using the SVM feedback method (FSVM) [6] and the related feedback algorithm FADM-SLLE proposed in this paper for image retrieval, SVM by gauss RBF kernel function, its parameter $\sigma = 3$, all 10 kinds of image respectively, the four feedback average precisions based on the top 25 images and 36 images are compared. the results is shown in figure 1.

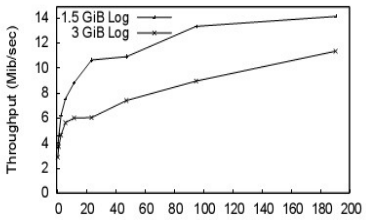

Fig. 1 Comparison result of F.25 and F.36

Graph starting point for no feedback in the original information retrieval results, as can be seen, the user for the first two rounds related feedback, the retrieval accuracy has the large scale enhancement, since then, the search precision ascension will gradually smooth. The proposed algorithm in overall scope are better than the SVM method, the two methods are significantly better than no feedback algorithm, it shows the users with feedback information related to improve retrieval performance is very good, with more feedback to explore a more relevant images, and improve the precision, the experimental results proved it.

Fig. 2 Original image

Fig. 3 Image produced by retrieval

Figure2 in terrain for image database of the arbitrary a original image, and figure 3 after ADM-SLLE method for image retrieval to create. The experiment results show ADM-SLLE method can more accurately according to the characteristics of the source image content retrieval to the outline of the source images.

6. Conclusions

How to use a lot of no label image point to improve learning performance has become a concerned problem about the image retrieval study. This paper is about a combination of the two - the strong generalization ability of the SVM and the LLE dimension-reduction methods, putting forward a new method of supervising and man folding learning algorithm, which can classify the interval between the two to maximize the local information and keep the data. The experimental results show that the method can improve the accuracy of image retrieval.

7.Reference

[1] J B Tenenbaum, V de Silva, J C Langford. A global geometric framework for nonlinear dimensionality reduction [J]. Science ,2010 , 290 : 2319 – 2323.

[2] S T Rowdies, L K Saul. Nonlinear dimensionality reduction by locally linear embedding [J]. Science , 2000 , 290 : 2323 – 2326.

[3] N. Cristianini and J. Shawe-Taylor, An Introduction to Support Vector Machines and Other Kernel-Based Learning Methods [M]. Cambridge,U.K.:Cambridge Univ. Press, 2000.

[4] Peng J, Heisterkamp D, and Dai H. LDA/SVM driven nearest neighbor classification [J]. Neural Networks, IEEE Transactions on, 2003, 14(4):940–942.

[5] Zhao Chengdong, Wang Xuhui, Lu Jianfeng, Image retrieval based on Improved supervised LLE Learning Method. Chinese Conference on Pattern Recognition 2010. pp513-516.

[6] S. Amari and S. Wu, Improving support vector machine classifiers by modifying kernel functions [J], Neural Netw, vol. 12, pp. 783–789, 2009.

Advanced Materials Research Vols. 989-994 (2014) pp 3679-3682
© (2014) Trans Tech Publications, Switzerland
doi:10.4028/www.scientific.net/AMR.989-994.3679

Study on Deep Structure of Extreme Learning Machine (DS-ELM) for Datasets with Noise

Mengmeng Ma[1, a], Bo He[1,b]

[1]School of Information and Engineering, Ocean University of China, Shandong, Qingdao, China 266000

[a]mmm_3462@163.com, [b]bhe@ouc.edu.cn

Keywords: Extreme Learning Machine (ELM), Auto-Associative Neural Network (AANN), Deep Structure of ELM (DS-ELM)

Abstract. Extreme learning machine (ELM), a relatively novel machine learning algorithm for single hidden layer feed-forward neural networks (SLFNs), has been shown competitive performance in simple structure and superior training speed. To improve the effectiveness of ELM for dealing with noisy datasets, a deep structure of ELM, short for DS-ELM, is proposed in this paper. DS-ELM contains three level networks (actually contains three nets): the first level network is trained by auto-associative neural network (AANN) aim to filter out noise as well as reduce dimension when necessary; the second level network is another AANN net aim to fix the input weights and bias of ELM; and the last level network is ELM. Experiments on four noisy datasets are carried out to examine the new proposed DS-ELM algorithm. And the results show that DS-ELM has higher performance than ELM when dealing with noisy data.

Introduction

Extreme learning machine (ELM) is a new algorithm proposed by Professor Huang in 2004 [1], which is a simple and efficient single-hidden layer feed-forward neural networks (SLFNs). In learning process of ELM, the input weights and hidden biases are randomly chosen and not need to be tuned, while the output weights are analytically determined by the Moore-Penrose generalized inverse. ELM algorithm can not only learn much faster with a higher generalization performance than those traditional gradient-based learning algorithms, but also avoid many problems such as stopping criteria, learning rates, learning epochs, local minima that are difficult to cope with by classical gradient-based learning methods. Over the next several years, the team led by Professor Huang has done many further development based on original ELM [2-4].

While there are so many competitive advantages for the ELM technology in comparison with other traditional neural network algorithms to lure people to explore it, many shortcomings are also supposed to be awarded: (1) ELM technology ignores the noise of data that can be found almost everywhere in the real world, which may be lead to instability of the system; (2) ELM algorithm sometimes makes the hidden layer output matrix not full column due to the random choice of input weights and biases which lowers the reliability of ELM. In this paper, a new algorithm named deep structure of extreme learning machine (DS-ELM) is proposed to deal with the noise data problems.

DS-ELM consists of two level networks: the first level network is trained by auto-associative neural network (AANN) aim to filter out noise as well as reduce dimension when necessary; the second level network is another AANN net to fix the input weights and bias of ELM; and the last network is ELM but input weights and bias are kept unchanged by the second AANN net to improve the effectiveness of the whole net. The outputs of the first level network are regarded as new input data for ELM. The difference between DS-ELM algorithm and ELM lies in removing noise of datasets and fixing input weights.

Methodology

In this part, we give a detailed introduction about the structure and main processes of ELM and DS-ELM algorithm.

A. Extreme Learning Machine (ELM)

Extreme learning machine (ELM) is a single hidden layer feed-forward neural network algorithm, which contains three layers: input layer, hidden layer and output layer. The following is a further detailed explanation of ELM algorithm.

For N arbitrary distinct samples (x_i, t_i), where $x_i = R^n$ and $t_i \in R^m$, standard SLFNs with k nodes and activation function $g(x)$ are mathematically described as

$$\sum_{i=1}^{k} \beta_i \, g_i(\omega_i \cdot x_j + b_i) = y_j, \; j = 1,2, \ldots, N \quad (1)$$

Where ω_i is the weight vector connecting the ith hidden neuron and the input neurons, β_i is the weight vector connecting the ith hidden neuron and the output neurons, then, b_i is the threshold of the ith hidden neuron. If the SLFNs can approximate these N samples with zero error, that is, $\sum_{i=1}^{n} \|y_i - t_i\| = 0$. And the equation can be expressed as:

$$H\beta = T \quad (2)$$

Where

$$H = \begin{bmatrix} g(\omega_1 \cdot x_1 + b_1) & \cdots & g(\omega_k \cdot x_1 + b_k) \\ \vdots & \ddots & \vdots \\ g(\omega_1 \cdot x_N + b_1) & \cdots & g(\omega_k \cdot x_N + b_k) \end{bmatrix}, \; \beta = \begin{bmatrix} \beta_1^T \\ \vdots \\ \beta_k^T \end{bmatrix}_{k \times m} \text{ and } T = \begin{bmatrix} t_1^T \\ \vdots \\ t_N^T \end{bmatrix}_{N \times m} \quad (3)$$

As mentioned in Huang et al. [5], H is named the hidden layer output matrix of the neural network; the ith column of H denotes the ith hidden node output with respect to inputs $(x_1, x_2, \ldots, x_N)$.

With these notations, the hidden-layer output matrix can be determined:

$$\beta = H^{\dagger} \times T \quad (4)$$

Where $H^{\dagger}$ is the Moore-Penrose generalized inverse of matrix H [6]. Owing to the Moore-Penrose generalized inverse, the learning speed of ELM net is dramatically increased.

B. Deep Structure Extreme Learning Machine (DS-ELM)

As ELM described above, it can avoid many difficulties faced by gradient-based learning technique. While, in order to improve the ability of removing noise of ELM, deep structure extreme learning machine (DS-ELM) is proposed, and this new algorithm can deal with the noisy data with very high accuracy. DS-ELM contains two subnets based on AANN and an ELM net. And Fig.1 shows the procedure of establishing the DS-ELM, and the following is the procedure of DS-ELM algorithm:

(1) Calculating the first hidden layer based on AANN algorithm aim to filter the noise of input data. Auto-associative neural network (AANN) was proposed by Kramer in 1992 [7], which is an unsupervised learning algorithm that applies back-propagation, setting the target values to be equal to the inputs. It tries to learn an approximation to the identity function, that is, the output is similar to the input, so as to filter the noise of input data and learn an equal representation of sample attributes. After the AANN net is trained well, the weights between the input layer and the hidden layer should be kept unchanged, and the output layer will be excluded, then, the remaining part of the well-trained AANN is used as the first net.

(2) Determining the weights and bias of input layer and hidden layer of ELM by the second AANN layer. The input output data of this AANN net is the output of hidden layer of the first AANN net. After the well-trained the second AANN subnet, the weights between the input layer and the hidden layer should also be kept unchanged, which will be used as the hidden weights and bias of ELM aim to avoid the hidden layer output matrix not full column rank.

(3) Training the ELM model. The output data of hidden layer of the first AANN net is regard as the input data of ELM. And the output data of ELM is the sample data. The weights and bias between input layer and hidden layer of ELM is that of the second AANN. After the well-trained ELM, the whole system of DS-ELM model is finished. It can be found the procedure of establishing the DS-ELM model is simple in implementation.

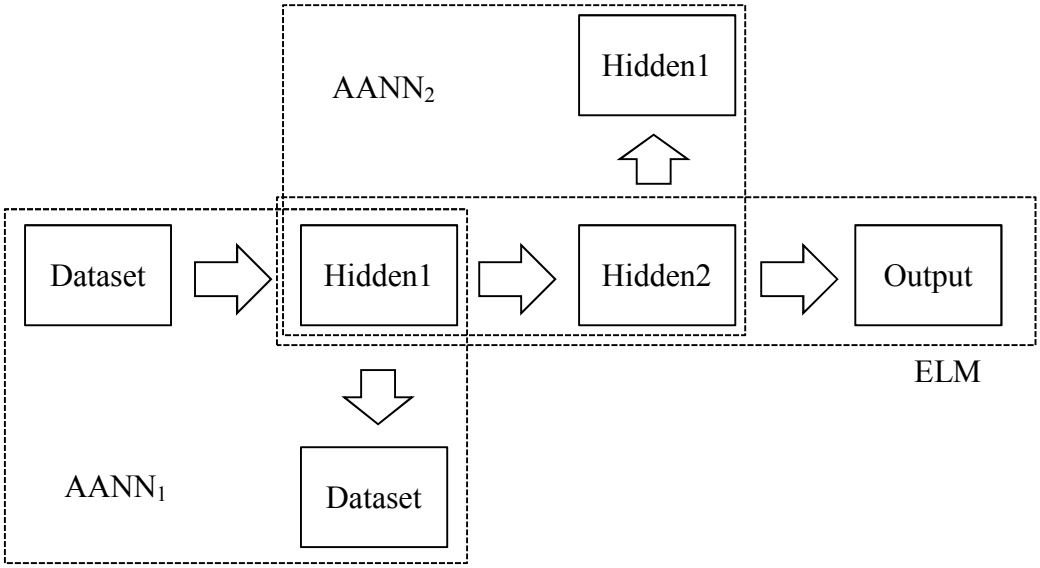

Fig.1 The structure of DS-ELM

Experiments

The DS-ELM model aims to improve the efficiency of ELM for noisy data. In this part, altogether four dataset are selected from UCI to examine the proposed DS-ELM model. In addition, 10 percent of white noise is added to all the four datasets. The different information for the datasets is summarized in Table 1.

Table 1 Information about the selected data sets.

Data set	# Attributes	# Train	# Test
Iris	5	120	30
Wine	13	89	89
Housing	13	338	168
Abalone	8	2000	2177

In order to compare the new proposed DS-ELM method with ELM method on classification and regression problems, an adequate error measure method must be selected. In this paper, the root mean squared error (RMSE) is used as the error criterion for regression problems, and accuracy of predict is used for the classification problems. And the RMSE is computed as follows:

$$\mathrm{RMSE} = \sqrt{\frac{\sum_{i=1}^{N}(y_i - t_i)^2}{N}} \tag{5}$$

Where N expresses the total number of samples in the test set, t_i is the real values and y_i is the output predicted by the DS-ELM model.

Table 2 The optimal results comparison between the proposed DS-ELM and ELM.

Dataset	Type	DS-ELM	ELM
		RMSE or Accuracy (%)	RMSE or Accuracy (%)
Iris	classification	96.67%	93.33%
Wine	classification	98.87%	96.63%
Housing	regression	6.0251	6.5237
Abalone	classification	96.46%	95.36%

Table 2 summarizes the type of problems (regression or classification) and the prediction performance (RMSE or accuracy) of DS-ELM and ELM model. Compared with ELM, it is obvious that DS-ELM provides a smaller value of RMSE or higher classification accuracy, that is, AD-ELM method outperforms the ELM method. That because AANN net removes noise of input data firstly, and then fixes input weights and bias of ELM which avoid the instability of ELM net.

Summary

In this paper, we have addressed the task of trying to improve the performance of ELM model for noisy data. ELM as a higher generalization performance than the traditional gradient-based learning algorithms, but when faced noisy data, the performance of ELM is needed to be improved. The new proposed DS-ELM model can filter noise of input data firstly, and then fix the input weights and bias of ELM, which makes the whole system becomes more stability and superior. So, DS-ELM is a better choice for the datasets with noisy.

References

[1] G.B. Huang, Q.Y. Zhu, and C.K. Siew, in: *Proceedings of International Joint Conference*, vol.2, Budapest, Hungary (2004), p.985-990.
[2] G.B. Huang, Q.Y. Zhu, and C.K. Siew: Extreme learning machine: theory and applications. Neurocomputing vol.70(2006), p.489-501.
[3] G.B. Huang, and L. Chen: Convex incremental extreme learning machine. Neurocomputing vol.70(2007), p.3056-3062.
[4] G.B. Huang, and L. Chen: Enhanced random search based incremental extreme learning machine. Neurocomputing vol.70(2008), p.3056-3062.
[5] G.B. Huang: Learning capability and storage capacity of two-hidden-layer feedforward networks. Neural Networks Vol.14(2003), p.274-281.
[6] D. Serre, in: *Theory and Applications*, edited by Springer, NY (2002).
[7] M.A. Kramer: Auto-associative neural networks. Computers in Chemicd Engineering, vol.16(1992), p.313-328.

Advanced Materials Research Vols. 989-994 (2014) pp 3683-3688
© (2014) Trans Tech Publications, Switzerland
doi:10.4028/www.scientific.net/AMR.989-994.3683

Design of 2_DOF Simulation Platform for the Testing of Airborne Laser Communication APT System

Lixin Meng[1,2,a], Dingxuan Zhao[1], Yangyang Bai[2], Lizhong Zhang[2]

[1]School of Mechanical Science and Engineering, Jilin University, Jilin .Changchun 130012

[2]Fundamental Science in Space-Ground Laser Communication Technology Laboratory, Chang chun University of Science and Technology, Jilin, Changchun 130022

[a]mengcust@163.com

Keywords: Motion simulation platform, Closed-loop vector method, Laser communication, Airborne.

Abstract. Lightweight, flexible motion simulation is the demand of airborne laser communication optical transceive when apply to outside test. A new parallel 2_DOF platform that has the function of azimuth and pitching is put forword based on the analysis of airplane position-pose changes affect the performance airborne laster communication APT system, and the kinematics model is established by using closed-loop vector method. Kinematics model is right through the comparison of mathematical model and simulation results of ADAMS, which provides the reference and basis for the design of control system.

Introduction

Wireless laser communication has the advantages of high-speed and large-capacity communication, anti-interference, anti-interception, security and the system needs small volume, small mass and low consumption. Meanwhile it is an important pattern in High-speed data transmission and wideband transmission in the future, also it's one of the most promising mode in communication. As the base of space laser communication, the acquisition, pointing and tracking subsystem is the first coming problem needs to be solved when starting the work on space laser communication.

Most of the laser communication platforms are mobile, the stability in motion and the change in gesture are two factors that restrict the performance of APT system. Among these mobile platform, the planes are the maximum mobility in the laser communication link. The effect of plane on tracking-pointing mechanism lie in high-frequency vibration and low-frequency posture change, and high-frequency vibration affect the stability of tracking-pointing mechanism while Low frequency swing affect the tracking performance [1,2]. Therefore, in the process of design and develop tracking-pointing mechanism, both low-frequency motion and high-frequency vibration in plane should be taken into consideration. Detecting the performance of APT system is an important method to improve the accuracy of APT system, and the best way is to detect its accuracy in real environment, however, it's almost impossible in the research on laser communication. The usual method is simulating movement characteristics of the carrier platform.

For far distance laser communication, a main factor affecting the performance of APT system is the posture change of carrier platform. Since laser communication is not imagining observation system, the effect of rotation of axis on performance of the system can be ignored, therefore the rotation of 2-DOF truly affect the performance of APT system. The common simulation platform in use are frame structure and parallel structure. Frame structure has advantage in control accuracy and velocity, but its structure is flexible and its capacity is small, also the location which place tasted parts is limited, the field of view can be occluded. Parallel structure is much compact and its capacity is bigger, in addition, the field of view can't be occluded, so parallel structure is first choice for simulating outfield motion.

Test about The Posture of Plane and Analysis of 2_DOF's Indicator

For control unit of coarse fine composite shaft of APT system, tracking accuracy,tracking velocity and tracking acceleration are mutual restraint. To acquire tracking accuracy, guaranteed precision angular velocity must be restricted [3,4]. When guaranteed precision angular velocity and guaranteed precision angular acceleration were given, the dynamic lag errors of the system is

$$\sigma_d = \sqrt{(\frac{\Omega}{K_v})^2 + (\frac{\varepsilon}{K_a})^2} \tag{1}$$

Where Ω is angular acceleration for relative movement, ε is angular velocity for relative movement, K_v is velocity quality coefficients for tracking system and K_a is acceleration quality coefficients for tracking system. As showing Eq. 1, the value of dynamic lag errors depends on both characteristics of tracking system and original incentive.

The low-frequency posture change of carrier platform can be measured by INS, the result is showed in Fig. 1.

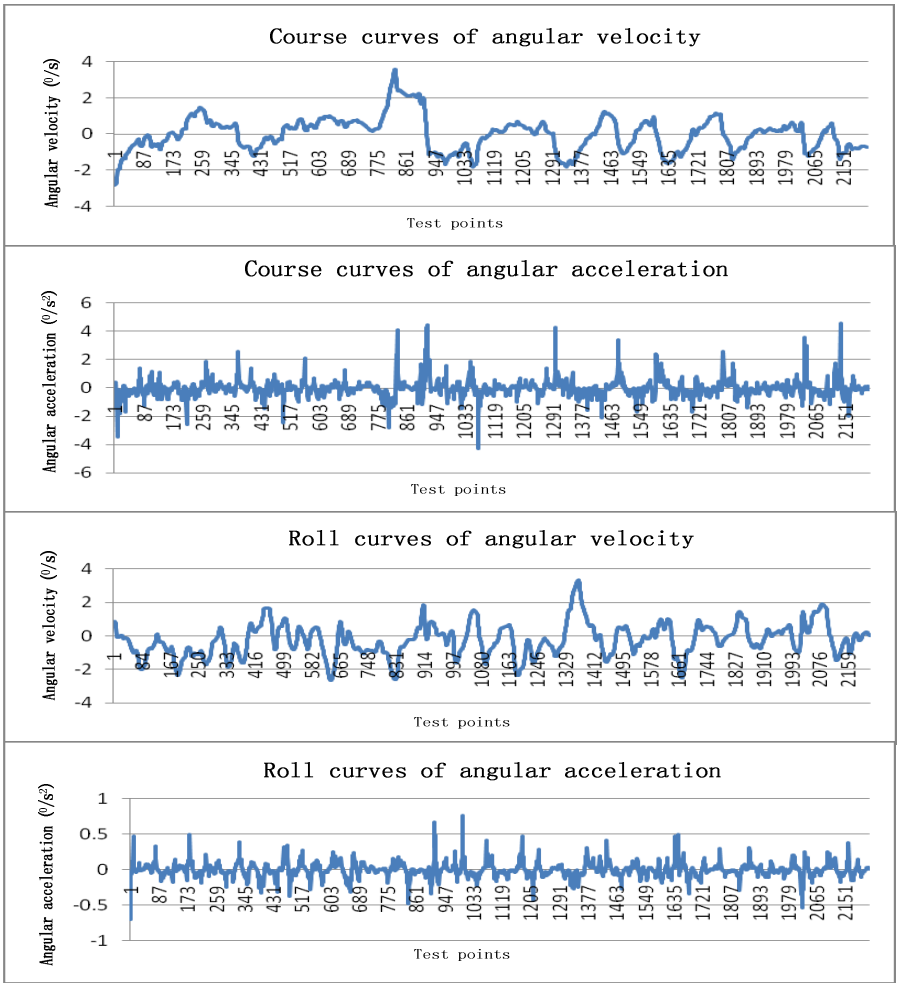

Fig. 1 Shows maximum posture change for tested carrier

Plane is about 6°/s ,and maximum acceleration is about 5°/s^2, in which, course correspond to direction of simulation platform and roll correspond to pitching of simulation platform. So considering the extension application of equipment, maximum simulating velocity of 2-DOF simulation tested rolling platform is 20°/s, maximum simulating acceleration is 20°/s^2, maximum range of motion is 15°.

2_DOF Parallel Simulation Platform's Design

Fig. 2 shows the structural diagram of the 2-DOF motion simulation platform, the system consists of moving platform, middle supporting platform (including 4 auxiliary support rods), center support, static platform, constraint rod A, servo electric cylinder A, B, C, and support beam of both ends (C_0C_1 and C_2C_3) plus 4 jointing hinges. The moving platform and middle supporting platform are connected by 4 support rods, the middle supporting platform and the static platform are connected by center support which installs the D2 self-lubricated spherical bearing, the center support link up to static platform by fixed point D1. The static platform, the self-lubricated spherical bearing, the middle supporting platform, and the moving platform are paralleled to each other, of which their centers are concentric. Constraint rod A and servo electric cylinder B are paralleled to the center axis O_1, O_2, O_3, O_4 of the simulation platform, perpendicular to the servo electric cylinder C. Joint A_2 and B_2 which connected to moving platform by spherical hinge are distributed at right angles in a circle which radius is R_0, joint C connected to the middle supporting platform by spherical hinge, joint A_1 and B_1 which connected to the static platform by Hooke through point C_1 are also distributed at right angles in the circle which radius is R_0. Servo electric cylinder B and C move at the same time to get the compound movement of azimuth and elevation of the simulation platform, this parallel mechanism has 2-DOF which is equal to the drive number, so there is no actuation redundancy.

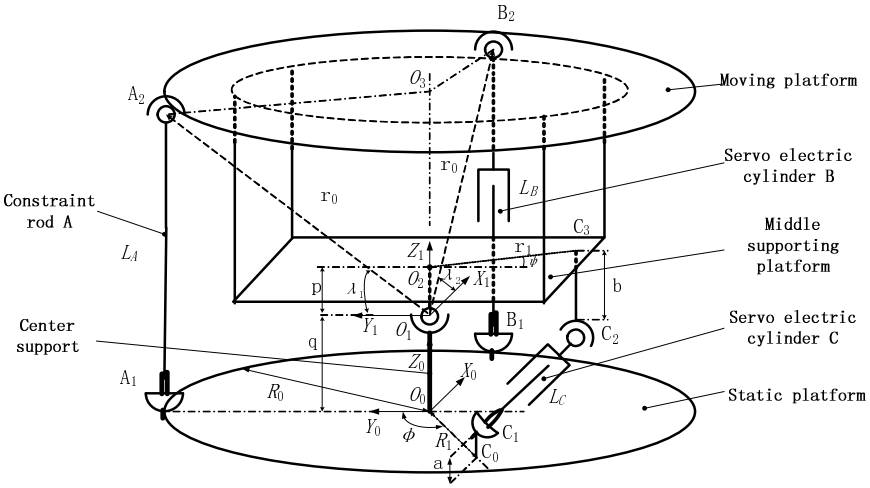

Fig. 2 2_DOF Structure of parallel simulation platform

We can establish a coordinate as shown in fig .2 firstly, then establish base coordinate O_0-$X_0Y_0Z_0$ in static platform and center coordinate O_1-$X_1Y_1Z_1$ in the center of the whole simulation platform of which the axes parallel to the other respectively in initial state. Supposing started at the initial position, the elevation rotates α degree around the Y_0 axis and the azimuth rotates β degree around the Z_0 axis then we get the current attitude coordinate (α,β), under Kaerdan angle coordinate transform relations [5,6,7] (Kaerdan angle applies to smaller angular transformation), in base ordinate any point E of the moving platform gets a coordinate vector $\overrightarrow{{}^0P_e}$:

$$\overrightarrow{{}^0P_e} = T\overrightarrow{{}^1P_e} + \overrightarrow{P_0} \tag{2}$$

Where, $\overrightarrow{{}^1P_e}$ is the coordinate degree of point E in the center coordinate, $\overrightarrow{P_0}$=(0,0,q) is the position vector of the center coordinate origin O_1 in the base coordinate, q is the vertical distance from O_1 to O_0, T is the direction cosine matrix from center coordinate O_1-$X_1Y_1Z_1$ to base coordinate O_0-$X_0Y_0Z_0$:

$$T=\begin{bmatrix}\cos\alpha\cos\beta & -\cos\alpha\sin\beta & \sin\alpha\\ \sin\beta & \cos\beta & 0\\ -\sin\alpha\cos\beta & \sin\alpha\sin\beta & \cos\alpha\end{bmatrix}$$

Setting the total length of the servo electric cylinder B and C at l_B and l_C respectively, and expressed as vector form is $\vec{l_B}=\overrightarrow{B_1B_2}$, $\vec{l_C}=\overrightarrow{C_1C_2}$, and we can get the position vector of points B_2 and C_2 in base coordinate O_0-$X_0Y_0Z_0$ according to closed loop vector method:

$$\overrightarrow{{}^0P_{B_2}}=\overrightarrow{O_0B_1}+\overrightarrow{B_1B_2}=\overrightarrow{O_0O_1}+\overrightarrow{O_1B_2} \tag{3}$$

$$\overrightarrow{{}^0P_{C_2}}=\overrightarrow{O_0C_0}+\overrightarrow{C_0C_1}+\overrightarrow{C_1C_2}=\overrightarrow{O_0O_1}+\overrightarrow{O_1O_2}+\overrightarrow{O_2C_3}+\overrightarrow{C_3C_2} \tag{4}$$

Simplify it we can get:

$$\vec{l_B}=T\overrightarrow{{}^1P_{B_2}}+\vec{P_0}-\vec{R_0} \tag{5}$$

$$\vec{l_C}=T\overrightarrow{{}^1P_{C_2}}+\vec{P_0}-\vec{R_1}-\vec{a} \tag{6}$$

Where, $\vec{R_0}$ is the direction vector from O_0 to B_1, $\vec{R_1}$ is the direction vector from O_0 to C_0, $\vec{a}$ is the direction vector from C_0 to C_1, modulus on both sides we can get :

$$\left|\vec{l_B}\right|=\left|T\overrightarrow{{}^1P_{B_2}}+\vec{P_0}-\vec{R_0}\right| \tag{7}$$

$$\left|\vec{l_C}\right|=\left|T\overrightarrow{{}^1P_{C_2}}+\vec{P_0}-\vec{R_1}-\vec{a}\right| \tag{8}$$

The coordinate degree of B_2 and C_2 in center coordinate is ${}^1P_{B_2}$ $(r_0\cos\lambda_2,0,r_0\sin\lambda_2)^{\mathrm{T}}$, ${}^1P_{C_2}$ $(r_1\sin\psi,-r_1\cos\psi,p-b)^{\mathrm{T}}$, among which r_0 represents the distance from the origin of center coordinate O_1 to hinge point B_2, r_1 represents the distance between the origin of center coordinate O_1 and hinge point C_2, b represents the vertical distance from hinge point C_2 to middle supporting platform, p is the distance from the center of middle supporting platform to the rotating center O_1 of simulation platform, λ_2 is angle between $\overrightarrow{O_1B_2}$ and X_1 axis, φ is angle between $\overrightarrow{O_0C_0}$ and -Y0 axis, ψ is angle between $\overrightarrow{O_2C_3}$ and -Y_1 axis, the rod length l_B and l_C changing with the angle formula can be settled when we substituting all above to Eq. 7 and Eq. 8:

$$\left|l_B\right|^2=\sqrt{\begin{aligned}&\left|\cos\alpha\cos\beta\cdot r_0\cos\lambda_2+\sin\alpha\cdot r_0\sin\lambda_2-R_0\right|^2+\left|\sin\beta\cdot r_0\cos\lambda_2\right|^2+\\&\left|-\sin\alpha\cos\beta\cdot r_0\cos\lambda_2+\cos\alpha\cdot r_0\cos\lambda_2+q\right|^2\end{aligned}} \tag{9}$$

$$\left|l_C\right|^2=\sqrt{\begin{aligned}&\left|\cos\alpha\cos\beta\cdot r_1\sin\psi+\cos\alpha\sin\beta\cdot r_1\cos\psi+\sin\alpha\cdot(p-b)+R_1\sin\phi\right|^2+\\&\left|\sin\beta\cdot r_1\sin\psi-\cos\beta\cdot r_1\cos\psi+R_1\cos\phi\right|^2+\\&\left|-\sin\alpha\cos\beta\cdot r_1\sin\psi-\sin\alpha\sin\beta\cdot r_1\cos\psi+\cos\alpha\cdot(p-b)+q-a\right|^2\end{aligned}} \tag{10}$$

Kinematics Simulation

According to technical indicators of the simulating platform, original structure parameters on simulating platform are setting as: the height between moving platform and static platform is(the length of restraint rod) 315mm, $R_0 = 185mm$, p = 33.5mm, through the simulation calculation and structure optimization, deducing the rest of the parameters: q = 106.5mm a = 85mm, $r_1 = 125mm$, b = 55, $r_0 = 278.7423mm$, $\lambda_2 = 48.41767^\circ$, $\phi = 110.6032^\circ$, $\psi = 53.1301^\circ$, $R_1 = 213.1320mm$.

To test the acquisition, pointing and tracking performance of airborne optical transmitter, 2-DOF simulation platform locomotes follows the change laws of azimuth α and pitching angle β. According to posture change of plane, equivalent sine for azimuth and pitch posture are:

$$\alpha = 12\sin(\frac{1}{2}t) \tag{11}$$

$$\beta = 5\sin(t) \tag{12}$$

Without considering error in joint clearance, setting up math model of simulating platform by numerical analysis software MATLAB, taking Eq. 11 and Eq. 12 into Eq. 9 and Eq. 10, we get change curves of the length of rod B, C in servo electric cylinder, meanwhile setting up 3D models of 2-DOF simulation platform by dynamics simulation software ADAMS [8,9], as showing in Fig. 3.

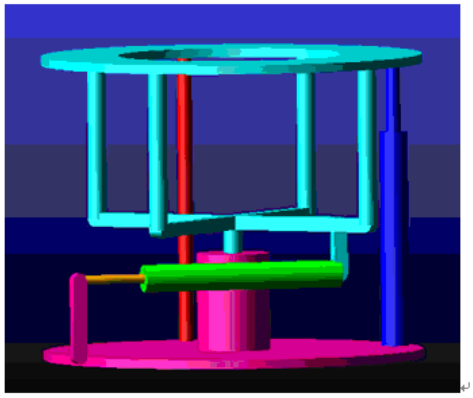

Fig. 3 The model of parallel simulation platform

Input the change laws of azimuth α and pitching angle β, simulation time is 30s, we get change curves of rod in servo electric cylinder by measuring the location changing of both ends. The computation result of maths model set by MATLAB and simulation result of 3D models set by ADAMS are shown in Fig. 4 and 5.

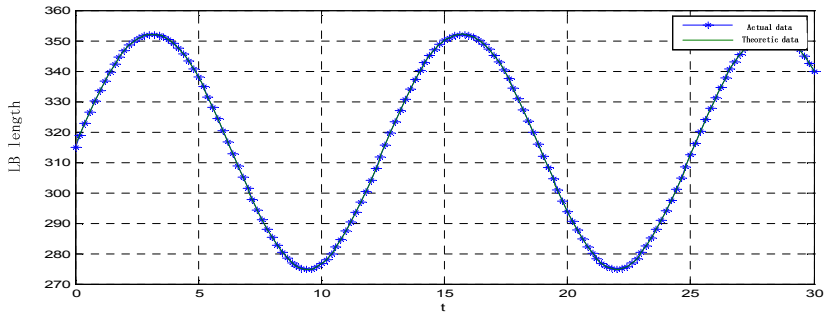

Fig. 4 The changing curve of servo electric cylinder B

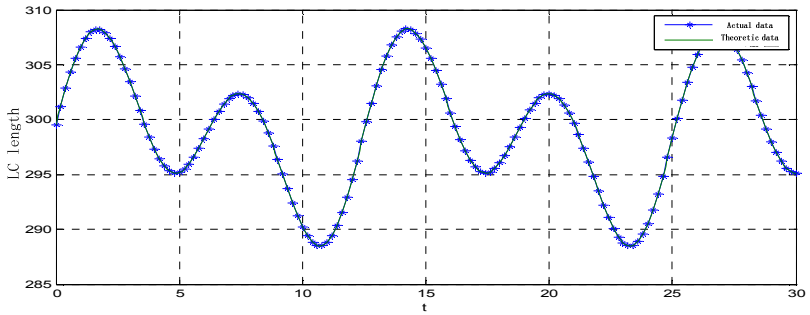

Fig. 5 The changing curve of servo electric cylinder C

The comparison analysis of length change get by mathematics modeling and physical machine simulating, two change curves of the length of rod in servo electric cylinder are consistent, indicating the setting maths model is right. Taking the data of the length change of rob calculated by MATLAB into spline made by ADAMA, loading the spline on two electric cylinders, measuring the change laws of azimuth and pitching angle, the result is exactly anastomotic with preestablished α and β. Through analyzing positive and negative solution of the results, it's indicating that the structure design of 2-DOF simulation platform is feasible both in theory and applications, providing math model for the design of next generation control system.

Conclusion

By setting and simulating math model of 2-DOF movement simulative platforms, the platform enable landing platform to motion in pitch and azimuth, meeting the testing requirements of posture change in APT system of airborne laser communication. In the meantime, since it has 2-DOF, controlling system is much simpler, the structure is light, small and simple, and it's very convenient for testing in external field.

References

[1] Huilin Jiang, Shoufeng Tong, etc. Space laser communication technology and the system (National Defence Industry Press, China 2010).

[2] Bobby.L and Ulich, "Overview of acquisition, tracking, and pointing system technologies",SPIE, 1988, Vol.887, pp.40-63.

[3] Lixin Meng, Lizhong Zhang, Xiaoming Li, Heyuan Sun: Automatic Control on Electrical Power System Vol.36,No.21(2012).

[4] Lizhong Zhang, Lixin Meng, Rui Xu, Huilin Jiang. Research of the Tracking Accuracy and Stabilization Accuracy Test on Airborne Platform. IEEE ICMA 2009 3201~3206.

[5] Zhen Huang, Lingfu Kong, Yuefa Fang. Parallel Robot Mechanism Theory and Control. (Machinery Industry Press, China 1997).

[6] Zhongbao Luo, Zhidong Yang, Dacheng Cong, Hui Zhang, Jia Guo: Robot.Vol.36,No.21(2012).

[7] Zhu.Z.s, Dou.R.l. Optimum design of 2-DOF parallel manipu-lators with actuationv redundancy[J]. Mechatronics, 2009, 19(5):760-768.

[8] Ying Qiu, Weimin Li, Tiehong Gao.The Simulation and Study on 2-DOF Parallel Mechanism. Advanced Software Engineering and Its Applications, 2008. ASEA 2008.

[9] Lining Sun, Qingyong Ding, Xinyu Liu. Chinese Journal of Mechanical Engineering, Vol.41, No.7(2005).

Advanced Materials Research Vols. 989-994 (2014) pp 3689-3692
© (2014) Trans Tech Publications, Switzerland
doi:10.4028/www.scientific.net/AMR.989-994.3689

The Method of Optimal Group Based on the Kernel Density Estimation and the Close Degree

YE Fei[1, a], WANG Xin[1, b], PENG Donghui[1, b], JIAO Chuanhai[1, d]

[1] New Star Institute of Applied Technology, Anhui Hefei, 230031, China

[a]yefeixyz@163.com, [b]wx245061@163.com, [c]354214520@qq.com, [d]jiao_chuanhai@126.com

Key words: kernel density estimation, histogram, optimal group, the close degree

Abstract. The optimal group is an important problem of histogram algorithm, and how to confirm group number has not a quantitative rule. So the concept of the close degree is imported to make the close degree between the upper contour line of histogram and the PDF(probability density function) of parameter as the judging criteria of optimal group. With the unknown of the PDF of parameter, the improved kernel density estimation algorithm can pre-select and estimate the PDF. This improved kernel density estimation algorithm combine the selection of fixed window and variable window's width to achieve the window's width automatic adjustment value between the different estimation points based on the sample distribution. In the parameter analysis of radar emitter signal, the algorithm based on improved kernel density estimation and close degree is used to determine optimal group, and the result indicate that this method is effective and can search the optimal group automatically.

Introduction

The histogram algorithm has visual concept and can achieve simply, but it need to solve two major problems: Data range extension and optimal group. The optimal group problem is more critical, because it is a complex and difficult problem by the effectiveness of histogram[1].So In the paper, the concept of close degree is introduced to solve this problem. According to the probability density curve that the parameters obey, the close degree between the histogram upper contour line and the parameter probability density function is calculated to be the judging criteria of optimal group. If the parameter probability density function doesn't know, kernel density estimation can be used.

The optimal group principle based on the close degree

A T is a set of a real parameter observation data, the interval A is the parameter range, $\delta_i (i = 1,2\cdots, N)$ is the subinterval of A and f_i called frequency is numerical number of which in interval T fall into the subinterval δ_i .Among them, δ_i and f_i respectively satisfy the following conditions:

(1)For arbitrary i and j $(i = 1,2,\cdots, N; j = 1,2,\cdots, N; i \neq j)$, the intersection between δ_i and δ_j is empty, that is $\delta_i \cap \delta_j = \phi, \phi$ is empty set.

(2) $\bigcup_{i=1}^{N} \delta_i = A$

According to specific situation, the width of $\delta_i (i = 1,2\cdots, N)$ can be equal and can also not be equal. To make N rectangles called histogram with the width of subinterval δ_i and f_i as side length. Taking the parameter values range as the transverse, the frequency as the longitudinal axis, and placing each histogram in transverse according to relevant δ_i, so the graphic made like this is called histogram.

Normalizing the histogram, and making $f_i' = \frac{f_i}{N}$,let the upper contour line of the normalized histogram function be $f(x)$, as shown in figure 1.The probability density function that the parameters obey is $p(x)$,and define the close degree between $f(x)$ and $p(x)$ is:

$$\sigma = \frac{\int_{-\infty}^{+\infty} \min[f(x), p(x)]dx}{\int_{-\infty}^{+\infty} \max[f(x), p(x)]dx} \tag{1}$$

The smaller close degree explains the upper contour line of histogram and parameter probability density function are closer and the group is better at the moment; the bigger close degree explains the upper contour line of histogram and parameter probability density function are far and the group is not optimal at the moment. If the probability density function of the parameters is unknown, kernel density estimation methods can be used to estimate.

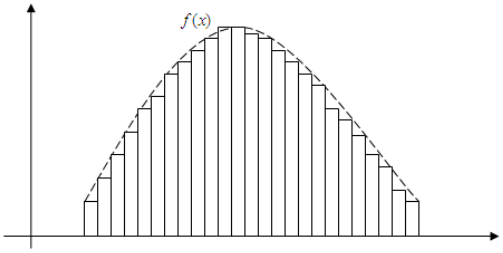

Figure1 The diagram of normalized histogram upper contour line

Improved kernel density estimation algorithm

$X_1, X_2, \cdots, X_n$ is the sample of the same independence distribution pumped from one dimension X , X has the unknown probability density function $p(x)$, $x \in R$,the kernel density estimation of $p(x)$ is[2]:

$$\hat{p}(x) = \frac{1}{nh}\sum_{i=1}^{n} K(\frac{x - X_i}{h}) \tag{2}$$

n is number of the sample set; $K(u)$ is the kernel density estimation function, referred to as kernel function; h is the window width that decides the variance of the kernel function. The selection of window width is the key to the success of the kernel density estimation. The selection of optimal window width can be divided into two categories: the fixed window width and the variable window width.

The fixed window width assumes that the real density $p(x)$ obeys the distribution of $N(\mu, \sigma^2)$ and make the error between density estimation and the real density minimum, then the optimal window width can be got[3] [4]:

$$h_{opt} = 1.059\sigma n^{-\frac{1}{5}} \tag{3}$$

$\sigma = [\frac{1}{n}\sum_{i=1}^{n}(x_i - \bar{X})]^{1/2}$, n is the number of the sample, $\bar{X}$ is the average of the sample set.

The variable window width begins from the error between the density estimation and the real density, makes minimum h of the mean square error between the density estimation and the real density as the optimal window width.

$$MSE(h_0) = E[\hat{p}(x) - p(x)]^2 \tag{4}$$

To get the optimal window width through the minimization of $MSE(h_0)$:

$$h^*(x) = n^{-1/5}[(k_2 p''(x))^{-2} p(x)\int_{-\infty}^{\infty} K^2(u)du]^{1/5} \tag{5}$$

$k_2 = \int_{-\infty}^{\infty} u^2 K(u)du$ .The value of $h^*(x)$ is related to the density estimation point x from equation (5) , its value changes with the different estimate points, when using the result of the above equation to solve the distribution density of x , the window width value changes with x, the variable window width can better reflect the smooth degree of the different points in estimated interval , reduce the fitting curve deviation in the top area and improve the flexibility of the fitting curve[5]. But the true density is unknown, or there is no need to estimate. So $h^*(x)$ can't be calculated. Another processing method is equal to the fixed window width selection, supposing a real density. Yet for an unknown distribution, the probability density function through the kernel density estimation, in most cases, should be closer to the actual than a hypothetical distribution. Therefore, the improved kernel density estimation method can be got through combining fixed window width selection and the variable window width selection, the specific steps are as follows:

(1)Calculating the fixed optimal window width h_{opt} according to formula (3);

(2)Calculating the real density estimation $\tilde{p}(x)$ according to formula (2);

(3)Calculating the variable window width $h^*(x)$ using $\tilde{p}(x)$ to replace the real density $p(x)$ according to formula (5);

(4)Calculating the final probability density estimation $\hat{p}(x)$ through using $h^*(x)$ as window width according to formula (2).

The simulation results

It is applied to analysis the basic parameters pulse repetition period of radar emitter signals (PRI) to test the validity of the histogram algorithm based on kernel density estimation. The value of the repetition cycle fixed type is set as 50 ms; The center value of repeat cycle jitter types is 50 ms; The values of repeat cycle three principal types are 50 ms, 100 ms, 150 ms; The values of repeat cycle agile or sliding variable are 40ms, 42.5ms, 45 ms,47.5 ms, 50ms ,52.5ms, 55ms, 57.5ms,60ms. Each type of simulation has 500 samples, and set the measurement error of 1%. The probability density function is estimated which the parameters are obeyed before analysis of the parameter by using the improved kernel density estimation algorithm.

The close degree is $\sigma_{th} = 0.85$ in the experiment. Using the following method to determinate data range extension: calculating the average of the samples $\overline{x} = \frac{1}{n}\sum_{i=1}^{n} x_i$ and the standard deviation $S_x = \sqrt{\frac{1}{n-1}\sum_{i=1}^{n}(x_i - \overline{x})^2}$, then the lower limit value of the parameters can be $(x_{\min} - w' \times S_x)$ and the upper limit value can be $(x_{\max} + w' \times S_x)$, $x_{\min}$ and $x_{\max}$ are the minimum and maximum of $x_i (i = 1, 2 \cdots n)$, $w' = 0.25$ in the experiment. There adopt equidistant grouping in experiment, when the close degree between the top contour line function of the histogram and the probability density function is less than the threshold σ_{th}, stop searching. At the moment, the close degree and the group number are as shown in table 1, the probability density curve and the histogram of the optimal grouping are as shown in figure 2 and figure 5. Histogram can clearly reflect the work type of parameters and the value when the optimal number is got from the graph.

Table1 The optimal group and close degree of different type PRI

Work type	Optimal group	Close degree
Fixed	7	0.8847
Stagger	21	0.8792
Jitter	16	0.9245
Agility	27	0.9143

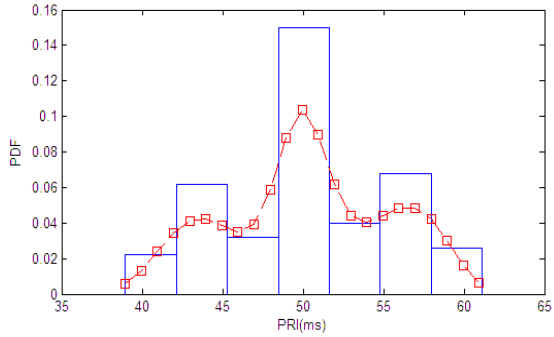

Figure2 The probability density curve and the histogram of the fixed PRI

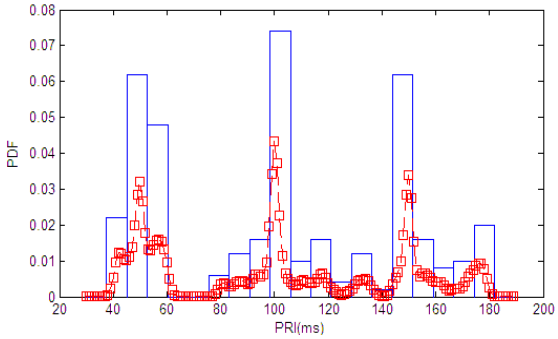

Figure3 The probability density curve and the histogram of the three stagger PRI

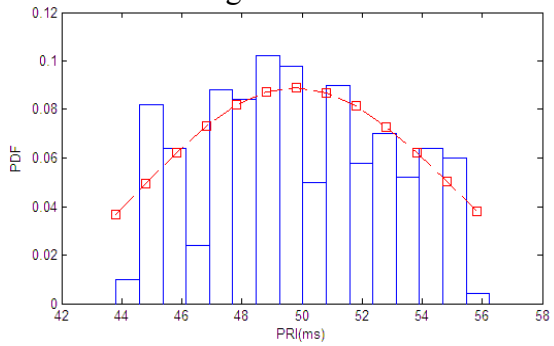

Figure4 The probability density curve and the histogram of the jitter PRI

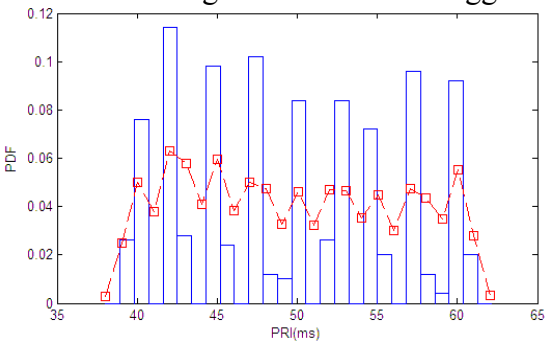

Figure5 The probability density curve and the histogram of the agility PRI

Conclusion

The concept of close degree is introduced to solve the problem of optimal grouping of histogram method. The close degree between the upper profile of histogram and the probability density function that parameters obey is the decision criteria of the optimal grouping. The probability density function of parameters can be primarily got by making use of the improved kernel density estimation algorithm with the variable window width. The histogram algorithm based on the improved kernel density estimate and the close degree is applied to analysis the basic parameters of radar emitter signals PRI, and the results show that this method can quantitatively get the optimal grouping number.

References

[1] LiuDianRui. A histogram of the optimal grouping problem [J]. Journal of geophysical and chemistry exploration , 1995, (1) : 62-67

[2] DengBiao, YuChuanQiang LiTianShi, SuWenBin, PanYangKe.The double window width kernel density estimation algorithm based on the estimation points [J]. Journal of instrument. 2001, 32 (1) : 615-620

[3] LiYun, HuangMinghui. The optimal window width choice improvement of Kernel density estimation point by point [J]. Journal of statistics and decision making. 2011, (14) : 28-32

[4] YuChuanJiang, GuoXiaoSong ZhangAn, WuHaiCheng.The sliding window width kernel density estimation algorithm based on the estimation points [J]. Journal of texas. 2009, 30 (2) : 231-235

[5] Lenk P J. Bayesian semiparametric density estimation and model verification using a logistic-gaussian model[J]. Comput.Graph.Stat,2003, 12: 548-565

Advanced Materials Research Vols. 989-994 (2014) pp 3693-3697
© (2014) Trans Tech Publications, Switzerland
doi:10.4028/www.scientific.net/AMR.989-994.3693

Research of Frequency-Hopping Communication for Arbitrary Array Based on Adaptive Beam-forming

Qiao Chenglin, Quan Houde, Cui Peizhang

Information Engineering Department, Mechanic Engineering College, Shijiazhuang 050003, China

email: qiaochenglin@126.com

Key words: FH communication; arbitrary array; CTMV; SINR

Abstract. Aiming at the problem of poor performance of suppressing the wide band jamming and fast following jamming in Frequency-Hopping(FH) communication system, a communication scheme by combination of the complementally transformed minimum variance with FH technique for arbitrary array(CTMV-FH) is proposed, based on the purpose to maximize the output Signal to Interference and Noise Ratio (SINR). Basic theory of CTMV is introduced. The algorithm is used to suppress the wide band jamming and fast following jamming. Simulation results show that the scheme can suppress the wide band jamming and fast following jamming effectively in FH communication system.

Introduction

Frequency-Hopping(FH) communication has strong ability of anti-jamming and anti-interception, which is widely used in the military communication, such as satellite FH communication and VHF radio FH communication. The wide-band jamming and fast follower jamming are the main threate for the FH communication [1]. The combination of adaptive nulling antenna with FH technique is first proposed to improve the ability of anti-jamming by Faik Eken [2]. Qiu and Montse Najar are further studying on the FH system with the wide-band jamming[3-5]. But they are not considering the case that the wide-band jamming and fast follower jamming are existing at the same time. In [6] [7], to this case, a combination of the eigenspace-based beamformer(ESB) with spatial smoothing algorithm(SS) is proposed [8]. The technique can suppress the wide-band jamming and fast follower jamming with array aperture reduction and effective element loss. An improved SS is proposed in [9] [10], which can suppress the wide-band jamming and fast follower jamming without array aperture reduction and effective element loss. But the technique of SS can only be used in the uniform linear array, it is invalid for arbitrary array. In [11], the complementally transformed minimum variance beamformer(CTMV) is used to suppress the coherent interference for arbitrary array, which obtains a well results.

In this paper, a communication scheme by combing of CTMV with FH technique for arbitrary array is proposed (CTMV-FH). Then system model of the scheme is introduced. Some necessary background is presented in next chapter. Then CTMV is presented for suppressing the wide-band jamming and fast follower jamming. Several simulation examples will illustrate the effectiveness of the proposed method. Conclusions are given in final chapter.

System model

The combination of adaptive nulling antenna with FH technique can discriminate the signal and interference in spatial-frequency domain, which can be further improve the ability of anti-jamming. The structure of CTMV-FH system is shown in Fig.1.

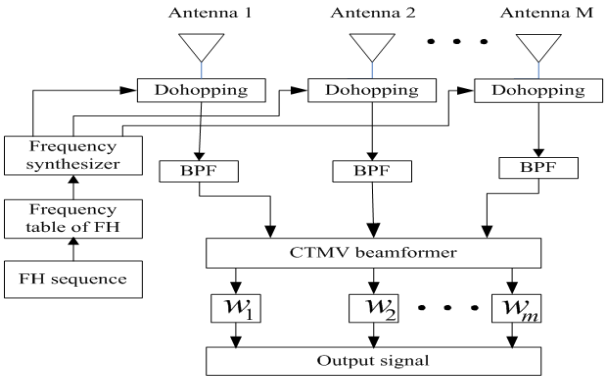

Fig.1 Structure of CTMV-FH system

The signal is received by RF of each array element. Firstly, the signal goes through the dehopping module. Secondly, the intermediate frequency signal is obtained by taking the dehopping signal through band pass filter(BPF). Finally sampling the intermediate frequency signal and taking it into adaptive beamforming module. Because the time-resident of each hop is very short, the adaptive beamforming algorithm must have fast convergence speed. So CTMV is used to suppress the wide-band jamming and fast follower jamming for arbitrary array.

Background

The wide-band jamming and fast follower jamming are seen as uncorrelated interferer and coherent interferer in the FH system, respectively. Consider a desired signal, P uncorrelated interferers and Q coherent interferers impinging on an M-element arbitrary antenna array from θ_0, θ_i and θ_j, respectively. The received complex-valued data vector $X(t)$ can be expressed as

$$X(t) = a(\theta_0)s_0(t) + \sum_{i=1}^{P} a(\theta_i)s_i(t) + \sum_{j=P+1}^{P+Q} a(\theta_j)s_j(t) + n(t) \tag{3-1}$$

Where $s_0(t)$, $s_i(t)$ and $s_j(t)$ denote the waveforms of the desired signal, the ith coherent interferer and jth uncorrelated interferer, respectively. $a(\theta)$ denotes the steering vector. $n(t)$ is an additive white Gaussian noise (AWGN) vector.

Based on the maximum SINR principle, the optimal weight vector can be given as

$$W_{opt} = \alpha R_{i+n}^{-1} a(\theta_0) \tag{3-2}$$

Where α is a constant and R_{i+n} is the interference-plus-noise covariance matrix.

So far, some adaptive beamforming algorithms such as direct matrix inversion(DMI) and eigenspace-based beamforming(ESB) can only obtain approximate value of R_{i+n} without the coherent interferer. SS and its improved algorithm can obtain a well approximate value with the coherent interferer, but these algorithms just apply to uniform linear array. For this purpose, CTMV is used to obtain R_{i+n} for arbitrary array with the coherent interferer.

CTMV

The desired signal is removed from the array data with other coherent interferers unchanged by using a linear transformation in CTMV[11].

Considering that there is a linear transformation $T(M \times M)$, it satisfying

$$Ta(\theta_0) = 0, Ta(\theta_i) = a(\theta_i), i = 1, 2, ..., P \tag{4-1}$$

The transformed data

$$TX(t) = \sum_{i=1}^{P} a(\theta_i)s_i(t) + \sum_{j=P+1}^{P+Q} Ta(\theta_j)s_j(t) + Tn(t) \tag{4-2}$$

Except for the desired signal, the only difference between (4-2) and (4-1) is the uncorrelated interference and noise. Thus, the transformation should minimize the impact on uncorrelated interference and noise. In other words, the transformation should minimize the error between the original data and the transformed data

$$E[\|TX - X\|^2] = tr[(T - I) R_x (T - I)^H] \quad (4\text{-}3)$$

Where R_x is the covariance matrix. $E[\bullet]$, $\|\bullet\|$ and $tr[\bullet]$ denote the expectation, the vector two-norm and trace operator, respectively.

The linear transformation can be solved by using Lagrange multiplier.

$$T = I - (A - B)(A^H R_x^{-1} A)^{-1} A^H R_x^{-1} \quad (4\text{-}4)$$

Where $A = [a(\theta_0), a(\theta_1), a(\theta_2), ..., a(\theta_P)]$ and $B = [0, a(\theta_1), a(\theta_2), ..., a(\theta_P)]$.

Then (4-5) is proved in [11]

$$Ta(\theta_j) = a(\theta_j) - (A - B)(A^H R_x^{-1} A)^{-1} A^H R_x^{-1} a(\theta_j) \approx a(\theta_j), j = P+1, P+2, ..., P+Q \quad (4\text{-}5)$$

Thus, the uncorrelated interference almost invariably by using the linear transformation .

To remedy the sensitivity problem, R_x should be modified into a better conditioned form. The diagonal loading algorithm is the simple method to decrease the sensitivity problem. Thus,

$$\overline{R}_x = R_x + \lambda I \quad (4\text{-}6)$$

Where λ and $I(M \times M)$ denote the diagonal loading factor and identity matrix, respectively. Finally, we obtain the linear transformation T

$$T = I - (A - B)(A^H \overline{R}_x^{-1} A)^{-1} A^H \overline{R}_x^{-1} \quad (4\text{-}7)$$

Combining with (3-2), the weight vector is

$$W = (TR_x T^H)^{-1} a(\theta_0) / (a^H(\theta_0)(TR_x T^H)^{-1} a(\theta_0)) \quad (4\text{-}8)$$

The weight vector is solved by (4-8) can raise two problems. Firstly, the correlation matrix $TR_x T^H$ is not always singular. Secondly, the noise component in $TR_x T^H$ is no longer the same as in the original R_x. So the noise part in $TR_x T^H$ should be replaced by $\sigma_n^2 I$

$$\widetilde{R}_x = TR_x T^H - \sigma_n^2 TT^H + \sigma_n^2 I \quad (4\text{-}9)$$

Finally, we obtain the weight vector

$$W = \tilde{R}_x^{-1} a(\theta_0) / (a^H(\theta_0) \tilde{R}_x^{-1} a(\theta_0)) \quad (4\text{-}10)$$

Through the above analysis, we can find that combining CTMV with FH can effective suppress the wide-band jamming and fast follower jamming. Computer simulation results will demonstrate performance of the proposed scheme in next chapter.

Simulations Results

In this section, simulation results are presented to demonstrate the performance of the proposed scheme. Considering a FH system, it works from 30MHz to 90MHz. Choose three points of frequency hopping random. Assuming the three points are {30, 40, 50} *MHz*. In order to compare with virtual spatial smoothing algorithm (VSS), the array element locations are {0, 3, 6, 9, 12, 15, 18, 21} *m*. The desired signal with SNR of 0dB impinges from $\theta_0 = 0^\circ$. The wide-band jamming and fast follower jamming with INR of 30dB impinge from $\theta_1 = 40^\circ$ and $\theta_2 = -20^\circ$, respectively. The diagonal loading factor is 10. The number of snapshots of each point of FH is 200. All results are averaged based on 100 independent Monte Carlo simulation runs.

A. Only existing the wide-band jamming

Tab.1 is the comparison of different algorithms with the wide-band jamming (the third point of FH for example). Clearly, the output of CTMV is higher than DMI and ESB, and it is closer to optimum value. Fig.2 shows the output SINR versus number of snapshots of different algorithms in three points of FH with the wide-band jamming. It can been seen that CTMV has a better

convergence speed than DMI and ESB. Fig.3 shows comparison of the beampatterns with the wide-band jamming(the third point of FH for example). Combining with Tab.1, the nulling of CTMV is deeper than DMI and ESB. Therefore, CTMV has a better performance than DMI and ESB with the wide-band jamming in FH communication system.

Tab.1 Comparison of different algorithms with the wide-band jamming

Gain/dB	DMI	ESB	CTMV	Optimum
$F(\theta_1)$	-57.1	-55.5	-59.7	-94.7
Output SINR/dB	7.9	8.5	8.8	8.9

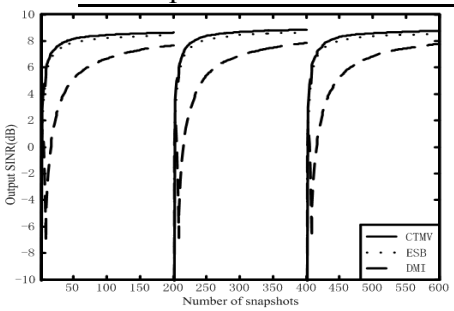

Fig.2 Output SINR versus number of snapshots with the wide-band jamming

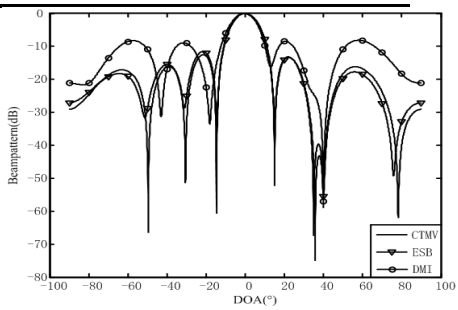

Fig.3 Comparison of the beam-pattern with the wide-band jamming

B. Existing compound interferences

Tab.2 is the comparison of different algorithms with the compound interferences (the third point of FH for example). Clearly, because of the coherent interferer, DMI and ESB can not obtain high output SINR. Opposite, VSS and CTMV can also achieve high output SINR and the latter is higher than the former. Fig.4 shows the output SINR versus number of snapshots of different algorithms in three points of FH with the compound interferences. It can been seen that CTMV has a faster convergence speed and higher output SINR than DMI, ESB and VSS. Fig.5 shows comparison of the beampatterns with the compound interferences(the third point of FH for example). Combine with Tab.1, it can be observed that the wide-band jamming can be suppressed by all algorithms, but the fast follower jamming can be only suppressed by VSS and CTMV. Furthermore, the nulling of CTMV is deeper than VSS. Therefore, CTMV has a better performance than DMI, ESB and VSS with the compound interferences in FH communication system.

Tab.2 Comparison of different algorithms with the compound interferences

Gain/dB	DMI	ESB	VSS	CTMV	Optimum
$F(\theta_1)$	-89.0	-47.8	-93.8	-75.0	-134.6
$F(\theta_2)$	-29.7	0	-43.0	-96.6	-90.6
Output SINR/dB	-0.6	-42.2	7.3	8.5	8.7

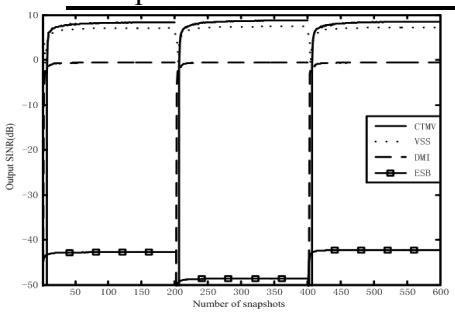

Fig.4 Output SINR versus number of snapshots with the compound interferences

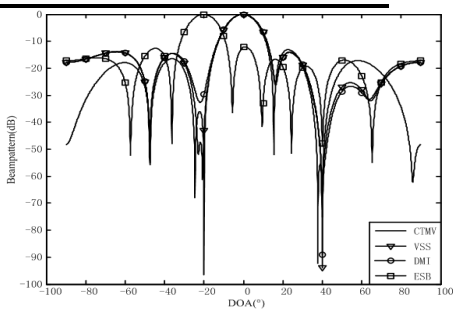

Fig.5 Comparison of the beam-pattern with the compound interferences

Conclusion

A communication scheme by combination of CTMV with FH technique for arbitrary array is proposed in this paper. Theoretical analysis and simulation results have been presented to demonstrate the wide-band jamming and fast follower jamming can be effective suppressed by

CTMV for arbitrary array in FH communication system. Furthermore, the scheme has a fast convergence speed. So it is suitable for FH communication and it can provide a reference for military FH communication, such as satellite FH communication and VHF FH communication. However the steer vector of desired signal always mismatch in the practice, which needs further research.

References

[1] Wenhua Mei, Shubo Wang, Yonghong Qiu. Frequency Hopping Communications[M]. Beijing: National Defense Industry Press, 2005.9.

[2] Faik Eken, Use of antenna nulling with frequency-hopping against the following jammer[J], Trans on Antenna and Propagation, 1991,39(9):1391-1397.

[3] Yonghong Qiu, Zhongmin Gan. Research of nullifying frequency-hopping jamming on the basis of adaptive digital beamforming[J], Journal of china institute of communications, 2000,21(7):39-44.

[4] Montse Najar, Miguel A. Lagunas, High Resolution Adaptive Arrays Based on Random Processing Technicals: Frequency Hopping Modulation[J], Acoustics, Speech, and Signal Processing, 1995,3:1737-1740.

[5] R.T. COMPTON, JR., Fellow. The Performance of an LMS Adaptive Array with Frequency Hopped Signals[J]. IEEE TRANSACTIONS ON AEROSPACE AND ELECTRONIC SYSTEMS Frequency Hopped Signals, 1985, 21(3):360-370.

[6] Zhiqiang Duan, Linrang Zhang, Yongchun Zhu. A jamming rejection method for FH system based on adaptive antenna[J], CHINESE JOURNAL OF RADIO SCIENCE, 2004,19(6):726-729.

[7] Zhiqiang Duan. Study on Adaptive Antenna for Frequency-Hopping System[D]. Xian: Xian Electronic Science &Technology University, 2004.

[8] S.U. Pillai, B.H. Kwon. Forward/backward spatial smoothing techniques for coherent signal identification[J], IEEE Transactions on Acoustics, Speech, and Signal Processing, 1989,37:8–15.

[9] Lei Zhang, Wei Liu. Robust beamforming for coherent signals based on the spatial-smoothing technique [J]. Signal Processing, 2012,92:2747-2758.

[10] Jiadong Shang, Zulin Wang. Research of Traching Interference Suppression in FH System Based on Two-dimensional Virtual Space Smoothing Algorithm[J]. Journal of Electronics & Information Technology, 2011,33(5):1193-1197.

[11] Ta-sung Lee, Tsui-Tsai Lin. Coherent Interference Suppression with Complementally Transformed Adaptive Beamformer[J]. TRANSACTIONS ON ANTENNAS PROPAGATION,1998,46(5):609--617.

Advanced Materials Research Vols. 989-994 (2014) pp 3698-3701
© (2014) Trans Tech Publications, Switzerland
doi:10.4028/www.scientific.net/AMR.989-994.3698

Research on Fabric Image Acquisition based on Compressed Sensing

Jicheng DONG[1, a] ,Shengqi GUAN [1, b]and Longlong CHEN[1, c]

[1]Department of Mechanical and Electrical Engineering , Xi'an Polytechnic University, Xi'an, Shanxi, 710048, China

[a]email: 421798321@qq.com, [b]email: sina1300841@163.com,

[c]email: chen40802040213@163.com

Keywords: Compressed Sensing; Fabric Image; Spare Representation; Sub-sampling

Abstract. Amount of data in collecting data of fabric image in the textile industry put forward a new challenge to sensor end. Compressed Sensing(CS) breaks limit of conventional Shannon's sampling theorem, so we can reconstruct a signal in Sub- sampling rate. In addition, theoretical analysis tells us that collecting the fabric image data by CS method have a better advantage than collecting the general image data. Having reconstructed three fabric images and one general image by CS method, we can easily find that the former have a high quality of reconstruction.

Introduction

Image signal is gradually favored by people owing to having rich information. As a key step to achieve textile machinery automation, collecting large amounts of image data is necessary. According to Shannon Theorem, to accurately reconstruct a signal, sampling rate must be 2 times higher than maximum frequency of the signal itself [1]. Image signal with high frequency will inevitably lead to sharp increasing in collecting data, and this must pose a severe challenge to the sensor which usually have a low operation rate.

In recent years, Compressed Sensing theorized by Candes, Tao and Donobo points out that sparse signal in a transform domain can be accurately or approximately reconstructed by a Sub-sampling rate which is lower than the Shannon sampling rate [2]. This theory has been widely used in Imaging, Sensor networks the, MRI, astronomy, and other fields, such as single-pixel camera made in Stanford University, magnetic resonance imaging, analog-digital converters.

CS requires signal sparsely in a transform domain, and CS sampling rate is negatively correlated with sparsity, fabric image should be lower CS sampling rate than usual because of it's higher sparsity [3]. we have a MATLAB text, and the result shows it works.

Compressed sensing analysis

Let's look at an intuitive example.Signal f has k nonzero values in Fig.1(here k = 2, f called k-sparse). We use a set of waveforms signals to measure f, in other words,we get five measurements through inner product between signal f and five waveforms signals according to the Eq.1:

$$y = \phi f \tag{1}$$

Above, ϕ is an matrix($M<N$,here $M= 5$, $N= 15$), f is an N-dimensional vector, y is a M-dimensional vector, any 2k columns are linearly independent, then the k-sparse vector f can be uniquely reconstructed. It is easy to know the number of measurements is less than the length of the signal itself, this may be the essence of CS [4].

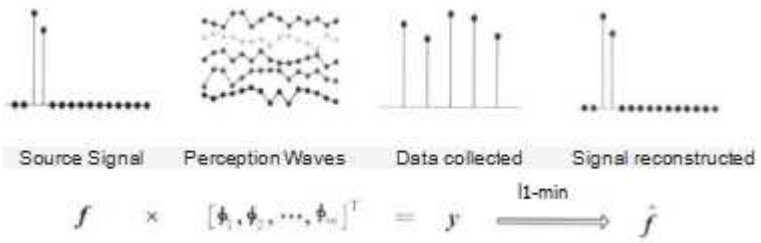

Fig.1. CS sampling mechanism flowchart

Spare representation. Image signal itself is hardly sparse, yet it has a high sparsity in a transform domain which can represent image signal features. CS asks signal being sparse in a transform domain, in other words, only few basis vectors can fully describe the signal. An N-length time signal can be described as follows:

$$X = \Psi S \tag{2}$$

Among above, each row of matrix Ψ called transformation matrix is the coordinate vector of this transform domain, and S is the coordinate value of signal in transform domain. Some transformation is often used such as DCT, DWT, DFT and so on.

Encoding measurement. Measurement matrix Φ is M x N(M<N), signal X is projected onto a set vectors based on each row in Φ. Assuming measurements is Y, which is presented as Eq. 3, Θ called sensing matrix, we can know:

$$Y = \Phi X = \Phi \Psi S = \Theta S \tag{3}$$

Decoding reconstruction. To reconstruct the signal exactly,matrix Θ must satisfy the Restricted Isometry Property (RIP) [5]. The main methods include Basis Pursuit and Greedy Algorithm [6], such as minimum 1-norm,orthogonal matching pursuit. Brief introduction to Minimum 1-norm as Fig.2, OMP introduction as Fig.3, we can easily get it.

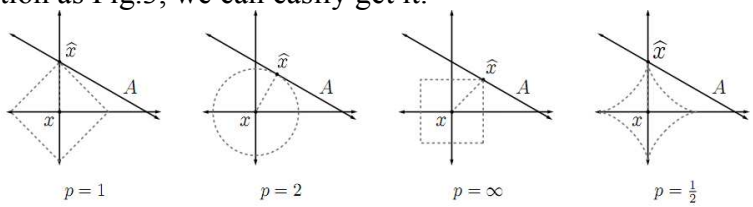

Fig.2. Best approximation of a point inby a one-dimensional subspace using the l_p norms for p = 1, 2, … and for the quasinorm with p = 1/2

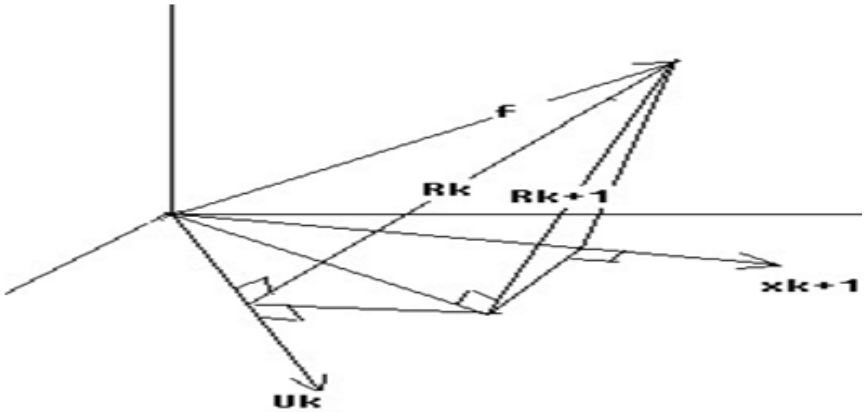

Fig.3. Fast approximation of f by combination of Component in subspace U_k and Projection in vector X_{k+1} which is independent on U_k

Test analysis

Here we have two experiments using DCT, Gaussian matrix, OMP algorithm, three fabric images and lena image. one is comparison of Nyquist method and CS method at same sampling rate, the other is comparison of the usual image and the fabric image by using CS method.

Test.1. Comparison of Nyquist and CS. We have a BROKEN END image reconstructed. In Fig.4, image above is obtained by Nyquist method, and image below is obtained by CS method .The PSNR of former is 34.6, however the latter is 41.

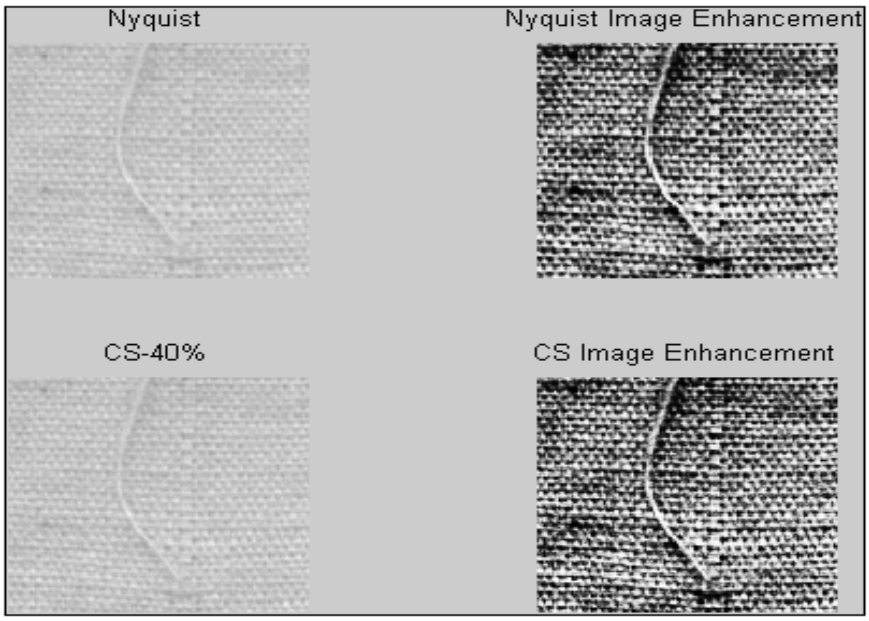

Fig.4. Comparison of Nyquist method and CS method at 40% sampling rate

Test.2. Comparison of usual image and fabric image. In Fig.5, (c)~(d) are fabric images whose left is source image, the other is reconstructed image,and (a) is a usual image. (e) is the Relative Error of each reconstructed image at different sampling rate, and (f) shows their PSNR .

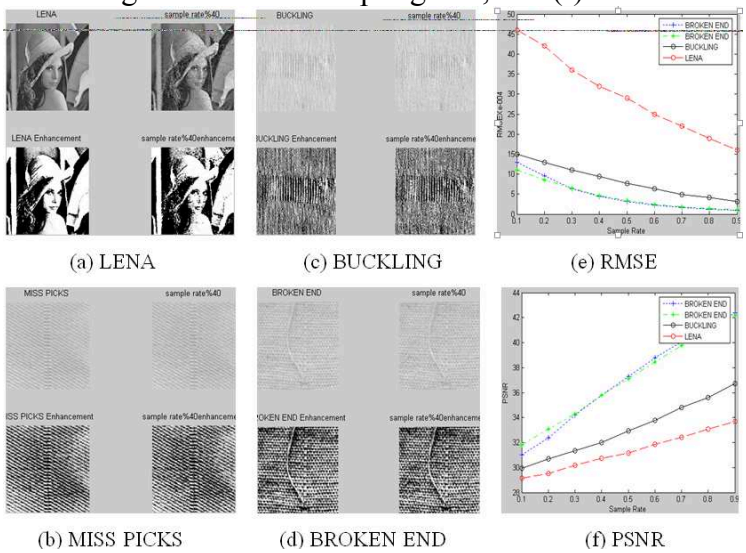

Fig.5. Fabric image comparison with usual image by CS at different sampling rate

From Fig.4 we can get a perfect image at a 40% Nyquist sampling rate. Fig.5 shows fabric image's PSNR is higher than usual image's, in other word, we can get the same level by reconstructing a fabric image at a lower sampling rate than reconstructing a usual image. In fact, the sparsity depends on the basis's selection.

Conclusion

We can not only reconstruct a signal accurately in Sub-sampling rate by CS, but also we can use fewer samples to reconstruct **f**abric image. In other word, it not only eases the contradiction between limited sensor computing speed and amount of data collected, but also breaks network bandwidth restriction. It is a great significant in terms of automated inspection of textile enterprise, such as reducing costs of sensor end, collecting more information under the same bandwidth.

References

[1] Stephane Mallat. A Wavelet Tour of Signal Processing: The Sparse Way, Third Edition. Beijing: China Machine Press, 2012.02.

[2] Lingjuan Yu, XiaoChun Xie. Introduction of Compressed Sensing [J]. Video Engineering, 2008.32(12).

[3] AlbertBoggess, FrancisJ, Narcowich. a first course in wavelets with Fourier Analysis. Electronic Industry Press, 2010.

[4] QiongHai Dai, ChangJun Fu and XiangYang Ji. Research on Compressed Sensing [J]. Chinese Journal Of Computers, 2011.34(3): 425-434.

[5] Richard G.Baraniuk. Compressive Sensing. IEEE Signal Processing Magazine [J], 2007.7:118-124.

[6] Yonina C. Eldar, Gitta Kutyniok. Compressed Sensing: Theory and Applications. New York: Cambridge University, 2012.

Advanced Materials Research Vols. 989-994 (2014) pp 3702-3705
© (2014) Trans Tech Publications, Switzerland
doi:10.4028/www.scientific.net/AMR.989-994.3702

Adaptive Equalization with Variable Step Size Algorithm Based on Gradient for HF Channel

Fang-Fang HAN[a], Zi-Hao LIN[b]

Urumqi Station of the State Radio Monitoring Center, Xinjiang Urumqi, China

[a]email:hanfangfang0993@163.com, [b]email:lin-zihao@163.com

Keywords: Adaptive Equalization; HF Channel; Variable Step Size; Iterative Gradient

Abstract. To further improve the performance of adaptive equalization in HF channel, a new variable step size algorithm is proposed based on the iterative gradient. The step size is set to a vector according to the weights of the equalizer, and it can vary with the iterative gradient during the equalization process. The algorithm overcomes the traditional variable step size with the constant scale for all the weights of the equalizer, thus it can obtain faster convergence rate and lower steady state error in HF channel. In the complex channel condition, the algorithm proposed in this paper can avoid the local minimum point of the objective function to obtain the global convergence performance. Simulation result shows the effectiveness in the Watterson channel model.

Introduction

The HF communication is very suitable for the middle or long distance communication [1]. The signal may include amount of inter-symbol interference (ISI) at the receiver due to the multi-path transmission, decline and time varying of the HF channel. Adaptive equalization is an effective technology to track and compensate the channel variation, which can eliminate the ISI to improve the communication quality [2]. Linear transversal equalizer with the gradient descent algorithm based on LMS criterion is simple and has the low computational complexity [3], so it is widely used in HF channel equalization. Adaptive equalization with variable step size is a compromise between large and small step size to obtain better performance of the equalization algorithm [4]. The traditional variable step size algorithm often use a constant scale for all weights of the equalizer, which use a step size decreased gradually during the iterative process. However the weights of the equalizer are not significant as the same to improve the equalization performance. Hereby, a new variable step size equalization algorithm is designed according to the iterative gradient, in which the step size is a vector but a constant value, and the variation of the step size is different for each weight of the equalizer. Therefore the equalizer can faster to convergence to the global minimum point of the objective function and obtains better performance. The simulation adopted the Watterson channel model and the results show the effectiveness of the algorithm proposed in this paper.

The HF Channel Model

The HF channel is a random parameters channel, and the characteristics vary with the time. The shortwave frequency has two transmission manners, one is shortwave ground wave transmission, and the other is shortwave space wave transmission. The shortwave space wave transmission manner implements the long distance communication, which the distance can spread from thousands to hundreds thousands meters. As a result, study on the equalization algorithm in HF channel to eliminate the ISI at the receiver is important. The characteristics of HF channel can be described by some parameters, the number of the multi-path, the time delay and the Doppler frequency shift. The signal transmitted through HF channel, the signal may reach to the receiver by different path, which is the multi-path transmission. Multi-path transmission results in frequency selective decline, and then there is aberrance in the waveform of the signal, which is the multi-path effect. Watterson model is recommended by CCIR [5], which can describe the HF channel

characteristics accuracy. The time varying frequency response function of Watterson model is given by

$$H(f,t)=\sum_{i=1}^{n}\exp\left(-j2\pi\tau_i f\right)G_i(t) \tag{1}$$

where i is the order of the multi-path, n is the total number of the multi-path. τ_i is the time delay of the i-th in the transmission path. $G_i(t)$ is the complex path gain function, which is a complex Gaussian function with independent Rayleigh distribution amplitude and uniform distribution phase. Based on the model of HF channel, the received signal can be given by

$$r_k=\sum_{i=0}^{g}s_{k-i}y_{ki}+n_k \tag{2}$$

where $\{n_k\}$ is the complex Gaussian noise with zero mean, $\{s_k\}$ is the send signal, $\{y_{ki}\}$ is the tap gain of the channel. The HF channel proposed by CCIR has two transmission paths, and the parameters of the channel for expressing the channel performance are shown in Tab.1.

Tab.1 The parameters of the HF channel

	Good condition	Moderate condition	Poor condition
Doppler shift	0.1 Hz	0.5Hz	1Hz
Time delay	0.5 ms	1 ms	2 ms

LMS Adaptive Equalization

In HF channel adaptive equalization algorithm, LMS and RLS is two main algorithms. Due to the RLS algorithm needs to calculate the inverse matrix of the input signal of the equalizer, which has burden computational complexity. Compared with RLS algorithm, LMS algorithm has lower computational complexity, and then LMS adaptive equalization algorithm is more suitable for the HF channel. LMS algorithm is educed from Wigner filter theory, which taken the mean square error as the objective function based on the MMSE to obtain the optimized solution. That is, the weights of the filter can be updated to obtain the minimum error between the output signal and the desired output signal. The adaptive equalization system is shown as Fig.1.

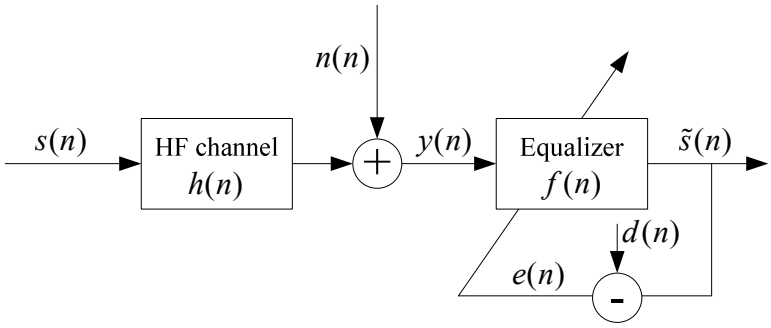

Fig.1 The basic adaptive equalization system

where $s(n)$ is the send signal, $h(n)$ is the HF channel response function, $f(n)$ is the linear transversal equalizer, $n(n)$ is the Gaussian noise. The objective function of LMS algorithm can be given by the output signal $\tilde{s}(n)$ and the desired output signal $d(n)$ as follow

$$J(n)=\frac{1}{2}E\left[d(n)-\tilde{s}(n)\right]^2 \tag{3}$$

LMS algorithm use the time mean instead of the expectation, so the objective function can be given by

$$J(n)=\frac{1}{2}\left[d(n)-\tilde{s}(n)\right]^2 \tag{4}$$

According to the gradient descent algorithm, the equalizer updating by

$$f(n+1) = f(n) - \mu \nabla J(n) \tag{5}$$

The output signal $\tilde{s}(n)$ is obtained by $y(n)$ passing through the equalizer $f(n)$ and can be given by

$$\tilde{s}(n) = f^H(n) y(n) \tag{6}$$

Then the objective function of LMS can be rewritten as follow

$$J(n) = \frac{1}{2}\left[d(n) - f^H(n) y(n) \right] \tag{7}$$

Based on Eq.7, $\nabla J(n)$ can be given by

$$\nabla J(n) = \frac{\partial J(n)}{\partial f(n)} = -\frac{1}{2}\left[d(n) - f^H(n) y(n) \right] y^*(n) \tag{8}$$

Let the error $e(n)$ is

$$e(n) = \frac{1}{2}\left[d(n) - f^H(n) y(n) \right] \tag{9}$$

The updating formula of the equalizer can be given by

$$f(n+1) = f(n) + \mu e(n) y^*(n) \tag{10}$$

where μ is the step size which control the convergence rate and convergence precision of the adaptive equalization algorithm.

Variable Step Size Algorithm

The parameter μ called step size has important influence on the performance of LMS algorithm. The larger step size can obtain faster convergence rate but bigger steady state error, and the smaller step size can obtain less steady state error but slower convergence rate. Variable step size LMS algorithm is a comprise between larger and smaller step size, and the traditional variable step size use the larger step size to speed up the convergence rate, and the step size decrease gradually during the iterative process to become smaller and smaller, and then the convergence precision is improved. However the step size is same for all weights of the equalizer, even for the variable step size algorithm, the step size is still same for all weights of the equalizer at the current iterative times. The weights of the equalizer provide different action to approach the inverse of the channel, some weights is redundant fully. Therefore the same step size for all weights of the equalizer is not an ideal method to further improve the performance of the equalization. Let the step size is a vector with the length N which is the length of the equalizer, according to the Eq.10 can give a relationship between the equalizer and the step size vector as follow

$$f(n) = f(n-1) + \mu(n) e(n-1) y^*(n-1) \tag{11}$$

Then the partial derivative of $f(n)$ to $\mu(n)$ is given by

$$\frac{\partial f(n)}{\partial \mu(n)} = e(n-1) y^*(n-1) \tag{12}$$

According to inner product operator, the partial derivative of $J(n)$ to $\mu(n)$ is given by

$$\frac{\partial J(n)}{\partial \mu(n)} = \left\langle \frac{\partial J(n)}{\partial f(n)}, \frac{\partial f(n)}{\partial \mu(n)} \right\rangle \tag{13}$$

Define the inner product operator of two vectors is computed by

$$\left\langle \frac{\partial J(n)}{\partial f(n)}, \frac{\partial f(n)}{\partial \mu(n)} \right\rangle = tr\left[\frac{\partial J(n)}{\partial f(n)} \times \frac{\partial f(n)}{\partial \mu(n)} \right] \tag{14}$$

Then the ideal step size $\mu(n)$ to minimize objective function can be updated by

$$\mu(n) = \mu(n-1) + \lambda \frac{\partial J(n)}{\partial \mu(n)} \tag{15}$$

The variable step size algorithm according to Eq.15 can drive the objective function to the global minimum point. The variable step size vector has different values for different weights of the equalizer during the iterative process.

Computer Simulations

The single carrier communication system with bit rate 2400bit/s is adopted in the simulations, and the send signal is modulated by 8-PSK. There are 56 symbols in one data packet, in which the user's data is 40 symbols and the training sequence is 16 symbols. The poor HF channel and the moderate channel are adopted to verify the effectiveness of the variable step size LMS adaptive equalization (VS-LMS). Simulation results are shown in Fig.2 and Fig.3 respectively.

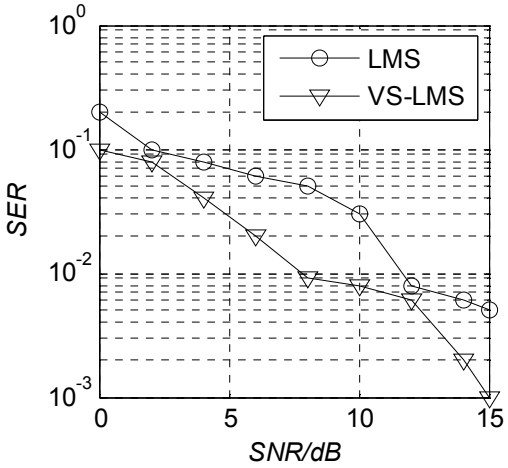

Fig.2 SER in CCIR moderate channel

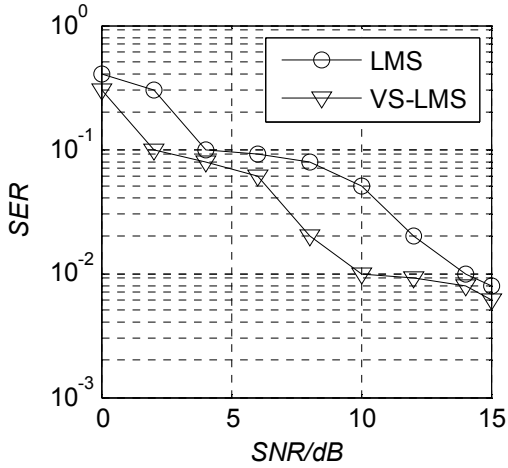

Fig.3 SER in CCIR poor channel

The results in Fig.2 and Fig.3 show VS-LMS can obtain lower SER both in the CCIR moderate and the CCIR poor channel, which proved the effectiveness of the variable step size equalization algorithm in this paper.

Conclusion

This work proposed a new variable step size adaptive equalization algorithm, in which the step size is a vector rather than a constant value. The step size is updated according to the iterative gradient based on the MMSE criterion, and it can drive the objective function convergence to the global minimum point. The simulation results show that, VS-LMS adaptive equalization can improve the performance in HF channel.

References

[1] JIANG Hong. Linear Equalization Methods under HF Channel [J]. Ship Electronic Engineering, 2013, 33(8): 85-87+112.

[2] Shukla P K，Turner L F．Channe1-estimation-based adaptive DFE for fading multipath radio channels [J]. IEE Proc. Pt, 1991, 138(6): 525-543.

[3] TIAN Wei, ZHOU Xin-li, CHU Jian-chong, YU Cheng-fei. Research into HF channel equalization based on DS-VCC-DDEA algorithm [J]. Journal of Circuits and Systems, 2013, 18(1): 390-396.

[4] GAO Ying, XIE Sheng-li. A variable step size LMS adaptive filtering algorithm and its analysis [J].ACTA Electronica Sinica, 2001, 29(8): 1094-1097.

[5] WATTERSON C C, JUROSHEK J R, BENSEMA W D. Experimental confirmation of an HF channel model [J]. IEEE Trans. On Commun. Technology, 1970, 18(6): 792-803.

Advanced Materials Research Vols. 989-994 (2014) pp 3706-3709
© (2014) Trans Tech Publications, Switzerland
doi:10.4028/www.scientific.net/AMR.989-994.3706

Joint Estimation of Doppler and Time Delay of Wideband Echoes for LFM Pulse Radar Based on Fractional Correlation in impulse noise environment

Li LI[1, a]

[1] Information Engineering College, Dalian University, Dalian 116622, China

[a]email: ffsimple@163.com

Keywords: fractional correlation; fractional lower order statistics;LFM Pulse signal, impulse noise

Abstract. A new method to estimate the Doppler and multipath time delay is presented in impulse noise environment. First, the Doppler is estimated by energy cumulation of multipath component based on fractional lower-order -frational correlation transform. Then, an order-reduced signal is reconstructed combining the Doppler with the prior knowledge of the transmitted signal, and the echoes signal is converted to many single-frequency signals. Finally, the multipath time delay is obtained by the fractional lower-order power spectrum method. The method is adapted for low SNR noise, can restrain the affection of the cross-items, and has a high time-delay estimation resolution. Some computer simulations are given in this paper and the results show that the new method is valid.

Introduction

At present, parameter estimation of the Doppler and time delay for LFM pulse radar echoes has received much research attention [1-2]. The broadband signals are frequently used in sonar and radar systems because of its good performance in both Doppler frequency and time delay estimation. In wideband sonar and radar systems, the echo from a wideband signal often contains a Doppler stretch (DS), not Doppler shift only, which results of difficulty in the parameters estimation [3-5]. Furthermore, in most parameter estimation methods for array signal processing, additive noise is assumed to be Gaussian, which has finite second-order statistics[7]. In some scenarios, it is inappropriate to model the noise as Gaussian noise. Therefore, this paper develops a new wideband signal model in impulsive noise.

The application of the fractional Fourier analysis in different areas has continuously increased during the last years. Fractional power spectra, which are the squared moduli of the fractional Fourier transform (FT), can be expressed in terms of the fractional correlation function. It is now a popular tool in optics and signal processing. In summary, this paper proposes a novel method, combining the fractional lower order statistics and fractional correlation, to suppress the impulse noise and estimate parameters.

This paper is organized as follows. Section Ⅱ presents a signal model in impulsive noise. In section Ⅲ, the analysis on the fractional correlation based on the fractional lower order statistics (FLOS-FC) is presented. In section Ⅳ, Doppler stretch and time delay are estimated by searching the peak of FLOSFC. In section Ⅴ, the performance of the proposed method is studied through extensive numerical simulations. Finally, conclusions are drawn in section Ⅵ.

The Proposed Signal Model

In radar or a sonar system, the received signal, in comparision with the transmitted waveform, often contains both time delay (TD) and Doppler stretch (DS). Let $x(t)$ be the transmitted signal having a constant propagation velocity. For improving the ability of anti-interference, transmitted signal is chirp signal as $x(t) = A\exp\left(j2\pi\left(f_0 t + \mu_0 t^2/2\right)\right)$ where A is the signal amplitude, f_0 is the

starting frequency, and μ_0 is the chirp rate. In wideband radar system, the received signal, in comparison with the transmitted waveform, contains both time delay and Doppler stretch. The echo $x_r(t)$ can be expressed as

$$r(t)=\sum_{l=1}^{L}\beta_l x\left(a_l(t-\tau_l)\right)+w(t) \tag{1}$$

where β_l denotes the complex constant accounting for the reflection of the l th multipath component, a_l and τ_l denote Doppler stretch factor (DS) and time delay (TD) of the l th multipath component, respectively. L is the number of multiple paths. The noise $w(t)$ is a sequence of i.i.d isotropic complex $S\alpha S$ random variable with $1<\alpha\le 2$.

Theory of Parameter Estimation based on the Fractional correlation based on the Fractional lower-order statistics

Fractional order signal processing is becoming an active research area in recent years, due to the non-stationary and non-Gaussian model in signal processing. This paper combines the fractional lower order statistics and fractional correlation[8] for suppressing the impulse noise and estimating parameters.

Fractional correlation function based on the fractional lower order statistics (FLOS-FC) $\hat{R}_{ss}^{(p)}(\rho,\varsigma)$ of the signal $s(t)$ is defined by

$$\hat{R}_{ss}^{(p)}(\rho,\varsigma)=\lim_{T\to\infty}\frac{1}{2T}\int_{-T}^{+T}R_{ss}^{(p)}(t+\varsigma,t)\exp(jt\varsigma\cot\rho)\,dt \tag{2}$$

where p is the order of the fractional lower order, and $1<p<\alpha\le 2$. $R_{ss}^{(p)}(t+\varsigma,t)=E\left\{s(t+\varsigma)[s(t)]^{<p-1>}\right\}$ denotes the fractional lower order correlation of the signal $s(t)$.

Joint Parameter Estimation Based on FLOS-FC

According to (1), we can obtain as

$$\begin{aligned}\hat{R}_r(\rho,\varsigma)&=\lim_{T\to\infty}\frac{1}{2T}\int_{-T}^{+T}r(t+\varsigma)r^*(t)\exp(jt\varsigma\cot\rho)\,dt\\&=\sum_{l=1}^{L}\lim_{T\to\infty}\frac{1}{2T}\int_{-T}^{+T}|\beta_l|^2\exp\left(j\left(2\pi\mu_0a_l^2+\cot\rho\right)t\varsigma\right)\exp\left(j2\pi\left(\left(f_0a_l-\mu_0a_l^2\tau_l\right)\varsigma+\mu_0a_l^2\varsigma^2/2\right)\right)dt+\hat{R}_{rw}(\rho,\varsigma)\end{aligned} \tag{3}$$

where $\hat{R}_{rw}(\rho,\varsigma)$ is treated as a random interference.

When $\cot\rho_l=-2\pi\mu_0a_l^2$, $\hat{R}_r(\rho_l,\varsigma)$ has the best energy-concentrated property. Therefore, we can obtain the estimator of Doppler stretch as

$$a_l=\sqrt{-\cot\alpha_{ql}/(2\pi\mu_{q0})} \tag{4}$$

Next, combining the estimator of Doppler stretch with the prior knowledge of the transmitted signal, an order-reduced signal is reconstructed as

$$g(t)=\exp\left(-j2\pi\left(\mu_0a_l^2/2\right)t^2\right) \tag{5}$$

According to the order-reduced function and the echo signal, we can obtain as

$$z(t)=r(t)\cdot g(t) \tag{6}$$

From (14),we find that the echoes signal is converted to many single-frequency signals. Finally, the multipath time delay is obtained by the dechirping method.

Assumed $R_z^{(p)}(t)$ as the fractional autocorrelation function of $z(t)$ and $\tilde{R}_z^{(p)}(u)$ as the Fourier transform of $R_z^{(p)}(t)$. So, we can obtain

$$u_l = \arg\max_u \left\{ \tilde{R}_z^p(u) \right\} \tag{7}$$

According to (14) and (15)，we can obtain the estimator of time delay as

$$\tau_l = \left(f_0 a_l - u_l \right) / \left(\mu_0 a_l^2 \right) \tag{8}$$

Test results

We performed two types of simulation experiments to assess the relative performance of the proposed method under $\alpha-$stable noise and Gaussian noise conditions respectively. In order to study the robustness of the propose method, complex isotropic symmetric $\alpha-$stable $(S\alpha S)$ noise [7] model is considered. We describe the signal-to-noise condition of $S\alpha S$ using the generalized signal-noise-ratio $\left(\text{GSNR} = 10\lg(\sigma_s^2/\gamma)\right)$, where, σ_s^2 is the signal power .

In the following simulation experiments, the number of multipath is $L=2$, and Doppler stretch and time delay are $a_1 = 0.9$, $\tau_1 = 20/fs$, $a_2 = 1.1$, $\tau_2 = 100/fs$ respectively, where the sampling frequency f_s is 1MHz The number of snapshots is 1000. The number of Monte Carlo iterations is 500 in all simulations. We considered the influence of the fractional lower order moment p and the GSNR to the performance of the proposed method.

Simulation 1: Generalized signal-noise-ratio GSNR

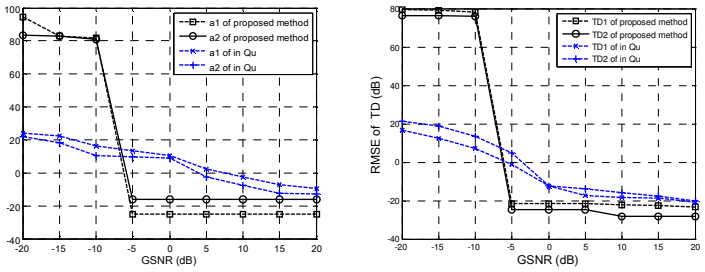

(a) (b)

Fig.1 Root mean square error versus GSNR

In this simulation, the noise is modeled as α-stable noise with $\alpha = 1.4$. Fig.1 (a)-(d) show the RMSE of the three algorithms for various values of GSNR when $p = 1.3$. From Fig.1, we can find that the estimation accuracy of the proposed method is higher than that of the method in the method of Qu.

Simulation 2: Characteristic exponent α

In this simulation, the generalized signal to noise ratio is set as GSNR=15dB, and the fractional lower-order moment is set as $p = 1.3$. Fig.2 shows the RMSE of the two algorithms for various values of characteristic exponent α.

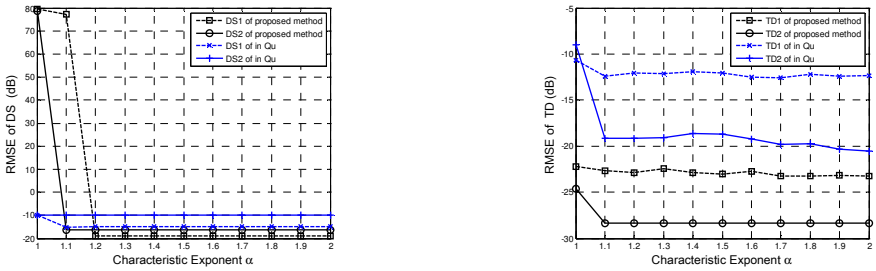

(a) (b)

Fig.2 Root mean square error as a function of the characteristic exponent α

From Fig.2, we find that FLOS-FC algorithm shows a significant performance improvement over the method in [13] in term of RMSE for values of α in the range (1, 2) in impulsive noise environments modeled under the stable law.

Conclusion

In this paper, we proposed a novel method for estimating unknown targets parameters in impulse noise environment. In wideband sonar and radar systems, the echo from a wideband signal often contains a Doppler stretch (DS), not Doppler shift only, which results of difficulty in the parameters estimation. For the determination of the range and the relative velocity of the target, the accurate estimation of these parameters is crucial. Furthermore, the echo signal may be corrupted by the non-Gaussian noise. The conventional algorithms and signal model degenerate severely in this case. The Alpha-stable distribution model is an ideal mathematical model for non-Gaussian impulsive noise. Thus, this paper proposes a novel method that combines the fractional lower order statistics and fractional correlation, for suppressing the impulse noise and estimating parameters in the impulse noise environment. First, the Doppler is estimated by energy cumulation of multipath component based on fractional correlation transform. Then, an order-reduced signal is reconstructed combining the Doppler with the prior knowledge of the transmitted signal, and the echoes signal is converted to many single-frequency signals. Finally, the multipath time delay is obtained by the dechirping method. Simulation results demonstrate that the proposed method still has good performance when poor GSNR condition exists.

Acknowledgement

This work is partly supported by the National Science Foundation of China under Grants 61172108, 61139001 and 60872122, and the National Science and Technology Support Program and the Grant 2012BAJ18B06.

References

[1] P. Stoica, J. Li, Y. Xie, On Probing Signal Design For MIMO Radar, IEEE Trans. Signal Process, 2007 55(8): 4151- 4161.

[2] S.Y. Chao, B.X. Chen, C.C. Li, Grid cell based detection strategy for MIMO radar with widely separated subarrays, AEU-International Journal of Electronics and Communications, 2012 66(9):741-751.

[3] C.C. Li, G.S. Liao, S.Q. Zhu, S.Y. Wu, An ESPRIT-like algorithm for coherent DOA estimation based on data matrix decomposition in MIMO radar, Signal Processing, 2011 91(8): 1803-1811.

[4] J.Y. Zhang, Z.D. Zheng, X.B. Li, An algorithm for DOD- DOA and Doppler frequency joint estimating of bistatic MIMO radar, Journal of Electronics & Information Technology, 2010 32(8):1843-1848.

[5] J. Li, P. Stoica, W .Roberts, On parameter identifiability of MIMO radar, IEEE Signal Processing Letters,2007 14(12): 968-971.

[6] J. Qu, M.W. Kon, Z. Q. Luo, The estimation of time delay and Doppler stretch of wideband signals, IEEE Trans. Signal Process, 1995 43(4):.904-916.

[7] C.L. Nikias, M. Shao, Signal processing with alpha stable distributions and applications, New York: John Wiley & Sons Inc,1995.

[8] H.M. Ozaktas, Z. Zalevsky, M.A. Kutay, The fractional Fourier transform with applications in optics and signal processing, Chichester: John Wiley& Sons, 2001.

Advanced Materials Research Vols. 989-994 (2014) pp 3710-3713
© (2014) Trans Tech Publications, Switzerland
doi:10.4028/www.scientific.net/AMR.989-994.3710

Parameter Estimation based on Fractional Correlation under Alpha-Stable Distribution Noise Environment in Bistatic MIMO Radar System

Li LI[1, a]

[1] Information Engineering College, Dalian University, Dalian 116622, China

[a]email: ffsimple@163.com

Keywords: fractional correlation; fractional lower order statistics; bistatic MIMO radar; α-stable distribution

Abstract. This paper takes the α-stable distribution as the noise model and works on the parameter estimation problem of bistatic Multiple-Input Multiple-Output (MIMO) radar system in the impulsive noise environment.This paper presents a signal model and a novel method for parameter estimation in bistatic MIMO radar system in the impulsive noise environment. Firstly, a signal array model is constructed based on the α-stable distribution model. Secondly, Doppler parameters are jointly estimated by searching the optimal rotation angle to meet concentrated-energy of the FLOS-FC. Furthermore, two algorithms are presented for the estimation of DODs and DOAs, including based on FLOS-MUSIC algorithm and FLOS-ESPRIT algorithm. Simulation results are presented to verity the effectiveness of the proposed method.

Introduction

Multiple-Input Multiple-Output (MIMO) system has attracted more and more attention for its ability to enhance system performance [1-6]. A MIMO radar system consists of both transmit and receive sensors, with the transmit sensors having the ability to transmit orthogonal waveforms.

The multi-target parameter estimation and localization is one of the most important aspects in bistatic MIMO radar. Most existing algorithms are divided into two categories. One ignores Doppler frequency and only estimated DOA and DOD as shown in [1-3]. The other estimates not only DOA and DOD but also time-invariant Doppler frequency as shown in [4-6]. The receiver signal expression shows that it has 3-Dimension array model characteristics. Three parameters are jointly estimated from three matrices obtained from low-rank decomposition. It is assumed that the Doppler frequency was time-invariant. In fact, the received signals contain time-variant Doppler frequency. In this case, these existing methods can not effectively solve this problem and provide an optimal solution.

Furthermore, in most parameter estimation methods for array signal processing, additive noise is assumed to be Gaussian, which has finite second-order statistics. In some scenarios, it is inappropriate to model the noise as Gaussian noise. To overcome these drawbacks, this paper proposes a novel method, combining the fractional lower order statistics and fractional power spectral density, to suppress the impulse noise and estimate parameters in the bistatic MIMO radar system.

The Proposed Signal Model

We assume that there are Q closely spaced transmit antennas and N closely spaced receive antennas, and L targets, with half-wavelength space between adjacent elements used for both transmit array and receive array. The transmit antennas emit orthogonal waveforms $x_q(t)$. The received signals contain Doppler frequency with time-variant. This paper presents a signal model of bistatic MIMO radar system. In general, the received signal from the nth antenna $y_n(t)$ can be expressed in (1)

$$y_n(t)=\sum_{l=1}^{L}\sum_{q=1}^{Q}\left\{\sigma_l x_q(t)\exp\left(j2\pi\left(f_l t+\mu_l t^2/2\right)\right)A_q(\varphi_l)B_n(\theta_l)\right\}+w_n(t) \tag{1}$$

where σ_l denotes the radar cross-section. f_l and μ_l denote the initial Doppler frequency (IDF) and Doppler frequency rate (DFR). $A_q(\varphi_l)=\exp\left(j2\pi(q-1)d_t\sin\varphi_l/\lambda\right)$ is the q th element of the transmitter steering vector, and φ_l is the DOD . $B_n(\theta_l)=\exp\left(j2\pi(n-1)d_r\sin\theta_l/\lambda\right)$ is the steering vector of the n th element of the receiver, and θ_l is the DOA. The noise $w_n(t)$ is a sequence of i.i.d isotropic complex $S\alpha S$ random variable with $1<\alpha\le 2$.

Since the transmitted waves are orthogonal with each other, there are $\langle x_q, x_k\rangle=0, q\ne k$ and $\|x_q\|^2=1$, for $k=1,...,Q$ and $q=1,...,Q$. The extracted signals from the q th matched filter can be expressed as

$$y_{q,n}(t)=\sum_{l=1}^{L}\left\{\sigma_l\exp\left(j2\pi\left(f_l t+\mu_l t^2/2\right)\right)A_q(\varphi_l)B_n(\theta_l)\right\}+w_n(t),\quad 0\le t\le T \tag{2}$$

Theory of Parameter Estimation based on the PLOS-FC

Fractional correlation function based on the fractional lower order statistics (FLOS-FC) $\hat{R}_{ss}^{(p)}(\tau)$ of the signal $s(t)$ is defined by

$$\hat{R}_{ss}^{(p)}(\tau)=\lim_{T\to\infty}\frac{1}{2T}\int_{-T}^{+T}R_{ss}^{(p)}(t+\tau,t)\exp\left(jt\tau\cot\rho\right)dt \tag{3}$$

where p is fractional lower-order moment and $1<p<\alpha\le 2$. $R_{ss}^{(p)}(t+\tau,t)=E\left\{s(t+\tau)[s(t)]^{<p-1>}\right\}$ denotes the fractional lower order correlation of $s(t)$.

Joint Parameter Estimation Based on FLOS-FC

In this section, study of parameter estimation is made by taking the signal $y_{qnl}(t)$ as an example.

$$y_{qnl}(t)=\sigma_l\exp\left(j2\pi\left(f_l t+\mu_l t^2/2\right)\right)A_q(\varphi_l)B_n(\theta_l)+w_n(t) \tag{4}$$

A. Doppler frequency parameters Estimation

According to (3) and (4), the FLOS-FC of $y_{qnl}(t)$ can be written as

$$\hat{R}_{yy,qnl}^{(p)}(\tau)=\lim_{T\to\infty}\frac{1}{2T}\int_{-T}^{+T}R_{yy,qnl}^{(p)}(t+\tau,t)\exp\left(jt\tau\cot\alpha\right)dt \tag{5}$$

where $R_{yy,qnl}^{(p)}(t+\tau,t)=E\left\{y_{qnl}(t+\tau)[y_{qnl}(t)]^{<p-1>}\right\}$.

When $\cot\rho_l=-2\pi\mu_l$, $\hat{R}_{yy,qnl}^{(p)}(\tau)$ has the best energy-concentrated property. Therefore, we can obtain the following expression as

$$\begin{cases}\hat{\mu}_l=-\cot\rho_l/(2\pi)\\ \hat{f}_l=\arg\max_f\left\{\tilde{R}_{y_1}^{p}(u)\right\}\end{cases} \tag{6}$$

where $\tilde{R}_{y_1}^{(p)}(u)$ is the Fourier transform of $R_{y_1}^{(p)}(t)$,and $R_{y_1}^{(p)}(t)$ is the fractional autocorrelation function of $y_1(t)=y_{q,n,l}(t)\cdot\exp\left(-\mathrm{j}2\pi(\hat{\mu}_l/2)t^2\right)$.

B. Joint DOA and DOD estimation

In this section, the DOD and DOA are estimated by employing the FLOS-MUSIC and FLOS-ESPRIT.

According to (2) and (6), both receive subarrays $\boldsymbol{R}_1$ and $\boldsymbol{R}_2$ constructed in this paper can be expressed by

$$\boldsymbol{R}_1 = \begin{bmatrix} \boldsymbol{y}_{11} & \boldsymbol{y}_{12} & \cdots & \boldsymbol{y}_{1L} \end{bmatrix}^{\mathrm{T}} = \boldsymbol{B}\boldsymbol{G} + \boldsymbol{N}_1 \tag{7}$$

$$\boldsymbol{R}_2 = \begin{bmatrix} \boldsymbol{y}_{q1} & \boldsymbol{y}_{q2} & \cdots & \boldsymbol{y}_{qL} \end{bmatrix}^{T} = \boldsymbol{B}\boldsymbol{A}\boldsymbol{G} + \boldsymbol{N}_2, \quad q \neq 1 \tag{8}$$

where $\boldsymbol{B} = \begin{bmatrix} \boldsymbol{B}_1 & \boldsymbol{B}_2 & \cdots & \boldsymbol{B}_L \end{bmatrix}$, $\boldsymbol{B}_l = \begin{bmatrix} B_1(\varphi_l) & \cdots & B_N(\varphi_l) \end{bmatrix}^{\mathrm{T}}$, $\boldsymbol{A} = \mathrm{diag}\left\{ A_q(\varphi_1), \cdots, A_q(\varphi_L) \right\}$, $\boldsymbol{G} = \begin{bmatrix} g_1(t) & g_2(t) & \cdots & g_L(t) \end{bmatrix}^{\mathrm{T}}$, $g_l(t) = \sigma_l \exp\left(j2\pi \left(\hat{f}_l t + \hat{\mu}_l t^2 / 2 \right) \right)$, $(\ )^{\mathrm{T}}$ and $\mathrm{diag}(\bullet)$ denote transpose and diagonal matrix respectively.

Spatial spectrum of FLOS-MUSIC can be got based on the classical MUSIC algorithm, which can be expressed as $P(\theta) = \dfrac{1}{\boldsymbol{B}^{\mathrm{H}}(\theta)\boldsymbol{U}_N\boldsymbol{U}_N^{\mathrm{H}}\boldsymbol{B}(\theta)}$. Searching spectral peak of $P(\theta)$, we can get the DOA estimator θ_l.

We define $\boldsymbol{C}_{11} = \boldsymbol{R}_{R_1R_1}^{(p)} - \gamma_1 \boldsymbol{I} = \boldsymbol{B}\boldsymbol{R}_{GG}^{(p)}\boldsymbol{B}^{\mathrm{H}}$ and $\boldsymbol{C}_{12} = \boldsymbol{R}_{R_1R_2}^{(p)} - \gamma_1 \boldsymbol{Z} = \boldsymbol{B}\boldsymbol{A}\boldsymbol{R}_{GG}^{(p)}\boldsymbol{B}^{\mathrm{H}}$, where $\boldsymbol{Z}$ is showed as $\boldsymbol{Z} = \begin{bmatrix} 0 & & & 0 \\ 1 & 0 & & \\ & 1 & \cdots & \\ 0 & & 1 & 0 \end{bmatrix}$. According to $\boldsymbol{C}_{11}$ and $\boldsymbol{C}_{12}$, we can get $\boldsymbol{A} = \boldsymbol{B}^{\#}\boldsymbol{C}_{12}\boldsymbol{C}_{11}^{\#}\boldsymbol{B}$.

Therefore, the DOD estimator φ_l is estimated by $\varphi_l = \arcsin\left(\arg(a_l) / (q-1)\pi \right)$, where a_l is the element of the principal diagonal of matrix $\boldsymbol{A}$, $\arg(a_l)$ stands for the phase of a_l.

Test results

In order to study the robustness of the propose method, complex isotropic symmetric $\alpha-$stable $(S\alpha S)$ noise[8] model is considered. We describe the signal-to-noise condition of $S\alpha S$ using the generalized signal-to-noise $\left(\mathrm{GSNR} = 10\lg(\sigma_s^2 / \gamma) \right)$, where, σ_s^2 is the signal power.

The considered bistatic MIMO radar is composed of $Q = 4$ transmit antennas and $N = 6$ receive antennas. Supposed the target locates at the positions $(\varphi_1, \theta_1) = (30°, 20°)$, $(\varphi_2, \theta_2) = (60°, 50°)$ and Doppler parameters are $f_1 = 8, \mu_1 = 1.2$, $f_2 = 10, \mu_2 = 2$. respectively. The number of snapshots is 1000. The number of Monte Carlo iterations is 500 in all simulations.

Simulation 1: Generalized signal-noise-ratio GSNR

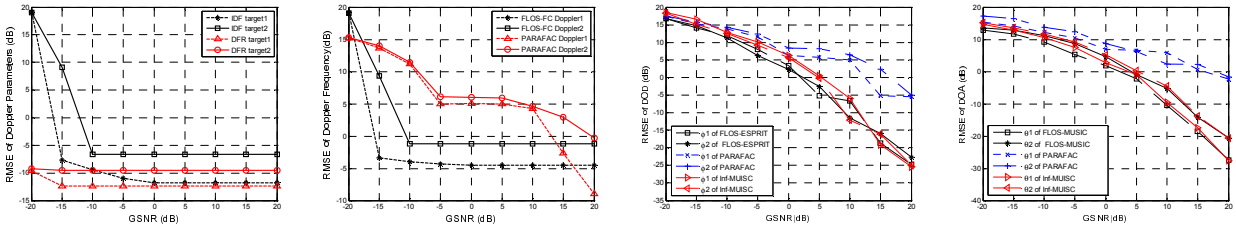

(a) (b) (c) (d)

Fig.1 Root mean square error versus GSNR

In this simulation, the noise is modeled as α-stable noise with $\alpha = 1.4$ and the fractional lower-order moment is set as $p = 1.2$. Fig.1 (a) depicts the RMSE of Doppler parameters. Fig.1 (b) shows Doppler frequency estimation performance of two algorithms for various values of GSNR.

Fig.1 (c)-(d) show the RMSE of three algorithms for various values of GSNR . From Fig.1, we can find that the estimation accuracy of the proposed method is higher than those of PARAFAC method.

Simulation 2: Characteristic exponent α

In this simulation, The generalized signal to noise ratio is set as GSNR=15dB, and the fractional lower-order moment is set as $p=1.2$. Fig.2 shows the RMSE of the three algorithms for various values of characteristic exponent α.

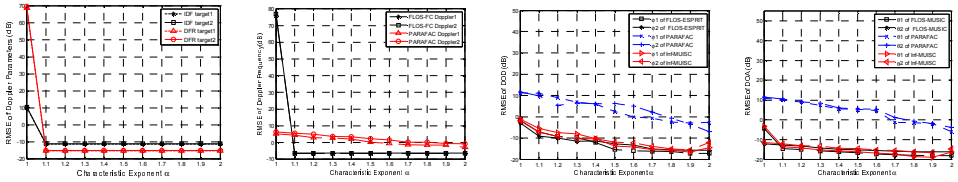

(a) (b) (c) (d)

Fig.2 Root mean square error versus α

From Fig.2 (a)-(d), we find that the proposed algorithm shows a significant performance improvement over the PARAFAC method and Inf-MUSIC method in term of RMSE for values of α in the range $(1,2]$ in impulsive noise environments modeled under the stable law.

Conclusion

In this paper, we proposed a novel method for estimating unknown targets parameters in impulse noise environment. Firstly, we present a signal model under Alpha-stable distribution noise in bistatic MIMO radar system. Secondly, Doppler parameters are estimated by the FLOS-FC algorithm. Thirdly, two subarray models are constructed and two algorithms are presented to estimate DOD and DOA. Simulation results demonstrate that the proposed method still has good performance when poor SNR condition exists.

References

[1] Chen ChunYang, and Palghat P. Vaidyanathan. MIMO radar space–time adaptive processing using prolate spheroidal wave functions[J]. IEEE Transactions on Signal Processing. 2008 56(2): 623-635.

[2] Li Caicai, et al. An ESPRIT-like algorithm for coherent DOA estimation based on data matrix decomposition in MIMO radar [J]. Signal Processing.2011 91(8): 1803-1811.

[3] Bencheikh Mohamed Laid, Yide Wang, and Hongyang He. Polynomial root finding technique for joint DOA DOD estimation in bistatic MIMO radar[J]. Signal Processing, 2010 89(9): 2723-2730.

[4] Lu Hui, et al. A novel method for target localization and doppler frequency estimation in bistatic MIMO radar[J]. Journal of Electronics and Information Technology, 2010, 32(9): 2167- 2171.

[5] Zhang JianYun, ZhiDong Zheng, and XiaoBo Li. An algorithm for DOD-DOA and Doppler frequency jointly estimating of bistatic MIMO radar[J]. Journal of Electronics and Information Technology,2010 32(8): 1843-1848.

[6] Zhang Xiaofei, et al. Direction of departure (DOD) and direction of arrival (DOA) estimation in MIMO radar with reduced-dimension MUSIC[J]. IEEE Communications Letters, 2010 14(12): 1161-1163.

[7] Nikias Chrysostomos L and Min Shao.Signal processing with alpha-stable distributions and applications. Wiley-Interscience, 1995.

[8] Almeida Luis B. The fractional Fourier Transform and Time-Frequency Representations[J], IEEE Trans. Signal Processing, 1994 42(11):3084-3091.

[9] Wang JuTing, et al. Subspace-based DOA Estimation in Impulsive Noise Environments for MIMO Radars[J], Journal of Astronautics, 2009 30(4):1653-1657.

Advanced Materials Research Vols. 989-994 (2014) pp 3714-3717
© (2014) Trans Tech Publications, Switzerland
doi:10.4028/www.scientific.net/AMR.989-994.3714

Multi-view video coding Based on video correction

Tao Yan[1, a], Xiaoxiong Zhou[1, b], Wenting Luo[2], Zeliang Liu[3], Pandong Zhang[1]

[1]School of Information Science and Technology, Jiujiang University, Jiangxi, 332005 China

[2]School of Literature and Communication, Jiujiang University, Jiangxi, 332005 China

[3]School of Electronic Engineering, Jiujiang University, Jiangxi, 332005 China

[a]email: yantaoshu@aliyun.com, [b]email: 48305311@qq.com

Keywords: Video Correction; The relation of inter-views; Multi-view video coding; View Scalability

Abstract. In order to enables the video to be displayed on a multitude of different terminals, Multi-view video coding (MVC) demands high compression rates as well as view scalability. A new the inter-view prediction structure with flexibility, MVC compatibility and view scalability is proposed. The proposed scheme first correct views. It then uses the position of the cameras and the relation of inter-views to divide all views into base view and enhancement views. Finally, the views quire by the viewers use scalable Multi-view Video Coding (SMVC). The main bitstream is the same as a H.264/AVC mono-sequence bitstream for H.264/AVC compatibility. The auxiliary bitstream come from enhancement views coding. We proposed SMVC scheme is tested with two Multi-view sequences to determine its flexibly view scalability, high coding efficiency and random access performance.

Introduction

Multi-view Video is proposed for interactive media, which mainly solves the problems of 3D interactive video performance, interactive and storage, transmission etc.. It is composed of a plurality of camera shooting from different angles to record multiple view data, which provided to the user to view selection and the scene roaming interactive ability[1] [2]. As with 2DTV, the 3DTV/FTV transmission system with the heterogeneity of network and terminal diversity. Due to its MVC data volume is much larger than the 2D video, makes the MVC in how to adapt to the network terminal degeneration, diversity, how to meet the low complexity and low delay, face greater challenges. Different users tend to use different terminals, they have different access bandwidth, different computing ability, different display capabilities. Multi-view stereo video only to the transmission mechanism more flexible to provide users with more degrees of freedom (for example, the general two-dimensional video or stereo video, a three-dimensional view of). Therefore, due to the JVT proposed Multi-view video coding [8] into view scalable coding, to meet different user needs at the same time, as far as possible to improve the coding efficiency.

At present, most of the existing MVC algorithm in a specific time and space resolution and fixed rate to get the best coding efficiency, and therefore can not be based on user terminal dynamic self-adapting coding different View number. Therefore, Lim first proposed the parallax view scalability characteristics of the support structure, and the realization of the MPEG-2 coding scheme based on [3], but the prediction structure of the program in terms of MVC, the compression efficiency is not high and are not compatible with the H.264/AVC; MIT Samuel L.Hill of the camera array shooting scalable[4], calibration but its focus on camera and display of the scalable coding; Ozbek et al. (Scalable Video Coding, SVC), and extend it to the scalable Multi-view video coding (SMVC) [5], but not on the view scalability; Yang[6] proposed a MPEG-4 compatible stereo Multi-view video coding scheme, in addition they also proposed a Multi-view video coding scheme based on wavelet, realize the time, spatial and PSNR scalability of[7], but which are not compatible with the H.264/AVC. Moreover, these methods have not considered the content correlation Multi-view video sequence with the camera placed between viewpoints and illumination and other factors varied phenomena.

In this paper, based on MVC, for Multi-view video signal sequence inter view correlation with the layout of camera and illumination and other factors varied phenomenon, given to predict the structure of a new inter viewpoint, to improve the coding efficiency while achieving scalable views, such as vertex classification can be combined with SVC together, provide a wider range of scalability. First we have the perspective correction for video sequences, the elimination of inter view image color and luminance inconsistency. Then according to the camera's position and inter view correlation effectively hold the view into basic viewpoint and the enhancement layer view, view the number of users required for scalable coding.

Video correction

Inter view image color inconsistency is a problem in urgent need to solve the Multi-view video coding in [8], the main causes of it are scene illumination, camera placement and exposure. Most of scholars, areper spective correction [9][10][11] by histogram matching, To eliminate the differences between the view image color, but there are differences between the views of brightness. Jae-Ho Hur et al [12] compensation in frequency domain, the brightness difference between the viewpoint that image macro block DC coefficients, such a treatment not only speed is larger and has achieved good results, but the difference between the color point of view is relatively large, the effect is not ideal for vision correction.

Fig.1 (a) Original images of 0^{th} and 4^{th} viewpoints in Flamenco2

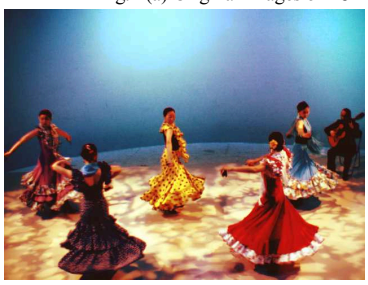

Fig.1 (b) Corrected images of 0^{th} and 4^{th} viewpoints in Flamenco2

Figure 1. The original image and the Corrected images

SMVC

MVC adopts a hierarchical B frame (Hierarchical B Picture) to realize the temporal scalability, inter view can also use a hierarchical B frame structure and a higher coding efficiency, coding delay, and is convenient for short random access to view scalability. Figure 4. shows the time hierarchical B frame inter view / prediction structure. According to the predicted sequence shown in Figure 6, each frame of video coding prediction can be adopted by the encoder reconstruction frame as the reference frame, and can easily achieve the view / temporal scalable coding. So you don't have MCTF (Motion Compensated Temporal Filtering) end reference frame inconsistency problem encoding and decoding structure.

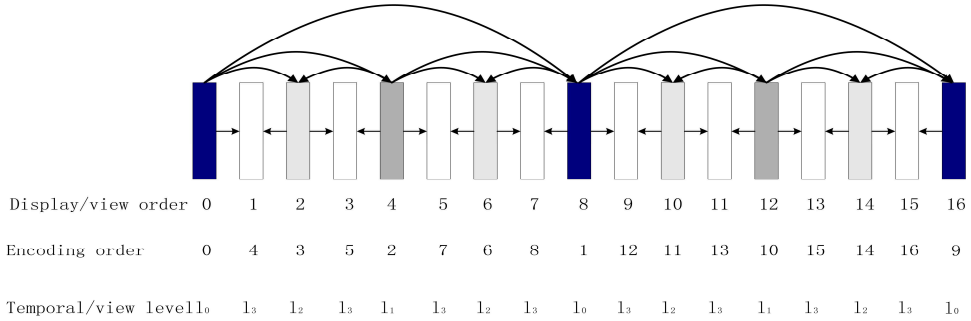

Figure 2 Hierarchical B frame inter view / prediction structure.

But such inter view prediction mode is single, it is difficult to adapt to the Multi-view video sequences with different. In the hierarchical inter view prediction structure, in order to get a better view of random access function usually lost to predict the relationship between the partial view, but such Multi-view video coding performance is low. For example, Simulcast code, using I-View code, the user can randomly access each viewpoint, however, did not use the inter view prediction,so the rate distortion performance is low. Generally speaking, when the inter view prediction structure layer is less, there will be more view video are encoded independently or only one view reference frame,disparity estimation so that the relationship between the loss of the more, random view access performance is better, but the overall coding performance is not high; with the increase in prediction of structural layers, independent encoding the video will be reduced, the overall coding performance will be improved, but the poor performance of random access.

Test results

In order to Multi-view coding and MVC to verify our proposed compatible, and flexible scalability and random access performance, we were on the two Multi-view video sequences were tested. .

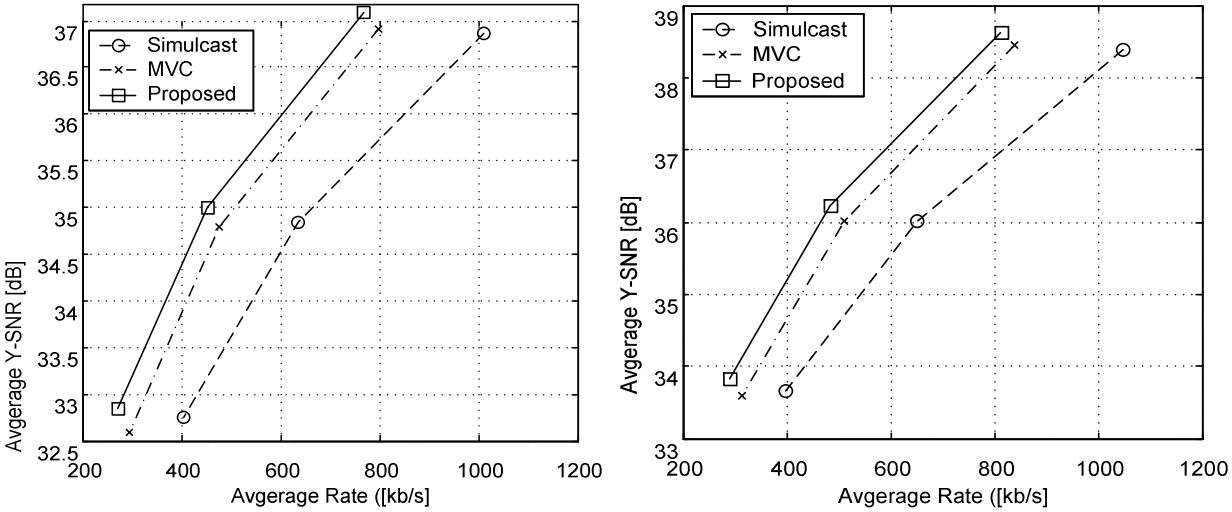

Figure 3. Rate distortion performance comparison

Figure 3. gives the best rate distortion performance comparison,Simulcast encoding the inter view prediction MVC said no, Multi-view video coding scheme is proposed by JVT. SMVC scalable coding methods for this view. On the difference in color between the sequences of Famecon2 and ballroom, through the perspective correction, the coding efficiency is improved obviously, We proposed SMVC scheme is tested with several Multi-view sequences to determine its flexibly view scalability, high coding efficiency and random access performance.

Conclusion

In this paper, based on MVC, for Multi-view video signal sequence inter view correlation with the layout of camera and illumination and other factors varied phenomenon, given to predict the structure of a new inter view, in ensuring the high rate distortion performance at the same time, improve the random access performance, we view scalability, and this view scalability can be combined with SVC, to provide a wider range of scalability. The coding, the perspective correction, and reduce the influence of the difference between colors as the coding, the view selection, and presents a reasonable inter view prediction structure, the coding efficiency is high, improve random access performance, support the view class. We will further study the view scalability in combination with SVC, to provide a wider range of scalability.

Acknowledgement

In this paper, the research was sponsored by the Natural Science Foundation of Jiangxi Province,China(Grant No.20132BAB211025). The Project Supported by Educational Commission of Jiangxi Province, China(Grant No.GJJ13716). This work is supported by the National Natural Science Foundation of China (Grant No.61362032). This paper is supported by the Humanity and Social Science Youth foundation of Ministry of Education,China (Grant No. 13YJC870007).

References

[1] Sullivan A, 2005, 3-Deep: new displays render images you can almost reach out and touch, Spectrum, IEEE Volume 42, Issue 4, April 2005 Page(s):30-35.
[2] Akira Kubota, Aljoscha Smolic, Marcus Magnor, Masayuki Tanimoto and Tsuhan Chen, 2007, Multi-View Imaging and 3DTV, IEEE SIGNAL PROCESSING MAGAZINE: Special Issue on Multi-View Imaging and 3DTV, 2007, 11.
[3] JeongEun Lim, King N. Ngan, Wenxian Yang, Kwanghoon Sohn, " A Multi-view sequence CODEC with view scalability ",Signal Processing: Image Communication, vol.19,no.3,pp:239-256,2004.
[4] Samuel L. Hill, 2004, Scalable Multi-view Stereo Camera Array for Real-Time Image Capture and Three-Dimensional Displays, M.S. Optical Sciences, Massachusetts Institute of Technology, 2004.
[5] Nukhet Ozbek, A. Murat Tekalp, and E. Turhan Tunali, "A new scalable multi-view video coding configuration for robust selective streaming of free-viewpoint TV", IEEE, ICME, 1155-1158. 2007.
[6] W. Yang, K. N. Ngan, J. Cai, "An MPEG-4 compatible stereoscopic/Multi-view video coding scheme" , IEEE Trans. on Circuit and Systems for Video Technology, vol. 16, no. 2, pp. 286-290, Feb. 2006.
[7] W. Yang, F. Wu, Y. Lu, J. F. Cai, K. N. Ngan, and S. P. Li, "Scalable Multi-view video coding using wavelet," IEEE International Symposium on Circuits and System, vol. 6, pp. 6078-6081, May 2005.
[8] P. Merkle, A. Smolic, K. Muller, and T. Wiegand, "Efficient prediction structures for multi-view video coding", IEEE Trans. on Circuits and Systems Video Technology, vol. 17, no. 11, pp. 1461-1673, Nov. 2007.
[9] F. Shao, G. Jiang, M. Yu, and X.Chen, "A New Image Correction Method for Multi-view Video System",ICME, 2006, IEEE International Conference on Multimedia and Expo, Toronto, Ontario, Canada, July 2006.
[10] Ulrich Fecker, Marcus Barkowsky, Andr e Kaup. Luminance and chrominance compensation for multi-view sequences using histogram matching. MPEG2005/ M12487, 2005, Nice, France
[11] U. Fecker, M. Barkowsky, A.Kaup. Improving the prediction efficiency for multi-view video coding using histogram matching [C]. Picture Coding Symposium. Beijing, China.
[12] J. Hur, S. Cho, Y. Lee, "Adaptive Local Illumination Change Compensation Method for H.264 AVC-Based Multi-view Video Coding", IEEE Trans. on Circuits and Systems Video Technology, vol. 17, no. 11, pp. 1496-1505.

Advanced Materials Research Vols. 989-994 (2014) pp 3718-3721
© (2014) Trans Tech Publications, Switzerland
doi:10.4028/www.scientific.net/AMR.989-994.3718

De-noising of Underwater Acoustic Weak Signals Based on Compressed Sensing Technique

Lili ZHAO, Xiaowei DAI

PLA 91550 Unit, Liaoning Dalian, China

email: 13904286205@139.com

Keywords: Compressed Sensing; Wavelet Transformation; Filter Design; Weak Signal De-noising.

Abstract. To remove the noise of weak signals detected in the underwater environment, the existing de-noising algorithms cannot perform satisfactorily. This paper aims to developing a new method to solve the problem, where the compressed sensing theory, wavelet transformation based filtering techniques and sparse signal reconstruction algorithm are employed. The simulation results show that the proposed algorithm performs favorably and has good potential to be used in some engineering applications.

Introduction

Periodic sound waves spread in water with the water pressure when the water to the surface acoustic wave propagates for time being, the joint action of this cyclical pressure, water surface tension and gravity of the original still water drives the jump-up and drop-down movement. If a laser shines on rough water surface which is excited by underwater sound field, the scattering beam bidirectional reflectance distribution function can be observed. While utilizing the optical system with a field of view to observe the surface, we can observe the entire process of the "rough" through the water surface mirror. The system receives the reflected light intensity and converted to the electrical signals of underwater sound field.

Wavelet analysis is an emerging technique over the past years, which has been rapidly developed due to its merits in data representation power and some nice properties for signal processing. Recently, wavelet transforms have been widely recognized and used in weak signal detection, feature extraction, data compression, fault diagnosis, and is playing a significant role in information technology and signal processing. Wavelet-based de-noising techniques can be currently clustered into three categories, which are presented in different forms according to the amplitude of the wavelet coefficients of the desired signal by selecting an appropriate threshold value. This way can remove effectively some high frequency noise and retain significant coefficients for approximate the original signals. As can be seen that the select of an appropriate wavelet threshold will play a key role in this approach for de-noising performance, hence so far, most studies have focused on optimizing the threshold value to achieve improved performance.

The basic idea behind the theory of compressed sensing is to find a better way to represent data with few parameters without loss of much information when the data is reconstructed [1]. A study in [2] pointed out that for noise-free signal the wavelet coefficients obtained by Mallat algorithm is sparse, that is to say, only few coefficients with significant values will be sufficient to represent signals. However, as noise presents, this sparse property of the wavelet coefficients does not hold. Therefore, the compressed sensing theory can be employed to achieve the goal for noisy reduction.

This paper considers a problem of de-noising underwater acoustic signal using wavelet compression-aware filtering method. A novel algorithm is proposed and some simulation results are reported. These primary results demonstrate that our proposed algorithm for noise removal of weak underwater acoustic signals is promising, and outperforms the wavelet-based de-noising method.

Compressed sensing theory

The compressed sensing theory is proposed by Candes and Donoho in 2006, the basic idea is non-adaptive linear projection signal acquisition, and then reconstruct the original signal by

reconstruction algorithm according to the corresponding values from the measured value [3]. It includes three aspects of the sparse representation of the signal, coding measuring coding and reconstruction algorithms. The Sparse signals represent that orthogonal projection transformation converted to vector signal group, and the vast majority of absolute value of the transform coefficients is small. The resulting is sparse or similar sparse, which can be viewed as a simple expression of the original signal. This is a priori condition of compressed sensing that the signal must be sparse representation under certain transformations. In the encoding measurement, first thing is to select a stable projection matrix. In order to ensure linearity of the signal to maintain the original structure of the signal, the isometric projection matrix must satisfy the restricted isometric property (RIP). And use the result of the original signal measured by the product of the matrix measurement to obtain a linear projection of the original signal. Finally, the original signal is reconstructed by the algorithm of the measured value and the projection matrix. The signal reconstruction process is generally converted into a minimum l_0 norm optimization problem.

One of the known measurement matrix is $\phi \in R^{M \times N} (M << N)$, as well as a signal $y \in R^N$ measured value in the measurement of linear matrix under $y \in R^M$, that is:

$$y = \phi f \tag{1}$$

Now consider the reconstruction f by signal y, apparently, because of the dimension of y is far less than the dimension of f, the above equation has infinite kinds of solutions. By theoretical proof, the signal from the measured values y, and f can be reconstructed accurately by solving the optimal l_0 norm:

$$\hat{x} = \arg\min \|x\|_0 \qquad s.t. \qquad \Phi x = y \tag{2}$$

where $\|\bullet\|_0$ is the l_0 norm of the vector, which represents the numbers of non-zero in vector x. However, the common natural signals are almost not sparse in the time domain, so that the signals need to be converted by some kinds of transformation Ψ to a sparse representation.

$$y = \Phi f = \Phi \Psi x = \tilde{\Phi} x \tag{3}$$

where $\tilde{\Phi} = \Phi \Psi$ is the $M \times N$ matrix, which was also called sensing matrix, y can be seen as the measured value of sparse signal x about the measured matrix $\tilde{\Phi}$. To reconstruct sparse signals, Candes and Tao presented and proved that sensing matrix must satisfy the constraint equally conditions. For arbitrary constants, if

$$(1-\delta_K) \| c \|_2^2 \leq \| \tilde{\Phi}_T c \|_2^2 \leq (1+\delta_K) \| c \|_2^2 \tag{4}$$

is established, which $T \subset \{1,...,N\}$, $|T| \leq K$ and $\tilde{\Phi}_T$ is the sub-matrix constituted by the column of the index T in the matrix $\tilde{\Phi}$. The signal reconstruction algorithm is the basic theory of compressed sensing. Candes and others proved that signal reconstruction problems can be solved by solving the problem of the minimum l_0 norm, but Donoho stated that the minimum l_0 norm problem solving is essentially an NP-hard problem, which usually required for conversion. Therefore, the researchers made a series of algorithms to obtain sub-optimal solutions, including the smallest l_1 norm method, match tracking series algorithm, iterative threshold method and the minimum variables analysis method [4][5].

De-nosing algorithm process steps

The wavelet filtering theory shows that the noise signal wavelet coefficients at each scale does not have sparse property. Therefore, it can be used to restore the sparse of wavelet coefficients by compressed sensing theory, in order to achieve the purpose of signal de-noising. The flow chart of the algorithm step is shown in Fig.1.

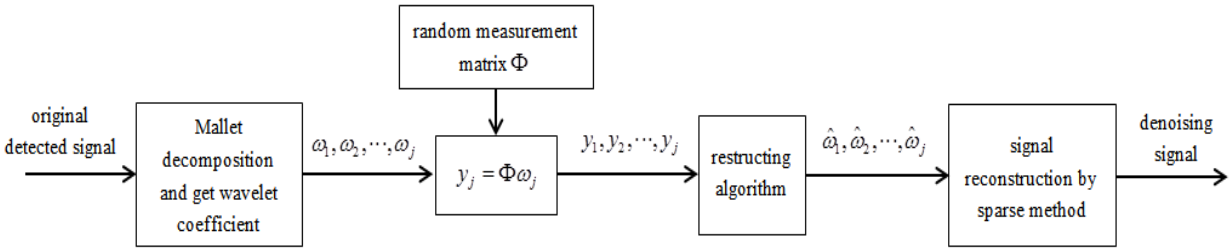

Fig.1 Underwater Acoustic Signal de-noising process steps

The random measurement matrix in the algorithm must meet the uniform uncertainty principle (UUP), that is, for any S-sparse vector x, if:

$$0.8\frac{M}{N}=\|x\|_2^2\le\|\varphi x\|_2^2\le 1.2\frac{M}{N}\|x\|_2^2 \qquad (5)$$

then the set of size S meets the UUP principle, where the perception matrix is currently used as a random matrix, such as Gaussian matrix, Bernoulli matrix, Fourier random measurement matrix and non-correlation measurement matrix [6].

Simulation results and analysis

The characteristics of the simulation processing signal of underwater acoustic signal are short time, low energy and transient. The original acquisition signal is $f(t)=s(t)+n(t)$, where $s(t)$ is the weak signal that will be extractive (as shown in Fig.2a), $n(t)$ is the signal of the system environment in the process of detection and the background noise, the signal-to-noise ratio of the detected signal $f(t)$ is set to -8.09dB (as shown in Fig.2b),which can be observed that the weak signals are submerged by noise signals[7][8].

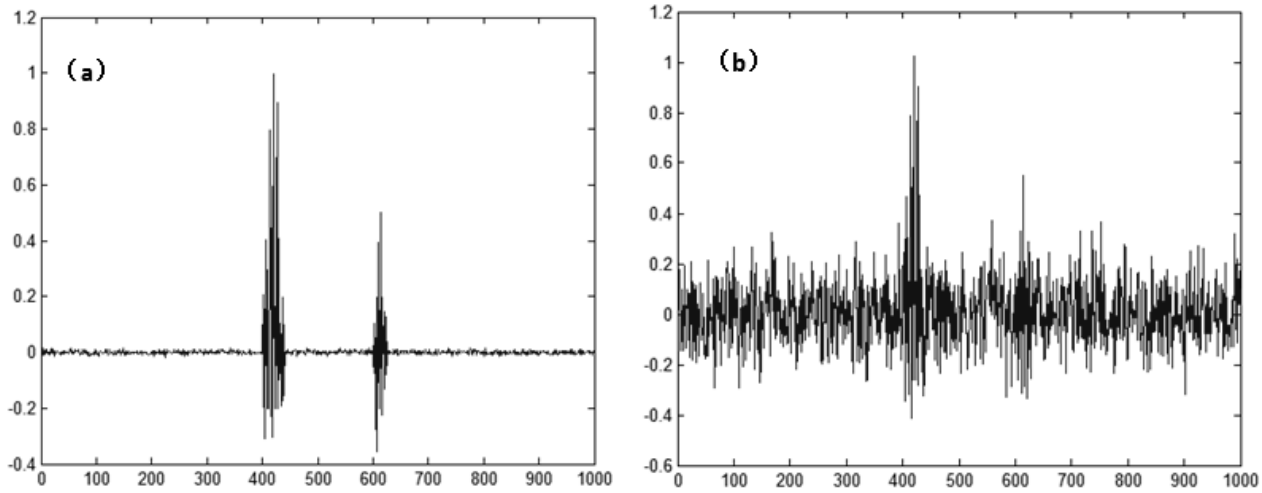

Fig.2 The original signal (a) and noise mixed signal (b)

When it has the strong noise interference, the traditional wavelet threshold algorithm can only detect a strong signal because of fixed threshold limitations, and the weak signal is cut as noise filtering (as shown in Fig.3a), the de-noising algorithm based on compressed sensing theory correctly detect the corresponding weak signals (as shown in Fig.3b).

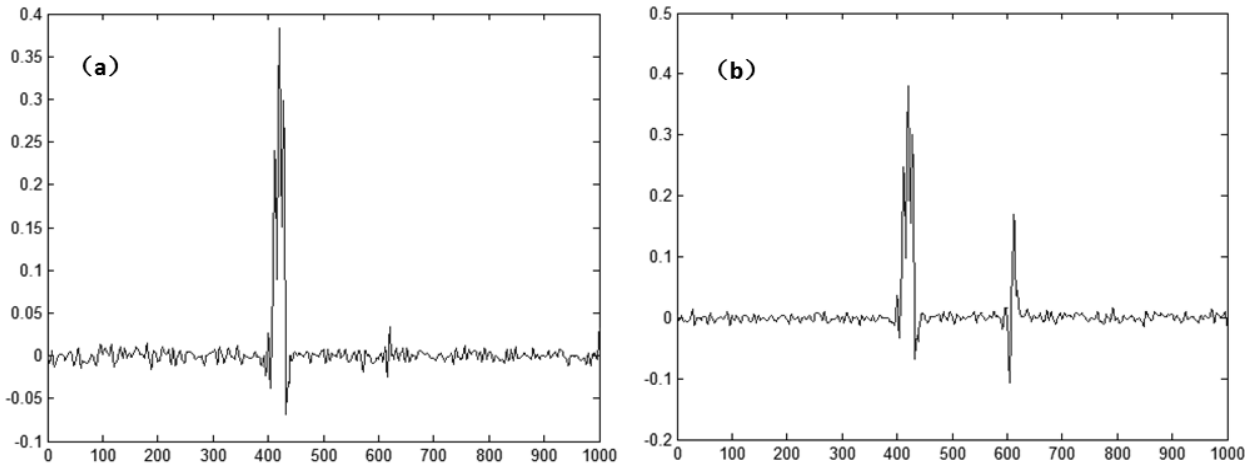

Fig. 3 The traditional wavelet de-noising (a) and compressed sensing theory based on improved effect (b)

This shows that with the deepening of decomposition scale, the wavelet coefficients of each scale only has a small number of large coefficients. When the signal has the noise, the wavelet coefficients corresponding to the noise reduced rapidly, but the wavelet coefficients of the signals are enhanced, so the sparse property of wavelet coefficients will be greatly reduced. Therefore, the methods of wavelet coefficient sparse property recovery based on compressed sensing theory can be used in weak signal detection, with the advantage of achieving the effective extraction of the useful signal and avoiding the difficult problem of threshold choice of wavelet threshold filtering.

Conclusions

This paper addresses a problem of removing weak noise from underwater acoustic signals. Our proposed algorithm is based on the well-known compressed sensing theory. A comparative study demonstrates that our proposed algorithm outperforms the wavelet based de-noising technique. Although the compression reduces the amount of information detail of the signals, it does not bring much negative effects on filtering noises.

References

[1] Candès E J. Compressive sampling[C]. Proceedings of the international congress of mathematicians. 2006, 3: 1433-1452.

[2] Mallat S, Hwang W L. Singularity detection and processing with wavelets[J]. IEEE Transactions on Information Theory, 1992, 38(2):617-643.

[3] Candès E J, TAP T. Near-optimal signal recovery from random projection: universal encoding strategies[J]. IEEE Trans. Inform. Theory, 2006, 52:5406-5426.

[4] Daubechies I. The wavelet transform, time-frequency localization and signal information theory, 1990,36(5):961~1005.

[5] Mallat S G, Sifen Z. On pattern analysis and machine intelligence[J]. IEEE Trans Information theory, 1992,14:710~729

[6]Hsung T C, Lun D P K. De-noising by singularity rejection[J], IEEE International Symposium on Circuits and Systems, 1997, 6: 205-208.

[7]Cheng Zh X. Wavelet analysis algorithm and application[M]. Xi`an: Xidian University Press,1998.

[8] Hu Ch, Li C, Design and system analysis based on MATLAB[M]. Xi`an: Xidian University Press,2004

Advanced Materials Research Vols. 989-994 (2014) pp 3722-3725
© (2014) Trans Tech Publications, Switzerland
doi:10.4028/www.scientific.net/AMR.989-994.3722

A Beam Forming Method Based on Amplitude Weighting of Uniform Circular Array

Jin-lin WANG[1,a], Yong-qing FU [1,b], Xue LIU[2]

[1]College of Information and Communication Harbin Engineering University, Harbin, China

[2]PLA 91550 Unit 94, Liaoning Dalian, China

[a]email: wangjinlin2003@qq.com, [b]email: fuyongqing@hrbeu.edu.cn

Keywords: Uniform Circular Array; Amplitude Weighting; Beam-forming; Side-lobe Suppression

Abstract. The uniform circular planar array (UCA) has lots of advantages what linear arrays and other surface arrays don't have. However, because of its limitations, such as the high side-lobe level and low zero depth, the application on controlling array space direction by beam forming has been limited. Considering the characteristics of UCA, the receiving UCA's signal model is established in this paper. The influence factors of UCA's beam will be found out on the basis of theoretical derivation. A new method, that can improve the performance of the UCA beam directivity by amplitude weighting, is proposed in this paper. The theoretical derivation results and simulation results improved that the method could have a better ability in side-lobe suppression, and the new method could make the UCA to have a good application prospect.

Introduction

In the fields of the modern wireless communication system, radar detection and navigation guidance, more and more UCAs appear due to their characteristics such as less elements then planar array antenna wind, easier to conform with carriers and its 360-degree angle range in azimuth [1][2]. In reference [3], the UCA is applied in wireless sensor networks and in reference [4] UCA is used for monopulse angle measurement. Beam forming technology is an important technology in array signal processing. Beam forming technology can delay and compensate the receiving signals what are from space sources, so the output of the UCA can be superposed in the same phase, and then we can get a peak on the angle of arrival (AOA) of the source. Applying the beam forming technology can also control the pointing angle of the UCA, which is the most used in phased array radar. The array directivity is an important indicator of beam synthesis technology, it determines the sensitivity of the array and the target resolution [5].Although UCA has many advantages, but there are also disadvantages such as the wider main lobe width , the higher side-lobe level and so on, what cause the UCA having a poorer directivity performance compared with uniform linear array(ULA).So it is more important to improve the directivity performance of the UCA. Weighted algorithm can effectively improve the uniform circular array directivity. A weighted algorithm of uniform circular array is systematically discussed in this paper. An improved weighted algorithm is proposedd based on the existing weighted algorithm, it is an effective method for suppressing the side-lobe, and it can effectively improve the directivity of UCA.

The Model of UCA

Uniform circular array（UCA），is an array antenna who's array elements are evenly distributed in on the circumference of a circle with a radius R. The number of the elements is M， and they are omnidirectional without cross coupling. The model is given in Fig.1.

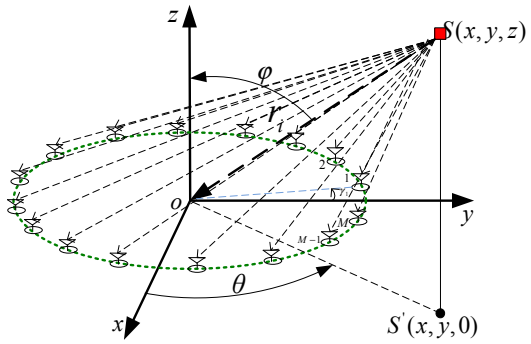

Fig.1 Uniform Circular Array Model

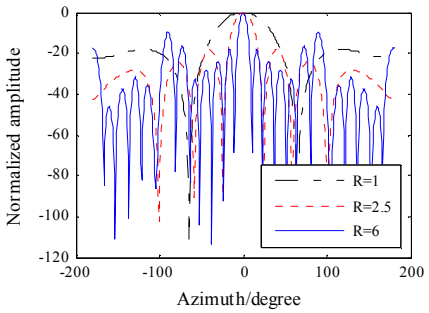

Fig.2 UCA Azimuth Pattern(M=16)

The elements of UCA in Fig.1 is considered as point elements. The far field narrowband source, s(t), spreads its energy to the UCA. We can also see the Azimuth, θ, the pitching angle φ and the source S with its incident angle (θ,φ) in Fig.1. We can set o as reference point, then the signal $s_l(t)$, which is get from the lth element of the UCA，where, $l=1,2,...,M$ (similarly hereinafter).

The direction vector of the array is an important parameter in array Analysis. Popularly, it is recorded as $\mathbf{a}$ .Hereby we give the direction vector of UCA directly as follow.

$$\mathbf{a}(\theta,\varphi)=[\exp[j\frac{2\pi R}{\lambda}\sin\varphi\cos(\theta-\gamma_1)],\exp[j\frac{2\pi R}{\lambda}\sin\varphi\cos(\theta-\gamma_2)],\\ ...,\exp[j\frac{2\pi R}{\lambda}\sin\varphi\cos(\theta-\gamma_M)]]^T \tag{1}$$

Influence Factors of UCA Pattern Performance

The width of main lobe determines the spatial resolution of the array，it is a key factor for the directivity of array. The spatial resolution of regular array is proportional with the array aperture [6]. The three UCA azimuth beam patterns is given in Fig.2. According to the simulation, we can find:

1) The width of main lobe. In Fig.2，when the radius of the UCA increasing，the width of main lobe narrows down, which appears the same regulation with regular array, such as ULA.

2) The side-lobe level. Different from the main lobe, the side-lobe level doesn't become lower when R increasing. When R is up to 2.5m from 1m，the side-lobe level becomes lower, but oppositely, when R=6, it becomes higher than the side-lobe level where the R=1,we call the unusual high side-lobe grating lobe.

To explain why the grating lobe appears and select a right R for the UCA, we quote a function from reference [1] as Eq.(2) as following

$$F_k(\theta)=\frac{M}{2\pi}j^kJ_k(\beta)\exp(jk\theta)+\frac{M}{2\pi}\sum_{i=-\infty}^{+\infty}j^{(k+iM)}J_{(k+iM)}(\beta)\exp[j(k+iM)\theta]=F_{Ek}+F_{Nk} \tag{2}$$

where， $\beta=2\pi R/\lambda$ and $J_k(\beta)$ the first class of Bessel functions of order k based on the variable β. By the nature of the first class Bessel function，we can find ,when $k>\beta$, $J_k(\beta)\approx 0$ .So, when $M>2K$,we have $|k+iM|>\beta$ and $|k|\le K$,where $K=\lfloor\beta\rfloor$. And then $F_{Nk}\to 0$, So, Eq.(2) can become as $F_k(\theta)\approx Mj^kJ_k(\beta)\exp(jk\theta)/2\pi$ .In the simulation , we had set $M=16$ and λ =3m, according to the constraint condition of $M>2K$,we can find $R_{\max}=1.2\lambda$ =3.6m, So we got a grating lobe when R=6m in the Fig.2.

Improved Symmetric Weighting method (ISWM)

To improve the directivity of the, In addition to selecting the right R, we can also array element weighted method. The formula is

$$G=\sum_{l=1}^{M} w_l g_0 \exp(-j\omega\tau_l)\ \ l=1,2,...,M \tag{3}$$

w_l can be divided into phase weighting and amplitude weighting. The phase weighting method can compensate signal phase, left the amplitude unchanged; The amplitude weighting method weights the amplitude left the phase unchanged. We can control the direction of the UCA by $w_l=\exp(j2\pi R\sin(\varphi_0)\cos(\theta_0-\gamma_l)/\lambda)$, which is the phase weighting.

To find a nice amplitude weighting method, we should consider two aspects. We must try to make the side-lobe level lower; otherwise, we shouldn't let the main-lobe much wider. The phase weighting for UCA has little influence on its side-lobe level. So, we must make the side-lobe level lower by amplitude weighting method. It is very complicated to suppress the side-lobe. Some researchers make it by changing the hardware structure of the elements [7], but there is little researcher make it by amplitude weighting method. And we can find out that the ordinary window functions, such as Hanning-window, make no use on suppressing the side-lobe level for UCA in Fig.3.

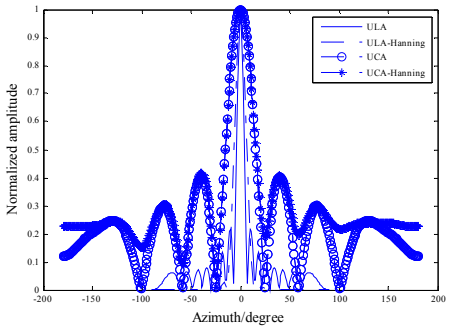

Fig.3 ULA&UCA Azimuth Pattern(M=16)

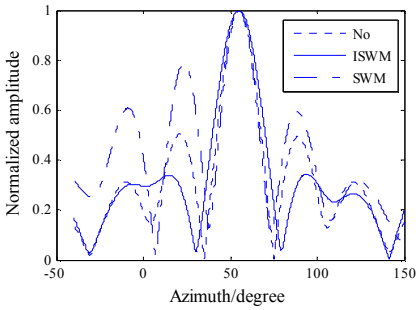

Fig.4 UCA Azimuth Pattern after ISWM

In this paper, An improved weighted algorithm is proposed for suppressing the side-lobe level of the UCA. The theoretical derivation is given as following.

1) The essential conditions of the improved amplitude weighting method

Condition 1: $w_l=w_{M+1-l}$; Condition 2: The elements position of the UCA showed in Fig.1 and $\gamma_l=[\pi+2\pi(l-1)]/M$, $l=1,2,...,M$; Condition3: $w_l^*=w_{2M_0+1-l}$, $l=1,2,...,M_0$, where, M_0 is the number of the elements in one quadrant in Fig.1.

2) The theoretical derivation

Based on the Eqs above, we can easily get the output of the UCA.

$$G(\theta,\varphi)=\frac{1}{M}\sum_{l=1}^{M} w_l \exp\left[j\frac{2\pi R}{\lambda}\sin(\varphi)\cos(\theta-\gamma_l)\right] \tag{4}$$

Step 1: Using condition 1 and condition 2, we can simplify the Eq. (4)

$$G(\theta,\varphi)=\frac{1}{M}\sum_{l=1}^{2M_0} w_l\left\{\exp\left[j\frac{2\pi R}{\lambda}\sin(\varphi)\cos(\theta-\gamma_l)\right]+\exp\left[j\frac{2\pi R}{\lambda}\sin(\varphi)\cos(\theta+\gamma_l)\right]\right\} \tag{5}$$

Step2: Using Condition 3 and condition 2, the Eq. (5) can be simplified as,

$$\begin{aligned}G(\theta,\varphi)=&\frac{1}{M}\sum_{l=1}^{M_0} w_l\left\{\exp\left[j\frac{2\pi R}{\lambda}\sin(\varphi)\cos(\theta-\gamma_l)\right]+\exp\left[j\frac{2\pi R}{\lambda}\sin(\varphi)\cos(\theta+\gamma_l)\right]\right\}\\&+\frac{1}{M}\sum_{l=1}^{M_0} w_l^*\left\{\exp\left[-j\frac{2\pi R}{\lambda}\sin(\varphi)\cos(\theta+\gamma_l)\right]+\exp\left[-j\frac{2\pi R}{\lambda}\sin(\varphi)\cos(\theta-\gamma_l)\right]\right\}\end{aligned} \tag{6}$$

Step3: $w_l=w_{lR}+iw_{lI}$, where, w_{lR} is real part, w_{lI} is the imaginary part. So

$$G(\theta,\varphi)=\frac{2}{M}\sum_{l=1}^{M_0}w_{lR}\left\{\cos\left[j\frac{2\pi R}{\lambda}\sin(\varphi)\cos(\theta-\gamma_l)\right]+\cos\left[j\frac{2\pi R}{\lambda}\sin(\varphi)\cos(\theta+\gamma_l)\right]\right\}$$
$$-\frac{2}{M}\sum_{l=1}^{M_0}w_{lI}\left\{\sin\left[j\frac{2\pi R}{\lambda}\sin(\varphi)\cos(\theta-\gamma_l)\right]+\sin\left[j\frac{2\pi R}{\lambda}\sin(\varphi)\cos(\theta+\gamma_l)\right]\right\} \quad (7)$$

3) Adaptive adjustment of the amplitude weighting

In order to satisfying condition 2，the amplitude weighting we chose should be adaptive to the searching angle. So we should adjust the amplitude weighting in ISWM.

Simulation Result and Analysis

According to the Eq.6，the complex exponential terms in the Eq.4 has been transformed to sine terms by using the three conditions; And the UCA output functions is an even function about azimuth θ, in other word, the UCA has the characteristics of the symmetry about azimuth, and we can find the symmetry of the beam pattern using ISWM obviously, through the simulation results showed in Fig.4. The simulation parameters are set as M=16, R=3.5, λ=3m , φ= 30°, θ=55°. From the simulation results by using different methods of amplitude weighting methods, we can find that the side-lobe can not be suppressed when using the SWM. But when using the methods of ISWM, which is proposed in this paper, the side-lobe was suppressed and the mainlobe was not broadened seriously. This could prove the effectiveness of the method of this paper.

Conclusion

This paper has proposed an improved method of weighting for uniform circular array, which is called ISWM. This method can suppress the side-lobe of the beam parttern effectively. With the constraint conditions of UCA aperture, the beam directivity of the UCA is improved significantly after the ISWM. The simulation results shows that the UCA ,horizontal, has the symmetry about azimuth for its beam pattern, and its amplitude weightings can be adaptive with the searching angle, so, the sidelobe can be reduced effectively, and the directivity of the UCA is improved significantly.

Acknowledgement

This paper is funded by the International Exchange Program of Harbin Engineering University for Innovation-oriented Talents Cultivation. I should express my sincere gratitude for this.

References

[1]Wang Yong-liang, Chen Hui , Peng Ying-ning，Wan Qun. Spatial spectrum estimation and algorithm[M].Beijing：Tsinghua University Press，2004:340-343

[2] Performance of ship-carried round super resolution direction estimation antenna array. Journal of Harbin Engineering University .2001, 22(4),33~36

[3]Wong C H, Siew Z W, Kiring A, et al. Distributed beamforming with uniform circular array formation in wireless sensor networks[C].Global High Tech Congress on Electronics (GHTCE), 2012 IEEE. IEEE, 2012: 75-80.

[4] ZHAO Ying-jun，LI Rong-feng，WANG Yong-liang，LIU Wei-jian. An adaptive monopulse angle measurement method for uniform circular array[J]. Journal of Naval University of Engineering. 2013, 25(4):103-107.

[5] Zhu Long-shi. A Weighting Method For Improving Beam Directivity of The Circular Array [J]. Journal of Electronics, 2000，22(4)，700-704.

[6] Li Ying. Analysis of the Systematic performance on Uniofrm Circuilar Ararys[D]. National University of Defense Technology, 2004.

[7]Zhang Zhi-ya.Research on Wideband Antennas and Shaped-beam Arrays Antennas [D]. Xi'an Electronic and Engineering University,2012.

Advanced Materials Research Vols. 989-994 (2014) pp 3726-3729
© (2014) Trans Tech Publications, Switzerland
doi:10.4028/www.scientific.net/AMR.989-994.3726

Impulse Noise Suppression Method for Telemetry Signal by Multi-scale Median Filtering

Xiu-fang LIU

PLA 91550 Unit 94, Liaoning Dalian, 116023, China

email: XiufangLiu@126.com

Keywords: Wavelet Transform; Median Filtering; Impulse noise; Telemetry

Abstract. The telemetry signal is often interfered with impulse noise, which results in difficulty in time domain and frequency domain analysis results. Hereby a new impulse noise suppression method based on wavelet transform and median filtering technique was proposed. The received signal is decomposed into detailed components and approximate components, and then the median filtering is carried on the wavelet decomposition components with vary filtering window size according to the wavelet transform scale respectively. This method can suppress the impulse noise effectively and keep the detail information of the signal from the loss at the same time. The simulation and experimental results prove the effectiveness of the method.

Introduction

In vehicle tests, the telemetry environmental parameters reflects the internal state of the aircraft in flight [1], processing and analysis of telemetry environmental parameters is an important work in the vehicle test and the results evaluation. Telemetry environmental parameters are often interfered by channel multipath and noise interference in the transmission process. The multipath transmission would induce inter-symbol interference and the adding Gauss noise may result in amplitude distortion. The receiver uses equalization or diversity technology, can generally get the original data is satisfactory. However, in the practical engineering, the noise interference by telemetry signal transmission process often exhibit impulse noise characteristics of [2], which includes short-term greatly impulse in the time domain waveform. Impulse noise interference results in the telemetry environmental parameters processing method failure, such as filtering, least square fitting, and the impulse noise [3] seriously affects the spectrum analysis in the frequency domain and the mean square error statistic in the time domain, and further affect the identification of the state in the process of aircraft reliability. Therefore, must find effective methods for impulse noise suppression in telemetry environmental parameters processing. The median filter is considered to be an effective nonlinear filtering method to eliminate the impulse noise [4], found in applications, the median filter window selecting has an important effect on the performance of impulse noise suppression. The larger median filtering window can suppress the impulse noise interference at the maximum extent, but the detail information of the received signal may loss, the smaller median filtering window can better keep the detail information of the signal, but the impulse noise suppression ability is weak. Therefore, combined with wavelet transform, this paper presents a multi-scale median filtering method, which uses the band-pass filter characteristics of the wavelet transform [5] to decompose the received signal into a series of detail components and approximate component, thus the impulse noise would distribute to each component in the signal. The median filtering window size is determined based on the wavelet decomposition components and the decomposition scale. Wavelet decomposition components finally reconstruct the original signal after median filtering. This method can effectively keep the signal details without loss and suppress the impulse noise interference. The results of computer simulation and the experimental data processing show the effectiveness of the method.

Impulsive Noise Model

De-noising is an important pre-processing in the process of the telemetry environment parameters. The traditional telemetry environmental parameter data processing often assume the noise meet the Gaussian distribution, which can be suppressed by the filtering or least square fitting method. Also the wavelet threshold de-noising is an effective de-noising method for Gaussian noise, wavelet de-noising does not need signal is stationary. However, with the multi-user interference, atmospheric noise (thunderstorms, lightning), discharge of car engines, and other natural and man-made electromagnetic interference, the noise in the telemetry received signals often exhibit impulsive noise characteristics. In recent years, impulse noise is widely regarded in some engineering applications, typically a microphone array speech signal acquisition system and the naval vessel sonar system, the noise shows typical characteristics of impulse noise. Impulse noise is different from the Gaussian noise, which has short greatly significant pulse in the time domain. In the engineering, the alpha stationary distribution is often used to describe the impulsive noise, which is an applicable to a wide range and has been widely used. The characteristic function can be given by

$$\phi(t) = \exp\{j\mu t - \gamma|t|^{\alpha}[1 + j\beta\,\mathrm{sgn}(t)\omega(t,\alpha)]\} \tag{1}$$

$$\omega(t,\alpha) = \begin{cases} \tan(\pi\alpha t) & \alpha \neq 1 \\ (2/\pi)\log|t| & \alpha = 1 \end{cases} \tag{2}$$

where α, γ, β and μ are the parameters to describe the alpha stationary distribution. α is the characteristic exponent, γ is the coefficient of dispersion, β is the symmetric parameter and μ is the mean or median of the alpha stationary distribution.

Wavelet Transform and Median Filtering

Wavelet analysis has been widely used in engineering for signal processing, and the wavelet threshold de-noising can obtain good performance for the Gaussian noise. However, if the noise does not meet the Gaussian distribution, the wavelet threshold de-noising performance would degrade, especially for the impulse noise. The median filtering is a kind of impulse noise suppression method as the nonlinear filtering techniques, but the median filtering with fixed window size has contradictory in the signal details protection and impulse noise suppression ability. In order to solve this problem, we can combine the median filtering with wavelet transform to construct a multi scale median filtering method.

Wavelet transform can be equivalent to a set of image filtering process, in which the signal through a decomposition of high pass filter and low-pass filter, and then the high frequency part of signal corresponding to the natural high pass filter, called the detail component, the output low-pass filter corresponding to the lower part of the relative frequency component signal, called the approximate components. The fast algorithm of wavelet transform is Mallat algorithm, which based on wavelet decomposition and reconstruction algorithm of wavelet theory respectively, as shown in Fig.1 and Fig.2.

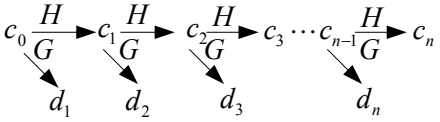

Fig.1 The tower decomposition algorithm

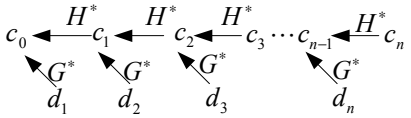

Fig.2 The tower reconstruction algorithm

where H and G are corresponding to the high-pass filter and the low-pass filter respectively, H^* and G^* are the dual operator of H and G. c_j and d_j （$j = 1,2,\cdots,n$） are the approximation component and detail components respectively.

Although wavelet decomposition is an iterative process, which can break down the infinite in theory, but in the practical application, it is decomposed into a finite number can meet the needs of the signal processing and analysis.

Median filtering is a nonlinear filtering method, in which the signal filtering based on the order statistics, and it has the advantages of simple and fast operation, with has excellent performance in impulsive noise suppression. For the one-dimensional median filtering, let the filter window length $n=2k+1$ or $n=2k$ and the sampling points $N \geq n$, when $U(t_1)$, $U(t_2)$, $\cdots$, $U(t_N)$ moving on the observation data, the output of the median filtering is given by

$$med(U(t_i))=\begin{cases} U(t_{k+1}) \\ \frac{1}{2}\left[U(t_k)+U(t_{k+1})\right] \end{cases} \tag{3}$$

where $U(t_k)$ is the k-th maximum or minimum in the window $n=2k+1$ or $n=2k$. According to this definition, the output $X(t_i)$ and the input $U(t_i)$ of the median filtering can be expressed as

$$X(t_i)=med\left[U(t_{i-k}),\cdots,U(t_{i+k})\right] \tag{4}$$

According to the process of the median filtering, the window size has an important influence on the performance. Typical if the median filter window smaller or equal to the width of the pulse, the pulse will be retained after filtering. If the pulse width is less than or equal to the window size, the pulse will be removed after filtering. Therefore, the median filtering window with better impulse noise suppression ability, the detail information of high frequency would loss seriously. Otherwise, the median filtering window is smaller can have the good protective capability for signal details, but the impulse noise suppression ability is weak, especially for some short impulse noise, often do not get ideal results.

Therefore, we can decompose signal into a series of detail components and approximate component by wavelet transform, and using different filter windows on the wavelet decomposition components for median filtering, as a result, a method can keep the detail information of signal and suppress the impulse noise as the same time is obtained.

The Simulation and Experimental Data Processing

The simulation signal is given by

$$x(t)=\sum_{i=1}^{3}\sin(2\pi f_i t)+n(t) \tag{5}$$

where the sample frequency $f_s=1000\,\text{Hz}$, the center frequency of is $f_1=50\,\text{Hz}$, $f_2=20\,\text{Hz}$, and $f_3=5\,\text{Hz}$. $n(t)$ is the impulse noise. The simulation results are shown in Fig.3a-Fig.3c. The results show that, the multi scale median filtering method can suppress the impulse noise and keep the detail information of the signal effectively. To further verify the effectiveness of the method, the vibration signal in a test is selected to process and the sampling frequency $f_s=5\,\text{Hz}$. The processing results are shown in Fig.4a-Fig.4c. The results can also show the effectiveness of the multi scale median filtering combined with wavelet transform.

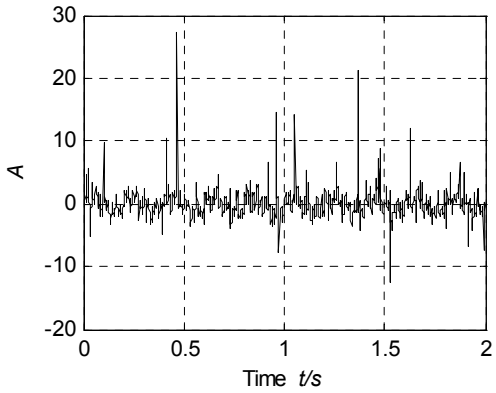

Fig.3a The simulation signal

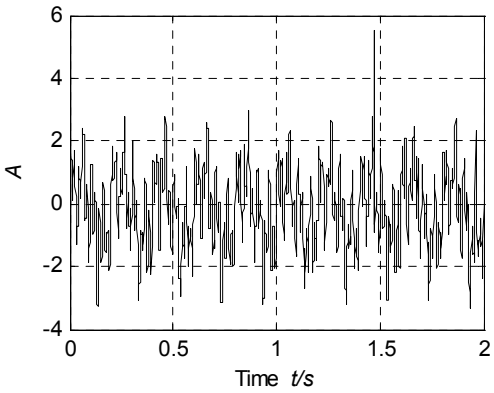

Fig.3b Median filtering result

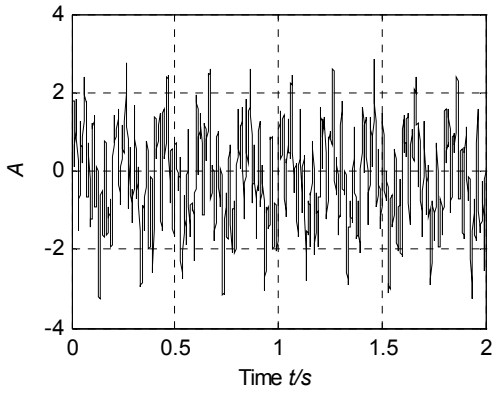

Fig.3c Multi scale median filtering result

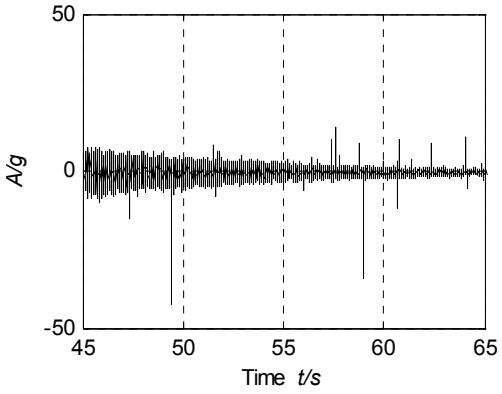

Fig.4a Vibration signal

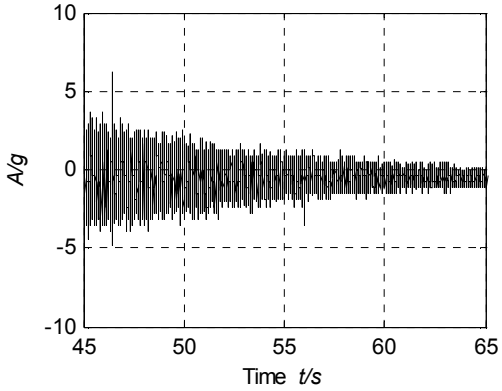

Fig.4b Median filtering result

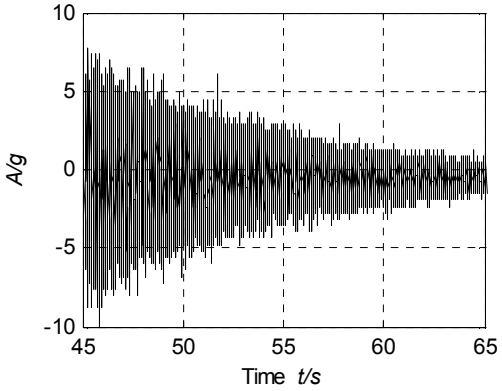

Fig.4c Multi scale median filtering result

Conclusion

This paper proposed a multi scale median filtering to suppress the impulse noise in the signal, which takes advantages of the wavelet transform and the median filtering to overcome the shortage of the median filtering with the fixed window size. The simulation and the vibration signal processing results show the method can suppress the impulse noise and keep the detail information of the signal effectively.

References

[1] XU Hong-tao, WANG Yue-gang. Noise cancellation for telemetry signal based on reconstructed phase space and principal component analysis [J]. Journal of Computer Application, 2010, 3: 793-795.

[2] YANG Hai-bao, ZHU Ya-jun, CHA Dai-feng, XIONG Mei-ying. STFT Time-frequency Analysis Method of Fractional Lower-order Alpha Stable Distribution [J]. Application Research of Computers, 2012, 29(8): 2915-2917.

[3] ZHANG Chen-rui, FAN Yang-yu, LIU Shu etal. Switching vector median filter based on fuzzy decision [J]. Application Research of Computers, 2013, 30(12): 3870-3873.

[4] GUO Ying, QIU Tian-shuang, ZHANG Yan-li. The fractional lower order cyclic statistics and its application in time delay estimation under impulsive noise conditions [J]. Signal Processing, 2008, 24(3): 407-410.

[5] WU YunJie, DENG Yu, DUAN HaiBin, ZHOU LinNa. Dual tree complex wavelet transform approach to copy-rotate-move forgery detection[J]. SCIENCE CHINA Information Sciences, 2014, 1:121-132.

Advanced Materials Research Vols. 989-994 (2014) pp 3730-3733
© (2014) Trans Tech Publications, Switzerland
doi:10.4028/www.scientific.net/AMR.989-994.3730

Research on color vegetable diseases in greenhouse image pretreatment and extraction method

Luo Xiao-li

Fuzhou Vocational and Technical College Fuzhou Fujian China

email:2416734036@qq.com

Keywords: Sobel-operator, channel, circular degree, weighted mean square error

Abstract. In order to realize the accurate identification of the image color vegetable diseases in Greenhouse, In this paper, by using computer image processing technology in the intelligent recognition of vegetable diseases in greenhouse leaf, First, the moving average method can effectively remove the noise by the image of R,G, B three channel gray level, Then separate three channel image using Sobel -operator and the 4 template based on the direction of gradient magnitude ,and then integrate the three channel edge ,it can overcome the shortcoming of traditional gray image information, and make up the deficiency of the traditional Sobel operator edge thinning geometric features.

Introduction

In abroad, [1] Shanwengang studied the infrared image of the harmful Sulfur dioxide gas pollution on crop In 1985 ;[2] later the Japanese Honami Nobuo separately samplied image to the arrowhead leaf of the lack of calcium, iron, magnesium nutrient elements by computer vision technology in the open , As the shape and position of the leaf image histogram a feature. But by the extracted features to distinguish the effect is not obvious.[3] At home, in the early 1990 s, the computer image processing technology applied in the field of agricultural engineering, mainly was used in the agricultural product quality inspection and grading, crop information retrieval. [4] Such as Jian Ping (1993) has used image processing technology to make more reasonable for tobacco appearance quality detection, synthesize variety of colorimetric system on the quantitative analysis of the quality of tobacco leaves.

The purpose of image processing is to get image edge from a true color image of plant disease. Through the disease imaged by CCD camera as the research material, have finished the output of plant disease image edge geometry information and prepared for the subsequent computer to diagnose diseases.

The research environment and technical methods

study Visual C++ software on Windows XP platform 6, 0 as a development tool, Edit programs to image preprocessing, Eventually form a complete image processing system. This project research method is based on digital image processing technology, as the theoretical basis of algorithm analysis, through the CCD camera image, study computer disease image edge scheme for greenhouse vegetables to achieve intelligent extraction disease geometric edge.

Image preprocessing

2.1 [6] channel separation:

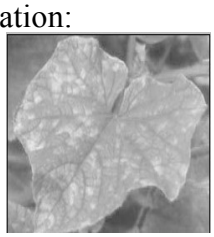

Fig.1Red channel

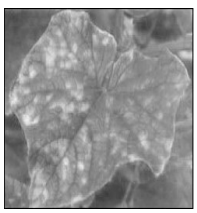

Fig. 2 Green channel

Fig. 3 Green channel

An image of RGB mode, with red, green and blue color values：True color RGB model with R, G, B three channel color, the color of each image channel window is displayed in gray image, the disease spot image edge and background will appear obvious gray contrast in each channel, and this provide the guarantee for the image edge extraction of the accurate. Use Photoshop to open the cucumber owny mildew leaf image into the channel view, get the following R, G, B three channel gray image as figure 1,2,3.

By contrast degree of three channels of gray image disease spot and leaves, set the weight of the red channel, the green channel, blue channel with 0.2, 0.7, 0.1set the weight of the red channel.

2.2 image denoising

[5]In the 3*3 area as the neighborhood of Z, the median filtering technology is on the basic principle of pixel numerical order except the center point of the median values, obtained The median values in the neighborhood, Gray pixel neighborhood center point values are replaced by the mid-value of group. The pixel of the centre is close to the real values, so as to eliminate the isolated noise points. f (x, y) is the original map images , F (x, y) two-dimensional median filter output , F (x, y) =med{f (x-m, y-l), (m, l ∈ Z)}. Out images using three channel gray on the separation based on the median filter, the median filter not only solves the problem moving smooth resulted in details but also solves overexpression of smooth and edge deletion etc by the traditional Gauss function .

Feature extraction,

First through image segmentation, using double threshold segmentation technique to remove background, so as to separate the image information and the background information, then by using four template Sobel-operator respectively calculated gradient amplitude of three-channel image edge detection, edge can be fully refined, finally, the geometrical characteristics of the disease spot can be fully extracted by fusing three-channel with weighted mean square erro.

3.1, the image segmentation

Due to the color of the leaf is darker than the disease spot, brighter than the background, so we can adopt double value binarization processing [6]

$$G(x,y)=\begin{cases} HIGH & (T1<F(x,y)<T2) \\ LOW & else \end{cases} \quad (1)$$

As an example of Green channel gray image, first, extract the image below a threshold value less than 128 as fgure 4; Then the image reversaed we can extract the image of threshold value larger than 140 as figure 5; Finally extract the image of threshold between 128 to 140 to get the following figure 6 which is the best effect:

Fig.4 Threshold < 128

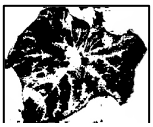

Fig.5 Threshold > 140

Fig.6Threshold of 128 ~ 14

3.2,Image edge detection:

use 4 template direction of Sobel-operator respectively calculate gradient amplitude of three-channel image edge detection.For Green channel gray image as an example, using the 3×3 matrix, the horizontal and vertical, respectively, with the image plane convolution, can be calculated the brightness of the horizontal and vertical difference approximation. [7] if A on behalf of the original image, Gx and Gy represent the horizontal and vertical edge detection of image, its formula is follows:

$$G_x = \begin{bmatrix} -1 & 0 & +1 \\ -2 & 0 & +2 \\ -1 & 0 & +1 \end{bmatrix} * A \text{ and } G_y = \begin{bmatrix} +1 & +2 & +1 \\ 0 & 0 & 0 \\ -1 & -2 & -1 \end{bmatrix} * A \qquad G_{45度} = \begin{bmatrix} -2 & -1 & 0 \\ -1 & 0 & +1 \\ 0 & 1 & +2 \end{bmatrix} * A \text{ and } G_{135度} = \begin{bmatrix} 0 & +1 & +2 \\ -1 & 0 & +1 \\ -2 & -1 & 0 \end{bmatrix} * A \quad (2)$$

Then the following formula can be used to compute the gradient direction.

$$\Theta = \arctan\left(\frac{G_y}{G_x}\right) \quad (3)$$

The image edge detection should has many directions: except in the horizontal directions , add the vertical directions and 45 degree, 135 degree directions, so as to improve the accuracy and can achieve real-time detection of edge effect .the image as the follows figure 7,8,9

THE FUSION OF THE THREE CHANNEL EDGE

Fig.7 G channel X and Y Sobel operator

Fig.8 G channel 45 ° and 35 ° Sobel operator

Fig.9 G channel four directions of 45 ° and 35 ° Sobel operator

Because of the B channel carrying more edge information of color image than R, G channels. Therefore, their right importance are larger.[8] So three channel fusion method set R, G, B channel weight fx respectively 0.7, 0.2, 0.1 by calculating the variance of three channel edge image, the deviation from the mean square variance, known as the standard deviation or variance, the variance to describe fluctuations. The more close to the true value if the fluctuation of small, obtain the value, or abandon, a point （x,y） in three channel edge image Gray value respectively is HR, HG , HB, There are：

Average Value: $E=0.2H_R + 0.7H_G + 0.1H_B$ (4)

Variance : $s_{R\wedge 2}= 0.2(H_R-E)\wedge 2 \quad s_{G\wedge 2}= 0.7(H_G-E)\wedge 2 \quad s_{B\wedge 2}= (H_B-E)\wedge 2$ (5)

Three channel edge images before image fusing as Figure10, Figure11, Figure12:

Fig.10 The red channel edge detection

Fig.11 The red channel edge detection

Fig.12 The red channel edge detection

Fig.13 The image after Three channels edges fused

So, with different weights to fuse the three edge detection image results information as the figure 13:

From the edge detection results as Figure 13, the closed area in the picture is the leaf spot, we can calculate roundness, area, perimeter as follows Table 1 :

TABLE .1 CUCUMBER LEAF DISEASE SPOT IMAGE CHARACTERISTICS

lesion area ID	Area Ar	Premeter Gir	Roundness Rou
0001	0.13	1.23	1.08
0002	0.10	1.17	0.91
0003	0.12	1.41	0.75
….	….	….	…..

Conclusion

If lesion area is small, it located at the blade tip, the circular degree nearly circular, damage to a lesser degree. When the area is large, the lesion area closed area, located at the blade tip round degree difference, the shape are irregular and the damage is more serious.

Project:Class A in Fu jian province department of education JA12400 topic: color image preprocessing and extraction method of greenhouse vegetable disease research project director: Luo Xiao-li

Luo Xiao-li, born in October 1971, native place, Wuchang city in Heilongjiang province in 1994, graduated from the university, fuzhou university software engineering master degree in 2010, research direction: software engineering. teaching in Fuzhou vocational college computer department, title: lecturer :Luo Xiao-li .

References

[1]Youwen Tian. Typical crop leaf diseases computer image recognition method research [J]. Journal of agricultural mechanization engineering 2005.
[2]Chunyan Xie and Keda Wu. Spectroscopy in the research development of crop pest and disease detection and prospects [J]. Journal of agricultural mechanization research, 2009 (9)
[3] Youwen Tian and Chenghua Li. Sunlight greenhouse cucumber disease recognition based on image processing research [J]. Journal of agricultural mechanization research, 2006
[4]Jianping Zhang ,Shouyi Wu , Ruming Fang and liangrun Gao tobacco leaf color measurement and analysis [J]. Journal of jiangsu university, 1994 (03)
[5]Wenpan Zhang,Junhui Wu,Zhen Zhu,Hua Li and Qiang Wan. Based on the quasi cross window median filtering method in the application of the infrared image processing [J]; Lightning and control; 2006 (1)
[6] Jingfu Li and Jinhui Zhao. Agricultural image segmentation method based on threshold study [J]. J AnHui agricultural science, 2010 (6)
[7]Yao Lang. An improved Sobel edge detection operator [J]. Computer and information technology, 2011 (5)
[8] Di ma and Wei Peng. Phase information of color image edge detection and mathematical morphology [J]. Journal of applied science and technology, 2010 (5)

Advanced Materials Research Vols. 989-994 (2014) pp 3734-3737
© (2014) Trans Tech Publications, Switzerland
doi:10.4028/www.scientific.net/AMR.989-994.3734

An Infrared and Visible Images Fusion Algorithm Based on Wavelet Multi-resolution Decomposition

Likun LIU, Zongjia WU

PLA 91550 Unit 94, Liaoning Dalian, China

tianyafc@163.com

Keywords: Image Fusion, Multi-resolution Decomposition, Bivariate Statistical Model

Abstract. Image fusion can be effectively utilized to obtain image redundant information from sensors, hereby improving the accuracy and reliability of information. Based on multi-resolution decomposition of the traditional image fusion method is vulnerable to high frequency noise, fusion is often ineffective. An improved image fusion algorithm has been studied based on the wavelet multi-resolution decomposition. The principle of the algorithm is regional energy maximum for low frequency decomposition image, and the bivariate statistical model for high frequency part. Experimental results show that the bivariate statistical model for the high frequency band is robust to noise based on the joint probability of wavelet coefficient in the conditions of Daubechies wavelet basis function with decomposing level 5 multi-resolution decomposition. Simultaneously, the regional energy maximum for low frequency band can be effective on the high frequency band based on the bivariate statistical model. Fusion image have a larger contrast, the preferred details and the higher gray level resolution.

Introduction

The basic idea of multi-resolution image fusion method is to use multi-resolution decomposition transformation of the source image, and then synthesized multi-resolution image fusion coefficient by some fusion rules, the final inverse transform using multi-resolution image fusion. However, the methods are susceptible to high frequency noise interference. To solve this problem, researchers proposed a fusion method based on the mathematical statistics of high-frequency image. Expectation maximization algorithm [3] for image fusion was used by Yang J. Lafert [4] has proposed statistical fusion model in different resolution image fusion.

In this paper, image multi-resolution analysis based on wavelet decomposition is firstly studied, then, image fusion algorithm has been proposed on multi-sensors image model, which is region energy maximum for low frequency band and bivariate model with the joint probability of wavelet coefficient pair(a wavelet coefficient and its parent) for high frequency band, lastly, with the inverse transform, the infrared and visible images fusion has been achieved.

Image Fusion based on Wavelet Transform

Multi-layer decomposition of the image, each layer produce four sub-images ILL, IHL, ILH, IHH, of which, ILL focus on the main low frequency part, IHL corresponds to the level of the direction of the high frequency information, and ILH corresponds to the vertical direction, IHH corresponds to the direction of 45 degrees.

Mallat proposed the fast algorithm of wavelet transform from the function of multi-resolution [5] [6].

Wavelet transform method generally has the following four steps.

Step1.To match two source images;

Step2. The wavelet decomposition of a source image to create an image wavelet pyramid image;

Step3. For each decomposition level fusion processing, the wavelet coefficients of each decomposition, according to the characteristics of the different frequency components, using different fusion rules for fusion, the formation of the wavelet decomposition pyramid image fusion;

Step4. Fusion of the wavelet pyramid, the inverse wavelet transform for image reconstruction, the formation of the fused image.

Fusion Rules of the Mathematical Model

Low frequency band of the fusion rules has been based on the largest regional energy integration rules. $E_{K,J}(x,y)$ Indicates that the size of the area (x, y) in the low frequency coefficient matrix $M \times N$ of energy, expressed as

$$E_{K,J}(x,y) = \sum_{m \in M, n \in N} \left[C_{K,J}(x+m, y+n) \right]^2 \tag{1}$$

Value in the region expressed as,

$$MED_{K,J}(x,y) = \sum_{m \in M, n \in N} \frac{C_{K,J}(x+m, y+n)}{M \times N} \tag{2}$$

If $Mat_{K,J} \le Thr$, low frequency coefficient is,

$$F_J(x,y) = \begin{cases} C_{A,J}(x,y), & \left(E_{A,J}(x,y) \ge E_{B,J}(x,y)\right) \\ C_{B,J}(x,y), & \left(E_{A,J}(x,y) < E_{B,J}(x,y)\right) \end{cases} \tag{3}$$

If $Mat_{K,J} > Thr$, low frequency coefficient is

$$F_J(x,y) = \frac{MED_{A,J}(x,y) + MED_{B,J}(x,y)}{2} \tag{4}$$

Where, Thr matches the threshold for the image, $Mat_{K,J}$ is the matching of two images corresponding to the regional energy, the size of the area is generally 3×3,5×5 or 7×7, in our study, 3×3 is selected.

The fusion of high frequency band is based on mathematical model [7] of the sensor and the bivariate statistical model [8][9]. In the case of not appear to be confused, in order to facilitate the derivation, the superscript H is omitted, and high-frequency part of the model rewritten in vector form, as shown below

$$\alpha = \beta s + \varepsilon \tag{5}$$

Where, $\alpha = \left[\alpha_1, \alpha_2, \cdots, \alpha_q\right]^T$, $\beta = \left[\beta_1, \beta_2, \cdots, \beta_q\right]^T$, $\varepsilon = \left[\varepsilon_1, \varepsilon_2, \cdots, \varepsilon_q\right]^T$.

Assume that the noise is no-correlative between each other in sensors. Then, we can get a diagonal noise covariance matrix $\sum_{\varepsilon} = diag\left[\sigma_{\varepsilon_1}^2, \sigma_{\varepsilon_2}^2, \cdots, \sigma_{\varepsilon_q}^2\right]$.

The Eq.5 can be used estimation theory to solve. The maximum a posterior estimator (MAP estimator) and bivariate statistical model will be used to solve this problem.

Based on the above assumptions, we can get

$$\alpha_1 = \beta_1 s_1 + \varepsilon_1 \tag{6}$$

$$\alpha_2 = \beta_2 s_2 + \varepsilon_2 \tag{7}$$

The two equations above can be rewritten in the following form

$$A = BS + n \tag{8}$$

Where, $A = (\alpha_1, \alpha_2), B = (\beta_1, \beta_2), S = (s_1, s_2), n = (\varepsilon_1, \varepsilon_2)$

Using MAP

$$\hat{S}(A) = \arg\max_S p_{S|A}(S \mid A) \tag{9}$$

With Bayes rule

$$\hat{S}(A) = \arg\max_S [p_{A|S}(A \mid S) \cdot p_S(S)] = \arg\max_S \left[p_n(A - BS) \cdot p_S(S) \right] \tag{10}$$

Noise probability density function can be written as

$$p_n(n) = \frac{1}{2\pi\sum_{\varepsilon}} \cdot \exp\left(-\frac{\varepsilon_1^2 + \varepsilon_2^2}{2\sum_{\varepsilon}} \right) \cdot \tag{11}$$

Then

$$\hat{S}(A) = \arg\max_{S}[\log(p_n(A - BS)) + \log(p_s(S))] \tag{12}$$

The above equation is equivalent to the solution of the following equation

$$\frac{\beta_1^T(\alpha_1 - \beta_1 \hat{s}_1)}{\sum_{\varepsilon}} - \frac{\sqrt{3} \cdot \hat{s}_1}{\sigma_s \sqrt{(\hat{s}_1)^2 + (\hat{s}_2)^2}} = 0 \tag{13}$$

$$\frac{\beta_2^T(\alpha_2 - \beta_2 \hat{s}_2)}{\sum_{\varepsilon}} - \frac{\sqrt{3} \cdot \hat{s}_2}{\sigma_s \sqrt{(\hat{s}_1)^2 + (\hat{s}_2)^2}} = 0 \tag{14}$$

Fusion Simulation

Fig.1 (a) and (b) are respectively the infrared and visible image (from the Dutch TNO Human Factors Research Institute) [10]. From Fig.1 (a), there are several residential buildings in the scene, on the lawn in front of the house to release smoke from the smoke source. In the infrared image, next to the houses there was a man can clearly be seen, but other scenes are rather ambiguous. In the visible image, the house behind the trees and the grass in front of the house and on the left side of the outline is very clear, but part of the structure behind the house and the smoke obscured completely invisible, due to smoke, visible image in Fig.1 (b) of the same scene, difficult to identify the target in Fig.1 (a), but the scenery of the grass, trees, sky. Using 3×3 local analysis size, the wavelet decomposition level of 5(Db3 wavelet basis function). The fusion results are shown in Fig. 2. Other methods of fusion images are shown in Fig.3 (a)-(f).

Fig.1 (a) IR image from UN Camp

Fig.1 (b) VI from UN Camp

Fig.2 using the proposed method

Fig.3 (a) Result using average

Fig.3 (b) Result using contrast

Fig.3 (c) Result using grads

Fig.3 (d) Result using MGA

Fig.3 (e) Result using DWT

Fig.3 (f) Result using LP

Conclusions

In this paper, image fusion algorithm based on multi-resolution decomposition was studied, which includes the low frequency band and high frequency band image fusion. Fusion rule is a very important in the image fusion algorithm, which relates to the stability of the fusion algorithm, efficiency and the image quality. The bivariate statistical model for the high frequency band is robust to noise based on the joint probability of wavelet coefficient pair. Experimental results show that, using the algorithm proposed can obtain good quality of the fusion image, compared with other algorithms, the effect of the proposed method is better.

References

[1] G. Piella. A general framework for multi-resolution image fusion: From pixels to regions. Information Fusion, 2003, 4(4): 259-280.
[2] Z. Zhang, R.S. Blum. A categorization of multi-scale-decomposition-based image fusion schemes with a performance study for a digital camera application. Proc. IEEE, 1999, 87(8): 1315-1326.
[3] J.M. Lafert, F.Heitz, and P.Perez. Hierarchical statistical models for the fusion of multir-esolution image data[C]. Proceedings of the international conference on computer vision. Cambrige, USA.1995.908-913.
[4] Costantiti M, Farina A, Zirilli F. The fusion of different resolution SAR images [A].Proceedings of the IEEE[C], 1997, 85(1): 139-146.
[5] X.Y. Huang, L.W. Zhou, Z.Y. Gao. Multispectral image fusion using wavelet transform[C].SPIE, 1996, 2898:35-42.
[6] G.X. Li. Fusion Technology of Infrared and Visible Images[D].Changchun,China.2008.
[7] R. K. Sharma, T. K. Leen, M. Pavel. Probabilistic Image Sensor Fusion. Advances in Neural Information Processing Systems, vol. 11, The MIT Press, 1999.
[8] L. Sendur and I. W. Selesnick, Bivariate shrinkage with local variance estimation, IEEE Signal Processing. 2002, Dec. 9(12): 438–441.
[9] L. Sendur and I. W. Selesnick, Bivariate shrinkage function for Wavelet-Based denoising exploiting interscale dependency. IEEE Transactions on Signal Processing,2002, 20(11):2744-2756.
[10] http://www.imagefusion.org/

Advanced Materials Research Vols. 989-994 (2014) pp 3738-3742
© (2014) Trans Tech Publications, Switzerland
doi:10.4028/www.scientific.net/AMR.989-994.3738

Simulation Research on Rolling Element Bearing Fault Signal Extraction Based on Blind Source Separation

Yongxiang Zhang[1,a], Jieping Zhu[1,b], Shuai Zhang[1,c]

[1]College of Power Engineering Naval University of Engineering Wu Han, 430033, China

[a]email: zyx6302@yahoo.com.cn,[b]email: 15172362010@163.com,[c]email: 414564787@qq.com

Keywords： blind source separation; rolling element bearing; fault diagnosis; Kurtosis

Abstract . In order to extract the fault information from rolling element bearing, combined with Kurtosis criteria and Hessian matrix. An improved rolling element bearing fault signal extraction method is proposed. Kurtosis is the cost function. The method is according to the construction principles of blind source separation (BSS), and it uses an analytically derived Hessian matrix in the maximization process of the cost function used. Then the impact signal is extracted successfully. The effectiveness of the method is demonstrated on simulated signal.

Introduction

Rolling element bearings are one of the most extensively used element in rotary machine, and they also play a key role and an easily damaged components in the whole system [1]. Vibration monitoring methods are more applicable to various kinds of rolling element bearings, and especially suitable for incipient fault monitoring and online monitoring. Vibration monitoring methods are widely used in the monitoring and diagnosis of rolling element bearing [2].

On the study of the rolling element bearing of general equipment many scholars have achieved valuable fruits from different angle of view. The common methods such as envelope analysis, wavelet analysis and so on have obtained a certain effect in engineering application [3]. However, because of multiple vibration exciting sources and the complex transfer path, the rolling element bearings fault diagnosis of the complex structure equipment belongs to the weak fault extraction field under multiple excitation sources and strong background noise. In addition, the transfer characteristics trend to unknown for engineering applications which make it hard to the fault recognition [4]. When the transfer characteristics and the number of signal resources are unknown, BSS is a method which utilizes the statistics feature of resource signals and the signals obtained by transducer to extract or separate the resource signals. The BBS method possesses superior performances because of it has taken full advantage of the independence between different resource signals. Hence we can use the BBS to extract the rolling element bearings fault feature of the complex structure equipment [5][6].

In this article, the structure and principles of BBS method is introduced. Kurtosis is regarded as the cost function and an analytically derived Hessian matrix in the maximization process of the cost function is used, and then the separation of rolling element bearing fault signal is achieved. Analysis results for the simulated signals show the effectiveness of the proposed fault extraction approach.

The basic principle and algorithm

Fundamental. The BBS method has good performance. $\mathbf{S}(k)=\left[s_1(k) \quad s_2(k) \quad \cdots \quad s_N(k)\right]$, where $s_n(k)$ is the nth input vibration exciting source, $\mathbf{y}(k)=[y_1(k), y_2(k),\ldots, y_M(k)]$, where $y_m(k)$ is the mth output measurement signal, at a sampling time k. The mechanical system is described as a discrete time system, and matrix $\mathbf{H}$ is the transfer function matrix between exciting and response. We define $\mathbf{y}(k)=\mathbf{H}(z)\cdot\mathbf{S}(k)$

$$y_i(k)=\sum_{i=1}^{M}\sum_{l=0}^{L_c} H_{i,j}(l)S_j(k-l),\ \ i=1,2,\ldots,M,\ \ j=1,2,\ldots,N \tag{1}$$

In the actual projects, multiple exciting sources and the transfer function of the mechanical system is unknown. The following four assumptions are made:

1. The exciting sources are zero mean and independent.
2. The fourth-order cumulants of all the components of the exciting sources are non-zero.
3. **H** is FIR.
4. No measurement noise is present.

When bearing surface defect is generated, impulse signal is excited and the value of Kurtosis increased along with it. We use Kurtosis as the cost function to construct the BBS algorithm, and the fault signal is separated. The Kurtosis is defined as:

$$\text{（Kurtosis）}\quad J=\frac{E(S_i^4)}{(E(S_i^2))^2}-3 \tag{2}$$

The basic approach is depicted in Fig. 1. This method uses independent inverse filter **W** to the measurements **y** resulting in the estimated separated sources S_e. The coefficients of **W** will be iteratively updated until the cost function is maximized. Finally, the fault signal is separated efficiently.

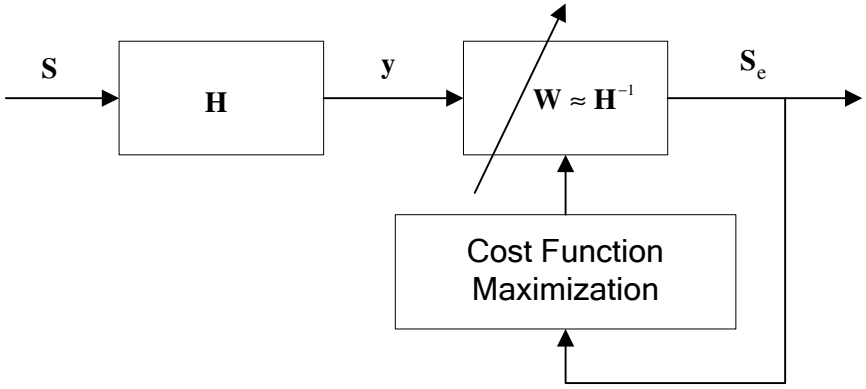

Fig. 1. The basic method

The inverse filter and its coefficients are defined as follows:

$$\mathbf{W}_{i,j}(z)=\sum_{l=0}^{L-1}W_{i,j}(l)z^{-l},\quad W_j=\begin{bmatrix}W_{1,j} & \cdots & W_{M,j}\end{bmatrix} \tag{3}$$

where L is sufficiently large for an reasonable approximation.

Applying the inverse filters to the measurements results in the estimated sources S_e. S_e is defined as:

$$s_{ej}(k)=\sum_{i=1}^{M}W_{i,j}(z)y_i(k)=\sum_{i=1}^{M}\sum_{l=0}^{L-1}W_{i,j}(l)y_i(k-l) \tag{4}$$

$$s_e(k)=\sum_{i=1}^{M}\sum_{l=0}^{L-1}W_i(l)y_i(k-l) \tag{5}$$

Newton iteration algorithm. The coefficients of inverse filter $W_i(l)$ can be obtained by Newton iteration algorithm. The Hessian matrix **H** is given by

$$H_{m,n}=H_{(i1\times l1)\times(i2\times l2)}=\frac{\partial^2 J}{\partial w_{i_1,j}(l1)\partial w_{i_2,j}(l2)},\quad i_1,i_2=1,\ldots,M,\quad l_1,l_2=1,\ldots,L \tag{6}$$

$$W_{i,j}^{q+1}(l)=W_{i,j}^{q}(l)-\left[H_j^q\right]^{-1}\frac{\partial J(W_{i,j}^q(l))}{\partial W_{i,j}^q(l)} \tag{7}$$

where q is the index of iteration.

The process of using Newton iteration algorithm to solve inverse filter $W_i(l)$ are as follows:

1. Initialize the inverse filter W_0.
2. Define q=0.
3. Calculate the Hessian matrix $\mathbf{H}$.
4. Define $Z^{(q)} = -\mathbf{H}^{-1}\frac{\partial J}{\partial W}$, the iteration stopped until $\left|\frac{\partial J}{\partial W}\right| < \varepsilon$, and the $W^{(q)}$ is obtained, otherwise goes to step 5.
5. Calculate S_k to makes $J(W^{(q)} + S_k \cdot Z^{(q)}) = \max(W^{(q)} + S_k \cdot Z^{(q)})$.
6. Define $W^{(q+1)} = W^{(q)} + S_k \cdot Z^{(q)}$, $q = q+1$, return to step 3.

After $W^{(q)}$ is obtained, we can also get $W_i(l)$. Namely use equation (6) to obtain S_e.

The above process, shown by Fig. 2 identifies a single estimated source.

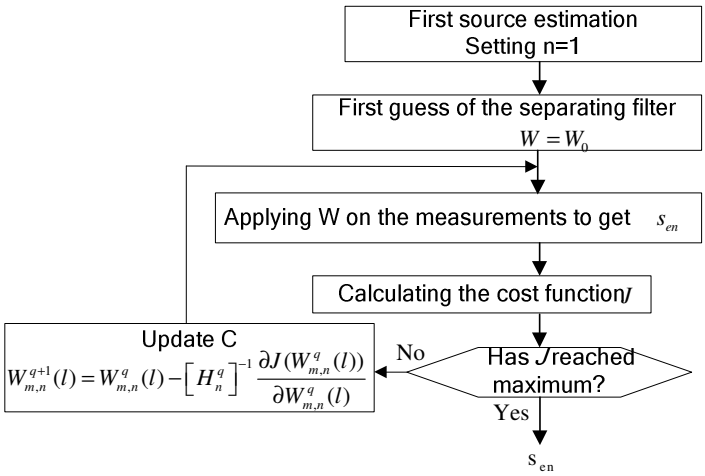

Fig. 2. Algorithm flow chart for single source estimation.

Using this known source, we now estimate the coefficient of the mixing matrix $\mathbf{H}$ related to this source.

The filters $f_{m,n}(l)$ are estimated from y_m and s_{en} using

$$\hat{f}_{m,n}(l) = \frac{E\{y_m(k)s_{en}(k-l)\}}{E\{s_{en}(k)^2\}}, \quad n = 1,2,\ldots,N, \quad m = 1,2,\ldots,M \tag{8}$$

The contribution of the estimated source to each measurement is now computed, as the component of s_{en} in y_m:

$$\hat{y}_{m,n}(k) = \sum_l \hat{f}_{m,n}(l)s_{en}(k-l) \tag{9}$$

Subtracting $\hat{y}_{m,n}(k)$ from y removes the nth source components from the measurements and thus allows the separation of the next (n+1) source in the same way. The process is stopped when no maximum is found.

Simulation studies

In order to validate the correctness and validity of the rolling bearing fault signal extraction method based on the BBS algorithm, the simulation signal of rolling bearing surface fault was studied and analyzed.

Simulated signal. The signals are typical of structural systems excited by impacts, i.e. periodic trains of decaying oscillations. These types of signals are often considered as models of faulty bearing vibrations. A rolling element bearing vibration model which is consist of three vibration

exciting sources is shown in Fig. 3(a). $s1(t)$ is the triangular-wave pulse, namely the impact pulse caused by bearing defect. $s2(t)$ and $s3(t)$ are sine wave, namely interrupt exciting sources. The three sources $s1(t)$, $s2(t)$ and $s3(t)$ are modified by structural resonances to nine signals which are shown in Fig. 3(b).

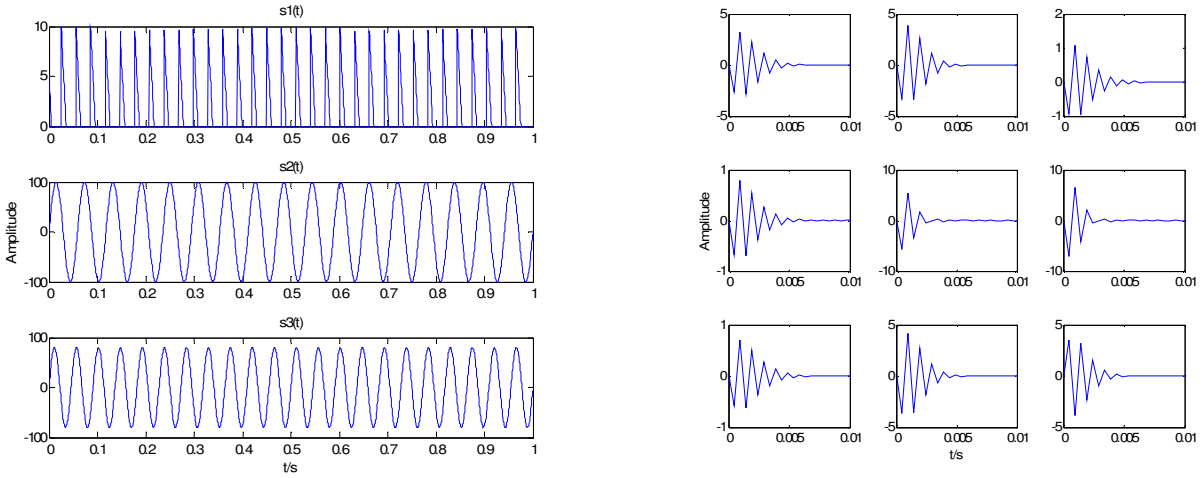

Fig. 3. (a) Vibration exciting sources (b) modified signals

In early stage of bearing failures, the feature information is usually buried by strong background noise coming from gear meshing vibration, mass unbalance, misalignment, etc. The three vibration exciting sources are modified by structure resonances and mixed in some arbitrary combination to produce the measured signals shown in Fig. 4, the fault impact can not be seen clearly from $y1(t)$.

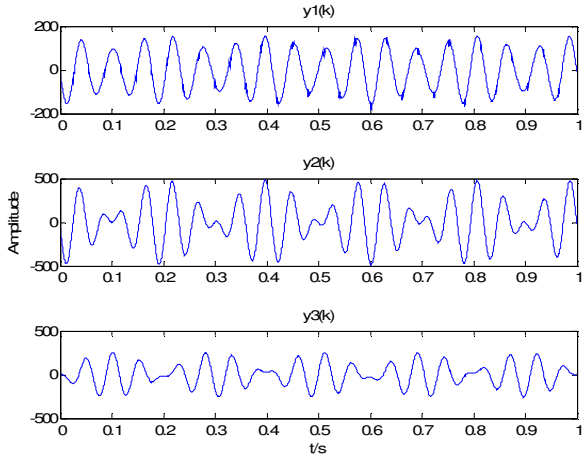

Fig. 4. Measured signals

Verification and analysis. The BBS algorithm is applied to simulation measured signals. Newton iteration algorithm is applied to calculate the inverse filter $W_i(l)$, namely it uses a Hessian matrix to maximize the cost function. This is a loop iteration process, and the inverse filter updating itself constantly until the Kurtosis reaches the maximum. Then the optimum inverse filter is obtained, and the optimum inverse filter is shown in Fig. 5(a). The fault signal S_e which is calculated with formula (6) is shown in Fig. 5(b). In the extracted signal, the fault impact can be seen obviously. The fault signal is obtained successfully through the BBS algorithm. Hence, the effectiveness of the method is demonstrated on simulation.

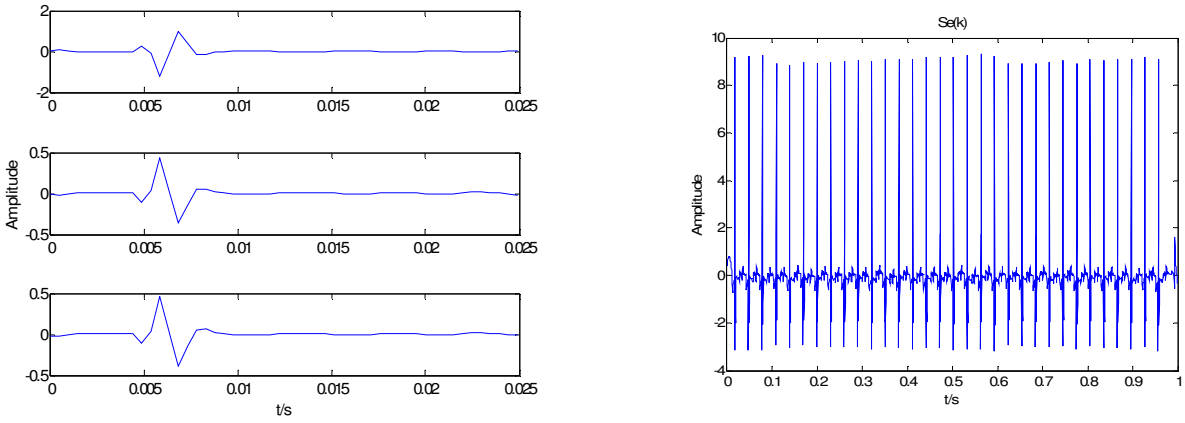

Fig. 5. (a) Optimum inverse filter (b) extracted signal

Conclusions

In this paper, the principle of BBS algorithm is analyzed at first. Then the method named rolling bearing fault signal extraction based on the BBS algorithm is proposed. In this method, Kurtosis is the cost function, and the inverse filter is obtained through the Newton iteration algorithm. Then the fault signal is obtained. The effectiveness of the method is verified by processing simulation signal of rolling element bearing. Future work should investigate the application of measured signals.

Acknowledgments

The author would like to thank the support of government (Funding ID 9140A27020413JB11076) and National Natural Science Foundation of China (Funding ID 50979109).

References

[1] Yanping Cai, Aihua Li, Linsuo Shi, Xiangfeng Bai, Jinwei Shen. Roller bearing fault detection using improved envelope spectrum analysis based on EMD and spectrum kurtosis[J]. Journal of Vibration and Shock, Vol.30(2011), p.167-172.

[2] Huiping Zhao,Ningyun Lu,Bin Jiang.Current Situation and Future Trends of Fault Diagnosis Methods for Steel Rolling Processes[J].Steel rolling, Vol.30(2011), p.48-53.

[3] Jing Wang. Research of the Key Technologies for the Train's Wheel Set Fault Vibration Characteristics and Diagnosis Method[D]. Central South University. 2012.

[4] Zhiqiang Zeng.Fault Diagnosis of Complex Mechanism Transmission System[D].North University of China.2007.

[5] Zhenmao Zhong, Jin Chen, Ping Zhong. On Blind Source Separation (BSS) and its Application to Fault Diagnosis of Machinery[J]. Mechanical Science and Technology, Vol.21(2002), p.282-284.

[6] Heping Shi, Jihua Cao, Xiao Liu. Blind source separation for non-stationary signal based on time-frequency analysis[J]. Journal of Computer Applications[J], Vol.31(2011), p.181-183.

[7] J.K. Tugnait, Identification and deconvolution of multichannel linear non-Gaussian processes using higher order statistics and inverse filter criteria, IEEE Transactions on Signal Processing, Vol.45(1997), p.658-672.

[8] R. Peled,S.Braun,M.Zacksenhouse. A blind deconvolution separation of multiple sources, with application to bearing diagnostic[J]. Mechanical Systems and Signal Processing, Vol.19(2005), p.1181-1195.

Advanced Materials Research Vols. 989-994 (2014) pp 3743-3746
© (2014) Trans Tech Publications, Switzerland
doi:10.4028/www.scientific.net/AMR.989-994.3743

The Improved Membership Matrix Initialization Method of FCM for Image Segmentation

Zong-jia WU, Li-kun LIU

PLA 91550 Unit 94, Liaoning Dalian, 116023, China

email: zjw1980221@126.com

Keywords: Membership Matrix; FCM; Initialization method; Image Segmentation

Abstract. The performance of FCM for image segmentation directly subjects to the initialized membership matrix. This paper proposed twice FCM method to solve the membership matrix initiation problem. The image is spared to a blurred image at first, and then uses the FCM for the blurred image to obtain an iterative result, in which the membership matrix is taken as the initialized membership function of the FCM for the original image processing. This method overcomes the random membership initialization method cannot convergence to the optimum point of the objective function of FCM for the image segmentation at some extend, furthermore, it can obtain better results than the traditional FCM method.

Introduction

Image segmentation is one of the most basic and important field in image processing, it is the basic premise for visual analysis and pattern recognition to the image. Image segmentation is based on some characteristics of an image is divided into several meaningful regions, the characteristics of identical or similar in a certain area, but in different regions are obviously different. Classical image segmentation methods include threshold method, region growing method, relaxation method, edge detection method and the split and merge method [1], modern methods include neural network and fuzzy clustering method [2]. Different methods are suitable for different fields of application, for the large scale image data mining research, the efficiency of the algorithm, automatically (without human intervention) ability is very important for classification and prediction. In essence, image segmentation is a process of classifying the pixel based on some attribute, and because of the image complexity of the clustering problem with uncertainty, so from the point of view of fuzzy clustering image segmentation problem is a feasible idea.

Fuzzy C means (FCM) algorithm [3] is a classical algorithm to solve the fuzzy clustering problem. The computational efficiency is robust and has good performance. Its disadvantage is that there is no general method to determine the weighted index and the number of clusters, it has more subjectivity [4], the clustering problem is only applicable to the class number is known, but the number of categories is one of the characteristics of the data structure, which is great importance to the image content understanding, and it is the goal of image mining. The performance of FCM for image segmentation directly subjects to the initialized membership matrix, if the membership matrix is random initialized, the iterative algorithm often drop into the local point of the objective function. Aiming at this problem, this paper proposes a membership initialization method to solve this problem. The image is spared to a blurred image at first, and then uses the FCM for the blurred image to obtain an iterative result, in which the membership matrix is taken as the initialized membership function of the FCM for the original image processing. The simulation results show the effectiveness of this method can avoid the local point of the objective function and obtain the better image segmentation result than traditional FCM method.

The Improved Fuzzy C Means Clustering Algorithm

Fuzzy C means clustering algorithm is proposed by Dunn [5], and Bezdek improved FCM algorithm by using the weighted index, which is the often used in the application. FCM algorithm is a clustering algorithm based on partitioning, which makes the idea is to be divided into the biggest

similarity between objects on the same cluster, while the minimum similarity between different clusters. Fuzzy C means algorithm is an improvement of common C means algorithm, C means algorithm for data classification is rigid, while the FCM is a flexible fuzzy partition. According to the weighted index FCM algorithm, the algorithm is to minimize the objective function which can be given by

$$J(U,c_1,\cdots,c_c)=\sum_{i=1}^{c}J_i=\sum_{i=1}^{c}\sum_{j=1}^{n}u_{ij}^m d_{ij}^2 \tag{1}$$

where n is the total number of samples, $U=(u_{ik})_{n\times c}$ is the membership matrix, u_{ik} is the element of the membership matrix with the constraint conditions as follow

$$\begin{cases}\sum_{i=1}^{c}u_{ik}=1 & k=1,2,\cdots,n\\ u_{ik}\geq 0 & i=1,2,\cdots,c\end{cases} \tag{2}$$

c_i is the clustering center of the fuzzy set i, $d_{ij}=\left\|c_i-x_j\right\|$ is the Euclidean distance between the clustering center and the j-th data point. $m>1$ is a weighted index. To minimize the objective function Eq.1, it can construct a new objective function which is the necessary condition of Eq.1.

$$\begin{aligned}\bar{J}(U,c_1,\cdots,c_c,\lambda_1,\cdots,\lambda_n)&=J(U,c_1,\cdots,c_c)+\sum_{j=1}^{n}\lambda_j\left(\sum_{i=1}^{c}u_{ij}-1\right)\\&=\sum_{i=1}^{c}\sum_{j=1}^{n}\lambda_j\left(\sum_{i=1}^{c}u_{ij}-1\right)\end{aligned} \tag{3}$$

where λ_j $(i=1,2,\cdots,n)$ is the Lagrange multiplier of the constrained Eq.1. Carry on derivation operator for all the input parameters, and the necessary conditions for minimizing the objective function can be given by

$$c_i=\frac{\sum_{j=1}^{n}u_{ij}^m x_j}{\sum_{j=1}^{n}u_{ij}^m} \tag{4}$$

$$u_{ij}=\frac{1}{\sum_{k=1}^{c}\left(\frac{d_{ij}}{d_{kj}}\right)^{2/(m-1)}} \tag{5}$$

The clustering problem can be formulated as a nonlinear optimization problem with constraints. Using general methods are difficult to obtain the global optimal solution in the complex constrained conditions. The usual practice method is to use alternating iterative algorithm to optimize the allocation of matrix U and the clustering center V to get an approximate local minimum. The FCM algorithm adopts iterative Eq.3 and Eq.4 to achieve the minimization of the objective function, and then implement the fuzzy clustering of the data sets.

The implement of FCM algorithm can be summarized as follow

Step 1. Determining the clustering number C, the weighted index m, and random initializing the membership matrix $U^{(0)}$;

Step 2. Let $b=0,1,2,\cdots$;

Step 3. Computing the clustering center $V_i^{(b)}$ according to the membership matrix $U^{(b)}$ and Eq.4;

Step 4. Updating $U^{(b)}$ and $U^{(b+1)}$ as follow

(A) For $k=1,2,\cdots,n$ calculate

$$\begin{cases}I_k=\{i\,|\,1\leq i\leq c,d_{ik}=0\}\\ \bar{I}_k=\{1,2,\cdots,c\}-I_k\end{cases} \tag{6}$$

(B) Computing the membership function value of x_k, if I_k is null, calculate u_{ik} according to Eq.5, otherwise, let $u_{ik} = 0$ for all $i \in \bar{I}_k$ and set $\sum_{i \in I_k} u_{ik} = 1$.

(C) Comparing $U^{(b)}$ and $U^{(b+1)}$, if $\left\| U^{(b)} - U^{(b+1)} \right\| < \varepsilon$, stop the iterative process, otherwise, return the step 3 and continue the iterative process.

Although the FCM algorithm is an unsupervised classification algorithm, the weighted index m and the clustering center number c must be given before the iterative process. Therefore, the effectiveness of FCM clustering often can be transformed into the optimal number of classes and the weighted index decision problems. In order to obtain these two parameters reasonable value, the researchers proposed some improved method from two angles preferably to determining the optimal clustering number and the weighted index by using discriminant function, such as the probability distribution based discriminant function, fuzzy correlation discriminant function and subset hood measure discriminant function etc. This paper focuses on the initialization of the membership matrix, and the clustering number and the weight index are not discussed here. In the FCM algorithm, the membership matrix is often random initialized, and then using the iteration to minimize the objective function to complete the classification. As a result, the classification performance directly subject to the initialization membership matrix. Form the other view point, the FCM algorithm carry on the calculation for all the data set during the one iterative process, so the computational complexity is large. To obtain an effective method to improve FCM algorithm, hereby, we proposed a new initialization method for the membership matrix.

In one image, lots of the pixels are redundant. For a gray image with size 256×256, the number of pixel is 65536, but the gray level is 256. So we can sparse the image to initialize the membership matrix to improve the FCM algorithm. Let the data set is

$$X = \{x_1, x_2, \cdots, x_n\} \tag{7}$$

Using the down sampling method to spare the data set, which is given by

$$\bar{X} = \{x_1, x_2, \cdots, x_q\} \tag{8}$$

And then using FCM algorithm on the data set $\bar{X}$ to obtain an initial membership matrix $\bar{U}_{n \times q}$, where $q < n$ due to the sparse operation, so the dimension of $\bar{U}_{q \times c}$ must less than the membership matrix $U = (u_{ik})_{n \times c}$. It can reshape the initialization membership matrix $\bar{U}_{n \times q}$ as the initial membership matrix $U^{(0)}$ by inserting zero.

The data set spare method for initializing the membership matrix in the FCM algorithm can overcome the local point of the object function, and further improve the clustering performance. If the down sampling rate is high, the computational complexity would increase a little compared the traditional FCM algorithm.

Simulation and Discussion

The image in the simulation is obtained from the internet, which is a plant image with the resolution 1024*735 as shown in Fig.1. The iterative threshold segmentation method and the maximum variance threshold segmentation method are done in the simulation for comparison. The down sampling rate is 4. Using the data set after down sampling to determine the initial membership matrix after 100 iterative times, and then use the traditional FCM for the image segmentation to obtain the result which is shown in Fig.4. The iterative threshold segmentation method result is shown in Fig.2 and the maximum variance threshold segmentation result is shown in Fig.3. Simulation results show that, the improved FCM algorithm has better segmentation and effect calculation efficiency, and more importantly, this method can obtain automatic image segmentation result, at the same time, it can give the target image data structure (classification) prediction, the prediction results can be further used to guide the image classification and image understanding.

Fig.1 The original image

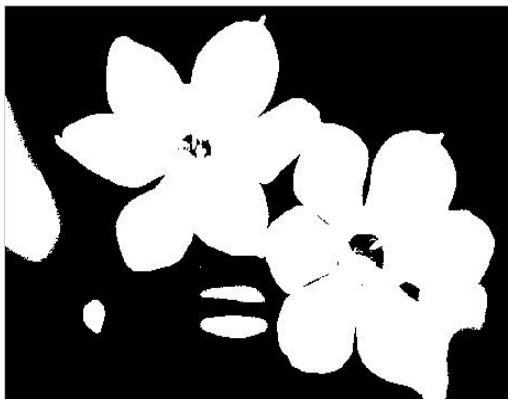

Fig.2 Iterative threshold segmentation

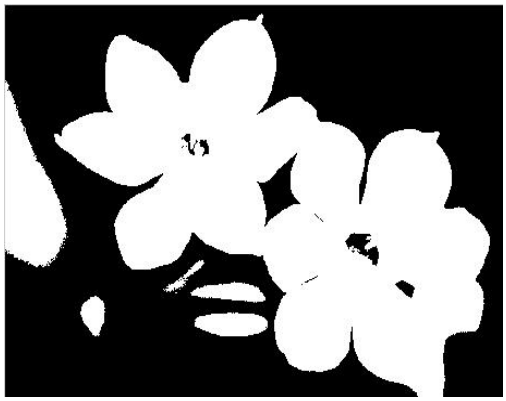

Fig.3 Between-cluster variance threshold segmentation

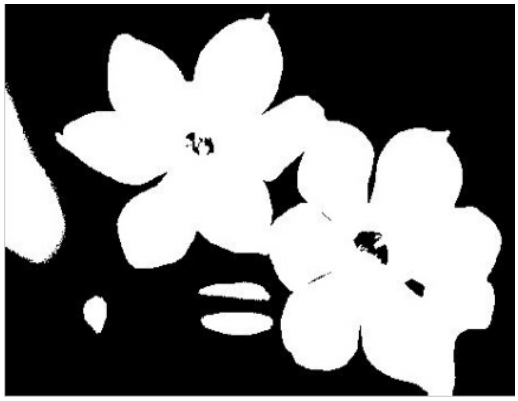

Fig.4 The improved FCM segmentation

Conclusions

This paper proposes an initialization method for the membership matrix in the FCM algorithm for image segmentation. The data set of image is down sampling to construct a new sparse data set, and the membership matrix is initialized by FCM on the sparse data set. This method can speed up the convergence rate of FCM and overcome the algorithm drop into the local minimum point of the objective function. As a result, the segmentation performance can be improved effectively.

References

[1] GONG Xue-Jing, CI Lin-Lin, YAO Kang-ze. Split-merge algorithm of image based on Morton code [J]. Computer Engineering and Design. 2007,28(22): 5440-5443.

[2] TAN Qing, HE Qing, ZHAO Wei-Zhong, SHI Zhong-Zhi. Evolutionary programming based FCMBP fuzzy clustering method [J]. Systems Engineering-Theory& Practice, 2011, 31(7):1363-1370.

[3] YU Jian. On the Fuzziness Index of the FCM Algorithms [J]. Chinese Journal of Computers, 2003, 26(8): 968-973.

[4] CHEN Song-Sheng, WANG Wei. Modified fast fuzzy C-means clustering algorithm [J]. Computer Engineering and Applications, 2007, 43(10): 167-169.

[5] BeZedk J. C. Patter Recognition with fussy objective function algorithms [M]. New York, Plenum Press, 1981.

Advanced Materials Research Vols. 989-994 (2014) pp 3747-3750
© (2014) Trans Tech Publications, Switzerland
doi:10.4028/www.scientific.net/AMR.989-994.3747

Discovering Frequent Itemsets an Improved Algorithm of Bit Vector and Graph

Naili Liu[1, a]

[1]Department of Information, Linyi University, Linyi, 276005, China

[a]email: lnl1999@163.com

Keywords: Data Mining; Association Rule; Frequent Item Set; Bit Vector; Graph

Abstract. Because of the weakness of traditional Apriori algorithm, this paper presents an improved algorithm for mining frequent itemsets, which constructs bit vector and graph, the algorithm deletes node and the adjacent edges according to the number of node's edges, which need traverse graph to generate candidate itemsets and verify candidate itemset by bit vector. Experimental results show that the improved algorithm has better efficiency than Apriori algorithm.

Introduction

The concept of association rules was proposed by Agrawal in 1993[1], it is an important field in data mining. Mining association rule is one of the important content of data mining; it reflects the interesting association or correlation between data items. So it is widely used in many industries [2-3]. In this field, the most famous algorithm is Apriori, which is an iterative searching process, but Apriori algorithm need scan database many times to mine frequent itemsets, so the efficient of Apriori algorithm is very low in mining frequent itemset, especially in large scale data. So how to improve the efficiency to mine frequent itemset is search hot in data mining field. In recent years, many improved algorithms [4-6] based on Apriori algorithm have been proposed. The main limitation of these algorithms is the need to scan database many times to generate frequent item sets and to generate a huge amount of candidate item sets.

Any kind of information is able to be representing as graphs of graph databases, where changes in data can be possible for naturally accommodation [7].

Literature [8] algorithm scans database only once, and then construct the correlation graph, and discovering frequent item sets through search graph, but it need many times to traverse the graph to generate candidate itemset. And soon many improvements have been proposed [9], but the algorithm need search graph many times.

This paper puts forward the improved algorithm to overcome the shortcomings of above algorithms, the algorithm need scan database only once. The algorithm generates bit vector when scanning database and generate frequent 2-itemset by using bit vector, and then constructs the graph, and compute the count of node's adjacent edges set for each node. The algorithm generates candidate itemsets by traversing graph, the algorithm verifies frequent itemsets by bit vector logic operation. So the improved algorithm is high efficient in mining frequent itemsets.

Basic Concepts and Theorems

Definition 1 Let $D = \{T_1, T_2, \ldots, T_n\}$ be a transaction database, let I be all items of transaction database D, $I = \{I_1, I_2, \ldots, I_m\}$, therefore, any of T_j $(1 \le j \le n)$, then exist $T_j \subseteq I$. where T_i $(1 \le i \le n)$ is a transaction which contains a set of items in I. Let A be an itemset, if $A \subseteq T_j$, then T_j contains A.

Definition 2 Let X be an itemset, the support of X is the proportion of transactions in D which contain X, denoted as sup(X); if $sup(X) \ge min_sup$, min_sup is given by user, then X is a frequent itemset and X is called frequent K-itemset, otherwise X is a non-frequent itemset. The set of all frequent k-itemsets is denoted by L_k.

Definition 3 Let I_i be an itemset, the bit vector of Ii is denoted by V_i. All itemsets are sorted by lexicographic order.

Definition 4 If there exists an edge N_i--N_j in graph, then the count of the adjacent edge of node N_i plus 1.

Property 1 If frequent itemset L_k contains I_i, then node N_i has at least k-1 edges.

Proof: if k=2, frequent 2-itemset contains I_i, then there exists an frequent 2-itemset (I_i,I_j), according to the rule of constructing graph, there exists an edge N_i-N_j, node Ni has at least 1 edge.

If k>2, the count of frequent k-itemset's subsets which contains I_i has k-1 itemsets, then there exists k-1 edges in graph. So node N_i has at least k-1 edges.

Let min_sup be the minimum support threshold.

Property 2 if X is a frequent itemset, then any subset of X must be a frequent itemset; if X is not a frequent itemset, then any super set of X must be not a frequent itemset.

Mining frequent itemsets algorithm-the improved algorithm

A. Relation Knowledge of the Improved Algorithm

We construct bit vector when scanning the database. According to the definition of bit vector, we generate bit vector for each item in database D, for each item I_i ($1\le i\le m$), if T_j($1\le j\le n$) contains I_i, then $V_i[j]$ will be set to 1,otherwise $A_i[j]$ will be set to 0. So there have m bit vectors, each bit vector's length is the length of transaction; the improved algorithm adopts binary to storage 1 and 0 in order to reduce space overhead.

Then computing the number of 1s in bit vector V_i($1\le i\le m$), denoted as C_i, if $C_i \ge$min_sup, then item I_i is frequent 1-itemset. So we can easily generate frequent 1-itemset by bit vector.

Then generate candidate 2 itemsets according to frequent 1 itemset by vector product, any candidate 2 itemset $\{I_i,I_j\}$($sup(I_i)\le sup(I_j)$), let $B=V_i\&V_j$, if the number of 1s in B is greater than or equal min_sup, then $\{I_i,I_j\}$ is a frequent 2-itemset.

We construct the graph by using frequent 2-itemsets. The idea of constructing the graph is: if $\{I_i,I_j\}$ is a frequent 2-itemset, then draw an edge N_i-N_j in graph. We draw an edge in graph for each frequent 2 itemset. Then compute the count of each node's edges in graph, we construct the array A, A_i is the number of node N_i's edges.

According to the graph and node edges set A, we generate candidate itemsets. We generate candidate 3 itemset, according to property 1, we delete all nodes which the count of nodes edges is less than 2, then delete node and adjacent edges of the node, and then we continue to delete node and adjacent edges of the node until the number of node's edges is not less than 2. According to the method, we can generate candidate k itemsets. Traversing the graph in lexicographic order. According to this method, we generate all frequent itemsets.

B.Algorithm decription

The steps of the improved algorithm are follows:

Input:transaction database D, the minimum support min_sup;
Output:Frequent itemset FS_D;

```
FS_D = ∅;
for each transaction T_j in D
  begin
    if   T_j contains item I_i then   V_i[j]=1;
   else     V_i[j]=0;
generate frequent 1 itemset L_1 according to the number of 1s in bit vector;
sort items in L_1 by lexicographic order;
generate frequent 2 itemsets L_2 according to frequent 1 itemset;
foreach(∀{I_i,I_j} ∈ L_2)
      draw the edge N_i-N_j in graph G
for (each node N_i in the graph G) {
      if there exists the edge N_i-N_j   then
         add the number of the edges of N_i plus 1;
 }
int k=3;
while (G!=null)
{
```

```
        delete all nodes which the number of node's edges is less than k-1;
        generating candidate k itemsets in graph;
        generating frequent k itemsets by bit vector;
        add frequent itemset to FS_D;
        k++;
    }
```

C.Algorithm example

For the transaction database D, transaction set $T=\{T_1,T_2,\ldots T_9\}$, item set $I=\{I_1,I_2,I_3,I_4,I_5,I_6\}$,specific data is shown in Table 1, the minimum support threshold is 2.

Table 1 Transaction Database D

TID	Item
T_1	I_1,I_3,I_5
T_2	I_2,I_4,I_6
T_3	I_1,I_3,I_5
T_4	I_3,I_5,I_6
T_5	I_1,I_3,I_6
T_6	I_1,I_3
T_7	I_2,I_4
T_8	I_1,I_3,I_5
T_9	I_3,I_4,I_6

Table 2 Bit vectors on D

TID	V_1	V_2	V_3	V_4	V_5	V_6
T_1	1	0	1	0	1	0
T_2	0	1	0	1	0	1
T_3	1	0	1	0	1	0
T_4	0	0	1	0	1	1
T_5	1	0	1	0	0	1
T_6	1	0	1	0	0	0
T_7	0	1	0	1	0	0
T_8	1	0	1	0	1	0
T_9	0	0	1	1	0	1

(1) All bit vectors of transaction database D are shown in Table 2.

(2) We can easily get frequent 1-itemset, $L_1=\{\{I_1\},\{I_2\},\{I_3\},\{I_4\},\{I_5\},\{I_6\}\}$, then we easily get frequent 2 itemset $L_2=\{\{I_1,I_3\},\{I_1,I_5\},\{I_2,I_4\},\{I_3,I_5\},\{I_3,I_6\},\{I_4,I_6\}\}$ by L_1.

(3) Construct the graph according to the frequent 2 itemsets, and compute the number of each node's edges. The graph is shown is Fig 1.

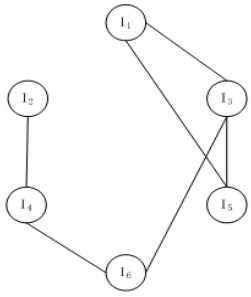

Fig 1. The graph

Construct the number of node, $A(I_1)=2$, $A(I_2)=1$, $A(I_3)=3$, $A(I_4)=2$, $A(I_5)=2$, $A(I_6)=2$.

(4) Generate candidate 3 itemsets. First, delete node N_{I2} and the adjacent edge N_2-N_4, then the number of node N_{I4}'s edges is 1, 1 is less than 2, so delete node N_{I4}, and delete the adjacent edge N_4-N_6, and then the number of node N_{I6}'s edges is 1, 1 is less than 2, then delete node N_6.so the graph has the remaining nodes$\{N_1,N_3,N_5\}$. Finally generate candidate 3 itemsets $C_3=\{\{I_1,I_3,I_5\}\}$.

(5) Because the number of each node's edges is less than 3, so candidate 4 itemsets is null. So the process of generating frequent itemset is over. Finally we get frequent itemset $FS_D=\{\{I_1,I_3\},\{I_1,I_5\},\{I_2,I_4\},\{I_3,I_5\},\{I_3,I_6\},\{I_4,I_6\},\{I_1,I_3,I_5\}\}$.

Analysis of algorithms

The improved algorithm need scan transaction database only once. The algorithm can generate bit vectors when scanning database. Time overhead depends on the length of transaction database, the average execution time is O(n); the number of the improved algorithm execution times by item decision, its average estimated execution time O (m*L), where m is the number of frequent itemset, L is the length of frequent itemset, its time complexity is much less than Apriori algorithm.

In order to verify the performance of the improved algorithm, this paper realized Apriori algorithm and the improved algorithm. Test database is mushroom database which is provided by Literature [10]. The experimental results obtained in the different support are shown in Fig 2.

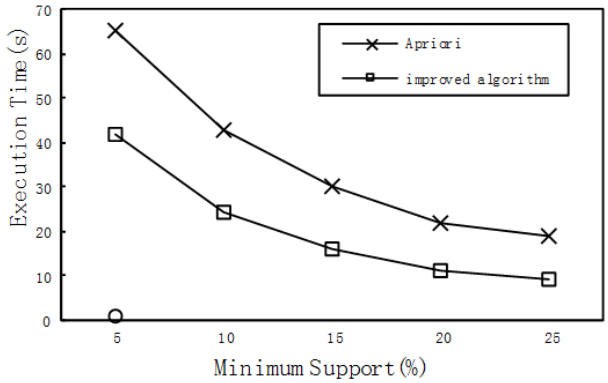

Fig 2. Performance comparison of two algorithms in different minimum support

Conclusion

This paper proposed the improved algorithm, the design idea of the improved algorithm is how to use bit vector and graph to generate frequent itemsets. The experimental results show that traditional algorithms take up too much memory; the improved algorithm uses bit vector of item to reduce memory overhead and delete useless node in generating candidate itemsets. The experimental results show that the improved algorithm has more obvious advantages compared to Apriori algorithm.

References

[1] Agrawal R, Imielinski T, Swami A, "Mining association rules between sets of items in large databases". In: Buneman P, Jajodia S,eds. Proc. of the ACM SIGMOD Conf. on Management of Data (SIGMOD'93). New York: ACM Press, 1993. 207-216.

[2] Jan M. Zytkow and Willi Klosgen, "Hand Book of Data Mining and Knowledge Discovery,"Oxford University Press, 2002.

[3] Tsai CF, Lin YC, Chen CP. A new fast algorithms for mining association rules in large databases. In: Kamel AE, Mellouli K, Borne P, eds. Proc. of the 2002 IEEE Int'l Conf. on Systems, Man and Cybernetics (SMC 2002). IEEE Computer Society Press, 2002.251-256.

[4] Balaji Raja.N and Balakrishnan.G, "Evaluation of Rule Likeness Measures for a Learning Environment," In: Proceedings of the ICOREM International Conf., 2009, pp: 1682-1690.

[5] Savasere A，Omiecinski E，Navathe S．An efficient algorithm for mining association rules in large databases[C].Proceedings of the2 1 st International Conference on Very Large Databases,1995:432-444.

[6] Park J S，Chen M S，Yu P S．An effective hash-based algorithm for mining association rules[C].Proceedings of the ACM SIGMOD．San Jose．1995：175-186.

[7] Sadhana Priyadarshini and Debahuti Mishra, "A Hybridized Graph Mining Approach," in proceeding of ICT2010,CCIS 101, 2010, pp. 356-361.

[8] HE Hao,WANG HAI-XUN,YANG JUN,et al. BLINKS: Ranked keyword searches on graphs[c]//Proceeding of the 2007 ACM SIGMOD International Conference on Management of Data. New York:ACM Press,2007:305-316.

[9] GUO Jing-feng, ZHANG Wei, CHAI Ran,"New Algorithm of Mining Frequent Subgraph",computer engineering,vol.37, issue.20 2011.10,pp.27-29.

[10] SCHLIMMER J.Mushroom data set[DB/OL].[2010-4-30].http://archive.ics.uci.edu/ml/ Machine -learning-databases/mushroom/agaricus-lepiota.data.

Advanced Materials Research Vols. 989-994 (2014) pp 3751-3754
© (2014) Trans Tech Publications, Switzerland
doi:10.4028/www.scientific.net/AMR.989-994.3751

An Improved Otsu Image Segmentation Algorithm

Yanxue DONG[1, a]

[1]School of Information , Linyi University, Linyi, 276000, China

[a]email: dyxtmb@163.com

Keywords: Otsu; Segmentation; Threshold

Abstract. Otsu segmentation algorithm is one of the most successful algorithms in the field of image processing,However, it has drawbacks such as it is poor in dividing small object in images. This paper propose a improved Otsu algorithm based on weighted smooth histogram which can ensure the location of threshold point is more near to the valley point of the image and at the same time ensure the ensure between-class variance maximum.The results show that the improved Otsu algorithm can effectively accomplish segmentation for multimodal image, and get better segmentation results for images added Gaussian noise.

Introduction

Digital image is an important means for people to get, express, and convey information, statistics show that more than 80% of the information humans get is from the visual perception. Image processing technology can be divided into three levels: image processing, image analysis and image understanding. Image segmentation is an important step from image processing to image analysis, it is not only the basis of object expression but also the precondition of image analysis and understanding, the segmentation results will directly affect the quality of image analysis and image understanding.

The uncertainty of image information increases the difficulty of image segmentation, the traditional segmentation method can hardly meet the demand of image processing nowadays, how to get an segmentation more accurate is still a hot spot of current research.

Thresholding technique has been widely applied in object recognition, medical image processing and remote sensing image processing because it is simplicity and easy to implement. The key point of thresholding algorithms is to determine the optimal segmentation threshold, and the processing object of threshold technology is mostly gray image such as MRI image, infrared image and so on.

$F=[f(x,y)]_{M\times N}$ is used to describe a gray-scale image and its size is $M\times N$, L represents the maximum gray value, typically 255. Thresholding segmentation is to find the optimal threshold t^*, which make the following formulation established.

$$\bar{f}(x,y)=\begin{cases}0 & f(x,y)<t^*\\ 255 & f(x,y)\geq t^*\end{cases} \tag{1}$$

$\bar{f}(x,y)$ represent the image after segmentation. Obviously, the process of thresholding is equal to the process turning a gray image into a binarizied image.

The traditional Otsu algorithm has some drawbacks, for example, it can not divide small object from an image effectively, so this paper presents an improved Otsu algorithm which is called Ostu thresholding segmentation algorithm based on Weighted neighborhood. The results of this algorithm used in medical images shows that it can divied small object in the image effectively.

Traditional Otsu Theory

In 1979, the Japanese scholar dajin proposed an adaptive threshold segmentation algorithm base probabilistic statistical theory, which is called Otsu algorithm. This segmentation algorithm considered each gray scale in the image as a possible threshold which can divides the gray scale into two categories, calculate the variancec between classes for each classification in proper

order, select a gray scale value as the optical threshold which make the value of variance between classes maximum. The principle of the algorithm is shown as follows:

$F=[f(x,y)]_{M\times N}$ indicates a digital image with size $M\times N$, in which $f(x,y)$ represents the gray value of pixel(x,y), $f(x,y)\in G$ $G=\{0,1,\cdots,L-1\}$, L is the value of gray scale. $f(g)$ indicates The number of pixels which has gray value g, and then $h(g)$ which indicates the probability gray value g appears in the image is expressed as follows:

$$h(g)=\frac{f(g)}{M\times N}, g=0,1\cdots,L-1 \tag{2}$$

and the averages of probability distribution μ_r is:

$$\mu_r=\sum_{g=0}^{L-1} gh(g) \tag{3}$$

Assuming that threshold t divides an image into two categories, object region and background region, denoted by C_0 and C_1:

$$C_0=[0,\cdots,t], C_1=[t+1,\cdots,L-1] \tag{4}$$

and the priori probabilities of these two categories are expressed as follows:

$$P_0(t)=\sum_{g=0}^{t} h(g) \qquad P_1(t)=\sum_{g=t+1}^{L-1} h(g) \tag{5}$$

The averagets of these two categories is :

$$\mu_0(t)=\sum_{g=0}^{t} g\,h(g)/P_0(t) \qquad \mu_1(t)=\sum_{g=t+1}^{L-1} g\,h(g)/P_1(t) \tag{6}$$

obviously, $P_0(t)\mu_0(t)+P_1(t)\mu_1(t)=\mu_r$, $P_0(t)+P_1(t)=1$

According to the given threshold t, we can get within-class variance $\sigma_W^2(t)$ and between-class variance $\sigma_B^2(t)$ of C_0 and C_1

$$\begin{aligned}\sigma_W^2(t)&=P_0(t)\sigma_0^2(t)+P_1(t)\sigma_1^2(t)\\&=\sum_{g=0}^{t} h(g)(g-\mu_0(t))^2+\sum_{g=t+1}^{L-1} h(g)(g-\mu_1(t))^2\end{aligned} \tag{7}$$

$$\begin{aligned}\sigma_B^2(t)&=P_0(t)(\mu_0(t)-\mu_r)^2+P_1(t)(\mu_1(t)-\mu_r)^2\\&=P_0(t)\mu_0^2(t)+P_1(t)\mu_1^2(t)\end{aligned} \tag{8}$$

and

$$\sigma_r^2(t)=\sum_{g=0}^{L-1}(g-\mu_r)^2h(g)=\sigma_W^2(t)+\sigma_B^2(t) \tag{9}$$

Three criteria is given in [1] ,according which we can choose the best threshold, expressed as follows:

$$\lambda(t)=\frac{\sigma_B^2(t)}{\sigma_W^2(t)}, k(t)=\frac{\sigma_r^2(t)}{\sigma_W^2(t)}, l(t)=\frac{\sigma_B^2(t)}{\sigma_r^2(t)} \tag{10}$$

According to the formula (9), we can know, the summation of within-class variance $\sigma_W^2(t)$ and between-class variance $\sigma_B^2(t)$ is a constant, so the minimizing within-class variance is equivalent to maximizing between-class variance. That is why the Otsu algorithm is often referred to as the maximizing between-class variance method or minimizing within-class method. Generally, between-class variance $\sigma_B^2(t)$ is used as the segmentationf unction, that is the optical threshold t^* is as follows:

$$t^*=Arg\max_{0<t<L-1}\sigma_B^2(t)=Arg\max_{0<t<L-1}\{P_0(t)\mu_0^2(t)+P_1(t)\mu_1^2(t)\} \tag{11}$$

The image can be divided into two categories according to formula (1) and get $\bar{f}(x,y)$.

The classic Otsu method can be easily extended to the case of multi-threshold,suppose that there are $M-1$ thresholds which divide the image into M categories,denoted by $C_1,C_2,\cdots C_M$, the optical thresholds $\{t_1^*,t_2^*,\cdots,t_{M-1}^*\}$ are expressed as follows:

$$\left\{t_1^*, t_2^*, \cdots, t_{M-1}^*\right\} = Arg \max_{0<t_1<t_2<\cdots<L-1} \left\{\sum_{k=1}^{M} P_k \mu_k^2\right\} \tag{12}$$

Otsu method is simple, relatively easy to implement, and has better adaptability, so it is one of the most commonly used segmentation algorithms in engineering practice.

However, Otsu method supposes that the grayscale distribution of object region and background region in the images meet mixed Gaussian distribution which means less variance and very different mean. So Otus can not obtain appropriate segmentation threshold in many cases, when the histogram of an image has two peaks differ more, the threshold obtained by Otsu algorithm is more close to the peaks with larger variance, but not the valley point.

Improved Otsu algorithm

In literature[2], point histogram weighted ostu method is put forward, and in this paper, a smooth histogram weighted Otsu method is proposed combining with point histogram weighted Otsu method. This method weighted by adopting smooth histogram, not only uses information of threshold point in histogram, but also considers the neighborhood information of threshold point, and then makes the weighted more effective.

Suppose that the original histogram of an image is denoted as $h(g)$, we can calculate the smooth histogram using the following formula:

$$\bar{h}(g) = \left[h(g-m) + h(g-m+1) + \ldots + h(g) + h(g+1) + \ldots + h(g+m)\right] \tag{13}$$

Assuming $n = 2m+1$, n is the length of the smoothing filter, and it is generally odd.

The objective function of Otsu method weighted by smooth histogram is expressed as follows:

$$\xi(t) = \left(1 - \bar{h}(t)\right)\left(p_0(t)\mu_0^2(t) + p_1(t)\mu_1^2(t)\right) \tag{14}$$

The optical segmentation threshold:

$$t^* = Arg \max_{0<t<L-1} \xi(t) = Arg \max_{0<t<L-1} \left(1 - \bar{h}(t)\right)\left(p_0(t)\mu_0^2(t) + p_1(t)\mu_1^2(t)\right) \tag{15}$$

Formula (15) shows that Otsu method weighted by smooth histogram requires not only the probability of threshold point small, but also the probabilities in neighborhood of threshold point small, what can further ensure that the location of threshold point is valley point of the histogram.

Test results

Dividing Figure1 applying traditional Otsu algorithm and improved Otsu algorithm,segmentation results are shown in Figure2 and Figure3, thresholds get by the two algorithms is 148 and 71(where the length of the smooth filter is 7) ,easily know from Figure1 and Figure2 that improved Otsu algorithm is more effective in dividing small object than traditional Otsu algorithm.

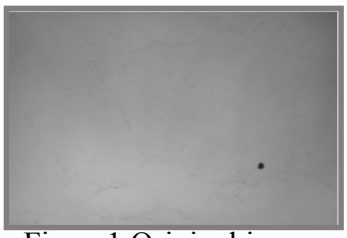

Figure1 Original image

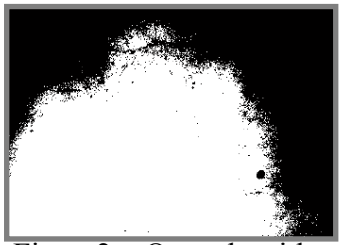

Figure2 Otsu algorith

Figure3 Improved Otsu algorithm

References

[1] Otsu N., A threshold selection method from gray level histograms[J], IEEE Transactions on Systems, Man and Cybernetics. SMC-9, 1979, 62-66.

[2] Ng H.F., Automatic thresholding for defect detection[J], Pattern Recognition Letters. 2006, 27:1644-1649.

[3] Yang Y., Yan H., An adaptive logical method for binarization of degraded document images[J], Pattern Recognition. 2000, 33: 787-807.

[4] Portes de AlbuquerqueM, Esquef IA, Gesualdi Mello AR, et a.l Image thresholding using Tsallis entropy[J]. Pattern Recognition Letters, 2004, 25: 1059-1065.

Advanced Materials Research Vols. 989-994 (2014) pp 3755-3758
© (2014) Trans Tech Publications, Switzerland
doi:10.4028/www.scientific.net/AMR.989-994.3755

Radar Compressed Sensing Imaging Method with Two-dimensional Separable Sampling

Shu-hong JIAO[1, a], Lin TANG[1, a], Xue LIU[2, a], Huan QI[1, a]

[1]college of Information and Communication Engineering, Harbin Engineering University, Harbin, 150001, China

[2]No. 92941 Army, Huludao 125000, China

[a]email: tanglinheu@163.com

Keywords: Radar Imaging; Compressed Sensing; 2-D Separable Sampling; 2-D Reconstruction Algorithm

Abstract. A radar compressed sensing imaging method with 2-D separable sampling is proposed in this paper. Instead of converting the radar imaging problem into two 1-D compressed sensing problem, we use the 2-D Separable Projections to solve it directly. Unlike the 2-D separable sampling in visible imaging, the range and azimuth which are the two dimensions of the radar imaging couple with each other. This Coupling increases the storage and computation in radar compressed imaging, therefore some de-coupling processing using in Range Doppler algorithm are adopted in the proposed method to construct the 2-D separable sampling data. Accordingly the two dimensional scene has been reconstructed with the proposed 2-D compressed sensing algorithms. Compared with conventional compressed sensing imaging methods, the new method has reduced the memory usage and complexity with imaging performance improvement.

Introduction

Radar imaging is an effective means to obtain information in all times and all weather conditions. Combined with the new emerging theory of compressive sensing (CS) technologies, the radar CS imaging can solve the acquisition, storing, processing and transmission problems caused by the demand for high-resolution [1][2].

Now, how to achieve better CS radar imaging has become a challenging problem. Alonso [3] proposed a novel imaging approach based on CS which is used to replace the traditional matched-filtering. It forms the basis of many 1-D CS imaging methods [4]. Some 2-D CS imaging methods are proposed in recent years [5]. Due to the existence of range and azimuth coupling, the memory usage and complexity of the recovery algorithms are very huge. Fang Jian [6] and Xiao Dong [7] proposed a 2-D CS imaging method which can solve this problem with traditional de-coupling operation. However, it needs to repeat the de-coupling operation in every iteration.

Some research results [6][8][9] suggested that the use of 2-D separable sampling observations in radar CS imaging can reduce both the memory usage and complexity in recovery algorithms. Meanwhile, since the de-coupling can be separated out alone with the two-dimensional separable observation, the repeat de-coupling operation can be avoided in the iterations.

In the proposed radar CS imaging method the imaging process is divided into two steps. In the first step, the Range Cell Migration Correction (RCMC) is processed in the Range Doppler domain, while the Secondary Range Compression (SRC) is conducted in the 2-D frequency domain. In the second step, the imaging scene is reconstructed by 2D recovery algorithm. The new method has reduced the memory usage and complexity with imaging performance improvement.

Signal models

Radar imaging system is a system that reconstructs the scene from the echoes. Supposing that the radar transmits LFM signals, then the echo signal of a point target can be written in equation(1).

$$S_0(t,\eta) = A_0 \cdot \exp\{j\pi K_r(t - 2\sqrt{R_0^2 + (v\cdot(\eta-\eta_0))^2}\ /\ c)^2\}\exp\{-j2\mathrm{m}\pi f_0\sqrt{R_0^2 + (v\cdot(\eta-\eta_0))^2}\ /\ c\} \quad (1)$$

Where (R_0, η_0) is the position of the point target; t is the fast time; η is the slow time; f_0 denotes the Carrier frequency; K_r is the range frequency modulation rate; c is the velocity of light and v is the carrier velocity. The pulse envelope and the antenna weighting are not considered here, so A_0 represents the scatter coefficient; m is depends on the imaging mode, if $\mathrm{m}=1$, it represents the forward-looking SAR imaging mode which proposed in [10], and if $\mathrm{m}=2$, it represents the normal side-looking SAR imaging mode. Considered that the imaging process is same，the side-looking SAR imaging mode here is enough.

2-D separable sampling data construction

The Traditional imaging algorithms will do some range compression which is achieved by matched filtering or compressed sensing before de-coupling operate. However it does not work here because the range chirp form is needed in the 2-D reconstruction. Thus the proposed method removes the effect of coupling on the range without range compression.

According to the stationary phase method, (1) can be translated to Range Doppler domain，

$$S_0(t, f_\eta) = A_0 \cdot \exp\{j\pi K_m (t - 2R_0 / c / D(f_\eta, v))^2\} \exp\{-j2\mathrm{m}\pi f_0 R_0 D(f_\eta, v) / c\} \exp(-j2\pi f_\eta \eta_0) \quad (2)$$

Where $D(f_\eta, v)$ is the Migration factor, with the analytic formulation(3).

$$D(f_\eta, v) = \sqrt{1 - c^2 f_\eta^2 / m^2 / v^2 / f_0^2} \quad (3)$$

The range frequency modulation rate has been modified to(4).

$$1 / K_m = 1 / K_r - 1 / K_{\mathrm{sec}} = 1 / K_r - 4cR_0 f_\eta^2 / m^3 / v^2 / f_0^3 / D^3(f_\eta, v) \quad (4)$$

Considering of the RCMC without range compression, the RCM is(5).

$$RCM = c \cdot t / 2 / D(f_\eta, v) \quad (5)$$

There are some differences from the traditional Range Doppler algorithm for that there is no range compression before RCMC. Generally, there are two methods to realize RCMC, one is interpolation, and the other is range scaling operation. Interpolation is used in the RCMC process here, the echo signal form changed.

$$S_1(t, f_\eta) = A_0 \cdot \exp\{j\pi K_m / D^2(f_\eta, v) \cdot (t - 2R_0 / c)^2\} \exp\{-j2\mathrm{m}\pi f_0 R_0 D(f_\eta, v) / c\} \exp(-j2\pi f_\eta \eta_0) \quad (6)$$

In view of equation(6), the range frequency modulation rate has changed again despite that these changes must be corrected effectively. Fortunately, these changes can be incorporated into Secondary Range Compression (SRC), meanwhile the SRC can be easily achieved by multiplying a phase in the 2-D frequency domain. According to the stationary phase method, equation (6) can be transformed to 2-D frequency domain

$$S_1(f_t, f_\eta) = A_0 \cdot \exp\{-j\pi D^2(f_\eta, v) f_t^2 / K_m\} \exp\{-j2\mathrm{m}\pi f_0 R_0 D(f_\eta, v) / c\} \exp(-j2\pi f_\eta \eta_0) \exp(-j4\pi f_t R_0 / c) \quad (7)$$

The phase function which is used to realizing the SRC can be represented as equation (8)

$$H(f_t, f_\eta) = (1 - D^2(f_\eta, v) f_t^2) / K_r - 4cR_{ref} f_\eta^2 / m^3 / v^2 / f_0^3 / D(f_\eta, v) \quad (8)$$

Where R_{ref} is the range of the scene center.

After the SRC, the influence of range by the coupling is eliminated completely. But the influence in azimuth frequency modulation rate still exists. Without the range compression, it can not be eliminated with the phase compensation in 2-D frequency domain. There are some methods can achieve it in spite of the difficulty. The easiest case is considering the azimuth frequency modulation rate as fix which equals to the azimuth frequency modulation rate in scene center on the condition that the scene is small enough. A harder one pre-compressed the range in 2-D frequency domain by multiplying a phase function initially， transformed to range Doppler domain and corrected the influence with another phase function sequently and transformed back to 2-D frequency domain and compensated the first phase function finally. These two methods can reduce the frequency modulation influence efficiently. The easier one is adopted here.

After transform to 2-D time domain, the echo signal gets the final form(9).

$$S_2(t,\eta) = A_0 \cdot \exp\{-j\pi K_r (t - 2R_0 / c)^2\} \exp\{-j2\mathrm{m}\pi f_0 \sqrt{R_{ref}^2 + v^2(\eta - \eta_0)^2} / c\} \tag{9}$$

The total echo signal can be written in the form of a double integral

$$S(t,\eta) = \int\int A(x,y) \cdot \exp\{-j\pi K_r (t - 2x / c)^2\} \exp\{-j2\mathrm{m}\pi f_0 \sqrt{R_{ref}^2 + v^2(\eta - y)^2} / c\} dxdy \tag{10}$$

2-D compressed sensing imaging

The 2-D compressed sensing is studied by some researchers. Rivenson [8] investigated the Compressed Imaging With a 2-D Separable Sensing Operator and deduced the reconstruction condition, Fang Yong [9] and Fang Jian [6] are applied the reconstruction algorithm in 2-D Separable Projections. All the work has shown that the 2-D compressed sensing especially the 2-D Separable Sensing can efficiently reduce the memory usage and complexity when applied to 2-D signal reconstruction. Recall (10), in fact, it can written as the 2-D Separable Sensing style. the discrete form of (10) can be written as (11)

$$S(m,q) = \sum_{n=1}^{N}\sum_{p=1}^{P} \exp\{-j\pi K_r \Delta t^2 (m-n)^2\} A(n,p) \cdot \exp\{-j2\mathrm{m}\pi f_0 \sqrt{R_{ref}^2 + v^2 \Delta\eta^2 (q-p)^2} / c\} \tag{11}$$

Rewritten it in matrix form

$$S = \Phi_r A \Phi_a^T \tag{12}$$

Where S is a $M \times Q$ matrix; Φ_r is a $M \times N$ matrix; Φ_a is a $Q \times P$ matrix; with

$$\Phi_r(i,j) = \exp\{-j\pi K_r \Delta t^2 (i-j)^2\} \tag{13}$$

$$\Phi_a(i,j) = \exp\{-j2\mathrm{m}\pi f_0 \sqrt{R_{ref}^2 + v^2 \Delta\eta^2 (i-j)^2} / c\} \tag{14}$$

So the scenes A can be reconstruction by the echo S using 2-D compressed sensing algorithm.

It is noteworthy that there is no coupling with the sampling matrix Φ_r and Φ_a. In other words, this is a 2-D Separable Sensing problem. Benefited from the Separable Sensing Operator and 2-D compressed sensing algorithm, the memory usage and complexity of reconstruction algorithm is reduced. Owe to 2-D joint reconstruction, the imaging performance will be improved effectively as well.

Experimental results

The simulation is conducted in three imaging methods, the first one is the traditional matched filter imaging with RD algorithm, the second one is the compressed sensing imaging using two 1-D reconstruction algorithms and the third one is the compressed sensing imaging using 2-D reconstruction algorithm which proposed in this paper. The targets are uniformly distributed on a circular that the Radius of the circle is growing in a step of 5m. The experiment is imaging with 25% data and results are shown in Figure1.

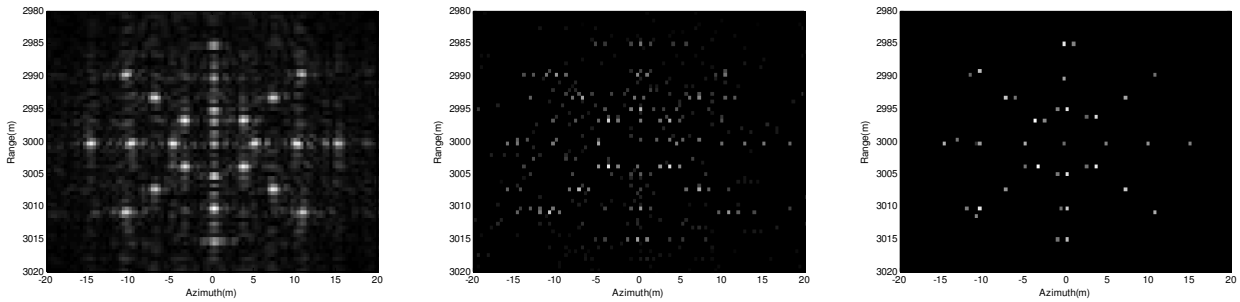

(a) Matched filter (b) 1-D reconstruction algorithm (c) 2-D reconstruction algorithm

Fig.1. The experimental results

As expected, the 2-D separable sampling compressed sensing with 2-D reconstruction algorithm obtained the best performance even with partial data. The reason for this is that the 2-D signal in

2-D reconstruction algorithm is much sparser than the 1-D signal in 1-D reconstruction algorithm. It is worth to note that 2-D separable sampling greatly reduces the memory usage and the 2-D reconstruction algorithm can reduced the reconstruction complexity efficiently in CS imaging. So the new method has several advantages over traditional CS imaging methods in performance of both memory usage and reconstruction complexity.

Conclusion

Based on 2-D separable sampling and 2-D reconstruction algorithm, a 2-D separable compressed sensing radar imaging method is proposed. The construction method of 2-D separable sampling data is investigated and an imaging model using two-dimensional reconstruction algorithm to process these separable sampling dates is showed. Compared with traditional methods, the proposed two-dimensional separable sampling method can effectively reduce the memory usage and complexity with imaging performance improvement.

Acknowledgement

This paper is funded by the International Exchange Program of Harbin Engineering University fo r Innovation-oriented Talents Cultivation.

References

[1] Potter L C, Ertin E, Parker J T, et al. Sparsity and Compressed Sensing in Radar Imaging[J]. Proceedings of the IEEE. 2010, 98(6): 1006-1020.

[2] Ender J H G. On compressive sensing applied to radar[J]. Signal Processing. 2010, 90(5): 1402-1414.

[3] Tello Alonso M, Lopez-Dekker P, Mallorqui J J. A Novel Strategy for Radar Imaging Based on Compressive Sensing[J]. IEEE Transactions on Geoscience and Remote Sensing. 2010, 48(12): 4285-4295.

[4] Xiao P, Yu Z, Li C. Compressive sensing SAR range compression with chirp scaling principle[J]. Science China Information Sciences. 2012, 55(10): 2292-2300.

[5] Patel V M, Easley G R, Healy D M, et al. Compressed Synthetic Aperture Radar[J]. IEEE Journal of Selected Topics in Signal Processing. 2010, 4(2): 244-254.

[6] Fang J, Xu Z, Zhang B, et al. Fast Compressed Sensing SAR Imaging Based on Approximated Observation[J]. IEEE Journal of Selected Topics in Applied Earth Observations and Remote Sensing. 2014, 7(1): 352-363.

[7] Dong X, Zhang Y. A Novel Compressive Sensing Algorithm for SAR Imaging[J]. IEEE Journal of Selected Topics in Applied Earth Observations and Remote Sensing. 2014, 7(2): 708-720.

[8] Rivenson Y, Stern A. Compressed Imaging With a Separable Sensing Operator[J]. IEEE Signal Processing Letters. 2009, 16(6): 449-452.

[9] Fang Y, Huang B, Wu J. 2D Sparse Signal Recovery via 2D Orthogonal Matching Pursuit[J]. 2011.

[10] Sutor T, Buckreuss S, Wendler M, et al. SIREV- Sector Imaging Radar for Enhanced Vision[C]. 2000.

Advanced Materials Research Vols. 989-994 (2014) pp 3759-3762
© (2014) Trans Tech Publications, Switzerland
doi:10.4028/www.scientific.net/AMR.989-994.3759

A MMSE channel estimation method in QC-LDPC coded OFDM systems

Sangirov Gulomjon[1, a], Fu Yongqing [1, b] and Fang Ye [1, c]

[1]Department of Information and Communication Engineering, Harbin Engineering University, Harbin, 150001 China

[a]email: gulomjons@hrbeu.edu.cn, [b]email: Yongqingfu@hrbeu.edu.cn [c]email: yefang@hrbeu.edu.cn

Keywords: MMSE channel estimation, QC-LDPC, OFDM;

Abstract. An orthogonal frequency division multiplexing (OFDM) is one of the effective techniques used in wireless communications. In OFDM systems, channel impairments due to multipath dispersive wireless channels can cause deep fades in wireless channels. The OFDM receiver also requires an accurate and computationally efficient channel state information when coherent detection is involved. Therefore, it needs a good robust estimation method of the channel in wireless communication for OFDM systems. And one of these channel estimation methods is minimum mean square error (MMSE) channel estimation. MMSE channel estimation one most used method in OFDM systems. In this work we enhanced robustness of MMSE channel estimation by using it in base of quasi-cyclic low density parity check (QC-LDPC) coded OFDM system.

Introduction

The OFDM is mostly used in wideband digital communications for splitting a high-rate datastream into a number of lower rate streams that are transmitted simultaneously over a number of subcarriers for easy transmission. The OFDM technique is applicable in digital terrestrial multimedia broadcast (DTMB) [1], digital subscriber line (DSL) broadband internet access, wireless networks, long term evolution (LTE) [2-3], and 4G mobile broadband communications [3]. In OFDM system, the transmitter modulates the message bit sequence into phase shift keying (PSK) / quadrature amplitude modulation (QAM) symbols, performs inverse fast fourier transform (IFFT) on the symbols to convert them into time-domain signals, and sends them out through a wireless channel. In order to avoid intercarrier interference (ICI) which caused by multipath fading channel. The OFDM system inserts cyclic prefix (CP) at the transmitter to provide high bandwidth efficiency and high wireless data transmission.

Channel estimation is an indispensable part of the OFDM system, which performance has a significant impact on system performance. MMSE channel estimation is one of the most used estimation methods in OFDM system. MMSE channel estimation outperforms the other estimator least square (LS) in [4-5]. MMSE estimator uses prior information about the channel statistics. In [6] MMSE channel estimation is modified for effective estimation of the effects of channel impulse response variations. Proposed approach has better bit-error-rate (BER) performance than conventional approaches for signal to noise rate (SNR) varying from 3 to 8 dB by using low-density parity check coded single-input single output OFDM system in [7]. Also a configurable high throughput QC-LDPC decoder architecture based on layered message described in [8]. In this work we have shown MMSE channel estimation in base of QC-LDPC coded OFDM system.

System Description

Considering OFDM system with size M OFDM symbol, the k^{th} block of OFDM symbols is expressed as $\tilde{\mathbf{S}}_M(k)=\left[\tilde{S}_1(k),\cdots,\tilde{S}_M(k)\right]^T$, where $(\cdot)^T$ denotes the operator of transpose. After inverse fast fourier transform

$$\mathbf{s}_M(k)=\left[s_1(k),\cdots,s_M(k)\right]^T=\mathbf{F}_M^H\tilde{\mathbf{S}}_M(k) \tag{1}$$

where $\mathbf{F}_M$ is the size M FFT matrix with entries $\mathbf{F}_M(m,n)=(1/\sqrt{M})e^{j2\pi mn/M}$

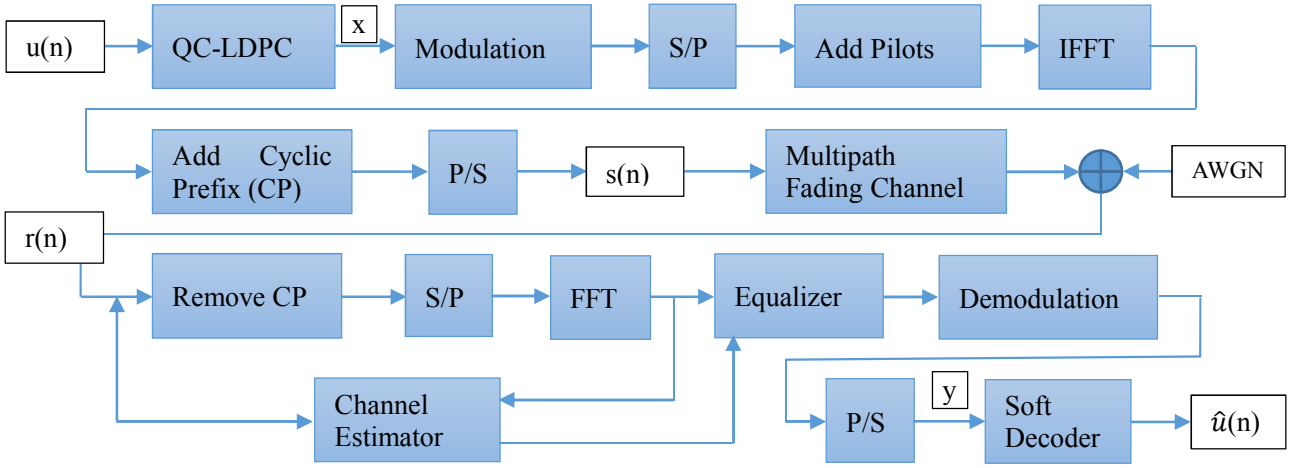

Fig. 1. Pilot sequence based single input single output OFDM system architecture

n figure 1 we showed simplified architecture from [7]. Let *Sdata=S(Id)* is a data symbols and *Spilot=S(Ip)*, *Id* and *Ip* are the vectors containing the indices of the subcarriers reserved for data and pilots respectively. The output of IFFT is

$$s(n) = IFFT(S) = \sum_{k=0}^{N=1} S(k) e^{i\frac{2\pi kn}{N}} \quad n = 0,1,...,N-1 \tag{2}$$

After CP adding into OFDM symbol through inserting the end *Lg* subcarrier to the start as per the following equation:

$$s(P) = \begin{cases} s(N - Lg + P) & P = 0,1,...,Lg-1 \\ s(Lg - P) & P = Lg, Lg+1,...,Lg+N-1 \end{cases} \tag{3}$$

where *Lg* is the length of the cyclic prefix, we assume that the cyclic prefix in each OFDM symbol is longer than the maximum delay spread. The received signal at the receiver can be expressed as:

$$r(n) = e^{i\frac{2\pi\omega n}{N}} \sum_{k=0}^{K-1} h(k)s(n) + w(n) \tag{4}$$

Where ω is the carrier frequency offset (CFO) normalized to the OFDM subcarrier spacing, $h(k)$ represents the kth tap channel impulse response, K is number of taps in the channel, and w(n) is a complex AWGN sample.

Quasi-Cyclic LDPC codes

According to [8] LDPC code is: $Hx = 0_{M\times 1}$; in (galious field) GF(2), where x is the *N*-dimensional binary-valued data vector, $0_{M\times 1}$ denotes an *M*-dimensional all-zero vector, and *H* is a sparse binary-valued $M \times N$ parity check matrix. QC-LDPC codes are described by a $M_p \times N_p$ LDPC matrix prototype H_p. The parity check matrix H in $Hx = 0_{M\times 1}$ is constructed from H_p by replacing each entry by $Z \times Z$ cyclic-shift matrices are defined as $P^c = \prod_{i=1}^{c} P^1$ (for *c*>0) with

$$[P^1]_{i,j} = \begin{cases} 1, & (i \bmod Z) + 1 = j \\ 0, & otherwise \end{cases} \tag{5}$$

$P^0 = I_z$, and $P^- = 0_{z\times z}$. Here entries of H_p satisfy $[H_p]_{m,n} < Z(\forall m,n)$.

Quasi -Cyclic LDPC decoding

The parity checks in $Hx = 0_{M\times 1}$ can be represented as a bipartite graph consisting of N variable nodes and M check nodes. Variable nodes are associated with transmitted bits x_n, $(n = 1,2,...,N)$.

The *m*th parity check node is connected to the *n*th variable node if $H_{m,n}=1$. LDPC decoding are represented as message passing (MP) on the bipartite graph and it consists of two phases. In the first phase, all messages from the variable to the check nodes (denoted by Q-messages) are computed with the aid of log-likelihood ratios (LLRs):

$$L_n \triangleq \log\left(\frac{P[x_n=0\,|\,y]}{P[x_n=1\,|\,y]}\right), \quad n=1,2,...,N \tag{6}$$

where y denotes the channel observation. In the second phase, all messages from the check to the variable nodes (denoted by R-messages) are computed. Both phases are repeated until $Hx=0_{M\times 1}$ is satisfied (i.e., the algorithm converges to a valid code-word) or a maximum number of iterations *I* has been reached.

Channel estimation

Suppose there are N_{pil} pilots in frequency domain signal at transmitter, denoted by $\tilde{S}=\left[\tilde{S}_{pil}(1),\cdots,\tilde{S}_{pil}\left(N_{pil}\right)\right]$. The corresponding frequency domain symbol in the receiver is $\tilde{R}=\left[\tilde{R}_{pil}(1),\cdots,\tilde{R}_{pil}\left(N_{pil}\right)\right]$ and **N** noise vector frequency domain. With the LS channel estimation, the channel frequency response is

$$\tilde{\mathbf{H}}_{LS}=\left[\frac{\tilde{R}_{pil}(1)}{\tilde{S}_{pil}(1)},\cdots,\frac{\tilde{R}_{pil}\left(N_{pil}\right)}{\tilde{S}_{pil}\left(N_{pil}\right)}\right] \tag{7}$$

According to [9], the MMSE channel estimation parameters as follows: $\widetilde{\mathbf{H}}_{\mathbf{LS}} \triangleq \widehat{\mathbf{H}}$; R_{HH} is autocorrelation of true channel $\mathbf{H}$; $R_{H\hat{H}}$ is the cross-correlation matrix between the true channel vector $\mathbf{H}$ and channel estimate vector $\hat{\mathbf{H}}$ in the frequency domain; $R_{\hat{H}\hat{H}}=E\left\{\hat{\mathbf{H}}\hat{\mathbf{H}}^{H}\right\}=R_{HH}+\frac{\sigma_N^2}{\sigma_S^2}\mathbf{I}$ is autocorrelation matrix of $\hat{\mathbf{H}}$. The MMSE channel estimation is:

$$\tilde{\mathbf{H}}_{MMSE}=R_{H\hat{H}}R_{\hat{H}\hat{H}}{}^{-1}\hat{H}=R_{H\hat{H}}(R_{HH}+\frac{\sigma_N^2}{\sigma_s^2}I)^{-1}\hat{H} \tag{8}$$

where σ_N^2 is frequency domain N noise variance, σ_S^2 frequency domain signal variance and **I** is identity matrix.

Let $\tilde{\mathbf{H}}_{pil}=\tilde{\mathbf{H}}_{MMSE}$ and $\mathbf{F}_{pil}$ denote FFT matrix at the pilot, which is constituted by first *L+1* columns of $\sqrt{M}\mathbf{F}_M$, and selects only the rows corresponding to the pilot carriers. Therefore, the channel impulse response can be expressed as

$$\mathbf{h}_{pil}=\frac{1}{M}\mathbf{F}_{pil}^{H}\tilde{\mathbf{H}}_{pil} \tag{9}$$

$\mathbf{h}_{pil}$ is the knowledge of channel time-domain attenuations afforded by pilot.

Simulation Results

During simulation process, each OFDM symbols occupied 64 subcarriers, 48 data and 16 pilot subcarriers with 16 CP. QAM 16 and QAM 64 modulations are used, and the simulation results are indicated in Fig.2 and Fig.3. We have evaluated the performance of MMSE channel estimation in OFDM systems and MMSE channel estimation in QC-LDPC coded OFDM systems. Furthermore we have compared the MMSE in traditional OFDM and in QC-LDPC coded OFDM systems over Rayleigh fading channel of 4, 16 and 36 taps. As the channel order is different for different environmental conditions and also with QAM 16 and QAM 64 modulations, these changings increase the adversity effects of the environment. It is clear that MMSE in QC-LDPC coded OFDM outperforms in different channel taps.

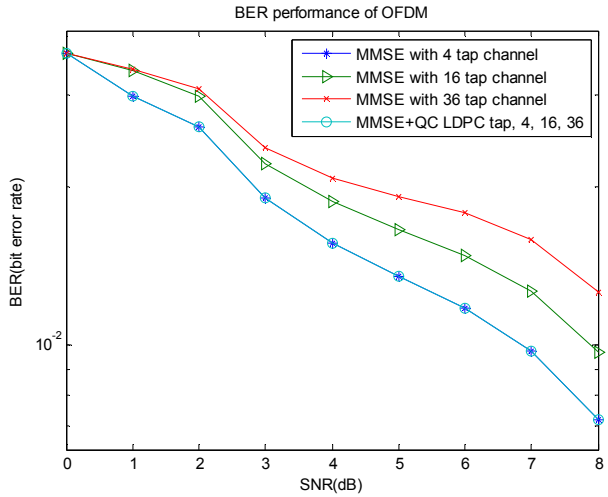

Figure.2 BER vs. SNR, QAM 16 modulation for channel tap 4, 16 ,36

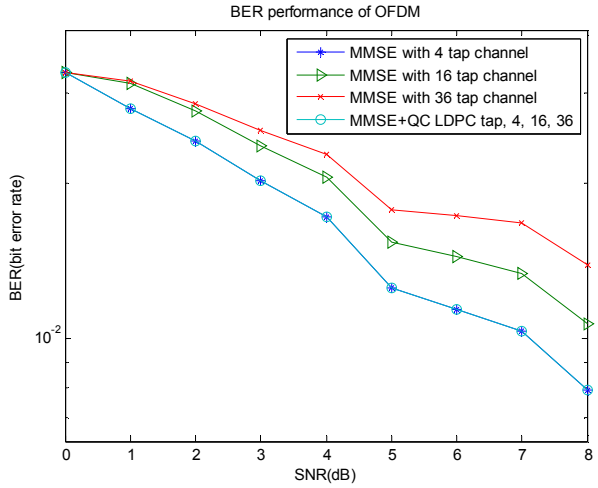

Figure.3 BER vs. SNR, QAM 64 modulation for channel tap 4, 16 ,36

Conclusion

In this paper we simulated MMSE in QC-LDPC coded OFDM systems over Rayleigh fading channel with 4, 16 and 36 taps. The QC-LDPC with ½ rate 5184 bits by QAM16 and QC-LDPC with 2/3 rate 5184 bits modulated by QAM64. It is observed that the performance of the these simulations MMSE in QC-LDPC coded OFDM system stays stable with increase in length of channel taps, however MMSE in OFDM system shows a significant performance degradation with an increase in channel taps.

Acknowledgement

This paper is funded by the International Exchange Program of Harbin Engineering University for Innovation-oriented Talents Cultivation.

References

[1] http://en.wikipedia.org/wiki/Digital_Terrestrial_Multimedia_Broadcast
[2] http://www.eventhelix.com/lte/lte-tutorials.htm
[3] E. Dahlman, S. Parkvall & J.Sköld, 4G LTE/LTE-Advanced for Mobile Broadband, Elsevier , 2011 ISBN: 978-0-12-385489-6
[4] Morelli, Michele, and Umberto Mengali. "A comparison of pilot-aided channel estimation methods for OFDM systems." Signal Processing, IEEE Transactions on 49.12 (2001): 3065-3073.
[5] Song, B., Gui, L., & Zhang, W. Comb type pilot aided channel estimation in OFDM systems with transmit diversity. Broadcasting, IEEE Transactions on, 2006 52(1), 50-57.
[6] L. U. Khan, M. I. Babar and Z. Sabir. Robust modified MMSE estimator for comb-type channel estimation in OFDM Systems. ICACT2013 (January 27-30, 2013) 924-928.
[7] T. L. Kung, K. K Parhi. Semiblind frequency - domain timing synchronization and channel estimation for OFDM systems. Advances in Signal Processing Journal on. Springer. 2013
[8] Studer, C., Preyss, N., Roth, C., & Burg, A.. Configurable high-throughput decoder architecture for quasi-cyclic LDPC codes. In Signals, Systems and Computers, 2008 42nd Asilomar Conference on (2008, October) (pp. 1137-1142). IEEE.
[9] Cho, Y. S., Kim, J., Yang, W. Y., & Kang, C. G. (2010). MIMO-OFDM wireless communications with MATLAB. John Wiley & Sons. pp.190-192

Advanced Materials Research Vols. 989-994 (2014) pp 3763-3767
© (2014) Trans Tech Publications, Switzerland
doi:10.4028/www.scientific.net/AMR.989-994.3763

Novel Infrared and Visible Images fusion algorithm Based on NSCT

Tan Hai-feng [1, a],Luo Tian-wen[1],Zhu Jing-jun[2],Li Guan-zhong[3],
Zhang Quan-xi[1]

[1] Aviation University of Air Force, Changchun, 130022, China

[2] Unit 93116, Shenyang, 110000, China

[3]Unit 93010,110000,China

[a]email: thffop@163.com

Keywords: Regional energy; Image fusion;NSCT

Abstract. A novel fusion algorithm based on Nonsubsampled Contourlet Transform (NSCT) is proposed, according to the characteristics of infrared and visible images. Firstly, the registered infrared and visible images from the same scene were transformed by NSCT transforms; then the low frequency coefficient is fused by the combination of local energy and normalised correlation matrix, the high frequency coefficient fusion is fused by regional energy matching with regional variance; finally, the target image is obtained by performing inverse NSCT transforms. experimental results indicate that the proposed algorithm can effectively get more detail information and the fusion performance is dramatically better than traditional fusion methods.

Introduction

Due to the different imaging mechanism and bands between different sensors, images of the same scene obtained by different sensors have complementary and redundant informations. Image fusion refers to the information processing of synthesizing an image or image sequence information about a specific scene obtained by two or more sensors at the same time or at different times[1] in order to generate new information about the scene. The mechanisms of visible light and infrared imaging sensors are different: Infrared imaging sensors generate images by using thermal radiation energy of the target scene; thus they have a certain ability to penetrate smoke, fog, etc. and a strong ability to recognize disguise. However, they are not sensitive to detailed changes of the scene and have low image resolution. Visible light imaging sensors generate images by using the reflectivity of light; thus they have a good spatial resolution and can well describe the environmental information of a specific scene. However, they can easily be influenced by light intensity and weather. By fusing images generated by infrared and visible light, we can make full use of their complementary information and improve the recognition and clarity of infrared targets in order to gain fusion images better for the observers to get an overall cognition of the scene.

In recent years, scholars have proposed a lot of methods to fuse infrared images and visible light images, mainly including: the method based on multi-resolution analysis, the method based on weighting a single pixel and the method based on regional segmentation[2][3].Because constructing a new multi-resolution structure is difficult and it may not be able to adapt to practical application, researches on fusion rules have always been the focus of study of such methods[4].At present, researches on fusion rules mostly focus on the fusion of high frequency coefficient, and the low frequency coefficient fusion methods mainly include the average method, ‘take the biggest’ method[5], and etc. Although to some extent these low frequency fusion rules have improved the efficiency of the algorithm, they have reduced the contrast ratio of these fusion images, which make the loss of some useful information in the source images.

According to the above situation, in order to make the details of the fusion image have better performance and further facilitate interpretation personnel and computers, this paper puts forward a kind of infrared and visible light fusion method in the NSCT domain based on local energy and the normalized correlation moments.

NSCT Transformation

Non-sampling Contourlet Transformation (NSCT) is proposed based on Contourlet Transformation. It not only inherits the multi-scale and multi-directional characteristics of Contourlet Transformation and good local features of space and frequency, which make it able to capture and track the important geometric features of images better, but also has the characteristic of translational invariance[6][7].Non-sampling Contourlet Transformation is also made up of two parts: Non-subsampled Pyramid(NSP) decomposition and Nonsubsampled Directional Filter Bank(NSDFB),which ensure the NSCT transformation decomposition characteristics of multi-scale decomposition and multiple directions. In the process of NSCT Transformation decomposition, there are no 'up and down' samples, and all the subgraphs of the decomposed are of the same size as the original images so as to make the NECT Transformation has the feature of translational invariance. Fig.1.(a)and Fig.1.(b)give the NSCT filter bank structure and frequency decomposition respectively.

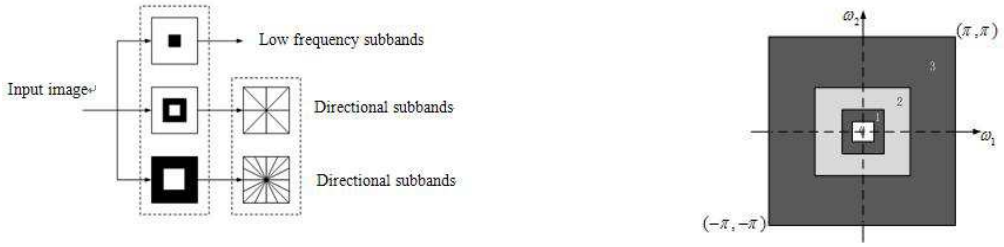

(a) NSCT filter bank structure diagram (b) NSCT frequency decomposition diagram

Fig.1. NSCT diagram

Fusion Methods of Infrared and Visible Light Images Based on NSCT Transformation

Fusion Rules of Low-frequency subband coefficients

After decomposition of the source image by the NSCT transformation, the low frequency subband image inherits the characteristics of the source image as a whole, determines the image contour [7] and occupies most of the image energy, which reflects how much information the image contains. Therefore, from the perspective of energy in the low frequency rules, this paper first calculates the contribution ratio of each pixel of low-frequency to the window as below:

$$F^X(x,y)=\begin{cases}\left|\dfrac{C^X(x,y)-\mu(x,y)}{\sigma_{xy}}\right| & \sigma_{xy}\neq 0\\ \dfrac{1}{M\times N} & \sigma_{xy}=0\end{cases} \tag{1}$$

Wherein, $M\times N$ refers to the size of the window, σ_{xy} refers to the deviation of each corresponding pixel of the window, $C^X(x,y)$ refers to the pixel value of each point in the window, $X=A,B$; and $\mu(x,y)$ refers to the average pixel value in the window. The energy of the local area window at the center of the low-frequency part is as below:

$$E_{LX}=\sum_{(x,y)\in K}F^X(x,y)\cdot\left|C^X(x,y)\right|^2 \tag{2}$$

Wherein, $K=M\times N$ refers to the regional window, $C^X(x,y)$ refers to the low frequency coefficient after the decomposition of the source image by the NSCT transformation. Energy difference defined by the normalization factor is $\Delta=\left|E_A(x,y)-E_A(x,y)\right|$, wherein

$$E_A(x,y)=\frac{E_{LA}(x,y)}{E_{LA}(x,y)+E_{LB}(x,y)} \tag{3}$$

$$E_B(x,y)=\frac{E_{LB}(x,y)}{E_{LA}(x,y)+E_{LB}(x,y)} \tag{4}$$

The threshod value is $T_1 \in (0.04, 0.1)$, so low frequency coefficients are fused according to the following fusion rule:

$$\begin{cases} D_{FL}(x,y) = C^A(x,y) & \Delta \geq T_1, E_A(x,y) \geq E_B(x,y) \\ D_{FL}(x,y) = C^B(x,y) & \Delta \geq T_1, E_A(x,y) < E_B(x,y) \\ D_{FL}(x,y) = E_A(x,y) \cdot C^A(x,y) + E_B(x,y) \cdot C^B(x,y) & \Delta < T_1 \end{cases} \tag{5}$$

Wherein, $D_{FL}(x,y)$ refers to the low-frequency coefficient of the point (x,y) in this fusion image.

Fusion Rules of High-frequency Bandpass Directional Subband Coefficient

As there is more energy at the corresponding image edges and other detailed parts reflected by the high efficiency coefficient and regional variance reflects the deviation degree of the pixel gray value to the average value in the area, the greater the variance, the greater difference between each pixel in the region and the more information this region contains. In this paper, the high-frequency coefficient fusion rules construct high-frequency coefficient of fusion images by constructing regional energy compatibility and taking the largest variance in this region.

The definition of regional energy matching degree is as below:

$$M_{A,B}(x,y) = \frac{\left| 2 \sum_{(x,y) \in K} w(m,n) \left| C_{j,l}^A(x+m, y+n) C_{j,l}^B(x+m, y+n) \right| \right|}{E_{j,l}^A(x,y) + E_{j,l}^B(x,y)} \tag{6}$$

Wherein, $E_{j,l}^X(x,y)$ refers to the regional energy of the $M \times N$ window centering on the (x,y) point at scale 1 section J and the definition is as below:

$$E_{j,l}^X(x,y) = \frac{1}{MN} \sum_{m=-(M-1)/2}^{(M-1)/2} \sum_{n=-(N-1)/2}^{(N-1)/2} w(m,n) \left(C_{j,l}^X(x+m, y+n) \right)^2 \tag{7}$$

$C_{j,l}^X, (X = A, B;\ j,l = 1,2,3\cdots)$ refers to the high frequency subband coefficients of the source image X at scale 1 section J after the decomposition by the NSCT. $w(m,n) = [1,2,1;2,4,2;1,2,1]/16$ refers to the window mask.

If $M_{A,B}(x,y) \geq \alpha$, then the weighted averages used to carry out the fusion, and the coefficient after the fusion is:

$$C_{j,l}^F(x,y) = q_A C_{j,l}^A(x,y) + q_B C_{j,l}^B(x,y) \tag{8}$$

Wherein, q_A, q_B refers to the self adaptive adjustment factor:

$$\begin{cases} q_A = \dfrac{E_{j,l}^A(x,y)}{E_{j,l}^A(x,y) + E_{j,l}^B(x,y)} \\ q_B = \dfrac{E_{j,l}^B(x,y)}{E_{j,l}^A(x,y) + E_{j,l}^B(x,y)} \end{cases} \tag{9}$$

If $M_{A,B}(x,y) < \alpha$, then the regional variance is defined as:

$$V_{j,l}^X(x,y) = \frac{1}{(M-1)(N-1)} \sum_{m=-(M-1)/2}^{(M-1)/2} \sum_{n=-(N-1)/2}^{(N-1)/2} \left| C_{j,l}^X(x+m, y+n) - \bar{C} \right|^2 \tag{10}$$

$$C_{j,l}^F(x,y) = \begin{cases} C_{j,l}^A(x,y) & if \quad V_{j,l}^A(x,y) \geq V_{j,l}^B(x,y) \\ C_{j,l}^B(x,y) & if \quad V_{j,l}^A(x,y) < V_{j,l}^B(x,y) \end{cases} \tag{11}$$

Simulation, analysis and evaluation

In order to verify the validity and effects of the algorithm, this paper uses MATLAB7.0 to carry out the simulation experiment, and compare the algorithm used in this paper with fusion rules like the commonly used ‘take the biggest’ method, the weighted average method and ‘take the biggest regional variance’ method, and etc. And the experimental data use two sets of images produced by

infrared and visible light. Figs. 2 are 'UN Camp' visible and infrared sequence diagrams provided by the Holland TNO Ergonomics Institute. The grey level of this image is 256, and the size is 360×270.

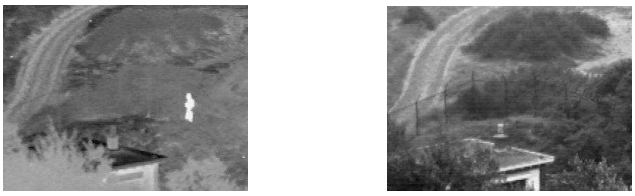

(a) Infrared Image (b) Visible Light Image

Fig.2. Infrared and Visible Light Images

In the simulation experiments, every fusion algorithm is taken out in the NSCT domain, using decomposition layer 3, and in accordance with the order from the senior to junior, the numbers of directional decomposition are 2, 4 and 8 separately. Scale decomposition filter group adopts '9-7', and directional decomposition filter group uses 'pkva'. The size of the neighbour is taken as 3×3,and T_1 taken as 0.05, α as 0.7.Definitions of the fusion rules are as follows:(1) For the low-frequency coefficients, take the average method, and for the high-coefficients, the 'take the largest regional variance' method;(2) For the low-frequency coefficients, take the average method, and for the high-frequency coefficients, the 'take the biggest absolute value' method;(3) For the low-frequency coefficients, take the 'weighted average' method, and for the high-coefficients, the 'take the biggest regional variance' method;(4)For the low-frequency coefficients, take the 'weighted average energy' method, and for the high-frequency coefficients, the 'take the biggest absolute value' method;(5)Fusion rules in this paper: The low-frequency coefficients are based on local energy and normalized correlation moments; for the high-frequency coefficients, the 'take the biggest regional variance with some regional energy matching degree' method is taken.

Fusion Rule (1) Fusion Rule (2) Fusion Rule (3) Fusion Rule (4) Fusion Rule (5)

Fig.3. Fusion Images Produced by Different Fusion rules

From a subjective visual perception, we can find that all these five ways can better keep the important information of the source image and integrate the features of the source image. And the fused image can better extract the scene information of the visible light images and the target information of infrared images. However, the contrast of the fusion result goals with the scene is small, which is due to the use of a simple average method to the low-frequency images. On the other hand, the contrast of fusion result details produced by using the fusion rules proposed in this paper is large, and the scene information is more abundant.

In order to evaluate the performance of different fusion methods of infrared and visible light images, this paper adopts the information entropy[9] , the standard deviation[9], the average gradient[9] and the mutual information[9] as the image fusion evaluation indexes. The bigger the entropy, the richer informations the image contains, and the better the quality of the fusion is. Standard deviation reflects the degree of dispersion of grey intensity of the image to the average grey value. If the standard deviation is large, then the greyscale of the image disperses; the image contrast is great, and more information can be seen. Average gradient not only reflects the clarity of the image, but also reflects the tiny contrasts in the image. The greater the average gradient, the more contrast details there are, and the higher degree of information retention. The greater amount of mutual information, the more information we can get from the source image. The comparison results are as follows:

Table.1. The Comparison of Performance of Different Fusion Algorithms Between Infrared and Visible Light Images

Evaluation Index	Ways of Fusion				
	Fusion Rule(1)	Fusion Rule(2)	Fusion Rule(3)	Fusion Rule(4)	Fusion Rule(5)
Information Entropy	6.3404	6.5926	6.6359	6.7241	6.8399
Standard deviation	24.7854	26.8564	27.1457	29.3654	29.5147
Average Gradient	5.3475	6.0214	5.4712	6.1243	6.1512
Mutual Information	1.0780	1.0990	1.3593	1.4628	1.4721

By analyzing the data in Table 1, it is not difficult to find that the fusion method proposed in this paper is superior to other fusion methods in the evaluation indexes information entropy and mutual information, indicating that the differences between the source image and the fusion image are small. Moreover, the average gradient of the fusion image is better than other methods, which shows that the tiny details of the image are better.

Conclusions

As a new kind of multiscale geometric analysis tool, NSCT has shown much superiority in the field of image fusion. Based on this, this paper presents a new fusion method in which low-frequency normalized moment is based on local energy and high-frequency coefficient uses the 'take the biggest regional variance in terms of regional energy matching' in the field of NSCT. This method has solved the problem that traditional average method and 'take the biggest' method are likely to reduce the contrast of the fusion images. Moreover, experimental statistics have further proved that the method proposed in this paper has a better visual effect and an objective evaluation indicator of quantity. However, when there are more NSCT decomposition levels and running codes, the method proposed in this paper remains to be improved.

References

[1] De I, Chnada B. A Simple and Efficient Algorithm for Multi-focus Image Fusion Using Morphological Wavelets. Signal Processing,2006,86(5):924-936.

[2] Shirin Mahmoudi. Contourlet-based image fusion using information measures[C]//Proceedings of the 2nd WSEAS International Symposium on Wavelets Theory＆Applications.2008:157-162.

[3] Cunha A L, Zhou J P, Do M N. The nonsubsampled Contourlet transform: theory, design, and applications[J]. IEEE Transactions on Image Processing,2006,15(10):3089-3101.

[4] Weiwei Kong, Yingjie Lei, Yang Lei,etc. Fusion Methods of Grey Visible Light and Infrared Based on NSCT and IHS Transformation Domain[J]. System Engineering and Electronics, 2010,32(7):1391-1393.

[5] Hai Peng. Researches on the Fusion Methods of Infrared and Visible Light Images[D]. Hangzhou: Master's Degree Thesis of Zhejiang University,2012:42-50.

[6] Li Wan, Yanxiang Hu, Xirong Ma, etc. Multi-focused Image Fusion Methods Based on Edge Enhancement[J]. Jornal of Tianjin Normal University(Natural Science Edition),2012,32(3):42-44.

[7] Yong Chai, You He, Changwen Qu. Multi-Scale Image Fusion Methods Based on the Characteristics of subpixel area weighted energy[J].Journal of Optics,2009,29(10):2732-2737.

[8] http://www.imagefusion.org

[9] Ying Zhang, Yanjun Li, Ke Zhang, etc.Image Fusion of Infrared and Visible Light Based on NSCT[J].Computer Engineering and application2011，47(3):196-198.

Advanced Materials Research Vols. 989-994 (2014) pp 3768-3772
© (2014) Trans Tech Publications, Switzerland
doi:10.4028/www.scientific.net/AMR.989-994.3768

A Novel Text Extraction Method from Pure Text Images Using Morphological Operations

Xuanqi Chen[1, a] Biao He[2, b] Guocheng Wang[3, c] Yaoxin Li[4, d]

[1,2,3]School of Microelectronics and Solid-State Electronics, [4]School of Optoelectronic Information, University of Electronic Science and Technology of China, Chengdu, China 610054

[a]email:chenxuanqi93@gmail.com, [b]email: 240743934@qq.com, [c]email: wgch19890113@163.com
[d]email: 380937887@qq.com

Keywords: Text Extraction; Mathematical Morphology; Skeleton; Document Image Process

Abstract. This paper presents a new method to achieve effective text extraction using mathematical morphology. Firstly, the document is segmented and divided into several parts based on the layout. And then, every part is dilated to big connected regions, whose biggest skeleton will be extracted and serve as a structure element(SE). Finally, a proposed region- concatenated operation with the SE will be employed, whose result can be the input of subsequent OCR system. Experimentally, the proposed method is robust to noise, the text orientation, font style and size, language and layout.

I.Introduction

Recent years, the text region extraction from document images has many practical meanings and provides many useful applications in image searches, optical character recognitions and compressions.Traditionally, methods of text extraction are commonly subdivided into three groups: top-down, bottom-up and hybrid techniques.

Bottom up techniques[1] based on connected components analysis to use merging and grouping from the thinnest elements. They do not make assumptions on size and about page layout，but they are computationally expensive and rely on the use of appropriate thresholds； Top-down techniques[2] are fast and efficient but the efficiency depends on priori knowledge .

Most methods do not fit into any of the two categories above were called hybrid.Typically, some methods based on edge information[3]have been proposed. But its process objective is limited that only Latin character can be handled. A method[3]subdivides the document into many small overlap column elements, then carries out a histogram analysis to connect them. It is able to work on low-resolution and is robust against skew, fast and very flexible. Unfortunately, it requires uniform background and approximately horizontal text. In [4], it proposes a mixed method which is independent from text orientation and is able to handle inverse text while its performance, unfortunately, depends on the quality of connected components strongly.

In this paper, a morphological method which focuses on the document's structure provides a new way to extract the text. The algorithm is straightforward in comprehension and processing while it is also robust against text orientation, font style and size, language . The algorithm is also fast and effective because of less multiplication, division.

II. Morphological Transforms

Mathematical morphology is a well-known technique based on set theory and lattice lgebr--a. It often includes many different standard morphological operations namely dilation, erosion, opening, closing etc. Structure element (SE) usually plays an important role in these transforms.

2.1 basis of MM transforms

The two most fundamental morphological operations are dilation and erosion. Erosion is used to delete the thin strokes and cause objects to shrink, Dilation is used to fill holes and narrow gulfs in objects and increases the object size. In gray scale they are defined by follows:

$$[\varepsilon_B(f)](x) = \min_{b\in B} f(x+b) \qquad (1) \qquad [\delta_B(f)](x) = \max_{b\in B} f(x+b) \qquad (2)$$

Opening (closing) is sequential combination of erosion (dilation) and dilation (erosion) with SE. The opening will remove all the pixels in the region that are smaller than SE. It tends to smooth outward bumps, break narrow sections, and eliminate the thin protrusion. However, the closing has same effect in the invert image.

$$\gamma_B(f) = \delta_{\tilde{B}}\left[\varepsilon_B(f)\right] \quad (3) \qquad \phi_B(f) = \varepsilon_{\tilde{B}}\left[\delta_B(f)\right] \quad (4)$$

Skeletonization is one of the characteristics to description the geometrical shape and property of topological for images (shown in figure 2a). It has many applications in image compress, character recognition, and image regenerate.

The convex hull of a set is defined as the smallest convex set that contains A. And the convex (shown in figure 2b) is one in which the straight line joining any two points in the set consists of points that are also in the set.

2.2 proposed region-connected operation

The region-connected operation can aggregate small connected domains to a big one. In this paper, it is required to concatenate small parts in a line. The proposed transform where B is a structure element, B1 is B's end points and f is figure:

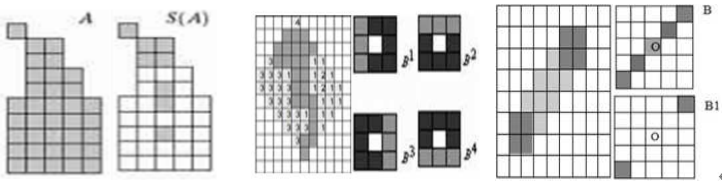

F2a F2b F2c

$$\delta_B\left(\varepsilon_{B1}(f)\right) \cup f \quad (5)$$

This transform guarantees the end points of the connected line are included respectively in the two regions so that regions only grow in a single direction, which reduces the overlap between two neighbor lines (view in figure 2c).

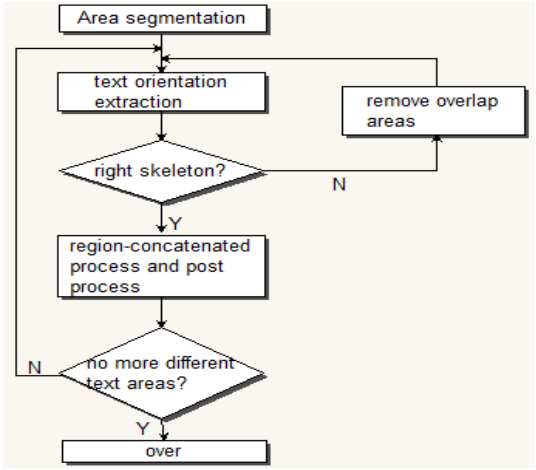

III. Proposed Methodology

The whole algorithm can be described as Fig.3:

3.1 Area Segmentation Based on Layout

The proposed methodology focuses on pure text while there are many other methods for mixed document embedded with graphs or tables, to achieve text and non-text separation, like [5].

A pure text commonly has a particular layout and its characters needs to be separated to different areas based on layout, because in each area, the text orientation, font style and size are not similar, which would add the difficulties of later processing. As for figure 3.1a, the document image consists of three different parts whose orientation is distinct. The text image, therefore, needs area segmentation based on layout to separate the image into several different subgraphs. And aim at each subgraph of same orientation and size for later processing.

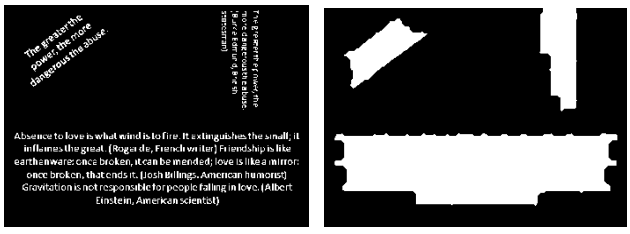

F3.1a F3.1b

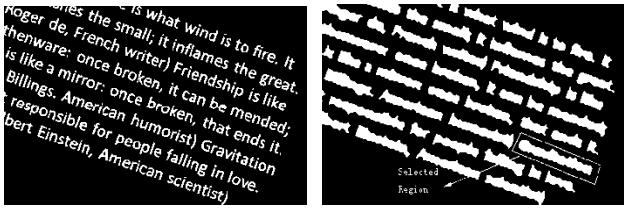

F3.2a F3.2b

This paper uses closing operation with a big SE to fill the regions of same text orientation, which makes each part become

a whole connected area. Then label these parts and get different subgraphs. The result of figure 3.1a is shown as figure 3.1b in which the text image is divided to three parts.

3.2 Text Orientation Extraction

After area segmentation in 3.1, separated areas with the same text orientation are extracted, which could be handled respectively. In this and following sections, a new image is used for deep illustration and discuss.

Typically, line spacing is greater than the character spacing, which provides a feasible way to tell characters' writing direction. Use the closing operation towards figure 3.2a to fill the regions of small character spacing in a line, while the gap between two neighbor lines is still big enough for distinction (shown as figure 3.2b). Therefore, neighboring characters are clustered to rectangle-like connected regions. Obviously, these regions include the information of text orientation which can be obtained by extracting their skeletons.

Long skeleton is needed because it would help to concatenate regions in 3.4. There are two ways to find the longest skeleton：

① Extract all regions' skeleton and then find the longest skeleton

② Find the biggest region and extract its skeleton as the longest skeleton

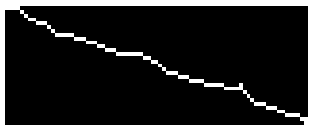

F3.2c

① may get the real longest skeleton but it causes more calculation consumptions than ② which only extract the skeleton of one connected region. In order to have a high speed performance, this paper adopts ② for the longest skeleton extraction.

The biggest region is defined as a region which has the maximum connected pixels (shown as the region in a square frame in figure 3.2b). After finding the biggest region, use the method in 2.2 and get its skeleton. Such skeleton has some small branches, which needs skeleton pruning to roughly remove these branches and get the main skeleton (shown in F3.2c).

3.3 Judge and Remove Overlap Areas

Problems may be caused by getting an incorrect skeleton when several skeletons would be considered as one skeleton by mistake due to the overlap of adjacent lines (in figure 3.3a). In the overlap situation, such false skeleton would be more likely to be found as the longest skeleton in 3.2 because its original connected region is usually bigger than others. Therefore, the process of judging and removing overlap areas is necessary to increase the algorithm's robustness.

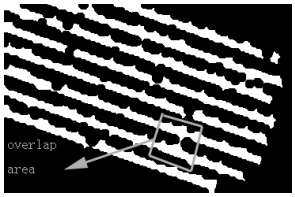

F3.3a

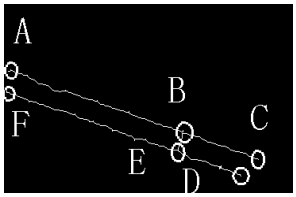

F3.3b

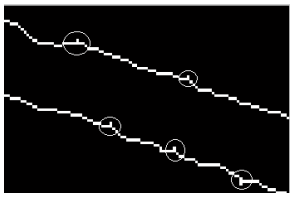

F3.3c

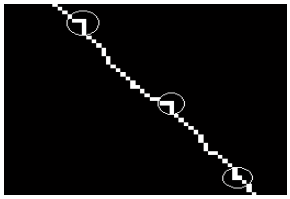

F3.3d

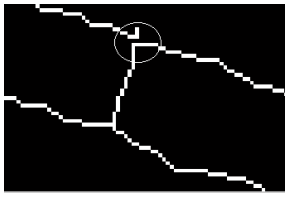

F3.3e

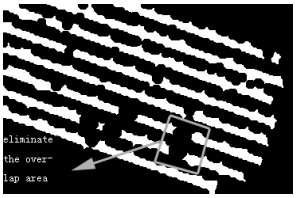

F3.3f

The incorrect skeletons have some common peculiarities (figure 3.3b):

①They contains branch points (B, E in Figure 3.3c)and more than two end points(A, C, D, F in Figure 3.3b).

②Their overlap-formed skeleton is usually smaller than the text line skeleton(BE is smaller than AC and FD in figure 3.3b).

The expense of skeleton analysis utilizing ② is high because some small branch points (figure 3.3c,figure 3.3d) and breaking points (figure 3.3e) may disturb the normal analysis. All these defects will increase the scale of question whose analysis is inevitably at the cost of the spacial and time complexity of algorithm while these defects are tolerant sometimes (see figure 3.3d, such branch points will not bring bad influence to the result).

This paper focuses ① to solve or lessen the bad effect. If the number of endpoints is more than two or the number of branch points is not zero, it will regard the skeleton as wrong skeleton and do the process of removing overlap areas as below.

It gets the skeleton's branch points, dilates and inverses the points, and then intersects them with the original (figure 3.3a). It will eliminate the effect and get figure 3.3f. Regard figure 3.3f as new input to operations in 3.2 excluding closing operation till find a no branch point or two end points SE.

F3.4a

F3.4b

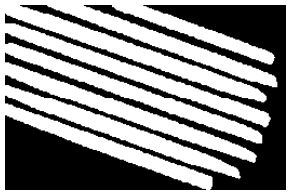

F3.4c

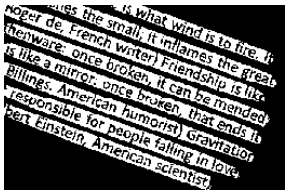

F3.4d

To avoid that skeleton pruning is too short to meet the subsequent actions' request, a maximum number of allowed loops is specified and the algorithm would then do the next process in 3.4 if it exceeds the number of cycles.

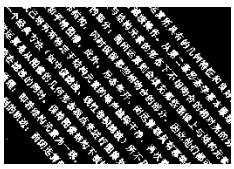

F4a

F4b

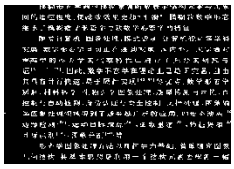

F4c

F4d

F4e

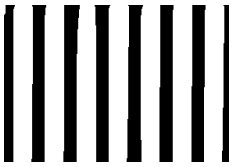

F4f

3.4 Region-Concatenated Process and Post Process

This step, at first, is making the skeleton as a SE and using a region-concatenated operation referred in part II towards figure 3.2b (the result is figure 3.4a). In order to eliminate the influence of picture's boundary, figure 3.4a is intersected with closing operation of figure 3.2a using a big SE whose result is figure 3.4b. Use a simple opening operation with the obtained SE to avoid new neighbor line overlap, and then generate convex hull image (figure 3.4c). This step will get a line region which can be analyzed and extracted to input into the OCR system (figure 3.4d). From figure 3.4d, the obtained domain nearly approach to the actual area of text.

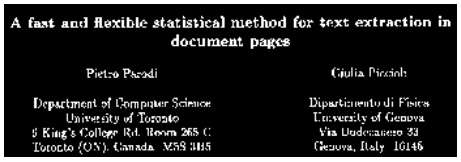

F4g

F4h

IV. Some other Experimental Results and Discuss

This section presents some results of the proposed text extraction algorithm on document images of various situations. Figure 4a, 4c and 4e are the inputs with the incline of 45^o ,0^o and 90^o . And figure 4b, 4d and 4f are the algorithm's output, which shows the suitable to a different language (Chinese) in different directions and sizes. Notably, the result of Chinese text is more parallel and regular than Latin's due to its character's peculiarity of equal height which reduces the overlap possibility and makes the line equal width without sharp fluctuation like Latin's.

Figure 4g whose font of characters is not same in different lines does not use area segmentation and employs the remaining steps deliberately. Its result (figure 4h) shows the algorithm's robust to more complex environment.

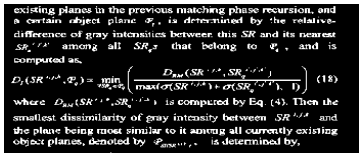

F4i

F4j

However, in some other situations especially when character spacing is less than line spacing (see in F4i with the irritation of expression), the discovered SE in 3.3 is strange or small because the overlap of neighbor lines is in an unquenchable state that causes more branch points to be found and strike themselves out in the original which means smaller connected regions and shorter skeleton found in the end. The result of figure 4i before the convex hull operation (see in figure 4j) shows the line's rupture area and holes due to the unfit skeleton.

V.Conclusions

This paper presents a new and effective method building on morphological image process which copes well with some usual occasions and is robust to the overlap between two neighbor lines. Text extraction in such a way can match the background detection and illumination normalization which also adopt the morphological strategy. It is also able to work on low- resolution.

The algorithm is concise and independent of text orientation, font style and size, language and layout, which adds its flexibility to most of specific situations with high calculation performance and compatibility with some morphological image preprocess operations; nevertheless, some improvements need to do for more sophisticated situation like grey or colorful images, font size excessively changed in a line, table-contained or formula-contained document and a text of slight contrast of line spacing and character spacing.

References

[1] LA. Fletcher and R.Kasturi., "A robust algorithm for text string separation from mixed text/graphics images," IEEE Transactions on Pattern Analysis and Machine Intelligence, 10(6):910918, 1988.

[2] Q. Yuan and C. L. Tan, "Text extraction from gray scale document images using edge information."

[3] Jisheng Liang ; Phillips, I.T. ; Haralick, R.M. , "An Optimization Methodology for Document Structure Extraction on Latin Charater Documents", Pattern Analysis and Machine Intelligence, IEEE Transactions on, page(s): 719 – 734,2001

[4]Parodi, P. ; Piccioli, G. "A fast and flexible statistical method for text extraction in document pages," Computer Vision and Pattern Recognition, 1996. Proceedings CVPR '96, 1996 IEEE Computer Society Conference on, page(s): 619 - 624

[5] A.K. Jain and S. Bhattacharjee.," Text segmentation using Gabor filters for automatic document processing." Machine Vision and Applications, 5:169-184, 1992.

[6] Clark, A. ;Filev, D. , "Clustering techniques for rule extraction from unstructured text fragments," Fuzzy Information Processing Society, 2005. NAFIPS 2005. Annual Meeting of the North American, page(s): 793 – 798, 2005

Advanced Materials Research Vols. 989-994 (2014) pp 3773-3776
© (2014) Trans Tech Publications, Switzerland
doi:10.4028/www.scientific.net/AMR.989-994.3773

Long-range communication scheme based on majority combing

Yuan PENG[1], Xing HUANG[2], Le HE[1], Yan Ping CUI[1]

[1] Wuhan Ordnance NCO Academy of PLA,Hubei,PR China. Wuhan,430070,China
[2,] No.722 Research Institute of CSIC,Wuhan 430079,China

Keyworks：HF communication, Majority combining, Multi-point receiving

Abstract: HF communication is a very important tactical communication method, which can achieve thousand-miles away communication through the ionosphere reflections without any infrastructure support. But HF communication quality is not stable for the ionosphere disturbance, multipath fading and propagation loss. In this paper, we propose a new long-range communication scheme based on majority combing. In the scheme, we use multi-point receiving and multi-copying transmission, which can significantly improve the communication success rate by utilizing the land-sites' space diversity and the multi-packet's time diversity.

0 Introduction

Satellite communications capacity and stable communication quality, has been favored by the military, as a major means of remote communication security. But relatively fixed, satellite orbit is in danger of being shot down in the war, In February 2008, the U.S. west coast emission standard in Hawaii - missile, shoot down a spy satellite USA193 successfully, this is a wake-up call to foreign military, it also makes the short-wave communication to high priority.

Short-wave communication is also called high-frequency (HF) communication, using the frequency range for 3 ~ 30 MHZ, the main advantage of sky-wave reflected by the ionosphere, relay stations can be achieved without creating thousands of kilometers of long-distance communication. Short wave is the only from the network hub and active relay institutional constraints of the remote communication means, and also has the advantages of circuit set up quickly, anti-destroying ability is strong.

But compared to shortwave communications satellite communications, there are still large gaps in communication reliability. Short-wave telecommunication relies on sky wave transmission mode. After sky wave transmitting need short wave signal by the antenna into the ionosphere, the ionospheric reflected back to the ground, and by ground reflected back into the ionosphere, reflect many times, and spread distance (hundreds or thousands of kilometers), and is not affected by the ground obstacles blocking. But the ionosphere poor stability, coupled with path attenuation, time delay, multi-path effects and other factors that could cause weakening and distortion of the signal, thus affecting the results shortwave communication. How to improve the reliability of HF communications, has been a hot issue in the countries industry, academia research.

1 Shortwave military communication research status

U.S. shortwave communication research is a world leader, its third-generation HF communication network has been put into use, based on the U.S. military standard MIL-STD-188-141B foundation for shortwave sky wave transmission characteristics, focusing on the design of adaptive frequency selection techniques, combined with channel sounding and evaluation, make both sides of communication can choose the optimal frequency of communication; And designed the automatic link establishment mechanism, make its reliability, ease of use and channel utilization efficiency is greatly improved.

Draw lessons from the third generation of shortwave communication network in China, similar adaptive frequency selection system is designed and put into use, makes the performance of the communication must be improved, but there are still problems in the long-distance communication is unstable sea shore communications, especially in the fleet is far way to the gulf of Aden and I first island chain ocean-going fleet over the Okinawa sailing on the way, it is the second island chain area were once an intermittent communication problem.

2 Long-range communication scheme based on majority combing

Coastal areas with a large number of sites, used for the investigation and communication security. Through the shore-based cable network connection between these sites, and data interaction between command posts, shown in Figure 1. Based on existing equipment and the existing communications site, design engineering means between the improvement of shore sea short-wave communication performance is a problem to be solved. The author's idea is to coastal stations networked communications, the use of space diversity advantage of each site, improving the success rate of ship traffic.

Command post can choose a site to establish communication with ship, if the land-based sites work at the same frequency, the data sent by ship multiple sites may receive. Each site location, radio, the antenna performance is not the same performance, the objective has geographical diversity advantage, short-wave communication error for sudden fault, if the site data fusion, is bound to improve the success rate of communication. Based on this consideration, combined with large numbers of ruling principles, designed for sea-multi-point delivery mechanism to receive and redundancy mechanisms.

2.1 Shore-to-ship multi-receiver mechanism

Currently the data packet contains a CRC, the receiver can determine the received message is wrong. When receiving ship, site A, B, C will play time stamp on the data received through the shore-based wired network transmission to the command post, the time synchronization between three sites can be through the network synchronization protocol.

Command post to receive three site data, first of all, according to the time stamp, judge for the same data, and then respectively for CRC check three site data. If there is any site message correctly, CRC check it send the data to the upper applications use; If all site message CRC errors, then the data on the three sites by large numbers of bits judgment. For example, one data packet, judging site A and C is 1, site B judgment is 0, argues that the bit is 1. To participate in more receiving site is not limited to three, shore to the ship's multipoint receives the essence is the use of the site space diversity advantage.

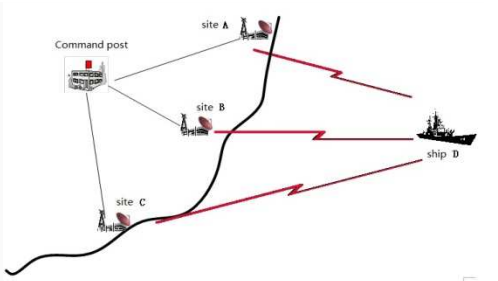

Figure.1 Shore sea communication diagram

2.2 shore to ship to send redundant mechanism

When sending data, no shore-to-ship between the ship station wired network connection or just a ship,not multi-point reception. However, the packet shore station can send multiple times in a row, after the ship station receives shore station data from the packet header sync start time set time window, the convention multiple packet data within the time window as the same packet data.

Assume that choose station B to ship station D communication command post, station B to ship station D continue to send the same package data, after you receive the ship station D, similar to receive more processing, will be 3 separate package data, respectively for CRC check, if any one pack of check is passed to the upper right agreement. If all the data packets are CRC errors, then the data bit by bit to three bags of Tarsus judgment, if two packets of data with a 1, then the judge is a bit, but after the data is transmitted to the upper layer protocol fusion . Redundancy is not limited to the number of sent three times, shore-to-ship redundant essence is the use of the time to send the packet diversity advantage.

3 Performance Analysis

in ship to receive the multipoint receives, using redundancy in the ship to send to send, with the need of ruling of large number, site and redundancy to send all can only take an odd number.

3.1 Multi-point performance

Assume that sends a packet length of L, m a shore-based sites at the same time receive ship station data, Ai represents the i-th station correctly receives the event data packets, the CRC check, B for each site receives data were wrong, bit by bit after the decision after receiving large numbers correct event, PM behalf of the packet error rate, which means that each site receives falsities, and by large numbers of probability judgment has still not correct [2].

There are: $P_M = 1 - \Pr\{A_1 \bigcup A_2 \bigcup \ldots \bigcup A_m \bigcup B\}$ (1)

Set any site k for Pk transmission error rate, the success rate of transmission of corresponding qk = 1 - Pk, right after receive more judgment of large number of conditions: the message in any one, if m, a site to receive the right site for more than half hour. Additional decision conditions of large number of formula 1, after receiving more still receive the error probability as shown in the Equation 2:

$$P_M = \sum_{k=0}^{m^*} (-1)^k \sum_{1\le i1<\ldots ik\le m} \cdots \sum (q_{i1}\ldots q_{ik})^L \left[1 - \left(\frac{q_1\ldots q_m}{q_{i1}\ldots q_{ik}} \sum_{s=0}^{m^*} \sum_{1\le j1<\ldots<js\le m} \cdots \sum \frac{P_{j1}\ldots P_{js}}{q_{j1}\ldots q_{js}}\right)^L\right] \quad (2)$$

Among them $m^* = \lfloor m/2 \rfloor$, for m half rounded down.

3.2 Redundancy send performance

If the ship station received m package data, a packet of data CRC checking them correctly, that the package is correct. If all packages of CRC errors, the ruling principle of large Numbers for error correction. Set all packages of CRC error probability for Psc, the probability of successful correction after a judgment of large number of Qmc | sc, the latter as a conditional probability. Finally after judgment of large number, packet transmission error rate expressed in Psc + Mc [3].

The three relations as shown in the Equation 3:

$$P_{SC+MC} = P_{SC} - Q_{MC/SC} \quad (3)$$

Is the conditions of success in judgment of large number of packet length L in any one, at least m, more than half a pack the bit transmission right, thus can get after the judgment of large number of packet error rate as shown in the Equation 4:

$$P_{SC+MC} = \sum_{k=0}^{\lfloor m/2 \rfloor} (-1)^k \binom{m}{k} \cdot q^{kL} \cdot \left\{1 - \left[\sum_{j=0}^{\lfloor m/2 \rfloor} \binom{m-k}{j} \cdot p^j \cdot q^{(m-k)-j}\right]^L\right\} \quad (4)$$

The p is the bit error rate, L is the packet length, m is the number of repetitions.

4 The simulation results

4.1 Multi-point reception

Matlab simulation on receiving multicast, fixed packet length L for 1000bit, m respectively 1, 3, 5, 7, 9, 11, the horizontal axis shows the bit error rate, longitudinal axis packet error rate, the simulation results are shown in figure 2:

With the increase of shore-based sites, performance gradually improved.When m = 5, the bit error rate is 0.001, the packet error rate is less than 10-5, its single point receiving the packet error rate nearly 100%, visible performance has improved.

4.2 Send redundancy

Fixed packet length L for 1000 bit, m respectively 1, 3, 5, 7, 9, 11, the horizontal axis shows the bit error rate, longitudinal axis packet error rate, the simulation results as shown in figure 3:

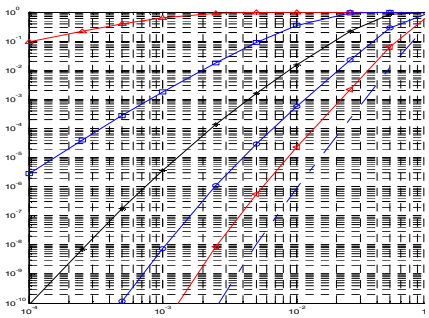

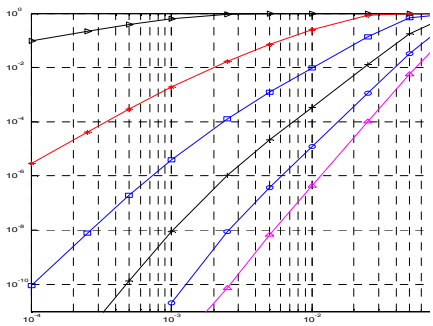

Figure 2 Fixed packet length multi-point emulation Figure 3 Fixed packet length redundancy send Simulation

With the increase of packet repetitions, the system performance improved significantly. When m = 5, the bit error rate is 0.001, the packet error rate is less than 10 to 5, the single point of single message when sending the packet error rate close to 100%, visible performance has improved.

From the simulation result shows that with the increase of the terminal points and the number of repeat sending message, communication performance improved significantly. But combined with the practical engineering application, take 5 site or send 5 repetitions can obtain satisfactory effect.

5 Conclusion

In this paper,Based on coastal both the shortwave communication site, the network use, take advantage of its geographical diversity, design the multipoint receiving mechanism, and the redundancy of ship station design send mechanism, by giving full play to the advantages of time diversity.

Theoretical analysis and simulation results show that, during the shore-ship communication packet length is set to 1000bit, the bit error rate of 0.001, the receiver-ship multi-receiver using five sites, to ship a single packet to send the case five times, the success rate of the ship receiving and sending better than 99.9999% success rate after large numbers verdict. The traditional single-point transceiver, the success rate for sending and receiving ship station success rate tends to zero. Visible, the scheme for communication between shore sea success rate improve significantly.

References:

[1] Binhong Dong, Shaoqian Li.Current Situation and Development Trend of short-wave communications Information and electronic engineering,2007(5):1-5.

[2] V. Vuković, G. Petrović, and Lj. Trajković.Packet error probability in a three-branch diversity system with majority combining.IEEE communication Letters,vol. 15, 2011.

[3] V. Vuković, G. Petrović. Packet Error Probability in Multi-Path Diversity Scheme with Majority Combining. IEEE communication Letters. 2013

Advanced Materials Research Vols. 989-994 (2014) pp 3777-3781
© (2014) Trans Tech Publications, Switzerland
doi:10.4028/www.scientific.net/AMR.989-994.3777

Electromagnetic scattering from perfectly conducting periodic rough surfaces using improved complex images method

Lin Li[1, a], Wenchao Zheng[2,b]

[1]School of Electrical and Electronic Engineering, Wuhan Polytechnic University, Wuhan 430023, P. R. China

[2]Department of Electronics and Information, Huazhong University of Science and Technology, Wuhan 430074, P. R. China

[a]lilin198509@126.com, [b]wenchaozheng@hust.edu.cn

Keywords: complex image method, periodic Green's function, perfectly conducting periodic surfaces, electromagnetic scattering.

Abstract. In this paper, an improved complex image method to derive closed form periodic Green's function for problem of scattering from perfectly conducting periodic surfaces is considered. The complex image technique represents a close-form periodic Green's function consisting of a finite series of real sources and two finite series of complex sources with complex locations and amplitudes. Then the integral equation with the complex images periodic Green's function in the kernel is solved by the method of moments. Results and computational times obtained by this improved complex image method and the previous one are compared with those obtained by the spectral Kummer-Poisson's method. Results show that the improved complex image method is more accurately than the previous one.

Introduction

The problem of evaluating the scattering of waves by periodic surfaces is one of fundamental importance in science and engineering [1-3]. Integral equation approaches in combination with the method of moments are among the most frequently used in the solution of scattering problems related to periodic surface due to their flexibility in modeling different geometries [4, 5]. The integral equation of electromagnetic scattering problems from periodic surfaces requires the efficient and accurate computation of periodic Green's functions [4]. The application of the Floquet-Bloch theorem reduces the computational domain of infinite periodic surfaces to a single unit period, but leads to results that involve the numerical evaluation of very slowly converging series [4]. This may cause serious difficulties in terms of the computational time, in order to speed up the evaluation of these series lots of acceleration techniques have been proposed in the literature [6-8]. Although these methods can be successfully applied to the periodic Green's functions, they are all derived no closed-form representation of the periodic Green's function. Since the periodic Green's functions are used in the kernel of the integral equations, it is necessary to derive closed-form periodic Green's functions.

In [9], a discrete complex image method was introduced to represent a closed-form periodic Green's function. However we have observed that the previous method fails to get accurate results when $2\pi h / p$ is much bigger than 0.448[10]. Here in this study an improved complex image method which is useful in deriving closed-form expressions to give more accurate results than previous results for the periodic Green's function, is considered.

Formulation of the Problem

The considered structure is represented in Fig.1. Consider a plane wave incident upon a periodic surface with height function z=f(x), such that f(x+p)=f(x). The period of the rough surface is p in the x-direction. The incident direction is in the x-z plane. The electric field of the incident wave is given by

$$\psi_{inc}(r) = \hat{y}e^{-jk_x x + jk_z z} = \hat{y}e^{-jk\sin(\theta_i)x + jk\cos(\theta_i)z} \tag{1}$$

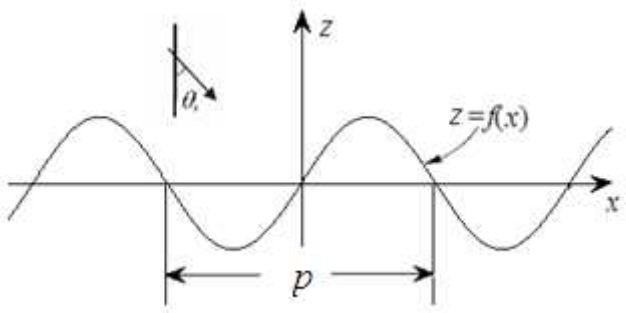

Fig. 1. The geometry of the problem

Applying the PEC boundary condition on the surface, the problem can be reduced to solution of the following integral equation [4]

$$\psi_{inc}(\overline{r}) - \int_{-\infty}^{\infty} G(\overline{r},\overline{r}')\hat{n}'\cdot\nabla'\psi(\overline{r}')d\sigma' = 0 \tag{2}$$

All the field points $\overline{r}$ are on the surface. The surface integral in (2) is over infinite surface. By applying the Floquet-Bloch theorem to limit the analysis to a representative unit period, the surface integral can be condensed into a single period [4]

$$\psi_{inc}(\overline{r}) = \int_{-p/2}^{p/2} G_p(\overline{r},\overline{r}')u(x')dx' \tag{3}$$

Where

$$u(x')dx' = (d\sigma'\hat{n}'\cdot\nabla'\psi(\overline{r}'))_{z'=f(x')} \tag{4}$$

$$\begin{aligned} G_p(x,z;x',z') &= \sum_{m=-\infty}^{\infty} G(x,z;x'+mp,z')e^{-jmpk_x} = \sum_{m=-M}^{M} G(x,z;x'+mp,z')e^{-jmpk_x} \\ &+ \sum_{m=-\infty}^{-M-1} G(x,z;x'+mp,z')e^{-jmpk_x} + \sum_{m=M+1}^{\infty} G(x,z;x'+mp,z')e^{-jmpk_x} \end{aligned} \tag{5}$$

where M is a positive integer, and the first term in the right side of (5) is the source point's effect in the middle 2M+1 periods, which will be preserved in the final representation. While the sources point's effect in the other two remaining infinite period can be represented by two finite series of complex images respectively using the complex image method. In order to derive the complex images representation of the last two infinite terms of (5) one can use the following identity

$$\begin{aligned} G(x,z;x'+mp,z') &= \frac{H_0^{(2)}(k\sqrt{(x-x'-mp)^2+(z-z')^2})}{4j} \\ &= \frac{1}{2\pi}\int_{-\infty}^{\infty}\frac{e^{-j\beta_x|x-x'-mp|}}{j2\beta_x}e^{-jk_z(z-z')}dk_z \end{aligned} \tag{6}$$

Where $\beta_x = \sqrt{k^2 - k_z^2}$. By substituting (6) in (5) and changing the order of summation and integration operators, the last two infinite series can be easily written as

$$\begin{aligned} \sum_{m=-\infty}^{-M-1} G(x,z;x'+mp,z')e^{-jmpk_x} &= \frac{1}{2\pi}\int_{-\infty}^{\infty}\sum_{m=-\infty}^{-M-1}\frac{e^{-j\beta_x|x-x'-mp|}}{j2\beta_x}e^{-jmpk_x}e^{-jk_z(z-z')}dk_z \\ &= \frac{1}{2\pi}\int_{-\infty}^{\infty}\frac{1}{j2\beta_x}e^{jMk_x p}e^{-j\beta_x(x-x'+Mp)}\frac{e^{j(k_x-\beta_x)p}}{1-e^{j(k_x-\beta_x)p}}e^{-jk_z(z-z')}dk_z \end{aligned} \tag{7}$$

$$\begin{aligned} \sum_{m=M+1}^{\infty} G(x,z;x'+mp,z')e^{-jmpk_x} &= \frac{1}{2\pi}\int_{-\infty}^{\infty}\sum_{m=M+1}^{\infty}\frac{e^{-j\beta_x|x-x'-mp|}}{j2\beta_x}e^{-jmpk_x}e^{-jk_z(z-z')}dk_z \\ &= \frac{1}{2\pi}\int_{-\infty}^{\infty}\frac{1}{j2\beta_x}e^{-jMk_x p}e^{j\beta_x(x-x'-Mp)}\frac{e^{-j(k_x+\beta_x)p}}{1-e^{-j(k_x+\beta_x)p}}e^{-jk_z(z-z')}dk_z \end{aligned} \tag{8}$$

The quotients in (7) and (8) can be approximated by a finite series of exponential as

$$\frac{e^{j(k_x-\beta_x)p}}{1-e^{j(k_x-\beta_x)p}}=\sum_{m=1}^{M1}a_m e^{b_m\beta_x} \tag{9}$$

And

$$\frac{e^{-j(k_x+\beta_x)p}}{1-e^{-j(k_x+\beta_x)p}}=\sum_{m=1}^{M2}c_m e^{d_m\beta_x} \tag{10}$$

Because the Generalized pencil-of-function method (GPOF) [11,12] has turned out to be quite robust and less noise sensitive when compared to the original and least-square Prony's methods [11-14], we using GPOF approximates the quotients. The parameters M1 and M2 can be determined by the GPOF method [14].

The spatial Green's functions can be obtained through the inverse Hankel transform, which is generally referred to as the Sommerfeld integrals. Substituting the above equation (9) in (7) and (10) in (8) respectively then using identity (6) the following results will be obtained:

$$\begin{aligned}G_p(x,z;x',z')&=\frac{1}{4j}\sum_{m=-M}^{M}e^{-jk_x mp}H_0^{(2)}(k\sqrt{(x-x'-mp)^2+(z-z')^2})\\&+\sum_{m=1}^{M1}a_m\frac{e^{jMk_x p}}{4j}H_0^{(2)}(k\sqrt{(|x-x'+Mp|+jb_m)^2+(z-z')^2})\\&+\sum_{m=1}^{M2}c_m\frac{e^{-jMk_x p}}{4j}H_0^{(2)}(k\sqrt{(|x-x'-Mp|+jd_m)^2+(z-z')^2})\end{aligned} \tag{11}$$

This completes the derivation of complex images representation of the periodic Green's function of (5). It can be seen that the first summation of terms in (11) corresponds to the sources points in the middle 2M+1 periods that have the most significant effects on the field points located in a unit period. The presence of these terms in the final result guarantees satisfactory results for the near fields especially in the vicinity of the unit period surface. While the other two summation of terms in (11) known as complex images correspond to the sources points in the two remaining infinite periods respectively have the same forms as real sources except their complex locations in space and complex values. They are more important when the field point is located far away from the surface within a unit period. The complex images representation in the previous method is a particular case when M is set to 1 of the one in this paper. When $2\pi h/p$ is much bigger than 0.448[10], the representation in the previous method wouldn't get accuracy results for the near fields because the real sources which guarantees satisfactory results for the near fields is not much enough. So big M is needed to get more accuracy results and the improved complex image method can deal with deep grating.

Numerical Results

In this section, we study the accuracy of the technique given in the previous section by considering some illustrative examples. The obtained results are compared with the previous complex image method and the Kummer-Poisson. In all cases, object is assumed to be located in free space illuminated by plane wave with frequency 400 MHz. First example is a periodic surface having sinusoidal variation of the form $f(x)=0.2\cos(\frac{2\pi}{L}x)$, incident angle is chosen as 60°, L=1 and scattered field are calculated on plane Zf =0.2 above the rough surface. Results are compared in Fig. 2. In Fig. 3, the real and imaginary parts of the scattered field calculated on plane Zf =0.8 for incident angle $\theta_i=45^\circ$ and roughness function of surfaces within one period are chosen as $f(x)=0.8\cos(\frac{2\pi}{L}x)$ with L=3.

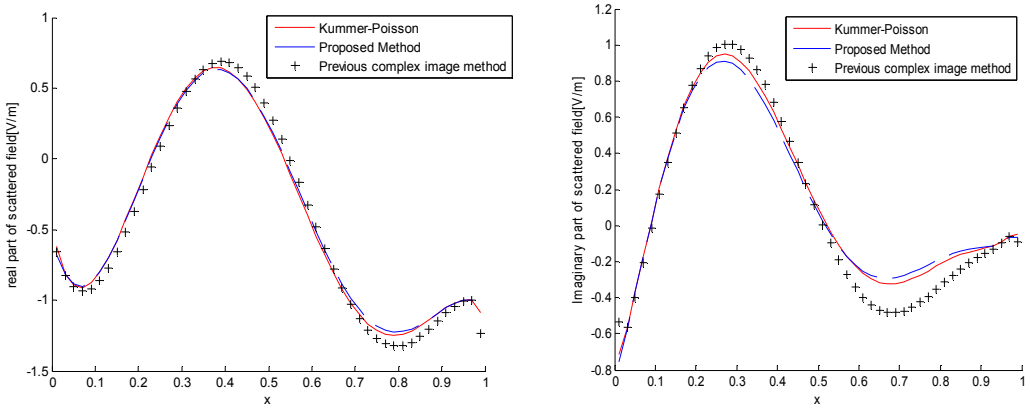

(a) (b)

Fig. 2. Scattered field above rough surface within one period(a)real part,(b)imaginary part(λ=0.75p, h=0.2p)

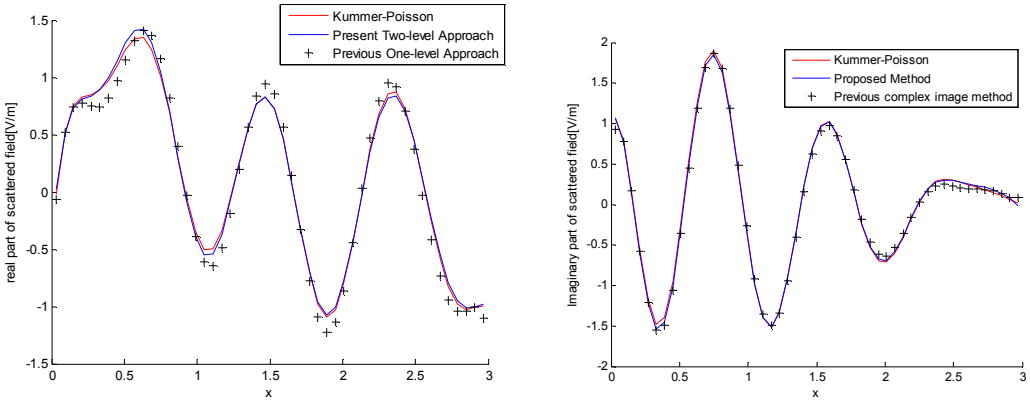

(a) (b)

Fig. 3. Scattered field above rough surface within one period(a)real part,(b)imaginary part(λ=0.25p, h=4p/15)

Conclusions

In this paper, an improved complex image technique has been presented for the calculation of periodic Green's functions for problem of scattering from perfectly conducting periodic surfaces. The complex image technique represents a close-form periodic Green's function consisting of a finite series of real sources in the middle 2M+1 periods and two finite series of complex images correspond to the sources points in the two remaining infinite periods respectively. The proposed method can give more accurate evaluation of the periodic Green's function than the previous method for the deep grating scattering problem. Numerical results show that the improved complex image technique has a better agreement with the spectral Kummer-Poisson's method than the previous one.

Acknowledgment

The research is supported by 2013RZ17 Wuhan Polytechnic University Scientific Research Foundation for the introduction of talent.

References

[1] R. Petit, Electromagnetic Theory of Gratings, Springer-Verlag, New York, 1980.

[2] T. Arens, S. N. Chandler-Wilde and J. A. DeSanto, On integral equation and least squares methods for scattering by diffraction grating, Comm. Comp. Phys. 1(2006) 1010-1042.

[3] J. DeSanto, G. Erdmann, W. Hereman and M. Misra, Theoretical and computational aspects of scattering from rough surface: one-dimensional perfectly reflecting surfaces, Waves Random Media 8 (1998) 385-414.

[4] L. Tsang, J. A. Kong, K. H. Ding, and C. O. Ao, Scattering of electromagnetic waves: Numerical simulations, Wiley, New York, 2001.

[5] R. Chen and J. C.West, Analysis of scattering from rough surfaces at large incidence using a periodic-surface moment method, IEEE Trans. Geosci. Remote Sens. 33(1996) 1206-1213.

[6] H. Rogier, New series expansions for the 3-D Green's function of multilayered media with 1-D periodicity based on perfectly matched layers, IEEE Trans. Microw. Theory Tech. 55 (2007) 1730-1738.

[7] A. L. Fructos, R. R. Boix, F. Mesa and F. Medina, An efficient approach for the computation of 2-D Green's functions with 1-D and 2-D periodicities in homogeneous media, IEEE Trans. Antennas Propag. 56 (2008) 3733-3742.

[8] S. P. Skobelev, A Modification of the Kummer's Method for Efficient Computation of the 2-D and 3-D Green's Functions for 1-D Periodic Structures, IEEE Trans.Antennas Propag. 60 (2012) 412-416.

[9] B. P. Saeedeh and A. S. Amir, Electromagnetic scattering from perfectly conducting periodic rough surfaces using complex images technique, Antennas and Propagation Society International Symposium, July 2010.

[10] S. L. Chuang and J. A. Kong, Scattering of waves from periodic surfaces, Proceedings of the IEEE 69 (1981) 1132-1143.

[11] A. J. Mackay and A. McCowan, An improved pencil-of-function method for extracting poles of an EM system from its transient response, IEEE Trans. Antennas Propagat. 35 (1987) 435-441.

[12] Y. Hua and T. K. Sarkar, Generalized pencil-of-function method for extracting poles of an EM system from its transient response, IEEE Trans. Antennas Propagat. 37 (1989) 229-234.

[13] H. Alaeian and R. F. Dena, A fast and accurate analysis of 2-D periodic devices using complex images Green functions, Journal of lightwave Technology. 27 (2009) 2216-2223.

[14] D. G. Dudley, Parametric modeling of transient electromagnetic systems, Radio Sci. 14 (1979) 387-396.

Advanced Materials Research Vols. 989-994 (2014) pp 3782-3785
© (2014) Trans Tech Publications, Switzerland
doi:10.4028/www.scientific.net/AMR.989-994.3782

Application and Analysis of the full-wave Band CCD System in ImageInterpretation Technology

Wei Han[1,a],Jun Xie[1,b],Jinhe Bao[1,c],Mei Zhao[1,d],

Xiuying Fan[1,e],Fei Guo[1,f]

[1]Aviation University of Air Force,Changchun,China,130022

[a]hwa3@163.com, [b]xiejun1981@gmail.com, [c]baojinhe57@sina.com, [d]jlzhaomei@sina.com, [e]fxy46100@163.com, [f]feer_2403@163.com

Keywords: Full-wave band CCD system; Image extraction;Image processing

Abstract. The full-wave band CCD system is widely used for military,civil or photography of criminal image and extraction analysis,its wavelength is range between 200 nm and 1200 nm,including ultraviolet,visible light and infrared.Through translating blanck visibleimage into optical image,and realizing collecting of weak signal under low illumination case and collecting and processing of high quality image,it makes Full-wavelength CCD system the powerful features such as the topography and landform scaning,traces exploration,file inspection,holographic photography and image processing.The whole band CCD system structure,characteristic and the application of the image interpretation technology were briefly introduced in this paper,and experiment band CCD selected was validated.

Introduction

The Full-wave band CCD camera is developed at first by U.S.A.,apply to study the technological field in spaceflight,army industry science at first,this equipment adopts and lengthens time for exposure and method to reduce noise mainly,in a situation that the intensity of illumination is low or the mark material evidence is very faint,can get the comparatively clear picture,at the same time,can comparatively lower the interference of the background of the object effectively too,it is one of the most advanced taking pictures tools at present.The Full-wave band CCD system shows and professional pattern process equipment in real time purple outside of one set,visible light,infrared picture high-resolution.It can visible light picture turn visible light picture into in real time,can realize faint collection and high-quality collection and processing of picture of signal under the low intensity of illumination situation, incorporate the verification of traces,file are examined,figure taking pictures and pattern process into an organic whole.

Images drawing and analysing

Introduction to the experiment platform. The size or picture of laser scanning based on CCD system shows measures the experimental provision.Three-dimensional laser scanning that device adopt this,overcome traditional vision machine succeed the two-dimentional picture three-dimensional scenery projection,cause and construct the three-dimensional scenery only defect again.Survey and draw and gather clicking more under this system,the depth of field of the picture is long,make the treated data true and reliable.The structure of the experimental provision and size of laser scanning of operation principle measure the device system and adopt the single track mere law of structure,this system including semiconductor laser instrument,CCD camera,picture gather card,computer , measuring platform,measuring and pattern process software etc.

The systematic flow chart is as Fig.1 shows.The system regards semiconductor laser instrument as the light source,its light beam is become on the fan-shaped level of the vertical direction only shone and examined the thing by the optical system,being examined and forming the stripe on the thing.Sloping and observing this stripe to get a stripe picture with CCD camera,the data information of the income is gathered the card by the picture and sent into the computer and dealt with from the

software of measuring, according to geometrical optics and this stripe deformation along z high change,axle of direction conversion of pattern triangular law.And is examined the thing and moved according to certain law in certain direction,so can receive the depth picture information on the object surface.

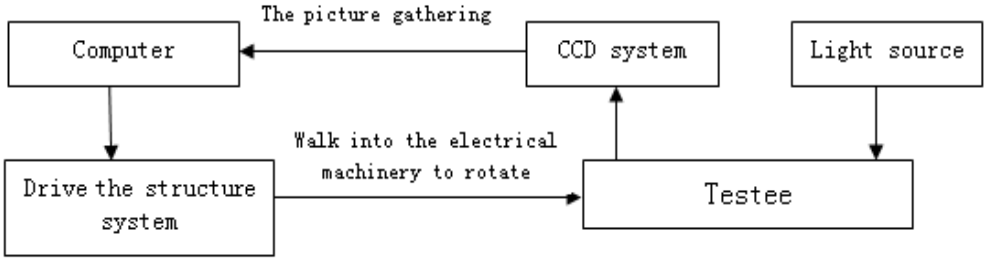

Fig 1. Systematic job flow chart

Measure the principle. In order to state the systematic measurement principle,introduce system of coordinates and position relation used in the system at first,as Fig.2 shows.

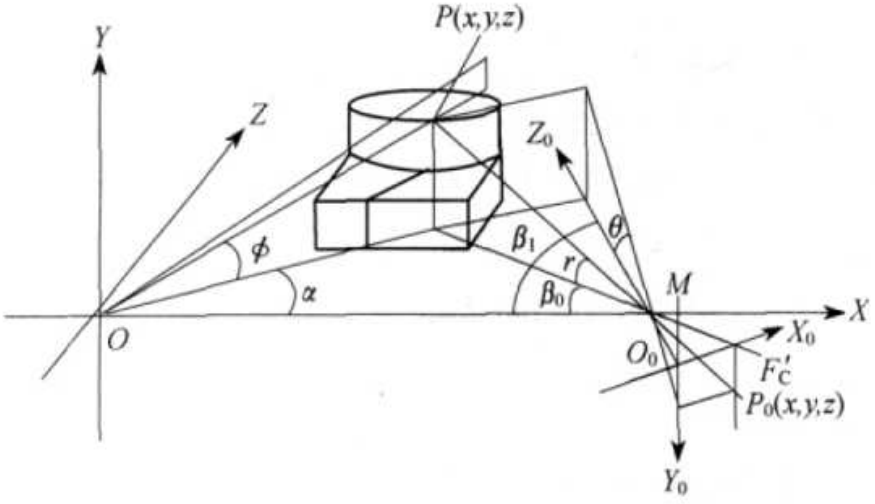

Fig 2.The systematic system of coordinates and position relation

The relation between the systematic system of coordinates of Fig.2 and these 3 kinds of coordinates of position relation is:System is it run to pass, receive goal thing and indicate picture yuans of screen coordinate that order at first,then change into a level coordinate of the image,could vary various kinds of with the square space coordinates of the thing finally,three-dimensional coordinate that thus it is superficial to get objects.

$$\tan(\beta_1-\beta_0)=\frac{O_0P_0'}{OM}=\frac{O_0P_0'}{f} \tag{1}$$

$$f=Nx\cot\theta_1\ ,Z=\frac{B}{\cot\beta_0} \tag{2}$$

$$Z=B\left(\frac{f-x\cot\beta_1}{f_x+f\cot\beta_1}\right)=B\frac{1-n\left(\cot\beta_1\tan\theta_1\right)/N}{\cot\beta_1+n\left(\tan\theta_1/N\right)} \tag{3}$$

Gather the card to a definite CCD camera and a definite picture,picture yuans of screen system of coordinates and image conversion,level of system of coordinates relation regular,as yuans of system of coordinates changed into a level coordinate of the image directly,but can read directly at the computer.The relation is between every parameter that can be won by the geometry principle of the camera.

$$f=Myx\cot\theta_2\ ,\tan\theta=\frac{my}{f}=\frac{my}{My\cot\theta_2}=m\tan\theta_2/M \tag{4}$$

$$X = Z\cot\alpha = 0, Y = \tan\theta\cos\left(\beta_1 - \beta_0\right)Z / M\left(\sin\beta_0\right) \quad (5)$$

$$Y = \frac{Z\left(\tan\theta_2\right)/M \cdot m}{\sin\beta_1 - \cos\beta_1\left(\tan\theta_1\right)/N \cdot n} \quad (6)$$

The experiment verifying. Measure the material object and adopt diameter 5 mm,the cylindrical part of high 80 mm,walking into amount 2 mm,the system adopts the standard volume one standardly,a distance clicked with consult coordinates of measuring amount is as the standard depth,measure a height and is regarded as the standard height.Can know from the result of measuring,the data measured move towards the form with the clause to accord with,can guarantee the precision.The three-dimensional laser scanning that the size of laser scanning based on CCD measures the experimental provision and adopts is different from simple survey and drawing technology,it can describe the intact attribute of the goal structure,is suitable for the original appearance of reducing the more goal.

Application of the Full-wave band CCD system in image technology

Inspection for the file or the fabrics. In writing the ink to examine,the ink of some brands displays the fluorescence under the circumstances that much wave band light sources shine,and have many kinds of colors changes.For example,the pen of different colors,ink of ball pen and signature pen are under the circumstances that indoor light and much wave band light sources shine separately,the fluorescence of some ink appears orange,some are partial and yellow.In addition,write the layer after the analytic approach of thin layer is divided layer of ink on the file and analyse and pursue,under many wave band light sources,some compositions will produce the strong fluorescence,and the difference exists in the position that the fluorescence will be brought,so can distinguish the ink of different brands conveniently.Equally,the fabrics fibre adhered to the clothes,some can produce the fluorescence too in specific wave band light.Utilize many wave band light sources to collect these fibres easily,and the dyestuffs in these fibres can adopt the analytic approach of thin layer to launch,and then shoot with the Full-wave band CCD system,thus differentiate the difference.

Inspection for the fingerprint,footprint or body fluid. In the course of using the Full-wave band CCD system and carrying on fingerprint to examine.The potential fingerprint on the plastic products after the cyanogen acrylic acid fat is dealt with,and then float and dye with Rodin bright 6G dyestuffs,observe under the indoor light and the Full-wave band CCD system separately,the latter fluorescence is strong,fingerprint appears clearly.Three ketone derivatives of indene developed in recent years,cooperate with the chlorine treated fingerprint of zinc solution,it will produce a lot of fluorescence results too that the Full-wave band CCD system is observed,it is with high efficiency that the fluorescence gives out light, traditional three ketone laws of indene that superior to.Equally,there is strong fluorescence too under the Full-wave band CCD system to examine chemical medicines DFO used in technology in laser fingerprint.In a word,use the Full-wave band CCD system to dispel the mark background to interfere effectively,strengthen image contrast.CCD system can be used for appearing to the footprint in addition.To the optics method,can all shoot appearing with the Full-wave band CCD system.As to ordinary camera, the Full-wave band CCD system is in the method of appearing of optics,it is quicker that it manifests the speed,and it is even more ideal to manifest the result,especially it is more obvious to reflect its advantage while taking pictures purple outside.

Inspection for the ammunition leftovers. Launch ammunition after remain mark have barium salt,appear orange fluorescence particle form distribute until the whole system,CCD of wave band, observe,but as differentiating the basis of launching the entry,the experiment indicates,adopt the Full-wave band CCD system to shoot apter existence of observing the barium salt particle in the room on the black carrier.

For fighting the inspection of place shape or ground form. The modern battle field is by enormous C4I system that light,electronics and information network disposing on the

multidimensional space make up, among them the information subsystem is one of the main backbones.Through adopting various kinds of and detecting and examining the characteristic information that technology and means obtain enemy's goal in one's own side's army,rely on the medium to convey to the acception station directly or in the form of sound,light,electric wave,processing,showing writing down,interpretation, the course of analysing etc.is turned into the available information.The modern battle field situation is fast changing,the commander will not establish in an unassailable position unless grasp enemy and our accurate situations of both sides in time.So the intelligence work must be continuous,real-time,information processing automation.No matter take any means,it is an essential procedure to detect and examine. According to the characteristics of the object and electromagnetic wave,scientific and technical personnel develop the varied reconnaissance means,for example:The visible light reconnoiters the technology and equipment,the shimmer reconnoiters the technology and equipment,reconnoiter the technology and equipment infraredly,reconnoiter the equipment and reconnoiter the technology and equipment,the sensor reconnoiters the technology and equipment,the satellite reconnoiters etc.

Discussing

With the development of science and technology,the digitized picture of direct output of the Full-wave band CCD system,can also be real-time check-up is revised,the digitized process of making the whole information reconnoiter is accelerated greatly.The appearance of this system,the network enabling interpretation personnel and pattern process personnel to totally realize the digitized picture is real-time and mutual.Take a picture while manifesting various kinds of topographical ground form or the mark material evidence with the Full-wave band CCD system,besides mixing the light and focusing,other work is finished in the computer,and the picture got is all right appear " real-timly " on the monitor.Especially to take pictures to purple outside and infraredly,all right to be " real-time " sees the picture ,so can adjust and match all angle according to the power of contrast,avoid " striking blindly ". But the one that need to pay attention to at the same time is,as the conditions,such as light source,illumination,etc.are limited and influenced,what a deep question that thinks that the effective one goes to make an uproar to become worth.

References

[1] Old banyan front yard,Peng MeiGui.CCD/CMOS picture sensor foundation and using [M].Beijing:Science Press,2006.

[2] Xu XiaoJing,Lin Jing.The material evidence of the Full-wave band examines application [J] in the field of criminal camera work of CCD system.Image technology,2003 (3).

[3] Nie XiaoXiao.Application [J] of the Full-wave band CCD system in criminal image technology.Legal system and society,2011 (2).

[4] Qiu Ying,Tan DingZhong,etc.Measure the reseach [J] of the experimental provision on the basis of CCD laser scanning measurement.Laboratory research and exploring,2011 (3).

[5] Zhang ShengYun,Zhang LiJiang.The Full-wave band CCD reflects the application [J] while taking pictures purple outside. Criminal technique,2008 (1).

[6] Luo Wen is rich.High-accuracy position of CCD measure [J] on the basis of line burst.Journal of Tsing-Hua University (natural science edition),2002,42 (9).

[7] Cao Ri gets up.Technical research of distance finding of laser scanning [D] on the basis of CCD.Harbin:Harbin Engineer University,2006.

Advanced Materials Research Vols. 989-994 (2014) pp 3786-3789
© (2014) Trans Tech Publications, Switzerland
doi:10.4028/www.scientific.net/AMR.989-994.3786

An improved DFT-based channel estimation algorithm for OFDM system on time-varying Multipath fading Channels

Xinli Ma[1, a], Tongliang Fan[1,b] and Yongfeng Du[1,c]

[1]China maritime police academy, Electronic Technology Department, 315801 Ningbo, China

[a]nbmaxinli@sina.com, [b]libufan432@163.com, [c]jdddyf@163.com

Keywords: channel estimation, OFDM, CIR (Channel Impulse Response), gate processing

Abstract. An improved discrete Fourier transform DFT-based channel estimation for OFDM systems is proposed. Conventional DFT-based channel estimator improved its performance by suppressing noise, but it does not completely suppress noise. In order to overcome the disadvantage, this paper proposed a gate method without requiring any channel statistical information. This method comprehensively considersthe effects of the power of the strongest path and the noises. Computer simulation demonstrates the performance of the proposed algorithms in terms of bit error rate.

Introduction

For coherent orthogonal frequency division multiplexing (OFDM) systems, a robust channel estimator is required critical to improve the performance of systems. By now, various OFDM channel estimation schemes have been proposed in the literature. In general, the least square estimator is the simplest channel estimation [1]. However, it is limited by the noise and inter-carrier interference.The minimum mean-square error MMSE [2] estimator is a well-known channel estimator. But the high computation complexity is a serious disadvantage. Zhao et al [3] introduced additional DFT processing to obtain the frequency response of LS estimated channel. Based on discriminant analysis, Fan [4,5] presented dynamic time-domain threshold for channel estimation.

By suppressing time domain noise, conventional DFT-based channel estimations improve the performance. However, in a multipath channel with non-sample-spaced time delays, this approach will cause power leakage and result in an error floor. After analyzing the property of Channel impulse response, an improved method based on gate processing is proposed. The gate value is got by the power of the strongest path and noises. The path whose power of CIR fails to reach the gate value is to be abandoned. So, the improved method can retain the CIRs and remove the noises at the same time, enhance the accuracy of estimation and the performance of system.

System description and channel model

OFDM System Model. We consider an OFDM system that consists of N sub-carriers. And each sub-carrier consists of data symbol $X[k]$, where k represents the sub-carrier index. The OFDM transmitter uses an inverse DFT of size N for modulation. Then the transmitted OFDM signals in discrete-timedomain can be expressed as:

$$x[n]=\frac{1}{N}\sum_{k=0}^{N-1}X[k]\exp(j2\pi\frac{nk}{N}),\qquad 0\le n\le N-1. \tag{1}$$

Where n is the time domain sample index of an OFDMsignals. In order to avoid ISI caused by multipath channel and consequent ICI [6], GI is appended to thebeginning of the N sample of IDFT. After passing through a time-varying multi-path fadingchannel and removing the GI, one receivedsignal $y[n]$ consists of channel distorted versionsof the transmitted OFDM symbols, which isrepresented by

$$y[n]=x[n]\otimes h[n]+w[n]\qquad 0\le n\le N-1. \tag{2}$$

Where $\otimes$ denotes cyclic convolution operation. $w[n]$ is iid additive whiteGaussian noise (AWGN) sample in time domain with zeromean and variance σ_{wt}^2. $h[n]$ is the discrete-time CIR.

$$\sigma_{wt}^2 = E[|w[n]|^2] \tag{3}$$

A tapped delay line channel model of wireless fading channel $h(t,\tau)$ can be expressed as:

$$h(t,\tau) = \sum_{l=0}^{L-1} \alpha_l(t)\delta(\tau - \tau_l) \tag{4}$$

Where, $\alpha_l(t)$ is the energy of l-th paths, and L is the total number of paths; τ_l is the l-th path delay. Assume T_s is the sampling interval, the CIR $h(t,\tau)$ is a time-limited pulse train, so the frequency response will span over the whole frequency domain. The OFDM signal is frequency limited. Hence, the receiver can only probe part of the frequency response. In this case, the CIR can be denoted as:

$$h(n) = \frac{1}{N}\sum_{l=0}^{L-1} \alpha_l \, \mathrm{e}^{-j\frac{\pi}{N}(n+(N-1)\tau_l)} \frac{\sin(\pi\tau_l)}{\sin(\pi(\tau_l - n)/N)} \tag{5}$$

For non-sample-spaced channel, τ_l isn't an integer. From Eq(5), the energy will leak to all taps $h(n)$.

DFT-based Channel Estimation

To perform the DFT-based channel estimation, the Least Square (LS) channel estimates on the pilots are first obtained. At the receiver, the received pilot signals are extracted from $Y[k]$. Then the channel frequency response in pilot sub-channels can be estimated by:

$$\hat{H}_{LS}[k] = Y[k]/X[k] = H[k] + W[k]/X[k] \qquad k \in K_P. \tag{6}$$

where K_P is the ensemble of all pilot indexes. The greatest advantage of LS algorithm is its simple structure and lowly complexity. The conventional DFT-based estimation reduces the noise power that exists outside of the CIR. An N-point IDFT is used to $\hat{H}_{LS}[k]$, to obtain an estimate of the CIR:

$$\hat{h}_{LS}[n] = IDFT\{\hat{H}_{LS}[k]\} = h[n] + \tilde{w}[n] \qquad 0 \le n \le N-1. \tag{7}$$

Where $\tilde{w}[n]$ is IDFT sample of noise. The CIR is typically limited to the length of CIR L which is less than the GI and much smaller the number of sub-carrier N. Because L is unknown, $L = N_{cp}$. By zero-padding for pure noise period, the conventional DFT-based estimator can be expressed as:

$$\hat{h}_{DFT}[n] = \begin{cases} h[n] + \tilde{w}[n], & 0 \le n \le N_{CP} - 1 \\ 0, & N_{CP} \le n \le N-1 \end{cases}. \tag{8}$$

N_{CP} is the length of CP. From (8), the DFT-based channel estimator is denoted as

$$\hat{H}_{DFT}[k] = DFT_N\{\hat{h}_{DFT}[n]\} \qquad 0 \le k \le N-1. \tag{9}$$

Proposed channel estimation

As mentioned before, the noise is eliminated based on the length of the guard interval. However, the energy of the corresponding path will leak to all the taps in the time domain when the channel path delay is usually non-sample-spaced. Then this method will not only eliminate the noise, but also lose the useful leaked channel impulse response. So the error floor is caused by loss of leakage power.

Even though the energy of non-sample-spaced path leaks to all the taps, but most of the energy is kept in the neighborhood of the original pulse locations. From Eq(5), we can see the energy concentrates at the ends of the sequences. To avoid the gate value setting too high or toolow, a newproposedmethod is in the following:

Step1: Compute the initial LS channel estimate HLS[k] from the Eq(6).

Step2: Take IDFT of the LS estimate, hLS[n] from the Eq(7).

Step3: As mentioned step1, the channel taps $\hat{h}_{LS}[n]$ can be divided into three groups: $0 \le n < N_{cp}$, $N_{cp} \le n < N - N_{cp}$, $N - N_{cp} \le n < N - 1$. In the region $N_{cp} \le n < N - N_{cp}$, the channel taps $\hat{h}_{LS}[n]$ can be handled as the taps of noise, $\hat{h}[n] = 0$. The noise power is estimated by:

$$\sigma_{wt}^2 = \frac{1}{N - 2N_{cp} - 1} \sum_{i=N_{cp}}^{N-N_{cp}-1} \left| h_{LS}[n] \right|^2 = \frac{1}{N - 2N_{cp} - 1} \sum_{i=N_{cp}}^{N-N_{cp}-1} \left| w[n] \right|^2 \tag{10}$$

Step4: In the region $0 \le n < N_{cp}$ and $N - N_{cp} \le n < N - 1$.We design the gate value λ based on the biggest tap value $h_{\max}$ and the power of noise. If $\left| \hat{h}_{LS}[n] \right| > \lambda$, $\hat{h}[n] = \hat{h}_{LS}[n]$ and $\hat{h}_{LS}[n] = 0$.

$$\lambda = (\varepsilon \left\| h_{\max} \right\|^2 + \gamma \sigma_{wt}^2) \big/ (h_{\max} + \sigma_{wt}) \tag{11}$$

The abovegate value avoids the case in which the gate value is setting too high or too low. when $\left\| h_{\max} \right\|^2 >> \sigma_{wt}^2$, ε value can be adjusted to maintain λ bigger to filter the majority of noises. When $\left\| h_{\max} \right\|^2 << \sigma_{wt}^2$, γ valuecan beadjusted to maintain λ smaller to keep usefulinformation as much as possible. The value ε and γ can be generated by Monte-Carlo simulation.

Step5: Finally, the channel estimation can be achieved by:

$$\hat{H}[k] = DFT_N \{ \hat{h}\ [n] \} \tag{12}$$

As mention above, channel estimation based on the gate value can eliminated the impact of the noise. The improved algorithm is gate processing method, and DFT-GP is its abbreviation.

Simulation results and analysis

In this section, we will investigate the performance of the proposed algorithm on non-sample-spaced multipath channels, and the bit-error-rate (BER) performance is examined. The simulations are concentrated on comparison between LS algorithm, conventional DFT algorithm and the proposed algorithm. For simulation, we have considered an IEEE 802.16e OFDMA system. Table 1 summarizes major system parameters. In our simulation, we test different algorithms under ITU-R M.1225 vehicular A channel model, which is applied assuming the maximum mobile speed of $v_{\max}$ =120 km/h. It is a typical non-sample-spaced multipath channels which have six paths. In addition, perfect synchronization is assumed, since it is hard to estimate the channel frequency response beyond guard band.

Table 1 Major system parameters

Parameters	Values
Carrier frequency	2GHz
Bandwidth	10MHz
Cyclicprefix	128
Sampling frequency	11.2 MHz
Sub-carrier spacing	10.94kHz
System period	102.86μs
Guard interval	11.43μs
Data modulation type	16QAM
Pilot sequence modulation	BPSK

In the simulation, gate factors ε and γ are $\varepsilon = 1.2$ and $\gamma = 0.2$ .Fig. 2 shows the BER performances ofthree different methods under non-sample-spaced multipath channels.As shown in Fig2, it is obvious that the performances of DFT-GP channel estimators are better than DFT-based channel estimator.At low signal-to-noise ratio (SNR), by suppressing time domain noise, the conventional DFT algorithm is better than the LS algorithm. At high SNR, the performance degradation is induced when low energy CIR samples containing useful channel information are discarded.There existsan error floor.

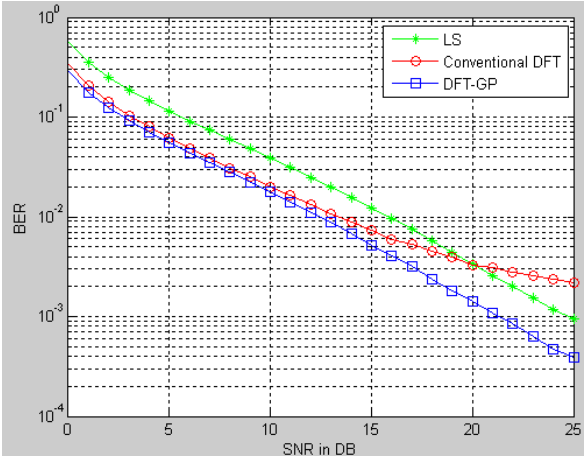

Figure1 BER performance with different channel estimation (CE)

Conclusion

In this paper, we proposed a gate processing channel estimation for OFDM system in non-sample-spaced multipah fading channel.Using two parameters threshold, this method can avoid the gate value setting too high or too low. The gate factors can be found by Monte-Carlo method. Simulation shows that the proposed method can achieve the better performance. In practice, the can be adjusted through feedback mechanism.

Acknowledgements

This work is supported by the research fund from China Maritime Police Academy (Grant No.2013XYPYZ010).

References

[1] Tong-liang, Fan, et al. An improved DFT-based channel estimation algorithm for OFDM system in Non-sample-Spaced Multipath Channels.Circuits Syst Signal Process 2014.33:1277-1288.

[2] J.-J. van de Beek, O. Edfors, etal. “On Channel Estimation in OFDM Systems, in Proc. IEEE Vehic. Technol. Conf., Volume 2, pp. 815–819, Chicago, IL, July 1995.

[3] Y. Zhao and A. Huang, “A Novel Channel Estimation Method for OFDM Mobile Communication Systems Based on Pilot Signals and Transform-Domain Processing,” Proc. IEEE Vehic. Tech. Conf., vol. 3, Phoenix, AZ, May 1997, pp. 2089–93.

[4] Tong-liang, Fan, et al. Two Novel Channel Estimation for OFDM Systems by Time-Domain Cluster Discriminant Analysis Based on Parametric Channel Modeling. Wireless PersCommun, 68, 349-360, 2013.

[5] Tong-liang, Fan, et al. DFT-based Cluster Analysis Channel Estimation Algorithm for OFDM Systems on Multipath Channels. IJFGCN.Vol.7. No. 1 2014. pp:225-234

[6] TL. Fan, HW. Wu, HC. Huang. Channel Estimation and Interference Cancellation for OFDM Systems Based on Total LeastSquares Solution. JOURNAL OF COMMUNICATIONS, VOL. 6, NO. 8, NOVEMBER 2011, pp:640-647

Advanced Materials Research Vols. 989-994 (2014) pp 3790-3793
© (2014) Trans Tech Publications, Switzerland
doi:10.4028/www.scientific.net/AMR.989-994.3790

Flattop Broadband Wavelength Conversion Based on Cascaded Second-harmonic Generation and Difference Frequency Generation in Step-Segmented Quasi-Phase Matched Gratings

Haidong Wu[a], Jinsong Guo[b], Yunwen Wu[c] and Zhaoxia Wang[d]

Leshan power supply company, Sichuan Leshan, 614000, China

[a]wu_hai_dong@163.com, [b]guojinsong118@126.com, [c]ywwu03@126.com, [d]wzx519@sina.com

Keywords: Wavelength conversion, Quasi-phase matching, Ccascaded second harmonic generation and difference frequency generation, Bandwidth

Abstract. Bandwidth enhancement and response flattening of wavelength conversion based on single-pass and double-pass cascaded second harmonic generation and difference frequency generation in step-segmented quasi-phase matched (QPM) gratings are investigated. For the same waveguide length, high conversion efficiency, flat response and broad signal bandwidth can be obtained simultaneously by optimizing the poling period of the step-segmented QPM structure. The conversion bandwidths in a 3-cm-long five-step-segmented waveguide are 134 nm for single-pass scheme and 132 nm for the double-pass one, respectively, which are both over the whole conventional band and long-wavelength band. The ripple on the matching response can keeps less than 0.2 dB as well.

Introduction

Wavelength converters based on second-order, $\chi^{(2)}$, nonlinear optical effect are important photonic devices being researched for wavelength division multiplexing (WDM) networks. These devices can be realized by difference frequency generation (DFG) or cascaded second-order processes in nonlinear-optical waveguides and can take advantage of quasi-phase matching (QPM) by reversing the ferroelectric domains to improve the conversion efficiency using the largest available nonlinear coefficient in a crystal[1, 2]. Moreover, ultrafast response, complete transparency, and the simultaneous up- and down-conversion of multiple channels can be realized. The simplest approach to wavelength conversion of signals near 1.55 μm relies on DFG from an intense pump wave in the 700- to 800-nm range outside the telecommunication band[3]. However, it is difficult to couple pump and signals into the fundamental guided-wave mode simultaneously without exciting higher-order modes which are not involved in the wavelength conversion process. This problem can be avoided in the cascaded second-harmonic generation (SHG) and DFG scheme since both the input pump and signals are in the 1.5 μm band and thus can be easily launched into a waveguide together[1]. Two kinds of configuration are employed to realize cascaded SHG+DFG wavelength conversion, which one is called single-pass since the second-harmonic (SH) wave propagates through the waveguide once, and another is called double-pass due to the SH wave propagates twice in the waveguide.

For multichannel conversion in WDM systems, the bandwidth is expected to be broad and flat. However, in uniform QPM gratings, the signal conversion bandwidth and the pump detuning bandwidth are very limited. Fortunately, chirped or segmented gratings, as well as phase shift method were theoretically proposed and/or experimentally realized to broaden the QPM bandwidth[1-5]. Almost all of the investigations, however, focused on how to widen the bandwidth efficiently, thus the response flatness, which is also an important quality parameter for the wavelength converters, is then neglected. In this paper, the step-segmented grating is used to flatten conversion efficiency response in single- and double-pass cascaded SHG + DFG wavelength conversion. Large signal bandwidth can be obtained simultaneously.

Theory and model

The device is proposed as a titanium diffused optical waveguide in a Z-cut lithium niobate crystal wafer, supporting only X-propagating quasi-TM mode at 1.55 m. With the slowly varying envelope approximation, the coupled-mode equations for single-pass configuration are expressed as

$$\frac{\partial E_p}{\partial x} = -i\omega_p \kappa_{SH} E_p^* E_{SH} \exp(-i\Delta k_{SH} x) - \frac{\alpha_p}{2} E_p , \tag{1a}$$

$$\frac{\partial E_s}{\partial x} = -i\omega_s \kappa_{DF} E_c^* E_{SH} \exp(-i\Delta k_{DF} x) - \frac{\alpha_s}{2} E_s , \tag{1b}$$

$$\frac{\partial E_c}{\partial x} = -i\omega_c \kappa_{DF} E_s^* E_{SH} \exp(-i\Delta k_{DF} x) - \frac{\alpha_c}{2} E_c , \tag{1c}$$

$$\frac{\partial E_{SH}}{\partial x} = -i\omega_p \kappa_{SH} E_p^2 \exp(i\Delta k_{SH} x) - i\omega_{SH} \kappa_{DF} E_s E_c \exp(i\Delta k_{DF} x) - \frac{\alpha_{SH}}{2} E_{SH} , \tag{1d}$$

where E_p, E_s, E_{SH}, E_c are the field amplitude of pump wave, signal wave, second-harmonic wave and converted wave, respectively, α_i (i = p, s, c or SH) is the propagation loss of ω_i . $\kappa_{SH} = d_{eff}\sqrt{2\mu_0} / \sqrt{CS_{SH}N_p^2 N_{SH}}$ and $\kappa_{DF} = d_{eff}\sqrt{2\mu_0} / \sqrt{CS_{DF}N_S N_C N_{SH}}$ are the nonlinear coupling constants, where N_i is the modal index at ω_i, C is the light speed in vacuum and $d_{eff} = (2/\pi)d_{33}$ is the effective value of the nonlinear coefficient and d_{33} of lithium niobate is $\approx$ 27 pm/V. Moreover, S_{SH} and S_{DF} are the effective interaction areas for SHG and DFG and are found to be $S_{SH} \approx S_{DF} \approx 47$ μm^2. The phase-mismatched terms for each segment L_l are $\Delta k_{SH} = \beta_{SH} - 2\beta_p - 2\pi/\Lambda_l$ and $\Delta k_{DF} = \beta_{SH} - \beta_s - \beta_c - 2\pi/\Lambda_l$, where Λ_l (l = 1, 2,…, m) is the QPM poling period of the l-th segment.

In double-pass SHG+DFG scheme, the processes of SHG and DFG are separated and, hence, their solutions can be dealt with independently. The SHG process is expressed as the following coupled equations:

$$\frac{\partial E_p}{\partial x} = -i\omega_p \kappa_{SH} E_p^* E_{SH} \exp(-i\Delta k_{SH} x) - \frac{\alpha_p}{2} E_p , \tag{2a}$$

$$\frac{\partial E_{SH}}{\partial x} = -i\omega_p \kappa_{SH} E_p^2 \exp(i\Delta k_{SH} x) - \frac{\alpha_{SH}}{2} E_{SH} . \tag{2b}$$

The DFG process is expressed as

$$\frac{\partial E_s}{\partial x'} = -i\omega_s \kappa_{DF} E_c^* E_{SH'} \exp(-i\Delta k_{DF} x') - \frac{\alpha_s}{2} E_s , \tag{2c}$$

$$\frac{\partial E_c}{\partial x'} = -i\omega_c \kappa_{DF} E_s^* E_{SH'} \exp(-i\Delta k_{DF} x') - \frac{\alpha_c}{2} E_c , \tag{2d}$$

$$\frac{\partial E_{SH'}}{\partial x'} = -i\omega_{SH'} \kappa_{DF} E_s E_c \exp(i\Delta k_{DF} x') - \frac{\alpha_{SH'}}{2} E_{SH'} , \tag{2e}$$

where the range of x' is from L to 0, and the subscript SH' denotes backward propagation of the second harmonic wave. The poling period of step-segmented gratings is arranged as shown in Fig. 1. For the first section, the period $\Lambda_1 = \Lambda_{SHG} + \delta\Lambda$, where Λ_{SHG} is calculated by finding the effective indexes of waveguides after using the Sellmeier expression for $LiNbO_3$ when $\Delta k_{SH} = 0$, and $\delta\Lambda$ is the period shift to control the period changing of the first section. The grating period of other sections changes according to $\Lambda_i = \Lambda_{i-1} + \Delta\Lambda$, where $\Delta\Lambda$ is the constant period change between two adjacent sections. Flat broadband response can be achieved by optimizing the poling period parameters $\delta\Lambda$ and $\Delta\Lambda$.

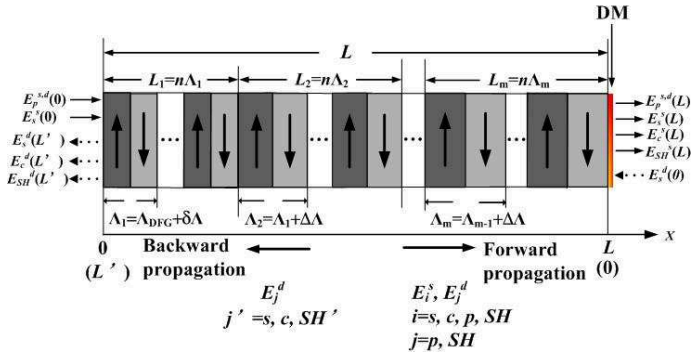

Fig.1 Model of step-segmented gratings for single-pass and double-pass cascaded SHG+DFG wavelength conversion. DM: dichronic mirror.

Results and discussion

High conversion efficiency, wide conversion bandwidth and flat response are needed for multichannel conversion in WDM systems. In this section, the step-segmented gratings is utilized and optimized to realize these characteristics. Neglecting the waveguide loss, optimal results of the conversion efficiency η and the 3-dB conversion bandwidth $\Delta\lambda_s$ for single- and double-pass schemes are calculated from equations (1)-(2) and shown in Fig. 2. Here the signal power is 1 mW, the pump is 100 mW at 1.55 μm, the waveguide total length is 3 cm. In the device, the response flatness is described by the difference between the maximum and center conversion efficiencies within the bandwidth. In order to achieve flat matching response, the fluctuation between the maximum conversion efficiency $\eta_{\max}$ and the center conversion efficiency η_0 is assumed less than 0.2dB (i.e., $\eta_{\max}-\eta_0<0.2$ dB).

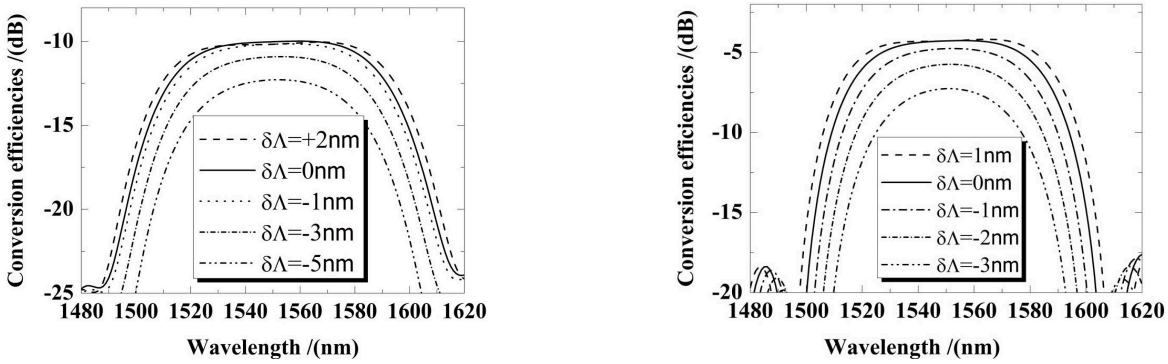

Fig.2 Conversion efficiency η and signal bandwidth $\Delta\lambda_s$ of (a) single- and (b) double-pass SHG+DFG scheme for uniform QPM structure with different $\delta\Lambda$.

It is easily seen Fig.2 that both the signal bandwidth $\Delta\lambda_s$ and the response flatness change with $\delta\Lambda$. The smaller the $\delta\Lambda$, the flatter the response and the smaller the $\Delta\lambda_s$. Under 0.2dB fluctuation assumption, the maximum $\Delta\lambda_s$ is 90 nm when $\delta\Lambda$ =+2 nm in single-pass scheme, while in double-pass configuration, that value is 80 nm when $\delta\Lambda$ =+1 nm. Although the signal bandwidth of double-pass is 10 nm less that of single-pass, the maximum conversion efficiency of the former of -4.26 dB is about 2 times greater than that of the latter.

Larger $\Delta\lambda_s$ can be obtained when dividing the nonlinear medium into 2 segments. Here both $\delta\Lambda$ and $\Delta\Lambda$ effect the conversion characteristics, as shown in Fig. 3. With the increase of $\delta\Lambda$ and $\Delta\Lambda$, $\Delta\lambda_s$ increases while the response flatness become worse. For 0.2 dB peak-to-peak ripple, 111nm signal bandwidth is obtained in single-pass scheme when $\delta\Lambda$ =3 nm and $\Delta\Lambda$ =-4 nm, while that value is 104 nm for the double-pass one when $\delta\Lambda$ =1 nm and $\Delta\Lambda$ =-1 nm.

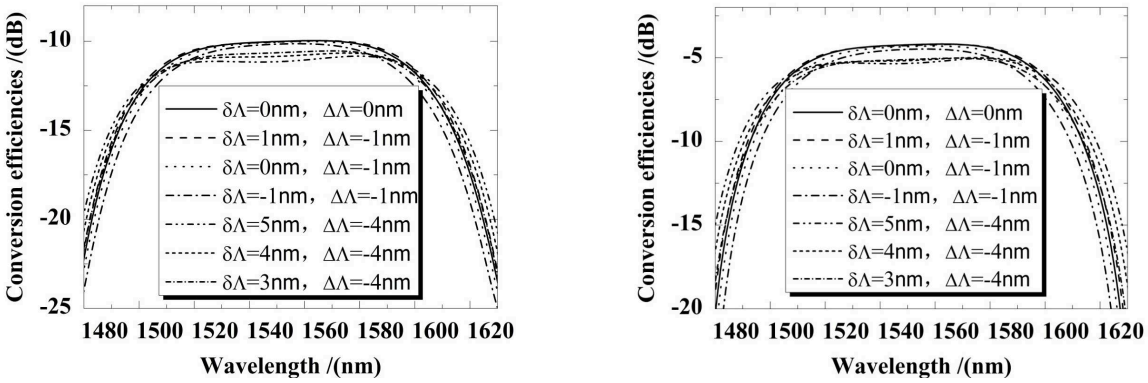

Fig.3 Conversion efficiency η and signal bandwidth $\Delta\lambda_s$ of (a) single- and (b) double-pass SHG+DFG scheme for two-step-segmented QPM structure with different $\delta\Lambda$ and $\Delta\Lambda$.

With the increase of the segment number, signal bandwidth can be widened further. If we divide the nonlinear medium into 3 segments, as shown in Fig. 4, $\Delta\lambda_s$ are 134 nm and 132 nm for single- and double-pass schemes, respectively. By comparison with Fig. 2 and Fig.3, adding segment number can efficiently broaden the signal bandwidth whereas rarely effect the maximum conversion efficiency.

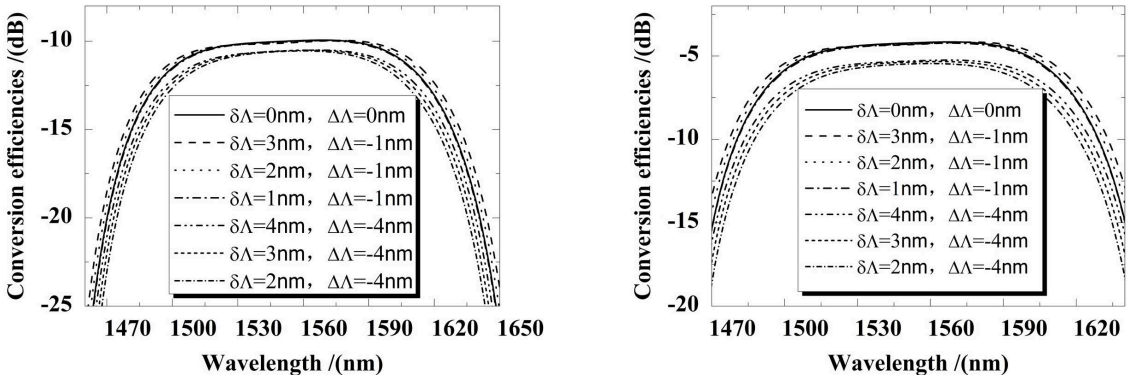

Fig.4 Conversion efficiency of three-step-segmented PPLN-based device versus (a) signal wavelength and (b) pump wavelength for different $\delta\Lambda$ and $\Delta\Lambda$.

Summary

The flat broadband wavelength converter for WDM application based on cascaded single-pass and double-pass SHG+DFG in step-segmented QPM waveguide has been analyzed numerically. The wavelength converter provides broader bandwidth and flatter response than uniform grating. In 3-cm-long three-segment channel waveguide, the signal bandwidths are 134 nm and 132 nm for single- and double-pass schemes, respectively. The ripple on the matching response keeps less than 0.2 dB simultaneously.

References

[1] Tao Liu, Yulin Qi, Linlin Che, *et al*.: Journal of Modern Optics, Vol. 59 (2012), p. 650.
[2] Song Yu, Wanyi Gu: IEEE J. Quantum Electron., Vol. 41 (2005), p. 1007.
[3] X. Liu, H. Zhang, Y. Guo, *et al*.: IEEE. J. Quantum Electron., Vol. 38 (2002), p. 1225.
[4] T. Kishimoto, K. Nakamura, H. Yaegashi, *et al*.: Photonics Technology Letters, Vol. 24 (2012), p. 228.
[5] A. Tehranchi, R. Kashyap: Optics Express, Vol. 19 (2011), p. 22528.

Advanced Materials Research Vols. 989-994 (2014) pp 3794-3797
© (2014) Trans Tech Publications, Switzerland
doi:10.4028/www.scientific.net/AMR.989-994.3794

Investigation of Efficient Wavelength Conversion Based by Difference Frequency Generation in Step-Segmented Quasi-Phase Matched Gratings

Jinsong Guo[a], Haidong Wu[b], Yunwen Wu[c] and Zhaoxia Wang[d]

Leshan power supply company, Sichuan Leshan, 614000, China

[a]guojinsong118@126.com, [b]wu_hai_dong@163.com, [c]ywwu03@126.com, [d]wzx519@sina.com

Keywords: Wavelength conversion, Quasi-phase matching, Difference frequency generation

Abstract. We report difference frequency generation-based wavelength conversion in step-segmented quasi-phase matched (QPM) gratings. It is shown that both the pump bandwidth and the signal bandwidth are efficiently widened by adding the segment number of QPM grating and optimizing the poling period of the first segment and the period shifts between adjacent sections. Especially, flattop conversion efficiency response with peak-to-peak ripples less than 0.2 dB, which is very helpful to multichannel conversion in WDM systems, can be achieved simultaneously. For 3-cm-long waveguide, the signal conversion bandwidth and the pump bandwidth reach 166 nm and 0.88nm, respectively, meanwhile the maximum efficiency is -0.55dB.

Introduction

Wavelength conversion is widely recognized as a key technology for future wavelength division multiplexed (WDM) networks and as an important method of enhancing routing optical network properties such as reconfigurability, nonblocking capability, and wavelength reuse[1]. Wave-mixing schemes due to second-order susceptibilities in QPM crystals are promising for all-optical wavelength conversion. They have ultrafast response and strict transparency. Difference-frequency generation (DFG) [2] and cascaded second-order interaction ($\chi^{(2)}$)[1, 3] are two important schemes to realize wavelength conversion in QPM crystals. The devices based on cascaded $\chi^{(2)}$ effect suffer from low conversion efficiency, because the effect consists of a second-harmonic generation (SHG) and a DFG processes. Direct DFG has high conversion efficiency in principle. However, it was difficult to couple pump and signals into the fundamental guided-wave mode simultaneously without exciting higher-order modes that are not involved in the wavelength conversion process. This problem can be solved by use of a subsequent adiabatically tapered periodic segmentation of channel waveguides [4].

In order to efficiently utilize the telecommunication band, flattened broadband wavelength converters are very attractive. However, in uniform QPM grating, the conversion bandwidth and the pump detuning bandwidth are very limited[1]. Many methods have been reported to broaden the bandwidth by chirping the optical superlattice period. By utilizing segmented gratings, Liu[1] obtained enhanced conversion bandwidth and pump bandwidth. Gao[3] reported a flat broad-band wavelength conversion in sinusoidally chirped optical superlattices (SCOS). However, the response flatness, which is also an important quality parameter for wavelength conversion as the bandwidth is, is a little worse in the above schemes. In this paper, step-segmented grating is used to fulfill wavelength conversion with high conversion efficiency, flat response and broad bandwidth.

Theory and model

In order to increase the conversion bandwidth and pump detuning bandwidth and enhance the flatness of response with high conversion efficiency, the step-segmented grating is employed in DFG-based wavelength conversion, as shown in Fig. 1. The Ep, Es, Ec in Fig. 1 are the field amplitude of pump wave, signal wave and converted wave, respectively. The step-segmented grating is implemented in a Z-cut and X-propagating lithium niobate channel waveguide, and it is formed by dividing the

nonlinear medium into *m* segments along *x* direction. The poling period of the first section is $\Lambda_1 = \Lambda_{DFG} + \Delta\Lambda_1$, where Λ_{DFG} is calculated by finding the effective indexes of waveguides after using the Sellmeier expression for $LiNbO_3$ when $\Delta k_{DF} = 0$[5], and $\Delta\Lambda_1$ is the period shift to control the period changing of the first section. The grating period of other sections changes according to $\Lambda_i = \Lambda_{i-1} + \Delta\Lambda_2$, where $\Delta\Lambda_2$ is the constant period change between two adjacent sections. Flat broadband response can be then achieved by optimizing the poling period parameters $\Delta\Lambda_1$ and $\Delta\Lambda_2$. In DFG wavelength conversion scheme, the signal wave and pump wave are injected from the same end of the waveguide and then propagate forward. The converted wave which carries is generated during the forward propagation by DFG process. With the slowly varying envelope approximation, DFG interaction can be described by the following nonlinear coupled-mode equations:

$$\frac{\partial E_s}{\partial x} = -i\omega_s \kappa_{DF} E_c^* E_p \exp(-i\Delta k_{DF} x) - \frac{\alpha_s}{2} E_s \tag{1}$$

$$\frac{\partial E_c}{\partial x} = -i\omega_c \kappa_{DF} E_s^* E_p \exp(-i\Delta k_{DF} x) - \frac{\alpha_c}{2} E_c \tag{2}$$

$$\frac{\partial E_p}{\partial x} = -i\omega_p \kappa_{DF} E_s E_c \exp(i\Delta k_{DF} x) - \frac{\alpha_p}{2} E_p \tag{3}$$

where α_i ($i = p$, s or c) is the propagation loss of ω_i. $\kappa_{DF} = d_{eff}\sqrt{2\mu_0} / \sqrt{CS_{DF}N_S N_C N_{SH}}$ is the nonlinear coupling constants, where N_i is the modal index at ω_i, C is the light speed in vacuum and $d_{eff} = (2/\pi)d_{33}$ is the effective value of the nonlinear coefficient and d_{33} of lithium niobate is ≈ 27 pm/V. Moreover, S_{DF} is the effective interaction areas for DFG and is found to be S_{DF} ≈47 μm^2. The conversion efficiency is defined as the ratio of the converted signal power with respect to the input signal power.

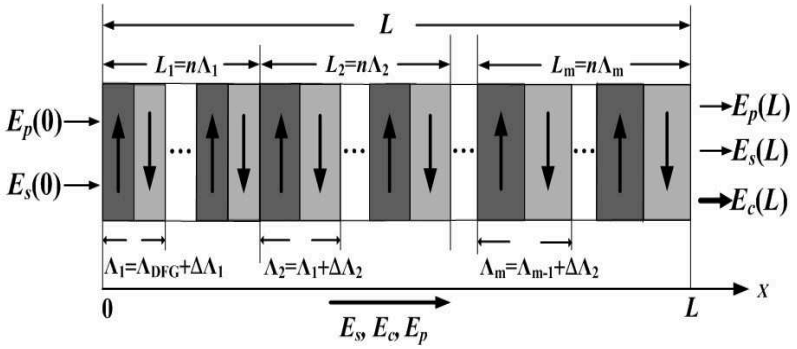

Fig.1 Schematic of the step-segmented structure.

Results and discussion

Neglecting the waveguide loss, Fig. 2, which comes from the calculation of equations (1)-(3), shows the optimal results of the conversion efficiency η, the 3-dB bandwidth of the signal and the pump in uniform QPM grating, respectively. Here the signal power is 1 mW, the pump is 100 mW at 0.775 μm, the waveguide total length is 3 cm. In the device, the response flatness is described by the difference between the maximum and center conversion efficiencies within the bandwidth. In order to achieve flat matching response, the fluctuation between the maximum conversion efficiency $\eta_{\max}$ and the center conversion efficiency η_0 is assumed less than 0.2dB (i.e., $\eta_{\max} - \eta_0 < 0.2$ dB).

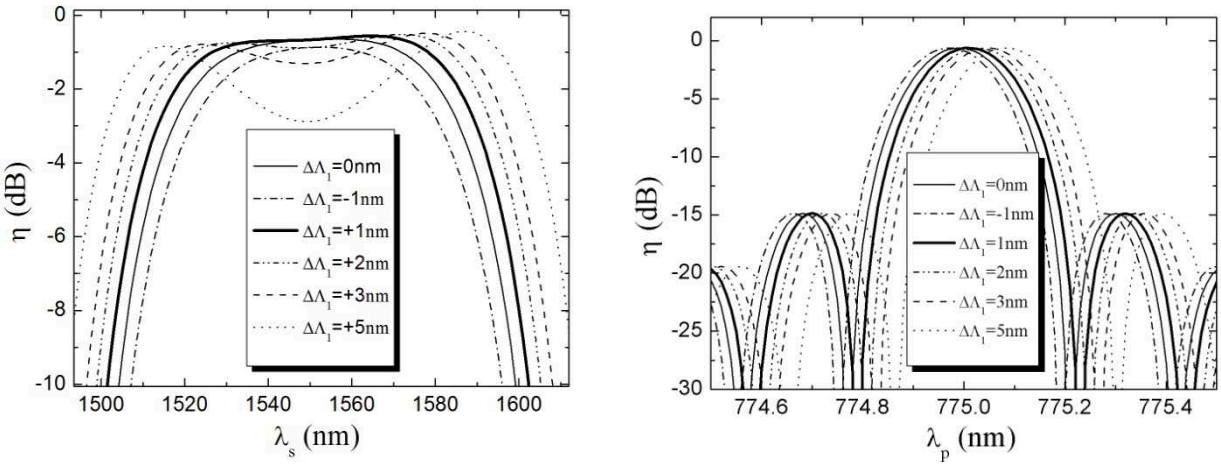

(a) (b)

Fig.2 Conversion efficiency of one-segment PPLN-based device versus (a) signal wavelength and (b) pump wavelength for different $\Delta\Lambda_1$.

It can be seen from Fig.2 (a) that both the signal bandwidth $\Delta\lambda_s$ and the response flatness change with $\Delta\Lambda_1$. Under 0.2dB fluctuation assumption, $\Delta\Lambda_1$ =+1nm is recommended because $\Delta\lambda_s$ can reach its maximum value 81nm under this condition. From Fig. 2 (b), one can seen that the pump bandwidth $\Delta\lambda_p$ =0.19 nm, which is remains unchanged when $\Delta\Lambda_1$ changes.

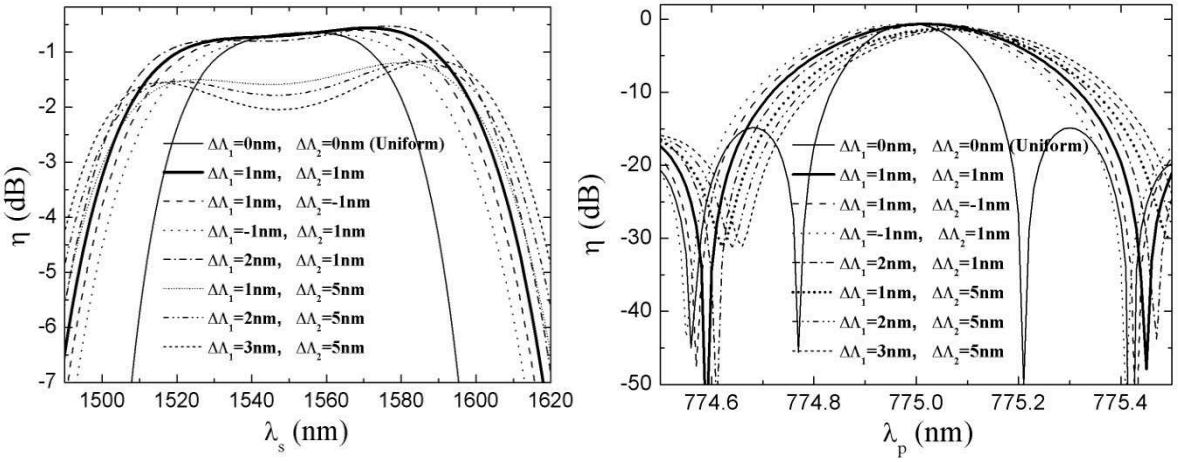

(a) (b)

Fig.3 Conversion efficiency of two-step-segmented PPLN-based device versus (a) signal wavelength and (b) pump wavelength for different $\Delta\Lambda_1$ and $\Delta\Lambda_2$.

When dividing the nonlinear medium into 2 segments and optimizing $\Delta\Lambda_1$ and $\Delta\Lambda_2$, both $\Delta\lambda_s$ and $\Delta\lambda_p$ can be broadened, as shown in Fig. 3. With the increase of $\Delta\Lambda_1$ and $\Delta\Lambda_2$, $\Delta\lambda_s$ increases while the response flatness become worse. For 0.2 dB peak-to-peak ripple, 111nm signal bandwidth and 0.34 nm pump bandwidth are obtained when $\Delta\Lambda_1$=1nm and $\Delta\Lambda_2$=1nm.

Both $\Delta\lambda_s$ and $\Delta\lambda_p$ can be further widened with the increase of the segment number. It can be seen from Fig. 4 that if we divide PPLN into 3 segments, $\Delta\lambda_s$ and $\Delta\lambda_p$ are 134 nm and 0.54 nm, respectively, which are 53 nm and 0.34 nm larger than those of uniform grating structure. As shown in Fig. 5, when the segment number increases to 5, $\Delta\lambda_s$ and $\Delta\lambda_p$ reach 166nm and 0.88 nm, respectively, which are not only greater than those of SCOS-based wavelength conversion[3] but also larger than those of segmented grating-based wavelength conversion[1]. Moreover, the 0.2 dB flatness obtained in step-segmented gratings in this paper is better than the above two kinds of QPM structure as well.

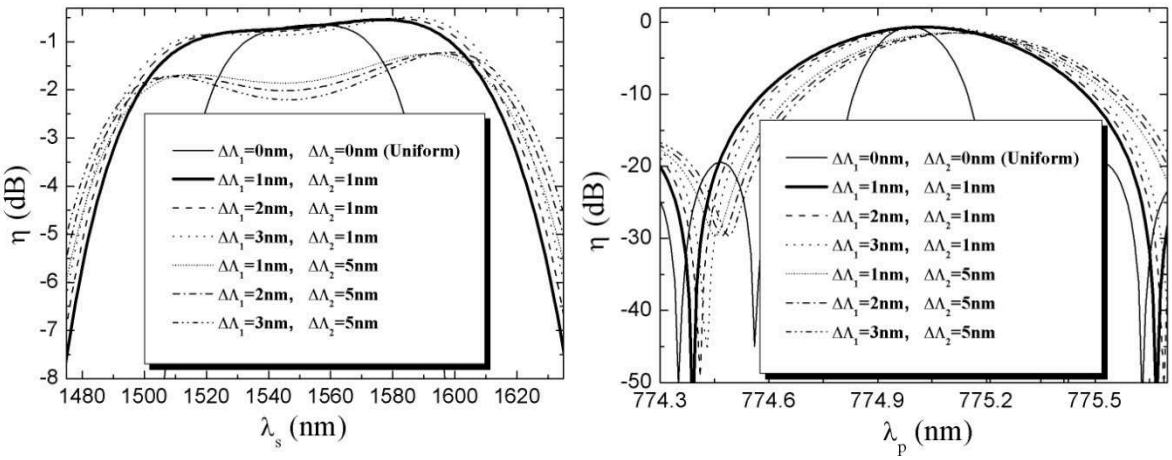

(a) (b)

Fig.4 Conversion efficiency of three-step-segmented PPLN-based device versus (a) signal wavelength and (b) pump wavelength for different $\Delta\Lambda_1$ and $\Delta\Lambda_2$.

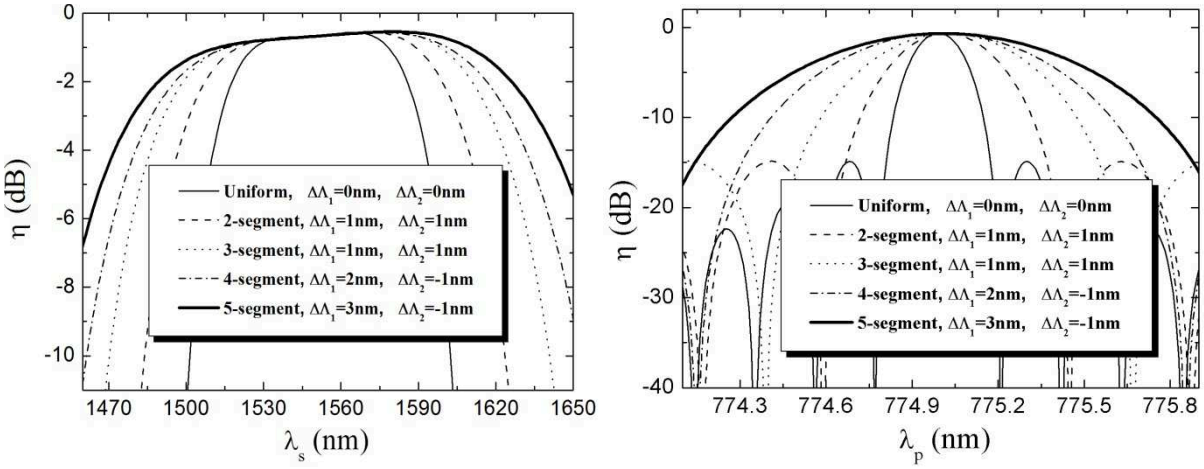

(a) (b)

Fig.5 Conversion efficiency versus (a) signal wavelength and (b) pump bandwidth for one- to five-step-segmented grating structures.

Summary

The flat broadband wavelength conversion based on DFG in step-segmented QPM waveguide is investigated. Both the signal bandwidth and the pump bandwidth can be efficiently broadened by increasing the segment number of QPM grating and optimizing the poling period of each segment. The ripple on the matching response of 0.2 dB is very small as well. Take 3-cm-long waveguide for example, the signal and pump bandwidths for five-segment step-segmented grating are 166 nm, 0.88 nm, respectively.

References

[1] Tao Liu, Yulin Qi, Linlin Che, *et al.*: Journal of Modern Optics, Vol. 59 (2012), p. 650.

[2] X. Liu, H. Zhang, Y. Guo, *et al.*: IEEE. J. Quantum Electron., Vol. 38 (2002), p. 1225.

[3] Shiming Gao, Changxi Yang and Guofan Jin: Optics Communication, Vol. 239 (2004), p. 333.

[4] M.H. Chou, M.A. Arbore, M.M. Fejer: Optics Letters, Vol. 21 (1996), p. 794.

[5] Dieter H. Jundt: Optics Letters, Vol. 22 (1997), p. 1553.

Advanced Materials Research Vols. 989-994 (2014) pp 3798-3801
© (2014) Trans Tech Publications, Switzerland
doi:10.4028/www.scientific.net/AMR.989-994.3798

Wavelet Transform Adjustment Method Study in Color Image Enhancement

[1,a] Zhang Zhigang,[2,b] Yan Shiqiang,[3,c] Geng Peng

[1,2,3] ShijiazhuangTiedao University(STDU)，Shijiazhuang，Hebei，China，050043

[a,b,c]zzg980910@126.com

Keywords: Color Image; Enhancement; Wavelet Decomposition; Homomorphism Decomposition.

Abstract. In order to improve the ensemble of color image, this paper proposes homomorphism decomposition—wavelet enhancement algorithm based on the basic principle of Wavelet Transform. We separate the incidence component and reflection component of the image by homomorphism decomposition, and then combine wavelet transform to enhance image as well as reserve details. The experimental result shows that the adaption and effect is obviously superior to MSRCR.

Introduction

Image enhancement based on wavelet Transform is still in exploratory stage in current picture processing research. Some scholars at home and abroad have begun to reach this method. Wavelet decomposition and composition included in image enhancement of wavelet analysis lead to huge data size and long operation time. Thus, in practical application, especially in real-time system, it doesn't gain acceptance and promotion, but this doesn't mean wavelet analysis is unsuitable for image enhancement. Because of the irreplaceable superiority of wavelet analysis, the processing result is much more satisfying comparing to the traditional methods. With the improvement of algorithm and successful development of high-speed chip, the speed problem can be solved. Therefore, image enhanced by wavelet analysis well gain attention and application. This paper introduces the true color image enhancement algorithm based on wavelet transform, defining a new incidence and reflection model by static wavelet transform and proposing a new thought that image enhancement is a process of image energy decaying and reamplifying. There are no restrictions for true color needs enhancing, and the adaptation and effect is obviously superior to MSRCR.

Basic Principles of Wavelet Analysis

The basic thought of wavelet transform is expressing or approaching signals by a family of functions, which is called wavelet function. It is constituted by wavelets generated by scaling and translating a small wave of generating functions. The original signals are described by its transformation coefficient.

A family of discrete wavelet functions $\{\phi_{i,j}(x) = 2^{j/2}\phi(2^j x - k)\}_{j,k\in z}$ we get by scaling and translating Function ϕ constitute the orthonormal basis of integrable function space L2(R). Admissible wavelet ψsatisfying the constraint condition $\int \frac{|\phi(w)|^2}{w} dw < \infty$ has enough decay rate with mean value of 0, then the wavelet transform is

$$W_\phi f(a,b) = < f, \phi_{a,b} > |a|^{-1/2} \int_R f(t)\phi(\frac{t-b}{a})dt \quad (1)$$

Map function f to the sequence in Z2 and if conversion has inverse, we can set up the figure method of accurately reconstructing f from wavelet coefficient < f，ψa，b>.

According to the Mallat pyramid decomposition algorithm, we can achieve the rapid decomposition of separable two-dimension orthogonal wavelet by utilizing biorthogonal filter with ∑hn=1，∑gn=0. Cj-1 is low-frequency image, namely the smooth version of pending image; DHL, DLH, DHH is high-frequency image, namely the detail version of original version; and different decomposition layers Dj-1, Dj corresponds to different resolution ratio, among which DHL is horizontal operation for original image, DLH is vertical operation, DHH is diagonal operation and the detail images are

separately obtained by original image passing high pass and low pass filter. j is the wavelet decomposition level. The number of levels of wavelet decomposition can be selected by needs, and each level corresponds to different frequency band and resolution ratio: the smaller the dimension is, the higher the resolution ratio can be. Rough resolution ratio corresponds to the main outline of the image and detail resolution ratio to some specific form.

Enhancing True Color Image by Homomorphism Decomposition---Wavelet

Color Retention the Selection of Color Coordinate System： The paramount consideration of enhancing true color image is color retention before and after enhancement. Most scholars' research fail to consider the sensibility human vision to spectral (namely that the sensibility human eye to visible light spectral is uneven), namely fail to consider the human visual system spectrum sense quality. What's more, the enhancement effect image enhancing method with well physical explanation to true color image is not very good and needs improvements.

HSV color coordinate system separates T Hue, saturation and value. Channel H can be keep the same; the energy of the saturation of Channel S can be adjusted by human visual system spectrum sense quality to suit human version. Conduct image enhancement to Channel S by homomorphism decomposition and wavelet transform.

Saturation Adjustment Algorithm and Homomorphism Decomposition -- wavelet Enhancing True Color Image： As for the scene with wild illumination space variation, human eyes can adjust automatically and is highly adaptive; especially they can realize multi-scale recognition to the details. The multiresolution analysis in wavelet transform shares many similarities with the crystalline lens in human eyes. The application in image enhancement can reserve the details well, overcoming the detail loss in Retinex effectively.

We can separate the incidence component and reflection component; compress the dynamic range of reflection component and then composite the deposed incidence component and reflection component. Separate the incidence component and reflection component and we can get:

$$g \approx r_o^{rH} i_0^{iL} \quad (2)$$

We adopt high pass filter in separation. When rH=1, rL=0, the image after filtering only contains reflection component r0; when rH=0, rL=1, the image after filtering only contains incidence component i0. Thus the incidence component and reflection component are separated effectively.

The highlight section in the image mainly distributes in the low-frequency section. According to the quality of pupil and black granulocyte and the incidence—reflection model, image dynamic range can be compressed well by decaying the energy in low-frequency section (highlight section) of attenuation image, Figure 1 is the original image and Figure 2 is the Fourier energy spectrum diagram (The abscissa and ordinate in Figure 2 is the frequency sampling value. The ordinate is the Fourier Spectrum in Figure 1). We can see from Figure 2 that the energy of low-frequency section mainly distributed in the four angular points in the image. Therefore the utilization of low pass filter can decay the low-frequency energy in the image well.

Figure 1: Original Image

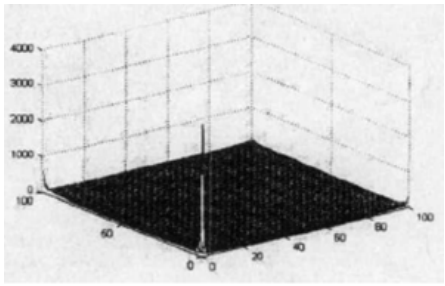

Figure 2: Spectrogram

The filtering effect of Butterworth low pass filter is well, as shown in Formula (3). In the formula, $D(u,v)=\sqrt{u^2+v^2}$ and rH are the coefficient of proportionalities; u, v are the frequency sampling value; D0 is the cut-off frequency and D0=1.2; the bigger n is, the more rapidly the decay rate of the filtering function is, and n=5. This low pass filter can enhance the wave form effectively.

$$H(u,v) = rHx\frac{1}{(D/D_0^2)^n + 1} \quad (3)$$

We can know from the incidence—reflection model that the compressed image within dynamic range can be get by multiplying the enhanced incidence component with reflection component. Because of the attenuation of the low-frequency energy, the overall brightness of the image is relatively dark, but we can conduct gamma correction by picture brightness formula（4）till the eyes feel comfortable. $\alpha = 0.35$, and the specific flow chart of homomorphism decomposition and wavelet decomposition image enhancement is shown in Figure 3.

$$g = g^{\alpha} \quad (4)$$

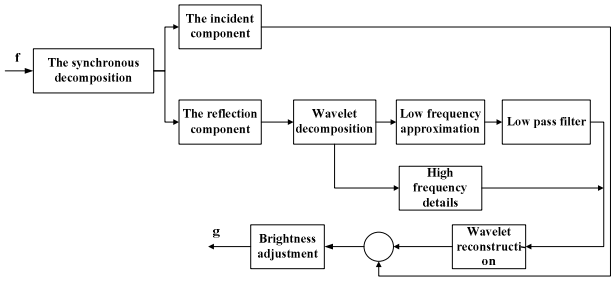

Figure 3: Image Enhancement of Homomorphism Decomposition and Wavelet Decomposition

The image color is determined by the wave length and frequency spectrum of catoptric light. Saturation reflects color category and chroma reflects shade, which is determined by color as well as the wave length and frequency spectrum of catoptric light. The sensibility of human to different spectrum is different as long as the catoptric light spectrum is different. Generally, human can sense the spectrum of wave length from 380nm to 780nm.

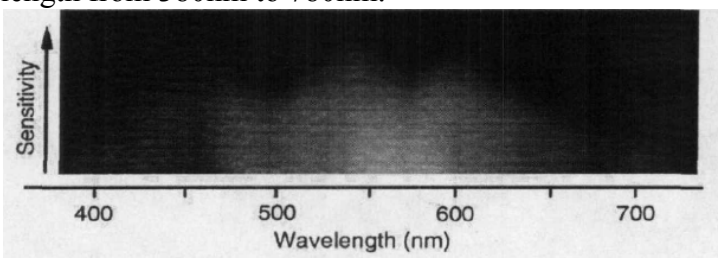

Figure 4: Human Visual System Spectral Sensibility Feature

From Figure 4, human most sensitive spectrum is between 425nm to 650nm; mainly the main colors are blue, green and light red. Frequency spectrum in other bands, namely the dark red, cannot be recognized easily. If the blue, green and light red dominate the true color image, the chroma and saturability can stay the same when enhancing, while if dark red dominates, dark red will turn into light red by adjusting saturation channel in formula (4) , which is good for observation.

$$H(u,v) = rH \times \frac{1}{1 + (\sqrt{u^2 + v^2} / D_0)^n} \quad (4)$$

rH is the proportionality coefficient determined by human eye observation, and we can select different rH to adjust the color purity of enhancement image.

Algorithm steps are as follows:

(1) read-in true color image;

(2) transform the true color image from RGB space into HSV space;

(3) enhance the true color brightness channel by Figure 3;

(4) saturation stays the same with blue, green and light red dominate; and adjust the image saturation by formula (4) if dark red dominates.

(5) the enhanced true color image will transform from HSV space to RGB space.

Example Verification

True color image enhancement of multiscale Retinex with color restore (msrcr) is the significant development of Retinex theory, and it is also one of the new-emerging classic algorithms of true color image enhancement. Thus, we conduct contrast experiment between the method in this paper and msrcr, and the experimental result is shown as follows:

Figure 5: Original Image

Figure 6: Image processed by msrcr

Figure 7: Image Enhanced by This Method

From the contrast experiment we can see that msrcr enhancement shows a lot halo and serious bleaching and loss details. The method in this paper is superior to msrcr in dynamic range compress, detail reserve and color maintaining. The image enhanced by this method is beautifully colored and is more close to the original color with moderate dynamic range comparing to msrcr. What's more, the application of human visual system spectrum sense quality moderately expands the spectrum sensitive range of human vision. True color images that enhanced by msrcr show obvious distortion. Observing the image border details after enhancement by these two methods, we can see that detail maintain of this method excel msrcr obviously. The true color image enhanced by this method is more suitable for human visual sense. It realizes the color constancy and the enhanced true color image is neat and clear. We cannot sense the halo and bleaching in human eye. The dynamic range compress, color and details maintaining is superior to msrcr.

Conclusion

From color constancy and the physical and spectroscopy qualities of true color image, we can get that the high dynamic of true color image is determined by the brightness. Separating brightness and color can reduce the impact on color when enhancing. Wavelet—energy enhancement has wide adaptation. It is flexible and the parameters can be adjusted according to needs and objective environment. The experimental result shows that this method is superior to MSRCR in maintaining color and details, removing bleaching and halo, and image clarity after enhancing.

References

[1] Ma Wenhui etc. A Survey of HDRI Range Compression Technology [J], Journal of Communication University of China (Natural Sciences), 2007, 14(4):66-72.

[2] Xue Dandan．The Research of Ultrasonic Testing Rail Defects and the Positioning [J]．Nuclear Electronics & Detection Technology, 2012, 32(9):1058-1061.

[3] Dong Hanli． Methods Study of Image Enhancement Based on Wavelet Transform[J]． Journal of Zhengzhou Textile Engineering Institute，1999，21(1) : 118-130．

[4] Xu Baochang．Dual-threshold Method of Flame Color Image Enhancement Based on Wavelet Analysis [J]．Optoelectronic Component, 2013，40(6) : 91-96．

[5] Chen Kai. Image Enhancement Based on Wavelet Transformation and Pseudocolor Coding with Phase-modulated Image Density Processing[J]. Journal of Tianjin University of Technology，2012, 28(3):71-74

[6] Han Lina. Real Color Image Denoising and Enhancement Based on Wavelet Transform[J]. Computer Engineering, 2010，36(12): 224-226.

[7] Ding Ximing. Image Enhancement Based on Wavelet Transformation [D]. Hefei： Anhui University，2010：36-39.

[8] Chen Wufan. Application of Wavelet Analysis in Image Processing[M]. Beijing：Science Press, 2003：108-118.

[9] Wang Huiqin. Wavelet Analysis and Application[M].Beijing： Beijing University of Posts and Telecommunications Press，2011：22-69.

Advanced Materials Research Vols. 989-994 (2014) pp 3802-3805
© (2014) Trans Tech Publications, Switzerland
doi:10.4028/www.scientific.net/AMR.989-994.3802

Accurate detection of fault signal in large-scale communication

Shu Na

Chongqing University of Posts and Telecommunications shuna@cqupt.edu.cn 400065

Keywords: fault signal; data mining; fault detection;

Abstract: Deep data-mining methods of fault signal in large-scale communication system are researched. Although with the characteristic of frequency uniformity as signals distribute in each reaction zone, common method of fault signal detection based on shortwave dispersing is invalid employing in large-scale communication system, which presents the absence or instability of fault signal. For this reason, a method based on particle swarm optimization is proposed for fault signal detection in large-scale communication system. As reaction speed and activity scope within the whole particle swarm are replaced, accurate results are achieved. Taking particle swarm optimization, it is detected that whether there is a fault in communication systems. The experimental results show that proposed method in signal fault detection process can greatly increase accuracy of signal fault detection, as plays a greater role in future.

1 Introduction

As fault detection techniques plays irreplaceable role in many fields, such as mechanic, electricity and control and has become core problem in exploring communication field [1]. For fault detection in large-scale communications systems, detection are achieved by comparison of fault signals collected in communication [2]. Fault signal detection has been the focal point of communication research and gotten attention of many researchers [3-5]. Currently fault signal detection methods are widely used, including PSO-based neural network algorithm, local wave analysis algorithms and wavelet decomposition algorithm [6]. Due to broad development of fault signal detection method in communication, it has become a major topic of inquiry for many experts with great prospects.

2 fault signal detection method

2.1 Particle update process

When a communication failure is detected, it must employ signal of all communication state as the particles. According to particle analysis, a communication failure is realized. Updating the particle, focus calculation of velocity and diffusion activities for particles are performed as Equation (1):

$$\begin{aligned} &x_k(m+1) = \xi x_k(m) + e_1 t_1 (R_k - Z_k(m)) \\ &+e_2 s_2 \left(R_i - Z_k(m)\right) \\ &Z(m+1) = Z_k(m) + x_k(m+1) \end{aligned} \tag{1}$$

In the process of updating the particles, the optimal particle swarm will find the optimal particle while speed and operating range of particle swarm are fully replaced and make it the optimal particle. The purpose of the non-optimal PSO is to find the operating range of other particles and then update the data.

Applying the above method, traveling range of other particles in the optimal particle swarm is obtained. By updating range, inconsistent occurs between updated range and activities range of optical particle swarm. Using equation (2) particle outside the optimal particle swarm can be updated:

$$\begin{aligned} &y_l(n+1) = \xi x(m) - e_1 t_1 \left(R_K - Z_K(M)\right) \\ &-e_2 t_2 \left(R_i - Z_K(M)\right) \end{aligned} \tag{2}$$

Employing above process, update process of optimal particle is completed. The particles become ideal value of the entire operating region, whose value are used to detect communication failures.

2.2 Achievement of communication signal detection

In the communication signal detection process, according to operating region and updated speed of optimum particle swarm, set the optimum area particle as b, $F_q > b$ shows activity range of optimal particles swarm are substantially the same and updating operation can be achieved so as to improve detection accuracy of communication failure signal.

When communication failure signal is in detection, optimal particle E_k is an enlarged particles appearing in the specified range, with the number of the particles is O. So the optimal and enlarged particles are combined to form a set of F. In this set, it is possible to obtain the optimal solution, employing transition between optimal particle and phase E_k. Then optimum value can be obtained in local range.

Assuming in communication particle swarm of fault signal the number of all particles is Q, the height of a single particle is N, using Equation (3) - (5) can calculate active area of particle swarm in communicate fault signal:

$$F_q = \frac{1}{1+G(Q)} \tag{3}$$

$$G(Q) = \frac{1}{N}\sum_{l=1}^{N} G_l(Q) \tag{4}$$

$$G_l(Q) = \sum_{j=1}^{P} -r_{kl} \log r_{kl} \tag{5}$$

All communication failure signal set is composed as set C, using the equation (6) it can be calculated for the k-th signal frequency of communication failure:

$$T(C_k) = \{T_l \,|\, 0 < \|C_k - T_l\| < t, T_l \in T\} \tag{6}$$

By the above methods, updated speed and activity scope of all particles in particle swarm are calculated to obtain the results, which are used as a basis for communication failure detection. Particle swarm updates to replace all the particles, as achieves fault signal detection in large-scale communication system.

3 Analysis of experimental results

To verify the feasibility and accuracy of proposed detection algorithm based on particle swarm optimization in large-scale communication system, an experiment is performed.

In the experiment, communication fault signal collected by a sensor is presented in Fig 1:

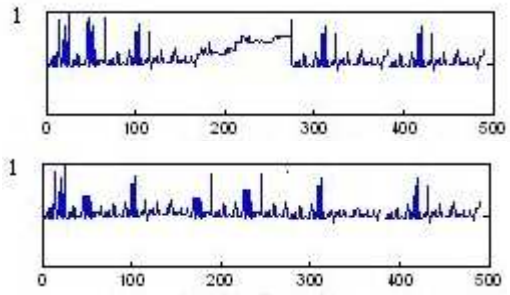

Fig1 Communication fault signal

Using the algorithm for detecting communication failure signal, the experimental results obtained are shown in Fig2:

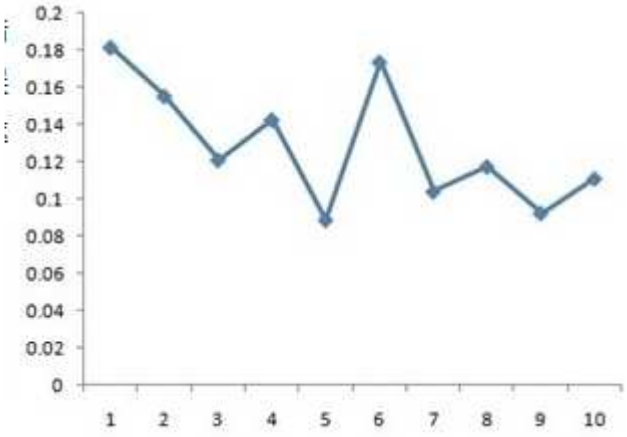

Fig2 Experimental results of communication fault signal

Analyzing with the above experimental results, it is possible to obtain the following table:

Table1 Experimental data of proposed algorithm

Experimental times	Correct judgment	Error judgment	Error rate（%）
1	33	6	0.181818
2	45	7	0.155556
3	33	4	0.121212
4	35	5	0.142857
5	45	4	0.088889
6	46	8	0.173913
7	48	5	0.104167
8	51	6	0.117647
9	54	5	0.092593
10	36	4	0.111111

Employing above experiment, the adopted algorithm for detection of communication fault signal can obtain accurate test results, which meets the communication requirements.

To verify the superiority of fault signal detection method proposed in this paper, traditional algorithms and improved algorithms are respectively performed for fault signal detection in large-scale communication system. Experimental results obtained are as follows:

Table2 Experimental data of different algorithms

Experimental times	Correct rate（%）	
	Traditional algorithm	Proposed algorithm
1	88	96
2	87	93
3	88	95
4	85	93
5	87	93
6	84	94
7	86	96
8	88	94
9	86	94
10	84	93

According to experimental results it is learned that proposed algorithm is performed for fault detection in large-scale communication system, detection accuracy is higher than traditional algorithms, demonstrating the superiority of the proposed algorithm.

4 Conclusion

Fault signal detection method in large-scale communication system is proposed based on particle swarm optimization. The reaction speed and activity scope of whole particles in particle

swarm are replaced, so that results of fault signal detection are accurate. Taking PSO method, it is demonstrated whether there is a fault in communication systems. The experimental results show that the proposed method in fault signal detection process can greatly increase accuracy of fault signal detection and will play a great role.

References：

[1] Xie Kefu, Luo An. Fuzzy diagnosis system optimized with genetic algorithm for power transformer[J]. Electric Power Automation Equipment, 2005,25(4): 55-58.

[2] Yan Xianglian, Wen YuangFang. Research on application of fuzzy neural network to transformer fault diagnosis[J].Transformer, 2002,39(7): 41-44.

[3] Wang Beibei, et al.. The power transformer fault site diagnosis based on information fusion technology [J]. High voltage apparatus, 2003,39(1): 49-52.

[4] Li Jingxiu, Ma Qinglin, Wangxin. Fault diagnosis of asynchronous induction motor based on fuzzy neural network [J].Colliery mechanical & electrical technology，2009，4：4-7.

[5] LiWei, Kuang Peng, Li Yang. A pipeline leak detection method based on fuzzy neural network[J].Computer simulation，2009，26（2）：190-192.

[6] Liang Wuke, et al.. Fault diagnosis method of hydroelectric units base on rough set & Rbf network[J]. Journal of Northwest A & F University (Nat. Sci. Ed.), 2007,35(7):223-227.

Advanced Materials Research Vols. 989-994 (2014) pp 3806-3809
© (2014) Trans Tech Publications, Switzerland
doi:10.4028/www.scientific.net/AMR.989-994.3806

Long Reach 10-Gbps WDM-PON Based on Carrier Distribution and Coherent Detection for Upstream Transmission

Jihong Liu[a], Yanping Ma, Shaorui Ren, Yang Yang and Bin Zhang[b]

Xi'an University of Posts and Telecommunications (XUPT), Xi'an, China

[a]ong1705@xupt.edu.cn, [b]zhangb@xupt.edu.cn

Keywords: WDM-PON, Coherent detection, Colorless ONU, Carrier contribution

Abstract. The wavelength division multiplexing passive optical network (WDM-PON) incorporated with colorless optical network units (ONUs) and centralized light source is the most promising approach for next generation PON. A cost-effective architecture utilizing coherent detection for upstream (US) signal is proposed to enlarge the reach of such WDM-PON systems. Simulation results show that a symmetric 10-Gbps WDM-PON with 80km error-free transmission is realized without using any optical amplifiers.

Introduction

WDM-PON has been considered as a promising candidate to meet the requirements of the future broadband access network solutions, owing to its advantages of broadband capability, free flexibility, and high energy efficiency etc [1]. To make the PON system cost effective and reduce the system maintenance cost, The WDM-PON using colorless ONUs with centralized light sources originated from the optical line terminal (OLT) is a desirable solution [2]. Furthermore, both downstream (DS) and upstream (US) transmission in a full duplex fashion using one single fiber is essential to further reduce the cost, complexity and size of WDM-PON plants [3]. However, the maximum reach of such a WDM-PON is often restricted by the power budget of the US signal. It seems to be possible to mitigate this limitation by increasing either the power of centralized light sources or the gain of US signal at ONUs. Unfortunately, signals propagating in opposite directions on the same wavelength in one single fiber suffer the impairment due to unavoidable Rayleigh backscattering (RB) and Fresnel back-reflections. Therefore, the backscattering noise will increasing proportionally, namely, the SNR of US signal will not be improved as expected [4].

Optical coherent detection technique has attracted great interest in the last decade for the prominent properties of its receiver sensitivity and frequency selectivity [5]. Thus, it may be possible to increase the maximum reach of WDM-PON by utilizing the coherent receiver. There have been some reports on using coherent technology in WDM-PON. But most of them are focused in using coherent receiver at both OLT and ONUs [6]. Although such proposals can increase the maximum reach of WDM-PON, the coherent detection at ONU requires local light source, therefore, the ONU is no longer cost-effective and colorless. Based on the fact that the maximum reach of WDM-PON is mainly determined by the US transmission, in this paper we propose a compromise architecture to realize long reach, single-fiber, full-duplex, centralized WDM-PON system incorporated with colorless ONU and coherent detection only for US signal, where 10-Gbps symmetric transmission are supported by quadrature phase-shift keying (QPSK) US signal and on-off keying (OOK) DS signal, respectively.

System Architecture

In general, carrier contribution [7] and remodulation [8] are the essential techniques to realize the colorless ONUs with centralized light sources. The principle of colorless ONU based on carrier distribution is shown in Fig. 1. Both DS and unmodulated carrier CW are transmitted towards the ONU in the single fiber on different wavelength. At ONU, they are separated by a demultiplexer

(DEMUX). Then the DS is demodulated by a PIN receiver, and CW is delivered by a circulator to the modulator through which the US data is loaded. The modulated CW (US signal) is transmitted again through the circulator, multiplexer (MUX), and towards OLT. Otherwise, in the remodulation-based WDM-PON , the DS signal and US signal are carried on the same wavelength, then the power of the DS signal is coupled to the receiver and reflective semiconductor optical amplifier (RSOA), respectively. The carrier for US transmission is recovered from DS signal by the saturated gain effect of RSOA. Meanwhile, the US data is modulated onto the recovered carrier in RSOA. Because of the reflection character of RSOA, the loop-back and circulator in Fig. 1 are no more used.

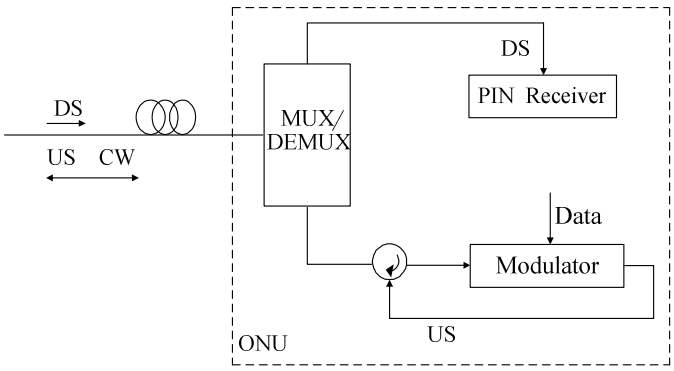

Fig.1. Principle of the colorless ONU based on carrier contribution

For both carrier contribution and remodulation, there is no extra local oscillator (LO) is needed if coherent detection is implemented at OLT. Although the complexity of the colorless ONU based on remodulatoin is a little simpler, and there is an enough margin in power budget because of the considerable gain of RSOA, the bit rate of US is hard to reach 10-Gbps due to the modulation nonlinearity of RSOA. In addition, the influence of Rayleigh backscattering noise is more serious if DS and US signals are at the same wavelength in the single fiber. For the above reasons, the carrier contribution technique is adopted in this paper to realize colorless ONU. Furthermore, the Mach-Zehnder modulator (MZM) is used to make the bit rate of US transmission up to 10-Gbps, which is important in the scenarios requiring symmetrical transmission.

The system architecture of proposed long-reach, bi-directional WDM-PON is shown in Fig. 2, where only one ONU is illustrated. The key features of the proposed scheme are (1) the upstream data is modulated onto distributed carrier using MZM at ONU, and (2) at OLT the US signal is demodulated by coherent detection without using extra LO.

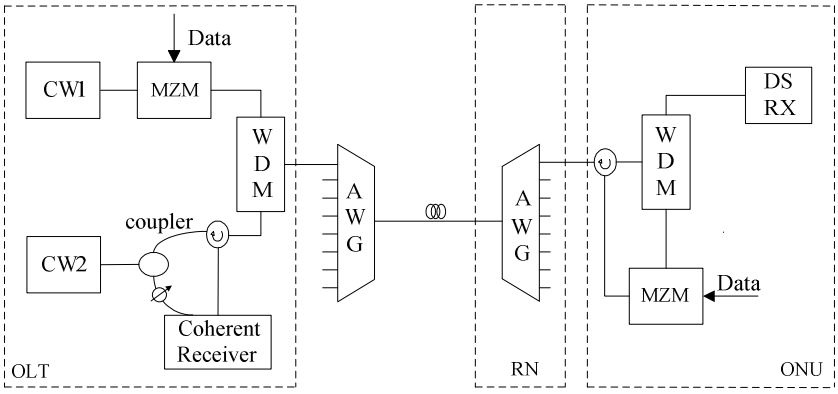

Fig.2. Schematic of the proposed long-reach centralized bi-directional WDM-PON using coherent detection for US transmission

At OLT, there are two continuous light sources (CW1, CW2) with different wavelengths. The MZM is used to generate the 10-Gbps OOK DS signal on CW1. A wavelength division multiplexer (WDM) is used to multiplex the DS signal with the distributed US carrier coupled the power from CW2 before they are passing an arrayed waveguide grating (AWG). After the AWG, the downstream

signal and the distributed US carrier are transmitted towards the ONU via remote node (RN) and a circulator.

At ONU, the WDM is used to separate the DS signal and distributed US carrier. Passing the WDM, DS signal is received by the downstream receiver (DS RX). The distributed US carrier is modulated 10-Gbps US data by a parallel MZM with the format of QPSK. The modulated US signal is then transmitted back to OLT. When the US signal reaches OLT, it passes through a WDM and a circulator, and then is delivered to the coherent receiver, where the undistributed part of CW2 acts the role of LO.

Results and discussion

The performance of the proposed system is simulated using Optisystem 8.0. In simulation system, the main parameters are set as following: The central wavelength of CW1, CW2 are 193.1THz and 193.2THz, respectively, and their linewidth is 0.1MHz. The standard SMF is used with loss and dispersion of 0.2dB/km and 16.75ps/(nm•km), respectively. Other parameters, such as the loss of WDM, AWG and MZM are default values in Optisystem 8.0. The optical power of distributed US carrier at the import of WDM is 2dBm, which is equal to that of modulated CW1. The US and DS data are pseudo-random sequences with length of 29-1 at the bit rate of 10-Gbps. No forward error correction and dispersion compensation are used in the simulation. Because the maximum reach of WDM-PON is limited by US transmission, here only the cases about US transmission are simulated and discussed.

The dependences of US transmission performance on the power of LO are simulated as shown in Fig. 3(a). It is obviously that the BER is decreased as expected when increasing the power of LO for any transmission distance. Even for error-free 80km transmission, the required LO power is still an available value of -2dBm.

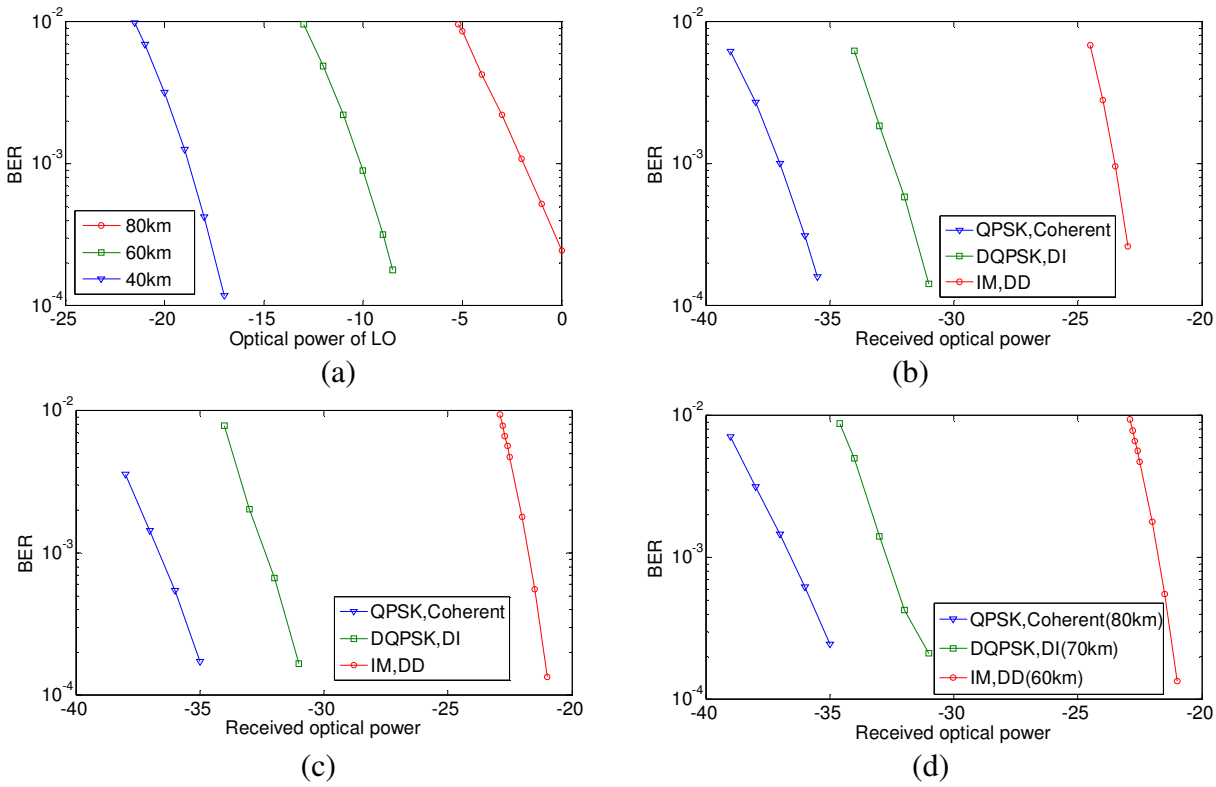

Fig.3. Simulation results of US transmission. (a) The dependences of BER on the power of LO. (b)-(d) BERs versus received powers of US signal for different modulation formats and detection techniques with the reach of 40km, 60km and 80km, respectively.

For comparison, the US transmissions of the WDM-PON using intensity modulation, direct detection (IM, DD) and DQPSK modulation, delay interferomenter based detection (DQPSK, DI) are also simulated here with the same simulation parameter sets. The simulation results under 40, 60, and 80km for US transmission are shown in Fig. 3(b), (c), and (d), respectively. The received power US signal is changed by the attenuator placed just in front of the coherent receiver and the power of LO is the constant value of -2dBm. For both 40km and 60km cases, it is found from Fig. 3(b) and (c) that the minimum allowed received power of coherent detection at BER=10-3 is 3~5dB and13~15dB lower than that of DI and DD, respectively. This will make an enough margin for power budget of the proposed WDM-PON. The maximum reaches supported by different detection schemes are also simulated as shown in Fig. 3(d). The maximum reach of IM-DD is about 60km, and DI can reach 70km. Otherwise, coherent detection can support 80km error free US transmission.

Summary

In this paper, a novel colorless ONU-based WDM-PON architecture is proposed to provide a long-reach, high speed US transmission by combing coherent detection with carrier contribution. The simulation results show that the maximum reach of error free transmission can over 80km with 10-Gbps QPSK US signal. Therefore, it provides a feasible approach to realize the symmetric WDM-PON with high bit rate (>10G-bps) and long transmission distance (>80km) without using any optical amplifiers.

Acknowledgements

This work was financially supported by the National High Technology Research and Development Program of China (2013AA014504), the Scientific Research Program of Shaanxi Provincial Education Department (2013JK1046) and the Young Teachers Research Funds of XUPT (ZL2012-08).

References

[1] E. Wong: J. Lightw. Technol. Vol. 20 (2012), p. 597

[2] J. Yu, M.-F. Huang, D. Qian, L. Chen, and G.-K. Chang: IEEE Photon. Technol. Lett. Vol. 20 (2008), p. 1545

[3] H.-C. Ji, I. Yamashita, and K.-I. Kitayama: Opt. Express. Vol. 16 (2008), p. 4520

[4] J. W. Simatupang, S.-L. Lee. Opt. Express. Vol. 21 (2013), p. 27565

[5] R. Gregory, A. Andrew, J. W. Peter, R. Sebastian, S. Luis, A. Konczykowska, J. Filip, J.-Y. Dupuy, L. B. Larry, C .Sethumadhavan, C. Xie, D. Steve, G. Marty, R. Kenneth, and U. Ruediger: J. Lightw. Technol. Vol.32 (2014), p. 824.

[6] D. Lavery, E. Torrengo, S. J. Savory. “Bidirectional 10 Gbit/s long-reach WDM-PON using digital coherent receivers”. Optical Fiber Comm. Conf., Los Angeles, CA, USA, Mar. 6-10, 2011

[7] Q. T. Nguyen, L.Bramerie1, P. Besnard, A. Shen, A. Garreau, C. Kazmierski, G.-H. Duan, J.-C. Simon. “24 channels colorless WDM-PON with L-band 10 Gb-s downstream and C-band 2.5 Gb-s upstream using multiple-wavelengths seeding sources based on mode-locked lasers”, Optical Fiber Comm. Conf., San Diego, CA, USA, Mar. 21-25, 2010

[8] R. D. Ulysses, S. P. Rivael, B. R. Joao, R.P. Fernando, F. P. Fernando, and A. R. Murilo. “Combined self-seeding and carrier remodulation method for reflective transmitters in WDM-PON”, Optical Fiber Comm. Conf., Anaheim, CA, USA, Mar. 17-21, 2013

Advanced Materials Research Vols. 989-994 (2014) pp 3810-3813
© (2014) Trans Tech Publications, Switzerland
doi:10.4028/www.scientific.net/AMR.989-994.3810

Analysis on Signal Extraction under Sudden Changing Noise Interference Based on Time Frequency analysis

Nie Shaohua[1]

[1]Elementary Education College of Linyi University, Linyi Shandong 273400, China
[a]Nshh98@163.com

Keywords: time frequency analysis; noise, signal extraction; network intrusion

Abstract. The illegal signal such as the intrusion signal which wanted to be embedded in the normal signal was analyzed for the extraction, and made the network environment be safe and pure, so the signal detection problem was shown as the key and important problem in the assurance of the safety of the network. The signal processing principle for the non stationary signal was analyzed firstly, and the new signal extraction method based on the Wigner Ville distribution and Hough transformation theory of the time frequency analysis. The original signal was filtered and detected, the spectrum analysis was got as the same time for the testing the detection property in the simulation. Simulation and experiment was implemented on the objects of the network intrusion signal with the real collection in the database. Simulation result shows that the performance of decreasing the noise and filtering is very good. The intrusion signal can be detected and extracted perfectly, and also it shows good value in the analysis of the network safety in practice.

Introduction

Facing the hackers attack means continuous hidden and sharp, the security threats of network system are increasing greatly, it is not enough to defeat the security threats just depending on the traditional firewall method. An effect Intrusion Detection System (IDS) needs be researched and the network security defense system needs to be studied and established for detecting and refuse the intrusion data for ensuring the network security[1,2]. Basically, the intrusion detection system is the application of the digital signal and information procession subject, and it is also the development and promotion of the signal and information procession subject in the modern network security subject. From the signal processing and data analysis point of view, the intrusion detection can be divided into two types as intrusion detection can be divided into expert knowledge of misuse detection and anomaly detection method[3]. The anomaly detection method is taken as the detection method in this paper, which based on the anomaly behavior detection method. Firstly, the normal behavior model system is built based on the mathematical method to detect the outlier pattern and abnormal model is going to be detected in the data by the anomaly detection method, and the anomaly model just is the intrusion feature[4,5].

In this paper, the detection problem of the network intrusion signal in deep camouflage is going to be analyzed in the signal analysis area, and it had become the problem of the signal extraction of the intrusion network signal in the interfering noise and is shown as the detecting, and filtering the signal. The illegal signal such as the intrusion signal which want to be embedded in the normal signal is analyzed for the extraction, and made the network environment be safe and pure, so the signal detection problem is shown as the key and important problem in the assurance of the safety of the network. The signal processing principle for the non stationary signal is analyzed firstly, and the new signal extraction method based on the Wigner Ville distribution and Hough transform theory of the time frequency analysis. The original signal is filtered and detected, the spectrum analysis is got as the same time for the testing the detection property in the simulation.

Non-stationary signal processing technology

A. Non-stationary signal

According to the many signal resources and disturbances, the signal is a non stationary signal including the network intrusion signal. The network intrusion signal is hiding in the common network signal which is referred as the interference noise. For extracting the intrusion signal, the

research and he application practice show that the statistics of the signal should be studied because it is playing an important role in the signal processing work.

The most common statistics are the mean value as the first-order statistics, and the correlative function, the power spectrum density (second-order statistics) and so on. If the joint distribution function of $\{x(t_1),\cdots x(t_n)\}$ and the joint distribution function of the $\{x(t_1+\tau),\cdots x(t_n+\tau)\}$ are equal for all the $t_1,\cdots,t_n$, and $\tau\in T$. The random process $\{x(t),t\in T\}$ is called strict stationary signal. It means that the distribution is constant with the change of time. If

$$E\{x(t)\}=m\in \mathrm{C},\quad \mathrm{E}\{\left|\mathrm{x(t)}\right|^2\}<\infty,\quad E\{[x(t)-m][x(s)-m]^*\}=R_x(t-s)-\left|m\right|^2 \tag{1}$$

Where $R_x(t-s)=E\{x(t)x^*(s)\}$, and the $x^*(s)$ is shown as the complex conjugate of $x(s)$, and the random process $\{x(t),t\in T\}$ is called generalized stationary process. A strict stationary process is always a generalized stationary process, and a generalized stationary process is not always shown as a strict stationary process. If a signal is not a generalized stationary process, then it is a non-stationary signal. The most common non-stationary signal is auto-correlative function and the power spectrum density.

B. Time frequency feature of the signal

The time frequency feature of the signal is researched for reflecting the intrinsic quality of the signal. In the time frequency analysis of the signal domain, the common features which can reflect the time domain and frequency domain information are including as follows: mean value of time, mean value of frequency, time distribution (standard deviation of time), and frequency distribution (standard deviation of frequency), the functions of them are shown as follows.

Principle of the time frequency analysis

Generally speaking, the Fourier transform is always used in the analysis and processing of the stationary signal, the Fourier transform algorithm is used as the signal processing method, and based on the Fourier transform, the signal can be analyzed both in the time domain and the frequency domain, the Fourier transform makes the signal which was shown in the time domain transferred in the frequency domain,, the Fourier transform is shown as follows:

$$S(f)=\int_{-\infty}^{\infty}s(t)e^{-j2\pi ft}dt \qquad s(t)=\frac{1}{2\pi}\int_{-\infty}^{\infty}S(f)e^{j2\pi ft}df \tag{2}$$

Because of the survival of the noise, the performance of the signal processing such as the signal extraction and signal filtering is affected to a great degree. For meeting the demand of the conditions, the time frequency distribution of the constant signal $s(t)$ defined as:

$$P(t,f)=\int_{-\infty}^{\infty}s(u+\frac{\tau}{2})s^*(u-\frac{\tau}{2})\alpha(\tau,v)e^{-j2\pi(vt+f\tau-vu)}dudvd\tau \tag{3}$$

In the design of the time frequency distribution, the core function should be designed according to the real application.

Feature extraction algorithm in the sudden changing interference

The maximum value of the WVD on some moment is not the instant frequency value of the signal, then the instant frequency is a slow change function, the basic concept of the algorithm is come from the digital image processing subject, the principle of the algorithm is that the length of the toe points in the two dimensions of the interface is demanded to be minimum, considering the time interval $n\in[n_1,n_2]$, all the paths between n_1 and n_2 points belong to K. the instant frequency is the minimum path shown as follows:

$$\hat{\omega}(n)=\arg\min_{k(n)\in \mathrm{K}}[\sum_{n=n_1}^{n_2}g(k(n),k(n+1))+\sum_{n=n_1}^{n_2}f(WVD(n,k(n)))]=\arg\min_{k(n)\in \mathrm{K}}p(k(n);n_1,n_2) \tag{4}$$

Where the $p(k(n);n_1,n_2)$ is the sum of $g(x,y)$ and $f(x)$, and the $g(x,y)$ is the cost price function of n_1 to n_2 along with path $k(n)$. The function $g(x,y)=g(\left|x-y\right|)$ is non decreasing function for the $\left|x-y\right|$, and the $f(x)$ is non increasing function for the $x=WVD(n,k(n))$. Then the maximum value of WVD on some moment is the instant frequency value of the signal.

Where the M is the points number of the signal frequency, the function $f(x)$ is defined as:

$$f(WVD(n,\omega_j)) = j-1 \tag{5}$$

If $g(x,y) = const$ the maximum value of WVD on some moment is the instant frequency value of the signal in the formula (5), the minimum value which is determined by the function $f(x)$.the $g(x,y)$ is shown as linearity form.

Simulation results and analysis

In the simulations, the signal is going to be extracted with the new algorithm for the intrusion network signal with sudden changing noise interference, and the DARPA database is taken as the object of study, the database can represent the real network data and it contains abundant intrusion signal types. The detected network intrusion signal is selected as the detection objective in the DARPA database, the test time is from 12:00 AM to 18:00 PM. The simulation parameters are set as follows: the network intrusion signal is taken as the simulation objective and the normalization original frequency $f_1 = 0.3$, and the normalization stop frequency $f_2 = 0.05$. In the sudden changing interference and the SNR is -5dB. The network intrusion signal is extracted based on the time frequency analysis method. The useful signal information is got though WVD algorithm, it can be shown in the WVD result plot as a line in the axis. In this paper, the WVD and Hough transform are combined together to detect the LFM signal. According to the two groups of the intrusion signal, the filtering extraction results are showed in the Figure2 as follows.

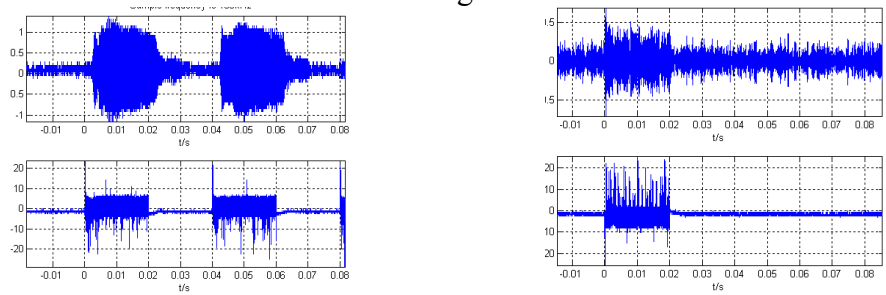

Figure1 Filtering result for the network intrusion signals

The WVD and Hough transform algorithm of the time frequency analysis method is proposed and simulated in the experiment, according to the collected network intrusion signal, the frequency spectrum is shown in the Figure 2. Where the SNR = -5dB. In the Figure 2, it is showing that there is massive interference information resulted from noise in the time and frequency interface, and there is a sharp peak shown as the power collection property. The spectrum figure shows that the signal is extracted and detected perfectly with nice performance.

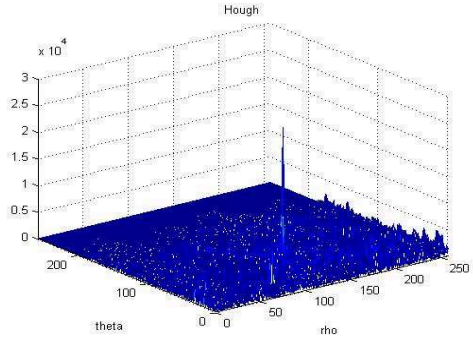

Figure 2 Signal extraction result based on WVD-Hough

Conclusions

In the paper, the signal detection and extraction problem of the network intrusion signal in deep camouflage was analyzed. Simulation and experiment was implemented on the objects of the network intrusion signal with the real collection in the database. Simulation result shows that the performance of decreasing the noise and filtering is very good in the interference of the sudden changed noise as the SNR is -5dB. The intrusion signal can be detected and extracted perfectly, and also it shows good value in the analysis of the network safety in the network safeguard application.

References

[1] Wei Xindan. Simulation Research on the Fuzzy C Algorithm In Network Intrusion Protection[J]. Bulletin of Science and Technology, 2012, 28(12): 221-223.
[2] SUI Xin. Study and Implementation on Host Characteristic Information Passively Identifying[J]. Science Technology and Engineering, 2013, 13(3): 652-658.
[3] WU Chun-qiong. Network Intrusion Detection Model Based on Feature Selection[J]. Computer Simulation. 2012, 29(6): 136-139.
[4] ZHANG Xu, ZHANG Yong-gang. Simulation for Acoustic Channel Influenced by Shallow Water Thermocline[J]. Journal of System Simulation, 2012, 24(10): 2167-2171.
[5] ZHANG Yi, ZHOU Bingyin, HU Guangbo. Hardware System Design of Underwater Motor Pump Faults Diagnose Detector[J]. Computer & Digital Engineering, 2012, 40(11): 162-166.

Advanced Materials Research Vols. 989-994 (2014) pp 3814-3817
© (2014) Trans Tech Publications, Switzerland
doi:10.4028/www.scientific.net/AMR.989-994.3814

Application and Research of Data Mining Technology in Communication Network Environment

Zhang Zhi[1,a]

[1]Jiangxi Science & Technology Normal University; Technique Center of Modern Education; Jiangxi Nanchang, 330013,China

[a]qfzz129225@163.com

Keywords: communication network; abnormal data recognition; data mining; fuzzy C-means clustering

Abstract. The abnormal data of communication networks are complex and diverse, it is difficult to recognize and mine the abnormal data accurately and effectively with traditional methods. In order to improve the recognition accuracy of communication network, a data mining algorithms based on the method of communication network abnormal data recognition is presented. Firstly, the communication network data samples are analyzed for fuzzy c-means clustering in order to obtain the degree of membership matrix. Secondly, the training samples of communication network abnormal data mining are selected according to the membership. At last, the training samples are put into the least square support vector machine learning, which establish the model of abnormal data identification in communication network. The performance of the algorithm was tested by simulation tests, and the results show that, the abnormal data recognition efficiency and accuracy in this paper was improved much more than the traditional identification methods.

Introduction

With the development of information technology, communication network security problems have become more serious, mainly for network intrusion, communication secrets leak and information warfare. Abnormal data recognition was defined to extract the abnormal data from a large number of data. Abnormal data recognition of the communication network and the security characteristics of the communication network has an important role on the protection of national communication secrets[1].

The abnormal data recognition of the communication network can be divided into non supervision recognition methods and supervision recognition methods. Non supervision recognition methods include K-Means method, FCM method[2], and supervision recognition methods include maximum likelihood method, and it is a good solution to the contradiction between the learning accuracy and generalization ability, so more and more scholars begin to apply LSSVM to abnormal data recognition of the communication network[3]. But the communication network data is quite large. Therefore, the selection of training samples becomes a difficult problem in abnormal data recognition of the communication network. In normal circumstances, the communication network data samples need manual's participation, which prevents the application of the LSSVM in the abnormal data recognition of the communication network. In order to solve the problem, some scholars proposed to select training samples using K-Means clustering, but the efficiency is low, it is difficult to obtain high recognition accuracy[4]. FCM algorithm using fuzzy theory can overcome the shortcomings. Some scholars have improved the FCM algorithm, which improved the precision of abnormal data recognition of the communication network[5].

In order to improve the communication network identification accuracy, the abnormal recognition method of data mining algorithms based on communication network data. First on the communication network data samples for fuzzy c-means clustering, obtains the degree of membership matrix, and then according to the membership degree matrix selection of abnormal data mining communication network training. The training samples to input the least square support vector machine learning, data mining model based anomaly of communication network, and the

simulation results on the performance of the algorithm was tested. The results show that this method can improve the data mining efficiency and accuracy of the communication network.

The principle of abnormal data recognition in communication network

Communication network security is affected by a variety of factors, and the abnormal data recognition of the communication network is to extract abnormal data using data mining methods. So the network security personnel can make effective prevention according to the recognition results in order to reduce the loss of communication network security problems. The input variable of communication network at i moment was $\{x_{i1}, x_{i2}, \cdots, x_{im}\}$, and the corresponding data type was y_i, which value was 1 or -1, and 1 represented normal, -1 represented abnormal, then the mathematical model of abnormal data recognition in communication network was expressed:

$$\hat{y}_i = f(x_1, x_2, \cdots, x_m) \tag{1}$$

If all the training samples are put input to the algorithm for learning, it is difficult to calculate. T herefore it is necessary to make cluster analysis on the sample data. FCM algorithm is adopted for c lustering analysis in this paper , and the training samples are sent to LSSVM to learn. The structure of abnormal data recognition in communication network based on FCM-LSSVM is shown in Figure 1.

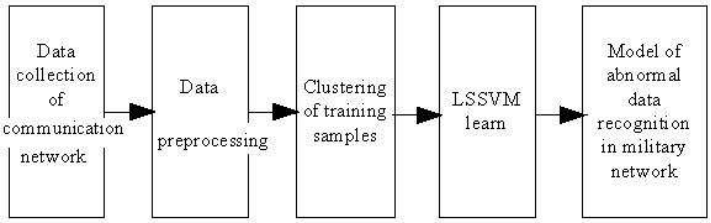

Figure 1 Structure of abnormal data recognition in communication network

The method of abnormal data recognition in communication network based on FCM-LSSVM

A. Least square support vector machine (LSSVM)

The training set of communication network data was supposed as {xi, yi}, so the linear function of optimal classification hyper plane of LSSVM in high dimensional feature space was:

$$f(x) = w^T \varphi(x) + b \tag{2}$$

In which, ω is the weight vector and b is the offset.

According to the structural risk minimization principle, type(2) can be expressed in a constrained optimization problem:

$$\min_{w,b,e} J(w,e) = \frac{1}{2} W^T W + \frac{C}{2} \sum_{i=1}^{n} e_i^2 \quad s.t. \;\; y_i = w^T \varphi(x) + b + e_i, i = 1, 2, \cdots, l \tag{3}$$

Where, C is the penalty parameter and ei is the prediction error.

The constrained optimization problem became a unconstrained optimization problem by introduc ing the Lagrange multiplier, and the Lagrange function was established as:

$$L(w,b,e,\alpha) = J(w,e) - \sum_{i=1}^{l} \alpha_i \left(w^T \varphi(x_i) + b + e_i - y_i \right) \tag{4}$$

In which, α_i is the Lagrange multiplier. According to KKT conditions, we select the radial basis kernel function as kernel function of LSSVM, the recognition decision function of LSSVM abnorm al data recognition in communication network is:

$$f(x) = \operatorname{sgn}\left(\sum_{i=1}^{n} \alpha_i \exp\left(-\frac{\left\| x_i - x_j \right\|^2}{2\sigma^2} \right) + b \right) \tag{5}$$

In which, σ is the width parameters of the radial basis kernel function.

B. The recognizer design of abnormal data

LSSVM is the two meta classifier, and communication network's abnormal data types, must con struct multiple recognizers to do the abnormal data recognition of the communication network, the " one to many" way was constructed multiple classifiers to identify the abnormal data. For example, t he abnormal data in communication networks has a total types of 4, and the abnormal data for +1, t he normal data for -1.

C. Fuzzy c-means clustering (FCM)

Supposing the data set in FCM algorithm is $X=\{x_1,x_2,\cdots,x_n\}$, and n is the number of data sets of X, which each element is a vector p, containing a class c, the class i center is $v_i=\{v_{i1},v_{i2},\cdots,v_{ip}\}$, the elements j in the X membership to the class centers of degree i is u_{ij}, $U=\{u_{ij}\}$, $V=\{v_{ij}\}$:

$$u_{ij}\in[0,1] \qquad \forall i,j,\sum_{i=1}^{c}u_{ij}=1 \qquad \forall j,\ \forall i,0<\sum_{j=1}^{n}u_{ij}<1 \tag{6}$$

The objective function for FCM algorithm is:

$$J(U,V)=\sum_{i=1}^{c}\sum_{j=1}^{n}u_{ij}^{m}\left\|x_j-v_i\right\|^2=\sum_{i=1}^{c}\sum_{j=1}^{n}u_{ij}^{m}d_{ij}^2\to\lim \tag{7}$$

Conditional extreme value of J function can be obtained by the method of Lagrange multipliers. First of all, the J function in the formula (7) under the extreme conditions can be expressed as:

$$J(U,V)=\sum_{i=1}^{c}\sum_{j=1}^{n}u_{ij}^{m}d_{ij}^2+\lambda\left(\sum_{i=1}^{c}u_{ij}^{m}-1\right) \tag{8}$$

In the formula (8), parameter λ is a constant. The two first order partial derivatives of J function is:

$$\frac{\partial J}{\partial u_{ij}}=mu_{ij}^{m-1}+\lambda,\frac{\partial J}{\partial v_{ij}}=-2\sum_{j=1}^{n}u_{ij}^{m}d_{ij} \tag{9}$$

Experiment and Analysis

Simulation experiment data is from the American DOD Lincoln Laboratory DARPA data set, which is composed of the normal data and the different types of abnormal data. And the abnormal behavior are: denial of service (DOS), remote unauthorized access attack (R2L), non authorized to obtain super user privileges attack (U2R), vulnerability detection and scanning attack (PROBE), each data consisting of 41 attributes, 7 of them are symbolic variables, 34 is a continuous variable. Because the DARPA data set is large, only 10% of the data was used in the experiments. The experiments are taken on the Intel Core4 2.8GHz, 2GB memory, simulation platforms are Windows XP and Matlab 2012.

The feature scope of DARPA data set is different, and the LSSVM is based on a sample and a h yper plane distance. A few characteristic has a strong influence on the performance of LSSVM, and the other characteristics have small influence. Therefore we need to eliminate the negative impacts. Comparison of the running time of algorithms, compared with K-Means, FCM and LSSVM, the run ning time of FCM-LSSVM is greatly reduced, and it greatly improves the recognition efficiency of communication network abnormal data. The data recognition results are shown in Figure 2, and it s hows that the method has good data mining and recognition performance in communication applicat ion.

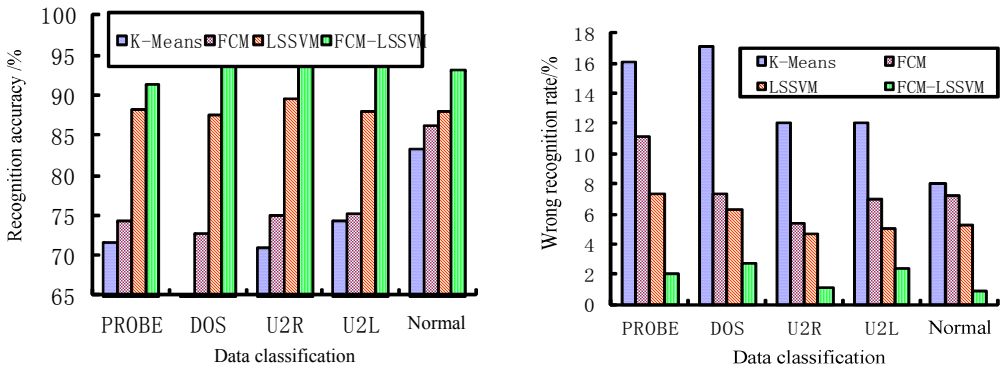

Figure 2 Data recognition results with different algorithms

Conclusions

In view of the abnormal data mining problems in current communication network, FCM-LSSVM mining algorithm was proposed in this paper. In the training sample extraction process, FCM-LSSVM only extracts the samples relatively close to the cluster center, which have representativeness and better performance. Combining with the LSSVM generalization ability, the mining accuracy can be improved very well. The experimental results show that the FCM-LSSVM classification was better than the unsupervised classification algorithm, and the extraction of training samples is more simple and reasonable. Comparing to the unsupervised classification and supervised classification algorithm, FCM-LSSVM need more time to classify, but data mining accuracy of communication network was increased greatly. FCM-LSSVM is suitable for the application of abnormal data mining in communication network, without complex process of training samples from supervised classification algorithm.

Reference

[1] CAO Jian, LI Hai- sheng, CAI Qiang. Research on Feature Extraction of Image Target[J]. Com puter Simulation. 2013; 30(1): 409-413.

[2] Wei Xindan. Simulation Research on the Fuzzy C Algorithm In Network Intrusion Protection[J]. Bulletin of Science and Technology. 2012; 28(12): 221-223.

[3] Xia K, Cai J, Wu Y. Research on Improved Network Data Fault-Tolerant Transmission Optimi zation Algorithm[J].Journal of Convergence Information Technology, 2012, 7(19):208-213.

[4] ZHENG Guo, WANG Bing, CUI Jun-. Generic prediction assisted single-copy routing in under water delay tolerant sensor networks[J]. Ad hoc networks, 2013, 11(3): 1136-1149.

[5] QIU Jing, WANG Ping. Encryption Algorithm for Compressed Image Based on Chaotic Maps[J]. Computer Science, 2012, 39(6): 44-46.

Advanced Materials Research Vols. 989-994 (2014) pp 3818-3822
© (2014) Trans Tech Publications, Switzerland
doi:10.4028/www.scientific.net/AMR.989-994.3818

Study on optimal design approach of one-card under multi-signal conflict

ZHU Heng-jun[1], WANG Zhuo[2]

[1]Communication and Electronics Engineering Institute of Qiqihar University，Heilongjiang Qiqihar 161006，China;

[2]Qiqihar Branch of China Telecom Corporation Limited,Heilongjiang Qiqihar 161000，China)

[a]18904621322@qq.com

Keywords: multi-signal conflict; one-card; optimal design

Abstract. IC card is a product of microelectronics, computer and information technology, with the development requirements of its wide application and digitized, one-card system will inevitably become a trend. The operation mode of one-card System with "one card, one database, one network", can both realize the norms for user management, but also provide important information for managers. Meanwhile, as an important part of digital one-card systems is one of the foundation works of information collection in the digital environment. It has the great significance for management and decision support of users.

Introduction

In the crowded environment, the designed one-card system based on multi-signal model is also being widely used [1]. Campus one-card system is one typical representative, which combines computer technology, network communication technology, automatic control technology and smart card technology. Various decentralized management and service facilities within the same system are fully integrated into computer management system to achieve the highly integration and full functionality of entire intelligence management system [2]. The main design idea is that by building standardized, secure, and scalable campus management system to fulfill informational, intelligent, self- oriented campus management [3]. The basic construction process is to solve the problem of campus electronic money, then according to the standards of educational industry information system construction and regulation of campus card to extend information technology applications and services to all aspects of campus management [4]. "Campus One-Card System" as an important part of digital campus, is one of the basic engineering of digital information collected on campus ,which has great significance for school management and decision support.

Multi-signal optimal design models

Chip and the antenna have no exposed parts, cards at a certain distance (typically 5-10mm) close to the surface of the reader, by passing radio waves to complete read and write operations of data. The technology succeeded in combining radio frequency identification technology and IC card technology together to solve the problem of no power supply in the card and non-contact, which is a major breakthrough in the field of electronic devices

A.operating principle of one-card

Currently, in one-card system, a contactless IC card with the carrier frequency of 13.56MHz generally is used, also known as radio frequency card or proximity card. It consists of inductive antenna and IC chips, packaged in a standard PVC cards. chip and antenna without any exposed parts card at a certain distance (typically 5-10mm) near the surface of the reader, the transmission by radio waves for reading and writing operation of data. It succeeded in radio frequency identification technology and IC card technology together to solve the passive (no power supply card) and avoid contact with this problem, a major breakthrough in the field of electronic devices.

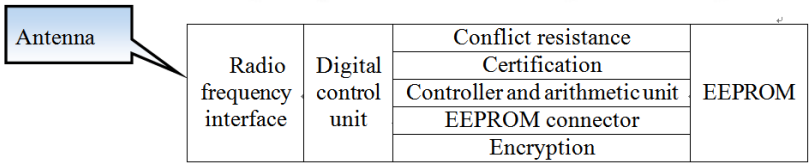

Figure 1 Logical block diagram of Mifare 1 S70 's

The non-contact IC card energy transfer process is as follows (Mifare example): the card itself is a passive member , when writing is operated on the card reader, the reader send a fixed frequency electromagnetic waves to the IC card, the card which has a L / C series resonant circuit , the frequency of it is same to the reader, thus generating an electromagnetic resonance, so that the capacitor has been charged. At the other end of the capacitor has a one-way electronic pump, which is used to transmit the charge in the capacitor to the other capacitor to store. When the charge storage accumulation reaches 2V, this power supply provides the operating voltage for the other circuits to transmit the data in the card or receive the data in reader (rate of 106kbps). Mifare 1 S70 has the logic diagram shown in Figure 1, the internal part mainly consists of the analog, digital section and the storage unit.

Non-contact reader includes two opposite paths flowing signal channel: the upper transmit channel and the lower receiver channel. Firstly, in the transmit channel, the corresponding frequency of carrier signal is generated from the quartz crystal oscillator with stable frequency. The signal will be made amplitude shift keying (ASK) modulation by the planned sending message which has been coded based on Manchester or variant Miller or the NRZ rules in the ASIC segment, and finally after a power output stage amplifier , it can be transmitted by the antenna . In receiving channel, interference and noise is filtered in input signal firstly. The weak response signal of non-contact type IC card is extracted from the high -intensity transmit driven signal, and then be amplified for further ASIC processing.

B.The realization of multi-signal Anti-collision operation

Setting the taken energy of signal transmission in one-card application process can be represented by y_T, the time consuming of this process can be with y_V , then, the following equation can be expressed the energy relationship:

$$y = y_T + y_V \quad (1) \qquad y_T = s_p(R_{Tv} + R_{Tt}H) \quad (2)$$

$$y_V = s_p R_{Vt} + wpR_{Vv} \quad (3)$$

Setting the number of all signals can be represented by p, the number of slots in signal transmission can be represented by H, the number of levels of the binary tree can be represented by N, then the number of time slots can be calculated using the following equation:

$$H = 2^N \quad (4)$$

The probability of a tag response can be calculated using the following equation when signal transmit in the designated channel,:

$$R(K) = \begin{cases} (1+D^N) & (N>0) \\ (H-1)^Q / H^Q & (N=0) \end{cases} \quad (5)$$

In this channel, there is no responding probability of tag can be calculated using the following formula:

$$R(U) = \sum_{m=1} R(m,p,N) R_{QE}(H,m) =$$

$$\begin{cases} \sum_{m=1} R(m,p,N) R_{QE}(H,m) & (N>0) \\ p(H-1)^{Q-m} / H^Q & (N=0) \end{cases} \quad (6)$$

Using the following equation, the probability of signal collision in this time can be calculated:

$$R(E)=1-R(U)-R(K)=1-R(U)-R(K)$$
$$=1-(1-D^N)-\sum_{m=1}R(m,p,N)R_{QE}(H,m) \quad (7)$$

Thereinto, $R_{QE}=H/H(H-m)$. In search process by using binary, the probability of signal collision occurs in specified channel can be calculated by the following equation:

$$Z_{y,N,p}=Z_{N,p}=1-(1-D^N)-$$
$$\sum_{m=1}R(m,p,N)R_{QE}(H,m)\ (N>0) \quad (8)$$

When the number of binary levels $N=0$, $z_{y,p}=1-R_{QE}(H,p)$. Using the following formula can calculate the probability of the N -layer binary occurs in the signal collision of y -th channel:

$$X_{y,N,p}=\begin{cases}1\ (N=0)\\ Z_{N-1,p}\ (N>0)\end{cases} \quad (9)$$

In the process of N -layer binary searching, it can use the following formula to calculate the number of slots:

$$v(p)=(H+1)\sum_{k=0,y=0}X_{y,N,p}$$
$$=(H+1)\left|1-\sum_{N=1}D^N X_{N,p}\right| \quad (10)$$

Assuming the specified tag is responding in the slot time, the collision problem of the nodes of a binary tree in this hierarchy exists in the signal channel, and the collision probability of the signal can be calculated using the following formula:

$$\mu_{y,q,p}=\sum_{m=1}mR(m,p,q)R_{QE}(H,m) \quad (11)$$

According to the above described, the signal can be made anti-collision operation, thereby reducing the probability of collision.

simulation experiment and results analysis

A. Structure of Campus Card System

In an example of a technical secondary school's campus card, the system function module mainly composes by the card system platform and application subsystems (shown in Figure 2) :

Application subsystem divides into logistics group , financial , academic , student office, and so on. in, the dual-use and compatibility of the network on / off is fully considered in the structural design of campus card system.

(1) Networking technology selection.

The fast Ethernet switching networking is used in the backbone network of campus card. it has the advantage of mature technology and low investment costs. Moreover, it can meet application needs of medium-sized network by combining with switching technology. RS485 star topology is used in Subnets, and seamlessly connected with Ethernet via protocol converter to ensure real-time data transmission.

(2) Network communication protocol selection.

In order to ensure openness and compatibility of networks, TCP / IP is selected as the communication protocol of network applications. TCP / IP can support different communication network between different types of operating systems and communication modes, including Ethernet, FDDI, Token Ring, X. 25 packet switch network and Frame Relay networks. RS485 communication protocol is selected in Subnet. The use of RS485 communication protocol can

reduce the cost. It can extend the communication distance of one terminal equipment to 1 200M, far exceeding the limit of 100M of Ethernet equipment.

B. operating mechanism of one-card system

Finally, all transactions occurred in card system will be collected to card data centers with the form of day-to-day. Therefore, the system should ensure the correctness and uniqueness upload of current count. It can neither lose any of transaction, nor upload the transaction repeatedly.

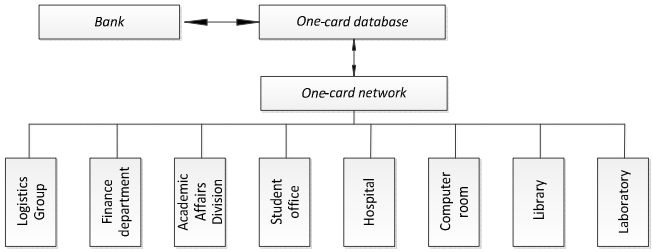

Figure 2 Function modules of one-card system

C device, application access and authentication

The access equipment includes a variety of card machines (eg POS, cash recharge machine, transfer machine, etc.). The access application includes various application systems, third-party integration system (libraries, schools hospitals, finance, etc.). It needs to prevent illegal equipment and illegal applications circulated into the network. All card machines must be authorized to use in the private card network. It has to carry through check-in and check-out and verify the legitimacy. All devices and applications are filed in the application management center. The cardholders system must have black and white lists inspection mechanism.

D.Experimental results and conclusions

According to multi-signals collision algorithm and the general algorithm, the data extracted from the card is for 10 times test generation respectively. As shown in Table 1, compared to the traditional algorithm, the performance of algorithm in this paper is with less time-consuming and high accuracy almost in all the circuits. The effects in some circuits are remarkable.

Table 1

	Time（ms）		accuracy rate（%）	
number of trials	traditional algorithm	algorithm in this paper	traditional algorithm	algorithm in this paper
1	53	32	84	93
2	56	33	86	94
3	54	35	87	95
4	53	32	84	93
5	55	33	86	94
6	54	35	86	93
7	55	33	85	95
8	52	34	85	94
9	54	35	85	95
10	56	34	87	93

Conclusion

Digital goal of building has two levels. Firstly, the goal of digitizing must follow and serve the overall development goals of constructing the high-quality, high-level, international and open-class multi-disciplinary university. Secondly, in the technology, it is to build unified data center, highly resource sharing business application platform, provide personalized information services and build digital management environment.

Testing indicators improved significantly through multi-signal collision optimal design, indicating that the optimal design is successful. If the optimization design can be carried out synchronously between the card system performance and the structural design, the system will be higher optimization levels.

References

[1] Somnath Deb, Krishna R, Pattipati et.al. Multi-signal flow graphs: A novel approach for system testability analysis and fault diagnosis[c]. IEEE Auto Test conference 1994: 361-373.

[2] Weiping Li, Guisheng Liao, Haihong Tao, and Ming Jin. Poly-phase Encoded Waveform Optimal Design for Space-borne MISO Radar Systems. Radar Conference. 2009 IET International, 2009:1-5.

[3] Hai D. Polyphase Code Design for Orthogonal Netted Radar Systems. IEEE Trans. on SP. 2004, 52(11): 3126-3135.

[4] Liu Bo, He zishu, Zeng jiankui et al. Polyphase Orthogonal Code Design for MIMO Radar Systems. Radar 2006 CIE' 06 International conference,Oct. 2006: 1-4.

[5] JOAN DAEMEN，VINCENT RIJMEN。Advanced Encryption Standard(AES)algorithm-Rijndael design [M]。 GU Da-wu，XU Sheng-bo，translation。Beijing：Tsinghua University Press，2003。(in Chinese) 205

Advanced Materials Research Vols. 989-994 (2014) pp 3823-3826
© (2014) Trans Tech Publications, Switzerland
doi:10.4028/www.scientific.net/AMR.989-994.3823

Design and Simulation of Wireless Communication System Channel in Coal Mine Based on OFDM Technology

Ma Ronghua[1,a]

[1]Computer Software and Theoretical Research, ZhengZhou Railway Vocational&Technical College ZhengZhouHeNan 450000, China

[a]50005280@qq.com

Keywords: channel; OFDM; delay spread

Abstract. The OFDM technology is applied in the mobile communication system of underground coal mine, the wireless communication system channel of underground coal mine is researched. The underground channel model is established, and the simulation is taken for testing the performance of system. The simulation results show that the OFDM technology can be applied in the mobile communication system in underground coal mine, and the transmission rate of the system and the ability of anti-interference are improved.

Introduction

In the underground coal mine, the mobile communication is playing an important role in mine scheduling, motor vehicle drivers communication, and the communication with other staff. It is the main means of communications for the mine operators, with the efficient communication system, the mine safety can be ensured. The efficient production can be obtained, and the disaster relief is realized. Electromagnetic wave is a multi-path propagation in the tunnel of coal mine, because of the mine environment is special and complex, the signal occurs delay spread, and the inter symbol interference (ISI) is occurred in the digital transmission system. The performance of digital communication system is affected seriously. Multi carrier orthogonal frequency division multiplexing (OFDM) technology is used to increase the symbol transmission time with parallel transmission, cyclic prefix is used to eliminate the inter symbol interference, and it can effective process the delay caused by multi-path transmission expansion.

Characteristics and model of wireless channel of underground coal mine

A.Characteristics of underground wireless channel

Because the coal production mainly is worked in underground, working environment is poor, the work area is narrow with poor lighting, and the humid and corrosive are serious. Security threats from water, fire, gas, roof accident are great, mobility of staff and equipments is great, and d other special factors are complicated.

(1) Multi-path propagation phenomenon of underground communication

The roadway of coal mine is relatively narrow in China, the length is up to several 10km, and it is distributed in different levels, section size usually reaches to tens of meters, tunnel wall rock and coal seam are rough, there are large number of dust, coal mining support, mechanical and electrical equipment, rail, power lines, and so on, the environment is very special and complex. Electromagnetic wave generates multi-path effect in communication, it affects the transmission quality.

(2) Received signal is time varying signal

In the underground wireless communication, due to antenna distribution in the tunnel, emission efficiency of the antenna is very low. The propagation velocity of electromagnetic wave is great. In addition, because of mine locomotive motion, the relative movement between the radio receiver and transmitter is occurred, there is Doppler effects. This leads to the signal receiving device is a time-varying signal, the amplitude fading is produced, and the signal to noise ratio of communication is low.

(3) Serious interference from underground electrical and mechanical noise

Electricity is the main power of the coal mine production, the main equipments are mine locomotive, excavator, fan relies on electricity to drive. The use of electricity is from the electromagnetic noise and electromagnetic radiation. The noise has become one of the important factors that influence the quality of communication.

B.Wireless channel model of coal mine

Most of coal mine roadway is flat, electromagnetic wave exists two kinds of fading propagation in this tunnel: one is the signal fading caused by the remote transmission for large scale fading, another kind is the signal fading arising from multipath propagation which is called the small scale fading. When frequency of wireless communication device above the cut-off frequency of tunnel, signal fading is decreased with the frequency increasing, it belongs to the large scale fading.

Table 1 Effect on the frequency of straight tunnel decay rate

Frequency(MHz)	40	60	150	470	900	1700
Attenuation (dB/km)	301	217	113	9.8	2	1.6

The system frequency is selected as is 1.8GHz, then the cause of signal attenuation is multi-path propagation. The statistical characteristics of small scale fading are analyzed. Assuming that the input signal into the channel is $s(t)=\mathrm{Re}\left(s_l(t)e^{j2\pi f_c t}\right)$, and the discrete multi-path channel can be expressed as $y(t)=\sum_{n=1}^{L}\alpha_n(t)s\left[t-\tau_n(t)\right]$.

Where, $s_l(t)$ is the equivalent low pass signal, f_c is carrier frequency, $\alpha_n(t)$ is the path delay with n paths, and $\tau_n(t)$ is the time delay of n paths, L is the number of paths. After low-pass equivalent, the

The carrier frequency, attenuation is the path, is a path delay, path number. After low-pass equivalent, $s(t)$ can be expressed as

$$s(t)=\mathrm{Re}\left[\tilde{s}(t)e^{j2\pi f_c t}\right] \tag{1}$$

Then, $y(t)=\mathrm{Re}\left\{\left(\sum_{n=1}^{L}\alpha_n(t)e^{-j2\pi f_c\tau_n(t)}\tilde{s}(t-\tau_n(t))\right)\right\}e^{j2\pi f_c t}$

The complex envelope of output signal is:

$$\tilde{y}(t)=\sum_{n=1}^{L}\alpha_n(t)e^{-j2\pi f_c(t)\tau_n(t)}\tilde{s}(t-\tau_n(t))=\sum_{n=1}^{L}\tilde{\alpha}_n(t)\tilde{s}(t-\tau_n(t)) \tag{2}$$

As formula (2) shows, the following complex time-varying low-pass equivalent impulse response $\tilde{c}(\tau;t)$ is used to describe multipath channel as:

$$\tilde{c}(\tau;t)=\sum_{n=1}^{L}\tilde{\alpha}_n(t)\delta(t-\tau_n(t)) \tag{3}$$

Where, $\tilde{c}(\tau;t)$ represents the added $t-\tau$ pulse channels in the t time response.

Because each path of discrete multipath channel can be regarded as the result of joint action of many scattering components, therefore, each tap of paths can be regarded as a complex Gauss random variables.

According to the channel model proposed by Bello, assume that the channel impulse response is wide sense stationary (WSS) random process, it meets:

$$R_{\tilde{c}\tilde{c}}(\tau_1,\tau_2,\alpha)=E\left\{\tilde{c}^*(\tau_1,t)\tilde{c}(\tau_2,t+\alpha)\right\} \tag{4}$$

Assumed the phase values are not correlated in different paths and different amplitudes, then:

$$R_{\tilde{c}\tilde{c}}(\tau_1,\tau_2,\alpha)=R_{\tilde{c}\tilde{c}}(\tau_1,\alpha)\delta(\tau_1-\tau_2) \tag{5}$$

The autocorrelation function of WSSUS channel can be expressed as:

$$R_{\tilde{c}\tilde{c}}(\tau,\alpha)=E\left\{\tilde{c}^*(\tau,t)\tilde{c}(\tau,t+\alpha)\right\} \tag{6}$$

The scattering function of the multipath channel is defined as:

$$S(\tau,\lambda)=F\left\{\left(\underset{\sim}{R}_{cc}(\tau,\alpha)\right)\right\}=\int_{-\infty}^{\infty}\underset{\sim}{R}_{cc}(\tau,\alpha)\exp(-j2\pi\lambda\alpha)\,d\alpha \tag{7}$$

Assume that the bandwidth of input signal $s(t)$ is W, according to the sampling theorem, the equivalent low pass signal can be expressed as:

$$\tilde{s}(t-\tau)=\sum_{n=-\infty}^{\infty}\tilde{s}(t-nT)\frac{\sin\left(2\pi B(\tau-nT)\right)}{2\pi B(\tau-nT)} \tag{8}$$

Where, $B=W/2$ is the equivalent baseband signal bandwidth, the sampling interval is $T=\frac{1}{2B}=\frac{1}{W}$, the output equivalent low pass signal is:

he equivalent baseband signal bandwidth, sampling interval. The equivalent low-pass signal output is:

$$\tilde{y}(t)=\int_{-\infty}^{\infty}\tilde{c}(\tau;t)\left\{\sum_{n=-\infty}^{\infty}\tilde{s}(t-nT)\frac{\sin\left(2\pi B(\tau-nT)\right)}{2\pi B(\tau-nT)}\right\}d\tau \tag{9}$$

Assumed the length of the channel impulse response is NT, if n<0 or n>N, the value of $\tilde{g}_n(t)$ is 0 approximately, the relation between input and output as above can be approximated as:

$$\tilde{g}_n(t)\approx T\cdot\tilde{c}(nT;t) \tag{11}$$

$$\tilde{y}(t)=\sum_{n=0}^{N}\tilde{s}(t-nT)\tilde{g}_n(t)\approx T\sum_{n=0}^{N}\tilde{s}(t-nT)\tilde{c}(nT;t) \tag{12}$$

The above model is firstly proposed by Kailath, called TDL channel mode, the structure is shown in Fgure 1.

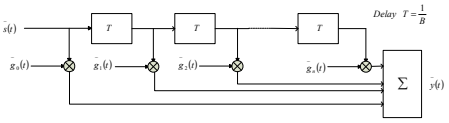

Figure 1 Tapped delay line (TDL) channel model

Communication system construction of underground coal mine and performance simulation

The OFDM physical layer parameters selection is very important to the performance of the system. According to the radio waves as above, the propagation channel model in the underground is calculated as 1.8GHz, the RMS delay spread of model 1 is $\tau_{rms}=46ns$, in the model 2, the RMS delay spread $\tau_{rms}\approx 62n$, the delay spread for indoor radio propagation is $60.6ns$, according to the IEEE802.11a standards, the OFDM physical layer parameters are expressed as follows: working frequency is 1800MHz, the bandwidth of the system is 20MHz, the number of subcarriers is 64, sub carrier spacing is 0.3215MHz(20MHz/64), the effective symbol period is $3.2\mu s(1/0.3125MHz)$, protection interval is 0.8 μs, modulation is 4QAM, the maximum transmission rate is $26Mbits/s(2\times 1/4\mu s\times 52)$. In order to facilitate the simulation, equivalent baseband model of OFDM system. In figure 2, the binary system simulation results is shown, the channel estimation uses LS estimation, the error rate results are calculated, it shows that the new method has better performance.

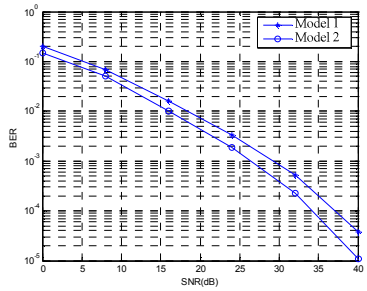

Figure2. Comparison of bit error rate of OFDM system in underground coal mine communication

References

[1] Zheng Baodao, Wang Huaijie. Design of Remote Image Alarming System Based on ARM/GPRS. Computer Measurement & Control. 2013; 21(1): 149-151, 159.

[2] MA Jian- hong，JI Li- xia. Study on Agent Immune Network Monitoring System Model[J]. Computer Simulation. 2013; 30(5): 213-216.

[3] Shen Yuan. Research on Intrusion Detection System Neural Networks and Principal Component Analysis[J]. Bulletin of Science and Technology. 2013; 29(6): 32-34.

[4] Yu Qingsheng. The Design and Implementation of Cloud Platform Based Building Algorithm for Logistic Regression Model[J]. BULLETIN OF SCIENCE AND TECHNOLOGY, 2013, 29(6): 137-139.

[5] Lin C W, Hong T P. A new mining approach for uncertain databases using CUFP trees. Expert Systems with Applications. 2012, 39(4): 4084-4093.

Advanced Materials Research Vols. 989-994 (2014) pp 3827-3833
© (2014) Trans Tech Publications, Switzerland
doi:10.4028/www.scientific.net/AMR.989-994.3827

Astronomical image matching based on the cross-correlation algorithm

JiJun Sun

(Department of mathematics and computer science, Panzhihua University, 617000, China)

405491737@qq.com

Keywords: Astronomical image, cross-correlation, medical image analysis

Abstract. Image registration is widely used in the areas of image fusion, target tracking, remote sensing data analysis, medical image analysis such as organization pathological changes, under the constantly exploring to the image registration technology. In this paper astronomical image matching based on the cross-correlation algorithm is proposed and we focuses on adopting the registration form using the cross-correlation method after segmenting the astronomical images. The method can effectively solve the difficulties of the overall matching, represent the salient regions of features and implement local matching.

1. Introduction

With the rapid development of science and technology, people desire to have a better knowledge of undiscovered areas and devote to the aerospace industry with full enthusiasm, so that the industry becomes a hot research topic. Aimed to obtain high-quality astronomical images, a large number of images are shot in a small time interval and registered. Astronomical images are mostly gray-scale images. With regard to the same image, multiple independent regions of interest co-exist, and the relative positions of interest region shot in a short time are so relatively fixed that large rigid movements are not easy to be generated in a short time. But when flipping images of the same group continuously, it is to find: a considerable problem of the local rigid movement exists in the images, that is to say, regions with rich information head for different directions at the same time. It makes overall matching for images difficult.

In the field of image processing, image segmentation as a key technology for image processing becomes increasingly important, and the segmentation results directly affect the quality of subsequent operations such as feature extraction and target recognition. The aim of image segmentation is to divide an image into several disjoint and a valuable collection of connected subregions in computer vision. The literatures [1][2] carry on a summary to image segmentation technology. Two segmentation methods adopted most frequently have: region-based segmentation and edge-based segmentation. The idea of region-based segmentation is to guarantee as far as possible that feature similarity within regions is greater than interregional that. The commonly used methods have: threshold method, region growing method and splitting and merging method. Generally, edge shows mutation or discontinuity of image features, and edge-based segmentation is to detect these features and form the boundary. The methods used mostly have: Robert operator, Sobel operator, Prewitt operator, Canny operator, Laplasse operator, differential operator [3] and boundary tracking method [4]. In addition, some new algorithms are proposed by combining image segmentation with some specific theories and methods. Regarding the possible solutions to the problem domain as the chromosome groups, the genetic algorithm [5] which has a global searching ability and can avoid the extremal solutions to a certain extent, is generated. In 1988, Osher and Sethia [6] firstly proposed a numerical method which can solve the problem of curve evolution effectively. Subsequently, relevant extensions and a summary of this algorithm were made by Oshe et al [7][8] again. Due to its stability and suitability for any dimensional space, this method is widely adopted at present.

The concept of mutual information from information theory, a measure of useful information, is used to measure the degree of correlation between two random variables. Woods et al [9] proposed and modified an automated method that allowed for cross-modality registration of MRI and PET brain images obtained from a single subject. Maes et al [10] investigated the performance

of various optimization methods and multiresolution strategies for maximization of mutual information, and pointed out that the multiresolution method can effectively overcome the local extremum. Maintz et al [11] proposed to use a global joint histogram based on optimized mutual information combined with a local registration measure to enable local elastic registration. Pluim et al [12] proposed to include spatial information by combining mutual information with a term based on the image gradient of the images to be registered, and made a clear improvement in robustness.

This paper focuses on adopting the registration form using the cross-correlation method after segmenting the astronomical images. Firstly, regions of interest in the images are extracted and segmented according to the principle of image segmentation. Then, the displacements are calculated by using the cross-correlation algorithm. Finally, the registered images can be obtained by performing the fusion of the obtained regions. The method can effectively solve the difficulties of the overall matching, represent the salient regions of features and implement local matching.

2. Extraction of region of interest

2.1 Experimental images

Figure 1 illustrates the experimental images of this paper, which is extracted randomly from 100 serial images shot continuously at the given points by the same sensor. Comparing three images with each other, tiny changes among them are difficult to be observed with human eyes. However, it is to find that regions of interest head for a tiny distance towards different directions if flipping the images continuously. In view of this, defects of the overall matching are considered to be eliminated from the standpoint of local registration.

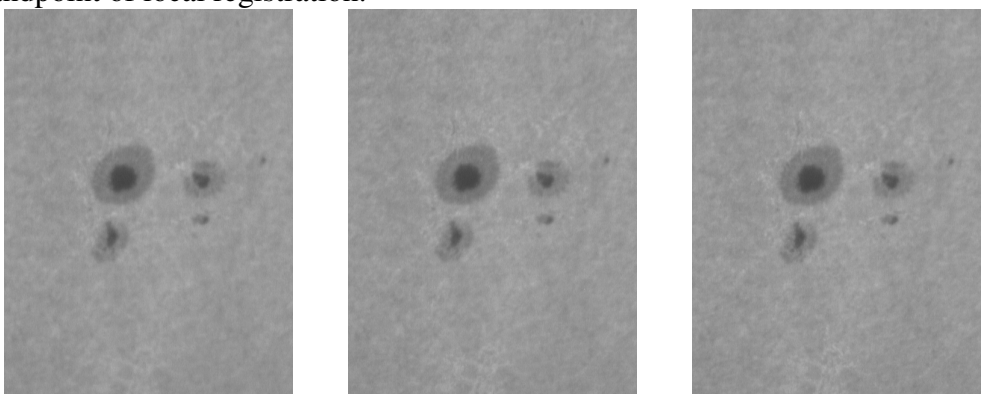

(1) A1 (2) A2 (3) A3

Figure 1 Experimental images (480*640 pixels)

2.2 Binarization processing

In this paper, the Otsu method7-8 is used to determine a binarization threshold value for image segmentation [13-16]. The Otsu method aims at obtaining the optimal threshold by traversing all the gray levels (i=1, 2,…, l) of an experimental image $f(x,y)$. By using the threshold value t, experimental images are divided into two target areas, C_0, C_1 respectively. P_i is the probability after normalizing the histogram. The optimal threshold is denoted as t*.

$$t^* = \arg\max_{i \in l} \delta^2{}_B$$

Where $\delta^2{}_B = \omega_0(\mu_0 - \mu_T)^2 + \omega_1(\mu_1 - \mu_T)^2$, and $\omega_0 = \sum_{i=0}^{t} P_i$, $\omega_1 = 1 - \omega_0$, $\mu_T = \sum_{i=0}^{l-1} iP_i$,

$\mu_0 = \sum_{i=0}^{t} iP_i$, $\mu_1 = \sum_{i=t}^{l-1} iP_i$.

Thus, after binarizing the experimental image $f(x,y)$, $g(x,y)$ is:

$$g(x,y) = \begin{cases} 0, f(x,y) < t^* \\ 255, f(x,y) \geq t^* \end{cases}$$

Figure 2 shows an image of the experimental effect after binarizing A1 of Figure 1 by using the Otsu method.

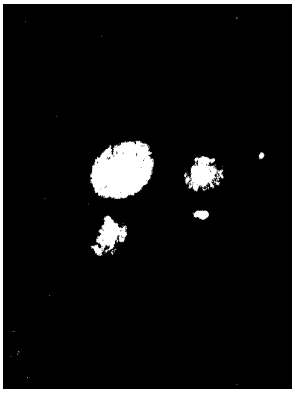

Figure 2

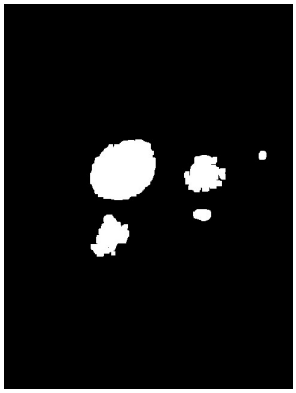

Figure 3

2.3 Morphological processing

Although the locations of five regions of interest can be distinguished clearly in Figure 2, their shapes are very irregular and a great number of holes exist, which makes subsequent cross-correlation registration inconvenient. In this paper, the morphology operations of dilation and erosion are used for image processing.

Pixels are introduced into object edges of images through the dilation operation. During this process, the value of output pixel is the maximum of all input pixels. A is dilated by structural element B, namely $A \oplus B$. Object edges of images are removed through the erosion operation. In contrast to the dilation operation, the value of output pixel is the minimum of all input pixels. A is eroded by B, namely $A \otimes B$.

There are three kinds of common operations by the combination of dilation and erosion operation in morphology, one of which is closed operation that is capable of filling effectively holes, linking notches and smoothing boundaries. The closed operation is named as: $A \bullet B$. And its principle is the result of A after being dilated and eroded by B. Therefore, $A \bullet B = (A \oplus B) \otimes B$. Figure 3 is an image of experimental effect of Figure 2.

3. Normalization of spatial segmentation

This paper focuses on using the method of boundary segmentation. However, when using the method, regions of interest is very irregular, which makes subsequent cross-correlation registration inconvenient. On this basis, we consider intercepting rectangular with the smallest area where regions of interest are included. On one hand, the operation makes cross-correlation registration of irregular images more convenient. On the other hand, registration time reduces when choosing the smallest area.

The normalized algorithm for spatial segmentation proceeds as follows:

(1) Find out the points whose value is 1 in Figure 3. If the points exist, record them. Otherwise, terminate the operation.

(2) Track and search in eight-connectivity and mark the path by choosing the right value. When the round points of tracking target's coordinate are all marked or their values are 0, stop tracking.

(3) Obtain the minimum and maximum of x-axis and y-axis directions in the marked area. When implementing the interception storage of the corresponding rectangular in A (1) of Figure 1, intercepting and st 1A (1) to the corresponding rectangular interception storage, matrix scope is to be appropriately extended around. Some black edges are generated in cross-correlation registration. And the integrity of region of interest can be guaranteed by extended rectangular.

(4) Go to step (1), continue to carry out inspection.

Figure 4 shows the effect images of normalized spatial segmentation for A (1) of Figure 1 according to the above algorithm.

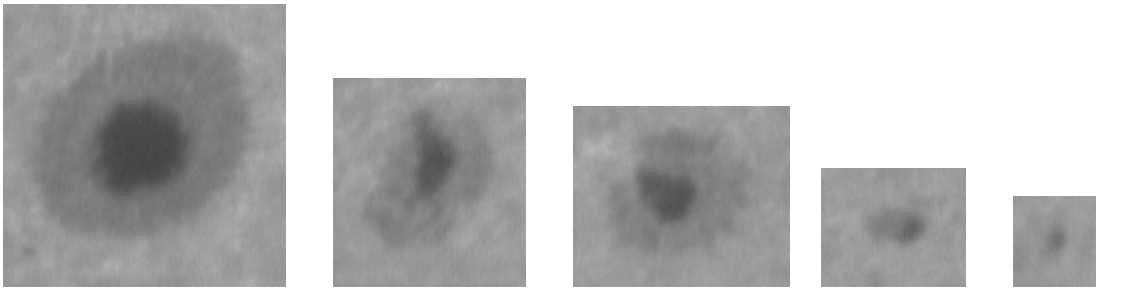

Figure 4 The effect images of normalized spatial segmentation

4. Cross-correlation registration and result analysis

4.1. Cross-correlation registration

In information theory [18], entropy, a measure of information, is usually used to represent the correlation degree between two random variables. Thus, the entropy of an image is a representation of random of the probability distribution to the image. Edge entropies and the joint entropies of images A and B are expressed as:

$$H(A) = -\sum_{a,b} p_A(a) \log p_A(a), \quad a \in A;$$

$$H(B) = -\sum_{a,b} p_B(b) \log p_B(B), \quad b \in B;$$

$$H(A,B) = -\sum_{a,b} p_{A,B}(a,b) \log p_{AB}(a,b), a \in A, b \in B;$$

Where $p_A(a)$ and $p_B(b)$ represent the probability distribution of image A and B, respectively, $p_{A,B}(a,b)$ represent the joint distribution of image A and B.

Accordingly, mutual information can be defined as:

$I(A;B) = H(A) + H(B) - H(A,B)$;

According to the Dobrushin formula, the formula of mutual information can be converted to a definition based on the probability distribution:

$$I(A,B) = \sum_{a,b} p_{AB}(a,b) \log \frac{p_{AB}(a,b)}{p_A(a) p_B(b)}, \quad a \in A, b \in B;$$

Cross-correlation algorithm for matching[19-22] is mutual information-based algorithm. It aims to find a transformation by which the largest amount of mutual information can be obtained when registration between the transformed image and another one are implemented. Figure 5 and 6 show the transform displacements based on *x* axis and *y* axis in the process of the cross-correlation registration for 100 images. Observing Figure 5 and 6, it is to find that: the trend curve of displacement of the local registration doesn't depend on the trend curve of the overall matching, a big deviation exists in movement distances, the deviation of directions even exists for some images. Obviously, the precision of the overall matching is lower than that of local matching when using the same method for registration. Figure 7 shows the effect image of the overall cross-correlation registration for A (1) of Figure 1. Figure 8 illustrates the images of local registration of each part after its spatial segmentation .

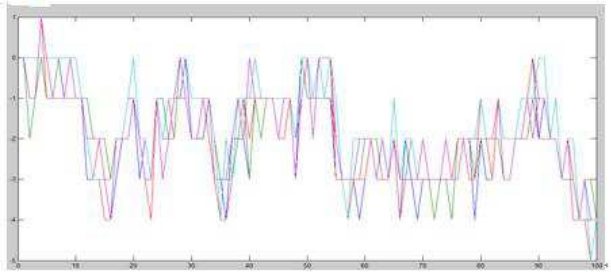

Figure 5 The displacement of *x*-axis direction

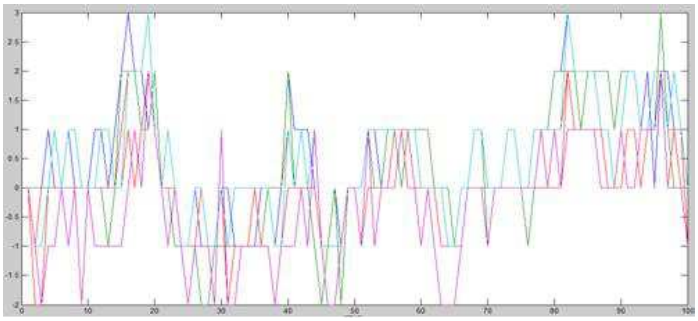

Figure 6 The displacement of *y*-axis direction

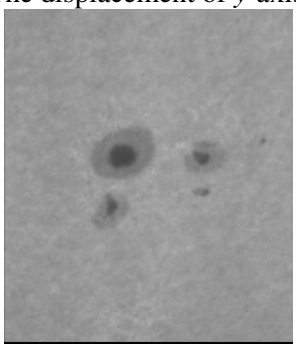

Figure 7 The effect image of the overall matching

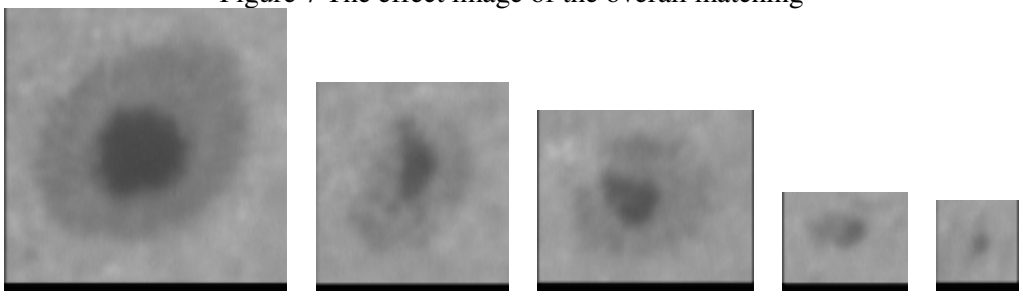

Figure 8 The local cross-correlation registration

4.2 Full-reference image quality assessment

Taking A1 as the standard image, the results in table 1 can be obtained. It can be seen from Table 1 that: the effect of peak signal-to-noise ratio, fuzzy coefficient and quality index of local registration is generally better than that of the overall registration.

Table 1 Results of full-reference image quality assessment

	Peak signal-to-noise ratio (PSNR)	Fuzzy coefficient	quality index
The overall registration	35.1575	0.6377	0.2068
The registration of Part a	38.4992	1.5424	0.6685
The registration of Part b	37.6040	1.5605	0.7760
The registration of Part c	39.2306	1.4929	0.7672
The registration of Part d	37.7845	1.4725	0.8693
The registration of Part e	39.0084	1.2685	0.9047

4.3 No-reference image quality assessment

Due to the inconveniences for selecting full-reference standard image, lots of experiments on quality assessment are performed according to the relevant methods of no-reference images in this paper.

Table 2 Results of no-reference image quality assessment

	Variance	Mean gradient	Fuzzy entropy	Information entropy
The overall registration	226.0073	1.3817	0.3074	4.7918
The registration of Part a	1087.1	2.9801	0.4963	6.1886
The registration of Part b	1001	3.1318	0.3010	5.9087
The registration of Part c	1303.6	4.7608	0.4911	6.1115
The registration of Part d	1975.1	6.7954	0.2488	5.6642
The registration of Part e	2643.7	10.865	0.1941	5.3816

5. Conclusion

Image registration is a hot topic in recent years, and various kinds of algorithms spring up constantly. In this paper astronomical image matching based on the cross-correlation algorithm is proposed and we focuses on adopting the registration form using the cross-correlation method after segmenting the astronomical images. The method can effectively solve the difficulties of the overall matching, represent the salient regions of features and implement local matching.

Although astronomical image matching based on the cross-correlation algorithm has strong flexibility, it has itself advantages, disadvantages and applicable scope. Therefore, besides the innovation, researchers should consider the integration of existing algorithms. The applicable scope of the algorithms can be expanded by collecting the advantages of existing algorithms. In addition, efficiency and robustness of registration need to be focused besides pursuit high quality registration. Some replacement through the registration process can be appropriately used to increase efficiency and enhance simultaneity of registration.

References

[1] Zhao C Y, Yan C Q and Shi X F 2009 Review on Image Segmentation *China Science and Technology Information* 1: 42-43

[2] Chen B Q, Liu H L and Meng F BCurrent Situation and Development Direction of Digital Image Processing Technology *Journal of Jishou University (Natural Science Edition)* 30(1): 63-70（ 2009）

[3] Ji H, Sun J X, Shao X F and Mao L The Algorithm for Image Edge Detection and Prospect *Computer Engineering and Applications* 14: 70-73 （2004）

[4] Liu J H, Yang J F, Shan X J and Yin J Y A Boundary Tracking Method Based on Preferential Direction for Searching *Remote Sensing Technology and Application* 19(3):209-213（2004）

[5] Zhou M and Zhou H An Adaptive Method of Clustering Image Threshold Segmentation Based on Genetic Algorithms *Computer Engineering and Applications* 18: 73-76 （2005）

[6] Malladi R, Sethian J and Vemuri B Shape modeling with front propagation: A level set approach *IEEE Transactions on Pattern Analysis and Machine Intelligence* 17(2): 58-174（1995）

[7] Osher S and Shu C W High-orderessentially nonoscillatory schemes for Hamilton-Jacobi equation *SIAM Joumal of Numerical Analysis* 28(4): 907-922（1991）

[8] Osher S and Sethian J A *Level Set Methods and Dynamic Implicit Surfaces* New York: Springer-Verlag: 22-114（2002）

[9] Woods R P, Mazziotta J C and Cherry S R MRI PET registration with automated algorithm *Journal of Computer Assisted Tomography* 17 (4): 536-546（1993）

[10] Maes F, Vandermeulen D and Suetens P Comparative evaluation of multiresolution optimization strategies for multimodality image registration by maximization of mutual information *Medical Image Analysis* 3(4): 373-386（1999）
[11] Maintz J B A, Meijer E H and Viergever M A General multimodal elastic registration based on mutual information *Proceedings of SPIE 3338 – Medical Imaging: Image Proessing San Diego* 144-154（1998）
[12] Pluim J P W, Maintz J B A and Viergever M A Image registration by maximization of combined mutual information and gradient information *IEEE Transactions on Medical Image* 19(8): 809（2000）
[13] Han S Q and Wang L A Survey of Threshold Methods for Image Segmentation *Systems Engineering and Electronics* 24(6): 94-102（2002）
[14] Liu J Z and Li W Q The Automatic Thresholding of Gray-Level Pictures via Two-Dimensional Otsu Method *Acta Automatica Sinica* 19(1): 101-105（1993）
[15] Zeng L Research on image segmentation based on Otsu adaptive threshold method *Information Technology* 10: 88-90（2008）
[16] Zhang X M, Sun Y J and Zheng Y B Precise Two-Dimensional Otsu's Image Segmentation and Its Fast Recursive Realization *Acta Electronica Sinica* 39(8): 1178-1184（2011）
[17] Wang J and Zhou Z J Research on morphological image processing based on Matlab *Computer Forum* 284:135-136（2010）
[18] Dobrushin R L General formulation of shannon's main theorem in information *Uspekhi Mat Nauk* 14(3): 92-104（1959）
[19] Ye B, LU X S, Zhang S and Chen Y Z Study on local extremum of object function in mutual information-based image registration *Computer Engineering and Applications* 43(6): 58-61（2007）

Advanced Materials Research Vols. 989-994 (2014) pp 3834-3837
© (2014) Trans Tech Publications, Switzerland
doi:10.4028/www.scientific.net/AMR.989-994.3834

Dynamic simulation of TT&C signal based on VFD filter

YANG Wen-ge[1,a], LI Wei[2] and ZHAO Jiang[2]

[1]Department of Optical and Electrical Equipment, the Academy of Equipment, Beijing 101416, China

[2]Company of Postgraduate Management, the Academy of Equipment, Beijing 101416, China

[a]loxwei@163.com

Keywords: VFD Filter; Dynamic Simulation; TT&C signal; High Dynamic

Abstract. A processing method based on VFD Filter is proposed in this paper for implementing the high dynamic simulation of TT&C signal. The method adopts the store-delay way which could implement integer delay for static data and adopts the VFD filter to implement high accuracy fractional delay for the integer delay signal. The simulation and analysis results show that the proposed method not only can accurately and commendably implement high dynamic simulation for TT&C signal, but also suits for different form signal. It provides a good way for dynamic simulation in the compatible test of TT&C equipment.

Introduction

Before the application of new type spacecraft or TT&C(telemetry track and command) equipment, the dynamic compatible test is necessary. Besides, the dynamic performance is an important norm in the test. One traditional test method is based on the flight experiment, however, the speed of airplane is always lower than the speed of missile or spacecraft, which makes the high dynamic performance of new equipment could not be tested. Another traditional test method is based on the dynamic signal simulation through the hardware platform, but this method can only realize integer delay dynamic simulation, which leads to the low precision.

In the application of dynamic compatible test, it is necessary to realize dynamic simulation of TT&C signal which based on the static digital data, frequency up-converter, down-converter and storage device. For this application, a dynamic simulation method for TT&C siganl based on VFD filter is proposed. Some numerical simulations are made to verify the proposed method could be used in the dynamic simulation of differrent form TT&C signal with high accurcy.

Design of dynamic simulation scheme

In the ideal case, the receipt signal $S_r(t)$ can be described by original signal $S_s(t)$ and delay τ as

$$S_r(t) = kS_s(t-\tau) \tag{1}$$

where k is the amplitude fading. It is obvious that the dymaic simulation conlude power and delay simulation by Eq.1. The power of singal is mainly depend on electromagnetic wave propagation distance and channel characteristics, which can be simulated easily by power attenuator. Therefore, the dynamic delay simulation is mainly researched in this paper.

Generally speaking, the signal would has group delay when it passes through the filter, and the group delay of digital filter is linear and controllable in the pass band. Therefore, the signal delay simulation could be realized by controlling the group delay of digital filter. If one want to realize the dynamic simulation of TT&C signal, the problem of fractional and continuous variable delay are necessary to be solved.

In order to solve the problem mentioned above, C.W.Farrow had put forward VFD(Variable Fractional Delay)filter[1], whose frequency response is related to delay. However, the filter coefficient is not related to delay, and the coefficient need be caculated and stored only one time in practice. All this advantages lead the filter was widely used in various signal processing applications, such as sampling rate conversion, time delay estimation and timing adjustment in digital receivers etc.[2-3].

Consider the characteristic of VFD filter, designing the scheme of dynamic simulation, which is shown in Fig. 1.

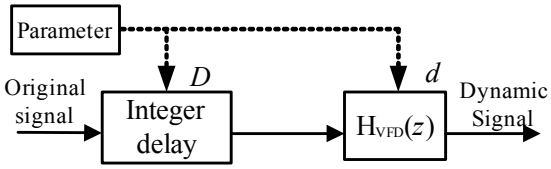

Fig.1. Dynamic simulation scheme based on VFD filter

The integer delay D and fractional delay d are given by parameter calculation module, where D is a positive real integer number and d is a fractional number. If the sampling interval is T_s, we can obtain

$$D = \left\lfloor \frac{\tau}{T_S} \right\rfloor \tag{2}$$

$$d = \tau - D, \quad 0 \le d < 1 \tag{3}$$

The integer delay module implements integer times of sampling interval delay for original siganl according to the parameter D. Besides, the VFD filter implements the fractional times of sampling interval delay for the integer delay signal according to the parameter d. Because of the integer delay is easy to be implemented, this paper is mainly introduces how to use VFD filter to realize accurate fractional delay.

According to the design method of VFD filter which is proposed by Deng T. B. in the Ref. [4]. The filter order N=65, the branch number M=8 and the weighting function $W(\omega, p)$ is assumed to be separable as

$$W(\omega, p) = W_1(\omega) * W_2(p) \tag{4}$$

where

$$W_1(\omega) = \begin{cases} 0.64 & \omega \in [0, 0.55\pi) \\ 4.9 & \omega \in [0.55\pi, 0.85\pi) \\ 37 & \omega \in [0.85\pi, 0.8996\pi) \\ 0 & \omega \in [0.8996\pi, \pi) \end{cases} \tag{5}$$

$$W_2(p) = \begin{cases} 53 & p \in [0, 0.1) \\ 0.2 & p \in [0.1, 0.9) \\ 8 & p \in [0.9, 1) \end{cases} \tag{6}$$

Fig.2 and Fig.3 depict the magnitude response of ideal VFD filter and the simulated VFD filter, respectively.

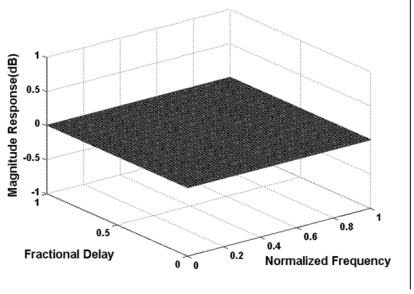

Fig.2. Magnitude response of ideal VFD filter

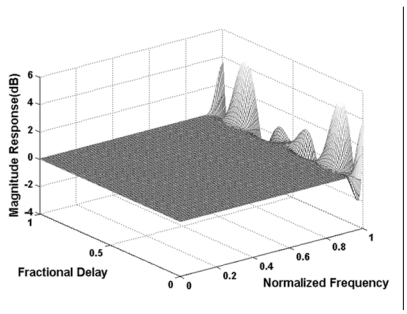

Fig.3. Magnitude response of simulated VFD filter

The results of Fig.2 indicate that the magnitude response of ideal VFD filter is fixed value in the whole frequency range, and no changes with the delay. In fact, it is impossible to achieve the ideal response in whole band, just as shown in Fig.3. Fig.4 depicts the absolute errors of the variable frequncy response that defined in Ref.[4] and Fig.5 illustrates the variable fractional delay response in the range $\omega \in [0, 0.9\pi]$ and $p \in [0,1)$. The results show that the absolute errors are less than -80dB, and the varible fractional delay response of the designed VFD filter is considerably flat in the pass band.

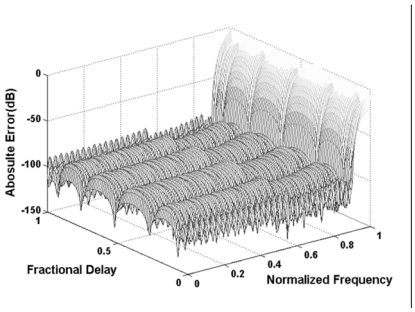

Fig.4. Absolute error of variable frequncy response

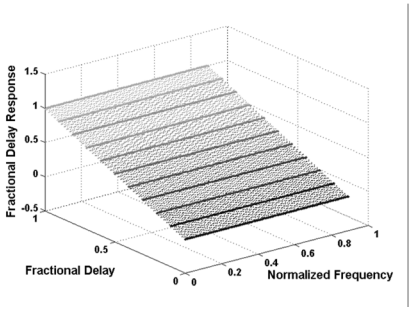

Fig.5. Variable fractional-delay response in passband

If combined with the use of the VFD filter and integer delay, it would be able to solve the problem of fractional and continuous variable delay and realize the dynamic simulation of TT&C signal.

Simulation and analysis

1) Fixed Doppler dynamic simulation

To verify the dynamic signal simulation scheme is correct and effective，the dynamic simulation of standard TT&C signal and PCM_FM signal are simulated. The simulation parameters are displayed in Table 1.

Table1 Simulation Parameters

Form of signal	Original signal parameters	Dynamic parameters	VFD filter parameters
Standard TT&C	Telemetry code rate =64kbps, Telemetry subcarrier frequency=512kHz High side tone frequency=100kHz Low side tone frequency=20kHz	Sampling frequency=56MHz Intermediate Frequency=70MHz Doppler=-800kHz SNR=20dB	Filter order=65 Branch number=8
PCM_FM	Code rate=2Mbps		

The simulation results show that integer delay signal which realized by the method of Ref.[5], the VFD filter delay signal and the ideal dynamic signal. The center frequency of the original signal(14MHz) is also marked in the figures.

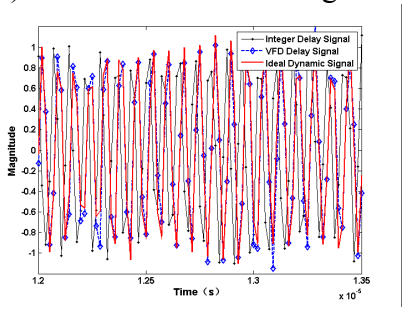

(a) Simulation results in time domain

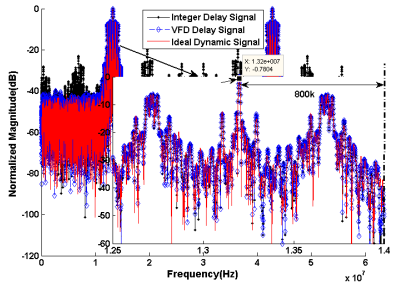

(b) Simulation results in frequncy domain

Fig.6. Fixed Doppler dynamic simulation of TT&C signal

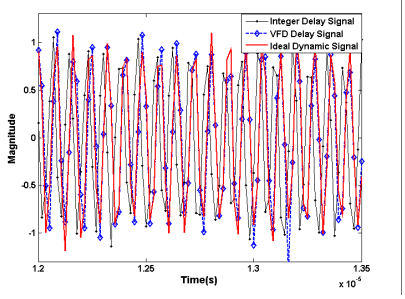

(a) Simulation results in time domain

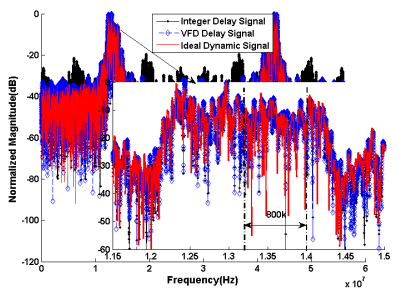

(b) Simulation results in frequncy domain

Fig.7. Fixed Doppler dynamic simulation of PCM_FM signal

As we can see from Fig.6 and Fig.7, there is a big error between integer delay signal and the ideal dynamic signal, but almost no error between VFD filter delay signal and the ideal dynamic signal. Moreover, the Doppler frequncy is in conformity with the preset information. Comparison shows that the dynamic simulation effect of the proposed scheme is obviously superior to the integer delay.

2) Varied Doppler dynamic simulation

For a comprehensive study of the dynamic simulation scheme, varied Doppler dynamic simulation of standard TT&C signal was used to verify the proposed scheme. The parameters are same as last simulation except the Doppler changed linearly with the first-order derivative is -200kHz/s.

Through the FFT(Fast Fourier Transformation) operation, we can achieve the Doppler frequency of dynamic signals, which were compared with the ideal Doppler, and the Fig.8 shows the comparison.

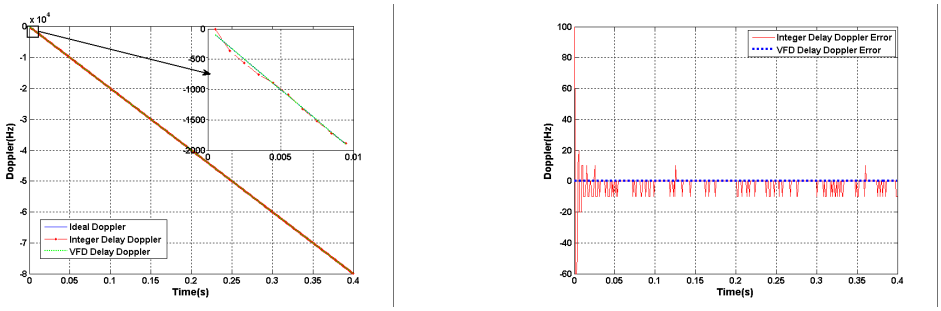

(a) Comparison of Doppler (b) Comparison of Doppler error

Fig.8. Varied Doppler dynamic simulation

As shown in Fig.8.(a), there is obviously difference between the integer delay signal's Doppler and the ideal Doppler, but almost no difference between VFD filter delay signal's Doppler and the ideal Doppler. By comparing the Doppler error as shown in Fig.8.(b), we can find that the Doppler simulation error of propose scheme is less than 10Hz and rather less than the error of integer delay.

In summary, all the results indicate that the proposed scheme could be used for dynamic simulation of TT&C singal and the performance of proposed scheme is superior to the traditional integer delay method.

Conclusion

A new scheme combinated with traditional integer delay and VFD filter has been deeply researched for dynamic simulation of TT&C signal in this paper. The simulation results show that the proposed scheme not only can realize high dynamic simulation with high precision, but also could be used in different form TT&C signal. Compared with the traditional demodulation dynamic simulation mode, it has better adaptability and provides an effective solution for the dynamic comptible test of new type spacecraft or TT&C equipment.

References

[1] Farrow C W. A continuously variable digital delay element[C]. IEEE International Symposium Circuits and Systems(ISCAS'88). 1988, 6: 2641-2645.

[2] Jong-Jy Shyu, Soo-Chang Pei, Cheng-Han Chan. Minimax phase error design of allpass variable fractional-delay digital filters by iteraive weighted least-squares method[J].signal processing, 2009:1774-1781.

[3] Tian-Bo Deng, Y.Lian. Weighted least squares design of variable fractional delay FIR filters using coefficient symmetry[J]. IEEE Trans. Signal Processing, 2006,54(8):3023-3038.

[4] Tian-Bo Deng. Discretization-free design of variable fractional-delay FIR digital filters[J]. IEEE Trans. Circuits Syst. Ⅱ, 2001, 48(6):637-644.

[5] LEI Ming, LI Ke. Design of dynamic simulatou scoure for deep space communication bu using close loop dual-port RAM[J]. Telecommunication Engineering, 2011,51(3):33-36.

Advanced Materials Research Vols. 989-994 (2014) pp 3838-3843
© (2014) Trans Tech Publications, Switzerland
doi:10.4028/www.scientific.net/AMR.989-994.3838

Enhancement Algorithm of Color Fog Image Based on the Adaptive Scale and Multi-parameter correction

Yin Gao[1], Li-jun Yun[2,*], Jun-sheng Shi[1] and Fei-yan Cheng[2]

[1] Color & Image Vision Lab, Yunnan Normal University, Kunming 650500, China

[2] College of Information, Yunnan Normal University, Kunming 650500, China

*Corresponding author：yunlj@163.com

Keywords: Image enhancement; Adaptive scale; Multi-parameter correction; Grayscale adjustment.

Abstract. To deal with the image contrast and color fidelity details problem in the traditional Center around the Retinex image enhancement algorithms, Enhancement Algorithm of Color Fog Image Based on the Adaptive Scale and Multi-parameter correction is proposed. First, the saturation component of the HSI color space is applied to the nonlinear correction. Then according to the brightness of the image pixel values, it can calculates the scale of the Gaussian kernel, and then proceeds to do the multi-parameter correction for the estimates of the reflection component, obtains the multi-scale image by the weighted average. At last, the obtained image is used to adjust the display correction, image sharpening and smoothing, and being superimposed reflection components, achieving the image enhancement. Through the subjective observation and objective evaluation, this algorithm is better than the traditional center around Retinex algorithm in treatment effect, and also saves a large amount of processing time.

Introduction

With misty weather conditions, the outdoor surveillance cameras and equipment with lots of interference [1], namely the contrast and color of recorded images are change and degradation; many features of image become blurred due to being covered with. Therefore, the fog image enhancement is more extra attention. Right now, the common fog image processing methods are mainly bilateral filtering, wavelet transform and Retinex algorithm. Bilateral filtering method can be widely noted due to maintaining the edge characteristic of image, but its treatment only has a significant effect on mist and has greater limitations. Wavelet transform have the characteristics of multi-resolution and the ability to the local signal in time-domain and frequency-domain, in which has been widely used in the image enhancement, but because of its two-dimensional image processing with isotropic, it means that it has limitation when representing the current characteristics and boundaries [2]. Retinex algorithm [3,4,5] is a new idea in image processing development, which is based on color constancy. The full name is the retina double cortex theory that the human eye perceiving an object depends on the color of light reflecting from the surface characteristics of the object and is irrelevant to the incident light. More common are the single-scale Retinex (SSR), multi-scale Retinex (MSR) and multi-scale Retinex with color restoration (MSRCR) algorithms. The MSRCR algorithm is better in these algorithms because of using color restoration, but not maintaining a constant tone, there is still a small color distortion.

In view of the above processing method, Enhancement Algorithm of Color Fog Image Based on the Adaptive Scale and Multi-parameter correction is proposed, which is depend on the nature of the hue, saturation and brightness from the perspective of machine vision in the HSI color space.

The MSRCR algorithm

According to the Retinex theory [6], the color of object is determined by the light reflection ability objects on long wave, medium wave and short wave, rather than by the reflection intensity, which is not affected by non-uniform illumination and is a consistency. The human eye perceiving the brightness depends on the ambient light and the irradiation light of surface reflection, its mathematical expression is:

$$I(x,y) = R(x,y) \times S(x,y) \ . \tag{1}$$

Taking the logarithm on both sides of equation (1), it is given such that:

$$\log I(x,y) = \log R(x,y) + \log S(x,y) \ . \tag{2}$$

where $I(x,y)$ is the image from observing or the camera receiving, $R(x,y)$ is the reflected component of the target object, $S(x,y)$ expresses the incident component of the ambient light.

Then using Gaussian filter to estimate the incidence of component $S(x,y)$ of the image, which is given such that:

$$R(x,y)^{'} = \log I(x,y) - \log[F(x,y) * S(x,y)] \ . \tag{3}$$

where $R(x,y)^{'}$ is the logarithmic of $R(x,y)$, and * denotes convolution, $F(x,y)$ expresses the surround function , here uses Gaussian function, which is defined as: $F(x,y) = K \times \exp(-\frac{x^2+y^2}{\sigma^2})$. σ represents the standard deviation, which is also the scale constant of Gaussian surround function.

According to the surround function, size of scale σ depends on the scope of the convolution kernel. the smaller a scale is, the greater the dynamic range compression is , the local details of the image is more prominent; the larger a scale is, the better the overall image is, the color is more natural and is close to the original color, but its local details is not clear [7]. K is a normalization factor and is now given by: $\iint F(x,y)dxdy = 1$. Single scale is difficult to achieve a large dynamic range compression and better color constancy at the same time. Therefore, it needs to adopt the MSR algorithm, which takes a plurality of single-scale to weight the processing results. The formula is given by:

$$R_{MSR}(x,y)^{'} = \sum_{i=1}^{n} \lambda_i \{\log I(x,y) - \log[F(x,y) * S(x,y)]\} \ . \tag{4}$$

Where n is a number of scales, the value is generally 3; λ_i represents a weight, and meets the equation, $\sum_{i=1}^{n} \lambda_i = 1$, the weight value is 1/3 under normal circumstances.

The multi-scale Retinex with color restitution is based on the results of color from consideration such that introduces a color restitution factor. Mathematically,

$$R_{MSRCR}(x,y)^{'} = \mathrm{C}_i(x,y) \times R_{MSR}(x,y)^{'} \ . \tag{5}$$

where $\mathrm{C}_i(x,y)$ is the color restitution factor , $\mathrm{C}_i(x,y) = \Gamma[\mathrm{I}_i(\mathrm{x,y})] = \Gamma[\frac{\mathrm{I}_i(\mathrm{x,y})}{\sum_{j=1}^{n} \mathrm{I}_j(\mathrm{x,y})}]$, and is used to adjust the proportion of three-channel color; $\Gamma[\mathrm{I}_i(\mathrm{x,y})]$ represents the i channel of the color mapping function, n value is 1,2,3.

Enhancement Algorithm of Color Fog Image Based on the Adaptive Scale and Multi-parameter

When traditional multi-scale Retinex algorithm processes a strong contrast edge region, it will appear the halo phenomenon. The scales are in a fixed number, it isn't free to determine the threshold value according to the features of fog image. After processing, there will be excessive contrast

enhancement. Given above situation, this paper studies the relationship between the image pixels and the scale in the MSR algorithm, and proposes the algorithm. The specific steps are as follows.

Original image conversion from RGB color space to HSI color space, the hue component remains unchanged, while the saturation component of Gamma Correction.

Due to the human visual sensitivity for brightness much stronger than the color shade, to facilitate processing and identification, it is often used the HSI color space, which is more consistent with the human visual characteristics than the RGB color space. Given the better visual processing effect while an appropriate increase in the saturation, the paper mainly uses Gamma correction [8] for the saturation component. Its formation is as follows:

$$S_1(x,y) = S_0(x,y).\hat{}\,\gamma. \tag{6}$$

where $S_0(x,y)$ is the saturation component of the original image; $S_1(x,y)$ is the processing saturation component; γ is the Gamma correction parameter, from lots of experiments, when the correction parameter is 1/1.3, it can accurately reflect the color image information.

The brightness component processing in the HSI color space

Given the flaw in the MSR algorithm, the paper introduces adaptive scale and a multi-parameter correction factor, which can better adjust a large halo phenomena and excessive enhancement phenomena.

With modern equipments diversification, people's choices have begun to tend to diversify, so the dimensions of the image pixel also begin to have more choices. To this end, it introduces the adaptive scale. The paper uses an algorithm which can be adaptive the size of the image pixel, and meet the details and overall requirements. The adaptive scales are chosen as follows:

(a) When the rows and columns of image pixel are even, it can directly obtain the Gaussian kernel from the above experiments: a small-scale is 2.5% of the product of rows and columns; a meso-scale is 12.5% of it, and a large-scale is 40 % of it;

(b) When the rows are even and the columns are odd, the value of rows does not change, and the value of column is decremented by one. The obtained is as a new Gaussian kernel: a small-scale is 2.5% of the product of rows and columns, a meso-scale is 12.5% of it, and a new large-scale is 40% of it;

(c) When the rows of image pixel are odd and the columns of image pixel are even, the value of rows is decremented by 1, the value of columns remains unchanged, The obtained is as a new Gaussian kernel: a small-scale is 2.5% of the product of rows and columns, a meso-scale is 12.5% of it, and a large-scale is 40% of it;

(d) When the rows and columns of image pixel are odd, the value of row and column minus one is as the new size of the image and obtains a new Gaussian kernel: a small-scale is 2.5% of the product of rows and columns, a meso-scale is 12.5% of it, and a large-scale is 40% of it.

Given the choice above the value of row and column, it is mainly based on the Gaussian kernel structure matching. When the selecting the Gaussian kernel is a size of a processed image pixel which is a fixed proportion value, the mismatch can be avoided.

In addition, when it estimates the reflection component of each luminance channel in a single-scale processing, it applies the multi-parameter correction factor [9], which enhances the proportion in the interest region of the entire image and improves the overall tone. The formula is following:

$$R(x,y)^{'} = \sum_{i=1}^{n} \lambda_i \left\{ \exp\left[\log I(x,y) - W(x,y) \times \log[F(x,y) * S(x,y)] \right] \right\} \tag{7}$$

where $W(x,y)$ is the pixel after the Butterworth filter processing. Each of the parameters is the same as the above.

After the MSR algorithm processing, the pixel will be negative and out of display range. Then it requires the pixel shift and compression to the display range. From lots of experiments, the gain/offset correction method is often mapped to display the grayscale range [10,11], the formulation is :

$$R_j(x,y) = G_1 \times R^{'}(\mathrm{x},y) + G_2 . \tag{8}$$

$$R_O(x,y) = 255 \times \frac{R_j(x,y) - R_{\min}}{R_{\max} - R_{\min}} . \quad (9)$$

where $R^{'}(\mathrm{x},y)$ is the input image; G_1 is the gain coefficient and G_2 is the offset, Thought lots of experiments, these two parameters may be a fixes value and does not affect the image processing effect, where the values are namely 3,50; $R_O(x,y)$ is the output image; $R_{\max}$ is the maximum value of the input image and $R_{\min}$ is the minimum value of it.

To make the details of images more prominent, this paper uses a Laplace operator custom filter to enhance edge profile details, after a Gaussian smoothing, and the overall integration of the image to achieve better processing effect. After the above processing, it is superimposed with the MSR algorithm processing image, and further uses the histogram equalization method in order to achieve the details more prominent and color more natural.

Experimental results and analysis

This experimental processing results shows in Fig. 1, Fig. 2, Fig. 3. In the experiment, the size of experimental image pixel are different, namely 669 × 1000, 900 × 651, 800 × 600, in which mainly contrast with the improved MSRCR algorithm (it mainly introduces adaptive scale).

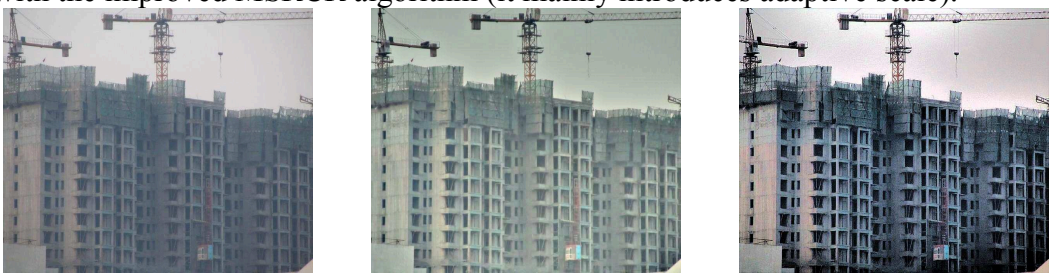

(a) An original image (b) An image after the improved MSRCR algorithm processing (c) An image after the new algorithm processing

Figure 1 Comparison of light fog image after processing

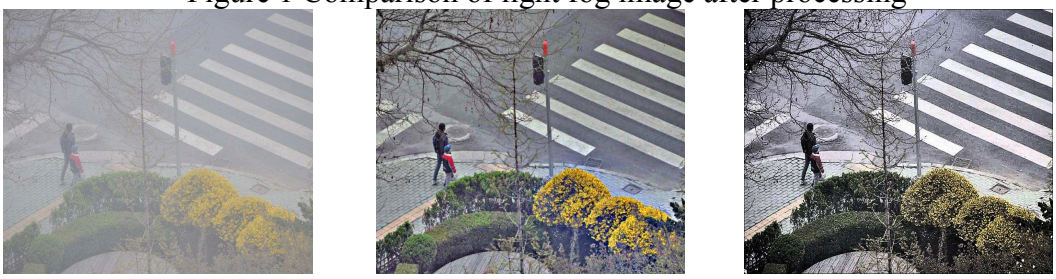

(a) An original image (b) An image after the improved MSRCR algorithm processing (c) An image after the new algorithm processing

Figure 2 Comparison of moderate fog image after processing

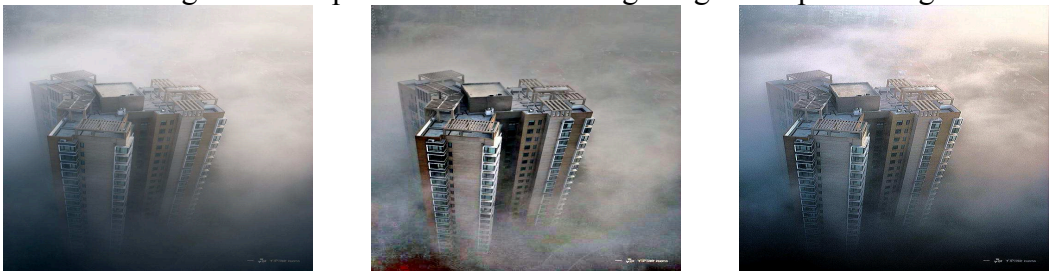

(a) An original image (b) An image after the improved MSRCR algorithm processing (c) An image after the new algorithm processing

Figure 3 Comparison of dense fog image after processing

From the results of the above, it can be seen that the algorithm can be adaptive adjustment in the different pixel and is better in details, brightness, contrasts and other aspects of processing. Although the improved MSRCR algorithm can meet with the change in the size of pixel, it introduces noise

after the Gaussian convolution processing. For the image processing effects, the paper will do comparison and evaluation from the contrasts (standard deviation), average gradient values and information entropy.

Table 1 The contrast of an image

The contrast of an image evaluation	The result of an original image	The result of the improved MSRCR algorithm processing	The result of the new algorithm processing
Figure 1	26.1528	43.2175	176.6955
Figure 2	32.3230	127.7746	373.7418
Figure 3	24.0906	71.5408	147.2442

The contrast of an image reflects the clarity. The greater the contrast is, the higher the sharpness of the image is, conversely, the lower [12] is. In Table 1, for the low-contrast image, the improved MSRCR algorithm improves the contrast 1.65-3.95 times, while the new algorithm improves 6.11-11.56 times.

Table 2 The average gradient of an image

The average gradient of an image evaluation	The result of an original image	The result of the improved MSRCR algorithm processing	The result of the new algorithm processing
Figure 1	0.7735	1.1939	3.4525
Figure 2	0.5835	2.3417	5.8337
Figure 3	0.6408	1.8165	2.3565

An important indicator is the average gradient in evaluation of image details. The average gradient can express the contrast of image details. In an image, when a gray level of an image has a large change rate, it is large [13]. From Table 2, after the improved MSRCR algorithm processing, the lowest increases 1.54 times, the highest increases 4.01 times; the image details have been greatly improved after the new algorithm processing, the lowest increases 3.68 times, the highest increases 10.00 times.

Table 3 The information entropy of an image

The information entropy of an image evaluation	The result of an original image	The result of the improved MSRCR algorithm processing	The result of the new algorithm processing
Figure 1	6.6930	6.9429	7.9873
Figure 2	5.9759	7.3924	7.9915
Figure 3	7.5855	7.1420	7.9805

For an image, the most important evaluation criterion is the information entropy, which reflects the average amount of information from the gray level of each pixel conveyed and can measure the importance of the target in the image. The higher the entropy is, the greater the amount of information containing is. From Table 3, the information entropy of the improved MSRCR algorithm can improve -5.8% -23.7% basically, which is mainly due to contain the color recovery coefficient and keeps the color of fog, also reduces the information entropy of an original image. But the information entropy of an image increases in the proportion of 5.2%-33.73% basically after the new algorithm processing.

Summary

In this paper, it proposes enhancement algorithm of color fog image based on the adaptive scale and multi-parameter correction. Combining with the characteristics of fog image, the saturation nonlinear Gamma correction can avoid the super saturation problem. In addition, multi-parameter correction for the tradition MSR algorithm, can reduce the noise from the Gaussian convolution, and avoids the halo phenomenon. Due to the algorithm processing only for the brightness, it saves much time. Through the subjective evaluation and objective evaluation, it is proved that the new algorithm

has a better effect on detail enhancement, color fidelity and clarity results comparing with the MSRCR algorithm processing.

Acknowledgement

This work is funded by grants from the National Science Foundation of China (No. 60963020) and Culture Program for Reserve Talents of Middle-Young Aged Academic Leader of Yunnan Province of China (No. 2010CI038).

References

[1] HUANG Li-hong: Journal of Applied Optics, Vol. 31, No. 5 (2010), p. 0728-0733.

[2] Xiao Ding, Sun Zi-qiang: Computer Engineering, Vol. 37, No. 17 (2011), p. 200-205.

[3] LIU Jia-peng, ZHAO Yu-ming, HU Fu-qiao: Journal of Shanghai Jiao Tong University, Vol. 41, No. 5 (2007), p. 0685-0688.

[4] J.M.Morel. A. B. Petro and C. Sbert: IEEE Transactions on Image Process, Vol. 19, No. 11 (2010), P.2825-2837.

[5] D Shaked: Proceedings of SPIE, the int Society for Optical Engineering, Bellingham:SPIE, 2007, 649312.1-649312.7

[6] Bo Sun, Weifang Chen, Hongyu Li, et al: Internationl Conference on Image and Graphics 2007, Chengdu: ICIG, 2007, 116-120.

[7] Zhao Xiao-xia, WANG Ru-lin: Computer Engineering, Vol. 37, No. 6 (2011), p. 209-211.

[8] ZHANG Shangwei, ZENG Ping, LUO Xuemei, ZHENG Haihong: Jouranal of Xi an Jiao Tong University, Vol. 46, No. 4 (2012), p. 0032-0037.

[9] SHA Junming, LIU Zeqian, PANG Shuai: Journal of Projectiles, Rockets, Missiles and Guidance, Vol. 32, No. 1 (2012), p. 003-006.

[10] Zhu Shuangzhi, Wen Jianguo, Yang Dong, et al: Remote Sensing Technology and Application, Vol. 27, No. 4 (2012), p. 549-554.

[11] FANG Shao-mei, GUO Chang-hong, WU Pei, LEI Jian-ping: Journal of Jishou university, Vol. 33, No. 4 (2009), p. 0037-0040

[12] Zhan Jie, Yan Fei: The Fourteenth National Conference on image and graphics, Beijing: China Society of Image and Graphics, 2008, p. 55-58.

[13] Li Guang-zhang, Luo Wu-sheng, LI Pei: Journal of Test and Measurement Technology, Vol. 23, No. 5 (2009), p. 445-451.

Advanced Materials Research Vols. 989-994 (2014) pp 3844-3850
© (2014) Trans Tech Publications, Switzerland
doi:10.4028/www.scientific.net/AMR.989-994.3844

3-D reconstruction of image sequence based on independent three-view

LI Cong[1,a], ZHAO Hong-rui[1,b] , FU Gang[1]
[1]Institute of Geomatics, Department of Civil engineering, Tsinghua University, Beijing China
[a]Licong1018@163.com, [b]zhr@tsinghua.edu.cn

Keyword: 3-D reconstruction; three-view; fundamental matrix; computer vision; photogrammetry; transformation parameters

Abstract. In order to realize efficient and stable 3-D reconstruction of image sequence, a novel 3-D reconstruction method is proposed based on independent three-view in this paper. Firstly, three-view is used as reconstruction unit. Consequently, robust fundamental matrix is calculated under the constraint of three-view. Then 3-D point cloud of 3-D scene corresponding to this three-view is rebuilt by triangulation. Because three-view point cloud is rigid body and local stable, 3-D point clouds of whole image sequence are unified to the same space coordinate system via calculating and using transformation parameters between adjacent three-view. Finally 3-D point cloud reconstruction of whole image sequence is achieved. As shown in experiment, method presented in this paper is simple, efficient and reliable.

Introduction

With the development of technology and the growth of demand about life quality, human have stronger and stronger desire to know and control the reality word. Obviously we are entering age of big data, which is thirsty for richer information about living environment extremely. As convenient is to realize objective digital description for real world, 3-D model has been getting widely attention, study and application in lots of fields. Consequently, acquiring of 3-D model, i.e. 3-D reconstruction, becomes an important fundamental task. 3-D reconstruction is a basic component both in computer vision and photogrammetry, and many methods have been proposed to achieved this goal. But, compared with classical reconstruction ways relying on modeling software or other expensive hardware equipment like 3-D scanner, method based on image sequence[1] has many advantages such as simple operation, Flexible application, and low cost. What's more, a vivid and objective result also can be obtained.

Key technologies related to 3-D reconstruction based on image sequence have been studied, summarized and realized in many articles[2,3]. And the whole process is mainly divided into four parts, they are feature points detecting and matching, robust calculation of fundamental matrix, camera calibration and 3-D reconstruction strategy. Striving to acquire improvement in fundamental matrix calculation and 3-D reconstruction strategy, a novel 3-D reconstruction method based on independent three-view is proposed in this article. Feature points detecting and matching is achieved using *sift*(Scale-invariant feature transform) algorithm[4] and Zhang Zhengyou method[5] is applied to get camera intrinsic parameters. Then the efficient and stable reconstruction of 3-D point cloud is achieved . Main innovations of this paper could be summarized as follows:

1 Fundamental matrix is computed robustly with high accuracy, using three-view as reconstruction unit and applying three-view constraint. What's more, there is no needs of calculating trifocal tensor any more.

2 3-D points cloud of each three-view is rebuilt and transformation parameters are obtained by common image between adjacent three-view. Finally, 3-D point clouds of whole image sequence are united into a completed point cloud model simply.

1 Introduction of 3-D Reconstruction Method Based on Independent Three-view

Calculation of fundamental matrix had been studied in lots of researches. *Ransac*（random sample consensus）algorithm is quite an useful robust approach, else some improved algorithms[6,7,8,9] based on it. However, most of those approaches are used under an assumption, that distribution of

matching point's residuals is changeless. So fundamental matrix could be computed robustly according to residuals' value. In fact, mismatch maybe also have little residual, and distributions of right matching points and mismatches are partially overlapping. Consequently, methods which use changeless residual distribution are not absolutely appropriate, because distribution of mismatches could not be adjusted based on actual situation. Advanced approaches[10] were proposed by researching distribution of matching points' residual. Methods [11,12]obtained improvement on accuracy and efficiency, selecting best matching point set via employing fuzzy clustering technology. Relying on constraint of epipolar geometry, those methods also have insufficient. When mismatches existing, those methods could not remove them absolutely, just getting a better matching point set as greater probability as possible. Trifocal tensor is a multiple view object in three-view, which could be described by geometry of "point-point-point" , owning stronger constraint ability than epipolar geometry. Fang Lei[3] excluded more mismatches between adjacent view in 3-D reconstruction process and achieved better results. As correctness of matching point has great influence in fundamental matrix calculation, the same way is employed to realize the robust correct computation of fundamental matrix by selecting more accurate matching point set.

In order to acquire 3-D point cloud of whole model correctly, 3-D point rebuilding form different three-view should be unified into the same coordinate system. Traditional iterative reconstruction method based on two-view is a common method. 3-D points' reconstruction of next image relies on accomplished points deeply. And matching point with next image and projection matrix must be computed for adding and reconstructing each image. It's not easy to get right matching points and projection matrix , so there are many disadvantages in such method. What's worse, there exists significant effect of error accumulation. A parallel iterative hierarchical reconstruction strategy[3] is presented, which is organized on the reconstruction unit of three-view. Compared with traditional iterative reconstruction method, it acquired improvement in accuracy and efficiency, with effective limit to error accumulation.

Regional network aerial triangulation algorithm[13] based on independent model is a classical strategy to realize 3-D reconstruction in photogrammetry. 3-D point cloud getting from independent image pair is a local and stable rigid body structure, so they could be unified by simple translation, rotation or scaling. Inspired by above two methods, a novel strategy based on independent three-view is presented. Considering local and stable point cloud structure could be obtained under three-view constraint, whole image sequence is divided into several three-views , also 3-D point clouds. Then transformation parameters are calculated by common image between adjacent three-view. Lastly, all of 3-D point clouds are unified into the final point cloud model. The whole process is shown as Fig. 1.

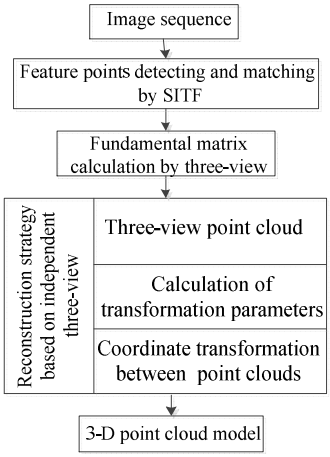

Fig. 1 Flow diagram of 3-D reconstruction

2 Calculation of Fundamental Matrix Based on Three-view

2.1 Three-view constraint

Three-view constraint - trifocal tensor, has analogous properties to the fundamental matrix of two-view geometry: it is independent of scene structure depending only on the relations between the views. The view matrices may be retrieved from the trifocal tensor up to a common projective transformation of 3-space, and the fundamental matrices for view-pairs may be retrieved uniquely.

The essence of the epipolar constraint over two views is that rays back-projected form corresponding matching points are coplanar, a weak geometric constraint, as left graph shown in Fig. 2.

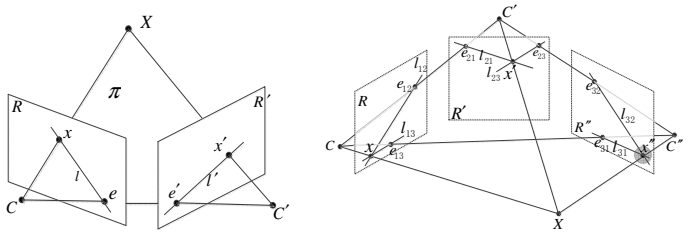

Fig. 2 Constraints of epipolar and three-view

C and *C'* are centers of the two cameras when getting images *R* and *R'*. Camera baseline *CC'* intersects each image plane at the epipoles *e* and *e'*, *x* and *x'* are image points which imaged by a 3-space point *X* in *R* and *R'*. Any plane π containing baseline *C C'* and point *X* is called epipolar plane, and interests image planes in corresponding epipolar lines *l'* and *l'*, *l'* is epiolar line of point *x*, and it passes through epipoles *e'* and point *x'*, corresponding point of *x* in another image. So, given a pair of images ,it was seen in Fig. 1, the epipolar geometry constraint can only guarantee that any point *x'* must lie on the epipolar line *l'*. But exact position where the point is could not be determined.

Compared with the epipolar geometry, three-view geometry owns ability to transfer from two views to a third: given a point corresponding over two views ,the position of the point in the third view is determined as the right graph shown in Fig. 2. e_{ij} represents epipole on the i^{th} image that is imaged from the j^{th} camera's center. Similarly, l_{ij} represents epipolar line on the i^{th} image of the projection point on the j^{th} image. *x*, *x'* and *x"* are the projection points of 3-space point *X* on the image *R*, *R'*, *R"*. they are corresponding points. So conclusion can be drawn from three-view constraint: any projection point on one image of three-view is the same with intersection of epipolar lines on the very image of its corresponding points.

2.2 Algorithm and experiment of the fundamental matrix calculation

To distinguish whether a pair of points are right matching points or not , distance(also called residual) form point to its matching point's epipolar line is always used as evaluation criterion in traditional robust algorithms. Guarantee that matching is right is not sure, even though the matching points have tiny residual. Suppose that there is a point *X* in 3-space, as shown in Fig. 3, *x* is its projection point in image *R* and *x'* should be another projection point in image *R'* . Because of detecting error, x_a' , x_b' and x_c' may be the undetermined points of *x'*. Distance of dotted line in Fig. 3 represents the magnitude of residual. Comparing residuals between x_a' and x_b' , it's easily to make sure that x_a' is the right one. Actually, x_c' has a smaller residual than x_a' ,and it's also possibly to be regarded as a correct matching point . But it is an error obviously.

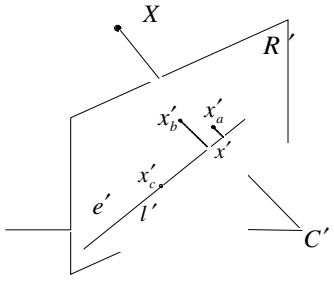

Fig. 3 Correctness judgment of matching points

Fig. 4 Three-view data for experiments

Three-view has stronger constraints between matching points. For an example as shown in Fig. 2 right, x and x' are the matching points, l_{31} and l_{32} are their epipolar lines on image R'', whose intersection should be the same point with point x'' in theory. Because of the noise produced during the extracting, shadow region as shown in Fig. 3, may be the area where real point x'' is. So distance between the intersection and real matching point should be limited to a certain threshold. In conclusion: distance between matching point and intersection of corresponding epipolar lines should be large, when matching points in three-view are not right. Based on that in this article, a more accurate matching point set is obtaining by getting rid of those mismatches .

Basic principle of this method could be described as follow. *Ransac* algorithm is frame of this approach, and matching point set is selected using constraint of three-view. Then fundamental matrix is acquired and used as initial value by M-Estimators method, to obtain higher accurate result. In order to verify the effectiveness of this algorithm, many experiments were conducted. 3 groups of experiment data are shown in Fig. 4, they were acquired using common fixed focus camera.

Because of the nonrepeatability of *ransac* method, result is averaged by 50 results for each experiment. What's more, the average distance between point to its epipolar line is used as evaluation criterion to describe algorithms' precision:

$$d = \frac{1}{N}\sum_{i=1}^{N} x_i' \boldsymbol{F} x_i \left(\frac{1}{\sqrt{(\boldsymbol{F}x_i)_1^2 + (\boldsymbol{F}x_i)_2^2}} + \frac{1}{\sqrt{(\boldsymbol{F}'x_i')_1^2 + (\boldsymbol{F}'x_i')_2^2}} \right) \tag{1}$$

N is number of right matching point. Experiments results are shown as Table. 1:

Table. 1 Results of the real images/pixel

Data	*ransac*		M-Estimators		Our Method	
	$\boldsymbol{F}_{12}$	$\boldsymbol{F}_{23}$	$\boldsymbol{F}_{12}$	$\boldsymbol{F}_{23}$	$\boldsymbol{F}_{12}$	$\boldsymbol{F}_{23}$
1st	0.3910	0.4070	0.3623	4.7255	0.2981	0.3253
2nd	0.4424	0.4159	1.8480	0.2714	0.2817	0.2590
3rd	0.3261	0.4338	0.2611	0.3133	0.2511	0.3124

Compared with *ransac* and M-estimators algorithm, method presented in this article gets obvious improvement in accuracy, being proved of an effective robust algorithm.

3 3-D Reconstruction of Image Sequence

For a image sequence containing n images, reconstruction strategy is mainly divided into 2 steps as shown in Fig. 5: (1) divide into several three-views and rebuild every point cloud;(2) calculate the transformation parameters between adjacent three-view.

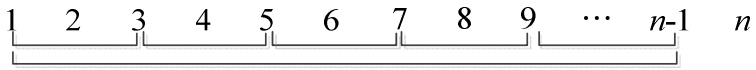

Fig. 5 Reconstruction strategy based on independent three-view

Firstly, image sequence is divided into several three-views(see Fig. 5), which have a common image with adjacent ones. (1,2,3)and (3,4,5) are adjacent three-views, image 3 is their common image. Fundamental matrix is acquired using method described in the 2nd section. Then 3-D point cloud is rebuilt by triangulation after getting projection matrix .Secondly, image point is selected on common image, whose 3-D coordinate should had been rebuilt in all the two three-views. Equations are formed according to selected points' transformation relationship. And then the transformation parameters are figured out simply. Now, the two key processes are going to be introduced in detail.

3.1 3-D point cloud reconstruction of three-view

Stable and accurate fundamental matrix has been obtained, then it can be upgraded to essential matrix with camera intrinsic parameters. We calculate and get the first two images' projection matrix by decomposing essential matrix[14]. Under the condition of central projection camera model, equation could be established without consideration of scale, for a image point $\boldsymbol{x}$ and its corresponding 3-D point $\boldsymbol{X}$, also its projection matrix $\boldsymbol{P}$:

$$\boldsymbol{x} = \boldsymbol{PX} \tag{2}$$

$\boldsymbol{x}$, $\boldsymbol{X}$ and $\boldsymbol{P}$ are expressed in homogeneous coordinates. One 3-D point has 3 elements, but only 2 equations can be established for one corresponding image point. So 3-D point must be computed when there exist at least a pair of corresponding points. For an example, there are a pair of corresponding points $\boldsymbol{x}=(x,y,1)$ and $\boldsymbol{x}'=(x',y',1)$ and projection matrices $\boldsymbol{P}$ and $\boldsymbol{P}'$, the 3-D point could be got by calculating following equations:

$$\begin{pmatrix} \boldsymbol{P}^1 - x_i\boldsymbol{P}^3 \\ \boldsymbol{P}^2 - y_i\boldsymbol{P}^3 \\ \boldsymbol{P}'^1 - x_i'\boldsymbol{P}'^3 \\ \boldsymbol{P}'^2 - y_i'\boldsymbol{P}'^3 \end{pmatrix} \boldsymbol{X}_i = 0 \tag{3}$$

i represents the i^{th} point, $\boldsymbol{P}^1$ is the 1st row of matrix $\boldsymbol{P}$. If corresponding points exist in every image of three-view, projection matrix $\boldsymbol{P}''$ of the 3rd image could be inversely calculated. Projection matrix has 11 elements and could be computed at the condition of points number no less than 6. Two equations could be established for each point.

$$\begin{bmatrix} X_i & Y_i & Z_i & 1 & 0 & 0 & 0 & 0 & x''X_i & x''Y_i & x''Z_i & x'' \\ 0 & 0 & 0 & 0 & X_i & Y_i & Z_i & 1 & y''X_i & y''Y_i & y''Z_i & y'' \end{bmatrix} \boldsymbol{p} = 0 \tag{4}$$

$(x'',y'',1)$ is the corresponding point on the 3rd image. $\boldsymbol{p}''$ is the vector representation for projection matrix, and $\boldsymbol{p}''$ could be calculated via SVD decomposition method.

3.2 Transformation parameters of 3-D point cloud

Coordinate transformation between different coordinate systems could be thoroughly described using 3 translation parameters, 3 rotation parameters and 1 scale parameter. Let's suppose that $\boldsymbol{X}=[X,Y,Z]^T$ and $\boldsymbol{X}'=[X',Y',Z']^T$ are the 3-D coordinates of a common image point in adjacent three-view structure, and the transformation relationship could be expressed as follow:

$$\begin{bmatrix} X \\ Y \\ Z \end{bmatrix} = \lambda \begin{bmatrix} a_1 & a_2 & a_3 \\ b_1 & b_2 & b_3 \\ c_1 & c_2 & c_3 \end{bmatrix} \begin{bmatrix} X' \\ Y' \\ Z' \end{bmatrix} + \begin{bmatrix} t_X \\ t_Y \\ t_Z \end{bmatrix} \tag{5}$$

λ is scale parameter. $\begin{bmatrix} a_1 & a_2 & a_3 \\ b_1 & b_2 & b_3 \\ c_1 & c_2 & c_3 \end{bmatrix}$ is rotation matrix constructed by that 3 rotation parameters. $[t_X\ t_Y\ t_Z]^T$ is translation vector. Describing 3-D point in homogeneous coordinates, equation could be simplified and rewritten as follow:

$$\begin{bmatrix} X \\ Y \\ Z \\ 1 \end{bmatrix} = \begin{bmatrix} a_1 & a_2 & a_3 & t_X \\ b_1 & b_2 & b_3 & t_Y \\ c_1 & c_2 & c_3 & t_Z \end{bmatrix} \begin{bmatrix} X' \\ Y' \\ Z' \\ 1 \end{bmatrix} \tag{6}$$

$\begin{bmatrix} a_1 & a_2 & a_3\ t_X \\ b_1 & b_2 & b_3\ t_Y \\ c_1 & c_2 & c_3\ t_Z \end{bmatrix}$ contains all parameters, spreading it and simpler expression is acquired: $\boldsymbol{W}=\boldsymbol{Ap}$.

$\boldsymbol{W}=[X,Y,Z]^T$, $\boldsymbol{A}=\begin{bmatrix} X' & Y' & Z' & 0 & 0 & 0 & 0 & 0 & 0 & 1 & 0 & 0 \\ 0 & 0 & 0 & X' & Y' & Z' & 0 & 0 & 0 & 0 & 1 & 0 \\ 0 & 0 & 0 & 0 & 0 & 0 & X' & Y' & Z' & 0 & 0 & 1 \end{bmatrix}$ is the vector and coefficient matrix constructed by 3-D point coordinates. Degree of freedom of $\boldsymbol{p}$ is 7, so it could be figured out when there exist 3 points at least. When number of points is more than 3, $\boldsymbol{p}$ also could be computed using SVD decomposition method ,or using following expression $\boldsymbol{p}=(\boldsymbol{A}^T\boldsymbol{A})^{-1}(\boldsymbol{A}^T\boldsymbol{W})$, relied on least square method principle.

4 Experiment and Summary

Image sequence shown in Fig. 6 is the input data used in our 3-D reconstruction experiment. 3 images in left of Fig. 6 are the enlarged display of three-view(1,2,3). Image sequence contains 35 images, whose size are 912×684, acquired using common fixed focus camera. Model of Camera is GR Digital III. Configuration of computer is *Intel* processor, with 2.00GHz clock speed and 2.00GB memory. All related algorithms are programmed by Matlab, using *matlab* vision 7.0.1. Whole process could be auto-completed by three steps after numbering for each image as shown in Fig. 6.

Fig. 6 Image sequence data and three-view (1,2,3)

Fundamental matrix of three-view (1,2,3) is calculated according to 2.2 section and 3-D point cloud is recovered according to method introduced in 3.1. 3-D point cloud is displayed form different angles as the 1st row shown in Fig. 7. Every 3-D point cloud of three-view is reconstructed with the same approach used in three-view (1,2,3). Transformation parameters between adjacent three-view are acquired using method described in 3.2. Regarding the 1st three-view coordinate system as datum, each three-view point cloud is transformed and unified. The 2nd row shown in Fig. 7 is the 3-D point cloud of whole image sequence.

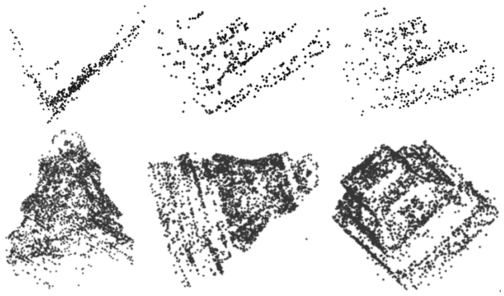

Fig. 7 3-D point cloud of three-view and whole image sequence

Actual image sequence data is experimented using method presented in this article and obtains ideal result. First step is feature points detecting and matching for 35 images, costs 11.7 minutes. The next step is recovering 3-D point cloud for each three-view, costs 2.5 minutes. The last step is computing transformation parameters between adjacent three-view, unifying point cloud and showing it. It costs 1.3 minutes. So the whole process costs 15.5 minutes altogether.

For each reconstructed 3-D point, its projective image coordinate could be calculated again by substituting itself into Eq. 2 with its corresponding projection matrix. Obviously, because of error, the reprojection image coordinate is generally not equal with its initial coordinate. So difference between them is commonly regarded as an evaluation criterion to prove method's performance, which also is called reprojection error. Average value of reprojection error for all 3-D points is computed on each image, and result is shown in Fig. 8. Most of the reprojection error is less than 1 pixel. What's more, the error accumulation is reduced effectively.

Image sequence used in our experiment is designed to be closed, that is to say, the 34th and 35th image are same with the 1st and 2nd image. If there is no error, 3-D point acquired from the 1st and 2nd images should has the same coordinate with that acquired form the 34th and 35th images. So difference between them also can be applied to describe method's performance. Because coordinate of 3-D point is relative, ratio of corresponding line segment is used as evaluation criteria instead of point's coordinate, whose value should be 1 in theory. 100 points are selected randomly existing on

image1, 2 and image 34, 35, accordingly C^2_{100} line segments are produced. Ratios of those corresponding line segments are computed and its statistics result is shown in Fig. 9.

Ratios between line segments mainly distribute around 1, and 96.4% of ratios locate between 0.94 and 1.03. However, there exist ratios bigger or smaller than1 obviously. Besides accuracy of algorithm should be improved further, distribution of points also is an important reason. If distance between points is little, tiny point error will produce huge influence on line segments ratio. But viewed as a whole, reconstruction realized by this method is reliable and ideal.

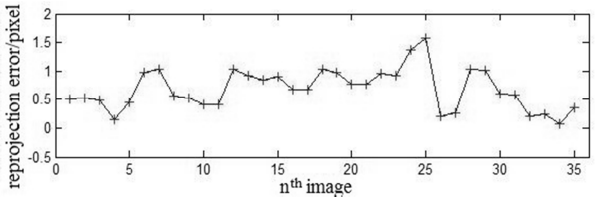

Fig. 8 Reprojection error of each image

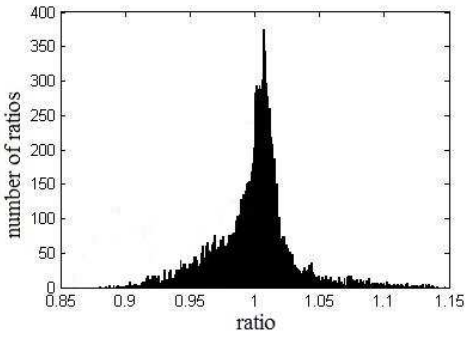

Fig. 9 Distribution diagram of line segments' radio

As reconstruction result and accuracy analyzing shown in Fig. 7,8,9, method proposed in this article acquires quite good 3-D point cloud reconstruction result, being proved to be a convenient, efficient, and reliable approach to realize 3-D reconstruction. Main advantages of this method can be concluded as follows:(1) three-view is used as reconstruction unit, acquiring accurate and robust fundamental matrix by three-view constraint , without calculation of trifocal tensor. what's more, stable and correct 3-D point cloud is obtained ;(2) reconstruction strategy based on independent three-view is proposed, which is simple and efficient. Of course, there also exist some insufficient need to be studied further, for example, the local optimization of independent three-view point cloud and the overall optimization of whole image sequence point cloud, also the implementation of parallel reconstruction strategy.

References

[1] R. Hartley, A. Zisserman: Multiple View Geometry in Computer Vision (Cambridge University Press ,UK 2004).

[2] H.T. Shan: The study on object 3D reconstruction theory and kty technology based on image sequences(PLA Information Engineering University, Zhengzhou,2011).

[3] L. Fang: Research on feature based 3D scene reconstruction techniques from image sequence (Huazhong University of science and technology, Wuhan 2006).

[4] D.G. Lowe: International Journal of Computer Vision (2004).

[5] Z,Y. Zhang,in:The Proceedings of the Seventh IEEE International Conference on Computer Vision, edited by IEEE, Kerkyra (1999).

[6] A.I. Carro, R. Morros, in: 3DTV-Conference: The True Vision - Capture, Transmission and Display of 3D Video , edited by IEEE, Zurich (2012).

[7] Y. Li, S. Velipasalar, and M.C. Gursoy, in: 10th IEEE International Conference on Advanced Video and Signal Based Surveillance, edited by IEEE, Krakow (2013).

[8] X.B. Shi, F. Liu, and Y. Wang, in: International Conference on Virtual Reality and Visualization, edited by IEEE, Beijing (2011).

[9] D.B. Calderon, T. Maria, in: 6th Colombian Computing Congress,edted by IEEE, Manizales(2011).

[10] S.S. Brant: Journal of Mathematical Imaging and Vision (2006).

[11] F.X. Chen, R.S. Wang: Journal of computer-aided design & computer graphics (2005).

[12] S. Lu, Y. J. Lei, and W. W. Kong: Control and Decision(2012)

[13] P. J. Wang, Y.M. Xu: Photogrammetry(Wuhan University Press, Wuhan 2010).

[14] N. David :IEEE Transactions on Pattern Analysis and Machine Intelligence (2004).

Advanced Materials Research Vols. 989-994 (2014) pp 3851-3855
© (2014) Trans Tech Publications, Switzerland
doi:10.4028/www.scientific.net/AMR.989-994.3851

Study on Enhancing Terminal Identification in Track and Field Using Digital X-ray Photography Image

Guangjin Lai

Department of Fundamental Courses, Jiangxi Institute of Economic Administrators, 330038, Nanchang, China

Keywords: Digital; X-ray photography image; Terminal of track and field; Image processing; Cluster algorithm; MATLAB software

Abstract. Digital X-ray photography technology is under the control of the computer, to use one-dimensional or 2D X-ray detector to convert the captured image into digital signals directly to using image processing technology. It can realize the function of image analysis. We introduce X-ray photography technology into the terminal identification in track and field, and use the clustering algorithm to improve computer image clustering algorithm. Through capturing the digital signal of human head, arms and legs, it enhances the terminal recognition method in track and field. Finally we use MATLAB to calculate the captured image value of X-ray photography. Through calculation, motion capture and recognition of X-ray image are enhanced obviously. It provides a theoretical basis for researching on motion capture technology in track and field.

Introduction

Digital X-ray photography is also called the DR system, the system is mainly composed of three parts: including control module, electronic magazine, scanning module and image processing module. This system can use electronic magazine to convert X photon into digital image, which realizes the X-ray photography. In this paper we introduce the technology into the terminal detecting in sports. As the sprint speed of athletes is very high, the general photography instruments are difficult to achieve high precision capture, but X-ray detection technology can enhance the image effect, namely realizing the transient capture function and improving the quality of the image [1, 2]. It provides technical reference for image capture and image processing technology in track and field.

Overview of Digital X-ray Photography Image Processing

Digital X-ray photography image technology is a new type of computer photography image processing technology. It uses computer digital automatic control mode, and uses of X-ray photography method to convert the captured image into mathematical information, directly displaying the effective information [3, 4]. In this paper, we introduce this method into the capture and recognition in track and field, which improves the quality of images and enhances terminal recognition for staff in track and field competition. The specific process is shown in Figure 1.

Figure 1 shows the flow chart of X-ray image processing. It includes image preprocessing of X-ray, pre-processing of track and field, image digital conversion [5]. After taking image of athletes sprint at the terminal, the computer can analyze the error in a very short period and discriminate the ranking finally.

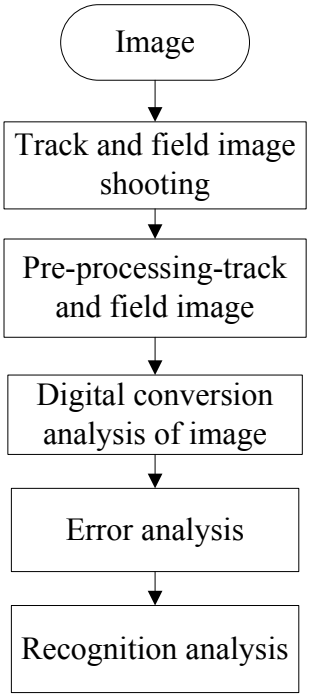

Fig. 1 Flow chart of X-ray image processing

Mathematical Model and Algorithms Design of Digital X-ray Image Processing

X-ray photography is mainly to capture the pixel; computer processing image mainly depends on the calculation of distribution and recognition error of pixel 6, 7]. The cluster algorithm is used to process the image, according to the distribution of pixels; the cluster formula is as shown in formula (1).

$$D=\frac{\sum_{j=1}^{m}\sum_{a_i\in b_i}K(a_i,b_i)}{\sum_{j=1}^{m}|B_i|}. \tag{1}$$

D is the clustering center function; m is the number of calculated pixel point; K is the distance of clustering center.

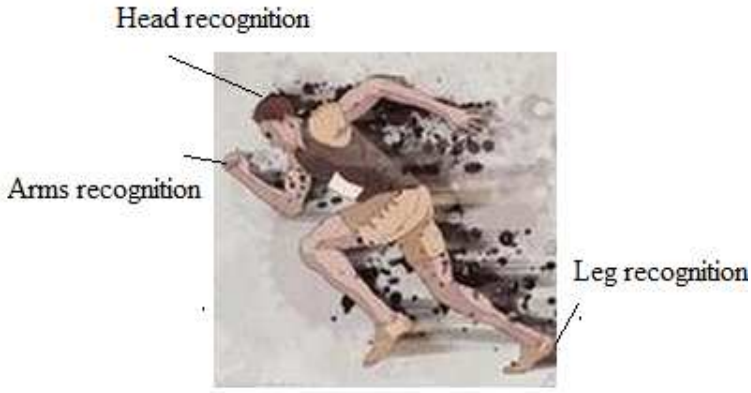

Fig. 2 Schematic diagram of gesture recognition in track and field sprint

Figure 2 shows the schematic diagram of 3D motion in the athletes' sprint. It uses X-ray photography to capture the motion of athletes, then uses computer to process image. In this paper, we establish digital output function of continuous two frames [8, 9]. Assume that continuous function of three parts of body is u,v. Then the similarity is as shown in formula (2).

$$W(u,v)=\begin{cases}s(u,v), & if \quad s(u,v)>2\\ 0\end{cases}. \tag{2}$$

$$s(u,v)=\sum_{p=1}^{5}s_p(u,v). \tag{3}$$

$$s_p(u,v)=\begin{cases}1 & if \quad u_p=s_p \\ & 0\end{cases}. \tag{4}$$

Among them, u_p and s_p are corresponding values of P item in u and s; $s(u,v)$ is the capture of successive frames. The specific process is as shown below:

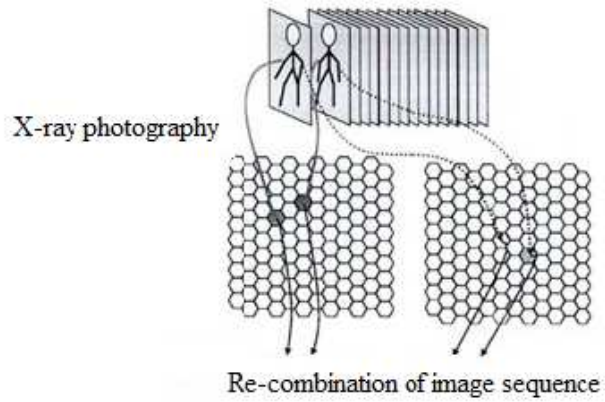

Fig. 3 Schematic diagram of motion decomposition data

Merging the frame, so the formula is as shown below:

$$U^p(t)=\bigcup_{r=1}^{K}Y_r^{\ p}(t), p=1,2...5, 1\le t\le l. \tag{5}$$

Among them, T is motion recognition function; l is the error range. In order to enhance the motion recognition at the terminal, we use MATLAB program to control the image recognition function. The main MATLAB programming is as follows:

```
unction f=myfun12(x)
f(1)=3*x(1)-2*x(2);
f(2)=-4*x(1)-3*x(2);
x0=[1;1];A=[2,3;2,1];
b=[18;10];lb=zeros(2,1);
[x,fval]=fminimax('myfun12',x0,A,b,[],[],lb,[])
goal=[18,10]; weight=[18,10]; x0=[1,1];
A=[2,3;2,1]; b=[18,10]; lb=zeros(2,1);
[x,fval]=fgoalattain('myfun3',x0,goal,weight,A,b,[],[],lb,[])
.....
```

Research on Application of MATLAB Image Processing in Image Enhancement at the Terminal of Track and Field

In order to verify the effectiveness and reliability of image processing cluster mathematical model and track pixel enhancement program designed in the second part, we use MATLABR2013a software to verify the effect of image processing, and design the computer system platform of X-ray photography image.

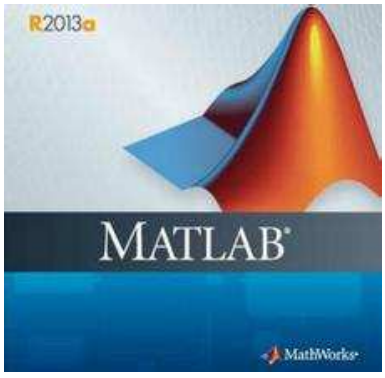

Fig. 4 Diagram of MATLAB starting window

Figure 4 shows schematic diagram of MATLAB starting window. In this paper we use the new version R2013a of MATLAB to capture the image shooting effect, and process the image effect of track and field terminal according to the distribution of pixels. The calculation process is as shown in Figure 5.

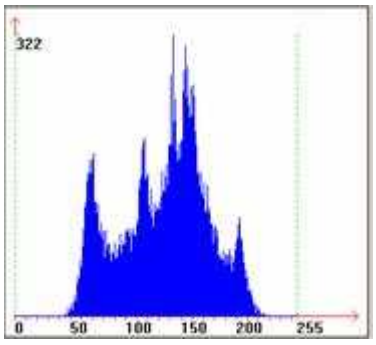

Fig. 5 Enhancement curve of pixel

Figure 5 shows the enhanced curve of pixel effect using MATLAB software. From it we can see, when the pixel is sparse, MATLAB will do enhanced curve encryption, and obtain the high pixel spectrum [10]. According to the position of spectrum we design the computer system platform of X-ray photography image, as shown in Figure 6.

Fig. 6 Computer processing image of X-ray photography image at the terminal of track and field

Figure 6 shows the computer processing image of X-ray photography image at the terminal of track and field. It use X-ray to capture the motion of the athletes at the terminal, and optimizes the system according to the shooting times and image processing time, which reduces the recognition error of the system.

Table 1. Calculation table of terminal error recognition using X-ray

Shooting times	Image processing time (s)	Error recognition rate (%)
1	0.128	99.28
2	0.179	99.35
3	0.098	99.47
4	0.146	99.59

Table 1 shows the calculation table of terminal error recognition using X-ray [11]. From the table we can see, the digital information processing speed of X-ray photography is more quickly, with only

0.098s; error recognition rate is up to 99.59%, . It is a efficient method of track and field terminal recognition.

Summary

In this paper we establish the cluster algorithm mathematical model of image processing, and introduce it into motion capture of consecutive frame, and use MATLAB programming to realize the function. In this paper, we introduce the X-ray photography technology into motion capture in track and field sports, and use the cluster algorithm to capture the motion continuously, and design using the clustering algorithm of image capture and image processing. We use the MATLAB to test the image effect captured by X-ray photography. Through calculation we find that image enhancement effect is obvious, and it reduces the error of motion capture. It provides a new method for computer image processing in track and field.

References

[1] Sun Jiping, Li Yingchun. Research on image boundary problem based on wavelet transform [J]. Journal of Xi'an University of Science and Technology, 2011, 3(3): 81-84.

[2] Bi Shu, Ren Ming, Wang Chengdao. Research on application of the wavelet transform in image mosaic technology [J]. Computer engineering and application, 2012, 2(21): 51-52.

[3] Gao Li, Wei Qun. Research and implementation of image mosaic fusion based on wavelet analysis [J]. Institute of command and technology, 2011, 2(10): 20-21.

[4] Wang Daliang, Tu Xuyan, Tong Zijian. Collocation extraction method of multi strategies fusion [J]. Journal of Tsinghua University (NATURAL SCIENCE EDITION), 2011, 48(4): 608-612.

[5] Wang Daliang, Zhang Dezheng, Tong Zijian. Collocation extraction based on relative conditional entropy [J]. Journal of Beijing University of Posts and Telecommunications, 2011, 30(6): 40-45.

[6] Ding Guodong, Bai Shuo. Query extending method based on the local co-occurrence [J]. Journal of Chinese information, 2012, 20(3): 84-91.

[7] Lou Luqun, Zhu Junjue. Research on language model in information retrieval [J]. Computer Engineering, 2011, 33(4): 49-51.

[8] Pu Qiang, He Daqing, Yang Guowei. Query language estimation model based on statistical semantic clustering [J]. Computer research and development, 2011(3): 45-49.

[9] Liu Zhiyuan, Sun Maosong. The small world effect and scale-free characteristics of Chinese word co occurrence network [J]. Chinese information technology, 2010, 21(6): 52-58.

[10] Zhong Maosheng, Liu Hui, Liu Lei. Calculation method of quantitative semantic relations between words [J]. Chinese information technology, 2011, 23(2): 115-122.

[11] Zhao Peng, Geng Huan, Cai Qingsheng, et al. K-means clustering algorithm based on weighted complex networks feature [J]. Computer technology and development, 2012, 17(9): 35-37.

Advanced Materials Research Vols. 989-994 (2014) pp 3856-3860
© (2014) Trans Tech Publications, Switzerland
doi:10.4028/www.scientific.net/AMR.989-994.3856

Track and Field Image Segmentation Technology of Automatic Multi-threshold Block Sampling Based on Matlab

Ali Yu

College of Physical Education, Jiangxi science and technology Normal University, Nanchang, 330013, China

Keywords: Block sampling; Genetic algorithm; Multi threshold; Image segmentation; Cross compiler; MATLAB programming

Abstract. Based on block sampling and genetic algorithm we improve the image segmentation technology, and obtain the new image processing method based on image pixel block cross reconstruction, and apply this algorithm to the block and the reconstruction calculation of track and field image. In order to verify the effectiveness and reliability of block sampling and genetic algorithm, we use MATLAB to test the algorithm. Through calculation, the number of 2D block is 20, the minimum number of 3D pixel array is 1259, and the calculation residual reaches the highest, with 0.0122. When the number of 2D block is 40, the maximum number of 3D pixel array is 3875, and the calculation residual reaches the lowest, with 0.0013. Therefore, according to the needs of computer hardware conditions, we can increase the 2D block number, improve the segmentation number of 3D pixel array for track and field image, which can reduce the residual and improve the precision of calculation.

Introduction

Multi threshold image segmentation has important applications in many fields in image compression, image analysis and pattern recognition, but the automatic selection of threshold has not been solved. In this paper, we use the block sampling technique to do image segmentation, and use copy and crossover of genetic algorithm to reconstruct the image, finally get the high resolution image. In this paper, we use MATLAB software to debug the algorithm, and through the image processing on the track and field running, get the residual curve changing with time [1, 2]. Finally, we do different 2D block processing on the image, get different 3D image array distribution point. It provides the theoretical reference for the study of sports image processing technology.

Application of Block Sampling Genetic Algorithm in the Image Segmentation of Track and Field

Image segmentation is split the image into a number of unique region, and extract the interested objects from the region. In order to analyze and identify the target, they need to be segmented and extracted [3, 4]. In this paper, we use the block sampling technique to do image segmentation, and reconstruct the image using the genetic algorithm. The specific process is as shown in Figure 1.

As shown in Figure 1, we use block sampling and genetic algorithm to calculate the image segmentation reconstruction algorithm, and use MATLAB to realize the genetic algorithm [5]. Finally we realize the optimization processing on the track and field sports image, and obtain high resolution images.

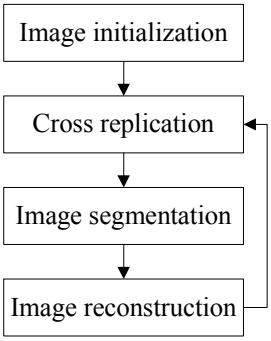

Fig. 1 The flow chart of image segmentation reconstruction

Block Sampling Genetic Algorithm Design of Track and Field Image Segmentation Reconstruction

Track and field image is mainly composed a series of pixels. Using block sampling technology can realize quick image division. Using the crossover and mutation feature of genetic algorithm can reconstruct image [6, 7]. First determining the image pixels set, pixel can be statistics to set boundaries. Pixel matrix can be written in formula (1) using the block principle.

$$\begin{matrix} 1 & a_{12} & \cdots & a_{1i} \\ a_{21} & 1 & \cdots & a_{2i} \\ \vdots & \vdots & \ddots & \vdots \\ a_{j1} & a_{j2} & \cdots & 1 \end{matrix} . \tag{1}$$

a_{ji} is block operation, the value of a_{ji} is greater, the higher accuracy of division. Based on genetic algorithm it can generate random sequence of image point, as shown in formula (2).

$$\{a_{t-1}, v_{t-1}^1, v_{t-1}^2, \cdots, v_{t-1}^n\}, a_{t-1} \in R . \tag{2}$$

Through the adaptive genetic algorithm we can do probability cumulative on the random sequence of pixel, finally get the cumulative formula as shown in formula (3).

$$b_c = \sum_{m=1}^{c} eval(\psi_m)(c = 1,2,\cdots,z) . \tag{3}$$

Doing cross operation on the random sequence of pixel. The cross process is as shown in formula (4).

$$\begin{aligned} \overline{a}_e^j &= xa_e^j + (1-x)a_e^j \\ \overline{a}_f^j &= (1-x)a_f^j + xa_f^j, j = 1,2,...,n \end{aligned} . \tag{5}$$

x is the cross coefficient, the coefficient is a random number, and $x \in [0,1]$.

Using genetic variation principle, we can do mutate operation on the pixel, as shown in the formula (5).

$$\{\overline{a}_e^1, \overline{a}_e^2, \cdots, \overline{a}_e^n\} = \{a_e^1, a_e^2, \cdots, a_e^n\} + N \bullet s . \tag{6}$$

N is a big positive number. S is random direction of n dimension space. In order to realize the genetic algorithm and block sampling of track and field image segmentation, this paper uses MATLAB to design the programming as below:

```
function [newpop]=crossover(pop,pc)
[px,py]=size(pop);
newpop=ones(size(pop));
for i=1:2:px-1
```

```
    if(rand<pc)
        cpoint=round(rand*py);
        newpop(i,:)=[pop(i,1:cpoint),pop(i+1,cpoint+1:py)];
        newpop(i+1,:)=[pop(i+1,1:cpoint),pop(i,cpoint+1:py)];
    else
        newpop(i,:)=pop(i);
        newpop(i+1,:)=pop(i+1);
end
end
Variation process MATLAB program
function
[newpop]=mutation(pop,pm)
[px,py]=size(pop);
newpop=ones(size(pop));
for i=1:px
    if(rand<pm)
        mpoint=round(rand*py);
        if mpoint<=0
            mpoint=1;
        end
.....
```

Application of Computer Image Processing Technology in Track and Field Image Segmentation

In order to verify the effectiveness and reliability of track and field image genetic algorithm designed in second part, we use genetic algorithm toolbox of MATLAB software to debug the program, and establish genetic algorithm system of track and field image processing [8]. The toolbox interface is as shown in Figure 2.

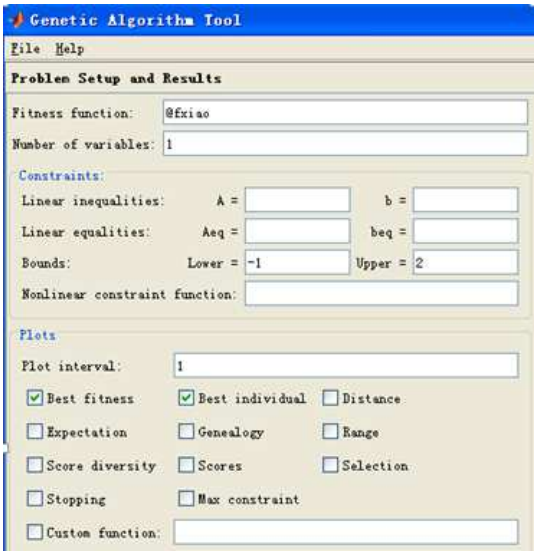

Fig. 2 Genetic algorithm toolbox of MATLAB

Figure 2 shows the genetic algorithm toolbox of MATLAB. It is in the MATLAB software. The module can achieve the genetic algorithm debugging function, where File can import the image processing program [8]. This paper uses the block sampling genetic algorithm to do segmentation reconstruction operation on the image. The residual convergence curve is as shown in Figure 3.

Figure 3 is the residual convergence curve computed by MATLAB. From the chart we can see, with the increase number of iterative, calculation gradually tends to be converge [9]. After 600 iteration, reconstruction iteration and segmentation iteration have reached a stable convergence

condition, the minimum residual is only 0.00016, which meets the requirements of design and calculation.

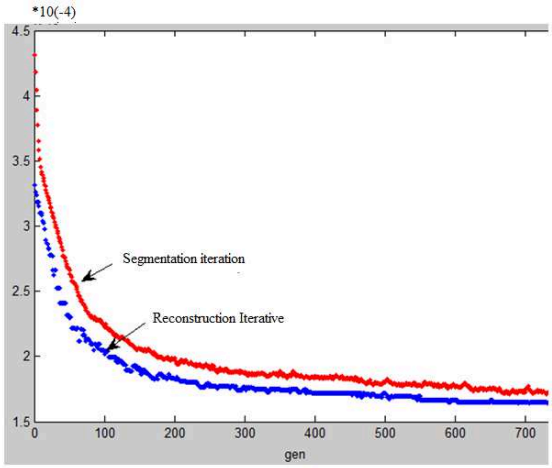

Fig. 3 The residual convergence curve

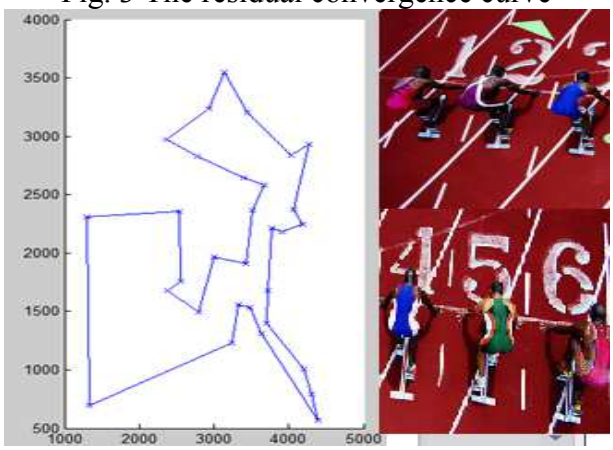

Fig. 4 The result of 2D image block

Figure 4 shows the 2D image block, MATLAB can achieve image block function. As shown in Figure 4, we do block segmentation on track and field image, use reconfiguration algorithm to synthetic images, and obtain 3D image point distribution as shown in Figure 5.

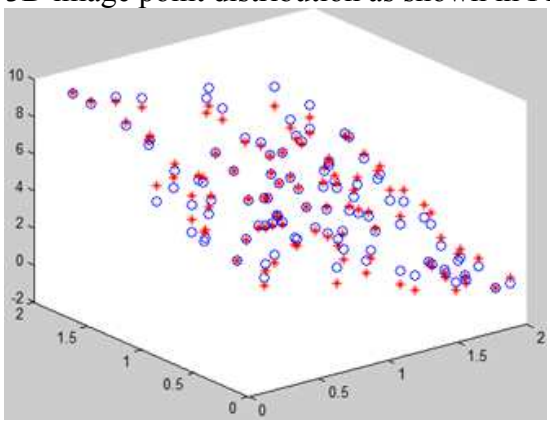

Fig. 5 The result of 3D image block

Figure 5 shows 3D image block sampling. It uses image segmentation theory to capture image sequences in 3D space, and maps pixel in 3D space. It uses crossover and mutation of genetic algorithm to reconstruct the pixel. The main data is as shown in Table 1.

Table 1. Result of image block segmentation

Number of 2D block	Number of 3D pixels	Residual
20	1259	0.0122
30	2456	0.0082
40	3875	0.0013

Table 1 shows the result of image block segmentation. From the table we can see, along with the increase number of blocks, the number of pixels increases gradually, but the residual is reduced. Through calculating we get the result of image segmentation reconstruction, as shown in Figure 6.

Fig.6 Diagram of track and field image diagram reconstruction

Figure 6 shows the effect of track and field image segmentation reconstruction using MATLAB genetic algorithm toolbox. From the chart we can see, the resolution of reconstructed image segmentation is improved, which is conducive to analyze the image details, and it improves the precision of image information processing.

Summary

In this paper we establish block sampling algorithm of image segmentation, and design the mathematical model of image reconstruction by using genetic algorithm, and obtain a new the block crossover reconstruction image processing of pixels. This method can realize the reconstruction calculation of the track and field image. We use MATLAB software to debug image segmentation reconstruction algorithm, obtain the residual curves changing with time. Combined with 2D block processing, we get the 3D pixel array distribution. Finally, we use the image block processing to optimize image, and get the high resolution images of track and field. It provides a new computer method for studying image processing technology.

References

[1] Lin Zhengchun, Wang Zhiyan, Zhang Yanqing. Threshold segmentation of image optimization [J]. Journal of computer aided design and graphics, 2012, 22(7): 1201-1206.

[2] Qiao Lishan, Chen Songcan, Wang Min. The image threshold technology based on relevance vector machine [J]. Journal of computer research and development, 2010, 47(8): 1329-1337.

[3] He Xiaojuan. Distribution Estimation algorithm and its application in production scheduling [D]. Lanzhou University of Technology, 2011: 2-14.

[4] Cao Song, Sun Fuchun, Hu Laihong. Distribution estimation algorithm based on flight optimization [J]. Journal of Tsinghua University (NATURAL SCIENCE EDITION), 2012, 52(1): 66-71.

[5] Zhuang Jian, Yang Qingyu, Du Haifeng, Yu Dehong. A higher efficient and complex system genetic algorithm [J]. Software, 2011, 3(13): 45-49

[6] Chen Hao, Cui Duwu. Population evolutionary algorithm [J]. Journal of software, 2010,21(5): 978-990.

[7] Yue Qian, Feng Shan. Calculation performance analysis of the genetic algorithm [J]. Journal of computer, 2011, 32(12): 2389-2392.

[8] Li Junhua, Li Ming, Yuan Lihua. The pseudo parallel genetic algorithm based on clustering [J]. Pattern recognition and artificial intelligence, 2011, 22(2): 188-194.

[9] Chen Shouwen, Li Mingdong. An improved genetic algorithm and its simulation [J]. Computer applications and software, 2012, 27(9): 100-102.

Advanced Materials Research Vols. 989-994 (2014) pp 3861-3864
© (2014) Trans Tech Publications, Switzerland
doi:10.4028/www.scientific.net/AMR.989-994.3861

The design of Image acquisition system based on CMOS image sensor USB interface

HU ZhiYu[1, a], LI Li[2]

[1,2] JINGDEZHEN UNIVERSITY, JiangXi JINGDEZHEN 333000,China

[a]huzhiyu29@yeah.net

Keywords: USB control transfer; Hub-and-spoke network model; Design an image acquisition system

Abstract. The system selected OmniVisiON company's CMOS chip OV7620, it is an integrated color camera chip, a 640 × 480 (300,000 pixels) image matrix. Considered that the CPLD control system is similar to the DMA mode of data transmission; Cypress's USB 2.0 chip is used by CY7C68013 chip. Finally, it is become the microcontroller firmware and device driver. The paper presents the design of Image acquisition system based on CMOS image sensor USB interface. Design an image acquisition and transmission system, and describes its firmware as well as the development of USB device drivers and PC-side application.

1. Introduction

Introduction of CMOS image acquisition system is the core of the CPLD con-trol, the system selects a colour image sensor OV7620 and fast image transmission through the USB interface which is similar to the DMA mode. Many applications of pattern recognition, computer vision, and multimedia ap-plications are increasingly have a high demands on the acquisition and transmis-sion of image data [1].

2. Image acquisition system

2.1 Image system acquisition

The system selected OminiVisiON company's CMOS chip OV7620, it is an integrated color camera chip, a 640 × 480 (300,000 pixels) image matrix in the interlaced mode, the operating frequency up to 60Hz progressive scan at 30/ s. Image plane size 1/3 inches to 8 or 16-bit digital signal from a single or dual channel output, the output signal type can be selected between YCrCb and RGB image matrix to support VGA or CIF regulations, the digital output format follow the the CCIR601 ZVPorts, CCIR656 or other standards [2].

The CPLD selection using ALTERA chip EPM7128S which is the core of the system that should not only be responsible for the OV7620 output video data are stored in SRAM, but also in conjunction with the MCU to complete the transmission of video data USB, as is shown by equation1.

$$M_{f,1} = \sum_{i=1}^{L} \sum_{j=1}^{L} h_{f,1}(i,j) \cdot \log_2 \frac{h_{f,1}(i,j)}{h_f(i) + h_1(j)} \tag{1}$$

MCU is the CIGNA company's high-performance microcontroller C8051F020, work and status of the CMOS chip via the I2C bus control, C8051F020 comes from SMBUS bus interface, I2C clock line SCL and the data line SDA can be assigned to the port pin through the crossbar [3]. MCU as the host of the I2C bus communication, using the OV7620 42H (Write), 43H (Read) as a slave address with the MCU communication.

$$f_c = \sqrt{\frac{1}{MN} \sum_{j=0}^{N-1} \sum_{i=1}^{M-1} [I(i,j) - I(i-1,j)]^2} \tag{2}$$

CMOS image sensors are larger due to the CMOS process technology which is not high, so that the sensor noise is in the application since the invention of the 1980s and the commercialization process has been slow. SRAM chip IS61LV5128AL, the chip for high-speed static RAM, storage time of about 10ns, and is enough speed to meet the requirements of OV7620, its 512KB of storage space is sufficient to store 30 million pixel video data (Bayer2pattern: each pixel consists of one word section of the RGB information) [4].The USB interface chip using the PHILIPS PDIUSBD12 chip, the chip supports USB 1.1 standard protocols and DMA transfer mode.

$$H_e = -\sum_{l=0}^{L-1} P(l)\log_2 p(l) \tag{3}$$

When the OV7620 set the stability for the work, it will output video data, as well as three important reference signals: frame synchronization signal SYNC, the HREF of the horizontal sync signal, and pixel clock signal PCLK. As is shown by equation4.

$$\begin{cases} C_{j+1} = HC_j H' \\ D^h_{j+1} = GC_j H' \\ D^v_{j+1} = HC_j G' \\ D^D_{j+1} = GC_j G' \end{cases} \quad (j = 0,1,2,\cdots,J-1) \tag{4}$$

In the low-end products, the quality of its picture is close to the low-grade CCD resolution, and related businesses hope to replace the CMOS device CCD so that efforts are being gradually become clear. CMOS sensor can be subdivided into: Passive Pixel Sensor CMOS and Active Pixel Sensor the CMOS.

2.2 The storage of the image

640 × 480 pixel output characteristics, 512KB of RAM is divided into 512 lines, each line 1KB space selected by the 10 address lines A0 ~ A9 passage within the address remember low-order address: the ADDR-L; high A18 ~ A10 a total of nineaddress lines strobe lines are recorded as high address: ADDR-H. Synchronized to ensure the OV7620 collection of data is written to the SRAM, CPLD macrocell design two address counters: ADDR-L low counters and high counters the ADDR-H.

$$\begin{cases} D^{\xi}_{j,F}(m,n) = w^{\xi}_{j,\max}(m,n)D^{\xi}_{j,A}(m,n) \\ \quad + w^{\xi}_{j,\min}(m,n)D^{\xi}_{j,B}(m,n) \quad E^{\xi}_{j,A}(m,n) \geq E^{\xi}_{j,B}(m,n) \\ D^{\xi}_{j,F}(m,n) = w^{\xi}_{j,\min}(m,n)D^{\xi}_{j,A}(m,n) \\ \quad + w^{\xi}_{j,\max}(m,n)D^{\xi}_{j,B}(m,n) \quad E^{\xi}_{j,A}(m,n) < E^{\xi}_{j,B}(m,n) \end{cases} \tag{5}$$

The high and the counter is cleared to 0, so that completion of an image data cache, detailed images acquisition signal timing shown in Figure 2. 512KB of SRAM chip is actually used and it has only 640 × 480 over 300 KB of storage space. Way the device works set to update the data on the falling edge of the PCLK signal: on the rising edge, the data is a period of stability, the falling edge of the PCLK signal to update the SRAM address signal ADDR; / WR signal at the rising edge of PCLK signal. CCD sensors combined with the analog signal generated by the component and then output to the third sensor followed by on, until the combination of the last sensor signal to form a unified output.

$$\begin{cases} D^{\xi}_{j,F}(m,n) = -(\left|w^{\xi}_{j,\max}(m,n)D^{\xi}_{j,A}(m,n)\right| \\ \quad + \left|w^{\xi}_{j,\min}(m,n)D^{\xi}_{j,B}(m,n)\right|) \quad D^{\xi}_{j,A}(m,n) < 0 \\ D^{\xi}_{j,F}(m,n) = \left|w^{\xi}_{j,\max}(m,n)D^{\xi}_{j,A}(m,n)\right| \\ \quad + \left|w^{\xi}_{j,\min}(m,n)D^{\xi}_{j,B}(m,n)\right| \quad D^{\xi}_{j,A}(m,n) \geq 0 \end{cases} \tag{6}$$

Then write data to the SRAM effectively. The CPLD control the SRAM write data logic using VHDL language, and finally achieve a continuous image data acquisition using MAX PLUS II tools for simulation design.

2.3 The storage of the image

The traditional USB transfer mode is the MCU start with SRAM data being sent to the PDIUBD12; by PDIUBD12 sent to the host. Regardless of the MCU to fetch data from the SRAM or to write data to the PDIUBD12 of the peripheral, the speed is slower. Therefore, we consider the CPLD control system is similar to the DMA mode of data transmission. In the working process, SCM is responsible for the interpretation of the USB control transfer.

$$\begin{cases} D_{j,F}^{\xi}(m,n) = \left| w_{j,\max}^{\xi}(m,n) D_{j,B}^{\xi}(m,n) \right| \\ + \left| w_{j,\min}^{\xi}(m,n) D_{j,A}^{\xi}(m,n) \right|) \quad D_{j,A}^{\xi}(m,n) < 0 \\ D_{j,F}^{\xi}(m,n) = -(\left| w_{j,\max}^{\xi}(m,n) D_{j,B}^{\xi}(m,n) \right| \\ + \left| w_{j,\min}^{\xi}(m,n) D_{j,A}^{\xi}(m,n) \right|) \quad D_{j,A}^{\xi}(m,n) \geq 0 \end{cases} \tag{7}$$

To be carried out from outside access number, the PDIUBD12 microcontroller allows the bus to complete the work by the CPLD. The CPLD generate external memory read signal and address to produce PDIUBD12 write signal and address, and the external memory data transmit to PDIUBD12 interface chip automatically.

2.4 The specific implementation of the data transmission

When a host needs to transmit data through the control pipe to send the request, the MCU receiving the order immediately after the OV7620 so that SRAM data bus, and to notify PDIUBD12 ready for the primary endpoint of the bulk data transfer, then the send TXCOM command signal to the CPLD,notify the CPLD to start transferring data; 64B of the data transfer is completed, the CPLD to the microcontroller send TXEND signal to show 64B transferred, and wait for next TXCOM signal, the next 64B transmission. MCU and CPLD through these two signals are in order to complete the handshake.

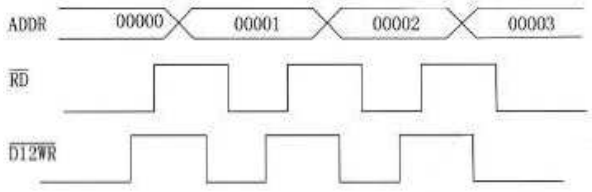

Fig. 1 Image transmission signal timing diagram

3.System software design

The system software includes a USB device firmware, device drivers and applications.

Device firmware is the core of the device when it is running, its main function is to control the interface chip PDIUBD12 and complete USB 1.1 protocol (including standard equipment request, vendor request processing, set the device interface, etc.).

What worth mentioning in the paper is that the microcontroller program of this system has an additional USB device firmware. The system also has single-chip OV7620 I2C control software and CPLD handshake procedure. All of the procedures is used the Keil C software to prepare for the programming, after the programming, we download it to the MCU in it.

$$\begin{cases} W_{\psi}^{H}(j,x_1,y_1) & \left| W_{\psi}^{H}(j,x_1,y_1) \right| \geq \left| W_{\psi}^{H}(j,x_2,y_2) \right| \\ W_{\psi}^{H}(j,x_2,y_2) & \left| W_{\psi}^{H}(j,x_1,y_1) \right| < \left| W_{\psi}^{H}(j,x_2,y_2) \right| \end{cases} \tag{8}$$

Second, we designed the device drivers in the Windows operating system within the running kernel level driver used to control the hardware, the USB device driver using standard WDM device driver while the WDM using the IRP as its drive mechanism.

In the development of this system, the driver DR IVERSTUD IO tools package provides a complete source code generation tool (DR IVER WIZARD) and the corresponding library.

$$w = \begin{bmatrix} 1 & 2 & 1 \\ 2 & 4 & 2 \\ 1 & 2 & 1 \end{bmatrix} * \frac{1}{16} \tag{9}$$

For the application of Win2 system, in each device abstraction for files, the data is transmitted through a few simple file operations AP function to communicate with a device driver.

$$\begin{cases} w^{\xi}_{j,\min}(m,n) = \frac{1}{2} - \frac{1}{2}\left[\frac{1 - M^{\xi}_{j,AB}(m,n)}{1 - T}\right] \\ w^{\xi}_{j,\max}(m,n) = 1 - w^{\xi}_{j,\min}(m,n) \end{cases} \tag{10}$$

4. Conclusion

Optimal adjustment of the 2G/3G switching to a longer include an analysis of the adjustment, observation, and then repeat the process of analysis cycle also to go through step by step in order to gradually adjust and optimize the place. The refined optimization analysis of 2G/3G Mode Switching provides an efficient and practical way for users for reference.

5. Acknowledgements

This paper is one of Application of Formal Schema JINGDEZHEN University"(Based on the modern computer technology and show the research of the cultural relics, ancient ceramics recovery - jingdezhen ancient kiln, for example project,2014). The project number is PT-1443.

Reference

[1] Zeng Cheng, Tonghe Li, Xiaoqing Zheng, "Implementation of Low Power Strategies in a Base-band Chip in 40nm CMOS Technologies", AISS, Vol. 4, No. 5, pp. 114 ~ 121, 2012.
[2] Ji-Woong Kim, Kyoung-Su Park, and Kae-Dal Kwack, "A 12-b Low Voltage CMOS Pipelined Analog-to-Digital Converter Without Sample and Hold Circuit", RNIS, Volume 5, pp. 28 ~ 30, 2010.
[3] Shi-gang HU, Xiao-Feng WU, Zai-fang XI, "Impact of Direct Tunneling Current on CMOS Logic Circuit ", JDCTA, Vol. 6, No. 8, pp. 231 ~ 238, 2012.
[4] Ni Haiyan, Li Zhenli, "The Layout Implementations of High-Speed Low-Power Sequential Logic Cells Based on MOS Current-Mode Logic", JCIT, Vol. 7, No. 10, pp. 1 ~ 10, 2012.

Advanced Materials Research Vols. 989-994 (2014) pp 3865-3867
© (2014) Trans Tech Publications, Switzerland
doi:10.4028/www.scientific.net/AMR.989-994.3865

Locating Method of DPM 2D Barcode Image

Zheng Herong, Shan Bing, Liu Zhi

College of Computer Science and Technology, Zhejiang University of Technology

288# Liuhe Road, Hangzhou, China, 310023

lzhi@zjut.edu.cn, hailiang@zjut.edu.cn

Keywords: DPM 2D barcode; Homomorphic filtering; Binarization; Convex hull algorithm

Abstract: This paper studies the positioning method of DPM 2D barcode image. Because of the reflective problems of metal surface, the barcode image gotten will have uneven illumination, high light issues. In this paper, the homomorphic filtering method is used to enhance the image. Then the gradient projection is used to positioning the barcode region preliminary. We use an adaptive threshold method composed of Otsu method and neighborhood threshold method to solve the error segmentation problem. Finally the convex hull algorithm is applied to locate barcode region. Experiment results show that this method can effectively locate the barcode region quickly.

Introduction

Direct Part Marking[1] is a permanent identification technique that will mark permanent words or symbols on the products. DPM 2D barcode is kind of the two-dimensional barcode which mark symbols on products by using DPM technique. Traditional Data Matrix 2D barcode positioning method cannot recognize the barcode effectively. This paper studies the barcode image enhancement and binarization method. A method to positioning the barcode image dotted Data Matrix 2D barcode marked on metal surface by laser is proposed in this paper.

Enhancement method of DPM 2D barcode image

Because of ambient light and surface quality of the metal, the barcode images gotten always are affected by uneven illumination and high light. So the barcode image need to be enhanced in order to be recognized. There are many uneven illumination image processing algorithms such as histogram equalization, homomorphic filtering and enhancement method based on Retinex theory. Classic homomorphic filtering is processed in the frequency domain. It will take a long computing time and need a large memory space. In this paper, we propose an improved spatial homomorphic filtering algorithm combined with the Kronecker product[2]. The algorithm procedure is shown in Fig. 1.

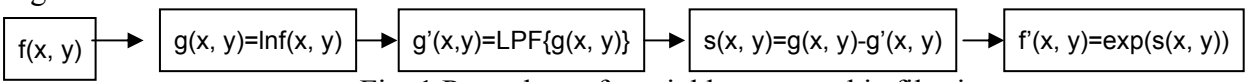

Fig. 1 Procedure of spatial homomorphic filtering

In order to approximate the low-pass filter using neighborhood average method, a larger range of neighborhood will be needed. This will definitely increase the computational complexity. Using Kronecker product principle, the two-dimensional array of neighborhood templates will be divided into two one-dimensional arrays. It will greatly improve computing speed. Fig. 2 is the result of this method.

(a) Original image (b) Enhanced image

Fig. 2 Image enhance by homomorphic filtering

Binarization method of barcode image

In order to get the binary barcode image, we use an adaptive binarization method composed of Otsu method and nearest neighbor pixels contributing threshold method[3]. In this way, all pixels of the image are divided into two groups by a sliding window firstly. Then we can move the sliding window from pixel to pixel. If the change of grayscale is great within the sliding window, the current pixel is divided to A group. Otherwise the pixel is divided to B group. The divide procedure is shown in Eq. 1.

$$\begin{cases} \frac{1}{\mathrm{N}}\sum_{i=-r}^{r}\sum_{j=-r}^{r}\left|g(x+i,y+j)-\overline{g}\right| \geq k*g' & g(x,y)\in A \\ \frac{1}{\mathrm{N}}\sum_{i=-r}^{r}\sum_{j=-r}^{r}\left|g(x+i,y+j)-\overline{g}\right| < k*g' & g(x,y)\in B \end{cases} . \tag{1}$$

Where r denotes the size of sliding window, g(x, y) denotes the grayscale value of each pixel and g' denotes the mean grayscale value in the sliding window, k is a ration of the average value and standard deviation of all pixels in the sliding window.

The result of segment is related to the size of sliding window. Table 1 shows the result of classification with different size of sliding window. Experiment results show that size of 7*7 is the best size of the sliding window.

Table 1 Classification result with different size of sliding window

Size of window	3*3	5*5	7*7	9*9
Result of classification		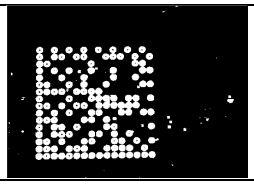	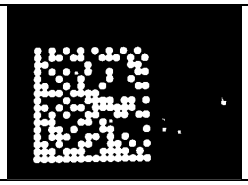	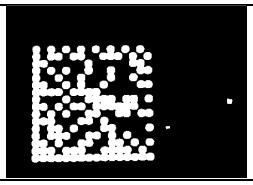

For the pixels in A group, the OSTU method is used to find the threshold T. If the grayscale value of the pixel is greater than T, the pixel can be marked as background pixel. Otherwise it will be marked as target pixel. For the pixels in B group, we use nearest neighbor pixels contributing threshold method. For one pixel in B group, search the 8-Neighbor pixels first. If the target pixels and the background pixels can not be found in the eight neighborhood, the scope of the search will be expanded. The search area will be enlarged to 16-Neighbor pixels, 24-Neidhbor pixels. The segmentation method is given in Eq. 2.

$$f(x,y)=\begin{cases} 255 & \left|f(x,y)-g'_b\right| > \left|f(x,y)-g'_w\right| \\ 0 & \left|f(x,y)-g'_b\right| \leq \left|f(x,y)-g'_w\right| \end{cases} . \tag{2}$$

Where g'_b denotes the average gray value of all pixels belong to background and g'_w denotes the average gray value of all pixels belong to target. According to the feature of dotted Data Matrix 2D barcode, we determine a threshold There. When search area is larger than the threshold T, searching process will be stopped. The current pixel will be marked as background pixel. Fig. 3 shows the comparison of different binarization methods.

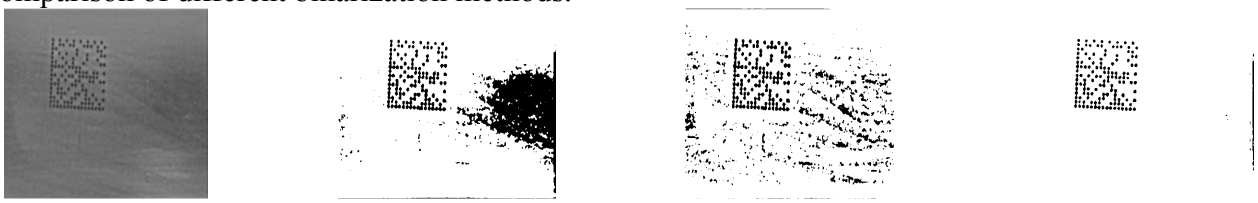

(a) Original image (b) One-dimensional Ostu (c) Two-dimensional Ostu (d) Method in this paper

Fig. 3 Comparison of different binarization methods

DPM 2D barcode localization

The Data Matrix barcode is composed of two solid adjacent borders in an "L" shape (called the "finder pattern"). In this paper, we locate the Data Matrix 2D barcode with convex hull algorithm[4].

Firstly, we use mathematical morphology to fit the “L” shape of the Data Matrix 2D barcode[5]. Fig. 4 is the result of closing operation.

(a)Original image

(b)Closing operation

Fig. 4 The result of closing operation

n this paper, we use Sobel operator to get the border of polygon. Then the convex hull points of polygon are calculated by using Graham scan method. In the standard Data Matrix 2D barcode, there will be 5 convex hull points. Because there are interference points around the areas of the image barcode, the amount final convex hull points detected may be much more than the expected points. It will reduce the locating accuracy. So these noise points should be removed. Finally, we can get the polygon which consisted of convex hull points. If “L” shape exists in the current convex hull polygon, stop calculating. Otherwise, the next polygon will be detected. The result is shown in Fig. 5.

(a) Original image

(b) Locating result

Fig. 5 Locating result by using Convex hull algorithm

Conclusions

In this paper, we use homomorphic filtering method to solve the issues of low contrast, uneven illumination in the DPM barcode image. Then we use an adaptive binarization method which combined the gray contribution information and space contribution of pixels. Finally, we use convex hull algorithm to locate DPM 2D barcode. The experimental results show the locating accuracy of this method is pretty high.

Acknowledgements

This work was financially supported by the Zhejiang Province Science and Technology Agency Project (2012C21046).

References

[1] Li Juan, Su Guanqun, Liu Limei. Research on DPM Technology Standardization Status Quo and Development Suggestion: Standard Science Vol. 10(2009)

[2] Xiao Jun, Song Shoupeng, DING Lijuan. Research on the Fast Algorithm of Spatial Homomorphic Filtering: Journal of Image and Graphics Vol. 12(2008)

[3] Jinrui Li, Aiqun Wang, Jianmei Li, Yusong Wu. An Adaptive Image Binarization Method for Laser Direct Marking Data Matrix Symbols on Metal Surface: Applied Mechanics and Materials Vol. 9(2013).

[4] Lu Jian, Liu Zhi. An approach for smart phone barcode positioning and correction based on an improved conve x hull algorithm: Journal of Zhejiang University of Technology Vol. 6(2010).

[5] Xie Junxi,Tang Zhaohui,Gui Weihua. Recognition of the Two-Dimension Barcode Based on Mathematical Morphology: Computer Engineering & Science Vol.31(2009).

Advanced Materials Research Vols. 989-994 (2014) pp 3868-3871
© (2014) Trans Tech Publications, Switzerland
doi:10.4028/www.scientific.net/AMR.989-994.3868

The simulation of DS-UWB RAKE receiver over the multipath channel

Zhang Ke [1, a], Cao Yu [1,b] Li Changfu [1,c] Liu Weiye[1d]

[1] College of information Engineering, Beijing Institute of Petrochemical Technology, Beijing, China, 102617

[a]zhangke@bipt.edu.cn, [b]525940677@qq.com, [c]lichangfu@bipt.edu.cn, [d]1034764204@qq.com,

Keywords: DS, UWB, Multipath channel, RAKE receiver

Abstract. Ultra-Wideband (UWB) wireless communication is a new potential communication technology currently in its field. It becomes very popular in the world since it's high performance, low radicalization and low cost. Currently UWB wireless system, we can call it Impulse Radio technology too, be invented in 20 century 1960s. But it was only used in military affairs field, bailout searching, radar location and so on. After civil using, it usually is used in indoor wireless LAN .In this paper, the development and application of UWB are introduced, the characteristic and limitation of UWB are simply analyzed. According to the simulating depending on Multipath channel, it shows increasing SNR about 1.5dB to the base of primary power district or increasing SNR about 1dB to primary power district and minor power district, we can get whole performance of RAKE receiver in perfect channel.

Introduction

UWB communication is also called the very narrow Pulse communication (Ultra Short Pulse), Impulse Radio (Impulse moisturizer Radio), etc. Tens of megabytes per second rate is used to transmit and receive no carrier frequency narrow pulse signal, the pulse width for less than 1 ns. Information communication is modulated to the precise time interval, including a Modulation method called Pulse Position Modulation (Pulse Position Modulation), due to cover many communication frequencies, it uses the random sequence jump time extension signal spectrum, makes the spectrum characteristics similar to white noise and has a very low power spectral density. Signal has low interference, low probability of intercept and time domain secret communication. As a kind of ultra wideband spread spectrum communication, it has more user capacity than now. Due to the use of less than 1 ns for narrow pulse signal of the carrier, it has the very good time resolution, almost not affected by multipath interference, and very suitable for indoor multipath environment complex applications of high-speed wireless local area network (LAN). From the existing technical indicators, in UWB wireless communication it has the most attractive index: high speed and low power consumption, so the research of UWB communication is of great significance [1].

UWB wireless communication can be divided into two kinds: carrierless UWB and carrier modulation UWB. Carrier modulation UWB has a variety of implementation scheme, the main two are based on DS - CDMA (Direct Sequence Code Division Multiple Access) and MB - based OFDM (Multi - Band Orthogonal Division Multiple). Different solution strengths and different applications may choose different scheme, other factors such as performance; complexity, price, etc will greatly affect the various solutions. There is still other UWB system scheme, especially in specific areas, such as military field. Research of UWB technology in our country and international standards, began almost at the same time, and get the support of national 863 plan, but compared with international advanced level, there are still a certain gap. In the set of standards/specifications, the United States, Europe, Japan and Singapore has carried on the related work, especially the United States, since releasing the preliminary rules of UWB communication, UWB technology research and development work has entered a new stage, many colleges and institutes are going on, and the UWB communications standardization of our country has not officially began to work. This work should be started as early as possible, so as to prompt the strength of research institutions and enterprises to participate in, to speed up the research and development work, to have more our own independent intellectual property rights related technologies and standards, to avoid more backward and huge losses in the international competition. In applications, according to the technical level of our country,

we can grasp the time to develop some low rate of product to seize the market first of all, we should constantly improve product performance, extend the range of products under the premise of stepping in technology research and development at the same time. In order to compete with the international advanced products [2,3].

In this paper we briefly introduce the development history of the concept of UWB content, the theory of ultra-wideband very narrow pulse signal is described and analyzed, through the computer simulation research of DS - UWB Rake receiver in multipath channel performance, finally draw the conclusion.

UWB system

An overview of the UWB system. According to the Shannon (c. E.Shannon) channel capacity

$$C = B\log_2(1+\frac{S}{N}) \tag{1}$$

We can increase the system transmission bandwidth B to keep the channel capacity C unchanged when the signal to noise ratio of S transmitted in Gaussian channel system falls, in order to achieve error-free communication channel. Step by step, it is from frequency hopping to spread spectrum communication, then to the ultra wideband (UWB) communication in the perspective of the development of communication technology. The bandwidth of the spread spectrum communication system is hundreds or even thousands of times greater than conventional communication system. Compared with the ultra wideband (UWB) communication, spread spectrum communication is a kind of narrow-band communication system, so the ultra wideband communications is bigger than the channel capacity of spread spectrum communication. Shannon also points out that under Gaussian noise interference, limited on the average power of the channel, to achieve effective and reliable communication signal is white noise statistical characteristics of signal, because Gaussian white noise signal has ideal autocorrelation properties. Gaussian white noise signal power spectrum is

$$s(\omega) = \frac{N_0}{2},\ -\infty < \omega < \infty \tag{2}$$

The autocorrelation function of it is

$$R(\tau) = \frac{1}{2\pi}\int_{-\infty}^{\infty} S(\omega)e^{j\omega\tau}d\omega = \frac{N_0}{2}\delta(\tau) \tag{3}$$

Ultra-wideband namely in the process of communication signal spectrum width is more than usually occupied bandwidth occupied the information system. According to the federal communications commission (FCC) definition of signal bandwidth is greater than 1.5 GHz, or the ratio of the signal bandwidth and center frequency is more than 20% for ultra broadband; The ratio of the signal bandwidth and center frequency between 1% ~ 20% for broadband, less than 1% for narrow band. The FCC then rule more than 500 MHZ bandwidth can be called ultra broadband [4].

The characteristics of the UWB wireless communication system. Modern UWB wireless communication technology has the excellent properties inherent resistance to multipath fading, it has a strong ability of market competition compared with the traditional wireless communication technology by the channel capacity of UWB, wide space, high Capacity (Spatial Capacity), low noise level of the power spectral density, strong anti-interference ability, dynamic adjustment data rate, power consumption and adaptive ability, almost all digital communication of simple structure, and thus can provide cost-effective wireless electric equipment. UWB pulse technology can be widely used in personal communication, high-speed LAN, cordless telephone, security detection, close to the high precision positioning etc.[5].

DS-BPSK modulated pulse ultra broadband simulation system.

Relative to the carrier system, pulse ultra wideband system is relatively simple and more. It realizes the most important is to solve the problem of precise timing and multi-user access, based on the timing of better, the system can provide multiple access good, better reflect pulse communication

advantage. The following part is to study the multi-user access timing good condition and receiving problems. Need to distinguish between different users in wireless communication.

The pulse waveform in Fig. 1 by the CM1-CM4 channel, because of the dense multipath channel, pulse waveform can no longer maintain visual shape, Fig. 2 shows in direct sequence spread spectrum pulse waveform of an chip by the corresponding waveform channel [6,7].

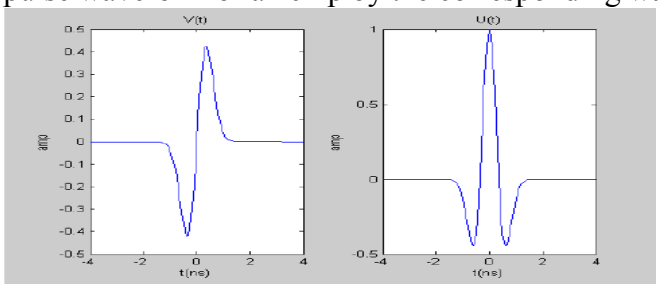

Fig.1 Gaussian pulse waveform and differential form Monocycle

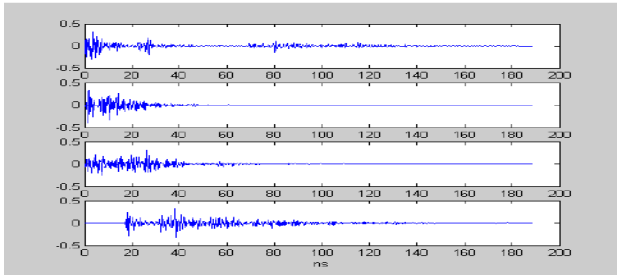

Fig.2 The direct sequence spread spectrum the differential form of Gauss is a channel impulse response chip

Now use that type, according to the selected Gold codes random equal probability binary sequence and baseband data rate, the ideal channel , Intel CM1-CM4 channel, statistics of a number of Monte Carlo simulation results on the same interval: $SIR \in (0,0.05)$

The results indicate that the actual chips interference is not serious, although the response waveform of CM1-CM4 channel is more complex and larger differences, but the performance under ideal received similar. The whole system simulation results also confirm that, in the ideal channel estimation for receiving, CM1-CM4 channel with similar performance, as a contrast, compare performance 63 bit Gold sequence and random binary sequence are three users, see Fig. 3 and Fig. 4

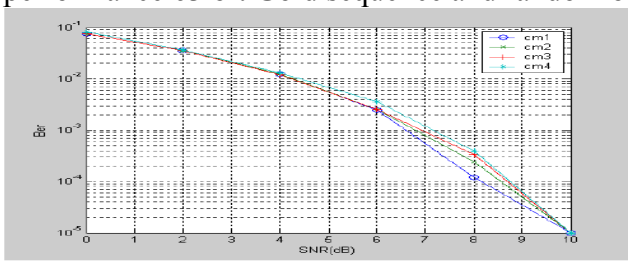

Fig.3 Gold sequence in CM1 - CM4 channel simulation results

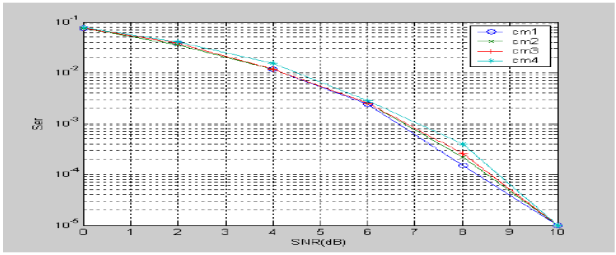

Fig.4 Random equal probability sequence in CM1-CM4 channel simulation results

In Fig.5, four curves were 63 bit Gold code as the user code, the simulation results in CM1-CM4 channel. Simulation results and theoretical analysis results are similar, namely, although four kinds of channel models in ultra wideband communication difference is bigger, but due to the interference between the chip produced by the multipath effect is small, the resulting four curve pretty close.

In Fig.6, the four curves are 63 bit equal probability random binary sequence as the user code, under CM1-CM4 channel simulation results, analysis as Fig.8.

At the same time, using the Gold code and the equal probability of random binary sequence as the user code, the curve is very similar. This shows that, in the channel condition and parameter selection, as long as the user code with pseudo random (random) characteristics and basic equal to the number of 0 and 1 in the code element, the bit error rate is very similar.

For comparison, Fig.6 shows the 63 bit Gold codes and equal probability random binary sequences of CM1 and CM4 bit error rate curve. Fig.9 can be seen, in the same channel, with two yards in the performance difference is small, only in different channels to different.

Research of Rake receiver performance. System simulation using low pulse transmission cycle, receiving the multipath energy .Although you can take small duty cycle to reduce chips interference, but in UWB communication, the channel response is more complex and the multipath

effect is relatively long, so it is necessary to study the Rank receiver receives the path number. This is a compromise between the receiving performance and receiving complexity [8, 9].

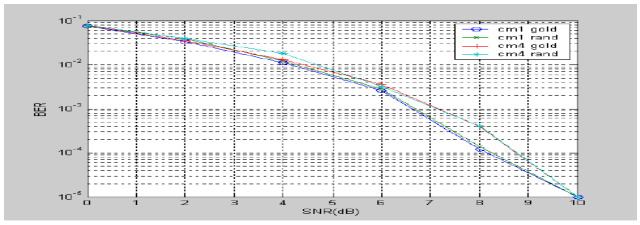

Fig.5 Gold codes and almost random binary code comparison

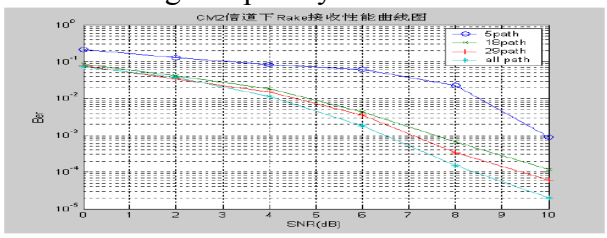

Fig.6 Rake receiver performances in CM2 channel

The simulation results in Fig.6. It can be drawn from the performance curve, as long as the receiving major path energy can achieve good effect. This is very useful for design of the receiver. From the curve in the graph can be seen, with a very small paths (5paths in figure) received, performance is not guaranteed, but the primary energy region receives (18paths in figure) can achieve better performance when receiving, the primary energy region and the secondary energy region receiving (29paths in figure) compared with the all Rake receiving (all paths in figure) has similar performance. As can be seen from the figure, on the basis of receives in the primary energy region increases 1.5dB, or on the basis of primary energy region increases in 1dB SIR, which can reach the performance of all Rake received under the ideal channel estimation.

Conclusions

The channel characteristics of UWB wireless communication system is dense multipath. Select the user code in UWB wireless communication system for system improvement is not obvious, the research results show that in choosing a random (pseudo random) characteristics of orthogonal user code, basically similar in performance .In our proposed MBOK (M-ary bi-orthogonal keying) scheme design in the future, by Walsh codes as multi user code. In the condition of big Duty ratio, direct selection of orthogonal code can get the best performance. In the chips interference can be used when the pseudo random sequence, such as Gold code, a little performance loss. At the receiving end, don't need to receive all the diameter of the energy, according to the statistical properties of the channel using appropriate tap number receiving multipath signal, can obtain a better signal-to-noise ratio, and simplify the design of the receiver.

References

[1] Ultra-wideband wireless communications Weihua Zhuang1,*,y, Xuemin (Sherman) Shen1and Qi Bi21Centre for Wireless Communications (CWC), Department of Electrical and Computer Engineering, Universityof Waterloo, Waterloo, Ontario N2L 3G1, Canada2Lucent Technologies Inc., 67 Whippany Road, Whippany, New Jersey 07981, USA

[2] .M.Maggio,N.RulkovandL.Reggiani,"Pseudo-chaotictimehop-pingfor UWB impulse radio, "IEEE Trans.Circuitsand Systems—I, vol.48,no.12,December2001.

[3] M.Z.Win and R.A.Scholtz, "Ultra-wide bandwidth time hopping spread-spectrum impulse radio for wirelessmultipleaccesscommu-nications,"IEEETrans.onCommunications, April 2000.

[4] G.DurisiandG.Romano, "On the validity of Gaussian approximation to characterize the multiuser capacity of UWB TH-PPM,"Proc UWBST2002, Baltimore(MD),May23-26,2002.

[5] D.Laney, G.M.Maggio,F. Lehmann,L.Larson, "Multiple access for UWB radio with pseudo-chaotic time hopping," IEEEJ-SAC, vol.20, no.9,pp.1692-1700,December 2002.

[6] C.J. LeMartret and G.B.Giannakis.All-digital pamimpulse radio for multiple-access through frequency-selective multipath. In MILOCM2000, volume2, pages655–659 2000.

[7] I. Bergel,E.Fishler, and H.Messer. Narrowband interference suppression in time hopping impulse radio systems to be submitted to the IEEE Trans on Communication, 2001.

Advanced Materials Research Vols. 989-994 (2014) pp 3872-3876
© (2014) Trans Tech Publications, Switzerland
doi:10.4028/www.scientific.net/AMR.989-994.3872

Video Sequences Foreground Enhancement using Hidden Markov Model

Dongyue Lv[1,2,a], Dongyan Liu[2], Zhipei Huang[2,b], Nenghai Yu[1] and Jiankang Wu[2,c]

[1] Institution of Electronics, Chinese Academy of Sciences, Beijing, 100190, China

[2] University of Chinese Academy of Sciences, Beijing, 100190, China

[a]lvdongyue_nuaa@126.com, [b]zhphuang@gmail.com, [c]jiankangwu@gmail.com

Keywords: Foreground enhancement, Hidden Markov Model

Abstract. Foreground detection is an important part in video surveillance system. The detection results will significantly affect the performance of tracking, abnormal behavior analysis and other following procedures. Many algorithms have been proposed to improve the detection performance. However, these algorithms simply focus on one single frame, ignoring the relationship among the detection results of one target in successive frames. This paper presents a novel foreground enhancement algorithm using Hidden Markov Model (HMM). In a video sequence, one target in successive frames usually has similar shape, size, et al. With this property, the target can be modeled by HMM and enhanced using the result of its prior frame. The observation of HMM is obtained by ViBe. The enhancement result is then estimated by using Maximum A Posteriori (MAP). Experimental results show that compared with the state-of-art algorithm, the proposed method can enhance foreground detection effectively.

Introduction

Foreground detection is an important technique in computer vision and have been widely used in different applications [1-5]. The simple methods [6-7] are basically based on subtraction of a fixed background image or certain simple background model. The complex methods build sophisticated models for every pixel or region in the frame, using parametric models[7-10] and non-parametric ones[11-13]. There are also other foreground detection techniques, such as using color and gradient information [14], Eigen-backgrounds [9] and recently proposed ViBe [15, 16].

The foreground detection techniques mentioned above have a common weakness: they all perform foreground detection procedure on a single frame and ignore the relationship between two successive frames of the sequence. In this paper, the relationship between two successive frames is considered and the Hidden Markov Model (HMM) is used to model the relationship. A foreground enhancement algorithm is proposed based on this model. After obtaining the foreground detection result, the HMM is used to update the detection result.

HMM in Video Sequence

Framework. The Hidden Markov Model (HMM) is a doubly stochastic model which consists of states and observations. The state X_k in time k only depends on the state X_{k-1} in time k-1. The observation Y_k in time k is depending on the state X_k. In a video surveillance system, each target has its own shape, and this state is related to the state that belongs to the same target in the prior frame. The foreground detection result of each frame is related to the shapes of the targets in the frame. So the detection result of one target in prior frame can be used to update the result of the corresponding one in the current frame. The detection procedure of each target can be modeled as a HMM which is shown in Fig. 1.

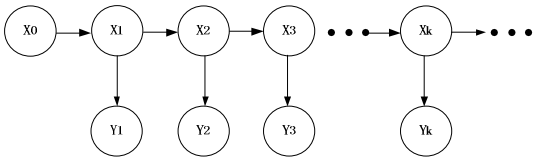

Fig.1 The HMM model of one target. X_k is the state and Y_k is detection result.

In practice, the enhancement of the whole target can be split into the updates of its pixels. Suppose x_k is the state of one pixel in time k, x_k is binary: 1 represents the pixel is foreground and 0 represents background; y_k is the observation result of the pixel in time k and is also binary.

To determine whether a pixel of one target in time k is foreground or not, the posterior probability $\Pr(x_k \mid y_{1:k})$ of the pixel must be calculated:

$$\Pr(x_k \mid y_{1:k}) = \frac{\Pr(y_k \mid x_k, y_{1:k-1}) \Pr(x_k \mid y_{1:k-1})}{\Pr(y_k \mid y_{1:k-1})} \tag{1}$$

In (1), the prediction probability $\Pr(x_k \mid y_{1:k-1})$ is sum of the production of posterior probability and transition probability in time k-1; the state x_k and the observations $y_{1:k-1}$ are independent given the state x_{k-1}, thus the posterior probability $\Pr(x_k \mid y_{1:k})$ can be rewritten as:

$$\Pr(x_k \mid y_{1:k}) = \frac{\Pr(y_k \mid x_k) \sum_{x_{k-1}=0,1} \Pr(x_k \mid x_{k-1}) \Pr(x_{k-1} \mid y_{1:k-1})}{\Pr(y_k \mid y_{1:k-1})} \tag{2}$$

Observation: Foreground Detection. The observation of the proposed HMM is obtained using the Visual Background Extractor (ViBe). It initializes the background model of one pixel from a single frame and randomly picks pixels from the pixel and its neighbors to build the model. When updating the model, it randomly updates one sample from the model and one from the model of its neighbors.

Enhancement: Using HMM. After detection and shadow elimination, the posterior probability $\Pr(x_k \mid y_{1:k})$ of one pixel can then be calculated by (2).The Maximum A Posteriori (MAP) estimation is used to determine the state of a pixel with $\Pr(y_k \mid y_{1:k-1})$ the same to both states (i.e. 0 or 1) of x_k in time k:

$$x_{\text{kmax}} = \arg\max_{x_k \in [0,1]} \Pr(y_k \mid x_k) \sum_{x_{k-1}=0,1} \Pr(x_k \mid x_{k-1}) \Pr(x_{k-1} \mid y_{1:k-1}) \tag{3}$$

The posterior probability is calculated after the corresponding blobs are found in two successive frames. The overlap region R of the bounding boxes of two corresponding blobs can be acquired after they are found using template matching. The enhancement procedure proposed here is processed in the overlap region. R can be divided into four parts:

$$\begin{cases} R_1 & y_k = y_{k-1} = 0 \\ R_2 & y_k = y_{k-1} = 1 \\ R_3 & y_k \neq y_{k-1}, \text{ surrounded by } R_1 \text{ or } R_2 \\ R_4 & y_k \neq y_{k-1}, \text{ surrounded by } R_1 \text{ and } R_2 \end{cases} \tag{4}$$

In these four parts, R_1 and R_2 represent confirmed background and foreground respectively; R_3 often represents holes in blob and noise in background; R_4 represents the region caused by shape difference between two frames.

In (2), the transition probability $\Pr(x_k \mid x_{k-1})$ of one pixel p is determined according to the region R. Pixels belong to R_1 or R_2 are definitely from background or foreground, the transition probabilities $\Pr(x_k = 0 \mid x_{k-1} = i)$ and $\Pr(x_k = 1 \mid x_{k-1} = i)$ are undoubtedly very high; pixels belong to R_3 are in a noise blob, the states will be changed or remained according to the surrounding region in a high

probability since the noise must be eliminated; pixels belong to R_4 are the shape difference between two frames, the states will be changed in a high probability.

The likelihood $\Pr(y_k \mid x_k)$ of one pixel p is determined according to the region R and "how deep" p is in the region. The observation of p in R_1 or R_2 is more likely to be the same with the state. The state of R_3 is determined by its surrounding region. The observation and state of p in R_4 will change simultaneously in a high probability. We assume the likelihood obeys the normal distribution of the distance from p to its nearest skeleton branch in the region.

Thus after the foreground detection, a foreground enhancement algorithm is proposed as follows:

Step1. Find the corresponding targets in two frames and acquire the overlap region R;

Step2. Enhance the pixels in R by calculating the posterior possibilities and use MAP to determine the state of the pixel.

For the first frame, the detection result is simply considered as the initial state. The foreground enhancement algorithm mentioned above can increase the quality of foreground detection and make the silhouettes of the targets more intact.

Experimental Results.

In this section, we compare three state-of-art algorithms (GMM [8], SOBS[13] and ViBe [15, 16]) with our algorithm in two difference video sequences (people in a shopping mall and pedestrians in a building). The two video sequences represent two typical circumstances respectively: a few people in scene and large amount of people. Some frames of the two video sequences and the foreground detection results using four algorithms are shown in Table 1 and Table 2, respectively.

Table 1 Foreground detection results (People in a shopping mall)

Original frame	
GMM	
SOBS	
ViBe	
Our algorithm	

Table 2 Foreground detection results (Pedestrians in a building)

Original frame	
GMM	
SOBS	
ViBe	
Our algorithm	

The frames in each table are chosen randomly. Compared with ViBe, SOBS and GMM, the proposed algorithm can describe foreground much more accurate since the HMM are used, however, since the observation of HMM is obtained by using ViBe, the results in illumination variation occasions are worse than those obtained by using GMM.

Conclusion and Discussion

In this paper a foreground enhancement algorithm based on HMM has been proposed. The corresponding targets in successive frames is modeled using HMM, the observation of HMM is acquired by ViBe (other effective algorithm can also be used), the detection results are then be enhanced by calculating the probability of being foreground or background of each pixel, then use MAP to determine the final state of the pixel. Experimental results have proved the effectiveness of proposed method.

Acknowledgements

This research is partially supported by National Natural Science Foundation of China (91024025) and the Ministry of Science and Technology (2011BAK07B00).

References

[1] L. Patino, H. Benhadda, N. Nefzi, et al. Abnormal behavior detection in video protection systems.International Workshop on Behaviour Analysis and Video Understanding (ICVS 2011), Sophia Antipolis : France, 2011.

[2] O. Otto, J. L. Gornall, G. Stober, et al. High-speed video-based tracking of optically trapped colloids.Journal of Optics, 13(2011)4, 40-51.

[3] Q. Luo, X. Kong, G. Zeng, et al. Human action detection via boosted local motion histograms.Machine Vision and Applications, 21(2010)3, 377-389.

[4] P. F. Felzenszwalb, R. B. Girshick, D. McAllester, et al. Object detection with discriminatively trained part-based models.Pattern Analysis and Machine Intelligence, IEEE Transactions on, 32(2010)9, 1627-1645.

[5] H. Zhou, Y. Yuan, C. Shi, Object tracking using SIFT features and mean shift.Computer Vision and Image Understanding, 113(2009)3, 345-352.

[6] C. R. Wren, A. Azarbayejani, T. Darrell, et al. Pfinder: Real-time tracking of the human body.Pattern Analysis and Machine Intelligence, IEEE Transactions on, 19(1997)7, 780-785.

[7] A. M. McIvor. Background subtraction techniques.Proc. of Image and Vision Computing, 1(2000)3, 155-163.

[8] Z. Zivkovic. Improved adaptive Gaussian mixture model for background subtraction.Pattern Recognition, 2004. ICPR 2004. Proceedings of the 17th International Conference on, 2004, 2, 28-31.

[9] M. Piccardi. Background subtraction techniques: a review.Systems, Man and Cybernetics, 2004 IEEE International Conference on, 2004, 4, 3099-3104.

[10] Y. L. Tian, M. Lu, A. Hampapur. Robust and efficient foreground analysis for real-time video surveillance.Computer Vision and Pattern Recognition, 2005. CVPR 2005. IEEE Computer Society Conference on, 2005, 1, 1182-1187.

[11] A. Elgammal, D. Harwood, L. Davis. Non-parametric model for background subtraction. Computer Vision—ECCV 2000, 2000, 751-767.

[12] A. Elgammal, R. Duraiswami, D. Harwood, et al. Background and foreground modeling using nonparametric kernel density estimation for visual surveillance.Proceedings of the IEEE, 90(2002)7, 1151-1163.

[13] L. Maddalena, A. Petrosino. A self-organizing approach to background subtraction for visual surveillance applications.Image Processing, IEEE Transactions on, 17(2008)7, 1168-1177.

[14] O. Javed, K. Shafique, M. Shah. A hierarchical approach to robust background subtraction using color and gradient information.Motion and Video Computing, 2002. Proceedings. Workshop on, 2002, 22-27.

[15] O. Barnich, M. Van Droogenbroeck. ViBe: a powerful random technique to estimate the background in video sequences.Acoustics, Speech and Signal Processing, 2009. ICASSP 2009. IEEE International Conference on, Taipei, 2009, 945-948.

[16] O. Barnich, M. Van Droogenbroeck. ViBe: A universal background subtraction algorithm for video sequences.Image Processing, IEEE Transactions on, 20(2011)6, 1709-1724.

Advanced Materials Research Vols. 989-994 (2014) pp 3877-3880
© (2014) Trans Tech Publications, Switzerland
doi:10.4028/www.scientific.net/AMR.989-994.3877

The study of a fast sub-pixel registration method for remote sensing image

Cui Zhou[1,2,a], Jinghong Zhou[2] and Donghao Fan[2]

[1]College of Traffic Information, Hunan Communication Polytechnic, Changsha Hunan 410132, China

[2] School of Geosciences and Info-physics, Central South University, Changsha Hunan 410083, China

[a]cuizhou@163.com

Keywords: Image registration, dimensional wavelet transform, cross power spectrum.

Abstract. We put forward a fast and efficiently sub-pixel registration method for solving the classical methods' problems of low efficiency, and use efficiently sub-images instead of original image to sub-pixel registration based on the Fourier transform phase correlation and matrix Fourier transform method. Effective sub-images are selected from the total size of the high-frequency energy after two-dimensional wavelet decomposition, then we use the phase correlation to calculate the pixel displacement and matrix Fourier transform to calculate the sub-pixel displacement. Not only the improved method is inherited the advantage of matrix Fourier transform sub-pixel registration, but also the registration speed is greatly improved. This is more applicable to massive remote sensing data. Through simulation and engineering practice, composited registration accuracy and speed, proved that the improved method is more efficient compared with the classical methods, and it's more suitable for real remote sensing image registration.

Introduction

With the rapid development of remote sensing technology, the technology of access to remote sensing data gradually incline to three multiples and three highs age with multiple platforms, multiple sensors, multi-angle and high time resolution, high spatial resolution, high spectral resolution[1]. Therefore, the amount of information for aerospace remote sensing data obtained increases exponentially [2], the magnitude of the remote sensing data obtained from high spatial resolution and high-precision surface information need efficient combination of theory with the hardware technology. The development of theory is often restricted by hardware technology updates. From hardware, The unit pixel size of CCD sensor can be limited access to shrink and expensive, which restricts the spatial resolution remote sensing image. By using one or more of the same scene in recent years, the low resolution of remote sensing image can be become a high resolution remote sensing image by the super-resolution reconstruction, which has become a research hotspot, and the subpixel registration accuracy of low resolution image and efficiency in image reconstruction process is particularly important

Subpixel image registration algorithm mainly include interpolation[3], extension of phase correlation [4] and settlement optimization problem [5-7]. Interpolation performance is affected by interpolation algorithm. Although accuracy of solving optimization problem is high, but the amount of calculation in the practical application is very large [8]. And the phase correlation method can integrate the performance of above two methods, which includes phase correlation in airspace and phase correlation in the frequency domain. Frequency domain phase correlation method is put forward by Kuglin [9] in parameter to solve the image translation at the earliest, the registration accuracy can reach pixel level. Alliney [10] and others use Fourier-Mellin transform to extends image registration to different conditions, such as rotation, translation, scaling and involved are pixel registration; and then Soummer [11] put forward the matrix multiplication Fourier transform which is used to image the subpixel registration, the method is based on phase correlation matching pixel level, and sample to the discrete Fourier transform after obtained the integral displacement field of a certain

range, the registration accuracy is better by comparing with traditional subpixel registration method [12]. Because the method has a calculation process of the phase correlation pixel displacement, when amounts of data is large, the amount calculated is larger, so this method is not very practical for the vast amounts of remote sensing data. The translation of image is a whole process, the translation of the whole image can represent the translation of the local area of the whole image, and partial translation information can reflect changes of the whole image translation.

An improved sub-pixel registration method is proposed for remote-sensing image, which use wavelet transform to select local effective subgraph to replace the original image, and use Fourier transform to calculate the matrix multiplication subpixel level displacement, so that through effective subgraph alternative to reduce the amount of calculation and improve the efficiency of registration. Effect of some existing method[13] is better in solving to match images of transformation on time with rotation, distortion and so on, but the essence of which is not in order to improve the accuracy and efficiency of registration, this improved method only consider a translational transform image registration.

In order to improve the registration efficiency, using effective subgraph instead of the original image to subpixel registration can greatly shorten the amount of calculation of the registration process. Compared with the traditional method, this method can satisfy the requirement of subpixel registration accuracy which can exponentially improve registration efficiency at the same time, and is suitable for remote sensing image registration of huge amounts of data.

Simulation experiment

Computing platform is a notebook computer with 4 GB RAM, Intel Core-i3 and 1.8 GHz CPU, The calculation software is Matlab7.0. The selected image is a Lena image with size of 512 × 512(Figure 2a). The image with sub-pixel displacement of $\triangle_1$(10.4857, 10.4857) in the experiment is shown in Figure 2b, Subpixel displacement image is realized by the Fourier transform phase displacement.

(a) The reference image (b) The image registration

Fig.1 Experimental images

We segment the image into 16 uniform sub-images, The size of each sub-image is 128×128, We use two-dimensional wavelet to each sub-images decomposition, when the sum of three decomposed high frequency component is maximum, the sub-images are effective sub-images.

The selection results of effective sub-images are shown in Figure 2a and 2b, such as the highlighted sub-block, Figure 2c is a magnified image of the highlight in Figure 2a, Figure 2d is a magnified image of the highlight in Figure 2b.

(a)The reference image (b) The image registration (c) The reference sub-image (d) The sub-image registration

Fig.2 Effective sub-images

The up-sample ratio k is set 100, and then we respectively use the WPM algorithm, the methods of Reference [9] and [12] to registration of effective sub-images Figure 2 c and 2d, the registration results are shown in Table 1. Coarse registration of normalized phase correlation method at pixel level by the WPM algorithm in the process of registration and spectrogram of matrix multiplication DFT subpixel level registration are respectively shown in Figure 3a and 3b,

Tab.1 The comparison of accuracy and speed between different methods

Registration parameters / Registration method	The X direction displacement/pixel	The Y direction displacement/pixel	Registration time/second
The standard displacement Δ_1	10.4857	13.7384	
WPM algorithm	10.49	13.74	0.244
Algorithm of Reference[9]	10	14	0.014
Algorithm of Reference[12]	10.49	13.74	0.465

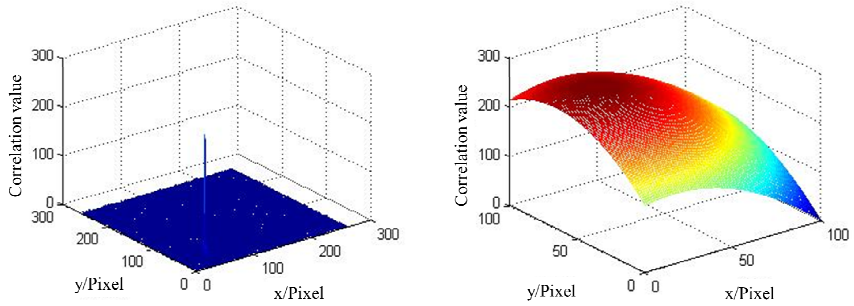

(a) Pixel registration (b) Subpixel level registration

Fig.3 The power spectrum of the image

Comparing with phase correlation method of the Reference [9], registration precision of WPM algorithm can reach 0.01 sub-pixel accuracy (from Table 1),which can well meet the requirements of sub-pixel registration, and comparing with the up-sample matrix multiplication DFT algorithm of the Reference [12]. When registration precision meet the requirements, computing time of WPM algorithm shorten half, and whole efficiency nearly doubled. The corresponding extreme value point of the coarse positioning and fine positioning has uniqueness by power spectrum diagram, which can be obtained corresponding image displacement accurately. Simulation experiments show that WPM algorithm can satisfy the sub-pixel registration precision and registration efficiency is very high, which can be well applied to engineering practice.

Summary

This paper puts forward a improvement registration method of effective subg-image instead of the original image, At the high-precision sub-pixel registration accuracy between images, the registration speed increases, the computational burden of the registration process reduce, which is suitable for remote sensing data processing. The innovation points are as follows in this paper: (1) We select effective subg-images instead of the original image in sub-pixel registration, the amount of calculation greatly reduce and the registration efficiency are greatly improved in the actual mass data of remote sensing image processing. (2) We use effective sub-images for registration phase correlation algorithm to obtain image pixel level displacement, and then use the up-sample matrix multiplication discrete Fourier transform to calculate displacement at pixel level for sub-pixel registration, the amount of calculation of improved algorithm combining the two steps is twice reduced. At improving efficiency, we ensure the sub-pixel registration accuracy,which can be widely used in remote sensing image processing.

References

[1] Li Deren. Change Detection from Remote Sensing Images. Geomatics and Information Science of Wuhan University, Vol. 28(2003), p.7-12

[2] Rong Yuecheng. A Dynamic Algorithm of Vectorization for Large Classified Remote Sensing Image. Acta Geodaetica et Cartographica Sinica, Vol. 41(2012), p.898-903

[3] Liu Weiguang, Cui Jiangtao, Zhou Lihua. Subpixel Registration Based on Interpolation and Extension Phase Correlation. Journal of Computer Aided Design & Computer Graphics, Vol. 17(2005), p.1273-1277

[4] Foroosh H, Zerubia J B, Berthod M. Extension of phase correlation to subpixel registration. Image Processing, IEEE Transactions on, Vol. 11(2002, p.188-200

[5] Yan Li, Hu Xiubing, Chen Changjun, et al. An Operator of Gradient Consistency for Multimodal Image Registration . Geomatics and Information Science of Wuhan University, Vol. 38(2013), p. 969-972

[6] Li Chang, LI Fangfang. Auto-extraction Sub-pixel Line Feature of Digital Image Based on Hypothesis Testing . Acta Geodaetica et Cartographica Sinica, Vol. 42(2013), p. 67-72

[7] Yue Chunyu, Jiang Wanshou. Registration Method for SAR Image Based on Cascade Filter and Relaxation Optimization Algorithm . Geomatics and Information Science of Wuhan University, Vol. 37(2012), p. 43-45

[8] Li Jun, Peng Qimin, Fan Zhihua. A Survey of Sub-pixel Image Registration Methods . Journal of Image and Graphics, Vol. 13(2008), p. 2070-2075

[9] Kuglin CD. The phase correlation image alignment method, Proc. Int. Conf. on Cybernetics and Society, p.163-165 (1975)

[10] Alliney S. Digital analysis of rotated images 1985 Medical Imaging Conferences. International Society for Optics and Photonics, 1985: 286-295.

[11] Soummer R, Pueyo L, Sivaramakrishnan A, et al. Fast computation of Lyot-style coronagraph propagation. Optics Express, Vol. 15(2007), p. 15935-15951.

[12] Guizar-Sicairos M, Thurman S T, Fienup J R. Efficient subpixel image registration algorithms. Optics letters, Vol. 33(2008), p. 156-158.

[13] Xu Liyan, Chen Yunjie, Qiu Jun, et al. Nephogram Nonrigid Registration Method Based on B-spline . Acta Geodaetica et Cartographica Sinica, Vol. 40(2011), p. 326-331.

Advanced Materials Research Vols. 989-994 (2014) pp 3881-3884
© (2014) Trans Tech Publications, Switzerland
doi:10.4028/www.scientific.net/AMR.989-994.3881

The Study of Combination Filtering for Removing Mixed Noise of Remote Sensing Image

Cui Zhou[1,2,a], Jinghong Zhou[2] and Donghao Fan[2]

[1]College of Traffic Information, Hunan Communication Polytechnic, Changsha Hunan 410132, China

[2] School of Geosciences and Info-physics, Central South University, Changsha Hunan 410083, China

[a]cuizhou@163.com

Keywords: Remote sensing image denoising, Combination filter, BayesShrink threshold, Adaptive median filter, Wiener filter, Gaussian noise, Impulse noise.

Abstract. The traditional combination filter method in the practical process is often two layers of composite filtering de-noising for the image containing the gaussian mixture noise and pulse noise. This paper proposes a three filter combination algorithm based on the two layers filters, To the Gaussian and pulse mixed noise of the remote sensing image, we use wavelet threshold de-nosing and adaptive median filter de-nosing, and then using the third layer adaptive Wiener filtering de-noising to remove the residual noise. Through theoretical analysis and practical application, the de-nosing results of this method is obvious in processing mixed noise of remote sensing image, this is a practical method of combination filtering de-noising, it can be widely used in the field of image processing.

Introduction

Remote sensing images are affected by noise pollution in the process of acquisition, transmission, etc, which lead the quality of the images to drop and affect the visual effect of image and data quality. The median filtering, average filtering, wavelet denoising and so on are main image denoising methods. Wang L.[1] has different improved median filtering methods based on the basis of the traditional median filter. Xing Z. [2] proposed a more windows median filtering method to overcome the disadvantage of separation of conventional adaptive median filtering between the image noise and median filtering process. Comparing with the traditional median filtering, these methods have obvious advantage. The wavelet threshold denoising algorithm is firstly proposed by Donoho [3], that is common Wavelet-Shrinkage algorithm. At the same time, Donoho [4] puts forward a VisuShrink method to compute the threshold, removal effect is obvious for Gaussian noise. Gonglin Gao [5] denoise for different image based on stationary wavelet transform method, due to reduced sampling which reduces the image edge information of the process, it is better than the wavelet transform. The above methods are all single filter methods, the limitations will appear in the face of a single the mixed noise. Therefore Wencheng Yuan [6] put forward a combination method of median filtering and adaptive Wiener filtering method, comparing the single filter method, it is more practical in actual situation contains the mixed noise such as Gaussian, pulse image. Hui Yang [7] used combination filtering method of adaptive median filtering and adaptive Bayes Shrink wavelet domain threshold filtering for image noise mixed processing, but the filtering process cause a certain degree of edge data smoothing and the resolution of the image is reduced. YouFu Wu [8] use a combination method of stationary wavelet and median filtering combined filtering approach to remove mixing noise, and the filter process is all the pixels in noise image, the process of non-noise pixel is the filter and introduces excess noise pollution.

By summing up the above single filtering de-noising characteristics and combination filtering denoising method, most combination filtering methods are available to two layer containing mixed noise of image filtering de-noising, denoising effect is not complete. In order to solve this problem, this paper put forward a kind of the combination of the three layers filter of denoising filtering

method, the algorithm firstly remove gaussian noise of the image based on the two-dimensional adaptive stationary wavelet transform BayesShrink threshold, and use the Gauss-Laplace operator to extract image edge after denoising. Then we take adaptive median filtering process for the rest of the image edge after extraction based on the number of judgment of impulse noise, and eliminate the pulse noise of image. And then we will use adaptive Wiener filter to smooth the image; Finally we will blend smoothed image and extracted edge.

Simulation and experiments

In order to verify effectiveness and superiority of the improved three-layer filter of the image denoising method, Lenna grayscale image size is set as 256 × 256 in the simulation experiment, we compared the experiment according to common hybrid noise in remote sensing image with different combination filtering method. The common mixed noise of remote sensing image mainly contains four types: 0.01/0.0005, 0.02/0.001, 0.05/0.001, 0.02/0.001, The former of the two data of each type data represents variance of the Gaussian noise, and the latter represents the density of impulse noise. Compared with the combination filtering methodreferences of [6], [7], [8], [9], [10], the combination of improved filtering method was carried out. The image denoising effect was quantitatively analyzed and compared by the peak signal-to-noise ratio (PSNR) and mean square error (MSE). Formulas of PSNR [11] and MSE [12] respectively type such as Eq. (1) and Eq. (2). The bigger PSNR values represents the better denoising effect, and the smaller MSE value represents the better denoising effect.

$$PSNR = 10\lg\frac{(M \times N)}{(f - \hat{f})^2} \tag{1}$$

$$MSE = \frac{1}{M \times N}\sum_{i=1}^{M}\sum_{j=1}^{N}[f(i,j) - \hat{f}(i,j)]^2 \tag{2}$$

Taking the 0.01/0.0005 mixed noise type as an example, the image mixed by Gaussian and impulse noise and the denoising image improved by combination filtering method in this paper were obtained, respectively, these images are shown in Figure 1. The removal effect of the different types of mixed noise by various combination filtering methods is shown in Table 1. According to Table 1.

The improved combination filter method in removing image of gauss noise and pulse mixing has better denoising effect than the combination of the traditional filtering method. From Table 1, when the image contains hybrid noise is smaller in each method, the denoising effect is better than that of bigger one, so the denoising effects are still affected by the amount of noise. Comparison in Table 1 shows target of the PSNR, the improved method is higher than the method of Ref. [9] a small amount of value. As shown in Figure 1, The denoising results of the method of Ref. [9] and improve the filtering method for the 0.1/0.01 type shows noise amplification, denoising effect is superior to the method of Ref. [9] from the contrast method. Comprehensive comparing the indicators, peak signal to noise ratio of improved filtering method is maximum and mean square error is minimum, the denoising effect is superior to traditional methods, which has obvious advantages in the visual effect of qualitative and quantitative analysis of data, and particularly suitable for remote sensing image which contains mixed noise removal.

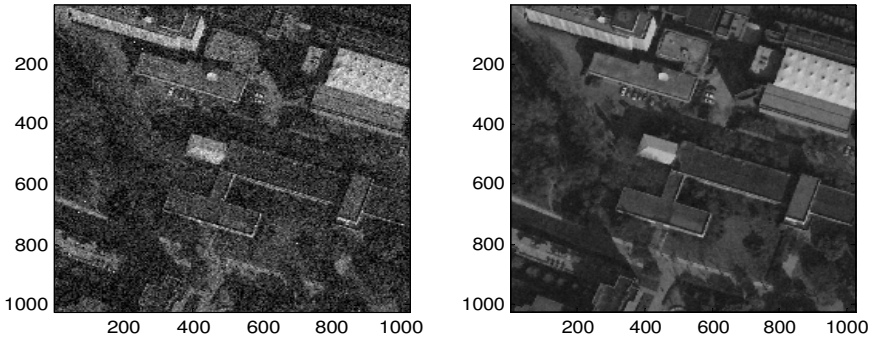

(a) The image mixed noise pollution (b) The denoising image by improved method

Fig.1 The effects of this method to remove mixed noise

Tab.1 The de-noising result comparison of various composite filters

Noise pollution / Denoising method (PSNR/MSE)	0.01/0.0005	0.02/0.001	0.05/0.001	0.1/0.01
The method of Ref.[8]	31.53/45.72	30.15/62.78	28.92/83.34	28.31/95.76
The method of Ref.[10]	32.35/37.86	31.72/43.73	30.71/55.21	30.01/64.95
The method of Ref.[7]	32.38/37.62	31.75/43.50	30.73/54.99	30.02/64.74
The method of Ref.[6]	34.03/25.67	33.01/49.69	31.31/48.14	30.14/62.95
The method of Ref.[9]	34.90/21.06	34.04/25.63	33.64/ 28.11	34.07/25.45
The method of this paper	35.06/20.26	34.31/24.13	33.92/26.38	34.38/23.75

Engineering applications

In order to further illustrate the improved combination filtering method applied to the actual remote sensing image denoising effect, we conducted a set of experiments for the actual remote sensing image. The experimental images cut out from the skies over an area of remote sensing images, the image size is 1024 × 1024. Taking the 0.01/0.0005 mixed noise type as an example, the image after mixed with Gaussian and impulse noise is shown in Fig. 2a and the images after denoising with the improved composite filter method is shown in Fig. 2b, we respectively use four common types in remote sensing image mixed with pulsed Gaussian noise experiment. The mixed types of noise is as follows：0.01/0.0005, 0.02/0.001, 0.05/0.001, 0.1/0.01.

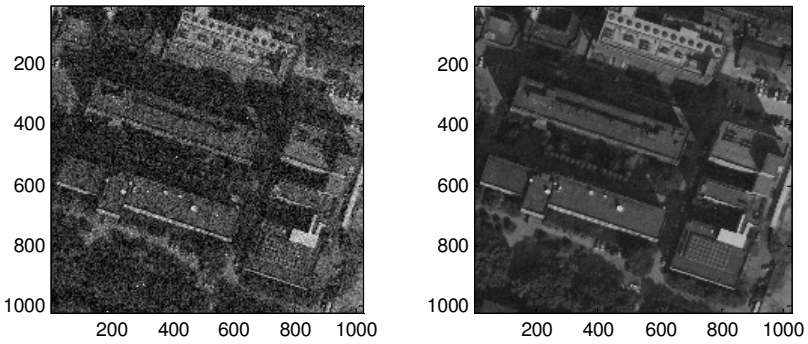

(a) The image mixed noise pollution (b) The denoising image by improved method

Fig.2 The effects of this method to remove mixed noise

Summary

Comparing with common filtering method, this method has obvious advantages in the human eye visual effect and the data quality of denoising: (1) The remote sensing image mixed noise removal is proposed by using the three layer filter method. The traditional methods are combination denoising of two layers for image with Gaussian and impulse noise denoising, although which has certain effect, but it is not sufficient because without taking into account the two layers of filter denoising. (2) This method is a new type of composite filtering denoising method. To greatest degree protection of useful information of the image, this new method can effectively remove common in remote sensing image with Gaussian mixture noise and pulse, and fully retained the image edge details, especially suitable for common types of mixed noise removing remote sensing images, which can be applied in practical applications.

References

[1] Wang LC, Wang YN, Mao LP, An algorithm of interferometric phase filter of insar based on wavelet analysis and median filter algorithm. Acta Geodaetica Et Cartographica Sinica, Vol. 34(2005), p. 108-112

[2] Xing ZJ, Qu YF, Xu J, et al. Multi-window adaptive filter for removal of impulse noise. Journal of Electronics & Information Technology, Vol. 24(2002), p.1912-1916

[3] Donoho DL, Johnstone IM. Ideal spatial adaptation by wavelet shrinkage . Biometrika, Vol. 81(1994), p. 425-455

[4] Donoho DL. De-noising by Soft-thresholding . IEEE Transactions on Information Theory, Vol. 41(1995), p. 613-627

[5] Gao QW, Li B, Xie GJ, et. Al. An image de-noising method based on stationary wavelet transform . Journal of Computer Research and Development, Vol. 39(2002), p. 1689-1694

[6] Yuan WC, Yang DX, Chen C. A synthetic filtering method for restoration of images contaminated by mixed noise . Microprocessors, Vol. 4(2007), p.78-80

[7] Yang H, Tang JF, Lu SZ. An effective method for removing mixed noise in images . Journal of Hengyang Normal University, Vol. 31(2010), p. 35-39

[8] WU YF. A adaptive de-noising method used to image with mixed noises . Information Technology, Vol. 8(2007), p. 76-77

[9] Hou JH, Tian JW, Liu J. An improved joint scheme for image denoising . Acta Photonica Sinica, Vol. 34(2005), p. 150-153

[10] Wan Q., Xue M. Mixed adaptive image denoising algorithm based on noise isolation and wavelet thresholding . Electronic Science And Technology, Vol. 24(2011), p. 94-96

[11] Ichigaya A, Nishida Y, Nakasu E. Nonreference Method for Estimating PSNR of MPEG-2 coded video by using DCT coefficients and picture energy . Circuits and Systems for Video Technology, IEEE Transactions on, Vol. 18(2008), p. 817-826

[12] Salman A G, Kanigoro B. Application Hiding Messages in JPEG Images with the Method of Bit-plane Complexity Segmentation on Android-based Mobile Devices . Procedia Engineering, Vol. 50(2012), p. 314-324

Advanced Materials Research Vols. 989-994 (2014) pp 3885-3888
© (2014) Trans Tech Publications, Switzerland
doi:10.4028/www.scientific.net/AMR.989-994.3885

Hyperspectral Image Classification via Discriminative Sparse Representation with Extended LBP Texture

Yuemei Ren[1, 2, a], Yanning Zhang[1,b] and Wei Wei[1]

[1]School of Computer Science, Northwestern Polytechnical Univeristy, Xi'an, P.R.China

[2] Department of Computer Engineering, Henan Polytechnic Institute, Nanyang, P.R.China

[a]renym2010@mail.nwpu.edu.cn, [b]ynzhang@nwpu.edu.cn

Keywords: Hyperspectral image classification, Sparse Representation, Dictionary Learning, Local Binary Patterns.

Abstract. Hyperspectral images (HSI) have rich texture information, so combining texture information and image spectral information can improve the recognition accuracy. Sparse representation has significant success in image classification. In this paper, we propose a new discriminative sparse-based classification framework using spectral data and extended Local Binary Patterns (LBP) texture. Firstly, we propose an extended LBP coding for HSI classification. Then we formulate an optimization problem that combines the objective function of classification with the representation error by sparsity. Furthermore, we use a procedure similar to K-SVD algorithm to learn the discriminative dictionary. The experimental results show that the proposed discriminative spasity-based classification of image including the extended LBP texture outperforms the classical HSI classification algorithms.

Introduction

Hyperspectral imaging technique is a great leap in the remote sensing techniques. The remote sensors capture digital images in hundreds of narrow spectral bands spanning the visible to infrared spectrum [1]. HSI has been found many applications in various fields, and the base one is HSI classification. However, the traditional HSI classification algorithms for will result in low classification precision and data redundancy. It is necessary to find an effective HSI classification algorithm. The high resolution HSI has rich space structure information [7]. Thus, combining texture information and image spectral information in HSI classification can improve the recognition accuracy.

In recent years, sparse-based techniques have a lot of successful applications in compute vision and image processing fields [2-6]. These applications are mainly based on the observation that the images in the same class usually lie in a low-dimensional subspace.

Considering the characteristic of HSI and the limitation of traditional classification techniques, based on sparse representation and LBP texture, a new effective HSI classification framework is proposed. Firstly, an extended LBP coding for HSI is proposed, and the LBP image and the original HSI are fused to obtain the fused HSI for classification. Then an discriminative optimization problem is formulated. Furthermore, we use a procedure similar to K-SVD algorithm to learn the discriminative dictionary.

Classification based-on Discriminative Sparse Representation and Extended LBP

Local Binary Patterns and the Extended LBP for HSI

The original LBP operator [7] is a powerful illumination invariant texture primitive. The operator describes each pixels of an image by the relative graylevels of its neighboring pixels. Then the histogram of the binary patterns computed over a region can be used as a texture descriptor.

However, in HSI, each pixel forms a spectral vector, we should analyse the LBP of every band image. This would result in low efficiency and poor effects. So we extend LBP for HSI by measuring it with the relation among spectral vectors instead of graylevel. The extended LBP defined as Eq. 1,

$$LBP_{P,R}(x,y)=\sum_{p=0}^{P}s(v_c,v_p)2^p,\quad s(v_c,v_p)=\begin{cases}1, & corr(v_c,v_p)>K\\ 0, & otherwise\end{cases}. \tag{1}$$

Where, v_c and v_p denote the spectral vector of the center pixel and P equally spaced pixels on a circle of radius R respectively. K is the threshold, and $corr\left(v_c, v_p\right)$ is the correlation coefficient of v_c and v_p.

Finally, the obtained LBP image is added to the original HSI as an extra band image. Then, the new HSI is used for the sparsity-based classification.

Discriminative Sparse Representation

The SRC algorithm assumed that the training samples of a particular class approximately form a linear basis set for any test sample belonging to the same class. However, the reconstructive dictionary in SRC is not the best for the classification problem. The training samples selected manually may not span the reasonable underlying subspace. Then, K-SVD algorithm which learns an over-complete dictionary with a fixed number k of atoms is proposed by solving the following minimization problem,

$$\min_{\alpha, D} \sum_{i=1}^{n} \left\| a_i - D\alpha \right\|_2^2 \quad \text{s.t. } \left\| \alpha_i \right\|_0 \le L. \tag{2}$$

But these dictionaries without discriminative power may not be optimal for a classification task. The main goal of our method is to learn discriminative dictionaries and not only reconstructive ones.

Thus, we design a discrimination function by the classical linear discriminant analysis

$$f(\bullet) = \frac{trace(S_b)}{trace(S_w) + \mu}. \tag{3}$$

Where S_b and S_w are the standard between-class and within-class scatter matrices, and μ is a regularization parameter. Then, we obtain the final objective function Eq. 4 is obtained by incorporating the discrimination function Eq. 3 into the objective function Eq. 2.

$$\min_{D, \alpha} \left\{ \sum_{j=1}^{c} \sum_{i=1}^{n_j} \left\| a_i^j - D\alpha_i^j \right\|_2^2 - \lambda \cdot f\left(\left\{ \left\{ \alpha_i^j \right\}_{i=1}^{n_j} \right\}_{j=1}^{c} \right) \right\}. \tag{4}$$

Discriminative Sparsity-based Classification

In order to achieve the classification goal, we try to seek the internal structure within each class and at the same time global discrimination among the classes. Now we optimize the dictionary that is reconstructive and discriminative, we rewrite the Eq. 4 as Eq.5,

$$\max_{D, \alpha} \left\{ \lambda \cdot f\left(\left\{ \left\{ \alpha_i^j \right\}_{i=1}^{n_j} \right\}_{j=1}^{c} \right) - \sum_{j=1}^{c} \sum_{i=1}^{n_j} \left\| a_i^j - D\alpha_i^j \right\|_2^2 \right\} \tag{5}$$

To solve the optimization problem, we extend K-SVD by instead the classical OMP of another better one improved from SOMP in the sparse coding stage. The whole process is shown as follows.

Initialization: Initialize $J = 0$, and

- Initialize dictionary: $D_{(0)} \in R^{B \times n}$, hyperspectral pixels $\left\{ \left\{ a_i^j \right\}_{i=1}^{n_j} \right\}_{j=1}^{c}$, sparsity level L
- Normalization: Normalize the columns of $D_{(0)}$

Main Iteration: Increment J by 1, and apply

- Sparse coding stage: Use the following procedure to compute the sparse coefficients $\left\{ \left\{ \alpha_i^j \right\}_{i=1}^{n_j} \right\}_{j=1}^{c}$ for each hyperspectral data $\left\{ \left\{ a_i^j \right\}_{i=1}^{n_j} \right\}_{j=1}^{c}$.

  Step 1: Set the class counter $q = 1$ and $\Gamma_0 = \varnothing$

  Step 2: Selection of L vectors according to the structure of the class q

  2-1. Initialize the residuals $r_i^{j(0)} = a_i^j$, the index set $\Lambda_0^q = \varnothing$, iteration counter $t = 1$

  2-2. Find the index ϑ_t^q by solving $\vartheta_t^q = \arg\max_{p=1,\ldots,n} \left\{ \sum_{i=1}^{n_q} \left| \left\langle r_i^{q,(t-1)}, d_p \right\rangle \right| + \lambda \cdot f\left(\left\{ \left\{ \left\langle r_i^{j,(t-1)}, d_p \right\rangle \right\}_{i=1}^{n_j} \right\}_{j=1}^{c} \right) \right\}$

2-3. Set $\Lambda_t^q = \Lambda_{t-1}^q \cup \{\vartheta_t^q\}, \Phi_t^q = \left[\Phi_t^q, d_{\vartheta_t^q}\right]$.

2-4. Calculate new coefficients and residuals $\alpha_i^{j,(t)} = \left(\Phi_t^{q'}\Phi_t^q\right)^{-1}\Phi_t^{q'}a_i^j, r_i^{j,(t)} = a_i^j - \Phi_t^q \cdot \alpha_i^{j,(t)}$

2-5. Set $t = t+1$. If $t \le L$, go to 2-2, else go to step 3.

Step 3: Save the estimates $\tilde{a}_i^{q,(L)}$ for class q, and its coefficients $\alpha_i^{q,(L)}$

Step 4: $\Gamma_q = \Gamma_{q-1} \cup \Lambda_L^q, q = q+1$. If $q < c$ go to step 2, else return.

- Dictionary update stage: Use the following procedure to update the columns of the dictionary and obtain $D_{(J)}$: repeat for $j_0 = 1,2,...,n$
  - Define the group of examples that use the atom d_{j_0}, $\Omega_{j_0} = \{i \mid 1 \le i \le n, d_j^{j_0}(i) \ne 0\}$
  - Compute the residual matrix $\mathrm{E}_{j_0} = a - \sum_{j \ne j_0} d_j a'_j$.
  - Restrict E_{j_0} by choosing only the columns corresponding to Ω_{j_0}, and obtain $\mathrm{E}_{j_0}^R$.
  - Apply SVD decomposition $\mathrm{E}_{j_0}^R = \mathrm{U}\Delta\mathrm{V}'$. Update $d_{j_0} = \mathrm{u}_1$, and $\alpha_{j_0}^R = \Delta[1,1] \cdot \mathrm{v}_1$
- Repeat until convergence.

Finally, we design a method to determine the class. For the samples in class i, we design an indicator operator $\delta_i(\bullet)$, which can keep the coefficients corresponding to class i and set all others to be zero. Then the residuals by each class are compute, and the class of the test sample is determined by the minimal residual.

Experimental Results and Analysis

In this section, we performed extensive experiments on a well known hyperspectral dataset AVIRIS Indian Pines image to evaluate the effectiveness of the proposed approach. We use 6 classes which have sufficient training samples in our experiment. The pseudo color image from the Geographic Information System (GIS) image is shown in Fig. 1(a) and Fig. 1(b). We compared our results with classical methods i.e. parallelepiped classifier (PPC), spectral angle mapper (SAM), maximum likelihood classifier (MLC), BP neural network (BPNN) and SRC without LBP.

The visual classification results obtained by different classifiers are shown in Fig. 1(c)~(h). It's easy to see that, our proposed algorithm got better performance than other methods mentioned above.

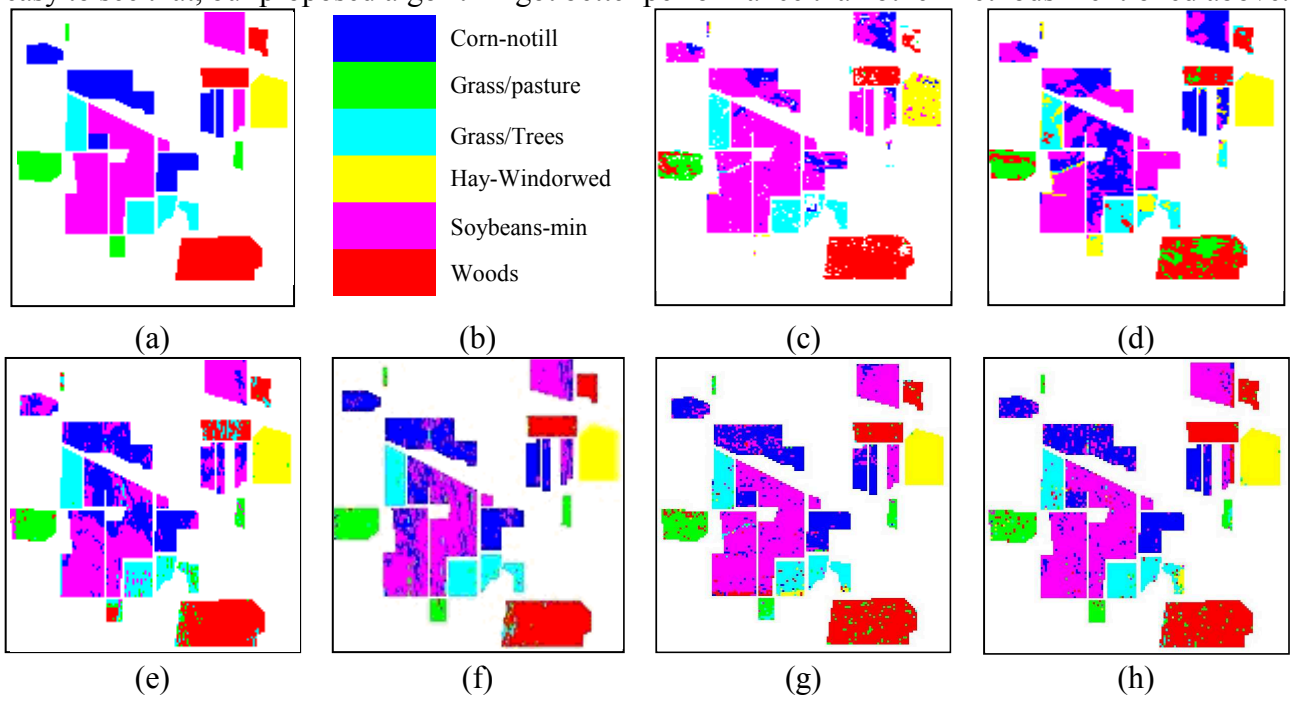

Fig. 1 The classification maps obtained by different classification methods. (a) The pseudo color image of the used 6 classes from the GIS image, (b) color map, (c) PPC, (d) SAM, (e) MLC, (f) BPNN, (g) SRC without LBP,(h) the proposed method

The classification accuracy for each class, the overall accuracy and the kappa coefficient are shown in Table 1. We can see that our proposed HSI classification algorithm competes against the others in either overall accuracy or kappa coefficient. That is because the proposed approach uses the rich texture information by the extended LBP image to improve the classification performance. Moreover, it uses the learned discriminative dictionary, not the reconstructive one.

Table 1. Classification accuracy (%) and kappa coefficient of these methods

Class	PPC	SAM	MLA	BPNN	SRC without LBP	Proposed method
1	18.41	49.75	82.33	83.26	79.63	86.40
2	39.24	57.68	83.75	94.82	81.27	88.13
3	82.06	74.97	87.92	94.25	90.38	89.83
4	88.55	99.59	89.93	98.74	99.64	99.39
5	86.83	61.86	82.29	74.26	89.59	91.05
6	84.62	77.74	87.06	95.89	92.55	95.05
OA	68.45	70.27	84.66	86.44	88.11	91.07
κ	0.5884	0.5864	0.8042	0.8221	0.8479	0.8847
Runtime(s)	1.1813	49.5869	3.0126	15.0944	40.2594	43.3426

Conclusions

In this paper, we have proposed an extended LBP coding for Hyperspectral images and added it to the original HSI as an extra band image. Furthermore, we proposed a new effective and discriminative sparse representation classification algorithm for HSI. In the proposed algorithm, we formulate an optimization problem that combines the objective function of classification with the representation error by sparsity, and use an improved K-SVD algorithm to learn the dictionary. The experimental results show that the proposed approch outperforms the classical HSI classification algorithms and the sparsity-based method without LBP image.

Acknowledgements

This work is supported by the National Natural Science Foundation of China (No.61231016, No.61303123, No.61272288, No.61201291), Key Science and Technology Program of Henan Province (No.142102210557), the NPU Foundation for Fundamental Research (No.JCT20130108).

References

[1] M. Borengasser, W. S. Hungate, and R. Watkins: Boca Raton, FL: CRC Press, 2008.
[2] H. Chavez-Roman, V. Ponomaryov: IEEE Geoscience and Remote Sensing Letters, vol.PP, no.99, pp.1-5(2014)
[3] Weisheng Dong, Lei Zhang, Guangming Shi, Xin Li: IEEE Transactions on Image Processing, vol.22, no.4, pp.1620-1630(2013).
[4] John Wright, Allen Yang, Arvind Ganesh, Shankar Satry, and Yi Ma: IEEE Transactions on Pattern Analysis and Machine Intelligence, vol.31, no.2, pp.210-217 (2009).
[5] Ehsan Elhamifar Ren´ e Vidal: 2011 IEEE Conference on Computer Vision and Pattern Recognition. pp.1873-1880(2011)
[6] H. Zhang, J. Li, Y. Huang, L. Zhang: IEEE Journal of Selected Topics in Applied Earth Observations and Remote Sensing. vol.PP, no.99, pp:1-10(2013).
[7] Li P J, Cheng T, Guo J C: Photo-grammetric Engineering and Remote Sensing. Vol.75, no.2, pp.147-157(2009)
[8] T. Ojala, M. Pietikainen, and D. Harwood: Pattern Recognition,vol. 29, no.1, pp.51-59(1996)

Advanced Materials Research Vols. 989-994 (2014) pp 3889-3892
© (2014) Trans Tech Publications, Switzerland
doi:10.4028/www.scientific.net/AMR.989-994.3889

Channel reservation strategies for Multiple Secondary Users in Cognitive Radio Networks

Qiang peng*, Yan Jiang†, Gan Liu‡, Fei Cui‡, Guobao He‡, and Weimin Wu‡

*Wuhan University of Technology, Wuhan, Hubei 430070, China

†Hubei Communications Technical College, Wuhan, Hubei 430079, China

‡Huazhong University of Science and Technology, Wuhan, Hubei 430074, China

e-mail: peng@whut.edu.cn; †beckyme0305@aliyun.com(Corresponding Author); liugan@hust.edu.cn; cuifei99@163.com; hegb2013@hust.edu.cn; wmwu@hust.edu.cn

Keywords: Cognitive radio networks; QoS; Markov chain; channel reservation.

Abstract. In cognitive radio networks (CRNs), improving the performance of SUs is the main aspect of present study. In this paper, we focus on the optimal access strategy to provide QoS guarantees for multi-services. The contribution of this paper is as follows. Firstly, we formulate and solve the optimal spectrum access problem with different channel reservation scheme. Secondly, we take account of buffer for handoff secondary users and propose a handoff scheme for multi-services. In addition, the computation complexity of solving the optimal channel reservation problem is simplified by a binary search. The system is analyzed using a continuous-time Markov chain model. The numerical results confirm the validity of the proposed scheme.

Introduction

In recent years, with the rapid development of wireless technology, spectrum resource is becoming more and more intense. One important reason is that the traditional static spectrum allocation has led to low utilization of the spectrum, as it is presented in [1]. In this case, the concept of Cognitive Radio Networks (CRNs) has been proposed to improve the spectrum efficiency. In spite of the fact that the cognitive radio technology can effectively address the scarce of spectrum [2] [3], however, due to the unpredictability of the dynamically changing network resources, it is a great challenge to guarantee the quality of service (QoS) of CRNs requirements.

To improve the performances, many models and algorithms have been proposed in CRNs these years (e.g. [4]-[9]). In [6], channel reservation has been proposed to reserve several channels only for handoff secondary users (SUs). In [7], the case of sub-channel reservation for high-priority SUs with buffer for handoff SUs has been investigated, nevertheless, the problem has not been solved. The authors in [8] proposed a framework to analyze call admission control for performance improvement. In order to reduce the dropping probability, [9] has proposed a channel reservation scheme for the primary system, it shows that how to compute the optimum number of reserved channels.

In this paper, we focus on the optimal access strategy to provide QoS guarantee for multi-services. Different from the existing models, the QoS guarantee for multiple services is considered in an overlay centralized cognitive radio network. We propose a channel reservation scheme for multi-services' QoS guarantee of SUs. We establish a multi-dimensional continuous-time Markov chain to calculate the steady-state probability. Then, we analyze the performance of the system. In addition, the computation complexity of solving the optimal channel reservation problem is simplified by a binary search. Numerical results show that our proposed channel reservation scheme can provide the QoS guarantees of multi-services.

System Model

The cognitive radio system is composed of N channels. Since the PUs enjoy absolute priority on using licensed channel, one ongoing SU using the channel reclaimed by a PU should be handed off. The SUs are classified into three priority classes： SU_1, SU_2 and SU_3, corresponding to voice, video and data. Each channel can only accommodate one PU or SU, and r_1, r_2, r_3 channels are reserved for

new SU_1, SU_2, SU_3 calls respectively. The handoff buffer is only available for handoff SU_2 and SU_3 calls. We assume that there are N buffers to accommodate handoff SUs being suspended.

Call arrivals occur independently as Poisson processes with mean arrival rates of λ_p, λ_1, λ_2 and λ_3 for PU, SU_1, SU_2 and SU_3, respectively. The service times independently follow exponential distributions with mean service rates of μ_p, μ_1, μ_2 and μ_3 for corresponding services, respectively.

A new SU call is blocked when the number of idle channels is less than that of reserved channels. Whenever the handoff buffer is unempty, new SUs will be rejected. The SU calls in the buffer will be reassigned to the resulting idle channel according to their priorities when an ongoing call completes service. These reassigned SUs resume transmissions for their remaining service times. When a new PU call arrives, the CR system works as Fig.1.

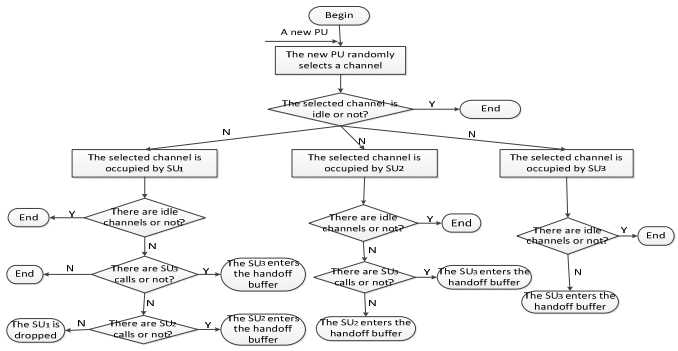

Fig.1. Flow chart of the system when a new PU arrives

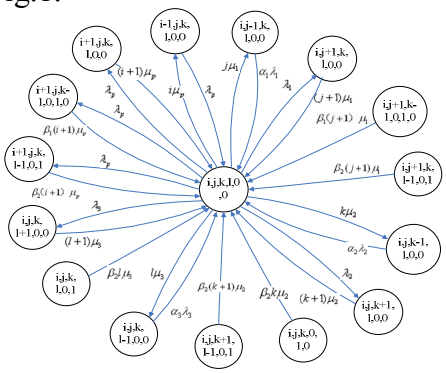

Fig.2. State transition graph when the buffer is empty

For this system, the state is denoted as $[i, j, k, l, k_q, l_q]$, where $i \in \{0,1,...,N\}$, $j \in \{0,1,...,N\text{-}r_1\}$, $k \in \{0,1,...,N\text{-}r_2\}$, $l \in \{0,1,...,N\text{-}r_3\}$ represents the number of ongoing PU, SU_1, SU_2 and SU_3 calls, respectively. And variables $k_q \in \{0,1,...,N\text{-}r_2\}$, $l_q \in \{0,1,...,N\text{-}r_3\}$ represent the number of SU_2 and SU_3 calls waiting in the buffer.

Fig.2 shows the state transitions graph when the buffer is empty. Specially, when $i+j=N$ and $j>0$ in current state, one of SU_1 calls will be dropped if a new PU arrives. Fig. 3 and Fig. 4 show the case that there are no ongoing SU_3 calls and there are ongoing SU_3 calls, respectively.

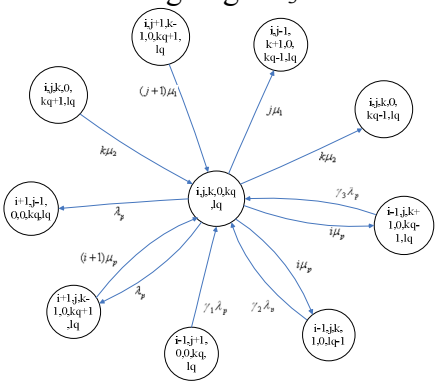

Fig.3. State transition graph when there are no SU3 calls

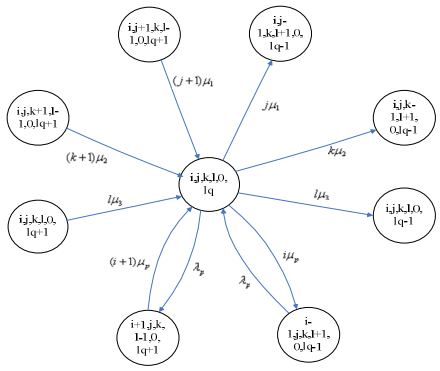

Fig.4. State transition graph when there are ongoing SU_3 calls

Performance Analysis

Let Y $(=i+j+k+l)$ denote the total number of busy channels at a given time instant. We can get the steady-state probability P_Z $(Z=[i, j, k, l, k_q, l_q])$according to the state transition graph. With the steady-state probability, we can derive the following performance measures.

1) The blocking probability.

$$p_{block(m)} = \sum_{\forall Z, Y \geq N - r_{(m)}} P_Z (m = 1,\ 2\ or\ 3). \tag{1}$$

2) The dropping probability.

$$p_{drop1} = \frac{\sum \lambda_p \cdot P_z}{\lambda_1 \cdot (1 - p_{block(1)})}. \quad (2)$$

3) Successful call completion rate. Successful call completion rate means without being blocked and dropped .The successful call completion rate of SU_1 , SU_2 and SU_3 is expressed as

$$R_1 = \lambda_1 \cdot (1 - p_{block1}) \cdot (1 - p_{drop1}). \quad (3)$$

$$R_{(s)} = \lambda_s \cdot (1 - p_{block(s)}) \ (s = 2 \ or \ 3). \quad (4)$$

The normalized successful call completion rate of SU calls denoted as R. ξ_1, ξ_2 and ξ_3 is the weight of the call completion rate of SU_1, SU_2 and SU_3, respectively. Then, R is expressed as

$$R = \xi_1 \cdot R_1 + \xi_2 \cdot R_{(2)} + \xi_3 \cdot R_{(3)}. \quad (5)$$

4) The mean handoff delay: the mean handoff delay for SU_2 (SU_3) calls is defined as the mean time taken by the SU_2 (SU_3) calls to perform successful handoff.

$$HD_2 = \frac{\sum_{\forall z, Y=N, l=0, k>0} P_z}{\sum_{\forall z, Y<N} \frac{k}{N-i} P_z + \sum_{\forall Z, Y=N, l=0, k>0} P_Z + \sum_{\forall z, Y=N, l>0} \frac{k}{N-i} P_z} \cdot \frac{\sum_{\forall z} k_q \cdot P_z}{\sum_{\forall z, Y=N, l=0, k>0} \lambda_p \cdot P_z}. \quad (6)$$

$$HD_3 = \frac{\sum_{\forall z, Y=N, l>0} P_z}{\sum_{\forall z, Y<N} \frac{l}{N-i} P_z + \sum_{\forall z, Y=N, l>0} P_z} \cdot \frac{\sum_{\forall z} l_q \cdot P_z}{\sum_{\forall z, Y=N, l>0} \lambda_p \cdot P_z}. \quad (7)$$

Results and Discussion

In this section, we evaluate the performance of this model. The accuracy of the analysis is verified through simulations. In our experiments, we use the following parameter settings: N=5, λ_1={0.6,0.8}, λ_2=0.8, λ_3=1, λ_p={0.1,0.2,...,1.1}, μ_1=0.6, μ_2=0.8, μ_3=0.8, μ_p=1.2, $r_1 \in$ {0,1,...,5}, $r_2 \in$ {0,1,...,5}, $r_3 \in$ {0,1,...,5}.

We assume the QoS threshold of dropping probability of SU_1, ς_1, is 0.01, and the QoS threshold of the mean handoff delay of SU_2, ς_2, is 0.025. Meanwhile, due to the priority, the weights of multi-services for normalized call completion rate of SU calls is reasonable to be set as ξ_1=0.45, ξ_2=0.4, ξ_3=0.15. For convenience, symbols<a>and<s>in the figures indicate analytical and simulation results, respectively.

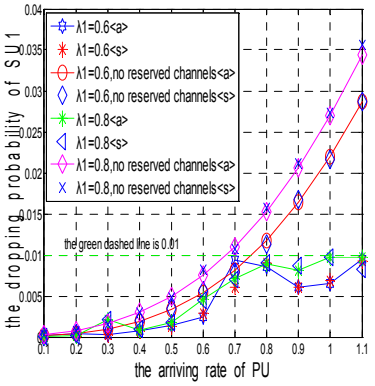

Fig.5.The arriving rate of PU vs. CDP of SU_1

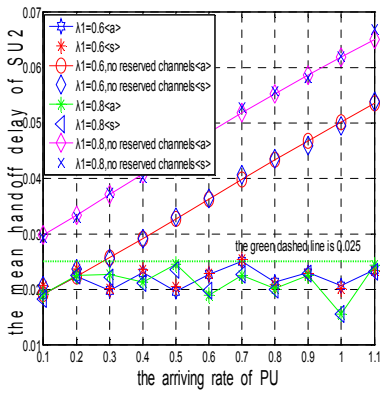

Fig.6.The arriving rate of PU vs. HD of SU_2

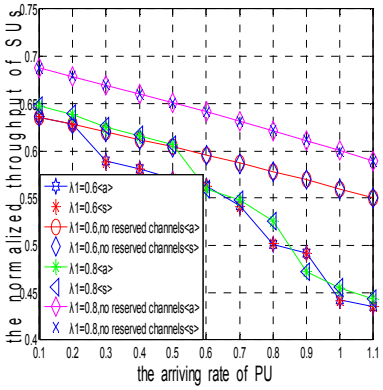

Fig.7.The arriving rate of PU vs. NT of Sus

Fig. 5 and Fig. 6 show the impact of the arriving rate of PU on the dropping probability of the SU_1 and the mean handoff delay of SU_2. By comparison, we present the results for the case that no channel reservation action is taken as well. As we know, when the traffic of PUs is low, the QoS of

SUs can be met, hence the traffic control is not necessary, as shown in Fig.5 and 6 when λ_1=0.6 and $\lambda_p \leq 0.2$, the dropping probability as well as handoff delay are the same for both cases with no traffic control. With the increasing of PUs traffic load, the dropping probability and handoff delay will increase due to less channels available for SUs, the dropping probability is higher than the threshold value (i.e., 0.01) if there is no reserved channel. Nevertheless, by using our optimal channel reservation scheme, no matter how high the PUs' traffic load is, the dropping probability and handoff delay can always be maintained below the predefined threshold value as shown in Fig.5 and 6. And in the case of λ_1=0.8, we can get the same conclusion.

In Fig.7, we give the relationship between normalized throughput and arrival rate of PU. As expected, no matter λ_1=0.6 or λ_1=0.8, the normalized throughput decreases with the arriving rate increasing. When there are reserved channels, the normalized throughput is lower than that of the case of no reserved channels, as the cost of guarantee the QoS of multi-services of SUs.

Summary

In this paper, a multi-dimensions stochastic model is proposed to analyze the performance of an overlay cognitive radio network. We have considered three levels of prioritization in the SU traffic, and the reserved channels for different types of new SU are different, which make us enable to not only provide the QoS guarantees of multi-services. As for performance analysis, we derived blocking probability, dropping probability, mean call completion rate and mean handoff delay for SUs. In addition, the computation complexity of solving the optimal channel reservation problem is simplified by a binary search. The analytical results have been verified through simulations. In the future, we will study the impact of the imperfect channel sensing on the optimal channel reservation and more accurate admission control.

This work has been supported in part by the National Natural Science Foundation of China (No.61071068), the National High-Tech R&D Program of China (No.2006AA01Z233, No.2012AA121604) and the International S&T Cooperation Program of China（No. 2012DFG12010). †Yan Jiang is the corresponding author

References

[1] W. Lehr and L. W. McKnight, "Wireless Internet access: 3Gvs.WiFi?" *Telecommun. policy, Competition Wirel., Spectr., Service Technol. Wars*, vol. 27, no. 5/6, pp. 351–370, 2003.

[2] S. Haykin, "Cognitive radio: brain-empowered wireless communications", *IEEE J. Sel. Areas Commun.*, vol. 23, no.2, pp.201-220, Feb.2005.

[3] I. F. Akyildiz, W. Y. Lee, M. C. Vuran, and S. Mohanty, "Nextgeneration/dynamic spectrum access/cognitive radio wireless networks:Asurvey," *Computer Networks,* vol. 50, no. 13, pp. 2127–2159, 2006.

[4] G. Liu, X. Zhu, and L. Hanzo,"Dynamic Spectrum Sharing Models for Cognitive Radio Aided Ad Hoc Networks and Their Performance Analysis", Proceeding of IEEE GLOBECOM 2011.

[5] G. Liu, X. Zhu, and G. Zhu, "Impact of Variance of Heterogeneous Spectrum on Performance of Cognitive Radio Ad Hoc Networks," Proceeding of IEEE ICC 2012.

[6] W. Ahmed, J. Gao, H. Suraweera, and M. Faulkner, "Comments on 'Analysis of cognitive radio spectrum access with optimal channel reservation'," *IEEE Trans. Wireless Commun.*, vol. 8, no. 9, pp. 4488–4491,Sep. 2009.

[7] P. Wang, D. Niyato and W. Song,"Performance analysis of cognitive radio spectrum access with prioritized traffic," *IEEE transaction on vehicular technology*, vol. 61, no. 4, May 2012.

[8] JianWang, Wei Wang, Tony Q.S.Quek, "Admission control in cognitive radio networks with finite queue and user impatience" *IEEE wireless communications letters*, vol.2, no. 2, April 2011.

[9] P. K. Tang, Y. H. Chew, L. C. Ong ,and M. K. Haldar,"Performance of secondary radios in spectrum sharing with prioritized primary access," in *IEEE MILCOM 2006* , Washington, DC, USA, Oct.2006,pp. 1 – 7.

Advanced Materials Research Vols. 989-994 (2014) pp 3893-3897
© (2014) Trans Tech Publications, Switzerland
doi:10.4028/www.scientific.net/AMR.989-994.3893

New enhancement algorithm of infrared images based on dual threshold of the exponential transform

Jing Lv [1, a], Jian Lv[1],Chuanfu Wu [1] ,Yun Zhou[1],Fengpei Sun[1],Kai Che [1]

[1] School of Optoelectronic Information, University of Electronic Science and Technology of China, Chengdu 610054, China.

[a]JingLv@126.com

Keywords: Infrared image, exponential transform, dual threshold, detail enhancement,grayscale transform.

Abstract. Since the thermal imaging system detection ability and spatial resolution is lower than visible light CCD array,the definition of the infrared image is lower than that of the visible light image, which needs enhancement to improve image quality and for human vision. This paper proposes an enhancement algorithm of infrared images based on dual threshold of the exponential transform, firstly the original image can be processed by median filter to reduce noise,next separate the detail information of the 14-bit infrared image after noise reduction; then deal the detail image with the double threshold method based on the exponential transform,retaining or enhancing the detail information;when it comes to the base image,deal it with the gray linear mapping method, compressing its dynamic range.Finally the detail image and the base image are composed together after processing,getting 8-bit infrared image which can display and be processed on an ordinary display.

Introduction

Along with the increasingly mature of uncooled infrared detector, the application of thermal imaging technology is more and more widely in military and civilian areas.Infrared thermal imaging technology[1] is a image information detection technology based on heat radiation,which performances the heat radiation of the target surface in the form of image.However the characteristics of infrared image, device processing technic and environmental factors result in infrared image with low contrast,low resolution and low signal-to-noise ratio. In order to accurately identify the target in a infrared image and improve the quality of the infrared image, the image should be enhanced appropriately,highlighting some interested parts selectively,such as the target in the infrared scene and the tiny structure on its surface. In addition,the noise often appears in the infrared thermal imaging system.When enhancing the infrared image,the noise which often is mistaken for details in the image,will be enhanced together,which eventually led to the decline in image quality.

At the same time,the infrared image has the characteristic of high dynamic range.In order to quantify the high dynamic range infrared image with sufficient accuracy, imaging system generally uses 14 bits or higher bits analog-to-digital(A/D) converter in the output signal of the detector for analog-to-digital conversion.While the conventional display device can only support 8-bit image, so it is necessary to compress the infrared image with high dynamic range properly. However, choosing irrelevant compression can easily cause the loss of detail information in the compression process and result in non-ideal effect in 8-bit image after compressing . Aimed at single frame infrared image,this paper proposes a new enhancement algorithm of infrared image. Firstly the original image can be processed by median filter[2] to reduce noise，next separate the detail information of the 14-bit infrared image after noise reduction by using high-pass filtering[3],obtaining the detail image;at the same time,the original infrared image after noise reduction subtracts the detail image to get the base image;then deal the detail image with the double threshold method based on the exponential transform processing,retaining or enhancing the detail information;when it comes to the base

image ,deal it with the gray linear mapping method[4],compressing its dynamic range . Finally the detail image and the base image are composed together after processing, getting 8-bit infrared image.

Algorithm description

Noise reduction on original image.

After non-uniformity correction, the noise mainly performancing as random disturbance is the high frequency information[5] in the original infrared image. On account of the goal of the system is detail enhancement, which inevitably will lead to noise enhancement and the decline in image quality. There are many effective solutions for reducing noise, but they are usually limited with a large amount of calculations and their feasibility. As is shown in figure 1, the 14-bit original infrared image is captured by the infrared thermal imaging system which is independently researched by our laboratory. In view of the single frame infrared image captured, it is proper to deal it with median filter, which can not only remove isolated noise, but also keep the edge feature of target and make the image not significantly fuzzy. So we select a median filter with window size w * w(w is an odd); then we scan the infrared image with w * w window,sort the datas contained in the window and get the median as the grey value of central point in the window,thereby reducing noise in the image. The advantages of this method is simple and fast computing speed,besides the simulation results show it has better effect on noise elimination and loss less useful detail information.

Fig. 1 The original infrared image

The separation of detail image and base image .

As is shown in figure 3(a),the infrared image after noise reduction contains rich detail information and has low contrast in detail part,having a gray scale range from 768 to 9788,about 9000 grayscale. Compressing and enhancing the whole image directly result in the loss of detail information and merging gray level of detail information to the adjacent grey level.As a result,the infrared image after noise reduction should be firstly separated to detail image and base image,the detail image and base image should be enhanced and compressed respectively.

Owing to the high frequency characteristic of the infrared target,it is proper to get detail information of high frequency by using high-pass filter.So the Butterworth high-pass filter is a good choice.Then the original infrared image after noise reduction subtracts the detail image to get the information of base image. Ideal high-pass filter and Butterworth high-pass filter can get better filtering effect in several high-pass filters. But because the images we need mostly contain complex background information,so the obvious "ringing" phenomenon of ideal high-pass filter is bad for target detection.The "ringing" phenomenon of Butterworth high-pass filter is usually smaller in comparison with that of ideal high-pass filter.In addition, Butterworth high-pass filter has a flexible filtering property.So it is necessary to transform the infrared image to frequency domain first by using fourier transformation,next Butterworth high-pass filter processes the infrared image in frequency domain.To get the detail information of the image,we must do Fourier inverse transformation.Then we decompose the detail image and the base image for subsequent processing.

The n order Butterworth high-pass filter transfer function is defined as follows:

$$H(u,v)=\frac{1}{1+[D_0/D(u,v)]^{2n}} \tag{1}$$

Where the bigger the cut-off frequency D0 is set, the more the low-frequency component is filtered out, the more the high-frequency component losses; The cut-off frequency D0 must be set a proper value,which can not only filter out low frequency component, but also can retain most detail information of the detail image.

The detail enhancement of detail image and the gray-scale compression of base image.

Since we can get the detail image by the above steps, the original infrared image after noise reduction subtracts the detail image to get the information of base image.Then we adopt different methods to process the detail image and base image respectively.

On the one hand the infrared image which doesn't contain color information records the temperature information,and on the other hand temperature corresponds with the brightness of pixels. As is shown in figure 3(a),the infrared image can be regarded as 14-bit gray-level information. The grayscale of the 14-bit detail image isolated from figure 3(a) ranges from 1197 to 2049,which is much smaller than that of base image. So in order to expand gray of target region, compress gray of background and transition region,while the whole gray mapped to the range 0 ~ 255,it is reasonable to choose double threshold method based on the exponential transform to map grayscale.The function $P\{f^{detail}(i,j)\}$ can be expressed as follows:

$$P\{f^{detail}(i,j)\}=\begin{cases}\dfrac{f^{detail}(i,j)-\min)\times(f^{detail}(i,j)+1)^{\gamma}}{f_{mid1}-\min} & f^{detail}(i,j)<f_{mid1}\\ \dfrac{(f^{detail}(i,j)-f_{mid1})\times(f^{detail}(i,j)+1)^{\alpha}}{f_{mid2}-f_{mid1}} & f_{mid1}<f^{detail}(i,j)<f_{mid2}\\ \dfrac{(f^{detail}(i,j)-f_{mid2})\times(f^{detail}(i,j)+1)^{\gamma}}{\max-f_{mid2}} & f^{detail}(i,j)>f_{mid2}\end{cases} \tag{2}$$

In eqution 2, min represents the minimum of grayscale in the image,max represents the maximum of grayscale in the image.In figure 3(b),max=2049,min=1197. The two proper threshold values f_{mid1} and f_{mid2} are choosen for splitting image,we choose f_{mid1}=min+(max-min)/5, f_{mid2}=min+3(max-min)/5. The values of f_{mid1} and f_{mid2} can be adjusted according to the image.

Generally speaking, the grayscale of infrared target is located in the high-level of gray histogram, we consider that gray values of the pixels greater than the threshold value belong to the target, other pixels belong to the background and transition region. Adopt different parameter functions to the target, background and the transition region separately , extending the gray of target region, compressing the gray of background and the transition region.With regard to target region ,the parameter of the exponential transform function α should be selected greater than 0.To expand the grayscale of target region,we take α=0.7.For the background and transition region, the parameter of the exponential transform function γ should be taken less than 0;To compress the grayscale of these regions,we take γ=-0.9. In other case, it is also available to choose any other suitable values.

The gray scale of the 14-bit base image isolated from figure 3(a) ranges from 2351 to 8475,which contains high dynamic range grayscale. In the premise of not affecting the imaging quality, we choose the simple linear mapping[4] to achieve the gray compression of non-detail information, reducing calculation and improving the processing speed. The gray linear mapping equation is defined as following:

$$Q\{f^{base}(i,j)\}=\begin{cases}0 & f^{base}(i,j)\le\min\\ \dfrac{f^{base}(i,j)-\min}{\max-\min} & \min<f^{base}(i,j)<\max\\ 255 & f^{base}(i,j)\ge\max\end{cases} \tag{3}$$

First count up the gray histogram of base image H(k),k=0,1,2,3...L-1;L stands for the gray-scale number of the base image. Then count pixels from the two ends of the gray histogram to middle individually, S_1=H(1)+ H(2) +…+H(min),S_2=H(L-1)+H(L-2) + …+H(max) , where 0 < min<max<L.

Estimate the values of S_1 and S_2, stop accumulating S_1 and save the value of min when S_1>T; stop accumulating S_2 and save the value of max when S_2>T,in which T is the preset threshold value.

After processing,we get max = 7695, min = 2562,thus we can combine the grayscale which contains less pixels at both ends together and map the concentrated region which contains great majority of pixels.

Linear compose the detail image and the base image after processing.

Compose the enhanced detail image and the compressed base image to obtain the composite image, which is our desired 8-bit enhanced output image.

To adjust the proportion of the two parts[2] in the result, multiply a factor of k to the base image, which called linear weighted composition method in the composite image:

$$f^{out}(i,j) = P\left\{f^{detail}(i,j)\right\} + kQ\left\{f^{base}(i,j)\right\} \quad (4)$$

Where the final 8-bit output composite image is $f^{out}(i,j)$, k is the weighting factor of base image in the output image,which can be adjusted according to actual situation. For example,a typical value of k is 0.8.

(a)The original image after noise reduction

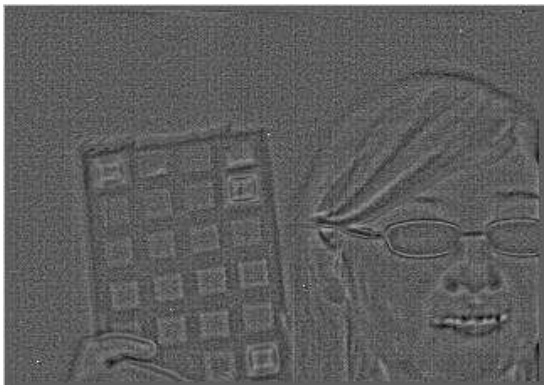

(b)The detail image

(c)The base image

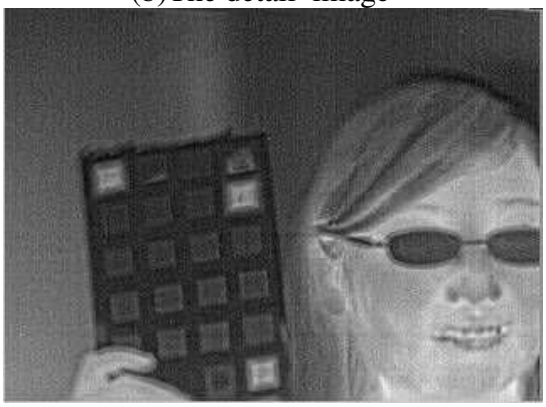

(d)The output image

Fig. 2 Image test result of demo 1

The result of experiment and analysis.

In the end，program the algorithm above-mentioned by using C++, and verify the processed image processing in Matlab simulation. As is shown in figure 1, the 14-bit original infrared image is captured by the infrared thermal imaging system which is independently researched by our laboratory. The infrared image after noise reduction, base image, detail image and enhanced detail image, which are processed from figure 1, are shown in figure 2. As is shown in Figure 3 (d), the detail information of the image has been preserved and enhanced obviously. In order to test the adaptability of the method further, we capture another group of infrared images with high dynamic range in different scenes by the infrared thermal imaging system which is independently researched by our laboratory. The group of infrared images shown in figure 3 contains abundant detail information, which has better enhancement effect after processed by the algorithm mentioned in this paper.

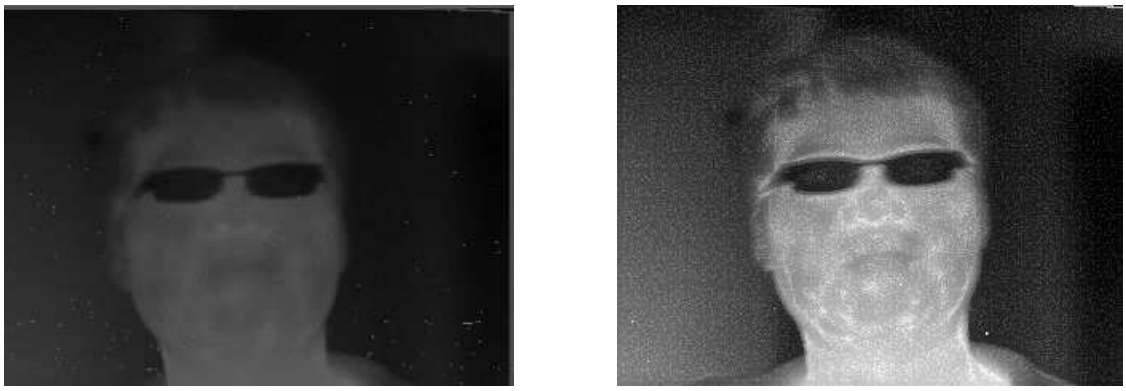

(a) The original image (b)The output image

Fig. 3 Image test result of demo 2

Summary

The new enhancement algorithm of infrared images based on dual threshold of the exponential transform mentioned in this paper, compresses scene information of the global large dynamic range reasonably ,on the basis of effective noise suppression;which not only compress the infrared image with large dynamic range,but also enhance the detail information of infrared image.Thereby the algorithm focus more on the extraction and enhancement of detail information, while improving the contrast of image,leading to the exaltation of the visual sense obviously.

References

[1] Scribner.D.A ,et al . Infrared focal plane array technology. Proc . of the IEEE, 1991.79(1):66-85.

[2] XiaoBo Chen, XinPing Lu, ZhiBo Liu,A DDE Algorithm Based on Hierarchical Data Processing of Image, MICROPROCESSORS,2013.

[3] Yang L, Yang J,Yang K.Adaptive detection for infrared small target under sea-sky complex background[J]. Electronics. Letters, 2004, 40(17).

[4] JiaHong Yang,Jin Xiang,CuiHong Li, DeYi Wei,Novel algorithm of detail enhancement for IR image,2012.

[5]XueMei Guan. Research on the technology of image enhancement based on frequency domain [J], Journal of Langfang Teachers College(Natural Science Edition),2012.12(2):27-32.

Advanced Materials Research Vols. 989-994 (2014) pp 3898-3901
© (2014) Trans Tech Publications, Switzerland
doi:10.4028/www.scientific.net/AMR.989-994.3898

Novel Single Image Dehazing algorithm

Chen Jian-Peng[1,a], Bi Du-Yan[1,b], Liu Chang[1,c], Fan Zhun-Lin[1,d]

[1]Air force Engineering University, Xi'an 710038, China

[a]1037348235@qq.com,[b]Biduyan@163.com,[c]yydyjjhnr@163.com,[d]FanZL@163.com

Keywords: dehazing; dark channel prior; LP filter; guided image filter

Abstract. In order to improve the quality of haze degraded image, a novel method is proposed combining dark channel prior and the atmospheric degradation model. Firstly, adaptive block is performed to acquire the dark channel image; then, in HSV space, laplacian pyramid filter is required to obtain the low pass portion of V, further compensated by the single scale Retinex to achieve the final atmospheric light; moreover, for the smoothness trait of guided filter and its fast operation rate, it is suggested to gain the optimal transmission map. Experimental results show that this algorithm can effectively improve the visibility of the optical imaging system.

Introduction

Images of outdoor scenes are usually degraded by the turbid medium which greatly affects the normal operation of most automatic systems. Therefore, the technique Dehazing of Atmospheric Degradation Image (DADI) improves the visibility of degraded images by weakening the effect of haze, having vitally important research meanings [1].

The dehazing methods can be divided into two categories: image enhancement and image restoration. The former enhances the color and contrast of the degraded images based on the human visual system [2], but may lose some information. While the latter establishes the atmospheric scattering model to obtain sharp image [3]. He [4] proposes a simple but effective DCP to remove haze from a single input image, while the method of fixed threshold to estimate atmospheric light is not accurate enough, and the soft-matting has high complexity in time and space .

In this paper, based on DCP, LP-filter[5] and SSR (Single Scale Retinex) compensation algorithm[6] is introduced to estimate the atmospheric light instead of fixed threshold in He's algorithm, and the guided filter is utilized to refine the atmospheric transmission map.

Monochrome atmospheric scattering model

McCartney put forward the widely used monochrome atmospheric scattering model

$$I(x,y)=t(x,y)J(x,y)+(1-t(x,y))A \tag{1}$$

Where the first term is the direct attenuation, and the second term is airlight. And $I(x,y)$ is the observed intensity, $t(x,y)$ is the atmospheric transmission, A is the atmospheric light, and $J(x,y)$ is the scene radiance. The goal of haze removal is to recover $J(x,y)$.

Our algorithm

2.1 Getting dark channel image based on adaptive partition

The dark channel image $J_{dark}(x,y)$ can be expressed as following:

$$J_{dark}(x,y)=\min_{c\in\{r,g,b\}}(\min_{\Omega}(J_c(x,y))) \tag{2}$$

Where $J_c(x,y)$ is a color channel of $J(x,y)$ and Ω is a local patch centered at (x,y), whose size is extremely important for the estimation of transmission. To seek the balance between abundance and distortion, we regard the maximum of row and column of 3% as the size of Ω.

$$block = round(\max(M, N) \times 3\%) \tag{3}$$

The transmission map from our adaptive blocking is more natural and real.

2.2 Estimating atmospheric light

The algorithm is as follows：

(1)Transform the hazy image from RGB space to HSV space to get V component,

$$V = \max(\boldsymbol{I}_R, \boldsymbol{I}_G, \boldsymbol{I}_B) \tag{4}$$

(2)Decompose V component to get VL using LP filter[4],

$$c[n] = \sum_{k \in Z^d} V[k] h[Mn - k] = \langle V, \tilde{h}[-Mn] \rangle \quad VL[n] = \sum_{k \in Z^d} c[k] g[n - Mk] = \sum_{k \in Z^d} \langle V, \tilde{h}[-Mk] \rangle g[n - Mk] \tag{5}$$

Where $h[-n] = \tilde{h}[n]$ is the impulse response of LPF, M is a $d \times d$ scale integral sample matrix；

(3)Employ SSR algorithm to compensate the luminance of VL to get VLC as the estimation of atmospheric light A.

$$F(x,y) = \frac{1 - \varepsilon((x - x_0)^2 + (y - y_0)^2 - 2)}{8} \tag{6}$$

Where (x_0, y_o) is the center point of the function， $\varepsilon(\cdot)$ is a step function.

2.3 Atmospheric transmission refinement

The initial atmospheric transmission is acquired as following:

$$t_1(x,y) = 1 - \omega \min_c (\min_{\Omega} \frac{I_c(x,y)}{A}) \tag{7}$$

Where ω is introduced to acquire more real dehazed image, which is set to be 0.95.

Now we define the following functions: the initial atmospheric transmission map t_1, guided image I, refining transmission map $\hat{t}$, where t_1 acts as the input image while I represents the original hazy image. When guided image I is a color image of multichannel, the local linear model can show as follows:

$$\hat{t}_i = \mathbf{a}_k^T \mathbf{I}_i + b_k, \forall i \in \omega_k \tag{8}$$

Where $\mathbf{I_i}$ and $\mathbf{a_k}$ are 3-by-1 vectors denoting color and linear coefficient, respectively, while $\hat{t}_i$ and b_k are all scalar quantities, which all can be obtained using the algorithm in [7].

(a1)He's refined map (a2)our refined map (b1)He's refined map (b2)our refined map

Fig.1 Comparison of refined map

When a refined transmission map is gained through guided filter, we can further achieve the final dehazed image $J(x,y)$:

$$J(x,y) = \frac{I(x,y) - A(x,y)}{\max(t(x,y), t_0)} + A(x,y) \tag{9}$$

A typical value of t_0 is 0.1, avoiding too small transmission value.

3 Experimental results and analysis

All the experimental data is based on Matlab R2010a.By comparison experiment of two haze degraded images, we can further confirm the performance of our algorithm. Results are shown in Figure 2:

(c1)Original image (c2)He's result (c3)Our result (d1)Original image (d2)He's result (d3)Our result

Fig.2 Comparison with He's result

After the subjective assessment, we quote [8] to make objective evaluation. We observed that the S component information entropy of original non-degraded images is much larger than that of haze degraded ones. Based on our observation, the overall color quality index Q can be expressed as its S component information entropy.

$$Q = \frac{-\sum_{i=0}^{255} p(x_i)\lg(p(x_i))}{m} \tag{10}$$

Where $p(x_i)$ defines the proportion of i-gray-level pixels in a whole image; m is a normalization factor with a value of 10. The result is demonstrated in Table 2. For the fastness of the proposed method, we make a comparison in calculation time. As shown in Table 3, our algorithm is far more efficient than He's.

Table 2 Image color quality index Q

Q	Degraded image	He	Our method
c	5.2849	6.5508	7.8809
d	4.1147	6.7613	7.2492

Table 3 Comparison in calculation time

Image number	He's method	Our method
c	48.075672	2.07955
d	44.585169	1.889495

4 Conclusions

In this paper, we propose a novel DADI algorithm based on DCP and with the combination of atmospheric scattering model. Firstly, we get the dark channel by adaptively blocking, and then obtain atmospheric light through LP filter and SSR compensation algorithm, and use guided filer to refine the transmission to achieve the vivid image. Whatever in subjective and objective evaluation, our results perform better than He's both in operation speed and image quality.

Acknowledgements

National Natural Science Foundation of China (No. 61175029).

References

[1]Bi Du-Yan, Li Quan-He and Chen Jian-Peng: Journal of Air Force Engineering University (Natural Science Edition) ,Vol. 14(2013) No.6, p.46.

[2]Ma Shi-Ping, Zhang Ming and Bi Du-Yan: Journal of Xidian University, Vol. 37(2010) No.3 , p. 541.

[3] Tarel J-P and Hautiere N: Proceedings of the IEEE Computer Society Conference on Computer Vision and Pattern Recognition(Kyoto, Japan)Vol. 2009, p.2201.

[4] He Kai-Ming, Sun Jian and Tang Xiao-Ou: Proc. of 27th IEEE Conference on Computer Vision and Pattern Recognition(Kyoto, Japan)Vol. 2009, p.1956.

[5] M. N. Do and M. Vetterl: IEEE Transactions on Signal Processing, Vol. 51(2003) No. 9, p.2329.

[6]Huang Li-Hong: Applied Optics, Vol. 31(2010) No.5, p.728.

[7]He Kai-Ming, Sun Jian and Tang Xiao-Ou: IEEE Transactions on Pattern Analysis and Machine Intelligence, Vol. 35(2013) No.6, p.1397.

[8]Nan Dong, Bi Du-Yan and Zha Yu-Fei: Journal of Electronics and Information, Vol. 28 (2013) No.9, p.245.

Advanced Materials Research Vols. 989-994 (2014) pp 3902-3905
© (2014) Trans Tech Publications, Switzerland
doi:10.4028/www.scientific.net/AMR.989-994.3902

Simulation and Application of Space-time Coding in OFDM System in Coal Mines

Jingxin Wei[a], Chun Sun[b]

NCIST Teaching Affairs Department, Bejing East, Yanjiao 101601

[a]weijing7703@126.com

Keywords: OFDM, Space-time Coding, channel estimation

Abstract. This research is conducted with the objective of improving the OFDM system in coal mines with regard to its defects and puts forward a structure diagram of STBC-OFDM transceiver for systems which require low complexity with a simulation of the system performance. Through the simulation, in which the STBC-OFDM communication system in coal mines is employed, the BER performance of the OFDM system is improved and the complexity and cost of the receiver is lowered with a significant reduction in daily maintenance.

1. Introduction

With added guard intervals in the OFDM system, the intersymbol interference in multipath transmission is eliminated with the spectrum efficiency enhanced, and the use of IFFT/FFT baseband reduces the complexity of the equipment. The OFDM system, however, is easily affected by frequency deviation and time-varying channels[1], yielding a high PAR and increased cost for equipments. Therefore, the combination of space-time coding[2] [3] [4] and OFDM technology[8] can promote the anti-fading ability of the system and lower the BER in transmission[5] [6].

2. Space-time Coding OFDM System

A space-time coding OFDM system with 4 emitting antennas and $p(p \geqslant 4)$ receiving antennas as is shown in Diagram 1.

In the moment n, either of the two data blocks $\{b_i[n,k]: k=0,1,\cdots\}$, $i=1,2$, when passing space-time coding, are converted into two different data sequences $\{t_{2(i-1)+j}[n,k]: k=0,1,\cdots, j=1,2\}, i=1,2$. After being space-time coded, the k[th] voice OFDM signal in the n[th] data block of the i[th] emitting antennas becomes $t_i[n,k]$.

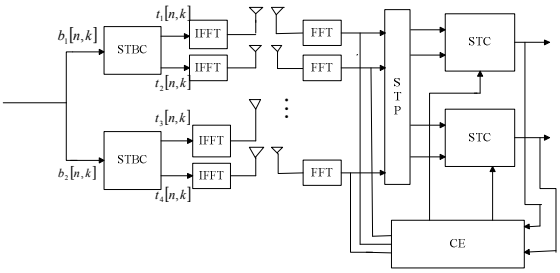

Diagram 1. Model of STBC-OFDM System

It can be seen from the diagram that the signal received by the receiving antenna is the superposition of 4 distorted signals from the transmitter, which can be expressed as

$$r_j[n,k] = \sum_{i=1}^{4} \mathbf{H}_{ij}[n,k] t_i[n,k] + w_j[n,k] \quad (j=1,\cdots,p) \qquad (1)$$

$w_j[n,k]$ represents that the mean of the is 0 with a variance of σ_n^2 and it also means the complex gauss noise which is additive and unrelated of different moments. $\mathbf{H}_{ij}[n,k]$ represents the frequency response of the k^{th} voice signal between the i^{th} emitting antenna and the j^{th} receiving antenna at the moment of n.

3. Statistical Features of MIMO Channel

The baseband signal in the impulse response of mobile wireless channels can be expressed as

$$h(t,\tau)=\sum_{k}\gamma_k(t)c(\tau-\tau_k) \quad (2)$$

τ_k is the delay of the k^{th} path, $\gamma_k(t)$ is the amplitude, and $c(t)$ is the shape of the impulse. With regard to the movement of the mine car in the tunnel, it can be assumed that $\gamma_k(t)'s$ is the complex gaussian process of the narrow band in Wide-sense stationary (WSS) and each path is independent. The average power of $\gamma_k(t)'s$ is determined by the distribution of channel delays, which is affected by the environment. For the convenience of research, it is assumed that the corresponding emitting and receiving antennas in the MIMO system have the same distribution of delays.

4. Enhanced Channel Estimation

$h_{ij}[n,l]$ is estimated in terms of time and frequency with the relevance of channel parameters. The channel frequency response of $\hat{h}_{ij}[n,l]$, the estimated $h_{ij}[n,l]$, is reconstructed as

$$\widehat{H}_{ij}[n,k]=\sum_{l=0}^{K_Q-1}\hat{h}_{ij}[n,l]W_K^{kl} \quad (3)$$

$\hat{h}_{ij}[n,l]$ contains the actual channel parameter $h_{ij}[n,l]$ and the estimated error $e_{ij}[n,l]$. That is

$$\hat{h}_{ij}[n,l]=h_{ij}[n,l]+e_{ij}[n,l] \quad (4)$$

The mean of $e_{ij}[n,l]$ is 0 and its variance is σ^2. $i's$, $j's, n's$, or $l's$ are independent gauss signals at different moments.

If the distribution of channel delays is given and when $l=0,\cdots,K_o-1\ \sigma_l^2$ are given and they are used to reconstruct the channel frequency response from $\hat{h}_{ij}[n,l]$, the Mean Square Error (MSE) of $\widehat{H}_{ij}[n,k]$ decreases rapidly. When α_l of the minimum NSME is selected at the moment

$$\widehat{H}_{ij}[n,k]\triangleq\sum_{l=0}^{K_Q-1}\alpha_l\hat{h}_{ij}[n,l]W_K^{kl} \quad (5)$$

Therefore, the optimal α_l after calculation is

$$\alpha_l=\frac{\frac{\sigma_l^2}{\sigma_l^2+\sigma^2}}{\sum_{m=0}^{K_o-1}\frac{\sigma_m^4}{\sigma_m^4+\sigma^2}} \quad (6)$$

And NMSE is

$$NMSE_O=\frac{\sigma^2\sum_{m=0}^{K_o-1}\frac{\sigma_m^2}{\sigma_m^2+\sigma^2}}{\sum_{m=0}^{K_o-1}\frac{\sigma_m^4}{\sigma_m^4+\sigma^2}} \quad (7)$$

The distribution of channel delays is partly dependent on the environment, so it is usually unknowable for users. For MIMO-OFDM system, however, different emitting and receiving antennas are considered to have the same delay distribution. Thus, $\sigma_l^2\triangleq E\left\|h_{ij}[n,l]\right\|^2$ can be estimated as

$$\hat{\sigma}_l^2=\frac{1}{4p}\sum_{i=1}^{4}\sum_{j=1}^{p}\left|\hat{h}_{ij}[n,l]\right|^2 \quad (8)$$

and σ_l^2 is further calculated.

Suppose the frequency of communicaton in the coal mine is 2GHz, it is considered that the noise in the system is additive white noise with a given variance so that the mechanical and electrical noises can be avoided. Enhanced channels are estimated to be not sensitive to noise variance, so this figure is considered to be σ^2 when the SNR (Signal to Noise Ration) is 10 dB.

5. Simulation Analysis

A simulation is conducted on the space-time coding of different numbers of antennas based on the simulated parameters in Diagram 1. It can be seen from Diagram 2 that the use of STBC-OFDM communication system in coal mines improves the BER performance of the OFDM system, and reduces the complexity and cost of the receiver with a significant reduction in the need for daily maintenance. See Table 1.

Table 1. Physical layer parameter of ofdm

Parameter	**Value**
Working frequency	2000MHz
System bandwidth	20MHz
Sub-carrier number	64
Sub-carrier interval	0.3215MHz(20MHz/64)
Valid symbol period	3.2us(1/0.3125)
Guard interval	8.0us
Symbol period	4us
Modulation mode	Qpsk
Maximum transmit speed	26Mbits/s □

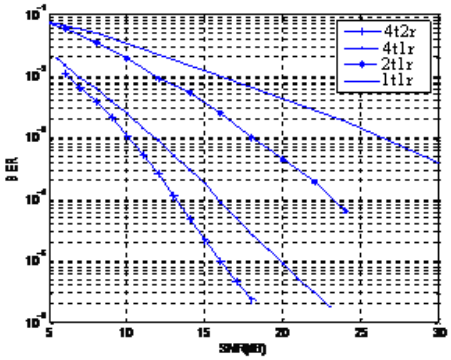

Diagram 2. BER Comparison of Space-time Coding of Different Numbers of Antennas in 3 Paths

References

[1]C.C.Yin:Multi-carrier broadband wireless communication technologies(Beijing University of Posts and Telecommunications Press,2004.)

[2] ALAMOUTI S M. A simplel transmit diversity technique for wireless Communications[J], IEEE Journal Select Areas Commun，1998，16 (8)：1451-1458.

[3] Z. Liu, G. B. Giannakis, S. Zhuo, B. Muquet, space-time coding for broadband wireless communications，Wireless Communications and Mobile Computing, Jan.2001,vol.1, no.1, pp. 35-53

[4] A. winttneben, A new bandwidth efficient transmit antenna modulation diversity scheme for linear digital modulation, IEEE International in Proc.1993

[5] Vahid Tarokh, Nambi Seshadri, A R Calderbank, Space-Time Codes for High Data Rate Wireless Communications: Performance Criterion and Code Construction, IEEE Transactions on Information Theory, Mar 1998, vol.1,pp744-765

[6] S. M. Alamouti., A simple transmit diversity technique for wireless communications, IEEE J. Select. Areas Comm., Oct., 1998, 16, pp. 1451-1458.

[7]Ye (Geoffrey) Li, Jack H. Winters, and Nelson R. Sollenberger, MIMO-OFDM for Wireless Communications:Signal Detection With Enhanced Channel Estimation, IEEE Transaction on Wireless communications, Vol. 3, NO. 3, May 2004

[8] Y. Li, N. Seshadri, and S. Ariyavisitakul, Channel estimation for OFDM systems with transmitter diversity in mobile wireless channels, IEEE J. Select. Areas Commun., vol. 17, pp. 461-471, Mar. 1999.

Advanced Materials Research Vols. 989-994 (2014) pp 3906-3909
© (2014) Trans Tech Publications, Switzerland
doi:10.4028/www.scientific.net/AMR.989-994.3906

Digital image technology mineral feature extraction method research

Peng Jian[1] , Li Dongbo[2]

[1,2] China University of Geosciences(WuHan), WuHan, HuBei province, 430074, China.

pengjian@cug.edu, lee_dongbo@126.com.

Keywords: Gabor wavelet, GLCM, SVM classifiers.

Abstract. This paper presents a texture classification algorithm using Gabor wavelet and Gray Level Co-occurrence Matrix as feature extraction method and Support Vector Machine as classifier. Gabor transform and Gray Level Co-occurrence Matrix are used to get the features of the digital images, SVM classifiers are followed to build image and realize classification. The results of the experiments have shown that the methods described in this paper can improve the rate of correct classification effectively than traditional method of classification.

1. Introduction

Image feature is the foundation of image understanding, the main features of image include color, texture and shape. Texture is an important feature of the image, which is the nature of spatial distribution characterization of pixel neighborhood gray level. Texture is texture primitive regular permutation and combination, texture element is a repetitive, consistent intensity of simple shape regional and image pixel is the smallest texture primitive. Domestic and foreign experts have conducted a lot of research on the image texture such as wavelet transform, texture, co-occurrence matrix and Markov random field. These methods can be roughly divided into statistical analysis method, model method, frequency domain analysis method, and structure analysis method. The statistical analysis method is most widely used, and fruitful research achievements have been made in the field of computer vision and pattern recognition. Mineral picture itself also has these characteristics. However, mineral structure differs in thousands of ways and the difference in impurity content of the ore lead the mineral difficult to recognize. A simple combination of simple texture, color, hardness and the color of texture is not enough to identify the complex image effectively, so, new image feature extraction method is needed.

2. Texture features extraction based on Wavelet Transform

Gabor wavelet is an important method of image texture feature extraction, with the good robustness of illumination and pose, Gabor wavelet is widely applied to the field of image recognition.

Definition of two-dimensional Gabor wavelet :

$$\psi(\kappa, z)=\frac{\|k\|^2}{\sigma^2}\exp\left[-\frac{\|k\|^2\|z\|^2}{2\sigma^2}\right]\cdot\left[\exp(ikz)-\exp\left[-\frac{\sigma^2}{2}\right]\right]$$

σ is a constant associated with the wavelet frequency bandwidth. $z=(x,y)$ is position coordinate space. k determines the direction and scale of the Gabor kernel. In the sample with 8 directions and 5 scales, scale and direction of the k can be written as $k_{\mu,\nu}=k_\nu e^{i\phi_\mu}$. $k_\nu=k_{\max}/f^\nu$ is sampling scale, $\nu\in\{0,1,\cdots,4\}$ is scale label. $\Phi_\mu=\pi\mu/8$ is sampling direction, $\mu\in\{0,1,\cdots,7\}$ is direction label. $k_{\max}$ is the maximum frequency, f is kernel interval factor in the frequency domain. Assume that $k_{\max}=\pi/2$, $f=\sqrt{2}$, $\sigma=2\pi$, the wavelet representation and identify will be better.

Gabor transform and convolution kernel is : $J_k(z) = \mathrm{I}(z) * \Psi(k, z)$

Assume that the amplitude of $J_k(z)$ is A_k and the phase of $J_k(z)$ is ϕ_k , $J_k(z) = \mathrm{A}_k e^{i\phi_k}$, so Gabor feature vector images in z position can be get by grouping different scales and directions of $J_k(z)$ together.

3. Texture feature extraction based on the gray level co-occurrence matrix

As the computation loads of the gray level co-occurrence matrix are still very high, for simplicity, five most commonly used features are used to extract image texture feature:

(1) Angle of second moment (energy)

$$ASM = \sum_i \sum_j p(i, j)^2$$

Angle of second moment is square of all gray level co-occurrence matrix elements, it is also known as energy. It is a measurement of image texture gray change uniform, reflecting the image gray distribution uniformity and texture coarseness. If all the values are equal in co-occurrence matrix, the value of ASM is low; on the contrary, if some values are large and others are small, ASM is high. A image with same gray level has only one value in its image gray level co-occurrence matrix, which is equal to the total number of pixels, it is also the largest ASM value. Therefore, the ASM value indicates that the change is uniform and in regular texture pattern.

(2) Contrast (moment of inertia)

$$CON = \sum_i \sum_j (i - j)^2 p(i, j)$$

The contrast is the gray level co-occurrence matrix main diagonal of the moment of inertia of nearby, it is a measurement of values distribution in matrix and local change in the image, reflecting the image clarity and the groove depth of texture. The groove depth of texture is large, contrast is also large, the image is clear; on the contrary, contrast is low, groove depth becomes shallow, the image is fuzzy.

(3) Entropy

$$ENT = -\sum_i \sum_j p(i, j) \log(i, j)$$

Entropy is a measurement of image texture stochastic. When all values in the spatial co-occurrence matrix are equal, it gets the maximum value; on the contrary, if the co-occurrence matrix values are not uniform, the value becomes smaller. Therefore, the maximum entropy implies that the image gray level distribution is completely random.

(4) Inverse Difference Moment (local stationarity)

$$IDM = \sum_i \sum_j \frac{1}{1 + (i - j)^2} p(i, j)$$

It is used to measure how much the texture local changes. The value is large indicates image texture between different region is lack of change, local region is very uniform.

(5) Variance of sum $f_{10} = p_{x-y}$

Figure.1 is the extraction algorithm based on features of gray level co-occurrence matrix. In the feature extraction of the texture, the brightness of the image is divided into 256 gray level and form a gray co-occurrence matrix in 4 directions, $p_{(1,0)}, p_{(0,1)}, p_{(1,1)}, p_{(1,-1)}$, computation loads of the co-occurrence matrix is determined by the gray level and size of the image. Assume that the image G has L gray level, and its size is R row and C column, the computation loads approximate to $L^2 * R * C$. Then calculating five texture features vectors of the co-occurrence matrix in 4 directions, second moment, entropy, contrast, inverse difference moment and the variance of sum. Finally, texture characteristic vectors are constituted by the five features.

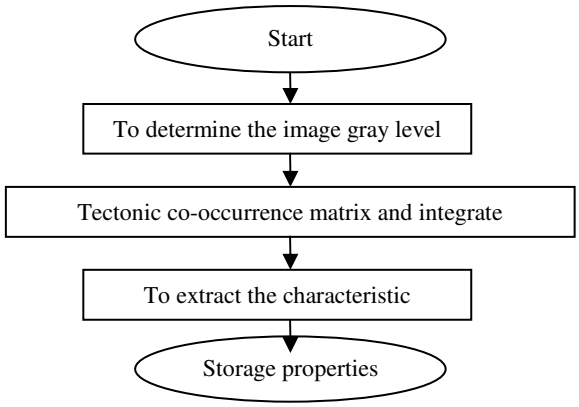

Fig. 1 Algorithm

4. Support vector machine (SVM)

Generally speaking, the support vector machine firstly transforms the input space into a high dimension space by a nonlinear transformation defined by the inner product function, then for (generalized) optimal classification level. SVM classification function is similar to a neural network, the output is a linear combination of several intermediate nodes, and each node in the middle layer of the input sample and a support vector inner product. Support vector machine is a process in which the image is divided into different classes, and makes the data objects in the same class with the higher similarity. Similar or dissimilar description is to determined by image description value. The classification of level is a nonlinear function, and in theory the input space should be mapped to a high dimensional feature space by a nonlinear mapping. There are linear categorization rules in this space, and you can construct a linear optimal classification hyperplane.

Firstly, the input vector x is mapped to a high-dimensional Hilbert space H by the mapping $\Psi : R^{\mathrm{n}} \to H$. A kernel function K satisfies: $K(x_i, x_j) = \Psi(x_i) \cdot \Psi(x_j)$.

The objective function of a quadratic programming problem into two: Maximize

$$W(\alpha) = \sum_{i=1}^{l} \alpha_i - \frac{1}{2} \sum_{i=1}^{l} \alpha_i \alpha_j \mathrm{y}_i \mathrm{y}_j \{\Psi(x_i) \cdot \Psi(x_j)\} = \sum_{i=1}^{l} \alpha_i - \frac{1}{2} \sum_{i=1}^{l} \alpha_i \alpha_j \mathrm{y}_i \mathrm{y}_j K(x_i, x_j)$$

$$s.t. \qquad \sum_{i=1}^{l} \alpha_i \mathrm{y}_i = 0 \quad C \geq \alpha_i \geq 0 \quad i = 1,2,\cdots,l$$

When the training is completed, the following function symbols are only needed to compute.

$$f(x) = \mathrm{sgn}\left[\sum_{\text{support vector}} \alpha_i \mathrm{y}_i K(x_i, x) - b \right]$$

In the formula, b is the offset value:

$$b = \frac{1}{2}\left[\sum_{i=1}^{l} \alpha_i \mathrm{y}_i \Psi(x_i) x^*(1) + \sum_{i=1}^{l} \alpha_i \mathrm{y}_i \Psi(x_i) x^*(-1) \right]$$

In the formula, $x^*(1)$ represents a support vector(everyone) belongs to the first class. $x^*(-1)$ represents a support vector belongs to the second class. Usually, it is no use to know Ψ and H directly. The support vector machine can be determined by selecting a appropriate kernel function K. The Mercer theorem points out the necessary and sufficient conditions that kernel function K must satisfy: for any function g (x) meets the condition: $\int g(x)^2 dx < \infty$, $\iint K(x, y) g(x) g(y) dx dy \geq 0$ is permanent establishment.

Different support vector machines can be made by selecting the kernel function K of different forms, common use are as follows:

(1) Polynomial SVM (when d=1, it is linear kernel): $K(x,y)=[(x\cdot y)+1]^d$.

(2) Radial basis function SVM: $K(x,y)=e^{-\|x-y\|^2/2\sigma^2}$.

(3) Sigmoid function SVM: $K(x,y)=\tanh(k(x\cdot y)+\delta)$.

As the RBF kernel has only two parameters, just C and G, which are needed to be defined with less computation loads. So this article uses the radial basis function.

4. Analysis of the experimental results

Selecting iron ore, copper ore and garnet images to test the image texture characteristics. Images of 10,5,3,1 were selected as the training samples, and according to the five characteristics of the calculated value, training in SVM classification machine based on kernel RBF. Then a test was applied according to other 30 obtained classification models. Test results are showed in Fig.2. This paper provides the method that based on Gabor wavelet and gray image co-occurrence matrix by training and classifying a support vector machine to realize the judging of image authenticity. The experimental results show that the classification effect of the five typical characteristics of the RBF kernel based on SVM is good. More samples will make the test accuracy be better. But the classified results also have some effects on the difference between typical and heterogeneous images samples. In this paper, the feature extraction is good. While processing different kinds of mineral image, it is clear to see that the extraction algorithm is general for ore image, the extraction algorithm has played a good role in understanding and classifying ore.

Samples	C	G	Accuracy
10	1.9	0.5	Three species are all 100%
5	7.8	0.5	Three species are all 100%
3	0.031	0.5	Iron ore：75%，Copper ore：80%，Garnet：87%
1	0.031	0.0077	Iron ore：70%，Copper ore：76%，Garnet：79%

Fig.2 Results

References

[1] Aksoy S, Haralick RM. Feature normalization and likelihood based similarity measures for image retrieval[J]. PRL,2001,22(5):563-582.

[2]ZHANG Zhi-an, LIN Li-hua. Image retrieval based on color and spatial features[J]. Journal of Xi'an University of Science and Technology,2007(3):35-39.

[3]GUO Jing, ZHOU Ming-quan, GENG Guo-hua. The fast retrieval algorithm for 3D based on shape[J]. Journal of Xi'an University of Science and Technology, 2007(1):12-16.

[4]LIU Wei-cheng, SUN Ji-hong. Image information retrieval based on content[J]. Information Science，2002(4):18-22.

[5]SUN Xing-hua. Research on image retrieval based on content[D]. Nanjing: Nanjing University of Science and Technology,2001.

[6]Haralick RM,Shanmugam. Texture featuers for image classification[J]. IEEE Trans, 1973, 3(6): 610 -621.

[7]Mallat S.singularity detection and processing with wavelets[J]. IEEE Trans Info Theory, 1990, 38 (2):617-643.

[8]ZHANG Yu-jin, XU Yin, LIU Zhong-wei. By extracting characteristics of image retrieval algorithm test platform[J]. Chinese Journal of Image and Graphics,2001(6):44-48.

Advanced Materials Research Vols. 989-994 (2014) pp 3910-3914
© (2014) Trans Tech Publications, Switzerland
doi:10.4028/www.scientific.net/AMR.989-994.3910

Image compression technology reseach based on lifting wavelet transform

Rui Guo[1, a], Yufeng Li[1, b] and Fei Liu[1, c]

[1]School of Electronics and Information Engineering, Shenyang Aerospace University, Shenyang, China

[a]suntrip@126.com, [b]li_yufeng@126.com, [c]385103193@qq.com

Keywords: Lifting wavelet transform, image compression, wavelet transform.

Abstract. Because the operational speed of the traditional image compression based on Mallat algorithm is slow, and auxiliary Storage space is occupied, image compressed method based on lifting wavelet transform is proposed, in order to realize its versatility, flexibility and high efficient. Experiments show that the lifting wavelet transform, is easy to realize integer wavelet transform can be used for lossless compression, and has higher compression ratio.

Introduction

The theory's basis of image compression is that there exists many redundant data[1] in the image. First, we need to know taht data and information are two different concepts. Data is the carrier of information and expression. Content as existing in the data which has nothing to do with the information is redundancy. Image compression is to reduce the redundant data to reduce the amount of data transmission and storage. Generally considered static image data redundancy mainly concludes the followings: (1) spatial redundancy; (2) visual redundancy; (3) coding redundancy[2-3].

Image coding mainly includes entropy coding, predictive coding, transform coding[4] and vector four basic coding methods. For all kinds of coding method to formulate unified specification, international telecommunication union and the international organization for standardization on the basis of the original static image compression standard JPEG, in 2000 a new generation of still image compression standard JPEG2000[5]. The standard use wavelet transform to replace discrete cosine transform (DCT), and makes the JPEG2000 standard can be applied to upon, including medical, remote sensing and mobile communications and other fields, all kinds of image compression, have become the 21st century the main static image compression standard.

Wavelet transform theory

In the field of image compression and coding, wavelet transform's basis idea is to decompose the image into different space and frequency of sub images, we called it a multiresolution decomposition[6-8]. After transformation the energy mainly concentrated in low-frequency subband image parts, high frequency subband energy is less. After wavelet transform of the image, all the sum total of the amount of image data in the subspace and the original image is equal to the amount of data, transform itself has no compression.Compression function is mainly in the subsequent quantization and coding and other steps.

Set function $\psi(t) \in L^2(R)$, if meet the permitting conditions $C_\psi \int_{-\infty}^{+\infty} \frac{|\phi(\omega)|}{|\phi|} d\omega < \infty$ $\psi(t)$ as a basic wavelet, the $\varphi(t)$ as the bits of Fourier transform $\psi(t)$.

Continuous wavelet transform is defined as:

$$W_f(a,b) = \frac{1}{\sqrt{|a|}} \int_{-\infty}^{+\infty} f(t) \psi^*(\frac{t-b}{a}) dt \tag{1}$$

For the scale factor of a, b for translation factor, a≠0,b, t are continuous variables, $\psi_{(a,b)}(t)=\frac{1}{\sqrt{|a|}}\psi(\frac{t-b}{a})$ is the mother wavelet $\psi(t)$ generated the wavelet, said $\psi^*(t)$ is the conjugate complex of $\psi(t)$.

The energy formula shows after wavelet transform the integration of signal amplitude square is proportional to the signal energy before ransform. Wavelet transform redistributes the energy of original signal, while the coefficient after wavelet transform completely retains the original signal information.

Discrete Wavelet Transform. In order to be able to apply wavelet transform on the computer, you need to discrete continuous wavelet operations and convert it into a binary wavelet. Make $a=2^{-m}, b=n2^{-m}\ \ n,m\in Z$ (Z is the set of integers), then the discrete binary wavelet is

$$\psi_{m,n}(k)=2^{m/2}\psi(2^m k-n), k\in Z \tag{2}$$

The signal $f(t)$ take discrete value $f(k)$, $k\in Z$,and $f(t)\in L^2(Z)$, that is $\sum_{k\in Z}|f(k)|^2<+\infty$, then wavelet transform of the discrete binary of $f(k)$ is:

$$A^0 f(x,y)=D^1 f(x,y)+D^2 f(x,y)+...+D^n f(x,y)+A^n f(x,y) \tag{3}$$

Accordingly, the inverse transform is:

$$f(k)=\sum_{m\in Z}\sum_{m\in Z}W_f(m,n)\psi_{m,n}(k)\ \ m,n,k\in Z \tag{4}$$

When a=2 and b=1, the Discrete Wavelet form is described as below.

$$\psi_{j,k}(t)=2^{-j/2}\psi(2^{-j}t-k)\quad j,k\in Z \tag{5}$$

And it is called Dyadic wavelet.

The Mallat algorithm of One-dimensional discrete wavelet transform. In the year of 1987, Mallat put forward the concept of multi-resolution analysis, and gave the method of orthogonal wavelet and its fast algorithm, that is the Mallat algorithm.

According to the theory of multiresolution analysis, we can conclude the fast decomposition algorithm expression of one dimensional discrete wavelet transform:

$$c_{j,k}=\sum_m h(m-2k)c_{j-1,m} \tag{6}$$

$$d_{l,k}=\sum_m h(m-2k)g_{j-1,m} \tag{7}$$

Where h and g are the decompositions of low-end, high-pass filter respectively. Its fast reconstruction algorithm can be expressed as

$$c_{j-1,m}=\sum_k c_{j,k}h(m-2k)+\sum_k d_{j,k}g(m-2k) \tag{8}$$

The $\overline{h}$ and $\overline{g}$ are the low, high-pass filter of reconstruction respectively. Where $c_{j,k}$, $d_{j,k}$ are respectively scale coefficients and wavelet coefficient of the scale j, and $c_{j-1,m}$ is the scale coefficient of the scale $j-1$.

The decomposition and reconstruction of two-dimensional discrete wavelet transform. Images of two-dimensional discrete wavelet transform are based on the one-dimensional discrete wavelet transform of signal. And it is the 2d extension of one-dimensional discrete wavelet transform. Each level of the image wavelet transformation can be divided into two steps. To begin with, we should make one-dimensional wavelet transform for the rows or columns of the image and then transform data in columns or rows in a one-dimensional wavelet transform. In the field of engineering application, we use digital filter and the sampling to realize two-dimensional discrete wavelet transform of the image.After wavelet transform, the original image is decomposed into four sub images, which are corresponding to the four zones respectively:

a) LL sub-band: low-frequency sub-graph, which is the overview of the corresponding image in the next dimension.b) LH sub-band: vertical high-frequency sub-graph, which is detail information of images in the horizontal direction of the scales.c) HL sub-band: level high frequency sub-graph, which is detail information of images in the vertical direction of the scales.d) HH sub-band: diagonal high-frequency sub-graph, which is detail information of images in the diagonal direction of the scales. As is shown in figure 1:

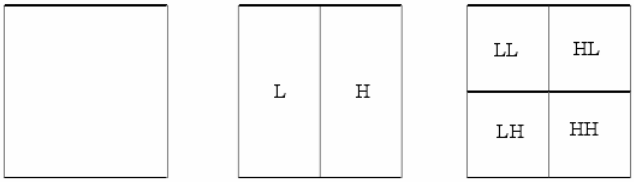

Fig.1, Schematic diagram of two-dimensional Wavelet transform

Fig.2, Decomposition example of two-dimensional Wavelet transform

Lifting wavelet algorithm

The basic idea of improving the algorithm is to break down finite lifting wavelet filters into some basic building blocks, and complete the wavelet transform step by step. Lifting algorithm is divided into three steps: division, forecast and update. Specific methods are as follows:

Division:

Set $x(n)\ (n=0,1,2\cdots,N)$ is the original sequence of discrete signals, which is divided into an odd sequence $x(2n+1)$ and an even-numbered sequence $x(2n)$ and they are two disjoint subsets mutually. As shown in this formula:

$$\{x(2n),x(2n+1)\}=Split(x(n)) \tag{9}$$

Forecast:

Because of the original data's dependencies, so you can take advantage of even-number $x(2n)$ to predict odd sequence $x(2n+1)$ .Set $p(\cdot)$ is predict operator, $p(x(2n))$ is the forecast value of even sequence, using the error between the value of $x(2n+1)$ and forecast value to represent detail information $d(n)$ .As shown in the formula (12):

$$d(n)=x(2n+1)-p(x(2n)) \tag{10}$$

In the lifting wavelet transformation, the prediction has the following two functions:It can represent the data in the form of a compact.Utilizing the local correlation of original signal sequence $x(n)$ during various elements, which can be used to predictive error $d(n)$ and predictive value of $p(x(2n))$ of even number sequence $x(2n)$ to predict the odd number sequence $x(2n+1)$.

It can isolate the high frequency component of signal $x(n)$ in the spatial domain:

We can predict that point by a smooth curve which goes through the near point of $x(2n+1)$ in the prediction, The smooth can be looked as the low frequency component of $x(n)$. The error of prediction $d(n)$ is the error after comparing a sequence $x(n)$ with their low frequency component in local area, so it can be viewed as the signal high frequency component of $x(n)$.

Update

For to maintain the overall of characteristics of the original sequence $x(n)$, $x(2n)$ must be updated. The purpose is to find out a subset of the data $c(n)$ which is able to maintain certain scale features of the original sequence $x(n)$ better. We can use the prediction error of d(n) to update even number

sequence $x(2n)$ to get data subset of $c(n)$. As shown in type (12), of which $U(\cdot)$ represents update operator.

$$c(n) = x(2n) + U(d(n)) \tag{11}$$

The reconstruction process of signal sequence $x(n)$ is the reversing process of above three steps, which are divided into three steps including anti update, anti prediction and merging.

1. Anti update

We can recover even number sequence by undo update formula (13) and sequence of $c(n)/d(n)$.

$$x(2n) = c(n) - U(d(n)) \tag{12}$$

2. Anti prediction

By the anti-prediction formula (14), sequence $x(2n)$ and $d(n)$ can restore the odd sequence.

$$x(2n+1) = d(n) - p(x(2n)) \tag{13}$$

3. Merger

We can restore the original signal sequence x(n) by the merger formula (14) and even.

$$x(n) = Merge\{x(2n), x(2n+1)\} \tag{14}$$

Lifting wavelet transform decomposition and reconstruction of the principle shown in Figure 3.

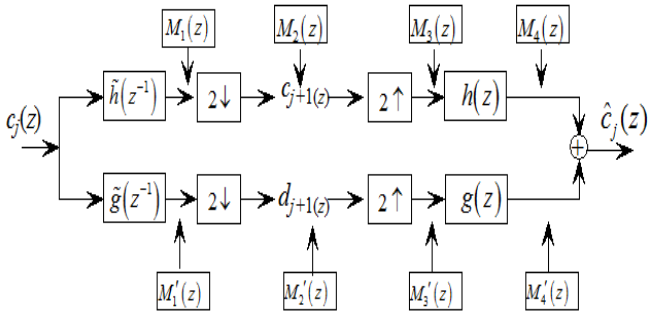

Fig.3,Lifting wavelet transform decomposition and reconstruction schematics

a.The original image b.Three decomposed image c. The final image

Fig.4, The image of using wavelet transform image compression

A. The original image B. The final image

Figure 5. The image of using traditional wavelet transform image compression

A is the original image, B is three layers of decomposition by the lifting wavelet transform, C is the image using the wavelet transform image compression in Figure 4.

In Figure 5, A is the original image and B is the final image by the traditional wavelet algorithm. The data are shown in Table I.

Compared with the wavelet transform, the lifting wavelet transform has the following main advantages:

A: The whole calculation process does not require auxiliary storage space, for this the lifting wavelet transform can operation in the situ. So compared with the additional Mallat algorithm, speed of wavelet transformation is significantly enhanced. And the lifting wavelet transform significantly enhance the computing speed is a repid and practical method of the wavelet transform.

B: Compared wavelet transform, the image reconstruction error by the lifting wavelet transformation is smaller, and the PSNR is larger than the traditional wavelet transformation to ensure integrity of image information.

Table 1 Arithmetic comparison of the image in to algorithms

Algorithm	The original size	Picture size after compression	Compression ratio	PSNR(db)	Time(s)
The traditional wavelet transformation	262144	154568	1.6959:1	25.78665	0.560248
This algorithm	262144	26208	10:1	33.168459	0.734843

Conclusion

As a key link in the process of information transmission, image compression and coding is a greatly key area of research in the field of communication. As one standard of image compression, The lifting wavelet transformation of JPEG2000 has more advantages than the traditional wavelet transformation in some aspects. Experiments show that, image compression of lifting wavelet transformation in this article is relatively improved than the traditional wavelet transform in both PSNR and the operation time.

References

[1] CONG Shuang, PU Ya-kun, WANG Jun-nan. “DCT based image compression algorithm and application” [J], Computer Engineering and Application, 2010, 46(18): 160-163.

[2] LI Ding-chuan.”JPEG2000 Image Compression Standard and Applications of Key Algorithm” [J], Image technology, 2010, 4(7):26-31.

[3] MA Yuan-yuan,YANG Feng,XIN Keand JIAO Fang-chao.”Research of JPEG Image Compression Based on DCT” [J], COMPUTER TECHNOLOGY AND DEVELOPMENT, 2011,21(8):133-136.

[4] ZHANG Jun, CHEN Li-Zhi, YANG Hai-Bin and HUANG Kui-Hua.”Adaptive Lifting Wavelet Transform and Image Compression Via Texture” [J], CHINESE JOURNAL OF COMPUTERS,2010, 33(1):184-191.

[5] ZHENG Wei, CUI Yue-li, WANG Fang,”A Review of Image Compression Coding Based on Wavelet Transform” [J], Communications Technology, 2008, 41(2):83-96.

[6] Pan Z G, Gao X. “An improved SPIHT algorithm for texture image compression” [J], Journal of Graduate School of the Chinese Academy of Sciences, 2010, 27(2):222-227.

[7] HAO Hong-Wei, JIANG Rong-Rong and SHI Ya-Shan “An Image Compression Algorithm for Circle Shaped ROI” [J], ACTA AUTOMATICA SINICA, 2008, 34(5):601-604.

[8] Tian Jiehua, Gu Xiaodong and Wang Yuanyuan,”Low-bit-rate wavelet-based image compression using human visual characteristics” [J], Chinese Journal of Scientific instrument , 2010, 31(11):2155-2159.

Advanced Materials Research Vols. 989-994 (2014) pp 3915-3918
© (2014) Trans Tech Publications, Switzerland
doi:10.4028/www.scientific.net/AMR.989-994.3915

Optimization of traffic signal timings based on surrogate measures of safety

Yi Zhang[1,2], Chaocheng Zheng[1,2,a], Li Zhang[1,2], Xinren You and Dongxiang Cheng[1,2]

[1]Nanjing Communications Institute of Technology, Nanjing 211188, China;

[2]Jiangsu province transportation energy saving engineering technology research center, Nanjing 211188, China.

[a]Corresponding Author E-mail: cczheng@njci.cn

Keywords: Signal optimization; Surrogate measures; objective optimizationl evolutionary algorithms

Abstract. One alternative mathod to improve safety of signalized arterials is to optimize signal timings. Historically, signal retiming tools were used to reduce traffic delay and stops and other measures of traffic efficiency such as closed-loop systems in California and United States. The concept of optimizing signal timings specifically to improve safety metrics, or their surrogate measures, is not common in current signal timing optimization practice. This study advocates a fresh approach to integrating VISSIM microsimulation software, Surrogate Safety Assessment Model, and VISSIM-based Genetic Algorithm for Optimization of Signal Timings to reduce surrogate measures of safety and thereby reduce risks of potential real-world crashes. In addition, a multiple-objective genetic algorithm is implemented to identify the optimal compromise between two competing objectives: surrogate safety and traffic efficiency.

1 Introduction

One way to improve safety of signalized arterials is to retime traffic signals. Well-coordinated traffic signals provide good progression for major vehicular streams previous to reducing the number of necessary stops and the potential for rear-end collisions. In addition, balanced splits provide more equitable green times for all traffic movements thus reducing potential for unsafe operations of 'unfairly treated' traffic movements. However, in spite of the common belief that proper signal timings promote safe traffic operations, evidence from the field to support this perception is lacking. The Highway Safety Manual states that several signal timing-related crash-reduction treatments (e.g. modifying cycle length and phase durations, and improving signal coordination) have unknown effects on crashes.

There are two major reasons for an inability to investigate impacts of signal timings on traffic safety at intersections on arterial streets. First, field evaluations of safety improvements obtained by tweaking signal timings are impractical and often inconclusive. Relationships between crash rates and potential causes are relatively low even when those causes (e.g. weather, geometrical design of the roads, and presence of work zones) have a much higher impact on traffic safety than signal controllers' timings. Second, unlike other traffic metrics which reflect efficiency of traffic operations, safety impacts have not been traditionally assessed by simulation tools.

An integrated simulation/signal optimization tool can generate, evaluate and fine tune signal timing plans in a cohesive manner. The advancement and deployment of telecommunication and ITS technologies make traffic and signal status data more readily available. These high-resolution data provide opportunities to allow closed-loop control systems to operate more adaptively and robustly to the changes in traffic demands and patterns. Recent research on the use of surrogate measures of safety to assess quality of various operational alternatives through micro-simulation has brought new perspectives to this field [1] . Several microscopic simulators are currently equipped to generate vehicular trajectory data that can be post-processed by the Surrogate Safety Assessment Model

(SSAM) to provide surrogate safety estimates [2]. Although the ability of micro-simulation tools to accuratly model safety aspects of traffic operations is still debated, the approach is gaining momentum and may result in further improvements to the fidelity of micro-simulation tools [3]. Also, estimating surrogate measures of safety is not necessarily equivalent to predicting accidents. Rather, it is a causal relationship similar to other conventional methods that estimate crashes [2].

The concept of optimizing signal timings to directly reduce safety metrics or their surrogate measures is not present in current signal timing optimization practice. Unlike metrics representing efficiency of traffic operations, commonly used signal timing optimization tools (such as Synchro, TRANSYT-7F, and PASSER) are not even equipped to evaluate impacts of signal timings on surrogate measures of safety. Although a recent study addressed impacts of signal timings on surrogate measures of safety, there are many related questions which remain unanswered [4].

This study essentially has two objectives, the first is to propose a novel approach to account for (surrogate) measures of safety when optimizing traffic signal timings on arterial intersections. This addresses a gap in the existing body of knowledge as no similar method has been documented in the literature. The second objective is to investigate the relationship between individual types of signal timings (cycle length, splits and offsets) and the total number of conflicts as estimated by SSAM. HSM (2010) clearly documents that such relationships are lacking.

2 Maximum and minimum green

Traffic demand at the intersection is critical in determining the number of timing plans needed and the actual timings of the phases. If the peak hour flows are significantly greater than off peak and weekend volumes, more than one timing plan should be considered and the maximum green times should be based on the volume splits.

The maximum green interval limits the time a phase can hold the green. When the signal is properly timed with appropriately short vehicle extensions, the maximum green interval will not consistently time out unless the intersection is significantly over capacity. The maximum green interval is typically determined based on a detailed capacity analysis of the intersection. With actuated operation, a maximum green interval of 1.25 to 1.5 times the maximum green time calculated by capacity analysis is generally desirable. This will allow the signal to better react to variations in traffic demand thereby maximizing the efficiency of signal operation. A maximum green interval that is set too low can significantly reduce the benefit of actuated operation. It should be noted that when a signal is running coordinated in a signal system, other considerations (cycle length) may take precedence in determining maximum green times.

The passage time or vehicle extension is the time required for a vehicle to travel from the detector to the stop bar or to the adjacent detector where multiple detection exists. The vehicle extension is also the time required to accommodate the gaps between vehicles. For maximum efficiency the vehicle extension should be set as short as practical to retain the green only as long as a real and consistent demand is present, but should not service vehicles straying behind. However, where detectors are located at some distance from the stop bar, the vehicle extension must be long enough to permit the vehicle to travel from the detector to the intersection without gapping out (See section on Vehicle Detection).

2 Traffic safety and traffic signal timings

When evaluating impacts of signal timings on road safety, the main focus is often on intergreen (yellow + all-red) times, while other signal timing parameters receive little attention.

The impact of intergreen on red-light running and dilemma zones is well documented [5]. However, very few studies have estimated the direct impact due to other signal timing parameters (such as cycle length, offsets, splits and phase sequence). One of the first such studies was conducted by Moore and Lowrie (1976), who investigated the impact of traffic signal coordination on number of traffic accidents in the field [6]. They compared the frequency of accidents from areas with and

without coordinated signals and estimated a 23% reduction in accidents following traffic signal coordination.

In practice, when signals are retimed, consultants usually apply a crash reduction factor to estimate the safety benefits of retiming. However, this approach is not very reliable because crash reduction rates may be based on a limited number of research studies[7]. Another study investigated, among other things, the impact of coordination of signalized intersections on the number of traffic crashes. The study was done for 170 signalized intersections in Florida. The results indicated that coordinated signals experience fewer crashes than isolated signals though the study did not address details of traffic progression between intersections [8]. Finally, the most recent research on safety evaluations of a traffic signal system represents an effort by Midenet et al. (2011) to investigate the exposure to lateral collisions at signalized intersections for two traffic control strategies [9]. The authors compared the timed exposure captured through video recordings from an intersection operating under both an adaptive real-time strategy called CRONOS and a time-plan strategy to vehicle-actuated ranges. The results showed that CRONOS reduced exposure to lateral collisions by roughly 5 min/h.

3 Surrogate measures of safety from microscopic simulations

One of the recent studies using a widely-available simulation model was conducted in 2002 by Drummond et al. when the authors found a high correlation between traffic efficiency performance measures (e.g. delays and stops) from simulation and field crash rates. A major breakthrough in research on surrogate measures of safety based on micro-simulation outputs was achieved when Gettman and Head (2003) developed functional requirements and algorithms for a software tool that analyzed surrogate measures of safety generated by a simulation model. This research led to development of publicly-available SSAM software a few years later [2].

Another recent study has furthermore investigated the impact of signal timings on surrogate safety measures using SSAM to evaluate simulated scenarios [4]. However, that study was performed within a framework limited by Synchro's inability to always find the best signal timings in VISSIM. Earlier studies have shown that when signal timings delivered by deterministic optimization tools are evaluated in stochastic environments their performances may not be optimal nor consistent. In addition, the goal of a Sabra et al. (2010) study was to conduct a sensitivity analysis and evaluate individual impacts of signal timings on surrogate safety measures rather than perform the optimization proposed in this study.

4 VISSIM–SSAM–VISGAOST framework

VISSIM is a microscopic, time step and behavior-based model developed to simulate urban traffic and public transport operations, while SSAM is a software application, sponsored by FHWA, that provides safety analysis for simulation-based comparative studies, and VISGAOST is an optimization program that optimizes signal timings of traffic controllers based on their performance in VISSIM microscopic simulation [2].

The program previously used for similar optimizations was modified to accommodate a new SSAM interface. The optimization process starts with VISGAOST generating an initial population of signal timings, which is seeded by the existing set of signal timings from the field. Each generated signal timing plan is evaluated in VISSIM, which generates both network-wide measures of effectiveness and trajectory data for each vehicle (where outputs are required for subsequent optimization steps).

The trajectory data file is processed by SSAM to identify the frequency, severity and types of conflicts [2]. In the next step the number of conflicts from SSAM is manipulated with some VISSIM performance measures to produce a meaningful objective function for ISGAOST optimization. This objective function is then minimized via the Genetic Algorithm iterative procedure by evaluating various combinations of signal timings from intersection controllers [10] . The whole process is then repeated until the predefined termination criterion is met (using a number of repetitions or convergence of solutions).

5 Acknowledgments

This work was supported by a grant from Transportation Scientific Research Project of Jiangsu Province, Jiangsu Provincial Communications Department (2013N02-3).

References

[1] Gettman, D., Head, L., 2003. Surrogate Safety Measures from Traffic Simulation Models. Report No. FHWA-RD-03-050, Federal Highway Administration, Washington, DC.
[2] Gettman, D., Pu, L., Sayed, T., Shelby, S., 2008. Surrogate Safety Assessment Model and Validation: Final Report. Report No. FHWA-HRT-08-051, Federal Highway Administration, Washington, DC. Goldberg, D.E., 1989. Genetic Algorithms in Search
[3] Archer, J., 2004. Methods for the Assessment and Prediction of Traffic Safety at Urban Intersections and their Application in Micro-simulation Modeling. PhD Thesis. Division of Transport and Logistics, Royal Institute of Technology (KTH), Stockholm, Sweden.
[4] Sabra, Z.A., Gettman, D., Henry R.D., Nallamothu, V., 2010. Balancing Safety and Capacity in an Adaptive Signal Control System – Phase 1. Report No. HRT-10-038, Federal Highway Administration, Washington, DC.
[5] Zimmerman, K.H., Bonneson, J.A., 2005. In-Service Evaluation of a Detection-Control System for High-Speed Signalized Intersections, Implementation Report No. 5-4022-01-1. Texas Transportation Institute, College Station, TX.
[6] Moore, S.E., Lowrie, P.R., 1976. Further on the effect of coordinated traffic signal systems on traffic accidents. In: Proc. of the 8th AARB Conference, vol. 8, No. 5, Session 26, pp. 10 – 15.
[7] Wong, S.C., Sze, N.N., Li, Y.C., 2007. Contributory factors to traffic crashes at signalized intersections in Hong Kong. Accident Analysis and Prevention 39,1107 – 1113.
[8] Guo, F., Wang, X., Abdel-Aty, M.A., 2010. Modeling signalized intersection safety with corridor-level spatial correlations. Accident Analysis and Prevention 42, 84 – 92.
[9] Midenet, S., Saunier, N., Boillot, F., 2011. Exposure to lateral collision in signalized intersections with protected left turn under different traffic control strategies. Accident Analysis and Prevention 43, 1968 – 1978.
[10] Stevanovic, A.Z., Martin, P.T., 2008. An assessment of the suitability of microsimulation as a tool for the evaluation of macroscopically optimized traffic signal timings. Journal of Transportation Engineering, ASCE 134 (2), 59-67.

Advanced Materials Research Vols. 989-994 (2014) pp 3919-3921
© (2014) Trans Tech Publications, Switzerland
doi:10.4028/www.scientific.net/AMR.989-994.3919

Research on the key technology of laser engraved image

Shaoqing Zhang[1, a], Dongmin Zhang[1, b], Quanhua Feng[1, c]

School of Mechanical Engineering, Shanghai Institute of Technology,Shanghai China

[a]Zhangshaoqing123@yeah.net, [b]dmzhang@sit.edu.cn, [c]946152050@163.com

Keywords : Laser engraving, Image processing, Process parameters.

Abstract. In 1960 the first ruby laser came out , after 40 years' development, laser engraving technology has been widely used in various areas. This paper describes the characteristics of laser engraving, the advantages and applications in industries and study images of laser engraving key technologies in-depth from image processing, laser engraving process parameters and clean carbide processing , and JK-2030 CO_2 laser engraving machines on paulownia color photos as examples for authentication, making laser engraving images more easily and efficiently .

Preface

Laser engraving is a new engraving technology , following the development of laser technology.Computer-controlled laser is a comprehensive application of computer technology, control technology and laser technology, the laser beam is focused on being irradiated surface sculpture, light energy transfer into heat energy , melting or vaporization instantly processed materials, the formation of holes, with the beam moving along a specific path, the photon interaction with the material, the material surface to form the final desired result kerf.[1-2]

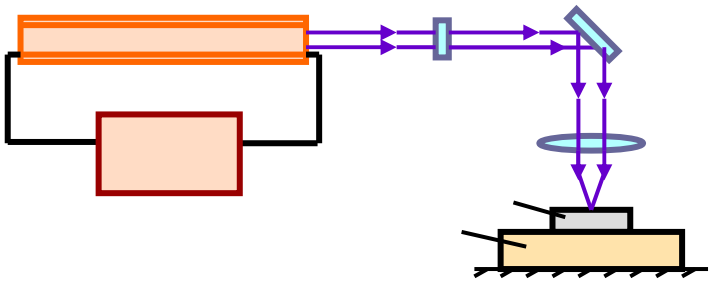

Fig. 1 The principle of laser engraving

Image processing is an important part of the laser engraving of the image, the image must be processed into that the laser engraving systems can identify the format. It's crucial in line with the characteristics of the laser engraving image processing methods, reasonable laser engraving process parameters.

Laser engraving characteristics and applications

Laser engraving characteristics

Laser has four major personalities : high brightness, high directivity, high pure, high coherence[2-5].Laser's personalities make laser engraving unique characteristics:

(1) non-contact processing, without special complex fixture, loss without tools, processing finished work without stress and deformation

(2) the minimum cut (CO_2 laser cutting slot < 0.5mm), improves the utilization rate of materials, material saving

(3) the accurate control, no inertia, high speed and in any position to start or stop processing

(4) the thermal deformation is small, the laser energy concentrated heat affected zone is very small, to prevent the heat diffusion of high speed machining.

Areas of laser engraving applications

In industry, lasers are used in four major processing areas:cutting,welding, marking and heat treatment. And laser carved of processing object also involves widely as organic board, cloth, paper, leather, rubber,various wood,intensive version, made bubble cotton, beauty resistance dish, glass, plastic, other non-metal,metal, ceramic, plastic,involves machinery industrial, steel industrial,ship industrial, car industrial, electronics,defense and people's life.

Study on the key technology of laser engraved image

Laser engraved image processing

An image is made up of red, green, and blue channels. According to the logarithmic relationship between white and black is divided into grades, image is divided into 256 levels of gray.Laser engraving is the density of points to reflect the outlines of pictures, a picture consistent with the characteristics of laser engraving gray image, higher resolution and clarity, better contrast ;

Fig.2 Raw image import software

(1)The original import Adobe Photo shop CS5 10.8MB pixel size, width 1456 pixels 2592 pixels high resolution 300 pixels/inch, click on the image-mode-gray(8 bits per channel) , initially gray, image pixels are calculated for 3.6MB at this time.

Fig. 3 Image gray preliminary processing

(2)Image bitmap output: 300 pixels/inch, halftone screen frequency 96 lines per inch, angle: 45 °, shape: round; output image pixel is important, characteristics of different materials is not set the parameters according to different materials and the results that you want to be, go through several tests, summarized the appropriate settings.

Fig. 4 Formation dotted gray bitmap processing

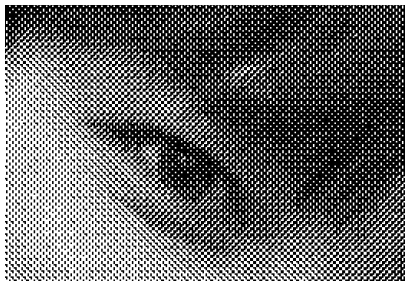

Fig.5 Local amplification effects

(3)Two times gray processing, according to the proportion of 1:1 output image, stored as *BMP format or JPEG format.

We can choose any bitmap as carved objects, but the laser itself condition is different, image processing parameter is different, finally carving effect will be very different[4]. Aiming at the character images, should pay attention to character outline clear process, characters and the background color and contrast, brightness.

Laser engraving technology

The performance of different materials, carving scheme adopted will be different. Engraving process parameters selection is the quality assurance of carving,there are many factors affect the quality of laser engraving, after repeated experiments, summarize the following points:

(1)Materials

Different materials absorb the energy different, lens together to the workpiece of laser energy can't all be absorbed.Thickness of carving, carving directions, materials, texture and other factors are taken into account.

(2)Laser ‘s output power

Laser’s output power and artifacts obtained by laser energy. When the focus is fixed on the workpiece surface, as the laser output power enhancement, carved by larger and deeper, carbonized black behavior occurs on the workpiece surface.

(3) The focal length focus on sculptured artifacts which form the shape of the pit depth has a major impact,.Engraving before experimenting prepare to determine the engraving effect, adjust the optimal focal distance to achieve the best engraving effect.

(4) Divergence angle of laser, engraving speed, exposure time, but due to the effect of carving power[2]

Professional engraving software Laser DRW will deal with image import, speed-carving speed: 180mm/s, carving the current: 14.2mA, carving area 90×90mm , engraving materials: 90mm paulownia in diameter wafers.

Fig. 6 Final carved effect

Cleaning the carbide processing

After engraving , use a damp cloth to clean the surface, charred parts available carbide surface oxidation and reduction of chemical materials and ultimately achieve bleaching effect, moderate concentrations of hydrogen peroxide.

Conclusion

Adoption of CO_2 laser carving on the paulownia color photo examples, discusses the key technologies of laser engraving the image. Expounded the principles and application of image processing technology, analysis of factors affecting the engraving effect, laser engraving and paulownia to find reasonable process parameter settings, provide technical support to ensure the quality of engraving is of great practical significance.

References

[1] Yuanji Tang,Laser Cutting In the Status of Industrial Application [J]. Laser & Optoelectronics Progress, 2002, 39(1): 53-56.

[2] JingZhao ,Wood Laser Engraving Technology, Beijing Forestry University, 2007.

[3] Xiaohua Tang , Honge Ren, Wood Molding Technology Laser Removal Method . Forestry Machinery & Woodworking Equipment, 2002, 30(7): 10-12.

[4] Jingfu Cai,and Fang Wen, and Qibin Liu, Image Processing Methods Conform to the Characteristics of Laser Engraving [J]. Computer Engineering and Design ,2009, 29(23): 6041-6043.

[5] Suqing Yang and Jiping Zhou, Laser Cutting Sheet Metal Key Technology [J]. Machinery Manufacturing and Automation2008, 36(6): 68-70.

Advanced Materials Research Vols. 989-994 (2014) pp 3922-3925
© (2014) Trans Tech Publications, Switzerland
doi:10.4028/www.scientific.net/AMR.989-994.3922

Study of PCM/FM Telemetry Sequence Soft Demodulation

Zhu Dongxu[1,a] , Fu Gang [1, a], and Feng Yue[1,a]

[1]China Satellite Maritime Tracking and Control Department, China
[a]348237548@sina.com

Keywords: synchronous, PCM/FM, MSD

Abstract. In order to improve the performance of PCM/FM signal demodulation system, this paper studies a kind of Symbol Detection more (Multi-Symbol Detection, MSD) technology. First for PCM/FM in hardware demodulation, a series of problems in the introduction of MSD software demodulation method; Then the MSD demodulation under low SNR synchronous implementation; The algorithm simulation, the results show that the bit error rate of 10^{-4}, detection performance than traditional non-coherent frequency discrimination algorithm can improve the nearly 3 dB, the performance is very ideal.

Introduction

With the rapid development of space technology, PCM/FM system get extensive application in the field of space remote sensing. In reference [1] proposed a method of using digital frequency demodulation realization of PCM/FM intermediate frequency signal demodulation, this demodulation method is helpful to reduce the error rate of signal demodulation, suitable for multi-stage assembly line's handling of the hardware, software radio processing platform is the most familiar demodulation method. And the use of software to realize signal processing has become the development trend of signal processing in the future.

The traditional discriminator is demodulation and detection for each symbol. For software demodulation, [2-3] and mentioned in the literature [4] using the short-time Fourier transform and instantaneous frequency measurement method for FM frequency estimation, thus the demodulating baseband signal. By further testing, short time Fourier transform method to the detection threshold improvement of bit error rate of 10^{-5} less than 3 dB, the instantaneous frequency measurement method when the signal-to-noise ratio is lower than 20 dB cannot achieve normal demodulation. This article in view of the traditional PCM/FM signal at low SNR is difficult to realize effective demodulation, symbol between before and after the combination of PCM/FM signal phase, the characteristics of the memory research a kind of method of demodulation and synchronization based on MSD.

1 The maximum likelihood algorithm of MSD

X for sending signals from the corresponding vector, r (t) for receiving signals, y for the receiver to receive signals of the verdict. Because of the symbol and noise are independent of each other, so are:

$$\begin{aligned} p(x/r(t)) &= p((x_1,x_2,\cdots,x_n)sent/(r_1,r_2,\cdots,r_n),n_r(t)) \\ &= \frac{p((x_1,x_2,\cdots,x_n)sent,(r_1,r_2,\cdots,r_n),n_r(t))}{p((r_1,r_2,\cdots,r_n),n_r(t))} \\ &= \frac{p((x_1,x_2,\cdots,x_n)sent,(r_1,r_2,\cdots,r_n))p(n_r(t))}{p((r_1,r_2,\cdots,r_n))p(n_r(t))} \\ &= p((x_1,x_2,\cdots,x_n)sent/(r_1,r_2,\cdots,r_n)) \\ &= p(x/r) \end{aligned} \quad (1)$$

Based on maximum a posteriori probability (MAP) criterion, observations of N symbols received conditional probability of r(t) are as follows:

$$p(r(t)/s(t),\theta)=\frac{1}{\sqrt{2\pi N_0}}\exp\{-\frac{1}{N_0}\int_{(n-N+1)T}^{(n+1)T}\left|r(t)-s(t)e^{j\theta}\right|^2 dt\} \quad (2)$$

To further simplify the above formula is:

$$p(r(t)/s(t),\theta)=Fe^{-NA^2T/N_0}\exp\{-\frac{1}{N_0}\int_{(n-N+1)T}^{(n+1)T}\left|r(t)\right|^2 dt\}\exp\{-\frac{2A}{N_0}\left|\beta\right|\cos(\xi-\arg\beta)\} \quad (3)$$

$$\beta=\int_{(n-N+1)T}^{(n-N+2)T}(r(t)e^{-j2\pi ha_{n-N+1}q(t-(n-N+1)T)})dt+e^{-j\pi ha_{n-N+1}}\times\int_{(n-N+2)T}^{(n-N+3)T}(r(t)e^{-j2\pi ha_{n-N+2}q(t-(n-N+2)T)})dt$$

$$+...+(\prod_{i=n-N+1}^{n-1}e^{-j\pi ha_i})\times\int_{nT}^{(n+1)T}(r(t)e^{-j2\pi ha_n q(t-nT)})dt \quad (4)$$

More symbol detection is to find the corresponding order, has absolute maximum likelihood. Detection algorithm is derived according to the many symbols, its implementation is shown in figure 1.

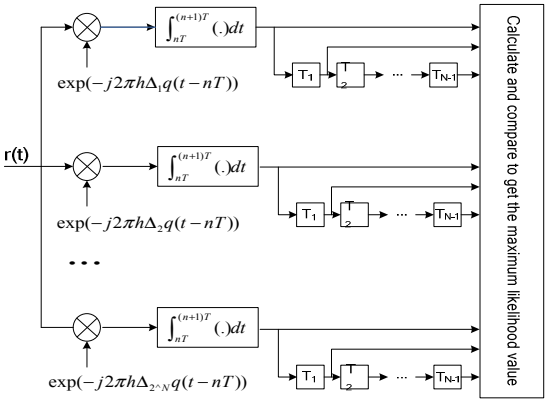

Fig1 Multiple symbol detection algorithm implementation block diagram

Further formula for computing the likelihood value is:

$$T_i=\sum_{n=1}^{N}\Gamma_{i_{n,N-n}}C_n \quad , \quad C_1=1 \quad , \quad C_k=\exp(-j\pi h\sum_{l=1}^{k-1}\Delta_{i_l})$$

2 Algorithm implementation process

Phase state transition diagram of PCM/FM signal can be expressed with grid, binary to the modulation index is equal to 0.5 PCM/FM signal, for example, the state grid as shown in figure 2, the abscissa for time, ordinate with phase.

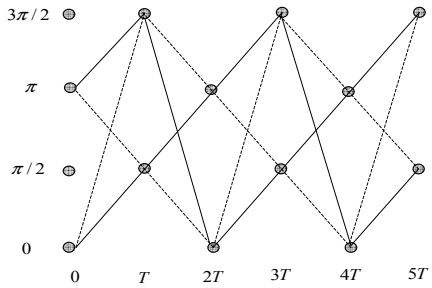

Fig2 h = 0.5 of PCM/FM signal phase grid figure

1, the t = 0 point set each state path metric is zero, the initial state is zero.

2, calculate all reach the measurement of the path. T = 3 t moment in figure 2, for example, a phase state of t = 3 t time for $s_3^{\pi/2}$, calculated from the time t = 0 to t = 3T time all reach the measurement of the path, a one-time completion of all of the metrics calculation, $s_1^{\pi/2}/s_0^0+s_2^0/s_1^{\pi/2}+s_3^{\pi/2}/s_2^0$, $s_1^{\pi/2}/s_0^0+s_2^{\pi}/s_1^{\pi/2}+s_3^{\pi/2}/s_2^{\pi}$, $s_1^{3\pi/2}/s_0^0+s_2^{\pi}/s_1^{3\pi/2}+s_3^{\pi/2}/s_2^{\pi}$, $s_1^{3\pi/2}/s_0^0+s_2^0/s_1^{3\pi/2}+s_3^{\pi/2}/s_2^0$.

3, screening and save the best path. Comparison in the previous step all reach the path measurement, the size of the selected measure minimum path, and save the path.
4, demodulation data obtained. To step on the best path to back the path through the element of $[x_{n-N},\cdots,x_{n-1},x_n]$, namely for the demodulation of the data.

3 Synchronization demodulation

Need to know the two symmetric points on either side of the maximum likelihood, can approximate a maximum likelihood to estimate the value of the frequency corresponding to the doppler frequency offset, and then to modify the signal carrier frequency, so as to eliminate the doppler frequency offset the impact on the decision. Figure 3 is a design using the curve fitting of the block diagram of corresponding frequency synchronization algorithm.

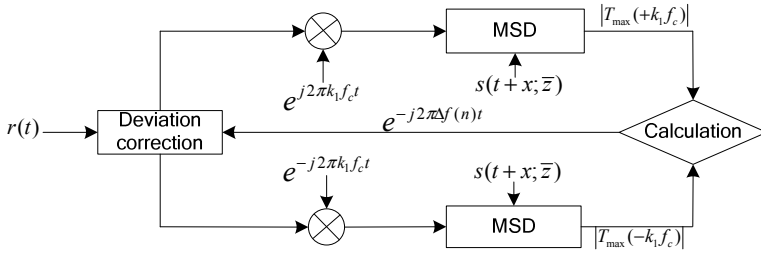

Fig3 Based on the MSD deviation compensation principle diagram

For after lifting the frequency of two-way signal to MSD after calculation, the two way likelihood value expressions for:

$$T_{\max}(\Delta f-\Delta f(n)+k_1f_c)=\max\{\int_0^{NT} r(t)e^{-j2\pi\Delta f(n)t}e^{j2\pi k_1f_ct}s(t+x;\bar{z})dt\}$$

$$T_{\max}(\Delta f-\Delta f(n)-k_1f_c)=\max\{\int_0^{NT} r(t)e^{-j2\pi\Delta f(n)t}e^{-j2\pi k_1f_ct}s(t+x;\bar{z})dt\}$$

The two likelihood value difference, is the measuring receiver frequency offset error metrics, and can feedback loop frequency deviation, the deviation correction to correct ring. Update deviation:

$$\Delta f(n+1)=\Delta f(n)-\frac{e(n)}{|e(n)|}\lambda$$

$$e(n)=T_{\max}(\Delta f-\Delta f(n)+k_1f_c)-T_{\max}(\Delta f-\Delta f(n)-k_1f_c)$$

4 Algorithm performance.

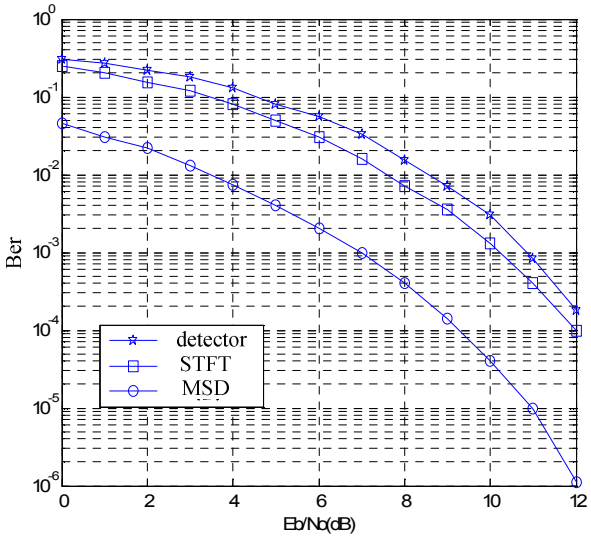

Fig4 Ber curve comparison diagram

Can be seen from the figure 4, the best method of MSD of demodulation, the bit error rate of 10^{-4}, compared to the noncoherent frequency demodulation can get about 3 db channel gain, performance is very ideal.

Summary

Study a relatively new FM signal demodulation technology, namely the MSD algorithm and the corresponding synchronization technology. Test results show that this method is illustrated in the aspect of improving channel gain performance advantages, make up for the low SNR telemetry signal demodulation error rate is higher, the shortcomings of traditional method of demodulation threshold and breakthrough. With the continuous development of software technology, PCM/FM software demodulation method based on MSD will have broad prospect of application.

References

[1] Zheng Ligang. PCM/FM telemetry digital intermediate frequency receiver design and implementation[J]. signal processing, 2004,20(2):122-126.
[2] Li Qiu-na,Yuan Si-jie,Zhang Lanying. Method of Demodulation for PCM/FM Signal Based on Virtual Radio[J]. JOURNAL OF SYSTEM SIMULATION. 2007.19(7):1617-1619.
[3] Liu Donghua. PCM/FM signal differential demodulation software research[J]. Equipment command technical college journals.2005,16(3):91-94.
[4] Liu Donghua, Wang Yuanqin etal. Research on Method of Demodulation for PCM/FM Signal Based on Instantaneous Frequency Measurement[J]. JOURNAL OF SYSTEM SIMULATION. 2005,17(10):2463-2466.

Advanced Materials Research Vols. 989-994 (2014) pp 3926-3929
© (2014) Trans Tech Publications, Switzerland
doi:10.4028/www.scientific.net/AMR.989-994.3926

Study of Reentry Telemetry Signal in The Environment of Soft Demodulation

Fu Gang[1,a], Tao Min[1, a], and He Qian[1,a]
[1]China Satellite Maritime Tracking and Control Department, China
[a]348237548@sina.com

Keywords: Reentry Telemetry, PCM/FM, Soft Demodulation

Abstract. PCM/FM system is one of the most widely used in the rocket telemetry system. Target spacecraft reentry telemetry telemetry signals in the process of low signal noise ratio (SNR), that the breakthrough tradition demodulation method of demodulation threshold problem, combined with the PCM/FM signal phase characteristic, the research based on a baseband complex rotating orthogonal symbol detection software (MSD) to solve method, and the corresponding synchronization algorithm is applied to ensure the smooth operation of the demodulation. The simulation and test results verified the soft demodulation algorithm can make the demodulation threshold effectively reduce.

Introduction

Remote sensing has a special channel is in the process of reentry telemetry channel, when the target aircraft on reentry telemetry channel, there are two main obstacles, namely again into the blackout and multipath effect. [1]Reentry black barrier is the main problem that bring on the aircraft surface to form certain thickness of the ionosphere, hinder the spread of the signal, the signal-to-noise ratio drops rapidly. And multipath effect, meaning that the channel is time-varying channel in the whole process of reentry telemetry from the sky to the ground, the channel parameters changed dramatically over time, the frequency spectrum of the received signal component will be subject to the influence of different gain level and nonlinear phase shift, that cause the receiving signal phase's serious distortion, bit error rate increased.

Above problem for PCM/FM telemetry signal demodulation method is selected to bring certain problems: in the low signal noise ratio (SNR), and complete normal demodulation signal distortion. This paper studies a demodulation method based on orthogonal complex baseband rotating MSD for PCM/FM telemetry signals under the environment of reentry telemetry demodulation. Similar to ordinary MSD, compared to the traditional non-coherent frequency demodulation method, to raise the channel gain nearly 3 dB[2], greatly reduces the threshold of PCM/FM telemetry signal demodulation. The simulation and test results verified the reentry telemetry channel environment effectiveness of the method.

1 Channel Model

In reentry telemetry channel, because the influence factors, such as multipath and platform of relative movement makes the mobile channel to transmit the signal in time, frequency and Angle caused the dispersion, so the multipath channel envelope statistical properties become the focus of our research. According to the statistical properties of different fading channel, the received signal envelope and several typical distributed generally, such as Rayleigh distribution, Rice distribution and the Nakagami -m distribution. In this paper, in accordance with Rayleigh distribution as a background for the multipath channel simulation.

Discrete multipath fading channel model is:[3]

$$R(t) = \sum_{k=1}^{N(t)} r_k(t) s_{FM}(t - \tau_k) \tag{1}$$

In order to show the multipath effect on telemetry signals, the Rayleigh channel characteristics, and through the Rayleigh channel of PCM/FM signal time-frequency characteristics of MATLAB

as shown in figure 1. Simulation conditions: the decline of path set to 6, intermediate frequency 70 MHz PCM/FM signal, code rate 2 Mbps, sampling rate and 56MSPS installed base, modulation index was 0.7.

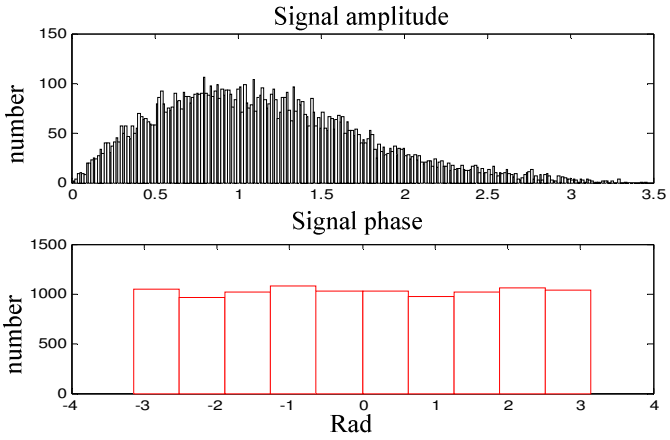

Fig1 Signal under the effect of Rayleigh channel amplitude and phase distribution

From figure 1, you can see, the received signal envelope obey Rayleigh distribution, phase in (0 ~ 2π) obey uniform distribution.Which conform to the Rayleigh distribution channel model.

2 Baseband complex rotating orthogonal MSD algorithm

Set the remote sensing observation period received can simplify the intermediate frequency signal is expressed as:

$$s(t)=\cos[w_c+f(t)+\theta_1] \tag{2}$$

Using the orthogonal digital frequency conversion technology to deal with $s(t)$, the received signal with local orthogonal carrier multiplication, respectively after the Hilbert transform of two orthogonal baseband signals (I/Q) :

$$I=\cos[f(t)+\theta_1] \tag{3}$$

$$Q=-\sin[f(t)+\theta_1] \tag{4}$$

When a local element combination and the received signal element phase at the same time, after two baseband signal resulting from the multiplication form of complex signals in the observation time remain the same. And when local other element combination of baseband after signal and the received after signal multiplication, the complex signals always changing.

According to the code rate and sampling rate can be observed within the length of the sampling points, set to N_C, the result of the product in integral operation, within the length of observation are:

$$M=N_C\cdot I_B+jN_C\cdot Q_B \tag{5}$$

Results modulus square, get:

$$S=N_C{}^2\cdot(I_B{}^2+Q_B{}^2) \tag{6}$$

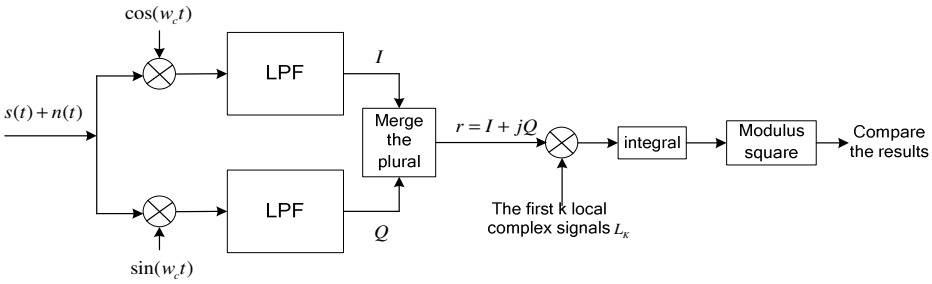

Fig2 Baseband orthogonal MSD principle block diagram

In figure 3 is only part of the local element corresponding to a group of complex signal and receiving orthogonal complex baseband signal block diagram of the baseband orthogonal MSD

decision, other local signal and received signal processing is similar, all is through relevant square to compare the result of the decision.

This more than symbols of orthogonal complex baseband signal detection, because of the baseband signal frequency is low, so the requirements of the processing speed is low, is advantageous to the computer software processing. But in terms of computational burden, there is still no fell, the intermediate frequency more casual and symbol detection algorithm is basically the same. So on this basis, the introduction of the complex spinning technology, namely the integral in a bit, then through after the way to realize the symbol detection, thus reduce the amount of calculation.

In a row in table 1 code sequences, on both sides of the two values are said to be on the current element before and after the disturbance of two element. Through the above analysis, the local can generate the initial phase element corresponding to the baseband signal $L_1, L_2, \cdots, L_8$. The 8 kinds of signal is the difference between the length of time is only one element width, and the eight kind of signal is a baseband modulation signal. A similar method respectively to the current received orthogonal complex baseband signal correlation processing in a symbolic, get eight plural $M_{10}(1), M_{20}(1), \cdots, M_{80}(1)$.

Table 1 Element combination and the corresponding phase

number	(1)	(2)	(3)	(4)
symbol sequence	-1 -1 -1	-1 -1 +1	+1 -1 -1	+1 -1 +1
corresponding phase	-0.7π	-0.58π	-0.58π	-0.47π
number	(5)	(6)	(7)	(8)
symbol sequence	+1 +1 +1	+1 +1 -1	-1 +1 +1	-1 +1 -1
corresponding phase	0.7π	0.58π	0.58π	0.47π

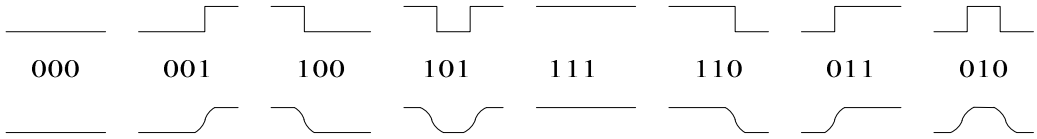

Fig3 Preset filter before and after eight possible code waveform comparison

Assume element observation length N = 5, 128 in observation length can be the local signal, and because the local signal phase change in the length of 5 yards yuan continuity, calculate the local 128 signals of each within the first four element length of the initial phase of local signal, can calculate the L_1 to L_8 may be the initial phase of the 8 kinds of local signal. Eight of the plural by allowing for $M_{10}(1)$ to $M_{80}(1)$ accordingly plural Angle rotation, get eight different symbol waveform corresponding to different initial phase values of local signal associated with the current signals as a result, $M_{11}(1), \cdots, M_{1p}(1), M_{21}(1), \cdots, M_{2p}(1), M_{81}(1), \cdots, M_{8p}(1)$.

According to the current element time of various local corresponding correlation matching value of the received signal waveform and $M_{10}(1)$ and $M_{80}(1)$ and before 4 yards yuan period have different code to local waveform and the initial phase of the correlation value between the received signal $M_{10}(k), \cdots, M_{1p}(k), M_{20}(k), \cdots, M_{2p}(k), M_{80}(k), \cdots, M_{8p}(k)$ $(k = 2,3,4,5)$ .Out of the 128 possible, recent five yards yuan period of approximate correlation value. Both before and after, for example, consider the symbol sequence element, the influence of length, we assume that the observation of element within the local signal sequence is -1+1+1-1-1-1+1 (the last but one to the current element), rotating through compounding technology and accumulation process, will be able to get this kind of circumstance the five element was used to observe the relative value in the length, expressed as:

$$M_n = M_{7a}(5) + M_{6a}(4) + M_{3c}(3) + M_{1d}(2) + M_{20}(1) \tag{10}$$

Among them a, b, c, d values range from 1 to P. Then to receive signal and local signal to calculate the complex signal, a total of 128 square arithmetic, then compare the verdict, get the final demodulation element.

3 Simulation result

In the baseband after rotating orthogonal MSD demodulation process on the basis of overall study, the following will be under the reentry telemetry channel environment, the parameters in the simulation according to the telemetry standard manual produce PCM/FM telemetry signals, using normalized SNR E_b/N_0 as main parameters, analysis of the BER and MSD demodulation and statistics, in the end, and then with traditional non-coherent frequency demodulation method[4] and short-time Fourier method demodulation performance comparison, the result is shown in figure 4.

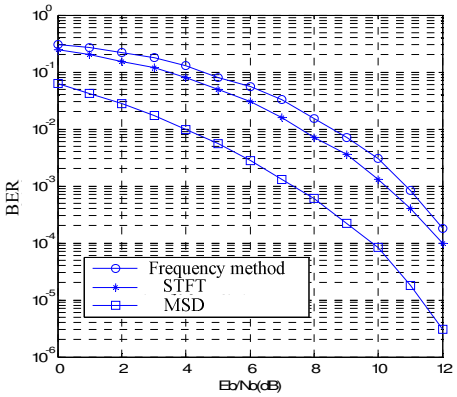

Fig4 Ber curve comparison chart

Can be seen from figure 4, MSD demodulation method of ber performance is much better than that of short time Fourier method and the traditional non-coherent frequency demodulation method. Compared to the traditional non-coherent frequency discrimination method, baseband complex rotating orthogonal MSD method can get the channel gain of about 2.4 dB.

Summary

Study a baseband complex rotating orthogonal MSD algorithm: first, the intermediate frequency PCM/FM signal under the digital frequency conversion processing, get the same phase and orthogonal subgrade with two orthogonal signal, again to two orthogonal signals in an integral element, and then through the complex spinning technology to compare with the size of integral value of the local signal to realize signal demodulation. Based on the MATLAB language to realize the demodulation system, under the environment of reentry telemetry channel, according to the telemetry standards manual test the simulation signal and the demodulation system. Test results show that this method can effectively solve the reentry telemetry environment SNR break the traditional problem of demodulation method of threshold. The reentry remote sensing signal demodulation has a certain reference significance.

References

[1] Huang Qiang. Waiting for receiving near-earth decline model of reentry telemetry channel[J]. Chinese Journal of Radio Science, 2007, 22(1): 53-58.
[2] Xu Xingyuan. Shipborne tt&c equipment based on MSD technology research rocket telemetry demodulation method[J]. Telemetry and Telecontrol, 2009, 30(5): 64-67.
[3] Tan Lixin. The statistical features of multipath fading channel and simulation research. [J]. Computer Simulation, 2010, 27(7): 96-99.
[4] Liu Donghua. Based on instantaneous frequency measurement of PCM/FM signal demodulation method research[J]. JOURNAL OF SYSTEM SIMULATION, 2005, 17(10): 2463-2466.

Advanced Materials Research Vols. 989-994 (2014) pp 3930-3933
© (2014) Trans Tech Publications, Switzerland
doi:10.4028/www.scientific.net/AMR.989-994.3930

Research on Continuous Phase FM Signal Demodulation based on STFT

Feng Yue[1,a], Fu Gang[1, a], Li Renlong[1,a] and Liping Wang[2,b]

[1]China Satellite Maritime Tracking and Control Department, China

[2]School of Computer Science, Engineering and Mathematics, Flinders University, South Australia 5042, Australia

[a]348237548@sina.com, [b]wlp2005518@gmail.com

Keywords: Virtual Radio, PCM/FM, STFT

Abstract. According to the characteristics of PCM / FM signals, we propose a new method based on STFT resolve tune software. Firstly, the spectral characteristics of PCM / FM signal is given use of the spectrum PCM / FM signal is demodulated theoretical basis. This paper discusses in detail the basic principles of this demodulation method and implementation process, analyze the demodulation performance and complexity of the method.

Introduction

PCM / FM signal is the current data transmission system is widely used as a signal type. Since the actual received PCM / FM signals and more non-stationary random signal, non-stationary random signal processing usually time-frequency analysis method. [1][2] proposed STFT and WD-based FM signal demodulation method has strong anti-noise and anti-fading, but the larger amount of computation, is not conducive to the realization of real-time processing software. With the continuous improvement of the performance of general-purpose computing, software-based radios (Software Define Radio-SDR) technology, signal processing modes are gradually departing from the dedicated hardware platforms (such as DSP or FPGA), digital signal A / D after the general-purpose computer on the platform, the signal "pure software" of the real-time processing by the application.

1 PCM / FM signal spectral characterization

PCM / FM telemetry signal field called continuous phase frequency shift keying (CPFSK) signal, the modulation method is the use of high frequency carrier moves to the first symbol representing a binary "1" state, moved to the second lower represents the frequency of the carrier wave binary symbol "0" state. Therefore, PCM / FM signals within one symbol can be regarded as the width of a single sinusoidal carrier frequency signals, by alternating two different carrier frequencies, digital data "0" "1" and transmission.

In a code width PCM / FM signal may be expressed as:

$$x(n) = A\exp[\ j(2\pi f_i n + \varphi)] + z(n) \qquad (n = 0,1,\cdots,N_w - 1) \tag{1}$$

And can be expressed as the formula $X = A_c E + Z$.

Among them,

$$\begin{cases} X = [x(0) \quad x(1) \quad \cdots \quad x(N_w - 1)]^T \\ E = [\quad 1 \quad e^{j2\pi f_i} \cdots \quad e^{j(N_w-1)2\pi f_i}\ ]^T \\ Z = [z(0) \quad z(1) \quad \cdots \quad z(N_w - 1)]^T \end{cases} \tag{2}$$

$$A_c = A\exp(j\varphi)$$

X signal A_c is obtained by the maximum likelihood (MLE) is estimated:

$$\hat{A}_c = \frac{E^H R_z^{-1} X}{E^H R_z^{-1} E} \tag{3}$$

And this estimate is unbiased.

$R_z = \sigma^2 I$ substituted into the formula (3) we have:

$$\hat{A}_c = \frac{E^H X}{E^H E} = \frac{1}{N_w} \sum_{n=0}^{N_w-1} x(n) e^{-j2\pi f_i n} \tag{4}$$

$\hat{A}_c$ is the amplitude of the signal amplitude A Unbiased MLE estimates.

$$A = \left| \hat{A}_c \right| = \frac{E^H X}{E^H E} = \frac{1}{N_w} \left| \sum_{n=0}^{N_w-1} x(n) e^{-j2\pi f_i n} \right| \tag{5}$$

So calculate the amplitude X signal f_0 / f_s, and f_1 / f_s as follows:

$$\begin{cases} a = \left| \dfrac{1}{N_w} \displaystyle\sum_{n=0}^{N_w-1} x(n) e^{-j2\pi (f_0 / f_s) n} \right| \\ b = \left| \dfrac{1}{N_w} \displaystyle\sum_{n=0}^{N_w-1} x(n) e^{-j2\pi (f_1 / f_s) n} \right| \end{cases} \tag{6}$$

In summary, according to the spectral characteristics of PCM / FM signal, the DFT method can be used by comparing the size of the amplitude of two frequency and demodulate the PCM / FM signal.

2 STFT demodulation method

Under the actual circumstances of the received PCM / FM signal is non-stationary random signal, the amplitude of DFT calculations cannot be used directly in a signal frequency point. Using short-time Fourier transform (STFT) method, the use of relatively narrow width of the window function for the interception of a time-domain signal, the signal thus obtained can be regarded as stable, and then the DFT. If you let the window function along the time axis signal continuously moving, you can get PCM / FM signals in two frequency energy over time, the process of change. PCM / FM signal using the signal frequency changes the transmission of digital information, you can compare the two by size variation frequency energy to achieve the demodulated signal. The length of the time window within the sampling points should be close to a symbol, it is a good frequency energy accumulation, improving the performance of signal demodulation.

$x(n)(n = 0,1,\cdots, N-1)$ DFT is defined as:

$$X(k) = \sum_{n=0}^{N-1} x(n) e^{-j\frac{2\pi}{N} nk} \qquad (\text{k=0,1,….N-1}) \tag{7}$$

The classic definition of DFT only an integer k, and if the test frequency does not correspond to integer values of k can be obtained from the amplitude of the frequency on the nearest integer k, which is the measured frequency energy Sinc function is not a peak, but rather a value near the peak, which affects the demodulation performance. To obtain the peak Sinc function, k is used when the DFT fraction, which corresponds to the first windowed taken after zero padding data, and then make DFT, which is equivalent to the interpolation in the frequency domain or the frequency domain is reduced when the discrete sampling interval.

$$x'(n) = \begin{cases} x(n), & n = 0,1,\ldots N-1 \\ 0, & n = N, N+1,\ldots rN-1 \end{cases} \tag{8}$$

$$X'(k) = \sum_{n=0}^{rN-1} x'(n) e^{-j\frac{2\pi}{rN} nk} = \sum_{n=0}^{N-1} x(n) e^{-j\frac{2\pi k}{N r} n} \tag{9}$$

Because of the increased sample values is zero, so does not greatly increase the amount of calculation. Calculation of energy and only a single frequency, greatly reducing the amount of calculation STFT. At this frequency is calculated by STFT energy by the formula f_i:

$$STFT_x(n, k_i) = \sum_{M=0}^{M-1} \tilde{x}(m, n) e^{-j\frac{2\pi}{M} k_i m} \qquad (k_i = M * f_i / f_s) \tag{10}$$

Among, $M = rN$, $\tilde{x}(m,n) = x(m) \cdot W(n-m)$.

Thus, a sequence of length N can be decomposed into operation DSTFT 1×N data vector with N×1 rotation coefficient vector, a calculation amount for the N complex multiplications, (N-1) complex additions. To further reduce the amount of computation processing can be used for the rectangular window DSTFT recursion method, see the derivation of equation (11). When the next DSTFT, you can use the results of the previous conduct DSTFT, greatly reducing the amount of computation. During the sliding of the rectangular window, for each quantitative calculation DSTFT 2 complex multiplications and two complex additions.

$$
\begin{aligned}
&DSTFT(n+1,\omega) = \sum_{m=0}^{M-1} x(n+1+m)e^{-j\omega m} \\
&= \sum_{m=1}^{M} x(n+m)e^{-j\omega(m-1)} \\
&= e^{j\omega}\sum_{m=1}^{M-1} x(n+m)e^{-j\omega m} + x(n+M)e^{-j\omega(M-1)} \\
&= e^{j\omega}\left(\sum_{m=0}^{M-1} x(n+m)e^{-j\omega m} - x(n)e^{-j0}\right) + x(n+M)e^{-j\omega(M-1)} \\
&= e^{j\omega}[STFT(n,\omega) - x(n)] + x(n+M)e^{-j\omega(M-1)}
\end{aligned}
$$

3 Algorithm performance.

Spectral energy calculated by STFT 0,1 frequency signal is:

$$
\begin{aligned}
a^2 &= \left| A\sum_{n=0}^{N_w-1} e^{j[2\pi(f_0/f_s)n+\varphi]} \cdot e^{-j2\pi(f_0/f_s)n} \right|^2 \\
&= \left| AN_w e^{j\varphi} \right|^2 = A^2 \cdot {N_w}^2 \qquad (11)
\end{aligned}
$$

$$
b^2 = \left| A\sum_{n=0}^{N_w-1} e^{j[2\pi(f_0/f_s)n+\varphi]} \cdot e^{-j2\pi(f_1/f_s)n} \right|^2 \qquad (12)
$$

$$
\Delta f = (f_1 - f_0)/f_s = 2K_{FM} \times R_b / f_s \qquad b^2 = A^2 \cdot \left| \frac{1-e^{j2\pi N_w \Delta f}}{1-e^{j2\pi\Delta f}} \right|^2 = A^2 \cdot \frac{1-\cos 2\pi N_w \Delta f}{1-\cos 2\pi\Delta f}
$$

$$
\rho_0 = \frac{b^2}{a^2} = \frac{1-\cos 2\pi N_w \Delta f}{{N_w}^2(1-\cos 2\pi\Delta f)} = \frac{\sin^2 N_w \dfrac{\Delta\omega}{2}}{{N_w}^2 \sin^2 \dfrac{\Delta\omega}{2}} \qquad (13)
$$

The relationship between ρ_0 and $\Delta\omega$ shown in Figure 1.

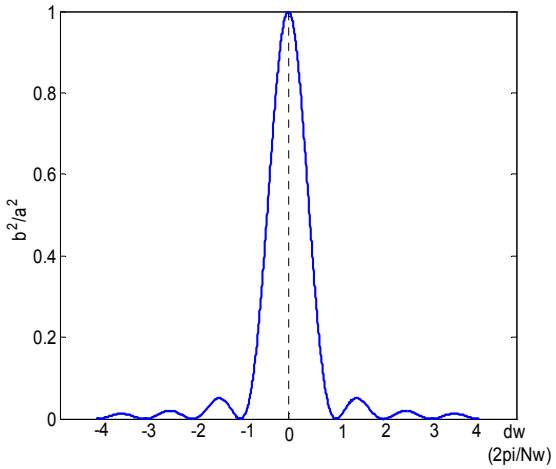

Fig 1 The relationship between ρ_0 and $\Delta\omega$

The relationship between ρ_1 and $\Delta\omega$ shown in Figure 2.

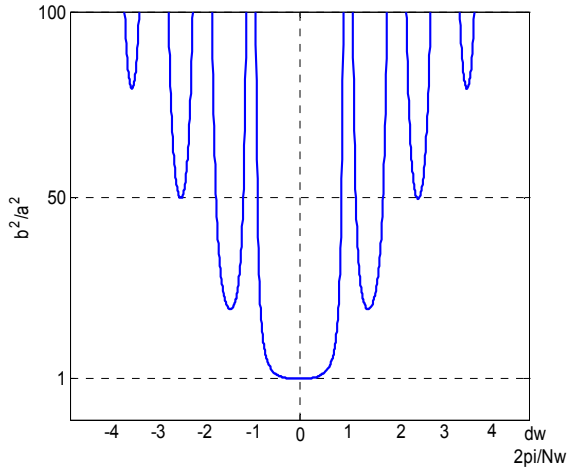

Fig 2 The relationship between ρ_1 and $\Delta\omega$

It can be seen that when the constant frequency offset PCM / FM signals, a method using STFT demodulating the best performance.

Summary

By comparing the two changes in the size and frequency energy law, the realization of the demodulated signal. Through the truncated data zeros ways to improve the impact of the barrier effect STFT window function brings the calculation frequency energy.

References

[1] Vanu Bose, Micha Isment, Matt Wellborn and John Guttag. Virtual Radio[J]. IEEE. select. Area Commun.17 (4).2009, 4.
[2] Vanu G B. Design and implementation of software radios using a general purpose processor[D]. Massachusettes: Massachusettes Inst Technol,2010.

Advanced Materials Research Vols. 989-994 (2014) pp 3934-3937
© (2014) Trans Tech Publications, Switzerland
doi:10.4028/www.scientific.net/AMR.989-994.3934

An adaptive filtering method for Chirp signal based on FRFT

Wu Yanjun[1, a], Fu Gang[1,a] and Cheng Gang[1,a]

[1]China Satellite Maritime Tracking and Control Department, China

[a]348237548@sina.com

Keywords: Chirp signal, FRFT, adaptive filter

Abstract. In this paper, an adaptive filter method for Chirp signal in additional white Gaussian noise (AWGN) is studied. First, we analyze conception and character of FRFT (Fractional Fourier Transform), and the results shows that Chirp signal has energy concentration character in FRFT domain. Then, an adaptive filtering method is introduced in FRFT domain, and a test is done for separating Chirp signal from AWGN by the filtering method. Last, performance of this filtering method is studied, and the SNR improvement expression is concluded to verifying its advantages, it depends on the performance of adaptive filter basically. At last, the results show that this filtering algorithm is simple in computation and easy in implementation.

Introduction

Chirp signal is a kind of non-stationary signal, it is applied in radar, sonar and communications widely. Hereby, it is important works to process Chirp signal in modern signal processing, where the shoe pinches is to rebuild Chirp signal from the polluted signal by noise, this problem can be concluded as the polluted signal filtering or wave form estimation essentially. We can use spectral line enhancement technique to improve SNR of sinusoid signal in AWGN, and the key part of this technique is adaptive filter.

Recent years, Fractional Fourier transform (FRFT) gained a lot of attention as a new time-frequency transform tool. It is put forward by V.Namias [1] and applied in non-stationary signal processing area. FRFT represents time-frequency distribution of a signal with a single variable and has no cross-term problem; hence, it is much well suitable to process non-stationary signal especially chirp-like signals. Some scholars proposed time-frequency filtering based on FRFT during the past years [2], and the FRFT domain filtering algorithm was ulterior consummated subsequently[3]. In this paper, an adaptive time-frequency filtering algorithm of Chirp signal based on FRFT is proposed to restrain noise.

1 Fractional Fourier transform

FRFT is generalization of Fourier transform (FT) with an order, and it is a one-parameter subclass of linear transform. The FRFT of $x(t)$ is defined as

$$X_p(u)=\left\{\mathcal{F}^p[x(t)]\right\}(u)=\int_{-\infty}^{+\infty}K_p(u,t)x(t)dt,\quad 0<|p|<2,0<|\alpha|<\pi$$
$$=\begin{cases}B_\alpha\int_{-\infty}^{+\infty}\exp\left(j\dfrac{t^2+u^2}{2}\cot\alpha-\dfrac{jtu}{\sin\alpha}\right)x(t)dt, & \alpha\neq n\pi\\ x(t) & \alpha=2n\pi\\ x(-t) & \alpha=(2n\pm1)\pi\end{cases}\tag{1}$$

Where $\mathcal{F}^p[.]$, $K_p(u,t)$, p, u and $\alpha=p\pi/2$ are the FRFT operator, kernel function, FRFT order, FRFT domain and rotation angle respectively, and coefficient $B_\alpha=\sqrt{(1-j\cot\alpha)\pi/2}$.

According to formula (1), we can easily know that the inverse FRFT can be defined as

$$x(t)=\mathcal{F}_{-p}[X_p(u)](t)=\int_{-\infty}^{+\infty}X_p(u)K_{-p}(t,u)du\tag{2}$$

Obviously, FRFT can be interpreted as a rotation in the time-frequency domain, and it can be also viewed as chirp-basis expansion according to formula (2). Therefore, FRFT is also called angular Fourier transform or rotational Fourier transform in some documents [4].

2 Chirp signal in FRFT domain

In this section, we analyze the impulsive characteristic of Chirp signal in FRFT domain. A general expression of Chirp signal is defined as

$$s(t) = A \cdot \exp[j(2\pi f_0 t + k\pi t^2 + \varphi_0)],\ T/2 < t < -T/2 \tag{3}$$

Where, A, f_0, k, φ_0 and T is Chirp signal parameters of amplitude, initial frequency, Chirp rate, initial phase and time duration.

We have noticed that a time limited chirp signal had energy concentrated in a certain FRFT domain. By applying equation (3) to equation (1), FRFT of Chirp signal is

$$\begin{aligned} \mathcal{F}^p[s(t)] &= A\sqrt{1-j\cot\alpha}\int_{-\infty}^{+\infty} e^{\left(j\pi(t^2\cot\alpha - 2ut\csc\alpha + u^2\cot\alpha)\right)} e^{\left(j(2\pi f_0 t + \pi k t^2 + \varphi_0)\right)} dt \\ &= A\sqrt{1-j\cot\alpha}\, e^{j(\pi u^2\cot\alpha + \varphi_0)} \int_{-T/2}^{T/2} e^{\left(j\pi t^2(\cot\alpha + k)\right)} e^{\left(j2\pi t(f_0 - u\csc\alpha)\right)} dt \end{aligned} \tag{4}$$

Evidently, when $k = -\cot\alpha$, $f_0 = u\csc\alpha$, the transformed result will gain the maximum value.

3 FRFT domain filtering

If the tested signal is Chirp signal polluted by AWGN, and it is expressed as

$$x(t) = s(t) + n(t) \tag{5}$$

Where $s(t)$ is time duration limited Chirp signal and shown as $s(t) = A\exp[j(2\pi f_0 t + k\pi t^2 + \varphi_0)],\ T/2 < t < -T/2$, $n(t)$ is AWGN.

According to equation (4), we know that Chirp signal will be transformed to a impulsive function in FRFT domain when the Chirp rate $k = -\cot\alpha$, the amplitude of Chirp signal in FRFT domain reach the peak at that time. Therefore, a Chirp signal with specified Chirp rate will produces energy concentration phenomenon in a specified FRFT domain, and Chirp signal with different Chirp rate will gather energy in different FRFT domain, the FRFT order p_0 correspond to its Chirp rate is called optimal FRFT order. The relationship between Chirp rate and optimal FRFT order theoretically can be expressed as

$$p_0 = 2arc\cot(k)/\pi \tag{6}$$

However, no mater what FRFT order are, the transforming results still be noise and never gather energy. Therefore, the work of extracting Chirp signal in AWGN can be instead of adaptive filtering of sinusoid wave in AWGN.

According to the description above, diagram of an adaptive filtering algorithm based on FRFT is shown as figure (1).

Fig.1 Adaptive filtering algorithm based on FRFT

The step of the adaptive filtering algorithm can be divided into four steps as follow

Step 1: calculate the optimal FRFT order of the specified Chirp signal according to equation (6), and do FRFT for the polluted Chirp signal;

Step 2: compute position of the energy concentration peak in optimal FRFT domain according to formula $u_0 = f_0\csc(arc\cot(k)/\pi)$ based on relationship between FRFT and Wigner distribution;

Step 3: pass a designed adaptive filter to do covering peak processing center with u_0 in the optimal FRFT domain;

Step 4: do order of $-p_0$ FRFT for the Chirp signal after passing adaptive filter, and transform it back to time domain Chirp signal.

In order to validate validity of the adaptive filtering algorithm, we do MATLAB experiment for the algorithm. Parameters of the Chirp signal are set as: amplitude A is equal to 1V，initial frequency f_0 is 30Hz, Chirp rate k is set to be 100Hz per second, initial phase is 0, time duration is 1 second, sample frequency is 6000Hz and SNR=-3dB.

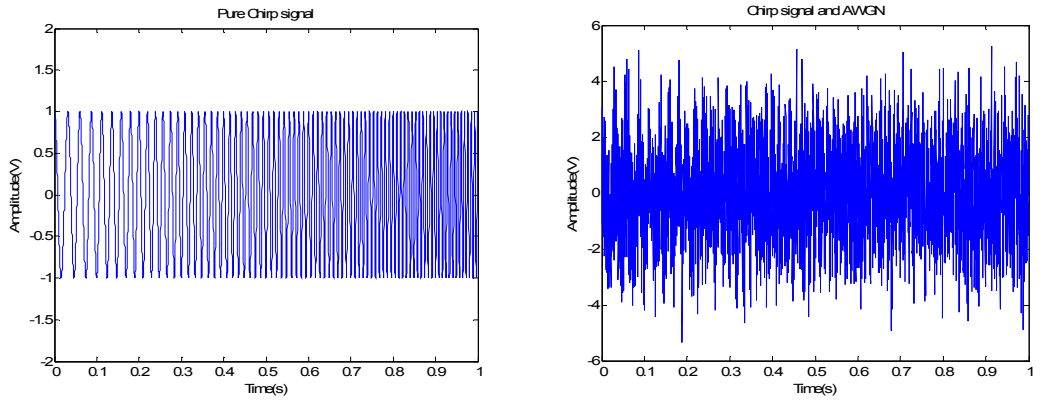

Fig. 2 The pure Chirp signal wave and polluted Chirp signal wave in time domain

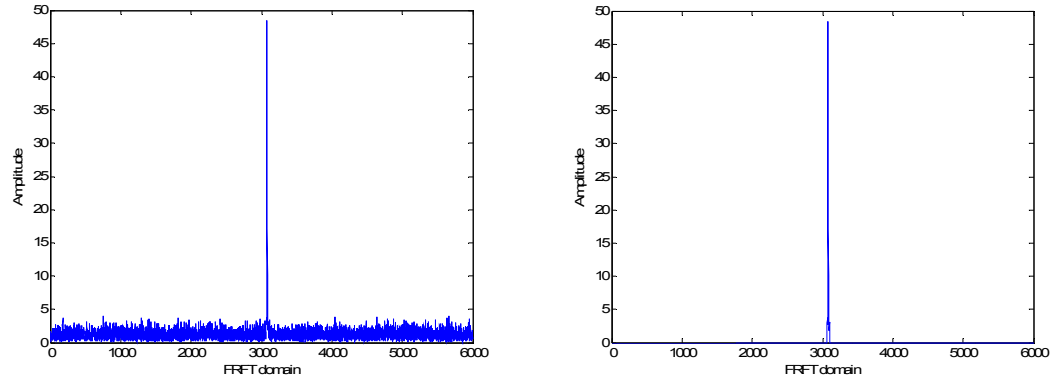

Fig. 3 Signal wave in its optimal FRFT domain before FRFT filtering and after FRFT filtering

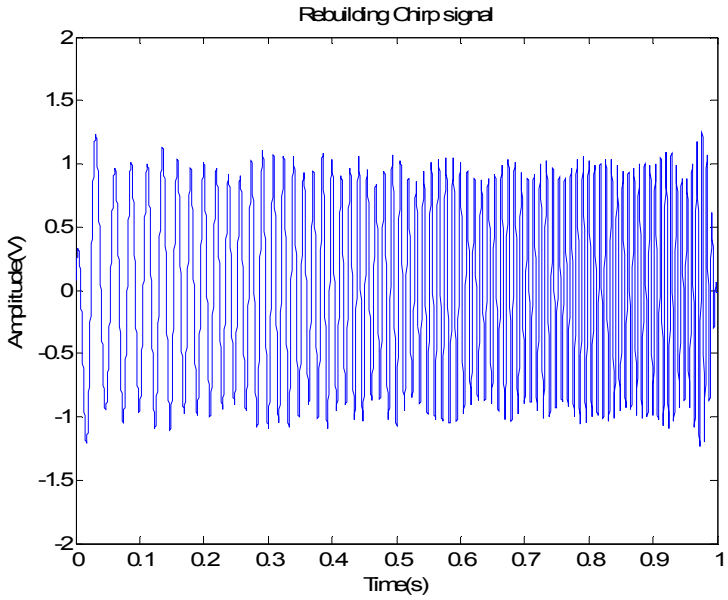

Fig.4 The rebuilding Chirp signal produced by FRFT domain filtering

5 Performance analyses

The complexity of Chirp signal adaptive filtering algorithm in this paper depends on the discrete FRFT algorithm, and there is several kind of fast algorithm corresponding to the discrete FRFT algorithm. Here, we select fast algorithm of discrete FRFT proposed by H.M.Ozaktas[4], and its computation complexity is equal to $O(N \lg N)$.

The effect of the filtering algorithm can be described by factor of SNR improving; it is defined as rate of the SNR before filtering and the SNR after filtering.

$$IF = \frac{SNR_{out}}{SNR_{in}} \tag{7}$$

After some approximately and series of complex computation, Qi Lin concluded that the expression of SNR improving factor IF can be described as [5]

$$IF = \frac{SNR_{out}}{SNR_{in}} \approx \frac{N}{\Delta n} \tag{8}$$

Where N is length of tested signal, Δn is bandwidth of band-pass filter in the optimal FRFT domain.

Summary

The aim of this paper is to propose an adaptive method for filtering Chirp signal embedded in AWGN. The idea that FRFT for a signal is equivalent to rotating the signal on time-frequency plane is used. First, a noisy Chirp signal rotated to a certain angle by FRFT will result in the least spectrum overlap between the signal and noise energy. Then, on the basis of dechirping the Chirp signal, a narrowband filter is exploited to extract the signal and depress most of the noise energy. Finally, the denoised Chirp signal is rotated back to the time domain using an inverse FRFT. Performance of the proposed method is seen through its simplicity in computation and in their improvement SNR.

References

[1] Namias V. The fractinal order Fourier transform and its application to quantum mechanics [J]. J Inst Math Appl, 1980, 25: 241~265.

[2] MCBRIDE A C, KERR F H. On Namias's fractional Fourier transform [J]. IMA Journal of Appl. Math,1987,39(9):159-165.

[3] ERDEN M F, KUTAY M A, OZAKAS H M. Repeated filtering in consecutive fractional fourier domains and its applications to signal restoration[J]. IEEE Trans. on SP, 1999, 47(5):1458-1462.

[4] Ozaktas H. M, Kutay M. A, Bozdagi G. Digital computation of the fractional Fourier transform [J]. IEEE Transactions on Signal Processing.1996, 44(9):2141-2150.

[5] Qi Lin, Tao Ran, etal. An adaptive time-frequency filtering method based on fractional Fourier transform for linear frequency modulation signal[J]. Journal of ordance. 2004,24(04):499-503.

Advanced Materials Research Vols. 989-994 (2014) pp 3938-3941
© (2014) Trans Tech Publications, Switzerland
doi:10.4028/www.scientific.net/AMR.989-994.3938

Research on FM Telemetry Software Demodulation Algorithms

Fu Gang[1,a] , Wu Yanjun[1, a], Li Renlong[1,a] and Liping Wang[2,b]

[1]China Satellite Maritime Tracking and Control Department, China
[2]School of Computer Science, Engineering and Mathematics, Flinders University, South Australia 5 042, Australia
[a]348237548@sina.com [b]wlp2005518@gmail.com

Keywords: maximum likelihood, PCM/FM, MSD, variable step length synchronization

Abstract. Aimed at the problem that the demodulation threshold of non-coherent demodulation technology of PCM/FM telemetry system using frequency modulation in the present situation of aerospace measurement and control is higher, research a kind of multiple symbol detection based on maximum likelihood thought (Multi-Symbol Detection, MSD) demodulation method. This paper introduces the principle of multiple symbol detection and aiming at the shortcomings of the previous synchronization method, studies a kind of symbol decision process and synchronization of the combination of synchronization method.

Introduction

At present our country aerospace measurement range rocket telemetry system mainly USES the noncoherent frequency discrimination method, because do not need coherent signal at the receiving end, thus is widely used. [1]But its drawback is that the band pass filter demodulation threshold to demand higher and higher, the threshold effect. As more and more electromagnetic interference, and the function of the spacecraft distance increasing, this method will no longer apply. In order to improve the performance of PCM/FM signal demodulation, American Nova Eng. Inc., the company in recent years has been studying a technology: more symbol detection (MSD), and successfully applying it to PCM/FM telemetry system, obtained the channel gain of nearly 3dB. [2]

1 Baseband complex rotating orthogonal MSD algorithm

Baseband complex rotating orthogonal MSD algorithm

$$s(t) = \cos[2f_c t + f(t) + \theta_1] \tag{1}$$

Orthogonal signal after frequency conversion components, constitute a complex baseband signal, the form of the complex signal for:

$$R = I + j.Q = \cos[f(t) + \theta_1] - j\sin[f(t) + \theta_1] \tag{2}$$

With exactly the same receiving signal elements that local signal can be represented as:

$$L = \cos[f(t) + \theta_2] + j\sin[f(t) + \theta_2] \tag{3}$$

$$\begin{aligned} R \cdot L &= \cos(\theta_2 - \theta_1) + j\sin(\theta_2 - \theta_1) \\ &= I_B + jQ_B \end{aligned} \tag{4}$$

In the result of the type (4) the product of the integral operation within the length of observation are:

$$M = N_C \cdot I_B + jN_C \cdot Q_B \tag{5}$$

$$S = N_C{}^2 \cdot (I_B{}^2 + Q_B{}^2) \tag{6}$$

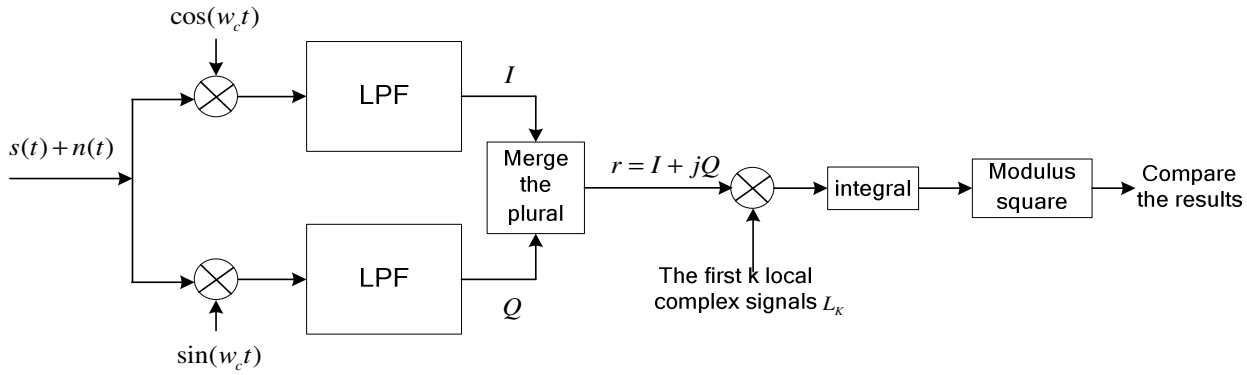

Fig1 Baseband orthogonal MSD principle block diagram

In a row in table 1 code sequences, on both sides of the two values are said to be on the current element before and after the disturbance of two element. Through the above analysis, the local can generate the initial phase element corresponding to the baseband signal $L_1, L_2, \cdots, L_8$. The 8 kinds of signal is the difference between the length of time is only one element width, and the eight kind of signal is a baseband modulation signal. A similar method respectively to the current received orthogonal complex baseband signal correlation processing in a symbolic, get eight plural $M_{10}(1), M_{20}(1), \cdots, M_{80}(1)$.

Table 1 Element combination and the corresponding phase

number	（1）	（2）	（3）	（4）
symbol sequence	-1 -1 -1	-1 -1 +1	+1 -1 -1	+1 -1 +1
corresponding phase	-0.7π	-0.58π	-0.58π	-0.47π
number	（5）	（6）	（7）	（8）
symbol sequence	+1 +1 +1	+1 +1 -1	-1 +1 +1	-1 +1 -1
corresponding phase	0.7π	0.58π	0.58π	0.47π

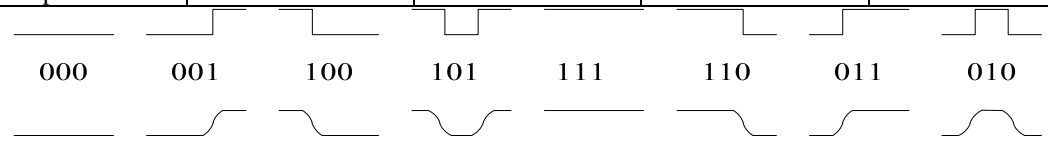

Fig2 Preset filter before and after eight possible code waveform comparison

Assume element observation length N = 5, 128 in observation length can be the local signal, and because the local signal phase change in the length of 5 codes continuity, calculate the local 128 signals of each within the first four element length of the initial phase of local signal, can calculate the L_1 to L_8 may be the initial phase of the 8 kinds of local signal. Eight of the plural by allowing for $M_{10}(1)$ to $M_{80}(1)$ accordingly plural Angle rotation, get eight different symbol waveform corresponding to different initial phase values of local signal associated with the current signals as a result, $M_{11}(1), \cdots, M_{1p}(1), M_{21}(1), \cdots, M_{2p}(1), M_{81}(1), \cdots, M_{8p}(1)$.

According to the current element time of various local corresponding correlation matching value of the received signal waveform and $M_{10}(1)$ and $M_{80}(1)$ and before 4 codes period have different code to local waveform and the initial phase of the correlation value between the received signal $M_{10}(k), \cdots, M_{1p}(k), M_{20}(k), \cdots, M_{2p}(k), M_{80}(k), \cdots, M_{8p}(k)$ $(k = 2,3,4,5)$ .Both before and after, for example, consider the symbol sequence element, the influence of length, we assume that the observation of element within the local signal sequence is -1+1+1-1-1-1+1 (the last but one to the current element), rotating through compounding technology and accumulation process, will be able to get this kind of circumstance the five element was used to observe the relative value in the length, expressed as:

$$M_n = M_{7a}(5) + M_{6a}(4) + M_{3c}(3) + M_{1d}(2) + M_{20}(1) \tag{10}$$

2 Synchronization variable step length

To step the same staircase tracking a sine wave as an example, as shown in figure 3.From top to bottom in turn for step size is too small, moderate step length, step size is too large. When the step length through the hours, means that the adjustment speed too slow, led to the capture time is too long. And when the amount being tracked changes fast, too slow adjustment speed can't timely tracking input, the tracking error is too big lead to can't really lock.

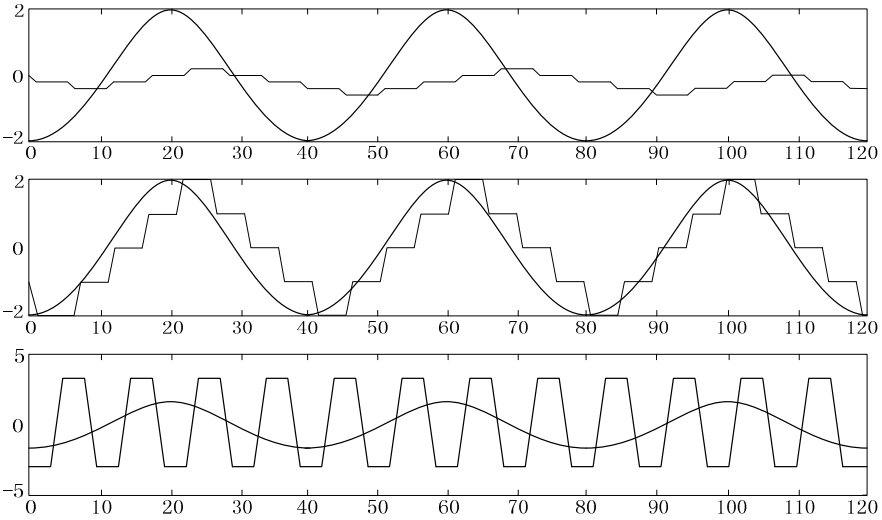

Fig3 Fixed step length schematic capture step speed, accuracy and long relationship

In order to improve the capture speed, the capture phase using larger iteration step length, inspired by speech signal delta modulation mode, designed the iteration step length controlled by the test statistic characteristics of the overall implementation scheme. The step length adjustment process as shown in figure 4.

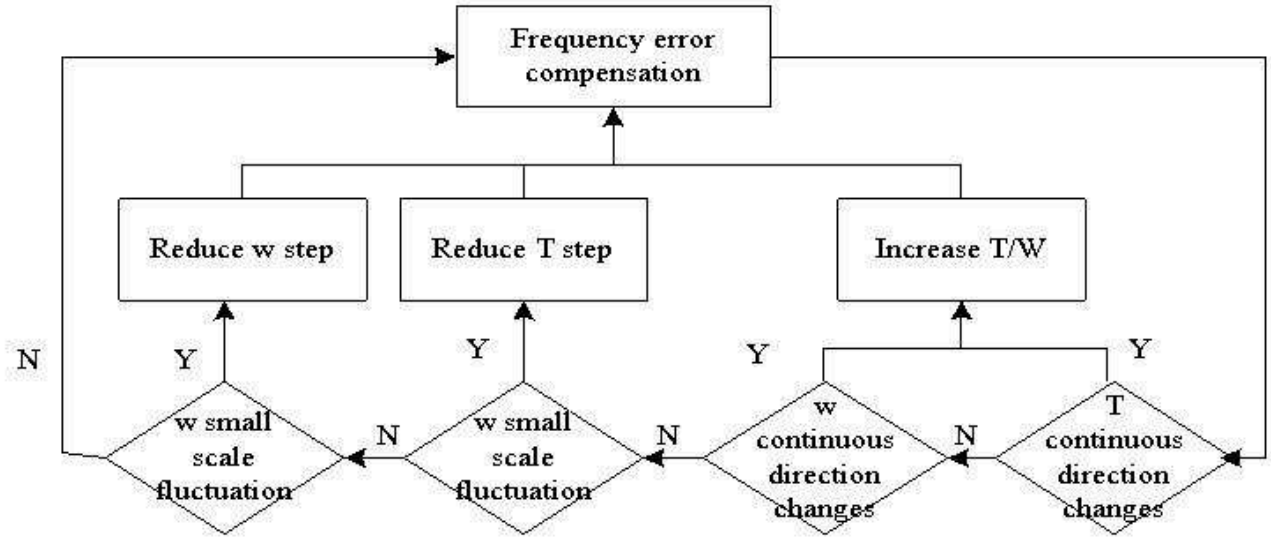

Fig4 Step length adjusting system state transition diagram

When the compensation value to a certain direction continuously increases, the system is still in the tracking status, the iteration step length need to be increased to reduce the iteration times; Compensation value fluctuate in a small scope, basic synchronization system, reduce the iteration step length needed to increase the tracking accuracy. When caught early, with big iteration step into near quickly achieve synchronization locks; Then, use less iteration step improve the synchronization accuracy.

3 Algorithm performance

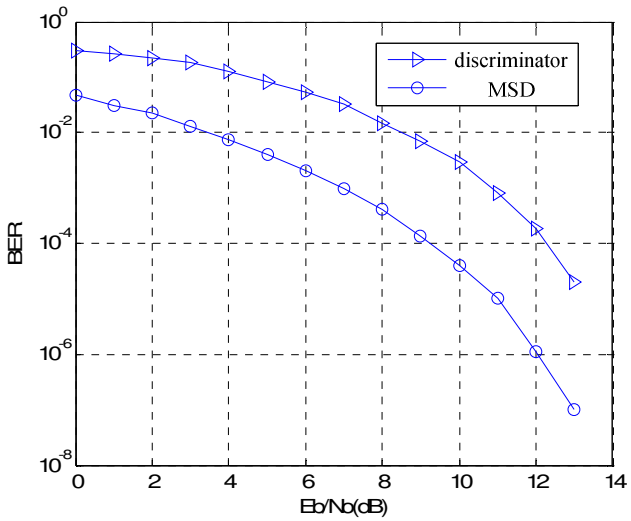

Fig5 The BER curve of MSD method with the conventional demodulation method

In bit error rate of 10^{-4} place[3], MSD technology can get about 3 dB channel gain, in this paper, the baseband pay after rotation MSD technology shows great superiority.

Summary

Through the baseband complex rotating orthogonal MSD technology and the corresponding synchronization method of research and testing shows that the technique can largely improve the performance of the shooting range PCM/FM telemetry system can effectively overcome the traditional technique of frequency discrimination threshold effect.

References

[1] Zhang Jun. Radio telemetry system and its application in weapon test[M]. Beijing: National Defence Industry Press, 2011.
[2] Xu Xingyuan. Shipborne tt&c equipment based on MSD technology research rocket telemetry demodulation method[J]. telemetry and telecontrol, 2009, 30(5): 64-67.
[3] IRIG 106-99，APPENDIX A FREQUENCY CONSIDERATIONS FOR TELEMETRY[S].

Advanced Materials Research Vols. 989-994 (2014) pp 3942-3945
© (2014) Trans Tech Publications, Switzerland
doi:10.4028/www.scientific.net/AMR.989-994.3942

Performance Analysis on Three Methods for Chirp Signal parameters estimation based on FRFT

Wu Yanjun[1, a], Fu Gang[1,a] and Yu Peng[1,a]

[1]China Satellite Maritime Tracking and Control Department, China

[a]348237548@sina.com

Keywords: Chirp signal, Fractional Fourier transform (FRFT), parameter estimation, peak searching

Abstract. Chirp signal has been used widely in radar signals, and the Fractional Fourier transform is one of the most effective tools to analyze Chirp signal. In this paper, the concept of FRFT and the estimation theory of Chirp signal are introduced firstly. Then, we study three Chirp signal detection algorithms based on character of Chirp signal energy concentrated in a certain FRFT domain. Finally, in order to test the estimation abilities of the frequency modulation rate and the central frequency of FRFT to Chirp signal, and compare the operation time of parameters estimation under different SNR of the three algorithms, we simulate performance of the Three methods, and the final simulation results show that the three method have remarkable capabilities of detecting Chirp signal with low SNR. In contrast, the two-searching method doesn't need planar search, consumedly reducing the computation cost at the same precision.

Introduction

Chirp signal occurs in modern radar commonly, it has a good time and frequency domain compression feature and excellent Doppler frequency shift characteristics .The routine processing method of Chirp signal in Radar is to doing impulse compression in time domain or frequency domain after go through a band pass filter. Radar receivers detect Chirp signal in receiving signal through threshold determination firstly, and then, extract target echo signal parameters including time delay, Doppler frequency shift and amplitude, this method can acquire higher processing gain and get target parameter accurately. However, when radar is in bad communication environment, especially in active jamming environment, the echo signal is commonly with low SNR, and conventional methods of detection and parameter estimation for these LFM signal is very difficult. Hence, it is an essential research subject of detecting and estimating the echo signal parameters with low SNR condition accurately and quickly.

For a long time, many scholars put forward corresponding methods to LFM signal detection and parameter estimation, Djuric P M and Barbarossa S solved the problem by using maximum likelihood estimation method to solve this problem, however, this method is with too large calculate amount, and make it difficult to put the algorithm into project implementation[1-2]. Haimovich A M took advantage of short time Fourier transform (STFT) and wavelet transform (WT) algorithm to the Chirp signal extimation, but the STFT is a very narrow window and WT time window width changes affect the resolution of the time-frequency domain[3].in additional, Rao P introduced Wigner Ville distribution of Chirp signal parameters estimation method[4], because of the cross terms obsession of Wigner Ville distribution in processing multi-component Chirp signal, therefore, this method is not ideal as well. So it is exigent to find a new fast effective Chirp signal detection and parameters estimation method.

1 Fractional Fourier transform

FRFT is a kind of generalized Fourier transform. it can be interpreted as signals in the representation domain which is generated by time-frequency plane circumrotate a certain Angle circling origin counterclockwise. When rotation Angle is 0, the FRFT result of Chirp signal is itself; when rotation Angle is π, then the FRFT will change into traditional Fourier transform. FRFT was

come up with point of characteristic value and characteristic function in form of pure mathematics by V.Namias in 1980[5], and then, Mcbride and Kerr studied it deeply and build a strict FRFT definition in mathematics. FRFT of a Time domain signal $x(t)$ is defined as

$$X_p(u)=\left\{\mathcal{F}^p[x(t)]\right\}(u)=\int_{-\infty}^{+\infty}K_p(u,t)x(t)dt,\quad 0<|p|<2,\quad 0<|\alpha|<\pi$$

$$=\begin{cases}\mathrm{B}_\alpha\int_{-\infty}^{+\infty}\exp(j\dfrac{t^2+u^2}{2}\cot\alpha-\dfrac{jtu}{\sin\alpha})x(t)dt & \alpha\neq \mathrm{n}\pi\\ x(t) & \alpha=2\mathrm{n}\pi\\ x(-t) & \alpha=(2\mathrm{n}\pm1)\pi\end{cases}\tag{1}$$

Where $\mathrm{B}_\alpha=\sqrt{(1-j\cot\alpha)/2\pi}$, $\alpha=p\pi/2$, and p is FRFT order.

2 Chirp signal detection and parameter estimation based on FRFT

2.1 Two dimension peak searching algorithm

If the rotation Angle is right, Chirp signal will display energy concentration character in corresponding FRFT domain. Hereby, we can take advantage of this feature to detect and estimate Chirp signal parameter. The step is: first, scanning rotation Angle with a step order, doing FRFT transform to the unknown parameters Chirp signal and taking its modulus square, so it will form a two dimension distribution of Chirp signal energy in (α,u) plane; Then, searching the peak value in the two-dimensional plane; Finally, we can estimate the Chirp signal parameters according to the relationship between parameters (α,u) correspond to the peak and initial frequency and the adjustable frequency of Chirp signal.

Chirp signals have a general expression as

$$s(t)=a_0\exp(j\varphi_0+j2\pi f_0t+j\pi\mu_0t^2),\quad \text{-T/2<t<T/2}\tag{2}$$

Where $a_0,\varphi_0,f_0,\mu_0,T$ are amplitude, initial phase, initial frequency, adjustable frequency and time duration. The relationship between Chirp parameters and the parameters (α,u) correspond to the peak value in the two dimension peak searching algorithm

$$\begin{cases}\hat{\mu}_0=-\cot(\hat{\alpha}_0)\\ \hat{f}_0=\hat{u}_0\csc(\hat{\alpha}_0)\\ \hat{\varphi}_0=\arg\left[\dfrac{X_{\hat{\alpha}_0}(\hat{u}_0)}{A_{\hat{\alpha}_0}e^{j\pi\hat{u}_0^2\cot(\hat{\alpha}_0)}}\right]\\ \hat{a}_0=\dfrac{\left|X_{\hat{\alpha}_0}(\hat{u}_0)\right|}{\Delta t\left|A_{\hat{\alpha}_0}\right|}\end{cases}\tag{3}$$

2.2 Two step maximum modulus searching algorithm

In order to improve the real-time performance and reduce calculation amount of Chirp signal detection and parameter estimation, in this section, we introduce a kind of two steps searching algorithm based on FRFT maximum modulus, the idea of algorithm can be divided into the following three steps:

Step 1: doing FRFT for certain Chirp signal on a larger order number step in the range of 0 to 2, and gain a vector of each FRFT order maximum modulus value.

Step 2: searching the maximum value and the minor maximum value, and then calculate FRFT order numbers corresponding to the two values.

Step 3: do FRFT for the Chirp signal between the two orders with smaller FRFT step value and search the maximum value in the two dimensional plane formed by FRFT order and FRFT domain, finally, we can detect and estimate Chirp parameters according to formula (1).

2.3 Pre-estimation algorithm

The idea of Chirp signal parameters estimation pre-estimation algorithm is based on bandwidth limited character of time duration limited Chirp signal. We do Fourier transform for a time limited Chirp signal and acquire its bandwidth from frequency spectrum; Then, we can easily figure out approximation of Chirp rate and initial frequency, so we can gain almost the best FRFT order; Finally, we do FRFT for the Chirp signal around the best FRFT order and gain the best FRFT order through peak searching, then estimate Chirp signal parameter based on the best FRFT order.

3 Simulation analyses

In this section, we compare estimation precision and calculation complexity of the three Chirp signal parameters estimation algorithms through MATLAB simulation. As shown the expression formula of Chirp signal as described above, parameters a_0, φ_0, f_0, k are equal to 1,,256 and -30 respectively, and time duration is between -1 second and 1 second. The simulation result is shown as follow.

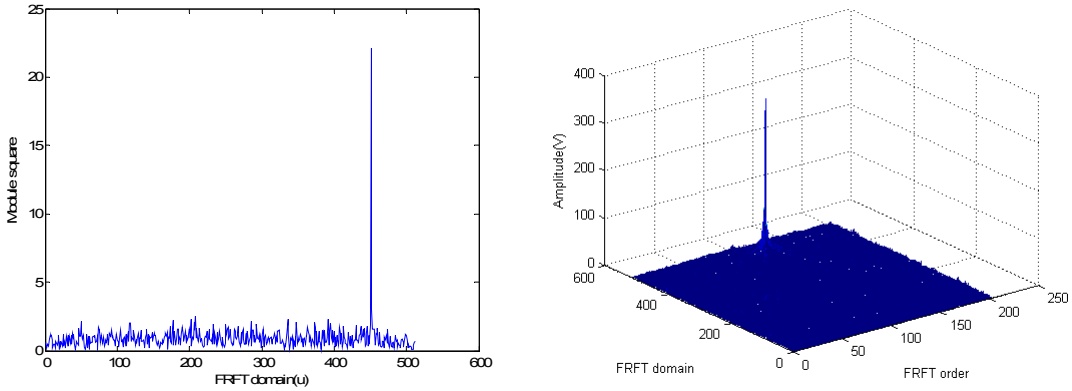

Fig 1 Three-dimensional energy distribution of Chirp signal and its form in best FRFT domain

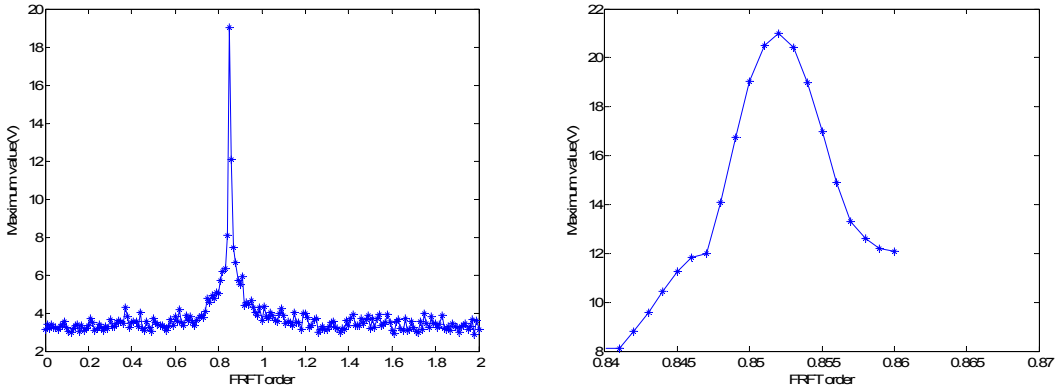

Fig 2 Relationship between maximum value and order in rough searching and refined searching respectively

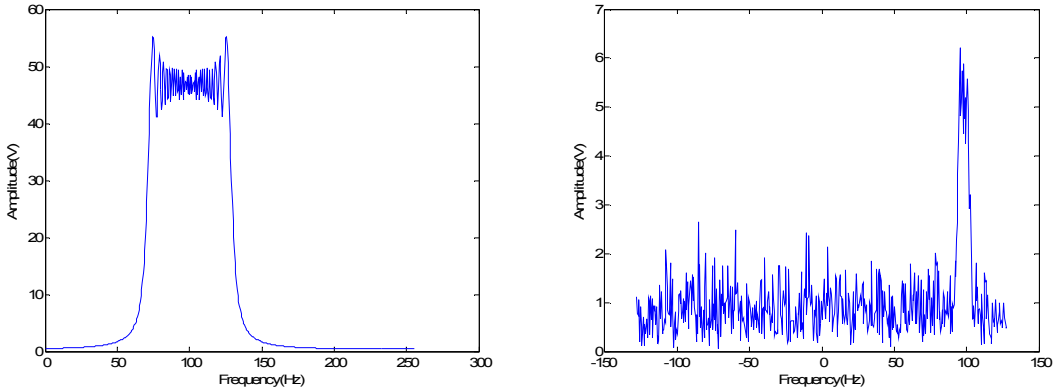

Fig 3 Chirp signal distribution in frequency domain and FRFT domain respectively

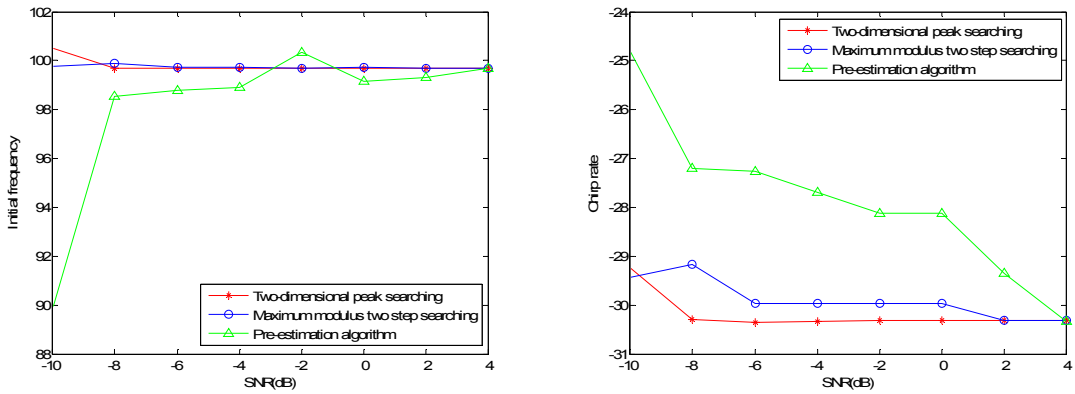

Fig 4 Chirp signal distribution in frequency domain and FRFT domain respectively

According Fig 4, it is easy to conclude that the two-dimensional peak searching algorithm has the best estimation precision, the pre-estimation algorithm is the worst, and performance of maximum modulus two step searching algorithm is close to the two-dimensional peak searching algorithm. However, the calculation complexity of the two-dimensional peak searching algorithm is decuple to the maximum modulus two step searching algorithm. Therefore, In contrast, we consider the two step maximum modulus searching algorithm as the most suitable algorithm in practice.

Summary

In this paper, we take advantage of energy concentration character of Chirp signal in FRFT domain to estimate radar echo signal parameters. Then, we introduce three Chirp signal parameters estimation algorithms based on FRFT. Finally, we compare estimation precision and computation complexity through MATLAB simulation under SNR range from -10dB to 4dB. In contrast, the two step maximum modulus searching algorithm is the most fitness Chirp signal estimation algorithm.

References

[1] Djuric P M, Kay S M. Parameter estimation of chirp signal[J]. IEEE Tans on ASSP,1990,38 (12):2118-2126.

[2] Barbarossa S. Analysis of multicomponent LFM signals by a combined wigner-hough transform [J]. IEEE Trans Signal Processing, 1995, 43(6):1511-1515.

[3] Haimovich A M ,Peckham ,Teti J G, et al. SAR imagery of moving targets: Application of time-frequency distribution for estimating motion parameter [C]//International Symposium on Aerospace and Sensing.Tokyo:IEEE Press,1994,22(38):238-247.

[4] Rao P, Taylor F J. Estimation of instantaneous frequency using the discrete wigner distribution[J]. Electronics Letters, 1990, 26(4):246-248.

[5] Namias V. The fractional order fourier transform and its application to quantum mechanics[J].Journal of Institute Applied Math, 1980, 25(3):241-265.

Advanced Materials Research Vols. 989-994 (2014) pp 3946-3951
© (2014) Trans Tech Publications, Switzerland
doi:10.4028/www.scientific.net/AMR.989-994.3946

Group Sparsity Regularization based Compressed Sensing MR Image Reconstruction

Xin Jin[1, a], Mingfeng Jiang[1, b] and Jie Feng[1, c]

[1]School of Information Science and Technology, Zhejiang Sci-Tech University,

Hangzhou, 310018, China

[a]2547950843@qq.com, [b]m.jiang@zstu.edu.cn, [c]arlose@zstu.edu.cn

Keywords: MR image reconstruction; group sparse; super-pixel

Abstract. Exploiting the sparsity of MR signals, Compressed Sensing MR imaging (CS-MRI) is one of the most promising approaches to reconstruct a MR image with good quality from highly under-sampled k-space data. The group sparse method, which exploits additional sparse representation of the spatial group structure, can promote the overall sparsity degree, thereby leading to better reconstruction performance. In this work, an efficient superpixel/group assignment method, simple linear iterative clustering (SLIC), is incorporated to CS-MRI studies. A variable splitting strategy and classic alternating direct method is employed to solve the group sparse problem. The results indicate that the proposed method is capable of achieving significant improvements in reconstruction accuracy when compared with the state-of-the-art reconstruction methods.

Introduction

MRI acquisition speed is usually limited by the large number of acquisitions needed along the phase-encoding direction [1]. With the advent of compressed sensing (CS) theory [2, 3], MRI with sparsity-promoting regularization criteria (e.g., ℓ1-based regularization), termed CS-MRI, have gained popularity [4-6]. CS-MRI [4] exploits the sparsity of the signal itself to reconstruct the MR images from far fewer samples than conventional methods require, thus significantly reducing the scan time. However, successful reconstruction from an undersampled MR signal using CS requires the satisfaction of two criteria: (a) the sparsity of the MR imaging introduced by a sparsifying transformation function; and (b) incoherency between the sampling matrix and the sparsity basis.

In the CS-MRI reconstruction, the method used to sparsify the MR images is very important. The most commonly used sparsity bases are predefined transforms, such as the discrete cosine transform (DCT), and the discrete wavelet transform (DWT). When using the above-mentioned sparsifying transforms in the CS-MRI reconstruction, it is often useful to include a Total Variation (TV) penalty as well [4]. The linear combination of total variation and wavelet sparse regularization, known as TVL1 problem, is very popular in many CS-MRI models[4,5], which can be considered as requiring the MR image to be sparse by both the specific transform and finite-differences at the same time. The non-linear conjugate gradient method (NLCG) with a backtracking line-search was first proposed to tackle the TVL1 problem for reconstructing the MR image in Sparse-MRI [4].In order to further enhance the reconstruction quality of CS-MRI, recent studies indicated the necessity of going beyond sparsity and taking into the structure information of sparse signals. In practice, a wide range of MR images are known to have certain "group sparsity" property, that is, the sparsity signals has a natural grouping of its components, and the components within a group are likely to have similar characteristics. The Group Sparse (GS) method has been introduced into one-dimensional signal recovery considering equal or unequal length groups [7, 8]. Experiment results have demonstrated that group sparse methods have advantages over standard CS reconstruction [7]. Usman et al. introduced the k-t group sparse method for dynamic MR images[9,10], which exploited not only the sparsity information as in the conventional compressed sensing, but also the spatial group structure in the sparse representation. Compared with the standard compressed sensing MR image reconstruction,

the group sparse method can improve the spatial and temporal quality of the MR image reconstruction. Typically, the group sparse method comprises three steps: prior information estimation, group assignment, and signal recovery.

Recently, a new super-pixel algorithm based on k-means clustering, simple linear iterative clustering (SLIC) [11], has been proposed for generating super-pixels, which has been shown to outperform other Super-Pixel methods with efficiency in computation and memory usage. In this work, we incorporate the SLIC-based super-pixel generating algorithm to implement the group assignment for a GS-enforced MRI reconstruction method, which is then solved using an efficient alternating direction method (ADM) with mixed $\ell_{2,1}$ regularization[8,12]. We refer to this approach as group sparse reconstructions using super-pixel algorithm, termed as SP-GS method. In order to compare with the state-of-the-art CS-MRI algorithms for reconstruction of the highly under-sampled MR imaging, we conduct extensive experiments to test the proposed SP-GS method.

Theory

Group Sparse Method

Suppose the reconstructed MR image u is partitioned into k groups by the super-pixel algorithm, the group sparse formulation can be described as:

$$\min_u \left\| u^{(g)} \right\|_{2,1} \quad s.t. \quad \left\| F_u u - f_u \right\|_2 \le \varepsilon , \tag{1}$$

where $\left\| u^{(g)} \right\|_{2,1}$ is the mixed $l_{2,1}$ norm defined as:

$$\left\| u^{(g)} \right\|_{2,1} = \sum_{i=1}^{k} \left\| u_i^g \right\|_2 \tag{2}$$

$\left\| u_i^g \right\|_2$ being the l2 norm of the vector of all elements of u assigned to the *i*th group (*i*=1,2,3,…,k).

In this work, alternating direction method (ADM) is applied to solve the group sparse problem in the form of Eq.(1). First, an auxiliary variable v is introduced to transform Eq.(2) into an equivalent problem as follows:

$$\begin{aligned} &\min_{u,v} \left\| v^{(g)} \right\|_{2,1} = \sum_{i=1}^{k} \left\| v_i^g \right\|_2 \\ &s.t. \quad v = u \text{ and } \left\| F_u u - f_u \right\|_2 \le \varepsilon \end{aligned} \tag{3}$$

The augmented Lagrangian problem of Eq.(4) can be formulated as :

$$\begin{aligned} &\min_{u,v} \left\| v^{(g)} \right\|_{2,1} - \lambda_1 (v-u) + \beta_1 / 2 \left\| v-u \right\|_2^2 \\ &-\lambda_2 (F_u u - f_u) + \beta_2 / 2 \left\| F_u u - f_u \right\|_2^2 \end{aligned} , \tag{4}$$

where λ_1, λ_2 are multipliers, and β_1, β_2 are penalty parameters. The multipliers λ_1 and λ_2 are updated in the following way:

$$\begin{cases} \lambda_1 \leftarrow \lambda_1 - \gamma_1 \beta_1 (v-u) \\ \lambda_2 \leftarrow \lambda_2 - \gamma_2 \beta_2 (F_u u - f_u) \end{cases} , \tag{5}$$

where γ_1, γ_2 >0 are step length.

Then, the ADM approach is employed to minimize the augmented Lagrangian problem, Eq.(4), with respect to *u* and *v* alternately[8].

B. Super-pixel based Group Assignment

A simple parameter of SLIC algorithm is the desired number of the approximately equally-sized super-pixels (ns). For grayscale MR image, the clustering procedure begins with ns initial cluster centers $C_i = [g_i, x_i, y_i]^T$, which are sampled on a regular grid spacing, where gi is the grayscale value and (x_i, y_i) is the position of the ith cluster center. To produce roughly equal sized super-pixels, the

grid spacing is set as $S=\sqrt{N/ns}$, and N is the total pixels of the MR image. The next step is to find the nearest cluster center for each pixel. Instead of searching over the entire image as in conventional k-means clustering methods, the SLIC algorithm adopts super-pixel search regions of $2S\times 2S$ pixels around the super-pixel centers, which significantly lessens the number of distance calculations and results in an obvious speed advantage. The distance measure D is an effective way to determine the nearest cluster for each pixel. To combine the grayscale distance d_g and spatial distance d_s between pixel *j* and pixel *i* into a single measure, it is necessary to normalize both distances by their respective maximum distance with in a cluster.

The distance measure D is defined as [11]:

$$D=\sqrt{d_g^2+(\frac{d_s}{S})^2 m^2}\ , \tag{6}$$

where *m* is the weighting parameter between the gray similarity and spatial proximity, and gray distance and spatial distance are calculated as:

$$\begin{aligned} d_g &= \sqrt{(g_j-g_i)^2} \\ d_s &= \sqrt{(x_j-x_i)^2+(y_j-y_i)^2} \end{aligned} \tag{7}$$

Once each pixel has been associated to the nearest cluster center, the cluster centers are adjusted to the mean $\overline{C}=[\overline{g},\ \overline{x},\ \overline{y}]^T$ vector of all pixels belonging to the corresponding clusters. The residual error E between the updated cluster center locations and previous cluster center locations is computed to evaluate the error convergence. The group assignment and update steps can be repeated iteratively until convergence. Finally, a post processing step using a connected component algorithm is designed to reassign the disjoint pixels to nearby super-pixels[11].

Materials and Methods

To compare the NLCG, method in the standard CS-MRI with the proposed SP-GS method, a brain MR image is used to test the reconstruction performance. The Fourier transform reconstructions of the fully-sampled k-space data are shown in Figure 1. To test the algorithms at various reduction factors, the k-space was under-sampled retrospectively. The sampling density of the 2D random pattern approximated the signal energy distribution. This sampling strategy has been widely used for compressed-sensing MR image reconstruction [4,5]. All the measured k-space data f_u are mixed with -20dB simulated Gaussian white noise compared with the maximum of the signal intensity.

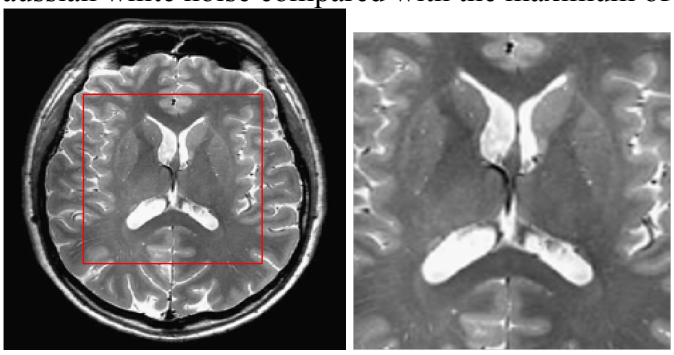

Fig.1 The Brain MR image. Left: Reference image; Right: Zoomed-in of the box in the reference image

The Daubechies-4 was used as the sparsifying transform ψ in the standard CR-MRI reconstruction problem (1), and its regularization parameters α and β are set as α=0.001 and β=0.035 respectively, which were used in the previous work [4,5]. The parameters for ADM-based group sparse method are set as follows: β_1=0.3/<abs(f_u)>,β_2=3/<abs(f_u)> and γ_1= γ_2=1.6, where <·> is the arithmetic average and abs(f_u) are the absolute values of k-space measurements . In the SLIC-based super-pixel generating method, the desired number of super-pixels is set as ns=200; the weighting

parameter between grayscale distance and spatial distance is set as m=10; and the threshold E in the algorithm 1 is set as 10-3. All reconstructions were implemented in the Matlab programming environment (Version 2008a, Mathworks, Natick, MA), and the experiments were performed on a ThinkPad laptop with 2.67 GHz Intel Core 2Duo processor, 3 G of memory and Windows 7 operating system.

To quantitatively evaluate the efficiency and accuracy of the reconstruction algorithms, three indexes were introduced: (i) the Signal-to-Noise Ratio (SNR); (ii) the image reconstruction time. Furthermore, the reconstructed images, zoomed-in regions and their error images (the absolute difference between reconstructed image and the original image) were also compared visually. The error images were magnified twice for better illustration. The SNR and RE were calculated as follows:

$$SNR = 10\log_{10}\frac{Var(u_0)}{MSE(u-u_0)} \tag{8}$$

where MSE is the mean squared error between the reconstructed (u) and the original image (u_0); $Var(u_0)$ denotes the variance of the values in u_0; u is the reconstructed image and u_0 is the original image.

Results

A. Super-Pixel based group assignment

After obtaining the prior information from the MR image reconstructions with 79.46% under sampling (using 20.54% of full data) by using the NLCG method, the simple linear iterative clustering (SLIC) was employed to generate the super-pixels. As shown in Figure 2, it can be found that the components within a group are likely to have similar grayscale values. The computed group numbers of the Brain image is 201.

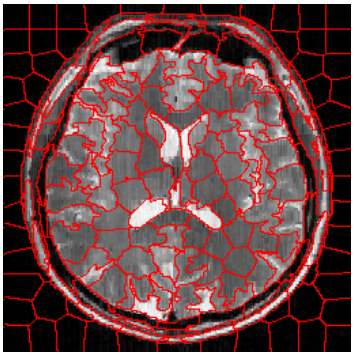

Fig. 2 SLIC based super-pixel method for assigning the groups from Brain MR image reconstruction with 79.46% under sampling by using the NLCG method.

B. MR image reconstruction

The brain image was obtained by scanning a healthy male volunteer's brain with a Bruker 2T whole-body MRI system. Figure 4 and Table 2 show the reconstructed brain MR image with different undersampling rate by using NLCG and the proposed SP-GS methods. For the 79.46% undersampling rate, Figure 4 displays the reconstructions, zoomed-in sections and the error maps, obtained by the use of NLCG method (Figure 3(a)), and the proposed SP-GS method (Figure 3(b)), respectively. As can be seen from Figure 3 and Table 1, the proposed SP-GS method provided better reconstruction quality than the NLCG method at all reduction factors.

Discussion and Conclusion

In this paper, a group sparse method was employed to reconstruct the highly under-sampled MR image. The group sparse optimization promotes group sparsity; however, the mixed $l_{2,1}$ norm

structure and possible grouping irregularity made the $l_{2,1}$ regularization problem more difficult to solve than the conventional l_1-regularized problem in standard CR-MRI reconstruction. simple linear iterative clustering (SLIC) based super-pixel generating method was incorporated to assign the groups. And the brain MR image with different undersampling rates was used to validate the performances of the proposed SP-GS method on reconstruction properties and computational efficiency.

In terms of the reconstruction quality with the three different MR data tested, it can be observed visually that the proposed SP-GS method significantly outperformed NLCG, in the case of 79.46% undersampling k-space data, as shown in Figure 3. Quantitative comparison, as summarized in Table I, suggested that the proposed SP-GS method improved the reconstruction SNR by 5~12dB and reduced the RE by 7%~34% when compared with the conventional CS-MRI reconstruction method.

In this paper, a novel group sparse based algorithm is demonstrated for reconstructing MR image with highly undersampled k-space data. The algorithm applies simple linear iterative clustering to assign the groups in the sparse representation, and then uses the alternating direct method to solve the group sparse problem. The experimental results indicate that the proposed method considerably outperforms the classic CS-MRI reconstruction methods in terms of the reconstruction quality.

TABLE 1 Comparisons of SNRs (dB), REs (%) and reconstruction time (in seconds) on NLCG and the proposed SP-GS method for reconstructing Brain MR image with different undersampling rates.

Undersampling Rate	Method	SNR(dB)	RE (%)	Time(s)
75.12%	NLCG	12.41	16.35	32.87
	SP-GS	18.42	8.18	10.84
79.46%	NLCG	10.52	20.32	32.21
	SP-GS	17.92	8.67	10.10
83.33%	NLCG	5.01	38.30	30.61
	SP-GS	16.99	9.64	10.01

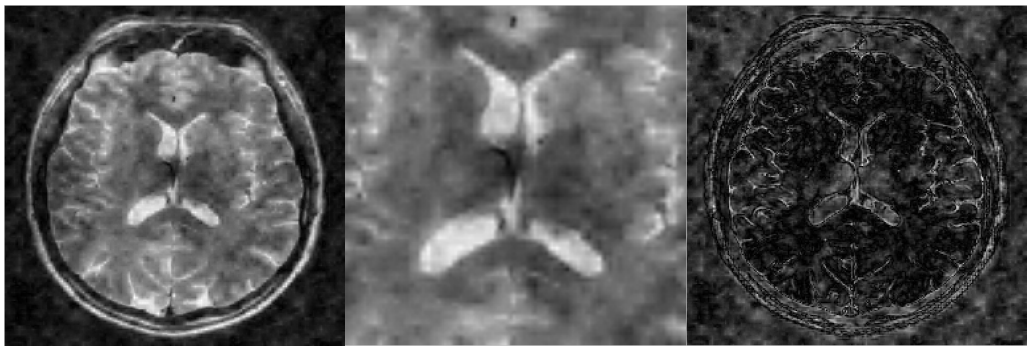

(a)

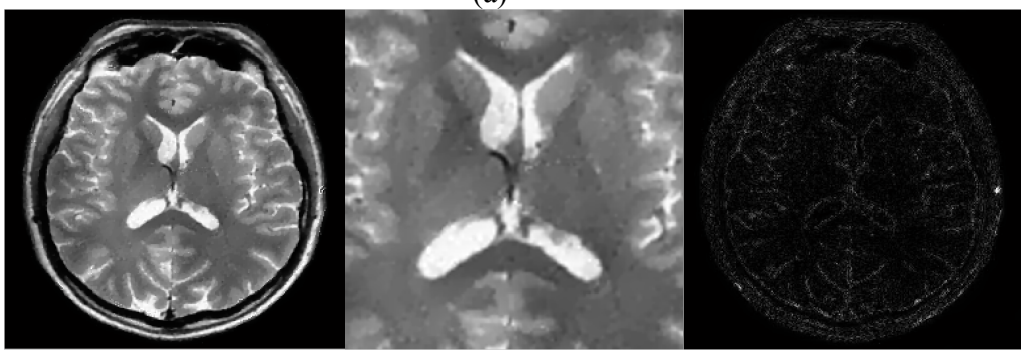

(b)

Fig. 3 Brain MR image reconstructions with 79.46% undersampling rate using the NLCG (a), and the proposed SP-GS method (b). The reconstructed images (left), the zoom-in of region of interest (middle) and the error maps (right) are shown.

Acknowledgment

This work is supported in part by the National Natural Science Foundation of China (61272311). This work is also This work is also supported in part by the science technology department of Zhejiang Province (2013C24019) and by Natural Science Foundation of Zhejiang Province (Y1100632 and LY14F010022).

References

[1] C. Westbrook, C. Roth K. and J. Talbot. MRI in Practice. 3rd edn, New York: Wiley-Blackwell, 2005.

[2] E. J. Candès, J. Romberg, T. Tao, Robust uncertainty principles: Exact signal reconstruction from highly incomplete frequency information, IEEE Trans. on Info. Theory. 52 (2006) 489-509,.

[3] D. L. Donoho, Compressed sensing, IEEE Trans. on Info. Theory. 52 (2006) 1289-1306.

[4] M. Lustig, D. L. Donoho, and J. M. Pauly, Sparse MRI: the application of compressed sensing for rapid MR Imaging, Magn. Reson. Med. 58 (2007) 1182-1195.

[5] J. Huang, S. Zhang, D. Metaxas, Efficient MR image reconstruction for compressed MR imaging, Med. Image Anal. 15 (2011) 670-679.

[6] H. Du, F. Lam, Compressed sensing MR image reconstruction using a motion-compensated reference, Magn. Reson. Imaging. 30 (2012) 954-963.

[7] M. Stojnic, F. Parvaresh, B. Hassibi, On the reconstruction of block sparse signals with an optimal number of measurements, IEEE Trans. Signal Process. 57 (2009) 3075–3085.

[8] W. Deng, W. Ying, and Y. Zhang, Group sparse optimization by alternating direction method, Technical Report TR11-06, Department of Computational and Applied Mathematics, Rice University, 2011.

[9] M. Usman, C. Prieto, T. Schaeffter, and P. G. Batchelor, k-t Group Sparse: A Method for Accelerating Dynamic MRI, Magn. Reson. Med. 66 (2011) 1163–1176.

[10] C. Prieto, M. Usman, J. M. Wild, S. Kozerke, P. G. Batchelor, and T. Schaeffter, Group Sparse Reconstruction Using Intensity-Based Clustering, Magn. Reson. Med., 69 (2013) 1169-1179.

[11] R. Achanta, A. Shaji, K. Smith, A. Lucchi, P. Fua, and S. Süsstrunk, SLIC Superpixels Compared to State-of-the-art Superpixel Methods, IEEE Transactions on Pattern Analysis and Machine Intelligence. 34 (2012) 2274-2282.

[12] Y. Xu, W. Yin, Z. Wen, and Y. Zhang, An Alternating Direction Algorithm for Matrix Completion with Nonnegative Factors, Front. Math. China. 7 (2012) 365-384.

Advanced Materials Research Vols. 989-994 (2014) pp 3952-3955
© (2014) Trans Tech Publications, Switzerland
doi:10.4028/www.scientific.net/AMR.989-994.3952

Pulse Coding Soft FM Telemetry Signal Demodulation

Wu Yanjun[1, a], Fu Gang[1,a] and Cheng Gang[1,a]

[1]China Satellite Maritime Tracking and Control Department, China

[2]School of Computer Science, Engineering and Mathematics, Flinders University, South Australia 5 042, Australia

[a]348237548@sina.com [b]wlp2005518@gmail.com

Keywords: demodulation, PCM/FM, MSD, synchronization

Abstract. The traditional method of demodulation for PCM/FM telemetry demodulation threshold is higher and the computation of the larger problem, research an orthogonal baseband after rotation, Symbol Detection (Multi - Symbol Detection, MSD) technology: the first frequency under the intermediate frequency digital telemetry signals processing, single sign on orthogonal baseband signal correlation matching, and then apply compound spinning technology to meet at the same time for multiple element symbols at the same time Detection, the purpose of the final design step length synchronization method with demodulation smoothly.

Introduction

PCM/FM telemetry signal demodulation is currently a hot research topic, the present stage space demodulation equipment is mainly used with orthogonal coherent demodulation method method, differential detection method, WD and DSTFT method, etc. However, all these demodulation method has certain limitation, such as orthogonal coherent demodulation needs strict synchronization; Digital FM signal demodulation based on DSTFT and WD algorithm is strong decay resistance, but the computation is too big. Boils down to a little[1] [2], the demodulation threshold causing high above the limitations of demodulation method. To this end, this paper adopts a orthogonal baseband after rotation symbol detection (MSD) method.

1 Traditional algorithms of MSD

Set the remote sensing observation period received can simplify the intermediate frequency signal is expressed as:

$$s(t) = \cos[w_c + f(t) + \theta_1] \tag{1}$$

The received signal with local orthogonal carrier multiplication, respectively after the Hilbert transform of two orthogonal baseband signals (I/Q).

$$R = I + j.Q = \cos[f(t) + \theta_1] - j\sin[f(t) + \theta_1] \tag{2}$$

So the corresponding local signal is also there are 2^N possible.

$$L = \cos[f(t) + \theta_2] + j\sin[f(t) + \theta_2] \tag{3}$$

$$\begin{aligned} R \cdot L &= \cos(\theta_2 - \theta_1) + j\sin(\theta_2 - \theta_1) \\ &= I_B + jQ_B \end{aligned} \tag{4}$$

The formula (5) the product of the result in integral operation within the length of observation, are:

$$M = N_C \cdot I_B + jN_C \cdot Q_B \tag{5}$$

Again to formulas (6) model of the complex signal results of square, get it:

$$S = N_C^{\,2} \cdot (I_B^{\,2} + Q_B^{\,2}) \tag{6}$$

So by the above process can distinguish the receiving signal element of positive and negative. Implementation block diagram is shown in figure 1.

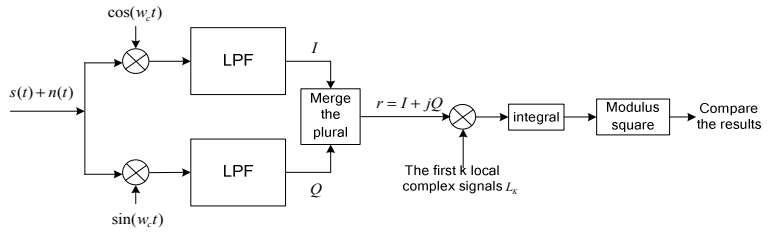

Figure 1 Baseband orthogonal MSD principle block diagram

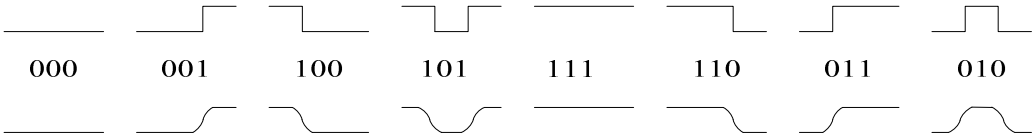

Figure 2 Preset filter before and after eight possible code waveform comparison

Eight of the plural by allowing for $M_{10}(1)$ to $M_{80}(1)$ accordingly plural Angle rotation, get eight different symbol waveform corresponding to different initial phase values of local signal associated with the current signals as a result, $M_{11}(1),\cdots,M_{1n}(1),M_{21}(1),\cdots,M_{2n}(1),M_{81}(1),\cdots,M_{8n}(1)$.

According to the current element time of various local corresponding correlation matching value of the received signal waveform and $M_{10}(1)$ and $M_{80}(1)$ and before 4 codes period have different code to local waveform and the initial phase of the correlation value between the received signal $M_{10}(k),\cdots,M_{1p}(k),M_{20}(k),\cdots,M_{2p}(k),M_{80}(k),\cdots,M_{8p}(k)$ $(k=2,3,4,5)$ .Out of the 128 possible, recent five codes period of approximate correlation value.

$$M_n = M_{7a}(5)+M_{6a}(4)+M_{3c}(3)+M_{1d}(2)+M_{20}(1) \tag{10}$$

2 Cascade type fixed step length synchronization

In the digital information transmission system, the accuracy of the synchronous is the basis of the correctness of the judgment, usually includes carrier synchronization and synchronization code. In the demodulation system, this paper design the cascade type fixed step length synchronizer can accurately fast local signal and the received signal to achieve the same frequency and phase.

First of all, only consider the deviation, will receive medium frequency signal in the form of a index for:

$$r(t) = e^{j(2\pi(f_c+\Delta f)t+\psi(t;z))} \tag{11}$$

At this point, with a maximum likelihood value expressions of deviation are as follows:

$$M = \max\left\{\int_0^{NT}\exp(j(2\pi(f_c+\Delta f)t+\psi(t;z)))s(t;\overline{z})dt\right\} \tag{12}$$

According to the type value of maximum likelihood (12) and the relationship between the deviation curve, the curve within the scope of 0.2 times the code rate on convex characteristics, according to the characteristics of intermediate frequency signal received at the same time A certain step fluctuation frequency processing, for after lifting the frequency of two-way signal to MSD after calculation, set by two way likelihood values for $M_{\max}(\Delta f-\Delta f(n)+k_1 f_c)$ and $M_{\max}(\Delta f-\Delta f(n)-k_1 f_c)$.

The two likelihood value difference, is the measure of synchronizer deviation error measurement, and can be feedback to the loop frequency offset correction to correct deviation loop.Update deviation:

$$\Delta f(n+1) = \Delta f(n) - \frac{e(n)}{|e(n)|}\lambda \tag{13}$$

Considering the influence of time delay below, only the presence of time delay, the presence of delay corresponding to the maximum likelihood expression is:

$$M_{\max}(\overline{z}) = \max\left\{\int_0^{NT}\exp(j(2\pi f_c(t-\Delta t)+\psi(t-\Delta t;z)))s(t;\overline{z})dt\right\} \tag{14}$$

Through (14) can draw the time delay effect on the likelihood value curve, and thus learned that the same curve with the convex properties, therefore, is similar to deviation, can be based on the idea of sooner or later, the door to receive the intermediate frequency signal simultaneously step must be A long time to add and subtract, and after MSD calculation, set by two way likelihood values of $M_{\max}(\Delta t-\Delta t(n)-k_2T)$ and $M_{\max}(\Delta t-\Delta t(n)+k_2T)$. Update time delay compensation value, namely:

$$\Delta t(n+1)=\Delta t(n)-\frac{e(n)}{|e(n)|}\lambda \tag{15}$$

In conclusion, through the analysis of carrier synchronization and code synchronization, design a step length of cascade type synchronizer is shown in figure 3.

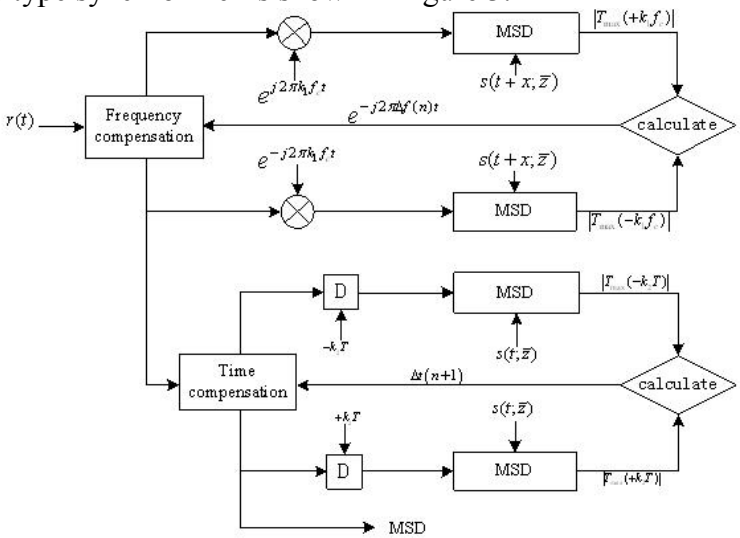

Fig3 Cascade type fixed step length synchronization principle block diagram

According to figure 3 design of synchronization method for frequency offset and time delay of synchronous simulation, get the estimates of variance and the SNR simulation diagram and the different time iteration step length and the relationship between the ber simulation diagram as shown in figure 4 and 5.

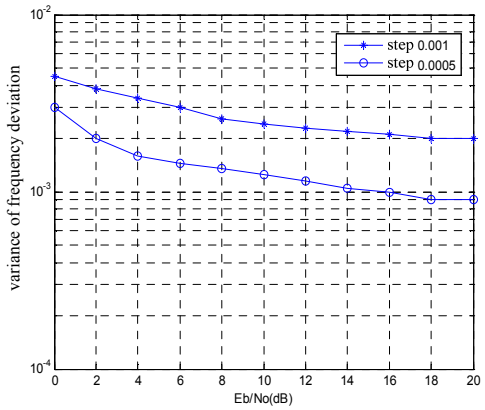

Fig4 Estimates of variance and signal-to-noise ratio

Figure reflects the achieve synchronization state 4, frequency offset estimation variance and the relationship between the SNR, it can be seen that with the improvement of signal-to-noise ratio, increase the stability of the estimates. The figure 5 shows, different time different iteration step length corresponding BER curve, namely under the condition of the same signal-to-noise ratio, different iteration step length error rate, with the decrease of the iteration step length, the bit error rate is reduced,

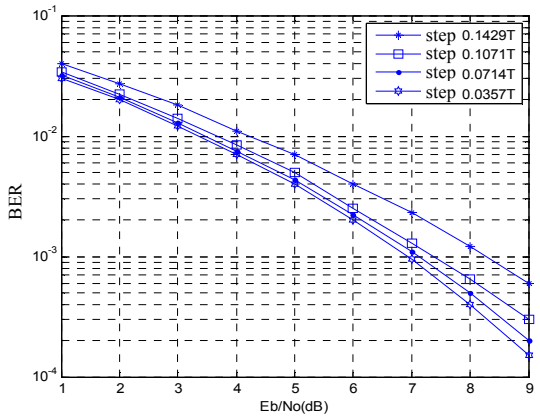

Fig5 The BER curves under different time iteration step length

3 Algorithm performance.

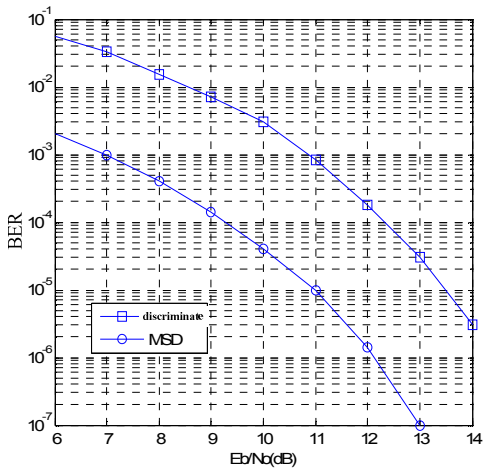

Fig6 The BER curves under different time iteration step length

Through the figure 6 shows that MSD demodulation method based on orthogonal baseband after rotating decoding performance is good, the method is feasible.

Summary

Test results show that the proposed method can effectively break the traditional problem of demodulation method of threshold.

References

[1] Feng Xiaoping. Discrete distribution of WV in the application of FSK signal digital demodulation[J]. Journal of xi 'an university of electronic science and technology (natural science edition), 2003, 30(2): 201-204, 250.

[2] YU Daquan. DSTFT FSK communication systems modeling and simulation and DSP code generation[J]. Microcontroller and embedded systems applications, 2011,1: 33-35.

Advanced Materials Research Vols. 989-994 (2014) pp 3956-3959
© (2014) Trans Tech Publications, Switzerland
doi:10.4028/www.scientific.net/AMR.989-994.3956

Design of High-Speed Data Collector of blast wave Signal Based on the Post-Trigger Principle

Xinger Tang

Electronic and Information Technology Department, Jiangmen Polytechnic, Jiangmen China

Keywords: post-trigged, blast wave signal, data sampling

Abstract: in view of the incomplete signal and other issues brought by the threshold trigger in the conventional blast wave signal test, this paper designed a post-trigger data high-speed collection method, adopted the ARM7 kernel MCU to complete the design of the hardware scheme and preparation of the corresponding test software, then developed the post-trigger data high-speed collector prototype, and completed the explosive shock wave signal collection through the test. Experiments show that the post-trigger high-speed data collector developed in this paper has the characteristics of simple interface circuit, high precision collection, good reliability, simple operation, which can meet the test requirements of blast wave.

1. Introduction

Blast wave refers to a high-speed high pressure wave spread in the medium (air, water) after the explosion of the explosive, with the characteristics of high transmission speed, instance increase of the pressure on the surface of the wave, the signal test has been the difficulty of dynamic testing technology in weapons industry. Usually, the test of the blast wave test collection is conducted by high-speed data collection instrument, while testing, turn on the collection in advance and then record the way of blast wave signal, which usually will cause the problems of redundant data, difficult to find, increase data processing difficulty and the cost of hardware. But if the data are collected after the threshold signal is triggered, which usually may cause the problem of the incomplete tested waveform caused by the instantaneous uncollected waveform of the pre-trigger point. Other scholars have proposed some solutions, but there are the problems of circuit design complexity and high cost.

Therefore, This paper put forward a data collection instrument design principle based on the post-trigger data high-speed data collection, namely once the collector is turned on, it will be in the normal working state, then it conducts continuous high-speed sampling for the tested analog signal, when the trigger signal comes, it stops the collection after some delay, and then it records the signal at a certain time before and after the trigger point by setting to complete the collection and recording of the waveform of the whole shock wave.

2. Design Principles

Principles of high-speed data collection instrument are usually as follows: the collector is normally in a wait state and it begins sampling measurement only when trigger signal produced by the blast wave arrives. So the weaker the trigger signal of the effective trigger is, the closer the test signal is to the complete blast wave. After all, the blast wave goes before the trigger signal, so no matter how little the trigger signal will produce effective trigger, which cannot obtain the complete shock waves.

2.1 External Trigger Modes and Defects of the Conventional Data Collection

In order to enable the external trigger signal to be effectively triggered, first of all, it is needed to set up a certain trigger condition, when the voltage of the input external trigger signal waveform exceeds the threshold voltage, it will produce the flip level of 0 to 1 or 1 to 0 to start the data collector to collect data.

External trigger signal is usually obtained through a trigger circuit; a simple triggering circuit can be achieved by using a comparator, as shown in Figure 1:

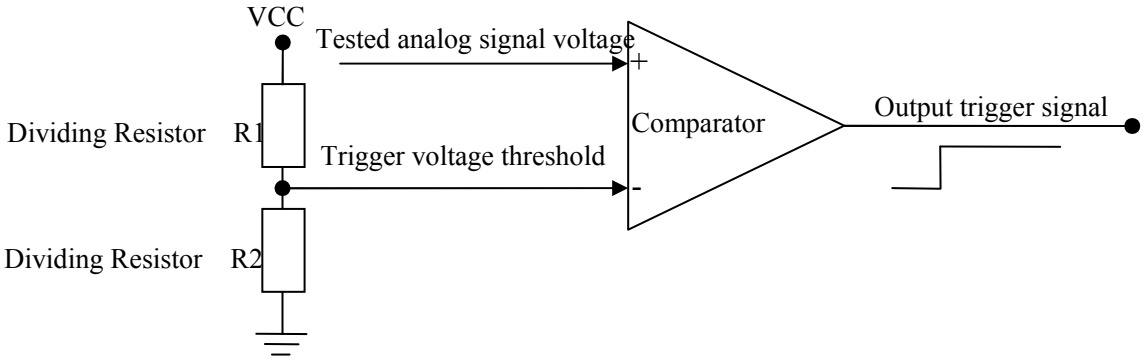

Figure 1: A Simple Trigger Circuit

Trigger voltage threshold can be obtained by the partial pressure of dividing resistor R1 and the dividing resistor R2 to VCC, the supply voltage, the required trigger voltage threshold can be set by changing the resistance ratio of the dividing resistor R1 and the dividing resistor R2.

When the voltage of the input tested analog input signal (i.e. external trigger signal) is compared with the trigger voltage threshold, if the voltage of the analog signal is greater than the trigger threshold voltage, the external trigger signal output by the comparator changes from "0" to "1", the trigger signal occurs a valid triggering, that is, the trigger signal starts the collector to begin sampling.

In response to the uncertainty of the trigger threshold voltage in the actual test situation, a digital analog converter (DAC) can be used to obtain the trigger circuit design of the voltage threshold, as shown in Figure 2.

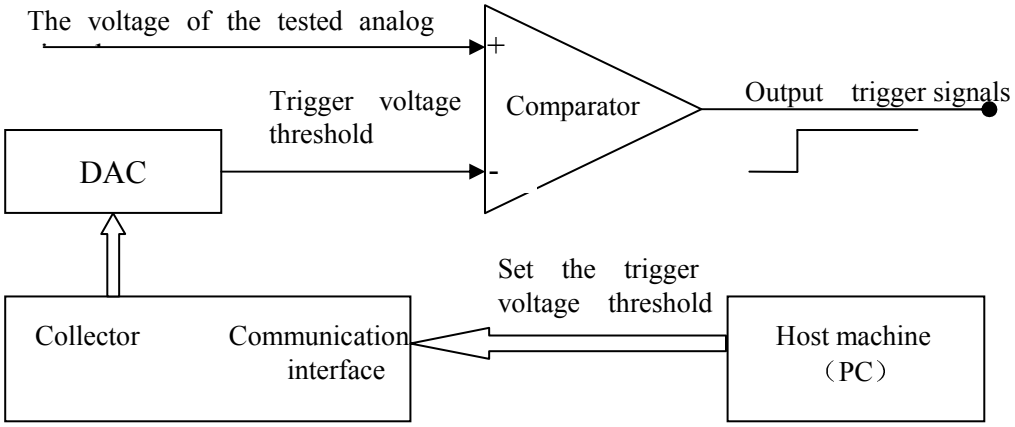

Figure 2: Triggering Circuit Design with DAC

General DAC receives the control and digital input on the host processor from the collector through data / address / control bus, or SPI bus receiver. After the digital quantity to achieve the corresponding required trigger voltage threshold is calculated, the background machine (PC) can send digital quantity to DAC through the UART communication interface to get the DAC output to trigger voltage threshold.

It can be seen that the method through the external trigger signal to start the collector sampling can only collect the waveform which the analog voltage signal is greater than the set threshold trigger voltage, so in order to measure the waveform signal of the complete blast waves as much as possible, it is needed to reduce the trigger voltage threshold as much as possible, but this will cause the occurrence of the false triggering.

2.2 Methods and Characteristics of the Post-Trigger High-Speed Data Collection

Therefore, in view of the above problems, this paper designed a method of post-triggering high-speed data collection, namely with the same external trigger signal, not with the trigger starting the collector to begin sampling operation, but with the trigger causing the collector to stop sampling operation. At this time, the collector usually works in the normal condition, constantly monitoring the input tested analog signal and the external trigger signal. Once the collector is turned on, it will be in the normal working state, the tested continuous analog signal will be high-speed sampled, and the data collected are stored in the collector, being composed of RAM memory in FIFO. After the sampling time of ΔT, the sampling data stored in FIFO will automatically cover before the sampling data before the sampling time of ΔT. Assuming the capacity of FIFO is X bit, the collector uses the ADC of 16 bit precision, the sampling rate is Y MB / sec. ΔT can be calculated:

$$\Delta T = \frac{X}{16 * Y}$$

The test method of post-trigger high-speed data collection is as follows: the same external trigger signal is used to start a delay circuit, after the Δt delay of the circuit. a jump signal is generated to end the high-speed data sampling operation of collector. It can be seen that if $\Delta t < \Delta T$, the sampling data in FIFO will not be covered; if Δt is greater than the time L cost from the beginning of the explosion to the end of the explosion, the collector will can completely collect the blast wave.

In practical design, the special delay circuit can be left out, and the external trigger signal can have direct access to some pin of the main processor, then the external trigger signal can start some timer of the processor, the time of the timer is set to be Δt. Then after the external trigger signal effectively starts the timer, the timer can interrupt after the Δt delay, high-speed sampling requesting the main processor to terminate the high-speed sampling operation of the collector.

3. High Speed Sampling Operation Used in the Measurement of the blast wave Signal

3.1 Introduction to MCU Chip

The main processor adopted in this design is STM32F103ZET6, the processor is the enhanced MCU, 32 bit RISC kernel of the high-performance ARM Cortex-M3 is used, with the frequency of 72M, a built-in high-speed 512K-bytes flash memory and 64K-bytes SRAM, which has a wealth of I / O ports and functions. Including three 12-bit precision A / D converter ; 4 16-bit general timers; 2 PWM timers; it also has a variety of communication interfaces, including two I2C bus interfaces, three SPI interfaces, two I2S interfaces, an SDIO interface, 5 USART / UART interfaces, a USB interface and a CAN interface. Meanwhile, the chip also integrates a FSMC module, which has four chip selective outputs, which support PC Card / CF card, SRAM, PSRAM, NOR and NAND.

3.2 Hardware Design

The overview of the working principle and hardware design of the high-speed post-trigger data collector using STM32F103ZET6 as the main processor is shown. After the signal conditioning of the tested analog signal, trigger signal is separated and be input into the STM32F103ZET6 analog sampling channel. STM32F103ZET6 achieves external RAM expansion via data /address /control bus.

As when the collector conducts high-speed data collection, the sampling data cannot be transmitted in real time, but chronologically stored inside the FIFO of the external SRAM. Only after the end of sampling, a host computer can be used (i.e. a PC in background services) to send commands to the collection via UART and other communication interfaces, taking the sample data existing in the RAM of the external collector.

3.3 Realization of the Function of Post-Trigger

The function of post-triggered of the collector can be realized by regarding one of the STM32F103ZET6 ADC channel to be simulated into watchdog, namely, one of ADC of the analog watchdog accurately monitors the external trigger signal, and the other ADCs collect the voltage of the selected and input analog signal.

When the external trigger signal monitored by the analog watchdog ADC exceeds a preset threshold, the STM32F103ZET6 will generate an interrupt signal to end the ADC sampling operation. An obvious advantage of such the ADC analog watchdog to monitor the external trigger signal is that it can conveniently precisely set the triggering voltage threshold according to the level of error of the actual external trigger signal, the sampling duration and anti-interference, accurate trigger voltage threshold setting of external trigger signal so as to facilitate the adjustment, be conducive to the collection of the sampling data of the complete waveform.

4. Conclusions

This paper used an ARM7 kernel MCU, developed a "post-trigger high speed data collector". The collector realized the functions of timely effectively and completely recording the explosion process by delaying the external trigger signal to end the working mode of the sampling process. And its interface circuit is simple with high precision, which is very suitable for the measurement of the explosion process, and has the widespread application prospect.

References

[1]Shouping Guan Fuqiang You.The design of high speed data acquisition system based on DSP,*Control Engineering of China,*55(6),2013,pp:53-57.
[2]Yang Zhao.Maxwell's equations on Cantor sets: a local fractional approach.*Advances in High Energy Physics,*2013(2013),2013,PP:1-7.
[3]Xingping Peng,Ningjun Fan.The design method of the special high speed data acquisition system.*Journal of Test and Measurement Technology*,31(4),1998,PP:38-43.
[4]Yang Zhao.Mappings for special functions on Cantor sets and special integral transforms via local fractional operators.*Abstract and Applied Analysis*, 2013(2013),2013,PP:1-6.
[5]Yang Zhao.Local fractional discrete wavelet transform for solving signals on Cantor sets.*Mathematical Problems in Engineering*, 2013(2013),2013,PP:1-6.
[6]Yang Zhao.Approximation solutions for local fractional Schrödinger equation in the one-dimensional Cantorian system.*Advances in Mathematical Physics*, 2013(2013),2013,PP:1-5.

Advanced Materials Research Vols. 989-994 (2014) pp 3960-3962
© (2014) Trans Tech Publications, Switzerland
doi:10.4028/www.scientific.net/AMR.989-994.3960

On Matlab's Simulations in Underground Mobile Multipath Channel

Jingxin Wei

NCIST Teaching Affairs Department，Bejing East, Yanjiao 101601

Keywords：Channel model, Simulation, multipath interference

Abstract: In underground channel environment, features of wireless mobile channel and channel modeling are discussed, and methods of calculating wireless channel model parameters by adopting even-interval tapped delay wire model are proposed. On this basis, Matlab simulation are carred out, whose results serve as theoretical foundation and criterion for further study of underground wireless communication system.

1 Features of communication in underground mine

The paths covered by signals from the transmitter to the receiver are called channel. In underground wireless communication, wireless waves are transmitted in non-free tunnel with frequent reflection, refraction and scattering. The underground situation is specifically complex due to the rugged seam around the wall and the tunnel-filled supports, electromechanical equipments, metals, power line, dust, and humid air, etc. Electromagnetic waves are transmitted with multiple refractions, reflection and scattering, making the signals reaching to the receivers the synthesis of multipath signals, which is called multipath effect. Multipath transmission will result in the frequency selective fading and delay expansion of received signals, leading to intersymbol interference, which affects the quality of communication directly. As a result, the electromagnetic waves can only be transmitted as far as hundreds of meters in mine tunnel, while the underground tunnel has an average length of several thousands meters, or even as long as ten thousands of meters.

Invisibility is caused by the curved floor and roof in the tunnel and working face, as well as the various kinds of varvature formed by directional changes of coal and rock horizontally. Wireless communication of invisibility greatly reduces the transmission distance of wireless signals in the tunnel and working face.

Therefore, the tunnel effect, limited space, distance and invisibility of underground transmission of the electromagnetic waves make it differ from the surface communication.

2 Underground channel model

The received signal of dispersed multipath channel can be represented[3] [4] :

$$y(t)=\sum_{n}\alpha_n(t)s(t-\tau_n(t)) \tag{1}$$

Where $s(t)$ is band pass received signal, $\alpha_n(t)$ is attenuation factor of Number n path, $\tau_n(t)$ is the corresponding transmission delay. By low pass equivalent effectivity, $s(t)$ can be represented:

$$s(t)=\mathrm{Re}\left[\tilde{s}(t)e^{j2\pi f_c t}\right] \tag{2}$$

$$y(t)=\mathrm{Re}\left\{\left(\sum_{n}\alpha_n(t)e^{-j2\pi f_c\tau_n(t)}\tilde{s}(t-\tau_n(t))\right)e^{j2\pi f_c t}\right\} \tag{3}$$

Then the envelope of attainable output signal is:

$$\tilde{y}(t)=\sum_{n}\alpha_n(t)e^{-j2\pi f_c\tau_n(t)}\tilde{s}(t-\tau_n(t))=\sum_{n}\tilde{\alpha}_n(t)\tilde{s}(t-\tau_n(t)) \tag{4}$$

(4)4indicates that multipath channel can be presented by $\tilde{c}(\tau;t)$, time-varying low pass equivalent impulse response:

$$\tilde{c}(\tau;t)=\sum_{n}\tilde{\alpha}_n(t)\delta(t-\tau_n(t)) \tag{5}$$

Where $\tilde{c}(\tau;t)$ refers to the channel response of $t-\tau$ -added impulse at the time of t.

Each path in the discrete multipath channel is commonly considered as the product of numerous scattering components, therefore, the tap of each path is regarded as one complex Gaussian random variable. In real channel simulation, it is commonly assumed that there a finite number of taps and the number is decided by the channel's delay extension value. To be simple, channel character is assumed to fit in with the character of WSSUS.

$$\tilde{g}_n(t)=\int_{-\infty}^{\infty}\tilde{h}(\tau;t)\left\{\frac{\sin(2\pi B(\tau-nT))}{2\pi B(\tau-nT)}\right\}d\tau \tag{6}$$

$$\tilde{h}(\tau;t)=\sum_{k=1}^{N}\tilde{a}_k(t)\delta(\tau-\tau_k) \tag{7}$$

Where the impulse response of discrete multipath channel is $\tilde{h}(\tau;t)=\sum_{k=1}^{N}\tilde{a}_k(t)\delta(\tau-\tau_k)$ Therefore,

$$\tilde{g}_n(t)=\sum_{k=1}^{N}\tilde{a}_k(t)\sin c\left(\frac{\tau_k}{T}-n\right)=\sum_{k=1}^{N}\tilde{a}_k(t)\alpha(k,n) \tag{8}$$

Where the envelope of $\alpha(k,n)=\sin c\left(\frac{\tau_k}{T}-n\right)$, $\alpha(k,n)$ decreases with increasing $|n|$. So the number of TDL's model taps can be described as $|n|\le m$, where $m>>T_{\max}/T$. When the maximum of delay expansion is within 3-4 symbol periods, the number of TDL taps is less than 20.

Table 1 TDL model of even interval

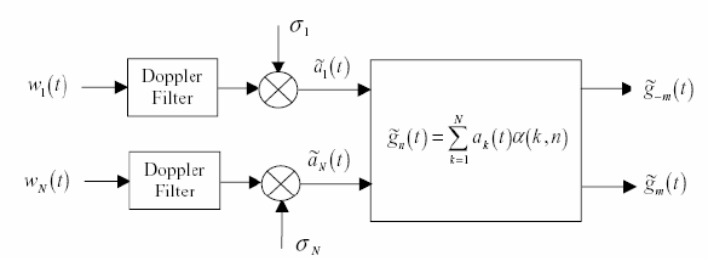

As Table 1 indicates, after input signal $w_1(t)\cdots w_N(t)$ (complex Gaussian random process with zero mean, unit variance) passes through the Doppler filter, $T^2p(nT)=\sigma_n^2$ is achieved, and then Doppler power σ_n, which is multiplied by output of Doppler filter to get $\tilde{a}_1(t)\cdots\tilde{a}_N(t)$, leading to $\tilde{g}_1(t)\cdots\tilde{g}_n(t)$, the tap coefficient.

3 Simulation of underground multipath channel

The underground supports, electromechanical equipments, rugged seam, humid air and dust leave no room for direct path between the transmitter and the receiver of wireless devices. So, underground wireless channel accords roughly with the character of Rayleigh channel. According to the documents, underground channel obeys the channel model of exponential decay, whose power delay spectrum decreases exponentially. The power delay spectrum of this model can be shown as:

$$p(\tau)=1/\tau_d\exp(-\tau/\tau_d) \tag{9}$$

To conclude, according to the data in the documents, the following underground wireless multipath channel model can be made:

Table 1: Channel model 1
(rms delay expansion=100ns)

path	delay（ns）	Average powerdB）
1	0.0	0.0
2	50.0	-1.6
3	150.0	-4.7
4	325.0	-10.1
5	550.0	-17.1
6	681.9	-21.7

Table 2: Channel model 2
(rms delay expansion=18ns)

path	delay（ns）	Average power（dB）
1	0.0	0.0
2	50.0	-9.4
3	100.0	-18.9

According to the data in the table, simulation is made as follows:

Table 2 Input spectrum and transfer function under two delays

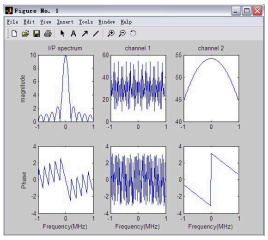

In Table 2, the upper line is magnitude function, while the lower line is phase function. The first column on the left shows that output spectrum is mainly distributed within the zone of [-200KHz,200KHz]. As to channel 2 (the right column), in this zone the magnitude of transfer function is almost flat and the phase of it is basically linear. So, channel 2 will lead to slight distortion, and this kind of channel is termed as flat fading channel. For channel 1 (the middle column), in this interval, the magnitude of transfer function is non-flat and the phase of it is non-linear. So channel 1 will suffer from severe distortion, indicating that underground channel is frequency selective fading channel. The change rate of transfer function (for specific frequency) is proportionate to the delay expansion — the bigger the delay expansion, the quicker the change rate of transfer function.

4 Conclusion

Considering the features of underground channel environment, this paper makes channel modeling and establishes the channel model according to the underground channel features. Moreover, computer simulation is carried out, laying theoretical foundation for further study on underground wireless communication system.

References

[1] Huangwei, Yao Shanhua. Discussion on the Problems and Solutions of Underground Mobile Communication Techniques. CoalMine Machinery. 2003.12.

[2]Li Bingyu, et al. Simulation of Microwave Multipath Communication Characters in the Tunnel. Microwave Journal. 19 vols. No.4,2003,12.

[3]W. H. Tranter, K. S. Shanmugan, T. S. Rappaport, K. L. Kosbar,Principles of Communication Systems Simulation with Wireless Applications,Prentice Hall, 2004.

[4]Tong Xuejian, Luo Tao. OFDM Mobile Communication Law and Application. Beijing: People Post Press, 2003,6.

[5]G. L. Turin et al.,“A Statistical Model of Urban Multipath Propagation,”IEEE Transactions on Vehicular Technology, Vol. 21, February1972,pp. 1－9.

[6]Zhang Yueping, Zhang Wenmei, Sheng Jianhuan, Wang Yongqiang. Characters of Transfer Channel of Broadband UHF Radio Waves in the Tunnel. Communication Journal. 1998,8, 19(8).

[7].Karen Halford, Mark Webster.Multipath Measurement in Wireless LAN. www.intersil.com.2000-5

[8].Chayat, Naftali.Tentative Criteria for Comparison of Modulation Methods. IEEE 802.11-97-96, 1997-9.

Advanced Materials Research Vols. 989-994 (2014) pp 3963-3967
© (2014) Trans Tech Publications, Switzerland
doi:10.4028/www.scientific.net/AMR.989-994.3963

Clutter Modeling and Characteristic Analysis for Airborne MIMO Radar

Hao Lin[1], Zhang Yong-shun[1], Li Zhe[1], Xu Jie[2]

[1]AFEU, School of air and missile defense, ShanXi Xi'an 710051, China;

[2]Unit 93617 of PLA, Beijing101400,China

Keywords: Airborne MIMO radar; Clutter modeling; Error conditions; Clutter characteristics

Abstract: For the issue of MIMO airborne radar clutter modeling in different environment conditions, a clutter modeling method based on composite model is proposed. It builds different types of clutter model through the changes of model parameters. The clutter model consists of clutter amplitude distribution model, and clutter cell scattering model. After considering the error factors such as element error, channel error, clutter fluctuation, a clutter modeling method based on composite model under error conditions is proposed. Finally, the computer simulation is made about the amplitude, the back-scatter coefficient, error factors, the space-time MV spectrum and the characteristic spectrum of different types of clutter through changing the model parameters. The simulation results show that: In ideal conditions, the Clutter Spectrum has good space-time characteristic, but in error conditions, the clutter fluctuates tempestuously, and in different environment conditions the fluctuation degree is different.

Introduction

How to suppress the strong ground clutter and other interference while the airborne radar is detecting moving target is the main problem now. Therefore，clutter modeling and simulation technology is always one of the research hotpots of radar application. The clutter modeling and simulation technology is always one of the research hotspots of radar application. Through deep research of clutter characteristic, the scholars obtained significative achievements. In [1-3],according to the radar resolution ratio and the amplitude modeling under different conditions, the Rayleigh model, Log-Normal model and Weibull model are proposed, they can match the amplitude data of the clutter properly. However, there are few research in the clutter modeling of MIMO radar, in[5]and [6],a clutter modeling method of airbore MIMO radar is proposed, but the element error, channel error and the gesture variation of the plane are not taken into account. In[7]a clutter model of airborne MIMO radar is established，but in this model ,the clutter has no fluctuation, non-Gaussian process is not under consideration.

Aiming at the limitation of the clutter model all above, this paper combines the common clutter amplitude distribution model, clutter cell scattering model and the radar parameter model ,considering the effect of element error, channel error and clutter fluctuation as well, a clutter modeling method based on composite model under error conditions is proposed .The model can reflect the generating principium and the statistical characteristic of clutter, in addition, it adapts to different environment and different error conditions.

The geometrical model of airborne MIMO radar

Fig.1 illustrates the geometrical model of Side-Looking airborne MIMO radar array antenna .The radar platform travels at velocity v in the positive direction of x axis, the altitude of the array phase center is H. The azimuth angle of the clutter scattering cell is θ,the elevation angle is φ,and the cone angle is ψ.We assume that during the Coherent Processing Intervals(CPI),the plane moving range is much more smaller than the slant range between the radar and the clutter source. Suppose that the antenna array has a side-looking uniform linear arrays configuration with M transmitting antenna elements and N receiving antenna elements. Let d_T be the space of each two adjacent

transmitting antenna elements while d_R be the space of each two adjacent receiving antenna elements. The ratio of space between each two transmitting and receiving elements is $\alpha = d_T / d_R$ .Let K be the number of radar pulses in one coherent processing interval (CPI).

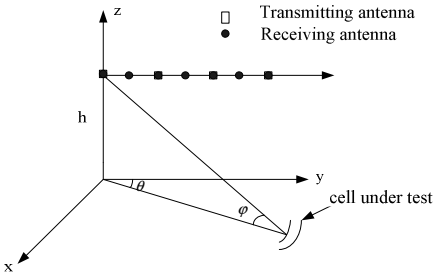

Fig.1 The model of airborne MIMO radar system

The amplitude distribution model of clutter

One of the nonhomogeneous performances of clutter is the clutter amplitude fluctuation. This fluctuation is stochastic, but taking one with another, such as Log-normal distribution：

$$p(X) = \frac{1}{2\pi\sigma X}\exp(-\frac{[\ln(X / X_m)]^2}{2\sigma^2}), (X \geq 0) \tag{1}$$

X_m is the median of X , σ is the standard deviation.

Another matching approximate distribution is Weibull distribution：

$$p(X) = \alpha\lambda X^{\alpha-1}\exp(-X^{\alpha}), (X \geq 0) \tag{2}$$

Here, α and λ are both constant, α is the parameter related to the distribution slope of Weibull., λ is called the Weibull parameter.

The scattering model of clutter cell

The radar cross section(RCS)is decided by the scattering model of the clutter cell, it can be defined as follow:

$$\sigma_c(R_S) = A_b \times \sigma_0(R_S) \tag{3}$$

A_b is the projection area of the clutter cell in the line of sight of radar, $\sigma_0(R_S)$ is the reflectivity . The strong and weak of radar clutter is always described by the reflectivity. A common reflectivity model is Morchin model0,which is given by:

$$\sigma_0(r) = \frac{A\sigma^0 \sin\theta_g}{\lambda} + \mu(ctg\beta_0)^2 \exp[\frac{tg(\beta_0 - \theta_g)^2}{tg\beta_0^2}] \tag{4}$$

λ is the wavelength of radar，θg is the grazing angle, A , B , β_0 , σ_m^0 , μ are the model parameter, Table 1 shows the typical simulation parameter of ground clutter.

$$\mu = \sqrt{f_0(GHz)} / 4.7 \tag{5}$$

f_0 is the frequency of radar.

Table 1 A set of typical ground clutters simulation parameter

	A	B	β_0	σ^0
desert	0.00126	$\pi/2$	0.14	F
farmland	0.004	$\pi/2$	0.2	1
hill	0.0126	$\pi/2$	0.4	1
mountain	0.04	$\pi/2$	0.5	1

$$\mathrm{F}=\begin{cases}\left(\dfrac{\theta_g}{\theta_c}\right)^k & \theta_g<\theta_c \\ 1 & \theta_g>\theta_c\end{cases} \tag{6}$$

θ_g is the grazing angle θ_c is the Transitional angle[11].

The composite model of airborne MIMO radar

The clutter signal of the i th gridding in the l th range ring can be denoted with the description of the amplitude distribution model of clutter, the scattering model of clutter cell and the radar parameter model:

$$\mathbf{c}_l(m,n,k)=\sum_{i=1}^{N_\theta}\frac{\sqrt{G}}{R_l^2}a_{il}e^{j\Phi}e^{j\alpha(m-1)\omega_s+j(n-1)\omega_s+j(k-1)\omega_t} \tag{10}$$

$m=1,2,\cdots,M$, $n=1,2,\cdots,N$, $k=1,2,\cdots,K$, M， Nand K are the amount of transmitting antenna ,receiving antenna and pulse respectively. R_l is the range between the l th range ring and the clutter cell. Φ is the random phase item， a_{il} is the sequence of clutter amplitude fluctuation. $\omega_s=(2\pi d/\lambda)\cos\theta_{li}\cos\phi_l$ and $\omega_t=2\pi f_{dl}/f_r$ are the airspace angular frequency and the time domain angular frequency respectively , d is the space of each two antenna， f_{dl} is the Doppler frequency of the l th range ring, f_r is the PRF. G is given by:

$$G=\frac{D_u P_t G_{t0} G_{r0}\lambda^2}{(4\pi)^3\Gamma}\sigma_c(r) \tag{11}$$

P_t is the radar pulsed power, $D_u=D\tau/T_r$ is the duty ratio, G_{t0} and G_{r0} are the power gain of the transmitting antenna and receiving respectively. Γ is the loss factor of the system, $\sigma_c(r)$ is denoted in formular(3).

Then element error of the transmitting antenna and receiving antenna is given by:

$$\rho_{p_1p_2}^{(\text{cell})}=\left(1+ea_{p_1p_2}\right)\exp\left(\mathrm{j}ep_{p_1p_2}\right) \tag{12}$$

$ea_{p_1p_2}$ ， $ep_{p_1p_2}$ is the element error， when $p_{1\neq}p_2, ea_{p_1p_2}=ep_{p_1p_2}=0$ 。

The channel error is given by:

$$\rho_{p_1p_2}^{(\text{channel})}=\left(1+ca_{p_1p_2}\right)\exp\left(\mathrm{j}cp_{p_1p_2}\right) \tag{13}$$

$p_1,p_2=n+(m-1)M,\ n=1,...,N,m=1,...,M$ $ea_{p_1p_2}$, $ep_{p_1p_2}$ denote the channel error between the p_1 th channel and the p_2 th channel .

The clutter fluctuation always obey the Gaussian distribution ,it can be expressed in:

$$\rho_{k_1k_2}^{(c)}=\exp\left(-B_c^2\left(k_1-k_2\right)^2/8\right) \tag{14}$$

$k_1=1,2,...,K,k_2=1,2,...,K$ 。

The clutter model can be expressed as follow after considering all kinds of the errors above:

$$r_l(\Delta m,\Delta n,\Delta k)=\sum_{i=1}^{N_\theta}\sum_{i=1}^{N_\theta}\exp\left(-B_c^2(\Delta k)^2/8\right)\left(1+ca_{p_1p_2}\right)\exp\left(jcp_{p_1p_2}\right) \tag{15}$$
$$\frac{\left(1+ea_{p_1p_2}\right)\exp\left(jep_{p_1p_2}\right)G}{R_l^4}a_{il}e^{j\Phi}e^{j\alpha\Delta m\omega_s+j\Delta n\omega_s+j\Delta k\omega_t}$$

Simulation results

In order to analyze the clutter distribution of airborne MIMO radar, a plenty of simulation has been processed. The parameter of the model are: the amount of transmitting antenna M= 8，the amount of

receiving antenna N= 8，the amount of pulses K= 16,the wavelength $\lambda = 0.23m$，the space of each two adjacent receiving antenna elements $d_R = \lambda / 2$, the ratio of space between each two transmitting and receiving elements is $\gamma = 10$，the velocity of the platform V= 140 km/h，the hight of the platform H=8 km，the PDF is f=2438. 8Hz，the transmitting power P= 180kW，the clutter-noise ratio $R_{CN} = 60dB$.Experiment 1: the clutter spectrum in different environment under ideal conditions

The simulation is implemented in two typical environments: desert and mountain. The clutter amplitude distribution obeys Log-normal distribution, while the clutter scaterring cell parameter refers to Table 1.

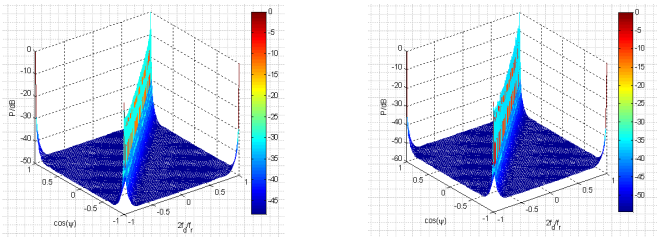

(a) The ground clutter in desert (b) The ground clutter in mountains

Fig. 2 The space-time MV spectrum plot of airborne MIMO radar under ideal conditions

Fig.2 shows that the clutter distribution has diagonal characteristic. By comparing Fig.2 with Fig.3, we can see that in desert environment, the fluctuation of the clutter spectrum is flatter, while in mountain environment, the fluctuation is more tempestuously.

Experiment 2: the clutter spectrum in different environment under error conditions

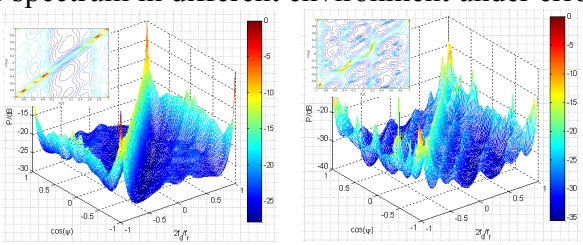

(a) The ground clutter in desert (b) The ground clutter in mountains

Fig. 3 The space-time MV spectrum and contour plot of airborne MIMO radar when the element error is 5

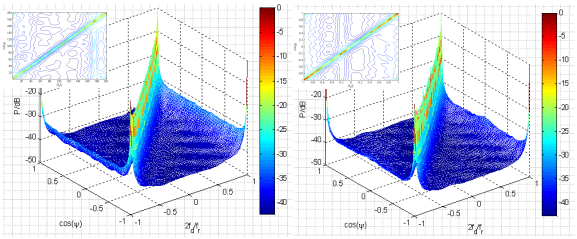

(a) The ground clutter in desert (b) The ground clutter in mountains

Fig.4 The space-time MV spectrum and contour plot of airborne MIMO radar when the channel error is 5%

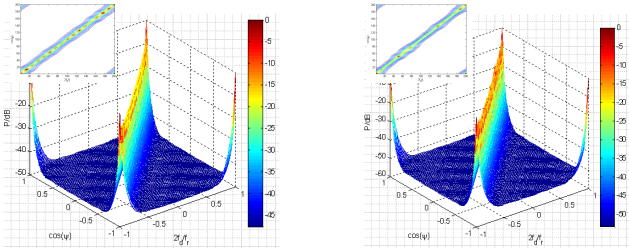

(a) The ground clutter in desert (b) The ground clutter in mountains

Fig.5 The space-time MV spectrum and contour plot of airborne MIMO radar when the clutter fluctuation is 5%

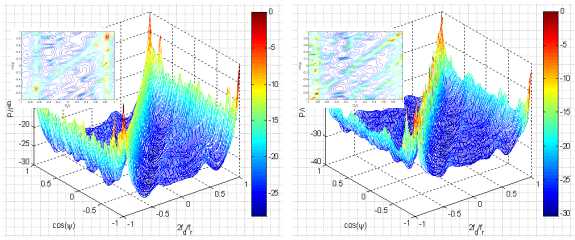

(a) The ground clutter in desert (b) The ground clutter in mountains

Fig.6 The space-time MV spectrum and contour plot of airborne MIMO radar under different kinds of errors.

Fig.3 shows that element error causes the clutter spectrum fluctuated tempestuously. Fig.4 shows that channel error causes the clutter spectrum extension and clutter fluctuation. Fig.5 shows that the main effect caused by clutter fluctuation is spectrum extension. Fig.6 shows that the space-time coupling characteristic is not obvious under different kinds of errors.

Conclusions

Aiming at clutter modeling of airborne MIMO radar in different geomorphic feature and different error conditions, a clutter modeling method based on composite model under error conditions is proposed .The simulation results show that the clutter spectrum of the airborne MIMO radar has good space-time two-dimensional characteristics and the element error, channel error, clutter fluctuation. etc make the spectrum wider, increase the degree of freedom of clutter as well, among all the errors, the element error has the strongest effect.

References

[1]Chengqing Lin,Xiubin Zhao,Guangjing Zhang.The modeling and simulations of radar[J].Modern Defence Technology, 2010,8（38）, 116-121.

[2] Baihua Zhang,Yongshun Zhang,Xingcheng Li,Hanjin Pan.Ground Clutter Characteristics of Airborne Bistatic Radar[J]. Modern Defence Technology, 2010, 6（38）, 132-138.

[3]Hu C，Long T，Zeng T. Statistic characteristic analysis of forward scattering surface clutter in bistatic radar[J]. Science China-Information Sciences, 2010, 53(12):2675-2686

[4] Hu Cheng, Long Teng, Zeng Tao, er al. Science China-Information Sciences, 2010, 53(11): 2310-2322

[5] Chen C Y and Vaidyanathan P P. A subspace method for MIMO radar space-time adaptive processing[C]. IEEE International Conference on Acoustics, Speech, and Signal Processing, Honolulu, Hawaii, April 15-20, 2007, (2):925-92A.

[6] Xichuan Zhang,Yongshun Zhang,Yongliang Wang,Pengfei Zhao. Journal of Air Force Engineering University(Natural Science Edition), 2010, 11(5):35-38

[7] Tao Yan,Wenchong Xie,Yongliang Wang.Model and Clutter Characteristics Analysis for Airborne MIMO Radar[J].Radar Science and Technology, 2010, 8(4):289-295

[8] Wenlin Hu,Yongliang Wang,Shouyong Wang.Performance of Ordered Statistic CFAR Detector Under Log-normal Distributed Clutter[j].Journal of Electronics&Information Technology, 2007, 35(3): 517-520.

[9] Wenlin Hu,Yongliang Wang,Shouyong Wang Wenchong Xie. Systems Engineering and Electronics, 2007, 29(6): 883-886.

[10] Pengfei Du.A study on constant false alarm rate detection of airborne early-warning radar[D].Changsha: National University of Defence Technology,2003,12.

[11] Ali Karimian, Caglar Yardim. Multiple grazing angle sea clutter modeling. IEEE. Transactions on antennas and propagation, Vol. 60, No. 9, 2012: 4408-4417

Advanced Materials Research Vols. 989-994 (2014) pp 3968-3972
© (2014) Trans Tech Publications, Switzerland
doi:10.4028/www.scientific.net/AMR.989-994.3968

Recognition of paper currency research based on AGA-BP neural network

Xue Xiao[1,a], Qinghong Wu[1,2,b] and Ying Zhang[1,c]

[1]School of University of Science and Technology LiaoNing, Anshan114051, China;

[2] National Financial Security and System Equipment Engineer, Anshan114051,China.

[a]876136660@qq.com,[b]aswqh@163.com,[c]yingzhang9118@126.com

Keywords: genetic algorithms; BP neural network; oriented identification

Abstract. The genetic algorithm is a randomized search method for a class of reference biological evolution of the law evolved, with global implicit parallelism inherent and better optimization. This paper presents an adaptive genetic algorithm to optimize the use of BP neural network method, namely the structure of weights and thresholds to optimize BP neural network to achieve the recognition of banknotes oriented. Experimental results show that after using genetic algorithms to optimize BP neural network controller can accurately and quickly achieved recognition effect on banknote recognition accuracy compared to traditional BP neural network has been greatly improved, improved network adaptive capacity and generalization ability.

Introduction

In recent years, paper currency image recognition technology is a more active issue in the field of pattern recognition, relying on image recognition banknote sorter at the core of the bill is playing an increasingly important role. Banknote sorter is a mechatronics financial instruments, has great market potential, and its main function is to identify the nominal value and for banknotes. For identifying the bill generally preclude the use of the current gradation weighting method accurate and convenient to implement. In addition, BP neural network has been facing in achieving recognition in the widely used, but due to the traditional BP neural network recognition of banknotes, while having good generalization ability, but the recognition rate is not very high[1]. Based on the banknote image recognition technology in-depth study and research, this paper proposes a genetic algorithm to optimize BP neural network to recognize banknotes oriented, the BP network weights and thresholds to optimize this method with the traditional BP neural network algorithm has improved significantly compared to the recognition accuracy.

1 Materials and Methods

1.1 Banknote image pre-processing and feature extraction

After this paper CCD image acquisition devices to get 100 RMB banknote images, we must first go through a series of image pre-processing, including image de-noising, image edge positioning, and tilt correction processing to ensure the accuracy of feature extraction. After the feature extraction, and then into the neural network.

In this paper, the method of adaptive median filter will be used to de-noise the 100 RMB banknote image, to give the image shown in the following Figure1. (a:the collected banknote image b:graphic containing salt and pepper noise c: median filtered image)

（a）Banknote image acquisition

Fig.1 Median filtered banknote image

The bill will go through de-noising images obtained, and then locate the edge of the work, mainly in the edge of goals and objectives between the target and the background, region to region. In this paper, the canny edge detection[2], shown in Figure 2.

Fig.2 Edge positioning image

In the banknote image acquisition process, there will be more or less inclined to some extent, it has a great impact on the banknote image for a correct recognition, and therefore, it is necessary to adjust the inclination of the banknote and the corrected image[3]. By the edge detection, and then use the Hough transform to detect we get four straight edges of the banknote, and the rotation correction in accordance with the bilinear interpolation and the horizontal angle between the straight line. Corrected image shown in Figure 3.

Fig.3 Tilt correction image

After a series of pre-processing, we can get the effective area of the image after the correction bill. Then you can banknote image feature extraction. The ranks of the image according to a certain number of segmentation, get a matrix-type sub-region, we can characterize an original feature in the promoter region of gray value[4]. The division method of the grid still does not have a theoretical guidance, is that we need to solve the problem. This paper uses a distance separability criterion to take all the appropriate size and number grid. To acquire a 100 RMB note positive positive image, for example, to take a fixed area renminbi center mesh partition, as shown in Figure 4. Now the central region 128 is divided into a rectangular region, this includes not only the banknote segmentation method substantially valid image information and image texture features, and in addition to containing a sawtooth edge noise and improve the accuracy of recognition.

Fig.4 Split feature block diagram

1.2 AGA-BP Network

Genetic algorithm GA (Genetic Algorithm) is based on Darwin's theory of evolution, a simulation of biological evolution mechanism robust optimization algorithm. Genetic algorithm based on sample questions for initial population fitness function selection, crossover and mutation, to guide learning and determine the search direction[5]. Simple genetic algorithm is a stochastic search algorithm probability evolution, it has a very good global search capability, but poor performance in terms of local search. In this paper, modified by genetic algorithm crossover and mutation probability, called adaptive genetic algorithm (AGA algorithm for short), the choice of an adaptive change important parameters rather than fixed to interact with the fitness function autoregulation. When an individual or similarity of the population tends to increase local minimal, crossover probability and mutation probability increases. When the population of individual fitness value is large, and the similarity of the population is low, the crossover probability and mutation probability decreases. Which not only improves search efficiency of genetic algorithms, but also effectively avoid local minimum. Crossover probability and mutation probability to make the following adjustments:

$$P_c = \begin{cases} P_{c1} - \dfrac{(P_{c1} - P_{c2})(f' - f_{\max})}{f_{\max} - f_{avg}} & f \geq f_{avg} \\ P_{c2} & f < f_{avg} \end{cases}$$

$$P_m = \begin{cases} P_{m1} - \dfrac{(P_{m1} - P_{m2})(f_{\max} - f'')}{f_{\max} - f_{avg}} & f \geq f_{avg} \\ P_{m2} & f < f_{avg} \end{cases} \qquad (1)$$

$f_{\max}$ the maximum fitness value; f_{avg} average fitness value; f' the larger of the two individual cross adaptation value, f'' for the variability of individual fitness value,In the above formula P_{c1} , P_{c2} , P_{m1} , P_{m2} Desirable value $P_{c1} = 0.9$, $P_{c2} = 0.6$, $P_{m1} = 0.1$, $P_{m2} = 0.0001$ .By AGA optimization algorithm to determine the weights and thresholds used in the initial space defined by the BP neural network for gene selection, crossover and mutation, and then the sample individual merit continued evolution, and ultimately chose the fitness of individuals to determine the maximum network structure, weights and thresholds.AGA-BP algorithm flow shown in Figure 5:

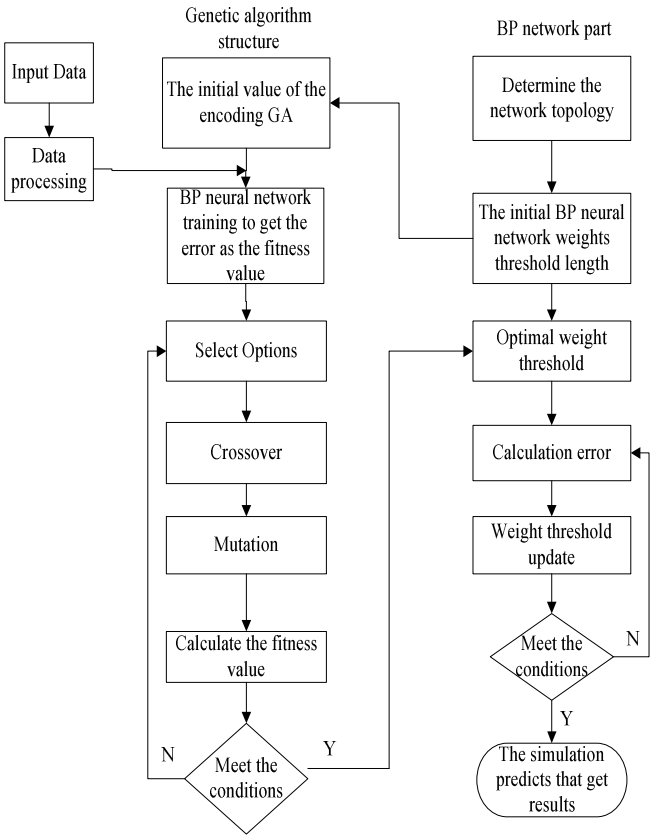

Fig.5 AGA-BP optimization algorithm flowchart

Firstly, the use of adaptive genetic algorithm to get the initial weights and structure of BP network, and then BP network training, choice of fitness as the biggest problem solution based on the results obtained in the final solution. Specific steps are as follows:

1) the use of three BP network , determine the number of nodes in the input layer BP network problems to be solved according to the number of output layer nodes. 2) real number encoding, in the basic solution space randomly generated set of neural networks have a real type of weight distribution, the value will cascade into the ownership of a long string in a certain order , each string is an individual, a group corresponding network weights and thresholds. 3) obtained by decoding the corresponding network weights and thresholds. 4) BP network samples were normalized , the right to use the threshold value obtained by decoding BP network training to get the output value is calculated for each individual's fitness. 5) to determine whether the population size, if not the genetic manipulation. Select the operation using the optimal selection strategy to select individual fitness highest remaining individuals using roulette method determines whether to enter the next generation. 6) The selection, crossover and mutation of the individual merged to form a new generation of the population, and set evolution algebra by 1, repeat steps 3-6 until the evolution algebra. Calculate the new population fitness value of each individual, to get the highest individual fitness. 7) for the largest individual fitness decode parameter combinations at this time was already sufficiently close to the optimum value, on the basis of learning with BP algorithm, the optimal weights and thresholds of the network. 8) obtained with the optimum weights and thresholds to identify training.

2 Experiments and results analysis

Before the neural network training, we must first select the training samples, in the paper, 100 RMB as the research object, whichever is different for each of the four samples of 3000, each class in the training and testing samples mixed with some slight cracks and noise banknotes. Each class in 1000 as training samples, each image has 128 eigenvalues for training artificial networks, a total of 128,000 eigenvalues. The remaining 2000 sample image as a test network.

Genetic algorithm parameter settings: initial population size of 230, crossover probability is 0.7, mutation rate of 0.03; Neural network parameter settings: network model is used in the BP network, and each layer activation functions are S-type function, input neurons BP network is 128, hidden layer nodes is 30, the output neurons of 4. After the network design is completed, the sample can be trained. After all samples positive input, if there is greater than the need to reverse the expected error correction weights. In the training process, the sample will be used repeatedly, it is best to change the order of input sample data at every training. When training a certain number of network errors will tend to a stable value. After the network training is complete, save the weights of the network, then the network performance test samples for testing, the results in Table 1 below:

Table 1 The simulation test results to identify

100 RMB face	The number of training samples	The number of samples tested	Successful identification number	Recognition rate
Positive forward	1000	2000	1991	99.7%
Positive reverse	1000	2000	1989	99.5%
Negative forward	1000	2000	1993	99.8%
Negative reverse	1000	2000	1987	99.3%

Experimental results show that: the use of adaptive genetic algorithm to optimize the BP neural network, BP neural obtain optimal structure of the network weights and thresholds, increasing the overall search capability and convergence speed of the network. BP neural network with adaptive genetic algorithm can greatly enhance the speed of the network and allows network to avoid falling into local minimal and improve the adaptive ability and generalization ability of the network.

3 Conclusion

This article describes an AGA-BP neural network recognition algorithm for banknote, through experimental analysis of the performance of the algorithm. The test results show that the algorithm can significantly improve the recognition accuracy proved adaptive genetic algorithm to optimize the BP network for the recognition of the practical application of the bill is feasible.

References

[1] Kong Fanhui. Research-oriented high-speed sorter RMB Par recognition technology [D]. Harbin Institute of Technology master's degree in theory Man,2004:30-35.
[2] Cui Mingxing. Research banknote recognition algorithm [D]. Harbin Industrial University, a master's degree thesis,2002:22-27.
[3]Rafael C.Gonzalez,Richard E.Woods,Steven L.Eddins. Digital image processing [M]. Electronic Industry Press .2009:117-121.
[4] Wei Zhengyi. Study notes image recognition algorithm [D]. Harbin Polytechnic University master's degree thesis, 2009.
[5] Cao Buqing. Based Currency Recognition GA evolution BP neural network [D]. Zhongnan University graduate dissertations pack, 2007.

Advanced Materials Research Vols. 989-994 (2014) pp 3973-3976
© (2014) Trans Tech Publications, Switzerland
doi:10.4028/www.scientific.net/AMR.989-994.3973

Wavelet De-noising Algorithm Based on OpenCV for Images Edge Detection

Yifan Ma[1, a], Shugui Liu[2, b]

[1,2]State key laboratory of precision measuring technology and instrument, Tianjin University, Tianjin 300000, China.

[a]mayifan1990@163.com, [b]sgliu@163.com

Keywords: Wavelet, image de-noising, canny edge detection, OpenCV.

Abstract. Image edge detection is easily affected by noise. Wavelet algorithm can divide the image into low frequency and high frequency. By the processing of high frequency signal and the reconstruction of wavelet coefficients, the purpose of removing noise can be achieved. In the environment of VC++6.0, an image de-noising algorithm based on the wavelet combined with the Canny edge detection is proposed, which obtains a good result. The above algorithms are implemented based on OpenCV, which is more efficient, providing the conditions for subsequent image analysis and recognition. Experiments are carried out and the results show that the proposed algorithm is available and has a good performance.

Introduction

Image edge is considered as an important basis for image analysis and recognition. An image is often corrupted by noise in its acquisition and transmission. Image de-noising is used to remove the additive noise while retaining the important signal features as much as possible [1]. The traditional edge detection algorithms mainly function as high pass filter simply by convolution using differential operator in spatial domain. They are generally sensitive to noise without accurate identification. Canny edge detection algorithm based on optimization theory [2] has been widely applied with the advantages of high signal-to-noise ratio, high detection precision and small computation. Traditional canny edge detection is based on Gaussian filtering, which can suppress the Gaussian noise to a certain extent. However, when dealing with images with heavy noise in the actual engineering application, the degree of filtering is always proportional to the blur of image. Wavelet transform can reflect the local mutation signal sensitively with its time-frequency localization and multi-scale resolution [3]. By decomposing the image into low frequency and high frequency at multiple scales, noise signal in high frequency can be suppressed at an appropriate scale. Then de-noise image can be obtained from the reconstruction of low frequency signal and the treated high frequency signal.

OpenCV is an open source library widely used in image processing and computer vision. It can operate on image data conveniently with powerful image processing function. This paper completes the configuration of OpenCV in VC++6.0, develops wavelet de-noising procedure with the database of OpenCV, and then uses the Canny operator in OpenCV for image edge detection. The obtained edge is effective against noise with rich information.

Image De-noising Algorithm Based on Wavelet Analysis

Wavelet Theory. In Fourier transform, time domain signal is written as a superposition of a series of simple waves mathematically represented by sines and cosines to realize signal localization in the frequency domain. But it can't reflect the time-varying signal frequency. Wavelet transform is a convolution of the signal by a cluster of oscillation functions with different frequency [3]. The window function can be changed according to signal variations in size, forming a variable time-frequency window. For the high frequency information, time interval is smaller, which is rich in details; for the low frequency information, time interval becomes large, showing more complete information.

The wavelet transform is defined as:
L2(R) is vector space of measurable, square integrable function *f (x)*, for any *f(x) ∈ L2(R)*, the continuous wavelet transform is:

$$W_{a,b}(x)=\int_{-\infty}^{+\infty}\psi_{a,b}(x)f(x)dx=|a|^{-1/2}\int_{-\infty}^{+\infty}f(x)\psi(\frac{x-b}{a})dx \tag{1}$$

where $\psi(x)$ is wavelet function, a is scaling factor, b is shifting factor.
It corresponds to the decomposition of *f(x)*. It can be proved that the original signal *f(x)* can be restored from $W_{a,b}$, when the decomposition satisfies the following admissible condition [3]:

$$W_{\psi}=\int_{-\infty}^{+\infty}\frac{|\psi(\omega)|^2}{|\omega|}d\omega<\infty \tag{2}$$

Then, the inverse transform of wavelet, namely reconstruction formula is:

$$f(x)=\frac{1}{W_{\psi}}\int_{-\infty}^{+\infty}\int_{-\infty}^{+\infty}W_{a,b}(x)\psi_{a,b}(x)dadb \tag{3}$$

Let *a, b* in a discrete form:$a=a_0^m$, $b=nb_0a_0^m$; where $a_0>1, b_0\in R$, $m, n\in Z2$, we can get discrete wavelet transform. For most purposes, the wavelet model is not required to keep continuous scale. To allow fast numerical implementations, we impose that $a_0=2$, $b_0=1$ to get dyadic wavelet transform, which is extended to the two-dimensional form, used for wavelet decomposition and reconstruction of image.

The Principle of Wavelet De-noising. The useful signal is usually the low-frequency part and the noise is shown as the high-frequency signal. Wavelet de-noising can be attributed to a kind of low pass filtering in a certain extent. But wavelet de-noising can keep the original image characteristics while de-noising comparing with traditional low pass filter, without causing excessive fuzz.

Wavelet de-noising process can be represented by the following figure simply.

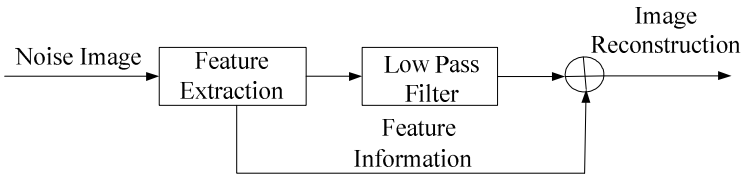

Fig. 2 Wavelet de-noising process

The first stage is the feature extraction. Select a suitable wavelet function to make wavelet transform of the image. The image is decomposed into low frequency and high frequency parts, as shown in the figure is one layer of decomposition and two layer of decomposition:

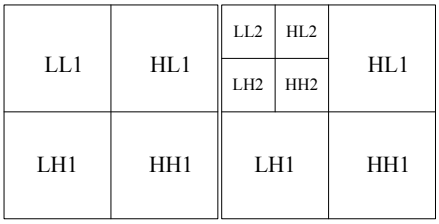

Fig. 3 One-layer and two-layer wavelet decomposition

One layer of decomposition divides the image into four parts, the low frequency image LL1, the high frequency detail image corresponding to the horizontal direction HL1, the vertical direction LH1, and the diagonal line direction HH1. Second layer decomposition only divides the low-frequency part of the upper layer, and so on. Feature extraction is to extract the high frequency part in an appropriate decomposition layer and direction according to the noise, to obtain the corresponding high-frequency coefficients.

The second stage is low pass filter. Select an appropriate threshold to quantify the extracted high frequency coefficients at each layer, and preserve the high frequency coefficients of suitable size, filter out the noise signal. The methods of threshold selection are usually hard thresholding and soft thresholding [5].

Hard thresholding formula:

$$W_{j,k} = \begin{cases} W_{j,k}, |W_{j,k}| \geq \lambda \\ 0, |W_{j,k}| < \lambda \end{cases} \quad (4)$$

Soft thresholding formula:

$$W_{j,k} = \begin{cases} sign(W_{j,k})(|W_{j,k}| - \lambda), |W_{j,k}| \geq \lambda \\ 0, |W_{j,k}| < \lambda \end{cases} \quad (5)$$

In the experiments, soft thresholding has been used over hard thresholding because it gives more visually pleasant images as compared to hard thresholding: reason being the latter is discontinuous and yields abrupt artifacts in the recovered images especially when the noise energy is significant.

The third stage is image reconstruction. Take the low frequency coefficients of the nth layer as the feature information and reconstruct the image together with the high frequency information at each layer after thresholding. Finally get the de-noise image.

Realization of Image Edge Detection Based on Wavelet De-noising

Algorithm Flow. The flow of this whole algorithm is as follows:

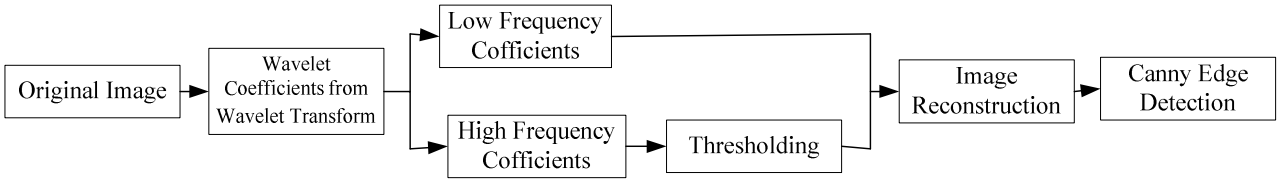

Fig. 4 Algorithm flow

OpenCV Implementation. OpenCV is an open source computer vision library written in C and C++. All images in OpenCV are operated in a same structure IplImage, which contains most of the required image information [6]. The main functions in program are:

Load an image: IplImage *cvLoadImage (const char *filename, int flags);

Allocate new image: IplImage *cvCreateImage (Cvsize size, int depth, int channels);

Define wavelet de-noising function: void cvWaveSmooth (const IplImage*src, IplImage*dst, int scale, int DecoWave, int RecoWave); DecoWave is decomposition wavelet, RecoWave is reconstruction wavelet.

Canny edge detection in OpenCV: Void cvCanny (const CvArr* image, CvArr* edge, double threshold1, double threshold2, int aperture_size=3);

Create a Window: int cvNamedWindow (const char *name, int flags);

Display an image: void cvShowImage (const char* name, const CvArr* image);

Wait and Clean: cvWaitKey (0); cvReleaseImage (&image); cvDestroyWindow ("source");

Experiment and Analysis of Results

In the OpenCV environment, extract the edge of the original image “lena.bmp” by cvCanny function. The two thresholds should be obtained according to the test. In this paper, threshold1=40, threshold2=100. The result is as figure 5.

Fig. 5 Left: original image. Right: Canny edge detection

Add a heavy Gaussian noise to the image, process the image by wavelet de-noising algorithm, then use the Canny algorithm for edge extraction. Contrast experiment: choose the traditional Gaussian filtering function for noise removal, and then Canny algorithm for edge extraction. The results are as follows:

Fig. 6 Left: noise image. Middle: Canny edge detection with Gaussian de-noising. Right: Canny edge detection with wavelet de-noising.

From the above experiments can be seen clearly, Canny algorithm can extract the coherent edge of the clear image with rich details in figure 5. But for the images with heavy noise, Gaussian filtering is difficult to ensure to suppress noise and preserve edge details in balance. Large threshold can remove noise, but obviously, lost a lot of details, and the edge is not consistent, as shown in the middle of figure 6. In contrast, combining wavelet de-noising with Canny edge detection can get the clear edge information, suppressing the impact on the edge detail information brought by noise well.

Summary

According to the characteristics of wavelet algorithm, the preprocessing of image with wavelet de-noising algorithm can largely eliminate noise effect in the latter part of Canny edge detection, which can obtain more rich real edge information. The algorithm is implemented in the OpenCV environment with its rich image processing library and the existing Canny algorithms. It makes a good foundation for further image analysis and recognition in the practical engineering with full use of the powerful vision library of OpenCV combined with wavelet algorithm.

Acknowledgment

We sincerely thank to the Natural Science Foundation of Tianjin for its financial support to the project. The granted project number is 13JCZDJC34500/E05020402.

References

[1] Kaur L, Gupta S. Image Denoising Using Wavelet Thresholding, ICVGIP. 2(2002) 16-18.

[2] Canny J, A Computational Approach to Edge Detection, J. Pattern Analysis and Machine Intelligence. IEEE Transactions on. 6(1986) 679-698.

[3] Mallat S. A wavelet tour of signal processing. Academic press, New York, 1999.

[4] Bradski G, Kaehler A. Learning OpenCV: Computer vision with the OpenCV library. O'Reilly Media, Inc., 2008.

[5] D L Donoho. De-nosing by soft-thresholding, J. Information Theory. IEEE Transactions on. 41.3(1995) 613- 627.

[6] Information on http://www.opencv.org.cn/

Advanced Materials Research Vols. 989-994 (2014) pp 3977-3980
© (2014) Trans Tech Publications, Switzerland
doi:10.4028/www.scientific.net/AMR.989-994.3977

A New Method of Multi-Component Chirp Signal Array Detection

Fu Gang[1, a], Wu Yanjun[1,a] and Tao HuaTang[1,a]
[1]China Satellite Maritime Tracking and Control Department, China
[a]348237548@sina.com

Keywords: Antenna array, Fractional Fourier Transform (FRFT); Chirp Signal; Parameter Estimation

Abstract. This paper presents a multi-component chirp signal detection with new methods of parameter estimation. The method using spatial characteristics of the antenna array. By array average fractional Fourier domain weighting function is introduced to reduce noise and suppress mutual interference between the signals from different sources. And compared to a single array element method. The proposed method greatly improves the multi-component chirp signal detection and parameter estimation performance. Simulation results show the effectiveness of the method.

Introduction

Chirp class is one common signal signal signal processing field, whether in the nature of a natural signal, or artificially generated signals are abound. Therefore, the detection and parameter estimation of multicomponent chirp signal has been people's attention. In recent years, with the rapid development of the theory of fractional Fourier transform to produce a variety of multi-component chirp signal detection and parameter fractional Fourier transform-based estimation algorithm. This class method can effectively achieve the chirp signal while four parameter estimation, performance analysis and simulation results demonstrate the accuracy of detection and estimation results are better than the original class of time-frequency algorithms.

However, the existing research results of such algorithms is for both single sensor signal, and the antenna with the development of technology, the current radar, communications systems are used in many array antenna to improve system performance. Therefore, we studied the performance of detection and parameter estimation how to use the array signal processing techniques to improve existing algorithms.

2 Preliminaries

2.1 Signal Model

As used herein, the following model:

$$\mathbf{X}(t) = \mathbf{A}\mathbf{S}(t) + \mathbf{N}(t) \tag{1}$$

Where: $\mathbf{S}(t) = [s_1(t), s_2(t), ..., s_N(t)]^T$ is N dimensional vector consisting of N source signal; $\mathbf{X}(t) = [x_1(t), x_2(t), ..., x_M(t)]^T$ for the M dimensional observation data to Volume, whose elements are M output signal sensing unit; $M \times N (M \geq N)$ dimensional matrix $\mathbf{A} = [\mathbf{a_1}, \mathbf{a_2}, ..., \mathbf{a_N}]$ is called mixing matrix, Sok said its yuan mixed signal, the spatial characteristics of the column vector $\mathbf{a_i} = [a_{i1}, a_{i2}, ..., a_{iM}]^T$ represents the ith signal source; $\mathbf{N(t)} = [n_1(t), n_2(t), ..., n_M(t)]^T$ is an $M \times 1$ dimensional Noise vector.

Meaning of formula (1) is N source signal $\mathbf{S(t)}$ by the spatial characteristic is $\mathbf{A}$ M-dimensional array to obtain the observed data vector $\mathbf{X(t)}$. To simplify the discussion, assume that $\|\mathbf{a_i}\|^2 = M$, this assumption does not affect the results discussed below.

1.2 Chirp signal parameters estimation based on FRFT

Multi-component chirp signal using the following model, said:

$$x(t) = \sum_{i=1}^{N} \xi_i e^{j\varphi_i + j2\pi f_i t + j\pi\mu t^2}, \quad -\frac{\Delta t}{2} \leq t \leq \frac{\Delta t}{2} \tag{2}$$

Wherein: ξ_i is the amplitude; f_i is the center frequency; μ_i is the Chirp rate and φ_i is the initial phase.

Define the fractional Fourier transform can be found in the literature [1][2]. The use of fractional frequency distribution relationship with the Fourier transform, chirp can achieve signal detection and parameter estimation:

$$\{\hat{p}_i, \hat{u}_i\} = \arg\max_{p,u} \left| X_p(u) \right|^2 \tag{5}$$

$$\begin{cases} \hat{\mu}_i = -\cot(\hat{p}_i \pi / 2), \hat{\varphi}_i = \arg\left[\dfrac{X_{\hat{p}_i}(\hat{u}_i)}{A_{\hat{p}_i} e^{j\pi \hat{u}_i^2 \cot \hat{\alpha}_i}} \right] \\ \hat{f}_i = \hat{u}_i \csc(\hat{p}_i \pi / 2), \hat{\xi}_i = \dfrac{\left| X_{\hat{p}_i}(\hat{u}_0) \right|}{\Delta t \left| A_{\hat{p}_i} \right|} \end{cases} \tag{6}$$

The above method can be extended to multi-component chirp signal detection and parameter estimation, the difference between the multi-component signal strength is large, can be affected by one from strong to weak elimination method to suppress strong component when the component is weak. Provided that the strength of multi-component chirp signal a larger difference between weak and strong component interference component is very small, and can more accurately eliminate strong component in turn. However, in practical application of the above conditions is often difficult to ensure, particularly when the signal component is more, the strength of each component of the difference between minimal and similar parameter. (5) modulo operation will lead to interactions between the various components of the enhancement. At this mutual interference between multiple components will greatly reduce the detection and parameter estimation performance.

To solve this problem, we use an antenna array to suppress the effects of noise and interference items by FRFD array weighting, which effectively improve the performance of existing methods.

3 Weighted array FRFT

Noise can also be seen as a source of the signal we are not interested, that is, in (1) $\mathbf{X(t)}$ of formula can be seen as the product of the $N+1$ signal source by the mixing matrix $\mathbf{A}$. So from this point of the analysis of multi-component mutual interference between the signals departure (also as a source of the noise signal analysis), you can simplify the formu la (1) is expressed as:

$$\mathbf{X(t)} = \sum_{i=1}^{N} [\mathbf{a_i} \cdot \mathbf{s_i(t)}] \tag{7}$$

Formula (7) in order to simplify the expression put, the summation symbol represents N s uperscript still use. Then the output of the sensor k as:

$$x_k(t) = \sum_{i=1}^{N} [a_{ik} s_i(t)],\ k = 1, 2, ..., M \tag{8}$$

As the FRFT is a linear transformation. So for a single sensor output x_k are:

$$F_{x_k}(p,u) = \sum_{i=1}^{N} a_{ik} F_{s_j}(p,u) \tag{9}$$

Then

$$\left| F_{x_k}(p,u) \right|^2 = \sum_{i=1}^{N} \sum_{j=1}^{N} a_{ik} a_{jk}^* F_{s_i}(p,u) F_{s_j}^*(p,u) \tag{10}$$

After each antenna element can be obtained by averaging the output signal:

$$\overline{\left| F_{\mathbf{X}}(p,u) \right|^2} = \sum_{i=1}^{N} \sum_{j=1}^{N} \left(\frac{1}{M} \mathbf{a}_j^H \mathbf{a}_i \right) F_{s_i}(p,u) F_{sj}^*(p,u) \tag{11}$$

Wherein: $\mathbf{a}_j^H \mathbf{a}_i$ is the inner product of $\mathbf{a}_j$ and $\mathbf{a}_i$.

Easy to prove: vwhen $i = j$, $\mathbf{a}_j^H \mathbf{a}_i = \left\| \mathbf{a}_i \right\|^2 = M$; when $i \neq j$, $\mathbf{a}_j^H \mathbf{a}_i \leq M$.

Defining a variable $\lambda_{ij} = \frac{1}{M} a_j^H a_i$, thus, the formula (11) can be written as

$$\overline{\left|F_{\mathbf{X}}(p,u)\right|^2} = \sum_{i=1}^{N}\sum_{j=1}^{N} \lambda_{ij} F_{s_i}(p,u) F_{sj}^*(p,u) \tag{12}$$

Where

$$\begin{cases} \lambda_{ij} = 1, & i = j \\ \left|\lambda_{ij}\right| \le 1, & i \ne j \end{cases} \tag{13}$$

The equation above shows that Each element antenna array output signal averaged square modulus is a linear combination FRFT FRFT interference term between FRFT square modulus of each source signal and the different source signals.

May be a further written as:

$$\overline{\left|F_{\mathbf{X}}(p,u)\right|^2} = U^H \left[F_{\mathbf{s}} F_{\mathbf{s}}^*(p,u) .* \Phi \right] U \tag{14}$$

Where, "$.*$" means multiplying the corresponding element in the matrix; U is a unit vector of dimension $N \times 1$; $\mathbf{\Phi} = \mathbf{A}^H \mathbf{A} / M = \left[\lambda_{ij} \right]$, $i, j = 1, 2, ..., N$.

In matrix $F_{\mathbf{s}} F_{\mathbf{s}}^*(p,u) .* \Phi$, the diagonal elements represent the squared modulus FRFT each source signal is a non-diagonal elements and the j th FRFT source signals and source sign als i th multiplied by the conjugate, it is the interference term.

Each element of the matrix former also has a weighting coefficient λ_{ij}, when $i = j$, $\lambda_{ij} = 1$; the time when $i \ne j$, $\left|\lambda_{ij}\right| \le 1$.

That is, the matrix of diagonal elements of the weighting factors are 1, the non-diagonal elements of the weighting factor is less than 1. Thus, by means of the output signal of the antenna array will be able to average a good source of suppressing interference with other signals.

4 The theory of algorithm

According to the foregoing, you can get new detection and parameter estimation algorithm steps are:

Step 1: The first step to strike its FRFT square modulus of the input signal for each sensor unit;

Step 2:The second step, the result of each array element obtained by summing the first step, the average, and the noise is suppressed by the interference term average of the array;

Step 3: A third step according to equation (5), (6), in a plane of the square (p,u) modulus of the average value obtained FRFT the two stage two-dimensional search, obtained from the peak position $(\hat{p}_1, \hat{u}_1)$ of the strongest signal component $(i = 1)$ parameter estimates $\left\{ \hat{\xi}_1, \hat{\varphi}_1, \hat{f}_1, \hat{\mu}_1 \right\}$;

Step 4: The fourth step is the use of parameter estimates to recover the first signal component is:

$$\hat{s}_1(t) = \xi_1 e^{j2\pi f_1 t + j\pi\mu_1 t^2}, \quad -\frac{\Delta t}{2} \le t \le \frac{\Delta t}{2} \tag{15}$$

Step 5: to get a result $\hat{s}_1(t)$ in accordance with equation (15) FRFT square modulus $\left|F_{\hat{s}_1}(p,u)\right|^2$, and subtracted from $\overline{\left|F_{\mathbf{X}}(p,u)\right|^2}$, that is:

$$\overline{\left|F_{\mathbf{X}'}(p,u)\right|^2} = \overline{\left|F_{\mathbf{X}}(p,u)\right|^2} - \left|F_{\hat{s}_1}(p,u)\right|^2 \tag{16}$$

Step 6: the result will be the fifth step into the third step, repeat the above steps, followed by the rest of the signal components to get an estimate $\hat{s}_i(t)$, until the rest of the square modulus of the average peak FRFT no longer exceeds a predetermined threshold.

5 Simulation

The sampling frequency is herein Simulation 1000 Hz, the sampling points is 1000, the array element number were taken 1,2 and 8, two chirp signals are used as follows:

$$\begin{cases} s_1(t) = \xi_1 \cdot \exp(j2 + j\pi 4t + j\pi 5t^2) \\ s_2(t) = \xi_2 \cdot \exp(j\pi 8t + j\pi 3t^2) \end{cases} \tag{17}$$

The spatial direction of arrival is $\pi/8$ and $5\pi/12$ respectively.

We may assume that $s_1(t)$ is a useful signal, $s_2(t)$ is the interference signal, the dry signal ratio $ISR = 20\lg(\xi_2/\xi_1)$, range from -16dB to 0dB.

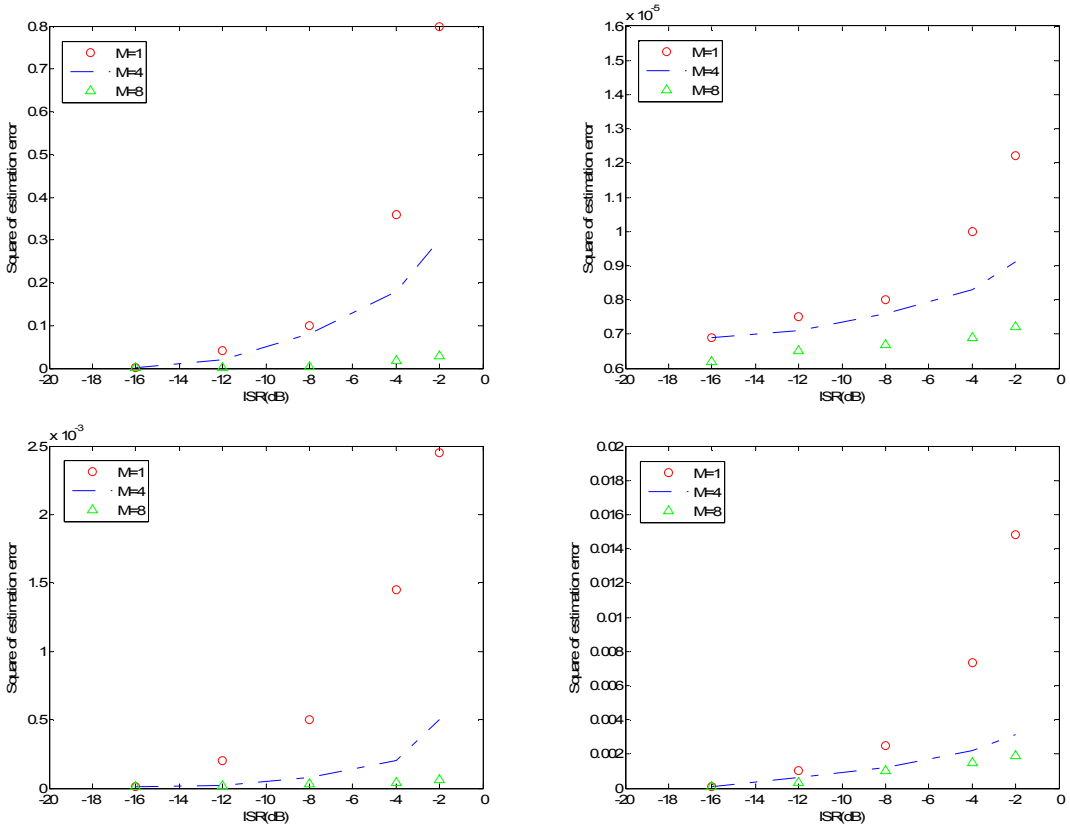

Fig3 The relationship with delay interval, code sequence and likelihood value

5 Summary

This paper proposes a multi-component chirp signal detection and parameter array FRFD new method based on the estimated weighted. Simulation results demonstrate the effectiveness and practicality of the method. And a single array element detection method, the new method can greatly improve the detection and parameter estimation performance, especially suitable for low signal to noise ratio, the number of components of the signal are more or less the intensity of each component and the parameters similar situation.

References

[1] Namias V. The fractinal order Fourier transform and its application to quantum mechanics [J]. J Inst Math Appl, 1980, 25: 241~265.

[2] Ozaktas H. M, Kutay M. A, Bozdagi G. Digital computation of the fractional Fourier transform [J]. IEEE Transactions on Signal Processing.1996, 44(9):2141-2150.

Advanced Materials Research Vols. 989-994 (2014) pp 3981-3984
© (2014) Trans Tech Publications, Switzerland
doi:10.4028/www.scientific.net/AMR.989-994.3981

Demodulation Method of Telemetry Signal Based on Virtual Radio

Yao Xuelu[1,a], Fu Gang[1, a], Li Renlong[1,a]
[1]China Satellite Maritime Tracking and Control Department, China
[a]348237548@sina.com

Keywords: DSTFT, PCM/FM, Demodulation

Abstract. According to the characteristics of PCM / FM signal demodulation method is proposed based on virtual radio platform. This paper discusses in detail the basic principles of this demodulation method and implementation process, analyze the demodulation performance and complexity of the method. Simulation results show that the method for actually received PCM / FM demodulation signal has better performance.

Introduction

At present, foreign countries have launched a software-based virtual radio station of GSM technology, virtual radar (virtual radar) GPS receiver and software aspects of the study, there have been domestic software of digital TV.[1-3]

PCM / FM signal is the current data transmission system is widely used as a signal type. Since the actual received PCM / FM signals and more non-stationary random signal, non-stationary random signal processing usually time-frequency analysis method. Based virtual radio signal demodulation technology, not only to reach a certain demodulation performance, but also to reduce as much as possible the signal demodulation algorithm and computation complexity, thus contributing to the signal processing software design and real-time signal processing.

1 PCM / FM signal characteristic analysis

PCM / FM telemetry signal field called continuous phase frequency shift keying (CPFSK) signals, the mathematical expression is:

$$S_{FM}(t) = A\cos\left[2\pi(f_c + f_d)t + K_{FM}\int f(t)dt\right] \tag{1}$$

Symbols "1" and "0" respectively corresponding to the carrier frequency:

$$f_1 = f_c + f_d + K_{FM} \times R_b \tag{2}$$

$$f_0 = f_c + f_d - K_{FM} \times R_b \tag{3}$$

Therefore, PCM / FM signals within one symbol can be regarded as the width of a single carrier frequency n (I) sinusoidal signals, by alternating two different carrier frequencies, digital data "0" "1" and transmission. Then, within one symbol width PCM / FM signal may be expressed as:

$$x(n) = A\exp[j(2\pi f_i n + \varphi)] + z(n) \qquad (n = 0,1,\cdots,N_w - 1) \tag{4}$$

Equation (4) and can be represented as $X = A_c E + Z$, where,

$$\begin{cases} X = [x(0) \quad x(1) \quad \cdots \quad x(N_w - 1)]^T \\ E = [\quad 1 \quad e^{j2\pi f_i} \cdots \quad e^{j(N_w-1)2\pi f_i}\ ]^T \\ Z = [z(0) \quad z(1) \quad \cdots \quad z(N_w - 1)]^T \end{cases} \tag{5}$$

$\hat{A}_c$ is the amplitude of the signal amplitude A Unbiased MLE estimates.

$$A = \left|\hat{A}_c\right| = \frac{E^H X}{E^H E} = \frac{1}{N_w}\left|\sum_{n=0}^{N_w-1} x(n)e^{-j2\pi f_i n}\right| \tag{6}$$

Since the PCM/FM signal represents "0" and "1" and a known carrier frequency, thus calculation of the signal amplitude X in f_0 / f_s , and f_1 / f_s are:

$$\begin{cases} a = \left| \frac{1}{N_w} \sum_{n=0}^{N_w-1} x(n) e^{-j2\pi(f_0/f_s)n} \right| \\ b = \left| \frac{1}{N_w} \sum_{n=0}^{N_w-1} x(n) e^{-j2\pi(f_1/f_s)n} \right| \end{cases} \tag{7}$$

In summary, according to the spectral characteristics of PCM / FM signal, the DFT method can be used by comparing the size of the amplitude of two frequency and demodulate the PCM / FM signal.

2 Demodulation method based DSTFT

$x(n)(n = 0,1,\cdots,N-1)$ DFT is defined as:

$$X(k) = \sum_{n=0}^{N-1} x(n) e^{-j\frac{2\pi}{N}nk} \quad (\text{k=0,1,....N-1}) \tag{8}$$

The x (n) make (r-1)N zero, r is an integer such as some integer $k = rN * f / f_s$, whereby rN point sequence x'(n):

$$x'(n) = \begin{cases} x(n), & n = 0,1,...N-1 \\ 0, & n = N, N+1,....rN-1 \end{cases} \tag{9}$$

$$X'(k) = \sum_{n=0}^{rN-1} x'(n) e^{-j\frac{2\pi}{rN}nk} = \sum_{n=0}^{N-1} x(n) e^{-j\frac{2\pi}{rN}nk} = \sum_{n=0}^{N-1} x(n) e^{-j\frac{2\pi}{N}\frac{k}{r}n} \tag{10}$$

At this point f_i by frequency DSTFT energy calculated by the formula:

$$DSTFT_x(n,k_i) = \sum_{M=0}^{M-1} \tilde{x}(m,n) e^{-j\frac{2\pi}{M}k_i m} \quad (k_i = M * f_i / f_s) \tag{11}$$

During the sliding of the rectangular window, for each quantitative calculation DSTFT 2 complex multiplications and two complex additions.

$$\begin{aligned} DSTFT(n+1,\omega) &= \sum_{m=0}^{M-1} x(n+1+m) e^{-j\omega m} \\ &= \sum_{m=1}^{M} x(n+m) e^{-j\omega(m-1)} \\ &= e^{j\omega} \sum_{m=1}^{M-1} x(n+m) e^{-j\omega m} + x(n+M) e^{-j\omega(M-1)} \\ &= e^{j\omega} \left(\sum_{m=0}^{M-1} x(n+m) e^{-j\omega m} - x(n) e^{-j0} \right) + x(n+M) e^{-j\omega(M-1)} \\ &= e^{j\omega} [STFT(n,\omega) - x(n)] + x(n+M) e^{-j\omega(M-1)} \end{aligned} \tag{12}$$

3 Performance Analysis

Assuming the frequency of the current signal is the width of the window f_0, the noise is not considered, namely:

$$x(n) = A \cdot e^{j[2\pi(f_0/f_s)n+\varphi]} \tag{13}$$

By DSTFT calculated the energy spectrum of the signal at the frequency of 0, 1:

$$a^2 = \left| A \sum_{n=0}^{N_w-1} e^{j[2\pi(f_0/f_s)n+\varphi]} \cdot e^{-j2\pi(f_0/f_s)n} \right|^2 = \left| AN_w e^{j\varphi} \right|^2 = A^2 \cdot {N_w}^2 \tag{14}$$

$$b^2 = \left| A \sum_{n=0}^{N_w-1} e^{j[2\pi(f_0/f_s)n+\varphi]} \cdot e^{-j2\pi(f_1/f_s)n} \right|^2 \tag{15}$$

Assuming $\Delta f = (f_1 - f_0)/f_s = 2K_{FM} \times R_b / f_s$,

$$b^2 = A^2 \cdot \left| \frac{1-e^{j2\pi N_w \Delta f}}{1-e^{j2\pi\Delta f}} \right|^2 \qquad = A^2 \cdot \frac{1-\cos 2\pi N_w \Delta f}{1-\cos 2\pi\Delta f} \tag{16}$$

So,

$$\rho_0 = \frac{b^2}{a^2} = \frac{1-\cos 2\pi N_w \Delta f}{N_w{}^2(1-\cos 2\pi\Delta f)} = \frac{\sin^2 \pi N_w \Delta f}{N_w{}^2 \sin^2 \pi\Delta f} = \frac{\sin^2 N_w \dfrac{\Delta\omega}{2}}{N_w{}^2 \sin^2 \dfrac{\Delta\omega}{2}} \tag{17}$$

The relationship between ρ_0 and $\Delta\omega$ shown in Figure 1. The relationship between ρ_1 and $\Delta\omega$ shown in Figure 2.

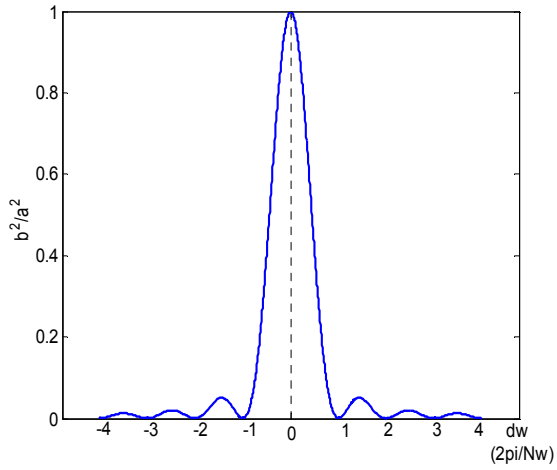

Fig1 The relationship between ρ_0 and $\Delta\omega$

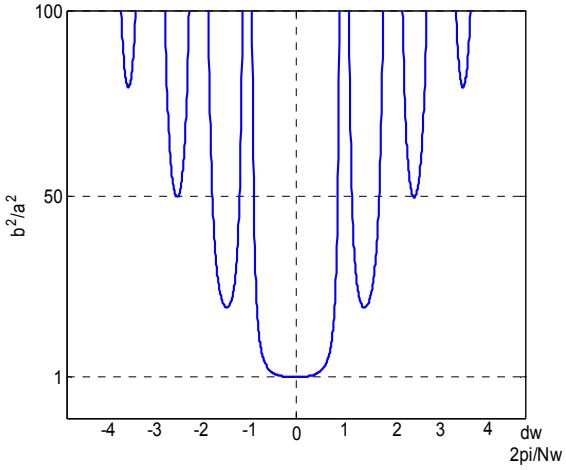

Fig2 The relationship between ρ_1 and $\Delta\omega$

Use MatLab simulation program written by computer demodulation actually received PCM / FM signal, the signal waveform shown in Figure 3, (a) represents the modulation symbols, (b) shows the modulation symbols corresponding PCM / FM time-domain waveform.

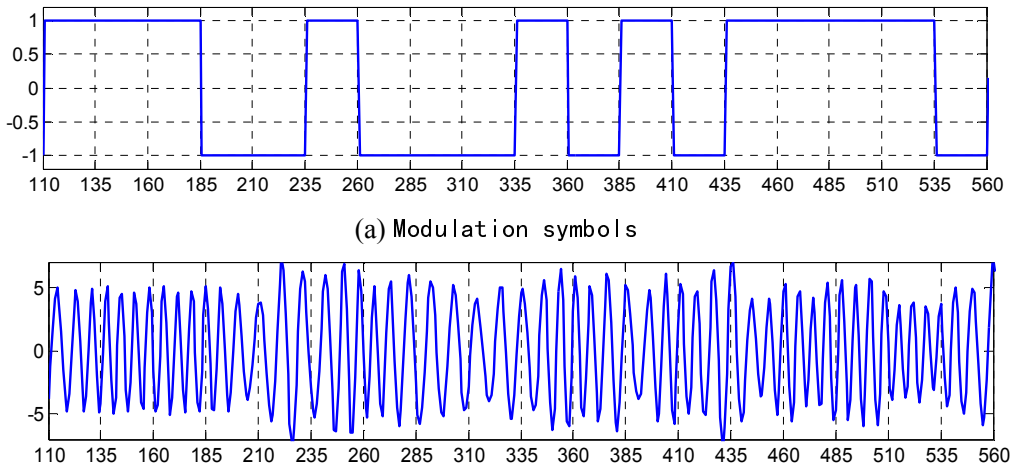

(a) Modulation symbols

(b) PCM/FM signal

Fig3 Ideal PCM/FM signal

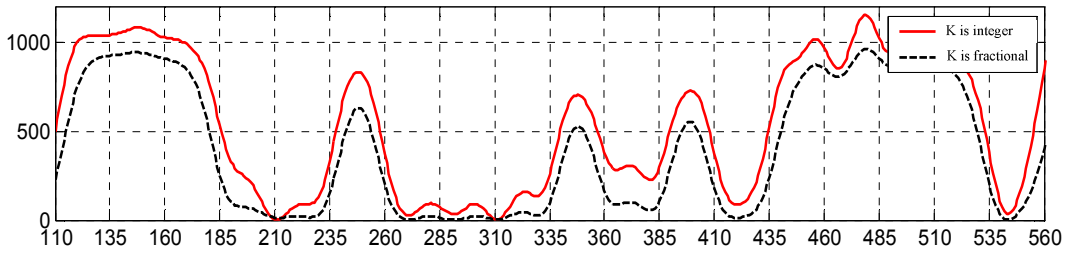

Fig4 Affect the value of K frequency energy

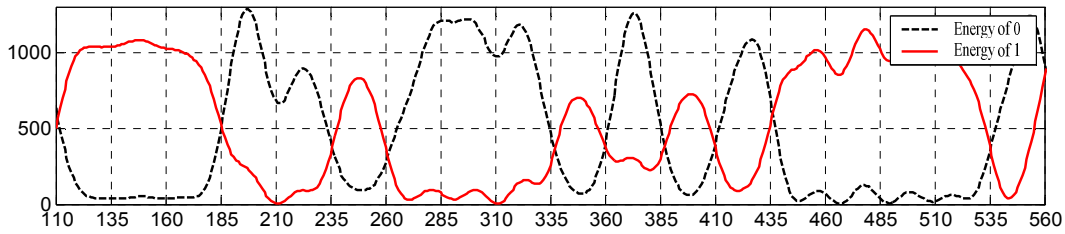

Fig5 PCM / FM signal frequency energy variation

According to "eye" in width and the size relationship between f_0 and f_1 energy can demodulate the PCM / FM signal.

Using current mainstream computer configuration, recorded on the hard disk where the data is processed using a signal demodulation speed of 1:5, the average SNR of 12.8dB signal error rate of 1.871×10^{-4}, to reach the current demodulation performance hardware devices.

Summary

According to the spectral characteristics of PCM / FM signal, the method used to calculate the energy STFT PCM / FM signal frequency points f_1 and f_0, by comparing the two laws of variation of size and frequency of energy, demodulate the signal. The demodulation method is simple, strong interference suppression capability, ease of computer software programming.

Reference

[1] Vanu G B. Design and implementation of software radios using a general purpose processor[D]. Massachusettes: Massachusettes Inst Technol,1999.

[2] T. Grydeland，F. D. Lind，P. J. Erickson，J. M. Holt. Software Radar Signal Processing[J]. European Geosciences Union 2004.

[3] John J. Schamus, Veridian Engineering, Dayton, OH. Real-Time Software GPS Receiver[J].ION GPS 2002,24-27.

Advanced Materials Research Vols. 989-994 (2014) pp 3985-3988
© (2014) Trans Tech Publications, Switzerland
doi:10.4028/www.scientific.net/AMR.989-994.3985

Multi-frequency Estimates Based on IIR Adaptive Frequency Estimator

Kou Mingxin[1,a] , Lin Jianhua[1, a], Fu Gang[1,a]
[1]China Satellite Maritime Tracking and Control Department, China
[a]348237548@sina.com

Keywords: Multi-frequency, IIR , Frequency Estimator

Abstract. Presents a IIR adaptive frequency estimator to achieve multi-frequency estimation algorithm. More traditional phase-locked loop algorithm, which has no mixing components, to achieve the advantages of full-band frequency estimation, frequency estimation accuracy under the same environment and phase-locked loop fairly.

Introduction

The traditional use of PLL frequency estimation, due to the transition from analog digital phase-locked loop is coming, there is a value to adjust the design parameters of the experience, it is difficult to establish a precise mathematical model. But most of the traditional methods for frequency estimator only a single point estimate frequency signal frequency range of applications is limited. This paper analyzes proceed from the IIR filter performance, making multi-point IIR adaptive frequency estimation frequency estimate possible.[1-3]

1 Adaptive filter theory and analysis of variance

Single-point frequency signal estimation commonly used second-order adaptive filters. As shown, the waveform of the original input signal and a noise is mixed, wherein the noise signal is not relevant; another path of the reference input signal is uncorrelated with the noise-related signals. IIR filter transfer function is:

$$H(z)=\frac{1+\rho_1 az^{-1}+\rho_1^2 z^{-2}}{1+\rho_2 az^{-1}+\rho_2^2 z^{-2}} \tag{1}$$

$0\le\rho_1\le 1$, $0\le\rho_1<\rho_2\le 1$.

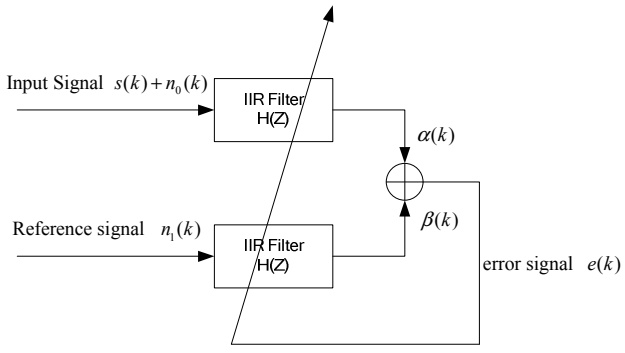

Fig1 Adaptive filtering schematics

The error signal may be obtained by Equation 2:

$$e(k)=\alpha(k)-\beta(k) \tag{2}$$

$$E[e^2]=E[\alpha^2]+E[\beta^2]-2E[\alpha\beta] \tag{3}$$

$$E[e^2]=\frac{1}{2\pi j}\{\oint P_{ss}|H(z)|^2\frac{dz}{z}+\oint P_{nn}|H(z)|^2\frac{dz}{z}-2\oint P_{sn}|H(z)|^2\frac{dz}{z}\} \tag{4}$$

Wherein, P_{ss} , P_{nn} and P_{sn} respectively of the input signal, the reference signal and their associated power spectrum.

$$E[e^2]=\frac{1}{2\pi j}\oint|H(z)|^2\{P_{ss}+P_{nn}-2P_{sn}\}\frac{dz}{z} \tag{5}$$

$$\frac{\partial E[e^2]}{\partial a}=\frac{1}{2\pi j}\oint\frac{|H(z)|^2}{\partial a}\{P_{ss}+P_{nn}-2P_{sn}\}\frac{dz}{z} \tag{6}$$

$$\frac{\partial|H(z)|^2}{\partial a}=\frac{\frac{\partial(AA^*)}{\partial a}BB^*-AA^*\frac{\partial(BB^*)}{\partial a}}{(BB^*)^2} \tag{7}$$

$$=\frac{BB^*[\rho_1 z^{-1}A^*+\rho_1 zA]-AA^*[\rho_2 z^{-1}B^*+\rho_2 zB]}{[BB^*]^2}$$

$$=\frac{2zA(\rho_1 B^*-\rho_2 A^*)}{|B|^2 B^*}$$

To analyze the extreme points, so $\frac{\partial E[e^2]}{\partial a}=0$, can be obtained:

$$\rho_1+\rho_1\rho_2 az+\rho_1\rho_2^2 z^2=\rho_2+\rho_1\rho_2 az+\rho_2\rho_1^2 z^2 \tag{8}$$

$$z=\frac{1}{\rho_1\rho_2} \tag{9}$$

As can be seen from Equation 9, Equation unconditional extremum exists. Figure 2 is a relationship between $H(z)$, a and ρ_2.

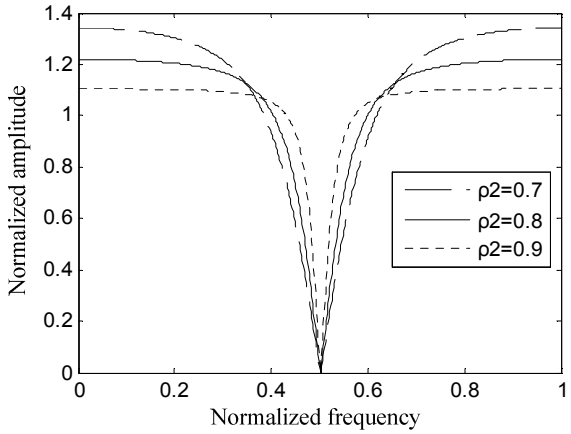

Fig2 Second-order filter frequency response ($f=0.5$， $\rho_1=1$)

Multi-frequency signal estimation must use higher-order adaptive filters. Through the two-channel adaptive filter performance characteristics of high-level analysis can be effectively overturned the adaptive filter. Dual-channel transfer function of the filter is:

$$H(z)=\frac{(1+\rho_1 a_1 z^{-1}+\rho_1^2 z^{-2})(1+\rho_1 a_2 z^{-1}+\rho_1^2 z^{-2})}{(1+\rho_2 a_1 z^{-1}+\rho_2^2 z^{-2})(1+\rho_2 a_2 z^{-1}+\rho_2^2 z^{-2})}$$

$$=\frac{k_0+\rho_1 k_1 z^{-1}+\rho_1^2 k_2 z^{-2}+\rho_1^3 k_3 z^{-3}+\rho_1^4 k_4 z^{-4}}{k_0+\rho_2 k_1 z^{-1}+\rho_2^2 k_2 z^{-2}+\rho_2^3 k_3 z^{-3}+\rho_2^4 k_4 z^{-4}} \tag{10}$$

Among, $a_1=-2\cos\omega_1$， $a_2=-2\cos\omega_2$， $k_0=k_4=1$， $k_1=k_3=a_1+a_2$， $k_2=a_1a_2+2$。

$$E[e^2]=\frac{C_1^2}{2}\left|H(e^{j\omega_1})\right|^2+\frac{C_2^2}{2}\left|H(e^{j\omega_2})\right|^2+\frac{1}{2\pi j}\oint|H(z)|^2\{P_{n_1n_1}+P_{n2n2}-2P_{n1n2}\}\frac{dz}{z} \tag{11}$$

$$\frac{\partial E[e^2]}{\partial k_1}=\frac{1}{2\pi j}\oint\frac{\partial|H(z)|^2}{\partial k_1}\{P_{n_1n_1}+P_{n2n2}-2P_{n1n2}\}\frac{dz}{z} \tag{12a}$$

$$\frac{\partial E[e^2]}{\partial k_2}=\frac{1}{2\pi j}\oint\frac{\partial|H(z)|^2}{\partial k_2}\{P_{n_1n_1}+P_{n2n2}-2P_{n1n2}\}\frac{dz}{z} \tag{12b}$$

Assume $\frac{\partial E[e^2]}{\partial k_1}=0$, $\frac{\partial E[e^2]}{\partial k_2}=0$,Can be deduced:

$$\oint \rho_2 \frac{Az^{-1}(1+\rho_2^2 z^{-2})+Az(\rho_2^2+z^2)dz}{BB^* z} = \oint \rho_1 \frac{AA^*[Bz^{-1}(1+\rho_2^2 z^{-2})+Bz(\rho_2^2+z^2)]dz}{BB^* BB^*}$$

$$\oint \rho_1^2 \frac{(A^* z^{-2}+Az^2)dz}{BB^* z} = \oint \rho_2^2 \frac{AA^*[Bz^{-2}+Bz^2]dz}{BB^* BB^* z} \tag{13}$$

Among, $A=1+k_1\rho_2 z^{-1}+k_2\rho_2^2 z^{-2}+k_1\rho_2^3 z^{-3}+z^{-4}$, $B=1+k_1\rho_1 z^{-1}+k_2\rho_1^2 z^{-2}+k_1\rho_1^3 z^{-3}+z^{-4}$.

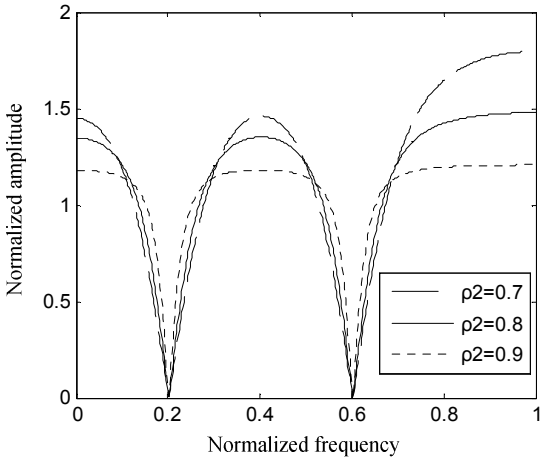

Fig3 Higher-order filter frequency response ($f_1=0.2$, $f_2=0.6$, $\rho_1=1$)

It can be concluded from Figure 4: High adaptive filter only when the signal carrier frequency and the center frequency of the narrowband process is controlled within a proper range away from the filter in order to achieve convergence.

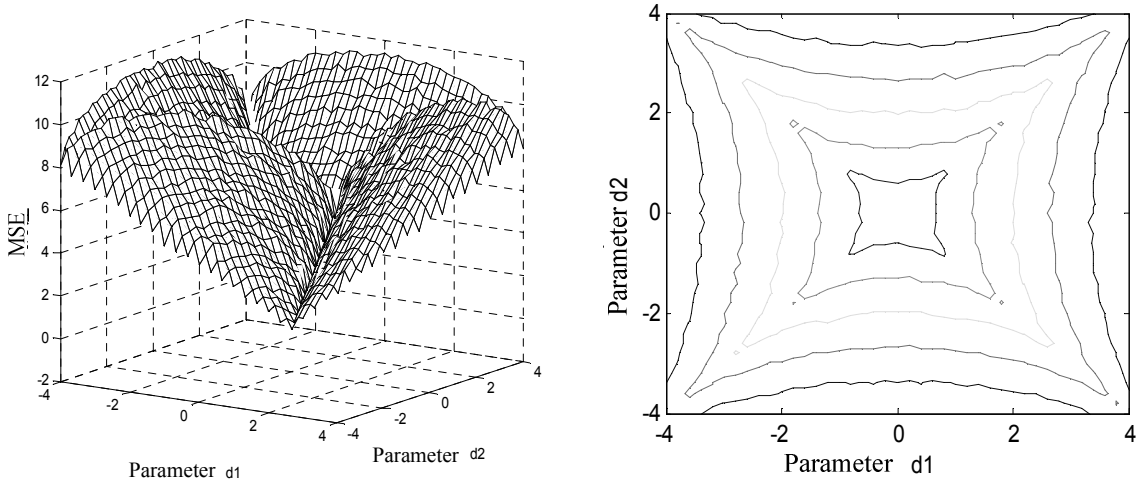

(a) Three-dimensional map (b) Contour map

Fig4 Effect of MSE of the parameters d_1 and d_2 of the adaptive filter

2 Performance Analysis

The main performance simulation using two-point and three-frequency signal frequency signal frequency estimation. Figure 5 is a carrier-to-noise ratio 30dBHz multi-frequency signal frequency tracking, the initial frequency of the filter has been estimated by the FFT. Figure 6 Comparison of IIR adaptive filter with conventional phase-locked loop tracking performance. Simulation results show that the FFT frequency assisted adaptive IIR filter may be implemented with an estimated multi-frequency signal frequency point; under different conditions IIR adaptive filter has a bandwidth of the phase locked loop similar to the tracking accuracy.

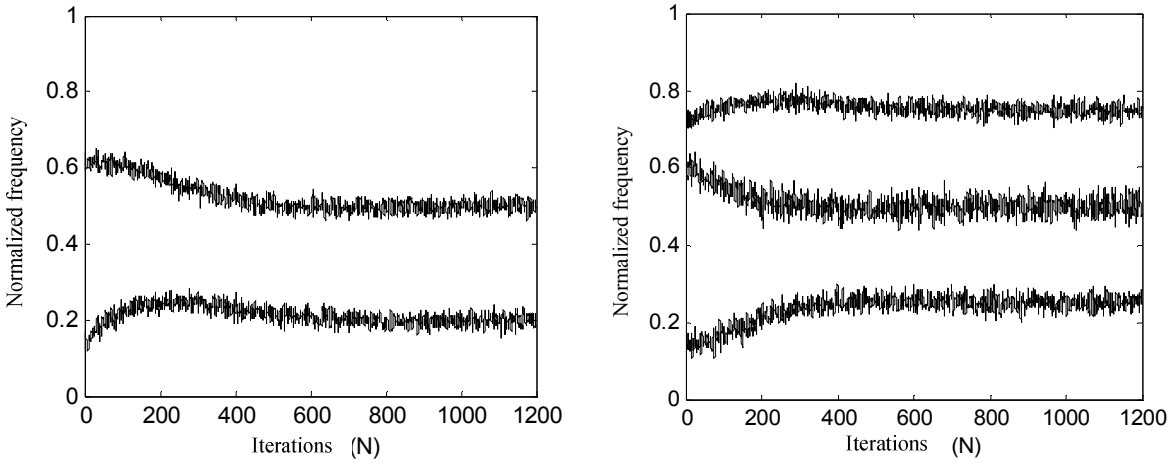

(a) Dual-band point signal($f_1 = 0.2$, $f_2 = 0.5$) (b) Three frequency signals ($f_1 = 0.3$, $f_2 = 0.5$, $f_3 = 0.8$)

Fig5 Multi-frequency signal parameter estimation curve

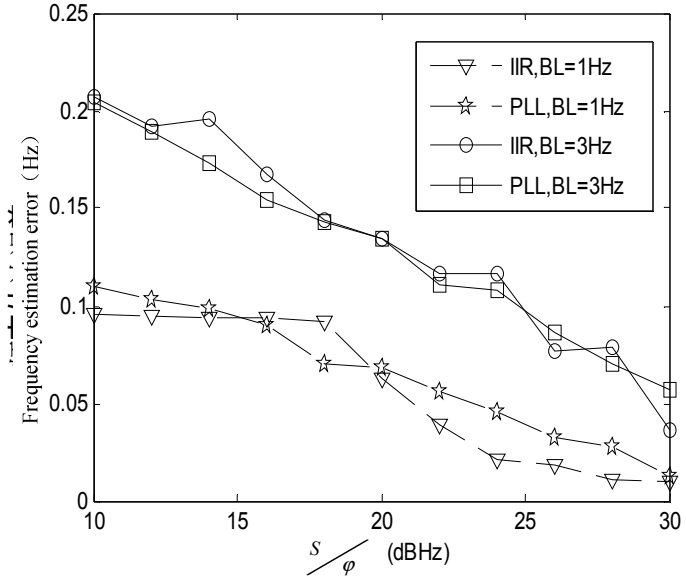

Fig6 Compared with different carrier-to-noise PLL frequency tracking error ratio IIR

Summary

By analyzing the second-order and fourth-order IIR filter that affect the variance adaptive prove second-order IIR model has a single peak characteristics, to achieve stable convergence; while the higher-order IIR model polymorphism, and therefore need to estimate parameters conclusions initialization.

References

[1]G W Lank, I S Reed, G E Pollon. A semi coherent detection and Doppler estimation statistic[J].IEEE Trans Aerosp Electron Syst,1973,9(2):151-165.

[2]S M Kay.A fast and accurate single frequency estimator[J] . IEEE Trans ASSP, 1989,37(12):1987-1990.

[3]L J Griffiths，Rapid measurement of digital instantaneous frequency[J].IEEE Trans ASSP, 1975,23(2),207—222.

Advanced Materials Research Vols. 989-994 (2014) pp 3989-3992
© (2014) Trans Tech Publications, Switzerland
doi:10.4028/www.scientific.net/AMR.989-994.3989

Detection and Parameter Estimation of Chirp Signal Based on Time-frequency Analysis

Wu Guangzhi[1, a], Fu Gang[1,a] and Wu Yanjun[1,a]

[1]China Satellite Maritime Tracking and Control Department, China
[a]348237548@sina.com

Keywords: Chirp signal; Wigner-Ville distribution(WVD); Radon-Wigner transform (RWT); fractional Fourier transform(FRFT)

Abstract. Based on the relationship between the Radon-Wigner transform and fractional Fourier transform and the time frequency distribution, using the property that Radon-Wigner transform has better performance in time and frequency domain, detection and parameter estimation of Chirp signal have been done by Radon-Wigner transform or fractiona1 Fourier transform. The theoretica1 analysis and simulation prove that two techniques are better than generic time-frequency transform, such as Wigner-Ville transform.

1 Introduction

In the time-frequency analysis, Wigner-Ville transform is a commonly used method, the analysis of non-stationary signals is very favorable. However, the definition of the Wigner-Ville transform apparent: it is essentially a bilinear transformation, the multi-component cross term signal will appear, especially when the signal contains two or more components, each of the components will produce cross between term, this is a major flaw in WVD. Radon-Wigner transform and fractional Fourier transform analysis of multi-component signals; you can effectively reduce or avoid the impact of such interference.[1][2]

Wigner-Ville distribution WVD ideal LFM signal was linear impulse function, finite length of Chirp signal is shaped dorsal fin, to its time-frequency plane along the corresponding WVD straight points to make smooth, energy WVD of the corresponding points in a straight line been gathered on, Radon-Wigner transform (RWT) is a linear integral projection transformation; fractional Fourier transform is the signal frequency distribution in the projection after the frequency axis of rotation, if the rotation angle is right, you can get LFM signal energy distribution of fractional gathered Fourier domain. Therefore, Radon Wigner transform and fractional Fourier transform for Chirp signal analysis is the ideal choice.

2 RWT and FRFT

2.1 Radon-Wigner transform

Radon-Wigner WVD of signal conversion is done straight integral projection of Radon transform, collectively referred to as the signal to make R a don transformation.

As shown in Figure 1, the original Cartesian coordinate system (t,ω) rotation angle α to obtain the new Cartesian coordinate (u,v) . u value at different time in parallel to the v axis points, the result is Radon transformation.

As we can be seen from Figure 1, Radon transform is actually equivalent to the generalized edge points, the equivalent of a projection points. Let two-dimensional plane (t,ω) has an arbitrary two-dimensional function (such as density function) $f(t,\omega)$, then the use of trigonometry, its Radon transform can be written as:[3]

Radon transform $P_\alpha(u)$ certain corner of α is a function u (equivalent to PQ line pan). For different values of α, $P_\alpha(u)$ is a function of the value change, and that it is a two-dimensional function of u and α .If R represents Radon transform operator, the transformation from the normal two-dimensional function $f(t,\omega)$ of the object instead of the signal $s(t)$ Wigner-Ville distribution

(WVD), converting the resultant Radon is the signal of Radon-Wigner transform(RWT), represented by a symbol $D_z(u,\alpha)$. By the formula (1) readily obtained:

$$P_\alpha(u)=\int_{PQ} f(t,\omega)dv=\int_{PQ} f(u\cos\alpha-v\sin\alpha,u\sin\alpha+v\cos\alpha)dv \tag{1}$$

$$\begin{aligned} D_z(u,\alpha)&=R_\omega[z(t)]=R[W_z(t,\omega)]=\int_{PQ} W_z(u\cos\alpha-v\sin\alpha,u\sin\alpha+v\cos\alpha)dv \\ &=\int_{-\infty}^{+\infty}\int_{-\infty}^{+\infty} W_z(u\cos\alpha-v\sin\alpha,u\sin\alpha+v\cos\alpha)\delta(u-u)dudv \end{aligned} \tag{2}$$

Where, $W_z(t,\omega)=\int_{-\infty}^{+\infty} z(t+\frac{\tau}{2})z^*(t-\frac{\tau}{2})e^{-j\omega\tau}d\tau$ is WVD of the signal $s(t)$; the real signal $s(t)$, $z(t)$ is the analytic signal of the signal $s(t)$, $z(t)=s(t)+j\cdot HLT(s(t))$; HLT represents signal indicates Hilbert (Hilbert) transformation.[4]

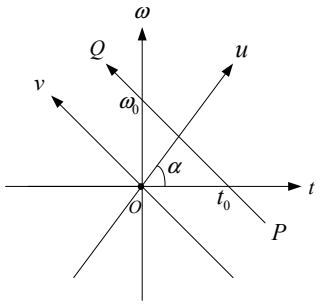

Fig 1 The axis of rotation of the coordinate geometry relations

Formula (2) represents signal $s(t)$ of Radon-Wigner transform that is represented by parameter (u,α). In Radon-Wigner distribution frequency plane, where the practice of using ω_0 and m of axes ω as a parameter to indicate the slope of the straight line. Therefore, when necessary points along a straight line $\omega=\omega_0+mt$, in Figure 1 may be integral path (straight line PQ) replace the parameters of (u,α) to (m,ω_0), and the relationship between the two parameters as follows:

$$m=-\cot\alpha,\quad \omega_0=u/\sin\alpha \tag{3}$$

Find a signal $s(t)$ of Radon-Wigner transform, and parameter (m,ω_0) represents the integral path, then

$$\begin{aligned} D_z(u,\alpha)&=\int_{PQ} Wz(t,\omega)dv=\int_{-\infty}^{+\infty}\int_{-\infty}^{+\infty} W_z(t,\omega)\cdot\delta(u-u)dudv \\ &=\frac{1}{|\sin\alpha|}\int_{-\infty}^{+\infty}\int_{-\infty}^{+\infty} W_z(t,\omega)\delta[\omega-(\omega_0+mt)]d\omega dt \\ &=\frac{1}{|\sin\alpha|}\int_{-\infty}^{+\infty} W_z(t,\omega_0+mt)dt\Big|_{\substack{\omega_0=u\sin\alpha\\ m=-\cot\alpha}} \end{aligned} \tag{4}$$

Formula (4) shows: If $s(t)$ is the parameters ω_0 and m are the Chirp signal, the maximum integral value; when the parameter ω_0 and m, when departing from the integrated value decreases rapidly, it is a certain Chirp signal, the Radon-Wigner transform spikes will appear at the corresponding parameter (m,ω_0), which can Chirp signal detection and parameters estimation.

2.2 fractional Fourier transform (FRFT)

Fractional Fourier transform (FRFT) is also based on the principle axes of rotation. Traditional Fourier transform function $g(t)$ is changed $\pi/2$ to ω rotational axis of said formula, denoted by $G=Fg$, the function of the angle $\pi/2$ of the ω axis of said shaft, is a function of converting the Fourier transform. It is easy to verify that: $F^2g(t)=FFg(t)=g(-t)$ and $F^4g(t)=g(t)$; where F^n represents the continuous use of the operator F n times. Figure 1 when the rotation angle α is not

equal to whole multiple of $\pi/2$, the function is obtained in the angle α of the axis u shaft of said fractional Fourier transformation. Let this time as a linear operator R, the function $x(t)$ fractional Fourier transform is defined as

$$X_p(u)=\left\{R^p x\right\}(u)=\int_{-\infty}^{+\infty}x(t)K_p(t,u)dt=\begin{cases}\sqrt{\dfrac{1-j\cot\alpha}{2\pi}}e^{j\frac{u^2}{2}\cot\alpha}\displaystyle\int_{-\infty}^{+\infty}x(t)e^{j\frac{t^2}{2}\cot\alpha}e^{-jut\csc\alpha}dt, & \alpha\neq n\pi\\ x(u) & \alpha=2n\pi\\ x(-u) & \alpha=(2n+1)\pi\end{cases}\tag{5}$$

Where: $\alpha=p\pi/2$, p is the order of FRFT, when $p=1$, the degradation of the traditional Fourier transform.

According to the concept of rotation, the operator R has the following properties: (1)zero rotation of $R^0=I$; (2)and Fourier transform equivalence $R^{\pi+2}=F$; (3) rotation addition $R^{\alpha}R^{\beta}=R^{\alpha-\beta}$; (4)the identity transformation $R^{2\pi}=I$.

Chirp signal when said frequency plane was inclined blade-like, with a clear time-frequency coupling characteristics. When the projector and fractional Fourier transform can be seen as a signal of the frequency distribution in the frequency axis rotated; conventional Fourier transform can be seen as a signal when the frequency distribution in the projection frequency axis, linear FM signal spectrum is broadened If the rotation angle is right, you can get the energy chirp signal gathering fractional Fourier domain distribution, which is the use of the basic principle of fractional Fourier transform to detect the chirp signal. For two different slopes FM chirp signal, choose a different rotation angles can be two separate, in order to estimate the parameters of the signal.

3 Chirp signal detection and parameter estimation

Chirp signal WVD for a good time and frequency aggregation, which is bilinear transformation. Due to the nature of the algorithm. The way to solve this problem is that demand for WVD LFM signal or directly to the Radon transform signal fractional Fourier transform.

Figure 2 shows the estimated flow detection and parameter time-frequency signal analysis ILFM based. The upper part of the figure has the upper and lower two-way, all the way to select any one time (controlled by a switch). The road to signal Radon-Wigner transform, the input signal is first calculated Wigner-Ville distribution, the time-frequency distribution after Radon transform signal can be obtained Radon-Wigner transformation; under way to signal the fractional Fourier transform, whichever is the square of the modulus value again. Upper and lower road use Radon-Wigner transformation respectively and fractional Fourier transform modulus squared value for signal detection and parameter estimation.

From the foregoing: Because Chirp signal in the time-frequency plane, the frequency is approximately linear variation with time $\omega=\omega_0+mt$, the value of the square modulus of its Radon-Wigner transform and FRFT, it will show a peak at the corresponding parameters (u,α), the peak corresponding value of the coordinate u and α ,we can calculated linear parameter $m=-\cot\alpha$, $\omega_0=u/\sin\alpha$.

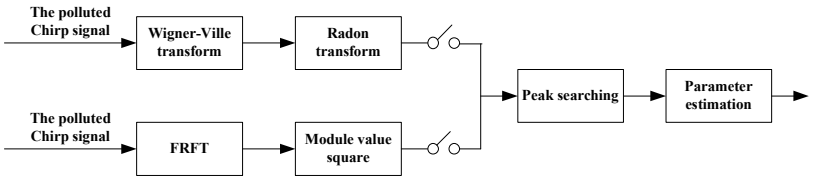

Fig 2 Flow chart of Chirp signal detection and parameters estimation based on time-frequency analysis

Assuming unknown signal $x(t)=s(t)+n(t)$, where, $s(t)=e^{j2\pi(f_0t+\frac{1}{2}mt^2)}$ is chirp signal, $n(t)$ is Gaussian white noise.

Table1 Chirp signal parameters estimation based on Radon-Wigner transform

The polluted Chirp signal	SNR(dB)	Parameter representation form					
		Parameters setting		Estimated parameters		Relative error(%)	
		$f_0(Hz)$	$k(Hz/s)$	$f_0'(Hz)$	$k'(Hz/s)$	$(f_0-f_0')/f_0$	$(k-k')/k$
Signal 1	-2	-30	100	-30.3051	99.6816	1.02	0.32
Signal 2	0	100	4000	98	4009	2.00	0.22
Signal3	4	300	-2000	303	-2020	1.20	0.17

Table2 Chirp signal parameters estimation based on FRFT

The polluted Chirp signal	SNR(dB)	Parameter representation form					
		Parameters setting		Estimated parameters		Relative error(%)	
		$f_0(Hz)$	$k(Hz/s)$	$f_0'(Hz)$	$k'(Hz/s)$	$(f_0-f_0')/f_0$	$(k-k')/k$
Signal 1	-2	-30	100	-29.9664	99.7265	1.12	0.27
Signal 2	0	100	4000	101	4008	1.00	0.20
Signal3	4	300	-2000	298	-1993	0.67	0.35

Set different chirp parameters (center frequency and frequency modulation), respectively, parameters and fractional Fourier transform detected (U, a) transform the Radon-Wigner, can estimate the center frequency and modulation frequency, as shown in Table 1 and Table 2 shown. The table also shows the relative error of the estimated parameters and the chirp parameter setting. Visible, the estimation error is small. This is because the cross-term Radon-Wigner distribution, affecting the resolution of the signal parameter estimation; while fractional Fourier transform is a linear transformation, without interference from cross-terms. Nevertheless, Radon-Wigner transformation is still an effective LFM signal detection and parameter estimation method.

4 Summary

By the theoretical analysis and computer simulation, we can see: the use of LFM signal Wigner-Ville distribution in the time-frequency plane is approximately linear relationship was characterized by its WVD seeking Radon transform of the signal with the direct fractional Fourier transform, not only can detect the noise LFM the existence and the number of component signals LFM signals, but also to estimate the parameters of each LFM signal components; especially for multi-component LFM signal detection and parameter estimation, Radon-Wigner transform and fractional Fourier transform more than Wigner-Ville transform effective.

References

[1] Namias V. The fractinal order Fourier transform and its application to quantum mechanics [J]. J Inst Math Appl, 1980, 25: 241~265.
[2] Ozaktas H.M, D.Mendlovic. Fractional Fourier Transform and their Optical Implementation (i and ii) [J]. Optical Society Am A.1993, 10(9):1875-1881.
[3] Almeida L. B. The Fractional Fourier Transform and Time-Frequency Representations [J]. IEEE Transactions on Signal Processing.1994, 42(11): 3084-3091.
[4] Shao Zhichao, Wu Yanhong, Jia Xing. Detection and Parameter Estimation of LFM Signal Based on Time-frequency Analysis[J]. Journal of the Academy of Equipment Command & Technology. 2004,15(2):71-75.

Advanced Materials Research Vols. 989-994 (2014) pp 3993-3996
© (2014) Trans Tech Publications, Switzerland
doi:10.4028/www.scientific.net/AMR.989-994.3993

Parameters Estimation and Waveform Reconstruction of Chirp signal Based on FRFT

Wu Yanjun[1, a], Fu Gang[1,a] and Liu Fei[1,a]
[1]China Satellite Maritime Tracking and Control Department, China
[a]348237548@sina.com

Keywords: Fractional Fourier Transform, Chirp signal, Wigner-Ville distribution, Waveform Reconstruction

Abstract: The fractional Fourier transform (FRFT) is a generalization of the Fourier transform. The article first introduces the definition of FRFT transformation; then analyzed FRFT Chirp signal based on this humble proposed restoration Chirp signal in a noisy background in two ways: one is based on parameter estimation, and the other is based on the scores Fourier domain filtering to achieve signal reconstruction; Finally, simulation verify the feasibility of the above analysis.

Introduction

Chirp signal is a special kind of non-stationary signals. As a large time-bandwidth product signals, it is widely in communications, radar, sonar and seismic exploration systems. In such systems, Chirp signal detection, parameter estimation and signal recovery is an important research topic. FRFT concepts from the field of optics was first introduced, it reflects the lens rear light intensity distribution in a plane perpendicular to the optical axis. In the mid-1990s, the method was introduced signal processing, and pointed out that it is the physical meaning of a given signal frequency distribution in the frequency domain with a timeline angled α integral projection axis. FRFT is a linear transformation, it wavelet transform, Wigner-Ville distribution (WVD) has a close relationship, so frequent in recent years, this method as a research tool to analyze the signals received wide attention of researchers, the corresponding discrete transform algorithms have been proposed.[1]

The article first introduces the definition and implementation of FRFT transform, and then analyzes the FRFT Chirp signal based on this proposed restoration Chirp signal in a noisy background of the two methods, verified by simulation analysis above.

1 Definition of FRFT

Fourier transform is a linear operator, the operator's role can be seen in the time-frequency plane rotation $\pi/2$, that is, from the timeline to the frequency axis. Understandably, if you find any angle $\alpha = p\pi/2$ can be used for a non-integer multiple (non-integer multiple of $\pi/2$, and p is a fraction) rotation operator,[2] the signal represented by the new operator is available, the so-called fractional Fourier transform (referred FRFT).

p th order FRFT of signal $x(t)$ is defined as

$$X_p(u) = \{F^p x(t)\}(u) = \int_{-\infty}^{+\infty} x(t) K_p(t,u) dt \tag{1}$$

Where $K_p(t,u)$ is a nuclear transformation, which is defined as

$$K_p(t,u) = \begin{cases} \sqrt{\dfrac{1-j\cot\alpha}{2\pi}} \exp[j(\dfrac{1}{2}u^2\cot\alpha - ut\csc\alpha + \dfrac{1}{2}t^2\cot\alpha)] & \alpha \neq n\pi \\ \delta(t-u) & \alpha = 2n\pi \\ \delta(t+u) & \alpha = 2(n+1)\pi \end{cases} \tag{2}$$

Where n is an integer number.

As can be seen from the definition, FRFT is generalized Fourier transform classic form, it contains a signal of time domain and frequency domain representation, when the rotation angle is $\frac{\pi}{2}$, that means the 1 order of FRFT is a traditional Fourier transform ; does not rotate when the rotation angle of 2π or an integer multiple of the result is the signal itself; when the rotation angle is not more than two positions, when p is a fraction numbet, it scores from the time domain and it also gives the frequency domain characteristics of the signal. FRFT corresponding inverse transform $-\alpha$ angle FRFT.[3]

2 Fractional Fourier Transform Chirp signal characteristics and recovery

Assuming a single frequency chirp signal $f(t)=\exp\left[2\pi j(f_0 t+\frac{1}{2}t^2)\right]$, Its Wigner-Ville distri -bution as

$$W(f,t)=\delta\left[f-(kt+f_0)\right] \tag{3}$$

According rotational invariance of Wigner-Ville distribution, as long as the rotation angle of the α and β FRFT orthogonal as shown in Figure1. Then the Chirp signal is projected onto a fractional Fourier domain should be gathered at one point. According FRFT definition, fractional Fourier transform domain decomposition based tone frequency is $-\cot\alpha$ ($\alpha=k\pi(k=0,\pm1,...L)$ here ignores the special circumstances), while the expression of available FM Chirp signal was $k=\tan\beta$, Chirp signal in order to achieve a base focus on the frequency must be adjusted to ensure equal as

$$\tan\beta=-\cot\alpha=k \tag{4}$$

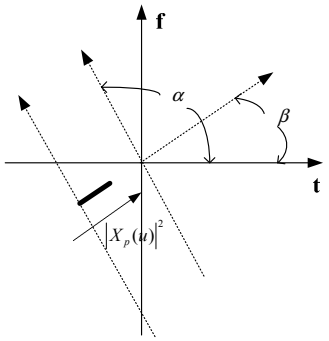

Fig1 FRFT of Chirp and its Wigner-Ville distribution

Here are Chirp signal recovery method.

The first method: Depending on the nature of the known FRFT it is a linear transformation, is a continuous function of p, so the fractional Fourier transform with $\alpha=p\pi/2$ angleis the angle $\alpha=-p\pi/2$ with the FRFT, that is

$$x(t)=\int_{-\infty}^{+\infty}X_p(u)K_{-p}(t,u)\,du \tag{5}$$

from a recovery directly out of the original signal.

If Chirp signal is finite length signal, then it's most of the energy in the u domain concentrated in u_0. Center within a narrow band, but there is no good time-frequency noise of focusing on fractional Fourier domain, so in the case of additive Gaussian noise conditions, the design of an appropriate bandpass filter centered in u_0, then the output signal can retain most of the energy and filter out most of the noise energy, then filtered output FRFT inverse transform, we can recover the original Chirp signal.

The second method: Chirp signal characteristics with energy gathered in FRFT certain angle, namely Chirp signal in the new coordinate system (u,v) has an impact alpha function and meet FM slope $k=-\cot\alpha$. Thus, the continuous search for α, once the shock exists, then the Chirp signal is present, and to meet FM slope $k=-\cot\alpha$; estimated slope of the FM signal k, you can calculate

the angle of its FRFT $\alpha = arc\cot(-k)$, and then seek the order of the FRFT, then search out the maximum point u_0 fractional coordinates on u, can be estimated Taking into account the initial beta frequency signal $f_0 = u_0 \csc\alpha$; Finally, according to the expression Chirp signal to recover the original signal.

3 Simulation analysis

To illustrate the effectiveness of the algorithm, the following assumes a bandwidth of $B = 200MHz$, FM was $k = 2\times10^{13} Hz/s$, initial frequency $f_0 = 100MHz$ of single-frequency Chirp signal, additive noise is zero mean Gaussian white noise. In the observation period $T = 10^{-6} s$, using the above two methods with different SNR, the simulation results shown in Figure 2.

When the SNR is equal to 12dB, the direct use of parameter estimates obtained: $k = 2.0001\times10^{13} Hz/s$, $f_0 = 9.9996\times10^{7} Hz$, relative error of k is 0.005%, the relative error of f_0 was 0.004%; frequency analysis of the signal obtained directly from the inverse transform filter were obtained $k = 2.002\times10^{13} Hz/s$, $f_0 = 1.0001\times10^{8} Hz$, the relative error of k is 0.001% and the relative error of f_0 is 0.01%.

When the SNR is equal to 12dB minus, the direct use of parameter estimates obtained: $k = 2.0003\times10^{13} Hz/s$, $f_0 = 1.0005\times10^{8} Hz$, relative error of k is 0.015%, the relative error of f_0 is 0.005% ; directly after the signal obtained using filtered back-transform time-frequency analysis and gained: $k = 2.0005\times10^{13} Hz/s$, $f_0 = 1.0006\times10^{8} Hz$, relative error of k and f_0 are 0.025%,0.06% respectively.

For multi-component signals $x(t)$, generally the first two-dimensional peak search method according to a first position (α_1, u_1) of the maximum peak point of the parameter estimates obtained strongest signal component corresponding to the signal , then calculated at the time of FRFT alpha α_1, in this case most of the energy of the first component is concentrated in a narrow band centered with u_1, u in the domain covered by the spike, and the method according to the second reverse rotation of the filtered signal back to the original time-domain α_1, detecting a second component; repeat the above process, to detect all detectable parameter estimation component until the average amplitude of the remaining signal components below a predetermined threshold.

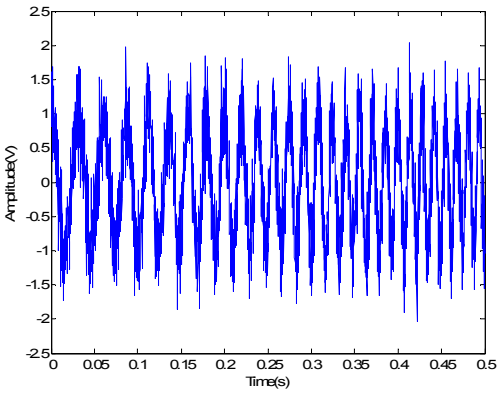

(a) Chirp signal waveform polluted by AWGN

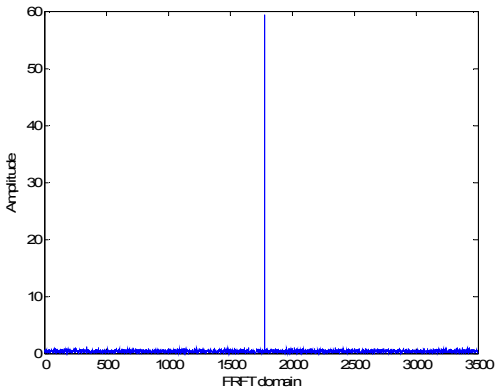

(b) The FRFT peak of two-dimensional peak search

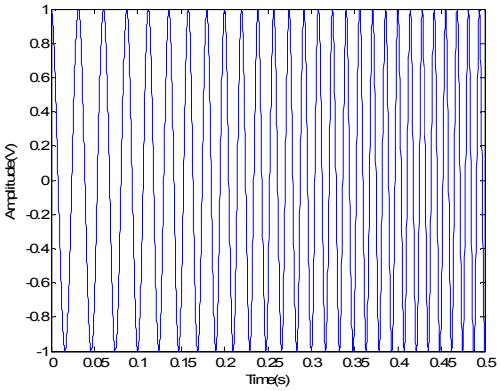

(c) Chirp signal waveform recovered by parameters estimation

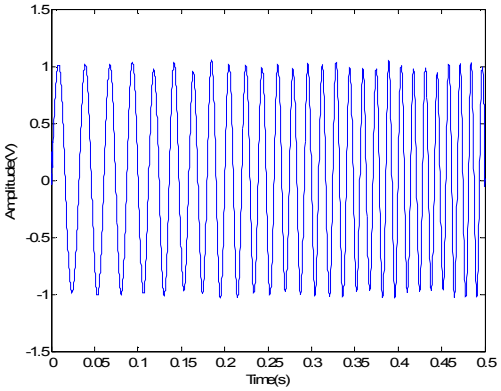

(d) Chirp signal waveform recovered by inverse FRFT

4 Summary

Article two methods have their own characteristics. Peak detection method for a more intuitive in principle, can be directly estimated parameters, but in the process variable rotation angle α scan, when the request parameter estimation accuracy is high, you must select a smaller scanning step, making computational complexity increases; followed in the multi-component detection, there is a strong influence on the weak component of the component, and therefore must be taken to suppress this interference, then you need to use the second method uses filtering successive elimination strong way to improve signal detection reliability. However, in the case of frequency modulation is unknown, the filtering method using the premise that accurately estimate a frequency swap, so the need for effective combination of both methods. Clear physical meaning of these two methods, the calculation is simple, no cross-infection, is a very effective method.

References

[1] Lohmann A .W. Image Rotation, Wigner Rotation, and the Fractional Fourier Transforms [J]. Optical Society Am A.1993, 10(10):2181-2186.
[2] Almeida L. B. The Fractional Fourier Transform and Time-Frequency Representations [J]. IEEE Transactions on Signal Processing.1994, 42(11): 3084-3091.
[3] Ozaktas H. M, Kutay M. A, Bozdagi G. Digital computation of the fractional Fourier transform [J]. IEEE Transactions on Signal Processing.1996, 44(9):2141-2150.

Advanced Materials Research Vols. 989-994 (2014) pp 3997-4000
© (2014) Trans Tech Publications, Switzerland
doi:10.4028/www.scientific.net/AMR.989-994.3997

Research on Demodulation of Pulse Code Modulated Signal Based on Instantaneous Frequency Measurement

Fu Gang[1, a], Wu Yanjun[1,a] and Feng Yue[1,a]
[1]China Satellite Maritime Tracking and Control Department, China
[a]348237548@sina.com

Keywords: PCM/FM, MSD, synchronous.

Abstract. According instantaneous frequency measurement theory, we propose a new PCM / FM telemetry signal demodulation method. This paper introduces the basic principles of this demodulation method and implementation process, the influence of instantaneous frequency measurement accuracy and the impact of factors on the Doppler frequency demodulation performance is proposed to improve the accuracy and instantaneous frequency measurement method demodulation performance .

Introduction

Currently, PCM / FM signal demodulation software commonly used methods are: using Wigner - Willie (WD) or on the distribution of discrete short-time Fourier transform (STFT),[1] frequency analysis of the signal when the signal is estimated using statistical methods the width of the frequency and the symbol realize PCM / FM demodulation signal; cycle using a sinusoidal model for precise slide fitting method demodulated PCM / FM signal. Although these methods must meet the accuracy of demodulation, but the complexity of the algorithm, a large amount of computation, the signal is not conducive to improved efficiency of the software demodulator.

Instantaneous frequency measurement capable of having a single carrier frequency signal for fast frequency measurement. In this paper, the theory of instantaneous frequency measurement is based on the characteristics of PCM / FM signal, the introduction of software demodulation principle and demodulation process and its performance analysis and simulation.

1 Instantaneous frequency measurement

Assuming a single frequency signal, denoted as:[2]

$$S(i) = A\sin(\omega T_S i + \varphi) \tag{1}$$

There are:

$$S_{i+1} + S_{i-1} = 2S_i \cos(\omega T_s) or \omega T_s = \arccos\left(\frac{S_{i+1} + S_{i-1}}{2S_i}\right) \tag{2}$$

Assuming $S_i \neq 0$, the use of three adjacent sample values, can calculate the frequency of the signal. In the quantization accuracy is high enough, the denominator is not zero in most of the conditions can be met. Practical applications, often with multi-point instantaneous frequency measurement, then equation (2) can be rewritten as:

$$y_i = Kx_i, \qquad y_i = S_{i+1} + S_{i-1}, \quad x_i = 2S_i, K = \cos(\omega T_s) \tag{3}$$

And obtaining the square of the distance:

$$\begin{aligned} &\frac{1}{1+K^2}\sum_{i=1}^{m}(y_i - Kx_i)^2 = m*\left[\frac{W}{1+K^2} - \frac{U*2K}{1+K^2} + \frac{V*K^2}{1+K^2}\right] \\ &\text{among:} W = \frac{1}{m}\sum_{i=1}^{m} y_i^2, U = \frac{1}{m}\sum_{i=1}^{m}(x_i y_i), V = \frac{1}{m}\sum_{i=1}^{m} x_i^2 \end{aligned} \tag{4}$$

The formula for the derivative gain K:

$$U * K^2 + (V - W) * K - U = 0 \tag{5}$$

And then solve:

$$K = \frac{-(V-W) \pm \sqrt{(V-W)^2 + 4U^2}}{2U}$$

By Equation (3) shows that: $|K| \le 1$, so:

$$K = \frac{-(V-W) + \sqrt{(V-W)^2 + 4U^2}}{2U} \tag{6}$$

2 Demodulation algorithm

PCM / FM signal is generated by two different frequencies to transmit information symbols. Therefore, the transition time is bound to two different symbols mutation frequency occurs, the frequency of the mutation point is also code synchronization position. Can be used instantaneous frequency measurement method by calculating the PCM / FM signal in continuous time sampling frequency, the frequency of mutations in the capture point, to achieve code synchronization.

Since actually received PCM / FM signal to the Doppler frequency shift, to improve the accuracy of code synchronization and demodulation performance in the demodulation process also requires the use of instantaneous frequency measurement method, Doppler frequency shift compensation, frequency measurement was corrected to "0" bit and the "1" code corresponding frequency. Doppler shift compensation from below, code synchronization and sentencing three aspects discussed in detail.

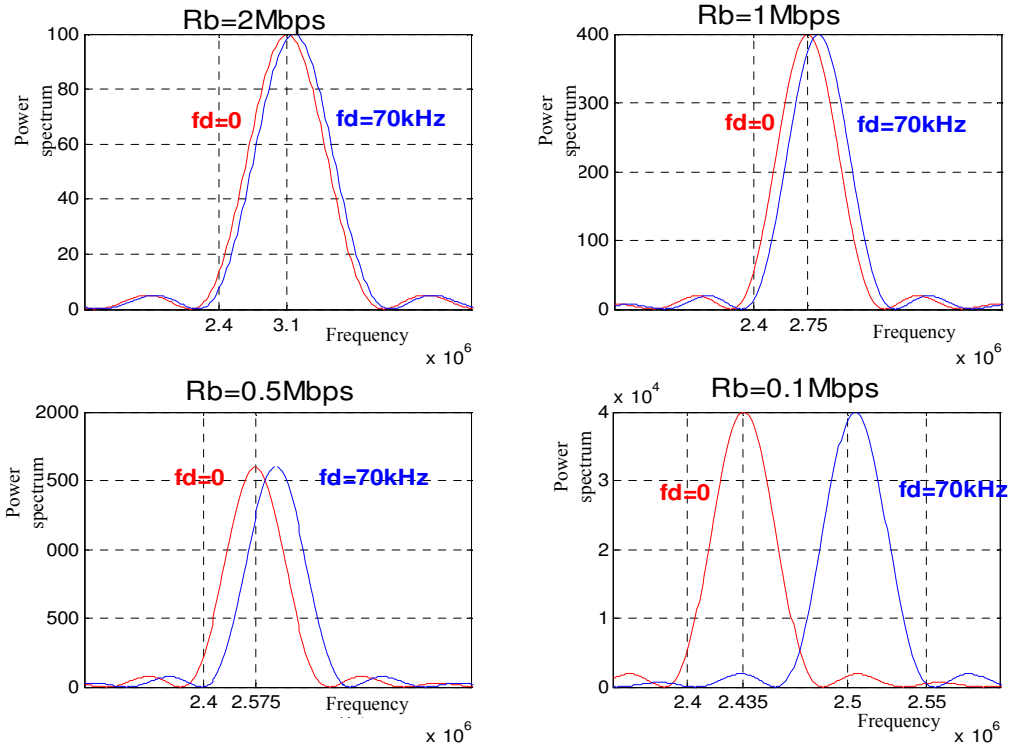

Fig1 Doppler frequency shift of the spectrum peak

Instantaneous Frequency Measurement Based on core PCM / FM demodulation method is that the instantaneous frequency of each symbol in accurate estimates and judgments. Received PCM / FM signal is always the Doppler frequency, this is reflected in the Doppler frequency PCM / FM signal carrier center frequency drift. Doppler positive bias 70KHz, different code rates, the "1" bit

corresponding to the frequency position, for example, analysis of the Doppler frequency shift of the maximum output position of the spectrum. The simulation results shown in Figure 1.

Can be drawn from Figure 1, the spectral Doppler shift effect on the maximum position with decreasing code rate is getting worse. Therefore, to reduce the error rates before demodulating the Doppler shift must be compensated.

The maximum instantaneous frequency corresponds to a "1" f_1 code of the actual frequency, minimum corresponds to the "0" code of the actual frequency f_0. Equation (8), (9) can be obtained after averaging the sum of:

$$\frac{f_1 + f_0}{2} = f_c + f_d \tag{10}$$

According to the Doppler frequency obtained corrected instantaneous frequency measurement results in "0" key and the "1" code corresponding frequency, thus avoiding the carrier frequency drift caused due demodulation error.

Receiving the synchronization accuracy of the transmission data in a data communication system is established on the basis of the correct synchronization. The hardware circuit is extracted synchronization code PLL core software demodulation code synchronization for the extraction process is the substance of each symbol, an optimal extraction processing start position starts from that position demodulating that demodulates achieve optimal performance.

Best code synchronization point PCM / FM signal is "0" key and the "1" code corresponding frequency hopping point. Instantaneous frequency measurement method, set a width (should be less than the width of a symbol sampling points) sliding window, calculate PCM / FM signal instantaneous frequency point by point, to capture the signal frequency hopping point, thus achieve code synchronization.

3 Performance Analysis

Instantaneous frequency measurement method throughout the demodulation process, including the estimated Doppler frequency and location code synchronization point, so instantaneous frequency measurement accuracy will directly affect the demodulation performance. Note that when you raise the following two aspects instantaneous frequency measurement accuracy:

1, the application frequency calculated instantaneous frequency measurement method is a prerequisite: the sampling signal is detected for a single carrier frequency, pure sinusoidal signal of constant amplitude, and does not contain a DC component.

2, the main parameters of the algorithm to the data window length, when selecting from two aspects: (1) Equation (6) actually uses the best approximation method, the more sampling points (ie the greater) for linear approximation, the better, the smaller the frequency measurement error.

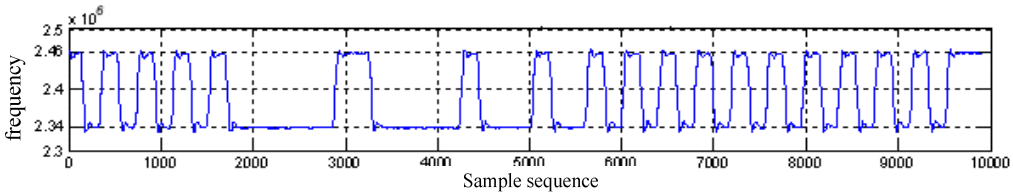

Fig2 PCM / FM signal instantaneous frequency measurement results

Can be clearly seen from Figure 2, since the waveform is similar to a rectangular pulse, when the decision threshold value for the carrier frequency, the positioning can be more accurate code synchronization point, to ensure the correctness of the demodulated result.

Figure 3 shows a comparison chart BER curves in the time code rate of 1.5Mbps. Demodulation performance can be seen that the method is relatively close to non-coherent demodulation performance under ideal conditions.

4 Summary

Instantaneous frequency measurement method for software demodulation PCM / FM signal can be corrected PCM / FM signal Doppler frequency shift caused by the carrier frequency, the more accurate the best position to extract the code synchronization is relatively simple to achieve demodulation symbol decision.

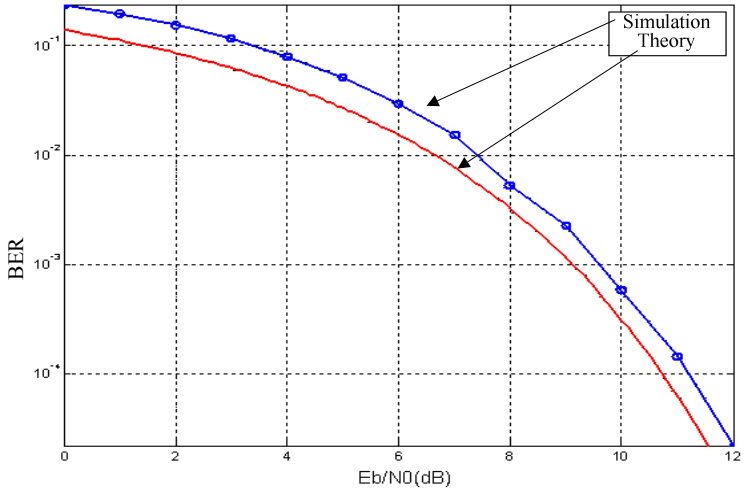

Fig2 BER curves

References

[1] Feng Xiaolin. WV distributed in discrete digital demodulation of the FSK signal applications[J]. Xi'an University of Electronic Science and Technology, 2008.04:201-205.

[2] Liang Zhiguo. An accurate digital FM signal demodulating method[J]. Measurement and Control Technology,2012.11:18-21.

Advanced Materials Research Vols. 989-994 (2014) pp 4001-4004
© (2014) Trans Tech Publications, Switzerland
doi:10.4028/www.scientific.net/AMR.989-994.4001

LFM Signal Detection Method Based on Fractional Fourier Transform

Wu Yanjun[1, a], Fu Gang[1,a] and Zhu Yuming[1,a]

[1]China Satellite Maritime Tracking and Control Department, China

[a]348237548@sina.com

Keywords: Time-frequency analysis, fractional Fourier transform (FRFT), discrete fractional Fourier transform (DFRFT), LFM signal

Abstract. As a generalization of Fourier transform, the fractional Fourier Transform (FRFT) contains simultaneity the time-frequency information of the signal, and it is considered a new tool for time-frequency analysis. This paper discusses some steps of FRFT in signal detection based on the decomposition of FRFT. With the help of the property that a LFM signal can produce a strong impulse in the FRFT domain, the signal can be detected conveniently. Experimental analysis shows that the proposed method is effective in detecting LFM signals.

Introduction

Fourier transform plays an important role in the continuous-time and discrete-time signal processing, analysis and processing is a powerful tool for stationary signals.[1] Fourier transform signal decomposition whole sinusoidal components having different frequencies get the whole spectrum of the signal, while the non-stationary signal processing becomes powerless.[2]

FRFT is a recently developed new time-frequency analysis tool, it is a generalized form of the Fourier transform, with many traditional Fourier transform are not available in nature, has been widely used in optical signal processing, signal analysis, differential equations, pattern recognition and other fields. Recent studies estimate and testing and other aspects of LFM signals based FRFT has been rapid development.

1 Radon-Wigner transform

Radon-Wigner transform is a linear integral projection transformation, is a signal of the Wigner-Ville distribution frequency plane straight line projection Randon integral transformation. As shown in figure 1, the time-frequency plane (t,ω) coordinate rotation angle α obtained a new Cartesian (u,v), with different values of u parallel to the v axis integral, Radon transformation result is obtained. (t,ω) and (u,v) are the coordinates of the relationship between the two planes is shown in formula (1).

$$\begin{cases} t = u\cos\alpha - v\sin\alpha \\ \omega = u\sin\alpha + v\cos\alpha \end{cases} \tag{1}$$

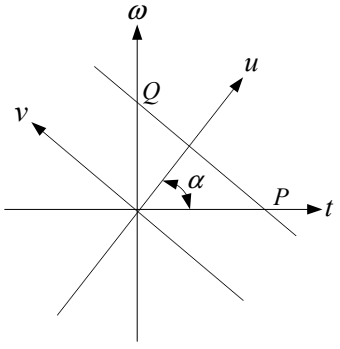

Fig 1 The geometrical explanations of Radon transform

Suppose an arbitrary two-dimensional function $f(t,\omega)$ on a plane (t,ω), which Radon transformation may be expressed as

$$P_\alpha(u) = \int_{PQ} f(t,\omega)dv \tag{2}$$

That is

$$P_\alpha(u) = \int_{PQ} f(u\cos\alpha - v\sin\alpha, u\sin\alpha + v\cos\alpha)dv \tag{3}$$

2 The definition of FRFT

Fourier transform is the time domain and frequency domain together; it shows the frequency components of the signal from the whole, it is suitable for stationary signal analysis and deterministic signals. For non-stationary signal frequency analysis, time-domain signal mapping it one-dimensional two-dimensional time-frequency plane, fully reflect the frequency distribution of the signal changes with time. Fourier transform as a linear operator, if it is seen from the perspective of a counterclockwise rotation $\pi/2$ to the frequency axis, the FRFT operator that can be rotated to any angle α of the operator. So combining Fourier Transform and Radon-Wigner transformation can be defined FRFT.[3]

p th order FRFT of signal $f(u)$ is defined as

$$f_p(u) = \int_{-\infty}^{+\infty} K_p(u,t) f(t)dt \tag{4}$$

Where the transform kernel function in Formula (4) is

$$K_p(u,t) = \begin{cases} A_\alpha \exp[j\pi(u^2\cot\alpha - 2ut\csc\alpha + t^2\cot\alpha)], & \alpha \neq n\pi \\ \delta(u-t), & \alpha = 2n\pi \\ \delta(u+t), & \alpha = (2n\pm 1)\pi \end{cases} \tag{5}$$

In formula (5), there is

$$A_\alpha = \frac{\exp[-j\pi\,\mathrm{sgn}(\sin\alpha)/4 + j\alpha/2]}{|\sin\alpha|^{1/2}},\ \alpha = \frac{p\pi}{2} \tag{6}$$

When the FRFT order $p=1$, there is $\alpha = \pi/2$ and $A_\alpha = 1$, then, according to equation (4), we can get

$$f_1(u) = \int_{-\infty}^{+\infty} e^{-j2\pi ut} f(t)dt \tag{7}$$

Therefore, $f_1(u)$ is the common Fourier transform of $f(t)$. Likewise, $f_{-1}(u)$ is an inverse Fourier transform of $f(u)$. Thus, it is considered that the fractional Fourier transform is a generalized Fourier transform. Because the kernel function $\alpha = \pi/2$, $\alpha_1 = p_1\pi/2$ only in the parameter of the trigonometric functions, so the cycle of the definition according to parameter p, therefore, we just need to examine the range $p \in (-2,2]$. When $p=0$, $f_0(u) = f(u)$, and when $p = \pm 2$, $f_{\pm 2} = f(-u)$.

3 DFRFT decomposition algorithm

In signal processing, we must adopt a discrete form of fractional Fourier transform (DFRFT), DFRFT can also be calculated using digital methods, commonly used algorithm is fast algorithm H.M.Ozaktas decomposition type proposed. The method is based on the so-called decomposition type FRFT expression, the FRFT decomposed into convolution signal, thus using FFT to calculate FRFT. The algorithm calculates the speed and the speed of FFT calculation rather, is a method of calculating the FRFT fast numerical methods. FRFT transformation matrix decomposition type as follows:

$$\mathbf{F}_p = \mathbf{D}\mathbf{K}_p\mathbf{J} \tag{8}$$

In formula (8), $\mathbf{D}$ and $\mathbf{J}$ is matrix of twice interpolation and decimation calculation respectively, $\mathbf{K}_p$ is transform kernel matrix of DFRFT, and its expression is:

$$K_p = \frac{A_\alpha}{2\Delta x}\exp[\frac{j\pi(\cot\alpha)m^2}{(2\Delta x)^2} - \frac{j2\pi(\csc\alpha)mn}{(2\Delta x)^2} + \frac{j2\pi(\cot\alpha)n^2}{(2\Delta x)^2}]|m||n| \le N \tag{9}$$

After one-dimensional normalized, the definition of DFRFT is

$$X_p(u) = \sqrt{\frac{1-j\cot\alpha}{2\pi}}\exp[j\pi\cot(\alpha)u^2]\int_{-\infty}^{+\infty} x(t)\exp[j\pi\cot(\alpha)t^2]\exp[-j2\pi\csc(\alpha)tu]dt \tag{10}$$

Do a discrediting processing to Equation (9) in FRFT domain u, we can obtain:

$$X_p(\frac{m}{2\Delta x}) = \frac{A_\alpha}{2\Delta x}\sum_{n=-N}^{N}\exp[\frac{j\pi(\cot\alpha)m^2}{(2\Delta x)^2} - \frac{j2\pi(\csc\alpha)mn}{(2\Delta x)^2} + \frac{j\pi(\cot\alpha)n^2}{(2\Delta x)^2}]x(\frac{n}{2\Delta x})$$

$$= \frac{A_\alpha}{2\Delta x}\exp[\frac{-j\pi\tan(\frac{\alpha}{2})m^2}{(2\Delta x)^2}]\times\sum_{n=-N}^{N}\exp[\frac{-j\pi(\csc\alpha)(m-n)^2}{(2\Delta x)^2}]\times\exp[\frac{-j\pi\tan(\frac{\alpha}{2})n^2}{(2\Delta x)^2}]x(\frac{n}{2\Delta x}) \tag{11}$$

Where $A_\alpha = \exp\left[j(p-1)\frac{\pi}{4}\right]/\sqrt{|\sin\alpha|}$, $0.5 \le p \le 1.5$, $\alpha = \frac{p\pi}{2}$, $N = (\Delta x)^2$.

The operation of sum can be seen as the convolution operation of two sequences $\exp[\frac{j\pi(\csc\alpha)n^2}{(2\Delta x)2}]$ and $\exp[\frac{-j\pi\tan(\frac{\pi}{2})n^2}{(2\Delta x)^2}]x(\frac{n}{2\Delta x})$.

4 Detection theory of LFM signal based on FRFT

The inverse FRFT expression can be written as

$$x(t) = \int_{-\infty}^{+\infty} X_p(u)K_{-p}(t,u)du \tag{12}$$

We can know that the FRFT can be seen as a signal $x(t)$ on a nuclear base in the inverse transform function $K_{-p}(t,u)$ space expansion, and the kernel function is a set of orthogonal chirp base on the domain u. Therefore, LFM signal at the appropriate FRFT domain will be expressed as a function of the impact that a certain order of FRFT FRFT domain of LFM signal given with good energy aggregation characteristics. The aggregation feature is the theoretical basis of FRFT LFM signal detection.

In one aspect, Wigner distribution of the signal at FRFT domain linear integral projection is that the signal on this domain FRFT Fractional square norm. If you find FRFT signals on a straight line perpendicular to the inclined fractional domain, obvious peak appears at a certain point the domain. And the noise energy is uniformly distributed throughout the time-frequency plane, in any domain FRFT energy concentration will not occur.

On the other hand, LFM signal on a different FRFT domains exhibit different characteristics of energy gathering, testing LFM signal containing location parameters is carried FRFT rotation angle α scanning, observing the signal, the signal energy in the form parameters (α,u) two-dimensional distribution of the plane, on this plane to the peak point of the two-dimensional search LFM signal detection and estimation of its parameters.

5 Simulation results

In FRFT domains, in their presentation accordingly chirp rate at the maximum, by simple thresholding, we can detect the existence of LFM signal and FM slope parameter estimates when rendered in accordance with the order corresponding to the maximum on FRFT.

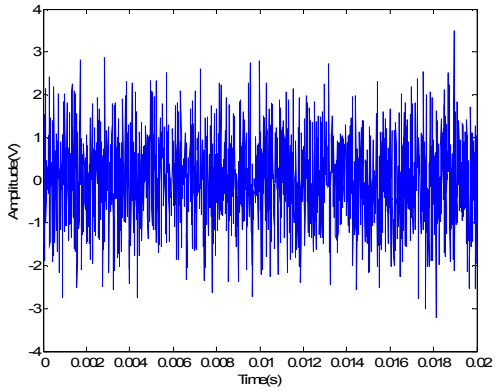

Fig2 Waveform of white Gaussian noise in time domain

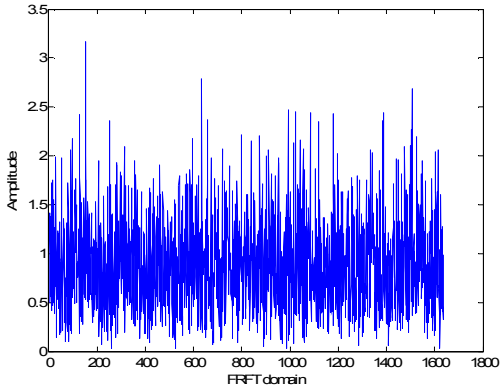

Fig3 Waveform of white Gaussian noise in FRFT domain

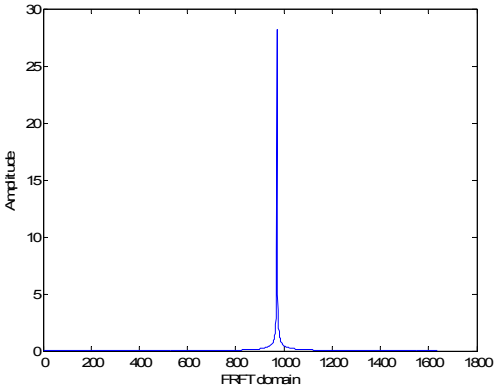

Fig4 Waveform of LFM signal in time domain

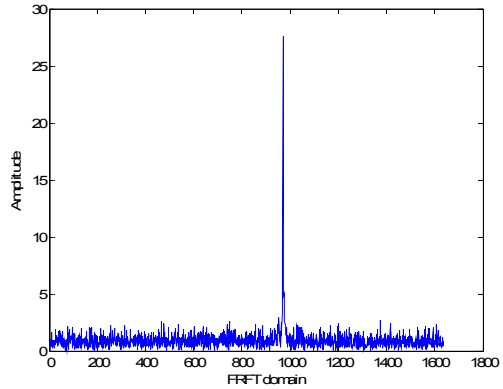

Fig5 The polluted LFM signal in FRFT domain

According to the four figure above, we can find that the waveform of white noise in FRFT domain still be noise wave and it cannot gather energy in any FRFT domain. Further more, the noise cannot influence the energy concentration of LFM signal in its best FRFT domain, and it is critical factor for LFM signal detection and parameter estimation in FRFT domain.

Summary

FRFT can be regarded as showing FRFT FRFT frequency domain signal after the plane at any angle of rotation about the origin constituted on the FRFT decomposed signal using FFT convolution calculation has the advantage of fast calculation. LFM signal with a non-stationary, stationary signal processing using methods often can not be satisfied with the results. Since the LFM signal FRFT domain impulse characteristics presented when the order chirp rate FRFT consistent with the LFM signal, the signal showing spikes, in order to achieve detection of LFM signal. Experimental results show that the signal detection method based on the LFM signal FRFT whether the noise can be satisfied with the results.

References

[1]Wood J C, Barry D T. Linear signal synthesis using the Radon-Wigner transform [J]. IEEE trans Signal Processing, 1994; 42(8):2105-2111.

[2]Djuric P M, Kay S M. Parameter estimation of chirp signals. IEEE Trans. ASSP,1990:38(12:2118-2126.

[3] Ozaktas H. M, Kutay M. A, Bozdagi G. Digital computation of the fractional Fourier transform [J]. IEEE Transactions on Signal Processing.1996, 44(9):2141-2150.

Advanced Materials Research Vols. 989-994 (2014) pp 4005-4008
© (2014) Trans Tech Publications, Switzerland
doi:10.4028/www.scientific.net/AMR.989-994.4005

Interference Suppression of VLF Communications in Atmospheric Noise

Wu Yanjun[1, a], Fu Gang[1,a] and Geng Wenjian[1,a]
[1]China Satellite Maritime Tracking and Control Department, China
[a]348237548@sina.com

Keywords: VLF Communication, FRFT, Chirp Spread Spectrum (CSS), Interference Suppression, Clipping

Abstract. This paper focuses on the weak signal reception and atmospheric noise suppression in VLF Chirp spread spectrum communication system. Due to interference of atmospheric noise generated by lightning phenomena, it makes the chirp signal detection under low SNR condition becoming more difficult. Therefore, we select alpha stable distribution noise model to generate noise to simulate the real atmospheric noise. Then, we introduced a new technique of Chirp Spread Spectrum (CSS) communication based on Fractional Fourier Transform (FRFT). Finally, we study a nonlinear processing interference suppression method of clipping in time domain. Simulation results verified its feasibility.

Introduction

VLF communication channel is with severe interference, narrow band, low antenna radiation efficiency and power-constrained characteristic. The Atmospheric noise generated by lightning phenomena is the main sources of interference in VLF communication, the receiving weak communicating signal is not only submerged by the strong background completely, but also jammed by atmospheric noise generated by lighting phenomenon and make it very difficult to detect communication signals under a low SNR condition. Thus, it is so necessary to study a new interference suppression method in VLF communication.

In the field of signal processing, Fourier transform is treating as a linear operator describes the characteristics of the signal in the frequency domain, if we think the Fourier transform as rotating angle from the axis to the frequency axis, the FRFT can be understood at any angle of rotation operator. Thus, we can get a new representation form of signal in a new domain and characteristics of the signal will also be reflected in the new axis. Therefore, FRFT is a uniform frequency conversion in essence. In addition, FRFT is a generalized Fourier transform, while retaining all the properties of the Fourier transform, the FRFT also has some new features.

1 Fractional Fourier transform (FRFT)

FRFT is defined as:

$$X_p(u) = \left\{\mathcal{F}^p[x(t)]\right\}(u) = \int_{-\infty}^{+\infty} K_p(u,t)x(t)dt \tag{1}$$

Where, the transform kernel function $K_p(u,t)$ is

$$K_p(u,t)=\begin{cases}\sqrt{\dfrac{1-j\cot\alpha}{2\pi}}\exp(A) & \alpha \neq n\pi \\ \delta(t-u) & \alpha=2n\pi \\ \delta(t+u) & \alpha=(2n\pm 1)\pi\end{cases} \tag{2}$$

Where $A = j\cdot\dfrac{(t^2+u^2)}{2}\cdot\cot\alpha - jut\csc(\alpha)$, $\alpha = p\pi/2$ represents the rotation angle of the transformed signal for pth FRFT.

According to formula (1), we can easily getting the inverse FRFT expression as

$$x(t) = \mathcal{F}^{-p}\left[X_p\right](t) = \int_{-\infty}^{+\infty} X_p(u) K_{-p}(t,u)du \tag{3}$$

So far, a lot of fast algorithms of FRFT were put forward to calculate discrete FRFT. Due to its low complexity and high precision, we select the fast algorithm of discrete FRFT presented by H.M.Ozaktas[1][2] to compute the discrete FRFT in this paper.

2 Chirp spread spectrum theory

A. Modulation

In this section, we study a binary orthogonal keying (BOK) communication system. The system communicates with others through using chirp rate of a Chirp signal to carry binary code information. The CSS communication system uses different chirp rate of chirp signal to modulation binary code, and it means code '1' is denoted by chirp signal with a positive number chirp rate μ ($\mu > 0$), and it is called up-chirp signal. Analogously, the chirp signals with negative number chirp rate $-\mu$ is called down-chirp signal, and it represents code'0'. Figure 1 shows theory of CSS modulator.

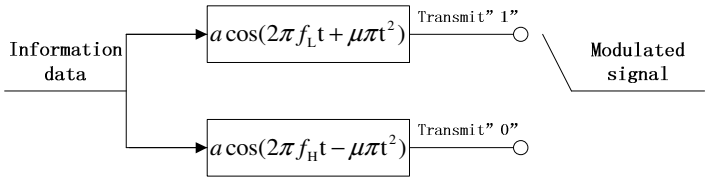

Fig1 The theory of chirp rate modulation

Where T , a , μ , f_L and f_H represent chirp duration, envelop, chirp rate, initial frequency and top frequency respectively, and $B=f_H - f_L = \mu T$ represents bandwidth of chirp signal [3].

B. FRFT Demodulation

According to formula (3), we known that chirp signal with specified chirp rate will gather energy concentration in a special FRFT domain, and when the transform order varies from 0 to 2, there is a one-to-one relationship between chirp rate and transform order as

$$\mu = -\cot(\alpha) \tag{4}$$

The transmitted Chirp signals are in forming of cosine function in CSS communication system. It can be divided into sum of a up-chirp signal and a down-chirp signal as follow

$$s(t) = a\cos(2\pi f_0 t + \pi\mu t^2) = \frac{a(e^{j(2\pi f_0 t + \pi\mu t^2)} + e^{j(-2\pi f_0 t - \pi\mu t^2)})}{2} \tag{5}$$

Therefore, we can deduce that up-chirp and down-Chirp signal gather energy in the same FRFT domain according formula (5), but the position of peak in FRFT domain is different. The wave form of up-chirp and down-chirp signal in FRFT domain as follow

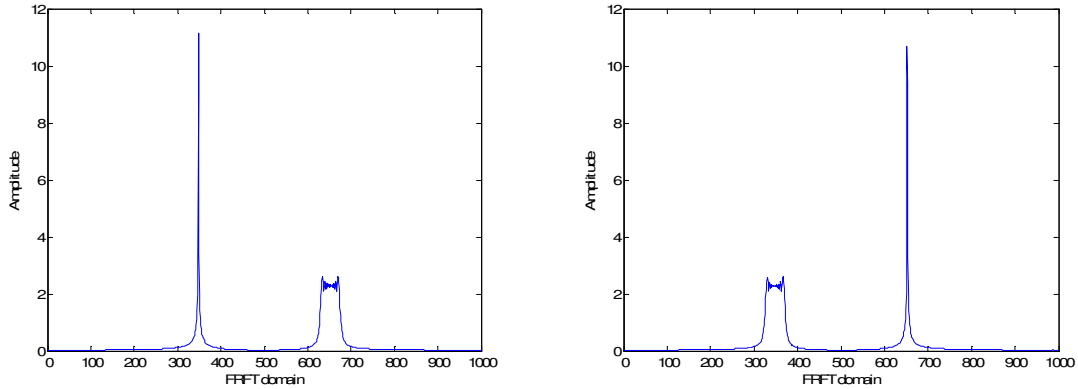

Fig2 Wave form of code "0"and"1"in p th FRFT domain

Observing the waveform of Up-chirp and Down-chirp signal in best FRFT domain, we can demodulate binary code according to peak position of chirp signal in FRFT domain. Figure 3 shows the diagram block of FRFT demodulation [4].

3 Clipping method

The transmitting VLF electromagnetic waves reaches receiver after a long-distance transmission is belonging to “weak signal" usually. This "weak signal" is not only means that the signal amplitude is low, but strong background noise and high amplitude impulse interference caused by the thundering near the receiver, and it makes the receiving signal low SNR. Therefore, in order to improve weak signal reception in VLF communication system, we need to find an effective weak signal detection and atmospheric noise suppression method.

In this section, we take advantage of Chirp Spread Spectrum communication in VLF communication system, demodulating binary code in FRFT domain, and it also suppresses atmospheric noise interference in a certain extent. In order to weaken atmospheric noise interference ulteriorly, we set a clipper in front of receiver according to the time-domain characteristics of atmospheric noise, and do nonlinear clipping to received signal and weaken high level spikes to improve reliability of receiver. Figure 3 shows character of clipper.

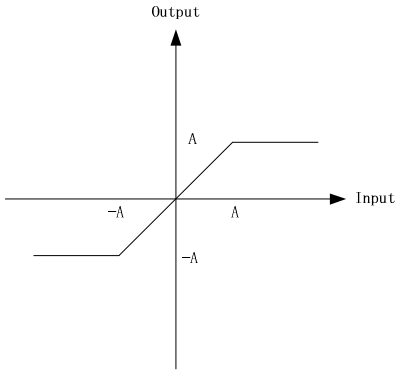

Fig3 The clipping input and output characteristic curve

According to Figure 3, it shows the received VLF signal after clipping is

$$s'(t)=\begin{cases} A, & s(t)\geq A \\ s(t), & -A<s(t)<A \\ -A, & s(t)\leq -A \end{cases} \tag{6}$$

4 Performance analyses

In this section, we simulate the performance of Chirp spread spectrum system in condition of interference suppression.[3][4] We treat alpha stable distribution noise model as the actual atmospheric noise model, and select symmetrical alpha stable distribution to generate atmospheric noise which is near the receiver. Due to inexistence of two rank squares in symmetrical alpha stable distribution, so, we set the SNR instead by mixture SNR, it is called signal to interference ratio and defined as follow

$$MSNR_{dB}=10\log_{10}(P_s/\sigma) \tag{7}$$

Where P_s is power of receiving chirp signal, σ is scale parameter of symmetrical alpha stable distribution.

The simulation parameter is set as: sample rate $f_s=81.92kHz$, central frequency of Chirp signal $f_0=7.6kHz$, bandwidth $B=1.2kHz$, code rate $R_b=50bps$, spread spectrum gain $G_p=13.8dB$.

Additionally, character parameters of symmetrical alpha stable distribution is set as $\alpha = 1.8$, scale parameter $\sigma = 1$, location parameter $\mu = 0$, and the mixture signal to noise ration is $MSNR = 0$ dB.

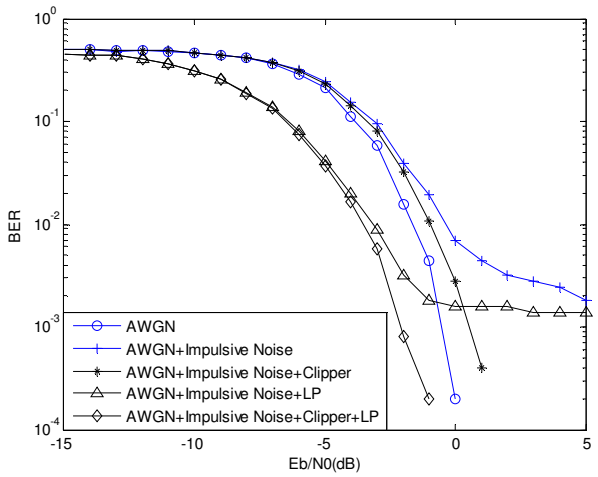

Fig4 VLF CSS System performance in clipper and low-pass filter

Where AWGN, Impulsive noise, Clipper is representing as environment of CSS system respectively.

According figure 4, we can easily know that the BER performance of low-pass filtering after clipping is better than the BER performance in AWGN. Further more, no matter what the SNR are, the performance of clipping after low-pass filtering has big improvement comparing with the BER performance in impulsive noise.

Summary

In this paper, we introduced theory of FRFT and technique of Chirp spread spectrum communication firstly, and then analysis the nonlinear time domain clipping algorithm of atmospheric noise interference suppression, the simulation results proved the nice performance of atmospheric noise interference suppression method. The conclusion in this paper is a useful method of VLF atmospheric noise interference suppression and it can play an important role in VLF communication.

References

[1] Namias V. The fractinal order Fourier transform and its application to quantum mechanics [J]. J Inst Math Appl, 1980, 25: 241~265.
[2] Ozaktas H. M, Kutay M. A, Bozdagi G. Digital computation of the fractional Fourier transform [J]. IEEE Transactions on Signal Processing.1996, 44(9):2141-2150.
[3] Tsai Y. R, Chang J .F. The Feasibility of Combating Multipath Interference by Chirp Spread Spectrum Techniques over Rayleigh and Rician Fading Channels[C]//Proceeding of IEEE 3rd International Symposium on Spread Spectrum Technique and Applications.1994:282-286.
[4] Xuejun Sha, Ronghui Wen, Xin Qin. A NEW MULTIPLE-ACCESS BASED ON FRACTIONAL FOURIER TRANSFORM. IEEE Conference,2009, 856-859.

Advanced Materials Research Vols. 989-994 (2014) pp 4009-4013
© (2014) Trans Tech Publications, Switzerland
doi:10.4028/www.scientific.net/AMR.989-994.4009

Research on Joint Time-Frequency Analysis Methods of Adaptive Radar Signal

Qiang Xing[1, a], Weigang Zhu[1, b], Yuan Bo[1, c] and Kang Wang[1, d]

[1] Equipment Academy, Beijing 101416, China

[a]xingyanqiang1989@126.com, [b]yi_yun_hou@sina.com, [c]boyuanxjtu@126.com, [d]wangkangdream@gmail.com

Keywords: Adaptive radar, FrFT, STFT, Joint time-frequency analysis.

Abstract. Faced with complex electromagnetic environment and varieties of adaptive radar waveforms, radar signal analysis and identification becomes more and more complex. Considering two important physical quantities - time and frequency in modern signal processing methods, this paper proposes that the joint time-frequency analysis (JTFA) method based on fractional Fourier transform (FrFT) and short-time Fourier transform (STFT) is applied to adaptive radar signal processing. The simulation results show that the joint time-frequency analysis method is superior to single short-time Fourier transform, getting a better analysis of results. The joint time-frequency analysis method provides the joint distribution of the time domain and frequency domain for adaptive radar signal analysis and describes the relationship between signal frequency and time.

1 Introduction

In 1960s and 1970s, the radar technology develops rapidly and a variety of new radars emerge in that period, such as synthetic aperture radar, pulse Doppler radar, phased array radar etc.[1]. In the new century, with the situation of various goals, complex environment and diverse tasks, people require performance of radar higher and higher [2] Meanwhile, the radars are faced with challenges of integrated interference, anti-radiation missiles, stealth technology and low altitude penetration [3]. Adaptive radar arises under this kind of background.

The so-called adaptive radar means that it can rapidly changes relevant parameters automatically, adjusting to the optimum working condition following the changes in the environment. Such radars usually use an adaptive antenna array [4]. Adaptive radar, with good anti-jamming capability, can automatically identify, judge, choose and track the target in the time domain and frequency domain. Adaptive radar does not refer to a particular radar, but a certain type of radar. They all belong to adaptive radar providing that they meet the definition of adaptive radar scope, such as phased array radar with adaptive beam-forming, digital array radar[5], software radar[6] and cognitive radar[7]. Phased array radar is a prototype of the adaptive radar, while the cognitive radar is the result of a higher level of the development of adaptive radar. Matching process of transmitter and receiver of adaptive radar with environment can greatly improve the performance of the radar.

Adaptive radars are usually multifunction radars. To adapt the complex electromagnetic environment and meet the requirements of different functions, the waveform design is complex and diverse, which makes it difficult for signal analysis and identification. In modern signal processing methods, time and frequency are two important physical quantities, and the relationship between time domain and frequency domain is closely. In the feature extraction process of the signal, combine the frequency domain characteristics if it can't obtain a good signal characteristic in the time domain. This tends to get a better effect. Time-frequency analysis method provides a joint distribution of the time domain and frequency domain for adaptive radar signal analysis, describing the relationships between signal frequency and time. In [8],Wang Xiaohua presents the radar signal intra-pulse analysis method based on FrFT and STFT, analyzing and simulating the chirp radar pulse signal.

Parameters of adaptive radar signals mainly include amplitude, phase, frequency, pulse width and so on. The radar pulse features are usually analyzed according to the pulse modulation type and the pulse modulation parameters. The radar signal is identified by extracting and separating these distributions and changes, and then the radar system, property and nature of the threat. This paper presents that JTFA is applied to adaptive radar signal processing, mainly studying four kinds of radar pulse signal, and the simulation results are given finally.

2 Principle of JTFA

Joint time-frequency analysis refers to the signal to go through fractional Fourier transform and then short-time Fourier transform, improving the resolution of the short-time Fourier analysis by adjusting the angle of rotation. It makes energy more concentrated and can effectively analyze the subtle characteristics of the signal.

2.1 Principle of FrFT

Fractional Fourier transform is a new time-frequency tool. It is the generalized form of the classical Fourier transform. Fractional Fourier transform is a signal representation method when the signal in the time-frequency axis in the plane rotates any angle around the origin counterclockwise. When the rotation angle is $\pi/2$, it is the traditional Fourier transform[9]. The fractional Fourier transform of signal $s(t)$ is defined as follows:

$$X_p(u) = F^p[s(t)](u) = \int_{-\infty}^{+\infty} s(t) K_p(u,t)\,dt \tag{1}$$

$$K_p(u,t) = \begin{cases} \sqrt{\dfrac{1-j\cot\alpha}{2\pi}} \exp\left[j\left(\dfrac{t^2+u^2}{2}\right)\cot\alpha - jut\csc\alpha\right] & \alpha \neq n\pi \\ \delta(t-u) & \alpha = 2n\pi \\ \delta(t+u) & \alpha = 2n\pi \pm \pi \end{cases} \tag{2}$$

α is the rotation angle, ie the angle between the fractional Fourier domain and time domain. The rotation angle $\alpha = p\pi/2$, p is the order of fractional Fourier transform. When $p=1$, it is the classical Fourier transform. Its rotational axis coordinate system shows in Figure 1. $F^p[]$ is the fractional Fourier transform operator, $K_p(u,t)$ is the transformation kernel, n is an integer, $\delta(\bullet)$ is the impulse function. The purpose of introducing the conversion axis coordinate system is to get the best signal time-frequency representation.

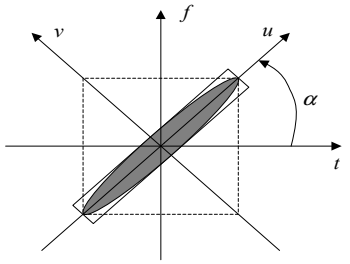

Figure1 Time-frequency plane rotation angle α coordinate

Figure 1 shows: $X_0 = s(\mu)$, $X_2(\mu) = s(-\mu)$, $X_1(\mu)$ corresponds to the classical Fourier transform of signal. Its rotational relationship is:

$$\begin{bmatrix} \mu \\ v \end{bmatrix} = \begin{bmatrix} \cos\alpha & \sin\alpha \\ -\sin\alpha & \cos\alpha \end{bmatrix} \begin{bmatrix} t \\ f \end{bmatrix} \tag{3}$$

FrFT is more flexibility compared to the traditional Fourier transform, suitable for processing non-stationary signals. Many properties of FrFT on the theoretical study are of great significance. When $\alpha \neq n\pi$, the calculation process can be broken down into the following four steps:

(1) The original signal is multiplied with a chirp function:

$$s0(t) = s(t)e^{-j\pi t^2 \cot\alpha} \tag{4}$$

(2) Do the Fourier transform:

$$s'0_\alpha(t) = \int_{-\infty}^{+\infty} s0(t)e^{-j2\pi ut \csc\alpha} dt \tag{5}$$

(3) Multiplied with a chirp function:

$$X'_p(u) = s'0_\alpha(t)e^{-j\pi u^2 \cot\alpha} \tag{6}$$

(4) Multiplied by complex amplitude factor:

$$X_p(u) = \sqrt{\frac{1-j\cot\alpha}{2\pi}} X'_p(u) \tag{7}$$

In the above definition, although p can be taken any real number, periods of the fractional Fourier transform is 4. So it is usually consider only in [0, 4].

2.2 Principle of STFT

The basic idea of short-time Fourier transform is that in the framework of the traditional Fourier transform, the non-stationary signals are viewed as superposition of a series of short-time stationary signal. Short of the time is achieved by adding windows and cover the entire domain by translating parameters. For a given non-stationary signals, $s(t) \in L^2(R)$, short time Fourier transform of signal $s(t)$ is defined as:

$$STFT_s(t,\omega) = \int_{-\infty}^{+\infty} s(\tau)h(\tau - t)e^{-j\omega\tau} d\tau \tag{8}$$

In general, $h(t)$ is the real function and its energy of Fourier transform concentrated in the low frequency. It can be viewed as the impulse response of a low-pass filter. As can be seen from the definition of formula, the signal $s(t)$ is divided by adding window functions $h(t)$ by translating parameter t:

$$s_t(\tau) = s(\tau)h(\tau - t) \tag{9}$$

Do Fourier transform for the signal $s_t(\tau)$ on the basis of obtaining signal in interval τ of original signal which is in near time t. With the changes of the translation parameters, time window determined by $h(t)$ moves on the timeline, so that the signal gradually go into the state to be analyzed. Since the segment signal $s_t(\tau)$ shows characteristics of the interval t of the original signal, so the Fourier transform of the segment signal reflects the frequency distribution of the original signal at the interval. Its advantage is simple and easy to implement the algorithm, the processing time is short and suitable for time-frequency of all non-stationary signal.

2.3 Principle of JTFA

Since the fractional Fourier transform can be rotated any angle compared to Fourier transform, it can improve the resolution of short-time Fourier transform on the basis of fractional Fourier transform. Joint -time Fourier transform is defined as:

$$\begin{aligned} STFT_s^\alpha(\mu,\nu) &= STFT_{X_p}(\mu,\nu) \\ &= \int_{-\infty}^{+\infty} X_p(\tau)h(\tau - \mu)e^{-j\omega\tau} d\tau \end{aligned} \tag{10}$$

$STFT_s^\alpha(\mu,\nu)$ calculations can be seen as general short-time Fourier transform of signal $s(t)$. The initial window uses the fractional Fourier transform. If the STFT window is too narrow, the resolution will be decreased in frequency domain; if the window is too wide, the resolution will decrease in time domain. Time domain and frequency domain can't get both high resolution simultaneously. The joint time-Frequency analysis enables the energy more concentrated in time-frequency domain. Selecting the appropriate angle of rotation can get the best time-frequency representation, meanwhile, this method is not affected by cross term interference, solving the problem that the resolution of single short-time Fourier transform is low.

3 Simulation

Signal forms of adaptive radar are various, and its waveforms are complex. According to the radar function, the waveform is usually designed on the basis of characteristics of the ambiguity function. Ambiguity function is mainly divided into four categories. The paper selected four kinds of signals according to ambiguity function, namely, single-frequency signal, LFM signal, BPSK signals and coherent pulse-sequence signal. Ambiguity function of these four kinds of signals represents four types of ambiguity function. Simulation of the joint time-frequency analysis is shown in Figure 2.

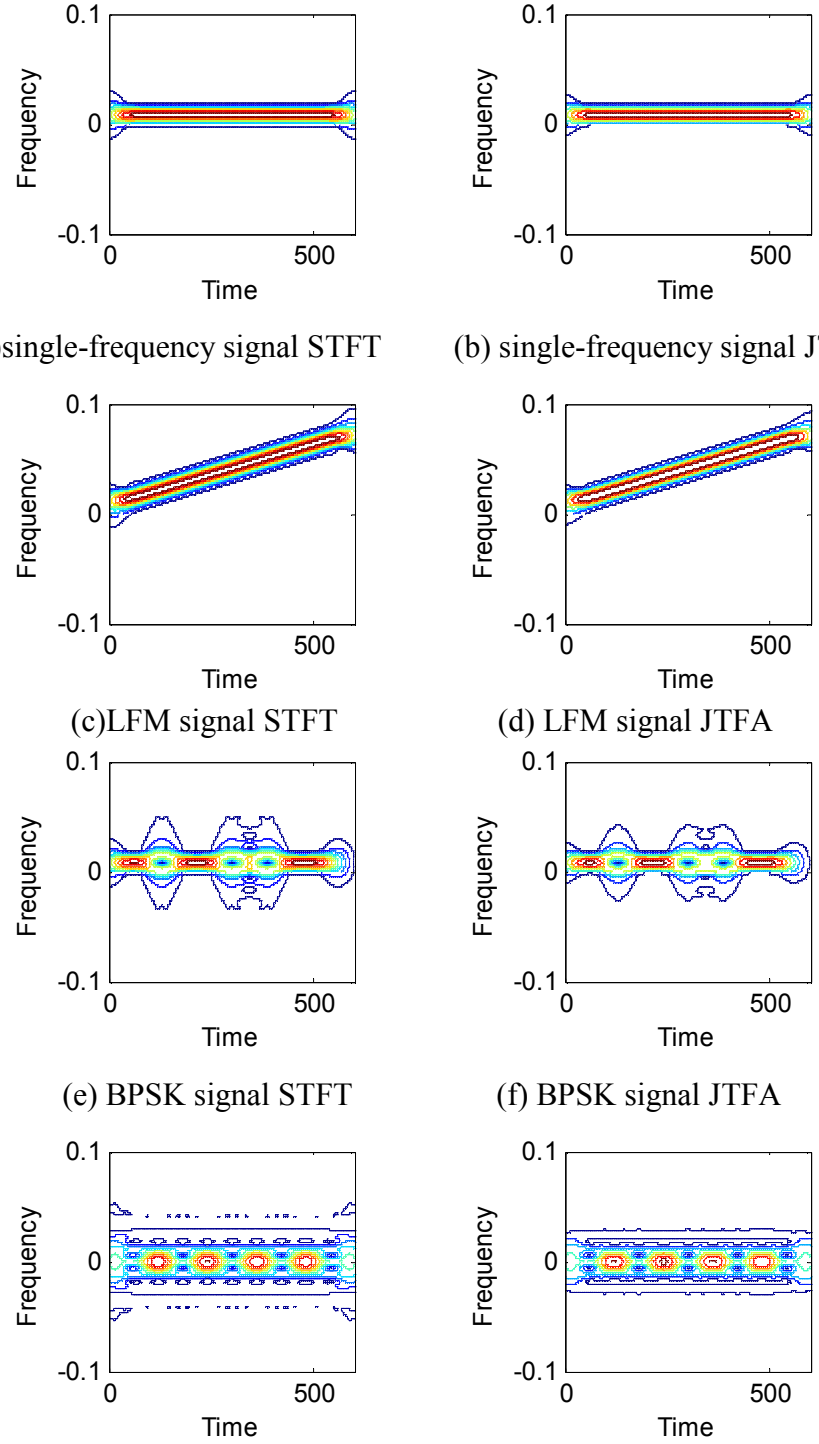

(a)single-frequency signal STFT (b) single-frequency signal JTFA

(c)LFM signal STFT (d) LFM signal JTFA

(e) BPSK signal STFT (f) BPSK signal JTFA

(g) coherent pulse-sequence signal STFT (h) coherent pulse train signal JTFA

Figure 2 Comparison of Signal STFT and JTFA

Simulation environment: Microsoft Windows XP Professional 2002, CPU: 2.6GHz, HDD: 150G, Memory: 2G. The simulation tool is MATLABR2009b. Simulation signal: pulse width T=2us, carrier frequency fc=2.5e6Hz, sampling rate: 300MHz. LFM signal modulation factor k = 1e13, coherent pulse-sequence signal PRI=4us.

Figure 2 shows that the joint time-frequency analysis method do have a better result than single short-time Fourier transform in the radar pulse signal analysis process. Energy of the joint time-frequency analysis is more concentrated in certain areas, therefore, the joint time-frequency analysis method can be appropriate to cover defects of STFT. In addition, the order of FrFT p will affect the signal analysis results when the window function is for fractional Fourier transform. To get the best effect of time-frequency representation, the frequency axis should rotate a right angle.

4 Conclusion

This article applies the joint time-frequency analysis method to adaptive radar signal analysis. Simulation results show that the joint time-frequency analysis method is better than the single short time Fourier transform. The joint time-frequency analysis method can effectively analyze the time-frequency characteristic of radar signals and improve the analysis resolution. This distribution can be more accurately reflects the frequency of the signal changes over time.

5 References

[1] Chen Boxiao, Modern radar systems analysis and design, Xi'an University of Electronic Science and Technology Press, 2012.

[2] Ding Lufei, Geng Fulu, Chen jianchun, Radar principle. Publishing House of Electronic Industry, 2011.

[3] D. Curtis Schleher, Electronic Warfare in the Information Age, Artech House, 2000.

[4] Luan enjie, National Defense Science and Technology Term, Aviation Industry Press, 2002.

[5] Wu Manqing, The development of Digital Array Radar, Journal of CAEIT, 2006,1 (1) :11-16

[6] Pongbo, Lin Xindang, Wanfu, The idea of Software radar, Radar and ECM, 2010,30 (1) :1-3

[7] Haykin S., Adaptive Radar: Evolution To Cognitive Radar, IEEE International Symposium On Phased Array Systems and Technology, 2003

[8] Wang Xiaohua, A new method for time-frequency analysis of intra-pulse radar signal. Shipboard Electronic Countermeasure, 2006,29 (6) :67-69

[9] Ping Xianjun, Tao Ran, Zhou Siyong, A Novel Fast Algorithm for Fractional Fourier Transform, ACTA ELELTRONIC SINCA, 2001,(3):406-408

Advanced Materials Research Vols. 989-994 (2014) pp 4014-4018
© (2014) Trans Tech Publications, Switzerland
doi:10.4028/www.scientific.net/AMR.989-994.4014

A Study on Same-beam Interferometry in Deep Space

Xiaoyu Wang[1, a], Jiacai Hong and Kai Hu [1]

[1]the Academy of Equipment, Beijing, 101416, China

[2]Department of Optical and Electrical Equipment, the Academy of Equipment, Beijing

[a]wangxy_ttc@126.com,

Keywords: same-beam interferometry; related processing; integer ambiguity

Abstract. Same-beam interferometry (SBI) has a wide range of applications and prospects in collocate geostationary satellites, space rendezvous and docking, landers and rovers positioning. The paper introduces the basic principles, underlying processing algorithms, ambiguity resolution solving, process flow comprehensively and systematically. Then use FX-related processing algorithms and integer ambiguity solution method step by step to process signals, draw process flowchart.

Introduction

With the deepening of deep space exploration in our country, a variety of new interference measure technologies are widely used in precise orbit determination and control. Thanks to its high-precision, real-time, flexible distribution network, and low baseline length requirements, SBI is more excellent to be widely used.

For example, there had been already 1120 geosynchronous satellites in an about 60km wide area in 2005[1], hence the orbital resources are becoming more and more tense. Collocated satellites technology is used to solve this [2]. This technology requires multiple satellites in a relatively small space to run, increasing their risk of collision. In the space rendezvous and docking [3], the ground should simultaneously monitor and control two or more spacecraft, and complete several precise orbit control and forecasting in a very short time, then measure relative positions precisely. If you want a more direct and richer understanding of target stars, soft-landing detection, patrolling and plumbing detection is essential. The precise measurements of the relative position of rovers and landers are important. In conclusion, we need to solve problems above. SBI can achieve high accuracy and relative position measurements accuracy can achieve within 10m with short baseline [4], and provide important complements and enhances of ground-based Doppler measurements, distance measurements of sight information and other control instruments.

SBI had already begun to be used in the detection of deep space in the 1970s in foreign countries, been listed as key development projects [5].Domestic research and applications should further improve and enhance. This paper introduces the principle, related processing algorithms, integer ambiguity solution, and process flow.

The Principles

When the two spacecraft in perspective are very close, you can use two antennas of two different ground stations to observe two spacecraft simultaneously in a beam, and get their dual differential interferometry volume. Then obtain high-precision relative distance information about two spacecraft in air plane. As shown in Fig. 1.

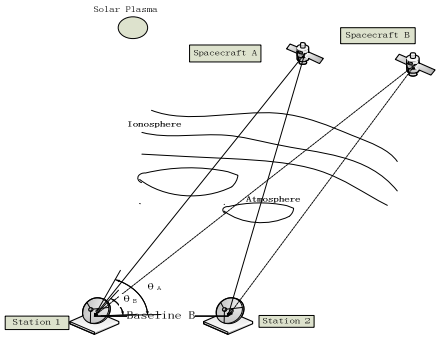

Fig. 1 SBI schematic diagram

SBI observation systems typically include two stations (station 1,2), two spacecraft (spacecraft A , B), and multi-frequency signals (typically more than three frequencies) [6].The station 1,2 receiving delay from spacecraft A,B:

$\tau_{ob_A1} = \tau_{g_A1} + \tau_{c1} + \tau_{s_A1} + \tau_{e_A1}$, $\tau_{ob_A2} = \tau_{g_A2} + \tau_{c2} + \tau_{s_A2} + \tau_{e_A2}$

Here: τ_g is the theoretical delay; τ_c the clock error between spacecraft and station; τ_s is the propagation delay introduced by atmospheric, plasma and other media; τ_e is device delay .The spacecraft B delay that the station 1， 2 receive are likewise:

$\tau_{ob_B1} = \tau_{g_B1} + \tau_{c1} + \tau_{s_B1} + \tau_{e_B1}$, $\tau_{ob_B2} = \tau_{g_B2} + \tau_{c2} + \tau_{s_B2} + \tau_{e_B2}$

The delay inequality between station 1 and 2 receiving from spacecraft A and B are

$\Delta\tau_{A12} = (\tau_{g_A1} - \tau_{g_A2}) + (\tau_{c1} - \tau_{c2}) + (\tau_{s_A1} - \tau_{s_A2}) + (\tau_{e_A1} - \tau_{e_A2})$, $\Delta\tau_{B12} = (\tau_{g_B1} - \tau_{g_B2}) + (\tau_{c1} - \tau_{c2}) + (\tau_{s_B1} - \tau_{s_B2}) + (\tau_{e_B1} - \tau_{e_B2})$

When the angular distance of two spacecraft is very small, propagation media delay and equipment delay of each spacecraft between stations can be considered to be equal. that is $\tau_{s_A1} = \tau_{s_B1}$, $\tau_{s_A2} = \tau_{s_B2}$; $\tau_{e_A1} = \tau_{e_B1}$, $\tau_{e_A2} = \tau_{e_B2}$. so double different time delay is $\Delta\tau_{AB} = (\tau_{g_A1} - \tau_{g_A2}) - (\tau_{g_B1} - \tau_{g_B2})$ 。

When the effect of thermal noise is not considered, Double differential delay measurements at any corresponding frequency will be equal to the theoretical delay measurements, and independent of frequencies. When making double-difference calculation, a number of system errors are eliminated. After getting the double differential delay, we can get high-precision angle measurements of two spacecraft separation in sky plane. The formulas are:

$\frac{B\cos\theta_A}{c} = \tau_{ob_A1} - \tau_{ob_A2} = \Delta\tau_{A12}$, $\frac{B\cos\theta_B}{c} = \tau_{ob_B1} - \tau_{ob_B2} = \Delta\tau_{B12}$

Here B is the baseline length, θ_s is the angle (S = A, B), c is the speed of light.

Double differential delay $\Delta\tau_{AB}$ can be written as $\Delta\tau_{AB} = \frac{B\cos\theta_A}{c} - \frac{B\cos\theta_B}{c}$

The two spacecraft should can be seen in a beam during same-beam observation, so $\Delta\theta = \theta_A - \theta_b$ may be small enough to make $\theta_A \approx \theta_B$,and $\sin\left(\frac{\theta_A - \theta_B}{2}\right) = \frac{\Delta\theta}{2}$, $\sin\left(\frac{\theta_A + \theta_B}{2}\right) = \sin\theta_A$. Thus

$\Delta\tau_{AB} = \frac{B\sin\theta_A \cdot \Delta\theta}{c}$

Therefore, the angle measurement accuracy of spacecraft is $\Delta\theta = \frac{c\Delta\tau_{AB}}{B\sin\theta_A}$. The measurement accuracy in the spatial position of the spacecraft is $\Delta l = c\tau \cdot \Delta\theta$.

Processing Algorithms

The paper describes how to get the double differential delay observations. In terms of the station 2 as the reference, the RF reception signal can be expressed as: $x_{h1n} = \exp(j2\pi f_{hn}(t + \tau_{ob_hn}(t)))$ $x_{h2n} = \exp(j2\pi f_{hn} t)$

Due to the relative motion between the spacecraft and the station, the delay difference between stations is time-varying, can be written as:

$$\tau_{ob_hn}(t) = \tau_{ob_hn} + v_{ob_hn} + v_{h1}t$$

Theoretical delay rate is only related with relative motion between the spacecraft and the station, nothing to do with frequency, but after effects of the ionosphere, delay rate and frequency are related, this impact reflected in the Doppler frequency is only mHz, we do not consider the relationship between the delay rate and the frequency. Therefore:

$$\begin{aligned} x_{h1n} &= \exp\left(j2\pi f_{hn}\left(t + \tau_{ob_hn} + v_{h1}t\right)\right) \\ &= \exp\left(j2\pi\left(f_{hn} + f_{d_h1n}\right)t + j2\pi f_{hn}\tau_{ob_hn}\right) \end{aligned}$$

Here $f_{d_h1n} = f_{hn}v_{h1}$ is Doppler frequency .After down-conversion, the two stations receive signals are as follows:

$$x_{h1n} = \exp\left(j2\pi\left(f_{Ihn} + f_{d_h1n}\right)t + j2\pi f_{Ihn}\tau_{ob_hn}\right), \quad x_{h2n} = \exp\left(j2\pi f_{Ihn}t\right)$$

Here f_{Ihn} is IF frequency of f_{hn} .According to the priori delay model $\hat{\tau}_{ob_hn}$ and the priori Doppler frequency model $\hat{f}_{ob_hn}$, the signal of station 1 can do streak rotation and time-delay compensation:

$$\begin{aligned} & x_{h1n}\exp\left(-j2\pi\hat{f}_{d_h1n}t\right)\exp\left(-j2\pi\hat{f}_{Ihn}\hat{\tau}_{ob_hn}\right) \\ &= \exp\left(j2\pi\left(f_{Ihn} + \Delta f_{d_h1n}\right)t + j2\pi\hat{f}_{Ihn}\Delta\tau_{ob_hn}\right) \end{aligned}$$

Here $\Delta f_{d_h1n} = f_{d_h1n} - \hat{f}_{d_h1n}$; $\Delta\tau_{ob_hn} = \tau_{ob_hn} - \hat{\tau}_{ob_hn}$ .and $\Delta\nabla\hat{\tau} = \hat{\tau}_{ob_An} - \hat{\tau}_{ob_Bn}$.

There are generally FX type and XF type two related processing methods [7]. Here the signal will use the FX-type processing method to deal with [8], as shown in Fig. 2.

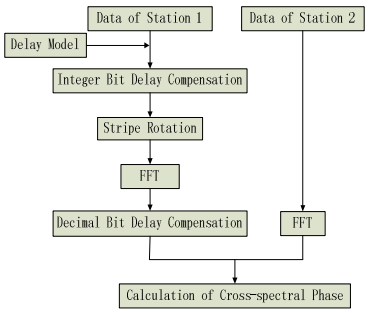

Fig. 2 FX type process's flow chart of SBI signals

The cross-spectral phases $\phi_{hn} = 2\pi f_{hn}\Delta\tau_{ob_hn} + 2\pi N_{hn}$ between stations can be obtained by FX-type processing method. N_{hn} is Integer Ambiguity. The cross-spectral phases make the difference. When the frequency resolution and reference station delay model error are small enough, you can get:

$$\phi_n = \phi_{An} - \phi_{Bn} = 2\pi f_{An}\Delta\tau_{ob_An} + 2\pi N_{An} - \left(2\pi f_{Bn}\Delta\tau_{ob_Bn} + 2\pi N_{Bn}\right) = 2\pi f_{An}\Delta\nabla\tilde{\tau} + 2\pi\Delta N_n$$

Here : $\Delta N_n = N_{An} - N_{Bn}$; $\Delta\nabla\tilde{\tau} = \Delta\nabla\tau - \Delta\nabla\hat{\tau} = \Delta\tau_{ob_An} - \Delta\tau_{ob_Bn}$ is remnant double differential delay.

If the integer ambiguity corresponding to a frequency is known and calculation accuracy of ϕ_n is equal, the double differential delay based on the highest frequency f_{A3} has the highest accuracy, expressed as follows:

$$\Delta\nabla\tau = \Delta\nabla\tilde{\tau} + \Delta\nabla\hat{\tau} = \frac{\phi_3 - 2\pi\Delta N_3}{2\pi f_{A3}} + \Delta\hat{\tau}_{ob_A3} - \Delta\hat{\tau}_{ob_B3}$$

Integer Ambiguity Solver

SBI Signals Processing Solutions can be implemented step by step. We can use group delay measurements to determine the ambiguity, and Japan's SELENE Program utilizes this method [9]. There are derivation steps and prerequisites as follows [10]:

As shown in Fig. 3, you can deduce $\Delta N_2 - \Delta N_1$ in a narrow 6 MHz band between f_{A1} and f_{A2} firstly. Referring the group delay of between f_{A1} and f_{A2}, adjust the integer phase of f_{A3}, then deduce the group

delay within the winder bandwidth of 75MHz between f_{A1} and f_{A3}, and get $\Delta N_3 - \Delta N_1$. Then the phase integer ambiguities $\Delta N_1, \Delta N_2, \Delta N_3$ can be solved.

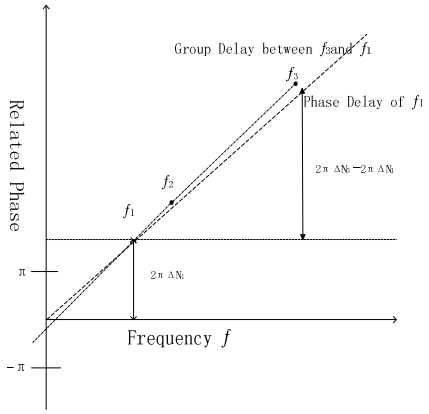

Fig. 3 Schematic diagram of SBI integer ambiguity solver

Processing Flow

According to the mathematical model derived previously, the algorithm processes can be divided: (1).Signals process between stations: divide different signals into groups , conduct delay compensation, Stripe rotation and gain the cross-spectral phases. (2).Signals process between spacecraft: the cross-spectral phases between stations make the difference, and get the double differential phase measurements.(3).Phases delay solution: conduct the integer ambiguity step by step, obtain the double differential delay residuals related to the highest frequency and get the double differential phases delay measurements by adding model values. As shown in Fig.4.

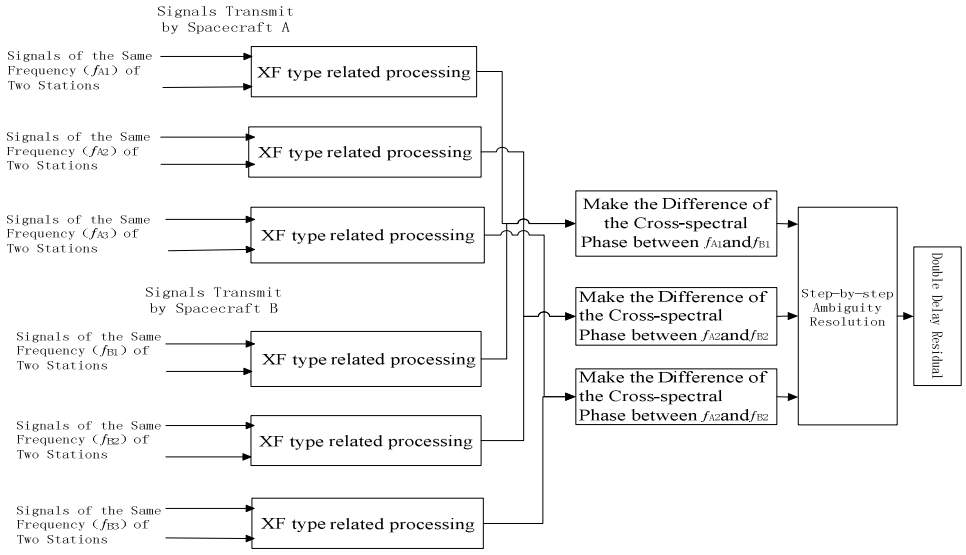

Fig. 4 Flowchart of SBI's processing algorithm

Conclusions

SBI has been recognized as the high-precision interferometric technology, and widely used. This paper describes the applications and prospects, such as Co-located satellites, space rendezvous and docking, landers and patrollers. In the meantime, the principle, processing algorithms, integer ambiguity solver and processing flow are described in detail. At present, China has already commenced the theoretical research and experimental verification. For example China has carried out with observation of SBI and obtained high precision measurements in Chang E III and Firefly One exploration missions. The research of SBI has far-reaching influence and significance.

References

[1] Juan Hu,Wenquan Chen. Position Determination for Co-located Geostationary Satellites[J].Electronic Sci & Tech,2012.25(7).
[2] Srinivasamurthy K N. Strategy Analysis for Collocation of INSAT-2 Satellites[J]. Acta Astronautica, 2002, 50(6):343-349.
[3] Dongxu Li, Zhi Li. The Technology of Autonomous Rendezvous and Docking of spacecraft [M].NUDT Press, 2009.
[4] Wenquan Chen, Jianwei Wu. Relative Position Localization Technology for Geostationary Orbit Collocation Satellites [J].Journal of Chendu Electromechanical College, 2010, 9. (13):3.
[5] Haitao Li,Huan Zhou. Development of Radio Interferometry and Its Prospect in Deep Space Navigation[J].Journal of Spacecraft TT&C Technology,2013,32(6).
[6] Lue Chen,Geshi Tang,etc. Multi-frequency Same-beam Interferometry on General TT&C Signal[J]. Chinese Space Science and Technology,2012, 42(6).
[7] Thompson A R, Moran J M, Swenson G W. Interferometry and synthesis in radio astronomy[M]. Florida: Krieger Publishing Company, 1994.
[8] Qinghui Liu,Ming Chen ,etc. Relative Position Determination of a Lunar Rover Based on Multi-frequency Same Beam Interferometry [J]. Science China: Phys, Mech & Astron,2009，39(10)：1410—1418.
[9] Shaowu Chen,Guangliang Dong. Research and Verification of Differential Phase Delay Measurement Model of Same Beam Interferometry[J]. Journal of Astronautics,2013,32(6):68—74.
[10] Chengbin Zhao,Xiaomin Hou. An Introduction to Application of High Accuracy Interferometric Techniques in Deep Space Navigation[J].Global Positioning System,2011(2).

Advanced Materials Research Vols. 989-994 (2014) pp 4019-4022
© (2014) Trans Tech Publications, Switzerland
doi:10.4028/www.scientific.net/AMR.989-994.4019

The Application and Simulation of OFDM Technology In Power Line Communication

Yiwen Chen[1, a], Bin Xu[2, b] and Jianhua Hao[2, c]

[1]Equipment Academy, Beijing 100000, China;

[2] Equipment Academy, Beijing 100000, China.

[a]ipad910913@163.com

Keywords: power line communication; OFDM; AR model; back noise; impulse noise

Abstract: Utilizing power line to transmit information speedily and safely is very important and significant. Whereas, the communication environment and construction of power grid are complex and hostile. The paper introduces the application, common modulation technology—OFDM and noise characteristics of PLC. The paper builds an OFDM input and output system and adds the power line noise into the channel, then compares and analyzes the difference between the OFDM output signals in common channel and PLC channel.

1. Introduction

The power line communication (PLC) is defined as a communication technology using power line to transmit data, and putting power grid into communication network. The following figure shows the PLC system.

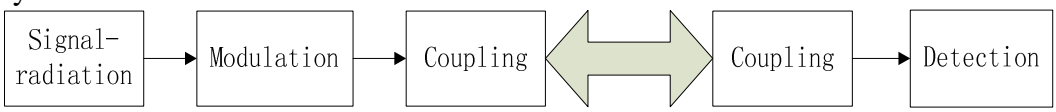

Fig.1 PLC signal system diagram

Nowadays, PLC has been widely used all over the world. Different countries have different applications for PLC. USA devotes PLC to smart home; for UK, PLC is used to automatic meter reading (AMR); and in China, PLC trial communities have been built in many cities.

2. PLC Modulation Method—OFDM

The physical environment of a power line channel is very poor. It is full of noise, interference, and fading, so the common signal is difficult to transfer in the power line. Orthogonal frequency division multiplexing (OFDM) technology can adopt this poor physical environment and fight against frequency selective fading and inter-carrier interference effectively. OFDM is the most common modulation method in PLC.

OFDM technology means converting serial data to parallel data after coding, and modulating N subcarriers in the interval of frequency respectively. Then add the N subcarriers and send then at the same time. In this way, the spectrum of each symbol represents only a small part of the available channel bandwidth. Through the choice of carrier spacing, the frequency orthogonality of each subcarrier in the whole symbol period assures that the receiving end received signal without distortion.

OFDM could be achieved through the IDFT/DFT transform. As shown in the fig.2.

There are N sub-channels in the system, the subcarrier of each sub-channel is

$$x_k(t) = B_k \cos(2\pi f_k t + \varphi_k) \qquad \text{k=0,1,2,3……N-1}$$

The sum of N carriers is

$$\mathrm{S(t)} = \sum_{k=0}^{N-1} X_k(t) = \sum_{k=0}^{N-1} B_k \cos(2\pi f_k t + \varphi_k)$$

Turning into the plural form:

$$S(t) = \sum_{k=0}^{N-1} \mathbf{B}_k e^{j2\pi f_k t + \varphi_k}$$

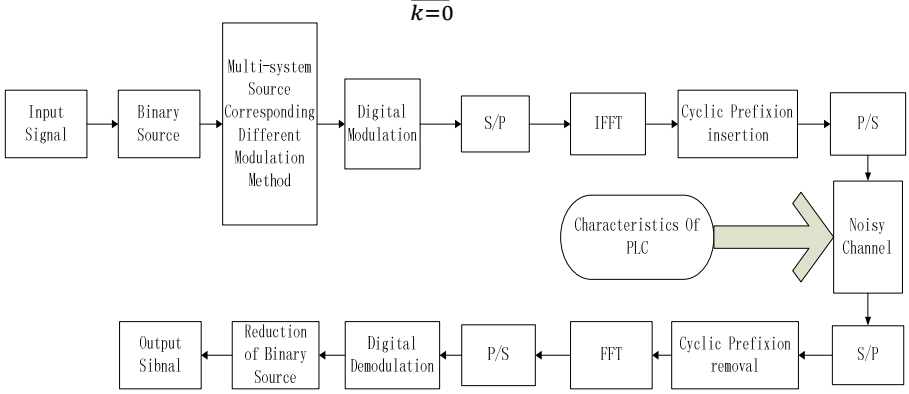

Fig.2 OFDM functional block diagram

$\Delta f = \frac{n}{T_s}$ The minimum separation of subcarrier frequency: $\Delta f_{min} = \frac{1}{T_s}$

Each subcarrier could be modulated in different method. Take QPSK modulation for example, the input signal after modulation, serial/parallel conversion, IFFT and prefixion as shown in the following figure:

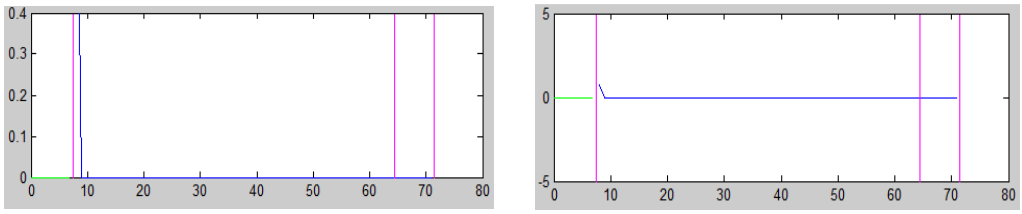

Fig.3 Modulated OFDM symbol amplitude and phase

In the same way, received signal as shown in the figure:

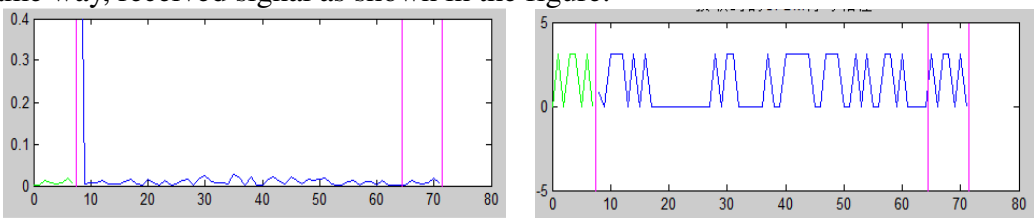

Fig.4 Received OFDM symbol amplitude and phase

The following figure shows the change of the constellation diagram of received signal:

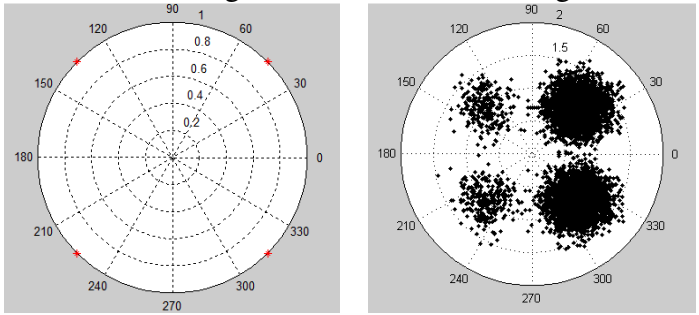

Fig.5 OFDM source QPSK modulation and demodulation constellation diagram

3. The Noise Characteristic of PLC

To build a power line communication system model, in addition to the OFDM signal, power line communication noise is a very important part. Different from command channel noise, the PLC channel noise derived from various electrical appliances, mechanical products and power line itself.

It is not additive white Gaussian noise (AWGN), and its characteristics can change in a short time period. The PLC noise is roughly divided into two categories-- background noise （including colored noises, narrow-band noise and power frequency asynchronous noise）and impulse noise （including power frequency synchronization noise and random impulsive noise）.

3.1 Background Noise

Background noise is a stationary random process and can be received by AR model as shown in the figure.

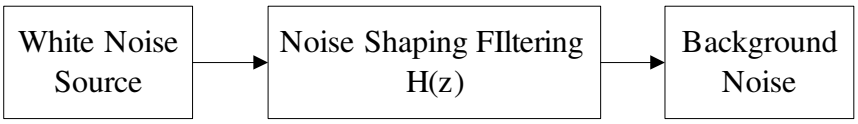

Fig.6 Background noise model

In the figure, the filter function can be described as

$$\mathrm{H(z)} = \frac{1}{\mathrm{A(z)}} = 1/(1 + \sum_{i=1}^{n} a_i\, z^{-i})$$

Utilizing the method of period gram, the formula of discrete series' power spectral density is

$$\mathrm{P}(\omega) = \frac{1}{N}|X_N(\omega)|^2 = \frac{1}{N}\left|\sum_{n=1}^{N-1} x(n)e^{-jn\omega}\right|^2$$

The power spectral density of the AR model background noise as the following figure:

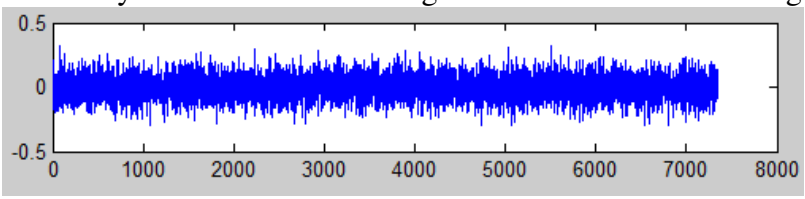

Fig.7 The AR model background noise

3.2 Impulse Noise

The power spectral density of impulse noise is 10 dB higher than the one of background noise. Through statistical analysis of a large number of actual data, we can find that the pulse intensity, pulse width, pulse interval and other parameters of pulse noise obey the exponential distribution, so a single pulse can be represented by a decaying sinusoidal signal.

$$N_{imp} = Ae^{-t/\tau}\sin(2\pi f(t - t_{arr}) + \varphi)$$

In this way, the construction impulse noise is shown in the following figure:

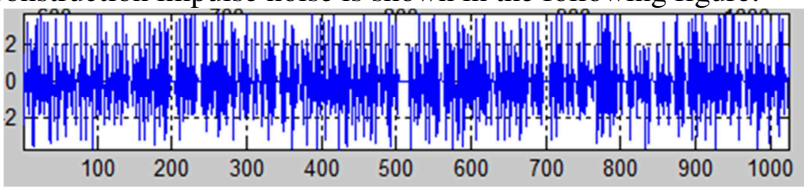

Fig.8 The impulse Noise

After adding the power line noise into the channel, the received OFDM symbol is:

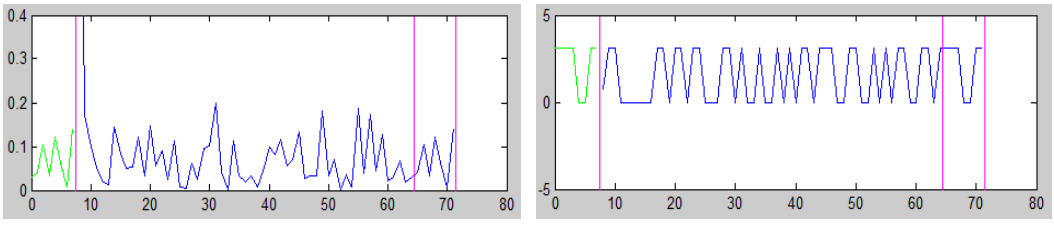

Fig.9 Received OFDM symbol amplitude and phase through PLC channel

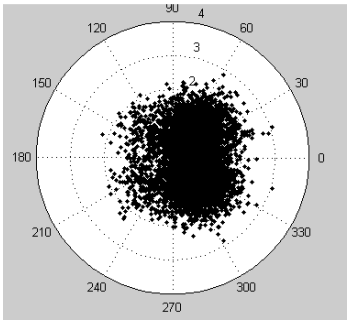

Fig.10 OFDM source QPSK demodulation constellation diagram through PLC channel

4. Summary

Under comparing and analyzing the difference between the OFDM output signals in common channel and PLC channel, we can find that the physical environment of a power line channel is very poor, and the background noise and impulse noise have bad effect on the transmission of OFDM signal.

Although OFDM signal is affected by the PLC noise, it fundamentally keeps the characteristic of input signal, and can be identified and demodulated finally. As a result, OFDM technology can adopt this poor physical environment and fight against frequency selective fading and inter-carrier interference effectively. It is a common and useful modulation method for PLC.

References

[1] Xavier Carcelle. Power Line Communications in practice. China Machine Press, 2011.6

[2] Meng H, Guan Y L, Chen S. Modeling and Analysis of Noise Effects on Broadband Power-line Communications [J]. Power Delivery, IEEE Transactions on, 2005,20(2): 630-637.

[3] Youbing Zhang and Shijie Cheng, A novel multi-carrier signal transmission system over multi-path channel of low-voltage power line, IEEE Trans on Power Delivery, VOL 19, NO.4, Oct 2004, pp. 1668~1672.

[4] Wang Bin, GE Lin dong. A novel algorithm for identification of OFDM Signal[C].Proceedings-2005 International Conference on Wireless Communications, Networkong and Mobile Computing, WCNM 2005.2005.6

[5] MA Qiang, CHEN Qi-mei, LI Bo. Predictive schemes for future power line communication: Part two PLC channel analysis and model [J]. Automation of Electric Power Systems, 2003, 27(4): 72–76.

[6] GUO Hao-kun, WU Jun-ji, LU Xian, et al. Research on noise model of power line communication's channel [J]. Telecommunications for Electric Power System, 2004, 32(8): 1–3.

[7] RAUGI M, TUCCI M. Power-line communications channel estimation and tracking by a competitive neural network [J]. IEEE Transactions on Communications, 2006, 52(4): 1213–1219.

[8] CAO Hui-bin. Survey of power line communication (PLC) technology [J]. Telecommunications for Electric Power System, 2004, 25(1): 1–6, 44.

[9] LAI Zheng-tian. Channel characteristics analysis and simulation of power line carrier communication system [J]. Telecommunications for Electric Power System, 2010, 31(10): 39–42.

[10] GUO Hao-kun, WU Jun-ji, YING Zhan-feng, etal. The application of improved Markov chain in power line communication channel's impulse noise modeling[J]. Power System Protection and Control, 2012, 40(5): 129–132.

Advanced Materials Research Vols. 989-994 (2014) pp 4023-4027
© (2014) Trans Tech Publications, Switzerland
doi:10.4028/www.scientific.net/AMR.989-994.4023

Research on Demodulation of High Bit Rate Telemetry Signal in FM Baseband

Yi Liang[1,a], Fu Gang[1, a], Wu Guangzhi[1,a]
[1]China Satellite Maritime Tracking and Control Department, China
[a]348237548@sina.com

Keywords: STFT, synchronization, PCM/FM

Abstract. According to the characteristics of PCM / FM signals, we propose a new software-based STFT Demodulation algorithm. This paper discusses in detail the basic principles of this demodulation algorithm and implementation process, analyze the complexity of the algorithm, proposed a new method for the extraction and correction code synchronization. Simulation results show that the algorithm not only can effectively suppress the influence of various disturbances in the actual signal synchronization accuracy of the code, with better demodulation performance, and realization of the principle is simple, high efficiency, easy to implement software-oriented real-time treatment.

Introduction

PCM / FM signal as a current standard aerospace monitoring system, at home and abroad have a wide range of applications. Because actually received PCM/FM signal non-stationary random signal, when dealing with non-stationary random signal frequency analysis method is often used, mainly the discrete Fourier transform (STFT) and Wigner-Willie distribution (WD). Related literature STFT algorithm is proposed to resolve the tone and WD-based digital FM signal, has strong anti-noise and anti-fading performance, but a large amount of computation is not conducive to improving the efficiency of software demodulation.[1][2] Signal Demodulation software realization requires not only have good demodulation algorithm performance, but also to the extent possible to reduce the complexity and dependency (such as frequency source) hardware circuit signal processing algorithms, thus contributing to the software environment under real-time signal processing. In this paper actually received PCM/FM IF signal point energy variation proposed algorithm STFT resolve tune of PCM / FM signal is software-based, software technology to achieve a fast, high-precision demodulation.

1 Demodulation algorithm

PCM/FM signal in the main section of a symbol can be approximated as a single carrier frequency sinusoidal signal, you can achieve demodulation PCM/FM signals by calculating the signal in two frequency energy approach. Since the received PCM/FM signal is non-stationary random signal processing method for non-stationary random signal is often used STFT, it is wide enough to use a narrow time window function of the time signal interception, signal thus obtained can be as is stationary, then the Fourier transform to obtain a frequency of the local energy. If you let time windowsill move the timeline, you can get a signal in a time-varying frequency energy in the process, so that you can achieve the demodulated signal. The length of the time window within the sampling points should be close to a symbol, it is a good frequency energy accumulation, improving the performance of signal demodulation.

As can be seen from the definition of short-time Fourier, the sliding time window so that the signal spectrum at the same time have a contact within a window to get the signal spectrum by the discrete Fourier transform (DFT). Due to the use of time windows of signal interception, influenced fence effect and truncated effect, the spectrum is the convolution of the spectral function of the time window and the signal spectrum function, the peak corresponding to the measured frequency energy at the point. DFT is defined as:

$$X(k)=\sum_{n=0}^{N-1}x(n)e^{-j\frac{2\pi}{N}nk} \quad (k=0,1,\ldots.N-1) \tag{1}$$

Seen through the use of a sliding window, a sequence of length N can be decomposed as STFT operation 1×N data vector with N×1 rotation coefficient vector, a calculation amount for the N complex multiplications, (N-1) complex additions. To reduce the amount of computation processing can be used for the rectangular window STFT, this can be achieved in the sliding window algorithm is recursive STFT process, see the derivation of the following formula. Therefore, during the sliding of the rectangular window, for each quantitative calculation STFT 2 complex multiplications and two complex additions.

$$\begin{aligned}
&STFT(n+1,\omega)=\sum_{m=0}^{M-1}x(n+1+m)e^{-j\omega m}\\
&=\sum_{m=1}^{M}x(n+m)e^{-j\omega(m-1)}\\
&=\sum_{m=1}^{M-1}x(n+m)e^{-j\omega(m-1)}+x(n+M)e^{-j\omega(M-1)}\\
&=e^{j\omega}\sum_{m=1}^{M-1}x(n+m)e^{-j\omega m}+x(n+M)e^{-j\omega(M-1)}\\
&=e^{j\omega}\left(\sum_{m=0}^{M-1}x(n+m)e^{-j\omega m}-x(n)e^{-j0}\right)+x(n+M)e^{-j\omega(M-1)}\\
&=e^{j\omega}\left[STFT(n,\omega)-x(n)\right]+x(n+M)e^{-j\omega(M-1)}
\end{aligned} \tag{2}$$

Computer simulation using the ideal PCM / FM signal (signal parameters: carrier frequency 2.4MHz, code rate 800Kbps, 0.7 constant frequency offset, the sampling rate is 20MHz), the signal waveform shown in Figure 1, (a) denotes a modulation symbol, (b) corresponding to said modulation symbol PCM / FM time-domain waveform.

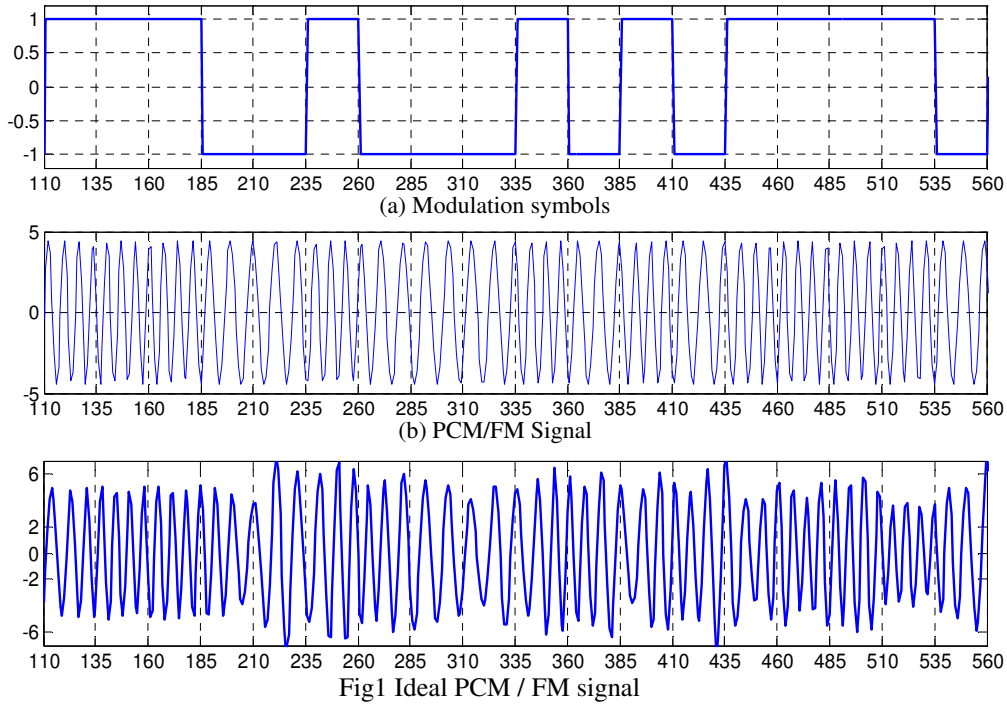

Fig1 Ideal PCM / FM signal

When K an integer and fractional both cases, the simulation calculations using STFT signal energy of the high frequency changes in the point shown in Figure 2.

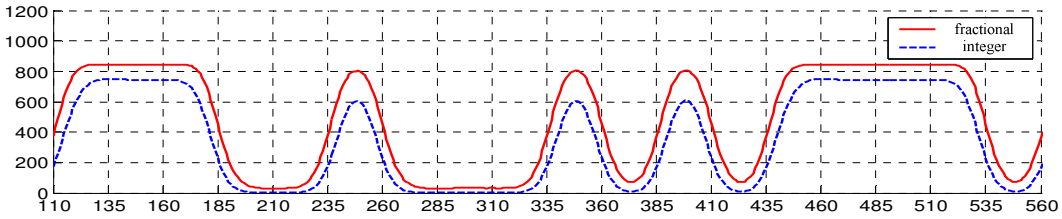

Fig2 Affect the value of K frequency energy

With the above method of calculating the STFT f_0 and f_1 in the case where the signal frequency energy changes with time, as shown in Figure 3.

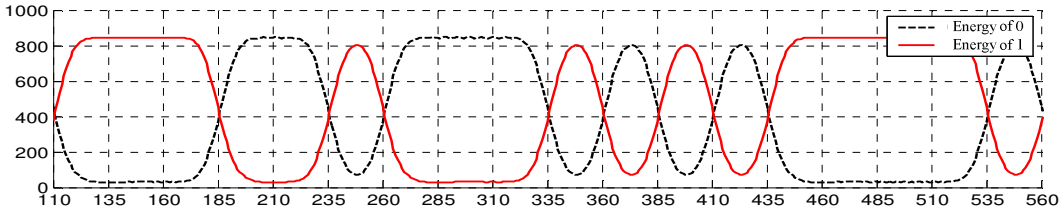

Fig3 Based on PCM / FM signal frequency energy variation method STFT

2 Code synchronization

Simultaneous transmission of a digital communication system, the data is correctly received based on the synchronization code based on the right. Code synchronization is receiving data, the symbol judgment must be tightly synchronized with the input symbol, namely the decision to synchronous clock signal must be consistent with the clock signal to send data, otherwise, it will cause even more than the demodulation error code less code. Hardware demodulation circuit method is commonly used to extract code synchronization using a frequency locked loop circuit control code synchronization clock symbol synchronization judgment. Demodulation environment software, hardware suitable for use in the method to establish synchronization codes only through the processing of the input sequence of discrete positioning an intermediate position of a symbol in each symbol of the judgment as the ideal position, to achieve code synchronization extraction and tracking.

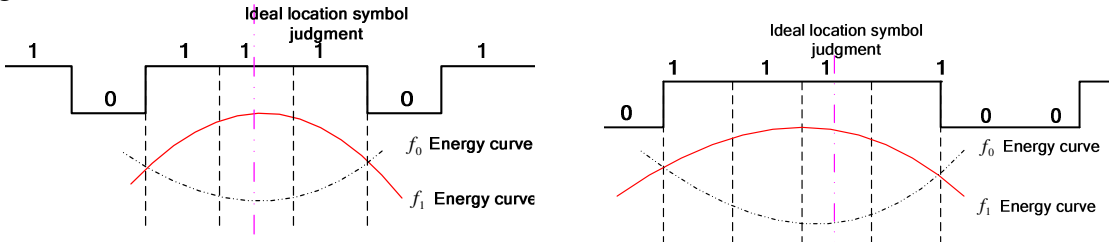

（a）Odd symbols ruling position （b）Even symbols ruling position

Fig4 Establishment code synchronization position

After positioning the first code synchronization point to the symbol width of the cycle, in the judgment of every ideal position by comparing the size of the two frequency energy relations, the judgment of the symbol.

Shown in Figure 5, the demodulation process performed in the correction code synchronization correction request of each match, "eye", it is possible to reduce the influence of interference on the code synchronization error, and to avoid the accumulation of errors caused in the demodulation process decreased demodulation performance.

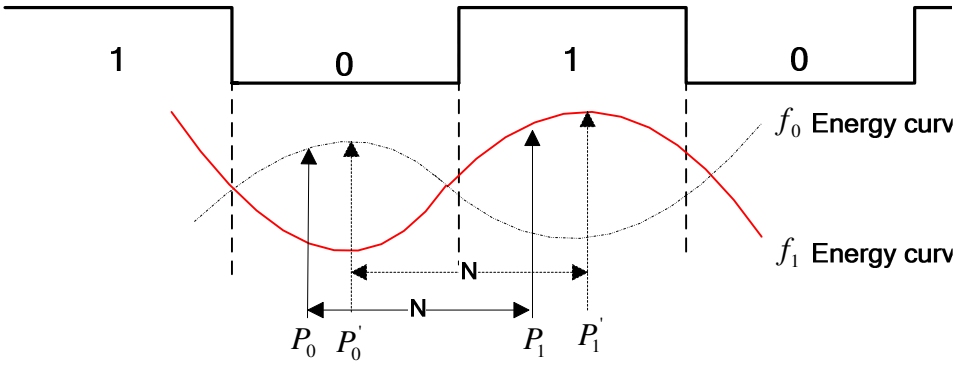

Fig5 Correction code synchronization

3 Performance Analysis

The actual received PCM / FM signal (SNR = 10dB, the code rate is 4Mbps, the carrier 2.4MHz, the sampling rate of 20MHz, the maximum Doppler frequency deviation 60KHz) code synchronization method according to the second part, made in different locations positioning a series of code synchronization point interval between two code synchronization points with the symbol of the relationship between the width of an integer multiple of any adjacent computing, simulation results shown in Figure 7. As can be seen, although the signal is subjected to serious disturbances, but by comparing the energy code synchronization method still has high positioning accuracy, the maximum deviation does not exceed 0.2 times the width of the symbol, the symbol is equivalent to the intermediate in the range of 0.3-0.7 judgment, will not have a serious impact on the verdict. And amended by the code synchronized and timely to avoid the accumulation of synchronization error, ensure that you understand tune performance. The actual received PCM / FM signal demodulation, the average error rate of 1.871×10^{-4}, meet or exceed the performance of the demodulation hardware.

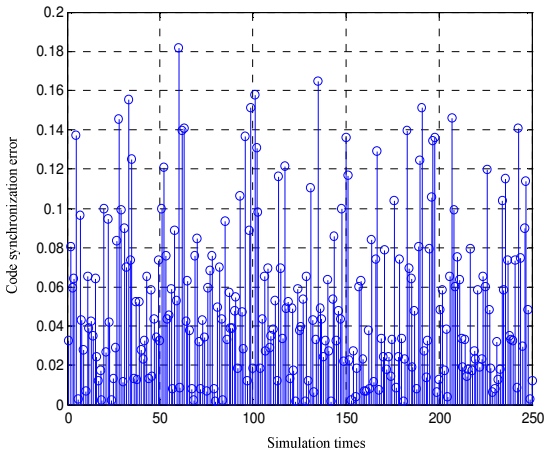

Fig6 Code synchronization performance

Summary

Using the method of calculating the STFT PCM / FM signal energy and frequency point by comparing two frequency energy to achieve the demodulated signal. Such demodulation algorithm can effectively suppress the influence of various disturbances PCM/FM code synchronization signal to the positioning accuracy, and ensure the performance of signal demodulation. Through the truncated data zeros STFT single method of calculating frequency energy, can effectively improve the impact of the fence on the effects brought about by the window function frequency energy. STFT rectangular window function using recursive algorithm greatly reduces the complexity of signal demodulation algorithm, is conducive to the software of the real-time demodulation.

References

[1] T. Grydeland，F. D. Lind，P. J. Erickson，J. M. Holt. Software Radar Signal Processing[J]. European Geosciences Union 2009.
[2] John J. Schamus, Veridian Engineering, Dayton, OH. Real-Time Software GPS Receiver[J].ION GPS 2007,24-27.

Advanced Materials Research Vols. 989-994 (2014) pp 4028-4031
© (2014) Trans Tech Publications, Switzerland
doi:10.4028/www.scientific.net/AMR.989-994.4028

Study on Identification Method of Zherong Radix Pseudostellariae with Near-infrared Spectroscopy

Yanping Pang[1, a] , Kun Liu[2,b], LiyaXia[1,c],Shaolong Yu[1,d]

[1]The College of Quality and Technology Supervision, Hebei University, Baoding, 071002, China;

[2] Tangshan city of Quaily and Technical Supervision, Tangshan, 063000, China

[a] pyp1982@163.com, [b]liukunqu@126.com, [c]xialiya@126.com, [d]yushaolong@168.com

Keywords: Near-infrared spectroscopy, Radix Pseudostellariae, Principal component analysis

Abstract. In order to identify the Zherong Radix Pseudostellariae, a geographical indication products, diffuse reflectance spectroscopy of came from ten different origins were collected by the Fourier near-infrared spectrometer. The spectroscopy was analyzed with Chemometrics method,and the spectroscopy was pretreated by the second derivative, first derivation and minus a straight line condition. The range of spectra was 3996.1-7282.5 cm^{-1}. The Calibration models of Radix Pseudostellariae were established by the qualification testing, principal component analysis, and cluster analysis respectively, and each model was verified. The results show that the optimal model established by the qualification testing, principal component analysis and cluster analysis can effectively identify authentic Zherong Radix Pseudostellariae , and accuracy rate was more than 97.5%. In conclusion, Zherong Radix Pseudostellariae can be identified accurately and quickly by the near-infrared spectroscopy technique.

Introduction

Radix Pseudostellariae is a traditional Chinese medicinal herb, belonging to the family Caryophyllaceae. Perennial herbs heterophylla Pseudostellaria root, Radix Pseudostellariae sweet, slightly bitter, flat. The spleen, lung. Body Moisturizing and nourishing fluid[1-3]. "Zherong Radix Pseudostellariae" is famous for its genuine medicinal materials, its yellow color, crystal, Ne Hoi, strongly smell are famous at home and abroad. The market price of the main Chinese medicinal materials regarded ‘’Zherong Radix Pseudostellariae price" as the standard, leading the domestic medicine market price of Radix Pseudostellariae. In 2007, Zherong Radix Pseudostellariae was implemented geographical origin protection by the State General Administration of Quality Supervision, Inspection and Quarantine. In order to identify the origin of Zherong Radix Pseudostellariae, protect the rights and interests of consumers, "Efficient Recognition Technology" of Zherong Radix Pseudostellariae is necessary to be established.

In recent years, Near- infrared (NIR) spectroscopy has become one of the most attractive and used methods for analysis of agricultural-related products and plant materials allowing for the simultaneous, rapid and nondestructive quantification of major components in the food matrix[4-6]. In order to identify the authentic Zherong Radix Pseudostellariae, Fourier near-infrared spectroscopy was used to collected diffuse reflectance spectra of Radix Pseudostellariae came from 10 different origins, and the analysis model established with the OPUS 6.5 metrology software.

Materials and methods

Materials

The collected Radix Pseudostellariae from different origins was purchased in the local and all products are grown in the year. The raw material was dried at 40 ℃ for 12 hours, pulverized, over a 60 mesh sieve, and equal amount of samples were tested. 94 samples of Zherong Radix Pseudostellariae from 20 plantations of origin protection and 63 samples of non- Zherong Radix Pseudostellariae came from other 9 origins were tested. Geographical origins of Radix Pseudostellariae samples are shown in table 1.

Table 1 Geographical origins of Radix Pseudostellariae samples

Province	Huna	Henan	Zhejiang	Jiangsu	Shandong	Guizhou	Anhui	Chengdu	Guangxi	Total
Sample size	6	6	6	6	6	15	6	6	6	63

Instruments and methods

Samples were scanned in diffuse reflectance mode (4000–12432 cm^{-1}) using a multi-purpose analyzer (MPA) spectrometer (Bruker Optics, Ettlingen, Germany) with a PbS detector and an internal gold background as the reference. NIR spectral data were collected using OPUS 6.5 (Bruker Optics, Ettlingen, Germany) and stored in absorbance format. Each sample was scanned in a quartz curette three times at room temperature with being stirred before each scanning. Then for each sample,three reflectance spectra were obtained and the average of them was used as the data of this sample in calibration or prediction. The scanning parameters were as follows: resolution of 8 cm^{-1}, scanner velocity of 10 kHz; 32 scans for each spectrum.

Results and analysis

Qualification testing

Zherong Radix Pseudostellariae spectra are used as the reference spectra, spectra of other origins were used as the test spectra, the spectral was pretreated by the Second Derivative with smooth point 13 condition, and the spectral range is 3996.1-7282.5 cm^{-1}. The eligibility test index range is selected of 3.6, and then it can be obtained the maximum eligibility index of the reference and test spectra, as shown in Fig. 1.

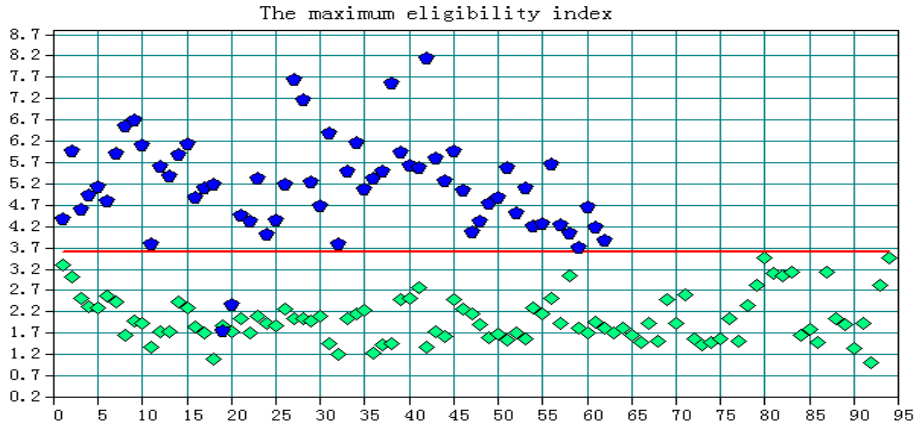

Fig. 1. The maximum eligibility index of the reference and test spectra

◆Zherong Radix Pseudostellariae

▲Other regions Radix Pseudostellariae

As shown in Fig. 1, the index value of the reference spectra was stable distribution near CI=3.6, and Zherong Radix Pseudostellariae is below the index line, it can be seen the Zherong Radix Pseudostellariae quality was stable; In addition, the spectral distribution of the test is clear. The accuracy rate of eligibility test was 98.7%. Therefore, the model can be used to identify the Zherong Radix Pseudostellariae from non- Zherong Radix Pseudostellariae.

Principal component analysis

Principal component analysis (PCA) is a multivariate statistical analysis method, which is to change the original variables, use fewer new variables to replace the old ones. And new variables can maximally express the data structure's characters of the original variables, and at the same time, wipe off useless message. For all spectra, the spectral was pretreated by first derivative and minus a straight line with smooth point 9 condition, the spectral range was 3996.1-7282.5 cm^{-1}, the principal component scores was shown in Fig. 2. The result showed that Zherong Radix Pseudostellariae in the region of the rectangle, and other regions were non- Zherong Radix Pseudostellariae. The

distance is long between Zherong Radix Pseudostellariae and non- Zherong Radix Pseudostellariae, it can be clearly identified, and it was shown quite different ingredients content between Zherong Radix Pseudostellariae and non- Zherong Radix Pseudostellariae.

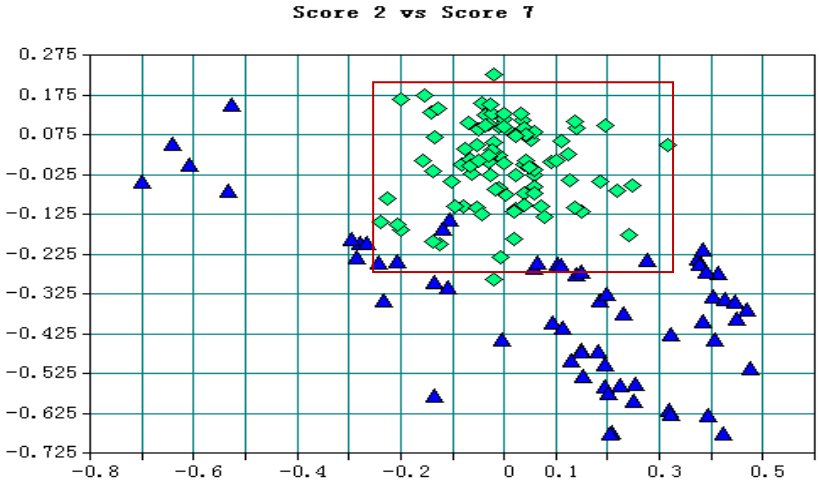

Fig. 2. Principal component scores
◆Zherong Radix Pseudostellariae
▲Other regions Radix Pseudostellariae

Cluster analysis

Second derivation and principal component analysis with smooth point 25 condition was used to pretreat the sample spectra, and the spectral range is 3996.1-12482 cm^{-1}.Samples were cluster analysis after pretreatments of spectra, and ward's algorithm was selected as cluster method, cluster analysis tree was shown in Fig. 3.

The near-infrared spectra between Zherong Radix Pseudostellariae and non- Zherong Radix Pseudostellariae can be clearly distinguished by the standard of cluster analysis, The distance of the spectra shows the similarity of the sample, and the distance of the spectra increased with the sample difference increased, the main component of Zherong Radix Pseudostellariae and other non-Zherong Radix Pseudostellariae was differences greatly.

As shown in Fig. 3, Cluster analysis diagnostic report as followed: all 94 Zherong Radix Pseudostellariae and 2 Jiangsu,1Guizhou,1Hunan sample in a class, 59 non-Zherong Radix Pseudostellariae in another class, The last fusion occurred at 1.910 and the identification of Zherong Radix Pseudostellariae accuracy rate was 97.5%. The identify results are accurate and reliable. Therefore, the method can be used to identify the Zherong Radix Pseudostellariae.

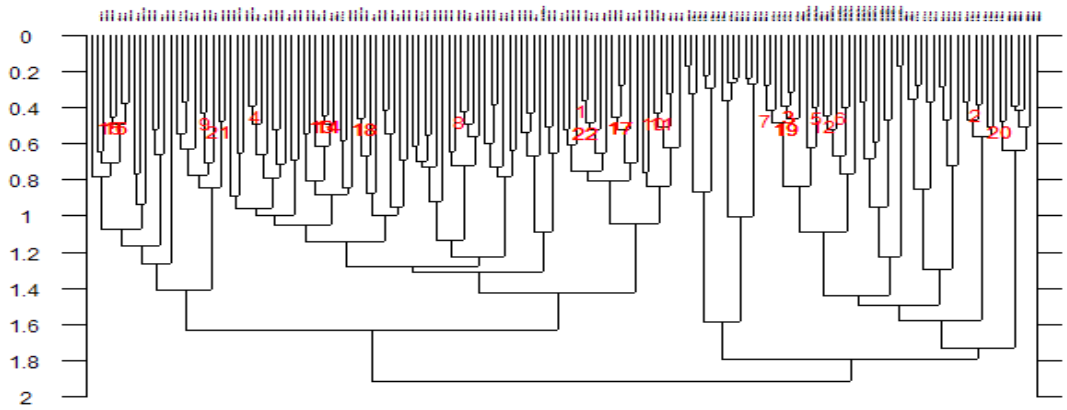

Fig. 3. Cluster analysis tree

Conclusions

The second derivative condition was used to pretreat the sample spectra. The identification models of Zherong Radix Pseudostellariae are established by the qualification testing in the range of 3996.1-7282.5 cm^{-1}, the accuracy rate is 98.7% . Cluster analysis and principal component analysis in the range of 3996.1-12482 cm^{-1} , the accuracy rate is 97.5%. Therefore, Zherong Radix Pseudostellariae can be identifiedeffectively, the near-infrared spectroscopy is combined with metrology methods, which can provide a reliable technique to identify the authentic Zherong Radix Pseudostellariae, and lay a foundation for the protection of the geographic indication products.

Acknowledgements

This work was financially supported by the Special Fund for Quality-Science Research project "doubles strike" key geographical indication protection technology on the origin of Chinese medicinal materials inspection appraisal method（2012104019-4）

References

[1] Li X, Wang Y R, Ma L, et al. Application of the Quality Evaluation of Traditional Chinese Herbal Medicines Using Chromatography of Fingerprints. *Journal of Biomedical Engineering*. *29* (2012), p.192

[2]Fang L and Lin N M. Quality Assessment of Spica Prunellaeby HPLC Fingerprint and Pattern Recognition.*Chinese Archives of Traditional Chinese Medicine*. *30* (2012), p.2034

[3] Tan N H, Zhao S X, Chen C X, et al. *Acta Botanica Yunnanica*.*13* (1991), P. 440

[4] Cozzolino, D, Heather E S, and Mark G : *Journal of Agricultural and Food Chemistry* ,. 26(2003), p. 7703

[5] Smyth H E, Cozzolino D : *Curr Bioact Comp*. *7*(2011), p. 66

[6] Cozzolino, Daniel : *Drug Development Research*. *8*(2012), p. 504

Advanced Materials Research Vols. 989-994 (2014) pp 4032-4037
© (2014) Trans Tech Publications, Switzerland
doi:10.4028/www.scientific.net/AMR.989-994.4032

Color Image Segmentation Based on Secondary Watershed and GrowCut Algorithm

Jianmei Chen[a], Haiying Lu[b]

College of Computer Science and Telecommunication Engineering, Jiang Su University, Zhenjiang 212013, China.
cjm@ujs.edu.cn,jsdxlhy@163.com

Keywords: image segmentation, cell automata, secondary watershed, GrowCut algorithm, mahalanobis distance, mathematical morphology.

Abstract. GrowCut algorithm is not only an interactive algorithm on the basis of cell automata, but also a multi-label algorithm based on seeds point. Aiming at the GrowCut algorithm usually asks users to partition foreground and background manually and mark a lot more initial seeds. This paper presents an automatic object segmentation method which combining secondary watershed and GrowCut algorithm, here in the following paper refers it to as SWGC algorithm. It firstly using the twice used watershed algorithm to partition the input image, the segmented regions are labeled using Mahalanobis distance, and merged according to the image color and space information, thereafter applying the GrowCut algorithm to perform globally optimized segmentation. The main contribution focuses on performing automatic segmentation which consist of obtain the foreground and background region and generate the seed template of GrowCut algorithm automatically. Thus not only leave out the constraints of user interaction operation, but also avoid the subjectivity and uncertainty. The proposed method reduces the runtime significantly as well as improves the segmentation accuracy and robustness of GrowCut algorithm. Experimental results show SWGC algorithm has superior performance compared to the other related methods.

1 Introduction

Image segmentation [1-2] is a technology and process that refers to make the image into regions with same characteristics and extract the interested objects, appropriate and accurate image segmentation can lay a good foundation for the higher image understanding, as a consequence realization of the real-time, automatic, robust and fast image segmentation. Color image segmentation [3] divide an image into several parts or subsets in accordance with the color rules of color image, extract the image features which are meaningful and need to be applied. It mainly has two main aspects: one is to select the appropriate color space, the other is the adoption of appropriate segmentation strategy and method. With the continual improvement of internet technology and imaging techniques, color image segmentation has become a new technology in demand in daily life, corresponding color image processing has attract more and more attention. In recent years, although there is a constant emerging of new methods in the field of color image segmentation, still it can not satisfy the needs of practical application, by means of a further research to the image segmentation method. It will be meaningful to improve the existing method and put forward more creative and effective method continuously, or that combine a variety of methods, take advantage of their own strengths perform image processing.

Watershed algorithm [4] is a common method for color image segmentation; it has the advantages of simple realization, rapid calculation speed, high precision for segmentation, a good response to the weak edge, can locate the target object accurately, also the object contour line is closed after processed; Faults is sensitive to the noise of the image, the segmentation results also too delicate, prone to over-segmentation, cannot split out the meaningful regions of the image. According to the above views, first conduct a relatively rough segmentation for a given image, preserving enough nodes and feature information which is the segmentation required, under the premise of the target edge line intact.

GrowCut algorithm is an interactive image segmentation algorithm on the basis of cell automata which introduced by Vezhnevets in 2006 [5], the algorithm possesses good robustness, it can be applied to any dimensional images, and complete the difficult segmentation tasks. Due to its distinctive advantages, GrowCut algorithm has attracted many researchers' attention recently [6-8]. The traditional algorithm requires user to mark the target foreground and background, literature [9]and literature[10] put forward the GrowCut algorithm which marked foreground and background by user's dotted line and rectangular marquee respectively, the former label foreground by light-colored dotted lines while dark line marks the background; The latter uses the rectangular marquee tool to surround the target area as the background, then conduct the same way to mark out the foreground in the surround area; For the two marking methods above, the correctly classified of foreground and background area determine the marker of initial seed accurate or not, seeds more or less, or even marker inaccurately will affect the convergence speed and segmentation result. To this end, in this paper we proposed a color image segmentation method that combining secondary watershed and GrowCut algorithm-SWGC algorithm, it marks out the foreground and background, generate the initial seed template of GrowCut algorithm without human interaction automatically. It can simplify user interactive operations, improves the segmentation accuracy of GrowCut algorithm, also reduce the computational complexity.

This paper is organized as follows. Section 2 is devoted to describing the designed approaches for the effective color image segmentation in detail. Section 3 illustrates the experimental results of different segmentation methods, followed by a discussion and comparison of these results. Finally the future work and conclusions are given in section 4.

2 SWGC for Color Image Segmentation

2.1 Secondary watershed

In view of the raw watershed algorithms are extremely vulnerable to noisy pictures; the subtle gray level change of object surface may produce over segmentation. There are several techniques [11] based on image preprocessing, mainly include median filter, low pass filter, Gaussian filter and color morphology et al. As the filters eliminate most of the high frequency from the image, they usually do not preserve borders of the objects. This paper adopts the common operation in morphology for gradient smoothing, Morphological opening and closing reconstruction operation is established on the basis of expansion and corrosion, corrosion before expansion for the open, expansion after corrosion is closed; closed and open operations not only can remove the specific image details which smaller than structural elements, but also avoid global geometric distortion.

To solve the color image gradient of the input image is the first step of pre-segmentation, then perform a segmentation on the color image gradient using watershed method, that is to say, put the minimum value of the gradient image as a starting point for submerged, so as to obtain the dividing line between each valley, this is a watershed process; In view of the large number of the separate area can not significantly reduce the computational complexity; And on this basis, employ the morphology close-opening operation smooth the color gradient image which obtain from a watershed manipulation, proceeding the secondary watershed segmentation, thus not only maintain an adequate amount of information, but also greatly reduces the number of regions.

2.2 Mahalanobis distance

There is a need to define the feature space prior to the calculation of Mahalanobis distance[12], the selection of color space is particularly important for merging the small areas accurately, the color difference of selected color space need to associated with Mahalanobis distance with the purpose of obtaining good segmentation results. CIE(*Luv*) is a kind of uniform color space, which can use the geometric distance of the color space compare different colors, and then measures the small chromatism effectively; Therefore this article adopts the *Luv* color model with linear mapping

properties, in which L represent the brightness, and u, v represent the chromaticity and coordinates respectively.

Mahalanobis distance was put forward by the Indian statistician P.C.Mahalanobis. It is an effective method to calculate the similarity of two unknown sample sets which means the data covariance matrix. Other than Euclidean distance, Mahalanobis distance considers the connection between the various characteristics; also it is independent of the units of measurement. For an average, $u=(u_1,u_2,u_3,...,u_p)$ multivariate covariance matrix vector $x = (x_1, x_2, x_3, \ldots, x_p)$, its Mahalanobis distance $D_M(x)=\sqrt{(x-u)^T\Sigma^{-1}(x-u)}$, not affected by the dimensions, able to eliminate the interference of the correlation between variables is an advantage of the Mahalanobis distance.

2.3 GrowCut algorithm

The core idea of GrowCut algorithm is using the cellular automata theory to calculate the strength relationship between cells and its neighbors iteratively, through the growth and repeated competition changing the state of the cell, and then achieve the foreground target segmentation. This algorithm adopts a new train of thought marking the pixel, specifically; it is not only a multi-label algorithm based on seeds point, but also an interactive algorithm on the basis of cell automata. Cellular automata (CA) [13] were introduced by Von Neumann in 1996, it can carry out complex calculation with the simple behavior rules.

GrowCut algorithm using cell automata as a framework for the segmentation process, a digital image is a two-dimensional array of $m\times n$ pixels; there is a one to one correspondence between pixel point and the cell in the cell automata. The cell state S_p in our case is actually a triplet $(l_p,\theta_p,\overrightarrow{C_p})$, where the label l_p of the current cell, "strength" of the current cell θ_p and cell feature vector $\overrightarrow{C_p}$ defined by the image. The growth process of GrowCut algorithm is an iterative process, in which each cell will have an impact on its neighbor cells, at each time step, the initial cells attempt to attack other surrounding cells, if the attack force is greater than defender's strength, the defending cells have their labels and strength changed to whichever cell originally conquered it. The result of these local competitions is that the strongest cell occupies the neighboring pixels and gradually spread over the image. This process repeats until the entire cell's states stop changing, or after a maximum number of iterations, all cells will reach an equilibrium state and then the algorithm converges, the end result is a set of foreground and background pixels that describe the object segmentation in the image.

2.4 Concrete algorithm design

In the light of above ideas, the main steps of SWGC can be concludes as follows:

Step 1. For a given color image, First pre-processed by the secondary watershed algorithm, acquire the rough segmentation of the image, then employ the close-opening operators in mathematical morphology do the smoothing, fusing some isolated points in the region, better to avoid over-segmentation and information loss, obtain a limited number of initial segmented small regions.

Step 2. Do the color image edge detection which based on canny operator in the first place, then take the center of the object as mask, use the mask to obtain the color information of the Luv feature space, and compared with other segments, which are taken from secondary watershed segmentation output. Afterwards, grow that mask on the basis of dissimilarity function named Mahalanobis distance between mask and other parts, if they are kind of similar then merge that region to the mask.

Step 3. The final mask which merged the most likely segments was set as the foreground information, and the remaining regions are utilized as background information in GC algorithm, so make a distinction between object and background without manual operation.

Step 4. According to the foreground and background information, employs morphological reconstruction technology manipulates the foreground and background, take its local maximum point

as the foreground and background seeds point respectively, generate the initial seed template of GrowCut method automatically, then perform the final segmentation for further.

3 Results and Discussions

SWGC algorithm proposed in this paper is applied for the object segmentation of the color images with natural scenes. The segmentation results are clearly illustrated step by step in Figure 1.

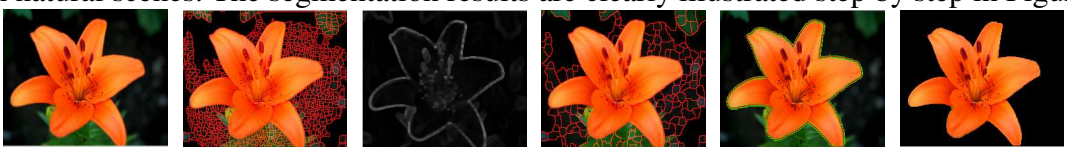

(a) (b) (c) (d) (e) (f)

Figure 1. (a) Original image (b) A watershed (c) Morphological smoothing (d) Secondary watershed (e) GrowCut segmentation (f) Extract the foreground object

Compared with traditional GrowCut algorithm's segmentation results, SWGC algorithm has a better performance which shown in Figure 2, Table 1 describes the runtime between GrowCut and SWGC algorithm. Thus it can be seen from that the proposed method can obtain the edge contour of the image accurately, also make the results tend to be more overall consistency; While traditional GrowCut algorithm existed over-segmentation and undivided regions, has a poorly effect; Meanwhile, Compared with the conventional manual marking GrowCut algorithm, SWGC can generate the desired foreground and background area automatically, has a faster execution time.

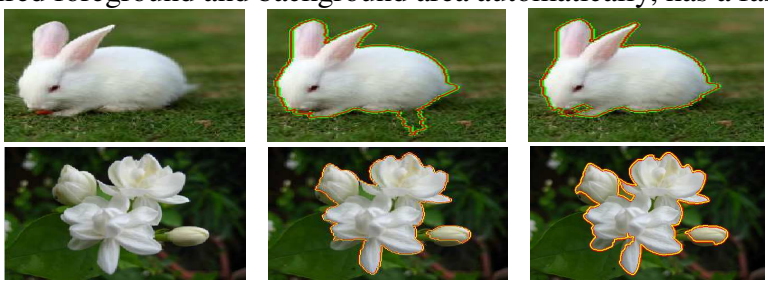

Figure 2. (a) Original image (b) GrowCut segmentation (c) SWGC segmentation

Table 1 Time comparison between GrowCut and SWGC algorithm

experiment image	Computational Time(s)	
	GrowCut algorithm	SWGC algorithm
White rabbit	5.8735	2.9219
jasmine	7.4688	4.7031

To further verify the validity of the proposed algorithm, this paper directly comparing the experimental results with the results of the algorithm in the related literature. The contrastive experiment results using the following three methods, MSNcut[14], MSAP [15] and SWNcut [16]. Figure 3-5 depict the test results of color images using four methods, and we can make the following observations from Figure 3-5 : The edge of the image obtained by MSNcut algorithm present obvious jagged, the effect is not ideal; MSAP algorithm segmentation generate quite smoother image edge, but there are quite a few small isolated area; SWNcut algorithm can accurately locate the image edge profile, yet the adjacent areas segment of multi-objective image is not quite accurate; For all the experimental results, SWGC algorithm, by contrast, partitions effectively the natural scenes into several meaningful regions and provides more accurate and complete object region. Time comparison between SWNcut and SWGC algorithm shown in Table 2, as can be seen both methods have performed pre-segmentation by secondary watershed, and got the same number of regions, under this condition, adopt the Ncut algorithm and GrowCut algorithm for re-segmentation respectively, GrowCut operation time is slightly less than the Ncut algorithm, thus the computing speed is improved.

Figure 3. (a) Original image (b) MSNcut segmentation (c) SWGC segmentation

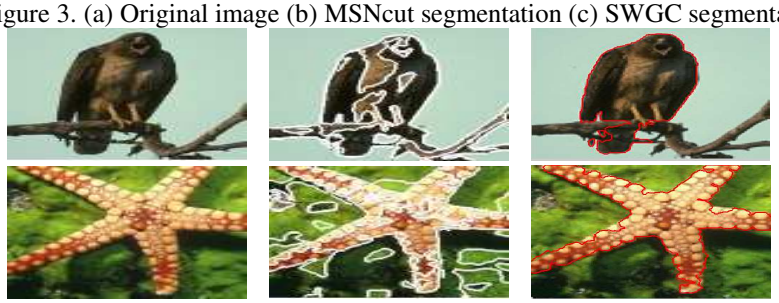

Figure 4. (a) Original image (b) MSAP segmentation (c) SWGC segmentation

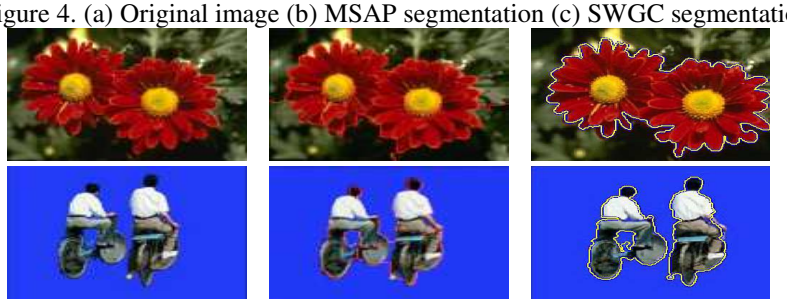

Figure 5. (a) Original image (b) SWNcut segmentation (c) SWGC segmentation

Table 2 Time comparison between SWNcut and SWGC algorithm

Number Figure 7	SWNcut algorithm	SW pre-segmentation		SWGC algorithm
	Ncut time(s)	Region number	Segment time(s)	GrowCut time (s)
1	6.737	238	0.2500	2.8281
2	5.796	88	0.3438	3.5750

4 Conclusions and Looking

A fast and effective SWGC method for color image segmentation has been designed in this paper. The strength of such approach is that it integrates the advantages of the two algorithms which have a faster processing speed and a more satisfactory segmentation result; it ensures the integrity and accuracy of the segmented regions and work well for all kinds of style images. In addition, compared with other related methods, such as the traditional GrowCut, MSNcut, MSAP, SWNcut et al, the SWGC algorithm indeed has a better performance. Experimental results verify the feasibility and practicality of the SWGC; it can be described as an efficient method for color image segmentation.

Future work will concentrate on exploring theoretical properties of the algorithm and seeking other algorithm which is simple, faster, obtaining better segmentation results as GrowCut algorithm's pre-processing in the first stage; In the next stage, the main task is to integrate the rich texture information of image, and apply to the segmentation algorithm while considering using color information.

References

[1] GUPTA P, SAXENA S, SINGH S, et al. Color image segmentation: a state of the art survey [J]. International Journal of Computational Intelligence Research, 2012, 8(1): 17-25.

[2] Wen Junling, Yan Zhuangzhi, Sun Yubiao, Lin Xiaoman.Image segmentation of integrated edge and region information by lattice Boltzmann model [J].Journal of Jiangsu University(Natural Science Edition) , 2013, 34(6):687-692.

[3] IVANOVICI M, RICHARD N, PAULUS D. Color image segmentation [M]//Advanced Color Image Processing and Analysis. Springer New York, 2013: 219-277.

[4] Zhang yi, Applied research in image segmentation used by the algorithm of watershed [D]. Guangdong University of Technology, 2013.

[5] VEZHNEVETS V, KONOUCHINE V. GrowCut: Interactive multi-label ND image segmentation by Cellular Automata[C]//proc. of Graphicon. 2005, Novosibirsk Akademgorodok, Russia: [s.n.] 2006:231-234.

[6] ARNDT O J, SCHEUERMANN B, ROSENHAHN B. “Region Cut”-Interactive multi-label segmentation utilizing cellular automaton[C]//2013 IEEE Workshop on Applications of Computer Vision (WACV). IEEE, 2013: 309-316.

[7] GHOSH P, ANTANI S K, LONG L R, et al. Unsupervised Grow-Cut: cellular automata-based medical Image segmentation[C]//Healthcare Informatics, Imaging and Systems Biology (HISB), 2011 First IEEE International Conference on. IEEE, 2011: 40-47.

[8] Phan R, Androutsos D. Interactive video GrowCut: A semi-automated video object segmentation framework using cellular automata [C]//Electrical and Computer Engineering (CCECE), 2011 24th Canadian Conference on. IEEE, 2011: 000081-000084.

[9] ROTHER C, KOLMOGOROV V, BLAKE A. Grabcut: Interactive foreground extraction using iterated graph cuts[C]//ACM Transactions on Graphics (TOG). ACM, 2004, 23(3): 309-314.

[10] Lan hong, Min-lequan. Interactive Segmentation Algorithm Optimized by Multi-threshold with Application in Medical Images [J]. Journal of Computer Applications, 2013, 33(5):1435-1438.

[11] BIENIECKI W. Over segmentation avoidance in watershed-based algorithms for color images [C]//modern Problems of Radio Engineering, Telecommunications and Computer Science, 2004. Proceedings of the International Conference. IEEE, 2004: 169-172.

[12] CHEN Bin, ZOU Xian-yong, ZHU Wen-jing. Eliminating outlier samples in near-infrared model by method of PCA-mahalanobis distance [J]. Journal of Jiangsu University (Natural Science Edition), 2008, 29(4):277-279.

[13] von NEUMANN J. Theory of self-reproducing automata [M]. Urbana-Champaign, Illinois, USA: University of Illinois Press, 1966.

[14] TAO W, JIN H, ZHANG Y. Color image segmentation based on mean shift and normalized cuts [J]. Systems, Man, and Cybernetics, Part B: Cybernetics, IEEE Transactions on, 2007, 37(5): 1382-1389.

[15] Xu Xiao-li, Lu Zhi-mao, Zhang ge-sen, Li chun, and Zhang qi. Color Image Segmentation Based on Improved Affinity Propagation Clustering, Journal of Computer-Aided Design & Computer Graphics, 2012, 24(4):514-519.

[16] Lu Zhi-mao, Xu Xiao-li, Fan Dong-mei, Li Hai-yan, Color Image Segmentation Based on Secondary Watershed and Ncut Algorithm, Journal of Huazhong University of Science and Technology (Nature Science), 2011, 39(z2):95-98.

Advanced Materials Research Vols. 989-994 (2014) pp 4038-4041
© (2014) Trans Tech Publications, Switzerland
doi:10.4028/www.scientific.net/AMR.989-994.4038

Tracking Optimization of FH signal based on Wiener Filtering

He Qian[1, a], Wu Guangzhi[1,a] and Wu Yanjun[1,a]

[1]China Satellite Maritime Tracking and Control Department, China

[a]348237548@sina.com

Keywords: FH (Frequency-Hopped), wiener filter, tracking accuracy

Abstract. Comparing with the traditional fixed carrier frequency signal, using FH (Frequency-Hopped) signals improved the performance of anti-interference of the TT&C system when bring the low signal tracking accuracy. In order to solve this problem, this paper proposed a loop structure of using wiener filter, the filter coefficient was deduced. Simulation results show that the loop tracking precision was increased after the optimization, and the improvement has relations with the filter order n. When $n=10$, the speed measuring precision reached 30cm/s which was increased about 3 times than did not use wiener filter.

Introduction

With the development of electronic warfare technology, it is a big challenge of communication in harsh environments for effective, in order to ensure the normal operation of the system in order to obtain favorable space superiority is the future development trend of the system. Using FH (Frequency-Hopped) spread spectrum signal is to improve the system in harsh conditions interfere with the satellite monitoring in effective monitoring system [1]. But using FH signal and brought the loop tracking accuracy is not high, so that the accuracy of measurement and control system is not high speed. Control signals for a fixed carrier frequency, using ordinary loop speed precision tracking signal about 2cm/s, measurement precision under the same circumstances hopping signals about 90cm/s.

In this paper, the monitoring system used in FH spread spectrum signal is not high speed precision problem, Wiener filter for tracking loop optimization.

1 Structural analysis

The so-called statistical filtering for random signals is to filtering from a mixture of random measurement error signal as close as possible to the true value of their estimated useful signal in factually. In the context of this article, because the characteristics of FH signals can not be used in case of PLL loop FLL loop with its tracking signal tracking, and adding auxiliary module hopping pattern in FLL loop to remove due to the hopping Carrier frequency agile problems caused[2]. But the tracking accuracy using frequency hopping signal tracking loop FLL limited Solutions to this problem is to use statistical filtering of the measured loop data estimates and projections, by this method to increase the frequency tracking accuracy, thus improving system The measurement precision. First through a Wiener filter, this article before using Wiener filter frequency tracking performance of the proposed method is mainly optimized for tracking the signal into the loop, the structure is shown in Figure 1.

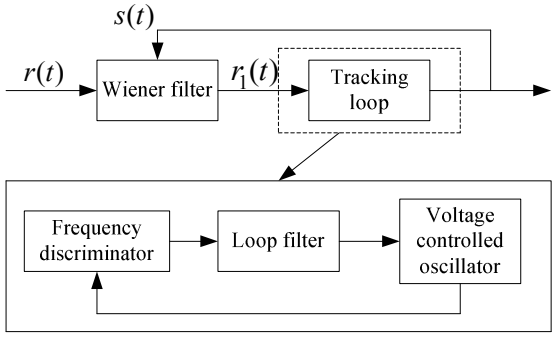

Fig 1 Tracking loop structure with Wiener filter

Where, the structure block diagram of the Wiener filter can be described in Figure 2.

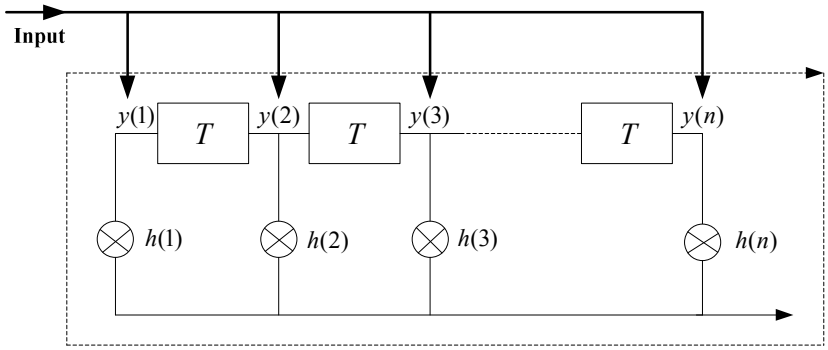

Fig 2 Non-Recursive Wiener filter structure diagram.

Assuming useful signal x is a random variable. $y(k)$ is sampled at different time points of the measured measurement values of the useful signal x, that is, the signal captured completed $r(h)$, $h(k)$ for the filter weighting coefficients. $v(k)$ is introduced in the measurement process additive noise, and uncorrelated with the random signal x, based on the above assumptions, we can get:

$$y(k) = x + v(k) \tag{1}$$

Suppose we have measured n samples value of $y(k)$ as $y(1), y(2), ..., y(n)$, then, the next step is to use a Wiener filter for further processing of these measurements, in order to make possible approximation to estimate x, we follow the statistical estimation theory habits, the estimated value of x is set to $\hat{x}$.

The purpose of the Wiener filter is thought captured by Wiener filter estimation completion signal, to produce a new received signal so that the signal obtained by the estimation as close to the useful signal. In essence, is removed by estimating the noise, thereby improving the signal to noise ratio of the received signal. Specific workflow:

First, the input signal has been captured to complete Wiener filter, a Wiener filter in accordance with the signal workflow $r(t)$ is processed, a new estimate of the signal $r_1(t)$, as estimated by remove noise and improve the signal to noise ratio.

Second, the estimated signal is input to the FLL loop, the traditional workflow lock loop tracking of the signal to obtain a frequency tracking loop to recover the received signal in the voltage controlled oscillator.

2 Filter coefficient optimization

The above section describes the structure of non-recursive type Wiener filter, which Wiener filter is the easiest way to achieve an average sample value estimator[3], which means that the weighted coefficients $h(1), h(2), ..., h(n)$ is equal to $\frac{1}{n}$, then the estimation value of x is arithmetic average of n sample value, and it is shown as

$$\hat{x} = \frac{1}{n}\sum_{i=1}^{n} y(i) \tag{2}$$

However, this is not a mean square estimation method to estimate the optimal sense of the estimation error is minimized, so next we mean square estimation error is minimized as an optimal criterion. The weighting coefficient $h(1), h(2), ..., h(n)$ is optimized such that the filter output the minimum mean square estimation error.

According to the filter structure shown in Figure 2, the general expression of the estimated value $\hat{x}$ of the Wiener filter is

$$\hat{x} = \sum_{i=1}^{n} h(i)y(j) \tag{3}$$

Where, $h(i)$ is the filter coefficient of the filter, and it is necessary to optimize section as well. From the following formula (3) starting under the minimum mean square error estimation criterion, the optimum filter coefficient calculating $h(i)$ such that the estimated mean square error filter is minimal, so that the loop tracking precision is optimum.

Due to the estimating value of random variable x is $\hat{x}$, therefore, the general expression for the mean square estimation error is

$$P_e = E[(\overline{x}\hat{x})^2] = E\left[\left(\overline{x}\sum_{i=1}^{n} h(i)y(i)\right)^2\right] \tag{4}$$

Because we need to strike the filter coefficients $h(1),h(2),...,h(n)$, and in accordance with the criterion of minimum mean square error estimation, so you can find the mean square error P_e partial derivative with respect to each of the weighting factors, and to make derivative value is 0, that is

$$\frac{\partial P_e}{\partial h(j)} = -2E\left\{y(j)\left[\overline{x}\sum_{i=1}^{n} h(i)y(i)\right]\right\} = 0,\ j = 1,2,...,n \tag{5}$$

Simplifying the formula (5), and we can obtain:

$$\sum_{i=1}^{n} h(i)E\left[y(i)y(j)\right] = E\left[xy(j)\right],\ j = 1,2,...,n \tag{6}$$

Wherein, $E\left[y(i)y(j)\right]$ is the autocorrelation sequence of measured values, and we denote it as $P_{xy}(i,j)$; $E\left[xy(j)\right]$ is the cross-correlation sequence between the random signal x and the measured value, and denoted by $P_{xy}(j)$.

Thus, the formula (6) can be written as:

$$\sum_{i=1}^{n} h(i)P_y(i,j) = P_{xy}(j),\ j = 1,2,...,n \tag{7}$$

Spreading formula (7) and we can get:

$$\begin{cases} P_y(1,1)h(1) + P_y(2,1)h(2) + ... + P_y(n,1)h(n) = P_{xy}(1) \\ P_y(1,2)h(1) + P_y(2,2)h(2) + ... + P_y(n,2)h(n) = P_{xy}(2) \\ \quad . \\ \quad . \\ \quad . \\ P_y(1,n)h(1) + P_y(2,n)h(2) + ... + P_y(n,n)h(n) = P_{xy}(n) \end{cases} \tag{8}$$

Where, $P_y(i,j)$ and $P_{xy}(j)$ are known parameters, $h(1),h(2),...,h(n)$ is willing to be solved. So the above formula can be determined by the filter coefficients $h(1),h(2),...,h(n)$, and we completed the minimum mean square error estimation filter criterion optimization.

According to the analysis above, and apply it into FH signal tracking, $y(k)$ is the received signal which is mixed with the noise, x is the useful signal, and we are aim reduced the difference of the them through using filter as far as we can.

3 Simulation results and analysis

According to deducing of filter coefficients $h(1),h(2),...,h(n)$ above, the derivation, such that the filter is estimated based on the minimum mean square error criterion optimization. In this section, the use of non-recursive type Wiener filter optimized by observing the actual simulation loop track after track results. First we observed in the remaining frequency difference $f_{in} = 20Hz$, Doppler rate of change $f_a = 5Hz/s$, preflight integration time $T_{coh} = 5ms$, loop bandwidth $B_L = 20Hz$, ratio of carrier to noise $C/N_0 = 35dB$, traditional FLL loop to jump the results of the tracking signals is shown in Figure 3.

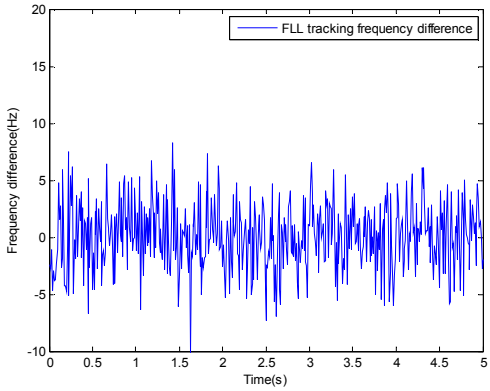

Fig 3 The relationship with delay interval, code sequence and likelihood value

Then, we simulate results of the loop after using wiener filter, and shown in figure 4.

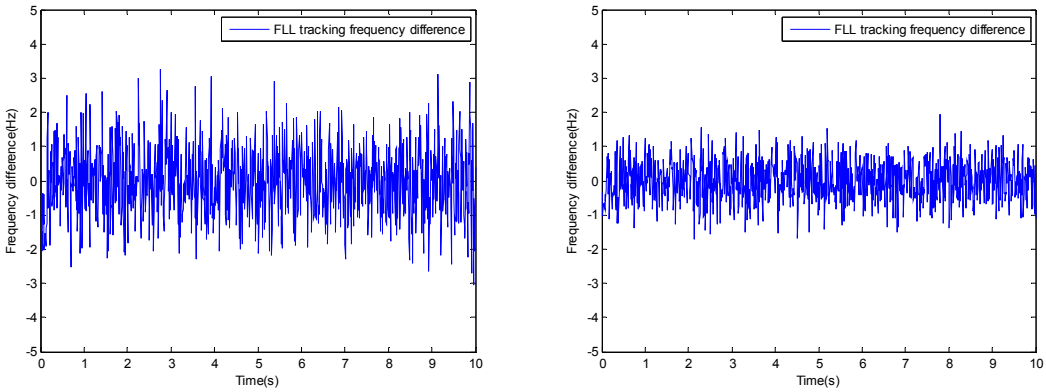

Fig 4 Loop tracking frequency difference of $n=5$ and $n=10$ respectively

Obviously, the tracking frequency difference is less than the original loop after using the optimizing loop, and with the processing number increasing of $y(k)$ each time in Wiener filter, the improvement effect of the tracking frequency difference is becoming better.

Summary

In this paper, we proposed a method of using wiener filter to optimize traditional carrier tracking loop, and derived the weighting coefficients of Wiener filter. Simulation results proved that the loop tracking precision improving accuracy is greatly increased for FH signal by using wiener filter. When the order of the filter is 10, the speed measurement accuracy of the system is 30cm/s, and it is three times accuracy improved than without using Wiener filter.

References

[1] SIMONE L, SALERNO N, MAFFEI M. Frequency-Hopping Techniques for Secure Satellite TT&C: System Analysis & Trade-Offs [C]. Proceedings of 2006 International Workshop on Satellite and Space Communications. IEEE, 2006:13-17.

[2]YANG W G, WEN Y J, MENG SH Y, et al. Performance analysis of a kind of DS/FH hybrid spread spectrum signal for telemetry [J]. Telecommunication engineering, 2009,49 (1):13-17.

[3] Mohinder S.Grewal, Angus P.Andrews. Kalman Filtering: Theory and Practice Using MATLAB [M]. The 3rd Revised edition. Wiley-IEEE Press, 2008.

Advanced Materials Research Vols. 989-994 (2014) pp 4042-4045
© (2014) Trans Tech Publications, Switzerland
doi:10.4028/www.scientific.net/AMR.989-994.4042

Detection of Nonlinear Frequency Modulated Signal Based on Fractional Fourier Transform

Wu Yanjun[1, a], Tao Min[1,a] and Zhou Minqi[1,a]

[1]China Satellite Maritime Tracking and Control Department, China

[a]348237548@sina.com

Keywords: Nonlinear frequency modulated signal, fractional Fourier transform (FRFT), linearly approximation approach, Wigner-Ville distribution

Abstract. Based on fractional Fourier transformation (FRFT), the feature of the signals which vary smoothly from time domain to frequency domain is given. The FRFT method is applied to the estimation and detection of nonlinear frequency modulated signals to which piecewise linearly approach. Wigner-Ville time frequency distribution of the signals is used after approaching and the masking results of the original signal accumulate energy as detecting statistic. A signal detector based on energy accumulation from time frequency domain in the angle of analysis of both time and frequency is proposed. Finally, a comparison with traditional non-coherent energy accumulation methods is made, which shows the proposed method has superior performance.

Introduction

Target detection in many areas (such as radar, sonar, etc.) has a wide range of applications. Traditional detection problem is divided into three parts [1]: the detection of a known signal in noise, random noise signal detection signal detection with unknown parameters and noise of. The former two problems were solved by a matched filter or a matched filter [2]. The third case is random since the signal waveform detection method is non-parametric method based on detection.

Time-frequency analysis is a useful tool for dealing with non-parametric detection problem. Its main idea is the one-dimensional time-domain transformation when the two-dimensional frequency distribution. The basic time-frequency distribution is divided into two types: atomic decomposition, such as short-time Fourier transform and wavelet transform; bilinear distribution, such as when the Cohen class frequency distribution [3]. In the past decades, the time-frequency detection theory of random signal had a rapid development. The fractional Fourier transform is applied to the signal detection and parameter estimation has attracted more and more attention, including linear FM signal (chirp signal) and so on. But these are the premise of linear signal to start, and in the actual signal processing, nonlinear signal occupies a large proportion, while the use of linear estimation method to detect non-linear signal is more practical application significance.

Fractional Fourier transform as a time-frequency analysis method has a number of excellent performance. In the text of the algorithm, using the Wigner-Ville distribution to indicate when the signal frequency distribution FRFT for piecewise linear approximation of the FM sub N section of the signal, then the signal will be approaching the Wigner-Ville transform, and finally results of two Wigner-Ville distribution a "mask processing", access to new distribution. According to the distribution of accumulated energy detection can be applied in order to take full advantage of the signal in the frequency domain information. In this paper the fractional Fourier transform and combine the energy accumulation and detection applied to estimate the unknown signals to analyze the detection performance of this approach. Experimental results show that the proposed method obtained good detection results.

1 FRFT and parameters estimation

1.1 Fractional Fourier Transform

Fractional Fourier transform by V. Namias in 1980 from a mathematical point given. It can be interpreted too frequent surface rotation operator, is about the axis signals in the time-frequency surface do rotate counter-clockwise. This property makes it suitable for analysis of LFM signal. Fractional Fourier transform is a generalized Fourier transform, the signal can be seen as representation on u axes counterclockwise rotation α axis on the timeline.

Fractional Fourier transform is defined as

$$X_p(u) = \{F^{\alpha}[x(t)]\}(u) = \int_{-\infty}^{+\infty} x(t)K_p(t,u)dt \tag{1}$$

The conversion kernel function is

$$K_p(t,u) = \begin{cases} \sqrt{\dfrac{1-j\cot\alpha}{2\pi}}\exp[j(\dfrac{1}{2}u^2\cot\alpha - ut\csc\alpha + \dfrac{1}{2}t^2\cot\alpha)] & \alpha \neq n\pi \\ \delta(t-u) & \alpha=2\mathrm{n}\pi \\ \delta(t+u) & \alpha=2(n+1)\pi \end{cases} \tag{2}$$

Where, p is the FRFT order, α is the rotation angle, and $\alpha = p\pi/2$.

The energy of white noise evenly is distributed over the entire time-frequency plane, the probability of the energy accumulation FRFD small. According to the nature of the fractional Fourier transform, chirp signal on FRFD energy accumulation appears, therefore, the position of the energy accumulation can occur via two-dimensional fractional plane to estimate the chirp signal the initial frequency and tune the frequency to complete the estimate of the parameters.

1.2 Dimensionless normalized and parameter estimation

Assumes that the original signal $f(t)$ is in the time interval $[-t_b/2, t_b/2]$, and the frequency domain is in the interval $[-f_b/2, f_b/2]$, t_b and f_b are the time width and bandwidth of the signal respectively. In order to transform the time domain into a domain of dimension 1, we introduce a normalized scale factor m, and define a new dimension following coordinates

$$x = t/m,\ v = fm \tag{3}$$

the new coordinate system realized normalized dimensionless, and $m = (t_b/f_b)^{1/2}$, the length interval of the two interval are $x = (t_b f_b)^{1/2}$, then the two normalized interval is $[-x/2, x/2]$, the sampling interval is $\frac{1}{x}$.

Expression of Chirp signal is defined as

$$f(t) = a_0\exp[j(\varphi_0 + 2\pi f_0 t + \pi\mu_0 t2)] + W(t),\ -t_0/2 \le t \le t_0/2 \tag{4}$$

Where $W(t)$ is additive Gaussian white noise, μ_0 is Chirp rate, f_0 is center frequency, and a is the FRFT order of the peak. The relationship expression between FRFT domain coordinate u and u_0, f_0 is defined as

$$\begin{cases} \mu_0 = -\cot(p\pi/2) \\ f_0 = u\csc(p\pi/2) \end{cases} \tag{5}$$

Assuming the signal frequency before normalization and after normalization is μ_0 and μ_0' respectively, the relationship between them is

$$\begin{cases} \mu_0' = \mu_0 m^2 \\ f_0' = f_0 m \end{cases} \tag{6}$$

2 Scheme of signal detection in time-frequency domain

Noise and clutter weak maneuvering target detection, radar and sonar has always been a challenging task in the field. Detect a weak goal requires a long observation time. However, in the long accumulation of target echo phase history is difficult to use a few parameters modeling. Thus, object detection becomes a non-parametric detection. Here, the echo can be assumed to be maneuvering target with unknown a smooth instantaneous frequency curve linear FM signal and noise can be modeled as a complex additive white Gaussian noise. Target detection can be equated to the complex Gaussian white noise in the background to detect unknown FM signal problems [4]. This is a typical binary hypothesis testing problems.

$$\begin{cases} H_0 : x(n) = w(n) \\ H1 : x(n) = s(n) + w(n) \end{cases} \tag{7}$$

Here, $x(n)$ is the time sequence of the tested signal; $s(n)$ is an unknown Chirp signal corresponding to the target; $w(n)$ is complex white Gaussian noise with mean zero and variance σ^2 independently.

2.1 Segmentation parameter estimation

Observation of the unknown signal x_1 (its length is M) is shown as

$$x_1 = [x_{11}, x_{12}, ..., x_{1N}]^T \tag{8}$$

Where N can be divided by M .

$$x_{i1} = \left[x_1\left((i-1)\frac{M}{N}+1\right), x_1\left((i-1)\frac{M}{N}+2\right), ..., x_1\left((i)\frac{M}{N}\right)\right]^{\mathrm{T}}, \ i = 1,2,...,N \tag{9}$$

Thus, the unknown signal x_1 is divided into N segments evenly, within the time-frequency plane is represented by Wigner-Ville distribution

$$W_{1i}(t,f) = \int x_{1i}(t+\frac{\tau}{2}) x_{1i}^*(t-\frac{\tau}{2}) e^{-j2\pi f\tau} d\tau, \ i = 1,2,...,N \tag{10}$$

Described in the previous section using the dimensionless normalized parameter estimation method, each signal can be approximated as a linear FM signal, the initial frequency of f_0, chirp rate μ_0. Thus, the segment of unknown chirp signal is approximately expressed as a form of formula (11) shown as follow.

$$x_{2i}(t) = \exp[j(\varphi_0 + 2\pi f_0 t + \pi\mu_0 t^2)] \tag{11}$$

2.2 Accumulation of energy detection based on Wigner-Ville distribution

Do Wigner-Ville transform for every segment signal and represented as

$$W_{2i}(t,f) = \int x_{2i}(t+\frac{\tau}{2}) x_{2i}^*(t-\frac{\tau}{2}) e^{-j2\pi f\tau} d\tau, \ i = 1,2,...,N \tag{12}$$

We use Wigner-Ville distribution to represent signal $x_{2i}(t)$, and then accumulated energy of all the tiny segment signal by using the “mask” method.

$$Y_i = \sum_f \sum_t W_{1i}(t,f) W_{2i}(t,f), \ i = 1,2,...,N \tag{13}$$

Where Y_i is energy of unknown signal in i th segment. the ”dot product” operation in the “mask” method can retrain noise very well and give prominence to the time-frequency distribution characters of the signal. For the new time-frequency distribution, it accumulates energy of all the N segments. As a inspection statistical variable, its computation formula is shown as

$$Y = \sum_{i=1}^{N} Y_i \tag{14}$$

3 Simulation and result analysis

In this section, we do FRFT for the unknown parameters nonlinear frequency modulated signal, and compute it by dividing it into N parts.

If the signal is separated by eight segments, the SNR is -5dB. We assume each segment of the nonlinear frequency modulated is Chirp signal, and it is restrained in range of $[-63/1024, 63/1024]$ according to discrete dimensionless scaling normalization method, the sample frequency is 512Hz, and length of noise is 512 equally. According to formula (4), we can calculate that the normalization scale factor is equal to $\sqrt{63}/512$ .Thus, we do FRFT for the sum of signal and noise in all the order in range of $[0,2]$ by the step of $1/180$ and searching the peak and its coordinate, then, estimate signal parameters according to the relationship between chirp rate, center frequency, FRFT order and the position of FRFT domain as shown is formula (6). This is the approximate expression of nonlinear frequency modulated signal by using chirp signal parameters estimation. Finally, we can find out performance of the method by comparing the original signal with the approximate expressing chirp signal, and it is shown in figure 1.

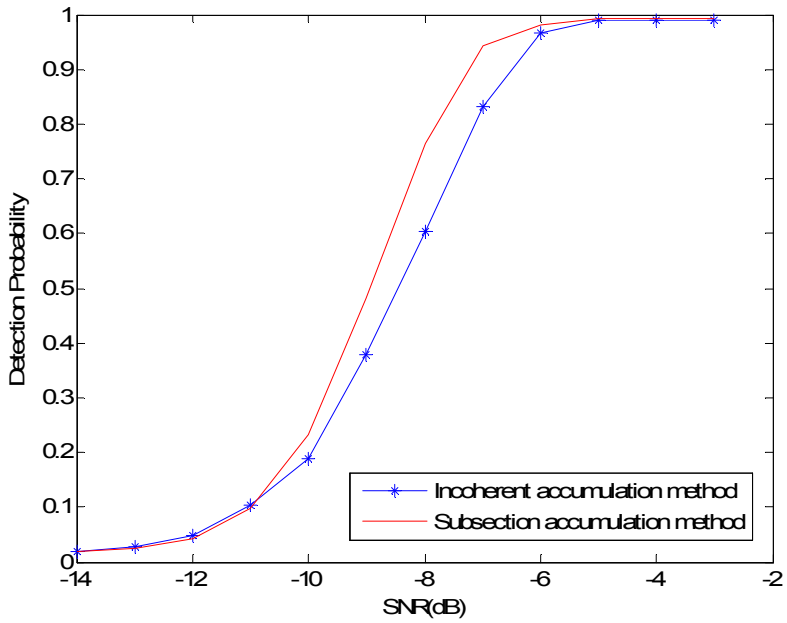

Fig1 Two nonlinear frequency modulated signal detection Probability curves

Summary

We present nonlinear frequency modulated signal detection method based on time-frequency analysis technique of parameters estimation by using FRFT in this paper. Piecewise parameter estimation method can be used in the piecewise linear approximation of nonlinear FM signal FM signal frequency curves. Based on the energy distribution and the resulting characteristics of the new mask, the unknown signal can be applied with a noise detection process, thus, it can improve the detection performance.

References

[1] McBride A C, Kerr F H. On Namias' fractional Fourier Transform [J]. IMA J Appl Math, 1987, 39:159-175.

[2] Ozaktas H. M, Kutay M. A, Bozdagi G. Digital computation of the fractional Fourier transform [J]. IEEE Transactions on Signal Processing.1996, 44(9):2141-2150.

[3] Chris Capus, Keith Brown. Short-time Fractional Fourier Methods for the Time-frequency Representation of Chirp Signals[J]. Acoustical society of America, 2003, 113(6):3253-3263.

[4] Qi L, Tao R, Zhou S Y, et al. Detection and parameter estimation of multi-component LFM signal based on the fractional Fourier transform [J]. Science in China, Ser F, 2004, 47(2):184-198.

Advanced Materials Research Vols. 989-994 (2014) pp 4046-4049
© (2014) Trans Tech Publications, Switzerland
doi:10.4028/www.scientific.net/AMR.989-994.4046

Detection of Chirp Signal with Time-varying Amplitude Based on FRFT

Wu Yanjun[1, a], Li Renlong[1,a] and Wang Xiao[1,a]

[1]China Satellite Maritime Tracking and Control Department, China

[a]348237548@sina.com

Keywords: Parameter estimation; fractional Fourier transform; chirp signal

Abstract. The general method time-varying amplitude linear FM signal parameter estimation, the proposed parameter fractional Fourier transform for time-varying estimates of the magnitude of the chirp signal, and the related issues of a more in-depth research. Study the time-varying amplitude of the initial phase chirp signal, the initial angular frequency, modulation frequency and amplitude information extraction and estimation methods, and the magnitude of the Gaussian function varies with the magnitude of random variation and chirp signal for the object properties (parameters on parameter estimation estimate the mean square error) were simulated.

Introduction

The fractional Fourier transform (FRFT) for linear FM (Linear Frequency Modulation, LFM, or Chirp) signal detection and parameter estimation in the past two years has attracted more and more attention. The literature [1-2] first studied the fractional Fourier transform in SAR radar moving target detection and imaging applications; The literature [3-4] The fractional Fourier transform is applied to spread spectrum communications broadband interference suppression and achieved good results; The literature [5] specifically studied the detection and parameter estimation based on fractional Fourier transform LFM signal, and gives a detailed performance analysis.

However, these studies are under constant signal amplitude of the fundamental hypothesis of unfolding. In fact time-varying amplitude chirp signal has a broader application background in engineering practice. In actual signal processing, the signal amplitude due to fading or other reasons not remain constant. For example, in mobile communication applications, a Gaussian minimum shift keying signal to band limit the radiated power of the base band signal generated Gaussian pulse, rather than a general rectangular wave, is a time-varying amplitude of the chirp signal. A class of radar echo signal detection system may be affected by two factors: the relative movement between the target and the receiver is Doppler shifted, the target range of the reaction medium, or scattered signal will be distorted, and therefore, echo signal is actually a time-varying amplitude of the linear FM signal, in addition, also in the presence of signal interference during transmission and recording modulation, such as the modulation caused by ionosphere domino offset in shortwave communication and civic electricity interference when a electrocardiograph is recording cordis electricity signal. All these cases show that when using variable amplitude chirp signal as engineering analysis model is more practical significance.

1 The main proposed methods of AM-FM signal detection and parameter estimation

Time-varying amplitude linear FM signal is actually an AM-FM (AM-FM) signal, its theory and methods for parameter estimation method usually include energy separation based Cyclostationarity methods and methods based on differential equations. Essence of the energy separation is to define a nonlinear signal operator (energy operator), it acts on the AM-FM signal, resulting in the energy function of the signal, they are used to the instantaneous amplitude and instantaneous frequency of the signal is estimated in the literature gives a statistic energy function additive noise. This method requires the use of discrete-time Teager-Kaiser energy function of AM and FM information in discrete time AM-FM signal is extracted, and the corresponding filter Group to digital implementation, which is a problem to be solved，furthermore, this method is just suit for single component.

Cyclostationary polynomial method is the use of reduced-order thinking, the polynomial phase signal (AM-FM signal) in the time domain with time-varying amplitude harmonic process becomes lag (A domain) with a time constant amplitude, so you can use solving harmonic retrieval method to get "harmonic amplitude", thus further AM-FM signal to make estimates. However, this method under consideration in the case of additive noise, modeling the signal is more complex, multi-component signal is even more difficult to operate.

In contrast, the method of difference equations can be used for multi-component AM-FM signal analysis. It is an AM-FM signal using a differential equation to describe, if the initial value of the differential equation pole coefficient and the characteristic equation can be informed, then the instantaneous frequency and instantaneous amplitude of the signal can be calculated. In practice, however, is not usually possible to know in advance the coefficient of difference equations. There are methods used to estimate the coefficients of the differential equation, but the application of it is very complicated.

Fractional Fourier transform is considered to be a time-frequency analysis method for the analysis of certain non-stationary signals (like LFM signal) has a very good performance, especially in that it has a linear characteristic can be easily used for multi-component LFM signal detection and parameter estimation, without cross-interference term, have been used constant amplitude chirp signals, and achieved good results. However, in many engineering applications, the use of time-varying amplitude LFM signal as a model more in line with actual engineering. Therefore, this work on the basis of this estimation problem revolves around some useful attempts were made based on the detection and parameter fractional Fourier transform variable amplitude chirp signal.

2 Time-varying amplitude chirp signal detection and estimation based on FRFT

The concept of fractional Fourier transform was first proposed by the V Namias, it can be comprehended as the generalized Fourier transform, and it can be interpreted as a signal of the axes in the time-frequency plane rotated counterclockwise about the origin as well. If the signal is an integer multiple of the rotation understood as a Fourier transform to the signal $x(t)$ from the time axis (time domain) counterclockwise rotation angle $\pi/2$ to the frequency axis (frequency domain), thus, is understood to mean any angle α except for integral times of $\pi/2$ FRFT obtained in the fractional Fourier domain (domain u) representation. It is defined as

$$X_p(u) = \{F^p[x(t)]\}(u) = \int_{-\infty}^{+\infty} x(t)K_p(t,u)dt \tag{1}$$

Where $K_p(t,u)$ is kernel function of FRFT, which is expressed as

$$K_p(t,u) = \begin{cases} \sqrt{\dfrac{1-j\cot\alpha}{2\pi}}\exp\left(j\dfrac{t2+u2}{2}\cot\alpha - jut\csc\alpha\right) & \alpha \neq n\pi \\ \delta(t-u) & \alpha=2\mathrm{n}\pi \\ \delta(t+u) & \alpha=2(n+1)\pi \end{cases} \tag{2}$$

Where p is the FRFT order, α is rotational angle and $\alpha = p\pi/2$.

A single component chirp signal with time-varying amplitude polluted by noise can be expressed as

$$\begin{aligned} x(t) &= s(t) + w(t) \\ &= a(t)\exp(j\varphi_0 + j2\pi f_0 t + j\pi\mu_0 t^2) + w(t), \ -T/2 \le t \le T/2 \end{aligned} \tag{3}$$

Where, $a(t)$ is a function of time, φ_0 , f_0 , and μ_0 is unknown initial phase, initial frequency and chirp rate of the chirp signal, E is an unknown parameter, $w(t)$ is the additive white Gaussian noise.

Wigner-Ville distribution of signal is considered to be the distribution of energy in the whole plane of the signal, which is defined as:

$$W(t,f)=\int x(t+\frac{\tau}{2})x^{*}(t-\frac{\tau}{2})e^{-j2\pi f\tau}d\tau \tag{3}$$

According to its edge characteristics, we known that the projection of WVD on the time axis represents the instantaneous energy $|x(t)|^2$ of signal, the projection on frequency axis represents the spectral density $|X(\omega)|^2$ of signal. As we extend the definition of signal into FRFT domain, then, we can get the projection of WVD in the u axis as:

$$P(u,\alpha)=\int_{L}W(t,f)dv \tag{4}$$

Where L is a straight line perpendicular with FRFT domain u , and it can be expressed as $f=kt+b$, $k=-\cot\alpha$, $b=u\csc\alpha$, and substituting it into formula (4) ,then we can get:

$$P(u,\alpha)=\int_{L}W(t,f)\int_{-\infty}^{+\infty}\delta(u'-u)dv'du'=\frac{1}{|\sin\alpha|}\left|\int x(t)e^{j2\pi(ut\csc\alpha+\frac{1}{2}t^2\cot\alpha)}dt\right|^2 \tag{5}$$

The square module for FRFT of the signal is

$$|X_p(u)|^2=|A_\alpha|^2\cdot\left|e^{ju^2\cot\alpha}\right|^2\cdot\left|\int x(t)e^{-j(ut\csc\alpha+\frac{1}{2}t^2\cot\alpha)}dt\right|^2=\frac{1}{|\sin\alpha|}\left|\int x(t)\cdot e^{-j(ut\csc\alpha+\frac{1}{2}t^2\cot\alpha)}dt\right|^2,\ \alpha\neq n\pi \tag{6}$$

Therefore, the projection of signal's WVD in FRFT domain is equals to module square of the signal's FRFT. When the signal is a chirp signal, it presents an oblique line dorsal fin distribution of its WVD in WVD plane. Chirp signal can generate energy concentration phenomenon only in the FRFT domain which is plumb with its time-frequency distribution. However, the white noise energy is evenly distributed over the entire time-frequency plane, and it will not gather energy in any FRFT domain as well.

With this obvious character, we can achieve the formula of chirp signal detection and parameter estimation as

$$\begin{cases}\hat{\mu}_0=-\cot\hat{\alpha}_0\\ \hat{f}_0=\hat{\mu}_0\csc\hat{\alpha}_0\\ \hat{\varphi}_0=\arg\left[\dfrac{X_{\hat{\alpha}_0}(\hat{u}_0)}{A_{\hat{\alpha}_0}e^{j\pi\hat{u}_0^2\cot\hat{\alpha}_0}}\right]\\ A_{\hat{\alpha}_0}=\sqrt{\dfrac{1-j\cot\hat{\alpha}_0}{2\pi}}\end{cases} \tag{7}$$

Where $\hat{\mu}_0$, $\hat{f}_0$, $\hat{\varphi}_0$ is the estimation value of μ_0 , f_0 and φ_0 respectively, and the estimated amplitude expression of chirp signal is shown as

$$\hat{a}(t)=\mathrm{Re}\left\{x(t)\cdot\exp[-j(\hat{\varphi}_0+2\pi\hat{f}_0t+\pi\hat{\mu}_0t^2)]\right\} \tag{8}$$

3 Simulation

In order to investigate the performance of parameter estimation, this gives the above algorithm Monte Carlo simulation. Simulation experiments were investigated using FRFT random variation of the amplitude and the chirp signal parameters change according to the law of the Gaussian function estimation performance, and were compared with constant amplitude, signal model is:

$$x(t)=a(t)\exp(j0.1t+j0.01t^2)+w(t) \tag{9}$$

Where $w(t)$ is additive white noise with zero mean, $a(t)$ is the amplitude of the signal.

The setting SNR range is from -2dB to 24dB, and the step is 2dB. We do 100 times Monte Carlo simulation, the mean square error curves of the estimated chirp rate value and the estimated initial frequency value (MSE(μ_0) and MSE(f_0))are shown in figure 1.

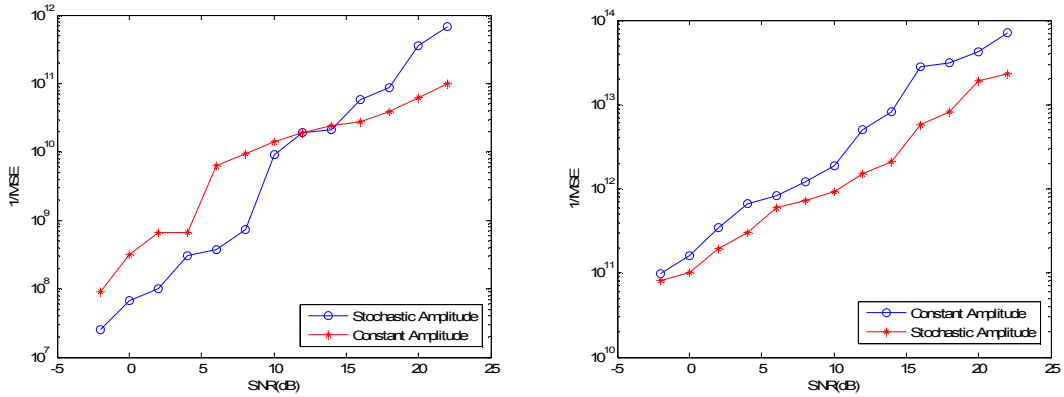

Fig1 Mean square error curves under different amplitude conditions of initial frequency and chirp rate

4 Results analysis

Simulation results from the foregoing, it can be seen: () a detection accuracy (both Reciprocal square error) with improved signal to noise ratio increases, indicating that changes in trend Potential is reasonable, FRFT can be used for time-varying amplitude linear FM signal Detection and parameter estimation. (2) the magnitude of random variation detection signal Compared with constant amplitude accuracy declined. This may be due to the amplitude Changes make signal changes in the spectral structure rather FRFD guide Cause. Inspection (3) the magnitude of change with Gaussian linear FM signal Compared with constant amplitude measurement accuracy declined, but with the amplitude attenuation factor Sub a, the increase is reduced. This is probably because the increase of al, The signal in the time domain is equivalent to the support area narrowed in the fractional Fourier Domain broadening, energy aggregation caused by deterioration.

5 Summary

This paper analyzes the general method of time-varying parameter estimates of the magnitude of the chirp signal, and then based on the parameters FRFT varying estimates of the magnitude of the problem of linear FM signal for a more in-depth research, study the detection and parameter estimation method to the results of the simulation parameter estimation performance, parameter changes and the magnitude of random Gaussian function varies with the chirp signal estimation mean square error. Theory and simulation show that, FRFT for the detection of varying amplitude linear FM signal is a convenient and effective tool.

6 References

[1] Sun Hong-bo, Liu Guo-sui. Application of the fractional Fourier transform to moving target in airborne SAR [J]. IEEE Transform on Aerospace and Electrnic Systems, 2002, 38(4):142-146.
[2] Olacy A. Broadband interference excision in spread spectrum communication systems via fractional Fourier transform [J]. Conference record of the Asilomar conference on Signals, Systems and Computer, 1998, 1:832-837.
[3] Qi Lin, Tao Ran, Zhou Siyong,et.al. Detection and parameter estimation of multicomponent LFM signal based on the fractional Fourier transform [J]. Science in China: ser.F, Information Science, 2004, 47(2):184-198.
[4] Bovik A C, Maragos P, Quatieri T F. AM-FM energy detection and separation in noise using multiband energy operators [J]. IEEE Trans. Sp, 1993,43: 3245-3265.
[5] Kayhan A S. Difference equation representation of chirp signals and instantaneous frequency hskip-0.1cm/amplitude estimation [J]. IEEE Trans. SP, 1996, 44:2948-2958.

Advanced Materials Research Vols. 989-994 (2014) pp 4050-4053
© (2014) Trans Tech Publications, Switzerland
doi:10.4028/www.scientific.net/AMR.989-994.4050

Analysis on Ranging and Velocity Measurement Performance of DS/FH Hybrid Spread Spectrum Signal

Wu Yanjun[1, a], Yao Xuelu[1,a] and Xia Jiang[1,a]
[1]China Satellite Maritime Tracking and Control Department, China
[a]348237548@sina.com

Keywords: DS/FH hybrid spread spectrum signal, interference, measurement performance

Abstract. The measurement performance with the interference is presented with the new DS/FH hybrid spread spectrum signal system. The DS/FH system model is established. The change of the SNR ratio is obtained by analyzing the characteristics of three kinds of interference signal such as partial-band noise jamming(PBNJ), wide-band noise jamming(WBNJ) and additive white Gaussian noise(AWGN). Then the ranging and velocity measurement performance is got through the simulation.

Introduction

With the continuous development of interference, the challenge facing the monitoring system is also growing [1-2]. It is a vital topic of ensure effective monitoring and control in harsh interference environments, which will be the future development trend of monitoring system. The proposed DS/FH hybrid spread spectrum monitoring system is to solve the interference in harsh conditions and effective monitoring and control [3-4]. It combines the advantages of DS and FH spread in two ways, capable of making the measurement and control system has a strong anti-jamming and interception capabilities.

1 System model

Send and receiver DS / FH hybrid spread spectrum system block diagram shown in Figure 1 and Figure 2, BPSK modulation input information, and then to DS and FH spread spectrum spreading processing. At the receiver, the transmitted signal by the blocking of broadband interference effects of partial-band interference and white Gaussian noise. Despreading processing of the useful signal is equivalent to the process of the interference signal and a Gaussian white noise FH and DS spreading.

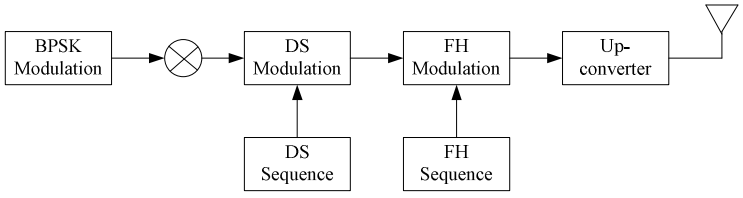

Fig1 Sending signal schematic diagram of DS/FH Hybrid Spread Spectrum Systems

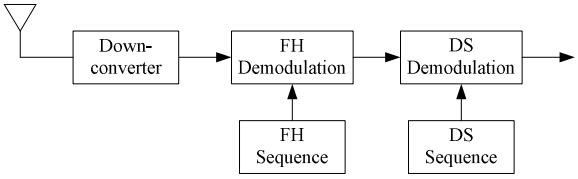

Fig2 Receiver block diagram of DS/FH hybrid spread spectrum system

2 SNR analysis

The signal jump after de-spreading and demodulating hopping process, the l th interval of the frequency hopping of the received signal after processed can be described as [5]:

$$r_l(t) = s_i(t) + n_l(t) + j_{\omega l}(t) + j_{pl}(t),\ (l-1)T_h \le t \le lT_h \tag{1}$$

$s(t)$ is the useful signal, $n_1(t)$ to be processed after the AWGN (White Gaussian Noise) signal, $j_{\omega l}(t)$ to be processed after the blocking wideband interference, $j_{pl}(t)$ is carried out after processing the sub-band interference. The useful signal is represented as:

$$s_i(t) = \sqrt{2E_b R_b}\cos(2\pi f_0 t + j\pi),\ j = 0,1 \tag{2}$$

E_b is the bit energy, f_0 is the frequency of the baseband useful signal. Due to the characteristics of the PN sequence spread spectrum signal, and therefore it does not produce anything during the time of the spreading influence of AWGN, so $n_1(t)$ can be considered zero mean and power spectral density N_0(W/ Hz). For broadband obstruction interference, assuming that its energy is J, the RF signal bandwidth of W_{ss}, you can think of it as a mean of 0, the power spectral density of $N_J = J / W_{ss}(W / Hz)$, for some band interference, assuming that the ratio of the interference band is $\eta = W_J / W_{ss}$, then it can be considered mean 0, power spectral density $N_J' = J / (W_J) = (J / W_{ss}) \cdot (W_{ss} / W_J) = N_J / \eta\ (W / Hz)$, Since the DS/FH hybrid spread spectrum system itself anti-jamming performance, so the baseband interference power output is reduced G_p times, so broadband blocking interference power spectral density after treatment for $N_{WJ} = J / (W_{ss} G_p) = N_J / G_P (W / Hz)$, part of the deal after the band interference power spectral density $N_{Pl} = N_J / (\eta G_p)\ (W / Hz)$, suppose that the parameters a, when $a = 1$, said first l hop interference, whereas when $a = 0$ is not disturbed. In summary, the equivalent system after processing the interference power spectral density is:

$$N_J = N_0 = \frac{N_J}{G_P} + a_l \frac{N_J}{\eta G_P},\ l = 1,2,...,L \tag{3}$$

So, we get the carrier to noise ratio of the system is

$$\frac{C}{N_0} = \frac{2E_b}{\frac{1}{L}\sum_{l=1}^{L} N_l} = \frac{2E_b}{N_0} \cdot \frac{1}{1 + \frac{JNR}{G_P} + \frac{k}{L}\frac{JNR}{G_P \eta}} \tag{4}$$

Where, $JNR = N_J / N_0$, a total of k jump is affected.

3 Ranging speed performance analysis

In order to determine the performance of different measurement loops must be analyzed carrier tracking loop (PLL) and delay locked loop tracking code (DLL) tracking performance. Since the receiver is nonlinear, the Monte Carlo simulator can be used to determine the circumstances under various stress factors expected to track the performance of the receiver, you can also determine the code and carrier tracking performance through a number of rules of thumb. We use rules of thumb to determine the spreading code and carrier tracking performance.

3.1 carrier tracking loop

Analysis of frequency locked loop with phase-locked loop, like locked loop can be directly read out copy of the carrier frequency, and thus deduce the receiver Doppler shift. PLL and the like, the total phase locked loop jitter variance are $\sigma_i = \sqrt{\sigma_{tFLL}^2 + \sigma_V^2 + \sigma_A^2}$, σ_{tLL} caused by the thermal noise of the frequency jitter. σ_V and σ_A are dynamic stress error, frequency error because the dynamic stresses induced jitter is relatively small, so the actual analysis time can be negligible.

Consider the tracking error of the measurement accuracy under the influence, regardless of each order loop, the loop order of the thermal noise, thermal noise variance are:

$$\sigma_{tFLL} = \frac{1}{2\pi T_{coh}}\left[\frac{4FB_L}{C/N_0}\left(1 + \frac{1}{T_{coh} C/N_0}\right)\right]^{1/2} \tag{5}$$

Where, B_L is loop bandwidth, C/N_0 is the carrier to noise ratio, T_{coh} is pre integral time, where the parameter F is set to 1, when C/N_0 is a higher value, otherwise F is set as 2.

Setting $F=1$, and then substituting formula(4) into formula (5), we can get:

$$\sigma_{tFLL}=\frac{1}{2\pi T_{coh}}\left[\frac{4FB_L}{C/N_0}(1+\frac{1}{T_{coh}C/N_0})\right]^{1/2}=\frac{1}{2\pi T_{coh}}\left[\frac{4B_L(1+\frac{JNR}{G_P}+\frac{k}{L}\frac{JNR}{G_P\eta})}{\frac{2E_b}{N_0}}\left(1+\frac{1+\frac{JNR}{G_P}+\frac{k}{L}\frac{JNR}{G_P\eta}}{T_{coh}\frac{2E_b}{N_0}}\right)\right]^{1/2} \quad (6)$$

Taken during the simulation loop bandwidth of 18 Hz, it can be deduced by the foregoing, the frequency curve of the jitter variance were affected to the number k of the frequency hopping shown in Figure 3.

As the carrier measurement accuracy can reach $\Delta f=\sigma_{tFLL}/T$, T is the Doppler integration period, then the velocity measurement accuracy is

$$\Delta v=\Delta f/f_0\cdot c=\frac{\sigma_{tFLL}\cdot c}{T\cdot f_0} \quad (7)$$

So we can know that when the carrier frequency f_0 is a certain number, the speed accuracy changes with σ_{tFLL}, and it is shown in Figure 3.

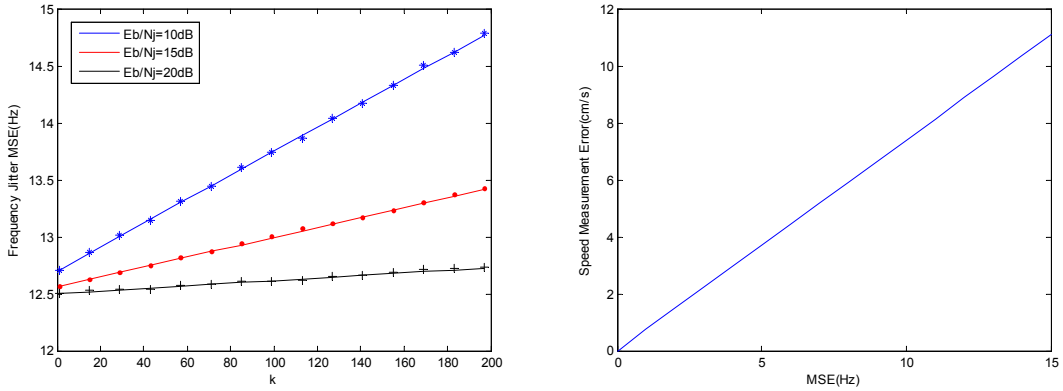

Fig3 Relationship between MSE of FLL tracking jitter variance with k and speed accuracy jitter respectively

3.2 Yards tracking delay locked loop

Receiver capture DS/FH signal, the received signal and the PN code is not fully aligned with the local code reproduced, it is necessary to further track DS/FH signal. And frequency-locked loop as an error code rings caused mainly by the thermal noise code phase jitter and dynamic stress error in two parts, regardless of the circumstances under dynamic stress of thermal noise tracking error jitter as

$$\sigma_{tDLL}=\left[\frac{dB_L}{2C/N_0}\left(1+\frac{1}{T_{coh}C/N_0}\right)\right]^{1/2} \quad (8)$$

Where, B_L is the loop bandwidth, C/N_0 is ratio of the carrier to noise, T_{coh} is pre integral time, D is the space between the former correlator with the later (generally taken to be 1).

As the same processing as the above, we can get:

$$\sigma_{tFLL}=\left[\frac{dB_L}{2C/N_0}(1+\frac{1}{T_{coh}C/N_0})\right]^{1/2}=\left[\frac{B_L(1+\frac{JNR}{G_P}+\frac{k}{L}\frac{JNR}{G_P\eta})}{\frac{4E_b}{N_0}}\left(1+\frac{1+\frac{JNR}{G_P}+\frac{k}{L}\frac{JNR}{G_P\eta}}{T_{coh}\frac{2E_b}{N_0}}\right)\right]^{1/2} \quad (9)$$

Similarly, the loop bandwidth is taken during simulation of 18Hz, the jitter can be obtained curves are affected by the variance of the number k of the frequency hopping shown in Figure 4.

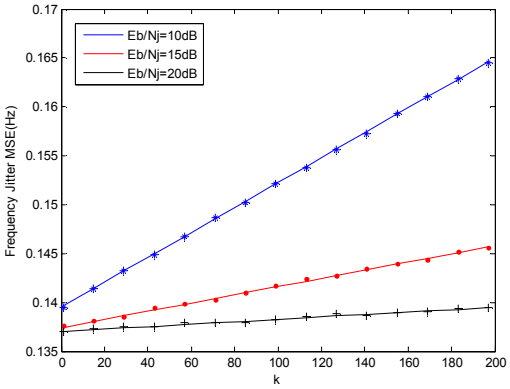

Fig4 Relationship with delay interval, code sequence and likelihood value

Chip tracking accuracy can be achieved $\Delta\tau = \frac{\sigma_{tDLL} \cdot T_c}{180^\circ}$, T_c is a chip period, the accuracy of distance measurements is

$$\Delta s = \Delta\tau \cdot c = \frac{\sigma_{tDLL} \cdot T_c \cdot c}{\pi} \tag{10}$$

So you can learn at the carrier frequency f_0 certain circumstances, with the change of σ_{tFLL}, the speed accuracy is also followed changes in trends and a similar effect on the measurement precision σ_{tFLL} is generated.

Summary

In this paper, the DS/FH hybrid spread spectrum signal speed ranging performance under interference conditions, through theoretical analysis and simulation shows that under the new system, and DLL FLL tracking loop jitter variance with both the number of interference by hopping points characteristics change, but also analyzes the impact velocity tracking jitter variance ranging performance are generated. After further study of DS / FH hybrid spread spectrum signal provides a foundation in the Satellite Control System.

References

[1] Yang Wen-ge, WEN Yi-jun, MENG Sheng-yun, et al. Performance Analysis of a kind of DS/FH Hybrid Spread Spectrum Signal For telemetry [J]. Telecommunication Engineering, 2009,1(49):13-17.

[2] NOVELLO R. The Korea sat 5 Secure Communication System: Design, Development & Performance[C]//Big Sky-2006, 2006: 99-102.

[3] CHERBINI G, MILSTENIN L B. Performance Analysis of Both Hybrid and Frequency-hopped Phase-coherent Spread spectrum System Part I: A hybrid DS/FH system [j]. IEEE Trans. Commun. 1989(37):600-611.

[4] CHERUBINI G, MILSTEIN L B. Performance Analysis of Both Hybrid and Frequency-hopped Phase-coherent Spread specTrum Systems Part II: An FH system [J]. IEEE Trans. Commun. 1989(37) : 612-622.

[5] SIMON M K, Polydoros A. Coherent Detection of Frequency Hopped Quadrature Modulations in the Presence of Jamming-Part: QPSK and QASK Modulations [J]. IEEE Trans. Commun, 1981(2): 1644-1660.

Advanced Materials Research Vols. 989-994 (2014) pp 4054-4057
© (2014) Trans Tech Publications, Switzerland
doi:10.4028/www.scientific.net/AMR.989-994.4054

Research of Image Denoising Method about Wavelet Transform with Neighborhood Average

Chen Huang

Department of Electrical Engineering, Guidaojiaotong Polytechnic Institute, Shenyang 110023, China

Email: huangchen054@163.com

Keywords: Wavelet transform, Neighborhood average filtering, Image denoising

Abstract. Because wavelet transform has good time-frequency characteristics, and its application in image denoising has been promising. Firstly, use the threshold method of the wavelet transform is used in removing image noise, and then the denoised image is smoothed using neighborhood average filtering with Gauss template. And wavelet denoising process and domain threshold selection principle are discussed. Simulation results show that this method can effectively reduce the noise and can remain most of image details better.

Introduction

The image denoising is very important for image processing, and the whole process of image with noise affects the image processing of the input, collection, processing and the output of the results. If there is too more input noise, the process and output results will be inevitably affected. So it is necessary to remove the image noise, lower noise affect, improve signal -noise ration.

Wavelet method characteristic has high frequency resolution and low time resolution in the low frequency part and has high time resolution and low frequency resolution in the high frequency part. Wavelet transform technique has unique time-frequency localization characteristic, so it has obvious advantages over the traditional denoising in discerning noise signal and image noise and effectively removing the noise and retaining useful information. It is well known that the wavelet denoising is superior. At the same time, wavelet denoising has certain limitations, and the better result can be obtained by neighborhood average filter to eliminate the sharp sense of denoised image.

Wavelet transform denoising principle

It is one of important applications that two-dimensional signal denoising for wavelet transform. The image is one kind of two-dimensional (2D) signal, and 2D multi-resolution is similar to one-dimensional signal. However, let the 2D space function be $L^2(R)$， and the scale function be $\varphi(x,y)$.

Let $\{V_j\}_{j\in Z}$ is a multi-resolution analysis of $\{V_j\}_{j\in Z}$, then it can be shown that tensor space $\{V_j^2\}_{j\in Z}$: $V_j^2 = V_j \oplus V_j$ compose a multi-resolution analysis of $L^2(R*R)$, Two dimensional scaling function $\varphi(x,y)$ is:

$$\varphi(x,y) = \varphi(x)\varphi(y) \tag{1}$$

Equation (1) shows the separability of two-dimensional scaling function. For each $j \in Z$, Function system $\{\varphi_{j,n,m}(x,y) = \varphi_{j,n}(x)\varphi_{j,m}(y) \,|\, (n,m) \in Z^2\}$, it constructs orthonormal basis.

$$\varphi_{j,n,m}(x,y) = 2^j \varphi(x - 2^j n)\varphi(y - 2^j m), (j \geq 0) \tag{2}$$

If $\psi(x)$ is one dimensional multi resolution analysis, the three wavelet function for two-dimensional multi-resolution analysis is formulated as follows:

$$\psi^1(x,y)=\varphi(x)\psi(y)$$
$$\psi^2(x,y)=\psi(x)\varphi(y) \quad (3)$$
$$\psi^3(x,y)=\psi(x)\psi(y)$$

Where $\psi(x)$ and $\psi(y)$ are $\varphi(x)$ and $\varphi(y)$ corresponding orthogonal wavelet functions respectively.

For each $j\in Z$, the integer translation system as follows:

$$\psi^1{}_{j,n,m}(x,y)=\varphi_{j,n}(x)\psi_{j,m}(y)$$
$$\psi^2{}_{j,n,m}(x,y)=\psi_{j,n}(x)\varphi_{j,m}(y) \quad (4)$$
$$\psi^3{}_{j,n,m}(x,y)=\psi_{j,n}(x)\psi_{j,m}(y)$$

Function system $\{\psi^{\varepsilon}{}_{j,n,m}(x,y)\}=\{2^j\psi^{\varepsilon}(x-2^jn,y-2^jm\}$, $j\geq 0,\varepsilon=1,2,3$ is $L^2(R*R)$ orthonormal basis, ε =1,2,3 is corresponding to three directions in the horizontal, vertical and diagonal.

For a two-dimensional image signal $f(x,y)\in L^2(R*R)$, in resolution 2^{-j} conditions, there is the following equation:

$$D^1{}_jf=\left\langle f(x,y),\psi^1{}_{j,n,m}(x,y)\right\rangle,(n,m)\in Z^2$$
$$D^2{}_jf=\left\langle f(x,y),\psi^2{}_{j,n,m}(x,y)\right\rangle,(n,m)\in Z^2 \quad (5)$$
$$D^3{}_jf=\left\langle f(x,y),\psi^3{}_{j,n,m}(x,y)\right\rangle,(n,m)\in Z^2$$

Wavelet threshold method is classical and general. The basic idea of wavelet threshold denoising is as follows:

(1) The signal $f(k)$ with noise is disposed with wavelet transform, and a set of wavelet coefficients $W_{j,k}$ are obtained;

(2) With the threshold processing for $W_{j,k}$, the estimated coefficient $\hat{W}_{j,k}$ is got to make the difference between $W_{j,k}$ and $\hat{W}_{j,k}$ be as small as possible;

(3) Using $\hat{W}_{j,k}$ wavelet reconstruction, we can get the estimation signal $f(k)$, which is the denoising signal.

Neighborhood average filtering

Neighborhood average method is a kind of image smoothing method using Box templates for the operation of the image, and Box template is a template in which all coefficients are the same values of the template. The template commonly used 3 × 3 template or 5 × 5 template. Box template does average processing for the current pixel and its neighboring pixels, so that it can filter out more noise in the image. The idea of smoothing template is based on that averaging one point and the 8 points around the point, thereby removing the sudden changes and filtering out the noise. As shown in Equation (6), let $f(i,j)$ be a given noisy image and $g(i,j)$ be the renoised image after neighborhood average filtering.

$$g(i,j)=\frac{\sum f(i,j)}{N},(i,j)\in M \quad (6)$$

Where M is the coordinate of the adjacent pixels in the neighborhood and N is the number of adjacent pixels contained in the neighborhood.

However, the image has a certain degree of ambiguity. While considering the points in the neighborhood, do not consider the impact of the 9 points location, and smoothing effect is not ideal. In fact we can introduce weighted coefficient, and form the new template called Gauss Template. This template is a common smooth template. This template is obtained by sampling 2 dimensional Gauss function. Use Gauss template to achieve the smoothing effect clearly. Therefore, we use the 3 × 3 Gauss template. In order to keep the average value of the smoothing image unchanged, the elements' sum is 1 within this template.

Filtering simulation and analysis

In this paper, MATLAB is used for simulation. Firstly, we could analysis the threshold effect of wavelet transform. Fig. 1 is the original signal and the noisy signal, and Fig.2 is the effect of four threshold methods selected for image denoising. In the process, the hard threshold function is used. As can be seen from Fig. 2, the denoising effect of sqtwolog and heursure is more thoroughly. And because rigrsure and minimaxi threshold rules are very conservative, and the noise cannot be completely removed, but in the high frequency and the weak signal can be separated from noise.

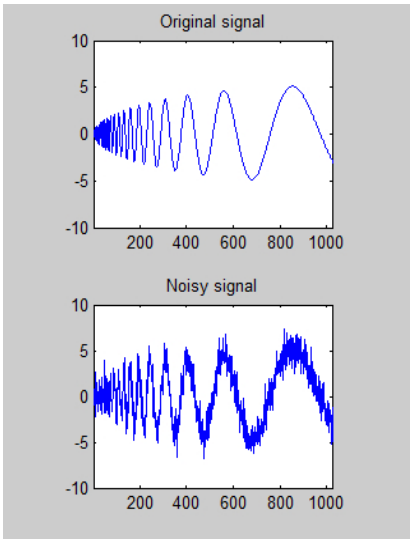

Fig. 1 The original signal and the noisy signal

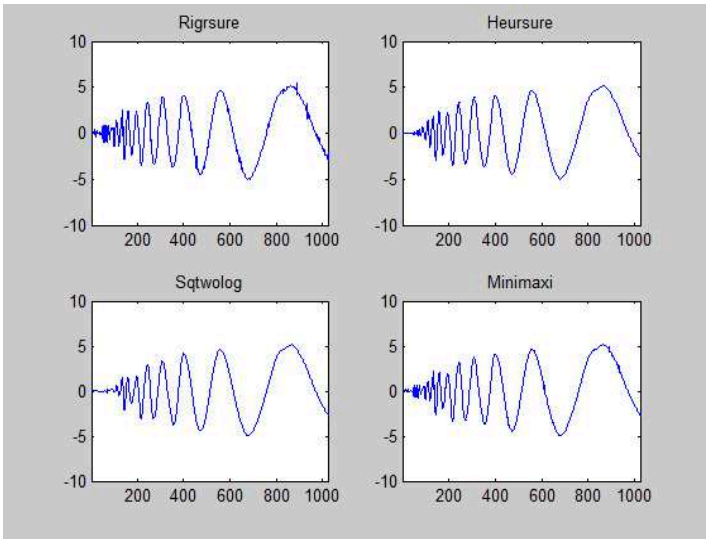

Fig. 2 The four threshold method of wavelet transform

According to the above analysis, in this paper the heursure method of wavelet threshold selection is used to remove the image noise. Choose figure 3 as the simulation object. First, add the random noise to the original image, as illustrated by Fig. 4. Secondly, using wavelet change to remove the image noise, as has been found that the result is not very ideal by Fig. 5.

Fig.3 Original image

Fig.4 Noisy image

Fig.5 Wavelet transform

In the second step, the neighborhood average with Gauss template is used to achieve image smoothing after denoising, and SNR is 30dB, as shown in Fig. 6 (d). At the same time, compare the different combination filtering method, Fig. 6 (a) shows the result of dual wavelet transform, (b)

shows the result of the mean filter and wavelet, (c) shows the result of the Wiener and wavelet, (d) shows the result of the neighborhood average and wavelet. According to Fig. 6, this method in this paper has certain advantages.

(a) (b) (c) (d)

Fig.6 Comparing results of various combination renoising methods

Summary

From the experimental results, the denoising effect of wavelet transform and neighborhood average described in this paper is much better, and it has strong adaptability and it is simple. Use wavelet transform and neighborhood average for denoising and it can maintain some image edge details. But there are still some shortcomings, therefore need further improvement for obtaining better effect.

References

[1] J Weaver. Filtering noise from images with wavelet transform[J]. Magnetic Resonance in Medicine, 1995, 21, 288-295.

[2] Selesnick I W, Baraniuk R G, Kingsbury N G. The dual-tree complex wavelet transform[J].IEEE Trans on Signal Processing,2005,22(6):123-151.

[3] Hu Yaobin, Chen Aihua, Zhang Chunliang Research of denoising technology about wavelet analysis with Wiener filter[J]. Telecommunications for Electric Power System.2006,162(27),42-44.

[4] Li Zhengfei. Image Noise Reduction Based 0n W avelet Transform[J], MECHAN1CAL ENGINEERING & AUT0MAT10N.2008,150(5),32-34.

[5] Peiyan Fei, Baolong Guo. Image denoising based on the dyadic wavelet transform[C]. ICCIMA 2003,9:402-406.

[6] Rafael C. Gonzalez. Digital Image Processing[M]. Publishing House of Electronics Industry, 2006.

[7] Astola J. Fundamentals of nonlinear digital filtering [M]. U.S.A: CRC Press, 1997.

[8] Le Yang. Image enhancement algorithm and its implementation[J], Modern electronic technology, 2008, 30(8): 133-134.

Advanced Materials Research Vols. 989-994 (2014) pp 4058-4061
© (2014) Trans Tech Publications, Switzerland
doi:10.4028/www.scientific.net/AMR.989-994.4058

Application and Debugging of All-digital Frequency Synthesizer

Hanbai Fan, Xian Meng, Junma Hou

North China Electric Power University, Baoding 071003,China

Keywords: SCM, Si4133, frequency synthesizer, Phase-Locked Loop.

Abstract: Presents the working principle of Integrated PLL chip Si4133, this paper presents the implementation of a 375MHz local oscillator for a super heterodyne transmitter/receiver by using Si4133.Using programming method to set the divider register Internal chip. In addition, this paper discuss the methods for decreases the phase noise. Debugging circuit using ICCAVR software , and show the debugging results. Facts show that the phase noise and spurious of the frequency synthesizer is low, and it is practical.

Introduction

Frequency synthesizer is used extremely broad in areas such as communications, radar, measurement and automation control, which has become essential basic components of various electronic devices[1]. With the development of electronic technology to digital direction, it requires digitally method to achieve the signal phase locking, so as to achieve the purpose of generating specific frequency. Traditional Phase-Locked Loop (PLL)is implemented by analog circuit. Digital Phase Locked Loop (DPLL) is high precision and not affected by voltage and temperature, compared to traditional analog circuit PLL. The loop bandwidth and center frequency is programmable .It's easy to build higher-order phase-locked loop. And more then when it is used in digital systems , with no need of A / D and D / A converter[2-4]. With the rapid development of communication technology, integrated circuit technology and system-chip (SOC) in-depth study, all-digital frequency synthesizer is bound to be more widely used.

Si4133 is production of Silicon Laboratories .It is an American company. Si4133 Contains an internal voltage controlled oscillators (VCO), loop filters, phase detectors, frequency dividers and other components. with only a small number of external components, it can constitute a PLL, which is the digital frequency synthesizer core. Figure 1 is the schematic diagram of Si4133. Two RF optimal center frequency of the VCO is between 947MHz ~ 1720MHz and 789MHz ~ 952MHz; IF center frequency of the VCO is 526MHz ~ 952MHz, can be achieved the minimum 62.5MHz by dividing.

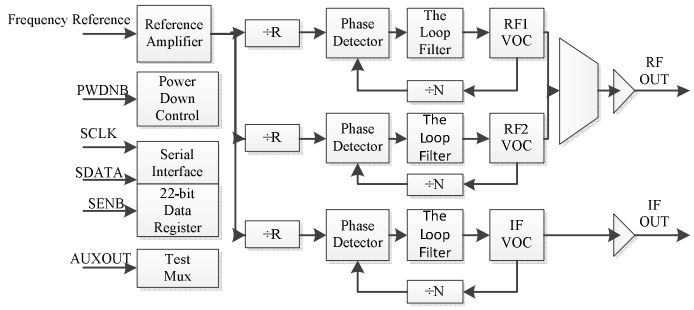

Fig.1 Block diagram of Si4133

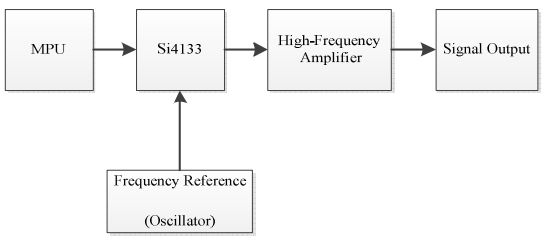

Fig.2 The overall circuit diagram

The chip has been widely used in electronic communications, GSM dual-band mobile phone and so on. This paper is used of Si4133 to design a frequency synthesizer to generate 375MHz frequency, as a super heterodyne transmitter / receiver local oscillator.

The overall design

Figure 2 is the overall circuit block diagram of the frequency synthesizer, the arrows represent flow of signals . We use AVR microcontroller. In this circuit we choose ATmage8. Compared to other 8bit MCU, the AVR has many advantages such as high computing speed, small object code, abundant internal resources, and so on[5]. The using of AVR can greatly improve the efficiency of debugging. AVR microcontroller sends out Control signals, to change the center frequency of the output signal of Si4133; This design uses 12.8MHz active high stability crystal oscillator as frequency reference source; The output signal through the Si4133 IF pin must be coupled to the next stage through a capacitor, that is, a high-frequency amplifier. After signal amplification, the signal can be obtained as the frequency synthesizer output signal. Finally, the signal through an coupling capacitor to the load.

In this frequency synthesizer, we use the Si4133 IF VCO generates a signal of 750MHz, then after frequency divider of the two obtained the 375MHz signal. Figure 3 is the interface circuit of Si4133. The 15 feet XIN connect oscillator frequency input. The 22 feet is the IF output terminal IFOUT.Si4133 via 1 feet SCLK (clock), 2 feet SDATA (data) and 24 feet SEN (Enable) the three pin connect to AVR microcontroller. It is effective when the enable terminal is low. The AVR microcontroller write the Internal registers of Si4133 through serial communication. A bit of data latched at each clock rising edge, and write into registers of Si4133 at falling edge of the clock. The AVR microcontroller writing data from the highest bit of register to the lowest bit of register. It is easy to change the frequency of the output signal. By setting 14 feet PWDN level and control relevant internal registers, you can set the low-power operating mode and choose the circuit that you need to work. The 13 feet AUXOUT can be output signal. When the pin is low , the output frequency is lock-lose. L2 in the Figure is the external inductor for Si4133, which ranges from 2.2nH ~ 12.0nH. It is primarily used to set the center frequency of the VCO output signal.

By the upper, it is can be seen that the digital frequency synthesizer design with Si4133 is easy to operate. Its external circuit is relatively simple. It can easily change the frequency of the output signal. So it is a practical frequency synthesizer.

2 Debugging and Implementation

Set the center frequency of VCO. Si4133 center frequency of the VCO output signal depends on the external connection inductor value. Taking into account the 10% error of an external inductor, Si4133 can be self-adjusting algorithm for compensating inductor error. Because the magnitude of the inductor value is nH, the packaging issues should be considered when determining the inductor value. Figure 4 is VCO connection with an external inductor. L_{PKG} is inside inductor of the package. L_{EXG} is external inductor; L_{LOT} is the sum of external inductance L_{PKG} and package inductance L_{EXG}. Si4133 VCO center frequency is calculated as:

$$f_{CEN} = \frac{1}{2\pi\sqrt{(L_{PKG} + L_{EXT}) \bullet C_{NOM}}} \tag{1}$$

The L_{PKG} of IF VCO is 2.1nH,the C_{NOM} is 6.5pF.We demand the frequency output of the IF VCO is 750MHz. Substituted into the formula (1) calculation shows L_{EXT} = 4.828nH, since the actual ,there is no such exact inductance. We chose the labeled value of 4.7nH wire-wound high Q values inductor, which can be calculated the center frequency is 757MHz.

Si4133 has sixteen 22 bits data registers, which comprises 18 bits data code and the 4 bits address code. registers 0 to 8 are programmable, they are : Main Configuration, Phase Detector Gain, Power Down, RF1 N-Divider, RF2 N-Divider, IF N-Divider, RF1 R-Divider, RF2 R-Divider, IF R-Divider. Register 9 to 15 is reserved. It set the division ratio and the frequency of RF VOC or IF VOC to obtain the final needed frequency. You can control the gain of the phase detector (also called phase sensitive). VCO gain and the LF gain can't set by programming. Unused registers are written to 0x00.

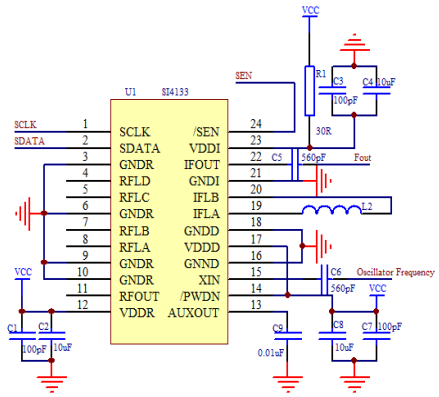

Fig.3 The Interface circuit of Si4133

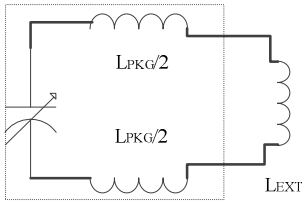

Fig.4 VCO connection with external inductor

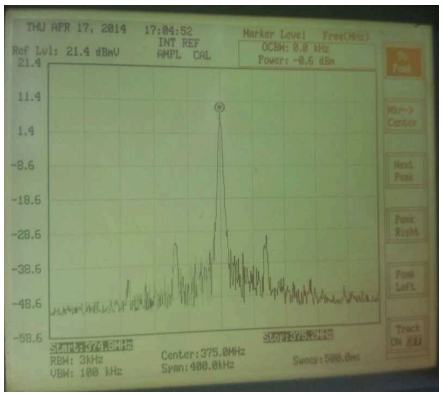

Fig.5 Test result

By setting R-Divider register and N-Divider register resulting output frequency is:

$$f_{OUT} = Nf_{IN} / R \quad (2)$$

f_{OUT} is the frequency output of the VCO. f_{IN} is frequency reference input the XIN pin. The reference frequency signal after R-Divider is f_{IN}/R. The VCO output signal after N-Divider is f_{OUT}/N. The two signals phase comparison in the PD, continuously control and correction, until both phases are identical, then the loop is locked when the output frequency is the setting value.

Tab.1 The set frequency compare with the actual frequency

Set frequency /MHz	The difference from center frequency (757)/MHz	The actual output frequency /MHz
710	-47	708.5562
720	-37	719.9981
730	-27	730.0015
750	-7	750.0013
770	13	769.9983
790	33	789.9978
800	43	798.6782

We use the digital oscilloscope observation frequency synthesizer output signal; the results are shown in Table 1. The set frequency comparison between the actual output frequency. When the center frequency is set to 757MHz, the set frequency is 720MHz, 730MHz, 750MHz, 770MHz, 790MHz, the error of the actual output frequency within ± 2KHz, within an acceptable error range. But in the 710MHz and 800MHz error increased significantly, phase-locked loop lost lock. Visible when setting the value of frequency adjustment doesn't exceed ± 5% of the center frequency, the frequency of output signal is accuracy. When the center frequency is set to 750MHz, it is accuracy, and then divides by 2, we can get an accurate 375MHz output signal.

The debugging of chip lock will come across some troubles ,which are caused by the problems of the parameters of peripheral devices or the Program. We found some rules, for example, the R-Divider register and N-Divider are not designed casually if we want to get the numerical value calculated by the formula (2), sometimes there will be some deviations. So we should choose some more data for testing and observing, and then select a group of optimal value.

The Control of phase noise. When design the PLL frequency synthesizer, we should consider the phase noise of the circuit to achieve the index, and eliminate the effects of phase noise. In general, the phase noise of loop in-band is determined by the noise of phase detector，divider and oscillator，and the out-band phase noise is mainly determined by VCO[6]. For the phase noise of crystal reference source, R divider, phase detector, N divider, their transfer function is low pass form. And for VCO, the phase noise form of transfer function is high-pass form. So the total output

phase noise is the sum of the product of noise source phase noise and their respective transfer function. In addition, we should consider that the loop bandwidth affects the noise within the band of loop a lot. So if the loop bandwidth is too narrow, the within band noise of VCO will not be ignored. But if it too wide, it could cause the deterioration of out-of-band noise.

Against the problem of phase noise, we adopted a series of measures to control .First of all, we choose a 12.8 MHz active TCXO as frequency reference source, whose frequency stability within the working temperature can reach ±0.5ppm, phase noise can be -100dBc/ Hz @100 Hz; We choose high Q value wire-wound inductance as the external inductance; Phase discriminator gain is not the bigger the better, we should set up it according to the size of the divider register. These measures can reduce the phase noise of the signal source greatly.

In addition, we adopt Gali-3+ which is a broadband high frequency amplifier as the last level of the frequency synthesizer. Its amplification at 375 MHZ can reach 17.5 dB ~ 22.4 dB, so that it can restrain low frequency noise well, and also increase the power of signal output.

Test Result

Figure 5 is the test result using the spectrum analyzer to test the finished circuit. When we set the update frequency (f_{IN}/R) 50KHz. We can obviously seeing in the test, there is some spurious frequency which stray away from the center frequency at 50kHz. When IF locked loop output signal is 375MHz,the power can reach-0.6dBm,the phase noise at 100kHz offset is -85dBc/Hz @ 100KHz.It can satisfy the receiver/ transmitter needs of the local oscillator.

Conclusion

The all-digital frequency synthesizer whose core is Si4133 can be designed simply. The frequency of output can be controlled by software, with the advantage of easy operational, low phase noise, low spurious, and very practical.

References:

[1] Yuqing Wen. Design and Application of Frequency Synthesizer [D]. Xi'an University of Electronic Science and Technology,2012.

[2] Kho. J, Loh. C.I, Wui Hung Moo, Chee Seong Fong, Man On Wong. Extended analysis of SSN effect on phase-locked loop (PLL) circuit. Electrical Design of Advanced Packaging & Systems Symposium, 2009. (EDAPS 2009). IEEE. 2-4 Dec. 2009.

[3] Yong Li, Lijun Zhu, Changhong Shan. Based on DSP Builder Bandwidth Adaptive DPLL Design and Implementation [J]. Modern electronic technology,2010,16:1-4.

[4] Sai. A, Kobayashi. Y, Saigusa. S, Watanabe . O, Itakura. T. A digitally stabilized type-III PLL using ring VCO with 1.01psrms integrated jitter in 65nm CMOS. Solid-State Circuits Conference Digest of Technical Papers (ISSCC), 2012 IEEE International. 19-23 Feb. 2012.

[5] Houliang Xie. AVR Microcontroller Serial Communication [J]. Computer Programming Skills & Maintenance,2011,12:79-80+85.

[6] HongTian Wu. PLL Frequency Synthesizer Research and Design [D]. University of Electronic Science and Technology,2013.

Advanced Materials Research Vols. 989-994 (2014) pp 4062-4068
© (2014) Trans Tech Publications, Switzerland
doi:10.4028/www.scientific.net/AMR.989-994.4062

Electronic Satellite Scheduling Problem and Its Heuristic Method

Jiangcheng Li[a], Lining Xing, Yingwu Chen and Xiangyu Wei

College of Information System and Management, National University of Defense Technology, Changsha 410073, China.

[a]18692205883@163.com

Keywords: Electronic satellite; heuristic algorithm; scheduling strategy; hierarchical optimization; roulette; TOPSIS

Abstract. The problem of scheduling for electronic satellites is a serious problem involving a lot of complex constraints. Considering the specific constraints of electromagnetic detection electronic satellite, on the basis of rational hypothesis, a multi-objective mathematic model was established. Several basic scheduling strategies were proposed. Based on the roulette method and hierarchical optimization method, a heuristic algorithm based on the rules was designed. A comprehensive evaluation with Technique for Order Preference by Similarity to Ideal Solution (TOPSIS) for the algorithm was offered. Finally, some experiments are conducted to verify the correctness and practicability of our scheduling model and algorithm.

0 Introduction

Electronic satellite is an artificial earth satellite detecting electromagnetic signal of the targets in which users are interested near satellite point by spaceborne remote sensing electronic equipment when flying around the earth. It has such advantages as covering a wide area, having a long lifetime, without area and weather condition limit, no need considering the safety of personnel. The information electronic satellite collects has important significance in industrial, scientific and military field. It also has great significance to research electronic satellite scheduling problem, maximize the profit of the tasks electronic satellite completes when expanding less resource, and make full use of electronic satellite resource.

So far, the vast majority related research that can be retrieved are for imaging satellites in the field of satellite scheduling. Literature [1] established ROCSAT-Ⅱ satellite programming model and proposed Lagrangian relaxation method based on single workpiece problem, Literature [2] solved the constellation planning problem for the Cosmo-Skymed using tabu search and random greedy algorithm Literature [3] established scheduling model for regional imaging satellites, and solved it by the use of neighborhood search methods. Literature [4] studied the scheduling problem for the sea and communications satellites and proposed task scheduling algorithm. Literature [5] established multi-objective model based on constraint Satisfaction for imaging satellites scheduling and solved it using SPEA2. Literature [6] studied the satellite application task planning problems and established directed acyclic graph model. However much less literature is able to retrieve in electronic satellite scheduling field. Literature [7] studied the multiple electronic satellites scheduling problem, and adopt genetic algorithm based on dynamic penalty function for solving. Literature [8] established a multi-objective mathematical model for electronic satellite integrated planning problems.

In the premise of in-depth analysis of the relevant literature for satellite scheduling, we study the scheduling model and give out the related solving algorithm. Firstly, according to the relevant characteristics of electronic satellite scheduling problem, extract the main constraints of the problem and make some reasonable assumptions and simplified, establish a multi-objective programming mathematical model for electronic satellite scheduling problem. Then propose several basic scheduling strategy, design rule-based heuristics under the idea of hierarchical optimization and roulette. We construct the index system for scheduling objective evaluation which is done by TOPSIS method. Finally, we give out our the simulation experiments and data analysis, and algorithm

comparison results proved that the proposed method can help effectively solve the electronic satellite scheduling problem.

1 Problem Analysis

Electronic satellite scheduling problem can be described as follows: Based on considering the electronic satellite detection capabilities and user needs, allocate resources to multiple competing tasks and determine the start and end time, work mode, and other related information. The target of this problem is that, considering the relevant constraints, the total value of the tasks scheduled successfully could be maximum and the need of users could be best meet.

Electronic satellite scheduling problem is a NP-Hard problem, involving a variety of complex constraints. To consider the main features of the issue, we make the following assumptions and simplifications:

(1)We only consider the payload of satellite, without regard to the other satellite service system.

(2)Assuming each satellite contains only one sensor, we could separate the satellite carry multiple sensors into multiple satellite carry only one sensor.

(3)The targets are fixed targets, and the electromagnetic characteristic parameters and other related information has been notified in advance, the work mode of electronic payload on satellite always is default accurate measuring mode.

(4)We would not consider the limitation of satellite storage capacity. That is, satellite has enough storage capacity to complete all tasks.

(5) The Duration of each frequency band is a fixed value. The transform time between different bands is so small that it could be neglected.

2 Model

2.1 Symbol Definition

(1) t_S represents the start time of scene, t_E represents the end time of scene.

(2) I represents the collection of tasks, $TaskNo$ represents the number of tasks, LP_i represents the priority of tasks.

(3) tw_i represents the feasible time windows of task i, ws_i and we_i represent the start time and end time of tw_i respectively, dt_i represents the duration of task i, st_i represents the start time of task i.

(4) o represents the virtual start task of satellite，whose start time is a and duration is 0; d represents the virtual finish task of satellite, whose start time is b and duration is 0.

(5) x_{uv} represents the satellite would continuously carry out task u and task v,when the satellite continuously carry out task u and task v, $x_{uv}=1$， otherwise $x_{uv}=0$.

(6) w_{il} represents the satellite would collect signal for task i by frequency band l,when the target frequency of task i is in frequency band l, $w_{il}=1$,otherwise $w_{il}=0$.L represents the collection of frequency band, t_l represents the duration of each frequency band, $lUpper_i$ and $lLower_i$ represent the upper and lower of frequency band l_i respectively.

2.2 Constraints

(1)Virtual task o and virtual task d would meet the conditions, which describe the satellite is available and virtual task o and virtual task d must be performed.

$$\sum_{v\in I\cup\{d\}} x_{ov}=1 \tag{1}$$

$$\sum_{u\in I\cup\{o\}} x_{ud}=1 \tag{2}$$

(2)Each task could be performed only once by satellite, and it must meet a certain order among the tasks.

$$\sum_{v\in I\cup\{d\}} x_{uv} \le 1, \forall u \in I \tag{3}$$

(3)When a task is performed in a time window of satellite, the start time and end time of this task could not beyond this time window range.

$$x_{uv}(st_u - ws_u) \ge 0, u \in I, v \in I \cup \{d\} \tag{4}$$

$$x_{uv}(st_u + dt_u - we_u) \le 0, u \in I, v \in I \cup \{d\} \tag{5}$$

(4) Here is the decision variable ranges.

$$x_{uv} \in \{0,1\}, u \in I \cup \{o\}, v \in I \cup \{d\} \tag{6}$$

$$w_{il} \in \{0,1\}, i \in I, l \in L \tag{7}$$

$$t_S \le st_i \le t_E, \forall i \in I \tag{8}$$

2.3 Index System

The indexes of the scheduling scheme of electronic satellite mainly include profit index, timeliness index and effectiveness index.

(1) Profit Index

For different tasks, users have different degree requirements. The more important the target is, the higher the profit (priority) of the task would be. Therefore, the profit index of scheduling scheme usually is measured by the sum of priority of tasks scheduled successfully.

$$V_1 = \max : \sum_{v\in I} \sum_{u\in I\cup\{o\}-\{v\}} \{x_{uv} \bullet LP_v\} \tag{9}$$

(2) Timeliness Index

Users have certain timeliness requirements for the task completion time, so scheduling scheme should make more important task to be performed as early as possible.

$$V_2 = \max : \sum_{v\in I} \sum_{u\in I\cup\{o\}-\{v\}} \{x_{uv} \bullet (t_E - st_v) \bullet LP_v\} \tag{10}$$

(3) Effectiveness Index

Limited resources could not meet the scheduling needs of all tasks. Efficient scheduling method should make more tasks to be executed. So we reflected the effectiveness of scheduling scheme by the rate tasks are scheduled successfully. The higher the rate is, the more effective the scheduling scheme is.

$$V_3 = \max : \sum_{v\in I} \sum_{u\in I\cup\{o\}-\{v\}} x_{uv} / TaskNo \tag{11}$$

3 Rule-based Heuristic Algorithm

Satellite scheduling problem is a NP-Hard problem. Given the complexity, scale and operability, rule-based heuristic method is still the most viable and effective solution method. The advantage is that such method does not require a lot of computing, which reduced configuration requirements of computing resources in work schedule; and also avoids the combinatorial explosion problem. Once the appropriate rules are chosen, corresponding scheduling strategy can be generated, which is quite easily performed. By analyzing the characteristics of the electronic satellite scheduling problem, based on previous experience of the planning and scheduling, proposed the basic rule of electronic satellite scheduling and designed rule-based heuristic algorithm.

3.1 Deterministic Strategy

(1) OPS Strategy

Determine the order of resources allocation according to the task priority and task list order sequentially. Allocate resources as early as possible so that the scheduling task executes as soon as possible. The realization process of the strategy is simple, algorithm ideas are easy to understand and

execution speed is relatively fast, which makes it suitable for the problems of resource "oversupply" and with less task time windows overlap.

(2) SEQ Strategy

Determine the order of resources allocation according to sequence of task starting time and task list order sequentially. This algorithm is based on OPS with some modifies. The realization process of the strategy is simple, algorithm ideas are easy to understand and execution speed is relatively fast(comparable with OPS), which makes it suitable for the problems of resource "oversupply" and with less task conflict.

(3) MPS Strategy

Applying the OPS strategy in multi-step repeatedly would generate a variety of initial scheduling scheme. Before each application of OPS, a list of tasks and the time window should based on expert system rule set in order to modify the sequence of tasks and the time window in scheduling data. Establish the evaluation index system, evaluate each scheduling scheme generated by OPS, choose the optimal one. Compared with OPS, the execution speed is a little slower, whereas the scheduling scheme generated is much better, which makes MPS suitable for problems of medium resource conflicts.

(4) RAN Strategy

Firstly, randomly generate an initial scheduling scheme of problems to be solved based on unbiased manner, allow the infeasibility of the initial scheme, then modify it to be feasible. The greatest feature of RAN strategy is the "unbiasedness", which makes such strategy suitable to solve those scheduling problem under situation of FOM hard to understand. Thus RAN strategy can provide some unpredictable scheduling scheme through the basic scheduling rules.

(5) Determined Mixed Strategy

Since performance of the scheduling rules is affected by various parameters, none heuristic algorithm based on single rule can exhibit good scheduling performance in all satellite scheduling problems. Based on simple scheduling rules, we construct determined mixed strategy MR. Strategy selection process is as follows:

$$MR(OPS,SEQ,MPS,RAN)=\begin{cases}OPS, 0\le x\le p_1\\ SEQ, p_1<x\le p_2\\ MPS, p_2<x\le p_3\\ RAN, p_3<x\le 1\end{cases} \tag{12}$$

where, x is a random number within the interval [0,1], and p_1, p_2 and p_3 are constants within the interval [0,1].

Repeat the process to obtain multiple scheduling schemes. Then evaluate each scheme based on TOPSIS, and give out the optimal scheduling scheme.

3.2 Stochastic Strategy

Based on deterministic strategies, design stochastic strategy according to the idea of roulette method. Roulette method randomly selects better individuals according to the fitness. The probability of the individual to be selected depends on its fitness.

$$p_i=\frac{f_i}{\sum_{i=1}^{n} f_i}, \sum_{i=1}^{n} p_i=1 \text{且} p_i\ge 0 \tag{13}$$

where, p_i is the probability of individual i to be selected, f_i is the fitness of individual i, n is the number of individual in group. Therefore, the larger f_i is, the larger p_i is, and the probability of this individual to be selected is higher.

In the NOPS, we take task priority as the task fitness; in the NSEQ, take the order of tasks start time as the task fitness; in NMPS, take the sort tasks from the expert system rule set as the task fitness; and in NRAN, take the initial unbiased task scheduling order as the task fitness. Calculate the probability range each task been selected according to the fitness, set a random number generator to drive the wheel rotation, which would generate a set of initial scheduling scheme. Evaluate

advantages and disadvantages of all initial schemes comprehensively through the method of TOPSIS, and choose the optimal scheduling scheme in them.

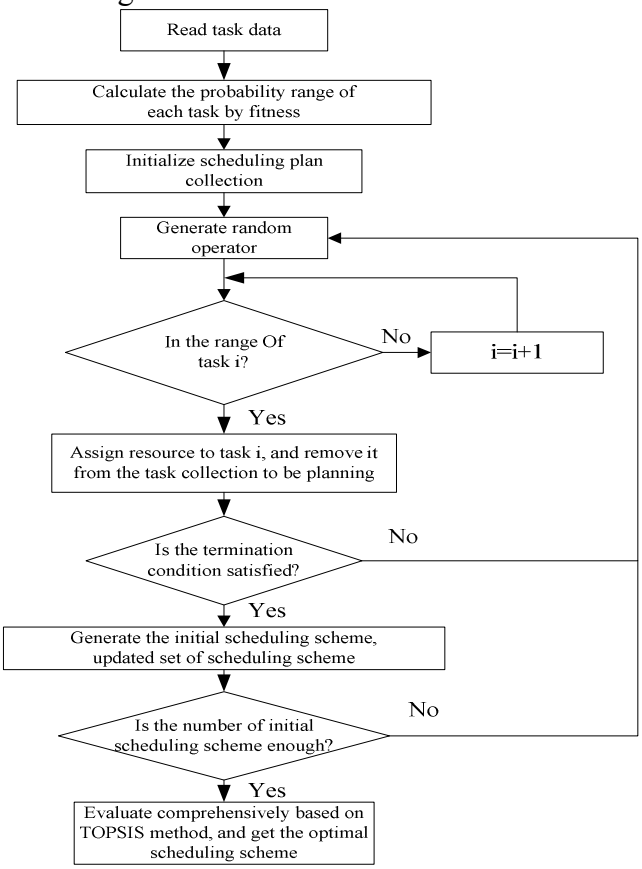

Fig. 1 Basic Flow of Stochastic Strategy

3.3 Stochastic Mixed Heuristic Algorithm

Taking these various stochastic strategy, based on the idea of hierarchical optimization, design Stochastic Mixed Heuristic Algorithm NMR, Algorithm is described as follows:

STEP 1. Determine the probability selecting range of each stochastic strategy, according to the specific circumstances of scheduling problems.

STEP 2. Initialization set of scheduling schemes.

STEP 3. Set the random number generator to drive wheel rotation, generate a random number to determine the type of stochastic strategy

STEP 4. Execute the strategy, obtain an initial scheduling scheme

STEP 5. Update the set of scheduling schemes, determine whether the number of scheduling schemes meet the demand, if meet, turn to STEP 6, otherwise back to STEP 3.

STEP 6. Evaluate each initial scheme based on TOPSIS, and give out the optimal scheduling scheme.

4 Experiments

To test and verify the effect of these methods for electronic satellite scheduling problem, we design several randomly generated examples of different size to conduct simulation experiments. There are 4 test examples with different task number of 50,100,150 and 200 respectively.

Assuming scheduling cycle is 24 hours, the priority of each task is a random number within the interval [1,10], and the duration of each task is a random number within the interval 100s~300s.

The results of example are shown in Fig.2~5. Among them, Fig.2~4 respectively show profit index, timeliness index and effectiveness index of 10 different algorithms to calculate each example. It can be seen that the five stochastic algorithms is generally optimum compared with its corresponding deterministic algorithm, however the advantage is not that obvious. Evaluation index

of NMR, MR, NRAN and RAN is superior to the others, while the rest six OPS, SEQ, MPS, NOPS, NSEQ and NMPS are of little difference generally. In fact, with the increasing scale of the problem, superiority of the former four is more obvious. Fig.5 shows the order indication value of different algorithm calculating each example. As can be seen, NMR is superior to the others, with MR, NRAN, RAN followed, and the rest are of little difference. Thus, by introducing the idea of random selection to consolidate variety of heuristic rules in scheduling, we can integrate the advantages of various algorithms, expand the space of feasible solutions, which enhance the algorithms' ability of searching optimization greatly.

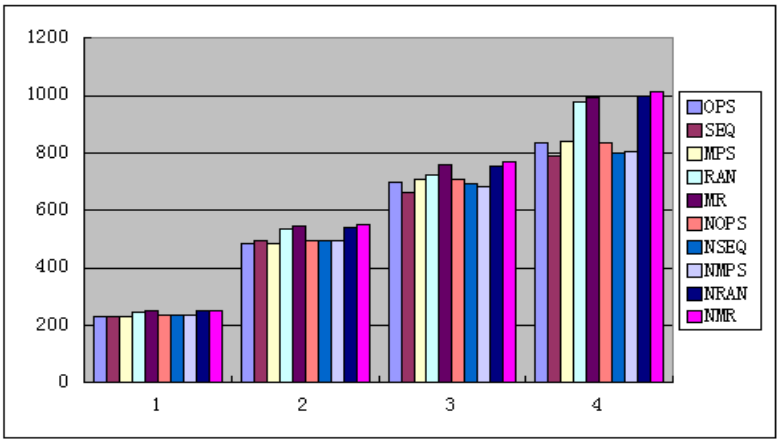

Fig. 2 Comparison Result of Profit Index

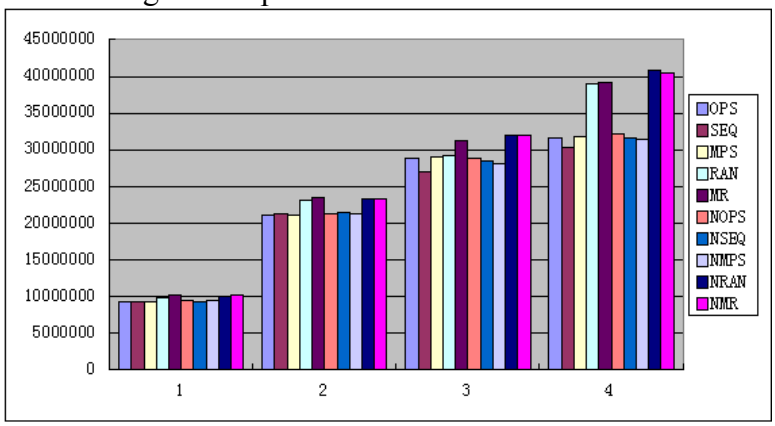

Fig. 3 Comparison Result of Timeliness Index

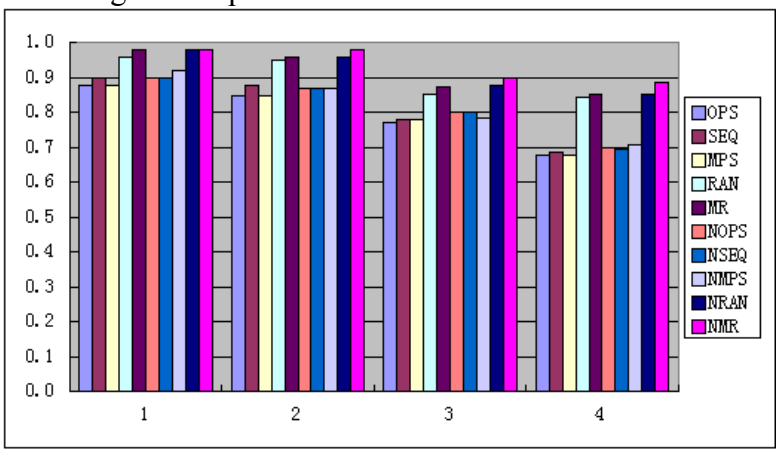

Fig. 4 Comparison Result of Effectiveness Index

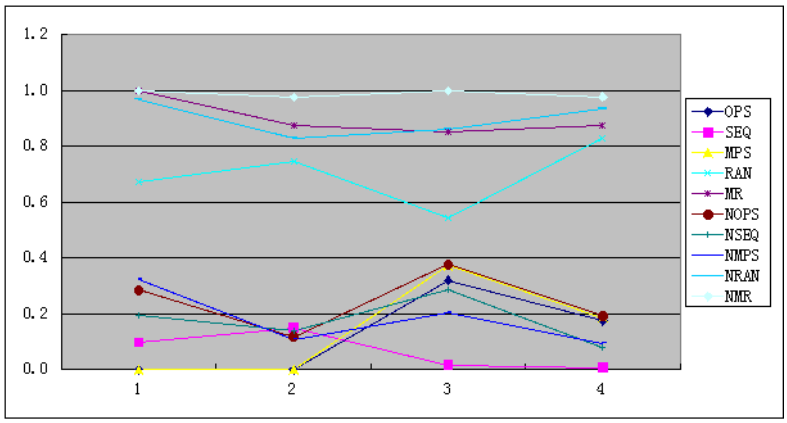

Fig. 5 Comparison Result of Indicated Value Sorted by TOPSIS

5 Conclusion

According to the relevant characteristics of electronic satellite scheduling problem, extract the main constraint, build a multi-objective programming mathematical model for electronic satellite scheduling problem. Propose several basic scheduling strategies, According to the hierarchical optimization ideas and thoughts of roulette, design rule-based heuristics, and comprehensively evaluate the solutions based on TOPSIS. Through comparative analysis of multiple test cases under different problem scale, it is shown that the introduction of the idea of random selection to consolidate variety of heuristic rules in scheduling can get on better scheduling result, which has some practical significance to solve practical problems.

Acknowledgements

Fund Project: National Natural Science Foundation of China (71101150, 71071156).

References

[1] W.C. Lin, D.Y. Liao, C.Y. Liu and Y.Y. Lee: Systems, Man and Cybernetics, Part A: Systems and Humans, IEEE Transactions on, Vol. 35 (2005) No.2, p.213.

[2] N. Bianchessi and G. Righini: Aerospace science and Technology, Vol. 12 (2008) No.7, p.535.

[3] Q.M. Ruan, Y.J. Tan, Y.T. Li, Y.W. Chen and R.J. He: Journal of Astronautics, Vol. 28 (2007) No.1, p.238.

[4] S. Lee, W.C. Jung and J. Kim: ETRI Journal, Vol. 30 (2008) No.1, p.1.

[5] J. Wang, J. Li, J. Chen, Y.H. Guo and N. Jing: Journal of Astronautics, Vol. 28 (2007) No.2, p.354.

[6] F. Zhang, J. Wang, J. Li and N. Jing: Journal of National University of Defense Technology, Vol. 27 (2005) No.6, p.61.

[7] H. Chen, J. Li, Y. Tang and N, Jing: Journal of National University of Defense Technology, Vol. 31 (2009) No.2, p.44.

[8] H.L. Wang, X.J. Huang, M.H. Ma and D.S. Qiu: Systems Engineering and Electronics, Vol. 32 (2010) No.8, p.1695.

Advanced Materials Research Vols. 989-994 (2014) pp 4069-4073
© (2014) Trans Tech Publications, Switzerland
doi:10.4028/www.scientific.net/AMR.989-994.4069

Recent improvements in Image Retrieval

Zeng Yansheng, XulinYing

ComputerScienceandTechnology, TianjinUniversity,Tianjin300072,China;

yhzys@sina.com

Keywords: image retrieval, TBIR, CBIR, annotation, automatic.

Abstract. The target of this paper is to introduce the improvement of the technique of image retrieval. At first, it comes up with the concept of image retrieval and shows the importance of this technique. As the techniques of multimedia and Internet are developing rapidly, the resources of images that users obtain are also extended. And then this paper gives the problem about the image retrieval, namely the information of images are disordering. As the result, it is significant to do the effective organization, management and retrieval based on the increasingly extensive image information storage. After that, this paper presents the concept of TBIR and CBIR and gives the definitions of them. It proposes an issue that CBIR is the improvement of TBIR. Based on CBIR, there are also some disadvantages that need to be improved. In terms of the main point of CBIR, the paper raises that the annotation is one of the most difficult techniques that need to be promoted. Then it describes some algorithms about the technique of automatic image annotation. After these algorithms, the paper shows the challenges and developing direction of the technique of image retrieval. At last, it presented the conclusion to emphasize the main points of this paper.

Introduction

The research of image retrieval has been started since 20th century. As the techniques of multimedia and Internet are developing rapidly, and the standard of people's life is promoted, various resources on the Internet are becoming abundant, especially the information of multimedia because its characteristic of visualized. For this reason, the resources of images that users obtain are also extended.

The target that the technique of image retrieval should accomplish is to make users find the image they need more exactly and quickly [1]. In terms of the theory of image retrieval technique, there are three aspects. The first one is to create a query to retrieve the index of database, based on the analysis of the users' demands. Second one is to collect and cure the image resource, extract the characteristics, analyze and create the index of database based on this picture. At last, the most popular algorithm is to use the vector space. This algorithm is according to the similarity algorithm，computing the similarities of users' query and the records of index database, extracting the records which is fit for the threshold value, and printing out these records as descending order.

There are two periods that the development of image retrieval technique passes by, namely the text-based image retrieval (TBIR) and the content-based image retrieval (CBIR) [2]. In the past, people only master TBIR while these days, as the technology developing, CBIR comes out and more people tend to choose this technique.

1.0 The development of image retrieval technique

Since the 20th century, as the promotion from the research realms in database systems and computer visual, the technique of image retrieval has become a more dynamic research field. In the past, the main technique of image retrieval is TBIR, using the text to describe the characteristics of an image and doing the retrieval. For example, the current search engine, such as Google and Being are all based on the text. Instead of the content of images, the results depend on the file names of images or the text descriptions of images. Because the method of retrieval is single and the description of images are not comprehensive, these image search engine will not be too precise. This means the user should select from such many results that the efficiency of retrieval are not high. As the result, CBIR is created as the improved technique. This technique is to analyze the

color, shape, texture and some other characteristics of the image, in order to make the retrieval more effective and precise.

1.1 Text-based image retrieval technique

The technique of image retrieval is begun with the research of TBIR. TBIR is to store images into a database, when retrieving a picture, users can access the file name or keywords as the image index, setting up relationship between the storage path of image and the keywords. It is general that the method to do the retrieval is to scan the classified catalogue or do the keyword query. In essence, these kinds of retrieval accomplish the accurate matching or the probability matching to the description of image [3].

As the quantity of images is rapidly increasing, the problem of TBIR has been coming out. First is the workload of marking all the images manually is quite large. Currently, the technique of computer visual and artificial intelligence cannot mark images automatically. This means the work of marking images will cost a lot of time. Second, because of the differences of personal subjective cognition, different people will have different comprehensions according to one image. However, the method of retrieval will use the keywords created from the marker to accomplish, which may generate some error matching, and will influence the reliability of the retrieval. At last, the visual features of images are various, such as shape, color, texture and some others, these will not be described by text objectively.

There are some typical applications that are based on the technique of TBIR, such as Yahoo! Picture-Gallery. Yahoo! Picture-Gallery has stored more than 40 thousand pictures. These pictures have been categorized and indexed according to art, technology, entertainment, animal, science, sport and some others. Users should scan, or input the keywords to do the image retrieval.

1.2 Text-based image retrieval technique

CBIR is based on feature of images, color, shape, texture and semantics respectively, is committed to query the image. It is aimed at querying the image that is similar to the typical example from the comprehension of image. This retrieval technology is different from the traditional one, which they use distinct method to accomplish retrieval task. The technology reflects quantized features that store the content of media and media. It uses the Query By Example based on similar measurement to come true the retrieval function. Compared to the traditional one, it adds some new technologies, such as technology of image comprehension, technology of pattern recognition, to offer the more powerful method of retrieval to the users.

In terms of CBIR, there are also some successful examples such as QBIC. QBIC is an image retrieval system developed by IBM company. It is the first CBIR system for business, and is one of the most popular image retrieval systems. This system is based on the image retrieval services of the web, using color, shape, texture and some other features as the characteristics of the query. The query is presented by drawing or any other imaging approaches [4].

2.0 The current situation of TBIR and CBIR

2.1 The comparison of TBIR and CBIR

Both TBIR and CBIR exist the advantages and disadvantages. It is supposed that CBIR is the improvement of TBIR.

In some extent, TBIR is more simple and flexible to operate and it is also accustomed for users to access it do the retrieval. In current circumstances, the majority of search engines have equipped with this function because this technology comes true simply. However, it also has a weakness, namely the limitation retrieval range of text. It is even easy to confuse about the description of words and languages. In addition, the annotation used to mark the image is different, which will decrease the rate of precision ratio and comprehensive of searching image.

[2] refers that CBIR improves the disadvantage of TBIR. First of all, as a kind of retrieval technique, it must provide the information or material of image recourses to users in a reasonable period from a large distributed database. Transparent is a characteristic in CBIR. Hence, the user need not understand the object of image and attempt to describe the format of text. User just needs to care about the way they prefer to query the information. It offers a quick way to find the object.

Secondly, CBIR adds the feature library and optimization algorithm. Feature library is going to store the visual feature, such as shape, color, texture and some others. The optimization algorithm is committed to increase the efficiency of query and the speed of matching. It is used the objective description of image of visual feature to increase the rate of query efficiency and accuracy.

2.2 The limitation of CBIR

The CBIR opens a more distinct and accurate approach to quickly query a large amount of image information online. However, it still has many imperfections, which can be:

1. **Low precision ratio.**
   Currently, most of all image retrieval engines cannot achieve the extent most of users are satisfied. As it queries the image, the user needs to query the object from thousands of images. Users cannot endure to spend long time on retrieving information. What's more, the worst thing is that sometimes the search engine cannot provide the information users want.
2. **The information of the image features extracted is not accurate.**
   In these years, the popular using in retrieval technique based on the content of image is mostly based on low-level visual feature. In fact, this is broken away from actual semantic of the image. If it just depend on low-level features to classify what the image includes, it is impossible. The low-level features do not have the ability to recognize the object. For example, usually the user wants to post an image as a query to do the retrieval, the system cannot find the one what the user wants to look for [5].
3. **The connection of user query is not ideal.**
   In the ideal image retrieval system, people can be active and the connection of user query can provide abundant interactive abilities. Furthermore, it also is a distinct and simple way to query image. However, the current technologies represent that the connection of user query in retrieval engine is still singleness and less interactive ability. In some case, the retrieval engine just offer the annotation of connection of query, dialog box of keywords.

3.0 The improvement of image annotation

The key techniques to realize CBIR are extracting the features of images and matching. There are two classifications according to the extraction of features, namely the low level features and the high level semantic contents. The low level features are some basic features of the image, such as color, shape and texture. The high level semantic contents are some high level of conception of the image, which need people to recognize and explain, and these will rely on the knowledge that people acquired. As the development of CBIR is limited, the CBIR cannot support the high level semantic contents. Currently, the mutual retrieval algorithms are most based on the low level features, namely using color, shape, texture and some other features to do the retrieval. After extracting, the data should do the operations such as index and dimensionality reduction.

As the importance of extracting features of the image, the technique of image annotation has become more and more significant.

1. **Automatic image annotation**

Automatic image annotation is to generate the text annotation automatically by the computer system according to the content of image visual. Generally, the annotation can be the category of the image, or some keywords. Thus, people can use a more mutual technique to do the index and retrieval for the image. For the cause that the quantity of images is increasing rapidly, the technique of manual image annotation has been more expensive [6]. As the result, the technique of automatic image annotation is becoming increasingly important.

2. **Different algorithms to realized the automatic image annotation**

In the automatic image annotation, the information to be marked is always the text words or some limited information of category. A simple way to accomplish is to train a corresponding binary classifier according to every word. When the system comes across a new image, it can use these classifiers to judge if this word should be an annotation of this image, and then it can create the image annotation.

In terms of the classification of information, one of the algorithms is to use the support vector machine (SVM) to categorize the area of the image [6]. Firstly, it uses several algorithms to do the image segmentation, in order to segment the image into different areas and recognize the salient regions of them [7]. And then the system will do the manual annotation to mark the category information to these salient regions, and regard them as training data. Each area should be departed into some tiles that can overlap with each other and every tile is include 4*4 pixels. The distribution information of the HSV color space and the relative gradient information are used as the features annotation of this tile. When training each binary classifier of a word, the system will use several tiles that are from the positive area and the negative area to do the training to SVM model. At last, collecting all the annotation information from different areas, and putting them together, after that, it will obtain the annotation of this image.

Another algorithm is to regard this issue as a point of translation between two languages: one is made by text words and the other is made by the vision words in order to describe the image. For the reason that the language translation model need to present these two languages as discrete symbols, the system regards the limited categories that are clustered by the image areas as the vision words. This algorithm firstly access normalized cut to segment the image into different areas that are not overlapping. And then use the K-Means method to do the cluster, and each of the result will be called as a kind of blob, namely the relative vision words category. And then this algorithm accesses a machine language translating method to build up the relationship between area categories and the text words. This method is called translation model (TM) [8]. To improve this algorithm, it is better to do the clustering for the text words. After that, it uses the TM into the translations between these conceptions and blob, and making the results more effective.

4.0 The challenges and developing direction of the technique

The most important keys of CBIR are two: one is to find the features of images that are suit for human being's vision while the other is to promote the speed of responses during the retrieval. In term of these two technologies, people should consider the following three aspects:

1. **Relevance.**
   The vision features of human beings are relative to the low-level image features, and more and more researchers have accepted the method of image retrieval turns to the direction of semantic. Relevance is a significant way to connect these two features.
2. **The performance evaluation criterion and the set of test**
   A positive evaluation criterion may lead the technique to a right direction while a negative one will mislead the research work. In terms of current situation, the performance evaluation criterion is the precision and recall. Moreover, to make a balanced, large-scale test database is also an important issue.
3. **The combination among the cross realms.**
   To accomplish a more effective technique of image retrieval，it seems need the efforts from cross realms.

Conclusion

In conclusion, as the unstructured resources have become increasingly abundant and the Internet have become more popular, it seems that users tend to access websites to retrieve the pictures what they want. This paper is based on the improvement of the technique of image retrieval, coming up with some kinds of techniques to make the image retrieval more effective. According to the analysis, image annotation is one of the most significant techniques. It is proved that automatic image annotation will bring more efficiency than the manual image annotation. Although the technique of image retrieval has been somewhat mature, there is still a large space to progress. Nowadays, the technique cannot accomplish to extracting the high level semantic content, to deal with these kinds of problems, people need to do more research.

Although this paper is relative comprehensively describing the improvement of technique of image retrieval, it seems need further research to make the research completed and comprehensive.

References

[1] D. Liu, "*Efficient Techniques for Relevance Feedback Processing in Content-based Image Retrieval"*. Florida, 2009, pp. 7-41

[2] Hernández-Gracidas, C. A., L. E. Sucar & M. Montes-y-Gómez "Improving image retrieval by using spatial relations", *Multimedia Tools and Applications*, vol.62, Nov.2, pp. 479-505, 2013

[3] D. Buffoni, S. Tollari & P. Gallinari, "A Learning to Rank framework applied to text-image retrieval", *Multimedia Tools and Applications*, vol.60, Nov.1, pp.161-180, 2012

[4] O. Marques & B. Furht, "MUSE: A content-based image search and retrieval system using relevance feedback", *Multimedia Tools and Applications*, vol.17, Nov.1, pp. 21-50, 2002

[5] Z. Shi, X. Liu, Q. Li, Q. He & Z. Shi , "Extracting discriminative features for CBIR", *Multimedia Tools and Applications*, vol.61, Nov.2, pp.263-279, 2012

[6] R. Zhang, "Combining visual features and contextual information for image retrieval and annotation", 2011

[7] A. Boucher, "Sub-pixel mapping of coarse satellite remote sensing images with stochastic simulations from training images", *Mathematical geosciences*, vol.41, Nov.3, pp. 265-290, 2009

[8] M. Y. Fang, Y. H. Kuan, C. M. Kuo & C. H. Hsieh, "Effective image retrieval techniques based on novel salient region segmentation and relevance feedback", *Multimedia Tools and Applications*, vol.57, Nov.3, pp.501-525, 2012

[9] I. Ahmad & M. Gabbouj, "A generic content-based image retrieval framework for mobile devices", *Multimedia Tools and Applications*, vol.55, Nov.3, pp.423-442, 2011

Advanced Materials Research Vols. 989-994 (2014) pp 4074-4077
© (2014) Trans Tech Publications, Switzerland
doi:10.4028/www.scientific.net/AMR.989-994.4074

Mineral belt image segmentation using firefly algorithm

Lifang He [1, a], Xiong Tong [2] and Songwei Huang [2]

[1]Department of Electronic Information, Kunming University of Science and Technology, Kunming, China

[2] Department of Mineral Processing Engineering, Kunming University of Science and Technology, Kunming, China

[a]843168660@qq.com, [b]xiongtong2000@qq.com, [c]594770837@qq.com

Keywords: Firefly Optimization (FA), Image segmentation, Otsu, Mineral belt image

Abstract. Otsu is one of better image segmentation algorithm, which obtains optimum threshold by maximizing the between-class variance of an image. However, computation time will sharply increase as the threshold increase. In order to greatly improve the problem, a new segmentation algorithm called firefly algorithm based on Otsu's method is presented in this paper, and applied the algorithm to segmentation of mineral belt image of shaking table, which lay the foundation for automation of shaking table. Experimental results show that the new algorithm can accurately segment different mineral belts and can obtain the same optimal thresholds and fitness values with Otsu's method.

Introduction

Image segmentation is an important step during the course of image processing, and thresholding is a simple and effective method, and the key technology is getting optimum threshold. At present, thresholding is widely used in some spheres [1], such as medical image segmentation, infrared thermal image segmentation, synthetic aperture radar image segmentation, moving object segmentation.

Otsu's method is one of commonly used thresholding algorithm, which can select an optimal threshold to maximize the between-class variance[2]. It can be easily extended to multi-level thresholding, but computation time will rapidly increase because it obtains optimum threshold by exhaust search[3]. To greatly improve the performance of the algorithm, Swarm intelligent optimization algorithm is combined with Otsu's method [4]. In 2008, Zhiwei Ye and others propose a new segmentation algorithm combining Otsu's method with particle swarm optimization algorithm to reduce computation [5].

Firefly algorithm is a new swarm intelligent optimization algorithm, which inspired by the social behavior of flashing of fireflies and presented by Xin-She Yang[6]. And it is compared to particle swarm optimization and genetic algorithm, the results of the experiment demonstrate that firefly algorithm is better than the two swarm intelligent optimization algorithm [7,8]. So we propose a new segmentation algorithm by combining firefly algorithm with Otsu's method in this paper, that is Otsu's method based on firefly algorithm.

At present, the position of mineral board and process variables is adjusted by artificial during the course of mineral dressing, which has wasted labor, the lower accuracy, real-time and separation indexes. In order to overcome the disadvantages, the new segmentation algorithm is used to segmentation of mineral belt image of shaking table in the paper.

This paper is describes the basic principles of Otsu's method in Section 2, introduces the firefly algorithm in Section 3, segmentation results of mineral belt image and analysis in section 4, followed by the conclusion in the section 5.

Otsu's method

Otsu's method was proposed by Japanese scholar Nobuyuki Otsu and is named after his namesake. Assume an image has N pixels and L gray levels, the number of pixels at level i is represented by f_i, then $N = f_1 + f_2 + \cdots + f_l$. The occurrence probability of level i is defined by

$$p_i = \frac{f_i}{N}, p_i \geq 0, \sum_{i=1}^{L} p_i = 1 \tag{1}$$

Assume the image contains two classes of pixels, the optimum threshold t divides the image into two classes, A and B, the cumulative probabilities and mean levels can be calculated respectively:

$$\omega_A = \sum_{i=1}^{t} p_i, \quad \omega_B = \sum_{i=t+1}^{L} p_i \tag{2}$$

$$\mu_A = \sum_{i=1}^{t} ip_i / \omega_A, \quad \mu_B = \sum_{i=t+1}^{L} ip_i / \omega_B \tag{3}$$

where ω_A is the cumulative probabilities of class A that contains of gray levels from 0 to t, ω_B is cumulative probabilities of class B.

Then the image of between-class variance is given by

$$\sigma^2 = \omega_A(\mu_A - \mu_T)^2 + \omega_B(\mu_B - \mu_T)^2 \tag{4}$$

where μ_T is the mean levels of whole image, $\mu_T = p_A\mu_A + p_B\mu_B = \sum_{i=1}^{L} ip_i$.

In Otsu's method the optimum threshold t^* is searched exhaustively by maximizing the between-class variance, then the optimal threshold is

$$t^* = \arg\max_{1 \leq t \leq L} \{\sigma^2(t) \left| \sigma^2 = \omega_A(\mu_A - \mu_T)^2 + \omega_B(\mu_B - \mu_T)^2 \right.\} \tag{5}$$

Firefly algorithm (FA)

In the firefly algorithm, fireflies are randomly placed in the search space by the following mathematical equation, which contain a light intensity:

$$x_i = rand \times (upper \quad range - lower \quad range) + lower \quad range \tag{6}$$

where x_i is the position of firefly i, upper range and lower range are respectively the upper range and lower range of search space.

Firefly algorithm has two important factors: the variation of light intensity and formulation of the attractiveness. Light intensity is associated with the position and objective function of firefly. The intensity of firefly can be presented by the following equation:

$$I = I_0 \times e^{-\gamma r_{ij}} \tag{7}$$

where, I_0 is the original light intensity , γ is the light absorption coefficient that is an constant parameter, and r_{ij} is the distance between firefly i and firefly j.

The attractiveness of firefly decides the direction of movement and the equation is as follows:

$$\beta = \beta_0 \times e^{-\gamma r_{ij}^2} \tag{8}$$

where, β_0 is the attractiveness at $r = 0$. The movement equation of firefly i to j is as follows:

$$x_i = x_i + \beta \times (x_j - x_i) + \alpha \times (rand - 1/2) \tag{9}$$

where, x_i and x_j is respectively position of firefly i and j, and firefly j is more brighter than firefly i. In the term, α is a randomization parameter, $rand$ is random number generator uniformly distributed in $[0,1]$.

During the course of movement, the fireflies with the lower light intensity move toward the brighter fireflies. After many movements, the majority fireflies gather the optimum value of the given objective function space.

Firefly algorithm based on Otsu's method

This section we apply firefly algorithm based on Otsu's method to segment mineral belt image of shaking table. The original images are shown in Fig.1, which are tin images from the concentrator. The experiments are carried out on a 2.70GHz CPU personal computer with 2G RAM under windows XP system. To ensure the validity, every experiment is done 20 times independent.

Table 1 The optimal thresholds and fitness values

Test images	Optimal thresholds		Optimal fitness values	
	Otsu	New algorithm	Otsu	New algorithm
image(a)	94,182	94,182	5464.4	5464.4
image(b)	95,183	95,183	5492.8	5492.8
image(c)	91,131,171	91,131,171	1255.9	1255.9
image(d)	118,150,180	118,150,180	1237.0	1237.0

(a)

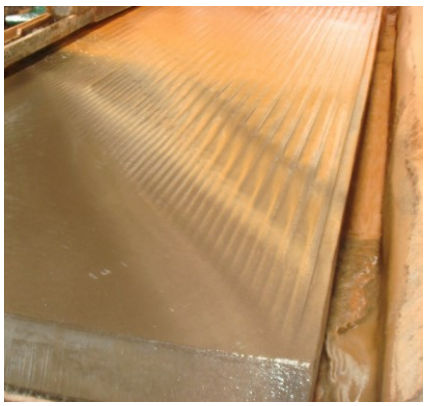

(b)

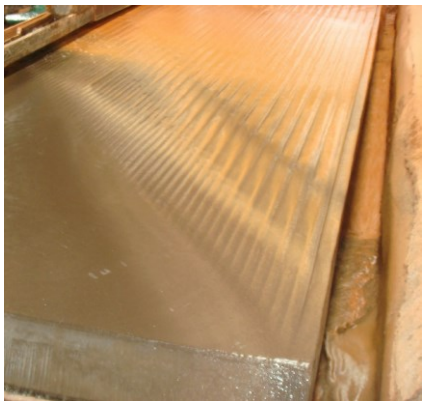

(c)

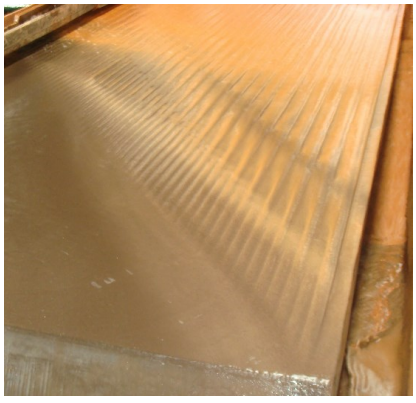

(d)

Fig. 1 Orginal image

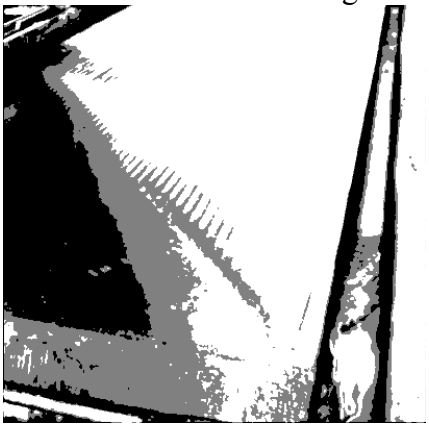

(a)

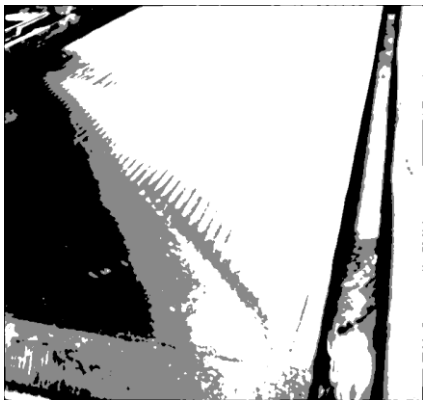

(b)

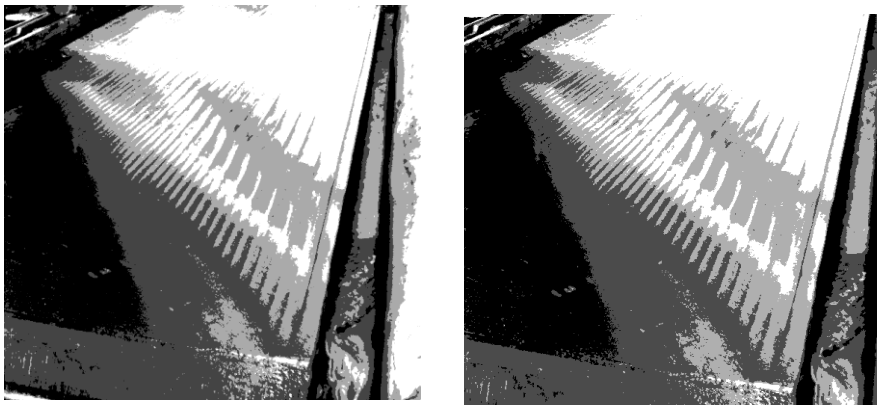

(c) (d)

Fig. 2 Segmented image used new algorithm

To test the performance of firefly algorithm based on Otsu's method, we execute the algorithm on the four images and compare the performance of the algorithm with Otsu's method. The optimal thresholds and fitness values are shown in Table 1. Obviously, the new algorithm can obtain the same optimal thresholds and fitness values with Otsu's method, and the new algorithm can divide the mineral belts into concentrate, middling and tailings for image (a) and image (b). And image (c) and image (d) are segmented into concentrate, time concentrate, middling and tailings.

Conclusions

To overcome the shortcomings of Otsu's method, we combine firefly algorithm with Otsu's method and present a new segmentation algorithm. Experimental results show that the new algorithm has good segmentation performance, which can segment different mineral belts and can obtain the same optimal thresholds and fitness values with Otsu's method, so it is suit for mineral belts image.

Acknowledgements

This work was supported by the National Nature Science Foundation of China (No. 51204077).

References

[1] Dengyuan Huang, Chiahung Wang: Pattern Recognition Letters. 30(2009)275-284.
[2] Nobuyuki Otsu: IEEE Trans. Sys., Man., Cyber. 9 (1979)62–66.
[3] Pingsung Liao ,Tse-sheng Chen , Pau-Choo Chung: Journal of informations science and engineering. 17(2001)713–727.
[4] Yong Zhao, Zongde Fang, Kanwei Wang, Hui Pang, Multilevel minimum cross entropy threshold selection based on quantum particle swarm optimization, In Proceeding of 8th ICSEAINPC. (2007) 65–69.
[5] Zhiwei Ye, Hongwei Chen, Wei Liu, Jinping Zhang, Automatic threshold selection based on particle swarm optimization algorithm, In Proceedings of international conference on intelligent computation technology and automation. (2008)36–39.
[6] Xin-She Yang. Firefly algorithms for multimodal optimization, Stochastic Algorithms: Foundations and Applications, SAGA 2009. Lecture Notes in Computer Sciences. 5792(2009) 169–178.
[7] Lukasik, S., Zak, S, Firefly algorithm for continuous constrained optimization task, ICCCI 2009,Lecture Notes in Artificial Intelligence. 5796(2009) 97-100.
[8] Ming-Huwi Horng, Ren-Jean Liou: Expert Systems with Applications. 38(2011)14805-14811.

Advanced Materials Research Vols. 989-994 (2014) pp 4078-4081
© (2014) Trans Tech Publications, Switzerland
doi:10.4028/www.scientific.net/AMR.989-994.4078

The Hidden Terminal Problem of 802.11 MAC and 802.15.4 MAC Protocols Based on NS2 Platform

Dong Qiu[1, a], Yanxiang Yang[2, b]

[1] School of Information and Electronics, Beijing Institute of Technology

Beijing 100081, China;

[2] School of Information and Electronics, Beijing Institute of Technology

Beijing 100081, China.

[a]qiudongbit@gmail.com, [b]yyx20091287@163.com

Keywords: IEEE 802.11 MAC, IEEE 802.15.4 MAC, Hidden Terminal, RTS/CTS.

Abstract: The IEEE 802.11 and IEEE 802.15.4 are two of the most popular wireless network protocols. And it is very important to look into the differences between IEEE 802.11 MAC and IEEE 802.15.4 MAC. The main goal of this paper is to look into the hidden terminal problem of the MAC layers of 802.11 and 802.15.4 based on NS2 platform. Through a dedicated experiment, the author compares the results based on the NAM animation and throughput and then explains the reasons respectively.

1. Introduction

The IEEE 802.15.4 [1] and IEEE 802.11 [2] are two of the most popular wireless network protocols. It is expected that low rate wireless personal area networks (LR-WPAN) will be used in a wide variety of embedded applications, in which numerous embedded devices running on batteries are distributed in an area communicating via wireless radios. While wireless local area networks (WLAN) aim to provide high throughput, low-latency for traditional file transfer and multimedia applications.

The MAC protocol plays a significant role in determining the efficiency of wireless channel bandwidth sharing and energy cost of communication. There have been some studies about the performance of IEEE 802.15.4 MAC and 802.11 MAC respectively. Gang Lu et al [3] evaluated the MAC performance of IEEE 802.15.4 in the simple star-topology. Hongqiang Zhai et al [4] analyzed a few performance metrics of the wireless LAN and give explanation to the performance degradation in delay and throughput at various traffic loads. There have been some studies about coexistence between IEEE 802.15.4 and IEEE 802.11 also. Sofie Pollin et al [5] studied the impact of a heavily loaded IEEE 802.15.4 network on an IEEE 802.11 network. But none of them look into the hidden terminal problem of IEEE 802.15.4 MAC and IEEE 802.11 MAC.

In this paper, a dedicated experiment of the same scenario with RTS/CTS mechanism enabled and disabled that uses IEEE 802.11 MAC protocol is used to compare the performance differences between RTS/CTS enabled wireless networks and RTS/CTS disabled wireless networks. The throughput is used as performance measure. Which is defined as the average value of the number of bytes of the current sampling time and the number of bytes of the previous sampling time, and the unit of throughput is Kb/s.

This paper is organized as follows. Section 2 brief overviews the IEEE 802.15.4 MAC and IEEE 802.11 MAC. In Section 3, the experiment is introduced and the results of NAM animation are given. The main performance measure throughput is used to analyze the differences between the two MAC protocols in Section 4. Finally, this paper concludes in Section 5.

2. Overview of the MAC protocol in IEEE 802.11 and IEEE 802.15.4

2.1 Overview of the MAC Protocol in IEEE 802.11

The 802.11 standard specifies a single Medium Access Control (MAC) layer and several physical layers. The MAC layer implements functions that enable the sharing of the common air medium [8].

The distributed coordination function (DCF) implements a carrier-sense protocol and supports only asynchronous communications. The DCF is suitable for sending information such as data files and bar codes, but it is not very efficient for sending broadband, time-critical information.

The 802.11 standard provides for an optional point coordination function (PCF) medium access mechanism, which is implemented in the access points and (in addition to the mandatory DCF) that provides delivery of time-bounded data via synchronous communications using station-polling mechanisms. This mechanism is capable of transporting video effectively as compared to the DCF.

2.2 Overview of the MAC Protocol in IEEE 802.15.4

In this section, we briefly review the MAC protocol specified in the IEEE 802.15.4 standard. More details of the protocol can be found in [6].

The MAC layer of IEEE 802.15.4 has two operating modes: beacon-enabled mode and non-beacon-enabled mode. In the beacon-enabled mode, a personal area network (PAN) coordinator transmits a beacon periodically to form the superframe time structure, as shown in Fig. 1. A superframe consists of a beacon that enables the beacon-enabled mode, contention access period (CAP), contention free period (CFP), and an optional inactive portion. The CAP and CFP together form the active portion of the superframe, during which all communication among the nodes should take place. In the CFP, the network coordinator controls entirely the contention free channel access by assigning guaranteed time slots (GTS) to those nodes with their GTS requests granted. Depending on the specific scheduling scheme used, the performance analysis of CFP is actually the same as that of the well-studied centralized scheduling schemes in cellular systems. And in the CAP, a slotted CSMA/CA is defined in the standard [7].

In the non-beacon mode, nodes use the carrier sense multiple access with collision avoidance (CSMA-CA) mechanism to contend for channel access. If the channel is idle, the transmission of a frame will begin immediately, otherwise the node will backoff and try to access the channel later.

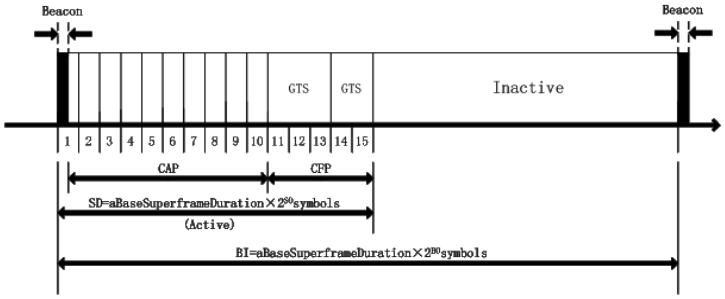

Fig. 1. IEEE 802.15.4 superframe structure in the beacon-enable mode

3. The Experiment: The Hidden Terminal Problem

The so-called hidden terminal problem, refers to a node, which is within the scope of coverage of the receiving node, but is outside the scope of the coverage of the sending node. Therefore, the node could not intercept the data sending of the sending node, and at the same time, transmit data to the same receiving node. At this time, it will make the data compete at the receiving node. After the competition has been generated, the node will retransmission the data that is not successful transmitted due to competition, thus lowering the coefficient of utilization.

Both IEEE 802.15.4 and IEEE 802.11 use the CSMA/CA mechanism, but their CSMA/CA mechanism has some difference. The main difference is that in IEEE 802.15.4, there is no RTS/CTS handshake mechanism, while in IEEE 802.11, it is possible to use the RTS/CTS handshake mechanism. So the hidden terminal problem could only be solved in IEEE 802.11.

This scenario includes three nodes, two nodes numbered 1, 2 act as the source nodes of data flow, while node 0 act as the destination node of date flow. Node 1 and node 0, node 2 and node 0 are two groups respectively. Each group of source node and its corresponding destination node are connected via UDP and bind with CBR application. Set reasonable topology, so that node 1 and node 2 are within the communication range of node 0. While node 1 and node 2 are out of the communication range of each other. The simulation time is 20 seconds. The topology of the three nodes is shown in Fig. 2.

Fig. 2. Topology of the three nodes

At 1.0, node 1 begins to send data to node 0. And at 2.0, node 2 begins to send data to node 0. At 15.0 stop sending data. Finally, end the simulation at the time of 20.0.

4. The Analysis of Throughput

Throughout is an important parameter to analyze wireless network. The experiment shows different results when the RTS/CTS mechanism is enabled and not enabled. It uses Phy/WirelessPhy as the network interface type and Mac/802_11 as the MAC layer type.

After running the Tcl file, two files are generated. Then they could be used to draw the throughput graph by using gnuplot. Fig. 3 shows the throughput graph that enables the RTS/CTS mechanism, while Fig. 4 shows the throughput graph that disables the RTS/CTS mechanism.

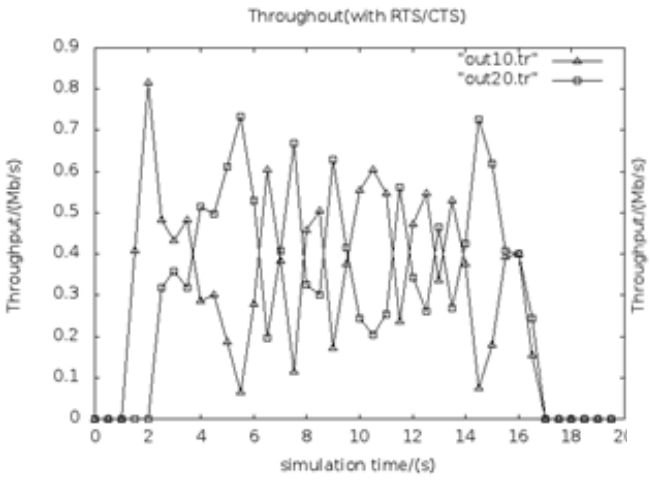

Fig. 3. Throughput(RTS/CTS enabled)

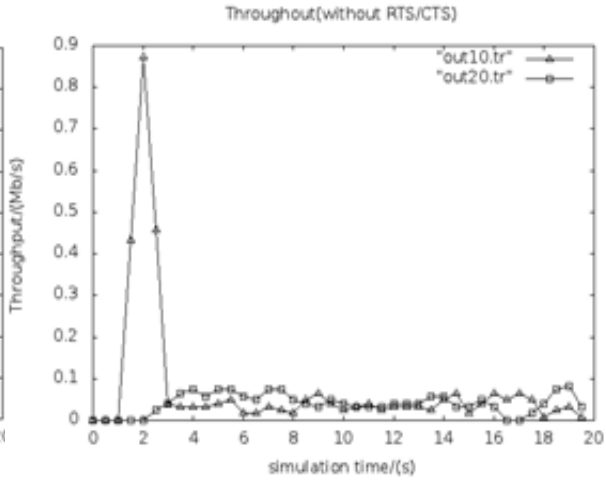

Fig. 4. Throughput(RTS/CTS disabled)

As shown in the figures above, when the second wireless transmission link begins data transmission at 2.0, both of the circumstance generate competition phenomena, but their results have

huge difference. In Fig. 3, that is, when the RTS/CTS handshake mechanism is enabled, through this mechanism, could avoid the hidden terminal problem. Through handshake signal, the two wireless transmission links could use the channel in turn. From the figure, we could see that when the throughput of one wireless transmission link fluctuate to its peak, the other wireless transmission link fluctuate to its trough. But in Fig. 4, that is, when the RTS/CTS handshake mechanism is disabled, the two wireless transmission links compete with each other, which reduce the transmission efficiency greatly.

From the experiment, it can be concluded that it is very effective to solve the hidden terminal problem by using the RTS/CTS mechanism. But it adds RTS frame and CTS frame. Therefore, this way will also increase the extra burden. As the length of them are 20 bytes and 14 bytes respectively. For IEEE 802.11, because the data transfer rate is higher, the length of the two kinds of control frame is not very great in comparison with the length of the data frame, and could avoid the greater waste of resend the data frame because of the conflict. But for IEEE 802.15.4, the data transfer rate is much lower than that of IEEE 802.11, the length of the two kinds of control frame is comparable to the length of the data frame, even greater than the waste of resend the data frame because of the conflict. So it is not very wise to use the RTS/CTS mechanism in this situation.

5. Conclusions

From the hidden terminal problem experiment, we observed the Different situations when enable and disable the RTS/CTS mechanism in IEEE 802.11 MAC. The hidden terminal problem could be solved in IEEE 802.11 by using RTS/CTS mechanism. And because the length of the two kinds of control frame is comparable to the length of the data frame in IEEE 802.15.4 MAC. RTS/CTS mechanism is not used in IEEE 802.15.4.

References

[1] IEEE P802.15.4/D18, Draft Standard: Low Rate Wireless Personal area networks, Feb. 2003.
[2] IEEE 802.11, Part 11: Wireless LAN medium access control (MAC) and physical layer (PHY) specifications, IEEE, Aug. 1999
[3] Gang Lu Bhaskar Krishnamachari, and Cauligi S. Raghavendra, "Performance Evaluation of IEEE 802.15.4 MAC for Low-Rate Low-Power Wireless Network" Performance, Computing, and Communications, 2004, pp.701-706
[4] Hongqiang Zhai1, Younggoo Kwon, and Yuguang Fang, "Performance analysis of IEEE 802.11 MAC protocols in wireless LANs" Wireless Communications and Mobile Computing, Volume 4, Issue 8, December 2004, pp. 917–931
[5] S. Pollin, M. Ergen, M. Timmers, L. VanDer Perre, F.Catthoor, I.Moerman, and A. Bahai, "Distributed cognitive coexistence of 802.15.4 with 802.11," in Proc. CrownCom, 2006, pp. 1–5.
[6] Wireless Medium Access Control (MAC) and Physical Layer (PHY) specifications for low-rate wireless personal area networks (LRWPANs), IEEE Std. 802.15.4 Std., 2003.
[7] X. Ling, Y. Cheng, J. W. Mark, and X. Shen, “A renewal theory based analytical model for the contention access period of ieee 802.15.4 mac,” IEEE Transactions on Wireless Communications, vol. 7, no. 6, 2008, pp. 2340–2349
[8] Jim T. Geier, Wireless LANs: Implementing Interoperable Networks, New Riders Publishing, Thousand Oaks, CA, 1998

Advanced Materials Research Vols. 989-994 (2014) pp 4082-4085
© (2014) Trans Tech Publications, Switzerland
doi:10.4028/www.scientific.net/AMR.989-994.4082

Research on Halftone Technique of Digital Images

Dai Wenbo[1,a], Chen Liang[1], Zhang Xinwei[2], Wang Le[1], Nie Shiyue[1], Yang Kaijie[1], Wang Yaowen[1]

[1]College of Communications Engineering, PLA University of Science and Technology, Nanjing, Jiangsu, China

[2]Xi'an Public Security Bureau Transportation Police Branch Science and Technology Department

[a]1534730024@qq.com

Keywords: Halftone; Error diffusion; Ordered dithering; Bidirectional feedback; Correction factor

Abstract. Halftone is the key technique for low-resolution equipment like fax machines and printers to reconstruct grayscale images with black and white binary data. Images produced by classic error diffusion algorithm have more abundant color than those made by ordered dithering method. But the problems still exits that there can distortions and false contour phenomenon and fuzzy edges. This paper puts forward an advanced error diffusion algorithm based on bidirectional feedback and improves its feedback type through adding correction factors. The simulation results show that the bidirectional feedback error diffusion algorithm with correction factors better inhibited the phenomenon of distortions and false contour. Directional texture is also improved greatly.

Digital halftone image technique is a technology that transforms an original image with continuous tone into discrete binary pattern of black and white so as to make it have subjective visual effects of continuous tone. It is widely used in printers, fax machines and other binary printing and display equipment.

Over the past twenty years, the digital halftone technique has made great developments by the advent of some good technique, such as ordered dithering[1], the error diffusion algorithm[2], DSB algorithm[2], point diffusion algorithm[3], etc. Among these algorithms, the error diffusion algorithm is widely used and studied because of its good image quality, rich color, anisotropy and no regularity of pixel distribution and its low computational complexity. But the halftone image processed by error diffusion method has the problems of moire and net dot phenomenon together with fuzzy edges and severely missed details. So T.D.Kite and others proposed the improved error diffusion algorithm by referring threshold parameters for threshold modulation of the original error diffusion algorithm. In this paper, with correction factor based on bidirectional feedback error diffusion method further inhibiting distortions and false contour phenomenon and improving directional texture, halftone images are made closer to the original images.

The principle and analysis of error diffusion algorithm

The basic idea of error diffusion algorithm is firstly to compare the current pixel of the grayscale image with a threshold to get a binary output, and then diffuse the pixel differences of input and output to the untreated area with a certain distribution coefficient. This method is an iterative method and there are very big differences compared with other non-iterative halftone methods. In error diffusion algorithm, the quantization error of each pixel of is not only related to the input and output pixel of the position, but is also affected by the quantization error of the treated area. Error diffusion algorithm is therefore a halftone algorithm based on region, and is no longer a point processing procedure[2].Compared with ordered dithering algorithm proposed by Bayer, the halftone images processed by error diffusion method have richer color and their pixel distributions are anisotropic and irregular. But there are still two problems, one is the phenomenon of distortions and false contour appearing in various zones of the halftone image, which means obvious artificial texture will appear in higher and lower brightness zones, as is called the "worm effect"[4]; another

one is that there is a severe loss of detail in the image and the color is inconsistent near fuzzy edges. Due to dot overlapping effect on output devices, it will make the phenomenon more obvious, making the overall image darker.

The improved error diffusion method based on the bidirectional feedback

In error diffusion process, the quality of halftone image varies due to different error filter coefficient. On the idea of error diffusion method of classical single feedback, two error filters are presented in this paper to change one-way feedback into bidirectional feedback. And the correction factor of the error diffusion filter is added to improve. Owing to the error distribution coefficient of each pixel is no longer a fixed value, the added filter and correction factor can adjust the error distribution coefficient in time, which makes diffusion coefficient of error diffusion in an area more reasonable.

In this paper, the filters added in bidirectional feedback error diffusion method introduce the middle frequency band between high frequency and low frequency, which makes the halftone image has a good transition on the band, so as to get a higher quality images.

Figure No.1 is the principle diagram of the improved error diffusion method.

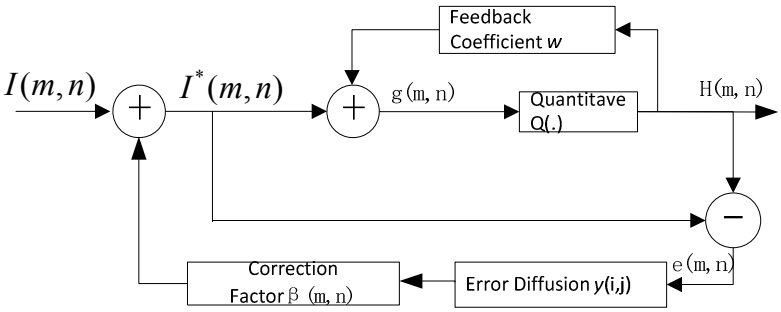

Fig.1 Principle diagram of the improved error diffusion method

Set I , I^* , H respectively represent the input of gray image, the input image after the diffusion of last step, the output of binary image. (m,n) means coordinates of pixel. The flow chart of error diffusion method can be expressed as:

$$I^*(m,n) = I(m,n) - \sum_{m,n} \beta(m.n) * y(i,j) * e(m-i, n-j) \quad (1)$$

()

$$H(m,n) = Q[g(m,n)] = Q[I^*(m,n) + \sum_{k,l} w(k,l) * e(m-k, n-l)] \quad (2)$$

$$e(m,n) = H(m,n) - I^*(m,n) \quad (3)$$

Apply filter y and filter w, in which filter y adopts the principle of diffusion in table 1 and the weight distribution coefficient. * * represents the pixel location of current dot; the arithmetic ratio in other positions represents the error diffusion weight of relative position with current pixel.

Table1 Error diffusion filter y

		**	5	7
3	7	5	7	3
3	3	7	3	3

In the classic error diffusion method, Floyd and Jarris-Judice-Ninke both used error diffusion filter with a fixed weight distribution, but in fact the human eye's sensitivity to noise of different detail areas in image and detail itself is different[5], then the fixed weight distribution cannot be processed very well in the detail part of the image. Here apply a correction factor $\beta(m,n)$ based on regional distribution of variance of a specific image to adjust the weight distribution of filter in time; therefore we make weight distribution better adapted to changes in the luminance values for each pixel.

Steps to determine the correction factor are as follows:

(1) Divide the area with the filter module width of 3×5, calculate the variance of each pixel region as variance of the area. The formula is:

$$p(m,n)=1/13\sum_{i,j}(I(m-i,n-j)-H(m-i,n-j))^2 \tag{4}$$

In which $p(m,n)$ means the regional variance of (m,n).

(2) Select the threshold point of region variance. We choose five characteristic value, as K_i（i=1,2,3,4,5）,from the regional variance as the threshold point of it, then on the basis of regional variance image can be divided into five detail areas. If $K_i < p(m,n) < K_{i+1}$, which means pixels at (m,n) belong to the area i, then we can decide the details area of each pixel by regional variance values;

(3) Calculate the correction factor $\beta(m,n)$ according to the following formula:

$$\beta(m,n)=\frac{p(m,n)-K_{i-1}}{K_i-K_{i-1}}\delta_i+(\delta_{i-1}-\delta_{i-2}) \tag{5}$$

In which δ_i means the experience parameter of correction factor. The choice of δ_i can be used to improve the quality of the halftone image according to the human visual characteristics and the experience of processing image.

Error diffusion filter w can help to introduce middle frequency band. It applies the diffusion principle and distribution weight in table 2:

Table 2 Error diffusion filter w

	**	7
3	5	8

In the table, * * represents the pixel location of current dot; the arithmetic ratio in other positions represents the error diffusion weight of relative position with current pixel.

The analysis of simulation and performance

Simulation based on Matlab platform, this paper uses lena.bmp and PEPPERS.bmp with 256 grayscales as the original image. Respectively we use the classic error diffusion method, error diffusion method based on the bidirectional feedback and error diffusion method with correction factors for image processing.

The classic error diffusion method chooses Floyd filter. The experience parameters δ_i used in correction factors are shown in table 3:

Table 3 Experience parameters

Area ID i	1	2	3	4	5
Experience parameters δ_i	0.05	0.7	0.5	-0.2	0.06

Figure 2 are a comparison for halftone image resulted from three kinds of algorithms and the original image.

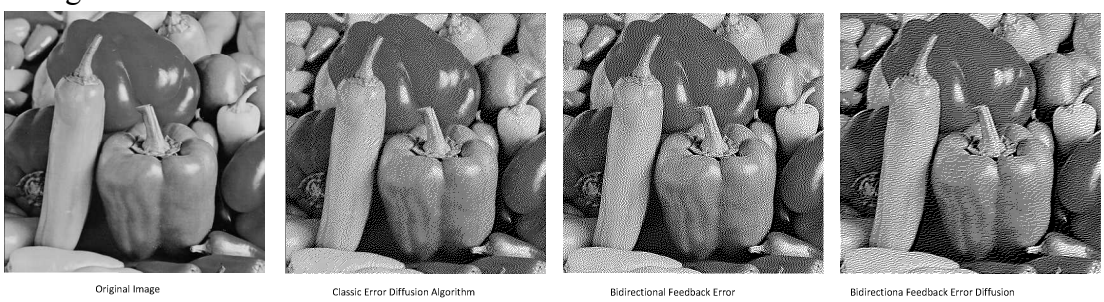

Fig. 2 Comparison of PEPPERS.bmp Quality between 3 Algorithms

The Image quality assessment is to measure the quality of representation by the error it deviates from the original image. Methods are divided into subjective assessment and objective assessment. From subjective view, images resulted from bidirectional feedback error diffusion method are superior to the ones from conventional error diffusion method. There is no clear directional principle. Tone appears more continuous after adding correction factor. We get better approximation to the original image and clearer edges thus retaining more details of the original image information.

In the simulation we use two indicators MSE(mean square error) and PSNR (peak signal-to-noise ratio), to evaluate image quality. The evaluation result is shown in table 4.

Table 4: Evaluation result

algorithm name		Classic algorithm （Floyd filter）	Bidirectional feedback error diffusion method	Bidirectional feedback error diffusion method with correction factor
Image of lena	MSE	17.5476	16.1370	15.4682
	PSNR	35.6886	36.3748	36.7693
Image of PEPPERS	MSE	18.2462	17.5274	15.4359
	PSNR	35.5191	35.6936	36.2455

By the evaluation results, the image effect received from bidirectional feedback error diffusion method is obviously better than that of the conventional error diffusion method, and the correction factor are introduced to further reduce the mean square error, which shows that the method of adding middle frequency band between low frequency and high frequency through double feedback and then using correction factor to adjust the weight of error diffusion based on region variance can effectively reduce the difference between the halftone image and the original image, which makes the halftone image closer to the original image.

Summary

The classic error diffusion method of Halftone algorithms are analyzed in this paper, and on this basis, by adding filter we introduce the middle frequency band and error correction factor to adjust weight distribution, thus we improve the phenomenon of "distortions ", "outline" and directional texture. The direction of next research is to use multiple sets of experience parameters δ_i in simulation test, and to find a set of correction factor of experience parameters δ_i which are more appropriate. Then we can make the processed image avoid the appearance of artificial texture in a larger degree.

Reference

[1] B.E.Bayer, An Optimum Method for Two Level Rendition of Continuous-Tone Pictures；Rec. IEEE Conf. ICC'73, 1973, pp.26-11-26-15.

[2] M.A.Seldowitz, J.P. Allebach, and D.E. Sweeney, Synthesis of Digital Holograms by Direct Binary Search; Appl.Opt., vol26, pp:2788-2798,1987.

[3] M.Mese and P.P.Vaidyanathan, Optimized Halftoning Using Dot Diffusion and Methods for Inverse halftoning, IEEE.Trans. Image Processing, Apr.2000, vol.9, pp.691-709.

[4] Yeyu Fen, GUO Bao, Ma Jia, error diffusion halftoning algorithms based on vision error, Computer Engineering, 2006

[5] Zhang Fang, research of halftone image detail reproduction techniquebased on error diffusion, Nanjing Normal University, 2010

Advanced Materials Research Vols. 989-994 (2014) pp 4086-4090
© (2014) Trans Tech Publications, Switzerland
doi:10.4028/www.scientific.net/AMR.989-994.4086

Research and Implement of Digital Image Watermark Based on DCT

Liyan Liu

Shandong University of Political Science and Law, Ji Nan, Shandong Province, 250014,China

email: Liuliyansd@163.com

Keywords: Digital Watermarking; Discrete Cosine Transforms (DCT); Robust

Abstract. With the rapid development of communication technology and Internet technology, as well as the popularization of computer, the application of digital multimedia technology is more and more widely, video, voice and image gathering, editing, storage, and dissemination of digital information has become more and more convenient. However, it is because of the computer and the network popularization and the fragility of the digital information itself, digital multimedia data are more vulnerable to attack, digital products is also very easy to forged and tampered with. According to these digital multimedia data more easily by illegal processing problem, people put forward the concept of digital watermark. Digital watermark technology is used to realize the protection of digital information. In this paper, the digital watermark technology research starting from the practical application, the digital image watermark based on DCT domain is studied.

Introduction

Digital media has been widely used on people's life, study, work and entertainment, and plays an increasingly important role. However, a number of important digital information may have been stealing, malicious attack and tampered with; Some digital products is easy to get the goods without owner's permission to reproduce and spread by people with the content of the copyright, and achieve the purpose of illegal. As a result, the enthusiasm of digital products producers is diminished, which hinder the development of information industry. To solve above problems, the original method is implemented by encrypting access control and security, but this method cannot completely solve the problem, on the one hand, the encrypted file due to the not understanding of itself in the transmission process will be blocked; On the other hand the encrypted file is easy to attract the attention of the attacker to attack, or cracked and file if the encrypted file is cracked and its protection also disappear, the file content can be arbitrarily unauthorized copying and transmission. Therefore, in the open network environment, the digital watermarking technology situational became a new kind of international copyright protection of digital products and data security maintenance technology effectively. For now, the digital watermark technology is a kind of effective measures and powerful means to realize the media information security, copyright protection and security products, widely used in anti-counterfeiting source, copyright protection, digital certification and safety communications and other fields.

Digital Watermark Technology

The basic principle of digital watermark

Digital watermark technology will directly embed the iconic information into the digital carrier (including software, video, documents, sound, image, etc.), such as: Logo, product serial number, Logo, etc of the individual, and usually does not affect the use value of the original digital carrier, also won't easily to detect and modify again. By hiding in the watermarking information in the digital carrier, can realize products anti-counterfeiting, copyright protection, data integrity, authentication, digital fingerprinting, radio listening, copy control, secure communication, etc.

The concept of DCT

Algorithm is the core of the digital watermark technology, with the continuous development of digital watermark technology, the kinds of watermark algorithm is also emerge in endlessly. Spatial

watermark algorithm, transform domain watermark algorithm and compressed domain watermark algorithm is one of the typical algorithms.

Nowadays, research mainly focused on the transform domain digital watermark algorithm. Based on the transform domain watermark algorithm embedded watermark information will not be easily detected. Because after transformation, the energy of the image become scattered, not easily perceived a single frequency. The typical algorithms of transform domain are discrete cosine transform (DCT Discrete Cosine Transform).

The basic idea of DCT decompose no embed watermark image into 8×8 small pieces, then respectively transform each small piece of DCT, then quantify the results of after transformation in turn, coding in the end. Each small piece of original image after DCT transformation, correction coefficient according to the watermark on the DCT, in order to ensure the correct watermark embedding, and then on each small piece of DCT inverse transformation, when all the sub-block is completed after the process after got the embedded watermark image.

Design and Implement of Image Digital Watermark algorithm based on DCT

The generation of watermark

Before making a watermark embedding, we choose suitable digital image for the laboratory as a watermark image, watermark image should be K×K binary image. This thesis, we select the school pin of Shandong University of Political Science and Law as a watermark image for this experiment. First of all, according to the requirements of this test, the image is set to 64 x 64 sizes and saved as a BMP format images. Secondly, using MATLAB tool to read images, the image grayscale and converted into a binary image. The original image and the converted binary image is shown by fig. 1 (a) and fig. 1(b).

Fig. 1 (a) Gray scale image

Fig. 1 (b) Binary image

Watermark embedding

1) The selection of location

Watermark embedding position should be able to make the watermark information to satisfy their invisibility and robust, and has strong ability against the attack. Due to the strength of the watermark too affected the image visual quality, the strength is too small will make the watermark information is easily damaged. Therefore, the strength of the watermark wants moderate is neither too big nor too small. Because the energy of image signal mainly concentrated in the low frequency part of the DCT domain, the signal energy of the low frequency part is more, so the watermark information should be embedded in the human feel the most important component in the low frequency region, so the watermark system has better resistance to attack. And when the image distortion happens, still can keep the main part of the image.

To sum up, the intermediate frequency part of DCT domain is regarded as the watermark embedded in the best location, can simultaneously satisfy the invisibility and robust of digital watermark

2) The embedding process

According to the selection of watermark embedding positions, we choose the watermark embedded into the intermediate frequency area of DCT domain. Choose a 512 x 512 image as a carrier of BMP format. The watermark embedding process is shown by fig. 2.

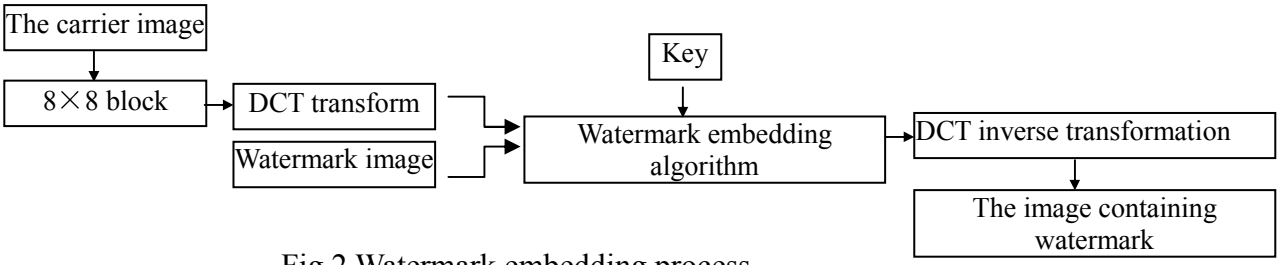

Fig.2 Watermark embedding process

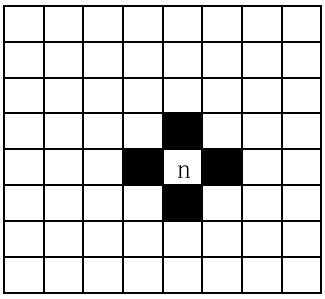

Fig. 3 The location of the n

Watermark embedding key code is as follows:

```
key = 32;
n = 5;

for p = 1:N
    for q = 1:N
        % computing block location information
        x = (p-1)*K+1;
        y = (q-1)*K+1;
        % Extract the piece
        BLOCK = I(x:x+K-1, y:y+K-1);
        % DCT transforms D
        BLOCK = dct2(BLOCK);
temp = mean(BLOCK(n,n-1)+BLOCK(n,n+1)+BLOCK(n-1,n)+BLOCK(n+1,n));
        if J(p, q) == 0
            % If the black pixels
        BLOCK (n,n) = temp + key;
        else
            % If not black pixels
            BLOCK (n,n) = temp - key;
        % dct
        %    dct
        BLOCK = idct2 (BLOCK);
        % Store watermark information
        I(x:x+K-1, y:y+K-1)=BLOCK;
    end
end
```

The analysis of experimental results

The robust verification

The robustness is one of the most important characteristics of digital watermark technology. The robustness of the watermark is refers to the original image containing watermark, after through some process, the watermark information is still able to maintain the integrity, and can be accurately identified. In the above experiments, the key value is different; its effect is also different. We choose

the key take 64 and 4 and the experimental results are analyzed. As shown by fig. 4 and fig. 5. Comparing the experimental results when the key take 4, 32, and 64, the quality of the image is lower, the value of key is smaller, the robustness of the watermark is lower.

The watermark image extracted

The image containing watermark

Fig. 4 Key=64

The watermark image extracted

The image containing watermark

Fig. 5 Key=4

Noise attack

In order to verify the watermark's ability to resist noise attack, to embed the watermark image respectively after joined the salt and pepper noise and gaussian noise, and the watermark image of after add noise watermark extraction. Among them, the salt and pepper noise intensity a is 0.005 and 0.01, the mean of gaussian noise is 0, variance b takes 0.001 and 0.005. Watermark image after add noises shown by fig. 6, the extracted watermark image is shown by fig. 7.

Salt and pepper noise a=0.005 a=0.01 Gaussian noise a=0.005 a=0.01

Fig. 6 The image containing watermark after noise attack

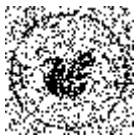

Salt and pepper noise a=0.005 a=0.01 aussian noise a=0.005 a=0.01

Fig. 7The extracted watermark image after noise attack

Filtering attack

In order to verify the Ability of watermark to resist filtering attack, we do to embed watermark image respectively linear filtering, median filtering and adaptive filtering processing, and the treated watermark image watermark extraction. The watermark image after filtering processing is shown by fig. 8, the extracted watermark image after filtering processing is shown by fig.9.

linear filtering median filtering adaptive filtering

Fig. 8 The watermark image after filtering processing

linear filtering median filtering adaptive filtering

Fig.9 The extracted watermark image after filtering processing

Conclusion

In the experiments, the main research problem is the watermark embedding location selection and the selection of embedding strength and watermark embedding algorithm selection. Found by experiment, the algorithm on the premise of meet the invisibility of watermark has a certain resistance to attack ability. Such as gaussian noise attack on watermarking image, the watermark can still under gaussian noise of a certain intensity attacks from primitive watermark extracted with high similarity watermark information, at the same time, the algorithm also has certain robustness

for filtering attack. But, at the same time we also see some disadvantages of the algorithm, such as watermark information has weak robustness under the image processing of increasing strength, we finally won't be able to extract the watermark information from the watermark image, lead to the watermark information was damaged. When used in actual system so need to further improve the performance of the algorithm is further perfect the watermarking scheme, thus improve their practical value.

Acknowledgement

In this paper, the research was sponsored by the Soft Science Research Grant of Shandong Province “On the Legalization of the Regulation of Public Security Video Information System in Shandong Province: Legislative Model and Proposals” (Research Grant No.2013RK01503) and Project of Shandong University of Political Science and Law “Research on P2P Downloading for Criminal Regulation”(Project No. 2011F22B).

References

[1] Chen Qixiang, Yan Cheng-hua, Xie Hui, Design and implementation of the Middle Frequency Hefts Algorithm about Digital Image of DCD domain [J]. IEEE Environmental Science and Information Application Technology (ESIAT), 2010:162 – 165.

[2] S.Tsekeridon, I.Pitas, Embedding Selg-Similar Watermarks in the Wavelet domain [C]. IEEE Int. Conf. On Acoustics: Systems and Signal Processing, 2007:1967-1970.

[3] Liang Tan, Zhi-jun Fang, An Adaptive Middle Frequency Embedded Digital Watermark Algorithm Based on the DCT Domain , IEEE Management of e-Commerce and e-Government, 2008:382 – 385.

[4] Tao Chen, research and application of Digital image watermarking algorithm based on DCT domain, [D]. Shandong Normal University, 2011.

[5] Embedding and Extraction of Digital Watermark Based on DCT [M]. Applied Mechanics and Materials, 2013:276-280.

[6] Jianfei Li , Digital Video Watermarking Algorithm Based on DCT Domain [M].Computational Sciences and Optimization (CSO), 2012:354-357.

Advanced Materials Research Vols. 989-994 (2014) pp 4091-4094
© (2014) Trans Tech Publications, Switzerland
doi:10.4028/www.scientific.net/AMR.989-994.4091

Face Recognition Based on Gabor Filter and Improved Linear Local Tangent Space Alignment Algorithm

Xueyan Xu[1, a], Jiaoyu Liu[1, b], Yuan Shi[1, c], Tuo Deng[1, d]

[1]School of Automation, Wuhan University of Technology, Wuhan, 430070, China

[a]email: XXYWUT@163.com ,[b]email:liujiaoyu_2006@163.com, [c]email: shiyuan0806@126.com,

[d]email: yodashine520@163.com

Keywords: Gabor Wavelet Transform; Improved Local Tangent; Face Recognition

Abstract. In this paper, Gabor filtering and linear local tangent space alignment algorithm and its improved algorithm are used on face recognition. The Gabor wavelet transform can detect the image information in different directions and scales, according to its selective direction and frequency characteristics. The LLTSA reduces the dimension of the sample while the LLTSA and the other improved algorithms extract secondary feature. Experiment and analyze the average recognition rate of the LLTSA and its improved algorithms with the variation of dimension. The experiment results show the effectiveness of the method, increasing the face recognition accuracy.

Introduction

Face recognition usually refers to capture images via smart devices, process image, extract effective identification information and finally identify the classification. Usually face recognition system is mainly divided into four stages. In the first stage we need to face detection, the second stage is to position the separated face feature point. The need for the third phase is to extract the feature from the extracted image. The final stage is a pattern classification of individual. [1]

This paper researches Gabor filtering and linear local tangent space alignment algorithm and its improved algorithm for face recognition. Since the linear local tangent space alignment algorithm may not be optimal projection direction and the field selection needs to be optimized, the linear local tangent space alignment algorithm has been improved in the paper. The experiment proved that the effects of the improved algorithm applied to the face may be raised.

Gabor Filter

Gabor wavelet [2] is proposed through the improvements of the Fourier transform. Fourier transform for the first time introduced the concept of frequency, making it a good solution to convert problems into the frequency domain which can be difficult in the time domain.

The definition of the two-dimensional Gabor wavelet transform and its core function are as follows:

$$\Psi(x,y,\omega,\theta)=\frac{1}{2\pi\sigma^2}\exp\left(\frac{-\left(x_0^2+y_0^2\right)}{2\sigma^2}\right)\left(\exp(j\omega x_0)-\exp\left(\frac{-\omega^2\sigma^2}{2}\right)\right) \tag{1}$$

Among the above formula, $x_0 = x\cos\theta + y\sin\theta, y_0 = -x\sin\theta + y\cos\theta$, x and y represent the spatial domain of the image, ω represents the center frequency, σ represents the standard deviation of Gaussian kernel function.. Moreover, $\exp\left(\frac{-\omega^2\sigma^2}{2}\right)$ represents the DC component. Since the existence of the DC component, the image will not be affected by the absolute values of the gray image and also be not very sensitive to light. $\exp\left(\frac{-\left(x_0^2+y_0^2\right)}{2\sigma^2}\right)$ is Gaussian kernel function and is limited by a Gaussian window function to observe its local information.

According to equation (1) we can know that Gabor filter [3] does well in the identification ability in the spatial domain and frequency domain. In the spatial domain, it changes the image direction by adjustment. Besides in the frequency domain, we can adjust it to have a good selectivity. Choosing different values of ω and θ extracts information on the different directions and scales. Figure 1-1 and Figure 1-2 shows the filtered schematic of the two-dimensional filter bank on the ORL .

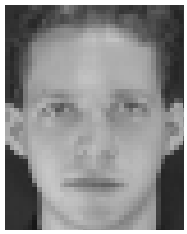

Fig.1. The original image in the ORL face database

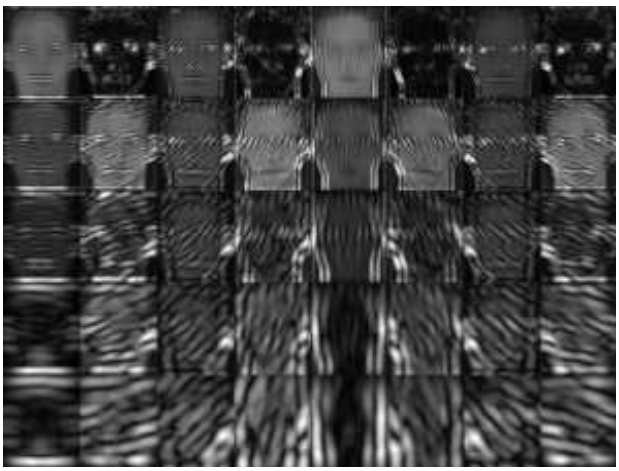

Fig.2. The real part after two-dimensional Gabor filters filter the original image

Linear Local Tangent Space Alignment Algorithm (LLTSA)

Linear local tangent space alignment algorithm (LLTSA) [5] is a linear optimization algorithm for LTSA. The algorithm projects the samples in that direction to reduce the dimension by finding the optimal projection direction. The following describes the algorithm:

Suppose there is a set of samples consisting of $\{x_1, x_2, \ldots, x_n\}$, X_i represents the sample matrix $X_i = [x_{i1}, x_{i2}, \ldots, x_{ik}]$ of k-nearest neighbor for sample points x_i. The aim is to try to find a projection matrix A so that the sample set projects according to the projection direction to obtain the sample points after the projection. The sample points matrix after the projection is configured as $Y = [y_1, y_2, \ldots, y_n]$, and the matrix meets the linear mapping $Y = A^T X H_N$, $H_N = I - e_n e_n^T / n$, e_n represents the column vector of all ones, the purpose of adding H_N is to make the mean be zero between each sample.

The Improvements of Linear Local Tangent Space Alignment Algorithm (LLTSA)

For popular learning, LLTSA will face the problem of adaptive selection. Literature [6] gives the standard for judging whether a neighborhood set of linear subspace determined by best-fit will approach the popular tangent space with high accuracy. According to the literature, the approximation standard of the tangent space is:

$$\left\| X_i - \left(x_i l_{k_i}^T + \tilde{Q}_i \Theta_i \right) \right\| \le \eta \left\| \Theta_i \right\|_F \tag{2}$$

In the formula, $X_i = \lfloor x_{i1}, x_{i2}, \ldots, x_{ik_i} \rfloor$; the right singular vectors of the largest d singular values of $Q_i = \left[x_{i1} - \tilde{x}_{i,}\ x_{i2} - \tilde{x}_i, \ldots, x_{ik_i} - \tilde{x}_i \right]$ consist of a matrix, $\Theta_i = \left[\theta_1^{(i)}, \theta_2^{(i)}, \ldots, \theta_{k_i}^{(i)} \right]$, $\theta_j^{(i)} = Q_i^T \left(x_{ij} - \tilde{x}_i \right)$; $\lambda_1 \geq \lambda_2 \geq \ldots \geq \lambda_{k_i}$ is the singular values in descending order of the matrix $X_i - \tilde{x}_i l_{k_i}^T . Q_i$ is the corresponding right singular vectors of the maximum d singular value. The original standard is equivalent to:

$$\sqrt{\sum_{j \geq d} (\lambda_j)^2} \leq \eta \sqrt{\sum_{j<d} (\lambda_j)^2} \tag{3}$$

According to the above criteria, it will be very easy to get the neighborhood selection criteria, making LLTSA algorithm be the adaptive neighborhood selection, so it is called the improved algorithm the adaptive linear local tangent space alignment algorithm (ALLTSA).

LLTSA algorithm is an unsupervised algorithm linear. As we know that the category information of training samples, we take its classification information into account to improve LLTSA algorithm. We call the improved algorithm discriminated linear local tangent space alignment algorithm (DLLTSA).

In order to eliminate the redundant information, one way is to take constraint of basis vectors on the orthogonal form so that the improved algorithm is called for the orthogonal linear permutation algorithm local tangent space (OLLTSA). The other way is to look for the best vector identification set with statistical uncorrelation, eliminating existed the redundant information of the base vectors, thus we call the improved algorithm unrelated linear local tangent space alignment algorithm (ULLTSA).

Face Recognition Algorithm Based on Gabor Filter and LLTSA

In this paper, integrating Gabor features and algorithms based on the linear local tangent space alignment algorithm for face recognition [7] and experimental comparison. Specific algorithm steps are as follows:

Suppose $X = \{x_1, x_2, ..., x_n\}$ as n pieces (c classes in all) of training images, x_i is the image matrix.

(1) Filtering each face images with Gabor filter in different frequencies and directions to get a lot of groups of Gabor features, n and m respectively represent number and frequency.

(2) Sampling for Gabor features of each group in groups and blocks to get lower dimension characteristics getting the composition of an image matrix c_i, the combination of methods is mentioned above.

(3)For the n samples set $C = \{c_1, c_2, ..., c_n\}$, use $(2D)^2 PCA$ to reduce dimension, then each image matrix is connected by line end to end, each image constitutes a column vector x_i, the matrix $X = [x_1, x_2, ..., x_n]$ is composed of n pieces of pictures.

(4) A secondary feature extraction is to use linear local tangent space algorithms for feature extraction.

(5)Classify the test samples using the above four steps to obtain a low-dimensional feature vector images and then use the classifier for classification.

Comparison and Analysis of the Experimental Results

In this paper, the experiment uses a self-built library of 120 individuals, 20 photos per person, including all kinds of information gestures, facial expressions and so on. For each person, we randomly sample 10 images as training samples, take the remaining 10 as test samples, cycle 20 times and take the average rate as the correct recognition rate. When adding adaption to the algorithm we use the letter A, when the discrimination we use the letter D, when orthogonal we use the letter O, adding no correlation with the letter U.

The results are the variation of dimension followed by the average recognition rate of the five algorithms (LLTSA, OLLTSA, DLLTSA, ALLTSA, ULLTSA) based on face database (abscissa represents the dimension, the vertical axis represents the average recognition rate of the algorithm, the following experiments are the same). The experimental results are shown in Figure 4-1:

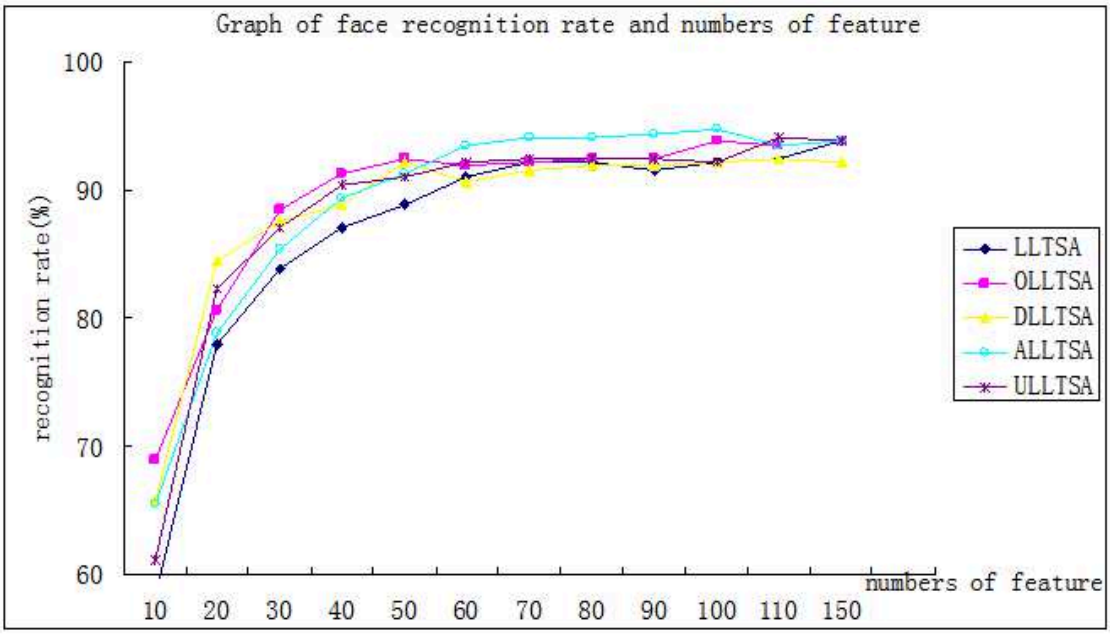

Fig.3.The variation of dimension followed by the average recognition rate of the five algorithms based on face database

From the figure above, between 10-60 dimension the algorithm OLLTSA, DLLTSA, ALLTSA, ULLTSA have improved the recognition rate compared to the linear local tangent space algorithm. After 60 dimensions their recognition rates approach a straight line basically reaching to the maximum recognition rate.

Conclusion

The model adopted and modified with the adaptive algorithm can play a great role in improvement. When adding class information, applying the priori knowledge will help improve the algorithm and recognition rate. After this, constraining the base vectors helps looking for the best vectors to improve algorithm, finding the optimal projection direction to improve the recognition rate, therefore, these improvements can well improve the performance and robustness of the algorithm.

References

[1] Xiangfei Nie. Recognition Review [J]. Chongqing Three Gorges University .2009.3:14-18]
[2] Gang Zhang, Zongmin Ma.A extraction method of sampling Gabor wavelet texture feature [J]. Chinese Journal .2010.15 Image (2):248-254
[3] Rui Sun. Recognition algorithm based on fast Gabor filter [J]. Computer Applications .2012.32 (4):1130-1136
[4] Yanchun Gu.An improved local tangent space alignment algorithm [J]. Application Research of Computers .2013.10:1-6
[5] Wenhua Li. Improved linear local tangent space alignment algorithm [J].Computer Applications .2011.32 (1):247-249
[6] Zheng Wang, Shuicheng Yan.Active learning with adaptive regularization[J].Pattern Recognition. 2011.44(10):2375-2383
[7] Tianhao Zhang, Jie yang. Linear local tangent space alignment and application to face recognition [J].Neurocomputing.2007.70(7):1547-1553

Advanced Materials Research Vols. 989-994 (2014) pp 4095-4099
© (2014) Trans Tech Publications, Switzerland
doi:10.4028/www.scientific.net/AMR.989-994.4095

A new way to optimize LDPC code in multiple access channel

Jingxi Zhang

School of Electrical and Electronic Engineering, North China Electric Power University, Baoding, Hebei, 071003, P.R.C.

zhjxbupt@eyou.com

Keywords: Low density parity check (LDPC) codes; additive white Gaussian noise(AWGN); multiple access channel(MAC); degree profile; density evolution; differential evolution

Abstract. A new way to optimize the degree profiles for irregular LDPC codes in MAC is presented. The combination technology of differential evolution and density evolution is applied in the optimizing of degree distributions. By using a greedy algorithm we show the differential evolution method to seek the maximum noise threshold in MAC channels under different degree number and maximum degree condition.

Introduction

Multiple Access Channel (MAC) is extensively used in modern communication systems. The classical MAC models a communication system in which independent transmitters send messages to a receiver, and Liao[1] derived the capacity region of the classical MAC. Haghi[2] investigates the capacity problem for some multiple-access scenarios with cooperative transmitters and proves a coding theorem.

The indispensable way to approach the capacity region of MAC is by means of coding. Low-density parity-check (LDPC) codes have been shown to achieve low bit-error rates (BERs) at signal-to-noise ratios (SNR) very close to the Shannon limits on many binary-input channels [3][4]. Therefore, LDPC codes are considered to be among the most power-efficient binary codes for digital transmission. If the degree profiles of LDPC codes are optimized, they can be used in MAC. Therefore, it is of great significance to make an attempt to design good LDPC code ensembles for MAC.

In this paper a method used to optimize the LDPC ensemble in MAC is proposed. And based on the method, both good LDPC code ensembles and threshold are obtained under different conditions.

Density Evolution Based on Gaussian Approximation

The design of good degree profiles which give asymptotically good performance in AWGN has been addressed in[5][6]. By approximating the messages passed between Variable Nodes (VN) and Check Nodes(CN), VN and Channel Function Node(CFN) as Gaussian, we have proposed a method to search the degree profile in MAC[7]. Now we will elaborate a way to find the degree profiles that maximize the standard deviation of noise.

Code restraint

The degree profile of LDPC codes is defined as

$$\lambda(x)=\sum_{i=2}^{dv_{\max}}\lambda_i x^{i-1},\ \rho(x)=\sum_{i=2}^{dc_{\max}}\rho_i x^{i-1} \tag{1}$$

Where dv_{max} and dc_{max} are the maximum degree of variable node and check node respectively. And $\lambda(1)=1 \quad \rho(1)=1$ is satisfied. The code rate R and the degree profiles satisfies the following constraint.

$$(1-R)\sum_i \frac{\lambda_i}{i}=\sum_i \frac{\rho_i}{i} \tag{2}$$

Therefore the dependency between them should be removed. By removing the dependency, we can get

$$\lambda_2 = 1 - \sum_{i=3}^{dv_{\max}} \lambda_i , \tag{3}$$

$$\rho_2 = 1 - \sum_{i=3}^{dc_{\max}} \rho_i \tag{4}$$

$$\lambda_{dv_{\max}} = \frac{\frac{R}{2} + \sum_{i=3}^{dc_{\max}} \rho_i \left(\frac{1}{i} - \frac{1}{2}\right) - (1-R) \sum_{i=3}^{dv_{\max}-1} \lambda_i \left(\frac{1}{i} - \frac{1}{2}\right)}{(1-R)\left(\frac{1}{dv_{\max}} - \frac{1}{2}\right)} \tag{5}$$

In this way we can ensure the independency of variable. Let D denotes the number of free elements of the degree sequence (λ,ρ), following the constraint(2),(3),(4), combined with the fact that $\lambda_1 = \rho_1 = 0$, it is easy to find that $L = dv\max + dc\max - 5$. We can form a D-dimensional parameter vector $p = (\lambda_3, \lambda_4, \ldots, \lambda_{dv\max-1}, \rho_3, \rho_4, \ldots, \rho_{dc\max})$ and our objective is to choose the elements of this vector so as to maximize the largest noise threshold.

For a variable node i with degree dv, it receives information from dv-1 neighboring check nodes and channel output, and sends extrinsic information to the target check node j.

Differential Evolution

This is a global optimization problem over continuous spaces, and differential evolution is quite suitable for it. Starting from an initial set of vectors, the algorithm iteratively updates each vector in the set until a vector is found which has the best cost function value. In the following, we briefly review it.

(1) Initialization

Starting from a certain noise level σ, which is the standard deviation of the noise, we randomly choose NP D-dimensional vectors $v_{i,G}$ (i=0,1,…,NP-1) for the first generation G=0, where NP = 20D is an integer that is a constant during the optimization process. Density evolution is run for each vector $v_{i,G}$ as in[7]and its residual error $Pv_{i,G}$,i.e. the fraction of incorrect messages is recorded. The vector with the smallest $Pv_{i,G}$ is labeled as the best vector, $v_{best,G}$.

(2) Mutation

For the next generation, i.e.G+1, new trial vectors are generated according to the following mutation scheme. For each i=0,1,…,NP-1, randomly choose distinct integers r_1,r_2 from [0, NP-1], each different from the index i, and define

$$v_{i,G+1} = v_{best,G} + F \cdot (v_{r1,G} - v_{r2,G}) \tag{6}$$

Where F is a real constant which controls the amplification of the differential variation, and F = 1.0 in our optimization. For each vector, the density evolution is run and its residual error, $Pv_{i,G+1}$, is recorded.

(3) Selection

For each i=0,1,…,NP-1, $v_{i,G+1}$ is obtained as follows:

$$v_{i,G+1} = \begin{cases} v_{i,G+1}, & if\ Pv_{i,G} > Pv_{i,G+1} \\ v_{i,G}, & if\ Pv_{i,G} \le Pv_{i,G+1} \end{cases} \tag{7}$$

Denote the vector with the smallest residual error by $v_{best,G+1}$..

(4) Stop condition

If the residual error $Pv_{best,G+1}$ of the vector $v_{best,G+1}$ is not zero (practically, it is not less than a very small value), return to step 2. Otherwise, increase the noise level by a small value, and return to step 2. If the noise level is increased to a value for which the residual error of the best vector does not converge to zero, the process is stopped. The vector whose residual error goes to zero at the highest possible noise level is labeled as the best vector v_{best}, and the corresponding noise level as the threshold σ*.

In the differential evolution process, a greedy algorithm is applied to search the maximum threshold for a given degree. The trial degree profile is generated in every generation for every population. And the optimum degree profile is obtained. The flow chart to seek the maximum threshold is illustrated in Fig.1. By this way, the degree profile and corresponding threshold are both obtained.

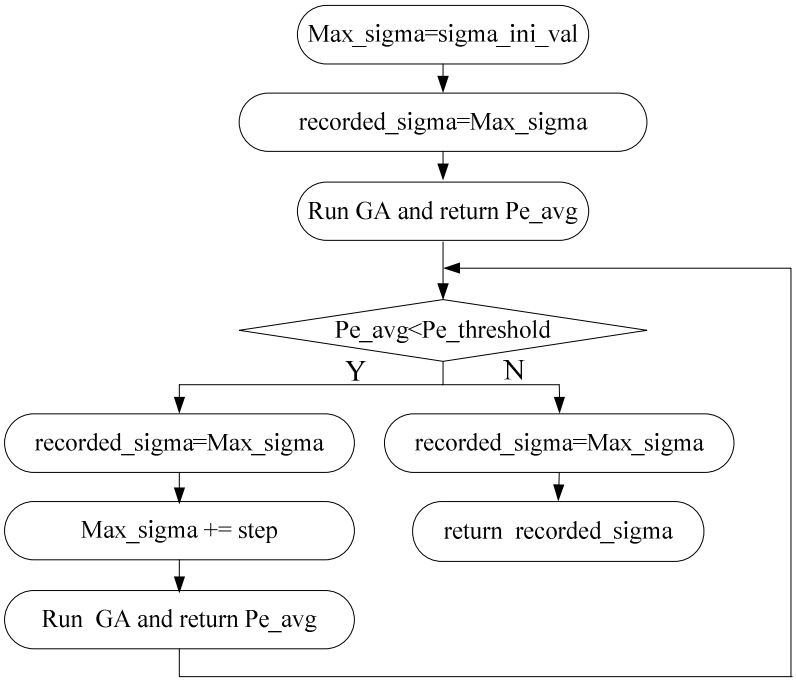

Fig.1 Flow chart to obtain the maximum sigma.

Results

In the differential evolution process, the parameter is set according to Tab.1.

Tab.1 The parameters used in differential evolution

dvmax	dcmax	gene_max	code_rate	Iteration_no	Sigma_ini_val	user_no
20/30/40	10	10	0.5	1000	0.0001	2

The dvmax and dcmax denotes the maximum degree of variable node and check node respectively. The gene_max denotes the maximum generation number of differential evolution. The code_rate denotes the code rate of LDPC code. The iteration_no denotes number of iteration in density evolution process, sigma_start user_no denotes the number of users in MAC.. The optimized degree profiles are shown in Tab.2, Tab 3 and Tab 4 with dvmax being 20, 30, and 40 respectively. The dv_no represents the number of variable node degree, and D(σ) in the table stands for the variation of the optimized threshold. It can be seen from these tables that the noise threshold varies slightly with the number of variable node degrees, i.e. the more the degree number, the higher the noise threshold. By comparison of Tab.2, Tab.3 and Tab. 4 we can see that the higher the maximum degree, the higher the threshold, and the variation is quite small. Considering the complexity in construction of LDPC code, four or five degree is enough.

Tab.2 The results of searched degree profile and the noise threshold with dvmax being 20

User no	2			
dv_no	3	4	5	6
dvmax	20			
(i)λ	(2) 0.2389	(2) 0.3325	(2) 0.2961	(2) 0.3127
	(3) 0.3315	(3) 0.05519	(3) 0.192	(3) 0.14
	(20) 0.4296	(4) 0.2648	(4) 0.04436	(4) 0.156
		(20) 0.3475	(5) 0.1002	(5) 0.0116
			(20) 0.3674	(6) 0.02292
				(20) 0.3567
(j) ρ	(7)0.03982	(7) 0.5103	(7) 0.3233	(7) 0.4483
	(8) 0.9602	(8) 0.4897	(8) 0.6767	(8) 0.5517
σ*	0.868	0.869	0.869	0.872
D(σ)	2.492e-005	2.126e-005	5.137e-005	1.888e-005

Tab.3 The results of searched degree profile and the noise threshold with dvmax being 30

User no	2			
dv_no	3	4	5	6
dvmax	30			
(i)λ	(2) 0.1815	(2) 0.2656	(2) 0.3079	(2) 0.2857
	(3) 0.2959	(3) 0.02292	(3) 0.03925	(3) 0.04322
	(30) 0.5227	(4) 0.2547	(4) 0.01466	(4) 0.0984
		(30) 0.4568	(5) 0.2831	(5) 0.1186
			(30) 0.3551	(6) 0.0517
				(30) 0.4023
(j) ρ	(9) 0.3049	(9) 0.87	(8) 0.6101	(8) 0.194
	(10) 0.6951	(10) 0.13	(9) 0.3899	(9) 0.806
σ*	0.868	0.881	0.884	0.885
D(σ)	0.03572	3.351e-005	1.465e-005	1.596e-005

Tab.4 The results of searched degree profile and the noise threshold with dvmax being 40

User no	2			
Dv_no	3	4	5	6
dvmax	40			
(i)λ	(2) 0.1307	(2) 0.1935	(2) 0.2213	(2) 0.3017
	(3) 0.3355	(3) 0.08914	(3) 0.005358	(3) 0.01729
	(40) 0.5338	(4) 0.1812	(4) 0.2145	(4) 0.0269
		(40) 0.5362	(5) 0.04813	(5) 0.01164
			(40) 0.5107	(6) 0.2841
				(40) 0.3584
(j) ρ	(10) 0.4796	(10) 0.1832	(10) 0.3655	(9) 0.9883
	(11) 0.5204	(11) 0.8168	(11) 0.6345	(10) 0.01174
σ*	0.869	0.881	0.889	0.893
D(σ)	0.06589	0.0006545	7.362e-027	2.045e-028

Summary

.Differential evolution is an optimized search technology and it is used in the search of good degree profiles of LDPC codes in AWGN MAC. In the search process, the target function is defined as the residual error and a greedy algorithm is proposed to seek the maximum noise threshold. Good degree distributions are obtained in MAC channels and these degree distributions are evaluated by density evolution algorithm to satisfy the error probability requirement.

Acknowledgment

The paper is supported by “the Fundamental Research Funds for the Central Universities (9161113003)”.

References

[1] H. Liao, “A coding theorem for multiple access communications,” in Proc. IEEE Int. Symp. Inf. Theory, Asilomar, CA, 1972.

[2] A. Haghi, The Capacity Region of p-Transmitter/ q-Receiver Multiple-Access Channels With Common Information, IEEE trans on information theory, VOL. 57, NO. 11, NOV. 2011,pp7359-7376

[3] T. J. Richardson, A. Shokrollahi, and R. Urbanke, “Design of capacityapproaching irregular low-density parity-check codes,” IEEE Trans. Inform. Theory, vol. 47, pp. 619–637, Feb, 2001.

[4] S. Y. Chung, G. D. Forney, T. Richardson, and R. Urbanke, “On the design of low-density parity-check codes within 0.0045 dB of the Shannon limit,” IEEE Commun. Lett., vol. 5, pp. 58–60, Feb. 2001.

[5] T. Richardson and R. Urbanke, “Capacity of low density parity check codes under message passing decoding,” IEEE Trans. Inf. Theory, vol. 47, no. 2, pp. 599–618, Feb. 2001.

[6] S. Y. Chung, T. Richardson, and R. Urbanke, “Analysis of sum-product decoding of low-density parity check codes using a Gaussian approximation,” IEEE Trans. Inf. Theory, vol. 47, no. 2, pp. 657–670, Feb. 2001.

[7] Jingxi Zhang, Zhisong Bie, Weiling Wu, “Enhancing the Performance of IDMA System by Irregular LDPC Codes”, ICWMMN2010, Beijing, China, Sep.2010

Advanced Materials Research Vols. 989-994 (2014) pp 4100-4103
© (2014) Trans Tech Publications, Switzerland
doi:10.4028/www.scientific.net/AMR.989-994.4100

A Study and Design of Compressed Encoder based on Neural Network for Remote Sensing Image

Ling Tao[1, a], Wenlong Li[1, a], Yanyan Yu[1, a], Jian Kang[1, a], Jun Yang[1, a]

[1]Department of Information Science and Engineering, Yunnan University, Kunming, China

[a]junyang@ynu.edu.cn

Keywords: remote sensing image, FPGA, neural network, compression encoder

Abstract. The characteristics of remote sensing image are big data volume and high resolution. It is difficult to meet actual demands by using traditional techniques for transmission and storage. This paper studies and designs remote sensing image compression encoder with FPGA technology and three-layer feedforward BP neural network. The neural network can parallelly process large amounts of data, and has a structural characteristic of self-learning and self-organizing. The encoder has a simple structure, safety, fast speed, good reconfiguration. It overcomes shortcomings of conventional compression techniques which compress high-resolution images ineffectively. The study has some theoretical values in the field of image compression.

Introduction

With the development of high-tech science and technology, satellite remote sensing technology will grow rapidly. That is, remote sensing data will grow exponentially, the current channel capacity and transmission capacity are difficult to reach its transport requirements. So the compression of remote sensing data is an effective method to solve the problem. It can effectively improve confidentiality and transmission rate of remote sensing data .

There are many traditional image compression methods, such as JPEG, effective wavelet compression method, etc. These methods only apply to some low-resolution ordinary images, but high-resolution remote sensing images which must get higher requirements of data compression. Traditional compression encoders are difficult to meet actual demands, so they are processed by a more efficient compression encoder.

This paper proposes a three-layer feedforward BP neural network algorithm, which uses its own characteristics to achieve remote sensing data compression encoder. The characteristics have the highly parallel, the synchronization information storing and processing, and the self-organizing and self-learning. Besides, it implements compression encoder with reconfiguration and flexibility of FPGA technology. The encoder has some characteristics of high compression ratio, high security and speed in order to meet actual needs.So it has some prospects in the field of image compression.

All manuscripts must be in English, also the table and figure texts, otherwise we cannot publish your paper.

BP neural network compression principle and algorithm

Remote sensing image compression principle: Fig.1, a set of input pattern is mapped to another set of output pattern by a small number of hidden layer units, and the output mode is equal to the input mode. The input layer is original image, the output layer is reconstructed image, the hidden layer is compressed image. In fact, the data processing between input layer and hidden layer is coding process, and decoding process is between hidden layer and output layer. Compression ratio is the ratio of input layer nodes and hidden layer nodes (less than input layer nodes).

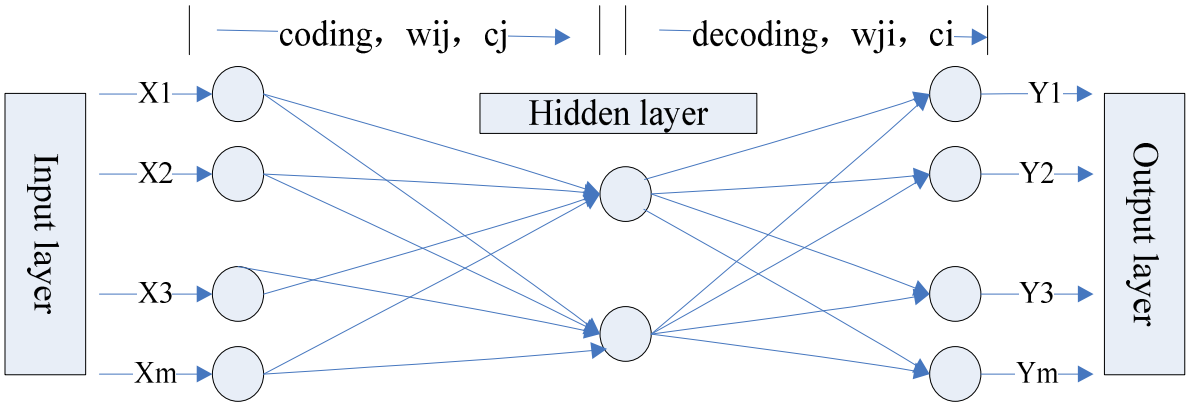

Fig.1, Three-layer feedforward BP neural network compression model

The input data of remote sensing image division and sample learning: image block of N×N pixels is divided into some same image blocks of P×P pixels. Each pixel point of the image block corresponds to an input/output neuron. The neural network selects P×P original image block as a sample by a random way. The sample repeats self-learning and self-organizing, and constantly corrects connection weights and thresholds between neurons, and which ultimately make the error between output values and desired output values of remote sensing image to a minimum. In this case, the hidden layer neuron vector is compression image data, the output layer neuron vector is reconstructed image data. Finally, the three-layer feedforward network will be used as a model of FPGA design. Input / output data model is shown in Fig.2.

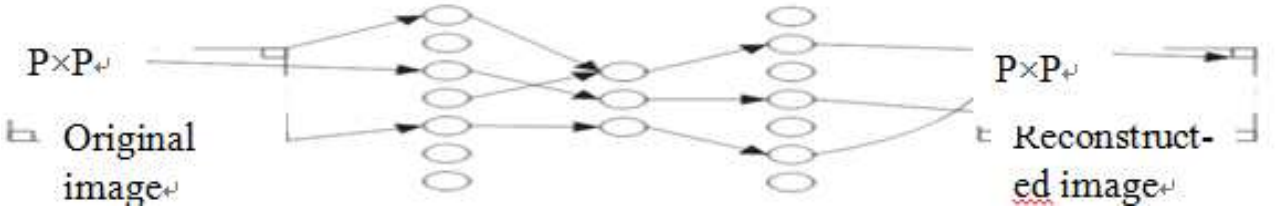

Fig.2, Input / output data model

BP neural network algorithm: Fig.1, Select a set of input values in the input layer, and then calculate the output values of hidden layer and output layer.
The j-th output value of hidden layer neuron:

$$h_j = f\left(\sum_{i=1}^{m} w_{ij} x_i + c_j\right), 1 \le j \le I \tag{1}$$

The i-th output value of output layer neuron:

$$y_i = g\left(\sum_{j=1}^{I} w_{ji} h_j + c_i\right), 1 \le i \le m \tag{2}$$

Hardware design principle of remote sensing image compression

Remote sensing image compression structural design. Design principle: Fig.3. First, in the compression coding process, input data of remote sensing image needs preprocessing, that is, it is divided into equal smaller blocks, data of each block will be transformed into a column vector. All column vector data need to be stored in the data buffer (fifo memory). Second, a set of input data is removed from the data buffer every time, and then forms image compressed data through BP network coding circuit. Finally, the compressed data will be stored in the compressed data buffer (fifo memory). Similarly, the compressed image forms reconstructed image through BP network decoding circuit.

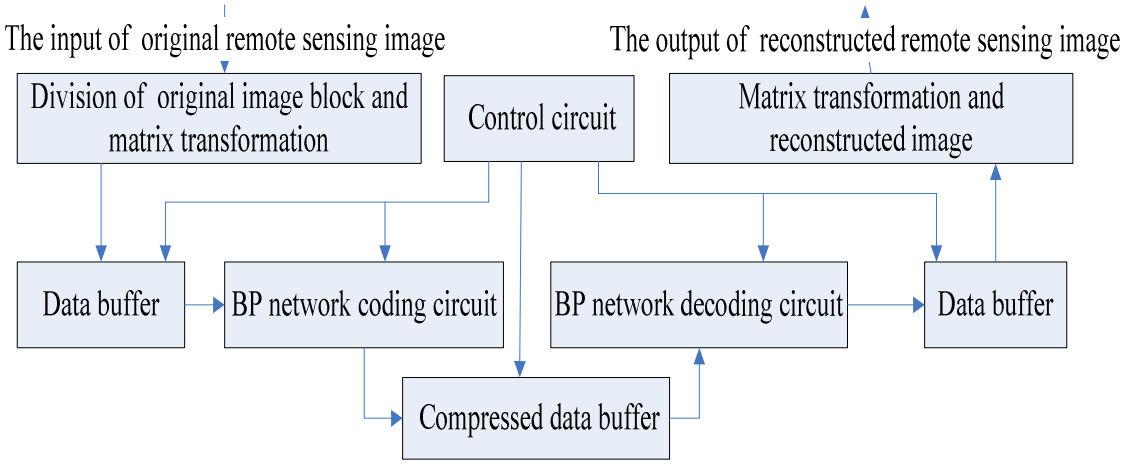

Fig.3. The overall structural design of image compression

FPGA design and implementation of BP neural network encoder. The main structure of encoder has MAC multiplier-accumulator and LUT lookup table. Fig.4, the input layer has four input values (x1, x2, x3, x4), the hidden layer has two output values (y1, y2). First, all weights are loaded from an input w, and shifted to each register according to the order, which reduces the number of chip pins and makes the chip integration become higher. And the corresponding weights and input values are multiplied and accumulated, the final results are output by LUT.

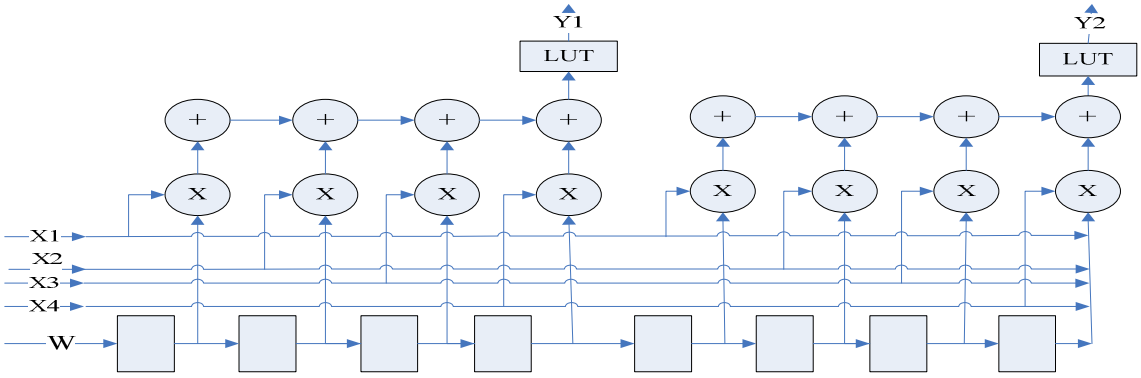

Fig.4,BP neural network coding structure

Waveform simulation of BP neural network encoder core circuit is shown in Fig.5. The input signal has a clock signal (clk), four input values (x1, x2, x3, x4), eight weights (w) which need eight registers to store. The input values and weights are 8-bit signed binary signal. The output signal has coding output values(y1, y2), test output signal (test) which checks all weights into these registers and outputs coding result.

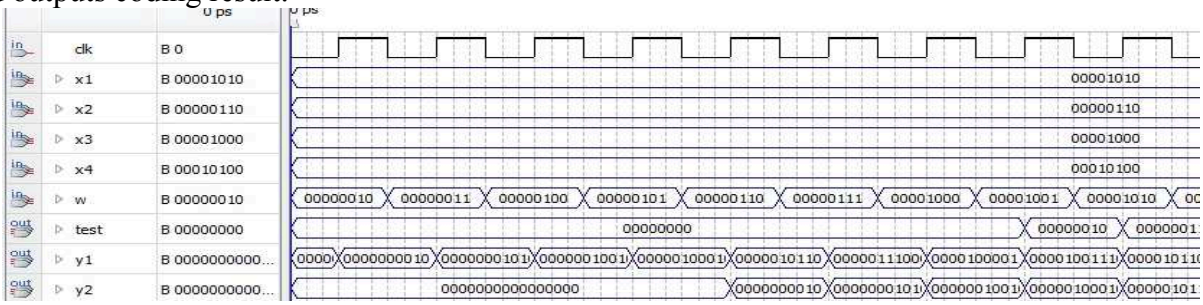

Fig.5, Waveform simulation of BP neural network encoder core circuit

The compression encoder calculates y1= 0000000100111010, y2 = 0000000010001010, that is, the simulation is correct. Then this paper does 4 times, 8 times, 12 times, 16 times compression experiments for remote sensing image. Conclusions: Table 1, compared with the traditional image compression encoders, less than 8 times, compression effect of BP neural network encoder has not

obvious advantages, however, more than 8 times, it has better compression effect. Therefore, transmission and storage of the compressed data have higher reliability and speed. Compression effect of the encoder based on FPGA has certain advantages.

Table 1 Compared with similar traditional encoders

Parameter	Less than 8 times	More than 8 times	Reliability	Speed
The encoder	Good effect	Better effect	Higher	Faster
Traditional encoders	Good effect	Poor effect	Lower	Slower

Conclusion

This paper studies and designs key technologies of remote sensing image compression based on three-layer BP feedforward neural network, and uses FPGA technology to design an encoder based on three-layer feedforward BP neural network. Compared with similar conventional encoders, the encoder has a higher compression ratio, more simple structure, good reconfiguration, higher security and speed. So the study in this paper has some theoretical values in the field of image compression.

References

[1] Yuanbin Hou, Jingyi Du, Mei Wang. Neural networks, Xi'an: Xi'an University of Electronic Science and Technology Press, 2007,08.(In Chinese)

[2] Yuzong Quan. Neural network control, Xi'an: Xi'an University of Electronic Science and Technology Press, 2009. (In Chinese)

[3] Jianbin Jin, Yuanqin Wang, Yuan Chen. Optimization strategies of BP neural network Based on Genetic Algorithm . Computer and Modernization, 2010,9:88-91. (In Chinese)

[4] Jun Yang. SOPC practice tutorials based on FPGA, Science Press, 2010. (In Chinese)

[5] Sun Jian, Zhang Xiong-wei, and Sun Xin-jian. A new training algorithm for quantum neural networks[J]. Signal Processing,2011, 27(9): 1306-1312. (In Chinese)

[6] Min Zhang. Improved image compression based on BP neural network, Liaoning Institute of Technology Journal, 2007,8,27 (4) :258-262. (In Chinese)

[7] Song Pan, Jiye Huang. EDA technology and VHDL (3rd edition), Tsinghua University Press, 2009. (In Chinese)

[8] Texas Instruments. TMS320DM642 Video/Imaging Fixed-Point Digital Signal Processor (SPRS200J), August,2005.

Advanced Materials Research Vols. 989-994 (2014) pp 4104-4106
© (2014) Trans Tech Publications, Switzerland
doi:10.4028/www.scientific.net/AMR.989-994.4104

A New Method of Image Matching in a Vision-Based Mobile Robot System

Cheng-Zhi CAO[1,a], Wen-Zheng GAO[2,b], Hui-Jun LI[1,c*]

[1]Center for Computer Fundamental Education, Jilin University, Changchun 130012, China

[2]Audi China Enterprise Management Co. Ltd, Building B6, 751D park,

Jiuxianqiao Road, Beijing 100000, China

[a]caocz@jlu.edu.cn, [b]wenzheng1010@live.cn, [c]lihuijun@jlu.edu.cn

[*] Corresponding Author

Keywords: vision-based, mobile robot, image matching, RANSAC, matched points

Abstract. In a vision-based system for mobile robot/human localization in the environment, extracting feature from images and image matching are important for the final results. Although there are many algorithms for image matching, they are not fit for this system. A new method is designed to improve image matching effect.

Introduction

In a vision-based system for mobile robot/human localization[1,2,3] in the environment, a fixed camera is used to supervise the environment where the robot works and moves around. Usually the robot motion is fixed, so the human target is needed to be estimated. The human and robot relative positions are estimated in the mobile robot frame by visual information. The probability of an accident is calculated by deriving a set of positions and relative velocities[4]. In such a system, extracting feature from images and image matching are important for the final results. There are several widely used algorithms for feature extraction. Features of an image usually are contours, straight lines and points. After extracting features from images, the next task is to match these features. Image matching is also a basic problem in the field of computer vision, such as object recognition, image stitching and motion tracking.There are many solutions for the matching problems,e.g. Random Sample Consensus[5] (RANSAC). The condition, on which RANSAC can fairly estimate the model, is contrast to the one in our system. With the general idea of RANSAC, a new method to eliminate incorrect matches is introduced.

Background and Related Work

RANSAC is an iterative method to estimate parameters of a mathematical model from a set of observed data which contain outliers. It is a non-deterministic algorithm in the sense that it produces a reasonable result only with a certain probability, with this probability increasing as more iterations are allowed. An advantage of RANSAC is its ability to do robust estimation of the model parameters, i.e., it can estimate the parameters with a high degree of accuracy even when amount of outliers are present in the data set. A disadvantage of RANSAC is that there is no upper bound on the time it takes to compute these parameters. When an upper time bound is used (a maximum number of iterations) the solution obtained may not be the optimal one, it may not even be one that fits the data set in a good way. A reasonable model can be estimated by RANSAC only with a certain probability, a probability that becomes larger the more iterations that are used. Another disadvantage of RANSAC is that it requires the setting of problem-specific thresholds.RANSAC can only estimate one model for a particular data set. As for any one-model approach when two (or more) models exist, RANSAC may fail to find either one.

Solution

Although RANSAC is robust to estimate the model parameters, and with a high probability to find the correct one, it has one condition that the correct matched points are in a high proportion in all matched points. And there should be more candidate matched points as input. If the missed matched points are the majority, RANSAC can not find the correct model with a high probability and the consensus will be a set of miss matched points.

The condition, on which RANSAC can fairly estimate the model, is contrast to the one in this project. With the general idea of RANSAC, a new method to eliminate incorrect matches is introduced.

Because the reconstruction of the model from 2D image to 3D world is a rigid-body transform, the distance between each two points, no matter it is in the model or in real world, is the same during rotation and translation. The proportion between the distance in model and the distance in real world is nearly the same if the matches are correct. So there is an algorithm based on the proportion of the distances among all matches.

There are some assumptions to be satisfied for this method:

1. The reconstruction of the model from 2D image to 3D world must be a rigid-body transformation. Otherwise the distance of any two points can change during the motion.
2. There should be not too few correct matched points among all matches.

The input of the proposed method is a set of matched points between the model and the captured image. The output is a set of correct matches. The method is depicted as follows:

1. Pick up all matched points and eliminate duplicated points.

Assuming the matched points in model are in the set S_M, and the correspondent matched points in matched image are in the set S_I. The definitions of the two sets are:

$$S_M = \{{}^M P_1, {}^M P_2, \ldots, {}^M P_i, \ldots, {}^M P_n\},$$

$$S_I = \{{}^I P_1, {}^I P_2, \ldots, {}^I P_i, \ldots, {}^I P_n\},$$

where ${}^M P_i$ is a point in model matched to the point ${}^I P_i$ in captured image. The entropies of the two sets are the same. The duplicated matches mean that the value of ${}^M P_i$ is the same as the value of ${}^M P_j$ while the correspondent ${}^I P_i$ is the same as ${}^I P_j$ and $i \neq j$.

There could be many duplicated matches with the same point in model and correspondent matches in captured image. We have to delete all such kind of data to make sure all the rest data are distinct to each other.

2. Pick up one point in model and compute the Euclidian distance between this selected point to the other points in model. The Euclidian distance in model ${}^M D_{ij}$ is defined as:

$${}^M D_{ij} = \sqrt{({}^M P_i.x - {}^M P_j.x)^2 + ({}^M P_i.y - {}^M P_j.y)^2}, \quad (1)$$

where $i \neq j$, and $i, j = 1, \ldots, n$.

3. Do the same calculation as in step 2 with the correspondent point in captured image. A set of distances between one point and the others are computed. The definition of Euclidian distance in image is defined as:

$${}^I D_{ij} = \sqrt{({}^1 P_i.x - {}^1 P_j.x)^2 + ({}^1 P_i.y - {}^1 P_j.y)^2}. \quad (2)$$

4. Calculate the proportion P between this distance in image and the correspondent distance in model.

For example, we have the distance ${}^I D_{12}$ of point **1** and point **2** in model image, and the distance ${}^M D_{12}$ between the matched points in captured image **1'** and **2'**. The proportion PP_{12} is ${}^I D_{12} / {}^M D_{12}$ (or ${}^M D_{12} / {}^I D_{12}$depends on the threshold you choose). These calculated proportions are in the set S:

$$S = \lfloor PP_{12}, \ldots, PP_{ij}, \ldots, PP_{n,n-1} \rfloor,$$

where n is the number of the calculated proportions in set S, and $i \neq j$.

5. Pick up one proportion PP_{ij} in S to calculate the difference between this proportion and the other proportion PP_{kl} in S where $ij \neq kl$.

If there exists a difference less than a desired threshold t, put these point numbers (which consist of the distances in model as i, j) into the set S^*. Recursively select proportions until S is empty.

6. Repeat step 2 to step 5 until all the matched points are calculated.

7. Find the point which identified in S^* most frequently. This point is regarded as a confident point which we believe is the correct match.

8. Compare this point with the other points in S^*, to make sure that the incorrect points are removed.

The set S^* contains all the possible models. Among these models, some are incorrect. But these incorrect models are generated by the previous procedures. This may be caused by the symmetric model which generates the same symmetric features on both sides of the symmetric line of the model. This kind of situation will be described in chapter 5. So we need to remove the wrong matched points. One possible method is to compare these missed matches with the most confident match. The points in model should be in the same relative position of the points in image. For example, assuming the directions of the model and the target are the same, and there is a match AB with point A in model and point B in image, and the most confident match CD with point C in model and point D in image. If A is top-left of C in model, B should be top-left of D in image when the match CD is correct. Otherwise, CD is an incorrect match and should be removed from set S^*.

This method is simple to understand and implement compared with RANSAC. There is no need to generate the transform matrix. It is not necessary to estimate a model to make other points to fit for this model.The time complexity of this method is $O(N^2)$. N is the number of matches. It is very fast when N is small. Compared with RANSAC, this method can pick out more correct matches. Because RANSAC works well when there is a large number of matches and the minority of matches are missed ones. But in our visual-based system, there are fewer matches and some of them are missed matches. So this method works well in this kind of condition.

The disadvantage of this method is that it can not recognize correct matches if they are too few among all matches. After all, this method is more suitable for the condition of our vision system.

References

[1] Richard M. Murray, Zexiang Li, S.Shankar Sastry: A Mathematical Introduction to Robotic Manipulation, Robotica, Vol. 18 Issue 1, January 2000.

[2] Dieter Fox, Wolfram Burgard, Sebastian Thrun: A hybrid collision avoidance method for mobile robots, Robotics and Automation, 1998.

[3] R.V. Bostelman, T.H. Hong, R. Madhavan, T. Y. Chang: Safety Standard Advancement Toward Mobile Robot Use Near Humans, 4th International Conference on Safety of Industrial Automated Systems, Chicago, IL, September 26-28, 2005.

[4] Ruslan Asaula, Daniele Fontanelli, Luigi Palopoli: A Probabilistic Methodology for Predicting Injuries to Human Operators in Automated Production lines, Emerging Technologies & Factory Automation, 2009.

[5] Martin A. Fischler and Robert C. Bolles, Random Sample Consensus: A Paradigm for Model Fitting with Applications to Image Analysis and Automated Cartography, Commun. ACM, Vol. 24, No. 6, pp. 381-395,1981.

Advanced Materials Research Vols. 989-994 (2014) pp 4107-4110
© (2014) Trans Tech Publications, Switzerland
doi:10.4028/www.scientific.net/AMR.989-994.4107

The research of Starry-sky image bright stray light background suppression method

Guo shao-jun[1, a], Wang-zhe[2,b]

[1] Graduate student 3th team of Navy aeronautical and astronautical university ,Shandong province Yantai City,264001,China

[2] Strategic missile engineering department of Navy aeronautical and astronautical university,Shandong province Yantai City,264001,China

[a] Email:guoba2000@163.com,[b] painel@sina.com

Keywords: bright stray light suppressed, targets submerge, background subtraction, target pixel extraction

Abstract. The space-based visible observation imaging platform for sky targets is influenced by many factors, a serious factor is the light of background too bright. A image with the bright stray light background has some high gray areas those may submerge the targets info. Aimed at the shortcomings of traditional background removal method in target extraction under the bright stray light background, according to the differences of bright stray light background and sky targets imaging characteristics, this paper has made some research of the algorithms about how to remove the bright stray light background but not delete the targets info. The algorithm we got that give us great results will be shown in the paper. It solves the problems of the bright background light removal and greatly retain the targets info which submerged in the bright areas.

Starry-sky image quality depressed by highlight background

Through the analysis of starry-sky image histogram, we found that the histogram distribute according to gauss curve, just as the figure 1(b) show us. The objects and stars have high gray scales but the background have low gray scales. Preference 1 has shown us how to fit the histogram as gauss curve, then get the background average and standard variance. Make $Threshhold = u + c * \sigma$ to subtract the image background so as to avoid the influence of the background. u is the average of background gray scales, c is a constant, σ is standard variance.

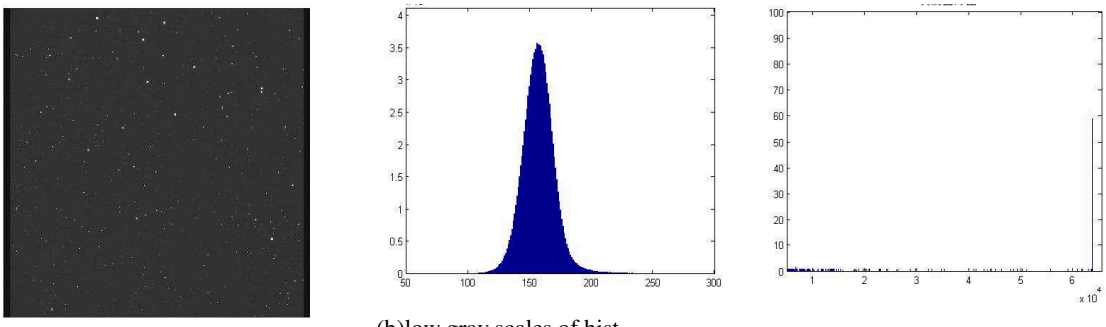

(a)starry-sky image (b)low gray scales of hist (c)high gray scales of hist

Figure 1 Starry-sky image gray histogram without highlight background

Unfortunately, because of the exist of bright stray light background in the starry sky, the gauss threshold cannot make the image background subtraction great enough to satisfy the need of stars detecting algorithm. Figure 2(c) gives the background subtraction result of a starry-sky image by gauss threshold without amelioration, where μ= 801.6136, σ= 49.7033, Figure 2(b) shows the gauss curve which we tried to fit the histogram gray scales.

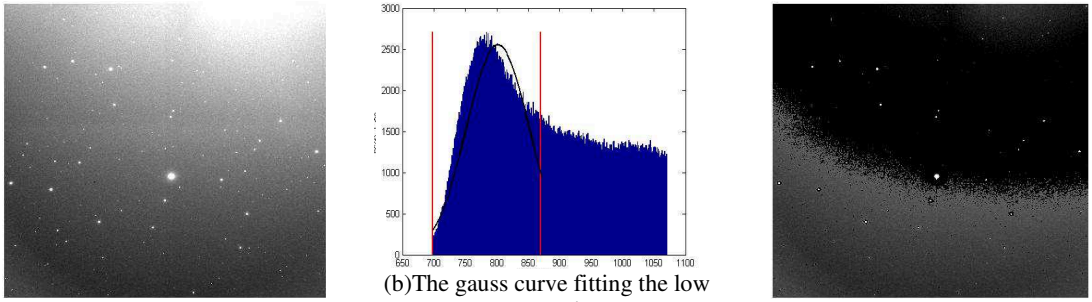

(a)starry sky image with highlight background

(b)The gauss curve fitting the low gray scales

(c)The background subtracting starry-sky image

Figure 2 Parameter estimation of starry-sky image by gauss curve fitting algorithm

The histogram of starry-sky image with bright stray light background doesn't fit the distribution of gauss curve any more, there are a lots of middle gray scale pixels between the background gray scales and objects gray scales, which is the influence of the bright stray light background. The background average value and standard variance will be a little small if using the gauss algorithm to fit the gray scales directly, consequently, the binary image based on gauss threshold will exist a lot of "1" area pixels which will affect the objects info detection.

Bright stray light restrain algorithm

For starry-sky images like figure 2, objects and stars info can not be detected effectively because of the background can not be entirely estimated. For this reason, the paper restrained the starry-sky background firstly, then tried to fit the background gray scales as gauss curve distribution. The steps:

(1)Processing the starry sky image with average filter. The template of the filter is $n\times n, n=3,5,7$ for this paper, $n=3$.

(2)Do morphologic operation to the step(1) images.

(a)Setting the radius, create the morphologic template.

Calculate the distant R of the template coordinate and the focus coordinate, make the value of the template coordinate "1" if the distance is less than R ,else "0".

$$dis[(x,y),(x_0,y_0)]=\sqrt{(x-x_0)^2+(y-y_0)^2} \qquad x,y=0,1,2,\cdots 2R \qquad (1)$$

$$if\ \ dis <= R \qquad x_0,y_0=R$$

$$temp(x,y)=1$$

$$else$$

$$temp(x,y)=0.$$

$(x,\ y)$ is the template coordinate and (x_0,y_0) is the focus coordinate, $temp$ is the matrix of template in formulae (1).

(b)Making the erode operation with template

Processing the image pixel $r(x,y)$ just follow the steps hereinafter:

Check the pixels with the coordinate which has the distant from the focus coordinate of the template less than *R* one by one, subtract the template value from the pixels value and record the numbers. Make the least value as $r(x,y)$.

(c)Operate twice with morphologic dilating operator of the template

Morphologic dilating operator is the counter operator of eroding operator, which add the template value and the the pixel value, and then make the largest value as $r(x,y)$.

(d)Another erode operation

(3)Subtracting the bright stray light after morphologic operation

(a)Calculate the average of the starry sky image, record as $avgval$.

(b)Add the pixels value of the origin image and $avgval$,then subtract the pixels values of image after morphologic operation and the last values of the matrix is the image without the stray light.

The results of experiment

The gauss curve fitting algorithm can estimate the parameters of the image which without bright stray light background, but parameters of images with the bright stray light background can not be rightly estimated by gauss curve fitting algorithm. This paper has brought forward the bright stray light restrain algorithm, the results of experiment as the figure 3 shows confirm the restrain algorithm can bring the great image matrix values those can rightly be fitted by gauss curve fitting algorithm.

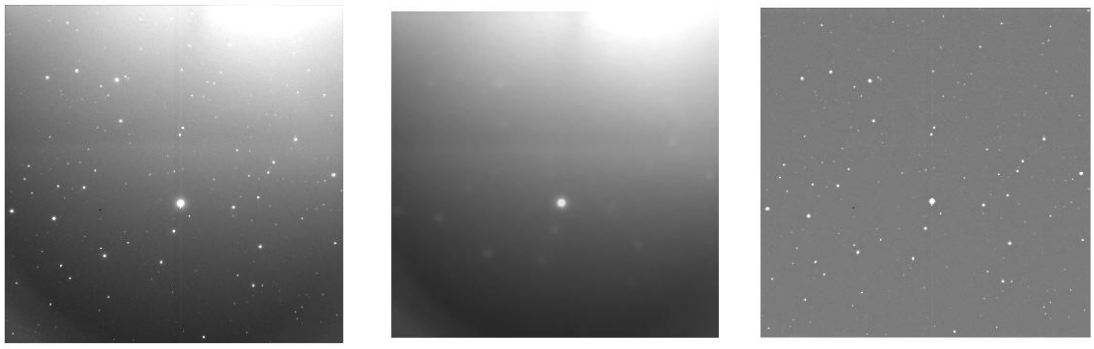

(a)Average filter result (b)Morphologic operate result (c)Subtract bright stray light result

Figure 3 Bright stray light restraining and subtracting results

The bright stray light restrain algorithm can bring the great effect as Figure 4 shows, where $\mu = 1058.9, \sigma = 8.5047$.

Figure 4 shows that we can get better objects and stars detecting results if the image with bright stray light background can be operated by the restrain algorithm of this paper.

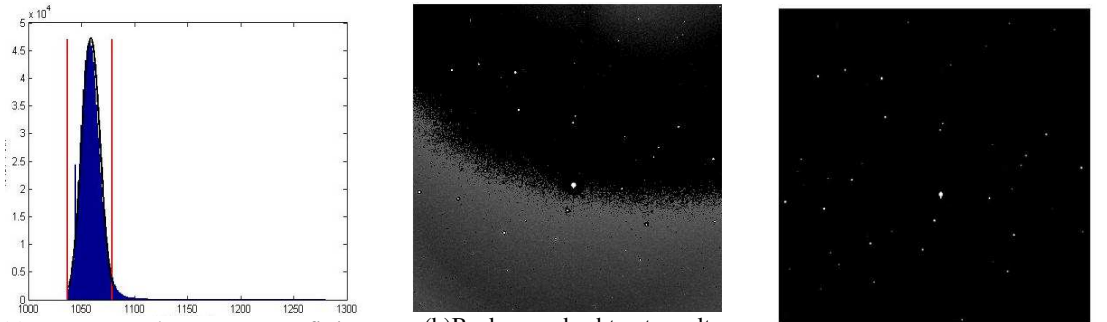

(a)Low gray scales gauss curve fitting after background restrain (b)Background subtract result without stray light restrain (c) Background subtract result with stray light restrain

Figure 4 The effect of restrain algorithm

Summary

The exist of bright stray light may effect the imaging of objects and stars, it can make stars and objects in the highlight area hard to detect. This paper has researched out the bright stray light restrain algorithm based on do not effect the stars and objects pixels info. The result of experiment has shown the advantage and reliability and practicability of the algorithm to the starry sky images with bright stray light background.

Reference

[1] Zhang Chunhua, ChenBiao, Zhou Xiaodong. Small target trace acquisition algorithm for sequence star images with moving background. Optics and Precision Engineering.2008,16（3）：524-530.

[2] Lincoln Laboratory. MASSACHUSETTS INSTITUTE OF TECHNOLOGY. Efficient Detection of Small Moving Objects. Technical Report 846.

[3] Yuping Lin· Qian Yu· Gérard Medioni.” Efficient detection and tracking of moving objects in geo-coordinates”. Machine Vision and Applications (2011) 22:505–520

[4] Brown, M., Lowe, D.G.: Recognizing panoramas. In: ICCV’03.

[5] Proceedings of Ninth IEEE International Conference on Computer Vision, pp. 1218–1225 (2003)

[6] Smith, K., Gatica-Perez, D., Odobez, J.-M.: Using particles to trackvarying numbers of interacting people. In: CVPR, pp. 962–969(2005)

[7] Yang, R., Pollefeys, M.: Multi-resolution real-time stereo on com-modity graphics hardware. In: CVPR, pp. 211–217 (2003)

[8] Lowe, D.G.: Distinctive image features from scale-invariant key-points. Int. J. Comput. Vis.60(2), 91–110 (2004)

[9] Khan, Z., Balch, T., Dellaert, F.: MCMC-based particle filtering for tracking a variable number of interacting targets. IEEE PAMI 11, 1805–1918 (2005)

[10]Kruger J., Westermann, R.: Linear algebra operators for gpu imple-mentation of numerical algorithms. In: International Conference on Computer Graphics and Interactive Techniques, pp. 908–916(2003)

Advanced Materials Research Vols. 989-994 (2014) pp 4111-4114
© (2014) Trans Tech Publications, Switzerland
doi:10.4028/www.scientific.net/AMR.989-994.4111

Body Surface to External Channel Modeling

YiHuai Yang[1, a], Lifang Wang[1, b*], DongYa Shen[2, c], Miao Yang[3,d]

[1]School of Automatic Control and Mechanical Engineering, Kunming University, 650214, China

[2]School of Information Science & Eng., Yunnan University, 650091, China

[3]Yunnan Testing Institute of Product Quality Supervision, 650231, China

[a]yyh_td@126.com, [b*]lfw2924@163.com, [c]shendy@ynu.edu.cn, [d]yangmiao216@sohu.com

Keywords: Wireless Body Area Network (WBAN); Channel Modeling; Time Variant Channel Fading; Channel Time-Coherence.

Abstract. In order to build WBAN devices and design WBANs, it is imperative to study the characteristics of WBAN channel and model the channel accurately. WBAN channel models are so different from the traditional mobile channel models and there are few publications on them. In this paper, we studied the statistic characteristics of the WBAN channel based on the IEEE 802.15.6 models. We focus on body surface nodes to external nodes, simulated the path loss models on 820 MHz and 2.36 GHz at both LOS and NLOS situations. We also used the Gauss model to fit the statistic results of the path loss and obtained coefficients of Gauss model.

Introduction

As an emerging application in short range wireless radio technology, WBANs have received a growing interest in scientific and industrial communities recently. It can be used for promising prospects across a range of applications, including military services, sport monitoring, personal entertainments, especially the healthcare. It provides an economical solution to rising costs in the healthcare system and promises unobtrusive ambulatory health monitoring for a long period of time and provide real-time updates of the patient's status to the physician.

An important step in the development of a wireless body area network is to design and evaluate specifications of PHY for WBANs, suitable channel models are necessary. However, due to the complexity of the human tissues structure and body shape, it difficult to drive a simple path loss model for WBAN.

There are been various analytical and experimental studies of propagation characteristics for WBANs during the past few years [1,2]. The IEEE 802.15 task group 6 was established in the year of 2007 to develop communication standard optimized for low power devices and operation both in-body and on-body. The channel modeling subgroup released the final channel model for WBAN in July 2010 [3].

In order to find more realistic channel models for WBANs, in this paper we studied IEEE802.15.6 WBAN channel models [3] based on statistical analysis method and used MATLAB software to do computer simulation. The scenarios we studied are body surface to external CM4, including scenario S6 and S7 situations for both LOS and NLOS circumstance. We did simulation at 820 MHz and 2.36 GHz medical frequency band. We statistic studied the characteristics of the path loss models and used the Gauss model to fit the statistic results of the path loss.

The remainder of the papers is organized into three sections. 'Model Description' presents channel models used in this study. Simulation results and corresponding parameters and coefficients are given in "Simulation Results". The final section concludes our work.

IEEE 802.15.6 Channel Models

In November 2010, according to the positions of transceiver nodes, the TG6 defined the WBAN channel models which covering seven scenarios [3]. They are Implant to Implant, Implant to Body

Surface, Implant to External, Body Surface to Body Surface (LOS), Body Surface to Body Surface (NLOS), Body Surface to External (LOS), and Body Surface to External (NLOS) scenarios. We have studied the first five scenarios in our previous papers. In this paper, we focus on Body Surface to External both at LOS and NLOS situations.

The details of experimental method and equipment used for these measurements can be found in [4]. This section presents summarizes of the channel path loss results. The transmitter is placed on the chest and the receiver is away from the body with various distances as outlined. Each channel measurement is of approximately 5 s in duration and consists of multiple 40 ¹s blocks that are separated in time by 2.5ms.

The channel path loss $PL(t)$ at a given time t is given by [4]:

$$PL(t) = P_{tx} - P_{rx}(t) + G_{amplifiers} - L_{cable} \quad (1)$$

where P_{tx} is transmitted power, $P_{rx}(t)$ is the RMS received power at time t, $G_{amplifiers}$ is amplifier gain, and L_{cable} is cable loss. The path loss sometime may decrease with increased distance in some measurements, but the general trend is increase. Table. 1 summarizes the average path loss results, Table. 2 summarizes the path loss variation. The transmitter was placed on the right wrist and the receiver was stationary.

Table. 1 Average Path Loss (dB)

		LOS				NLOS			
	Distance (m)	1	2	3	4	1	2	3	4
820MHz	Standing	47.84	65.29	65.72	70.72	60.27	65.60	70.94	74.43
	Walking	48.12	57.42	59.02	58.65	51.85	57.51	63.19	62.51
2.36GHz	Standing	59.78	73.04	67.20	63.61	69.30	72.62	73.72	74.40
	Walking	55.68	58.90	61.92	65.18	58.26	60.89	61.92	63.15

Table. 2 Path Loss Variation(dB)

		LOS				NLOS			
	Distance (m)	1	2	3	4	1	2	3	4
820MHz	Standing	0.49	0.77	1.09	1.13	0.34	0.81	1.42	1.25
	Walking	20.59	9.28	21.18	14.48	17.78	16.73	16.63	12.75
2.36GHz	Standing	1.38	1.36	3.95	0.81	2.11	0.84	0.92	1.36
	Walking	24.71	24.23	20.21	15.52	24.62	21.83	20.05	16.54

The path loss of NLOS is larger than the LOS situation, because the signal is shadowed by the human body.

Simulation Results

In this section, we give the simulation results of nodes on body surface to body surface external nodes CM4 (Scenario S7 & S8) for 820MHz and 2.36GHz.

A. CM4 for 820MHz （LOS）

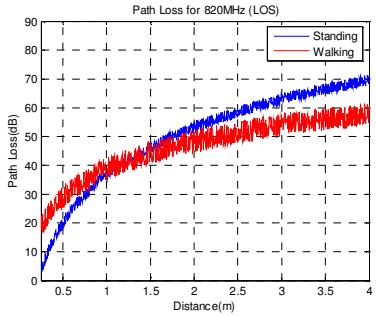

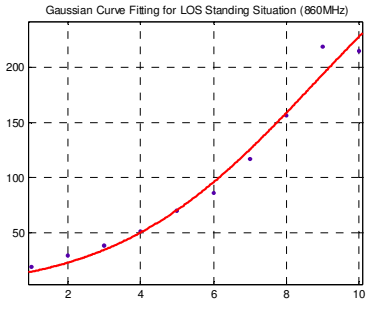

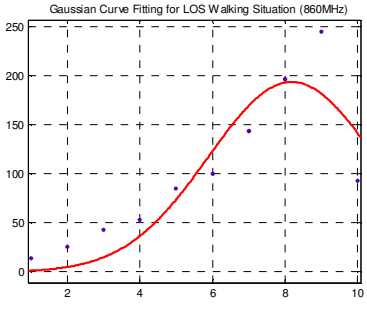

Fig. 1 Path Loss for 820MHz Fig. 2 Curve Fitting for Standing Situation Fig. 3 Curve Fitting for Walking Situation

B. CM4 for 820MHz （NLOS）

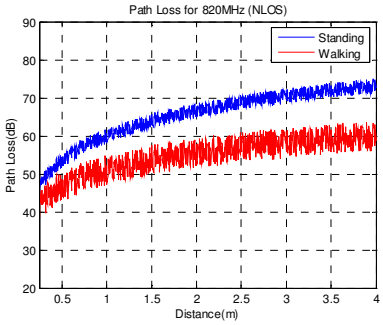

Fig. 4 Path Loss for 820MHz

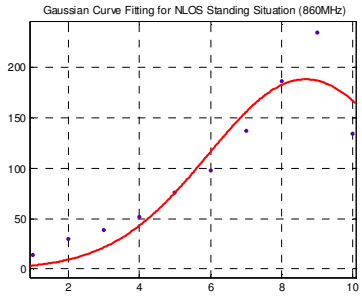

Fig. 5 Curve Fitting for Standing Situation

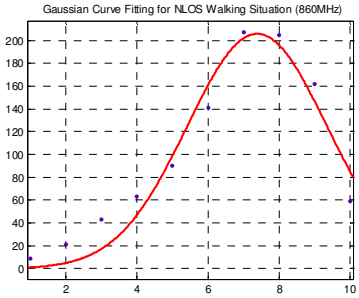

Fig. 6 Curve Fitting for Walking Situation

C. CM4 for 2.36GHz （LOS）

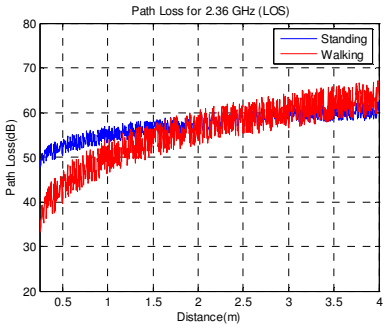

Fig. 7 Path Loss for 820MHz

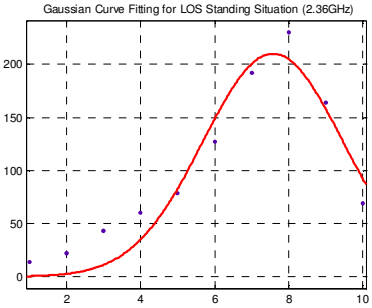

Fig. 8 Curve Fitting for Standing Situation

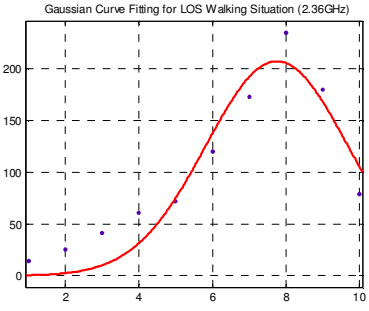

Fig. 9 Curve Fitting for Walking Situation

D. CM4 for 2.36GHz （NLOS）

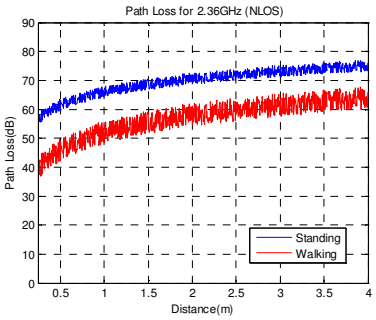

Fig. 10 Path Loss for 820MHz

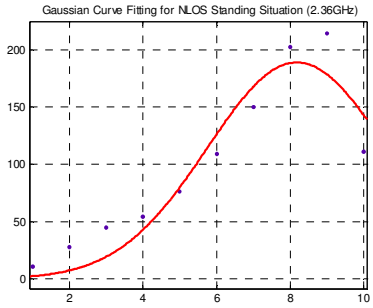

Fig. 11 Curve Fitting for Standing Situation

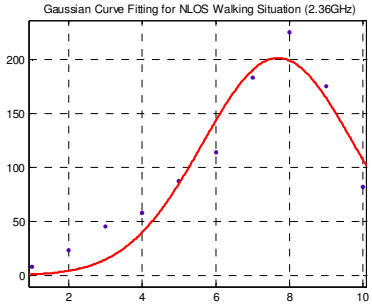

Fig. 12 Curve Fitting for Walking Situation

Fig.1, Fig. 4, Fig.7 and Fig. 10 are path loss curves for LOS 820MHz, NLOS 820MHz, LOS 2.36GHz and NLOS 2.36GHz respectively. Fig. 2, Fig. 3, Fig. 5 and Fig. 6 show Gauss curve fitting of the statistic characteristics of path loss for LOS 820MHz of standing situation, LOS 820MHz of walking situation, NLOS 820MHz of standing situation and NLOS 820MHz of walking situation. Fig. 7, Fig. 8, Fig. 11 and Fig. 12 show Gauss curve fitting of the statistic characteristics of path loss for LOS 2.36GHz of standing situation, LOS 2.36GHz of walking situation, NLOS 2.36GHz of standing situation and NLOS 2.36GHz of walking situation respectively.

We use the Gauss general model: $f(x) = ae^{-\left(\frac{x-b}{c}\right)^2}$ to fit the statistic characteristics of path loss. The coefficients (with 95% confidence bounds) and the goodness of fit are shown in the Table 3.

Table 3. Coefficients of Gauss model and the Goodness of fitting

			Coefficients of Gauss model			Goodness of fitting			
			a	*b*	*c*	SSE	R-square	Adjusted R-square	RMSE
860MHz	LOS	Standing	307	14.1	7.502	1061	0.9787	0.9726	12.31
		Walking	193.8	8.185	3.247	9316	0.8172	0.765	3648
	NLOS	Standing	188	8.674	3.851	4941	0.8944	0.8642	26.57
		Walking	205.8	7.383	2.785	2727	0.9443	0.9283	19.74
2.36GHz	LOS	Standing	210	7.577	2.674	3942	0.921	0.8985	23.73
		Walking	207.6	7.753	2.733	4898	0.9013	0.873	26.45
	NLOS	Standing	188.9	8.185	3.438	4361	0.9029	0.8752	24.96
		Walking	201.4	7.694	2.905	3965	0.9174	0.8938	23.8

Conclusion

Channel models of WBANs can be used to understand wave propagation in and around the human body and they are essential for antenna design, protocol design and the design of front-end RF hardware and modulation schemes. In order to obtain a sophisticate wireless technology and design WBANs with high efficiency and high reliability, the knowledge about the propagation characteristics of WBANs must be thoroughly investigated. In this paper, we studied the path loss models of body surface to external CM4 (Scenario S6 & S7) for 860MHz and 2.36GHz and obtained coefficients of Gauss model.

Acknowledgement

This paper is supported by National Science and Technology Major Project (2010ZX03007-001); Yunnan Natural Science Key Foundation of China (2013FA027); Yunnan High-Tech Top-Talents Recruitment Project (2012HA005) and Kunming University Scientific Research Project (XJL12006).

References

[1] Sana Ullah, Pervez Khan, Niamat Ullah, Shahnaz Saleem, Henry Higgins, and Kyung Sup Kwak: *A Review of Wireless Body Area Networks for Medical Applications*. ArXiv:1001.0831v3 [cs.NI] 3 Aug 2010.

[2] Harri Viittala, Matti Hämäläinen, Jari Iinatti, Attaphongse Taparugssanagorn: *Different experimental WBAN channel models and IEEE802.15.6 models: comparison and effects*. ISABEL 2009, Bratislava, Slovakia, Nov. 24-27, 2009.

[3] IEEE 802.15 WPAN Task Group 6 (TG6) Body Area Networks. [Online] Available: http://www.ieee802.org/15/pub/TG6.html.

[4] Dino Miniutti, Leif Hanlen, David Smith, Andrew Zhang, Daniel Lewis, David Rodda, Ben Gilbert, "*Narrowband on body to off body channel characterization for ban*," IEEE 802.15-08-0559-00-0006, August 2008.

[5] Jung-Hwan Hwang, Il-Hyoung Park, and Sung-Weon Kang: *Channel model for human body communication*. IEEE 802.15-08-0577-01-0006, July 2010.

[6] Zasowski T, Althaus F, Stäger M, Wittneben A, Tröster G. *UWB for noninvasive wireless body area networks: channel measurements and results*. IEEE Conference on Ultra Wideband Systems and Technologies (UWBST) 2003.

[7] Fort A, Desset C, Ryckaert J, De Doncker P, Van Biesen L, Wambacq P. *Characterization of the ultra wideband body area propagation channel*. International Conference ICU 2006; 22-27.

[8] Molisch A. *Statistical properties of the RMS delay-spread of mobile radio channels with independent Rayleigh fading paths*. IEEE Trans. Veh. Technol; 45: Feb. 1996.

Advanced Materials Research Vols. 989-994 (2014) pp 4115-4118
© (2014) Trans Tech Publications, Switzerland
doi:10.4028/www.scientific.net/AMR.989-994.4115

Research and Solution on Bottleneck Problem in Zigbee

Jianping Zhang, Xiaoling Zeng

Chongqing Creation Vocational College, China

mybaoer@126.com, zenxiaoling123@163.com

Keywords: Converge Cast, Bottleneck, Scheduling.

Abstract. When the root is collecting data at a tree-based network, more upper nodes is usually with more packets usually. We called this bottleneck problem. The goal of this paper is to solve the bottleneck problem in ZigBee tree network. We use The Beacon-Only Period Approach which has been proposed by IEEE802.15.4b to avoid the collision caused by beacon frame. Moreover, we propose a centralized algorithm (TDMLF) that enables the nodes to fully use the GTS transmission. TDMLF not only avoides the hidden node problem which occurs in IEEE802.15.4, but also enables the entire network to achieve a more effective parallel transmission. Simulation results show that the TDMLF algorithm effectively reduces the bottleneck problem, and thus achieves a high delivery ratio. Moreover, because of no collision, the TDMLF also reduces the waste of time and energy by retransmission.

Introduction

The ZigBee standard provides three kinds of network topology: star, tree and mesh. In order to enhance expandability and apply electric power effectively, this paper selects cluster tree network for discussion. When network performs data collection, there is higher flow and bottleneck problems occurs easily because inner layer nodes must help outer layer nodes deliver data. When data collection is carried out for ZigBee cluster tree, there is no handshaking mechanism in IEEE802.15.4 standard. Thus, when the number of child nodes of ZigBee Router (ZR) is large, competition will be quite fierce so that ZR fails to receive data effectively and the bottleneck problem occurs. To address this problem, this paper puts forward a new scheduling method, i.e. Top Down Maximum Load First (TDMLF), and uses Guaranteed Time Slot (GTS) that will not cause collision to transmit packets.

A ZigBee network consists of three different types of nodes: ZigBee Coordinator (ZC), ZigBee Routers (ZRs) and ZigBee End Devices (ZEDs) [1]. IEEE802.15.4b task group has two main jobs: explaining ambiguous parts in the IEEE802.15.4 standard and improving shortages of the standard [2]. Reference [3] puts forward scheduling algorithm which transmits nodes at the bottom layer first and make data achieve the effect that they are transmitted from bottom to upper layer. Thus, the delay time from the moment when nodes transmit data to the time at which ZC receives data can be reduced. However, the method sets the time at which all nodes are awake as the same. If so, nodes on the upper layer, which hope to help nodes on the lower layer to transmit data, may suffer the bottleneck problem. Reference [4] puts forward a new Active Period collocation method that is called Time Shift Grouping Access (TSGA). To make ZC be able to receive data constantly during the whole Beacon Interval (BI) at which beacon frames are transmitted, the method divides the whole network into two sub-trees. When the first sub-tree transmits data to ZC, the second sub-tree can make full use of this time to collect data; vice versa. This transmission mode is similar to D-MAC [5]. However, length of the activity interval of each node in this method may not be able to accord with their flows. To ensure each ZR has enough time to transmit all data that need be delivered, TDBS proposes an approach in which work cycle can be decided according to data size [6]. In TDBS, the work cycle of each ZR is exponential power of 2 and must be larger or equal to sum of all sub-ZRs. When ZC extends its work cycle to 1, its activity interval will occupy the whole BI, which makes the activity interval of ZRs on the first layer fail to be staggered from ZC. This will disobey principles of the Time Division Approach.

In order to solve the bottleneck problem, this paper puts forward a new scheduling algorithm, i.e., TDMLF. In TDMLF, ZC will configure appropriate GTS according to flow of each node, which makes nodes that have higher flow can obtain more opportunities of transmission.

The Algorithm

This paper considers environment of periodic return and assumes that ZC knows topology and interference conditions of the whole network. The bottleneck problem is not serious in network with small scale and flow is not serious, so this paper focuses on analyzing network with large scale and flow. Our designed protocol adopts the Beacon-Only Period (BOP) approach that all nodes can enter the activity interval simultaneously, as shown in Figure 1.

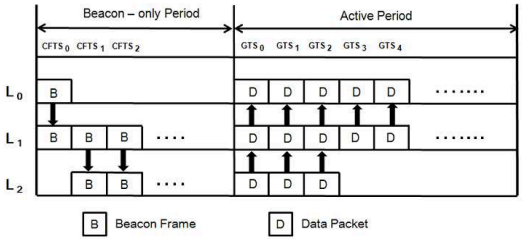

Fig. 1 Proposed superframe format

In Fig. 1, one BI is divided into two parts, i.e., BOP and Active Period, which is composed of Contention Free Time Slots (CFTS) and GTS, respectively. It is set that the time that ZC takes to implement one data collection is one BI, it will imply that ZC cannot finish all data collection within one BI and the bottleneck problem will occur if the time at which nodes generate a group of data is too short. To reduce occurrence rate of this situation, we aim at increasing parallelization transmission and making ZC can receive data constantly in order to shorten length of BI.

In BOP, ZC allocates CFTS to each ZR, which makes it be able to transmit Beacon frames in CFTS that it belongs to instead of causing collision. The algorithm used to allocate CFTS is shown as follows.

Algorithm 1: CFTS allocation
Step 1, ZC sorts all ZRs in the network according to following conditions:
(1) Height of sub-trees (in descending order)
(2) The number of ZRs (in descending order)
(3) ID (in ascending order)
Step 2, ZC checks whether ZRs that have been sorted accord with following specifications or nor:
(a) Have received but not transmitted Beacon frames
(b) Neighboring father nodes are not allocated with CFTS
(c) Neighbors of sub-nodes are not allocated with CFTS
If the ZR passes the inspection, it can be allocated with CFTS.
Step 3, if all ZRs are allocated with CFTS, end the algorithm. Otherwise, i+1 and return to Step 2 to continue implementation.

The Beacon-Only Period Approach proposed by IEEE802.15.4b will cause much collision during Active Period. To avoid collision, we let all nodes transmit data by using GTS. However, in the standard, length of a GTS is (1/16) *k (k is a positive integer from 2 to 15) of the activity interval. However, the length is too large and it is not divided specifically. In this paper, we fix the size of a GTS as the time that complete transmission of a data packet needs. This period of time contains four parts, including transmitting a packet, waiting for Ack, time used to transmit Ack and a LIFS. In detail, the LIFS directs at making MAC layer have time to process data received from PHY layer. Thus, when a packet is received, a period of waiting time about LLIFS is needed. At initialization of network, ZC will implement TDMLF algorithm proposed by us to allocate GTS transmitted by all nodes in the network. The algorithm about allocation GTS is shown as follows.

Algorithm 2: TDMLF algorithm
Step 1: ZC sorts all ZRs in the network according to following conditions:
(1) The number of hops of ZC (in ascending order)
(2) The number of packets in buffer (in descending order)
(3) ID (in ascending order)
Step 2: check whether ZRs that have been sorted accord with following specifications or nor:
(a) There are packers that wait for being transmitted in buffer.
(b) All neighboring sub-nodes are not allocated with GTS.
(c) Father nodes and neighbors of father nodes are not allocated with GTS.
If the node passes the inspection, it can be allocated with GTS and the number of its buffer packets will reduce by 1 and the number of its buffer packets in its father nodes will increase 1.
Step 3: if ZC receives data of all nodes, end the algorithm. Otherwise, i+1 and return to Step 1 to continue implementation.

Simulation and Analysis

To verify the foregoing algorithms, we carry out simulation to comparie the two protocols TDMLF and TDBS By comparing the following three indexes, performance of the network is measured.

Goodput (kbps): average amount of the information that ZC receives each second correctly.

Delivery Ratio (%): the ratio of data generated by all nodes and transmitted to ZC successfully.

Power Consumption per Packet (mJ): the electric power consumed by transmitting one packet to ZC averagely.

Artificial network scene is in a 100*100m^2 square area. 100 ZRs and 200 ZEDs are deployed evenly and randomly [7]. To make ZED help us detect a larger scope, we deploy 88 ZEDs in the scope of a hop, which is obtained via extending original area outward, as shown in Fig. 2. Draw a grid line each 10 meters on x axis and y axis. Besides, node reservation is arranged at intersection of grid lines. However, each node and grid point will have a random displacement about 0-3 meters at x axis and y axis, which makes topology different when simulation is carried out each time.

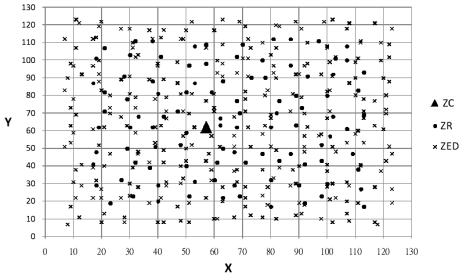

Fig. 2 Network stationing method

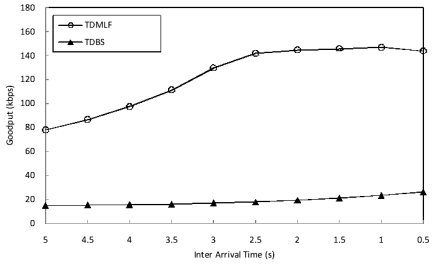

Fig. 3 Date size received by ZC under different flows

Parameter settings used by the simulation are shown as follows: *Cm*=6, *Rm*=4 and *Lm*=10, the maximum communication distance among nodes is 15m, size of data packet is 127 Bytes and rate of data transmission is 250kbps. Besides, power consumption of a transceiver follows setting of CC2420 single chip [8], current under a sending mode is 17.4mA, the current under a receiving mode is 18.8mA, the current under an idle mode is 426uA and the current under a power saving mode is 20uA. Besides, simulation time is 600s. All simulation data are average value of 20 simulations.

IN TDBS, there is no detailed description about how ZR can receive data of each sub-node in the activity interval. To compare with TDMLF fairly, we amend TDBS: each ZR also uses GTS to transmit data, while 7 GTSs can be allocated to different sub-nodes at least according to standard specifications. In order to ensure each ZR can be allocated with GTS, we let father nodes allocate minimum GTS (2 slots) to each ZR.

Fig. 3 shows data size received by ZC under different flows. According to the figure, it can be found that there is much difference between TDBS and the proposed TDMLF algorithm. The reason for this is that TDBS is subject to limitations of the standard for length of GTS. Thus, length of the allocated GTS cannot accord flow of each node accurately. If a certain sub-node fails to transmit all of its data, the bottleneck problem will occur. If a certain sub-node sends all of its data too early, wasting

of resources will be caused. In addition, the work cycle of ZC is limited to be less than 1/2, which reduces growth of Goodput to a large extent. In TDMLF, Goodput will increase with traffic load. Nevertheless, when inter arrival time reaches 2.5 seconds; increase in Goodput will tend to be mild.

Fig. 4 displays the ratio at which data are passed back to ZC under different flows. According to the figure, it is shown that TDMLF can nearly reach 100% of date loopback rate before the inter arrival time is 3 seconds. Similarly, the loopback rate begins to reduce later because Goodput of ZC has been saturate.

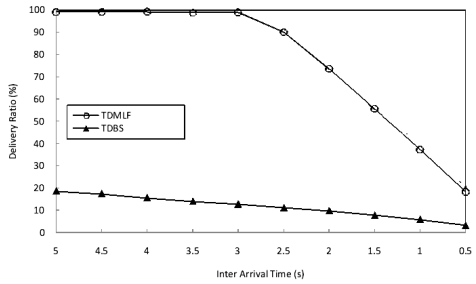

Fig. 4 Ratio of data passed back to ZC

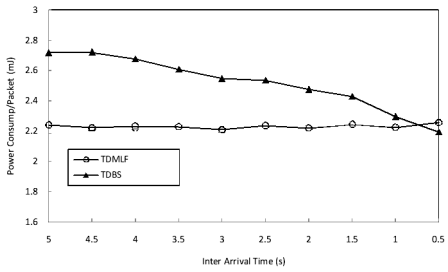

Fig. 5 Average power consumption need by transmitted a packet

Fig. 5 illustrates average power consumption need by transmitted a packet under different flows. According to the figure, we can find that TDMLF algorithm is better than TDBS. Power utilization efficiency of TDBS is in direct proportion to flow because the size of data that ZC receives from sub-ZED is small in TDBS with low flow. However, when the flow is high, ZC receives a large number of data from sub-ZEDs. Data of TDMLF algorithm is sent to ZC directly. Compared with data that are transmitted layer by layer, the power consumption needed by transmission of these data is low. Thus, average power consumption can be reduced.

Conclusions

First of all, this paper procided definition of the bottleneck problem in ZigBee tree network. To reduce the complexity of the bottleneck problem, we put forward a centralized TDMLF algorithm to make nodes by using GTS to achieve better parallelization transmission. At the same time, we re-adjusted the length of GTS, which enabled more efficient resource allocation. Simulation results showed that the proposed algorithm proposed is better than existing methods in the aspects of both data loopback rate and electricity saving efficiency. Therefore, it should be a scheduling protocol with huge potential for ZigBee cluster tree network.

References

[1] X.P. Gao and D.Y. Luo: Microcomputer & Its Applications. Vol. 29 (2010), p. 42-45

[2] Information on http://grouper.ieee.org/groups/802/15/pub/TG4b.html

[3] M.S. Pan and Y.C. Tseng: Computer Communications. Vol. 25(2012), p. 999-1011

[4] Y. Yamao and S. Takagishi: *Proc. IEEE Consumer Comm. and Networking Conf* (Las Vegas, 2008), p. 338-342

[5] Q.L. Liu, L. Wang, Y. Li and Y.J. Pan: Computer Engineering and Applications. Vol. 32 (2011), p. 91-93

[6] A Koubâa, A Cunha, M Alves and E Tovar: Real-Time Systems. Vol. 6 (2008), p. 312-354

[7] X. Zhou and Y. Lin: Science Technology and Engineering. Vol. 32 (2013), p. 8722-8725

[8] W.Z. Song, R.J. Huang, B. Shirazi and R.L. Husen: Pervasive and Mobile Computing. Vol. 6 (2009), p. 750-765

Advanced Materials Research Vols. 989-994 (2014) pp 4119-4122
© (2014) Trans Tech Publications, Switzerland
doi:10.4028/www.scientific.net/AMR.989-994.4119

A Image Decomposition Method Based on Euler Mapping for Face Recognition

Zhaokui Li[1,2,a], Yan Wang[1,b]

[1] Shenyang Aerospace University, School of Computer, Shenyang, China, 110136

[2] Wuhan University, School of Computer, Wuhan, China, 430072

[a] lmy52wy@163.com, [b] wy4615@sina.com

Keywords: Image decomposition, linear discriminant analysis, Euler mapping, face recognition.

Abstract. This paper presents a robust but simple image feature representation method, called image decomposition based on Euler mapping (IDEM). IDEM firstly captures the orientation information by implementing arctangent operator for each pixel. Then, the orientation image is decomposed into two mapping images by executing Euler mapping. Each mapping image is normalized using the "z-score" method, and all normalized vectors are concatenated into an augmented feature vector. The dimensionality of the augmented feature vector is reduced by linear discriminant analysis to yield a low-dimensional feature vector. Experimental results show that IDEM achieves better results in comparison with state-of-the-art methods.

Introduction

Face recognition is a popular research field in pattern recognition, and has attracted much attention in many areas, such as information security, law enforcement, and surveillance. Many face representation approaches have been introduced, including holistic feature representation approaches and local feature representation approaches. The holistic representation methods take a single feature, which is extracted from the whole face image, as input for face recognition. Among them, principal component analysis (PCA)[1] and linear discriminant analysis(LDA)[2] have become the most popular techniques for face recognition. The performance of the holistic matching methods obviously degrades with variations in expressions, poses, illumination conditions, etc. Increasing attention recently has been put into the local matching methods. The local binary pattern (LBP) [3] and Gabor wavelets [4] are two of the most popular local representation methods for face recognition. Recently, Qian et al. propose a simple but effective feature representation method called image decomposition based on local structure (IDLS) [5] . They consider decomposing an image into a series of sub-images which contain different structural information. In this paper, we propose a simple but effective local feature representation method called image decomposition based on Euler mapping (IDEM). IDEM first captures the orientation information by implementing arctangent operator for each pixel. After that, we obtain an orientation angle for each pixel. Then, motivated by the recent work on robust cosine-based dissimilarity measure [6], we show that a cosine-based dissimilarity measure has a functional form, which enables us to define an explicit nonlinear Euler mapping from the input space into a complex space. Each orientation image is therefore decomposed into two mapping images, which contain the imaginary part image and the real part image. For an orientation image, the imaginary part image retain the main information and smooth the higher value information, and the real part image mainly enlarges the lower value information and reduces the higher value information. Finally, each mapping image is normalized using the "z-score" method and we concatenate all normalized vectors into an augmented vector. The dimensionality of the augmented vector is further reduced by LDA to yield a low-dimensional feature vector.

Image Decomposition based on Euler mapping

Assume that we are given two images $F_j \in \Re^{h\times l}$ and $F_k \in \Re^{h\times l}$, we compute their orientation images Φ_j and Φ_k according to (1). let b_j and b_k be the D-dimensional ($D = h \times l$) vector obtained by writing Φ_j and Φ_k in lexicographic ordering.

$$\Phi = \arctan(F) \tag{1}$$

Motivated by the recent work on robust correlation-based translation estimation [6], we replace the l2-norm with the following dissimilarity measure:

$$d(b_j, b_k) = \sum_{q=1}^{p} \{1 - \cos(b_j^{(q)} - b_k^{(q)}))\} \tag{2}$$

where $b_j^{(q)}$, $b_k^{(q)}$ are, respectively, the q-th dimension column vector b_j and b_k.

Next, we will show that how to get a new mapping image by utilizing the robust dissimilarity in (2). We make the following derivation:

$$\begin{aligned} & d(b_j, b_k) = \sum_{q=1}^{p} \{1 - \cos(b_j^{(q)} - b_k^{(q)})\} \\ & = \frac{1}{2} \sum_{q=1}^{p} \{2 - 2(\cos b_j^{(q)} \cos b_k^{(q)} + \sin b_j^{(q)} \sin b_k^{(q)})\} \\ & = \frac{1}{2} \sum_{q=1}^{p} \{(\cos b_j^{(q)} - \cos b_k^{(q)})^2 + (\sin b_j^{(q)} - \sin b_k^{(q)})^2\} \\ & = \frac{1}{2} \left\| (\cos b_j + i \sin b_j) - (\cos b_k + i \sin b_k) \right\|_F^2 \\ & = \left\| \frac{1}{\sqrt{2}} e^{ib_j} - \frac{1}{\sqrt{2}} e^{ib_k} \right\|_F^2 \end{aligned} \tag{3}$$

We map the orientation vector b_j onto the complex representation $z_j \in C^p$,where

$$z_j = \frac{1}{\sqrt{2}} [e^{ib_j^{(1)}}, e^{ib_j^{(2)}}, ..., e^{ib_j^{(p)}}]^T = \frac{1}{\sqrt{2}} e^{ib_j} \tag{4}$$

The vector z_j can be thought of as the special features in complex space C. Because of (4), we coin this mapping as Euler mapping. Actually (4) is also rewritten as：

$$z_j = \frac{1}{\sqrt{2}} e^{ib_j} = \frac{1}{\sqrt{2}} (\cos b_j + i \sin b_j) \tag{5}$$

According to (5), we can get a real part mapping feature vector and an imaginary part mapping feature vector:

$$\begin{aligned} & \xi_j^{real} = real(z_j) = \frac{1}{\sqrt{2}} \cos(b_j) \\ & \xi_j^{imag} = imag(z_j) = \frac{1}{\sqrt{2}} \sin(b_j) \end{aligned} \tag{6}$$

where $\xi_j^{real} \in (0, 1/\sqrt{2}]^D$, $\xi_j^{imag} \in (-1/\sqrt{2}, 1/\sqrt{2})^D$, and the real part corresponding to the cosine function, the imaginary part corresponding to the sine function.

Given an input image F, we can compute its orientation image Φ by executing arctangent operator. The orientation image is decomposed into a real part image and an imaginary part image by implementing Euler mapping. For an orientation image, the imaginary part image (sine transformation) retain the main information and smooth the higher value information, and the real part image (cosine transformation) mainly enlarges the lower value information and reduces the higher value information.

Assume that we are given a set of n images $\{F_i\}$,we can obtain $N(=2\times n)$ sub-images $\{\Theta_i^s\}$ by decomposing image. Let Θ_i^s ($i=1,...,n; S=1,\ 2$) represents the *S*-th sub-image of the i-th sample image. Let ξ_i^s be the *D*-dimensional column vector obtained by writing Θ_i^s in lexicographic ordering. We can obtain matrix of the decomposed data $B=[\xi_1^S...\xi_n^S]\in\Re^{D\times n}$. Each mapping image is normalized using the "z-score" method. We denote by δ_i^s the normalized vector of ξ_i^s . The *q*-th dimension of δ_i^s can be calculated according to (7).

$$\delta_i^{S,(q)}=(\xi_i^{S,(q)}-\mu^{S,(q)})/\sigma^{S,(q)}\ ,\ i=1,...,n\ ,\ q=1,...,D \tag{7}$$

where $\xi_i^{S,(q)}$, $\delta_i^{S,(q)}$ are , respectively, the q-th dimension of column vector ξ_i^S and δ_i^s , $\mu^{S,(q)}=\frac{1}{n}\sum_{i=1}^{n}\xi_i^{S,(q)}$, $\sigma^{S,(q)}=\sqrt{\frac{1}{n}\sum_{i=1}^{n}(\xi_i^{S,(q)}-\mu^{S,(q)})^2}$. We can compute all D dimensions of column vector δ_i^s according to (7).

For an input image F_i , we can obtain its two normalized vectors, and concatenate them into an augmented feature vector $\chi_i=[(\delta_i^1)^T(\delta_i^2)^T]^T\in\Re^L$ ($L=2\times D$). The dimensionality of the augmented vector is reduced by LDA to yield a low-dimensional feature vector.

LDA searches for feature vectors in the underlying space that best discriminate among classes. More formally, given a number of independent features relative to which the data is described, LDA creates a linear combination of these which yields the largest mean differences between the desired classes. Mathematically speaking, for all the samples of all classes, we define two measures: 1) one is called within-class scatter matrix S_w. 2) the other is called between-class scatter matrix S_b. The goal is to maximize the between-class measure while minimizing the within-class measure. The discriminative projection basis W and eigenvalues Λ are obtained by solving the thin Linear Discriminant Analysis(LDA) eigendecomposition:

$$(S_w+\varepsilon I)^{-1}S_bW=W\Lambda \tag{8}$$

where ε is a small regularization constant (10^{-3} below) and I is the identity matrix. Thus, the original L-dimensional space is projected onto a final d-dimensional space using LDA.

Experiments

In this section, we will evaluate the performance of IDEM and compare it with some state-of-the-art methods by experimenting on Extended Yale B[7].

In the following experiments, we choose the regularized parameter in feature extraction as $\varepsilon=0.001$ in our IDEM method. The extended Yale B face image database contains 38 human subjects under 9 poses and 64 illumination conditions. All frontal-face images marked with P00 are used in our experiment, and each is resized to 96×84 pixels. Some sample images of one person are shown in Fig. 1. In our experiment, we randomly choose K samples from each class for training and the remaining images for test. Here, K varies from 4 to 20 with interval of 4. For each K, we perform 10 runs of tests for each method mentioned above. The average recognition rates and std of each method across 10 tests are shown in Table 1. The recognition results of compared methods are reported in [5]. As we can see, the recognition rates of PCA and TPLBP are relatively poor. The performances of LTP/DT, LTP plus Chi2, LDA , Gabor plus FLDA, LARK and IDLS-Distance are not very satisfying. ID-LARK,LBP+Chi2 and IDLS achieve better results than the above methods. However, in this experiment, IDEM achieves better results in comparison with state-of-the-art methods, and is the most stable method.

Fig. 1. Partial face images of the same subject taken from the Extended Yale B database.

Table 1. The average recognition rates(percent) and std of different methods

Methods	4	8	12	16	20
PCA	41.6 ± 5.77	59.7 ± 6.26	65.5 ± 7.11	70.6 ± 2.86	75.2 ± 3.09
LDA	57.3 ± 11.8	77.5 ± 7.91	86.7 ± 4.10	91.1 ± 2.86	92.3 ± 3.21
LARK	84.5 ± 5.30	90.6 ± 2.20	92.2 ± 2.83	92.6 ± 3.20	93.7 ± 3.06
ID-LARK	86.8 ± 4.73	91.3 ± 3.43	96.4 ± 1.63	96.9 ± 0.88	97.7 ± 0.54
LBP+Chi2	84.2 ± 8.59	93.2 ± 1.68	95.3 ± 1.71	96.3 ± 1.02	96.6 ± 0.91
LTP+Chi2	62.1 ± 8.79	76.7 ± 5.08	81.9 ± 3.76	84.5 ± 3.75	85.3 ± 2.52
LTP/DT	64.3 ± 10.8	80.8 ± 5.08	86.6 ± 3.73	89.6 ± 3.55	91.1 ± 2.14
TPLBP+Chi2	50.3 ± 11.7	66.3 ± 5.67	71.8 ± 5.42	75.4 ± 2.81	76.5 ± 3.36
Gabor+LDA	60.3 ± 3.94	78.2 ± 3.98	85.2 ± 3.10	91.2 ± 3.48	93.3 ± 2.83
IDLSDistance	74.9 ± 7.49	84.4 ± 4.16	91.3 ± 2.10	93.5 ± 2.01	93.9 ± 1.69
IDLS	95.8 ± 1.73	96.9 ± 0.72	97.9 ± 0.50	98.0 ± 0.66	98.0 ± 0.75
IDEM	**96.13±1.39**	**97.78±0.65**	**98.75±0.15**	**98.98±0.056**	**99.32±0.059**

Conclusions

We propose a novel image feature representation method coined IDEM and apply it to face recognition. Given a face image, we first captures the orientation information by implementing arctangent operator for each pixel. Then, by executing Euler mapping, each orientation image is decomposed into two mapping images. Finally, each mapping image is normalized using the "z-score" method and we concatenate all normalized vectors into an augmented vector. The dimensionality of the augmented vector is further reduced by LDA to yield a low-dimensional feature vector. Our experimental results show that IDEM achieves better results.

Acknowledgements

This work has been partially supported by the National Natural Science Foundation of China under contract No. 61170185.

References

[1] M. A. Turk and A. P. Pentland, "Face recognition using eigenfaces," in Proc. IEEE Comput. Soc. Conf. Comput. Vis. Pattern Recognit., Jun. 1991, pp. 586–591.

[2] J. P. H. P. N. Belhumeur and D. J. Kriengman, "Eigenfaces versus Fisherfaces: Recognition using class specific linear projection," IEEE Trans. Pattern Anal. Mach. Intell., vol. 19, no. 7, pp. 711–720, Jul. 1997.

[3] T. Ahonen, A. Hadid, and M. Pietikainen, "Face description with local binary patterns: Application to face recognition," IEEE Trans. Pattern Anal. Mach. Intell., vol. 28, no. 12, pp. 2037–2041, Dec. 2006.

[4] C. Liu and H. Wechsler, "Gabor feature based classification using the enhanced fisher linear discriminant model for face recognition," IEEE Trans. Image Process., vol. 11, no. 4, pp. 467–476, Apr. 2002.

[5] Jianjun Qian, Jian Yang, and Yong Xu. "Local Structure-based Image Decomposition for Feature Extraction with Applications to Face Recognition." IEEE Trans. Image Process., vol. 22, no. 9, pp. 3591–3603, Sep. 2013.

[6] G. Tzimiropoulos, V. Argyriou, S. Zafeiriou, and T. Stathaki. Robust FFT-Based Scale-Invariant Image Registration with Image Gradients. IEEE Trans. Pattern Analysis and Machine Intelligence, 32(10):1899-1906, Oct. 2010.

[7] K. C. Lee, J. Ho, and D. J. Kriegman, "Acquiring linear subspaces for face recognition under variable lighting," IEEE Trans. Pattern Anal. Mach. Intell., vol. 27, no. 5, pp. 684–698, May 2005.

Advanced Materials Research Vols. 989-994 (2014) pp 4123-4126
© (2014) Trans Tech Publications, Switzerland
doi:10.4028/www.scientific.net/AMR.989-994.4123

Color Space Comparison Between RGB and HSV Based Images Retrieval

Ching-Hung Su[1,3,a], Huang-Sen Chiu[1,b], Jui-Hung Hung[3,c], Tsai-Ming Hsieh[2,d]

[1]Dept. of Electronic Engineering, Lunghwa University of Science and Technology 33306, Taiwan

[2]Dept. of Information and Computer Engineering, Chung Yuan Christian University 32023, Taiwan

[3]Dept. Of Electronic Engineering, Chung Yuan Christian Univerity 32023, Taiwan

[a]chsu@mail.lhu.edu.tw, [b]sam@mail.lhu.edu.tw, [d]hank40hank40@hotmail.com
[d]hsieh@cycu.edu.tw,

Keywords: HSV color space, RGB color space, quantized color code

Abstract. The visual attributes of color are suitable for human perception and computer vision. A Color space is defined as a model for representing the intensity value of color. We propose a color space comparison and analysis between RGB and HSV based images retrieval. We succeed in transferring the image retrieval problem to sequences comparison and subsequently using the color sequences comparison between the color featurs of RGB and HSV to compare and analyze the images of database.

Introduction

As rapid growth of internet, digital acquisition of images prevails over the world, the traditional text-based retrievals based on keywords are not sufficient to resolve image retrieval. Content-based image retrieval (CBIR) is a technique used for retrieving similar images from an image database. The query image which based on user orientation to search the most similar images from database. The CBIR system retrieve relevant images from images database by the means of derived features to enhance the accuracy and efficiency of image retrieving. In this paper we describe both color space based method to retrieve images from database [1, 2, 3]. The features of Content-based image such as color, shape, texture and outline are used for image retrieval. Among these features, color is an important feature in CBIR, which is invariant on size, orientation and relatively robust to background complication. A color space is a multidimensional space in which the different dimensions represent the different components of color [7, 8, 9, 10]. The generic model which in terms of mathematical value to describe the representation of color space consist of RGB, CYMK, YCbCr, HSV and so on. In this paper, we proposed the features extraction techniques comparison and analysis between HSV and RGB color space to solve the images retrieval.

RGB Color Space

RGB color space is defined by the three chromaticities of the red, green, and blue primary colors, and can produce any chromaticity that is the triangle defined by those colors, serve as local descriptors of color and texture. Since RGB color space is a 3-dimensional vector space, and each pixel, *p(i)*, is defined by an ordered triple of red, green, and blue coordinates, *(r(i), g(i), b(i))*, which represent the intensities of red, green, and blue light color respectively [6]. We realize that the values of r, g and b are totally different with the altered illumination conditions shown as Fig. 1. However, the relative values between *r(i), g(i)*, and *b(i)* are very similar . Moreover, the number of the permutations of R, G, and B is only 6 (RGB, RBG, GRB, GBR, BRG, and BGR). We append white color series and black color series to let them become 8 series. We utilize 8 rules to transfer each cartoon image to a color sequence as below:

1. If a pixel 235 <= r(i) <= 255, 235 <= g(i) < =255 and 235 < =b(i) <= 255,
then assigns the pixel as 'W';

2. If a pixel 0 <= r (i) < =20, 0 <= g (i) < =20, and 0 <= b (i) < =20,
then assigns the pixel as 'K';
3. If a pixel r (i) > g (i) >= b (i), then assigns the pixel as 'R';
4. If a pixel r (i) >= b (i)> g (i), then assigns the pixel as 'S';
5. If a pixel g (i) > r (i) >= b (i), then assigns the pixel as 'G';
6. If a pixel g (i) >= b (i) > r (i), then assigns the pixel as 'H';
7. If a pixel b (i) > r (i) >= g (i) , then assigns the pixel as 'B';
8. If a pixel b (i) >= g (i) > r (i), then assigns the pixel as 'C';

We can obtain the impression of the characters "G" and "H" present two series of green colors. Subsequently, each image will become a 2D sequence array, and then we will convert the 2D sequence array to a 1D sequence as RRRRRRRGGGCCCHCBCCCCC…RRHHHRRWWWWRRR (20 x 20 =400 characters). An instance illustrates how to obtain a 2D color cipher is shown as Fig. 1 (a) An original frame of sport videos (352X 240 pixels); (b) Resized frame of sport videos (20X 20 pixels); (c) Resized the 20 X 20 pixels frame of sport videos to 322 X 322 pixels) to be seen clearly by readers; (d) Transfer the frame of the resized frame of sport videos (20 X 20 pixels) to a 2D color cipher array. From the 1D cipher array, you can see the layout of the sportsman with a gesture of victory. We compare each element of cipher of the query to the same location element in of the frame in the database. Where two ciphers are equal, increases weight value. If the matching weight value is 400(20 X 20 pixels), then the distance is 0, as shown retrieved image (1) in Fig. 2.

HSV Color Space

The HSV color space is fundamentally different from the RGB color space since it separates out the intensity from the color information. In our efficient alternative system, we employ the HSV color space instead of the RGB color space in two reasons. One is the lightness component is independent factor of images and second is the components of hue and saturation are so closely link with the pattern of human visual perception. The HSV model, defines a color space in terms of three constituent components: Hue, the color type range from 0 to 360 relative to the red primary at 0°, passing through the green primary at 120° and the blue primary at 240°, and then back to red at 360°. Saturation, the "vibrancy" of the color: Ranges from 0 to 100%, and occasionally is called the "purity". Value, the brightness of the color: Ranges from 0 to 100%. For the HSV color space, we map the original image into the HSV color space. We propose the scheme to produce 14 non-uniform colors. The proposed scheme contains three phases. First of all we resize all images to reduce the size of images and processing time. Secondly we convert each pixel of resized image to quantized color code. Finally we compare the quantized color code between the query image and database image. The formula that transfers from RGB to HSV is defined as below:

$$H = \cos^{-1} \frac{\frac{1}{2}[(R-G)+(R-B)]}{\sqrt{(R-G)^2+(R-B)(G-B)}} \quad (1)$$

$$S = 1 - \frac{3}{R+G+B}(\min(R,G,B)) \quad (2)$$

$$V = \frac{1}{3}(R+G+B) \quad (3)$$

For each color's scope of images is nonuniform, the three primary colors of R, G and B possess more scope than the other colors, we segment the scope of the hue which the components of HSV color space into six nonuniform classes including three primary color and the scope interposed between two primary colors, each class depending on the value of saturation of the components of HSV color space divides two subclasses along with the color of "white" and "black" according to the value on saturation and value of the components of HSV color space, the total is 14 classes. Each

pixel of the images from query and database assigned the quantized color code. Compare quantized color code between each pixel of three components of HSV color space of the images (20x20 pixels) from query and database, we obtain the weight of the quantized color code has compared. Sort the weight value of similarity feature vector and the retrieval images are presented.

Results and Conclusion

In this paper, a comparison and analysis for Content Based Image Retrieval using color space features between HSV and RGB is proposed.. The performance of an information retrieval system can be measured in terms of its recall and precision. Precision is the fraction of retrieved documents that are relevant. Recall in information retrieval is the fraction of the documents that are relevant to the query that are retrieved correctly. The experimental database contains MLB sports frames and test images from Wang's image data base. The MLB sports frames are taken from TV video programs. The Wang's images database including animals, sceneries, plants and flowers taken from SIMPLIcity paper[5]. The RGB color space illustrates the system is more robust and reliable, not only can handle different size, miscellaneous color saturation, blurred(as shown in Fig. 2), noise conditions, dissimilar illumination circumstances, and partial occlusion, but also consider the layout or spatial relation of the color. As shown in Fig.2 demonstrates retrieval results of the RGB based system are remarkable even in occlusion situations. On the alternative efficient scheme, we employ the HSV color space instead of the RGB color space in two reasons. One is the lightness component is independent factor of images and second is the components of hue and saturation are so closely link with the pattern of human visual perception. The HSV color space which we proposed as shown in Fig. 4, demonstrates that the retrieved results are more precise than RGB color space scheme as shown in Fig.3.

Acknowledgements

This work was partially supported by NSC of Taiwan under Grant No. NSC 102-2221-E-033-067

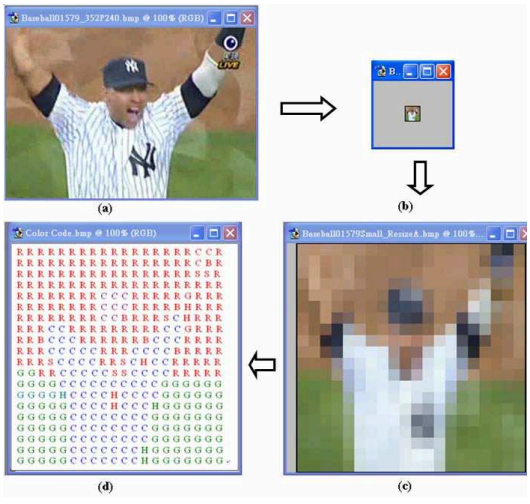

Fig.1 RGB based color cipher processing procedure

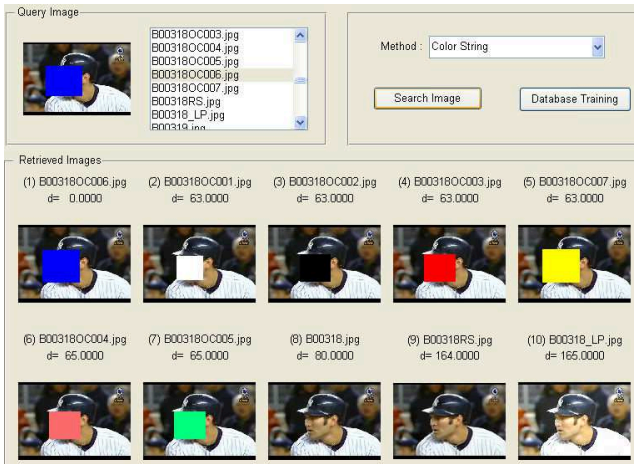

Fig.2 RGB based retrieval in occlusion situations.

Fig.3 Retrieval result based on RGB color space

Fig.4 Retrieval result based on HSV color space

References

[1] P. Aigrain, H. J. Zhang, and D. Petkovic, “Content-based representation and retrieval of visual media: A state-of-the-art review”, Multimedia Tools and Applications, 3:179–202, 1996.

[2] Sameer Antani, Rangachar Kasturi, Ramesh Jain, “A survey on the use of pattern recognition methods for abstraction, indexing and retrieval of images and video”, Pattern Recognition Volume: 35, Issue: 4, April, 2002, pp. 945-965

[3] Torres, R. da S.; Falcão, A.X., "Contour salience descriptors for effective image retrieval and analysis ", Image and Vision Computing Volume: 25, Issue: 1, January, 2007, pp. 3-13.

[4] Sameer Antani, Rangachar Kasturi, Ramesh Jain, “A survey on the use of pattern recognition methods for abstraction, indexing and retrieval of images and video”, Pattern Recognition Volume: 35, Issue: 4, April, 2002, pp. 945-965

[5] James Z. Wang, Jia Li, Gio Wiederhold, ``SIMPLIcity: Semantics-sensitive Integrated Matching for Picture LIbraries," IEEE Trans. on Pattern Analysis and Machine Intelligence, vol 23, no.9, pp. 947-963, 2001

[6] Chiunhsiun Lin, Ching-Hung Su, Hsuan Shu Huang, and Kuo-Chin Fan “MLB Sports Frames Retrieval Using Color Cipher Similarities” INTERNATIONAL JOURNAL OF CIRCUITS, SYSTEMS AND SIGNAL PROCESSING Issue 6, Volume 5, pp. 565-580, 2011

[7] J. R. Smith, “Integrated spatial and feature image system: Retrieval, analysis and compression “ PhD dissertation, Columbia University, New York, 1997

[8] W. Rasheed , G. Kang, J. Kang, J. Chun and J. Park, “Sum of Values of Local Histograms for Image Retrieval,” in Proc. International Conference on Networked Computing and Advanced Information Management, vol. 2, pp. 690- 694, 2008.

[9] R.Datta, D. Joshi, J.Li, J.Z. Wang, " Image retrieval: ideas, influences, and trends of the new age ", ACM Computing Surveys 40(2), 2008, pp. 1-60.

[10] V.N. Gudivada, and V.V. Raghavan, “Content based image retrieval systems", IEEE Computer, Vol. 28, No. 9, 1995, pp.18-22.

Advanced Materials Research Vols. 989-994 (2014) pp 4127-4131
© (2014) Trans Tech Publications, Switzerland
doi:10.4028/www.scientific.net/AMR.989-994.4127

Blind Detection of Copy-Move Forgery in Digital Images Based on Dyadic Wavelet Transform

Ruifang Zhang, Hanmin Ye, Zihang Song and Min Wang

Guangxi Scientific Experiment Center of Mining, Metallurgy and Environment,Guilin University of Technology, Guilin, Guangxi, China

tdrf@sina.com,yehanmin@163.com

Keywords: Dyadic wavelets transform. Copy-move forgery. Edge handling.

Abstract. This paper proposed a detection algorithm for copy-move in same image based on dyadic wavelet transform. First of all, four sub images could be got through the decomposition of detecting image by dyadic wavelet transform. Secondly, high-frequency and low-frequency sub image were decomposed into blocks without any overlap and two sub image's dyadic wavelet coefficients were regarded as the eigenvalue of the image block. At Last, both the high similarity among the low-frequency sub image blocks and the low similarity among the high-frequency sub image blocks were selected as a distorted image block. A kind of image edge processing methods was used to improve the tampering region at the same time. Through the experiments, it shows that the algorithm got the higher detection rate and lower error rates.

Introduction

With the rapid popularization of digital products and the fast development of the Internet, digital images have become an important part of the Internet and been applied to media and administration areas. But with the appearance and powerful functions of image processing software, even an amateur can forge images easily and the forged images can not be distinguished by eyes. Thus, the identification technology of digital images has become the hot topic.

The image identification technology can be divided three classes: digital signature, digital watermaking and digital image blind forensic. The digital signature and the digital watermaking need preprocessing and they are initiative forensic technologies. The digital image blind forensic can detect whether images have been forged without no preprocessing and it is a passive forensic technology and becoming more and more popular.

Copy-move is the most common forgery way. It copies some regions of the image to other regions to cover up. J. Fridrich has proposed the block idea and designed to detect image copy forgery areas based on image block DCT coefficient algorithm. Hany Farid and A.Popescu has proposed the analysis methods based on main components. Weiqi Luo has proposed a robust forgery detection algorithm and it uses the main transfer vector to remove wrong similar blocks and get tampering regions. Guohui Li has proposed a detection algorithm based on DWT an SVD and this algorithm can lower the dimension of images and fetch singular value in low-frequency wavelet coefficient moments as eigenvalues of every block to ensure copy-move regions.

The representative algorithms which are motioned above have achieved some results when detecting the same image copy-move. But they also have some problems in detection rate and error rate. Some algorithms have no powerful resistance. The detection rate and error rate is mainly determined by the chosen eignevalues. So this paper proposes a detection algorithm based on dyadic wavelet to improve detection rate and reduce error rate. It also improves the detection time efficiency by using no overlap blocks.

Dyadic Wavelet

Dyadic Wavelet Theory. Generally speaking, if something can use Fourier transform in the analysis, it can also use wavelet transform instead. But the wavelet analysis has better localization features in time domain and frequency domain, so it has more advantages when analyzing object details. Continue Wavelet Transform (CWT) is defined as follows:

$$Wf(a,b)=\int_R f(t)\frac{1}{\sqrt{a}}\psi^*(\frac{t-b}{a})dt=<f,\psi_{a,b}> \tag{1}$$

The parameters a and b in (1) need discretization and $a=2^j$, $b_{j,k}=2^jk$, among them, $j,k\in Z$, the equation of Discrete Wavelet Transform (DWT) corresponding to the arbitrary function $f(t)\in L^2(R)$ is shown as follows:

$$Wf(j,k)=\int_R f(t)\frac{1}{\sqrt{2^j}}\psi^*(\frac{t}{2^j}-k)dt=<f,\psi_{j,k}> \tag{2}$$

There is the fast algorithm Mallat which is corresponding to DWT, but here we don't talk about it in detail. During the fast realization process of DWT, many singular points which are on the edge of images can be gone when sampling. There will be the Gibbs phenomenon during the images reconstruction. It looks like the distortion of image edges. During the process of discrete continuous wavelet transform, if there is the character of translation invariance when transforming, the problems which are mentioned above can be solved. That is DWT.

In the wavelet transform of (1), a=2j, $j\in Z$, b is still the continuous changing values, just like it is in the wavelet transform. About the arbitrary function $f(t)\in L^2(R)$, dyadic wavelet transform can be defined as follows:

$$Wf(2^j,b)=\int_R f(t)\frac{1}{\sqrt{2^j}}\psi^*\left(\frac{t-b}{2^j}\right)dt=<f(t),\psi_{2^j,b}(t)> \tag{3}$$

In that equation, $\psi_{2^j,b}(t)=\psi_{2^j}(t-b)=\frac{1}{\sqrt{2^j}}\psi\left(\frac{t-b}{2^j}\right)$

Essentially, dyadic wavelet can be regarded as the transformation between continuous and discrete wavelets. CWT makes the dimension parameter a and the translation parameter b continuous. Conversely, DWT needs to discretize the two parameters. But the dyadic wavelet transform just discretizes the dimension parameter and the translation parameter in time domain is still continuous. That is the main distinction with DWT. The corresponding fast algorithm of dyadic wavelet transform is the atrous algorithm.

Application of Dyadic Wavelet in This Algorithm. Supposing I is the image which need detection, h[k] and g[k] are low-pass filter and high-pass filter. When j=0, making $I^0=I$, when j=1, 2, J, the corresponding coefficient calculation methods can be get by the equations as follows:

$$c^{j+1}[n]=\sum_k h[k]c^j[n+2^jk] \tag{4}$$

$$d^{j+1}[n]=\sum_k g[k]c^j[n+2^jk] \tag{5}$$

The filter $h^j[k]$ and $g^j[k]$ is determined after every sample is inserted into 2^j-1 pieces of 0 by the filter h[k] and g[k]. The dyadic wavelet transform filtering is described as follows: when j=0, we make $I^0=I$. when getting the dimension function coefficient and wavelet function coefficient of I^J and D^J, we can use $h^{j-1}[k]$ and $g^{j-1}[k]$ to filter I^{j-1}. The corresponding tow-dimension dyadic wavelet decomposition is shown in Fig. 1.

After the dyadic wavelet first level decomposition, the image will obtain four sub images: LL, LH, HL, HH. They are the same side as the original image. The sub image LL is the approaching image of the original image, and HH contains amounts of high-frequency information. The algorithm will choose these two images for analysis.

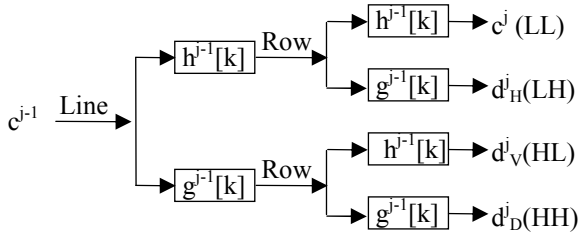

Fig. 1 Two-dimension dyadic wavelet first level decomposition

Detection Alglrithm

Image Block. After dyadic wavelet first level decomposition of the image, we choose LL and HH to do image segmentation. Because the general tampering regions are not very small, it is not necessary to move a pixel. The algorithm in this paper will not divide the image into blocks by movements. It will divide the image into R×R image blocks directly which are adjacent. M×N image is the same as that. After segmentations, there will be $\lceil M/R \rceil \times \lceil N/R \rceil$ pieces of image blocks. Meanwhile, we hypothesis first: copy-move forgery regions are connected instead of very tiny fragment image blocks or even pixel points. The size is at least four times of image blocks. Here, choosing image blocks which are 16×16 size to do the whole image fragmentation can make some image blocks contains a part of image forgery regions entirely.

Similar Region Matching. In LL and HH, we suppose that the size of every image block is R×R and they are all transformed into the matrix form: $1\times R^2$. That is, every image block is transformed into one line. Every image block is act as a vector, all image blocks of LL and HH are transformed into a matrix. The equation of defining the distance between vectors is shown as follows:

$$d(p,q)=\sqrt{\frac{1}{N}\sum_{i=1}^{n}(p_i-q_i)^2} \tag{6}$$

In the above equation, N is 256. It means standardizing the distance between vectors. The corresponding distance value is converted between 0 and 1 to make the setting of threshold value easy. Before dictionary ranking, we define two threshold values Th1 and Th2. Because LL is the approaching image of the original image, we save all the image blocks which d<Th1 in Llist according to dictionary ranking algorithm. The main information in HH is the noise, edge and other high-frequency information of image blocks. As soon as the image is forged, this sensitive information must change and all image blocks whose distance d>Th2 in HH will be saved in Hlist. It will choose image similar blocks pairs in saved image block pairs. The image similar block pairs which are chosen from K_{LL} and K_{HH} are listed Llist and Hlist. If image block pairs appear in the two lists at the same time, that image block will be similar image blocks.

Confirmation of Tampering Regions. After finding out similar image blocks through similar region matching, some image blocks which only contain a part of tampering regions and can not be enough similar may not be detected. That is because it is not the overlapping image segmentation. The detected image blocks almost contain tampering regions. Thus, confirmation of tampering regions is necessary. There is an edge handling method of image blocks and it is shown in Fig. 2.

In Fig. 2, a grid represents an image block. Assuming the part comprised of X and Y is the similar image which has obtained just before. It is also the region which X edge contains. The specific steps are as follows:

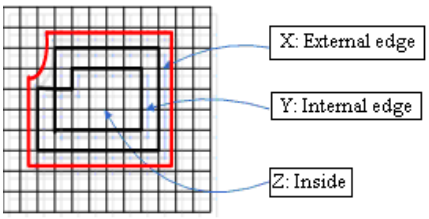

Fig. 2 Edge handling of tampering regions

(1) Conformation of inner edges of image blocks. To the former similar image blocks, every detected similar image blocks will be judged in four domains (up, down, left, right) image blocks. If all the four domains are in distorted image blocks, it will be grouped in Z (inside) in the Fig. 2. If one to three domains are image blocks, then they will be grouped in Y (internal edge). Nonexistent image blocks will do nothing.

(2) Conformation of external edges. All the eight domains image blocks in Y image blocks will be marked. The image blocks which are already in Y and Z will do noting. The rest are grouped in X (external edge).

(3) Improvement of tampering regions. The former internal edge image blocks are overlapping according to the movement of pixel whose step side is 1. The biased direction is from Y to X and they are all in X. Eventually, the tampering regions are confirmed.

Algorithm Flow. (1) Supposing the size of detecting image I as M×N, we transform it into 256 level grey spaces;

(2) After dyadic wavelet first level composition of images, we can get sub image LL and HH;

(3) LL and HH will do the non-superimposed image block. The size of every image block is 16×16 and they are adjacent;

(4) To LL and HH, every image block eigenvalue of every sub image will be in line to establish feature vector matrix and constitute the K-D tree KLL and KHH of LL as well as HH;

(5) Set threshold value Th1 and Th2. KLL tree will be saved in Llist by searching every image block pair that the node distance is less than Th1. KHH tree will be saved in Hlist by searching every image block pair that the node distance is more than Th2;

(6) Choosing the image block pairs which are in both Llist and Hlist as distorted image blocks;

(7) Do the image edge handling and improve tampering regions;

(8) The algorithm ends.

Experiment Results and Analysis

The environmental parameters of this experiment are: Pentium (R) Dual-Core CPU T4200 @ 2.00GHz, 2.00GB memory, the OS is Windows XP and the formulation platform is Matlab R2009b.

In the experiment processing, the equations of defining detection rate r and error rate w is as follows:

$$r = \frac{\sum_i |A_i \cap P_i| + |B_i \cap Q_i|}{\sum_i |A_i| + |B_i|} \tag{7}$$

$$w = \frac{\sum_i |A_i \cup P_i| + |B_i \cup P_i|}{\sum_i |A_i| + |B_i|} - r \tag{8}$$

In equation (7) and (8), A_i and B_i are copy-move regions of detecting images. P_i and Q_i are detected regions.

The experiment uses grey images. If the images are colorful, it will transform color images into grey images firstly and then begin handling. The image size of the experiment is 320×320. The original image is copy-move forged by Adobe Photoshop CS. the parameters in the experiment are: the size R of image block is 16, the domain value Th1 is 0.72 and Th2 is 0.29.

An original image is shown in Fig. 3. The image after copy-move forging by photo editor is shown in Fig. 4. The result which is detected by our algorithm is shown in Fig. 5. We can see that the two white regions are the copy-move regions.

To compare the algorithm in this paper with the DCT coefficient algorithm based on image blocks, we have performed an experiment as follows. We have used 500 pieces of 320×320 images and forged them and then use the above algorithms to do forge detections. The statistical data are shown in Table 1.

From Table 1, the algorithm in this paper has improved detection rate and reduced error rate. Thereason is the comprehensive analysis of sub images LL and HH after dyadic wavelet decompositions

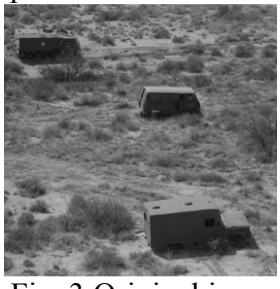

Fig. 3 Original image

Fig.4 Distorted image

Fig.5 Detected result

Table 1.Comparison of Detected Results

	Algorithm in this paper	DCT coefficient algorithm
Detection rate	93.0%	91.6%
Error rate	5.2%	9.4%

Conclusions

This paper proposed a detection algorithm for copy-move based on dyadic wavelet transform. This algorithm has image blocks without any overlap and analyses low-frequency and high-frequency sub images after dyadic wavelet decompositions. It has improved the detection rate and reduced the error rate. But this algorithm also has some disadvantages. For example, it can no resist the handling ways of rotations, zooms and so on. Those are the further investigative orientations.

Acknowledgment

This work is financially supported by the foundation of Guangxi Postgraduate Education Innovation Project in 2013 (Grant No. YCSZ2013078) and the open foundation of Guangxi Scientific Experiment Center of Mining, Metallurgy and Environment (Grant No. KH2001YB007).

References

[1] Linna Zhou, Dongming Wang. Digital Image Forensics Technology, Beijing: Beijing Post and Telecommunication Press. (2008).

[2] Fridrich J,Soukal D,Lukas J. Detection of copy-move forgery in digital images, Cleveland: Proceedings of Digital Forensic Research Workshop :DFRWS , 2003.M. King and B. Zhu, “Gaming strategies,” in Path Planning to the West, vol. II, S. Tang and M. King, Eds. Xian: Jiaoda Press, (1998), p. 158-176.

[3] Popescu A C,Farid H. Exposing digital forgeries by detecting duplicated image regions. Dartmputh College, Hanover New Hampshire, USA: TR2004-515, (2004).J.-G. Lu,”Title of paper with only the first word capitalized,”J. Name Stand. Abbrev. In press.

[4] Weiqi Luo, Jiwu Huang, Guoping Qiu. Robust Detection of Region-Duplication Forgery in Digital Image. Chinese Journal of Computers. 30(11), (2007).11: p. 1998-2007

[5] GuoHui Li, Qiong Wu,Dan Tu, Shaojie Sun, A sorted neighborhood approach for detecting duplicated regions in image forgeries based on DWT and SVD,IEEE International Conference on Multimedia & Expo, ICME: , (2007).p. 1750-1753

[6] Shanshan Jiang. A Study on Image Adaptive Threshold Denoising Based on Dyadic Wavelet Transform. Master’s thesis. Xinjiang Normal University. (2010).6

[7] Guanghui Zhang, Hangjun Wang. Quick Detection of Copy-Move Forgery Based on FMT. Computer Engineering and Design. 2010, 31(15): p. 3530-3532

Advanced Materials Research Vols. 989-994 (2014) pp 4132-4135
© (2014) Trans Tech Publications, Switzerland
doi:10.4028/www.scientific.net/AMR.989-994.4132

The realization of receiving and reporting the HARQ-ACK information in LTE system

Peng Sun[1, a*], Jing Yang[2, b], Yajie Chen[3, c], Chun Zhou[3, d]

[1]Chongqing Key Lab of Mobile Communications, Chongqing University of Posts and Telecommunications (CQUPT), Chongqing 400065, China

[2]School of Communication and Information Engineering, Chongqing University of Posts and Telecommunications (CQUPT), Chongqing 400065, China

[3]School of Automation, Chongqing University of Posts and Telecommunications (CQUPT), Chongqing 400065, China

[a]sunpeng05321@163.com,yj920628@sina.com,[c]nostalgia19921212@gmail.com, [d]372011198@qq.com

Keywords: LTE; HARQ; PUSCH; PUCCH

Abstract. A brief introduction of hybrid automatic repeat request (HARQ) is given first, and then a description of physical uplink shared channel (PUCCH) or physical uplink shared channel (PUSCH) receiving and reporting the HARQ-ACK information in bundling mode or multiplexing mode is made in detail. Based on the principle, a scheme is designed to solve the problem of receiving and reporting the HARQ-ACK information.

Introduction

HARQ (hybrid automatic repeat request), which is forward error correction (FEC) applied in automatic repeat-request (ARQ) system .while the FEC can be used to correct the data error in transmission process, that is if the error is in the error correction range of FEC, then the FEC can correct it, if the error is beyond that scope, then the retransmission from the receiver will be made .In the receiver module, the CRC check is usually used to detect the error of the received data packet. If there is no fault, a positive acknowledgment (ACK) will be sent, otherwise, the data packet will be dropped and a negative acknowledgment (NACK) will be sent. The data packet will be retransmitted when the NACK is received. Therefore, the scheme not only increases the reliability of the system but also increases the transmission efficiency of system, it is has been applied to the LTE system.

Feedback of HARQ-ACK Information in bundling mode

The generation of HARQ-ACK feedback information needs the some parameters in bundling mode, while V_{DAI}^{UL} is the value of the downlink assignment index (DAI) in downlink control information (DCI) format 0 detected by UE, V_{DAI}^{DL} is the value of DAI in DCI format1/1A/1B/1D/2/2A/2B, U_{DAI} is the number of physical downlink control channel (PDCCH) released, N_{SPS} is the number of physical downlink shared channel (PDSCH) without PDCCH indicated[1]. For time division duplexing (TDD), when in the HARQ bundling mode or the HARQ multiplexing mode with M equals to 1, while M is the number of downlink subframes that need to report feedback information in an appointed subframe, if the HARQ-ACK feedback information is sent via physical uplink shared channel (PUSCH), the parameters above can be used to detect whether the downlink tasks are lost, the method is as follows [2].

When the uplink and downlink configuration is set to 0, if the PDSCH transmission is detected in the subframe $n-k$, whether there is corresponding PDCCH indicated or not, N_{bundled} is set to 1.When the uplink and downlink configuration is set to 1-6, the HARQ-ACK information is transmitted via PUSCH and the transmission is made according to the detected DCI format 0,if

$V_{DAI}^{UL} \neq (U_{DAI} + N_{SPS} - 1) \bmod 4 + 1$, it means at least one downlink assignment has been lost and then UE will generate NACK for all codewords ,at the same time set $N_{\text{bundled}} = V_{DAI}^{UL} + 2$ [3]. UE shall not transmit HARQ-ACK information when $U_{DAI} + N_{SPS} = 0$ and $V_{DAI}^{UL} = 4$.From the above analysis, it can be seen if the downlink task is lost, NACK will be sent via PUSCH and $N_{\text{bundled}}$is also determined, otherwise, the M downlink subframes' feedback information of each codewode will do the operation of Logic and, one or two HARQ-ACK bits will be generated. When the HARQ feedback information is sent via PUCCH [4], the difference is that the value of N_{bundled} is not needed. In the realization of the process, if the PUSCH transmission is scheduled in the uplink HARQ process, it can be considered that that the HARQ information sent via PUCCH is placed by PUSCH, besides, an array is defined to record the process ID in the process, when in bundling mode, the uplink and downlink configuration 5 should be considered specially, as the uplink and downlink configuration 5 support bundling mode only and all the downlink subframes should be considered in this configuration, then corresponding process ID can be read from the array and the final feedback information is generated ,at last, the right channel is selected to send the final information. The PUCCH or PUSCH receiving and reporting the HARQ-ACK information in bundling mode process can be seen in Fig1.

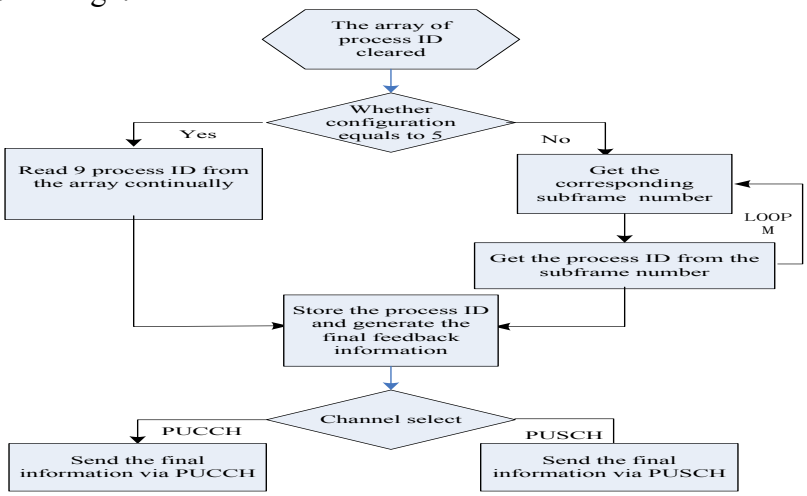

Fig1 Ttion in HARQ multiplexing

When the HARQ-ACK feedback information is sent via PUSCH, for the case M>1 in HARQ multiplexing mode, independent ACK/NACK information of different codeword do the operation of logic and, then UE will determine the feedback ACK/NACK bits when the information is sent via PUSCH[5].

If the transmission through PUSCH is adjusted according to the DCI 0 of PDCCH, unless it satisfies $V_{DAI}^{UL} = 4$ and $U_{DAI} + N_{SPS} = 0$, UE will not send the HARQ-ACK information, or $O^{ACK} = V_{DAI}^{UL}$. While $o_{DAI(k)-1}^{ACK}$ means the PDCCH indicated by PDSCH or released by semi-persistent scheduling (SPS) in subframe n-k, DAI (k) is the value of DAI detected in DCI format 1A/1B/1D/1/2/2A/2B, the information placed order is in accordance with Table 1 that whose distance with subframe n is far. When $N_{SPS} > 0$, it means a PDCCH transmission without PDSCH, then the ACK/NACK information can be mapped to $o_{O^{ACK}-1}^{ACK}$, if there is no PDSCH transmission or SPS indicated by PDCCH detected, set this task is set to NACK [6].

Table 1: Downlink association set index K : $\{k_0, k_1, \cdots$ for TDD

UL-DL Configuration	Subframe *n*									
	0	1	2	3	4	5	6	7	8	9
0	-	-	6	-	4	-	-	6	-	4
1	-	-	7, 6	4	-	-	-	7, 6	4	-
2	-	-	8, 7, 4, 6	-	-	-	-	8, 7, 4, 6	-	-
3	-	-	7, 6, 11	6, 5	5, 4	-	-	-	-	-
4	-	-	12, 8, 7, 11	6, 5, 4, 7	-	-	-	-	-	-
5	-	-	13, 12, 9, 8, 7, 5, 4, 11, 6	-	-	-	-	-	-	-
6	-	-	7	7	5	-	-	7	7	-

If the transmission of PUSCH is not adjusted according to the DCI 0 of PDCCH, then $O^{ACK} = M$, o_i^{ACK} is the ACK/NACK information corresponding to subframe $n - k_i$ ($k_i \in K$)in Table 1. If there is no PDSCH transmission or SPS indicated by PDCCH detected, the result is NACK. When HARQ-ACK feedback information is sent via physical uplink shared channel (PUCCH) and M=1, it can be done as the operations in bundling mode. When M>1, the final two bits are generated according to the tables in protocol. The PUCCH or PUSCH receiving and reporting the HARQ-ACK information in multiplexing mode can be seen in Fig 2.

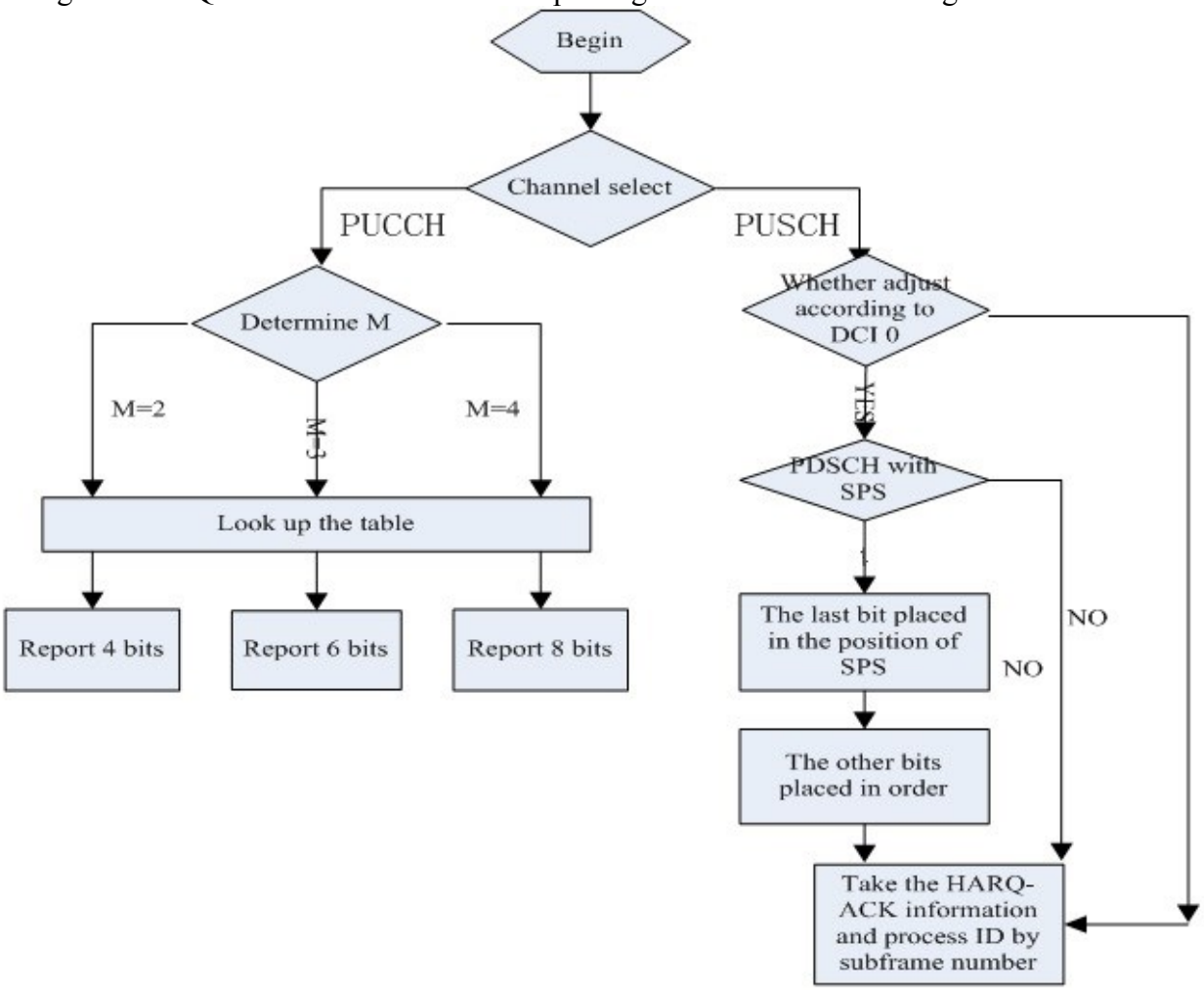

Fig2 The process in in multiplexing mode

Conclusions

This scheme is designed to solve the PUCCH or PUSCH receiving and reporting the HARQ-ACK information in bundling mode or multiplexing mode, when applied in the system through the realization of DSP, the result is reliable; the reliability of the scheme is proved.

References

[1] 3GPP TS 36.213 v11.6.0, Physical layer procedures[S], 2012-06

[2]3GPP TS 36.213 v11.4:Evolved Universal Terrestrial Radio

[3] Xiaowen Li, Shaoxu Wu and Taotao Liang. The Research and Improvement of HARQ in TD-LTE Systems. 2011 3rd IEEE International Conference on Information Management and Engineering (ICIME 2011) VOL.05

[4] Zukang Shen, Aris Papasakellariou, Juan Montojo. Overview of 3GPP LTE-advanced carrier aggregation for 4G wireless communications. IEEE Communications Magazine 2012.

[5] Iwamura, M., Etemad, K., Fong, M.-H., Nory, R., and Love, R.: 'Carrier aggregation framework in 3GPP LTE-Advanced', IEEE Commun. Mag., 2010, 48, (8) pp. 60-67

[6] R1-120122, "Motivations on UL signaling enhancement", Huawei, HiSilicon, Dresden, Germany, February 6- 10, 2012

Advanced Materials Research Vols. 989-994 (2014) pp 4136-4139
© (2014) Trans Tech Publications, Switzerland
doi:10.4028/www.scientific.net/AMR.989-994.4136

NSCT-Based Image Enhancement Combing Homomorphic Filtering With Fuzzy theory

Kai Wen[1,2,a], Bin Sun[1,b], Jing Yang[3,c]

[1]Research Centre for Application of New Communication Technologies,
Chongqing University of Posts and Telecommunications Chongqing (CQUPT), 400065, China

[2]Chongqing Information Technology Designing Co. , LTD Chongqing, 400065, China

[3]School of Communication and Information Engineering,
Chongqing University of Posts and Telecommunications (CQUPT), Chongqing 400065, China

[a]wenkai@cqcyit.com,[b]824941854@qq.com,[c]yj920628@sina.com

Keywords: image enhancement; homomorphic filtering; NSCT; fuzzy enhancement

Abstract. Proposed is an algorithm of NSCT-Based Image Enhancement Combing Homomorphic Filtering With Fuzzy theory to improve the performance of traditional algorithms in the expression of the image edge detail and contrast. With the NSCT, both the low and high frequency sub-band components can be extracted. We dispose of the low frequency sub-band components of the decomposed image by homomorphic filtering and enhance the high-frequency sub-band components with fuzzy sets theory. Then the reconstructed image after above enhancement is obtained by using NSCT inverse transform.

Introduction

Image enhancement is a processing method which to highlight some certain information according to the specific needs and to weaken or eliminate some certain information of an image. Usually, the main purpose of the image enhancement has the following: enlarging the contrast of interest structure of an image and increasing the comprehensibility; reducing or suppressing all the noises mixed in an image in order to enhance the visual effect to some extent[1,2].Generally, image enhancement technology mainly includes two categories: airspace method and frequency method. In recent years, the image enhancement method which is based on wavelet transform, fuzzy set theory, mathematical morphology and multi-scale analysis is wildly used and make a good performance[3-5]. All these methods have achieved a certain performance to some extent.

Image enhancement algorithm

NSCT Transform

NSCT transforming is one of the Multiscale Analysis methods. This method subtitute Nonsubsampled Pyramid Filter Banks and Nonsubsampled Directional Filter Bank for the LP and DFB part of Contourlet transforming[6]. Under the premise of ensuring the original properties of Contourlet, NSCT gets a a fully shift-invariant without downsamplers and upsamplers. Thus, essentially, The NSCT is a fully shift-invariant, multi-scale, and multi-direction expansion that has better directional frequency localizationand a fast implementation[7].

Fig.1 illustrates the struction of NSCT decomposed. At first, the image is decomposed by NFPFB in multiscale, both the lowpass and highpass sub-band can be extracted.And then,NSDFB decomposes the highpass subband into several directional subbands, The scheme is iterated repeatedly on the lowpass subband. At last, we can get the different directional subbands. As a result, it is easier to get the property information of the image using NSCT method.

Fuzzy Enhancement

Pa1.King as a traditional fuzzy edge detection algorithm has some defects. Owing to that transit point got relied on our past experience and several attempts, a large number of gray values in original image are set to 0 rigidly, and the edge information of lower gray values are lost[8]. Therefore, these affect the quality of image enhancement seriously. Based on the shortcomings of traditional algorithms, we use the new membership function as follow:

$$U_{\mathrm{ij}} = \mathrm{T}(g_{ij}) = \log_2\left[1 + \frac{g_{ij}-g_{min}}{g_{max}-g_{ij}}\right] \quad (1)$$

In which, $g_{\min}$ and $g_{\max}$ are the minimum and maximum, respectively. The new membership function values are distributed in [0, 1]. After this treatment, we can save the edge information of lower gray values. We define new non-linear transformation to enhance the blurred image as:

$$\mathrm{U}'_{\mathrm{ij}} = \mathrm{F_r}(\mathrm{U_{ij}}) = \mathrm{F_r}\left(\mathrm{F_{r-1}}(\mathrm{U_{ij}})\right) \quad \mathrm{r} = 1,2,3 \ldots \quad (2)$$

$$F_r(U_{\mathrm{ij}}) = \begin{cases} \frac{\sin\left(\pi(U_{\mathrm{ij}}-0.5)\right)+1}{4} + {U_{\mathrm{ij}}}^2 & 0 \le U_{\mathrm{ij}} \le 0.5 \\ \frac{\sin\left(\pi(U_{\mathrm{ij}}-0.5)\right)+1}{4} - {U_{\mathrm{ij}}}^2 + U_{\mathrm{ij}} & 0.5 < U_{\mathrm{ij}} \le 1 \end{cases} \quad (3)$$

The key of fuzzy enhancement is to increase the membership values higher than 0.5 and decrease the membership values lower than 0.5.Do inverse transform with blurred image and generate the new gray scale. The equation of inverse transform as written:

$$g'_{ij} = g_{min} + (g_{max} - g_{min})\left(2^{U'_{\mathrm{ij}}} - 1\right) \quad (4)$$

From the equation (4), because $2^{U'_{\mathrm{ij}}} - 1 \ge 0$,then $g'_{ij} \ge g_{min}$It also retains the edge detail information of low gray values. Experiments show that the new algorithm is better than the Pa1.King algorithm.

Homomorphism filtering

The classic homomorphism filtering algorithm is compared by establishing lighting reflection model[9],and an image is mainly represented by its incident and reflection components. The equation can be expressed as

$$\mathrm{f}(\mathrm{x},\ \mathrm{y}) = \mathrm{i}(\mathrm{x},\ \mathrm{y}) * \mathrm{r}(\mathrm{x},\ \mathrm{y}) \quad (5)$$

In which, the incident and reflection component is relevance to the low-frequency and high-frequency component in Fourier plane, respectively. However, due to the Fourier transform of the two functions is not separated, so makes the multiplicative components turn into the additive component using logarithmic operation (Formula 6), and then Fourier transform to do it again (Formula 7).

$$\mathrm{z}(\mathrm{x},\ \mathrm{y}) = \ln\left(\mathrm{f}(\mathrm{x},\ \mathrm{y})\right) = \ln\left(\mathrm{i}(\mathrm{x},\ \mathrm{y})\right) + \ln\left(\mathrm{r}(\mathrm{x},\ \mathrm{y})\right) \quad (6)$$

$$\mathrm{Z}(\mathrm{u},\ \mathrm{v}) = \mathrm{I}(\mathrm{u},\ \mathrm{v}) + \mathrm{R}(\mathrm{u},\ \mathrm{v}) \quad (7)$$

Since the transfer function $\mathrm{H}(\mathrm{u},\ \mathrm{v})$ has different effects on the low-frequency and high-frequency components, so selects the appropriate transfer function is critical. In this paper, we use the Butterworth high-pass filter function, it is defined as follows:

$$\mathrm{H}(\mathrm{u},\mathrm{v}) = (r_H + r_L)\left[1 - \exp\left(-c\frac{D^2(u,\mathrm{v})}{D_0^2}\right)\right] + r_L \quad (8)$$

In which $\mathrm{r_H}$and $\mathrm{r_L}$ is defined the high-frequency and low-frequency gain, respectively. $\mathrm{D_0}$ is the cutoff frequency, $\mathrm{D}(\mathrm{u},\mathrm{v})=\sqrt{\mathrm{u}^2+\mathrm{v}^2}$is the distance from point（u, v）to frequency plane origin. The value of Butterworth high-pass filter function dropped the half-maximum when $\mathrm{D}(\mathrm{u},\mathrm{v})=\mathrm{D_0}$. Then it was treated with filtering function:

$$\mathrm{S}(\mathrm{u},\mathrm{v}) = \mathrm{H}(\mathrm{u},\mathrm{v})\mathrm{Z}(\mathrm{u},\mathrm{v}) = \mathrm{H}(\mathrm{u},\mathrm{v})\mathrm{I}(\mathrm{u},\mathrm{v}) + \mathrm{H}(\mathrm{u},\mathrm{v})\mathrm{R}(\mathrm{u},\mathrm{v}) \quad (9)$$

In which, $\mathrm{S}(\mathrm{u},\mathrm{v})$is the Fourier transform after filtered.We can get the enhanced image after the inverse transform.

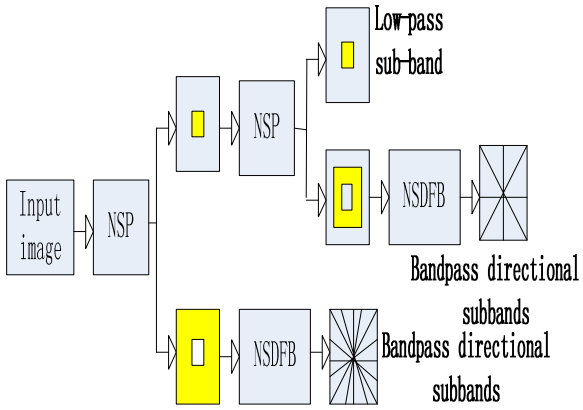

Fig 1. The struction of image decomposed

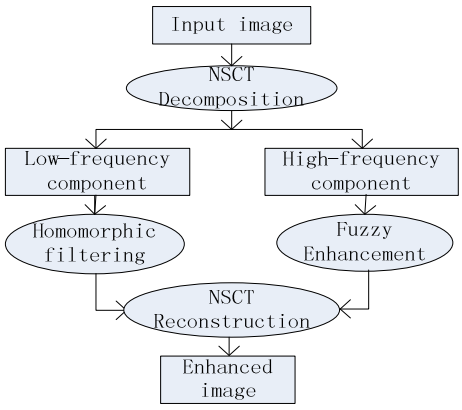

Fig. 2 Flow chart of the proposed algorithm

Steps of the enhancement algorithm

Based on Combing theory and algorithms of 3.1 and 3.2 mentioned, the specific execution steps are as follows and the flow chart of the proposed enhancement algorithm is shown in Fig 2.

(1) Decompose the image by NSCT transform to obtain the the low and high frequency sub-band components.

(2) The high-frequency sub-band components of image were decomposed by fuzzy sets theory According to the formula (1) to the formula (4)

(3) The low frequency sub-band components of image were decomposed image by homomorphic filtering According to the formula (5) to the formula (9)

(4) Reconstruct the image by inverse NSCT, so as to achieve the purpose of the image enhancement.

Experimental results

The experimental results are also compared with three different methods. Fig.2(b)–(d) shows the different enhanced images by the Fuzzy based enhancement method , the homomorphic filtering based on wavelet enhancement method and this peper proposed based enhancement method, respectively. For NSCT, we use three scales of decomposition and 4, 8, 16 directions in the scales from coarser to finer, while for the wavelet we choose the" db4" and six scales of decomposition. Fig.2(b) shows sample of encouraging result enhanced by Fuzzy based enhancement method .It obviously that the edge detailed information of enhanced image is improved while gray contrast is not discernible. Fig.2(c) shows the experimental results in which $r_H = 1.2$, $r_L = 0.5$ and c=2.Both edge detailed information and gray contrast of enhanced image are improved but a little blurred. From Fig. 4(d) it is evident that the proposed algorithms have been strengthened to increase the contrast and brightness by preserving the general shape of the original peppers.jpg image. Moreover the enhanced image is more smooth than the figure (b) and (c), and effectively keep the direction and the edge information of original image. So we can draw conclusion that the proposed algorithm is better in the favorable visual effect of image enhancement

(a) (b) (c) (d)

Fig. 1. (a) Original "peppers" image. (b) Enhanced by the undecimated wavelet transform. (c) Enhanced by the homomorphic filtering based on wavelet .(d) Enhanced by the proposed enhancement algorithm

Table 1 Comparisons of image enhancement results

Methods	Fuzzy Enhancement	Homomorphic filtering	The algorithm proposed
MSE	53.358910	30.322326	31.002238
PSNR	28.523295	51.763686	64.552629

To further evaluate the performance of the different enhancement methods objectively. we use mean square error(MSE) and Peak Signal to Noise Ratio (PSNR) to evaluate the different enhanced images. MSE and PSNR are is expressed in (10) and（11）respectively, and the corresponding values are presented in table.1:

$$\mathrm{MSE} = \frac{1}{mn}\sum_{i=0}^{m-1}\sum_{j=0}^{n-1}||I(i,j) - k(i,j)||^2 \tag{10}$$

$$\mathrm{PSNR} = 10\log_{10}(\frac{\mathrm{MAX}_I^2}{\mathrm{MSE}}) = 20\log_{10}(\frac{\mathrm{MAX}_I}{\sqrt{\mathrm{MSE}}}) \tag{11}$$

Where m, n denotes the number of matrix rows and columns, respectively. MAX ,representing the grayscale image, is usually 255.The lower the value of MSE, the larger the value of PSNR, the greater the quality of enhanced images. Table 1 show performance measure values obtained after Applying different enhancement techniques on images. From the table values, it is evident that the proposed method gives higher PSNR compared to other image enhancement value methods. Though the homomorphic filtering based on wavelet enhancement method give Lower MSE values, the visual quality of the resultant image are not comparable with the proposed method.

Conclusion

An algorithm of NSCT-Based Image Enhancement Combing Homomorphic Filtering With Fuzzy theory has been proposed in this paper. Experimental result of comparative analysis concluded the algorithm proposed achieves better enhancement results than traditional image enhancement algorithms. So as to a fast and efficient image enhancement algorithm, how to reduce the complexity of the algorithm and improve the operational efficiency becomes the next focus of the study.

References

[1] Chang D-C, Wu W-R. Image contrast enhancement based on a histogram trans-formation of local standard deviation. IEEE Trans Med Imaging 1998;17(August(4)):518–31.

[2] Wan Y, Chen Q, Zhang B-M. Image enhancement based on equal area dual-istic sub-image histogram equalization method. IEEE Trans Consum Electron1999;45(February (1)):68–75.

[3] S. Mallat, A Wavelet Tour of Sinal Processing, 2nd ed. Academic Press, 1999.

[4] Hanmandlu, M., Jha, D.: An optimal fuzzy system for color image enhancement. IEEE Trans. Image Process. 15(10), 2956–2966 (2006)

[5] Xiang Jingbo，Su Xiuqin，Lu Tao.Image enhancement based on the contourlet transform and mathematical morphology[J].Acta Photonica Sinica，2009，38（1）：224-227.

[6] M. N. Do and M. Vetterli, “The contourlet transform: An efficient directional multiresolution image representation,”IEEE Trans. Image Proc., 2005, to appear.

[7] da Cunha A L, Zhou Jianping, Do M N. The Nonsubsampled Contourlet Transform: Theory, Design and Application[J]. IEEE Trans. on Image Processing, 2006, 15(10): 3089-3101.

[8] Nair MS, Rekha L, Wilscy M, Tatavarti R. Fuzzy logic based automatic contrastenhancement of satellite images of ocean. Signal Image Video Process, Springer-Verlag 2011;5(March (1)):69–80.

[9] Holger G. Adelmann.Butterworth equations for homomorphic filtering of images. Computers in Biology and Medicine, 1998, Vol.28 (2), pp.169-81.

Advanced Materials Research Vols. 989-994 (2014) pp 4140-4142
© (2014) Trans Tech Publications, Switzerland
doi:10.4028/www.scientific.net/AMR.989-994.4140

Realization of Book Locating by RFID Technology in Mobile Phone Libraries

Yingpei Wang [1, a]

[1] Jilin Agricultural University library, 130118, Changchun, China
[a] 1228185392@qq.com

Keywords: Mobile phone library; Radio Frequency Identification(RFID); Book positioning Book Positioning by Radio Frequency Identification Technique in Mobile Phone Libraries

Abstract. Book positioning in mobile phone libraries could make readers acquire books conveniently andquickly. Readers could use mobile phone access to OPAC system, and apply to book positioning systemwhich is based on RFID system for book positioning. The book positioning system combines with the RFIDsystem to fix the position of books, converts spatial information of books to geographic location information,then feedbacks the information to readers by mobile phone.

Introduction

Along with the popularization of mobile phones and their increasingly powerful functions, mobile phone libraries come into being. As long as the Internet is available, readers can enjoy the corresponding services of mobile phone libraries through mobile phones. The shift from desktop terminal to mobile terminal truly realizes readers' dream of "having" a library. Therefore, this paper combines mobile phone libraries with RFID technology so as to realize the book locating function of mobile phone libraries.

Summary of Mobile Phone Libraries' Book Locating System Scheme

As to the book locating through mobile phones, mobile phones firstly access the OPAC (Online Public Access Catalog) system of libraries through the network, and then the OPAC system initiates a book locating request to the book locating system which locates books by combining the RFID system and then converts the spatial information as located to geographical information before feeding back to readers through mobile phones [1].

The book locating through mobile phones should meet the following 3 conditions: (1) Mobile phones have the function of connecting to the Internet and can access a library's OPAC system through the website to search books and initiate a book locating request. (2) Libraries have the RFID-based automated book circulation system. (3) The book locating system can convert the spatial information as located to geographical information and present it in a graphical way to readers.

Basic Components and Operating Principle of the RFID System

The RFID system includes a reader-writer, antennas, electronic tags, and a control terminal.

The reader-writer sends a radio-frequency signal through transmitting antenna. When the passive RFID tag enters into the working area of transmitting antenna, induced current is generated, and then the passive RFID tag sends out the information of its code (carrier signal) through tag. After receiving such carrier signal from the passive RFID tag, the system sends it to the reader-writer which further sends the signal to the backstage main system for processing [2]. as shown in Fig.1.

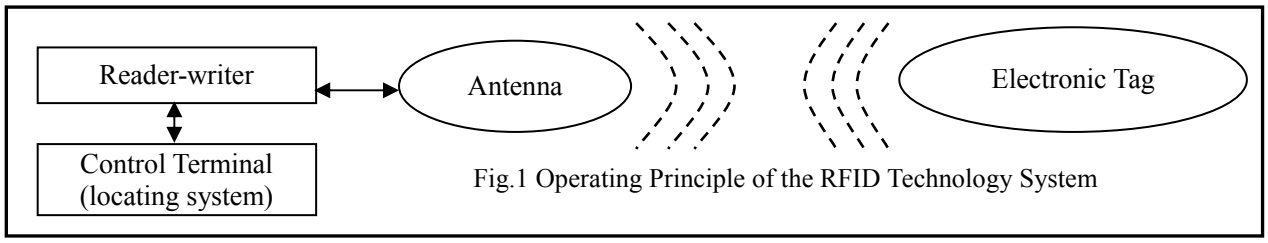

Fig.1 Operating Principle of the RFID Technology System

Realization of Mobile Phone Libraries' Book Locating System Scheme

Proposal of the Location Method of Priority Local Search

The traditional indoor location method is usually based on the TOA (Time of Arrival). Generally it estimates the distance between the tag on books and the reader-writer according to the time of arrival of the signal between the two, thus confirming the location of books. The delay of the transmission time of the signal between reader-writer and book tag will lead to poor location results. Another location method is that the passive RFID tag each book carries will receive the trigger pulse sent by reader-writer antenna to locate books. However, because of the large number of books, these two methods are both time-consuming.

According to the characteristics of library books, this paper puts forward the implementable location method of priority local search. The so-called location method of priority local search means that when locating books, the reader-writer does not search passive RFID tags in sequence, but first conducts local search from a certain location. Since the reader-writer stores the shelf information of any books, it can activate the antenna closest to the book's passive RFID tag as soon as possible to locate the book [3]. This location method of priority local search saves both time and labor and is more feasible than the traditional location method of full-range search.

Implementation Process of the Locating Scheme of Priority Local Search, as shown in Fig.2.

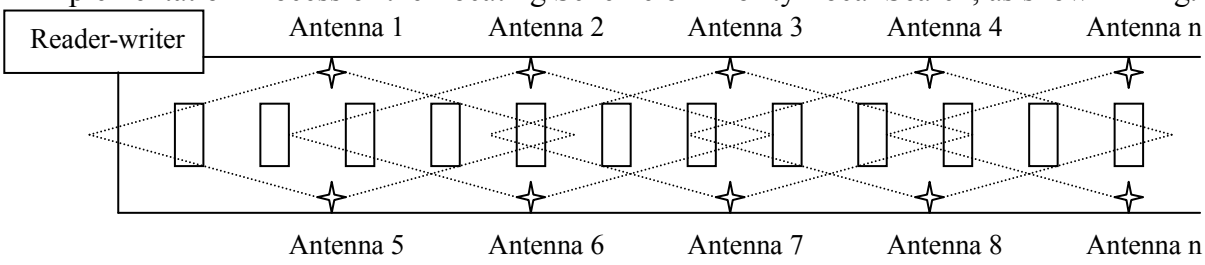

Fig.2 Book Locating System Architecture

In the process of priority local search, the RFID reader-writer in Graph 2 can control multiple antennas that could be activated in sequence. The reader-writer sends the trigger pulse to the first antenna close to it. The built-in antenna of the passive RFID tag tuned to the same frequency "collects" the magnetic field generated by the first antenna. After rectification, the energy received is stored in the capacitor inside the RFID tag. Then the RFID tag immediately sends back the data which is received by the receiving antenna and decoded by the reader-writer.

If no target RFID tag is detected within the read range of the selected antenna, the reader-writer will disconnect the power supply of the selected antenna and then activate each indoor antenna in sequence. If the reader-writer detects the target passive RFID tag, it will record the signal strength it receives and then activate the next antenna to conduct the same detection. If the target tag is detected, it will record the signal strength at the time as well until all antennas are covered. Afterwards, all of the detected signal strengths will be compared and the TOA method will be applied to conduct accurate locating [4].as shown in Fig.3.

The locating system transfers the result of book searching to readers through graphic information so that readers can find the books they need quickly. Since each book shelf is equipped with at least one antenna, the comparison between the coordinate of the target book and the coordinates of the three antennas with the strongest signal can indicate which of the three antennas is closest to the location of the target book. Furthermore, since the bookshelf number of the three antennas is known and the spatial information of the book is also confirmed, the book's bookshelf number can be basically inferred through antenna. Then the general location of the book is further detailed

according to the information of the location and length of the bookshelf, and the finally confirmed location is marked in a graphical way (see Fig.4) and sent back to readers' mobile phones through the website[5] .

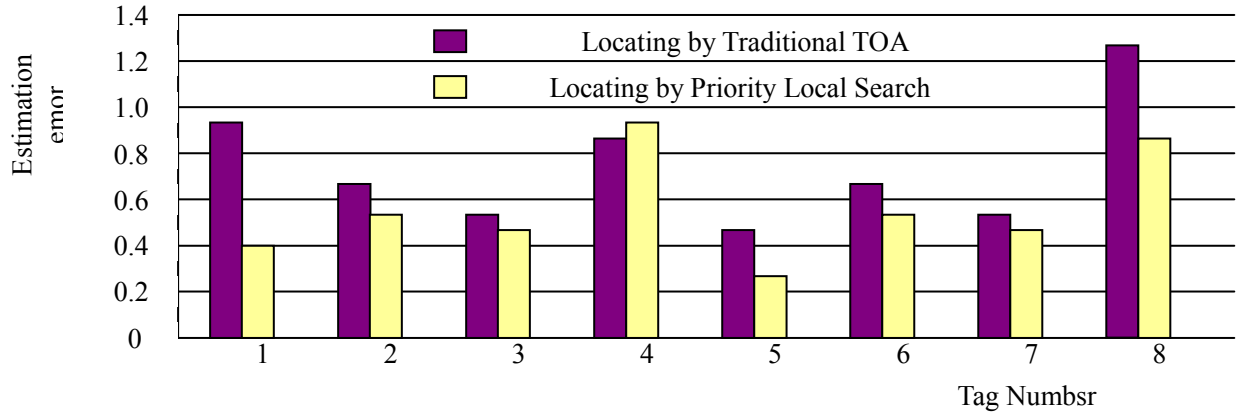

Fig.3 Comparison of Location Error Feed the Locating Information back to Mobile Phones

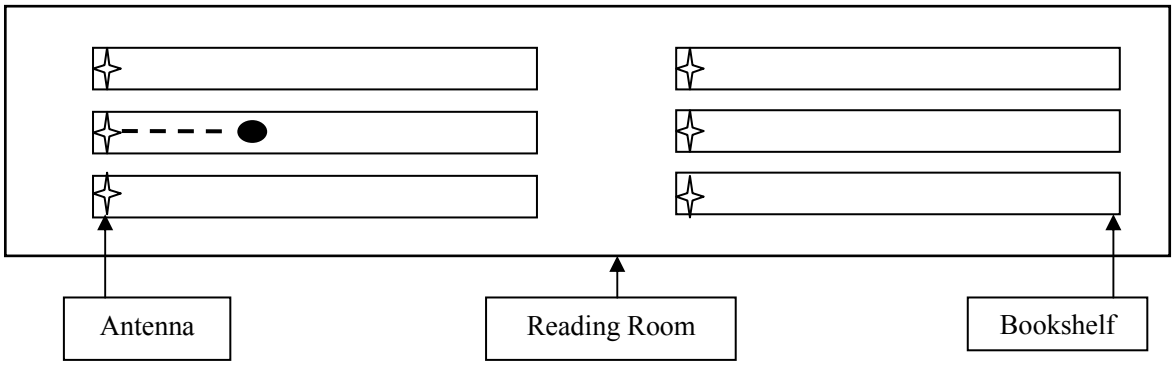

Fig.4 Books' Location Information Obtained by Mobile Phones

Conclusion

In combination with the RFID technology, this paper proposes the location method of priority local search to rapidly locate RFID books. Through the bookshelf information stored in the book locating system and by referring to the historical shelf information of finding the target book, the search scope is narrowed so as to ensure accurate locating. This paper selects the three antennas with the strongest signal to locate books to improve the accuracy.

References

[1] Zhu Juan, Zhou Shangwei, Ma Qiping. Indoor Location Algorithm based on the RFID Technology [J]. 2009 (23): 160-162..

[2] Pahlavan K,Li Xinrong. Indoor Geolocation Science and Technology[J].IEEE Communications Magazine,2002(2):112 -118.

[3] Jaegeol Y. Introducing a Decision Tree-based Indoor PositioningTechnique [J].Expert Systems with Applications, 2008(2):1296-1302.

[4] Yang Tianchi, Jin Liang, Cheng Juan. A CHAN Improved Algorithm based on TOA Location [J]. Chinese Journal of Electronics, 2009 (4): 819-822.

[5] Yuan Zhengwu, Chu Jingjing. Development Status and Tendency of Mobile Terminal Location Technology [J]. Application Research of Computers, 2007 (11): 1-6

Advanced Materials Research Vols. 989-994 (2014) pp 4143-4146
© (2014) Trans Tech Publications, Switzerland
doi:10.4028/www.scientific.net/AMR.989-994.4143

Design of a Novel Variable Bit Rate Video Traffic Prediction Model Based on Neural Networks

Lian Zuozheng[1,a], Wang Haizhen[2,b] and Li Dahui[2,c]

[1]Compute Center, Qiqihar University, China

[2]College of Computer and Control Engineering, Qiqihar University, China

[a]lianzuozheng@163.com, [b]wanghaizhen1976@163.com, [c]lidahui1968@yahoo.com

Keywords: Neural network, Multi-fractal Wavelet model, VBR Video Traffic Prediction, Wavelet reconstruction

Abstract. The video business has gradually become the main business of the network traffic, video traffic is Variable Bit Rate (VBR), which has nonlinear and sudden features, a single prediction model is not fit for describing those features, and prediction accuracy is not high. Because of wavelet analysis has advantages of multi-resolution and dealing with unexpectedness, and the neural network has better nonlinear fitting characteristics, in order to improve the prediction performance, the paper researched on the problem of VBR video traffic prediction based on neural networks, a novel prediction model AMWM is proposed, the model firstly introducing BP neural network to multi-fractal wavelet model, and designing prediction method, which introduced multi-fractal wavelet model to model VBR video traffic, and then applying BP neural network to forecast scale coefficient decomposed, and forecast multiplier using AR model, and predict traffic generated by wavelet reconstruction. Finally, the model is built and simulated. The experimental result shows that prediction performance based AMWM is better compared with multi-fractal wavelet model.

Introduction

With the discovery of VBR video traffic multi-fractal characteristics, people begin to research on VBR video traffic and network traffic modeling using multi-fractal theory. In addition, the wavelet transformation can analyze multi-fractal features of video traffic, therefore, multi-fractal wavelet model (MWM) is proposed in view of current internet increasingly complex network business and video traffic in [1], the model better descript various time scales of wavelet coefficients, but it is a kind statistical model.

As research on prediction model in the previous known, the single model is not suitable for predicting complex VBR video traffic. Therefore, the paper proposed a novel VBR video traffic prediction model AMWM combining with the neural network based on multi-fractal wavelet model, the model may more effectively and really predict VBR video traffic, and improve the prediction performance.

Multi-fractal wavelet model principle

Discrete wavelet transformation may conduct multi-scale analysis on signal $\mathrm{X(t)}$, its expression is as follows [2].

$$\mathrm{X(t)} = \sum_{k} U_{\mathrm{J}_0,k}\phi_{\mathrm{J}_0,k}(t) + \sum_{\mathrm{j}=J_0}^{+\infty}\sum_{k} W_{j,k}\psi_{j,k}(t) \tag{1}$$

Where J_0 is the largest scale, $U_{\mathrm{J}_0}{}'_k$ is the wavelet transformation scale coefficient, $W_{j,k}$ is wavelet coefficients, for Harr wavelet transformation, the scale coefficient and wavelet coefficient can be calculated by equation (2,3), $\phi_{\mathrm{j},k}(t)$ is the mother wavelet function, and it can be expressed as equation (4), $\psi_{j,k}(t)$ is scale function , and it can be expressed as equation (5) [3].

$$U_{j-1,k} = 2^{-\frac{1}{2}}(U_{j,2k} + U_{j,2k+1}) \tag{2}$$

$$W_{j-1,k} = 2^{-\frac{1}{2}}(U_{j,2k} - U_{j,2k+1}) \tag{3}$$

$$\phi_{j,k}(t) = 2^{j/2}\phi(2^j t - k) \tag{4}$$

$$\psi_{j,k}(t) = 2^{j/2}\psi(2^j t - k) \tag{5}$$

Where $\phi(t)$ is defined by equation (6), and $\psi(t)$ is defined by equation (7).

$$\phi(t) = \begin{cases} 1, & \text{when } 0 \leqslant t < 1 \\ 0, & \text{when } t < 0 \text{ or } t \geqslant 1 \end{cases} \tag{6}$$

$$\psi(t) = \begin{cases} 1, & \text{when } 0 \leqslant t < 1/2 \\ -1, & \text{when } 1/2 \leqslant t < 1 \\ 0, & \text{when } t < 0 \text{ or } t \geqslant 1 \end{cases} \tag{7}$$

Therefore, equation (2) addition equation (3) launches (8), namely

$$U_{j+1,2k} = 2^{-\frac{1}{2}}(U_{j,k} + W_{j,k}) \tag{8}$$

Equation (2) reduction equation (3) launches (9), namely

$$U_{j+1,2k+1} = 2^{-\frac{1}{2}}(U_{j,k} - W_{j,k}) \tag{9}$$

it can use a multiplier $A_{j,k}$ to descript the relationship between the wavelet coefficient at the same level and scale coefficient by equation (4) ~ (9), namely

$$W_{j,k} = A_{j,k}U_{j,k} \tag{10}$$

So the multi-fractal wavelet model modeling process can be described as flows: to conduct Haar wavelet transform on video traffic data, firstly getting the biggest scale coefficients $U_{0,0}$, and then turning out various time scales $A_{j,k}$, passing out smallest scale coefficient U_N by equation (8) and equation (9), U_N was the final output results.

Design of Prediction Model AMWM

In this section, a novel VBR video traffic prediction model AMWM is designed, specific steps are as follows:

Step 1: Let scale j is 0, and then computing scale coefficient;

Step 2: Generating a random number between minus one and positive one as a multiplier $A_{j,k}$ ($0 \leq k \leq 2j$), on scale j, and then calculating $W_{j,k}$ by equation (10);

Step 3: Let j= j + 1, calculating $U_{j,k}$ by the equation (8) and equation (9);

Step 4: Repeating from step (2) to step (3) until j = N;

Step 5: Let SUCj=[Uj,k]

Step 6: Introducing SUC_0, SUC_1, …, SUC_N to neural network, getting the scale coefficients SUC'_0, SUC'_1, …, SUC'_N corresponding adjacent sequence scale, that is to predict the next set of corresponding scale coefficients by the scale coefficients of the last set of data. Because of neural network is the teacher learning, it must be trained, in order to speed up the training speed, the paper trained by the parallel method.

Where M is the number of BP neural network training data, N is the smallest scale, namely, to predict the scale coefficient of the first M+1 data by the scale coefficient of the last M data; BP neural network 1 to N can use the same structure, parallel processing the N sets of data at the same time, so generating a new set of scale coefficient of each layer, as well obtaining the scale coefficient prediction output value by means of the trained network.

Step 7:Getting the multiplier by the above step 2 to step 3, then using it for the actual data to initialize the AR model, estimating parameters of AR model, and then according to (11), getting the prediction multiplier;

$$X_t - \phi_1 X_{t-1} - ... - \phi_p X_{t-p} = a_t \tag{11}$$

Step 8: Calculating $W_{j,k}$ on the basis of prediction multiplier, and to conduct wavelet inverse transformation combining with the scale coefficient, generating prediction data, as shown in fig. 1. Predicting the first M data by the the scale coefficient prediction value of last M data and multiplier AM + 1, and so on, the first M+2 data can be predicted, etc.

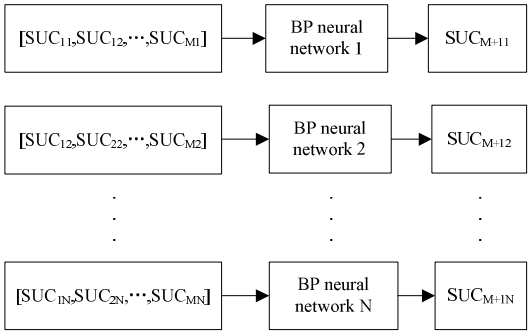

Fig. 1 Predicted data generation method

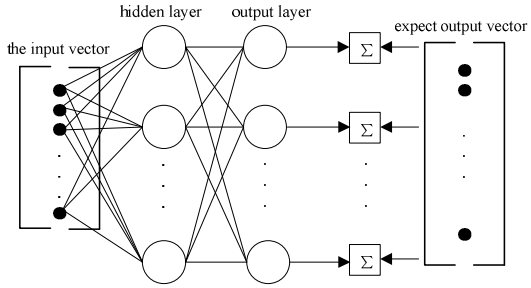

Fig. 2 BP neural network structure

Three layers BP neural network can approximate any nonlinear function [4], as shown in fig. 2, the circles represent neurons nodes, number of nodes in each layer references experience value and the experiment value. The transfer function of hidden layer uses the hyperbolic tangent sigmoid transfer function tansig, and the transfer function of output layer uses linear transfer function purelin, weights and threshold learning function use the gradient descent method, network training function use momentum BP algorithm and it conducts correction on weights and threshold of the neural network, error performance function uses normalized mean square error (NMSE) performance function.

Because the scale coefficient of model proposed in the paper are obtained by Haar wavelet decomposition, they can meet the absolute value of Uj,k less than one, that is as the scale coefficient of the Haar wavelet function and wavelet coefficients nature known, so it isn't necessary to preprocess data before they inputting the network.

After training data in neural network, the output of the network function is linear function, the output value is likely to be between -∞ and ∞, the processing method of Uj,k is as follows:

Step 1: Finding the maximum number of less than one between all the scale coefficients, and replacing the Uj,k, of absolute value greater than positive one.

Step 2: Finding the minimum number of greater than one between all the scale coefficients, and replacing the Uj,k of absolute value is greater than minus one.

Experimental Simulation and Performance Analysis

we carry on experiment confirming the references of three layers BP neural network, the results show the number of input layer nodes are ten, hidden layer nodes are six, output node is one; M is ten, N is three, analysis data length is twenty-forth, so the neural network input vector array was 10*3 dimensional, 10*6 dimensional, 10*12 dimensional, learning rate is 0.04.

We conduct on experiment by "the Silence of the lambs" (from the university of Berlin mpeg-4 video tracking database [5]), As known in fig. 3, it may be observed that when the size of a video

frame doesn't change sharply, the difference is small between the predicted values and the real value; When the amount of data change severely, the difference between the predicted values and the real value also increases, but predicted value can reflect the change trend of real data to a certain degree.

Fig. 4 shows the video predict performance of MWM model and AMWM model in the case of single layer VBR encoding, horizontal axis is preliminary step length, and vertical axis is NMSE values. When the prediction step length was small, the performances of the two methods were close, but, with the increase of prediction step length k, AMWM has smaller error and higher prediction precision.

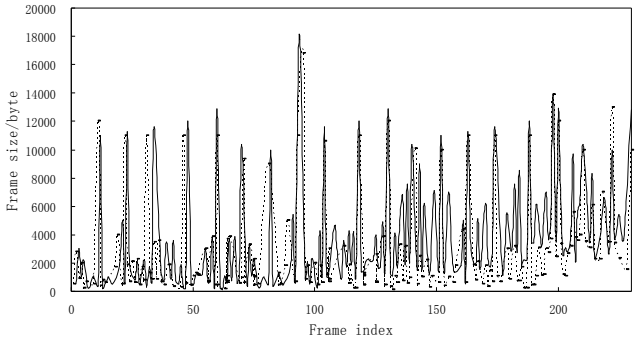

Fig. 3 Simulation results

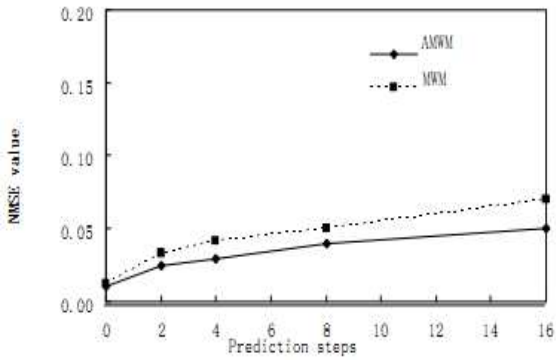

Fig. 4 Prediction performance analysis

Conclusions

The paper studies multi-fractal wavelet model, and then establishes a VBR video traffic prediction model combining wavelet and BP neural network, and the prediction method is designed, and conducted on modeling analysis by Matlab. Fig.3 shows that AMWM prediction model can reflect the change of the original video streams, fig. 4 shows relative to the MWM model, forecasting method proposed in the paper introduces the neural network and can undertake multi-step prediction, and the prediction precision is improved.

Acknowledgements

This work was financially supported by the Heilongjiang Natural Science Foundation (F201218) and Qiqihar university young teachers' scientific research started to support projects foundation(2011 k - M05).

References

[1] (In Chinese)Xiaoan MA, Hongguang LI, A New Multi-step Predictive Algorithm for Network Traffic, Journal of Computational Information Systems. Vol.7 (2011), p. 1116.

[2] (In Chinese)Huachuan Zhang, Research on Traffic Simulation System based on Multi-fractal Wavelet Network Nankai University, May 2010.

[3] (In Chinese)Lu Zhao, Guangwei Bai, Yong Sun. MPEG Video Traffic Prediction Model based on Wavelet Transform, Computer Engineering and Design. Vol. 32(2011), p.1531-1534.

[4] Ke Guo, Ye San, Yi Zhu: Journal of Electronic Engineering Design.Vol. 20(2012), p. 63.

[5] Patrick Seeling, Martin Reisslein, Beshan Kulapala: A Tutorial IEEE Communications Surveys and Tutorials.Vol. 6(2004), p. 58.

Advanced Materials Research Vols. 989-994 (2014) pp 4147-4151
© (2014) Trans Tech Publications, Switzerland
doi:10.4028/www.scientific.net/AMR.989-994.4147

The application of physical layer network coding in the UAVs

Zhimin Yang[1,a], Yongjiang Hu[2,b], Changlong Wang[3,c], Quansheng Yuan[4,d]

[1]Mechanical Engineering College, Shijiazhuang, 050003, P. R. China

[2]Mechanical Engineering College, Shijiazhuang, 050003, P. R. China

[3]Mechanical Engineering College, Shijiazhuang, 050003, P. R. China

[4]Mechanical Engineering College, Shijiazhuang, 050003, P. R. China

[a]email:yangzhiminmimi@163.com

Keywords: physical layer network coding ;UAVs; modulation

Abstact. In order to improve the network throughput and anti-jamming capability of UAV communications, physical layer network coding is applied in the UAV communications. Simulation results show that: the use of physical layer network coding can not only improve network throughput greatly, reduce the error rate of communication, but also enhance its anti-jamming capability,which satisfy UAVs' requirements in modern warfare.

Introduction

In some long-distance wireless communication scenarios,the communicating parties do not have the direct path due to mountains and other obstacles blocks.It is necessary to establish a reliable communication link through a high-altitude relay platform. UAVs become the appropriate high-altitude relay platform because of its good performance, low cost, deploying and controlling easily, flexible communications networking and communications equipment[1].

But the UAV as a relay platform needs to meet the following requirements: first, it needs to have a large throughput and high speed to ensure real-time network; second,it needs to have a good anti-jamming capability to ensure the reliability of the network. Most communication system designs try to either reduce or avoid interference (e.g., through receiver design or transmission scheduling [2]). However, instead of treating interference as a nuisance to be avoided, we can actually embrace interference to improve throughput performance.

The scheme of jointing the physical layer network coding with UAV communication meets the above requirements.Compared with the traditional means of communication and the straightforward network coding[3],the network throughput is increased by 100% and 50% respectively,which greatly improves the transmission rate.On the other hand, the interfere becomes part of the algorithm,as a result,it improves its anti-jamming capability.

The design of system model

The communication models of UAVs include communication between the UAVs and the ground, as well as between UAVs and UAVs.

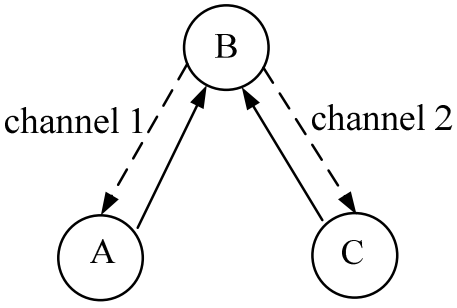

Fig.1. Two-way relay system model

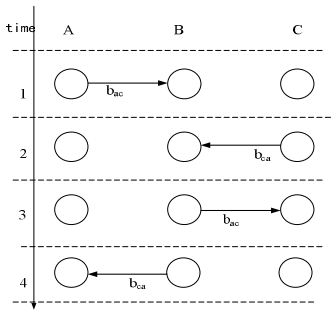

Fig.2. Traditional means of communication

To simplify,following model is extracted which is named the two-way relay system model[4]as shown in figure1:First,two source nodes which are A and C send information to the relay node B separately or simultaneously (this process is called the uplink).Second, the relay node broadcast information to the destination nodes which are node A and C (this process is referred to downlink). Channel between A and B is set to channel 1, channel between B and C is set to channel 2. The relay node deals with the signals differently when the channels are different.

Figure2 shows the traditional means of communication[5]. In the first time slot, the source node A transmits information b_{ac} to the relay node B.In the second time slot, the source node C transmits information b_{ca} to the node B.In the third time slot,the relay node B transmits information b_{ac} to the destination node C.In the fourth time slot,the relay node B transmits information b_{ca} to the destination node A. Node A and node C complete an information-exchange over four time slots.

Figure3 shows the straightforward network coding. Unlike the traditional method,in the third time,the relay node B transmits information $b_{ac} \oplus b_{ca}$ to two destination nodes.It takes three time slots to complete information-exchange.

The main idea of PNC is to create an apparatus similar to that of network coding, but at the physical layer that deals with EM signal reception and modulation. Through a proper modulation-and-demodulation technique at the relay nodes, additions of EM signals can be mapped to $GF(2^n)$ additions of digital bit streams, so that the interference becomes part of the arithmetic operation in network coding[6].

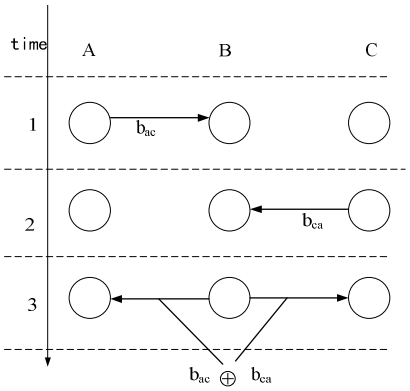

Fig.3. Straightforward network coding

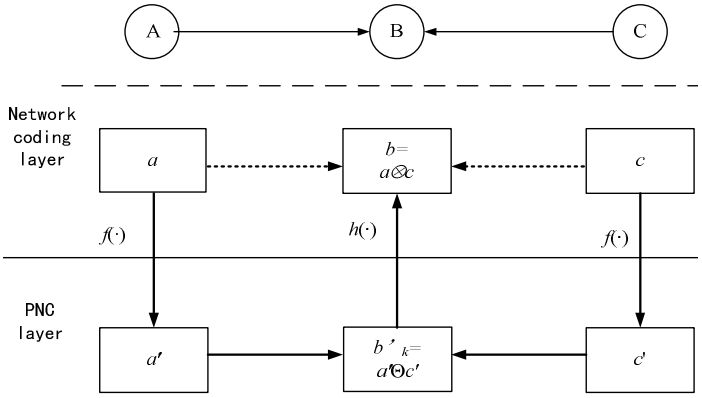

Fig.4.Physical layer network coding flowchart

As shown in Figure3: Let a and c denote the digital symbols, and let $\otimes$ be the general binary operation for network-coding arithmetic (note that $\otimes$ is not necessary the bitwise XOR hereinafter). That is, applying $\otimes$ on a,c.Next,let a' and c' denote the set of modulated symbols in the EM-wave domain. a,c is mapped to a modulated symbol a',c'.Let $f(\cdot)$ denote the modulation mapping function and it is a one-to-one mapping.In the PNC layer,two signals may combine to yield a composite signal at the receiver.Let Θ represent the binary combination operation.That is,combination of a' and c' yield $a' \Theta c' = b'_k$.Note that b'_k is not the same as b and has a higer cardinality than b,and $h(\cdot)$ is a many-to-one demodulation mapping.

In order to research easily, we make the following assumptions:node A and node C exchange information with the help of relay node B.All nodes are half-dulplex,i.e.,a node cannot receive and transmit simultaneously.This is an assumption arising from practical considerations because it is difficult for the wireless nodes to remove the strong interference of its own transmitting signal from the received signal.There is no direct link between node A and node C.The signals transmitted by node A and node B are perfect synchronization,which includes symbol-level time synchronization, carrier-frequency synchronization and carrier-phase synchronization.

Let $s_1(t)$ and $s_3(t)$ denote the signals sent by the node A and node C which have the same phase and amplitude.The received combined signals $r_2(t)$ by the relay node B is

$$\begin{aligned} r_2(t) &= s_1(t) + s_3(t) + w(t) \\ &= a_1\cos(wt) + a_3\cos(wt) + w(t) \\ &= (a_1 + a_3)\cos(wt) + w(t) \end{aligned} \tag{1}$$

In the type(1):The packets of two source nodes are mapped to PNC layer after they are modulated.They reach the relay node after two same channels.$w(t)$ is additive white Gaussian noise (AWGN) with double-sided power spectral density $S_w(f)=N_0/2$. A form is used for a exhaustive description.

TABLE1.PNC mapping

Modulation mapping at node A and node C				Signal processing at B		
Input		Output		Input	Demodulation mapping	Output
s_1	s_3	a_1	a_3	a_1+a_3	r_2	a_2
1	1	1	1	2	0	-1
0	1	-1	1	0	1	1
1	0	1	-1	0	1	1
0	0	-1	-1	-2	0	-1

In the TABLE1,BPSK is used and the noise is ignoring.Next we analyze the bit error rate (BER) performance.

When the noise is added, the relay node in the mapping process need to consider the various threshold values.The maximum a posteriori probability criterion[7]is used to find the decision threshold. The conditional probability density at the relay node is

$$p(\mathrm{r}\,|\,\mathrm{s}_x) = \frac{1}{\sqrt{\pi N_0}}\exp[\frac{-(\mathrm{r}-\mathrm{s}_x)^2}{N_0}] \tag{2}$$

Then find the two decision point

$$r_1 = -1 - \frac{N_0}{4}\ln 2 \tag{3}$$

$$r_2 = 1 + \frac{N_0}{4}\ln 2 \tag{4}$$

Let the received signal be r.When the r is less than r1, declaring a1+a2 to be -2. When the r is more than r2, declaring a1+a2 to be 2.Otherwise, declaring a1+a2 to be 0.Thus, the BER can be derived as follows:

$$\begin{aligned} P_{up} = {} & \frac{1}{2}\int_{-\infty}^{r_1}\frac{1}{\sqrt{\pi N_0}}\exp(\frac{-r^2}{N_0})\,\mathrm{dr} + \frac{1}{2}\int_{r_2}^{\infty}\frac{1}{\sqrt{\pi N_0}}\exp(\frac{-r^2}{N_0})\,\mathrm{dr} \\ & + \frac{1}{4}\int_{r_1}^{r_2}\frac{1}{\sqrt{\pi N_0}}\exp(\frac{-(r+2)^2}{N_0})\,\mathrm{dr} + \frac{1}{4}\int_{r_1}^{r_2}\frac{1}{\sqrt{\pi N_0}}\exp(\frac{-(r-2)^2}{N_0})\,\mathrm{dr} \end{aligned} \tag{5}$$

Above we describe the derivation of uplink.In the following,we will get the derivation of downlink.The relay node broadcast the information processed to node C and node B.

TABLE2.Modulation mapping at B ; Received at C,A

Modulation mapping at B		Received at C		Received at A	
Input	Output	Input	Output （-1 correspondence to same，1 correspondence to same difference）	Input	Output （-1 correspondence to same，1 correspondence to same difference）
r_2	a_2				
0	-1	-1	1	-1	1
1	1	1	0	1	1
1	1	1	1	1	0
0	-1	-1	0	-1	0

In the TABLE2, $r_2 = a_1 \oplus a_3 \in \{0,1\}$ .The signals processed by the relay node B reach the destination node after the channel.Node C and A recover the signals by the information in the cache.

Use the methord as in the uplink,we can get the bit error rate by

$$P_{down} = \frac{1}{2}\int_{-\infty}^{r} \frac{1}{\sqrt{\pi N_0}} \exp(\frac{-(r-1)^2}{N_0})\,\mathrm{dr} + \frac{1}{2}\int_{r}^{\infty} \frac{1}{\sqrt{\pi N_0}} \exp(\frac{-(r+1)^2}{N_0})\,\mathrm{dr}$$
$$= \frac{1}{2}Q(\sqrt{\frac{2}{N_0}}) + \frac{1}{2}Q(\sqrt{\frac{2}{N_0}}) = Q(\sqrt{\frac{2}{N_0}}) \tag{6}$$

Then,we get

$$P_e = \max(P_{up}, P_{down}) \tag{7}$$

Numerical simulation and verification

For details, we make the following simulation graphics.

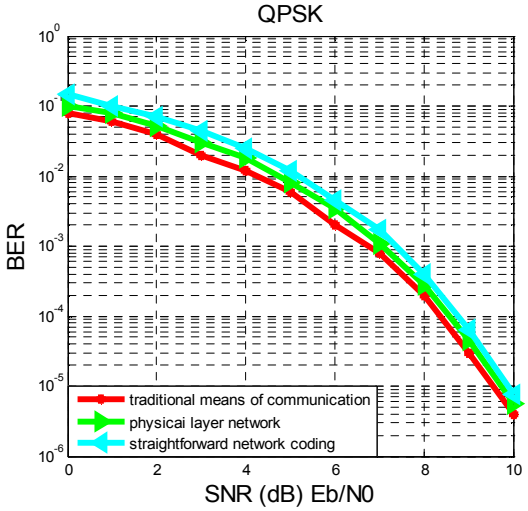

Fig.5. Three different communication methords

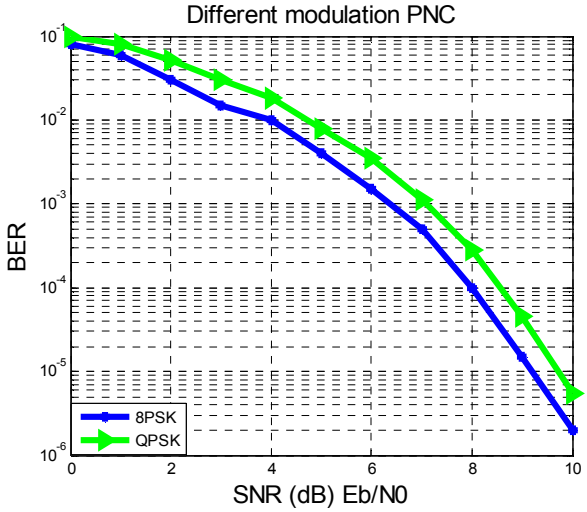

Fig.6. Two different modulation

As the Figure5 shows the BER of the PNC, straightforward network coding,and the traditional means of communition.The BER of PNC is slightly worse than the traditional means of communition,but is slightly better than straightforward network coding.

In the Figure6,we plot the BER of PNC under different modulation.The result shows that the higher the modulation order, the lower the error rate.The reason is that the MPSK modulation increase the euclidean distance.But the higher the modulation order number, the longer relay node data processing.So we must choose the right order number according to the practical situation.

Conclusion

Based on the above numerical analysis,we discover that the use of physical layer network coding in UAV communication systems is an appropriate choice. In terms of network throughput, compared to traditional physical layer network coding communications and direct network coding it increases 1 times and 0.5 times; in terms of the error rate, compared to the direct network coding,the physical layer network coding is lower. Therefore,the UAV communication which uses physical layer network coding will meet the needs of modern warfare.

Acknowledgements

In this paper,we are very grateful to Professor Zhang Shengli and Ph.D. LU LU in Chinese University of Hong Kong for theoretical guidance.

References

[1] Xumeng Yuan.UAV network and related technology[J].Science for development,2009:27-28.
[2] T. Ojanpera, and R. Prasad, “An over view of Air Interface Multiple Access For IMT 2000/UMTS,” IEEE Communication Magazine, pp. 82-91, Sep. 1998.
[3] Ahlswede R, Cai Ning, Li S Y R, et al. Network InformationFlow[J]. IEEE Trans. on Information Theory, 2000, 46(4):1204-1216.
[4] Hausl C,Hagenauer J. Iterative network and channel decoding for the two-way relay channel [C]. In Proc IEEE International Conference on Communications (ICC), Istanbul,June 2006: 1568-1573.
[5] Matthew C,Valenti.Don Torrieri,Terry Ferrett. Noncoherent Physical-Layer Network Coding Using Binary CPFSK Modulation[J]. Lane Department of Computer Science and Electrical Engineering, West Virginia University,2009.
[6] Shengli Zhang, Soung Chang Liew, Patrick P.Lam. Physical-layer network coding[C]. The Annual International Conference on Mobile Computing and Networking (ACM Mobi-Com). 2006:358-365
[7] J. R. Proakis, Digital Communication. New York: McGraw Hill,1989.

Advanced Materials Research Vols. 989-994 (2014) pp 4152-4156
© (2014) Trans Tech Publications, Switzerland
doi:10.4028/www.scientific.net/AMR.989-994.4152

Study on the Implementation of RAKE Receiver in 4G System

Haiyang FU[1, a], Churong ZHU[1, b], Xiangdong JIA[2, c]

[1]College of Telecommunication and Information Engineering,

Nanjing University of Posts and Telecommunications, Nanjing, P. R. China

[2] College of Mathematics and Information Science,

Northwest Normal University, Lanzhou, P. R. China

[a]fuhy@njupt.edu.cn, [b]zhuchurong1989@163.com, [c]jiaxd@nwnu.edu.cn

Keywords: Multi-path; 4G; RAKE; Coherent Demodulation

Abstract. The RAKE receiver has must been used in CDMA or 3G systems for its function to form the diversity reception of signals resulting from multi-path propagations. The basic condition for the implementation of RAKE receiver is that the spectrum spreading (SS) must be used in those systems. But that SS would not be existed in 4G system continuously, and OFDM and QAM would be used in that system instead. So the new method should be found to replace that SS code to separating those multi-path signals, making the RAKE receiver in 4G could be realized. This new method for the implementation of RAKE receiver in 4G System would be introduced in the paper, as well as the performance difference between those two kinds of Rake receiver.

Introduction

There must be multi-path interferences (MPI) existed in any radio channel, which is same for 3G and 4G mobile communication system. Also there is multi-access interferences (MAI) existed in the radio channel of CDMA system. The classical RAKE receiver (CLRAKE) is the basic component of CDMA system. Making use the spectrum spreading (SS) code, which must be included in the CDMA systems, the separation, time-delay adjustment and superposition of signals resulting from multi-path propagations could realized by the RAKE receiver, making the diversity reception being completed. Those signals were considered as MPI in CDMA system, but now the energies of those multi-path signals could be made used. Comparing with the receiver without RAKE, the signal to noise ratio (SNR) of RAKE receiver could be upgraded a lot, as well as the efficiency of the power transmitted. Also the RAKE receiver could be used to restrain the effect caused by MAI in CDMA system, but there is no such MAI similar to that in CDMA system in 4G OFDM system. Upon the important function of RAKE receiver in 3G system there is enough reason to expect that the RAKE receiver should be used in 4G mobile communication systems continuously since the environment of radio wave propagation for 4G is almost the same as that of 3G.

Several block diagrams of RAKE receiver have been given in [1], which are in the configuration of delay reference. Really, RAKE receiver is a kind of diversity reception hidden in time domain, which could be known by the block diagram of RAKE receiver given in [2]. Comparing the configuration in [2] with that in [1], it could be known that the fixed time delay given in the block diagrams in [1] is unsuitable.

One important problem existed in those block diagrams given by the above references is that the input signals of those block diagrams are always a path signal in base-band, meaning that the phase relation among those multi-path signals received by a RAKE receiver has not been considered enough, whose influence has been analyzed in [3][4] specifically, in which a new named as coherent RAKE receiver (CORAKE) is introduced. Now, those RAKE receivers introduced in [1][2] would be named as classical RAKE receiver (CLRAKE) in this paper. Comparing CLRAKE with CORAKE, it could be found easily that the SS code in CLRAKE is substituted by the local coherent carrier in CORAKE. It is well known that the key function of SS code is to separate different path signals from a signal with several path signals. Now, the local coherent carrier in CORAKE could be used for the separation of signals resulting from MPI without SS code such as the OFDM system

[5][6]. Also it would be introduced in the paper how to use the local coherent carrier for the separation of signals resulting from MPI in the OFDM system.

The Principles of Classic RAKE Receiver and Coherent RAKE Receiver

A scheme of CLRAKE receiver for 3-path signals received is shown in Figure 1, and the scheme in [2] is similar with that in Figure 1, in which the third path $PN_{I3L}W_{3L}$ is assumed with the maximum delay.

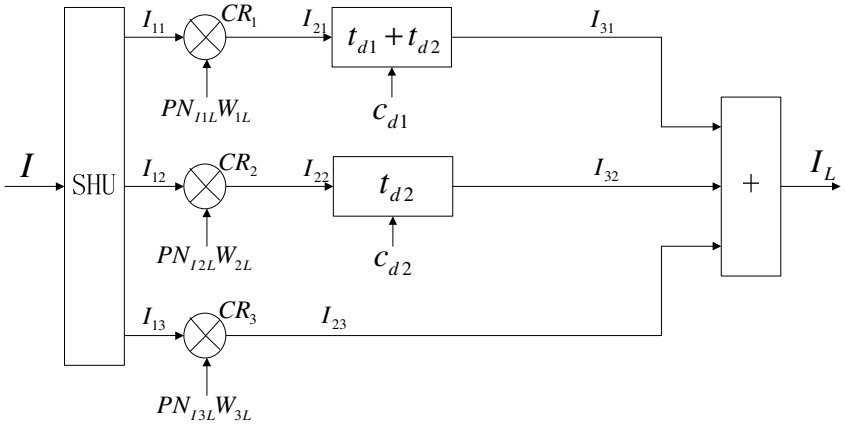

Fig.1. CLRAKE receiver

After the down-conversion in the receiver of CDMA system, the first path signal of some user could be expressed as follows,

$$x_1(t) = D_1(t)W_1(t)PN_{I1}(t)\cos(\omega_1 t + \varphi_{11}) + n(t) \quad (1)$$

In which some user's data is denoted by $D_1(t)$, cell address-code by $PN_{I1}(t)$, the SS code for the uplink channel by $W_1(t)$, the carrier phase of the first path signal received by φ_{11}, and the noise by n(t). The main component of the noise in CDMA is the self-interference formed by MAI and MPI. To simplify the derivation process, only the MPI has been considered.

In Figure 1, $PN_{I1L}W_{1L}$ is the local address-code sequence recovered. Assuming that local coherent carrier $\cos(\omega_{1L}t + \varphi_{11})$ is synchronized to the carrier in the first path signal received. Corresponding to $PN_{I1L}W_{1L}$, the input signal of SHU in Figure 1 is that

$$I = I_1 + I_2\cos\theta_2 + I_3\cos\theta_3 \quad (2)$$

In which I_1 is the output of the coherent demodulating of the first path signal received, θ_2 and θ_3 are the phase differences between the carriers of the second, third path signals received and the carrier of the first path signal received respectively.

The output I_{21} of correlator CR_1 in Figure 1 is that

$$I_{21} = PN_{I1L}W_{1L} \bullet I = D_1(t) + PN_{I1L}W_{1L} \bullet \left[I_2\cos\theta_2 + I_3\cos\theta_3\right] \quad (3)$$

In equation (2, 3), due to the asynchronous between PN_{I1L} and those PN sequences in I_2 and I_3, so these two signals will be treated as self-interference in I_{21}. This noise could be expressed as

$$n(t) = PN_{I1L}W_{1L} \bullet \left[I_2\cos\theta_2 + I_3\cos\theta_3\right] \quad (4)$$

Similarly, assuming PN_{I2L} in Figure 1 is synchronized with $PN_{I1}(t - t_{d1}) = PN_{I2}$ in I_2, there is

$$I_{22} = PN_{I2L}W_{2L} \bullet I = D_1(t - t_{d1})\cos\theta_2 + PN_{I2L}W_{2L} \bullet \left[I_1 + I_3\cos\theta_3\right] \quad (5)$$

In which θ_2 is determined by the delay between those carriers in those two path signals received. While $\cos\theta_2$ is a negative value, the polarity of signal I_{32} is inverted to I_{31}. So it will reduce part of the signal in I_{31}, making the signal amplitude of I_L in Figure 1 be decreased.

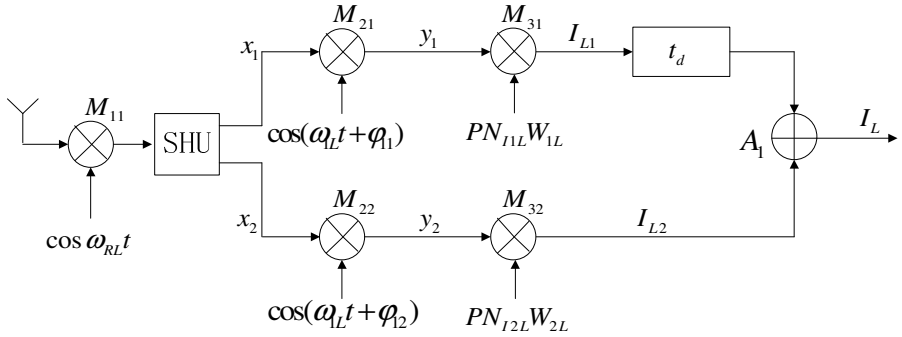

Fig.2. CORAKE demodulator

The scheme of CORAKE receiver for the receiving of two-path signals is shown in Figure 2. Similarly, there are the same assumptions about $\cos(\omega_{1L}t+\varphi_{11})$ and $\cos(\omega_{1L}t+\varphi_{12})$. So there is

$$I_{L1} = PN_{I1L}W_{1L}y_1(t) = D_1(t) + PN_{I1L}W_{1L}\left[I_2\cos\theta_2\right] \tag{6}$$

In which $I_2 = D_1(t-t_d)W_1(t-t_d)PN_{I1}(t-t_d)$, $\theta_2 = \varphi_{11}-\varphi_{12}$, and the last term is the self-interference in CDMA. Similarly, the following could be derived,

$$I_{L2} = PN_{I2L}W_{2L}y_2(t) = D_1(t-t_d) + PN_{I2L}W_{2L}\left[I_1\cos\theta_2\right] \tag{7}$$

In which $I_1 = D_1(t)W_1(t)PN_{I1}(t)$. After signal I_{L1} being delayed by circuit t_d and being summed with I_{L2} in A_1, there is

$$I_L = 2D_1(t-t_d) + n(t) \tag{8}$$

It is clear that the amplitude of I_{L2} would be larger than that of composing output for the corresponding parts in Figure 1.

The Principle Model of OFDM

The principle model of OFDM is given in Figure 3, in which the scheme for modulator of multi-carrier is given really. There S/P means to transform a series of input data stream into several parallel data streams, and that constellation mapping (MAP) means to transform several parallel data streams with two levels in two groups into two amplitude modulation signals with multi-level, and that symbol "+" means a kind of complex adding of those signals of I and Q, which would be used to modulate a pair of quadrature sub-carries denoted by $e^{j\omega_n t}$. That constellation mapping means that some kind of digital modulation such as BPSK, QPSK, 16-QAM or the other similar modulations may be produced. Any OFDM symbol means a QAM or PSK symbol, which is composed of a pair of quadrature sub-carries modulated.

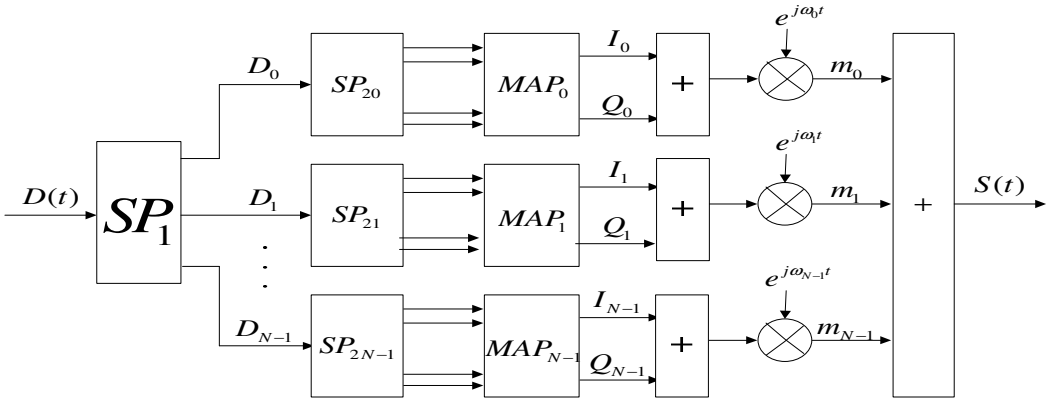

Fig.3. The principle model of OFDM

The expression for MQAM in a symbol could be given as follows,

$$y(t) = I_m\cos\omega_0 t + Q_m\sin\omega_0 t \qquad 0<t<T \tag{9}$$

In which T is used to denote the duration time of a symbol, and I_m or Q_m would with multi-level of amplitude. The number of levels would be decided by that M in MQAM.

The neighboring carrier frequencies in OFDM system must be quadrature which could be defined as follows,

$$\frac{1}{T}\int_0^T \exp(j\omega_m t)\exp(-j\omega_n t)dt = \begin{cases} 1, & m = n \\ 0, & m \neq n \end{cases} \tag{10}$$

It could be known that the receiver scheme of OFDM signal should be similar to that of classic MQAM signal since the feature of quadrature neighboring carrier frequencies, which could be used to save the required bandwidth for the system, would not change the characteristic of MQAM signal, so classic coherent demodulation receiver could be used for the OFDM signal.

The RAKE Receiver for OFDM Signal

The scheme for RAKE receiver of OFDM signal is given in Figure 4, in which $S_r(t)$ is used to denote that received OFDM signal, but it could be processed as an MQAM signal. Since assuming that OFDM signal come from 3-propagation paths, there are 3-path signals included in $S_r(t)$ with different time delay, and only the signal carried by sub-carrier ω_0 is considered. So in Figure 4 there are three MQAM demodulators for those 3-path signals. For example, that $DQAM_0$ is used to denote the MQAM demodulator for the 1st path signal, DEL_0 the time delay needed for the 1st path, and cd_0 the controlling signal for the time delay needed. Here assuming that the 1st path signal has minimum time delay compared with the other path signals. The local coherent carrier $\cos\omega_{01L}t$ is synchronized with that $\cos\omega_0 t$ in the 1st path signal received in phase. Similarly, assuming that 6-path local carriers are synchronized with those corresponding carriers in the multi-path signals received in phase and according to Figure 4, there are

$$I_{01}=I_{r01}+I_{r02}\cos\theta_2+I_{r03}\cos\theta_3+Q_{r02}\sin\theta_2+Q_{r03}\sin\theta_3 \tag{11}$$

$$Q_{01}=Q_{r01}+Q_{r02}\cos\theta_2+Q_{r03}\cos\theta_3-I_{r02}\sin\theta_2-I_{r03}\sin\theta_3 \tag{12}$$

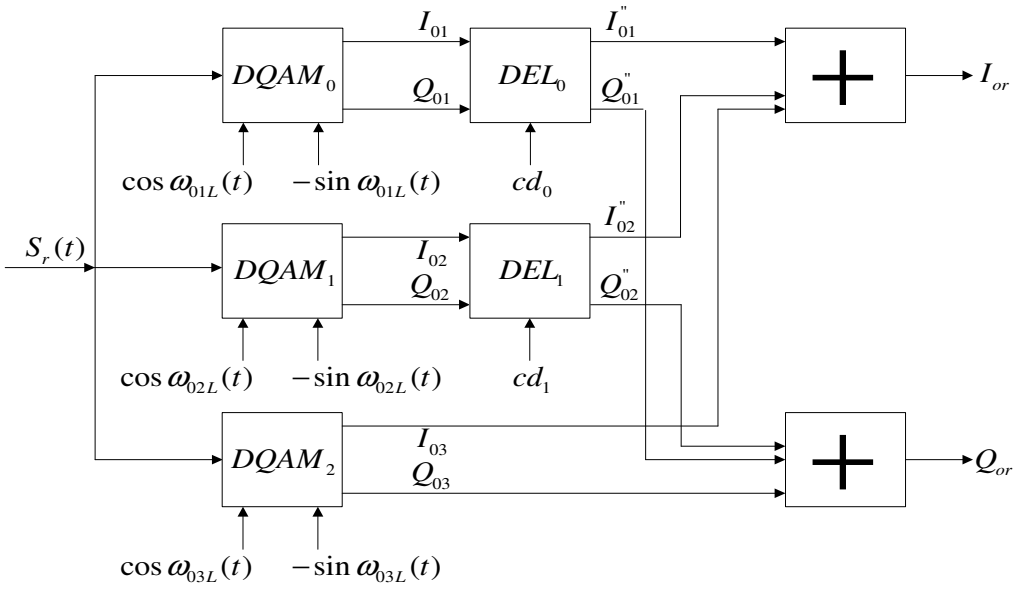

Fig.4. The RAKE receiver for OFDM signal

In which I_{r01} being used to denote the signal received in the 1st path carried by ω_0 is corresponding to I_m in Eq.(9), θ_2 and θ_3 to denote the phase differences between the carrier of 1st path signal and the carriers of 2st path or 3st path signal respectively. Similarly, the equations for $I_{02}, Q_{02}, I_{03}, Q_{03}$ given in Figure 4 also could be deduced. Analyzing the Eq.(11) and Eq.(12) further, it could be found that apart from I_{r01} there are many other terms to be considered as noise

resulting from MPI. Generally speaking, such kind interference should be restrained by some method. According to Eq.(11),

$$I_{0r} = I_{r01}(t - t_{d0} - t_{d1}) + I_{r02}(t - t_{d1}) + I_{r03} \quad (13)$$

In Rayleigh fading conditions, assuming that all amplitudes of 3-paths signals received are the same in Figure 4, the amplitude of I_{0r} would be 3 times of that for a single path receiver. It is easy to derive that the SNR gained by the scheme in Figure 4 is 4.8 dB about.

It has be shown in Figure 4 and by Eq.(11) or Eq.(12) that the separation of 3-path signals received could be realized by the coherent demodulations for different path signals separately, separation and coherent demodulation being realized simultaneously. Also the defect of CLRAKE resulting from the phase difference θ_2 and θ_3 among carries in 3-path signals received could be removed.

Conclusions

Before it is well known that RAKE receiver must be used in CDMA system since that receiver must be constructed on the basis of spectrum spreading communication. But according to the method, presenting by us before in [3], of to separating different path signals confused in a signal received by coherent demodulation, the RAKE receiver could be used in any communication system almost, and significant SNR gain would be obtained. Limiting by the space of this paper, such as how to recovering the local coherent carrier and how to produce the control signal of time delay component have not been discussed in the paper, and they should be studied further.

Acknowledgment

This work was supported by the Research Fund for the Doctoral Program of Higher Education of China under Grant 20113223110001.

References

[1] John G. Proakis, “Digital communications”, 4th edition, Boston: McGraw-Hill, 2001, pp.842-853.

[2] I. Matsunami, A. Kajiwara, Rake reception of UWB-IR indoor radio with reflector, ICC2007 Proceedings, IEEE International Conference on Communication, IEEE, 2007: 5781-5786.

[3] Fu Hai-yang, Dai Zhen-hua, Zheng Jian-guang, Jia Xiang-dong, RAKE receiver with carrier coherent demodulation for multi-path signals, 33(3), Journal of Beijing University of Posts and Telecommunications, pp.30-33.

[4] Jia Xiang-dong, Fu Hai-yang, Yang Long-xiang, Implementation Scheme of Rake Receiver in Base Band and Phase Difference Estimation of Multi-path Signals, 34(4), Journal of Beijing University of Posts and Telecommunications, pp.97-100.

[5] 3GPP Technical Specifications 36.301, Version 9.1.0, User Equipment (UE) radio transmission and reception, 2009.9.

[6] Astély D., Dahlman E., Furuskar A., et al., LTE: the evolution of mobile broadband, Communications Magazine, IEEE, 2009, 47(4): 44-51.

Advanced Materials Research Vols. 989-994 (2014) pp 4157-4160
© (2014) Trans Tech Publications, Switzerland
doi:10.4028/www.scientific.net/AMR.989-994.4157

The Research of M-learning Platform Based on 4G Network

Haiyun LIN[1, a] , Yujiao WANG[1,b,*]

[1]Department of Physical Science and Technology, Kunming University, Kunming, 650214,China

[a]lhy198@163.com, [b]tjwyj817@163.com

* Corresponding author: tjwyj817@163.com

Keywords: mobile learning; 3G; system design; 4G

Abstract. By analyzing mobile learning application mode of 4G network, combining with the technical characteristics of 4G network , a mobile learning system based on 4G was proposed. We described the architecture of system and found a solution to the flexibility question of multimedia service development in mobile learning.

Introduction

As an effective combination of mobile communication technology with the digital learning ,Mobile Learning is considered to be a future learning mode, or a kind of learning mode indispensable in the future, bringing learners a brand new feeling whenever and wherever learning is possible. Being flexible, convenient, and “random-access", Mobile Learning has become a hot topic in the research of modern educational technology. Learners can learn shortly and quickly at any time, anywhere without being constricted by desktop. In the afternoon of December 4, 2013, the Ministry of Industry and Information Technology officially issued 4G licenses, announcing China’s communication industry entering into the 4G era, which also marking that the mobile learning platform, based on 4G network, will bring a brand-new feeling for teachers to learn whenever and wherever .

3G and 4G

Compared with 3G mobile technology, the fourth generation communication network can connect different fixed and wireless platform across different frequency bands, truly providing consistent and seamless mobile computing environment and supporting high-speed data transferring capacity in high-speed mobile environment, with lower network expense to realize high quality transmission of voice, data and image. In addition, 4G can provide users with personalized service defined by themselves, which precisely meets the requirements of high quality and large data for mobile learning in the modern sense. In order to reflect more directly the significant improvement in performance and service of 4G communication technology, this paper is about to make a comparison between 4G and existing 3G technology in the service, network structure, transmission speed, frequency range, connecting method and module design [1].

Service, 3G focuses on voice, with video-calling, while 4G can realize voice, video-calling, video conference and multimedia communication.

Network architecture, 3G is a WAN mode of base-station tower with high costs, complicated construction, and incomplete coverage. While 4G is a mixed mode of LAN and WAN with low costs and integration with existing network construction. Its network capacity is 5-10 times more than that of 3G, also its transmission quality is better than that of 3G.

Transmission speed, 3G is 2Mbs (actual deployment 384Kbps),and the speed can be even lower where interference is strong. However, 4G is 20-100Mbps; its speed can be as fast as being connected.

Frequency range, 3G is 1.8-2.5GHz, which means that bandwidth and frequency range is too narrow. As all mobile users occupy the same frequency and bandwidth, the "near-far effect" problem is quite serious. However, 4G is 2-8GHz. Its power control is more precise than that of 3G, and mobile and the base station use power control simultaneously and strictly, thus solving the "near-far effect" problem.

Connecting method, 3G is CDMA, based on wireless technology. It needs to adopt expensive and complex adaptive anti-interference device, whereas 4G uses OFDM which is a kind of high speed transmission technology, which can effectively resist signal interference. And the cost is low.

Module design,3G adopts wireless optimization design, lacking enough IP support, wireless transmission technology with a unified format, and a core network. While 4G uses smart antenna which is adaptive to low adjustment direction for tracing signal changes, thus gain signal coverage, system capacity, service quality etc. at a lower cost.

In addition, 4G communication technology has a significant improvement in communication, coverage method and tariff etc..

Communication becomes more flexible, Mobile phone function, based on 4G communication technology, will not only be limited to phone call, message, Internet etc. The phone can also be used for two-way downloading data, image, video, all kinds of entertainment and learning information, which can be compared to a tiny computer.

Seamless coverage. 4G communication system will implement global-unified standards, allowing "seamless connection" among all kinds of media, communication equipment and network. Besides, 4G communication technology allows using wireless network unlimited by time and space.

Low cost. 4G communication not only has a good compatibility with 3G communication for users to upgrade easily, but also introduces many advanced communication technologies to ensure a highly flexible system operation mode. Thus compared with other technologies,4G communication deployment can be far more easy and fast [2]. Also, communication operators would consider directly construct 4G network communication system based on 3G infrastructure step by step, so that it can effectively reduce costs from both operators and users. The cost of instant wireless connection and some other services in 4G communication will be cheaper than 3G communication.

Application mode of mobile learning based on 4G

A. Mobile learning mode based on 4G real-time mobile video service

4G real-time mobile video is one of the core application of 4G service, sending users video content through mobile network and mobile terminal. 4G network is capable of transmitting high quality video image in parallel with HDTV. To some extent, mobile learning based on 4G real-time mobile video service will have a great impact on mobile learning based on 3G [3]. Because with the help of network bandwidth provided by 4G technology, learners can get a higher network transferring bandwidth no matter in indoor, outdoor or in mobile learning. Mobile learners access gateway when wireless network is accessible through mobile terminal, so as to achieve teaching video on demand, live or download, enjoying the fast surfing experience of mobile learning; Providers provides the teaching video content through wireless access mode which has greater flexibility and mobility compared with the mobile learning mode based on 3G and thus realize the real-time interaction between teachers and students whenever and wherever possible.

B. Mobile learning mode based on 4G and cloud computing

The use of expanded 4G network will make the data and application for online storage in cloud computing become more attractive than today. 4G-based cloud services will have a significant improvement in the aspect of reliability, functionality and safety for mobile users. Schools and teachers will use "cloud services" supported by “cloud computing" in education and in construction of information environment of individualized teaching. It also supports teachers' effective teaching and students’ active learning, and provides teaching with resource sharing and unlimited storage space and other convenient conditions. So teaching activities will not be restricted by time, space and region, and will get high quality assurance.

C. Mobile learning mode based on 4G multimedia messages

Message service is the most common function of telephone. Applying this function to mobile learning can not only meet the communication requirement from learners, but also be used in the work arrangement, teaching schedule and notice etc. Under the technical conditions of 3G, message can be used to send multimedia messages with text, sound, image, video, thus transferring learning information and develop mobile learning. By way of message, information can be transmitted at any

time between learners and learners, learners and teachers. Information can be transmitted between learners and the Internet as well. In this mode, learners send messages to the teaching server, the intelligent system then changes the message content into a data request based on analysis of the content, and then through analyzing and processing, automatically replies to learners.

Architecture design

Mobile Learning platform refers to the software system providing learners with mobile learning information and learning service support by the use of wireless communication technology and wireless network technology [4]. The architecture of this platform from low to high order is: the presentation layer, the network layer, the business logic layer and the data layer as shown in figure 1,within which the presentation layer is located on the client-side, the network layer is based on mobile communication network and Internet, and the business logic layer and data layer is located on the server.

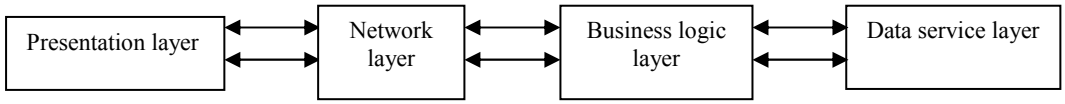

Fig.1. M-learning Platform Based on 4G Network

Based on 4G, Mobile Learning platform uses J2EE (Java 2 Platform Enterprise Edition) database as a permanent data support, integrating large amounts of data for visitors. The system includes mobile phone and some other client-side devices based on J2ME (Java Micro Edition), J2EE server and wireless service provider (China Mobile or Unicom), as shown in figure 2. The require digital education resources are searched through the information channel (4G accessing server) of wireless service provider, and mobile phone client devices access the information on the server. The interaction of the general wireless mobile phone devices and enterprise level application is promoted by the use of underlying data communication technology of wireless field, thus allowing client devices gain access to the server and complete the feedback of data information to the server [5]. This system dynamically separates wireless client and server by using establishment and component technology: sending the information to the server by the wireless client search engine, then processing the return information, and then accessing the corresponding digital educational resources information.

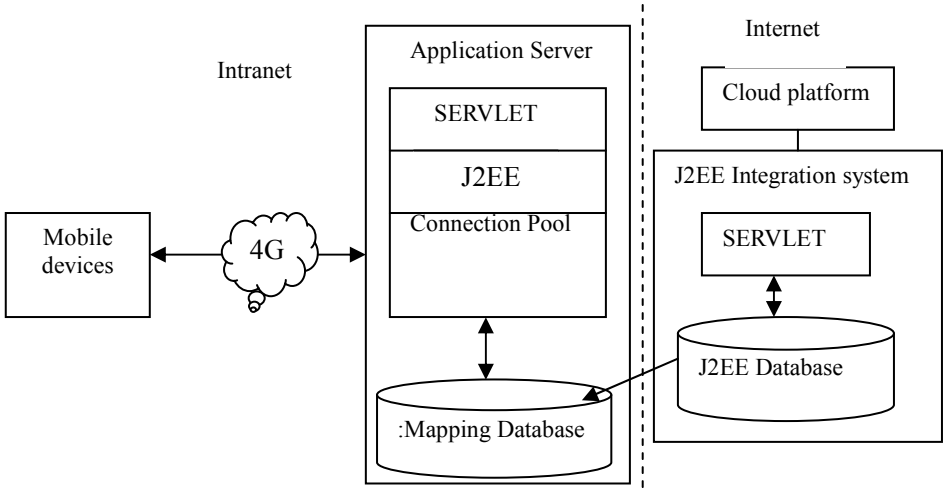

Fig.2. The modules of M-learning Platform

Conclusion

With the development and improvement of 4G network technology and 4G mobile terminal equipment, Mobile Learning helps us realize our dream of lifelong learning whenever and wherever. With the implementation of Mobile Learning platform based on 4G, the complexity of network structure and maintenance cost of operation will be reduced, thus improving the flexibility of multimedia service development in Mobile Learning.

References

[1] Yulong Zhang, Zhifeng Li, Xun Zhao. 4G mobile communication technology application and development prospect. [J]. Information and Communications. 2013 (1) 45-50.

[2] Minghai Yi. 4G study on characteristics and development status of mobile communication system. [J]. Science and Technology for China's Mass Media, 2013 (6) 179-180.

[3] Lin Haiyun, Zhao Qingjiang, Wang Yujiao, Li Xiaofeng. Mobile Learning System Based on 3G Core Network IMS. [J]. Computer and Digital Engineering. 2011 (3) 69-71.

[4] Li Chuanzhi, Chen Yong, Xu Ming. Software engineering design and implementation of case teaching resources system based on 4G. [J]. Research on Library Science. 2012 (8) 27-30.

[5] Xue Yan. To explore the mobile tourism electronic commerce platform based on 4G network technology. [J]. Electronic Test, 2013 (7) 51-52.

Advanced Materials Research Vols. 989-994 (2014) pp 4161-4164
© (2014) Trans Tech Publications, Switzerland
doi:10.4028/www.scientific.net/AMR.989-994.4161

3D Human Body Data Acquisition and Fit Evaluation of Clothing

Zhen Wang[1], Yueqi Zhong[1,2,a], Kaijie Chen[1], Jiayi Ruan[1], Jincheng Zhu[1]
[1]College of Textiles, Donghua University
[2]Key Lab of Textile Science and Technology, Ministry of Education, China
[a]Corresponding author: zhyq@dhu.edu.cn

Keywords:3D data acquisition, Body scan, Body measurement, Residual space, Clothing fit

Abstract. This paper presents the method of 3D human body data acquisition based on 3D scanning and the non-contact fit evaluation of clothing based on the distribution features of residual space between clothing and human body. A Kinect camera is employed to collect point cloud data. The points cloud is treated by Geomagic for noise reduction and surface reconstruction. By analyzing the residual space between clothing and human body, the fit distribution of scanned clothing can be achieved. The fit evaluation will make contributions to clothing design, online sales of clothing and virtual try-on.

Introduction

There are two major methods of body measurement in use, one is contact body measurement, and another is non-contact body measurement[1]. The method of contact measurement does not fit for soft materials and ultrathin things for its low measuring speed and inaccuracy.The application of non-contact measurement effectively avoids the disadvantages of low efficiency and poor objectivity.

Non-contact measurement has been widely accepted by companies and scientific research institutions in collecting 3D body data[2], including college of Loughborough, Marks & Spencer, Courtaulds, etc. The common problems exist in 3D scanning includes the cost of device is barely afordable for average customers, and the installation is quite complicate.

As an effort to tackle these problems, we use single Kinect camera to scan body for intact 3D body data[3]. We then process the data through Geomagic software[4] to obtain a triangulated surface model. Different from the work reported by Chen[5], we analyze the dimensional features at key points of human body[6]. We obtain the fit evaluation of clothing through data analysis. The scanning system has the characteristics of simple operation, low cost with fast speed

3D data acquisition

In this investigation, we use Kinect camera (RGB-D sensor) to scan the human body. The RGB-D sensor can obtain RGB color and depth information at the same time. With Kinect fusion algorithm[7], we can effectively decrease the error when measuring body by two-dimensional image and perspective image. RGB-D sensor used in the test can provide serried and accurate gap information, collect 3D point cloud of original clothing, and then it can get high-precision 3D garment prototype.

The test needs to be conducted in an closed environment with stabilized light to decrease noisy points and frame skipping during scanning, as shown in Figure 1. The temperature and relatively humidity are set at 18-25℃, 45%-75% RH respectively according to occupant comfort.

The process of scanning. The common procedure of body scanning follows.

Step1. Identify the position. We regard a fixed standing point as center of a circle whose radius is 1.5 meters, the circle provides a track for Kinect to scan around body.
Step2. Identify scanning point. We set eight equidistant points on the track, when device arrives at each point, we move the camera up and down slowly to obtain high-precision 3D body data.

Step3. Consulting Kinect device with computer. We keep the camera at a settled height, and swing the camera to identify the whole body has been captured. Meanwhile, we observe the point cloud image on the screen for fear of frame skip.
Step4. We keep the body in a settled posture with body standing uprightly, arms stretched and legs separated slightly. We scan the body along the circle, at the starting location we need to move the camera up and down to 'fuse' the points cloud. We move Kinect at constant speed and swing the camera at each point to obtain intact point cloud of human body. The total time to finish one round of scanning is about 2-4 minutes.
Step5. For fit evaluation, we put the clothing (in this paper, we use a shirt as an example) onto the human body, and repeat step4.

Figure 1.Test environment. Figure 2.Original point cloud data. Figure 3.Data after noise reduction.

Data process and fit evaluation of clothing

Data process. We use the Geomagic software to denoise the 3D point cloud data, then we change the surface of point cloud into triangulation structure, the process is called surface encapsulation.

The Geomagic software has the function to finish point cloud data of hook face rapidly, and to generate gridding automatically. In order to shrink the range of point cloud we have measured, we need to wipe them off by using the noise reduction of Geomagic software (Figure 3) to remove the side effects caused by slight shaking of device, bad treated body surface, and inaccurate calibration.

After noise reducing and encapsulation, we have a triangulated model with holes on it (Figure 4).These holes are the data we missed in the scanning process. The little holes can be filled based on the surrounding surface curvature directly. The bigger holes need to be filled from the edge, or the filling will not conform to the actual surface morphology (Figure 5).

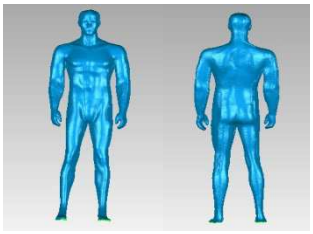

Figure 4.Triangle facet model. Figure 5.The process to fill holes.

To improve the arithmetic speed and enhance operational precision, we reduce the number of surface facet around 20,000 triangles, as shown in Figure 6. Eventually we obtain smooth triangle facet model to analyze the characteristic of the dimension in different parts of body.

Fit evaluation of clothing. Between body and clothing, there are the residual space. This is the foundation of fit/ease evaluation, i.e., we can obtain the fit information by the contact relation between body and clothing, and the size of key points can ascertain major characteristics of body, as shown in Figure 7.

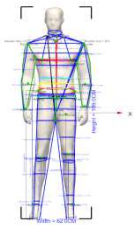

Figure 6.Simplified triangle facet model. Figure 7.Key points of body.

Using the scanned shirt as an example, we calculate the profile distribution characteristics of shirt and body contour along body from bottom to top, as shown in Figure 8.

We segment the dressed and undressed model into many slices horizontally (Figure 9), then we can get fit evaluation through the contact relation between shirt contour and body contour. When shirt contour is smaller than body contour, we think that the shirt doesn't fit for body or the shirt is too tight, on the contrary, when shirt contour is larger than body contour, the shirt fits for body exactly or the shirt is loose.

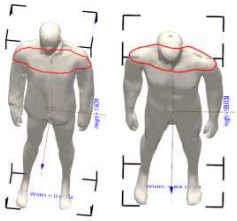

Figure 8.Shirt contour and body contour.

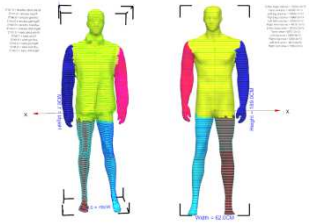

Figure 9.Slices in horizontal.

Therefore, based on the difference of each slice between shirt contour and body contour, we can plot the contact relation between them (Figure 11). Figure 11 shows the data of torso, we have also measured arms and legs (Figure 12, Figure 13). These three figures constitute the complete data of shirt. We can obtain the fit evaluation of clothing from them.

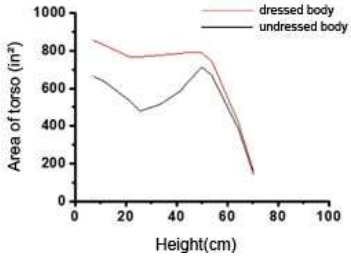

Figure 10.Data of torso.

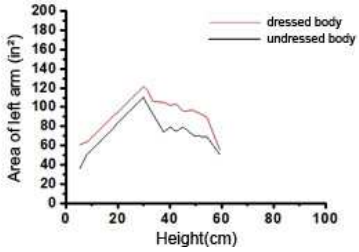

Figure 11.Data of left arm.

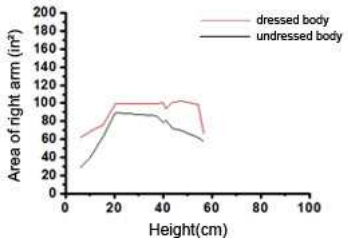

Figure 12.Data of right arm.

We use these curves to evaluate the fit between body and clothing preferably, mixing with subjective feeling to the clothing fits.

The method of getting the contour of body and clothing is shown as follows (Figure 14):

1. Based on the spatial position of the slice I, we can obtain the central location c through weighted average.
2. Set a scanning radius r based on the maximum distance from central location to the edge of the contour, $r = 1.5\max$.
3. Form a circle on the plane of the slice. Make rays from circumference to the center c of the circle, the area between two lines is small enough, we can regard it as a small triangle. We mark the area of the small triangle as S_t, therefore, the area of the whole slice can be calculated by Equation 1.

$$S = \sum_{i=0}^{n} S_t \quad . \tag{1}$$

4. The vector lines intersect the triangles of the slice of body or clothing. Link the points of intersection, we can obtain the contour of the slice.

The advantage of this method is that circular projection points have been ranked, so the sorting of space contour line can be avoided. Meanwhile, accuracy and speed are ensured. In our practice, we divide each contour into 360 points to maintain the accuracy of every slice.

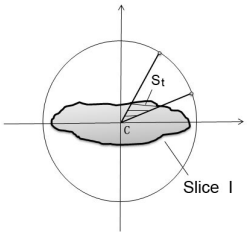

Figure 13.Method of getting the contour.

Result and discussion

The curves mentioned above show the area of the same slice of undressed body and dressed body. We can calculate the difference value of the two areas, then we conclude the minimum and maximum difference value. Mixing with subjective feeling, we can acquire fit evaluation of clothing preferably.

As limited by the test condition, error is inevitable in the original data. This is mainly on account of the low resolution of the RGB-D sensor or heavy noise during the scanning process. Compared with method of two dimensional images, this method breaks the tradition to make it possible to measure virtual models.

Conclusion

In this paper, we introduce a method to collect 3D point cloud data and to obtain fit evaluation of clothing. We calculate the area of slice between body and clothing in limbs and torso area respectively, and conclude the difference value to get fit evaluation method. When subjective feeling is in consideration, the evaluation would be more accurate. The method of collecting 3D point cloud data can also be widely used in fields of clothing online sales, virtual fit, garment customization, medical service and electronic commerce. The fit evaluation will make contributions to clothing design, online sales of clothing and virtual try-on.

Acknowledgments

This work is supported by Undergraduate Innovative Test Program (201210255025) and the Fundamental Research Funds for the Central Universities (11D10122, 13D110111)

References

[1]Xiaolin Zhang, Guowen Yuan. Treatment of non-contact measurement point cloud data [J] Journal of Guilin College of Aerospace Technology, 2010, 15 (3): 289-291.

[2]Yan Chen. Progress and application of non-contact three-dimensional body measurement technology [J] Progress in Textile Science and Technology, 2010 (006): 88-90 .

[3]Chao Song, Suping Yu, Wujun Xu. Study on 3D body scanning, reconstruction and measurement technology of the Kinect [J] Tianjin University of Technology, 2012, 31 (5): 34-37.

[4]Han Xia. Based Imageware, Geomagic Studio reverse engineering products [J]. Beijing Institute of Clothing Technology, 2010, 30 (3).

[5]Wenfei Chen. Study based garment fit female human body [J]. Donghua University, 2001.

[6]Yueqi Zhong and Bugao Xu. Automatic Segmenting and Measurement on Scanned Human Body. International Journal Clothing Science and Technology (2006).19-30.

[7]Shichao Song. Study on three-dimensional human modeling and measurement of the Kinect [D]. Donghua University, 2013.

Advanced Materials Research Vols. 989-994 (2014) pp 4165-4168
© (2014) Trans Tech Publications, Switzerland
doi:10.4028/www.scientific.net/AMR.989-994.4165

Design and Implementation of Telemetry Data Post-processing System

Wu Xingcun[1,a], Fu Gang[1, a], Li Renlong[1,a]

[1]China Satellite Maritime Tracking and Control Department, China
[a]348237548@sina.com

Keywords: Post-processing, Telemetry data, Synchronous

Abstract. This paper presents a post-hoc analysis of telemetry data processing systems, introduces the design ideas and composition structure of the system, discussed in detail the design and implementation of key technologies demodulation processing module and the module frame involved. System to achieve a recording deal with post hoc analysis of telemetry data, to solve the current telemetry signal reception playback devices, high maintenance costs, has some economic benefits.

Introduction

At present, domestic and foreign telemetry data recording equipment are high-density tape drive (HDDR) and disk arrays (RAID) two kinds. In recent years, the use of disk arrays to achieve real-time telemetry data recording has become the development trend of satellite ground receiving equipment.[1] The next satellite pass through the high-speed digital data stream collection, storage in the form of data files directly to disk array. With the extensive application of the rapid development of software radio technology and high-performance computers, can adopt high-level computer programming language software system, post-hoc analysis and processing telemetry data.

1 Design ideas

Later analysis of telemetry data processing system through software algorithms programmed manner, the telemetry signal processing applied in the form of digital signal processing program package, to become an independent function modules. In order to meet the needs of different modes telemetry data processing, this system has a modular and reconfigurable features through a combination of a number of functional modules to achieve multi-mode recording after the telemetry signal analysis, processing, display and save.[2]

Telemetry data in accordance with the recording data format, post-hoc analysis of telemetry data processing system reads information recorded on the disk first telemetry data, including telemetry signal and when the system signal. Telemetry signal through the bit synchronization and coherent demodulation, the composition of the telemetry frame has a data structure; through search telemetry frame header, frame synchronization. According to the data structure when the system signals, read B code time records each frame. When the lock header, the B time code added to the header of each frame position to achieve the reorganization of the frame structure. Finally, each frame of the processed data in a format of data stored as files. In the process system, by displaying the window in different display modes to observe the telemetry data frame of each branch. After completion of data processing, data files can be read by processing the waveform data of each branch playback telemetry frame.

Process flow of the entire system is shown below.

In order to improve the operating efficiency of the system, give full play to computer resources, on the basis of the optimization algorithm to simplify logical judgment on the use of multi-threading technology. The whole system includes three threads, one is the main thread, the data processing, set the parameters, control of the whole system running; another two threads for processing data in the background, they are also controlled by the main thread.

To ensure stable system operation, before the data processing system, we must first apply for and initialize memory, ensure that the system memory space effectively throughout the course of the

operation. To prevent memory leaks, each time the system exits normally or abnormal, should release have already requested memory space. Second, the input parameters (example: frame period, the frame code group, etc.), to determine the validity, the input parameters cause the system to prevent unstable operation.

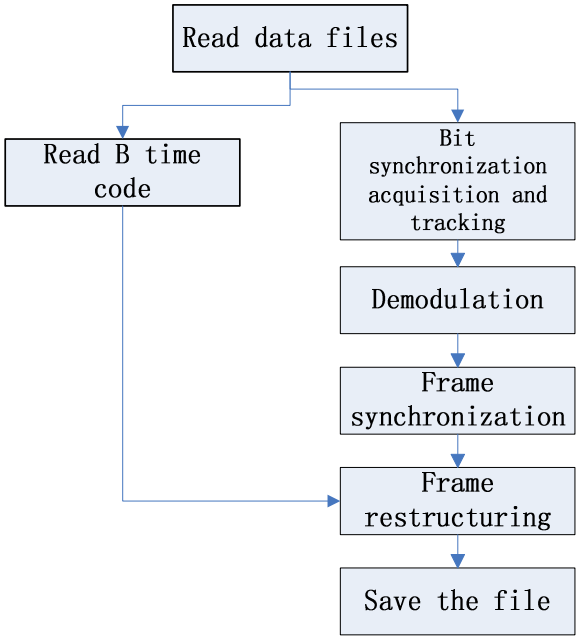

Fig1 System operation flowchart

2 System Architecture

Telemetry data analysis later processing system can be divided into six major functional modules: the main control module, data reading module, timing signal reading module, bit synchronization and demodulation module, frame synchronization module, display and storage module.

The main control module is the main frame system, which controls the running state of the whole system, at the same time, it provides a human-computer interaction interface, realize telemetry data parameter selection and Settings.In order to facilitate the process of observation of the shunt signal telemetry frame in different state, can also through the waveform display window, choose three different display modes.

Data reading module is the input of the whole system, it implements the function is: according to the records of the telemetry data formats, read the telemetry data stored in hard disk and timing signals.For telemetry intermediate frequency sampling signal and pass the cascade extraction about wave, realize the data extraction, reduce the module at a lower level of data processing.

In recording the telemetry signal, in order to reduce the requirement of storage capacity, adopting the structure of parallel branch store, after B code time sampling, in the form of the signal of single bitstream, together with the telemetry data, according to certain data structure stored in the disk.Timing signals read module is on the basis of the data reading module, will read the timing signal, according to the structure of B code decipher the size B time information.

Bit synchronization and demodulation module is the most complex is the most important module in the system.According to the different type of telemetry, first of all, to implement a synchronization.Then, on the basis of the implementation of coherent signal demodulation, and send the results to the frame synchronization module.

Frame synchronization module function is: in the demodulation search frame element in the head and under the conditions of the frame head lock according to the given read shunt data telemetry signal frame structure, and information into the frame head of the time B code, complete the restructuring of the frame structure.

The frame structure of the reorganized in accordance with the certain data types, in the form of files stored on disk.In the process of system processing, according to the user action, can in a variety of display mode at the same time, according to multiple data users select shunt data.

3 Key technology

Intermediate frequency sampling the results of the greatly increased amount of telemetry data record, a lot of redundant data to the system efficiency of pressure.In order to solve this problem, before the telemetry data demodulation, first of all, the high sampling rate after the frequency to baseband signal extraction filter, in meet the Nyquist law under the premise of minimizing baseband signal data, and then after extraction of the baseband signal demodulation.

Due to the input signal of narrow-band digital intermediate frequency processing the sampling rate is very high, but also requires the extraction filter passband bandwidth and transmission belt is very narrow, this will make the filter section number is large, operational efficiency is very low.Therefore, in order to effectively realize the sampling rate conversion, can adopt the method of multistage sampling.Digital cascade extraction filter in general can be divided into three:Comb sampling filter 3~7 times the signal extraction;Half take twice extraction filter signal extraction;Are usually performed low-pass filter compensation filter.

At present, used in the digital frequency measurement algorithm is more, including time domain, frequency domain algorithm time-frequency analysis, algorithm, feature subspace decomposition algorithm, etc.Principle of time domain algorithm is simple, high operation efficiency, therefore, is suitable for the signal of digital frequency measurement.This system USES a time-domain algorithm of instantaneous autocorrelation algorithm for digital frequency measurement.Below is the actual record of a remote sensing signal to digital frequency measurement result, figure dashed range caused by the phase jump in carrier frequency of mutations.We can find that, under the condition of the signal-to-noise ratio of 10 db, via digital frequency measurement method, the location of the change in phase and frequency of sampling data corresponding with the carrier frequency deviation.By judging the frequency transformation range, more quickly to achieve bit synchronization capture and correction.

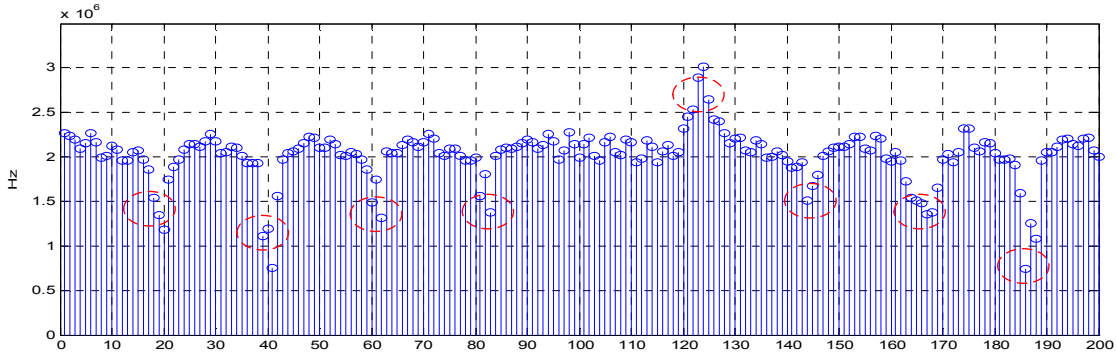

Fig12 Digital frequency measurement results

The telemetry data signal flow to frame as a general identifiable transmission unit, a frame and a frame to transmit sequence.Is placed at the beginning of each frame frame synchronization code (hereinafter referred to as the frame code) as this frame.Select the best correlation between fixed code as a general frame.In order to more accurately identify from the random signal stream frame size, the length of the frame size n (digits) is generally not less than 16.At the same time, in order to facilitate computer processing, the whole frame length of S (hereinafter referred to as the frame length) and the length of the frame size should be set to 8 n integer times.

This system, the frame synchronization locking process is divided into the frame head identification and protection of frame synchronization.Frame code identification of the work process is divided into the following two steps:1, the frame code search: with a known frame code group and demodulation of PCM data are compared, and bit by bit to calculate the number of each phase of ectopic, set by the system fault tolerance for a (i.e., allow with the frame code group has a

different), the system frame head search stage.2, search check: when the first find no fault tolerance after a block of frames, and then to frame by frame, which is in the position to compare the length of the interval of a frame, the system is in search for checking stage.In the process of comparison, once found in the location element is inconsistent with the frame size group, started from the first frame search frame size.If three consecutive frame data are meet the requirements, at this time to get into with gait (i.e., lock the position of the frame head).

Frame synchronization protection work process is divided into two steps: 1, the synchronization protection: system after entering with gait, due to the interference or interrupt may be located in a good frame have appeared over fault-tolerant code position, at this time will need to determine whether really has been out of step, in order to avoid mistakes directly into the search state, the judge also will check after 3 times.If there is no more than 3 times in a row fault-tolerant (set by the system fault tolerance for b), indicating that the frame head positioning is accurate, and can extract each frame of shunting signal, the system is in synchronous protection stage.2, frame head to fish: if in three consecutive frame synchronization protection state is more than fault-tolerant b, frame head position is not correct, the system has entered the stage of out-of-step, and at the same time from the first frame to frame head to search again.

Summary

Telemetry data after the analysis processing system for remote signal analysis and processing provides a new method, solve the current domestic telemetry ground station receives playback telemetry signals of the high cost of equipment operation and maintenance problems, have a certain economic benefits.Because of the characteristic of the software itself is flexible, can achieve a variety of post-processing pattern telemetry signals.Compared with the hardware processing, improve the accuracy of the telemetry data processing, can completely satisfy the DQPDK post-processing, telemetering BPSK and FSK signal.With the rapid development of software radio technology and its application to the software processing of telemetry data later will become the future development trend in the field of remote sensing.

Reference

[1]Sun Xiurui.The design of filter medium frequency soften PCM/DPSK demodulator [J].Telecommunications technology,2008,9(1):42-45.

[2]Yan Junhui.Digital frequency measurement algorithm research[J].Radar and Confrontation, 2009,4(15):24-29.

Advanced Materials Research Vols. 989-994 (2014) pp 4169-4174
© (2014) Trans Tech Publications, Switzerland
doi:10.4028/www.scientific.net/AMR.989-994.4169

An Energy-efficient Three-dimensional Positioning Technology for Underwater Acoustic Wireless Sensor Network

Xiangyu Wei[1], Cheng Zhu[1], Shidong Qiao[1]

[1]Science and Technology on Information Systems Engineering Laboratory, National University of Defense Technology, Changsha, Hunan, 410073, China

wxyrc5@163.com

Keywords: WSN; Positioning Technology; non-ranging; RSSI; energy efficiency

Abstract. The self-positioning for the nodes is the prerequisite for wireless sensor network to work, especially considering that the deployment of underwater node changes rapidly in position. Taking the issue of energy efficiency and prolong the network lifetime into account, the energy-efficient positioning technology of the underwater acoustic sensor network is studied in this paper .Brief introduction of the current node positioning technology is concluded in this paper too. Similarly to the overlapping ideological positioning algorithm FTPL we introduce RSSI but not for the ranging. Also discuss the inadequacies of our new algorithm, and the possible improvements. Simulation results show that the improved algorithm has good improvement in both the accuracy and the energy efficiency.

Introduction

The underwater wireless anti-submarine sensor network has received great attention by the navy for its acclimatization in the information-based war, and thus has developed rapidly in recent years. Self-positioning for the nodes is the foundation for the anti-submarine network to achieve its tactical ability, and the precondition for the network's efficacy, therefore positioning technology is extremely crucial in modern war.

So far, there are various classifications for the node localization algorithms [1]. Below are the most common classification methods:

- Range-based v. Range-free localization algorithms [2]
- Anchor-based v. Anchor-free localization algorithms [3],
- Incremental v. Concurrent localization algorithms [3],
- Centralized v. Distributed localization algorithms [4],
- Fine-grained v. Coarse-grained localization algorithms [5] ,
- Physical v. Symbolic location algorithm [6].

Among them, the most widely accepted classification is range-based and range-free localization algorithms. There are four kinds of commonly used measuring technique: Time of Arrival (TOA), Time Difference of Arrival (TDOA), Angle of Arriva (AOA), Received Signal Strength Indication (RSSI), among them the RSSI application is the most widely used. Range-based algorithms require more hardware support, such as transmitting and receiving equipment, clock synchronization equipment etc. while range-free localization algorithms usually use the connectivity and geometric relations of the nodes to determine the location, instead of measuring the distance between the nodes. Thus range-free localization algorithms are of smaller hardware requirement and more energy saving. Centroid method [6], DV-Hop [7], Amorphous and APIT algorithm are some of the typical range-free algorithms. Under ideal conditions, range-based algorithms are more accurate than range-free algorithms, whereas for the anti-submarine network located underwater, clock synchronization in real situations can hardly be accurate. Thus, given the restriction of hardware and energy, range-free algorithms perform much better when the accuracy can be improved through the optimization method, which makes them widely used in underwater acoustic sensor localization.

FTPL Algorithm

Flexible Transmission Power for Localization algorithm (FTPL) [8] is a sensor node localization algorithm bring forward by Danlin Yao of National University of Defense Technology. FTPL suffers no influence of ranging error, and also consumes low communication overhead. The basic idea is to assume all anchor nodes in the wireless sensor network are the same with variable transmit power $(P_1, P_2, ..., P_n)$, and communication radius $(R_1, R_2, ..., R_n)$ corresponding to the anchor nodes' transmit power $(P_1, P_2, ..., P_n)$ of all the unknown nodes have been stored prior to network deployment. Each anchor node transmits a beacon signal at the minimum transmit power, and gradually increases the power. When the unknown node firstly received the anchor nodes' signal, the corresponding arc can be the outer boundary of possible regions for the unknown nodes, and the circle corresponding to the last launching signals as the inner boundary. When three or more such anchor nodes are found, centroid can be calculated as the position of unknown nodes.

The algorithm has obvious advantages, for those unknown nodes are totally inactive, thus the energy cost and communication overhead can be saved. If the network is in ideal condition, and the function between RSSI attenuation and the distance is well, FTPL is of high precision and easy performing.

However, this algorithm has the following problems:

1. FTPL takes no consideration of the uncertain signal attenuation problem. In fact, the attenuation of either underwater acoustic signal or ground electromagnetic wave signal, is largely caused by other uncertain factors in addition to the natural decay of distance, especially the underwater acoustic environment is indeed complex, when the uncertain issues are ignored, would certainly lead to the weaker received signal strength of the unknown nodes than the emission intensity, thus the radius calculated would be smaller. Once this happens, the positioning error can be quite big.
2. FTPL would discard the received signal when nodes receive signal, thus wasting the data, which is not expected during the data processing.
3. When an unknown node receives beacon message for a large number of anchor nodes, FTPL handle the case too simple by overlying these different circles.
4. FTPL takes no consideration of the sensitivity of nodes signal receiving. When the sensitivity of a node is low, it may miss the signal of weak strength, which thereby leads to the radius calculated bigger than real.

FTPL-3D

In this paper, we intend to locate the underwater nodes in three-dimensional space; however the original algorithm FTPL is based on two-dimensional plane. Whereas the basic overlapping idea of the original algorithm can be used for reference; here this algorithm is overlapping spherical shell.

FTPL-3D (Flexible Transmission Power for Localization in three-dimension space) stores the ID of anchor nodes and the signal strength corresponding to the transmission distance in advance, installs the pressure sensor to measure the depth information of the node. The anchor node broadcasts beacon information to the space instead of transmitting beacon signal to the plane, while the unknown node completely receives passive signal. When catch the anchor node A for the first time, mark the radius R_i corresponding to the firstly received signal as the outer radius of spherical shell, and R_{i-1} as the inner radius. Similarly, when received the signal of anchor node B, the inner and outer radius of another spherical shell can be gotten. Then modify the distance information to get more precise distance. Store the information of first received for later use.

As the entire anchor nodes are deployed at the bottom of the sea, none of connection between two nodes is vertical to the surface. According to the geometric relations, there must be three-dimensional rings not parallel to the surface of sea. Thus the pressure sensor measures the depth information, getting the plane overlap in the ring, calculate the centroid as the position of the node.

What need point out is, that the algorithm assumes that the sea anchor nodes have receiving device which can accept echo, which can help find which octant the unknown node is in the three-dimensional coordinate system which makes its own as the origin.

(1) Spherical Shell Radius Correction Algorithm

The underwater acoustic signal is inevitably influenced by lots of disturbance when propagating in water, thus the attenuation is very fierce, and the most causes of the decay are uncertain. Therefore we can only get the empirical formula of underwater acoustic signal propagating attenuation in the shallow water, obviously determining acoustic wave propagation distance would produce a big error only by experience formula, that is the factors the original algorithm takes no consider. This section will focus on solving the problem. We introduce the energy-consumption model of Cao Zhixin [9] as a reference.

The following is the empirical formula of acoustic signal propagation loss:

(1) Water absorption loss model:

$$\alpha = \frac{0.1f^2}{1+f^2} + \frac{40f^2}{4100+f^2} + 2.75\times10^{-4} f^2 + 0.003; \tag{1}$$

(2) Mixed layer channel propagation loss model:

$$\begin{cases} TL = 20\log r + (\alpha+\alpha_L)r\times10^{-3} \quad when \quad r < 350H^{1/2} \\ TL = 10\log r_0 + 10\log r + (\alpha+\alpha_L)r\times10^{-3} \quad when \quad r > 350H^{1/2} \end{cases} \tag{2}$$

(3) Propagation loss model of uniform shallow water channel:

$$\begin{cases} r < H: \quad TL = 20\log r + \alpha r\times10^{-3} + 60 - k_L \\ H \le r \le 8H: \quad TL = 15\log r + \alpha r\times10^{-3} + \alpha_r(r/H - 1) + 5\log H - k_L \\ r > 8H \quad TL = 10\log r + \alpha r\times10^{-3} + \alpha_r(r/H - 1) + 10\log H + 64.5 - k_L \end{cases} \tag{3}$$

where TL is the propagation loss, r is the effect distance(kilometer), α is sea absorbing coefficient(dB/km), H is the transition distance(kilometer), $H = [(D+L)/2]^{1/2}$, D is the depth of the sea water, L is the thickness of mixed layer channel(meter), α_r is the shallow water attenuation coefficient, k_L near field attenuation coefficient, α_r, k_L can be queried from the database according to the sea states and the geology.

Anti-submarine sensor network typically is deployed in coastal, and most of our China's offshore are shallow, which makes it possible for the formula (3), of course under the ideal sea state. Suppose that the attenuation caused by uncertain issues is $LOSS$, we can modify the algorithm as follow.

Considering that the different strength signals from one same anchor node to another same unknown node have the same propagating ways, thus the same interferences they would experience, that will make the same attenuation which is $LOSS$, then followed such formula:

$$P_i = P_{Ri} + \mathrm{TL}_i + LOSS \tag{4}$$

Where P_i represents the signal strength of the anchor nodes send, P_{Ri} represents the signal strength of position nodes received. As those unknown nodes have already stored the ID of anchor nodes and the signal strength in advance, P_{Ri} is known as a result. Thus among the propagation loss TL only R remains unknown, P_i is unknown either.

According to the idea of mathematical equations, simultaneous any three of them can help get the real distance R. In the actual operation of the process, we calculate arithmetic mean of the multiple sets of numerical result, which would help to make the result closer to the actual value.

(2) FTPL-3D-F

FTPL-3D-F (Flexible Transmission Power for Localization in three-dimension space based on data fusion), the algorithm is the further upgrading to FTPL-3D after taking data fusion in account. FTPL-3D-F behaves well as it can handle many issues such as distance from different anchor nodes to the unknown nodes, or the self-construct of anchor nodes.

When an unknown node received signal from many (no smaller than 4) anchor nodes, each three of the spherical shell can built an enclosed area, plus the depth information measured, that is each three anchor nodes gives out a centroid. The question is which one is the optimal; do we need comprehensive treatment to all the results; and how to choose anchor nodes from the candidates. That's what we are trying to solve in this chapter.

Two conclusions emerge from these general statements:

1) When the exact location cannot be found, then the smaller region the point may exist, the higher possibility the true location it can be.

2) Under the same area, shapes close to the equilateral triangle, square and other similar angles about the size, capered with those of narrow angle, angles in different size of more, the former can provide more accurate location estimated than the latter. At least in the probabilistic perspective, possibility of the former position is more accurate and higher.

The estimation of unknown nodes in the former location is more accurate than the latter, at least in the probabilistic perspective, possibility of the former position information more accurate and higher.

There are obvious geometrical meanings of the above conclusion, here without proof.

The basic idea of FTPL-3D-F is: when the unknown node can receive the signal from a lot of anchor nodes, exhaustive three combinations, judge the shape that every three anchor nodes formed from the overlapping region shape, calculate the centroid of the region as a possible location point; then give different weights to the results according to their shape and area, calculate the weighted average as the final result.

(3) Weight selection

As in the model of underwater acoustic signal propagation path loss, numerical value of RSSI is similar inverse proportion function with the distance between, that is the value decrease with distance. At the same time, there may be more interference of underwater acoustic signal propagation process. Attenuation compensation mentioned above is just an experience formula, may not be perfect compensation. Therefore, in the actual process of anchor nodes positioning, the closer the distance, the smaller the radius error. So when setting the weight, we assume it inversely proportional to the ball shell radius, which makes the positioning accuracy proportional to $1/R_1 + 1/R_2 + 1/R_3$.

The larger the overlap area is, and the more long and narrow shape is, the bigger the node location measuring error is, that is the weight is inversely proportional to the area. We can judge the shape from the point's distance deviation of the overlap region boundary. The bigger the distance deviation is, the narrower the shape is. That is the positioning accuracy is proportional to the overlap area S, proportional to $1/(L_{\max} - L_{\min})$, where $L_{\max}, L_{\min}$ represents the maximum and minimum value of the overlapping regions vertex distance.

What need point out is that the process of weight selection is lack of rigorous mathematical reasoning calculation; we estimate the weight according to the geometric intuition, for the lack of good methods of selecting weight as to the information available at present. Our assumption is yet helpful to enhance positioning accuracy.

Here are the operation steps of the algorithm of FTPL-3D-F:

Step 1.Determine the depth information of the unknown nodes;

Step 2.After the unknown node receives the signal, judge the anchor node ID and the inner and outer radius of the spherical shell;

Step 3.Catalogue all combination of each three anchor nodes, get the coordinates of boundary points for each overlapping area according to the depth of the plane where position nodes identify , each anchor node position and radius of the spherical cavity;

Step 4.Judge the shape of each overlap region, and calculate the area;

Step 5.Calculate centroid of each anchor nodes combination overlap region, serve as an unknown node coordinate values, obtain a set of coordinate values;

Step 6. Calculate the weighted average of the resulting data as the node coordinates.

Simulation Test

The simulation conditions are: in a room of 100*100*100, generate a random coordinate of unknown nodes, and then randomly generate four anchor nodes coordinates (Z=0, means the anchor nodes usually deployed at the bottom of the sea), add in random interference. We did multiple tests for location calculation using FTPL algorithm and the FTPL-3D-F algorithm respectively. Figure 1 below gives the comparison of positioning accuracy of the two algorithms, where the *vertical axis* represents the error, which is defined as the distance from the actual location to the calculated location while the *horizontal axis* represents the difference of different radius. Compared of precision curve of the two algorithms, it is obvious that the FTPL-3D-F algorithm significantly improves the positioning accuracy.

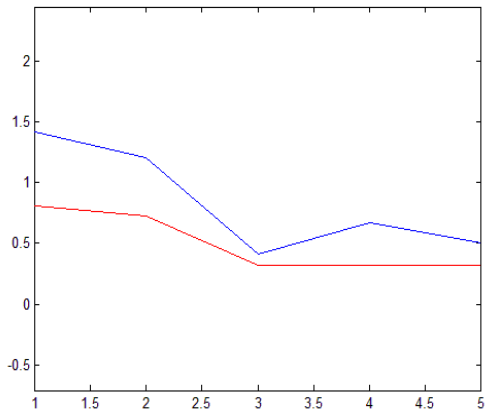

Fig. 1 Comparison of positioning accuracy of FTPL and FTPL-3D-F

Notes: Blue curve represents the error of FTPL while red curse represents the error of FTPL-3D-F

As is shown in the figure, our accuracy of the FTPL has directed relationship with the difference of radius. The smaller the difference is, the more accurate the result is. Theoretically, the smaller the radius difference is set, the smaller the volume of the sphere overlap is, and thus more accurate the centroid as the node's coordinates. When the radius difference is infinitely small, FTPL-3D turns out to be range-based Three-point positioning method, which has the highest accuracy in theory. However such infinite can hardly be reached, for the difference of power cannot be that small, let alone that such difference set would increase the economic costs for the excessive demands on the hardware. Then more information to be saved for the smaller difference, and nodes burdened with heavy storage is not suitable for underwater acoustic wireless sensor network.

FTPL-3D-F is an improvement for FTPL-3D based on data fusion, however compared with FTPL, under the situation of same difference; FTPL-3D-F has a more obvious improvement than FTPL for larger one. FTPL-3D-F takes the shape of the overlap area, the volume size and other issues into consideration, which makes it less sensitive to the change of radius difference. Numerous tests proved our conclusion with larger radius difference.

After large number of experiments, we found FTPL-3D-F is not always better than FTPL-3D. The former consider the issue of the shape and volume size of the overlap area and the distance to anchor nodes, but these can only improve the possibility of high accuracy, thus low accuracy turns out occasionally. We state that not an error in our data fusion but the shortage of algorithm.

Conclusions

To improve the accuracy of range-free localization algorithms, we expand FTPL algorithm, continue to use the idea of RSSI strength but abandon the idea of practically measuring distance, and therefore avoid the complex problem of clock synchronization effectively. Meanwhile our algorithm conquers the limit of localization algorithm caused by the influence of uncertain issues such as complex underwater acoustic environment and large quantitates of noise and interference. We improve the FTPL algorithm, and do the processing of data fusion aimed at the multi anchor node localization algorithm, and after experimental verification, both improvements help to improve the accuracy and adaptability of the algorithm.

There are still improvement rooms for the algorithm we give out for data fusion. Our algorithm can improve accuracy in most cases in many measurements, however further study is focus on the higher accuracy for each of the measurement. Besides, for the nodes with low sensitivity , the nodes can only receive Signals with high strength, that would cause large error. Both algorithm are weak in this case, method to improve the sensitivity and the auxiliary positioning of AUV and UUV may help.

References

[1] J. LI and Y.Y. Li: A Review of Localization Algorithms in Wireless Sensor Network [J]. Journal of Changzhou Institute of Technology, Vol. 23 (2010) No.5, p.51

[2] T. He, C.D. Huang, B.M. Blum, J.A. Stankovic, and T. Abdelzaher: *Proceedings of the 9th annual international conference on Mobile computing and networking ACM* (New York, NY, USA, 2003) Vol. 1, p.1

[3] N.B. Priyantha, H. Balakrishnan, E. Demaine, and S. Teller: *Proceedings of the 1st international conference on Embedded networked sensor systems ACM*, (New York, NY, USA, 2003) p.340

[4] R. Want and A. Hopper: Falcao V, et al. The active badge location system [J]. ACM Transactions on Information Systems (TOIS), Vol. 10 (1992) No.1, p.91

[5] N. Bulusu and J. Heidemann: Estrin D. GPS-less low-cost outdoor localization for very small devices[J]. Personal Communications, IEEE, Vol. 7 (2000) No.5, p.28

[6] J. Hightower and G. Boriello: Location Systems for Ubiquitous Computing [J]. Computer, Vol. 34 (2001) No.8, p.57

[7] D. Niculescu and B. Nath: DV Based Positioning in Ad Hoc Networks [J]. Journal of Telecommunication Systems, Vol. 22 (2003) No.1-4, p.267

[8] D.L. Yao and Q.M. DuanMu. A Study of the Localization Algorithm for Wireless Sensor Network [J].Computer Engineering & Science, Vol. 30 (2008) No.3. p.82

[9] Z.X. Cao, Y.M. Zhou and J.H. Chen: Simulation Study on Forecast of Warship Sonar Distance [J]. Military Operations Research and Systems Engineering, Vol. 21 (2007) No.3. p.31

Advanced Materials Research Vols. 989-994 (2014) pp 4175-4178
© (2014) Trans Tech Publications, Switzerland
doi:10.4028/www.scientific.net/AMR.989-994.4175

Electric power communication network alarm data acquisition system based on CORBA northbound interface

Yujun He [a], Yu He [b], Peng Peng [c] and Ran Chen [d]

North China Electric Power University, Baoding 071000, China

[a] 38341828@qq.com, [b] 491481152@qq.com, [c] 619696687@qq.com,

[d] 783915643@qq.com

Keywords: Power system communication network, alarm management, CORBA

Abstract. With the development of communication technology, the increasing scale of power communication network is bigger and bigger. Based on the important significance of electric power communication network to establish an alarm information acquisition system is necessary. CORBA, as a distributed processing environment interconnect solutions in hardware and software, is widely used in the field of network management for its high versatility. In this paper we use real-time CORBA platform TAO as a network management platform to develop a kind of electric power communication network alarm acquisition system.

Introduction

Electric power communication network is one of the national special communication network and an indispensable important part of power system. It is the foundation of the power grid dispatching automation and marker-oriented operation [1]. Therefore, on the basis of original network management system to establish integrated alarm information processing platform is very important.

The article is as an example of CORBA northbound interface and detailed analysis the application of CORBA technology in the northbound interface. So we put forward a design scheme based on CORBA northbound interface and realize the acquisition of SDH transmission network alarm information in the TAO platform.

CORBA overview

Common Object Request Broker Architecture (CORBA) defined by the object management group (OMG) is a language-independence object interoperation model in heterogeneous environment platform. In an object-oriented distributed computing environment, an object request proxy can provide key communication facilities between applications, servers and network facilities for distributing message.

The design of northbound interface based on CORBA system. The overall structure of northbound interface is mainly divided into two layers. Near the EMS is data adapter layer. The layer mainly realizes EMS package and information model processing. Near the NMS is agreement processing layer. The layer mainly realizes the CORBA object implementation, parameter analysis and report processing module. In addition, the layer can generate structured events and passes the events to the client through Event Channel [2]. The structure of northbound interface is shown in figure 1.

The overall design of system. The realization of alarm acquisition function is the foundation of alarm integrated management system. According to the alarm information processing, the function structure of whole system can be divided into three layers, including: alarm information collection layer, alarm information analysis processing layer and alarm information reporting storage layer.

Alarm information collection layer

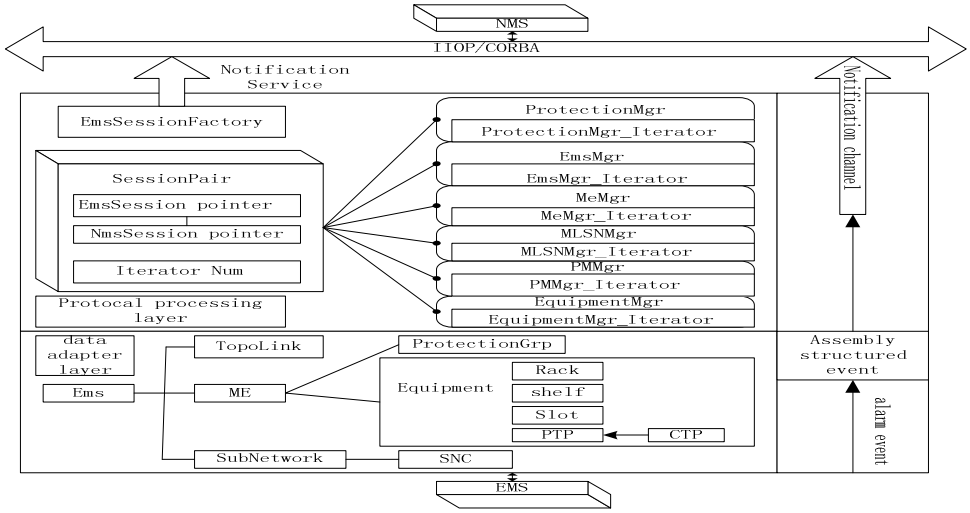

Fig. 1 The structure of northbound interface

Establish session interface. To complete alarm information collection, the system first needs to realize communication between NMS and EMS. In the building of session interface, EmsSessionFactory interface calls the only function getEmsSession to get EmsSession interface. Each manager can be obtained through EmsSession. In the meantime, NmsSession parses names by naming service and gets object reference registered under EmsSessionFactory to realize the establishment of the NMS - EMS session [3].

The process of alarm information acquisition. The system mainly realizes electric power communication network alarm information acquisition based on CORBA northbound interface. The main means used in collecting alarm interface are naming service and notification service in CORBA interface mode.

In the network management of alarm collection, alarm information collection can be divided into two parts, for respectively the real-time alarm collection and the non real-time alarm collection. The alarm information collection process is shown in figure 2.

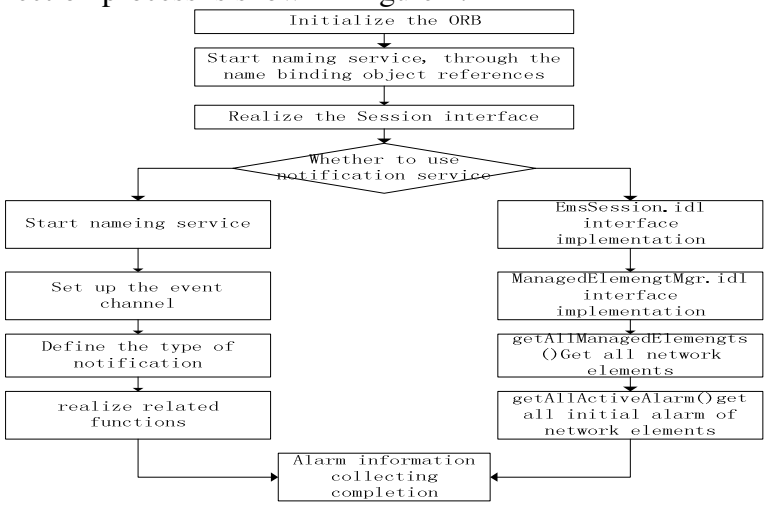

Fig. 2 The process of alarm information collection

CORBA notification service can realize real-time alarm information collection. Notification service with its own unique management quality of service can obtain real-time alarm information collection to establish event buffer queue.

Using the method of ManagedElement_I can realize non real-time collection of alarm information network elements. The ManagedElement interface provides getAllManagerElements and getAllActiveAlarms function to realize alarm collection[4] . Function call sequence diagram is shown in figure 3.

Alarm information analysis processing layer. The collected alarm information can give operation staffs huge interference because of its rich content. You have to gather alarm data of refining and normalized for pretreatment. As a result, the different formats of alarm information can be converted into key alarm information's unified format which is needed by the system and then passed key alarm information to the application server. Key alarm information mainly includes network elements ID, alarm name, alarm object name, alarm object type, alarm time and alarm status.

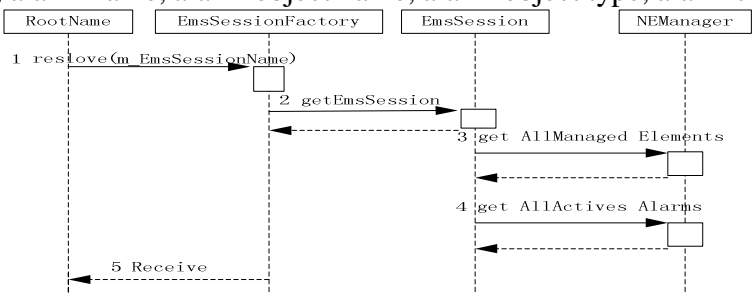

Fig. 3 The function call sequence diagram

Alarm information reporting storage layer. In the completion of alarm information analysis processing, the alarm information is stored in the database by the ODBC source for later alarm statistical analysis and then send the unified format of alarm information to the cache space which will form alarm sent queue [5]. By using CORBA notification service event channel can realize the alarm information sequentially take the initiative to report to the backend server.

Notification service inherits the event service of Push and Pull two communication modes. In Push mode, notification provider actively push notification to consumers; In Pull mode, notification consumer pull the notification from the providers .In actual system we usually choose Push mode. Realizing a Push mode for events sending contains two aspects. First, connect provider to the event channel. Second, connect consumers to the event channel [6]. This process is shown in figure 4.

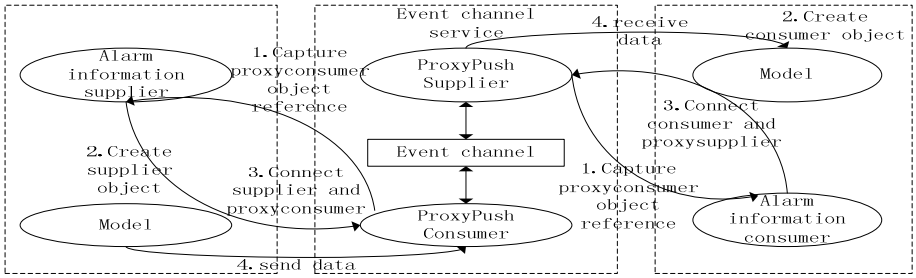

Fig. 4 The process of push model event transmission

The result of alarm acquisition system

The TAO platform can realize the alarm data collection. The alarm collection display interface is shown in figure 5.

	AlarmSerialNo	NOTIFICATIONID	OBJECTNAME	NATIVEEMSNAME	NATIVEPROBABLECAUSE	OBJECTTYPE	EMSTIME	NETIME	ISCLEARABLE	LAYERRATE
31	24061980	41218400334559	EMS =	Huawei/T2000;1000-	CP_SER_NOT_OR	9	20130415043506	20130415043504	1	1
32	24061981	41218400334490	EMS =	Huawei/T2000;1000-	CP_SER_NOT_OR	9	20130415042444	20130415042442	1	1
33	24061980	41218400334489	EMS =	Huawei/T2000;1000-	CP_SER_NOT_OR	9	20130415042443	20130415042441	1	1
34	24061949	41218400334469	EMS =	Huawei/T2000;1000-	CP_SER_INT	9	20130415042443	20130415042441	1	1
35	24061950	41218400334470	EMS =	Huawei/T2000;1000-	CP_SER_INT	9	20130415042443	20130415042441	1	1
36	24061949	41218400334464	EMS =	Huawei/T2000;1000-	CP_SER_INT	9	20130415042442	20130415042440	1	1
37	24061950	41218400334465	EMS =	Huawei/T2000;1000-	CP_SER_INT	9	20130415042442	20130415042440	1	1
38	24061782	41218400334268	EMS =	Huawei/T2000;1000-	CP_SER_NOT_OR	9	20130415034109	20130415034107	1	1
39	24061781	41218400334267	EMS =	Huawei/T2000;1000-	CP_SER_NOT_OR	9	20130415034108	20130415034106	1	1
40	24061782	41218400334179	EMS =	Huawei/T2000;1000-	CP_SER_NOT_OR	9	20130415033028	20130415033026	1	1

Fig5. The display of collection interface

Alarm information collection display interface shows the alarm information according to the standardized format. Putting alarm ID in the first place can improve the processing efficiency of alarm information. The real-time display of different network management alarm information can accomplish the alarm information collection which will achieve the purpose of the system.

The test of alarm acquisition system

In order to verify the design of CORBA northbound interface alarm data acquisition system, it is necessary to carry out the functional test. It is mainly from the alarm reporting function to carry on the CORBA alarm interface test so that the correctness of the interface can be well verified.

Test project: alarm report function. Testing purposes: northbound interface should support manufacturer network management system report all real-time alarm to transmission network management system, the creation and disappearance of alarm should come in pairs.

Testing expected results: northbound interface supports manufacturer network management system report all real-time alarm to transmission network management system, the creation and disappearance of alarm come in pairs [4].The content of test is shown in Table 1.

Table 1.Details of alarm report function test

Parameter name	Interface parameter names	Date type	Value instructions	Test result
Event type	Event_type::type_name	String	Type_name must be NT_ALARM	OK
Alarm identifer	NotificationId	String	Notification event unique ID number	OK
Alarm source object types	ObjectType	Notifications::ObjectType_T	The reported alarm of object types	OK
Alarm level	PerceivedSeverity	Notifications::PerceivedSeverity_T	Critical alarm Major alarm Minor alarm Warning	OK
Alarm reason	Probablecause	String	Defined alarm probable cause	OK
Alarm time of ems	Globaldefs::Time_T	String	The time value of EMS to report events	OK

Summary

Based on the reusability and portability of CORBA, the TAO platform realizes alarm information collection, alarm processing and alarm report management .The implementation of alarm information acquisition system can improve the reliability of electric power communication network which will promote the automation and centralization of power grid.

Reference

[1]Lijing Zhang. Electric power communication and information basis. Beijing: China electric power press, 2010, 106-115

[2]Yanpen Xiao. The SDH network management system northbound interface based on Visibroker . Optical communication technology, 2011,Vol.11 18-20

[3]Miao Zhang, Chenqun Yin, Yujun He: Power system communication, Vol.33 (2012) no. 238, p. 17-21.

[4]Qikun Yu.Network management alarm interface based on CORBA. The master thesis of East China University of Science and Technology (2013).

[5]Miao Zhang. Research and implementation of the power communication alarm information acquisition system. The master thesis of North China Electric Power University (2014).

[6]Leishen Qi,Yan Zhang, Xiaona Zhang. The analysis and design of communication confrontation training simulation system based on CORBA. Modern electronics technique.2011,Vol.34(2) 42-45

Advanced Materials Research Vols. 989-994 (2014) pp 4179-4182
© (2014) Trans Tech Publications, Switzerland
doi:10.4028/www.scientific.net/AMR.989-994.4179

Robustness Analysis of Telecommunications Customer Service System

WU Bo[1,a]

[1]Department of Computer Science , Harbin Finance University, Harbin Heilongjiang 150030, China

[a]wubomail@126.com

Keywords: communication networks; complex networks; robustness

Abstract. The robustness of customer service system for telecommunications industry is researched. To overcome existing robustness defect of node failure in current network robust research model, node efficiency assessment of robustness is employed, generalized evolution theory is taken into, and changes process of telecommunications customer service systems is simulated. In analysis of conditions in different interference, robustness performance is presented. Simulation results show that the method considering the telecommunications industry to build robust customer service system is feasible and effective for large, complex networks, which has a good capability of computing power.

Introduction

Robust has meanings of a rugged, durable, robust. Capacity, reliability, redundancy is conducive to improve the robustness enhancement [1]. In operation, communication network is usually disturbed or damaged, leading to loss of function or decrease of performance. Robust communication networks become an important feature of network research [2]. At present, robust wired networks is mostly focused on in international field, but wireless communication network nodes become failed node due to random failures or malicious attacks [3]. Wireless failed node will lead to networks split, leading to network performance degradation and even complete loss of the network [4-6]. Measurement robustness method is presented, considering the efficiency of communications networks. Firstly, it employs efficiency of original network nodes to define to load of each node and limit load, according to changes in the network before and after the attack to determine load function of node failure model; then gives robustness assessment algorithms of network function and optimizes. Finally, experimental analysis is used to verify its effectiveness and feasibility.

Construction of communication system network model

A.Theoretical support of network communication system

Current research methods of robust communication system are based on the shortest path of network nodes, based on network connectivity, which are both based on research of network topology but ignoring network functions robustness. It is affected by not only actual operation of network system topology, but also capacity constraints of the node itself. For example, information transmission of in communication network should consider load information of each node. Once transmission overloads of information node in communication network, it will also lead to collapse of the entire network. For a simple communication network (side right of adjacent nodes are l) shown in Fig 1 if failure of the node V1 occurs, communication load of subnet A and B on the entire are superimposed on V2, communication network connectivity will be destroyed.

It is seen that in study process of complex networks robustness, network topology considerations alone is not enough, because removing nodes or edges can lead to redistribution of flow information throughout network and node load changes in the information transmission process. For actual network system, node failure on the network is global, and not just affects neighbor nodes. As FIG l node V1 failure affects node V2. Connectivity is not just the physical connectivity, but also considers in the actual system load range of capacity constraints. Even

physical side suffers a blow, as long as the node has sufficient resources, it will maintain its existing function by other means. However, if the node is overloaded, it will also lead to collapse of network.

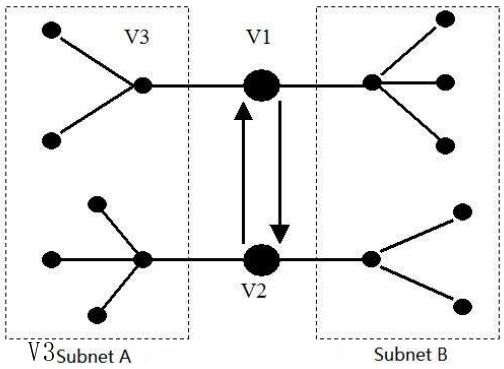

Figure1 Information distribution of schematic communications network

B.Establishment of a communication system network model

Figure G = (V, E) represents a communication system network, wherein V means the set of nodes, E represents a set of edges. | V | is number of nodes in the set, considering edges in the graph is undirected edges. If a subgraph G '= (V', E '), V' ∈ V, in V 'between any two points there is an edge, G' is a connected subgraph of G. If the graph G = (V, E) consists of connected subgraph structure, denoted G1 = (V1, E1), G2 = (V2, E2), ..., G1 = (V1, E1), then G1, G2, ... , G1 of G is called connected component. If V '∈ {V1, V2, ..., V1} and

$$|V'|=\max\{|V_1|, |V_2|, \ldots, |V_1|\} \tag{1}$$

Called G' = (V ', E') is the largest connected component of the graph G. Note

$$C=\frac{|V'|}{|V|} \tag{2}$$

G′ is coverage rate of G.

Definition1: In the node network model G = (V, E), number of nodes | V | = n, delete Nr (n) node, the remaining sub-graph consisting of m-branch communication, G1 = (V1, E1), G2 = (V2, E2), ..., Gm = (Vm, Em), 1 ≤ m ≤ Nr +1, the number of nodes available to Am (n) = max {| V1 |, | V2 |, ..., | Vm | }, if the coverage Cm (n) satisfies the equation:

$$\lim_{n\to\infty} C_m(n)= \lim_{n\to\infty} \frac{A_m(n)}{n}=1 \tag{3}$$

It is claimed that Figure G = (V, E) can tolerate the failure of Nr (n) nodes.

Assuming activity cluster head node proportion of all points is p(n), recording number of failure nodes as Nr (n), failure nodes may be a cluster head node or may be an ordinary node. Set number of failure cluster head node as N_{r1} (n) and number of failure ordinary nodes as N_{r2} (n). The N_r(n) can be expressed as:

$$N_r(n)=N_{r1}(n)+N_{r2}(n) \tag{4}$$

Failed cluster head node is represented as the proportion of total number p_1 (n), namely:

$$p_1(n)= \frac{N_{r1}(n)}{N_r(n)} \tag{5}$$

When failure is caused by random failures, failure probability of all nodes are the same, so p1 (n) = p (n); When the failure is caused by malicious attacks, failed nodes are mainly in the cluster head, so p1 (n) = 1.

Definition2: In the node network model G = (V, E), number of nodes V = n, the probability of active nodes is p(n), optionally N_r (n) nodes, wherein the proportion of active nodes is p1 (n), p_1 (n) is determined by the formula(4), (5). If Figure G = (V, E) can tolerate Nr (n) failure nodes, when p1 (n) = p (n), figure G = (V, E) is the Nr (n) fault-tolerant, when p1 (n) = 1, Figure G = (V, E) of Nr (n) invasion-tolerant.

Simulation experiments and result analysis

In the telecommunications industry, customer service system, for example, employs simple communication network structure as shown in Figure 1. With network connectivity and maximum size of subnet connectivity indicators, customer service system robustness of telecommunications network are simulated while V1, V1 and V2 both fails, experimental results are shown in Table 1 (average of multiple simulation).

Table1 Robustness results of telecom customer service system

Assessment index	Failure nodes	V1	V1，V2
Topological robustness	Network Connectivity	connected	disconnected
	Maximum Connectivity subnet model	14	12
Functional robustness（α=1， β=1.5）	Network Connectivity	disconnected	disconnected
	Maximum Connectivity subnet model	15	0
Functional robustness（α=∞）	Network Connectivity	connected	disconnected
	Maximum Connectivity subnet model	15	14

As can be seen from Table 1, when α=∞, robustness results of network function and assessment results of topology robustness are the same; Whenα=1，β=1.5, above results are different. The reason is that robustness of network function considers withstanding load of communication network node. It can be seen that, it is more accurate to consider network topology, capacity of nodes and robust assessment.

For robustness of complex networks, it is generally considered in the random attack. Random scale-free networks have a stronger network fault tolerance; but in a deliberate attack, scale-free network is extremely fragile. Experimental results of function robustness for communication network can be shown in Figure 2.

As can be seen from Figure 2, when tolerance factor α of network node load and load limit of coefficient β increases, function robustness of communication network is gradually increased. When α=∞, function robustness of communication network is stabilized, indicating that there is no failure node caused by overload in communication network. Besides hit node, the other nodes can maintain its existing communications capabilities, in communications networks at this time functional robustness is strongest.

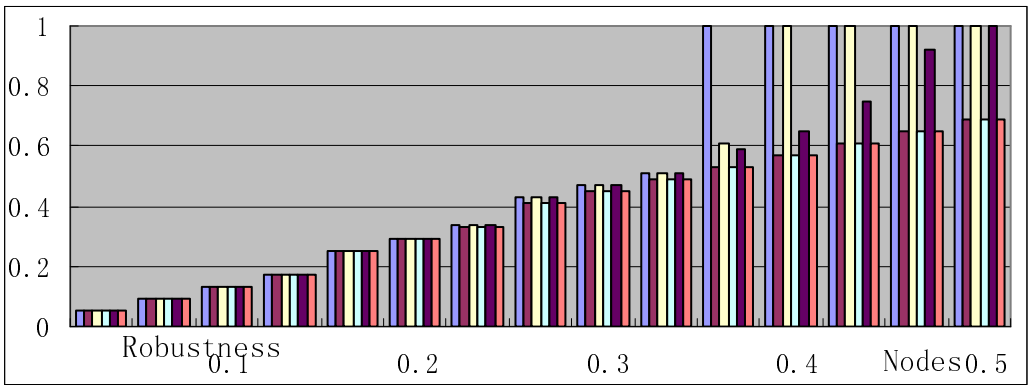

Figure 2 Robust schematic of communications network

When α and β values are fixed, on the whole: communication network in response to deliberate attack on its functional robustness is low with strong fault tolerance; different ways of attacking is little affected to random communication network, which is consistent with the conclusions of classic experiment, indicating the effectiveness of this method.

Conclusions

Detailed analysis is performed for robustness of telecom customer service system. In view of network robustness assessment model, assessment of network robustness is presented considering nodes efficiency of global network information. Experimental results show that of telecommunications customer service system is constructed, not only assessment of actual network topology, but also withstanding load of nodes. This method can be used to guide the telecommunications industry to build customer service system and solve specific issues in system control of telecommunications industry customer service.

Acknowledgement

supported by science and technology research project of Heilongjiang's educational committee, project number:12521064

References

[1] Dodds S P，Watts D J，Sabel F C.Information exchange and robustness of organizational networks[J].Proceedings of the National Academy of Sciences， 2003， 100(21)： 12516-12521.

[2] Kwon Y K，Cho K H. Analysis of feedback loops and robustness in network evolution based an Booleam model[J].BMC Bioinformatics，2007，8(9)：430-48

[3] ASH J ， NEWTHD.Optimizing complex networks for resilience against cascading failure[J].Physical A：Statistical Mechanics and its Application， 2007， 380(7)： 673-683.

[4] Newman M E J，Barabasi A L，Watts D J.The Structure and Dynamic of Networks[M]. Princeton， NJ，USA：Princeton University Press，2006.477

[5] Nafday A M. System safety performance metrics for skeletal structures [J]. Journal of Structural Engineering， 2008， 134(3)： 499—504.

[6]Song Minghong,Yu Huafeng,Chen Haiyan. Application of Improved Quantum Evolutionary Algorithm in Computer Network's Routing Choice[J]. Bulletin of Science and Technology, 2014, 30(1): 170-173.

Advanced Materials Research Vols. 989-994 (2014) pp 4183-4186
© (2014) Trans Tech Publications, Switzerland
doi:10.4028/www.scientific.net/AMR.989-994.4183

A Novel Public Key Image Cryptosystem Based on Elliptic Curve and Arnold Cat Map

Ling-jiao CHEN[1,a] and Ao-dong SHEN[2,b]

[1]Chien-Shiung Wu Honors College, Southeast University, Nanjing, 210096, China.

[2]Laboratory of Image Science and Technology, Southeast University, Nanjing, 210096, China.

[a]Cljmyth@gmail.com, [b]Shen.list@seu.edu.cn

Keywords: Cryptosystem, Image encryption, Elliptic curve, Arnold cat map.

Abstract. For decades, symmetric cryptosystems, such as chaos-based ones, are designed for image encryption. In this paper, a novel public key scheme for image encryption is presented. Based on the improved elliptic curve cryptosystem and Arnold cat map, the novel scheme can offer high security while avoid exchange and distribution of secret keys. The experiments illustrate that the presented scheme is computationally less complex than the traditional asymmetric cryptosystems and suitable for large image encryption.

Introduction

Nowadays, images play a critical role in people's private life. Consequentially, efficient image encryption methods are in great demand. Asymmetric cryptosystems, such as RSA [1], can hardly be directly used for image encryption because of the large image size. On the other hand, a number of symmetric image cryptosystems are developed [2]. Most of them rely on chaos-based maps [3]. However, chaos-based symmetric cryptosystems have intrinsic difficulty of exchange and distribution of secret keys [4]. In addition, most chaos-based maps require floating point operation and considerable iterations which is time consuming.

In this paper, a novel public key image scheme is proposed to overcome the problems above. Based on the elliptic curve cryptosystem (ECC), our scheme can solve the difficulty of secret keys management. Also, our scheme requires much less time and storing space than typical ECC because of the use of nonlinear operation as well as Arnold cat map.

This paper is organized as followed: in the next section, ECC and Arnold cat map is briefly reviewed. In section 3, our scheme is put forward. In section 4, experimental results are discussed. In section 5, we give the conclusion.

Elliptic Curve Cryptosystem (ECC) and Arnold cat map

ECC was developed by Koblitz [5] and Millier [6] in 1980s originally. Its security is based on the difficulty of solving the Elliptic Curve Discrete Logarithm Problem (ECDLP). Let p be a large prime number, and$E(F_p) = \{(x,y)|y^2 \equiv x^3 + ax + b(mod\ p), x, y \in F_p\} \cup \{O\}$. The parameters $a, b \in F_p$, *s.t.* $4a^3 + 27b^2 \not\equiv 0(mod\ p)$. O is the point at infinity. $E(F_p)$ is called an elliptic curve in finite field F_p. ECC is established based on elliptic curve $E(F_p)$ and point addition together with scalar multiplication defined on $E(F_p)$. Compared to RSA, ECC requires much shorter keys to maintain a same security level [7]. Hence, ECC occupies smaller space and consumes less time than RSA. However, the typical ElGamal ECC has two difficulties. One is that the message must be represented by a point in $E(F_p)$. The other is that ECC should not reuse keys to assure the security. As a result, it is still inefficient to apply ElGamal ECC directly for image encryption.

Arnold cat map is a two-dimensional invertible chaotic map [8] for an *N*x*N* image. In Arnold cat map, there are three parameters, *c*, *d* and *s*. *c* and *d* are integers in *{0, 1, 2,..., N-1}*. *s* is the number of iterations. Arnold cat map has high computational efficiency, though, its periodic property and disability of changing the histogram weakens its security.

In the next section, we propose a novel public key cryptosystem based on improved ECC and Arnold cat map to cipher large image more effectively without compromising the security.

The Proposed Image Encryption Scheme

In this section, we propose a public key scheme for large image. Suppose Bob wants to send a large image $X_{n\times n}$ to Alice, and that the dimension of the image is $n \times n$.

Key Generation. Alice chooses a large prime p, an Elliptic Curve $E(F_p)$ and a point $P \neq O \in E(F_p)$ carefully. Then she chooses a large secrete random number $k_a \in [2, p-2]$ and computes $Q = k_a P$. $(E(F_p), P, Q)$ is the public key and k_a is the private key. Alice should keep k_a secret.

Encryption. Bob encrypts the image as followed:

1) Select two large random numbers k_b and k_c as his private keys.

2) Compute

$$K_0 = k_b Q = (x_0, y_0). \tag{1}$$

$$L = k_c Q = (x_L, y_L). \tag{2}$$

$$R = k_b P. \tag{3}$$

$$S = k_c P. \tag{4}$$

3) Generate the key matrix K_M_{nn} with the following algorithm:

Algorithm 1 *Key Matrix Generation*

Input	***Output***
$K_0 = (x_0, y_0), L = (x_L, y_L), n$	K_M_{nn}

```
1:  Keyseq ← null
2:  i ← 0
3:  K = (K1, K2) ← (x0, y0)
4:  while length(Keyseq) <n^2 do
5:      i ← i + 1
6:      K ← K + K
7:      l ← length(K1⊕yL)
8:      Keyseq ← shiftleft(Keyseq, l)
9:      Keyseq ← Keyseq + K1⊕yL
10:     l ← length(K2⊕xL)
11:     Keyseq ← shiftleft(Keyseq, l)
12:     Keyseq ← Keyseq + K2⊕xL
13: end while
14: for i ← 1 to n do
15:     for j ← 1 to n do
16:         ptr ← (i − 1)n + j
17:         K_Mnn[i, j] ← Keyseq[ptr]
18:     end for
19: end for
20: return K_Mnn
```

4) Compute

$$c \equiv x_0 (mod\ n). \tag{5}$$

$$d \equiv x_L (mod\ n). \tag{6}$$

$$s \equiv y_0 \oplus y_L (mod\ n). \tag{7}$$

$$C_{nn} = \big(Arnold\ cat\ map(X_{nn} + K_M_{nn}, c, d, s)\big) \oplus K_M_{nn}. \tag{8}$$

Now, Bob can send (R, S, C_{nn}) to Alice.

Decryption. Once received (R, S, C_{nn}), Alice decrypts the image as followed:

1) Compute

$$K_0 = k_a R = (x_0, y_0). \tag{9}$$

$$L = k_a S = (x_L, y_L). \tag{10}$$

2) Apply *Algorithm 1* to obtain the key matrix K_M_{nn}.
3) Use (5), (6), and (7) to obtain *c, d* and *s*. Then compute

$$X_{nn} = \left(Inverse\ Arnold\ cat\ map(C_{nn} \oplus K_M_{nn}, c, d, s)\right) - K_M_{nn}. \tag{11}$$

Experimental Analysis

In this section, some experimental results are discussed to illustrate the security and efficiency of our scheme.

Security Compared to Arnold Cat Map. In Fig.1, LENA.BMP, a 256x256 size gray picture, is encrypted within our scheme and directly using Arnold cat map, respectively.

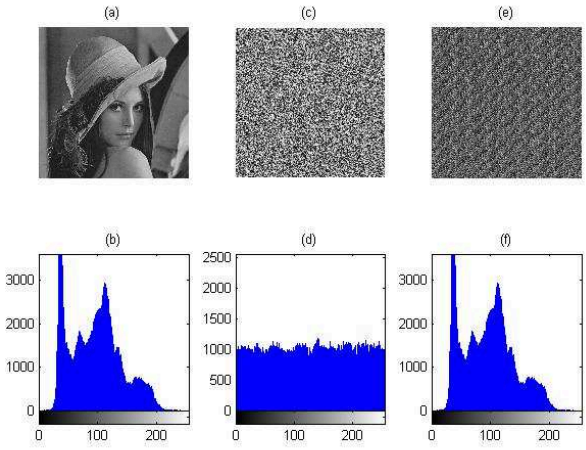

Fig.1 (a) original-image LENA; (b) the histogram of LENA; (c-d) Encryption of LENA using our scheme and the histogram; (e-f) Encryption directly using Arnold cat map and the histogram

Fig.1 shows that our scheme is more secure for image encryption than Arnold cat map. The histogram of the encrypted image resulted from our scheme is like white noise while that generated directly by the Arnold cat map is exactly the same as that of the original image.

Efficiency Compared to ECC. Our scheme and ECC are used for encryption of four different images, respectively. Fig.2 shows the comparison of encryption time and cipher image size.

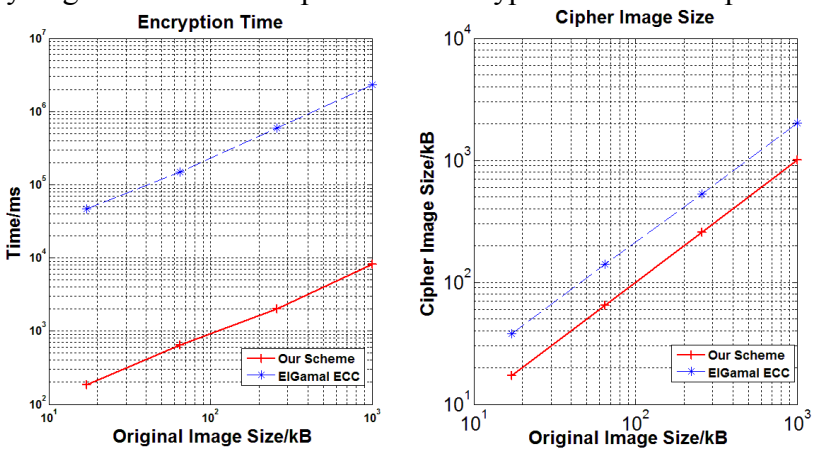

Fig.2 The comparison between our scheme and ElGamal ECC

Fig.2 demonstrates that our scheme requires much less encryption time and occupies smaller storing space than ECC. The larger the image is, the more efficient our scheme will be.

General Security Analysis. The security of the presented scheme essentially relies on ECDLP. Thus, it is difficult for an intruder to compute k_a, k_b and k_c from public keys. Because of the XOR operation and Arnold cat map, even if the adversary knows a part of the original image, he/she can hardly obtain the key matrix so that no other parts can be acquired. Therefore, our scheme can resist chosen-plaintext attack.

Conclusion

In this paper, we propose a fast public key scheme for large image encryption. The scheme is based on improved ECC and Arnold cat map. It is shown that our scheme can avoid the exchange and distribution of private keys, require much less time than typical ECC and guarantee a high security level. This scheme is suitable for massive confidential image exchange in open network.

Reference

[1] R.L. Rivest, A. Shamir, and L. Adleman, *A Method for Obtaining Digital Signatures and Public Key Cryptosystems*, Comm. ACM, 21(2):120-126, 1978.

[2] Rajput A. S. et. al.,, *Towards the Growth of Image Encryption and Authentication Schemes,* International Conference on Advances in Computing, Communications and Informatics, 454-459, 2013

[3] Matthew R, *On the derivation of a chaotic encryption algorithm.* Cryptologia 8(1):29-42,1989

[4] Wade Trappe and L.C. Washington, *Introduction to Cryptography with Coding Theory*. Prentice Hall, 2002

[5] Koblitz. *Elliptic Curve Cryptosystems*. Mathematics of Computation. 203-209, 1987.

[6] V. Miller. *Uses of e1liptic curves in cryptography*. Lecture Notes in Computer Science, 417-426, 1986.

[7] Torri, N. and Yokoyama, K. *Elliptic Curve Cryptosystem*. FUJITSU, 36(2) :140-146, 2000.

[8] Mao-Yu Huang et. al., *Image Encryption Method Based on Chaotic Map*, International Computer Symposium (ICS), 154-158, 2010.

Advanced Materials Research Vols. 989-994 (2014) pp 4187-4190
© (2014) Trans Tech Publications, Switzerland
doi:10.4028/www.scientific.net/AMR.989-994.4187

Research on Adaptive Face Gender Recognition Based on Compressive Sensing

Zhang Lin

Jiangxi Science & Technology Normal University, Nanchang, China

zlhaze@aliyun.com

Keywords: Compressive Sensing, Adaptive, Feature Extraction, Gender Recognition

Abstract. An adaptive gender recognition method is proposed in this paper. At first, do multiwavlet transform to face image and get its low frequency information, then do feature extraction to the low frequency information using compressive sensing (CS), use extreme learning machine (ELM) to achieve gender recognition finally. In the process of feature extraction, we use genetic algorithm (GA) to get the number of measurements of CS in order to gain the highest recognition rate, so the method can adaptive access optimal performance. Experimental results show that compared with PDA and LDA, the new method improved the recognition accuracy substantially.

Introduction

The rapid development of computers has had a huge impact on human society today. In many areas, the computer is increasingly toward intelligent, and gradually replace humans do a lot of challenging work. In order to be more flexible and convenient communication between computers and humans, to achieve human-computer interaction is inevitable development. As the most obvious biological features of human, face image contains a lot of information, we can get gender, age, race, identity and other information [1]. Compared with other biological features, face features are naturalness, convenience and non-contact [2] which make gender recognition based on face features got some development. Gender recognition research has a very wide range of applications [3-5]. Firstly, gender recognition is an important research field of intelligent man-machine interfaces which let the computer to understand face information and classify. If it can achieve a certain degree of intelligence, the current inflexible, inconvenient interactive environment will be improved greatly. Secondly, gender recognition can provide the necessary sex information for a number of users which provide the basis for the user to make decisions based on the information. Thirdly, with the increasing emphasis on security, gender recognition can also play a huge role in security systems, authentication, etc. In addition, gender recognition has good application prospects in population information collection, population statistics, image retrieval, ect.

Therefore, a series of studies on gender recognition and further improve is very necessary. In this paper, we consider using CS in feature extraction of face gender recognition. The appearance of CS brought great changes to feature extraction. Optimal feature selection is no longer a key issue, substantial decline of calculation and good discrimination of sparse representation of signal is very exciting [6]. This paper is organized as follows. Section 2 introduces some background information of this method including CS and ELM. Section 3 gives a detailed description of the proposed method. Experimental results and analyses are shown in section 4. Section 5 gives the conclusion.

Background Information

Compressive Sensing. CS is proposed by proposed by Candes and Donoho in 2006 [7] which revolutionized the tradition. This theory combines with sampling and compression to break through the bottleneck of the Nyquist-Shannon sampling theorem. The advantage of CS is that the number of measurements of signal is far less than the Nyquist-Shannon sampling theorem which makes the process of broadband signals is more efficient. Therefore, the theory will help people easing the pressure of hardware facility from the requirements of the huge amount in information processing

[8] and can effectively carry valuable information in the signal which ensures accuracy in signal transmission, signal processing and reconstruction.

Extreme Learning Machine. Most existing learning algorithms are much slower and cannot satisfy the requirement. Aiming at this shortcoming, Huang and Zhu proposed Extreme Learning Machine (ELM) in 2006. Comparing with most learning algorithms, ELM has extremely fast learning speed, better generalization performance and is much simpler. ELM works for generalized single-hidden layer feedforward networks (SLFNs) which randomly chooses hidden nodes and analytically determines the output weights of SLFNs [9,10]. ELM tends to reach the smallest training error and norm of output weights [11]. Different from the traditional learning algorithm, the hidden layer in ELM need not to be iteratively tuned. ELM requires milder optimization constraints and less human intervention [12].

Based on the advantage of ELM, we consider using ELM in our new method. ELM can be described as follows [10,13]: Suppose given a training set Y, activation function G and hidden node number M. At first, randomly assign input weight a and bias Ψ. Secondly, calculate the hidden layer output matrix H. Finally, calculate the output weight ω via ordinary least-square.

The Proposed Method

Multiwavelet is developed on the basis of wavelet, it is a wavelet generated by scaling function which is composed of more than one function. Multiwavelet expands multi-resolution analysis of space generated by single scaling function of wavelet to space generated by several scaling functions of multiwavelet. Multiwavelet retains many of the advantages of wavelet and perfectly combines smoothness, short support, orthogonality, symmetry, ect. [14], so it has gained widespread attention. GA is proposed by Holland in 1975 which is an optimization method that simulates the natural selection of Darwin's evolution theory and biological evolution process of genetic mechanism which combines the survival of the fittest theory of Darwin and random exchange theory. The survival of the fittest theory can eliminate the inappropriate factor of solution and random exchange theory use existing knowledge of the original solution which speed up the search process for the optimal solution [15].

We know that most important information of a signal after multiwavelet transform focus on low frequency information. So we can directly extract feature from low frequency information replacing original signal to reduce the computational time of algorithm. In CS, the number of measurements M has a great influence to performance. Because the value of M must be integer, we use integer programming GA to ensure the value of M in our method.

The proposed method can be described as follows:

Given some face images, multiwavelet basis, a measurement matrix Φ

Step 1: read training images and testing images, do pre-treatment and normalized to them

Step 2: do multiwavlet transform to training images and testing images, gain low frequency information, we select Sa4 multiwavelet basis here

Step 3: create a N*M measurement matrix Φ obeying Gaussian distribution (0,1/M) , do CS to low frequency information to extract feature. In this step, the selection of the number of measurements M will ensure via GA which will be described below

Step 4: enter feature of training images into ELM to do learning, then enter feature of testing images into ELM to do face gender recognition, output the recognition rate

The process of GA in step 3 is shown as follows:

Step 1: determine the parameters set of the actual problem, we need find the optimal solution or approximate optimal solution of M, so the parameters set of the actual problem is M, use integer programming to generate initial population, choose 10 as the size of initial population

Step 2: define fitness function, we select face gender recognition method proposed in this paper which make M as input parameter and recognition rate as output parameter as fitness function

Step 3: use optimal individual preservation method to select individuals, arithmetic crossover to recombine individuals and non uniform mutation method to preserve diversity in the population

Step 4: set mutation rate, we choose 0.1 as mutation rate to avoid premature convergence

Step 5: evaluate offspring, we select excellent individuals, discard bad individuals and preserve excellent individuals as parents in next iteration

Step 6: judge ending condition, stop if condition is satisfied, else go to step 2. According to many times of experiments, choose 25 as the number of iteration is suitable for our method.

Experimental Results

We select FERET face database as simulation data which is a standard dataset used for face gender recognition. The FERET database which is shown in Fig.1 includes multi-pose and multi-illumination images of person. Before the experiments, we prune training images and testing images into the size of 80*80, and then normalize the gray value of them into 0 to 1.

Fig. 1. Some face images in FERET database

GA optimization trace of the new method is shown in Fig. 2. The horizontal axis represents the number of iteration of algorithm, and the vertical axis represents recognition rate of the new method. The figure shows that the trace is steady after 10 iterations, so selecting 25 iterations as ending condition is suitable for our method. Add up the recognition results which are shown in Table 1. The results illustrate that the new method has higher recognition rate. Compared with PCA and LDA, accuracy of the new method has been improved substantially.

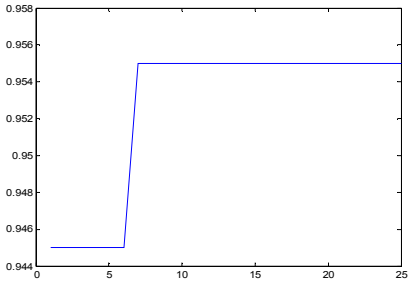

Fig. 2. GA optimization trace of the new method

Table 1. Results of gender recognition rate

A.	R.
PCA	75.5%
LDA	81%
CS+GA	95.5%

Conclusion

Aiming at low recognition accuracy of face gender recognition method currently, we proposed an adaptive recognition method. The new method gain low frequency information of original signal via multiwavelet transform firstly. Then we used CS to extract feature. Finally, ELM is used to achieve gender recognition. To achieve the purpose of adaptive recognition, the new method ensures the value of M according to integer programming GA to achieve the optimal recognition rate. The experimental results tested on a large database showed that the new method can find the value of M with the optimal accuracy adaptively and improved the recognition accuracy substantially compared with traditional methods.

Acknowledgement

This paper is supported by the Youth Foundation of Jiangxi provincial education department (GJJ13562)

References

[1] X.Q.Chen, Z.Y.Xu, L.Lu and P.F.Shi: Gender Recognition Based on Face Features, Journal of Data Acquisition & Processing, Vol.25 (2010), p.595-599.
[2] X.Bai: Gender recognition research based on face image, thesis of master degree, Taiyuan University of Science & technology, 2013.
[3] W.W.Pei: Gender Studier Based on the Feather Extraction of Face Images Analysis, thesis of master degree, Taiyuan University of Technology, 2010.
[4] T.Q.Zhang: Multi-view Face Gender Classification and Feature Selection, thesis of master degree, Shanghai Jiao Tong University, 2010.
[5] Z.Yang: Research on the Technology of Gender Recognition Based on Face Image, thesis of master degree, Jiang Su University, 2009.
[6] N.Sun, C.Zhang, X.Y.Zhu, R.Dai and S.Wei: Survey of face gender classification using compressed sensing, COMPUTER ENGINEERING AND DESIGN, Vol.33 (2011), p.4382-4385.
[7] E.Candès and M.Wakin: An introduction to compressive sampling, IEEE Signal Processing Magazine, Vol.25 (2008), p.21-30.
[8] F.Yang: Research on Image Reconstruction of Compressive Sensing, thesis of master degree, Jiangxi Science & Technology Normal University, 2010.
[9] M.Zhai, R.Zhang and Y.Wang: A Summary of Network Structure Adjustments of Extreme Learning Machine, Journal of Xi'an University of Arts & Science (Nat Sci Ed), Vol.17 (2014), p.1-6.
[10] G.B.Huang, Y.Z.Qin and C.K.Siew: Extreme learning machine: theory and applications, Neurocomputing, Vol.70 (2006), p.489-501.
[11] G.B.Huang, D.H.Wang and Y.Lan: Extreme learning machines: a survey, International Journal of Machine Learning and Cybernetics, Vol.2 (2011), p.107-122.
[12] G.B.Huang, H.M.Zhou, X.J.Ding and R.Zhang: Extreme Learning Machine for Regression and Multiclass Classification, ieee transactions on systems, man and cybernetics, part b: cybernetics, Vol. 42 (2012), p.513-529.
[13] H.F.KE and J.Ying: Real-time license character recognition technology based on R-ELM, Journal of Zhejiang University (Engineering Science), Vol.48 (2014), p.1-8.
[14] P.Y.Fei and B.L.Guo: A study on multiwavelet based image denoising, Journal of Image and Graphics, Vol.10 (2005), p. 107-112.
[15] L.Zhang, Z.J.Fang, S.Q.Wang, F.Yang, G.D.Liu: Multiwavelet Adaptive Denoising Method Based on Genetic Algorithm, Vol.28 (2009), p. 77-80.

Advanced Materials Research Vols. 989-994 (2014) pp 4191-4194
© (2014) Trans Tech Publications, Switzerland
doi:10.4028/www.scientific.net/AMR.989-994.4191

The Application of A New Demodulation Technology in The Telemetry System

Tao Min[1,a] , Fu Gang[1, a], Wu Guangzhi[1,a]

[1]China Satellite Maritime Tracking and Control Department, China

[a]348237548@sina.com

Keywords: PCM/FSK, demodulation, self-adaptive

Abstract. This paper presents a new PCM / FSK digital signal demodulation method. By using an adaptive least mean square error algorithm consider wave single frequency, the tracking signal, analyzes the envelope of the output signal, demodulate the PCM / FSK signal. This paper introduces the basic principles of this demodulation method and implementation process, analyzes the factors that affect the demodulation performance. Simulation results show that this method is superior to the differential demodulation performance, strong anti-jamming capability, ease of software programming and DSP devices achieve a certain value.

Introduction

PCM / FSK telemetry as a current standard system, at home and abroad have a wide range of applications. It transceiver simple, the detection efficiency and spectrum occupancy is more reasonable. With the rapid development of modern digital signal processing methods and computer technology, implemented by software methods for PCM/FSK signal demodulation is not only possible, but also very urgent. [1] proposed a signal-based WD distribution in time-frequency two-dimensional plane of the FSK signal analysis , digital signal resolve to achieve FSK modulation method. [2] proposed a short-term based on the discrete Fourier transform in the frequency domain for the FSK signal analysis , digital signal resolve to achieve FSK modulation method . Both methods of calculation amount than the larger, the signal applied to the inconvenience software demodulation. In recent years, with the rapid rise and development of adaptive signal processing method can consider the use of adaptive signal wave frequency tracking algorithm, the realization of the demodulated signal . This paper presents an adaptive demodulation method is to consider wave LMS adaptive filtering algorithm to track the frequency of the signal based on the information detected by the phase FSK signal demodulation in order to achieve better results.

1 Adaptive consider wave device

Adaptive consider wave is a wave refers to consider the parameters can be updated with adaptive recursive way, it can be divided into the number of adjustable parameters into account wave and adaptive algorithm in two parts.

LMS algorithm is one of the steepest descent method type adaptive algorithm, due to its simple and efficient, easy to implement, is commonly used in adaptive algorithms consider wave. The basic idea of the LMS algorithm is a series of operation by adjusting the parameters, the linear combiner and the error output signal in response to a desired value between the minimum mean square, and the basic block diagram shown in Figure 1.

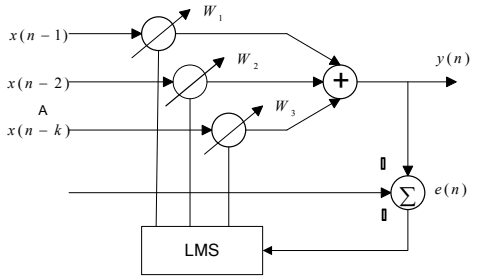

Fig 1 Schematic of adaptive consider wave

The input is $x(n-1), x(n-2), \ldots, x(n-k)$. The output is $y(n)$ weighted linear combination of these inputs, namely:

$$y(n) = \sum_{i=1}^{k} W_i x(n-i) \tag{1}$$

In response, the error signal $d(n)$ representative of the expected:

$$e(n) = d(n) - y(n) \tag{2}$$

According Window and Hoff proposed in 1960 the steepest descent method, the next time the weight coefficient vector A should be:

$$W(n+1) = W(n) + 2\mu e(n)x(n) \tag{3}$$

2 Adaptive demodulation principle

FSK is the continuous phase frequency shift keying, the mathematical expression is:

$$S_{FSK}(t) = A\cos\left[\omega_0 t + \omega_d \int_{-\infty}^{t} f(t)dt + \varphi_0\right] \tag{4}$$

Instantaneous frequency of the FSK signal is:

$$\omega_i = \frac{d}{dt}\left[\omega_0 t + \omega_d \int_{-\infty}^{t} f(t)dt + \varphi_0\right] = \omega_0 \pm \omega_d \tag{5}$$

ASK and FSK signal can be regarded as two signals of different carrier frequencies, the mathematical expression is:

$$S_1(t) = A\cos(\omega_s t + \varphi);\quad S_2(t) = A\cos(\omega_M t + \varphi) \tag{6}$$

With symbols "1" signal corresponding to an example, this time in the form of the signal can be further simplified as:

$$S_2(t) = A\cos\varphi\cos\omega_M t + A\sin\varphi_n \sin\omega_M t \tag{7}$$

Assuming $W_1 = A\cos\varphi, W_2 = A\sin\varphi$,there are:

$$S_2(t) = W_1\cos\omega_M t + W_2\sin\omega_M t \tag{8}$$

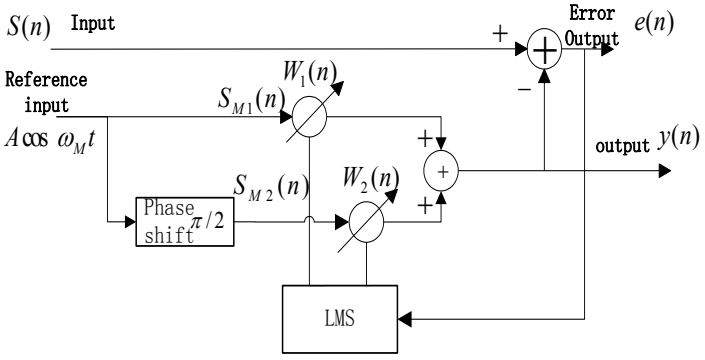

Fig 2 Schematic adaptive demodulation

$$S_{M1}(n) = A\cos\omega_M T_S n$$
$$S_{M2}(n) = A\sin\omega_M T_s n \quad (9)$$
$$y(n) = W_1(n)S_{M1}(n) + W_2(n)S_{M2}(n) \quad (10)$$
$$e(n) = S(n) - y(n) \quad (11)$$
$$W_1(n+1) = W_1(n) + 2\mu e(n)S_{M1}(n) \quad (12)$$
$$W_2(n+1) = W_2(n) + 2\mu e(n)S_{M2}(n) \quad (13)$$

Adaptive implementation process FSK signal is demodulated into account wave: first by the LMS algorithm, tracking mark frequency signal components or space frequency, and then to take into account the output of the absolute value of the wave, and then after removing the median consider wave packet envelope, the envelope waveform of the analysis, the result of demodulation. Taking into account the value of the mathematical expression for the wave:

$$M(n) = \frac{1}{2m+1}\sum_{i=-m}^{m}|y(n+i)| \quad (14)$$

Figure 3 shows a waveform of the demodulated signal at different stages of the process.

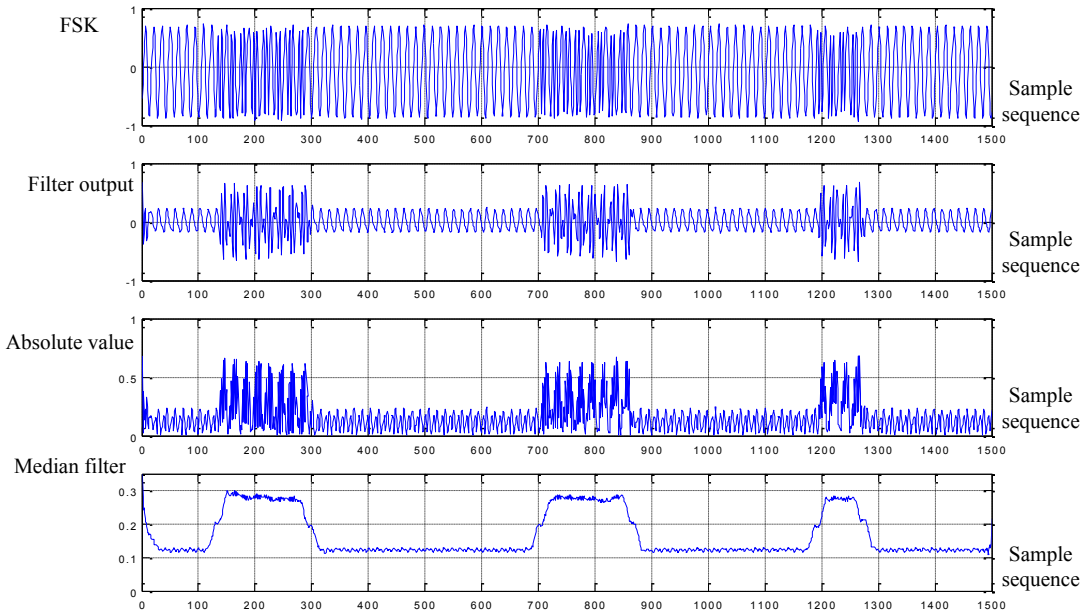

Fig 3 FSK demodulation process adaptive curve

Can be derived from Figure 3, after the absolute value, the value considering the wave, the envelope signal is obtained, then the decision threshold distinguished by the symbol "1" or "0", thereby achieving demodulation of the FSK signal.

3 Performance Analysis

Adaptive consider wave pair FSK signal tracking results will directly affect the outcome of demodulation. LMS adaptive algorithm key is to choose the learning rate parameter. Large learning rate can improve tracking performance oscilloscope into account, but the steady-state performance of the system will be reduced; Conversely, when steady state in order to improve the system performance and the use of small learning rate, the convergence performance will be affected. Therefore, in order to solve the contradiction between convergence rate and steady-state performance, time-varying learning rate can be used.

In the maximum-likelihood ratio criterion derived FSK demodulation method used (non-coherent demodulation) theoretical BER curve, as measured by the theoretical basis for such a demodulation method performance. Since the FSK modulated signal is "1" bit energy, and "0", the correlation coefficient between the energy of the code with a code rate of change varies, the correlation

coefficient will affect the BER, therefore, the code rate corresponds to a different type of BER theoretical curve. In a certain code rate (2Mbps) premise calculate different SNR BER simulation results shown in Figure 4. Visible, adaptive demodulation method is superior performance than non-coherent demodulation performance, especially in the low SNR, demodulation performance is significantly better than non-coherent demodulation.

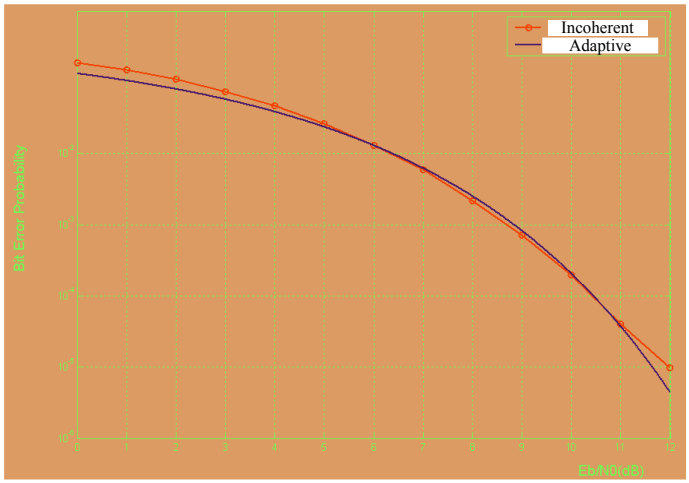

Fig 4 BER curves

Summary

Adaptive consider wave PCM/FSK signal demodulating FSK signal demodulating method is another method. The principle of this method is simple, relatively small amount of computation to facilitate the realization of software programming, suitable for the application of DSP chip to build a software radio system. BER performance and superior anti-interference ability, can effectively suppress the influence of the Doppler frequency of the received signal demodulation.

Reference

[1] Zhao Xiaoping. WV distributed in discrete digital demodulation of the FSK signal applications[J]. Xi'an University of Electronic Science and Technology,2008,30(2):201-205.
[2] Zhao Xiaoping. The FSK signal discrete STFT digital demodulation method[J]. Xi'an University of Electronic Science and Technology,2007,28(6):812-815.

Advanced Materials Research Vols. 989-994 (2014) pp 4195-4199
© (2014) Trans Tech Publications, Switzerland
doi:10.4028/www.scientific.net/AMR.989-994.4195

Digital Signal Processing Approach of Dithered RLG Based on IFIR Digital Filter

Zhang Kui[1, a], Yang Gongliu[1], Zheng Weizhen[1] and Ma Rendong[1]

[1]School of Instrumentation Science and Opto-electronics Engineering, Beihang University, Beijing, China

[a]encyclopedicchris@163.com

Keywords: Interpolated Finite Impulse Response; IFIR; RLG; Digital Signal Processing

Abstract. An interpolated finite impulse response (IFIR) digital filter approach was purposed to improve the demerits of traditional finite impulse response (FIR) digital filter in the case of noise attenuation for dithered Ring Laser Gyroscope (RLG). Concentrated on the time delay and computation complexity, a comparison of FIR and IIR digital filter was illustrated. By optimizing the *stretch factor* L, an IFIR digital filter was designed to reach the requirements of a typical RLG. The static experiment results show that the impulse number is decreased from 250 to below 0.15, attenuation of the dither noise is nearly 100 dB and group delay remains the same level by 11.25ms.

Introduction

With dynamic range input, high-reliability, and long working lifespan, Ring Laser Gyroscope (RLG) is widely applied into Strapdown Inertial Navigation System (SINS) , which is utilized for various backgrounds owing to its high-precision and cost-effective performance. The RLGs are dithered to prohibit the effect known as lock-in. However, mechanical dither introduces high frequency noise, which distorts the signal of angular rate from RLGs. By sampling at high rate, a commonly method to remove the noise is applying digital filters.

According to the length of its impulse response sequence, digital filter is classified into the Finite Impulse Response (FIR) digital filter and Infinite Impulse Response (IIR) digital filter. FIR filter enjoys its advantage on the behavior of the strict linear phase response, but acquires higher order to reach the effective performance on magnitude frequency response, which leads to not only an increasing amount of computational operations for two-input adders and multipliers but also an undesirable long time delay. Unlike the linear phase of FIR digital filter, the nonlinearity of IIR filter gives rise to a time delay ripple when the input signal contains different frequencies, which cannot guarantee a real-time output. As a mainstream approach, a lowpass FIR digital filter is designed to remove the dither noise [2], and some methods demonstrate a well-designed cascade of IIR digital filter [3, 4] also satisfy the requirements.

After analyzing of traditional approaches, a method based on Interpolated Finite Impulse Response (IFIR) digital filter is established to demodulate the output signal of dithered RLG. Static experiment results prove that the magnitude response of the filtered signal on the bandwidth of dithered noise is attenuated to 100dB, and it is a compromising solution to ensure the performance on both low group delay and computation complexity reduction.

Filter Analysis

Time delay analysis. There are two types of time delays considering a multi-frequency input signal processed by a digital filter, i.e time delay for operations and group delay. Group delay reflects each component of a broadband signal goes through different phase delays when filtered. For high-order digital filters, time delay for operations is comparative count for little, so the major concern goes to minimize group delay.

For an FIR digital filter which phase function $\theta(\omega_{in})$ is at the frequency ω_{in} of the input signal, the group delay is defined as below

$$\tau_g(\omega_{in}) = -\frac{d\theta(\omega_{in})}{d\omega_{in}} \tag{1}$$

In the case of a linear-phase FIR digital filter, the phase response is given by

$$\theta(\omega_{in}) = -\omega_{in}(N-1)/2 \tag{2}$$

Therefore the group delay

$$\tau_g(\omega_{in}) = -d\theta(\omega_{in})/d\omega_{in} = (N-1)/2 \tag{3}$$

The unit of Eq. 3 is measured by sampling period. Due to the nonlinearity of the phase of an IIR digital filter, which the group delay is variable, the real-time accuracy of RLGs is greatly distorted.

Therefore, the *exclusive* approach to minimize group delay of an FIR digital filter is to reduce the order.

Computation Complexity Analysis. The computation complexity of digital filter structure depends on the sum of two-input adders and multipliers to realize the structure. Table 1 illustrates the computation complexity of N-order of FIR digital filter and IIR digital filter. Under the same requirements of digital filter specifications, FIR digital filters generally load a considerably higher order comparing IIR digital filter, which leads to a heavy workload of computation complexity; the ratio of N_{FIR} / N_{IIR} is always in two-digits.

Table 1. Computation Complexity of N-order FIR and IIR Digital Filter

Digital Filter Structure	Amount of Multipliers	Amount of Two-input Adders
FIR Direct Form	$N+1$	N
FIR Linear Phase	$\left\lfloor \frac{N+2}{2} \right\rfloor$	N
IIR Direct / Cascaded Form	$2N+1$	$2N$

Principle and Design of IFIR Digital Filter

Principle of IFIR Digital Filter. Improvements should be done to solve the dilemma between time delay and computation complexity. The major drawback of FIR digital filter is the heavy computational workload and comparative long time delay on demand of the specification. [6]

As an approach to cut down the workload of traditional FIR digital filter, Interpolated Finite Impulse Response (IFIR) digital filter is an ideal adder-less and multiplier-less solution for filtering output signal of RLGs.

Shown in Fig. 1, the basic structures of bi-stage IFIR digital filter $H_{IFIR}(z)$ comprises of a linear-phase periodic FIR *model filter* $F(z^L)$ and a linear-phase FIR *image-suppressor* $I(z)$. Known as *stretch factor* L, there inserts $L-1$ units of zeros between the prototype samples in the first subfilter $F(z^L)$. As we could expect, a L-fold expansion of time-domain filter impulse response leads to an L-fold shrink in frequency-domain, meaning the transfer function $\widetilde{F}(L\omega)$ in magnitude frequency response is a periodic function with a period of $2\pi / L$. The effect of interpolation sharply shrinks the band edge of transition without employing any adders and multipliers.

The impulse response and magnitude response are shown in Fig. 2 assuming $L = 3$.

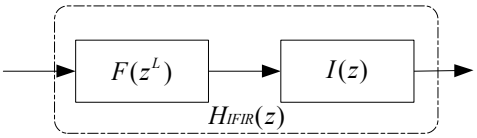

Fig. 1. Structure of $H_{IFIR}(z)$

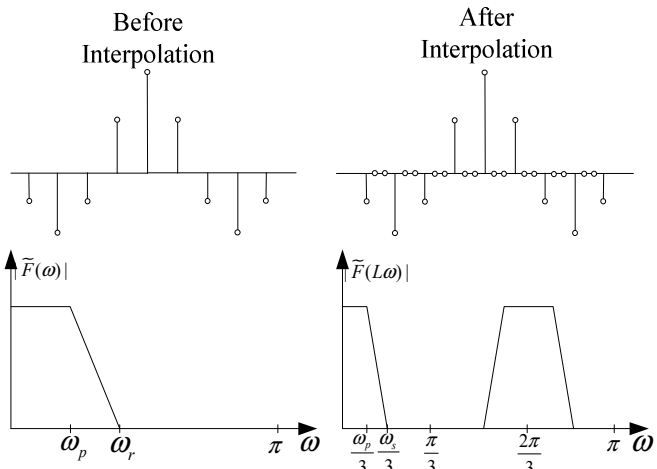

Fig. 2. Impulse Response and Magnitude Response before and after Interpolation

Design of IFIR Digital Filter. A vital step in the development of a digital filter is to determine the specifications given realizable parameters. The frequency domain of output angular rate signal from the typical RLG we focused is below 100Hz, and the high-frequency dithered noise is around 350Hz. Hence, a lowpass digital filter is feasible to attenuate the noise theoretically. According to Nyquist sampling theorem, we set the sampling rate as 4000Hz. To guarantee the efficient of attenuation, the magnitude response of the dither noise should be an order or higher than the one of angular rate [2], i.e the minimum stopband attenuation A_s should be 60dB at least. In the case of this design, specifications of the IFIR digital filter $H_{IFIR}(z)$ are given in Table 2

Table 2. Specifications of the Lowpass IFIR Digital Filter

Passband Edge Freq. ω_s [Hz]	Stopband Edge Freq. ω_p [Hz]	Peak Passband Ripple. A_p [dB]	Minimum Stopband Attenuation. A_s [dB]
100	300	0.01	80

Here, we develop the IFIR digital filter using an *ifir* Matlab function to obtain the coefficients. A standard syntax is written as [H, I, D] = ifir(L, TYPE, F, DEV, STR) where L stands for *stretch factor* and using STR to choose the algorithm level of optimization. Here, we select *advanced* option to fulfill the design. By relying on the well-established the formula of Kaiser for estimating order N of an FIR filter as

$$N = \frac{D(\delta_p, \delta_s)}{\Delta\omega} \tag{4}$$

$$\Delta\omega = \omega_s - \omega_p \tag{5}$$

As illustrated in Table 1, the total multipliers R of the FIR is calculated as

$$\mathrm{R} = \left\lfloor \frac{N+2}{2} \right\rfloor \tag{6}$$

Therefore, the total number of multipliers in the IFIR $\mathrm{R}_{\mathrm{IFIR}}$ can be approximated as

$$\mathrm{R}_{\mathrm{IFIR}} = \frac{D(\frac{\delta_p}{2}, \delta_s)}{\Delta\omega} + \frac{D(\frac{\delta_p}{2}, \delta_s)}{2\pi/\mathrm{L} - \omega_s - \omega_p} = D(\frac{\delta_p}{2}, \delta_s) \cdot f(L) \tag{7}$$

Where

$$f(L) = \frac{1}{\mathrm{L}(\omega_s - \omega_p)} + \frac{1}{2\pi/\mathrm{L} - \omega_s - \omega_p} \tag{8}$$

Assume the derivative function of $df(L)/dL = 0$. It yields

$$L_{optimum} = \frac{2\pi}{\omega_p + \omega_s + \sqrt{2\pi(\omega_s - \omega_p)}} \tag{9}$$

Specifically speaking, after normalizing the desired passband edge and stopband edge respectively to $\omega_p = 0.05\pi$, $\omega_s = 0.15\pi$ and we obtain $L_{optimum} = 3.09$. By adopt $L = 3$ to realize the specifications listed in Table 2, and shown in Fig. 3 here comes the magnitude responses of 82-order linear phase FIR digital filter as the *model filter* and 10-order linear phase digital filter as the *image-suppres*

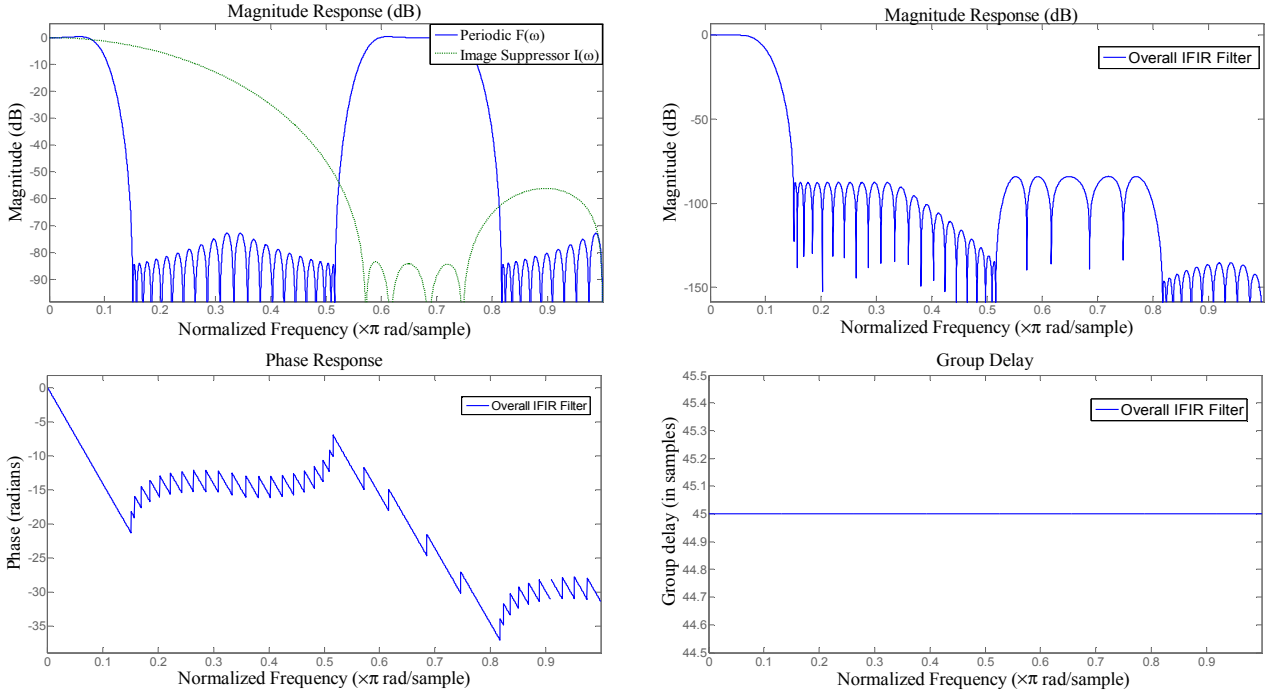

Fig. 3. The Magnitude Responses of $F(z^L)$ and $I(z)$ and the Magnitude Response, Phase Response, Group Delay of the Overall IFIR Digital Filter

Experiments and Test Analysis

To prove the feasibility of the IFIR digital filter, static experiments are implemented. Initially, we design an 81-order lowpass FIR digital filter as a contrast listed as Table 3. Next, set the RLGs IMU on a standard marble platform and keep power-on for 1 hour. Then sample the output signal using an upper IPC by the frequency of 4000 Hz.

Table 3. Specifications of Lowpass IFIR and FIR Digital Filter

Filter Structure	Order N	Passband Edge Freq. ω_s [Hz]	Stopband Edge Freq. ω_p [Hz]	Peak Passband Ripple A_p [dB]	Min. Stopband Attenuation A_s [dB]
Lowpass IFIR	82 & 10	100	300	0.01	80
Lowpass FIR	81	100	300	0.01	80

As shown in Fig. 4, the Power Spectral Density (PSD) and impulse numbers of output signal of designed filters are comparing with input signal before filtered. The impulse number results indicate that IFIR filtered signal acts a similar efficient noise-removal performance as FIR by reducing the impulse number from 250 to below 0.15. From the aspect of PSD, the IFIR filtered signal realizes the purpose of attenuating the dither noise by nearly 100 dB.

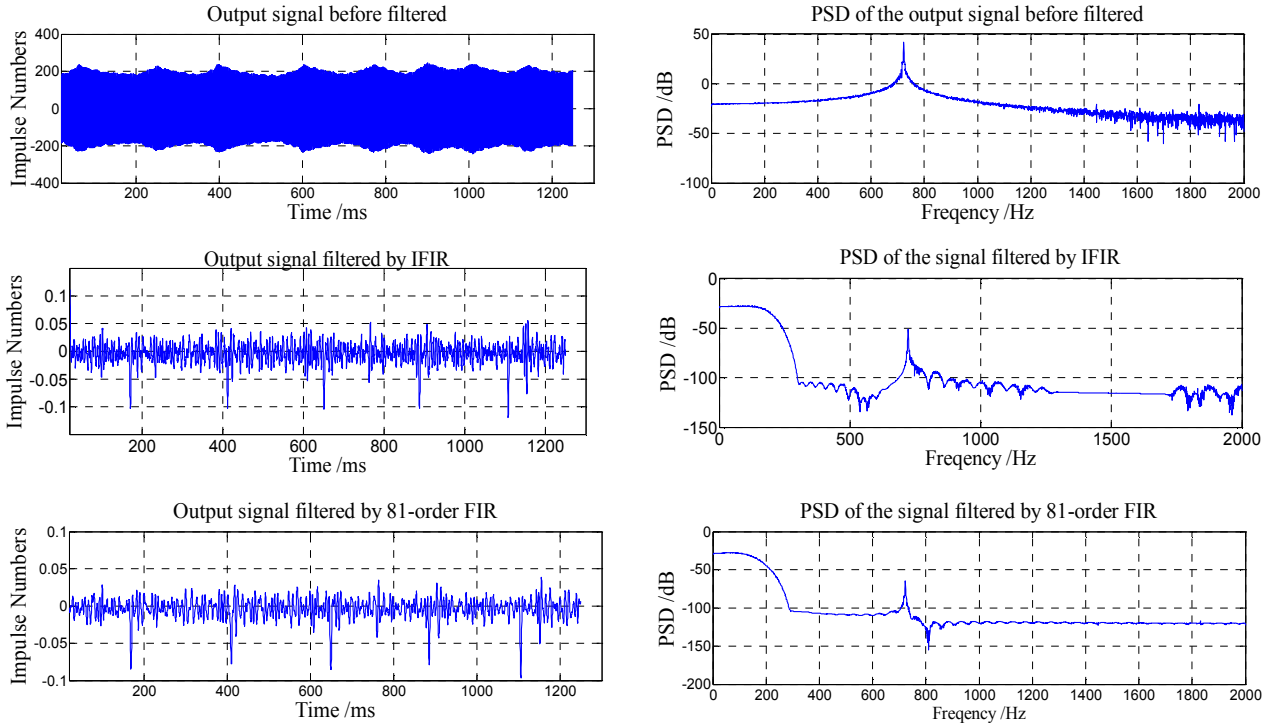

Fig. 4. The Magnitude Responses of $F(z^L)$ and $I(z)$ and The Magnitude Response, Phase Response, Group Delay of the Overall IFIR Digital Filter

As shown in Table 4, in contrast of FIR, the computation complexity of IFIR approach is reduced by around 54% and group delay almost remains the same by 11.25ms.

Table 4. Group Delay and Computation Complexity of IFIR and FIR Digital Filter

Filter Structure	Group Delay [ms]	Computation Complexity	
		Multipliers	Adders
Lowpass IFIR	11.25	38	36
Lowpass FIR	10.125	82	81

Conclusion

An IFIR digital filter is designed to solve the dilemma between time delay and computational complexity to eliminate dither noise of RLGs. In contrast of the previous FIR method, the static experiment results show IFIR digital filter has a cost-efficient performance: the computational complexity is decreased by 54% and group delay stays in the same level by 11.25ms.

References

[1] G. T. Schmidt, INS/GPS Technology Trends, RTO-EN-SET-064 p. 1-12 (2006)
[2] M. Y. Zhong, D. K. Yan, in: Research on Predictive Filtering and Delay Compensation of RLG POS. Journal of Chinese Inertial Technology, Vol. 12, 6 (2011), p. 670-675 in Chinese.
[3] Y. Q. Cheng, D. M. Xu, in: Digital Signal Processing Algorithm of Laser Gyro Based on Digital Filter. Journal of Chinese Inertial Technology, Vol. 21, 1 (2013), p. 112-116 in Chinese.
[4] J. L. Li, in: Low Time Delay De-noising Method for Mechanically Dithered RLG POS Based on Linear Phase Infinite Impulse Response Filter. Vol. 20, 6(2012), p. 644-649 in Chinese.
[5] S. K. Mitra: Digital Signal Processing: A Computer-Based Approach 4th Edn. McGraw-Hill Companies, Inc. New York, NY (2011).
[6] A. Mehrnia, A. Willson JR, in: On Optimal IFIR Filter Design. Circuits and Systems. ISCAS04 Proceedings of the 2004 International Symposium on. Vol. 3, IEEE (2004).

Advanced Materials Research Vols. 989-994 (2014) pp 4200-4204
© (2014) Trans Tech Publications, Switzerland
doi:10.4028/www.scientific.net/AMR.989-994.4200

A New Framework for Churners' Influence Analysis using Call Data Records

Georges Olle Olle[1, a], Cai Shuqin[1, b], Yuan Qian[1, c]

[1] School of Management, Huazhong University of Science and Technology, Wuhan, Hubei 430074. P.R.China

[a]georgesdelortolleolle@gmail.com, [b]caishuqin@hust.edu.cn, [c]hustyuanqian@gmail.com

Keywords: Call Data Records, Churn Prediction, Telecommunication, Influence Analysis

Abstract. Predicting customer churn is of paramount importance in telecommunication companies. The taxonomy of churn reports that, not only individual constraints but also social factors can create users' propensity to churn. This study uses real world call data records (CDR) to extract the social relationships among mobile phone users and build a multi relational social network, where the influence of users diffuses. The research is conducted to propose a framework that enhances the actionable value of social influence of predicted churners and to examine the parameters that control the churn information diffusion in the telecommunication networks.

Introduction

Nowadays, every business employs customer retention strategies in order to gain competitive advantage and ultimately to survive in a saturated and fiercely competitive environment. Behavioral science is the path that many businesses have adopted as the best lever of retention to yield advantages [1,2,3]. The focus is on understanding the customer attitude and interactions with the organization. Thus, it consists of predicting or describing a particular subscriber's future events based on his or her historical data [4,5,6]. *Customer Churn* prediction is the detection of customers with high propensity to leave the service in the near future. It is the utmost concern of mobile telecommunication operators, as they register more than 30% of annual churn rate. The principle of customer churn prediction is to build a general and simplified process that will classify the subscriber as either churner or non-churner. There are numerous researches on data mining (DM) that study the prediction of churn. A typical DM model for churn prediction includes: The identification of most suitable data for the business task; the data semantics or data preprocessing; the feature selection and building; the model development using DM methods; such as: support vector machine (SVM), neural networks (NN), logistic regression (LR), etc. A validation of the results is required before implementation [6,7,8,9]. Social influence of users has recently been introduced to the research of churn prediction to resolve some limitations of traditional predictive models. Some obvious relevant shortcomings are that: They do not provide an adequate time frame between the detection time and the moment when retention campaign can be successfully deployed. It is necessary to notice that, sufficient long forecast horizon is an advantage; since the further away the customer is from making the decision to churn, the easier it is to retain him at a significantly low cost. Also, traditional churn prediction models do not provide any information about the influence that a user can receive from other users. When people are socially connected, they can imitate behaviors that are not related to their individual patterns [9,10,11], but that are based on the influence they receive from their friends.

In this research, we use call data records or CDR, that are the characteristics of calling traffic (caller receiver IDs, date, duration etc…); to propose a framework research and conduct some experiments on the churn influence diffusion in a multi relational social network. The model is constructed based on different behaviors observed on users' interactions. We are motivated by the fact that: The number of retained or left potential churners can create an impact on the network. We also consider that the diffusion of churn influence should not only consider the growing number of churners but also the structure of the affinities linking users. To the best of our knowledge this

research is one of the first to consider a heterogeneous behavior to build a communication network based CDR.

Research Framework and Description

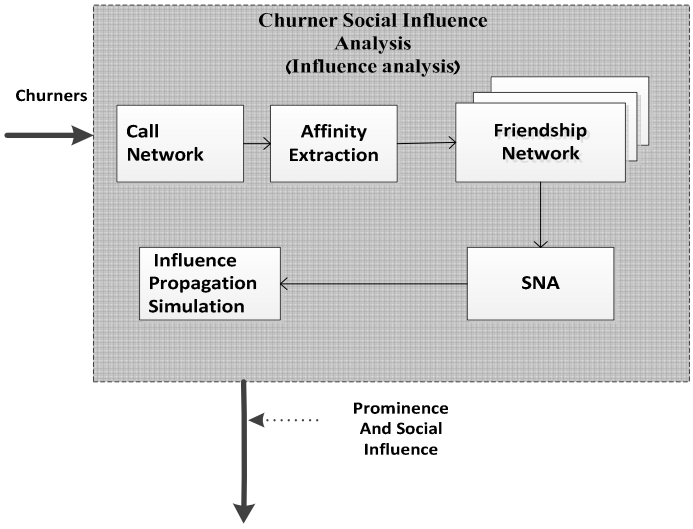

Fig.1 Churner Social Influence Analysis Framework

A call network or call graph is considered as a directed weighted graph $G = (V, E)$, where V is a set of vertices representing individual subscribers, and E is the set of directed edges representing interactive calls among the subscribers. A pairwise is formed for every two subscribers' IDs, where reciprocal calls are registered. Multiple calls between one pairwise constitute the same edge or relationship. Affinities hidden in a single relationship between 2 nodes of a pairwise are extracted using an edges clustering method. The attributes of the edges are constructed based on the call characteristics. Attributes are built targeting particular affinity behaviors. Social network analysis is performed on the multi relation call network obtained whereby churners' influence diffuses based on a diffusion model.

Datasets

The dataset used in this study represents CDR of more than 9 thousand users of one of the main telecom companies in China. It expands a whole month chronological communications of the selected subscribers, all belonging to the city area of Wuhan-Hubei Province. The data contains all the details of the communication (IDs of caller and of receiver, period of call , duration, start time and end time.); the data does not include SMS communication. Content of communication and user real ID where protected as the work where done with the collaboration of the data provider.

Table 1. Data statistics

Total number of valuable calls traffic	303257
Total number of nodes from the local network	9752
Total number of links established within the local network users	26244

Table 2. List of built edges-variables

Edges variables and definitions
Total number of calls by the pair within a month
Average Number of calls per day
Call Duration in seconds within the month
Number of calls Direction (IN)
Number of calls direction (OUT)
Call Period Percentages A { count monthly calls number during P1 [6am-11:30 am and 2-5pm],P2 [5pm-7pm], P3 for [7pm-10pm[, P 4 for [10pm-12pm[, P5 for [12pm-6am]
Number of Calls Period B (count monthly calls number during W1=Weekdays [Monday 2am-Friday 5pm[or W2= Weekend [Friday 5pm-Monday 2am[

Ratio (PD) Average duration of calls at period A / Total duration per month
Ratio :average duration of calls at period B-Total duration per month
Ratio : Number of Calls made at period A /Total Number of calls by the pair within a month
Ratio: Number of Calls made at period B / Number of calls made at period B
Ratio: number of calls made at period P1, P2,P3,P4,P5 / total number of call within a month
Reciprocity ratio(Compute Number of mutual Calls/total Number of total calls within a month)
Total number of mutual correspondents (count how many numbers call both users)

Experiment and Results

Fig.2 represents the social network obtained with the nodes of our mobile telecommunication network. Fig.3 is the node distribution of the network. The network is scale free and the degree distribution follows the power law. The diffusion of churn information can be modelled in our network, where highly connected subscribers that are churners or for whom churners are close friends, are expected to convey the churn influence. Fig.4 represents the clusterring results based on the attributes in Table 4, showing different behaviors patterns in the communications of the subscribers.

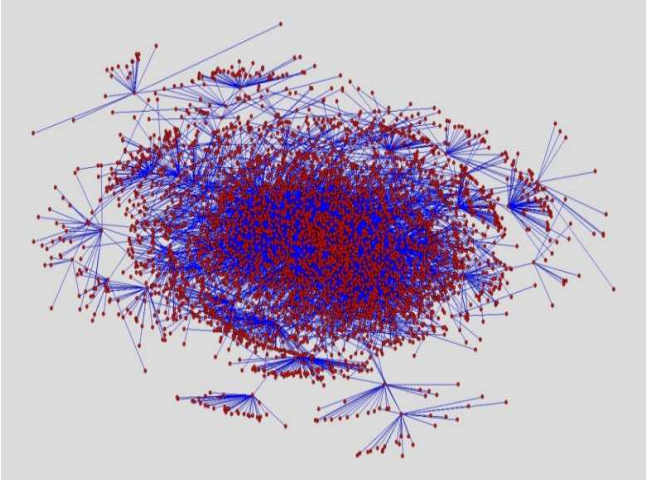

Fig. 2 Call Network

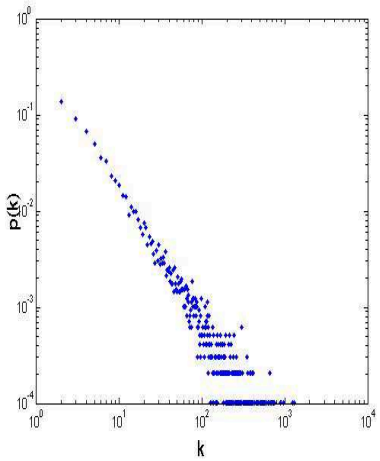

Fig. 3 Node Degree Distribution

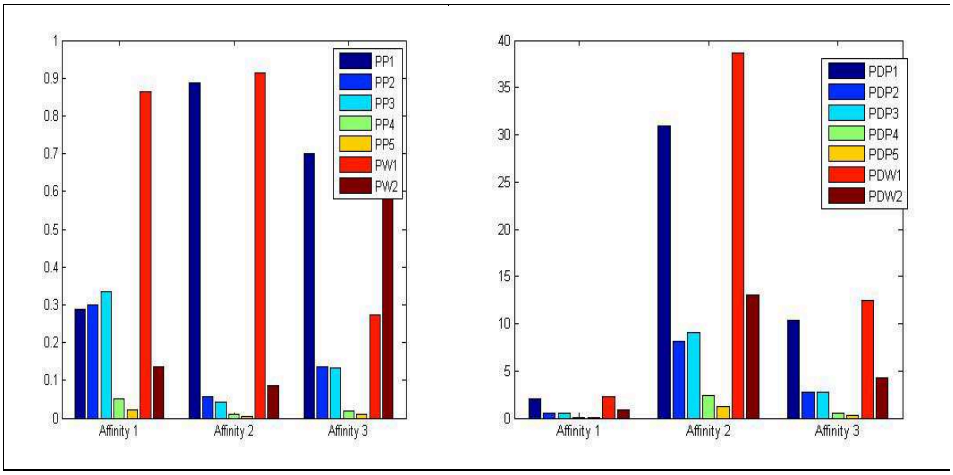

Fig. 4 Affinities Extraction based Edges Clustering: Call Frequency (L) and Call Duration (R)

Influence Diffusion

We use the linear threshold model (LT) in this study to analyze the diffusion of churn information in the different affinity networks. More details on the LT model can be found in [12,13]. Each edge $(u, v) \in E$ has a weight $\omega_{uv} \geq 0$, indicating the power of u influencing v. For convenience, we set for each $(u, v) \notin E$, $\omega_{uv} = 0$; and for each $v \in E$, we have:

$$\sum_{u \in V} w_{uv} \leq 1 \; ; \tag{1}$$

$$\sum_{u \in S_{t-1}} w_{uv} \geq \theta_v \; , \tag{2}$$

where $S_{t-1} \subseteq V$ is the seed set at the time $t-1$ with $S_0 = S$, $\sum_u w_{uv} \in [0,1]$ and $\theta_v \in_R [0,1]$
The weight of the ties is obtained by computing the characteristics of the calls between 2 nodes and the Jaccard coefficient of the similarity in their contacts.

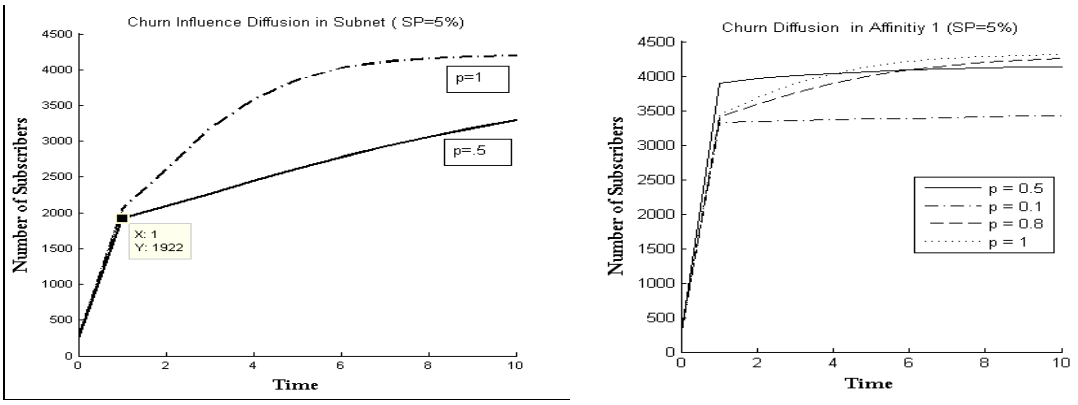

Fig. 5 Churn Diffusion in: Random network (Left) and Affinity Network(Right)

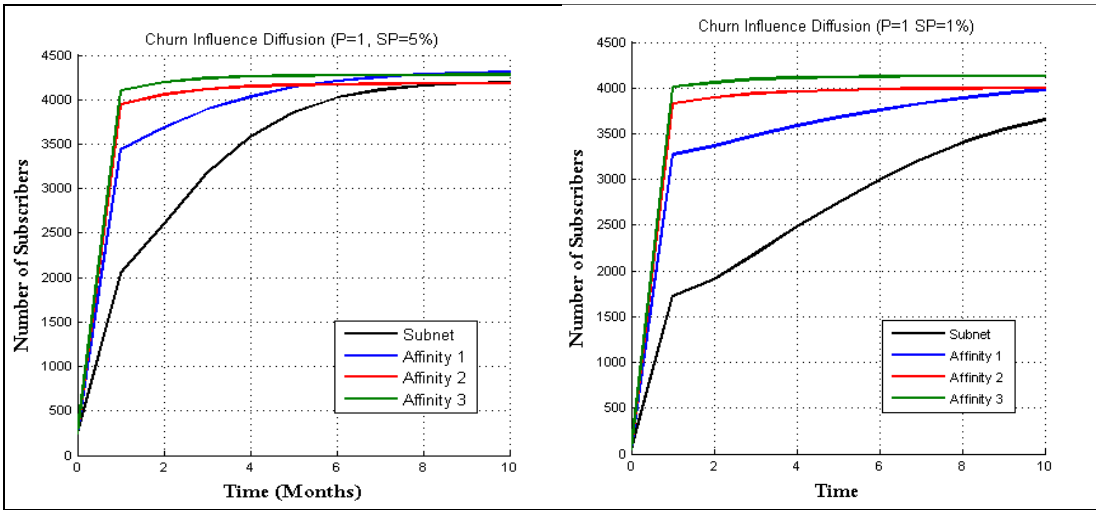

Fig. 6 State of diffusion with initial number of churners (5% and 1% spreaders)

Discussion and Conclusion

Churn happens when the telecom company loses an inherent customer. Based on social evaluation, a subscriber who has many contacts that have churned is expected to have a high propensity to also churn [11]. Current researches on that realm propose that the tie strength should be enhanced and the diffusion should be analyzed to better target churners with long forecast and introduce targeted incentives and applications [14]. We have extracted 3 different users communication behaviors based on the input data sets and have obtained a multi relational call network. All the subscribers of the networks exhibit one or all the behaviors targeted in our clustering methods. Therefore, the obtained tie structure between any two nodes reflects a particular influence weight that is based on the affinity and the similarity between the two nodes. The number of potential future churners increases faster after the first period of the diffusion. This increase is more important in a network where affinities are represented, than in a random network. This means that connectivity plays an ambiguous role in the diffusion of churn influence. This result is consistent with the online social networks. When churn diffuses over a particular behavior group, there is a good probability that most actors will be exposed as churn easily expands in a close community than in a random network (Fig 5, and Fig. 6). Churners that belong to communities represent a risk to the network. The number of initial churners (SP), the probability of transmission (p) and the affinity shared by users all co-contribute to evaluate the true influence received by the future churners. Our proposed framework can be integrated in the overall hybrid churn prediction model which would combine DM and social network analysis for a better accuracy. This

methodology will also provide a better manoeuver on the time aspect for the implementation of retention campaigns.

Acknowledgements

This research was supported by the National Natural Science Foundation of China under Grant 71071066 and 71371081; and by the Social Science Foundation of Ministry of Education of China under the Grant 11YJA630098. This work was also supported by the Doctoral Fund of Ministry of Education of China (Grant No.20130142110044); and by the Technology Innovation Foundation of Innovation Institute of Huazhong University of Science and Technology (Grant No. CXY13Q033). The authors would also like to thank the Chinese Mobile Telecommunication Company which provided the dataset and Ms. Pinar Kisioglu for the provision of materials that we've used in another complementary study.

References

[1] Cheng, L. C., & Sun, L. M. Exploring consumer adoption of new services by analyzing the behavior of 3G subscribers: An empirical case study: *Electronic Commerce Research and Applications*, 11(2), 89-100. (2012).
[2] Hohwald, H., Frias-Martinez, E., & Oliver, N. User modeling for telecommunication applications: Experiences and practical implications: *User Modeling, Adaptation, and Personalization*, 327-338. (2010)
[3] Stroele, V., Zimbrão, G., & Souza, J. M. Modeling, mining and analysis of multi-relational scientific social network: *Journal of Universal Computer Science*, *28*(8). (2012).
[4] Qi, J., & Li, Y. A novel and convenient variable selection method for choosing effective input variables for telecommunication customer churn prediction model: *In Systems, Man and Cybernetics, 2009*. SMC 2009. IEEE International Conference on (pp. 3217-3222). IEEE. (2009, October)
[5] Peng, J., Quan, J., & Zhang, S. Mobile phone customer retention strategies and Chinese e-commerce: *Electronic Commerce Research and Applications*, 12(5), 321-327. (2013).
[6] Long, X., Yin, W., An, L., Ni, H., Huang, L., Luo, Q., & Chen, Y: Churn Analysis of Online Social Network Users Using Data Mining Techniques: In Proceedings of the International Multi-Conference of Engineers and Computer Scientists (Vol. 1). (2012).
[7] Datta, P., Masand, B., Mani, D. R., & Li, B: Automated cellular modeling and prediction on a large scale: *Artificial Intelligence Review*, 14(6), 485-502 (2001).
[8] Bin, L., Peiji, S., & Juan, L: Customer churn prediction based on the decision tree in personal handyphone system service: *Service Systems and Service Management,* 2007 International Conference on (pp. 1-5) IEEE. (2007, June).
[9] Dasgupta, K., Singh, R., Viswanathan, B., Chakraborty, D., Mukherjea, S., Nanavati, A. A., & Joshi, A: Social ties and their relevance to churn in mobile telecom networks. In Proceedings of the 11th international conference on extending database technology: *Advances in database technology* (pp. 668-677) (2008, March).
[10] Zhu, T., Wang, B., Wu, B., & Zhu, C: Role defining using behavior-based clustering in telecommunication network: *Expert Systems with Applications*, 38(4), 3902-3908 (2011).
[11] Richter, Y., Yom-Tov, E., & Slonim, N: Predicting Customer Churn in Mobile Networks through Analysis of Social Groups. In SDM (pp. 732-741). (2010, April)
[12] Gomez Rodriguez, M., Leskovec, J., & Krause, A: Inferring networks of diffusion and influence. In Proceedings of the 16th ACM SIGKDD international conference on Knowledge discovery and data mining (pp. 1019-1028). ACM (2010, July)
[13] Kempe, D., Kleinberg, J., & Tardos, É: Influential nodes in a diffusion model for social networks. In *Automata, languages and programming* (pp. 1127-1138). Springer Berlin Heidelberg. (2005)
[14] Phadke, C., Uzunalioglu, H., Mendiratta, V. B., Kushnir, D., & Doran, D. Prediction of Subscriber Churn Using Social Network Analysis. *Bell Labs Technical Journal*, *17*(4), 63-75. (2013)

Advanced Materials Research Vols. 989-994 (2014) pp 4205-4208
© (2014) Trans Tech Publications, Switzerland
doi:10.4028/www.scientific.net/AMR.989-994.4205

A Robust Image Preprocessing Algorithm for Face Recognition

Yan Wang[1, a], Zhaokui Li[1, b]

[1] Shenyang Aerospace University, School of Computer, Shenyang, China, 110136

[a] wy4615@sina.com, [b] lmy52wy@163.com

Keywords: Average gradient angle, image preprocessing, robust dissimilarity, face recognition.

Abstract. In order to obtain more robust face recognition results, the paper proposes an image preprocessing method based on average gradient angle (AGA). It is based on the fact that the central pixel and its neighbors are similar in the local window of an image. AGA firstly calculates the ratio between the relative intensity differences of a current pixel against its neighbors and the number of its neighbors, then employs the arctangent function on the ratio. The dimensionality of the AGA image is reduced by linear discriminant analysis to yield a low-dimensional feature vector. Experimental results show that the proposed method achieves more robust results in comparison with state-of-the-art methods in AR face database.

Introduction

Various methods have been proposed for facial feature extraction and classification, among which the representatives include subspace learning methods, local binary pattern (LBP) methods, Gabor feature based classification methods, preprocessing based approaches[1,2,3,4,5]. While most of these methods in controlled conditions has already achieved impressive performance over large-scale galleries, there still exist many challenges for face recognition in uncontrolled environments. This paper focuses mainly on the image preprocessing technology, and the issue of robustness to facial expression varying, lighting variations and partial occlusions. Zhang et al. develop a novel technique called Gradientfaces (GF) by extracting the illumination insensitive measure from the gradient domain. Wang et al. use a similar idea in the Self Quotient Image. Gross and Brajovic (GB) developed an anisotropic smoothing method that relies on the iterative estimation of a blurred version of the original image. More recently, Xiaoyang Tan and Bill Triggs (TT) present a simple and efficient preprocessing chain that eliminates most of the effects of changing illumination while still preserving the essential appearance details that are needed for recognition, and B. Wang et al. present a novel Illumination normalization technique called weberfaces(WF) by using weber's law. In order to get robustness to facial expression varying, lighting variations and partial occlusions, in this paper, we propose an image preprocessing method based on AGA. It is based on the fact that the central pixel and its neighbors are similar in the local window of an image. AGA firstly calculates the ratio between two terms: One is the relative intensity differences of a current pixel against its neighbors, the other is the number of its neighbors, then employs the arctangent function on the ratio. AGA captures the orientation information for each pixel of an image and finally generates an AGA image which achieves a more robust image dissimilarity between images. The dimensionality of the AGA image is reduced by linear discriminant analysis to yield a low-dimensional feature vector. Experimental results show that AGA achieves more robust results in comparison with state-of-the-art methods in AR face database.

Image preprocessing method based on AGA

Consider a set of images $\{\Gamma_i\}, \Gamma_i \in \Re^{h\times w}, i = 1,2...,n$. At each pixel location, we estimate its AGA. We denote by $\{\alpha_{st}\}, \alpha_{st} \in [0,255], s = 1,2,...,h; t = 1,2,...,w$ the pixel in the two-dimensional image Γ. We denote by $\{\Psi_i\}, \Psi_i \in \left(-\frac{\pi}{2}, \frac{\pi}{2}\right)^{h\times w}, i = 1,2...,n$ the set of gradient images, and by $\{\beta_{st}\}, \beta_{st} \in \left(-\frac{\pi}{2}, \frac{\pi}{2}\right), s = 1,2,...,h; t = 1,2,...,w$ the image local approximate gradient in the gradient image Ψ.

Definition 1. Neighbor pixels. We denote by $\Omega=\{b_1,b_2,...b_l\},l=\#(\Omega)$ the neighbor pixels of α. Ω is a collection of the pixels of the surrounding α in the two-dimensional image.

Definition 2. AGA. We denote by β the image average gradient angle of α. β reflects the average gradient angle between α in Ω. The formula is as follows:

$$\beta=\arctan\left(\frac{1}{l}\left(\sum_{m=1}^{l}b_m-\alpha\right)\right),\quad \Omega=\{b_1,b_2,...b_l\},l=\#(\Omega) \tag{1}$$

Expressed in Eq (1) is only an approximation of the average gradient angle. Substantially, it is reasonable to consider a gradient. Usually, the pixel values of the local region in the image tend to be relatively close. For dramatic change of the local area pixels, it often implies the emergence of contour. The contour may be the general contour of the image (such as the face, mouth, eyes, nose, etc.), and may also be caused by outlier pixel (such as sunglasses, scarf). Through the calculation of the gradient values, on the one hand the local image similarity is retained, on the other hand, the outline of the image information is also retained. In the following, we will compare the difference dissimilarity between the pixel intensity values and the local approximate gradient values by different distance metric. Let x_j be the *p*-dimensional column vector obtained by writing image Γ_j in lexicographic ordering. The same is to let y_j be the *p*-dimensional column vector obtained by writing image Ψ_j in lexicographic ordering. where the pixel values of the corresponding images Γ_j,Γ_q are represented in the range $[0,1]$. The local approximate gradient values of the corresponding images Ψ_j,Ψ_q are represented in the range $(-\pi/2,\pi/2)$.

Let us consider a motivating example in which different dissimilarity measures are applied to the images shown in Fig. 1. In Fig.1, the resolution of all images resolution is adjusted to 128×128 ,and the pixel neighbor layer is set to 2. As can be seen in Table 1, the pixel intensity values associates a smaller distance between the original image and an image from a different subject. The distance between the original and the same image with occlusion is larger. In contrast, the use of the AGA values results in a large distance between the original image and the image of a different person.

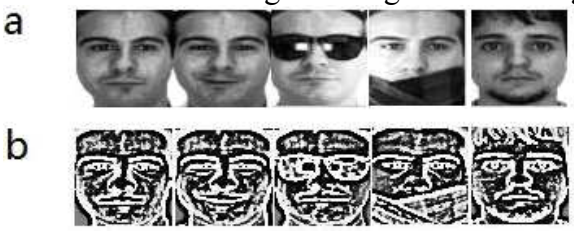

Fig. 1 Images used for the dissimilarity measurement. (a)Original images (b) AGA images. Each row from left to right in turn is the neural expression, smiling expression, occluded (sunglasses), occluded (scarves) and another person's neural expression.

Table 1 Dissimilarity comparison between neural image and the other images with different measures

	Euclidean		Cosine	
	Intensity	AGA	Intensity	AGA
Neural-Smile	0.14	1.02	0.09	0.55
Neural-Sunglasses	0.51	1.09	0.54	0.70
Neural-Scarves	0.39	1.14	0.78	0.62
Neural-Different person	0.32	**1.28**	0.39	**0.85**

Assume that we are given an images Γ ,we can obtain its AGA images Ψ by calculating AGA value. Let y be the p-dimensional column vector obtained by writing Ψ in lexicographic ordering. The dimensionality of the p-dimensional column vector is reduced by LDA to yield a low-dimensional feature vector.

Linear Discriminant Analysis

Linear Discriminant Analysis (LDA) searches for those vectors in the underlying space that best discriminate among classes (rather than those that best describe the data). More formally, given a number of independent features relative to which the data is described, LDA creates a linear combination of these which yields the largest mean differences between the desired classes. Mathematically speaking, for all the samples of all classes, we define two measures: 1) one is called within-class scatter matrix, as given by

$$S_w = \sum_{c=1}^{C} \sum_{h=1}^{l^c} (y_h^c - m^c)(y_h^c - m^c)^T \tag{2}$$

where y_h^c denotes the hth training sample in class c, l^c is the number of training samples in class c, m^c is the mean of the training samples in class c, and C is the number of class. 2) the other is called between-class scatter matrix

$$S_b = \sum_{c=1}^{C} l^c (m^c - m)(m^c - m)^T \tag{3}$$

where m represents the mean of all classes.

The goal is to maximize the between-class measure while minimizing the within-class measure. The discriminative projection basis W and eigenvalues Λ are obtained by solving the thin Linear Discriminant Analysis(LDA) eigendecomposition:

$$(S_w + \varepsilon I)^{-1} S_b W = W\Lambda \tag{4}$$

where ε is a small regularization constant (10^{-3} below) and I is the identity matrix. Thus, the original p-dimensional space is projected onto a final d-dimensional space using LDA.

Experiments

In this section we evaluate the robustness of our method for the application on face recognition. A publicly available face databases, namely, AR [6] is used for experimental evaluation. The AR database consists of more than 4,000 frontal view face images of 126 subjects. Each subject has up to 26 images taken in two sessions. The first session contains 13 images, numbered from 1 to 13, including different facial expressions(1-4), illumination changes (5-7), and different occlusions under different illumination changes (8-13). The second session duplicates the first session two weeks later. Fig. 2 shows a sample of images used in our experiments. For AR, we resize them to 128×128. To verify the effectiveness of the proposed method, in this series of experiments we evaluate the performance of the proposed method and compare it to that of several methods using the LDA and 1-NN classifier.

Fig. 2 Face images of the same subject taken from the AR database.

We investigate the robustness of our scheme for the case of facial expression varying, illumination variations, occlusions(sunglasses)-illumination changes, and occlusions(scarves)-illumination changes. Table2 provides the detailed information of each experiment. The best recognition rates are shown in Table 3. From Exp.1 to Exp.4, we use images 1-4 of session 1 for training. As our results show, AGA-LDA achieves better recognition rate compared with other methods. AGA-LDA achieves approximately 93.27% recognition rate for different expressions(Exp.1). For Exp.2, AGA-LDA achieves approximately 89.45% recognition rate for the case of illumination changes. For Exp.3 and

Exp.4, which are more difficult experiment on the AR database, AGA-LDA achieves approximately 68% recognition rate for the case of occlusions(sunglasses)-illumination changes, and achieves approximately 67.45% recognition rate for the case of occlusions(scarves)-illumination changes.

Table 2 The detailed information of different experiments

Exp.	Training Set (session 1)	Test Set (session 2)
Exp.1	1-4	1-4 expressions(neural, smile , anger and scream)
Exp.2	1-4	5-7 illumination variations
Exp.3	1-4	8-10 sunglasses-illumination
Exp.4	1-4	11-13 scarves-illumination

Table 3 Best recognition rate comparison on different experiments

Method	Exp.1	Exp.2	Exp.3	Exp.4
LDA	88%	51.33%	16%	34%
GF-LDA	88.25%	82%	39%	45.33
GB-LDA	61.5%	52.33%	20.33%	36.33%
MSR-LDA	71.75%	68.3%	12%	27%
TT-LDA	76.25%	73.67%	25.67%	50%
WF-LDA	68.5%	62.67%	31.67%	35.67%
AGA-LDA	**93.27%**	**89.45%**	**68%**	**67.45%**

Conclusions

In this paper, we propose an image preprocessing method based on AGA. AGA captures the average gradient angle for each pixel of an image and finally generates an AGA image which achieves a more robust image dissimilarity between images. The dimensionality of the AGA image is reduced by linear discriminant analysis to yield a low-dimensional feature vector. Our experiments show that the proposed method is robust.

Acknowledgements

This work has been partially supported by the National Natural Science Foundation of China under contract No. 61170185.

References

[1] T. Zhang, Y. Y. Tang, B. Fang, Z. Shang, and X. Liu,"Face recognition under varying illumination using gradientfaces,"IEEE Trans. Image Processing, correspondence, vol. 18, no. 11, pp. 2599-2606, 2009.

[2] H.Wang, S. Li, and Y.Wang, “Face recognition under varying lighting conditions using self quotient image,” in Proc. IEEE Int. Conf. Autom. Face Gesture Recognition, 2004, pp. 819–824.

[3] R. Gross and V. Brajovic, “An image preprocessing algorithm for illumination invariant face recognition,” in Proc. AVBPA, 2003, pp. 10–18.

[4] Xiaoyang Tan and Bill Triggs, "Enhanced Local Texture Feature Sets for Face Recognition Under Difficult Lighting Conditions," IEEE Trans. Pattern Anal. Mach. Intell., vol. 19, no. 6, pp.1635-1649,June 2010.

[5] B. Wang, W. Li, W. Yang, and Q. Liao, “Illumination normalization based on Weber’s law with application to face recognition,” IEEE Signal Process. Lett., vol. 18, no. 8, pp. 462–465, Aug. 2011.

[6] A.M. Martinez and R. Benavente, “The AR Face Database,” CVC technical report, 1998.

Advanced Materials Research Vols. 989-994 (2014) pp 4209-4212
© (2014) Trans Tech Publications, Switzerland
doi:10.4028/www.scientific.net/AMR.989-994.4209

Feature Representation Method Based on Kirsch Masks Filter for Face Recognition

Zhaokui Li [1, a], Yan Wang [1,b]

[1] Shenyang Aerospace University, School of Computer, Shenyang, China, 110136

[a] lmy52wy@163.com, [b] wy4615@sina.com

Keywords: Kirsch masks filter, direction image, decision level fusion, linear discriminant analysis, face recognition.

Abstract. In this paper, a feature representation method based on Kirsch masks filter for face recognition is proposed. We firstly obtain eight direction images by performing Kirsch masks filter. For each direction image, the low-dimensional feature vector is computed by Linear Discriminant Analysisis. Then, a fusion strategy is used to combine different direction image according to their respective salience. Experimental results show that our methods significantly outperform popular methods such as Gabor features, Local Binary Patterns, Regularized Robust Coding (RRC), and achieve state-of-the-art performance for difficult problems such as illumination and occlusion-robust face recognition.

Introduction

Face recognition (FR) has received a great deal of attention from the scientific and industrial communities over the last three decades due to its wide range of applications in entertainment, smart cards, information security, law enforcement, access control and video surveillance. Various methods have been proposed for facial feature extraction and classification, among which the representatives include subspace learning methods [1], [2], local binary pattern (LBP) methods [3], Gabor feature based classification methods [4], the recently developed sparse representation based methods [5], and the like. While most of these methods in controlled conditions has already achieved impressive performance over large-scale galleries, there still exist many challenges for face recognition in uncontrolled environments. In this paper, we propose a feature representation method based on Kirsch masks filter for face recognition(abbreviated as FRKMF). Given a face image, for each pixel we compute its eight direction information by performing Kirsch masks filter operator. We can obtain eight direction images. LDA is performed to extract the corresponding low-dimensional features. A fusion strategy is used to combine different images according to their respective salience. The experimental results show that the proposed method significantly improves recognition performance under partial occlusions, varying illuminations.

Kirsch Masks Filter

For an input image, we can calculate eight directional edge response value of a particular pixel using Kirsch masks in eight different orientations (M0~M7) centered on its own position. These masks are shown in the Fig. 1. Applying eight masks, we obtain eight edge response value m0, m1, …, m7, each representing the edge significance in its respective direction. The presence of corner or edge show high response values in particular directions. By performing Kirsch masks filter, an input image is decomposed into eight direction images.

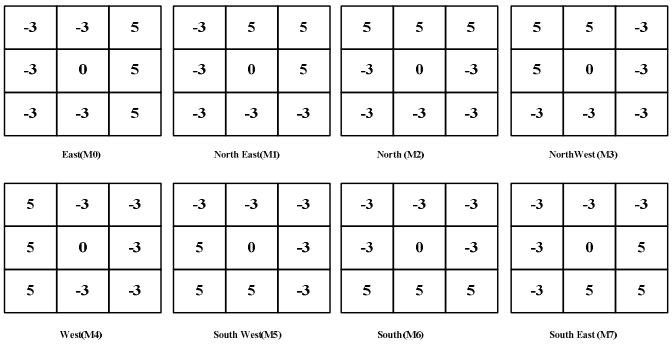

Fig. 1 Kirsch edge response masks in eight directions.

Linear Discriminant Analysis

Linear Discriminant Analysis (LDA) searches for those vectors in the underlying space that best discriminate among classes (rather than those that best describe the data). More formally, given a number of independent features relative to which the data is described, LDA creates a linear combination of these which yields the largest mean differences between the desired classes. Mathematically speaking, for all the samples of all classes, we define two measures: 1) one is called within-class scatter matrix, as given by

$$S_w = \sum_{c=1}^{C} \sum_{h=1}^{l^c} (\xi_h^{\ c} - m^c)(\xi_h^{\ c} - m^c)^T \tag{1}$$

where $\xi_h^{\ c}$ denotes the hth training sample in class c, l^c is the number of training samples in class c, m^c is the mean of the training samples in class c, and C is the number of class. 2) the other is called between-class scatter matrix

$$S_b = \sum_{c=1}^{C} l^c (m^c - m)(m^c - m)^T \tag{2}$$

where m represents the mean of all classes.

The goal is to maximize the between-class measure while minimizing the within-class measure. The discriminative projection basis W and eigenvalues Λ are obtained by solving the thin Linear Discriminant Analysis(LDA) eigendecomposition:

$$(S_w + \varepsilon I)^{-1} S_b W = W\Lambda \tag{3}$$

where ε is a small regularization constant (10^{-3} below) and I is the identity matrix. Thus, the original D-dimensional space is projected onto a final d-dimensional space using LDA.

Multiple Direction Images Fusion

Assume that we are given a sample $F \in \Re^{M \times N}$. We can obtain eight direction images Φ^s by performing Kirsch masks filter. Let x^s ($s = 1,..,8$) be the D-dimensional vector obtained by writing images Φ^s in lexicographic ordering. We can compute the average feature vector $\overline{y^{s,c}}$ of the cth person of the sth training sample set.

$$\overline{y^{s,c}} = \frac{1}{l^c} \sum_{j=1}^{l^c} W^T x_j^{s,c}, \quad c = 1,2,...C \tag{4}$$

where $x_j^{s,c}$ is jth training sample of the cth person of the sth training sample set. Then, we compute the average cosine distance $\overline{d^{s,c}}$ between $\overline{y^{s,c}}$ and $\overline{y^{s,j}}$ ($j = 1,2,...C$).

$$\overline{d^{s,c}} = \frac{1}{C}\sum_{j=1}^{C}\left(1 - \frac{(\overline{y^{s,c}})^T \overline{y^{s,j}}}{\left\|\overline{y^{s,c}}\right\|\left\|\overline{y^{s,j}}\right\|}\right) \tag{5}$$

For the *c*th person, we obtain s between-class distances which are sorted according to descending order. Each $\overline{d^{s,c}}$ characterizes the weighted coefficient of the *s*th gradient orientation feature of the *c*th person. Given a test image $F_{test} \in \Re^{M\times N}$, We can compute the corresponding eight orientation images Φ_{test}^{s}. Let x_{test}^{s} ($s = 1,..,8$) be the *D*-dimensional vector obtained by writing images Φ_{test}^{s} in lexicographic ordering. We can compute the *d*-dimensional vector $y_{test}^{s} = W^T x^s$ using LDA. The projected feature vectors y_{test}^{s} are classified using the nearest neighbor rule and the cosine "distance"

$$d^{s,c}(y_{test}^{s}, \overline{y^{s,c}}) = 1 - \frac{(y_{test}^{s})^T \overline{y^{s,c}}}{\left\|y_{test}^{s}\right\|\left\|\overline{y^{s,c}}\right\|} \tag{6}$$

When a face image is presented to the system, its eight direction images are computed, separately projected into their optimal discriminant spaces and used to compute the corresponding distance scores. Each score is normalized using the "*z-score*" method

$$z^{s,c} = \frac{d^{s,c} - \mu^{s,c}}{\sigma^{s,c}} \tag{7}$$

where $\mu^{s,c}$, $\sigma^{s,c}$ are, respectively, the mean and standard deviation of over the training set.

Finally, the eight scores are fused at the decision level. We fuse the eight similarity scores using the simple sum rule, and F_{test} is classified by solving the following optimization problem:

$$k = \arg\min_{c} \sum_{s=1}^{8} (\omega^{s,c}) z^{s,c} \tag{8}$$

where $\omega^{s,c}$ is the weighted coefficient ,and $\omega^{s,c} = \overline{d^{s,c}} \Big/ \sum_{s=1}^{8} \overline{d^{s,c}}$.

Experiments

The AR database [6] consists of more than 4,000 frontal view face images of 126 subjects. Each subject has up to 26 images taken in two sessions. The first session contains 13 images, numbered from 1 to 13, including different facial expressions (1-4), illumination changes (5-7), and different occlusions under different illumination changes (8-13). The second session duplicates the first session two weeks later. To verify the effectiveness of the proposed methods, in this series of experiments we evaluate the performance of the proposed methods and compare them to that of several methods using the simplest nearest neighbor (1-NN) classifier with the cosine distance. For LBP, the χ^2 histogram distance is used. In order to evaluate the performance of our algorithm for the case of synthetic occlusions. A series of similar experiments were also performed. In these experiments, all test images were artificially occluded by a "Dinosaur" patch at random position. We used "Dinosaur" patch of resolution 35×35. For all experiments, we used manually aligned cropped images of resolution 64×64. We carried out the following 3 experiments in AR database. In experiment 1, we used images 1-4 of session 1 for training and images 1-7 of session 2 for testing. In experiment 2, we performed a similar experiment with the experiment 1, and the only difference is that all test images were artificially occluded by a "Dinosaur" patch at random position. In experiment 3, we used images 1-4 of session 1 for training and images 8-13 of session 2 for testing. Fig. 2 shows a sample of images used in our experiments. Table 1 tabulates the best recognition rates of different methods about experiment 1,2 and 3. As shown in Table 1, the proposed FRKMF consistently outperform the other compared methods. As we can see, for the non-occluded facial experiment (experiment 1), FRKMF performed the best. For experiment 2 and 3, which are the most difficult experiments on the AR database, FRKMF largely outperformed all other methods. More specifically, the gain in recognition accuracy goes up to 5.58 and 7 percent on artificial occlusions and original occlusions. In contrast to experiments 1, these results are statistically significant.

Fig. 2 Face images of the same subject taken from the AR database.

Table 1 Recognition Rates on the AR Database for Experiment 1, Experiment 2, and Experiment 3

Methods	**Exper.1**	**Exper.2**	**Exper.3**
PCA	54.86%	25.85%	14.17%
LDA	69.57%	21.00%	25.83%
Gabor-PCA	66.43%	43.00%	14.83%
Gabor-LDA	86.14%	22.57%	45.67%
LBP-8	95.14%	84.71%	78.00%
RRC-L_1	75.57%	58.57%	39.5%
FRKMF	**96%**	**90.29%**	**85%**

Conclusions

We propose a feature representation method based on Kirsch masks filter for face recognition. Given a face image, we firstly compute its eight direction images by performing Kirsch masks filter operator. For each direction image, the low-dimensional feature vector is computed by Linear Discriminant Analysisis. Then, a fusion strategy is used to combine different direction image according to their respective salience. The experimental results show that the proposed method significantly improves recognition performance under partial occlusions, varying illuminations.

Acknowledgements

This work has been partially supported by the National Natural Science Foundation of China under contract No. 61170185.

References

[1] M. Turk and A. Pentland, ”Eigenfaces for Recognition, ” J. Cognitive Neuroscience, vol.3, no.1, pp.71-86, 1991.

[2] P.N. Belhumeur, J.P. Hespanha, and D.J. Kriegman, ”Eigenfaces vs. Fisherfaces: Recognition Using Class Specific Linear Projection,” IEEE Trans. Pattern Analysis and Machine Intelligences, vol.19, no.7, pp.711-720, July 1997.

[3] T. Ahonen, A. Hadid, and M. Pietikainen, ” Face Description with Local Binary Patterns: Application to Face Recognition, ” IEEE Trans. Pattern Analysis and Machine Intelligence,vol.28, no.12, pp.:2037-2041, December 2006

[4] L. Chengjun, ”Gabor-Based Kernel PCA with Fractional Power Polynomial Models for Face Recognition, ” IEEE Trans. Pattern Analysis and Machine Intelligence, vol.26, no.5, pp.572-581, May 2004.

[5] M. Yang, L. Zhang, J. Yang and D. Zhang, ”Regularized Robust Coding for Face Recognition, ” IEEE Trans. on Image Processing, vol.22, no.5, pp.1753-1766, 2013.

[6] A.M. Martinez and R. Benavente, ”The AR Face Database, ” CVC technical report, 1998.

CHAPTER 8:

General Principles of Information Technology, WEB and Networks Engineering, Information Security, E-Engineering, Software Application and Development

Advanced Materials Research Vols. 989-994 (2014) pp 4215-4218
© (2014) Trans Tech Publications, Switzerland
doi:10.4028/www.scientific.net/AMR.989-994.4215

Research to household sub- network development based on Bluetooth control technology

QIAN Long[1, a]

[1] School of international education, Wuhan University of Technology, Wuhan 430070, China

[a] QianLong@yeah.net

Key words: household sub- network; Bluetooth control technology; embedded; universal device control protocol

Abstract. With the development of household appliances, the short of communication among them is more and more becoming a problem. At present there is no central point of control among the traditional home appliances, and we cannot access them through Internet. To solve these issues, home network is proposed to connect all the appliances, home PC and portable devices together using network technology. Controlling all the appliances through one single node(the home network gateway), home network makes life much simpler and convenient. There are several local area network technologies applicable to home network. Bluetooth technology is chosen in this paper as the home networking technology due to its many advantages over others. The implementation scheme of home control sub- network based on Bluetooth serial part profile(SPP) and the standards of Home Network Platform in China is proposed. According to actual application fields, the communication protocol architecture for this scheme is established by using appliance control protocol promoted by the manufacturers and universal device control protocol(UDCP) over SPP. Many management functions of appliance terminals are realized such as appending, login, operation, logout and alarming. Implementation methods of appliance terminal based on an entirely embedded single- chip manner and mobile control terminal which is realized by computer simulation are proposed. Analysis and solution of baud rate error brought by inaccurate crystal frequencies are presented. Further discussion about applying ad hoc technology to home control sub- network is carried out.

Bluetooth

Bluetooth is a wireless technology standard for exchanging data over short distances(using short wavelength UHF radio waves in the ISM band from 2. 4 to 2. 485 GHz) from fixed and mobile devices, and building personal area networks. Invented by telecom vendor Ericsson in 1994, it was originally conceived as a wireless alternative to RS- 232 data cables. It can connect several devices, overcoming problems of synchronization.

Bluetooth is managed by the Bluetooth Special Interest Group(SIG), which has more than 19,000 member companies in the areas of telecommunication, computing, networking, and consumer electronics. Bluetooth was standardized as IEEE 802. 15. 1, but the standard is no longer maintained. The SIG oversees the development of the specification, manages the qualification program, and protects the trademarks. To be marked as a Bluetooth device, it must be qualified to standards defined by the SIG. A network of patents is required to implement the technology, which is licensed only for that qualifying device.

The use of Bluetooth

Bluetooth is a standard wire- replacement communications protocol primarily designed for low consumption, with a short range based on low- cost transceiver microchips in each device. Because the devices use a radio(broadcast) communication systems, they do not have to be in visual line of sight of each other, however a quasi optical wireless path must be viable. Range is power- class-dependent, but effective ranges vary in practice; see the table on the right.

The effective range varies due to propagation conditions, material coverage, production sample variations, antenna configurations and battery conditions. Most Bluetooth applications are in indoor conditions, where attenuation of walls and signal fading due to signal reflections will cause the range to be far lower than the specified line- of- sight ranges of the Bluetooth products. Most Bluetooth applications are battery powered Class 2 devices tends to set the range limit. In some cases the effective range of the data link can be extended when a Class 2 devices is connecting to a Class 1 transceiver with both higher sensitivity and transmission power than a typical Class 2 device. Mostly however the Class 1 devices have a similar sensitivity to Class 2 devices. Connecting two Class 1 devices with both high sensitivity and high power can allow ranges far in excess of the typical 100m, depending on the throughput required by the application. Some such devices allow open field ranges of up to 1 km and beyond between two similar devices without exceeding legal emission limits.

While the Bluetooth Core Specification does mandate minima for range, the range of the technology is application specific and is not limited. Manufacturers may tune their implementations to the range needed for individual use cases.

class	Max. permitted power		Typ. Range
	(mW)	(dBm)	(m)
1	100	20	~100
2	2.5	4	~10
3	1	0	~1

Version	Data rate	Max. application throughput
1.2	1 Mbit/ s	>80 kbit/ s
2.0 + EDR	3 Mbit/ s	>80 kbit/ s
3.0 +HS	24 Mbit/ s	See Version 3.0 + HS
4.0	24 Mbit/ s	See Version 4.0 LE

As a new idea, family network that represents family informatization has already obtained more and more attention by people. Generally speaking, family network is a combination which contains processing, governing, transmitting and storing the information that have the capability to connect and integrate so many devices in one' s family, like calculating, controlling, guarding and communicating. After that, household sub- network is in charge of controlling and governing with the relevant network parts like the family appliance, the energy resources and the security. Because Bluetooth technology has a lot of advantages like lower prime cost, lower consumption, better security, superior transmitting function and flexible network form, it has already become one of the most important wireless technology part to fulfill the family network.

The structure of family network

According to two different types, physical transmitting medium and bottom protocol, when connect devices or gateways, family network can be divided into two different network parts, one is the major family network, the other is household sub- network.

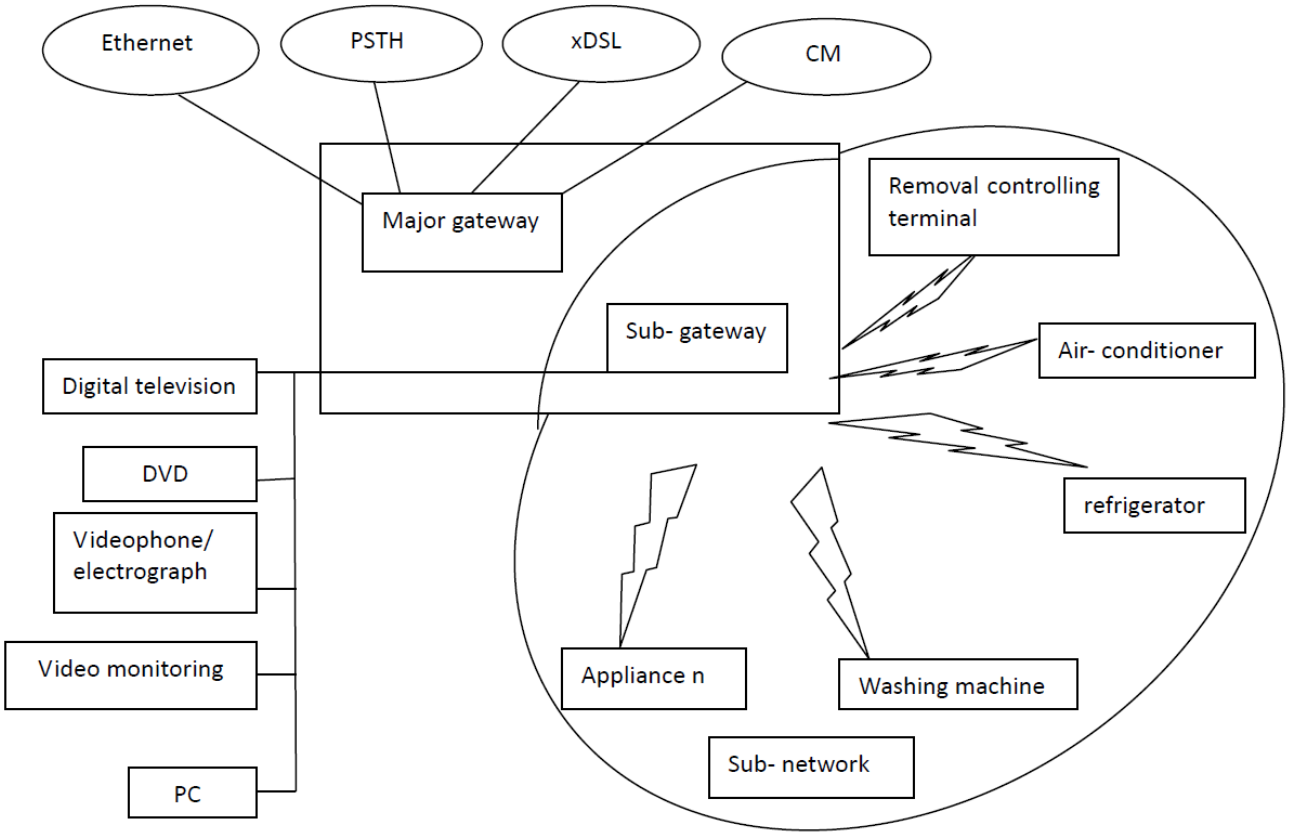

Figure 1. The structure of family network

The major family network is a network part which has the fast information transmitting rate device, including information device, amusement device, communication device, the major family network gateway(major gateway), household sub- network gateway(sub- gateway), etc. Its main function includes providing the communication with all the public network, family intelligent governing and family electrical amusement. The major gateway is a kind of gateway device in the major family network, it can accomplish the communication with the high speed information transmitting device in family network, provide the exterior network joggle to all kinds of insert devices, and as a servicer to be interviewed by the interior devices and exterior network in the meantime. However, household sub- network includes some lower speed devices network parts, like subsidiary gateway, removal controlling terminal, three expression and three prevention devices, information appliance, etc. The subsidiary gateway can accomplish the communication with household controlling sub- network and provide the major network joggle for all kinds of insert devices.

The accomplishment of household controlling sub- network hardware

Household controlling sub- network is composed of three logic substances by subsidiary gateway, removal controlling terminal and IA.

Removal controlling terminal adopts the scheme of flushbonading single chip, connecting with RS232 joggle and Bluetooth module by PC. IAC Application, working on PC, provide the user interface and accomplish UDCP(universal device control protocol), and fulfill the data communication with users and all kinds of sub- network devices by the flushbonading program of Bluetooth receive and dispatch module. Appliance controlling circuit, centralized controlling center, commonly provides by the appliance factories and makes of a mini- processor and a series of number, analogous circuit, in charge of collecting appliance' s all kinds of controlling process and data, and by universal asynchronous receiver transmitter to communicate with Bluetooth receive and dispatch module with 19.2 kbit/ s. Their communication obey the family controlling protocol.

The use of UART joggle completely obey this lower speed scene and allow the appliance manufacturer to use low side mini- processor to reduce prime cost in the process of appliance controlling circuit. Appliance controlling circuit supply electricity together by the source unit of Bluetooth receive and dispatch module. BlueCore2- Exernal cover with 8 MB Flash which consists of the smallest Bluetooth system of the complete flushbonading single chip scheme design. In the process of the actual research, we found that it must pledge both sides to have certain timing precision by using UART joggle to achieve the communication with the appliance controlling circuit and Bluetooth receive and dispatch module. Because the accumulation of timing plus- minus deviation will probably be defeated of serial communication. In general, calculating Baud rate use this formula:

$$B = \frac{f_{osc}}{kN}$$

f is the frequency of crystal oscillator; N is the factor of integer frequency division; k is the times of collecting one information code.

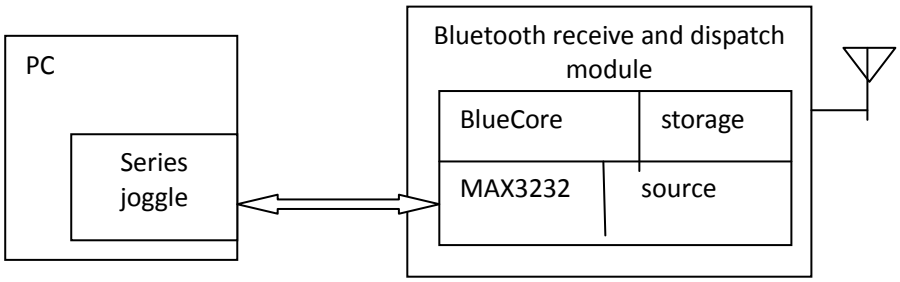

Figure 2. Removal controlling terminal

Conclusion

To use Bluetooth wireless technology, a device has to be able to interpret certain Bluetooth profiles, which are definitions of possible applications and specify general behaviors that Bluetooth enabled devices use to communicate with other Bluetooth devices. These profiles include settings to parameterize and to control the communication from start. Adherence to profiles saves the time for transmitting the parameters a new before the bi- directional link becomes effective. There are a wide range of Bluetooth profiles that describe many different types of applications or use cases for devices.

Reference

[1]. Bluetooth, Wikipedia

[2]. Yuan yuheng, Ye Zhihui, Shen Lianfeng, Design and development of home control sub-network base on Bluetooth, National Mobile Communication Research Laboratory, Southeast University, Nanjing 210096.

[3]. Cambridge Silicon Radio Limited. BlueCore2- External Product Data Sheet, 2003- 03- 28.

Advanced Materials Research Vols. 989-994 (2014) pp 4219-4222
© (2014) Trans Tech Publications, Switzerland
doi:10.4028/www.scientific.net/AMR.989-994.4219

The archives management in the environment of office automation

Hanqing Zhou[1, a], Ling Huang[2, b]

[1] Archives, Jiangxi Science & Technology Normal University, Nanchang, China

[2] Basic Teaching Department, Jiangxi College of Foreign Studies, Nanchang, China

[a]zhouhq123456789@163.com；[b]huangling0828@163.com

Keywords: document, archives management, office automation

Abstract. History archives, an important part of archives, records the historical process of social development and objectively reflects the process and outcome of problem-handling, decision-making, construction, research and development. With the development of reform, how to improve the management level of archives to provide the file information timely, accurately and completely to meet the demand and adapt to the new situation of development is a new topic in the archives work. The paper introduces advantages and problem brought by archives management in the environment of office automation, as well as suggestions to develop archives management.

Introduction

History archives, an important part of archives, records the historical process of social development and objectively reflects the process and outcome of problem-handling, decision-making, construction, research and development. With the development of reform, how to improve the management level of archives to provide the file information timely, accurately and completely to meet the demand and adapt to the new situation of development is a new topic in the archives work. Thus automation of files management opens a new chapter for archives work.

Advantages of office automation for archives management

Efficient and convenient filing rate. Powerful information processing ability is the biggest advantage given by computer to office automation. The archives management in the environment of office automation is fully integrated with information technology, maximizes the cumbersome procedures of traditional paper files to a minimum, and does related work of archiving. These advantages can effectively guarantee resource better utilized.

Comprehensively and efficiently realize the sharing of resources. Records management in the environment of office automation can give full play to the role of information technology, effectively implement the system of file management, and realize the resource sharing, reading and searching conveniently and quickly. At the same time, the promotion of the network and information transmission technology make the electronic archives management search, classify, arrange, optimize and filter according to different circumstances, which is conducive to strengthen the archives management and play the role of those advantages, such as high transmission speed, strong use ability and large amount of information. It is also able to share resources. Especially in government organs and institutions, the utilization of information is more comprehensive and efficient.

Storage is more stable. Compared with paper archives, electronic archives can make full use of modern science and technology to store and transmit, such as DVD disk, U disk, mobile hard disk, memory card, and so on. These equipments' advantage is not easy to be affected by object environment, but also has the characteristics of long-time storage, a large amount of information, strong stability. Transferring document resources directly through the network tool make the stability and safety of documents greatly improved.

Archives management in the environment of office automation is simpler. The traditional archival management has a complicated process, from the document information collection, classification, sorting, filing to the end. Each step not only needs a lot of manpower, material resources, but also is easy to make mistake. But in the environment of office automation, the assistance of computer make the complicated work simple and the operation not need too much time and energy, but also improve the quality of document and reduce the time and space.

The main problems existing in office automation of archives management

The security of electronic document becomes vulnerable. The biggest difference between electronic culture and paper file is that electronic culture has no fixed form and is easy to change, without traces even after being modified. However, once paper file is modified, the traces are obvious. Therefore, the confidentiality of electronic documents is not good as paper documents. Because electronic document make some file with high confidentiality become weaker, this is not conductive to safety management of file information. At present, although some related technology can prevent others increase, delete, or change the original forgery, but can not effectively identify original document. Paper draft can pass through the seal or signature. These are severe test electronic culture suffered in security aspect. In anther word, electronic culture's security exist hidden risk.

The quality of archives managers is high. The application of office automation system in archives management needs to strengthen archives personnel's quality. The theory, method and technology related to archive management is not enough, excellent computer technology is necessary. So archives management personnel not only need to reach a certain level of knowledge, but also need to master modern high technology and ability to handle related issues. At present, most archives management personnel are deficient in technology, related theoretical knowledge, and initiative in the use of office automation equipment, which is not conductive to the electronization of archives management.

The network environment of the document information exist security risks. Because the document generates in the computer, transmits and processes through the network, it is vulnerable to multiple threats from the computer and network. On one hand, illegal access on the internet is unquantifiable, the firewall is impossible to guard against the hacker master; on the other hand, internal personnel often unauthorized spread out data of document information management system through the USB flash drive, WIFI tuning demodulator, a smart phone, Bluetooth adapter, digital music player, infrared transmission, e-mail, FTP and other ways. In bad network environment attacked by both inside and outside, the document information cannot insulate itself, and document management always face security risks.

Authenticity identification and maintenance of document information become more difficult. The essential attribute of archives is the original record of the carrier, while the carrier of paper document is inseparable with the external characteristic recorded, such as handwriting, signature, and seal and so on. Electronic document is restricted in confidentiality. Due to the characteristics of electronic documents, electronic files are not only easy to be modified and without any traces, but also can be transferred and replicated between different computers and carrier. Although some technology can prevent electronic file to be increased, cut or copied in the manuscript, the content is more possible to change than paper document. People can not tell the original from the handwriting, and seal or signature for each document, so they cannot determine what is the original electronic document from seal or signature. All the problems above are severe test of authenticity, reliability, confidentiality of electronic documents.

Suggestions can be adopted on file management in the environment of office automation

Improve the comprehensive quality of archives managers. Firstly, start from hardware construction and input to continuously improve the hard environment and the business skills of personnel files. Only increasing modernization hardware facilities, can archives personnel recognize

these devices, learn to enhance the business skills, and improve the management level. Second, the mode of "self-study, training supplemented" gradually form lifelong education mechanism and guarantee the quality of archivists changed with the times. Getting knowledge by constantly study is the fundamental way to improve the quality, so set up the incentive mechanism of the unit personnel files and consider the file service learning as a part of performance evaluation. Third, strengthen cooperation between archives departments to expand communication itself. Through the exchange, learn successful experience and methods of brother units, use the network and modern communication to expand file management information source and innovative thinking.

Make efforts to solve standardization problem of electronic archives management. The appearance of office automation, paperless and other things bring great changes in the formation of archives, such as document issued, reminders, filing and other process are carried out in computer and communication line. So archives must be readable file and their management mode has big difference with paper carrier archives. This change indicates that file worker will face more machine-readable form files. Setting normative, open, service, sharing file management system and standardization of basic business is a necessary prerequisite for electronic document management.

Set up unified standard. To do the archival filing management in office automation environment, we must proceed from the following aspects. First, set up standard system of document management. At present, records management and archives management of many units are separated and belong to different management departments. Archives department are often difficult to carry out early control, which accidentally become "ultra vires". Therefore, it must be regulated from the management system, and implemented unified leadership and planning in document management and archives management in the unit. File management-guidance and control should be took into the responsibilities of archives departments, which can ensure that the file forming, processing, archiving management, consult and other aspects are carried out under the supervision of archives departments. In system design, use the software system with strong compatibility and good application performance; regulate the related technical parameters and technical standards, including the standard of data interface, data security standard and different types of data transformation standard, which can ensure different types of sub files smoothly circulate and safely manage from office automation system to archives management system.

Formulate the corresponding file management law. The automation of archives management process is more and more quickly and also the general trend of archives management in the future. The advantage of managing archives through computer is very obvious. Compared to the old paper records, electronic files have great potential of development. The managers should be active to solve the corresponding constraints, because our country is ruled by law and everything should be carried out in accordance with the relevant legal provision, but also for the future of the archives management. The electronic archives can be modified easily and difficulty to be found, so the relevant departments should formulate corresponding laws to regulate these behaviors. Only the legal norms all details of electronic archives management, electronic archives can develop better. In addition, the corresponding penalties should be set up to the personnel violating the law. Then the related laws should be resolutely implemented. Electronic archives law should conform to the national idea of the rule of law, which has a very important value for the development of electronic files management.

Conclusion

In short, in order to better carry out the archives management in the environment of office automation, we must change the thought, use scientific minds to improve the level of management, keep pace with the times, and constantly put new technology in archives management. At the same time, we should adopt a variety of ways to overcome the drawbacks brought by office automation, which can improve the utilization rate of documents and serve better for daily work and management decision-making layer.

References

[1]Ninghong Zhang. The applicaton of office automation on the management of archives[J]. Archives of Heilongjiang, 2011(10).

[2]Wenshan Chen. The integration of archives management and office automation[J]. Information and Computer(theory edition), 2012(1).

[3]Weiyan Ren. The application of office automation in the documents and archives[J]. Heilongjiang History, 2010(7).

[4]Wei Chen. How to do archives management in new period[J]. Office Business, 2012(5).

[5]Ying Tang. On the application of office automation in archives management[J]. Technology Wind, 2010(24).

Advanced Materials Research Vols. 989-994 (2014) pp 4223-4225
© (2014) Trans Tech Publications, Switzerland
doi:10.4028/www.scientific.net/AMR.989-994.4223

Analysis of application of digital media arts

Sen Nie[1, a], Yan Liu[2,b]

[1] Department of Media and Art Jilin Business and Technology College Changchun, China.

[2] Department of Hand Surgery The China-Japan United Hospital of Jilin University Changchun,China.

[a]e-mail: 49006309@qq.com [b]e-mail:yayouliuyan@163.com

Key word: Digital Media Arts;disputed;development;application ;effect

Abstract. In 21st century, with the leaping advances in science and technology, computers and the rapid development of science and technology industry, formed by combining human intelligence and high-tech digital content industry that corresponds to the rapid development, and developing at an astonishing speed into a pillar industry of the knowledge economy in the new century. It is well known that digital media are based on digitized text, sound, images, Graphics, animation and video images as information carriers, through means of dissemination and development of science and technology. Basic characteristics of digital media arts: Cross uses online media which contains computer-animated production, the television advertising shoot, digital music player, there are activities such as online games, virtual reality, network, performance art, video, interactive installations and DV (digital video). This paper discusses the present status of digital media art, features, applications in education, vocational orientation and analysis of the development trend.

The rapid development of science and technology promote the application and development of digital media. Humans to combine high-end network technology and digital communications technologies effectively, gradually replacing traditional radio, television, film, and quickly towards the development of digital audio, video and film industries. Therefore, computer animation, virtual reality, digital industry information industry constitutes a new world, new digital media, and gradually developed into a huge industrial chain and ultimately progressive digital media arts industry occupies a pivotal position in knowledge economy.

An Overview of Digital Media Arts

Throughout recent years, digital media arts in a swift development in the era of knowledge economy. Digital media art concepts into people's hearts, we disagree, but for the most part the understanding is the same. Simply put, digital media creation and formation process of art is art. It depends on the development of computer technology and existing scientific research achievements in the field of information, images, artistic process them, to spread use of modern media, creating a digital media art. And other arts Compared to digital media art unique is its form of expression and artistic creation, in whole or in part based on digital technology. Produced by digital media or digital art design or Visual Arts are one of its manifestations. For now, vibrant digital media art is the art design and development potential of art. With the development of society and technology, digital media technology will render more unique and attractive to everyone.

Applied to Features of Digital Media Art

2.1 creation of digital media arts

Creation of digital media art not blindly rely on exclusive old crafts techniques, but use digital platforms to create unique and self-contained works of art. It's digital art works enable the audience to get involved and into the role 。 Interactions can subvert the role of public participation, public works not only effect change and have an opportunity to become part of the work.

2.2 performance characteristics of digital media art

Digital media art can be a simple split into "digital" and "digital art". Application of existing digital and computer technology can be understood as "digital". "Digital art" through "digital" works they create. The "media" is one of the digital art media.

Digital Media Arts Employment Orientation and Development Trend

3.1 employment development of digital media technology

Digital media art talent cultivation direction of talents of both technology and art, technology and art in digital media arts and complementary. Traditional education lacked both technology and art in digital media talent and training of such personnel in line with demand from emerging markets, their career major TV stations, film and television animation producers at all levels, Art, digital media and advertising company corporate image planning, exhibit design firms, branching, multimedia and Web design, interior design, product design and other popular industry. Exposure to developments in the field of digital media art is a wise choice, because it hides the huge potential for development. Digital Media Arts undergraduate approval formally adopted at the end of 2002 the Ministry of education, become subject to a new direction for the development of Arts and culture. After approval by, Tsinghua University, Beijing University, Zhejiang University, Guangdong University of technology and other colleges and universities started adding digital media art-related professions, to meet market demand. According to who statistics reveal that China's annual Digital Arts talent gap is 150,000. TV cartoon industry will see an annual market of 20 billion yuan. Broad markets and demand for multimedia industry evolved into huge economic industry 。 Some experts pointed out that, along with the development of science and technology, and also gradually raise the public requirements for Visual beauty.

3.2 industrial background of digital media arts

United Kingdom in developed countries, for example, in 2000 alone, the digital technology industry (including digital content) of annual output value of more than NT $ 60 billion pounds, while export value far more than £ 8 billion. Digital technology industry employs a total of approximately 1.95 million people, account for one third of GDP 7.9%. Data indicate that the digital technology industry is the United Kingdom's largest industry. United States, as the world's only superpower, to films and computer software as the main industries of digital technology, an annual turnover of more than $ 400 billion, 4% per cent of GDP. Even more striking is the digital technology industry (media art, video games, anime cartoons, and so on) in Japan's output more than twice times the GDP of this steel industry output in Japan of the digital technology industry has become the second largest industry after the auto industry. According to relevant statistics show that up to now, work directly with digital art with computers of nearly 100,000 people. In addition, more than 300,000 people a year receive digital industry related vocational skills training. Korea's digital technology industry with game industry is particularly famous, and has jumped among Korea's largest industry, even the car industry has followed. Digital technology industry's development in China is quite optimistic, and online games in this sector is particularly prominent. According to the international data Corporation (IDC) concluded that China's online game market compared with 2002, 2003 online game of rapid advancement of market development, reached 3.91 billion production value reached 1.32 billion RMB,2004 year RMBB net rose 2.59 billion RMB from 2003 to 2004, production value has quadrupled over b which data indicate that China's online game market potential, hides enormous business opportunities. In terms of animation, the Expert predicts: China's cartoon industry has a huge market, the output value is expected to reach 20 billion yuan. Merely developed cities in China, such as Shanghai, Beijing and Guangzhou youth anime consumption will reach 1.3 billion yuan. Consumers aged between 13 to 30 years of age. In addition, the animation industry could promote the development of industries associated with it, such as stationery, children's food, children's clothing, children's audio and various children's publications. The annual output value of the industry total was 205 billion yuan. The output was brought about by the animation industry, is a considerable income.

3.3 development of digital media arts

New aesthetics of digital media art features is its breaking into difficult and mysterious one thing everyone can accept and understand what forms of artistic expression, giving a visual feast. Digital media art art combines elements of science and scientific elements on a simple way of deciphering appeals to many people. Works downtown and brilliant, amazing and beautiful, is for digital media art through computers programmed to automatic interpretation and understanding. Both the art form and the content on your computer they all have the same sex. In the field of art, the development of digital media art is revolutionary in the field of subversion, with milestone significance. Different art information conversion can be achieved and everyone will enjoy the extraordinary Visual effects and artistic vision.

Digital media art with a triangular prism have striking similarities. Prism from different angles to the observer, which correspond to refracted rays are also different. Digital media art as well. Digital media art as a new art form, relies on digital technology and modern media technology, human rational thinking and perceptual thinking of art as one, given as a new and unique. It consist of art, science and technology layer, the media layer, the application layer overlapping compositions, includes a wide range of commercial design and popular art. Digital media authoring tool works of digital works interactive, polymorphism, and breadth of subject characteristics. Is rendered as: was the creation by all art forms (synthesis of art, video art, net art, etc) with a combination of computer technology, the Internet as a dissemination medium, the final step is combined with intelligent software, final artwork. Technological progress and innovation will be the concept of promoting the power of digital media art development, digital media and creative industries and information design is the art of the mainstream development, leading the artistic innovation of digital media art to the more extraordinary unique and wider, broader horizons of thought.

Conclusion

Derived from review on, development on both the means of digital media technology, transmission and dissemination of space provides a broader space for artistic creation. Digital media art will accompany humanity into "being digital" era gradually become the most representative form of art. Prospects for the development of digital media technologies will be invaluable. Based on this situation, productivity in the age of new media and digital information technology and penetration of digital media art have a growing impact on the development, so that the traditional art and traditional art and aesthetics of digital media more closely.

References

[1]Li Sida. Theoretical research of digital media arts[J].，2006（3）.

[2]Li Sida. image-----After the image age of new media art exploration, digital media and Contemporary Art[J].,2007（4）.

[3]Gui Yuhui. Development of digital art design facing the new century[J].Journal of Wuhan University (engineering),2003,36(2).

[4]Xiao Yongliang. The education of digital media art[A].The second session of national digital art education and Cooperation Symposium[C].2006

[5]Li Xueming. Location of digital media arts from information communication to digital content[J].Chinese employment of College Students,2007(22).

Advanced Materials Research Vols. 989-994 (2014) pp 4226-4228
© (2014) Trans Tech Publications, Switzerland
doi:10.4028/www.scientific.net/AMR.989-994.4226

Discussion on the digital cinema technology and its development trends

Sen Nie[1, a], Yan Liu[2,b]

[1] Department of Media and Art Jilin Business and Technology College Changchun, China.

[2] Department of Hand Surgery The China-Japan United Hospital of Jilin University Changchun,China.

[a]e-mail: 49006309@qq.com [b]e-mail:yayouliuyan@163.com

Keyword: The film; digital technology; development trend

Abstract. With the rapid development of modern science and technology, the development of digital movie is increasingly fast, digital film technology has gradually become the mainstream trend in the development of film technology.And its significance for regulating the film industry and promoting the sustainable development of the film industry is very important.The standards of digital cinema technology and traditional film technology are different, and grasp the full digital film technology standards, to fully improve on it and in the practice of the implementation is very important for the development of digital film. Therefore, we must attach great importance to the digital film technology, to enhance the capability of independent innovation of our country, and constantly improve after repeated practice, make contribution to the promotion of China's movie industry prosperity

One, foreword

The development of science and technology makes digital and film industry more quickly, the digital process of the film industry is irreversible, digital film technology thanks to the development of information technology and the rapid development of modern high-tech industry, which is leading the current society in many industries in a huge change. Digital technology, network technology and information technology deeply reflect the connotation of this change. As an important part of cultural industry, in the promotion of digital technology, the film industry has also launched a digital revolution in the global range, film of past is gradually began to change and the change was very rapidly. At present, the worldwide digital building of traditional film cinemas is faster and faster, after years of exploration and development, digital film technology in equipment, specifications, technical standards, the market management is more perfect.We can foresee, digital film technology in the near future will replace the traditional film and become the mainstream of modern film industry.

Two, digital film technology overview

Digital film technology standard ranges wider, it includes many aspects of filming, post production, data transmission, film screenings, safety management and other aspects. In order to have a better understanding of digital cinema technology standard, we must first fully understand the basic process of digital cinema system processes, drawings for digital cinema system, from the figure we can clearly see that, digital cinema system is fundamentally a typical multimedia information communication system, this system not only has the characteristics of multimedia information communication system, also has the movie's own characteristics, the basic process of the system is composed of a receiver, digital program source program and program transmission and digital cinema program receiving, storing and showing the program consists of four aspects.

Receiving the so-called digital program source usually covers photography, film digital program to digital, computer processing these three kinds of means; then the digital program post processing, there are usually nonlinear editing, color correction, subtitle synthesis and effects processing and other aspects. At present, a digital intermediate (Digital Intermediate) technology is gradually being used in digital film processing process; after the digital movie DCDM arises, digital cinema parent

version (Digital Cinema Distribution Master) is the non compressed picture, sound and letter data., it must formate Digital Cinema Package by JPEG2000 image compression,AES data encryption, MXF/XML package. AES data encryption technology (Advanced Encryption Package) is the advanced encryption standard, MXF are an emerging media formats (Material Exchange Format) represents the material exchange format, XML (Extensible Markup Language) Extensible Markup Language. DCP (Digitally Controlled Potentiometers) can be transferred via satellite, hard drive and optical fiber channel to digital cinema, when digital programming is transmitted to movie theaters, the first step will be stored, and then by playing a server solution for packaging, data decryption as well as processes such as image compression processing, after which you can use with digital projectors and other equipment for the audience playing digital movies. This entire process can be referred to collectively as digital film technology.

Three, the development trend of digital film technology

First of all, construction of digital cinema will be broadcast from a single digital storage devices into technology and equipment, management and services in one integrated solution. With the development of digital film technology, converging trends are bound to have a profound effect on digital cinema system as a whole, thereby allowing digital cinema with a deep and rich connotation, is a more accurate concept, with more robust capabilities. Digital cinema is not just for the future of digitizing broadcast system upgrades, but the entire upgrade digital theater systems, namely digital film programs are provided for digital cinema sets receive digital broadcast, digital storage, as well as services such as operations management, content of an integrated total solution. In order to adapt to this shift, the digital cinema should be the focus of future development and reform trend from digital theater systems and related equipment to the transformation of information management services. Construction and development of digital cinema will broadcast equipment from the past provide only a movie store provides a high quality service system and standard system changes, which includes storage and viewing of digital programming, broadcast quality, TMS digital cinema (Theater Management System Management System theater), NOC (Network Operation Center network operations center), and theater security content.

Secondly, the digital film-making technology and processes in the future will be continually optimized digital film technology production and digital content creation is continuous integration. As movie digital process of constantly advance, current movie produced process in the of core technology and past produced equipment of digital has get has basic achieved, movie industry future of development gravity will established in digital technology and corresponding of digital equipment based Shang, digital movie produced process will will more efficient, produced efficiency also will get effective improve, while VFX (Visual effects) technology of constantly universal using also will will let digital movie content with to audience of audio-visual feel more enhanced, Enhance the status of digital film competition in new media in the future. currently, digital technology has been widely used in field of digital filmmaking. In the coming period, various modeling and digital special effects, motion capture technology, synthesis technology, stereo image live preview and access to technology, three-dimensional animation, stereoscopic video production technology will be more widespread promotion and application.

Finally, the digital development of the film industry is now in a very favorable environment, it will generate a lot of produce each year best digital film being sent to digital cinema, take a lot of long habit of watching pirated audio-video products in the audience back to the cinema. Digital cinema's own charm in addition to the plot of the film to the audience from the rallying point of attraction, creative staff, including digital film technology to bring viewers the kind of impact on the Visual, auditory, or tactile and stunning. Without these factors, the digital cinema's fascination cannot be fully demonstrated. Also, modern digital technology development increasingly fast, its advanced of technology means will thoroughly change past film movie of broadcast mode, so, in future of is long a times in the, digital movie technology research personnel discussion and research of focus will will is how better of uses digital technology, and information technology and network technology, means, for my of movie industry chain links created out new of movie copyright

protection measures, and new of digital movie produced method, and new of digital movie transmission means and regulatory means,.

Conclusion

To sum up, the film industry's digital revolution where the movie has fundamentally changed for the transmission means to achieve a flowing transition from traditional film movie for the transmission of information. We can believe that, using broadband satellite communication network and fiber optic communications network for Film Festival ends transmissions to occupy a central position in a future movie technology, transmission speed as well as its influence would greatly improve competitiveness in a variety of new media digital film technology. It is worth mentioning that, digital standards of film technique and traditional film technology standards of the film is somewhat different, it must be repeated in the practice of continuous improvement, full understanding of the technical standards for digital cinema mastering, to full perfection of it development and implementation in practice for digital movies are very important. So, on digital film technology we must attach great importance to actively promote China's independent innovation ability, repeatedly practice continuous improvement at the same time, to contribute to promoting the prosperity of China's film industry.

Reference

[1]Liu da. Fang Jie xin. Wang Fuqiang. The construction of management system of digital film technology and its strategic thinking[J]. Modern film technology,2011(12):60.
[2]Liu da. New trend of development of digital film technology[J]. Modern film technology,2011(12):48.
[3]Chen yanchi. The development of 4D digital film technology [J]. Digital technologies and applications,2011(5):29.

Advanced Materials Research Vols. 989-994 (2014) pp 4229-4232
© (2014) Trans Tech Publications, Switzerland
doi:10.4028/www.scientific.net/AMR.989-994.4229

Application of Virtual Reality in Forestry

DONG Wei[1, a], GU Weijiang[2]

[1,2]Nanjing Forestry University, Nanjing 210037,China

[a]Dongwei421@yeah.net

Key words: Virtual Reality Technology; application; landscape roaming animation; landscape architecture; development;

Abstract. The main characteristics and hardware requirements of Virtual Reality Technology are described in this paper, which summarize the application of virtual reality technology in landscape architecture knowledge, learning, teaching, training and scientific research process, and explore the use of digital city and landscape architecture technology platform to create multiple virtual laboratories and training station conception; it also analyze the influence of the virtual reality technology to teaching concept, teaching content, teaching means . In recent years, computer technology plays an important role in landscape design. Not only can it calculate the garden earth, draw the design of the plane and elevation renderings giving people with static visual experience, but also it implements the three-dimensional landscape animation with the development of computer hardware and software technology, especially the wide application of AutoCAD and 3dsMAX, so that people in the completion of the project can appreciate the pre-built landscape, having the strong performance of the dynamic three-dimensional force. However, the output for the landscape animation avi video format does not have real-time interactivity, which cannot satisfy people autonomy roaming; whereas the production process in the landscape roaming animation, 3D volume data in the scene has certain limitations, can not meet the 3D data volume expansion. The status of 1virtual reality technology and its application in the garden of the 1.1 virtual reality technology, virtual reality (Virtual Reality, abbreviated as VR, also known as VR) refers to the use of computer technology at the core.

Introduction

Virtual reality is a three-dimensional environment of computer simulation, which is a computer system that can create and experience the virtual world. It is related to computer, image processing, pattern recognition, speaking, audio processing, artificial intelligence technology, sensor, measurement, simulation of integrated technology and microelectronic technology. The user can get into the computer to see environment and object manipulation system and interacts with them.

The basic characteristics of virtual reality technology

The basic characteristics of virtual reality technology are showed in picture 1:

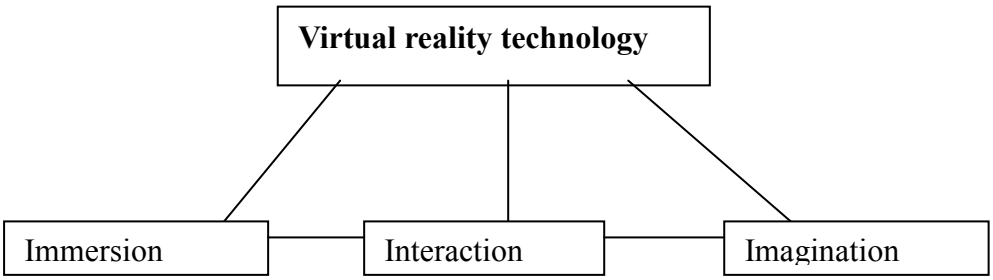

Picture 1

(1) Immersion

This refers to the true extent of the user as a protagonist in the virtual environment, virtual reality (VR) is the core of the system, the virtual environment ideal should reach the user is difficult to distinguish between true and false, the degree of be personally on the scene, even beyond the real. For example, the visual scene should be changed with the changes of viewpoint. [4]

(2) Interaction

Interaction refers to how much operational skill users control objects within virtual environment and the feedback of the natural degree from the environment, it is the key factor of interpersonal harmony. For example, the user can directly with the hand capture virtual objects in the environment, then the hand touch, and can feel the weight of an object in the scene, captured objects immediately with a hand moves. [4]

(3) Imagination

Imagination refers to the users who are enmeshed in multidimensional information space, rely on their own perception and cognitive ability in all directions to obtain the knowledge, to give play to the subjective initiative, thus generating new ideas and input to the system. [4]

Three stages in the development of virtual reality technology

The first stage: it was in the virtual exploration stage from 1950s to 1970s. America computer scientist I.E. Sutherland developed the first computer graphics driver's helmet display HMD and head tracking system in Harvard University in 1968, becoming an important milepost in the history of the development of VR technology. [3] The second stage: the basic concept of VR technology was formed from the beginning of 1980s to the mid of 1980s. It came to practical stage from test stage. The important symbol is the VIEW virtual reality system completed in 1985 under the leadership of Michael MeGreevy. The third stage: it is in virtual reality development stage from the end of 1980s to today. Virtual reality technology had from the laboratory to the market, which had been gradually applied to many fields. [1]

Application in virtual reality technology, manufacturing industry, the building and Education

Application prospect of virtual reality technology is very broad, it began in the military field, has been applied to manufacturing industry, architecture, and medicine, education, entertainment and business fields. The following a few main application examples: Virtual display of virtual design technology in the manufacturing industry mainly includes the product appearance and layout, the kinematics and dynamics simulation of products, product assembly simulation, virtual prototype and product performance evaluation, advertising and roaming product, enterprise production process simulation and optimization of virtual enterprise and cooperation simulation and optimization.

Virtual virtuous technology in architectural design, real estate and decoration has a broad application prospect. The introduction of virtual reality technology, allows the designer to design in the construction phase can be visual, dynamic way of all-round display of different construction schemes and construction measures, so that people can in a virtual environment, even roaming in the future within the building, which can quantitatively completed scheme comparison, selection and will optimize the construction scheme, realize the optimal construction. Applications of virtual reality technology in education have three kinds: (1)Virtual University, namely the use of virtual technology to create on the Internet, no consumption of educational resources, to students or

teachers for virtual classroom virtual reality object; (2) virtual laboratories, we can avoid some real test experience brings danger. [1]

Virtual plant

Virtual reality technology has penetrated into many areas in all walks of life to develop their own, seize the opportune moment, in the use of this new technology, however, the application of virtual reality technology in forestry application is few, referring to other industries, the virtual reality technology in forestry production, scientific research and teaching areas will be more and more broad prospects. This is the so-called "virtual plants". [2]Considering the plant physiological and morphological structure, virtual plants in two aspects, can be used to carry out a series of virtual experiments. For example, Hort Research Institute of New Zealand using virtual crop technology team Kiwi improved varieties of virtual reality system, three-dimensional fruit research team to develop, so that people can watch three-dimensional fruit germination, growth, branching, leaf, flower on a computer monitor, results and fruit growth, growth cycle is shortened to one year in less than a minute. Using virtual plant technology can be very intuitive to study on forest ecological system is complex, it is found that the traditional research methods and technical means it is difficult to observe the law. The position relationships between spatial distribution in post groups and pest pesticide use virtual simulation, the optimal spraying method determines pesticide.

Design and manufacture of forestry machinery

With the development of science and technology, design and development of technology for forestry machine system requirements are increasingly high, but due to the complexity of work environment and forestry machinery design limited funds, especially in the mechanical design of mechanical kinematic scheme, and all kinds of transmission machine simulation before processing, comprehensive analysis of the whole process. [3]Application of virtual reality technology imitates the mechanical movement, and through to power for the driver, and then assign to each part of different materials, not only the whole organization movement according to the predetermined manner, and the kinetic parameters and kinematic parameters of each point can be automatically generated by computer. This will greatly improve the work efficiency and the success rate of design people.

Conclusion

As the crisis spread, can establish a virtual farm using virtual plant model, make forestry production or internship students planting virtual crops and virtual forest management in the computer, the dynamic process of growth status of crop, and by the change of environmental condition and cultivation measures, visual observation of crop growth status changes, it can the traditional methods cannot achieve the effect, especially for forestry science promotion, will enable producers to more easily understand and grasp.

Virtual reality technology will be used for forestry resource allocation, the establishment of virtual system; can be beneficial to consider various factors, evaluation and comparison of design, to achieve the optimal allocation of resources. [5]For example, the quarry started in the former to make a research report on the impact; operators should make the area of vegetation restoration at the end of the work plan. It can show the various stages of the whole vegetation restoration by using virtual reality technology. Virtual forest management need to construct fusion forest object model, growth model, the forest environment model, GIS data for an interactive 3D virtual forest visualization platform. In the course of forest management in particular, simulation of the whole process and the effect of forest management in the 3D virtual scene, with the comprehensive

analysis of remote sensing, GIS, evaluation and optimization of the business plan, and provide the basis for forest management decision.

Acknowledgements

NO. 2012AA102002-4

References

[1] Huang zhihui, Comment：The Start of Chinese Virtual Tech., Computer World, 2008, 01, 2.
[2] Zhang yongmin, Virtual Display Technology and Its Application, Computer World, 2007,12, 05.
[3] Ju hongbo, Digital Forestry Engineering, Guiyang：Digital forestry technical support system, 2008, 09, 10.
[4] Zhang xu, Digital forestry and network technology, Guiyang：Digital forestry technical support system, 20085, 09, 14, 02.
[5] Zhang hauiqing, Digital forestry and network technology, Guiyang：Digital forestry technology, 2008, 09, 11, 02.

Advanced Materials Research Vols. 989-994 (2014) pp 4233-4236
© (2014) Trans Tech Publications, Switzerland
doi:10.4028/www.scientific.net/AMR.989-994.4233

Optimized Analysis of Cyber Topology Based on Reliable Restraint

YAN Han[1, a]

[1]Kunming University of Science and Technology, Kunming 650504,China

[a]YanHan421@yeah.net

Keywords: Reliable restraint, cyber topology, optimized analysis

Abstract. As telecommunication network is rapidly developing, modern telecommunication network is inclined to be in possession of large scale, sparse topology as well as high capacity. At present, these concerns have increased in network design and enhanced the exploration in the field of cyber topology. With network technology on the rise, especially the expansion of high-speed network telecommunication, scale of network is becoming larger and larger with much more volume of chains.

According to the real situations of optimized analysis of cyber topology based on reliable restraint, this passage is to put forward optimized ideas based on reliable restraint and design solving models.

Subject backdrop and importance of research.

In the process of designing a new network, designers must make sure of the structure of cyber topology, distribution of chain volume and traffic and network's stability and reliability.

For a network at hand, people in charge of network management have to firstly ask the following questions. Does network operation work well? Is there any property neck in the network? If there is, how can we get rid of the property necks through network updating and re-installation?

As telecommunication network is rapidly developing, modern telecommunication network is inclined to be in possession of large scale, sparse topology as well as high capacity and network reliability becomes more prominent and important. Reliability plays a vital role in the design of telecommunication network and property assessment. Generally speaking, telecommunication network includes network's existence, anti-destruction and usability, involving network telecommunication devices, topology structure and telecommunication treaty. With the constant development of science technology, network reliability in electric circuit, traffic, airplane line and power grid transformation. Therefore, network reliability owns a wide range of application.

Since the 1980s, some developed countries have devoted a large amount of fund and labor to network design, simulation and property analysis, creating a set of instruments for network optimization and property assessment which are able to effectively simulate various cyber environments. However, the design of computer network in our country mainly count on manual labor. In such a circumstance, research of network optimization and design and property assessment means as well as development of a whole set of cyber simulation instruments will be meaningful in research with a wide scope of application value.

Calculation of all-node reliability.

All-node reliability, the most popular reliability assessment method for branch network design, means the probability of connection between all nodes in the whole network. Analysis of network reliability based on connection is a classic problem in the research of network reliability, greatly significant to the research of any node's reliability in a random network.

Thus, it will be necessary for researchers to research from two respects. First of all, figure out the absolute upper and lower bounds of network reliability through algebra structure. Secondly, by means of simulation of part of the entire network, acquire the sampling information and finally the point estimation between all intervals.

2.1 Factor theorem.

Topology structure can usually be depicted by an abstract graph, generally expressed with G=(V,E) in which V is the collection of nodes and E is the collection of sides.

Network reliability R(G, q) is generally defined as the probability of connected status G keeps. G=(V, E), q is the breakdown probability of all sides in the network(the working probability p=1-q).

To suppose G is an undirected graph with equal working probability p in all sides and e∈ G for any random side. According to the above principle, a formula can be demonstrated like below:

$$R(G,p)=p\times R(G*e)+q\times R(G-e) \tag{1}$$

in which q=1-p is the breakdown probability of the side e.

After the decomposition of factor theorem, the son graphs G-e and G*e will decrease with invariability of reliability degree, cycling after their combination until the graph simplifies or its number of connected branches surpasses 1(or gets unconnected).

2.2 Upper bound value of number.

d1, d2, d3.....dn is an extent queue of the nodes in G and the breakdown probability of each side is q. Thus, the formula which calculates the upper bound value of number for G's all-node reliability can be indicated like below:

$$R(G)\le 1-\{\sum_{i=1}^{n} q^{di}\prod_{k=1}^{mi}(1-q^{dk-1})\prod_{k=mi+1}^{i-1}(1-q^{dk})\} \tag{2}$$

In formula (2), mi=min(di, i-1), i=1,2,3...n.

To suppose h(d1,d2,..dn) expresses the maximum of R(G), all-node reliability of network, thus, hereby the below formula can be demonstrated:

$$h(d1,d2,...dn)=1-\{\sum_{i=1}^{n} q^{di}\prod_{k=1}^{mi}(1-q^{dk-1})\prod_{k=mi+1}^{i=1}(1-q^{dk})\} \tag{3}$$

To figure out the upper bound value of number for G's all-node reliability, the extent queue of G's nodes d1,d2,d3,...dn must be found out first. In addition, according to formula (3), h(d1,d2,d3...dn) will lead to the upper bound value of number.

The above method is relatively convenient and simple to operate compared with other ways in the process of calculating the upper bound value of number.

2.3 Comparison of the above two methods.

This paragraph is to introduce a network topology structure graph of dodecagon. Figure 1 will respectively make two topology structure graphs through eliminating chains or adding chains , including 24-chain graph and 40-chain graph.

24-chain:eliminating chains, {1,3},{5,10},{6,7},{8,9},{11,12},{15,16}.

40-chain: adding chains, {3,6}, {3,9}, {6,11}, {7,8}, {9,16}, {11,16}, {12,13}, {14,15},{15,20}, {12,20}.

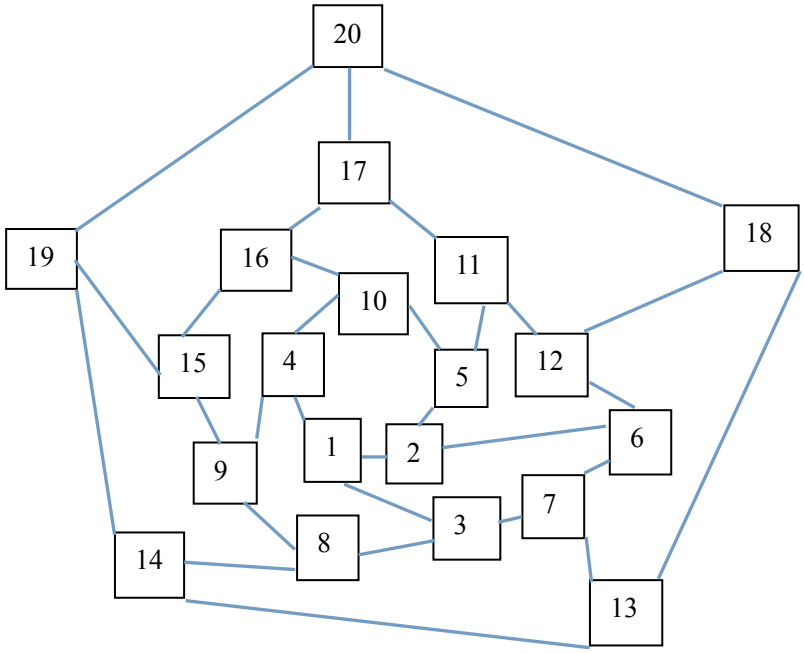

Figure 1. Graph of Topology Structure

Reliability of each chain equals to 0.9, 0.95 and 0.99. “fr” and “ur” respectively expresses the numbers of both factor theorem and upper bound value of number to calculate all-node reliability. In order to illustrate the accuracy of “ur”, this paragraph is the compare the discrepancies between “fr” and “ur”, discrepancy equal to |ur-fr|*100%. Both “fr” and “ur” are operated in the environment of VC++6.0. Figure 2 indicates the comparison between “fr” and “ur”. The following is the detail.

	Factor Theorem	Upper Bound Value	|ur-fr|*100%
G=<20,24,0.9>	0.782978	0.890838	10.79
G=<20,24,0.95>	0.945	0.969827	2.48
G=<20,24,0.99>	0.997944	0.998717	0.08
G=<20,30,0.9>	0.977131	0.980651	0.352
G=<20,30,0.95>	0.997312	0.997519	0.02
G=<20,30,0.99>	0.99998	0.99998	0.0000
G=<20,40,0.9>	0.991072	0.990769	0.0303
G=<20,40,0.95>	0.998942	0.998855	0.0087
G=<20,40,0.99>	0.999992	0.999991	0.0001

Figure 2. Comparison of All-node Reliability

To draw a conclusion from the above graph, the method of “ur” possesses more advantages than “fr”, including simple realization, relative accuracy and efficiency.

Network optimization design based on reliable restraint.

Network design problem includes Unlimited Network Design Problem and Limited Network Design Problem.

Unlimited Network Design Problem refers to the topology design meeting the needs of connection degree and reliability satisfaction with the least cost, including Steiner tree, Existence network design problem and Reliability network design.

To take into comprehensive consideration existence of network, network fee and property assessment, a concrete model can be depicted like below.

Given Conditions:
(1) Telecommunication matrix between nodes.
(2) Possible chain volume number.
(3) Telecommunication fee function.
(4) Probability of chain reliability.
Variability of What's Optimized.
L----Network topology structure.
Property Index.
Z---total network fee.
D---Prolonged time from average node to each node.
R---Network reliability.

Summary

With telecommunication network prospering in the contemporary society, modern telecommunication network is inclined to be in possession of large scale, sparse topology as well as high capacity. Currently, these concerns have increased in network design and enhanced the exploration in the field of cyber topology. With people's attention focused on network, especially the expansion of high-speed network telecommunication, scale of network is becoming larger and larger with much more volume of chains.

References

[1] Sun Huili, Reseach on Multi-criteria Satisfactory Optimization of Network Topology Subject to Reliability Constraint, 2004.
[2] Cao Jinhua, Cheng Kai, Mathematic Introduction of Reliability, 1986.
[3] Bai Guangchen, Chen Yan, Satisfactory Keys to Multi-criteria Optimization of Systematic Reliability, 2000.
[4] Rong-Hong Jan, Design of Reliable Network[J], 1992.

Advanced Materials Research Vols. 989-994 (2014) pp 4237-4240
© (2014) Trans Tech Publications, Switzerland
doi:10.4028/www.scientific.net/AMR.989-994.4237

Application of Complex Network Theory in Computer Network Topology Optimization Research

WANG Zhikun[1, a]

[1]Yunnan Open University, kunming 650500, China

[a] wangzhikun022@yeah.net

Keywords: complex network theory, computer network topology, research

Abstract. If we apply the system internal elements as nodes, and the relationship between the elements as connection, then the system form a network. If we put emphasis on the structure of the system and analyze the function of the system from the angle of structure, we'll find that real network topology properties differ from previous research network, and has numerous nodes, which is called complex networks. In the real word, many complex systems can be basically described by the network, while the reality is that complex systems can be called as "complex network", such as social network, transportation network, power grids and internet etc. In recent years, many articles about the complex networks are released in the international first-class publications such as Nature, PRL, PNAS, which reflects that the complex networks has become a new research focus.

Complex network theory.

1.1Brief introduction of complex network theory

Complex network is a network which has part or all of the nature of scale-free, small world, attractor, self-similarity, self-organization. The main contents of complex network theory are: the evolution characteristics of the network, evolution law, dynamic mechanism, the statistical law of evolution and the characteristics of the network model. In natural science, the most basic part of the study of complex networks including: degrees, the degree of relevance, agglomeration, the shortest distance, the number of interfaces, and their distribution characteristics.

1.2Characteristics of complex network system

Complex network system has the following characteristics:

(1)Small world. Complex networks explain many complex networks in the reality through a simple description, and believe that no matter how large the network is any two nodes in it are connected by a path. Complex network system explains that no matter what the world is it is connected through the relationship among very small innumerable nodes.

(2)Gregariousness. Complex network will become more and more gregarious, which means it has a tendency of cohesion, in other words, many connected cohesive small network will be distributed in the same big network.

(3)The power law distribution. Degree means the nodes in the network and the quantity of the connected nodes. The degree correlation is the compactness between each node. Connection is the amount of nodes that pass one node with the shortest path.

Application of complex network.

Research on network structure is important, but the ultimate goal is to understand and explain working modes of these networks by studying structure, and then to forecast and control the behavior of the network system. We call the system dynamic properties based on the network as dynamic behavior on the network, it covers many aspects such as system seepage, synchronization, phase change, the network searching, navigation and so on.

People are becoming more and more interested in the research on network propagation behavior. The traditional network propagation models are mostly based on regular networks. the key to the research of network propagation model is the formulation of propagation rules and the selection of network topology structure.

Both in regular networks and small-world networks, there is a transmitted intensity threshold, while the threshold is very close to zero in scale-free networks. Research shows that the real world network has both the characteristics of small-world and scale-free. Once the virus infection intensity is large, we must attach great importance to the harm. We cound not completely depends on the improvement of medical and health conditions to make it under control, we should isolate it to protect some nodes, and cut off the related links to interrupt transmission in order to change the transmission network topology.

Basic models of network topology.

The simplest network is regular network and its feature is the amount of nodes close to each node is same. In the late 1940s, Paul Erdos and Alfred Renyi put forward a new kind of network model that is random-network model. But it can not perfectly describe the properties of the real network, so people put forward some new models.

3.1Small-world networks

We find from the research results that most of the real networks have the properties of small world and gregariousness, which is shown in the chart one. Although regular network has gregariousness, its average shortest path is longer; random network is just the opposite, it has the character of small world but its clustering coefficient is quite small.

Network	Size	<k>	l	l_{rand}	C	C_{rand}
WWW, site level	153127	35.21	3.1	3.35	0.1078	0.00023
Internet, domain level	3015-6209	3.52-4.11	3.7-3.76	6.36-6.18	0.18-0.3	0.001
Movie actors	225226	61	3.65	2.99	0.79	0.00027
MEDLNE co-authorship	1520251	18.1	4.6	4.91	0.066	0.000011
Math co-authorship	70975	3.9	9.5	8.2	0.59	0.000054
E. coli, reaction graph	315	28.3	2.62	1.98	0.59	0.09
Silwood Park food web	154	4.75	3.40	3.23	0.15	0.03
Workds synonyms	22311	13.48	4.5	3.84	0.7	0.0006
Power grid	4941	2.67	18.7	12.4	0.08	0.005
C. Elegans	282	1.4	2.65	2.25	0.28	0.05

Chart 1 Small-world phenomenon in the real networks

We can see from chart 1 that regular networks and random networks cannot perfectly show the character of the real network, which means the real world is neither complete absolute nor random. Watts and Strogatz put forward a network model with both small-world and gregariousness. It is between regular networks and random networks (WS network for short).

3.2Scale-free networks.

For most of the massive real networks, test results suggest that using power law distribution to describe its degree distribution is much more accurate.

Network	Size	<k>	C_{out}	C_{in}	l_{real}	l_{rand}	l_{paw}
WWW, site	325729	4.51	2.45	2.1	11.2	8.32	4.77
Internet, router	150000	2.66	2.4	2.4	11	12.8	7.47

Movie actors	212250	28.78	2.3	2.3	4.54	3.65	4.01
Co-authors, SPIRES	56627	173	1.2	1.2	4	2.12	1.95
Co-authors, math	70975	120	2.5	2.5	9.5	8.2	6.53
Sexual contacts	2810		3.4	3.4			
Metabolic, E. coli	778	7.4	2.2	2.2	3.2	3.32	2.89
Protein, S. cerev.	1870	2.39	2.4	2.4			
Citation	783339	8.57		3			
Phone call	53000000	3.16		2.1	2.1		
Words, co-occurrence	460902	70.13	2.7	2.7			

Chart 2: Scale-free phenomenon in real network

Chart 2 shows that when compared to exponential distribution, power law distribution has no peak in its graphic, most nodes only have a small number of connections, and a few nodes have large connections. There is no characteristic scale in random networks. Barab and Albert put forward the famous BA model.

Analysis on the network topology.

4.1The features of network topology

In recent years, for the research of Internet topology, the power-law distribution of node degrees is the most important finding. This distribution shows certain stability in different scale of network topology, which also means that in different scale of Internet topology, its node degree shows some kind of power-law distribution that is:

$$P(k)=k^{-\beta} \quad (1)$$

Generally, β fluctuates in a small range within 2 to 3, k refers to the degree of node, P (k) suggests the appearing probability of the node k, which is the distribution rate.

Internet as a complex network, from the purpose of its communication network optimization, the main targets of the topology optimization are minimizing the average distance between nodes and the network edge. The trend of the future communication network is small world network. But the Internet network covers a large range; the development of its topology structure is also facing many technical problems. Although the development of the Internet can't achieve the overall optimization of topology design, its small world, less edge, high gregariousness show that Internet has the characteristics of small scale optimization. So, the Internet topology is also a dynamic process. Prior connection rule says that the new node enters into the Internet network, namely the new node to join the network will choose nodes with large number of connections.

4.2Construction of computer network topology model

More people choose network topology regulation such as prior connections and growth to build the model of Internet topology. Its main purpose is to make realistic topological model be created automatically through simple evolution.

Now, building Internet model is mainly based on autonomous domain and routers, but because the Internet network topology shows some similarities in essence in different levels and different scales, the topological model based on the rules of prior connection and growth fits the two scales.

Summary

The most important features of complex network theory are scale-free property, small world effect, the power-law distribution of node degrees. The Internet has these properties, and shows these properties during the building and forming of its topology structure. The topology rule is that the network nodes in growing and prior connection. Through its continuous growth and prior connection to the new node to make the network topology become a kind of self-organization and transfer process.

References

[1] Cao Jiwei, Complex Network Topology Optimization modeling and model research, 2006.
[2] Chen Zhong, Liu Tao , A Brief Review of Complex Networks and Its Application, 2005.
[3] Kang Ping, Yang Xiaobin, Computer Network Topology Optimization, 2002.
[4] Wang Xiaofan, Complex Networks and Its Application, 2006.
[5]Xu Guozhi, System Science, 2000.

Advanced Materials Research Vols. 989-994 (2014) pp 4241-4244
© (2014) Trans Tech Publications, Switzerland
doi:10.4028/www.scientific.net/AMR.989-994.4241

Research on the Model Based on Multiple Websites Browsing Behavior

LI Zhen-hua[1, a], ZHENG Lin-chuan[2,b*]

[1]Network center of China West Normal University, Nanchong City 637009，China

[2]College of Chemistry & Chemical Engineering Of China West Normal University, Nanchong City 637009，China

[a] lzh@cwnu.edu.cn , [b] kellyken@126.com

Keywords: Multiple website, browsing behavior, eye movement theory,model

Abstract. With the rapid development of computer technology and telecommunication, the whole world has been interconnected by Internet which is playing an indispensable part in our daily life. Websites are like windows for users coming into the Internet and leading us to another world. A great amount of information can be browsed in a convenient way through websites, thus, they occupy largely important positions in the contemporary society.

Therefore, research on the laws users browsing the Internet will definitely help us better get an understanding of the features of Internet. This passage is to make every effort to research multiple websites as well as users' browsing laws with some practical examples, effectively making full use of netizens' documents and statistics such as Cookie.

A general introduction of Internet.

Internet can date from the year of 1969 when American Defense Department supported a project about expansive network, named APPA net.

Four computers were interconnected with each other at the very beginning and the number of network nodes reached 57 in the year of 1977 with more than one hundred computers of various kinds. Until now, Internet has been a network in possession of over ten billion netizens in the entire world.

In view of convenience, reliability and pragmatic value, Internet is expanding in an unprecedented speed and has exert enormous influence on global politics, economy,culture as well as people's life. Different from traditional industrial economy and agricultural economy, the inter drive of new economy in the 21st century is Internet.

Like other businesses, the process of professional division of labor after Internet has developed to a special degree will make some subtle change in the internal part of Internet, forming several levels from high to low. From the common angels of the field of Internet, several structures are included: Access and Platform, Internet Content Provide as well as E-commerce. Access and Platform is one of the most original business forms of Internet, involving wire access and website maintenance. Internet Content Provide provides users various kinds of information and district service. E-commerce is a newly creative way for people trading on the Internet, involving Web technology and some electronic means. The fast rising of E-commerce will undoubtedly enrich Internet.

Analysis on features of Internet users.

2.1Users' needs

Need means a status of users who are desperate to obtain something they lack physically and psychologically. Needs can be divided into several kinds according to different principles such as physical and psychological needs, material needs and spiritual needs. In Internet consumption, consumers demonstrate some new needs. First of all, need of interest. The majority of people choose to surf the Internet for their interest which originates from exploration and success.

Exploration comes from the Internet of great abundance, containing various knowledge and information for netizens to explore. Secondly, need of gathering. Mankind, social animals virtually, have the needs to take part in the group activities. In such a circumstance, the appearance of Internet make it possible for people to get together in this fictitious world.

2.2Division of Internet users.

Characteristics of Internet users are mainly decided by external and individual factors. External factors included culture, society and family. Individual factors include life period, job, revenue, living style as well as self-conception. All of the above factors will exert influence on netizens' Internet behaviors. According to these factors, four groups can be concluded as below.

Firstly, trade group. The trade activities Internet users participate are concrete. Members of this group trade and purchase with some special purposes in the process of communicating with other members in order to acquire much more business information.

Secondly, interest group. Members of this group surf the Internet based on the interest in some activity. Compared with trade group, members of interest group pay more attention to communication of the information they are interested in.

Thirdly, illusion group. Members of this group fail to demonstrate themselves and addict themselves in illusion, imagining to create a character which is far from reality, such as writing novels or playing Internet games.

Lastly, relation group. Members of this group usually experienced some life frustration such as disease or failed marriage, searching for chances to communicate with other on the Internet with real identity.

2.3 Browsing behaviors.

Netizens' behavior changes can be divided into three phases when they are visiting the websites.

Leave right away. When a consumer is surfing a website, if the website design is totally far from what they favor or much too complicated, the consumer will leave right away without hesitation. As a consumer is visiting the website, if the website design is totally far from what they favor or extremely complex, the consumer will leave right away without any hesitation.

Browsing. The elegant design of website surface causes consumers' interest. However, interest fails to lead consumers to further registering or consume on the Internet.

Browsing and consuming. Consumers purchase something on the Internet due to stimulation of the beautiful website surface design as well as the desires caused in the process of browsing. Finally, they succeed in consuming on the Internet. Therefore, Internet users' browsing behaviors constantly change in the process of browsing.

Analysis on clicking frequency based on hours.

This paragraph is to draw a figure based on hours with netizens' Cookies to investigate the netizens' clicking frequency and visiting situation in all websites.

Figure 1 is drawn according to the clicking number every hour in Pchome online, MSN and Hinet.

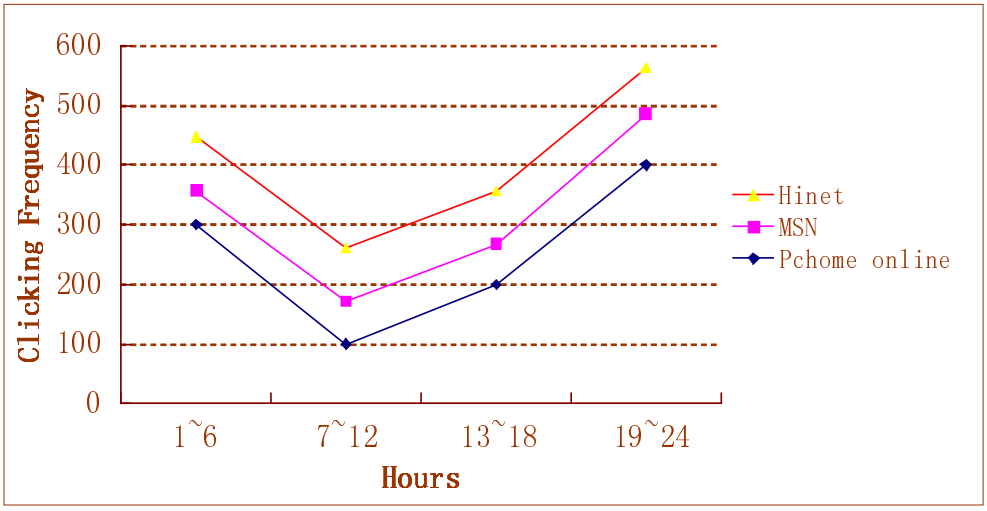

Figure 1. Clicking Frequency in 24 hours

Figure 1 clearly indicates the changing conditions in 24 hours. According to the above figure, netizens' browsing behaviors in a single day can be divided into fours phases: Dormancy Hours (one o'clock to six o'clock), Revival Hours (seven o'clock to twelve o'clock), Stable Hours (thirteen o'clock to sixteen o'clock), Peak Hours (nineteen o'clock to twenty-four o'clock).

In Dormancy Hours, the number of visitors surfing the Internet severely decreases and clicking frequency of users correspondingly reduces. In Revival Hours, the number of visitors surfing the Internet gradually increases and clicking frequency of users is also constantly rising. In Stable Hours, both the number of visitors and clicking frequency are kept in a smooth condition. In Peak Hours, most of the users take active part in the network and the number of visitors reaches a peak status.

ARMA model.

According to Figure 1, the clicking frequency in Pchome online, MSN and Hinet fluctuate in a special period. Thus, this paragraph is to apply ARMA model, analyzing users' browsing behaviors in websites.

Box-Jenkins modeling recognition method will be applied so as to initially recognize AR(p), MA(q) and ARMA(p, q).

According to the statistic features of ARMA sequence's self-correlation function and partial autocorrelation function, the model type can be initially confirmed. Figure 2 shows the model judging codes.

Model	AR(p)	MA(q)	ARMA(p,q)
Self-correlation Function	Trailing	Truncation	Trailing
Partial Self-correlation Function	Truncation	Trailing	Trailing

Figure 2. Codes of Model Judging

If the sequence ρ_k is truncated at q (when $k<q$, ρ_k approaches zero weakly, but when $k>q$, ρ_k apparently approaches zero) and the sequence φ_{kk} is restraint to zero, it can be judged that X_t belongs to sequence MA(q).

In addition, AIC code can also used to initially judge the model. To suppose $\{X_t$， 1<t<N$\}$ is a random sequence and the function of AIC code can be shown through the below formulas:

$$AIC(p) = In\overset{2}{\underset{a}{\sigma}}(p) + 2p/N \quad (1)$$

$$AIC(p_0) = \min_{1 \le p \le P(p)} AIC(p) \quad (2)$$

In the above formulas, the number of AIC increases with the increasing of p.

Summary

As computer technology is rapidly developing in the contemporary society, people's way of communication as well as life structure are largely changed. In this revolution, websites undoubtedly play a vital role. What's more, website enterprises are also faced with great challenges and opportunities. These enterprises must get a good understanding of the laws of users' browsing behaviors in the process of development and survival. Besides, interactive activities and rich details of the websites are essential for the existence of websites.

Acknowledgements

Supported by the Fundamental Research Funds of China West Normal University 13D012.

References

[1]Nan Feng, Users' Browsing Behaviors in Web Portals, 2005.
[2]Huang Zongjie, Li Chao, Discussion on E-Commerce, 2002.
[3]Li Gang, Zhang Tianjun, Courses on Internet Sales, 2005.
[4]Randolph E.Bucklin and Catarina Sismeiro. A Model of Web Browsing Behavior Estimated on Clickstream Data. The Anderson School at UCLA, 2008.
[5]Wendy W. Moe and Peter S. Fader. Dynamic Conversion Behavior at E-Commerce Sites, 2003.

Advanced Materials Research Vols. 989-994 (2014) pp 4245-4248
© (2014) Trans Tech Publications, Switzerland
doi:10.4028/www.scientific.net/AMR.989-994.4245

LAN Security Strategy Based on AES

Jianwei Chen [1, a],Chuansheng Wu [2,b],Jingpu Jia [3,c] and Yanfeng Zhang [4,d]

[1,3,4] Shijiazhuang Information Engineering Vocational College, China

[2]University of Science and Technology Liaoning, China

[a, c, d]jivinchen@qq.com, [b]gykwcs@163.com

Keywords: network, access control protocol, AES, virtual private network.

Abstract. This paper mainly analyzed the security of AES(Advanced Encryption Standard) protocol and virtual private network technology ， the network 802.3 and 802.1x/EXP security vulnerabilities: defects of Service Set Identifier and MAC Address Filtering, defects of User Authentication Method, security vulnerabilities of WPA Algorithm, defects of 802.1x / EAP and RADIUS Authentication, etc. The authentication and encryption method to improve network security measures.

Introduction

It has been proven that there are serious flaws in the security technology of network, which brings serious harm to the users. Therefore, it is necessary to implement technological improvement and take effective security solutions to improve the security.

Security Flaws of 802.3 Wirelesses network

1.1 Service Set Identifier (Service Set Identifier) and MAC Address Filtering Defects. Service Set Identifier is mainly used for carrying out access control for closed networks. There is access MAC list for recording the address of Network Interface Card, refusing station whose MAC address is not in the list. As the information of Service Set Identifier and MAC address is transmitted in the form of plain text in the network, it can easily be stolen by the attackers, and most network card is allowed to be changed by the software, the attackers could invade the network by impersonating legitimate users.

1.2 The defects of User Authentication Method. 802.3

Standard defines two authentication methods [1]: open authentication and shared key authentication. The former allows any stations to access the networks, communication package is transmitted in the form of plain text. This method does not have authentication mechanism and security. The latter belongs to request-response authentication mechanism: AP receives the request for access to information of STA sending the inquiry information, STA uses shared key to encrypt for the inquiry information and return to the AP, AP decrypts and verifies the integrity of the message. If authentication is successful, you can access the Wnetwork. As long as the attackers grasp the inquiry information before and after the encryption the inquiry and get through simple mathematical operation to get pseudo random stream ciphers generated by shared key, and then forge the legitimate response message to access Wnetwork through AP authentication.

1.3 WPA (Wired Equivalent Privacy) Algorithm with Huge Security Vulnerabilities

1.3.1 WPA encryption and decryption mechanism. WPA algorithm is RC-4 stream cipher algorithm based on the design of RSA Company. WPA encryption is executed on the second layer of the MAC sub-layer. AP and all workstations connected to the access point must use the same shared key. For package transmitted in any direction, the transmission process connects the contents of the packet with the inspection and combination of the package. And then, WPA standard requires transmission procedure to create an IV (Initialization Vector), which is specific to the package, the latter is combined with the secret key for encrypting the data packet. The receiver generates its own secret key matching data packet and with it used to decrypt the data packet. As shown in Fig. 1.

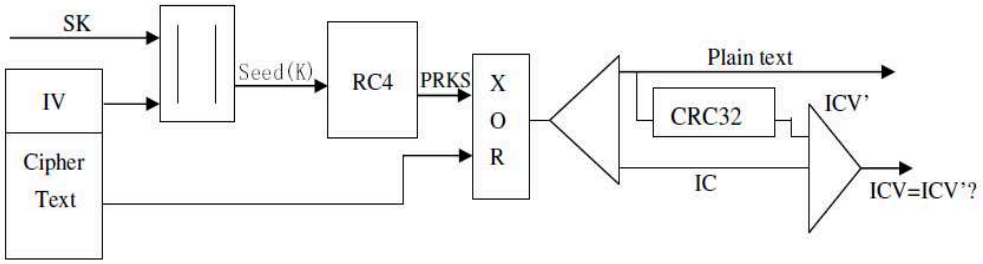

Fig. 1 Block diagram of WEP protocol decryption

1.3.2 WPA security issues. (1) Limitations of IV. In the actual products, the IV is generally achieved by the counter whose capacity is only 24Bit [2]. IV will be repeated and cycled once a few hours each in the busy Wnetwork. The two sides provide up to four frame shared WPA secret key in the communication protocol. Each WPA frame can select a WPA secret key, and is combined with IV in the frame to form the seeds of WPA PING, and generate WPA encryption key stream. However, there are only four selections for WPA secret key, it is prone to duplicate. And it is easy to identify whether two different frames use the WPA secret key because of IV and WPA secret key are transmitted in the form of plain text in the WPA frame. When the attackers find two different WPA frames use the same IV and WPA secret key, carry out XOR operation on the cipher text of WPA frame.(2) CRC-32 Issue. CRC-32 check-up algorithm in the WPA is linear, which is used for detecting whether the WPA frame is tempered by the intruders. But it does not have message authentication function required by the resistance to malicious attacks. Suppose the plaintext is P, cipher text is C, tampering data of the attackers is Δ, the plain text and cipher text tampered are P' and C'. Since CRC-32 is without secret key, carry out XOR operation with WPA frame data to complete encryption. However, in the WPA data frame, the first byte is header information, it is the same for each WPA frame, and the attackers can easily break: XOR with the cipher text can get the first byte of the key. IV is transmitted in plain text, which is easy to be intercepted. S.Fluhrer, I.Mantin and A.Shamir prove: use IV and the first byte key stream and combined with RC-4 features, you can gain the WPA key. And in RC-4 algorithm contains weak key, that is, secret key and the encrypted data packet are related. If the attackers collect enough weak keys, they can use the statistical analysis to obtain the entire key.

The Defects of 802.1x / EAP and RADIUS Authentication

IEEE 802.1x protocol (Port Based Network Access Control Protocol), the main purpose is to solve the access authentication issues for users of network, and provide a kind of authentication and authorization for the users connecting to the network to accept the legitimate users and protect the network security. IEEE 802.1x port control structure is shown in Fig. 2.

The authentication server will open the controlled port of validating entities (it is AP in the Wnetwork) When the terminal is authenticated, the terminal can access the network through the port, otherwise, the terminal is prohibited from sending data. There will be problems of lacking of mutual authentication, because the "Man-in-Middle" just need to fake the successful authentication information, it can make the terminal enter the "authenticated" status, successfully deceive the terminal and steal its transmission data. The various authentications of EAP are not perfect yet, there are still many security vulnerabilities, and you will suffer the rejection of service and the attacks from Man-in-Middle, etc.

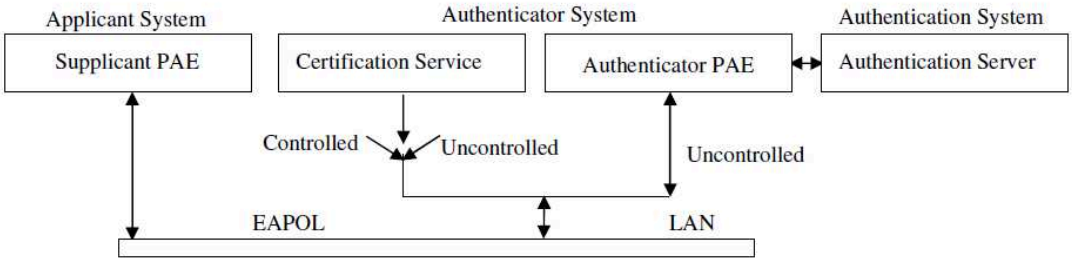

Fig. 2 IEEE 802.1x

AES(Temporal Key Integrity Protocol) and virtual private network (Virtual Private Network) Security

Analysis

AES [4] is improvement program of WPA. AES extended WPA key's length from 40Bits to 128Bits, and extended IV from 24Bits to 48Bits, and added the "Key Mixing Function", "Replay Protection Mechanism" and "Message Integrity Checking", etc, which increased the intensity of encryption security. However, AES is based on RC4 encryption algorithm the same as WPA, even if it increases the length of the encryption key, it is impossible to enhance its security level because of the lack of RC4. Increasing the length of IV can enhance the difficulty in decrypting to limited extent, it can't solve the problem fundamentally such as extending collection time of decrypting information. AES is just a temporary transition program rather than a final program.

Development and Security Strategy of network Security

There are more security flaws in the security mechanism based on WPA protocol and security risks in AES protocol applied in network, which make many security threats to current network. A new generation of security technology IEEE802.1 II protocol proposes a long-term and complete security assurance framework of network.

4.1 Improved Data Encryption Protocol. Given there are various security flaws in WPA, WI-Fi Alliance releases a interim agreement WPA (Wi-Fi Protected Access), WPA uses a new algorithm to solve the flaws of WPA on encryption and data checking. WPA mainly completes the following tasks: solve the main security issues of WPA, especially for its vulnerabilities on shared key: Add user-level authentication measures; solve the problem of system upgrade. The existing Wi-Fi certified products of network can achieve WPA through software upgrade.

4.2 Improved Authentication Mechanism. Since the basic authentication mechanism specified by IEEE 802.3 standard is too simple to provide the reliable security defense for network. 802. Ix authentication protocol uses EAP to handle the authentication request of client. Authenticators create a logical port for them according to association ID of each applicant; each logical port has two states: unauthorized and authorized. When the port is unauthorized, it can only send and receive 802.Ix protocol data packet, while data packet of other protocol type is blocked.

Conclusions

For continuing expansion and increasing demand of network, it puts forward higher requirements for network security. It is impossible for simple enhancement of security protocol of single layer or using one kind of means to solve all security issues of the network. Therefore, the network can use various technologies, such as IPSec virtual private network, Service Set Identifier access control, upgrade Wi-Fi encryption, MAC address filtering, firewall and intrusion detection, etc. to protect network security. Using various security technologies to establish multi-level security system is developing direction of network security.

References

[1] Xiuying Cao etc. Security System of network, Electronic Industry Press, 2009.

[2] Xiaodong Zuo. Analysis of network, Telecommunications Science, 2010.

[3] Yinchun Yang. Analysis of WAPI security mechanism [J], Computer Engineering, 2011.

[4] (English) Edney, (American) Al Pau writes, Zheng Zhou, etc. Security Practice of network -WPA and 802.3i, People's Posts and Telecommunications Publishing House, 2010.

[5] Haiying Gao, Yuanxing Xue,etc. virtual private network Technologies, China Machine Press, 2012.

[6] Yurzin Bogdanov,Valeri Chipulis. Information-analytical systems of thermo-power engineering[A]. Proceedings of The First International Conference on Wireless Communications and Applications[C]. 2011

Advanced Materials Research Vols. 989-994 (2014) pp 4249-4252
© (2014) Trans Tech Publications, Switzerland
doi:10.4028/www.scientific.net/AMR.989-994.4249

A radio Link Logical Relationship Between And One Network Apparatus

Wu Chuansheng

Software College, University of Science and Technology Liaoning,China

gykwcs@163.com

Keywords: radio Link,network apparatus,network, handling barred ,cell

Abstract. MAC layer, a radio link control (RLC) layer and a broadcast and multicast control (BMC) layer exist in a second layer. The MAC layer maps various logical channels to various transport channels and performs logical channel multiplexing to map a plurality of logical channels to one transport channel.The MAC layer is connected to the RLC layer, which is a higher layer, through a logical channel. The logical channel is divided into a control channel for transmitting information on a control plane and a traffic channel for transmitting information on a user plane, according to the kind of transmitted information.

0 Introduction

The MAC-b sublayer is responsible for management of a Broadcast Channel (BCH) which is a transport channel for broadcasting system information, the MAC-c/sh sublayer is responsible for management of a Forward Access Channel (FACH) common transport channel shared with the other UEs, and the MAC-d sublayer is responsible for management of a Dedicated Channel which is a dedicated transport channel of a specific UE. In addition, the MAC-hs/ehs sublayer manages a High Speed Downlink Shared Channel (HS-DSCH) for high-speed downlink data transmission and the MAC-e/es or MAC-i/is sublayer manages an Enhanced Dedicated Channel (E-DCH) which is a transport channel for high-speed uplink data transmission.The RLC layer guarantees Quality of Service (QoS) of a Radio Bearer (RBs) or data transmission. The RLC has one or two independent RLC entities for each RB in order to guarantee the QoS of the RB. In order to guarantee various QoSs, three operation modes, i.e., a Transparent Mode (TM), an Unacknowledged Mode (UM), and an Acknowledged Mode (AM), are provided. In addition, the RLC is responsible for adjustment of a data size to suit data transmission over an air interface and is responsible for segmentation and concatenation of data received from a higher layer[1,2].

1 The relationship between the wireless network andwireless link

The A cell, on which a general UE cannot camp in order to enable a network manager to utilize the cell for a special purpose, is referred to as a reserved cell and the other cells are referred to as non-reserved cells. In the cell selection process and the cell reselection process, the UE does not regard the barred cell as a selectable cell. The UE regards a non-barred cell or a non-reserved cell as a selectable cell.[3]

A suitable cell refers to a cell in which the UE can receive a public-use service. A suitable cell is a non-barred cell in which the intensity of a signal measured by the UE is greater than the intensity of a signal of a cell, which currently provides a service to the UE, by a predetermined value, which belongs to a Public Land Mobile Network (PLMN) which can be accessed by the UE, and in which a location area updating process or a tracking area updating process of the UE is not inhibited.[4]

From the viewpoint of the UE which uses a plurality of frequencies as in the dual cell HSDPA, the

cell includes one downlink and one uplink associated therewith. However, in the system using the plurality of frequencies, the cell does not always include one uplink and one downlink. The UE may include two downlinks or four downlinks and one uplink. In this case, a downlink without an uplink associated therewith may be present. That is, a cell including only downlinks or a cell including uplinks may be present.[5]

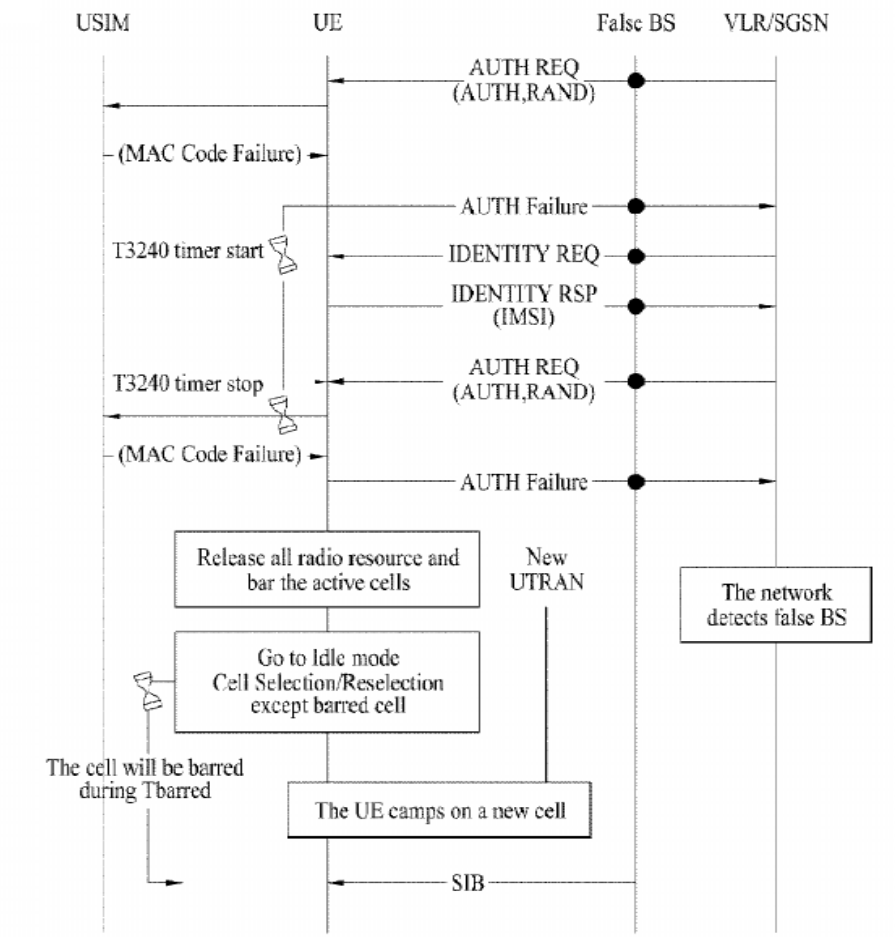

FIG. 1

Next, the active set will be described with reference to FIG. 1.

A radio link is a logical relationship between one UE and one network apparatus.

A downlink radio link is identified by a frequency and a cell identifier, and the frequency is at least one of a Universal Mobile Telecommunications system (UMTS) Terrestrial Radio Access (UTRA) Absolute Radio Frequency Channel Number (UARFCN) and an Evolved Absolute Radio Frequency Channel Number (EARFCN), and the cell identifier is at least one of a Primary Scrambling Code (PSC) and a Physical Cell Identifier (PCI).

An uplink radio link is identified by a frequency and a cell identifier. The frequency is at least one of a UARFCN and an EARFCN which are uplink frequencies to transmit data through the uplink radio link. In the UMTS, the cell identifier is an uplink scrambling code or a Physical Random Access Channel (PRACH) scrambling code. In the LTE system, the cell is identified by a PCI and a Cell Radio Network Temporary Identifier (C-RNTI).

Alternatively, the uplink radio link may be identified by the frequency and the cell identifier of the downlink radio link to receive control information necessary for uplink transmission.

The active set refers to a set of radio links for performing a specific communication service between the UE and the network, and a cell present in the active set is a cell located in an area in which soft

handover is possible. Due to handover, during actual data transmission, data transmission may be performed through one or more radio links.

FIG. 1 is a diagram showing an E-DACH active set if a UE uses one frequency. The active set includes an active set for DCH transmission and an E-DCH active set for E-DCH transmission. The active set generally refers to an active set for DCH and E-DCH transmission. The E-DCH forms a pair with a HS-DSCH. For E-DCH transmission, the UE receives a grant through an E-AGCH and receives an ACK/NACK signal of the transmitted data through an E-HICH. If the UE can receive data using three radio links C1, C2 and C3 through the HS-DSCH, radio links C1 and C2 which can perform E-HICH reception are present and a radio link C1 through which the UE receives the E-AGCH is present, C1 and C2 are included in the active set of the UE and C3 are not included in the active set of the UE.

Diagram showing an E-DCH active set of a UE which performs dual cell HSDPA. If the UE uses a plurality of frequencies, a cell having both an uplink radio link and a downlink radio link is included in the active set, but a cell having only an uplink radio link or a downlink radio link is not included in the active set. The active set of the E-DCH transmission is a radio link to receive a downlink control signal for uplink transmission. Accordingly, when data transmission is performed using one uplink frequency and two downlink frequencies, the radio link may be set as shown in FIG. 8. In this case, downlink radio links for receiving the E-HICH are included in the active set and all the other radio links are not included in the active set.Next, a cell selection method according to an embodiment of the present invention will be described with reference to is a flowchart illustrating a cell selection method according to an embodiment of the present invention.

2 Design of wireless network and wireless link

In some instances, well-known structures and devices are omitted in order to avoid obscuring the concepts of the present invention and the important functions of the structures and devices are shown in block diagram form. The same reference numbers will be used throughout the drawings to refer to the same or like parts.In the following description, it is assumed that a terminal includes a mobile or fixed user end device such as a user equipment (UE) and a mobile station (MS), and a base station includes a node of a network end communicating with a terminal, such as a Node-B, an eNode B, and a base station.First, dual cell High Speed Packet Access (HSPA) will be described with reference to FIG. 3.is a diagram showing a dual cell HSPA.As shown in FIG. 3, in the related art, a UE transmitted an Enhanced Dedicated Channel (E-DCH) using one frequency. However, in the dual cell HSPA, the UE simultaneously transmits data using two frequencies such that data transfer rate increases to twice that of the related art. In the dual cell HSPA, the UE may transmit data at a maximum rate of 20 Mbps, and an operation for transmitting data using two frequencies by the UE is referred to as a dual cell E-DCH operation. In addition, even in a downlink, in the related art, the UE received a High Speed Downlink Shared Channel (HS-DSCH) using one frequency. However, in the dual cell HSPA, one UE receives data using two frequencies so as to double a data reception rate. In the dual cell HSPA, the UE may receive data at a maximum rate of 80 Mbps, and an operation for simultaneously receiving data using two frequencies is referred to as a dual cell HSDPA operation. One UE may simultaneously receive data using four frequencies so as to increase a data reception rate to four times that of the basic HS-DSCH. This is referred to as a four-carrier HSDPA operation.

A cell which receives a downlink control signal necessary for data transmission through a primary uplink frequency of a UE in a dual cell HSPA is referred to as a serving HS-DSCH cell or a primary serving HS-DSCH cell. In addition, cells other than the serving HS-DSCH cell among cells in which a UE receives data are referred to as secondary serving HS-DSCH cells. At this time, the

primary uplink frequency is an uplink frequency in which a HS-DPCCH channel for transmitting an acknowledgement/non-acknowledgement (ACK/NACK) of the received downlink data exists.

Next, Carrier Aggregation (CA) of an LTE-A system will be described with reference to is a diagram showing the CA of the LTE-A system.

3 Summary

A cell is a wireless network object for transmitting a broadcast message from one UTRAN access point to all UEs present in one specific area and is identified by a cell identifier. A cell, on which the UE camps, refers to a cell selected after a UE successfully completes a cell selection process and a cell reselection process.Next, a cell state and cell reservation will be described. The network identifies a cell state by a barred cell and a non-barred cell in order to control the cell selection process and the cell reselection process of the UE. The barred cell indicates a cell on which the UE cannot camp and the non-barred cell indicates a cell on which the UE can camp.

Reference

[1] Intelligent fuzzy controller design of pressure ball drying system[A]. Proceedings of 2011 IEEE International Conference on Computer Science (CSAE 2011) VOL01[C]. 2011

[2] The Dairy Cattle Data Acquisition System Based on PDA[A]. Computer and Computing Technologies in Agriculture-Ⅰ--Proceedings of the Third IFIP International Conference [C]. 2009

[3] The Research of Distributed Power Quality on-line Monitoring System Based on GRPS[A]. Proceedings 2010 IEEE International Conference on Software Service Sciences[C]. 2010

[4] Amir Haghbinshomali,Naser Valaei,Mehrnaz Fahimirad,Kamarulzaman Ab. Aziz. A Conceptual Model for an Efficient Personnel Monitoring System using Radio Frequency Identification (RFID) Technology.[A]. Future Information Technology--International Proceedings of Computer Science and Information Technology[C]. 2011

[5] Kannan Rathimala,Govindan Marthandan. A Conceptual Model for Information Navigation Structure of E-Commerce Websites[A]. Computer and Software Modeling--International Proceedings of Computer Science and Information Technology[C]. 2011

Advanced Materials Research Vols. 989-994 (2014) pp 4253-4260
© (2014) Trans Tech Publications, Switzerland
doi:10.4028/www.scientific.net/AMR.989-994.4253

Real-time Cluster Resources Scheduling Strategy in WIA-PA Networks

Yuping Sun [1, a], Mingjie Fang [2,b] and Jianhua Sun [3,c]

[1] Wuhan Second Ship Design&Research Institute, Wuhan, China

[a] sun-198192@163.com, [b] fangmingjie@webmail.hzau.edu.cn, [c]4.ttpconference@163.com

Keywords: real-time communication; resources scheduling; edge-coloring; low latency

Abstract. WIA-PA network is a kind of multi-hop wireless network, which is specially designed for industrial process automation control. It uses hybrid management pattern with star and mesh structure. Intra-cluster and inter-cluster communication is scheduled simultaneously based on TDMA as well as FDMA. In this paper, a real-time cluster resources scheduling strategy for WIA-PA networks is proposed and the specific algorithm is implemented by edge-coloring. Our algorithm combines with optimal routing mechanism and arranges the order of links reasonably, resulting in avoiding conflict and improving the original communication success rate. Furthermore, the algorithm makes full use of channel resources, which greatly reduces end-to-end delay. The performance analysis shows that our algorithm is close to optimal for WIA-PA networks. In addition, compared with RSCA algorithm, our algorithm has lower latency and higher network throughput.

Introduction

Due to the huge advantage over wired communication, wireless communication technology has been a hot spot in the field of industrial automation control. Wireless process automation system can save costs and reduce the difficulty of connection among devices, which is applied to the complex industrial environment. What's more, it is easy to be maintained and very flexible, which hence has a broad prospect [1]. However, because the wireless channel is sensitive to interference, the specific requirements of industrial control application bring some challenges to wireless networks, especially in terms of strict real-time, reliability, security, low power consumption and time synchronization. These issues must be solved urgently when wireless technology is applied to industrial process automation.

Based on the IEEE 802.15.4 standard, WIA-PA (Wireless Networks for Industrial Automation-Process Automation) is the wireless communication specification used for industrial process automation and accepted by IEC in 2008 [2], which became the second Wireless industry standard after Wireless HART. WIA-PA networks adopt layered hybrid organization, divided into star and mesh structure. In the star network, router devices, as the cluster head, gather the data information from field devices and forward to the gateway. With centralized management, the network manager manages the entire network by collecting information of all devices and issuing commands, and allocates time slots and channels to clusters in mesh network. which can ensure normal communication. It accesses channels randomly with TDMA/CSMA mechanism, and supports periodic or non-periodic communication loads. Besides, frequency hopping spread spectrum and automatic retransmission technology improves the reliability of networks. WIA-PA has 16 available physical channels in all. Intra-cluster communication uses the same channel only while inter-cluster communication can use either the same or different channels, but conflict avoidance must be concerned. In this paper, according to the need of real-time communication in WIA-PA networks, time slots and channels are arranged orderly for links between each cluster, greatly improving the network performance.

The rest of this paper is arranged as following: In Section II, WIA-PA network architecture and superframe is introduced, and the relate work is summarized. Our scheduling algorithm is proposed

and the scheduling result of a specific network is given in Section III. In Section IV, compared with RSCA, we evaluate the performance of our algorithm. Finally, this paper is concluded in Section V.

BACKGROUND AND RELATED WORK

A. WIA-PA network architecture

WIA-PA network architecture is shown in fig. 1, which combines star structure with mesh structure.

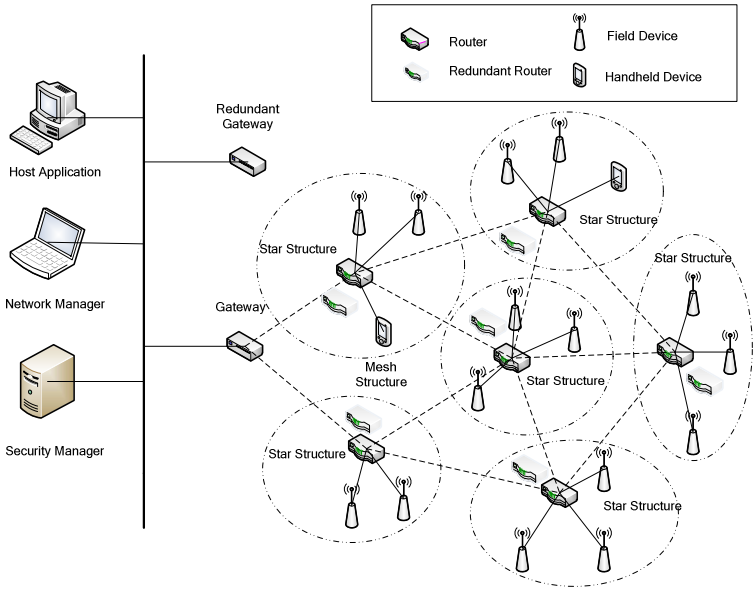

Fig. 1 WIA-PA network infrastructure

Routers, field devices and handheld devices constitute the star topology, regarded as a cluster. Field devices, as members of the cluster, collect data information and transmit to the cluster head. A handheld device is used to configure and diagnose the network. The reliable mesh network is composed of routing devices and the gateway. Routers transfer data information to the gateway which connects WIA-PA network with the upper management and application network. As the hinge, network manager is responsible for organizing the entire network, distributing communication tasks, establishing routing table and allotting communication resources. In addition, because cluster heads and the gateway may malfunction or die under very heavy loads, there are a large number of redundant equipments in WIA-PA networks, which can replace the dead nodes timely.

B. Superframe structure

WIA-PA networks coordinate communication between various devices through TDMA technology. Links are specified in time slots and channels, which ensure communication without conflict. Time synchronization is necessary among all devices.

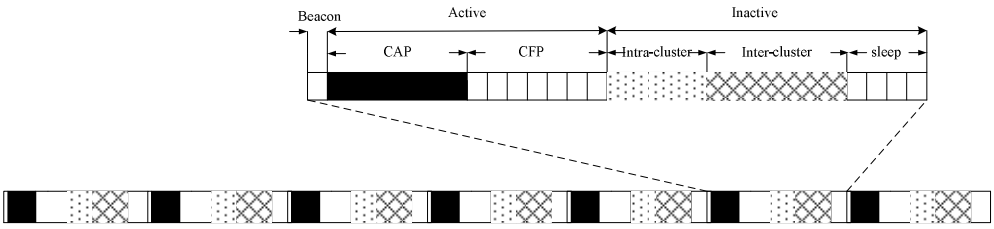

Fig. 2 WIA-PA superframe

WIA-PA superframe consists of cyclic time slots in fig. 2. The number of slots is the length of superframe. In order to facilitate the new devices joining, beacon frame is placed at the beginning of

each time slot. All routers send beacon frame through their own channel, while field devices can only receive beacon. New devices can get relevant network parameters from beacon. Next is active period, including CAP (Contention Access Period) and CFP (Contention Free Period). CAP is devoted to new devices joining, intra-cluster management and information retransmission. In CFP, communication between the cluster head and mobile devices is processed. Inactive period is used for intra-cluster and inter-cluster communication as well as sleep.

WIA-PA has rich network resources. Network manager is responsible for allocating resources to each device reasonably and the distribution result will affect the performance of network. There are two types of communication in WIA-PA networks. With intra-cluster communication, each member sends data information to the cluster head through the same channel in different time slots. Inter-cluster communication can be achieved through different channels, which also makes full use of network resources and reduces end-to-end delay. This paper mainly studies inter-cluster resource scheduling in WIA-PA networks, which assigns time slots and channels for each link in mesh network.

C. Relate work

Link scheduling strategies based on TDMA in wireless multi-hop networks have been widely researched [3,4], and many scholars propose a number of classic algorithms. However, to our knowledge, resources scheduling algorithms for WIA-PA networks are few. In [5], a cluster channel assignment strategy in WIA-PA networks is studied and a scheduling algorithm based on vertex-coloring is proposed, which can satisfy the demand of real-time communication. However its algorithm is too simple and reliability as well as throughput isn't considered. [6] describes an adaptive timeslot scheduling strategy for long cycle data in WIA-PA networks, which allocates resources for star and mesh network uniformly. Conflict is decreased owe to feedback mechanism, but isn't avoided completely. In [7], distributed and dynamic TDMA channel scheduling algorithm is presented, which reduces the channel interference by using blacklist technology. It also reduces data retransmission times effectively and improves the network throughput. [8] puts forward an improved adaptive channel hopping scheme in WIA-PA networks. The network reliability is greatly improved by the way of channel assessment and reasonable arrangement of channels sequence, but there are no specific optimization measures for network latency and network throughput is not evaluated either. In [9], a resources scheduling algorithm for multi-hop mesh networks is implemented by vertex-coloring. This algorithm avoids conflict, but the order of links is not arranged properly, leading to a high delay. In [10], a superframe scheduling algorithm for high reliability in Wireless HART networks is given. As a result of retransmission mechanism for each link, the network has a very high reliability, but the excessive consumption of network resources causes low throughput and high time-delay, which is not suitable for WIA-PA networks.

At present, most scheduling algorithms for wireless sensor networks are realized by graph theory, aimed at optimizing network performance. However, due to the special structure and application requirement of WIA-PA networks, few scheduling algorithms are satisfactory. According to the characteristics of WIA-PA networks, a resources assignment algorithm by edge-coloring is presented in this paper. Combining with optimal routing algorithm, we reasonably arrange the link order, which greatly improves the network performance.

Resources Scheduling

A. Network model and definitions

Here we only consider cluster heads and gateway nodes in mesh network which can be modeled as a simple acyclic graph G = (V, E). V = {v0,v1,v2,…,vn} is the set of all nodes, where each node vi, $1 \le i \le n$, denotes a routing device and v0 is the gateway. E = {e0,e1,e2,…,em} is the set of all links, and the link ek = (vi, vj), $0 \le k \le m$, $0 \le i \le n$, $0 \le j \le n$, can be built if and only if vi and vj are in the range of

communication between each other. The set of time slots is defined as T = {t1, t2, t3,... , tl}, and the frame length is l. A kind of color corresponds to a time slot, which can be defined as S = T. Channel set is C = {c1,c2,c3,…,cr}. Scheduling issue can be regarded as assigning links to the plane composed by l slots and r channels.

In a real network environment, it is very necessary to create an optimal network topology and remove suboptimal links for network manager. If network nodes route packets through the shortest path, the network delay and power consumption can be reduced. In [9], the optimization method for mesh networks based on breadth-first search is described.

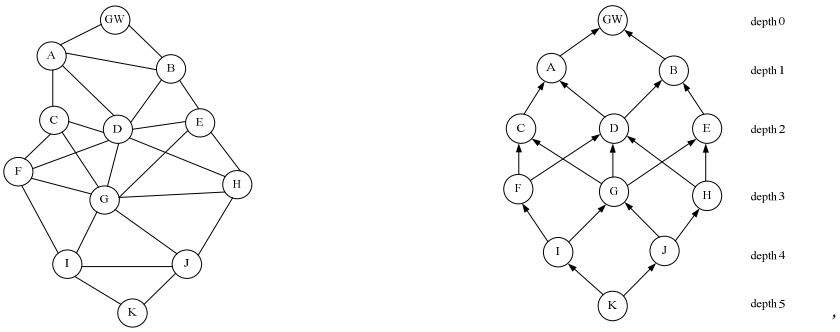

(a)The original graph G (b)The optimized graph G'

Fig. 3 Network model

Fig. 3a illustrates an original network topology G and its optimized topology G' is drawn in fig. 3b. Uplink data is transferred from low-layer to high-layer gradually, so routing path of each node is the shortest. What's more, links between the children nodes and their uncle keep the network redundancy.

B. Scheduling algorithm

WIA-PA is applied in industrial process control, which requires real-time and reliability. Therefore, we consider the following strategies in our scheduling algorithm:

1) Based on graph routing. Graph routing contains multiple paths from the source to the destination. Data can be transmitted through other paths when a certain path is blocked. In order to ensure the fair communication opportunities of all devices and the redundancy of graph routing, resources should be allotted to each link. All links in the network graph are dyed with one colour at least.

2) Conflict avoidance. There are two types of conflict in WIA-PA networks: explicit conflict and implicit conflict.

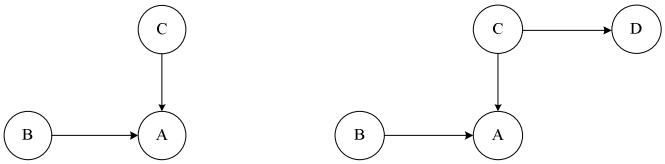

(a)Explicit conflict (b)Implicit conflict

Fig. 4 Conflict in mesh network

As shown in fig. 4a, when the node B and C send packets to the node A at the same time, explicit conflict will appear. In order to avoid it, the links B->A and C->A should be assigned to different time slots. In fig. 4b, if the node A and C in the range of communication, and the node B communicates with A and meanwhile the node C send packets to D, then implicit conflict will occur in the node A.

We can allot the links B->A and C->D to different channels in the same time slot, which also ensures the utilization of network resources. Therefore, with the purpose of conflict avoidance, links with public node must be dyed in different colors while others can be dyed with the same color which should be arranged to different channels.

3) Reasonable links sequence. The sequence of time slots in a superframe corresponds to the order of communication, which will affect the communication latency greatly. A node should be arranged for the transmission slot as soon as possible to transfer packet when it receives a packet, which also saves the storage space of devices. Furthermore, due to real-time communication in WIA-PA networks, an edge can be colored only when its starting point has memorized received packets.

4) Optimal routing mechanism. Our resources allocation strategy combines with optimal routing algorithm. Data packets will be transferred through the best route preferentially, so links on the best route should be allocated in earlier time slots. In other words, they must be colored firstly. Here we selected a WIA-PA network oriented routing algorithm ORBV in [11], which has low latency and energy consumption.

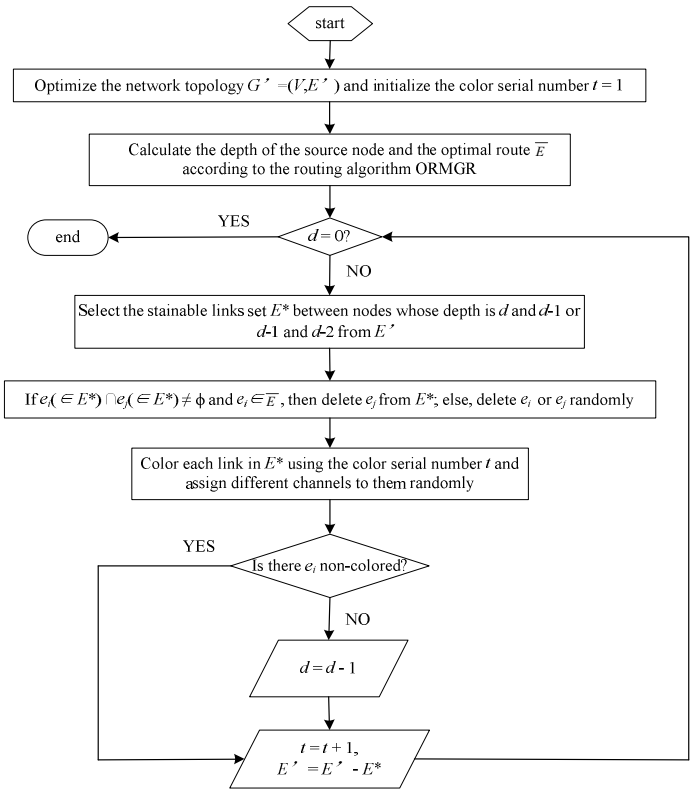

Fig. 5 Our scheduling algorithm

Our algorithm is implemented by edge-coloring which starts from the source node. An edge denotes a link and each color corresponds to a time slot. The specific scheduling algorithm is shown in fig. 5, where d is the network layer number and ei represents a link between the current layer and the upper.

C. Resources allocation

In accordance with our algorithm, the scheduling result of the graph G' in fig. 3b is showed in fig. 6. We assume that the optimal route is K->I->G->C->A->GW according to the routing algorithm ORBV.

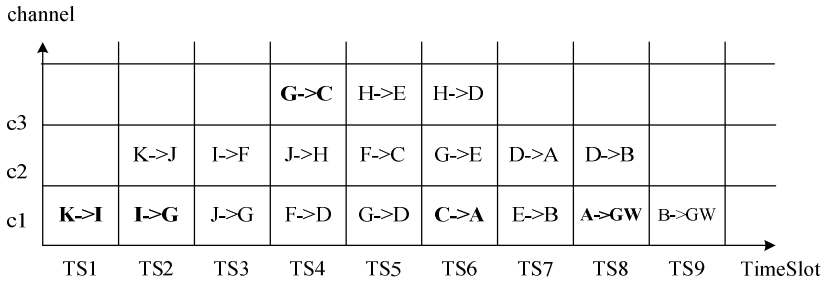

Fig. 6 The example of our scheduling result

We assign resources for each link in the mesh network, which guarantees the redundancy. In every time slot, any node appears at most once and all links are arranged to different channels, so as to avoid conflict completely. Moreover, we arrange links orderly and allocate the earliest time slots to links on the best route. For example, when the node K sends packets to the gateway, the links K->I at TS1, I->G at TS2, G->C at TS4, C->A at TS6 and A->GW at TS8 are used firstly.

Analysis and Evaluation

Our resources allocation strategy reasonably arranges time slots and channels for each link in the mesh network, resulting in conflict avoidance. Furthermore, considering limited buffer memory resources of devices, we arrange a transmission slot to the node immediately when it has received packets. The maximum of packets in each node is less than the number of its children. It can save the cost of devices and meet the requirements of industrial application.

In order to evaluate our strategy entirely, a route-based scheduling algorithm in wireless multi-hop mesh networks for collision avoidance (RSCA) proposed in [9] is compared with our scheduling algorithm. Its superframe result of the network graph G' in fig. 3b is presented in fig. 7. RSCA algorithm assigns communication resources to nodes in mesh network by the way of vertex-coloring which avoids conflict completely, but it does not arrange links orderly.

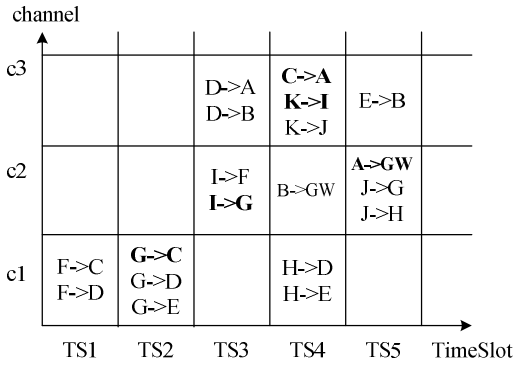

Fig. 7 The example of RSCA scheduling result

Our algorithm is based on graph routing, which rich redundant paths exist in the mesh network. Compared with multi-path routing, graph routing can effectively improve the robustness of the network [10]. Besides, because the transmission success rate on the optimal route is higher than that of other routes, the original communication success rate is greatly improved as a result of scheduling links on the optimal route preferentially. We assume that the loss probability of packets for each hop on the best route is pl = 0.05 and that on other routes is pl' = 0.1. Then the transmission success rate of our scheme shown in fig. 6 is 89.44%, which can ensure successful communication between the source and the gateway through a superframe. While RSCA arranges links with the common start to the same channel, leading to random links sequence for communication, so its transmission success rate is obviously lower than ours.

WIA-PA is applied in industrial process control which needs real-time communication. Our scheduling scheme decreases the transmission delay substantially because links are arranged in order and channel resources are made full use. In fig. 6, it takes eight or nine time slots to transfer data to the gateway from node K according to our algorithm. For RSCA algorithm shown in fig. 7, the shortest time is nine time slots, which the corresponding route is K->J->G->D->B->GW. However, in the practical application environment, wireless channel interference is generally strong. As mentioned before, our schedule has very high reliability and can guarantee successful communication through a frame. While RSCA algorithm can't ensure successful transmission through the fastest path from the source to the destination, which often requires several superframe cycle scheduling, so the network delay is very high. In addition, owe to optimal routing mechanism, our algorithm greatly improves the success rate of original communication, which also reduces the retransmission delay.

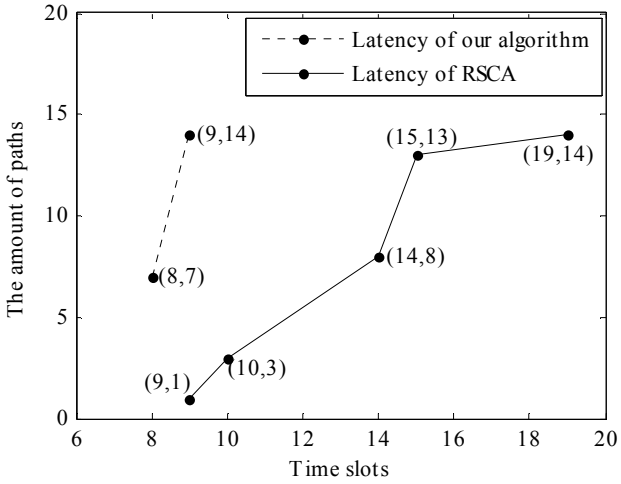

Fig. 8 The relationship between network latency and redundancy

There are 14 paths from node K to the gateway in fig. 3b. It's obvious that the network reliability is proportional to the amount of available paths from the source to the gateway which corresponds to redundancy. The relationship between network latency and redundancy is illustrated in fig. 8. The horizontal axis represents the total slots spent by transmission from node K and the gateway. And the vertical axis is the amount of homologous available paths. We can see that our algorithm has much lower latency than RSCA on the premise of the same redundancy.

Network throughput is also an important performance for WIA-PA, which is defined as the average number of packets received successfully by the gateway in each time slot. It can be expressed as following,

$$NT = \frac{n - n_l}{l}$$

Where n is the number of packets sent by all nodes in a superframe, n_l is the amount of loss packets in a superframe and l is the amount of time slots. For a specific network, n_l is fixed. However, the loss probability of packets with our strategy is lower than that of RSCA, so n_l of our scheme is smaller. In fig.6, our superframe length is 9 and node K can transfer data packet to the gateway through a superframe. While a successful communication between node K and the gateway needs twice superframe scheduling at least for RSCA in fig.7, which the total slots is 10. Thus, our algorithm improves the network throughput compared with RSCA. For the practical WIA-PA network, when cluster heads transmit data packets simultaneously, we can schedule their superframe at the same time by using channels parallelly which can achieve a high convergence speed. It's our future work.

Conclusion

A cluster resources scheduling algorithm for WIA-PA networks is implemented by edge-coloring in this paper. Communication resources are assigned to each link reasonably, which makes conflict avoidance. Based on graph routing, our strategy combines with optimal routing algorithm ORBV, which improves the success rate of original data transmission. Analysis shows that our algorithm improves the reliability and network throughput effectively, and save the storage resources of network devices. Compared with RSCA, our algorithm has lower latency and can satisfy the requirement of real-time communication in WIA-PA networks.

References

[1] Willig A, Matheus K, Wolisz A. Wireless technology in industrial networks[J]. Proceedings of the IEEE, 2005, 93(6): 1130-1151.

[2] Wireless Industry Automation Specifications for Process Automation, IEC/PAS 62601, Oct. 2008.

[3] Wang W, Wang Y, Li X Y, et al. Efficient interference-aware TDMA link scheduling for static wireless networks[C]//Proceedings of the 12th annual international conference on Mobile computing and networking. ACM, 2006: 262-273.

[4] Ergen S C, Varaiya P. TDMA scheduling algorithms for wireless sensor networks[J]. Wireless Networks, 2010, 16(4): 985-997.

[5] Yue F, Liu F. Research for cluster channel assignment in WIA-PA[C]//Proceedings of the 5th International Conference on Wireless communications, networking and mobile computing. IEEE Press, 2009: 2852-2855.

[6] Zhang X, Liang W, Yu H. Adaptive Timeslot Scheduling of Long Cycle Data in WIA-PA network[C]//Computational Intelligence and Industrial Applications, 2009. PACIIA 2009. Asia-Pacific Conference on. IEEE, 2009, 1: 267-271.

[7] Zhang X, Liang W, Zheng M, et al. Distributed and dynamic TDMA channel scheduling algorithm for WIA-PA[C]//Intelligent Computing and Intelligent Systems, 2009. ICIS 2009. IEEE International Conference on. IEEE, 2009, 3: 462-466.

[8] Wang P, Pan Q, Wang H, et al. An improved adaptive channel hopping scheme for WIA-PA industrial wireless networks[C]//Advanced Computer Theory and Engineering (ICACTE), 2010 3rd International Conference on. IEEE, 2010, 1: V1-596-V1-600.

[9] Jindong Z, Qin W, Feng Y. A route-based scheduling in wireless multi-hop mesh networks for collision avoidance[C]//Wireless Communications, Networking and Mobile Computing, 2009. WiCom'09. 5th International Conference on. IEEE, 2009: 1-4.

[10] K. Dang, J. Shen, L. Dong, Y. Xia. A Graph Route-Based Superframe Scheduling Scheme in WirelessHART Mesh Networks for High Robustness[J]. Wireless Personal Communications, 2012: 1-14.

[11] Yi X, Jiang P, Wang X, et al. A WIA-PA Network Oriented Routing Algorithm Based on VCR[M]//Recent Advances in Computer Science and Information Engineering. Springer Berlin Heidelberg, 2012: 39-44.

Advanced Materials Research Vols. 989-994 (2014) pp 4261-4264
© (2014) Trans Tech Publications, Switzerland
doi:10.4028/www.scientific.net/AMR.989-994.4261

Research on Security Issues of the Internet of Things

Xiaofeng Wang

Langfang Teachers University, Mathematical and Information Sciences Institute, Langfang, China

Wangxiaofeng7654@126.com

Keywords: the Internet of things; information security; security policy; privacy protection

Abstract. According to the current mainstream architecture of the Internet of Things, Makes research on security threat of the Internet of things from the perception layer, network layer and application layer, Gives the corresponding security policies and measures. It provides the theoretical reference for security of the Internet of things and privacy protection.

Introduction

In recent years, with the rapid development of Internet technology and a variety of network access and intelligent computing, the Internet of Things as a new technology is being more and more concerned by people, and continues to be applied and promoted in all walks of life. The Internet of things connects the reality physical space and virtual information space, Its ubiquitous data awareness, information transmission based on wireless, intelligent information processing, can be used in all aspects of daily life, it is closely related to the national security and economic security, and has become an important factor of the competition of comprehensive national strength among countries. With the continuous development and application of the Internet of things, its own hidden security problems increasingly appear.

The Architecture of the Internet of Things

The Internet of things is a network based on the Internet, through the radio frequency identification (RFID), infrared sensors, global positioning systems, laser scanners and other information sensing device, according to the agreed protocol, connects anything with the Internet, to exchange information and communicate, to achieve intelligent identify, locate, track, monitor and manage . The Internet of Things architecture can be divided into three layers: the perception layer, network layer and application layer. It is shown in Fig. 1.

The Perception Layer. In the overall structure of the Internet of things, the perception layer exists as a basis, has a very important role. The perception layer is the beginning of the Internet of Things overall structure, its main task is to collect and transmit the data. Data is collected by GPS, camera and other reader tools, and the data is transferred to the associated device by means of short-distance transmission technology, such as ZigBee, Bluetooth and other wireless technologies or industrial field bus technology, so the device can process the data.

The Network Layer. In the overall architecture of the Internet of things, the network layer is based on the Internet. The network layer generally transmits the collected data, plays a very important function in the overall system of the Internet of things. The network layer requires the Internet of good performance; however, the situation of today's Internet can not meet the demand of data transmission. So, if we want the Internet of Things deeper and more long-term development, we need to re-integrate the current Internet, to improve performance.

The Application Layer. The ultimate aim of the Internet of things is to develop applications. Therefore, the application layer is the core of the Internet of things architecture .The application layer receives the data of collection and transmission, and then processes data through certain techniques, in order to have the right judge and control for the Internet of things. The Internet of things application

layer can be divided into the terminal device layer and application layer, which together take up the work of the Internet of things in different industries and different areas.

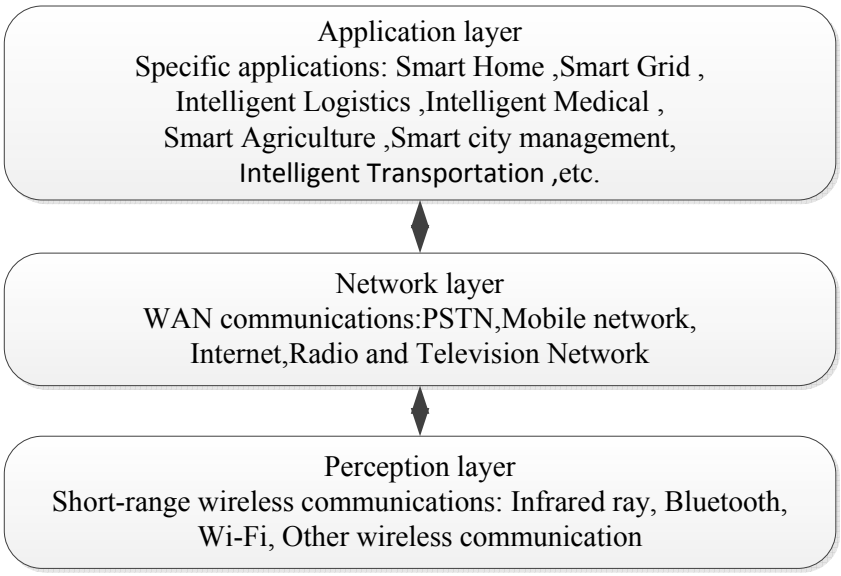

Fig. 1. The Architecture of the Internet of Things

Security Threats and Countermeasures of the Internet of Things

Perception Layer Security Threats. It is mainly related to RFID security, sensor nodes security, and intelligent terminal security.

Denial of Service: electronic tags respond to a lot of malicious requests without differentiate, resulting in not responding to legitimate requests. Safety measures: use intrusion detection techniques to identify attacks.

Node Failures: due to the destruction of the environment or the physical, leading to the perception node failure, resulting in inaccurate data, or even false data. Safety Measures: use the fault detection and tolerance techniques.

Message Damage: intruder between the source node and the destination to insert itself, tampering message content. Safety measures: use lightweight or super lightweight encryption and authentication mechanisms.

Physical Damage: sensor nodes are in the unattended state may be damaged or stolen. Safety measures: establish a remote device management platform for sensor nodes to monitor and manage.

User Privacy Violations: sensor nodes transmit information stored indiscriminately to the reader. Safety Measures: Since node computing and storage capacity constraints, can use lightweight or super lightweight encryption and authentication techniques.

Packet Loss: at the sensor network aggregation node, due to the large amount of data, is prone to channel error, the node congestion, and packet loss and packet collisions. Safety measures: use data fusion and security control techniques to improve fault tolerance of the network.

Node Camouflage: the perception layer nodes and devices are typically deployed in an open environment, the attacker obtains node identity information through the analysis of node, and then captures the nodes, masquerading as legitimate users; or posing by using other nodes. Safety measures: use access control technology for sensor nodes to verify the legality of the node.

Channel Interference: radio frequency signals and wireless network are vulnerable to interference, the attacker can issue a large number of repeat visit request, leading to the depletion of energy of active tags or the gathering node of gateway type is submerged, blocked, so that the work of the perception layer becomes failure. Safety measures: use electrostatic shielding, active jamming, and blocking labeling technology to protect the communication channel.

Information Theft: Since sensor nodes computing and storage capacity limits, unauthorized RFID reader communicates with the label directly, read, tamper or delete data. Safety measures: use lightweight access authentication control; allow only certified reader to access the label.

Security Threats and Countermeasures of the Network Layer. Network layer security issues are mainly related to transport security for wireless sensor networks, mobile communications networks, the Internet, private network and other networks, and secure issues of heterogeneous networks.

Routing Attacks: selective delivery attacks and false network routing attacks cause waste of resources and changing of the routing path or circuit. Safety measures: use secure routing protocols, routing information authentication, intrusion detection, etc.

Middle Attack: The attacker posing as an intermediate node, destruct information confidentiality, integrity and availability. Safety measures: use encryption and authentication measures to protect the network.

Information Tampering: data transmitted over the network is vulnerable to tampering. Safety Measures: use the message authentication technologies, such as digital summaries integrity protection technology.

Replay Attacks: an attacker sends a packet has been received over, to achieve the purpose of deceiving the system. Safety measures: use the time stamp, serial number, and response mechanisms to prevent replay attacks.

Across Heterogeneous Network Attacks: network interconnection of different protocols and different security domains can cause serious safety problems, such as cross-border two-way attacks, protocol conversion reliability, disclosure of sensitive information and so on. Safety measures: divide security domain, protocol conversion, isolation protocols, information ferry and other technical measures.

General Protocol Attacks: SYN Flood, ARP Spoof, Ping of Death, IP fragment and other network attacks may make the network device or transmission network in response to a service request rejected. Safety measures: enable the appropriate security module on the network devices such as intrusion prevention, packet filtering to block these conventional network attacks.

Information Disclosure: the attackers obtain confidential information, such as user privacy information on unencrypted network. Safety measures: use VPN, TLS and other security technology to protect the confidentiality of information.

Transmission Performance is Limited: node scale becomes larger, sends large amounts of data, and then lead to network congestion, resulting in intolerable delays or even denial of service. Safety measures: use data fusion and intelligent processing technology to reduce network redundant data.

Security Threats and Countermeasures of the Application Layer. Mainly related to the terminal application layer security, data confidentiality, integrity, availability, Auditability and application systems own security.

Information Disclosure: disclosure of confidential or private information in the data processing, transmission and storage. Safety measures: use encryption technology to ensure confidentiality of data transmission, processing and storage.

Access Control Vulnerabilities: access control logic confusion or control failure, may lead to serious security problems. Safety measures: use discretionary access control, mandatory access control, role-based access control, attribute-based access control policy.

Software Vulnerabilities: memory leaks, buffer overflows, SQL injection, XSS injection and other application vulnerabilities are seriously affecting the safe operation of the system. Safety measures: In software design, use technologies to avoid security loopholes. Before the on-line operation, should carry out the vulnerability scan.

Security Audit Vulnerabilities: security audit functions miss, don't audit important security event, auditing data protection is improper and so on. They may make potential or occurred security incidents not be effectively tracked. Safety measures: improve security audit function; allow users to be responsible for their actions.

Integrity Destruction: data is modified, inserted, deleted, etc. in the processing, transmission and storage. Safety measures: use cryptographic technique and hashing technology to protect data integrity.

Denial of Service: When a large-scale concurrent access, low hardware configuration or software design flaws can lead to system response slow or even denial of service. Safety measures: the application of the Internet of things should be considered in the performance and capacity of the system to avoid performance bottlenecks. Before on-line operation, the performance of stress tests should be carried out.

Insecure Terminals: mobile operating terminal and PC have not security reinforcing, security scanning, may pose security vulnerability. Safety measures: carry out terminal security checks, security certification, and prevent illegal end user to use system.

Summary

Currently the Internet of things has started preliminary development and pilot, but security and privacy protection of the Internet of things is one of the decisive factors that determine the rapid development of the Internet of things. From the three-layer structure of the Internet of things, analyzes the security threats of the Internet of things, and gives solutions, at today of the rapid development of the Internet of things, hope to provide help for the country's development and construction of the Internet of things and protect our security of the Internet of things and national security.

References

[1] Yong Peng, Research on security problem countermeasure based on the Internet of things, information network security, 2011.10: 4-6. (In Chinese)

[2] Haixiao Han, Research on safety analysis of the Internet of things, computer security, 2012.08:61-64. (In Chinese)

[3] Guang Yang,Guining Geng,Jing du,Chaohui Liu,He Han, Security threats and measures of the Internet of things, Journal of Tsinghua University (Natural Science), 2011, Vol.51, No.10 :1335-1340. (In Chinese)

[4] Changxing Zheng, Discussion on Safety problems and countermeasures of the Internet of things, computer security, 2012.10:70-75. (In Chinese)

[5] Daoyin Zhang, Wei Wang, Security threats and countermeasures of the Internet of things, information technology and standardization,2012.4:21-23. (In Chinese)

[6] He Wang,Hua Yang,Fubing Gao,Security of the Internet of things, Journal of Sichuan Ordnance,2011.10:90-91. (In Chinese)

Advanced Materials Research Vols. 989-994 (2014) pp 4265-4268
© (2014) Trans Tech Publications, Switzerland
doi:10.4028/www.scientific.net/AMR.989-994.4265

Research on Network Control Based on QoS of the Network

ZHOU Yang[1, a]

[1]Beijing University of Posts and Telecommunications International School, Beijing 102209,China

[a]ZhouYang2015@yeah.net

Keywords: network control, QoS, controller

Abstract. With the technology improvement of computer communication and multimedia coding, real time communication such as audio and video is introduced to networks and become a dominant way of communication. In the control of network, the optimization problem of the network controller based on network Quality of service (QoS) is a very important problem in the research of network control. Considering the influence of network quality—of service(QoS)on the control performance，a system model combining the network parameters and the control parameters is established for networked control systems(NCSs). Based on this, the condition dependent on the network parameters and control parameters is presented for the existence of guaranteed cost controllers. LMI). Within the scope of QoS perturbation，the designed controller can not only make the system as hypnotically stable but also guarantee that the system performance index is not greater than the upper bound.

1.The brief introduction of QoS.

As the name suggests, the Quality of Service often reflects the consumer's satisfaction with the services provided by servers. In computer systems, especially the Computer Network System, as a provider of calculation and information services also has the same quality problems of quality of service (QoS). From the appearance of computer system, people are tirelessly focused on working to improve service performance and service quality of the system. For present, definition of the QoS has a various forms. We see from chart 1 that RFC2386 describes QoS as: network needs to meet a series of service requests in data transmission flow, such as bandwidth, delay, delay jitter, drop rate, throughput and complexity etc. QoS reflects the ability of network in guaranteeing information transmission and meeting the services.

Types of application	Requirements for QoS	Range
FTP	bandwidth	0.2-10Mbps
Telnet	Relevant delay	<=800ms
Telephone	bandwidth	16kbs
	End-end delay	0-150ms
	End-end jitter	1ms
	Drop rate	<=le-2
HDTV	bandwidth	>=1Gbps
		500Mbps
		20Mbps
	End-end delay	250ms
	End-end jitter	1ms
	Drop rate	<=le-2
		<=le-11

Chart 1:QoS requirements of several applications

Quality of Service (QoS) is a set of service requirements, which the network must meet these requirements in order to ensure the appropriate service level of the data transfer. QoS draws a distinction between the business flow and customizes different strategies through various kinds of ways in the process of data transmission in the network, such as immediate sending, sending later,

discarding the different strategies to protect different quality service requirements of the data of different priority level .

2.Network control system.

The improvement of the performance of the network control depends not only on the algorithm design but also closely related to the shared network transmission resource scheduling. Scheduling problem of network control is based on transfer order assigned by the transmission scheduling algorithm for each entity (such as sensors, controllers and actuators, etc). Scheduling algorithm is actually a series of rules which decides the delivery order.

2.1Intrduction of the network control system.

In the network control system, we assume that the controlled object is a invariant continuous system, which can be described as:

$x(t)=Ax(t)+Bu(t)$ (1)

$y(t)=Cx(t)$ (2)

$x(t)\in R^n$ and $u(t)\in R^m$ is the state vector and controlled input vector respectively. A and B is constant. Assume that the sensor is clock-driven; controller and actuator are event-driven and single packet transmission. Data type (1) maintains and realizes the real control input must be piecewise continuous function by the zero order. In addition, considering network latency and packet loss in the process of network control, the actual network control system can be expressed as:

$x(t)=Ax(t)+Bu(t), t\in(i_kh+T_k, i_k+_1h+T_k+1)$ (3)

$u(t+)=Kx(t), \quad t\in(i_kh+T_k, k=1,2\cdots)$ (4)

H is the sampling period, K is feedback gain for the network controller, i_k (k=1, 2,...) are integers, T_k is network induced delay which shows the time interval needed from the time when sensor samples from the control object to the time when controller sends controlling signal to the actuator.

2.2QoS and network controller.

At present, research about controller design method based on the Network Quality of service (QoS) mainly focuses on two aspects: (1) according to the QoS parameters measured online to dynamically adjust the output of the controller gain; (2) to complete collaborative design of controller along with QoS in the design phase of Network control systems. The two methods are consisten twith respect to their esence, which dynamically adjust the output of the controller gainis according to off-line table controller gain parameters under different Network QoS and Network QoS.

Under the network environment, the joint control of network parameters and parameters of the control system can be described as the following general form:

$x(t)=f(x(t)),u(t),p_{x(t)},g(QoS)$ (5)

$x(t)=y(t),t\in[-d,0]$ (6)

$x(t)\in R$ ， $u(t)\in R^m$ are state vector and controlled input vector respectively, $p_{x(t)}\in R^m$ is object parameters from remote control, and quality of service (QoS) is related parameters about network services, $f\in R^m$ is conversion function of the network system, d is network system delay and (t) is the system initial state functions. Further, if the sensor system is time-driven, controllers and actuators are the event-driven, single packet transmission and the system state data are fully measurable, the state feedback controller output u (t) maintains and realizes through the zero order and discretization, then type (5) and type (6) can be described as:

$x(k+1)=f(s(k)),Kx(k-tik),px(k),y(QoS)$ (7)

And ik(k=1,2…) and are integers.

2.3Network service quality of real-time data .

From chart 1 we see that the network control system has more than more one network node and the sending node pi. In addition, according to business characteristics of network control system,

its data mainly divided into two categories: (1) real-time data with periodicity; 2) non real-time data amd non-periodicity mainly the control parameters' setting, the switch command and data report forms etc. For not the real-time data can go with dynamic input bandwidth scheduling according to the network quality of service and using "breakpoint continuingly" network technologies.

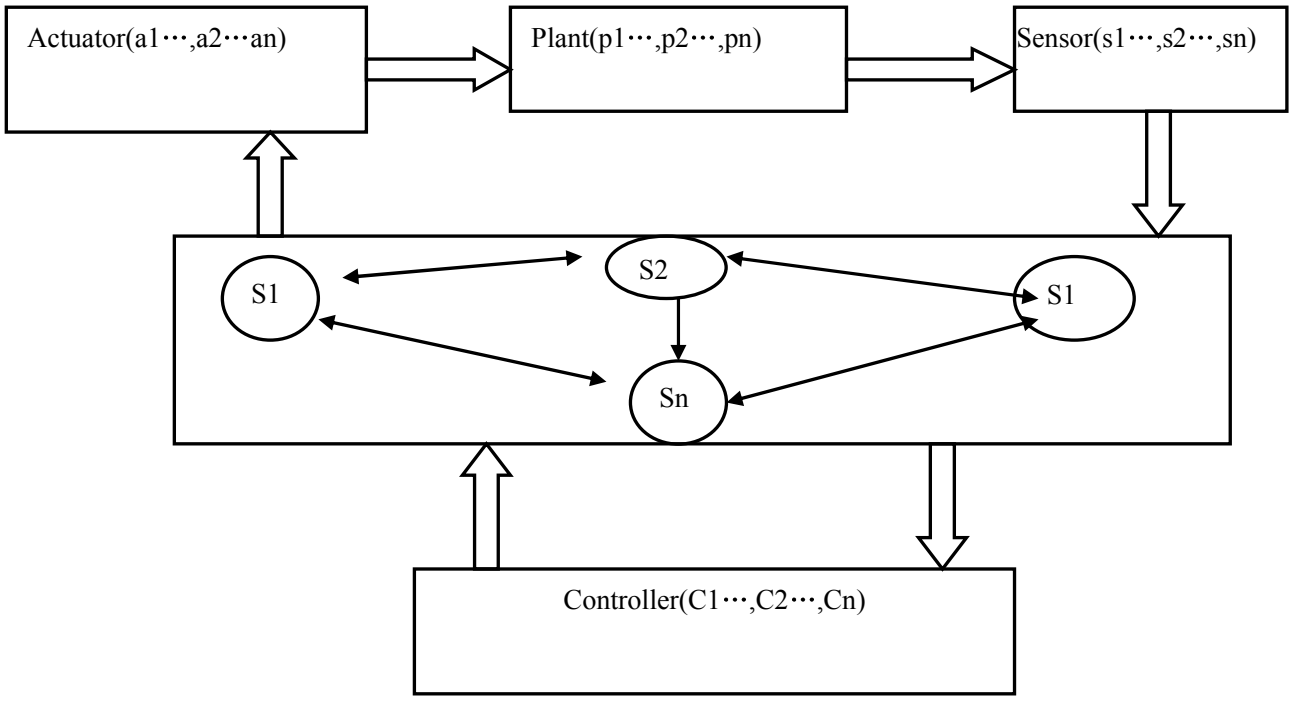

Chart 1: Network control system

3.**Numerical simulatin.**

From chart 2 we can see that with the change of the network parameters, the performance of the closed-loop system will decline, this is because different loop network parameters and control system can lead to a drop in the quality of network service and affect the performance of the closed-loop system. the Network controller design method based on the network quality of service gives the regulation of network parameters and control with the change of system parameters on the control system performance attenuation, and can provide certain theory basis for further network scheduling.

T(s)	P(k)	C(kbps)	£(kbps)	J	K
0.8	8	10	[0.1,8]	20.1655	[-1.461,-1.3395]
0.75	8.5	9.8	[0.1,8]	39.8903	[-1.8903,-1.7037]

Chart 2: Numerical simulation

Summary.

In network control problem, the collaborative problem of control and scheduling is mainly aimed at choosing the appropriate signal transmission network and designing a suitable controller according to control performance requirements. In the network, selected cases are external disturbances and network QoS is time-varying. If with the same controller gain to deal with the time-varying network control, the control performance will become worse. So according to the network QoS parameters such as transmission delay, combining network controller design and network scheduling, effective measures are taken to improve the comprehensive performance of the network control. The research questions are interaction design and scheduling of many objects of network controller and network QoS, and network quantitative and robust controller design etc.

References

[1] Bran icky M S，Liberatore V，Phillips S M ． Networked control system co-simulation for co-designed．In：Proceedings of the American Control Conference．Colorado，USA：IEEE，2003．

[2] Man F L．Analysis Design，Modeling and Control of Networked Control Systems，University of Michigan，USA，2001.

[3]Peng Chen, Yue Dong, Optimization Design in Network Environment Based on QoS Network Control, 2007.

[4]Yishuang Geng, Yadong Wan, Jie He, Kaveh Pahlavan, An Empirical Channel Model for the Effect of Human Body on Ray Tracing, 2013 IEEE 24nd International Symposium on Personal Indoor and Mobile Radio Communications (PIMRC), London,Britain Sep. 2013 pp. 47-52.

[5]Yishuang Geng, Jie He, Kaveh Pahlavan, Modeling the Effect of Human Body on TOA Based Indoor Human Tracking,International Journal of Wireless Information Networks (IJWIN) 20(4), 306-317, Dec. 2013

Advanced Materials Research Vols. 989-994 (2014) pp 4269-4272
© (2014) Trans Tech Publications, Switzerland
doi:10.4028/www.scientific.net/AMR.989-994.4269

Research on Computer Cluster Load Balancing Mechanism

LI Xingyu [1, a], JIANG Tingting [2]

[1]Heilongjiang University, Harbin 150080,China

[2]Heilongjiang Polytechnic, Harbin 150080,China

[a]LiXingyu09@yeah.net

Keywords: Computer cluster; Load balancing; Oscillating; Adaptive

Abstract. Currently it is difficult to use a single network computer application server to meet the demand of concurrent access to a large number of users. It is an ideal way to introduce in the cluster technology in the network for a computer system to solve this problem. In this paper, network computer server cluster on the basis of the existing network computer system is designed and key issues are studied.

Network computer system

With the development of computing technology, personal computing provides users with an increasingly rich personalized graphics interface and application, but costs of personal computer installation, deployment, maintenance and management continue to increase, the PC calculation mode put forward a huge challenge for users, especially for business users. Network computer system not only allows the user to use the applications and personalized settings of the server by service agreement, but also allows multiple users to share the application computing and storage resources, thus greatly reduces the installation, deployment, maintenance and management costs. The calculation mode that provides users with remote service network computer through network computer is becoming increasingly popular; its products are increasingly rich.

Basic principle

The so-called network computer system generally consists of three parts: the application server, the client and the application service agreement. The design of the application service agreement is the core of the network computer system. The application of the service agreement here refers to the mechanism of interaction between the client and server in particular. In network computer systems, multiple clients communicate with the server system through application service agreement thus be able to shared server the application service. Application logic, including window systems are running on the server side, the client only has a simple input and output capacity. Compared with the traditional mode of application, application mode based on network computer system has some typical features.

ASPNC

ASPNC system is the foundation of this article. The system is for different applications, such as the electronic government affairs, network education, financial services and software factory. With the support of all kinds of application server, it provides high cost performance, convenient solution that easy to use. Multiple users can use a variety of clients through the network to access application server and the X window system under various applications, such as office software and Internet software, etc that remote operation application server provides. In more advanced cases, the client's external equipment can automatically register as a server operating system peripherals, making the client an advanced network terminal. The application of the system model is shown in figure 1.

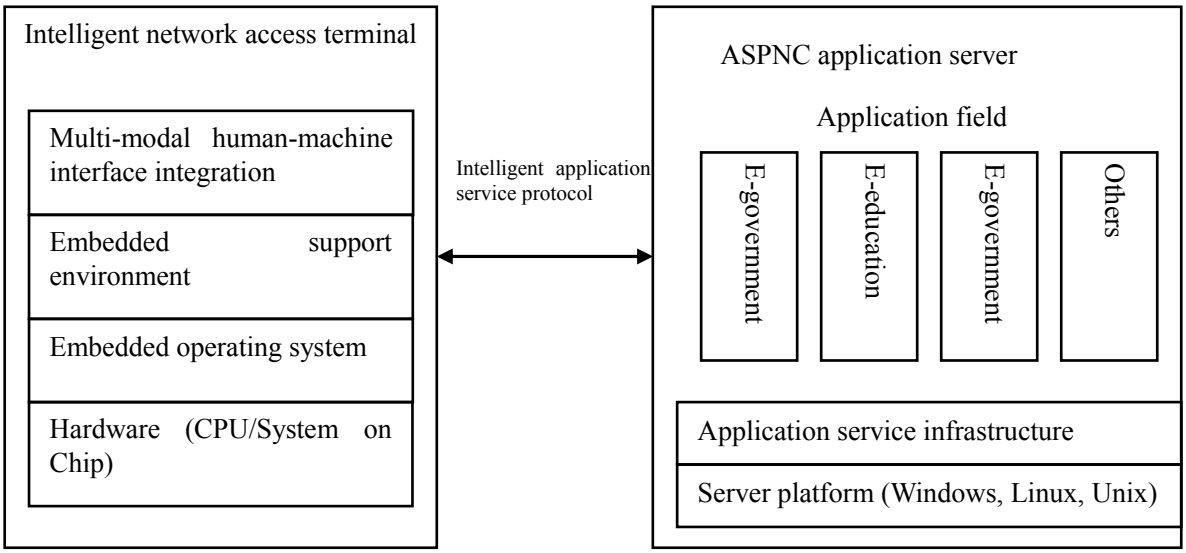

Fig1. ASPNC application mode

This paper will introduce the system from two aspects of application service protocol and system architecture.

Intelligent application service protocol (IASP)

Intelligent application service agreement (hereinafter referred to as the IASP) is the core content of ASPNC system. IASP protocol sequence consists of two parts: initialization protocol handshake and message content delivery phase. In initial handshake agreement, negotiations at the ends of the client and the server is initialized, specific work are as follows: protocol version number consultation, certification, session management, information, graphics configuration system, terminal initialization messages and server initialization. When it is in the message content it is transmitted in accordance with the input and output content categories of the transmission.

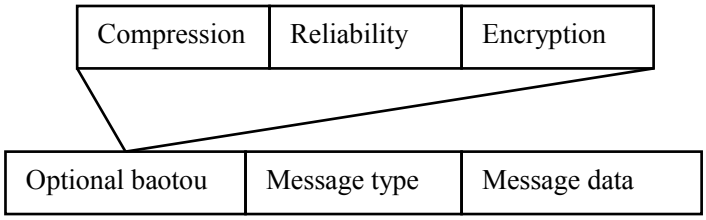

Fig2. IASP protocol message format

IASP agreement is as shown in figure 3, including four sub-protocols: user interface protocol, input information protocol, parameter control protocol and voice transmission protocol.

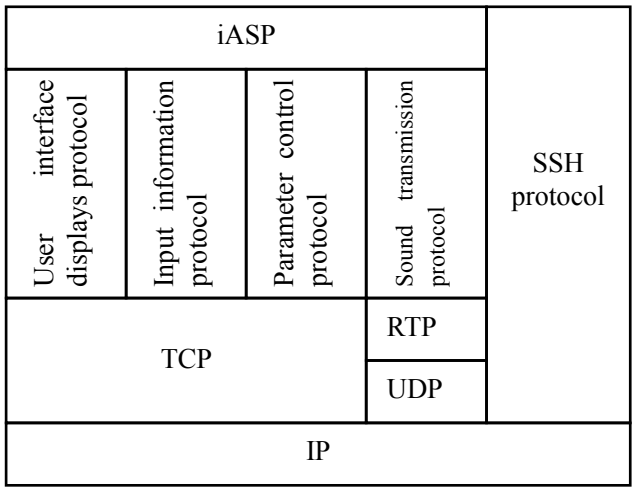

Fig3.IASP agreement

ASPNC architecture of the system

Structural view of the system structure that can only access network terminal system about IASP protocol can be abstractly divided into two key parts: one part is for processing the system input and output data on the server; output data gotten in application system will be stored in the data buffer, or input data in protocol processing engine from the client application transmitted to the system. On the client side, this section will export output data from protocol processing engine in the corresponding client module, or get the keyboard and mouse input information and then transmits it to the protocol processing engine. Another key part is for protocol processing engine, this section transmit input and output data according to certain data encoding format and strategy on network transmission.

The algorithm based on the load weight

Calculation of node performance and load

Nodes in the cluster system $S=(S_1,S_2,...,S_n)$ is often heterogeneous, so task allocation must consider the performance of different nodes in order to achieve the effect of load balance. The performance $C(S_i)$ of the node S_i is mainly evaluated from CPU number n, frequency of CPU $C(C_i)$, memory capacity $C(M_i)$, rate $C(D_i)$ of disk I/O, network throughput $C(N_i)$ and other indicators, using the type (1) to calculate.

$$C(S_i)=k_1\times n\times C(C_i)+k_2\times C(M_1)+k_3\times C(D_i)+k_4\times C(N_i) \qquad i=0,1,...,n-1,\sum k=1 \qquad (1)$$

Load $L(S_i)$ of node S_i is mainly considered from the CPU utilization $L(C_i)$, memory utilization rate $L(M_i)$, utilization $L(D_i)$ of disk I/O, network bandwidth occupancy rate $L(N_i)$ and other indicators. Use formula (2) to calculate.

$$L(S_i)=k_1\times L(C_i)+k_2\times L(M_i)+k_3\times L(D_i)+k_4\times L(N_i) \qquad i=0,1,...,n-1,\sum k=1 \qquad (2)$$

Load weight and load difference

Node load weight $W(S_i)$ is defined as the ratio of node loads $L(S_i)$ with node properties $C(S_i)$, using type (3) to calculate. The greater the weight, the heavier node load is, according which task allocation may be determined according to the size of the load weight.

$$W(S_i)=L(S_i)/C(S_i) \qquad i=0,1,...,n-1 \qquad (3)$$

Node load difference $\Delta L(S_i)$ refers to minus the difference between it from the maximum load weight $W_{\max}$ of the node load weight and then the performance of the node, using type (4) to calculate.

$$\Delta L(S_i) = (W_{\max} - W(S_i)) \times C(S_i) \qquad i = 0,1,...,n-1 \tag{4}$$

Load incremental load nodes load and correction

Because the system is updated regularly, it is unable to get the actual load of each node the update cycle; we need to introduce the load increment to forecast the node load. Load incremental δ refers to the node load type brought by some kind of a request assigned. Type (5) is used to calculate. It is associated with the type of service request, so need to calculate load increment for the different service.

$$\delta = L(S)/n \tag{5}$$

Summary

Load balancing algorithm is the core part of load balancing cluster, excellent equalization algorithm can play the advantages of cluster, make full use of the resources of the cluster, to provide users with high quality service. By analyzing the advantages and disadvantages of the commonly used load balancing algorithm, this paper proposes a dynamic feedback load balancing algorithm based on the load weight, and the algorithm of the main features are: full application node the actual load and performance of two factors, the guidance task allocation, through the load correction to ensure system stability and the experimental results show that the arithmetic
Method can better improve the efficiency of equilibrium, to improve the stability of the load balance cluster.

References

[1] Tadao Murata, Boris Shenker, Sol. M.ShaZt, Detection of Ada Static deadlocks using Petri net invariants[J],EIEE transactions on software engnieering,15(3),1989,31-326.
[2] Kmael Barkaoui and jean-Francois Pradat-Peyre, Verification in concurrent programming with Petri nets structural techniques [J], Washington. DC, Proc 3rd Int, IEEE High-Assurance Systems Engineering Symposium, 1998, 124-133.
[3] B.C. Cumberland, G.Carius, and A.Muir, Microsoft Windows NT Server 4.0, Terminal Server Edition: Technical Reference. Microsoft Press, Redmond,1999
[4] Citrix. Citrix MetaFrame 1.8 Backgrounder, Citrix White Paper. Boca Raton, Fla, 1998.

Advanced Materials Research Vols. 989-994 (2014) pp 4273-4276
© (2014) Trans Tech Publications, Switzerland
doi:10.4028/www.scientific.net/AMR.989-994.4273

Improvement of Cluster-head Selection Mechanism Based on LEACH Protocol in Wireless Sensor Networks

Shiping Fan[a], Xiaodi Zhang[b], Haili Wang[c]

Department of Communication and Information Engineering, Chongqing University of Posts and Telecommunications, Chongqing 400065, China

[a]email: 1026791137@qq.com, [b]email: 903766647@qq.com, [c]email: wanghaili0524@163.com

Keywords: LEACH protocol; residual energy; density; distance

Abstract. In order to prolong the lifetime of wireless sensor networks, improvement of cluster-head selection mechanism based on LEACH protocol is proposed. To make the energy distribution more uniform, we consider the relationship of the density of nodes, residual energy of nodes and distance between nodes and Sink node. It eliminates the defect of energy consumption imbalance in the network caused by random position of cluster-heads and the problem of premature death of nodes caused by low energy nodes becoming cluster-heads. Simulation results show that compared with LEACH algorithm, the improved algorithm extend the network lifetime.

Introduction

A wireless sensor network is composed by a large number of cheap micro sensor nodes in the monitoring area, which is a multi-hop self-organization system by wireless communication method. Its purpose is to sense cooperatively, collect and process the sensing target information within coverage area and send it to the viewer. Due to the limited resources of a single node in wireless sensor networks, reducing energy consumption and prolonging the survival time of the network have become the primary purpose of wireless sensor networks routing protocol design. Routing protocols are divided into plane routing protocol and cluster-based routing protocol [1]. Common plane routing protocols include DD [2], SPIN [3], etc.. Plane routing protocols need to maintain a large number of routing table and take up large storage space, so it is not suitable for large-scale networks [4] [5]. Currently, cluster-based routing protocol for wireless sensor networks is the mainstream protocol, this paper analyzes the advantages and disadvantages of a representative cluster-based routing protocol-LEACH protocol, and proposes an improved routing protocol. The main goal is to balance the network load, and extend the network lifetime.

LEACH Protocol

Low Energy Adaptive Clustering Hierarchy(LEACH)is the first cluster-based routing protocol proposed by Heinzelman [6]. The basic idea of the protocol is to randomly select cluster-heads by means of circulating, and cluster-heads fuse the information from the nodes in the cluster, then the cluster-heads send the information to Sink node, which reduces the transmission capacity and data transmission distance, reduces the energy consumption of the network, and extends the network lifetime [7] [8].

Algorithm description. The cluster-head selection principle of LEACH algorithm is: a sensor node generates a random number between (0,1), if it is less than the threshold T (n), then this node is selected as the cluster-head node. T (n) is defined as:

$$T(n)=\begin{cases}\dfrac{p}{1-p*[r \bmod(1/p)]} & n\in G\\ 0 & otherwise\end{cases} \tag{1}$$

Where, p represents the percentage of cluster-heads, r refers to the current round, G denotes the collection of the nodes which have not been selected as cluster-head in the past 1/p rounds.

Analysis of algorithm. LEACH algorithm selects nodes randomly as cluster-heads to balance the whole network load. But the cluster-head selection is random, node with less energy may become a cluster-head, thus it may cause the depletion and premature death of node. The cluster- head distribution is not uniform, there may be a high density of nodes where no cluster-head or cluster-heads in the network edge, which increases the communication distance. It leads to increase the energy consumption and reduce the lifetime of the network greatly [9][10][11].In view of such defects, cluster-head selection mechanism should be improved. In order to prolong the network lifetime, the residual energy, density and location of the nodes must be considered when choosing a cluster-head.

Improvement of Cluster-head Selection Mechanism

Network model. In this paper, we use the node energy consumption model shown in Fig.1:

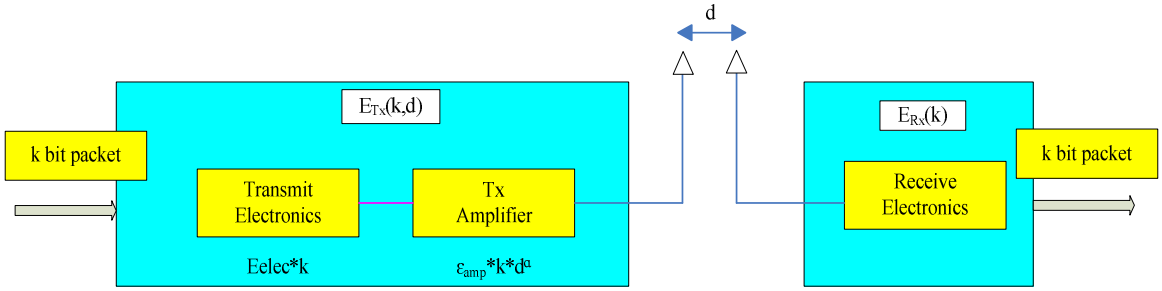

Fig.1 Node energy consumption model

The energy dissipation of the sensor nodes sending k bit data consists of two parts, one is used to produce signals, the other is used to amplify the signal. Energy is calculated by:

$$E_{Tx}(k,d) = E_{Tx_elec}(k) + E_{Tx_amp}(k,d) = \begin{cases} kE_{elec} + k\varepsilon_{fs}d^2, d < d_0 \\ kE_{elec} + k\varepsilon_{amp}d^4, d > d_0 \end{cases} \quad d_0 = \sqrt{\frac{\varepsilon_{fs}}{\varepsilon_{amp}}} \tag{2}$$

Eelec represents the circuit energy consumption, ε_{fs} and ε_{amp} are energy of the power amplifier magnification in the free space model and the model of multi-path fading, respectively.

The energy consumption of receiving k bits of data is given by:

$$E_{Rx}(k) = E_{Rx_elec}(k) = kE_{elec} \tag{3}$$

Cluster-head fuses the cluster membership information and its own data, and data fusion energy consumption is:

$$E_{fuse} = (I+1) * E_{DA} * k \tag{4}$$

I represents the node number of a cluster, E_{DA} is energy consumed by unit data fusion.

Definition. Neighbor nodes: the nodes that node i can communicate with directly in a hop range.

Node density: The number of neighbor nodes of node i.

Radius of investigation: $R = \sqrt{\frac{M}{p * N * \pi}}$, M represents the area of the detection region, p represents the probability of selected cluster-heads, N represents the number of nodes in the detection zone.

Improved of cluster-head selection mechanism.In LEACH algorithm, whether a node becomes cluster-head or not has something to do with the percentage of cluster-heads and whether the node has served as a cluster-head. It has nothing to do with node's residual energy, density and location. In the improved algorithm, the node's residual energy, density and location are considered as the threshold's impact factors. So it can increases the probability of the node becoming cluster-head which has more residual energy, greater density, shorter distance from Sink node . Improved threshold is defined as:

$$T(n) = \begin{cases} \frac{p}{1 - p*[r \bmod (1/p)]}[(\alpha \frac{E_{current}}{E}) + (\beta \frac{N(i)}{\pi R^2}) + ((1-\alpha-\beta)\frac{\overline{D_{i_\sin k}}}{D_{i_\sin k}})] & if\ n \in G \\ 0 & otherwise \end{cases} \tag{5}$$

Where, p represents the percentage of cluster-heads in all nodes, r refers to the current round, G denotes the collection of the nodes which have not been selected as cluster-head in the past 1/p rounds. $E_{current}$ represents residual energy of the current node, E represents the initial energy of the node, N (i) represents the number of neighbor nodes of node i, R represents radius of investigation, D_{i_sink} indicates the distance between node i and Sink node, $\overline{D_{i_sink}}$ shows the average distance between i's neighbor nodes and the Sink node, α, β are weighting factors, respectively.

Simulation Results and Analysis

The energy consumption of the network is mainly used for data transmission, data reception and data fusion. The LEACH algorithm and the improved algorithm are compared by simulation using MATLAB in this paper. Parameters are set as: E=1J, monitoring area is 100m*100m, Sink node location is (50m,175m), E_{elec}=50/nJ(bit)$^{-1}$, ε_{fs}=10pJ/bit/m^4, ε_{amp}=0.0013nJ/bit/m^2 ,E_{DA}=5nJ.

Through simulation, we found that the best performance can be attained when the parameters are set as $\alpha = 0.6, \beta = 0.2$.

It can be seen from the simulation Fig.2 that the distribution of cluster-heads is more uniform in improve-LEACH protocol, which reduces the communication distance between nodes in the cluster and the cluster-head, so that the energy consumption is reduced.

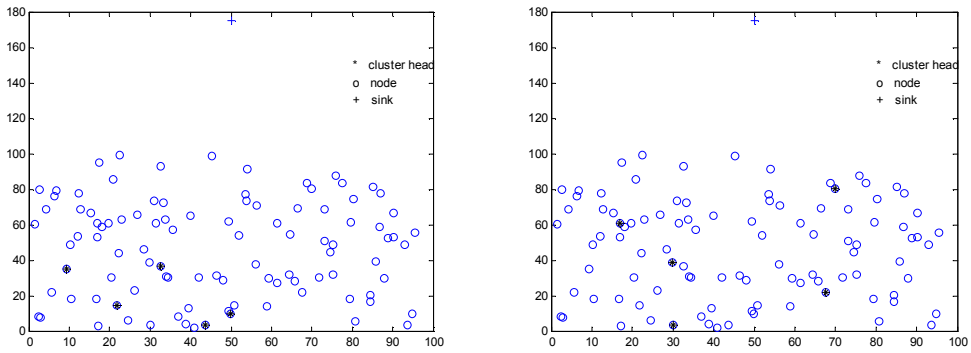

(a)LEACH cluster-heads distribution (b)improve-LEACH cluster-heads distribution

Fig.2 LEACH protocol and improve-LEACH protocol cluster-heads distribution map

As we can see from Fig.3, the first node's death occurred in the 1580th round in improve-LEACH protocol, while 1377th round in LEACH protocol, that is, 15% delay than LEACH. The fiftieth node's death occurred in the 2245th round in improve-LEACH while 1680th round in LEACH protocol, which is 33% extend than LEACH. The reason why improve-LEACH is better than LEACH protocol lies in that when selecting a cluster-head, improve-LEACH protocol considers the residual energy of nodes, the density of nodes, and the distance between the node and the sink node, which ensure the optimal node is selected as the cluster-head so that the cluster distribution is more uniform, the energy load is more balanced.

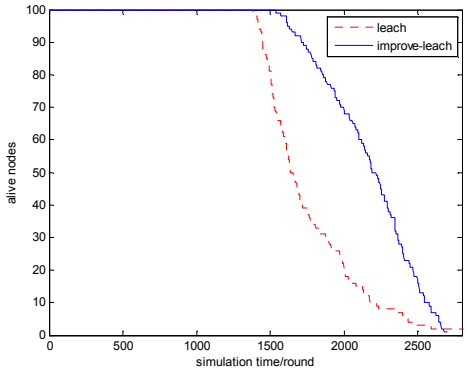

Fig.3 Relationship between survival nodes number and the simulation time

Conclusion

For the uneven distribution of nodes and random selection of cluster-heads and other defects of wireless sensor networks, this paper presents an improved cluster-head selection mechanism, that is, considering the residual energy of nodes, the density of nodes, and the distance between the node and the sink node when selecting a cluster-head, in order to solve the node load imbalance problem in LEACH algorithm. MATLAB simulation results show that compared with the LEACH algorithm, the improved algorithm balances the network load effectively, reduces the network energy consumption, and prolongs the network life cycle.

Acknowledgement

This research was financially supported by National Natural Science Foundation of China (Grant No.61171190).

References

[1] Haosong Gou,Younghwan Yoo.An energy balancing LEACH algorithm for wireless sensor networks. Seventh International Conference on Information Technology. 2010.

[2] Intanagonwiwat C, Govindan R, Estrin D, et a1．Directed Diffusion for Wireless Sensor Networking[J]．IEEE/ACM Transactions on Networking, 2003, 11(1):2-16.

[3] Kulik J, Heinzelman W, Balakrishnam H．Negotiation based Protocols for Disseminating Information in wireless sensor networks[J]．Wireless Networks，2002, 8(2—3): 169—185.

[4] KATIYAR V, CHAND N, Gautam G C, et al. Improvement in LEACH protocol for large-scale wireless sensor networks[C]. Emerging Trends in Electrical and Computer Technology (ICETECT), 2011International Conference on. IEEE, 2011: 1070-1075.

[5] LI HUI, SHI JIANGHONG, YANG QI, et al. An Energy-efficient hierarchical routing protocol for long range transmission in wireless sensor networks[C]. Education Technology and Computer (ICETC), 2010 2nd International Conference on. IEEE, 2010, 4: 45-48.

[6] Heinzelman W, Chandrakasan A, Balakrishnan H. Energy-efficient Communication Protocol forWireless Micmsensor Networks[C]. In Proceeding of the 33rd Annual Hawaii Int't Conf. on System Sciences. Maui：IEEE Computer Society，2000: 3005—3014.

[7] Muruganathan S D,Ma DCF,Bhasin PI,and et al, A centralized energy-efficient routing protocol for wireless sensor networks. IEEE Communications Magazine, 2005, 43(3):8-13.

[8] e Mao, Li Cheng-Fa, Chen Gui-Hai, Wu Jie. An energy efficient clustering scheme in wireless sensor networks. Ad Hoc & Sensor Wireless Networks.2007.

[9] Zhang R B,Cao J F.Uneven clustering routing algorithm for wireless sensor networks based on ant colony optimization[J].Journal of Xi'an Jiaotong University,2010,44(6):33-38.

[10] PENG D, CAO M. An Energy Efficient Routing Protocol for Wireless Sensor Network[C]. Internet Technology and Applications, 2010 International Conference on. IEEE, 2010: 1-4.

[11] Muhammad Haneef,Zhou Wenxun,Zhongliang Deng.MG-LEACH:Multi group based LEACH an energy efficient routing algorithm for wireless sensor network. International Conference on Advanced Communication Technology . 2012

Advanced Materials Research Vols. 989-994 (2014) pp 4277-4280
© (2014) Trans Tech Publications, Switzerland
doi:10.4028/www.scientific.net/AMR.989-994.4277

The Development of Interactive Marine Incinerator Operational Training System based on Web3D

YAO Wenlong[1, 2]

[1] Department of Marine Engineering, Qingdao Ocean Shipping Mariners College, Qingdao, China

[2] College of Marine Engineering, Dalian Maritime University, Dalian, China

yaowl@coscoqmc.com.cn

Keywords: marine incinerator; operational training system; scene simulation; web3D modeling

Abstract. In this paper, the design scheme, technical route and system structure of the interactive marine incinerator operation training system based on Web3D are proposed based on the study of the marine engine room simulator project. The virtual reality technique, visual C# and IE real-time interaction technology are introduced to the marine incinerator operation training system and the development thoughts of the interactive marine incinerator operation training system based on Web3D are elaborated based on the 3D modeling optimization and real-time interaction technology. This study is a new type of marine engineering training mode, it can better meet the STCW convention in Manila amendments on incinerator equipment management requirements.

Introduction

Large marine simulation system plays a very important role in terms of training high quality crew, it has become the effective means and methods for the maritime education and training. The STCW convention stipulated that crews can obtain certificate of competency though by undergo a certain time of simulator training[1]. But it can not satisfy the needs of student with the increasing of maritime colleges and training institutions because of the high cost of large marine simulation system were limited, the training ground were fixed, the training time was very limited. In recent years, with the rapid development of network technology and the performance improvement of personal computers, the maritime universities have established the campus network, most of the students also have a personal computer. These basic conditions makes the distributed simulation system based on Web is feasible.

At present, the simulation based on web3D attracts more attention, the simulation system based on Web3D were established in many fields, but it still very few in the field of navigation[2]. This project will combine the web3D technology closely with the marine incinerator plant simulation system. A new training pattern that the interactive marine incinerator operation training system based on Web3D is proposed, it makes that more students can perform certain online training course anytime and anywhere through the browser. This project has the properties of mobility and high interactivity, openness, easy maintenance and cost saving, etc., so that the students can easily connect to the specified Web site for training during any time any place, it can effectively make up the shortfall that the traditional remote education was limited to the predetermined learning program[3].

Overall Design

Developing the interactive marine incinerator operation training system based on Web3D is the purpose of this research by using virtual reality technology and combining with the teaching and training practice of marine engineering technology. In this paper the marine incinerator plant, web3D technology, virtual reality technology were studied, and the realization of the key research of training system based on web3D were developed, and the ActiveX control technology, server technology and multithreading technology were utilized for the operational training system. The idea is to realize the use of desktop machine and web browser to access the lifelike marine training through the network

environment. It can meet the international maritime organization and the national maritime bureau about the seafarers' training, certification and standards of the international convention on duty "competency assessment project" and "to demonstrate" continuous proficiency requirements. The concrete research content is as follows:

Mathematical Model Establishment and Optimization

The mathematical model of the marine incinerator plant was established and verified the related optimization according to the working principle structure characteristics of marine incinerator plant and the basis of thermodynamics and dynamics knowledge.

Implementation of Virtual Reality Simulation

The 3-D modeling for marine incinerator plant was realized by the 3dmax and SolidWorks[4], the virtual reality simulation of the Marine incinerator plant was accomplished by using VRML and then through the establishment of two-dimensional three-dimensional scene for communications between the interaction.

Marine Incinerator Plant Dynamic Process Simulation

On the basis of the system global model, the dynamic model simulation was realized by utilizing Matlab M-file function and by using the experimental data to validate the simulation value, correction algorithm, improve the system mathematical model, the correctness and efficiency of model were analyzed by SIMULINK software simulation.

Marine Incinerator Plant Fault Simulation Visualization Interface Development

The various fault phenomena or characteristics are analyzed though the established dynamic model of marine incinerator plant. The dynamic model was solved by VC# programming, and the correction coefficient was introduced, the value were tested for many times. Each subsystem and fault training system of marine incinerator plant were researched and developed, the results were called to monitor the system.

The Software Design and Implementation of Marine Incinerator Plant Simulation System based on Web3D

The interface design and development of marine incinerator plant simulation software were completed by combining with the established mathematical model of marine incinerator plant though Visual Studio.net 2010 that was act the development environment, with Visual computer programming language Visual c # as the programming tool, combining with VRML and Java technology solutions ,utilize GDI + technology to create control library. It adopt VRML for client interactive 3D graphics display of virtual Marine environment, and it adopt Java technology for network communication responsible, distributed simulation to more user interaction, marine simulation training and 3D scene data encoding decoding, and other functions[5].

Technical Implementation

According to the ship equipment data and practical investigation, combined with the marine incinerator plant training programs, the B/S frame was adopted to develop the simulator. The realistic 3D model of the equipment are established based on the virtual reality software, the function of virtual roaming and remote real-time interaction are developed by ActiveX technology and visual C# technology. Overall study plan is as follows:

(1).The realistic 3D model of the marine incinerator plant are established based on the actual size of the equipment by utilizing the Converse3D modeling tool and its development kit;

(2).For function simulation part, we utilize ActiveX of Converse3D by embedding C# language to develop the interactive marine incinerator operation training system based on Web3D combined with the practical of the training.

(3).For the multi-engineer cooperative training based on IE browser, we utilize the converse3D three-dimensional network platform and virtual community functions and embedding visual C# language to develop the remote visualization interactive control module[6].

(4).This paper makes some improvements aimed to the traditional B/S model: first programmed by the socket and run it in the client port to achieve real-time transition of the dynamic data, then realized the display of dynamic data in browses port by adopting ActiveX technique. Provide concrete resources for browses by using HTTP protocol to ascertain Web server through unified resources localizes. The mode of the improved project still through browses to visit embedded Web server, yet which combined the advantages of B/S and C/S.

System Structure

In order to make the engineers to simulate marine incinerator management status as far as possible, the interactive marine incinerator operational training system based on Web3D must have enough simulation environment, which can enable trainees to get and show the skills required by the training objectives. The operational training system should include simulation equipment: incinerator ontology, burner, exhaust fan, damper regulator, dirty oil circulation pump and other ancillary equipment, it can produce the random operation equipment sound simulation at the same time. It can not only more visually on a single engineer for regular working conditions and deal with the emergency case training through the operational training system[7], it can realize remote real-time operation and more engineers interaction. The software architecture is showed as Figs.1-3.

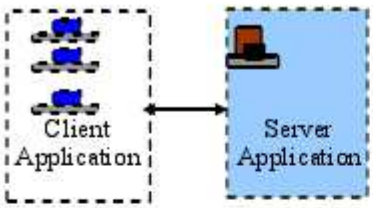

Fig 1 C/S

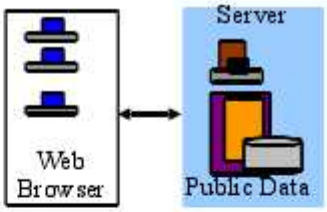

Fig 2 B/S

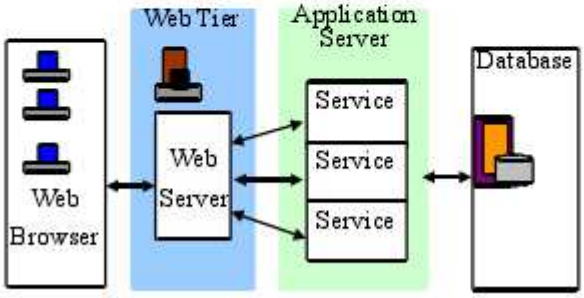

Fig 3 Multi-layer architecture based on web

Major Training Content Include:

(1) The operational training mode based on Web can be achieved;
(2) The 3D visual of marine incinerator plant can be provided;
(3) The operation control panel of marine incinerator plant can be provided in the client;
(4) The accurate mathematical model of marine incinerator plant can be provided in the client;
(5) The corresponding various operations of software control panel can be provided in the client;
(6) The fault setting and find the training function can be realized;
(7) The different training patterns can be chosen according to the requirement.

Conclusions

At present, with the rapid development of 3D virtual reality technology and the network technology, its application is becoming more and more widely in the field of education and training. It will have broad prospects to develop the online edition of the two-dimensional control system

combined with 3D simulation model of the comprehensive training of software though combining the advanced technology and marine simulator. This technology will be the focus direction of the marine engine room simulator in the future. It is believed that with the progress of science and technology, the development of shipping industry and the rapid development of virtual reality technology, the project studied operations training system will have a bigger development space, it will be more and more widely used because of its beyond the traditional simulation, and the advantages of the marine simulation training system based on Web has wide prospect of market demand and development, its role in the crew training will be more and more widely.

Acknowledgment

This work is supported by the Shandong Province Higher Educational Science and Technology Program under Grant J13LN72, COSCO Science and Technology Development Project 2012-1-H-004, and the National Natural Science Foundation (NNSF) of China under Grant 61104187 and 51179102,promotive research fund for excellent young and middle-aged scientists of Shandong Province under Grant BS2012NY003 and Science and Technology Development Project of Qingdao City (13-1-4-227-jch).

References

[1] Interpretation Group of STCW. The interpretation of STCW Manila convention amendment [J] . Maritime Education Research, (2011), p.10-14.

[2] Wenlong Yao, Dezhi Jiang, Yuan Liu and Jundong Zhang. The Research and Development of Remote Interactive Engine Room Resource Management Simulator, Electronic &Mechanical Engineering and Information Technology,2012(11):1906-1910

[3] Horn D.Stream reduction operations for UPUPU applications[C].USA:Addison-Wcslcy Publishing Company, 2005:573-589.

[4] DeZhi JIang, Research of Engine Department Team Based on Engine Room Resource Management, ECWAC 2012,Wuhan, China,(2012), p. 35-40

[5] Covindaraju N K, Lin M C,Manocha D, et al. Quick-CULLIDE; Fast inter-and intra-object collision culling using graphics hardware[C]// Proceedings of IEEE Virtual Reality. USA:IEEE Press,2005:59-66.

[6] Yao Wen-long,Tu Zhi-ping, Fault analysis of PWM control circuit for high-power switching power supply of ship, Marine Technology,2010, pp.56-58

[7] Distributed Simulation Technology Inc. GL Studio User's Guide[M]. 2000.

Advanced Materials Research Vols. 989-994 (2014) pp 4281-4285
© (2014) Trans Tech Publications, Switzerland
doi:10.4028/www.scientific.net/AMR.989-994.4281

A Review of Cluster based Routing Protocols in Wireless Sensor Networks

Jing WU[1,2,a] , Guo-Zhao HOU[3,b]

[1]College of Computer, North China Institute of Science and Technology, Yanjiao Hebei 101601, China

[2]College of Computer, Qinghai Normal University, Xining Qinghai 810008, China

[3]Department of Basic, Army Aviation Institution of PLA, Beijing 101123, China

[a]99061632@163.com, [b]wonderh@yeah.net

Keywords: Wireless sensor networks, Cluster based routing protocol, Review

Abstract. At present, cluster based routing protocols have been the main solution of routing scalability problem in wireless sensor networks. Based on the deep research on cluster based routing protocols, cluster based routing protocols were divided into two parts. The main routing protocols of each part were reviewed and analyzed. This work will contribute to the further study of cluster based routing protocols.

Introduction

In recent years, Internet of things has become a hot research topic in the academic and business circles. The wireless sensor network is the development core of Internet of Things in the current stage[1]. The research of wireless sensor networks has very high value. At present, applications of large-scale wireless sensor networks become more and more, such as coal mine environment detection, ecological monitoring of the Three Rivers Origin, etc[2-4]. Therefore, it becomes more and more urgent to research the scalability problem of wireless sensor networks. At present, cluster based routing protocols have become the main solution of routing scalability problem. Based on the deep research on cluster based routing protocols, cluster based routing protocols are divided into two parts. The main routing protocols of each part are reviewed and analyzed. This work will contribute to the further study of cluster based routing protocols.

Cluster based Routing Protocols and the Classification

The cluster based routing protocols in wireless sensor networks are routing protocols based on cluster structures. The protocols select cluster heads through some strategy. A cluster head and some cluster members constitute a cluster structure. The cluster members are responsible for collecting monitoring data and transmitting them to the cluster head. The cluster head is responsible for fusing the received monitoring data and forwarding them to the sink node. Compared with the flat routing protocols [5-9], cluster based routing protocols perform more prominent in network topology management, energy minimization and data fusion. At present, cluster based routing protocols have become the main solution of routing scalability problem. Cluster based routing protocols are divided into two-layer cluster based routing protocols and multi-layer cluster based routing protocols. We will review and analyze the above two kinds of protocols separately in this paper.

Review and Analysis of Two-layer Cluster based Routing Protocols

Two-layer cluster based routing protocols are routing protocols based on two-layer cluster structures. A two-layer cluster structure is shown in Fig.1.

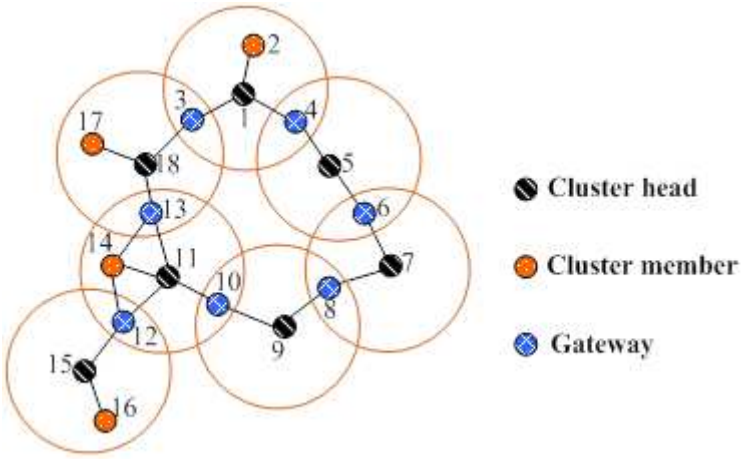

Fig.1 A two-layer cluster structure

At present, two-layer cluster based routing protocols have matured. For example, the LEACH protocol[10] is the first two-layer cluster based routing protocol in wireless sensor networks. It focus on solving the load balancing and energy control. But there are some problems in LEACH, such as "single hop communication mechanism between the cluster head and the sink node increases the energy of the cluster head" and "cluster head election strategy imbalances the energy of the cluster head". The most of the two-layer cluster based routing protocols after LEACH protocol are evolved based on LEACH protocol. They improve LEACH protocol from different angles. For example, the sink node elects the cluster heads consentrately by combining the energy and locations of all the nodes in LEACH-C protocol[11], which can solve the problem of unbalanced energy consumption of cluster heads. In HEED protocol[12], two decisive parameters are introduced during cluster constructing, such as node residual energy and intra-cluster communication cost, which can solve the problem of unbalanced energy consumption of cluster heads. The clustering method adopted by TEEN protocol[13] is the same with that adopted by LEACH protocol. And TEEN protocol adds two thresholds to reduce data amount, but it is not suitable for the application of periodic reporting data. Aiming at the problem that expensive cost is produced during the cluster constructing in LEACH protocol, PEGASIS protocol[14] is proposed. In PEGASIS protocol, only one cluster (chain) is formed in the network, and then the cluster head and the sink node communicate with each other. Aiming at the problem of "single hop" mechanism in LEACH protocol, RPBC protocol [15] is proposed in which "multiple hop" mechanism is adopted. Each cluster head establishes their own route to the sink node when the sink node broadcasts interest messages. The multi-hop communication from each cluster head to the sink node is achieved by the single-hop communications between cluster heads. Aiming at the same problem, LEACH_CHMST protocol [16] is proposed in which the minimum spanning tree of cluster heads is taken as the inter-cluster routing tree. And it can achieve the multi-hop communication between the cluster head and the sink node. HRPBC protocol [17] is proposed in which the cluster head finds the route to the sink node by broadcasting. And the cluster head arrives at the sink node with multiple hops, in which the communications between cluster heads are conducted by their common gateways.

The two-layer cluster based routing protocol is more suitable for large-scale wireless sensor networks than the flat routing protocol. But its backbone network still has the scalability problem. The routing protocol who can really solve the routing scalability problem of large-scale wireless sensor networks is the multi-layer cluster based routing protocol.

Review and Analysis of Multi-layer Cluster based Routing Protocols

Multi-layer cluster based routing protocols are routing protocols based on multi-layer cluster structures. A multi-layer cluster structure is shown in Fig.2.

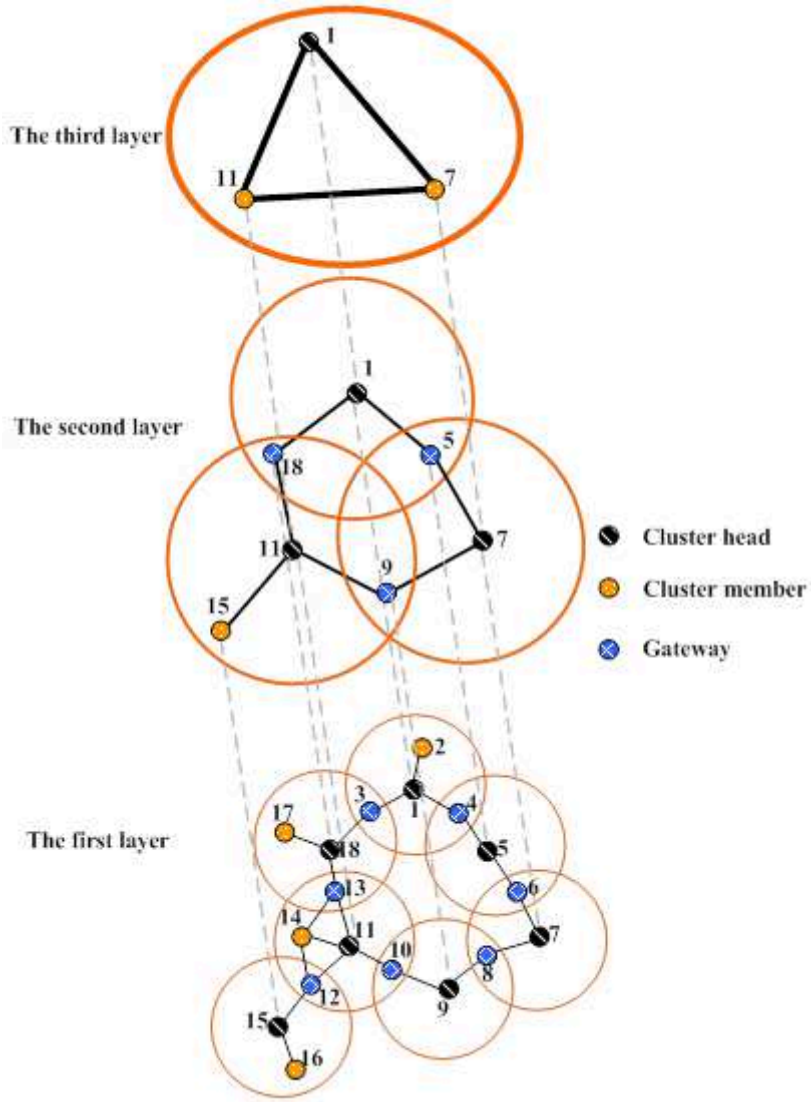

Fig.2 A multi-layer cluster structure

At present, the research results of multi-layer cluster based routing protocols are very seldom. It has not formed a perfect theory system. For example, CAMHP protocol[18] set up a context-aware cluster based routing protocol which is based on a three-layer cluster structure. But the network scalability is still limited. DETA protocol[19] is three-layer cluster based routing protocol. The constructing process of the three-layer cluster structure is that the network is divided into several square areas, which are equal size, adjacent and non-overlapping, according to the geographic location firstly; the bottom-layer cluster heads and upper-layer cluster heads are selected secondly. But the network scalability is still limited. The three-layer cluster structure constructed in literature [20] also exists the scalability problem. The constructing methods of the multi-layer cluster structure are presented in literature [21-23]. But the appropriate layers have no way to determine. The routing algorithms proposed in literature [24,25] present the methods of constructing the multi-layer cluster structure to the top layer. And they adopt multi-hop forwarding mechanism between the top-layer cluster head and the sink node. The design is complete. But the strategy "direct communication between cluster heads" makes the scalability of these algorithms limited. Therefore, the researches on multi-layer cluster based routing protocols for large-scale wireless sensor networks at home and abroad have many problems. It is necessary to carry out innovative theory researches.

Conclusion

In this paper, cluster based routing protocols of wireless sensor networks are deeply researched. The cluster based routing protocols are divided into two parts. The main routing protocols of each part are reviewed and analyzed. Cluster based routing protocols are divided into two-layer cluster based routing protocols and multi-layer cluster based routing protocols. The two-layer cluster based routing protocols have matured, but protocols still have the scalability problem. The multi-layer cluster based routing protocols take better scalability. But the relative researches have many problems. It is necessary to carry out innovative theory researches. We wish that the review and analysis in this paper will contribute to the further study of cluster based routing protocols.

Acknowledgements

This work was financially supported by the Fundamental Research Funds for the Central Universities(3142014087,3142013098,3142014125,3142014096,3142014085),Natural Science Fou ndation of Qinghai Province of China (2012-Z-935Q,No.2012-N-525), Key Prevention and Control Technology of Major Safety Accidents in Production(2013).

References

[1] The white paper on the Internet of Things (2011). http://wenku.baidu.com/view/0d2b5e20482fb4daa58d4b70.html. (In Chinese)
[2] L.M. Sun, J.Z. Li, Y. Chen, et al. Wireless sensor networks. Beijing: Tsinghua University Press, 2005. (In Chinese)
[3] J.Z. Li, H. Gao. Survey on sensor network research. Journal of Computer Research and Development, 2008, 45(1): 1-15. (In Chinese)
[4] F.Y. Ren, H.N. Huang, C. Lin. Wireless sensor networks. Journal of Software, 2003, 14(7): 1282-1290. (In Chinese)
[5] S.M. Hedetniemi, S.T. Hedetniemi, A.L. Liestman. A survey of gossiping and broadcasting in communication networks. Networks, 1988, 18(4): 319-349.
[6] Z.J. Haas, J.Y. Halpern, L. Li. Gossip-based ad hoc routing. Proceedings of the IEEE INFOCOM, 2002: 1707-1716.
[7] J. Kulik, W. Heinzelman, H. Balakrishnan. Negotiation-based protocols for disseminating information in wireless sensor networks. Wireless Networks, 2002, 8(2/3): 169-185.
[8] C. Intanagonwiwat, R. Govindan, D. Estrin, et al. Directed diffusion for wireless sensor networking. IEEE/ACM Transactions on Networking, 2003, 11(1): 2-16.
[9] D. Braginsky, D. Estrin. Rumor routing algorithm for sensor networks. Proceedings of the 1st ACM International Workshop on Wireless Sensor Networks and Applications, 2002, 10: 22-31.
[10] W.R. Heinzelman, A. Chandrakasan, H. Balakrishnan. Energy-efficient communication protocol for wireless microsensor networks. Proceedings of the 33rd Annual Hawaii International Conference on System Sciences, 2000: 3005-3014.
[11] W.B. Heinzelman, A.P. Chandrakasan, H. Balakrishnan. An application-specific protocol architecture for wireless microsensor. IEEE Transactions on Wireless Communications, 2002, 1(4): 660-670.
[12] O. Younis, S. Fahmy. HEED: A hybrid, energy-efficient, distributed clustering approach for ad hoc sensor networks. IEEE Transactions on Mobile Computing, 2004, 3(4): 366-379.
[13] A. Manjeshwar, D.P. Agrawal. TEEN: A routing protocol for enhanced efficiency in wireless sensor networks. Proceedings of the 15th International Parallel and Distributed Processing Symposium, 2001: 2009-2015.
[14] S. Lindsey, C.S. Raghavendra. PEGASIS: Power-efficient gathering in sensor information systems. Proceedings of IEEE Aerospace Conference, 2002, 3: 1125-1130.

[15] P. Yue. The research on a multi-hop routing protocol based on clustering in wireless sensor networks. Master Degree Thesis in University of Electronic Science and Technology, 2010. (In Chinese)
[16] Y.M. Fan, Q.Z. Chen, J.J. Yu. New routing protocol for wireless sensor networks based on the minimum spanning tree of the cluster head. Chinese Journal of Sensors and Actuators, 2008, 21(12): 2067-2072. (In Chinese)
[17] B.L. Chen. Research on hierarchical routing protocol based on clustering for wireless sensor network. Master Degree Thesis in Southwest Jiaotong University, 2007. (In Chinese)
[18] M.E. Haque, N. Matsumoto, N. Yoshida. Utilizing multilayer hierarchical structure in context aware routing protocol for wireless sensor networks. International Journal of Computational Science, 2010, 4(1): 23-37.
[19] J.N. Al-Karaki, R. Ul-Mustafa, A.E. Kamal. Data aggregation in wireless sensor networks-exact and approximate algorithms. 2004 Workshop on High Performance Switching and Routing, 2004: 241-245.
[20] A.R. Masoum, A.H. Jahangir, Z. Taghikhani, et al. A new multi level clustering model to increase lifetime in wireless sensor networks. Second International Conference on Sensor Technologies and Applications, 2008: 185-190.
[21] G.S. Tomar, S. Verma. Dynamic multilevel hierarchical clustering approach for wireless sensor networks. 11th International Conference on Computer Modelling and Simulation, 2009: 563-567.
[22] A. K. Thomas, R. Devanathan. Energy efficient dynamic multi-level hierarchical clustering technique for network discovery in wireless sensor networks. The 3rd International Congress on Ultra Modern Telecommunications and Control Systems and Workshops, 2011: 1-5.
[23] D. Estrin, R. Govindan, J. Heidemann, et al. Next century challenges: scalable coordination in sensor networks. Proceedings of the 5th Annual ACM/IEEE International Conference on Mobile Computing and Networking, 1999: 263-270.
[24] K.H. Xu, Y.C. Jia, Y.H. Liu. A novel hierarchical clustering routing algorithm for wireless sensor networks. Proceedings of International Conference on Internet Computing in Science and Engineering, 2008: 282-285.
[25] X.H. Wang, G.R. Zhang. The HEED based multi-layer cluster-based routing algorithm in wireless sensor networks. Journal of Gansu Lianhe University (Natural Sciences), 2011, 25(1): 78-81. (In Chinese)

Advanced Materials Research Vols. 989-994 (2014) pp 4286-4289
© (2014) Trans Tech Publications, Switzerland
doi:10.4028/www.scientific.net/AMR.989-994.4286

Analysis of the Technologies for Host and Port Scanning

ZHU Nafei, ZHOU Yue, WANG Wei and LOU Li

National Application Software Testing Labs, Beijing, China

{znf, zhouyue, wangwei, louli}@bsw.net.cn

Keywords: Host Scanning, Port Scanning, ICMP, TCP, UDP

Abstract. Host scanning and port scanning are the basis for attacking information system. The technologies commonly used in these scans can be classified as ICMP scanning, TCP scanning and UDP scanning. We analyze these technologies and make comparisons among them. Totally, ICMP are mainly used to discover the host, while the TCP and UDP are mainly for port scanning, except for ACK. At the same time, using certain special TCP datagram such as SYN packets and ACK packets, and UDP datagram, we can make a host scanning in a secret manner.

Introduction

Network scanning mainly includes host scanning, port scanning, service detection, operating system identification, and vulnerability scanning. Host scanning refers to host discovery and port scanning finds out the port is open or close. They are the basis for other scans and exploration in the following attack stages. The technologies commonly used in host and port scanning can be divided into three categories, which are ICMP scanning, TCP scanning and UDP scanning. We will analyze these three types of technologies and make comparisons among them. This paper is organized as following: In section 2, we introduce the ICMP scanning technologies; in section 3, scanning technologies based on TCP protocol are analyzed; in section 4, UDP scanning technologies are related; in section 5, we make comparisons among these scanning methods; we conclude this paper in section 6.

ICMP Scanning

Internet Control Message Protocol (ICMP) messages, delivered in IP packets, are used for out-of-band messages related to network operation or mis-operation. It is a key protocol to exchange control and error messages over the Internet [1].

2.1 ECHO Scanning

ECHO scanning is also called as ping. ECHO scanning works by sending specific types of network traffic, called ICMP Echo Request packets(ICMP type 8), to a specific interface on a computer or network device. If the device (and the attached network card) that received the ping packet is turned on and not restricted from responding, the receiving machine will respond back to the originating machine with an Echo Reply packet(ICMP type 0) . From this reply, we can say that the host is alive.

2.2 ICMP Sweep

An ICMP sweep is a series of pings that are automatically sent to a range of IP addresses, rather than manually entering the individual target's address. This type of scanning is suitable to scan a middle size of computer network.

2.3 Broadcast ICMP

Broadcast ICMP sets the aim of the ICMP Echo Request packets as a broadcast address or a network address, so the on-line host in this address will reply to the request packets and tell us that they are alive. But this method is only suitable to UNIX/Linux system, because the windows system will not replay to the broadcast ICMP Echo Requests. So we can identify the operating system according to this characteristic.

2.4 NON-ECHO Scanning

Except for the ECHO scanning, the ICMP Timestamp Request (ICMP type l3) and ICMP Address Mask Request (ICMP type l7) are also can be used to discover host. If the host is alive, it will reply with the ICMP Timestamp Reply (ICMP type l4) and ICMP Address Mask Reply (ICMP type l8).These methods can be used to discover host when the firewall blocks the ICMP ECHO packets.

2.5 Parameter Problem on a Datagram

If we send an IP datagram with wrong header length filed to a destination, the on-line host will reply with "Parameter Problem on a Datagram" ICMP packets (ICMP type l2). If no reply back, we can label the host as down or a firewall is in front of it.

2.6 Fragment Reassembly Timeout

If the IP datagram is fragmented, the destination host will start a timer when it gets the first fragment. In the following, if not all the fragments are received in the restricted time, the receiver will discard all the fragments and send back a "Fragment reassembly timeout" ICMP packet (Type 11, code 1) to the sender. According to this, we can discover a host by sending an incomplete IP fragments and receiving the "Fragment reassembly timeout" ICMP packet. If no reply back, we can label the host as down or a firewall is in front of it.

2.7 Protocol Unreachable

Sending an IP datagram with the wrong protocol to the destination, then the destination host will return the "Protocol Unreachable" packet which is one of the "Destination Unreachable"ICMP message. But if there is a firewall or a filter device in front of the target host, this reply will be flitted and no response will return to the source. So when sending an IP datagram with a large protocol number at least not used nowadays, the destination will return "protocol Unreachable" to the source, if so, we can get that the host is alive. Otherwise, if no "Destination Unreachable" ICMP data returned, we can infer there is a firewall in front of the host or the host is down. At the same time, we can deduce what protocols are in use according to the returned ICMP error messages. If "Destination Unreachable" is returned, the host is not using this protocol. On the contrary, if nothing back, the host may use this protocol, or the reply may be filtered by firewall, etc.

2.8 Port Unreachable

When sending a packets to unused port of the destination host, the host will reply with the "Port Unreachable"（ Type = 3, Code = 3） which is also one of the "Destination Unreachable" ICMP message. So when sending an IP datagram with a large port number little chance used, the destination will return "port Unreachable" to the source, if so, we can get that the host is alive. Otherwise, if no "Destination Unreachable" ICMP data returned, we can infer there is a firewall in front of the host or the host is down.

TCP Scanning

TCP provides reliable, ordered and error-checked delivery of a stream of octets between programs running on computers connected to a local area network, intranet or the public Internet. Resident at the transport layer, it casts congestion may happen in high-bandwidth and low-latency networks when multiple synchronized servers send data to the same receiver in parallel [2].

3.1 TCP Connect Scanning

The scan host establishes a connection to a port on the destination host based on Three-Way Handshake principle which is shown in Fig.1. In detail, this connection is started by calling the function "connect ()". If the port is open, the connection will be established. Otherwise, it will return -1 for the calling, indicating the port is closed [3].

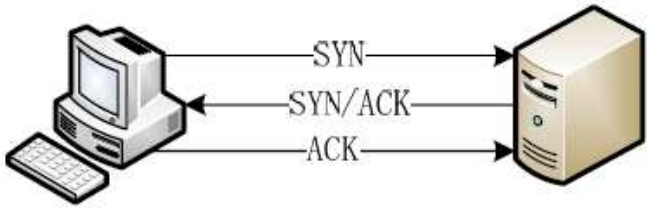

Fig.1 Three-Way Handshake

3.2 SYN Scanning

In a SYN scan, the scanning host sends a SYN packet, only with the SYN tag labeled, to the destination. If the target responds with a SYN/ACK, we can get the port is in use and then the scanning host discontinues the process by sending a "RST" to the target. Otherwise, when sending the SYN to the target, if it responds with a RST, we can get the port is close. At the same time, if we get nothing after sending the SYN to the target, we can mark the host as down. Because this process does not establish a connection, so it may not be record by some application and logs and it provides a level of obscurity or stealth [4].

3.3 ACK Scanning

The same with SYN scan, in an ACK scanning, the scanning host sends an ACK packet, only with the ACK tag labeled, to the destination. Whether the port is open or close, as long as the target host is alive, the destination will responds with a RST, for it has not sent a SYN to that scanning host and feels obscure to this ACK. If nothing back, we can label the target host as down. According to whether the ACK packet can pass the firewall, we can identify the packet filtering firewall with state inspection firewall [5,6]. This type of scan also has obscurity.

3.4 FIN Scanning

Sending a FIN packet to a certain port on the destination, if nothing replied back, we can get the host is alive and port is open. If the target replied with RST, we can get that the host is alive but the port is close. This type of scan also has obscurity. The theory basis of this scan method is the TCP RFC, which says that if a closed port receives a packet that does not have a SYN, ACK, or RST flag set, the port should respond with an RST packet of its own. Furthermore, the RFC states that if the port is open and it receives a packet without a SYN, ACK, or RST flag set the packet should be ignored.

3.5 NULL Scanning

In a NULL scans, which is also an obscures scan, the scan host sends a packet devoid of any flags to a certain port on the destination. Given TCP RFC, a NULL packet should be replied with RST when the port on the destination is close and should be replied with nothing when the port is open.

3.6 Xmas Scanning

In an Xmas scans, the scan host sends a packet with the FIN, PSH, and URG packet flags are all set to "on"to a certain port on the destination. Given TCP RFC, an Xmas packet should be replied with RST when the port on the destination is close and should be replied with nothing when the port is open.

UDP Scanning

The User Datagram Protocol (UDP) is one of the core members of the Internet protocol suite.With UDP, computer applications can send messages, in this case referred to as datagrams, to other hosts on an Internet Protocol (IP) network without prior communications to set up special transmission channels or data paths. We use UDP other than TCP for video and audio streaming service or online gaming where data travel speed or bandwidth has more priority compared to reliability [7].

For UDP is a connectionless protocol, when sending packets to a UDP port, it will return nothing to the source if the port is open, while if the port is closed, some systems will reply with ICMP Port Unreachable. It is the same with section 2.8. But since UDP is not a reliable connection-oriented protocol, this scanning method is easy to get wrong conclusion with packets dropping.

Comparisons of the Methods

Here, we make comparisons among all these 15 scanning methods related above to show for what tasks these methods can be used. The tasks refer to host scanning and port scanning. The results are shown in Table 1. As the principle of "Port Unreachable" is the same with that of "UDP Scanning", we merge them into "UDP/Port". In this table, the name of every scanning is demonstrated by the main part of its original name to save space. If the scanning method is suitable for such task, we label

a " √ " in the corresponding blank. From this table, we can see that (1) Totally, ICMP are mainly used to discover the host, while the TCP and UDP are mainly for port scanning, except ACK. (2) Though belong to the TCP datagram, ACK packets only can be used for host scanning, for it cannot tell the difference between the open and close ports. (3) SYN scanning and UDP scanning can be used for both port and host scanning. (4) SYN, ACK, FIN, NULL, Xmas and UDP scanning can complete their tasks in a secret way, which may not be logged by applications or systems.

Table 1 Comparisons among Scanning Methods

	Ping	Sweep	Broadcast	Non-echo	Parameter	Fragment	Protocol
Host	√	√	√	√	√	√	√
Port							
	TCP	SYN	ACK	FIN	Null	Xmas	UDP/Port
Host		√	√				√
Port	√	√		√	√	√	√

Conclusion

Network protocols such as ICMP, TCP and UDP can be used for host scanning and port scanning. Some of the scanning methods are elaborately designed to pass the examinations of firewalls. So, comprehensively using these methods can give us a more accurate and complete knowledge of the hosts and their ports. Totally, ICMP are mainly used to discover the host, while the TCP and UDP are mainly for port scanning, except for ACK. At the same time, using certain special TCP datagram such as SYN and ACK packets, and UDP datagram, we can make a host scanning in a secret manner.

Acknowledgement

The work in this paper has been supported by Research, Development and Application Verification of Performance Testing Tools for Highly Concurrent Internet Application Service Systems (Z131100005313010).

References

[1] L. Jacquin, V. Roca, M.A. Kaafar and F. Schuler, IBTrack: An ICMP black holes tracker, IEEE Global Communications Conference (GLOBECOM), Dec., (2012), P. 2827-2833.

[2] H.T. Wu, Z.Q. Feng, C.X. Guo and Y.G. Zhang, CTCP: incast congestion control for TCP in data-center networks, IEEE/ACM Transactions on Networking, 21(2), (2013), P. 345-358.

[3] C. McNab, J.X. Wang, in: Network Security Assessment, China Electric Power Press (2005).

[4] P. Engebretson, in: The Basics of Hacking and Penetration Testing, Elsevier, Waltham, 2011.

[5] U. Thakar, L. Purohit and Pahade, An Approach to Improve Performance of a Packet-filtering Firewall, Ninth International Conference on Wireless and Optical Communications Networks (WOCN), Indore, Sept. (2012), P. 1-5.

[6] H.Q. Mao, L. Zhu, M.B. Li, Current State and Future Development Trend of Firewall Technology 8th International Conference on Wireless Communications, Networking and Mobile Computing (WiCOM), Shanghai, Sept., (2012), P.1- 4.

[7] V. Verma and S. Dhawan, Comparison and Assessment of TCP& UDP Protocols in Different Network Scenarios, International Journal of Software&Hardware Research in Engineering, 2 (2), (2014), P. 112-115.

Advanced Materials Research Vols. 989-994 (2014) pp 4290-4293
© (2014) Trans Tech Publications, Switzerland
doi:10.4028/www.scientific.net/AMR.989-994.4290

The Application of Multicarrier Code Division Multiple Access System in the Internet of Things

Hancheng Liao

School of Software and Communication Engineering

Jiangxi University of Finance and Economics

Nanchang, China, 330013

Liaoemail@163.com

Keywords: Multicarrier, CDMA, Internet of Things

Abstract. Massive amounts of data frequently need to be communicated in the internet of things where the channel is wireless. CDMA is a good technology to combat fading. In order to improve the system capacity or the spectrum efficiency, more than one carrier can be employed. Both the transmitter structure and that of the receiver are given in this paper. The interference item, as well as the received signal, is carefully analyzed. A summary, after some simulation results is given in the end.

Introduction

Recently, the internet of things (IOT) is one of the research hotspots [1-2]. Being a successor of internet, it has broader use. After massive data are obtained from lots of sensor nodes, communication with high quality becomes indispensable. More often than not, wireless or mobile application accounts for a large proportion. Code division multiple access (CDMA) system is famous for combating multipath fading in wireless communication [3]. Large-area-synchronized (LAS) codes are very suitable to act as the multiple access codes (MACs) due to their good auto-correlation property and cross-correlation property [4-5]. In our research, the multicarrier technology is applied to CDMA system using LS codes which is the specific LAS codes in one cell situation.

System Model

At first, we talk about the correlation function between LS code c_m and c_n, named $R_{mn}(p)$. If the absolute value of p is not greater than the width of the zero correlation zone (ZCZ), $R_{mn}(p)$ is zero except $R_{mm}(0)=1$ for normalization. Suppose that the unit pulse response function of the wireless fading channel is $h_{ku}(t)=\sum_{l=1}^{L}\alpha_{ku}^{l}\delta(t-\tau^{l})$, where α_{ku}^{l} is the fading coefficient, τ^{l} is the time delay and L is the number of multipath.

The transmitter of user k is shown in Fig. 1. The frequency of the carrier u is $f_u, u=1,2,\cdots,U$. The data of the user k is $d_k[i], i=0,1,2,\cdots$. The multiple access code of user k is c_k. So that the signal of user k corresponding to carrier u is $d_{ku}(t)=\sum_{i=-\infty}^{+\infty}d_{ku}[i]p_{T_s}(t-iT_s)$, where $d_{ku}[i]=d_k[i]\big|_{(i \bmod U)+1=u}$ and $p_{T_s}(t)$ is the forming pulse with duration time of one symbol. Therefore the transmitting signal of user k is $s_k(t)=\sum_{u=1}^{U}d_{ku}(t)c_k(t)e^{j2\pi f_u t}$, where $c_k(t)=\sum_{n=0}^{N_c}c_k[n]p_{T_c}(t-nN_c)$, $p_{T_c}(t)$ is the (rectangular) pulse with duration time of one chip and N_c is the length of MAC sequence.

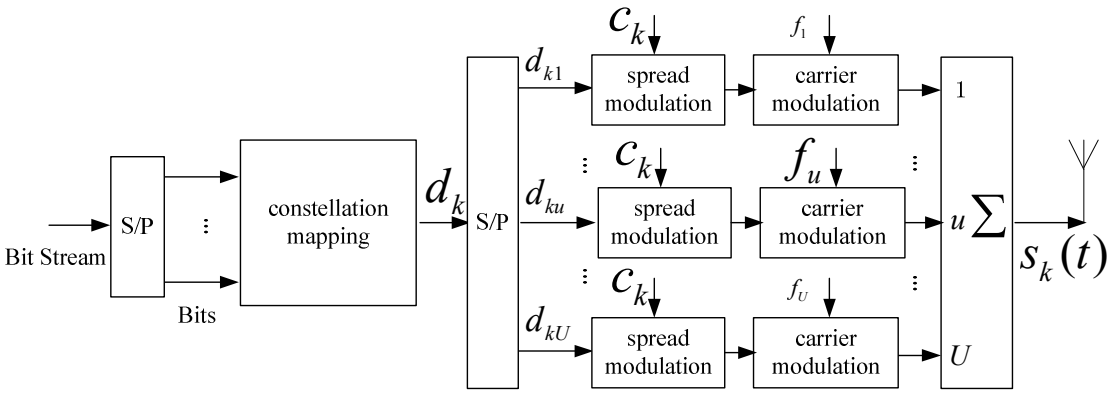

Figure 1. The transmitter model of user *k*

The receiver model of any given user *n* is showed in Fig. 2, where g_{nm}^{v} ($m=1,2,\cdots,U$; $v=1,2,\cdots,L$) are the coefficients of multipath combination.

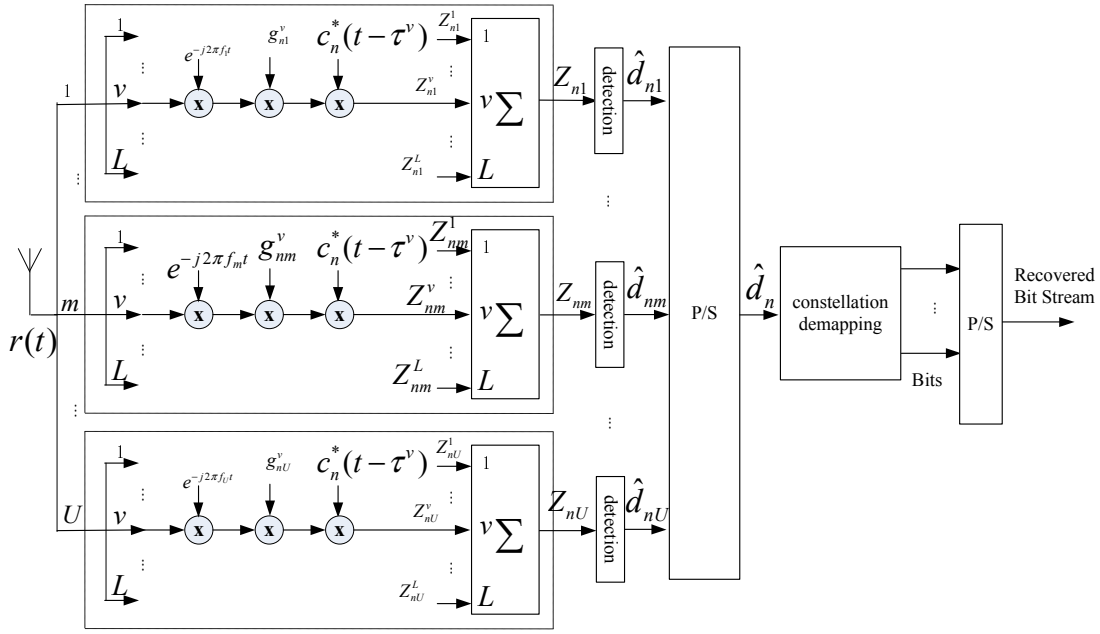

Figure 2. The receiver model of user *n*

The received signal $r(t)$ can be notated as follows, where $n(t)$ is the Gaussian noise

$$r(t)=\sum_{k=1}^{K}\sum_{u=1}^{U}\sum_{l=1}^{L}\alpha_{ku}^{l}d_{ku}(t-\tau^{l})c_{k}(t-\tau^{l})e^{j2\pi f_{u}(t-\tau^{l})}+n(t) \tag{1}$$

Thus, the *m*-th output of user *n* on decision time $T_s+(L-1)T_c$ is $Z_{nm}=\sum_{v=1}^{L}Z_{nm}^{v}$ $n=1,2,\cdots,K;m=1,2,\cdots,U$ where

$$Z_{nm}^{v}=\frac{1}{T_s}\int_{\tau^{v}}^{T_s+\tau^{v}}r(t)g_{nm}^{v}c_{n}^{*}(t-\tau^{v})e^{-j2\pi f_{m}(t-\tau^{v})}dt$$

$$=\sum_{k=1}^{K}\sum_{u=1}^{U}\sum_{l=1}^{L}\left\{\frac{1}{T_s}\int_{\tau^{v}}^{T_s+\tau^{v}}\left[g_{nm}^{v}\alpha_{ku}^{l}d_{ku}(t-\tau^{l})c_{k}(t-\tau^{l})c_{n}^{*}(t-\tau^{v})\ c_{n}^{*}(t-\tau^{v})e^{j2\pi[f_{u}(t-\tau^{l})-f_{m}(t-\tau^{v})]}\right]dt\right\}+\eta_{nm}^{v}$$

$$\eta_{nm}^{v}=\sum_{k=1}^{K}\sum_{u=1}^{U}\sum_{l=1}^{L}\frac{1}{T_s}\int_{\tau^{v}}^{T_s+\tau^{v}}n(t)g_{nm}^{v}c_{n}^{*}(t-\tau^{v})e^{-j2\pi f_{m}(t-\tau^{v})}dt \tag{2}$$

Therefore $Z_{nm}=\sum_{v=1}^{L}\sum_{k=1}^{K}\sum_{u=1}^{U}\sum_{l=1}^{L}\left\{\frac{1}{T_s}\int_{\tau^v}^{T_s+\tau^v}\left[g_{nm}^{v}\alpha_{ku}^{l}d_{ku}(t-\tau^l)c_k(t-\tau^l)\ c_n^*(t-\tau^v)e^{j2\pi[f_u(t-\tau^l)-f_m(t-\tau^v)]}\right]dt\right\}+\sum_{l=1}^{L}\eta_{nm}^{v}$.

When the width of the zero correlation zone of LS code is great enough, we obtain

$$\begin{aligned}&\sum_{v=1}^{L}\sum_{k=1}^{K}\sum_{u=1}^{U}\sum_{l=1}^{L}\Psi(n,m,v,k,u,l)\\&=\sum_{v=1}^{L}\Psi(n,m,v,k,u,l)\big|_{k=n,u=m,l=v}+\sum_{v=1}^{L}\sum_{\substack{l=1\\l\neq v}}^{L}\Psi(n,m,v,k,u,l)\big|_{k=n,u=m}+\sum_{v=1}^{L}\sum_{\substack{k=1\\k\neq n}}^{K}\sum_{l=1}^{L}\Psi(n,m,v,k,u,l)\big|_{u=m}+\sum_{v=1}^{L}\sum_{k=1}^{K}\sum_{\substack{u=1\\u\neq m}}^{U}\sum_{l=1}^{L}\Psi(n,m,v,k,u,l)\\&=D_{nm}+\Upsilon_{nm}^{(1)}+\Upsilon_{nm}^{(2)}+\Upsilon_{nm}^{(3)}\end{aligned}\tag{3}$$

where $\Psi(n,m,v,k,u,l)=\frac{1}{T_s}\int_{\tau^v}^{T_s+\tau^v}\left[g_{nm}^{v}\alpha_{ku}^{l}d_{ku}(t-\tau^l)c_k(t-\tau^l)\ \ c_n^*(t-\tau^v)e^{j2\pi[f_u(t-\tau^l)-f_m(t-\tau^v)]}\right]dt$

The information signal transmitted exists in D_{nm}, spoiled by channel fading of course. The last three interference items in equation (4) are respectively as follows: $\Upsilon_{nm}^{(1)}$ is the interference between paths having different delay within one user of the same carrier, $\Upsilon_{nm}^{(2)}$ is the interference between different users that use the same carrier, $\Upsilon_{nm}^{(3)}$ is the others interference that is not included in the former two interference items.

Remembering that $R_{nn}(0)=1$, we obtain the first item

$$\begin{aligned}D_{nm}&=\sum_{v=1}^{L}\Psi(n,m,v,k,u,l)\big|_{k=n,u=m,l=v}=\sum_{v=1}^{L}\frac{1}{T_s}\int_0^{T_s}g_{nm}^{v}\alpha_{nm}^{v}d_{nm}(t)c_n(t)c_n^*(t)dt=\sum_{v=1}^{L}\frac{1}{T_s}\int_0^{T_s}g_{nm}^{v}\alpha_{nm}^{v}d_{nm}[0]c_n(t)c_n^*(t)dt\\&=\sum_{v=1}^{L}g_{nm}^{v}\alpha_{nm}^{v}d_{nm}[0]R_{nn}(0)=\sum_{v=1}^{L}g_{nm}^{v}\alpha_{nm}^{v}d_{nm}[0]\end{aligned}\tag{4}$$

The last item is worked out as

$$\begin{aligned}\Upsilon_{nm}^{(3)}&=\sum_{v=1}^{L}\sum_{k=1}^{K}\sum_{\substack{u=1\\u\neq m}}^{U}\sum_{l=1}^{L}\Psi(n,m,v,k,u,l)=\sum_{v=1}^{L}\sum_{k=1}^{K}\sum_{\substack{u=1\\u\neq m}}^{U}\sum_{l=1}^{L}\frac{1}{T_s}\int_{\tau^v}^{T_s+\tau^v}\left[g_{nm}^{v}\alpha_{ku}^{l}d_{ku}(t-\tau^l)c_k(t-\tau^l)\,c_n^*(t-\tau^v)e^{j2\pi[f_u(t-\tau^l)-f_m(t-\tau^v)]}\right]dt\\&=\sum_{v=1}^{L}\sum_{k=1}^{K}\sum_{\substack{u=1\\u\neq m}}^{U}\sum_{l=1}^{L}\frac{1}{T_s}\int_0^{T_s}\left[g_{nm}^{v}\alpha_{ku}^{l}d_{ku}(t+\tau^v-\tau^l)c_k(t+\tau^v-\tau^l)\,c_n^*(t)e^{j2\pi[f_u(t+\tau^v-\tau^l)-f_m t]}\right]dt\approx\sum_{v=1}^{L}\sum_{k=1}^{K}\sum_{\substack{u=1\\u\neq m}}^{U}\sum_{l=1}^{L}\frac{1}{T_s}\int_0^{T_s}\left[g_{nm}^{v}\alpha_{ku}^{l}d_{ku}[0]c_k(t+\tau^v-\tau^l)\,c_n^*(t)e^{j2\pi[f_u(t+\tau^v-\tau^l)-f_m t]}\right]dt\end{aligned}\tag{5}$$

In the same way, we can get

$$\begin{aligned}\Upsilon_{nm}^{(1)}&=\sum_{v=1}^{L}\sum_{\substack{l=1\\l\neq v}}^{L}\Psi(n,m,v,k,u,l)\big|_{k=n,u=m}\approx\sum_{v=1}^{L}\sum_{\substack{l=1\\l\neq v}}^{L}g_{nm}^{v}\alpha_{nm}^{l}d_{nm}[0]e^{j2\pi f_m(\tau^v-\tau^l)}R_{nn}^*(\tau^l-\tau^v)=0\\\Upsilon_{nm}^{(2)}&=\sum_{v=1}^{L}\sum_{\substack{k=1\\k\neq n}}^{K}\sum_{l=1}^{L}\Psi(n,m,v,k,u,l)\big|_{u=m}\approx\sum_{v=1}^{L}\sum_{\substack{k=1\\k\neq n}}^{K}\sum_{l=1}^{L}g_{nm}^{v}\alpha_{km}^{l}d_{km}[0]e^{j2\pi f_m(\tau^v-\tau^l)}R_{nk}^*(\tau^l-\tau^v)=0\end{aligned}\tag{6}$$

So we get $Z_{nm}\approx d_{nm}[0]\left(\sum_{v=1}^{L}g_{nm}^{v}\alpha_{nm}^{v}\right)+\Upsilon_{nm}^{(3)}+\sum_{l=1}^{L}\eta_{nm}^{v}$. The first two items $\Upsilon_{nm}^{(1)}$ and $\Upsilon_{nm}^{(2)}$ are little and many parts of $\Upsilon_{nm}^{(3)}$ can be counteracted, which leads to greatly decrease the interference. The recovered signal of user n corresponding to carrier m, i.e. $d_{nm}[0]$ in equation (4) can be easily achieved. Therefore, the system performance of such multicarrier CDMA system increases greatly.

Performance Simulation

The main simulation parameters used in the computer experiments are shown in table 1.

The bit-error-rate versus signal-to-noise ratio performance simulation results of this kind of multicarrier CDMA are shown in Fig. 3. From this figure, we can easily notice that, when the number of subcarrier is relatively small, the performance is almost equivalent to that of the single carrier system. In the same time, the system capacity almost enhances linearly to the number of carriers.

Table 1. The main simulation parameters

Parameters	Values
Spread factor	512
Channel model	ITU-VA
Velocity	70 km/h
Number of carrier	1,2,4,8,16
Channel estimation algorithm	Ideal channel estimation
Mapping constellation	64QAM
Equalization algorithm	MMSE equalization

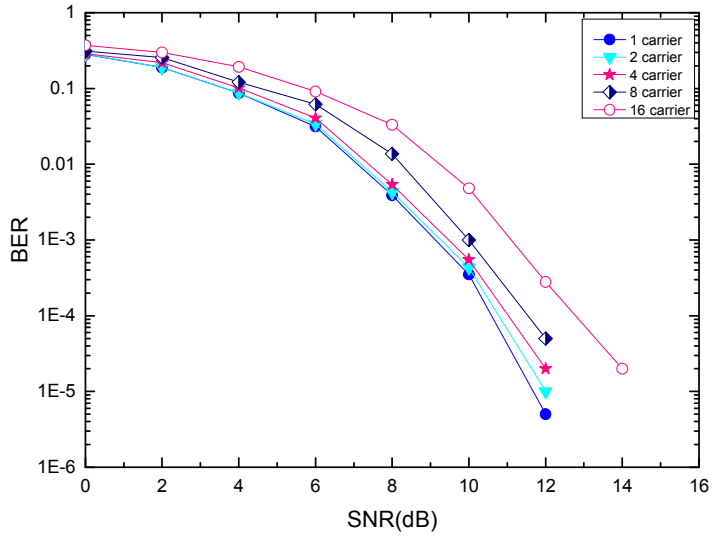

Figure 3. The bit-error-rate performance of the multicarrier CDMA system

Summary

On the one hand, thanks to the existence of zero correlation zones in the correlation functions of the LS codes, the system capacity of such kind multicarrier CDMA system can be greatly increased by employing multicarrier technology. On the other hand, the system bit-error-rate performance has little loss as compared with that of single carrier system. As the system performance of such kind of multicarrier CDMA system using LS codes is excellent, all the merits of such system make it suitable to future IOT wireless application.

References

[1] ITU Internet Reports 2005: The Internet of Things (2005)

[2] Information on http://www.smart-systems-integration.org/public/internet-of-things

[3] L. Hanzo, L. L. Yang, E. L. Kuan and K. Yen, *Single and Multicarrier DS-CDMA*, IEEE Press (2003)

[4] Hancheng Liao, Daoben Li and Qingrong Zhang: An example of LS codes, 16th International Conference on Computer Communication, Beijing, China (2003), p. 918

[5] Daoben Li: A spread spectrum coding method possessing interference free window, Chinese Patent PCT/CN00/0028.(1999)

Advanced Materials Research Vols. 989-994 (2014) pp 4294-4297
© (2014) Trans Tech Publications, Switzerland
doi:10.4028/www.scientific.net/AMR.989-994.4294

Improved Ant Colony Algorithm and Its Application on the Routing Selection of Stable Clusters in Wireless Sensor Networks

Hai Yang[1, a]

[1]College of Information Science and Electricity Engineering, Shandong Jiaotong University, Jinan, Shandong, China 250023

[a]yanghai_sdjtu@163.com

Keywords: wireless sensor networks; ant colony algorithm; energy consumption; stable cluster

Abstract. Aiming at the shortcomings of slow convergence speed and instable optimal routing which will occur when ant colony algorithm is applied in wireless sensor networks, an improved algorithm is proposed in this paper, which can be used to optimize cluster heads number, cluster unequally and keep the majorizing clusters stable. In addition, the improved ant colony algorithm is used for routing in the majorizing cluster. Simulation experiments show that the stable cluster colony algorithm is useful in reducing the energy consumption and improving the speed of data package transmission.

Introduction

Wireless Sensor Network (WSN) is a new research area of computer science and technology. It consists of the convergence of sensor, micro-electro-mechanism system and network technologies. Wireless sensor network is supposed to have a variety of applications in the future [1].

A wireless sensor network (WSN) is consist of many spatially distributed autonomous sensors. It can monitor physical or environmental conditions, such as temperature, sound, pressure, etc. and cooperatively pass their data through the network to a main location. The development of wireless sensor network was motivated by military applications such as battlefield surveillance [2]. Today wireless sensor networks are used in many industrial and consumer applications, such as industrial process monitoring and control, machine health monitoring, and so on.

The WSN is built of nodes which are from a few to several hundreds or even thousands, where each node is connected to one (or sometimes several) sensors. Each such sensor network node has typically several parts: a radio transceiver with an internal antenna or connection to an external antenna, a microcontroller, an electronic circuit for interfacing with the sensors and an energy source, usually a battery or an embedded form of energy harvesting.

Because of the useful characteristics, including easy to be realized, supporting multi-path, ant colony algorithm was introduced into the routing selection of stable clusters in wireless sensor networks. Then an improved ant colony algorithm based on stable clusters was proposed in this paper. Simulation experiments show that the stable cluster colony algorithm is useful in reducing the energy consumption and improving the speed of data package transmission.

Ant Colony Algorithm

The ant colony algorithm (ACO) is a probabilistic technique for solving computational problems which can be reduced to finding optimal paths through graphs.

The first version of ant colony algorithm, which is initially proposed by Marco Dorigo in 1992 in his PhD thesis [3], was aiming to search for an optimal path in a graph, based on the behavior of ants seeking a path between their nest and a source of food. The original idea has since diversified to solve a wider class of numerical problems, and as a result, several problems have emerged, drawing on various aspects of the behavior of ants.

In the natural world, ants initially wander randomly, and upon finding food return to their nest while laying down pheromone trails. If other ants find such a path, they are likely not to keep

travelling at random, but to instead follow the trail, returning and reinforcing it if they eventually find food. When the ant k moves to the next node j from node i, the node j can be decided with the probability $P_{ij}^{k}(t)$ which can be calculated by formula (1):

$$P_{ij}^{k}(t)=\begin{cases}\dfrac{\tau_{ij}^{\alpha}(t)\eta_{ij}^{\beta}(t)}{\sum_{s\in A_k}\tau_{is}^{\alpha}(t)\eta_{is}^{\beta}(t)} & j\in A_k\\ 0 & otherwise\end{cases} \tag{1}$$

Where $\tau_{ij}(t)$ denotes the pheromone density, A_k is the set of optional nodes adjacent to node i. α is the heuristic factor of pheromone. β is the heuristic factor of expectation. $\eta_{ij}(t)$ is the distance function which denotes the heuristic information of path. $\eta_{ij}(t)$ can be described as formula (2):

$$\eta_{ij}(t)=\frac{1}{d_{ij}} \tag{2}$$

Where d_{ij} denotes the distance from node i to node j.

Over time, however, the pheromone trail starts to evaporate, thus reducing its attractive strength. The more time it takes for an ant to travel down the path and back again, the more time the pheromones have to evaporate. A short path, by comparison, gets marched over more frequently, and thus the pheromone density becomes higher on shorter paths than longer ones. Pheromone evaporation also has the advantage of avoiding the convergence to a locally optimal solution. If there were no evaporation at all, the paths chosen by the first ants would tend to be excessively attractive to the following ones. In that case, the exploration of the solution space would be constrained.

Local pheromone updating strategy is regarded as follows:

$$\tau_{ij}(t+n)=(1-\rho)\cdot\tau_{ij}(t)+\Delta\tau_{it}(t) \tag{3}$$

Where ρ is the evaporation rate of pheromone. $\Delta\tau_{it}(t)$ denotes the increment of pheromone on path (i , j) during once iteration. $\Delta\tau_{it}(t)$ can be gain by formula (4) as follows:

$$\Delta\tau_{it}(t)=\begin{cases}Q/L_k & (i,j)\\ 0 & otherwise\end{cases} \tag{4}$$

Where Q is the pheromone density and L_k denotes the total length of the route ant k passed by.

Improved Ant Colony Algorithm Based on Stable Clusters (ACA-SC)

There are several limitations when ant colony algorithm is applied in wireless sensor networks. The priority of the specific node is not focused well enough when the amount of nodes is too big. So that the optimal routing selected by ant colony algorithm is instable, and what's worse, the convergence speed is slow and energy consumption is high.

The improved ant colony algorithm (ACA-SC) proposed in this paper selects the cluster-heads based on energy. The cluster-heads exchange the information of its distance and remaining energy with its neighborhood [4]. Then the distance and remaining energy of the neighborhood are integrated into the computation of pheromone concentration. Finally the data packet will choose its next hop with probability, which is computed on the basis of pheromone value [5].

Cluster-heads Selection. The improved cluster-heads selection strategy consists of two stages including primary selection of cluster-heads and cluster-heads adjustment.

Primary Selection of Cluster-heads. First of all, set an energy threshold E_{th}. During the procedure of primary selection of cluster-heads, one node will be chosen as the candidate cluster-heads only if its energy is greater than the threshold E_{th}. The energy threshold E_{th} can be calculated as follows:

$$E_{th} = E_0 \times (1 - \frac{R}{N}) \tag{5}$$

Where R is the number of rounds being executed, E_0 is the initial energy of every node, E_{th} denotes the limiting value of energy on the cluster-heads at the Rth round.

Introducing the energy threshold into cluster-heads selection strategy can effectively prevent the nodes with low energy from being chosen as cluster-heads and void the problems that cluster-heads die and stable cluster disappear.

Cluster-heads Adjustment. In the procedure of cluster-heads adjustment, one normal node sends candidate cluster-heads broadcasting message to other normal nodes within communication radius after it has been chosen as a candidate cluster-head. The message includes the label of the new candidate cluster-head and the remaining energy value of it.

Each candidate cluster-head establishes the list of neighbor candidate cluster-heads which includes the labels of neighbor candidate cluster-heads, remaining energy values, the times being chosen as cluster-head and the adjacent relationship among other candidate cluster-heads.

If one node is near enough with another neighbor node so that the distance from the node to its neighbor is less than the distance threshold, these two nodes are called close nodes. The weight of close nodes can be calculated by formula (6) as follows:

$$W_{cn} = a \times \frac{E_r}{E_{node}} + b \times C_{cn} \tag{6}$$

Where E_r denotes the remaining energy of neighbor node, E_{node} denotes the initial energy of node. Both a and b are weight factors. The node with the maximal energy will be chosen as the final cluster-head at this round.

Improved Method for Choosing Normal Nodes into Cluster-heads. The criterion of cluster selection only focuses on the distance between normal nodes and cluster-heads according to LEACH protocol. If one normal node with the nearest distance from the cluster-heads, it can be joined into the cluster.

Suppose every distance between one cluster-head and sink node is greater than d_0. The much nearer the distance between cluster-heads and sink node is, the less energy consumed when transporting data [6]. Therefore the distance from one normal node to sink node should be considered when choosing normal node as a cluster-head.

The formula of improved method for choosing normal nodes into cluster-heads is:

$$COST\ (ch) = \begin{cases} f\ (d_{ch}) & d_{ch} > d_0 \\ g\ (d_{ch}) & d_{ch} \le d_0 \end{cases} \tag{7}$$

$$f\ (d_{ch}) = \frac{d_J - d_{\min J}}{d_{\max J} - d_{\min J}} \tag{8}$$

$$g\ (d_{ch,bs}) = \frac{d_S - d_{\min S}}{d_{\max S} - d_{\min S}} \tag{9}$$

Where d_j denotes the distance from the normal node to the temporary cluster-head, d_S denotes the distance from cluster-head to base station, $d_{\max J}$ denotes the expectation maximization distance from the normal node to temporary cluster-head, $d_{\min J}$ denotes the expectation minimization distance from the normal node to temporary cluster-head. $d_{\max S}$, $d_{\min S}$ separately denote the maximal and minimal distance from the cluster-head to base station.

ACA-SC and Its Application on Stable Cluster. Through the steps mentioned above, the wireless sensor network is divided into several small clusters. Then we apply ACA-SC to select optimal routing in small clusters and the convergence speed is quicker than before.

The improved transition probability is described as follows:

$$P_{ij}^{k}(t)=\begin{cases}\dfrac{\tau_{ij}^{\alpha}(t)\omega_{ij}^{\beta}(t)}{\sum_{s\in A_k}\tau_{is}^{\alpha}(t)\omega_{is}^{\beta}(t)} & j\in A_k\\ 0 & otherwise\end{cases} \tag{10}$$

Where $\omega_{ij}(t)$ denotes the energy grade which is calculated by formula (11):

$$\omega_{ij}(t)=\frac{(I-e_j)^{-1}}{\sum_{n\in R_s}(I-e_n)^{-1}} \tag{11}$$

Where I denotes the initial energy of nodes, e_j denotes the current energy of the receiving node.

Furthermore, ACA-SC uses local memory of each node to save the messages passing by it. If the new message received is already saved in the local memory, the repeated message will be omitted.

Experimental Results

The simulation experiments are carried out in the MATLAB by using ACA-SC and basic ant colony algorithm (ACO) separately. The simulation data include: base station position is at (50,175), sensor region is 100m×100m, the number of nodes is 300, initial energy of nodes is 0.5J, length of message is 4000bits. The experimental results are shown in Fig.1 and Fig.2.

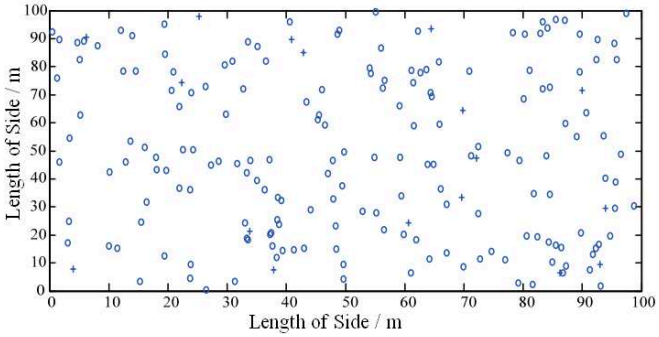

Fig.1 Topological Structure of ACA-SC

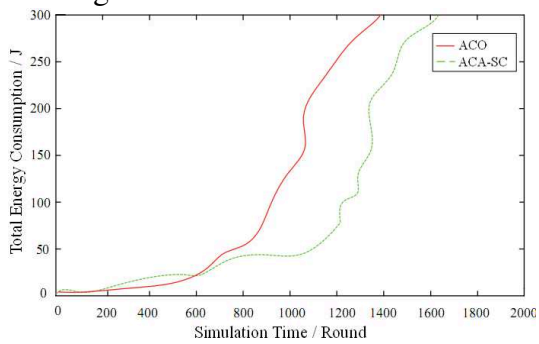

Fig.2 Comparison of Energy Consumption

Conclusion

In this paper an improved ant colony algorithm based on stable cluster was proposed. The improved algorithm takes advantages of optimal number of cluster-heads and optimal method for choosing normal nodes into cluster-heads to gain the stable clusters, and then applies ACA-SC in clusters to find the optimal routing. Furthermore the energy consumption of wireless sensor network has been decreased.

References

[1] Tilak S, Abu-Ghazaleh NB, Heinzelman W. Taxonomy of wireless micro-sensor Networkmodels. Mobile Computing and Communications Review, 2002, 1(2): 1-8.

[2] Akyildiz LF, Su WL, Sankarasubramaniam Y. A survey on sensor networks. IEEE Communications Magazine, 2002, 40(8): 102-114.

[3] Marco Dorigo. Ant colonies for the traveling salesman problem [J]. Biosystems, 1997, 43, pp.73-81.

[4] Pottie G. J., Kaiser W.J. Wireless integrated network sensors [J]. Communications of the ACM, 2000, 43(5): 51-58.

[5] Braginsky D, Estrin D. Rumor Routing Algorithm For Sensor Networks [J]. Proceedings of the 1st ACM international workshop on Wireless sensor networks and applications, 2002: 22-31.

[6] Wenyu Cai,Xingyu Jin,Yu Zhang,et al.. ACO based Qos routing algorithm for Wireless Sensor Networks [J]. A Survey Computer Networks. 2002, 38(4): 393-422.

Advanced Materials Research Vols. 989-994 (2014) pp 4298-4301
© (2014) Trans Tech Publications, Switzerland
doi:10.4028/www.scientific.net/AMR.989-994.4298

Research the architecture of a new Leisure Agriculture Intelligent System Base on the Internet of Things

Lin Yuan-guai

College of Electronics Information and Engineering, Qiongzhou University Technology, SanYa, Hainan, 572022, China

email: lyg_top@163.com

Keywords: Leisure agriculture; intelligent system; internet of thing; intelligent Cultivation Device; J2EE

Abstract. According to Hainan smart tourism problem characteristic, a new leisure agriculture intelligent system was proposed combining agricultural technology and the Internet of Things technology. The paper illustrates the overall structure of the system, then design the software platform frame of the system which on Struts, Hibernate, Spring Framework for J2EE technology. The system may provide an effective solution for leisure agricultural intelligent; the intelligent data center analyzes and processes the data, combine with the expert decision-making system, providing support for the user to better understand, then real-time tracking, make cultivation strategies or control online, the user can browse the information via the Internet .

Introduction

In recent year, leisure trips have been bloom. Leisure agriculture is a new kind of industry which combined agriculture with tourism [1]. The development of agriculture fallow and sightseeing tourism plays an important role in promoting the new rural construction, is also response to the specific implementation of the national 12th five-year plan [2]. At present, the focus of loyal tourism is being transferred to a leisurely vacationing tour with the target of building the Hainan Island into a tropical beach holiday resort in an eco-friendly environment. The Hainan international tourism island construction brings good opportunity for the development of leisure agriculture. Sanya is the most popular tourist area in Hainan, the development of leisure agriculture has the advantageous conditions, where has rich tropical agricultural landscape and varieties of agricultural resources. At present smart tourism relatively falls behind actually in Hainan province.

With the development of Internet of Things (IOT), it has become increasingly important for agricultural modernization and tourism intelligent. The development of leisure agriculture in Sanya needs the network platform based on IOT. The paper in view of the actual situation of leisure agriculture development based on the Internet of Things technology, combined with the agricultural technology, analyzes and studies the IOT application in leisure agriculture, then designs the architecture of a new leisure agricultural intelligent system. Anybody can browse the reality scenic of leisure agriculture. The system can remote manage the reality farm crops through the internet. The application of the internet of things in leisure agriculture not only meet the "low carbon" concept, but also can greatly improve the efficiency of management.

Related Theories

Internet of Things is a new research in the field of Internet. In IOT billions of objects can communicate, recognize and respond without human intervention and it is actually an internet of thing and thing. It has many examples of application in our real life, such as equipment inspection, intelligent fire protection, industrial monitoring, smart tourism, smart home, smart grid, intelligent transport, etc. IOT is the network that connects everything with internet, through various types of information sensor devices, such as radio frequency automatic identification (RFID), microwave

sensor, global positioning systems (GPS) and laser scanner, exchange information, and its final aim is to achieve intelligent identification, location tracking, monitoring and management [3]. Current research projections estimate that within 5-10 years, 100 billion devices will be connected to the internet [4].

WSN is an important wireless technology that has wide variety of applications and provides unlimited future potentials for IOT [5]. Wireless sensor network (WSN) is an important wireless technology that has wide variety of applications and provides unlimited future potentials. A WSN can have from a few to several thousand collaborating nodes with computing, data processing, and communicating components.

Tourism information in the process of advancing, the smart tourism is the advanced stage development. The Internet of things technology used in the tourism industry can accelerate the tourism information; make the tourism more intelligent, make people travel more comfortable.

Design of the Architecture of a new Leisure Agriculture Intelligent System

The Internet of Things is acted as the indispensable foundation link of terminal information sensing and will be given wide application space in the tourism management [6]. The intelligent system of leisure agriculture based on the internet of things completely changed the traditional management mode of tourism and agriculture. The proposed intelligent system for leisure agriculture based on IOT is illustrated in Figure 1. The system consists of wireless sensor networks (WSNs) in leisure agriculture scenic spot, video monitoring equipment, cultivation device, gateway, transmission network and intelligent data center.

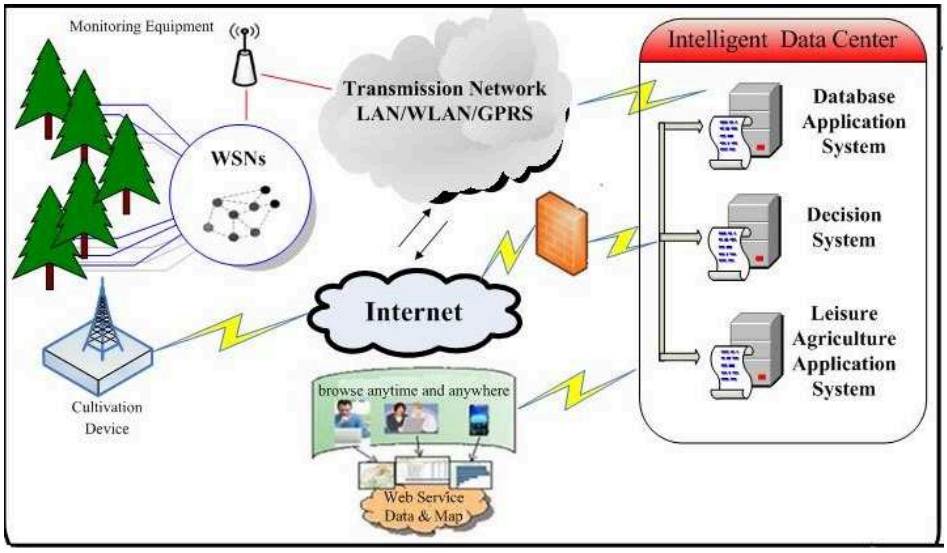

Fig.1 The architecture of the new leisure agriculture intelligent system

WSNs are composed of a great number of tiny low cost and low power consumption sensing nodes based on Zigbee technology [7]. The node is made up of four main sub modules [6]. The sensing module consists of several sensors chip as humidity, temperature sensor and On-board interfaces for optional sensor; two AA-batteries are used as power supply. The RFID reader interface can connect the RFID reader and complete the RFID cards and labels reading and writing capabilities. A great many such nodes, deployed in the leisure agriculture tourism scenic spot to be detected. The data from the monitoring nodes is transferred to the intelligent data center by the gateway via a transmission network (LAN/WLAN/GPRS). The gateway can realize the seamless access and adaptive switch through WLAN/Ethernet/cellular network.

Cultivation equipment integrated with embedded TCP/IP protocol; access the Internet through wired or wireless way, which can perform the breeding strategy on by remote control. When the Cultivation equipment receives the control command from remote intelligent center, it will make

response, such as adjusting the light intensity and irrigation time. Video monitoring equipment can transport the scene of the leisure agriculture parks in real time.

The intelligent data center analyzes and processes the plant growth quality parameters, combine with the expert decision-making system, providing support for the grower and tourist to better understand, then real-time tracking, make cultivation strategies or control, who get the information via the internet anytime and anywhere, how each factor affects growth and how to manage maximal crop productiveness. It can realize to move the physical world of farmland into the network, then manage real-time online through internet.

The intelligent data center software platform frame is shown in figure 2, which based on Struts, Hibernate, Spring Framework for J2EE technology, designs each module function of the system according to the idea of modularization. And using the method of system engineering, combine with the multiple subsystems, forming a reusable, extensible and replicable system. It includes main three parts: the leisure agriculture application system, database application system and the decision system.

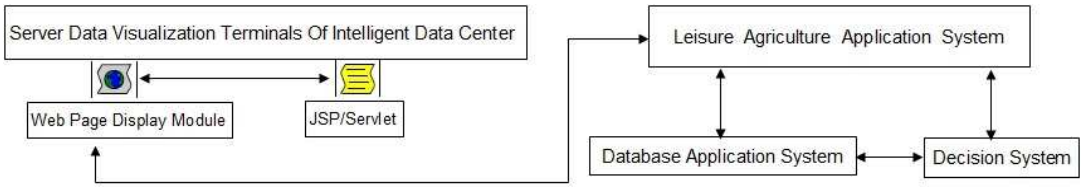

Fig.2 Intelligent Data Center Software Platform frame

The leisure agriculture application system faces to users group; this system is used for collecting new data and shows out in the website form. It can build a stable and safe bridge between intelligent data center and gateway. The database application system is used for classifying and saving the different information in the database. It mainly has three son databases: the information from leisure agriculture farmland son database, the information of communication son database and the user information son database. This system stores the data, then provides to other applications. The decision system mainly collects agricultural domain knowledge, intelligent system model and expert experience, which provide advisory services to agricultural production and management, guide the scientific farming.

Design of the leisure agriculture application system

The leisure agriculture application system includes four parts: Server data visualization terminals, data transmission module, data collection transfer module and the backstage management module. The server data visualization terminals include web page display module and JSP/Servlet. The server data visualization terminal is one part of the leisure agriculture application system, which are the interface of user and the intelligent data center.

The data transmission module includes the tripartite function mainly: Building connection element; receive data and upload element; dispatching terminal data element [8]. The data collection transfer module is mainly responsible for connecting database application system with customer data display web page.

The web page display module is used to demonstrate relevance information, which function structure chart is shown in figure 3. This module introduces the factory pattern, analyze and expand it. Based on the module, users can make online planting plan and implementation, realize remote real farm management via the Internet, and according to their own favor and need to choose the field of personalized cultivation; when the user is planted in the network, the real farm will have staff on-site service, thus it can combine virtual and reality. After planting, the customer can browse the growth of their crops and cultivate their farm online. Of course, the user can also choose to plant personally on-site in the farm. It not only enrich the farm, but also can loosen body and mind, o achieve the combination of leisure and entertainment. When the crop is mature, can be obtained by way of self pick or entrust, comfortable taste of green food.

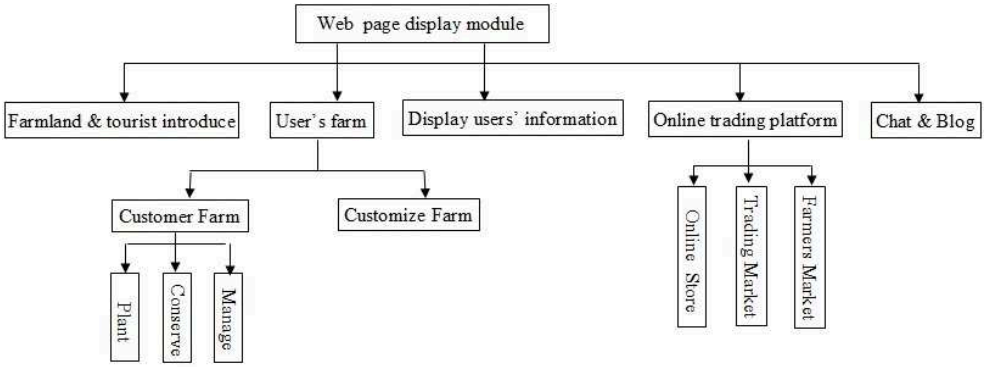

Fig.3 Web Page Display Function Structure

Conclusion

With the development of intelligent agriculture and smart tourist application of the Internet of things, based on the Internet of things the new leisure agriculture intelligent system can remote manage the reality farm, browse the live of the farm, combine virtual and reality. Therefore, based on the Internet of things the new leisure agriculture intelligent system has very big prospect and space on intelligent leisure agriculture.

Acknowledgement

In this paper, the research was sponsored by university and local government technological cooperative of SanYa (project No. 2013YD22) and science research of education of Hainan province (project No. Hjkj2013-43) .

References

[1] Chang H M, Liao F H. A study of development model for leisure agricultural farm localization[C]//Business Innovation and Technology Management (APBITM), 2011 IEEE International Summer Conference of Asia Pacific. IEEE, 2011: 338-340.

[2] Gu Liang, Research and Design of Leisure Agriculture System Based On the Internet of Things [D].Suzhou: SoocHow University, 2012. (In Chinese with English abstract).

[3] Yingying Lei , Pingchuan Ma and Lili Zhao, The Internet of Things Brings New Wave of the Information Industry [J].International Journal of Computer Science and Network Security, VOL.11 No.5, May 2011:15-21.

[4] Prasad S S, Kumar C. A Green and Reliable Internet of Things[J]. Communications and Network, 2013, 5: 44.

[5] Virkki J, Chen L, Zhu Y, et al. Challenges in Qualitative Accelerated Testing of WSN Hardware[J]. Engineering, 2011, 3(12).

[6] Lin Yuanguai. The application of the internet of things in Hainan tourism scenic spot[C]. Computational Intelligence and Security (CIS), 2011 Seventh International Conference on. IEEE, 2011:1549–1553.

[7] Lin Yuanguai. An Intelligent Monitoring System for Agriculture Based on Zigbee Wireless Sensor Network [J]. Advanced Materials Research, Vols. 383~399，4358–4364.

[8] Z. Y. Li, LINQ from the Foundation to the Project Development Proceeding of LINQ to SQL [M], Chemical Industry Press, Beijing, 2010, 174-263.

Advanced Materials Research Vols. 989-994 (2014) pp 4302-4305
© (2014) Trans Tech Publications, Switzerland
doi:10.4028/www.scientific.net/AMR.989-994.4302

Technical Framework and Functional Framework on Sports E-government Platform

Lixia Wang[a], Ligong Zhao[b]

Physical Education College, Shijiazhuang University, Shijiazhuang, P.R. China

[a]smilexia1225@163.com, [b]1213552916@qq.com

Keywords: sports; E-government; development platform; technical framework; functional framework

Abstract. Constructing sports e-government platform is an important content that all levels sports departments carry out sports optimal allocation of resources, expand the development and use of sports information resources and to improve the level of development of sports undertakings. For difficult problems in the construction of sports e-government platform, this paper studies the technical framework and functional framework. The technical framework is composed of seven sub-systems that Infrastructure layer, Database layer, Basic components layer, Core services layer, Application system layer, Portal layer, Access channel layer and so on. The functional framework is composed of five sub-systems that Sports information distribution system, Sports transverse application system, Sports office automation system, Sports management information system, System maintenance management system and so on. Contents of this paper focus on improving the level of application, government information resources development and utilization as the main line, for enhancing sports work management, promoting the development of sports undertakings plays an important role.

Introduction

E-government is the application of modern information and communication technology, make management and services through network technology integrate, on the Internet to implement optimal reorganization of the organizational structure and workflow restructuring, Beyond time and space and the separate limitations of departments, to provide quality and comprehensive, standardized and transparent, in line with international standards of management and services [1, 2] to the society. With the development of information technology and application level awareness continues to improve, many local governments to upgrade and update the system, adding a new operational rules and regulations, strengthen inter-departmental coordination between regions, promoting development of China's sports undertakings.

With the development of software development technology, in multi-software development project, reusable, easy to expand, and is well-tested software components, more and more people favored. It will be ample time to analyze, build on the application of the business logic, rather than the code works complex [3]. So make same type of problem solving approaches abstract, extraction into an application framework, that framework are some proved through practice, it can be used to develop technology of highly efficient application systems, through the design and application of the framework to achieve the control software to improve the quality of software production efficiency. For existing problems in the sports e-government construction process, this paper studies its technical framework and functional framework to provide support for system construction.

Technical Framework

Technical framework is the basis of the framework supporting software development; developers accomplish specific business processing functions on the technical framework. Sports e-government technical framework is composed of Infrastructure layer, Database layer, Basic components layer, Core services layer, Application system layer, Portal layer, Access channel layer, Safety and security, Management and regulation and so on. The structure is shown in Fig. 1.

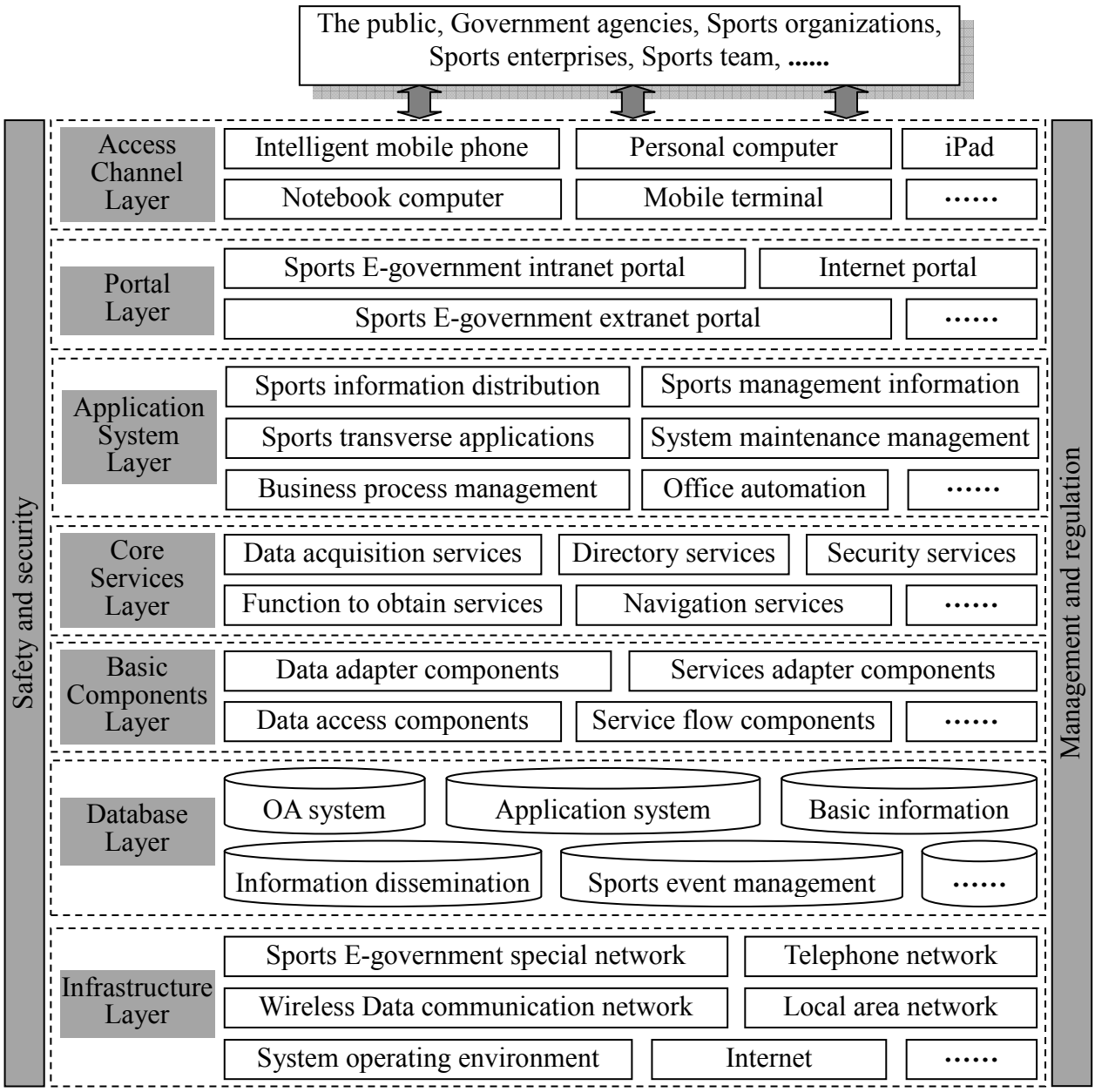

Fig. 1. Technical framework on sports E-government platform

In Fig.1. each layer is described as follows [4,5]: Infrastructure layer, provides support for the system operation, including data communications network infrastructure, the system runs the software and hardware environment; Database layer, various data storage system operation, the database management system and the various databases configured; Basic components layer is encapsulation of data and methods, you can drag and drop programming, fast processing and properties of the real object-oriented design; Core services layer, providing a variety of different applications for different services, including search services, and intelligent search engine services, data acquisition services, features access to services; Application system layer, the functional departments building e-government applications including functional departments of internal office systems, vertical industry applications, cross-sect oral leadership-oriented applications and integrated decision support systems; Portal layer, e-government portal is a variety of applications in various application systems integration and deployment platform components, the different functions of each system to effectively organize themselves to provide a unified entry information publishing and services for all types of users. Access channel layer, the user can use a variety of terminal equipment, through a variety of access channels to achieve any person at any time, any place can enjoy Licenses personalized e-government services; Management and regulation,

including dedicated e-government standards and comprehensive standard specification of existing IT two parts, it is to ensure that e-government application system design, construction and operation comply with the relevant standard security system.

Functional Framework

Combined with results of previous studies [6, 7], sports e-government platform functional framework shown in Fig. 2.

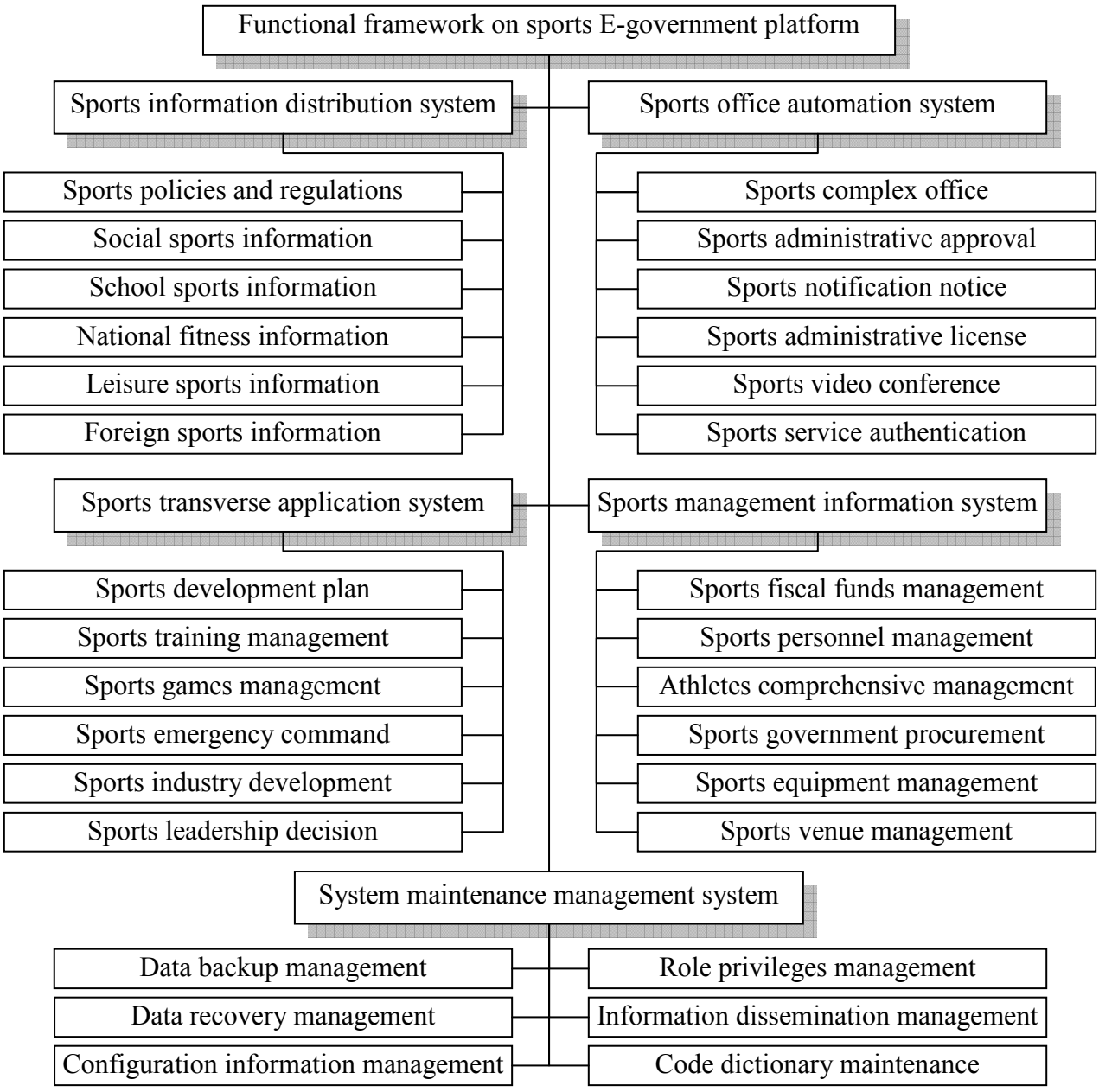

Fig. 2. Functional framework on sports E-government platform

For a brief description of each function in Fig. 2. as follows: Sports information distribution system, it integrated diversity and vivid multimedia video information, and achieved remote centralized management and content of the new information published at any time, so that the audience for the first time to receive the latest information on all kinds of sports, not only to provide timely, comprehensive, high quality and efficient information services and the new sports culture, but also can greatly enhance the overall image of the sports management department; Sports transverse application system, combining sports and generic e-government actual situation, depending on the sports management department of information technology related guidance on the

development of scientific and rational information system implementation plan, to avoid duplication and investment, primarily to establish a collaborative management system covering business areas; Sports office automation system, using Internet / Intranet technology, based on the concept of workflow, the internal staff to quickly and easily share information, work together effectively to achieve a full range of information collection, information processing, to provide a scientific basis for government management and decision-making; System maintenance management system, only to do system maintenance, sports e-government platform that has the vitality of a planned, organized and carried out the necessary changes to the system to ensure that the various elements of the system along with changes in the environment is always in the latest, correct operating state [8].

Conclusion

Implementation of e-government is the focus of the national information work; it is an important measure to deepen administrative reform. The main purpose of sports e-government construction is to promote sports management department office automation, network, electronic, use of information technology to break the organizational boundaries of sports executive, establish electronic virtual office to achieve widespread sense among government departments and government and sports communication between the community and contact information [9]. Sports functional framework and technical framework of sports e-government platform in this study, it focus on improving the level of application, government information resources development and utilization as the main line, establish mechanisms for information sharing and business collaboration, focusing on improving social management and public service role, for better enhancing physical work management, promoting the development of sports, and then stimulating development of information technology has an important role.

References

[1] Mick Green, Shane Collins. Policy, Politics and Path Dependency: Sport Development in Australia and Finland[J].Sport Management Review, 2008, 11(3): 225-251.

[2] W. W. Jia, G. X. Xu, "Establishment on Software Scheme Evaluation Index System of Sport E-government Platform," Computer Technology and Development, vol. 23, no. 11, pp. 121-123, 2013.

[3] Electronic fancier, "What is the framework technology," http://www.elecfans.com/dianzichangshi/2009061769504.html, 2014-3-20.

[4] Information technology center of Hubei university of technology, "The overall framework of national e-government," http://itc.hbut.edu.cn/kuaixun/n166/index.html , 2014-3-22.

[5] Baidu library, "Beijing City E-government Architecture," http://wenku.baidu.com/link?url=27NmZK4DucOONe3CO0WWdxyK5kEPvRJUqAapPvyoYEO-9lQpc209GWT3eRD9U1mbE4tU6lb-V2EqPs47I3LMY1YA0IrF1IBCDvzFVcfVMm3, 2014-3-25.

[6] X. B. Xong, "E-government system functional design," Science and Technology Communication, vol. 3, no. 16, pp. 200-202, 2011.

[7] Jun Zheng, Ying Chen, Cheng Li, "Based on the Lotus Domino in OA System Security Mechanism Research," AASRI Procedia, vol. 1, no. 1, pp. 416-421, 2012.

[8] Y. J. Hao, "Research enterprise computer management system maintenance," Software Guide, vol. 12, no. 9, pp. 19-20, 2012.

[9] S. M. Yang, H. K. Si, "The Analysis of Present Situation and Tactics of Sport Electronic Government of China" Journal of Guangzhou Sport University, vol. 30, no. 3, pp. 12-15, 2010.

Advanced Materials Research Vols. 989-994 (2014) pp 4306-4309
© (2014) Trans Tech Publications, Switzerland
doi:10.4028/www.scientific.net/AMR.989-994.4306

Design and Implementation of Portable Software System

CHEN xiuyu[a], WAN hongli[b] and GUO minghao[c]

Dalian Neusoft University of Information ,Dalian, Liaoning, China,116023

[a]chenxiuyu@neusoft.edu.cn,

[b]wanhongli@neusoft.edu.cn

[c]guominghao@nou.com.cn

Keywords: boost, CIP, portable

Abstract. The paper explains the Ethernet/IP and CIP communication protocol and its application in the industrial automation systems, and designs a software system based on many construction cases,which can be transplanted to variety of the medium.

Introduction

In the industrial automation systems, network management need to control the internet in real time, and get the production process data in order to meet the different needs of management. Since DCS, PLC and other intelligent instrumentation in the control line often from different factory, so the communication between each other is very complicated. Because of the less flexible communication interface , traditional automation systems which is based on the communication between the network and data management leads to low flexibility and bad extension.So that, How to effectively get the data needed in the management of internet from the control network, is an issue of common concern in enterprise automation implementation process.

As the industrial portable communication software, which can implement the data collection and data confusion.This involves three problems: the communication protocol, the design of data collection server software, and the software design of data collection of client terminal.

This software to imitate the OPC of C/S architecture ,and can provide the function of OPC, but the communication method of the client and server use and implementation is different from the existing OPC design[5].

Portable Software Design

Software portability is refers to the code can be transplanted between different platforms; hardware portability refers to transplant between different hardware (such as different CPU architecture). To be able to obtain a wide range of code portability, two aspects need to pay attentions. First is the selection of the development of language. Currently, all interpreted languages, such as Java, etc., based on the design of its managed execution, are able to have a good portability [2,4]. However, its disadvantages are also obvious, because of the need to have the support of the Java virtual machine, its performance is poor, so it is difficultly to meet the need of data exchange industry. Therefore, This software uses the language is a standard C+ +,G++ compiler and some C++ library STL, Boost, etc. Since the industrial software commonly uses C++ language, so that makes the code developed for a wide range of portability and the costs are relatively small.

Another need to avoid the problem is to avoid using platform in the program directly related API functions. For example, if you use too many Windows API functions in the program, when the program transplanted to Linux direction, will be very difficult. So, this software enables logical separation of the data access and data entity tiers. Commonly used API is packed into DLL module for using the functions of the device by particular interface in experiments.In other parts of the software, you only need to call these defined interfaces. As the porting software, each of the modules is

independent so that the user can amend and perfect any incomplete module according to his requirement without influencing the function of the others.

Based on the idea of design is proposed,the paper selected C++Boost libraries ,Boost library for these platforms,so that files,or network communications,or thread can be managed from an API. This software embodies the portable design idea, and has been successfully applied to several projects. This means that the code for these applications does not have to be changed or recompiled to run in compatibility mode.

Software Design

Overall Architecture. Based on distributed design, this software is divided into two parts: client and server, each part of the process runs as an independent. As the core of the software, server is in charge of protocols package of Ethernet and TCP/IP, and communication with equipment. Server processes these requests and also communicates with the back-end server to gather the necessary response data[1].

In the software design, the design plan and function are given and all server programs were completed by C++ language. In the network communications and multi-threaded processing, based on the principle of reducing the correlation system, the Boost IO libraries can be called.

With good human-computer interface feature, this software can display various data completely, such as: specify the data device, select the data points, observations, and so on. Communications between the client and the server can be configured according to the requirements of customers. If the server program and client program running on the same machine, the user can choose the way of shared memory communication in order to get the higher efficiency. If the server and client programs running on different machines, the user can select a network socket communication.

The architecture of the software as shown in figure 1:

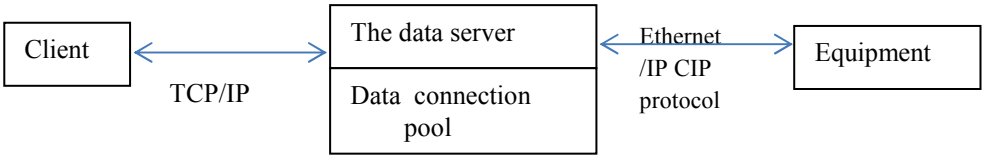

Fig.1. Software architecture chart

Detailed Design

Client /Server interface and Communication. In this software, server participating in communication work in two ways: one of which is accomplish data gathering, the other is complete the data communication. This module allow encapsulation of a piece of functionality in a standalone module with an explicit list of
C ++ functions that are available for external users. Interface of this module,which resembles a OPC standard interface functions, mainly includes adding Group and specify the refresh rate of Group , add or delete item about Group list items , read or write data item data and so on. A client application can call on the module to perform Communication between the server and equipment. This module needs to design a perfect communication protocol, in which client and server group can complete the communication . The system needs to be composed of a series of calls to existing backend databases and commands.

As described in the previous section, there are two ways to complete the communication between server and client :share memory and network socket . According to the the principles of object-oriented programming, communication between the server and the client in the underlying implementation is based on the abstract data flow(stream). According to the user's choice, the software applies it to memory stream or network transmission flow. In order to limit the communication congestion, which can dramatically degrade the system performance, it is

important to using asynchronous IO mechanism, and according to the different usage of the signal synchronous or asynchronous network I/O mechanism.

Realization of data collection service

(1) Ethernet / IP protocol stack and CIP

The server communication protocol stack architecture based on the layering thought. The Ethernet / IP connection layer and CIP protocol layer are designed, and each layer includes a series of class. The following focused on not only the design of key classes and the realization of system's flexibility, but also the realization of key functions.

(2)The management of connection pool

To communicate more than one local area network devices requires an additional module, such as connection pool , which ensure a connection for each communication equipment correspondence in the pool. The connection will be automatically deleted as soon as the connection pool without any data transmission over a period of time to decrease overhead and increase performance, references are timeout management mechanism.

(3) The management of data pool

Typically, data collection program communicates with the hardware equipments according to the refresh rate specified by the client, and gets the value of some of Tag. Because of some changes in the Tag value may be very frequent, and contain a lot of noise. This software, like the OPC standard ,provides user subscription service[3]. The client software is usually only need to care about its value exceeds a certain threshold. That is, the service provider will need access to the parameters given by the customer to determine where to send the response to the client. So, we need to cache data from a database or other backend data store that needs to save the certain historical data, up to achieve the above purpose. In order to achieve efficient data search, the data pool is based on the connection, that is to say, each connected active and equipment room, will be corresponding to a data pool. Simple codes as follows:

```
server = new DataServer();
error = server->Connect(addr);
error = server->AddGroup(group.Handle, group.Rate);
   BOOST_FOREACH(Item&item, items)
{
Item.GroupHandle = group.Handle;
}
error = server->AddItems(items);
for (int i = 0; i < 1000; i++)
{
  error = server->WaitUpdates(C__INFINITE);
  ItemUpdate buffer[100];
  int n = sizeof(buffer);
  error = server－>ReadItems(&n, buffer);
   // parse the buffer and output result…….
}
Server->DeleteGroup(group.Handle);
Server->Disconnect();
```

Software operating results

Finally, create a simple client program under Linux platform to test software. After running the client program and provide the necessary parameters, it can get a value from the server regularly. Operating results shown in Figure 2.

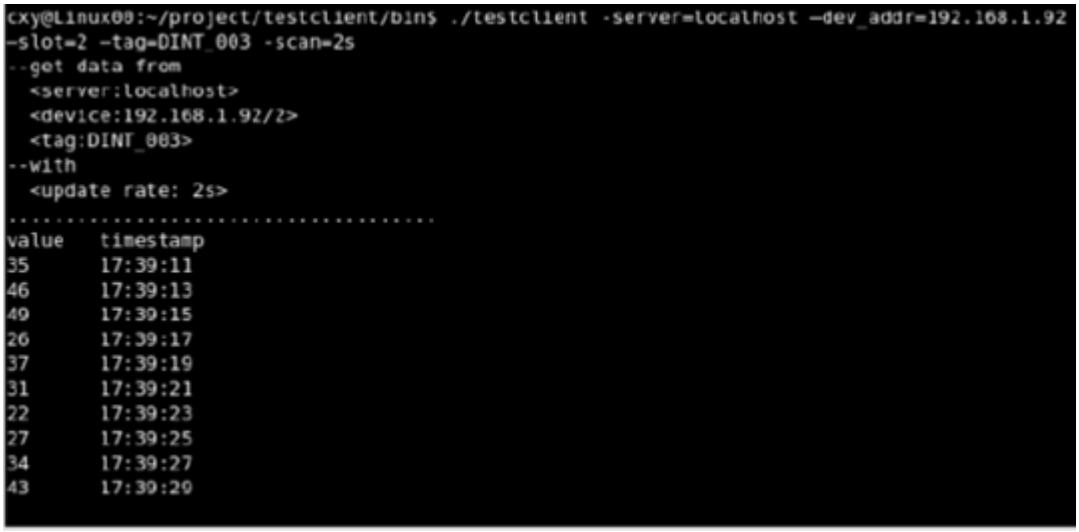

Fig. 2. Software running effect diagram

Conclusions

This paper describes some key techniques in design and implementation of portable software system, including the realization of interfaces and communication module, which makes portable industrial communication software possible. Future will further study on how to develop OPC server under Linux.

References

[1] Zhou Hao, Zhou Jun, in: Analysis of industrial Ethernet standard EtherNet /IP, Information Technology,(2009) ,p. 1

[2] Wu Xin, Gong Liang, Yang Yu-Pu: Implementation method of OPC cross platform communication , Computer engineering, (2009),p. 7

[3] Gao Fei: Application of OPC technology in enterprise integrated automation [J] , Southern Steel and Tube Technology Li, (2008),p.3

[4] Jiao qingsong, Wu yingliang: The Realization of Client Application Bas ed on OPC Specification using Java. Microcomputer Information, (2006), p. 60

[5] OPC Foundation: OPC Data Access Custom Interface Specification 3.0(2003).

Advanced Materials Research Vols. 989-994 (2014) pp 4310-4313
© (2014) Trans Tech Publications, Switzerland
doi:10.4028/www.scientific.net/AMR.989-994.4310

Design and analysis of a reliable group signature scheme based on discrete logarithm

Hongli Wan[a], Guijuan Song[b] , Yanhui Chen[c]

Dalian Neusoft University of Information

[a]wanhongli@neusoft.edu.cn,[b]songguijuan@neusoft.edu.cn,[c]chenyanhui12@nou.com.cn

Keywords: Discrete logarithm, Group signature, Signature scheme.

Abstract. Through the analysis, a group signature scheme based on discrete logarithm is put forward in this paper. strengthen the validation of the members when they join the group; Records the time stamp of the revoked member into the database, to prevent the forged signatures; To recognize the forge the signature of the revoked and illegal members. Finally, analysis shows the scheme satisfies correctness and security.

Introduction

In 1991, the group signature scheme is put forward for the first time by Chaum and Van Heyst [1]. This scheme allows group legal members signature in the name of the group. The administrator can reveal the signer when dispute occurs. A security plan should be non-forge ability in addition to anonymity, trustworthy and Coalition-resistance [2-5]. All the group members cannot forge a valid group signature; the revoked members can't signature with previous legal status [6-9].

Through the analysis, a group signature scheme based on discrete logarithm is put forward in this paper. strengthen the validation of the members when they join the group; Records the time stamp of the revoked member into the database, to prevent the forged signatures; To recognize the forge the signature of the revoked and illegal members. Finally, analysis shows the scheme satisfies correctness and security.

New Signature Scheme

This scheme includes three entities: Certificate Authority (CA), Group Member and Group Administrator. The mutual information between CA and group members will be validated by signature algorithm. The algorithm has a certain security because of the discrete logarithm.

System Establishment

Assuming the group center is trusted. It chooses two max prime numbers p and q secretly, and a public hash functions $H(.)$. Let $n = pq$, $\varphi(n) = (p-1)(q-1)$. Random select an integer $e < \varphi(n)$. Meet the condition $ged(e, \varphi(n)) = 1$. Calculate the integer d, meet the condition $ed = 1 \bmod \varphi(n)$. The public parameters of CA are *n* and *e*, the private parameter is *d*.

Add Member

When the *n+1* member want to join the group, firstly, choose a integer $e_(k+1) < \varphi(n)$ randomly, meet the condition $get(e_(k+1), \varphi(n)) = 1$, calculate the integer *d*, meet the condition $e_(k+1)d_(k+1) = 1 \bmod \varphi(n)$. Use the $e_(k+1)$ as public key, the $d_(k+1)$ as the private key. The number *k+1* member applies to the group center, sends $e_(k+1)$ to CA. After CA to verify their identity, the identity ID of $e_(k+1)$ and the *k+1* member are stored in the database.

Delete Member

To delete member *i*, calculate $y_i = (ID_i)^{d_i} \bmod n$. Member *i* will send the $Sig(ID_i)$ and the withdraw application to the CA together. CA verifies the identity of the applicants:

$$Ver(ID, y) = TRUE \Rightarrow y^{e_i} = ID_i (\bmod n) \quad (1)$$

CA use the formula (1) to verify the membership of group member *i*. if the result is true, then validation passes, the cancel application is made by group member *i*. CA will set the abolish timestamp of the information map (e_{k+1}, ID_{k+1}) as the current time in the PB.

Generate signature

Group member *i* signs for message m by the sign secret key d_i, calculate: $y = (m)^{d_i} \bmod n$, send y_i and message *m* to CA. CA verify the legitimacy of the identity, then verify the correctness of the signature using the formula $Ver(m_i, y_i) = TRUE \Rightarrow y^{e_i} = m (\bmod n)$. If the result is true, the signature is correct and send by member *i*, CA will send signature *y*, ID_i and the signature timestamp to the group administrator. The group administrator will record it in the signature list, in case of a dispute open signature use in the future.

In order to prove that the CA has reviewed the signature, CA will sign on it:

$y_{CA} = (m \cdot ID_{CA})^{d_{CA}} \bmod n$. Then y_{CA} will be sending to group member *i* by CA.

The member will send the final signature (y_i, y_{CA}) to the signature receiver.

validate signature

CA is trustable; the group member who receive the signature will validate the signature by the public key of CA:

$$Ver(ID_CA, y_CA) = TRUE \Rightarrow y_CA \wedge (e_CA) = ID_CA (\bmod n) \quad (2)$$

If the verification passes, prove that the signature has been approved by CA, and has been recorded in the CA database. Here, to verify the signature is correct, and issued by CA：

After verification of $Ver(ID_i, y_i) = TRUE \Rightarrow y_i \wedge (e_i) = ID_i (\bmod n)$, proved that the signature is generated by the legal group member *i*.

Open signature

When the dispute occurs, need to open the signature. Send the signature to group administrator, the administrator will verify the signature is generated by the legalgroup members through the formula(1) and the information stored in PB. If the signature is send to administrator, the administrator will search the signature list, find the ID_i of the corresponding signature, then send the ID_i to CA. CA sends ID to the requester who open the signature.

Scheme analysis

Correctness

Based on the discrete logarithm, If the signature of *Y* received by CA is produced by the legal group members according to the algorithm, then the signature can be verified by CA.

Prove:

Only the signature verified by formula (1) can be recognized by the CA.CA calculation process is as follows:

Premise: $e_i d_i = 1 \bmod \varphi(n)$; $y_i^{e^i} \equiv (ID_i)^{d_i e_i} \bmod n \equiv ID_i (\bmod n)$

Therefore: The formula was established, CA can confirm the legal status of members.

Prevent forgery attack

When the user *i* cancellation, CA will let the abolished timestamp of the information map (e_i, ID_i) as the current time in the database. If other members forged the signature of *i*, will be identified.

Prove: proof by contradiction, Assume that the user can forge a signature; the signature will pass by CA validation. CA validate the signature of user *i* by formula (1), the forger *j* resolve the private key of member *i* successfully. That is forger *j* resolve the discrete logarithm problem; this is conflict to the fact that the discrete logarithm is intractable. So, if the other members forge the signature of *i* after the member *i* sign out, it will be distinguish. QED.

Above is analysis of revoked member forge legal signature. For all the illegal members, to forge the member's signature, have to work out the private key, which solves the discrete logarithm problem. Because of the discrete logarithm is hard, so any illegal members can forge the signature of legitimate member *i*.

Conclusion

This paper proposes a group signature scheme based on discrete logarithm. Members to join the group, strengthen the validation of the members. Record the timestamp of the sign out member in the database, prevent its signature was forged. Be identification to the sign out member and all the other illegal members. Finally, analysis the scheme satisfies from the correctness and safety. When the group member withdraws, only record its timestamp, but do not update the private key of other group members, to improve operation efficiency.

References

[1] Chaum D, Heyst E V: Group Signatures[C] Proceedings of Eurocrypt. Berlin: Springer-verlag, (1991),p. 257 265.

[2] Nakanishi T, Funabiki N: Group signature schemes with membership revocation for large groups[J] IEICE Transactions on Fundamentals of Electronics, Communications and Computer Sciences,(2006), 89(5),p. 1275-1283.

[3] He G, Tate S R: A group signature scheme with signature claiming and variable linkability [C] 25th IEEE International Performance, Computing and Communications Conference.Washington: IEEE Computer Society, (2006),p.497-504.

[4] Zhang Jian-hong, Geng Qin: On the security of group signature scheme and designated verifier signature scheme[C] Proceedings of the 2008 IEEE International Conference on Networking, Architecture, and Storage. Washington: IEEE Computer Society, (2008),p. 351-358.

[5] LiJun,Cui Guo-hua, Liu Zhi-yuan: Cryptanalysis and improvement of a group signature scheme[J]. Chinese Journal of Electronics，(2007),35(4),p.778-781.

[6] Zhou S, Lin D: Group signatures with reduced bandwidth[J].IEE Proceedings: Information Security, (2006), 153(4) ,p.146-152.

[7] Kim K, Lim S, Yie I, et al: Hierarchical identity based group signature with enhanced privacy of the signers[C]Proceedings of the 7th WSEAS International Conference on Applied Informatics and Communications. Greece: World Scientific and Engineering Academy and Society, (2007),p.29-33.

[8] Nakanishi T, Funabiki N: A short anonymously revocable group signature scheme from decision linear assumption[C]Proceedings of the 2008 ACM Symposium Information, Computer and Communications Security. NewYork: ACM Press, (2008),p.337-340.

[9] Contini S , Yin Y: Forgery and partial key-recovery attacks on HMAC and NMAC using hash collisions[C] Lecture Notes in Computer Science. Berlin: Springer-Verlag, (2006), 4284,p.37-53.

Advanced Materials Research Vols. 989-994 (2014) pp 4314-4317
© (2014) Trans Tech Publications, Switzerland
doi:10.4028/www.scientific.net/AMR.989-994.4314

The Solution of Safety of Electronic Cash in E-Commerce under Cloud Computing Environment

Songjie Gong, Liping Zeng

Zhejiang Business Technology Institute, Ningbo 315012, China

zengliping1208@163.com

Keywords: cloud computing, electronic commerce, electronic cash, safety.

Abstract. Electronic commerce system is now developing at a huge speed, whose final objective is to electronize every phase of commercial activity. Electronic payment is the heart of electronic commerce. Along with electronic commerce development, electronic cash payment systems are also developing. How to achieve safe electronic transactions is the key to the development of electronic cash payment systems. There are two kinds of electronic cash system, on-line and off-line. As the security and effective electronic payment system has become an important part of electronic commerce, according to the new character of cloud computing, it can solve the problems that the electronic cash systems exist leakage of privacy, non-standard transactions and high cost in the traditional network. The paper describes the types of electronic payment and discusses the electronic cash payment safety based on cloud computing. The presented solution can reduce the hardware and software systems cost, particularly for the current electronic commerce security, with efficient and convenient interactive response to the trend.

Introduction

Electronic commerce is to the Internet as a platform, formed through the integration of business information, business flow, logistics system and the payment system of the new business operation mode, can also think that electronic commerce is e-Business. Electronic commerce is an important part of the electronic payment system. Technically speaking, the most critical problem in the electronic commerce is how to achieve the safe payment functions, and ensure the security of the parties to the transaction. Therefore, online payment security and efficiency is the key link of the electronic commerce, electronic commerce is the fundamental condition of the smooth development of.

The so-called electronic payment, refers to the parties to the transaction by electronic means, such as bank electronic deposit system and electronic clearing system to record and transfer of funds, electronic payment is the key part of electronic commerce, the electronic payment is the key link in e-commerce, because of the different mode of operation, various payment systems different characteristics in the aspects of safety, risk and efficiency of payment. But the real money is more convenient, effective. In its simplest form, consists of three main and four protocols. The three parts is the business, customer and bank; four security protocols is initialization protocol, withdrawal protocol, payment agreement and deposit agreement.

As the security and effective electronic payment system has become an important part of electronic commerce, according to the new character of cloud computing, it can solve the problems that the electronic cash systems exist leakage of privacy, non-standard transactions and high cost in the traditional network. The paper describes the types of electronic payment and discusses the electronic cash payment safety based on cloud computing.

Electronic Payment in E-Commerce

Electronic payment is to the business of electronic tools and all kinds of electronic money as the media, computer technology and communication technology as a means, realize the flow of capital and payment in computer network system.

Electronic payment system based on credit card

In this system, consumers first in the bank to have the credit card number and password to open an account. When consumers in the open network environment for shopping or service, he need your credit card number and the password is encrypted and transmitted to the merchant, through the Internet, and then forwarded to the bank by the merchants, and then in accordance with the special protocol for online payment. The model is shown in Figure 1.

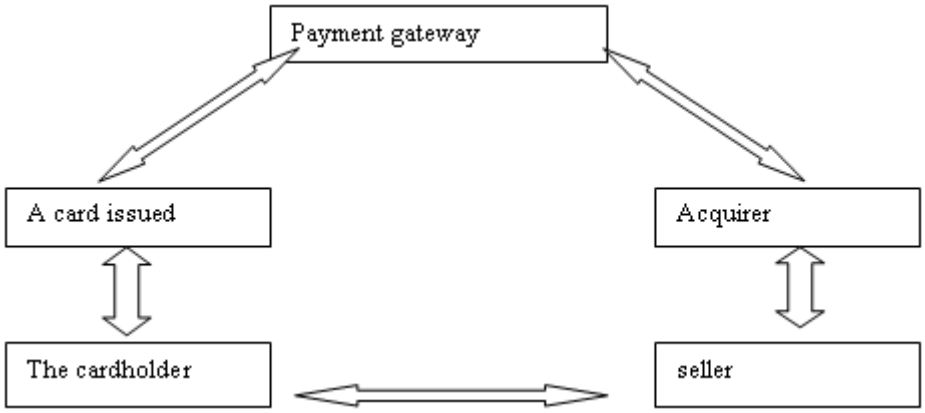

Figure 1 Electronic payment system based on credit card

Payment system based on e-cash

Consumers to open an account in the provision of electronic cash service bank, and pre deposit funds, so as to achieve the same electronic cash and cash value (usually memory smart card or a pure form of electronic hard disk file), and then use the electronic cash terminal software download to your computer hard disk backup, to pay subsequent purchases cost, electronic cash bank businesses and authorized finally received the consumer electronic cash settlement, the bank will consumers to purchase goods or claim service fees to merchants, the model shown in figure 2.

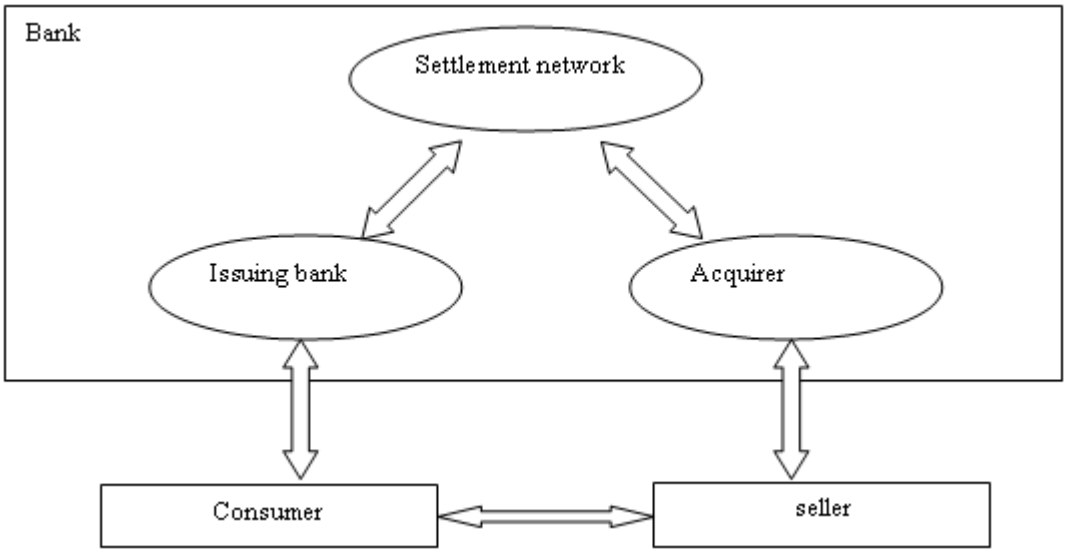

Figure 2 Payment system based on e-cash

Mobile payment system

Consumers through mobile phone wireless internet access browse the service provider's Web site, produce the order information and the digital certificate, payment information to the service provider. Service providers will consumer payment information for payment gateway, and a payment gateway transmits it to the financial institutions. The model is shown in figure 3.

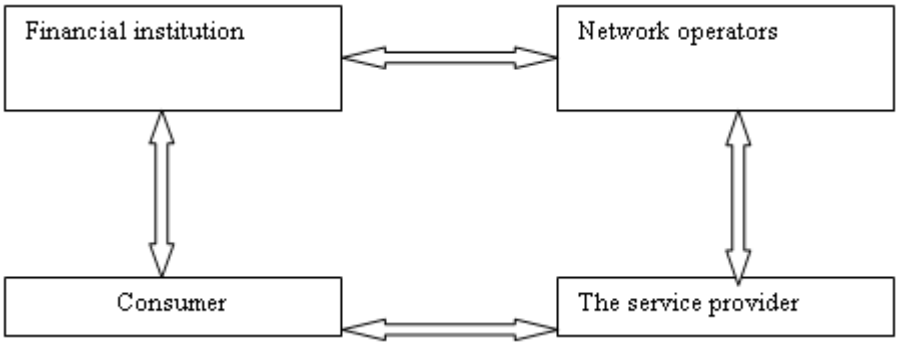

Figure 3 Mobile payment systems

Safety of E-Cash in Cloud Computing Environment

The solution of participation in the main banks, businesses, users and cloud service providers, terminal system and assume that all subjects are embedded in the electronic commerce module. A group of several cloud of electronic banking, by a cloud service provider management, any one bank can issue electronic cash. Business users and can not in the extraction and deposit the same bank electronic cash operation. The model is shown in figure 4.

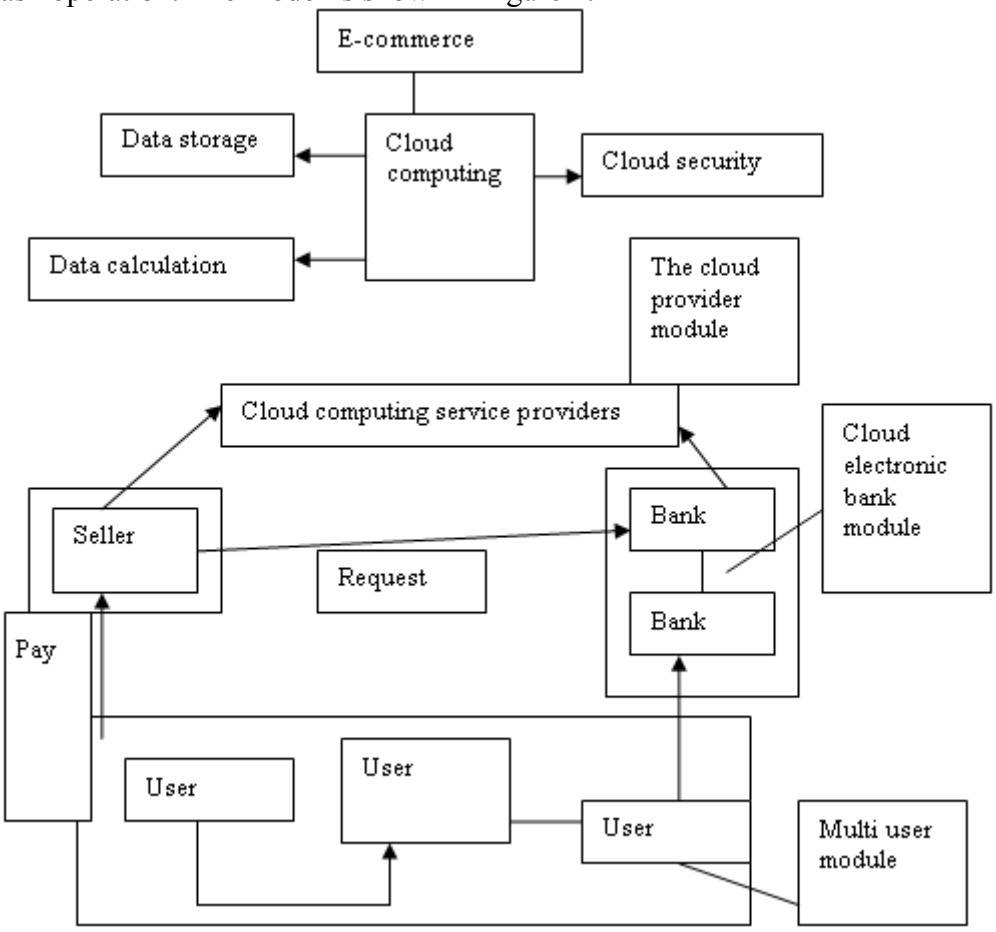

Figure 4 Safety of E-Cash in Cloud Computing Environment

Cloud computing electronic commerce electronic cash model environment are as follows:

1) Cloud electronic bank module: many electronic bank formed groups, group manager GB Bi, group member, and the group of public and private key pair (PK-Bi, SK-Bi). The module has the function of deposits and withdrawals.

2) The user module: formed by multiple users, groups, group manager GU. The user Ui (your bank Bi), platform attestation identity key AIK (PK-AIK public key, private key SK-AIK), the identity of the user's ID IU, and the system terminal of each user with an embedded TPM module is used to protect the terminal security.

3) Business module: business S (your bank Bj), the public and private key pair (PK-S, SK-S). Businesses in order to reduce the cost, hire a cloud service.

4) The cloud service provider module: a cloud service provider for businesses and banks offer cloud services.

5) Encryption scheme subject interaction by using E representation.

6) Security system under the cloud computing environment.

7) Security system of electronic payment in electronic commerce.

Summary

In this paper, it describes the types of electronic payment and discusses the electronic cash payment safety based on cloud computing. The presented solution can reduce the hardware and software systems cost, particularly for the current electronic commerce security, with efficient and convenient interactive response to the trend.

Acknowledgment

This research is supported by University Students' Innovative Undertaking Project of Zhejiang Business Technology Institute

Programs Supported by Ningbo Natural Science Foundation (Grant No. 2013A610072).

References

[1] Fan C I, Chen W K, Yeh Y S. Randomization enhanced Chaum's blind signature scheme[J]. Com- puter Communication,2000, 23(13): 1677-1680.

[2] S. Canard and J. Traoré, "On fair e-cash systems based on group signature schemes," ACISP2003 , 2003, pp. 219-219.

[3] Hung-Yu Chien, Jinn-Ke Jan, Yuh-Min Tseng. RSA-based partially blind signature with low com- putation [C]//Proceedings of the eighth international conference on parallel and distributed systems, 2001. 385--389.

[4] P. Tsang and V. Wei, "Short linkable ring signatures for e-voting, e-cash and attestation," Information Security Practice and Experience, pp. 48-60, 2005.

[5] Xiaoya Liu ,Xiaolong Xin . Improved blind signa- ture electronic cash scheme [J]. Computer Engineering and Applications ,2011,47:114-116.

[6] Zhang, YH; Rao, YB; Zhou, MT, "A E-cash scheme base on structured multi-signature" , IC-BNMT 2007, pp. 98-102 , 2007.

[7] M. Au, W. Susilo, and Y. Mu, "Proof-of-Knowledge of Representation of Committed Value and Its Applications," INFORMATION SECURITY AND PRIVACY, pp. 352-369, 2010.

[8] Ziba Eslami , ehdi Talebi . A new untraceable off-line electronic cash system [J]. Electronic Com- merce Research and Applications,2011, 10:59-66.

[9] Tian Yuan, Wen Xiaojun, Gong Yanju. Applica- tion of quantum blind and group signature in e-payment systern [J].Computer Engineering and Ap- plications,2011, 47:108-112.

[10] G. Fuchsbauer, D. Pointcheval, and D. Vergnaud, "Transferable constant-size fair e-cash," Cryptology and Network Security, pp. 226-247, 2009.

[11]J. Camenisch, S. Hohenberger, and A. Lysyanskaya, "Compact e-cash," Advances in Cryptology–EUROCRYPT 2005, pp. 302-321, 2006.

Advanced Materials Research Vols. 989-994 (2014) pp 4318-4321
© (2014) Trans Tech Publications, Switzerland
doi:10.4028/www.scientific.net/AMR.989-994.4318

On the China Tourist Hotel E-Business management

Feilong Liu

School of Economics and Management Hunan Institute of Science and Technology, 414006,Yueyang,Hunan, China

E-mail:liufeilong12@126.com

Key words: China; Tourist Hotel; E-Business; operating models

Abstract. Along with the market competition intensifying, the hotel industry has begun to pay more attention to how to create new competitive advantage to increase or maintain the hotel's comprehensive competitiveness, and the development of modern information technology, to create new competition carrier for the hotel industry, so the Tourist hotel to implement electronic business management is the trend of The Times. At present China's hotel industry to carry out the practical effect of electronic business is far from the ideal requirements compared. From three aspects to build and perfect the hotel e-Business is the overall framework of the management model is very necessary: one is set up and improve the customer relationship management system as the center, based on hotel resource planning system of hotel management information system; Second, supply chain management system, set up and improve the hotel in order to realize the hotel e-business B to B mode; Three is to establish and perfect the hotel website or homepage, build hotel network e-business platform to achieve the hotel e-business B to C mode.

For over 30 years reform and opening up, China's hotel industry obtained rapid development. So far, according to statistics, China has reached about 15000 star-rated hotels, there are several times in this hotel. As a whole, China's hotel industry has been in a state of oversupply. Between competing for customers, improve occupancy rates, hotel has become very competitive. In the process of operating practice, restaurant operators have become increasingly aware that competition is the purpose of profit, and not at the expense of profits for the improvement of occupancy. And the product price discount and is no longer the most effective way to the hotel to expand patrons. Price competition as the main means to obtain competitive advantage has clearly not adapt to the reality of the current market development. Therefore, the hotel industry has begun to pay more attention to how to create new competitive advantage to increase or maintain hotel's comprehensive competitiveness, so as to gain higher than the industry average profit margins.

In an increasingly tend to be more open environment, the management of the hotel will be more detailed content, The network can greatly simplify and standardize all of this, but also can greatly reduce the cost. In addition, as an important component of the tourism industry, hotel industry also must try to blend in their whole business chain, more through the network to expand the business. Hotel must be able to grasp at any time from the customer's need, and can meet the needs of all kinds of personalized, only to set up and improve the modern hotel electronic business management system, to make the hotel to adapt to these troublesome and require absolutely in a timely manner the needs of the hotel management operation.[1]

E-Business and its basic characteristics

we usually discuss the e-business generally refers to a way of using the Internet for business activities. From the macroscopic view, E-business is a direct product of information technology led to the network revolution , is the establishment of a new economic form networks through electronic means. It involves not only IT and business transaction itself , but also involves other levels , such as government, finance, education and other social . From the microscopic point of view, e-business refers to the ability of various entities with commercial activities , such as production companies, commercial enterprises , financial institutions, government agencies, individual consumers using advanced computer and network technologies in the commercial trade activity , is a specific form of IT enterprise applications.

Internet itself has an open , global , low cost, high efficiency, also an inherent feature of e-business and e-business far beyond making as a new form of business has value , it will not only changing the enterprise itself production, operation and management activities , and will affect the operation and structure of society as a whole economy. In particular, e-commerce has five basic characteristics:

First, the traditional e-business business process digitization, on the one hand to the digital stream instead of real logistics, can significantly reduce the manpower, resources, reduce costs ; on the other hand it can break through the restrictions of time and space, so that you can in any trading activities time and any place , which can greatly enhance the efficiency ;

Second , e-business they have to open and global nature , able to create more trade opportunities for businesses ;

Third , e-business allows businesses to cost close to enter the global electronic marketplace , making it possible for SMEs and large enterprises have the same information resources , help to improve the competitiveness of SMEs ;

Fourth, redefines the traditional e-Business business and circulation patterns , reduce intermediate links , so that producers and consumers to deal directly as possible, to a certain extent, can change the entire social and economic mode of operation ;

Fifth , e-business on the one hand to get rid of the barriers of time and space , on the other hand can provide a wealth of information resources, it offers more possibilities for the re- combination of various socio-economic factors and factors of production , and thus will affect the community economic layout. With the improvement of the further development of information technology and network infrastructure , e-business will become mainstream business in the form of the information age. Therefore, the implementation of e-Business business management will be its future strategy to create a competitive advantage in important ways and means.[2]

China 's hotel industry to implement e-Business management major problems facing

China 's hotel industry on the application of information technology, time is not long , but now there are many hotels have set up their own business website , or have their own independent website. Many hotel managers also want to quickly improve their competitiveness and economic hotels through e-Business activities , it is actually the lack of a thorough understanding of the overall framework and specific hotel e-Business operation methods. Therefore, the industry believes that the current requirements of the actual results and the ideal e-Business in China's hotel industry is also a far cry compared .

A very real problem is : the application of information technology in the hotel industry offset a widespread understanding, did not really take it as an integral part of the business development strategy , without a profound understanding of hotel e-Business is a systematic project , it involves many aspects of computer hardware and software , hotel property management philosophy and management processes. We find : a considerable number of hotel companies just opened a home page on the Internet , neither the use of web development and integration of various resources , nor conduct business online . Some hotel website or home page for a long time can not update the information , but a lack of hotel communication and interaction with customers , in fact, has become a figurehead for the empty station .[3]

From objective reality , the majority of e-Business service provider fore-businesssoftware and hardware solutions provided by hotel companies can only belong to e-business technology solutions , computer hardware and software systems which simply reflected an overall e-business technology platform concept , service providers difficult enterprise business operations from a specific property characteristics and needs of departure for the complete design and planning. The resulting hotel business e-business applications , can not make the technology platform and business processes to form a perfect combination. In other words , China's hotel business e-business technology solutions based on actual generated e-business application operations management and e-Business software and hardware solutions based on e-business application service provider operating programs are generally difficult to form a perfect combination of form .

To improve measures and countermeasures of Chinese tourist hotel e-business management

Hotel e-business management final solutions from the hotel business and e-business service providers two aspects, but also embodied the two basic elements of e-business. How hotel companies should design and plan their e-Business applications , to finally put forward a set of practical e-business application operation of the program , through the establishment and improvement of hotel e-Business model with universal significance to achieve. Combined with the management of the hotel industry specific reality , in the hotel business and e-Business software and hardware enhanced service providers full communication and collaboration throughout the premise , we can consider the following three levels to build and perfect the Chinese e-business , management and operation of modern hotel the overall framework of the model.[4]

1.To establish and improve customer relationship management system as the center, Hotel Resource Planning -based hotel management information system

Customer Relationship Management system is an important tool for hotel customer resource management. CRM from the hotel at all levels of contact with the customer , the customer's data of all backgrounds and behavioral data collected and together, these operational data , and external market data through the integration and transformation, then loaded into the data warehouse , OLAP and use data mining techniques to analyze and master the relevant laws , patterns or trends from the data. Finally, the hotel Resource Planning , etc., the relevant customer information and knowledge effectively transfer and sharing throughout the hotel . The information and knowledge will translate into strategic and tactical actions hotels , help improve the relevance and effectiveness of hotels across all channels of communication with customers , thus bringing the right products and services , through appropriate channels , at the right time , provided to the appropriate customers.

The so-called property resource planning system, refers to the use of database technology and specialized user interfaces to control processing center hotel business information, is uniform for the entire property transaction processing systems. It features a variety of business hotels such as customer resources, human resources, finance, services, accounting , distribution and other links to a common system, so that the hotel business process management and service data sharing and integration in order to achieve automated transaction processing and customer , financial , service and distribution of resources and effective tracking.[5]

2.To establish and improve the hotel supply chain management system, in order to achieve the hotel 's B to B e-business model

Hotel Supply Chain Management comes to hotels material suppliers , distributors (travel agents , online distributors, airlines , exhibition companies, etc.) , rental companies , scenic (attractions) , and other partners and end customers , is a hotel integrated system of external supply chain management . Under the trend of economic globalization and the development of market integration , the market will no longer be a competitive advantage companies have many material resources , but in their many social resources can be integrated to increase their market competitiveness. Hotel supply chain management system is to optimize and improve the hotel supply chain activities . Hotel Supply chain management is the organization of the supply chain objects (business) and information flow , capital flow and material flow between them. Methods are integrated and coordinated , the goal is to meet the needs of users hotels to ultimately improve the overall competitiveness of the supply chain hotel . Supply chain management is not another name for supplier management , but a new organizational strategies , which integrate the different companies in order to increase the efficiency of the entire supply chain , focusing on cooperation between enterprises. Relevant stakeholders in the supply chain with multiple parties competing relationship led to the arrival of the era of mass customization supply chain has a strong randomness. Establish and improve the hotel supply chain management system enables hotel companies with the fastest speed through the supply chain to effectively respond to the specific needs of customers, the entire supply chain to maintain continuous dynamics , which can more effectively ensure adequate to meet the needs of hotel customers .

3. establish and improve the hotel website or home page , e-commerce platform to build the hotel network in order to achieve the B toC hotel e-business model

Core Hotels is to create a network of e-business through the hotel website building a good network marketing environment , you can always receive hotel reservations around the world and sales information , and feel free to send information about this hotel in order to facilitate the selection and booking guests . This necessarily involves several important aspects : first, online room reservation system ; Second important domestic and international tourist hotels electronics market ; third is to provide property -related information and services ; Fourth, online customer surveys and consulting , as well as mailing lists and forums and other interactive features.

Many hotel managers tools just as a publicity hotel Hotel website corporate image , released hotel advertising , this is a big misunderstanding.Because network marketing is completely different from traditional marketing target object.The main factors involved are traditional marketing 4P, namely product , price , Place and promotion; while in the network environment, the elements involved in network marketing is 4C, that the Consumers Wants and Needs,Cost to Satisfy Want and Needs and to Convenience to buy and communication. Therefore, the positioning of the hotel e-business website should solve problems for customers around the needs of customers to solve problems , rather than according to their own needs to build hotel site, which is a major principle of network marketing. Only under this precondition site targeting , hotel managers will consider such questions in the website content design : layout and offers hotel rooms distribution, electronic map showing location of the hotel and the surrounding environment , the hardware facilities such as room decoration style , bedding and other customers may be asked to change or choose to provide weather forecasts Check for booking customers, to provide pick-up or car rental , hotel or surrounding scenic attractions, providing customers with discount tickets , providing customers with local terroir human introduce major economic and cultural activities and local reports , and so on . Hotel industry is an open industry at different levels , different grades of hotels will have to face different target markets. Hotel impossible to meet the diverse needs of all customers , but must endeavor to provide services to their target customer groups , in order to fully meet their needs.[6]

All in all, only from the above three levels to build and improve the overall framework of Chinese tourist hotel management and operation of e-business model , was better able to form a complete e-business value chain hotel . China 's hotel industry on the application of e-business is still in the exploratory stage, the hotel industry there is not a specific reference to a successful business model . How to effectively use e-business to enhance the competitiveness and economic hotel , hotel business depends on continuous learning and practice.

Reference

[1] Xu Rui, Zhuolin Mao: E-Business Journal Vol.6 (2013) (In Chinese)

[2]WangJue:Jiangxi Social SciencesVol. 10(2001)(In Chinese)

[3]Junliang Lu, Mingkui Yang:China Computer & CommunicationVol.7(2004)(In Chinese)

[4] Jinjin Wan,Zehua Liu:Inquiry into Economic IssuesVol.11(2009)(In Chinese)

[5] GengshengTang: science and technology enterpriseVol.19(2012)(In Chinese)

[6] Shuling Yan:Journal of Leshan Teachers CollegeVol.12(2007)(In Chinese)

Advanced Materials Research Vols. 989-994 (2014) pp 4322-4325
© (2014) Trans Tech Publications, Switzerland
doi:10.4028/www.scientific.net/AMR.989-994.4322

Design and Implementation of Web Extraction System of Ceramic Products' Information in the Business Website

Muqing Zhan[1,a] and Ronghua Lu[2,b,*]

[1]Modern Education Technology Center, Jingdezhen Ceramic Institute, Jingdezhen, China

[2]College of Information and Engineering, Jingdezhen Ceramic Institute, Jingdezhen, China

[a]mushi3609@sina.com, [b]lrhlucy2003@163.com

Keywords: Ceramic Products' Information; Web Information Extraction; Extraction Rules

Abstract. In the means of getting information from the Internet, the Web information extraction technology which can get more precise and more granular information is different from Search Engine, this article presents the technical route of Web information exaction of ceramic products' information on the basis of analyzing the developing status of Web information extraction technology at home and abroad, and makes the extraction rules, and develops a set of extraction system, and acquires the relevant ceramic products' information.

Introduction

With the application and promotion of Internet technology, and the explosive growth of information, the World Wide Web has become the massive information repository. Confronted with such massive data of huge and varying structures, how to get useful information rapidly and accurately from the Internet? The common method is that users look for, according to their requests, a large number of relevant web page information with the aids of well-known SEs like Google, Baidu, Yahoo, etc. . Because the structure of these web page information is different, and the content is independent from the database, the SE crawler can not find the information in the back-end database, so it needs manual interpretation. In order to get more precise and more granular information from the Internet, meanwhile transforms the received crawler information into database, so as to make further analysis, and the Web information extraction technology is born at the right moment.

The information extraction research started in the 1980s, the typical extraction system at that time were Linguistic String System, FRUMP System and ATRANS System[1], etc.; with the prosperous development of the Internet in the 1990s, the information extraction developed into Web information extraction, the high-profile project was the Web Excavation Project of Carnegie Mellon University "Center for Automated Learning and Discovery"; American Stanford University developed the extraction tool of extracting semi-structured information from Web[2]. Now the Web information extraction technology has developed into the automatic phase. But the rub is: due to the poor adaptability of the extraction rules, the accuracy rate of the extracted data will become lower as the automation degree becomes higher. As a result, the practicability of the technology is poor.

The earliest domestic documentation that involved in Web information extraction system research was *Semantic Tracing Analysis Algorithm in Information Extraction*[3], published in Apr. 2001. The latest documentation was *Web Information Extraction Based on Mutual Information Metric*[4], published in Dec. 2013, in the article the author presented the Web information extraction method which was on the basis of mutual information measure, could identify the noise information automatically and keep the key information. This method analyzes web pages by making them into DOM trees, and calculates the mutual information values of the leaf nodes. Then it gathers the leaf nodes block by block according to the DOM tree structure, and acquires recursive upwardly the mutual information value of tag <body> as the threshold value to distinguish noise and non-noise. Yang Shaohua, etal, of the Chinese Academy of Sciences presented the new method of generating the data template firstly, then automatically extracting the data from the web page by the detected

template; Institute of Artificial Intelligence, Zhejiang University proposed the Web information extraction which was on the basis of ontology[5], etc..

After checking the documentation we knew that no matter at home or abroad there were less researches which really involved the applications of ceramic products in the researches of Web information extraction system, and this article conducts the research on Web extraction of the ceramic products' information in the Business Website.

Technical Route of Web Extraction of Ceramic Products' Information

A. Determination of Web Extraction Model of Ceramic Products' Information

The structures of internet and its websites are diversify, standards are different, and the sites' scripting codes have no uniform layout, so you can not directly adopt the X path to locate node and extract information. The design idea of this article is to use the advantages of structured XHTML, by introducing the PHP open-source database SimpleDOM to carry out the HTML page analysis, the DOM tree is formed. And according to the specific rules of DOM tree on different websites, the products information on the web pages and page turning linkages can be analysed, realizing the extraction of related information from the Web page document. All the results that are extracted in accordance with the inquired conditions are all saved in the founded database of websiteextraction. Therefore, the Web extraction model of ceramic products' information which is established in this article is showed in Figure 1:

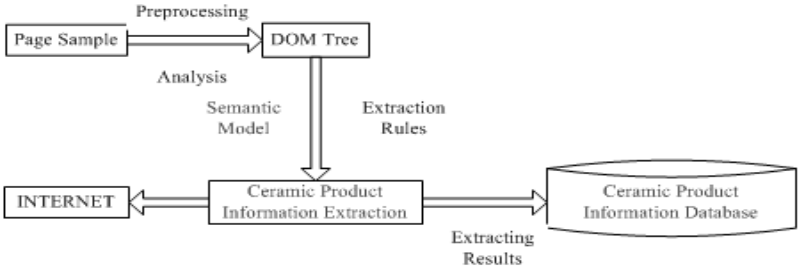

Fig.1 Web Extraction Model of Ceramic Products' Information

B. Preprocessing of Web Document

Most of the data on the Web is described by HTML, the HTML mingles data content and pattern of manifestation, which is adverse to the extraction, therefore to carry out the preprocessing of Web document, the treating process is generally subdivided into three steps: first transfer the HTML document into XHTML document; then analyze the XHTML into DOM tree; finally filter the DOM tree by the method of matching, to get rid of the irrelevant nodes and its content in the DOM tree.

C. Determine the Extraction Rules of Products' Information

To form the extraction rules of products' information in accordance with websites, for example, the rules of website http://www.ccmall.cn/ are as the following:

A. Find the first table with the ID of TableList on the web page

B. Loop gain the first table cell of tr on each line in the table

a) [Product's Picture Linkage]: the SRC property of the first IMG Tag

b) [Product's Name]: the first linking characters with A tag in the DIV classified as "namelist"

c) [Linkage of Product's Detail]: the first href linkage with A tag in the DIV classified as "namelist"

d) [Product Manufacturer]: the characters after "Shop Name" in the DIV classified as "namelist"

e) [Release Date]: the characters after "Release Date" in the DIV classified as "namelist"

f) [Place of Origin]: the inner characters of the DIV classified as "namelist"

g) [Price]: the inner characters of the SPAN classified as "price"

To build the matching web site extraction database, to determine the information extraction process, to retrieve data model mapping library, and make use of the website corresponding data model mapping rules, and to lead the information in the XML document into websiteextraction database.

Concrete Realization of Web Extraction of Ceramic Products' Information

A. Database Design

To build web site extraction database by using the development tool of Eclipse PDT, and the result is showed in Figure 2:

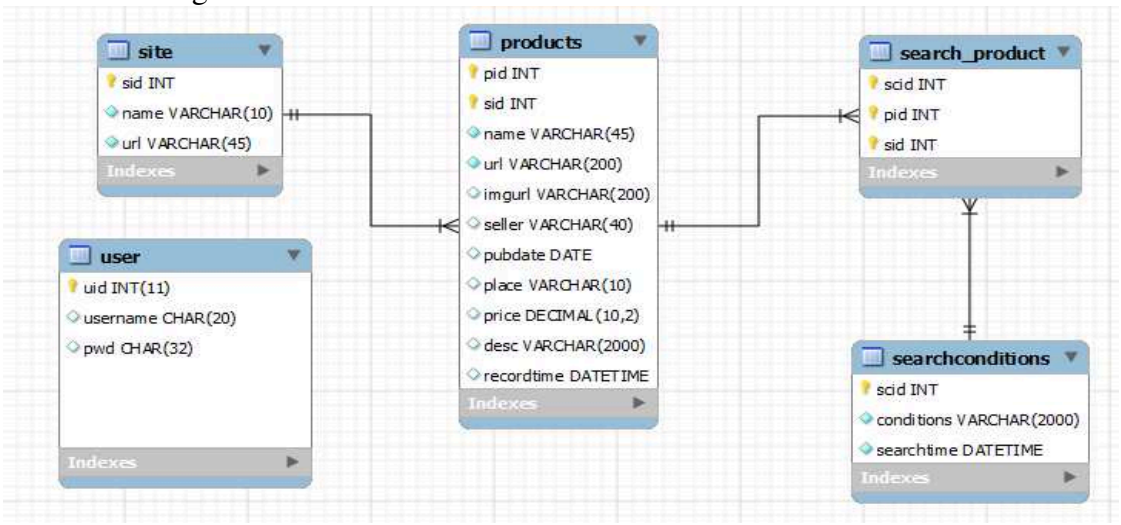

Fig.2 WebSiteExtraction Database

Site: Site information table, which is used for saving the basic information which is extracted by the web page from the site.

Products: Product information table, which is used for saving the products' information which is extracted by the web page.

Search_product: Extraction results' relationship table, which is used for saving extraction conditions and products' interacted system.

Searchconditions: Extraction condition table, which is used for saving extraction conditions.

B. Web Information Extraction

This system mainly through constructs five functional modules to realize the entire system functions, respectively are: Login function module(index.php), Information Extraction function module(search.php), Display module of extraction results(result.php), class of SiteProductSearch and class of MyDb.

a) Login function module(index.php): this module is mainly used to realize the function of login and register.

b) Information Extraction function module(search.php): this module is mainly used to input information extraction conditions, for example, to classify the ceramic in accordance with its usage, which can be classified into domestic ceramics, art (display) ceramics, sanitary ceramics, building ceramics, electrical ceramics, chemical ceramics, textile ceramics, etc.. Then we could extract according to customers' requirements. Part of the functional codes on web extraction of ceramic products information as the following:

```
function genSearchParams ($queryArr){      $sps = array();
  if(array_key_exists('querytext', $queryArr)){
        $sps[] = new SearchParam('NAME',$queryArr['querytext']);        }
  if(array_key_exists('price1', $queryArr) || array_key_exists('price2', $queryArr)){
        $p1 = array_key_exists('price1', $queryArr) ? $queryArr['price1'] : '';
        $p2 = array_key_exists('price2', $queryArr) ? $queryArr['price2'] : '';
        $sps[] = new SearchParam('PRICE',array($p1,$p2));      }
  return $sps;    }
```

c) Display module of extraction results(result.php): this module is used to display the products' information extraction results, and supports the EXCEL export function. How to display the products' information which is acquired in accordance with the inquiry conditions is also the important content of the extraction system. For example, the above EXCEL figure, which we get

according to the condition of “Bone China”, is classified by site, product, price, picture linkage, product linkage, release date, manufacturer, place of origin, and introduction.As is showed in Figure3, Figure 4:

d) Class of SiteProductSearch: this class is extracted in accordance with each site’s corresponding condition, and to analyze the products’ information from the results’ web page.

e) Class of MyDb: this class is to realize the read and write function of the database. Part of the functional codes are as the following:

```
private function connectDb(){          $dsn = array(       'phptype'    => 'mysql',
  'username' => $this->dbUser,        'password' => $this->dbPassword,
  'hostspec' => $this->dbHost,        'database' => $this->dbName,
            'new_link' => true         );
        $res = DB::connect($dsn);
        if(PEAR::isError($this->pearDbObj)){      $this->throwException($res);     }
          else{    $this->pearDbObj = $res;      }
```

Summary

With the high-speed development of information, ceramic products’ information has played a more and more important role in the development of ceramic enterprises, this article provides a new thinking for acquiring the ceramic products’ information, however it is far from enough, we shall excavate the customer’s needs in depth, to develop more reasonable and applicable Web information extraction system which is on the basis of ceramics’ E-commerce websites, strengthen the access to and the sorting out of the ceramic products information, standardize the information resources, and provide decision-making basis for ceramic enterprises to make product development strategy.

Acknowledgment

The research leading to these results has received the support of science and technology project of Jiangxi province education department "The application of Web information extraction technology in the ceramic e-commerce" (NO.GJJ13623) and Humanities and Social Science Research Project in Colleges and Universities of Jiangxi Province “Network group events countermeasure research based on web mining”(NO.JC1221） and Scientific Research Project of Jingdezhen Ceramic Institute “Text information filtering system based on Web”.

References

[1] Y.Yu. *Design and Implementation of Web Information Extraction System SEU-WIE*[D]. Southeast University. 2006.

[2] ARASU Arvind, GARCIA-MOLINA Hector. *Extracting structured data from Web pages*. New York: Proc of the Int Conf on Management of Data, 2003.

[3] Q. Q. Jiang, Z. Gong and Y. Xin. Design and Implementation of BBS Information Extraction System Based on HTML Parser. Techniques of Automation and Applications, vol.1(2012), p.32-37.

[4] Z. Y. Hu and Y. S. Hu. Design of Information Extraction System Based on Domain Main Body. Value Engineering, vol.14(2010), p.158-159.

[5] D. C. Guo. *Based on the Web server's Android mobile phone management system design and implementation*[D]. University of Electronic Science and Technology of China, 2013.

Advanced Materials Research Vols. 989-994 (2014) pp 4326-4331
© (2014) Trans Tech Publications, Switzerland
doi:10.4028/www.scientific.net/AMR.989-994.4326

An improvement for fully homomorphic encryption over integers with shorter public keys

Zetao Jiang [1, a], Xiaote Huang [2,b]

[1] Guilin University of Electronic Technology ,Guilin,China

[2] Nanchang Hangkong University,Nanchang,China

[a]zetaojiang@126.com, [b]906127779@qq.com

Keywords: fully homomorphic encryption;approximate GCD;sparse subset sum problem;public key size

Abstract. This paper puts forward a more efficient fully homomorphic encryption scheme with a view to improving the oversized public key based on the Dijk's scheme.Encrypted with a cubic form in the public key elements instead of quadratic form by adopting Gentry's fully homomorphic techonology.The results show that the public key size reduce from $\widetilde{O}(\lambda^7)$ to $\widetilde{O}(\lambda^6)$ compared to the Coron's scheme.The security of the proposed scheme is based on both the approximate GCD problem and the sparse-subset sum problem.

Introduction

Homomorphic encryption is also called privacy homomorphism.The notion was suggested by Rivest,Adleman and Dertouzos[1] back in 1978 which allows computation on encryption data without decryption.Although these relevant papers to this field had been put forward continuously in the later 30 years,there had been no breakthroughs[2-6].In 2009,Gentry described the first encryption scheme[7],which based on the fully homomorphic encryption scheme over ideals,making the fully homomorphic encryption come true in theory using of ideals[8].In 2010,Dijk,Gentry,Halevi and Vaikuntanathan made an improvement based on the fully homomorphic encryption over ideals and proposed a scheme over integers which could achieve fully homomorphic encryption without using of ideals,that is,fully homomorphic encryption over integers[8].Moreover,there were continuous many improved papers later[9-12].In 2011, Coron put forward a scheme of having shorter public key size[13] ,which reduced the public key size from $\widetilde{O}(\lambda^{10})$ to $\widetilde{O}(\lambda^7)$ by encrypting with a quadratic form in the public key elements,instead of a linear form.The idea consisted in storing only a smaller subset of the public key and then generating the full public key on the fly by combining the elements in the small subset multiplicatively.This paper reduces the public key size by encrypting with a cubic form in the public key elements and the result shows that the public key size is compressed from $\widetilde{O}(\lambda^7)$ to $\widetilde{O}(\lambda^6)$.

Preliminaries

1.1 Basic Notation

For a real number z ,we denote by $\lceil z \rceil, \lfloor z \rfloor, \lfloor z \rceil$ the rounding of a up,down,or to the nearest integer.Namely,these are the unique integers in the half open intervals $[z, z+1), (z-1, z]$ and $\left(z-\frac{1}{2}, z+\frac{1}{2} \right]$,respectively.For a real number z and an integer p ,we use $q_p(z)$ and $r_p(z)$ to denote the quotient and remainder of z with respect to p ,namely $q_p(z)=\lfloor z \rceil$, $r_p(z)=z-q_p(z)\cdot p$.

In this paper we usually denote parameters by Greek letters.Specificlly, we give some descriptions about the parameters:

λ : the security parameters of this scheme
γ :the bit-length of the integers in the public key
η :the bit-length of the secret key
ρ : the bit-length of the noise
τ :the number of integers in the public key
ρ' :the bit-length of the second noise

1.2 Related Definitions

Definition 1(Approximate GCD).Given a random set of integers S=$\{x_0, x_1, ..., x_n\}$,every x_i is close to the big prime number p and p is the most closed common factor of these integers.The problem of finding the most closed common factor p is the Approximate GCD.

Definition 2 (Sparse Subset Sum Problem(SSSP)).Given a set of integers S=$\{a_1, a_2, ..., a_n\}$and a integer x,whether exit a none-empty subset H$\in$ S satisfy that the sum of all elements in H is equal to x.The problem is called SSSP.

Definition 3 (Homomorphic Encryption Scheme). A homomorphic encryption (denoted by ε)is composed of the following four algorithms:

KeyGen:According to the security parameter λ,generate pk and sk of the scheme.

Enc:Given a plaintext $m \in \{0,1\}^*$,encrypt plaintext m with pk and get ciphertext c.

Dec:Input sk and c and run Dec,output m.

Evaluate:Input pk , circuit C having t inputs（be composed of addition gate and multiplication mod 2） and a string of ciphertexts **c**= $(c_1, c_2, ..., c_t)$ (c_i is the encryption of plaintext m_i),output $c^* = Evaluate(pk, C, c)$,

moreover,satisfy $Dec(sk, c^*) = C(m_1, m_2, ...m_i)$.

Definition 4 (Fully Homomorphic Encryption Scheme)If a scheme satisfy the contidition that the result of decrypting after arbitrary conputation on encrypted data is equal to the outcome of the same computation on plain data,the scheme is called fully homomophic encryption scheme.

Definition 5 (Augmented Decryption Circuits).Define following two augmented decryption circuits:

Dec-Add:Input sk and two ciphertexts c_1、c_2 and compute Dec（sk, c_1）+Dec（sk, c_2）mod2.

Dec-Mult: Input sk and two ciphertexts c_1、c_2 and compute Dec（sk, c_1）× Dec（sk, c_2）mod2.

We denote by $D_\varepsilon = \{$ Dec - Add, Dec - Mult$\}$the set of the two kind of circuits.

Definition 6 (Bootstrappable Encryption).Let $\varepsilon = (KeyGen, Encrypt, Decrypt, Evaluate)$ be a homomorphic encryption scheme,and for every value of the security parameter λ let $C_\varepsilon(\lambda)$ be a set of circuits with respect to which ε is correct.We say that ε is bootstrappable if $D_\varepsilon(\lambda) \subseteq C_\varepsilon(\lambda)$holds for every λ.

1.3 Gentry's ideological frame of fully homomorphic encryption scheme.

(1)Construct a somewhat homomorphic encryption scheme,which can evaluate a limited computations of polynomial.

(2)Control noise using the technology of ciphertext refresh.

(3)Squash the Decryption Circuit.

(4)get the fully homomorphic encryption scheme.

Coron's scheme with shorter public keys

2.1 Constructing ideas

Coron and Mandal proposed a fully homomorphic encryption scheme with shorter public keys with a view to improving the oversized public key based on the Dijk's scheme. The improved scheme reduced the public key size from $\tilde{O}(\lambda^{10})$ to $\tilde{O}(\lambda^7)$ by encrypting with a quadratic form in the public key elements,instead of a linear form.,

2.2 concret algorithm

KeyGen (1^λ)**.**Genenrate a random prime $p \in \left[2^{\eta-1}, 2^\eta\right)$.Let $x_0 = q_0 \cdot p$ where q_0 is a random square free 2^λ-rough integer in $\left[0, 2^\gamma / p\right)$.Generate integers $x_{i,b}$ for $1 \le i \le \beta$ and $b \in \{0,1\}$:

$$x_{i,b} = p \cdot q_{i,b} + r_{i,b}, 1 \le i \le \beta, 0 \le b \le 1$$

Where $q_{i,b}$ are random integers in $[0, q_0)$ and $r_{i,b}$ are integers in $\left(-2^\rho, 2^\rho\right)$.Let sk^*=p and pk^* = $(x_0, x_{1,0}, x_{1,1}, ..., x_{\beta,0}, x_{\beta,1})$.

Encrypt $(pk, m \in \{0,1\})$**.**Generate a random vector **b**=$\left(b_{i,j}\right)$ of size $\tau = \beta^2$ and with components in $\left[0, 2^\alpha\right)$.Genenrate a random integer r in $\left(-2^{\rho'}, 2^{\rho'}\right)$.Output the ciphertext:

$$c^* = m + 2r + 2\sum_{1 \le i,j \le \beta} b_{ij} \cdot x_{i,0} \cdot x_{j,1} \bmod x_0$$

Evaluate $(pk, C, c_1, c_2, ..., c_t)$**:**Given the (binary) circuit C_ε with t inputs,and t ciphertexts c_i,apply the (integer) addition and multiplication gates of C_ε to the ciphertexts,performing all the operations over the integers,and return the resulting integer.In addition,ciphertexts are reduced modulo x_0 after addition and multiplication.

Decrypt (sk, c)**:** Output $m \leftarrow (c \bmod p) \bmod 2$.

The scheme of this paper

In this paper,we reduced the public key size to $\widetilde{O}(\lambda^6)$ by encrypting with a cubic form in the public key elements.

3.1 Somewhat homomorphic encryption scheme

Our technique consists in working with integers $x'_{i,j,k}$ of the form $x'_{i,j,k} = x_{i,0} \cdot x_{j,1} \cdot x_{k,2}$ mod x_0 for $1 \le i, j, k \le \beta$.Then only 3β integers $x_{i,b}$ need to be stored in the public key in order to generate the $\tau = \beta^3$ integers $x'_{i,j,k}$ used for encryption.The public key size from τ down to $3\sqrt[3]{\tau}$ of γ bits.

We set the constrains on the scheme as follows:

$$\gamma = \omega(\eta^2 \log \lambda)$$
$$\eta \ge (3\rho + \alpha) \cdot \Theta(\lambda \log^2 \lambda)$$
$$\rho = \omega(\log \lambda)$$
$$\rho' = 3\rho + \alpha + \omega(\log\lambda)$$
$$\alpha\beta^3 \ge \gamma + \omega(\log \lambda)$$

keygen (1^λ). Genenrate a random prime $p \in \left[2^{\eta-1}, 2^\eta\right)$.Let $x_0 = q_0 \cdot p$ where q_0 is a random square free 2^λ-rough integer in $\left[0, 2^\gamma / p\right)$.Generate integers $x_{i,b}$ for $1 \le i \le \beta$ and $b \in \{0,1,2\}$:

$$x_{i,b} = p \cdot q_{i,b} + r_{i,b}, 1 \le i \le \beta, 0 \le b \le 2$$

Where $q_{i,b}$ are random integers in $[0, q_0)$ and $r_{i,b}$ are integers in $\left(-2^\rho, 2^\rho\right)$.Let sk =p and pk = $(x_0, x_{1,0}, x_{1,1}, x_{1,2}, ..., x_{\beta,0}, x_{\beta,1}, x_{\beta,2})$.

encrypt $(pk, m \in \{0,1\})$**.**Generate a random vector b=$(b_{i,j,k})$ of size $\tau = \beta^3$ and with components in $\left[0, 2^\alpha\right)$.Genenrate a random integer r in $\left(-2^{\rho'}, 2^{\rho'}\right)$.Output the ciphertext:

$$c = m + 2r + 2\sum_{1 \le i,j,k \le \beta} b_{i,j,k} \cdot x_{i,0} \cdot x_{j,1} \cdot x_{k,2} \bmod x_0$$

evaluate and decrypt: same as in the Coron's scheme.

3.2 Correctness

Permitted Circuits （C_ε）: the definition is same as the literature[13].

According the encryption algorithm of the scheme in this paper,we know:

Exit an integer k,make $c = m + 2r + 2\sum_{1\le i,j,k\le\beta} b_{i,j,k}\cdot x_{i,0}\cdot x_{j,1}\cdot x_{k,2} + k\cdot x_0, |k| \le \tau$

Because $x_{i,b} = p\cdot q_{i,b} + r_{i,b}, x_0 = q_0\cdot p$,we can derive

$$c = m + 2r + 2\sum_{1\le i,j,k\le\beta} b_{i,j,k}\cdot r_{i,0}\cdot r_{j,1}\cdot r_{k,2} \bmod p$$

This gives using $\rho' \ge 3\cdot\rho + \alpha$:

$$|c \bmod p| \le 2^{\rho'+1} + 2\tau\cdot 2^{3\rho+\alpha} \le \tau\cdot 2^{\rho'+2} \quad (1)$$

Let $C \in C_\varepsilon$ be a permitted circuit with t inputs and let C' be the corresponding circuit oprating over the integers rather than modulo 2.Let $c_i \leftarrow Encrypt(pk, m_i)$ .We have :

$$c \bmod p = C'(c_1,...,c_t) \bmod p = C'(c_1 \bmod p,...,c_t \bmod p) \bmod p \quad (2)$$

From (1) and the definition of permitted circuits,we obtain:

$$|C'(c_1 \bmod p,...,c_t \bmod p)| \le 2^{\eta-4} \le p/8$$

Therefore $C'(c_1 \bmod p,...,c_t \bmod p) \bmod p = C'(c_1 \bmod p,...,c_t \bmod p)$,which implies from (2): $c \bmod p = C'(c_1 \bmod p,...,c_t \bmod p)$

and eventually:

$$(c \bmod p) \bmod 2 = （ C'(c_1 \bmod p,...,c_t \bmod p) \bmod 2 = [C'([c_1 \bmod p]_2,...,[c_t \bmod p]_2)]_2$$

So, $[c \bmod p]_2 = C(m_1,...,m_t)$,that is,the scheme is correct.

3.3 Making the Scheme Fully Homomorphic

In this paper,we still adopt the techonology of SSSP like [4] to compress the decryption circuit and finally get the fully homomorphic encryption scheme,because the large complexity in computing $\lfloor c/p \rceil$ of decryption algorithm.

Concrete algorithm is as follows:

keygen（1^λ）.Call the sk=p and pk=（$x_0, x_{1,0}, x_{1,1}, x_{1,2},..., x_{\beta,0}, x_{\beta,1}, x_{\beta,2}$）,which is generated in above-mentioned somewhat homomorphic scheme.Let M= $\lfloor 2^\kappa / p \rceil$ .Choose a random number $q_0 \in [0, 2^\gamma / p)$,and let $x_0 = q_0\cdot p$ .Generate integers $x_{i,b}$:

$$x_{i,b} = p\cdot q_{i,b} + r_{i,b}, 1 \le i \le \beta, 0 \le b \le 2$$

Where $q_{i,b}$ are random integers in $[0.q_0)$ and $r_{i,b}$ are integers in $(-2^\rho, 2^\rho)$.Let $pk^* = (x_0, x_{1,0}, x_{1,1}, x_{1,2},..., x_{\beta,0}, x_{\beta,1}, x_{\beta,2})$.

Additionally generate random bit vectors $s^{(0)}$, $s^{(1)}$ and $s^{(2)}$ of length $\lceil \sqrt[3]{\Theta} \rceil$,subject to the conditions that $s_1^{(0)} = s_1^{(1)} = s_1^{(2)} = 1$, $\mathbf{S} = \{(i,j,k) : s_i^{(0)}\cdot s_j^{(1)}\cdot s_k^{(2)} = 1\}$.

Initialize a system-wide pseudo-random number generator f with a random seed **se**,and use $f(se)$ to generate integers $u_{i,j,k} \in [0, 2^{\kappa+1})$ for $1 \le i,j,k \le \sqrt[3]{\Theta}$, $(i,j,k) \ne (1,1,1)$ .Then,set $u_{1,1,1}$ such that

$$\sum_{(i,j,k)\in S} u_{i,j,k} = M \bmod 2^{\kappa+1}$$

Where $M \leftarrow (z_{i,j,k})$.

Compute encryption $\sigma^{(b)}$ of the vectors $s^{(b)}$,by picking,for each $i \in \left[1, \lceil \sqrt[3]{\Theta} \rceil\right]$ and $b = 0,1,2$,random integers $r'_{i,b} \in (-2^\rho, 2^\rho), q'_{i,b} \in [0, q_0)$,and setting:

$\sigma_i^{(b)} = s_i^{(b)} + 2r'_{i,b} + p \cdot q'_{i,b} \bmod x_0$

Finally,output the secret key as sk= （ $s^{(0)}$, $s^{(1)}$, $s^{(2)}$ ） and the public key as pk=$\left(pk^*, se, u_{1,1,1}, \sigma^{(0)}, \sigma^{(1)}, \sigma^{(2)}\right)$.

encrypt （ *pk,* $m \in \{0,1\}$ ） *and evaluate* **:** Choose a random integer matrix $b=\left(b_{i,j,k}\right)1 \le i,j,k \le \beta \in \left[0, 2^{\alpha}\right)^{\beta\times\beta\times\beta}$ and a random integer r in $\left(-2^{\rho'}, 2^{\rho'}\right)$.Output the ciphertext: $c^* = m + 2r + 2\sum_{1\le i,j,k\le\beta} b_{ijk} \cdot x_{i,0} \cdot x_{j,1} \cdot x_{k,2} \bmod x_0$

Let $y_{i,j,k} = u_{i,j,k} / 2^{\kappa}$ and $z_{i,j,k} = \left[c^* \cdot y_{i,j,k}\right]_2$ .For every $z_{i,j,k}$,keeping only $n = \lceil \log_2(\theta+1) \rceil$ bits of precision after the binary point.Define the matrix z= $\left(z_{i,j,k}\right)$ .Output the expanded ciphertext c= （c^*,z）.

decrypt（*sk,* c^* ,*z*）**:**Output $m \leftarrow \left[c^* - \lfloor \sum_{i,j,k} s_i^{(0)} \cdot s_j^{(1)} \cdot s_k^{(2)} z_{i,j,k} \rceil\right]_2$.

Comparision of public key size in several schemes

The fully homomorphic encryption scheme in this paper is proposed based on Dijk's scheme and Coron's scheme with a view to improving the oversized public key,so we compare the public key size in the three schemes.The result is shown in Table 1.

Table1

Scheme	Based the assumption of hard problem	Public key size
Dijk's scheme	GCD and SSSP	λ^{10}
Coron's scheme	GCD and SSSP	λ^{7}
The scheme in this paper	GCD and SSSP	λ^{6}

Conclusion

The scheme in this paper is proposed based on Dijk's scheme and Coron's scheme,constructing fully homomotphism by adopting Gentry's fully homomorphic idea frame.Reduce the public key size by encrypting with a cubic form in the public key elements and the security also depends on GCD and SSSP.Comparing to the first two scheme,the scheme in this paper have shorter public key size and higher computing efficiency.

Acknowledgements

This paper is sponsored by science and technology planning project of jiangxi province(CA201304033) and science and technology key project of Education Department of jiangxi province(Kj201109091788) and fall to the ground planning project of Education Department of jiangxi province(KJLD12029).

References

[1]Rivest R L,Adleman L,Dertouzos M L.On data banks and privacy homomorphisms[Z]. Foundations of Secure Computation,1978.

[2]Lipton B.Searching for Elements in Black Box Fields and Applications[C]//Proc.of Cryptology-Crypo'96.[S.I.]:Springer-Verlag,1996:283-297.

[3]Domingo-Ferrer J.A Provably Secure Additive and Multiplicative Privacy Homomorphism [C]//Proc.of the 5th International Conference on Information Security. [S.l.]: Springer-Verlag,2002:471-483

[4]Brickell E F,Yacobi Y.On Privacy Homomorphisms[C]//Proc.of Cryptology-Euro Crypt'87. Berlin,Germany:Springer-Verlag,1987:117-126.
[5]Feigenbaum J,Merritt M.Open Question,Talk Abstracts,and Summary of Discussions [EB/OL].(1991-12-05).
[6]Fellows M,Koblitz N.Combinatorial Cryptosystems Galore![Z].1993
[7]C.Gentry.Fully homomorphic encryption using ideal lattices.In STOC'09,pages 169-178. ACM,2009.
[8]C.Gentry,A fully homomorphic encryption scheme.Ph.D.thesis,Stanford University, 2009. Available at http://crypto.stanford.edu/craig.
[9] M.van Dijk,C.Gentry,S.Halevi and V.Vaikuntanathan,Fully homomorphic encryption over the integers.In H.Gilbert(Ed.),EUROCRYPT 2010,LNCS,vol.6110,Springer,2010,pp.24-43
[10] C.Gentry and S.Halevi.Implementing Gentry's fully homomorphic encryption scheme.In K.Paterson(Ed.),EUROCRYPT 2011,LNCS,Springer,2011.
[11]D.Stehle and R.Steinfeld,Faster fully homomorphic encryption.In M.Abe(Ed.),ASIACRYPT 2010,LNCS,vol.6477,Springer,2010,pp.377-394.
[12] Nigel P.Smart and Frederik Vercauteren. Fully homomorphic encryption with relatively small key and ciphertext sizes. In Public Key Cryptography-PKC'10,volume 6056 of Lecture Notes in Computer Science,pages 420-443.Springer,2010
[13] J.S.Coron,A.Mandal,D.Naccache and M.Tibouchi,Fully Homomorphic Encryption over the Integers with Shorter Public Keys.In P.Rogaway(Ed.), CRYPTO 2011,LNCS,vol. 6841, Springer, 2011,pp.487-504. Full version available at IACR eprint.

Advanced Materials Research Vols. 989-994 (2014) pp 4332-4337
© (2014) Trans Tech Publications, Switzerland
doi:10.4028/www.scientific.net/AMR.989-994.4332

Design and implement an application development platform based on open source technology

TIEBIN LIU

University of Chinese Academy of Sciences, China Futures Association

liutiebin@cfachina.org

Keywords: open source; J2EE; application development platform.

Abstract. This paper design and implement a J2EE application development platform based on open source technology by studying on Paoding-Rose, Spring, Mybatis, Activiti and other open source technologies. The platform can improve enterprise capabilities of independent research and development IT system.

Background

It is necessary to build enterprise independent R & D capacity , and the reasons are listed below: 1) we need a unified IT architecture and management of enterprise application development; 2)improve the response speed of business requirements; 3) ensure information system security and stability; 4)protect existing IT investment; 5)reduce the developer's skill requirements and employee turnover risk. This article based on depth study on open source technology platform which domestic mainstream software vendors and large financial institutions use. We use Paoding-Rose, Spring, Mybatis, Activiti and other open source technologies to design and implement a set of J2EE-based application development platform. This platform comply with software lifecycle management specification and business-centric. This platform also combine business processes and provide the major functions required for enterprise application R & D system.

Introduction to the relevant open source technology

The platform mainly use the Spring Framework and Paoding-Rose, combined with MyBatis persistence mapping technology,， Activiti workflow technology and other open source technology as the core design. This section briefly Introduce related technologies.

2.1 Paoding-Rose Development Framework

Paoding-Rose Development Framework (hereinafter referred to as the Rose) is released by Renren website and Sticky website. It's a Java web development framework based on open source Spring specification and Servlet specification[1]. This development framework has the following advantages[2]:

1．Convention over configuration: package path, class name and class method name do not require declaration in configuration file, as long as the name contains specific keywords and Annotation keywords. As long as this condition is satisfied, the other naming parts can easily be modified and do not require to modify any configuration .

2．Automatic Binding: This is a very useful feature. In Struts2, we need to use struts2 tags and "set" to automatically bind form data. But Rose doesn't. It has no label restrictions, free to binding properties, and pass parameters directly through "Annotation" without "set" data. The data persistence layer of Jade Framework also provide automatic binding properties. It does not require any set or get methods, so it's greatly enhance the development efficiency.

3．REST style: As the development of Rose is based on Spring, so it use a lot of Spring MVC components. It also brings the Spring MVC REST style for Rose. It has a lot of advantages of Spring MVC. Rose optimizes the URL mapping and page-value operations of Spring MVC, so it's more elegant and full support for REST.

4. Minimalist Jade: Jade framework greatly enhance the efficiency of development. DAO interface method plus an SQL statement can implement database operation and assignment.

5. Portal Technology: This is one of the original JAVA background technology created by architects of Renren website. The basic principles to implement this technology is module segmentation of page which requires a lot of data for rendering it (such as public home page). Each module as a "Window" access data from concurrent database, and then re-integrate data, and ultimately presented to the user. Back office operations similar SCALA concurrent algorithms that block the data and concurrent computing. Foreground effect is similar with page fragment loading technique that SINA Weibo used. In order to ensure that the user's response speed, the first part of the page is loaded clip, and gradually display the entire page. Facebook also have a similar solution.

6. Compatibility: Rose use filters instead of intercepting the request by Servlet. Currently, most of the framework intercept requests by filter. The benefit is that you can easily be compatible with other frameworks. Based on this point, Rose has REST style and coexist with Struts which intercept requests based on Servlet, so we can reform legacy systems.

2.2 MyBatis framework

MyBatis framework collects multiple concepts and methods of operational relations data. It's a powerful data access tool and solution[3]. It's an excellent persistence framework which supports the common SQL queries, stored procedures and advanced mapping. MyBatis framework mainly consists of two categories: DAO components and SQL Map components. The common tools include Log management, etc. Its structure is shown in Figure 2-1.

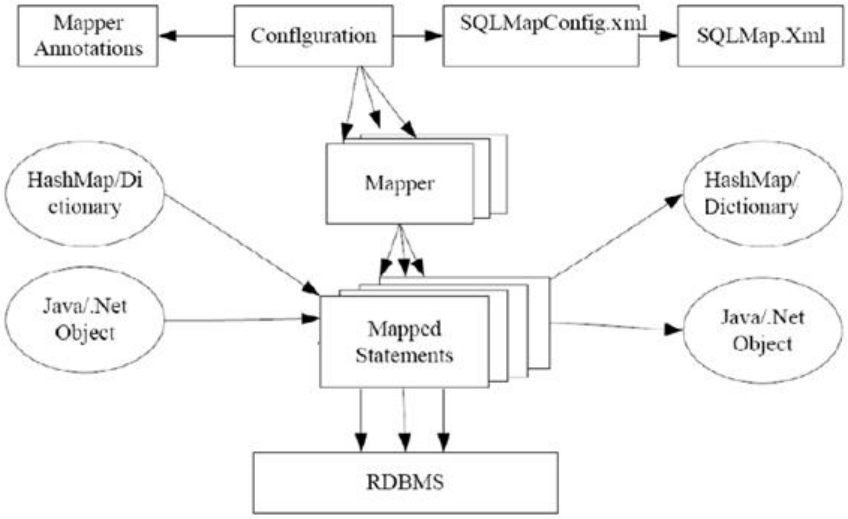

Figure 2-1 MyBatis component architecture diagram

Since MyBatis supports developer write SQL statements, so developers can flexibly use SQL statements to query different objects. But Hibernate framework has no ability to do that. Also MyBatis performance is much higher than ORM framework. Those are main reasons why a lot of developers choose MyBatis currently [4].

2.3 Activiti technology

Activiti technology is from the JBoss jBPM4 project which is dedicated to collaborative management among business people, developers and system managers . Activiti is an open source lightweight workflow and BPM platform product [5] and the latest version of Activiti is 5.8. Activiti is a scalable workflow management system, using an intuitive process language to describe business processes. Activiti abstracts part of the business process or factors into tasks, wait states of asynchronous communication, timers, automatic operation, etc. These operations are bundled together by Activiti, so Activiti has a powerful and easy control flow mechanisms which can be configured in any database or can be deployed on any application server [6].

Analysis and design of the application development platform

3.1 Requirements Analysis

As a development platform, it must provide technically efficient , easy , reusable, monitoring and manageable development platform for enterprise IT R&D staff. The purpose of the development platform is to improve the abilities of enterprise IT project management and independent R&D capabilities. Its functional requirements include providing design and development tools, run-time environment and management monitoring tools. Design and development tools are mainly based on eclipse visual mode which integrate design, development, assembly, testing, maintenance, deployment, management in one integrated development environment. Also it provides guided business object development, visualization, process and report design, rapid deployment capabilities. The development platform have run-time environment which are provided by J2EE container, workflow engine, reporting engine, basic services and other core modules, etc. These modules provide the necessary running environment for applications and services. To facilitate system debugging for R&D staff and run-time monitoring for maintenance staff, the development platform should provide graphical management and monitoring capabilities.

From the perspective of good performance and advanced technology, its non-functional requirements include: a modular platform architecture, loosely coupled and high performance design; based on J2EE standards, easy to use, easy to build efficient development system, improve application development efficiency.

3.2 Functional Design

Demand for self-development requirements, the development platform functional design include:

1. Code Generator: Using Eclipse plug-in, building the code, graphical reporting tools and other features, developers can set up service and entity to meet the business requirements through visual way, and automatically generates all files (including configuration files, JAVA code and SQL scripts) from the page to the persistence layer.

2. Support System: a complete object-oriented support system which provides buffer management, workflow engine, etc. and a large number of API for JAVA code and JS. In order to ensure the platform itself scalability, stability and flexibility, the platform should provide maximum abstraction whether its on the page presentation, or on any layer in CURD.

3. Component Services: Provides a set of component-based services, including organizational management, rights management, menu management, application configuration management, page assembly and other functions.

3.3 Architecture Design

Technical architecture of the development platform fully consider modularity, low coupling , high performance requirements of hierarchical design, and its provide a hierarchical bottom-up support for the system. To reduce the complexity of system integration and application deployment, the base layer use packaging technology to shield storage, computing, transfer and other technical details. Based on above mentioned, the development platform clearly defines a common service layer, application layer and the business component layer, and provide application software development life-cycle management capabilities, shown in Figure 3-1.

3.4 Security Design

Security is an essential part of the development platform. Good security design can protect applications and data security and ensure stable running of the system. So we should fully consider the problems and prevent it from system data layer, application layer, network layer, and maintenance, etc.

From application security aspect, development platform is designed to use dedicated login control module which provides identity and authentication features for access control. Its use the MD5 encryption algorithm[7] to provide the user password encryption feature, and use combination of two or more identification techniques to achieve user authentication. Its use encryption technology to ensure security of data transmission and verification. The application platform use the targeted improvement and configuration middleware to allow the server provide stronger enforcement of access control based on the user's identity, security and policy. In order to prevent cross-site scripting

and SQL injection attacks, the development platform filter and background process the data which are submitted by the users.

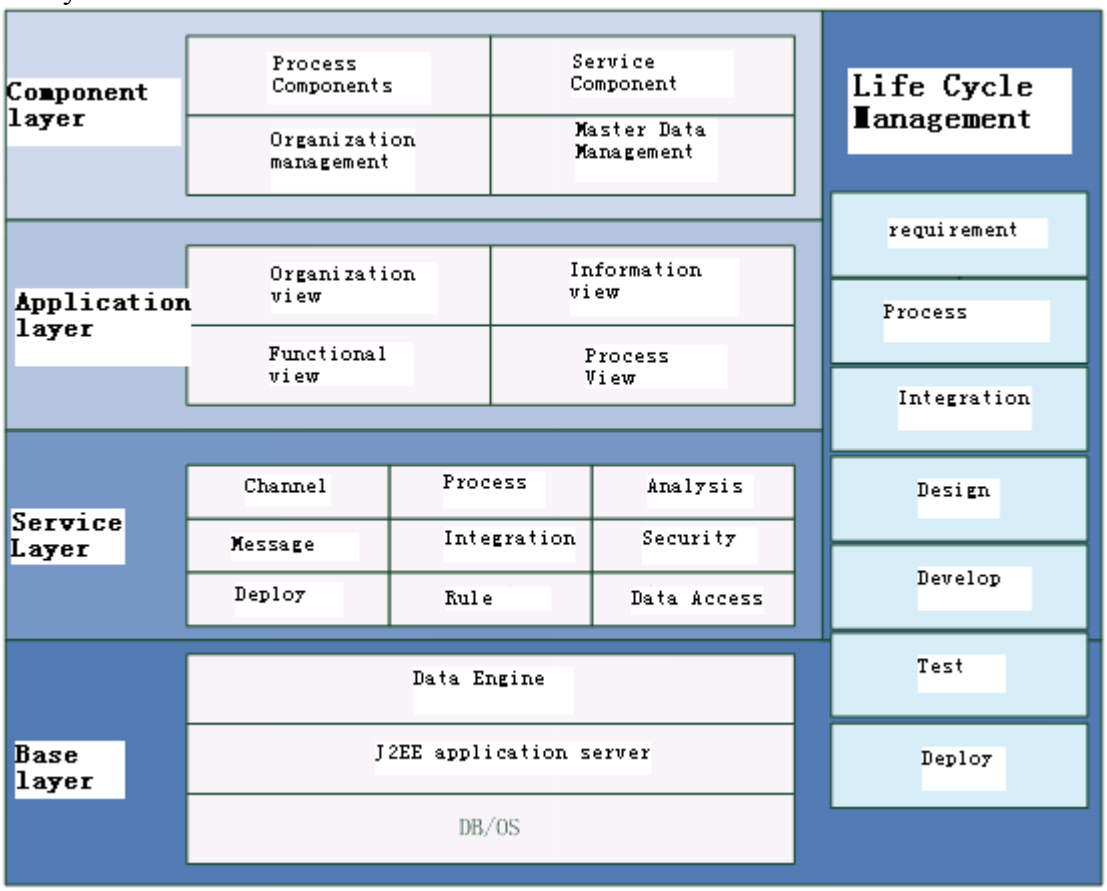

Figure 3-1 System architecture of the development platform

Implement the application development platfrom

4.1 Selection of open source technology Experiment design

To ensure openness of the application development platform, we determine use mainstream mature open source frameworks and development tools in terms of platform technical realization.

After integration testing, we determine use JDK1.6 as the basic framework of JAVA development compiler environment, use Servlet-2.5 as the intermediate layer, use Spring-3.0.3 as JAVA development framework, use MyBatis-3.0.6 as persistence layer, and use Paoding-Rose as Java Web development framework.

Java Web development tool use Eclipse Java EE IDE for Web Developers, use Indigo Service Release 2 as the communications infrastructure components, use PL / SQL as the database programming tools, and use Tomcat as Web-based server.

4.2 Implement the architecture of application development platform

The application development platform is based on J2EE, Eclipse and other open source technology. Its use mainstream MVC design framework and its functions cover design, development, testing, deployment, operation , monitoring and other aspects. Entire technology architecture consists of three layers: the data access layer, business logic and page presentation layer.

1. Data Access Layer

It use Mybatis framework, use SQL statements to access the database and SQL statements can be easily be optimized. It can also implement Mybatis-based database cache.

2. business logic layer

(1) use Paoding-Rose (Lightweight J2EE Framework) which is based on open source Spring and use "convention than configuration" principle, almost zero-configuration, enable developers to quickly develop the background service.

(2) use Spring's transaction management

(3) use standards-based open source Activiti Spring framework which supports BPMN2.0 processes as the workflow engine.

(4) use birt [8] which can be integrated with Paoding-Rose as reporting engine.

3. Page presentation layer

Using JSON format data exchange with back system, we can diversify front display mode and use different styles or different topics foreground template engine on display. It also supports both desktop and PAD terminal adapter to facilitate the development of mobile Internet applications.

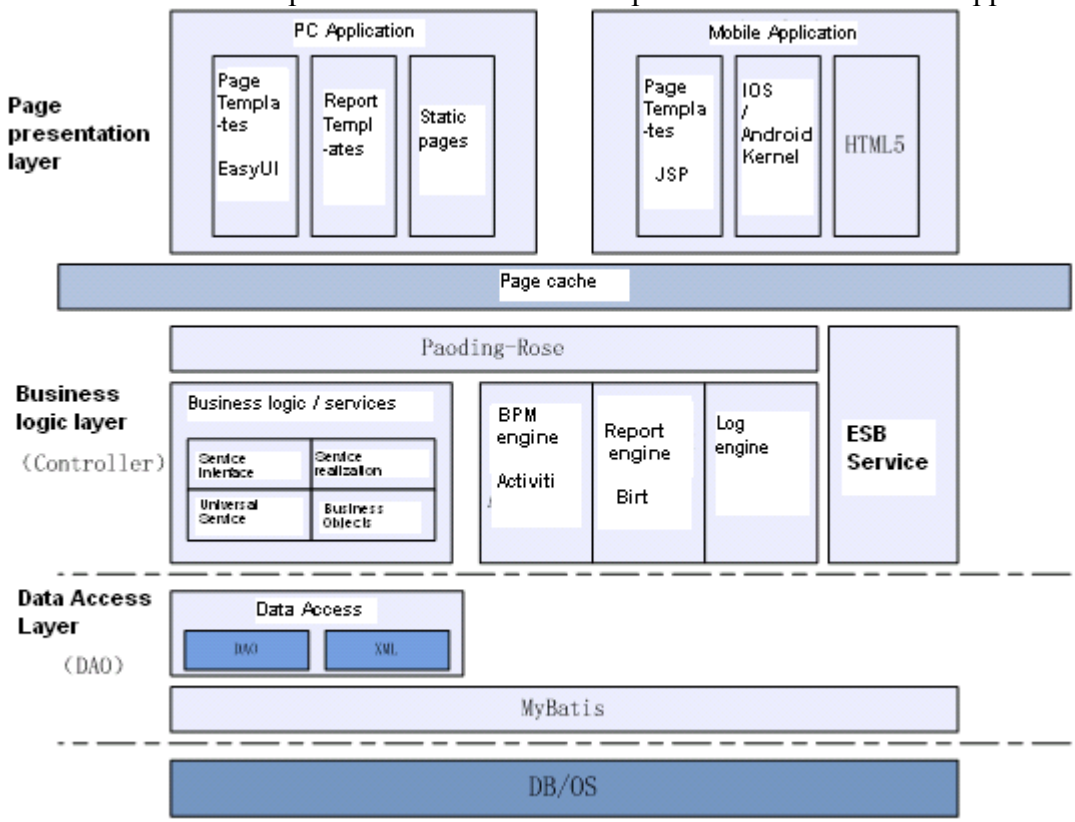

Figure 4-1 The Application Development Platform Architecture

4.3 Implement the critical functions of application development platform

4.3.1 Modular Rapid Development

According to the certain rules interconnection， application development platform use the standard interface and other same subsystems to compose more complex systems. Public modules and core modules which abstract from the system functions form the platform API. It reduces the complexity of application and makes the applications simplification and standardization in design, testing and maintenance operations.

4.3.2 Business Process Management

Application development platform uses BPMN2.0 business process definition model to achieve business process lifecycle management, including design modeling business processes, testing and debugging, deployment, operation, monitoring and management. This function consists of routing which is responsible for parsing the definition of business processes and coordinate activities, orchestration engine which process client requests, visual business process modeling designers and process management monitoring module which based on the Eclipse plug-in technology.

4.3.3 Access Management

Based on security design model, the development platform use role-based access control (RBAC) model. It establishes a set of access management functions including user management, role management, organization management, data rights , functions management, menu management, etc.

4.3.4 PAD terminal adapter

With the rapid development of mobile Internet, the application development platform achieve the PAD terminal application development capability. By defining a unified front end data transmission

protocol, it realizes server side sharing between mobile devices and PC, so as to achieve cross-platform, cross-terminal synchronous project development.

4.3.5 One-click deployment

The application development platform design a solution for one-click rapid deployment. It intergates software compiler , test step, deploy step, etc. to an automated tool. One-click rapid deployment use pure JAVA language and generate XML schema documents which can be integrated into the development environment by given template, with good cross-platform and convenience.

4.3.6 Old module rapid death mode

For previous problems that internal application can not quickly offline outdated or useless business function modules, the application development platform introduces the concept of "old module rapid death". By sufficiently reduce coupling of modules, the application development platform achieve the old module simple, fast and no risk peeling, so that internal applications can be maintained in spite of application increasingly large and complex .

Summary

Using open source technology to build the application development platform can provide openness, flexibility, autonomy and other advantages. On the basis of this foundation form a set of development operating system , and it can support from concept, development, maintenance of IT products R&D process. The application development platform can effectively enhance the enterprise IT R&D capabilities.

References

[1] [1] http://baike.baidu.com/view/23694.htm [EB/OL]. 2013.
[2] http://baike.baidu.com/view/1632686.htm [EB/OL]. 2013.
[3] Clinton Begin, Brandon Goodin, Larry Meadors. iBatis in Action [M]. Manning publications Co. Chero Station, 2007.
[4] MyBatis: new home of the world’s most popular SQL mapping framework [M]. Chuck Cavaness Programming Jakarta Struts, OŔeilly Media, June 2004, Second Edition.
[5] Jie Gao. Shen Ru Qian Chu jBPM[M]. Beijing:People You Dian Press, 2009.
[6] TIJS RADEMAKERS, Activiti in Action[M]. Manning Publications Co, 2012, Third Edition.
[7] Ming Mao,Zhiguang Qin,Shaohui Chen. Research of Key technology of Recognize and interpret MD5 Algorithm [J]. Computer Apply. 2009(12).
[8] http://baike.baidu.com/view/425694.htm [EB/OL]. 2013.

Advanced Materials Research Vols. 989-994 (2014) pp 4338-4341
© (2014) Trans Tech Publications, Switzerland
doi:10.4028/www.scientific.net/AMR.989-994.4338

Research on Network Management Network

Wang Liangrun [1, a], Wu Chuansheng [2,b] , Zhao Shicheng [3,c], Liu Fanghui [4,d]

[1,2,4]University of Science and Technology Liaoning, China

[3]Dalian University of Technology,, China

[a] wlrun@163.com,[b,d]gykwcs@163.com ,[c]liufanghuidl@gmail.com

Keywords: network, network management, switching nodes, node server;

Abstract. Where in a metropolitan area server controls the network management process and the service process of a node switch and a node server under it, while the node server controls the network management process and the service process of an access switch and a terminal under it. Where in the metropolitan area server or the node server allocates an address to each network device by sending a query packet to each communication port, and establishes a clear network topology on the main control server side during the allocation process, in a main control mode. Thus, during the transmission process of a specific data packet, the main control server (metropolitan area server or node server) directly allocates a corresponding communication link (because it clearly knows the device topology of the whole network), without the need of carrying out route negotiation between each network device, thus a stable transmission rate may be guaranteed, and delay may be avoided.

Introduction

The current network technicians seem to miss a basic theory: the root of network packet loss phenomenon is flow non-uniformity. Macroscopically, when the sending speed is high in one time period, it is certain to cause jam in another time period; no upper limit can be given to the peak flow of the network so long as the network flow is non-uniform, and any arbitrary large bandwidth may be occupied in a short time[1].

At preset, device manufacturers recommend ultra-wideband access networks of tens or even hundreds of Megabit to each household. However, even if optical fiber enters each household, it is difficult to exhibit a video communication service with good QoS to the consumers. In spite of what complex QoS measures are taken, the transmission quality of IP Internet can only be "improved", and no quality of network transmission can be "guaranteed"[2].

The Network Access Process of a Metropolitan Area Network

The Network Access Process of a Metropolitan Area Server and a Node Switch, a Node Server

Firstly, each switch that is allowed to access the network must be registered on a server, the registration information of an switch includes the device type and device identification of the switch, and an switch that is not registered will be unable to access the network.

As shown in FIG. 1:

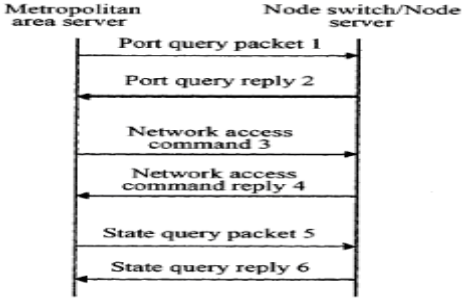

FIG. 1 A node server

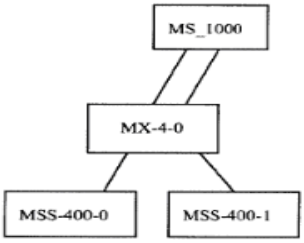

FIG. 2 Schematic diagram

1). a server sends a query packet to each port, after a switch receives the query packet, it sends a reply (the reply contains the device type and device identification of the switch, which is the intrinsic information of each switch);

2). after the server receives the reply issued by the switch, it knows that the current port is connected with a switch, then it finds the switch information in an internal registration information table of the server, and sends a network access command to the switch (informing the metropolitan area network address and label of the switch), and after the switch receives the network access command, it accesses the network and sends a network access command reply to the server at the same time;

3). after the server receives the network access command reply issued by the switch, it knows that the switch has accessed the network, and then a state query packet is sent to the port each second to check whether the switch works normally; and at the same, a port query packet is sent to other ports of the switch to check whether other devices are connected under the switch. If the switch works normally, after it receives the state query packet, it will sends a state query reply to the server. When the server does not receive a state query reply in a certain period of time (for example, in 6 seconds), it will be considered that the switch has been removed from the network, and no state query packet will be sent any longer; instead, it continues to send a query packet to the current port[3,4].

An Example of Network Access Interaction Between a Metropolitan Area Server and a Node Switch, a Node Server

All devices on the metropolitan area network are described with a device information table, and a device may be uniquely identified by a device type of 2 bytes and a device identification of 6 bytes; generally, it will be described according to that different device types have different device information tables, for example, node switch information table and node server information table. The items of a device information table are consisted as follows:

1) device identification: 6 bytes, which is written into a hard disk or flash of a metropolitan area server when a device is registered, and imported to the CPU memory after the metropolitan area server is powered on;

2) device state: 2 bytes, wherein 0x0000 represents that the device does not access the network, and 0x0001 represents that the device is to be accessed to the network (the metropolitan area server issues a network access command packet, but no network access command reply is received), 0x0002 represents that the device has accessed the network (set by the metropolitan area server after receiving a network access reply packet);

3) device address: 2 bytes, the metropolitan area network address allocated to the device.

The metropolitan area network address has a length of 16 bits, all devices on the metropolitan area network have a unique access network address (including metropolitan area server, node switch and node server). A table with a size of the sixteenth power of two, i.e., 64K, is maintained by a CPU module of the metropolitan area server, which is called metropolitan area address information table, and each item of the table is consisted as follows:

Similarly, a metropolitan area query label describes the connection from a metropolitan area server to a node switch or a node server, while a metropolitan area reply label describes the connection from a node switch or a node server to a metropolitan area server. In order to simplify the design, it is hypothesized that the two has a one-to-one correspondence, for example, if the metropolitan area query label from the metropolitan area server to a node switch is 0x0008, the metropolitan area reply label from the node switch to the metropolitan area server is also 0x0008; moreover, OUT label equals to IN label. Thus, another table with a size of the sixteenth power of two, i.e., 64K, is maintained by a CPU module of the metropolitan area server, which is called metropolitan area protocol label information table, and each item of the table is consisted as follows:

1) label occupation descriptor: 2 bytes, wherein 0x0000 represents that this label is not used, 0x0001 represents that this label is standby (the metropolitan area server issues a port query packet

by this label, but no network access reply packet is received), and 0x0002 represents that this label is used (set by the metropolitan area server after receiving a network access reply packet);

2) label descriptor: 2 bytes, the metropolitan area network address of a device corresponding the label;

3) label route description information: 4 bytes, for describing the metropolitan area network address and port number of the previous-hop switch of the metropolitan area query label packet, wherein the first 2 bytes represents the metropolitan area network address of the previous-hop switch, and the last 2 bytes represents the port number of the previous-hop switch.

Network Interactive Process Instance

As shown in FIG. 2 for example, it is hypothesized that the metropolitan area server has four 1000M fiber interfaces and one CPU module interface. If the four 1000M fiber interfaces are in turn defined as port 0 to port 3 and the CPU module interface is defined as port 4, the type of the metropolitan area server will be MS-1000, and port 0 and port 1 of MS-1000 are respectively connected with port 2 and port 3 of MX-4-0, and port 0 of MX-4-0 is connected with MSS-400-0, and port 1 of MSS-400-0 is connected with MSS-400-1.

The network access interaction process is as follows

1) After server MS-1000 is powered on, it initializes the hardware and imports a configuration file from the hard disk to the CPU memory (for example, the registration information of a node switch and the registration information of a node server, etc.), server MS-1000 initializes the metropolitan area address information table and the metropolitan area protocol label information table, and all the items are cleared (which represents that all addresses and labels are not used), and server MS-1000 configures its own metropolitan area network address as 0x0000, that is, item 0x0000 of the metropolitan area address information table is configured as follows:

address occupation descriptor: 0x0002 represents that the address is used;

device descriptor: 0x0000 represents metropolitan area server;

device resource description information: the metropolitan area server has four 1000M fiber interfaces, which are in turn defined as port 0 to port 3, and the CPU module interface is defined as port 4, the type of this node server is MS-1000, the metropolitan area network address of a device connected to a network port thereof is not allocated, and downlink flow count of each of its network ports is 0;

The next available address is 0x0001, and the next metropolitan area protocol label is 0x0000;

Server MS-1000 initializes tables 4, 5, 6 and 7

configuring table 4 as "0 0000 0000 0000 0000 0000" to "0 0000 1111 1111 1111 1111", i.e., the transmission of all metropolitan area query label packets is shut down;

configuring table 5 as "1 0000 0000 0000 0000 0000" to "1 0000 1111 1111 1111 1111", i.e., all metropolitan area reply label packets are oriented to the CPU;

configuring tables 6 and 7 as "0 0000 0000 0000 0000 0000", i.e., the transmission of all unicast or multicast data packets is closed;

Port 2 of switch MX-4-0 receives a query packet with a metropolitan area protocol label of 0x0000 according to the topological graph, then:

configuring table 5 "101 0000 0000 0000 0000"=>"0 0100 0000 0000 0000 0000", i.e., a reply packet with a metropolitan area protocol label of 0x0000 is oriented to port 2;

Port 3 of switch MX-4-0 receives a query packet with a metropolitan area protocol label of 0x0001 according to the topological graph, then:

configuring table 5 "101 0000 0000 0000 0001"=>"0 1000 0000 0000 0000 0000", i.e., a reply packet with a metropolitan area protocol label of 0x0001 is oriented to port 3;

Two reply packets (which contains the device type and device identification of the current switch and the port number that receives the query packet) are sent, wherein the header of one packet is 0x0900 0x0000 0x0000 0x0000 0x0000 0x0000 0x0000 0x0000 0x0000 0x0000 0x0000, and at the same time, it marks in the packet that the port number receiving the query packet is port 2;

The header of the other packet is 0x0900 0x0000 0x0000 0x0000 0x0000 0x0000 0x0000 0x0000 0x0000 0x0000 0x0001, and at the same time, it marks in the packet that the port number receiving the query packet is port 3;

After port 0 of server MS-1000 receives a query reply packet with a metropolitan area protocol label of 0x0000,

1) according to the device type in the reply packet, server MS-1000 knows that it is a node switch, and compares the device identification in the reply packet with the device identification items in the device information table on the node switch one by one, until a totally identical item is found, this indicates that the device has been registered, and it finds that the device state item is 0x0000, so it knows that the device does not access the network;

2) it checks item 0x0000 of the metropolitan area protocol label information table according to the metropolitan area protocol label 0x0000 in the reply packet, and knows that the previous-hop switch is server MS-1000 (with an address of 0x0000), and the port number is port 0;

3) according to field number 5 in the reply packet PDU (which indicates the switch port number that receives the query packet), server MS-1000 knows that port 0 is connected with port 2 of an switch.

A network access command is sent (informing that the metropolitan area network address of the switch is 0x0001), the head of the packet is 0x9000 0x0000 0x0001 0x0000 0x0000 0x0000 0x0000 0x0000 0x0000 0x0000 0x0000;

Conclusion

As can be seen from the above description, the node server can know flow information of its port, so can report itself flow information in the metropolitan area network, and then respective node switches and metropolitan area server can know the flow information of its port because the flow information of respective ports may be simply added. Because the floe information of each port can be known, so when the metropolitan area server set metropolitan area network communication link, the metropolitan area server can perform control according to flow information to achieve path control and transmission effect well

References

[1]Ayan Banerjee,,John Drake,Jonathan Lang.“Generalized Multiprotocol Label Switching: An Overview of Signaling Enhancements and Recovery Techniques,”. IEEE Communications Magazine . 2011

[2]Paul Bonenfant and Antonio Rodriguez-Moral.”Generic framing procedure (GFP): The catalyst for efficient data over transport network,”. IEEE Communications Magazine . 2012 , pp.111–123

[3Lili Ran,Minxiang Bian,Hongling Li,Rong Chai,Qianbin Chen. Load Balancing Based Accessing Scheme for Multi-hop WLAN[A]. Proceedings of 2013 22nd Wireless and Optical Communication Conference[C]. 2013, pp.26–33

[4]Paul Bonenfant and Antonio Rodriguez-Moral.”Generic framing procedure (GFP): The catalyst for efficient data over transport network,”. IEEE Communications Magazine . 2012 , pp.111–123

[5]WANG Jian,LIANG Zheng. An Advocacy Coalition Approach to Global Governance on Technology Standard Evolution: The Case of WLAN Standards[A]. Proceedings of 2007 International Conference on Public Administration（ICPA 3rd）(Volume Ⅰ)[C]. 200, pp.611–633

Advanced Materials Research Vols. 989-994 (2014) pp 4342-4345
© (2014) Trans Tech Publications, Switzerland
doi:10.4028/www.scientific.net/AMR.989-994.4342

The application research of Lightweight J2EE security framework

An Ming Hu

Tianhe College of Guangdong Polytechnical Normal University GuangZhou 510540

E-mail:anminghu@hotmail.com

Key words: Spring Security;Information Security;Access Authorization

Abstract. Lightweight J2EE framework to actually use efficiency, has been widely used in all kinds of information system development,However ,Spring is open source framework, its security and access control has been problem of concern,How to construct safe and effective Web applications, is the development process of the important link must be thinking。Based on the Spring frame structure technology on the basis of summing up the access authorization control methods and strategies, highlights the Spring framework in the development process of the advantage technology.

Introduction

In the framework of SSH information system software development process, effective control of access to resources, has always been an important part of the development process. How to build a secure, efficient Web applications, developers must consider the problem.

At present the mainstream development technology, the access control model, is usually divided into two parts to realize, namely, user authentication and user authorization. User authentication, which verify the identity of the user information in the system is legal; user authorization, verify that users have to perform the operation of power.

In the early days, Spring Acegi frameworks usually used in the development of Spring, the Spring Acegi framework while powerful, But it is not based on the AOP thought development, And Spring Acegi applications in a large number of the filter, the filter needs maintenance chain, complex configuration. While the new version of the Spring Security framework, based on AOP technology, have complete access control capacity increases at the same time a series of new function, For example: a simplified configuration, inheritance OpenID; support single sign on; support Aspectj pointcut expression language etc.. The development efficiency makes the Spring Security framework has a higher and broader application of space.

The Realization Of The Spring Security Framework

Spring Security framework mainly contains: authentication management, access control security agent, decision-making, operation of identity management and call management etc..

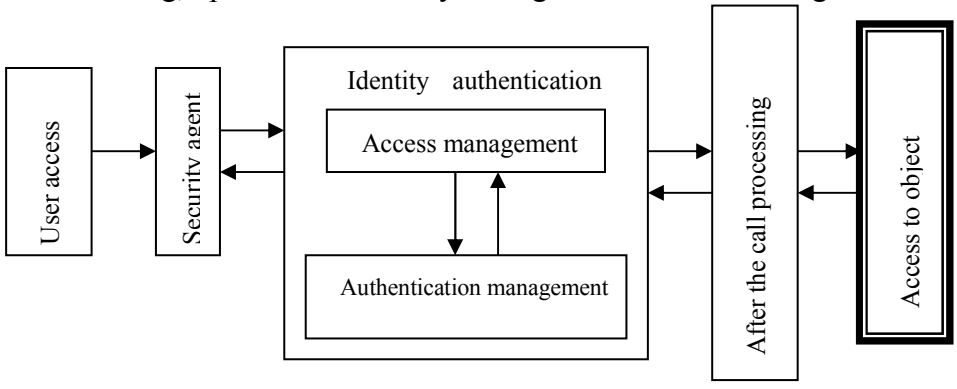

.

Fig.1 Spring Security Framework Access Process

Spring Security framework configuration consists of 2 parts, storing the user account information database and Web.XML file, applicationContext-security.xml file configuration.

1) to realize user authentication database

User authentication database contains 2 database table, user table and user permissions list. One user table is used to record the user name and password, password using MD5 encryption; user permissions table is used to record the user of the role, is used to configure the limit user access; The table structure as shown in Table 1, shown in table 2.

Table 1. The user information table

The field name	Type	Explain
UserName	Varchar(20)	User name
Password	Varchar(15)	password;
Enable	Boolean	user mode

Table 2. The table of user role

The field name	Type	Explain
UserName	Varchar(20)	User name
authority	Varchar(15)	authority

The simulation data are as follows:

```
+-----------+---------------+
| username  | authority     |
+-----------+---------------+
| admin     | ROLE_ADMIN    |
| manager   | ROLE_MANAGER  |
| user      | ROLE_USER     |
+-----------+---------------+
3 rows in set (0.00 sec)

mysql> select * from users;
+-----------+----------------------------------+----------+
| username  | password                         | enabled  |
+-----------+----------------------------------+----------+
| admin     | 21232f297a57a5a743894a0e4a801fc3 |        1 |
| manager   | 21232f297a57a5a743894a0e4a801fc3 |        1 |
| user      | 21232f297a57a5a743894a0e4a801fc3 |        1 |
+-----------+----------------------------------+----------+
```

2）The Web.XML file, applicationContext-security.xml file configuration

The Web.Xml file configuration consists of 2 points, the standard 1Spring frame start listener, 2 on the Spring Security framework to achieve Spring filter SpringSecurityFilter AOP startup configuration. Configuration list as follows:

Spring framework listener code list:

```
<context-param>
        <param-name>contextConfigLocation</param-name>
        <param-value>classpath:applicationContext*.xml</param-value>
    </context-param>
```

SpringSecurityFilter class configuration：

```
<filter>
        <filter-name>springSecurityFilterChain</filter-name>
        <filter-class>
            org.springframework.web.filter.DelegatingFilterProxy
        </filter-class> </filter> <filter-mapping>
        <filter-name>springSecurityFilterChain</filter-name>
        <url-pattern>/*</url-pattern>
<!—According to the needs for access control can be set here to filter -->
    </filter-mapping>
```

DelegatingFilterProxy is a Spring class, the configuration is designed for Spring Security boot provides a guide, to implement filtering using SpringBean through the proxy class form.

applicationContext-security.xml configure.

applicationContext-security.xml, The file is Spring important Securit file, for each resource configuration Web site access, configuration code list is as follows.

<http auto-config="true" access-denied-page="/accessDenied.jsp">
<intercept-url pattern="/AdminManager" access="ROLE_ADMIN" />
<intercept-url pattern="/UserManager" access="ROLE_USER" />
<form-login login-page="/login.jsp" authentication-failure-url="/login.jsp?error=true" default-target-url="/index.jsp" />
<anonymous/.><http-basic/><logout/></http>
The validator configuration:
<jdbc-user-service data-source-ref= " dataSource "
users-by-username-query= " SELECT u. UserName,u.Password,u.enabled FROM users u where u.username=? "
authorities-by-username-query= " SELECT u.username,a.authority
FROM users u JOIN authorities a ON u.username=a.username WHERE U.username=? " /></authentication-provider>

In the applicationContext-security.xml file, the access control under the HTTP node for each allocation site, For example, assume that there are two directory sites AdminManager and UserManager were assigned to the ROLE_ADMIN and ROLE_USER permissions user access, while the system login page and image resources is to allow anonymous access, then filter configuration none without permission check.

The above code list there are two points to note: the specified login failed to access the page access-denied-page properties for the HTTP node, the access to the page must enable anonymous access.The <form-login/> node is used to specify the login page, by default Spring Security framework will be easy to generate a login page, it is recommended to design the login page.

To design the login page should pay attention to submit form form action address is j_spring_security_check, list the code as follows:

```
<form action="${pageContext.request.contextPath}
/j_spring_security_check" method="post">
      User name:<input type="text" name="j_username"></input><br/>
    The code:<input type="password" name="j_password"></input><br/>
        <input type="submit" value=" Sign in"></input>
</form>
```

Spring Security tag library

Spring Security framework JSP tag libraries according to the user's permissions to control the display of some part of the page and hide, such as a ERP system, management interface can distinguish between the interface and the group manager department general manager interface through the label.

Spring Security framework tag library contains 3 tabs, which are authorize, authentication and accesscontrollist.

Authorize tag: used to determine if contains the content should be displayed

Authentication tag:Used to obtain the current certification object content.

Accesscontrollist tag: to protect the content based on access control lists.

Controls whether the content should be displayed. The attribute domainObject the label represents the domain object, and the hasPermission property to check permissions, so as to achieve a deeper level of protection object.

Method of use are as follows.

The first in the JSP page into <% @ taglib prefix= "sec" uri= "http://www.springframework.org/security/tags"%>

Security/tags "% >

In the JSP page in the application for example:

```
 <sec:authorize ifAllGranted="ROLE_ADMIN">
<a href="admin.jsp"> Enter the admin.jsp page
```

```
! </a><br/> <hr/>      <a href="DocumentServlet?method=add"> New documents
 </a><br /></sec:authorize>
```

Conclusion

In this paper, user authentication, access control on the Spring Security framework application configuration method of authorization and commonly used functions were discussed.

The Spring Security framework provides a complete and practical Web authorization and access control model, the URL access control, can control access to the Web application system resources, can meet the development needs of the majority of application system.

References

[1] Zengguang Yu, Zhusong Liu. Extension and application security framework based on SpringSide[J]. Modern computer, 2010(7):210-212.

[2] Peng Lu, Zhaolin Yin. Analysis and extension of authentication and authorization of Acegi security framework based on Spring[J]. Computer engineering and design,2007(3):1313-1316.

[3] Shifei Luo. Proficient in Spring[M]. Beijing: Publishing House of electronics industry,2005.

[4] Yingjie Zhang, Wanjun Liu. Research on Application of Spring AOP technology in the security of J2EE system in the verification[J]. Computer engineering and Science,2008,30(8) : 137 – 138

[5] Lianghui Shi. Design and application of a framework of role based access control[J]. Computer application technology, 2007. 3: 22 - 26

[6] Peng Wang, Yun Peng, etc. An extended role-based access control model[J]. Journal of Wuhan Bioengineering Institute, 2010. 6(2) : 113 -116.

Advanced Materials Research Vols. 989-994 (2014) pp 4346-4349
© (2014) Trans Tech Publications, Switzerland
doi:10.4028/www.scientific.net/AMR.989-994.4346

The Solution of P-Teredo Service Traversing Symmetric NAT

Fuyang Xia

Wuxi Professional College of Science and Technology, Wuxi, China

email: xfy016@126.com

Keywords: Teredo; P-Teredo; IPv6; NAT; success rate

Abstract. P-Teredo is a service that enables IPv4 nodes behind of the symmetric NAT to acquire the IPv6 connection by the arithmetic of port prediction and tunnel technology. The theory of Teredo service and classes of NAT was introduced in this paper. It describes the structure of P-Teredo service and the method of acquiring the client's address which applies the algorithm of port prediction. Some methods which can improve the success rate of port prediction were proposed. Finally, the success rate of network connectivity and the analysis of performance were given.

Preface

IPv6 as the core technology of the next generation internet provides nearly infinite address space which improved the security and data integrity, with automatic address configuration, mobile computing and data multicast, etc., the application of IPv6 provides more efficient service quality. But IPv6 couldn't replace IPV4 in the short time. IPv4 and IPv6 networks coexist in the application. Now, NAT has been used to solve those problems of public IP address lack and network security, so how to make IPV4 nodes behind of NAT communicate with IPV6 nodes has become the focus of research. Teredo service has realized the IPv4 nodes behind of NAT communicating with IPv6 nodes by encapsulating IPv6 data packets in the UDP packets of IPv4.But Teredo service can not traverse Symmetric NAT, because the client host transmits packets to different address will be mapped into different address and port, so its problem of traversing NAT is very difficult. Aiming at the problem, the prediction algorithm based on Teredo (P-Teredo) service has been used to traverse Symmetric NAT, then the IPv4 node behind of Symmetric NAT to acquire the network connection of IPv6 easily.

Teredo service

Teredo is a service which can make IPv4 node behind of NAT to acquire the network connection of IPv6.Teredo service has the Teredo client, Teredo server and Teredo repeater. The Teredo client can access the IPv4 network by sending a Teredo service request to the Teredo server to acquire IPv6 network access. The Teredo server can access the IPv4 network through the global routing address and it provides IPv6 connections for the Teredo client. Teredo repeater locates between Teredo client and IPv6 network; it performs data processing and data forwarding through the Teredo service.

The operation rules of Teredo service: firstly, the Teredo client generates an IPv6 request packet, then encapsulates it in an IPv4 UDP packet, and then sends the packet to Teredo server through the IPv4 network. When the server received the router request packet of IPv6, it will send the response packet the client, the response packet includes a prefix and the public IP address and port number which are mapped by the Teredo client through the NAT. The Teredo client generates its own IPv6 address according to the response packet, and uses the address to communicate with IPv6 node. The IPv6 address format is shown in Figure 1.

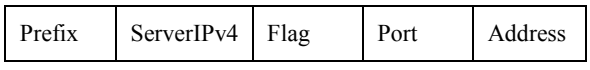

Fig.1 The format of IPv6 address

Prefix: 32bit address of Teredo service; Server IPv4: IPv4 address of Teredo server; Flag：16bit address and NAT device type; Port: UDP port of client; Address：IPv4 address of client.

NAT Device Type

(1) Full cone NAT: All requests from the same internal IP address and port are mapped to the same external IP address and port. And any external host can send a message to the internal host by sending a message to the mapping external address.

(2) Restricted NAT: All requests from the same internal IP address and port are mapped to the same external IP address and port. But unlike the former is that the external host sends back the packet to internal host when it has received the packet from the internal host.

(3) Port Restricted NAT: It is similar to restricted NAT. But an external host sends the packet to the internal host using external address X and port P on condition that the internal host has sent packet to the IP address X and port P.

(4) Symmetric NAT: The address from same internal IP address and port to different destination IP address and port will be mapped different external IP address and port. And the external host will send back UDP packet to internal host when it has received a packet.

Teredo service can traverse the former three type of NAT, but it can't traverse the Symmetric NAT, because the external address will be mapped to different port when the host sends the packet to different IP address and port in the Symmetric NAT. So the client host can't acquire the effective port information from the response information of Teredo server. This paper proposes a prediction algorithm of P-Teredo traversal NAT method based on Teredo for solving the problem of traversing Symmetric NAT.

The P-Teredo Service Based on Port Prediction

A. P-Teredo Architecture

The reason of Teredo service can not traverse the Symmetric NAT is that it can't predict the assigned IP address and port when the Teredo client will send data at the next time. The idea of P-Teredo is that the Teredo client acquires the enough prediction information by sending many times request to Teredo server. The service can predict the possible assigned port according to the information, so it will finish the traversing of Symmetric NAT. The system architecture of P-Teredo service is shown in figure 2.

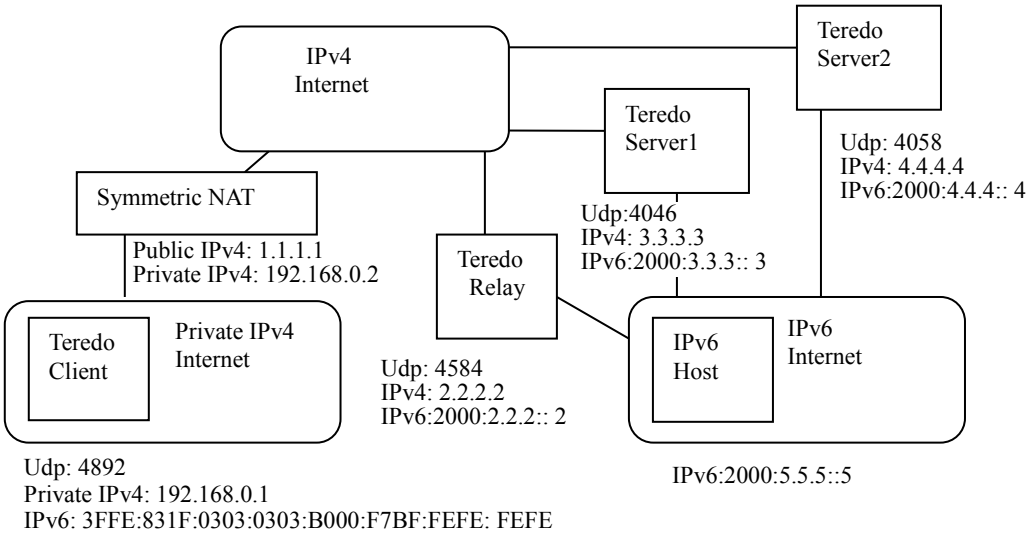

Fig. 2 Module structure of TCP protocol

The mapping port of Teredo client in NAT is changing because the Teredo client is in Symmetric NAT, so you must know the port allocation strategy for NAT if the Teredo client will communicate with the external network host. The Teredo client is located in the Symmetric NAT as shown in figure 2.There are two Teredo server, including Teredo Server1 and Teredo Server2,in the system. The two servers are used for returning the corresponding response message when the Teredo client send routing request message to them. Teredo relay is to realize the function of packet

forwarding. Teredo relay encapsulates the IPv6 data packets from Teredo host into IPv4 UDP data packets, and then sends these packets in IPv4 network. Contrarily, Teredo relay unpacks the IPv6 data packets from the IPv4 data packets of the Teredo client, and then sends them to IPv6 host.

B.Port Prediction algorithm

The linear growth port allocation strategy is used in the port of Symmetric NAT. The mapping ports in NAT exists the relationship of linear growth when the same IP address in Symmetric NAT sends data to different destination address. The port prediction algorithm by using the P-Teredo service traversing the Symmetric NAT is described as follows.

(a)Teredo client sends the request message to Teredo server1 and Teredo server2 respectively. The mapping external addresses of Teredo client are 1.1.1.1：4096 and 1.1.1.1：4098 from the two times response message.

(b)According to the acquired two ports, the port assigned spacing could be calculated as ΔP=4098-4096＝2.

(c)When Teredo client connects the network, the prediction assigned port is P=Pl+ΔP=4098+2 =4100(including P1 is the last mapping port).

(d)Teredo client acquires the mapping IP address in NAT according to the response message from Teredo server1.Teredo prefix of 32 bits is 0x3FFE:831F, Teredo server IPv4 address of 32bits is 0x03030303,flag of 16 bits is 0xB000,external port of 16 bits is 4100 xor 0xFFFF=0xF7BF, external address of 32 bits is 0x01010101 xor 0xFFFFFFFF =0xFEFEFEFE .The IPv6 address of Teredo client is 3FFE:831F:0303:0303:B000:F7BF:FEFE:FEFE.

(e)Teredo client sends the connection request message to IPv6 host according to the IPv6 address. The IP address is 2000:5.5.5::5.Then the IPv6 host sends the responding response message to Teredo client for confirmation connection.

C．Improve Success Rate of Port Prediction

There is problem about critical time period and port distribution in the port allocation strategy based on prediction. The critical time is from the client sends the connection request message to the client sends the connection request packets to the destination host. Application A1 and application A2 are the two applications which run in the Symmetric NAT. First, A1 respectively sends the request message to the two Teredo servers at t0 time. Then the external mapping address and the spacing of port distribution of Teredo client could be acquired according to the response message from server. The possible allocation port could be calculated in the process of data transmission by the mapping address. Then A2 sends a packet to the remote host at t1 time, the prediction port of A1 may be used when the packet goes through the NAT. Then there is error when A1 sends packet to the remote host at t2 time according to the recent prediction port, because the prediction port of A1 has been used by A2.So the correct prediction critical time period is timeΔt which is between t0 and t2.Therefore,in order to improve the accuracy of the prediction, the critical period of Δt should be minimized. The range of port allocation is that the Symmetric NAT allocates the port between a range such as oxa000~0xafff.These ports are the circular distribution. The reason of failure port prediction in P-Teredo service is the follows.

(a) There is another request occurs between the critical time period t0 and t2.

(b) The distribution port arrives at the bottom of port scope in the port restrict scheme.

(c) The use rate of UDP in the local network.

There are several improvement methods for the reason of failure port prediction.(a)Reduce the use rate of UDP. Minimize the number of applications in the Symmetric NAT.(b)Minimize the critical time period. Through optimizing the algorithm allows the t0 to T2 interval of time as short as possible, and to reduce the probability of the occurrence of another request in the critical period of time, so the accuracy of prediction of port should be improved.(c)Multi-port prediction strategy. To set a status table of port use information in NAT. The port use information could be found from the table when creating a new connection. The host should use the next prediction port if the port has been used and create the new IPv6 address according to the new port. Then the host sends the request to Teredo host to establish a connection between each other using the new IPv6 address, until the successful establishment of the network connection. The successful rate of network connection could be improved by multi-port prediction strategy.

Performance Analysis

To test the performance of this method in the practical application, we wrote a test program to test the method.The test of successful rate of network connection. The performance of port prediction algorithm has a great deal to do with the use frequency of UDP in client, so we tested the success rate of client network connection at different rate of UDP load. In the case of the low load (two applications), the medium load (six applications) and the high load (twenty applications), the network connections has been acquired using the prediction algorithm. Thirty times network connections were tested at each kind of load. The test results as shown in table I.

Table I. Network connections at each load

	Connections times	Successful times	Success rate %
Low load	30	30	100
Medium load	30	30	100
High load	30	27	92

The algorithm works well at the low load and the medium load, and the success rate of network connection is 100%.But the success rate of connection declines under the high load, because the increasing probability of new request occurs at the critical time period and the probability of hit port at one time declines. According to the prediction of the port to establish new client IPv6 address and port connection attempt, which increases the system cost, reduce the network connection success rate.

Prediction algorithm of P-Teredo service is a good solution to the problem of Teredo service cannot traverse Symmetric NAT, the prediction algorithm using multi-port, improve the success rate of the network connection, and make the Teredo service to use more widely. However, P-Teredo service exist some problems. It can traverse the NAT of UDP type and can not traverse the NAT of TCP type because it is based on Teredo service. In the algorithm we set the Symmetric NAT port assignment rule is a linear growth strategy. it has some limitations, because if the NAT port assignment rule is random distribution, it can not traverse the NAT. But the port allocation strategy in Symmetric NAT was linear in fact, so the algorithm is practical.

Conclusions

This paper presents the P-Teredo service used to traverse the Symmetric NAT, which realizes by the port prediction algorithm based on Teredo service. We should find the address mapping rules and build the network connection using IPv6 address according to the prediction port. Meanwhile the multi-port prediction strategy has been used to improve the hit rate of port prediction. So it can ensure the validity and high efficiency of the algorithm. P-Teredo service can traverse the symmetric NAT and acquire the high success rate of network connection. So it has high useful value in the future.

References

[1] Huitema. Tunneling IPv6 over UDP through NATs[C], IETF, 2004.12
[2] Shiang-Ming Huang, Quincy Wu, Yi-Bing Lin, Tunneling IPv6 through NAT with Teredo Mechanism [J], IEEE, 2005
[3] Midcom WG,Y.Takeda. Symmetric NAT Traversal Using STUN [C], IETF, 2003.6
[4] J. Rosenberg, J. Weinberger. STUN - Simple Traversal of User Datagram Protocol (UDP) Through Network Address Translators (NATs) [S], RFC 3489, 2003.3
[5] Al-tamimi, B.N.A. Protecting teredo clients from source routing exploits, Distributed Framework and Applications, 2008
[6] Elich, M. An investigation into teredo and 6to4 transition mechanisms: Traffic analysis. Local Computer Networks Workshops , 2013 IEEE

Advanced Materials Research Vols. 989-994 (2014) pp 4350-4354
© (2014) Trans Tech Publications, Switzerland
doi:10.4028/www.scientific.net/AMR.989-994.4350

Design and Implementation of Dynamic Web Services Publishing Software Based on CXF

Chun Shan[1,a], Luxia Wu[1,b], Yang Yang[1& 2,c] and Jingfeng Xue[1,d]

[1]School of software, Beijing Institute of Technology, Beijing100081, China

[2] Information Systems Department, China Mobile Group Ningxia Co., Ltd., Yinchuan 750002, China

[a]sherryshan@bit.edu.cn, [b]wuluxia1990@163.com, [c]bitss.yang@gmail.com, [d]xuejf@bit.edu.cn

Keywords: Enterprise Application Integration, Web Service, CXF

Abstract. Communication between heterogeneous systems is difficult to be achieved without affecting the existing systems in Enterprise Application Integration. A kind of dynamic web services publishing software based on CXF is proposed in this paper. The purpose of this software are twofold. Firstly, it encapsulates specified data called by other systems into web service published dynamically which unifies customization among heterogeneous systems. Secondly, the function of service monitoring provided allows users to get the real-time information of published web services. The proposal software has been deployed in a Chinese large-scale military enterprise. Practice in the enterprise shows that the software can simplify web service development, quickly build a web service which encapsulates large amounts of data, and achieve information sharing within the enterprise environment.

Introduction

In the past few years, various information systems have been applied in a Chinese large-scale military enterprise. These information systems, such as Human Resource Management System, ERP, Financial System and Positional Titles Declaration System, have been developed by different techniques, programming languages, and databases. At the same time, one of the central activities in enterprise software development is the continuous process of integration of various technologically heterogeneous parts into an evolving system. EAI projects have a very high failure rate due not only to technological complexity, but because the systems being integrated are critically tied to the business process itself [1]. So the enterprise introduced an ESB model based on SOA infrastructure to meet the integration needs.

The key step for integration based on SOA in this enterprise is how to achieve effective communication between heterogeneous systems quickly and easily. Supporting the shift toward service-oriented development and SOA is Web services [2]. A dynamic web services publishing software solution based on Apache CXF is proposed in this paper. It minimizes heavy workload and accelerates application integration process. The encapsulation of specific application data will be in the form of Web Service, which can be called by other applications. In addition, the software also implements the management and monitoring to all services within domain.

Related Research

Enterprise Application Integration (EAI) is the process of integrating multiple applications that were independently developed, may use incompatible technology, and remain independently managed [3]. It improves competition by integrating the heterogeneous systems according to business requirement. Service Oriented Architecture (SOA) is the best way to utilize existing IT systems to meet new challenges.

SOA is a solution for designing and setting up the loosing coupling software system, it can publish business functions in the manner of programmable and accessible services, and the other application can use these services by using the published and findable interface [4]. SOA can use Web Services to allow standards-based applications to interact over the Internet. This enables machine-to-machine

communication, speeding the application-interaction process and eliminating the need for human intervention [5]. Enterprise Service Bus (ESB) is one mode of SOA infrastructure. ESB acts as the middleware glue infrastructure that holds SOA parts together and integrates and manages the communication between different Web Services, applications, and data sources [6].

Apache CXF is an open source services framework that makes web service development easy, simplified, and standard based. CXF provides many features such as fronted programming, support for different transports and data bindings, support for different protocols, and other advanced concepts like Features and Invokers [7]. More specifically, it has become the preferred in the domain of building Web Services using Java language.

Dynamic Web Services Publishing Software

Requirements analysis. Current information systems mostly use different databases to store data. If we can bypass the complicated business logic and define the encapsulation of Web Service data to database level directly, it will be possible to unify customization among different systems. This method may be implemented by extracting and encapsulating sharing data from original data. For example, staff basic information of Human Resource Management System which is developed in Delphi language is stored in the Mysql2000 database. In that case, using the original method to do Web Service development on the system is cumbersome. As we know, the use of Web Services as an infrastructure of service sharing has made it possible to provide collaboration and interoperability in distributed system [8]. We can acquire staff basic information and encapsulate it as web service, so that it can be called by other applications without changing Human Resources Management System. The target of this paper is to complete the operations by simple connection configuration to system database.

The original data encapsulation can solve the drawback that heterogeneous systems are difficult to be united. Once web service is configured by users, service engine will publish the service, and then other applications can invoke it with the addresses of web service at this point. For web service that has been published, the system provides query operation to find service by service address, name, description or other information. The system also provides the function of service monitoring, so that users can get the real-time information of published web services. In addition, users can use the system to test web service. Enter the requested values for each parameter, appropriate web service is invoked and the result will be returned for review. Meanwhile, the test cases also can be saved to achieve test cases management. Each test case is bound to the appropriate web service for multiple tests. Considering data security, the system should achieve full rights management, prevent data leaks and misuse occurs. System use case diagram is shown in Fig.1.

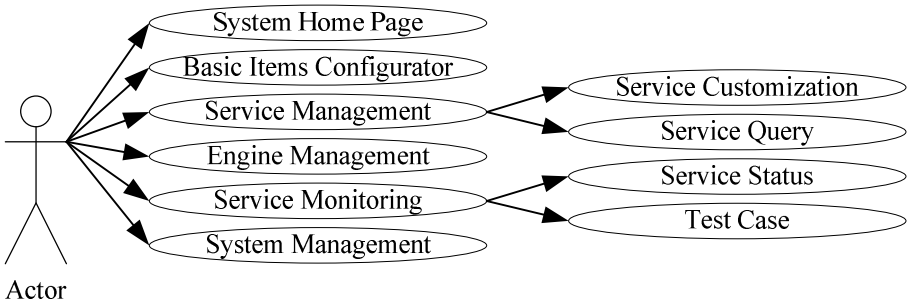

Fig.1 System Use Case Diagram

Software Architecture. The system is divided into three parts: foreground management, core database and background service engine. Foreground management maintains data in core database and queries service information stored in core database. Core database is a bridge between foreground and background, which stores basic information. Background is a service engine based on CXF, including service publication and customization, service monitoring. Background gets service information from core database to complete service creation and publication, thus other applications on the integration platform of enterprise applications can call the service. System architecture design is shown in Fig.2.

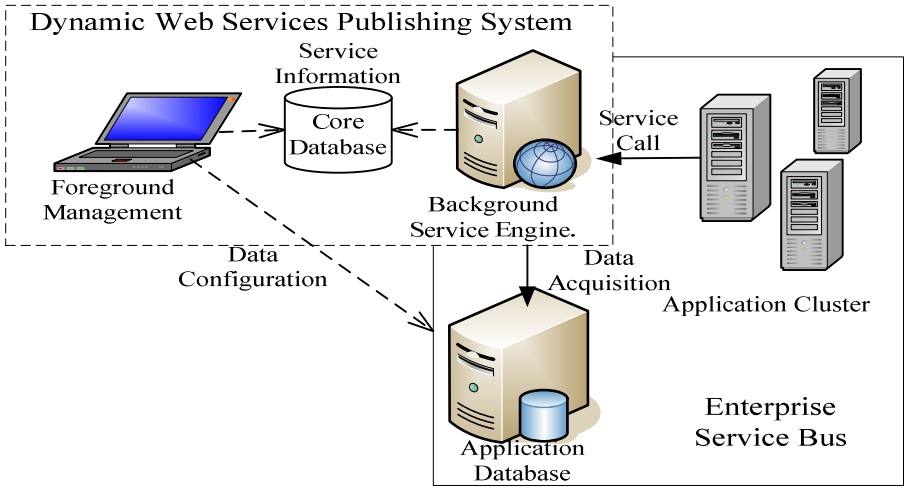

Fig.2 System architecture design

The integration of information systems can be regarded as data synchronization among databases. From this perspective, the software can also been seen as a data synchronization tool of databases [9]. The basic information of web service created and customized by foreground is stored in core database, and background service engine gets service information from database to complete service creation and publication. The server updates service information in real time for users to view from foreground.

According to the architecture and application background, MVC architecture is used. View is user interface which is mainly made up of Html elements; Model represents the business rules and business data, and can be reused by multiple views; Controller is responsible for receiving users' input and then calling appropriate models and views to complete the operation. The software is further extended on the base of MVC architecture that divides the whole system into 5 levels: data link layer, data encapsulation layer, controller layer, function layer, interface layer. It is relatively independent between the various layers. Upper layer achieves specific function by calling lower interface. The system overall structure is shown in Fig.3.

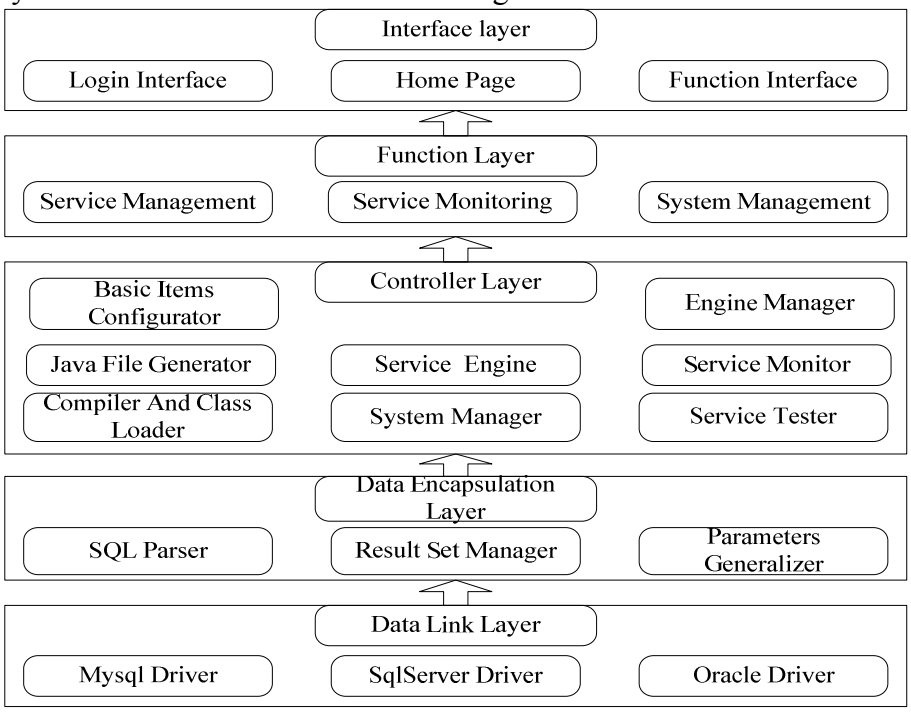

Fig.3 System overall structure

Data link layer uses Java simple factory design pattern, create corresponding database connection driver for database connection according to incoming database type parameter. Data encapsulation

layer uses standard J2EE design pattern - DAO pattern, including SQL parser, result set manager, parameters generalizer etc. SQL parser verifies and tests SQL query; result set manager can carry out advanced operations; parameters generalizer determines the parameter type according to the information of database table. Controller layer is divided into multiple functional components according to different business needs and composed of relatively independent processors, such as basic items configurator, Java file generator, engine manager, service monitor and so on. Function layer mainly achieves complex business logic and completes corresponding business processes through controller. Interface layer achieves complex business presentation and interactive support under different browsers. Each functional interface corresponds to an implementation class, such as service customization, service management, service monitoring, system configuration etc.

Design and Implement of Service Engine. Service engine is the background application based on CXF written in Java language. Service engine is the core of the system, including database connection pool, service management thread and service monitoring thread. Database connection pool supports Oracle, SqlServer, MySql and other types of databases; service management thread takes charge of service customization and publishing. Core technologies related include multiple threads, binary access, dynamic compilation and loading of Java file, etc. Service engine uses a structure that separates data link layer and logical layer to avoid compatibility problems caused by different database types. The layered architecture is shown in Fig.4.

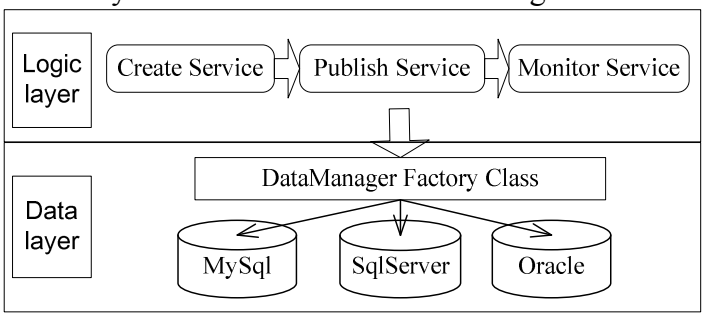

Fig.4 Service engine layered architecture

Data link layer is responsible for the interaction of different types of databases. This layer creates and returns appropriate database driver and connection on the basis of database type contained in service information.

Logic layer can be divided into two parts: Server and Monitor. Server is responsible for service creation and publishing while Monitor takes charge of service monitoring. Server thread notifies Monitor thread to start and monitor service after finishing the service creation.

Service creation is the first step, and also the most crucial step in building web service. After users finishing web service customization and configuration in foreground, information related to corresponding service is stored in the database including service name, address, port number, and parameter, and then service engine will acquire and publish the information to make it a real Web Service. In the implementation process of this system, Web Service is published based on JAX-WS standard.

Service class generated by compiler is stored in a specific directory after service creation. Next, URLClassLoader class loads the service class into main thread and generates corresponding instances. At this point, relevant service class and its instances have already existed in the thread, then use the CXF engine to publish them. After the successful service publishing, Server thread will be responsible for updating service address information in database.

Service monitoring is completed by a specialized thread. Main thread hangs and starts a specialized Monitor thread for monitoring service. Once all services have been created and published, Monitor thread will acquire all published service information and store it in memory first, then visit each service every certain time (60s) to get status information, and write it to corresponding database field to update service in real time at the end.

Software Deployment

Runtime environment. System runtime environment is composed of foreground manager runtime environment and background service engine runtime environment. Foreground database management system needs the support of JDK1.6, SqlServer and Tomcat server, and uses B/S architecture and Justep X5 studio development tool. Background service engine is also developed in Java language with Eclipse development tool. In addition, enterprise internal LAN and network environment of other heterogeneous systems running are still needed for the system to run.

Practice Situation. This system achieves the comprehensive management and maintenance of Web service in a large-scale military enterprise. It can be used by system developer, tester and maintainer as an assistant during the building of enterprise ESB. This system has been well-received in the commissioning phase.

Conclusions

This paper proposes a dynamic web services publishing software solution based on CXF in Enterprise Application Integration. The solution completes Web Services dynamic customization, management, testing, monitoring and other functions through the use of JAX-WS and provides a strong support in building the enterprise ESB information platform.

The innovation of this solution is that users are liberated out from traditional web service development pattern. Users have no need to pay much attention to different technical solutions of different systems. They focus on business level and finish web services customization and publishing just by simple service configuration which reduces much work.

Though this software plays an important role in the Web services management and monitoring, there are still some shortcomings and deficiencies, such as operation efficency. It will be upgraded and improved according to the concrete conditions in the future. So the system has better usability, efficiency and robustness, direction and difficult it is to continue to study.

References

[1] Vitomir Kovanovic, and Dragan Djuric: ISEC, 2012. Proceedings. India Software Engineering Conference, 2012: 22-25.

[2] Eric Newcomer and Greg Lomow, in: Understanding SOA with Web Services, Introduction, Addison-Wesley Professional (2004).

[3] Christopher A. Motur, Gabriel Githehu Kinu and Andrew Mwaura Kahonge,: submitted to International Journal of Applied Information Systems (2013).

[4] Wu Deng, Xinhua Yang, Huimin Zhao, Dan Lei and Hua Li: Electronic Commerce and Security, 2008. International Symposium, 2008: 95-98.

[5] Ortiz, S.: Computer Vol. 40 (2007), p. 15-17.

[6] Suhail Madoukh and Rebhi Baraka: submitted to International Arab Journal of e-Technology (2014).

[7] Naveen Balani and Rajeev Hathi:,Apache CXF Web Service Development, chapter, 1, Packt Publishing Ltd. (2009).

[8] Ruixuan Li, Zhi Zhang, Zhigang Wang, Wei Song and Zhengding Lu: Services Computing, 2005. Proceedings. International Conference on IEEE, 2005.

[9] Xianwang Li, Yuchuan Song, Ping Yan and Xuehai Chen: submitted to Journal of Networks (2014).

Advanced Materials Research Vols. 989-994 (2014) pp 4355-4357
© (2014) Trans Tech Publications, Switzerland
doi:10.4028/www.scientific.net/AMR.989-994.4355

The Design And Implementation Of Micro Player

Hui e Chen

Tianhe College of Guangdong Polytechnical Normal, University GuangZhou 510540

E-mail: yifanchenchen@163.com

Keywords: micro player;Function Realization

Abstract. Windows Media Player developed by Microsoft Player, it is a component of Microsoft Windows, can support through plug-ins enhancements. In this paper, by applying the ActiveX control, design a set play audio files, MIDI files and Windows Media files, movies (MPEG), such as video files as one of the players play a variety of Media files.

Introduction

Visual C++ 2010 can be used to create Windows platform Windows applications and network applications, is one of the most popular Windows platform application development environment, compared with the previous version, the new added several new features introduced in the C++11 standard support. "Reflect the diverse functions of micro player program is a comprehensive application of new features in Windows applications.

Ideas Of The Program Design

The website often give us free to download the player with the storm video, Mplayer player, Flash player, video, QQ, mainstream video formats are supported, most player software size there are dozens of MB- hundreds of MB, taking up a lot of resources, this paper optimized the player occupied resources and support video format based on the points of design, a mini player 160KB, resources, and through the creation of application program, application program interface design, application functions of three parts in-depth analysis of the implementation of the new function of micro player.

The Steps Of Program Design

1) To Create The Application Project

First create a dialog box MFC application based on micro player; the "file | new | project" menu, open the "new project" dialog box, select the project template for the "MFC application", and in the name of the project, add micro player to preserve the path, click "next"; in "MFC the application wizard" "application type" options "dialog based; in" the MFC Application Wizard "" advanced "options, select the" ActiveX control "to support ActiveX controls, and finally click" finish "button.

2) Application Program Interface Design

In the VS2010 integrated development environment, add Windows Media Player control to the application of the project, design of main program dialog box.

The first choice the "view", select the item micro player resources under the Dialog, double-click the dialog resource IDD_MICRO PLAYER_DLALOG, open the dialog box resource editor. From the "toolbox" the shortcut menu, select "options", will pop up "Choose Toolbox" dialogue ActiveX controls. Choose to add ActiveX controls from the "COM" list, click "OK", complete the ActiveX control to the toolbox, you can see the toolbox on a Windows Media Player control, and can be put to use the control as a standard control.

The second step is shown in the dialog box, select a name for the Windows Media Player ActiveX controls, click "OK" button, to complete the "toolbox" add "Windows Media Player" controls. As shown in the dialog box, select a name for the Windows Media Player ActiveX controls, click "OK" button, to complete the "toolbox" add "Windows Media Player" controls.

The third step is to add the Windows Media Player controls the menu resource. Open the "resource view", click the right mouse button on the Menu, select "add resources" in the pop-up menu, select Menu in the pop-up dialog box, click the "new" button, the Insert menu resource. Among them, the Popup attribute in the Menu to False, can change ID to ID_OPEN or ID_CLOSE.

Table 1. Add menu item attribute table

The Menu Item	ID	Property
OPEN	ID_OPEN	Open the media file
CLOSE	IDCANCEL	quit

Table 2. Modify the properties of the value of the properties dialog box

Property Value	Property	Set up
Menu	IDR_MENU1	True
Style	Popup	True
Border	Resizing	True
Minimize Box	True	True
Maxminze Box	True	True

The Function Of The Application Program Realization

Add the appropriate class for the Windows Media Player control, close the dialog resource (avoid mistakenly believe that the dialog box to add class), click the "project", "add", "ActiveX controls in the MFC class", such as the pop-up dialog box, select the CMICRO PLAYERPlayer4 interface class here is generated, and add a header file #include "CMICRO PLAYERPlayer4.h" in MICRO PLAYERDlg.h in the statement, At the same time to declare the control object(public: CMICRO PLAYERPlayer4 m_micro player;)

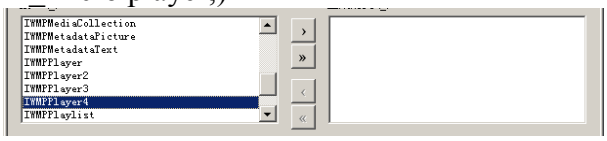

And then in the MICRO PLAYERDlg.cpp file in the location to DoDataExchange () function, ID number manually add the associated control DDX_Control IDC_OCX1 Windows Media Player control (pDX, IDC_OCX1, m_micro player); location: OnInitDialog () function to CMICRO PLAYERDlg:, add the following code.

```
BOOL CMICRO PLAYERDlg::OnInitDialog()
{   CDialogEx::OnInitDialog();
…
    CRect re;// Set the MediaPlayer control's size
    GetClientRect(&re);
    m_MICRO PLAYER.MoveWindow(&re,TRUE);
    SetWindowText(_T("My player")); //set the title
return TRUE;   // Unless you set the focus to the control, otherwise it returns TRUE   }
```

When dragging the dialog,In order to realize the MediaPlayer control with the dialog box the size of synchronous change,In the class wizard "message" tab, choose WM_SIZE, OnSize function overloading the system, add the following code:

```
void CMICRO PLAYERDlg::OnSize(UINT nType, int cx, int cy)
{   CDialogEx::OnSize(nType, cx, cy);
    // TODO: Add to this the extra initialization code
    if(IsWindowVisible())
    {    m_MICRO PLAYER.MoveWindow(0,0,cx,cy,TRUE);  }   }
```

MoveWindow(0,0,cx,cy,TRUE), The function is to realize the change of the specified window location and size.

The function prototype for:BOOL MoveWindow(HWND hWnd, int X, int Y, int nWidth, int nHeight, BOOL bRepaint);

Parameters:

hWnd: The window handle for the specified

x（0）:The new CWnd position on the left side of the specified.

Y（0）:The new CWnd position at the top of the specified.

nWidth:The new CWnd width of the specified.

nHeight: A new highly specified for CWnd.

Brepaint: specifies whether to redraw CWnd. If TRUE, then CWnd as usual in the OnPaint message processing function receives a WM_PAINT message..

Use the wizard to "open" menu to add a message response function, ID_OPEN, for the CMICRO PLAYERDlg menu item under the add command message response function, navigate to the CMICRO PLAYERDlg.

```
void CMICRO PLAYERDlg::OnFileOpen()
{   // TODO: Add to this the extra initialization code
    CString fileName;
CFileDialog fileDialog( TRUE,NULL,NULL,OFN_HIDEREADONLY | OFN_OVERWRITEPROMPT,_T("Audio files, video files, movie file, all files(*.*)|*.*||"),this);
    if (fileDialog.DoModal() == IDOK)
    {   fileName=fileDialog.GetPathName();
        m_MICRO PLAYER.put_URL(fileName);     // Open play   }   }
```

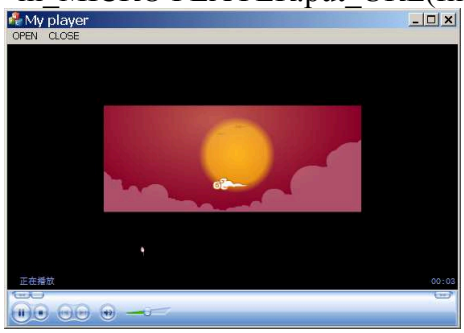

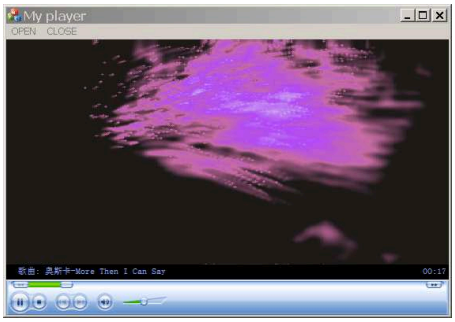

Research Prospects

This paper designed the mini player to play flash files, midi files,mp3 files, avi files, support of the mainstream media files, meet the optimization function, use the player needs. In addition, can also study based expansion, more functions, improve the utility efficiency optimization player, playback.

References

[1]Zhi Bo Chen. Visual C++ program design. Beijing: China Railway Publishing House(2008) , p. 12

[2]Xin Sun. VC++ in-depth Detailed. Beijing: Publishing House of electronics industry (2012)

[3]Horton, I.，Translated by Zheng quan Su. Visual C++2012 Introduction to the classic. Beijing: Tsinghua University press(2012)

[4]Per Cold, Min Fang. Windows program design. Beijing: Tsinghua University press, (2010)

[5]Hart, Feng Dai. WINDOWS system programming. Beijing: mechanical industry press(2010)

Advanced Materials Research Vols. 989-994 (2014) pp 4358-4361
© (2014) Trans Tech Publications, Switzerland
doi:10.4028/www.scientific.net/AMR.989-994.4358

The Application of Digital Information Technology in the Volleyball Game

Bai Zhen, Zhang Qiang

Student Physique Health Research Institution of Henan University Kaifeng 47500

Keywords: Digital Information Technology; Application; Course Selection; Training

Abstract. In this paper, the author starts from the application of digital information technology in making a further promotion of the scientific development in the China's volleyball game, exploring the application of digital information technology in our scientific volleyball course selection, training and matches. At the final conclusion, the author thinks that digital information technology will achieve a better, faster, more precise and stronger development in our volleyball game.

Foreword

At present, some foreign companies have already brought digital information technology into the volleyball game. For example, the DOTEPROJEETS (Italy) has developed the volleyball program; in China, there are few studies about the application of digital information technology in the volleyball game. The information technology will determine the development of the volleyball game and the increasing performance of the athletes to a great extent. The application of digital information technology is playing a greater auxiliary role in the volleyball training and matches. For our volleyball game, the author is going to discuss the application of digital information technology in terms of the scientific volleyball course selection, training and matches.

Digital information technology is a comprehensive application science that is integrated with mathematics, optics, electronics, photography, computer science technology and biotechnology, including the acknowledgment of digital information, message delivery and information processing, etc. The acknowledgment of digital information is to collect the index on the related physical training and competitions by means of the digital information technology. For example, it is able to collect the data about the athletes' physical quality, mechanisms and fighting ability as well as the volleyball game skills and tactics, etc; message delivery is an input and output process in view of the obtained data and analysis results by means of the wireless network access; information processing is to make the mathematical statistics on the image, digital information or the transferred digital information.

Scientific Course Selection

In the 21sth century, the studies about the scientific volleyball course selection is the comprehensive multi-disciplinary studies as well as the actual results of the comprehensive application on the course selection, combining with the coaches' training experiences, establishing the scientific and simple course selection ways; while the advanced technology is integrated with the research achievements of all the subjects, it is possible to set up the effective course selection model for the athletes. Meanwhile, it is able to simplify the complicated course selection ways, establish the fast feedback system for the athletes in each sports program so as to improve the talent rate. The digital information technology is applied into the course selection for the athletes, integrating all kinds of the multi-disciplinary research results into one, adopting the comprehensive research plans with the multi-disciplinary and indicators, and establishing the efficient and scientific course selection model. The digital information technology on the course selection for the volleyball athletes is to collect the comprehensive index about their physical shapes, physiology mechanism, biomechanics, psychology and genetics and others for the foreign and domestic excellent athletes. On the basis of the mathematical statistics, it is able to build up the talent cultivation database for the domestic and foreign excellent athletes; with the growth standards of the children and the juveniles, it is able to set up the scientific course selection model database. And

then the comprehensive indexes for the corresponding children and juveniles will be stored in directly going on with the database processing for the scientific volleyball course selection. The final research conclusion will provide the evidence for the volleyball course selection in improving the talents rate.

Scientific Training

3.1 Physical Quality Training

The application of the digital information technology on the physical quality training draws support from the advanced scientific technology like bio-sensing technique and remote sensing technology to test the changing index of the physical mechanism for the athletes. The test results will be stored and processed. There comes the final feedback information that is used to monitor the athletes' physical quality training.

In the volleyball game, the application and construction of digital information technology in the physical quality training starts from the remote test of the physiology index by means of bio-sensing technique and remote sensing technology in the game. In this way, it is able to collect the changing index of the athletes' body mechanism of which the corresponding data will be stored in making the mathematical statistics, revealing the energy metabolism characteristics and rules and setting up the databases for the changing index of the athletes' body mechanism; and then it is able to monitor the athletes through bio-sensing technique and remote sensing technology so as to acquire the changing physiology data about the athletes in the training. The obtained index and rules about the athletes' body mechanism will be processed of which the final feedback will provide the scientific evidence on the reasonable control and training for the coaches.

3.2 Skills & Tactics Training

3.2.1 Single Skill Action Training

On the basis of the three-dimensional camera technology and sports biomechanics, the application of digital information technology on the single skill action training is to analyze the single skill action, presenting the improvements on the reasonable skill action. The construction of digital information technology on the single skill action starts from the three-dimensional camera technology for the athlete's skill action. And then it is possible to enter the obtained image in the computer so as to make the sports biomechanics analysis. There comes the final analysis results. The coach will be able to give the intuitive guide for the athletes based on the analysis result of the image and skill action so that the athlete will find out the primary issue in the process, have the efficient understanding on the skill action concept and present the right movement. For some athlete, the special trainings are necessary to correct the wrong movements as soon as possible. In this way, the athlete will present the right dynamic modes about the movements in improving the athlete's single technique standards. According to the analysis results of the skill action as well as the characteristics and rules of the single skill action, it is able to assign the scientific and reasonable training and make the special training (for example, it is allowable to develop the muscle training that is affective to the single skill action, etc). In this way, it will improve the athletes' special quality and techniques in presenting the reasonable and scientific skill action. The efficiency of skill action is also increased.

3.2.2 Team Skills & Tactics Training

The application of digital information technology in the team skill and tactics training starts from the collection of the volleyball skills and tactics and write the statistics system about the volleyball skills and tactics; through the three-dimensional camera technology and voice control, it is able to obtain the team skills and tactics training materials, make the statistical analysis of the field tactics based on the action skill statistics system, seek for the more reasonable tactics so as to improve the team skills and tactics level. The coaches will not only give the more precise field guide with the analysis results, but also make the immediate training discussions with the team members in the ending of the game so that the team members will illustrate their performances outside the field, discover, consider and solve the problems in the role of the coach so that they will have the good

understanding about their performances and the opponents' performances. In this way, it will improve the team fighting ability and the athletes' skills and tactics.

Scientific Matches

4.1 Preparation Stage

Before the match, it is known that the preparation meeting is necessary to analyze the skills and tactics of the competitors and the team. The traditional way is to watch the previous videos about the competitors for the coach and the team members. The coach will analyze the competitors' performance and the tactics. However, this kind of analysis is usually rough of which it will be hard to get the particular and exact conclusion. In this case, it will not be able to foresee all kinds of the complicated situations in the official match. The team members will be hard to completely understand the characteristics of the competitors. Especially, there are deadlock to open up a new prospect.

The application of the digital information technology will make a complimentary to the deficiency to the great extent. In the preparation meeting, the coach and the team members will be able to watch the video about the actual situations of the entire match. As well, it is able to analyze the digital information about the obtained image and message from the skill and tactics system. It is possible to present the skills & statics and team member performance at each turn and stage in the form of the digits. The team member and coach will get the particular and exact result. Hereby the coach and the team members will make the efficient thought preparation in adopting the team advantages and avoid the shortcomings. According to the condition of the competitors, it is able to design the tactics, enhancing the athletes' confidence and mental quality and making the enough preparation to win the game.

4.2 Underway

Sometimes, it is not satisfying to get the guide upon the observation of the coaches outside the field. Even the issue is discovered, it is hard to find out the solutions. In terms of the application of the digital information technology in the game, it is much clear to compare the skills & tactics and powers at both sides, put forward the reasonable tactics and provide the theoretical evidence for the field guide on the skills and tactics.

In the game, the application of digital information technology starts from the obtained match images through the three-dimensional camera technology. The stored image will be transferred into the digital information. The information will be sent to the computer by means of the wireless digital transmission system. With the application volleyball program software, all the field data will be got at the both side. The coach will achieve the final information to adjust the field arrangement in view of the analysis results. In this way, it is able to defend the opponents' offensive strengths and attack the vulnerability in arranging the reasonable skills and tactics.

4.3 Summary Of The Post-Matches

After the match, the summary is unavoidable in each match. In this way, it will discover the existing problem in a better way, propose the greater count measures, and make the preparation for the success of the following matches. With the digital information technology, the team members' performance and skills and tactics will be recorded in making the mathematical statistics and providing the reliable data analysis. The coach and the members will be able to propose the reasonable suggestions about the post-match in a better way. The team members will have a full understanding about their performance and find out the existing issues in offering the evidence for the training and the match. Therefore, it is better to enhance the athletes' volleyball skills and tactics.

Conclusions

The digital information technology will promote the volleyball game in an accurate, efficient and scientific way. The application of the high technology on the promotion of the skills and tactics will become the trend to develop the modern volleyball game. With the continuous improvement of our

volleyball game, it is required to set up the corresponding and suitable volleyball software in view of our skills and tactics. The application of the high technology will promote our volleyball game in a better, faster and stronger way.

References

[1] Tian Maijiu, Wu Fu Quan. Scientific Sports Training Exploration [M] Beijing: People's Sports Publishing House, 1989, 5.

[2] Qin Ling, Hu Shengyu, Chen Qiming. Basic Research and Development of Sports Biomedicine [M]. Beijing: People's Sport Publishing House, 2001, 2009.

[3] Xue Weichen, Liu En. The Application of Digital Graphics Technology in the Civil Engineering Structure Test [J]. Experimental Technology and Management, 2004 9 a 44.

[4] Qian Jin. The Application of Modern Information Technology in the Competitive Sports (J). Fujian Sports Science and Technology, 2002, 21 (4) : 3 a 5.

[5] Chirac,Translated by Ma Tie. The Application and Development of Modern Information Technology in Sports [J]. Sports Science, 1997 (2) : 92 - a - 94.

Advanced Materials Research Vols. 989-994 (2014) pp 4362-4366
© (2014) Trans Tech Publications, Switzerland
doi:10.4028/www.scientific.net/AMR.989-994.4362

The Application of Computer Digital Simulation Technology in the Technical Structure Study of the Martial Arts

Gao Meihong

(Sports Department of Zhengzhou Normal University Zhengzhou 450044)

Keywords: Computer Digital Simulation; Martial Arts; Action Technology Structure

Abstract. In this paper, the author adopts the literature review research methods, starting from the perspective of the sports science research methodology, and discussing the research methods and procedures of the computer digital simulation technology in the technical structure study of the martial arts. In the martial arts study, the author expounds the application methods, procedure, steps and functions of the computer digital simulation technology in terms of the establishment of the structural digital models of the human body, the procedures, data input, data pre-treatment and calculation of the computer digital simulation technology, the structure models modification of the martial arts, the new action skill model design as well as the application value of the computer digital simulation technology in the skill training.

Introduction

With the science and technology development and the demands of the modern sports development, the fast development of computer technology has laid the scientific foundation for the comparison, overlay, dynamics test, calculation and automatic analysis and others about the structural image of the action as well as the quantitative analysis and researches of the action technology structures. In particular, the computer digital simulation technology is accessible for the martial arts experts and the coach to foresee the function and results of the action skills in the design stage. In this way, it has created a scientific and practical road for the researches of the martial arts technology structure characteristics as well as the best action technology structure. In light of the improvements of the martial arts technology structure or its re-construction, the application of the computer digital simulation technology in the martial arts action technology structure researches. Therefore, its research cycles will be greatly shortened in enhancing the feasibility or the actual application value of the martial arts technology structure design scheme, as well as the control level and training efficiency of the martial arts skill training.

The Establishment of the Digital Simulation Model of the Martial Arts Technology Structure

The computer digital simulation technology is the powerful tool to analyze, investigate and design the complex system for the human body motion in the computer. This technology has affected numerous scientific researches of the sports programs, such as. This technology has fully revealed the links between its external forms and the inherent nature, the principles, the establishment of the action technology structure and its development rules. In the martial arts technical structure studies, the human body is usually simplified as the multi-particle model or the digital model of the multiple rigid systems in light of the characteristics of the human body movements, the purpose, the rules and characteristics of the martial arts technology. The motion system like bones, muscles, tendons and other organizations will be processed as the forces in many links so as to have the multiple factors to affect the action skill structure in the model. In this way, it is able to establish the kinematics equation, dynamics equation and biology equation for the martial arts technology structure. For the independent generalized coordinates, the ordinary differential equations is often adopted in the skill action studies; for the dependent generalized coordinates, the differential algebraic equation is often adopted. These equations are high-order and highly coupled nonlinear. At very rare cases, the results are artificially solved. Typically, the final answer is got through the computer.

The Methods & Procedure of the Computer Digital Simulation Technology

3.1 The Methods of the Computer Digital Simulation Technology

The computer digital simulation procedures and methods in the models of the martial arts action structure include the original parameters input and calculation, the partial skill actions, the description of the entire motion dynamic (static) structure characteristics, the principle of the formation of the martial arts technology structure, etc. This kind of procedure is called as computer digital simulation procedures or numerical simulation technology. In the practice, there are forward or reverse calculation issues on the application of the computer digital simulation technology. For example, when the motion state of the human body (such as the motion space and time characteristics of the partial action) is known in each part, it needs to solve the mechanical conditions (such as myotility resistance, link resistance, the internal force transfer and the transfer of the human body angular momentum, external force, etc.) during the formation process of the skill action structure.

During the calculation process of the computer digital simulation technology, the additional constraints on the mechanics shall be increased so as to ensure the best combinations about the input value, and complete the best design about the martial arts action technology structure. With the accurate parameters in the digital simulation models, the final results will be reflected as the real structure characteristics of the motion state. The received results in the martial arts action skill researches will be featured as the strong predictability and the extremely practical guidance. For example, the American sports biomechanics experts Dr Lille had made the technical diagnosis for the throwing athletes Wilkinson. Through the computer numerical simulation technology, he had simulated and calculated the action space, velocity, force and momentum transfer parameters in the process. These high-orders, highly coupled nonlinear equations had offered the optimized action technology plans for Wilkinson during the process of throwing. With the scientific theory, these researches have provided the scientific guide for the optimization of the athletes' movements. It is significant to improve the sports science.

3.2 The Computer Digital Simulation Application Process

The computer digital simulation process is involved into many aspects. For instance, according to the investigated subjects and tasks of the martial arts action technology structure, it has created the digital models, the sports biomechanics equation, software application or writing, debugging, data checking and correction, feedback adjustment or control and others in the multiple rigid body system and in a continuous and dynamic way. The working flows of the best action technology structure of the finally established martial arts are stated as follows:

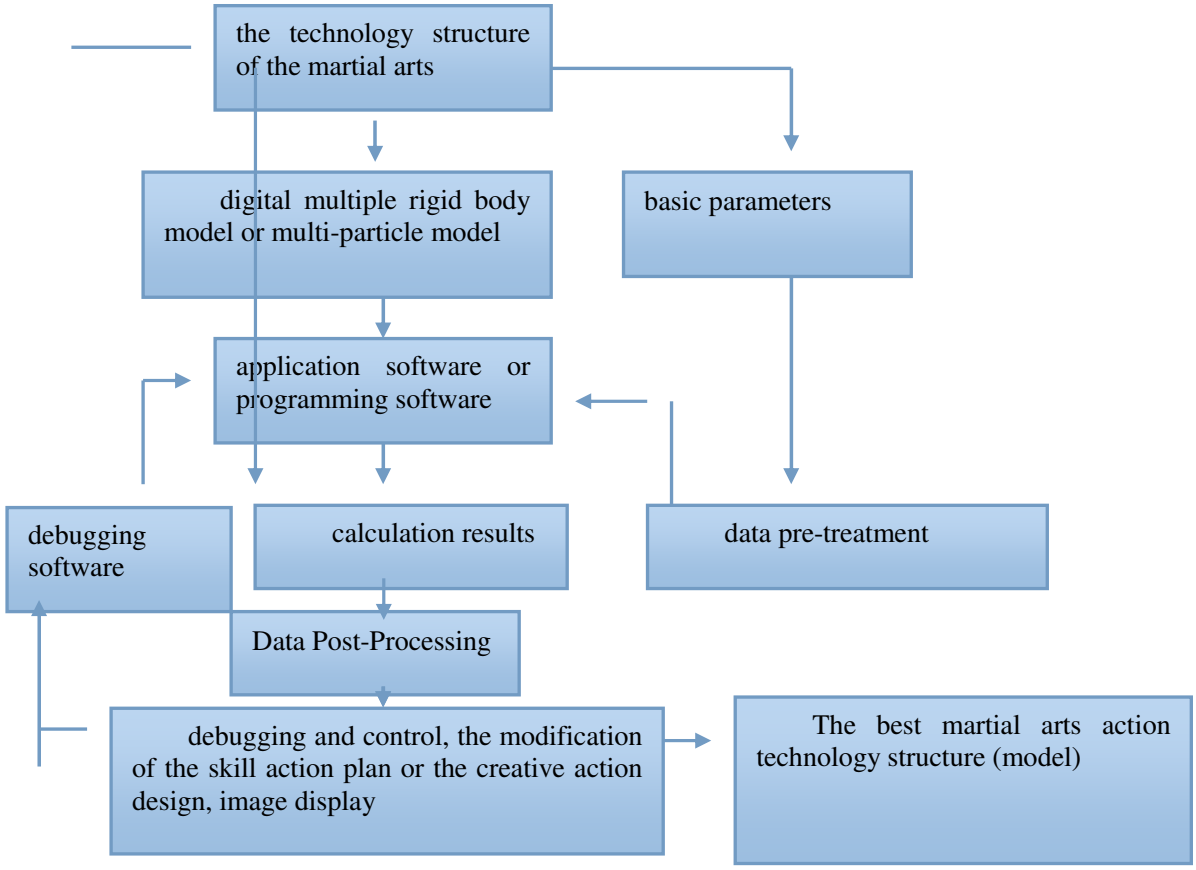

Figure 1 The working flow chart of the computer digital simulation technology

The Simulation Procedure and Steps of Computer Digital Technology

With the rapid development of the modern electronic computer technology, much computer application software is developed in relation to the rigid system mechanics model in the current market. This software is used to solve the forward and reverse issues about the multiple rigid system of the human body in terms of kinematics and dynamics. Since all the movements are constrained by the basic mechanics and biology principles in the martial arts, the digital simulation technology is good at solving the quantitative analysis of the martial arts action technology structure. The steps of the computer digital simulation technology include data input, data pre-treatment, simulation calculation, post-processing, the skill action plan modification, the creative movement design as well as the post-processing and the image display.

4.1 Data Input

Data input are comprised of the kinematics parameters of the martial arts technology structure from the three-dimensional photographic films or the plane videos, the kinetic parameters and inertia, moment inertia and other biomechanical parameters from the electronic loading system. The data are statistically entered. Its filtering, modification and smoothing procedure can be re-confirmed and modified on account of the wrong or suspicious data.

4.2 Pre-Treatment Data

The data pre-treatment refers to the conversion of the data coordinates, error processing, time synchronization processing, etc. According to the films or videos, the action space is generally featured as the inertia and inertial reference coordinates (such as background reference mark, human body structure axis, etc). The coordinates of the computer simulation calculation is usually based on the principle inertial axis of the human body rigid model. Therefore, it needs to transform the coordinate of the original data in the earlier stage, make the statistics, eliminate the singularities in the error processing, and smooth the complete data set. Time synchronization processing refers to the coincidence of the plane image space data and time characteristics, or the synchronization

correction of the mutually perpendicular plane image data in the three-dimensional photographs. The data pre-treatment works produce the direct influence for the accuracy of the system calculation results.

4.3 Computer Simulation Calculation

Upon the correct data pre-treatment stage, it is able to get the whole space motion process of the martial arts actions on account of the dynamics calculation equation, verifying the accuracy of the simulation program by comparison of the data with the actual image. By comparison of the simulation calculation images with the real motion images, the basically matching track indicates that the computer numerical simulation calculation is consistent with the actual situations. The results will offer the great guidance function for the improvement and re-engineering of the martial arts action technology structure as well as the sports training and practices.

4.4 Martial Arts Action Technology Structure Modification & New Action Technology Structure Design

The computer numerical simulation technology is an important solution to modify the partial actions and design the new optimization action skills. Since the changes of the images can be described by the mathematics, the automatic computer identification system is accessible for the entire motion image to change with the modification of the partial actions. If the observed results are satisfying in the computer display, it is worth to try the modification or new action design about the martial arts skill actions. It is much helpful for the coach and the athletes in the martial arts training process, especially for the basic action confirmation of martial arts and the design of the high, difficult and new movements. While the coach has some new ideas, it is able to prove the feasibility and efficiency of the simulation program, and then make the actual attempts so as to decrease and prevent the sports trauma, enhance the feasibility and safety of the martial arts action training.

4.5 Data Post-Processing& Image Display

According to the research contents and task requirements, the obtained computer digital simulation data shall be displayed in the different ways. The computer digital simulation procedure is featured as the data conversion functions of which the results will be shown in various kinds of the images. The procedure is called as data post-processing. The final technical motion images shall be much intuitive and reasonable. During the process of the optimal technical solutions, these connective images from the computer digital simulation calculation will have the important and direct effect on the modification and innovation of the martial arts action technology structure solutions.

The Application Value of Computer Numerical Simulation in the Skill Training

The application and function of the computer digital simulation and the animation technology researches on the skill actions are featured as: (1) The computer digital simulation takes use of the three-dimensional ways for the martial arts space structure, explaining its kinematics, dynamics and biological characteristics in the animation form. The athletes are easier and quicker to master the essentials of the skills so as to greatly enhance the overall training level and action skills

（2）Action choreography, simulation and reasonable action design system can design the new action technology scheme and standardize the action skills. Through the computer numerical simulation technology, it is able to edit, modify and design new action, choosing from the various scheduling results, and giving the optimization technology solutions, establishing the martial arts action technology structure modes and conducting the skill teaching and training.

（3）Through the comparison of the simulation results and the skill action training, it is able to make the quantitative and comparative analysis on the martial arts action technology structure, make the technique diagnosis, and display the analysis results in the form of the images of which the results are comprised of the human body space state changes, focus trajectory changes, displacement, velocity, acceleration, force and moment function, etc. In this condition, it is able to make a deep comparison analysis about the action mode and the athletes' technical action. The

athlete's training action and standard analog action will be shown in the same screen so as to make the technical diagnosis from the same view point to the synchronous contrast way. According to the martial arts action technology principle, it is able to design the directive scheme for the athletes.

Conclusions

The computer digital simulation technology is still a great topic in the martial arts action technology researches. The counterparts at home and abroad have achieved some successes in the computer digital simulation technology and calculation of the human body motion analog. Due to its complexity, the artificial tedious parameters are hard to fully meet the requirements in the sports practice. With the high-speed development of the modern science and technology, the computer digital simulation technology will play a greater role upon the combination of the constant martial arts action technology structure researches.

References

[1] Zheng Xiuyuan. Modern Sports Biomechanics [M]. Beijing: National Defence Industry Press, 2002.

[2] Feng Genquan. Human Body Engineering [M]. Lanzhou: Gansu People's Publishing House, 1980.

[3] Li Liangbiao. Sports Biomechanics [M]. Beijing: Beijing Sports University Press, 1991.

[4] Tian Maijiu. Sports Training [M]. Beijing: People's Sports Publishing House, 2000.

[5] Wei Wenyi. F. Sports Biomechanics [M]. Beijing: Tsinghua University Press, 1989.

Advanced Materials Research Vols. 989-994 (2014) pp 4367-4370
© (2014) Trans Tech Publications, Switzerland
doi:10.4028/www.scientific.net/AMR.989-994.4367

The Application of Computer Numerical Simulation in the Sports Science Study

Shangguan Yiqin

(Sports Department of Henan Agricultural University Zhengzhou 450002)

Keywords: Computer Numerical Simulation; Action Skill; Rigid Body Models

Abstract. In this paper, the author uses the literature review methods to talk about the application of the computer numerical simulation technology, combining the research methods and features of the sports science. In the sports science study, the author expounds the application methods, procedure, steps and functions of computer numerical simulation in terms of the establishment of the digital simulation model of the human body motion, the procedures, data input, data pre-treatment and calculation of computer numerical simulation, the technical plan modification of the human body movement, the new movement design as well as the application value of computer numerical simulation in the skill training.

In the sports teaching and training, the athletes' skill action are usually photographed and analyzed through the camera. However, it only makes the simple review on the athlete's single skill action. It is undesirable on the quality and comparative analysis in terms of the kinematics, dynamics, biology of the action skills. With the high development of the modern computer technology, it has laid the scientific foundation for the comparison, overlay, dynamics test, calculation about the images of the skill action. In particular, the computer numerical simulation technology is accessible for the coach to foresee the results of the action skills in the design stage so that the coach will be able to give the best action skill design. In view of the action skill improvement or re-construction, the study cycles are greatly shortened in enhancing the feasibility of the action skill design plan and its actual value.

The Establishment of the Digital Simulation Model of the Human Body Movements

System simulation is the powerful tool to analyze all kinds of the complex system in the computer. This technology has affected numerous scientific researches, engineering areas and non-engineering areas. For the action technology research, the human body is usually depicted as the multiple rigid system models in light of the characteristics of the human body movements, the purpose, the rules and characteristics of the action skills. The motion system like bones, muscles, tendons and other organizations will be processed as the mutual force and kinematics of the rigid body system so as to establish the kinematics equation, dynamics equation for the human body movements. For the independent generalized coordinates, the ordinary differential equations is often adopted in the skill action study; for the dependent generalized coordinates, the differential algebraic equation is often adopted. These equations are high-order and highly coupled nonlinear. At very rare cases, the results are simplified. Typically, the value is got through the computer.

The Methods and Procedure of Computer Numerical Simulation

2. 1 The Methods of Computer Numerical Simulation

Through the computer, the human body motion methods include the original parameters input and calculation, the technical action, the principle formation, etc. This kind of procedure is called as numerical simulation. There are forward or reverse calculation issues. For example, when motion state of the human body (such as the motion space and time characteristics) is known in each link, it needs to solve the mechanical conditions(such as myotility resistance, link resistance, the internal force transfer and momentum transfer of the human body, external force, etc.) during the formation process of the skill actions. In the computer numerical simulation calculation process, the additional constraints on the mechanics shall be increased so as to ensure the best combination about the input

value, and complete the best design about the action skills. With the accurate parameters in the numerical simulation models, the final results will be reflected as the real motion state. The received results in the action skill research will be featured as the strong predictability and the extremely practical guidance. For example, the American sports biomechanics experts Dr Lille had made the technical diagnosis for the throwing discus athletes Wilkinson. Through the computer numerical simulation technology, he had simulated and calculated the action space, velocity, force and momentum transfer parameters in the process. These high-orders, highly coupled nonlinear equations had offered the optimized action technology plans for Wilkinson during the process of throwing the discus. With the scientific theory, these researches have provided the scientific guide for the optimization of the athletes' movements. It has played a significant role for the improvements of the sports science.

2. 2 The Computer Numerical Simulation Process

The computer numerical simulation process is involved into many aspects. For instance, according to the investigated action skill subjects, purpose and tasks, it has created the digital model, the sports biomechanics equation, software application or writing, debugging, data checking, feedback adjustment or control and others in the multiple rigid body system and in a continuous way.

The Computer Numerical Simulation Steps

With the rapid development of the modern electronic computer technology, many computer application software are developed in relation to the rigid system mechanics model in the current market. This software is used to solve the forward and reverse issues about the multiple rigid system of the human body in terms of kinematics and dynamics. Since all the movements are abide by the basic mechanics and biology principles, the numerical simulation is good at solving the action skill issues of the human body. Its simulation steps include data input, pre-treatment, simulation calculation, post-processing, the skill action plan modification, the creative movement design as well as the post-processing and the image display.

3. 1 Data Input

Data input are comprised of the kinematics parameters from the three-dimensional photographic films or the plane videos, the kinetic parameters and inertia, moment inertia and other biomechanical parameters from the electronic loading system. The data are statistically entered. Its filtering, modification and smoothing procedure can be re-confirmed and modified on account of the wrong or suspicious data.

3. 2 Pre-Treatment Data

The data pre-treatment refers to the conversion of the data coordinates, error processing, time synchronization processing, etc. According to the films or videos, the action space is generally featured as the inertia and inertial reference coordinates (such as background reference mark, human body structure axis, etc). The coordinates of the computer simulation calculation is usually based on the principle inertial axis of the human body rigid model. Therefore, it needs to transform the coordinate of the original data in the earlier stage, make the statistics, eliminate the singularities in the error processing, and smooth the complete data set. Time synchronization processing refers to the coincidence of the plane image space data and time characteristics, or the synchronization correction of the mutually perpendicular plane image data in the three-dimensional photographs. The data pre-treatment works produces the direct influence for the accuracy of the system calculation results.

3. 3 Computer Simulation Calculation

Upon the correct data pre-treatment stage, it is able to get the whole space motion process of the human body on account of the dynamics calculation equation, verifying the accuracy of the simulation program by comparison of the data with the actual image. By comparison of the simulation calculation images with the real motion images, the basically matching track indicates that the computer numerical simulation calculation is consistent with the actual situations. The results will offer the great guidance function for the improvement and re-engineering of the action technology as well as the sports training and practices.

3. 4 Human Body Motion Changes & New Action Design

Computer numerical simulation technology is an important solution to modify the partial actions and design the new optimization action skills. Since the changes of the images can be described by the mathematics, the automatic computer identification system is accessible for the entire motion image to change with the modification of the partial actions. If the observed results are available in the computer display, it is worth to try the modification or new action design. It is much helpful for the coach and the athletes in the training process, especially for the basic action confirmation of human body and the design of the high, difficult and new movements. While the coach has some new ideas, it is able to prove the feasibility and efficiency of the simulation program, and then make the actual attempts so as to decrease and prevent the sports trauma, enhance the feasibility and safety of the skill training.

3. 5 Data Post-Processing& Image Display

According to the research contents and task requirements, the obtained computer numerical simulation data shall be displayed in the different ways. The computer numerical simulation procedure is featured as the data conversion functions of which the results will be shown in various kinds of the images. The procedure is called as data post-processing. The final technical motion images shall be much intuitive and reasonable. During the process of the optimal technical solutions, these connective images from the computer numerical simulation calculation will have the important and direct effect on the modification and innovation of the action technology solutions.

The Application Value of Computer Numerical Simulation in the Skill Training

The application of the computer data simulation and the animation technology researches are featured as:

(1) The computer data simulation takes use of the three-dimensional ways for the skill action analog, explaining its kinematics, dynamics and biological characteristics in the animation form. The athletes are easier and quicker to master the essentials of the skills so as to greatly enhance the overall training level and action skills.

(2) Action choreography, simulation and the reasonable action design system can complete the new action technology scheme and standardize the action skills. Through the computer numerical simulation technology, it is able to edit, modify and design new action, choosing from the various scheduling results, and giving the optimization technology solutions, establishing the action skill modes and conducting the skill teaching and training.

(3) Through the comparison of the simulation results and the skill action training, it is able to make the quantitative and comparative analysis on the skill action, make the technique diagnosis, and display the analysis results in the forms of the images of which the results are comprised of the human body space state changes, focus trajectory changes, displacement, velocity, acceleration, force and moment function, etc. In this condition, it is able to make a deep comparison analysis about the action mode and the athletes' technical action. The athlete's training action and standard analog action will be shown in the same screen so as to make the technical diagnosis from the same view point to the synchronous contrast way. According to the action technology principle, it is able to design the directive scheme for the athletes. The computer numerical simulation calculation technology is still a difficult and hot issue in the sports science researches. The counterparts at home and abroad have achieved some successes in the computer numerical simulation calculation science researches of the human body motion analog. Due to its complexity, the artificial tedious parameters are hard to fully meet the requirements in the sports practice. With the high-speed development of the modern science and technology, the computer numerical simulation technology will play a greater role upon the combination of the constant action technology researches.

References

[1] Zheng Xiuyuan. Modern Sports Biomechanics [M]. Beijing: National Defence Industry Press, 2002.

[2] Feng Genquan. Human Body Engineering [M]. Lanzhou: Gansu People's Publishing House, 1980.

[3] Li Liangbiao. Sports Biomechanics [M]. Beijing: Beijing Sports University Press, 1991.

[4] Shi Xuehuang. Sports Biomechanics [M]. Beijing: Tsinghua University Press, 1985.

[5] Wei Wenyi. F. Sports Biomechanics [M]. Beijing: Tsinghua University Press, 1989.

[6] Wu Xuguang. Computer Simulation Technology [M]. Beijing: Chemical Industry Press, 2005

Advanced Materials Research Vols. 989-994 (2014) pp 4371-4374
© (2014) Trans Tech Publications, Switzerland
doi:10.4028/www.scientific.net/AMR.989-994.4371

Security Protection Model of QR Code Scanning Software[1]

Zhu Lei

Central University of Finance and Economics Beijing 100086, China

iamzzzz@163.com

Keywords: Attack, QR code,Security Model

Abstract. A QR code is more and more widely used in recent years. The two-dimensional bar-code can be seen in business cards, advertising, or web page and everywhere. But there exist some potential security dangers behind scanning those codes. Hence it have being obstacles to the widely using of QR code scanning software in some degree. This article analyzes several kinds of known attacks tricks through the QR code, and puts forward that the most efficient technology in protect the QR code scanning software is code encryption and white list . Finally An Android security protection model is given.

Introduction

In recent years, two-dimensional code has become one of the most important entrance of mobile internet. The two-dimensional code is convenient to connection freely online and offline; therefore wins users' praise highly and popular increasingly . Two dimensional code is very simple to use, as long as the user scans the the two-dimensional bar-code with the camera of a mobile phone installed with scanner software. Information of pictures can quickly display on the mobile phone screen, avoiding the tedious operation and error input. But it is very easy to be infected with the virus when the user scans some unknown two-dimensional code, which may racking up big bills for user, or leaking privacy information property information. Therefore, how to strengthen the security protection ability of this kind of scanning software is becoming increasingly concerned problem of the software developers[1].

Theory of two-dimensional code

Many kinds of two-dimensional code exist, such as: PDF417, Code 16K, Data Matrix, Maxi Code etc.. But the basic principles of two-dimensional code are the same. QR code [2]is a matrix two-dimensional code, originally developed by the Japan Inc., and finally become a standard. Two dimensional QR standard code is square, with black and white color. At the 3 corners of the QR code square are image like Chinese "回" word. The 3 image can help software locating the correct position of two-dimensional code. The user does not need to complete alignment, and the scanning angle is not restricted. The data can still be read correctly. Elsewhere in the QR code is black and white, indicating the 1 and 0 in binary system. In order to improve the fault tolerance, QR code include more bits information besides the real meaningful words. This technical is called Reed -Solomon coding. This code can correct many unexpected errors.

In addition, many color blocks are used to correct, and determine the copyright information. The scanning process of two-dimensional code is to translate the information contained in the image; the complete decoding process is as follows.

Location. The three angles of QR code are "回" like images,which can be seen as a mark.The size and location of the"回" like image are required by the QR code standard; Therefore, no matter how image rotation, it can rotate the QR code image to the standard forward position,through matching the mark position.The original and rotated image are shown in figure 1.

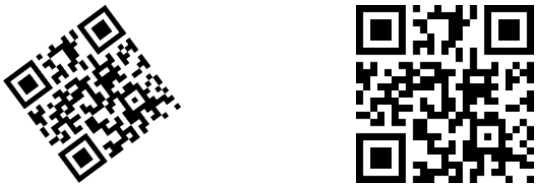

（a）original image （b）rotated image

Fig 1 The operation of location

Calibration. The shooting angle of the QR code image can be arbitrary. Therefore the forward image after locating may be not a standard square, which is likely to be beveled, one side large and the other short, as shown in figure 2. Calibration process use the mark of the QR code in the middle left lower side positon to enlarge the image to a suitable size.

Fig 2 Beveled QR code

Decoding. In this process the software read the contents of the image according to the image of the black and white color block. Every black and white block represents a binary "1" and "0". Hence the process of decoding is to read these the binary data according to its position in the image.

Error correction. The data cannot be directly used after decoding, because most of the QR code achieved by decoding process contain errors.Error correction process can remove these errors in binary, and provide a correct binary data.

Translate. Binary data will be converted into the text messages that can be recognized.

Attacking ways

People cannot directly read the information in the QR code image, but it is very simple for scanning software; Most scanning software provides intellisense and content recognition after getting the QR code image information, so greatly improve the user experience.But it also give the attacker a opportunity to attack.At present, the common attack ways are list below.

Trojan attack. Trojan embedded into the normal web pages is commonly known as the Trojan horse attack. Infected Trojan web pages,and even those seemingly normal web, can be downloaded by the user's browser, while users know nothing.The purpose of Trojan distributors allure the users to download these web pages to its local computer, so as to attack and control the user's computer.Trojan attack have different ways, among them the easiest way is to insert a hidden frame in the web page.For example, inserting the following HTML code into a normal web page.

<iframe src=http://dangerous website width=0 height=0></iframe>

In the web frame, the properties of width and height are equal to zero, which means that the frame are invisible. While the victims visit a seemly normal web page, the hidden dangerous http://dangerous website is visited at the same time unwittingly.

Phishing attack. Phishing is the ancient attack way . By sending a large number of deceptive information, the attacker is intent to induce the recipient to give sensitive information (such as user name, password, account ID and credit card details).The most typical QR code phishing attack way is the way by sending a coupon fishing users scan QR code to access the website.The web address (URL) are encoded into QR code, so the user is convenient to visit the web site by just scanning. The fishing site intent to imitate the URL and outlooking of famous sites. So it is easy to leak their personal information to the attacker, if you think the fishing web site is the real web site in your impression.

Inject attack. Command injection attacks has two ways, one is to attack mobile system itself, the other one is to attack the database system . Attacks on mobile phone system can take advantage of the mobile phone system engineering code. Most of the engineering code are harmless. But if a QR code

contains some important system engineering operation code, the user may suffer user data loss and the system reset.

Another kind of injection is against the database. The same attacks as that of website, the place where need input from a keyboad changes into scanning QR code. If there have no validity detection to the QR information, it might cause problems with executing query command in the database. For example: to construct the SQL query statement

SELECT a,b FROM c WHERE a_id = '123';DROP DATABASE pubs.

In this query, the former part is normal SQL query, ";" semicolon marks the end of the SQL statement. Behind the semicolon is a very dangerous operation SQL statements, it will clear away the pubs table in the database. User accidentally scan the QR code, if he has the authority, *pubs* table will be cleared, then the entire database will collapse. Therefore command injection attack need to strictly guard against.

These are a kinds of used attacking way by the QR code at present. In essence, the QR bar code is only a type of encode, and itself does not contain a virus. But some malicious information may be embeded into a QR code, then attack can be conductted.

Protect Module

The application scenario of QR bar code scanning software has two kinds: one is on a handheld device, another is on the scanning terminal. Command injection attacks are the main attack method in the scanning terminal, while handheld devices receive a variety of attacks, most of which are Trojan attack. In order to protect the 2D bar code scanning software, we introduce the encryption technology and the white list technology in our model.

QR code encryption. The most effective way to prevent QR code command injection attacks is to use the encryption code[3]. Anyone can use the software to generate QR code image, thus the attack code is very easy to be added in the 2D QR image. Once the two-dimensional codes are encrypted, scanning software needed to decrypt and then run; without proper encryption the information cannot be correctly interpreted, not up to attackking. Process of two-dimensional code decryption can be carried out after reading the information of cameras, and then the decrypted information can be pass on the other modules.

White list. QR code encryption technology is very effective to prevent injection attack. Only people who holds the key can generate QR code recognized by the software system, but this technical are not suitable for some third party application. These third party software usually adopt plain code, such as scanning and download software etc.., hence it must be at the risk of being attacked when read these QR code images.

The conservative security way is white list technology, which is simple but effective for software.The software application only redirects to the specified websites (white list), while the other web sites are not permit to redirects. On the software design, white list filtering works behind the step of the scanning.

System Frame. The position of the two kinds of technology use the same position, so you can build a unified model for protection the scanning software.

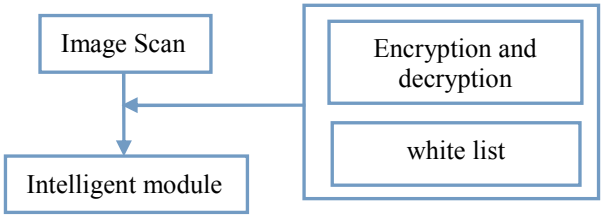

Fig. 3 Security Protection module

After reading the information in the QR code image by opening the camera of the phone, the software can't directly jump to the websites or intelligent processing. It need to go through the security encryption or white list processing contained in the protection module.The System Frame and the security model as shown in figure 3.

Key technical. A lot of QR code scanning software are designed with the help of the public API or a software package[4][5]. Among them the ZXing bar code image processing library is an open source software package that is very easy to implement the QR code scanning and decoding. The function's calling way and security module code position are set as follows:

```
//QR CODE SECURITY SCANNING MODULE
private PreviewCallback mPCallback = new PreviewCallback() {
  public void onPreviewFrame(byte[] data, Camera camera) {
    int pWidth = camera.getParameters().getPreviewSize().width;
    int pHeight = camera.getParameters().getPreviewSize().height;
    PlanarYUVLuminanceSource source = new PlanarYUVLuminanceSource(
      data, pWidth, pHeight, 0, 0, pWidth, pHeight, false);
    BinaryBitmap bitmap = new BinaryBitmap(new HybridBinarizer(source));
    Reader reader = new QRCodeReader();
    try {
       Result result = reader.decode(bitmap);
       String text = result.getText();
       ...//security processing function
       Intent intent = new Intent();
       ...//intelligent processing function
       ...;
    } catch (Exception e) {
  ...
```

The above code gives the location of the security processing function and the intelligent processing function. Due to the different way of the QR bar-code encryption and decryption, we can not give detailed processing code. However, after security processing, the program returns either errors or correct useful string which could be used for the following intelligent processing.

Conclusion

The article discusses a variety of attack types which are easy to be suffered by the QR code scanning software. And a software security model is accordingly put forward . In general, the more security designing in the software, the worse programming efficience and worse use experience. On the contrary, the software will be easily attacked if there have no security protection.Appropriate and targeted design is the starting point of this safety model proposed in the paper. With the wide application of two-dimensional code technology, more and more special 2D bar-code scanning software will be boomed in the market. An excellent security protection designing will make the application of this kind of software more wide.

[1]Supported by Discipline Construction Foundation of Central University of Finance and Economics

References

[1] Kieseberg, Peter, et al. "QR code security." Proceedings of the 8th International Conference on Advances in Mobile Computing and Multimedia. ACM, 2010.

[2] Jean-Pierre Lacroix, Shikatani Lacroix. QR Codes whitepaper, (2011)

[3] Dey, Somdip. "SD-EQR: A New Technique To Use QR Codes in Cryptography." arXiv preprint arXiv:1205.4829 (2012).

[4] Vidas T, Owusu E, Wang S, et al. QRishing: The Susceptibility of Smartphone Users to QR Code Phishing Attacks[M]//Financial Cryptography and Data Security. Springer Berlin Heidelberg, 2013: 52-69.

[5] Ramachandran R, Oh T, Stackpole B. Android Anti-Virus Analysis[J]. ASIA and SKM, (2012).

Advanced Materials Research Vols. 989-994 (2014) pp 4375-4378
© (2014) Trans Tech Publications, Switzerland
doi:10.4028/www.scientific.net/AMR.989-994.4375

Based on SVM Tibetan Web public opinion sentiment classification

Li Yingxing[1, a],Zheng Zongjun[2,b], Yani E[1,c]

[1] College of Mathematics & Computer Science North-West University for Nationalities

Lanzhou 730124, P.R.China

[2]Lanzhou Railway No.3 Primary School ,Lanzhou 730000 , P.R.China

[a] liyx555@126.com, [b]zhengzongjun@tom.com, [c] 436048536 @qq.com

Keywords: Tibetan,web public opinion,SVM,sentiment classification

Abstract. Tibetan Web text has increased rapidly in recent years. According to mining and analyzing the data about user's comments, we could identify the Sentimental tendency and evolution. Therefore we can better understand the user's behavior. Hot Tibetan public opinion analysis at the same time also can give enterprise, government and other institutions to provide important decision-making basis. The paper first describes SVM algorithm. Then the study of public opinion and target Tibetan Web Sentiment classification is defined and described, after that the paper gives the basic ideas and experimental research program. Finally, we summarize the achievements and shortcomings of Tibetan sentiment classification, as well as describe the challenges and the prospects of its development prospects.

Introduction

With the popularity of the Internet and the development of the Tibetan information technology, more and more Tibetan websites appeared. Nowadays,a large number of people choose the network to publish their attitude. Network comments are as a kind of UGC (User Generated Content) data, the user's perception of an event and point of view, and a kind of network public opinion information. However, faced with a flood of information of Tibetan review, it is very difficult to get information about the actual about what we really need. Therefore, people often classify the Tibetan website according to Sentimental content. With respect to the relevant technical research increasingly sophisticated Chinese and English text processing techniques, Tibetan corpus construction, Tibetan word segmentation, Tibetan text classification and text clustering are still in the early stages[6,7].

SVM Algorithms

SVM (support vector machine) is based on a statistical learning method, which is the basis of the VC dimension theory and theoretical knowledge of the theory of structural risk minimization in statistical theory [1, 2, 3].

The actual problem is rarely linearly separable problems. Most of them are relatively complex non-linear separable problems. For simple linearly separable problems, we can use a linear function $f(x) = w \bullet x + b$ to classify the sample. For complex nonlinear problems by introducing a nonlinear mapping function to map the data from low-dimensional space to a high-dimensional space, then we could find the best hyper plane in a high-dimensional space. When looking for the best super-plane only need for inner product operation between samples, high-dimensional inner product space can be calculated using the favorable kernel function $K(x_i, x_j) = \phi(x_i) \cdot \phi(x_j)$ .You can say that the introduction of kernel function makes the support vector machine classifier into a generic classifier.

For a given sample: $\{(x_1, y_1), (x_2, y_2), ...(x_n, y_n)\}$, $x_i \in R^d$, $y_i \in \{+1, -1\}$. We adopt an effective nuclear function $K(x_i, x_j)$, and then a linear classification can be achieved after non-linear

transformation. It makes the problem of complexity greatly reduced. Nonlinear problem can be divided as follows:

$$\min_{w,b,\varepsilon} \frac{1}{2}\|w\|^2 \quad s.t. y_i(w \cdot x_i + b) \geq 1, i = 1,2,...l \tag{1}$$

According to Wolfe duality theory, we can get the following formula of the dual problem:

$$\max_a w(a) = \sum_{i=1}^{l} a_i - \frac{1}{2}\sum_{i,j=1}^{l} a_i a_j y_i y_j K(x_i, x_j) \quad s.t. \sum_{i=1}^{l} a_i y_i = 0, a_i \geq 0, i = 1,2,...l \tag{2}$$

Solving these Dual optimal solution $a*$, if $a*>0$, x_i is called Support Vector; if $a*_i = C$, x_i is called Border Support Vector; if $0 < a*_i < C$, x_i is called True Support Vector. Resulting in the decision-making function of the high-dimensional space:

$$f(x) = \mathrm{sgn}(\sum_{i=1}^{l} a_i^* y_i K(x_i \cdot x_j) + b^*) \tag{3}$$

$K(x_i, x_j)$ is called kernel function, when it satisfies Mercer condition and at the same time $K(x_i, x_j) = \phi(x_i) \cdot \phi(x_j)$, we can introduce kernel function method to solve the reality of complex nonlinear separable problems.

Algorithm Implementation

3.1 Tibetan text preprocessing

Experiment texts get from Qinghai Tibetan network broadcasting network, people's Tibetan network, China netcom, Tibetan xinhuanet multilingual Tibet channel.

Tibetan texts must be handled as follows: transcoding, segmentation, redundancy removal, in order to take over the text for further processing.

A text after processing as shown in figure 1:

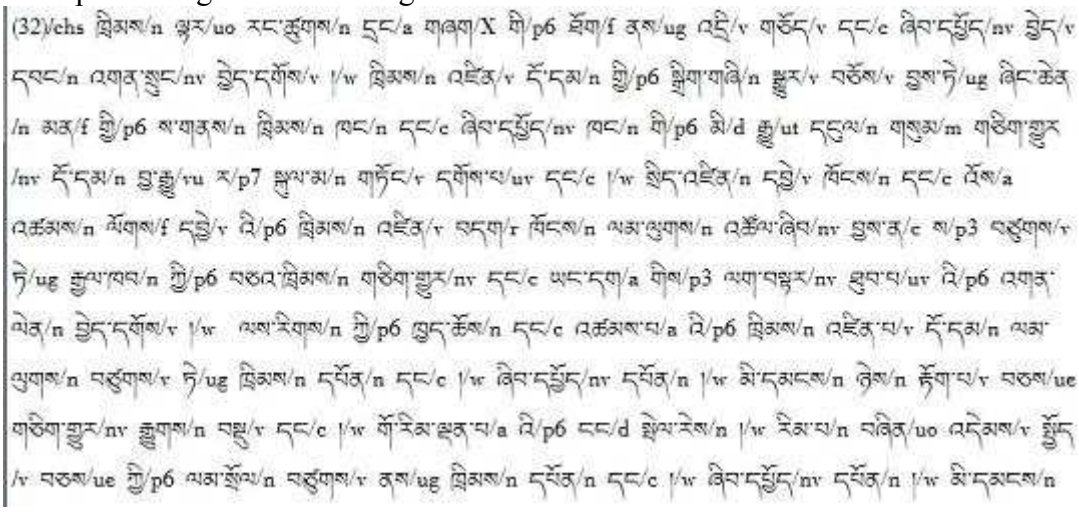

Fig.1

3.2 Tibetan text feature extraction and text representation

For all of the text sets extracted thesaurus created, if the text of a word as a feature, hundreds of thousands of feature is very common. How to distinguish a high degree on the category chosen words

is important. Firstly, it can reduce the amount of computation. Secondly, it could be able to improve the classification results.

The number of statistics for every term in documents is called terms frequency (TF). Calculated for each term of A, B, C, D.

A is the number of documents under this category contains the term;

B is not the number of documents under this category contains the term;

C is the number of documents under this category does not contain the term;

D is the number of documents not under the classification, and does not contain the term.

Each term eigenvalue calculated according to the formula:

$$x^2(C_j, t) = \frac{(AD-CB)^2 \times (A+B+C+D)}{(A+C)\times(B+D)\times(A+B)\times(C+D)} \quad (4)$$

All the eigenvalues order from big to small, and take out 1000 terms before each category. Cycle each category, the terms eigenvalue in all categories are merged into one text.

3.3 The data processing

The 700 documents is coming from the website by Web crawler, including 550 as a training set for classifier learning, and the remaining 150 as the test set. All the documents divided into political, economic, military, cultural and legal five categories by professionals. After handding the documents,such as transcoding, segmentation, redundancy removal ,we use Libsvm classification tools for data processing. Libsvm is an open source support vector machine (SVM) software package. It is developed by Professor Lin Chih-Jen and available for use. Libsvm is able to quickly and effectively classify and regress.

The data format of Libsvm is:

lable1 index1:featureValue1 index2:featureValue2 index3:featureValue3 ...

lable2 index1:featureValue1 index2:featureValue2 index3:featureValue3 ...

So,Tibetan text vector space model is expressed as follows:

3 11:0.136432 134:0.102896 162:0.368742 191:0.093873 273:0.334915 313:0.062247 385:0.103369 417:0.02399 470:0.317241 501:0.004156 ...

For example 3 11:0.136432 . Arabic numerals 3 representatives category ID, 11 representatives the term which the feature number is 11, 0.136432 is the features value (already scaled between 0 and 1 by svm-scale function)

Summary

Through experiment results, we found that the choice of the type of kernel function impact on the classification not so much. When we selected RBF kernel function we could get better classification results than we choose others type of keener function. From the beginning of this century, sentiment analysis on text information extraction gradually becomes a hot research field so that it is drew more and more attention. Meanwhile, with the continuous development of natural language processing techniques and machine learning techniques, subjectivity text sentiment analysis become possible else, and it would be gradually widely used.

Acknowledgements

This work was financially supported by Humanities and Social Sciences Planning Projects of the Ministry of Education of PR China under Grant No.11YJAZH053 and the Humanities and Social Sciences Youth Projects of the Ministry of Education of PR China under Grant No. 12YJCZH027 and No.13YJCZH029.

References

[1] Hayes, Steven P, Weinstein. A System for Content-Based Indexing of a Database of News Stories[C]. Proceedings of The Second Conference on Innovative Applications of Artificial Intelligence, 1009: 54-56.

[2] Cortes C. Vapnik V. Support-vector networks [J]. Machine Learning,1995,20(3): 73-297.

[3] Vapnik Vladimir N. Overview of statistical learning theory [J]. IEEE Transactions on Neural Networks, 1999, 10(5): 988-999.

[4] Yan Chao, research and implementation of SVM Chinese text automatic classification system [D], based Taiyuan: Taiyuan University of Technology, 2010.

[5] Zhu Shuxian, Zhang Renjie, research SVM kernel function selection [J]. Science Technology and Engineering, 2008.8,8 (16).

[6] Jia Huiqiang, Li Yonghong. design and implementation Tibetan text classifier [J]. Technology rich wizard, 2010, (4) :30-31 under.

[7] Xu Guixian. Tibetan web-based text automatic classification column [J]. Chinese Information Technology 2011 (4) :20-23.

[8] Li Y X, Deng K Y. User browsing interest in the propagation of public opinion in Tibetan internet to determine research[C].CISP,2012, pp.859-862.

[9] Deng J W, Deng K Y, Li Y S, Li Y X. Opinion Spreading Models on Tibetan Networks [J], Computer Systems & Applications. 2013, 22(3), pp.209-211.

[10] Li Y X, E Y N. The Research on Learning Behavior of Tibetan Network Teaching Systems[C]. IERI Procedia (2012) pp.127-132

[11] Deng J W, Deng K Y, Li Y S, Li Y X. Study on Evolution Model and Simulation Based on Social Networks[C]. ICNC (2012) pp.1249-1252.

Advanced Materials Research Vols. 989-994 (2014) pp 4379-4382
© (2014) Trans Tech Publications, Switzerland
doi:10.4028/www.scientific.net/AMR.989-994.4379

Web-based Data Translation for a Resource Management Grid

Lin Zhang

School of Mathematic & Computer Science, Wuhan Polytechnic University,
Wuhan, 430023, China

email: zhl_wh@sina.com

Keywords: Web; semantic; grid environment

Abstract. Grid environment as the cross field of semantic web and grid computing, has received significant attention recently. Our workgroup develops a resource management semantic grid named RM-Grid to enhance information process accuracy and efficiency in heterogeneity environment. This paper describes the architecture of RM-grid, mainly introduces the data translation service of RM-Grid. It puts forward an ontology based common semantic model and an XML based data model, presents the data translation algorithm between different data sources and an adapter framework for accessing distributed heterogeneous resources as well.

Introduction

A multi-institutional semantic grid environment will contain many data sources, which maintain different types of data using different storage mechanisms. Data collection, translation and retrieval are the major tasks in such systems. So far, there have been several projects on service infrastructure for data management, such as Storage Resource Broker [1], Metadata Catalog Service [2], etc. Our workgroup develops a resources management semantic grid named RM-Grid, which aims to improve the ability of processing heterogeneous sources under dynamic, distributed environments. In this paper, we will introduce the architecture of RM-Grid and discuss the data translation service emphatically.

Architecture of RM-Grid

The logical architecture of RM-Grid is divided into three layers.

1) Client Layer

RM-Grid is presented to the users with client Layer. Grid Portal provides the users with graphic interfaces. Users could browse domain ontology and describe their requirement, Grid Portal will send the user request to RM-grid, and the grid then invokes a series of corresponding services and presents the result to user in Grid Portal.

2) RM-Grid components

The RM-Grid core components include:

a) Semantic Registry Service. It is used to the registry and discovery of services. Referring to the Web service registry center, we add the metadata to RM-Grid for service descriptions. The service metadata is saved in registry center in form of XML. When a grid user wants to create a service, he should adopt the concepts in ontology to describe it. So that, the users can make use of semantic matching to search services accurately.

b) Ontology Service. In order to support semantic process, we make use of ontology to translate between semantically heterogeneous XML data. Ontology provides a formal, shared specification of concepts, their relationships, and other realities of some domain, which can reduce or eliminate confusion of terminologies, enable computers to process domain knowledge more precisely and conveniently [3]. RM-Grid provides ontology service for the grid consumers to maintain and search ontology.

c) Data Translation Service. It will often be the case that institutions will have different methods for modeling data, which may be conceptually or semantically the same. It would be beneficial to both institutions to be able to translate between one another's data models such that each can leverage the other services. Data translation service is the way to share data and services using common models. This, of course, does not mean that the automatic structural or semantic data translation problem is solved. This simply gives a service architecture where data translation services are published and can be trusted between the two domains in which the data is translated and potentially accepted by others as the standard.

d) Agent Service. It is responsible for assisting consumers to make use of grid resource and services. Agent service generates for each user an agent service instance, which interacts with Grid Portal and invokes the service on behalf of the user.

e) Global Model Management Service. In order for services on the grid to communicate with each other, their data must be described in a format that is understood by each involved component. Referring to the multi-level models theory of database field, the RM-Grid provides a method for defining an XML schema based data model derived from an ontology conceptual model. The Global Model Management Service provides for the consumers some methods to create and register their models, i.e. the XML schemas. The consumer can search the Global Model Management for existing XML schemas and may use one that suits their need; He can version an existing schema by adding or deleting data attributes. Once the schema is created, it is registered with the Global Model Management so that other consumers can search for it.

f) Data Instance Management. Services on the grid will need a method for storing and querying data. This will be integral for service communication on the grid. Given valid credentials, data should be able to be stored across a series of heterogeneous loosely-coupled machines. The RM-Grid also provides the ability to allow trusted users to update, query and delete the data. Data are in form of XML.

g) Domain Specific Service. Domain Specific Service is a series of services abstracting from the usual domain specific functions. A domain specific service could accomplish a relatively complete function by invoking the corresponding services in the grid. In the running process of RM-Grid, it could add services dynamically.

h) Common Data Service. Common Data Service is a series of grid services providing for the whole virtual organization with common data process functions. It will be invoked by other grid services frequently.

i) Task Monitor and Management Mechanism. It is responsible for monitoring, scheduling and supervising the programs running in the RM-Grid, make the grid right and efficient.

j) Grid Qos Mechanism. It is designed for tracing the running status of RM-Grid and recording the quality of the grid services.

k) Grid Security Mechanism. It is responsible for supervising the security of RM-Grid

3) Resource Layer

Resource of RM-Grid is the autonomic systems, such as enterprise information system, file system servers, relation or object-oriented database system and so on. Since these systems present different structures and semantics result from that distinct data sources may use different modeling methods, making very difficult to share and exchange information, RM-Grid provides resource service to encapsulate heterogeneous resource, they have uniform interfaces, which make it easier to manage. The RM-Grid will allow the grid consumer create schemas which describe their data models, register and share these data models with other collaborators, manage and version them while new data types are added or deleted, facilitate translation between data models that have the same semantic meaning, but different structure, and create, integrate, and manage databases and data that conform to these data models.

Common data model

The Data Translation Service is responsible for managing the translation between heterogeneous representations. In RM-Grid, we make use of ontology to translate between semantically heterogeneous data. Ontology is the key technology to describe the semantics of information exchange. It is defined as "specifications of a shared conceptualization of a particular domain" [4]. Ontology specifies a common understanding of certain domain in terms of concepts, attributes, and relations that can be communicated across people and application systems, thus they facilitate knowledge sharing and reuse. Both ontology and XML schema [5, 6] provide vocabulary and structure to describe information, the difference is that ontology languages specify domain theories and XML schema provides integrity constraints for information sources. With regard to the relationship between them, we refer to the multi-level models theory of database field. Correspondingly, we could consider ontology is analogous as conceptual model, and XML Schema is analogous as data model, therefore, an XML-orient semantic data model can be derived from an ontology conceptual model by designing a mapping algorithm originating from ontology to XML schema. Deriving XML Schema from ontology means to map ontology concept entities, attributes and is-a hierarchy to XML document structure and tag set, and forming a new schema-level specification. As a consequence, XML documents validated by the XML schema will be compatible with ontology. Since XML tags and structures can express explicit domain knowledge, our approach improve information from the syntactic or representational level to the more abstract level of concepts and relationships, avoids semantic heterogeneity efficiently and realizes the consistent representation of unstructured information. Meanwhile, using standard semantic level tags based on ontology to annotate content can help the computers to extract semantic of information from XML documents automatically.

To solve the data translation in semantic heterogeneity environment, RM-Grid firstly makes use of ontology to provide a machine processable semantics that can be communicated between different data sources, and then translates between different data referring to the semantic data model deriving from ontology. The general idea can be expressed as follows:

–Each concept from the ontology generates an element type in the XML Schema.

–For each attribute the XML Schema defines a sub element or, an attribute of element.

–If the attributes represents a relation to another concept the attribute element has as content the respective concept element, otherwise its content model is simply atomic.

Data translation service

Semantic data model derived from ontology in above subsection is a common data model register in RM-Grid. Model translation service will translate the heterogeneous model in resource layer into the common data model, so that the systems in resource layer could realize data sharing and cooperation. Original systems in resource layer of RM-Grid have their own understand about domain knowledge. Each system uses different language or syntax to represent knowledge, which forms respective local semantic schema. Before discussing the model translation, we require that the resource layer could output data in XML. The information providers need to wrap their own unstructured information with XML. What we want to emphasize is the hypothetical heterogeneity, i.e. XML documents need not abide to any certain structures. So resource providers can implement the wrapping process easily.

There is an adapter framework, which is responsible for the translation.

1) Extract local semantic model. This step analyses XML documents and their XML Schema submitted by resource providers, extracts the XML elements and attributes tags from the documents, finds the meanings and characters.

2) Concept matching. The generation of semantic knowledge and integration of different local models depend on the result of concept matching to a great extent. Different from keywords matching, concept matching is the consequence of local semantic models. It is matched by attribute

and content. Initial stages of the process need human interference, which involves semantic knowledge construction. At first, we can construct a semantic knowledge base making use of synonymous dictionary and train it subsequently, expand fresh knowledge continuously. Concept matching produces vocabulary-mapping table.

3) Generation of semantic XML documents. According to VMT, adapter translates heterogeneous XML documents. Then referring to XML Schema derived from ontology, realizes the transition from local XML documents to global ones with XSLT programming.

Conclusions

This paper presents a resource management grid. Mainly introduce the data translation service of it. The main objective of the architecture is to improve the capabilities of semantic processing and the translation between ontology based semantic model and local data models, which contributes to the flexible information extraction, information integration and knowledge acquisition from heterogeneous, distributed, autonomous information sources. In the next phase of the project, other issues should be considered. Since RM-Grid is a research effort still under active development, we will work on the organization of RM-Grid architecture with the ongoing technology, so as to this architecture could be compatible with the advanced open standards, services and tools.

Acknowledgements

This work was partially supported by a grant from the NSF of Hubei Education Agency of China (grant No. Z2014). Thanks to Dr. Guan Hua for his valuable discussions on this paper.

References

[1]SRB. Available: http://www.npaci.edu/DICE/SRB/index.html.

[2]Metadata Catalog Service (MCS). Available: http://www.isi.edu/ deelman/MCS/.

[3]Mike Uschold, Michael Gruninger. “Ontologies: Principles, Methods and Applications”, Knowledge Engineering Review Vol II (2), June 1996.

[4]Gruber. T. R. “Toward Principles for the Design of Ontologies Used for Knowledge Sharing”, International Journal of Human and Computer Studies, Vol 43(5/6), pp. 907-928.

[5]David C. Fallside, “XML-Schema Part 0: Primer”, W3C Working Draft, 7 April 2000. http://www.w3.org/TR/2000/WD-xmlschema-0-20000407/

[6]H. S. Thompson, D. Beech, M. Maloney, and N. Mendelsohn, “XML Schema Part 1: Structures”, W3C Working Draft, 7 April 2000. http://www.w3.org/TR/2000/WD-xmlschema-1-20000407/.

Advanced Materials Research Vols. 989-994 (2014) pp 4383-4387
© (2014) Trans Tech Publications, Switzerland
doi:10.4028/www.scientific.net/AMR.989-994.4383

Design and Implement of Decision Support System in the Ceramic Information Technology Integration Service Platform

Hua HUANG [1,2,a], Yi-Lai ZHANG [1, b], Min ZHANG [1, c]

[1]Jiangxi Ceramic Enterprise Information Technology Engineering Research Center, Jingdezhen Ceramic Institute, Jingdezhen, 333001, China

[2]State Key Laboratory of Software Engineering, School of Computer, Wuhan University, Wuhan 430072, China

[a]jdz_hh@qq.com, [b]tyzyl@qq.com, [c]191148074@qq.com

Keywords: Information Technology Integration Service Platform; DSS; Data Warehouse; Data Mining.

Abstract. Based on the introduction of DSS (Decision Support System) development, the paper discusses the function, structure, key technology and realizing approaches of DSS supported by data warehouse technology according to the characteristic of ceramic information technology service integration platform. Finally, the development direction is prospected.

Introduction

With the application of collaborative management ideology, based on information sharing and collaborative technology, the ceramic information technology service integration platform (CITSIP is called for short) supporting business collaboration of the industrial clusters is researched and developed. The goal of this platform is to provide a scalable, ease using and low cost integrated solution with business collaboration feature for small or medium ceramic enterprises within the region, to improve the capability of independent innovation and business responsiveness, and reduce production costs and enhance the core competitiveness of the whole cluster region. This provides a successful case and demonstration of the regional information service mode and platform operating mechanism for the homogeneous class enterprise clustering area. And the DSS (Decision Support System) is a sub-system of the CITSIP.

Based on the introduction of DSS development, the paper discusses the harmonizing mechanism, function, structure, key technology and realizing methods of DSS supported by data warehouse technology according to the characteristic of CITISP. At last, the development direction is prospected.

Development of DSS

Since DSS's appearing, its development from managing semi-structured problem by using interaction technology to assist managers, to infiltrating computing science, decision science and a variety of AI techniques to the various practical DSS which have appeared, its application involves various areas , and become one of the hot areas of information systems. However, the success examples of the traditional DSS applications are very little. On the one hand the DSS based on traditional DBMS supporting can only provide a data-level support in assisting decision-making process, and the reality data for decision-making is often distributed and heterogeneous; on the other hand the most practical application of DSS have high requirements on decision-makers, who not only need to have professional knowledge but also have a higher DSS modeling knowledge. In order to meet different social needs, a variety of types of DSS is appearing, e.g., intelligent decision support system, distributed decision support system, group decision support system, organizational decision support system [1], adaptive decision support systems [2], strategic decision support system, etc., with the implementation of these systems, each is suitable for different occasions, in different degree to meet the new needs of the decision-making situation.

DSS based on Data Warehouse

Data Warehouse is not a single technology or software, which combines a number of areas, such as database theory, statistics, data visualization and artificial intelligence technology and so on, whose goal is to find a valuable knowledge for supporting decision and predicting the future in the large amounts of data. So the decision support system based on this technology provides a desirable way of data organization for DSS and a powerful decision support tools for decision-makers, and effectively promotes the modernization of decision-making process.

The research and development of DSS based on the theory and technology of data warehouse is still in its infancy[3], but has received the attention of many scholars, Its main research topics includes: ①DW(Data Warehouse) applications in the establishment of DSS, and the structure of DSS based on DW's framework; ② How to enhance knowledge source of DSS by adopting data mining techniques or knowledge discovery methods; ③ Organization and design of DW in DSS and Design of DW's management system. In general, the research of DSS based on DW focuses on how to use DW and related technologies to discover knowledge and how to interpret and express knowledge to users, to provide stronger supporting data of decision support, effectively overcome the difficulties of traditional data management and the issues of ignoring historical data by DSS.

Design and Implementation of Decision Support System for CITISP

The product development of ceramic manufacturers in the ceramic cluster region requires comprehensive, large amounts of information, including the demand information, competitive intelligence, management information, product data, etc., and a lot of information will be obtained from distributed, heterogeneous mass of data by mining, the traditional DBMS cannot meet this need. Therefore, the DSS ceramic cluster region Information service platform based on data warehouse comes into being. Data warehouse system is a subject-oriented, integrated, stable in a certain period, and over time data collection of decision analysis for companies or organizations, which can be carried out to integrate much information from various databases, to organize and store data according to the history and development perspective of things, for users to do data analysis and assist decision support, finally to provide some useful information and knowledge of decision support for decision-makers [4].

A. Design ideas of this system

The DSS based on the data warehouse of platform mainly includes two modules: user information inquiry and fuzzy information inquiry. The module of user information inquiry mainly makes use of text data mining method to search information, according to information provided by the user or enterprise; and in order to facilitate users to quickly find key information needed, the module of fuzzy information inquiry is to simulate the query way of Baidu, search some effective text information, provide available information with a greater match degree to users.

The main design idea of user information inquiry module is shown in Figure 1.

In the design process, using two tables to store related information, respectively, the table "Msg" in the database "AspServer" is used to stored information target data and information word data; enterprise user information is stored in the table "InteractMsg". As known from the design, the information of the table "Msg" comes from network resources, which will be converted into the information used in the module through a series of change. However, the web is a dynamic massive resource, which determines the amount of information resource library is changing with time, and this database used is also dynamically updated. Because of large amount of text information and computing capacity, the time complexity and space complexity will be high in data mining algorithm for mining text, and the processing time of text word segmentation will lag, in the design procedure, if to use directly B/S Architecture for users' communication, the transaction time of the system will be longer, resulting in the situation for waiting the affairs of other users and the performance degradation of the system. Therefore, in order to resolve this problem, an idea of intermediate service is proposed, which is that by making use of segmentation technology the target

data database and enterprise user information technology are converted into the library of information words and the calculation process of implementing matching sets is separated from the system, allowing a stand-alone program “AspServer.exe” to calculate the matching set in advance, so that the performance of this system will be improved.

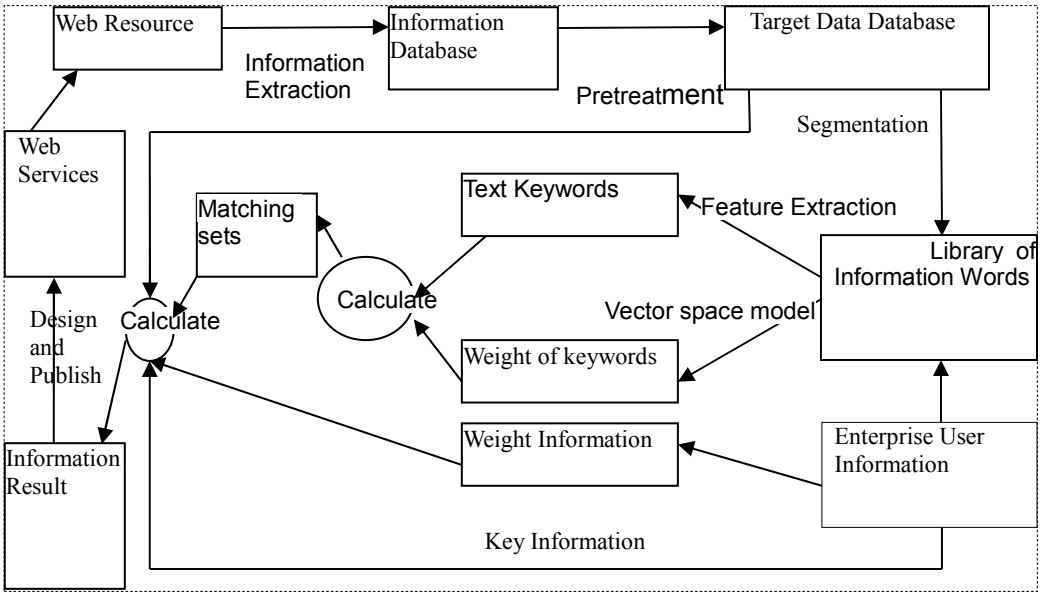

Fig.1. Design idea of user information inquiry

The application is to prevent repeating the calculation processes of matching sets，improve system performance and make some results to be reused. Because of a large amount of data calculation, the procedure in the calculation process will take a lot of CUP and memory, so the system administrator who is implementing the program on the server needs to set a free time to calculate this process, which is the reason for designing this middle service application.

The matching sets obtained by calculating in “AspServer” procedure is stored in the "New" property of table “InteractMsg”. Taking advantage of the property to describe what information extracted is close to the information provided by enterprises (Company Profile) then order them by descending of text message number. For example, the number of the current information are 16, 30, 101, 102, 1976 ,1977, 1980, 1981, 1983, 1988, 1989, 1991, 2001, 2002, 2003, 2006, 2009, 2014, 2017, 2020, 2026, 2033, 2038 and 2052,which are similar with the information submitted by Pengfei Building Ceramic Co., Ltd, other information should be ignored. However, seen from the example, the amount of information is relatively large, as to users’ demand, it is necessary to do further calculating, and make the text messages searched to mostly meet user's requirements.

“AspServer” procedure is to extract information matched in larger degree with enterprise profile; there are still some distances to users’ specific needs. Therefore, more specific information should be provided to further extract relevant information. The decision support system mainly provides some information, such as enterprise products, main material source, other key information and the associated weights, based on this information and the previously extracted information, using relevant algorithm to match with information submitted by users, then order them by descending of information, and finally submit to users.

Fuzzy information inquiry module is designed primarily for users to quickly search some key information. This module also uses word segmentation technology, it can intelligently recognize the information entered by user, then split it into a number of words, according to the frequency and the associated weight of these words in the text message, the importance of text and information submitted is obtained by calculating, then by which to set a threshold level to divide class, e.g. a user submits the information "I love china ceramic", through the segmentation program, two words "china" and "ceramic" are got, making use of fuzzy matching method to calculate the frequency of two words appearing in all text, eventually arranging them according to certain rights of these texts to get the maximum extent of the information related.

If a user submits the information "I love " china ceramic "" ,that means the word “china ceramic” is in quotes, "china ceramic" is only as one word, so there will be three words: china, ceramic, china ceramic. In order to facilitate further search for relevant information in the existing results, the module also provides a function of "search within results", this function is achieved by operation of key words "and", therefore, space can be added behind the keyword existing, then the query keywords should be filled, e.g., "I love china Jiangxi ceramic ".

B. Key technology of implementing system

Data Warehouse Design. The structure design of platform data warehouse needs to arrange reasonably various elements for the goal of decision-making, and ensure the standardization and integrity of the data warehouse system. Definition of various data in data warehouse design is stored in metabase. Data structure of data warehouse commonly makes use of star-shaped model and data model. Firstly it is necessary to define each theme and data source; the data source is divided into internal and external data sources, the properties related with which include a computer platform, data owners, data structure, processing of this data source, storage update plans, etc. Secondly to define the principles of data extracting, refining and loading. Finally, to extend topic, form a theme table and define a data mart.

Data pre-processing. The main task of data pre-processing is to analyze and conduct the data from different platform enterprise database, to identify the inconsistent data used for cleaning, conversion and reprocessing, etc., and then load them into the data warehouse. The concrete method includes two steps: Firstly it is necessary to do extraction, cleansing, standardization, integration for DB1, DB2... DBn data, and convert inconsistent data into consistent data; in this process, a table of mapping name will be created. Secondly, in the process of organizing data from different sources, the data is changed into an intermediate model, and then moved them to a temporary work area. Finally, the inconsistent data is converted into a standard and consistent data, which will be deposited in data area of the data warehouse.

Data Administration. The scale of data warehouse is generally large, at the beginning of establishment, it is necessary to ensure that it should be managed; several data warehouse or data mart may be created in this service platform, which shares a metabase for managing them. First, to inquiry the required metadata element in metabase, and then to do updating operations of the data warehouse, after ending updating operations, the updating situation will be recorded in the metabase. When the operating environment and structure of data source and the maintenance program of the objective data is changing, the metadata is needed to modify. Metadata is an important part of the data warehouse, the quality of which determines the quality of the data warehouse.

Conclusion

The decision support system based on the data warehouse built in this service platform support a variety of knowledge representation and reasoning methods, allow structured data and unstructured data to exist together, various types of distribution, and heterogeneous knowledge sources are integrated for providing various types of effective data for decision-makers to analyze them, which plays a role of supporting decision. Data Warehouse provides an effective and workable system solution for the research and development of decision analysis system. According to a statistic, 98% of top 500 enterprises have established some applications based on the data warehouse, but in our country there is a big gap in this respect. With the growing of China's overall national strength and the rapid development of information technology, more and more successful applications of decision support system will appear. A solution of complete decision support system should integrated data warehouse, OLAP, data mining, and other information processing technology, if this solution is widely adopted, the research and development work of decision support system will be promoted into a higher leveraged on the analysis of the mechanical theory as the foundation, designed the soccer robot pick the ball institutions optimal design process, found aim function, select design variables and the corresponding optimization algorithm to optimize a complete set of institutions, then through the test to get the final performance parameters of the institution. Experiments show that the system has higher accuracy and stability.

Acknowledgement

In this paper, the research was sponsored by National Science and Technology Support Program (NO.2012BAH25F02 and No. 2013BAF02B01).

References

[1] Gottschlich Jörg, Hinz Oliver. A decision support system for stock investment recommendations using collective wisdom. Decision Support Systems, v9, n1,p52-62, 2014.3.

[2] Razmi Jafar, Sangari Mohamad Sadegh. A comprehensive decision support system for ERP. European Journal of Industrial Engineering,v7, n4,p 475-496,2013.1

[3] Rong Xie. Decision Support System Based on Data Warehouse. System Engineering Theory & Practice, 2008, 4:27 ~ 30.

[4] Chao-zhen GUO, Jun-jie YANG. Decision support systems Based on data warehouse and OLAP,System construction, 2007, 1: 11 ~ 13.

[5] J. Dong, H.S. Du, S. Wang, K. Chen, X. Deng, A framework of Web-based Decision Support Systems for portfolio selection with OLAP and PVM, Decision Support Systems 37, 2004,367–376.

Advanced Materials Research Vols. 989-994 (2014) pp 4388-4391
© (2014) Trans Tech Publications, Switzerland
doi:10.4028/www.scientific.net/AMR.989-994.4388

Design of Campus E-Commerce Platform Based on MVC Model

Zhao Sheng[1,a], Sun Yongdao, Shi Xuekui

[1]Department of Information Engineering, Xingtai Polytechnic College, Xingtai, 054035, China

[a]e-mail: joson1026@sina.com

Keyword: Campus E-Commerce; MVC; N-layer Framework model

Abstract. Electronic Commerce is now spreading into all sorts of economic activities.Therefore, The E-commerce System call be applied extensively on Campus，aiming at the practical needs of campus business activities．This dissertation ion is going to study the"E—commerce System on campus"based on the project．The system adopts N-layer framework model, realizes its elasticity and expansion and lays a solid foundation for system maintenance and secondary development.

Campus E-Commerce

The development of e-commerce has changed the traditional commercial model. E-commerce itself is equipped with a great advantage and development prospect. In China, developing e-commerce can promote internal reform of enterprises, accelerate information construction of enterprises, improve quality service of enterprises and lay a solid foundation for China to participate in international competition. However, the development of Chinese e-commerce is currently restricted by a variety of factors such as safety certificate, logistics distribution and consumption concept, etc. These problems can be solved to a large extend if e-commerce is developed in university campus.

Campus e-commerce platform refers to a computer system equipped with high availability, elasticity and safety, which is constructed in campus by making use of infrastructure network, computer hardware and software and electronic communication, for the purpose of catering to all the aspects of activity needs of units, enterprises or individuals in campus for handling business, working, studying and living. Relying on campus network, it serves all the teachers and students. In recent years, all walks of life in the society have started construction of e-commerce, and campus e-commerce has also begun to enter the popularization stage. Though construction of Chinese e-commerce has achieved some results, a huge gap still can be seen compared with developed countries. At present, China has not had practical platform of constructing campus e-commerce and even lacked mature campus e-commerce software. Therefore, how to grasp the opportunity brought by global informatization, adopt Internet technology and construct campus e-commerce platform according to characteristics of campus to meet the needs of modern management of campus will be a chance and challenge that educational circles and even the whole world are faced with.

MVC (Model-View-Controller) Framework Model

MVC model is very suitable for software framework with strong interactivity. Campus e-commerce platform is a kind of typical interactive system whose inner core usually keeps stable. For instance, its model of domain data (such as order and commodity) is often unchanged, but the interface of data used for observation is changeable. For example, with regard to checking order data, ordinary users want to check their own orders and see which goods are delivered while clients opening shops would rather check some statistical data of their orders. Under the circumstances, though users see different external forms, actually their internal data models are consistent. MVC framework model can provide such interactive system with a basic structured organization.

The full name of MVC is Model-View-Controller, namely model-view-controller framework mode. The model divides an interactive application system into three layers:

Model Layer: It encapsulates domain data and informative function. Independent of given output representation and input mode, model is an invisible object which includes all the data and conducts except for the data and conducts of UI and belongs to an object of domain model.

View Layer: It is responsible for demonstrating information to users mainly through interfaces. View obtains data from models. A model consists of many views.

Control Layer: Controllers usually accept user input and are usually taken as the activities of mouse move and mouse button or events of keyboard input. The event is translated into the server request of models or views. Users only interact with system via the controller. Each view invokes the corresponding controller and completes displayed data input. Views take charge of display output function of data. They together constitute the interface of users.

The relationship of the three is as shown in Figure 1:

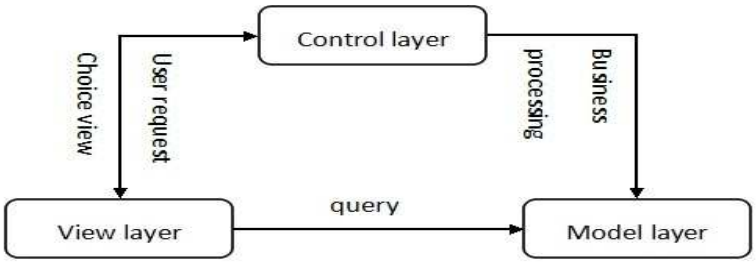

Figure 1:MVC model

It is because of separation of models, views and controller components that realize a model and many views. If users change models through the controller of a view, other views relying on the data can also reflect such change. In other words, once data of models changes, models will report to all the views. In reverse, views recover new data from models and update the information displayed.

The advantages of MVC design mode:

Allow expansion of many user interfaces: In MVC model, views and models do not have necessary connection and interact with each other via controllers. In this way, changing corresponding views and controllers instead of models can add new type of user interfaces.

Effectiveness of modules: Program change of controllers, models and views will not influence other layers and components. Additionally, different component development can occur simultaneously.

Reusability of code and design: Extensively adopting reusable components can make communication among development teams convenient and system designed easy to understand and reduce development cost of projects.

Ease of maintenance: Controllers and views can accordingly expand following expansion of models. Keeping a common interface, old version of controllers and views can also be used continuously.

Strong user interfaces: Invocation and combination of user interfaces and model methods enable program to release more clearly and friendly interfaces to users.

In conclusion, MVC is a good design mode of constructing application framework, which can separate business process from display, divide application into controllers, models and views and increase expansibility, robustness and flexibility of application.

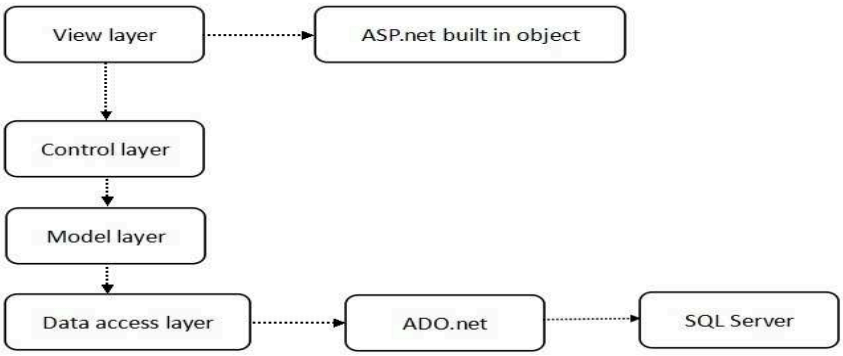

Figure 2： Model Framework of Campus E-Commerce Platform

Model Framework of Campus E-Commerce Platform Based on MVC

Campus e-commerce software system framework diagram is as shown in Figure 2, which combines the characteristics of campus e-commerce system, adopts advantages of layer model, designs and realizes campus e-commerce platform software framework and puts forward soft framework schemes. The framework takes advantage of MVC model to design four-layer framework. The top layer is view layer which mainly displays data, acts as the interface through which software users make contact with software, deals with layout by using elements like HTML and CSS and captures and presents event response of user operation by means of Asp.net object and JavaScript. Event handling achieves its goal through invoking business logic function of the controller layer which provides the interface of invoking business logic and realizes separation of display and logic. In addition, the controller layer provides lower layers with the interface of handling business logic. The interface is just abstract statement and is realized through data access. Data access layer meets the needs of data access aimed at specific database platform. The system realizes operation of SQL-Server database through ADO.NET interface, which returns data to padding model layer. The domain models of the system layer are commodity, order and users. Domain model is the projection of data entity of database. In every layer, there is internal system structure. The specific description of collaboration diagram of various components of campus e-commerce software system is as shown in Figure 3.

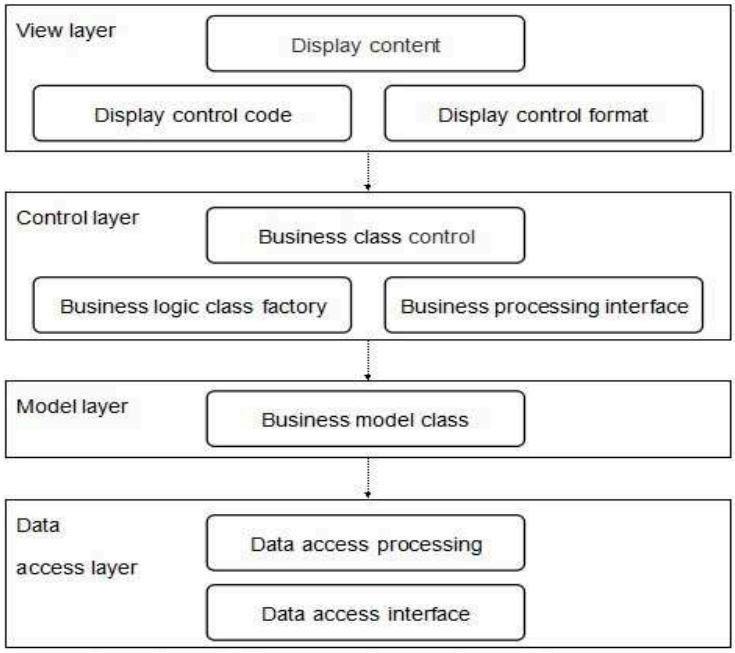

Figure 3: Campus E-Commerce Platform Component relationship

View Layer

It is actually class package of interfaces of system. It plays a role in setting up the interface used by user window of the system and supporting system. The layer is made up of three aspects including displaying format control, user content pages and control codes.

Display format control package: It mainly controls various page formats and sets up page layout to control display modes of interfaces and display styles of webpage.

Display content pane: It is mainly responsible of setting of webpage content and sequence and is taken as the main part of webpage display.

Display control interface: It mainly makes use of models separated by means of code of net platform to control dynamic display of page contents.

The layer separates format, content and control so as to make system easy to maintain, expand and control.

Control Layer

In fact, it is the domain logic layer of business object of system, connects pages and the interface of realizing specific functional service of system and provides functional service of system through

managing business object of system. It is composed of three parts including commercial control logic function, commercial logic class factory and business process interface.

Business logic control: It directly offers domain service of system and plays a transitional part in connecting setting pages and various interfaces of realizing specific functional service.

Business logic processing interface: It provides an abstract interface for invocation of commercial logic. It is usually functional class inheritance of specific system business. The type of object realizes database operation and actually processes specific and practical business.

Actual business logic object package: Its formation can realize actual business object set of various functions of system including business object and external business object newly constructed by system.

Business logic class factory: It realizes dynamic creation of actual business object.

The layer provides the upper layers with a unified interface for invocation and the lower layers with a unified interface for realization. Such design makes the interfaces stable, lessens range of fluctuation of system and facilitates its maintenance.

Model Layer

As the projection of database table, the layer mainly realizes data storage of business class object, provides a container for managing the class object and data support of business logic based on the business model.

Data Access Layer

Closely related to specific database, the layer provides specific operation and access methods of database. Here, it invokes the interface of ADO.NET and realizes persistent object access to database of SQL-Server.

All the persistent data of the system is stored in database

Conclusion

Electronic Commerce is now spreading into all sorts of economic activities. Therefore, The E-commerce System call be applied extensively on Campus, aiming at the practical needs of campus business activities. Campus e-commerce platform takes all the teachers and students as the main customer base, construct e-commerce platform as per their needs and determine transaction contents and forms. The system adopts N-layer framework model, realizes its elasticity and expansion and lays a solid foundation for system maintenance and secondary development.

Reference material

[1] JiangXue, ASP.NET MVC Model Binding validation extension application[J], Information & Communications, 2012, 002

[2] PengXia, Construction Scheme of University Scientific Research Management Platform Based on MVC Model [J] , Computer Technology and Development,2013,004

[3] ZhangYuan ,Modular design of virtual experiment system based on MVC design model[J] ,Computer Engineering & Science,2013,008

[4] HuangPeipei, Design of Campus E-commerce System Based on Web[J] ,Computer & Telecommunication,2010,001

[5] LiLi,Teaching Practice Platform's Design and Accomplishment about Campus E-Commerce Based on Web[J] , Computer Knowledge and Technology,2011,35

[6] LiShaowei , On the Design and Construction of Campus E-commerce Platform[J],Office Automation,2010,008

Advanced Materials Research Vols. 989-994 (2014) pp 4392-4395
© (2014) Trans Tech Publications, Switzerland
doi:10.4028/www.scientific.net/AMR.989-994.4392

The Study on the Improvement of Observer Pattern based on .net Framework

Zhenjun Fan

College of Computer Science, Tonghua Normal University, Tonghua, 134002, China

email:jlthfjq@163.com

Keywords: Object-oriented Programming; Observer Pattern; Delegate; Event

Abstract. This paper introduces the relevant concept of observer pattern and realized method. Based on .net framework, we make detailed discussion about the principle and method of observer pattern, which is simplified and improved by delegate and event mechanism.

Introduction of Observer Pattern

A design pattern is a set of objects. The main function of design pattern is to solve a kind of special problem and it is the optimal method to solve the problem [1]. Software will have excellent reliability, expandability, reusability and maintainability using design pattern. Design pattern is a summary of experience of designing and developing software, a sort of expert knowledge.

Definition of Observer Pattern

Observer pattern is a classical design pattern. It defined a dependency relationship from one to many among objects. All dependency objects will be noticed and automatic updated when an object alter its state [2], where the dependency objects are called observers, and another one is named subject. Observer pattern allows many observers to monitor the same subject. All observers will be noticed and responded when the subject changes. The relationship between observers and subject is loose coupling. Subject can increase and decrease observers at any time and it cannot be affected. Observer pattern aims at decreasing the degree of coupling among components and decreasing dependency relationship among objects.

Roles in observer pattern

There are four roles in observer pattern [3].

Abstract subject role:

Subject role preserves all citation of observer objects into an accumulation, and every subject can own any quantity of observers. Abstract subject provides an interface which can increase or delete observer object. Subject role is also named abstract observable role; generally, it is realized by an abstract class or an interface.

Abstract observer role:

It defines an interface for all specific observers and it will be updated when it is noticed by subject. This interface is called updated interface. In general, abstract observer role is realized by an abstract class or an interface. Only one method is performed to update interface and this method is called updated method.

Concrete subject role:

All registered observers are informed when internal state of the concrete subject changes. In addition, concrete subject is also called concrete observable and it is realized by a specific subclass.

Concrete observer role:

It realizes the update of interface asked by abstract observer role to guarantee that the state of observer is coordinated with the state of subject. Concrete observer is normally achieved by a concrete subclass.

Main operation of observer pattern

Three kinds of operations are included in observer pattern, i.e. register, notice and cancel.

Register:

Observer calls the registration method of subject, so that it can be registered in the subject.

Notice:

Subject sends messages to inform the data changing for all registered observers when the state of subject alters.

Cancel：

Observers will cancel the subject if it does not need to observe the subject, so the observation of subject is cancelled.

Universal implementation method of observer pattern

Traditional implementation method

Interface is generally adopted traditionally. Class is regarded as observers or subject role through realizing corresponding interface. Abstract observer class provides the updating method which is coordinated with the data changing of subject. All observer demand realizing such interface to correspond the changing behavior of subject. Subject interface provides three methods to perform registering, cancellation and notice to all observers. Subject class must realize these methods.

Analysis of traditional implementation method

We know that concrete subject is realized by subject class from traditional implementation method. A private Hash table object is involved and it is a container to store observer objects. Observers are added to Hash table using register method, the relationship between observers and subject are cancelled using Un-Register method. There is a method to notify observer the corresponding data changing when the state of subject changes. Each observer object must inherit observer interface, which is inflexible and inconvenient. It is necessary to create a new method when developers hope to realize observer, but the interface isn't realized, or the realized interface is incorrect. Subject should preserve list of observer to realize registration, cancellation etc., so, there are undirected relationship between subject and observer. It is time-consuming to inform all observers if an Subject object own many directed and undirected observers, for all list of observer has to be searched through as a loop, so the efficiency is determined by the scale of observer list.

Realizing observer pattern using delegate and event mechanism in .net program

For the purpose of realizing low coupling, we can take advantage of delegate and event technology to realize observer pattern [4].

Delegate

Delegate is a class. It defined the type of a method and passed a method as parameters of another method. This kind of dynamic parameter can avoid using many selected statement, so the program has better expandability [5].

Delegate may not know detailed information on the class of capsulation method. This method can be called as long as the parameter types and return type match delegate. We can make full use of the important property of delegate and event mechanism to complete observer pattern. Thus, coupling among objects is decreased, and static combinational relationship is altered to dynamic one. The other significant property of delegate is multicast, which can help realizing registration and cancellation of observers.

Event

Event is further capsulation of delegate in .net framework. Event can be easily grouped into two parts: the class of event occurring and the class of event processing [6].The class of event occurring is to trigger an event in this class but the class doesn't know which object or method will receive and handle the event. The class of event occurring is treated as observable, and the class of event processing is regarded as observer. Sender and receiver accomplish the event processing through delegate.

Realizing observer pattern using delegate and event mechanism

Subject class doesn't need to realize any interface or inherit from abstract class，an agency and an event is only needed to provide when .net application program adopts agency and event to realize observer pattern. For observer class, it only needs to provide an updating method [7].

In the process of using delegate and event mechanism, observer establishes an agency, then, it passes the name of updating method to the agency and registers this agency to the event of subject class.

The improvement of observer pattern based on .net technology

There are no linked list and traversal operation in these codes using .net framework technology. Subject class and observers do not require any interface. Subject class provides an agency and an event to send data updating information to every observer object. It can simply add new different observer objects even though it does not know where these observer objects inherit from and doesn't need to unify their interface method. Observer class only realizes updating method corresponding to the changing of subject and registers this method to the event provided by subject class. Observers can employ "-=" operation to cancel when they do not need observing the changing of subject class. Traditional observer method realized by interface can decrease coupling between observer and observer object, while agency and event almost remove coupling between these two modules. So, flexibility is enhanced.

Conclusions

Registration, cancellation and notice in observer pattern can be performed by dynamic combination between delegate and event mechanism based on .net framework. Thus, it unchains dependence of goal object on observer, and decrease the coupling of them, so flexibility of design is enhanced.

Reference

[1] Biying Lin,Junhua Qu.The application of design mode based on e-commerce website [J] .Computer System Application ,2005(1).

[2] Erich Gamma, Richard Helm, Ralph Johnson: Design Mode: The Basis of Reusable Object-oriented Software, translated by Yingjun Li, Xiaoxing Ma, Min Cai, China Machine Press Beijing 2005:194.

[3] Litao Xiao,Changsong Qi.The application and Extension about Observer Design Pattern Based on MVC[J].Computer and Moderization,2012(5).

[4] Jinping Yu , Xiaohui Liu. Research on Application of Delegate of C# in Observe Design Pattern [J].Software Publications, Vol.9 No.11.

[5] Farong Zhan. The Application of The Delegate and Event of C#.net [J]. Journal of NiXia Normal University, 2009(6).

[6] Ying Gao,Yizhi Luo , Chulin Liu. The Analysis' of Event Mechanism of C# [J]. Network and Computer Security, 2010(12).

[7] Zhenxin Zhang, Yu Song, Lisheng Han , Jianfeng Liu. Analysis and Improvement in .net of Observer Pattern [J].The Development of Microcomputer, Vol. 13 No. 8.

Advanced Materials Research Vols. 989-994 (2014) pp 4396-4399
© (2014) Trans Tech Publications, Switzerland
doi:10.4028/www.scientific.net/AMR.989-994.4396

Design and Implementation of an Intelligent Cross-Platform IaaS

Fen GUO [1, a], Qing DU[2, b], Jie YANG[3, c]

[1, 2, 3] School of Software Engineering, South China University of Technology, Guangzhou, 510006, China

[a]email: csguofen@scut.edu.cn, [b]email:duqing@scut.edu.cn, [c]email:yjclear@scut.edu.cn

Keywords: Cloud Computing; Virtualization; IaaS

Abstract. Cloud computing is considered to be the next generation of IT service model, and the virtualization technology is the key technology of it.The paper focuses on the design and implementation of an intelligent cross-platform IaaS platform which is called ICIaaS. It is based on the existing open source platform technology, while its deploying and scheduling strategy for virtual machines (VMs) is self-owned. The ICIaaS is compatible with the current mainstream commercial VM, and has applied in the current research project. It is concluded that it has achieved heterogeneous virtualized computing platform integration and intelligent VM management strategy.

Introduction

Cloud computing [1] is considered to be the next generation of IT service model, which has got a lot of attention from academia and industry. Virtualization technology is one of the key technologies of cloud computing, and it has greatly improved the utilization of computing resources, reduced the physical infrastructure, and implemented the on-demand deployment. Infrastructure as a service (IaaS) is an important branch of service delivery model of cloud computing. Various virtualization vendors have various independent management platforms. The different management way has brought great inconvenience for the application of IaaS. What's more, most VM deploying and scheduling strategy is too simple to meet the real-time requirements.

Most designs of the IaaS have been emphasized with the merchant's profits but the research value. Studies of these effects covered various aspects, and the subject is concerned chiefly with the design and implementation of an intelligent cross-platform IaaS (Infrastructure as a service) platform which is named as ICIaaS. It is based on the existing open source platform technology.

This paper is divided into four major sections as follows. Section 1 opens with the design architecture of the ICIaaS. Section 2 shows the self-owned virtual resource scheduling strategy. Section 3 provides the implementation and application of the ICIaaS, and section 4 draws a conclusion.

Design Architecture

The main goal of ICIaaS is to achieve heterogeneous virtualized computing platform integration and intelligent VM management strategy, so as to meet the needs of laboratory teaching and research and promote the combination of intelligent computing and cloud computing.

The ICIaaS invoked various virtualized computing resources through the API.It used a new IP address assignment technology basing on VM images injection[2], which has improved the polling host distribution[3] method. The user can use the underlying computing resources with the Web management end, and the platform is compatible with the current mainstream types of VM.

The mail goal of the intelligent VM management strategy is: to choose the most appropriate scheduling policies dynamically to deploy VM according to user requirements and the real-time monitoring data. And a new load balance deployment strategy is developed.

As in figure 1, the ICIaaS consists of three layers as follows.

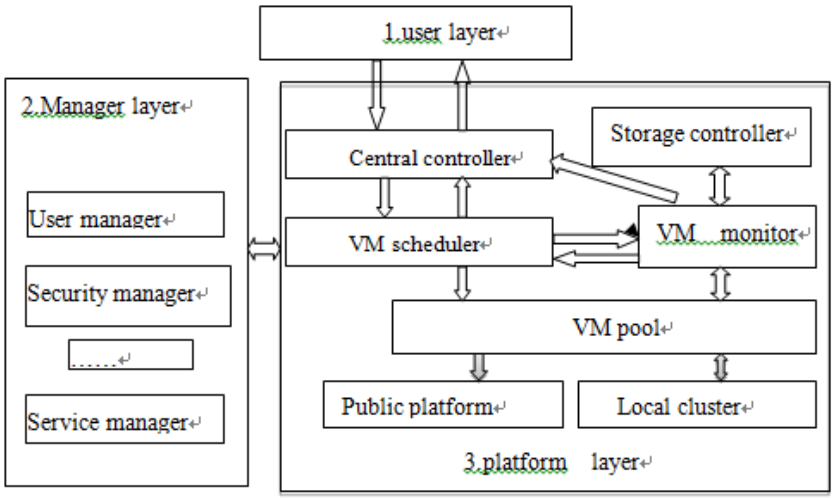

Fig. 1 The architecture of ICIaaS

1) The user layer: It is the interface that the user can interact with the ICIaaS conveniently.
2) The manager layer: It includes service management, user management, security management, etc. For example, the user manager is in charge of user information and rights .The service manager modules provide the service components which encapsulate services and functions of the underlying, and users can customize the service according to the needs on the Web interface.
3) The platform layer: It includes Central controller, memory controller, the VM scheduler, and the VM monitor, etc. The details are as follows.
   a) Central controller: It is composed of a set of services which coordinate the whole intelligent system. These services will response all the user requests ,validate and maintain system and user metadata .It employs the main standby server hot backup mode to ensure the security, which does not need to stop the system when failure appears.
   b) VM scheduler: It will deploy and schedule the VMs dynamically by analyzing the real-time data from the monitor. It has the function of static distribution and dynamic allocation. The details are in section 3.
   c) VM monitor: This module is in charge of monitoring the real-time usage of the service and resource, and then offers the reference to the scheduler. In order to generate resource allocation proposal, the monitor should summarize and analyze the surveillance data. It provides the user layer with a report, which will be helpful for the further task optimization.
   d) Storage controller: It is responsible for cloud storage management, including storage application, recovery of free space, access control, etc.
   e) Virtual resource pool: It encapsulates different kinds of VM. The module integrates local private cloud and public cloud. Firstly, it selects a virtualization platform type automatically. Secondly, it creates a VM by invoking the corresponding public API of various open source platform or private function provided by ICIaaS.

Resource Scheduling Strategy

The VM deploying and scheduling strategy is composed of the static and dynamic parts. The ICIaaS selected the BFD [4] strategy as the static one, and designed an intelligent deployment optimal selection and dynamic VM migration strategy as the other one. The process of the Strategy is noted in figure 2. The details are as follows: Firstly, to choose the best appropriate strategy, combining with the user demand and the current load value of the ICIaaS. Secondly, to choose the appropriate VMs to be migrated to rearrange the current request when there is no host to meet the requirement on the current scheduling domain.

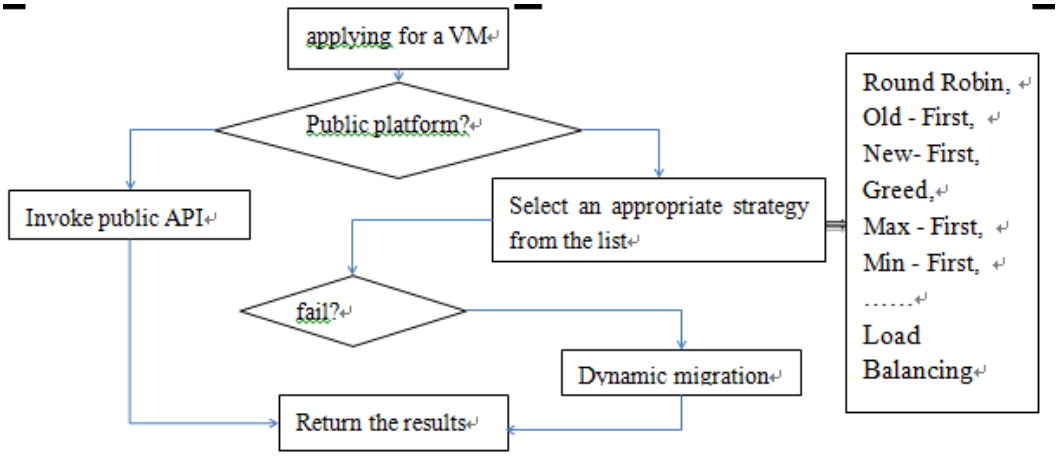

Fig. 2. The process of the strategy

1. Mathematical Describing

The objective of the strategy is as follows: (1) to meet the existing load request, and maximize the load balancing on each physical server scheduling domain. (2)to minimize the number of hosts to start on ICIaaS on the basis of 2.(3)to control the load rate of all hosts in each scheduling domain not higher than the specified threshold system.

Let $bl(j)(j \in [1,m]$(m stands for the number of the hosts in the scheduling domain) be the load performance value of the host p_j, O as the load performance value of the scheduling domain. Function f returns the number of the VMs deployed on the host p_j, while $H_p(P_j)$ represents the performance value of host p_j ,and $H_v(j,i)$ stands for the performance value of the VM V_{ji} . $\overline{W_x}$ (X can be a VM or a host) represents the performance weight vector, while $\overline{S_x}$ stands for the real-time performance vector. The performance weighted strategy calculates the load performance according to the following formulas.

$$H(x) = \overline{W_x} \times \overline{S_x} \quad (1)$$

$$bl(j) = \sigma \times H_p(p_j) + (1-\sigma) \times \sum_{i=1}^{f_n(j)} H_v(j,i)/f_n(j) \quad (2)$$

$$O = \sqrt{\sum_{j=1}^{m}(bl(j) - |bl|)^2}/m \quad (3)$$

2. Algorithm

If (m> threshold number)
return the first j in $\{j|j \in min_{j\in[1,l]} \Delta bl(j)\}$
else return the first j in $\{j|j \in min_{j\in[1,l]} \Delta O(j)\}$

The $\Delta bl(j)$ stands for the predicted change value of the load balancing performance of host p_j if the new VM is deployed on p_j.And the $\Delta O(j)$ stands for the predicted change value of the load balancing performance of the current scheduling platform.

Implementation and Application

The ICIaaS is compatible with the current mainstream commercial VM such as KVM[5], XEN[6], and has applied in the current research project.

1) Server virtualization: The basic part (such as VM application, destroy, etc.)adopts a mature virtualization management – libvirt, the advanced part (such as a balloon native memory drift technology) is developed by C language.
2) Network virtualization: It uses fixed IP allocation mechanism basing on the libguestfs VM images injected technology.
3) User's Web interface: The Central controller provides command interface for Web interface, so user can interact with it. The Central controller will check the legitimacy of

the command and parameter after accepting commands, and then return the results to the Web interface.

Conclusion

The research we have done suggests an increase in the VM deploying and scheduling strategy and various IaaS integration, which achieves the Qos and the good performance of cloud to some degree. The ICIaaS did provide a module of IaaS,which took the customer requests and the weight of performance parameters into account. What's more, it unified the virtualization resources view.We will improve the dynamic migration strategy to the platform to enhance the system reliability in the future work.

Acknowledgement

This work is supported by the national science of nature fund project (x2jsb55101680) and the guangdong province science of nature fund research group project (x2jsb6110010).

References

[1] http://en.wikipedia.org/wiki/Cloud_computing

[2]Theng, D., Hande, K.N.VM Management for Cross-Cloud Computing Environment. Communication Systems and Network Technologies (CSNT), 2012 International Conference .

[3] Iftikhar, M., Imran, M. , Al-Naymat, G., Alnuem, M.A. , Mathkour, H.Performance analysis of mixed polling schemes with multiple classes of self-similar traffic input to build comprehensive SLAs .Local Computer Networks Workshops (LCN Workshops), 2013 IEEE 38th Conference.

[4] Weiwei Lin, Baoyun Peng , Chen Liang, Bo Liu. Novel Resource Allocation Model and Algorithms for Cloud Computing. Emerging Intelligent Data and Web Technologies (EIDWT), 2013 Fourth International Conference.

[5] http://www.linux-kvm.org/page/Main_Page.

[6] http://wiki.xensource.com/.

Advanced Materials Research Vols. 989-994 (2014) pp 4400-4404
© (2014) Trans Tech Publications, Switzerland
doi:10.4028/www.scientific.net/AMR.989-994.4400

A network information filtering method based on node energy transfer

Ji LIU

Institute of statistics and information, Xinjiang university of finance and economics, Urumqi, china, 830012

email: liuji5000@126.com

Keywords: network information filtering; overlapping node; redundant recommendation energy; nonnegative matrix

Abstract. Network information filtering can be projected into link prediction in bipartite network to alleviate information overload. The paper discovers that node transfers redundant recommendation energy in network and gives bad effect on information filtering efficiency. Gathering node's overlapping degree by factorizing negative matrix, redundant energy is reduced with overlapping degree and initial recommendation energy. The method endows information filtering system with dynamic recommendation prediction, the empirical results indicates the method can enhance information filtering performance.

Introduction

The amount of information increases far more quickly than our ability to process it. Information filtering technology came into being as an effective method to alleviate the problem of "information overload"[0]. LIU mei-lian0 proposed a scheme of combining the shopping preferences of consumers and network behavior information to make information filtering. YUAN xiao-fang0 combined case-based reasoning and ontological structure to enhance the information filtering quality. With development of social networks, users can not only create information nodes, but also change the network links between them. Netizens' activities would have impact on information filtering results for others. ZHOU tao[4,5,6] projected information filtering system into user-object bipartite network and proposed information filtering algorithm based on network structure.LIU jian-guo[7][8] improved the computing similarity based on character of node . Some other researchers filtered information according to behaviors of online netizens0,the sparsity of recommendation data with tagged network[0]is reduced and revising the method of resource allocation[0] is revised. As a result, the quality of recommendation is partially improved. ZHANG Chu-xu0 combined rating information of netizens and clustering information of netizens, refining information of collaborative filtering commendation . Considering the effect of time window on reducing the complexity of information filtering computation and storing data, GUO qiang0 presented recommendation method based on time window. Although the above methods improved information filtering quality based on diffusion kinetics of netizen behaviors, the recommendation energy is amplified in the information filtering network .In addition, the recommendation energy of node is not stay at a static value with time, how to depict the transfer of recommendation energy in network is new problem facing us.

Resource allocation in bipartite network

Users and resource objects construct selecting (rating) relationship network in information filtering system, meanwhile, recommendation energy of objects can allocate and flow on network. The main target of information filtering system is providing new resource object for user based on users' information of selected resource object. Information filtering system can be projected in bipartite network is composed of users and objects, and the task of the recommender system is to provide new objects for user based on historical information of collecting. The object-set can be denoted as $O=\{o_1,o_2,o_3,\ldots o_n\}$,and user-set as $U=\{u_1,u_2,u_3\ldots u_m\}$, So we can get a $m\times n$ matrix $A=\{a_{ij}\}$,where $a_{ij}=1$ if u_i collected o_j, and $a_{ij}=0$ otherwise. Typically, bipartite network can be set as

G(X,Y,E), E denotes set of edge, X,Y can be denoted as $\{x_1,x_2,x_3,\ldots x_n\},\{y_1,y_2,y_3,\ldots y_m\}$,X's i-th node 's initial resource energy is $f(x_i)\geq 0$.

Tao Zhou[0] presented a weighted resource-allocation network to describe the relation of different resource. We can use the method to compute the allocation relation between objects in information filtering system. In the first stage, we can compute the recommendation energy of objects collected by user with edge in user-object network, In the second stage, user allocates he or her own energy to different objects, $f'(o_i)$ denotes the cumulated energy of o_i from all objects at last

$$f'(o_i)=\sum_{l=1}^{m}a_{il}f(u_l)/k(u_l)=\sum_{l=1}^{m}\frac{a_{il}}{k(u_l)}\sum_{j=1}^{n}\frac{a_{jl}f(o_j)}{k(o_j)} \tag{1}$$

Then ,we can draw,
$$f'(o_i)=\sum_{l=1}^{n}w_{ij}f(o_j) \tag{2}$$

where
$$w_{ij}=\sum_{l=1}^{m}\frac{a_{il}a_{jl}}{k(o_j)k(u_l)} \tag{3}$$

The weight denotes the degree of resource object o_j allocated to o_i, based on this weight and the initial recommendation energy of object that user collected, we can predict the final energy of each object by

$$\vec{f}'=W\vec{f}\ . \tag{4}$$

The top N objects can be obtained by sorting final recommendation energy in descending order, and we can recommend those N objects to active user.

The reduction of recommendation energy transfer in network

Resource allocation method allocates recommendation energy on network by transferring nodes twice, and draws transferring weight of recommendation energy between different resource objects, the matrix weight is denoted as W in eq.3. Since some resource objects are similar while some users are also resemble ,there is some redundant energy that transferred from similar objects(see[6]). The ability of transferring recommendation energy of node depends on the location of node in communities, we can see in graph 1.

From graph 1,we can see that m_1 is a core node in the community c_1,while m_2 also is a core node in the community c_2,$o_1$is an overlapping node of C_1 and C_2.

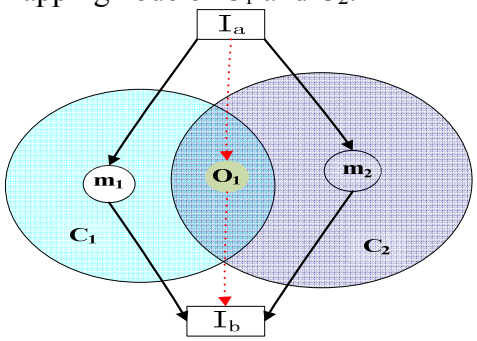

Graph.1 The transfer of recommendation energy in network community

The ability of transfer energy of Node m_1 and node m_2 is low. As an overlapping node, the node o_1's ability of transfer redundant recommendation energy between I_a and I_b is bigger than node m_1 and m_2.If we can get overlapping degree of node ,we can reduce the redundant recommendation energy in transfer process partially.

Computing overlapping degree of network node

The matrix that made up of user and object is a large scale non-negative matrix. We can use matrix factorization to reducing dimension of matrix and study character of overlapping node . see[14] . NMF can be looked as optimal problem.

$$E = \|V - QH\|^2 = \sum_{ij} (V_{ij} - QH_{ij})^2 \tag{5}$$

Lee[14] proposed a new update algorithm, the update rule is:

$$H_{au} \leftarrow H_{au} \frac{(Q^T V)_{au}}{(Q^T Q H)_{au}} \qquad Q_{ia} \leftarrow Q_{ia} \frac{(V H^T)_{ia}}{(Q H H^T)_{ia}}$$

Here if h_{ij} is the largest element in column j，the object j probably belongs to community i. If the second largest correlation value is similar to the largest ones, the node is probably overlapping node . we define overlapping degree as：

$$od_j = \frac{h_j^{**}}{h_j^{*}} \qquad ODM_{ik} = \begin{cases} 0, i \neq k \\ od_i, i = k \end{cases}$$

H* denotes the biggest correlation value in column j, while h** is the second largest correlation value in column j. The bigger overlapping degree value a node has, The bigger redundant energy the node transfers. The overlapping degree of all nodes can be set as overlapping degree matrix(ODM).

The reduction of recommendation energy transfer

Because some redundant recommendation energy can be transferred by overlapping node,we can use overlapping degree to reduce redundant recommendation energy(RRRE), the original weight matrix can be update as:

$$WED = W - W \times ODM \times W \tag{6}$$

For a given u_l, the different initial configuration will process on the network. In general, recent collecting activity can reflect a user's current preference accurately, the recommendation energy of node will decay with time .If the current time is t, the energy of initial configuration for u_p is

$$f^{t}_{u_p, o_j} = e^{\left[-\gamma \frac{(t - t_{u_p, o_j})}{\max_n (t_{u_p, o_n}) - \min_n (t_{u_p, o_n})} \right]} \tag{7}$$

γ is time attenuation coefficient of initial object. In this paper we set it as $\ln[\max_n(t_{up,on}) - \min_n(t_{up,on})]$,From above equation, the energy of resource objects in uncollected set is

$$\tilde{f}^{t}_{u_p, o_i} = \sum_j wed_{i,j} \times f^{t}_{u_p, o_j} \tag{8}$$

The top N resource objects can be obtained by descending energy of recommendation and be recommended to target user.

Empirical result

In order to test the accuracy of algorithm, we use MovieLens as benchmark data sets. The data set 1 consists of 10^5 ratings for 1682 movies by 943 users, the data set 2 consists of approximately 10^6 ratings for 3952 movies by 6040 users. We divided each data set into two parts based on rating time, which can be distinguished by the timestamp of the movieLens data. Typically, as for the two different data sets, we selected 30% records for each user that occurred in recent time as testing data, others 70% as training data.

For a given length L, the prediction list of user ul contains L objects. For each pair of relationship between a user u_l and objects on the list, o_j item in testing data，if o_j is also in the prediction list of u_l, we say the pair of user–object be hit in the given prediction list by system. The ratio of hit entries to the length of L is called the "hitting rate". Generally, for a given L, the algorithm with higher hitting rates is better prediction algorithm.

Table 1. The hitting rates for some typical lengths of prediction list.

Dataset	Length	GRM	CF	NBI	RRRE
Data set1	**10**	4.74%	6.26%	5.93%	8.11%
	50	16.78%	21.02%	21.45%	26.95%
	100	27.55%	32.72%	33.85%	41.68%
Data set2	**10**	2.98%	3.33%	3.40%	3.93%
	50	11.19%	12.38%	12.77%	15.11%
	100	18.74%	20.84%	21.61%	25.39%

The hitting rates of some typical lengths of prediction list are shown in table 1. When the length of list is 10，the merit of RRRE(reduce redundant recommendation energy) is obvious. The accuracy of information filtering is promoted by 70.25% higher than GRM(Global Ranking Method), and 28.91% than CF(collaborative filtering), and 31.65% than NBI(network-based inference) in dataset1, while promoted by 36.24% higher than GRM, and 21.92% than CF, and 19.41% than NBI in dataset2.

Conclusion

Based on network energy transfer, the paper proposes information filtering method recommends resource objects for users in dynamic environment. The redundant energy of recommendation has much business with the node overlapping degree. With a non-negative matrix factorization method, we get the overlapping degree and reduce the redundant recommended energy transfer and reduce initial energy of different objects according to time. Experimental data show that this method results in hit rate is better than other traditional methods.

Acknowledgement

We acknowledge GroupLens Group for providing us the data set MovieLens. This work is partially supported by MOE (Ministry of Education in China) Project of Humanities and Social Sciences (Project No. 11YJC630129), the National Science Foundation of China under Grant No. 71261025,the Fund of the Key Research Center of Humanities and Social Sciences in the general Colleges and Universities of Xinjiang Uygur Autonomous Region(NO. 050312B01)

References

[1] LY Lü, M. Medo, C H Yeung, et al. Recommender systems[J]. Physics Reports, 2012,519(1):1–49

[2] M.L LIU,T.C. Liu , W. P WU. Recommendation Algorithm Based on Web Consumer Preference Prediction[J].Library and information service.2012,56（4）:120-124

[3] X.F. Yuan, J.H. Lee, S. J. Kim, Y.H. Kim . Toward a user-oriented recommendation system for real estate websites. Information systems. 2013,38:231-243

[4] T Zhou, J Ren, M Medo, Y C. Zhang Bipartite network projection and personal recommendation [J] .Phys Rev E,2007, 76(4) :046115

[5] T, Zhou L L Jiang, R Q, Su Y C Zhang. Effect of initial configuration on network-based recommendation [J].Europhysics Letters,2008, 81(5):58004

[6] T Zhou, R Q Su, R R Liu et al. Accurate and diverse recommendations via eliminating redundant correlations[J]. New Journal of Physics 11 (2009) 123008

[7] J G Liu, T Zhou, B H Wang,et al .Highly accurate recommendation algorithm based on high-order similarities[J].Physica A ,2010,389:881-886

[8] J G Liu, B H Wang, Q Guo. Improved collaborative filtering algorithm via information transformation [J].International Journal of Modern Physics C ,2009,20(2): 285-293

[9] C J Zhang, A Zeng. Behavior patterns of online users and the effect on information filtering[J]. Physica A 391 (2012) 1822-1830
[10] Z K , Zhang T Zhou, Y C Zhang. Tag-aware recommender systems: A state-of the art survey [J]. Journal of Computer Science and Technology 26,2011 :767-777.
[11] J Ren, T Zhou , Y C Zhang. Information filtering via self-consistent refinement[J].EPL,2008, 82(5):58007-1--58007-5
[12] Zhang CH. X., Zhang Z K, Yu L, Liu CH., Liu H, Yan X. Y. Information filtering via collaborative user clustering modeling[J].Physica A: Statistical Mechanics and its Applications, 2014,396(15):195–203
[13] Q Guo., W. J. Song, L. HOU Y. L. ZHANG, J. G LIU. Effect of the time window on the heat-conduction information filtering model[J].Physica A: Statistical Mechanics and its Applications,2014,401:15-21
[14] D D Lee, H S Seung. Learning the parts of objects by non-negative matrix factorization [J]. Nature,1999,401(6755):788-791

Advanced Materials Research Vols. 989-994 (2014) pp 4405-4408
© (2014) Trans Tech Publications, Switzerland
doi:10.4028/www.scientific.net/AMR.989-994.4405

Improved HEED based Trust Routing Algorithm for WSNs

WANG JunWei[1, a], SUN WenYi[1,b]

[1] Department of control engineering, Northeastern University at Qinhuangdao, Qinhuangdao, hebei Province, China

[a]wjw0331@163.com, [b]sunwenyi@126.com

Keywords: Wireless sensor networks; HEED; Trust routing; QoS; energy efficient.

Abstract. In Wireless Sensor Networks (WSNs), besides the energy efficient, trust and Quality of Service (QoS) supported should be considered under some circumstances. All of them unveil additional challenges for routing scheme design. Based on Hybrid Energy - Efficient Distributed clustering (HEED) protocol, this paper presents a trust QoS routing algorithm for WSNs. Hierarchical structure is adopted and the trust value of the node is constructed by the direct trust value and the indirect trust value. In HEED, the combination of the trust value and residual energy as the main parameter and the propagation delay as the secondary parameter. The former guarantees the credibility of the data transmission, and the latter ensures the load balance of the entire network. Compared to typical routing algorithms of sensor networks, the proposed algorithm has better performance.

Introduction

Wireless Sensor Networks (WSNs) have got more and more attentions by people. However, WSNs are often placed in hostile environments and operated on an unattended mode in order to cooperatively monitor physical or environmental conditions. Due to the Characteristics of restricted by the limited resources of sensor node, WSNs can only support inherently unreliable communication [1]. Moreover, under some circumstances, nodes may suffer from malicious attacks such as denial of service (DoS) or packet modifications. Hence, the trustworthiness of routing information is an additional important parameter of it.

However, the existing routing protocols always pay more attention to energy efficient and Quality of Service (QoS), they rarely take the credibility into account. Providing trust guarantees in WSNs is a very challenging problem, but several approaches have been proposed in the literature. Related literature can be found in paper [1]-[3]. However, all of them cannot scale large networks due to the computation of trust value and no QoS parameters are considered.

Trust QoS Routing Model

WSNs can be modeled as a connected, undirected and weighted graph $G(V,E)$, where V denotes the set of nodes (sensor nodes and sink node) and E depicts the set of bi-directional links between nodes. For a pair of nodes $v_i, v_j \in V$ if the link $e_{ij} \in E$, then (v_i, v_j) are treated as a pair of adjacent nodes. Each node $i \in V$ in the graph, includes a set of three QoS metrics elements: $\{dl(i), re(i), tr(i)\}$. Where $dl(i)$ expresses the queuing delay, which can be obtained by the distance between two nodes, $re(i) = E_{res}(i) / E_{init}(i)$ denotes the remaining energy with respect to the initial energy and $tr(i)$ indicates the trust value.

Trust evaluation mechanism. Trust value of network nodes consists of direct trust value and indirect trust value. Direct trust value is determined by the node status and routing behavior, indirect trust value is determined by the interactions with the neighbor nodes.

Direct trust value. For the *n* recent historical records of a node, a triple $< td_i, time_i, td_m_i >$ is stored. Here, td_i refers to the initial trust value, $time_i$ refers to the time of inserting behavior,

td_m_i refers to the modified trust value. Set effective time window, the behavior record over the effective time will be removed from the window. Trust nodes using information of the recent behavior to take trust evaluation. Each behavior trust value of the record $td_i \in [0,1]$.

Computing trust value of node *i* in the recent period:

$$T_dir_i = \begin{cases} \sum_{i=N-n}^{n} \frac{time_i - time_{N-n}}{\sum_{i=N-n}^{n} (time_i - time_{N-n})} * td_i & n \neq 0 \\ 0 & n = 0 \end{cases} \quad (1)$$

Indirect trust value. The trust values of neighbor nodes to the evaluated node are used to calculate the indirect trust value. Any neighbor nodes of the trusted node *i* calculate its trust value t_ind_i recommended by the trust node:

$$t_ind_i = \begin{cases} r_i & td_i \geq \beta \\ td_i * r_i & 0 < td_i < \beta \\ 0 & td_i \leq 0 \end{cases} \quad (2)$$

td_i refers to the trust value of the neighbor nodes of the trusted nodes, r_i refers to the direct trust value of the neighbor nodes of the trusted nodes to the trusted nodes, β refers to the trust threshold. Indirect trust value defined as the mean value of all neighbor nodes to the trusted node:

$$T_ind_i = \frac{\sum_{i=1}^{n} t_ind_i}{n} \quad (3)$$

n refers to the number of neighbor nodes of the trusted nodes.

Comprehensive trust value. Comprehensive trust value reflects the trust of the node to the trusted node, consists of direct trust value and indirect trust value, calculated as follows:

$$tr(i) = (1 - \frac{init_n}{N}) * T_dir + \frac{init_n}{N} * T_ind \quad (4)$$

$init_n$ refers to the number of initial behavior records in a sliding window.

Delay Estimation. Wireless sensor nodes are scattered over a two-dimensional plane following a uniform distribution. Assume energy consumption follows free space model [4], then:

$$r = \frac{\lambda \sqrt{P_t / P_r}}{4\pi} \quad (5)$$

Here, P_r is received power of destination node, P_t is transmit power of source node, λ is the wavelength of signal, r is the distance between the two nodes.

Then the propagation delay between the two nodes is:

$$dl_{tr}(i) = r / c = \frac{\sqrt{P_t / p_r}}{4\pi f} \quad (6)$$

Here, f is the frequency of electromagnetic wave.

Because TDMA strategy is used to packet transmit, there is no queue delay in the procedure. Then the data processing delay $dl_{dp}(i)$ is fixed and depends on the node processor and packet length. The delay of the path is constructed by two parts: from general node to cluster head node $dl(s)$ and from cluster head node to base station $dl(b)$.

$$dl(P) = dl(s) + dl(b) \quad (7)$$

Algorithm Description

3.1 Cluster Head Node Selection

Hybrid Energy - Efficient Distributed clustering (HEED) [5] protocol is proposed in 2004. In order to prolong the network lifetime, it periodically selects cluster heads according to a hybrid of a main parameter (such as residual energy) and a secondary parameter (such as intra-cluster communication cost). The modified expression of main parameter is:

$$P(i) = \alpha tr(i) + \beta re(i) \tag{8}$$

Here, $P(i)$ is the probability of the node i being chosen as a cluster head node, α, β are weighted factors and $\alpha + \beta = 1$. The node which possesses more trust value and more residual energy will have more probability to become a cluster head temporarily.

3.2 Clustering Process

Once the cluster head nodes are selected, each of them will send a broadcast package to the other nodes along with the delay information $dl(s)$. In the proposed algorithm, the transmission delay from the regular node to the base station $dl(P)$ is chosen as the secondary parameter. If a node can't receive any of the broadcast information, then it is forced to become a cluster head nodes. If a node may receive more than one of the broadcast information, according to the received $dl(s)$, the node computes the path delay $dl(P)$. Under the premise of meeting delay requirement, the node decides to join the cluster through the trust value.

3.3 Packet Transmission

After the period of clustering process, the cluster head node adopts TDMA strategy to assigned time slot to the other node inside the cluster. The other node can send packet just in their respective slot, and in the rest of time, it is in the sleep state to reduce energy consumption. In order to ensure credibility of packer transmission, CRC check mechanism is used. Whenever packet transmission completed, the cluster head node verifies the packet and if it is validity, ACK packet is send back, and the other node increases its trust value in its time slot, otherwise, NAK packet is send back, and the trust value of the other node decreases. Over a period of time of data transmission, the cluster head nodes will send the results to the base station after data fusion.

3.4 Algorithm Design

Step 1. Initialize trust value of the node and a timer. Generate a random number, each node compute it's $P(i)$ according to the formula (8). Choose the cluster head nodes.

Step 2. Compute the delay of cluster head nodes to the base station according to formula (7), deliver the clustering packet RREQ and delay information.

Step 3. Compute the delay information from the other node to the neighbor cluster head nodes. Under the condition of meeting user's delay requirement, compute the trust value of the neighbor cluster head nodes.

Step 4. Send the request join packet RREQ from the general node to the cluster head node which has the maximum trust value.

Step 5. Under the control of the cluster head nodes, the regular node transmits its packet in its time slot. Update its trust value according to formula (4), the cluster head nodes exchange information with base station and update its trust value.

Step 6. If time out, go to Step 2, otherwise, go to Step 5.

Performance Evaluations

Simulations have been done on NS (Network Simulator) 2 platform. It was assumed that 200 sensor nodes were distributed randomly over a square area of 10 m× 10 m. Our proposed algorithm (Called HEED-T) was compared to AntQA[6] and LEACH. Same as [6], the initial energy of the sensor nodes was 0.5 J. Comparing the above algorithms through three aspects: node survival ratio (NSR); packet delivery ratio (PDR) (malicious nodes may refusal to retransmit packets) and packet

validity ratio (PVR) (malicious nodes may modify the real data). Simulations are shown in Fig. 1, Fig. 2 and Tab. 1. It can be found that the proposed algorithm has better performance.

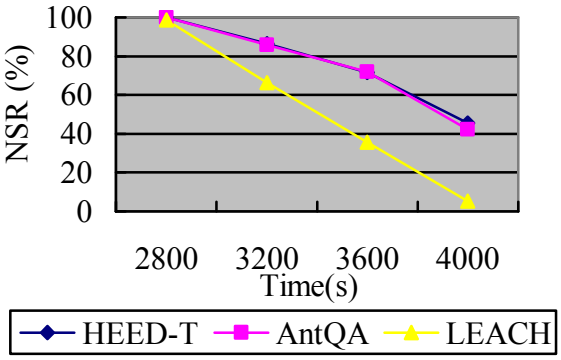

Fig.1 Comparison of Node Survival Ratio

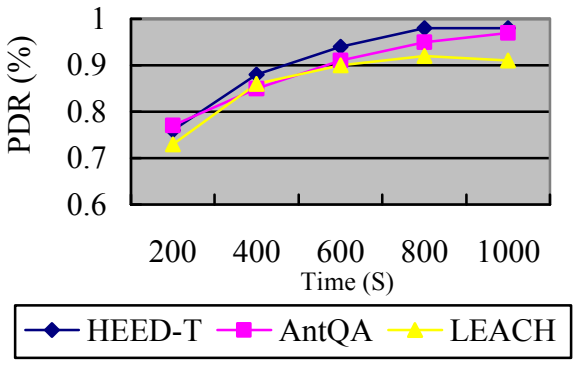

Fig. 2 Comparison of Packet Delivery Ratio

Tab.1 Comparison of PVR

Time(s) / Algorithm	2800	3200	3600	4000
HEED-T	100%	100%	100%	100%
AntQA	100%	97.6	91.2	87.8
LEACH	95.7	93.2	86.5	81.0

Conclusion

In this paper, a trust-based QoS routing algorithm is proposed. Three factors: Energy efficient, packer validity and QoS constraints are considered to modify the HEED protocol. Simulations have shown that the proposed algorithm is both feasible and effective.

Acknowledgment

This work is supported by the Fundamental Research Funds for the Central Universities under Grant No. N100423004 and Research Funds of Northeastern University at Qinhuangdao under Grant No. XNK201304.

References

[1] F. Bao, I. Chen, M. chang, et al, Hierarchical trust management for wireless sensor networks and its applications to trust-based routing and intrusion detection, IEEE transactions on network and service management, Vol. 9, No. 2, (2012), pp. 169-183.
[2] L. J. Li, L. J. Sun, R. C. Wang, et al, Energy efficient routing reliable protocols in WSNs, Systems Engineer ing and Electronics, Vol. 32, No. 12, (2010), pp. 2711-2715.
[3] K. N. Kiran, D. Mallapur, S. Hiremath, Trust based secured routing in wireless multimedia sensor networks, Fourth international conference on computational intelligence, communication systems and networks, (2012), pp. 53-57.
[4] H. K. Wang, Y. P. Li, L. Y. Zhang, et al. Mobile communication principle and technology, Tsinghua university press, 2009.
[5] O. Younis, S. Fahmy. HEED: a hybrid, energy - efficient, distributed clustering approach for ad-hoc sensor networks[J].IEEE Trans on Mobile Computing, 2004, 3(4): 660- 669
[6] L. Cobo, A. Quintero, S. Pierre, Ant-based routing for wireless multimedia sensor networks using multiple QoS metrics, Computer networks, Vol. 54, (2010), pp. 2991-3010.

Advanced Materials Research Vols. 989-994 (2014) pp 4409-4412
© (2014) Trans Tech Publications, Switzerland
doi:10.4028/www.scientific.net/AMR.989-994.4409

Self-certified ring signcryption scheme based on discrete logarithm problem

Haisheng QIN[1], Zhongxia JIANG[1,a], Maokui GENG[1], Jie LUO[1], Shulun ZHOU[1]

[1]School of Computer, Electronics and Imformation, Guangxi Univrsity. Nan-ning, China, 530004

[a]email: jiangzhongxia2008@163.com

Keywords: Self-certified Public Key Cryptology; Discrete Logarithm Problem; Ring Singcryption; Bilinear Parings

Abstract. This paper analyzes and summarizes existing ring signcryption schemes, combined with self-certified cryptosystem and ring signcrypption, we proposed a self-certified ring signcryption based on Discrete Logarithm Problem. The scheme proposed not only guaranties ring signcrption's anonymity, confidentiality, unforgeability and other security features, but also solves certificate management and key escrow issues, which can save storage space and communication cost. By removing bilinear pairings in the process of design, the efficiency of this scheme has been greatly improved. Concluded from the experimental results, this scheme has the advantages of high computational efficiency, high security, and low communication cost.

Introduction

In 2001, the concept of ring signature was first proposed by Rivest et al[1]. Ring signature is similar to group signature, which was proposed to leak information anonymously. Any user in the ring can use their private key and public key of other members to sign messages without all members' consent. The message receiver can only determine the signature from which groups but don't know the actual signer, only the actual signer can reveal its true signer identity, so the signer's anonymity is fully realized. Since then, some effective ring signature schemes were proposed by scholars.

Two of the most basic and most important services of Public key cryptography are secrecy and authentication, and usually both properties are required in many cryptographic applications. The traditional approach is signature then encryption, while in 1997, Zheng[2] introduced the concept of signcryption for the first time, which enabled us to achieve both encryption and signature in a single logical step, it was more efficient compared with the traditional signature-then-encryption approaches. Since then many effective signcryption schemes have been proposed.

The concept of Self-certified public key was first proposed by Girault[3] in 1991. It has two advantages as follow: (1)Save storage space and communication cost by not using certificates. (2)Reduce the quantity of calculation by not applying additional verification using public key. On this basis, scholars have proposed some self-certified signcryption schemes.

Ring signcryption was proposed in 2003, it not only has the functional features of ring signature, but also it is equally efficient as signcryption. Under such circumstances, scholars proposed many ring signcryption schemes[4], for example Yu[5] proposed the first self-certified ring signcryption scheme which combined the concept of ring signcryption and self-certified cryptosystem, but it is based on bilinear pairings, so the computational efficiency of scheme is decreased.

To improve the efficiency of ring signcryption, so we proposed a self-certified ring signcryption without paring which is based on the intractability of the discrete logarithm problem in the finite field.

Preliminaries

Related complexity assumptions

p, q are two prime numbers and satisfied the conditions of p | q-1. Let G be a cyclic additive group of prime order q, and g $\in F_P^*$ be a generator of G. At first, this paper assumes that for any polynomial time algorithm, the following problems do not have advantages that cannot be ignored to solve it.

(1) The discrete logarithm problem (DLP): Given element g, $g^a \in F_P^*$, and we need to compute a $\in F_P^*$.

(2) The computational Diffie-Hellman problem (CDHP): a, b $\in F_P^*$. Given g, g^a, $g^b \in F_P^*$, and we need to compute $g^{ab} \in F_P^*$.

Self-certified signcryption scheme based on discrete logarithm problem

Description of Scheme

(1) Setup: ① PKG chooses p_1 and q_1 as two large prime numbers, and they are both satisfied $p_1 = 2p' + 1$, $q_1 = 2q' + 1$. p' and q' are large prime numbers too. PKG computes $p = p_1 q_1$, choose g as a generator which prime order is $p'q'$. Then, KGC chooses some cryptographic hash functions as follows: $H_0 : \{0,1\}^* \times F_P^* \to F_P^*$, $H_1 : F_P^* \to \{0,1\}^n$, $H_2 : \{0,1\}^* \to \{0,1\}^L$, $H_3 : \{0,1\}^* \to Z_q^*$, $H_4 : Z_q^* \to \{0,1\}^n$, $H_5 : F_P^* \to F_P^*$.

② Then PKG randomly selects a secret value $x \in F_P^*$ as a master key of system, and compute its public key $y = g^x \bmod p$.

③ PKG keep (p_1, q_1, p', q', x) as secret. And publishes the system parameters （p, g, y, H_0, H_1, H_2, H_3, H_4, H_5） for the use of all users.

(2) Key Generation: The identity of the user U_i is d_i. User U_i romdomly selects a secret value $r_i \in F_P^*$, and computes $y_i = g^{ri}$. Then Ui send （d_i, y_i） to the PKG through a safe channel. After received（d_i, y_i）, PKG computes $Q_i = H(d_i, y_i)$ and $X_i = g^x Q_i$, and transmits it to the user Ui through security channel. After received （Qi, yi）, The user U_i can verify the legitimacy of the X_i by computing $y^{Qi} = X_i \bmod p$. If equation is holds, the user U_i computes $Si = r_i H_5(X_i)$ as his private key, and yi as his public key.

User's identity, public key and private key are （d_i, y_i, S_i）.

(3) Ring signcryption: There are user group U= {U_1, U_2, …. U_n}. Let user U_s who stands for the group U signcrypt message m. the user U_s as a member in the ring to signcrypt message m. The user U_s's identity is d_s, public key is y_R , and the private key is S_R. User U_s sends ciphertext to receiver whose identity is U_R. Then, the user U_s performs as follows.

1). User U_S randomly chooses k$\in F_P^*$, and compute $R = g^k \bmod p$.

2). User U_S selects r$\in \{0, 1\}^L$, keep r secret, then compute t=H(y_1... y_{s-1}, y_{s+1}... y_n, r).

3). For any i≠s, choose $U_i \in F_P^*$, then compute $h_i = H(d_R, y_R, U, U_i, t, m)$.

4). If i=s, compute $U_s = r_s Q_s - \sum_{i=1, i \neq s}^{n} (u_i + h_i Q_i)$, $h_S = H(m, U_S, U, y_R, d_R)$.

5). Compute $V = y_R^{h(y^{QR})(r_s + X_s)}, c = H_4(V) \oplus m$.

6). Compute $S = H_1(m, R) g^{-k} g^{S_s(r_R + X_R)}$.

Then send the ciphertext Ω={t, S, U, c, U_1, U_2,….U_n} to user U_R.

(4) Unsigncrypt: When the user whose identity is d_R receives ciphertext Ω={t, S, U, c, U_1, U_2,….U_n}, the receiver decrypts the ciphertext as follows.

1). For all i$\in$(1, n), check whether $hi = H(d_R, y_R, U, U_i, t, m)$, if all the equations hold, go to the next step. Otherwise reject the ciphertext Ω.

2). Compute $V' = y_s^{h(y^{Q_S})(r_R + X_R)}$, and recover the message by computing $m' = H(V') \oplus c$, If m= m′, means that the received message is correct.

3). Compute $V = R^{S_R(r_s+X_s)}$

4). Check that the equation $RS = H(m,R)\, y_s^{h(y^{Q_s})(X_R+r_R)} \bmod p$.

Correctness Analysis.

$$V = y_R^{kh(y^{QR})(r_s+X_s)} \bmod p = g^{r_R kh(y^{QR})(R_s+X_s)} \bmod p$$

$$= R^{r_R h(X_R)(r_s+X_s)} \bmod p = R^{S_R(r_s+X_s)} \bmod p$$

$$RS = g^k H(m,R) g^{-k} g^{S_s(r_R+X_R)} \bmod p = H(m,R) g^{r_s H_3(X_R)(r_R+X_R)} \bmod p$$

$$= H(m,R) y_s^{H_3(y^{Q_s})(r_R+X_R)} \bmod p$$

Security Analysis

Unforgeability.

PKG is credible: when an external attacker wants to signcrypt by faking a user in U, in order to construct a signature S which receiver can accept it. He must know the private key S_S of sender U_S .When attackers don't know private key of any member of user group, he want to solve S_S must faces discrete logarithm problem. and we all know it is difficult.

PKG is not credible: If PKG reveals part of private key X_s of signer U_s to attacker, but due to $S_s = r_s H_5(X_s)$, r_s in the equation is the secret value selected randomly by user, so it has a certain randomness, getting r_s also belongs to the difficulties of CDH problem through $y_s = g^{r_s}$, So it is hard to get the private key of signer, the attacker can't forge the signature.

Anonymity.

The design for this scheme is symmetrical, so as to attacker, any user in the users group U has the same power to signcrypt message, their probabilities are equal and they are 1/n. The probability that an attacker guesses signer correctly is not exceed 1/n .So the scheme satisfies anonymity.

Confidentiality.

Assuming attackers obtained ciphertext, If he wants to extract the message m from the ciphertext Ω={t, S, U, c, U_1, U_2,….U_n }. Attacker must know the value of V, but $V' = y_s^{h(y^{Q_s})(r_R+X_R)}$, and it is not feasible to get the value of V by this equation. because this procedure belongs to the difficulties of DLP. Therefore, in addition to any attacker outside user U_R can not recover the message m from the ciphertext Ω. So the scheme satisfies the confidentiality.

Authentications.

Through the scheme shows that any other users except U_s in user group can not prove that he is a real signer, because verify information(y_1... y_{s-1}, y_{s+1}... y_n, r)through equation t=H(y_1... y_{s-1}, y_{s+1}... y_n, r),it belongs to the problem of original image of hash function, and it is very difficult on the calculation. So in this scheme, only signer himself can prove his real signer identity.

Efficientibility.

With this scheme with [4] [5] comparing their efficiency, and H stands for Hash operation, P stands for bilinear operation, E stands for exp operation, G_{1M} stands for scalar multiplication of G_1, G_{2M} stands for multiplication of G_2, G_{1A} stands for addition of G_1. Comparative analysis of results are shown in Table 1 as follows:

Table 1.The results compared with [4-5]

scheme	Ring signcryption	unsigncryption
scheme[4]	2nP+(n+3)H+2G_{1M}+nG_{1A}+nG_{2M}	(n+2)P+3H+nG_{2M}+n G_{1M}
scheme[5]	(n+3)G_{1M}+(n+1)H+P+E+nG_{1A}	(n+1)H+3P+(n+1) G_{1A} +n G_{1M}
Our scheme	5E+4H+3 G_{1M}+(n+2) G_{1A}	(n+3)H+5E+3 G_{1A}+5 G_{1M}

Analysis in Table 1, we can see , our scheme does not use bilinear pairings. And compare with other operations such as pow operation , scalar multiplication and other operation, bilinear pairings is still are time-consuming and complex operation. In the whole ring signcryption and unsigncryption procedure, both scheme[4] and [5] used bilinear operation. And we all know the

bilinear pairing computation efficiency is relatively low, so our scheme is more efficient in calculation compared with scheme[4][5].

Conclusions

On the basis of intractability of discrete logarithm in the finite field, and combined with self-certified cryptosystem and ring signcryption, this paper proposed a self-certified ring signcryption. The scheme has the following characteristics: KGC only has part of users' private key, so it can't impersonate the user and forge signature; this scheme realizes the confidentiality and authenticity of the message within a logical step, and realizes full anonymity of the signcrypter. If necessary the signcrypter can publicly verify its true identity; The efficiency of the scheme has been improved by not using bilinear pairings. Through comparative analysis, this scheme we proposed has greatly improved the efficiency of signcrption.

Acknowledgement

In this paper, the research was sponsored by the Nature Science Foundation of China (Project No. 61262072).

References

[1] Rivest R L, Shamir A, Tauman Y. How to leak a Secret[c]. Advances in Cryptolopy-Asiacrypt'01, Springer-Verlag, Berlin, 2001: 552-565.

[2] Zheng Y. Digital signcryption or how to achieve cost (signature & encryption)[C]. Advances in Cryptology—CRYPTO′97，LNCS1294． Berlin: Springer—Verlag, 1997: 165—179.

[3] M. Girault. Self-certified public keys[C]. Advances in Cryptology-EUROCRYPT' 91, LNCS547, Berlin: Springer-Verlag, 1991:491-497.

[4] Hongxia Hou, Yefeng Hou. A new certificateless ring signcryption scheme[J]. Computer Technology and Development, 2012, 22(7):151-153.

[5] Huifang Yu, Bo Yang, Yi Zhao, Jiali Dang. Tag-KEM for Self-certified Ring Signcryption[J]. Journal of Computational Information Systems 9: 20 (2013) 8061-8071.

Advanced Materials Research Vols. 989-994 (2014) pp 4413-4416
© (2014) Trans Tech Publications, Switzerland
doi:10.4028/www.scientific.net/AMR.989-994.4413

Research on Ontology Based Government Affair Workflow

Shuxia WANG[1,a] Zengqiang WANG[2,b]

[1]College of Computer, Tonghua Normal University, Tonghua 134001, Jilin, China

[2]Qinghe Middle School, ji'an 130021, Jilin, China

[a] email: wsx1652@163.com, [b]email:zhong2004@163.com

Keywords: Ontology, Electronic Government, Workflow, Meta-Model

Abstract. The paper, in which Government Affair Workflow Model as an illustrated application is discussed, clarifies nature and concept of Ontology. Based on the characteristics of the workflow model and application of Government Affair Workflow , this paper puts forward Government Affair Workflow Model and creates a Workflow Meta-Model, Document Meta-Model and Determent Meta-Model and offers framework of OWL+RDF+XML. It is proved in the experiments that Ontology can be applied effectively in Government Affairs Workflow.

Introduction

With the rapid development of the technology of computer hardware and software and Internet, OA has been widely studied and applied. To fit political system reform and government innovation, electronic government has also become a research focus. For the government, different from the common OA system, electronic government not only needs to attain simplifying structures and increasing work efficiency of the government after finishing routine work, but also tries to serve the people to the utmost extent and establish a good image in their hearts for the government. So the construction of electronic government includes the construction of internal and external information of the government and better integration of these systems.

In addition, due to relatively clear intelligence division in the current government, it needs the cooperation among several government departments to finish a task. To improve work efficiency of the government, not only the cooperation among the departments should be enhanced but the parallelism of work should be increased. As core technology of a process modeling and a process management, management technology of workflow can be effectively combined with other applied systems, and produce various vocational management systems which meet the demand of the government such as OA, project management software and PDM system etc. Therefore, electronic government system suits for adopting workflow technology to build system model. A large number of different government processes exist in government departments, and there are different ways adopted to depict government processes. At present, the most promising technology about the communication of common concept is Ontology which is based on RDF semantic network of W3C company.[1] Therefore, as Government Affairs Workflow Meta-Model, Ontology technology can be used as the main described technology.

The Whole Hierarchical Structure

Workflow is a computerized model reflecting vocational process. It is also a vocational model operated by Workflow management system to achieve business process integration and process automation in the advanced computer environment. Workflow technology is a core technology which realizes business process modeling, business process simulation analysis, business process optimization, business process management and integration and ultimately accomplishes business process automation. In government affairs process, putting Workflow into business process modeling and deep analysis can standardize the government business process, discover the unreasonable parts in business process and optimize and restructure government business process. Moreover, business process model itself is the important knowledge base and rule base, so it can be a model directing to operate computer management information system.[2]

Philosophically, Ontology studies nature of objective things; in the engineering sense, Ontology refers to a concept or a terms in a field. According to W. N. Borst, Ontology is defined as a formal, explicit specification of a shared conceptualization. [3]The purpose of constructing Ontology is to achieve Knowledge sharing and reuse to some extent. Combining with multilayer technology framework and Workflow model developed and supported by W3C, the paper puts forward layer framework structure of Ontology model (see Fig. 1).

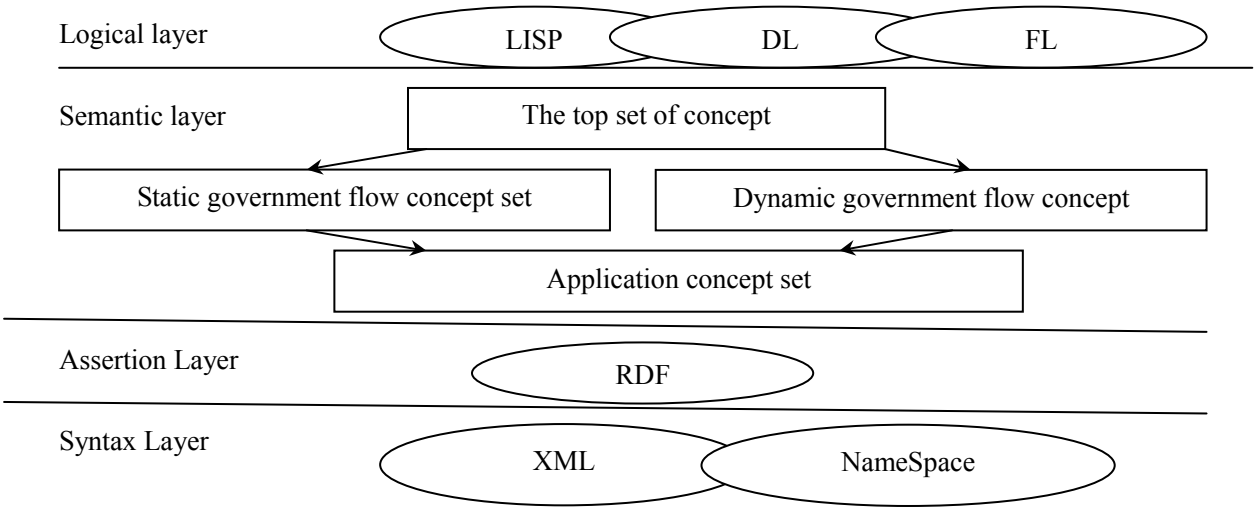

Fig. 1.The Model Framework of Government Affair Workflow Ontology

(1) Logical Layer: It is the foundation of achieving the reasoning function of Government Affair Workflow Ontology Model. It inquires of the concepts of semantic layer, property and example by Artificial Intelligence such as DL, FL, and Lisp etc. and logically reasons them, ultimately forming Government Affair Workflow expert system with reasoning function.

(2)Semantic Layer: It is the core of Government Affair Workflow Ontology Model and includes The top set of concepts, Static workflow concept set, Dynamic workflow concept set and Application concept set, among which Static workflow concept set and Dynamic workflow concept set belong to intermediate concept set. These concepts have nothing to do with government departments, but are the concept sets which Government Affair Workflow model mainly studies. The top set of concepts chiefly involves the most basic concepts, properties and semantic relations connected with government activities such as time, space, object, event and behavior etc; Static workflow concept set mainly refers to the most basic concepts about time, space and object in government field such as civil servants, government institutions, working documents and various archives; Dynamic workflow concept set mainly shows the most basic concepts about event and behavior in government field such as official document circulation, civil servant switch and document classification; Application concept set indicates the concepts connecting with government department resources and government transfer activities.

(3)Assertion Layer: It establishes the connection between metadata and described resources in a standard way, thus ensuring that computer is able to clearly identify the meaning of metadata and its relation with the resources. Currently, RDF is becoming a basic assertion mechanism in a network environment.

(4)Syntax Layer: It is a markup language standard, which marks the above three layers in a way computer can understand and handle. At present, as the markup language of network resources, XML is becoming the basic markup language of semantics and knowledge. Furthermore, it also needs data encoding and the standard which the resources show such as Unicode and URL.

Government Meta-Model and Ontology Description

Basic Meta-Model made by WFMC is a model used to depict the internal connection of workflow model. It describes different objects, the relations among different objects and their properties. In addition, using this Meta-Model helps to establish model which is able to exchange information among many workflow products.[4]

In terms of modeling approach of workflow model and combining with the process of government work, the paper presents the abstract Government Affair Workflow model in Fig.2. Two main parts are included here: The first part finishes the design of government process, and the second part finishes the execution of government process. The paper researches the main applied method of Ontology in the design stage of government process. The paper won't focus on the fact that the popular frameworks such as J2EE, Struts and NET are adopted to accomplish the run phase of government process.

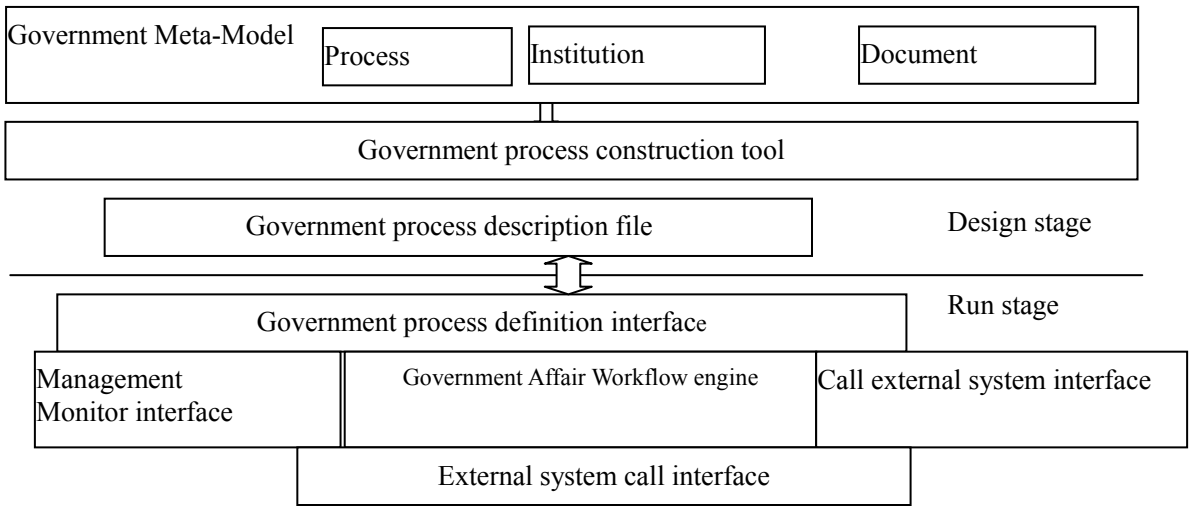

Fig. 2 The abstract Government Affair Workflow model

3.1 Government Meta-Model

Government Meta-Model is composed of three parts: process Meta-Model, institution Meta-Model, document Meta- Model.

Government process Meta-Model uses process object, activity object, route object and control object etc. to depict a government process. As for the characteristics of government process, we need extend and simplify the basic Meta-Model in some fields. We lead a series of relevant concepts into the study and remove some objects and properties used less in government process definition.

Since government authorities have clear division, special staff administrates special tasks, which contributes to government administration, but also increase the flexibility of work. The reengineering of government process is put forward on such a kind of premise. Moreover, how to reengineer government process and what kind of model will be r reengineered have been the issues which need to be discussed deeply. Based on Government Affair Workflow model mentioned here, the paper also presents government institution Meta-Model and government document Meta-M model. Government institution Meta-Model is used to describe the relations of various staff, departments, and posts in the government. Government document Meta-Model is used to depict the composition of using documents, the types of different elements constituting documents and permissions in government process.

Government process Meta-Model is the core in these three parts and builds the link with government institution Meta-Model and government document Meta-Model. To enhance the flexibility of government process description, we have some expansion in government Meta-Model: (1) in government circulation Meta-Model, activity object and control object are separated and the information, concerning with process control information such as convergence and divergence structures, is described by control object in order to increase the flexibility and modifiability of process description. (2) Different objects in government Meta-Model needn't give a complete definition at the moment of process definition. According to the practical process running state, evaluation can be provided during the course of process running, which can increase the flexibility of government process. Through government Meta-Model, we needn't define completely the activity at the definition stage, but can finish handling it at the running period in terms of the property of activity object when touching different sub-processes of government. (3) In government Meta-Model, the relevance between activity object and document object leads to the connection

between government process Meta-Model and government document Meta-Model. In the process of government circulation, the information on the direction of circulation and the participants of activities can be dynamically determined in terms of the contents of government documents. (4) In government Meta-Model, the relevance between activity object and character results in the relations between government process Meta-Model and government institution Meta-Model. Government Meta-Model can adopt dynamic character to describe activity participants. Dynamic character possesses a certain generating rule, so according to the information about government institution and the choice of participants at the stage of process execution, participants will be automatically generated in the next activity, and that way process user can dynamically change process participants according to the actual situation. At the same time, it can ensure that the optimization of government institution can't influence process structure.

3.2 Ontology Description of Government Meta-Model

To adopt to he complexity and polytrope of government work, a government process construction tool is added in government Meta-Model and government process description document. The tool will provide a graphical interface to directly finish the direct allocation of government process description document and then the allocated document will achieve the alteration and reconstruction of relevant tasks in government Meta-Model to increase flexibility of handling tasks. In the paper, government process description document chiefly uses Ontology language to construct, and it possesses the main functions as follow:

(1)At the initial design stage of government process, Ontology can conserve the design result of government process and put it into the file so that it can present shared knowledge data and indication to get better allocation and government process installment in addition to a certain intelligence decision instructions. In the phase of government process execution, corresponding data can be checked and conserved. As the input of Government Affair Workflow engineer, Ontology language can provide workflow engineer with control information and correctly control government process and make it follow the plan to execute normally. (3) During the course of government circulation, Ontology language establishes own Government Process Description Document for every circulation process. In addition, workflow can finish the dynamic revision and allocation of description documents. The accomplishment of the revision and allocation of government process doesn't influence the circulation and allocation of the other business process.

Conclusion and Outlook

With the idea of workflow, the main tasks in government departments are applied to the consolidated shared platform Ontology provided, thus making government leaders and the common civil servants work better and effectively avoiding the appearance of the isolated information island.

In our opinion, Ontology is an effective knowledge indication and shared way, and is able to organize knowledge in a field better; Workflow management technology is a core technology of process modeling and process management, and conveniently integrates task process of government. Government Affair Workflow model which Ontology is used to show possesses a certain reference significance for achieving government management system and electronic government system.

Based on the above research results, we are developing and designing protosystem and deeply discussing electronic government model based CSCW.

Reference

[1] http://www.w3china.org

[2]FanYusun. the base of Workflow management technology. Beijing: Tsinghua University press, 2001:32

[3] W. N. Borst. Construction of Engineering Ontologies for Knowledge Sharing and Reuse. PhD thesis, University of Twente, Enschede, 1997.

[4] Workflow Management Coalition. The Workflow Reference Model, Version 1.1 [EB/OL]. http://www.wfmc.org/atandards/docs/tc003vl.pdf ; 2002.10.27/2004.06.05

[5]Bi Jianxin, Zhu Shuyuan etc. E-government and government process reengineering. Modern intelligence, 2004 (4)

[6] Zhaowen,Hu Wenhui, Zhang Sikun etc. Research and application of workflow Meta-Model [J].Journal of software,2003,14(2)

Advanced Materials Research Vols. 989-994 (2014) pp 4417-4420
© (2014) Trans Tech Publications, Switzerland
doi:10.4028/www.scientific.net/AMR.989-994.4417

The robustness and mutual information entropy of random modular Boolean networks

Nan ZHAO[1,2,a], Binghui GUO*[1,2,b] , Fanchao MENG[1,2]

[1] LMIB & School of Mathematics and System Sciences, Beihang University, Beijing 100191, China

[2]State Key Laboratory of Software Development Environment, Beihang University, Beijing 100191, China

[a]email: nancyzo1990@gmail.com [b]email: binghuiguo@gmail.com * corresponding author

Keywords: Boolean Network; Dynamical Analysis; Information Entropy

Abstract. Random Boolean networks have been proposed as a basic model of genetic regulatory networks for more than four decades. Attractors have been considered as the best way to represent the long-term behaviors of random Boolean networks. Most studies on attractors are made with random topologies. However, the real regulatory networks have been found to be modular or more complex topologies. In this work, we extend classical robustness and entropy analysis of random Boolean networks to random modular Boolean networks. We firstly focus on the robustness of the attractor to perturbations with different parameters. Then, we investigate and calculate how the amount of information propagated between the nodes when on an attractor, as quantified by the average pairwise mutual information. The results can be used to study the capability of genetic information propagation of different types of genetic regulatory networks.

Introduction

Networks' normal performance are essential to the stabilization of nature and human society such as random Boolean networks (BNs) [1]. BNs have been used to study global dynamic properties of biological networks, particularly as models of gene regulatory networks. In this context, the Boolean variables are used to represent the genes [2].

There're many kinds of BNs, one of them is random Boolean networks (RBNs) [3]. RBNs behave a rich variety of dynamical preferences, which don't assume any particular functionality or connectivity of the random generated nodes and are generic. The properties and abundance of attractors have been focused by much work. The RBNs' topologies with one input per node can be looked as graphs of random maps. Due to the corresponding topology, there's an access to investigating random maps and finding analytical results for attractors in RBNs. At the same time, there's some strong differences that emphasize the difficulties in making direct comparisons between RBNs and real systems [4].

The asymptotic dynamics of RBNs subjected to random fluctuations is investigated. Under the effects of noise, the system can escape from the attractors of the deterministic model, and a thorough study of these transitions is showed. The sets of attractors can more properly describe dynamics rather than single ones. Through interpreting RBNs as models of genetic regulatory networks, it suggests the threshold ergodic sets [3].

According to a Boolean function and the current state of its input nodes, all nodes are synchronously updated at every time in synchronous networks. RBNs present a rich boundary of dynamics. In particular, groups of BNs fall into two broad dynamical regimes: order and chaos [5]. The dynamic regime of the network can be determined from its response to perturbations, such as a deviation from the behavior prescribed by the topology and logic of the network. In general, ordered RBNs are very robust to perturbations – they behave similarly to the unperturbed network – however they lack the ability to respond differently to different perturbations. RBNs in the chaotic regime tend to magnify small perturbations until the entire behavior of the network changes. Because of that, their responses to similar perturbations differ widely.

The most usual method to measure the response to perturbations is to assess the number of nodes which are in different states. These assessments of robustness studied the response of RBNs to perturbations, starting from random states [6]. Information propagation in RBNs also has been assessed by other methods, which also found maximization at the critical regime [7].

So far, there are some researches on the RBNs and they have gotten some results [8]. In a large, complex network of interacting elements, such as a genetic regulatory network, the average of the mutual information over all pairs is a global measure of how well the system can coordinate its internal dynamics. They study this average pairwise mutual information in random Boolean networks RBNs as a function of the distribution of Boolean rules implemented at each element, assuming that the links in the network are randomly placed [9].

Based on the fact that real RBNs are modular [10] and most studies have been made over random topologies, it is important to study the properties of robustness and information propagation in RBNs with modular topologies. Therefore, in this paper, we extend classical robustness and entropy analysis of random Boolean networks to random modular Boolean networks. In one hand, we focus on the robustness of the attractor to perturbations with different parameters. In another, we investigate and calculate how the amount of information propagated between the nodes when on an attractor, as quantified by the average pairwise mutual information.

Definition of the robustness and mutual information entropy

In a biological setting or genetic regulatory system, we expect that both the ability of the network to process information and its robustness. Particularly for RBNs, it is important to calculate these two different indices. Based on the work in [9], we extend their methods to the random Boolean networks with modular topologies.

Firstly, we define the robustness index of an attractor, *RA*, which can be quantified by the fraction of the number of single-node perturbations from all states of all the possible attractors after which the network returns back to the original attractors. Here, we use single-node perturbations, which could be formally defined as the probability that a trajectory starting from a state on an attractor with one node perturbed, will return to that attractor.

Then, we define another index, mutual information entropy, *IA*. The different levels of mutual information entropy are defined as follows.

Let S_a be a process that generates a 0 with probability p_0 and a 1 with probability p_1. We define the information entropy of S_a as

$$H[S_a] = -p_0 \log_2 p_0 - p_1 \log_2 p_1 \tag{1}$$

Similarly, for a process sab that generates pairs *ab* with probabilities p_{ab}, we define the joint information entropy as

$$H[S_{ab}] = -p_{00} \log_2 p_{00} - p_{01} \log_2 p_{01} - p_{10} \log_2 p_{10} - p_{11} \log_2 p_{11} \tag{2}$$

For an instance of RBNs, we may consider running the dynamics for finitely long times and starting from all possible initial configurations which can be evolved to some attractor. The value of p_{ab} for the process is given by the fraction of time steps for which node *i* has the value a and on the next time step node j has the value *b*. Then, the mutual information entropy of the pairwise *ij* could be defined as

$$M_{ij} = H[S_i] + H[S_j] - H[S_{ij}] \tag{3}$$

Therefore, the mutual information entropy between the time series of two nodes of a Boolean network with modular topologies, with the output time series shifted by one time step *IA*, can be used as a measure of the amount of dynamical correlation between an input and an output. We use the average mutual information between all nodes as a measure of the average efficiency of information propagation in the network as following equation

$$\langle IA \rangle = \left\langle N^2 \sum_{i,j} M_{ij} \right\rangle \tag{4}$$

It has previously been observed that $\langle IA \rangle$ is maximized near the critical regime in numerical simulations of random Boolean networks with a small number of nodes.

Algorithms and numerical simulation results

As the state of the Boolean network may have kinds, therefore, we need to use backtracking search. It is about the current state and status before looking for ways to compare iterative sequence repeat state to find the attractor. Depending on the nature of synchronous RBNs, if there are duplicate states in the iterative sequence, all the subsequent states are repeated. Therefore, in order to reduce the computational complexity, every T iteration step can conduct a retrospective search.

When calculating the robustness, we use this method to search the attractor: T is taken as 1/10 of iterations of having been conducted attractors, and keeps on updating constantly. After searching the attractor, we keep the current state as a starting point for half of the nodes are applied perturbation, and iteration. If the iteration to the previous state of a disturbed state with the same step, then stop the iteration, remember back to the times of the original disturbance attractor. If the iteration has reached the attractor, but still did not appear the state of disturbance before, then stop the iteration, the second disturbance failed to remember back to the original attractor. Counting the proportion of the times that disturbed status come back to the original attractor add up to account for the disturbance times， then we get the robustness index

When calculating the mutual information entropy, in order to search for duplicate state for the first time the iterative sequence, we shall fetch as 1 T, or search by tracing each iteration step. At the same time, record the number of nodes to take the number of "0" and "1" and take "00", "01", "10" and "11" .After the search to the attractor, according to the records of each node and node, the number of the various values obtained by the probability of their various values, then the probability of their various values are put into mutual information entropy formula, we can get the mutual information entropy.

The calculation results are in the following graphs.

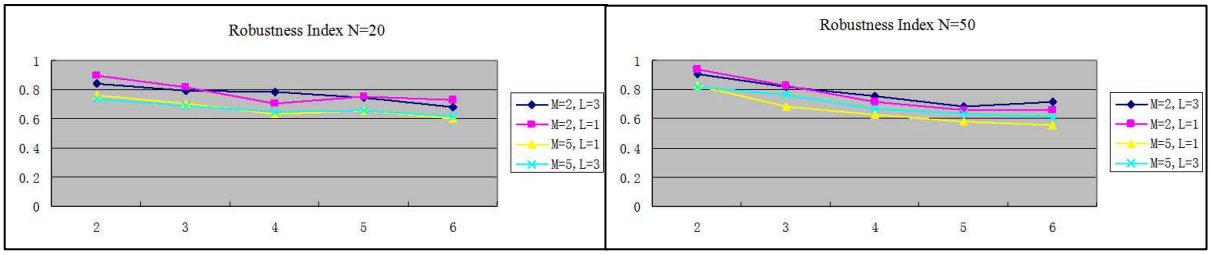

As we can see, robustness index decreases with the increasing of K value. When the module is strong, that is, the value of M is larger, there has less robustness index. With respect to K, M, L has the less effect in the robustness index, but we can see that when the module is strong, the test group which L is larger has the higher robustness index than the smaller one.

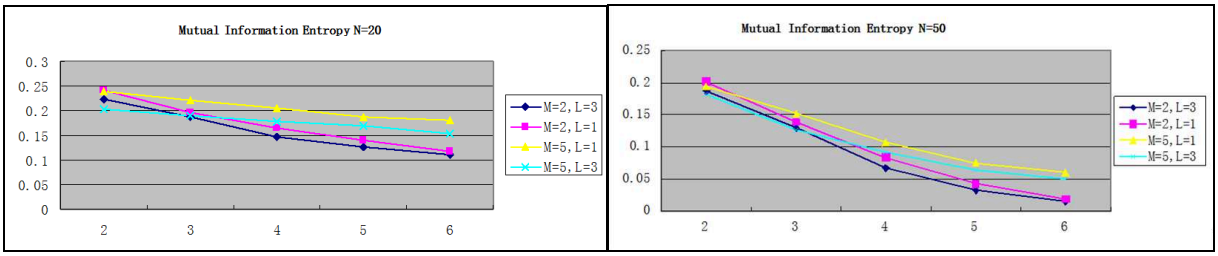

We can see from the figure that the mutual information entropy increases with the K value decreases. When L is small, mutual information entropy is larger. The modularity of mutual information entropy affect y related to the K value. When K = 2, the interactive of low entropy test module set is large, and when K> 2, the interactive of the high entropy test module set is large. In other words, high modularity reduces the speed of the mutual information entropy decreases with the increase of K. Besides these, we also found that when the larger network size, the N value larger, and the value of mutual information entropy decreased greatly.

Conclusion

Since the modularity plays an important role in evolution of biological systems, it is necessary to extend classical robustness and entropy analysis of random Boolean networks to random modular Boolean networks. Based on the analysis and calculation of the robustness and pairwise mutual information entropy in this work, we find that the dynamical behavior and properties of attractors in random Boolean networks are quite different from those in random modular Boolean networks. This investigation of the robustness of the attractor to perturbations and the capability of genetic information propagation with different parameters could be the new viewpoint to explore the mechanism of realistic genetic regulatory systems.

Acknowledgement

In this paper, the research was supported by State Key Laboratory of Software Development Environment (Project No. SKLSDE-2012ZX-09) and NSFC Project 11290141.

References

[1] Grefenstette J, Kim S, Kauffman S (2006) An analysis of the class of gene regulatory functions implied by a biochemical model. Bio Systems 84: 81–90.

[2] Kauffman SA (1969) Metabolic Stability and Epigenesis in Randomly Constructed Genetic Nets. J Theor Biol 22: 437–467.

[3] Ribeiro AS, Kauffman SA, Lloyd-Price J, Socolar JES (2008) Mutual information in random Boolean models of regulatory networks. 77: 011901.

[4] Shmulevich I, Kauffman SA (2004) Activities and Sensitivities in Boolean Network Models. Phys Rev Lett 93: 048701.

[5] Bertschinger N, Natschlaäger T (2004) Real-time computation at the edge of chaos in recurrent neural networks. Neural computation 16: 1413–1436.

[6] Krawitz P, Shmulevich I (2007) Basin Entropy in Boolean Network Ensembles. Phys Rev Lett 98: 1–4.

[7] Nykter M, Price N, Larjo A, Aho T, Kauffman S, et al. (2008) Critical Networks

Exhibit Maximal Information Diversity in Structure-Dynamics Relationships. Phys Rev Lett 100: 1–4.

[8] Derrida B, Weisbuch G (1986) Evolution of overlaps between configurations in random Boolean networks. J Physique 47: 1297–1303.

[9] Lloyd-Price J, Gupta A, & Ribeiro A S. (2012) Robustness and information propagation in attractors of Random Boolean Networks. PloS one, 7(7): e42018.

[10] Segal E, Shapira M, Regev A, Peer D, Botstein D, Koller D, & Friedman N. (2003) Module networks: Identifying regulatory modules and their condition-specific regulators from gene expression data. Nature Genetics, 34: 166–176.

Advanced Materials Research Vols. 989-994 (2014) pp 4421-4426
© (2014) Trans Tech Publications, Switzerland
doi:10.4028/www.scientific.net/AMR.989-994.4421

Research and Design of Network Instruction Interaction Mode

Cong LIU[1, a]

[1]Information Technology Center, Tsinghua University, Beijing, 100084, China

[a]email: liuc@tsinghua.edu.cn

Keywords: Network Instruction; Interaction; Interaction Mode; Network Instruction Platform

Abstract. The quality and effect of network instruction is largely affected by the effectiveness of network instruction interaction. Firstly, we explain the definition and elements of network instruction interaction, as well as the concept of interaction of network instruction platform. Then, we focus on the overall analysis of network instruction interaction from the horizontal and longitudinal aspects. In the horizontal analysis, we discuss the network instruction interaction mode in detail. In the longitudinal analysis, we integrate all the instruction modes to introduce the instruction interaction hierarchical model. As the network instruction platform is a key element in the implementation of network instruction, its interactivity greatly affecting the effectiveness of network instruction as well, we finally design network instruction interaction mode including interactive classification and overall architecture of network instruction platform, in order to provide information technology support to create flexible network instruction interaction environment.

Introduction

Interaction is one of the basic characteristics of instructional activities. In the various forms of instructional activities, interaction approaches are different. With the rapid development of information technology, advances in network technology, communication technology and multimedia technology have not only promoted the changes of instruction form, but also have promoted the development of instruction interaction theory. Interaction has become the term widely used in the field of network instruction. Research scholars [1-3] argue that many new technologies own interactivity and make it easier to create instruction environment. In such kind of environment, students can learn through practice, get feedback, continue to improve their understanding and build new knowledge. Network instruction based on Internet and multimedia must and only has rich interaction mechanisms in order to truly achieve the goal of network instruction, to inspire the power and desire of students to explore knowledge, and to intuitively provide learning contents.

Network instruction platform with rich interactivity is the demand of network instruction, and is the necessary requirement to play the effectiveness of network instruction. How to fully understand and design interaction mechanisms of network instruction platform has become an important part of design, development and evaluation of this platform. Currently, researches on interaction of network instruction platform mostly focus on the analysis from the technical point of view on how to design and develop interactive means, and have less analysis from the instruction application level point of view on meanings and characteristics of interactivity. In this paper, based on the related concepts we focus on network instruction interaction from two aspects of horizontal and longitudinal analysis, and design network instruction interaction mode.

Related Concepts

The meaning of network instruction interaction. In the researches on the instruction interaction under the network environment, the explanations and descriptions of its meaning mainly include as follows.

- Merrill, LI and Jones believe that learning interaction is a real-time, dynamic and mutual giving extraction process including the exchange of relevant information between instruction system and students [4].

- Gilbert and Moore believe that instructional interactivity based on computer-media refers to information exchange between students and technology [5].
- Professor Wagner believes that interaction is the mutual influence and information exchange between individuals and groups, requiring interaction between two subjects and two kinds of activities [6].
- Chen Li believes that instruction interaction is an event occurring between students and learning environment, which includes students and teachers, as well as exchanges between student and student, and includes mutual exchange and interaction between student and a variety of physical resources [7].

Taking these above descriptions, we can conclude the definition of network instruction interaction. Network instruction interaction refers to under the network environment for the realization of the instructional target interactive events between students, network instruction resources and teachers. The events include social interaction between student and teacher as the subject, the interaction and communication between subject and network instructional resources as the object, as well as the dynamic change process of network instructional resources.

Element analysis of network instruction interaction. Any instruction system includes three elements, i.e. teachers, students and curriculum resources. Curriculum resources include instructional media and instructional information. Network instruction system as a special instructional system contains three factors, i.e. teachers, students and network instruction platform. In fact, network instruction interaction shown in Fig.1 refers to the interaction and relationship between teacher, student and the network instruction platform.

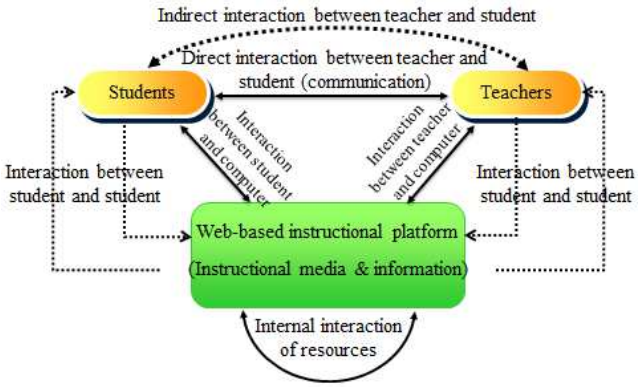

Fig.1. The interaction between the various elements of network instruction

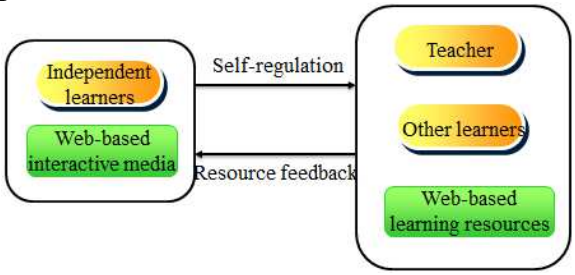

Fig.2. Individual independent interaction mode

The interaction definition of network instruction platform. The interaction of network instruction platform one hand refers to dynamic representation and generation of instruction information, on the other hand refers to information and emotion exchange activities formed by interaction between students and teachers in the network instructional process.

The interaction purpose of the network instruction platform is to enable students to change their behaviors through mutual communication and interaction in the network learning process in order to achieve network instruction goals. When this interaction enables students to respond to students' behavior toward the direction of instructional objectives, the network instruction is effective. Therefore, the interaction of network instruction platform is focused on how interactive activities make an effect on the meaning of student learning.

Horizontal Analysis of Network Instruction Interaction Based on Network Instruction Interaction Mode

Individual independent interaction mode. In the individual independent interaction mode shown in Fig.2, instruction interaction includes three main elements, i.e. independent learners, web-based interactive media and web-based learning resources. Independent learners through web-based interactive media conduct self-regulation to web-based learning resources. Then, according to learners' self-regulation these resources generate learners' requirements of learning resources as called resource feedback.

Cooperative interaction mode. The elements of cooperative interaction are learners, web-based interactive media, teacher and web-based learning resources. Learners are members of a learning community, and are the main aspects of interaction. There exists collaboration and equal communication between learners, as well as a competitive and opposite relationship. Teachers are responsible for the monitoring and guidance of the entire group interaction process, and undertake to establish learning goals, to assign learning tasks and to divide into groups. Web-based interactive media and web-based learning resources constitute learning environment for entire team to cooperate and interact. Learner can communicate with other cooperative members through interactive media and can obtain learning tips or advices from the teacher. Web-based learning resources can provide a wealth of learning information for learners in a team. Therefore, the learner according to his own learning task assigned in a team selects his desired contents from these resources and cooperates with other group members to complete the learning tasks. The specific interaction mode is shown in Fig.3.

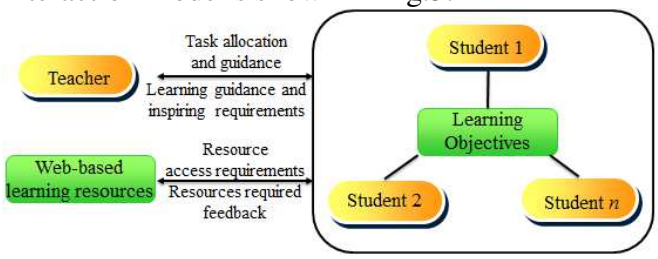

Fig.3. Cooperative interaction mode

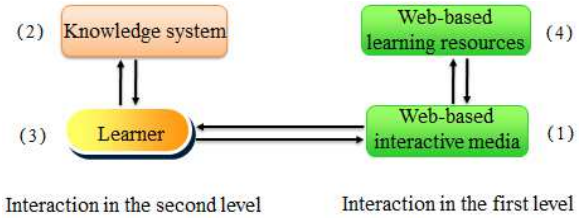

Fig.4. Individual interaction mode

Interactive-object-based interaction mode. The interaction mode based on interactive object mainly includes three aspects as following.

1) *Individual interaction mode*. The elements of individual interaction mode include learner and web-based learning resources. Teacher and web-based interactive media are only in a supplementary role, not as the main factors to be considered.

The learner gets new knowledge and information data from web-based learning resources through interactive media. Then, the learner will compare his acquired information with his existing knowledge system, in order to make his original knowledge assimilate new information through applying interaction mode between learner and teacher. When new information cannot be assimilated by learner's knowledge system, the learner should be required to get more information from learning resources to support assimilation or reconstruction of knowledge architecture. Finally, the learner continues to draw more relevant knowledge and information from web-based learning resources through interactive media. The specific interaction mode is shown in Fig.4.

In these four steps, (1) and (4) is an external exchange process between learner and web-based learning resources, whereas (2) and (3) is an internal communication process of learner himself. It is obvious that the basis of (2) and (3) is (1) and (4), thus we define (1) and (4) as interaction in the first level, and (2) and (3) as interaction in the second level.

2) The interaction mode between students and teacher. Learners and teachers are the two most important factors of network instruction activities. The interaction between them is an essential part of instruction. Teachers are the designer and organizer of web-based learning resources. In fact, even in the individual interaction process, learners are inevitably affected by the impact of teachers. Web-based learning resources have been infiltrated by the teachers' instruction intention and other important information. Certainly, we not only pay attention to those information included in the learning resources, but also will be more focus on the ability of teachers to provide effective learning support services for learners. Teachers will help students to identify that curriculum content is the information, skills, attitudes or values. Teachers will organize students to apply what they have learned including practice skills and knowledge. Teachers will organize formal or informal quizzes to find out whether the students make progress, thus helping students whether they need to change strategy. Finally, teachers also need to provide advice, support and encouragement for students, whose extent and nature depends on the education level of learners, educational philosophy of educational institutions, teachers' personality and social environment and other factors.

With the wide application of network technology in the information interaction between teacher and student, the exchange content may be more than the curriculum content itself, even with personalized trend. Many students may discuss other issues professionally with teachers, even privacy problems. This is the emotional support provided by the teacher. The specific interaction mode is shown in Fig.5.

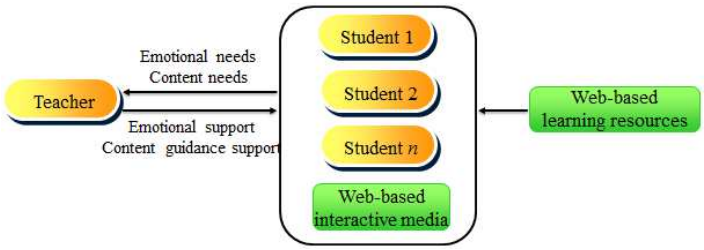

Fig.5. The interaction mode between students and teacher

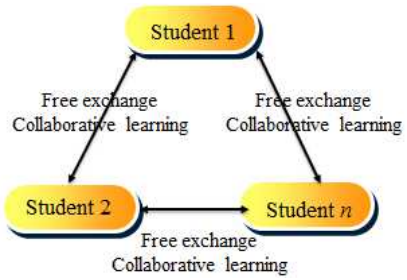

Fig.6. The interaction mode between student and student

The interaction mode between student and student. The interaction between the learner and the learner is a new dimension of network education. This interaction is the interaction between learners, which can occur between individual learners, as well as learners in the collective, and can or cannot have teachers to organize or participate in. In the course design including instruction objectives and content to train collective spirit, to explore community features and collaborative relationships, it is necessary to organize learners to gain collective interaction experience and to make it as a way of learning. At present, the main form of information interaction between student and student in the network learning includes free exchange, consisting of defining theme or non-defining theme, and collaborative learning, i.e. task-based cooperation. The free exchange can be individualized, and can be collective as well, in which the teacher is only as an equal participant and facilitator. A large number of studies show that the free exchange has a great role in promoting learning for students. The specific interaction mode is shown in Fig.6.

Media-based interaction mode analysis. We have analyzed network instruction interaction mode from the perspective of interactive subject mentioned above. This section will feature from media as called network interactive bridge to start with research on network instruction interaction mode. According to its functions, web-based media can be divided into synchronous media and asynchronous media. The synchronous media refers to interactive media with a consistent time, such as web chat room, videoconferencing system, audio conferencing system. The asynchronous media refers to interactive media with an inconsistent time, namely exists a delay in the information dissemination, for example e-mail, online forums, web pages. Correspondingly, media-based network interaction mode shown in Fig.7 can be divided into synchronous-media-based interactive mode and asynchronous-media-based interactive mode. Due to both of interactive mode above with its own advantages and disadvantages, the combination of two kinds of interactive mode will play a greater role in the actual network instruction process. The elements of media-based network interaction include learners, teachers and web-based synchronous/asynchronous media. Specially, asynchronous media is not only the exchange bridge of the other two elements, but also is a log carrier of exchange information.

Longitudinal Analysis of Network Instruction Interaction Based on Instruction Interaction Hierarchical Model

Network instruction interaction is a hierarchical model described in Fig.8, from operation interaction, information interaction to conceptual interaction, gradually from concrete to abstract, and also from junior to senior. The junior instruction interaction is the condition and foundation for the senior instruction interaction.

Operation interaction is the basis of information interaction, information interaction is the basis of conceptual interaction, and conceptual interaction is the highest level of interaction. Information interaction includes three kinds of interaction forms, such as interaction between student and

teacher, interaction between student and student, and interaction between student and learning resources. The interactive feature of media is the basis of all instruction interaction, because media is the platform and carrier of all the instructional interaction.

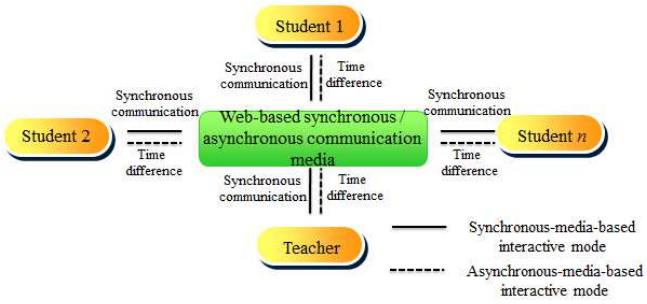

Fig.7. The interaction mode based on synchronous/asynchronous media

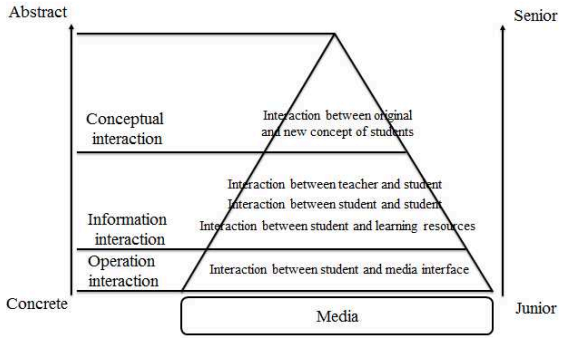

Fig.8. Instruction interaction hierarchical model

The Design of Network Instruction Interaction Mode

From the perspective of system theory, the interaction objects of network instruction platform can be divided into two elements, i.e. subject and object. The subject including teachers and students is the core part of the interactive system. The object including network instruction platform and those interactive means which act on the platform is a necessary condition for interactive system. From the perspective of teaching effectiveness, the interaction of network instruction platform can be regarded as the epitome of the network instructional system, which can also be regarded as the subject and object relational system. According to the interaction function established between the subject and object, the interaction of network instruction platform can be divided into the following three categories.

The interaction in navigation respect. The interaction in navigation respect refers to the network instruction platform how to present the teaching content and their relationships, including student subject how to browse and select information from the foreground and teacher subject how to control the structure and framework of instructional contents from the background and so on. Such kind of interaction is to enable students to master the learning content quickly including knowledge structure, learning paths and specific learning content through the foreground, and is to enable teachers to quickly generate network learning resources from background using clear navigation.

The interaction in feedback and reinforcement respect. The interaction in feedback and reinforcement respect refers to control mechanism between network instruction platform and the student subject. When students enter certain information, the system can be feedback response according to the input conditions. Feedback response may be dominant and may be recessive. The dominant response manifests that students through the user interface can see the response, such as test results feedback and learning feedback. The recessive response manifests that the system will respond to the results transmitted to the back-end database to be stored or processed, and students can not directly see these results because these results are not apparent directly on the user interface, such as learning process tracking, learning pace, control strategies of learning content and so on.

The interaction in functional operation respect. The interaction in functional operation respect refers to the network instruction platform to provide methods and interface interaction techniques for student subject using the platform, in order to enable students to familiarize the basic network learning methods and techniques, to reduce the difficulty of computer operation for students and to enhance friendly interactive interface. For example, platform provides help module, interactive downloads for special teaching resource player plug, etc.

The overall architecture design of the network instruction platform is shown as Fig.9.

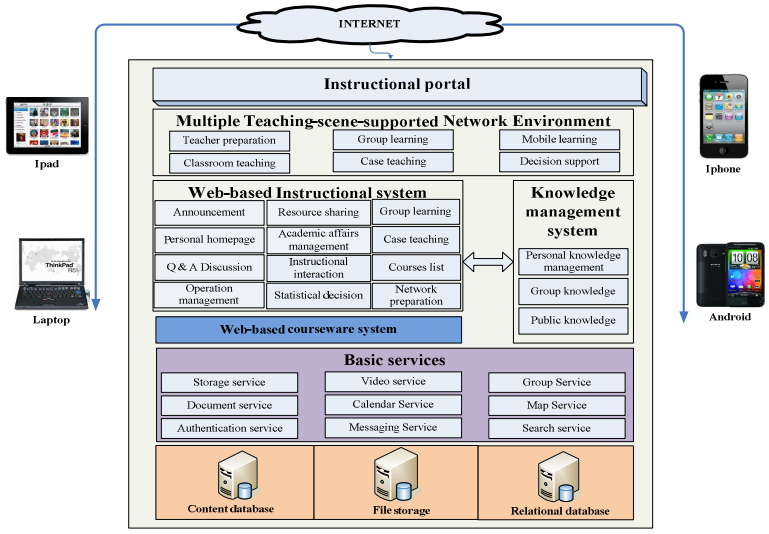

Fig.9. The architecture design of network instruction platform

Conclusion

Due to the spatiotemporal separation of teachers and students in the network instruction, web-based instruction interaction is essentially different from the face to face interaction in a traditional classroom. The learning quality of learns on the Internet depends largely on their level of interaction with the online courses. The interaction of network instruction platform is the main way to connect instructional contents, students and teachers, and also is the main channel for the implementation of the teaching process. In the research and design of interaction of network instruction platform, we use system approach, from the perspective of the relationship between subjective and objective comprehensively analyze design strategies of interaction including navigation, feedback and reinforcement, and functional operation, and fully consider characteristics of teachers and students, learning resource type, network own characteristics and other influence factors. Therefore, we rationally apply interactive means and methods of network instruction platform to improve the effectiveness of network instruction.

References

[1] Hillman D.C.A. and so on. Learner-interface interaction in distance education: an extension of contemporary models and strategies for practitioners [J]. American Journal of Distance Education. 1994:8 (2):30-42.

[2] Sims R. An interactivity conundrum: Constructs of interactivity and learning theory [J]. Australian Journal of Educational Technology. 2000 (16) 45-57.

[3] Rose E. Deconstructing interactivity in educational computing [J]. Educational Technology. 1999:39 (1):43-49.

[4] M. David Merrill, Zhongmin Li and Mark K. Jones. Second Generation Instructional Design [J]. Educational Technology. 1991: 30 (1):7-11 and 30 (2):7-14.

[5] Larry Gilbert, David R. Moore. Building Interactivity into Web Courses: Tools for Social and Instructional Interaction [J]. Educational Technology. 1998:38 (3):26.

[6] Ellen D. Wagner. In support of a functional definition of interaction [J]. The American Journal of Distance Education. 1994:8 (2):6-29.

[7] Li Chen. A Hierarchical Model for Student and Teacher Interaction in Distance Learning [J]. Distance Education in China. 2004 (5) 24-28.

Advanced Materials Research Vols. 989-994 (2014) pp 4427-4431
© (2014) Trans Tech Publications, Switzerland
doi:10.4028/www.scientific.net/AMR.989-994.4427

Research on TCP Congestion Control Mechanisms

Shuguang Zhang[1, a], Qiaoyun Sun[1, b], Qinghua Gao[1, c], Min Wang[1, d], Yu Zhang[1, e]

[1]Information Department, Beijing City University, Beijing, 100083, China

[a]email: shugzhang@163.com, [b]email: sunqy@bcu.edu.cn, [c]email: qhuagqhuag@126.com, [d]email: wm983100@163.com, [e]email: sunqy@bcu.edu.cn

Keywords: TCP; Congestion Control; Sliding Window; Algorithm

Abstract. With the rapid development of information society, the number of information data transmitting in the Internet is growing quickly, so congestion control becomes very important and it is a hot research field on the Internet now. In this paper, the sliding window, reasons and TCP algorithms of congestion control such as slow start, congestion avoidance, fast retransmit and fast recovery are discussed. Different TCP versions about congestion control are studied and analyzed. As a result, improvements on the congestion control algorithm and the research is still an important topic in the study of Internet congestion control.

Introduction

Most of the work for congestion control is done by TCP protocol, which contains some network congestion control algorithms. The reliability and stability of the Internet today is closely connected with TCP congestion control mechanism, and the success of TCP owes to its stable congestion control mechanism. Along with more and more applications and continuous development of technology, it is very difficult to meet the requirements of quality of service (QoS) relying on terminal systems' strategy and algorithm only. Relevant network technology gradually turns to the middle network nodes such as routers, by enhancing their functions to realize what the end-to-end technology cannot achieve, so as to realize effective congestion control, maintaining good performance of the network.

The original TCP has only flow control and doesn't have congestion control. The receiver uses TCP header to notify it's receiving capacity to the sender. Such control mechanism only considers the receiver's capacity and doesn't consider network transmission ability, causing network breakdown (Congestion Collapse).

Reasons of congestion

If the transport entities on many machines send too many packets into the network too quickly, the network will become congested, with performance degraded as packets are delayed and dropped. This situation is called congestion [1]. Congestion is a state of continuous overload of network, since the demand for network resources is over its inherent capacity, which is the most important reason of congestion. There are some other reasons of congestion, mainly including: 1) Relative insufficient buffer space. Mainly on the router, while increasing the buffer space sometimes can relieve congestion, but sometimes it will aggravate congestion. 2) Insufficient bandwidth for high rate data stream. Low-speed link can also cause congestion on high rate data stream input. 3) Link mismatch to the processing speed of CPU, causing weak processing capacity and congestion.

Link capacity, buffering space in switching nodes, processors and so on, are the resources of the network. In a certain period of time, if the demand for available resources in the network is more than what it can provide, the network performance will be worse. If there are many resources leading to congestion at the same time, the performance of the network will degrade obviously. The network throughput will decline along with the increase of input load. Since the congestion is derived from the imbalance of the network resources and network traffic distribution, congestion will not be eliminated with the increase of network capacity.

Congestion control mechanisms of TCP

1. TCP's sliding window mechanism

Like many of the flow control protocols, TCP is also using the sliding window mechanism, but there are still some differences from other protocols, such as LLC, HDLC and x.25. Data receiving acknowledgement and data sending notice are processed separately. Every byte is assigned a sequence number. When the sender transmits message segment, each byte of the data gets a sequence number, using ($A = i, W = j$) message form to confirm data transmission. The specific meaning is as follows:

(1)If the sequence number of *i-1* has been confirmed, the sequence number of the following byte which is expected to receive is *i*;

(2) The receiver permits the other party to send *j* bytes of data (*j* is window size). The sequence number of those bytes is from *i* to *i + j-1*.

In TCP, the sending rate of data is determined by the slowest part among the hosts and other network nodes. The receiver needs some strategies to decide how many bytes the sender sends. A conservative method is permitting the sender to send message segments that the buffer space can just accommodate. Under the condition of bigger delay bandwidth, the receiving party can improve the throughput by advancing cache space.

2. Additive increase multiplicative decrease (AIMD) algorithm

TCP is the most widely used end-to-end transport protocol on the Internet, and its congestion control mechanisms are mainly based on additive increase multiplicative decrease (AIMD) algorithm. The algorithm defines three window variables:

(1) Congestion window (*cwnd*): it limits the maximum number of data transmitted by the sender in a timeframe, which is a sender-side limit on the amount of data the sender can transmit into the network before receiving an acknowledgment (ACK).

(2)Advertised window (*awnd*): after the connection is established between the receiver and the sender, the receiver notify the sender its maximum receiving rate, which is a receiver-side limit on the amount of outstanding data.

(3) Effective window (*win*) : the actual window size that the sender sends data. The sender's actual (usable) window *win* is then written as the minimum of the receiver's advertised window *awnd* and the congestion window:

$$win = \min(cwnd, awnd)$$ [2].

The working process of AIMD can be divided into two steps:

(1)Once the sender receives an ACK for the receiving confirmation, congestion window increases according to the formula $cwnd = cwnd + mss * (mss / cwnd)$, in which *mss* is the maximum message length. It means that if the packets sent by the sender are confirmed in the recent round-trip time (RTT), the sender's *cwnd* add 1, namely Additive Increase idea.

(2)When a timeout occurs at the data transmission, TCP considers congestion appearing on the link, and begins to decrease data sending rate. Once a timeout occurs, the sender will recalculate the value of the congestion window, formula is as follows:

$$cwnd = cwnd / 2,$$

This thought is the congestion window decreases to a half of the original *cwnd*, namely the Multiplicative Decrease idea.

Four congestion control stages of TCP

TCP congestion control can be divided into four stages of slow start, congestion avoidance, fast retransmit and fast recovery, reflecting the basic idea of TCP congestion control.

(1) Slow Start

When starting a connection old TCP sends many packets to the network, lots of packets may run out of buffer space of routers, resulting in the throughput of TCP connection fall sharply. The algorithm to avoid is slow start.

When the connection has just established, or a timeout occurs, the network is at the stage of slow start. Congestion window has been initialized to a packet size (a packet with default size of 536 or 512 byte). The sender is allowed to send only one message. When a message receives an ACK from the receiving end, *cwnd* adds 1, which is to add a message segment to send. Obviously, the *cwnd* will grow exponentially depending on the RTT (an exponential growth: 1, 2, 4, 8...). Thus the the amount of data sent into the network will increase sharply.

By using slow start TCP can prevent sending too much data and causing data loss and network congestion when starting a new connection. At the same time, because the *cwnd* actually grows exponentially, the problem of throughput increasing slowly caused by the pure AIMD algorithm is avoided.

Infinite growth of *cwnd* will lead to network congestion, so a state variable should be introduced: slow start threshold *ssthresh*.

When *cwnd* < *ssthresh,* TCP implements slow start algorithm, *cwnd grows* exponentially with RTT;

When *cwnd* > *ssthresh,*, congestion avoidance algorithm is adopted to slow the growth of the *cwnd* [3].

(2) Congestion Avoidance

When a timeout occurs or three same ACK frames are received, congestion happens. At this time the network enters a stage of congestion avoidance.

At congestion avoidance phase, when TCP detects congestion is happening, it does not reset *cwnd = 1* directly and apply slow start method. Because it takes a long time to recover in case of congestion and *cwnd* exponential growth in slow start algorithm appears radical, it is likely to increase the congestion. Therefore, a relatively more conservative regulatory mechanism is used to change *awnd* growth way, makeing it become linear growth from exponential growth at this stage, the specific process is as follows:

The slow start threshold *ssthresh* is set to a half of the current *cwnd*, namely the *ssthresh = cwnd / 2;*

When a timeout occurs, setting *cwnd = 1*, TCP implements slow start algorithm under the condition of *cwnd*< ssthresh;

Under the condition of *awnd* ≥ ssthresh, congestion avoidance algorithm is implemented. After receiving each of ACK, *cwnd* add only 1 / *cwnd* packets, making *cwnd* grow linearly with RTT.

(3)Fast Retransmit and Fast Recovery

When a timeout occurs at the congestion avoidance phase, *cwnd* is reset to 1, entering the slow start stage. This will lead to decrease send window size excessively and reduce the throughput of TCP connection. In order to improve the performance of TCP, the fast retransmit and fast recovery mechanisms are introduced.

At the fast retransmit phase, when the sender received 3 or more duplicate ACKs, it judges that the packets are dropped. The *ssthresh* is set to one half of the current *cwnd* (i.e. *ssthresh = awnd/2)*, and the dropped packets are retransmitted, entering the stage of fast recovery.

At the fast recovery phase, when the sender receives each of a repetitive ACK, the *cwnd* adds 1; If the sender receives a different ACK, *cwnd = ssthresh*, the network transfers to congestion avoidance stage; When a retransmission timeout occurs, *ssthresh = cwnd / 2, cwnd = 1,* the network enters the stage of slow start.

Fast retransmit and fast recovery mechanisms avoid entering slow start stage directly while a timeout occurs, which improves the performance of TCP and throughput to a great extent.

Analysis and comparison of TCP congestion control algorithms

Van Jacobson pointed out the shortages of TCP in network congestion control in 1988. He put forward the "Slow Start" algorithm and "Congestion Avoidance" algorithm. TCP Reno version in 1990 added the "Fast Retransmit" algorithm and "Fast Recovery" algorithm, which avoid the phenomenon of excessive reducing send window size because the slow start is implemented when

the congestion is not severe. TCP congestion control is made up of the above four core parts. Improved TCP versions have been emerged in recent years, such as New - Reno, SACK, Vegas and so on, each of which has advantages and disadvantages.

(1) TCP Tahoe algorithm

TCP Tahoe is the version joined Van Jacobson's algorithm of slow start, congestion avoidance, fast retransmit in 1988 after 4.3 BSD or similar TCP implementations[4]. The core idea of Tahoe algorithm is that the *cwnd* rapidly approaching available channel capacity in exponential growth way, then slowly close to equilibrium. It includes three basic congestion control algorithm: slow start, congestion avoidance, fast retransmit. The shortcomings of Tahoe lie in low efficient network bandwidth utilization and long delay while transferring from slow start to fast retransmit.

(2) TCP Reno algorithm

Aiming at the shortcomings of the algorithm of Tahoe, improved algorithm of Reno was proposed. The improvements mainly includes two aspects: One is, the algorithm directly enters congestion avoidance after receiving three consecutive duplicate ACKs without entering low start; The second is, fast retransmit and fast recovery mechanisms were added. Reno algorithm has become the mainstream in TCP source algorithms for its simplicity, efficiency and robustness, being used widely. But Reno algorithm has also performance problems under the condition of losing multiple segments in the same window. The dropped messages will make TCP implement fast retransmit and fast recovery, and the *cwnd* and *ssthresh* will be halved for many times, greatly reducing the throughput.

(3) TCP New - Reno algorithm

New - Reno added fast recovery algorithm into Reno, it takes into account that multiple packets dropped within a send window of data at the same time. In Reno algorithm, the sender quits from fast recovery after receiving a non-duplicate reply. However, in New - Reno, only when all the packets are replied does the sender quit from fast recovery. It is very easy to realize New Reno, as long as modifying TCP sender’s implementation code.

(4) TCP Sack algorithm

SACK algorithm was improved to solve the problem of multiple packets dropped in a window of data for Reno algorithm. A variable of SACK pipe is defined to estimate the numbers of packets appearing on routers. The TCP receiver sends SACK packets to notify the sender it’s data receiving, so that the sender knows exactly what data is correctly received, so as to avoid unnecessary retransmission, reduce delay and improve the network throughput. But the realization of the SACK algorithm need to modify TCP sender and the receiver implementation code, increasing the complexity of TCP, therefore it is not easy for large-scale of applications [5].

(5) TCP Vegas algorithm

Vegas is different from the above algorithms, it adjusts sending rate based on the change of RTT as congestion signal, by monitoring the change of RTT to change the size of the *cwnd*. Since Vegas use RTT to determine the available network bandwidth, it can well predict the usage of network bandwidth with good fairness and efficiency. However, it is some unfair for Vegas compete bandwidth with other algorithms, thus it fails to use widely on the Internet and needs to improve continuously.

Conclusions

With the increasing of network scale, the most efficient way to improve congestion control is introducing router queue management congestion control algorithm based on the traditional end-to-end TCP congestion control, which will improve the congestion control on the network. On the basis of the existing congestion control mechanism, an effective congestion control algorithm will bring huge advantage for the development of the Internet.

Acknowledgement

This work was supported by the non-governmental education promotion project of Beijing: Construction of new specialty -- communication engineering specialty in Beijing City University and the comprehensive reform project of communication engineering specialty in Beijing City University (Project No. zy2014102).

References

[1] Andrew S. Tanenbaum and David J. Wetherall: *Computer Networks, Fifth Edition* (China Machine Press, China 2013)

[2] Kevin R. Fall and W. Richard Stevens: *TCP/IP Illustrated, Volume1, The Protocols, Second Edition,* (China Machine Press, China 2013)

[3] Xie Xiren: *Computer Networks, Sixth Edition* (Publising House of Electronics Industry, China 2013)

[4] Kevin R. Fall and W. Richard Stevens: *TCP/IP Illustrated, Volume1, The Protocols, Second Edition,* (China Machine Press, China 2013)

[5] William Stallings: *Data and Computer Communications, Ninth Edition,* (Publising House of Electronics Industry, China 2011)

Advanced Materials Research Vols. 989-994 (2014) pp 4432-4436
© (2014) Trans Tech Publications, Switzerland
doi:10.4028/www.scientific.net/AMR.989-994.4432

Research on Forensics Method based on Log on SaaS

Gang Zeng

Police Information Department, Liaoning Police Academy, Dalian, China

Email:dlzenggang@126.com

Keywords: log; digital forensics; SaaS; user behavior sequence

Abstract.Cloud computing is getting more and more attention from the information and communication technologies industry recently, security issues is becoming more important. Forensics technology on cloud computing is becoming a researched focus. In this paper, we discuss the impact and challenges to digital forensics, finally we present the improved measure of log and forensics system based on logs on SaaS.

Introduction

Cloud computing is getting more and more attention from the information and communication technologies industry recently, because of its key characteristics: agility, low cost in using, device and location independence, Virtualization, Reliability, scalability and etc. It has three delivery model: Infrastructure as Service (IaaS), Platform as a Service (PaaS), and Software as a Service (SaaS). Now we use cloud computing universally, but there is also attack in cloud computing environment, forensics is the effective way to deal with the security question.

It is very difficult to collect evident in cloud computing environment, but we can do some work by logs, logs exist anywhere in cloud computing, it records evidence with security. In this paper, we mainly discuss logs, firstly, we introduce digital forensics and the impact and challenges to traditional digital forensics in cloud computing environment; In section II, we discuss Log System and Improvement; In section III, we design a system, which collect logs from cloud computing, then analyze it.

Digital Forensics and the impact and challenges

1.1 Digital Forensics

Digital forensics is a branch of forensic science encompassing the recovery and investigation of material found in digital devices, often in relation to computer crime. It was originally used as a synonym for computer forensics but has been expanded to cover investigation of all devices capable of storing digital data. Therefore, it is called digital forensics[1].

A digital forensics investigation commonly consists of 4 procedures: identification, evidence collection, analysis, and reporting. Acquisition involves creating an exact sector level duplicate of the media, often using a write blocking device to prevent modification of the original data. Both acquired image and original media are hashed (using SHA-1 or MD5) and the values are compared to verify the copy's accuracy.

The evidence is analyzed to reconstruct events or actions, and to reach conclusions. When an investigation is completed, the data is presented, usually in the form of a written report in lay persons' terms.

1.2 Impact and Challenges to traditional digital forensics

With the development of cloud computing, it has been found that traditional digital forensics is not suitable for cloud computing, This is the methods of traditional digital forensics: create an image of the media seized from the crime scene, and at the same time the data mustn't be modified, then analyze on the image to find evidence. But it is realistic in cloud computing environment, because it meets challenges coming from cloud computing.

The first challenge is multi-tenancy and resource sharing. Many users use the same cloud, who uses it, when, where is it being used? What the users have done? To answer these questions, it is

easier in past, because the environment was simple than now, but it is difficult in cloud computing environment which is multi-tenancy and resource sharing.

The second challenge is that Cloud computing is more vulnerable to attack. Users access the cloud computing by internet, new attack methods to cloud computing keep popping up excepting the original attack mode, some attacks use the security vulnerabilities of cloud computing, other attacks are deformation of the traditional methods of attack. The following are some of the attacks:

- Wrapping Attack
- Malware-Injection Attack
- Flooding Attack
- Browser Attack
- Insecure Interfaces and APIs
- Malicious administrators
- Data Stealing
- Data Leakage

The third challenge come from Other technical matters .

Traditional forensics is impotent in cloud computing environment, in IaaS model, we may get a complete image of a virtual machine, but we don't know that the evidence we focused on is in which one of all virtual machines, in PaaS or SaaS model, we can't get a complete image of hard disk.

Cloud computing is running uninterruptedly, if the cloud is shutdown, the data that can be relevant to an investigation may be lost, and parallel or unrelated services may be interrupted, This is fatal for Business Companies, is not allowed[2][3][4].

Challenges come from log of cloud computing at the same time. Log is recorded in different format in different environment, and different content is record by different applications. Now the problem that we have to solve is where we can find the log, how to analyze them, what does log mean? How to link them together? What is more serious is that non existence of logs and absence of critical information in logs.

Log System and Improvement

2.1 present situation of log analysis

We often hear the term called "log", what does the log contain, Why we study it? Log has recorded some important information: who used the cloud, when and where did he login(IP), which service did he use, when did he logout? These information is very helpful for tracking the attack.

Log is important , but our understanding about the log is one-sided, when it comes to log, it is deemed the system log by a lot of people. The log that we discus, Includes not only the cloud server log, including the client log, cloud service providers operating billing log; also includes network equipment log, includes log that is beneficial to digital forensics[5].

Now, many questions exists in log analysis, there is redundant information, even self-contradictory records in the log, these information is useless for us to collect evidence.

By the log, we can find the time when the user use cloud, particular IP that user accessed, services that users have used. We can find the relationship between the multiple log events by Statistic and analysis of log and mining, and then find the cloud service mode and the user usage mode, find out the clues and evidence of the cases by Analysis on user behavior pattern. But analysis of the log is not deep enough, correlation degree between evidences is not enough too.

2.2 Improvement of log system

It is because of the above reason, we propose an improved measure for log system. What problem the improved measure can solve, what principles should be followed in log management, what is recorded in log, what is the format of log, where log stored is safe, these problem is very important, now we discuss these problems.

First of all, the basic principles of log management guide our actions, it guides us what should be done and what should not be done. The principles are as follows:

- Log is recorded when and where we need it.
- Logs should be centrally managed.
- Content of log is what we need.
- Format of log can be understood by us.

Now many system do not record logs because of performance or storage capacity, When an event occurs, no logs is available for analysis, therefore, we should record logs as much as possible.

Many systems do not record logs for performance or storage capacity, so we propose a solution of centralized log management. Logs are transferred from the sources to a central log server, the application server need not high capability and big storage capacity any more.at the same time, logs is more safety than on the application server. When logs are transferred to log server, we should solve the following questions:

- Reliable transport protocol
- How to encrypt the log
- How to compress log to save bandwidth.

Our focus is what should be recorded in the log, This is directly related to what we can get in the future. At a minimum, the following fields need to be present in every log record: user_id, session_id, client_ip, application, activity, timestamp, Severity, Reason, Categorization. These fields help answer the questions: when, what, who, and why.

The format of log is one of the challenges to digital forensics, the format that the record is made up key-value pairs, it is suitable for MapReduce mode, and is based on standards work and the study of many existing logging standards.

user_id=zhangsan_ram_010,session_id=05BaswoGGQgQQDVDG3IEEEEED,
client_ip=1.2.3.4,object=sales, action=insert, status=failure,
severity=ERROR,reason= syntax error,time=2014-05-3 16:25:47.123231PDT.

Log Analysis System Based On Hadoop

3.1 Structure of the System

The log of cloud computing is very important, and includes helpful evidence for digital forensics, but the cloud computing is multi-tenancy and Resource Sharing, and many tasks are running on it, so massive logs is stored in the cloud, their format is different. It is very difficult to analyzing on log by traditional methods, we designed a forensics system based on Hadoop for SaaS.

The forensics system is composed of the following function modules: evidence collection module, evidence processing/analysis module, reporting module. The evidence collection module is responsible for the collection of logs from the target cloud computing, it is a plus-in or an application, and easy to deploy. The log processing module is the core module of the system, it includes two functions: pre-processing and analyzing. Reporting module has a graphic user interface, users can execute all kinds of commands includes querying data, cluster analysis, association analysis, etc.

The structure of system consists of the following layers[5]:

1.Hadoop cluster layer, It consists of many virtual machines, Hadoop service is been installed in the virtual machines.

2.Distributed file system layer, we use HDFS file system, the massive log files will be stored in it, its duplicate strategy and load balancing strategies can provide reliable service.

3.Database layer, it provides data storage service, by the reasonable arrangement of the primary key and indexes, it provides data access for the upper layer. We use HBase as database, It can meet the high concurrency, high scalability requirements. All log data is stored in HBase.

4.Business processing layer, a variety of business logic is performed here, includes query, analysis, association and so on, these business processing can be transformed into Map/Reduce model.

5.user interface layer, the interface is is a graphical user interface, simplified operation.

3.2 Pre-processing of log

1. The module of log collection, we use the open source components for log collection, it can real-time or periodically collect log files from SaaS system.

2. The module of data-processing, As the number of users in SaaS systems is very large, the log is massive and miscellaneous, it often contains noise, missing data and inconsistent data, in order to improve the quality of log data, and improve the quality of the data analysis, improve the efficiency of log mining, the data processing is needed.it includes：

Data cleaning：to remove duplicate data, inconsistent data, impossible or incorrect data.

Data transformation: to transform the log on a system to the data that can be identified on another system, to transform log into the model that is easy to mine, transformation methods include clustering, normalizing, etc.

3.3 Analyzing of log

Combined with the characteristics of SaaS, we adopted the analysis method based on user behavior pattern.

1.The log collection：We can collect log information in the key points of the system by the log collection module. The key points include SaaS application system, operation system, the network device, the safety system, etc.

2. Users' behavior modeling：The traditional method of behavior modeling is based on the statistical results，Including the frequency of access, access time，etc. This method describes the behavior patterns statically，and these descriptions lack the ability to describe the behavior of semantic information. Aiming at this problem, This paper proposes a behavior element model of log based on Metadata.

According to the characteristics of user behavior, behavior pattern can be divided into three layers: the key point, activity and the session.

The key point is the users access Location in the system, it includes: Function modules in SaaS and equipment where users have accessed; User location, etc. we can use the following tuple to describe it[6].

(user_id, request_id, Time, Delay, Stateset);

Activity not only describe the semantic information of user access sequence, such as keywords, links, abstract, and corresponding operations, such as search, login, add, modify, delete , logout, etc.

(Userid, Activity_id, ActivityNane, Time, Delay, StateSet)

A session is a series of activities to achieve specific objectives, and it is described by the following tuple,

(User_id, Session_id, Time, Delay, StateSet, Activities)

Algorithmic thought：

This algorithm uses the depth first search strategy, checks prefix subsequence frequently, divide the corresponding postfix subsequences into projection sequence database according to the length, these postfix are mutually independent and does not affect reciprocally. Then constantly recursion, generate multiple smaller sequence databases from sequence database, finally, digging one by one in the projection database.

User behavior pattern clustering

According to the user access behavior, the user behavior is divided into login, query, add, modify, delete, logout, calculation, report, etc. Along with the increase of the using time, the user behavior pattern must be integrated a variety of behavior. According to changes of behavior sequence model on a time axis, by sequence similarity calculation method, finally cluster on behavior sequence model[7].

Conclusion

This paper analyzes first the characteristics of cloud computing and challenges to cloud computing forensics, then proposes the improved method for SaaS system log, finally proposes forensics method on SaaS based on user behavior sequence model. But the forensics method needs changes in log system, this is the shortage of the method, and it is also the place to improve in the future.

Acknowledgement

This work was partly supported by general scientific research project of education department of Liaoning Province of China (No. L2013490), by project of State Key Laboratory Of Information Security(No. 2013-3-4).

References

[1] ROGERS, M. K. & SEIGFRIED, K. The Future of Computer Forensics: A Needs Analysis Survey. Computers & Security, Volume 23(1), 2004. pp. 12-16.

[2] TREACY, B. & BRUENING, P. Cloud Computing –data protection concerns unwrapped. Privacy and Data Protection PDP, Volume 9(3), 2009. pp. 13.

[3] L. Pimlott, An Investigation of the Impact of Cloud Computing on the Association of Chief Police Officers (ACPO) 'Good Practice Guide for Computer-Based Electronic Evidence, University of Derby, 2010.

[4] VACCA, J. R. COMPUTER FORENSICS Computer Crime Scene Investigation. 2nd edn. Charles River Media Inc. Hingham, Massachusetts. 2005.

[5] J. Dykstra and A. T. Sherman, "Understanding issues in cloud computing: Two hypothetical case studies," Digital Investigation, vol. 3, no. 1, pp. Pages: 19-31, 2011.

[6] K. Kent, S. Chevalier, and T. Grance, "Guide to Integrating Forensic Techniques and Incident Response," National Institute of Standards and Technologies (NIST), 2006.

[7] L. Zhao. The Design and Implementation of Massive Scarch Logs Analysis Platform Based on Hadoop[D]. Dalian: Dalian University of Technology,2013.

Advanced Materials Research Vols. 989-994 (2014) pp 4437-4440
© (2014) Trans Tech Publications, Switzerland
doi:10.4028/www.scientific.net/AMR.989-994.4437

Complexity Analysis of Neural Network Using First Category Orthogonal Weight Functions

Daiyuan Zhang [a], Jianhui Zhan [b]

College of Computer, Nanjing University of Posts and Telecommunications, Nanjing, Jiangsu 210003, China

[a]email: dyzhang@njupt.edu.cn, [b]email: hui6075@163.com

Keywords: Algorithm Complexity; Neural Network; Weight Function; Orthogonal Approximation

Abstract. To describe the performances of a new kind of neural network, the complexity for training neural network using orthogonal weight functions is analysed. The full adders are used as the neurons of the neural networks, and the weight functions are orthogonal functions. We derive the relationships of the iteration time with the number of input dimensions, output dimensions and training patterns. Finally, some simulation examples verified the theoretical results obtained in this paper.

Introduction

Traditional neural network algorithms (such as BP or RBF) have some shortcomings such as local minima, slow convergence and initial sensitivity, these shortcomings can impede the development and application of neural networks [1]. To overcome those shortcomings mentioned above, Literature [2] proposed a new kind of neural network's learning algorithm, named as weight function neural networks, which makes the training weights as functions of the input samples called weight functions, rather than a set of constants used in conventional algorithm.

Based on spline weight function neural networks, this article introduces the topology of first category orthogonal weight function neural network, then gives the algorithm to solve the orthogonal weight functions and analyses its time complexity, finally verifies the theoretical results through MATLAB simulation experiments.

First Category Orthogonal Function Neural Network Topology

Literature [2] gives the topologies of first category and second category spline weight function neural network. Topology of first category orthogonal weight function neural network with m-dimensional input layer and n-dimensional output layer in this article is shown below:

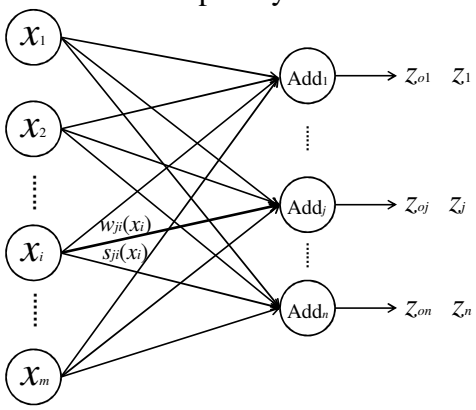

Fig. 1 First category orthogonal weight function neural network with *m* input layer and one output layer.

The network has *m* input nodes that directly connect with output nodes which are adders by weighting functions $w_{ji}(x_i)$ i=1,2,…,m; j=1,2,…,n. Each component z_j (j=1,2,…,n) of the network output $\boldsymbol{z}$ is the sum of all input samples' weight function value, namely

$$z_j = \sum_{i=1}^{m} w_{ji}(x_i) \ \ (i = 1,2,...,m; \quad j = 1,2,...,n) \tag{1}$$

The First Category Orthogonal Weight Function Neural Network Training Algorithm

Literature [2] gives the first category spline weight function neural network training algorithms. According to theories in literature [2] we give the training algorithm for first category orthogonal weight function neural network. Suppose there are N training samples, input for i-th node can be expresses as a vector $x_i = (x_{i0}, x_{i1}, \cdots x_{i(N-1)})$, target vector can be expressed as $z = (z_0, z_1, \cdots, z_{N-1})$, where z_j (j=0,1,$\cdots$,N-1) is a n-dimensional column vector. Orthogonal weight function neural network algorithm is to solve the orthogonal functions $S_{ji}(x_i)$. The neural network training interpolation points are as follows:

$$\mathbf{Ip}_i = \left\{ (x_{i0}, \eta_i z_0), (x_{i1}, \eta_i z_1), \cdots, (x_{i(N-1)}, \eta_i z_{N-1}) \right\} \tag{2}$$

According to least-squares fitting theory [3], weight functions can be written as:

$$S(x) = a_0\varphi_0(x) + a_1\varphi_1(x) + \cdots + a_n\varphi_n(x) \tag{3}$$

Least-squares fit is defined by minimizing the square error of the data and to find the best match function, using the least squares method can be easy to obtain unknown data, making the square error between the obtained data obtained with the actual data is minimized. Using mathematical language can be describes as:

$$\|\boldsymbol{\delta}\|_2^2 = \sum_{i=0}^{m} w(x_i)\left(S(x_i) - f(x_i)^2\right) \tag{4}$$

Orthogonal function means for a function set $\phi_1(x), \phi_2(x), \cdots, \phi_r(x) \in [a,b]$, any two functions satisfies $a_i = (f, \phi_i) = \int_a^b f(x)\phi_i(x)\mathrm{d}x, i = 1,2,\ldots$. When using orthogonal polynomials $g_k(x)$ (k=0,1,$\cdots$,l) to solve the least squares fit polynomial as the neural network weight functions, the resulting $S^*(x)$ is called orthogonal weight function.

We use Chebyshev orthogonal polynomial $\{g_i(x)\}_{i=0}^{l} \subset H_l$ and $\rho(x) = 1/\sqrt{1-x^2}$ to solve weight functions $S^*(x)$ in the interval C[-1,1], then

$$S_l(x) = \sum_{k=0}^{l} a_k g_k(x) \tag{5}$$

where

$$a_k^* = \frac{(f, \varphi_k)}{(\varphi_k, \varphi_k)} = \frac{\sum_{i=0}^{m} \omega(x_i) f(x_i) \varphi_k(x_i)}{\sum_{i=0}^{m} \omega(x_i) \varphi_k^2(x_i)}, \quad (k = 0,1,\cdots,n) \tag{6}$$

Algorithm Complexity Analysis of the First Category Orthogonal Weight Function Neural Network

For the structure shown in Fig. 1, give the algorithm pseudo-code.

Algorithm Input: Point out to be fit ($\boldsymbol{x}$,$\boldsymbol{z}$) ($\boldsymbol{x}$=[x_1,x_2,…,x_N],$\boldsymbol{z}$=[z_1,z_2,…,z_N]), orthogonal polynomials weight $\rho(x)$, maximum permissible error *mpe*, maximum order of fit *Max_n*;

Algorithm Output: Orthogonal basis function coefficients.

Algorithm Steps:

Step1 set $\varphi_0(x) = 1$; $a_0 = (\varphi_0, y)/(\varphi_0, y0)$; $P(x) = a_0\varphi_0(x)$; $err = (y, y) - a_0(\varphi_0, y)$;

Step2 set $a_1 = (x\varphi_0, \varphi_0)/(\varphi_0, \varphi_0)$; $\varphi_0(x) = (x - a_1)\varphi_0(x)$;

Step3 set $k = 1$;

Step4 while (($k \le Max_n$) && ($|err| \ge mpe$))

Step5 k++;
Step6 $a_k = (x\varphi_1, \varphi_1) / (\varphi_1, \varphi_1)$; $\beta_{k-1} = (\varphi_1, \varphi_1) / (\varphi_0, \varphi_0)$; $\varphi_2(x) = (x - a_k)\varphi_1(x) - \beta_{k-1}\varphi_0(x)$;
$a_k = (\varphi_2, y) / (\varphi_2, \varphi_2)$; $P(x) += a_k\varphi_2(x)$; $err -= a_k(\varphi_2, y)$;
Step7 set $\varphi_0(x) = \varphi_1(x)$; $\varphi_1(x) = \varphi_2(x)$;
end;
Step8 output( ); end.

Where in, solving $(\varphi_j, \varphi_k) = \sum_{i=0}^{N} \omega(x_i)\varphi_j(x_i)\varphi_k(x_i)$ need to call the child algorithm 2:

Step1 set $(\varphi_j, \varphi_k) = 0$;
Step2 for ($i = 0$; i != N; i++)
for ($k = 2$; k! = N-1; k++)
$\varphi_0(x_i) = 1$; $\varphi_1(x_i) = x_i$; $\varphi_k(x_i) = [(2k-1)\varphi_{k-1}(x_i) - (k-1)\varphi_{k-2}(x_i)] / k$;
end;
end;
$(\varphi_j, \varphi_k) += \omega(x_i)\varphi_j(x_i)\varphi_k(x_i)$;
Step3 output((φ_j, φ_k)); end;

Main algorithm include a *while* loop which contains several (φ_j, φ_k), to solve (φ_j, φ_k) need to call algorithm 2 that have a *for* loop which solve k-order orthogonal polynomials and should be execute k times. Analysis of the above algorithm time complexity [4] [5] we find in the worst case time complexity is

$$T(N) = O(N^2 \log N) \tag{7}$$

Where N is the number of training samples. For m input, n output first class orthogonal weight function neural network, need to solve each weight function connected input and output neurons, the time complexity is

$$T(m, n, N) = mnO(N^2 \log N) \tag{8}$$

Experimental Methods and Results

Experiment I:

Select appropriate network topology: input layer with two nodes and output layer with two nodes; objective function $x_1^2 + x_2^2$; learning curve: $x_1 = f_1(t) = t$, $x_1 = f_1(t) = t$; number of samples N with 100, 200, ..., 1200 ; multiplication factor takes equal distribution. Count the training times of first category orthogonal weight function neural network under different training numbers.

Experiment II:

Select appropriate network topology: input layer with 2,4,6,8, ... 30 nodes; output layer with two nodes; objective function: $x_1^2 + x_2^2$, $x_1^2 + x_2^2 + x_3^2 + x_4^2$ ..., $x_1^2 + x_2^2 + \cdots + x_{30}^2$; learning curve: $x_1 = f_1(t) = t$, ..., $x_{30} = f_{30}(t) = t$; number of samples N with 400; multiplication factor takes equal distribution. Count the training times of first category orthogonal weight function neural network under different input layers.

Experiment III:

Select appropriate network topology: input layer with two nodes; output layer with 2,4,6, ..., 30 nodes; objective functions of each output layer depends on the number of nodes; each input layer node with objective function $x_1^2 + x_2^2$; Learning curve: $x_1 = f_1(t) = t$ $x_2 = f_2(t) = t$. number of samples N with 400; multiplication factor takes equal distribution. Count the training times of first category orthogonal weight function neural network under different output layers.

Experiment results:

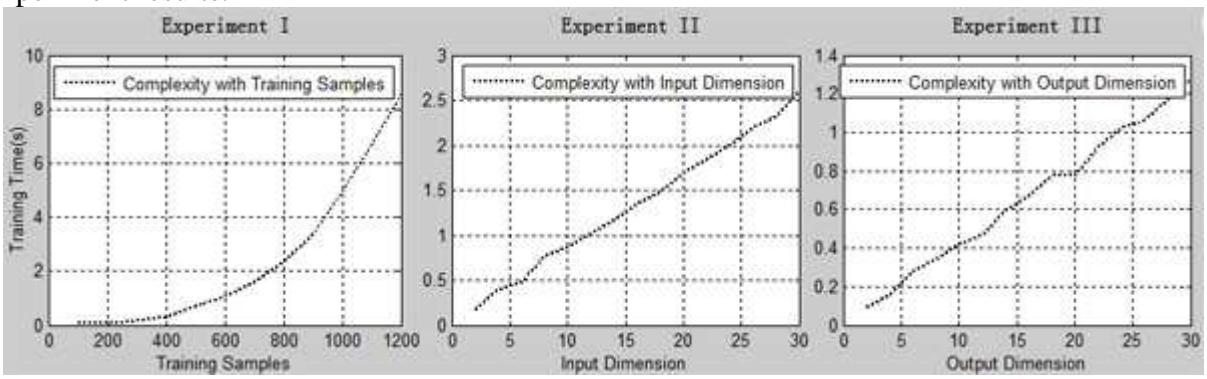

Fig. 2 The first category orthogonal weight function neural network algorithm on the number of sample complexity of the training experiment

Experimental Analysis

Experimental results show that the first class to see the complexity and number of samples right orthogonal function neural network algorithm in line with the curve of a quadratic function, and the input and output dimension linear relationship. As can be seen from these three experiments the time complexity of the first class of orthogonal function neural network algorithm right in line with the conclusions previously deduced: $mnO(N^2 \log N)$.

Summary and Conclusions

This paper first introduces the right of the first class of orthogonal function neural network topology and training algorithm; then according to the algorithm complexity of knowledge, a key step in the analysis of network training the number of operations to derive the first class of orthogonal function neural network training right time complexity. Finally, the time complexity of the algorithm to verify the theoretical training results of the first class of orthogonal function neural network right through the experimental accuracy, the simulation results show that the right of the first class of orthogonal function neural network has a faster learning and training capabilities, and its training time complexity degree and the number of training samples, the input layer and output layer nodes nodes about which the input samples was proportional to the square of the relationship, with the input layer nodes and output layer nodes is linear.

References

[1] Martin T.Hagan，Howard B.Demuth. Neural Network Design [M]. Beijing: Machinery Industry Press, 2006

[2] Zhang Daiyuan. New Theories and Methods on Neural Networks[M]. Beijing: Tsinghua University Press,2006

[3] Li Qingyang, Wang Nengchao, Yi Dayi. Numerical Analysis (4th edition) [M]. Wuhan: Huazhong University of Science and Technology Press, 2006

[4] Shiow-Shung Yang, Ching-Shiow Tseng. An Orthogonal Neural Network for Function Approximation [J]. Systems, Man, and Cybernetics, Part B: Cybernetics, IEEE Transactions on, 1996, 26(5):779-785

[5] Thomas H.Cormen, Charles E.Leiserson. Introduction to Algorithms [M]. Cambridge: The MIT Press, 2009

Advanced Materials Research Vols. 989-994 (2014) pp 4441-4446
© (2014) Trans Tech Publications, Switzerland
doi:10.4028/www.scientific.net/AMR.989-994.4441

Crowdsourcing software development process study on ultra-large-scale system

Xu Xiaolan[1, a], Wang Ya[2, b]

[1]BeiHang University XueYuan Road No.37,HaiDian District,Beijing,China

[2]BeiHang University XueYuan Road No.37,HaiDian District,Beijing,China

[a]xuxiaolan@cie-info.org.cn, [b]wangya@buaa.edu.cn

Keywords: ultra-large-scale system;Software Crowdsourcing;Process management

Abstract. Software Crowdsourcing development model shows the increasingly strong advantage in solving the development of ultra large scale system, mode of development of this new software development process chang to mass, openness and community. At the same time, Software Crowdsourcing development process also reflects the strong competitive, crowdsourcing software development mode is a periodical process of releasing requirement-bidding competition-software review.In order to promote the community members to collaborate, compete and develop, and to improve the software development efficiency and quality,This paper discusses the group in the process of Software Crowdsourcing development, reward and remuneration of reputation and ranking, corporate governance.thus,we can Improve process management, improve the quality and efficiency of software development.

Introduction

The ultra-large-scale system has unprecedented complexity, variability and uncertainty, bringing huge challenge on traditional software engineering method. The ever-increasing Software Crowdsourcing practices, for example App Store of Apple Inc and Android Market of Google Inc, have revealed feasible program on solution of ultra-large-scale system structure problem. These new software engineering practices embody brand new software development mode: from elite researchers to public researchers, from closed and planned software development to opened and competitive software development, from workshop development environment to community development environment. In the whole ultra-large-scale system ecological environments of technology, the user will play a more and more important role.

Crowdsourcing software development mode

The basic software element in the ultra-large-scale system is defined as crowdsourcing software in this article, that is, the crowdsourcing software is the basic software entity in crowdsourcing software development method. During the crowdsourcing software development process, the basic crowdsourcing software development mode is a periodical process of releasing requirement-bidding competition-software review (as shown in Fig.1). Once the end-user proposes a specific requirement for the system, he may achieve it according to the following steps. Firstly, he can explain the specific requirement in natural language, and release it in the crowdsourcing software environment, and then ask for solutions from developers of the whole community. His requirement will be converted to design program by community members, and the best design program will be selected by collective review and prioritizing. Secondly, the winning program will be published to community members, and members with competence and development technology will be selected to participate in development competition. Finally, the created software entity will be performed collective review and user group trial, and each user can perform review and evaluation on each aspect of the software entity, and the related trial report will be generated. A new round of crowdsourcing software designing-realizing-testing and application will be performed according to review and trial result, and further improvement on the crowdsourcing software will be performed.

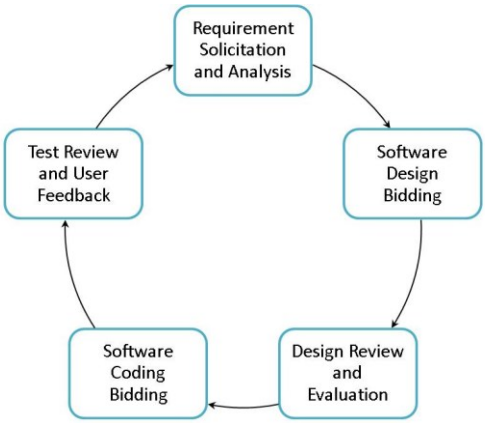

Fig.1 Crowdsourcing software development process

The above crowdsourcing software development process usually shows very strong competitive characteristic, similar to the contribution and appointment process in high level academic conference. Different from classical software development process, the crowdsourcing software task will not be assigned to a appointed developer in the company or epibolic contract engaged developer. On contrast, the crowdsourcing software task criterion containing technical requirements, development schedule and accomplishment reward will be released to the whole community in an open and transparent form, to admit the best by competition. The community members who are interested in the crowdsourcing software development task will accept the released task, set out to the coding work for the crowdsourcing software, and then submit their development results to the community review committee. The committee is responsible for the evaluation on their results and the selection of the best work as well as its developer. All the crowdsourcing software entities need to pass the competitive process and be designed and developed, and then pass the social test and integration. Similarly, the test and integration task should be organized and accomplished in a similar competitive method, to call upon the members with test and integration experience to participate. Therefore, the cooperative type competition mode is the main way to generate high quality software product in crowdsourcing software ecological environment. We can analogy the structure and evolutionary process of crowdsourcing software system to the compiling course of Wikipedia: each community member can contribute chapters or sentences in Wikipedia entry. And the entry is jointed and combined by basic character element and compound sentences and paragraphs in a recursion way.

Governance on crowdsourcing software development process

We need to perform scientific governance on crowdsourcing software development process, in order to promote the community members to collaborate, compete and develop, and to improve the software development efficiency and quality, and this involves in how to design a reward system to stimulate the crowd to participate in ultra-large-scale system development project; how to construct a ranking mechanism to ensure the crowdsourcing software developer have sufficient competence and quality to successfully accomplish the crowdsourcing software task; how to manage the social structure of the ultra-large-scale ecological system to regulate the development activity, balance the conflicts among project development cost, time schedule and project task complexity.

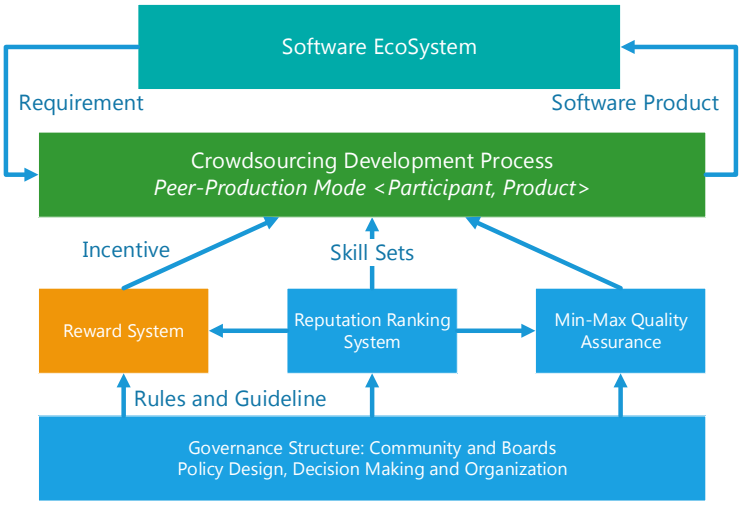

Fig.2 Crowdsourcing software engineering governance structure: reward mechanism, reputation mechanism and governance organization

Fig. 2 shows the basic governance structure of crowdsourcing software development, which consists of three sub-systems: reward system, reputation ranking system and top leading organization. The core of the overall governance structure is the relevance and interaction between grouped members. The community governance committee is the top leading organization, in charge of policy design, strategic decision making, structure planning and behavior standardizing. The governance committee has two necessary methods to cultivate healthy and energetic ecological system: the reward mechanism and the reputation mechanism. The reward mechanism provides incentiveness for crowdsourcing software, promotes them to participate in crowdsourcing software development; and the reputation mechanism provides quantitative basis for competence analysis of each community member, and also is the basis of reward mechanism.

3.1 Reward and compensation system

Crowdsourcing software development can't be separated with effective reward mechanism, and it is very important to attract wide range participation of community members to keep the vigor of crowdsourcing software platform. In traditional open source software community, the "Hacker" culture is usually known as the important factor to motivate people to participate in, because people wish to improve their coding competence and enjoy the challenging coding task[1]. Besides, people wish to make more contribution in the community, to acquire or enhance their popularity. Although these social reward mechanisms are still effective in crowdsourcing software development, it is far insufficient for them to mobilize people to accomplish complicated task such as ultra-large scale system. At the same time, the economic incentive method has powerful and effective power to promote community development activity[2]. According to the traditional economic theory, when the money reward is linked up with working performance, the rational workers will improve their working performance to improve product quality. This market-oriented incentive method can be adopted in the reward mechanism of crowdsourcing software community, to provide reasonable compensation for each crowdsourcing software task, and to encourage community developers to acquire the reward compensation by competitions.

3.2 Reputation and ranking system

The main functions of reputation system embody in two aspects: the first one is, to rank the intelligence and competence of participants, to guarantee the software product quality; the second one is, to promote the sufficient trust and positive interaction between the requester and the developer of the crowdsourcing software task. It is very difficult for the requester of the crowdsourcing software to find out skillful developer to accomplish the request, and exclude poor crowdsourcing software products. On the contrary, the ranking of the crowdsourcing software requestor will help the developer to select the task released by the requestor with high reputation, according to their history.

A reputation system can collect, release and aggregate the latest behavior and history of the requestor and the executor, and a ranking algorithm is adopted to perform quantitative score for

them. This kind of ranking method is usually established on basis of user evaluation and third party review. The main parts of online reputation mechanism include: crowdsourcing software task evaluation system, the accumulator and reputation engine fed back by crowdsourcing software. Firstly, the reputation ranking evaluation index can be subjective or objective. The quantitatively measured performance index of each community developer can embody his coding competence and the seriousness degree of executing the development task, for example, his successful submission number of times, the reward and corresponding user download rate of the crowdsourcing software entity created by him. And the information such as third party evaluation and user review can be analyzed as the crowdsourcing software entity quality and the basis of reputation subjective evaluation of crowdsourcing software task requestor. Secondly, all the collected information related to reputation are collated and sorted to establish detailed document for each community member, and to analyze their knowledge structure, competence degree and experience collection. Thirdly, the reputation engine can be used to synthesize the history and recent working performance, to give quantitative evaluation on the developer.

At present, the ranking algorithm research in crowdsourcing software calculating system is still in immature stage. It should be pointed out that the competition ranking research has been conducted for several decades. For example, the classical Elo ranking mode, which calculates the chess skill of each international chess player based on the statistic method, has been widely applied in various types of athletic contests. The improvement works on the basis of the mode enhance the accuracy of ranking algorithm and also introduce other statistic methods, for example: the player's performance fluctuation and Bayesian reasoning frame, to deal with the competition situation with multiple players[3][4]. We abstract the reputation system, apply them in crowdsourcing software engineering methodology, and define competitive software development principle.

Input: define a sequence S = { R1, R2, R3 }, in which each R is a six-tuple: (C, P, T, X, Y, Z), in which C is the criterion required by crowdsourcing software, P is the assemblage of participants, T is the assemblage of crowdsourcing software development tasks. The remaining functions: X, Y, Z defines ranking mechanism and reward system respectively.

X is the mapping function of crowdsourcing software product submission and its score in this round of the crowdsourcing software competition. Its definition is $X: P \times T \rightarrow Score$, in which P and T representatives the two assemblages of the participants and the tasks respectively. The score is a group of evaluation indexes, including: download counting, positive or negative evaluation from users as well as expert opinions of the review committee. Each participant can be ranked based on the score.

Y is the function used to calculate the reputation in the competition, defined as follows:

$Y: P \times Rating \times Rank \rightarrow Rating$,

In which two inputs are included, input variable Rating representatives the past competition result, and the other variable Rank is the ranking of this round of competition.

Z is the reward function that the winner of this round of competition should obtain, defined as follows: $Z: P \times Rating \times Rank \rightarrow Reward$.

The reward obtained by a developer is decided by the developer and the task requestor based on the crowdsourcing software accomplishment quality as well as the reputation ranking of the developer. Usually, the programmer with relatively high raking can obtain more compensation. In this way, the community members participate in competitions actively, to promote their ranking and coding skills.

3.3 Governance organization

The governance mode of crowdsourcing software engineering is an assemblage of organizations, processes and policies, to guide and control the grouped development of the community, and maintain the common community value. With the support of open technology platform and transparent software frame, the governance organization can persistently coordinate the relationship between manpower, knowledge and resources of the community, to promote the development and progress of ultra-large-scale system in a prompt and adaptive way. The main body of governance organization is the community governance committee, the members of which are experts with

application field and software engineering background. The committee is in charge of sketching the overall shape and strategic decision of the project, to guide system development and achieve risk control. The governance committee should formulate and optimize correct policies and regulations on reward and reputation mechanisms, to enlarge the scale of community network, and maintain a team of developers with high quality. At the same time, the most powerful method of the governance committee is to set rules and development guides, to effectively standardize the development activity of the community. The governance committee must listen to suggestions and modifications of the stakeholder of the project, to formulate regulations which can be widely accepted by community members.

The governance committee needs to lead a working team, follow the policies of the governance committee and coordinate between various independent developers in the community. The working team members can be directly selected from the community members. Their responsibilities include:

1) Organize software requirement analysis: the working team should communicate with key stakeholder, to determine main function requirements and define preliminary requirement criterion. As for the ultra-large-scale system, the stakeholder must be very large scale community. The working team needs to adopt the grouped calculation mode of Wikipedia, collect requirement information by online human network, and generate complete analysis report[5][6]. Once a new requirement point is found by the software requirement analysis, the working team needs to update requirement analysis in time, and start a new round of competitive development, to achieve the new function requirement in a high priority.

2) Design software system structure and lead ecological platform development. After determining the requirement criterion, the working team can start to perform preliminary stage software system structure design, and define main function components and software structure style. After the structure planning, the primary task of the working team is to achieve the core general function of the system, to construct a solid and reliable open platform, to achieve the sustainable development of the whole software ecologic system. In some cases, the working team even needs to develop related software tool and environment in different levels, to support the corresponding community members to perform grouped development work. The working team can fully reference the past software project achievements or open source achievements, to improve the present platform and increase characteristic function.

3) Resolve the overall design and release crowdsourcing software development guide; the preliminary design detailed specification document can be released by the working team to the community, to mobilize community members to achieve the needed crowdsourcing software entity. The working team must at the same time create online coordination tool, to achieve collaborative design and discussion, to encourage the community to participate.

4) Review the intelligence of grouped developers; one of the main tasks of the working team is to find suitable developer in the community to achieve each crowdsourcing software entity. According to the detailed record and ranking provided by the reputation system, the working team can screen out the optimized member with development competence and field knowledge from the applying developers.

5) Review the crowdsourcing software product quality; it is very important for the success of grouped development project's success to review all the submitted crowdsourcing software, examine them whether in accordance with the criterion, and whether to achieve the quality requirement. The working team members are all programming experts, with the competence and experience of testing the crowdsourcing software's correctness and quality. At the same time, except for the expert review, the working team should encourage the end-user of the community to perform function test to crowdsourcing software entity and compile feedback opinions. With the evaluation of the crowdsourcing software from the comprehensive experts and general users, the working team can ultimately determine the best crowdsourcing software achievement, and provide the developer with reward.

The governance organization of the App Store of Apple Inc partly realizes the above described organization mode, especially on crowdsourcing software review aspect. It has a review committee consists of 40 people, perform analysis and test on each provided ISO application according to the review guide of App Store. But the review course of Apple Inc is neither open nor transparent; the review is totally performed inside of the company to guarantee the mobile phone application quality. This behavior causes some disputes, and the American FCC even performed survey and inquiry on it. Besides, the closed behavior brings abundant workload to the review committee, and greatly delays the passing time of crowdsourcing software.

Conclusion

The crowdsourcing software engineering method shows increasingly powerful advantage on the development problem of ultra-large-scale system; on this overall background, this article firstly discusses on the development mode of crowdsourcing software development basic element, and the coordinative competition mode is the main way of crowdsourcing software development. In order to better coordinate the competition relationship of crowdsourcing software development, this article discusses three governance problems of reward, ranking and top layer governance in software process governance, to better mobilize the enthusiasm of community members, improve the condition of the overall software ecological system, and promote software development efficiency and quality.

References

[1] Karim R. Lakhani, Robert G Wolf, Why Hackers Do What They Do: Understanding Motivation and Effort in Free/Open Source Software Projects, (September 2003). MIT Sloan Working Paper No. 4425-03. Available at SSRN: http://ssrn.com/abstract=443040 or http://dx.doi.org/10.2139/ssrn.443040

[2] Nikolay Archak , Money, glory and cheap talk: analyzing strategic behavior of contestants in simultaneous crowdsourcing contests on TopCoder.com, Proceedings of the 19th international conference on World wide web, 2010.

[3] Parameter estimation in large dynamic paired comparison experiments, Applied Statistics 48 (1999), 377-394.

[4] Ralf Herbrich and Thore Graepel, TrueSkillTM: A Bayesian Skill Rating System, Tech. report, 2006, MSR-TR-2006-80.

[5] Carlos Castro-Herrera, Chuan Duan, et al, A recommender system for requirements elicitation in large-scale software projects, Proceedings of the 2009 ACM symposium on Applied Computing.

[6] S.L. Lim, D. Quercia, and A. Finkelstein, StakeSource2.0: using social networks of stakeholders to identify and prioritise requirements.

Advanced Materials Research Vols. 989-994 (2014) pp 4447-4451
© (2014) Trans Tech Publications, Switzerland
doi:10.4028/www.scientific.net/AMR.989-994.4447

The implement of a Linux database data processing mechanism based on cache

Yongjun Zhang[1, a], Chunhui LI[1,b]

Photonics and Optical Communication and Optoelectronics, Beijing University of Post and Telecommunication, Beijing, China

yjzhang@bupt.edu.cn

lichunhui1014@163.com

Keywords: database; cache; IOT(Internet of Things); gateway; embedded Linux operating system

Abstract. Although the simple structure and easy operation of completing data process depending only on the real-time request of database, the database call time is far longer than the lookup time. If the database is called too frequently, the processing speed will surely be cut down and the real-time performance will be degraded. Based on the situation, this paper will put forward one method, which combined cache with database can improve the performance of the system in the main controller of integrated security system of equipment management.

Introduction

Database is an important tool to store, share, dispose data and even manage information now. Database performance optimization has become an important topic.SQlite which is contained in a C programming library is a relational database management system.In contrast to other database management systems, SQlite is not a separate process that is accessed from the client application but an integral part of it. The operation is faster than the current most popular database. Provide support for the transaction function and concurrent processing. The application of the transaction, not only ensure the integrity of the data, will also improve the running speed.

Cache is a memory chip in the hard disk controller which has extremely fast access speed. It is the buffer for the interior memory and the external interface, and is usually used in RAM to save temporary data, which can be missed once it is powered off.

Theoretically, base on the high access speed of cache, the method embedded database combined with cache can optimize the traditional great. This paper presents the integrated security system of equipment management, in which the embedded service gateway combines the traditional internet with the new type of sensor network. In this system the embedded service gateway plays the role of the coordinator gateway of wireless sensor network, and becomes the remote web client, which makes it possible to communicate between two different protocols. Because of the hardware characters of Reader in the bottom layer and the inflexibility of handling with data, we can only pass the status information to the embedded service gateway directly. It analyzes the data with information in the database to get the relevant signal. The signal will be saved in the record and post to web server.

The realization of the processing mechanism

This system adopted the wireless sensor, the embedded system and some other techniques. From the beginning of equipment distribution, it took the real-time monitor and protection for the needed equipment, which made the superiors be able to master the subordinate equipments status. When one moved with illegality or violation, it would get the alarm message. As a result we could avoid the equipment accident occurrence.

Fig. 1 shows, the integrated security system of equipment management was divided into three layers [1-2]: the perceptual layer, the transport layer, and the presentation layer. The perceptual layer received information from the active label RFID(Radio Frequency IDentification), which included

labelID, the current energy, position and other related information. The reader made all the data about labels in combinations and then encapsulated in certain rules, finally post to the main controller. The transport layer was the main controller which received and analyzes data, and then produced register, loss, return, lowpower, access door, on-off of the safe signal, finally reported to the web server. The presentation layer was the web server. It received signal from the main controller, and can also make remote alarm if needed.

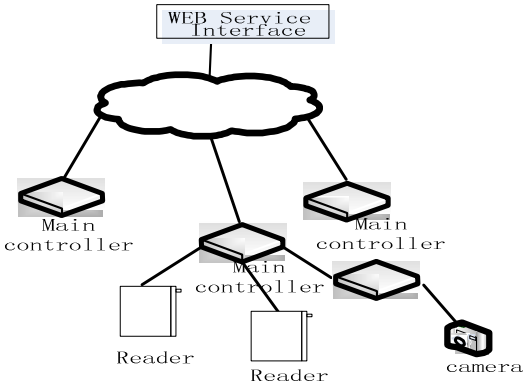

Fig. 1. The Structure of the Integrated Security System of Equipment Management

The main controller code of this system was achieved by Qt. It is a fully objected-oriented, easy to expand and allows a true component programming c++ application framework. And it encapsulates the access detail which adapts to the different operation system, which makes it be able to deploy with a variety of desktops and embedded systems quickly [3].

The main controller core was divided into two modules [4-6]: communication module and data processing module. The former was corresponding to the input and output of the central processor in figure2; the latter was corresponding to the handling part between central processor and database.

Communication module

Communication module was the basic module in completing the function of main controller. It included two sub-modules, multi-threaded server and the client of http. The former was used to communicate with multiple readers, get RFID information, listen and get connected with QTcpSocket and QTcpServer and so on. The latter, was used to report the effective information to web server.

Multi-threaded server. Fig. 2 shows the data processing flow:

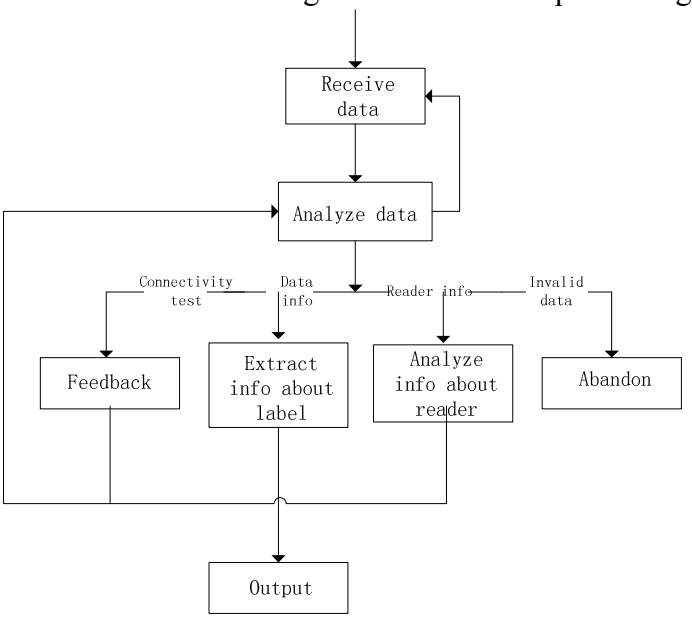

Fig. 2 Data Processing Flow

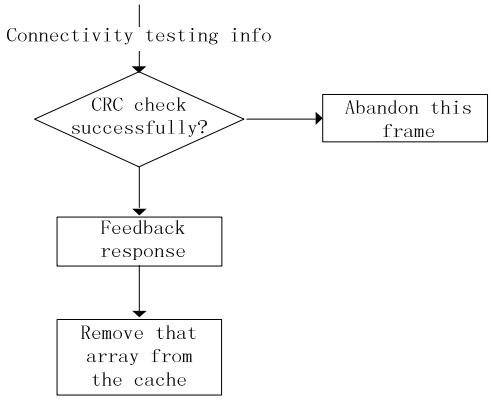

Fig. 3Connectivity Testing Part

Connecting part for testing is shown in Fig. 3.After connected with main controller, we could make sure whether the line is alive or not, through receiving and sending connectivity testing information. If the line was normal, we could switch the available message. Because of the smaller length of frame and the simpler structure than the normal data frame, on one hand it might reduce unnecessary traffic, on the other hand as it was easier to parse, it could reduce the handling stress.

As for the message about label in Fig. 4, we needed to get the Reader ID, and acquire the message about Reader. And then stored labelList, lopedList, and some other lists in the cache, passed them to the database. Finally took the corresponding disposition.

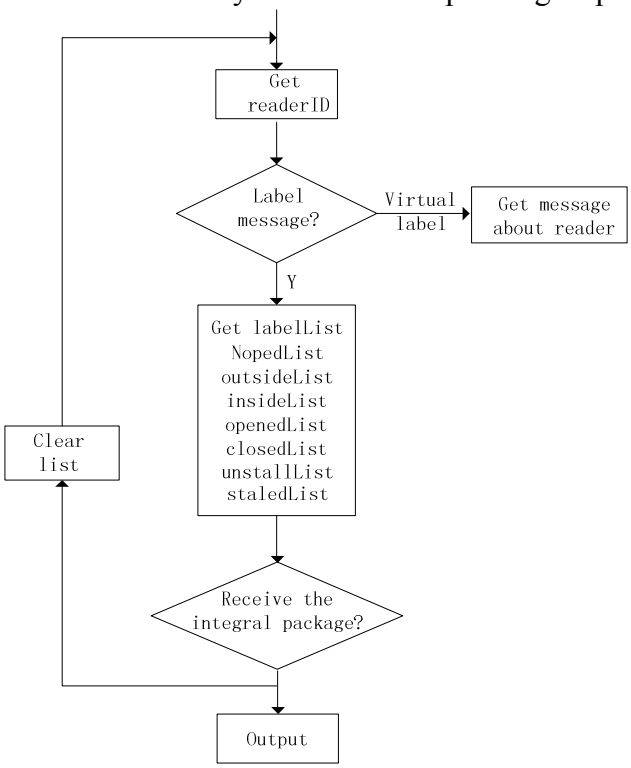

Fig. 4 Get Message about Label

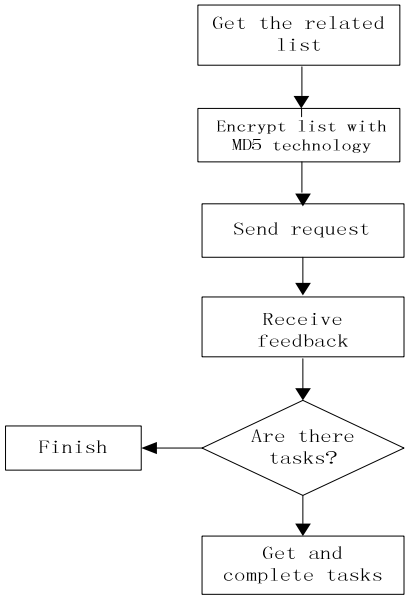

Fig. 5 Heartbeat Message Flow

HTTP Client. There are three interfaces to connect with WEB Server, register, status, and heartbeat message. To enhance the safety, we employed MD5 encryption technology.

Register message was the same as status message: got the related list->encrypted List with MD5 technology->sent request->received feedback. Fig. 5 shows the heartbeat message flow.

Data processing module

It was the core module to achieve the function of main controller. Data processing module summarized data from the transport module, and analyzed with database, then passed them on transport module.

We could get such signals as: register, loss, return, go out, enter the door, open the door, close the door, and temper signals.

Get register, loss, return signals. Fig. 6 shows report process. Implementation approach: First, we could get labelList through labelID in transport module, then after compared with data in the database, we got the related message.

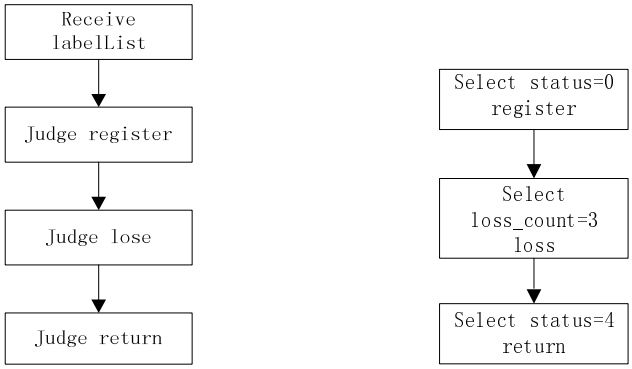

Fig. 6 Report Process

We got these three signals by comparing the LabelList with data in database, as is shown in Fig. 7 and Fig. 8.

(1) Register signal

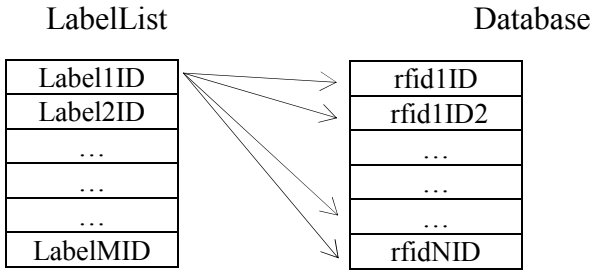

Fig. 7 Register Match

Find every item that from LabelList in database. If

Successfully: Leave alone.

Unsuccessfully: Insert that item into database. Set status = 0;

In this part we bring in status row, which is used to record rfid status, as Table 1 shows.

Table 1 The position status value

0	1	2	3	4
Register but not report	normal	Lose but not report	Lose and reported	Return

Report process

Start the timer, and report every three seconds. Find the items with status = 0, and then put them in the regiList, finally report them to the server, and set status = 1.

(2)Lose signal

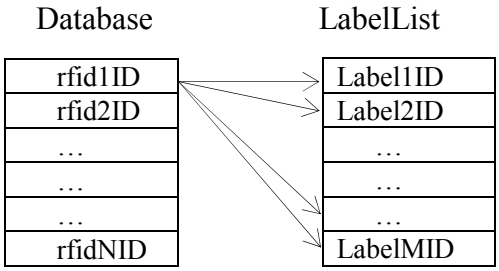

Fig. 8 Loss Match

Find every rfidID item from the database in the LabelList.

Successfully: Leave alone.

Unsuccessfully: Set status=2, and increase loss_count value by 1.

When the reader receives message from the label, it is impossible to receive all the label message at any time, because of the obstacles. To avoid the misinformation, we make the reader report lose signal, only if it does not receive that label in three consecutive times.

Report process

Start the timer, and report every three seconds. Find the items with loss_count = 3, and then put them in the lossList, finally report them to the server, and set status = 3, loss_count = 0.

(3)Return signal

To dissolve the misinformation:

Find the items with status = 2->Find that items in LabelList

Successfully: Set status = 1, label_count = 0 in database.

Unsuccessfully: Leave alone.

Return signal:

Find the items with status = 3->Find that items in LabelList

Successfully:Set status = 4, label_count = 0 in database.

Unsuccessfully: Leave alone.

Report process

Start the timer, and report every three seconds. Find the items with status = 4, and then put them in the retuList, finally report them to the server, and set status = 1, lo**ss**_count = 0.

Power, access door, opening and shutting door and tamper. Implementation thought: Firstly, we can get the position, power of the label and the state of the door the tamper state. That is, we can get these lists, such as, insidList, outsideList, lopList, nopList, openedList, closedList, instList, uninstList. Then, we find every list labelID in the database, if the status changes, we should make out the related signal.

The related keyword in database is as table 2 shown.

Table 2 The other status value

Lowpower(int)	Position(int)	Uninstall(int)	Door_state(int)
0-low power 1-normal power	0-out of the door 1-inside of the door	0-installed 1-uninstalled	0-shut down 1-open

Conclusion

When applying the mechanism which combines cache with database to main controller of integrated security system of equipment management, it can not only control the delay in 0.001 second or so, but can also run stably in the system.

References

[1]Zhongke. The design and implementation of Iot gateway based on ARM [D] .Chengdu: Southwest Jiaotong University. 2012.(In Chinese)

[2]ASleman and R． Moeller, SOA Distributed Operating System for Managing Embedded Devices in Home and Building Automa

[3]Liqiang, Guo Weichang, Guanxin, Infrared focal plane digital video image processing system, based on general DSP[J]. Journal of Tianjin university. 2005, 38(10): 904-908(In Chinese)

[4] ZhongLiping, Zhang Yongjun, GuWanyi. The design and implementation of smart home gateway server software [J]. Journal of Central South University. 2013, 44(supplement 1):333-336(In Chinese)

[5]Anoop Gupta, Wolf-Dietrich Weber, Todd Mowry. Reducing Memory and Traffic Requirements for Scalable Directory-Based Cache Coherence Schemes.Computer Systems Laboratory, Stanford University. 1994

Advanced Materials Research Vols. 989-994 (2014) pp 4452-4455
© (2014) Trans Tech Publications, Switzerland
doi:10.4028/www.scientific.net/AMR.989-994.4452

Experimental Data Publishing Based on Browser/Server for Neutral Beam Injection in EAST

Rui Zhang[1, a], Chundong Hu[1, b], Peng Sheng[1, c], Xiaodan Zhang[1,d], Yuanzhe Zhao[1,e], Deyun Wu[1, f], Qinglong Cui[1, g] and Yulian Lin[1, h]

[1]Institute of Plasma Physics, Chinese Academy of Sciences, Hefei 230031, China
[a]rzhang@ipp.ac.cn, [b]cdhu@ipp.ac.cn, [c]shengpeng@ipp.ac.cn, [d]zhangxd@ipp.ac.cn, [e]zyz@ipp.ac.cn, [f]wdyun@ipp.ac.cn, [g]qlcui@ipp.ac.cn, [h]yllin@ipp.ac.cn

Keywords: NBI, B/S, data, experimental results, publishing, AJAX, JFreeChart.

Abstract. In the experiment of Neutral Beam Injection (NBI), Experimental Data Publishing Software (EDPS) is developed to get experimental data monitored remotely. Adopting B/S module, EDPS publishes information, such as experimental configurations and results on the Internet dynamically. The design and implementation of how EDPS uses the present information source in NBI Control System (NBICS), the procedure EDPS handles the requests from clients and displays the information on web pages are introduced in this paper.

Introduction

NBI system is employed on Experimental Advanced Superconducting Tokomak (EAST) for plasma heating and plasma current driving to support the steady-state operation and physical research [1]. NBICS is a subsystem which takes charge of monitoring the experimental operation process and interlock protection. Besides, it implements data collection processing and network communication [2]. During the experiment, NBICS collects experimental configuration, current value and voltage value of magnet power supply, gas valve, arc power supply, etc. This information makes great contribution to experimental result analysis.

EDPS acquires experimental data and publishes them on the Internet. With the implementation of EDPS, users who cannot get access to the Local Area Network (LAN) of NBI system can get an approach to experimental data acquisition.

Requirement and Analysis of EDPS

NBICS consists of four levels: remote control level, main control level, field control level and video monitoring level [3]. In each discharge, Main Control Console (MCC) in remote control level sends configuration to Main Control Server (MCS) which is located in main control level. Then MCS transits the command to subsystems and acquires the results collected in field control level. In this process, MCS saves all configurations and results. For the sake of analyzing the data, this information needs to be published beyond the LAN. Take security into consideration, MCS needs to be isolated from Internet in case that the data are modified illegally. So a platform connected with main control net and Internet is established. EDPS is software running on this platform, collecting experimental data and publishing them on the Internet. EDPS is implemented with the following specific functions:

a. During the experiment, EDPS displays the current configurations of the experiment, including shot number, voltage, and amplitude and pulse width of each sub-system.
b. EDPS displays experimental results collected by different channels in the form of waveform dynamically.
c. EDPS offers inquiry service for historical data, such as experimental configurations, spectrum results, etc.

Implementation

EDPS adopts B/S model. Clients can access data on the server by using a browser. This model decreases the burden of clients and developers. Besides, it provides an easier way to update software. The architecture of EDPS is shown in Fig. 1 (parts in dotted box). Data acquisition module takes charge of the communication with MCS to acquire experimental data. Request processing module processes requests from clients and transmits data between server and web page display module. Web page display module displays experimental data in appropriate forms on web pages.

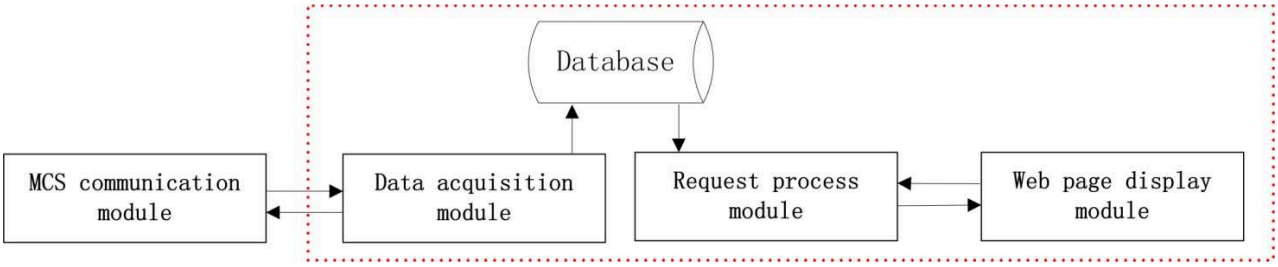

Fig. 1 Architecture of EDPS (parts in dotted box)

Design of Data Acquisition Module

In this module, programs are developed in C/C++ language, with a C/S program model based on standard TCP/IP protocol and multi-threading technology. The NBI TCP communication data structure is defined as it is shown in Fig. 2. The numbers at the top of figure express the size of bytes in different fields [4]. In every discharge, MCS sends information under this structure to EDPS, then EDPS analyzes the information and saves the data into MySQL database thus to provide an interface for request processing module.

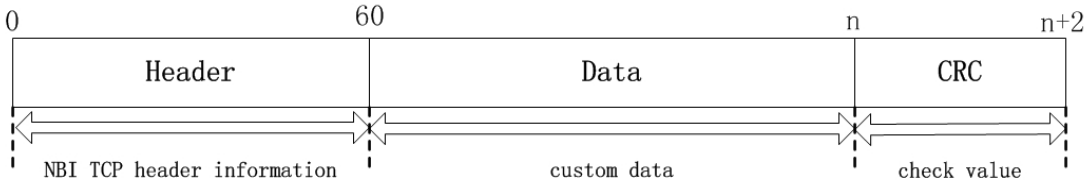

Fig. 2 Definition of the NBI TCP communication data structure

Design of Request Processing Module

In this module, Java Web techniques, especially servlet, Asynchronous JavaScript and XML (AJAX) are applied to process requests from clients. Taking advantages of specific class, servlet based on Java checks whether the requests is legal, then servlet invokes specific Java Bean to handle the requests and transmits responses to Web page display module or AJAX programs. Java Bean mainly handles the database by taking advantage of the application of connection pool. The work procedure of Java Bean is shown in Fig. 3.

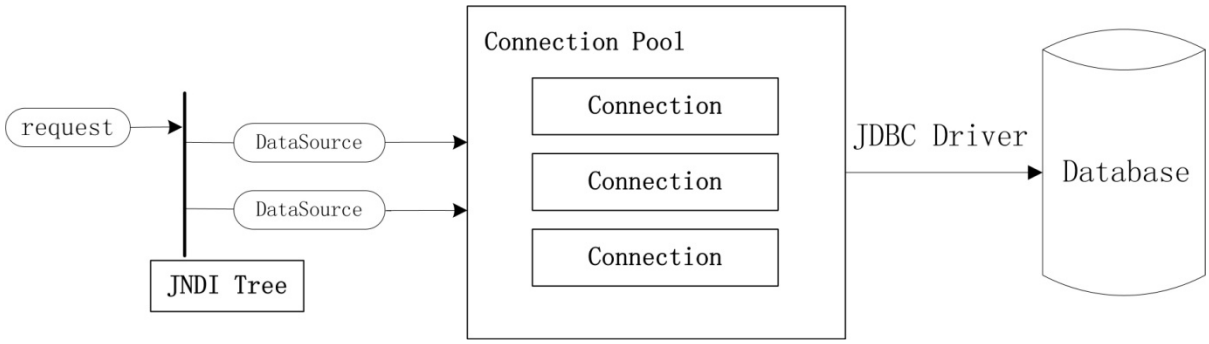

Fig. 3 Work procedure of Java Bean

AJAX is adopted to implement partial update of web pages in order to avoid the waste of bandwidth [5]. The programs are developed by JavaScript which are embedded into Hypertext Markup Language (HTML) or Java Server Page (JSP). Since experimental data change dynamically, AJAX programs send requests to servlet in every period to get the new information from database. In this way, web pages are refreshed dynamically to show the changes. The application of AJAX frameworks optimizes this module.

Design of Web Page Display Module

Experimental data are published in the form of table and waveform. This module is developed mainly relying on JSP and HTML. Some configurations are shown in the form of tables which can be directly printed on web pages, while other data, such as the amplitude and pulse wide of power supply, results collected from different channels are better to be displayed in the form of waveform.

Waveform is generated by JFreeChart, which is a library developed by Java. This library supports for many output types, including Swing components, image files (including PNG and JPEG), and vector graphics file formats (including PDF, EPS and SVG) [6]. In this module, waveform is imported by image files. Apply data by using the Class 'chartUtilities' and use the method 'writeChartAsJEPG' to output image in format of JPEG. Using the method 'writeRenderingInfo' can generate MAP data. MAP data enables clients to read the accurate value of each point of the waveform by keeping the mouse pointer staying. The work flow of generating waveform by JFreeChart is shown in Fig. 4.

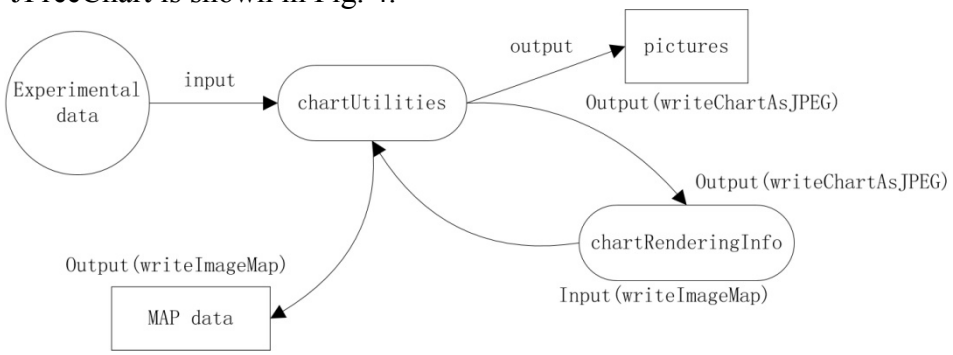

Fig.4 Work flow of generating a waveform by JFreeChart

Conclusion

The design and implementation of each sub module of EDPS are described in this paper. EDPS meets the requirements of publishing configuration and experimental results dynamically and providing service for inquiry. By adopting B/S, EDPS provides a method to analyze experimental data for those people on the Internet network.

References

[1] Hu Chundong, Xie Yahong, 2011, Plasma Science and Technology, 14:75

[2] Sheng Peng, Hu Chundong, Song Shihua, et al. 2013, Plasma Science and Technology, 15:6

[3]Sheng Peng, Hu Chundong, Song Shihua, et al. 2010, Asia Pacific conference on plasma science and technology, Jeju Island, Korea, pp. 4-8

[4] Wu Deyun, Hu Chundong, Sheng Peng, et al. 2013, J Fusion Energy, 1:5

[5] Huang X T, Yang B Z, et al. 2010, Computer Engineering and Design, 31:2629

[6] D. Gilbert, 2002, “The jfreechart class library,” Developer Guide. Object Refinery

Advanced Materials Research Vols. 989-994 (2014) pp 4456-4460
© (2014) Trans Tech Publications, Switzerland
doi:10.4028/www.scientific.net/AMR.989-994.4456

Three Networks Convergence Analysis Based on SWOT Theory

Zhang Rui[1], An Ying[2]

Harbin University of Science and Technology, School of Management, Heilongjiang Harbin, 150040, China

zhangrui0619@163.com

Keywords: three networks convergence; SWOT theory; information industries

Abstract. With the development of information technology, the three networks convergence are making progress on technology, policy and market fields in China. This research analyzed the CATV, telecommunication and internet industries based on SWOT theory. It found they have different strengths, weakness, opportunity, threats in different industries. So we found the problems on three networks convergence and proposed the suggestions.

Introduction

Three networks convergence has developed for over ten years. It refers to the convergence of CATV, telecommunication and internet on the physical layer. With the development of the industrial chain of vertical and horizontal in China, the network system, terminal, business, institution and policy and so on, which have shown the trend of convergence. The subjects of three networks convergence make technology convergence through the interconnection, use the same IP protocol, and strengthen their infrastructures' construction. The subjects of three networks convergence take the method of mutual penetration and mutual cooperation in the business aspects, take the mode of coexistence of competition and cooperation to promote the development of the three networks convergence, thus provide superior service for people with low cost, diversification and humanization, personalization, multimedia service and so on.

According to the present situation of three networks convergence in China, the technology has been no longer the main factors influencing the three networks convergence. In terms of CATV, telecommunication and internet who have their own customer groups, and occupy a certain market share, CATV and telecommunication with monopoly management system lasted for decades, so the two major subjects are conservative. They also think that they have vast domestic market and customers. When three networks convergence begin, they are worried that their own interests will be affected. On technical and business aspects, each operator of them will keep some secrets, therefore, which is not conducive to the development of three networks convergence.

SWOT analysis is first proposed by K.J. Andrews who is a professor in Harvard Business School. SWOT was mentioned in his book "company strategic concept" in 1971 [1]. SWOT analysis tool is a kind method of enterprise strategy analysis S represents strength and advantage, W represents weakness, O represents opportunity, T represents threat. The S and W are the internal factors. O and T are external factors.

According to the SWOT model, this research mainly analyzes the present situation of three networks convergence as well as the present problems in China, and give some policy suggestions to promote three networks convergence.

Analysis of the telecommunication industry based on SWOT model

Before 2008, the telecommunication industry was composed of China Telecom, China Railway Telecom, China Network Communication, China Unicom and China Mobile. Due to the competition mechanism becomes more and more invalid in the telecommunication industry. The services of fixed telephones gradually declined, more and more users turned to mobile services; so it needs to create a better network to communicate, to resolve consumers' complaints, to carry out the "full-service" for telecommunication. Therefore, the companies were restructured, and they are known as the China Telecom, China Unicom and China Mobile.

On the background of three networks convergence, the method of SWOT analysis was carried out on the telecommunication. The advantages of telecommunication networks (S) as followed. Telecommunication has wide coverage, advanced technologies, perfect equipment, high qualities, abundant talent employees, well-managed, gradually improvement of service qualities, plentiful and valuable experience in market, diverse business model, and a certain of monopoly. Telecommunication's weaknesses (W) are that telecommunication has still provided telephone calls which has become saturated, and telecommunication is lack of the operating experience in content. Enterprise's strategic management and innovation are inconsistent with trend of development. To draw lessons from advanced system, telecommunication companies need innovate on telecommunication business and explore a profitable business model [2].Telecommunication's opportunities (O) are huge market, improved laws and regulations, and strategic made by Chinese government. With the sustained and rapid development of national economy, a huge demand of potential market is formed, and provides a greater opportunities for the development of Chinese telecommunication companies. The laws and regulations of telecommunication industry have constantly improved, telecommunication industry will enter a new stage. Chinese government promotes strategic decision-making of the national economy and social information, and creates the opportunity for the development of telecommunication companies. Telecommunication's threats (T) are employees and regulations. The competitive structure of telecommunication competition has switched from locally to comprehensively, from simple to diversity; the talent drain in industries is very serious. The influences of asymmetric regulation are also very serious. They are influenced by on business license, connectivity, telecommunication charges, universal service and so on [3].

Analysis of the CATV industry based on SWOT model

SWOT analysis was carried out on CATV. The advantages of CATV(S) include that penetration rate of CATV users is very high, and CATV has the advantage of the monopoly operation. It also has the advantage of the cable TV network, rich spectrum resources, and the advantage on technology research and development. CATV has advanced hardware and many financing methods. CATV also has a strict management system. The weaknesses of CATV (W) as followed. CATV has been in a state of self-sufficiency, and its profit model is single which needs to be innovated. Cable TV broadband network is seriously impacted by "multi-business bundling" of the telecommunications, leading to the growth of business slow. At the same time, the system of customer service is not perfect. The majority of users are the single mode, and the convergence with telecommunication business and Internet business is slow. The social welfare is strong, CATV is hard to achieve full market-oriented operation. The main opportunity of CATV (O) is policy. Under the environment of three networks convergence, CATV has more opportunities than challenges with the policy support. CATV should cooperate with telecommunication to develop the value-added businesses of bidirectional interaction, high-definition television, video on demand, broadband services, and to promote the transformation to the multimedia service provider and establish a new

development mode. The threat of CATV (T) is only one network. CATV does not form a "national network". Monopolization makes CATV be short of market competitive abilities and completely regulated by the state policy. Other enterprises have the advantages of full-service management. The user's mind about the service of CATV is free or low-cost. Market competition is becoming more and more intense [4].

Analysis of the Internet industry based on SWOT model

SWOT analysis was carried out on the Internet. The advantages of the internet (S) are that the scale of Chinese internet users is enormous. The rate of internet penetration is very high, most of people have computers, and almost all of adults have mobile phones, as a result, the penetration rate of user is very high. The physical infrastructure system of Internet is comprised of individual terminals, family terminal and industry terminal. IP address and domain name are the core resources of Internet. We can use IP address and domain name to perform dynamic addressing, and it can provide many business application, such as public cloud, private cloud, support cloud etc.. The main weakness of the internet (W) is broadband. The broadband of the internet is not enough, the speed of the internet is not enough; the credibility of the Internet is relatively low. A lot of bad events usually happen on the internet, such as Trojan virus, account stolen, information disclosure, consumer fraud etc.. The government is in favor of CATV and telecommunication, therefore, the government will give some additional support on policy to CATV and telecommunication, but the internet does not have such preferential support. The opportunities (O) of the Internet are about company. The Internet company arose that can provide the service of the world. To a certain extent, a number of shops and enterprises gain new business opportunities, and they can transfer the business pattern from offline to online. Meanwhile, they provide more job opportunities for people, such as the generations of logistics company, the third-party payment etc.. The position of the Internet is to become the information infrastructure of the society. Technological breakthrough of "terminal and cloud applications" promotes the explosive growth of mobile internet, Internet application is facing new innovations and more opportunities. The fusion of mobile, social networking, and big data etc. will produce some new business models, those industries are very promising in China [6]. The threats of the Internet (T) will gradually change the model of competition. Internet needs higher technologies and more secure platform than before. Many internet companies cannot reach the standards, so many companies will go to abroad which results the scale of market is smaller in China. It's an enormous challenge to improve this situation for us. Determine how to improve the reliability of network is also a huge challenge.

Policy proposal

In terms of policy, we give some suggestions

Firstly, establish a united regulatory system which is benefit to the real realization of three networks convergence. Only when the government builds a united regulation for the businesses of CATV, telecommunications and the internet, it can make progress of technology and the development of the market.

Secondly, propel and establish full-service operators for three networks. The scale of Cable TV network operators is different which needs to be integrated. The government should take some measures to separate government from the enterprises, separate program from broadcasting, and separate network from platform. It impels and sets up full-service operators, and builds a fair and healthy environment for market competition and cooperation by the reform and recombination of the telecommunications.

At last, develop and introduce a relatively perfect legal protection system. In order to promote the sustainable development of three networks convergence, the government and related departments should speed up to develop related legislation, and provide the perfect legal protection system.

In terms of technology, we give some advices

The first one is to integrate the networks. The network of traditional communication in China means that the government and related departments put the network into hierarchical construction, management, deployment and operation. Because of the communication network scattered, there are some contradictions of the transmission in terms of the business of voice, video, data etc.. Therefore, the system should be reformed, and the technology should be transformed in the large-scale to achieve the effective integration for the network, realize the connectivity of technology, business, market, policy etc..

The second one is to increase the validity bandwidth of broadband network. The bandwidth of access network has become an important condition which restricts the entrance of telecommunication industry network and the internet into the business of CATV. The operators of telecommunication industry should modify current data network to increase the validity bandwidth of broadband network.

In terms of market, we give some recommendations

Develop the competition environment of market. Relevant departments and government should build a fair and just market competition mechanism, regulate the competition of CATV and telecommunication, and cultivate a good market environment. The development of the three networks convergence, CATV and telecommunication should put aside of their own interests. It is important for all of them that share the technology and business, collaborate actively, and achieve the further development of three networks convergence.

Increase the investment, improve the quality of the business, and expand the scope of the business. They must take some measures to attract more customers and sponsors if the enterprise wants to increase the share of market. The business should change from simplification to diversification so that improve the enterprises' competition ability.

Acknowledgement

This research was financially supported by Harbin Special Fund for Science &Technology Innovation Talents (2013RFXJ009), Humanities and Social Science Program of Department of Education of Heilongjiang (11552039), and Harbin university of Science and Technology Fund for Young Scholars.

References

[1].Renfang Ni, Xiaobo Wu. The evolution of the management thoughts of enterprise strategy [J].Economics and Management，2001，(6). (in Chinese)

[2].Xiaofang Pan. Based on the theory of SWOT analyze the influences of three networks convergence for the traditional fixed-line operators [J]. Modern Marketing, 2012(7)：216.(in Chinese)

[3].Weijiang Xu, Hao Wang . The SWOT analysis of China telecom [J].Squawk Box,2002 (11): 77-78.(in Chinese)

[4].HuaZheng. Under the background of three networks convergence, the development strategy research of CATV networks company of D town [D]. Nanchang University. 2013,5 (25).(in Chinese)

[5].Kai Wei. The key technologies and development trend of Internet TV face three networks convergence[J]．Telecommunications Network Technology,2010(9)：42—46. (in Chinese)
[6].Wei Mao. The analysis and prospect of the development situation of Internet in China[J]．Scotland China Education Network ,2013(7)：39-42.(in Chinese)
[7].Mingdong Fang, Rui Chen. Three networks convergence and cultural construction[J]．Journal of Chinese radio and TV,2009：13-14.(in Chinese)
[8].Leping Wei. The thoughts of three networks convergence [J]. Telecommunications Science, 2010（7）：11-13．(in Chinese)

Advanced Materials Research Vols. 989-994 (2014) pp 4461-4465
© (2014) Trans Tech Publications, Switzerland
doi:10.4028/www.scientific.net/AMR.989-994.4461

The Research of Multi-network Switching Model for Power Communication Network Based on Analytic Hierarchy Process

Gangjun Gong[1, a], Guilin Song[2,b] ,Dangke Hao[3,c],Jianhong Hao[4,d],Gang Xu[5,e]

[1,2,3] School of Electrical and Electronics Engineering, North China Electric Power University, Beijing102206, China

[a]gonggangjun@126.com,[b]songguilin0422@163.com,[c]hdk613@163.com

[d]jianhonghao@ncepu.edu.cn, [e]xugang@ncepu.edu.cn

Keywords: Power Distribution and Utilization Business; Analytic Hierarchy Process; Weights; Quality of Service

Abstract: To further improve the quality of service of communication business for power distribution and utilization, and to meet the needs of communication network for smart power distribution and utilization, we propose a multi-network switching model based on AHP; First, this model analyzes the performance of LTE, WCDMA and WiFi, to determine the integrated weights of optional network by solving the relative weight of rules and index, then select a network which is based on guarantee the performance index of QoS; In the process of transmission of power distribution and utilization business, take the transmission efficiency as the optimization target, the network of which weight is larger is priority to transfer power distribution and utilization business; Simulation results show that the model can improve the quality of service of communication business for power distribution and utilization.

Introduction

For power communication systems, no one single communication system can fully meet the communication requirements. Under the current power system, data acquisition, remote transmission, video surveillance and load management, of which is the multi-mode multi-service environment, then it is necessary to take an integrated communications system while according to the specific conditions and make mutual integration between the various networks, which can meet the requirements of the power communications system [1, 2].

For many types and complex communication business for power distribution and utilization [3, 4], this paper proposes a multi-network switching model algorithm based on AHP in order to avoid the data backlogs, transmission delays and others. The algorithm is aimed at improving the network efficiency, and using AHP to analyze the QoS performance of these three wireless networks. This paper studies bandwidth, economy, transmission distance of an optional network, and then determine the weights of the three networks under different criteria; Since the transmission business requires different bandwidth, economy and transmission distance, and determine the integrated weights of the three networks. The larger weight is priority to transfer power distribution and utilization business, which can effectively improve the quality of services of communication business for power distribution and utilization.

Network Environment

To improve the quality of service of communication business for power distribution and utilization, this paper puts forward a multi-network switching model, while is transporting the business data, the multi-mode terminal can real-time detect whether the current network environment in which a variety of wireless network coverage, and search the various network performance parameters, determine the comprehensive weights of each network, it priority to switch to the larger weight of the wireless network. As shown in figure 1, this paper studies the environment located in three overlapping coverage area of the network, namely, LTE, WCDMA and WiFi.

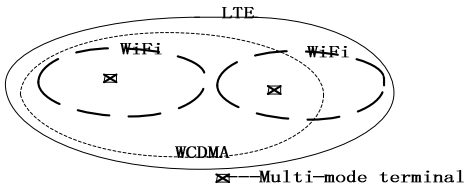

Fig. 1 The study environment

In order to further determine the relative importance of each network performance, this article adopts the analytic hierarchy process (AHP) to analyze the performance index of LTE, WCDMA and WiFi.

Construct the hierarchical structure model

Using the analytic hierarchy process (AHP) to deal with multi-attribute decision making problems, first of all, clear objectives, construct the hierarchical structure model, then determine the subordinate relations between adjacent level elements. Target layer as the highest level indicates that problems needed to be solved, the problem needed to be solved in this paper is to determine comprehensive weight of three networks; Rule layer usually indicates influencing factors of bidding decision, we choose a transmission bandwidth, efficiency and the transmission distance as the three factors in this paper; Index layer indicates specific indicators or parameters of the project evaluation, namely, various specific indicators under the rule layer, such as the three kinds of wireless networks in this paper [5,6]. In a variety of wireless network environments, this paper constructs the hierarchical structure is shown in figure 2.

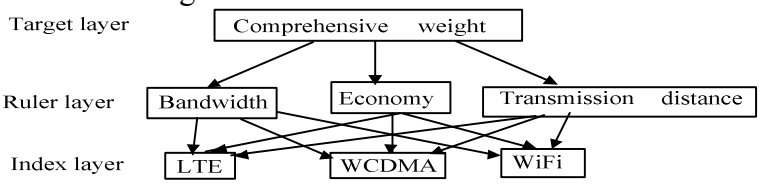

Fig. 2 The hierarchical structure model

As the comprehensive weight of target layer is determined, multi-mode terminal can choose the network of high weight to switch, and make the best network access.

Construct judgment matrix

Set ruler layer has n elements, $x_1, x_2, \cdots, x_n$ which affect the choice of the target layer. First compare the relative weight between n elements, then select two elements x_i, x_j and comparison, a_{ij} indicates the importance ratio between the two elements, and finally, after all the factors pairwise comparison, $A=(a_{ij})_{n\times n}$ indicates the comparison results, called the judgment matrix.

According to Satty table 1~9 scale and its inverse to determine the elements of judgement matrix, Satty table is shown in table 1.

Tab.1 The Satty list law

Importance (compare A with B)	explanation
1	the same
3	a little
5	obviously
7	highly
9	extremely
2,4,6,8	the middle

Consistency check

Calculated the largest eigenvalue $\lambda_{\max}$ and the corresponding characteristic eigenvector W of the judgement matrix, then characteristic eigenvector is normalized processing, the consistency ratio CR is calculated by the type (1) and type (2).

$$CI = \frac{\lambda_{\max}(A) - n}{n-1}. \tag{1}$$

$$CR = \frac{CI}{RI}. \tag{2}$$

Among them, RI is the average random consistency index of same order matrix and RI is generally known, when $CR < 0.1$, determine the consistency of judgment matrix is satisfied, otherwise reconstruct the judgment matrix.

The relative weight between the various rules

Suppose the power distribution and utilization business demand for broadband and transmission distance requirements are the same, and bandwidth demand and the requirements of the transmission distance slightly higher than the economy. Bandwidth demand, economy and transmission distance affect the weight of the power distribution and utilization business, in different levels, so according to the Satty list method, the judgment matrix is:

$$A=\begin{pmatrix} 1 & 3 & 1 \\ 1/3 & 1 & 1/3 \\ 1 & 3 & 1 \end{pmatrix}$$

Calculated the maximum eigenvalue of the judgment matrix is λ_{max}=3, then the characteristic vector is normalized processing, get the weight vector $q=[0.43 \ \ 0.14 \ \ 0.43]$.

The relative weight of between optional networks under the rule of a single

Assumes that the user is currently having three kinds of network can choose, have two kinds of wide area coverage of LTE and WCDMA, and there is a smaller coverage of wireless local area network (WLAN) WiFi, we use C1, C2 ,C3 stand for these there network respectively. When multi-mode terminals detected these three optional networks, began to implement the analytic hierarchy process to determine the weights of optional network, then switching access. Judge the QoS performance parameters, mainly need to consider bandwidth, economy and transmission distance, we use X1, X2, X3 stand for these performance parameters respectively.

Bandwidth of wireless network can be measured by the transmission rate. According to statistics, these three networks transmission rate of LTE, WCDMA and WiFi is shown in table 2.

Tab.2 Transmission rate

category		LTE	WCDMA	WiFi
rate	uplink	50Mbps	5.76Mbps	11~54Mbps
	downlink	100Mbps	14.4Mbps	

Economy of wireless network can be measured by the reciprocal of the investment cost. According to statistics, cost of WiFi is low, WCDMA is higher, and LTE is higher than the 3G.

According to statistical analysis, although the current WiFi technology transfer rate quickly, but can only achieve short-range wireless transmission; Although LTE tariff is high, but the transfer rate is high, and can achieve the function of long-distance wireless transmission; Compared with LTE, 3G coverage more widely, the transmission distance is farther. When the business is transmitted to a certain distance, signal strength of 3G is better than that of LTE, and signal strength of LTE is superior to the WiFi.

This paper mainly studies how to select the optimal wireless network, and then to transmit power distribution and utilization business, so consider the uplink rate f selected network mainly. In conclusion, three kinds of network parameters is shown in table 3.

Tab.3 Network parameters

Parameter / network	X_1	X_2	X_3
C_1(LTE)	50Mbps	low	long
C_2(WCDMA)	5.76Mbps	high	longest
C_3(WiFi)	54Mbps	highest	close

With Satty table 1~9 scaling method for the analysis of table 3, pairwise comparison of optional network of LTE, WCDMA and WiFi, the judgment matrix of bandwidth is A_1; the judgment matrix of economy is A_2; the judgment matrix of transmission distance is A_3.

$$A_1=\begin{pmatrix} 1 & \frac{50}{5.76} & \frac{50}{54} \\ \frac{5.76}{50} & 1 & \frac{5.76}{54} \\ \frac{54}{50} & \frac{54}{5.76} & 1 \end{pmatrix} \qquad A_2=\begin{pmatrix} 1 & 1/5 & 1/7 \\ 5 & 1 & 1/3 \\ 7 & 3 & 1 \end{pmatrix} \qquad A_3=\begin{pmatrix} 1 & 1/5 & 5 \\ 5 & 1 & 9 \\ 1/5 & 1/9 & 1 \end{pmatrix}$$

Calculated the maximum eigenvalue of A_1, A_2, A_3 respectively, we acquire λ_1=2.6248, λ_2=3.06, λ_3=3.12. Then the corresponding characteristic vector is normalized processing, get the weight vector $q_1=[0.559 \quad 0.064 \quad 0.377], q_2=[0.072 \quad 0.279 \quad 0.649], q_3=[0.207 \quad 0.735 \quad 0.058]$.

Comprehensive weights of optional network

In the process of transmission of power distribution and utilization business, the relative weight of optional network can be calculated using the weighted average method. Sort of optional networks by using the weight averaged method, the greater the value, the higher the priority. The relative weight between optional networks can be expressed as:

$$\begin{aligned} N_\omega &= [q_1^T \quad q_2^T \quad q_3^T] \bullet q^T \\ &= \begin{pmatrix} 0.559 & 0.072 & 0.207 \\ 0.064 & 0.279 & 0.735 \\ 0.377 & 0.649 & 0.058 \end{pmatrix} \bullet \begin{pmatrix} 0.43 \\ 0.14 \\ 0.43 \end{pmatrix} \\ &= [0.3395 \quad 0.3826 \quad 0.2779]^T \end{aligned}$$

The simulation and results

In this article, the weight of judgment matrix is calculated by using MATLAB software. In the process of running the program, always does not appear “The matrix does not pass the consistency check”, which explain that the judgment matrix all pass the consistency check, so the order weight calculated by the program is acceptable.

For different business, the degree of requirements of the transmission bandwidth, economy and the transmission distance is not the same. And this degree can be represented by the size of the weight, and the sum of the three weights is one. Therefore, simply select two variables in the process of simulation. First of all, in this paper, transmission bandwidth, economy and transmission distance of three kinds of optional network can be determined. Then to simulate the comprehensive weights of three kinds of network by MATLAB software, as shown in figure 3, figure 4 and figure 5 respectively. The X-axis represents the bandwidth, the Y-axis represents economy and the Z-axis represents the comprehensive weight of network.

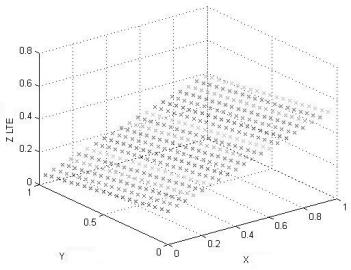

Fig.3 The weight of LTE

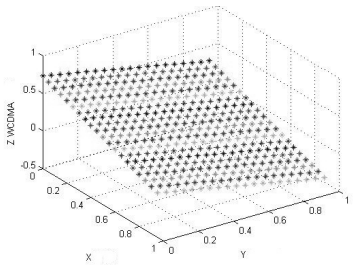

Fig.4 The weight of WCDMA

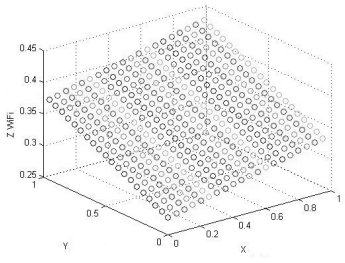

Fig.5 The weight of WiFi

Figure 3 shows that the weight of LTE increases along with the requirement of transmission bandwidth increases, increases along with the decrease of the economy. Figure 4 shows the weight of WCDMA increases along with the decrease of the transmission bandwidth and increases along with the decrease of the economy; Figure 5 shows the weight of WiFi increases along with the requirement of transmission bandwidth increases, increases along with increase of the economy. When choosing a network, only need to make sure that the user requirement for transmission bandwidth, economy and transmission distance, can be concluded from the simulation diagram of three optional network weights, finally choose the optimal network.

Conclusion

The simulation results show that make sure the level of requirements of the network performance, this algorithm can determine weights, can this algorithm can determine weights, can choose the best access networks according to the different needs of users, so as to achieve maximum transmission efficiency.

Acknowledgements

The work was supported by a general program from the Basic Science Research Fund of Central Universities (No.JB2014048).

References

[1] Intel. Understanding Wi-Fi and WiMAX as MnD-Access Solutions[z].2004.

[2] Huibin Cao. The Summary of “12th Five-Year” Telecommunication Network Plan of SGCC[J]. Tele Communications for Electric Power System.2011, 32(223):1-6. (In Chinese)

[3] Mengchao Li, Yunping Wang. Smart substation and technical characteristics analysis[J].Power System Protection and Control. 2010, 38(18):59-62. (In Chinese)

[4] Zhi Dong. A Study on Urban Power Network Cabling Reconstruction Based on Analytic Hierarchy Process. Tianjin University[D]. 2005. (In Chinese)

[5] Qiang Sun, Jiguang Yue. Electrohydraulic system reliability allocation based on interval analytic hierarchy process with correction[M]. 2013, Page(s): 1823 - 1828

[6] Gangjun Gong, Chen Xiong. The Research of Communication Business Model of Power Distribution and Utilization Based on the Analytic Hierarchy Judgment Matrix[J]. Power System Protection and Control .2011, 41(21):19-239. (In Chinese)

Advanced Materials Research Vols. 989-994 (2014) pp 4466-4469
© (2014) Trans Tech Publications, Switzerland
doi:10.4028/www.scientific.net/AMR.989-994.4466

Active Online Thematic Map Cartography Based on Network

SU Deguo[1,a], WANG Liang[1,b], CUI Ximin[2,c],YUAN Debao[2,d]

[1]28, Lianhuachixi Road, Haidian District, Beijing,China

[2]11, Xueyuan Road, Haidian District, Beijing,China

[a]sdg@casm.ac.cn, [b]wl@casm.ac.cn, [c]cxm@cumtb.edu.cn, [d]yuandebao@cumtb.edu.cn

Keywords: Online Thematic Map; RIA; Active; Knowledge

Abstract. This paper analyzes two important problems of thematic map cartography facing, namely which technique solution is appropriate and how to simplify the cartography process. Firstly, contrasts some popular technique solutions of thematic map, and points out the bottlenecks and inconveniences of thematic map cartography process nowadays, then brings out active online thematic map cartography based on the technique solution of RIA (Rich Internet Applications). In addition, this paper gives out RIA-based implementation framework of active online thematic maps mapping, which is contrasted with RIA-based implementation framework of general online thematic maps mapping, and main methods of building knowledge of active cartography of thematic map.

Introduction

Thematic maps have been an ordinary application in various industries with its intuitive, efficient and novelty. From the application demand, online thematic cartography can meet the needs of user's real-time mapping and personalized mapping. With the popularization of network and network application requirements of thematic mapping, online thematic cartography becomes an important direction of geographic information science development, thus every one on the web can cartography thematic maps themselves anywhere or any time.

Firstly, from the perspective of software development, with B\S structure of the software model used widely, the original stand-alone thematic cartography has been converted as service-oriented and network based, which is the initial model of online thematic maps. At present, four technique solutions have been formed, that is, images of thin client, vector of thin client, vector of fat client and vector of rich client-side (RIA).

Nowadays, the modes of images of thin client and vector of fat client have been used in the LAN, WAN applications in many areas. But the mode of vector of thin client has many limitations for no unified standard of multiple browsers (IE, FireFox, etc.), which prevents it developing quickly, though it has good prospects for development because of its OGC Standards. Last technique solution in Table 1, namely vector of RIA, which is based on the mature lightweight plug-in technology to satisfy the demands of network and stand-alone application, such as flash technology, can address the needs of increasingly demanding from the beautiful graphics, high efficiency and good experiences of online thematic mapping.

The basic work of online mapping of thematic maps, namely the process of thematic cartography is not avoided, and the intelligence and complexity of this process have a direct impact on the effects of online mapping applications. At present, many software have done a lot of work in this area, such as sophisticated template technology mapping, which builds some steps to allow the user to select various parameters, then get the thematic maps, even though, which still having a big gap from easy mapping of thematic maps for persons without professional knowledge. So the author brings out the idea of active online thematic map cartography with reliable knowledge of thematic cartography, which can do lots of work for user as many as possible to reduce the complexity of thematic cartography, especially selecting confused, professional mapping parameters, such as thematic symbols, colors, grade num, etc.

This paper will talk about the realization method of RIA in active online thematic cartography and how to build the system's main knowledge to improve the practicality of online thematic cartography.

Framework of Active Online Thematic Cartography Based on RIA

On the basis of the application framework as Figure.1, we try to add the data search services, including search map data services and thematic data search service. When users needs only a thematic map drawing without their own mapping data and thematic data, the data search service will be available and using, which can search suitable data for users. In addition, thematic mapping symbol type, grade classification of data, data classification and the number of color choices can be fixed or judged based on user demand by active system to provide proactive service. In short, the initiative of active thematic cartography can be reflected in the two aspects as follows:

1) Searching data: active thematic cartography can search required data to the user initiatively, including the map data and thematic data, thematic data resources and various types of commonly used statistics, such as agriculture statistical data, industry statistical data.

2) Finding optimal parameters: active thematic Cartography can construct suitable parameters, and different requirements may construct different mapping parameters, including the mapping symbol type, data classification or grading methods, and the color or hue.

Obviously, to achieve the two purposes above, thematic map cartography knowledge and knowledge learning are necessary. Later in the article will introduce the process of main knowledge building.

The user interface can be designed as GOOGLE search engines (this is suitable to users without their own data especially)， which has input box only, and when users input some key words, then the cartography system gives the proper mapping results for users according to existing knowledge. Active Framework for online thematic cartography can be described as Fig.1.

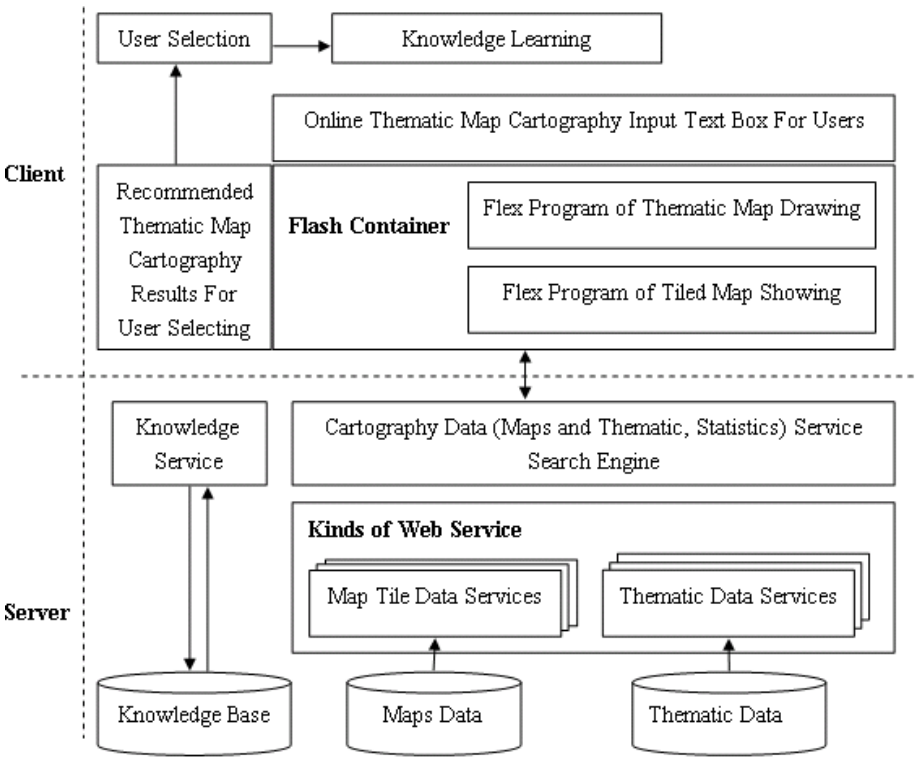

Fig.1 Technical framework for active online thematic cartography

The Main Knowledge Building for Active Thematic Cartography

In general, thematic map cartography can be divided into four processes: understanding，solution，evaluation and learning. Thus, analysis of thematic map data features is the first step in mapping, and the follow processes of knowledge building are closely linked with the data properties. The following describes the knowledge construction process with symbol types and colors to choose as examples.

The original adaptive knowledge building between thematic mapping Symbol type and data. First of all, thematic data is divided into one-dimensional, two-dimensional and multidimensional, with different dimensions of the data set can be divided into categories (qualitative schemes), sequencing (with order), fixed pitch (which can add and subtract), fixed ratio (which can multiply and divide) and irregular quantitative data, while the irregular quantitative data also can be approximated by different linear function or multiple functions by fitting or interpolation. In the five data types, the first two categories are qualitative data, the latter three are quantitative data. The quantitative data also shows the distribution of a variety of complex features.

Then, through study of thematic mapping symbol type, thematic mapping symbol type (histogram, pie chart, line chart, pyramid, etc.) can also be classified according to the dimension and data characters, namely, one-dimensional symbols, two-dimensional symbol and multi-dimensional. Further more, according to adaptability to classes, thematic map symbol types can get correspondence relationship with data classes. Given qualitative schemes, sequencing schemes, fixed pitch, fixed ratio and irregular quantitative coded with the A, B, C, D, E to indicate, adapting relationship table is achieved showing in Table 2.

Table 1 Adapting relationship between data and thematic mapping symbol type

Data / Sysmbol	One Dimension (A)					Two Dimension (B)					Multi Dimension (C)				
	A	B	C	D	E	A	B	C	D	E	A	B	C	D	E
Bar Chart(1)	✓		✓		✓	✓		✓		✓	✓		✓		✓
Pie Chart(2)						✓	✓	✓			✓	✓	✓		
…															
Pyramid Chart (N)						✓	✓	✓	✓	✓					
Color/Texture Map (N+1)	✓	✓	✓	✓	✓										

According to adapting relationships table above, when getting a group of data, by computing data statistical characters, some suitable thematic map cartography types are shown for users. To simplify the explanation, condition-action or condition-result mode can be used to describe the knowledge, such as Table 3, which gives some cases as examples.

Table 2 Some relationship knowledge cases with condition and action mode

Knowledge Type	Condition	Action
Initial	AC	1,n+1
Initial	BA	1,2,N
Initial	CE	1

The table above gives out knowledge type, knowledge condition and action (or result), which contains application examples from Table 1. In this way, the right type of thematic mapping symbol type is obtained to meet the expressed needs of the display of thematic data, which is helped by original knowledge, knowledge tested and Knowledge learning. On the original knowledge to pass the test of practice, validation, updates, and accumulation, that is, knowledge learning, are not discussed in this article in detail, and irregular quantitative data is also not discussed for further detail.

The original adaptive knowledge building between colors and data character and properties. Color is an important aspect of thematic cartography, how to select the color needs relevant knowledge. Different from thematic mapping symbol types, colors dimension is only the length of color group, even though, the dimension of colors is also the important element to color group's design, and color groups of different dimension have different color selection policy. In

addition, to highlight the special nature of industry-need, special data type parameters are needed, which describes data's thoughts features, e.g., fire as the emergency should be emphasized on red, but agricultural production and other green plants can use green. Similar ideas can be used as described in the original knowledge of color selection, which delegates experiences. According to the analysis results above, the following can be constructed to adapt to relationships between the data and the thematic color, as shown in the Table 3.

Table 3 Relationship between data type and color group

Data / Type	Qualitative	Categorical	Sequence	Diverging
Fire	S8,S10,S12	S4,S9,S11	S3,S12,S22	S21,S32,S52
Water	S9,S11,S16	S1,S2,S21	S6,S8,S15	S4,S5,S17
Plant	G3,G7,G8	G12,G19,G23	G23,G36,G68	G1,G2,G5
....	....	....	....	....

According to the relationship in the table above, some original knowledge of color choice can be formed. Table above lists the different color categories and data nature (type), which can find different group of color template code. In fact, user demand is sophisticated and different knowledge will be obtained from different angles, e.g., from the perspective of the display device, including CRT-Friendly, LCD-Friendly, Print-Friendly, etc., color schemes are also different. This needs further study.

In addition to the above, of course, there are other aspects of thematic cartography also need similar studies, and the formation of the corresponding knowledge helps to build a more reasonable active thematic cartography.

Summary

With the development of online thematic maps, and increasingly high demand of thematic map cartography, this paper discusses two important aspects of thematic maps cartography, namely technology routes and active cartography process, brings out RIA technology has practical significance for online thematic cartography, and probes the methods of knowledge building of Active online thematic cartography. By means of efficient RIA technology platform, active online thematic cartography can easily realize the beauty and animation of thematic cartography, including efficient user interaction. Active Online thematic cartography is a upgrade project of cartography of template, which can help cartographer without professional knowledge to quickly build thematic maps of professional level, promoting the wide use of online thematic maps applications.

Further study will be still needed about knowledge, learning system, detailed technique solution route and also application model, which is the important base of active online thematic map cartography with high efficient, convenient, and easiness.

References

[1] Otakar Cerba, 2008. Application of Markup Languages in Cartography . GIS Ostrava 2008, Czech Republic

[2] Michael Friendly, October 16, 2008. Milestones in the history of thematic cartography, statistical graphics, and data visualization

[3] Robinson, Arthur H., 1982. Early Thematic Mapping in the History of Cartography. Chicago:University of Chicago Press. ISBN 0-226-72285-6

[4] Otakar Cerba, 2009. Thematic Maps in Browser. GIS Ostrava 2009, Czech Republic

[5] Mark Harrower, 2003. Tips for Designing Effective Animated Maps. Cartographic Perspectives, Issue 44 (Winter 2003): 63-65

Advanced Materials Research Vols. 989-994 (2014) pp 4470-4473
© (2014) Trans Tech Publications, Switzerland
doi:10.4028/www.scientific.net/AMR.989-994.4470

Study on One Generating Method of Digital Painting Patterns

Weidong XU[1,a], Jianfei QIN[2,b], Jinsong ZHU[3,c], Xuliang LU[4,d]

[1,2,4] Key Lab, Institute of Field Engineering, Science and Technology University, PLA

No. 1 Haifuxiang, Qinhuai District, Nanjing, Jiangsu, China.

[3] Institute of Sciences, Science and Technology University, PLA

No. 60 Shuanglong Road, Qinhuai District, Nanjing, Jiangsu, China

[a]xweibing1968@aliyun.com, [b]qjfth@163.com, [c]zjsleon68@sina.com, [d]xllu1957@126.com

Keywords: painting pattern digital camouflage camouflage design military camouflage

Abstract. Military camouflage is one of the critical measures taken by some key military forces to disguise weapons and facilities, military projects and combat fighters. Digital camouflage is a novel form in this field. Preliminarily verified by Edge Detection, one method is proposed to digitize large- spot painting patterns, to generate random spot-modification and richer patterns.

1. Introduction

Camouflage is the technology to change the color, pattern and distribution characteristics of the target surface, with the application of dyeing, painting and other materials, which is easy to process, quick in effect and low in cost. Currently, there are three categories, i.e. protective, distortive and imitative painting patterns. The distortive camouflage is to segment and distort the regular outline of the target by utilizing irregular multi-color patterns, with some spots consistent with and the others contrasting to the background. It is normally employed to disguise weapons and facilities in multi-color mottled settings [1]. Digital camouflage refers to the complicated painting patterns, which is generated by computer and composed of rectangular painting pixels with different sizes. It is also known as pixel camouflage, digitized camouflage or mosaic camouflage due to its similarity to the randomly printed output of pixels in different colors [2]. Digital camouflage first appeared in Canada in 1995 and was officially adopted by Canadian Army in 1997. CADPAT TW entered into trial in 1998, followed by the research and development of urban and desert battledress, which ran through all the tests and was granted the patent in the year of 2001. Tests run by the Canadian National Defense Research Base revealed that at the range from 50m to 300m, the disguise effect of digital camouflage battledress is 45% higher than the Olive-Green, and the detecting distance reduced by 35%. Likewise, NATO field test indicated that digital camouflage was obviously superior to the U.S. jungle, German small-spot and U.K. distortive [3]. Later, the employment of digital camouflage by the Royal Canadian Air Force and Navy also obtained good effectiveness. Jungle, urban and desert camouflage battledress were sequentially developed by the U.S. Armed Forces. Some other countries like Finland and Australia produced their own digital camouflage battledress [4]. China began late in this filed. In addition to the military battledress, some weaponry with digital camouflage demonstrated in the Military Parade on the 60th Anniversary National Day indicated the employment of digital camouflage in the Chinese Armed Forces. Nevertheless, basic research concerning the CAD design of digital painting patterns still remains to go further.

In terms of the design of digital painting patterns, there is no unified and definite conclusion so far [1~5]. This paper tries to propose one method to convert the large-spot to digital painting pattern,

with the basic perception that both large-spot and digital are in the same nature of camouflage, the imitative camouflage is achieved by painting the background patterns on the target, and the distortive camouflage by painting the irregular multi-color patterns composed of color block units. Hence, it is feasible to digitize the existing large-spot painting patterns to obtain digital camouflage.

2. Digitization of Large-Spot Painting Patterns

Large-spot painting patterns are composed of segmented and unshaped color blocks, each containing only one single color inside and smooth curves around to segment and distort the original outline of the target. Despite single color inside, each block is filled with many color block units, which are surrounded by dentate curves and contain some spot patterns for modification. Compared with large-spot painting patterns, the blocks of the digital painting patterns are weak in contrast and natural in transition, which is more likely to distract the attention from the observers. The digitizing process is to convert the original large-spot painting patterns to the ones composed of color units. To begin with, large-spot painting patterns are input to array pix (x, y, z) to conduct color space conversion for the purpose of algorithmic operation. Next, the whole large-spot painting pattern is segmented according to the size of color unit, to gain the respective average values of color pixel. Then the pixel values, either of the whole or of the selected part, are replaced by the computed average values. And finally, the digitized output is displayed. The procedure is shown in Fig. 1.

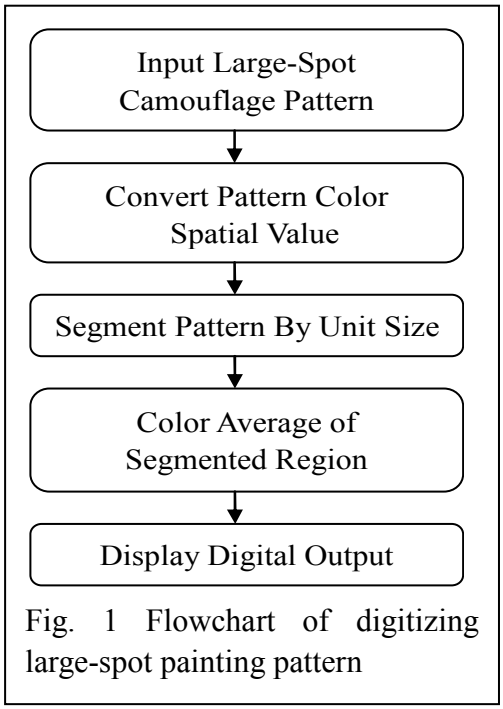

Fig. 1 Flowchart of digitizing large-spot painting pattern

The computed outcome shows that the original large-spot painting pattern (shown in Fig. 2) is segmented to pattern composed of color block units (shown in Fig. 3) surrounded by dentate boundaries.

However, it can be found that many new color blocks appear in Fig. 3, which did not exit and are not identical in color with the original large-spot pattern. In this paper, they are named as "newly-emerging spots", which require to be processed to avoid future trouble in painting.

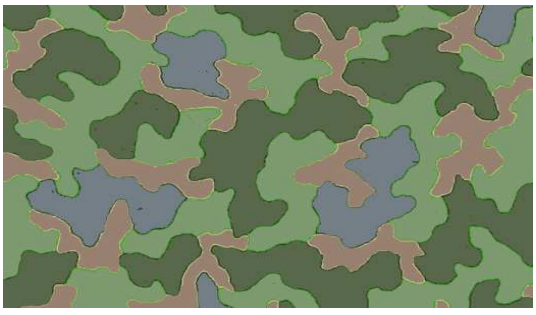

Fig. 2 Original large-spot painting pattern

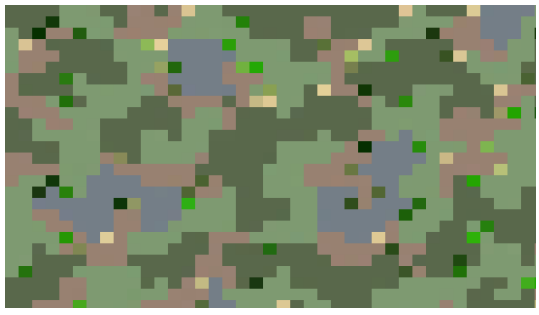

Fig. 3 Digitized painting pattern

3. Processing of "Newly-Emerging Spots"

These "newly-emerging spots" result from the two (or even more) color averages on the edge of the large-spot painting patterns when segmented by color block unit. In fact, they play important roles in enriching digital painting patterns and enhancing pattern randomicity. The processing procedure is to locate them first by comparing each segmented block of the whole pattern or of the

selected part with the existing color. Then identify one after another to check if the color of the segmented block is identical with at least one of the existing spot colors. If not, a random number from 1 to n (n stands for the number of painting color kinds) is generated, according to which the corresponding color is given to the segmented part. Complete the identification process to cover all "newly-emerging spots", which is named as "spot modification" in this paper (shown in Fig. 4).

Owing to the additional randomicity while processing the "newly-emerging spots", different patterns are generated in the final output, especially on the edging parts of different color block units. These new patterns enable the large-spot to segment and distort the regular outline of the target, and at the same time enhance the disruptive effect by their diversity and variability.

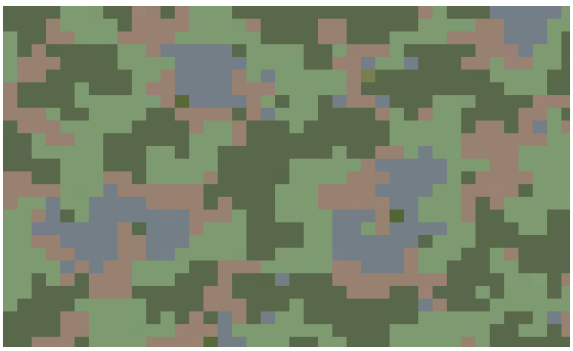

Fig. 4 Digitized painting pattern with "newly-emerging spots" modification

4. Camouflage Effectiveness Simulation Test by Edge Detection Method

To make the preliminary assessment of the camouflage effectiveness generated by the proposed method, the original large-spot and digitized painting patterns are respectively set into the same background (shown in Fig. 5 and 6). And Edge Detection method is applied to make the assessment.

Fig. 5 Original large-spot painting pattern

Fig. 6 Digitized painting pattern

In the digital image processing technology, Edge Detection method intends to extract the target boundaries from the background to separate the target. In this case, both the large-spot and digital painting patterns are required to possess the ability to segment and distort the straight outline of the original target. The main operators involved are Sobel, Roberts, Prewitt, Log and Canny. Fig. 7 and Fig. 8 respectively demonstrate the result of large-spot and digital painting patterns operated by Sobel, and Figure 9 and 10 by Canny. All the rectangular outlines are segmented and distorted, which reveals that camouflage effectiveness is somewhat achieved by both. However, with the comparison between Fig. 7 and 8, large-spot painting pattern still retains some large-spot patterns while the digital does not when operated by Sobel.

The comparison between Fig. 9 and 10 shows that, when operated by Canny, the large-spot presents less quantity and larger size than the digital, which implies, from the Edge Detection point of view, that the latter is better in camouflage effectiveness.

Fig.7 Large-spot painting pattern operated by Sobel

Fig. 8 Digital painting Pattern operated by Sobel

Fig. 9 Large-spot painting pattern operated by Canny

Fig. 10 Digital painting pattern operated by Canny

5. Conclusion

The generation of digital painting pattern is the worldwide focus in its field. Based on the principle of large-spot painting pattern, either by segmenting the whole large-spot painting pattern into color block units, or by averaging the colors of each segmented unit in selected parts, the proposed method successfully digitizes the large-spot painting patterns, eliminates the "newly-emerging spots" by randomly painting them the same color as the original spots, and enriches the patterns with the random modification spots. Edge Detection test also preliminarily verifies that digital camouflage method is able to segment and distort the original regular straight outline of the target, and weaken the visibility further for better integration into the background settings.

References

[1] Jianghua HU: *Camouflage Techniques* (National Defense Industry Publications, Beijing 2012)

[2] Jun YU: *Study on Generating Algorithm of Digital Camouflage Pattern,* Opto-Electronic Engineering (2010)

[3] Mengqi QU, *Study on Digital Camouflage Color Blending*, Master Dissertation of Xi'an Technological University (2011)

[4] Jun YU, *Digital Camouflage Design on Disguising Fixed Target*, Computer & Digital Engineering (2010)

[5] Lei QIN, Jianghua HU, Tianqi FU: *A New Method to Generate Digital Camouflage,* Electro-Optic Technology Application (2013)

Advanced Materials Research Vols. 989-994 (2014) pp 4474-4477
© (2014) Trans Tech Publications, Switzerland
doi:10.4028/www.scientific.net/AMR.989-994.4474

A Wavelet Kernel-Based Support Vector Machine for Communication Network Intrusion Detection

Ying Zhan

School of Mathematics &Computer Science, Jiangxi Science &Technology Normal University, Nanchang 330038, China

zhanyingg@sina.cn

Keywords: wavelet kernel, data mining methods, communication network, intrusion detection.

Abstract This study is to propose a wavelet kernel-based support vector machine(SVM) for communication network intrusion detection. The common intrusion types of communication network mainly include DOS, R2L, U2R and Probing. SVM, BP neural network are used to compare with the proposed wavelet kernel-based SVM method to show the superiority of wavelet kernel-based SVM. The detection accuracy for communication network intrusion of wavelet kernel-based SVM is 96.67 %, the detection accuracy for communication network intrusion of SVM is 90.83%, and the detection accuracy for communication network intrusion of BP neural network is 86.67%.It can be seen that the detection accuracy for communication network intrusion of wavelet kernel-based SVM is better than that of SVM or BP neural network.

Introduction

In the few years, lots of data mining methods have been applied to communication network intrusion detection because of the advantages of discovering useful knowledge from large data sets[1-4]. SVM is based on statistical learning theory and executes structural risk minimization, thus it can provide better generalization ability than the conventional methods[5], such as artificial neural network which uses the empirical risk minimization[6,7]. This study is to propose a wavelet kernel-based SVM for communication network intrusion detection.

120 testing samples from KDDCUP99 datasets are employed to study the communication network intrusion detection performance of wavelet kernel-based SVM. The common intrusion types of communication network mainly include DOS, R2L, U2R and Probing. SVM, BP neural network are used to compare with the proposed wavelet kernel-based SVM method to show the superiority of wavelet kernel-based SVM.

The detection accuracy for communication network intrusion of wavelet kernel-based SVM is 96.67%, the detection accuracy for communication network intrusion of SVM is 90.83%, and the detection accuracy for communication network intrusion of BP neural network is 86.67%. It can be seen that the detection accuracy for communication network intrusion of wavelet kernel-based SVM is better than that of SVM or BP neural network.

Wavelet kernel-based SVM

SVM is based on statistical learning theory and executes structural risk minimization, thus it can provide a better generalization ability than the conventional methods, such as artifical neural network which uses the empirical risk minimization.

Given a training set $\{(x_1,y_1), (x_2,y_2), \ldots, (x_n,y_n)\}$, where $x_i \in R^n$ denotes the ith input vector and the corresponding target denotes $y_i \in \{+1,-1\}$, the margin between the input data in the high-dimensional feature space can be maximized to be $1/\|w\|$.

The classifier function of SVM is described by

$$f(x) = w' \cdot \varphi(x) + b \tag{1}$$

The optimal classifier function of SVM can be gained by minimizing the quadratic problem:

$$\frac{1}{2}\|w\|^2 \tag{2}$$

Subject to the constraints $y_i(w' \cdot \varphi(x_i) + b) \geq 1$. We introduce the positive slack variables ξ_i and the optimization problem can be transformed into the minimizing the following formula:

$$\frac{1}{2}\|w\|^2 + C\sum_{i=1}^{n}\xi_i \tag{3}$$

Subject to the constraints $\begin{cases} y_i(w' \cdot \varphi(x_i) + b) \geq 1 - \xi_i \\ \xi_i \geq 0 \end{cases}$, where C denotes the positive constant parameter.

Then, SVM is trained as a Lagrange optimization problem by introducing the Lagrange multipliers:

$$W(a) = \sum_{i=1}^{n}\alpha_i - \frac{1}{2}\sum_{i,j=1}^{n}\alpha_i\alpha_j y_i y_j x_i' x_j \tag{4}$$

Subject to the constraints $\sum_{i=1}^{n}\alpha_i y_i = 0$ and $\alpha_i \geq 0$, where α_i is the Lagrange multiplier. The above formula can be transformed into the following formula:

$$W(a) = \sum_{i=1}^{n}\alpha_i - \frac{1}{2}\sum_{i,j=1}^{n}\alpha_i\alpha_j y_i y_j k(x_i, x_j) \tag{5}$$

Subject to the constraints $\sum_{i=1}^{n}\alpha_i y_i = 0$ and $\alpha_i \geq 0$. In the above formula, $k(x_i, x)$ is the kernel function, and the value of $k(x_i, x)$ equals to $\varphi(x_i) \cdot \varphi(x)$, which is described by

$$k(x_i, x) = \varphi(x_i) \cdot \varphi(x) \tag{6}$$

where $\varphi(\cdot)$ denotes the transformation function. The decision function of SVM is described by

$$f(x) = \text{sign}\left[\sum_{i=1}^{n}\alpha_i y_i k(x_i, x_j) + b\right] \tag{7}$$

where $k(x, x_i) = \exp\left(\frac{-\|x_i - x\|}{2\sigma^2}\right)$, σ is the width of the kernel function. Here, the Morlet wavelet kernel $\Theta(x) = \cos(1.75x)\exp\left(-\frac{x^2}{2}\right)$ is employed as the wavelet kernel function of SVM. Thus, the corresponding wavelet kernel function is

$$k(x,x') = \prod_{j=1}^{m}\left(\cos\left(\frac{1.75\left(x_j - x_j'\right)}{a}\right)\exp\left(-\frac{\left\|x_j - x_j'\right\|^2}{2a^2}\right)\right) \tag{8}$$

Finally, the classification function of wavelet kernel-based SVM can be written as

$$f(x) = \mathrm{sign}\left[\sum_{i=1}^{n}\alpha_i y_i \prod_{j=1}^{m}\left(\cos\left(\frac{1.75\left(x_j - x_{ij}\right)}{a}\right)\exp\left(-\frac{\left\|x_j - x_{ij}\right\|^2}{2a^2}\right)\right) + b\right] \tag{9}$$

Experimental analysis for communication network intrusion detection by using wavelet kernel-based SVM

120 testing samples from KDDCUP99 datasets are employed to study the communication network intrusion detection performance of wavelet kernel-based SVM. The common intrusion types of communication network mainly include DOS, R2L, U2R and Probing.

SVM, BP neural network are used to compare with the proposed wavelet kernel-based SVM method to show the superiority of wavelet kernel-based SVM.

Fig.1 gives the communication network states of 120 testing samples, where normal state, DOS, R2L, U2R and Probing are denoted as "1~5". Fig.2 gives the detection results for communication network intrusion of wavelet kernel-based SVM, and the detection accuracy for communication network intrusion of wavelet kernel-based SVM is 96.67%. Fig.3 gives the detection results for communication network intrusion of SVM, and the detection accuracy for communication network intrusion of SVM is 90.83%. Fig.4 gives the detection results for communication network intrusion of BP neural network, and the detection accuracy for communication network intrusion of BP neural network is 86.67%.

It can be seen that the detection accuracy for communication network intrusion of wavelet kernel-based SVM is better than that of SVM or BP neural network.

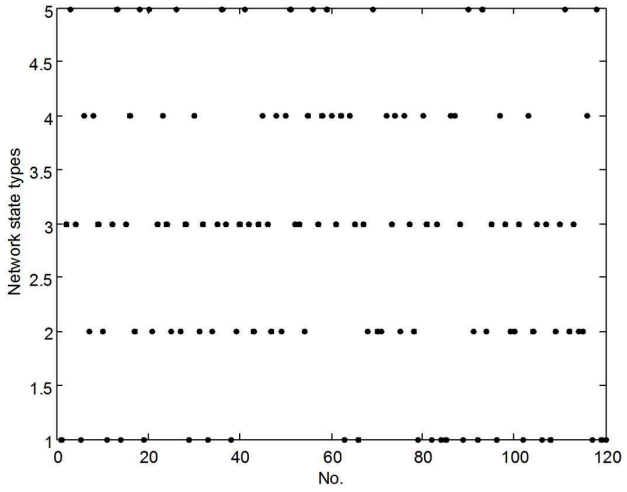

Fig.1 The communication network states of 120 testing samples

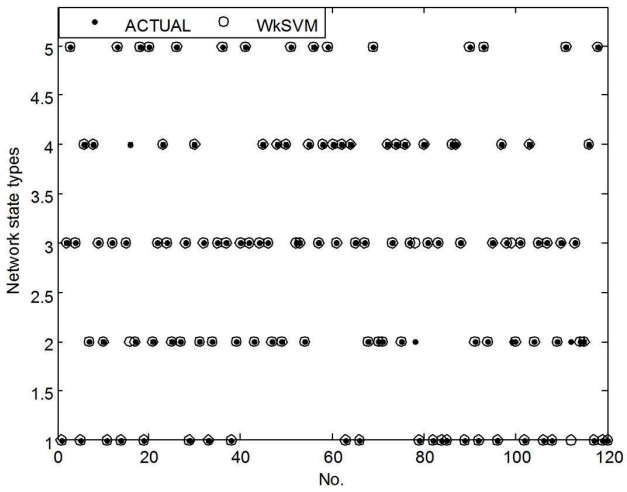

Fig.2 The detection results for communication network intrusion of wavelet kernel-based SVM

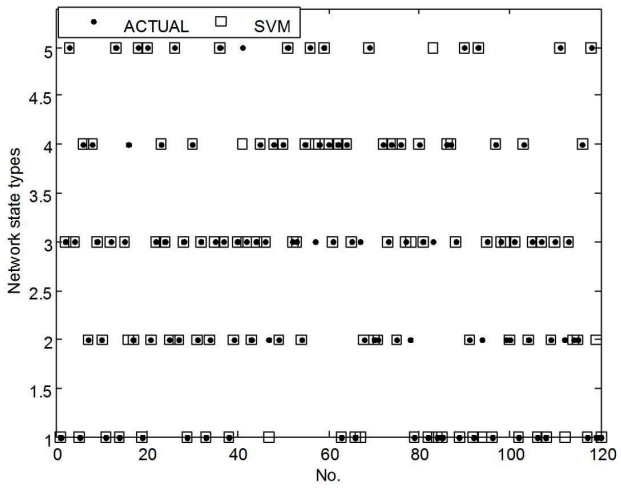

Fig.3 The detection results for communication network intrusion of SVM

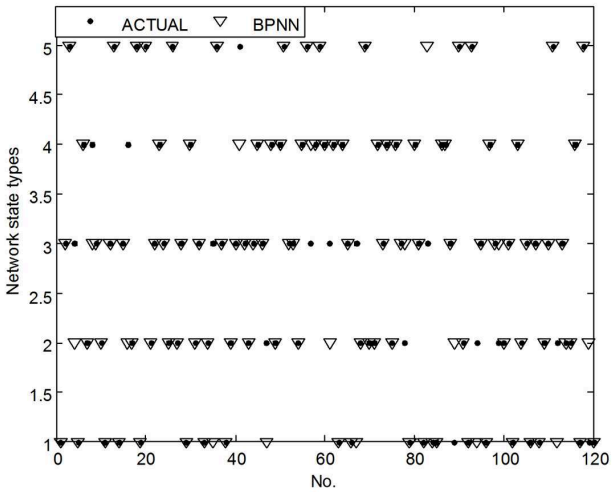

Fig.4 The detection results for communication network intrusion of BP neural network

Conclusion

This study is to propose a wavelet kernel-based SVM for communication network intrusion detection. 120 testing samples from KDDCUP99 datasets are employed to study the communication network intrusion detection performance of wavelet kernel-based SVM. The detection accuracy for communication network intrusion of wavelet kernel-based SVM is 96.67%, the detection accuracy for communication network intrusion of SVM is 90.83%, and the detection accuracy for communication network intrusion of BP neural network is 86.67%. It can be seen that the detection accuracy for communication network intrusion of wavelet kernel-based SVM is better than that of SVM or BP neural network.

References

[1] Chenfeng Vincent Zhou, Christopher Leckie and Shanika Karunasekera: Computers & Security, Vol.29(2010) No.1, p.124-140.

[2] Mrutyunjaya Panda, Ajith Abraham and Manas Ranjan Patra: Procedia Engineering, Vol.30(2012), p.1-9.

[3] M.Govindarajan and RM.Chandrasekaran: Computer Networks, Vol.55(2011) No.8, p.1662-1671.

[4] Saurabh Mukherjee and Neelam Sharma: Procedia Technology, Vol.4(2012), p.119-128.

[5] Yuan-Hai Shao and Nai-Yang Deng: Neural Networks, Vol.25(2012) No.1, p.114-121.

[6] Unal Akdag, M.Aydin Komur and A.Feridun Ozguc: Advances in Engineering Software, Vol.40(2009) No.9, p.864-870.

[7] Meiqin Liu: Neural Networks, Vol.22(2009) No.7, p.949-957.

Advanced Materials Research Vols. 989-994 (2014) pp 4478-4481
© (2014) Trans Tech Publications, Switzerland
doi:10.4028/www.scientific.net/AMR.989-994.4478

The Attendance Management System Based on Micro-cellular and GIS technology

Zhu Jian-Feng[1, a], Wang Fang[2,b], Zhang Kun[3,c]

[1] Qiongzhou University, Yucai Rd. 1, Sanya City, Hainan Province, P.R. China

[2]Northeast Dianli University, Changchun Rd. 169, Jilin City, Jilin Province, P.R. China

[3] Qiongzhou University, Yucai Rd. 1, Sanya City, Hainan Province, P.R. China

[a]zhujianfeng@live.jp, [b]767433095@qq.com , [c]zk0588@163.com

Keywords: G-XML; GIS; Attendance Management System; PHS.

Abstract. This paper puts forward the composition of geospatial information and its definition. The author designed and implemented the attendance management system based on Micro-cellular and the geographic information system (GIS) technology. The function of the geographic information system (GIS) was achieved by transforming Japan Geographical Survey Institute's Digital Map 2,500 base plate data into G-XML data. The function of location information system was accomplished according to micro-cellular mobile terminal-in the GIS's Real-time positioning and tracks. At last, the attendance management system based on micro-cellular and GIS technology was implemented by comparing the work schedule with the mobile tracks of its related mobile handheld terminals.

Introduction

Recently, many companies have introduced a variety of attendance management system. For example, IC card accesses control system, IC card attendance management system [1], radio frequency identification RFID card attendance management system [2]. The applicable object is the attendance of employees at fixed work time and fixed work place. However, when work time and work place change, the problem of employees' attendance is still difficult to resolve. The attendance management system is based on the combination of PHS (Personal Handy-phone System) location and geographic information system, it makes the information query function which includes where the holder is at a time become true. According to comparing the field operations staff work schedule (place, time) which was pre-entered in the database with the trajectory (place, time) of PHS (Personal Handy-phone System), the attendance management system automation is achieved.

The Components OF Attendance Management System based on Mobile Handheld Location Information

The attendance management system which is based on mobile handheld location information consists of the following components:

Mobile Handheld (such as PHS)

Micro-cellular base station

Mobile Handheld location information service center

Attendance Management System

Terminal PC

Mobile Handheld location information service center sometime is responsible for the timely and regular collection of Mobile Handheld location information (longitude, latitude coordinates) and sends them timely and regularly to attendance management system. According to the demand of PC side for real-time and regular employees' attendance, the attendance management system is responsible for sending requests for information about location of the current mobile handheld to

locate information service center timely and regularly, receiving mobile handheld location information (longitude, latitude coordinates) at a time from service center timely and regularly, indicating the mobile handset location information in the GIS, and transmitting it to the Terminal PC. At the PC side, the terminal PC sends the mobile handheld's attendance requirements to the Attendance Management System, receives the immediate and regular mobile handset location information which is marked on the GIS, then, according to the schedule information which is the same as accepted mobile handset, We can determine the attendance results and achieve attendance management after comparing with time and location.

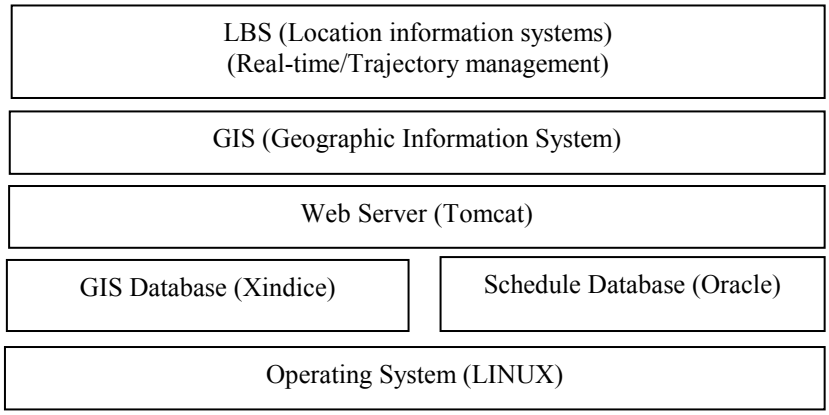

Figure 1. Mobile handheld location information-based attendance management system

The Implementation of Mobile Handheld Location Information System (LBS)

The mobile handheld terminal location was marked in corresponding position on the vector map accurately by the mobile handheld location information system (LBS), which is mainly implemented by the following function modules.

The coordinate conversion function module is responsible for transforming the location of mobile handsets longitude coordinates and latitude coordinates which are received from the mobile handset service center location information into the plane rectangular coordinates. It means that the location of mobile handsets is the actual location of the base station which is the nearest from the mobile handset. The maximum theoretical error of using the base station is 500 meters. Of course, the error is determined by the distance between base stations. The closer the distance between the base stations, the smaller the error.

The figure sector inquiry function module inquires the Xindice database to get the figure pages (G-XML[3] file) which contains the plane rectangular coordinates according to the plane rectangular coordinates of the location of mobile handsets. In order to mark the location of mobile handsets in the central region, the most relevant 9 figures need to be checked out.

The position coordinates conversion function module is responsible for transforming the plane rectangular coordinate of the location of mobile handsets into the coordinates system of the computer screen coordinates.

The figure-depicting function module is responsible for transforming the most relevant 9 figure (G-XML files) into a file group, which is composed of 9 SVG (Scalable Vector Graphics) files, and depicting the vector group according to the file group.

The mobile handset location identification module is responsible for marking the location of mobile handsets (including the date and time information), in corresponding position on the vector map with a small icon.

The Attendance Management System

The Preconditions for achieving this system are as follows: First, employees switch on the mobile handsets and set the location information query function to be effective status; Second, the enterprise of attendance management system and the mobile handheld location information service center sign the contract as follows: the center of location information service should collect location information of the mobile handheld terminal regularly and irregularly and send them to the enterprise timely.

Collecting mobile handset location information regularly is that the service center of mobile handset location information collects the location information of mobile handset in a specified time interval everyday. For example, at 08:00 am~18:00 pm from Monday to Friday, collecting location information of the mobile handheld terminal one time every 20 minutes. For one of the mobile handsets, the location information of mobile handsets needs to be collected 31 times regularly everyday.

Collecting mobile handset location information irregularly is that the service center of mobile handset location information collects the required location information of mobile handset instantly according to the temporary requirements from the side of attendance management system. For example, the service center of mobile handset location information receives a requirement of attendance management system at 10:17 on Saturday which requires inquiring about the location information of three mobile handsets owned by attendance management system side immediately. Then the service center of mobile handset location information collects the location information of the three mobile handheld terminals soon and sends it to the attendance management system side immediately.

The attendance management system mainly consists of the function modules as follows:

The mobile handset location information request module is responsible for sending the requirement which can obtain real-time location information of mobile handset to the location service center. The sending format is HTTP file, the contents are phone number, request time, request type of the mobile handset and so on.

The mobile handset location information response module is responsible for translating the location information (latitude and longitude, time, etc.) of the mobile handset which is received from the service center of location information into plane rectangular coordinates (time, location). After that, this module inquires GIS databases to obtain the location information (administrative location, etc.) of the coordinates, and inputs the spatial location information (time, administrative position, etc.)to the schedule database of the employee attendance management system.

The schedule management function module is responsible for inserting, updating and deleting the work schedule record of the employee. The work schedule mainly consists of employee names, phone numbers of the mobile handsets, address of workplace, working hours and other projects.

The attendance management function module is responsible for comparing the work schedule with the actual action trajectory (time, location) of the mobile handheld according to the work schedule. If the location of the actual action matches with the schedule address (in the range of allowable error), the attendance result is normal, otherwise, the attendance result is abnormal.

The location-expressing function module of mobile handsets is responsible for expressing the current position and the trajectory of mobile handsets.

The current location expressing function of mobile handsets is responsible for marking the present position of the specific or complex real-time mobile handsets on the vector map.

The mobile trajectory-expressing function module of the mobile handset is responsible for marking the passed location information and time information on the vector map.

Conclusion

The mobile handheld location information attendance management system is an attendance management system based on Micro-cellular technology substantively which has resolved the employees' attendance when work time and work place constantly change.

Ultimately, it can achieve providing services for all the people and all the things at any time (anytime) and anywhere (anywhere) [4]. However, the in depth discussion and consensus standard which is about geographic information system in China have not formed yet. In order to be geared to international standards, the international standards of GIS and LBS (location based on service) should be translated into the Chinese national standard as soon as possible [5].

Acknowledgements

This work was financially supported by the Hainan Natural Science Foundation (611132).

References

[1] S. Lu, L. Pan, Non-contact IC card attendance management system [A], China Institute of Metrology, 2001,12 (3): 59-63. (in Chinese)

[2] L. Wang, R. Qin, Accesses control system based on RFID technology, access control system [J], Microcomputer Development, 2003,13 (11): 59-60 +63. (in Chinese)

[3] G-XML, http://www.jipdec.or.jp/archives/dpc/gxml/contents/

[4] D. Li, Q. Li, Z. Xie, Y. Zhu, On the spatial information and the integration of mobile communications applications [A], Information Science of Wuhan University, 2002,27 (1): 1-8. (in Chinese)

[5] J. B. He, J. T. Jiang, Standardization of Geographical Information Review and Consideration [J], Surveying and Mapping, 2006, 31 (3): 9-12 +3. (in Chinese)

Advanced Materials Research Vols. 989-994 (2014) pp 4482-4487
© (2014) Trans Tech Publications, Switzerland
doi:10.4028/www.scientific.net/AMR.989-994.4482

A Prevention Scheme for Black Hole Attack Based on NS2[1]

Xiaojing Meng[1,a],Deyu Lin[2,b],Deqin Lin[3,c],Rong Hua[3]

[1]Shandong University of Science and Technology,College of Information Science and Technology, No.579, Qianwangang Road , Economic & Technical Development Zone, Qingdao, Shandong, China.

[2]Xidian University,College of computer, No.2, South Taibai Road ,Yanta District, Xi'an, Shannxi, China.

[3]Division of Social Science and Management,Graduate School at Shenzhen,Tsinghua University.

[3]Shandong University of Science and Technology,College of Information Science and Technology, No.579, Qianwangang Road , Economic & Technical Development Zone, Qingdao, Shandong, China.

[a]jack.meng@263.net, [b]ldy19880210@126.com, Keimmy@126.com

Keywords: Ad Hoc network; black hole attack; AODV; NS2

Abstract. Mobile Ad Hoc network is a self-composing network with a highly dynamic network topology. Although it has many advantages, there are still some safety problems in it. One of these problems is the black hole attack. The black hole attack is a typical attack to the Ad Hoc network and is also the main threat facing it. In this paper, the safety problems exist in the AODV protocol, which is a kind of routing protocol in the Ad Hoc, has been analyzed in detail. In the meanwhile, an improved Secure Ad Hoc On-Demand Distance Vector Routing called OSAODV has been proposed and realized based on the NS2. Finally, three set of experiments have been made, the results have shown that the OSADOV can avoid the black hole attack very well.

Introduction

Mobile Ad Hoc network is a temporary multi-hop autonomous system that consists of a group of movable nodes with wireless transmitting /receiving devices. At present, there are mainly three kinds of routing protocols applied in the Ad Hoc network. They are Destination-Sequenced Distance Vector Routing (DSDV), Dynamic Source Routing (DSR) and Ad Hoc On-Demand Distance Vector Routing (AODV). AODV is currently the most frequently used protocol. However, without any safety mechanism, AODV is vulnerable to the attack from malicious nodes. The common attacks include the black hole attack, the routing table overflow attack, the information disclosure attack and the energy-depletion attack.

In order to avoid the black hole attack, a lot of solutions have been advanced. A very effective methods was advanced by Hongmei Deng, Wei Li and Dharma P. Agrawal, who are in University of Cincinnati. They came up with a protocol which is a security extension of the AODV protocol. In this protocol, each intermediate node is required to send back the nexthop information when it send back a RREP message. Since every source node must send an extra packet to the next hop node of the intermediate nodes, then it surely causes some overhead to the network and increases the network delay. Therefore, there is still some shortcoming in it.

This paper focused on the safety holes in the AODV, discussion of the working process of AODV and analysis of the causes of the black hole attack. Finally an improved solution was proposed based on the existing solution to the black hole attack. A series of experiments have been made and the results shown that this method is somewhat effective. Of course, as a result of personal knowledge and information Limited, there still may be some shortcomings in this paper.

Ad Hoc On-Demand Distance Vector Routing

AODV is a common on-demand protocol of the Mobile Ad Hoc network. It includes the route discovery and route maintenance functions.

1A node disseminates a RREQ when it determines that it needs a route to a destination and does not have one available. The node that receives the RREQ first creates or updates a route to the previous hop without a valid sequence number. It then checks to determine whether it has received a RREQ with the same Originator IP Address and RREQ ID within at least the last PATH_DISCOVERY_TIME. If such a RREQ has been received, the node silently discards the newly received RREQ, otherwise it replies with a RREP message. Once the RREP received, the process of route discovery will be completed and the routing information will be recorded.

2A node may offer connectivity information by broadcasting local Hello messages periodically. If, within the past DELETE_PERIOD, it has received a Hello message from a neighbor, and then for that neighbor does not receive any packets (Hello messages or otherwise) for more than ALLOWED_HELLO_LOSS * HELLO_INTERVAL milliseconds, the node should assume that the link to this neighbor is currently lost. When links break, AODV causes the affected set of nodes to be notified so that they are able to invalidate the routes using the lost link and repairs the link.

The Secure Problem and Black Hole Attack exist in AODV

The characteristics of AODV make the Mobile Ad Hoc network be able to dynamically organize network and function well. However, there are some problems hidden in it. Normal operation of this protocol bases on the premise that all the nodes would be cooperative and authentic. Once the malicious node appears, the protocol may be destroyed. It is just this shortcoming of AODV that is taken advantage of by the malicious node to implement attack. Black hole nodes reply a RREP message to all the nodes generated RREQ and claim that they have the “shortest” route to destination. As the malicious nodes usually give a reply without looking up their route tables or comparing the sequence of the destination, their replies often arrive first. After the node which received the RREP message establishes the route according to the RREP message, its routing path includes the black hole nodes as intermediate nodes. Then when the source node sends data, all the packets will be taken in by the malicious nodes. Thus the black hole nodes become “black hole” which will gobble up all the packets and destroy the normal function of AODV, even makes the Ad Hoc network paralysis.

As the Figure 1 shows, node A wants to communicate with C but doesn’t have the valid route to C, so it sends RREQ message. Both B and D receive the RREQ message, then B replies and claims that it has the fresh enough and shortest route to C immediately without checking its route table. A compares the RREP messages from B and D, it chooses B as the next hop to C and then sends data packets to it. Then B discards all of the data packets, as a result, the black hole attack actualizes successfully.

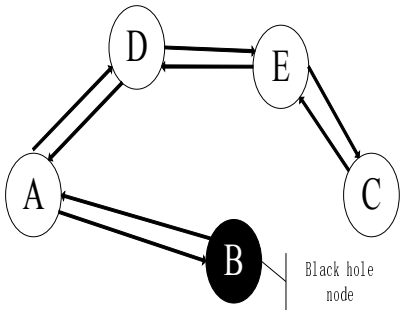

Fig.1. Black hole happens when B is a malicious node

[1] Mobile Ad Hoc Networking Working Group. Secure ad hoc on-demand distance vector(SAODV)routing [EB/OL]. http: www.ietf.org/internet-drafts/draft-guerrero-manet-saodv-06.txt.2006

[2] Mobile Ad Hoc Networking Working Group. Secure ad hoc on-demand distance vector(SAODV)routing [EB/OL]. http: www.ietf.org/internet-drafts/draft-guerrero-manet-saodv-06.txt.2006

Solution

Existing Solutions.[3]Hongmei Deng, Wei Li and Dharma P. Agrawal, who are in University of Cincinnati, came up with a solution to avoid the black hole attack. Its main idea is that an intermediate node B must put its next hop node C's information into the RREP message which is sent to the source node A when it replies. Then the node A which sent the RREQ message will generate an additional packet to C to check whether the route from the intermediate node exists or not. If the node C really has fresh enough route to the destination node and the intermediate node B, then the node A will trust B as well as its RREP message and start to send data packet to the destination node. If not, it will notify all the nodes in the whole network that B is a black hole node to isolate the node B.

This method still has some problems. Since every source node must send an extra packet to the next hop node of the intermediate nodes, then it surely causes some overhead to the network and increases the network delay.

New Solution. In order to avoid the black hole attack as well as reducing the network delay, the above scheme must be improved. Specific improvement scheme is as follows: two kinds of control packets should be added to the original control messages. They are Confirmation Route Request Message (CRREQ) and Confirmation Route Reply Message (CRREP). Whenever an intermediate node B replies with a RREP message, it must send a CRREQ message to its next hop node C at the same time. Then C which receives the CCERQ message will firstly look up its route table, if it really has the valid route to the destination, it must send a CRREP message to the source node which sends the RREQ message. If not, it just discards the CRREQ message. After receiving both RREP message and CRREP message, the source node starts to send packets to its destination. If only receiving RREP message from an intermediate node, it will send a REEQ message once again and notifies all the nodes to beware of the intermediate nodes from which it receives the RREP message. The new solution can be seen as the following figure 2, figure3 and figure 4.

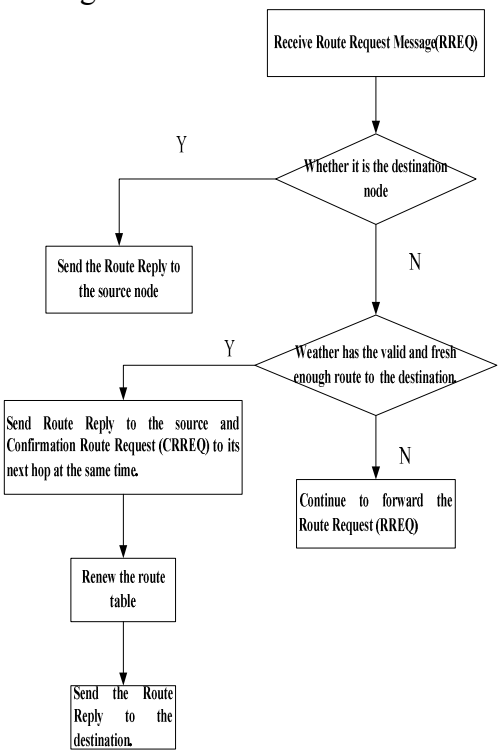

Fig.2. A flow diagram of the process when a node receiving the Route Request Message

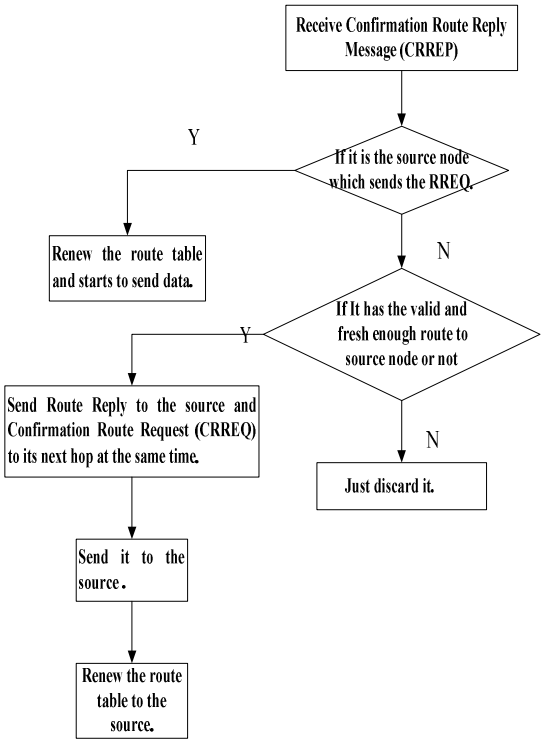

Fig.4. A flow diagram of the process when a node receiving the Confirmation Route Reply Message

[3] Sanjeev Rana, Manpreet Singh: I-SAODV: Improving SAODV to Mitigate Hop-Count Attack in Mobile Adhoc Network.A. Abraham et al. (Eds.): ACC 2011,Part Ⅰ,CCIS 190, pp.91-100,2011

.

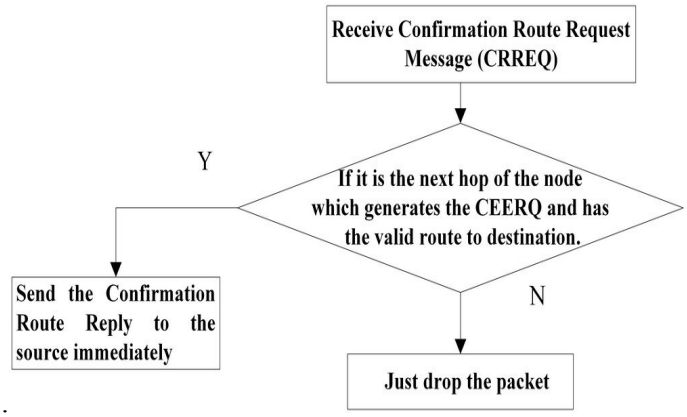

Fig.3. A flow diagram of the process when a node receiving the Confirmation Route Request Message

Realization and Simulation Experiment Based on NS2

In order to achieve the above scheme, two more packets and four more functions must be added. Meanwhile, the original function sendRequest(nsaddr_t dst)should be set one more parameter to carry warning information when a malicious node was found. The main codes are as follow:

```
#define OSAODVTYPE_CRREQ        0x12    // I add
#define OSAODVTYPE_CRREP        0x14    //    I add
#define HDR_OSAODV_CREQUEST(p)    ((struct
hdr_osaodv_crequest*)hdr_osaodv::access(p))
#define HDR_OSAODV_CREPLY(p)    ((struct      hdr_osaodv_creply*)hdr_osaodv::access(p))
struct hdr_osaodv_crequest {
            …
   inline int size() {
  …
   }
};
struct hdr_osaodv_reply {
            …
               inline int size() {
   …
   }
};
void      sendCRequest(osaodv_rt_entry *rt,nsaddr_t ipdst, u_int32_t hop_count,nsaddr_t crqdst,
nsaddr_t crqsrc, u_int32_t crqseq, u_int32_t lifetime);        //      I add
void      sendCReply(osaodv_rt_entry *rt,nsaddr_t ipdst, u_int32_t hop_count,nsaddr_t crqdst,
nsaddr_t crqsrc, u_int32_t crqsequ_int32_t lifetime);
void            recvCRequest(Packet *p);
void            recvCReply(Packet *p);
```

After finishing all of these, I recompiled the NS2 and wrote a tcl script file for verification. In this paper, I used a kind of simulation software named NS2 to simulate the AODV and OSAODV protocols, and compared the mean network delay and packet loss rate when using the different protocols.

The network model includes eleven nodes which distributed in a square field of 1000m×1000m. Every node used the same configuration except the routing protocol, the time of simulation lasted 65 seconds. Three sets of experiments were made when using different data send rates, which ranged from 150 Kb/s to 300 Kb/s. Two used AODV or OSAODV when there was a black hole node in the network, and the last used AODV when there was no malicious node.

After the experiments, the mean network delay was compared. The results showed in the figure 5 and figure 6 in the following.

The Figure 5 showed the mean delay when using AODV and not having malicious nodes or OSADOV protocols and having malicious one node. As we could see, the mean delay of OSADOV was a slightly greater than that of AODV. Extra packets such as CRREQ and CRREP caused longer time to find a valid route.

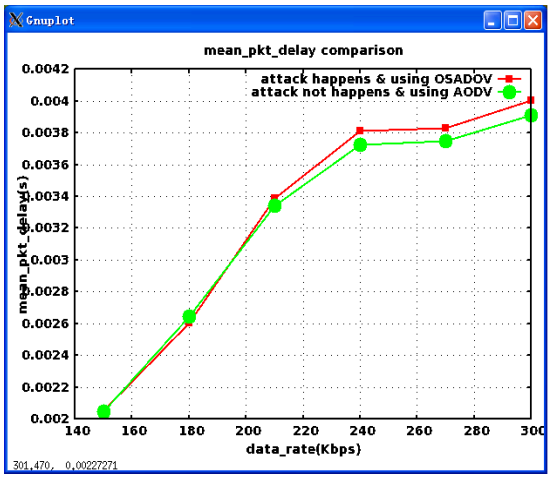

Fig.5. Network delay comparison when using AODV & notexisting malicious nodes and using OSADOV & existing a malicious node

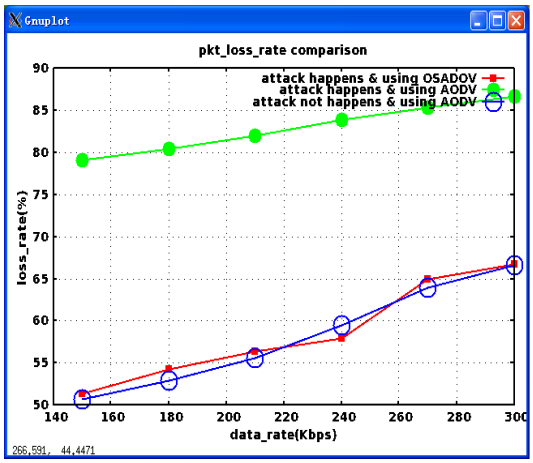

Fig.6. Packet loss rate comparisonbetween three sets of experiments

The Figure 6 showed the packet loss rate of three sets of experiments. When having a black hole node, the packet loss rate of AODV was rather high, while the packet loss rate of OSAODV was just slightly higher than that of AODV when not having malicious nodes

Conclusion

Mobile Ad Hoc network is a developing wireless network and attracts more and more attention. So does the safety problems caused by it own weakness. The basic principle of black hole attack has been introduced in this paper. Besides, an optimization secure protocol called OSADOV has been realized based on the platform NS2 and an Ad Hoc network black hole attack simulation model has been established to make experiments. The results of the experiments have shown that the black hole attack can be effectively prevented when using OSADOV. The packet loss rate can be reduced notably; meanwhile the overhead as well as network delay will not be so large.

Due to personal knowledge and information Limited, there may be some shortcomings in this paper. For example, there is just one black hole node in these experiments. In order to prevent the black hole attack caused by many cooperative nodes more effectively, much work must be done.

[1]This work was financially supported by the Shandong Science and Technology Development Project (13GGX10118), Key Technology Development Project of Qingdao Development Zone (2012-2-50, 2012-2-48, 2013-1-65), and the Open Research Fund from Shandong provincial Key Laboratory of Computer(SDKLCN-2012-01).

Reference

[1] Mobile Ad Hoc Networking Working Group. Secure ad hoc on-demand distance vector (SAODV) routing [EB/OL]. http:www.ietf.org/internet-drafts/draft-guerrero-manet-saodv-06.txt. 2006

[2] Eric Lee: Security in Wireless Ad Hoc Networks. Science Academy Transaction on Computer and Communication Networks. Vol.1,pp.29-36,2011

[3] Cayirci,E. and Rong, C. Security in Wireless Ad Hoc and Sensor Netwokr.John Wiley and sons. Chichester, West Sussex,United Kingdom,2009

[4] Zhang, H., Olariu, S., Cao, J: Mobile Ad-Hoc Seneor Networks: Third International Conference (Page: 12-14 Year of Publication: 2007 ISBN: 3-905084-33-3)

[5] Sanjeev Rana, Manpreet Singh: I-SAODV: Improving SAODV to Mitigate Hop-Count Attack in Mobile Adhoc Network.A. Abraham et al. (Eds.): ACC 2011,Part Ⅰ,CCIS 190, pp.91-100,2011

[6] Wu, B., Chen, J., Wu, J., Cardei, M.:A survey of attacks and countermeasures in mobile ad hoc networks. Wireless Network Security vol.30,n.3, pp.103-105,2007

[7] Hu,Y., Perrrig, A., Johnson, D.B,.: Wormhole attacks in wireless networks. IEEE Journal On Selected Areas in Communication vol.24,n.2,2006

[8] Liu Wei, Chai Qiaolin: Prevention of black-hole attacks using worn-holes theories. Computer Engineering and Design. Vol.28,pp. 4888-4890,2007

[9] C. Perkins, E. Belding-Royer:Ad Hoc On-Demand Distance Vector (AODV) Routing. IETF RFC 3561,2003

[10] Manel Guerrero Zapata: Secure Ad hoc On_Demand Distance Vector Routing. Mobile Computing and Communications Review, vol.6, pp.106-107,2002

Advanced Materials Research Vols. 989-994 (2014) pp 4488-4492
© (2014) Trans Tech Publications, Switzerland
doi:10.4028/www.scientific.net/AMR.989-994.4488

Design and Implementation of A Software Automation Development Framework for Management Information System

Cheng Xiao[1,a], Qiu Xingxing[1,b]

[1]School of Information Science and Technology, Jiujiang University, Jiujiang Jiangxi 332005, China

[a]410290@qq.com, [b]920708@qq.com

Keywords: Three-tier Architecture, Code Template, Automated Code Generation, Generation Engine

Abstract. To solve the problem of user demand dynamics in the development of management information system, an automation development framework based on database is proposed. Software code is generated automatically in the framework that includes three-tier software architecture design, code generation engine, the common code template design and the constraints of the conceptual models design, thus adjusts to change in demand and increases development efficiency. The comparison between the test and analysis shows that the layered architecture can meet the requirements of software applications. The application in the actual project shows that automation development framework can reduce development cost and promote software quality effectively.

Introduction

With the development of information technology, more and more government departments and enterprises use information technology and establish their own Management Information Systems[1](MIS) to improve their management level. During the process of development and practice of MIS, we find user demand dynamics obvious[2] and the user can not present the complete system function demand. It is a cognitive process from vague to increasingly clear, user can understand the function displayed by the software interface well and propose purposeful opinion and suggestions. During the development of MIS based on database, the changes of the user demand may cause the changes of database design.

Based on .NET development platform, this paper presents a MIS software automation development framework which takes the database as the core and is based on code generation engine, paper also describes the implementation of web automation development under the three-tier software architecture, thus in actual application it can improve the efficiency of software development, reduce development cost and able to deal with user changing demand flexibly.

MIS Software Automation Development Framework

The data acquisition, processing and use in MIS can be manifested as taking the database as the core. Therefore, software automation development framework which is oriented management information system and is based on a data model-driven[3] style is implemented in this paper. The MIS software automation development framework consists of four parts, it is shown in Fig. 1.

To apply the framework in MIS development, first, analyze and design the database conception model according to the demand and obtain physical model[4]; then, the code generation engine generates three-tier architecture source code automatically through common code template and database physical model; finally, develop user interface based on the functional demands. MIS software automation development framework mainly works on designing database conception model and writing code for the three-tier architecture with new function.

In the .NET-based platform web system development, the hierarchical approach can be adopted to realize the high cohesion and low coupling[5]. ASP.NET use the simple layers that is code-behind[6] technology. Thus, development efficiency is improved in some degree. The three-tier architecture in MIS automation development framework divides the whole implementation of

system into presentation layer(Web User Interface, Web UI), business logic layer(BLL) and data access layer(DAL). The approach calling these layers one after another has an impact on system performance. Data is transfered among WebUI, BLL and DAL by Entity Layer(Model).

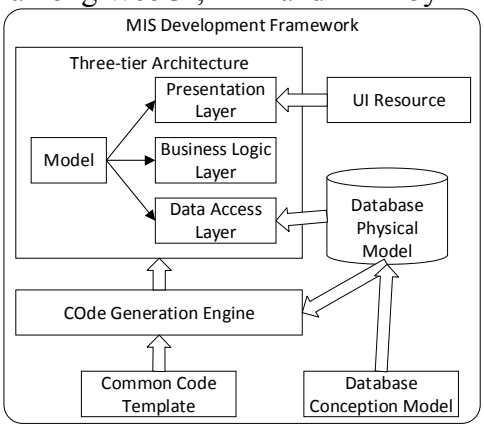

Figure 1 MIS software automation development framework

CodeSmith[7] is a template-based code-generation tool. Through custom templates[8], developer can generate anything from a simple strongly typed collection to an entire application, and do not be required to subscribe to a particular application design or architecture. CodeSmith provides an assembly called the SchemaExplorer which encapsulates all the database objects and supports connection to multiple data sources.

In MIS, database is the core content, its basic database operations consist of four parts, namely INSERT, UPDATE, DELETE and SELECT. The common code model is designed around the four operations. Thus Model, DAL, BLL and WebUI the four common templates are implemented through MIS software automation development framework.

Implementation of Common Code Template

Development framework generates automatically a corresponding source code to each table name of physical database model. According to Table 1 definite relevant rule and obtain source code under the three-tier Architecture. The main generation algorithm pseudo code is as follow:

```
Tables = TableUtilities.FilterTables(Tables); //Obtain table collection from data source
//Obtain code template
CodeTemplate ObjectTemplate = GetCodeTemplate("<template>.cst");
string Directory = OutputDirectory + "\\<directory>\\";//Obtain path
foreache(<table name> in <table collection>){//Generate source code file
    RenderFileUsingProperties("<filename>.cs",true,ref <template>,<data table>)
}
// Generate DALFactory class
RenderFileUsingProperties("DataAccess.cs",true,ref DALFactoryTemplate);
```

Table 1 The rules of code automatic generation

Layer	Rules
Model	“\Model\” + “tablename” + “Info.cs”
DBUtility	“\DBUtility\” + “MySQLHelper.cs”
<xxx>DAL	“\<xxx>DAL\” + “tablename” + “.cs”
IDAL	“\IDAL\”+ “I” + “tablename” + “.cs”
DALFactory	“\DBLFactory\” +”DataAccess.cs”
BLL	“\BLL\” + “tablename” + “.cs”
Web	“\Web\” + “\tablename\” + “<operation>.aspx.cs”

A. Model Template

A model corresponds to a table name in physics database model. Through the model template entity class code is generated, including member variables and relevant get/set method. During the code generation, correspondent relation between the database field type and C# data type is established. The main generation algorithm pseudo code is as follow:

```
foreach(<field> in table){
    // Obtain definition statement of member variable, Called GetCSharpVariableType() and
    // GetCSharpVariableType()
    GetMemberVariableDeclarationStatement(<field>)
}
```

B. DAL Template

DAL template is designed around four operations, that is INSERT, UPDATE, DELETE, SELECT. To separate from concrete database access, the operations are abstracted as a separate interface module IDAL. The design which has nothing to do with the implementation assures the system's expansibility and database's portability as well. During the realization of access to the database, MySQLDAL, SQLServerDAL and OracleDAL common data access templates are provided; the corresponding Helper class is also provided to encapsulate the database operation in DBUtility. In DALFactory, a definition about sealed class implement Abstract Factory pattern is given. Then dependencies are reduced through configuration file and reflection. The main generation algorithm pseudo code about Insert in MySQLDAL is shown in the following:

```
public int Insert(<Model Object>){
    createInsertSQL();// Generate insert statement according to filed
    createMysqlParameter();// Generate MySQL param according to field
    //Obtain result by call ExecuteNonQuery() in MySQLHelper class
      MySQLHelper.ExecuteNonQuery(MySQLHelper.ConnectionString, CommandType.Text,
strSQL, _params);
}
```

By similar approach, MySQLDAL provides Update, Delete, Get<table name>, Get<table name>All, Get<table name>By<field> etc. to implement data basic operations. At the same time, the template defines the method of execSQLForResult and execSQLNoResult to deal with the special SQL requirement in BLL.

C. BLL Template

BLL is the part which reflects the core value of system structure, mainly concerns with defining business rules and implementing of the business process. Therefore, BLL template designs basic data operation business logic, which needs to be implemented in BLL module. The main generation algorithm pseudo code is as follow:

```
DataAccess.Create< tablename >();//Create instance of I<table name> interface
public static int Insert(<tablename >Info){ //Basic business handle : Insert
    _dal.Insert(<tablename>Info); //DAL handle: Insert
}
```

Similar with IDAL, BLL also provides implementation of data basic operation with approaches, including: Update, Delete, Get<table name>, Get<table name>All, Get<table name>By<field>, execSQLForResult, and execSQLNoResult.

D. WebUI Template

WebUI is the layer needs to write the most lines of code in MIS development framework, including script files, style file, image files and media files etc.. Therefore the template design only generates addition, modification, delete, querying (listing) these four standard pages in which the three basic Web controls （Button, TextBox, GridView）are adopted. Here Add.aspx and Add.aspx.cs main generation algorithm pseudo code is as follow:

```
foreach(<field name> in <field collection>){//Create Add.aspx
    "<asp:TextBox ID="TB< field name >" runat="server"></asp:TextBox>"
}
<asp:Button ID="Button1" runat="server" Text="OK" onclick="Button1_Click" />
//Create Add.aspx.cs
protected void Button1_Click(object sender, EventArgs e) {//Button event handle
    create <table name>Info object _obj;
    foreach(<field name> in <field collection>){
        object assignment
    }
```

<table name>.Insert(_obj) //execute Insert method in BLL
}

The design of creating other pages is basically the same, using GridView control to show data list in query interface.

Application Analysis

A. Performance analysis

The hierarchical design of MIS development framework reduces coupling and generates code automatically, which enables developers to focus more on business logic and implementation of interface display in the process of development, but it also imposes a performance penalty. A comparison experiment is carried out between system code generated from the framework and non-layered code. Aiming to MIS with the database as the core, there are four operations are made out to test.

Test environment for this paper: CPU Core i5-3230M, Memory 4GB, HD 1TB，Web platform .NET Framework4.0 and VisualStudio2012（built-in IIS Express)，Database MySQL. To different implementation way execute data-operation test of different magnitude record collection (10, 100, 1000, 10000, 100000, 1000000). Test result is shown in Table 2 and Table 3.

Table 2 MIS development framework layered architecture

Record collection	Average of ten times [second]			
	Insert	Update	Delete	Select
10	0.00540402	0.00810554	0.00620414	0.00140159
100	0.05083377	0.04683117	0.04252775	0.00299833
1000	0.5261511	0.43699134	0.39066053	0.01651062
10000	5.10500705	4.2398297	3.71547944	0.17111395
100000	44.27965447	36.56134138	38.97659102	1.39092815
1000000	354.5257415	383.3854963	298.7542193	16.20891126

Table 3 ASP.NET code-behind architecture

Record collection	Average of ten times [second]			
	Insert	Update	Delete	Select
10	0.00468688	0.00360248	0.00310217	0.00120084
100	0.01562204	0.02071429	0.01661065	0.00250166
1000	0.12096958	0.15670435	0.12368224	0.01140744
10000	1.12094686	1.42805171	1.1365568	0.11957963
100000	11.15363613	14.68989249	11.5336883	1.27084694
1000000	132.2544559	154.6008215	126.9883284	12.06444252

The comparison of tested data is shown in Table 4

Table 4 Result

	Insert	Update	Delete	Select
10	1.15	2.25	2	1.17
100	3.25	2.26	2.56	1.2
1000	4.35	2.79	3.16	1.45
10000	4.55	2.97	3.27	1.43
100000	3.97	2.49	3.38	1.09
1000000	2.68	2.48	2.35	1.34
Average	3.33	2.54	2.79	1.28

Table 4 illustrates that Insert, Update and Delete operational performance reduces to 200 to 300 percent, Select operational performance reduces to 30 percent. Considering that the query operation accounts for the large proportion in the real application of MIS, the code generated through the development framework is able to meet the demand.

B Case Study

The paper presents that software automated development framework has already been successfully applied in Jiujiang agricultural products monitoring platform system. To obtain citywide agricultural products data, step up monitoring and improve time effect of data, Jiujiang agricultural products monitoring center needs to establish an effective data transfer, analysis and statistical system.

First, communicate with consumer to get initial demand, according to which build a conceptual database model and generate quickly prototype system through development framework. Second, by using and test, consumer clarifies demand; a more satisfied demand analysis will be obtained after many repetitions. Finally, take this as milestone proceed into stable system development. Through code statistics tool, the number of lines of all software code and lines of automatically generated code are obtained respectively. Statistics result is shown in Table 5.

Table 5 Percentage of automatically generated code

	Model	DAL	BLL	WebUI	Software
total	5726	16594	6921	15502	44743
generation	5726	14962	5171	9658	35517
percentage	100%	90.1%	74.7%	62.3%	79.4%

The code of Model is generated automatically 100 percent, the code of DAL is generated automatically 90.1 percent, the code of BLL is generated automatically 74.7 percent, and the code of WebUI is generated automatically 62.3 percent. The average automatic generation rate is 79.4 percent. According to the above statistics, application of the software automated generation technology presented in this paper improves development efficiency, makes developer focus on solving main problems of demand and respond timely when user's demand changed, thus debases the workload of developer.

Conclusions

This paper presents a software development automation technology oriented MIS, and gives a development framework not only is suitable for medium or small MIS but also can respond to user dynamic demand. By testing and analyzing, we find the data which accounts for a large portion in MIS has little querying performance loss, test results show that it has better performance. The analysis of the actual application results shows that it has better practicability and maneuverability.

Acknowledgment

This work has been supported by Jiangxi Provincial Education Department Youth Science Fund Project, No.GJJ12623.

References

[1] LAUDON K C, LAUDON J P. Essentials of management information systems [M]. Pearson Upper Saddle River, 2011

[2] XIAO-MING M Y D. Study on the Application of Evidence Theory in Software Requirements Engineering [J]. Computer Science, 2012, S3.

[3] PARADA A G, SIEGERT E, DE BRISOLARA L B. Generating Java code from UML class and sequence diagrams; proceedings of the Computing System Engineering (SBESC), 2011 Brazilian Symposium on, F, 2011 [C]. IEEE.

[4] YU-HONG Z, FENG-XIN Y. Design and Implementation of a Cross-platform Digital Resource Integrated System [J]. Computer Technology and Development, 2010, 20 (1): 243-246.

[5] ZHI-JIE Z. Architecture Design of Management Information System Based on Layered-Structures [J]. Computer Technology and Development, 2010, 20 (10): 146-149.

[6] BOEHM A, MURACH J. Murach's ASP. NET 4 Web Programming with C# 2010 [M]. Mike Murach & Associates, 2011

[7] JIE-HUA Z X-H W, SU-RONG S Z-G C. Software Automation Development Technology by PowerDesigner and CodeSmith in .NET Framework [J]. Computer Science, 2010, 37 (007): 156-159.

[8] YU-XIN L, KAI-XUE Y, DAO-YUN X. Automatic Code Generation Based on Template on.Net Framework of Three Layers Architecture [J]. Computer Technology and Development, 2012, 22 (8): 13-16.

Advanced Materials Research Vols. 989-994 (2014) pp 4493-4496
© (2014) Trans Tech Publications, Switzerland
doi:10.4028/www.scientific.net/AMR.989-994.4493

Study on the Adaptive Congestion Control Algorithms for Wireless Sensor Networks

Zhijing Zhang [1,a], Zengxin Xie[2,b]

[1]Department of Information Engineering Jilin Business and Technology College, Changchun, China

[2] Department of Accounting, Changchun Finance Institute, Changchun, China

[a] 2986557@qq.com, [b]275096208@qq.com

Keywords: Wireless sensor network; congestion control; RED

Abstract. As the study on and promotion of wireless sensor networks (WSN) are deepening, people have increasingly higher requirements for the transmission speed and transmission performance of wireless sensor networks. Network congestion is an important factor of the transmission performance of a network, so congestion control becomes a hot research topic in the studies on the improvement of WSN services. Based on the study on WSN congestion control mechanism, this paper proposes an adaptive congestion control algorithm and simulates the algorithm. The simulation result shows that this algorithm can ensure stable network performance.

Introduction

Compared with the congestion caused by performance degradation which results from insufficient resources in traditional networks, the coexistence of various network environments is a key problem in WSN congestion control mechanism. How to keep smooth data transmission among multiple networks has become a significant bottleneck in WSN development. Therefore, how to solve the congestion problem of WSN is a major direction of the future network studies. This paper improves existing congestion control methods to adapt to the changeable WSN environment.

Wireless sensor networks and their congestion control mechanism

1. Causes of WSN congestion

The causes of WSN congestion vary with different modes of network transmission.

(1) Congestion of wired network transmission

Its cause is not essentially different the cause of traditional network congestion. Network performance declines because of insufficient storage space, limited processor capacity and narrow bandwidth. When a subnet forwards too many packets, the load exceeds the network capacity and congestion occurs, which is manifested as longer transmission delay, packet loss and performance decline, etc.

(2) Congestion of wireless network transmission

The wireless network environment is characterized by limited bandwidth, bit error rate, high packet loss rate, long time delay, random loss of data, linkage interrupt and limited energy. The congestion of wireless networks is mainly caused by the lack of efficient mechanism of error processing, the lack of effective recovery of unexpected errors, frequent switching of network transmission data as well as frequent changes in the locations of mobile terminals and destination node.

(3) Congestion of hybrid network transmission

A WSN is a hybrid network, including local area networks composed of different devices, in addition to wired networks and wireless networks. The complex network environment leads to diverse causes of congestion. The congestion of hybrid networks is manifested as data package loss when transmission data are switched in different networks, data piling up when data is transmitted from a high speed network to a low speed network, waste of bandwidth when data is transmitted from a low speed network to a high speed network, etc.

2. Manifestations of WSN congestion

When the load of a network increases to a certain degree, the available resources on the network decrease, which causes network congestion or even collapse. In a complex network environment, there may be diverse causes of WSN congestion or collapse, and congestion or collapse may occur even though the above conditions are met. The failure of packets to arrive at the source and the loss of data packages in network transmission are the main manifestations of congestion and collapse. Moreover, TCP's repeated transmission of the data packages which are not yet lost may also lead to collapse. Due to the particularity of WSNs, it is cannot be determined under what circumstances data packages do not to arrive, so repeated transmission is more likely to result in WSN congestion.

3. Evaluation criterion of congestion control algorithms

A criterion is required to evaluate the performance and practical significance of congestion control algorithms. An algorithm is evaluated from its feasibility, reliability and execution efficiency, and it is usually analyzed from the aspect of the user, i.e., to evaluate whether the congestion control algorithm is effective through the processing capability of the end system, and from the aspect of the system, i.e., the feasibility and effectiveness of the algorithm.

4. Congestion control strategy

Due to the special environment of WSN, there is no specific and concrete algorithm to effectively solve the problem of congestion control. The study on, analysis and comparison of traditional congestion control algorithms indicate that Random Early Detection (RED) algorithm has a good performance in wired and wireless network environments. With the combination of the advantages of RED algorithm, this paper proposes an improved adaptive congestion control algorithm—a RED algorithm based on semi-normal distribution function, which can effectively solve the WSN congestion control problem in the wired, wireless and hybrid network environments.

Study on congestion control queue

1. Queue management

A new concept of queue management is developed after the queue management based on tail drop algorithm is improved. That is, queue management is a management mechanism of transmission control on the packets of router in the form of queues, and it is composed of data packet forward and buffer queue management. Queue management mechanism plays an important role in congestion control, and according to certain principles, determines whether a data package enters the forward queue, i.e., whether a data package is to be dropped.

2. Queue management control strategy

The researchers have studied and improved the queue management mechanism to deal with complex and changeable networks, and have proposed various new methods and strategies. Such studies are embodied in two levels:

(1) Data packet level: Queue management determines the packet drop strategy from the perspective of packet control.

(2) Congestion control at the data flow level: The resources in the buffer area are fairly allocated to each data flow.

3. TCP congestion control mechanism

The studies show that the maximum bandwidth B available to data flows in congestion control phase is

$$B < \frac{1.45 \times M}{R \times \sqrt{P}} \quad (1)$$

Where, M refers to the maximum segment size, R is the round-trip delay, P is the drop probability of data packages in congestion state. Thus it can be seen that the effective bandwidth available to data flows is proportional to the segment size, but is inversely proportional to the round-trip delay, the drop probability.

In a real network environment, N links share Mmb bandwidth; assuming that each link has identical bandwidth, the bandwidth available to each link is

$$B_n < \frac{M}{N} < \frac{1.45\times M}{R\times\sqrt{P}} \quad (2)$$

The drop probability P of data packages can be derived from the above formula:

$$P < \left(\frac{N}{M}\times\frac{1.45\times M}{R}\right)^2 \quad (3)$$

It can be seen from the above formula that the drop probability of data packages is proportional to the square of the maximum segment size, the square of link number, but is inversely proportional to the round-trip delay. That is, when there are more link connections, the increase in P can release serious network congestion; when there are fewer link connections, the decrease in P can adapt to the mild network congestion.

4. Congestion control algorithm

RED algorithm calculates the drop probability of data packages according to the average queue length, and packets, marks and drops data according this drop probability so as to effectively prevent the congestion of the source. RED adopts FIFO queue scheduling strategy to drop the data packages which have not entered the router yet. However, this algorithm has sensitive parameter setting; the average queue length changes little and the heavy network load likely adds delay jitter; it cannot estimate the severity level of congestion and cannot ensure fair use of bandwidth.

Improvement of WSN congestion control algorithm

Compared with the previous packet algorithms, RED algorithm has improved performance and stability, but poor adaptive adjustment capability. This paper proposes a DRED algorithm based on semi-normal distribution.

1. Improvement strategy

Based on the above analysis of RED algorithm, this algorithm can be improved from the following three aspects:

(1) The drop probability of data packages adjusts dynamically and adaptively with the change in the average queue length to increase network flexibility;

(2) Use curve to describe the drop probability of data packages, reduce the influence of threshold value on P to increase the pass probability of packet;

(3) Adjust P to 1 quickly to avoid entering the drop phase of all data packages when the packet is between the maximum threshold value of the queue length and the buffer size;

2. Algorithm improvement

The fuzzy semi-normal distribution membership function is as follows:

$$u\wedge(\mu)=\begin{cases}0 & \mu\le\alpha\\ 1-e^{-\alpha(\mu-\beta)^2} & \mu>\alpha,\ \alpha>0,\ \beta<0\end{cases} \quad (4)$$

Assuming that μ refers to the average queue length; β is the minimum threshold value, the formula for the drop probability of data packages is

$$P(Q_{av})=\begin{cases}0 & Q_{av}\le Q_{min}\\ 1-e^{-\alpha(Q_{av}-Q_{min})^2} & Q_{av}>Q_{min}\end{cases} \quad (5)$$

When the queue length equals the maximum threshold value, the drop probability of data packages is P_{max}, and thus α is:

$$\alpha=-\frac{Ln(1-P_{max})}{k^2} \quad (6)$$

Where, k is $Q_{max}-Q_{min}$, and the value of α is determined by P_{max}. Thus it can be concluded that the drop probability function of data packages based on semi-normal distribution is as follows:

$$P(Q_{av})=\begin{cases}0 & Q_{av}\le Q_{min}\\ 1-(1-P_{max})^{-\left(\frac{Q_{av}-Q_{min})^2}{k}\right.} & Q_{av}>Q_{min}\end{cases} \quad (7)$$

3. Simulation and performance analysis of the algorithm

To verify the effect of DRED algorithm, three sending endpoints and one receiving endpoints were set in NS2, and each link had the same sending speed and could be adjusted according to the experiment requirements so as to set bottleneck link between the nodes. The following figures are the

specific parameters: P_{max}update time: 0.05S; Q_{min}:100 packets; Q_{max}:300 packets; weight:0.002; buffer size:400 packets; simulation time:50S.

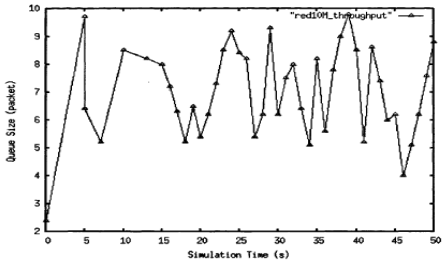

Figure 1 Queue length change in RED algorithm

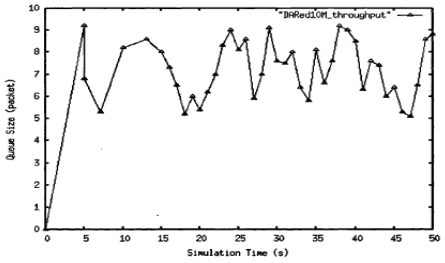

Figure 2 Queue length change in DRED algorithm

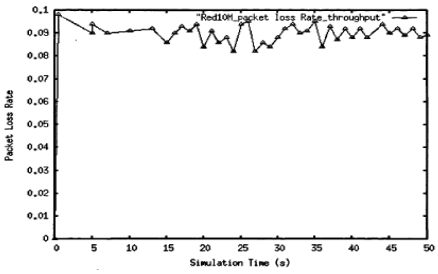

Figure 4 Change in the drop probability of data packages in RED algorithm

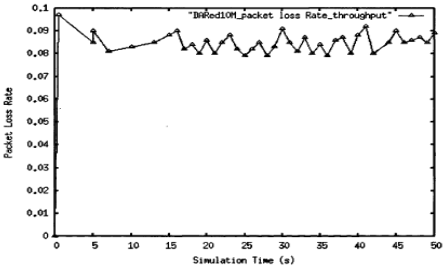

Figure 3 Change in the drop probability of data packages in DRED algorithm

When the sending rate is 10mb/s, DRED algorithm can adjust the drop probability of data packages according to the change in network environment, promptly notify the sending endpoints to change their sending rate and adjust the various parameters in the network so as to maintain the queue length in a faster and better way, prevent congestion, effectively prevent the drop of many data packages, keep good throughput capability and performance and satisfy the complex WSN environment.

Conclusion

This paper conducts a in-depth analysis and study on the complex WSN environment and the causes of WSN congestion, analyzes the application of active queue management mechanism to complex network environments. It also proposes an adaptive control algorithm based on semi-normal distribution, builds a transmission model, and conducts a simulation and a comparative analysis. The simulation and analysis results prove the effectiveness of this algorithm in the adaptive control of WSNs on congestion.

References

[1] S. Soro, W. Heinzehnan, Prolonging the lifetime of Wireless Sensor Networks via Unequal Clustering. In Proceedings of the 19th IEEE International Parallel and Distributed Processing Symposium(IPDPS).2011.

[2] M. Ye, J. Wu, EECS: An Energy Efficient Clustering Scheme in Wireless Sensor Networks. In Proceedings of IEEE Int'1 Performance Computing and Communications Conference (IPCC)2012. PR1388—1397.

[3]P. Mohapatra, J. Li, Analytical modeling and mitigation techniques for the energy hole problem in sensor networks. Pervasive Mobile Computing, v01, 3, no.3, PP.233-254, 2011.

[4] T. Camilo, C. Carreto, An Energy-Efficient Ant-Based Routing Algorithm for Wireless Sensor Network. Lecture Notes in Computer Science, Springer, 2012.

Advanced Materials Research Vols. 989-994 (2014) pp 4497-4500
© (2014) Trans Tech Publications, Switzerland
doi:10.4028/www.scientific.net/AMR.989-994.4497

An Approach to Describing Software Logic Model

Xiaoguang An

Department of Information Engineering Jilin Business and Technology College, Changchun, China

34233682@qq.com

Keywords: software logical model, structure of software, security of running software, performance of software

Abstract. This paper proposes the concept of software logical model, the basic idea and the approach of constructing the model. It describes the structure of this model, the ways of expression and the related definitions in detail. At the same time, it has also analyzed the application direction of this model. It discusses the roles playing on the aspects of research and the analysis detailedly, in which this model improves the performance of software, optimizes the structure of software and guarantees the software will run in security. Based on this model, a kind of early security warning mechanism of software is proposed.

Introduction

At present, some security management technologies and products have been developed in the field of computer network security, and many software development models have been advanced and fully discussed. However, there are few studies on software logic models, which affect further studies on the optimization of logical structure, improvement of performance and security of software.

This paper attempts to advance an approach to describing software logic models and aims at using this model to carry out further studies on the optimization, performance improvement of the related software as well as on the security of software operation so as to make computer software better serve customers.

Software logic model

Introduction of the software logic model

From the perspective of software function, any software can be described as a simple model: input—processing—output, as is shown in Figure 1 Diagram of Software Function Model. Input is responsible for acquiring the data necessary for the operation of the software; processing is to process the entered data according to some given rules; then output is to output the processed results.

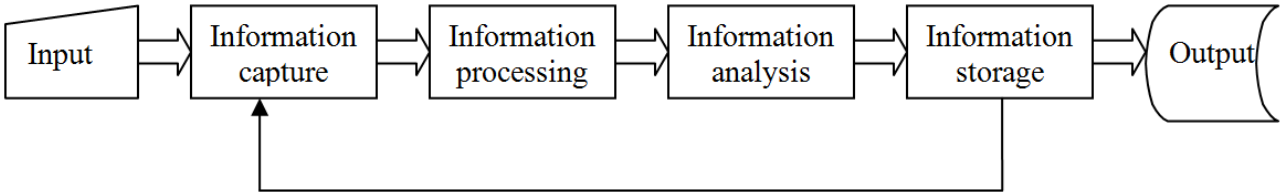

Figure 1 Diagram of Software Function Model

In terms of a specific application program, the ordered arrangement of input, output and processing can make the application program perform its special function. If the program's stable state of waiting for input is defined as State I, the stable state of output completion is defined as State O, and processing is defined as State transition C, then the above model can also be described as State I—State transition C—State O, as is shown in Figure 2 Diagram of Software Logic Model. The ordered arrangement of State I, State transition C and State O fulfils the software function. According to this idea, a program may be considered consist of a state set, a state transition set and a function set.

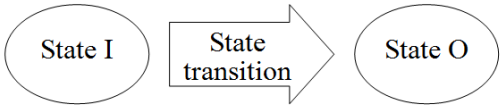

Figure 2 Diagram of Software Logic Model

The state set includes all stable states of an application program, i.e., state; the state transition set consists of all available routes for state transition. All subsets of the set of the staggered and ordered arrangements between state and state transition constitute all possible functions of the program.

The following algorithm can be obtained based on the above study.

Algorithm 1：If the state set of a program is S={s0, s1,…si…, sn-1}, the state transition set is C={ c0, c1, …ci…cm-1 },where cj (si, p0, p1,…pi…, po-1)=sk∈S, p0, p1,…pi…, po-1 are transition parameters; the function set of the program is F={f0, f1,…fi…, fr-1}, where fi is a subset of S⊕C, then the logic model of a program can be defined as follows:

P=(S, C, F), where S is the state set of a program, C refers to its state transition set and F is its function set.

Notes: A⊕B={all subsets of the staggered and ordered arrangements between A and B elements}, where A and B are finite sets.

Expression of the software logic model

According to Algorithm 1, the software logic model can be dealt with in the following way. States can be abstracted as points, and the transitions between different states are abstracted as arcs, then the logic model of a program can be expressed by a digraph. In this way, the studies on software logic model turn into the studies on the digraph, the optimization problem of software structure into the spanning tree problem of the digraph, the software performance problem into the network flow problem and the access control problem of software operation into the isomorphism problem of the digraph. Therefore, digraph and network theories can be used for further studies on the structure optimization, performance and detection of legal operation of software.

After the introduction of the software logic model, this model is then used to carry out quantitative analysis on the optimization, performance and access control of software, and then the expression of the logic model will be handled. With reference to the incidence matrix of digraph, matrix can be used to express software logic model. Algorithm 2 is described as follows:

Algorithm 2：If the software logic model is P= (S, C, F), S={s0, s1,…si…, sn-1}, C={ c0, c1,…ci…cm-1 }, F={f0, f1,…fl…, fr-1}, matrix M(P)=[aij] is the incidence matrix of P, where,

$$a_{ij}=\begin{cases}0, & \text{when there is no transition between } s_i \text{ and } s_j\\ 1, & \text{when there is transition betweens}_i \text{ and } s_j\end{cases}$$

, M is clearly a n×n matrix.

If the cost of transition between different states is considered as weight, then the digraph of software performance and performance matrix can be obtained.

Algorithm 3：If the software logic model is P= (S, C, F), S={s0, s1,…si…, sn-1}, C={c0, c1,…ci…cm-1 }, F={f0, f1,…fl…, fr-1}, matrix Mp(P)=[pij] is the performance matrix of P, where,

$$p_{ij}=\begin{cases}\infty, & \text{when there is no transition between } s_i \text{ and } s_j\\ v, & \text{when there is transition cost between } s_i \text{ and } s_j\end{cases}$$

, Obviously, Mp is also a n×n matrix.

The incidence matrix of the software logic model lays a foundation for the quantitative studies on the relationship among the sub functions of the software function, software structure optimization analysis and performance analysis, software access control and other problems.

After the expression of the software logic model is determined, the relationship among the sub functions of the software function is studied, which is significant for the optimization of software structure as well as for the judgment of whether an operator operate legally in software operation. In order to achieve the above-mentioned aim, the algorithms for describing the relationship among the sub functions are as follows:

Algorithm 4：If ci exists, ci (si, p0, p1,…pi…, po-1)=sk, then si and sk constitute the context of ci, si is the preceding part, while sk is the following part.

Algorithm 5：If the sequence sj0,…sji, sji+1…, sjn exists, where, sji∈S, then sji is the preceding part of sji+1, sji+1 is the following part of sji; if so∈S-{sj0,…sji, sji+1…,sjn} does not exist, and so has the preceding part or the following part in S, then the sequence sj0,…sji, sji+1…,sjn is a maximum ordered sequence of S.

For a specific program, a specific function can actually be understood as a maximum ordered sequence of its state set, and all of its functions belong to the set of all maximum ordered sequences in its state set. Since software operates in strict compliance with the maximum ordered sequences, and if this rule is violated, the software will end in an abnormal state. For example, forced shutdown, logical errors lead to the outage of the software.

Step 1. In software logic model P= (S, C, F), all maximum ordered sequences with S0 as the original state constitute the set of all functions of P, and S0 is the first stable state in the software operation.

The state S in the logic model P= (S, C, F) is abstracted as a point, and transition C is abstracted as a directed arc, then logic model P can be converted into a digraph G.

(1) With S0 as the root node, construct the spanning tree G' of Digraph G;

(2) In G', the nodes in the route from the root node (serving as the initial node) to any leaf node constitute a node sequence. According to Definition 4, this sequence is a maximum ordered sequence of the node sequences of G';

(3) Since G' is the spanning tree of G, the set of node sequences from the root node of G' to each leaf node is equal to the set of all maximum ordered node sequences in G;

It can be concluded from the above description that all maximum ordered sequences of S in the logic model P= (S, C, F) constitute the set of all functions of P.

Step 2. Software operates in strict compliance with the maximum ordered sequences of the state set in the logic model.

(1) Assuming that software operation is not in strict compliance with the maximum ordered sequences of the state set in the software logic model, there must be a state Si which belongs to the software state set. When the software is in the state Si, it does not belong to the maximum ordered sequences of any software state set;

(2) Since all maximum ordered sequences of the software state set S contain the state set S'=S, and Si does not belong to S', Si does not belong to S;

(3) On the basis of (2), it can be concluded that Si is not a stable state in the software state set, so Assumption (1) is false;

(4) The above discussion proves that software operation complies strictly with the maximum ordered sequences of the state set in the software logic model.

In software operation, if transition ci exists, ci (si, p0, p1,…pi…, po-1)=sk, while si and sk are not the maximum ordered sequences of the same software state set, then the software operation is illegal.

Application of the software logic model

With the software logic model, software with complex logical relationship can be abstracted into a digraph, and thus digraph theory can be used to study the logical structure of software. This assumes significance for logical structure optimization, performance improvement as well as operation security of software.

The software logic model can be used to identify the redundant states and calls in software, to integrate software functions so as to achieve their optimization, to predict the software function which is about to run, which is meaningful for fulfilling the pipelining call of software functions, and thus helps improve its operation performance. With increasing importance attached to software security application, this model can also be used to secure legal users' safe access to the system resources and prevent illegal visitors' intrusion in the operation process of software.

Conclusions

Currently, the object-oriented software development technology is the mainstream software development technology, and it encapsulates the details implemented by software, which tends to make software development have integrated components. This tendency accords with the logical structure of the software logic model, and proves the reasonability of this model from the practical perspective of software development. It is worth noting that in C/S software, because the states which constitute the logical structure of software are in a stateful relationship, on the premise of not ignoring the stateful property between the states, the analysis of the logical structure with the software logic model is limited. However, in B/S software, such characteristics as the independence of requests, connectionlessness and statelessness of software make the software logic model very suitable for this kind of software. Therefore, it is very appropriate to use this logic model to represent the logical structure of B/S software. With its convenient use and excellent maintainability and expandability, Web application is becoming the mainstream in the development of application system, which further reflects the value of the logic model.

This paper introduces the concept of the logic model of Web application programs, and presents the related expressions and algorithm rules. This logic model provides a new solution to the performance analysis, structure optimization and security of Web application programs and new development space for our studies on security.

The accuracy of this logic model still needs further improvement. Since Web application programs have big granularity, our further studies will focus on the division of security granularity.

Acknowledgements

The authors gratefully acknowledge the fund of this study by Jilin province science and technology department soft science research project（20130420026FG）"Study of Jilin province engineering and technology talent support for strategy emerging industry" and the Jilin province talent development project in 2013 (20131079) and the Jilin Province Department of Education research project (2012366).

References

[1] Xu Wenjun. Analysis of computer network security management. Henan Science and Technology, 2013(2).

[2] Li Ying, Han Dianguo. On network security management technology. Software Guide, 2013 (2).

[3] Pan Bo. On the detection methods of computer software security. Computer Knowledge and Technology, 2013 (13).

[4] Fan Yile. Application of the active defense network security configuration technology to computer forensics. Software Guide, 2011.

[5] Wang Shuang. On the detecting technology of computer software security [J]. China Computer & Communication, 2011(11).

Advanced Materials Research Vols. 989-994 (2014) pp 4501-4505
© (2014) Trans Tech Publications, Switzerland
doi:10.4028/www.scientific.net/AMR.989-994.4501

Software Platform of Home-Based Community Care for the Old Based on jQuery Mobile

Hui-min XIN[1,a], Sheng-wei LI[1,b], Meng-zhen FU[1,c]

[1]Department of Information Engineering, China University of Geosciences(Beijing), Beijing , 100083, China

[a]email: xinhuimin_0502@126.com, [b]email: 996377284@qq.com, [c]email: 694036177@qq.com

Keywords: Home-Based Community Care for the Old; Mobile web; jQuery Mobile; Software Platform

Abstract. "Empty nest" is increasingly serious and jQuery Mobile (JQM) has become a mainstream UI framework for Mobile web development. According to which phenomenon, formulate 18 kinds of service items according to the practical needs of the old. Build modular interface by means of JQM, and then fill detailed function in each module combining with MySQL database. The content of the database includes service resources and information about the old, which need to be updated in real time. Realize foreground-background communication through SOCK_DGRAM. Results show that the platform can accomplish the prospective service for the old. This mode has low cost and strong scalability, and it is a new socialization care for the old platform which is clear to operate, supporting the use of resources and multi-party benefit.

Introduction

The data shows that the rate of “Empty Nest” reaches up to 49.7% in China and there are even more than 80% in foreign countries [1].The phenomenon of “Empty Nest” is a social issue as well as an symbol of social progress .The old man play an important role in society and their wisdom, knowledge and experience are thought to be great wealth of the society [2]. Therefore, government and people should show solicitude and respect to the old, protect the rights and interests of the elderly, made it achieved for them to get welfare medicine, accomplishment, knowledge and entertainment. We need to help them be healthy in both physical and psychology. What’s more we should make sure the insurance of their life and they should have their own dignity and the sense of safety.Home-based community care for the old means a social service which takes the family as the core with community service network, and with pension system to guarantee [3]. It`s also a social service which the main content is solving the Old’s difficulties in daily life. Compared with the institutional care, the home-based community care has many advantages such as low cost, wide coverage, flexible service and so forth. It can also offer the service to the old with less cost. The more important, it can even take care of the old who lack of money but in need of care. So we can use the home-based community care to support the solid family and stable society [4].

Although the Home-Based Community Care of the Old has developed rapidly in recent years. And there are more and more pilot projects in local which are used for searching the innovation mode. But the system was just stared at present said many scholars [5]. The home-based care services in these areas are lack of a platform which is complete, operable and visible. As a result, this bad condition may lead to a tedious process or even missing some services when the old seeking for help. Therefore, the purpose of this topic is using the technology of jQuery Mobile (JQM) to construct an intelligent platform for many pension communities to use which aims to make the care service more convenient and effective.

Correlation Technique

1) jQuery Mobile

JQM is an open source JavaScript library framework and a mobile version of jQuery. The programmer can develop mobile website which runs across mainstream mobile platforms as well as

major mobile browsers with less cost. JMQ has been paid close attention by the mobile technology developers since 2010, when the JMQ was invented [6]. It's because that JMQ has the features such as: First, it`s easy to learn, which means we can develop a pleasing-looking mobile web programs swiftly by grasping some basic contents like pages and dialogue; Secondly, it's outstanding compatibility which means we can uniform the unified user's UI in the different diligent mobile phones and computers' web browsers which can help us to use some of the basic content like JQM box, the toolbar, button, content formatting, form elements, lists, APT and so on; Thirdly, it`s small scale, which means it contains only tens KB except icons after decompression; Fourth, it can support diverse input methods, including touch screens, mouse and the cursor on user inputs focus; Last but not least, we have custom theme, which means we can delimit various kinds of theme pattern easily by using the Theme Roller applications.

2) MySQL

MySQL is an open source of relational database management system (RDBMS). The MySQL database system manages the database by using the most common data management language--structured query system (SQL) [7]. The main features of the MySQL are small scale, quick running and open resource. Therefore, it's the first choice for many companies which have small or medium scale. At the same time, MySQL always comes out with Navigate which is a graphical management tool , so even a novice can do some basically operations on database management, which can greatly reduce the cost of database management.

3) Socket Communication

Socket is also called "socket", which is the API of TCP/IP, establishing a really stable and safe point-to-point communication. At present, most of the network use the Socket for interposes network communication. Socket appoints the specific IP and definite port for communication, and it would generate a Socket instance on each end of the application once connected correctly [8]. There are two types of Socket, connect-oriented flow socket and connectionless datagram socket.

4) JSON

JSON, a lightweight data-interchange format, which is easy for reading and writing, and computers can also digest and generate easily [9]. It can be used to write very practical, beautiful and readable code. The writing form of JOSN is name/value. The data format of JSON is very simple. It can transfer an easy String, Number, Boolean and an array, or even a complicated Object.

Function Partitioning

1) Requirements division

The need of the old people can divide into six parts: Economic Requirements, Consumption Requirements, Medical Requirements, Mental Requirements, Amusement Requirements and Social Activity Requirements. Among them, mental requirement on caring aging people is closely related to the quality of life and the happiness index which is significance for family stability and social harmony [10]. At recent stage, the coverage of the home-based community care services is still relatively narrow. The old people should be considered by not only the government but also the communities and families. And we should continue expending the content of service and guide the elderly to participate in social development so as to help them to realize their self-value.

2) Service Programming Established

According to the elderly questionnaire and a great deal of information from the Internet, we made 18 service items for old people which can be altered, added or subtracted in the future.

Theses 18 items are as follows: Key for Help; Family Hotline; Community Concur; Community Shopping, Community Service, Daily Reminders, Nutritious Meals, Medical Health, asking medicine, Health Topic, Brain Games, Weather Conditions, Traffic Conditions, connection to everything, Elderly University, Deposit and Investment, and Furniture Control. The medical health is a distinctive item which combine of remote medical technology comes from Italy ADiTech Company. And the ADiTech said they are willing to have a long-term cooperation with China in the construction of community home endowment.

Design of Software Platform

Based on the multi content of service, communities need a visual sense of software platform which can set out the content of services clearly.

1) Framework of Software System

The system architecture can be divided into four layers: Presentation Layer, Network Layer, Business Logic Layer and Data Layer，as shown in figure 1. In order to separate the function module and display module，the system use MVC as its design pattern, which can improve the system in maintainability, scalability, portability and reusability. The Presentation Layer just like the View in MVC, users uses the handset 'Browser' to surf different types of Webpage. HTML document prepared for static Webpage. ASP, JSP, PHP are Dynamic Webpage Languages which can be embedded into HTML. Next the Interpreter will interpret these words and return the result to the Browser; XML is a kind of data source like the File Database. Signals can be transferred through wireless network or wired network between users and the server. The network can be a LAN or WAN.But LAN will be the preferred for most users within the community. Business Logic Layer is similar to the Model in MVC. It used to handle the data of logic in applications, and its main task is to manage the equipment, network configuration, and business processing and user information. The resource of data used in Business Logic Layer is from Data Layer. The data is called by MySQL through WebService. And MySQL is managed by Navicat which is graphical software.

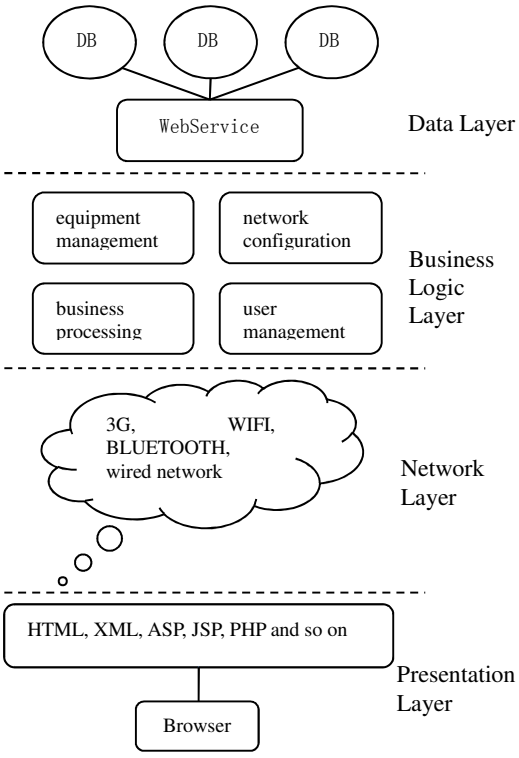

Fig.1. System architecture diagram

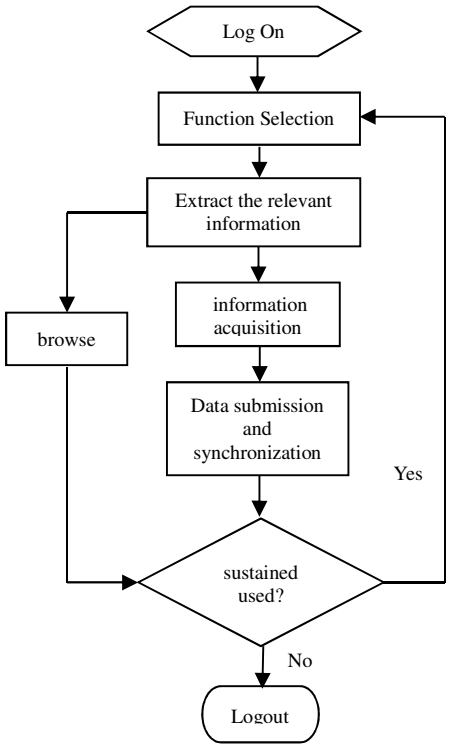

Fig.2. Flow chart of software operation

2) Scheme of Software Design

This topic uses NetBeans IDE 7.3 as the development environment. NetBeans is a tool for software developed which open its source code. It is a development framework which can be extended, also used for the development of program in Java, C / C++, PHP, HTML5 [11]. You must install JDK before installing NetBeans, and configure the system environment variables. For our topic is a design of a web site, so what we need is to use the web function of the application program in the NetBeans. And we should choose the default GlassFish Server as the web server. We create a web which should contain three files: jQuery JS, jQuery Mobile JS, jQuery Mobile CSS because we apply JQM framework since the initial interface. In addition, another important work is to establish a database which has a clear hierarchy layout through MySQL. Database will give all aspects of data resources like transportation, culture and life which are provide for the old. It need

to be updated in time and also includes the old own information. Such as name, phone number, ordering, part-time appointments, health indicators and treatment records. The old submit service orders to the background, as well as the background feedbacks the information confirms are both based on the Socket communication. In order to improve efficiency, we use Socket which is for connectionless datagram, and JSON structure.is used in data formats.

3) Flow Char of Software Operation

Figure 2 presents the software the chart of operation flow. The first step for the old to use the platform is to log in and the system will automatically turn in their relevant information. Then they can enter the main interface. The main interface is composed of 18 sub modules. If someone only wants to browse information, the system will display the corresponding data from the backstage database. When someone need to submit the order, shopping request or upload the measure data of health indicator (some of the relevant instrument can submit the data automatically), he/she should submit information so that the system can synchronize the database after receive the data. If the operation is completed, he/she can log off or continue to use other functions.

4) Function Module

Figure 3 and Figure 4 listed 2 modules from the 18 modules in the platform of home-based community care for the old. The topic use JQM plugins to reduce the complexity of program. Such as the Photo Gallery plugin Photos wipe which makes the picture and the operation more bright and colorful based on HTML, CSS, and JavaScript. It can be seen that even the illiterate old man can find the related services through these images.

Fig.3. Module of Elderly University

Fig.4. Module of Transport Guide

5) Software Equipment

In order to improve the service efficiency, the topic has some supporting software. Android application software is equipped for service personnel to use. There are different services with different icons, including ordering a meal, shopping, property, family therapy. Modeled on the QQ and chat in the upper right corner of which icon there will be pop-up unfinished message number. And it will renew timely after the staff deal with the event. In addition, in order to improve the compatibility and transmission efficiency supply video, we need to covert the format of the original video. So we use java to develop software of video format conversion. Its ‘features are different from those existing software. It can batch convert video formats, conversion result will level with the original folder hierarchy in corresponding. Each video file will be saved in a folder which using the same name with the video at the bottom. The folder will contain the new video format and three random screenshot. Select open-source ffmpeg as video compression solution. It supports many video compression standards including MPEG series and dozens of common AV file formats [12]. And it has high portability and codec quality. If we master the command set of ffmpeg we can get the specific quality and format.

Conclusion

The test shows that the software platform of home-based community care for the old based on JQM is a new type of pension platform which has social resources, can be clear operated and support multi benefits. Through this platform of elderly service can improve the quality of the old. What`s more it has positive significances because it can promote the reemployment of laid-off workers, perfect minimum subsistence guarantee system and promote the community integration. The platform is highly scalable and it can used in hospitals, trains and some other occasions in the future. So we need continual exploration and improvement to achieve a higher value with low cost.

Acknowledgement

In this paper, the research was sponsored by the National Natural Science Foundation of China (Project No. 41374185).

References

[1] Xiaobo Wang. Develop Home-based Care for the Old to Cope with Aging[N/OL]. BUSINESS TIMES, 2011-01-12[2014-01-21].

[2] Manyun Lin. Competitiveness Analysis of Aging Human Resources[J]. Fujian BBS (Humanities and Social Sciences Edition),2008,25(S3):15~16.

[3] Linling Xu. Status and Development of Home-based Care for the Old[J]. Law and Social, 2009,4(18):216~217.

[4] Baidupedia. Home-Based Care for the Old[EB/OL]. 2013-12-26[2014-01-21]. http://baike.baidu.com/link?url=kPA5EMEtOGF0JBro_xNSRKmf-RbEf0aEkJTim9SMBKh3tw67xqI7dxmCEbDrbSS4

[5] Zhao Qing. Status and Problem Analyses of the Mode of Chinese Home-Based Community Care for the Old[J]. The South of China Today,2010,3(7):4~6.

[6] Xiao Zhi,Wenjun Yang. Design and Development of Mobile Information Publicity System of Universities Based on jQuery Mobile[J]. Library Science Research,2012,33(23): 47~51.

[7] Guanghua Yu. Analysis and Design of E-education Platform System Based on MySQL[J]. Computer & Telecommunication, 2011,17(6):47~48.

[8] Wenjuan Shao. Design and Implementation of Mobile Phone Image Acquisition and Transmission System Based on Socket[J]. Wireless Interconnected Technology,2013,10(11):48~49.

[9] Lingyu Zhou. Design and Implementation of Front-End Page Effects Based on jQuery[J]. Computer and Modernization,2013,29(1):61~63.

[10] Congzheng Lu. Attaches Importance to the Spirit of "Provision for the Old" Manifest Humanistic Care[J]. Economic Research Guide,2012,8(22): 21~22.

[11] Wikipedia. NetBeans[EB/OL].2014-01-08[2014-01-21]. http://zh.wikipedia.org/wiki/NetBeans

[12] Ruipeng Gao,Jialing Liu. General Video Plug-in Based on FFMPEG[J]. Computer Knowledge and Technology, 2010,10(6):2475~2476.

Advanced Materials Research Vols. 989-994 (2014) pp 4506-4509
© (2014) Trans Tech Publications, Switzerland
doi:10.4028/www.scientific.net/AMR.989-994.4506

Design and Implementation of Personalization Recommendation System in Mobile E-Commerce

Jinfeng MIAO

Xingtai polytechnic college, Xingtai, 054035,China

email: mjf0901@126.com

Keywords: Mobile E-Commerce; Personalized Recommender Systems; Design

Abstract. The purpose of this paper is to basing on the design of the mobile e-commerce personalized recommender systems, presents a method of personalized recommendation product information, and makes every effort to provide effective personalized service solutions for mobile e-commerce sites.

Introduction

Recent years, with the rapid development of the Internet technology, information technology and mobile communication technology, mobile e-commerce has become the new direction of the electronic commerce development. According to the requirement of the mobile e-commerce on personalized recommendation system, and combining content filtering technology with collaborative filtering technology, the author puts forward a weighted combination filtering recommendation system in this article.

1 The composition of the mobile e-commerce personalized services recommendation system

According to the working process of the personalized recommendation system in mobile e-commerce, the whole system is mainly made up of input function module, the function module of recommendation method and output function module.

1.1 Input function module

Its role is to collect information customer's personal and community groups. Customer's personal inputs, that is, target users Input evaluation project including the customer's personal attributes, purchase history, page browsing history, explicit browse input, keywords, and the project properties, etc. This information can help mobile business enterprise analysis of target customers' preferences, and then enterprises can recommend a suitable for their goods. Community inputs, namely the collective form of evaluation data, which includes the project properties, corporate purchase history, text evaluation and grade, etc. The information is the basis of social collaborative recommendation.

1.2 The function module of recommendation method

It is the core part of the recommendation system, and determines the performance of recommendation system. The main task of this module is to establish customer behavior model, analyze customer behavior characteristics or preferences, and then according to the results of certain recommendations have recommended.

1.3 The output function module

It is the content from the recommendation system to the user after the system input information. The main forms of module:

(1) Suggestion, Divided into single Item, unsorted suggestion List and ordered List. A typical such as Top-N, Namely according to customer's preferences, then the system recommends the most likely to attract customers' N pieces of goods to the customer.

(2) Prediction, Including: system overall score for a given project, the individual rating of goods from other customers， review about the goods from the customers.

2 Recommended technology and ideas about mobile e-commerce personalized service system

2.1 Recommendation technology

2.1.1 Filtering technology based on content

In the recommendation system, the objects of interest to the user are defined by feature. The method is based on the content and no memory; it can only recommend the related content to the customer based on the features of user previously seen or evaluation, etc.

2.1.2 Collaborative filtering technology

It recommends contend to the user based on the same interests or program. The basic starting point of induction:

(1) According to the classification of preference;

(2) If the user rating of some projects is similar, they also similar to the evaluation of certain projects.

2.2 Ideas about personalized services recommendation system

This article analyzes user forecasts by content filtering and collaborative filtering technology, and then uses the weighted sum method. First of all, according to the mobile users purchase history log data and browsing behavior, to extract the characteristics of potential information and then form a user interest model. Second, given the similar interest, the similarity about characteristics of the same goods evaluation from the users, the users are divided into category. Finally, to combine the weighted sum of contribution to the recommended, so as to form the final recommendation results.

3 The basic framework and process of personalized recommendation system

3.1 The basic framework of personalized recommendation system

As shown in Fig.1, after the user login page, the system will analysis, recommend the results to the user by information collection.

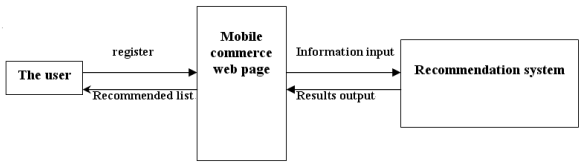

Fig.1. The basic framework of personalized recommendation system

3.2 The process of personalized recommendation system

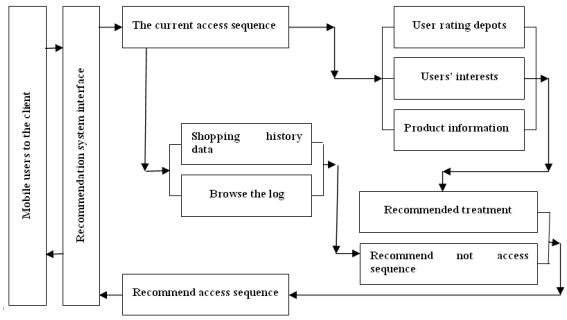

Fig.2. Personalized recommendation system process

As shown in Fig.2, the basic process of recommendation system is: First, the content, such as the customer shopping history data, the current access sequence and browse the log, are processed in advance. Second, through data processing, the system creates content filtering recommendation module; Finally, two recommendation modules are weighted summation, and related products in the product information database are generate a variety of recommended access sequence, which are recommended by moving the personalized interface on the server to the user.

4 Algorithm design about the personalized recommendation system

4.1 Algorithm design about content filtering recommendation module

In this module, the user's current access sequence is converted to interest topic vector. Customer shopping history data and browsing log, which are formed the feature vector by weighting computation. Then they form the initial recommendation model vector. By calculating the degree of similarity between the current access sequence and the initial vectors, the system finally set initial similarity values for interest topic of everyone.

Assumption: I-the user's interest; Pf0(I)-the initial I recommend model vector about I;P0-interested topic vector about users; P1- feature vector from shopping history data of customer; P2-feature vector from browse the log of customer; wi- the Ith interest in vocabulary; X,Y,Z for the respective weight.

$$Pf_0(I) = \mathrm{X} \times P_0(I) + \mathrm{Y} \times P_1(I) + \mathrm{Z} \times P_2(I) \tag{1}$$

Based on the formula in the smart recommendation system，which was build by Buckley

$$\mathrm{P_{0i}} = \begin{cases} \log（\mathrm{N}/\mathrm{d}f（\mathrm{w_i}））,\text{if } \mathrm{w_i} \in \mathrm{I} \\ 0, \quad \text{otherwise} \end{cases} \tag{2}$$

$$\mathrm{P_{1i}} = \begin{cases} \mathrm{logMI}（\mathrm{w_i},\mathrm{rel(I)}）,\text{if logMI}（\mathrm{w_i},\mathrm{rel(I)}）\geqslant 3 \\ 0, \quad \text{otherwise} \end{cases} \tag{3}$$

$$\mathrm{P_{2i}} = \begin{cases} \mathrm{logMI}（\mathrm{w_i},\mathrm{pseudo\text{-}rel\ (I)}）,\text{if logMI}（\mathrm{w_i},\ \mathrm{pseudo\text{-}rel(I)}）\geqslant 3 \\ 0, \quad \text{otherwise} \end{cases} \tag{4}$$

In the recommendation system, the threshold is adjustable.

4.2 Algorithm design about collaborative filtering recommendation module

According to user's interest in similarity, the interest is classed as a kind of similar users, thus gain n content clustering(C_1,C_2,C_3,……,C_n).

Ci=(Ui1,Ui2,Ui3,……,Uili),li-The number of users

A user feature vector:Uij=(tij1, tij2, tij3, ……,tijk),j=1,2,3,……,li

Category feature vector:

$$C_i = \frac{1}{l_1}\left\{ \sum_{j=1}^{l_1} t^{ij}{}_1, \sum_{j=1}^{l_i} t^{ij}{}_2, \ldots \sum_{j=1}^{l_i} \mathrm{t}^{ij}{}_k \right\} \tag{5}$$

The similarity of feature vectors between the text information and the clustering content.

$$\mathrm{sim}_{CE}(U,T) = \mathrm{sim}_{CE}(C,T) = \cos(C,T) = \frac{\sum_{\mathrm{j=1}}^{\mathrm{ili}} C_{\mathrm{j}} \times \mathrm{T_j}}{\sqrt{\left(\sum_{\mathrm{j=1}}^{\mathrm{ili}} C_{\mathrm{j}}^2\right)\left(\sum_{\mathrm{j=1}}^{\mathrm{ili}} T_{\mathrm{j}}^2\right)}} \tag{6}$$

The division of collaboration clustering can consult content clustering. The average of interest strength is regarded as intensity of interest from text in cooperation clustering.

4.3 The results from the weighted combination recommend

$\mathrm{sim}_U(\mathrm{U},\mathrm{T})$ -the similarity between Text feature vector and the user vector

$\mathrm{sim}_{CE}(\mathrm{U},\mathrm{T})$ -the similarity

$G_{DE}(\mathrm{U},\mathrm{T})$ -the similarity about user content clustering between Text feature vector and the user vector

$\mathrm{S}(\mathrm{U},\mathrm{T})$ -the relevance of user and the text

$$\mathrm{sim}_U(\mathrm{U},\mathrm{T}) = sim_U(\mathrm{pf},\mathrm{T}) = \cos(\mathrm{pf},\mathrm{T}) \tag{7}$$

$$\mathrm{sim}_{CE}(\mathrm{U},\mathrm{T}) = sim_{CE}(\mathrm{pf},\mathrm{T}) = \cos(\mathrm{C},\mathrm{T}) \tag{8}$$

$$G_{DE}(\mathrm{U},\mathrm{T}) = \frac{1}{MN_U}\sum_{i=1}^{MN_U} g(T,B_i,\mathrm{U}_i) \tag{9}$$

$$S(U,T) = \alpha\times\mathrm{sim}_U(U,T) + \beta\times\mathrm{sim}_{CE}(U,T) + \gamma\times\mathrm{G}_{DE}(U,T) \tag{10}$$

α,$\beta$and γ is for the adjustable weight parameters.

5 The recommended method of personalized recommendation system

This system can realize the four kinds of personalized recommendation method.

(1) Recommend in response to user requests.

This is the most basic of personalized recommendation service. As long as the system thinks that is associated with user interest, is to form a recommended sequence to the user, and then the users determine whether is effective. Its characteristic the similarity is whether is greater than or equal to the threshold.

(2) The most popular recommendation.

According to all the user's preferences, the system shows the most popular, the same product category. This recommendation does not consider the current user’s interest preference, but determined by the degree of sales.

(3) The latest recommendation.

This recommendation does not consider the current user interest preference. As long as within the scope of a certain amount of time, the system recommends these commodities to the customer.

(4) The user personalization recommendation.

According to corresponding user customization service, system will recommend the customize product information to the users. In the accurate identification of the user's identity and customization service type, according to the different customize service, the system can do different recommendation to users in response.

References

[1] Niknama T, Amiri B, An Efficient Hybrid Approach based on PSO, ACO and K-means for Cluster Analysis [J]. Applied Soft Computing, 2010, 10(1):183-197.

[2] J.W.Han, H.Cheng, D.Xin and X.F.Yan, Frequent pattern mining; current status and future directions[J]. Data Mining and Knowledge Discovery, 2007,15(1):55-86.

[3] C.M. Wu, Y.F. Huang, Generalized association rule mining using an efficient data structure[J]. Expert Systems with Applications, 2011,38(6):7277-7290.

[4] Bobadilla J, Ortega F, Hernando A and et al. A collaborative filtering approach to mitigate the new user cold start problem, Knowledge-Based Systems, 2012,26:225-238.

[5] X.Yi, Z.L.Whang, W.S.Guo, E-commerce Personalized Recommendation Technology Based onExpert System [J]. Bulletin of Science and Technology, 2014,30:98-99.

Advanced Materials Research Vols. 989-994 (2014) pp 4510-4513
© (2014) Trans Tech Publications, Switzerland
doi:10.4028/www.scientific.net/AMR.989-994.4510

A Novel Feature Selection Method Based on Principal Component Analysis for Network Traffic Classification

Hongzhi WANG[1, a], Jianping ZHANG[1, b], Zunyi SHANG[1, c]

[1]Network & Information Center, Dalian Jiaotong University, Dalian, 116028, China

[a]email:1064776788@qq.com, [b]email:zhangjp@djtu.edu.cn, [c]email:szy@djtu.edu.cn

Keywords: PCA; Feature Selection; Maxima-order; Network Traffic

Abstract. In network traffic classification, by conventional PCA method, more features still exist due to uniform contribution rates for most of features. To overcome this problem, in this paper, a novel feature selection method is proposed to reduce data dimension of network traffic. A contribution rate of various features in each component is calculated by a new weight criterion. A maxima-order principle is proposed to determine feature selection. Based on three multi-class classification methods, performance comparison is conducted by actual traffic data with 10-fold cross-validation. Experiment shows that the proposed method has higher classification accuracy than conventional PCA method.

Introduction

Network traffic monitoring is an important way to keep network security and management [1]. Network traffic classification is a key for network traffic monitoring [2]. According to traffic classification, we can identify various applications, monitor and control the whole network, optimize network performance and improve the quality of service while keeping the network security. Network traffic contains many attribute features, e.g. the standard Moore set [3] selects the TCP flows with complete semantics (start with 3 TCP handshakes, end with 3 TCP handshakes) as network traffic samples, each sample contains 248 attribute features. Obviously the number of attribute feature is too big to be use, and it leads to heavy computation. At the same time, the redundant and related features may be included. So it is very important to reduce the attribute dimensions.

Feature selection is vital to reduce attribute dimensions. Literature [4] proposed a feature selection method by integrating filter and wrapper models. [5] used two filter-based feature selection methods for classification algorithms. [6] proposed a lightweight for intrusion detection system based on filter mode and feature selection.[7] proposed a set of features for P2P internet traffic detection and classification using Support Vector Machine by analyzing different types of features. [8] used fast correlation based filter (FCBF) for feature reduction and naive bayes algorithm to assess the reduction effect. [9] applied two optimal features subsets to provide better result in term of accuracy. [10] used random search algorithm for features reduction to identify P2P traffic by using SVM.

The principle of PCA is to convert the original data into a new coordinate system through linear transforming [11]. Literature [12] proposed a method to select informative object features using a sparse PCA. Network traffic has so many features that conventional PCA still provide more features due to uniform contribution rates for most features.

To overcome this problem, in this paper, a novel feature selection method is proposed. Firstly, according to contribution rate of principal component, the key principal components are chosen. A contribution rate of various features in each component is calculated by a new weight criterion. Secondly, a maxima-order principle is proposed to determine feature selection. Experiments show that our proposed method can greatly reduce feature dimension and obtain better recognition results.

A Novel Feature Selection Method based on Modified PCA

We assume the sample set is X, i.e. the feature set of network traffic can be denoted by $X^{n\times p}$ where n is the number of samples and p is feature number of network traffic. First, to keep uniform of network traffic data, we normalize X as follows:

$$x_{ij}^{*}=\frac{x_{ij}-\bar{x}_j}{\sqrt{\mathrm{var}(x_j)}} \qquad (i=1,2,\cdots,n; \quad j=1,2,\cdots,p) \tag{1}$$

Where $\bar{x}_j$ is mean value of jth column of X and can be expressed by

$$\bar{x}_j=\frac{1}{n}\sum_{i=1}^{n}x_{ij} \tag{2}$$

$\mathrm{var}(\cdot)$ is variance of X and can be depicted as

$$\mathrm{var}(x_j)=\frac{1}{n-1}\sum_{i=1}^{n}(x_{ij}-\bar{x}_j)^2 \qquad (j=1,2,\cdots,p) \tag{3}$$

And then we get the correlation coefficient matrix R. We assume the normalized data is still represented by X, so the correlation coefficient of X is presented as follows:

$$r_{ij}=\frac{1}{n-1}\sum_{t=1}^{n}x_{ti}x_{tj} \qquad (i,j=1,2,\cdots,p) \tag{4}$$

Through the Jacobi method, we can get the eigenvalues ($\lambda_1,\lambda_2\cdots\lambda_p$) and the corresponding eigenvectors $a_i=(a_{i1},a_{i2},\cdots a_{ip}),i=1,2\cdots p$ of the correlation coefficient matrix R, and then obtain p principle components. All these p principle components are obtained in descending order, so the amount of information they contained are obtained in descending order too. The variance of a principal component accounts for the proportion of total variance (i.e. the corresponding eigenvalue account for the proportion of total eigenvalues) is called the contribution rate; bigger contribution rate means that the principal component contains more original information and is shown as:

$$\mathrm{k}r=\frac{\lambda_i}{\sum_{i=1}^{p}\lambda_i} \tag{5}$$

The sum of contribution rate for the first k principal components is called cumulative contribution rate and is expressed as $cumcontri$, the selection of k depends on the actual needs, and generally the cumulative contribution rate should be more than 85%.

We assume the sample set is $X=[x_1,x_2,...,x_p]$, its eigenvectors matrix which satisfies the contribution rate is $U=[u_1,u_2,...,u_k],k<<p$; its principle component can be expressed as follows:

$$Y=U^TX=\sum_{i=1}^{k}u_ix_i \tag{6}$$

The purpose of network traffic feature selection is to select the main features from X which can represent the principal component. So how to choose the main features from matrix U is very important. Here we propose a criterion based on feature contribution rate on principle components.

We define the eigenvectors $u_i=[u_{i1},u_{i2},...,u_{ip}]$, and get the contribution rate of u_i and can be expressed by

$$cr=\frac{u_i}{\sum_{j=1}^{p}u_{ij}} \tag{7}$$

Arrange the above cr in descending order and then get u_i which satisfies the accumulative contribution rate $cumcontri$ between 85% and 95%, the first i components of u_i is the feature selection result of X. We express the feature label set as $index$ and it can be depicted by

$$index = \{i, 1 \le i << p, cumcontri = \sum_{k=1}^{L} contri_k \ge T\} \quad (8)$$

But the amount of components that satisfies the $cumcontri$ is often too much, the features are still too many, i.e. the dimension reduction is not satisfactory. In order to reduce the dimension further, our approach is to search the components in u_i which has the maximum magnitude and can be depicted as:

$$u_i^* = \left\{u_{ij}^*, \max(\lfloor u_i * 10^m \rfloor) \le 10, m = 1,2,...\right\} \quad (9)$$

Then select the corresponding feature label set from X, and expressed as ind

$$ind = \left\{i, 1 \le i << p, u_i == u_i^2\right\} \quad (10)$$

According to formula (9) and (10), we can get the feature selection of network traffic, expressed as X^{Sel}

$$X^{Sel} = X(ind) \quad (11)$$

Through the above process, we effectively reduce attributes of network traffic, and achieve the purpose of dimension reduction and features selection.

Algorithm Description of Proposed Feature Selection Method

We briefly describe the proposed algorithm as follows:

1) Normalize the network traffic data according to formula (1);
2) Calculate the correlation coefficient according to formula (4);
3) Build corresponding eigenvector matrix through formula (5) and (6);
4) According to formula (7) and (8), get the feature label set of eigenvector columns;
5) Obtain the minimum feature set from formula (9) and (10);
6) Get the result of feature selection from formula (11).

Experimental Results

We conduct experiments to test the feasibility of the proposed method with 10-fold cross-validation. Three classification methods are used to conduct comparisons between proposed method and conventional PCA method. They are One-Against-One (OAO) [13], One-Against-All (OAA) approach [14], Binary Multi-class classifier [15]. Experiment data is selected randomly from the Moore set used in [3]; there are totally 10280 samples be selected and each sample includes 248 features. The experiment data is divided into 10 equal parts; we choose one part in turn as testing set and the rest 9 parts as training set, and conduct classification. Then repeat the above experiment 10 times; the average classification accuracy of each method is recorded in table 1. Using our proposed method, the number of selected features is 25. Comparison result shows that the proposed method increases the classification accuracy in contrast with conventional PCA method.

Table 1 Average classification accuracy with each method

	OAO	OAA	Binary Multi-class
Conventional PCA	85.50%	88.51%	91.17%
Modified PCA	89.33%	91.01%	93.17%

Conclusion

In this paper, a novel feature selection method based on PCA is proposed. A contribution rate of various features in each principal component is calculated by a new weight criterion. A maxima-order principle is proposed to determine feature selection. Experiments show that our proposed method can reduce feature dimension and obtain better classification accuracy.

References

[1] Feihu Yang. Research on Feature Selection Approach and its Application in Network Traffic Identification[D]. Nanjing:Nanjing Communication University,2012.
[2] He Deng. Research on Network Traffic Classification Based on Machine Learning Method[D]. Zhuzhou:Hunan Industrial University,2009.
[3] Moore A W, Zuev D. Internet traffic classification using bayesian analysis techniques[C].International Conference on Measurement and Modeling of Computer Systems (SIGMETRICS). Alberta (Canada), 2005:50-60.
[4] Yang Aimin, Zhou Yongmei, Deng He, et al. Method of feature generation and selection for network traffic classification[J]. Journal of Shandong University,2010,40(5):1-7.
[5] Huang Junyi, Wu Jing, Zhang Hui. Analysis of Feature Selection Effect on IP Traffic Classification Algorithms[J]. Computer Engineering,2010,36(16):68-70.
[6] Huang Hongyan. Lightweight Intrusion Detection System Based on Feature Selection. [D]. Baoding: Hebei University, 2009.
[7] Haitham A. Jamil, Roozbeh Zarei, Nadir O. Fadlelssied, et al. Analysis of Features Selection for P2P Traffic Detection Using Support Vector Machine[C]. International Conference of Information and Communication Technology.Bandung, 2013:116-121.
[8] A. W. Moore, D. Zuev. Internet traffic classification using bayesian analysis techniques[C]. Proceedings of the 2005 ACM SIGMETRICS international conference on Measurement and Modeling of Computer Systems. USA(New York), 2005:50-60.
[9] Li Jun, Zhang Shunyi, Liu Shidong, et al. P2P traffic identification technique[C]. Computational Intelligence and Security, 2007 International Conference on. China(Harbin), 2007:37-41.
[10] Yuexiang Yang, Rui Wang, Yang Liu, et al. Solving P2P traffic identification problems Via optimized support vector machines[C]. Computer Systems and Applications, 2007. AICCSA'07. IEEE/ACS International Conference on. Amman,2007:165-171.
[11] Pascoal C, Rosario de Oliveira M, Valadas R, et al. Robust Feature Selection and Robust PCA for Internet Traffic Anomaly Detection [C]. INFOCOM, 2012 Proceedings IEEE. Orlando,2012:1755-1763.
[12] Naikal N, Yang A Y, Sastry S S. Informative feature selection for object recognition via sparse PCA[C]. Computer Vision (ICCV), 2011 IEEE International Conference on. Barcelona, 2011:818-825.
[13] J Friedman. Another approach to polychotomous classification, Technical report [R] Stanford University, Department of Statistics, 1996.
[14] V N Vapnik. Statistical Learning Theory[M]. Wiley Inter-Science, 1998:493-520.
[15] Ran Wang, Sam Kwong, Degang Chen. A new method for multi-class support vector machines by training least number of classifiers[C]. Proceedings of the 2011 International Conference on Machine Learning and Cybernetics. China(Guilin),2011:648-653.

Advanced Materials Research Vols. 989-994 (2014) pp 4514-4518
© (2014) Trans Tech Publications, Switzerland
doi:10.4028/www.scientific.net/AMR.989-994.4514

A Security Compliance Based Mobile User Authentication Scheme

Yifei Yuan [1, a], Lianzhong Liu [1, b], Chunyan Han[1, c]

[1] Beijing Key Laboratory of Network Technology of Computer Science and Engineering, Beihang University, Beijing, 100191, China

[a]email: ifay.yuan@gmail.com, [b]email: lz_liu@buaa.edu.cn, [c]email: hanchunyanbupt@gmail.com

Keywords: BYOD; compliance strategy; authentication

Abstract. The BYOD (Bring Your Own Device) scenario puts traditional two-factor authentication into great security challenge. To strengthen the authentication in BYOD scenario, we propose a security compliance based mobile user authentication scheme, which includes a novel calculation method for device identifier, and a fine-grained compliance strategy and its management. The scheme provides a secure authentication mechanism for BYOD scenario and satisfies the requirements of device authentication in mobile user authentication.

Introduction

With the fully developed techniques of intelligent devices and its widespread, personal intelligent devices represented by mobile phones and tablets has come to enterprise area, which is called as BYOD mode. The diversity of employees' devices makes it difficult to manage and authenticate mobile devices. Thus how to protect enterprises' sensitive data from illegal access has become an important issue [1, 2].

Traditional two-factor authentication (2FA) scheme has two main drawbacks [3]. First, it can only authenticate the users, but can do nothing about the devices, so employees are able to use unregistered devices to access business data, which may cause data leakage. Second, it cannot control the security of employees' devices, that is, an unsecure device may be allowed to get access to the sensitive business data and the uncertain functions and applications on the device may get the corporate data illegally [4]. In this paper, we improve the traditional 2FA, and propose security compliance based mobile user authentication scheme.

Background and Related Research

There are three authentication factors that are typically used to authenticate users: proof-of-knowledge, proof-of-possession, and proof-of-characteristics [2].

Much work around authentication factors and their security has been done. As to the proof-of-knowledge factor, traditional user-defined password is either easy to guess or subject to brute force attacks. In mobile times, researchers start investing the use of OTP (One Time Password) technology [5].

The proof-of-possession factor is most frequently strengthened in banking systems and e-commerce systems, which requires strict security. Jhe-Yi used a three-factor authentication combines PIN code authentication, USIM (Universal Subscriber Identity Module) card authentication and facial biometric authentication [6]. However, the USIM card only exists in UMTS (Universal Mobile Telecommunications System) phones and cannot be a universal identifier for BYOD scenario.

Paper [7] focused on strengthening the "something you are" factor and proposed a multi-factor authentication method combined facial, voice and iconographic biometric factors to strengthen the mobile authentication. Three bio-factors may be secure enough for enterprise usage, but its high precision will also lead to a low recall rate, which will cause inconvenience in practice.

Besides the three factors mentioned before, there are additional authentication factors like location and time added to authentication systems. Paper [8] proposed a location-assured,

multi-factor authentication on smartphones via LTE communication. To guarantee the security and reliability of location information, they use both device-collected location and LTE-provided location.

The previous research work mostly focused on the strengthening of authentication factors, which is not enough for BYOD scenario. The BYOD scenario stresses the importance of authentication of both user and device, and requires more on additional authentication factors such as location and application-state on device. So we propose a security compliance strategy to limit the additional authentication factors and use a novel calculation method for device identifier to adjust the diversity of devices.

Authentication Scheme Overview

In this section we will discuss the factors needed in our authentication scheme, and give a formalize description of mobile user authentication. We use a two-tuple $< \text{FACTORS}, \text{RULES} >$ as authentication vector. The explanation of each item is described as below:

FACTORS : the authentication factor set, $\text{FACTORS} = \{\text{DEID}, \text{PWD}, \text{OPTION}\}$, in which DEID denotes the device's unique identifier, PWD represents the password set by users and OPTION means a configurable option set for enterprises to adjust to their own security requirements.

$\text{OPTION} = \{\text{TEL}, \text{JMUN}, \text{BIO}, \text{TOKEN}\}$, the elements in set refer to employee's telephone number, job number, biological features and hardware token respectively. All the elements except for $DEID$ are configurable[9], that enterprise can define their own method to generate PWD, such as OTP (one time password) or SMS-based password, and decide whether to use more factors to strengthen the authentication scheme according to their security requirements.

As to $DEID$, researchers have proposed different methods to select the most suitable one. Steven Furnell disscussed the feasibility of using PIN code to authenticate and suggested that flexible, multi-level authentication of the user [10]. Before we decide which to choose as $DEID$, lets first check and discuss different devices' identifiers adopted by vendors.

Table. I Identifiers of mobile devices

Identifier	Meaning	Usage	Storage Location	Length
IMSI	International Mobile Subscriber Identification Number	Identifier for mobile device subscriber	SIM card	15-digit
IMEI	International Mobile Equipment Identification Number	Identifier for mobile device	GSM&WCDMA network device	15-digit
ESN	Electronic Serial Numbers	Identifier for mobile device	CDMA network device	8-digit
MEID	Mobile Equipment ID	Strengthened ESN	CDMA network device	15-digit
MAC address	Media Access Control	Network device identifier	NIC	48bit

From table 1 we can see that different devices use different identifiers. For the devices with SIM card, such as mobile phones, IMSI may be used as $DEID$ if we ignore the fact that CDMA devices' IMSI cannot get through program. But for devices without SIM card, such as tablets and mobile phones without SIM card, we may use IMEI or MEID or ESN as $DEID$. The length of identifiers mentioned in above table are also different to each other, thus the $DEID$ cannot be unified, so we proposed a novel calculate method for $DEID$, which will be described in II.A section.

RULES: the compliance strategy set, defined as:

$$RULES = \{rul_1, rul_2, \ldots, rul_n\} \quad (1)$$

The RULES is compliance strategies set by enterprise administrator, aiming at checking devices' security state and users' state. Thus the RULES includes two main parts: the compliance strategy for devices and the compliance strategy for users, and each rule is composed of compliance items and logical operators. Table. II describes the items in compliance strategy.

Table. II Description of compliance strategy items

category	compliance item	description
device	dOwnership	device ownership type: employee-owned, corporate-owned or shared device
	dVersion	device's platform and version
	dState	device state: whether has got the super user permission
	dType	device type: mobile phone or tablets
	dFunction	device function, includes WiFi, 2/3/4G, camera, Bluetooth, GPS etc.
	dLocation	device's location
	dWLApp	whether device includes all of White List Apps
	dBLApp	whether device includes none of Black List Apps
	dMax	max number of simultaneously online device
user	uPwdLength	user password length
	uPwdStrength	user password strength
	uPwdValid	whether user password is in valid period
	uAttempt	the login attempt times
	uValid	user account validity

Here is an example of compliance strategy:

$$RULE1 = (dOwnership = employee\ owned)\ AND\ (dVersion > Android4.0)\ AND\ (dState = NotRoot)\ AND\ (dType = phone)\ AND\ (dFunction = wifi\&GPS) AND\ \big(dLocation = (116.00E, 40.90N)\big) AND\ (dWLApp = true) AND\ (dBLApp = true)\ AND\ (dMax \leq 3) AND\ (uPwdLength \in [10,16]) AND\ (uPwdStrength = Char\&Num) AND\ (uAttempt < 4) AND\ (uPwdValid = valid)$$

The RULE1 means when authenticate user devices, the compliance strategy requires that device is employee owned phone, and the version of device platform is higher than Android 4.0, and is not rooted, and device's Wi-Fi and GPS functions are enabled, and device's location is at 116.0 east longitude and 40.9 north latitude, and ALL the white list apps have been installed on the device and none of the black list apps is installed, and no more than three devices can be online simultaneously. Also RULE1 requires user password length should between 10 and 16 characters and the password should include both characters and numbers, and total trial time should less than 4 times, and password is valid.

A. The calculation method for $DEID$

As one of the most important factors in 2FA scheme, $DEID$ is quite different between devices, and the length of device identifiers cannot be unified. Here we propose a SHA1-based calculation method for DEID, which is unique for device and is calculated from device hardware to guarantee that the $DEID$ will not change with reboot or factory reset.

$$DEID = SHA1\big(IMEI\,|MEID|\,ESN + MACAddress + BlueToothAddress\big) \quad (2)$$

The IMEI|MEID|ESN means the first calculate factor is IMEI(for GSM devices) or MEID|ESN (for CDMA devices), the second factor is MAC address of device's NIC, and the third factor means the device's Bluetooth address if exists. The $DEID$ will be of 160-bit length after the SHA1 algorithm.

B. The management of compliance strategy

Compliance strategy must be defined in the enrollment procedure. When a user registers into enterprise system, the enterprise administrators must allocate or define a proper compliance strategy for the user according to his or her role in the company. Each time the device connects the internet, it is automatic to check the local compliance strategy's integrity and update. The integrity check's object is the MD5 of local compliance strategy file, and if it differs from the MD5 of server's compliance strategy file, which may be caused by illegal operation from local device or the update of server's compliance strategy, then the local enterprise application will download and apply the

newest file from server. Also, when an employee's working role changes, his or her compliance strategy will also be changed by the enterprise administrator.

Design

The authentication procedure involves four entities: user, device client, authentication server and enterprise service. In BYOD scenario, users refer to employees, and device client include mobile device and the applications installed on it, especially the enterprise application.

Step 1: The employee request to access to enterprise service client (such as an app) on mobile device, and type in password to get through.

Step 2: After the employee passed the app's authentication, he (she) is authorized the permission to operate the enterprise client.

Step 3: The employee requests to access enterprise service through the client.

a)The client queries the server to check local compliance strategy's integrity and updates.

b) The enterprise server replies and client synchronizes local compliance strategy to server.

c)Then device client does self-check according to compliance strategy.

d) Then the device client sends employee's request to authentication server where employee's compliance will be checked.

Step 4: After all compliance strategies are meet, employee can commit business operations and communicates with enterprise service.

Fig.1 shows the sequence of mobile user authentication scheme.

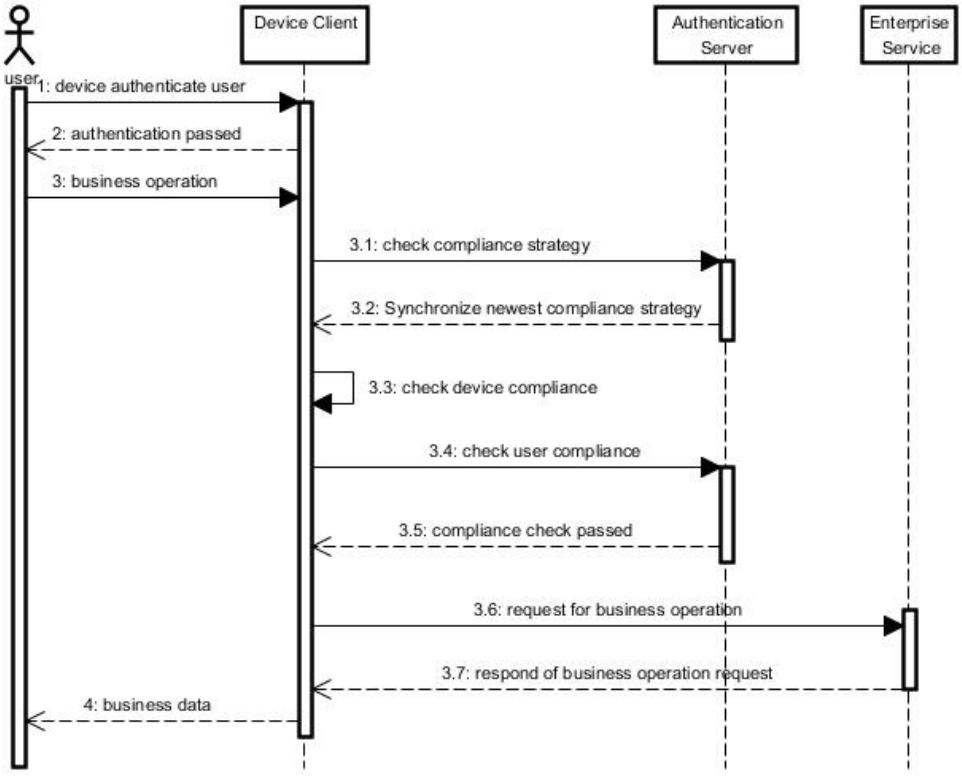

Fig. 1 Sequence diagram of the authentication procedure

The table below shows the algorithm in Step 3. The algorithm includes compliance-checking part and the logging part, which is an important part for enterprise to do auditing later.

Table. III Check Compliance Algorithm

Algorithm：CheckCompliance
Input： None
Output：Success|Fail, ResultList
Condition precedent:

```
1. Synchronize Local Compliance Strategy
2. Synchronize Black and White App List
Initialization:
ResList=null
Process：
For each item in ComplianceStrategy
    If ItemType(item)=Device
        itemVal=getItem(item)
         ResList.put(item,itemVal)
        If Compare(itemVal,item.restriction)=true
            Log(item,itemVal)
            Continue
        else
             LogError(item,itemVal)
    If ItemType(item)=User
        sendCheckRequest(item.val)
        result=getCheckResponse(item.val)
         ResList.put(item,result)
        If result=false
            LogError(item,itemVal)
        else
            Log(item,itemVal)
  Return List
```

Conclusion

In this paper, we focus on the drawbacks of traditional two-factor authentication scheme and make two main improvements to fulfill the requirements of mobile device authentication. First, we propose a calculation method of device's unique identifier to unify the authentication factor of device identifier. Secondly, we support a fine-grained compliance strategy for enterprises to strengthen the security of their authentication procedure.

Acknowledgement

In this paper, the research was sponsored by Co-Funding Project of Beijing Municipal Education Commission under Grant No.JD100060630.

References

[1] B. Morrow, "BYOD security challenges: control and protect your most sensitive data," *Network Security,* vol. 2012, pp. 5--8, 2012.
[2] S. Holtmanns, V. Niemi, P. Ginzboorg, P. Laitinen, and N. Asokan, *Cellular Authentication for Mobile and Internet Services*: Wiley. com, 2008.
[3] A. Kemshall, "Why mobile two-factor authentication makes sense," *Network Security,* vol. 2011, pp. 9--12, 2011.
[4] A. Scarfo, "New Security Perspectives around BYOD,", 2012, pp. 446--451.
[5] G. Yang and F. Zhou, "Trusted Computing-Based Double Factor Authentication for Mobile Terminals,", 2010, pp. 683--685.
[6] J. Hu, C. Sueng, W. Liao, and C. C. Ho, "Android-based mobile payment service protected by 3-factor authentication and virtual private ad hoc networking,", Hong Kong, China, 2012, pp. 111 - 116.
[7] B.A.P. Botelho, D.G.A.E. Pelluzi and E.T. Nakamura, "A versatile access control implementation: secure box,", 2013, pp. 249--252.
[8] T. Kuseler, I. A. Lami and H. Al-Assam, "Location-assured, multifactor authentication on smartphones via LTE communication,", 2013, p. 87550B--87550B.
[9] S. Furnell, N. Clarke and S. Karatzouni, "Beyond the pin: Enhancing user authentication for mobile devices," *Computer fraud \& security,* vol. 2008, pp. 12--17, 2008.
[10]B. Arkin, "The case for mobile two-factor authentication," *IEEE Security \& Privacy,* 2011.

Advanced Materials Research Vols. 989-994 (2014) pp 4519-4523
© (2014) Trans Tech Publications, Switzerland
doi:10.4028/www.scientific.net/AMR.989-994.4519

An IPv6 Security Multicast System Based on CA Authentication

LI Jian-bing[1,a], LI Xiao-ping[1], YANG Fan[1], Dong Qing-kuan[2]

[1]School of Aerospace Science & Technology, XiDian University., China,710071)

[2]State Key Lab. Of Integreted Services Networks; XiDian University, China,710071)

[a]email: jbli@mail.xidian.edu.cn

Keywords: CA authentication; IPv6; security multicast; system

Abstract. To deploy network components of a security multicast which is based on the multicast group security architecture and its key management architecture, an IPv6 security multicast system using CA authentication is designed. The multicast group members use CA certificate to access network, while the role of Group Controller/key Server deployed in the network is to establish and manage the group key and negotiate SA with multicast source. The proposed scheme solves the problem of components deployment of multicast system with security, and has strong scalability as well which means various multicast protocols and group management protocols can run on this system.

Introduction

Multicast is an important supporting technology for the next generation Internet applications. The security problem hinders the widespread use of multicast technology. Secure multicast system includes multicast security architecture and group key management framework, and key management protocols and algorithms. Secure multicast architecture and usage of the GSA group key management protocol is proposed by the Internet Engineering Task Force (IETF) in RFC3740, RFC4046. However, combined with the existing multicast routing protocols such as Protocol Independent Multicast (PIM), group management protocols such as Internet group management protocol (IGMPv6) and Multicast Listener Discovery (MLDv2), and using a efficient group key management algorithm, the design of safety and ease of deployment of multicast system is still a challenge. Based on the comprehensive consideration of secure multicast architecture, multicast security key management architecture, protocol and algorithm, a security multicast system is presented in this paper.

The hierarchical architecture Iolus[1] is suitable for dynamic multicast applications, but its decryption efficiency is low, and it is difficult to play a role in large dynamic multicast environment. The distributed architecture[2] can avoid single point of failure, but due to the adoption of policy based mechanism, it lacks of flexibility in a large and dynamic environment. A two layer of mobile multicast key management architecture and algorithm is proposed in reference [3]. According to the mobile environment, by the number of subgroup member is saturated or not to determine whether to generate a new subgroup. However, this method itself and the moving member dynamics are contradictory. The logical key tree includes the group key management algorithm of LKH, TOFT, CGKA are proposed in the reference [4-6], respectively. They all have their own advantages, and the requirement of secure multicast key management can be satisfied in a certain environment. But their common weaknesses that focuses on the algorithms themselves, rather than to consider how to deploy the device when the algorithm is implemented.

Therefore, we need to design an efficient key management system that can adapt to the application of large dynamic environment and a security multicast system that can be convenience to the implementation of variety group key management algorithm

This system is put forward in RFC3740 multicast security framework and RFC4046 definition of group key management framework. Multicast communication protocol mainly includes the routing protocol and group management. A typical multicast routing protocol is PIM[7] protocol with various models for different applications such as Dense Mode (DM), Sparse Mode (SM), and a

protocol for source specific multicast (SSM). The MLDv2 protocol sub protocol of IGMPv6 is used for group management protocol in IPv6. The system will run the above protocol to realize multicast communication.

Secure Multicast Architecture

As shown in Figure 1, the system mainly consists of 4 parts, which is CA center, multicast, group members and GCKS. The CA center authenticates multicast source, GCKS and group members. Multicast source is multicast data sender, which can be a member in the group that receives multicast data, also may be an outside group member. GCKS is the group controller and the policy server, which is responsible for the consultation of group management key generation with multicast source.

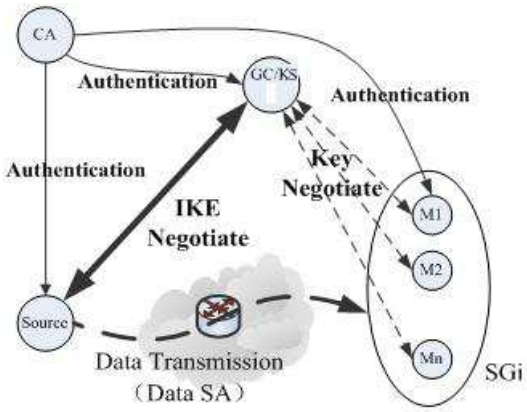

System Function Module and Deployment

As shown in Figure 2, the system consists of three parts divided from the function modules, which is multicast communication module, key management module, and authentication module. I is the IP multicast module, and the thick solid line represents the path of multicast data transmission. II represents a group key management part, main including the group key foundation, distribution, and group key management. Dotted lines refer to the possible key negotiation between GCKS, and a GCKS may correspond to multiple routers. III is authentication module, and the arrows indicate the authentication of the GCKS and group members by the CA center. In this system, CA authentication is a authentication mechanism to provide the required safety, and it is safe and credible.

Routers support multicast in the IPv6. Routers support and run the IGMPv6 and related protocols such as MLDv2. Therefore, the deployment of IP multicast module for general network deployment do not need to set up additional components. The core component of multicast key management is GCKS. The deployment of GCKS adopts distributed deployment mode, and the higher performance of the host or server is selected as the GCKS in a certain range. The authentication module bases on the current mature CA certification deployment method.

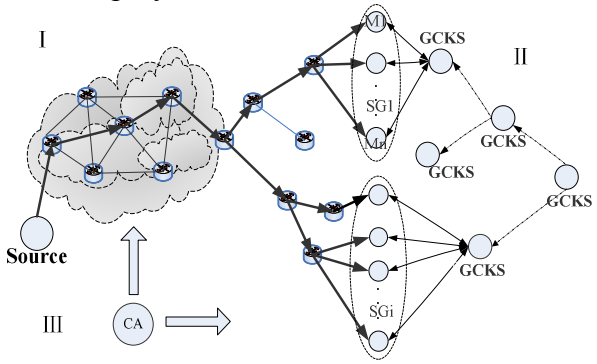

Fig.2 System function module

Multicast Communication Process

"Query and response" communication mode is adopted in the IP multicast communication. The foundation of a multicast group is an important process of multicast communication. Firstly, the query router is determined by election mechanism in the access router. The query router periodically sends query messages to the local link, and the host on the link decides whether to join multicast groups though its response to the query message. Then, the query router founds multicast listener query list according to the received response message, and Multicast data forwarding is decided by the router MLD list. Another important process of multicast communication is to determine the multicast routing, which is the process of multicast data transmission from the multicast source to the access router. For the multicast from single point to multipoint, a source specific multicast routing protocol such as PIM-SSM, has the high efficiency of the host to join a multicast group in PIM-SM mode, skips the shared tree and Rendezvous Point (RP) rules in PIM-SM mod, and uses the Channel to uniquely identify a group communication. Therefore, PIM-SSM routing protocol is adopted in the routing process of this system.

In secure multicast system, the protection of end-to-end data and the multicast distribution tree, and the access control of membership in subnet hierarchies need to be provided. IPSec is employed to provide the above safety requirement in this system, which is the frame of Group Security Association (GSA) proposed by RFC4046, including register SA, update key SA, and data SA. The register SA provides information a protection for GCKS registration from group members. Key update SA offers a protection of key update material for group members updating. Data SA protects the multicast data flow from the source to the group members. Due to the IPSec is a kind of point to point protocol designed for the unicast system, compatibility problems exist between the secure multicast protocol and the IPSec protocol suite, which performs mainly in the establishment of data SA in the GSA.

In this system, related parameters of GCKS and multicast source negotiation data SA are used, and GCKS implements group key generation and group key management. Firstly, GCKS consults with group members on the group key. Then, as the group agent GCKS negotiates with the multicast source on the data SA. The certification part of the system bases on CA authentication certificate mode.

The process of security multicast communication for this system is shown in figure 3. After the encrypted multicast data are obtained by the group members, the multicast data can be decrypted by group key obtained from the GCKS.

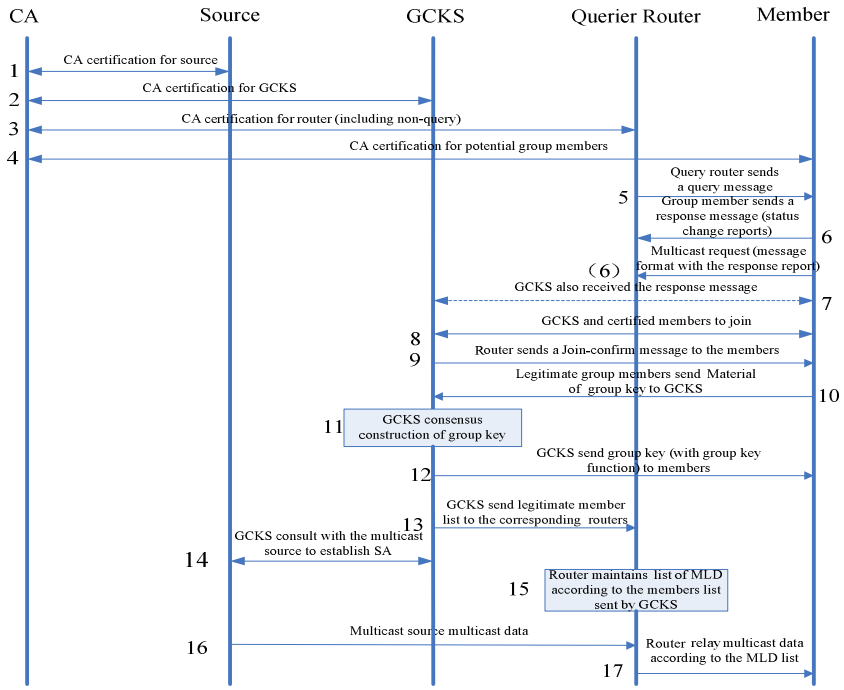

Fig3. Processing system

System Performance Analysis

The system provides a method for the secure multicast establishment and the equipment deployment. The security, deployment and other advantages of this system are shown below.

Security: the most important work in the system is that the data send from the multicast source is in protection by the data SA in GSA and it ensures the confidentiality of the data of the group members. Moreover, when members join multicast groups, it needs to use the certificate with GCKS mutual authentication, and the access control mechanism reduces the possibility of denial of service attacks (DoS) to a certain extent.

Deployment: multicast communication module and group key management module is relatively independent. In a secure multicast system, according to the required level of security requirements, appropriate GCKS level is set and connected to the network system, solving the function node entity deployment problem in the group key management algorithm. Meanwhile, this key management set independent to the multicast communication module is easy to use various group key agreement algorithms and has good scalability.

Efficiency: Compared to the security multicast management system proposed in patent [8], this system adopts the access authentication based on Certificate in real time through GCKS generating and distributing group key, and has a better dynamic. Moreover, this system considers the routing protocol and group management protocol of the current multicast, avoiding extra overhead.

Conclusion

The system can meet the safety requirement of multicast communication. Though the use of the certificate authentication mode, the problem of the use of SA in the multicast is solved, and the system has high security. Meanwhile, deployment of group key management is convenient and efficient, and has a good scalability. The equipment deployment is convenient to use the different key generation and management algorithm, getting good efficiency of the algorithm.

Acknowledgement

In this paper, the research was supported by the National Natural Science Foundation (Project No.61301173).

References

[1] Mittra S. Iolus: A Framework for Scalable Secure Multicast[C], In pro. Of ACM SIGCOM, France: Cannes, 1997,277~288
[2] Hardjono T, Dondeti R. Multicast and Group Security. London: Artech House Boston, 2003
[3] Yiling Wang, Phu Dung Le and and Balasubramaniam Srinivasan. Efficient Key Management for Secure Wireless Multicast[C], Third 2008 International Conference on Convergence and Hybrid Information Technology. 2008:1131-1136
[4]Wong C K, Gouda M, Lam S S. Secure Group Communications Using Key Graphs[C]. IEEE/ACM Trans. On Networking, 2000,8(1):16~30
[5] Fucai ZHOU , Jian XU , Long LIN , Haifang XU. Multicast Key Management Scheme Based on TOFT[C]**,** The 10th IEEE International Conference on High Performance Computing and Communications, 2008:1130-1135
[6]Elisavet Konstantinou. Cluster-based Group Key Agreement for Wireless Ad hoc Networks[A]. The Third International Conference on Availability , Reliability And Security, 2008 550-557
[7]Fenner B, Handley M, Holbrook H. Protocol Independent Multicast - Sparse Mode (PIM-SM): Protocol Specification (Revised) [S], RFC4601, IETF, 2006
[8]WU Wei, LI Xiao-jian， SHEN Ling. A Security Multicast Management System and Method[P]， CHINA, CN1588839A, 2005.3.2

Advanced Materials Research Vols. 989-994 (2014) pp 4524-4527
© (2014) Trans Tech Publications, Switzerland
doi:10.4028/www.scientific.net/AMR.989-994.4524

Research on SIQRS Spreading Dynamic Model with Feedback Mechanism on Scale-free Networks

Tao LI[a], Yuanmei WANG[b], Youping Yang[c]

School of Electronics and Information, Yangtze University, Jingzhou, 434023, China

[a]email: taohust2008@163.com, [b]email:yuanyzq@163.com, [c]email: youpingyang@126.com

Keywords: Model; Scale-free Networks; Feedback Mechanism; Threshold; Equilibrium

Abstract. A modified *SIQRS* spreading dynamic model with feedback-mechanism based on scale-free networks is presented in this study. Using the mean field theory, the spreading dynamics of the model is analyzed. The spreading threshold and equilibriums are derived. The relationship between the spreading threshold, the epidemic steady-state and the feedback-mechanism is analyzed in detail. Theoretical results indicate the feedback-mechanism can increase the spreading threshold, resulting in effectively controlling the epidemic spreading.

Introduction

The studies of complex network have attracted much interest since the seminal works on the scale-free property [1]. In the study of scale-free networks, a good example is to inspect the effect of the scale-free features on the epidemic spreading [2-9]. Using SIR and SIS models [6, 8], the absence of a spreading threshold has been observed. Currently, many of these results are based on the unchangeable topology structures of networks. For instance, a *SIQRS* epidemic model on scale-free networks without considering the change of topology structures [2]. In reality systems, people will decrease the contact with other people consciously while there is a disease spreading in crowd and the number of infections is growing. On the contrary, people will increase the contact with others people while the number of infections is going down [9]. That is to say, the structures of networks will be changed according to the feedback information. So the feedback mechanism is introduced in the study. The article is organized as follows. In Section 2, the establishment of scale-free network model is described. A modified *SIQRS* epidemic model with feedback mechanism on scale-free networks is proposed in Section 3. In Section 4, we conclude the paper.

The Network Model

In the paper, we focus on the Barab´asi and Albert (BA) model, which incorporates growth and preferential attachment. Starting with m_0 fully connected nodes, every time step a new node is added, with m edges that are connected to an old node with probability $\prod_{k_i}=k_i/\sum_j k_j$, where k_i is the connectivity of the ith node. After a long period of evolution, this network organizes itself into a scale-free stationary state, in which the probability that a node has k edges $P(k)=2m^2k^{-3}$, $k \geq m$, the mean number is $\langle k\rangle=\int_m^\infty kP(k)dk=2m$, the variance of node connectivity is $\langle k^2\rangle=+\infty$.

A Modified *SIQRS* Epidemic Model

In the proposed modified *SIQRS* epidemic model, the nodes can only exist in one of the four discrete states, namely, susceptible, infected, quarantined and removed, denoted respectively by S, I, Q, and R. Let $S_k(t)$, $I_k(t)$, $Q_k(t)$, $R_k(t)$ be the densities of nodes with degree k at time t. In the course of disease transmission, a susceptible node is vaccinated with probability α and infected with probability λ. Infective nodes are quarantined with probability σ or recover spontaneously with probability γ. Some useful management is employed on the quarantined nodes

so that they leave for the removed state with probability ε. Due to loss of immunization removed nodes join the susceptible nodes again with probability δ. For feedback mechanism we suppose the node disconnects his connection with the infected nodes with probability μ [9]. So the probability of the node disconnects with his neighbors is $\mu I(t)$. Based on the above hypotheses, using the mean field theory the dynamic mean-field equations can be written as

$$\begin{cases} \dfrac{dS_k(t)}{dt} = -\lambda k(1-\mu I_k(t))S_k(t)\theta(t) - \alpha S_k(t) + \delta R_k(t) \\ \dfrac{dI_k(t)}{dt} = \lambda k(1-\mu I_k(t))S_k(t)\theta(t) - \gamma I_k(t) - \sigma I_k(t) \\ \dfrac{dQ_k(t)}{dt} = \sigma I_k(t) - \varepsilon Q_k(t) \\ \dfrac{dR_k(t)}{dt} = \gamma I_k(t) + \varepsilon Q_k(t) + \alpha S_k(t) - \delta R_k(t) \end{cases} \tag{1}$$

The probability $\theta(t)$ describes a link pointing to an infected node, which satisfies the relation

$$\theta(t) = \frac{\sum_k kP(k)I_k(t)}{\sum_s sP(s)} = \frac{1}{\langle k\rangle}\sum_k kP(k)I_k(t) \tag{2}$$

Let $I(t)$ be the density of all infective nodes of the whole network at time t. Obviously, $I(t)=\sum_k P(k)I_k(t)$ is the density of infected nodes of the whole network. For $(1-\mu I_k(t))S_k(t) = (1-\mu I_k(t))(1-I_k(t)-R_k(t)) \approx S_k(t) - \mu I_k(t)$ the system (1) can be simplified as

$$\begin{cases} \dfrac{dS_k(t)}{dt} = -\lambda k(S_k(t)-\mu I_k(t))\theta(t) - \alpha S_k(t) + \delta R_k(t) \\ \dfrac{dI_k(t)}{dt} = \lambda k(S_k(t)-\mu I_k(t))\theta(t) - \gamma I_k(t) - \sigma I_k(t) \\ \dfrac{dQ_k(t)}{dt} = \sigma I_k(t) - \varepsilon Q_k(t) \\ \dfrac{dR_k(t)}{dt} = \gamma I_k(t) + \varepsilon Q_k(t) + \alpha S_k(t) - \delta R_k(t) \end{cases} \tag{3}$$

Theorem 1. There always exists a disease-free equilibrium $E_0(\delta/\delta+\alpha, 0, 0, \alpha/\delta+\alpha)$. Define $\rho = \dfrac{\delta\lambda}{(\alpha+\delta)(\gamma+\sigma+\mu)}\dfrac{\langle k^2\rangle}{\langle k\rangle}$. If $\rho > 1$, then system (3) has a unique endemic equilibrium $E_+(S_k^\infty, I_k^\infty, Q_k^\infty, R_k^\infty)$.

Proof. To get the equilibrium $E_+(S_k^\infty, I_k^\infty, Q_k^\infty, R_k^\infty)$, the equilibrium should satisfy

$$\begin{cases} -\lambda k(S_k^\infty - \mu I_k^\infty)\theta^\infty - \alpha S_k^\infty + \delta R_k^\infty = 0 \\ \lambda k(S_k^\infty - \mu I_k^\infty)\theta^\infty - \gamma I_k^\infty - \sigma I_k^\infty = 0 \\ \sigma I_k^\infty - \varepsilon Q_k^\infty = 0 \\ \gamma I_k^\infty + \varepsilon Q_k^\infty + \alpha S_k^\infty - \delta R_k^\infty = 0 \end{cases}$$

where $\theta^\infty = \dfrac{1}{\langle k\rangle}\sum_k kP(k)I_k^\infty$. One has

$$\begin{cases} S_k^\infty = \dfrac{\lambda\mu k\theta^\infty + \gamma + \sigma}{\lambda k\theta^\infty} I_k^\infty \\ Q_k^\infty = \dfrac{\sigma}{\varepsilon} I_k^\infty \\ R_k^\infty = \dfrac{(\lambda k\theta^\infty + \alpha)(\gamma+\sigma) + \alpha\lambda\mu k\theta^\infty}{\delta\lambda k\theta^\infty} I_k^\infty \end{cases} \tag{4}$$

According to the normalization condition $S_k^\infty + I_k^\infty + Q_k^\infty + R_k^\infty = 1$, we can obtain

$$I_k^\infty = \frac{\lambda k \delta \theta^\infty}{\lambda k \theta^\infty \left[\delta(1+\sigma/\varepsilon)+(\gamma+\sigma)\right]+(\alpha+\delta)(\gamma+\sigma+\mu)} \tag{5}$$

Inserting (5) into (2), we can obtain the following equation

$$\theta^\infty = \frac{\sum_k kP(k)I_k^\infty}{\langle k\rangle} = \frac{\sum_k k^2 P(k)\dfrac{\lambda\delta\theta^\infty}{\lambda k\theta^\infty\left[\delta(1+\sigma/\varepsilon)+(\gamma+\sigma)\right]+(\alpha+\delta)(\gamma+\sigma+\mu)}}{\langle k\rangle} \triangleq f(\theta^\infty) \tag{6}$$

Obviously, $\theta^\infty = 0$ is a solution of (6), i.e., $f(\theta^\infty) = 0$. We suppose that $f(\theta^\infty)$ is a continuously smooth function and then we can easily demonstrate that $f(\theta^\infty)$ is a strictly monotonic increasing function. To ensure (6) have a nontrivial solution the following condition must be satisfied, i.e., $\left.\dfrac{df(\theta^\infty)}{d\theta^\infty}\right|_{\theta^\infty=0} > 1$. So, we have

$$\left.\frac{d}{d\theta}\left(\frac{1}{\langle k\rangle}\sum_k k^2 P(k)\frac{\lambda\delta\theta^\infty}{\lambda k\theta^\infty\left[\delta(1+\sigma/\varepsilon)+(\gamma+\sigma)\right]+(\alpha+\delta)(\gamma+\sigma+\mu)}\right)\right|_{\theta^\infty=0} \geq 1$$

Then, we obtain $\dfrac{\lambda\delta}{(\alpha+\delta)(\gamma+\sigma+\mu)}\dfrac{\langle k^2\rangle}{\langle k\rangle} > 1$. Let $\rho = \dfrac{\lambda\delta}{(\alpha+\delta)(\gamma+\sigma+\mu)}\dfrac{\langle k^2\rangle}{\langle k\rangle}$, a nontrivial solution exists if and only if $\rho > 1$. The epidemic threshold can be defined by

$$\lambda_c = (1+\frac{\alpha}{\delta})(\gamma+\sigma+\mu)\frac{\langle k\rangle}{\langle k^2\rangle} \tag{7}$$

Namely, the epidemic incidence will die out if $\lambda < \lambda_c$, and it will break out if $\lambda > \lambda_c$. Substitute the nontrivial solution of (6) into (5), we can get I_k^∞. By (4) and (5), we can easily get $0 < S_k^\infty < 1$, $0 < I_k^\infty < 1$, $0 < Q_k^\infty < 1$, $0 < R_k^\infty < 1$.

Therefore, the equilibrium $E_+(S_k^\infty, I_k^\infty, Q_k^\infty, R_k^\infty)$ is well-defined. Hence system (3) has a unique endemic equilibrium $E_+(S_k^\infty, I_k^\infty, Q_k^\infty, R_k^\infty)$ when $\rho > 1$. This completes the proof.

Now, consider the BA scale-free network model. As a matter of fact, the mean number of node degree and the degree distribution satisfy $\langle k\rangle = \int_m^\infty kP(k) = 2m, P(k) = \dfrac{2m^2}{k^3}$. Inserting this into (6), by integrating with respect to k the following can be obtained

$$\frac{1}{m} = \int_m^\infty \frac{\lambda\delta}{k\left\{\lambda k\theta^\infty\left[\delta(1+\sigma/\varepsilon)+(\gamma+\sigma)\right]+(\alpha+\delta)(\gamma+\sigma+\mu)\right\}}dk$$

which yields

$$\theta^\infty = \frac{(\alpha+\delta)(\gamma+\sigma+\mu)}{m\lambda\left[\delta(1+\sigma/\varepsilon)+(\gamma+\sigma)\right](e^{\frac{(\alpha+\delta)(\gamma+\sigma+\mu)}{m\lambda\delta}}-1)} \tag{8}$$

By (5) and (8), we get the density of infected nodes in the steady state of the whole network

$$I^\infty = \sum_k P(k)I_k^\infty = \frac{2\left[m\lambda\delta(e^{\frac{(\alpha+\delta)(\gamma+\sigma+\mu)}{m\lambda\delta}}-1)-(\alpha+\delta)(\gamma+\sigma+\mu)\right]}{m\lambda(e^{\frac{(\alpha+\delta)(\gamma+\sigma+\mu)}{m\lambda\delta}}-1)^2\left[\delta(1+\sigma/\varepsilon)+(\gamma+\sigma)\right]}$$

Remark 1. With changes of disconnect probability, we can get different values of threshold and densities of infected nodes in steady state. When μ increases, the corresponding λ_c rises and I^∞ decreases significantly, which shows that feedback mechanism helps contain the epidemic.

Remark 2. When $\mu=0$, the model yields the *SIQRS* epidemic without feedback mechanism, which shows the valid epidemic threshold consists with [2]. When $\mu=0$, $\sigma=0$ and $\alpha=0$, the model yields the standard *SIRS* epidemic with the valid threshold consists with [6]. Apparently, in the eco-limits of infinite network size the nodes grows to infinity, i.e. $N\to\infty$, then $\langle k^2\rangle\to\infty$, so the absence of an epidemic threshold is observed.

Conclusion

A modified *SIQRS* epidemic model with feedback-mechanism on the scale-free networks is presented. By mean-filed theory, we obtain the threshold and the endemic prevalence of infection. Theoretical analysis shows the epidemic threshold and the steady infection density of the system is virtually correlated with the feedback mechanism. Moreover, increasing the disconnect probability can result in the raise of infection threshold and the decrease of the population finally infected.

Acknowledgement

In this paper, the research was sponsored by the Science and Technology Development Project of Jingzhou (Project No. 2012CA20).

References

[1] Albert Barabasi, Reka Albert. Emergence of scaling in random networks [J]. Science, 1999 (286) 509-512.
[2] Tao Li, Yuanmei Wang, Zhi-Hong Guan. Spreading dynamics of a SIQRS epidemic model on scale-free networks [J]. Communications in Nonlinear Science & Numerical Simulation, 2014 19(3) 686-692.
[3] Robert M. May, Alun L. Lioyd. Infection dynamics on scale-free networks [J]. Physical Review E, 2001 64(6) 066112.
[4] Romualdo Pastor-Satorras, Alessaudro Vespignani. Epidemic spreading in scale-free networks [J]. Physical Review Letters, 2001 86(14) 3200-3203.
[5] Romualdo Pastor-Satorras, Alessaudro Vespignani. Epidemic dynamics in finite size scale-free networks [J]. Physical Review E 2002 65(3) 035108.
[6] Yamir Moreno, Romualdo Pastor-Satorras, Alessaudro Vespingani. Epidemic outbreaks in complex heterogeneous networks [J]. The European Physical Journal B, 2002 26(4) 521-529.
[7] Guanghu Zhu, Xinchu Fu, Guanrong Chen. Global attractivity of a network-based epidemic SIS model with nonlinear infectivity [J]. Communications in Nonlinear Science and Numerical Simulation, 2012 17(6) 2588-2594.
[8] Romualdo Pastor-Satorras, Alessaudro Vespignani. Epidemic dynamics and endemic states in complex networks [J]. Physical Review E, 2001 63(6) 066117.
[9] Guoji Lin, Xun Jia, Qi. Quyang. Predict SARS infection with the small world network model [J]. Journal of Peking University (Health Sciences), 2003 35(66) 66-69.

Advanced Materials Research Vols. 989-994 (2014) pp 4528-4532
© (2014) Trans Tech Publications, Switzerland
doi:10.4028/www.scientific.net/AMR.989-994.4528

Research on Web Service-oriented Access Control Model

Meng Liu[1, a], Lianzhong Liu[1, b], Yu Zhang[1, c]

[1]Beijing Key Laboratory of Network Technology School of Computer Science and Engineering, Beihang University, Beijing, 100191 China

[a]email: liumengtw@gmail.com, [b]email: lz_liu@buaa.edu.cn, [c]email: yzhang1077@gmail.com

Keywords: Web Service; Access Control

Abstract. Access control is an important technique which is used to protect system resources from damage by unauthorized users. With the advantage of web services, the access control module was released as web services interfaces. In order to control accessing to system resources and take advantage of web services，this paper proposes the web service-oriented access control (WSOAC) model. The development of access control is firstly introduced; after that the authors describe this model with two levels—platform and tenant and then present the execution process. At last, the paper summarizes the characteristics of the model and the next step.

Introduction

Service-oriented architecture (SOA) can greatly enhance collaboration and information sharing capability of the companies or organizations. Its ideology is widely used in cloud computing—the emerging business model; however, there are still many critical issues that should be solved during the development especially the security in it [1]. Therefore, with the cloud computing technology to be applied to large-scale production, it is necessary to fully analyze and address security issues. However, in security field, there is still not a sound theoretical model to meet the needs of multi-tenant environment for accessing control services.

Researches on access control date back to the models of discretionary access control and mandatory access control addressed by U.S. Department of Defense. After that, Farraiolo et al [2] proposed RBAC model (role-based access control) in 1992; this model introduced the concept of roles between the user and the permission and soon became the research focus. On this basis, Sandhu et al [3] have proposed model ARBAC02 and model ARBAC97 [4]. For the SaaS model which enjoys the rapid development at present, the three current mainstream access control technologies (ie, DAC, MAC and RBAC) have their limitations. Literature [5] adopted a layered approach and proposed an access control method for SaaS platform on the basis of RBAC. Literature [6] also proposed an access control method for SaaS platform; this method disabled the role of inheritance and showed the user the accessing processes by UML diagram, but roles and tenants were in a multi-to-multi relationship and they might easily suffer from conflicts. A multi-tenant access control model was introduced in literature [7], but could not achieve role inheritance on the level of tenant.

In this paper, the authors design a web service-oriented access control model (WSOAC) against the weakness in multi-tenant cloud environments of the traditional RBAC model. This model, consisting of the platform level and the tenant level, efficiently deals with users' accessing public resources and tenants' exclusive resources and solves accessing isolation when users get access to different tenants' inner resources.

Web Service-oriented Access Control Model

Access control is to ensure that resources are only granted to authorized users, programs, and processes, and to protect resources from unauthorized access. Model is a simplified representation of objective entities in words, graphics, symbols, formula and solid models through people's thinking abstraction of the objective reality when they study and solve various problems in the

objective world. Access control model is the basic abstraction of access control fundamentals, including User, Roles, Permissions and Sessions.

Based on ARBAC02 model, this paper presents a web service-oriented access control (WSOAC) model to satisfy complex cloud system resource access control requirements under the cloud environment. Different from local systems, web service system realizes the isolation and share of resources access not only on tenants layer, but also on the platform layer. The overall configuration of a model is shown in the following figure.

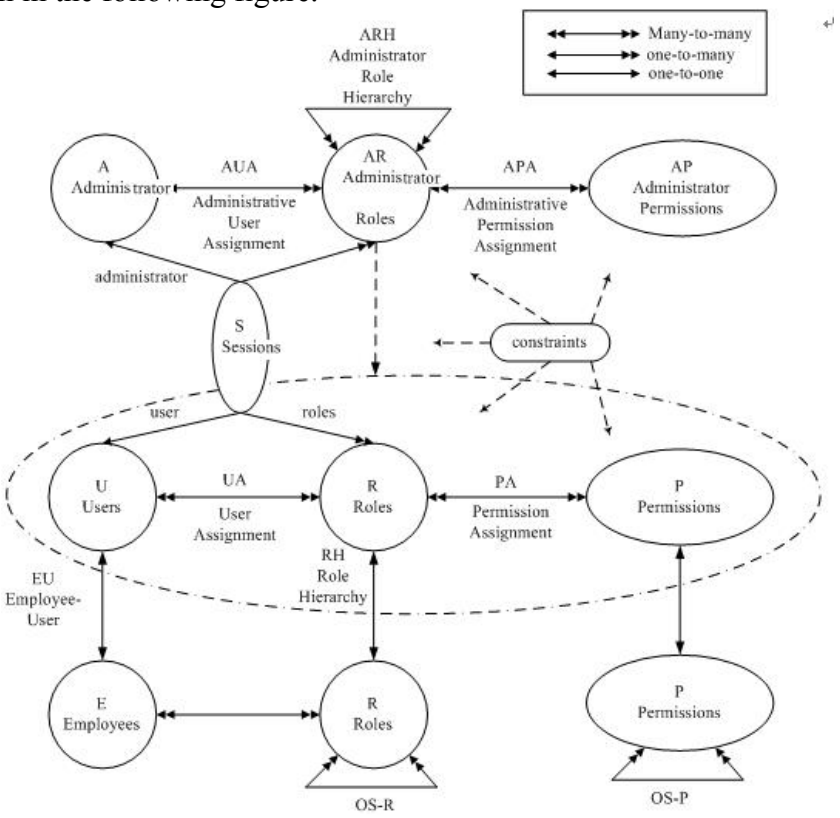

Fig.1 Web Service-Oriented Access Control Model

Web service-oriented access control model is divided into the platform layer and the tenants layer. The platform layer is responsible for tenant-level distribution of permissions and roles but can not operate within the system; the tenant layer empowers users to operate within the system via the user-role-permission mapping mechanism.

Tenant layer model

Firstly, the authors give the following definitions:

Def.1 Role

<Role>:=<r_ID, r_name, company_ID, roleList > (r_ID∈ComID ⋃ DeptID ⋃ PosID; r_name∈ComName ⋃ DeptName ⋃ PosName; company_ID∈ComID, roleList ⊆ roleSet)

Def.2 Permission

<Permission>:=<p_ID, p _name, resource_ID, description, company_ID, p_role>(p_ID∈PID; p_name∈PName; resource_ID∈ResID, company_ID∈ComID,p_role∈role_Set)

Def.3 User

<User>:=<u_ID, u_name, company_ID, u_role > (u _ID∈EmployeeID; u_name∈EmployeeName; company_ID∈ComID,u_role∈roleSet)

Resource directory, user and role management: the operation of their information-----create, retrieve, update and delete, and add the user to the role. After that, the permission of resource to the user or the role is authorized.

Platform layer model

In the service-oriented access control model, in order to assign a user within the tenant the roles and permissions, WSOAC model creates a manager-management role-management permission mapping relationship on the platform layer. The platform layer only implements the distribution and control of management role and management permission, and should not be to implement the distribution and control of operation role and operation permission. The definitions are as follows:

Def.4 AdminRole, inherited from Role

<AdminRole>:=<r_ID, r_name, company_ID, roleList > (role_ID∈AdminRoleID;

r_name∈AdminRoleName; company_ID∈ComID∪PlatformID, roleList ⊆ AdminRoleSet)

Def.5 AdminPermission, inherited from Permission

<AdminPermission>:=<p_ID,p_name,resource_ID,description,company_ID,

p_role>(p_ID ∈ AdminPermID; p_name ∈ AdminPermName; resource_ID ∈ ResID, company_ID∈ComID∪PlatformID, p_role∈AdminRole_Set)

Def.3 AdminUser, inherited from User

<AdminUser>:=<u_ID,u_name,company_ID,u_role>(u_ID∈AdminUserID;u_name∈AdminUserName;company_ID∈ComID∪PlatformID,

U_role∈AdminRoleSet)

Model execution process

As shown in Figure 2, the access control process perform as follows:

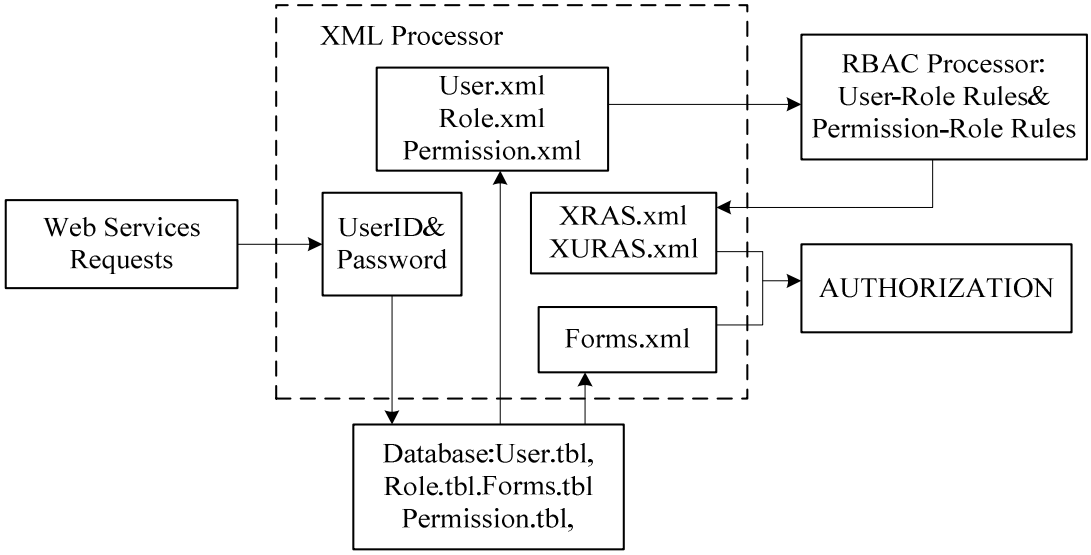

Fig.2 The architecture of web service-oriented access control

The dotted line is XML Processor. It processes the information in XML documents, extracts association as well, and then generates the corresponding XML document based on the XML schema. Once successfully checking each relevant XML document, XML Processor generates DOM tree, and then assigns the role permissions checking tasks to RBAC Processor. RBAC Processor contains RBAC module and associates the data items that are generated by RBAC. RBAC Processor implements the policy management and policy enforcement.

Policy management means that it will resolve DOM tree generated by the XML Processor to an internal data model in RBAC Processor, extract the information related to the user rights and then check the consistency principle of RBAC for verification. Policy enforcement means that RBAC module uses the legal information to manage the user's session. The initial session is automatically generated when a user just logs into the system, the initial session only activates the essential role currently, that is, the minimum set of roles.

The complete process of users' requested services is as follows:

(1) After receiving request by the user, the application service passes the request to XML Processor, and then analyzes it to obtain the user ID and password from the message and gets the appropriate rights from the database.
(2) XML Processor, after processing users' permission information, generates corresponding User.xml, Role.xml, Permission.xml according to various XML Schema, and passes these three XML documents to RBAC Processor.
(3) RBAC Processor passes the request and permission to access control system and checks the permission with the RBAC rules, then passes the processed result back to XML Processor and generate XRAS.xml, XURAS.xml
(4) Get the information of all the forms of enterprise application system from the database and generate Form.xml via XML Processor, and then generate the function tree corresponding to all the forms in users' permission scope by integrating XRAS.xml, XURAS.xml and Forms.xml.

The model involves service users, service developers and system administrators. Service users send requests with the information about their rights; service developers will write their own service permissions policy, no longer concern about the identity of the requester; the system administrators set up policy system of resources rights.

Characteristics of the model

Compared with other access control models for web services, WSOAC model has the following advantages:

(1) The role of inheritance and role management capabilities:
Role inheritance is intact and adapts to multi-tenant environment
(2) The independence&scalability of the system and flexibility&portability of security management:
WSOAC model is a model of a generic framework for web services applications, and does not depend on the structure of XML documents and concrete realization of the code. With the growth of Web services, system scalability increases. Meanwhile, the model adopts the service and service attributes to encapsulate; in this way can a more flexible and portable security management be achieved.
(3) Satisfy web services security applications:
Previous researches focused on the structure of an XML document, and the system did not focus on independence and scalability. In view of this weakness, this research, focusing on web services application environment, proposes service-level access control and service attribute-level access control mechanisms, thus making access control more granular in order to meet the practical application of the characteristics of Web services to work better.

Epilogue

Based on traditional RBAC model, this paper proposes a service-oriented access control (WSOAC) model. The model is divided into platform level and tenant level to meet the need of multi-tenant environment for multi-user access control, and then introduces the execution process of the model. However there is the drawback of not achieving the role's autonomous management. This is the focus of follow-up work.

Acknowledgement

In this paper, the research was sponsored by Co-Funding Project of Beijing Municipal Education Commission under Grant No. JD100060630.

References

[1] Feng Dengguo, Zhang Min, Zhang Yan, et al. Study on cloud computing security[J]. Journal of Software, 2011, 22(1):71-83.

[2] Ferraiolo, Barkley, Kubn. A role based access control model and reference implementation within a corporate intranet[J]. ACM Trans on Information Systems Security，1999，2(1) :34-64.

[3] Sandhu R, Bhamidipati V, Munawer Q. The ARBAC97 model for role-based administration of roles[J]. ACM Trans on Information and System Security, 1999, 2(1) : 105-135.

[4] Zhang Xinwei. A role administration model based on organization structure[J]. ACM Trans on Information and System Security, 2006, 9(2) : 113-137.

[5] Li Dancheng, Liu Cheng, Wei Qiang. RBAC-based access control for SaaS systems[C], 2010: 1-4.

[6] Jing Xu, Tang Jinglei, He Dongjian. Research and implementation on access control of SaaS[C]. 2010: 388-392.

[7] Tong tong. Research and application based on extended RBAC model in SaaS systems [D]. Zhengzhou: Zhengzhou University, 2011.

Advanced Materials Research Vols. 989-994 (2014) pp 4533-4537
© (2014) Trans Tech Publications, Switzerland
doi:10.4028/www.scientific.net/AMR.989-994.4533

Network security technology research in the process of art e-commerce transactions

Yanli Li

Yunnan Arts University, No.1577 Yuhua Road, Chenggong District, Kunming 650500,Yunnan Province, P.R. China

99eve@163.com

Keywords: Art e-commerce; Trade process; Network; Security technology

Abstract. This paper expounds the concept of art electronic commerce, analyzes the connotation of art e-commerce, and introduces some related security technology from security problems in e-commerce transactions so as to effectively eliminate safety troubles in e-commerce activities, guide and promote healthy and rapid development of art electronic commerce in our country.

Introduction

21st century is an information century. The development of computer network makes further change in the connotation of information society. “Digital life would bring human into the information age. All kinds of modes are changing rapidly in the current society, forming a new pattern based on ‘bits’ thinking. ”said by American Negroponte in the book "Being Digital". Network is a 24-hour-open space, and its potential customers are throughout the world. Under the environment of network economy, e-commerce is the inevitable choice of our country’s enterprises, traditional industry in particular, for their integration into the global economy.

With the popularity of network technology and the development of art trades, the role of e-commerce in the field of art trades is becoming more and bigger. Through the network, art trades are going from professionals to folks. As the segmentation of electronic commerce, art e-commerce has changed the traditional art business operation mode, which greatly improved the efficiency of art business, and reduced the cost of art trade. It has gradually become a striking new art trading mechanism, and causes consumers’ attention. The analysis, comparison and research of art electronic commerce gradually become hot topics nowadays. However, due to the internet characteristics of openness, security problem has become the bottleneck which restricts the development of further electronic commerce. As a result, building a safe and reliable art electronic commerce application environment has become the key issue affecting art e-commerce development.

The connotation of art e-commerce

In the increasingly detailed social labor division, art e-commerce is like clothing e-commerce and tourism e-commerce, which belongs to the segmentation of e-commerce in concrete industry. We can refer to the concept of e-commerce for preliminary concept of art e-commerce definition, that is to say that art e-commerce refers to the business system with network as the main body, the Internet technology, art information database, electronic commerce bank or the third party payment as the foundation, using the most advanced electronic means to operate art industry and its distribution system. In essence, art e-commerce can be understood as an Internet platform provided for general art industry peers. Although art e-commerce is applied in art industry for only a few years, it has very strong development momentum. Art e-commerce has become a new mode of art information age, and the requirements of e-commerce security technology are growing in the process of art electronic trading.

From the above definition of art e-commerce, we can conclude that the connotation of art electronic commerce is that the emergence and development of information technology, especially of the Internet technology are the premise of art e-commerce carrying out; Masters of modern

information technology and art business theory and practice are the core of art electronic commerce activities; Series and systematic information base and electronic payment tools are the foundation of art e-commerce activities; Economic affairs activities with art trade as the center are the objects of e-commerce; Network security technology in the process of art e-commerce transactions is the key to art e-commerce activities.

Art e-commerce security issues

Generally, the information in art electronic commerce system can be divided into public information and private information. Public information refers to the information which need no encrypt in art e-commerce trade, such as art introduction and promotion information in art e-commerce site. Conversely, private information refers to as confidential information, for example, a customer's personal information or net bank password, etc. Art electronic commerce security problems are mainly for private information or confidential information.

A. Information disclosure, damage, and been tampered

Information disclosure mainly displays as the leakage of business secrets in art e-commerce, which includes two aspects: one is that trade content of both trade parties is stolen by a third party; the other is that the file one trade party provided for the other party is used illegally by a third party. Information destruction is mainly reflected in network hardware or software problems which may lead to trade information loss, fallacies and destruction of computer network itself by some malicious programs, such as virus, hacker intrusion, etc. In addition, in the process of art e-commerce transactions on the computer network, information transmission may be unauthorized tampering, deleted, or be used multiple times because the network has the characteristics of openness, and thus lose information’s authenticity and integrity.

B. Identification

Identification in art electronic commerce involves two problems: first is that without identification, the third party is likely to counterfeit trade party’s identity, destroy trading, and corrupt one fake party's credibility or steal art trading results; second is non-repudiation. Both parties should bear some responsibility for their actions, and the information sender and recipient cannot deny that. Identification is to prevent the denied behavior of counterfeit and trading in art e-commerce activities.

C. Art e-commerce transaction security

Art e-commerce transaction security refers to all kinds of security problems of art business activities in the process of online transactions. In order to ensure orderly art e-commerce activities, implement the electronic commerce’s confidentiality, authenticity, integrity, reliability, and prevent the denying, real-name system, certification system and certification system, accelerate the construction of legal system, promote blacklist system, and intensify illegal punishments, etc.

Main security technologies used in art electronic commerce

According to the domestic and foreign academic research on e-commerce security issues, there are many corresponding solutions to a lot of security threats in the process of art e-commerce transactions, which involves mainly security technologies like data encryption technology, firewall technology, digital signature technology and security agreement, etc.

A. Data Encryption

So-called data encryption is to transform an information (or called plain text) by encrypted key and encryption function transformation to meaningless cipher text, and the receiver decrypts cipher text by decryption key to reform plain text. In art e-commerce, data encryption technology is the basis of other security technologies, and is the most main security measure. Trading party may use it in information exchange stages according to needs. At present, there are two types of encryptions, namely, symmetric encryption and asymmetric encryption.

(1) Symmetric encryption

Symmetric encryption is also called private key encryption, which refers to the both sides of the encryption method use the same key for encryption and decryption. Key security exchange is the core of symmetric encryption, and private keys are exchanged. Symmetric encryption method is used to simplify the processing of encryption. Every trade party doesn't need to study and exchange dedicated encryption algorithms, but to use the same encryption algorithm and only exchange sharing private keys. Commonly used symmetric encryptions are DES, IDEA, RC2, RC4, SKIPJACK, RC5, and AES algorithm, etc. More famous symmetric encryption algorithm is proposed by the national bureau of standards DES (Data Encryption Standard). DES belongs to grouping encryption algorithm, namely data encryption in 64 bits for the grouping. Its symmetry displays in using the same algorithm for encryption and decryption. Its key length is 56 bits (because each 8 bits are used for parity). The key can be any number of 56 bits, and it can be changed at any time.

A problem of symmetric encryption is that it is unable to identify the initiator or trade final party. Because the two sides share the same private key, so any information of both trade sides is sent by this encrypted key to each other.

(2) Asymmetric encryption

Asymmetric encryption is also known as public key encryption and asymmetric encryption system is put forward with the fatal weakness of symmetric encryption system. Unlike symmetric encryption algorithm, asymmetric encryption algorithm needs two keys: public key and a private key. Public and private keys are a key pair. If use public key to encrypt data, it can be decrypted only with the corresponding private key; If use private key to encrypt data, it can be decrypted only with the corresponding public key. The public key is open outward and the private key is reserved. RSA (Rivest Shamir Adleman) algorithm is the most famous within the territory of symmetric encryption algorithm. The basic process of users' exchange of confidential information by using this scheme is: trade party A generates a pair of keys and take one of those as a public key to other trade party publicly, and trade party B gets the public key and encrypts the confidential information by using it and then sends to trade party A; Trade party A uses the other private key to decrypt the encrypted information. Trade party A can only use its private key to decrypt any information encrypted by the public key.

In order to give full play to symmetric and asymmetric encryption systems' respective advantages, these two kinds of encryption systems are usually applied together in actual application, such as: using DES to encrypt information, and RSA is used to transmit the keys in symmetric encryption system.

B. Firewall technology

Firewall is to establish the corresponding network traffic monitoring system in network boundary to ensure the security of computer network. It is a kind of control technology, which can be either a software product, or make or be embedded in some kind of hardware products. All transport information or information issued from the Internet must go through a firewall. So the firewall will protect the security of e-mail, file transfer, remote login, and exchange of information between particular systems. The main ways to realize firewall technology are: packet filtering and proxy service.

(1) Packet filtering

Packet filtering is a firewall based on the router. It sets a access list or blacklist in the network router according to network security policy, namely with the help of IP address in data packet to determine what type of information to be allowed to get through the firewall, and what kind of information to be avoided to pass. The responsibilities of the firewall are to check in and out of the router's grouping and filtering according to accessing table (or blacklist). The firewall is simple, but can't effectively prevent illegal attacks. At present, 80% of the firewalls use the technology.

(2) Agent service

Agent service is a kind of firewall based on proxy service. It has high safety, strengthens the function of identity authentication and audit trail, but it is slower. The audit trail is to provide a

complete record about the usage of network resources in order to complete supervise and control the network. Through continuous collection and accumulation of complete event records accessing network, perform audit trail selectively on some of them, find possible illegal acts and provide strong evidence, then sent the relevant information such as the blacklist secretly to firewall on the net. Although the firewall can implement effective protection of external network blows, the safety of internal information transmission network is powerless. There must be some dynamic security technologies to realize the security of e-commerce.

C. Digital signature technology

Encryption technology only is not enough to ensure the security of business information. To ensure information integrity, digital signature technology occupies an irreplaceable position. At present, the applications of digital signature are mainly digital abstract, digital signature and digital time-stamp technique.

(1) Digital abstract

Digital abstract is to get information of certain length based on one-way Hash function transform operation to an original message. The abstract is one-to-one correspondence with the original information, that is, different original information is bound to get a different abstract. If the integrity of the information is destroyed, the information will not be able to get through the original information verification, and become invalid information. The recipient can then choose to no longer trust the information.

(2) Digital signature

Digital signature is actually using non-repudiation information of public and private key encryption technology and its concrete process is: the file sender generate a digital abstract from a file, encrypt it with its own private key, and form a digital signature. The encrypted digital signature file is send to the receiver with the original file as attachments. After the receiver receives information, decrypt it with the sender's public key. If the correct summary is worked out, this abstract can make sure that the original file has not been changed. So the information is true to be sent by the sender. Then it realizes the identification and non-repudiation of the original documents.

(3) Digital time-stamp

Digital time stamp technology or DTS is a third party service to sign date for digital file or trading information. Essentially digital time-stamp technology is the same as digital signature technology. After sealed by digital time-stamp, information cannot be forged, tampered with, and denial and it provides reliable information time information for the reference.

D. Security protocol

In addition to various security control technology, the operation of electronic commerce also needs a set of perfect security trading agreement. The complexity and the security of each different deal are not identical, so different applications have different requirements for the agreement aims. At present, more mature agreements are SET, SSL, S - HTTP, etc.

(1) SSL protocol

Secure Sockets Layer (SSL) protocol is between TCP/IP and various application Layer protocols to provide security support for data communication, which is a network security protocol firstly applied in international electronic commerce. Because SSL is located between the transport layer and application layer, SSL is a good way to encapsulate application layer data without changing the application program in application layer, and it is transparent to the user. At the same time, SSL needs only one "handshake" process to build a secure communication channel between client and server, and ensure the safety of data transmission. The SSL protocol, however, has some problems, such as only support both sides certification. When multiple electronic trading is involved, SSL protocol cannot coordinate various security transmission and trust relationship.

(2) SET protocol

Secure Electronic Transaction (SET) protocol is a safety standard used in the Internet on the basis of bank card online trading. SET is mainly designed to solve the users', businessmen's and banks' payment transactions through credit card, and to ensure the secret command, payment process, legal status of merchants and cardholders, and its operability. SET provides authentication

between consumers, businessmen and banks, ensures the safety of transaction data, complete reliability and non-repudiation of the deal, and especially avoids the bank card number exposed to businessmen and consumers and supports the three parties' authentications etc. So it is widely applied in the field of e-commerce security, but SET protocol is too complex, and there are still many problems in actual application.

(3) S-HTTP protocol

S-HTTP (Security HTTP) is a high-level protocol constructed on HTTP protocol. S-HTTP supports a variety of ways to encapsulate information which includes encryption, signature, and certification based on the content of MAC, and supports that one message is repeatedly encapsulated and encrypted. In addition, S-HTTP protocol supports RSA and Kerberos key exchange, and provides a flexible programming environment for programmers. S-HTTP allows the user to generate a digital signature on each message, but S-HTTP protocol is powerless for the attacks from the bottom.

Conclusion

This article mainly expounds the concept and connotation of art e-commerce, analyzes the security technologies in current art e-commerce: data encryption, firewall technology, digital signature technology, as well as security agreement, and points out their use range and their advantages and disadvantages. Of course, the security of art electronic commerce is complicated system engineering. Only to guard from a technical point is not enough. In addition to technical research and application, the construction of social cultural environment should also be included, that is the Internet culture construction and spread of art e-commerce legislation and information morality and ethics to regulate all kinds of problems in the rapid development of art e-commerce in the real world, so as to guide and promote healthy and rapid development of art electronic commerce in our country.

References

[1] Liu Minghua, Yang Mi. E-commerce security technology research status and development trend abroad. Overseas Viewpoint, 2009, 08.

[2] Mao Liping. E-commerce security issues. Small and Medium-sized Enterprise Management and Technology, 2011, 04.

[3] Zhang Likun, Yang yong. E-commerce security issues and solutions. National Business (Theory), 2011, 204.

[4] Yang Yingmei. China's e-commerce security issues and security environmental construction. China Commerce. 2010, 04.

[5] Yuan Fang. E-commerce security technology analysis and application research. Science and Technology Information, 2013,09.

[6] Zhou Hui . E-commerce security research based on chaotic encryption. Dalian Maritime University, 2013,06.

[7] Zhang Qingli. E-commerce security policy research. Henan University, 2012, 05.

Advanced Materials Research Vols. 989-994 (2014) pp 4538-4541
© (2014) Trans Tech Publications, Switzerland
doi:10.4028/www.scientific.net/AMR.989-994.4538

The Application Design of Personalized Recommendation system Based on Data Mining to E-commerce

Li Sun

Hang Zhou Vocational & Technical college, Hang Zhou City, China

E-mail: lisun30@163.com

Keywords: Data mining, E-commerce, System architecture, Freakommendation

Abstract. Personalized recommendation application system of product and service is a valid tool to boost sales in both online and offline business. It has been reported and has been our experience that algorithmic –modeling phase occupies at most 20% of the effort in a data–mining project. The other 80% is how to put the "model" into practical application. The implementation process of personalized recommendation system based on data mining to E-commerce was discussed in this paper. We also proposed architecture of the system, described the application of technology, designed some features of the function modules.

1. Introduction

As IT technology accelerating, the world's economic modes have been undergoing tremendous changes. E-commerce, which brings all types of business activity online, is the most significant reform in recent 20 years that changing human's life greatly. While huge business user data accumulated, the owner will face losing control of the store online. And as salesman can not give customers suggestion face to face in E-commerce dealing, so we turn to data mining technology for personalized product recommendation [1]and business process transformation, which compares multiple customers' data, collected via registration record, questionnaires, web log files, basket-to-buy rate, and finds those with similar tastes. Generally the typical recommendation tasks in E-commerce include: helping new and infrequent visitors, building credibility through community, enticing customers to come back, cross-selling, and building long-term relationships.

2. Introduction of data mining techniques for achieving recommendation system

Data mining is sorting through data to identify patterns and establish relationships. Data mining techniques are used in a many research areas, including mathematics, cybernetics, genetics, marketing, Web mining, enterprises' management information system and so on. The Cross Industry Standard Process for Data Mining (CRISP-DM) defines six phases for data mining that is business understanding, data understanding, data preparation, modeling, evaluation, deployment. Six common algorithms are involved in data mining, they are:

(1)Association rule learning looks for patterns where one event is connected to another event.

(2)Collaborative filtering is a method of making automatic predictions (filtering) about the interests of a user by collecting preferences or taste information from many users (collaborating). The underlying assumption of the collaborative filtering approach is that if a person A has the same opinion as a person B on an issue, A is more likely to have B's opinion on a different issue x than to have the opinion on x of a person chosen randomly.

(3)Classification is the task of generalizing known structure to apply to new data. For example, an e-mail program might attempt to classify an e-mail as "legitimate" or as "spam".

(4)Clustering is the task of discovering groups and structures in the data that are in some way or another "similar", without using known structures in the data.

(5)Sequence or path analysis looks for patterns where one event leads to another later event.

(6)Forecasting aims to discover patterns in data that can lead to reasonable predictions about the future.

Recommended system must take into account the accuracy and timeliness. A good system may be combined with a variety of methods and techniques and let them learn from each other.

3. Characteristics of data mining in E-commerce

Data mining to E-commerce is the process to discover and extract implicit marketing mode by collecting website documents and services information. It targets at a large number of heterogeneous, distributed web documents which might be web log files or figures logically consisting of document nodes and hyperlinks.

As compared to ancient or shielded legacy systems, data collection to E-commerce can be controlled and reliable to a larger extent. We have the opportunity to design systems that collect data for the purposes of data mining, which will ease the integration with existing processes. Data are collected electronically, rather than manually, so less noise is introduced from manual processing. E-commerce data are rich, containing information on prior purchase activity and detailed demographic data. But on the other side, unlike fully structured data in traditional databases, the data of E-commerce platform has small correlation with data mining content, and highly dynamic. Its greatest feature is semi-structured without strict structure model. Data mining to E-commerce is more complicated than to a single data warehouse.

4. The implementation process of personalized recommendation system based on data mining technology

A typical recommendation system includes online interactive data collection, database processing, understanding of business rules, data mining process, recommendation model establishing, recommendation engine [2], as Fig.1 below. The form of recommendations, including recommended product to the customer, providing personalized product information, and other customers likes and dislikes and so on. Data mining part is the analysis of customer profiles generation process, using data mining techniques to identify customer data rules and patterns for recommendation system. The commercial domain knowledge and methods require the interactivity. The precise rules and patterns is crucial, and should be interacted with involving business domain knowledge and methods.

4.1 Data sources and arrangement

Personalized customer recommendation data source has the following three categories: one is the kind of content and product data capacity, including login records, click rates, browse paths and purchase records, etc., which exist in the E-commerce platform database with daily size of the TB bytes; The second category is the customer preference data on the partner network, such as browsing, collection, purchase and other data. This part of the data has the daily volume of the GB level scale. This two types of the most recent data mentioned above from the consumer are the core of e-commerce data. The third category of data is from the SCM, ERP, CRM information systems' historical data, such as customer transaction records, vendor records, assessment records, product costs, standard costs, forecasted orders costs, inventory, logistics information, orders forecasting, profitability analysis, etc.

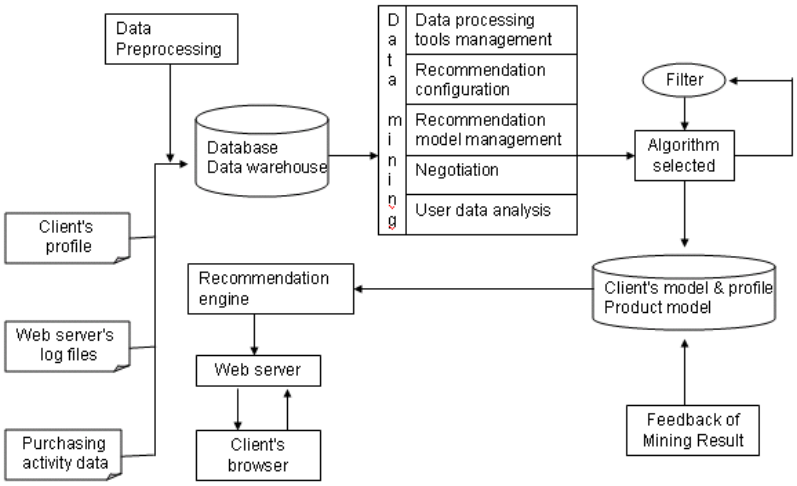

Fig1 The system architecture of E-commerce recommendation system based on data mining

We arrange the data above to establish commodity data item file with commodity characteristic number and feature weights. Also we build customer profiles database. It is composed of customer feature information and behavior data. Customer feature data items' files include user registration information, user access path to business platform, server logging files, recording customer inquiries, status. Customer behavior data items' file consists mainly of market data, including user purchasing behavior, commodity item information, E-commerce site information and etc.

4.2 Building customer prediction model

This work is providing a static data set, removing some of them, thinking of ways to use the remaining portion of the data to recover the removed data while making recovery error to the minimum. According to algorithm thinking, we build customer prediction model based on collaborative filtering algorithm and content-based algorithm. In practice, these two ideas can be further classified into black box and white box recommended modes. Black box mode does not consider any specific recommended content, but take the use of machine learning, data mining and other statistical methods and artificial intelligence methods [3] to analysis the data, establish relevant models and optimization objectives. The white box recommended process also uses machine learning and data mining algorithms.

Black and white box recommendation mode does not require too much knowledge of the field or manual intervention to build such a prediction model. But we meet challenges of freakommendation, macro and micro paradox while running black box recommendation mode. Freakommendation refers to the strange recommended result, such as. a similar association of flowers and horror films which leads to a lot of users recommended discomfort. It has a very negative impact on trust and psychological feelings. Macro and micro paradox refers to the phenomenon that as data growing, the entire recommendation system indicators will be getting better and better, but the prediction model inclines to give some mediocre and conservative recommended contents to the VIP. So in practice, we tend to take a so-called mixed models with the integration of two modes' advantages in order to achieve a better recommended results.

4.3 Forecasting the next change in the system by taking the given data set as a self-consistent system.

This step is to form knowledge from information. Forecasting will optimized the forecasting indicators in the time dimension based on prediction model [4]. It is more complicated than building prediction model because psychological and social factors must be considered as time going. To solve forecasting problems, it is not enough to start only from the given data and prediction models, but also needs to integrate data from other sources, require prior knowledge, or even take a little user's cognitive and mental models.

4.4 Making personalized recommendation

According to customer requests and recommendation strategies, we call the relevant data processing tools to get recommendation result by considering customers' background information. Input elements include customer identification mark, customer type, customer score sheet, customer profiles, commodity item files, customer specified number of neighbors and the maximum recommended number. Output elements include recommended product group and promotional strategies. This step is to form business process system from knowledge. The system should have the recommended areas of knowledge, but also be able to understand its every customer. The system is able to self-start while being able to grow, evolve and learn by itself. The system is not strictly defined, and its basic technical architecture may not be limited to the current popular personalized recommendation system frameworks, techniques and algorithms [5].

4.5 Design of recommendation engine

In actual operation of e-commerce, the data mining algorithms need to be planted into the bottom frame of recommendation engine from basic forms of service which means recommendation engine does not directly provide recommended result. Because precise marketing recommendations vary greatly according to the scenarios and requirements. So users need to add recommendation dimension parameters to recommendation engine to reach customer's true needs. It aims to provide solutions of achieving personalized, intensive level service concept for the seller.

5. Suggestion and conclusion

We noticed that E-commerce recommendation framework would surely increase personalization by collecting and processing additional data of customer's behavior automatically which also affects the actions of customers. However in the future of the internet era, personalized recommendation system may not become platforms like Amazon, Facebook, Google etc., but it surely become the core competitiveness for all the E-commerce platforms.

References

[l] Ronny Kohavi, Foster Provost ,Applications of Data Mining to Electronic Commerce ,Kluwer Academic Publishers; Reprinted from DATA MINING AND KNOWLEDGE DISCOVERY, 2001, 5:1-2

[2] Terveen, Loren; Hill, Will (2001). "Beyond Recommender Systems: Helping People Help Each Other". Addison-Wesley. p. 6. Retrieved 16 January 2012.

[3] G. Adomavicius, A. Tuzhilin, "Toward the Next Generation of Recommender Systems: A Surveyof the State-of-the -Art and Possible Extensions," IEEE Transactions on Knowledge and Data Engineering 17 (6), 2005, pp. 734-749.

[4] Yao Gang, Mai Yong-hao,Dang Xuan-ju, "The Design of E-commerce Recommendation Applications using Data Mining", Computer and modernization,2012, 12, P39-40,50

[5]Xiaogao Yu, Distributed Data Mining-based E-commerce Recommendation System, Computer system applications, 2009,11, 34-37

Advanced Materials Research Vols. 989-994 (2014) pp 4542-4546
© (2014) Trans Tech Publications, Switzerland
doi:10.4028/www.scientific.net/AMR.989-994.4542

Research on combine White-box testing and Black-box testing of Web Applications security

Jie Fan[1, a], Peng Gao[1, b], Congcong Shi[1, c], Nige Li[1, d]

[1] Institute of Information and Communications t, Nanjing Branch of China Electric Power Research Institute, Nanjing, 210000, China

[a]email: fanjie@epri.sgcc.com.cn, [b]email:gaopeng2@epri.sgcc.com.cn, [c]email:shicongcong@epri.sgcc.com.cn, [d]email:linige@epri.sgcc.com.cn

Keywords: White-box testing; Black-box testing; Web Application; Security

Abstract. Contrary to high false positives rate of use White-box testing tools for Web application source code security and unable to locate vulnerabilities of use Black-box testing tools for Web application security, propose an effective method for combine White-box and Black-box testing tools of Web applications. This method will put the new technology of "Associated Files Matching Engine" into White-box testing tools, this test result and Black-box test result will be statistical analyzed and combined. Argumentation show, this method reduce the positives rate of White-box test result and be able to locate vulnerabilities where it is in file.

Introduction

Continuous innovation and development of Internet applications has greatly promoted the development of social progress and human civilization, has become one of the main driving force of social development. Information and network security is also facing unprecedented serious problems, the challenge facing the network security become increasingly severe, people increasingly focus on the network security issues.

With the threshold of excavating operating system vulnerabilities have gradually increased, application security has become short board. Network intrusion, large-scale worm propagation, denial of service system such as other issues are triggered by the application software vulnerabilities. Current software development model is a very important reason of arising vulnerabilities, for example, architecture design flaws, coding vulnerabilities, inadequate safety testing. Simultaneously, code security detection technology uneven. In security code detection method, definition of code defects, code defect classification, code defect risk level and other aspects did not unified. In support environment, it still stay on the basis of common defects library, it cannot combine with existing application systems. And cannot trace the code vulnerabilities of between different versions of the application system, cannot effectively control code security. This is an urgent need to strengthen the system security testing work, to detect system vulnerabilities, improve system security.

In the usual sense, threaten of network security is the vulnerabilities of Web application. Currently, Web application vulnerabilities detection methods are Black-box testing and White-box testing. Black-box testing [1] detect Web application security when Web application run, this detection dependence on external environment and test cases, and it has a certain degree of uncertainty, but it has the advantage of low false positives rate. White-box testing is static source code analysis technology, it progressive analyze the source code of Web application, use symbolic executing techniques [2], data flow analysis [3] other analytical methods find out security flaws of code, this detection can avoid these shortcomings, but it has the disadvantage of high false positive rate.

Evaluating the White-box testing has two important indicators [4]:

(a) False negatives rate, the rate of the tools cannot find the security problems of Web application system.

(b) False positives rate, the rate of the tools find the security problems what it is not really problems in Web application system.

According to the above two criteria, existing white-box testing tools are present its own deficiencies and defects. How to effectively reduce the rate of false positives White-box testing? How to effectively locate the vulnerabilities of Black-box testing? This article discusses these two issues, and proposes solution.

The White-box testing

White-box testing mainly refers to the source code static analysis detection [5]. The Static analysis method scans the program code directly, extract the crucial grammar, explain the grammar, and understand the behavior of program. Then according to the preset vulnerability signatures, safety rules detect vulnerabilities [6].

(a) The lexical analysis

The lexical analysis is the earliest one of the source code analysis technology, it only detects the grammar. The lexical analysis divides the program into a fragment, then every fragment with a "suspect database" to compare, if it belongs to suspect, then further implementation of heuristic judgment.

(b) The rule checking

The program itself security is described by safely rules. The program itself exists some programming rules, these are some general safety rules, also known vulnerabilities mode. The rule checking will describe these rules by specific syntax, received by the rule processor, and converted to the date what it can be accepted by analyzer, then be compared and tested to the behavior of the program.

(c) The type inference

Automatic deduce the type of the program variables and functions to determine whether access to variables and functions in line with type rules. The type inference of static vulnerabilities is derived by stereotypes assertions, deduction and checking rules of three parts. The stereotypes assertions defines the initial type of variables, the deduction rules provide the rules set of inference system, the checking rules judge determination corollary is "good behavior".

(d) The symbolic executing

The basic ideal of symbolic executing that it converts the value of the variable in the program logic into abstract symbols, simulate path sensitive program control flow, constraint solving method, tests whether there is the possibility of error. Starting from conditions before the execution of the program P, in a program point in a program, can launch the constraint c1^c2^…^cn, so at this point have P^c1^c2^…^cn->R, R is meet the conditions when the program end.

Existing white-box testing tools are contains one or more of the combination of static source code security detection technology. For example Fortify SCA tool, contains the data flow engine, semantic analysis engine, the configuration analysis engine, etc. Because after the White-box testing , lack of the source code to verify safety defects. So the White-box testing can detect a lot of vulnerabilities of source code, but do not know what loopholes are real, what loopholes are important, what loopholes need to repair immediately. See Figure 1.

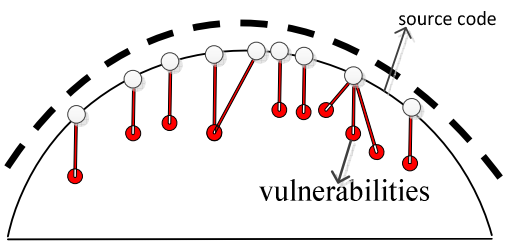

Fig.1. The abstract model of White-box testing

The Black-box testing

The Black box testing is the program as a cannot open the box, regardless of the program's internal logical structure and internal characteristics, tests program directly [7]. Black-box testing tool is tested in the absence of the source code, soon after get the test result cannot determine the cause of the vulnerabilities, produces by which a piece of code? See Figure 2.

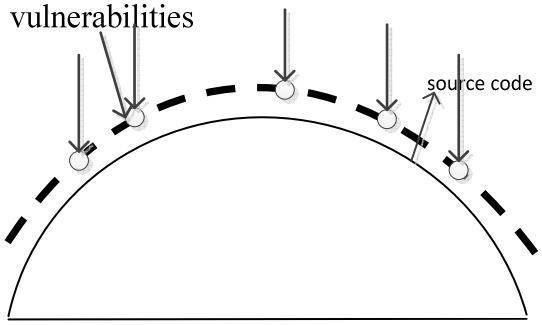

Fig.2. The abstract model of Black-box testing

Combining White-box and Black-box testing

Aiming at the shortcomings of the above white box testing and black box testing, Design a kind of white and black box combination analysis method, the analysis method is mainly the result of white box testing and black box testing effectively, quickly locate a vulnerabilities on the number of lines of code rule out false positives. See Figure 3.

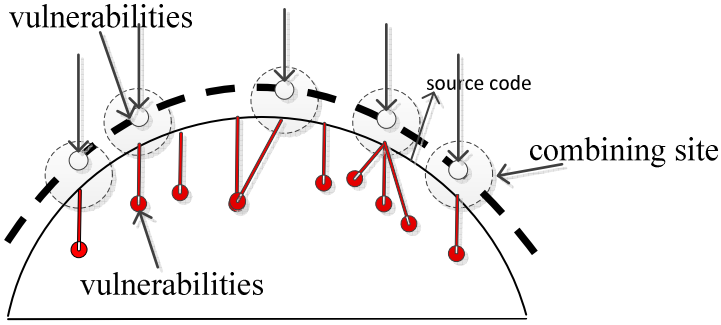

Fig.3.The abstract model of combining White-box and Black-box testing

The White-box testing results contain {the vulnerability type, the file where the vulnerability locate, the line of the file where the vulnerability locate} this several important conclusions. The Black-box testing results contain {the vulnerability type, the files where the vulnerability locate} this several important conclusions.

Here we have an example of SQL Injection result:

The SQL Injection result what tested by White-box testing, a set W is {{SQL Injection, file 1, line n},{SQL Injection, file 2, line n}……}.

The SQL Injection result what tested by Black-box testing, a set B is {{SQL Injection, file a}, {SQL Injection, file b}……}.

The set W and the set B have a certain intersection, but the existing methods cannot be selecting the intersection of set W and set B.

In the White-box testing, to scan the file where the SQL Injection vulnerability locates and uses the technology of “Associated Files Matching Engine” to scan the whole project. Then enumerating file collection F {file n1, file n2, file n3……} what relate to the file where the SQL Injection vulnerability locates.

The "Associated Files Matching Engine" mainly uses the file scanning, rules checking such as technology, to scan the entire project and find out other files which are associated with the file where the vulnerability locates.

(a) The file scanning

Through the file with the formation of a file stream to read out, and then to traverse the entire file. Using fuzzy matching technology to look for the file which contains the keyword (in file 1 of vulnerability). If the file includes the keyword, the file will be selected out. If the file does not includes the keyword, then scanning the other files in the program.

(b) The rule checking

Through the file scanning technology, to find out the key words related files collection {file f1, file f2……}. Then check the each file which is in the collection using the rules. First, selecting file f1, then locating the position of the keywords in the file f1 and checking use the rules. Centering on the position of the keyword, rule checks within a certain range. If within the scope of the definition, look for to the keyword matching rules, will file selected. If there are no rules in the library to find keywords, to file scanning techniques of other files in the collection of rule processing. Finally it is concluded that the associated files collection {file a1, file a2……}.

The flow chart of "Associated Files Matching Engine" sees Figure 4. Using the keyword to scan the all file in whole project and simultaneously using the rule base (the keyword of struts and spring) to matching. Last enumerating the associated files.

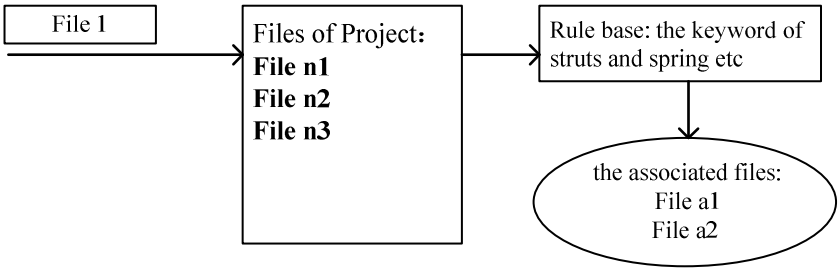

Fig.4.The flow chart of "Associated Files Matching Engine"

See Figure 5. Black-box testing results, White-box testing results, files associations through vulnerability type to match, White-box testing results and files associations through the file (file 1) where the vulnerability locates match. Finally, iterating through all the black box testing results (SQL Injection). Using the file (file b) which is tested by Black-box testing compares to the file which associates with file 1, if traversing all the Black-box testing results do not find out the file which associates with it, so the vulnerability which is tested by White-box testing is not real.

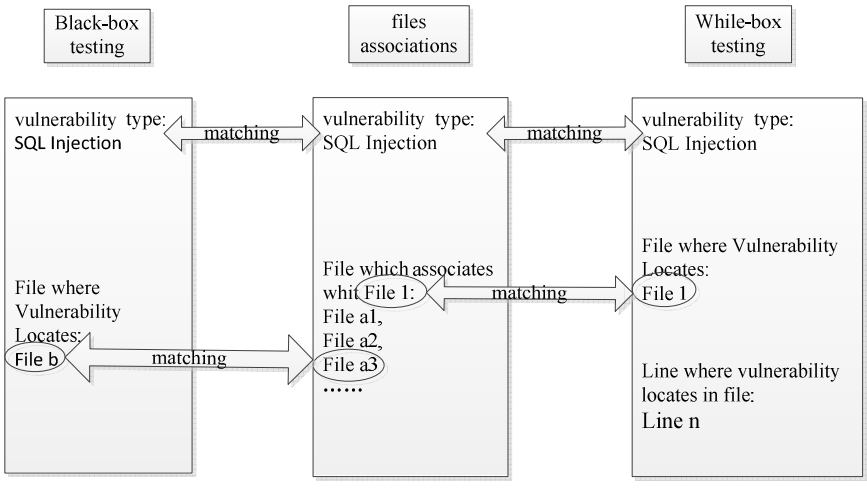

Fig.5.The chart of matching

Conclusion

This paper proposes a method which is combining White-box testing and Black-box testing of Web Applications security. This approach has been demonstrated on. The method can effectively reduce high false positives rate of use White-box testing tools. The next step of research is focused on the technology of “Associated Files Matching Engine”, through into different technology, To effectively improve the efficiency and accuracy of “Associated Files Matching Engine”.

References

[1] LIANG Jie, ZHANGMiao, XUGuo-ai, YANG Yi-xian. New static analysis model in source code. APPLICATION RESEARCH OF COMPUTERS, 2008 25(9).
[2] Jinbin Lin, Xiaofei Zhang, Hui Liu. Research Symbolic Executing. China's information security. 2008 3.
[3] Honglu Yang, Yunzhan Gong, WenLing Gao, Lege Bai. Software security static testing techniques and tools. Microcomputer & Its Applications. 2009 28(9).
[4] BRIAN C. Static analysis for security [J]. IEEE Security & Privacy. 2004 7(4) 32-36.
[5] Xia Yiming. Security Vulnerability Dection Study Based on Static Analysis. [J]. Computer Science. 2006 33(10) 279-283.
[6] Lin Zhang, Qingkai Zeng. The static testing technology of software security vulnerabilities. Computer Engineering. 2008 34(12) 157-159.
[7] Jiangguang Yang, Dacheng Mei. Black-box testing method and the comprehensive strategy research. Computer CD Software and Application. 2012 4 121-122.

Advanced Materials Research Vols. 989-994 (2014) pp 4547-4550
© (2014) Trans Tech Publications, Switzerland
doi:10.4028/www.scientific.net/AMR.989-994.4547

Performance Comparison Based-RSSI for Sensor Networks in Different Environments

Yan FENG[1, a], Bo YI[2]

[1]Department Information Engineering, Hunan Mechanical & Electrical Polytechnic, Changsha, 410151, China

[2]College Information Science and Engineering, Hunan University, Changsha, 410082, China

email: fpyan2014@163.com

Keywords: Received Signal Strength Index; Performance Comparison; Wireless Sensor Networks; Distance Estimation

Abstract. A lot of the wireless sensor network applications call for sensor nodes to be applicable to any environment. RSSI-based measurements implement conveniently and are cost-efficient and power-efficient in practice. This paper compares the distance estimation performances based RSSI in three different environments by experiments and discusses their characteristic in detail. We carry out a large amount of repeated experiment based on RSSI in three kinds of environments over the 2.4GHz wireless channel. Subsequently, we focus on studying and discussing data analyses of RSSI and possible improvements in each environment. Experimental results demonstrate availability and feasibility of RSSI in outdoor and indoor environments.

Introduction

A lot of the wireless sensor network(WSN) applications, for example, intrusion detection[1], fire prevention[2], environmental monitoring, and military safety[3], call for sensor nodes to be applicable to any environment[4]. Location of sensor nodes is a fundamental issue in WSN. In the last few years, localization of WSN has attracted a large amount of interests for researchers range from wireless communications to data processing[5]. Nevertheless, range estimation is foundational to a location based service system. A lot of distance estimation methods such as time of arrival(TOA)[6], time difference of arrival(TDOA) [7], angle of arrive(AOA)[8], and received signal strength indicator(RSSI)[9] are proposed. RSSI-based measurements implement conveniently and are cost-efficient and power-efficient in practice, because it doesn't require extra hardware design. Others approaches are costly and need extra hardware embedded in device.

RSSI-based localization is an simple techniques to infer the location of the unknown sensor nodes because they has merely low demand on the hardware module[10]. In the field of RSSI-based localization, considerable amount of research has been done. In different environments, RSSI-based localization suffer from a variety of effects. In this paper, we compares the distance estimation performances based RSSI in three different environments by experiments and discusses their characteristic in detail. We use many sensor nodes, which employ a 2.4GHz low power radio chip CC2430 based ZigBee[11]. We carry out a large amount of repeated experiment based on RSSI in three kinds of environments over the 2.4GHz wireless channel[12]. Subsequently, we focus on studying and discussing data analyses of RSSI and possible improvements in each environment. It is shown that distance estimation based RSSI is availability and feasibility in outdoor and indoor situation.

The remainder of this paper is organized as follows. In Section II, we introduce the Measurement equipment, environment and propagation model, Section III presents experimental performance evaluation, conclusions will be given in Section IV.

Measurement & Methodology

For our Experiment, The sensor node uses the reinforced 8051 processor which can run in high energy efficiency and low power dissipation, and have 128kB flash memory and 8kB RAM. Each

sensor nodes employs a CC2430 transceiver, which is a system-on-chip solution and use O-QPSK modulation with DSSS at 250kbps, as its radio frequency and was assigned to transmit continuously with a data packet in the 2.4 GHz band. As the receivers, we put to use other sensor nodes to gather the RSSI of the packet. CC2430 is computed over 8 symbol periods, which possess a integrated register named RSSI_VAL to store RSSI value, and can extract the power value on RF pin using the following equation:

$$RSS = RSSI_VAL + RSSI_OFFSET[dBm] \tag{1}$$

(a) Playground

(b) corridor

Fig.1. Measurement Environment

The RSSI_OFFSET is set to -45dBm that is popularly used in WSN. The receiver sensor nodes is designed to collect the RSSI every 0.5 seconds that achieve a continuous sampling of the channel.

We implement the experiments in three different environments as described in detail next.

Location I: One playground fields measuring 200×200 m. As shown in Fig.1.(a), the playground are flat and planted with short grass.

Location II: A corridor area measuring 150×1.5 m. As shown in Fig.1.(b), the corridor have occasionally people walk through.

Location III: One indoor rooms is a three dimension structure measuring 7.5m(L)×5.3m(W)×2.89m(H). there are several desks, chairs and cabinet on the wall in room.

To measure the communication characteristics at a local area, we firstly estimate parameters of the radio propagation model. Assuming the m reference nodes are positioned at (x_r, y_r), r=1,2,…,m. and the n unknown nodes are positioned at (x_u, y_u), u=1,2,…,n. The log-distance path loss signal propagation model is given as follows .

$$P_t - P_0(d_0) - P_r(d) = 10\eta \log(\frac{d}{d_0}) + X_\sigma \tag{2}$$

Where, P_t is the transmitted power at transmit node, $P_0(d_0)$ is the path loss at the reference distance d_0, $P_r(d)$ is the received signal strength at distance d, d is the distance between the reference nodes and unknown node, d_0 is the distance between the reference nodes and reference point, which is common assigned to be 1m. η is the path loss exponent varying with different environment and X_σ is a Gaussian random variable.

Assuming P_t-$P_0(d_0)$=A, each unknown sensor node (x_u, y_u) have k reference nodes, Using Equation (2) ,we can have matrix equation as follows.

$$\begin{bmatrix} P_{r_1}(d) \\ P_{r_2}(d) \\ \dots \\ P_{r_k}(d) \end{bmatrix} = \begin{bmatrix} 1 & -10\log d_1 \\ 1 & -10\log d_2 \\ \dots & \dots \\ 1 & -10\log d_k \end{bmatrix} \begin{bmatrix} A \\ \eta \end{bmatrix} + \begin{bmatrix} X_{\sigma_1} \\ X_{\sigma_2} \\ \dots \\ X_{\sigma_k} \end{bmatrix} = BX \tag{3}$$

By least-squares resolution, we obtain as follows.

$$X = (B^T B)^{-1} B^T P \tag{4}$$

From equation (4), we can solve vector X. The parameters of communication model, A and η can be obtained from X. The more is the number of reference nodes, the higher accuracy is the result for A and n.

Performance comparison

We quantify the performance of RSSI employing our sensor nodes based ZigBee. To reduce the RSSI instability and attenuation, the nodes, which attach to a height of 1.2m tripod over the ground, equip with omni-directional antenna that can transmit signal in all directions with 0 dBm. Each measurement situation is deployed a lot of sensor nodes to transmit data packets and other neighbor nodes senses the packets containing the RSSI information and forwards this packets. In each of experiment, we use coordinator node gather packet ,via USB interface, to laptop.

In our experiments, repeated observations about RSSI is measured from one meter to eleven meters spaced 0.1m for one hour. we analysis distribution of RSSI from different environments. The figure is obtained with range(m) along x-axis and RSSI along y-axis. Fig.2 show that the RSSI values were observed in outdoor and indoor and RSSI varies with distance, which shows that RSSI value in different environments has much fluctuation. We select different environments to analysis relation between RSSI and distance. In Fig.2(a), it is to be observed that the RSSI value vary dramatically with distance increasing under flat open square. It is noticeable that from the range of RSSI at each distance point only few different values were measured. However, In Fig.2(b) , It is obvious that a lot of different RSSI values were measured and that the RSSI values vary a few extent under identical conditions at corridor. Fig.2(c) show similar characteristics. Fig.2(b) and Fig.2(c) also show too much fluctuation between RSSI and distance in indoor and corridor which exist a few obstruction and walking men. However, The data analyses in above section have similarity and imply that using RSSI is availability and feasibility in outdoor and indoor environments.

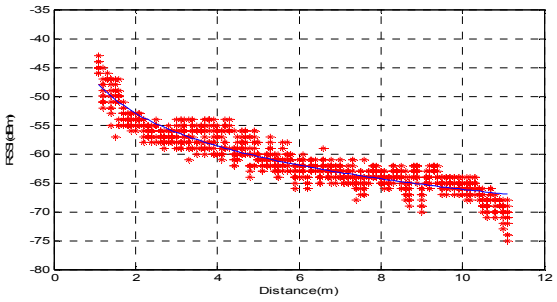

(a) Playground

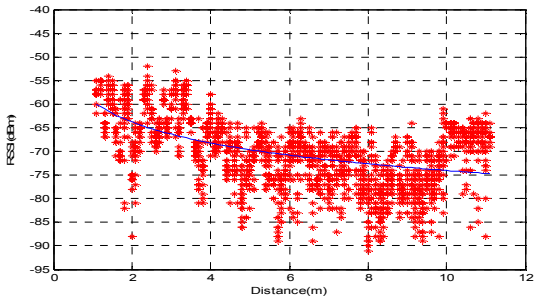

(b) corridor

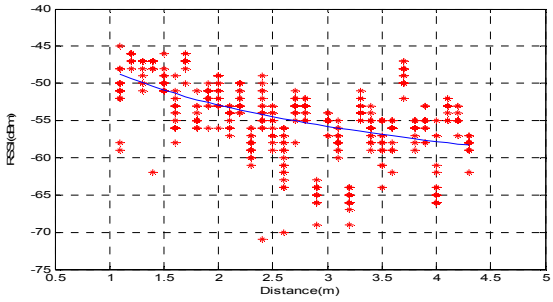

(c) Indoor

Fig.2. RSSI distribution in different environment

In different environments, the statistical properties require to be measured. A comparison of the statistical terms shows that three kinds of measurements exhibit similar characteristics as depicted in Table1.

Table 1. RSSI with different orientation

Statistics	playground	corridor	indoor
A(4.3m)	-47.8549	-60.0172	-48.0518
A(11.1m)	-47.2205	-59.3701	-
n(4.3m)	1.7254	0.9494	1.6204
n(11.1m)	1.8893	1.4680	-
correlation	0.9619	0.6053	0.5958

Conclusion

We have carry on an substantial study of RSSI using the widely used TI CC2430 radio. Our experiments in outdoor and indoor environments have shown that the RSSI can provide information for deriving distance estimation and localization. Our experience experimental result demonstrate that RSSI is a feasible method in complex environment.

Acknowledgement

In this paper, the research was sponsored by the General Project of Hunan Provincial Education Department (Project No. 12C1064)

References

[1] M. sepulcre, et al. Wireless connectivity for mobile sensing applications in industrial environments [C]. Proc. IEEE Symposium on industrial Embedded Systems(SIES), 2011, 111-114.

[2] Akyildiz, I.F., Su, W., Sankarasubramaniam, Y., And Cayirci, E. Asurvey on senor neworks [J]. IEEE Commun. Mag. 2002, 40: 102-114.

[3] A. Hossain, Y. Jin, W. Soh, and H.Van. Ssd: A robust rf location fingerprint addressing mobile devices' heterogeneity [J]. IEEE Transactions on Mobile Computing, 2011,99, 1-7.

[4] P. Chen et al. Instrumenting Wireless Sensor Networks for Real-time Surveillance [C]. In Proc. IEEE ICRA'06, Orlando, Florida, USA, 2006, May 15-19: 3128-3133.

[5] J.Xu, M. Ma, and C. Law. Performance of time-difference-of-arrival ultra wideband indoor localization [J]. Science, Measurement Technology, IET, 2011,5(2): 46-53.

[6] T. Antoine-Santoni, J.F. Santucci, E. de Gentili, X. Silvani, and F. Morandini. Performance of a Protected Wireless Sensor Network in a Fire [J]. Analysis of Fire Spread and Data Transmission. in Sensors, 2009, 9(8): 5878-5893.

[7] C.-Y. Chong and S.P. Kumar. Sensor networks: Evolution, opportunities, and challenges [C]. Proc. IEEE, 2003, Aug: 1247-1256.

[8] G.S. Kuruoglu, M.Erol, M. and S.Oktug. Localization in Wireless Sensor Networks with Range Measurement Errors [C]. In Proc. IARIA AICT'09, Venice, Italy, 2007, October 8-11: 1-3.

[9] Ferrigno L., Paciello V., Pietrosanto A. Experimental Characterization of Synchronization Protocols for Instrument Wireless interface [J]. IEEE Transactions on Instrumentation and Measurement, 2011, 60(3): 1037-1046.

[10] Mohit Saxena, Puneet Gupta, Bijenda Nath Jain. Experimental Analysis of RSSI-base Location Estimation in Wireless Sensor Networks[C]. 3rd International ICST Conference on Communication, 2008, January.

[11] P.K.Chong, D.Kim, Kaist. Surface-Level Path Loss Modeling for Sensor Networks in Flat and Irregular Terrain [J]. ACM Transactions on Sensor Networks, 2013.

[12] SUZ.A, ELBATSH.K.A, MAC.E. Gradient RSSI filter and predictor for wireless network algorithms and protocols[J]. Network Protocols and Algorithms, 2010.

Advanced Materials Research Vols. 989-994 (2014) pp 4551-4555
© (2014) Trans Tech Publications, Switzerland
doi:10.4028/www.scientific.net/AMR.989-994.4551

Research of Virtual Simulation Scenario Editor for Earthquake Tabletop Exercise

Bojia Zhou[1, a], Qunlin Jia[2,b] and Kuang Cen[3,c]

[1]No.1, Yuquanxi street, Shijingshan district, Beijing city, China

[2]No.1, Yuquanxi street, Shijingshan district, Beijing city, China

[3] Earth Resource and Environment School, China University of Geosciences, Beijing, China

[a]zhoubojia@126.com, [b]jql2005@126.com, [c]cenkuang@126.com

Keywords: Virtual Simulation, Earthquake Emergency Drill, Scenario Editor, Scenario System

Abstract. Earthquake is a small probability of unexpected events. Most of the emergency management personals did not experience the earthquake. They may cause flaws in the post-earthquake emergency response process, if they do not take part in earthquake emergency exercise. Traditional tabletop exercise, however, cannot provide a relatively realistic earthquake disaster scenes and vivid emergency background, so they need the virtual simulation exercises and drills for emergency management personnel to provide a real disaster site that is very similar to a drill. This paper presents system structure, function composition, scenario editing process of virtual reality simulation of earthquake emergency exercise and discusses a scenario editor based on OSG. Scenario Editor of earthquake emergency can control the drill and quickly rebuild the drill scene and improve emergency management personnel to design urban 3D scenes and earthquake and secondary disasters events.

Introduction

Earthquake is a small probability of unexpected events. Most of emergency managers do not have experience of the earthquake. They may cause flaws in the post-earthquake emergency response process, if they do not take part in earthquake emergency exercise. Traditional tabletop exercise does not provide realistic disaster scenes and vivid emergency backgrounds. Simulation of earthquake emergency response exercises can provide a relatively realistic virtual three dimensional earthquake scene, through numerical simulation of earthquake and secondary disasters and conduct simulation digital simulation, simulating real situations in which the maximum in the virtual space, development process, as well as the possible responses in disaster environments. The trainee can be immersed in this virtual earthquake disaster scene, discussion and deduction emergency decision-making and on-site disposal process, thereby enhancing the training staff ' feeling, promote relevant personnel to master the emergency plan prescribed duties and procedures, improve emergency command decision and coordination ability.

Virtual simulation scenario concept [1] extended from traditional military training exercise scenario concept, is the traditional military thinking to further expand. Virtual simulation scenario includes both traditional military scenario exercise background, exercise process, content description also includes a pair of visual simulation system and simulation end condition description. Earthquake emergency response exercises virtual simulation scenario is for earthquake emergency exercise, exercise virtual simulation system for earthquake emergency response required space, time, and in order to achieve the required background, conditions, constraints, rules and the simulation resource set.

Domestic and foreign researchers in the field of virtual simulation to sudden events made much research. Such as the United States of America ETC company ADMS for city emergency management at all levels and departments command personnel in key action planning, resource management, emergency response capacity assessment and cooperating with many departments in response to training provides practical experience. The national earthquake emergency rescue training base for the development of earthquake rescue virtual simulation scenario system can construct macro earthquake disaster scenario, earthquake rescue scene, and one-man operation ruins

scene of different resolution virtual training scene [2], can meet the earthquake rescue virtual simulation and training needs.

In this paper, we design virtual simulation scenario according to the earthquake emergency exercise platform on virtual simulation scenario generation system needs. The system is based on OSG (Open Scene Graph) for rendering platform, using XML as the structure of scene description language an application in virtual simulation scenario editor of earthquake emergency exercise. It provides visual manner, support a variety of customized training City and emergency practice content, including virtual earthquake disaster scene size, location and range of secondary disasters, victims of the position and number of tasks and goals. In this paper the design of simulation scenario system and emergency exercise system independent, without requiring the user to modify the program code to set of exercise. When adding new training task, users only need to modify by visualization of the exercise to exercise platform, without the need to modify other functional module.

Structure of scenario system

Concept scenarios edit system. Concept scenario edit subsystem is responsible for the scenario concept model development, it does not relate to a specific entity model. It is based on the emergency drill field uniform concept description library. It includes descriptions of entities, aggregation entities and processes and other elements of the concept of information, the information to be able to identify and describe these elements may state, tasks, events, behavior and performance, parameters and attributes etc.. Concept scenario model is to establish the relationship of elements, constraints, assigned tasks etc. It described include: scenario model hierarchy, synthetic natural environment description, drill entity and configuration, entity relationship, a collection of tasks and so on. Concept scenario model not only need a unified concept description for the foundation, but also used by the environment editor for generating synthetic natural environment data. Concept scenario modeling supported the scenario model of hierarchical, support collaborative modeling process, supported the scenario model coupling, in order to meet the development of large-scale scenarios.

Simulation scenarios edit system. Simulation scenario editor system is responsible for management and the establishment of simulation scenario. Simulation scenario is mainly considered simulation model resource mapping. Scenario concept model into the simulation scenario editor system, add the necessary information, into a simulation scenario model. Mappings include model mapping, model parameter mapping, mapping task of mapping, etc. Simulation scenario modeling process absorbed the concept scenario modeling features, and provides to the user a modified to function, the user can not only on the original concept to be mapped, but also on the scenario model two, add, delete, modify modeling original scenario model, and allows the user to build this directly simulation scenario. Simulation scenario editor subsystem is divided into to input module, scenario data rendering module, to cut and a reconstruction module.

Three-dimensional scenarios database. Three dimensional data is the base of simulation. Scenario database storage " three-dimensional " scenario, not only for the user study provides three-dimensional exercise scene scenario, but also embodied the staff, resources, command and control, exercise process in time, space constraints, but also easy to make and reconstruction. Three dimensional scenario databases include scenario database, standard alias called database, and model database. Scenario database save scenario description file and corresponding attachments contains information about the scenario 3D environment description, scenario basic assumptions, task scenario content. The rules database is to make the general and reusable, for trying to develop a set of specification language. Three dimensional scenario database models is the main earthquake disaster scene, emergency equipment, a character of visual physical model and its related parameter, function, behavior, audio description. Training evaluation database for virtual simulation effect, operators and agents or operation would be within the scope of assessment, to make emergency managers to better understand the scenario execution or inspection training effect.

Scenario operation management subsystem. Scenario operation management subsystem is responsible for the scenario query, maintenance, and to organize and control the process to run. Based

on the scenario of various data tables, model base and process parameter management data interpretation, real-time generation scenario 3D virtual environment, and the corresponding control parameter or parameters obtained from the interface module data real-time modification of the corresponding 3D virtual environment or to content and modify the corresponding database files, has to achieve constant operation of the process control and scenario database content modification. It contains three parts: like the retrieval module, to set the process management module, scenario database management and maintenance. [4]

Interface. Interface subsystem provides interactive interface between 3D scene and simulation application system. Interface subsystem is the communicate bridge between scenario subsystem and each simulation subsystem. It realizes the scenario parameters simulation data and corresponding data between conversion and exchange, which is mainly divided into man-machine interface and simulation application system interface.

Function composition of Earthquake exercise scenario editor

In this paper, scenario generation system is independent of earthquake emergency exercise simulation. Scenario generation system separate into scenario and simulation phase, keeps the scenario data independence, to make a set of input, storage and processing independently of the simulation based on typical cases, allowed to cut and reconstruction, promote scenario, simulation model and Simulation of the reusable member. The system is based on OSG (Open Scene Graph) for rendering core, taking XML as the structure of scene description language[5], operating system using Windows7. The function of the system mainly includes walkthrough city 3D environment scenario and earthquake and secondary disaster scenario.

Scenario of exercise city environment. Scenario of exercise city 3D environment mainly editing basic city scene, with emphasis given to the embodiment of scene in the terrain display and combinatorial logic, including city factors, social environment, the type of terrain complexity, road, climatic conditions, for a scene in one entity, can drag the mouse to a certain position, and can be directly input latitude and longitude position, the entity is automatically moved to this location. It includes not only a realistic topography and surface cultural characteristics of the terrain, but also can reflect all kinds of natural scenes and climate phenomena, such as water, trees, sky, rain, snow, fog. [6] At the same time the terrain environment also includes a number of 3D models, these models can be divided into static model and dynamic model. Static solid model refers to the ground some cultural characteristics such as buildings, trees, etc.; dynamic model refers to a variety of simulation entity model such as cars, pedestrians, such as a river[7].

Fig.1 The demo of exercise scenario

Scenario of earthquake disaster and second disaster. The system according to the levels of seismic hazard index and influence range, were used to build the four earthquake disaster events (especially major earthquake disaster, major earthquake disaster, earthquake disaster, generally larger earthquake disaster), each seismic disaster events influence field can and 3D virtual medium city model, 3D virtual city model small overlay display, display different city types at different magnitudes of city disaster damage, virtual city scene can pre-disaster contrast display and related city data comparison, match the seismic process demonstration, in the visual and sensory on trainees caused the most close to the real disaster shock effect, deepen the emergency management of earthquake disaster cognition degree[8].

The system can be set in accordance with the prior to the basic parameters of the earthquake data simulation of city buildings and infrastructure of the city disaster situation, provide different levels a

range of buildings, lifeline engineering damage status and distribution, direct economic loss, the casualties and homeless numerical and spatial distribution.

In the earthquake disaster scenario simulation basis, choose a dam height, hydrological, spillway, depressions distribution and upstream reservoir earthquake induced flood information, simulation of flood range model, by using the scene provides a three-dimensional reality and spatial analysis function, simulation of flood embankment somewhere once burst, flooding break into the city along the urban, flood submerged area, the submerged city of three-dimensional landscape and city infrastructure damage.

Scenario of second disaster fire is achieved by processing the input information, modeling, analysis and result output simulation link, through the qualitative model of fire scene simulation display and data description. According to different height of building structure, materials, construction of buildings, covering fire scene model, scene of each model are maintained in a predetermined scene database, through scripting and event information into a call and display[9], as shown in figure 3.

Fig2. Scenario of earthquake secondary fire

Earthquake secondary geological disaster scene model can describe in detail the disaster of topographic and geomorphic features, such as the slope of the terrain, length, size, shape, area of slope geological composition, gully characteristics and vegetation characteristics, while the use of 3D remote sensing image, describe the geological disaster type, location, boundary, size, activity mode, steady state, and show their on the surrounding environment and personnel activity areas of influence degree.

Before exercise, the director control group members can be dynamically constructed virtual 3D city and choose a different damage degree of buildings, the delineation of different secondary disaster distribution range, and the specific exercise add corresponding trigger events and set event influence scope, in order to drill the trigger operation. A virtual disaster scene through three-dimensional, all-round display of an emergency, disaster on city scene effects and damage degree, the influence scope and landforms, construction, population, traffic and other virtual situations, and support for dynamic adjustment of disaster information.

Earthquake emergency response exercises virtual simulation scenario system may wish to set already in the database to be indexed, and provides two ways to establish the scenario. System editor four typical scenario templates(Wenchuan city earthquake,Bachu-Jiashi city earthquake, Xingtai city earthquake, Liyang city earthquake) to deposit into a case file. On one hand, in the template based on modified, cut. In the edit new to timing, just out of similar scenario template was modified, which can avoid repeated input, shorten the scenario editing time, improve work efficiency. On the other hand is to edit a new scenario.

Fig3. Scenario interface

The system renders script data to speech, music, color, graphics, 3D model, with OSG as rendering platform, and build 3D virtual reality scenes, giving a good human-computer interaction interface to meet in various contexts exercise deduction need.

Conclusion

Earthquake emergency exercise is an important application domain of virtual simulation. Virtual simulation scenario of earthquake emergency response exercises provides a real disaster scene which is very similar to the exercise environment for emergency management personnel to carry out earthquake emergency exercise. In this paper, the realization of a desktop earthquake emergency exercise meet requirements of the virtual simulation scenario editor system for earthquake drill needs, and apply to the actual earthquake emergency drill. The system can be repeated fast reconstruction drilling scene, improve managing groups of drill city 3D scene scenario and earthquake and secondary disaster scenario. However, how to design the structure more reasonable, realistic rendering, interactive processing and deducing the rationality are in need of further study. In the later work constantly improve, in order to make the system better adapted to the earthquake emergency exercise of simulation system requirements. [10]

References

[1] Cui Zhonghui, Xu Yongzhi, Zhang Maojun :Research and implementation of the earthquake rescue virtual simulation scenario editor. micro computer information, volume twenty-second(2006),p298-301.

[2] Jia Qunlin, Chen Xin, Zhou Bo Jia; Earthquake rescue training the application of virtual simulation technology ;. Beijing: Contemporary World Publishing House.(2009)

[3] Xiao Tianyuan, Zhang Yanyun, Chen Jiadong: introduction to system simulation. Tsinghua University press, 2000

[4] Li Ni, Tang bravery, Lei Zhengdong Web based simulation scenario management system :Chinese Journal of Stereology and image analysis, p.335-338.(2010)

[5] Peng Chunguang, Qiu Xiaogang, Zhang Ke . Simulation environment based on XML model research of the script generate system. Computer simulation, 2006 (08),p403-405.

[6] Arul Asirvatham, Hugues Hoppe. based on GPU geometry shear map terrain rendering. Tsinghua University press .(2007)

[7] Zhao Qinping. DVENET distributed virtual reality application system operation platform and development tool . Beijing: Science Press.(2005)

[8] Wang Dongming:Earthquake disaster simulation and rescue virtual simulation training system based on. Institute of engineering mechanics, China Earthquake Administration.(2008)

[9] Reeves William T: Particale systems-a technique for modeling a class of fuzzy objects;.Computer Graphics,1983,17(3),p.359-376.

[10] Duchaineau Mark A, Wolinsky Murray, Sigeti David E. ROAMing Terrain:Real-time Optimally Adapting Meshes; .IEEE Visualization 1997. Los Alamitos:IEEE Computer Society Press, (1997),p.81-88

Advanced Materials Research Vols. 989-994 (2014) pp 4556-4561
© (2014) Trans Tech Publications, Switzerland
doi:10.4028/www.scientific.net/AMR.989-994.4556

HIPPO: an Adaptive, Scalable, Hierarchical P2PLive Streaming System

Kai Lei[1, a], Lihua Li[2, b], Cheng Peng[3, c], Longyu Yu[4, d]

[1, 2, 3, 4]The Shenzhen Key Lab for Cloud Computing Technology and Applications (SPCCTA) School of Electronic and Computer Engineering, Peking University (Shenzhen) Shenzhen 518055, P. R. China

[a]leik@pkusz.edu.cn, {[b]lihua, [c]pengcheng, [d]1201213683}@sz.pku.edu.cn

Keywords: P2P, Streaming media, Hierarchical, Adaptive

Abstract. P2P live streaming is a hot research topic of Internet, but for the defective of system architecture and scheduling policy, P2P streaming applications have poor user experience, such as long start-delay, long play-delay, and low play-continuity and so on. Firstly, based on the analysis of the advantages and disadvantages of previous works, this paper designed and implemented a hierarchical P2P streaming system. The system is composed by three layers: source management servers, region management servers, and peers. The underlying P2P overlay network is organized through Mesh-pull mechanism. We propose a new scheduling strategy to utilize the capacity of the peer. The new adaptive scheduling strategy considers the urgency and scarcity of the data blocks, and selects the appropriate neighbor nodes by monitoring neighbor nodes' the maximum load. The study of a real-life system provides valuable insights for the future development of P2P live streaming systems.

Introduction

In recent years, with the increasing demand for streaming application, peer-to-peer (P2P) techniques have been studied and deployed in live streaming systems. P2P techniques play a leading role in the Internet and are widely applied to many multimedia applications, such as PPStream [1], PPLive [2], QQLive [3]. P2P technique has the higher continuity with lower deployment overhead because it fully utilizes the upload bandwidth of other clients to reduce the server's bandwidth cost. Unfortunately, it adds more challenges including the playback continuity, the startup time, and suitable peering and scheduling strategies.

In a real-time application, the source server generates a live streaming which is divided into chunks with fixed size and some latest chunks are cached in the local buffer. All the clients can exchange the chunks with a small subset among the participating peers. Peers involved in these systems have heterogeneous uploading bandwidth capabilities while the average uploading bandwidth capability of the participating peers constrains the maximum service rate of the video stream that can be delivered successfully to all peers [4]. Accordingly, peers deployed in these live streaming systems need to receive a video stream with a service rate close to the average upload bandwidth of the neighbor peers with small delay.

In the P2P live streaming service, the video stream is diffused by the topologic overlay that constituted by these nodes which join in the distributed streaming system. The live stream is spreading in the network through the scheduler in every node. Peers connect each other and select some as its neighbors. Then each node will maintain a list of neighbors. The scheduler in a peer is running to exchange chunks with other peers. In the precious work, the content retrieval is based on three steps at each hop: Swapping buffer bitmaps with neighbors, analyzing and requesting content and finally sending data block [5]. Peers select neighbors based on a quantity of chunks which the neighbor sends to peer in every certain period. In a precious work [6], we indicated that constructing a good topology is a necessary way to minimize the playback delay. This paper will propose a peering strategy to reduce the difference of the video quality of peers and react quickly enough to the dynamic behavior of the participating peers and the fluctuation of underlying network. The main research

direction of P2P streaming is overlay organization. Numerous related strategies are proposed to optimize the overlay topology [7][8].

In this paper, we conduct a hierarchical P2P live streaming system. The rest of this paper is organized as follows. Section Ⅱ describes the design principle of the architecture and the detailed design of each module. Section Ⅲ proposes a new scheduling policy of the Mesh-pull mechanism P2P streaming media system and summarizes the advantages and disadvantages of other strategies [9-12], putting forward the optimization scheme, and applying to the Hippo system. In Section Ⅳ, Real-life measurement data were collected from the deployed live streaming system. We analyze the different scheduling strategies by the collected data. Finally, we discuss related work and conclusions.

Ⅱ Hierarchical P2P Live Streaming System

A. Major Components Of The System

This paper presents a hierarchical P2P live streaming system—Hippo. The system supports large-scale applications and multifunction (live, download) P2P streaming system. In this section, we first briefly introduce some terms.

SM (Source Manager): responsible for the entire network resources scheduling and querying. **RM (Region Manager)**: responsible for the scheduling of some a certain media resource and node. **Peer**: a kind of node, it a peer entities in P2P networks, including Speer and Dpeer. **Speer (Static Peer)**: a static node deployed as data source in the system. It's always online once launched. **Dpeer (Dynamic Peer)**: the user node, the state of this kind of node will follow the users' action. **Admin**: Provide the administration on the system and the management of resource scheduling. **LiveSvr**: the live server, responsible for the data downloading, packaging, identifying, and distribution to Speer. **LogSvr**: the log server, record the key log for issue tracking and data mining. **Segment**: media is cut to some piece according to a certain size; every piece of it is called a segment. They have the same size except the last one. **Block:** cutting the resources on the basis of segment, each called block. The size of it is fixed; the last one will be filled with empty content.

B. The framework of Hippo

The framework of Hippo including SM, RM, Speer and Dpeer, they form hierarchical service architecture, as shown in the Figure 1:

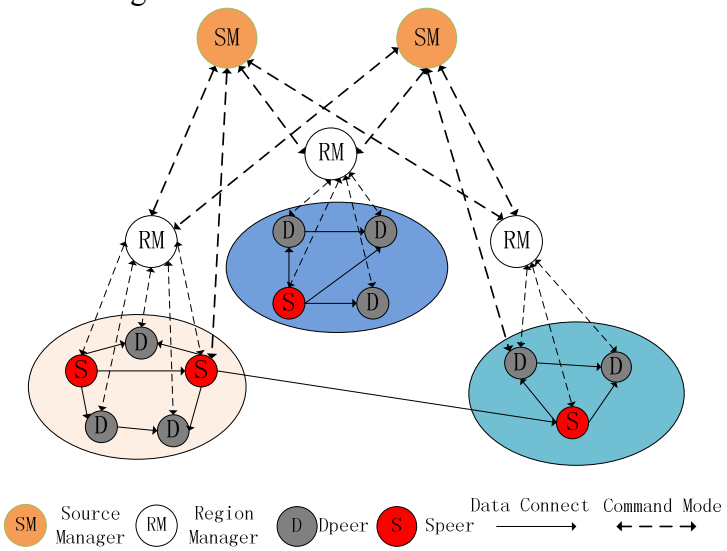

Fig.1. Hierarchical P2P architecture

SM is located on the top. It's responsible for the managing schedule (online, offline and copy) and queries of the media resources in the entire network. A SM represents a content publisher. It is

independent between different issuer of SM. SM is only concerned with resource distribution in what areas and don't care about specific storage location of resources. SM also can provide resources query service.

RM is located in the middle tier, which is divided according to region. Each RM is responsible for the Scheduling management of all resources and nodes in the area. RM concerns not only which resources can be getting in a certain area, but also which node they distribute.

SM and RM are fully connected. For any resource management server SMi and any area management server RMj, SMi will set up an interactive channel with the RMj, RMj report the resource information within the jurisdiction of the SMi to SMj, and receive news resource scheduling from SMi. RM record all the node information in this area, and responsible for the node scheduling and retrieval. RM is equal and divided. There is no direct interaction between each other.

A lot of nodes located at the bottom, they are Speers and Dpeers. When nodes are online, they will report the resource information to the belonging RM, and send heartbeat packet to the RM in its whole life. Speer provides data service and the object is other Speer and Dpeer. Dpeer enjoys media services as well as servicing for other Dpeer at the same time.

Upper is a Mesh structure organized by Speers, there are two factors lead to this Mesh structure, the first is that Admin sends the resource scheduling command. The second is that RM will monitor resources heat and Speers' load balancing, which will decide the movement between Speers.

Ⅲ The Design of Priority-based Adaptive Scheduling Algorithm

The task of scheduling is to choose a suitable partner in h from partner nodes set H for each request block b in request block set B, and request b. Then process request block according to a certain order. From this perspective, we propose a priority-based adaptive scheduling algorithm (PBASA). We defined a request as ask for a particular piece of data. Assume that

$$B=\{b[i] \mid i=0,1,2,\ldots,n-1\},H=\{h[j] \mid j=0,1,2,\ldots,m-1\}$$

The number of request blocks in the system is n; Partner node collection contains m elements.
Define the following functions:
Φ: N->B, Φ (i) means the i-th block.
Ψ: B->H, Ψ (b[i]) means the partner b[i] should request.
ζ: N->B×H, ζ(i)=<Φ(i),Ψ(Φ(i))>, mean the i-th request if request from partner Ψ(Φ(i)) to block Φ(i).
This article briefly describes the order of the request, namely the choice of function Φ.

As is described above, the request order of greedy method arranged mainly based on the "urgency". The least copy priority arranges the order according to "scarcity", hybrid scheduling algorithm is a combination of greedy method and the least copy priority. We combines the greedy method and the least copy priority algorithm, take both "urgency" and "scarcity" into consideration, and set a priority p[i] for each block b[i], decide the request order of b[i] according to the priority. t[i] is the expected play time of i-th block, we use it to represent the "urgency" of the request block b[i], it's the sooner the urgency higher. d and M in the formula are fixed for the same file, so the urgency can be simplified as t[i] =b[i] – play.

The parameter α is between 0 and 1, when α equal to 1, the priority only reflects the request of scarcity; when α equal to 0, priority is only calculated according to urgency of the request block; when α is between 0 and 1, both the urgency and scarcity are considered in the priority.

$$p[i]=-\alpha \bullet t[i]+(1-\alpha)\bullet r[i] \qquad (1)$$

FBSA [14] unified set for each node limit of simultaneous requests, which for the presence of heterogeneous network and node heterogeneity P2P overlay network is unreasonable and cannot achieve truly adaptive. In this paper, we adopt a dynamic approach to monitor partner nodes' the maximum load max_req. The procedure of monitoring the entire partner nodes' max_req is shown in

Algorithm 1.

Algorithm 1 Dynamic adaptive monitoring partner node's the largest load max_req

```
Set(λ, μ)
For each partner node:
    Initial (max_req)
For each partner node:
    if  req_T0 − req_T1 ≥ λ  then
        max_req ++
    else
        if  req_T1 − req_T0 ≥ μ  then
            max_req - -
        end if
    end if
```

Ⅳ Measurement Results and Analysis

1. Experiment and Setup

Parameter	Value	Parameter	Value
SM	1	Speer Bandwidth	1 Gbps
RM	3	Dpeer Bandwidth	10 Mbps
Speer	6	Maximum neighbor	10
Dpeer	500	Channel A rate	5128 Kbps
Block Size	64KB	Channel B rate	2128 Kbps
Dpeer Buffer	200*64KB	Channel C rate	400 Kbps

2. *α* settings

We can see that α value range is [0, 1], and α values determines the influence of the "urgency" and "scarcity", combined the advantages of greed and RF. Greed has lower start-up delay and RF has better playback continuity and higher utilization rate of P2P, the following will determine the value of α from these three indicators.

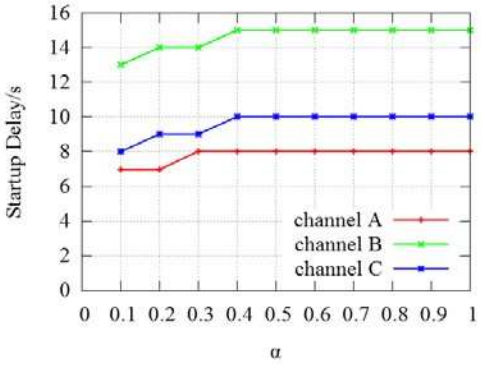

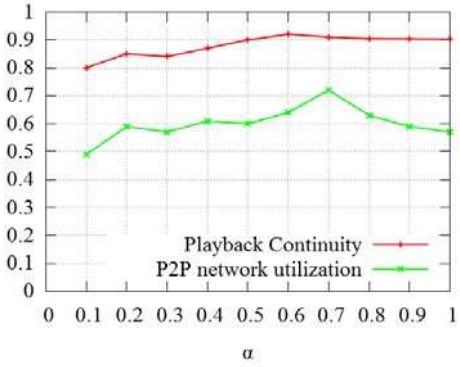

Fig.2. Alpha Setting Fig.3. Playback continuity and network utilization of Channel B

3. Performance Comparison Of Different Strategies

We can see from Figure 2, the higher the code rate is the higher the start-up delay. This is due to the higher code rate the larger data flow is. Start-up delay is smaller, along with the change of alpha, when α≥0.3, start-up delay is similar. This is because of the retransmission mechanism; the block in retransmission interval is first downloaded from Speer, which reduces the start-up delay.

This article use the definition of playback continuity in citation [13], which is the "persisted time/full time (including the pause time)"and defines the P2P network utilization as "blocks number downloaded from Dpeer/Total download blocks". Figure 3 is the experimental results of channel B, we can see that network utilization is better when alpha=0.7, and when alpha is 0.7 or higher, P2P utilization began to decline because of the retransmission mechanism. This article set the alpha value to 0.7.

It can be seen from Figure 4, PBASA algorithm has great advantage start-up delay compared with FBSA [14], and also has the advantage compared with MIX [15], reflect the flexible of combination of greed and RF. In the aspect of sustainability, we get the result in Figure 5, based on the experiment statistics of channel B. PBASA playback continuity remain at around 0.99 and has a less volatile, Mix algorithm remain above 0.9, and FBSA has a bigger volatility, the continuity is sometimes less than 0.9.

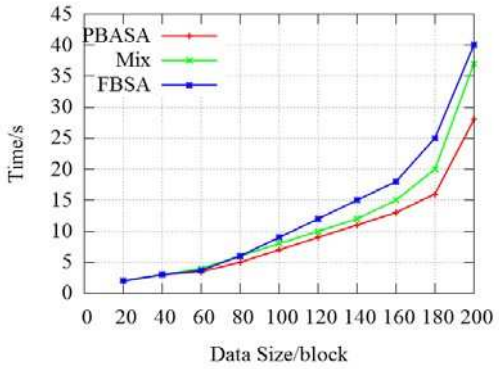

Fig.4. Start-up delay of different Scheduling Strategies

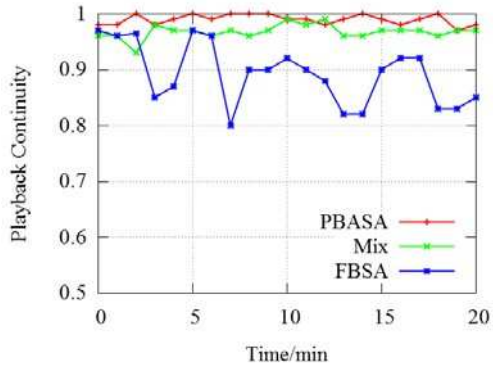

Fig.5. Playback continuity of different Scheduling Strategies

After comparing and analyzing the P2P network utilization in different scheduling algorithm using 3 different test channels, result is shown in Figure 6. For channel C with a low bit rate, Mix and PBASA showed a higher P2P network utilization (greater than or equal to 80%). Along with the rising of the bit rate, three kinds of algorithm of a P2P network utilization ratio become lower, but reduction of PBASA is minimum. It's easy to say PBASA has a better adaptability to different bit rate. Overall, PBASA reflects the higher utilization rate of P2P network.

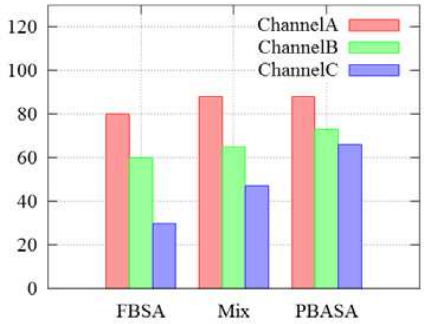

Fig.6. Comparison of network utilization

Summary

P2P live streaming system is an up and coming for the internet. Significant amount of research has been conducted in assessing the viability of peer-to-peer live video streaming, and some encouraging results have been reported. However, most of these systems have been tested only in research environments, and the deployment experience of these applications is very limited. In this paper, we design and implement a real-life hierarchical P2P streaming media system Hippo. It has three layers including SM (top), RM (middle) and Peer (bottom). We make a thorough research at live scheduling strategy and then present an adaptive scheduling optimization algorithm. In the end, we demonstrate the advantages of improved algorithm through experiments.

Acknowledgement:

This research was financially supported by NFSC project (Grant No: 61103027), 973 project (No: 2011CB302305) and Shenzhen Gov Projects (JCYJ20130331144541058 and JCYJ20130331144416448).

References

[1] PPStream, http://www.ppstream.com/
[2] PPLive, http://www.pplive.com/.
[3] QQLive, http://v.qq.com/
[4] R. Kumar, Y. Liu, and K. W. Ross, Stochastic "Fluid Theory for P2P Streaming Systems", INFOCOM 2007, Anchorage, Alaska, 2007
[5] D.Ren, Y.-T, H. Li, and S,-H, G. Chan, "On reducing mesh delay for peer to peer live streaming" , in proc. of IEEE INFOCOM, 2008.
[6] A. Ouali, B. Kerherve, and B.Jaumard, "Toward new peering strategies for push-pull based p2p streaming systems," to apper in P2PNet' 09, October 2009, St.Petersburg, Russia
[7] Nazanin Magharei, "PRIME: Peer-to-Peer Receiver-Driven Mesh-based Streaming", INFCOM Anchorge, Alaska, 2007
[8] Meng Zhang, Yongqiang Xiong, Qian Zhang, and Shiqiang Yang,"On the Optimal Scheduling for Media Streaming in Data-Driven Overlay Networks", in proc. of IEEE GLOBECOM 2006, Novemember 2006
[9] Zhou Y, Chiu D M, Lui J C S. A simple model for chunk-scheduling strategies in P2P streaming [J]. Networking, IEEE/ACM Transactions on,
2011, 19(1): 42-54.
[10] Zhou Y, Fu T Z J, Chiu D M. A unifying model and analysis of p2p vod replication and scheduling[C]//INFOCOM, 2012 Proceedings IEEE. IEEE, 2012: 1530-1538.
[11] Sanu C, Deepa S S. Chunk Scheduling Strategies In Peer to Peer System-A Review[J]. International Journal of Advanced Research in Computer Engineering & Technology (IJARCET), 2013, 2(3): pp: 1041-1045.
[12] Hu C, Chen M, Xing C, et al. EUE principle of resource scheduling for live streaming systems underlying CDN-P2P hybrid architecture[J]. Peer-to-Peer Networking and Applications, 2012, 5(4): 312-322.
[13] Tom Z. J. Fu, D. M. Chiu and Z. Lei. Desining QoE Experiments to Evaluate Peer-to-Peer Streaming Applications. In SPIE Visual Communications and Image Processing, 2010.
[14] S. Chen, L. Huo, Q, FU, R. Guo and W. Gao. FBSA: A Self-adjustable Multi-source Data Scheduling Algorithm for P2P Media Streaming. In MCAM, 2007.
[15] Y.P. Zhou, D.M. Chiu and J.C.S. Lui, A Simple Model for AnalyzingP2P Streaming Protocols. In IEEE ICNP, October 2007, pp. 226-235.

Advanced Materials Research Vols. 989-994 (2014) pp 4562-4565
© (2014) Trans Tech Publications, Switzerland
doi:10.4028/www.scientific.net/AMR.989-994.4562

About the Requirement Analysis Changes of ERP Software Project

Wenjing Liu[1, a], Yingying Song[2,b], Man Zhao[1, c] , Peng Wang[3, d] and Xin Wang [1,e]

[1]2222 East Nanhu Road, Nanguan District, Changchun, Jilin, 130000, China

[2]46 South Zhongguancun Street, Haidian District, Beijing, 100081, China

[3]7186 Weixing Road, Chaoyang District, Changchun, Jilin, 130000, China

[a]liuwenjing130@sina.com, [b]songyingying@huafeng.cma.gov.cn, [c]xman@126.com, [d]wpeng@cust.edu.cn, [e]wangxin.ccut@163.com

Keywords: Software Requirement, Secondary Development, Requirement Process, Requirement Management Tools.

Abstract. Requirement change is always a serious problem for developers and Software companies. Especially in putting ERP software into effect or ERP software secondary development, the requirement change has brought great disaster. The requirement process is not in-depth understanding and having no standard management mechanism are the main reasons for requirement changes. For ERP software companies, they must pay more attention to the requirement process and requirement changes.

Introduction

The ERP software which each company used to manage its resource nowadays is composed with standard product and secondary development. Standard product is the software that developed for common use. Secondary development is developed for satisfying the individual requirement of each company, Different from the all-developed-software.

The process of the secondary development exist a obvious problem. Before we develop the software, we must find out the requirement firstly. Not all these requirements can be solved by the standard product. We should develop the secondary development software to solve the other requirements. The requirements we finding out are changed frequently. The influence of the change is huge for the ERP software company and the client company. For ERP company, requirement changes lead to more expanding workload, project postponed, cost inflation, bad maintainability, and so on. In lifecycle of the software, the later requirement changes appeared, the more charge we cost (Table 1). If we find out the requirement changes early, we will save the cost.

Table 1. Restore cost of the Software lifecycle

Moment	Restore Cost
Requirement Moment	0.1~0.2
Design Moment	0.5
Coding Moment	1
Cell Test Moment	2
Thermoscope Test Moment	5
Maintenance Moment	20

There are many reasons results in the changes: an insufficiency of investigate, half_baked requirement understanding, disaccord requirement understanding, increasing of the users' requirement, changes of users' operation, changes of users' management system, and otherwise. These reasons can be carved up to two parts: one part is avoidable changes, the other part is unavoidable changes. In order to saving cost and enhancing the efficiency, we must put an end to avoidable changes and decrease unavoidable changes.

The process we capture and analyse the requirement is called “requirement process”. The requirement process is composed by requirement development and requirement management. (Fig.1)The requirement development is composed by problem capture, analysis, making standard explain and validate. The requirement management is composed by changes manage, edition manage, requirement slot and requirement estate slot.

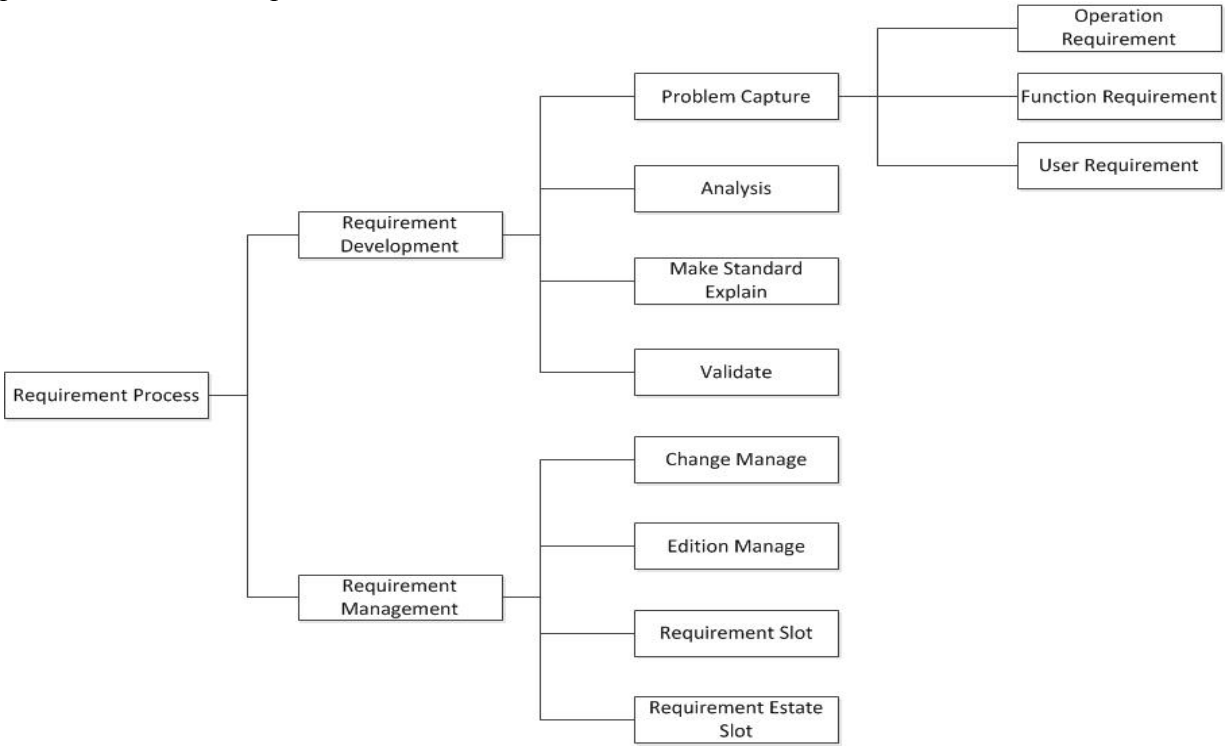

Figure 1. Requirement Process

ERP software second developers also use this requirement process as common software. Many ERP software second developers make a point of capturing problem in the requirement process. The problems include operation requirement, function requirement and user requirement. Operation requirement is the requirement of the aim that the client or the company wanted. This kind of the requirement is shown in item view and system bound documents. User requirement describe that users make use of the ERP system to accomplish the work and the task. This kind of the requirement is shown in user case. Function requirement define the software function that the developers must make it true. This kind of requirement make users can operate the ERP software. Because the ERP software is used to manage the enterprise resource, the developers pay much attention to the operation flows, the way of management, the ideology of management and the demand of the terminal users.

But ERP software second developers take no account of the analyse and other nodes of the requirement process. Analyse is an important node. In this node, developers first find out which requirement can be solved by standard product, which is not true of the ideology of management, which is disobedient to the modern logos of the requirement , finally which is must be developed by the developers. Then the developers analyse the requirement that need second develop with the requirement process. Nest nodes of the requirement process nodes are omitted. This nonstandard requirement process result in the frequently changes of ERP software project.

How to put an end to avoidable changes of ERP software? How to reduce unavoidable changes of ERP software?

The secondary developers or the ERP software companies should pay more attention to each node of the requirement process, Build a standardized system to control the requirement process. They also can use some requirement management tools. These requirement management tools divide into two parts. One is requirement content management tools, the other part is requirement process management tools. Requirement content management tools can manage the entry of the requirement,

follow up the requirement, manage the base line of the requirement. These tools include IBM DOORS, IBM Rational Requestpro, Borland CalibraRM, Hanskey Dragonfly, etc. Requirement process management tools mainly manage the requirement changes. These tools contain IBM Clearquest, Butterfly of Hanskey, IBM Change, etc.

Rational Requestpro, is a familiar requirement content management tool that manage the requirement and the use case. This tool is easy used and compositive. This tool expand its function with its integration. It can work with Rational software products. It can manage the requirement by making the requirement like the item. It also brings a lot of functions like information query, slot and management in the lifecycle of the software. With these functions, the tool can help us to evaluate the effect of the changes and manage the requirement changes. It also can recede the project risk.

IBM Rational DOORS, at one time called Telelogic DOORS. DOORS is a oldest company requirement management software. It can help the corporation to communicate effectively and enhance the collaboration by using DOORS/ERS. It can use different methods to manage different structures. That make the management process more crystal. It also can make the corporate out of the zone restrictions.

Borland CaliberRM, is a requirement define and manage tool that based on Web and collaboration. It is very helpful for distributed development team. It can raise the delivery schedule of the application system. CaliberRM gathered many developed tools: project planning tool, software configuration management tool, the analysis and design tool, object modeling tool and test management tool, etc. A collection of these tools can understand the requirement and the influence of the requirement changes better.

Besides these famous requirement management tools, the ERP companies can develop a little requirement management tool. This tool is faced to the secondary developers. By using these requirement management tools, we can control all the nodes of the requirement process and make all the requirement change process normative.

The first and the second node of the requirement process are the most important nodes in all of the nodes. If we want to put an end to avoidable changes of ERP software and to reduce unavoidable changes of ERP software thorough, we should pay more attention to the first two nodes: capture the problem and analysis.

Capture the problem is the requirement search process, the developers communicate with the client. Talking for the requirement of the ERP software. This process is the process of communication. For the customer psychology, their ideal state is coordinating with our research. But unfortunately, in the process of real research, customers are different. Many of them have unrealistic ideals, what they expect in ERP software is imaginary mode. The requirement cannot realize. Many of the customers present the requirement that not the operation and the flow path of the routine work. They are not the actual operator. Instead of the actual operator, they tell the requirement by their imagination and understand. Many of the customers have psychological conflict on enterprise informatization construction. They think that the ERP software may increase their workload. They also maybe don't want to change their mode of operation. Many of the customers shirk their responsibility when talk about the key point of the software process. They don't confirm the main flow path.

When the features above appeared, our developers should have good communication skills. We can take the following measures to solve the above features. Talking to the customers from different level and different department, because the people from different organization level , different business department and different computer level, have the different requirement. For example, the customers like general manager level maybe interested in macroscopic report, they have no suggestion on the details of operation. While the department managers may pay more attention on daily work report, the function of the system and the expansion of the function. Ordinary business operation personnel may interesting in the mode of operation, interface style and easy-to-use. So, group the customers becomes very valuable. We should talk to many customers ,then find out the difference between the description of the requirement from each customer. Finally we let the leader to

confirm the different requirement. We can make friend with the customers, this way can reduce the psychological reactance of the customers.

Summary

Requirement changes cost much resource of the ERP companies. To save the cost, the ERP corporation must pay more attention to the requirement process. The requirement process have many nodes. We can use requirement management tools to control the requirement process. Especially, the problem capture is the process of the communication. Developers should have the good communication skills. We hope the ERP secondary development may have a useful requirement management system. By using the system, we can reduce the requirement changes and finish the ERP project successfully.

References

[1] IBM Rational Software innovation forum, IBM Rational requirement.pdf(2010).

[2] Project Management Institute Standards Committee. Aguide to the proect management body of knowledge. USA: Pennsylvania, 2008 .

[3] Jones C. Software Quality in 2000: What Works and What Doesn't[M].McGraw Hill,2000.

[4] Information on http://www.cloudtopo.com

[5] Information on http://www.borland.com/us/products/caliber/index.html.

Advanced Materials Research Vols. 989-994 (2014) pp 4566-4569
© (2014) Trans Tech Publications, Switzerland
doi:10.4028/www.scientific.net/AMR.989-994.4566

The study on optimization of energy consumption for nodes ZigBee wireless sensor networks based on library information service

Zhang Junsong Sun Bao Liu Dongmei

North China Institute of Science and Technology,CHINA

Keywords: optimizing, node's dormancy ,quality of network communication

Abstract：This paper studies the key issues of how to reduce the energy consumption of the ZigBee nodes, through optimizing node's dormancy mechanism without affecting the quality of network communication.

1 The Introduction

Owing to the wireless sensor node is powered by battery, we need to consider the energy consumption of these nodes if many sensor nodes are decorated in the practical application.[1] If the energy consumption is small, we can use nodes at a long time without replacing battery; but if the power consumption is big, replacing numerous battery at a short time will increase human burden. Under this application background, this paper establishes an energy saving strategy, based on ZigBee wireless sensor network , which can accomplish timing measurement.

2 Zigbee technology application in library information service

ZigBee[2] technology is a new type of short distance wireless communication technology,and this technology is considered most likely to be used in industrial control occasions.And it also can use the 2.4 GHz frequency band for free.[3]

From the network configuration，there are three types of ZigBee network nodes: ZigBee coordinator nodes, ZigBee router nodes and ZigBee terminal nodes.[4]

Special attention should be paid that the specific architecture of the network will dramatically affect the resources required for equipment. ZigBee network main support three kinds of topology structure: the Star, Mesh and Cluster-Tree structure. In this several kinds of topology structure, the star network requires minimum resources.[5]

If the zigbee technology is applied to library information service, the library information designated collection will come true.The collection system generally use star network.

3 Full symmetric transmission model of competition for channel resources based on CSMA/CA algorithm (Model one)

In this article, model adopts star network, with the fixed device nodes distibuted in the scene。That is，the coordinator in the center, the surrounding is uniformly distributed with N terminal nodes .

In this model, node 1 to node N will upload the data, which is collected by themselves, to the coordinator within the prescribed period of time T.Because the position of each node is symmetrical and send data may happen at any time within the 0~T, there may be multiple nodes upload data at the same time . ZigBee protocol uses the CSMA/CA technology to solve the above problems.

Under the CSMA/CA algorithm of ZigBee protocol, when receiving the beacon frame, the node detects CCA idle channel before sending data. The node will send data if the channel is empty, otherwise the backoff counter randomly generates one number in 1~5, the number minus 1 after a time slot until it reduces to 0 ,then the next CCA detection begins. In the process of uploading data, node includes the states: CCA idle channel detection or retreat, data transmission, receiving the ACK response frame, successful transmission . State transition diagram is shown in Figure 1:

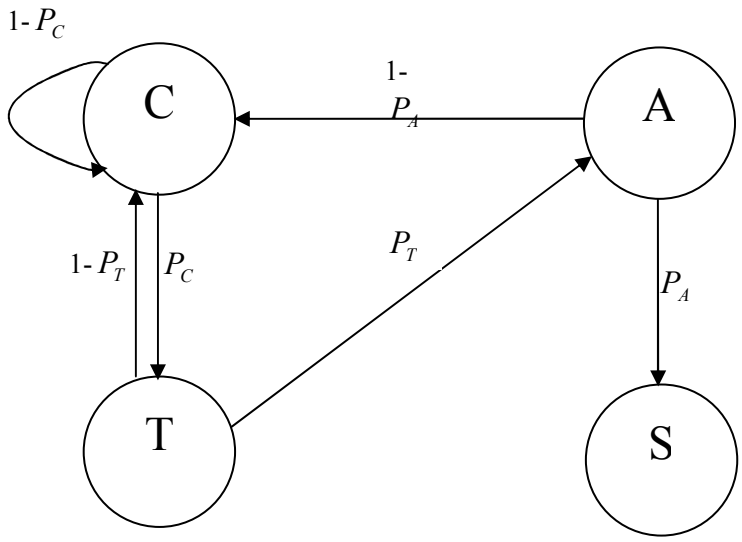

Figure1:State transition diagram of node in the process of uploading data

4 Communication as planned model based on CSMA/CA algorithm (Model two)

In this model, node is scheduled to communicate, every two nodes wake up successively, at the same time the two nodes'position is centrosymmetric, with the coordinator at the center.

State transition matrix of node 1 are as follows:

$$P_1 = \begin{array}{c} \\ C \\ T \\ A \\ S \end{array} \begin{array}{c} \begin{array}{cccc} C & T & A & S \end{array} \\ \begin{pmatrix} \frac{1}{2} & \frac{1}{2} & 0 & 0 \\ 1-P_T & 0 & P_T & 0 \\ 1-P_A & 0 & 0 & P_A \\ 0 & 0 & 0 & 1 \end{pmatrix} \end{array}$$

In the model one, the state transition matrix of any node is:

$$P = \begin{array}{c} \\ C \\ T \\ A \\ S \end{array} \begin{array}{c} \begin{array}{cccc} C & T & A & S \end{array} \\ \begin{pmatrix} 1-P_C & P_C & 0 & 0 \\ 1-P_T & 0 & P_T & 0 \\ 1-P_A & 0 & 0 & P_A \\ 0 & 0 & 0 & 1 \end{pmatrix} \end{array}$$

In this model system, the probability of any node grabs channel through the CCA is P_C. If the channel is busy, then the node will transfer to the retreat state with the probability of 1- P_C, and will wait for the next CCA detection until grabs the channel. Therefore, a node grabs channel based on the CSMA/CA algorithm so as to enter into the state of transmission state, which need $\frac{1}{P_C}$ times.

Expectations of power consumption in this process is: $\frac{1}{P_C} \times E_C$

N nodes' expectations of energy consumption in this process is : $N \times \frac{1}{P_C} \times E_C \times N$

Under the worst communication condition, in the N communication time, any node state transition matrix is :

$$P_N = \begin{array}{c} \\ C \\ T \\ A \\ S \end{array} \begin{array}{c} \begin{array}{cccc} C & T & A & S \end{array} \\ \begin{pmatrix} 1-P_{NC} & P_{NC} & 0 & 0 \\ 1-P_T & 0 & P_T & 0 \\ 1-P_A & 0 & 0 & P_A \\ 0 & 0 & 0 & 1 \end{pmatrix} \end{array}$$

Expectations of power consumption in this process is: $k \times \frac{1}{P_{NC}} \times E_C$

N nodes' expectations of energy consumption in this process is: $k \times N \times \frac{1}{P_{NC}} \times E_C \times N$

Under the same conditions, that is,the quality of communication channel is the same, comparing the model two and model one's power consumption is the same as the comparison of $\sum_{i=1}^{\frac{N}{2}} \frac{2i}{P_{2iC}} \times E_C$ and $N^2 \times \frac{1}{P_{NC}} \times E_C$.

In this paper, the model N is even. When N is an even number, $\sum_{i=1}^{\frac{N}{2}} \frac{2i}{P_{2iC}} < \sum_{i=1}^{N} \frac{i}{P_{iC}}$

As $P_{iC} \geq P_{NC}$, so $\sum_{i=1}^{N} \frac{i}{P_{iC}} \leq \sum_{i=1}^{N} \frac{i}{P_{NC}} = \frac{1}{P_{NC}} \times \sum_{i=1}^{N} i = \frac{1}{P_{NC}} \times \frac{(1+N) \times N}{2}$

As $N < N^2$, so $\frac{N^2+N}{2} < N^2$

The conclusion is as follows, $\frac{1}{P_{NC}} \times \frac{(1+N) \times N}{2} < \frac{1}{P_{NC}} \times N^2$

Under the good condition of communication channel quality, in model 2, each node can transfer the data in their own planning time N, therefore, the expectation of nodes' power consumption is: $2N \times E_C$

Under this condition,N nodes' expectations of energy consumption in model one has been computed: $N \times \frac{1}{P_C} \times E_C$

As $\frac{1}{P_C} \geq 1$, $N \geq 2$, so $N \times E_C < N^2 \times \frac{1}{P_C} \times E_C$

The above results simulation by matlab,as shown in figure 2:

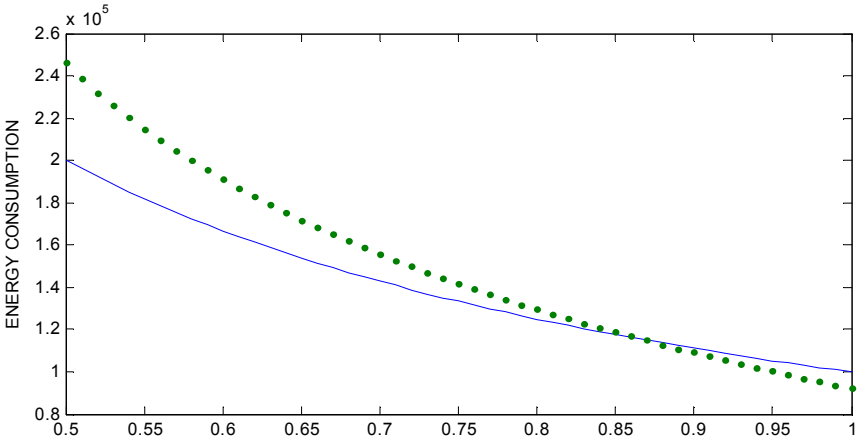

Figure 2:Comparison of energy consumption of the two kinds of model

In conclusion, under the same channel quality conditions, the power consumption of the entire network in model 2 is smaller than model 1 , which can achieve expected purpose——node optimization, reducing power consumption.

Acknowledgements

This paper is supported by the Fundamental Research Funds for the Central Universities(3142014013).

Reference:

[1]LU Ke-zhong,HUANG Liu-sheng,WAN Ying-yu,XU Hong-liDeploying.Sensor Nodes in Wireless Sensor Networks.Journal of Chinese Computer Systems2006,11(27):2003-2006.

[2]ZigBee Alliance. ZigBee Specification 2006. [2010-08].http://www.zigbee.org

[3] CC2530 A TrueSystem-on-Chip solution for 2.4GHz IEEE 802.15.4/ ZigBee [EB/OL].[2011-05-16].http//www.TI.com.

[4]LEI Chun, He Xiao-yang, Su Sheng-hui. Based on zigbee more temperature gathering system design and realization [J]. Automation technology and applications,2010,29(2):43(in Chinese)

[5]ZHOU Xue, Zhang Yun-Gui, Xiao Zheng-Yu based on zigbee technology. The temperature and humidity of the design and application of sensor nodes [J]. Jmetallurgy Since The move,2008,2(45):765.(in Chinese).

Advanced Materials Research Vols. 989-994 (2014) pp 4570-4572
© (2014) Trans Tech Publications, Switzerland
doi:10.4028/www.scientific.net/AMR.989-994.4570

On the model analysis of wireless sensor networks based on library information service

Liu Dongmei Zhang Junsong

North China Institute of Science and Technology,CHINA

KeyWords：model analysis,wireless sensor networks,communication as planned

Abstract：In wireless sensor networks based on ZigBee,we often see such a model that full symmetric transmission model of competition for channel resources based on CSMA/CA algorithm. For the purpose of reducing the energy consumption of entire network,this paper establishes a model that communicate as planned which based on CSMA/CA algorithm.

1 The Introduction

With the rapid development and increasingly mature of communication technology, embedded computing technology and sensor technology,Micro Sensors, which has the perception, the computing power and communication ability,began to appear around the world.[1] This kind of sensor networks is made up of sensor technology, embedded computing technology, distributed information processing technology and communication technology, which can cooperation to real-time monitor, perceive and gather information of various environment or monitored objects in the network distribution area. They can process this detailed and accurate information and transmit the information to users in need.[2]

2 Zigbee technology application in library information service

ZigBee technology is a new type of short distance wireless communication technology,and this technology is considered most likely to be used in industrial control occasions.And it also can use the 2.4 GHz frequency band for free.[3]

From the network configuration,there are three types of ZigBee network nodes: ZigBee coordinator nodes, ZigBee router nodes and ZigBee terminal nodes.[4]

Special attention should be paid that the specific architecture of the network will dramatically affect the resources required for equipment.ZigBee network main support three kinds of topology structure: the Star, Mesh and Cluster-Tree structure. In this several kinds of topology structure, the star network requires minimum resources.[5]

If the zigbee technology is applied to library information service, the library information designated collection will come true.The collection system generally use star network.

3 Communication as planned model based on CSMA/CA algorithm

In this model, node is scheduled to communicate, every two nodes wake up successively, at the same time the two nodes'position is centrosymmetric, with the coordinator as the center. That is to say, the time T_X is assigned to each node,the centrosymmetric two nodes awaken, receiving beacon signal from the coordinator, and communicate with it, as all the other nodes in the sleep state. For example,a coordinator (node 0) and six nodes (node1 - node6) compose the star topology network,which are evenly distributed.Node 1 and 4 wake up at the same time and communicate with the coordinator , node into the sleep state after the communication; In the second T_X , node 2 and 5 wake up at the same time, receiving beacon signal from the coordinator, and communicate with it , as all the other nodes in the sleep state. After the node 2, 5 communicate with the coordinator , the two nodes enter the sleep state; When the third T_X coming , node 3 and 6 wake up, receiving the beacon signal from the coordinator , and communicate with it... and so on. In the period of time T_X , every node has k superframes, that is to say, each node in the allocated time

T_X has k chances to transmit data. Each superframe accounted for $1/k$ of the the entire time T_X. If the node transfers date successfully in the first superframe, it will in a dormant state in the rest of the k-1 superframes, no longer wake. If the node within its distribution time T_X transmit data unsuccessfully with the coordinator, then when the next node wake-up time arrival, the two nodes will compete for channel resources.

State transition matrix of node 1 are as follows:

$$\mathrm{P}_1 = \begin{array}{c} \\ C \\ T \\ A \\ S \end{array} \begin{array}{c} \begin{array}{cccc} C & T & A & S \end{array} \\ \begin{pmatrix} \frac{1}{2} & \frac{1}{2} & 0 & 0 \\ 1-P_T & 0 & P_T & 0 \\ 1-P_A & 0 & 0 & P_A \\ 0 & 0 & 0 & 1 \end{pmatrix} \end{array}$$

In the ideal situation, the product of the node's state at any moment and the state transition matrix is also the state.The state of node at any moment may be in CCA detection or retreat, data transmission, receiveing the ACK response frame, the data packet transferred successfully ,node comes into dormant state. The state of node at any moment is υ, according to the node state transition matrix of transport matrix P_1, calculating the ideal steady state transfer state:

Ideal steady state transfer status, namely:

$$\begin{pmatrix} \frac{1}{2} & 1-P_T & 1-P_A & 0 \\ \frac{1}{2} & 0 & 0 & 0 \\ 0 & P_T & 0 & 0 \\ 0 & 0 & P_A & 1 \end{pmatrix} \times \begin{pmatrix} x_1 \\ x_2 \\ x_3 \\ x_4 \end{pmatrix} = \begin{pmatrix} x_1 \\ x_2 \\ x_3 \\ x_4 \end{pmatrix}$$

Calculating the ideal steady state transfer status is = (0,0,0,1). Therefore, successful dormancy is the absorbing state of the whole system. The energy consumption of the node in each state is written as .The initial state of node 1 is $\mu = (1, 0, 0, 0)$, that is to say, the node 1 can access channel after receiving the beacon frames, because there is no other nodes to compete. The allocation of node 1's transmission time divides into n time slots.,every once in a time slot, the power of the node can be calculated according to the state transition matrix in this state. That is,

$$\begin{aligned} &\mu \times \bar{E} \\ &\mu \times \mathrm{P} \times \bar{E} \\ &\mu \times \mathrm{P}^2 \times \bar{E} \\ &\cdots \\ &\mu \times \mathrm{P}^{n-1} \times \bar{E} \\ &\sum_{i=1}^{n} \mu \times \mathrm{p}^{i-1} \times \bar{E} \\ &= \sum_{i=1}^{n} [(\mu \times \mathrm{P}^{i-1} \times \bar{E} - \upsilon \times \bar{E}) + \upsilon \times \bar{E}] \\ &= \sum_{i=1}^{n} (\mu \times \mathrm{P}^{i-1} \times \bar{E} - \upsilon \times \bar{E}) + n \times \upsilon \times \bar{E} \end{aligned}$$

$$\left| \sum_{i=1}^{n} \mu \times \mathrm{P}^{i-1} \times \bar{E} - n \times \upsilon \times \bar{E} \right| = \left| \sum_{i=1}^{n} (\mu \times \mathrm{P}^{i-1} - \upsilon) \times \bar{E} \right| \le \sum_{i=1}^{n} e^{-C(i-1)} \| \bar{E} \| = \frac{1-e^{-C \times n}}{1-e^{-C}} \| \bar{E} \|$$

In this model, the communication time assigned to each node relative to the data transmission time is relatively long, through the steady state transition probability we can calculate that the successful dormancy is the absorbing state of the whole system. But the possibility of a node unsuccessful in its transmission data can not rule out within the allotted time, such as the channel quality is poor，may exist in this case. As the next node communication period, the case that four

nodes compete in the channel resources may exist. If four nodes transmit data at the same time data , the four nodes state transition matrix is:

$$\mathrm{P}_2 = \begin{array}{c} \\ C \\ T \\ A \\ S \end{array} \begin{array}{c} \begin{array}{cccc} C & T & A & S \end{array} \\ \begin{pmatrix} 1-P_{4C} & P_{4C} & 0 & 0 \\ 1-P_T & 0 & P_T & 0 \\ 1-P_A & 0 & 0 & P_A \\ 0 & 0 & 0 & 1 \end{pmatrix} \end{array}$$

According to the communication situation in the worst case, that is,in the last node's plan communication time data,all the nodes compete for the channel resources,the energy consumption under the condition of mathematical expectation is:

$$k \times （2 \times \frac{1}{P_{2C}} \times E_C + 4 \times \frac{1}{P_{3C}} \times E_C + \cdots + N \times \frac{1}{P_{NC}} \times E_C ） = \sum_{i=1}^{\frac{N}{2}} \frac{2i}{P_{2iC}} \times E_C \times k$$

4 Summary

This paper analyzes the wireless sensor network based on ZigBee. To reach the aim of reducing the energy consumption of entire network，this paper establishes a model that communicate as planned which based on CSMA/CA algorithm.

In the future,we will compare this model with the full symmetric transmission model of competition for channel resources based on CSMA/CA algorithm,to study the superiority of this model in terms of energy consumption of entire network.

Acknowledgements

This paper is supported by the Fundamental Research Funds for the Central Universities(3142014013).

References

[1]QU Lei,Liu Cheng-de, Hu Cheng-bin. ZigBee technology and application [M].beijing:Beijing aerospace university press, 2007.(in Chinese)

[2]LV Zhi-an.ZigBee network principle and application development [M].beijing: Beijing university of aeronautics and press, 2008:12.(in Chinese)

[3] CC2530 A TrueSystem-on-Chip solution for 2.4GHz IEEE 802.15.4/ ZigBee [EB/OL]. [2011-05-16].http//www.TI.com.

[4]LEI Chun, He Xiao-yang, Su Sheng-hui. Based on zigbee more temperature gathering system design and realization [J]. Automation technology and applications,2010,29(2):43(in Chinese)

[5]ZHOU Xue, Zhang Yun-Gui, Xiao Zheng-Yu based on zigbee technology. The temperature and humidity of the design and application of sensor nodes [J]. Jmetallurgy Since The move,2008,2(45):765.(in Chinese).

Advanced Materials Research Vols. 989-994 (2014) pp 4573-4576
© (2014) Trans Tech Publications, Switzerland
doi:10.4028/www.scientific.net/AMR.989-994.4573

Comparative Study of Construction and Operation of the Domestic Famous Park Platform

Yi Wu [1,a], Tian Xu [2,b], Yexiang Fang[3,c], Shuhai Fan[4,d,*]

[1] Wuxi software industry development co., LTD, Wuxi, 214000, China

[2,3,4] Department of Industrial Engineering, Nanjing Tech University, Nanjing 210009, China

[a]yi.wu@263.net, [b]xutian107107@126.com, [c]285487987@qq.com, [d]fanshuhai@tsinghua.org.cn

Keywords: Cloud Platform; Integrated Management; IT Services

Abstract. Introducing the background of domestic park cloud platform. Comparing the Platform construction operations of Suzhou Software park, Hangzhou east software park, Beijing Zhongguan Village software park, Chengdu Tianfu software park and Dalian software park platform construction operation comparison. Through the study, we concluded that park's cloud platform was more than just an IT service platform. It was also a park assets and service of integrated management platform and learning and employment platform. Cloud platform will support park characteristic industry and provide information for the development of the park's industry.

Introduction

These years, under great support of governments at all levels, our country has been integrating regional software industry superiority. Not only does it create favorable hardware and software environment for hardware industry, but it does great contribution to establishing professional creative service system, talent strategy, medium-sized and small enterprises incubation, scale expansion and internationalization of software enterprises, financing and transforming traditional industry.

As IT applications deepen, the quantity of data is certain to increase day by day. Cloud computing, as a burgeoning commercial computing model, gives up a new inspiration [1-3].

Domestic famous parks speed up in building up cloud computing in the process of construction. It will not only improve comprehensive problem solving ability and enhance the orientation of service-providing park, but it can improve intelligence of park management.

The comparative analysis of famous park clouds' construction and operation

Suzhou industry park

These years, Suzhou Industry Park has been focusing on software, monolithic circuit, bio-pharmaceuticals, animations and games, NT, telecommunication of next generation under the aim of technology spanning plan and creating creative science and technology park. Also it creates support ability of industry development, improves self-dependent innovation ability of enterprises and promotes industry development environment. [4]

(1)Industry technology service platform

Surrounded by software, monolithic circuit, bio-pharmaceuticals, animations and games, NT and new materials, it has completed all coverage of key industries. It has established software rating public service platform, software as a service (SaaS) platform, monolithic circuit design and testing

platform, bio-pharmaceuticals experiment platform, antibody profession technology service platform, NT process platform, NT detection platform and animations and games public technology service platform. Also it will lay out to integrate telecommunication industry service platform, embedded software platform, biological new drugs security rating platform, GMP platform, NT photoelectron and NT manufacturing technology platform.

(2)Supporting service platforms

Centering on science and technology innovation, science and technology innovation integrated service center is set up. It integrates Suzhou Industry Park enterprises, colleges and universities within district, Suzhou NT institute, intermediaries at the aim of professionalization, marketization, socialization service. Also a integrated service platform is built up, covering investing and financing of science and technology, industry-university-research cooperation, technology achievement transformation, scientific information and information services, project application service, policy consulting, market channels and promotion, intellectual property, talent training, integrated supporting and so on.

Hangzhou east software park

The east software park has been exploring a sustainable development mode in its developing process, which can help the park of science and technology develop successfully. From the point of this strategy's aim, it puts forward 2 requests, which can be describe below: one is to solve the problem of how to achieve low carbon, high effective, sustainable development; the other is the growing problems of medium-sized and small enterprises. It's construction centering on new service system of scientific innovation, which will quicken the development of science and technology industry.

The service contents from wisdom park cloud platform mainly include 5 aspects. The first one is flexible computing cloud, flexible computing service based on Ali cloud. The second one is testing cloud, which can simulate real users' operation and conduct real time function tests so that the cost pressure of enterprises will be reduced. Thirdly, developing cloud includes integrated circuit and software developing collaboration platform. ALL sorts of public technology platforms co-build developing environment to help medium-sized and small enterprises grow quickly. Fourthly, cloud official business can provide cloud desk renting service, which is safer, more reliable, easy to manage and quickly arranged, extensible. The enterprises don't need to apply resources to operation and maintenance of desk system. So it improves IT efficiency and reduces TCO. The fifth one is application of web of things. The management system based on web of things in wisdom park arranges and achieves resources management, intellectual lighting, intellectual air-conditioner, equipment inspecting.

Beijing Zhongguancun software park

Zhongguancun software park service cloud was officially released online in 2011 cloud world conference. The platform serves more than 50 enterprises in Zhongguancun software park with Iaas service (cloud server, cloud storage), SAAS (CRM, e-mail system, online network disk), basic PAAS service and so on. As Xiangyun project and the first arrival industry park cloud service platform in domestic, it insists on the idea of "the government guides strategically, the professional companies operate, leading enterprises drive, public platforms support". It gathers core enterprises

from every link of industry chain and establishes \industry innovation eco-system, which will play an important role in setting new standards, new industry condition incubation and cultivation of new leading enterprises. [5]

As the first park cloud service platform with independent intellectual property rights in domestic, now Zhongguancun cloud service platform has achieved flexible computing and storage with webs which is typical IaaS service ability. What's not the same implementation model with foreign public clouds such as Amazon is that Zhongguancun cloud service platform achieves arrangements of end to end and localization delivery. And it gets support from distributed visualized data center of China Netcom broadband MAN at the same time. So it solves thoroughly the problems which domestic cloud service delivery quality can not be guaranteed such as cloud service's availability, reliability and safety.

Chengdu Tianfu Software Park

At present, Chengdu is managing to create the wisdom and modern garden city of the world. Smart City will be an important direction of the city's development when the city develops economy and information technology. As China's largest professional software park, Chengdu Tianfu Software Park is also accelerating the pace of constructing smart park. Information construction is the carrier. The manager will strive to connect resources within the park with external resources. New a park one-card-through system and Chengdu Tianfu card is integrated. User can own e multifunction card and combine other redundant cards [6].

"Network E-School" established by Tianfu Software Park is a new online learning platform. It uses professional courses of world-renowned education services provider in order to provide an interactive and new "E-learning" training model for all businesses online in park. Tianfu Software Park also offers a number of public platform resources to enterprises. Among them, the moat famous is national public platform software technology resources spend billion to build. The managers can rent a variety of development equipment and software after enterprise applications are put forward. For entrepreneur teams and the developing enterprises, such platforms will largely reduce development costs on businesses.

Dalian Software Park

Dalian Software Park is a service-oriented company that manage science and technology, real estate and park management services. Service system includes investment development, project management, investment management, customer service, property management and human resource services . The departments of investment development and project management are body of work in Dalian Software Park. They are responsible for the park's construction planning and project management services on site. Most department personnel are represented the number of company staff.

Dalian Software Park is not involved in the construction of smart metering systems and smart card system. The managers use Kingdee system to integrate internal company information. The system belongs to the ERP system. It mainly has the finance function and CRM management functions. It covers a single function that involves the projects, finance, procurement, CRM, and part of the company management process. There is no professional team to construct and maintain the information systems. They use professional systems such as human resources service platform and campus portal to provide relevant information about the park's corporate information system.

Summary

Cloud platform is established in order to improve efficiency and reduce costs. In this context, the integration of resources and building of public service platform is extremely important. Through cloud solutions, physical separation can be realized just in logic [7]. Also through virtualization, we can make a substantial increase in efficiency. Therefore, we can reduce a lot costs of operation, hardware software, and so on.

Through comparing the construction and operation of the domestic famous park platform, we know cloud platforms could be able to manage park resources. In the development process, the platform can learn management experience. Based on the principle called "resource sharing, business cooperation, complementary advantages, value-added innovation and sustainable development", we can achieve the goals that integrating public service resources, configuring and scheduling uniformly and building intelligence platform. Park's cloud platform is not only an IT services platform, but also a comprehensive platform that manages park's assets and services. We can learn and find jobs on the platform. The cloud platform would be a support platform that has characteristic industry. It will provide strong support for the development of the information industry park [8-9].

Acknowledgements

The research work was supported by National Natural Science Foundation of China under Grant No. 71171110 and No. 71371097.

References

[1] Liang Yong, Zhang Panxiang, Chen Qiuhua. Construction and Operation Program of Enterprise-Class Database Cloud Platform. Telecommunications Science Vol.28 (2012), p. 146-155

[2] Jiang Wuxue, Zhang Jing, Wang Zhiming. Cloud computing and its architecture model. Journal of Liaoning Engineering Technical University (Natural Science Edition) Vol.30 (2012), p. 575-579

[3] Yin K, Cloud Computing: Concept, Model, and Key Technologies. ZTE Technology Vol.8 (2010), p.21-26

[4] Wang Shoubin, Gao Hongtao. Foreca st & Ana lysis of Demand for Skilled Personnelof the Suzhou Industr ia l Park Ba sed on Industr ia l Structure Adjustment. Journal of Hunan Industry Polytechnic Vol.10 (2010), p. 17-19

[5] Cheng Juhua. High-tech industries of China's economic transformation roadmap. Zhong Guancun Vol.4(2007),p. 26-29

[6] Shellhammer S J, Goren D P, Pavlidis T. Novel signal-processing techniques in barcode scanning. Robotics & Automation Magazine Vol. 6(1999),p. 57-65

[7] Liu Yue. Reviews of Cloud Computing and Research on the Application of Mobile Cloud Computing. Information and Communications Technologies Vol.4(2010),p. 15-20

[8] Zhou Yang. SaaS Model to Build E-government Services Cloud Platform. China Management Informationization Vol.15(2012),p.43-44

[9] Wang Xiaoqin, Zhao Gang. The Research of Architecture in IT Service Management Enterprise Center. Informatization Construction Vol.5(2006),p. 53-54

Advanced Materials Research Vols. 989-994 (2014) pp 4577-4580
© (2014) Trans Tech Publications, Switzerland
doi:10.4028/www.scientific.net/AMR.989-994.4577

Discussion on the micro-blog information resources in disseminating the local image

Luo Zixin[1, a], Li Siyi[2,b]

[1] Sichuan Academy of Social Sciences, Chengdu, P.R.China, 610071；

Sichuan University, Chengdu, P.R.China, 610041

[2] Chengdu University of Technology, Chengdu, P.R.China, 610059,

[a]luozixin21@aliyun.com, [b]ceciliasiyili@hotmail.com,

Keywords: Agenda setting; micro-blogging; information resources; local image

Abstract. This article studies the characteristics of agenda setting and mode of transmission, which are presented in the micro-blog information resources in spreading the local image. Discovers the operation pattern, at the same time, tries to seek the common pattern of local image communication in new media times through micro blogging, which on behalf of the local social media, and then use the micro-blog information resources to shape and optimize the local image.

Traditionally, people always do research on the information resources sharing from two aspects: one is to consider information resources from the rational distribution and configuration in the geographic area to achieve maximum sharing; the other is to share information resources through cooperation between the information providers [1]. Micro-blogging is a derivative of personal blog. It is a We-Media form, “Users can send short messages with maximum 140 words to their micro-blog through cellphone, IM(such as QQ, MSN, Gtalk, etc.), email and web”[2]. These short expressions might be catharsis, inspiration catching, just forward something, or self-entertainment, are all shown in public. It is clearly that to disseminate the micro-blogging information, the geographic area has merely no influence on the micro-blogging information resource flows. But “the cooperation between information providers” is more prominent in the micro-blogging information, which carries out mass information and has characteristics of interpersonal communication. With the popularization of 3G technology, tablet PC and other clients have become the popular platform for publishing micro-blogging information. Micro-blogging information is the very influential information resources on the public. Its’ agenda setting function is highlighted in disseminating local image in public place, and has further development Political scientists, Bernard Cohen, stated in the book, The newspaper and foreign policy, that “the press may not be successful much of the time in telling people what to think, but it is stunningly successful in telling its readers what to think about”. In the 1968 presidential elections study, by comparing “what the voters thought was the most important election issue” and “what the Media reported was the most important issue in the same period”, American Communication experts Maxwell McCombs and Donald Shaw found a strong correlation between them. In 1972, they first put forward the agenda-setting function of mass media in The Agenda Setting Function of Mass Media. They believed that “news reports by the Media and information convey activities influence the salience of topics on the variety of public agenda, affects the judgment of people around the world to the 'event' and the degree of its importance”. This theory also stresses that agenda setting is the media’s ability to transfer salience issues through their news agenda so the public agenda can form their understanding of the salience issues [3]. Agenda setting means that the media, an institution engaged in “environment reconstitute”, is not only the important information source, but also the important impact source. In micro-blogging information resource dissemination, the increase of communication subject let every micro-blogging users become information receiver, commenter and transmitter. The decentralized the speaking rights make micro-blogging users having the same potential audience the traditional media has and build a community of discourse focus with the traditional media and Internet media (in other application form). Therefore, compared with the

traditional agenda-setting theory, micro-blogging information resources agenda-setting has widen its scope, and could achieve through the interaction between the institutional or personal micro-blogging and user.

(1) Institution Micro-blogging Information Resource Sharing

At the early stage of blog, the representative of the We-Media, blog website usually made judgment of what topic the public might be interested based on the news event happened recently, and took the active planning way to arrange, recommend or post the context published by blogger, or set some discussion topics on the webpage to let the user participate in topics through blog context, and these blog context often get higher clicking rate and reading rate because of edit settings to set the agenda of the role. The 2006 year China's blog survey report published by China Internet Network Information Center (CNNIC) showed that over 40% readers read blog through the blog home page [4]. This creates a blog channel editor for the audience agenda setting， and this agenda setting dominated by web site and agency blog still work in nowadays.

The appearance of "micro-blogging square" [5] displaces the original agenda-setting function of the blog portal. But this function is been diluted in a certain extent because of the limitation on word amount, and replaced by the information released by every institution and media's micro-blog. For local image, these institutions do a micro-blogging follow-up for the local image campaign. For example, during the Western Fair, Chengdu People's Government Information Office official micro-blog "Chengdu Release" posted series of news related to this event with the form of "focusing on the Western Fair" column, and there were some positive comments on Chengdu from the guests, such as "Chongqing Mayor Huang Qifan visited and observed Chengdu tourism and leisure, cultural and creative industry development and he stated that the Easter park keeps authentic industrial elements, and also fully integrates into the most modern music elements, it's so creative". And former Japanese Prime Minister Hatoyama Yukio commented that Chengdu is a beautiful and modernized city. For "Chengdu Release" which has over 1,600,000 followers, this information undoubtedly did a positive spread of local image, and played a role in agenda setting to its followers.

The institutions' blogs with a large number of followers have a very good agenda setting effect. They play an important role in the daily dissemination of information and the local image building. And the institutions (especially the media) also can reflect local image through micro-blogging the news events. For example, on October 21st 2011, "Xiao Yueyue Event", a 2 year old girl was successively crushed by two cars at Foshan. In 7 minutes, there were 18 strangers passing all turn a blind eye, nonchalance but go. At last, a scavenging woman approached to lend a helping hand. This event led a widely debate by micro-blog users. About Foshan local image, several representative comments from micro-blogging users were collected by the writer: "A fresh life had been ruined by rich Guangdong, Foshan people", "The apathy of Cantonese, it's time to rethink the market economy society! Foshan's apathy, Guangdong's apathy, the indifference of the people! We can't tolerate it and it's time for us to rethink the market economy society". "Foshan really deserves to be China's most apathy city!" "Foshan, a place you can choose not to live, live in the death is a continuation of Life. It should just call "Shan" (mountain) instead of "Foshan" (Buddhist Mountain)." Obviously in this event Foshan people's apathy reflects the business atmosphere of this city, which is sorely lacking the most basic moral conscience and human kindness.

（2）Agenda Orientation of Personal Micro-blogging Information Resources

Although most micro-blogging audiences are influenced by institutions' micro-blogging information, the interpersonal communication advantage reflected in the personal micro-blogging information resources can't be ignored. The followers, as the receiver, repeatedly refresh the information of the people they care about to get the update information from communication subject. By this way, audiences will inevitably be influenced by individual micro-blogging agenda-setting. The information released by micro-blogging users in their own interest or attention may not get into

audience view from micro-blogging square and also did not get strong communication effect because of lacking fans. But after the interpersonal communication and group transmission, it is also possible to obtain a higher degree of the attention between acquaintances and have a certain impact.

Of course, there is also some celebrities will conduct the agenda setting for fans through consciously talking about the topic. Such as they will release some topics or questions they thought valuable to interact with fans or increase the influence of the issues though the form of releasing series of the micro-blogging, or through the fans forwards, comments, or hyperlinks expansion to the relevant topic, attract the audiences' attention. For example, some reporters often release some news which could not be seen in traditional media for various reasons, or express their views and opinions to attract the attention and response of internet users. In this way the content they spread can often receive attention quickly, and quickly become a hot discussion.

In addition, the communication subject of the micro-blogging information resources can "weaken or strengthen the topics taking about" though some technical methods. Such as delete, add special symbol (for example in sina weibo, the symbol "#" is used to mark the scope of topics), transmit repeatedly, and forward audience comments to achieve agenda setting.

（3）The Interaction between the User "Strengthening" the Information Resource Agenda Settings

The spillover effects, formed by the city's political, economic and cultural aggregation function, and the reality demand or imagine consumption from the individual and organizational, make the city, individual and organization connected to each other becoming a reality or potential, direct or indirect benefited party and risk taker. This community relationship of interests is a mutual stakeholders' relationship. They embody the partner relationship with the public interests as its axis which is formed by local image communication in the social favorable development and related groups and organizations. Therefore, after the information resources forwarded by the institutions or personal micro-blog, or whether consciously or unconsciously set the agenda for visitors, it usually leads some audiences to have a further discussion around the issue by the way of giving some comments or forwarding. The spillover effects, formed by the city's political, economic and cultural aggregation function, and the reality demand or imagine consumption from the individual and organizational, make the city, individual and organization connected to each other becoming a reality or potential, direct or indirect benefited party and risk taker. This community relationship of interests is a mutual stakeholders' relationship. They embody the partner relationship with the public interests as its axis which is formed by local image communication in the social favorable development and related groups and organizations. Therefore, after the information resources forwarded by the institutions or personal micro-blog, or whether consciously or unconsciously set the agenda for visitors, it usually leads some audiences to have a further discussion around the issue by the way of giving some comments or forwarding.

Some scholars believe that We Media can make the "noise" reduced to a minimum level in the communication process. Because micro-blogging information recourses have a strong interaction, the audiences can directly access the information which is released by communication subject at first time. Even though the audiences may have different understanding, they can eliminate the "noise" in time through the interaction with the author. Therefore, during micro-blogging transmission, the information released by opinion leader may minimize misunderstandings. On the other hand, audience can through forwarding of the information to contact the information source directly, which guaranteed the authentic and comprehensive of information in a great degree. Audiences can directly express their own opinions or provide some supplementary information of the issues. These timely, sufficient and free expressions make the opinions of communication subject and audience shown in public. Different opinions mutually penetrate, fuse and extend, which will affect other visitors' focus, understanding and judgment of the issue. This process not only "strengthens" the agenda-setting

function of institution and personal micro-blogging, but also provides the space to form the new agenda, and plays a more effective role in the local image spreading as well.

Acknowledgement

This paper is funded by Sichuan province philosophy social sciences planning program (SC11C023), general achievements of Sichuan province philosophy social sciences popularization planning program, Academic and technical outstanding youth leaders program in Sichuan province, and Statistical scientific research projects in Sichuan Province (2011sc126), Chengdu Science department's soft science project, Science and technology plan projects in Sichuan province (2013ZR0116, 2014KZ0008, 2013ZR0177), Chengdu soft science project (13RKYB059ZF-041), Sichuan province philosophy social sciences key research base (Li Bai culture research center) project (LB13-11), Sichuan province education department's humanities and social science key research base (Xihua university's local cultural resources protection and development research center) project (13DFWH006.1) , general project of cultural industry development research center of Sichuan province philosophy social sciences key research base (WHCY2013B05), and Youth develop program of Sichuan academy of social sciences. Thanks all.

References

[1] F.C.Ma, L.Pei: *Overviews on Information Resources Sharing Theory and Practice in China* [J], Journal of The China Society For Scientific and Technical Information, 2005(3). (In Chinese)

[2] W.H.Sun, Q.Y.Zhang: *Micro bogging communication pattern analysis* [J], Media observation, 2008. (In Chinese)

[3] S.A.Lowery, M.L.DeFleur writes, H.L.Liu translates: *Milestones in Mass Communication Research: Media Effects* (Third Edition)[M].China Renmin University Press, 2009. (In Chinese)

[4] C.Q.Xu, L.Y.Ruan: *Analysis the function of the network media in the public domain--In the blog, as a representative of the network space analysis of public opinion*, Journal of Fuqing Branch of Fujian Normal University ,2009(5). (In Chinese)

[5] Micro-blogging plaza is selected by the editor appear on the landing page, the user of the latest release some information can lead to mutual concern, comment on the news or event-based, such as Sina micro-blogging "we are talking about", and Phoenix micro-blogging "hot micro-blogging"

Advanced Materials Research Vols. 989-994 (2014) pp 4581-4584
© (2014) Trans Tech Publications, Switzerland
doi:10.4028/www.scientific.net/AMR.989-994.4581

Design of Multi-functional Gateway in Mine Internet of Things

Yuqin Su[1,a], Ying Liang[1,b], Zhao Xu[2,c]

[1]Communication Company of Lu'an Mine Group Ltd,ChangZhi 046204,China

[2]China University of Mining and Technology, Xuzhou 221008,China

[a]suyuqin@126.com，[b]lynncumt@163.com,[c]xuzhao551@163.com

Keywords: Mine Internet of Things; Multifunction Gateway; Optical fiber Ethernet; WiFi; ZigBee

Abstract. Mine Internet of Things can be divided into 3 layers: sensing layer, network layer, application layer. Multi-functional gateway of Mine Internet of Things works at the edge of the network layer, and it both has access and transmission functions. It can make use of various communication media like optical fiber, cable and radio waves. It also adapts to a variety of protocol interfaces like industrial ethernet, WiFi, ZigBee, CAN, RS485, RS232 and so on. It can convert information of sensing layer into ethernet data which can be transmitted by Gigabit fiber ring network.

Introduction

Internet of Things is the network of "thing to thing", whose access of information and transmission need a ubiquitous network. The ubiquitous network needs to be interconnected and fused by all kinds of existing or newly-built medium, protocols and heterogeneous networks[1]. Because of the high speed, high reliability and intrinsic safety, optical fiber communications has been the first choice of transmission media for mining backbone transmission network.

There are as many as dozens of monitoring and controlling systems in mine. Networking equipments of the systems are not almost the same, particularly networking protocol. Therefore, during building Internet of Things in mine, we urgently need the sub-station and multifunctional network node equipment that can be compatible with a variety of monitoring and controlling systems. The basic features of the equipment include: 1) easy accessing voice, video, and various monitoring and controlling data; 2) achieving transmission media flexible adapter from wired and wireless to optical fiber; 3) offering a variety of standard transmission interfaces, such as RS485, RS232, CAN, Ethernet,WiFi, ZigBee, etc.

According to this demand, this paper design multifunctional, multi-media, multi-interface gateway in mine Internet of Things based on optical fiber GbE (Gigabit Ethernet), in order to achieve a variety of Monitoring and controlling data access high-speed fiber-optic transmission network, which is real-time, long-distance, without distortion transmission.

Corresponding to three layers of functional structure of IOT[2]: sensing layer, network layer and application layer, the gateway in Mine Internet of Things mainly works at the edge of network layer, and it both has sensory information access and transmission network functions. Because the gateway in Mine Internet of Things has diversity function and flexibility interface matched and used which can cover the basic requirements for the various requirements of transmission in mine.

Overall Architecture of Gateway in Mine Internet of Things

The gateway in Mine Internet of Things utilizes embedded systems, FPGA and ASIC technologies integrated overall program which is modular, building-block design structure. The main function modules of it include embedded control management module, FPGA interface conversion module, Gigabit Ethernet switching module, WiFi high-speed wireless communication module, ZigBee/IEEE802.15.4 wireless sensor access module and power module. The specific architecture is shown in figure 1.

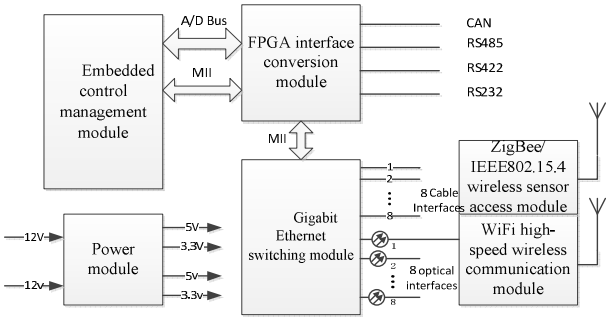

Fig.1 Overall architecture of gateway in mine Internet of Things

Wired communication is the primary means of transmission in mine. The optical fiber industrial Ethernet has been widely used as backbone transmission ring network in mine. Therefore, the sub-station takes Gigabit Ethernet switch module as core. The configure interface converter module achieves data conversion between Ethernet and other industrial field bus (wired) interface, and embedded control management module is responsible for the entire sub-station configuration management, protocol conversion, and remote control management. The above three modules and power modules constitute the motherboard of gateway Internet of Things.

WiFi and ZigBee module are designed as wireless boards. They can work independently, and to be used to access voice, video, other high-speed mobile data, and wireless sensor nodes, personnel position data, etc.

Ethernet switch module selects VSC7429 which is carrier-class Ethernet switch chip of Vitesse. VSC7429 is a complete system on a chip, and integrated processor MIPSTM in a single chip, that provides 8 electrics, 8 fibers and 16 Gigabit Ethernet interfaces. It has capabilities of networked timing and performance monitoring, and supports storm suppression, port mirroring, LACP link aggregation protocols and RSTP spanning Tree Protocol, and has 4096 VLAN, rich QoS and ring protection feature. It aims at multi-fiber Ethernet ring network interconnection and access application, fully functional, and low-power of Ethernet switches.

The power board is made up of two DC/DC modules which are respectively 12V to 5V and 12V to 3.3V. This paper focuses on embedded control and management module, FPGA interface converter module and hardware configuration and design of wireless boards of motherboard.

Hardware Design

Design of Embedded Controlling and Management Module.

See diagrams 2 for the formation principle of embedded control and management module. As shown, with MPC8308 of PowerPC as its core, matching 16M Nor Flash and 1Gbit DDR2, so it can run the embedded operating systems and the minimum embedded system in the software of the communication, management and controlling working in various of networks. Take advantage of the MII interface of network controller eTsec0 within the MPC8308, which can extend the common Ethernet transceiver IP101A to form the adaptive Ethernet interface with the rate of 10/100Mbps and regard as the interface of remote managements, network debugging and data communications. The A/D Bus (address/databus) and the MII interface of eTsec1 should be connected to the FPGA at the same time, so it can not only ensure that the data and the management, controlling channels of the MPC8306 to Ethernet switch going ahead, but also ensure that the RS232/RS485/CAN Ethernet monitoring data which is packaged by the FPGA hardware to access to Ethernet rapidly.

The Console interface is used exclusively for proximal configuration and management of the switch. The other ways to configure and manage the switch, such as Web, Telnet and so on, must be used after the basic configuration relying on the Console. Because they often need the help of the IP address, domain name, equipment name to realize, but the newly purchased switch containing these parameters is apparently impossible.

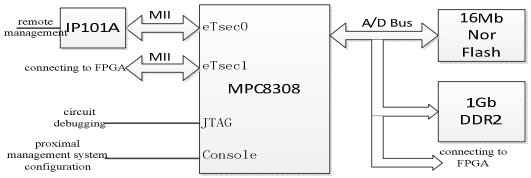

Fig.2 The hardware of embedded control and manage module

Design of Interface Conversion Module on FPGA.

The interface conversion function of gateway is mainly realized by FPGA, which has two advantages: firstly, the standard interfaces in the design are RS232/485/422 and CAN, but the sites of mine might use other protocols and standards, the FPGA is field programmable, so it can provide various conversion interfaces what we needed; secondly, if we convert and package by software after CPU, could not ensure the real time data when the rate of the monitoring data more than 100kbps.

With reference to Fig.1 we can see that the FPGA module has a lot of interfaces and wide kinds. The kinds include the address/databus and MII bus connected to the MPC8306, the UART, SPI connected to various monitoring equipment and field bus, which should be realized through hardware description language within FPGA. There also has an important task in FPGA, which is to assemble Ethernet packet after the multiplex serial data multiplexed and send to Ethernet switch directly through MII interface, in order to achieve high-speed data transferring with hard real-time guarantees. All the related design work has immature VHDL language module in the authors' laboratory, readers are referred to Reference［3-5］ and will not be described here.

Design of Wireless Board.

The wireless board with Wireless Routing switch chip RT7620A of Ralink as the core, which supports three modes of 802.11b/g/n and the maximum transmission rate up to 300Mbps, having five Ethernet switch internally installed, supporting HNAT function, and having strong routing transmit capability. It also supports two UART (the serial port). One is regarded as console debugging interface, the other is connected to CC2530 to form wireless communicating interface of ZigBee/IEEE802.15.4[6].

The WAN port and one of the LAN ports in the built-in switch are connected with Ethernet transceiver AR8033 and optical fiber transceiver module, forming two fiber communication interfaces, so that the board has a Gigabit WAN interface when the board is connected with the main board. When used independently, concatenation of multiple boards through fiber can form a linear network even ring.

In Figure 3, the electrical interface consists of Ethernet line transformer and related resistance-matching circuit, signal indication LED for communicating and RJ45 joint. The optical interface mainly consists of fiber communication transceivers and related resistance-matching circuit, power filtering circuit.

The main performance indexes of wireless board:

1) Supporting 802.11b/g/n and the wireless maximum transmission rate up to 300Mbps;

2) Supporting three adaptive electrical interfaces with the rate of 10/100Mbps, one optical interface with the rate of 100Mbps, one optical interface with the rate of 1000Mbps;

3) Supporting the WDS function, this can realize the concatenation of wireless;

4) Supporting the AP Client mode, this can be connected to wireless AP;

5) Supporting no longer more than eight SSID;

6) Supporting the mutual switching and transmission between Wife, Ethernet and ZigBee.

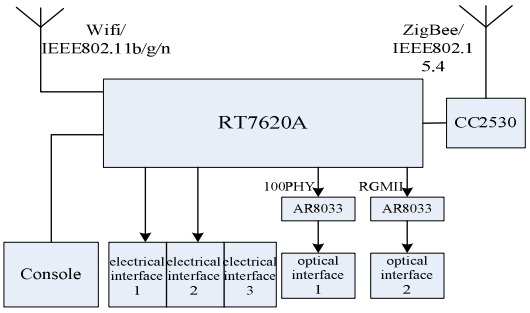

Fig.3 The principle of wireless router board

Summary

Using a variety of advanced technologies and sophisticated results, we design a gateway in mine internet of things, which can adapt to a variety of the transmission mediums and protocols. The gateway includes two independently running boards: the main board and the wireless communication sub-board. The main board takes the Gigabit Industrial Ethernet as the core, which has a variety of interfaces used in optical fiber communication and cable communication which is needed in coal mine underground. It can complete the real-time transfer between gigabit Ethernet based on optical fiber, cable and field bus. The wireless sub-board achieves the interchangeable data transmission between WiFi, ZigBee and Ethernet. Therefore, the gateway in mine internet of things can almost meet the demands for every aspect of networking communication in coal mine underground.

References

[1] Wei Wu, Lianhe Luo. Internet of Things and ubiquitous communication technologies[M]. Beijing: Publishing House of Electronics Industry, 2012, 16-17.

[2] Shen Zhang, Enjie Ding, Zhao Xu. Part I of Lecture of Internet of Things and Sensor Mine-Basic Concept of Internet of Things and Its Typical Application[J]. Industry and Mine Automation , 2010(10),104-108.

[3] Zongyi Chen, Zhao Xu, Chongxun Wei. FPGA implementation of optical GbE+TDM communication technology[J]. Optical Communication Technology, 2011, Vol. 35(9),15-18.

[4] Jie Chen. FPGA implementation of Real-time Communication Interface of Coal-mine Rescue Robot[D].Xuzhou: China University of Mining and Technology, 2009.

[5] Qiang Zhang, Hongdang Zheng. Synchronous transmission principle and implementation of asynchronous data base on FPGA[J]. ELECTRONIC ENGINEERING & PRODUCT WORLD, 2005,10.

[6] Weicong Zhang,Xinwu Yu,Zhongcheng Li.Wireless Network Sensor Node design base on CC2530 and ZigBee protocol stack[J]. Computer Systems & Applications,2011,Vol.20(7) ,184-187+120.

Advanced Materials Research Vols. 989-994 (2014) pp 4585-4589
© (2014) Trans Tech Publications, Switzerland
doi:10.4028/www.scientific.net/AMR.989-994.4585

The Research and Design Based on IntelliJ IDEA+Oracle Measuring Management System

Li Zhu[1, a], Lan Bai[2,b], Rui Ying Zheng[1,c]

[1] Jiangxi Science and Technology Normal University Nanchang, China

[2] Jiangxi Modern Polytechnic College

[a]bailan_1982@sina.com, [b]ilovexz0802@163.com, [c]zhengruiying@sina.com

Keywords: Measurement; Business systems; JSP; IntelliJ IDEA; The oracle database

Abstract. On basis of the need of measurement, this paper is dedicated to build the IntelliJ IDEA + Oracle based metering management information system mainly in computing process. According to the needs of the business, we designed the multiple functional modules, gave the system architecture, develop platform and the database design strategy and completed the overall design of the system. Meanwhile we also made the profound discussion on some key technologies in the metrology management system. The research and design of the system thoroughly transforming the existing operation and service mode, fundamentally realize enhancing the scientific and technological content of department of metrology by means of computer science and promote the management standardization and efficiency of measurement work

Introduction

Along with the development of economic globalization, rapid expansion of enterprises, great improvement in operating efficiency, measurement testing department transformation from the original FaZhiXing technology supervision and management institutions to service-oriented institutions, measurement testing department is getting unprecedented development in the process of meet the testing needs of enterprise. Accordingly, the rapid development of computer technology also makes the measurement business management gradually transform from manual management mode to the computer automation. The design of the measurement of business management information system with the development of the informatization construction of legal metrology institutions across the country, as well as a variety of software and hardware facilities, measurement management system has become more and more urgent to research and design requirements. Construction of measurement management system is in order to improve the efficiency and the purpose of promotion. However only through the planning and development of information resources it can play its role to the greatest extent. In this paper, design and research of metrology management system requirements for measurement, as well as the measuring mechanism of daily office, personnel management, file system to be able to realize integration, standardization, unification, so as to realize the real office automation.

The Related Background of Metering Management System Research

The Related Technology Applied by System

This system uses the development pattern which is the JSP reception combined with the background of ORACLE database B/S structure taking JAVA as a development language so that the program code and structure are optimized, and also can improve the efficiency of program. This system is developed in IntellijIDEA7.0.1.In this paper, the development environment is IntelliJ IDEA7.1 with Oracle11g. IntelliJ IDEA, one of the most useful Java development environments, is a relatively new Java IDE. Highly optimized IntelliJ Idea makes it much easier to common tasks, the Idea support many integration function, it is more important that they designed very easy to use. Idea support XML code

in the implementation, the Idea and correction of XML, the Idea of support structure of the JSP.ACTS on the many functions of ordinary Java code applies to the JSP (such as the integration of functions), at the same time support the JSP debugging; Support the EJB, although it does not include the special support to individual application server. Idea to support the Ant build tool is not only the target it support to compile and run the program before and after the operation target, but also support the binding keyboard shortcuts. When editing an Ant build an XML file, the Idea of the Ant project also part of the XML to provide support. IntelliJ IDEA is known as a development platform is the best JAVA IDE. Oracle oracle11g is the latest company to launch a database, support for UNIX platform has the very good database management functions such as processing speed, high level of security, support flash and perfect recovery, do a few database load database, can be done within 30 s failover, grid control, and data warehouse is also very strong so this design USES the oracle. At the same time the system development environment also provides a large number of alternative data control, we can easily establish the connection between the database and on the basis of this connection, use a variety of common data components for database operations.

The Feature of the System

Traditional manual processing data is very complicated, and the efficiency is very low, while with the present rapid development of network technology, and through modern network management system, It can be dealt with related business anytime and anywhere by passing the shared information measurement. The present application of network technology in measuring work for effective management, control, can improve work efficiency, and it is a good way to standardize business processes, conducive to more effective management of metrological work. In order to adapt to the new situation of the need of measurement management and service work, we make the measurement work further to a higher level and development of the new field, introduced in the informatization construction of metrological work is particularly necessary.

This system is to establish a complete and orderly metering management system, and fundamentally change the existing operation mode and service mode, basic implementation using computer technology on the analysis of original data processing, the measurement of management and service implementation of computerized management, to serve by units or individuals provide standard calibration certificates and test reports and calibration certificates and relevant conclusions and data, upgrading of the technological content of metrology department service, promoting the administration of metrological work standardization and high efficiency.

The System Planning and Analysis

Developing measurement management system needs to analysis the demand and design overall, use the analysis system objects, design the system architecture and database structure, decide to use the development tools and background database, and plan and project development progress. This work is very important in the actual project development process.

The Design of System Structure

In this system, the core technology need to be solved is how to access data, by appropriate means. And for different needs, we should choose what kind of data the collocation of components to achieve a specific purpose. The data access is as shown in figure 1. The picture data in this system is to access the operation process of abstraction. The above takes data principle as the foundation combines with the characteristics of the measurement management system, the whole system will be divided.

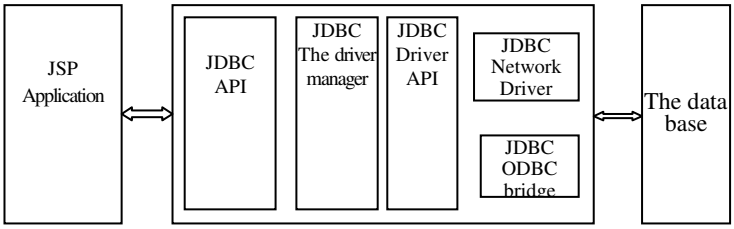

Figure 1. Data deposit and take out picture

The Analysis of System Function

The main purpose of measurement system is to improve the working efficiency of the staff, make itself equip a shared information platform for personal office. A preliminary set of main function modules includes: login module, my work, data maintenance, customer service, interactive platform. When the user login successfully into the measurement business system after first saw four big modules, And then in each module is divided into several small modules. They completed the corresponding increase respectively, query, modify, delete messages, and other functions. Users can easily query, modify the corresponding information. As is shown in figure 2:

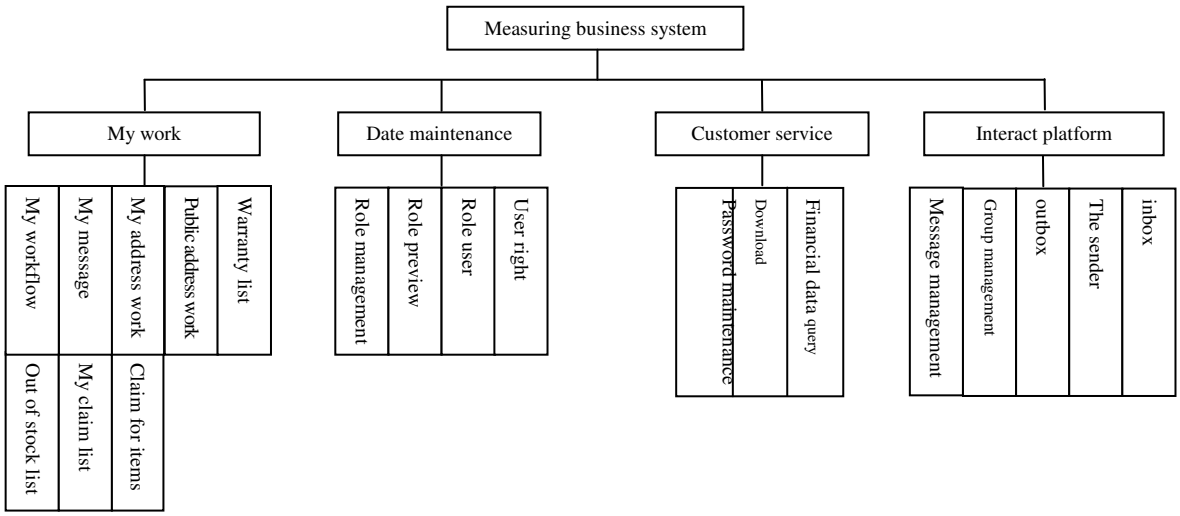

Figure 2. The system function module chart

System is the first impression to the user interface, the user has a close relationship with whether to choose to use this system, so the design and implementation of related becomes very important. The system has designed the a series of modules, namely, the user login module, address list module, sending information module, the register of products shortage module, the input of repair form information module as well as various kinds of solution to deal with the condition when abnormalities occurs.

In multiple modules, take the current shortage of supplies register module as an example, we defines a public DBUtil class, it respectively achieve the current database connection, release a database connection, released a statement, and closed results function. If you want to connect to the database, only to call get Current Connection DBUtil class () method.

Then is the Dao class to realize database operations, Dao class it first call to get Current Connection DBUtil class () method, which connect to the database then define the database query, modify, delete, and insert a series of operations. As long as the corresponding methods of the Dao can be used in Action, the database can make operation. For example the user who selects good claims department, choose the type of products, fill out the required information (add an asterisk behind for mandatory

fields) and then click the submit the data of the page will be submitted to the database. The interface as is shown in figure 3:

The Test Of The System

Under carefully controlled system environment, by using the corresponding technical means, a set of good structure in advance to execute a program test cases we can find the problems existing in the system, and finally confirm the system function. The performance is in line with the requirements. Again and determine the test objectives and methods, as well as the test cases used in this system and the test report. After several rounds of testing, by correcting the error code, ensuring the measurement management system we can achieve high quality, high efficiency operation.

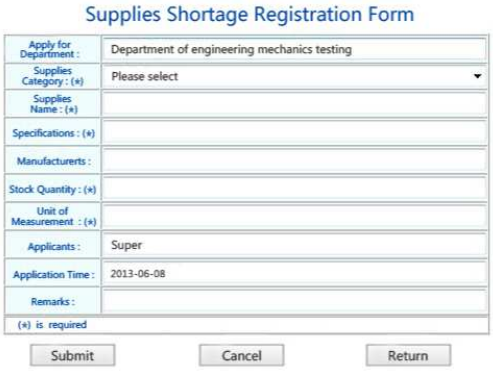

Figure 3. Shortage of products interface

Unit test Cases

Unit testing is testing each module individually, it is an important work before the unit test that make sure the authentication module interface and design specifications are consistent, all the major processing path of module testing and comparing with the expected results, but also for all the wrong path test. To review the source code, reference design specifications, statements to check whether the source program is conform to the requirements of the function of logic. As is shown in figure 4:

The test case number	Name of test cases	conditions	The output
1	Input the correct common user name and password, login successfully	1) user name = '800' 2) the password = '123123'	The test pass
2	Enter incorrect normal user name and password, login failed	3) user name = "mm..." 4) password = "11"	The test pass
3	Click on the public address book information query. Choose the department name to query, display the related information	5) department name = "department of medical equipment testing"	The test pass
4	Click the repair button to add the relevant information in my report, according to the modified successfully	6) to fill in and select the relevant information	The test pass
5	Delete the inbox information, select the relevant information to delete, delete successfully.	7) such as "delete titled": 'QQQ' information	The test pass
6	Change the password input relevant information, according to modify success.	9) the username = 800 10)Old password = 123123, 11) the new password = 123 12)Confirm new password = 123,	

Figure 4. The test use case diagram

The Test Report

After two rounds of testing, This system has implemented a total of 15 cases, found a problem, and solved a problem, There is no legacy, no denial. After fully test, the quality of the system is reliable, and can be released. As is shown in figure 5:

Rounds	Find the problem	Resolve problem	The solution	Deny problem	Leftover problem
1	1	1	Check the code, find the error code	0	0
2	0	0		0	0

Figure 5. Test report

Conclusion

In this article, we made a elaborate conception for IntelliJ IDEA + Oracle based on the general structure. Measurement management system, throughout the whole business process as the main line, according to the demand of the measurement test, design the function of each module, and construct a complete measurement management system, make use of several key technologies in the design and research has been fully reflected. In this paper, the design and research of the system is convenient to efforts to develop the masses of users to use a function of the perfect measurement management system, the system operating efficiency of above 90% has the very good practical value.

References

[1] Zhang Anyang. Based on the interface between inner and outer net FX2 ez-usb isolation transmission system design and implementation[D].Nanjing: nanjing university of technology,2009.
[2] ZhengWei，Xuwenbo. The design and implementation of a physical cars brake[J]. Micro computer information，2005，（25）：131~134.
[3] ZhangJinkun.Lightweight container J2EE Web application research[D]. Chengdu: Sichuan University，2005.
[4] YaoChongdong. Multi-source heterogeneous data integration based on XML, the implementation of the method research [D]. Harbin: Harbin engineering university, 2007.
[5] KeZicong. Ajax Development essence - concept, case and frame [M]. Beijing: electronic industry press, 2006.
[6] SongHutao. Heterogeneous data integration system based on SDO is the design and implementation of [D]. Beijing: Beijing university of posts and telecommunications, 2009.

Advanced Materials Research Vols. 989-994 (2014) pp 4590-4593
© (2014) Trans Tech Publications, Switzerland
doi:10.4028/www.scientific.net/AMR.989-994.4590

Analysis of conflict resolution model in Campus WLAN wireless network

ZHU Heng-jun[1,a], WANG Rui[2,a]

([1.] Communication and Electronics Engineering Institute of Qiqihar University, Heilongjiang Qiqihar 161006, China;
[2.] Qiqihar Branch of China Telecom Corporation Limited,Heilongjiang Qiqihar 161000, China)
[a]2976838@qq.com

Keywords: wireless networks; conflict prevention;channel

Abstract. In the campus WLAN wireless networks, transfer speed of network data is attracted great attention of users. How to solve conflict problem occurred in the network data transmission process has become the main goal of the campus WLAN network optimization. This paper presents campus WLAN wireless networks conflict resolution based channel mapping anti-collision algorithm. According to the amount of data to be transmitted in the network, the data length is estimated to provide conflict resolution with support data. On the basis of the channel mapping anti-collision algorithm related theory, conflict resolution model is established. Experimental results show that the proposed algorithm used in resolving conflict in campus WLAN wireless network can reduce the probability of data conflict happened in channel, so as to improve the performance of campus WLAN wireless network.

Introduction

With the campus WLAN wireless networks widely used in universities, the data transmission problems in the network has become the core issue need to be resolved during the operation of the network[1]. Assuming task load need to be transmitted is large, task conflict tends to happen [2]. Therefore, the campus WLAN Wi-Fi conflict resolution has become a hot issue need to be studied in computer field, and attracts the attention of many scholars[3]. At this stage, the main resolution of campus WLAN wireless network conflict includes conflict resolution method based on non-uniform distribution algorithm, conflict resolution method based on ant colony algorithm and conflict resolution method based on decision tree algorithm[4]. Among them, the most commonly used method of conflict resolution is based on decision tree algorithm[5]. As the campus WLAN wireless networks conflict resolution method has a very broad space for development, itbecomes an important research topic in the field of computers and has a brilliant future[6] .

Relevant principle of conflict resolution in campus wireless network

A. Estimation of data length in campus WLAN wireless network

During the process of campus WLAN wireless network conflict resolution, the length of data needs to be predicted, thus providing the basis for the campus WLAN Wi-Fi conflict resolution. Details of which are described below:

Time interval of campus WLAN wireless network data transmission is set $e=[e(0),e(1),\cdots,e(P-1)]^T$ per frame, the number of all data can be describedby q . Time interval of campus WLAN wireless network data transmission needs to obey the distribution $d \sim p(e,q)$, based on the distribution data, the prediction of data length can be achieved.

The following formula can be used to calculate data transmission time interval in campus WLAN wireless network:

$$\hat{p} = arc\min_{\overline{n}\in\chi} \sum_{p=1}^{+\infty} K(\overline{p},p)p(p|d) \tag{1}$$

In the above formula, $L(\overline{q},q)$ can be utilized to describe the distribution of time interval of the campus WLAN wireless network data transmission, δ is the set constituted of all data, the contents as follows:

$$\varepsilon = \{\overline{r} \,|\, f_1 + 2f_r \le \overline{r} \le R\} \tag{2}$$

Wherein, Q can be used to describe the maximum value of all data size which needsto be transmitted in campus WLAN wireless network.The following equation can be employed to describe Bayesian cost function in the data length forecasting process:

$$L(\overline{q}, q) = (\overline{q}, q)^2 \tag{3}$$

According to the following formula to calculate the maximum value of posterior probability prediction :

$$L(\overline{q}, q) = \begin{cases} 1 & |\overline{q}, q| > \dfrac{\Delta}{2} \\ 0 & |\overline{q}, q| \le \dfrac{\Delta}{2} \end{cases} \tag{4}$$

In the above formula, Δ can be used to describe the transmission state parameters of campus WLAN wireless network data. According to the description above, the following formula can be applied to predict data transmission length in campus WLAN wireless network:

$$\overline{q} = arc \max_{\overline{q}} p(\overline{q} \,|\, e) \tag{5}$$

According to the above- described method , capable of predicting length of campus WLAN wireless network data, thus provide the basis for the campus WLAN Wi-Fi conflict resolution.

B. The establishment of conflict resolution model

The task load transmitted in campus WLAN Wi-Fi channels per unit of time is set to be z, the channel transfer efficiency blurred value is u, $u \in [0,1]$, the following formula can be utilized to calculate service efficiency incremental coefficient of channel:

$$u \in [0,1] \tag{6}$$

According to the method outlined above, mapping relationship between task scheduling and the channel transmission is established. In this mapping relationship, the data set constituted of entire campus WLAN wireless networks transmission tasks is $u = \{u_1, u_2, \cdots, u_q\}$, where constitute that which is the task of the first channel needs to be passed. Setting, where u_k is task need to be transmitted in k-th channel.Setting, w_k is transmission requirement for channel T exerted by task waiting for transmission, and the requirement of $U_k, w_k \in [0,1]$ needs to be hit. y_k is priority of massive tasks in the campus WLAN wireless network data transmission process. The higher priority task will be transmitted in prior, $y_k \in [0,1]$. During the data transmission process, task quantity can be transmitted in channel is limited,it is necessary to meet the following requirement:

$$y_k \in [0,1] \tag{7}$$

Efficiency of scheduling tasks can be calculated using the following equation:

$$f = |u - w| = \sqrt{(u_1 - y_1 w_1)^2 + (u_2 - y_2 w_2)^2 + \cdots + (u_q - y_q w_q)^2}$$
$$= \sqrt{\sum_{k=1}^{q} (u_k - y_k w_k)^2} \tag{8}$$

Wherein, f is the efficiency of task scheduling, and the greater the dispersion u and w are, the higher efficiency of task schedulingis.

The following formula is employed to establish a conflict resolution model in campus WLAN wireless network:

$$\min f = \sqrt{\sum_{k=1}^{q} (u_k - y_k w_k)^2}$$
$$s.t. h(u_1, u_2, \cdots, u_q) = 0$$

$$u_k, w_k, y_k \in [0,1]$$
$$k = 1, 2, \cdots, q \quad (9)$$

According to the method described above, it is possible to estimate the length of transmitted data during the campus WLAN wireless network data transmission process. . Based on the results of estimation, the conflict resolution model is founded to prevent conflict happened in campus WLAN wireless network.

Simulations and Results Analysis

In order to verify the effectiveness of the proposed method, an experiment was conducted. During the experiment,it is necessary to establish a campus WLAN wireless network simulation environment, the distribution channel in the campus WLAN wireless network can be described by the following figure:

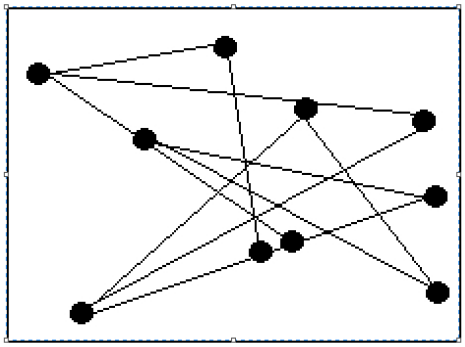

Figure 1 Channel Distribution

In the process of campus WLAN Wi-Fi conflict resolution experiments solved with different methods, the probability of channel conflict tasks happens can be described by the following figure:

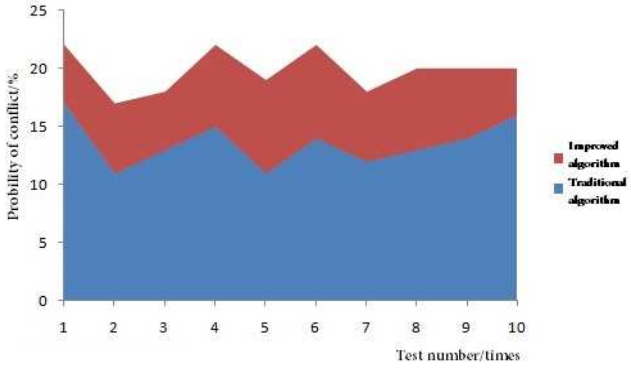

Figure 2 Comparison of channel conflict probability with different algorithms

According to the figure above, it can be learned that by using proposed algorithm to conduct the campus WLAN Wi-Fi conflict resolution experiment, assuming the campus WLAN wireless network task size is too large, caused an augment in the probability of channel conflict.

The above experimental data were analyzed, and Table 1 can be obtained as follows:

Table 1 Channel conflict probability table

The amount of data (ten thousand)	Conflict probability of traditional algorithm (%)	Conflict probability of proposed algorithm（%）
1	17	5
2	11	6
3	13	5
4	15	7
5	11	8
6	14	8
7	12	6
8	13	7
9	14	6
10	16	4

According to the above experiment, it can be learnt that the use of this algorithm for solving conflict in campus WLAN wireless network, can greatly reduce the probability of channel conflict, showing a strong advantage.

Conclusions

In the paper, the campus WLAN wireless networks conflict resolution based channel mapping anti-collision algorithm is raised. According to the amount of data to be transmitted in the network, the data length is estimated to provide conflict resolution with support data. On the basis of the channel mapping anti-collision algorithm related theory, conflict resolution model is established. Experimental results show that the proposed algorithm used in resolving conflict in campus WLAN wireless network can reduce the probability of data conflict happened in channel, so as to obtain the satisfactory results .

References

[1] P. Xie, Z. Zhou, Z. Peng, H Yan, T.S. Hu, J.-H. Cui, Z.J. Shi, Y.S. Fei and S.L. Zhou, Aqua-Sim: A NS-2 Based Simulator for Underwater Sensor Networks[C], IEEE/MTS OCEANS, 2009:1-7.

[2] Su K. F ,Ou C. H, Jiau H. C. Localization with Mobile Anchor Point s in Wireless Sensor Networks[J]. IEEE Transactions on Vehicular Technology, 2005.54: 1187-1197.

[3]B Waters. Efficient identity-based encryption without random ora-cles[C].Advances in Cryptology-EUROCRYPT 2005. Berlin: Springer-Verlag, 2005.114-127.

[4] Akyildiz I F, Pompili D, Melodia T. Under-water acoustic sensor networks: research ch-allenges [J]. Ad Hoc Networks (S1570-8705), 2005, 3(3): 257-279.

[5] Li J, Ning T, Pei L, et al. Millimeter-wave radio-over-fiber system based ontwo-step heterodyne technique. Optics Letters, 2009, 34(20):3136-3138.

[6] Shih P T, Chen J, Lin C, et al. Optical millimeter-wave signal generation viafrequency 12-tupling. J LightwTechnol, 2010, 28:71-78.

Advanced Materials Research Vols. 989-994 (2014) pp 4594-4597
© (2014) Trans Tech Publications, Switzerland
doi:10.4028/www.scientific.net/AMR.989-994.4594

Large-scale data mining and distributed processing in big data Internet

XING chun-zhi[1,a]

[1]Henan Radio & Television University, Zhengzhou Henan 450008, China
[a]hndd2013ks@163.com

Keywords:big data internet; data mining; distributed

Abstract. With the development of Internet， various Internet-based large-scale data are facing increasing competition. With the hope of satisfying the need of data query, it is necessary to use data mining and distributed processing. As a consequence, this paper proposes a large-scale data mining and distributed processing method based on decision tree algorithm.

Introduction

With the continuous development of computer data processing technology, the application of this technology in data mining has become increasingly widespread [1]. Thus, large-scale data mining and method of distributed processing has become the core problem of data management, raising widely attention among many scholars [2]. At this stage, the major methods for large-scale data mining and distributed processing include the data mining and distributed processing method based on BP neural network algorithm, means clustering algorithm and variety constraint model [3-4].Among them, the most commonly used method is based on variety constraint model. Due to the distributed data mining and processing methods have broad space for development in data management, therefore, has been a great concern, has a huge potential for development[5].

Large-scale data mining and distributed processing methods revenant principles

A. fuzzy clustering on large-scale data processing

Let $Z=\{z_1,z_2,\cdots,z_q\}$ is the set of the large-scale data in big data Internet, using the following formula to describe the target function of large-scale data analysis,

$$L_p(Y,B)=\sum_{k=1}^{q}\sum_{l=1}^{e}y_l^p f_{kl}^2(z_k,b_l) \tag{1}$$

Let the state parameters of large-scale data are $e,q,p,d=1$, the set of the clustering center of all large-scale data is $B_{(d)}=(b_1,b_2,\cdots,b_e)$. Based on the following formula, the update and transition of the large-scale data in big data Internet can be manipulated.

$$y_{kl}=\frac{1}{\sum_{m=1}^{e}\left[\frac{f_{kl}}{f_{km}}\right]^{\frac{2}{p-1}}} \text{ when } f_{kl}\neq 1$$

$$y_{kl}=0 \text{ when } e_{kl}=0, l\neq m$$

$$y_{kl}=1 \text{ when } e_{kl}=0 \tag{2}$$

According to the following formula to calculate the average property features large-scale data:

$$b_l=\frac{\sum_{k=1}^{q}y_{kl}}{\sum_{k=1}^{q}y_{lm}} \tag{3}$$

Compare the above conclusion with the next the average property features, assuming following conditions are met, then complete the clustering large-scale data processing in a bigdata Internet, otherwise repeat the above steps until it reaches the maximum number of iterative processing.

$$\left|b_d - b_{(d+1)}\right| \le \varphi \tag{4}$$

B. Achievement of large-scale data mining

Let the set of known large-scale data can be described as $Y = \{(y_j, z_j) \mid j = 1, 2, \cdots, total\}$, among them, $y_j = (y_{j1}, y_{j2}, \cdots, y_{je})$ can be used to describe the element in the set, $(B_1, B_2, \cdots, B_e)$ can be used to describe the corresponding properties. Using the following formula can calculate the expected information of the large-scale data

$$J(p_1, p_2, \cdots, p_n) = -\sum_{k=1}^{n} \frac{p_k}{total} \log_2 (\frac{p_k}{total}) \tag{5}$$

Using the following formula an optimal decision tree can be built based on the above data:

$$B_j = MIN + \frac{MAX - MIN}{P} \times j \tag{6}$$

, where $j = 1, 2, \cdots, P$.

For each data which reaches the maximum information gain ratio, regard it as the branch of the decision tree and build a node of decision tree. Build the corresponding branch based on the different weight of data properties, by querying the leaf node to finally complete the building of decision tree.

According to the method described above can build an optimal decision tree. Based on the decision tree, classify the data so that query the needed types of data and finish the data mining finally.

Experiment of Simulation and the Analysis of the Result

In order to verify the correctness of large-scale data mining algorithm proposed by this paper, it is necessary to perform an experiment. During the experiment, the big data Internetis usedas the object and the large-scale data in the Internet are used as the sample data.In the case that the sample amount in the Internet is under 50 thousand, respectively using traditional algorithm and proposed algorithm for large-scale data mining, the results obtained can be described by the following figure.

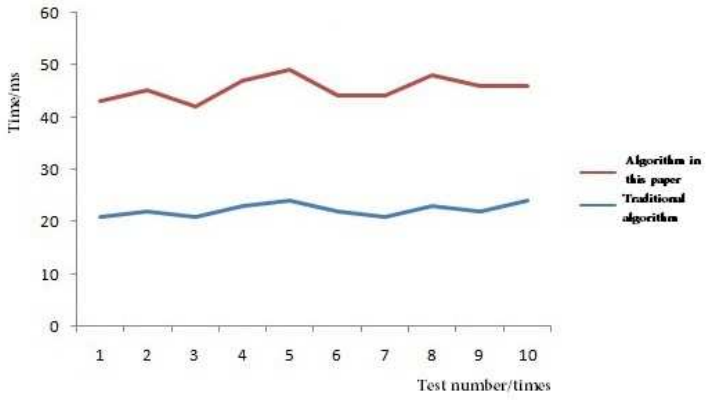

Figure 1, Time consumption when the amount of data is 50 thousand

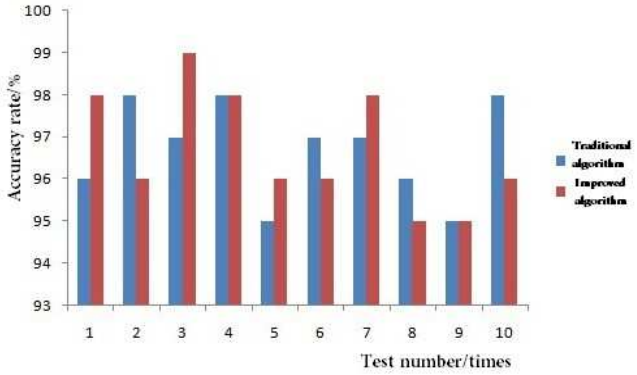

Figure 2, The accuracy of different algorithms when data amount is 50 thousand

Organize and analyze the above data, the following table 1 can be obtained:

Table 1, Experiment data table when the data amount is 50 thousand

No.	Time（ms）		Accuracy（%）	
	Traditional	Proposed	Traditional	Proposed
1	21	22	96	98
2	22	23	98	96
3	21	21	97	99
4	23	24	98	98
5	24	25	95	96
6	22	22	97	96
7	21	23	97	98
8	23	25	96	95
9	22	24	95	95
10	24	22	98	96

Based on the table above, when the amount of data is under 50 thousand, using the proposed algorithm by this paper, the time used by data mining and the accuracy are approximately the same as the traditional algorithm.

When the amount of sample in big data Internet is 100 thousand, respectively use the traditional algorithm and the proposed algorithm to perform large-scale data mining, the obtained data is shown as following graph:

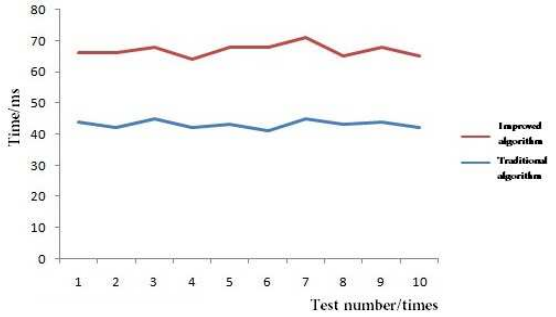

Figure 3. Time consumption of different algorithm when the amount data is 100 thousand

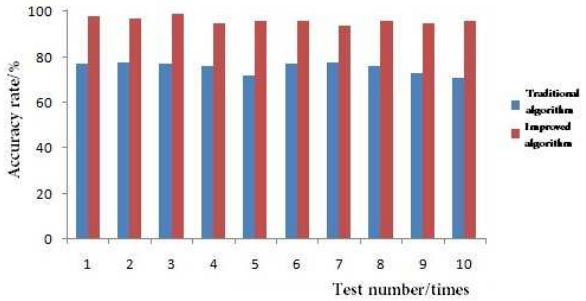

Figure 4.Accuracy of different algorithm when the amount data is 100 thousand

Organize and analyze the above data, the following table 2 can be obtained:

Table 2. Experiment data table when the data amount is 100 thousand

No.	Time（ms）		Accuracy（%）	
	Traditional	Proposed	Traditional	Proposed
1	44	22	77	98
2	42	24	78	97
3	45	23	77	99
4	42	22	76	95
5	43	25	72	96
6	41	27	77	96
7	45	26	78	94
8	43	22	76	96
9	44	24	73	95
10	42	23	71	96

According to the above data, when data amount is 100 thousand, using the proposed algorithm to perform large-scale data mining, the consumption of time is slightly shorter than the traditional algorithm.

Conclusions

This paper presents a large-scale data mining and distributed processing method based on the decision tree algorithm. For large-scale data, using fuzzy clustering process to obtain a big data Internet that highly related to the search target. According to the decision tree mining algorithms and its related theory, a large-scale data mining decision tree can be built and achieve big data Internet data mining. Experimental results show that using the improved algorithm, the time consumption of data mining can be shorten and accuracy of data mining can be improved.

References

[1] Han J W,KamberM.DataMining:Concepts and Techniques. 2nded[M].Morgan Kaufmann Publishers,2001:223-250.

[2] Wei Zhang, Michael S. Branicky, Stephen M. Phillips. Stability of networked control systems [J]. IEEE Control Systems Magazine, 2001, 21(1): 85-99.

[3] Guo Lin-sun and Wei Guo. Comparison of Distributed Localization Algorithms for Sensor Network With a Mobile Beacon[C].Networking, Sensing and Control, 2004 IEEE International Conference. Taiwan, 2004: 536-540.

[4] AbdelhamidBouchachia, WitoldPedrycz. Data Clustering with Partial Supervision [J]. Data Mining anf Knowledge Discovery, 2006, (12): 47-48.

[5] Vilalta R, Stepinski T, Achari M. An Efficient Approach to External Cluster Assessment with an Application to Martain Topography [J]. Data Mining and Knowledge Discovery, 2007,(14): 21-23.

Advanced Materials Research Vols. 989-994 (2014) pp 4598-4602
© (2014) Trans Tech Publications, Switzerland
doi:10.4028/www.scientific.net/AMR.989-994.4598

Design of Smart Household Monitoring Platform Based on Internet of Things

[1,a] Yang Xu

[1,] Yunnan Vocational college of Mechanical and Electrical Technology，Kunming，YunNan，China，650203

[a]4066614@qq.com

Keywords: Internet of Things (IOT), smart home, monitoring platform, ZigBee.

Abstract. In order to popularize the intelligent monitoring in households, this thesis is aimed to conduct researches on“Household Monitoring System based on the Internet of Things (IOT)”and starts with the design of this system. General technology concerning household video monitoring and home appliance controlling in computers, mobile phones, etc. is explored in this thesis and a household monitoring system based on IOT is set up. According to experiments, the household monitoring system has various functions such as operating once plugged, ad hoc network, various and interactive controlling methods and friendly serial ports.

Introduction

Along with the rapid development of computer technology, sensor technology, communication technology and Internet technology, smart home has become the trend of our future life, which connects all the household items through the network and conducts remote monitoring and intelligent management of the household so as to create a safe, comfortable and convenient environment. The smart household with the application of Internet of Things is a highlight of China's current economic and social development. With the theme as “Research and Development on the Household Monitoring System Based on the Internet of Things”, this thesis starts with general technology concerning household video monitoring and home appliance controlling in computers, mobile phones, etc. to explore a household monitoring system based on Internet of Things. This paper is contributive to the development and practical application of measurement and control, promotion of the Internet of Things technology, development of the Internet of Things discipline and improvement of smart households.

Design of the Framework of Household Monitoring System based on Internet of Things

Based on system requirements and the Internet of Things technology, the framework of household monitoring system is designed in Figure 1. The whole system architecture is divided into three layers: perception layer, network layer, application layer. The perception layer connects all the household items through sensors, actuators, etc on wireless network. The network layer is the information transfer media between the other two layers. And the application layer is sort of monitoring operation for users to connect with the system and to operate household items.

ZigBee equipment in this system is JENNIC JN5139 module. The system adopts a fully functional device JN5139 Z01 - M02R1 as ZigBee network coordinator to receive instructions from upper machine and send information back to the machine. Three simplified function equipments JN5139 Z01 - M01R1 are adopted as a network node to control home equipments and upload information. The whole work is operating in a star network structure.

The etwork layer supports RS232, RS485, ZigBee, WIFI, Internet and mobile communication network etc. ZigBee and WIFI can connect home appliances with the monitoring center. The mobile communication network can connect users with the monitoring center. Mobile phone users can be connected to the smart household system by the mobile communication network such as 2 G, 2.5 G and 3 G technology.

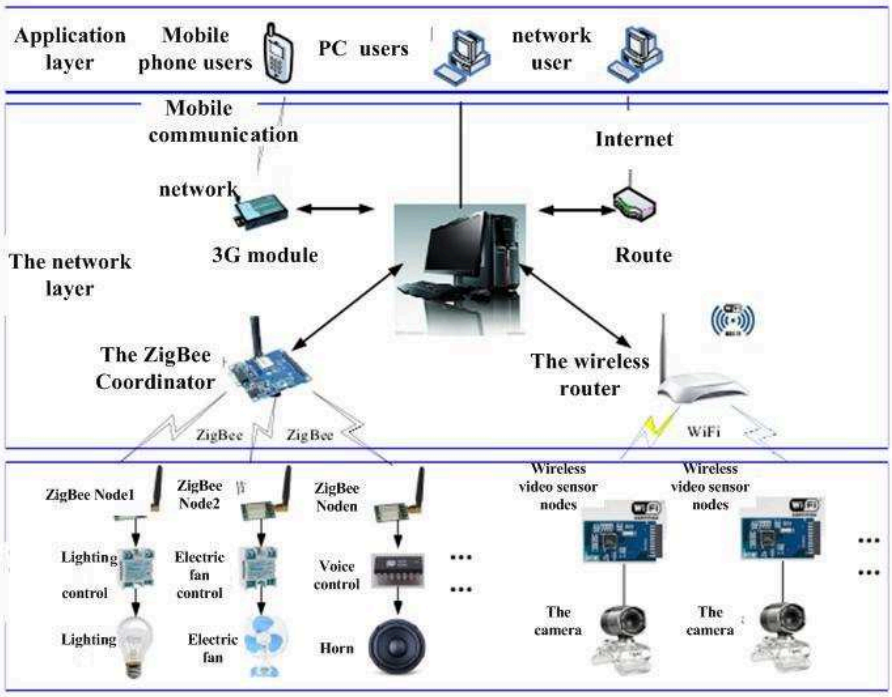

Figure 1 Overall Framework of the Monitoring System

Considering the expansion needs, this thesis chooses 3 G technology. 3 G module selects the Huawei EM560 module, which supports TD-SCDMA(3G) and GSM(2G) , a only TD module that supports both A frequency band (1880-1920 MHZ) and B frequency (2010-2025 MHZ) in the present world. EM560 supports mini PCI Express and UART serial port and functions such as text messaging, voice, the phone book, supplementary services, etc. With the center of the master machine, this thesis designs a ZigBee coordinator responsible for the node communication with ZigBee home appliances, a wireless video acquisition center to communicate with WIFI cameras and provide text messaging service to monitor home appliances with 3G modules.

2. Design of Hardware of Smart Household Monitoring System

This household monitoring system based on IOT in this thesis adopts the ZigBee star network, the household monitoring system uses JN5139 chip ZigBee star network. The household monitoring system ZigBee wireless coordinator provides a network for home wireless network and family network. ZigBee coordinator is aimed to start and maintain wireless network, connect with home PC through serial ports, receive and process commands from family gateways, send command data frame to the terminal node of ZigBee and receive and process data to familiy gateways through serial ports. More details can be seen in Figure 2.

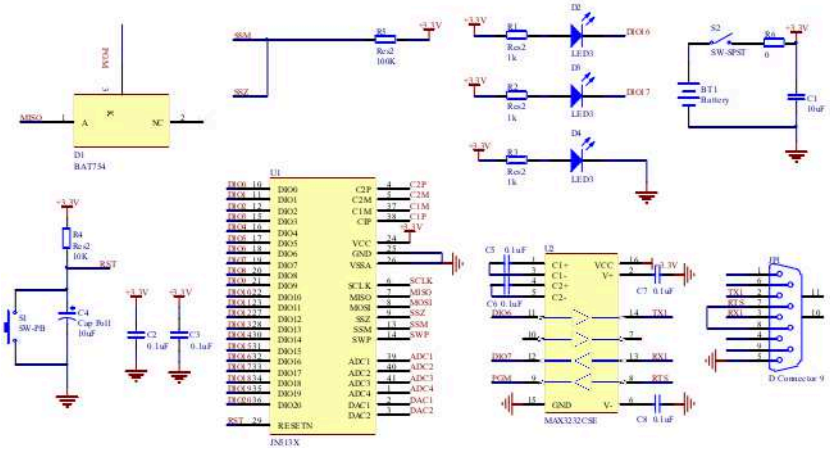

Figure 2 Schematic Circuit Diagram of ZigBee Wireless Coordinator

Schematic Circuit Diagram of ZigBee Wireless Terminal Nodes in this paper is shown in Figure 3. As ZigBee wireless terminal nodes exist in a wireless manner, there are not extra wired network serial ports in those nodes. In order to ensure home appliances under small signal control and high voltage, wireless terminal nodes need corresponding household control circuit. To better know household environment conditions, the corresponding intelligent temperature sensor DS18B20 collecting circuit is added. As ZigBee wireless terminal nodes and ZigBee wireless coordinator both use the same control kernel, thus batteries are also used in wireless terminal nodes. This system is compatible with the IEEE 802.11 b/g and allows interoperability among multiple vendors. It also supports Wi-Fi access protection, 802.11 I safety standards through the implementation of WEP security mechanism under AES/TKIP, 802.11 e quality of service (QoS). More details are introduced in Figure 4.

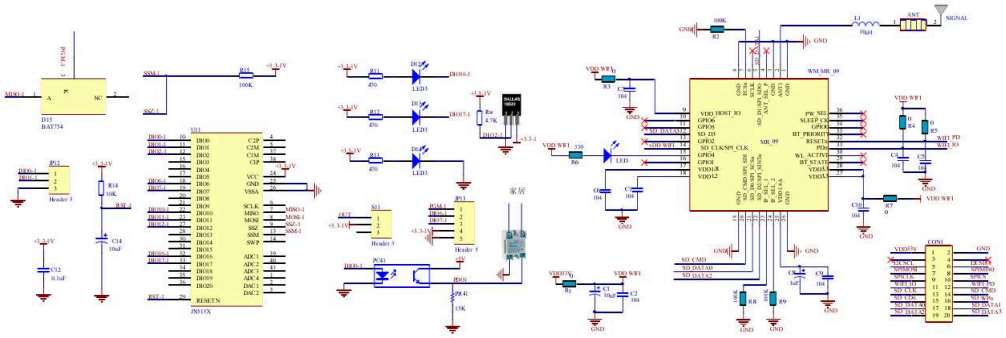

Figure 3 Schematic Circuit Diagram of ZigBee Wireless Terminal Nodes
Figure 4 Schematic Circuit Diagram of WIFI Video Receiving and Sending

Design of Software of Smart Household Monitoring System

The master software is developed by C# language in Visual Studio 2008 environment. Visual Studio is the most popular Windows platform development environment of Microsoft's that supports Visual Basic, Visual C# and Visual C++ development language, etc. The working process of the system control center is shown in Figure 5.

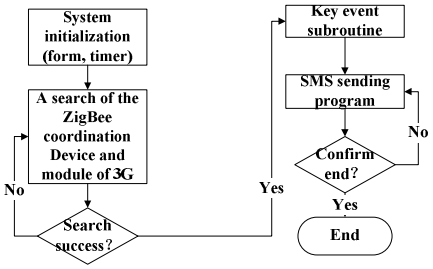

Figure 5 Working Process of Master Software

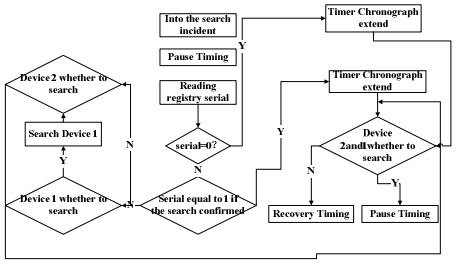

Figure 6 Automatic search algorithm

The master software and the ZigBee coordinator are connected with serial ports and the NET platform provides SerialPort class operation serial ports. The main control software and the 3G module EM560 are connected with USB and the registry of the PC operating system will create a virtual serial port to control EM560 through commands. While operating SerialPort, users can firstly configurae PortName, BaudRate, Parity, DataBits and StopBits. Then open the serial port under the command of Open(), close the port with Close(), read the port with Read() and write the port with Write().The serial port only needs to use SerialPort. DataReceived event to adopt event trigger methods.

Another vital technology to program the master is software multithreaded programming. "Threaded" is named by the System. Threading. Set up with new (), start with the start (), suspend with sleep (), end with abort (). It is noticeable that calling abort () often causes System. Threading. Thread AbortException, which is a system of .Net. It usually occurs if users give forced termination to an operating thread. At that time, the method of "try…catch…"is needed. What's more, the thread in the outside form can not get direct access to the form object but needs to used the method of delegate. It is

an important method for thread communication. The automatic search algorithm is shown in Figure 4-5.

Testing and Application of Smart Household Monitoring System Based on Internet of Things

Put one SI4432 module in a room and the other SI4432 module in the second room to test whether two sides can keep communication. Change the distance of two modules (increasing transmission distance and numbers of the walls) if the communication can be kept. Test again until two sides can not keep normal communication. Test results are shown in table 1. With the results, it is obvious that SI4432 has enough communication distance, which is applicable to this thesis.

Table 1 Test for Indoor Wireless Communication Distance

The test conditions	The test results
1 wall, spacing of 5 m	Able to reliable communication
3 wall, spacing of 23 m	Able to reliable communication
8 wall, spacing of 75 m	Able to reliable communication
9 wall, spacing of 85 m	Can't reliable communication, loss of data

Monitor the sensor nodes through the monitoring software in the monitoring center. If the monitoring center can collect data of sensor nodes, the wireless communication can be achieved in that distance. Then extend the distance between nodes and the center. Test results are shown in table 2.

Table 2 Test for Indoor Wireless Communication Distance

The test conditions	The test results
Outdoor, stadia barrier-free, 50 m	Able to reliable communication
Outdoor, stadia barrier-free, 100 m	Able to reliable communication
Outdoor, stadia barrier-free, 300 m	Able to reliable communication
Outdoor, stadia barrier-free, 500 m	Able to reliable communication
Outdoor, stadia barrier-free, 1000 m	Able to reliable communication

The monitoring interface is shown in figure 4 and the data uploaded by the monitoring software will be transmitted into real-time temperatures display. After receiving the monitoring data uploaded by a node, the state light will be up indicating the active state. Data uploaded includes time of data collecting and will be displayed on the interface after analysis.

Conclusion

This thesis, supported by general technology of video monitoring of household items through computers and mobile phones, designs a household monitoring system based on Internet of Things. This household monitoring system mainly focuses on general technology of video monitoring and controlling of home appliances by computers and mobile phones. This thesis also offers new ideas to the application and development of the IOT monitoring and pragmatic application of integrating smart households and the IOT monitoring. There are still some limitations and further researches are needed. Works such as optimizing the interface, upgrading the working process of the household monitoring system and developing wireless termination controlling software needs to be finished.

References

[1] Ye Xinggi. Smart household system based on IOT [J]. Modern Architecture and Electronics, 2010(9):25-28。

[2] Shen Subin. Researches upon the system of IOT and relevant technology [J]. Journal of Nanjing Post and Communication University,2009,29(6):1-11.

[3] He Dongzhi. Researches of smart household controlling system based on encircling intelligence [J].Computer Engineering,2007,33(10):261-273。

[4] Xu Zhenhao. Researches upon IOT routing technology [J]. Scientific and Technological Information, 2010(5)：86-87
[5] Sun Jing, Yu Yang. Researches on routing agreements of Zigbee arborescence wireless sensor network [J]. Journal of Tonghua Teachers College,2011(6).
[6] He Xiang. Design and application of terminal man-machine interface of flushbonading smart households [J]. Computer Engineering and Design,2010(10):2166-2168.
[7] Jiang Xiaoluo. Development of smart home long-distance monitoring system [J]. Observation and Control Technology, 2006(12):160-163
[8] Miao Shuo. Research and design of long-distance smart home managing system [D]. Xi'an: Xi'an University of Architecture and Technology,2006
[9] Zhang Yunyong. Standard situation and developing suggestions of smart home system based on Internet of Things [J].Mobil Communication, 2010(15): 25-29.
[10] Zhu Hongbo,Yang Longxiang,Yu Quan. Researches on technological thinking of Internet of Things and application strategies [J]. Communication Journal, 2010(11): 2-9

Advanced Materials Research Vols. 989-994 (2014) pp 4603-4607
© (2014) Trans Tech Publications, Switzerland
doi:10.4028/www.scientific.net/AMR.989-994.4603

GNS-based Simulation and Analysis of OSPFv2 Neighbor Authentication

Xiaohua Li [a], Renlong Zhang, Yujie Wang, Li Yang, Juan Nie, Quanyue Yang

School of Computer and Information Engineering, Beijing University of Agriculture, Beijing, China

[a] lixiaohua_bj@163.com

Keywords: OSPFv2; neighbor authentication; GNS; MD5

Abstract. Routing information release is a kind of promise from the router for network reachability. Illegal routing information may have disastrous effects on the normal work of the network. Open Shortest Path First (OSPF) protocol provides authentication methods to protect the authenticity and integrity of the routing traffic. This paper describes two authentication types of OSPFv2, analyzes the realization mechanism and packet header format of each authentication respectively. Based on GNS3, a typical network topology was designed, and with the aid of it functional verification and security analysis are carried out. The simulation can provide a reference for building an OSPF network. Experimental results show that the configuration of OSPFv2 routing authentication can effectively prevent the router from receiving unauthorized or malicious routing updates, thereby improving network safety.

1.Introduction

To feasibly protect the authenticity and integrity of the routing traffic and provide the means to verify the authority of the participating routers, Open Shortest Path First protocol version 2 [1-3] (OSPFv2) supports two types of authentication. In this paper, we focus on the simulation and analysis of OSPFv2 routing authentication. We discuss the two authentication types of OSPFv2 in section 2, and carry out GNS-based simulation and analysis in section 3. Finally conclusions are given.

2.OSPFv2 Authentication

OSPFv2 supports two types of authentication [3-5]: one is simple password authentication and the other is MD5 cryptographic authentication. The authentication type is configurable on a per-interface basis and the 2-byte authentication type field (*AuthType*) in the OSPFv2 packet header should be set accordingly. Different type of authentication has different packet header format and realization principle. We will discuss it in the following.

2.1. Simple Password Authentication

In simple password authentication, the *AuthType* field in the OSPFv2 packet header (shown in Fig. 1) should be set to 1. At the same time, a 64-bit clear text password can be configured and all packets sent on a particular network must have this configured value in their OSPFv2 header. The received OSPFv2 packets will be authenticated according to the following rules. Packets which fail authentication will be discarded.

- The *AuthType* field in the received OSPFv2 packet header should match the setting of *AuthType* for the receiving OSPFv2 interface.
- The 64-bit *authentication* field in the received OSPFv2 packet header must be equal to the 64-bit password (i.e., *authentication* key) that has been configured for the interface.

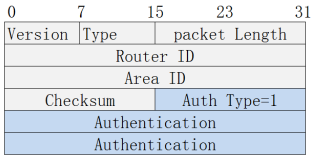

Figure 1. OSPF packet header in simple password authentication.

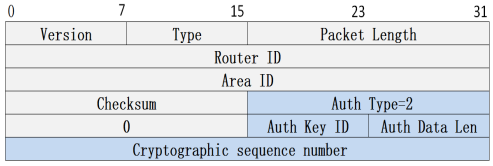

Figure 2. OSPF packet header in MD5 authentication.

2.2. MD5 Cryptographic Authentication

In MD5 cryptographic authentication, the *AuthType* field in the OSPFv2 packet header should be set to 2. In addition, the 64-bit *Authentication* field in the standard OSPFv2 packet header is redefined as shown in Fig. 2 and a 64-byte *crypto authentication TLV* (message digest) will be appended to the OSPFv2 packet as well. The new field definitions are as follows:

- *Key ID*: This field identifies the algorithm and secret key used to create the message digest appended to the OSPFv2 packet. Key Identifiers are unique per-interface (or equivalently, per-subnet).
- *Auth Data Len*: The length in bytes of the message digest appended to the OSPFv2 packet.
- *Cryptographic sequence number*: An unsigned 32-bit non-decreasing sequence number. Used to guard against replay attacks.

The received OSPFv2 packets will be authenticated according to the following rules. Packets which fail authentication will be discarded.

- Locate the receiving interface's configured key having *Key ID* equal to that specified in the received OSPFv2 packet. If the key is not found, or if the key is not valid for reception, the OSPFv2 packet is discarded.
- If the *cryptographic sequence number* found in the OSPFv2 header is less than the *cryptographic sequence number* recorded in the sending neighbor's data structure, the OSPFv2 packet is discarded.
- Verify the appended message digest. Calculate a new digest and let it compare with the received one. If they do not match, the OSPFv2 packet is discarded. If they do match, the OSPFv2 protocol packet is accepted as authentic.

3. Simulations and Analysis

In this section, a typical network topology is designed and with the aid of GNS3, we carry out simulation and analysis. GNS (Graphical Network Simulator) is a very good graphical network simulator that can simulate the real IOS and complex networks. It is visual and accurate, with friendly interface, convenient operation, and strong interactivity. It can be said to be one of the most popular network simulators. It is also an excellent complementary tool to real labs for network engineers, administrators etc. It is an open source, free program that may be used on multiple operating systems, including Windows, Linux, and MacOS X.

3.1. Experimental Network Topology and Configurations

We design such a network topology as shown in Fig. 3, which is a two-level hierarchical routing scheme. It consists of three areas and 10 C7200 routers. Through serial and fastEthernet connections the routers are connected and compose a typical LAN network. In this topology, R3 and R2 are *Area Border Routers*: through R3 area 0 and area 2 is connected, whereas area 0 and area 1 is connected through R2. The *router ID* and other corresponding configurations for each router are set and marked in the figure.

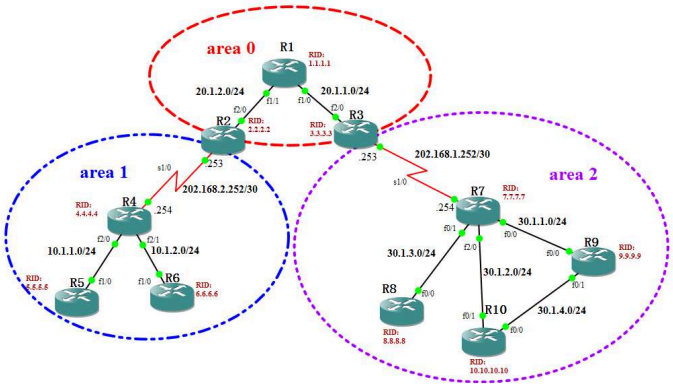

Figure 3. Experimental network topology.

3.2. Simulation and Analysis of Simple Password Authentication

Router R3 and R7 are connected through serial connection. We will enable simple password authentication to this connection and capture the data packets on this route using Wireshark software. We will unpack and analyze the captured packets to discuss the behaviour of OSPFv2 and analyze the security of OSPFv2 authentication.

By default, OSPFv2 employs *Null* authentication, meaning that all the routing exchanges over the network/subnet are not authenticated. In this case, when R3 and R7 runs, after sending *hello* messages periodically in the network, they can find each other as their neighboring router, establish full adjacency and synchronization with each other. Fig. 4 demonstrates the packet series for database synchronization in OSPFv2 *Null* authentication. From this series of operation, R3 can learn the routes in area 2 from R7, thus, all the routers in the topology can *Ping* and communicate with each other. When simple password authentication is configured on R7, as for the mismatch authentication type, the neighbor relationship between R3 and R7 is broken. Examine the neighbor list of R3, we find that only R1 is the neighbor of R3.The topology at this time becomes isolated and routers in area 2 cannot communicate with other routers in area 0 and area 1. But if we set the same password and enable simple password authentication on R3, we can see the full adjacency between R3 and R7 is established again (shown in Fig. 5).

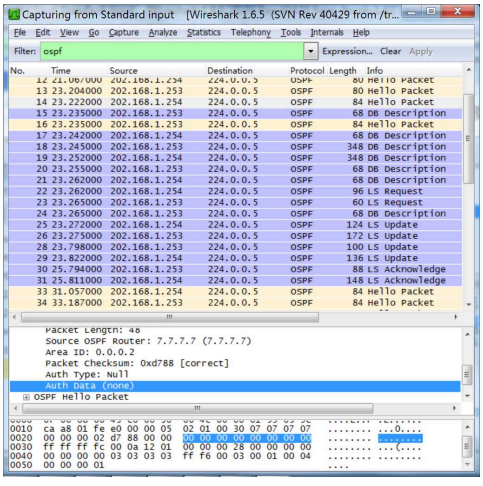

Figure 4. Database synchronization in OSPF Null authentication.

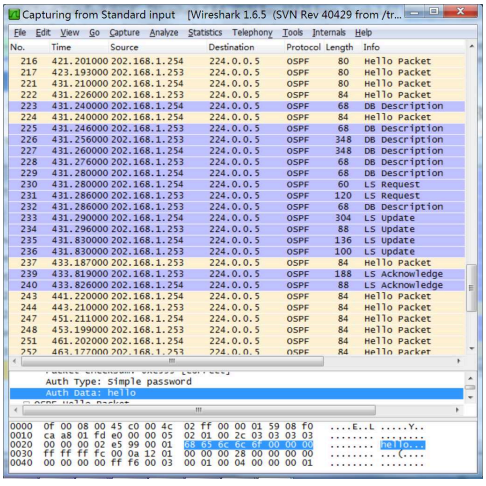

Figure 5. Database synchronization in OSPF simple password authentication.

Examine the neighbor list and route table of R3 (shown in Fig. 6), we can see R7 becomes its full adjacent neighbor and R3's route table is complete and convergent.

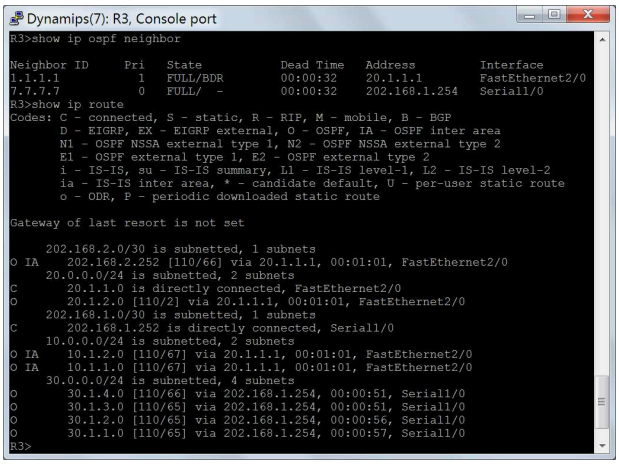

Figure 6. Route table of R3 in simple password authentication.

3.3. Simulation and Analysis of MD5 Cryptographic Authentication

We will enable *MD5 cryptographic authentication* to the serial connection between R2 and R4. By default, OSPFv2 employs *Null* authentication. In this case, after sending *hello* messages periodically in the network, R2 and R4 can find each other as their neighboring router. After the establishment of full adjacency, their link state databases are synchronized. When *MD5 cryptographic authentication* is configured on R2, packet series captured using *Wireshark* (shown in Fig.7) demonstrate that the neighbor relationship between the two routers is broken due to the mismatch of authentication type, but when we enable MD5 cryptographic authentication on R4, full adjacency and synchronization between the two routers is established again (shown in Fig. 8).

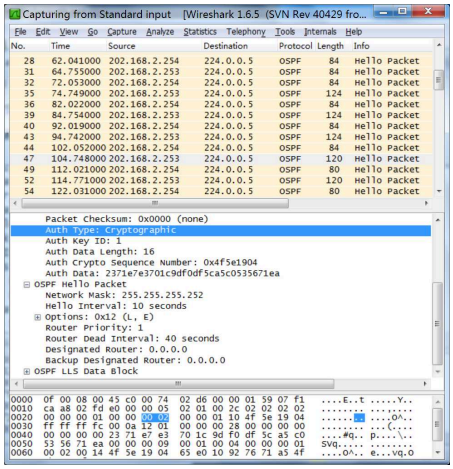

Figure 7. Neighbor relationship breaks in MD5 cryptographic authentication.

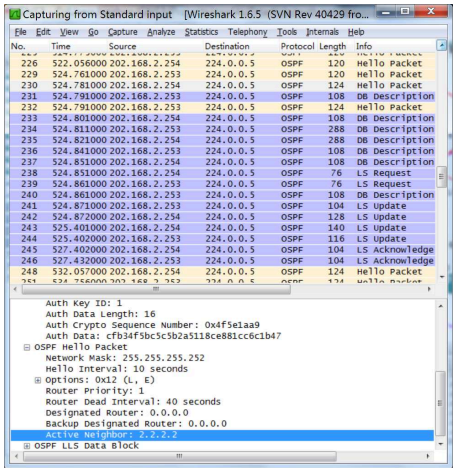

Figure 8. Establishment of full adjacency in MD5 cryptographic authentication.

Examine the route tables of R4 (shown in Fig. 9), we can see it is complete and convergent.

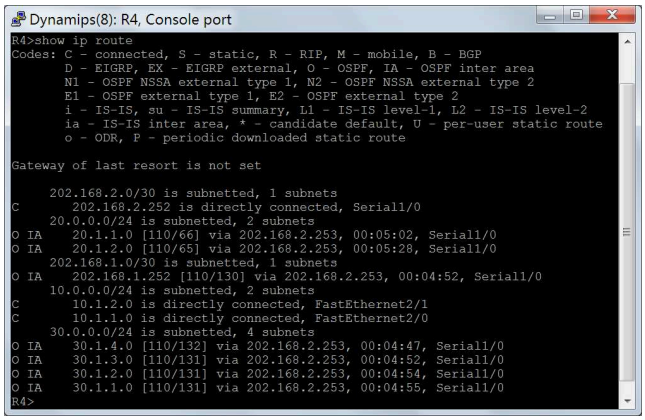

Figure 9. R4's Route table in MD5 authentication.

Summary

This paper makes a study of OSPFv2 neighbor routing authentication, analyzes the realization mechanisms and packet header formats of the simple password and MD5 cryptographic authentication. Based on GNS, simulation and analysis are carried out. Experimental results show that the configuration of the OSPFv2 neighbor routing authentication can prevent the router from receiving unauthorized or malicious routing updates, thereby improving network safety. Using Wireshark to capture OSPFv2 packets and analyze the security of OSPFv2 authentication, we can see simple password authentication can guard against routers inadvertently joining the routing domain, but it is vulnerable to passive attacks. Anyone with physical access to the network can learn the password. MD5 cryptographic authentication is much safer than simple password authentication. It can prevent eavesdropping on the line to obtain the authentication key phenomenon effectively.

Acknowledgment

This work is sponsored by the project of Beijing Committee of Education (KM201210020004). Renlong Zhang is the corresponding author.

References

[1] D. Bauer, et al., "A case study in understanding OSPF and BGP interactions using efficient experiment design," Proc. 20th Workshop on Principles of Advanced and Distributed Simulation, PADS, May 24, 2006 - May 26, 2006, Institute of Electrical and Electronics Engineers Computer Society, 2006, pp. 158-165.

[2] Y.N. Krishnan and G. Shobha, "Performance analysis of OSPF and EIGRP routing protocols for greener internetworking," Proc. 2013 International Conference on Green High Performance Computing, ICGHPC 2013, March 14, 2013 - March 15, 2013, IEEE Computer Society, 2013.

[3] G.P.S. Kalyan and D.V.V. Prasad, "Optimal selection of Dynamic Routing Protocol with real time case studies," Proc. 2012 International Conference on Recent Advances in Computing and Software Systems, RACSS 2012, April 25, 2012 - April 27, 2012, IEEE Computer Society, 2012, pp. 219-223.

[4] P. Li, et al., "Research on security of OSPF routing protocol with digital signature," Nanjing Youdian Xueyuan Xuebao/Journal of Nanjing Institute of Posts and Telecommunications, vol. 25, no. 2, 2005, pp. 86-90.

[5] D.-F. Li, et al., "Secure protection mechanism for OSPF protocol with sinitizable signature scheme," Beijing Youdian Daxue Xuebao/Journal of Beijing University of Posts and Telecommunications, vol. 34, no. 3, 2011, pp. 79-83.

Advanced Materials Research Vols. 989-994 (2014) pp 4608-4611
© (2014) Trans Tech Publications, Switzerland
doi:10.4028/www.scientific.net/AMR.989-994.4608

Study on the Design of Mobile Digital Library based on 3G Mobile Internet Technology

Jing Zhao

Library, Handan College, Handan, 056005, China

Keywords: 3G technology; Mobile library; VC software; MATLAB software; Hierarchy analysis; Data mining

Abstract. We use hierarchical data mining to compress the mobile communication data, which improves data transmission rate of 3G mobile internet. Based on this, combining the advantages of VC and MATLAB, we design the digital library architecture of 3G mobile internet model. This model has the functions of inquiry, backstage management, and mobile data optimization and so on. In order to verify the effectiveness and reliability of the model, we use network testing of small digital library as an example to test the library query function with mobile phone. By using the Android test terminal we get the library query process curve and the data flow transmission characteristics. It provides technical support for 3G on mobile internet technology and innovative design of library.

Introduction

With the development of the 3G mobile internet technology, mobile internet is able to meet the digital library needs of text, pictures, video and audio transmission [1, 2]. But in the design process of the mobile digital library it will produce a lot of data redundancy, so it needs to compress the data, so as to reduce the packet loss rate and delay characteristics of files, and improve the data transmission rate. In this paper we use hierarchy analysis process to do mining on the transmission data, and use conversion functions of HTML and WML to establish the mobile internet platform, and eventually develop WTA mobile library based on Android intelligent terminal, which is an innovation application of computer and communication technology.

Research on Application of 3G Mobile Internet in the Construction of Digital Library

With the popularization of 3G mobile internet technology, mobile technology is applied in mobile phone terminal and portable terminal device [3]. We use the protocols of WML and HTML to design mobile network and establish a digital library model, as shown in Figure 1.

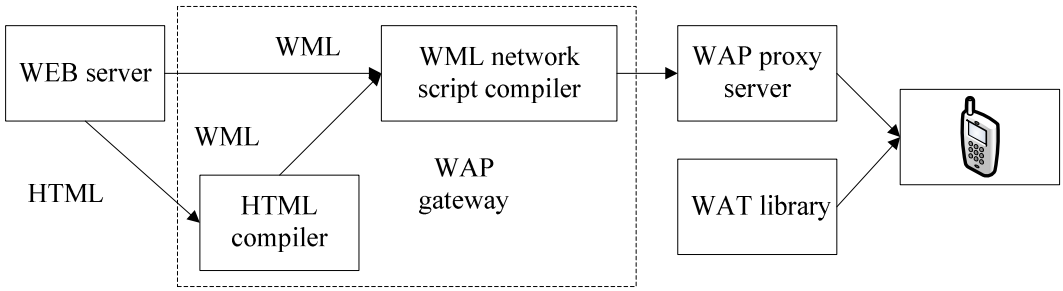

Fig. 1 Digital library mobile network model

Figure 1 shows the digital library by using HTML protocol and WML technology, and it realizes the data conversion between protocols [4]. The library can use WAP gateway to establish mobile network terminal of WEB server, and also use WAP proxy server to realize the request and authentication of mobile terminal, which ensures the stability and reliability of the network.Figure 2 shows the architecture diagram of 3G mobile digital library [5]. As shown in the diagram, it uses 3G mobile network access stations to connect many devices, including 3G mobile phone, 3G portable computer and 3G internet terminals.

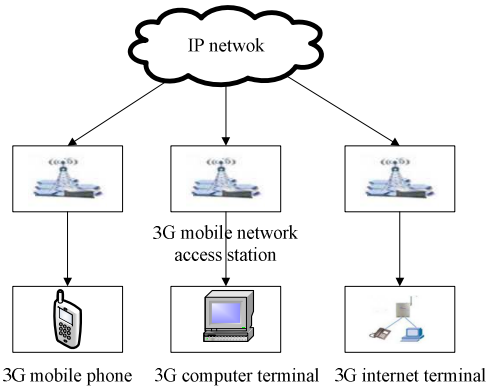

Fig. 2 Architecture diagram of 3G mobile digital library

Mathematical Model and Algorithm Design of Mobile Digital Library based on Data Compression Technology

In the constructing process of 3G mobile digital library, due to limitations of mobile communication hardware, it needs to compress the transmission data [6, 7]. We use the hierarchical data mining to compress the mobile communication data. Assume that the initial inputting sequence is $M, C1, C2$, so:

$$\{K_{M,m}\}, -C1 < m < -C2. \tag{1}$$

Compression of 3G mobile data can be expressed as shown in formula (2).

$$\begin{aligned} x_{m,\frac{n}{2}} &= \sum_{i=-M+n}^{n} b_{i-n}, d_{m+1,i} \\ y_{m,\frac{n}{2}} &= \sum_{i=-M+n}^{n} u_{i-n}, d_{m+1,i} \end{aligned}. \tag{2}$$

In order to improve the data compression quality, we use hierarchy method to analyze the data, as shown in formula (3).

$$f_{o,p}^{(n)} = f_{o,p}^{(n-1)} - [\sum_{o} u_{o,p+1}^{(n)} G_p^{(n)} + \frac{1}{2}]. \tag{3}$$

G_p is the lift coefficient of B/S frame data algorithm. According to the level compression model, the data compression can be written in formula (4).

$$\begin{array}{l} G_{p1}^{\ i} \quad \ldots \quad G_{p\,n/2i}^{\ i} \\ \quad \ldots \\ G_{p1}^{\ 2} \quad \ldots \quad \ldots \quad G_{p\,n/2i}^{\ 2} \\ G_{p1}^{\ 2} \quad G_{p2}^{\ 2} \quad \ldots\ldots\ldots \quad G_{pn}^{\ 1} \\ \Rightarrow \quad \Rightarrow \quad \Rightarrow\Rightarrow\Rightarrow\Rightarrow\Rightarrow\Rightarrow\Rightarrow\Rightarrow\Rightarrow\Rightarrow. \\ S1 \quad S2 \quad \ldots\ldots \quad \ldots \quad \ldots\ldots \quad \ldots\ldots \quad S_n \end{array} \tag{4}$$

S is the level and number of calculation. In order to realize the data compression process, we use VC and MATLAB joint programming way to control level compression model. The main program is as follows:

```
#include <stdio.h>
void main()
{Again:
{    int large(int x,int y);
     int a[10],b[10],i,n=0,m=0,k=0;
     printf("\n starting:\n mobile library a:\n");
     for(i=0;i<10;i++)
          scanf("%d",&a[i]);
     printf("\n search directory b:\n");
```

```
for(i=0;i<10;i++)                                    else
        scanf("%d",&b[i]);                                  if (large(a[i],b[i])==0)
printf("\n");                                                       m=m+1;
for(i=0;i<10;i++)                                           else
{if (large(a[i],b[i])==1)                       k=k+1;}
                n=n+1;
```

Research on Application of 3G Technology in Digital Library Construction

In order to verify the effectiveness and reliability of multi hierarchical analysis model designed in the second part, based on the WCDMA single carrier bandwidth, we use the MATLAB platform to do simulation calculation on the test data [8, 9]. The MATLAB interface is as shown in Figure 3.

Fig. 3 MATLAB interface

In this paper, we use the Matlab2011 version as the numerical calculation and the Custom version. We use the Fdatool tool to design the original peak signal in MATLAB, and test the transmission process of the signal, as shown in Figure 4.

Figure 4 shows the test schematic diagram of 3G signal transmission using MATLAB software. The Structure uses the Direct-Form model, order selects 255. Using 3G base station as a signal source, we can obtain visualization curve of signal transmission process.

Table 1. Data transmission testing table of digital library

Data type	Transmission time (s)	Transmission speed (kb/s)	Packet loss rate (%)
Original data	15.8	12.5	2.5
Compression data	11.5	24.6	1.2

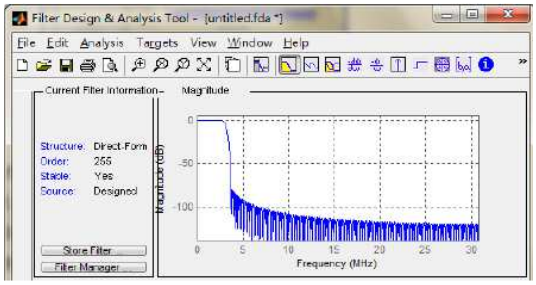

Fig. 4 MATLAB data signal transmission test

Table 1 shows the data transmission testing table of digital library by using Android intelligent terminal. From it we can see, the video compression algorithm can improve the data transmission speed, reduce the packet loss rate and improve the delay performance of data.

Figure 5 shows the query process curve of mobile digital library.We use the Android intelligent terminal to realize data transmission and visual interface [11]. From the chart we can see, when the query produces results, the data transmission amount is relatively large, and the entire query process curve is relatively smooth, which meets the design requirements.

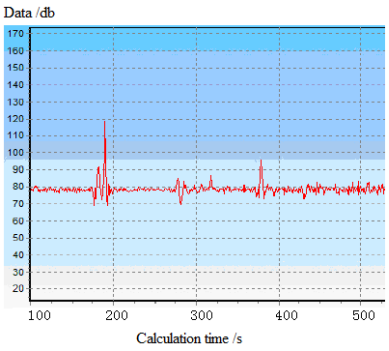

Fig. 5 Data transmission curve of Android intelligent terminal

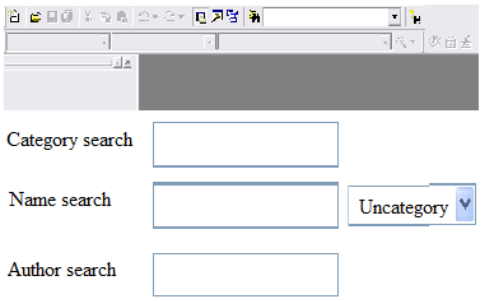

Fig. 6 Interface diagram of 3G digital library

Figure 6 shows a schematic diagram of 3G digital library using VC and MATLAB [12]. According to the user demand, using characteristics of Android intelligent terminal, users can access the literature of 3G digital library from three aspects of category, name and the author, which improves the efficiency of literature search.

Summary

In this paper we establish a mathematical model of 3G mobile internet digital library, and use multi hierarchy data mining technology to improve the model, which improves the signal transmission speed, improves the signal delay and achieves the design process of digital mobile library. We use VC and MATLAB joint programming control to establish 3G mobile internet digital library model, which realizes the function of digital library inquiry, backstage management and mobile data optimization. We use the Android intelligent terminal to test the performance of library. Through the results we find that the data transmission process of digital mobile library designed in this paper is steady, fast running speed, which can meet the needs of different users.

References

[1] Ren Haifeng, Zhao Jun. Mobile learning of domestic and foreign research present situation [J]. Adult education, 2010(1): 14-19.
[2] Ni Xiaopeng, Zhang Jingran. The development and trend of mobile learning - an interview with expert Dr. Fant Hofit [J]. Chinese audio-visual education, 2012(7): 45-49.
[3] Bian Jie. Research and implementation of semantic retrieval model based on Jena [D]. Xi'an Electronic and Science University, 2012: 3-15.
[4] Zhang Xiaojuan, Zhang Gantao, Zhang Jieli et al. Study on the hotspot of information resources integration in China [J]]. Information journal, 2011(10): 34-38.
[5] Tan Lei. A personalized mobile search technology [J]. Computer application, 2010(5): 78-81.
[6] Liu Bingli, Wang Li. The introduction and enlightenment of foreign mobile learning project - analysis of mobile project framework based on Frohberg [J]. Chinese audio-visual education, 2010(4): 34-38.
[7] Shang Jianyu. Using 3G communication technology to build the future of mobile phone library [J]. Depth map communication, 2012(3): 15-17.
[8] Xu Xin, Lou Lu. Study on construction of mobile phone library service system based on 3G [J]. Books and information, 2012(3): 50-54.
[9] Gao Feng. Application of mobile library online information retrieval system based on 3G [J]. Modern information, 2011(10): 218-220.
[10] Du Liang, Wu Fang, Zeng Qiang. The construction of mobile phone library based on 3G technology [J]. Jiangxi Library Journal, 2011(4): 12-13.
[11] Wang Liang, Gao Ling. The design and function realization of digital library based on 3G technology [J]. Journal of Fuyang Normal College (NATURAL SCIENCE EDITION), 2011(4): 60-62.

Advanced Materials Research Vols. 989-994 (2014) pp 4612-4616
© (2014) Trans Tech Publications, Switzerland
doi:10.4028/www.scientific.net/AMR.989-994.4612

Research on Key Technology of Web Network based on Mobile Computing

Rong Deng

Institute of Information Engineering, Chongqing Institute of Engineering, Chongqing, 400037, China

Keywords: Mobile computing; Web network; VC software; Network node; Spatial statistics; 3G base station

Abstract. Mobile computing environment is relatively complex, and the structure dynamic degree is high, and the heterogeneous is changeable. Therefore, the development of mobile network based on web techniques must be adapted to the complex environment. In order to get a better network structure supporting mobile computing, based on the context aware consciousness theory, combined with the VC programming software, we design the algorithm of mobile computing network node, obtain the spatial statistical node model of mobile network, and use GPRS/3G base station to establish mobile network model based on the core of multimedia services. In order to verify the effectiveness and reliability of mobile computing algorithm, we calculate the network performance using VC programming software, obtain the network data transmission and delay results, and use mobile algorithm to develop multimedia licensing scheme. It provides a new algorithm for researching on mobile computing.

Introduction

Due to the rapid development of wireless communication facilities and continuous expansion of mobile devices, mobile computing has rapid development as a new network computing technology[1,2]. Mobile computing access information on the moving, and it can coordinate distributed work and spread the field of distributed computing [3, 4]. The running network node has characteristics of space free moving, so that it makes network environment complicated. Combined with context awareness learning principle, we design the Web engine and network components. The framework structure is as shown in Figure 1.

Figure 1 shows schematic diagram of mobile computing Web engine design. From the chart we can see, the design of network is mainly based on the awareness learning theory. The main part of the network is composed by the Web engine, conscious learning and context aware component. Between Web engine and every member there is a great relationship [5]. In order to synergy mobile knowledge base, we need to optimize the design of network nodes, and coordinate performance of each component in space domain.

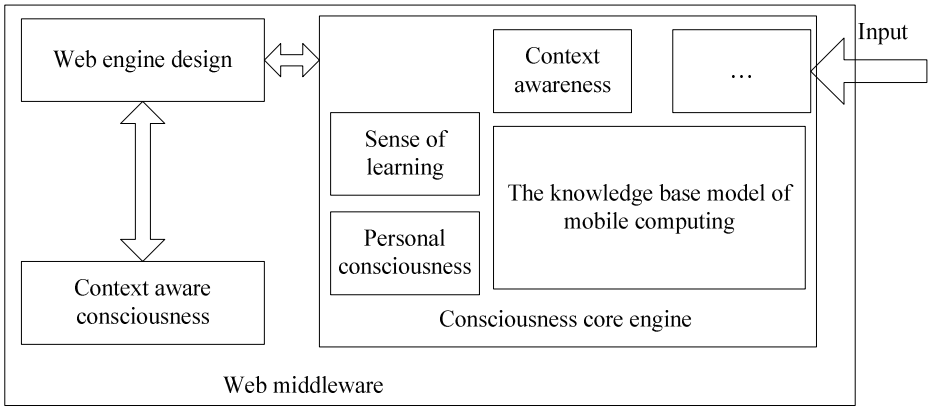

Fig. 1 Schematic diagram of mobile computing Web engine design

Mathematical Model and Algorithm Design of Mobile Computing Web Network

The primary basis for the design of mobile web network is optimization of network nodes. The node optimization can speed up the mobile computing speed, which realizes the effective transmission of information. We use the spatial statistical analysis of Web node as base, assume that the space matrix of mobile computing network node is Q, and the matrix is symmetric [6, 7]. The n-dimensional proximity relation of mobile web space can also be expressed with matrix, in order to simplify the calculation; the formula is as shown in formula (1).

$$Q=\begin{bmatrix} q_{11} & q_{12} & \cdots & q_{1n} \\ q_{21} & q_{22} & \cdots & q_{2n} \\ \cdots & \cdots & \cdots & \cdots \\ q_{n1} & q_{n2} & \cdots & q_{nn} \end{bmatrix}. \tag{1}$$

q_{ij} is network space adjacent relation between node i and node j . If x_i is reference values of position i, so similarity between nodes can be represented as shown in formula (2).

$$I=\frac{n\sum_{i=1}^{n}\sum_{j=1}^{n}q_{ij}(x_i-\bar{x})(x_j-\bar{x})}{\sum_{i=1}^{n}\sum_{j=1}^{n}q_{ij}\sum_{i=1}^{n}(x_i-\bar{x})^2} =\frac{\sum_{i=1}^{n}\sum_{j\neq i}^{n}q_{ij}(x_i-\bar{x})(x_j-\bar{x})}{S^2\sum_{i=1}^{n}\sum_{j\neq i}^{n}q_{ij}}. \tag{2}$$

S is the variance of node displacement distance, and the formula is as shown in formula (3).

$$S^2=\frac{1}{n}\sum_{i}(x_i-\bar{x})^2. \tag{3}$$

$\bar{x}$ is the average value of node distance, and the formula is as follows:

$$\bar{x}=\frac{1}{n}\sum_{i=1}^{n}x_i. \tag{4}$$

We introduce the optimization parameters to represent the optimization performance of clustering, and its expression is as shown in formula (5).

$$Y=\frac{(n-1)\sum_{i=1}^{n}\sum_{j=1}^{n}w_{ij}(x_i-x_j)^2}{2\sum_{i=1}^{n}\sum_{j=1}^{n}w_{ij}\sum_{i=1}^{n}(x_i-\bar{x})^2}. \tag{5}$$

In order to realize the optimization mathematical model of web network mobile computing, we use VC programming to design the algorithm. The main program is as follows:

```
#include <stdio.h>
#include <math.h>
void main(){Again:{
int rand(void);int max_valud;int a[4][4];int m,n,restart;
    printf("\n start:\nWeb mobile computing array:\n")
    for (m=0;m<4;m++)
        for (n=0;n<4;n++)
```

```
            {if (n=0) printf("\n");
                    a[m][n]=rand();
                    printf(" %5d",a[m][n]);}
        scanf("%d",&restart);
        if (restart==1) goto Again;}}
    int max_value(int array[][4])
    {int i,j,max;max=array[0][0];
        for (i=0;i<4;i++)
            for (j=0;j<4;j++)
                if (array[i][j]>max)
                    max=array[i][j];
        return (max);
    }
```

The Design of Web Network Mobile Computing System

In order to verify the effectiveness and reliability of web mobile computing model and algorithm, we use multimedia web network as architecture model to verify the performance of mobile computing. The overall network structure is as shown in Figure 2.

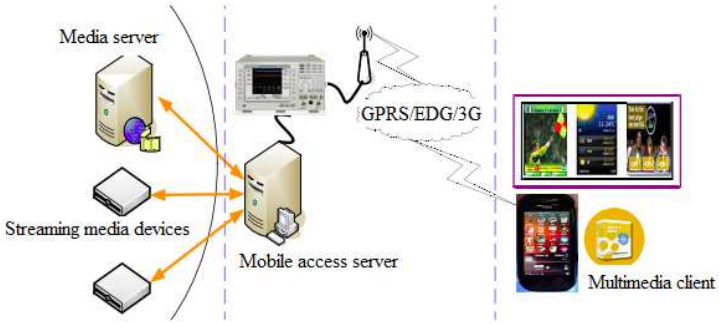

Fig. 2 Integration model of mobile computing web network

Figure 2 shows the architecture model of mobile calculation web network. In order to realize multimedia mobile service, the user can connect multimedia client by mobile phone, access multimedia network through the mobile server and the GPRS/3G base station [8]. The multimedia network terminal is composed of video and audio servers.

Figure 3 shows the test results of the web platform using VC software. The curve represents the sensitivity of the QoE on the QoS network. QoS parameters mainly include network delay, network packet loss rate and mobile call error rate and success rate [9]. For different mobile computing service, curve form is different. As shown in Figure 3, the curve has three relatively flat areas, which represents the QoE portion is not sensitive to QoS part.

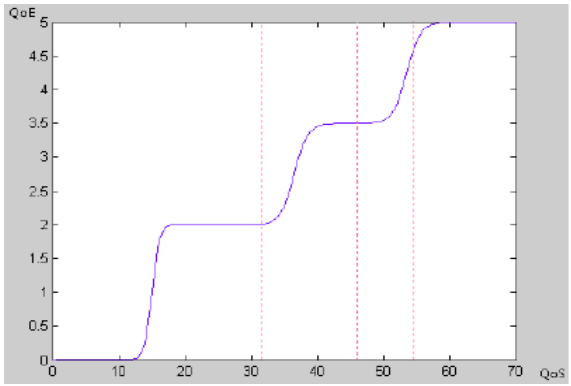

Fig. 3 The curve calculated by VC software

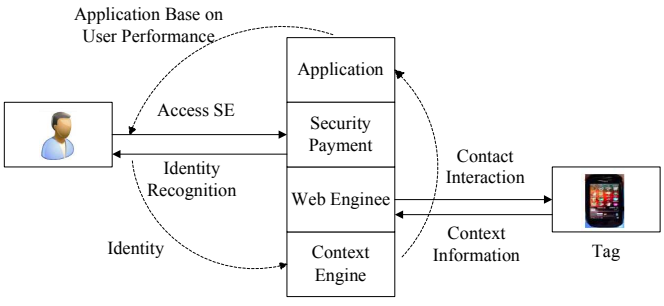

Fig. 4 The design of multimedia services mobile computing

Figure 4 shows the design of multimedia services mobile computing. According to the design in the scene graph, mobile user can get all kinds of services from the cinema, and can check all the information tags in the web page [10]. When the user enters the page and finds a poster, poster interior is embedded in NFC tag which can access webpage. When a mobile device selects it, it will respond to the corresponding information, and we can obtain film information from the label.

Fig. 5 Privacy protection technology of mobile video

Figure 5 shows schematic diagram of video protection using mobile computing network node. Video in the figure is transformed and applied the jamming technology. According to the context awareness principle, when the video decoding, video can be clear; when the video encryption, video will produce distortion effect.

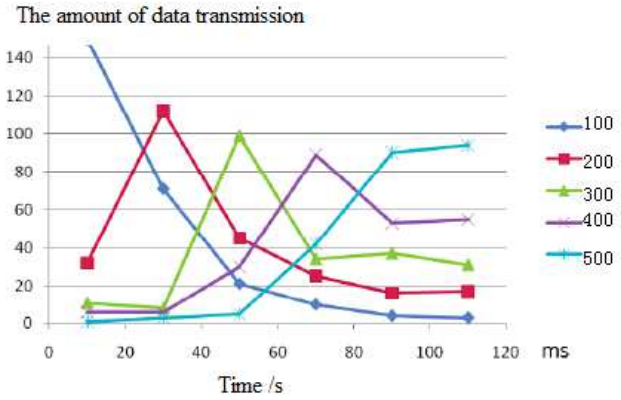

Fig. 5 Statistical graph of data transmission amount

Figure 5 shows data transmission amount and data search of web network engine in the mobile computing process. From the figure we can see, with the increasing of network node data, the data transmission amount will increase rapidly [11]. In order to study the influence of network nodes on data transmission, we list the network optimization, time delay characteristics and the comprehensive evaluation results in Table 1.

Table 1. Network node optimization table

Number of network node optimization	Delay characteristics (ms)	Comprehensive evaluation score
200	50.1	3
300	40.2	5
400	38.5	6
500	32.1	8

Table 1 shows the delay characteristics and comprehensive evaluation results through network nodes optimization. From the table we can see, as the increasing number of network node optimization, network delay reduces gradually, with lowest 32.1ms. Comprehensive evaluation score also increases with the increasing number of network node optimization [12]. So the design of network node optimization improves the performance of mobile computing, and optimizes the network architecture. It verifies the effectiveness and reliability of the network optimization model.

Summary

Through the improvement of mobile calculation environment, we propose a spatial web mobile internet node model, and use the matrix theory to establish the optimization mathematical model of node, and use VC programming software to design the algorithm. Using VC programming control method, combined with the GPRS/3G base station, we establish the mobile web internet architecture model of multimedia service, and develop multimedia licensing scheme. In order to verify the effectiveness and reliability of multimedia mobile internet architecture model, we use the VC visualization technology to statistics network data transmission and time delay characteristics. It provides the theory reference for the application of web technology in mobile computing.

Acknowledgments

The work was supported by the science and technology research projects of Chongqing Education Commission with its project number KJ132001 and its project name Research on Fixed Assets Management System Based on Internet of Things.

References

[1] Deng Haisheng, Li Junhuai. Mobile calculation model based on reflective middleware [J]. Computer engineering, 2012, 38(20): 278-281.

[2] Zheng Di, Wang Jun. The member adaptation model supporting context aware [J]. Computer engineering, 2012, 38(2): 39-41.

[3] Wang Huajin. Review of visualization technology in data mining [J]. Science Plaza, 2011(1): 235-237.

[4] Li Na. Overview of data mining software products [J]. The popular science, 2010(1): 22-24.

[5] Deng Qianni, Chen Quan. Cloud computing and its key technology [J]. Application and development of high performance computing, 2012, 26(1): 2-6.

[6] Li Xiaopeng. Electronic purse system design and security research based on NFC technology [D]. Beijing University of Posts and Telecommunications, 2011: 2-15.

[7] Xia Wendong, Lin Kai. 3G smart card system fused NFC [J]. Computer engineering, 2011(37): 230-239.

[8] Wang Yuwei, Zhang Hui. Study on the application of NFC based on mobile phone [J]. Chinese radio, 2011(6): 4-8.

[9] Yao Gang. The popularity of NFC technology through the Android platform [J]. Electronic design technology, 2011(3): 69-73.

[10] Zhang Jixian, Luo Lei, Jiang Fan. Rich media scene rendering optimization strategy in mobile device [J]. Computer aided design and graphics, 2010, 22(8): 1272-1278.

[11] He Gaoqi, Pan Zhigeng, Zhang Mingmin. Vector graphics rendering based on mobile devices technique [J]. Journal of Zhejiang University, 2011, 42(11): 1856-1864.

[12] Zhang Jixian, Luo Lei, Jiang Fan. Stroke font storage research and outline algorithm based on the mobile terminal [J]. Journal of computer aided design and graphics, 2010, 22(12): 2125-2132.

Advanced Materials Research Vols. 989-994 (2014) pp 4617-4620
© (2014) Trans Tech Publications, Switzerland
doi:10.4028/www.scientific.net/AMR.989-994.4617

Jess-based Argumentative E-commerce Negotiation System

Wei Zhang[1] ,Ya'nan Zhang[2] ,Shaosheng Guo[1] ,Xianzhen Ma[1]

[1].School of Information Science and Technology, Qingdao University of Science and Technology, Qingdao, 266062, China,zhangweisimt@163.com

[2].School of Computer Science and Technology, Beijing Institute of Technology, Beijing,100081, China

Keywords: argumentation, E-commerce, negotiation, Jess

Abstract: Based on Dung's argumentation framework, using Dung's extended argumentation semantics, importing reasoning argument and fact argument, design and implementing Jess-based argumentative E-commerce system, the system has important significance and high reference value for studying E-commerce argumentative negotiation systems.

Introduction

At the end of 1980, researchers began to study E-commerce negotiation system; multi-agent technology is mainly adopted in the study of negotiation system, in which agent partly or wholly represents human negotiation. Intelligent E-commerce negotiation and argumentation-based negotiation theory has became one of the hotspots in artificial intelligence. Multi agent based negotiation refers to the interactive action between the agents who have conflict interests and have desire to corporate with each other in order to reach both accepted agreement in the limited resource and information[1].

In this paper we design and implement a negotiation algorithm based on E-commerce alternating negotiation applied in E-commerce negotiation. In the negotiation system agent will negotiate with the opposite side and present arguments to persuade the other to accept his proposals. In the end of the negotiation agents will reach agreement on a certain proposal or quit the negotiation without agreement. We use Jess language simulate negotiation process.

Argumentation theory

In the field of automatic negotiation field, there are three kinds of negotiation mechanism and method[2], game theory based, heuristic-based and argumentation-based negotiation. Argumentation based negotiation is one of the research hotspots in negotiation field.

Besides proposals argumentation based negotiation permits agents exchange extra information in the form of arguments to defend some behaviors by arguments, so as to dynamically affect other agent's attitude and knowledge. Argument has two basic functions, one is declaration of self negotiation position; the other is affect the other agent negotiating position.

Argumentation based negotiation framework

In 2003, Rahwan etc. presented a relatively comprehensive concept framework[3], and described argumentation based negotiation external factors and internal factors. According to the negotiation concept framework of Rahwan, we define proposal, argument, the functional relation between argument and proposal and the binary preference relations between agents as the internal elements of agent. We also specify the interactive environment: primitives and their meanings of interactive agent are defined; negotiation data is stored in working memory and we use fact base in the simulated program.

We define preference based argumentation framework. Supposing two agents, ag_i *and* ag_j correspondingly refer to negotiation agents. P represents the proposals set, and $P = \{P_1, P_2, ...P_n\}$. Assuming exists $P_c \in P$, in which P_c is preserve proposal and other proposals are preferred to P_c.In the proposal set P all the proposals are mutually exclusive.

Definition1 Abstract argumentation framework[4] is a binary relation $(Arg, attacks)$, Arg is the infinite set of arguments, $attacks \subseteq Arg \times Arg$ is the binary relation on Arg. Suppose $X, Y \subseteq Arg$, X attacks Y iff $x \in X$, $y \in Y$ and $(x, y) \in attacks$. $Args$ is the conclusion set of arguments and $Attack$ is the conflict set in logic.

Definition2 Argument extension set X is a set of arguments

i) X is an admissible set iff X does not attack itself and attacks every argument set Y which attacks X.

ii) X is a preferred set iff X is the maximum admissible set.

iii) X is a complete set iff X is admissible and for $\forall x \in X$, X attacks all the arguments which attack x.

iv) X is a grounded set iff X is minimum complete.

v) X is an ideal set iff X is admissible and is contained in arbitrary preferred set.

Argument type

Using logic language ξ to construct arguments set $Argu(\xi)$. We present two kinds of argument: reasoning argument and fact argument.

Definition3 Reasoning argument A_R support proposal trying to justify the proposal.

Definition4 Fact argument A_F represent agent's belief.

And the two kinds of arguments satisfy:

(1) $Argu(\xi) = A_R \cup A_F$

(2) $A_R \cap A_F = \varnothing$

Argument and function are function mapping relation. G is the function, which is a mapping from a proposal to its supporting arguments, i.e. $\forall P_i \in P, G(P_i) \subseteq A_R$ and $\forall P_x, P_y \in P, P_x \neq P_y$, $G(P_x) \cap G(P_y) = \varnothing$.

Argumentative negotiation protocol

Amgoud[5]etc. defined negotiation protocol: negotiation protocol is a set of rules to control dialogues between agents who have well active ability. In a negotiation round the proponent and opponent agent can defend its own arguments and attack the others arguments. Each round includes negotiation behaviors of the agents.

Definition5 Argumentative negotiation is a non-empty dialogue sequence $N = \{n, ..., r_n\}$ between two agents.

Primitives

In the negotiation process, agents propose and exchange argument by primitives.

Definition6 A primitive is defined as $B_{r,t}$ which is the behavior of the agent in r round and the first t times in this round.

There are also some function, such as $Primitive(B_{r,t})$ returns r round the first t times primitive; function $Agent(B_{r,t})$ returns r round the first t times negotiating agent; function $Argument(B_{r,t})$ returns the r round the first t times argument; function $Target(B_{r,t})$ returns r round the first t times primitive; function $check()$ update negotiation theory to decide whether agree the other or find a new argument to attack it; function $defend()$ defend own proposal when opponent returns Argue.

Protocol include interact agreement and dialogue rules which is a formal constrain of interactive agents.

Negotiation protocol

In the negotiation process, the proponent and opponent alternating propose their primitives. The proponent agent has primitive set $\{Offer, Argue, Agree, Exit, Pass\}$ and the opponent has primitive set $\{Argue, Refuse, Pass, Accept, Exit\}$.

The needed sets in the program (1) A_{rec} is the received argument set; (2) P_{off} is the proposed proposal; (3) Att_{use} is the used attack set.

Table 1. Communication primitives and their meanings

primitives	meanings
$Offer(ag_i, ag_j, \mathrm{P}_x, \mathrm{A}_R)$	The proponent propose Px and its reasoning argument A_R
$Argue(ag_i, ag_j, a, T\arg et)$	ag_i present argument a attack agent ag_j 's proposal or argument
$\mathrm{Re}\,fuse(ag_i, ag_j, \mathrm{P}_x)$	ag_i refuse ag_j 's proposal P_x
$Pass(ag_i, ag_j)$	ag_i say nothing
$Accept(ag_i, ag_j, P_x)$	ag_i accept ag_j proposal P_x
$Agree(ag_i, ag_j)$	ag_i agree with ag_j
$Exit(ag_i, ag_j)$	ag_i raise to exit the negotiation

Firstly, begin with $B_{1,1}$ and all the sets initiate to empty sets.

Secondly, computing their proposal sets respectively, then the proponent agent proposes. We define a variable mark, $mark = \{1,0\}$ when $mark = 1$ the proposal is proposed by him, or else $mark = 0$ the proposal is the opponent's. At the beginning $mark = 1$.

Then agent sends primitive Offer, and function $\mathrm{Pr}\,imitive(\ )$ captures its return value. According to the return value agent make decision for next step. The whole process depicted in figure 1.

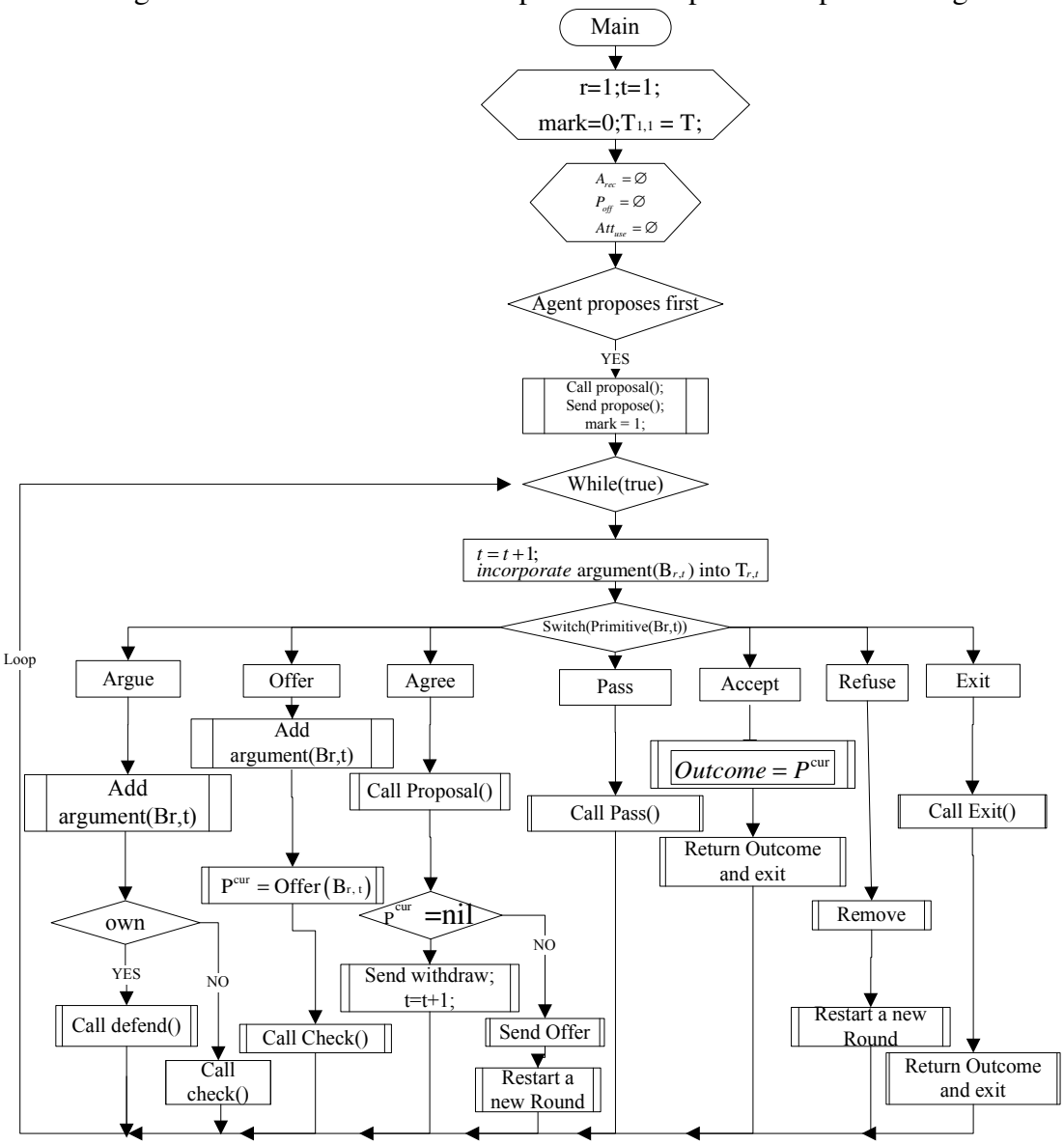

Fig.1. Negotiation main algorithm flow chart

Prototype design and implement

There are two main approaches: the structured approach and the abstract approach for argument implementation[6-7]. Jess is the kernel of expert system developed by Java. Java Expert System Shell is an extend rule engine based on Java platform. The prototype embedded Jess in Java, and we can create an example of Rete class as following: import jess.*; myrete = new Rete();

As depicted in figure 2, argument template and rules are defined ; output interface is displayed.

Argument template is defined as:

```
(deftemplate Ap (slot id) (multislot supportlist) (slot conclution))
(deftemplate Ae (slot id) (multislot supportlist) (slot conclution))
```

Rules are defined as::

```
(defrule compute-ESA-remove
(declare (salience 16))
(compute-esa yes)
(MAIN::Ap (conclution ?PH&:(not (myeq ?PH od))))
?tempESA <- (MAIN::ESA (offer ? PM&:
 ( myeq ?PH ?PL) ))=> (retract ?tempESA))
```

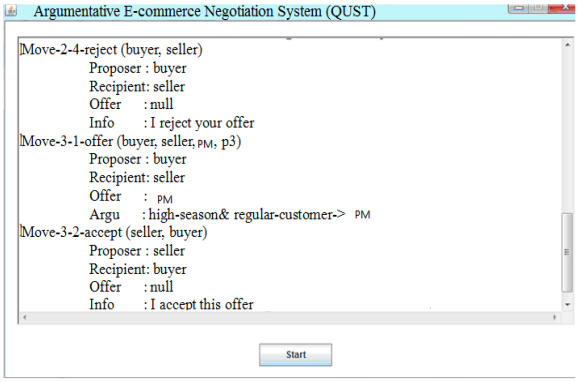

Fig.2. Argument template definition and output interface

Conclusion and discussion

Jess based e-commerce argumentative negotiation system is implemented; the prototype can process argument-based negotiation and output the proposals and arguments. Using argument easier to persuade the other agent accepts opinion and reach agreement. In the future we should use the knowledge base and belief base predict adverse belief and behavior and revision the agents' belief.

Acknowledgement

In this paper, the research was sponsored by the Nature Science Foundation of Shandong Province (Project No. ZR2009GQ013 , ZR2011FQ005 and ZR2012FQ021).

References

[1] N.R.Jennings, K.Sycara, M.Wooldridge.A roadmap of agent research and development [J]. Autonomous agent and Multi-agent Systems, 1998, 1(1):7-38.

[2] A. Kakas and P. Moraitis. Adaptive agent negotiation via argumentation [R]. In 5th International Joint Conference on Autonomous Agents and Multi-Agents systems, 2006: 384–391.

[3] I. Rahwan, L. Sonenberg, and F. Dignum. Towards interest-based negotiation.In J. Rosenschein, T. Sandholm, M. J. Wooldridge, and M. Yokoo, editors, (AAMAS-2003) : 773–780.

[4] P.M. Dung, On the acceptability of arguments and its fundamental role in non-monotonic reasoning, logic programming and n-person games[J]. Artificial Intelligence, 1995,77(2):321–357.

[5] L. Amgoud, S. Belabbes. A formal general setting for dialogue protocols[C]. ArtificialIntelligence: Methodology, Systems, and Applications, Proceedings. Berlin, Springer-Verlag Berlin. 1998，4183: 13-23.

[6] Bas van Gijzel .Tools for the implementation of argumentation models[C]. 2013 ICCSW, London, United Kingdom, Dagstuhl Publishing .September 26–27, 2013:43-48.

[7]Günther Charwat, Wolfgang Dvorák, etc. Implementing abstract argumentation - a survey[C]. Technical Report DBAI-TR-2013-82, Vienna University of Technology, 2013.

Advanced Materials Research Vols. 989-994 (2014) pp 4621-4624
© (2014) Trans Tech Publications, Switzerland
doi:10.4028/www.scientific.net/AMR.989-994.4621

The Application Research of Information System in the Information Pipe

Huang Zhijun[1, a]

[1]Long communication service co. , ltd, Guangzhou 510507,China

[a] huangzhijun@yeah.net

Keywords: Information system; Information security risk management; Information pipe

Abstract. Applying the computer technology to the real management is the development trend of today's society. The popularization of computer technology has brought great convenience for managers. As a large application field of the computer, information system plays an important role in the information management. The application of information system in information management makes the spread of information and information utilization improved. This paper discusses related questions of information system in information management.

Research status of information security risk management method

Risk management is the overall process to identify, evaluate and control information system security risk, which includes risk identification, risk analysis, security selection, implementation and test security, security evaluation and so on.

ISO 13335 gives safety management relational model taking risk as the core. It assumes that the safety management of the main elements include assets, threats, vulnerabilities, and impact, risk, protective measures and residual risk; the main safety management process include risk analysis, risk management, safety awareness to maintain, monitor and consistency check; four risk management strategy risk avoidance, risk transfer, risk elimination are taken in the process of risk management to curb risk.

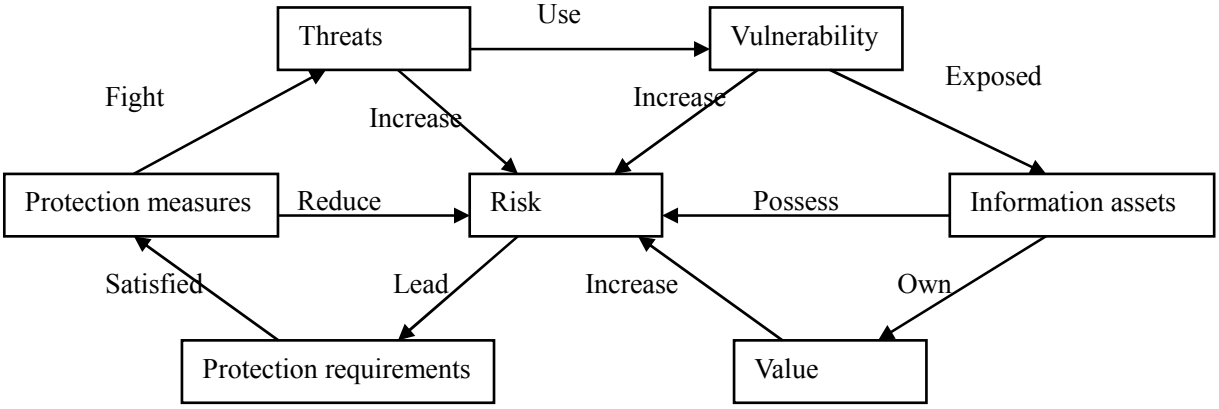

Figure1. Risk management relationship model diagram of ISO 13335

System security engineering capability maturity model SSE - CMM put forward by the United States at Carnegie Mellon university the defines four risk management process: PA04 - evaluation of security threats, PA05 - evaluation system vulnerabilities, PA02 - to assess impact of the event and PA03 - evaluation of security risks. [1] The relationship between them is shown in figure 2. It requires in the initial stages of information system security engineering, developers should first risk take analysis and assessment according to the risk management process.

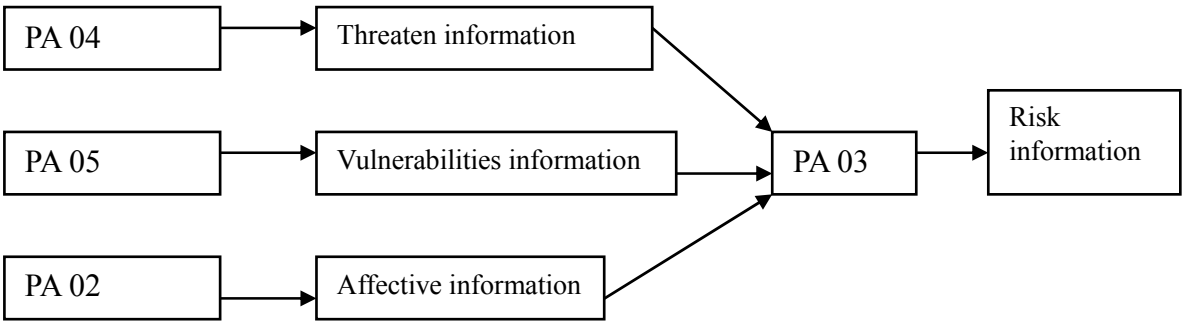

Figure2. Risk management process defined by SSE - CMM

Multilevel security model of information system

Security requirements

For important information system, the users have different level of security permissions. Information stored, processed and transferred in the system is of different level of sensitive and part of the equipment for processing the information also has the sensitive of different level. Therefore, realize the multilevel security is the basis of the information system requirements. [2] Multilevel security refers to the information system can allows users to access with different level of security permissions to have information of different sensitive level, and also can prevent unauthorized users to access information.

A multi-level security information system must at least meet the following requirements:

(1) Conduct reliable identification and authentication to users on the system;

(2) Data is transferred safely on the communication network;

(3) Allow users of the different level of security permissions to access information of different sensitive level at the same time;

(4) Prevent users from accessing to unauthorized information;

(5) Share information with the appropriate user safely.

Basic security assumptions

In order to simplify the description of information system security model, before the establishment of the formal security model, we put forward the following basic assumptions:

(1) Information system has reliable identification and authentication mechanism;

(2) Information system can provide secure data transmission channel;

(3) All entities of information systems have comparable sensitivity level;

(4) All the entities of information system have a need-to-know category and a need-to-share category, but the need-to-know category and need-to-share category of the same object is no intersection;

(5) Information system has a single security management center. Security management center is credible and the security administrator can correctly distribute the subject and object in the information system security level through the security management center;

Model elements

(1) Entities: resources in the information system (processes, files, equipment, etc.) and users.

(2) Object: abstract network connection to information systems in other computer system resources, remembered as $O=\{O_1,O_2,...,O_m\}$. [3] Connection security level is equal to the connection of the security level of resources.

(3) Main body: users or equipment in the information system, remembered as $S=\{S_1,S_2,...,S_N\}$. Use two functions $sdr,rcr:O\to S$ to respectively connect the sender $sdr(O)$ and receiver $rcr(O)$.

(4) Level of security permissions: trust level of when access to confidential information.

(5) Confidential categories: the confidentiality level of information stored in the object.
Security permission levels and the classification show the sensitive level of the subject and object, respectively, $C=\{C_1,C_2,...,C_q\}, C_1>C_2>...>C_q, C$ as poset.

(6) Categories need to know: based on the Need-to-Know principle, it is noted as. $K=\{K_1,K_2,...,K_r\}$.

Categories need to know principle means unless subject is to complete certain operations that need to access the object, subject to access object is prohibited. The category set each subject can access is a category set power set. For example: there are three need to know categories: K_1, K_2, K_3, then the category collection subject can access is one of the following set: $\phi, \{K_1\}, \{K_2\}$, $\{K_3\}, \{K_1, K_2\}, \{K_1, K_3\}, \{K_2, K_3\}, \{K_1, K_2, K_3\}$.

(7) Need to share: access restrictions based on the Need-to-Share principle is remembered as $H=\{H_1,H_2,...,H_w\}$.

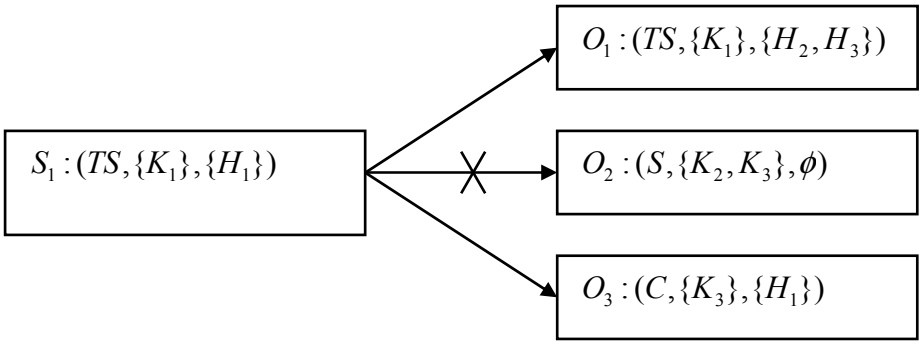

Figure3.An example of information sharing

Definition 1: In addition to have its own security permission $level(S)$, a body has two other levels of security permissions: the max security permission $v-\max(S)$ and minimum security permission level. The sensitive level scope of main body is $ran(S)=\{C: v-\max(S)\geq level(S)\geq a-\min(S)\}$.

Definition 2: Security level of subject S controls that of object O, if and only if

(i) $v-\max(S)\geq e-\max(O) and f_3(S)\supseteq f_4(O)$, or

(ii) $v-\max(S)\geq e-\max(O) and f_6\supseteq f_5(S)$

The domination relationship of subject to the object is $SL(S) dso SL(O)$.

Definition 3: Security level of object O controls that of subject S, if and only if

(i) $i-\min(O)\geq a-\min(S) and f_4(O)\supseteq f_3(S)$, or

(ii) $i-\min(O)\geq a-\min(S) and f_6(O)\supseteq f_5(S)$

Definition 4: Security level of Object O_1 controls that of subject O_2, if and only if $i-\min(O_1)\geq e-\max(O_2) and f_4(O_1)\supseteq f_4(O_2)$, remembered as $SL(O_1) doo SL(O_2)$.

Definition 2-6: Security level of subject S is equal to that of object O, if and only if

(i) $level(S)=level(O) and f_3(S)=f_4(O)$

(ii) $level(S)=level(O) and f_5(S)=f_6(O)$

The domination relationship of subject S to the object O is $SL(S)=SL(O)$.

Summary

The rapid development of computer technology and network technology accelerate and deepen the process of social informatization, also makes the organization and information system become

increasingly close. However at the same time of improving organizational information resources sharing and information systems business operation efficiency, it also brings information security problems. Therefore, as the basis of information system construction and safety management, a comprehensive and systematically information security risk management to organize information system has very important practical significance.

References

[1] Levin, D. Lessons Learned in Using Live Red Teams in IA Experiments. DARPA Information Survivability Conference and Exposition (DISCEX'03), Washington, D.C.: IEEE Computer Society. 2003, 1: p110-119.

[2] Steffan, J., Schumacher, M. Collaborative Attack Modeling. Proceedings: 2002 ACM Symposium on Applied Computing (SAC 2002), Madrid, Spain: ACM/SIGAPP. 2002: 253-259.

[3] Cha, S. S., Leveson, N. G., T. J. Shimeall. Safety Verification in MURPHY Using Fault Tree Analysis. Proceedings: 10th International Conference on Software Engineering, Singapore. 1988: p377-386

Advanced Materials Research Vols. 989-994 (2014) pp 4625-4628
© (2014) Trans Tech Publications, Switzerland
doi:10.4028/www.scientific.net/AMR.989-994.4625

Research on the Information Push System Using Case-based Reasoning

Huailiang Shen, Lingping Fu

Zhejiang Business Technology Institute, Ningbo 315012, China

huailiang_shen@163.com

Keywords: information recommendation, push system, case-based reasoning.

Abstract. Information push systems play an important role in reducing information overload for people visiting online sites, but their services could be improved by using data from online social networks, electronic communication tools and others. Information push systems are used by electronic commerce sites to suggest products to their customers and to provide consumers with information to help them determine which products to buy. There are many electronic commerce applications on the Web. A common shortcoming is the lack of customer service and marketing analysis tools in most electronic commerce websites. The paper presents the information push system using case-based reasoning. It introduces the case-based reasoning technology and analyzes the case representation, case library and case search. Lastly, it gives the architecture of the information push system using case-based reasoning.

Introduction

With the rapid development of Internet technology, people want to find, collect and maintain their information need to spend a lot of time and energy from Internet. Traditionally, there are many methods of WWW information retrieval. The first is accessed through the web site address; the second is to use multiple search engine queries; third is the production of the professional company database query database. The traditional information retrieval technology has certain insufficiency. Firstly, the user must take the form of keywords summed up their information requirements. Secondly, because the network is constantly updated information, the user to obtain the latest information needs to be with the same key words repeated query.

Information filtering technique is proposed for this problem, it is aimed at different user; provide different service, to meet different needs, to learn the user's interests and behavior by collecting and analyzing user information, so as to achieve the purpose of the initiative recommendation.

Intelligent information recommendation technology is to learn the user's interests and behavior through the collection and analysis of customer information, and timely update, the realization of active recommendation information to the user. At present, the intelligent information recommendation system can be divided into two types: content based recommendation and recommendation system based on collaborative. Similar recommendation system content resources and based on the interests of the user to filter information. Recommendation system based on content has the advantages of simple, effective, the disadvantage is difficult to distinguish between resource content quality and style, but not for the user to find new resources of interest, can only be found and the user has a similar interest in information. The similarity between users in the recommendation system is based on collaborative filtering to filter information. Its advantage is to discover new information of interest to the user, but in the use of the initial system, because the system does not get the user evaluation enough, it is difficult to give a similar recommendation.

Case-based reasoning

Case based reasoning is accumulated in the case of experience as stored knowledge foundation, defines and describes the new problems, in order to capture the information to solve the new

problems. This method in the automatic correction system industry, auxiliary medical system, comprehensive evaluation and decision making has been widely applied in the field.

The premise of the CBR is to establish a case based experiences. According to the characteristics of specific areas, each experience is represented as a case. The main idea is based on experience, searched and the new question similar case, and then adjusts the draw solution to new problems for the solution according to the similar case. Visible, in the whole process of CBR, including the important part of the following: the case representation, case searching, case solution.

Case representation

The existing knowledge or experience needs to be represented as a case base, can play a role on the basis of CBR. A case can be represented as a feature vector of the form. For example, a digital camera price is determined by its brand, how many pixels, decision, optical zoom, then the brand, pixel and optical zoom can be used as features from the extracted feature space problem, is used to describe the specific characteristics of each camera to determine its price. The Olympus camera as an example, if it is known pixel is 20000000, is 3 times optical zoom, the price is 3000 Yuan, then such an experience can be expressed as a case, as shown in table 1.

Table 1 Using the feature vector representation of case

Brand	Pels	Optics	Price
Olympus	2000	3	3000

Case library

In the case of descriptive features are usually called attributes, such as the brand, pixel and optical zoom; case results or decision scheme called decision-making features, such as price. After determining the attributes, each one's previous experience can be accurately represented as a case, and thus form a case base. Table 2 shows a case base of library.

Table 2 An example of case library

Brand	Pels	Optics	Price
Olympus	2000	3	3000
Cannon	3000	5	3500
Sony	2500	3	2700

Case search

Given an unknown problem, first of all, to the given problem is expressed as the form of case, known as the case. This case is a feature vector, but because the decision value is unknown, the eigenvalue includes only the attributes and does not include the decision-making characteristics. For example, there are people who want to buy a digital camera, the requirement is Olympus, 30000000 pixels, optical zoom is the 3, want to estimate how much is the price. This problem can be expressed as shown in table 3.

Table 3 Case representation

Brand	Pels	Optics	Price
Olympus	3000	3	?

According to the principle of CBR, to solve the new problem, is found from the case base and the problem of feature values in the case of vector most similar, then use the similar case results to make a decision. Take the above example, now is to estimate the camera price, then from the case base and the case to find the most similar cases. As can be seen, where the need to measure similarity of a given. The commonly used similarity measurement method is based on the "distance" of similarity

calculation method has been widely used. "Distance" is that similarity is small. Here is the commonly used distance measure.

If the case base represented by a CB, CB ={e1, e2,... , eN} N contains a case, EI (I =1,2, -, N). Each case with n attribute Fj (1 ≤ J ≤ n) and a decision characteristics of D. In each case the case base in EI (I =1,2,... , N) can be expressed as a (n +1) dimensional feature vector, i.e., EI = (Xi1, xi2,... , Xin), Xij is corresponding to the j features of Fj (1 ≤ J ≤n). Assume that for each attribute of Fj (1 ≤ J ≤ n), a weighted WJ (WJ ∈ [0,1]) specifies the importance to measure the characteristics of the. The weighted Euclidean distance:

$$d(x,y)=\sqrt{\sum_{i=1}^{n} w_i*(x_i-y_i)*(x_i-y_i)}$$

The Information Push System Using Case-based Reasoning

The information push system using case-based reasoning is shown as figure 1.

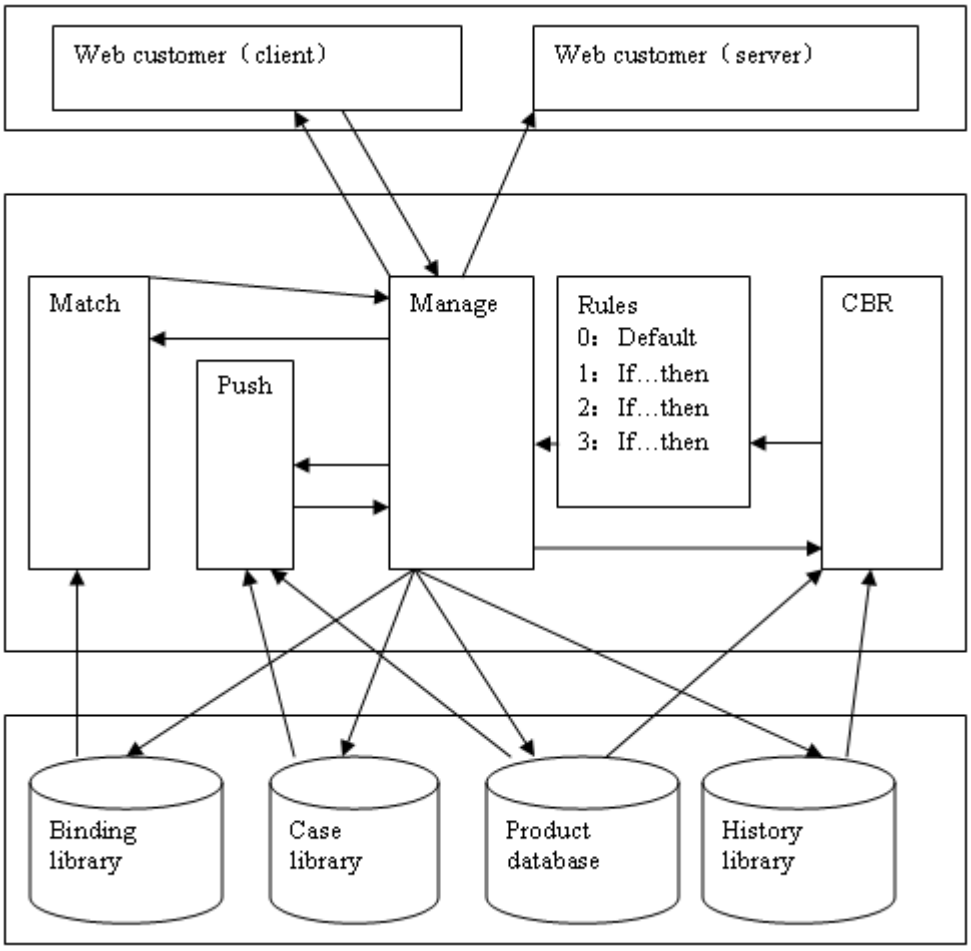

Figure 1 The information push system using case-based reasoning

First, a large number of existing, mature case previously stored in the case library. Then, according to the requirements and characteristics of the customer, according to similarity are retrieved from the case library as a case. Then, modification, composition and processing is the necessary. Finally, may be formed for different customers with new recommendations.

(1) Cases were collected and said. The typical case, collect past problem solving, is in each case by the individual characteristics, customer demand information and consumer behavior.

(2) Case retrieval. Retrieval of case base, case extraction similar to those of the problem domain and target problem, according to the customer demand information, dynamic weight adjustment characteristics and related attributes to provide recommendation results.

(3) Case matching. Calculation case similarity, the similarity measure and the results of sequencing, retrieve the matching case from the case base.

(4) Case solution. Modify and adjust the scheme for solving the best similar case as the target case solution.

(5) Cases update. The adjusted target case recommendation result as the target case solution is added to the case base, accumulate experience for the future to solve the new problems.

Summary

Information push systems play an important role in reducing information overload for people visiting online sites, but their services could be improved by using data from online social networks, electronic communication tools and others. Information push systems are used by electronic commerce sites to suggest products to their customers and to provide consumers with information to help them determine which products to buy. There are many electronic commerce applications on the Web. In this paper, we present the information push system using case-based reasoning. Then we introduce the case-based reasoning technology and analyze the case representation, case library and case search. Lastly, it gives the architecture of the information push system using case-based reasoning.

Acknowledgment

This research is supported by University Students' Scientific and Technological Innovation Project of Zhejiang Business Technology Institute.

References

[1] Hyung Jun Ahn, A new similarity measure for collaborative filtering to alleviate the new user cold-starting problem, Information Sciences 178 (2008) 37-51.

[2] Songjie Gong, Learning User Interest Model for Content-based Filtering in Personalized Recommendation System, International Journal of Digital Content Technology and its Applications, Vol. 6, No. 11, pp. 155 ~ 162, 2012.

[3] Jong-Seok Lee, Chi-Hyuck Jun, Jaewook Lee, Sooyoung Kim, Classification-based collaborative filtering using market basket data, Expert Systems with Applications 29 (2005) 700–704.

[4] Songjie Gong, A Collaborative Filtering Recommendation Algorithm Based on Trust Network and Trust Factor, Journal of Convergence Information Technology, Vol. 8, No. 5, pp. 1111 ~ 1118, 2013.03.

[5] George Lekakos, George M. Giaglis, Improving the prediction accuracy of recommendation algorithms: Approaches anchored on human factors, Interacting with Computers 18 (2006) 410–431.

[6] Songjie Gong, Research on Attack on Collaborative Filtering Recommendation Systems, AISS: Advances in Information Sciences and Service Sciences, Vol. 5, No. 10, pp. 938 ~ 946, 2013.05

[7] Manos Papagelis, Dimitris Plexousakis, Qualitative analysis of user-based and item-based prediction algorithms for recommendation agents, Engineering Application of Artificial Intelligence 18 (2005) 781-789.

[8] JIANG Lihong, XU Boyi, XI Junhong, CBR filtering algorithm and intelligent information recommending system, J Tsinghua Univ (Sci & Tech) , 2006, 46(S1):1074-1077.

[9] Zeina Chedrawy, Syed Sibte Raza Abidi, An Intelligent Knowledge Sharing Strategy Featuring Item-Based Collaborative Filtering and Case Based Reasoning, 5th International Conference on Intelligent Systems Design and Applications (ISDA'05), 2005,pp.67-72.

Advanced Materials Research Vols. 989-994 (2014) pp 4629-4632
© (2014) Trans Tech Publications, Switzerland
doi:10.4028/www.scientific.net/AMR.989-994.4629

Analysis of Wireless Mesh Network Routing

Xiaolong Tan[1], Jia Zhou[1], Wenbin Wang[1,a]

[1] Yalong River Hydropower Development Company LTD, Chengdu, 610051, China

[a] email: wangwenbin@ylhdc.com.cn

Keywords: Mesh Network, Routing Overhead, Network Topology

Abstract: Since the wireless mesh network topology dynamics and the radio channels instable, the design of wireless mesh network routing protocol become one of the key factors to determine the performance. This paper mainly studied the existing several kinds of typical three-layer mesh network routing protocol (DSDV and AODV), aimed at the defects of three-layer routing limited to the network topology changes, the paper proposed a network model based on two-layer routing. Forwarding the packet, establishing and maintaining the communication links are accomplished on the Mac layer. Simulation tests showed that two-layer routing has a big improvement on the efficiency of packet forwarding, and it effectively reduced the routing overhead and end-to-end delay simultaneously.

Introduction

Wireless mesh network (WMN) is a dynamic self-organizing, self-configuring network. WMN is mainly composed of mesh routers and mesh clients. All the nodes in a mesh network automatically establish a dynamic network and maintain network connectivity[1]. Wireless mesh network become one of the hot spots in current research due to its wide range of applications and network flexibility, low cost, easy to expand and so on. WMN routing algorithm must be based on the characteristics of multi-hop wireless networks to satisfy requirements.

Routing protocol analysis

DSDV protocol is a distance vector protocol. The design idea is to maintain a monotonically increasing sequence number of the destination node for each route. In the case of don't need to collaborate with adjacent nodes, contrast the serial number of nodes to prevent appearing routing loops[2] . DSDV protocol stipulates that the destination node serial number stored in the routing table entry of each network node. By joining in packet destination node domain, the destination node distance information exchanged mutually in the adjacent nodes with each routing updates. In this way, each node using the distance vector received from the neighbor node to update their routing table, to make sure the current routing is latest and best.

But in the condition of network topology changes frequently and high-speed mobile nodes, the convergence performance of DSDV protocol will worsen sharply. Whether the node needs to send data or not, it requires broadcasting updating information to the adjacent nodes periodically. So, the more nodes join in the network, the larger the network traffic density, and the capacity, cost of the routing table and bandwidth increasing will increase network load[3] . Limited network scale is the main drawback of DSDV protocol.

AODV is a typical on-demand routing protocol. It is proposed based on the DS-DV algorithm and combined the on-demand routing mechanism of DSR algorithm.

Design of routing scheme

In fact, the performance of the variety three-layer routing protocols are different in the specific different networks, the complexity of the network topology has a lot to the conditionality of marketable by the performance of the agreement, The complexity of the network topology has a lot conditionality to the performance of the protocol.

Two-layer routing protocol is the proactive routing protocols based on node topology. It can be implemented by either centralized or distributed strategies. The differences between two-layer routing protocols and traditional protocols are: the two-layer protocols address by the MAC address and forward through two layers[4] . The upper layer protocol stack do not need for additional splitting and encapsulation. Neighbors, topology built and maintained in MAC layer, requires no additional sending notice, updating routing messages to create and maintain the routing. This can reduce the system overhead brought by the routing protocol, save bandwidth, and reduce the delay[5] . Especially suitable for the multi-hop networks with high real-time demand of data transmission, large number of nodes and complicated network structure.

Here discussed the mesh node routing, assume a neighbor relationship table:

	1	2	3	4	5
1	0	1	0	0	0
2	1	0	1	1	1
3	0	1	0	1	1
4	0	1	1	0	1
5	0	0	1	1	0

Node 1 as an example to describe the process of routing path discovery:

(1) The neighbor of node 1 (level 1) is node 2, record the arrival path:

1－＞2

(2) The neighbor of node 2 (level 2) is node 3, 4, record the arrival path:

1－＞2－＞3

1－＞2－＞4

(3) The neighbor of node 3 (level 3) is node 2, 4, 5, the arrived is no longer record:

1－＞2－＞3－＞5

Now found that all nodes have finished traversal, so the final routing information of node 1 is as follows:

1－＞2

1－＞2－＞3

1－＞2－＞4

1－＞2－＞3－＞5

Routing addressing and data forwarding

Packet routing mainly involves the following several modules: Mac Layer, Mesh Route and IPFM. The protocol stack is shown in figure 1:

(1)MAC Layer mainly responsible for the allocation of resources, time slot and conflict avoiding and maintain network topology table topo_table and the neighbor table neighbour_table;

(2) Mesh Route is mainly responsible for network topology table obtained from the MAC Layer, and calculates the two-layer routing and selects the path.

(3) IPFM forwarding management for IP, The main function is the forwarding of host routing and the maintenance of host routing table host_table.

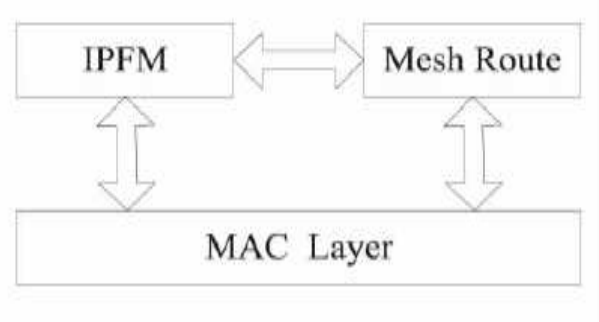

Fig.1 Protocol stack model

In order to reduce the processing delay, we can use the mixed two-layer and three-layer mode to forward. Increase the target node identification in forwarding data. If the destination node is not itself after the receiver receives the data, then check the next-hop node of the target node by Mesh Route, forwarding on the second layer and don't need to check routing; If the destination node is itself, then send to IPFM routing module to discover route and forward.

Test result

In this paper, we use NS2 software to simulate under the Linux operating system. 1000m×1000m simulation area uniformly distributed 50 wireless Mesh nodes. The distance between each test nodes is larger than 100 m, and the maximum rate of mobile node is 25 m/s. Under the same simulation scenario, by changing the movement speed of test node, we compare the routing overhead and the average delay of typical three-layer AODV and two-layer routing algorithm, and simulated the network throughput under different network topology.

Routing overhead refers to the amount of the average control group used to transmit a group successfully. The selection of routing algorithm greatly influences the routing overhead.

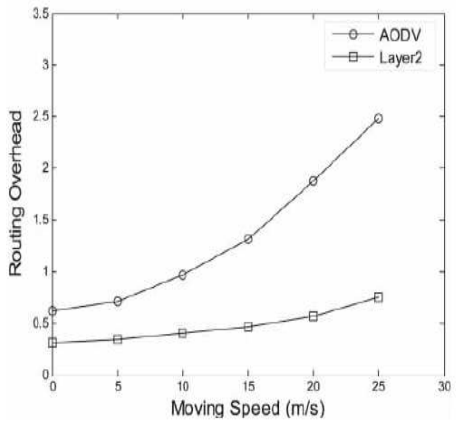

Fig. 2 Routing overhead

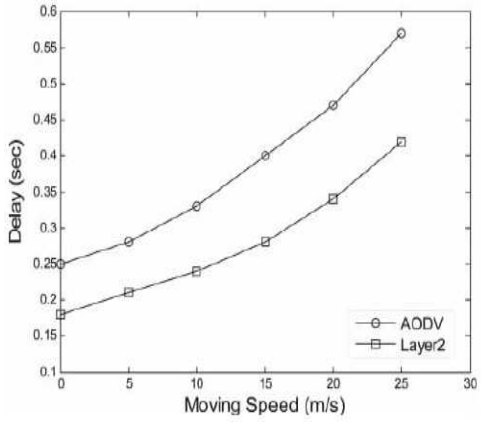

Fig.3 Average end-to-end delay

As shown in figure 2, two-layer routing has obvious more advantages in routing overhead than AODV routing. The increase of node speed leads to greater risk of link disconnected, at this moment need more system overhead to repair links. Since the stability of the node topology built and maintained on MAC layer in the two-layer routing scheme, requires no additional sending notice, updating routing messages to create and maintain the routing, improving the efficiency of the routing and packet delivery success rate, also lower the number of the fixed link simultaneously, thus largely reduces the network routing overhead.

The end-to-end delay is the time difference value of data packets from the source node to destination node. It can effectively measure the time efficiency of the routing algorithm. The delay jitter is particularly important for voice video stream demanding high real-time requirements.

As shown from the figure 3, with the change of node location and increase of speed, the possibility of the routing path breakage increases and needs more extra time for topology stability and routing reconstruction. So the end-to-end delay also increases accordingly. While the two-layer routing forward the packet on the Mac layer. On the one hand, it reduced the encapsulation and

splitting of protocol, and forward faster. On the other hand, maintain the link stability on Mac layer is more quickly and efficiently than on the IP layer, so obviously reduces the end-to-end delay.

Conclusions

This paper studied and analyzed the characteristics and defects of the existing typical Ad Hoc network/Mesh structure routing protocols, proposed the scheme design based on the two-layer routing to forward the packet and establish and maintain communication links on the Mac layer. Simulation tests show that packet forwarding on the second layer improving the efficiency of the system delay and forwarding efficiency, especially suitable for complicated multi-hop networks.

References

[1]. I.F.Akyildiz, X. Wang, "A Survey on wireless mesh networks," IEEE Commun. Mag, vol.43, no.9, pp. 523-530, Sep. 2005.
[2]. P. Gupta, P.R. Kumar, "The capacity of wireless networks," IEEE Trans. Inf. Theory, vol.46, no.2, pp.388-404, Mar. 2000.
[3]. I. Akyildiz, X. Wang and W. Wang, "Wireless Mesh Networks: a Survey," Computer Networks, 2004.
[4]. R. Draves, J. Padhye and B. Zill, "Routing in Multi-Radio, Multi-Hop Wireless Mesh Networks," Proc. ACM MobiCom '04, pp. 114-128, 2004.
[5]. R.W. Yeung, S.-Y.R. Li, N. Cai, Z. Zhang, "Network coding, theory", Foundation and Trends in Commun. Infor. Theory, vol.2, no.4-5, pp.241-381, 2005.

Advanced Materials Research Vols. 989-994 (2014) pp 4633-4636
© (2014) Trans Tech Publications, Switzerland
doi:10.4028/www.scientific.net/AMR.989-994.4633

Research of Ad Hoc Network Routing Based on NS2 by Performance Comparison

Xiaolong Tan[1], Jia Zhou[1], Wenbin Wang[1,a]

[1] Yalong River Hydropower Development Company LTD, Chengdu, 610051, China

[a] email: wangwenbin@ylhdc.com.cn

Keywords: Ad hoc Network, Self-Organization Network, Packet Delivery Ratio

Abstract: In recent years，the ad hoc network has been paid extensive attention due to its characteristics of non-center and self-organization．Firstly this paper introduces three typical routing protocols AODV，DSDV，DSR，and the principles of them; then，adopts the NS2 simulation platform to simulate the performance of end-to-end delay，routing overhead and packet delivery ratio by changing the number of nodes and the paused time of nodes．Finally，by comparing the simulating results, the comparison conclusion is provided．

Introduction

Ad hoc network is a distributed wireless multi-hop networks without central control nodes. It does not need the support of fixed infrastructure. Each user can network automatically and forward data through other nodes.

According to the characteristics of the ad hoc network, a variety of ad hoc protocols has been developed, such as AODV, DSDV, DSR, TORA and so on[1] . This paper analyzed the performance of the end-to-end delay, normalized routing overhead and packet delivery ratio for AODV, DSDV, DSR, and made a comparative analysis.

Ad hoc network routing protocols

Existing ad hoc routing protocols are mainly including table driven routing protocols and on-demand routing protocols. DSDV belongs to table driven protocols, and DSR, AODV belongs to on-demand protocols[2] .

The exchange of message occurred between adjacent mobile nodes in DSDV, if the routing information of destination nodes which send a packet is unknown, the groups will be buffered, and the routing query message RREQ sent at the same time until receiving the route reply message RREP.

The DSR is mainly divided into two parts, route discovery and route maintenance. When the source node send data to the destination node, first check the route buffer if there is a route to the destination node[3] . If there is, send data using this routing, otherwise starting routing discovery process. Routing maintenance completed by routing error group and acknowledge group.

AODV is essentially the combination of the DSR and DSDV, it has the routing discovery and routing maintenance function of DSR, at the same time adopt hop-by-hop method of DSDV[4] .

The performance indicators and the selection of simulation parameters

(1) The average end-to-end delay: it represent the average time of source node sends the packet to the destination node.

(2) Normalized routing overhead: the total number of packets used for route discovery and route maintenance divided by the number of received packets, during the process of packets from the source node successfully transmitted to destination node.

(3) Packet delivery ratio: successfully received packet number of destination node in proportion to the number of packets sent by source node[5] .

The performance comparison under different number of nodes

Simulation scenario: 600m×400m area respectively distribute 25, 50, 75, 100, 125, 150 mobile nodes, there are 10 pairs of communication links, sending TCP business.

(1) End-to-end delay

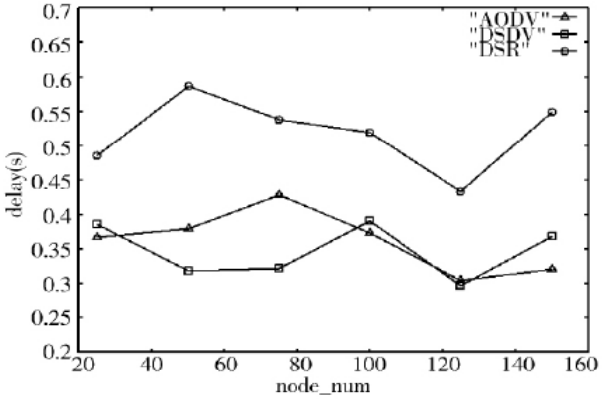

Fig. 1 The average delay under different number of nodes

Figure 1 shows the average end-to-end delay of communication nodes under different number of nodes. It can be seen that the DSR's average delay is generally greater than AODV and DSDV, AODV and DSDV delay value is relatively closely. Because DSR search the best routing in the routing cache, the large cache and routing errors will cause the large end-to-end delay.

(2)Normalized routing overhead

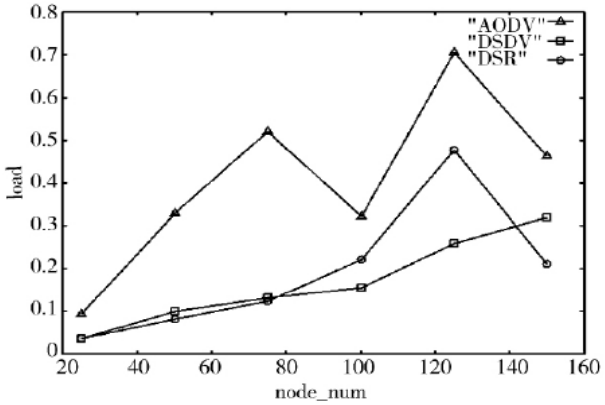

Fig.2 The normalized routing overhead under different number of nodes

Figure 2 shows that with the number of nodes increase, routing overhead of the protocol is increase overall. When the node number is large, the routing overhead of DSR is lower than AODV. Because the DSR protocol uses the routing cache technology, intermediate nodes do not need to maintain routing tables like AODV protocol. DSDV routing overhead is least, because each node in the network have kept a routing table recording the destination node and the hops to the destination node, the routing hops of each node is already determined in the process of sending messages.

(3) Packet delivery ratio

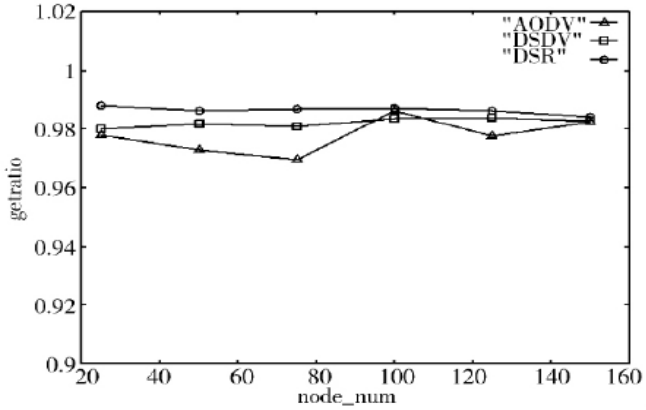

Fig.3 The packet delivery ratio under different number of nodes

Figure 3 is the comparison of the data packet delivery ratio for variety protocols. It shows that the changes of packet delivery rate for DSDV and DSR protocol is closely.

The performance comparison under different paused time

(1) end-to-end delay

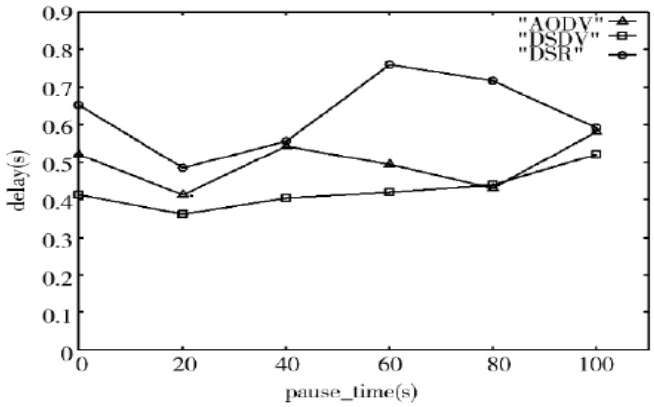

Fig. 4 The average delay of nodes for different paused time

Figure 4 reflects the average end-to-end delay under different paused time. The average delay of DSR and AODV value higher than DSDV, and DSDV delay value increased with the extension of paused time. In the DSDV protocol, each node maintains the routing information table of other nodes, it can be sent immediately via lookup table, without time consuming of looking for routing on demand.

(2)Normalized routing overhead

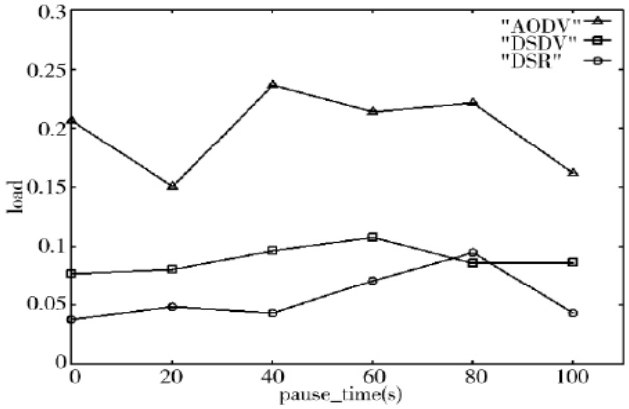

Fig. 5 The normalized routing overhead for different paused time

Figure 5 shows the relationship of routing protocol overhead among three kinds of routing protocols. It can be seen that the overhead of DSR is least. For the DSR, when the paused time of nodes increases, the dynamic topology of network abated, so routing overhead reduced. the overhead of DSDV has less relationship with node mobility, so the influence caused by node paused time is not obvious. AODV is an on-demand routing protocol, the large routing request increased the routing overhead.

(3) Packet delivery ratio

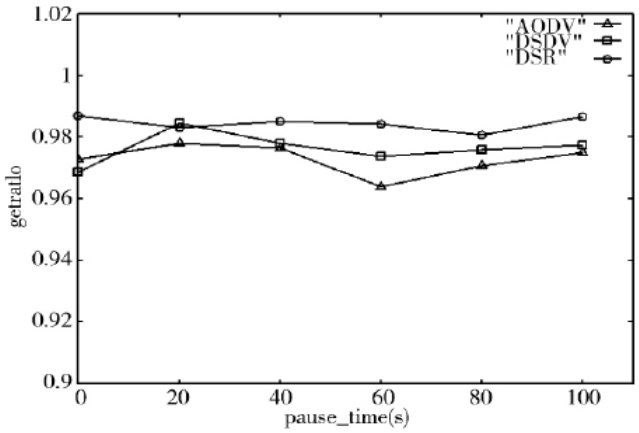

Fig.6 The packet delivery ratio for different paused time

Figure 6 is the comparison of packet delivery ratio for various routing protocols. It can be seen from the diagram that the packet delivery rate dynamic changed with the change of paused time, and the packet delivery ratio of DSR and DSDV is better than AODV. DSR is the on-demand protocol. It can be rapidly find a route to the destination from the routing buffer. But DSDV is the table driven protocol, each node must form routing tables include the routes to all nodes of the entire network, so the network resources consumed too much and packet delivery ratio is not high.

Conclusion

This paper introduced the NS2 simulation and performance comparison of ad hoc network routing protocols DSDV, AODV and DSR. The DSR protocol has maintained high packet delivery ratio and low routing overhead, but the average end-to-end delay is large; The influence of DSDV performance caused by the number of nodes and the change of paused time is relatively stable; The delay of AODV is relatively small and routing overhead is large. The overhead increases with the increase of network density. Visible, the different routing protocol has its own advantages and disadvantages and applications, separately using a routing protocol may not be able to meet the various requirements, at the same time. Therefore, hybrid routing protocols can be considered.

In addition, in the process of construct actual wireless network need to consider the particularity, the network scale and extensibility of ad hoc network. Select the appropriate network topology contributes to designing appropriate protocols for specific network structure and maximize the performance of the entire network.

References

[1]. Seawright, L., MacKinnon, R.: VM/370 a study of multiplicity and usefulness. IBM Systems Journal, pp. 4-17 (1979)

[2]. D. B. Johnson and D. A. Maltz Mobile computing, pp.153 -181 1996 :Kluwer Academic Publishers

[3]. "RFC2290", RFC 2002: IP mobility support, 1996

[4]. K. Fall and K. Varadhan ns Notes and Documentation

[5]. C. E. Perkins "Mobile IP", IEEE Communications Magazine, pp.84 -99 1997

Advanced Materials Research Vols. 989-994 (2014) pp 4637-4642
© (2014) Trans Tech Publications, Switzerland
doi:10.4028/www.scientific.net/AMR.989-994.4637

Research of the Computer-aided-translation Software

Su Han[1,a] and Xindai Zhang[2,b]

[1,2] Department of Basic Courses, Shandong University of Science and Technology, Tai'an, 271000, China

[a]email:hs56923@163.com, [b]email:1561750710@qq.com

Keywords: Computer-aided translation; Research; Software

Abstract: In recent years, with the rapid development of computers, computer-aided-translation software has been used more often, which can improve the efficiency and quality of translation. This paper analyzes the characteristics of the four commonly used computer-aided- translation software at home and abroad--SDL Trados, Déjà Vu, Wordfast and Yaxin in satisfying different users' needs, points out their characteristics and provides reference for those who are interested in computer-aided- translation technology.

Introduction

Computer-aided translation has originated from machine translation, but there is a sharp difference between the two. Machine translation attempts to replace translators by means of completely automated translation process, but computer-aided translation is to utilize computer technology to improve translation efficiency and quality, in which a translator still plays the decisive role. In a broad scene, computer-aided-translation tools refer to all the computer tools which can assist the translators with their translation. They include word-processing software, grammar checkers, e-mails and the Internet [1]. In a narrow sense, they refer to the special computer-aided-translation software designed for improving the translation efficiency and optimizing the translation process[2],which includes translation memory system, terminology management tools, the alignment tools and project management tools.

Brief Introduction to Computer-aided-translation Software

It was in the 1970's that the first translation memory tools came into being. But it was not until the middle of the 1990's that they began to develop commercially. Afterwards a lot of translation-aided-translation software has poured into the markets like mushrooms and been recognized and utilized by more and more translators. Now in the international arena, there are such famous CAT(computer-aided-translation) software as Déjà Vu, Wordfast, Idiom, Catalyst etc besides the leading brand-SDL Trados. In 1998 the foreign CAT software came into China's translation market. In 1999, the CAT software of the China's Yaxin Company came into the market. Afterwards Chuanshen, Yongli, Saidi, Xueren and other companies have researched, developed and put out their own CAT software one after another.

According to the network investigation of the application status quo of CAT in the Chinese translation industry made by Xiaochen Hou and Yuzuo Yan of the CAT Department of Beijing University in 2008, about 66% translators used CAT tools in their work, 85.8% of whom used Trados, 29, 68% of whom used Yaxin CAT 3.0+CAM (Computer-aided Match), 26.45% used Déjà Vu X and 20.65% used Wordfast. According to the investigation result, now SDL Trados, Déjà Vu, Wordfast and Yaxin are the four commonly used CAT software both at home and abroad[3].

Research Base

Researchers at home and abroad have made many valuable research into the CAT technology. For example, Quah [4] and Duoxiu Qian [5]have introduced many aspects of knowledge which CAT technology involves. Lisong Lv and Lei Mu [6]have put forward paying great attention to the training of translation talents from the angle of combining translation teaching with the translation market. Jun Wen and Yan Ren [7] have made more comprehensive commentaries on the history and the present situation of China's CAT research and predicted its future direction of development. But the researches have seldom probed into the evaluation of CAT software and have not formed a uniform assessing standard.

As we know, CAT technology is mainly concerned about how to use computer software to realize automatic translation process, improve the efficiency of artificial translation process, guarantee the quality of manual translation and efficiently control the whole translation process. Therefore translation memory system, terminology management tools, the alignment tools and quality assurance tools are the four big modules to guarantee that CAT tools realize their main functions. On the basis of users' concept of quality, combined with our using experience of SDL Trados Studio 2009, Déjà Vu X 7.5, Wordfast series and Yaxin CAT 3.5, we'll make a comparative study of the four common software's functionality and usability. The functional index mainly probes into their differences and similarities in the four main functional modules of translation memory system, terminology management system, the alignment tools and project management tools. The usability index is mainly concerned about the effective working area of software interface and whether it has a Chinese interface. Then we'll further point out their characteristics so as to provide some reference for those who are interested in CAT technology when choosing CAT software.

Result of Comparative Research

A. Functionality

(a) The comparison of translation memory systems

The above four commonly used CAT software at home and abroad are all functional rich, including such functional modules as translation memory system, terminology management system, the alignment tools, automatic translation, file filter, electronic dictionary and the spelling and grammar checker. Because all the CAT software is established on the basis of translation memory technology, the translation memory bank is the core of CAT software. The translation memory systems of the above four tools can all establish and guide-in one or more translation memory banks, and the operating procedures are almost the same.

When a translation memory bank is established, the language and other parameters should be determined in advance. The file extension of the translation memory bank, which SDL Trados Studio 2009 generates when the translation memory bank is established, is .sdltm. When the related translation memory files are guided into the established translation memory bank, it can be compatible with the files which comply with the standard of translation memory exchange. It can also guide in the bilingual files of SDL XILFF and the translation memory files which the former editions of TRADOStag and SDL Edit software have customized according to their own standards. Other forms of translation memory files need to be changed into TMX(Translation Memory eXchange) form, then can be guided into translation memory bank. The file extension of the translation memory bank established by Déjà Vu X 7.5 is .dvmdb, which is the typical mdb database formatted file and has the strong compatibility. Its memory bank can directly guide in the delimited text file, the Access 9X/2000/XP and Excel 9X/2000/XP files of Microsoft Office Software, the translation memory document of Trados translators' station and TMX format

documents. In addition, it can also use the file format conversion function owned by the 7.5 edition to change the translation memory files of the Déjà Vu 2.X/3.X into the new edition of the translation memory document for the use of translators. What the translation memory bank of WFC 6.0 uses is Wordfast's own translation memory format, which is compatible with TMX format translation memory bank document. The translation memory bank documents established by WFP 2.1.8 are test files, into which Wordfast itself free format can be guided, and at the same time are compatible with TMX format. Besides guiding-in the early edition of Wordfast translation memory files, WFA 1.5.0 is compatible with the translation memory file format of Trados, Idiom and SDLX tools. The generated file extension of Yaxin CAT 3.5 is. mem. It is compatible with the forms of Excel 8.0 text file, TMX file and Yaxin 2.5 translation memory files. As far as the service conditions of translation memory banks are concerned, WFC 6.0's compatibility is the worst and Déjà Vu X 7.5's compatibility is the best.

(b) The comparison of alignment tools

Only when the content of its translation memory bank constantly increases can CAT tools play a more and more important role. There are two methods for translation memory banks to enlarge the contents: 1. To deposit the translated text and the source text into the translation memory bank. 2. To guide the collected source texts of all fields and their corresponding translated texts into the translation memory bank. The successful guiding-in of these documents can't do without another important module-alignment tools. The users of SDL Trados Studio 2009 need use WinAlign Module of SDL Trados 2007 to align the original with the translation in the unit of a sentence before guiding them into the translation memory bank so as to make them into the translation unit of translation memory bank.

Déjà Vu X 7.5 itself has the alignment tools which can be used directly. WFC 6.0 has no alignment tools itself. If needed, Plus Tool free of charge must be installed, which can be used for the alignment process as a plug-in of Word, but it can only work in Word 2003 and the former editions. WFP 2.1.8 has no alignment tools either, its later edition has Wordfast Aligner but isn't integrated in WFP interface and need start alone. WFA 1.5.0 uses its own Wordfast AutoAligner still in the experimental stage for alignment. The user can upload the document to be aligned free of charge, the module can align it through intelligent judgment, then send the alignment result to the user's registered mail in the three formats of text file, Excel file and TMX form. Yaxin CAT 3.5 doesn't have the alignment tools and need be installed the independent CAM module for the alignment. The operating procedures of the four above tools are almost the same all through certain separation signs to segregate text and then align it, but all of them can't deal with the situations of one-to-many and many-to-one, so the aligned text need the manual correction.

(c) The comparison of terminology management tools

Terminology management tools are used for establishing, maintaining and managing the Term Bank. The translators can store the technical terms of specific industry into the Term Bank, extract and use them in later translation.

Yaxin CAT 3.5 has 74 specialized term banks but the term banks of the other three software require the translators to add or guide the existing nomenclature made by other people into the local term bank to increase its capacity.

MultiTerm, the terminology management tools of SDL Trados Studio 2009, is a separate module, providing a converter which can convert the nomenclature in the Excel format into TBX format and the term extraction tool. It has powerful functions.

The terminology management tools of Déjà Vu X 7.5 have special features, including Terminology and lexicon. Lexicon is closely linked with the ongoing translation project and more targeted. Therefore in the process of actual translation, Déjà Vu would first search for lexicon, then search for terminology and at last search for translation memory bank. This hierarchical searching, querying and managing system is more suitable for the actual situation of translation.

WFC and WFP all carry out terminology management through the menu of Terminology, while WFA adds terminology through "Glossary Panel".

Yaxin CAT 3.5 manages the term bank through the Tab of Database Maintenance. "Database Maintenance" can not only add a single term, but also add term entries in batches.

(d) The comparison of project management tools

Translation project management refers to the process of guiding-in, analysis, pre-translation, grammar and spelling checking and export. The standardized project management process is very important for improving translation efficiency.

After creating a project, SDL Trados Studio 2009 guides-in the file to be translated, makes use of the tab of "Analyzing File" to analyze and determine translation's amount of work and repetition rate and utilizes the existing translation memory bank and term bank to pre-translate and carry out the translating word count of the project. After finishing the translation project, "the functions of spelling check" and "verification" can be used to check the translation in spelling, the consistence of grammar and terms. Then we can export well-translated file.

When using Déjà Vu X 7.5 to finish a new translation task, the translator must build a translation project folder, guide the file to be translated into CAT tools and keep all the results of the translation project management activity in the project folder. Déjà Vu X 7.5's functions of word count, pre-translation and quality check are the same as those of SDL Trados Studio 2009, but its "Analysis" menu can not only count the repetition rate but also show the situation of fuzzy matching so as to help the translator to better predict the translation process.

WFP 2.1.8 must be installed Project Manager to realize the complete project management function. The related icons of the respective software must be clicked to set parameters for the quality assurance function of WFC 6.0 and WFA 1.5.0; for WFC6.0, the tab of "Setup" need be clicked then, afterwards the tab of "QA" need be selected to set quality assurance parameter; for WFA 1.5.0, "Pandora's box" need be opened, then the fourth functional parameters setting variables "Configure Document's translation with proofreading" is clicked to pop-up proofreading function dialog box to set for its use. There is no pre-translation function in WFC 6.0's functions, while WFA 1.5.0 can carry out pre-translation after guiding-in translation memory files and nomenclature.

With the help of grammar and spelling checkers owned by Word Software, Yaxin CAT 3.5 doesn't have the functions of word count and pre-translation. The project management of Yaxin belongs to an independent function module, which the project manager completes utilizing Yaxin's relative software.

B. Usability

(a) The effective working area of interface

Interface is the important parameter to evaluate the usability of CAT software. Most of the office software is Microsoft Office, especially the Word file format, so all kinds of CAT software is compatible with the format.

When SDL Trados 2007 is used to translate, the software is cooperatively used with Word. It belongs to semi-independent interface. When a translator uses the CAT software, the main

translation work is finished in the Word interface, while the translator's working station operates as a background program. But the translator's working station and Word operate at the same time, which evidently brings inconvenience to the translation, because translator's working station probably occupies one-fourth of the whole screen. SDL Trados Studio 2009 integrates workbench with Word in the same interface, which overcomes the inconvenience which the interface of 2007 edition brings to translation activity.

WFC's interface has no independent interface. Its software agent is a Word plug-in component, and operates completely on Word's macroefficiency. All the translator's work is finished in Word. Both WFP and WFA take an independent interface. WFP requires users to translate in the independent interface of the software, while WFA requires the translator to use browser to do translation work in webpage.

The different versions of Déjà Vu software have not depended on Word software. All of its translation activities are finished in its own independent interface. In the working interface of Déjà Vu X 7.5, all the functions are centered on the inside. It is as clear as a form, the leftmost side is the original, the middle is the translation and the rightmost side is the other auxiliary translation functions.

Yaxin CAT 3.5 can work cooperatively with Word. The layout of its interface has four parts: the original zone, the translation zone, reference example zone and Word Window. In such an interface, it operates more intuitively and conveniently to synchronously finish translation in the translation zone and Word interface.

(b) The Chinese interface

Besides the effective working area, it is an important reflection of the CAT software's usability whether the interface can be set to Chinese for the Chinese users, because the Chinese interface can make the operation of CAT software and the system setting easier. Both SDL Trados Studio 2009 and Yaxin CAT 3.5 have Chinese interfaces, Déjà Vu X 7.5 has no Chinese interface and must be installed the Chinese language pack to show the Chinese interface, while all the versions of Wordfast don't have a Chinese interface.

C. Characteristics

The above four CAT tools have their own characteristics.

SDL Trados Studio 2009 is the only CAT software of directly processing PDF document without the file format conversion. In addition, it is sold together with a local tool software-SDL Passolo 2009 and can translate the executable file, resource file and the file in XML format in the visualization window of "WYSLWYG "(what you see is what you set) ,saving the complicated process of taking the words of source language out, guiding them into the CAT tools to translate and then guiding the translation into the original document. That is to say, SDL Passolo can let the translators directly carry out the translation in the document, then directly compile the document which has the same function as the original document.

When adding the translation memory and terms of Déjà Vu X 7.5, we can use the automatic transmission mode to add, which is convenient and fast and its translation memory bank and term bank are stored in the form of data file and can be transplanted, which helps to guarantee the uniformity of terms and the translation style through exchange when the team works. At the same time it is compatible with the translation memory bank and term bank of SDL Trados.

In Wordfast series software, it is its online version that has the most features, i.e. WFA, which the translators can register and use free of charge, not limited by any version or time. But only 500 translation units can be added to its translation memory bank once a time, which is not very suitable

for the operation of big translation project. The registered user of WFA can not only use his own local translation memory bank, but also anonymously use the very large translation memories free of change.

When a translator uses CAT 3.5 to do translation work, the screen can take the word and insert the explanation given by the term bank and lexicon into the place which needs to be edited, which is unique in the whole field of CAT software. The words in its English-Chinese, Chinese-English dictionary amount to more than 7 million. When we meet the sentence to be translated which is beyond the matching values of the system settings, Yaxin's computer-aided software would give the reference sentence for us.

V. Summary

From what has been said above, we can understand the functionality, usability and characteristics of the 4 commonly used CAT tools. We hope that they will be helpful to the translators in choosing the software so as to efficiently finish the translation work..

References

[1]Bowker, L: Computer-aided Translation Technology: A Practical Introduction (University of Ottawa Press, Ottawa 2002).

[2] Bin Xu, Hongmei Guo and Xiaoli Guo: submitted to Shandong Foreign Language Teaching Journal(2007)

[3] Xiaochen Hou and Yuzuo Yan: "A research report of the application status quo of CAT in Chinese translation industry" The Software Department ,Beijing University, Beijing 2008

[4] Quah, C.K: Technology and Translation (Shanghai Foreign Language Education Press, Shanghai 2008)

[5]Duoxiu Qiao:Computer-Aided Translation (Foreign Language Teaching and Research Press, Beijing 2011)

[6] Lisong Lv and Lei Mu: submitted to Foreign Language World (2007)

[7]Jun Wen and Yan Ren: submitted to AFLE(2011)

Advanced Materials Research Vols. 989-994 (2014) pp 4643-4649
© (2014) Trans Tech Publications, Switzerland
doi:10.4028/www.scientific.net/AMR.989-994.4643

Design and realization of Alfresco database of the micro-information system

Xiaoyang Yan[a], Zhipeng Lin[b], Xingming Zhang[c] and Wenchao Yang[d]

School of Computer Science and Engineering, South China University of Technology, Guangzhou, China，510640

[a] xiaoyyan@scut.edu.cn, [b] scut_linzhipeng@foxmail.com, [c] cszxm@scut.edu.cn, [d]727421835@qq.com

Keywords: Alfresco database; Data management; Lucene search engine

Abstract. The Alfresco development tool, which includes Apache Tomcat, MySQL and WebService, is an open platform for building a functional database system in a Java website. In order to improve the enterprises' management efficiency in specialized industrial townships, a micro-information system based on Alfresco development tool has been proposed. In the construction of the micro-information system, Alfresco database exhibits great superiority in network database architecture, data query with Lucene search engine, data management and data security. In this paper, the general design ideas, functions, key technologies and realization methods of the Alfresco database are introduced.

Introduction

Since the opening-up policy has been carried out in China, Guangdong province has developed quickly in the last 30 years and acts as the forerunner of china's economic reform. In the past ten years, there are more and more specialized industrial townships with characteristics of Guangdong's economical model founded. Since specialized industrial townships develop persistently and rapidly, it is prominent and essential to strengthen the ways to promote the brands and exchanges for enterprises in specialized industrial townships. However, for enterprises in specialized townships recently, no such efficient platform has achieved these functions. In order to achieve more effective ways for these enterprises to promote their information communication, it is required to construct a micro-information system platform for these enterprises. Data storage, data management and data mining are the key technologies to the micro-information system.

Alfresco is an open source development tool for Enterprise Content Management (ECM). It adapts to MVC pattern which divides a given software application into three interconnected parts. Alfresco development tool manages all the contents, such as documents, images, records, web pages, or any other unstructured or semi-structured file. Alfresco is functional in controls and services, such as version control, meta-data management, workflow, search, life-cycle management, associations to other content, tagging, commenting and so on. For the mountain of information which is accumulated in enterprises, you can find the content you want with these services easily and can ensure its accuracy. Alfresco that runs as a web application within an application server is composed of some open source components, and exposes repository through many different protocols and APIs.

In this paper, Alfresco database of the micro-information system is introduced in terms of the basic concept of Alfresco development tool, operation of Alfresco SDK, for the purposes of improving the enterprises' management efficiency. Furthermore, the conclusion will be obtained in the end of paper.

Development of Alfresco database

Alfresco is an open source Enterprise Content Management system. It's primarily implemented in Java, suited to a number of environments including J2EE. It is not tied to any particular web browser, operating system, application server or database. The binary streams of content are stored in the

Alfresco database and the associated full-text indexes are maintained by the Lucene indexes. The actual binary streams of the content are stored in files managed in the Alfresco database, although these files are for internal use only and do not reflect what you might see through the shared drive interfaces. The Alfresco database also holds the associations among content items, classifications, and the folder/file structure that is maintained in the database and not reflected in the internal file storage structure. The Alfresco database implements and exposes these services through an Alfresco API and the Java API. The storage engine of the Alfresco database stores and retrieves content, metadata, and relationships, and operates on the nodes and contents.

1. Alfresco SDK configuration

Alfresco provides a developer oriented download bundle, known as the Alfresco SDK (Software Development Kit) to complement the Alfresco release bundle. The Alfresco SDK provides support for developers who wish to extend or customize the Alfresco database. In order to use Alfresco SDK, we should do the following things. First of all, ensure the development tools such as JDK and Eclipse IDE are installed. Then download the Alfresco SDK and import the whole project to the Eclipse IDE.

2. Operating Alfresco SDK

(1) Identity Authentication: Before operation being done on the Alfresco development tool, the identity authentication is required . The project AuthenticationUtils in Alfresco SDK provides a utility class which manages the privileges. For this purpose, function StartSession and EndSession ensure the security of the system. The source code likes as follows.

```
1 AuthenticationUtils.startSession("admin", "password");
2 AuthenticationUtils.endSession();
```

Here the function StartSession() gets the authentication and verify its authority. In this way, the safety of system can be guaranteed. The function EndSession() ensure the security when logging out the system.

(2) Node creation: The project CML, which is short for Content Manipulation Language, provides a set of statements to update Alfresco database. And we can use the following code, in which the function CMLCreate() and CMLWriteContent() realize the main function, to create a node in the database.

```
1 cml.setCreate(new CMLCreate[]{create});
2 cml.setWriteContent(new CMLWriteContent[]{writeContent});
3 UpdateResult[] result = WebServiceFactory.getRepositoryService().update(cml);
```

In this code, the function CMLCreate() initializes the class and the function setWriteContent() sets up the creation information. And then the function UpdateResult() is used to perform the create operation. These three statements insert data into the database while the data are stored in Alfresco database as nodes.

(3) Content creation: In order to insert the content to the node, the following classes are needed. The Reference class is used to describe the address of the node. And the format of content including the type and encoding is determined by the ContentFormat class. The byte stream of the content is described in the Content class. The content can be created into the database using the following code.

```
1 Contentcontent=WebServiceFactory.getContentService(). write(referenceForContent,
2 Constants.PROP_CONTENT,"This is the content for the new node".getBytes(), format);
```

Here the content, which can be pictures, a list of string and so on, to the node we defined is inserted. And These contents of the node would be stored in the folder of the Alfresco server instead of the database. Therefore the efficiency of the search in database will be improved greatly.

(4) Node deletion and updating: The CMLDelete class achieves the delete operation to the nodes in the database, the code of deletion and update operations likes as following:

```
1 cmlRemove.setDelete(new CMLDelete[]{delete});
2 WebServiceFactory.getRepositoryService().update(cmlRemove);
```

Here a node defined in the database will be deleted, after the position of the node is defined in the line 1 and the delete operation is executed in the line 2.The CMLUpdate class is used to achieve the update operation to the nodes in the database like this:

```
1 cmlUpdate.setUpdate(new CMLUpdate[]{update});
2 WebServiceFactory.getRepositoryService().update(cmlUpdate);
```

In this codes, the node defined in the database will be updated, after the updated information is entered in the line 1 and the update operation is implemented in line 2.

(5) Lucene search engine: Alfresco development tool queries the data we need in the database system with Lucene search engine. Lucene, that provides search operations using the Lucene search syntax, is an open source information retrieval software library. The code used likes as follows.

```
1 String luceneQuery = "PATH:\"/app:company_home\"";
2 Query query=newQuery(Constants.QUERY_LANG_LUCENE,luceneQuery);
3 QueryResultqueryResult=WebServiceFactory.getRepositoryService().query(spacesStore,
query, false);
```

Here when the search range described as a directory is needed to be defined in line 1, the query results will be returned in line 3 after the search operation is executed in line 2. And also the conditional search with the keyword such as and and or can be used in Lucene grammar.

Design and realization of Alfresco database

1. Structure of Alfresco database

The database system of the micro-information system is constructed based on the Alfresco development tool, and the structure of the Alfresco database is shown in Fig.1. Storage and content of data is provided by persistent back-ends such as databases and file systems, in the meantime the application server houses both the Alfresco Application and the Alfresco API. An Alfresco Application provides a complete solution tailored for a specific area of Content Management such as Document Management (DM), Web Content Management (WCM) and Records Management (RM). The Alfresco API offers a set of reusable cross-cutting Content Management services such as content storage, query, versioning and content transformation. Furthermore all these services may be utilized by multiple applications.

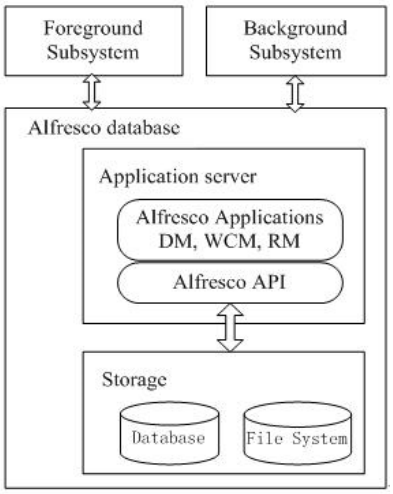

Fig.1 Structure of Alfresco database

2. The design of the micro-information system

(1) The foreground subsystem: In the micro-information system, the main role of the foreground subsystem is to demonstrate the content in the database system. After following the agreed protocol interfaces, the useful information from the database system could be gotten in the foreground subsystem, the MVC pattern of which is shown in Fig.2. Actually, the system manager does not need

to fully understand database techniques, while they just build the database by importing the required data of company in the management system through visualized operation which separates techniques and operation so as to reduce the technique requirement of manager.

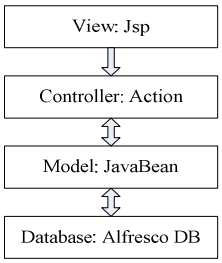

Fig.2 MVC pattern of the system

(2) The background subsystem: In the micro-information system, the background is designed to manage the system, in which the system administrators manage the database system and decide which would be shown in the foreground system. The basic function of the background subsystem in the Alfresco development tool is shown in Fig.3. In Alfresco database, both the database and the tables ,which include images, WIKI Encyclopedia and the market information database are stored as folders. The market information database contains information related to industry exhibition and some other latest information on the market.

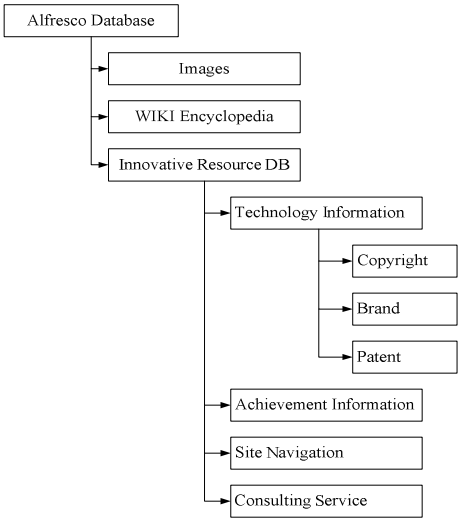

Fig.3 Basic function of background

(3) Design of Alfresco database: In this system, the databases, the data item of which can be either structured data, semi-structured data or unstructured data, such as images, sound and videos and so on, are designed as four groups, that are innovative resource database, market information database, enterprise technology database and user database. The innovative resource database contains the information such as patents, the latest researches which promote technological progress for enterprises, and so on. In the meantime the market information database includes information related to industry exhibition and some other latest information on the market, etc. The enterprise technology database consists of the information concerning recruitment, facilities rental and so on. In the user database there are all the information of users. The hierarchical contents of database system is shown in Fig. 4.

3. Realization of Alfresco database

(1) Table creation and editing: In Alfresco database development environment, it is convenient to create a table by visualized operations. First of all being token creating the table copyright that likes a table in other database as an example, after a new folder named Innovative_Resource_DB as one database of forth groups of this system in the Alfresco database development tool will be created after

log in the system as administrator, a new sub-folder named Achievement_information inside the Innovative_Resource could be created. Using the same method, the folder structure same as the relational database in other database system like SQL could be established successfully for the database of this system according to the hierarchical contents of database system in Fig. 4.

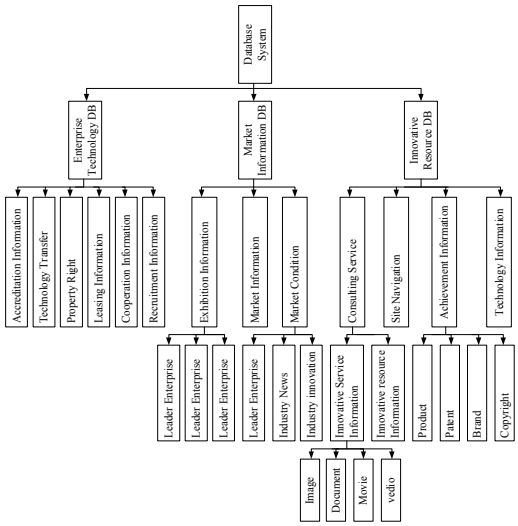

Fig.4 Hierarchical contents of database system

Editing a table is also convenient in Alfresco database by visualized operations too. For example in order to edit the table copyright, after logging in the system successfully and obtaining the permission to the table, we can create a file in the folder and edit the attribute of the file similar to the data item in traditional SQL.

(2) Data query: Suppose we want to search SONY in table brand, after getting permission to connect to the Alfresco database, we can use the following commands to realize this search function step by step like below:

To get permission to connect to the Alfresco database at first:

```
1  AuthenticationUtils.startSession("name", "passport");
```

To Set the search scope secondly:

```
1  path="PATH:\"/app:company_home/cm:InnoResource /cm:Achievement/cm:brand/*"";
2  factor1="@fdk\\:"+name+":\""+SONY+"\"";
3  luceneQuery = "" + path AND factor1;
```

To execute the query command thirdly:

```
1  Query query = new Query(Constants.QUERY_LANG_LUCENE,luceneQuery);
2  ResultSet resultSet = queryResult.getResultSet();
```

To obtain the query results at last.

```
1  ResultSetRow[] rows = resultSet.getRows();
```

(3) Data update: In order to update the attribute of the item SONY in table brand, the following steps can be used to update the data in the database after there being the permission to connect to the Alfresco database.

To get permission to connect to the Alfresco database at first:

```
1  AuthenticationUtils.startSession("name", "passport");
```

To set update information.

```
1  CMLUpdate update = new CMLUpdate();
2  update.setProperty(mySet("Name"， "Attributes"));
```

To set the node location.

```
1  update.setWhere(myWhere("File"， "Name"));
2  CML cmlUpdate = new CML();
3  cmlUpdate.setUpdate(new CMLUpdate[]{update});
```

To execute the update operation.

```
1  WebServiceFactory.getRepositoryService().update(cmlUpdate);
```

4. Superiority of Alfresco database

(1) Table operations: In order to create a new table in traditional database, the "CREATE TABLE" command, that should specify a set of attributes of the new table: the name of the table, the location of the new table, the name of each column in the table and so on, is needed in the professional database management system such as SQL. And the UPDATE statement to update records in a table is the same. Although all these operations can be done by the professionals, they can be easily implemented through visualized operations by customer only in the Alfresco database after designed by the professionals.

(2) Native file system support and Hot Backup: Alfresco database manages all kinds of content including documents, XML documents, photos, images, records, Web pages, or any other unstructured or semi-structured file. Users can get documents into and out of the repository easily. It needs to scale in order to support several hundred or more users and hundreds of thousands or even millions of documents with some percentage of growth each year. In this deployment, one Repository Server is designated as the Master host and another completely separate Repository Server is designated as the Slave machine. The application is hosted on the Master and as it is used, synchronous and asynchronous replication updates are made to the Slave i.e. the backup which remains in read-only mode. If for some reason, the Master breaks down, it is a relatively simple task to swap over to the Slave to continue operation. The Hot Backup of the system is shown in Fig.5.

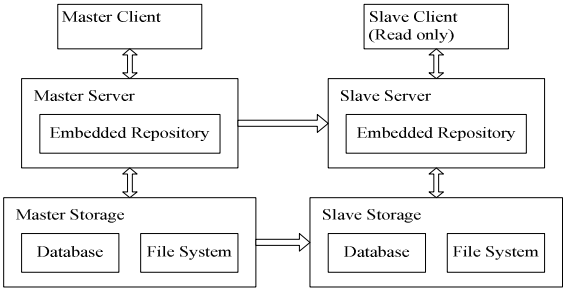

Fig.5 Hot Backup

(3) Other advantages of Alfresco database: In addition to above features described, there are many other advantages in Alfresco database. It gives fine-grained permissions which can be used to partition data, or to control access for "non power users" which can limit the damage they can do. It also owns high-level content management services such as transformation and meta-data extraction. It is deployable to any environment, including any application server, database and operating system. Besides these, Alfresco database supports workflow which can be used to streamline and automate manual business processes by letting the document management system keep track of who needs to do and what to a document at any particular time. The comparison between traditional database and Alfresco database is shown in Table.1.

Table.1 Comparison between traditional database and Alfresco database

	Traditional database	Alfresco database
Access Authority	Yes	Yes
Data Access Technology	JDBC	Alfresco SDK
Search Language	SQL	LUCENE
Data Encryption	No	Yes
Visualized Operations	No	Yes
Workflow support	No	Yes
Hot backup support	No	Yes
File System Support	No	Yes

Conclusion

In this paper, the Alfresco database of the micro-information system has been designed and realized. Construction and putting into operation of the micro-information system shows that the effect of Alfresco database is good in accordance of above ideas. Compared with traditional database system, Alfresco database provides better performances for construction of micro-information system for the small enterprises, which mainly reflects in higher security data, faster development speed and more stable performance. All these greatly improve data management and statistics of enterprises in specialized industrial townships. Through study and application of Alfresco database in this paper, it will be helpful for the developers to implement the management system with high efficiency.

Acknowledgements

This paper is supported by the project of Guangdong provincial department of science and technology.

References

[1] Clare Churcher, Beginning Database Design: From Novice to Professional [M], Apress, 2007, (ISBN 1590597699).Jeff Potts, Alfresco Developer Guide[M], Packt Publishing, 2008, (ISBN 1847193110).

[2] Munwar Shariff, Amita Bhandari, Alfresco 3 Enterprise Content Management Implementation[M], Packt Publishing, 2009, (ISBN-1847197361).

[3] David Caruana, John Newton, Professional Alfresco: Practical Solutions for Enterprise Content Management[M], Wrox, 2010.

[4] Hu Bin, Zhu Lidong, The design and realization of the information system of geological profiles based on ArcEngine, Computer Science and Network Technology (ICCSNT), 2011:1307-1310.

[5] Jeff Potts, Alfresco Developer Guide[M], Packt Publishing, 2008, (ISBN 1847193110).

Advanced Materials Research Vols. 989-994 (2014) pp 4650-4653
© (2014) Trans Tech Publications, Switzerland
doi:10.4028/www.scientific.net/AMR.989-994.4650

An Improved RBAC Model and its Application in Development of Information System

SONG Wan Li[1,3,a], ZHANG Hai Fei[2,3,b], WU Wei Feng[1,c], HE Wen Jie[3,d]

[1]Nanjing Communications Institute of Technology, Nanjing, 211188, China

[2]Nantong Textile Vocational Technology College, Jiangsu Nantong, 226007, China

[3]College of computer and information, Hohai University , Nanjing, 210098, China

[a]swlhhu@hhu.edu.cn, [b]0820705005@hhu.edu.cn, [c]wwf@njci.edu.cn, [d]wenjiehe@hhu.edu.cn

Keywords: RBAC; control strategy; fine-grained access control; personalized operation; information system.

Abstract. Aiming at the deficiencies of traditional RBAC model, on the basis of studying of the models introduced in the literatures published, this paper puts forwards an improved model--MR-RBAC, including its concepts and design. This model is implemented by adding restriction strategy on the operation objects and data objects, assignment different privileges to different users via configuration mapping of functions and menus. The implementation and practice indicates that the MR-RBAC model not only simplifies privilege management, but also improves the system security and privileges management flexibility.

Introduction

Access control is an important means to realize safe access and operation on information system. Role Based Access Control, RBAC [1-3] is relatively mature and widely used in information system. With increasingly awareness of intellectual property and innovation, security for information system are more concerned and more requirements. Therefore, the researchers have been improving the mode of RBAC to realize better effect. Three major improving methods are as follows: (1) Aiming at operation targets of the model. Literature [4] proposed a RBAC authority management model by data limitation, adopting a kind of data limitation mode similar SQL to separate authority targets from data targets. (2) Aiming at role configuration of the model. Literature [5] improves the concept of role in RBAC, providing role property definition and validation mode based on property strategy. (3) Aiming at user operation in the mode. Literature [6] proposed correlation model of user interface and operation authority which enables automatic interface configuration according to users' authority.

Though the research improved the deficiency of RBAC, the requirement for authority management is not only complicated but changeable because of complex application and changeable management requirement. The above methods cannot solve complicated and changeable management requirement for authority distribution and are mainly reflected as follows: (1) Restriction on operation objects often leads to too high link between authority management and database structure, and increases coupling and extra risks like SQL injection attacks. (2) Improvements on role configuration simply integrate authority and separates resource range. But it cannot simplify configurations of operation interface, and can neither substantively change authority sets nor thin authority granularity. (3) Restrictions on users' operation, which merely relies on visiting pages. If data is operated by artificially constructing URL, it will lead to unauthorized use and less rigorous implementation. This paper puts forward an improved strategy based on RBAC model by regarding operation objects, users' role and users' operation as an organic whole to realize granularity control of object authority and automatically configure menu interface of different functions according to different roles and verify operation authority as well. Formalized definition of improved model (Menu and Restriction-RBAC model) is given in the paper and an implementation of general authority access control system---GAACS is provided as well.

MR-RBAC Model

Model Description. This model improves RBAC role by adding the menu configuration item to realize dynamic allocation of system operation authority. This model decouples authority management and system data. Through above improvements, users are assigned function privilege. Detailed model description as shown in fig. 1.

Related Concepts. The related concepts added in this model are illustrated here. Menus: menu set, personalized interfaces set of the access system operating. Objects: object set, the set of data and resources in the system. Operations: operation set, the set of functions that users can use. Op Restrictions: operation restriction set. Ob Restrictions: object restriction set, security level for example. RO: the mapping of many-to-many relationship in roles and operations. MR: the mapping of many-to-many relationship in menus and roles. OO: the mapping of many-to-many relationship in operations and objects. OPOR: the mapping of many-to-many relationship in operation restrictions and operations. OBOR: the mapping of many-to-many relationship in object restrictions and objects.

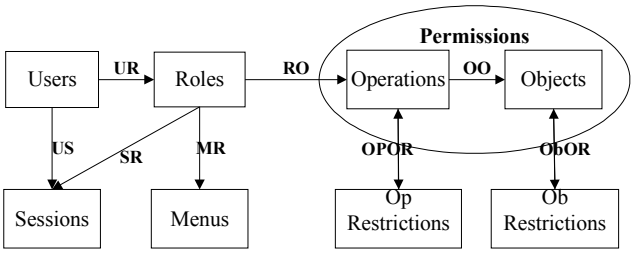

Fig. 1 MR-RBAC model

Model Implementation Approach. Here we present an approach for implementing MR-RBAC model that enables the user to reuse. We first give an overview of the approach and explicate its design in next section. The menu configuration realizes dynamic binding of authority and menu by configuring mapping relationship between role and menu first. Then it realizes dynamic binding of users and authority by configuring mapping relationship between user and role, and then realizes binding of user and menu. In order to avoid unauthorized operation on data by artificially construct URL, this model imposes further restrictions on user operation and examination on operation data. We take IP restriction as a user operation example. It can be realized by setting operation name in the database, corresponding IP validation and IP scope. The approach of data restrictions is similar to the operation restrictions. Dynamic binding of users and restrictions is realized by configuring mapping relationship between role and constraint. When performing an action, the model will verify the operation authority. Then to execute the operation on a data or not depends on whether the user has access to the operation of the data. Thus menu interface, restrictions on operation and restrictions on data, the three-layer authentication mechanism ensure the full restriction on user operation and guarantee system security.

Model Design and Realization

In this section we present the design of GAACS. The improved model consists of users' identification module, menu generation module, constraint strategy management module, authority management module and access control module.

Database Model Design. The database model design of general authority access control system is based on the thought of MR-RBAC model and analysis of module function demand. Fig. 2 only shows the main property of each related table in the model.

Function Design. Main functions of the system include user creation, menu generation, restriction verification and authority verification. Users' access control can be realized by organic organization of these functions.

User Creation. User creation is an essential function, which is the foundation of system operations. Firstly this function obtains user information to fill user object, then configures menu items and corresponding restrictions, lastly assigns corresponding role to the user.

Menu Generation. Menu as an entrance to system is very important. First acquiring all menu of the system from the database, and order according to the menu level, and then configure according to

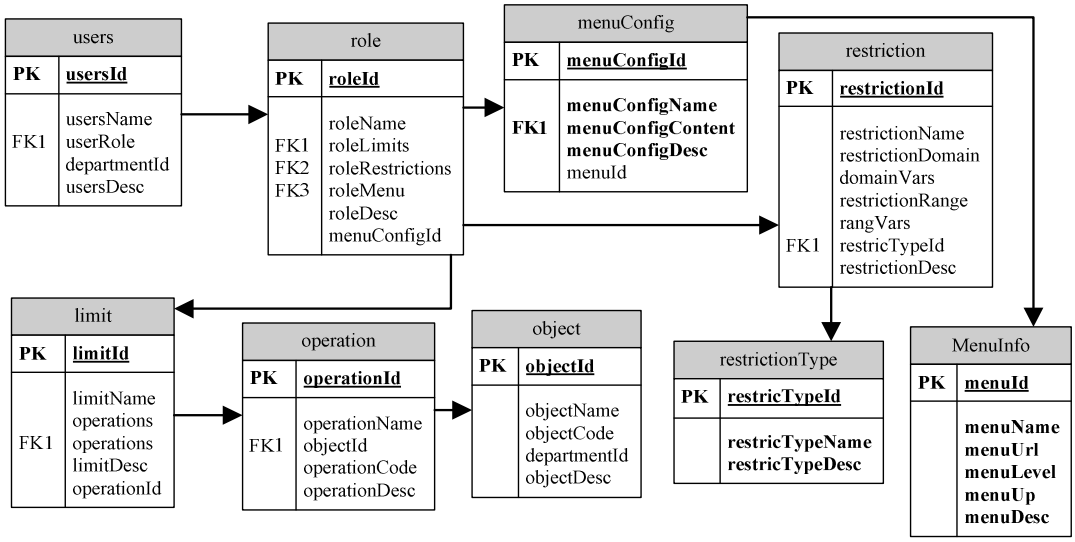

Fig.2 Database model of general authority access control system

subordinate relationship among menus. After all menus are configured, menu configuration data is persistently input menu configuration information list. When the system configures, menu configuration information corresponds to role, and then the generation of personalized interface is realized.

Restriction Verification. Restriction verification is introduced to manage access control for resource and data granularity management. Restriction strategy is a solution to strictly constrain system security level. Corresponding restriction information is acquired from user information after logging (the principle of acquiring restriction information refers to the implementation principle of above). When users implement a certain operation on an certain object, users' operation condition should be matched firstly. If the match is successful, it indicates that the user cannot implement the operation under this condition. It's the same case that if object match is successful, object cannot be operated under restriction condition. If the matches are all unsuccessful, corresponding object operation will be implemented.

Authority Verification. Authority verification is the core module of verification system and the control center of user access authority. First of all, acquire user information. If empty, enter logging page and acquire operation menu item corresponding to user and then dynamically generate user interface. Acquiring users' operation information after logging in and then load and intercept to judge whether it is in White List. If it is in White List, related operation is directly implemented. If not , verify user operation authority , operation object authority, operation restriction information and operation object restriction information. If there is authority and no related restriction, related operation should be implemented. Otherwise, unauthorized access will be reminded and the back. Authority verification flow chart is as Fig. 3.

Model Implementation and Application

Based on above design and approach, we develop a general authority access control system namely GAACS, based on Java EE 6.0 platform, use Oracle11g as database and MVC as system structure. GAACS is a Web application being deployed in Apache Tomcat 7.0 server. It is a non-invasive system, too. The front-end of this system is implemented with JSP combining Ajax technology to realize menu display. The back-end is coded base on Struts2 framework (using Actions to control user creation, menu generation, restriction verification and etc. and using interceptors to control authority verification) and Hibernate framework which is used to realize objectification access operation of Oracle database. Java reflection mechanism is used to realize decoupling of authority management

and thinning operation access granularity. Finally we use Spring framework to integrate each function module to complete all the GAACS functions of MR-RBAC model.

We use GAACS to conduct experiments to verify the effectiveness of MR-RBAC model. We apply this system to the Management Information System of College Communist Youth League and the network curriculum system of Java EE Framework Technology. Users can realize dynamic assignment of operation authority by configuring the mapping of menu items and user roles. They can add restriction strategy of operation and object to further guarantee system security. When operation management demands or data changing, users can directly adjust restriction strategy in authority configuration instead of readjusting program code. This improves authority configuration flexibility in the process of system operation and development efficiency of information system. The applications in the real-life information system development verify the effectiveness of our proposed model.

Summary

Access control is one of the most important parts of information systems. This paper puts forward an improved model--MR-RBAC model which can be reused in developing of various information systems. This model provides improvement strategies regarding operation object, user role and user operation as an organic whole instead of separated ones to realize granularity control of object authority. And it can automatically configure menu interface with different functions according different roles and verify operation authority. The implementation and successful applications indicate that the proposed model is achievable and the model proves to be effective in the practice and improves development efficiency of information system.

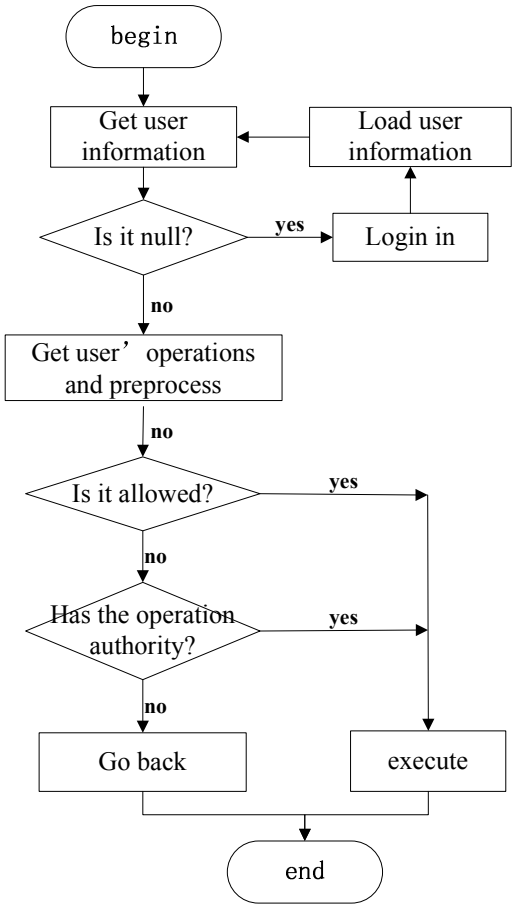

Fig.3 Authority verification flow chart

Acknowledgements

This work was financially supported by Research Foundation of Nanjing Communications Institute of Technology (JY0810, JY1108) and College Students Practice and Innovation Training Project of Nanjing Communications Institute of Technology (CX1326).

References

[1] Ferraiolo, David, Janet Cugini, and D. Richard Kuhn. Role-based access control (RBAC): Features and motivations. Proceedings of 11th Annual Computer Security Application Conference. (1995), pp. 241-48

[2] Sandhu, Ravi S., et al. Role-Based Access Control Models. IEEE computer 29.2 (1996), p. 38-47

[3] Ferraiolo, D. F., Sandhu, R., Gavrila, S., Kuhn, D. R., & Chandramouli, R. Proposed NIST standard for role-based access control. ACM Transactions on Information and System Security (TISSEC) 4.3 (2001), p. 224-274

[4] S. P. FAN, Y. GAO. Extended RBAC rights management model based on three management roles separation and data constraints. Journal of Computer Applications. 31(S2), (2011), pp. 112-115.

[5] W. G. LI, F. Y. ZHAO. RABC Permission Access control Model with Attribute Policy. Journal of Chinese Computer Systems. 34(2), (2013), pp. 328-331.

[6] Y. WANG, M. WANG, M. LI. Research on Configuration of Custom UI in MIS. Science and Technology Management Research. 32(17), (2012), pp. 220-224.

Advanced Materials Research Vols. 989-994 (2014) pp 4654-4656
© (2014) Trans Tech Publications, Switzerland
doi:10.4028/www.scientific.net/AMR.989-994.4654

Research on ASP.NET-based task management platform

Fengwei Wang[1, a], Zhihong Xing[1,a] and Chen Liu[1,a]

[1]Liaoning institute of measurement, China

[a]250178551@qq.com

Keywords: task management; ASP.NET; Visual Studio 2005

Abstract. With constantly expansion of companies, more and more woks on communication become the managers' top issue. It is urgent to use computer technology to improve work efficiency and achieve of information sharing as much as possible. The managers need a platform to keep their information updated real-time, statistics tasks information at any necessary times, and the staff also need platform to record the task process, make schedule to alarm. Therefore, ASP.NET-based task management information system is designed and implemented. The system is developed with Visual Studio 2005 and SQL Server 2005, including task management module, file management module, schedule management module and background management module. With running in practical, it is proved that the system improved working efficiency greatly and implemented work information sharing effectively..

Introduction

With constantly expansion of companies, managers play more and more important role and undertake heavier and heavier work on the development and management part. The managers arrange a lot of tasks everyday, but the work progress cannot feedback to the managers in time and effectively. On the other hand, the feedback information and work records in the form of printing paper and copying paper are not easy to manage, find and statistics, which wastes a lot of human resources and greatly decrease the working efficiency. The root of the root-causes, it is not that the managers and staff are lazy on the job, but lack of an effective information communication and management platform which provides the foundation to achieve the right decision for manager.

Therefore, a ASP.NET-based task information management platform is designed and implemented based on the actual demands of work, which consists of task management module, file management module, schedule management module and background management module. With this system, the information communication between managers and staff improve effectively, which inevitable increases the working efficiency and management level.

Key Technology

.NET Framework. .NET Framework developed by Microsoft Corporation is a platform applied to Agile software development, Rapid application development, it is a programmed platform running in virtual machine which is based on the Common Language Runtime (CLR), and supports programming with Visual C#, Visual Basic, Visual C++ and so on.

The task management information system is developed with C# language and based on .NET Framework.

ASP.NET. As part of Microsoft .NET Framework, ASP.NET is a computing environment that simplifies application development in the highly distributed Internet environment. Besides simplicity, good usability, scalability, manageability as well as high efficiency, it is also known for its well-defined structure, good extensibility, powerful development tool support and security, and thus has become one of the most popular Web development technologies.

ASP.NET provides component-based, event-driven, programmable Web Form as a great simplification in programming. In addition, ASP.NET is capable of building Web Services. The main difference between ASP.NET and ASP lies in that the former requires compilation before execution

while the latter is interpreted during execution, so ASP.NET is much better in efficiency. In fact, we can consider the execution process of ASP.NET as CLR (Common Language Runtime) code working as an application that interacts with the front-end web browser and the middleware to accept requests from the user and output HTML stream to the user[1].

System Design

Workflow design and module design. The routine works in "Quality and Technology" department consist of many parts, such as QS (quality system) management, scientific research management, purchase management, train management and others, and work of each part consist of many items. Everyone in the department takes charge of many items which belong to different parts. On the other hand, there are many files on each item of work, including working guidance, common forms, and reference documents and so on. In order to increase the flexibility of system, the work items management is designed.

The system is developed to manage work in "Quality and Technology" department, implement effective communication between manager and staff. In this system, manager input work task first, and then staff input task progress according to actual work. After the task completed, staff click in the system, and manager input evaluation.

File management is also main function in the system, including attachment file management and reference file management. Firstly, everyone could query and download file to guide the work, and secondly, the manager could upload the reference file, and staff could upload the attachment file when report the process in the system. The file management flow is distinct and easy to execute.

Schedule management is auxiliary function of task management. Everyone could record and manage own schedule which will remind in time. Not only schedule can bind to work task, but also schedule can exist alone.

The function modules of system include task management, file management, schedule management, and background management.

(1) Task management module: publish task, input task process, edit task information, confirm the task has completed, evaluate and so on.

(2) File management module: upload reference file, delete file, search file and so on.

(3) Schedule management: make schedule, delete schedule, alarm at the homepage and so on..

(4) Background management: manage users information, manage task classed and file classes and so on..

Database design. Database design is a process to construct database structure. The system is developed with Microsoft SQL Server 2005 and based on the relational database. The entities in the system include task, task classes, file, file classes, schedule, evaluation, task process and others[2].

The relation between task and other entities is shown as Fig. 1.

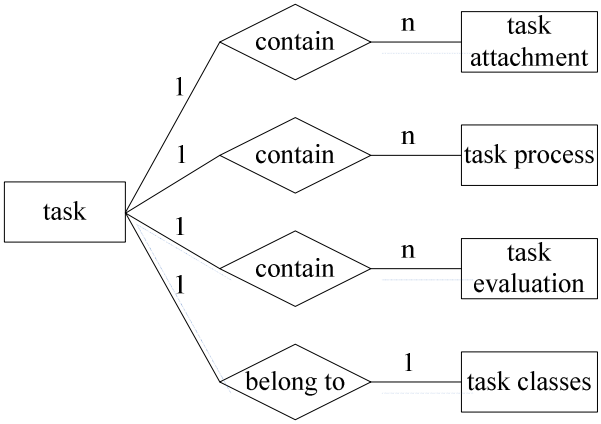

Fig. 1 The relation between task and other entities

System Implementation

Data Access Layer. To implement data access, a class named "DBOperation" is established and the data access string used is set in the file "web.config". The data access string is set as below[3]:

<appSettings>
<add key="ConnectString" value="server=(local);database=Task; UserId=sa; pwd = 123456"/>
</appSettings>

In the "DBOperation" class, many methods to access database are defined, such as:

(1) the methods open database connection and close database connection;
(2) the methods execute SQL command to insert, update, delete records;
(3) the methods execute SQL command to select records.

In addition, a class named "SQLString" is established to form SQL string based on the input values and validate the SQL strings which can increase the safety of database access[4].

Implementation of task management platform. Task management module include publish task, input task process, edit task information, confirm the task has completed, evaluate and so on. The flow chart of publish task is shown as Fig.2.

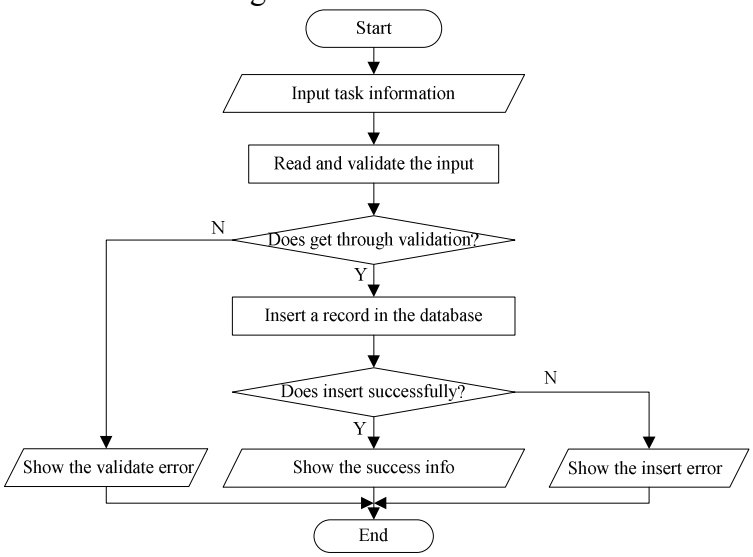

Fig. 2 The flow chart of publish task

System test and conclusion

The test is executed with each function by "Black Box Testing" method[5]. A lot of detail test prove that the system run with no breakdown in usual.

(1) The functions mentioned in the requirement document are implemented.
(2) The system is easy to use, easy to maintain.
(3) With running in practical, it is proved that the system improved working efficiency greatly and implemented work information sharing effectively.

References

[1] Shen Jun. Electronic Measurement Technology. 2008, 31(2), p.76-79. In Chinese.
[2] Information on http://www.cnblogs.com/wuhenke/archive/2010/08/11/1797307.html
[3] Han Shuangwang.. Automation & Instrumentation, 2011(5)，p.15-16. In Chinese.
[4] MA Baoguo, WANG Wen-feng, HOU Cun-jun, QIAN Fang-zheng. Computer Technology and Development, 2006, 16(3), p. 50-55. In Chinese.
[5] Information on http://www.buzzle.com/editorials/4-10-2005-68349.asp

Advanced Materials Research Vols. 989-994 (2014) pp 4657-4659
© (2014) Trans Tech Publications, Switzerland
doi:10.4028/www.scientific.net/AMR.989-994.4657

Research on Application Technology of Body Area Network and the Internet of Things Connection

Liu Xue-feng[1],Liu Chen[2]

[1,2] (Chongqing ZhengDa Software Vocational and Technical Institute, ChongQing ,400056, China)
E-mail:zhengjian.002@163.com

Keywords: Body Area Network, Internet of Thing, Combination

Abstract: with the rapid development of body area network technology and the internet of things technology, makes the effective combination of these two techniques. Scientific connection method of study of this two kinds of techniques in this paper, to solve the core problems of these two kinds of technology association, and proposed solutions. The combination of these two techniques, and provide the technical support is widely used for applications of the Internet of things technology development and body area network.

1. Introduction

The Internet of things is also known as the sensor network, a vast network of the various information sensing equipment combined with Internet. The Internet of things is considered to be following the computer, the Internet, mobile communication, a new round of information technology revolution,it is the driving force of the core competition in the future information technology field and the commanding heights of industry upgrading. With the rapid development of information collection and intelligent computing technology,and wide use of the Internet and mobile communication network, large-scale development of the Internet of things and related industries the opportunity is becoming mature, developed countries such as America and Europe will network as an important area of future development. Our country began the research of the Internet of things as early as ten years ago, formed a certain scale of the industry, and has made certain discourse power in international standard setting, the application of Internet of things is initially started.

Biological recognition in twenty-first Century was named one of the ten major high-tech. As body communication technology of biological recognition technology, as early as in 1996, IBM first unveiled the human communication technology. Now study abroad, to the skin surface of human body as the data bus HAN (HAN, Human Area Network) technology has been gradually moving towards the commercial application. Japan has developed a data bus in communication technology with skin and skin 20CM distance. China has started, the scope of its application are remote medical treatment, digital intelligence, automatic safety communication, identity authentication etc.

In recent years, with the development of microelectronic technology, the wearable , the implantable and can invade of service device has appeared: for example, worn on a finger of quality sleep blood oxygen sensor, wrist watch type glucose sensor, watch type measuring device, sleep physiology checker, implantable identification components etc. If there is no body area network, these sensors and actuators are all can work independently, to bring their own respective communication components, so the communication resources can not effectively use. Visible, body area network and the Internet of things is a combination of natural in technology.

2. Wireless Body Area Network

BAN (BAN, Body Area Network) is usually regarded as a solution, wireless standards organizations and IEEE are in the development of BAN technology.Sensors collect information through wireless transmission to the terminal processor. Then the processor through the traditional data network (for example: Ethernet, Wi-Fi or GSM), will all send information to the specified server. Sensor of BAN will generally require high precision, low power signal processing level, and require a wireless connection.BAN is the sensor system to a configuration, low cost, low power and high reliability. The packaging and operation must be sterile for human peripheral or internal. In addition, the wireless communication must be enough robust to prevent the RF interference in various environments,for example: Wi-Fi network, microwaves and cordless phones.

BAN design should meet the following conditions:

(1)Low power consumption and low current consumption. Use time of the battery should be considered in design of BAN node.

(2) High reliability. The system must be able to provide sufficiently high data accuracy and reliability.

(3) High security. The BAN node must have adequate safety measures, to protect patient privacy and prevent hacking.

Red Tacton technology is a kind of wireless transmission technology of BAN technology, to transmit data through the skin of the human body. Red Tacton is used in weak electric field, so wear or implanted in the body of Red Tacton transmitter produce much weaker electric fields on the surface of the human body, the human skin as the data transmission channel and media.

In order to develop an suitable low power consumption device and optimized communication standard for BAN application, IEEE has developed the IEEE802.15.6 standard.Compared with the existing standards, IEEE802.15.6 has many advantages. It focuses on the short distance, low cost, low power consumption and low implementation complexity. IEEE802.15.6 standard on the PHY (PHY, physical layer), MAC (MAC,media access control layer) protocol and security layer are defined.

IEEE802.15.6 consists of a PHY layer and a public MAC and a security layer.The PHY layer is designed to meet the needs of different data rate requirements of the application, it is divided into three bands:narrow band, ultra wide band and human body communication band. Its target communication distance is 3 meters,support 100kbit/s to various data between 1Mbit/s rate.The maximum power consumption for the 3mA.

3 The Internet of things Modeling

The internet of things not only provides the connection of the sensor, its also has the ability of intelligent processing, to implement the intelligent control of objects. The internet of things sensor and intelligent processing combination, the use of cloud computing, pattern recognition and intelligent technology, expand its application areas.

The internet of things is a information carrier based on the internet and the traditional telecom network etc. It makes all independently addressable physical object to realize interconnection. The related technology of the Internet of things related to many fields,its technology often has the application demand in different industries[1], the internet of things can be roughly divided into three layers.

Among them, the perception layer is responsible for perception the physical world data information, With gathering information on the real world or RFID terminal sensor node.

The network layer is responsible for solving the perception layer for data transmission problem, and to provide the service to the upper layer.

The application layer is responsible for processing information and user interface management. Through analysis and processing of sensory data, provide the application interface and support services for the user. The current typical applications such as logistics monitoring[2][3], furnishing asset statistics[4], intelligent Home[5]， remote meter reading[6] etc.

Hypothesis the communication channel is a N independent channel,let X and Y are independent of each other and mean value is 0, variance σ^2 of Gauss random variables, received terminal signal can be expressed as:

$$Z=Xi+Y \tag{1}$$

Among them,the joint probability density function for X and Y:

$$f_{(x,y)}(x,y)=\frac{1}{2\pi\sigma^2}e^{-\frac{x^2+y^2}{2\sigma^2}},-\infty<x,y<\infty \tag{2}$$

Hypothesis the signal phase is θ, and the amplitude is ω,according to the formula (2) may be marginal probability density function of phase and amplitude :

$$\begin{cases} f(\theta) = \int_{-\pi}^{\pi} f_{(x,y)}(z,\theta)d\theta = \frac{\omega}{\sigma^2} e^{-\frac{\omega^2}{2\sigma^2}}, 0 < \omega < \infty \\ f(\omega) = \int_{0}^{\infty} f_{(x,y)}(z,\theta)dz = \frac{1}{2\pi}, -\pi < \theta < \pi \end{cases} \quad (3)$$

Then using formula (3) to calculate the amount of the received signal average value:

$$E(\omega) = \eta \int_{0}^{\infty} \omega f_{(x,y)}(\omega)d\omega = \eta\sqrt{\frac{\pi}{2}}\sigma \approx 1.26\sigma * \eta \quad (4)$$

Among them, η is model correction coefficient.

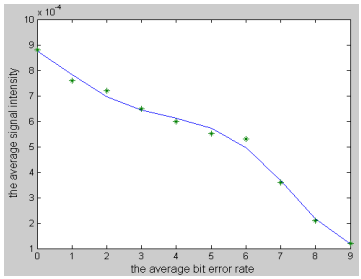

Figure 1. Relationship between signal intensity and the bit error rate

This paper did a study on the relationship between the signal intensity and the bit error rate, shown in figure 1 is the signal in different intensity through the channel the bit error rate. It can be seen that the signal intensity increased but the bit error rate reduced gradually. There is requires the channel transmission code accuracy in BAN protocol. As can be seen from figure 1, as long as the signal strength is large enough, maybe satisfy the requirements of the BAN protocol agreement.

4 Conclusion

The internet of things is a new technical system of multiple information fusion, as a connection Things—Things the relationship between network, include a variety of network, has a key role in communication technology and wireless sensor network. The body area network and the Internet of things combined has important practical significance.

Acknowledgement

Research on Application Technology of Body Area Network and the Internet of Things Connection(Project ID: KJ123501)

REFERENCES

[1]LiuQiang,CuiLi,ChenHaiming.Key technology and application of the Internet of things[J].Computer Science,2010,3(6).
[2]Tae-Hong Shin,Sangyoon China,Su-Won Yoon.A service-oriented Integrated information framework for RFID/WSN-based intelligent construction supply chain management.Automation in Construction,2011,20(6):706-715.[3]DaiDingyi. The internet of things and intelligent logistics. China logistics and procurement,2010,(08):34-36.
[17]Detlef Zuehlkea.SmartFactory-Towards a factory-of-things.Annual Reviews in Control,2010, 34(1):129-138.
[4]DanCheng,PengBiche,XueYuan.The realization of intelligent home furnishing completely gateway based on the SOC8200 industrial plate. Journal of Wuhan University,2010,(05):672-676.
[5]LiKaicheng,PanLanlan,LiuBin etc.Research on remote meter reading based on wireless communication. Electrical Automation,2005,(01):41-42.

Advanced Materials Research Vols. 989-994 (2014) pp 4660-4664
© (2014) Trans Tech Publications, Switzerland
doi:10.4028/www.scientific.net/AMR.989-994.4660

A SVM Reliability Evaluation Framework for the Component-based Web System

NIE Peng[1, a]

[1]Jiangxi University of Finance and Economics, Nanchang, China

[a]zeanet@163.com

Keywords: component; Web system; reliability evaluation; support vector machine

Abstract. In the reliability evaluation studies of the component-based Web system, the stated-based models and the path-based models suffer from the high time-consumption for the high complex web structures. In this paper, a SVM Reliability Evaluation Framework for the component-based Web system (SVMREF) with a low computational complexity is presented. SVMREF employs the Web component reliabilities as the SVM inputs and outputs the final reliability evaluation after the well-trained learning process. Our proposal has a low evaluation complexity and outperforms the state-based model and the path-based model. The experiment results and the analyses show that SVMREF has a better reliability evaluating convergence and SVMREM is evidently lower than the contrast models when the Web system structure is complex .

Introduction

With the development of software technology, software grows both in functions and complexity. Adapting to the trend, the ideas of the component-based software design and reuse have been widely used in the enterprise information platform constructions and become one of the important methods in software development. The enterprise Web application is an instance of the component-based idea. The Web application is usually divided into several subsystems, and the subsystems are split into the components charging different functions. The white box models are used in the component-based Web software reliability evaluation. Further more, the white box models includes the state-based[1-3] and the path-based[4-5].

A SVM Reliability Evaluation Framework for the component-based Web system (SVMREF) is proposed for the component-based Web systems in this paper. Our proposal obtains the Web component reliability based on the system logs and learns the implicative complex knowledge between the component reliability and the overall software system reliability. Based on that knowledge, the final evaluated result is output.

The rest of this paper is organized as follows. Section 2 presents the related works on the Web component-based software evaluation. The SVMREF notations, definitions are presented in Section 3. Our proposed model SVMREF in detail is presented in Section 4. Section 5 gives the experiments and the performance analyses. Finally, Section 6 concludes this paper.

Related works

Musial[6] proposed a heterogeneous architecture reliability model based on the discrete time Markov chain for service-oriented applications. Eaton[7] designed a learning mechanism that inductively acquires knowledge of tag support criteria based on observed samples of accessible and inaccessible web page source code. Leticia[8] gave a methodology for improving the reliability of web-based software systems by the traditional analytical model. Karambir[9] summarized the relevant aspect of reliability issues and estimated the reliability of Web application using Markov model. Rohini[10] used the doubly stochastic model to access the website current reliability.

The major drawback of Markov Model is the explosion of number of states as the size of system increases. The resulting models are large and complicated. The analytical models suffer from the model assumptions[11].

SVMREF notion

Notation

N_i	a specific component	R_i^k	the reliability of N_i on the k-th execution
R_s^k	the software system reliability on the k-th execution	R^k	the software system reliability set on the k-th execution
R_T , R_E	the observed software system reliability and the evaluated reliability	ε	the error between R_T and R_E

SVM reliability evaluation framework

In our proposal, we employ SVM based on the component historical reliability to construct the software system reliability evaluation. Fig. 1. presents the overview of SVMREF. The elements in the SVMREF are introduced in detail as follows.

- Web log collector analyses the Web logs, and collects the faults logged in the system.
- Component reliability constructor constructs the component reliabilities according to the result given by the Web log collector.
- Reliability converger reports the component reliabilities to the reliability database center.
- SVM Reliability Input Vectors are set up based on the reports from the reliability converger.
- SVM Reliability Training uses the reliability input vectors as its input, and trains itself to learn the implicative complex knowledge between the component reliability and the overall software system reliability.
- SVM Reliability Evaluating uses the desired Web component reliabilities and outputs a abecedarian value. The SVM error between the real value and the evaluation are checked, and SVM is trained again until the SVM error is minimized to a given value.

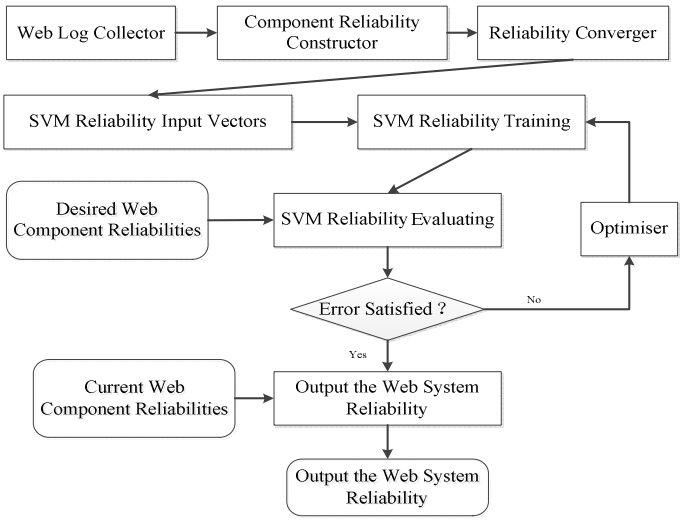

- SVMREF loads the current Web component reliabilities to evaluate the Web system and outputs the evaluation result after the SVM is well-trained.

Figure 1. Overview of SVMREF

Assume $\{((R_1^1,\cdots,R_n^1),R^1),\cdots,((R_1^k,\cdots,R_n^k),R^k)\}$ be the given training datasets where each $(R_1^i,\cdots,R_n^i)$ shows the SVM reliability training data vector in the *i*-th iteration for the nodes from 1 to n. R^i is a corresponding target system reliability value in the *i*-th iteration where $i=1,\cdots,k$. k represents the iteration number of the software reliability testing. The support vector regression solves an optimization problem:

minimize: $\frac{1}{2}\|w\|^2 + C\sum_{i=0}^{l}(\xi+\xi^*)$

$$\text{subjected to } \begin{cases} R^i - \langle w,(R_1^i,\cdots,R_n^i)\rangle - b \le \varepsilon_i + \xi \\ \langle w,(R_1^i,\cdots,R_n^i)\rangle + b - R^i \le \varepsilon_i + \xi^* \\ \xi_i,\xi_i^* \ge 0 \; i=1,\cdots,l \end{cases} \quad (1)$$

where ξ_i is the upper training error (ξ_i^* is the lower) subject to the ε insensitive tube $R^i - \langle w,(R_1^i,\cdots,R_n^i)\rangle - b \le \varepsilon$. The parameters which control the regression quality are the cost of error C, the width of the tube and the mapping function ϕ . The constraint simply that we would like

to put most data $(R_1^i,\cdots,R_n^i)$ in the tube $R^i-\left\langle w,(R_1^i,\cdots,R_n^i)\right\rangle-b\le\varepsilon$. If $(R_1^i,\cdots,R_n^i)$ is not in the tube, there is an error ξ_i or ξ_i^* which we would like to minimize in the objective function. For the traditional least square regression, ε is always zero and data are not mapped into higher dimensional spaces. Hence, SVM is a more general and flexible treatment on regression problems. Dibike et al. demonstrated that the radial basis function (RBF) outperforms other kernel functions, and is expressed as

$$k(R_i^j,R^j)=\exp\{-\gamma\left|R^j-R_i^j\right|^2\} \tag{2}$$

where γ is the parameter of RBF which gives the width of the kernel. In general, γ varies from 0 to 1. The SVM model used herein has three mutually dependent parameters, namely C,ε,γ, thus changing the value of one parameter changes the other parameters too. A common way to estimate the SVM parameters C,ε,γ is to separate the data into two sets, namely a training dataset and a validation dataset. The prediction accuracy of this validation dataset reflects the accuracy of the model, and SVM parameters which are able to give minimum prediction error are considered to be the optimal parameters.

Experiments and performances

The Online Course Choosing Web System(OCCWS) in Jiangxi University of Finance and Economics was employed for the SVMREF experiments and the performance analyses. The classical stated-based CUORM model and the path-based HARAM model were used as the baselines for SVMREF software reliability assessment.

OCCWS

The component list of OCCWS and the visit statistics are shown in Table 1.

Table 1 OCCWS components list and visit statistics

Function	Component ID	Description	Visits	Cumulative errors
User Login	C_1	Login interface	26430	0
	C_2	Login capacity controller	1163327	3025
	C_3	Authenticode creator	182227	1002
Certificate	C_4	Certification	697246	1046
	C_5	Certification Ending	165545	762
Privilege Assign	C_6	Personal information controller	39328	12
	C_7	Privilege assignment	23090	5
Course Choosing	C_8	Course selected visitor	95083	1008
	C_9	Course pool visitor	194525	992
	C_{10}	Course retaken controller	45905	1001
	C_{11}	Book subscription controller	40163	3000
	C_{12}	Course resource auditing	28171	1000
	C_{13}	Course resource submission	27398	649
	C_{14}	Course information edition	18032	400
Exit	C_{15}	Logout controller	18597	7

OCCWS workflow is shown as Fig. 2.

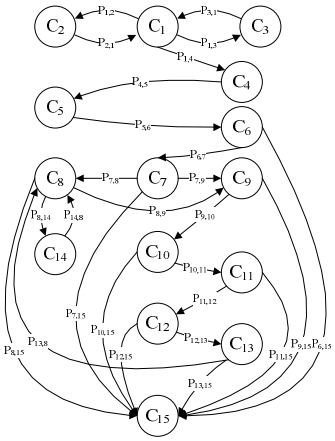

$P_{1,2}$=1	$P_{1,3}$=1	$P_{1,4}$=1	$P_{2,1}$=1
$P_{3,1}$=1	$P_{4,5}$=1	$P_{5,6}$=1	$P_{6,7}$=0.5868
$P_{6,15}$=0.4132	$P_{7,8}$=0.5063	$P_{7,9}$=0.4935	$P_{7,15}$=0.0002
$P_{8,9}$=0.7953	$P_{8,14}$=0.1896	$P_{8,15}$=0.0151	$P_{9,10}$=0.236
$P_{9,15}$=0.764	$P_{10,11}$=0.875	$P_{10,15}$=0.125	$P_{11,12}$=0.7014
$P_{11,15}$=0.2986	$P_{12,13}$=0.9726	$P_{12,15}$=0.0274	$P_{13,8}$ = 0.9834
$P_{13,15}$=0.0166	$P_{14,8}$=1		

$P_{n,m}$ presents the reliability transition probability from C_n to C_m

Figure 2. OCCWS workflow

The reliability curves evaluated by CUORM, HARAM, SVMREF and the observed real reliability in OCCWS are shown in Fig. 3-(a). The evaluating time-consumptions are show in Fig. 3-(b).

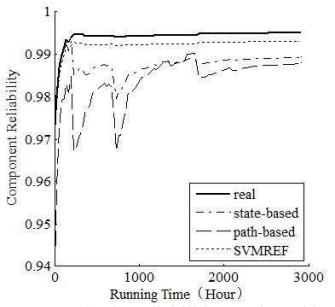

(a) the reliabilities evaluated by CUORM, HARAM, SVMREF

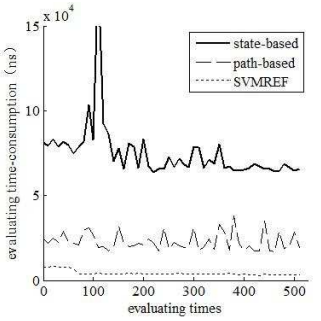

(b) the evaluating time-consumptions

Figure 3. Reliability evaluated curves and the evaluating time-consumptions

Model comparisons

For the model comparisons, the relative error (ε) as Eq. 3 is used to evaluate the accuracy of models.

$$\varepsilon = \frac{R_T - R_E}{R_T} \tag{3}$$

R_T denotes the observed reliability, and R_E alternatively uses R_{HARAM}, R_{CUORM} or R_{SVMREF}. Average $|\varepsilon|$ is used to calculate the average relative error in the experiments of OCCWS. Table 2 presents the evaluated reliability comparisons in OCCWS.

Table 2 Evaluated reliability comparisons for OCCWS

$\lvert\varepsilon\rvert$						Average $\lvert\varepsilon\rvert$		
R_{HARAM}		R_{CUORM}		R_{SVMREF}		R_{HARAM}	R_{CUORM}	R_{SVMREF}
min	**max**	**min**	**max**	**min**	**max**			
0.010	0.034	0.011	0.015	0.000	0.008	0.011	0.007	0.001

OCCWS have been executed more than 500 times to reach their stable reliabilities. As Table 2 shows, in most cases, the average $|\varepsilon|$ of R_{HARAM} is much greater than the other two. The accuracy of R_{CUORM} is relatively smaller than R_{HARAM}, around 1% on average of $|\varepsilon|$. However, the cost is the complexity of $O(n^3)$. The reliabilities evaluated by the proposed model SVMREM are closer to R_T than those of R_{HARAM}, and R_{SVMREM} around 0.1% $|\varepsilon|$ on average.

Time-consuming comparison

Fig. 3-(b) shows that HARAM has a less time consuming. However, HARAM suffers from nesting one sub-structure within another sub-structure. As the software system becomes complex, such nesting sub-structure combination makes HARAM rather complex. SVMREF benefits from its

low computing complexity and outperforms the other two models in the reliability evaluation for the Web system.

Conclusion

This paper presents SVMREF for the reliability evaluation for the Web system constructed by the components. SVMREF enhances the time-consumption and outperforms the state-based and the path-based models in the evaluation accuracy. Our analysis and experiments show that the proposed scheme consumes less time and has a better reliability accuracy in the Web reliability evaluation.

References

[1] R. C. Cheung. "A user-oriented software reliability model". IEEE Transactions on Software Engineering, 1980, vol. 6, pp. 118-125.

[2] J. Tian, S. Rudraraju, and Z. Li. "Evaluating Web Software Reliability Based on Workload and Failure Data Extracted from Server Logs". IEEE Transactions on Software Engineering, 2004, vol. 30, pp. 754-769.

[3] W. Wang, D. Pan, and M. Chen. "Architecture-based software reliability modeling". Journal of Systems and Software, 2006, vol. 79, pp. 132-146.

[4] C. Hsu, and C. Huang. "An adaptive reliability analysis using path testing for complex component-based software systems". IEEE Transactions on Reliability, 2011, vol. 60, pp. 158-170.

[5] N. F. Schneidewind. "Integrating testing with reliability". Software Testing, Verification and Reliability, 2009, vol. 19, pp. 175-198.

[6] E. Musial, and M. Chen. "Effect of Data Validity on the Reliability of Data-centric Web Services", Proc. IEEE 19th International Conference on Web Services, IEEE, 2012: pp. 576-583, DOI 10.1109/ICWS.2012.95.

[7] C. Eaton, and A. Memon. "Evaluating Web Page Reliability across Varied Browsing Environments" Proc. the 15th IEEE International Symposium on Software Reliability Engineering, IEEE, 2004: pp. 198-209.

[8] L. Dávila-nicanor, and P. Mejía-alvarez. "RELIABILITY IMPROVEMENT WITH PSP OF WEB-BASED SOFTWARE APPLICATIONS". Computer Science & Engineering: An International Journal, 2012, vol. 2, pp. 9-25.

[9] M. Karambir, and J. Tamak. "A Review of Fault Detection Techniques to Detect Faults and Improve the Reliability in Web Applications". International Journal of Advanced Research in Computer Science and Software Engineering, 2013, vol. 3, pp. 14-21.

[10] P. Rohini, C. Jayaprakash, and R. Ganesh. "Reliability Enhancement from http Log Files In Composite Web Services". International Journal of Engineering and Advanced Technology, 2013, vol. 2, pp. 464-468.

[11] J. Geng, P. Nie, and Z. G. Qin. "Status and Research of Software Reliability Models". Journal of University of Electronic Science and Technology of China, 2013, vol. 42, pp. 565-570.

Advanced Materials Research Vols. 989-994 (2014) pp 4665-4668
© (2014) Trans Tech Publications, Switzerland
doi:10.4028/www.scientific.net/AMR.989-994.4665

The Design and Realization of Virtual Editing Environment for News Release

ChengJiong-wang

School of computer engineering WeiFang University WeiFang China

wcjsdwf@126.com

Keywords: Virtual editing, News gathering and editing, Network officing.

Abstract. As the development of modern information technology, the digitization, mobilization and networking of working environment have become the general trend, directly from which the virtual editing environment cooperatively supported by the computer comes. The realization of mobile officing and home officing through VIEW makes the editing of news agencies virtual and links news gathering and editing with network to fully enhance the efficiency of news publishing and provide better working environment for editors and reporters.

1. Background of the Subject

As the constant progress of the society and rapid development of the technology, the social value and economic value of news information have been widely recognized and higher demands for timeliness of news are made. How to enhance the working efficiency of news gathering and editing process has become another focus in news publishing world. Establishing news gathering and editing all-in-one system through modern information technology to realize the digitization of news gathering and networking of news releases greatly enhance publishing efficiency. However, as one of the key links for news publication, relay mode in composition system and manual processing mode in layout planning, layout proofreading, layout editing, layout delivery and layout issuing have become the main bottleneck for enhancement of efficiency. Moreover, it is hard to develop new generation layout production system based on network environment for single machine system and news gathering and editing network which has become an urgent mission[1][2][3].

In recent years, modern information technologies such as computer, exchange network and multimedia database have developed rapidly and entered realization stage, influencing people's life styles and working styles and promoting the formation of many a brand-new conceptions such as home officing, mobile officing, video conference and computer supported cooperative work-CSCW, besides information consumer electronic such as information household appliances, intelligence terminal, VOD, WebTV are in line with the developing trend[4][5].

Using information technologies to create efficient and comfortable working environment and living environment has become the theme of information development, traditional working geographical attribute is vanishing gradually, and virtual working environment characterized by digitization, mobilization and networking is going to be the main stream. Above all, all the conditions that using modern information technologies to reform news publication process, fully enhancing the timeliness of news and providing convenient and fast digital working environment for editors and reporters are ready and time is propitious.

2. System Demands

Layout production is the one main influencing efficiency and quality in the process of news publication; it includes layout planning, typesetting, proofing, proofreading, submission and issuing. Different from gathering and editing, it includes not only serial work flow process but also collaborative parallel processing by dynamic working team comprising responsibility editor, operator,

director and chief editor, which is a layout design and editing process according to different operation authority. In details it has the following functions:

Selecting a Template. It is mainly used to complete the traditional layout production, including the following aspects:

Layout Planning. It is divided into two steps: the first one is to draw up the framework of news releases and advertisement regions by general editing office; the second one is to partition the layouts according to the news by responsibility editor to confirm the position and relevant attribute and to confirm the advertisement arrangement according to the demands of the subscribers by advertisement editor[6].

Regional Subject Editing . Set up regional subjects and select and post the picture-text news from the issuing ones. Typeset according to the confirmed attribute (font, size) and decorate for readability and aesthetic (lace, underpainting). Regional contents editing includes adding, deleting, revising and changes of regional position, sizes and decorations.

Collaboration Function. Using video, audio, e-mail and electronic white board for multi real-time collaboration in the process of layout production, which includes: parallel processing of different regional subjects in the same layout and interactive processing of the same regional subjects by different persons.

Controlling Function. It is used to control the layout quality and layout processing procedure.

Layout Processing Procedure Monitoring. It can real-time track the regional subject processing and know the schedule of the whole layout at any time and offer relevant comments.

Layout Proofreading. Using network printing device to output layout (also called proofing) and evaluate the output effects, including fonts quality, color quality and layout arrangement etc.

Another important one for layout proofreading is to check the news release itself, including words, phrases, structure and logic, besides the factuality and legality, in order to guarantee quality[7].

Proofreading requires the support of news material management and service system.

Layout Submission and Issuing. According to the work process, designate authority for different persons, and layout shall be submitted for check step by step after completion, at last signed and issued by chief editor. The final version could be in the form of PS, EPS, PDF and HTML. The layout could be handed for printing and sent to different printing agencies through Internet or satellite and could be published on the Web in the form of electronic newspaper. The sign and issuing of the layout requires the support of digital signature technology.

Revision Process Record. Make detailed and correct record of revision on layout elements in the process of layout production for inspection.

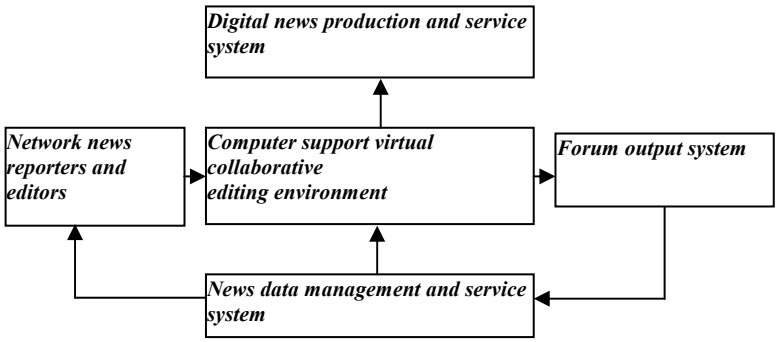

Fig.2 The Relationship of Other System in View System and News Press Process

Maintenance Function. Complete the management of different persons and their access rights and back-ups of core data. Especially the maintenance of font library makes the layout results independent of specific output platform for better applicability, which is the difference between the east and west languages.

Non-function Demand. Besides above function demands, VIEW has following non-function demands:

Good Integration. Integration has two aspects:

VIEW system could be an independent running entity, at the same time it also should combine with news gathering and editing system and output system.

VIEW system is only a basic frame system and mainly used for organization and management of layout. Some regional subjects of different type can be completed by relevant components which can be integrated with frame system as required to simplify the complexity and guarantee the openness of system to meet the individual needs of different users.

Convenient Operation Mode. Layout production process is a highly interactive one. Design quality of interactive process and interface influence operation efficiency directly and are closely related to the work intensity, so convenient operation mode is the key point for success.

Manageability. Mobile officing and home officing editorial office supported by VIEW is not geographical conception but a dynamic working team on the Net. People may be working everywhere, traditional software management is no longer suitable for the work management and new software structure is taken for zero management of working platform. Available technologies right now include CORBA, JINI and DCOM.

High Safety and Reliability. Due to the particularity of news publishers, the safety and reliability are demanding. It requires strict operation authority for different persons to unify the power and responsibility, and also to guarantee the printing and publication in time. Every technology should be used in the system to guarantee the normal operation of software and hardware devices, even under extreme circumstance; single machine is able to be used to complete the layout production.

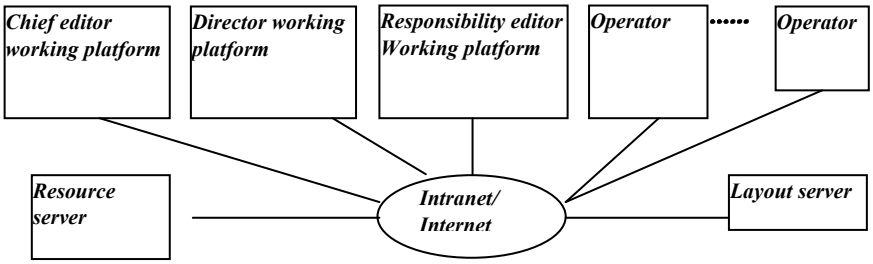

Fig.1 The system structure

3. The System Structure

The structure of virtual editing system is as Fig.1. The relationship of other system in VIEW system and news press process is as Fig.2.

According to the business features of news press, collaborative roles are operator, responsibility editor, director and chief editor. Every role corresponds to one working platform to complete his function in his own right management.

The layering model of virtual editing environment is as Tab.1

TABLE1 THE LAYERING MODEL OF VIRTUAL EDITING environment

Chief editor working platform	Director working platform	Responsibility editor working platform	Operator working platform
Editing environment general components			
Video, audio	Electronic white board	E-mail	Components integration support	database
Operating			
Hardware Platform			

Operator Working Platform. The platform is mainly used to make layout subjects, including news posting, subject decoration, contents editing and layout submission to the responsibility, according to responsibility editor's design plan.

Responsibility Editor Working Platform. It is mainly used to complete layout planning, layout check, layout elements revision, region locking and layout submission. Real-time alternation between responsibility editor and operator is the most frequent.

Director Working Platform. It is mainly used to monitor the layout schedule, layout sign and issuing and submit the completed layout to the person in charge.

Chief Editor Working Platform. It is mainly used to read the layout, check important news releases and general effect and offer revision comments to responsibility editor (including the change and revision of layout elements), even adjust or revise the layout and its elements directly if necessary.

Besides above functions, every platform supports on-line news material search.

4. Difficulties In System Research

The Research on virtual editing environment collaboratively supported by computer consists of information processing technologies such as computer, exchange network, multimedia and database and psychology and behavior, which is a very complicated information processing system, mostly in following aspects:

Establishment of Editing Environment Model. It includes the recognition in editing process, drawing in behavior model and information procedure establishment driven by roles. The establishment of editing environment model is the basic of system research, which is involved in decomposition in business process and requirement of behavior mode. Due to the relationship with psychology, it is hard to establish a stable model.

Materials Distribution and Management. VIEW system is different from the normal shared application, which can not be easily controlled by "virtual pen". Fully considering network reliability and transport efficiency, make a reasonable compromise between concentrated materials management mode and distributed materials management mode to guarantee the conformity and completeness and enhance transport efficiency.

Establishment of Collaboration Conversion Model. For many different roles are involved in VIEW system, the operations influence each other and single working platform includes many parallel processing, unified conversion model must be taken into consideration to guarantee the stability of the whole system at the time of parallel processing for order and efficient operation of the system.

5. Conclusion And Expectation

News press model consists of news gathering and editing, network composition, parallel output, digital news production etc. We put forward the conception of virtual editing environment and complete it in network environment. The spread and application will improve the modernization of news press technologies [8].

References

[1] Jia-dong Ruan, Web Database Technology (3rd edition). Beijing: Science Press, January,2010.

[2] Hong Jiang, Qing-song Yu, Practical Course Based on. NET's Web Database Development Technology. Beijing: Tsinghua University Press, April, 2007.

[3] Cheng-Jun Wang, etc. Web Database Application Course (2nd edition). Beijing: China Water Power Press Shan-pei Wei, Practical Course of Web Database Technology. Beijing: Tsinghua University Press,Mrch 2007.

[4] Jun Tie, Web Database Technology. Beijing: Tsinghua University Press, July,2008.

[5] Hong-liu Cai, Xinhua He, Information Security Technology and Application Experiments Beijing Kehai Electronic press, December,2004

[6] Xin-yan Liao, ASP.NET WEB Interactive Database Programming. Beijing: China Railway Press, January,2003.

[7] Xin-gwei Hao, Web Development Technology. Beijing: Higher Education Press, December 2006.

Advanced Materials Research Vols. 989-994 (2014) pp 4669-4674
© (2014) Trans Tech Publications, Switzerland
doi:10.4028/www.scientific.net/AMR.989-994.4669

Reliable Node based Multipath QoS Routing Protocol on Opportunistic Networks

Xuebin Ma[1, a], Liting Wang[1, b] and Zhenchao Ouyang[1, c]

[1]Department of Computer Sciences Inner Mongolia University Hohhot, China

[a]csmaxuebin@imu.edu.cn, [b]wanglt99@gmail.com, [c]ouyangkid@gmail.com

Keywords: routing; multipath; QoS; reliable node; opportunistic networks.

Abstract. Opportunistic networks are similar to the mobile ad hoc networks (MANETs) that does not have fixed infrastructure, and the messages can be transmitted by nodes in a "store - carry - forward" approach. The mobile nodes randomly move, which result in a constantly changed network topology and frequently interrupted link. Thus, multipath routing has been proposed to improve the stability of link, extend path lifetime and reduce packet loss rate. The paper first analyzes the traditional multipath routing protocol and its path selection theory, and then investigates quality of service (QoS) metric to improve transmission efficiency of opportunistic networks, and finally proposes a reliable node based on multipath QoS routing protocol, named as RNMR. In RNMR, the stable path contains primary path and two backup paths. The primary path consists of reliable nodes and intermediate nodes, and the two backup paths are formed by two disjoint sub-paths selected from two adjacent and reliable nodes. By comparing with the backup source routing (BSR) protocol and greed -based routing (GBR-WB) protocol, the paper proves RNMR protocol has longer path lifetime, deliver rate and relay are also improved.

Introduction

Opportunistic networks are class of mobile ad hoc networks (MANETs) and do not necessarily have a complete path between source and destination. An opportunistic network utilizes encounter chance of mobile nodes to realize communication each other [1]. Delay tolerant network (DTN) [2] is first proposed by tolerant network research group for communication of interplanetary network (IPN), and its main objective is to support inter-connection of heterogeneous network which has intermittent connectivity, large delay and high error rate, such as Internet and sensor network, mobile ad hoc network (MANET). Thus, the opportunistic network can be treated as a wireless ad hoc network with the general characteristics of the DTN network.

The traditional MANET [3] routing protocol exists at least a complete end-to-end path when transmits messages. At some point, MANET network may be divided into unconnected sub-regions. When source node and destination node are in different domains, MANET routing protocol cannot find the path to the destination node. However, this does not represent without any communication. Since the nodes are moving, and two nodes within radio communication range can exchange data in a hop-by-hop method. Thus, in opportunistic networks, the network is not required to be fully meshed which is more suitable for ad hoc network. Opportunistic networks take the "storage - carry - forward" approach as the means of information transmission. Because the opportunistic networks rely on nodes to complete the end-to-end message transmission, and thus it is necessary to consider three questions in the information transmission process: reliable node selection, transmission reliability control and buffer management and scheduling.

Through the deep research, extensive usage of the MANET and Wireless Sensor Network (WSN) [4], opportunistic networks deny routing model in the traditional network, and improve the stability of path. Although Epidemic routing protocol [5], Spray and Wait routing protocol [6] that are based on encoding routing protocol can reduce TTL, they can cause much network overhead and ignore to improve QoS [7]. Probabilistic Routing Protocol using History of Encounters and Transitivity (PROPHET) is a kind of probabilistic routing protocol, which can transmit messages by encountering

probability of nodes. There is a shortcoming that it cannot guarantee messages successfully to transmit from source to destination.

In order to improve the stability of the routes and QoS of network, this paper proposes a reliable node based on multipath QoS routing protocol (RNMR). We determine the zone of reliable nodes in the research workplace, and select reliable nodes by battery model. Then we can use encountering probabilistic model to establish one major path and two backup paths. At the same time, there are two disjoint sub-paths between adjacent reliable nodes. RNMR routing protocol has many advantages: (1) the primary path is the shortest path, which composes of reliable nodes and intermediate nodes; (2) when major path interrupted, backup paths can continually transmit messages; (3) it can reduce routing overhead. Through theoretical analysis, RNMR routing protocol can acquire longer path lifetime so that improving the path stability and QoS.

The rest of this paper is organized as follows: Section II describes RNMR routing protocol in detail. Section III discusses the performance of the RNMR protocol through theoretical analysis. Finally, we conclude the characteristics of RNMR.

RNMR routing protocol

Initial position coordinates of the nodes in the research scene are determined by the Global Positioning System (GPS). We use power model to find the reliable node for message transmission, and to utilize encountering probability mode for route discovery. In addition, mobility model is used to determine link expiration time of nodes, and confirm expiration of paths.

Reliable node region. We analyze the mobile of students at school; mobile nodes have certain regularity. We record initial position of nodes and collect position of others.

Reliable node selection. We will assume a university as the research scene and choose one of the buildings within the university as a region. We draw a circle with the centre and width of the building. It is the size of the selected area. At the same time, we choose a small circle again from the selected circle. Assume O and R represent the centre and radius of the circle, respectively. The small circle is the selection area for reliable node whose radius is r (r=0.5R). The initial position of every node is acquired by GPS, and new position of these nodes is determined by mobility node at time t.

Power model. In order to select the optimal reliable node from the reliable area, the power model is used to determine its remaining battery power, and its power ratio is calculated to select the best reliable node.

Let F be battery full charge of the portable communication device of node. At time t, the remaining power of node i is as follows:

$$W_i^{rem}(t) = W_i^{rem}(t-1) - N * W_i^{tr}(t-1,t) - M * W_i^{re}(t-1,t) - W_i^{\text{int}}(t-1,t). \quad (1)$$

The related parameter of the formula is shown in Table 1.

At $t=0$, $W_i^{rem}(t) = F$. It is assumed that the remaining power of a battery lies in two ranges based on power ratio [8].

$$Power\ ratio = \frac{W_i^{rem}(t)}{F}. \quad (2)$$

Then,

$$W_i^{rem}(t) = \begin{cases} low\ \ range, & 0 < Power\ \ ratio < 0.3 \\ high\ range, & 0.3 \le Power\ \ ratio \le 1 \end{cases}. \quad (3)$$

Through the above judgment, when the remaining power of node i is in the high range, it is set as a reliable node; otherwise, it is not.

Table 1 The related parameter of the formula

$W_i^{rem}(t)$	remaining battery power of node *i* at time *t*
$W_i^{rem}(t-1)$	remaining battery power of node *i* at time *t*-1
$W_i^{tr}(t-1,t)$	the power required to transmit a data packet from *t*-1to*t*
$W_i^{re}(t-1,t)$	the power required to receive a data packet from *t*-1to*t*
$W_i^{\text{int}}(t-1,t)$	power required to perform node's internal operations for the duration *t*-1 to *t*
N	the number of transmitting data packet
M	the number of receiving data packet

Mobility model. The initial position of node *i* and *j* is (X_i, Y_i) and (X_j, Y_j) respectively, at the same time, their speed constantly changes, and the nodes are moving in a particular direction. Assumed that the node moves in the X-axis positive direction, the angle of node *i* and *j* is $\theta 1$ and $\theta 2$ respectively. At time *t*, the moved distance of node *i* and *j* is $d1$ and $d2$, and their new position is (X_i', Y_i') and (X_j', Y_j'), is shown in Fig.1[8].

$$X_i' = X_i + d1Cos\theta_1, \quad Y_i' = Y_i + d1Sin\theta_1, \quad X_j' = X_j + d2Cos\theta_2, \quad Y_j' = Y_j + d2Sin\theta_2. \tag{4}$$

In practice, it is not possible for nodes to move in a constant velocity. So average speed is presented for distance calculation. Let V_i , V_j as the average speed of node *i* and *j*, then $d1 = V_i \times t$, $d2 = V_j \times t$.

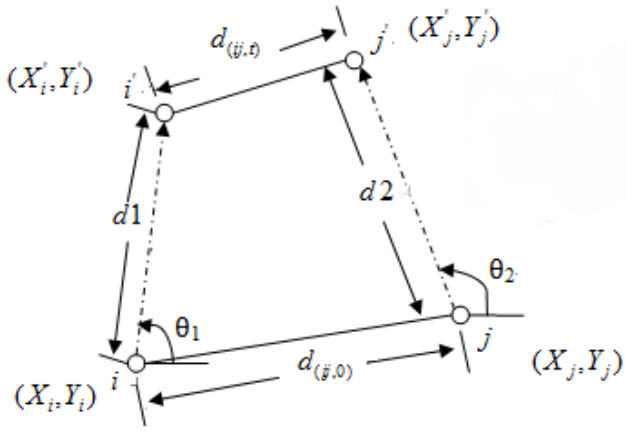

Fig.1 A pair of nodes: before and after mobility

Expiration time of full path. Aussmed that nodes' communication radius is *R*, the link expiration time is $LET(i,j)$, and the path expiration time is *PET*.

$$LET(i,j) = \frac{-(mn+pq) + \sqrt{(m^2+p^2)R^2 + (mq-np)^2}}{m^2+p^2}. \tag{5}$$

Where $m = V_i Cos\theta_1 - V_j Cos\theta_2$, $n = X_i - X_j$, $p = V_i Sin\theta_1 - V_j Sin\theta_2$, $q = Y_i - Y_j$.

Since the entire path is composed of many links, the path expiration time is determined by the following equation.

$$PET = \min_{i\in(1,2,\ldots,k)}(LET(i,j)). \tag{6}$$

Encounter probability model. The optimal path of two adjacent reliable nodes is computed by encountering frequency of nodes. Since the nodes are independent each other, the maximum delivery rate of data packet can be calculated. Reliable nodes split paths into the number of disjoint sub-paths. R_i^* represents the optimal path in the ith sub-path.

$$R_i^* = \max\left\{\frac{\sum_{l\in R_i} f(t)}{nR_i} \middle| R_i \in R_{s,d}\right\}.$$

$$s.t. \quad R_i^* = \{s = A_i, a_i, a_{i+1}, A_{i+1} = d\}. \tag{7}$$

Where the i presents the ith optimal sub- path, A presents reliable nodes, a presents intermediate nodes, $f(t)$ is frequency of the received data packets which equals to node encounter probability. $f(t)$ is as follows:

$$f(t) = m/M . \tag{8}$$

Assuming node is randomly mobile and mutually independent. Maximum probability of data packet delivery from source node S to destination node D is as follows:

$$P_{\max} = \prod_{i=1}^{n} R_i^* . \tag{9}$$

Analysis and discussion

Expected path lifetime of RNMR. Path lifetime can be judged by the path stability and its Cumulative Distribution Function (CDF), and it can be obtained by mathematical derivation. Between the source node S and the destination node D, there are three paths: a primary path and two corresponding backup paths. The three paths are composed of link-disjointness multipath, the common nodes in the links are reliable nodes, and the backup path length between two adjacent reliable nodes is 3 hops. The primary path is the shortest distance path connected by reliable nodes and intermediate nodes. Reliable nodes will split the whole path into m-1 sub-paths, the ith path is expressed as the L_i (i =1, 2... m-1) and has the lifetime X_{L_i}. L_i has two backup paths represented as $BP_{(i,1)}$ and $BP_{(i,2)}$, respectively. The corresponding link of $BP_{(i,1)}$ is $BP^1_{(i,2)}$, $BP^2_{(i,2)}$ and $BP^3_{(i,2)}$ which have lifetime of $X^1_{(BP_i,2)}$, $X^2_{(BP_i,2)}$ and $X^3_{(BP_i,2)}$. The corresponding link of $BP_{(i,2)}$ is $BP^1_{(i,2)}$, $BP^2_{(i,2)}$ and $BP^3_{(i,2)}$ which have lifetime of $X^1_{(BP_i,2)}$, $X^2_{(BP_i,2)}$ and $X^3_{(BP_i,2)}$, the lifetime of backup path is $X_{(BP_i,1)}$ and $X_{(BP_i,2)}$.

$$X_{(BP_i,1)} = \min(X^1_{(BP_i,1)},\ X^2_{(BP_i,1)},\ X^3_{(BP_i,1)}). \tag{10}$$

$$X_{(BP_i,2)} = \min(X^1_{(BP_i,2)},\ X^2_{(BP_i,2)},\ X^3_{(BP_i,2)}). \tag{11}$$

The two backup paths are represented as $LBR_{(i,1)}$ and $LBR_{(i,2)}$ which has the lifetime of $X_{(LBP_i,1)}$ and $X_{(LBP_i,2)}$ respectively. When the primary path connection fails, it selects an optimal path of two backup paths for message transmission. X_{LBR_i} is the longest lifetime of backup paths.

$$X_{LBR_i} = \max(X_{L_i}, X_{(BP_i,1)}, X_{(BP_i,2)}). \tag{12}$$

The lifetime T of the path from S to D is expressed as follows:

$$T = \min(\max(X_{L_1}, X_{(BP_1,1)}, X_{(BP_1,2)}), \max(X_{L_2}, X_{(BP_2,1)}, X_{(BP_2,2)}), ..., \max(X_{L_{m-1}}, X_{(BP_{m-1},1)}, X_{(BP_{m-1},2)})). \tag{13}$$

The CDF of path lifetime T is as follows:

$$\begin{aligned} F_T(t) = P[T \le t] &= P[\min(\max(X_{L_1}, X_{(BP_1,1)}, X_{(BP_1,2)}), \max(X_{L_2}, X_{(BP_2,1)}, X_{(BP_2,2)}), ..., \\ &\qquad \max(X_{L_{m-1}}, X_{(BP_{m-1},1)}, X_{(BP_{m-1},2)})) \le t] \\ &= P[\min(X_{LBR_1}, X_{LBP_2}, ..., X_{LBP_{m-1}}) \le t] \\ &= 1 - \prod_{i=1}^{m-1} (1 - P[X_{LBR_i} \le t]) \\ &= 1 - \prod_{i=1}^{m-1} (1 - F_{X_{LBR_i}}(t)). \end{aligned} \tag{14}$$

Assuming X_{L_i} (i=1, 2, ... , m-1) is independent and identically is distributed random variables. Its probability density function is approximately equal to exponential distribution. The probability density function of X_{LBR_i} is $f_{X_{LBR_i}}(t) = \lambda_i e^{-\lambda_i t}$ [9], where $\lambda_i = (m-1)/l$, l is the average lifetime of the link. CDF of X_{L_i} and X_{LBR_i} are as follows:

$$F_{X_{L_i}}(t)=1-e^{-\frac{1}{l}t},\quad F_{X_{(BP_i^1,1)}}(t)=1-e^{-\frac{3}{l}t},\quad F_{X_{(BP_i^1,2)}}(t)=1-e^{-\frac{3}{l}t},\quad F_{X_{LBP_i}}(t)=(1-e^{-\frac{1}{l}t})(1-e^{-\frac{3}{l}t})^2. \tag{15}$$

We obtain the CDF of T as follows:

$$\begin{aligned} F_T(t) &= 1-[1-F_{X_{L_i}}(t)F_{X_{(BP_i^1,1)}}(t)F_{X_{(BP_i^1,2)}}(t)]^{m-1} \\ &= 1-[1-F_{X_{LBR_i}}(t)]^{m-1} \\ &= 1-[1-(1-e^{-\frac{1}{l}t})(1-e^{-\frac{3}{l}t})^2]^{m-1} \\ &= 1-(e^{-\frac{1}{l}t}+2e^{-\frac{3}{l}t}-2e^{-\frac{4}{l}t}-e^{-\frac{6}{l}t}+e^{-\frac{7}{l}t})^{m-1}. \end{aligned} \tag{16}$$

Path lifetime comparison of several routing protocols: RNMR, GBR-WB and BSR. In order to study the path lifetime of RNMR, the paper conducts the comparison with GBR-WB and representative multipath routing protocol BSR. GBR-WB is a GBR routing protocol without local backup path. Its lifetime is approximately equal to l/h, where l is the lifetime of average link, h is the path length [10].

BSR [11] is a multipath routing protocol and may have common nodes or links among the paths. It obtains the similarity cost function by similarity of links and nodes and construct backup path.

CDF of BSR lifetime is as follows [9]:

$$F_T(t)=1-e^{-kt}\prod_{j=1}^{w}(e^{-h_jt}+e^{-h_j't}-e^{-h_jt-h_j't}). \tag{17}$$

Where k represents the number of the same link between the primary path and the backup path, w represents the number of disjoint sub-paths, $h_j$and h_j' (j = 1, 2, ⋯, w) indicate the corresponding length of disjoint paths.

In order to verify the performance of RNMR routing protocol, it will compare with GBR-WB and BSR. the setting of parameters is shown in Table 2.

Table2 Setting of parameters for RNMR, GBR-WB and BSR

l	1s
k	0
h=m-1	2,3,4,5,6,7,8
h_j	2
h_j’	3

Acoording to the theory analysis, when the primary path length of RNMR, GBR-WB and BSR changes, the corresponding path lifetime can be obtained.

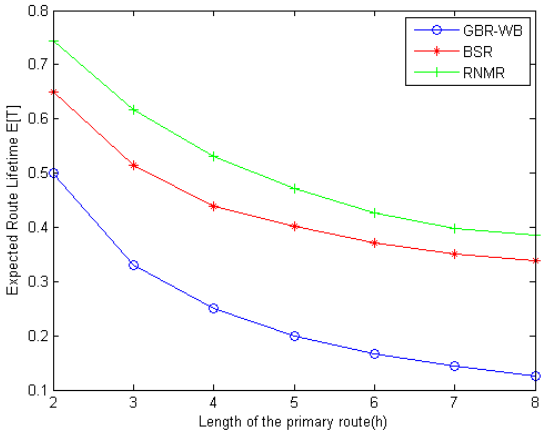

Fig.2 Expected route lifetime of different primary route length

Fig. 2 shows that, with the increase of primary route length, the route lifetime is reduced. There are two main reasons for the phenomenon: One reseaon is that with the increase of path length , the stability of the path is reduced; the other reseaon is that with the increase of the primary path length,

the length of the corresponding backup path will also increase. Seen from the figure, it is obvious that the lifetime expectancy of RNMR routing protocol is significantly higher than GBR-WB and BSR.

Conclusions

In opportunistic networks, nodes move which make the dynamic topology change constantly and the path be frequently interrupted. Therefore, it cannot guarantee successful transmission of message from the source to destination. This paper presents RNMR routing protocol to improve the path stability of the opportunistic networks. RNMR routing protocol selects the best reliable node by power model in reliable region. Through the introduction of reliable nodes, the primary path is divided into several disjoint sub-paths. The backup paths of each sub-path exist independently. This improves the lifetime of the entire route as well as reduces packet loss rate and delay so that QoS of network has been obviously improved. Primary path is the shortest distance path chosen between reliable nodes and intermediate nodes, while the backup paths are two selected best backup paths calculated by the nodes' encounter probability model. When a link of the primary path fails, the upstream node of the link could continue to find path through backup paths.

By comparing RNMR with GBR-WB and BSR, it turns out that RNMR routing protocol has a longer path lifetime, which further reduces the packet loss rate and delay, thus makes the QoS of opportunistic networks be guaranteed.

Acknowledgements

This work was financially supported by the Foundation of Inner Mongolian Autonomous Region Educational Committee (NJZY11017), "Spring Sunshine Program" of the PRC Ministry of Education (z2009-1-01011), National Natural Science Foundation of China (61162006) and Research Program of Institutions of Higher Education of Inner Mongolia Autonomous Region (NJZZ12005).

References

[1] Yongping Xing, Limin Sun, Jianwei Niu, Yan Liu: Opportunistic Networks. Journal of Software. Vol.20 (2009), p.124-137. inChinese.

[2] Yunsheng Wang, Wei-Shih Yang, and Jie Wu: Analysis of a Hypercube-based Social Feature Multi-Path Routing in Delay Tolerant Networks. TRANSACTION ON PARALLEL AND DISTRIBUTED PROCESSING (2013).

[3] Mina Masoudifar: A review and performance comparison of QoS multicast routing protocols for MANETs. Ad Hoc Networks 7 (2009) , p.1150-1155.

[4] Jennifer Yick, Biswanath Mukherjee, Dipak Ghosal: Wireless sensor network survey. Computer Networks. 52 (2008), p.2292-2330.

[5] Vahdat A, Becker D: Epidemic routing for partially connected ad hoc networks. Department of Computer Science, Durham (2000).

[6] Spyropoulos T, Psounis K, Raghavendra CS: Spray and wait: an efficient routing scheme for intermittently connected mobile networks. ACM (2005), p.252-259.

[7] S.Venkatasubramanian, N.P.Gopalan: Multi-path QoS Routing Protocol for Load Balancing in MANET. International Journal of Networking & Parallel Computing (2013).

[8] Rajashekhar C. Biradar and Sunilkumar S. Manvi: Neighbor supported reliable multipath multicast routing in MANETs. Journal of Network and Computer Applications 35 (2012).

[9] S. Ross.Introduction to Probability Models.Academic Press, 1989.

[10] A. Nasipuri R. Castaneda and S. R. Das, Performance of multipath routing for on-demand protocols in mobile ad hoc networks, Mobile Networks and Applications 6 (2001), p.339-349.

[11] Song Guo, Oliver Yang and Yantai Shu: Improving Source Routing Reliability in Mobile Ad Hoc Networks. IEEE TRANSACTIONS ON PARALLEL AND DISTRIBUTED SYSTEMS 16(2005), p.362-373.

Advanced Materials Research Vols. 989-994 (2014) pp 4675-4679
© (2014) Trans Tech Publications, Switzerland
doi:10.4028/www.scientific.net/AMR.989-994.4675

Privilege Separation in Browser Extensions Based on Web Workers

Chunmei Yu[1,a], Jianhua Sun[2,b] , Hao Chen[3,c], and Xianghua Xu[4,d]

[1,2,3]College of Information Science and Engineering, Hunan University, Changsha, China

[4]Zhejiang Provincial Key Lab of Data Storage and Transmission Technology, Hangzhou Dianzi University, China

[a]lantianxia@hnu.edu.cn, [b]jhsun@aimlab.org,[c]haochen@aimlab.org,

Keywords: Privilege Separation, Web Workers

Abstract. In this paper, we propose to use Web Workers [1], isolated parallel threads in current browser working in the background, to enforce privilege separation in chrome extensions. Our tests show that our design is applicable to most chrome extensions (those not using the jquery library) and achieves a reduction in TCB up to 77 percent for our examples. Our implementation shows that our design is efficient enough to enforce privilege separation in chrome extensions and not needs to modify the browser or learn new high-level languages.

Introduction

With Web applications and browser extensions becoming more and more popular, the web vulnerabilities are still pervasive [2]. The Web applications that own the elevated privileges are the main target of attackers.

The Google Chrome Extension platform has recognized the necessity to enforce privilege separations in the chrome extensions. The Google Chrome Extension platform divides a chrome extension into two components: the core extension that runs in an isolated sandbox and content scripts that are in charge of interacting with the browser [4]. The permission mechanism enforces restrictions on the privileges the extension requires [7]. However, this design that needs to modify the browser and its permission mechanism is not sufficient enough to enforce privilege separation because of its coarse grained policies.

Recently, the paper [3] proposes a language-based approach to isolate an application by assigning every component a minimum of privileges of a Web application, each of which forms an isolated domain. But, in this approach, it is necessary for developers to learn a new high-level language that is time consuming and can't maintain completed compatibility with legacy code.

In 2012, iframes are proposed to enforce privilege separation in Web applications. But it has a shortcoming that the script code in an iframe may impact the main page's liveness, if the script code consumes the resources of the browser or goes into a dead loop [6].

In this paper, we proposed to use Web Workers to enforce privilege separation in Chrome extensions. Web Workers provide completely isolated JavaScript environment and work in the background, which can't impact the main page's liveness. In our system, we create a common privileged master and a few unprivileged workers. How many components a chrome extension can be divided is decided by the number of the extension pages, e.g., we divide an extension owning background.html, popup.html and options.html into three components. We just put all the functional JS files from an extension page into an unprivileged Web Worker and other HTML and CSS files still execute in the extension page. The workers communicate with the master with postMessage [6]. The master interposes on all the privileged calls from workers by enforcing a fine-grained policy code that is application-specific and can be modified freely by developers.

We show that our proposal is practical for most existing chrome extensions. We retrofit two Google Chrome extensions to use our design. Its overhead for memory consumption is a little high, but the absolute costs are tolerable (no human perceivable latency). In our examples, the trusted

computing base (TCB) [8] reduces by up to 77 percent and no more than 18 lines of code need to change. And, there is no need for developers to learn new languages.

There is a limitation to use our design. Since Web Workers can't access the DOM, the library jquery will not work in them. As a result, our design is only applicable to these chrome extensions that not using jquery.

Design

In this section, we describe our privilege separation architecture for chrome extensions.

In our design, an extension has a common privileged master and an arbitrary number of unprivileged Web Workers [6]. The privileged master is loaded in every extension page before the extension is packaged. Each unprivileged Web Worker is created by the privileged master in each extension page and all JS files from an extension page execute in its own Web Worker. Since jquery library is invalid in a worker, our design is only applicable to those chrome extensions without using jquery. Figure 1 shows our proposed model for privilege separation.

Master. The master mediates all the privileged calls from the unprivileged Web Workers. The privileged master has four components:

(1) Startup Code. After the extension is loaded, the startup code begins to create a Web Worker and imports all the JS files hosted in the extension page into the worker.

(2) Master Shim. When the script code in a worker makes privileged calls to the privileged master in the extension page, the master shim is in charge of all the privileged calls on behalf of the workers and returns the required results to the corresponding workers.

(3) Policy Code. The policy code specifies what kinds of privileged operations the worker code can ask the master to perform. It is application-specific. The developers can add additional essential restrictions on these extensions or modify some privileges.

(4) Proxy. Since the Web Workers do not have access to DOM, we have to virtualize the DOM （VDOM）[6]. The proxy is in charge of disposing the DOM modification messages from workers.

Workers. Our system moves all functional JavaScript files from different components of an extension to Web Workers. Each worker consists of three components:

(1) JavaScript Code. JavaScript code means the JavaScript files that render operations from the extension page, e.g., popup.js and other JavaScript libraries the page needs.

(2) Worker Shim. The worker shim consists of a wrapper module. It wraps all the privileged functions. When a call is invoked, its corresponding wrapped function marshals the function as a message and posts this message to the master. On receiving respond from the master, the worker shim also deals with the execution of the callback with the results to complete the original call.

(3) Monitor. Since workers have no access to the real DOM, the monitor is in charge of 1) exporting to the Web Worker a Virtual DOM (VDOM) [6], 2) listening to the VDOM modifications, 3) applying the modification events to the master. The VDOM can be implemented by *Jsdom* [9], a JavaScript implementation of the DOM. Besides, we also use the libraries *underscore* and *RequireJS* to complement the JavaScript functionality. The VDOM contains subtrees of the real DOM (the extension's JavaScript code decides which subtrees are used).

Implementation

To integrate our design into a chrome extension, before an extension is packaged, the developer needs to include the master code as a JavaScript file inside every extension pages. When the packaged extension loaded, the startup code in every page creates an unprivileged Web Worker respectively and executes the extension script code in it.

In this section, we focus on the procedure of implementing a privileged call and DOM modification.

(1) Implementing a privileged call. When a privileged API (e.g., chrome.tabs.getSelected) is called, its wrapped function begins to executes, which asks the master to perform the correct function by 1) marshaling the privileged function name and all its arguments as a message, 2) saving the privileged function's callback in

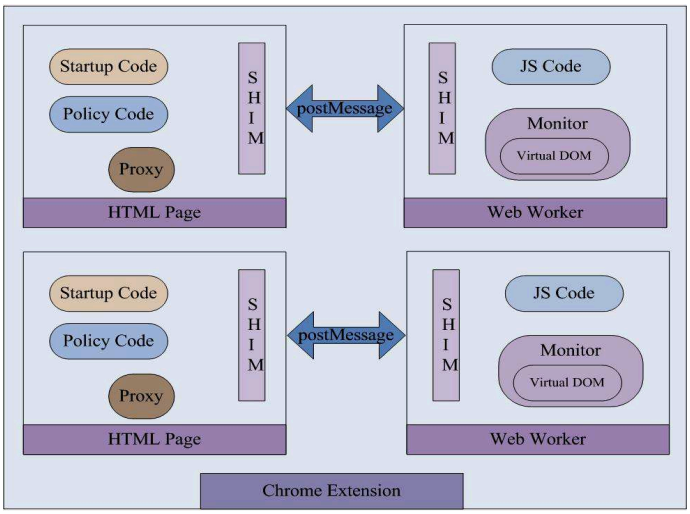

Figure 1: High-level of our architecture

an array, 3) sending the messages to the master, 4) waiting for respond from the master, 5) executing the saved callback with the parameters from the master. Listing 1 is the wrapped function for the chrome.tabs.getSelected.

On receiving a message from a Web Worker, the master shim 1) demarshals the message from the worker, 2) checks with the policy code to see if the call is allowed, 3) executes the correct function if allowed, 4) marshals the results as a message, 5) sends the message back to the worker. Listing 2 shows the master shim for the chrome.tabs.getSelected.

(2) Implementing a DOM modification. When the VDOM is modified, the monitor 1) serializes the events, 2) marshals it as a message, 3) sends the message to the master using postMessage.

Upon receiving this message, the proxy 1) demarshals the message, 2) deserializes the modification event, 3) applies the modification event to the real DOM.

Examples

We apply our design to two chrome extensions to demonstrate that our architecture is efficient enough in privilege separation.

In the two examples we measure (a) the reduction in TCB after using our architecture, (b) the amount of code need to be changed in order to retrofit the application, and (c) performance overheads (load latency, communication time, the interposition time by policies, and memory consumption). Table 1 lists our examples and summarizes our results.

TabJump. We apply our design to a chrome extension called TabJump, which can help a user to easily access most used tabs, associated tabs, and closed tabs, and allow a user to lock the current tab in case of accidentally clicking the close button. This extension has two components: background.html and popup.html. The functionality of background.html is to get tabs information, consisting recently closed tabs, related tabs, and frequently used tabs, then send these tabs to popup.html; when a user click the TabJump button, popup.html opens, which shows all these tabs' link and provide the lock feature.

(1) Unbundling and Example Policy: In the original version of TabJump, popup.html receives the tabs information from background.html and allows users to open, update, or lock these tabs, but runs with full privileges of the extension. Under our design, the popup.js code runs within an unprivileged worker and the policy only gives the popup.js access to the sendMessage API to send and receive the

tabs information from the background page as well as only tabs.create, tabs.update, tabs.getSelected and tabs.getAllInWindow chrome APIs.

PanicButton. PanicButton is a chrome extension that can be used to hide all tabs in the browser just clicking the hide button and restore them by another click. This extension has three components:

```
chrome.tabs.getSelected=function(windowId,callback){
                    var callbackctr = -1;
                    if(typeof callback !== 'undefined'){
                            callbackctr = callbackID++;
                            cached_callbacks[callbackctr] = callback;
                    }
                    var temp = {"type":"chrome.tabs.getSelected",
                                "callbackid":callbackctr,
                                "windowId":windowId};
                    postMessage(temp);
                    };
```

Listing 1: Wrapped function for chrome.tabs.getSelected

```
var msg=event.data;
  if(!policy.allowcall(msg)){return;}
    if(msg.type===" chrome.tabs.getSelected" )
      {
        chrome.tabs.getSelected(msg.windowId,function(tab){
            postMessage({ "type" :" cb_chrome.tabs.getSelected" ,
                          "callbackid" :msg.callbackid,
                          "tab" :tab});
        });
      }
```

Listing 2: Master shim for chrome.tabs.getSelected

background.html, popup.html and options.html. The functionality of background.html is to hide or restore all tabs; a user also can set a shortcut for this button and set a password to manage these hidden tabs in options.html. When a password is set, a user must enter the password in the popup page to restore these hidden tabs.

(1) Unbundling and Example Policy: This extension uses options.html to set a shortcut for the hide button and enter a password in the popup.html to manage the hidden tabs. But these two pages have full privileges of this extension. In our architecture, popup.js and options.js execute in different unprivileged Web Workers, the policy only gives the popup page the privilege to call sendMessage API and the options page the privileges to call chrome.tabs.create and sendMessage APIs.

Evaluation

Our approach has four possible overheads: 1) latency of loading Web Workers; 2) the overhead caused by the parent's mediation on privileged APIs; 3) the overhead on each call crossing the sandbox boundary; 4) the memory consumption of the redesigned extensions. We measure the impact of each below.

Latency. To measure the time overhead, we include two scripts in an extension page's different places, measuring the time elapsed between them. For example, one script is in the page's header and the other at the end of its body to measure the load latency. We perform 10 runs in each extension page, using the JavaScript's Date.now() API to collect the average time . For TabJump, the background load latency is about 319ms, and the VDOM size is 9 KB with 61ms to populate it. The average time on each call crossing the sandbox boundary is about 14ms, and with 13 lines of policy code, the average interposition time is less than 1ms.

As shown in Table 1 and Table 2, without VDOM, our extension runs nearly at a local speed; even with VDOM, we do not observe any user-perceivable increase in latency. The VDOM population time is affected by its size more or less. However, unless the chrome extensions spend most of its time in DOM operations and the VDOM size is not too big, and the total overhead should be tolerable.

Memory. We evaluated the memory overhead by observing the increase in memory consumption caused by creating web workers. We found that with the two extensions, the memory increase is 2.8M and 2.3M respectively. We believe that this level of overhead should be acceptable to enforce privilege separation in chrome extensions. Besides, it's up to a user to close these Web Workers after the chrome extensions exit, since it will not be automatically garbage collected.

Conclusion

We propose a new design that uses Web Workers to partition a web application into an arbitrary number of unprivileged components. Our evaluation shows that we can apply our architecture to most chrome applications and achieve significant reduction in TCB with no more than 18 lines of change for the chrome extensions we studied. However, those extensions that use jquery library do not fit with our model.

Acknowledgements

This research was supported in part by the National Natural Science Foundation of China under grants 61272190 and 61173166, the Program for New Century Excellent Talents in University, the open research fund of Zhejiang Provincial Key Lab of Data Storage and Transmission Technology, Hangzhou Dianzi University（No. 201302）

Reference

[1] HTML5 living standard. http://www.whatwg.org/specs/web-apps/current-work/multipage/.

[2] Google Inc., “Google chrome webstore.” https://chrome.google.com/webstore/.

[3] A. Krishnamurthy, A. Mettler, and D. Wagner. Fine-Grained Privilege Separation for Web Applications. In Proceedings of the International Conference on World Wide Web, pages 551–560, 2010.

[4] A. Barth, C. Jackson, C. Reis, and T. G. C.Team, “The security architecture of the chromium browser,” 2008.

[5] Privilege Separation in HTML5 Applications, Devdatta Akhawe, Dawn Song, Prateek Saxena, 2012.

[6] TreeHouse: JavaScript sandboxes to help Web developers help themselves, Lon Ingram, Michael Walfish, 2012.

[7] N. Carlini, A. P. Felt, and D. Wagner, “An evaluation of the google chrome extension security architecture,” in Proceedings of the 21st USENIX Conference on Security, 2012.

[8] http://en.wikipedia.org/wiki/Trusted_computing_base

[9] https://github.com/tmpvar/jsdom.

Advanced Materials Research Vols. 989-994 (2014) pp 4680-4683
© (2014) Trans Tech Publications, Switzerland
doi:10.4028/www.scientific.net/AMR.989-994.4680

Bayesian Inference of Information Theoretic Metrics of Anonymity

Han-Ru Pei[1], Zhi-Jian Wang[1] and Yu Wang[1]

[1]College of Computer and Information, Hohai University, China

Keywords: Bayesian inference, Anonymity, Anonymous Communications, Metrics

Abstract Information theoretic metrics is popular theory to measure anonymity. However the difficulty in getting the probability distribution of subjects hampers its practical usage. In this paper we propose a Bayesian inference method to tackle this problem. Our method makes it possible to compare the anonymity of different anonymous systems. We use this method to analyze Threshold Mix and point out different system parameters which do and do not have influence on anonymity.

Introduction

Metrics of anonymity has long been a hot research area. Metrics of anonymity is the quantitative analysis of the degree of anonymity provided by an anonymous communication system. It's used to evaluate the security of anonymous communication technologies. Information theoretic metrics [1] [2] has been widely acknowledged since its inception. However, there are some obstacles in utilizing this theory, among which is one of its assumptions that attackers can build a probability distribution of all subjects using the system. This distribution is very difficult if not impossible to get in practice. In this paper, we propose a method to systematically solve the problem. We first build a statistical model of anonymous communication being studied. By utilizing Bayesian inference and sampling technology, we then get a sampling probability distribution of subjects which can be applied to information theoretic metrics of anonymity.

The remaining paper is organized as follows: we introduce how to measure anonymity using Bayesian inference in section 2; section 3 is experiments and evaluations where we describe our experiment setup in detail and discuss the results; we conclude in the last section.

Anonymity Metrics using Bayesian Inference

Threat Model. We use Mix [3] to provide anonymous communication service; we only focus on traditional Threshold Mix. The attacker is a Global Passive Adversary (GPA) [4]. The attacker is able to monitor all links and connections during the lifetime of the system, intercept and record the metadata of traffic. The attacker is unable to modify, block and replay recorded traffic.

There are N_{mix} mixes (servers) providing anonymous service and N_{user} users using the system. There is also a GPA monitoring the system. Mix works by storing and forwarding users' messages. Messages are flushed in a batch when a mix received N_{t} messages. Mix obfuscates the messages by some cryptographic operations to ensure the attacker cannot find out the relationship between messages it receives and sends. Mixes can be cascaded to further improve security. When a user starts to use the system, first she chooses a user among the $N_{\text{user-1}}$ users as her communication partner. Then she determines the path length L where $L_{\min} \le L \le L_{\max}$. L mixes are selected randomly next to form a cascade path P. Finally her message is sent through the path to its receiver anonymously.

Bayesian Inference Overview. Let's assume an abstract anonymous communication system C. Its traffic flow is composed of observed data O and a set of unobservable hidden states H. The attacker is interested in H. By applying Bayes' rule, we can compute the probability distribution of H:

$$\Pr(H \mid O, C) = \frac{\Pr(O, H \mid C)}{\Pr(O \mid C)} = \frac{\Pr(O \mid H, C) \times \Pr(H \mid C)}{\sum_H \Pr(O, H \mid C) = Z} \tag{1}$$

In theory, knowing how C – the anonymous communication system – works is all we need to perform analysis by utilizing Bayesian inference technique. In practice however, $\Pr(H \mid O,C)$ is hard to compute directly due to the immense number of possible hidden states H. We have to resort to Markov Chain Monte Carlo (MCMC) methods to approximate $\Pr(H \mid O,C)$.

MH Algorithm Overview. It has been noted before that the aim of the attacker is to find the probability of sender S_x corresponds to receiver R_y given observations O and constraints C. This problem can be transformed to the problem of finding the probability of input corresponds to output of every mix in the system, notated as H. Unfortunately, for complex systems, it is infeasible to enumerate all H . We know $\Pr(H \mid O,C) \propto \Pr(P \mid C)$, so this problem can be transformed again to the problem of finding the probability of any possible path in the system. We use MH algorithm [5] to get path samples. For any sender S_x and any receiver R_y, we approximate:

$$\Pr(S_x \to R_y \mid O,C) = \Pr(H \mid O,C) \propto \Pr(P \mid C) \approx \frac{\sum_{i \in N_{\text{sample}}} \mathrm{I}_{S_x \to R_y}(\text{Sample}_i)}{N_{\text{sample}}} \tag{2}$$

where Sample_i is one separate sample from the sample set. N_{sample} is the sample size. $\mathrm{I}_{S_x \to R_y}$ is an indicator function on whether S_x corresponds to R_y in the sample.

We randomly choose an initial state MH_0. Then we do random walk on the Markov chain until we get a steady state which correctly reflects our target distribution, that is $\Pr(P)$. Two transform functions are defined. T_1 doesn't change current state. Current state will be the candidate state. T_2 randomly exchanges two inner links of a mix. The proposal distribution of MH algorithm depends on the transform functions as well as the probability of choosing which transform function. Clearly, $\Pr(T_1)+\Pr(T_2)=1$. Proposal distribution is defined as follows:

$$\mathrm{Q}(MH' \mid MH_j) = \begin{cases} \Pr(\mathrm{T}_1) & \mathrm{T}_1 \\ \Pr(\mathrm{T}_2) \times \dfrac{1}{|\mathrm{Mix}|} \times \dfrac{1}{N_t} \times \dfrac{1}{N_t - 1} & \mathrm{T}_2 \end{cases} \tag{3}$$

Given current state MH_j, proposal distribution Q and candidate state MH', we determine whether to accept candidate state as the next state:

$$\alpha = \frac{\Pr(MH') \times \mathrm{Q}(MH_j \mid MH')}{\Pr(MH_j \mid \times \mathrm{Q}(MH' \mid MH_j)} \tag{4}$$

If $\alpha \geq 1$, MH' is accepted as the next state; otherwise MH' is accepted as the next state with probability α.

Entropy Anonymity Sampling. For any sent message S_x, let the distribution of N possible corresponding received messages R_y(y=1,2,…,N) be Φ_x, the entropy anonymity of message S_x is:

$$H(\Phi_x) = -\sum_{y=1}^{N} \Pr(S_x \to R_y) \times \log_2 \Pr(S_x \to R_y) \tag{5}$$

It should be emphasized that the distribution from Eq. (2) is only the sampling distribution of Φ_x which is derived from paths data from samples, rather than the actual distribution of Φ_x. There may be paths haven't been sampled that have non-zero probability. We resort to Bayesian inference again to evaluate Φ_x. We model Φ_x as a multinomial distribution of R_y. In Bayesian statistics, Dirichlet distribution is a conjugate prior of multinomial distribution. For a given S_x, we assume the attacker has no prior knowledge about R_y, i.e., the prior distribution of Φ_x is Dirichlet(1,1,…,1). We define an auxiliary function $\mathrm{C}(S_x \to R_y)$ which equals the number of samples in which S_x corresponds R_y. Thus the posterior of Φ_x is:

$$\Phi_x \sim \text{Dirichlet}(\mathrm{C}(S_x \to R_0)+1, \mathrm{C}(S_x \to R_1)+1, ..., \mathrm{C}(S_x \to R_N)+1) \tag{6}$$

We retrieve N_D samples per Eq. (6). For each sample, we compute its sampling entropy anonymity $H(\Phi_x)$ according to Eq. (5). We order N_D $H(\Phi_x)$ in decreasing order and take the bounds the anonymity offered by system as the confidence interval of S_x.

Experiments and Evaluations

Experiment Settings. We use effective anonymity set size [1] as the tool to measure anonymity. Since this metrics doesn't normalize, a busy system is sure to have a higher degree of anonymity than an idle system. In order to eliminate this factor, experiments are being conducted under identical number of messages, which is 50. We conduct three experiments which test the anonymity implications of three different parameters, namely the number of mixes N_{mix}, the threshold N_t and the maximum path length L_{max}. They are summarized in Table 1.

Table 1. Experiment Parameters

	Exp1	Exp2	Exp3
N_{msg}	50	50	50
N_{mix}	**3-8**	5	5
N_t	3	**3-8**	3
L_{max}	3	3	**1-5**

N_{obs}=10 observations of message flow in the system are randomly generated for each experiment. For each observation, we get 500 path samples. For every sent message S_x, we record the number of times received messages in samples R_y (y=1,2,…,N_{msg}) correspond to it as C($S_x \rightarrow R_y$). We generate 1000 samples from the posterior distribution Dirichlet(C($S_x \rightarrow R_y$)+1) (y=1,2,…N_{msg}) of $S_x \rightarrow R_y$. We calculate the entropy anonymity of every sample. We then order the results in decreasing order to find the 95% confidence interval of message S_x. We repeat the above steps for every message in every observation and get N_{msg}*N_{obs} confidence intervals. We average on the upper and lower bound of intervals as the final 95% confidence interval of anonymity the system provides.

Results and Evaluations. Since the number of messages is fixed at 50, its maximum entropy is $\log_2 50 \approx 5.644$. There are three graphs below plotting the 95% confidence interval of entropy anonymity under 3 different parameters. H(min) and H(max) are the upper and lower bound of intervals. We can see from the left part of Fig. 1 that N_{mix} has little impact on the entropy anonymity. For N_{mix}=3 and N_{mix}=8, the entropy only increased from 2.844 to 3.104. In other words, by adding 5 mixes, the effective anonymity set size only increased $2^{3.104} - 2^{2.844} \approx 1.4$.

From the right part of Fig. 1 we can see that N_t has significant impact on the anonymity. For N_t equals 3 and 8 respectively, the entropy increased from 3.061 to 4.106. The effective anonymity set size increased by approximately 8.9. When N_t becomes larger, the mixes have to store more messages before flushing them. Also messages will be delayed for more time. So by increasing N_t, we get better anonymity with the price of worse delay and more storage resources.

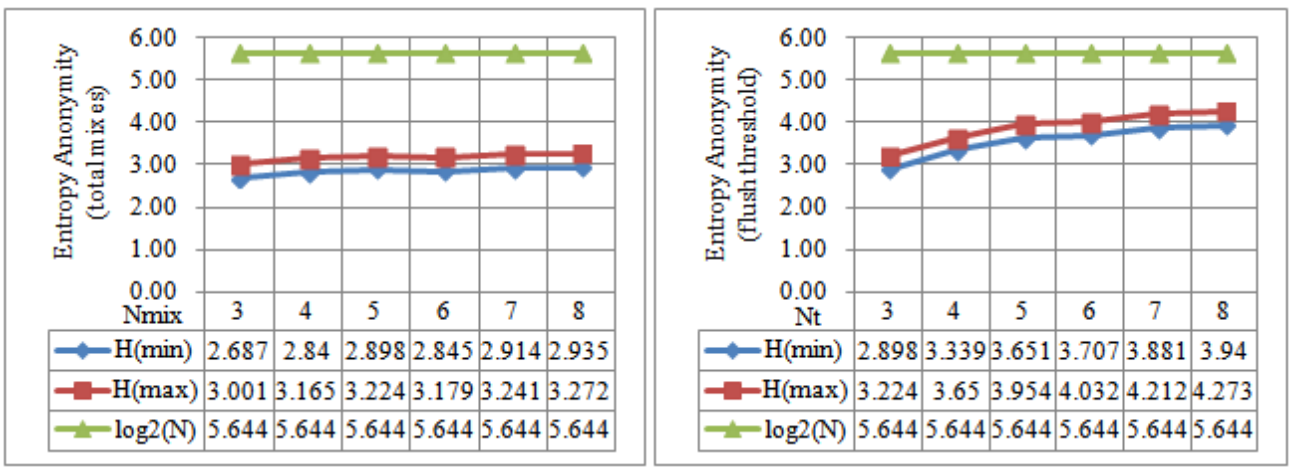

Figure 1. Entropy anonymity under different total number of mixes (left) and different flush threshold (right)

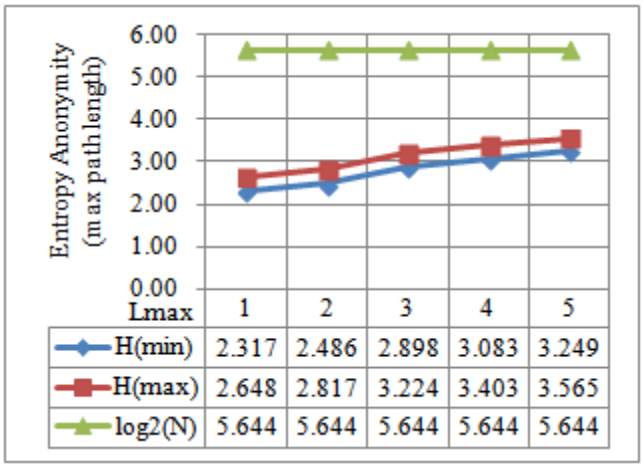

Lmax	1	2	3	4	5
H(min)	2.317	2.486	2.898	3.083	3.249
H(max)	2.648	2.817	3.224	3.403	3.565
log2(N)	5.644	5.644	5.644	5.644	5.644

Figure 2. Entropy anonymity under different path lengths

We find from Fig. 2 that L_{max} also has obvious impact on the anonymity. When L_{max} is 1 and 5 respectively, the entropy increased from 2.482 to 3.407. The effectively anonymity set size increased by approximately 5.0. As with larger N_t, larger L_{max} also increases message delay. Besides, larger L_{max} means more mixes are involved in the activity a message travelling though the system, this adds up to the whole load of the system. So by increasing L_{max}, we have better anonymity with the price of worse delay and more computation resources.

Conclusions

The main contribution of our work is the proposal of a Bayesian framework to measure anonymity. The framework is composed of three steps. First we built a probability statistical model of the anonymous communication system under study. Second we simulated the running of the system, got the path samples of messages in the system, and computed the probability distribution of all senders and receivers in the system. Since what we got is statistical distribution rather than actual distribution, we sampled the results of second step again and finally were able to measure the system under study. We used this method to analyze Threshold Mix. We found that different threshold and different path lengths have significant influence on the anonymity of the system. We also found that contrary to common knowledge, more mixes in the system only has neglectful influence on the anonymity.

Acknowledgements

This study is co-sponsored by Project The key technologies research of information metadata applications based on volunteer computing (NSFC NO.61103017), The Internet of things in Jiangsu Province demonstration "The intelligent environment monitoring of water and emergency treatment demonstration project and standardization construction" 2011.12-2013.1(Su property industry NO.[2011]209) and The Natural Science Foundation of Jiangsu Province BK2012807.

References

[1] A. Serjantov and G. Danezis, "Towards an Information Theoretic Metric for Anonymity," in *Proceedings of Workshop on Privacy Enhancing Technologies (PET 2002)*, San Francisco, CA, USA, 2002, pp. 259–263.

[2] C. Díaz, S. Seys, J. Claessens, and B. Preneel, "Towards Measuring Anonymity," in *Proceedings of Workshop on Privacy Enhancing Technologies (PET 2002)*, San Francisco, CA, USA, 2002, pp. 184–188.

[3] D. L. Chaum, "Untraceable Electronic Mail, Return Addresses, and Digital Pseudonyms," *Commun. ACM*, vol. 24, no. 2, pp. 84–90, Feb. 1981.

[4] J.-F. Raymond, "Traffic Analysis: Protocols, Attacks, Design Issues, and Open Problems," in *Proceedings of Designing Privacy Enhancing Technologies*, 2000, pp. 10–29.

[5] W. K. Hastings, "Monte Carlo sampling methods using Markov chains and their applications," *Biometrika*, vol. 57, no. 1, pp. 97–109, Apr. 1970.

Advanced Materials Research Vols. 989-994 (2014) pp 4684-4689
© (2014) Trans Tech Publications, Switzerland
doi:10.4028/www.scientific.net/AMR.989-994.4684

Software safety analysis based on Multiple state transition

YuLong-Wang [1, a], JinLong- Xiao [2,b], YuKun-Liu[1,a], TianQi- Li [1,a] , Wei Wu [1,a]

[1] Information Center of north china industry group corp ,BeiJin, china,100089

[2] Jinshan branch of shanghai public security bureau,shanghai, china,200540

[a] yulongwangmr@163.com, [b] xiaojinlong@21cn.com

Keywords: multitasking; software failure model; high-risk ; military software

Abstract. At present, existing methods are difficult to analyze the Safety of Multitasking and complex timing sequence software. In order to overcome this difficulty, a new analysis method of multiple state transfer and real-time logic analysis method (MSTRT-TPN) is proposed. This method extends the time Petri net analysis rules and proposes the concept of synchronous synthesis and sharing synthesis. It combines temporal logic and state transition, establishes software failure model. Through the model, the possibility of high-risk state of software can be analyzed. The effectiveness of the proposed method is verified through application in three protection device software which is typical safety-critical military software.

Introduction

With the development of weapons intellectualization and information, software has become an indispensable part of tank and armored vehicle equipment, helicopters, artillery and so on. And with the increase of military software function, software data flow and control flow are becoming more complex.

At the same time, the major accidents caused by the failure of the software are becoming more and more. Software security not only seriously affects the weaponry operational effectiveness, but also disastrous consequences, which causes the loss of our personnel casualty and equipment. The key of military software security research has become an urgent problem.

Software safety definition in academia has several different versions. The military standard GJB142-2004 defines software safety "The software has the ability, which does not lead to accidents". It emphasizes two aspects. On the one hand, software safety is the decomposition of the system safety, due to system security. On the other hand, software safety closely associated with the hardware, because software shows failure through hardware. Software alone is not an accident。 Software safety is different from security and software reliability.

Safety analysis methods include the fault tree analysis, *SFMEA* and *Petri* etc.. These methods have certain help for software safety analysis which are single task or a serial task , but there are some difficulties on the analysis of multitasking software safety. This paper puts forward a kind of new analysis method which provides an effective way to solve this problem.

The principle of TIME Petri nets

Petri network is an information flow model of mesh structure, it describes the relationship between conditions and events. The Petri net is composed of five parts :

$\phi = (P, T, I, O, \mu)$, Among them, $P = \{p_1, p_2, ..., p_m\}$ is a finite set position, $T = \{t_1, t_2, ..., t_n\}$ is a finite set of transfer; I: $T \to P^{\infty}$ is the input function by transfer to the location package (from P to T directed arc); O： $T \to P^{\infty}$ is the output function from the transfer to the position package (from T to P directed arc); Mark μ is assigned to a set of tokens in the Petri network, $\mu : P \to \{0, 1, 2, ...\}$ is a function from the position set P to the non negative integer N

A Petri network structure can be used in an equivalent Petri net picture to express. In the Petri network, "O" indicates the position, "1" indicates transfer,Twhe position and transfer connect through directed arc. Token is represented by "• ". The mark is used to represent the distribution state of

the token. By the ignition of the transfer and position change of the token, Petri nets describe the system dynamic behavior.
It finds out the conflicting state and analyzes the causes according to the operating results.

MSTRT-TPN MODEL

A. The definition of single task time Petri nets

Definition 1.1: If $\varphi=(P,T,I,O,\mu)$ is a Petri net (PN), $P=\{p_1,p_2,...,p_m\}$, $p_i=(b_{i1},b_{i2},...,b_{ik})$, Among them $b_{ij}=0,1(j=1,2,...,k;\ i=1,2,....m)$ .When Transfer $t_i\in T$,Transfer conditions is as follows.

The input domain :

$$t=(p_{i_1},p_{i_2},...,p_{i_r})=\begin{pmatrix}(b_{i_1}1,b_{i_1}2,..b_{i_1k}),\\(b_{i_2}1,b_{i_2}2,..b_{i_2k}),\\...,\\(b_{i_r}1,b_{i_r}2,..b_{i_rk})\end{pmatrix} \quad (1)$$

The output domain:

$$t=(p_{j_1},p_{j_2},...,p_{j_r})=\begin{pmatrix}(b_{j_1}1,b_{j_1}2,..b_{j_1k}),\\(b_{j_2}1,b_{j_2}2,..b_{j_2k}),\\...,\\(b_{j_s}1,b_{j_s}2,..b_{j_sk})\end{pmatrix} \quad (2)$$

The transfer occurred right (i.e: T in μ initiative under) condition is: all input position of input domain have the same component 1, and the output position in the corresponding component is zero.

After $\mu[t>\mu']$ $\mu'(p_{i_ch})=(c'_{i_c1},c'_{i_c2},...,c'_{i_ck})$ Among them

$$c'_{i_ch}=\begin{cases}0 & c_{i_1c}=c_{i_2e}=...=c_{i_rk}=1\\ c_{i_ch}\end{cases} \quad (3)$$

$h=1,2,...,r$ output domain $\mu'(p_{j_d})=(b'_{j_d1},b'_{j_d2},...,b'_{j_dk})$

$$b'_{j_dh}=\begin{cases}1 & b_{i_1h}=b_{i_2h}=...=b_{i_sh}=0\\ b_{jdh}\end{cases} \quad (4)$$

$d=1,2,...,s\quad h=1,2,...,k$

This Petri net is named one-dimensional Petri Net of single-task (i.e: $MSTRT-PN$) , marked: $\phi_{k(0,1)}=(P,T,I,O,\mu)$

Definition 1.2: $\phi_{k(0,1)}=(P,T,I,O,\mu)$ is MSTRT-PN Net,

$$\Phi_{k(0,1)}=(P,T,I,O,Min,Max,\mu) \quad (5)$$

Then it is named one-dimensional time Petri net of single-task (i.e $MSTRT-TPN$) , $P=\{p_1,p_2,...p_m\}$, $T=\{t_1,t_2,...,t_n\}$, $p_i=(b_{i1},b_{i2},...b_{ik})$ among them, $b_{ij}=0,1(j=1,2,...,k\ \ i=1,2,...,m)$

$t_{i'}=((t^1_{i'1},t^2_{i'1}),(t^1_{i'2},t^2_{i'2}),...,(t^1_{i'k},t^2_{i'k}))\qquad i'=1,2,...,n$

, $(t^1_{i'j'},t^2_{i'j'})=(\mathrm{mint}_{i'j'},\mathrm{maxt}_{i'j'})\quad j'=1,2,...,k\quad i'=1,2,...,n$

Min and Max are respectively the minimum time function and time function.Transfer t_j t can be multiple times ignition.

The prerequisite is the existence of multiple components 1, and output the corresponding component position in the domain of zero

The rule of multiple times ignition:

1, $t_{i'}=((t^1_{i'1},t^2_{i'1}),(t^1_{i'2},t^2_{i'2}),...,(t^1_{i'k},t^2_{i'k}))$

If Each component is active and $\left(t_{i'1}^1, t_{i'1}^2\right) \cap \left(t_{i'2}^1, t_{i'2}^2\right) \cap \ldots \cap \left(t_{i'k}^1, t_{i'k}^2\right) = \phi$

Then ignition carried out according to the numerical size

2, If $\left(t_{i'1}^1, t_{i'1}^2\right) \cap \left(t_{i'2}^1, t_{i'2}^2\right) \cap \ldots \cap \left(t_{i'k}^1, t_{i'k}^2\right) \neq \phi$, Ignition carried out according to the numerical size of $t_{i'1}^2, t_{i'2}^2, \ldots t_{i'k}^2$;

If $t_{i'1}^2, t_{i'2}^2, \ldots t_{i'k}^2$ is equal Ignition carried out according to the numerical size of $t_{i'1}^1, t_{i'2}^1, \ldots t_{i'k}^1$;

3, If $\left(t_{i'1}^1, t_{i'1}^2\right) = \left(t_{i'2}^1, t_{i'2}^2\right) = \ldots = \left(t_{i'k}^1, t_{i'k}^2\right)$, Ignition carried out At the same time。

B. Sharing synthesis of Petri net operation

The synthetic operation is the synthesis of one-dimensional Petri network as a multi-dimensional network Through the method of sharing the synthetic operation or synchronous synthesis operation

There is a public transfer (or position) in subnet that is a prerequisite for synthesis applications. The public transfer (or position) can be one or more.

Definition 3.5 ： if $\phi_i = \left(P_i, T_i, I_i, O_i, \mu_i\right) \quad i = 1,2 \quad P_1 \cap P_2 \neq \phi$, $T_1 \cap T_2 = \phi$, then $\Phi = \left(P_1 \cup P_2, T_1 \cup T_2, I_1 \cup I_2, O_1 \cup O_2, \mu_1 \cup \mu_2\right)$ is named Sharing synthesis net of subnet ϕ_1 and subnet ϕ_2 [4]。marked： $\Phi = \Phi_1 C_P \Phi_2$

Sharing synthesis requires sub network have a common position, network system after synthesis connect the network through mutual position Sharing synthesis of

C.Sharing synthesis of Petri net operation

The synthetic operation is the synthesis of one-dimensional Petri network as a multi-dimensional network Through the method of sharing the synthetic operation or synchronous synthesis operation

There is a public transfer (or position) in subnet that is a prerequisite for synthesis applications. The public transfer (or position) can be one or more.

Definition 3.5 ： if $\phi_i = \left(P_i, T_i, I_i, O_i, \mu_i\right) \quad i = 1,2 \quad P_1 \cap P_2 \neq \phi$, $T_1 \cap T_2 = \phi$, then $\Phi = \left(P_1 \cup P_2, T_1 \cup T_2, I_1 \cup I_2, O_1 \cup O_2, \mu_1 \cup \mu_2\right)$ is named Sharing synthesis net of subnet ϕ_1 and subnet ϕ_2 [4]。marked： $\Phi = \Phi_1 C_P \Phi_2$

Sharing synthesis requires sub network have a common position, network system after synthesis connect the network through mutual position Sharing synthesis of network can be extended to subnet synthesis of more than two, When combined with the public part of the position, new sharing synthesis of net forms。

D. The synchronous synthesis operations of Petri nets

Definition 3.6：if $\phi_i = \left(P_i, T_i, I_i, O_i, \mu_i\right) i = 1,2$ $P_1 \cap P_2 = \phi$, $T_1 \cap T_2 \neq \phi$, then

$\Phi = (P_1 \cup P_2, T_1 \cup T_2, I_1 \cup I_2, O_1 \cup O_2, \mu_1 \cup \mu_2)$ is named synchronous synthesis net of subnet ϕ_1 and subnet ϕ_2 。marked： $\Phi = \Phi_1 C_T \Phi_2$ 。

Because they do not relate to the position synthesis, token set is not changed compared with the atomic。And the network system of synchronous synthesis can maintain some dynamic properties which system shared. For the complex system modeling, which can be divided into several simple subsystems, each subsystem is constructed one-dimensional model separately, then the whole model is obtained by computing the synthesis of Petri nets.

The establishment of MSTRT-TPN Model

MSTRT-TPN model is established as the following step :

1) Creating the system workflow including software system by Analysis system design documentation and user manual,

2)Writing each subsystem software flow chart. According to the system function realization condition to the state transition process, the task is divided into a number of process. Thus the software system is divided into several sub system (each sub system is a relatively independent).

3）Analysising the software flow chart, listing the process state of each subsystem, and then forming a software feature set。Naming each characteristic state set, determine its meaning, symbol name, scope, initial value

4) According to the time conditions and state transition conditions, each subsystem software characteristic state is organic combined, then a one-dimensional Petri network formed. Then extracting the intersection part of the software flow diagram and the system flow chart, as associated with the software interface of the system input or time conditions to the time Petri net, forming a one-dimensional software K_1 (0,1) -TPN. According to this method, the system of time Petri nets is established.

5）Subnet synthesis shared operation and synchronizing operation is carried. P and t of each subnet is merged to form of multidimensional k_n (0,1) –TPN.

6）Comparing with the actual application, checking Rules of modeling TPN model, including consistency, consistency and completeness.

7）According to the meaning of system symbol name, domain, the initial state, the transfer time threshold, recalibrating of the k_n (0,1) -TPN network

8）According to the actual physical background, The system risk is determined. the dangerous state, can be divided into three levels of risk. Dividing of the risk status classification can refer to GJB /Z 102 - 1997 [7]

9）reachability analysis of dangerous state. Given the network position variable and transfer the meaning of T and range table, get the state reachability graph and Petri net operating table by Petri network model, analysis of high, low risk; to pay attention to every high risk condition, the key state method [8] and the critical transfer node sequence analysis of the state in the back, and find out the key state; by analysis of high risk of path [9], the key reasons put forward high risk path

10）Analysis and modification of the problem. Aiming at the problem, put forward the improvement proposal, modify the system Petri net model.

Verification of engineering cases

A. Safety overview of Three protection device software

Protection device is a device for preventing nuclear, biological, chemical weapons, which is mainly used for the overall protection of tanks and armored vehicles. Through the establishment of high air pressure values in the car, it protects the occupant and vehicle parts which are not or less affected by nuclear radiation, biological, chemical weapon damage. It maximizes the occupant and vehicle survivability, avoides the occurrence of accidents. It is a safety critical software.

B. Safety analysis based on MSTRT-TPN

According to the MSTRT-TPN modeling steps, and combined with the protective device software mission profile, as shown in Figure 1 protection device four-dimensional MSTRT-TPN model.

Figure 1，P_{4i}（i=1…22），Subscript 4 represents the four-dimensional variable input, a represents the gas, B represents a nuclear explosion, C represents the radioactive contamination, D represents the fire. Abstract analysis of the protection device software features state of ZT={chemical gas type, concentration, working mode, actuator state}, the largest state in theory for 64 ={4 222 2}. But considering the actual logic system constraints and the characteristic state stultify oneself, can analyze the 48 state actually can not reach, the actual reachable state only 16.

The executive mechanism is the main hazard protection device. Danger is the executing agency error opening or drain opening, resulting in the potential accident. Risk analysis is to analyze the possibility which appear at the same time, alarm and no protection. In terms of software high risk refers to the warning condition and not the protection state of coexistence. Low risk is no warning and protection status coexist. The key state method

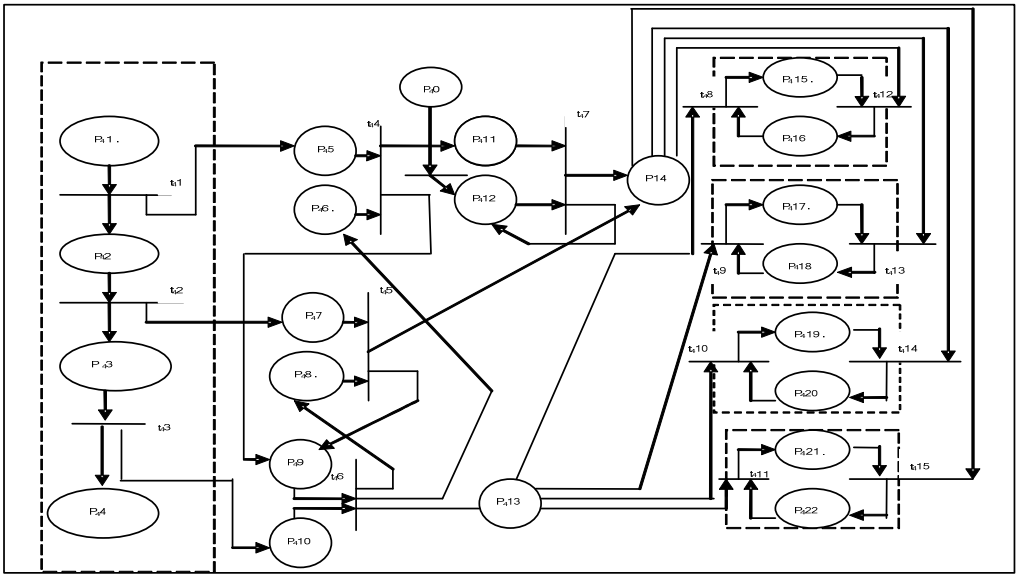

Figure 1 Time Petri net of Three Defense Control System

Using the key state analysis, the reachable state, there are several dangerous:

a. when there are more than 2 kinds of chemical weapons at once, the same execution mechanism is required in the two states which mutually contradictory, it is in a dangerous state.

b. when the alarm, protection mechanism is closed but not in the open state, can lead to casualties.

c. interlock status of P8 and P9 co existing state, it is not logical, not to protect the expected.

d. in manual mode, P411 can not alarm in a specified period of time, while the mechanism is not automatic implementation of protective measures, leading to dangerous state.

e. when the chemical weapons disappeared, protection mechanism not open and remain closed, resulting in low risk status

C. Problem analysis and improvement

In order to limit the high risk, time constraint method is applied to constrained sequence of occurrence, thereby limiting the unsafe state, Petri net model is modified as shown in Figure 2. The following solution is taken:

a, By modifying the software ,four kinds of alarm signal processing priority is added. Software alarmes according to the priority;

b. On the one hand, modify the code execution time (t44+t47+t412) which is less than T42, on the other hand, modify the Petri network, the requirements of T42 transfer ignition after transfer of t412, t413, t414, t415. This design ensures the safety interlock.

c. Modify the design of the software, to avoid the interlocked together.

d. The default state is set to automatic mode; when in manual mode, increase the timer interrupt in software, when in a specified time range no alarm, automatic alarm protective effect, and prompts the operator.

D. Safety analysis based on other methods

At the same time, other traditional methods of safety analysis also are used to analyze three protect software, Result contrasts are shown in Tab1.

Tab 1 Analysis results comparative table

analysis method	The number of software defect	cost of Time and manpower	Analysis ability of Multitasking and timing sequence
MSTRT-TPN	five	low	strong
Time Petri	four	high	middle
The fault tree	three	middle	poor
FMEA	two	middle	poor

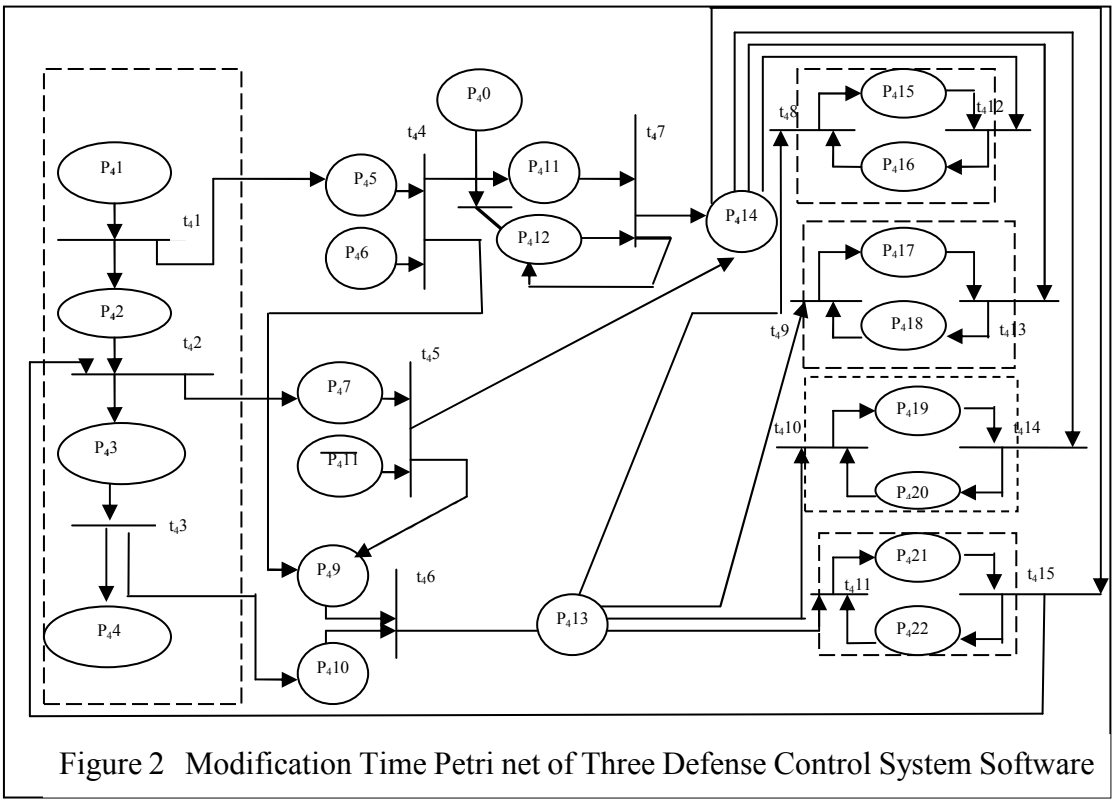

Figure 2 Modification Time Petri net of Three Defense Control System Software

Conclusion

Because of the lack of effective methods of software safety analysis and verification, it is a common practice to rely solely on the latter software testing. It led to pay too high price. We should propose more efficient methods to analyze software security. MSTRT-TPN is a good practice.It makes up the defects of traditional methods and improves the effect of the software security analysis.

References

[1] Li DeBao,Lu QiuHai.Engineering vibration test[M].Beijing:Tsinghua University press, 2004:250—255.

[2] Shi Yang,Liu GuangBin.The GPS digital satellites IF signal simulator design based on FPGA technology[J]. AEROSPACE CONTROL. 2007, 25(6)75-89.

[3] Zhao JunXiang.The study on mathematical model of high dynamic and intelligent GPS satellite signal simulator's software[D].Beijing : School of Electronics and Information Engineering, Beijing University of Aeronautics and Astronatics, 2003.

[4] Liu ShuShi, Tang Bing, Tang WeiTao. IF GPS signal simulator software implementation. 14th National remote sensing and control technology papers, 2011.

[5] Lei Dong,IF GPS Signal Simulator Development and Verification. December 2003.

[6] IS-GPS-200, Navstar GPS Space Segment / Navigation User Interfaces[S].USA: Navstar GPS Joint Program Office, 4 December 2004.

[7] WU You-nian. Invalidation mode research [D]. Beijing: School of Electronic Engineering,Beijing university of Aeronautics and Astronautics, 2007:45-65(in chinese).

[8] Wei JenYeh ,Michal Young. Compositional Reachbility Analysis using Process Algebra. In Proceedings ofthe symposium on Testing, analysis, and very- fication, pages 49–59, 1991.

[9] SONG Xiao-qiu, Software security analysis of Petri net method [D], China's Defense Science and Technology Report, Beijing: Aerospace software evaluation center 1998:32-38 (in Chinese).

Advanced Materials Research Vols. 989-994 (2014) pp 4690-4693
© (2014) Trans Tech Publications, Switzerland
doi:10.4028/www.scientific.net/AMR.989-994.4690

Security Framework based on SDN

Yang Yu, YuNan Wang and Wei Yang

School of Software Engineering of Beijing University of Posts and Telecommunications, Beijing, China

fishoutsider@gmail.com, wangyunan1992@gmail.com, danielxy0215@gmail.com

Keywords: SDN, Security, Framework, IDS, Firewall

Abstract. With the growing demand for information, it has a strategic importance for the future of sustainable development how to create a safe and robust network system to ensure the security of important information. Intrusion detection technology can proactively react against intrusion behavior and adjust its strategies in time. So it provides an effective means for network security to minimize or avoid loss when network system is attacked. It is an important part of network security system. This article first explains the current framework and the working principle of SDN. Then it explains the existing security threats of current framework. Next intrusion detection system based on SDN is proposed after the introduction of the intrusion detection system. And we made experiments to verify it. Finally we analyze the lack of the structure and propose some improvements.

Introduction

SDN consists of decoupling the control and data planes of a network. It relies on the fact that the simplest function of a switch is to forward packets according to a set of rules. However, the rules followed by the switch to forward packets are managed by a software-based controller.

The logical architecture of SDN is shown in Fig. 1. It consists of application layer, control layer and infrastructure layer.

According to the architecture, we can find that the most important feature of SDN is the use of a centralized approach to forward data. Even though the individual device fails, the entire network still has a very good performance. On the other hand, the openness and centralized management brings an urgent problem, the security problem. Meanwhile, the target of attack is now turned to the control layer and the application layer from physical device.

Traditionally firewall is the first line of defense security. Intrusion Detection System (IDS) makes network security defense more active. Therefore, we apply this technology to the emerging network architecture to resolve some security problems of SDN and make the SDN's architecture safer.

Existing problems of SDN

Major work of SDN:

1. Users define network control and network services network logically through software in application layer so that they can manage routes and network strategies.
2. Control layer receives call from upper layer through application-control interface and is responsible for controlling the forwarding equipment of the underlying intensively.
3. Infrastructure layer receives control message from control layer. It also can process and forward the date packages.

It can be found security needs mainly in the application layer and control layer.

Threats of control layer

1) Sniffer: The attackers forge and modify the signaling after getting network entry point of controller.
2) IP address spoofing: The attackers change the IP address of forged signaling to the controller's IP address through sniffer to defraud switches' trust so that they can destroy the network.

3) DDoS attacks: The attackers send multiple service requests to the controller until the controller refuse to provide services due to overload and all return addresses are forged.
4) Viruses, worms and Trojan attacks: The attackers obtain the control right of controller to execute malicious code through the vulnerabilities existing in the controller.

Threats of application layer

1) Malicious applications: The attackers can implanted worms and spyware applications in the application layer to interfere the normal work process in control plane, including stealing the network information, changing the network configuration, occupying the network resources etc.
2) Applications' safety rules conflict: Application layer need develop security rules to access some security interfaces for providing a wide range of network services. Safety rules conflict occurs between multiple applications because applications become more and more complex. It brings chaos to network services and make management more complicated.

Improvement of SDN framework

Most scholars believe that the current cumulative network security technology is fully capable of SDN security requirements, but we should also consider the following three questions:

1. How to implement traditional network security applications on the SDN architecture.
2. How to define the relevant API of SDN controller to achieve the above functions.
3. Select which network security applications implemented on SDN architecture

Through analysis of these three questions, we get a new framework for SDN.
The improved SDN framework is shown in Fig. 2. The deployment of the overall structure is shown in Fig. 3.

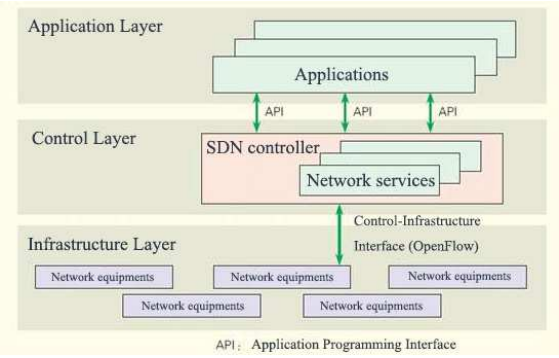

Fig.1 The logical aichitecture of SDN

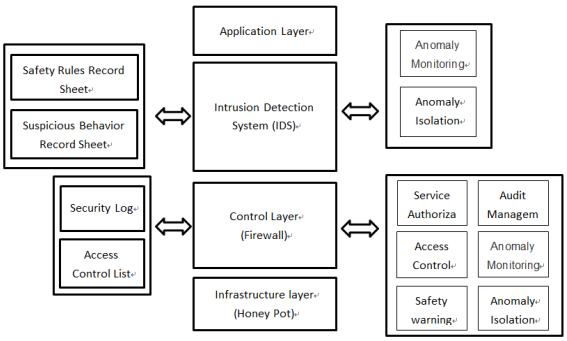

Fig.2 The improved SDN framework

Intrusion Detection System (IDS)

Rules of NIDS based on SDN

The rule is shown as follows: alert tcp 192.12.1.32 :80 -> 192.168.1.12 111
The first item is the conduct of the rule. It defines how the package should be handled when the package matches the rule. There are five default handling: alert, log, pass, activate and dynamic.
The second item is the agreement. The agreements that Snort can analyze are TCP, UDP and ICMP.
The third item is the IP address of the sender. It can be some IP or a range of IP address. It can be presented as 192.12.1.3:192.12.1.15.
The fourth item is the port number of the sender. It is just like the IP. There are three kinds of expression. 12 means the port 12. :80 means the port number can't be greater than 80. Similar, 80: means the port number can't be less than 80. The last one is 80:100, it means the port number must be between 80 and 100.
The fifth item is the direction operator. One-way operation (->) represents the flow direction of the data package. Two-way operation (< >) represents that the system should record and analyze the bi-directional data transferred between the two hosts.
Then they are the IP address and port number of the receiver.

Structure of NIDS based on SDN and functions of each part

It consists of three subsystems:

1) Capture and parsing subsystem
2) detection subsystem
3) log and alarm subsystem

The function of the capture and parsing subsystem is to capture data transferred on the network and parse the package according to different protocols.

Detection subsystem is the core of the IDS's implementation. Accuracy and speed are the important measures of its performance

The former mainly depends on the accuracy of summarizing the intrusion features and the practicality of rules. We should summarize the intrusion features as different eigenvalues of different field. Then we can determine whether the intrusion occurred through the eigenvalues. The latter depends on the organizational structure of the detection subsystem.

The log refers to the ability to promptly record in the simultaneous detection of intrusion. The alarm means the system can timely notice when an intrusion occurs.

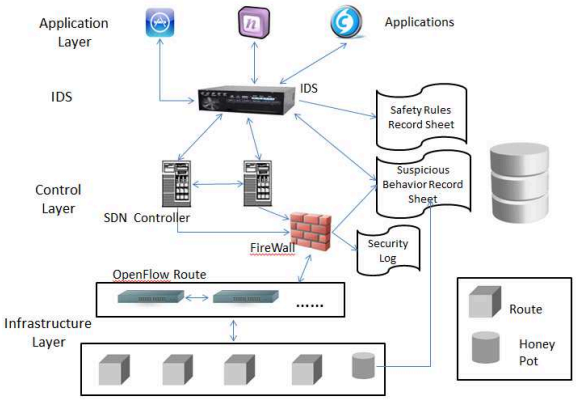

Fig.3 The deployment of the overall structure

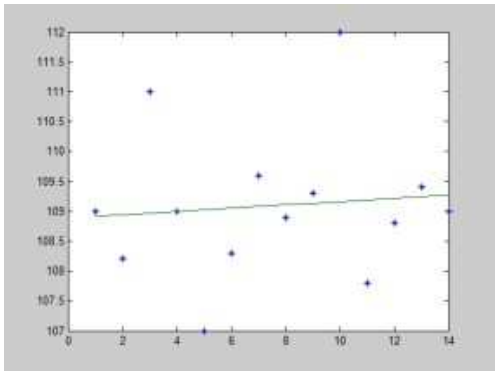

Fig.4 The delayed time's average value of different data packages' number under duplicating process

(Abscissa unit: dozens of data package; Vertical unit: millisecond)

Implementation and verification

Experiment environment

Operating system: Linux Fedora 18
CPU: Intel Core i7-2670QM
Main memory: 4GB
Open source SDN controller: Floodlight
Firewall: Linux Iptables
IDS: Snort

Verification procedures

1) Application layer send PACKAGE IN to Snort
2) Snort executes intrusion detection. If the data package is safe, send it to the controller of Floodlight.
3) Floodlight controller issues instructions to switch based on policy, and redirects PACKAGE IN to the firewall.
4) If the data package is legal, it will be forwarded normally. Otherwise, it will be handled according to the existing rules.

Experiments

We conducted two experiments. The first one is to test the delayed time of 20 times separately in the packet forwarding process and duplicating process and normal transmission process under the new structure. Then take the average of it. The second one is to test the delayed time of different data

packages' number under duplicating process. We also averaged the delayed time. Then we used Matlab to fit curve.

The result of the first experience is shown in Tale 1. The second experience's result is shown in Fig. 4.

Table 1 The average value of delayed time under different operations

Operation performed by the controller	The average value of delayed time (/ms)
Duplicating	1.796
Forwarding	3.656
Normal transmission	0.4526

Considering the results of two experiments, we can conclude that the delayed time won't increase at a high rate of speed with the increasing number of data packages. So when the number is small, the framework doesn't have too much advantage. But the framework may have a good performance when the number of packages is large. Nowadays, people's demand for information is increasing. And big data has become a hot research topic. So our frame can suit the future's network well.

Conclusion

This paper describes how SDN works and the security challenges of SDN. Then it introduces IDS and explains what the frame structure of IDS based on SDN should be and how to deploy. Finally we build environment through open source software and make experiences to verify the framework.

Obviously, there are still some deficiencies. I picked out the following urgent problems as the focus of the next phase of research.

1. IDS can only detect intrusions whose features have been existed in the datebase.
2. If we want to use data mining to obtain the features of intrusions in time. How to design data mining algorithms?
3. The loss of a package will affect the transmission of the file. So what can we do to improve the accuracy of detection.

So, in the next stage of the research, our main goal is to study mining algorithms to make the characteristics obtained through data mining as close to the real situation. And we need design safeguards to ensure proper packet forwarding rate.

References

[1] Qiu Xiaofeng, Zhao Liang, Gao Teng, VSA and SDS: A research of two kinds of network security architecture based on SDN [J], JOURNAL OF CHINESE COMPUTER SYSTEMS, 2013, 34 (10).

[2] Open Networking Foundation. Software-defined networking: the new norm for networks[R]. ONF White Paper, April 13, 2012.

[3] Chung-Shen, Liao Li, Wan Jiun. Software defined networks[J]. Communications Magazine, IEEE, 2013, 51(2): 113.

[4] Zuo Qing-yun, Chen Ming, Zhao Guang-song, et al. OpenFlowbased SDN technologies[J]. Journal of Software, 2013, 3(29): 1078-1097.

[5] Shin S,Gu Guo-fei. CloudWatcher: network security monitoring using OpenFlow in dynamic cloud networks (or: How to provide security monitoring as a service in clouds?)[C]. 20th International Conference on Network Protocols (ICNP), 2012: 1-6.

Advanced Materials Research Vols. 989-994 (2014) pp 4694-4697
© (2014) Trans Tech Publications, Switzerland
doi:10.4028/www.scientific.net/AMR.989-994.4694

Research of Application of 3D Pipeline in Mobile E-commerce

Zhang Jianqing[1,a], Wu Ping[1,a], Yu Tao[1,a], Cao Qianqian[2,a] and Xiong Feng[1,a]

[1] School of Mechatronics Engineering and Automation, Shanghai University, Shanghai

[2] E-commerce center, China mobile Shanghai Company ltd, Shanghai

[a]wuping526@163.com

Keywords mobile e-commerce; 3D Pipeline; nature of the pipeline; 3D Pipeline's application

Abstract. In recent years, the OTT (Over The Top) was very popular in the communications industry and the mobile Internet industry. The behavior of Internet companies such cross operators, to develop a variety of value-added services and products Internet-based or mobile-Internet-based poses a serious threat to the operators' benefits. In order to change this situation and enhance their competitiveness, it is necessary for the operators to find new interests growth point. So the concept of three-dimensional mobile operators is proposed, and the nature of the pipeline, such as systematicness, spatiality and openness were studied. Finally, the application of 3D pipeline in mobile e-commerce is researched.

Introduction

In recent years, the OTT (Over The Top) concept is very popular in the communications industry and the mobile internet industry. This word comes from basketball and other sports, which means that the ball players pass the ball to another to make it reach the destination back and forth over their heads [1]. Now it refers to the internet companies across the operators to develop value-added services and products based on internet or mobile internet, reflecting the independence of the services in the internet or mobile internet environment and the physical network of operator [2].

Currently the OTT services appear extensively in the field of ICT, for example abroad such as Google, Apple, Skype, Netflix, domestic as Tencent and other companies use the operator's broadband network to develop their own business, such as Apple relying on its smart terminal iPhone, iPad, ITV launch of the iTunes App Store services, voice services provided by Skype, Tencent QQ and WeChat business and so on. The OTT service providers directly provide services to users and charge, enabling operators to become mere 'transmission channel' and cannot obtain benefits which correspond to their heavy investment. It also constitutes a certain threat to the operators' future development [3][4].

Facing the rapid development of OTT services, how to deal with it and achieve transformation has become a key to the operator. 3D pipeline is advanced to avoid mobile operators to become mere "transmission channel" and to seek new growth points of interest, while the realization of restructuring and development.

3D Pipeline

The concept of 3D pipeline. The term of pipeline mostly appears in the industry, and is given its national standard concept in the industry, which is composed of piping components, pipe hangers and other components for transmission, distribution, mixing, separation, discharge, measurement or control fluid flow [5]. Now we have to define the pipeline in the eyes of operators, combined with the operator's industry characteristics, it can be defined as an invisible virtual pipeline for transporting wireless network signals to achieve connection between people.

In the traditional era, the operator's pipeline means voice channels, message pipes and traffic pipes, but with the mobile internet era comes, the traditional pipeline is no longer applicable and will hinder the development of operators, so the operators are in urgent need of transformation. The mobile internet with its characteristics of 'mobilize', 'randomization', 'fragmentation' and 'trust'

becomes a strongly support to the operator to achieve the transformation and increase capacity. Thus, for purpose of fitting the development of mobile e-commerce, the operator proposes a 3D pipeline theory, which is constituted by the connection pipe connecting the enterprise with the operator, channel pipeline providing service for sales and intelligent pipeline managing traffic intelligent.

The nature of 3D pipeline.

1) systematicness

3D pipeline is a system, more precisely, it is an associated pipeline system which consists of three dimensions pipelines. Thus, 3D pipeline has the relationship of the system theory.

The relationship refers to the three dimensions pipelines relating to each other. Only after offering the merchants to come together in the poly platform, it can establish a more generalized cloud sales channel; last the intelligent traffic management is a more commercial value after customers reaching a certain size.

2) spatiality

3D pipeline mainly consists of three dimensions in space,

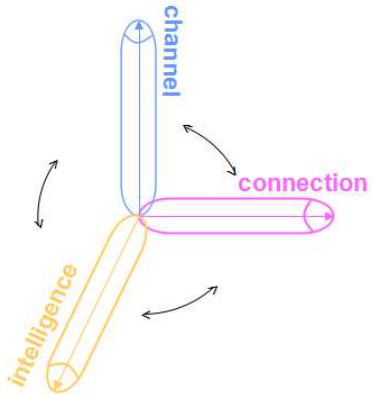

Fig. 1 The spatiality of 3D pipeline

① Connectivity, 3D pipeline connection dimension provides an access to all kinds of businesses, instead of building B2C system by themselves, the merchants can put their goods in the mobile e-commerce platform built by mobile operators, then they are provided display of all kinds of SKU, sales(pre-sale), order, warehouse, logistics (sale) and other after-sales service.

② Cloud Channel, it provides SMS services, ability opening up and distribution in sales channels to merchants. After the Connectivity solves the problem of the merchants to quickly access, the operators help businesses get through customer-oriented services and sale channels by generalization capability.

③ Intelligent, after merchants completing access, settled and sales, the intelligent dimension provides further flow data analysis based on intelligent pipe and decision support capabilities to help businesses better understand customers' behavior and better serve customers. This is a unique characteristic of the operators of mobile e-commerce model.

3) Openness

3D pipeline exists in a certain network environment (such as 2G, 3G, 4G, etc.), so it inevitably exchanges data and information with the other systems in the network. And in the process of exchange, 3D pipeline will experience the dynamic development process which is from junior to senior, from simple to complex and continuously optimized. In order to better realize the self-renewal and self-improvement, 3D pipeline must have a good foreign scalable and open interface.

3D Pipeline's application in mobile e-commerce

The application model of 3D pipeline consists of three parts, shown in figure 2, from the enterprise merchants settled, operator and finally value achievement, this process completely presents the application model of the 3D pipeline.

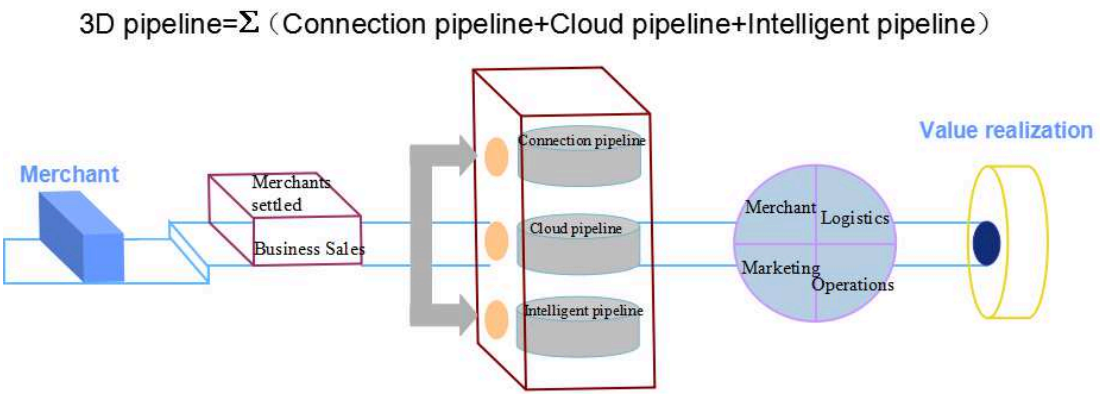

Fig. 2 The application model of 3D pipeline

Connection pipeline - The poly platform

Through Poly platform provided by connection pipeline, it can accomplish merchants settled, product display and sales. In poly platform, 3D pipeline can achieve unified management of businesses and resources, and it also can help the businesses to achieve the management of orders, logistics and payment of the front-end applications.

Cloud pipeline - SMS cloud channel

Cloud platform based on SMS ability opening up can provide such as customer service, marketing and business acceptance and other business operation functions. Cloud channel is dominated by message piping, business templates and other components. The ability to quickly generate data services through business templates, including custom, quizzes, sweepstakes, etc., while providing a unified API, can further support the development and operation of the respective businesses.

Intelligent pipeline - Accurate operation

Accurate operation model based on flow analysis can be said to be the operator characteristics of big data business marketing. And intelligent pipeline can personalize recommendations and provide strong marketing support to merchants through the depth collection of the flow of all kinds of Internet applications, scenario analysis, preferences analysis, and ultimately setting up ability open data by pipeline intelligence.

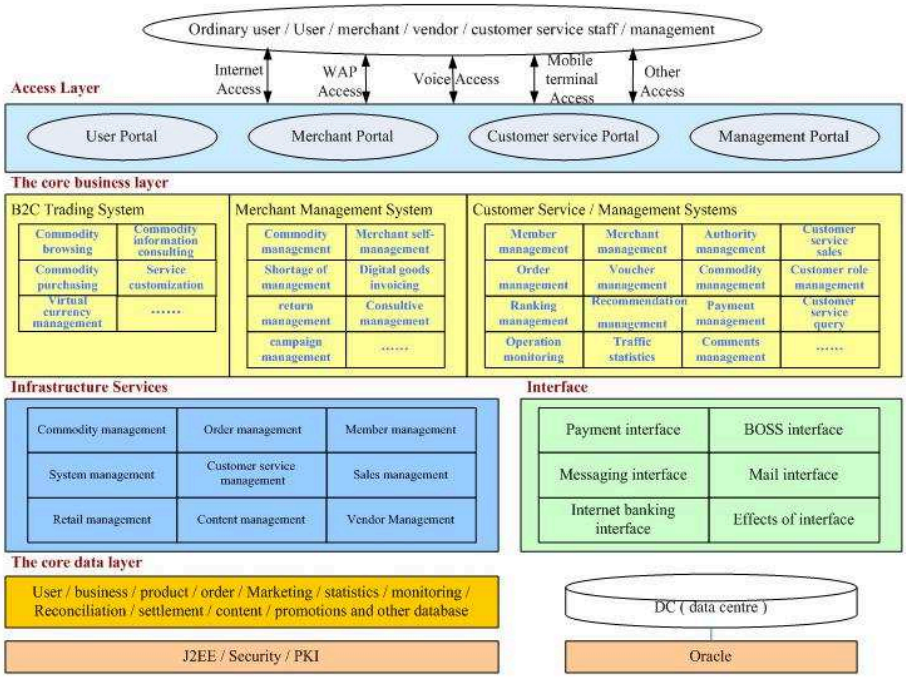

Fig. 3 The mobile e-commerce platform architecture based on 3D pipeline

Summary

With the popularity of smart phones, PDA and other mobile terminals, as well as the development of 3G/4G networks, mobile e-commerce has to show expansive growth in the world, and the

opportunities for people to use mobile devices for business activities will be greatly increased. And the 3D pipeline applied in the mobile e-commerce, will further enrich the mobile e-commerce services, promote market more subtle, rational division to meet the different needs of different people.

References

[1] Lv Pin. Intelligent terminal and OTT services [J]. Video Engineering, 2012, 36(A01): 34-36.
[2] Information on http://baike.baidu.com
[3] Ye Xiaoyang, Wang Liang. Opportunities and Challenges for Equipment Vendors Brought by OTT Service[J]. Telecommunications Network Technology, 2013(1): 12-16.
[4] Liu Jiuping, Wang Zhengjun and Wang Bingfeng. Radio and television operators OTT strategy analyses [J]. Cable Television Technology, 2012 (10): 49-53.
[5] GB 50316-2008, Design code for industrial metallic piping[S].

Advanced Materials Research Vols. 989-994 (2014) pp 4698-4703
© (2014) Trans Tech Publications, Switzerland
doi:10.4028/www.scientific.net/AMR.989-994.4698

Research on the Structure of Authentication Protocol Analysis Based on MSCs/Promela

Chao Zhang[a], Yu Wangb[b]

Equipment Academy of PLA, Beijing 101416

[a]zhang_zsazc@126.com, [b]duanyu_gogo@163.com

Keywords: Authentication Protocol Analysis; MSC2Promela; Structure of Protocol Analysis

Abstract. To discover the existing or possibly existing vulnerability of present authentication protocol, we proposed a structure of authentication protocol analysis, which consist of white box analysis, black box analysis and indicator system as the three main functional components. White box analysis makes use of the transformation from MSCs (Message Sequence Charts) to Promela (Process Meta Language), the input language of the remarkable model checker SPIN; black box analysis is based on the attack platform of authentication protocol analysis; indicator system is decided by deducibility restraint methods. Compared with the UML modeling methods based on Promela, the MSC2Promela methods we figured out on the context have more advantages than its disadvantages. Finally, we proposed a structure of authentication protocol analysis based on the transformation from MSC2Promela, which makes sense to the later work on the area of authentication protocol analysis.

Introduction

With the growing seriousness of the situation of network confrontation, most authentication protocols[1] at present find it difficult to meet the requirement of confidential information security. Many authentication protocols were found vulnerable after versions of publication and years of use. To figure out the existing or possibly existing vulnerability of present authentication protocol, we should focus on authentication protocol analysis. In this paper, we proposed a structure of authentication protocol analysis, which consist of 3 main functional components as follows:

a) white box analysis of known authentication protocol; b) black box analysis of unknown authentication protocol and c) indicator system of authentication protocol under the environment of network confrontation, which main properties and their measurement were reached using the method of deducibility restraint due to different aspects of different authentication protocol.

White box analysis is mainly supported by the transformation from MSCs (Message Sequence Charts) to Promela, the input language of model checker SPIN. By the use of the transformation, user difficulty of modeling authentication protocol by SPIN can be reduced. We proposed an analysis platform of protocol attack, which contains single or multi ways of attack method, to generate black box analysis. With the development of rules of simplifying restraint, indicator system can be decided by the 'solved-form', which was the simple form of authentication protocol simplified by the deducibility restraint. The mentioned structure of authentication protocol is shown in Fig.1.

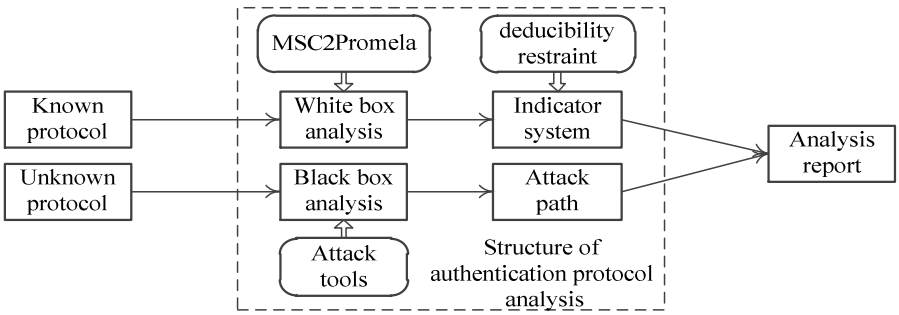

Fig.1 Structure of authentication protocol analysis

Key Technology

Structure of Authentication Protocol Analysis based on MSCs/Promela. Informal analysis of authentication protocol is both difficult and fallible. So it can no longer satisfy the need of security application requirements. Formal analysis, however, is the more rigorous, trusted and standard way to analyze authentication protocol.

MSC[2] is a formal language based on finite communication sequence composition, and plays an important role in the field of visual formalism application of distributed interactive systems. System behaviors, standard test generations and test cases can be depicted using MSCs. Describing in detail the interactions between messages of objects[3] rather than focusing on sending and receiving messages between objects itself is the main specialty of MSCs. MSCs is simple, intuitive, full of readability and easy to learn and practice.

SPIN[4] is a stable and reliable model checker which was widely used in the area of formal analysis, and is one of the most successful open source tools for formal verification of distributed systems. SPIN sets advantages of three kinds of formal analysis methods such as modal logic, model checking and theorem proving methods. The advantages of SPIN, like small memory, original manners of working and high efficiency verification, make it popular in the academic field and engineering field among researchers and engineers. As the input language of SPIN, Promela is a description language that makes it possible to assign behavior of senior system and is the kind of process algebraic language that possesses the function of variable expansion and the structure of programming language. SPIN has been widely applied in the analysis of concurrent systems. However, modeling authentication protocol in Promela, the language which lacks of available tools that act as its auxiliary modeling utilities to translate from other modeling languages, is relatively cumbersome.

To model authentication protocol more clearly and easily for users that have less knowledge about Promela, MSCs can be put forward to associate with model checker SPIN. We may translate authentication protocol model described in formal graphical language MSCs into protocol model in Promela, the input language of SPIN, thereby reducing the difficulty of directly modeling authentication protocol using the Promela, and then use the SPIN model checker to analyze the carried out authentication protocol model. Finally, the analysis results will be displayed respectively in the form of text and graphical MSCs at the same time. The block diagram of authentication protocol analysis based on MSC/Promela was shown in Fig.2, and the two main stages of the analysis process such as modeling-translation and model checking was shown too.

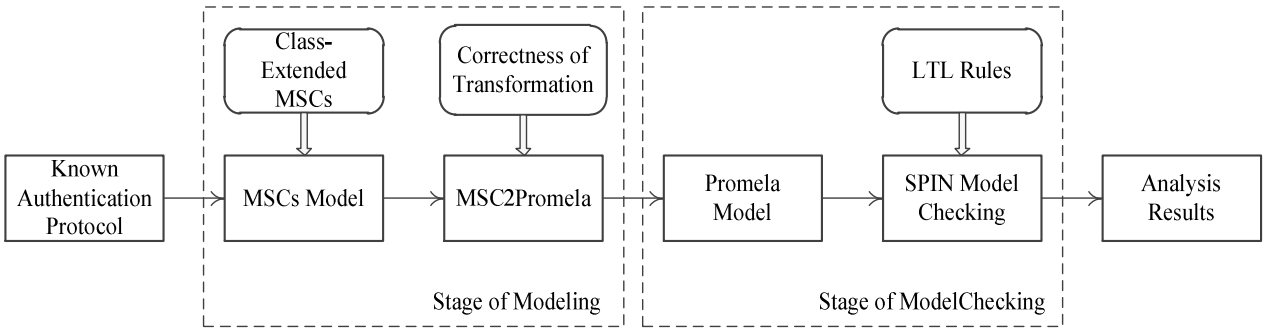

Fig.2 Structure of authentication protocol analysis based on MSCs/Promela

Transformation from MSCs to Promela: MSC2Promela. The main purpose of this transformation is based on the invariance of the semantic of MSCs, during the process of converting MSCs structure to Promela structure. The structure of MSCs is made up of the concurrent object (INIT) that encapsulates process states. Object responds to the received message (MSGS) according to the rules (RULES) defined by the class (PROC), making the corresponding processes. Promela abstracts the concurrent execution of processes, which can communicate through message channels. More than the similar points, the definition of the transformation from MSCs class to Promela process is feasible. MSCs class states can be translated to internal variables of Promela process. Each process instance in Promela has a connected input channel associated to it. All input messages that enter the

process will transmit through the specialized input channel, which can be done by the reference of each MSCs object. The main body of Promela process can be represented as the evaluation cycle applied by process rules. The main compositions of the transformation from MSCs to Promela are shown in Fig.3:

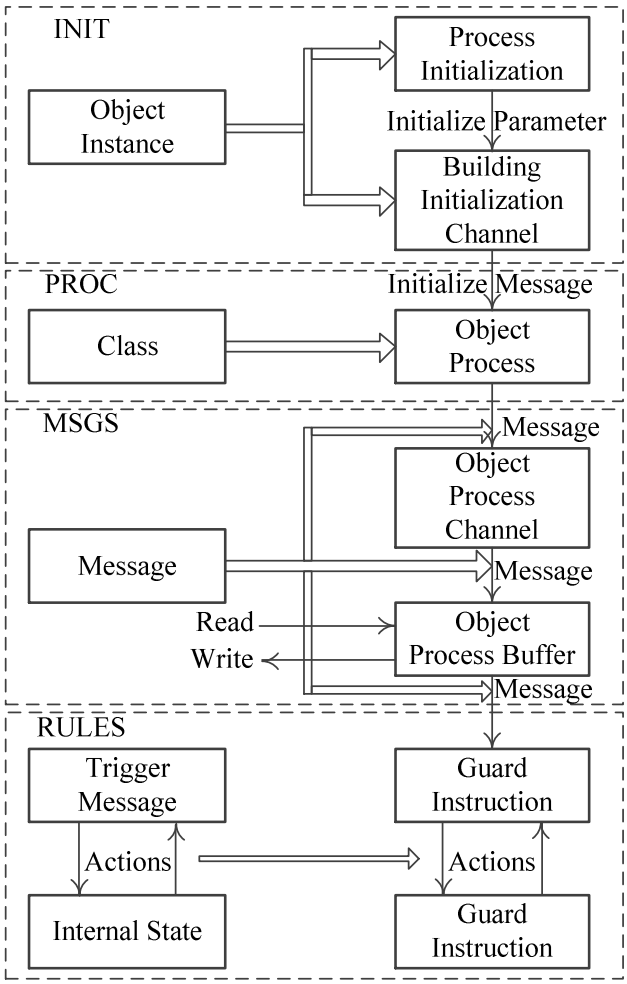

Fig.3 Main compositions of MSCs2Promela

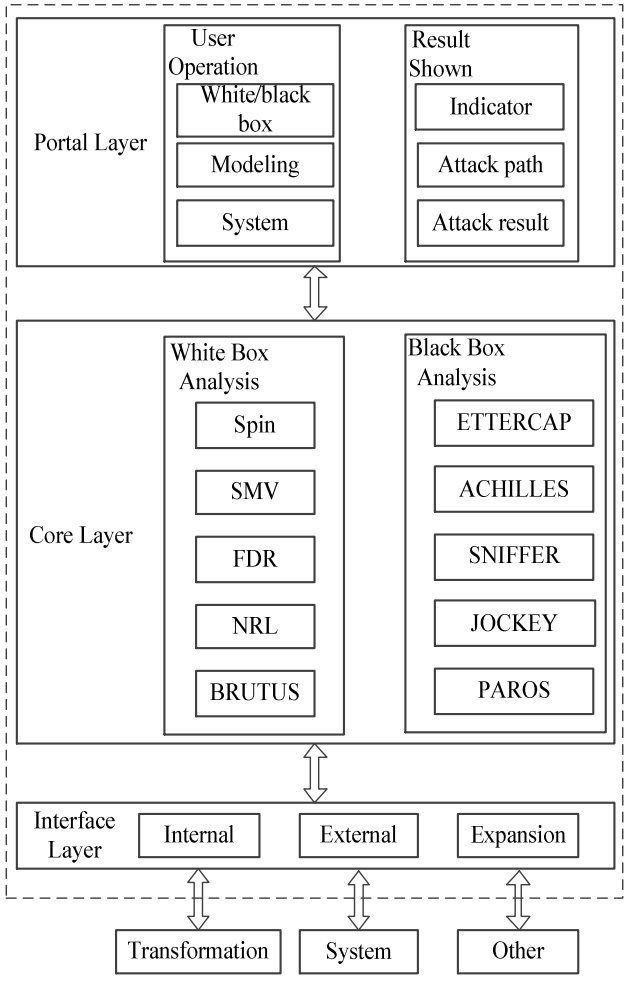

Fig.5 Structure of authentication protocol analysis

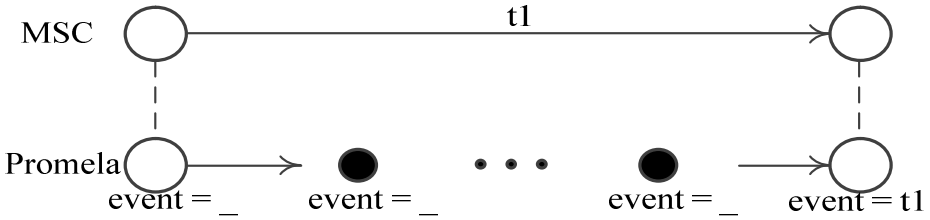

Fig.4 Well-formed states

INIT: The initialization chart of MSCs can be transferred to the INIT process of Promela, and object instances of MSCs can be translated into corresponding creation of input channel and initialization of process in Promela. Messages in initialization chart are transformed to the messages of input channel. Through the above initialization settings, each process can react to the messages from the input channel to make corresponding processes. INIT describes the transformation from the initialization chart of MSCs to the INIT process of Promela. The transformation is implemented by the creation of object process channel. Transferring the relevant parameters of the initialization of object process to the message channel and transferring initialization message to object process through object process channel can respectively activate the object process and its channel.

MSGS: The strategy of transferring messages through message channel in Promela follows FIFO, and there is no concept of message order in MSCs. In the transformation, each process(object process) sends messages to an object process buffer that can execute evaluation and disorderly deal with

messages through input channel (object process channel). Object process buffer has two operations: read (READ) operation and non-deterministic write (WRITE) operations.

RULES: rules of MSCs describe the trigger message (and parameter) and internal state that can be correctly used by rules, and action that can properly apply the rules. Those described by rules of MSCs include the repeat of trigger message, the change of object state, and the generation of new message and object instance. Using guard instructions in Promela can properly correspond to these semantics: evaluations of guard instructions about available messages and current state can be used to detect if rules are correctly applied. The corresponding actions of guard instruction are expressed by the cost of message forwarding and the change of state of process variables as well as the possible generation of new information and processes. The non-deterministic choice of MSCs rules can be mapped into non-deterministic choice of several corresponding guard instruction of Promela.

PROC: MSCs class can be mapped to the static definition of Promela processes. Each MSCs class is mapped to the definition of a process. MSCs object is corresponded to process instance of Promela, namely object process. The body of object process contains the loop of actions such as choosing the message to be executed, evaluating, and applying rules. When object process channel receives a message, the message will be moved to the object process buffer and wait for the process. When the message is selected, an executable rule of the message will be applied.

Correctness proof of MSC2Promela. In order to make sure that MSCs model effectively and correctly transferred to Promela model, we must ensure that the generated sequences of events of the two models are the same, that is, the sequence application of rules generated by MSCs is consistent with the corresponding Promela migration sequence variable. Ensuring the basis of the correctness of model transformation is to ensure that MSCs object state is consistent with Promela process states. This means that at the same time the MSCs object state transferred to Promela process state, the Promela process state can be fully converted to the original state of MSCs object. We call the state that can be transferred in two directions the ‘well-formed’ state.

As shown in Fig.4, the hollow circle represents the ‘well-formed’ state that can be transferred bidirectionally; Solid circle represents the mutual transformation state, that is, in the MSCs people can't find the object state of the corresponding Promela process state. In the operation of protocol, if all protocol steps can be described as a corresponding set of qualified state transition, then we can deduce that the transformation from MSCs model to Promela model is correct.

Contrastive analysis. Modeling method proposed in [5] is aiming at the complementation of formal method and visual UML method, and deal with the transformation UML model to Promela model. Finally they proved the effectiveness of the proposed method. This method slightly lacks advantages in UML modeling, especially the need to generate requirements specifications. Modeling by UML requires the use of class diagram, state diagram and collaboration diagram, respectively. Using this transformation method to model authentication protocol is relatively complicated in general

In this paper, the MSC2Promela modeling method we gave is relatively simple and clear. Authentication protocol can be directly described using class-extended MSCs. At the same time, the accuracy of transformation method of MSC2Promela, on the premise of which MSCs model can be achieved by promela model and the other way around, can be assured. Finally, after authentication protocol modeled by MSC2Promela is analyzed, the result of the analysis of model checker SPIN will be displayed through text and MSCs graphical. But the transformation method of MSC2Promela is only currently applicable for authentication protocol analysis, and the requirement of class extension of MSCs is indispensable, which increases the difficulty of modeling authentication protocol. Comparison results are shown in table 1:

Table 1 Difference between MSC2Promela and Promela-based UML

Modeling Method	Difficulty	Principal	Direction	Result form	Scope
MSC2Promela	Convenient	Correctness	Two-way	Graph/Text	Protocol Analysis
Promela-based UML	Complicated	Effectiveness	One-way	Text	Software Development

Design of Structure

As shown in Fig.5, the structure is overall divided into three layers: portal layer, core layer and interface layer. Portal layer provides interoperable ports and results for users and administrators. Core layer conducts the actual operation and processing while interface layer provides supporting interfaces for internal model language translation and external connections of the measured system and API. Before the execution of analysis, the structure provides modeling interface of authentication protocol by MSCs and interface of attack analysis respectively in view of the white/black box analysis methods. At the end of the white box analysis, the structure shows accordingly the indicators of analyzed authentication protocol, its measurement, and possible attack path depending on feedbacks. At the end of the black box analysis, attack results and available attacker instances will be displayed.

White box analysis. Knowing the authentication protocol in detail, the integrated use of various automated formal analysis tools, such as SPIN, SMV, FDR, NRL and BRUTUS was carried out on the deal. Especially the use of MSC2Promela can be applied to modeling and transformations. By using SPIN, transformed Promela model is analyzed, decreasing the difficulty of modeling authentication protocol so as to improving the efficiency of authentication protocol analysis.

Black box analysis. By the single use or combination approaches of freshness attacks such as type flaws, parallel session attacks, implementation dependent attacks, binding attacks and encapsulation attacks and attacking tools like Ettercap, Achilles, Sniffer, and Paros Jockey, we constructed the platform for attack analysis on authentication protocol to perform the actual attack on unknown authentication protocol.

Indicator system. To analyze authentication protocol, one needs to go deeply through the security nature like confidentiality, integrity, and availability for further research. By giving a simple set of simplified rules to simplify any deduction constraints, a set of "solved-form" that represents all actions of protocol is generated. In the case of finite number of sessions, any deducibility restraint system can be transformed into a simple combination of several "solved-forms". By analyzing the characteristics of "solved-forms", we can decide the main indicators of the protocol and the different indicators according to different authentication protocol.

Conclusions

Methods and tools of formal analysis for authentication protocol have considerably accumulated. Particularly, the application with respect to the SPIN/Promela model checking method is very popular. However, the transformation method based on SPIN/Promela language is in research. This paper described exploringly the transformation from graphical language MSCs to the input language Promela of a universal model checker SPIN, greatly reducing the difficulty of modeling and possibility of making error. Finally, we gave a structure based on the transformation method of authentication protocol analysis, which has certain reference significances for the related work of authentication protocol analysis and validation in the future.

References

[1] Clark J A, Jacob J L. A survey of authentication protocol literature: Version 1.0[J]. 1997.
[2] Recommendation I. Z. 120: Message sequence chart[R]. Technical report, ITU-T, Geneva, 2011.
[3] O M Mendizabal, F L Dotti, L Ribeiro, Stochastic object-based graph grammars, Electronic Notes in Theoretical Computer Science 184 (2007) 151–170. doi:10.1016/j.entcs.2007.03.020.
[4] Holzmann G J. The model checker SPIN[J]. IEEE Transactions on software engineering, 1997, 23(5): 279-295.
[5] Liangchun Shu, et al. Promela-based UML Modeling Methods and Its Application [J]. Computer and Modernization, (2010) 2: 101-104. In Chinese.

Advanced Materials Research Vols. 989-994 (2014) pp 4704-4707
© (2014) Trans Tech Publications, Switzerland
doi:10.4028/www.scientific.net/AMR.989-994.4704

Hot News Recommendation System across Heterogonous Websites Using Hadoop

Shengwu Xu, Zhengyou Xia

Department of Computer Science and Technology Nanjing University of Aeronautics and Astronautics Najing City, China

cocafriend@sina.com, zhengyou_xia@nuaa.edu.cn

Keywords: News Recommendation;Hadoope;Bbig datastyling;Bayesian Mdoel.

Abstract. The current most news recommendations are suitable for news which comes from a single news website, not for news from different news websites. Little research work has been reported on utilizing hundreds of news websites to provide top hot news services for group customers (e.g. Government staffs). In this paper, we present hot news recommendation system based on Hadoop, which is from hundreds of different news websites. We discuss our news recommendation system architecture based on Hadoop.We conclude that Hadoop is an excellent tool for web big data analytics and scales well with increasing data set size and the number of nodes in the cluster. Experimental results demonstrate the reliability and effectiveness of our method.

Introduction

Owing largely to the ever-increasing volume and sophistication of information on the web, we are able to access an enormous amount of information from around the globe[1,2,3].Recommender systems are usually classified into three categories, based on how the recommendations are made[4,5]:content-based recommendation ,collaborative filtering and hybrid. Content-based recommender systems: These recommender systems recommend an item to the user similar to the ones the user preferred in the past [6,7]. Collaborative recommender systems: These systems recommend an item to the user based on the people with similar tastes and preferences have liked in the past. They have the advantage that they can recommend items for which little or no semantic information is available (music, movies, products)[8,9]. Hybrid recommender systems: These systems combine both the collaborative and content-based recommendation techniques in order to improve the accuracy of the recommendation [10].

In this paper, we propose to develop News recommendation system based on Hadoop platform for handling web big data. The remainder of this paper is organized as follows: in section 2 we discuss the architecture of Hadoop. We discuss the news recommendation system on Hadoop in section 3. Finally, we present the results of our experiments in section4.

HADOOP ARCHITECTURE

Hadoop is a distributed file system where files can be saved with replication. It provides high fault tolerance and reliability. The technology has been well received by the community which handles large amount of data. Google uses it for web indexing, data storage, so-cial networking [11]. It is being used to scale up classifiers for mining peta-bytes of data [12]. Data mining algorithms are being rewritten in different forms to take the advantage of MapReduce technology [13]. Figure 1 is the architecture of Hadoop., which is consisted of Name node, Datanodes and HDFS Client[14-15].

1). NameNode : Files and directories are represented on the NameNode by inodes. NameNode records attributes like permissions, modification and access times, namespace and disk space quotas. The data file is split into large blocks (typically 128 M) and each block of the file data is independently replicated at multiple DataNodes (generally three). The NameNode maintains the namespace tree and the mapping of file data blocks to DataNodes.

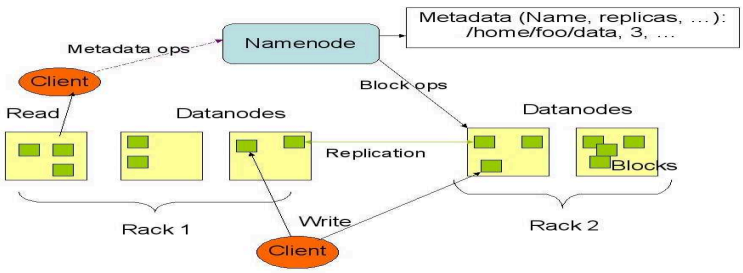

Figure1. Hadoop Architecture [18-19]

2). DataNodes: Each block replica on a DataNode is represented by two files in the local host's native file system. The first file contains the data itself and the second file is block's metadata including checksums for the block data and the block's generation stamp. The size of the data file equals the actual length of the block and does not require extra space to round it up to the nominal block size as in traditional file systems. Thus, if a block is half full it needs only half of the space of the full block on the local drive.

3) HDFS Client :User applications access the file system using the HDFS client, a code library that exports the HDFS file system inter-face. Similar to most conventional file systems, HDFS supports operations to read, write and delete files, and operations to cre-ate and delete directories. The user references files and directo-ries by paths in the namespace. The user application generally does not need to know that file system metadata and storage are on different servers, or that blocks have multiple replicas. When an application reads a file, the HDFS client first asks the NameNode for the list of DataNodes that host replicas of the blocks of the file. It then contacts a DataNode directly and requests the transfer of the desired block.

NEWS RECOMMENDATION SYSTEM USING HADOOP

In this paper, the design of the system is based on the Hadoop platform news recommendation system, which mainly includes several important functional modules. Figure 2 shows the main modules of the system as follows: Data capture engine, automatic segmentation, Semantic, Hbase, Bayesian model. We will detail discuss the main functions and role of these modules. Data Capture Engine is responsible for crawling web data (news or topics) from hundreds of different websites. We design the Data Capture Engine based on Hadoop and the flowchart is as follows. 1) Injector Job: get a group of seed pages from the file, put them to crawl database; 2) GeneratorJob: generate pages to crawl into the crawl queue to grab the database from;3) Fetcher Job: crawl web pages to crawl queue, using the producer / consumer model in the reducer;4) Parser Job: completed pages to crawl parsed to produce analytical results of some new links and web content;5) DbUpdaterJob: the newly generated link the database to be updated to crawl; 6) SolrIndexerJob: be parsed for content indexing.

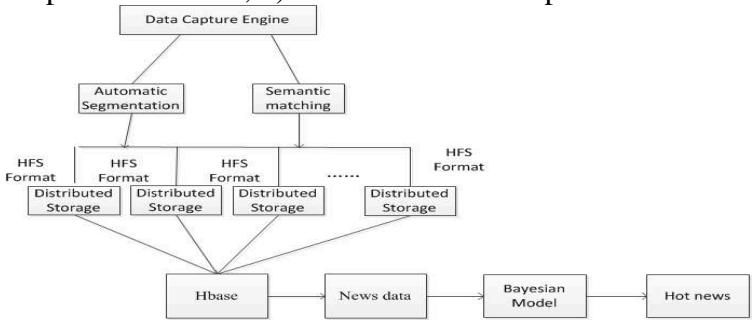

Figure 2. News recommendation system using Hadoop

Chinese automatic segmentation techniques based on "word" as the basis, but not the Chinese written language as a natural separator (space) like the Western text, but in a statement to the characters as a unit, no clear boundaries between words. Idea of the semantic matching algorithm is established in advance thesaurus, let it be according to certain policies will be analyzed. Our system uses and reverse matching methods in this paper. All web data is stored in HFS format and placed in

Hbase database. We propose a novel hot news recommendation model based on Bayesian, which is from hundreds of different news websites. In the model, we determine whether the news is hot news by calculating the joint probability of the news. News headlines are generalization of news contents. Readers often can know the news content through these headlines. This is because news headlines contain highly relevant keywords about news content.Therefore, we firstly preprocess news headlines. In this paper, we use the word segmentation technology to preprocess news headlines. Each headline will be divided into vocabularies with not fixed length and we statistic the frequency of occurrence for each vocabulary. Therefore, we should select appropriate number of vocabularies to analyze the news headlines. Because length of every news headline is different, according to our practical experience data, we select four vocabularies with higher weight as keywords for a news headline (we will discuss the reason of selecting four vocabularies in the next section). For some news headlines, their lengths are relatively short, and could not be divided into four vocabularies. In this case, we add the default vocabularies to these news headlines. The probability of default vocabularies that exist in hot news is set to 0.4, which means that the default vocabularies is not important and is less than 0.5. The 0.4 is set by experience. Calculation equation of hot news probability finally is shown in equation (1).

$$P = \frac{P_1 P_2 P_3 P_4}{P_1 P_2 P_3 P_4 + (1 - P_1)(1 - P_2)(1 - P_3)(1 - P_4)} \quad (1)$$

where, probability of four vocabularies is respectively $P_1 P_2 P_3 P_4$, and P represents the probability of hot news.

EXPERIMENTAL RESULT AND ANALYSIS

In order to verify the reliability of our system we do experiments on real data sets. We collected news from 55 different news websites from 2013.10 to 2013.12, which includes 15243 news. Because there is different updating frequencies from news website, news from different websites have different proportion of the total number of news as shown in Figure 3.

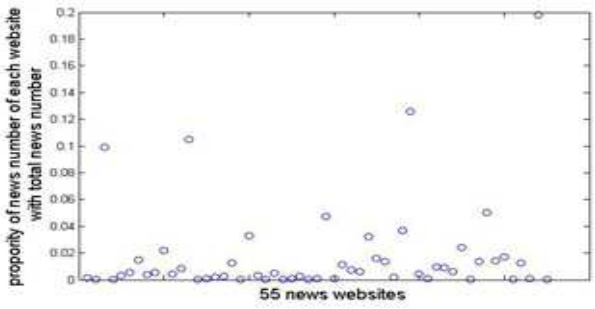

Figure 3. Distribution of news number for 55 different news websites

In Figure 3, only a few websites publish more news . The vast majority of websites publish a few news and the proportion of news number from these websites is below 0.06. This means that the number of news published and updated is less in most websites. We invited five news staffs to select Top 10,20,30,40,50,60,70,80,90,100 hot news from the 2000 news data set. We compare similarity of these two result sets, as shown in Figure4.In Figure 4, when we select the hottest Top 10 news, similarity of the result of our method and human experts is relatively low. Because when the news quantity is less, the human experts' subjective influences will make a difference for hot news. And with the increase of number of news, human experts' subjective influences will decrease accordingly. Therefore, while the number of hot news reaches a certain value, the result of our model and human experts is similar. For these 2000 news, when the Top number of hot news is 100, precision of results are ideal.

CONCLUSION

Hadoop is capable of processing large amounts of data distributed software framework. But Hadoop is a reliable, efficient, and scalable way process. Hadoop is reliable, because it assumes that

computing elements and storage will fail, so it maintains multiple copies of data, to ensure against the failed node can be re-distributed processing. Hadoop is a framework that allows users to use of distributed computing platforms.In this paper, we discuss our new recommendation system based on Hadoop platform and propose our system architecture. We do plenty of experiments on real data sets and compare the result of our model with the result of human news staffs. The experimental results show that our model can effectively extract top hot news from news data sets which are collected from different websites.

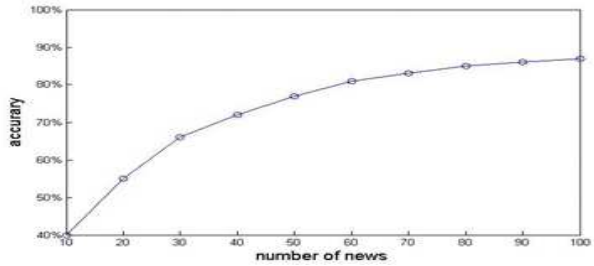

Figure 4. Similarity results of our model and human experts

References

[1]. Xia, Zhengyou, and Zhan Bu. "Community detection based on a semantic network." Knowledge-Based Systems 26 (2012): 30-39.

[2]. Xia, ZhengYou. "Fighting criminals: Adaptive inferring and choosing the next investigative objects in the criminal network." Knowledge-Based Systems 21.5 (2008): 434-442.

[3]. Bu, Zhan, Zhengyou Xia, and Jiandong Wang. "A sock puppet detection algorithm on virtual spaces." Knowledge-Based Systems 37 (2013): 366-377.

[4]. A. Tuzhilin and G. Adomavicius, “Toward the Next Generation of Recommender Systems: A Survey of the State-of-the-Art and Possible Extensions,” in IEEE Transactions on Knowledge and Data Engineering, pages 734-749, New Jersey, USA,2005.

[5]. M. Balabanovic and Y. Shoham, “Fab: Content-Based,Collaborative Recommendation,” in Communications of the ACM, pages 66-72, New York, New York, USA, March 1997.

[6]. J. Ahn, P. Brusilovsky, J. Grady, D. He, S.Y. Syn, Open user profiles for adaptive news systems: help or harm? in: Proceedings of 16th InternationalWorld Wide Web Conference, Banff, AB, Canada, 2007, pp. 11–20.

[7]. J. Wang, Q. Li, Y.P. Chen, , News recommendation in forum-based social media, in: Proceeding of the 24th Conference on Artificial Intelligence, Atlanta, GA, USA, 2010, pp. 1449–1454

[8]. Y. Seroussi, F. Bohnert, I. Zukerman, Personalised rating prediction for new users using latent factor models, in: Proceedings of the 22nd ACM Conference on Hypertext and hypermedia, New York, NY, USA, 2011, pp. 47–56.

[9]. Rosa M. Rodríguez, Macarena Espinilla, ,Using linguistic incomplete preference relations to cold start recommendations,Internet Research Volume: 20 Issue: 3 2010

[10]. Hensinger E, Flaounas I, Cristianini N. Modelling and Explaining Online News Preferences[M]//Pattern Recognition-Applications and Methods. Springer Berlin Heidelberg, 2013: 65-77.

[11]. Duen-Ren Liu, Wei-Hsiao Chen, Po-Huan Chiu,Recommending quality book reviews from heterogeneous websites,Internet Research Volume: 23 Issue: 1 2013

[12]. Chang, F., Dean, J., et al.: Bigtable: A Distributed Storage System for Structured Data. In: OSDI Seventh Symposium on Operating System Design and Implementa-tion (November 2006)

[13]. Moretti, C., Steinhaeuser, K., Thain, D., Chawla, N.V.: Scaling Up Classifirs to Cloud Computers. In: IEEE ICDM (2008)

[14]. White, T. (2009). Hadoop: The Definitive Guide: The Definitive Guide. O'Reilly Media.

[15]. Hadoop official websites: http://hadoop.apache.org/

Advanced Materials Research Vols. 989-994 (2014) pp 4708-4712
© (2014) Trans Tech Publications, Switzerland
doi:10.4028/www.scientific.net/AMR.989-994.4708

On the Process Modeling of Software Crowdsourcing Based on Competitive Relation

Xu XiaoLan[1, a], Wang Ya[2,b]

[1]BeiHang University XueYuan Road No.37,HaiDian District,Beijing,China

[2]BeiHang University XueYuan Road No.37,HaiDian District,Beijing,China

[a]xuxiaolan@cie-info.org.cn, [b]wangya@buaa.edu.cn

Keywords: Crowdsourcing QCV model verification

Abstract: With the increase of the scale and complexity of software system software crowdsourcing development have gradually favored by the industry and scholars, to solve the large-scale, large system to develop effective solutions. In this background, this article first introduces the crowdsourcing the basic framework of the development process of software, the basic framework of crowdsourcing and then based on the software development process of put forward a comprehensive software Quality (Quality), the software task Cost (Cost) and software (Value) of a reward QCV model. Finally, this paper, by using data from the topcoder, the QCV process model is verified, it is concluded that the software quality, software cost and interaction relationship between reward.

1. Foreword

Along with asoftware system characterized by growing vast scale and complexity day by day, innovation power and creativity is desiderated in consideration of its demand analysis, function design,functional modeling, code design, functional test and performance evaluation in the development process. In addition, more and more software developers urgently hope their software developed could meet the diversified demands of customers with realized tremendous and multiple functions, which could simulate diversified usage scenario and present the work load distribution of business and measure the acts of employees from various aspects etc. Therefore, crowdsourcing emerges at the right moment in recent years.

Crowdsourcing[1] means a reform of production mode and the software development based on which is to open the process of software development to the public and any software development team and individual could participate in. Its development process is dispersed, which could be allocated to any participant in the development process. Also, it provides some specific mechanism to encourage participants and the participants fulfil the task for the sake of abundant rewards and well-deserved reputation. Furthermore, in crowdsourcing, the mode organizing software development will be transformed from traditional software plants and distributed program development teams to the scattered and mass production mode based on software development ecosystem. Firstly, crowdsourcing opens its development process to the mass organizations on the internet, which means the masses could freely take part in the process shows different open nature comparing from open source. Secondly, it depends on the dispersive development process of the labor force in community.The traditional tasks of software development are often be done by the interior employees of software company or its contractors.However,all the tasks will be allocated to anyone in ordinary people. Finally, outsourcing offers specific rewards to the developers from community and the open source programs usually relies on the fame-oriented volunteers to complete tasks. Consequently, crowdsourcing enlarges the concept of open source community to the software ecosystem driven by market.

Based on the above-mentioned discussion, the text firstly introduces the basic frame of crowdsourcing process and then puts forward a software system model based on crowdsourcing and takes advantage of the data from TopCoder to verify the model of crowdsourcing process.

2. Basic Frame of Crowdsourcing Process

The core of crowdsourcing is to reward the developers in community to participate in mass production tasks and provide software products for the software ecosystem[2]. Therefore, modeling

and the optimization for the modeling for the process of crowdsourcing becomes a focal point of the research. The figure 1 introduces the basic frame including reward system, fame evaluating system, quality assurance system (QAS) and management mechanism of the process of crowdsourcing.

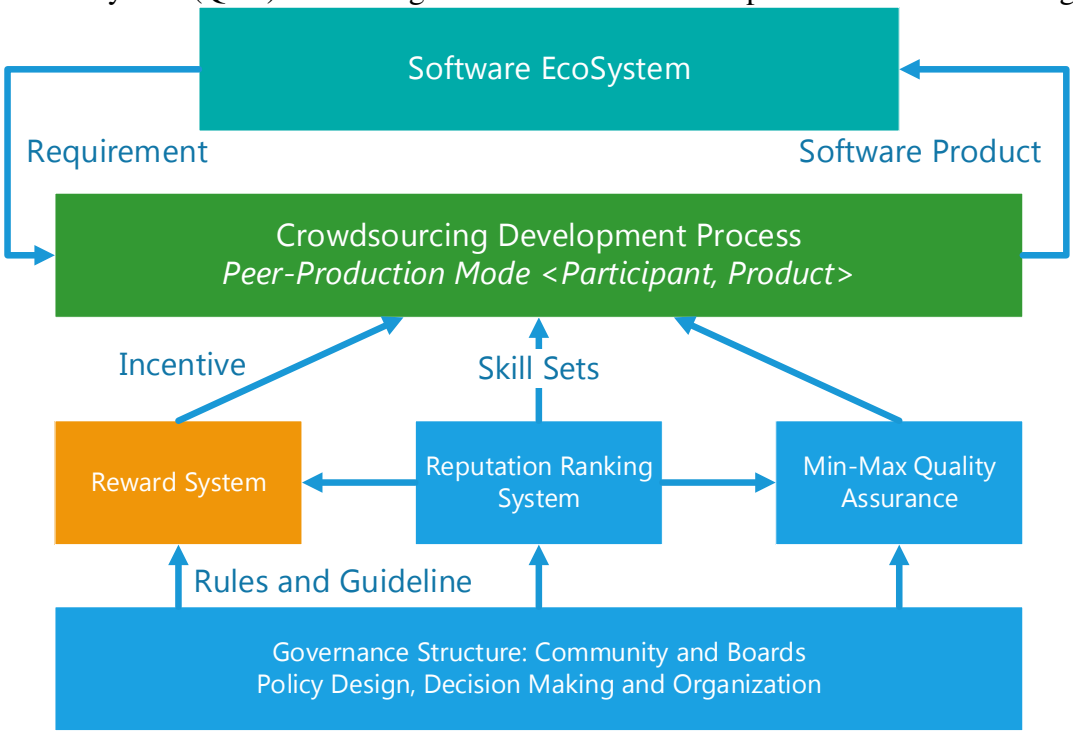

Fig1.Software Crowdsourcingfor developing Software Ecosystem

Management mechanism mainly includes the design of strategy and summary realization, which encourages community people to participate in the development tasks with reward system; ranks the skill of each participant with fame evaluating system;evaluates the products provided and chooses classic ones to software ecosystem with QAS. Crowdsourcing[3] needs an efficient mechanism to encourage the developers in community to participate in its process and provide qualified software products, acting as the major components of the process. Hence, the problem how to optimize reward mechanism becomes the subject we study.

The traditional reward system is designed by taking static business process as the principal thing with limited business environment. However, the systems could not be suitable for crowdsourcing development process and[4] other social computing platform due to the dynamic cooperation modes frequently seen in these platforms and numerous participants. So, in these environments, the results of reward schemes will be even unexpected and claim much higher costs than traditional companies.

3. Crowdsourcing Process Modeling (QCV Model)

The text maps crowdsourcing as a mass production model with competitive mechanism.All software products like demand analysis, scheme design and software composition and so on will be completed through a way of mass production. If there are N development units in the development and they provide M solutions and P products in the crowdsourcing process, manager will select the best one from the P products. Thus, $P \leqslant M \leqslant N$.

So, the optimal object of mass production process is to reduce the costs in encouraging community developers to participant in the crowdsourcing process[5]; enhance the diversity of developers to excavate more innovative ideas and improve the product quality adopted in the end. With the competitive model and optimal object assumption theory, the crowdsourcing process will be modeled. The text puts forward a QCV process model including software quality, task costs and value.

In the competitive relation, each work defined by mass software project could be considered as the work containing competitive nature. Provided that a number of developers take part in the work, the quality of scheme provided by each developer will decide his rewarding possibility[6].

In the QCV model, the text defines$l_{\mathrm{i}} = l_{\mathrm{i}}(\mathrm{Q}_1, \mathrm{Q}_2, \ldots, \mathrm{Q}_{\mathrm{i}}, \ldots, \mathrm{Q}_{\mathrm{n}})$ as developer d_i'possibility in winning crowdsourcing competition when his product is rated as Q_{i}.The$C_i(Q_i)$ is the costs brought by the completion of crowdsourcing task. The $V_i(Q_1, \ldots, Q_n)$ is the reward for the winners[7].

Hence, the income expected by developers is:

$$e_i(Q_1, \ldots, Q_n) = l_i(Q_1, \ldots, Q_n) \times V_i(Q_1, \ldots, Q_n) - C_i(Q_i) \quad (1)$$

When the income expected by developers is higher than zero, developers will have motivation to participate in crowdsourcing. On the contrary, they will not. For simplifying the analysis for the task participation of N developers, we define:

$$l_i = \frac{\phi(Q_i)}{\sum_{j=1}^{n} \phi(Q_i)} \text{if } \sum_{j=1}^{n} \phi(Q_i) > 0,\ l_i = \frac{1}{n} \text{ if } \sum_{j=1}^{n} \phi(Q_i) = 0 \quad (2)$$

Define $x_i = \phi(Q_i)$ and assume $C_i(Q_i) = C_i(\phi^{-1}(x_i)) = r_i x_i$,

The definition of r is the ratio of developers between their costs and winning possibility. So, the r will be determined by the skills of the developers. With the help of Nash Equilibrium Theory [1], the developers in the process of crowdsourcing could be divided into active and passive ones. For the active m developers, the formula $\forall r_i\, i = 1, \ldots m, \sum_1^m r_j > r_i(m-1)$ is to describe competitive mechanism. Let's assume ten developers take part in the mass production competition.

Assume$r_i = \sigma \times i,\ \ i = 1,2, \ldots 10,\ the\ \sigma$ is the minimum spacing in quantizing r_i.

m>1

Thus,$\frac{\sigma m(m+1)}{2} > \sigma m(m-1)$ (3)

Hence, m<3.That means two developers will do active contributions to the task.

Let's assume r obeys two distribution patterns like uniform and normal ones. When the number of competitors changes, the corresponding number of m could be calculated and a changing curve of m following n will be drawn accordingly.

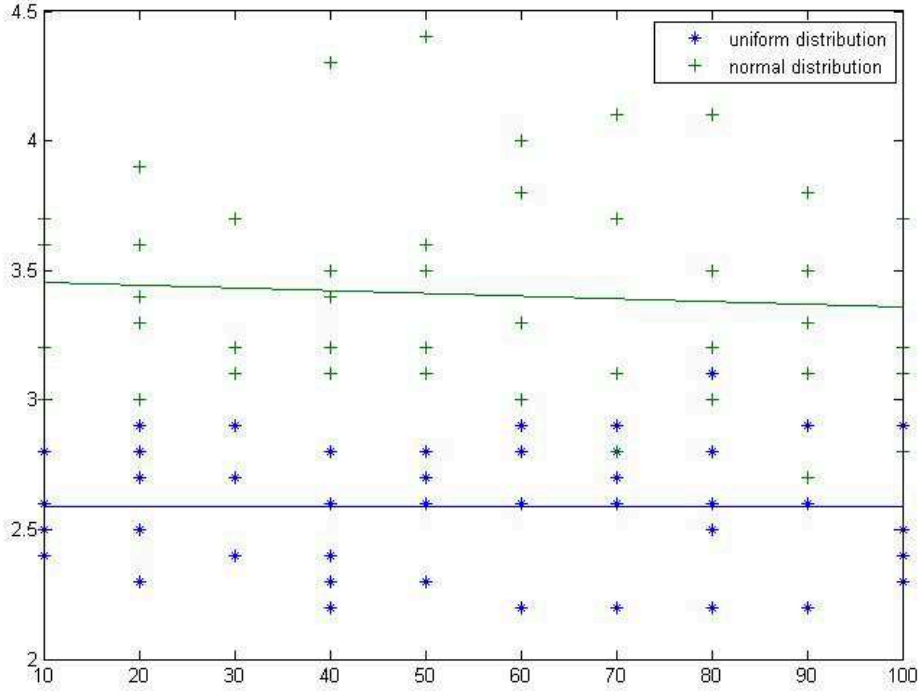

Fig2 M-value under different R values (uniform vs normal distribution)

Known from the figure, based on the QCV model, the range of value m is 3-4.5 when the value of m is determined by the distribution of r and ther obeys the normal distribution$r\sim N(0.5,1)$.When r obeys uniform distribution $d\sim U(0,1)$, the value range of m is 2-3.

4. QCV Model Verification

Based on the above model, the text verifies the data from the TopCoder and the data sets include 1734 software design cases and 910 software development cases. With the data sets, a changing curve is simulated and drawn including registrants, the schemes submitted and the reliable scheme number following rewards.

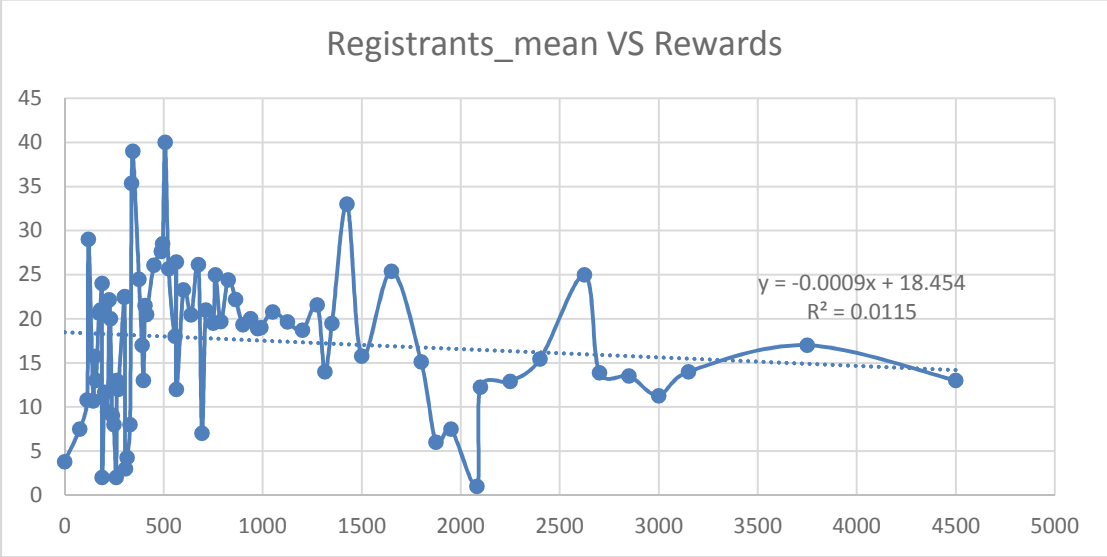

Fig3. Registration-Reward Curve in Development contests of TopCoder

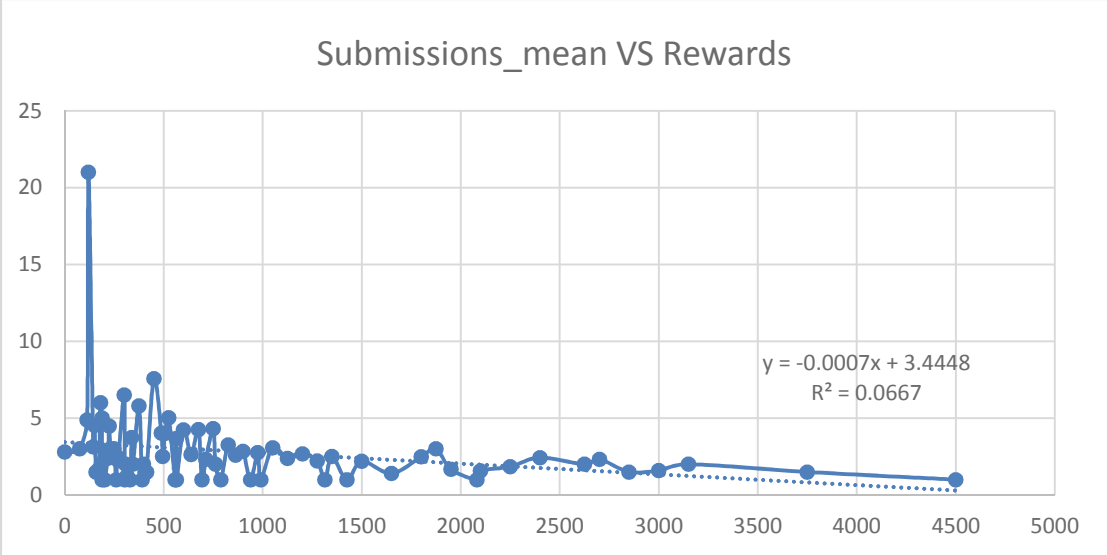

Fig4.Submission-Reward Curve in Development contests of TopCoder

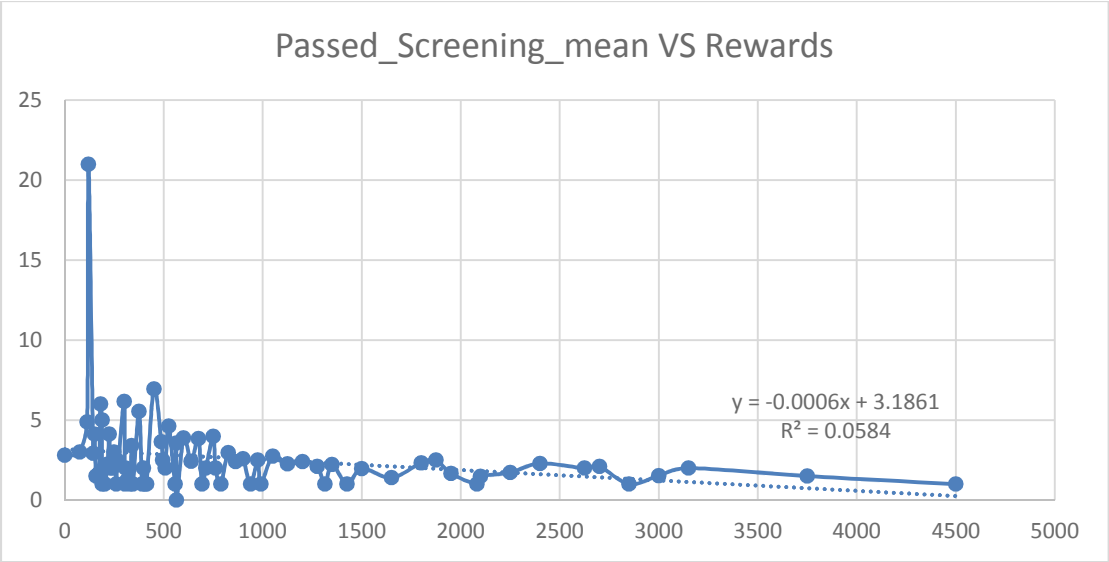

Fig5.Effective-Reward Curve in Development contests of TopCoder

Obviously, the qualified products number submitted finally is greatly less than registered ones. Meanwhile, bonus amount shows little influence to the motivation of the workers in community and more bonuses shall not bring about more participants. According to the statistical data from TopCoder, the average time for completing the tasks of TopCoder is about two weeks. So, those urgent challenging tasks and time limit may make most developers feel too much risk. For this reason, more data is needed in verifying it.

5. Conclusion

Based on the discussion for the crowdsourcing process, the text raises a QCV model including quality, cost and value.Then, taking advantage of TopCoder, the text verifies the QCV process model and gets the mutual effect among software quality, costs and rewards.

References

[1] A. Doan, R. Ramakrishnan, and A. Y. Halevy, "Crowdsourcing Systems on the World-Wide Web," Communications of ACM, Vol. 54, No. 4, April 2011, pp. 86-96.

[2] Jan Bosch, From Software Product Lines to Software Ecosystems, SPLC '09 Proceedings of the 13th International Software Product Line Conference.

[3] E. Schenk and Claude Guittard, “Crowdsourcing: What can be Outsourced to the Crowd, and Why?” Workshop on Open Source Innovation, Strasbourg, France. 2009.

[4] Nikolay Archak, A. Sundararajan, “Optimal Design of Crowdsourcing Contests,” Proc. of International Conference on Information Systems (ICIS), Association for Information Systems, 2009, pp. 1-16.

[5] C.Y. Baldwin, K.B. Clark, “The Architecture of Participation: Does Code Architecture Mitigate Free Riding in the Open Source Development Model?”, Management Science July 2006 vol. 52 no. 7, pp 1116-1127.

[6] Nikolay Archak, Money, “Glory and Cheap Talk: Analyzing Strategic Behavior of Contestants in Simultaneous Crowdsourcing Contests on TopCoder.com,” Proceedings of the 19th international conference on World Wide Web, 2010.

[7] Dominic DiPalantino, Milan Vojnovi´c, “Crowdsourcing and All-Pay Auctions,” EC '09 Proceedings of the 10th ACM conference on Electronic commerce.

Advanced Materials Research Vols. 989-994 (2014) pp 4713-4716
© (2014) Trans Tech Publications, Switzerland
doi:10.4028/www.scientific.net/AMR.989-994.4713

On Application of E-Government 2.0 in Basic Public Services

Hua Yanhui[1,2,a],Li Pengfei [b],Wang zhijian[c],Liu Bangfan[2,d]

[1]Qinhuangdao Vocational and Technical College，Qinhuangdao China 066004
[2]Humanities-law College Yanshan University，Qinhuangdao China 066004
[a]email:ysdxwenfa@126.com, [b]email:ysu888@yeah.net,
[c]email :ysdxwenfa@163.com , [D]email :liubangfan@sina.com,

Keywords: E-Government 2.0; Basic Government; Public Service

Abstract: Although the construction of E-government in our country has advanced into the era of E-government 2.0 from E-government 1.0, whose development greatly promotes the integration and improvement of governmental public service and management ability. Basic government is the main supplier of lots of public services,and for basic government,using E-government 2.0 to provide and to improve public service is an important mean to improve service quality and efficiency.However,in practice,E-government still faces obstacles in aspects of concept,institution and resource in the application of basic public service.Eliminating these obstacles,and promoting E-government 2.0 to function,will further improve the efficiency and level of basic public service.

Introduction

The so-called "E-government 2.0",is to apply one or several kinds of techniques of Web2.0 in E-government[1].E-government is a platform and mode where application information communication technology conducts network integration and flat management of public management matters,and government can use E-government to reform traditional government into electronic government.The incipient E-government cannot satisfy technically the interaction between the public and the manager,which can be achieved by E-government2.0,thus achieving electronic service which confronts the public and orients the public as the core.

1. Application of E-government2.0 in Basic Public Service

E-government2.0 applies new concepts and technical support of Web2.0,improves the efficiency of basic government, and transforms the relation between the public and government.E-government2.0 is the upgraded version of E-government1.0.E-government2.0 will not only link government departments with each other,government with enterprises,and government with the public through network communication technology,establish a new ,interactive and ever-present service form,but also achieve one-station and timely public application platform around satisfying public demand.At the same time government can also publish information by E-government2.0,obtain various feedback information and the demand for service of the public,manage public matters and provide public service. The specific application forms of E-government2.0 in basic public service are shown as following aspects：

1.1 Information Release Window of Basic Public Service

The function of government portal website is to publish public service information,but the current construction of electronic government certainly demands fundamental construction and development in the prophase of E-government,which makes closer information transmission window relation between E-government construction and information platform,and thus is beneficial for the achievement of mutual assistance function between the two.Basic public service relies on government portal website to publish and to open up public service and public policy through the medium of information service,thus making cut the distance between government and the public,which delivers duly social service value loaded by information service.For instance,RSS in E-government2.0 is a kind of Web2.0 content syndication format and possesses a set of bidirectional and interactive linkage applications program which can achieve Web content among

content consolidators,content providers and final users.If the public relies on RSS service in E-government,the public takes RSS reader as carrier to browse and to criticize views,policies and regulation,etc.of government,thus establishing electronic service information integrated world of society and government.

1.2 Coordination Office Platform of Basic Government Departments

E-government takes information technology of that period as carrier,and merely drives directly the artificial way into automation stage.It is thus clear that the process is to extract operation staff from the stage of conducting repeated work step by step,and then to simplify its work layer and to perfect work flow[2].Through using network technology such as Blog,Wiki,etc.,on the basis of E-government1.0,E-government2.0 will establish some inter-departmental and inter-organization communities.It will rebuild business flow,and thus conduct foreground government integration of original decentralized government.And it will also conduct cross-foreground-background cooperation and inter-departmental coordination office of background business departments drove by service administration.For instance,administration service center,one-station service and citizenry card are all typical cases of applying cooperation office mode.

2. Obstacles of E-Government2.0's Application in Basic Public Service

The application of E-government2.0 in basic governments can strongly promote the quality an efficiency of basic public service. However,in practice,the whole application rate of E-government2.0 in basic public service is low,and the application of E-government2.0 of basic governmental departments is insufficient,and governments are still accustomed to the traditional monomial mode where governments provide public services directly to the public.E-government2.0 cannot function fully because of the presence of obstacles in the aspect of concept,institution and resource.[2]

2.1 Conceptual Obstacles of E-Government2.0's Application in Basic Public Service

The leaders and the administrative staff do not value sufficiently E-government2.0,and are affected by official standard and the thinking of monopoly on governmental information,thus making low the degree of E-government's usage in basic governments.Affected by traditional administrative culture,bureaucrats in basic governments do not change official-standardized thinking fundamentally,whose bureaucracy and privilege thinking are ingrained.In their thinking,they think that the government rules the people,so they are accustomed to regulating the public rather than providing service.The construction of government portal websites-as the carriers of E-government public service-do not reflect the central concept which takes the public as the core and serves the public,but the social public service information cannot be found. The most prominent flaw of basic government's portal websites is that the content is incomplete, and the update speed is slow,and the websites cannot meet the timeliness demand of the public for information.Some basic government's websites also set columns such as message boards for communicating with the public,but many comments and problems of the public do not receive timely treatment,which cannot function to communicate with the public.On the one hand,basic governments's monopoly of information makes congested the way of public participation in administration and discussion of politics, which cannot know the demand of the public,thus causing the divorce between administrative decision and real demand,and poor effect of implementation.On the other hand,information disclosure is limited,and the public cannot effectively supervise government's administrative activities,thus making possible the abuse of administrative power.

2.2 Institutional Obstacles of E-Government2.0's Application in Basic Public Service

Institutional obstacles of E-government2.0's application in basic public service are shown in two aspects including segmentation of trap and block of governmental organizational mechanism and disperse information.Current governmental administrative structure in our country is matrix organizational structure,however,what must be considered is that matrix structure under segmentation of trap and block will certainly increase node departments and possibility that the local protectionism of departmental head occurs,thus causing further the phenomenon of institutional corruption.At the same time,each node department will formulate decision and take

action from their own interests,and every government and every department are insufficient in interaction and communication,which causes the increase of administrative cost and the decrease of administrative efficiency. Fragmentation among governments is not conducive to the construction and development of E-government2.0.Each department uses different standard from their own business demand,thus causing the phenomenon of information interaction absence among each node department and between upper government and basic government,and thus finally making relatively low sharing degree of public service information.E-government2.0,a systematic and compositive program,needs a unified plan to achieve the sharing of information resources .Meanwhile, absence of sharing system of public service,will certainly affect the construction process of E-government2.0 in basic government,and will also cause lots of repeated construction and waste of resources.

2.3 Resource Obstacles of E-Government2.0's Application in Basic Public Service

Resource Obstacles of E-Government2.0's Application in Basic Public Service are shown in the absence of material resources and human resources.On the aspect of material resources,because of insufficiency of basic government's monetary expenditure,insufficiency of investment of hardware and software,and,the backwardness of electronic information facilities in remote region such as villages,application rate of E-government2.0 is low,which causes each government to provide service mainly by traditional method and to be unable to represent convenient and timely effect of network service.The basic government's construction of database is not mature enough,and data is incomplete, and information is confused,and,the update and maintenance of database are insufficient,which causes the absence of vast information and the disarray of management,thus making the level of public service low.[3] Because internet coverage rate and home networking rate in remote areas such as villages are low, acceptance of network path of government information is low,thus making inaccessible to obtain network service and even more to participate in government-society bidirectional management through the network.Requirements of E-government2.0's construction for administrative staff is not only to master the basic knowledge of computer operation,but also to possess some application skills of E-government software system.However,currently,staff who can apply proficiently E-government operating system are very small in civil servants system of basic government .

3. Measures to Promote the Application of E-Government2.0 in Basic Public Service

Conceptual, institutional and resource obstacles of E-government2.0's application in basic public service seriously hamper the development of basic public service.The advanced technology of E-government2.0 cannot be capitalized fully and cannot reflect its advantages.Therefore to make efforts in the following aspects eliminates obstacles of E-government2.0's development,in order to create conditions for improving level of basic public service.

3.1 Transforming Service Concept of Basic Governmental Service

To transform consciousness of government departments and the role location,converts from original administration into service.E-government2.0,taking the public as the dominant,provides new concepts for basic government.When basic governments take advantage of E-government2.0 to transform governmental functions,basic governments need to consider demand of people, in order to better provide the most urgent service for people.When governments formulate policy and make decision,governments can take advantage of political and public communication channels to carry out research, solicit public opinion,know public demand,and optimize constantly basic public service.[4] Basic government should set up a transparent administrative concept,to let the government's rights operate under the sun.Basic governments should make greater breakthrough in information disclosure,and open up all information which can be published to the public.The application of E-government2.0 provides smooth, convenient channel for the public to obtain government information,and satisfies the citizen's right to know and participate.Basic governments through E-government2.0 expose behaviors under the sun, conducting transparent administration.

3.2 Promoting the Cooperation among Basic Governments and Realizing Information Sharing

Cooperation among basic governments facilitates the sharing of information between the government and the Department and the information sharing among institutions will promote the smooth development of cooperative service among basic governments,both of which are mutually functional and mutually stimulative relation.To improve the level of information sharing,needs to make efforts in two aspects.On the one hand, the depth and breadth of information resources are the key task in the current information construction.Public service of basic governments should establish a wealth of information database through collection and integration of information,expand the amount of information and optimize quality of resource through resource allocation,and establish information base about population, cadaster,economy, community, environment and transportation,etc.to provide a rich source for information sharing.On the other hand,establishing the integrated information resource management system unifies data standard and operation mechanism,to let governments at all levels and each department obtain the data they need in information database and to reduce administrative cost,and to improve administrative efficiency.

3.3 Increasing Investment and Enriching Material and Human Resources

The central authorities and basic governments at all levels should increase the investment of developing E-government,for the rural areas set basic hardware and software facilities,and comprehensively realize online office of basic governments,thus further developing towards E-government2.0 system.Equipping with professional technical staff to help basic governments to establish the basic information database about population,cadaster and economy,etc.,ameliorates the situation of information absence.Country should accelerate network covering every village project,to let farmers surf the Internet home and share equally network service with city residents.The lack of professional E-government talents in basic governments is caused mainly by two reasons:firstly,the supply shortage of talents and secondly,the neglect of E-government skills in civil servants selection.Therefore,to meet the demand for E-government human resource should begin from the two aspects.On the one hand,to increase the supply of professional E-government talents can be achieved through school education and on-the-job train.School education is to set up major and courses related to E-government in colleges and universities,which lets students master the basic knowledge of E-government and smoothly conduct online office when they enter into governments afterwards.E-government2.0 can promote the improvement of level of basic public service,and thus further promote the construction of service government in our country.Currently,in our country,the development of E-government in central authorities and provincial and municipal governments is relatively fast.Therefore what should be done is to move the construction center of E-government2.0 down into base course,which realizes comprehensive and balanced development from the top to the base,and which accelerates the construction process of government administrative information,modernization and service in our country.

References

[1]Wang Congxia &Fang Jie.*Study on Application Field of Web2.0 in E-government and its problems*.*Library theory and Practice,*2010,02:53-55.

[2]Wang Jianfeng.*On Basis of Web2.0 the Application of Virtual Community in Academic Research*.*Information Technology*,2013,01:184-187.

[3]Tian Peng,Wang Weijun&Liu Rui.*Study on the Influence of the Application of Web2.0 Technology on the Behavior of Knowledge Sharing*.*Information Science*,2011,05:647-651.

[4]Xu Hongyu.*Web2 0 Application Technology Integrated with Knowledge Management*.*Modern Information*,2012,01:44-47.

[5]Jing Peidong&Wang Ying.*The Application of Web2.0 in Government Information Work*.*Science Development: Social Management and Social Harmony -- 2011 Academic Essays (I)*:2011:7.

Advanced Materials Research Vols. 989-994 (2014) pp 4717-4722
© (2014) Trans Tech Publications, Switzerland
doi:10.4028/www.scientific.net/AMR.989-994.4717

The Big Data How to influence the development of E-government

Li Bo[1,2,a],Liu Bangfan [2,b],Liu Naixi[2,c]

[1]Qinhuangdao Vocational and Technical College, Qinhuangdao China 066004
[2]Humanities-law College Yanshan University, Qinhuangdao China 066004
[a]email:ysdxwenfa@126.com, [b]email:liubangfan@sina.com, [c]email :ysdxwenfa@163.com

Keywords: Big Data;Cloud Computing;E-government

Abstract: Big data is an emerging concept in the field of computer and E-government recently,but research institutions and scholars have different opinions in the content and understanding of big data.In the era of big data,E-government is facing great challenges and tests,and the processing of complex data in the era of big data will become the main theme of the development of E-government in our country.Through analyzing processing mode of big data,and on this basis,this thesis discussed the influence of the era of big data on the development of E-government,in order to find an effective path under the mode of big data to develop E-government.

1. Overview of Big Data and Big Government

1.1 Big Data

Big data is an emerging concept in the field of computer or E-government.For the content of big data,enterprises and the academic circles have not yet formed an accurate definition.Wikipedia defines big data as "a collection of data sets so large and complex that it becomes difficult to process using on-hand database management tools or traditional data processing applications"[1];the authority of IT research and advisory consulting company Gartner defined big data as"a matter of extreme information management and processing,which exceeds the processing capacity of traditional information technology in one or more dimensions "[2];moreover USA National Science Foundation(NSF) defines big data as "large-scale, diversified, complex, long-term distributed data sets generated by various data sources including scientific instruments, sensing devices, the Internet trading, e-mail,audio and video software, web click stream "[3].

1.2 Big Government

Now the development of E-government has brought many new changes.In the past the E-government is the application using the Web1.0 by PC computer connected to the Internet,while now along with the development of information technology including mobile Internet,the Internet of things and cloud computing,etc.,and the popularization of mobile terminal equipment,more network application and a large amount of data have been produced,indicating the arrival of the era of big data.Under the context of big data,E-government will certainly move on to a new stage,i.e. the stage of "Big Government".Big government can be defined as:in the context of development of new generation of information technology including mobile Internet, Internet of things, and cloud computing,etc.,along with the context where increasing mobile terminal equipments and increasing software applications produce a large amount of data,the government makes full use of the change of the context(mobility,openness),uses a variety of techniques of the era of big data,has the aid of the character that the analysis techniques of big data locate precisely, achieves the optimization and reorganization of the governmental organizational structure and the work flow,exceeds the limits of time,space and department separation,and establishes a streamlined, efficient, honest, fair governmental operation mode,so as to provide high-quality,standardized,transparent management and service conforming to the international standard in all directions."Big Government" is the manifestation of E-governmental "Big Wisdom",and will better support the national wisdom city construction.Moreover relying on big data to construct the "Big Government",the method's advantages and characters are showed in Figure 1.

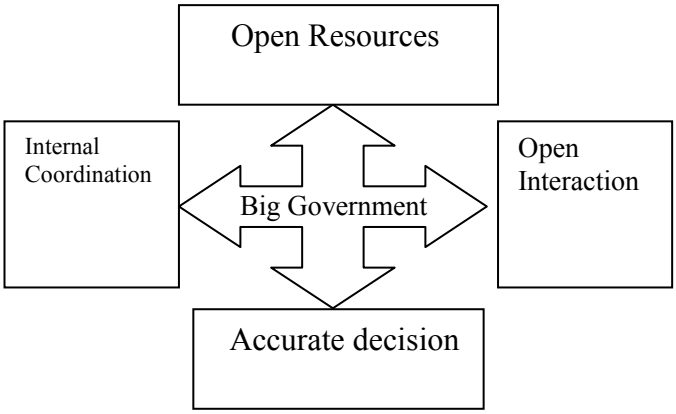

Figure 1 The advantages and characters of Big Government

1.3 the Relationship between Big Data and Cloud Computing

Big Data and Cloud Computing complement each other.Cloud Computing is the IT basis of Big Data,and Big Data is a killer application of Cloud Computing.Cloud Computing is the driving force for growth of Big Data.In the other hand,because data are becoming more and more complex and increasingly real-time,it is more necessary for mining,analyzing and processing.

At present,Cloud Computing has popularized and become the mainstream technology of IT industry.Its essence is a basic architecture and business model generated in the demand context where computation becomes more and more huge,and data becomes more and more,increasingly dynamic and increasingly real-time.

The emergence of Big Data is causing worldwide profound transformation of technology and commerce.On technology,Big Data has changed the conventional way of extracting information from data.In the field of technology,in the past relying more on the way of model,now we can borrow large scale of data,and use method based on statistics,hoping to make new progress in areas including speech recognition, machine translation in this Big Data era.On the business model,for the participants of commercial competition,Big Data means the exciting innovation opportunities of business and service.Retail chain enterprises and electric business tycoons have had a lot of successful cases in big data exploring and marketing innovation.

Overall,Cloud Computing and Big Data differ mainly in two aspects in application:Firstly,they are different in concept.Cloud Computing changes IT,while Big Data changes business.However, Big Data must have the cloud as infrastructure to smoothly operate.Secondly, the target audience of Big Data and Cloud Computing is different.Cloud Computing is the technology and product sold to CIO,and an advanced IT solution.However Big Data is the product sold to CEO and business layer and the policymaker of Big Data is business layer.Because they can directly feel the pressure from market competition,they must beat rivals by means more competitive in business.

2. The Processing Mode of Big Data

The processing mode of Big Data evolutes from traditional database cluster to Cloud Computing MapReduce massively parallel processing structure,and achieves the decomposition process of task and the merger of result,so as to achieve unlimited extension of scale of disposable data. Barge Data processing techniques have been considered another subversive technological change after cloud computing,Internet of things in IT industry.

2.1 Mode of Database Cluster

Cluster means loosely-coupled sets of computing nodes which constitute from running the same set of applications through the cooperative work, providing a single system image for clients and applications,and using specific way of connection to make hardware equipment combined.It has the following advantages:performance lifting,extensibility lifting,reliability lifting.Database cluster introduces the cluster technology into the database[6].Database cluster has some limitations in technology,specifically introducing as follows:

Using PC server as a function node,too many system cables,too high complexity of hardware,and pretty difficult implementation of erection,make extensibility limited;High speed interconnected devices must be connected with main engine through the PCI of main engine,but the transmission rate of PCI cannot meet the demand of data communication among the nodes of parallel database cluster;Space for improvement of the database security and extensibility of data sets is minimum,and four technical indicators including all-round speed promotion,data synchronization,security guarantee,and extensibility,are huge problems;As the increase in amount of equipment and the complexity of application,it is necessary to rapidly superadd investment to solve all kinds of problems of compatibility and reliability,etc.;Parallel database mainly uses shared-nothing structure,and is insufficient in aspects of extension, fault tolerance, cost, and ability to support heterogeneous environment and interacts,thus extensibility is very limited and at present, there is still no application case of a scale of thousands of nodes.

2.2 MapReduce Framework Mode

Cloud Computing Structure forms server cluster by large-scale low-end servers, provides vast storage space and processing capacity of large-scale data,and has reliability, extensibility and high availability.Therefore electronic business platforms including Institute of Computing Technology, Chinese Academy of Science(ICT),China Mobile,Baidu,Taobao and Netease, use mainstream Cloud Computing platform-Hadoop Structure-to conduct Web search and analysis of Big Data,etc.MadReduce Structure includes:Distributed File System(HDFS),Parallel Programming Model MadReduce,and Parallel Execution Engine.

From the perspective of HDFS,Hadoop's node consists of data node which stores and provides location service, and name node which manages namespace of distributed file system.Structure design of HDFS host-guest structure greatly simplifies distributed system structure.The design features of its file system:centralized management of metadata,scattered storage of data block（64 MB） to guarantee security of data,and data replication(at least three backups for every data) to achieve high fault tolerance[3].The traditional database system has high real-time responsibility,but for Big Data of Class TB or Class PB,search speed of data mining fells sharply.However introducing mechanism where HDFS and RDBMS combine can make full use of advantages of the two,and achieve highly-efficient data mining and decision support[9].

MadReduce,designed by Google and used to process parallel computing on big data sets of cluster,is a typical representative of non-relational data management and analysis technology.MadReduce makes data processing task abstracted into a series of map and reduce operation, completes respectively filtration and aggregation operation of data,and conducts management through simple interface.Simply put, its calculation process and basic principle are to make big data sets decomposed into hundreds of small data sets,each(or some) data sets processed by a node of cluster and to generate intermediate results.These intermediate results are merged by a lot of nodes,and form the final results. As shown in Figure 2.

Main coding work,based on computing model writing distributed parallel programs ,is to achieve map and reduce function.Other complex problems such as distributed storage, job scheduling,load balance,fault tolerant processing and internet communication,etc.,is in the charge of MadReduce to process.MadReduce has simple principle,simple technology and high efficiency in data processing,and in the system level solves the stubborn problems of database cluster such as extensibility, fault tolerance.MadReduce opens resource for free,builds large-scale cluster elastic to stretch out and draw back on the basis of heterogeneous cheap server,and processes and analyzes large-scale data parallelly in distributed way.Its cost of construction is far lower than that of parallel database used by database cluster[9].Comparative analysis of several kinds of big data processing mode is shown in Table 1.Therefore MadReduce big data processing mode has relatively noticeable advantages.

Table 1. Comparative analysis of big data processing mode

Character	Database Cluster Mode	MapReduce Structure Mode
Extensibility	very limited, hundreds of nodes	extensible to exceed platforms, thousands of nodes
Integrity	poor on fault tolerance,task processing,and disaster recovery	high fault tolerance,robustness
Security	failing node to affect entirety	failing node not to affect entirety
Flexibility	low	high
Data Processing Ability	mainly supports structural data	supports complex data processing,including structural data and non-structural data
Processing Efficiency	relies on optimized distributed programming design	high
Heterogeneous Storage	unsufficient	highly supportive
Cost	high complexity of hardware, and rapid increase of additional investment	low demand of hardware, and low cost of extension

3. The Influence of Big Data on the Development of E-Government

The development of big data will greatly change the managerial mode of government.Its inclusiveness will blur the borders among various government departments and between government and citizenry.The phenomenon of information island will reduce greatly,and data sharing becomes possible,thus improving coordinative office efficiency and civil service efficiency,and promoting the government's ability of social management and public service.Specifically, relying on the development of big data will be in favor of saving government investment and strengthening market supervision,thus improving the decision-making ability of government,promoting ability of public service and realizing regional management.

Capitalizing big data to integrate information and to share and compare enterprises fundamental information collected by departments such as Department of Industry and Commerce, National Tax Bureau, Local Tax Bureau,and quality inspection department, through analysis,can discover regulatory loopholes,raise the level of law enforcement and achieve the objective to promote fiscal income and to improve the level of market supervision.Establishing the center of Big Data,strengthening the acquisition, organization, analysis, decision-making of government data,achieving unified management of large data for government information resources by Cloud Computing Techniques,and conducting exploitation and utilization of government resources according to the laws and regulations and the demand of each department,can improve the utilization rate of equipment resources,avoid overlapping projects and reduce maintenance cost.

Big data will also further improve the efficiency of decision-making,improve the accuracy and scientificity of government's decision-making,improve the government's ability of forecasting and warning and of emergency response,and save cost of decision-making.Taking the fiscal department for example,on the basis of Cloud Computing and Big Data Techniques,the fiscal department can handle data of every department according to demand and analyze the data.Thus the decision can be more accurate and more efficient.In addition,the fiscal department can also promote fiscal innovation on the basis of data,thus making fiscal work more efficient,more open and pore transparent.Capitalizing Big Data,can also gradually achieve three-dimensional, multi-level, comprehensive public service system of E-government, promote openness of information,drive service functions such as real-time receiving online service,cooperative sector management and feedback on the Internet query, accelerate the intelligent E-government services and preliminary application of mobile E-government service new mode,expand personalized service constantly,and further enhance the direct two-way interaction and synchronous communication among government,society and citizenry.

Management based on city grid requires a unified and coordinated integration of management information,and all kinds of basic resources and information should be shared commonly.Big Data can achieve that.By making full use of various resources of Big Data,playing the managerial utility of city grid will achieve the greatest degree of shared application,in order to improve the service

quality city and community, to improve the service ability,to strengthen the service management and to create a service-oriented society,thus making the level of city management and community service to a higher class.

4.In the Era of Big Data the Development Path of E-Government in Our Country

Although at present the information sharing construction based on Big Data in our country was partly successful.However,in general,the cross-sector utilization system of information resource is still limited in small parts of the government's business scope and, the depth and breadth of applications are still far sufficient,which cannot meet the requirement of development of modern society.Therefore we need to conform to the trend of Big Data,build online business hall,exchange and sharing platform, social credit system,disaster recovery backup system and open platform on the basis of Big Data,build Cloud Computing platform of government,and actively promote the construction of E-government.

Building Province-Municipality-County tri-level unified online business hall which sets information disclosure, online processing, convenient service, electronic monitoring in one,by virtual service window,provides one-station, cross-regional, all-weather, and transparent various social service and management matters.At the same time,promoting all classes of substantive administrative service hall to move to online business hall,achieves effective integration of cross-department online matters and promotes online affairs of the whole process.

Entirely building Province-Municipality-County tri-level exchange and sharing platform of Big Data,perfects the coverage of exchange and sharing platform,opens up the horizontal and vertical sharing channel of information,and promotes cross-regional,cross-department information resource sharing and business collaboration.At the same time,perfecting information resource catalog system of the whole province,formulating information resource sharing catalog of the whole province and data criteria,and strengthening the integration of various information resources,provide cross-layer,cross-department data support for provincial,municipal and county governments to deepen the application of E-government.Building mechanism of exchange, integration, comparison, update, maintenance among data centers and among database of all-class government,and building fundamental database of natural person, legal person, spatial geography,etc.,provides data support for social management,public service and macro-control.

Integrating credit and information resources from government functional departments,enterprises and institutions, guilds, and intermediary organizations,and promoting and regulating the construction of credit institution,provide complete, accurate, and timely credit information of enterprise and individual.At the same time,building individual credit information platform, exploring the construction mode of individual credit system,and promoting the exploitation and utilization of individual credit information,lay a solid foundation for building credit society.

Carrying out the top-level design of E-government public service platform based on Cloud Computing,and building centralized and unified regional E-government Cloud platform,provide server resources, huge storage space, high bandwidth of network and safe network environment for government departments.E-government Cloud platform will be built in accordance with unified criteria,which can be plug-and-play.Government departments can also customize and use the E-government Cloud platform according to their own demands.Creating a new situation where information is shared jointly,and resources are shared jointly,and operation and maintenance are managed jointly, gradually achieves the goal that government departments unify server management,generator room,operation and maintenance,in order to fully integrate resources, improve utilization rate of resources,and reduce overlapping investment.

Building disaster recovery backup facilities,provides unified disaster recovery backup service for users of party and government.Through techniques such as data backup and data duplication,achieving data-level disaster recovery, ensures the integrity,consistency and availability of business data of each department.At the same time,achieving fast-switching and zero-data-loss application-level disaster recovery for some important application system,thereby provides disaster backup and recovery service of network,data and application system for government departments of the whole province.

5.Summary

Through construction of Big Data center,after processing summary, cleaning, comparison and analysis of government department's data,forming information resources and building a public platform of Big Data, hence open up government data jointly to society and promote exploitation and utilization of information resources by the whole society.

References

[1] http: / / en. wikipedia. org / wiki / Big_data.
[2] http: / / www. gartner. com / it-glossary / big-data.
[3] http: / / www. nsf. gov / funding / pgm_summ. jsp? pims_id = 504767.
[4]Li Minghua. *Big Data to the E-Government*. *Information Construction,*2013,01:18-19.
[5]Huang Huahuan & Xue Lifang. *Big Data,Big Government,New Network—The Development Direction of E-Government Network in the Era of Big Data*. *E-Government*,2013,05:104-109.
[6]Gan Lixin & Tu Wei. *Discussion on Chance and Challenge of E-Government in th Era of Big Data*. *Technology Square*,2013,03:137-140.
[7]Quan Shifeng. *The Function of Big Data Processing on the Development of E-Business under the Environment of Cloud Computing*]. *Knowledge and Technology of Computer*,2013,20:4762-4763+4770.
[8]Wang Jin & Shu Baoqi. *Discussion on E-Government in the Era of Big Data*. *New Century Library*, 2013,07:24-26.

Advanced Materials Research Vols. 989-994 (2014) pp 4723-4726
© (2014) Trans Tech Publications, Switzerland
doi:10.4028/www.scientific.net/AMR.989-994.4723

Design and Implementation of Topology Management Based on EPON Network Management System

YangZhiguo [1, a], LiuDongfei [2,b], GaoYu[3,c(*Corresponding author)]

[1]College of Computer Science and Technology,Wuhan University of Technology,Wuhan,China
[2]College of Computer Science and Technology,Wuhan University of Technology,Wuhan,China
[3]College of Computer Science and Technology,Wuhan University of Technology,Wuhan,China
[a]327723312@qq.com, [b]1073770191@qq.com, [c]490913741@qq.com

Keywords: EPON; topology discovery; topology management; memory management

Abstract

The network bandwidth has been expanded after EPON(Ethernet Passive Optical Network)came.So a topology management for EPON System is needed.In this paper, methods of topological data collection is analyzed, the form of topological data structure object is designed , and topological structure is displayed in the terminal by coding. With introducing in improved memory object and caching techniques, system performance was significantly improved through experiments.

Introduction

EPON(Ethernet Passive Optional Network)solve the problem of limited access network bandwidth.Integrity and vitality of the network topology plays an important role in performance inspecting, event analysis ,fault localization and resource management in terms of network management.Also,it responses to the network service quality intuitively.

Idea of Design

Function

Topology management features include :

1.Topology Discovery, to automatically search the entire EPON network for OLT(Optical Line Terminal) and ONU（Optical Network Unit)and so on ,which support the SNMP,and get informations about the devices.

2.Topological construction, to construct the logical topology graph consistent with the actual network topology in network management system,according to the informations we get.

3.Topology display,to build a topology form of memory objects by informations that found ,and display to the user in a graphical way.

4.Topology edit,users can operate easily and intuitively,including creating a domain, creating a group, creating OLT network elements,creating segments and creating ONU device operations.

Architecture

Topology management is designed as three layers :data acquisition layer, data manipulating layer, and topology display layer. Data acquisition layer is responsible for collecting topology data,including informations of the status of the devices and informations of topology between them,supporting data acquisition methods of multi-thread, multi-point collection and multi -gathering instrument.In data manipulating layer ,the topology data is filtered and assembly to the

topological data structure object needed by topology display layer,and then be passed to the foreground display layer.Topology will be displayed in various styles in topology display layer. Fig. 1 shows the architecture.

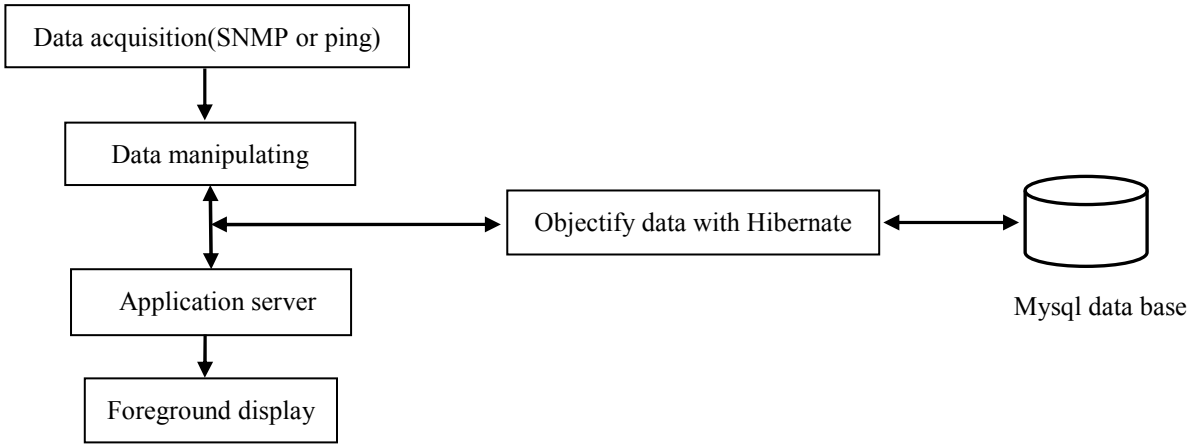

Fig. 1 Topology management architecture diagram

Realization and Improvement

Memory Objects and Database

Data model will be used in interacting with the database persistence layer by business logic layer of the system and foreground display,known as memory object. Memory object is used to implement a topology memory object data model, including *Domain,Group,TopoNeInfo,CardInfo,PortInfo,TopoLinkInfo,OnuDiscoverInfo* and *OnuSearchFilter* etc.Let's take *TopoNeInfo* for example.

As a network element memory object,*TopoNeInfo* inherited base class *BaseObject*,and has properties and behavior of a normal network element *NeInfo*,also it has its own character such as coordinate positions etc.

Design of the table of the database(Mysql) contains all of the memory object corresponds to the data model.Table 1 describes *Domain* as a database table.

Table 1 Database table of *Domain*

Property / field name	field type	field description
domainId	varchar(255)	primary key
domainName	varchar(255)	Domain name
xCoordinate	long	Coordinate x
yCoordinate	long	Coordinate y

How to Realize

Fig. 2 is a flowchart of topology discovery algorithm ,which discovers OLT and ONU devices and their interconnection in the network of EPON.

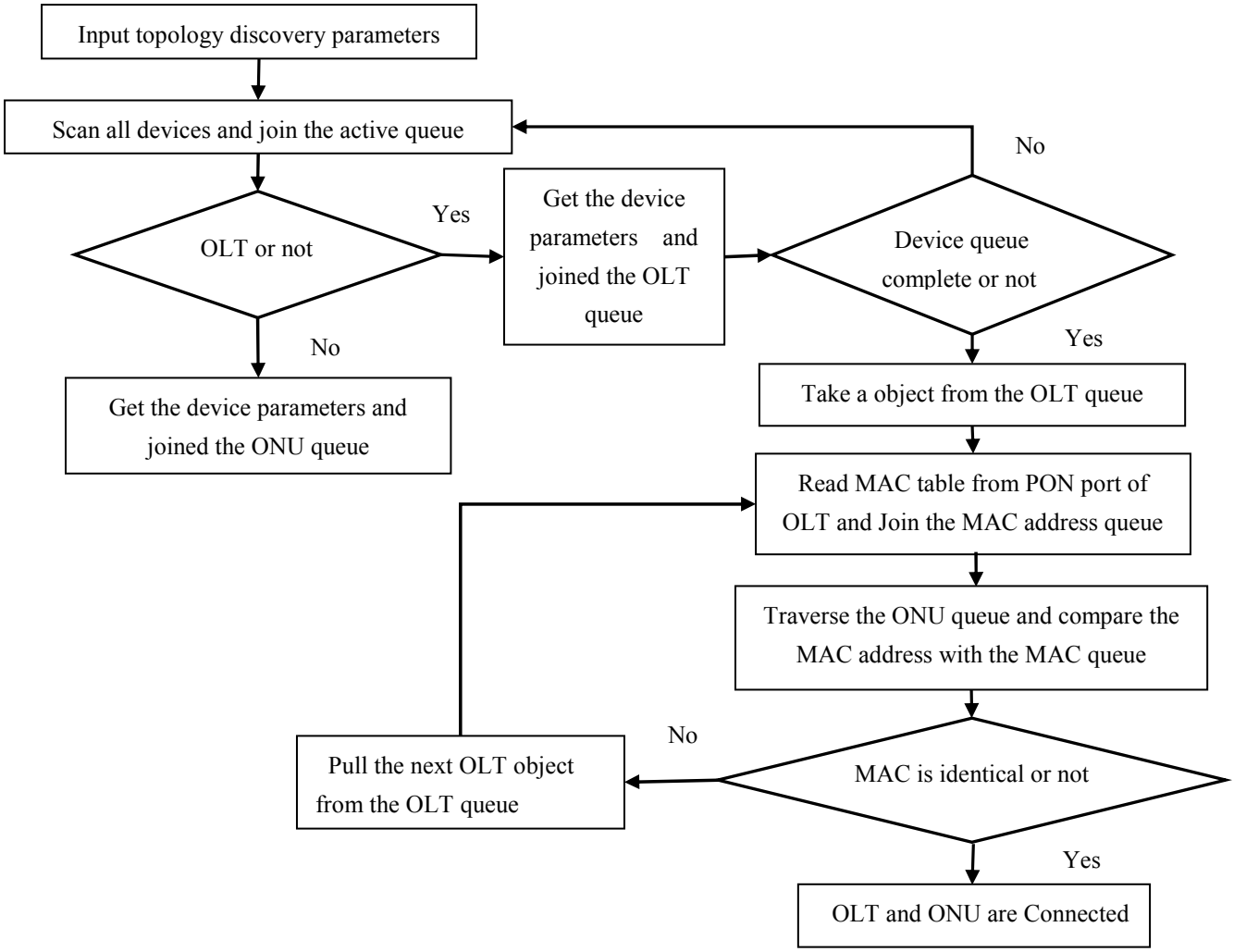

Fig. 2 Flowchart of topology discovery algorithm

In this topology discovery process,ICMP and SNMP are used as data acquisition method. Device state information can be quickly got by *ping* method of ICMP ,and more information about the device can be received by means of *get* method of SNMP.

Gateway network element successive discovery of topology is the method used to discover topology rapidly. First,get the NNI（Network Node Interface）information of gateway network elements from the local connection connect to the elements,and join in the NNI queue,until all the interfaces are found.Then,pull a interface object from the NNI queue and find the interface of the adjacent element *A* ,join in the corresponding interface queue of *A*, and traverse the NNI interface of *A* to find adjacent network element *B* ,then iterate,similar to the thought of Depth - First walk of the tree-structure,until loop through all the network elements for NNI interface informations to discover the entire EPON network topology.

Realization of Topology Display

Considering the scale of EPON network and features,the overall layout is designed as relative layout, which is the hierarchical display;while absolute layout is taken within every subnet,meaning that change the actual information of the node and link locations into the form of the coordinate(x,y)corresponds to the origin (0,0)of the topological interface,also supports the user to manually adjust the layout and save the adjusted results.

Improvements to Memory Object

Split API property supplied by hardware provider into smaller objects,and distinguish important properties and general properties according to the actual needs of customers,meanwhile

the content of the table of the database is modified.The only one property of the main object is the main key corresponds to the primary table,and other properties are scattered in more than one table as the foreign key.

The Result of the Test

All of the three types of OLT devoices are found by network elementdiscovery,but before that domain, subnet, and groups should be created,so that network elements in a certain category can be distinguished. After improvements to the memory object,redundant data that occupied the memory space is reduced significantly.Table 2 shows the result of in a certain test environment(12 sets of network element equipment ,26 paths between the network elements).

Table 2 Result of test

business situation	network element discovery (before the improvements)			network element discovery(after the improvements)		
	number of equipments	number of paths	elapsed time (seconds)	number of equipments	number of paths	elapsed time (seconds)
null	12	26	3.8	12	26	3.0
1000 business	12	26	5.6	12	26	4.3
3000 business	12	26	7.8	12	26	6.0

Summary

This paper focus on algorithm of topology discovery,including architecture, functionality, structure, memory objects, topology discovery and topology display.But inadequacies remain,system should be expended to perform topology discovery of new type of equipment.Also,the system structure should develop from c/s to b/s .

References

[1] Zhang Hongwu,Shan Rong:*Researching the EPON Technology in the Intelligent Communication Network* (Information Science and Technology (ICIST), March,2011[C]. Wuhan: Information Science and Technology,2011).

[2] Ioalis P.Chochliouros,George A.Heliotis:optical Access Networks and Advanced Photonics:Technologies and Deployment Strategies(2009).

[3] Sun Zhongwei,Ma Yaning,Sun Fengjie,Wang Yirong:*Access Control For Distribution Automation Using Ethernet Passive Optical Network*(Power and Energy Engineering Conference2010).

[4] Glen Kramer,in:Ethernet Passive Optical Networks(first edition) .USA:McGraw-Hill Professional,Vol.45-83(2005).

[5] Li Lin in:Research on Technology of Network Topology Discovery. Central South University, 2008.5

Advanced Materials Research Vols. 989-994 (2014) pp 4727-4732
© (2014) Trans Tech Publications, Switzerland
doi:10.4028/www.scientific.net/AMR.989-994.4727

The research and application based on competitive scheduling mechanism in Mine Based Wireless Mesh Networks

Qi Shen

School of Software Engineering Beijing University of Technology, Beijing, China

shenq@bjtu.edu.cn

Keywords: self-organizing network; scheduling algorithm; media access control

Abstract.This paper analyzes the current MAC layer protocol for wireless sensor networks based scheduling, according to the transmission of mine environment signal needs, around the traditional CSMA / CA technology, a scheduling algorithm is proposed adjustment factor based on the contention window to more effectively avoid data collisions at the MAC layer transmission process. In order to ensure more equitable sharing of all nodes in wireless link bandwidth. Simulation results show that the algorithm can effectively improve the information in the MAC layer transmission reliability.

1.Introduction

Wireless Mesh network can build multipoint to multipoint network architecture, RFID technology is generally responsible for the deployment of information nodes in the network, While the location aware system can be achieved by using ZigBee, the integration of these three can build an omnipresent information network environment. Based on the mine wireless mesh network architecture, Use of RFID the non-contact automatic identification technology, transmission a frequency of the signal, after treatment and then transmitted to the location aware systems, precise positioning can be achieved in real time, then determine the specific location information. ZigBee is based on the IEEE802.15.4,this is based on the IEEE wireless networking standard security technology, is also an IEEE standard for wireless personal area network working group, has the most power saving, the advantages of maximum network node number and minimum cost, designed for low-cost, low-power multi-node network, this fully satisfy the requirements of the Mine Mesh Networks, so the fusion of ZigBee technology and RFID technology, can greatly improve the performance of mine Mesh network.

ZigBee is based on the IEEE802.15.4,while 802.15.4 MAC layer is based on the 802.11 wireless LAN standard, a good MAC layer protocol for network traffic, capacity and stability has a direct impact. Mine environmental transmission of signals need excellent anti-interference ability, although the 802.15.4 MAC layer protocol combines CSMA / CA (Carrier listening Multiple Access) anti-jamming technology, but the application environment in the mine can not achieve satisfactory results.

2.MAC layer protocol

The MAC layer protocol for wireless Mesh networks need to make the appropriate changes according to the characteristics of wireless Mesh network. Despite the presence of a centralized entity (gateway), however, the gateway will not be able to coordinate the MAC layer node a few hops away. An important problem in wireless Mesh MAC is how to efficiently use multiple physical channels. In the infinite Mesh network, all the access nodes compete for the use of a wireless LAN link resources. Therefore, the need for a queue scheduling mechanism to ensure fairness of all nodes to access resources. Therefore, the need for a queue scheduling mechanism to ensure fairness of all nodes to access resources.

2.1.MAC layer overview

MAC layer is mainly responsible for dealing with tasks of access the physical channel, it provides 2 kinds of services: the MAC layer data transmission service and MAC management service.MAC layer data transmission services primarily to ensure that the correct MAC protocol to send and receive data at the physical layer, while MAC layer management services is responsible for the management and function achieve of MAC layer, including channel scan and access, association of network and exit, synchronization between devices, transport management and other things. Where the MAC layer during data transmission, since the physical transmission media is information sharing, each slot can have only one physical channel occupied physical signal to transmission channel, therefore, the data to be transmitted during the access physical channel will collisions. Although the 802.15.4 MAC layer protocol combines CSMA / CA (Carrier listening Multiple Access) anti-jamming technology, to avoid a collision when data is transmitted.MAC IEEE802.n provides two kinds of media access control mechanism, they are called Distributed Coordination Function(DCF， Distributed Coordination Function)And Point Coordination Function(PCF，Point Coordination Function).

PCF also called uncondensed services. Specifically, PCF uses AP (Access Point) access algorithm in centralized control will send the data right turns to each site, thus avoiding the generation of conflict. On the other hand, DCF is also known as contention Services, that is DCF using CSMA / CA (carrier sense Collision Avoidance) mechanist each node for distributed access method, let each site by the contention channel to get sent right. In Wireless Mesh Networks, the main uses of this competition mechanism, the core algorithm of DCF system is the binary exponential back off algorithm (BEB),to avoid collision between nodes back and forth.

DCF is also the main as a basic control mechanism, is widely used in wireless Mesh networks. However, the core of this algorithm is binary back off algorithm, many drawbacks exist, this paper presents an improved method based on the competition window, to improve the overall performance of the MAC layer.

2.2 The basic scheduling algorithm

In the whole network has many processes responsible for ensuring the efficient operation of network, they are running on different time level, they were: scheduling and buffer management (microseconds), Feedback control (ms), re-negotiation (s), call control - Routing (minutes).

The scheduler acts on each packet, acts as a coordinating role of the minimum strength, its features include: Ensure that different types of services with different QoS, determine whether the network is fair, and allocate bandwidth to different business, to ensure delay, packet loss, to restrictions delay jitter .

Reasonable scheduling algorithm is to determine the key factors that network quality of service. One of the most common algorithms include queue scheduling algorithms including FIFO queue (FIFO), Round Robin (Round Robin), and PF (Proportional Fair) algorithm.

FIFO queue is the most simple scheduling algorithm based on priority. Time stamp packet data in the FIFO queue is the packet arrival time. FIFO queue provides basic storage forwarding function, is currently the most widely used method, it uses queuing method by default, do not need to configure. Its advantages are simple, low cost; on the other hand, its drawback is unable to provide QoS features and isolation technology, lack of fairness, vulnerable to attack illegal users.

First put forward in the scheduling model in the scheduling model is the Round-Robin model, as shown in Figure 1 the principle of the model.

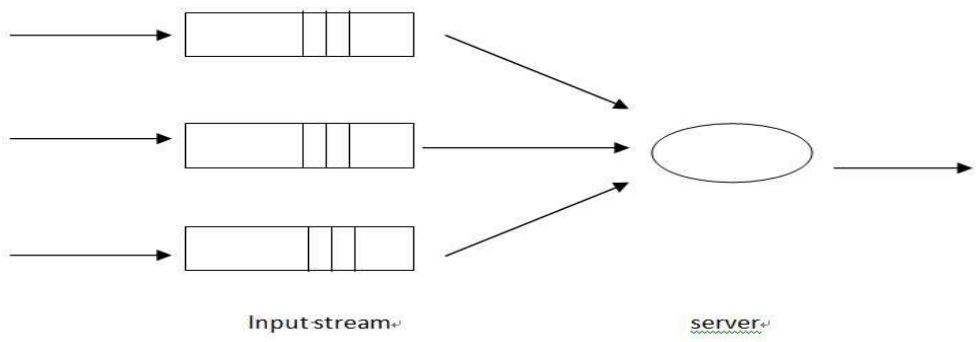

Fig. 1 Robin scheduling model

A scheduler flow to maintain a queue for each service, Round-Robin algorithm sent out a packet from every business stream in the scheduling architecture, Until an empty traffic before transferring to the next traffic. However, when the packet size in the service stream is variable, this method does not provide a fair allocation of bandwidth, Traffic larger obviously get more bandwidth than the small one. Therefore, researchers have proposed an algorithm called Bit-By-Bit Round Robin's. The algorithm assumes that a packet service stream can be divided into a one bit to transmit, the scheduler still turn each of a traffic service. In this model, we assume that $R(t)$ indicates the number of polling algorithm , $N_{ac}(t)$ indicates the number of business activities, business activities in the queue means a bit of business to be transferred. Suppose μ is a scheduler exit rate, there is the following formula:

$$\frac{\partial R}{\partial t} = \frac{\mu}{N_{ac}(t)} \tag{1}$$

After integrating both sides of the equation, we can get

$$R = \int \frac{\mu}{N_{ac}(t)} dt \tag{2}$$

It represents the more the business activities, the slower growth in the number of rounds.

Holzman presents a classical proportional fairness algorithm(PF) in reference [3],the expression of PF algorithm used in the scheduling judgment:

$$i = \arg\max \frac{R_i(t)}{T_i(t)} \tag{3}$$

Wherein, $R_i(t)$ is the transmission rate of user i in timeslot t.the throughput$T_i(t)$ of user i (Equation 3) has been update in each slot by the exponential smoothing process:

$$T_i(t) = \left(1 - \frac{1}{t_c}\right) T_i(t-1) + \frac{1}{t_c} R_i(t) \cdot I(t) \tag{4}$$

Wherein, $I(t)$ is the indicator function: If the user i get scheduled at time slot t, $I(t) = 1$,otherwise, $I(t) = 0$. Where the time constant of the smoothing process (unit: slot), the specific values decided by the maximum access delay of the user i can be tolerated, t values usually between 100 to 1000. As can be seen from Equation 3 and 4,the scheduling verdict of PF algorithm is determined by the transmission rate and throughput: When the transmission rate of a

user is larger or throughput smaller, it can be easier to obtain a certain scheduling. Furthermore, since a low value t_c can speed up the update speed of the $T_i(t)$, when a user does not get any more service at timeslots continuous, the smaller $T_i(t)$ can make $T_i(t)$ decrease rapidly, Allowing the chance of users access to scheduling increased greatly, this shows that the PF algorithm can provide some small-scale service time guarantee for users.

2.3 Packet scheduling algorithm based contention window

In this paper, start with the single FIFO queue mechanism used in the MAC layer protocol. Around the MAC layer protocol. We study the packet scheduling algorithm based on the contention window, and we add a control factor based on the original algorithm, making a better scheduling effect. Assuming all nodes are within transmission range of the other node[4].MAC layer queuing model shown in Figure 2.

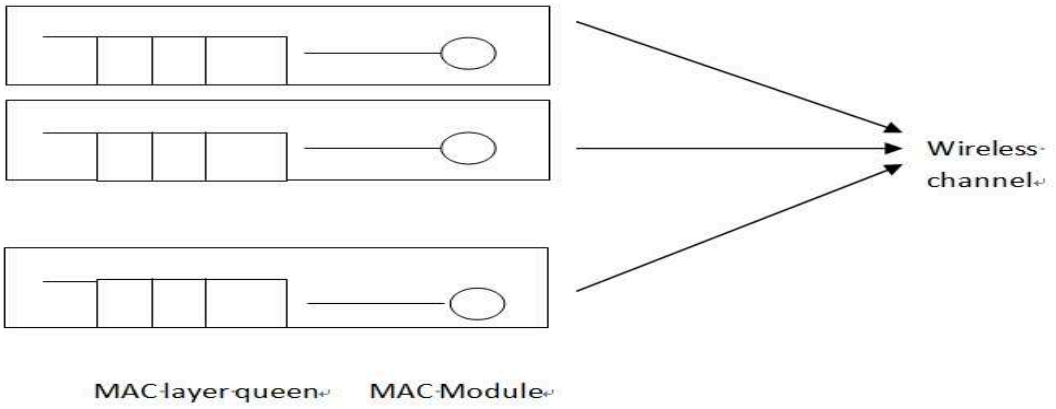

Fig. 2 MAC layer queuing model

The following describes directly a packet scheduling algorithm based on the competition of the window: The main difference between this algorithm and IEEE 802.11 DCF is that collision resolution algorithm. In addition to the original agreement back off window has added a new competitive window. Thus, competition between nodes is divided into two stages: When the channel is free, the node sending data goes into the first back off stage. Only the nodes completed the first phase of retreat can goes into the second stage. Same as IEEE 802.11,The second back off stage can only start after the data channel is idle. However, after the competition of first back off stage, there will be only part of the node enters the second stage back off. This will reduce the probability of collision between the nodes and the new range of back off window can be relatively small.

From the above analysis we can see the advantages of contention window algorithm is significantly reduce the collision probability in the new stage. Its downside is that when there are small number of nodes, to a certain extent, increased channel idle time.

A retreat from the first stage of the competition node using the back off counter BC_1 competition began retreating to solve the problem of collisions.

If BC_1 is nonzero, then BC_1 will randomly select from within $[0, CW_1]$, CW_1 is the contention window of the first stage. If the channel is idle, BC_1 minus 1 per time slot. when channel is idle, and BC_1 minus to 0,The winners advance to the next stage.

BC_2 is the second stage of the competition back off counter, it randomly select from within $[0, CW_2]$, CW_2 is the contention window of this stage. BC_2 minus 1 per time slot. The first one reduced to 0 nodes start access channel, others stops back off activities.

If a node sending the packet successfully, it returns the first back off stage. In fact the channel collision happen in the second stage, and when a collision occurs at this phase, CW_1 and CW_2 are exponentially increased power 2,until reach their maximum.

CW_1 select from within $[CW_{1,\min}, CW_{1,\max}]$, CW_2 select from within $[CW_{2,\min}, CW_{2,\max}]$.After the successful transmission of data packets, the competition window will return to their minimum, waiting for the next delivery.

3.Regulators scheduling algorithm based on the contention window

In order to effectively solve problems related to performance caused retracted, MILD back off algorithm combined with traditional algorithms and different performance in achieving fairness. Inspired by the MILD, This paper attempts to modify the CW reduce and growth in back off algorithm and rules to improve the algorithm. Second window back off counter is no longer a process for reducing the integer 1,But a characteristic combination MILD algorithm-back off diminishing negative exponent form, Corresponds to the inverse of the original protocol retracted, this approach can effectively inhibit the fairness issue, but also to the network quickly tracking system frequency conflicts.

3.1 scheduling algorithm based on the Reusable contention window

A brief description of the principle of improvement: Retracting the first stage described as above. When retracted into the second stage, Back off counter BC_2 value from $[CW_{2,\min}, CW_{2,\max}]$,after a node clashes, contention window CW_2 is multiplied by two, waiting to be sent back. If the conflict continues to occur, repeat until get the window limit values. If the channel is idle, then reduced according to the following formula until reduced to 0;In this algorithm, CW mode are still rising contention window-based approach, using the drop method corresponds to the inverse of the rising process in the second back off stage. CW Rise way based on the contention window, drop method using the inverse process of the process corresponds to rise in the second stage of retraction. It is not difficult to get to this conclusion: If the BC_2 is too small, the possibility of the collision between the entering node of the evacuation second stage will increase. There appears a phenomenon a node can not be serviced. So, BC_2 value from $[CW_{2,\min}, CW_{2,\max}]$;Thus, BC_2 Smooth fast diminishing, can reduce system latency also reduce the network system to track the frequency of conflict, "the response speed."

Therefore, according to the above analysis, we adopt the following strategy.

$$BC_{2,new} = \left\lceil BC_{2,old} \cdot \left(1 - \frac{1}{\log(BC_{2,old})}\right)\right\rceil \tag{5}$$

$\lceil \bullet \rceil$ Said the rounding operation, $BC_{2,new}$ represents BC_2 after the update. $BC_{2,old}$ represents the original BC_2.On the other hand, the multiplicative factor $1/\log(BC_{2,old})$, ensures the drop-off time stationary of the second phase, at the same time, reduced the time BC_2 reduces to 0, thereby increasing the overall response speed.

3.2 Simulation and Analysis of Algorithms

Simulation performance of the algorithm by MATLAB, the window is set as follows: $CW_{1,\min}$ is 31, $CW_{1,\max}$ is 1023, and $CW_{2,\min}$ is 63, $CW_{2,\max}$ is 511, through research the saturation throughput (As the load increases and the system can carry a maximum throughput)to research channel utilization, and assuming that each node always has data waiting to be sent, traffic sources has constant bit rate, and data packet fixed, this paper use 512-byte as sizes of different Data packets, the number of simulation nodes changes from 2 to 64. The following figure shows the throughput comparison of different algorithms.

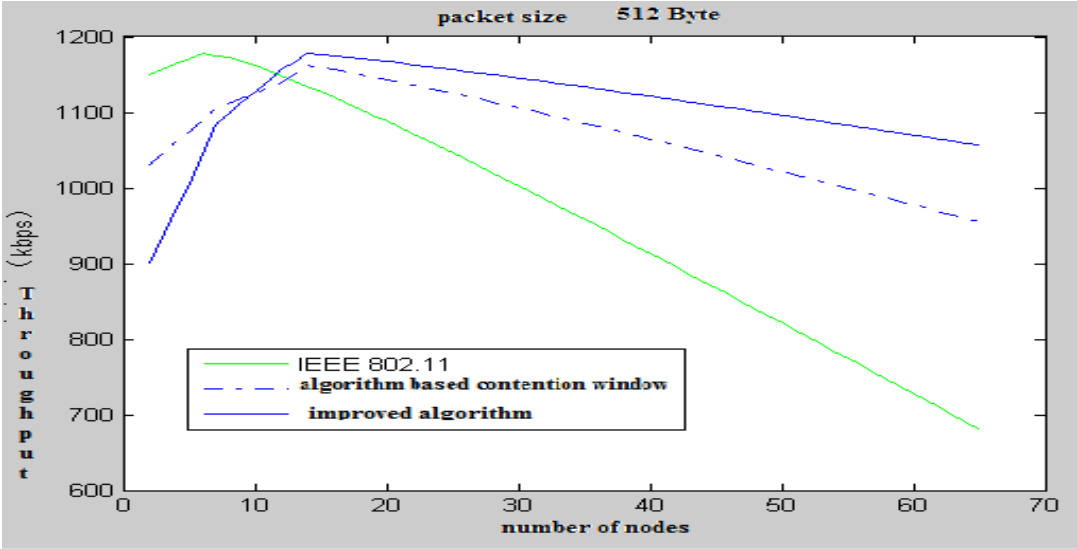

Fig. 3. IEEE802.11 and Comparison of saturation throughput based saturation throughput packet scheduling algorithms

By MATLAB simulation results, we can see, adjustable factor contention window scheduling algorithm based on this article, it can improve anti-jamming capability of wireless Mesh networks, give full play to the advantages of ZigBee technology, provides technical support for the construction of the mine network.

4.Conclusion

On the basis of service and data provided by the MAC layer transmission mechanism and the traditional scheduling algorithm analysis, we propose a new scheduling algorithm to more effectively improve the reliability of data transmission of MAC layer. By adding a new layer of back off window on back off process, you can reasonably control reasonable order what needs simultaneously transmitted data packets need to wait. While since the addition of the back off window, the considerable possibilities of all packets to be sent in the collision new avoidance factor becomes lower, while reducing the probability of collisions occurring again, accelerate the transmission of the data and to ensure the reliability of the MAC layer data.

References

[1] Ergen S C, Varaiya P. TDMA Scheduling Algorithms for SensorNetworks[J]. Wireless Networks, 2010, 16(4): 985-997.

[2] Rui Ding, Jian Guo Nan. Research and Analysis of MAC protocols for wireless sensor networks [J] Computer Engineering, 2009, 35(19): 105-107.

[3] Vaidya NH，Bahl P，Gupta S.Distributed fair scheduling in a wireless LAN.Proc.of MOBICOM，Boston，August 2000:167-168

[4] ZHAO Yizhi，NGUYEN Thuy Ngoc，MA Maode，et al．An Energy-Efficient MAC Protocol with Adaptive Scheduling for Wireless Sensor Networks［C］//IEEE.International Conference on Industrial Informatics Cardiff UK: IEEE Press，2009: 446-451．

Advanced Materials Research Vols. 989-994 (2014) pp 4733-4736
© (2014) Trans Tech Publications, Switzerland
doi:10.4028/www.scientific.net/AMR.989-994.4733

Study on the Technologies of Operating System Scanning

ZHU Nafei, ZHOU Yue, LOU Li and WANG Wei

National Application Software Testing Labs, Beijing, China

{znf, zhouyue, louli, wangwei}@bsw.net.cn

Keywords: Operating System Scanning, Operating System Fingerprinting, TCP/IP Protocol Stack

Abstract. Operating system (OS) scanning makes it possible to focusing further attacks to known weaknesses of that system. The principle of OS scanning is that different OS vendors may make different implementations for the TCP/IP protocol in their OS products. IP, UDP and TCP as well as application layer protocols are can be used for OS scanning. These methods can be used in active ways sending probes to the targets or passive ways only listening without probes. Totally, whether it used in an active or passive way, the essence for OS scanning is analyzing the characteristics of the packets sent by the targets and matching the characteristics with certain operating system. So, in some cases, we need two or more of these methods together to determine the type of the OS for the target.

1 Introduction

Network scanning can be divided into four steps which are host scanning, port scanning, operating system detection and vulnerability scanning. Each of these scans has its own aim and technology. Host scanning determines whether the target host is alive and port scanning detects the open port on the target host. And then, OS detection and vulnerabilities scanning are conducted based on the results of the port scanning. Host and port scanning have been already related in paper [1]. In this paper, we will analyze the technologies of OS scanning, and then make a comparative study among these 15 scanning methods, especially focusing on the active or passive way it takes. This paper is organized as following: In section 2, we introduce the purpose and principle of OS scanning; in section 3, scanning technologies including 15 methods are analyzed; in section 4, we make comparisons among these scanning methods; we conclude this paper in section 6.

2 Purpose and Principle of OS Scanning

Operating system scanning is handy for determining if the attacking target is a Windows, Linux, or other type of machine. Knowing the operating system of the target will save time by focusing attacks to known weaknesses of that system. There is no use in exploring exploits for a Linux machine if the target is running Windows [2].

Operating system scanning has two purposes: obtaining the OS information of the target host and the program information of the services. The principle of OS scanning is that different OS vendors may make different implementations for the TCP/IP protocol in their OS products. Thus, these differences can be used to identify different systems.

3 Technologies of OS Scanning

Totally, the technologies of operating system scanning can be classified as three types, which are banner information detection, HTTP response analysis and TCP/IP stack fingerprinting identification.

3.1Banner Information Detection

Connecting to certain open ports of the host, these service programs, such as FTP, Telnet and Sendmail, often show their Banners, the basic information of these applications, so we can directly get the type of the OS, version number and so on. This may be the simplest method for OS scanning.

3.2 HTTP Response Analysis

After establishing the HTTP connection to the target host, its OS information can be analyzed from the target host responses.

3.3 TCP/IP Stack Fingerprinting Identification

TCP/IP stack fingerprinting is the process of determining the identity of a remote host's operating system by analyzing packets from that host [3]. This process is to scan TCP/IP stacks, shown in Fig.1, efficiently by quickly matching query results against a database of known operating systems. Though the TCP/IP is a standard for network communication, certain parameters within it are left up to the implementation. Different operating systems, even different versions of the same operating system, set different defaults for these values. By collecting and examining these values, one may differentiate among various operating systems, and implementations of TCP/IP.

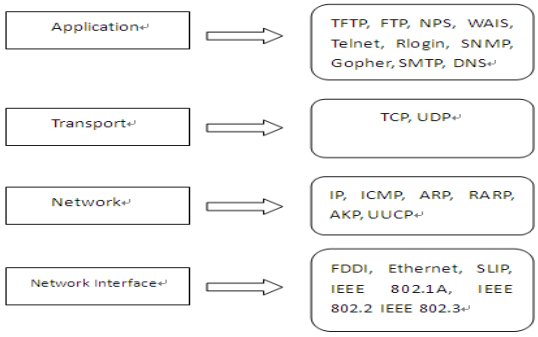

Fig. 1 TCP/IP Protocol Stack

(1) Acknowledge Number

Different OS handles the ACK number in different ways. Sending a FIN/PSH/URG packet to a close the TCP port, most OS will set the ACK number of the response packet (RST packet) as the initial number of the sending packet, while Windows and some printers will send a RST packet with ACK number set to be the initial sequence number added 1.

(2)Type of Service

For ICMP port unreachable message, the TOS (type of service) value of this message package is different among different operating systems. Most operating systems will set the TOS to be 0x0000, while the Linux sets it to be 0xc0.

(3) ICMP Address Mask Request

For ICMP address mask request, only a few operating systems will send back the corresponding responses. These systems include OpenVMS, Windows 95/98/98 SE/ME, Windows NT below 4 SP, and SUN Solaris machines. Furthermore, in the reply to fragment ICMP address mask request, sun system is not the same to others, so we can identify the SUN.

(4) Responding to the FIN

Sending a FIN packet, only the FIN flag set to 1, to an open port, Linux will reply nothing, while other systems, such as MS Windows, CISCO and HP/UX, will responds with a RESET packet.

(5) Fake SYN Packet

Setting an undefined TCP flag in the TCP head of the SYN packet is referred as the fake SYN packet. Sending such a fake packet to the target system, some operating systems, such as Linux machine before 2.0.35, will keep this flag in the responses, while some operating systems will not. Also, some systems will reset the connection when receive this packet.

(6) Initial Sequence Number

Different systems choose TCP ISN (Initial Sequence Number) in different ways [4]. Some UNIX systems adopt the traditional method of 64k progressive increase. New Solaris, IRIX, FreeBSD, Digital UNIX and Cray systems adopt the method of random increment. Linux 2.0, OpenVMS and AIX system use true random methods. Windows system adopts a kind of time correlation model. Some systems use the constant, such as 3com hub uses 0x803, Apple LaserWriter printer uses 0XC7001, etc.

(7) ICMP Error Message
RFC 1812 specifies the sending speed of the ICMP error message. Linux sets the maximum unreachable message (type 3) speed to 80 per 4 seconds. So we can detect the OS by sending a large number of packages to the high UDP ports, and then calculate the number of the unreachable message. But this method need to send a lot of package which is time cost and not credible for the package may be lost in the communication.
(8) ICMP Message Quoting
RFC specifies that ICMP error messages can quote part of the original message caused the error. For the port unreachable messages, the reply packages of the most systems quote the IP request header plus 8 bytes. Solaris quotes a bit more and Linux even much more. Some systems, such as FreeBSD, OpenBSD, ULTRIX, will change the head of the message causing the error and then send it back to the source. This method is still effective to identify Linux and Solaris, even when the target host does not open any port.
(9) Maximum Segment Size
Maximum Segment Size (MSS) represents the maximum package length in a TCP connection, and it is controlled by the initial socket by negotiation during the TCP connection establishment [5]. Different operating systems have different MSS values, and their responses to different MSS values are not the same during the negotiation in the connection establishment. If send a small MSS value to Linux host, it will generally send back this value unchanged, while some other systems will return different values.
(10) SYN Flood Limitation
Different operating systems deal with the SYN flood in different manners [6]. Many systems can only deal with 8 SYN packets at the same time, and they will refuse new TCP connection requests if they are handling more than 8 SYN packets.
(11) TCP Initial Window Size
It is more reliable to estimate the OS by analyzing the initial window, because many operating systems are different in the initial window size. Such as AIX set the initial window size to be 0x3f25, while Windows NT5, OpenBSD, FreeBSD x402E set a value of 0. Analyzing the initial window size in the response packet is another way to estimate the type of the operating system.
(12) DF Flag
In order to improve performance, certain systems set the DF (Don't Fragment) flag "on" when sending the data package, so we can estimate on the type of operating systems according to this.
(13) Time to Live
Each operating system has its own constant TTL (Time to Live) value, such as TTL of LINUX Kernel 2.2.x&2.4.x is 64 , while TTL of FreeBSD 4.1,4.0,3.4 as well as Sun Solaris 2.5.1,2.6,2.7,2.8 is 255, at the same time, TTL of Windows NT and Windows 2000 is 128. So, we can make estimation about the type of operating systems according to this characteristic.

4 Comparisons of the Methods

Here, we make comparisons among all these 15 scanning methods related above to show whether it is an active or passive scanning. Active scanning sends probe packet to the target and estimate the type of the OS by comparing its replies with the operating system database. Passive scanning sniffs the target communication packet instead of sending probe packets to the target. It estimates the type of operating system by analyzing the grasped packet in the same way as the active scanning analyzes the replies. The results are shown in Table 1. In this table, the columns represent the 13 scanning methods and the name of every scanning is demonstrated by the main part of its original name to save space. The rows demonstrate the active and passive ways. If the scanning method can be implemented in such way, we label a " √ " in the corresponding blank.

From this table, we can see that (1) The methods can be used in a passive way are can be used in an active way. (2) ICMP packets are mostly used for active ways, for they are requests and replies in

couples. (3) TCP and UDP protocols can be used by active ways and passive ways. (4) Application layer protocols such Telnet or HTTP are used for active ways. Totally, whether it used in an active or passive way, the essence for OS scanning is analyzing the characteristics of the packets sends by the targets and matching the characteristics with certain operating systems. So, in some cases, we need two or more of these methods together to determine the type of the OS for the target.

Table 1 Comparisons among Scanning Methods

	Banner	HTTP	ACK	TOS	ICMP17	FIN	SYN	ISN
Active	√	√	√	√	√	√	√	√
Passive			√	√				
	ICMP 3	ICMP Quoting	MSS	SYN Flood	Window Size	DF	TTL	
Active	√	√	√	√	√	√	√	
Passive					√	√	√	

5 Conclusion

Operating system scanning is handy for determining if the attacking target is a Windows, Linux, or other type of machine. Knowing the operating system of the target will save time by focusing attacks to known weaknesses of that system. The principle of OS scanning is that different OS vendors may make different implementations for the TCP/IP protocol in their OS products. IP, UDP and TCP as well as application layer protocols are can be used for OS scanning. These methods can be used in active ways sending probes to the targets or passive ways only listening without probes. Totally, whether it used in an active or passive way, the essence for OS scanning is analyzing the characteristics of the packets sent by the targets and matching the characteristics with certain operating system. So, in some cases, we need two or more of these methods together to determine the type of the OS for the target.

Acknowledgement

This research was supported by the Research and Demonstration on the Information Technology Specifications for the Operation Dispatching Command System of the Urban Rail Transit (D141100000714003).

References

[1] N.F. Zhu, Y. Zhou, W. Wei and L. Lou, Analysis on the Technologies of Host and Port Scanning, 2nd International Conference on Computer Software, Data Handling and Applications (CSDHA 2014), April, (2014).

[2] P. Engebretson, in: The Basics of Hacking and Penetration Testing, Elsevier, Waltham, 2011.

[3] M.A. Rahman, M.H. Manshaei, E. Al-Shaer, A Game-theoretic Approach for Deceiving Remote Operating System Fingerprinting, 2013 IEEE Conference on Communications and Network Security (CNS), Oct., (2013), P.73-81.

[4] H. Zhao, Y.Q. Shi, Detecting Covert Channels in Computer Networks Based on Chaos Theory, IEEE Transactions on Information Forensics and Security, 8(2), (2013), P. 273-282.

[5] G. Gómez, J. Lorca, R. García, and Q. Perez, Towards a QoE-Driven Resource Control in LTE and LTE-A Networks Journal of Computer Networks and Communications, (2013), P. 1-15.

[6] J.X. Tao, L. Zhou, Z. Zhou, R. Yang, Defending Against SYN Flood Attack under Asymmetric Routing Environment, International Workshop on Cloud Computing and Information Security, (2013), P. 165-168.

Advanced Materials Research Vols. 989-994 (2014) pp 4737-4741
© (2014) Trans Tech Publications, Switzerland
doi:10.4028/www.scientific.net/AMR.989-994.4737

Design and Implementation of IPv6 Border Router For Wireless Sensor Networks

Heng Wang[1, a],Baoguo Wang[1,b],Shiqiang Zhao[1,c] and XiafuLv[1,d]

[1]Key Laboratory of Industrial Internet of Things and Networked Control, Chongqing University of Posts and Telecommunications, Chongqing, China

[a]wangheng@cqupt.edu.cn, [b]18716321733@163.com,

[c]13629713141@163.com, [d]Lvxf@cqupt.edu.cn

Keywords: 6LoWPAN, border router, wireless sensor networks, IPv6

Abstract. With the rapid development of Internet of things, IPv6 has been introduced into wireless sensor networks and widely used in many areas. It is significant to develop routing devices to connect wireless sensor networks and the Internet based on IPv6 technology. In this paper, we present a 6LoWPAN (IPv6 over Low power Wireless Personal Area Networks) border router scheme. The hardware design and software design are discussed and the experimental results demonstrate the feasibility of the router scheme. By using the proposed border router, the network can achieve end-to-end communications between 6LoWPAN nodes and IPv6 hosts in a universal method.

Introduction

In recent years, with the rise of Internet of things and Wireless Personal Area Networks (WPAN), an important research focus is to combine WPAN with the next generation Internet technology-IPv6. Wireless sensor network is widely used in areas such as smart home, industrial inspection and so on for its short-range and low-power characteristics. The IPv6 technology has huge address space and simplified packet header format, which makes low-speed wireless personal area network nodes connect to the Internet and has its own IP address. As 6LoWPAN utilizes standard IPv6 protocol in the network layer [1], 6LoWPAN nodes can be connected with public IPv6 network hosts through 6LoWPAN (IPv6 over Low power Wireless Personal Area Networks) border router, which can achieve the end-to-end communications.

In this paper, we present a border router aiming to collect data of wireless sensor network and transmit data to public IPv6 hosts if the destination address is known. The function of configuration and management of wireless sensor networks is another aim of 6LoWPAN border router in order to satisfy different application requirements. And users can access the subnet nodes to get information locally or remotely.

System Architecture

6LoWPAN provides a kind of simplified adaptation layer which works between network layer and data link layer. The adaptation layer is used to encapsulate and compress the IPv6 header to allow IPv6 packets to be sent and received over IEEE 802.15.4 based networks. When the border router receives anIPv6 packet, it disassembles the IPv6 packet，compacts it into a shorter 6LoWPAN header and forwards this packet to a sensor node in wireless sensor network. When the border router receives a 6LoWPAN packet from wireless sensor network, it decompresses 6LoWPAN header to full IPv6 header and forwards this packet to IPv6 Internet [2, 3].

The border router presented in the paper consists of two parts, one is a sink node as a gateway and the other is a Linux host. The gateway is used to receive sensor data which is sent periodically by wireless sensor network nodes [4]. When the gateway receives the data sent to remote public IPv6 host, the gateway deliver the data to the Linux host via a SLIP interface. Then the Linux host handles these packets and decides to forward or to discard the packets.

The convergent gateway and Linux host can be connected with any communicated interface [5]. However, we use serial interface in this paper. If Linux host is connected to Internet, then wireless sensor network nodes are able to communicate with IPv6 hosts by end-to-end, which can greatly reduce network complexity and improve communication efficiency. The architecture of 6LoWPAN border router is shown as Fig. 1.

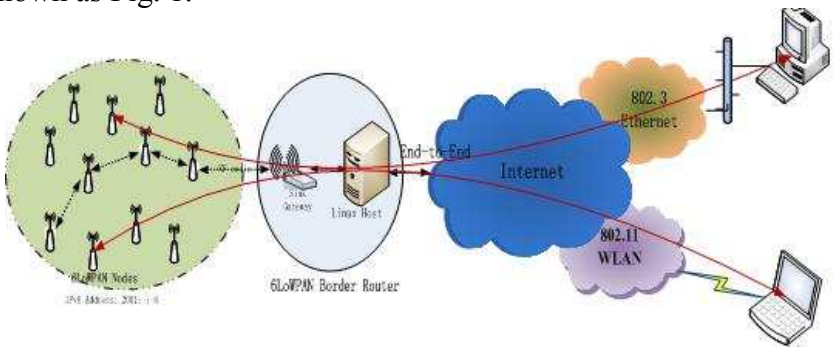

Fig.1 Architecture of 6LoWPAN border router

Design and Implementation

In this section, the detail of design and implementation of the 6LoWPAN border router is discussed.

Hardware Design. It is known from the system design scheme above that the 6LoWPAN border router presented in this paper is made up of a convergent gateway and a Linux host. The hardware design is mainly for the convergent gateway. Considering the convenience and generality of connecting gateway with Linux host, hardware design should be simplified as much as possible to minimize volume. The core part solution is a STM32 chip plus a 2.4 GHz RF module. Other modules include power supply circuit design, debug circuit design and interface circuit design, etc. The architecture of hardware design is shown as Fig.2.

We use STM32F103RB as master control chip for its low price and rich resources, and UZ2400 as wireless RF module of 6LoWPAN border router. UZ2400 is a kind of standard solution conformed to the IEEE 802.15.4 to meet the needs of low cost and low power wireless applications. The master controller connects the RF module by SPI bus.

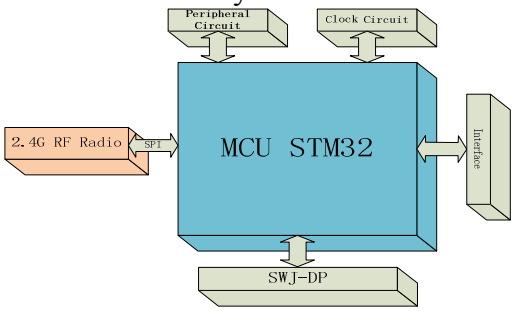

Fig.2 Hardware design of border router

Software Design. The software design of protocol stack is based on Contiki 2.6 operation system. Making full use of existing resources on Contiki, we can improve development effectively. Architecture of protocol stack is shown as Fig.3.

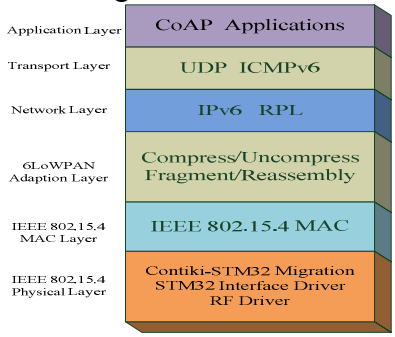

Fig.3 Architecture of protocol stack

There are several mainly sub-modules have to be designed in protocol stack, and they are described as follow.

a) First of all, we use STM32 chip as border router microcontroller. Since the ordinary development environment of this chip is IAR or Keil, we must transplant Contiki operation system to STM32 microcontroller by IAR in order to meet our development habits.

b) Secondly, we use UZ2400 as border router RF module. SinceUZ2400 radio is not supported by Contiki, we should develop the driver in Contiki using STM32 as master controller. We use SPI interface to control RF radio and to send and receive data normally.

c) And then, we use serial interface to communicate with upper computer. So the serial interface of STM32 must be driven in Contiki OS.

d) Finally, we use RPL and CoAP in protocol stack of border router. RPL and CoAP are supported by Contiki 2.6, but how to use it in border router is an actual problem. We integrate CoAP in the application layer in order to make remote hosts access the wireless sensor networks by border router. RPL is used as routing protocol which has the ability to form network and forward packets automatically.

There are two parts of tasks have to be done in 6LoWPAN border router software development. One is protocol stack designed in the sink node for wireless sensor network, and the other is the design and implantation of daemon in Linux host. 6LoWPAN protocol stack running on the sink node, it can compute the data of wireless sensor network and then judge to forward, route or discard them. However, the daemon of Linux host is made for complete the task of driving the sink gateway and forwarding data.

1) Design and Implementation of Protocol Stack. Nodes communicate with each other by RPL protocol in the subnet of wireless sensor networks. So the implementation and use of RPL is very important to the wireless sensor network subnets. RPL is a Distance Vector IPv6 routing protocol for LLNs that specifies how to build a Destination Oriented Directed Acyclic Graph (DODAG) using an objective function and a set of metrics/constraints. The objective function operates on a combination of metrics and constraints to compute the ‘best’ path. There could be several objective functions in operation on the same node and the mesh network because deployments vary greatly with different objectives.

The core function of sink node of 6LoWPAN is to process the received data when it is work as a convergent gateway. The hardware, Contiki operation system and protocol stack need to be initialized when equipment powers on, and then the sink node begin to form and configure a wireless sensor network, finally it is able to receive data of sensor nodes. The convergence gateway can receive data via RF or slip interface. When the data is coming from RF, we analysis the packets step by step according to protocol stack and decide how to deal with them, received, forwarded or discard. When the data is received from SLIP interface, we must judge which type the data is, if command packet is coming, we do what the command required. However, if the packet is the common IPv6 packet that sends to the remote host, then the border router will forwards it according to its destination address.

2) Background Program Design. We must design background program in Linux in order to realize the function of IP routing of 6LoWPAN border router and driving the sink gateway in Linux operation system. The background program Parsing packets and decide how to deal with these packets, so it looks like a transport channel. Daemons are virtually seen as a network interface by Linux operation system via the sink node. So you don’t have to consider how to realize the wireless sensor network sink gateway, just routing, forwarding and dealing with the packets as it should be done. We can implement it by global ways as shown in Fig.4.

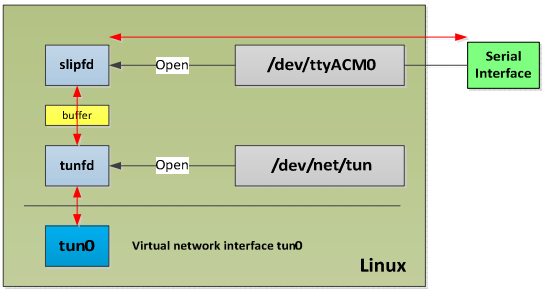

Fig.4 Background program of Linux host

The background program begins to initialize the corresponding interface and network socket when we start it. The daemon must keep listening on multiple interfaces (file descriptor) at the same time, so we can achieve the monitoring on more than one interface by calling select function which is offered by Linux operation system.

Experiment and Evaluation

In order to validate the function of 6LoWPAN border router presented in this paper, we deploy a wireless sensor network on a scale of twenty nodes. Each node reports environmental data once a minute, and then the sink node decides how to deal with these packets when it receives the data. At the same time, we use ping command in the IPv6 host of external network to test the connectivity with 6LoWPAN subnet nodes. As the ping command is an ICMP message sent from the network layer, border router will be routed to forward it when received. If the ping command test passed, we can prove the border router works properly. The test topology is show as Fig.5.

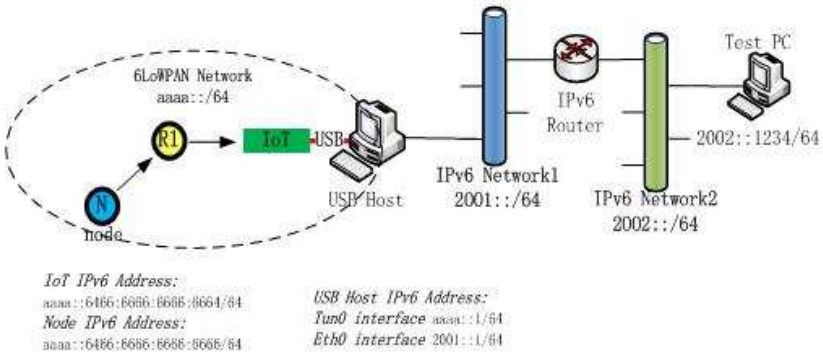

Fig.5 The test topology of 6LoWPAN border router

The network prefix is configured as aaaa::/64, the convergence gateway and 6LoWPAN subnet nodes generate its own IPv6 address according to this prefix , for example, the IPv6 address of one node is aaaa::6466:666:666:666/64. We set the IPv6 address of the Linux host's USB virtual interface aaaa::1/64. Moreover, hosts connect to the Internet by Ethernet. And these two IPv6 networks join each other by IPv6 routers. The test results are show as Fig.6.

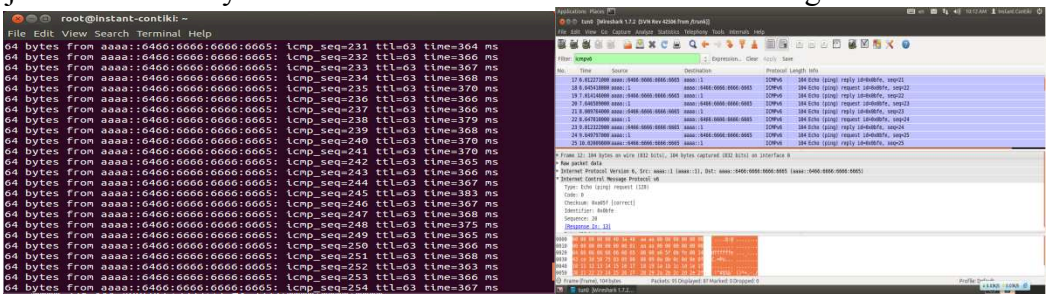

(a) Ping command test (b) Sniffer analysis

Fig.6 6LoWPAN border router Ping command test

We use sniffer in Linux such as Wireshark to analysis the packets received by Linux host. The Wireshark in Linux host can capture these packets. Ping command is an ICMP packet which is sent and forwarded in network. If we use ping command, it will generate request packets firstly, then the

request packets will arrive at the 6LoWPAN border router, since the packets is not sent to border router, then they would be routed and forwarded by border router according to their destination addresses, and the border router will sent the packets to final destination if the network is connected. On the other side, if a terminal node in wireless sensor network receives these request packets, it will reply them, and the response messages will backtrack. According to this experiment, we can test and verify the connectivity of downstream and upstream by 6LoWPAN border router.

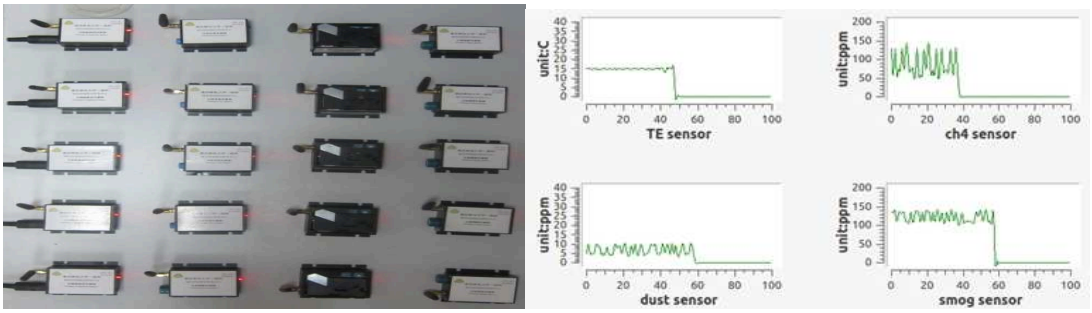

(a) Photo of wireless sensor network nodes; (b) Plots of sensor data

Fig.7 6LoWPAN border router packets forwarding test

In Fig.7, we show photos of 6LoWPAN border router test platform. There are twenty sensor nodes in our demonstrate system, and all data are actually measured. Moreover, the plots of sensor data show that the remote IPv6 host has received the sensor data of 6LoWPAN subnet through the forwarding of the border router. There are four kinds of sensor data shown on the plot which are arranged by time sequence. According to the result, we can prove that the 6LoWPAN border router enables interconnect between wireless sensor network and extern IPv6 network effectively.

Conclusion

This paper developed a prototype of 6LoWPAN border router aiming at seamlessly connecting 6LoWPAN subnet to the public IPv6 networks. The border router consists of a wireless sensor network convergence gateway and a Linux host. It could route and forward the packets between the 6LoWPAN nodes and any IPv6 host with end-to-end communications.

Acknowledgements

This work was supported by the Fundamental and Advanced Research Program of Chongqing (Grant No. cstc2013jcyjA40008), the National Natural Science Foundation of China (Grant No. 61301125), and the Youth Top-notch Talent Support Program of Chongqing.

References

[1] 6LoWPAN Working Group, in: *Transmission of IPv6 Packets over IEEE 802.15.4 Networks*, edited by IETF, (2007).
[2] ROLL Working Group, in: *RPL: IPv6 Routing Protocol for Low-Power and Lossy Networks*, edited by IETF, (2012).
[3] Jonathan W. Hui and David E. Culler.IPv6 in Low-Power Wireless Networks. Proceedings of the IEEE, Vol. 98(2010), p. 1865-1878.
[4] S. Oh, C. Lee. u-Healthcare Sensor Grid Gateway for connecting Wireless Sensor Network and Grid Network. Advanced Communication Technology, 10th International Conference, Vol. 1(2008), p. 827-831.
[5] H. Kang, H. Hong, S. Sung, and K. Kim. Interference and sink capacity of wireless cdma sensor networks with layered architecture. ETRI Journal, Vol. 30(2008), p. 13.

Advanced Materials Research Vols. 989-994 (2014) pp 4742-4746
© (2014) Trans Tech Publications, Switzerland
doi:10.4028/www.scientific.net/AMR.989-994.4742

Design and Realization of On-line Uyghur Handwritten Character Collection System

Halmurat Dilmurat[1, a], and Kurban Ubul[1,2,b *]

[1]School of Information Science and Engineering, Xinjiang University, Urumqi, China

[2] Xinjiang laboratory of multi-language information technology, Xinjiang University, Urumqi, China

[b *]Corresponding author mail: kurbanu@xju.edu.cn

Keywords: Uyghur, handwritten character, stroke, on-line collection

Abstract. Data collection is the first step in handwritten character recognition systems, and the data quality collected effects the whole systems efficiency. As the necessary subsystem of on-line handwritten character/word recognition system, a Uyghur handwritten character collection system is designed and implemented with Visual C++ based on the nature of Uyghur handwriting. Uyghur handwritings is encoded by 8 direction tendency and stored in extension stroke file. And they are collected based on the content of Text Prompt File. From experimental results, it can be concluded that the handwriting collection system indicates its strong validity and efficiency during the collection of Uyghur handwriting.

Introduction

Handwritings has continued to persist as a means of communication and recording information in day to day life even with the introduction of new technologies and design new products [1]. The machine recognition of handwriting has practical significance and successfully applied in reading handwritten notes in a PDA, in document digitization and retrieval, in bank check processing, in postal mail sorting, in pen-based text input, and so on[1,2].

Handwriting data is converted to digital form either by scanning the writing on paper or by writing with special pen on an electronic surface. The two approaches are distinguished as off-line and on-line handwriting separately [1]. In the on-line approach, the two-dimensional coordinates of successive points of the writing as a function of tine are stored in order, i.e., the order of strokes made by the writer is readily available. In the off-line approach, only the completed writing is available as an image.

Early research works for handwriting recognition begin 1960s [3]. Nowadays, the handwriting technologies for English and Chinese character is nearly get mature, and it is being used in practical applications. Studies for on-line and off-line handwriting recognition until 2000 year is summarized in survey paper [1]. Liu et.al [2] evaluated state-of-the-art on line and off line handwritten character recognition methods on the new large scale, unconstrained Chinese handwriting databases CASIA-HWDB and CASIA-OLHWDB. Report [4] present an efficient system that automatically generates prototypes for each word in a lexicon using multiple appearances of each letter. So, research works about handwriting recognition mostly based on English handwriting, Chinese handwriting and Arabic handwriting, but there are a few works for Uyghur handwriting recognition.

Uyghur is the official character of Xinjiang Uyghur Autonomous Region (hereafter: XUAR) in China. Research and development on identification system of Uyghur character plays an important role not only on the improvement of technical level of information processing of Xinjiang ethnic minority, but also on the using Uyghur character, and keep its strong applicability and commonality in XUAR. The features of Uyghur character bring difficulties on Uyghur character identification system, such as scarce abstracted information for its simple structure and little stroke; extremely high similar degree for its many similar subclasses; many printed character and certain typeface is similar to handwritten cursive script; common word size is small etc. Now, Uyghur character identification is

on the research period. There no specific report about realization of on-line Uyghur handwriting collection system, and a Uyghur handwritten character collection system is presented in this paper.

Building of Uyghur Handwritten Characters Model

The Nature of Uyghur Character. Uyghur character used in XUAR in China are all alphabetically writing based on Arabic characters and some Persian characters. Uyghur character is composed of 32 letters, in which 8 vowel letters, and 24 consonant letters. Each Uyghur character has 4 types of different forms, thus, these 32 letters have more than 120 character styles [6], and they are indicated as the following Fig.1.

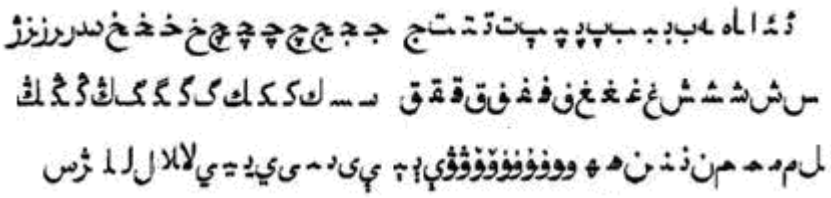

Fig.1 Character set of Uyghur character

Uyghur character is written from right to left, and from left down right for the line progression. There are 4 different writing forms for Uyghur letter: “initial form”, “intermediate form”, “final form”, and “isolated form”. Only the suffix connects with the next character with “initial form”, and initial and suffix connect with adjacent letter to “intermediate form”. Only the initial connects with the above letter with “final form”, and initial and suffix does not connect with adjacent letter to “isolated form”. The selection of writing form in Uyghur character is confirmed as the location of letters in the characters, but Chinese character adopts the same form, and English has two forms, capitalization and small letter.

The vocabulary of Uyghur is composed of one or several letters. According to rules of Uyghur writing, these letters will form one or several letter passages by initial and suffix connection. Uyghur letters connect along a horizontal level in writing, which is called base line [5].

Uyhgur letters are not equal in width. This situation happens not only on different letters, but also on the 4 different forms of a certain letter. Even more, a straight line will be adopted to fill in the spaces among the letter to let a line of text distribute uniformly [5]. The features of Uyghur character bring difficulties on character/word identification.

Basically, vocabulary of Uyghur is composed of syllables, which is generally constituted by the combination of vowels and consonants, and vowel is the center of them. It is sure that constitution of syllable and vocabulary is regular in Uyhgur. There is blank among vocabularies, which is basically same as English and Arabic, but different with Chinese.

Usually, there are two types of strokes: one-way stroke and turning stroke. One-way stroke means that the direction of stroke keeps on a certain direction; turning stroke means that the direction of stroke does not keep on a certain direction, it may be two or more direction. Turning stroke includes order stroke, counter stroke and composite stroke. They all exist in Uyghur stroke, of which order stroke appears more

Creation of Uyghur Handwritten Characters Model. The handwriting point and time series date used for online handwriting is relevant with stroke. It is encoded the stroke direction for 8 directions to the Uyghur handwritten characters, refer to as Fig. 2(a). It divides the coordinate plane into 8 areas to encode successively, and the code is called stroke direction code. The effect of handwriting characters encoded as stroke direction referred to as Fig.2 (b) set a Uyghur character “ئا” as an example. The code changed tendency is shown by the direction code series, where “12345678” is just stroke tendency.

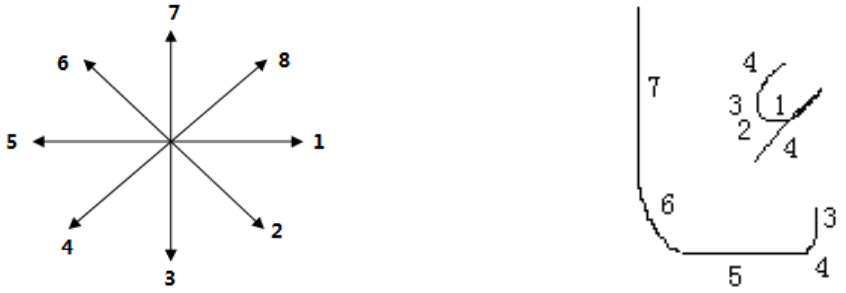

(a) 8 direction code (b) Sketch of stroke direction code

Fig. 2 Direction definition of model building of handwritten Uyghur characters

It is Created strike direction code based on the fix of input point as the following formula:

$$K=(Y_{\mu}-Y_{p(t-m)})/(X_{\mu}-X_{p(t-m)}) \quad (1)$$

Where, k is the alternation gradient between two points, and it confirm the relevant direction code according to the gradient. "*m*" refers to the selected coordinate of the *m*th point as calculating the direction code at *t*. The concrete value is confirmed as the collection frequency in actual handwritten input, if the value is too small, it is difficult to overcome the noise caused by tremble and lead to direction code alternation frequently. It is easy to neglect the key point and make false decision, if the value is too big. To meet with the requirement of difficult samples, set *m*=1 in this work, and the noise caused by this will be removed by the filtering treatment hereafter.

File Storage Organization

The collected Uyghur text is stored by the extension stroke file. It contains file header at the beginning, then the texts collected are saved by their order. The descriptor is a character string, and carriage return character is adopted to divide every information is divided by the string '\n', and it is ended with '\0'. The structure of the file is illustrated as the following Fig.3.

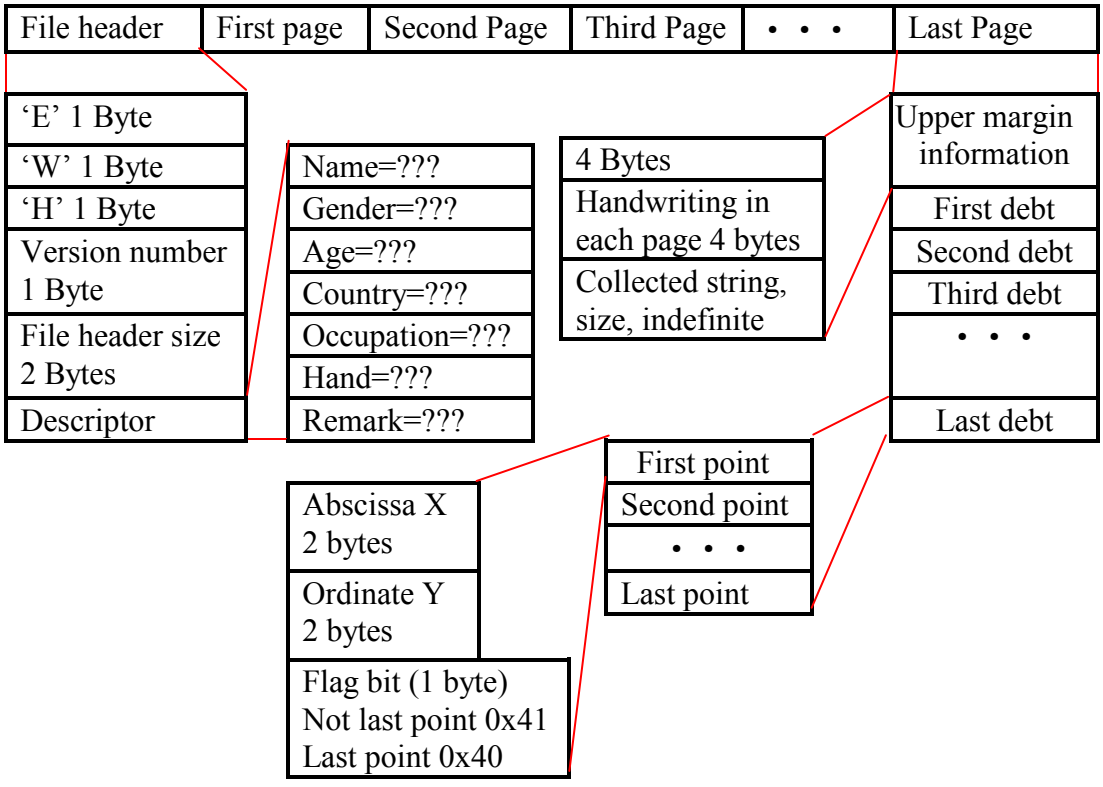

Fig. 3 Structure of extension stroke file

Total numbers of bytes in extension stroke file refer to the byte numbers engaged by the whole page of text, which contains page heading and strokes:

$$N=4+4+N_h+Lc \quad (2)$$

Where N is the total numbers of bytes in the file, N_h is refer to total numbers of bytes for handwriting, and L_c is the character string length. If the character string has no the string '/0' at the end, its length can be obtained by calculation using Equation (2) above. The right side of the coordinate X is positive, and the downside of Y is positive, time refers to the relative time from the beginning of the first point of the first stroke, and the time value of the starting point is 1. The time is invalid if the time value of this point is 0.

System Architecture

The on-line Uyghur handwritten character collection system is composed of Handwriting Collector, Prompt Maker, Text Prompt file and the extension stroke files, which is used for collecting handwritten point and time series data.

Creation of Text Prompt File. The text prompt file is text file, which contains character content need to be collected; its format is described as the following:

[Section###]
Content1
[Section###]
Content2
⋮

Where '###' is digital number increased from 0 as pages. Content1, Content2 are the contents in each page, and it can be characters, punctuation and so on. If the content contains multi-row of text, the collection program will neglect line feed character, and connect them as a whole row. The text prompt file can be created by hand, and produced by Prompt Maker. The flowchart of creating Text Prompt File by using Prompt Maker is presented as the following Fig.4:

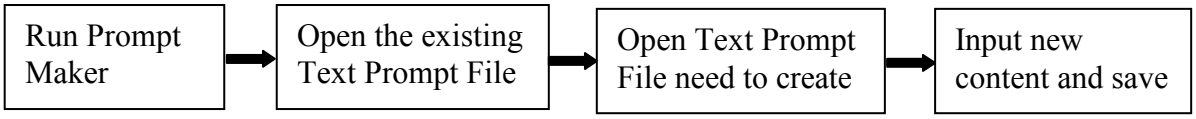

Fig. 4 The flowchart of creating Text Prompt File by using Prompt Maker

A new Text Prompt File is created after clicking "save" (ساقلاش) button on the Prompt Maker. The system asked to save all the Text Prompt Files at the assigned space.

Handwritten Sample Collection. It is collected 1356 Uyghur words, 522 Uyghur simple sentences which each sentence includes 3~7 words by using the implemented handwritten character collection system**.** Handwritten sample collection process is as follows: firstly, the collection program is started, and a new sample dialog is built by double clicking "open" buttons in client area. Then, it is saved the path for handwritten sample after filling in writer information, and the Text Prompt File is opened, and it is entered the sample collection interface. Finally, the Uyghur characters shown in the writing frame, indicated as the collection system frame as Fig.5. The next sample words are presented in the system after clicking the "next page" button. It can be exit the collection system by clicking "finish collecting" when all the samples are collected.

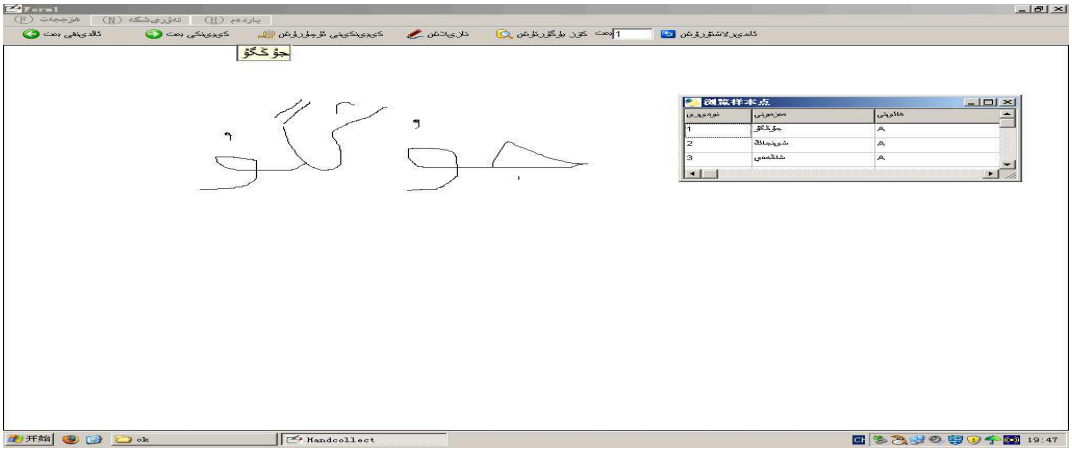

Fig.5 The collection system frame

The collection method used in this system can overcome effects caused by different font style, stroke thickness and font size. However, the twisting on left and right sides and up and down sides of font style shall not change the vector of vertical and horizontal cross feature code. Therefore, this method is very applicable for identifying characters of different size written in different writing habit (left inclined, right inclined, broad or narrow) by different people.

Summary

This paper presents an on-line Uyghur handwritten character collection system. Considering the needs of Uyghur handwritten character/word recognition system (or Uyghur handwritten input system), it is emphasized that the character need to be written from right to the left, and the character size is selected moderate. From experimental results, it can be concluded that the system shows its strong efficiency during the collection of Uyghur handwriting. Besides, the system function is further improved by strengthen editional function, even adding some preprocessing steps for Uyghur handwritten character /word recognition system.

Acknowledgment

This work is supported by the College Scientific Research Plan Project of Xinjiang Uyghur Autonomous Region (No. XJEDU2013I11), Special Training Plan Project of Xinjiang Uyghur Autonomous Region's Minority Science and Technological Talents (No. 201323121), and the Open Projects Program of National Laboratory of Pattern Recognition (No. 201306321).

References

[1] R. Plamondon, S. N. Srihari: On-Line and Off-Line Handwriting Recognition: A Comprehensive Survey, IEEE Transactions on Pattern Analysis and Machine Intelligence, Vol. 22 (2000), p. 63
[2] Cheng-Lin Liu, F. Yin, Da-Han Wang, Qiu-Feng Wang: Online and off line hand written Chinese character recognition: Benchmarking on new databases, Pattern Recognition, Vol. 46 (2013), p. 155
[3] M. Eden, Handwriting and Pattern Recognition, IRE Trans. Information Theory, Vol. 8 (1962)
[4] R. M. Saabni, , J.A. El-Sana. Comprehensive synthetic Arabic database for on/off-line script recognition research, in: International Journal on Document Analysis and Recognition, Vol. 16 (2013), p. 285
[5] K. Ubul, A. Hamdulla, A. Aysa, A. Raxidin, R. Mahmut. Research on Uyghur off-line handwriting based writer identification. Proceeding of International conference of signal processing (ICSP2008), Beijing, China, 26-29 October 2008, p. 1656.

Advanced Materials Research Vols. 989-994 (2014) pp 4747-4750
© (2014) Trans Tech Publications, Switzerland
doi:10.4028/www.scientific.net/AMR.989-994.4747

Researching of Project Management Information Systems Based on WBS

Wan-yin Du

Department of Information Management, The Central Institute for Correctional Police, Baoding, China

duwanyin96@126.com

Keywords: Work Breakdown Structure (WBS), Project Management Information Systems, Planning, Control.

Abstract. This paper takes project management information systems as the main object of studying，it applies the theory and means of Project Management Knowledge System，and the specific features of construction project management on the research. It makes detail analysis and deep study to the application of WBS for project management and construction project information classification system.

Introduction

Computers are seen to have the potential to make a significant contribution to the project. The use of information technology has rapidly increased due to its efficiency and effectiveness. In the initial stages of its development, project management information systems main purpose and usage was to improve the efficiency. The value of management information was recognized during its integration stages. Work breakdown structure (WBS) is a one “procedure, concept or technique” utilized for project planning and control.

The use of information technology in project management has rapidly increased due to its efficiency and effectiveness. The project managers are used to spend large amount of time in solving complex allocation problems. Information technologies facilitate the decentralization of work tasks and their coordination in an interactive network of communication in real time.

Project planning is one of the important steps in the process of project management, which impacts many of the steps to follow. The main goal of project planning is to develop the project work plan, considering various aspects. The project work plan could be used to predict the situation of project during its lifecycle, and enables the control of its progress trend.

Project Management Information Systems

The “Management Information Project” is one of the recent methodologies for planning projects. The main concern of this methodology is to offer some special tool s and techniques, to ease the planning of project work breakdown structure and activities. We have assumed that the title of any project could be illustrated by the combination of a” Master Function” (MF), and the “Information Deliverable”. For example the combination of “Construction” and “Information Product ion Complex” which results “Construction of Gas Product ion Complex”, could be considered as the title of a project. According to AMPM, any project “Work Breakdown Structure” (WBS), consists of three different structure s including “Project Control Work Breakdown Structure”, “Functional Work Breakdown Structure” (FWBS), and “Relational Work Breakdown Structure”. As these structures have been used to form the output s of the proposed patterns of neural networks, they have been described in the following sub sections.

PMIS — features, strength and drawbacks

There are numerous different PMIS available on the market that can be used by any industry with respect to the scope of their projects and to their specific necessities. Also, some companies can purchase specifically tailored solutions. Therefore, depending upon the company and the type of projects they will be addressed to, PMIS can vary significantly from one another. However, it is important to note that all projects include several basic elements and that these elements become key requisites of any PMIS:

• Resource allocation, to define teams and individual assignments along with materials;
• Time and Deliverables;
• Assignments;
• Risk management, to deal with uncertainty and control the project flow effectively;
• Monitoring and Quality control.

Owing to the above mentioned considerations, it is possible to individuate several benefits deriving from the adoption and the correct use of PMIS:

•projects can be managed from within integrated and coherent applications;
• tasks and task assignments can be created, updated and tracked in real-time;
• real time completion control gives a justification for the eventual re-scheduling of the project itself;
• individuals are allowed to communicate with one another in real-time. All communications can be logged and tracked from within the software.

At present both small and large firms may adopt project management tools to increase efficiency, productivity and transparency, making the most of a single application which allows them to manage and track their projects. One of the most interesting and valuable aspects is the possibility for the involved managers to act proactively on tasks if resources are behind schedule, increasing the chances that the project will be completed on time and profitably. This is particularly true for companies that run multiple projects at the same time. Additionally, PMIS become essential when teams are made up of people who are dispersed across multiple locations, as it provides them with access to a centralized information database that reflects real-time updates. In brief, they can be effective if any of the WBS statements apply.

Work Breakdown Structure

A work breakdown structure element may be a product, data, service, or any combination thereof. A WBS also provides the necessary framework for detailed cost estimating and control along with providing guidance for schedule development and control.

History

The concept of work breakdown structure developed with the Program Evaluation and Review Technique (PERT) by the United States Department of Defense (DoD). PERT was introduced by the U.S. Navy in 1957 to support the development of its Polaris missile program. While the term "work breakdown structure" was not used, this first implementation of PERT did organize the tasks into product-oriented categories.

The document has been revised several times, most recently in 2011. The current version of this document can be found in "Work Breakdown Structures for Defense Materiel Items" (MIL-STD-881C). It includes WBS definitions for specific defense material commodity systems, and addresses WBS elements that are common to all systems. Elements of each WBS Element:

• The scope of the project, "deliverables" of the project.
• Start and end time of the scope of project.
• Budget for the scope of the project.
• Name of the person related to the scope of project.

Design Principle

An important design principle for work breakdown structures is called the 100% rule. It has been defined as follows: The 100% rule states that the WBS includes 100% of the work defined by the project scope and captures all deliverables – internal, external, interim – in terms of the work to be completed, including project management. The 100% rule is one of the most important principles guiding the development, decomposition and evaluation of the WBS. It is important to remember that the 100% rule also applies to the activity level. The work represented by the activities in each work package must add up to 100% of the work necessary to complete the work package.

Mutually exclusive: In addition to the 100% rule, it is important that there is no overlap in scope definition between different elements of a work breakdown structure. This ambiguity could result in duplicated work or miscommunications about responsibility and authority. The WBS Dictionary

describes each component of the WBS with milestones, deliverables, activities, scope, and sometimes dates, resources, costs, quality.

Plan outcomes, not actions: When a project provides professional services, a common technique is to capture all planned deliverables to create a deliverable-oriented WBS. Work breakdown structures that subdivide work by project phases must ensure that phases are clearly separated by a deliverable also used in defining entry and exit criteria.

Coding scheme: It is common for work breakdown structure elements to be numbered sequentially to reveal the hierarchical structure. The purpose for the numbering is to provide a consistent approach to identifying and managing the WBS across like systems regardless of vendor or service.

Application in the information management system

In order to better solve the deficiency and defect management information system by using the WBS method. The principle of this method is simple, convenient operation, easy application. The following is a example, that example is the management of project management information system with WBS method:

This system is mainly aimed at the general project management business enterprise,and the development of the system will use the Browser/Server model. Then the paper uses C# to describe them.

```
ListItemit=newListItem;
it.Seleeted=rue;
this.dropType.Item.Items.Insert(0,it);
If(Request.Paranms[“jxNo”]!=NULL)ProjcetType=;
Ruquest
TreeNodeRootNede=newTreeNod;
RootNode.ImageUrl=”../IResource/images/ieon05.gif”;
if(ProjeetTyPe=””)
{       RootNode.TeX=”All of them ”;
ROOtNode.NedeData=””;
ROOtNode.ID=f,TreeViewRoot,,;
InitTyPe(RootNede);
}
Else
{       RootNode.Tex=Type;
RootNode.NodeData=””;
RootNode.ID=”TreeviewProject”;
try
{       //XML Data
catch(Exceptionex)
}       ;{
ResPonse.Write(ex.ToString());
}
InitTree(RootNode,RootNode.NodeData);       }
TreeNodetmpProjectNd;
DataTabledt=newDataTable();
Dt=conn.GetTable;
foreach(DataRowdrTyPeindt.Rows)
{
tmpProjectNd=newTreeNode();
tmpPfojectNd.Text=drType[“DBI_2”].Tostring();
tmpProjectNd.NodeData=””;
tmpProjectNd.ID=”TreeViewProject””;
tmpProjectNd.ImageUrl=””;
tmpProjectNd.SelectedImageUrl=””;
treenode.Nodes.Add(tmpProjectNd);
tmpProjectNd.Expanded=true;
try
{
dtblsProject=conn.GetTable();
}
Catch(Exceptionex)
   {
      Response.Write(ex.ToString());
   }
InitTree(tmpProjectNd,tmpProjectNd.NodeData);
}
```

Running the program could get the more whole graph about the WBS. And you can read the graph to help yourself catch the final goal easier.

Conclusion

In the guidance of the theoretical frame of project management information system based on the WBS, the paper made an example to illustrate. The paper considers the user requirement, analysis system. And there are the compilation code they are the way to catch the goal by using the software. Studies on PMIS should focus on finding ways of enhancing its use by the project principals and administrators. Appropriate training and effective leadership could escalate the benefits of PMIS in the area of project management.

Reference

[1] An integrated approach to implement Project Management Information Systems within the Extended EnterpriseM. Braglia, M. Frosolini / International Journal of Project Management 32 (2014) 18–29 19)

[2] P. Nitithamyong, M.J. Skibniewski, Web-based construction project management systems: how to make them successful? Automation in Construction 13 (4) (2004) 491–506.

[3] Towards a conceptual reference model for project management information systems. Ahlemann , F., International Journal of Production Management 2009.27, 19–30.

[4] R.Alan Bowman. Developing activity duration specification limits for effective project control [J].Europe and Journal of Operational Research 2006,174:1191.1204.

[5] Rodney Anthony Stewart. IT enhanced project information management in construetion: Path ways to improved performance and strategic competitiveness [J].Automationin Construetion.July2007,16(4):511 一 517.

Advanced Materials Research Vols. 989-994 (2014) pp 4751-4754
© (2014) Trans Tech Publications, Switzerland
doi:10.4028/www.scientific.net/AMR.989-994.4751

Research of Access Control Models in Personal Networks

Yulan Zhao[1, a], Chunfeng Jiang[1, b]

[1]Jilin Agricultural Science and Technology College, Jilin, China

[a]llbird@126.com, [b]hero_jcf@126.com

Keywords: access control; role; task; personal networks

Abstract.How to prevent illegal users from sharing system resources was one of the main purposes for MAGNET Security Group. This paper introduced some major access control models such as traditional access control models, role-based access control model (RBAC), task-based access control model (TBAC) and role-task-based access control model (T-RBAC). In the end, a feasible scheme PN_T-RBAC was proposed at the base of the T-RBAC model in existence, which was suitable for the coalition environment of personal networks.

Introduction

MAGNET was a large integrated project in the field of information society technology of the EU's sixth framework programme for research, FP6, which means My Personal Adaptive Global NET. MAGNET started around the concept of personal networks. PN was a network that all devices belonged to a particular user, which the personal devices might be local also remote. There was a typical PN contained four clusters as Fig. 1. The first cluster A was around the user's own local cluster, the second cluster B was located in the home, the third cluster C was located in the office, the forth cluster was located in the car, and B,C,D were remote clusters. As communication was between people, there also were dialogue and sharing of resources between the PN. While other PN exchanged through cluster A with this PN, how to ensure secure access to resources in each cluster was one of the goals for MAGNET security working group.

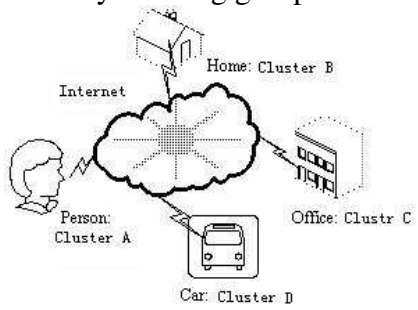

Figure1 a Typical Personal Networks

Access Control Model

Access control model was main method to secure access for networks. Access control model included subject, object definition and authorization policies. The core technology of Access control was licensing strategy, which provided the scheme where the main obtained accessed ability to the object. According to different authorization policies, access control model was divided into MAC-Mandatory Access Control, DAC-Discretionary Access Control, RBAC-Role-Based Access Control, TBAC-Task-Based Access Control and more popular lately T-RBA, which mint Task-Role-Based Access Control. Normally, MAC was too simple and poor flexibility, the principal permission of DAC was too large, to insecure security, gradually being replaced by other models. This article would focus on the analyzing RBAC, TBAC and T-RBAC, and constructed an access control model which fit for PN coalition based on them.

Role-Based Access Control Model. The basic idea of RBAC model was introduced the concept of roles between user and permissions, which achieved logical isolation between users and permissions. The role was a collection that operation could be executable or service could be accessed by the main in system. The biggest advantage of RBAC was its simplified management, the major management of RBAC system was authorization or canceling use's role. RBAC model had a variety of structures, RBAC96 models was widely recognized. In the RBAC system, permissions were not assigned directly to the user, but first assigned to roles, and then the system assigned a role to the user, so user got appropriate access authority according to their roles. When the system function changed or evolved, it would only delete the old character features, add new functions, or define a new role, without having to update each user permission settings, and greatly simplifies permissions management.

Task-Based Access Control Model. Access control model usually achieved secure access control of resources from the perspective of the system, without considering the context of the specific operation during the authorization. The TBAC model changed its attention for security access control from the protection of static subject and object in independent system to the protection of dynamic authorization carried out with the tasks executing. The task was a logical unit in workflow, for a specific function. TBAC model had the advantages of active control, dynamic allocation of permissions, especially fit for security management of workflow, distributed processing and multi-point access control.

In TBAC model, authorizing was described by five tuple (*S, O, P, L, AS*). Where *S* represented the subject, *O* described object, *AS* said the step of authorization, *P* was the permissions activated by *AS*, *L* was survival period of *AS*. *L* and *AS* were notable features of TBAC, which were different from other access control model. When *AS* was triggered, its agent began to have centralized authority that it commissioned, while its life cycle started countdown. During the lifetime, the granted permissions to user depended on not only the subject and object, but also the currently executing task, the task status, the user's permissions during task was active. When the task suspend, permissions were frozen; task resumed execution, permissions were restored; when the task was terminated, permissions were revoked.

Task-Role-Based Access Control Model. RBAC and TBAC in some specific situations would expose their flaws, for example, RBAC could not forwardly control the sequence of task execution, could not cope with the control requirements of workflow system either; compared to the system with high requirements of the overall structural stability, TBAC seemed powerless, it was not suitable lonely as a general policy framework for more complex systems. So many scholars put forward the access control model based on the task and role, aimed at task and roles were referred to the centrality of access control strategy, combined with their advantages, to make up for lack of both. How to achieve the perfect combination of TBAC and RBAC, and build access control model, which had become a hot topic in recent years, the main models were RTBAC and T-RBAC, showed relatively good performance T-RBAC as Fig 2.

The main idea of T-RBAC was the overall framework based on RBAC, while introduced the concept of task, and assigned roles related tasks, then gave the task relevant authority, to achieve dynamic management of permissions. T-RBAC authorization represented with quintuple (*U*, *O*, *P*, *T*, *R*), where *U* was subject who could independently access system resources ; and *O* was the physical

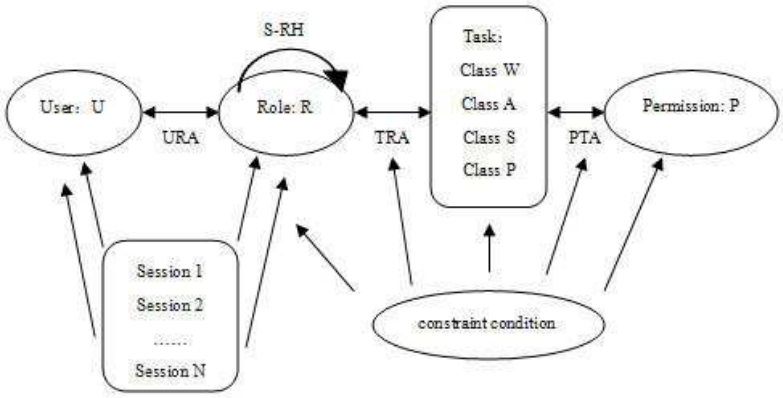

Figure 2 Task-Role-Based Access Control model

resources passive acceptance of other body movements. *P* indicated the role permissions to perform tasks; *T* mint task; *R* were a set of roles which could perform tasks with hierarchical relationship. Before *T* was activated, the privileges of *R* were not available. *URA* was to assign many to many relationships from users to roles, *TRA* was to assign one to many relationships from tasks to roles, *PTA* was to assign many to one relationship from permissionss to task. When *T* was active, *R* began to have permissions, and the permissions would change based on context with *T* performing tasks, then be recycled accordingly as task completed. Therefore, in T-RBAC model, users accessed specific object resources in the system during only the execution of specific orders.

Personal Networks Coalition

PN coalition refers to a temporary commonwealth formed by several independent PNs for current common interests or task. The biggest feature of PN union environmental was resources belonged to several independent PN network systems.

Access Control Model of PN Coalition. While the existing access control technology solved the access control issue of resource in a separate system. For this conflict, PN_T-RBAC, an improved model program was proposed, it could reflected the advantages of existing T-RBAC technology in the PN league environment, shown as Fig 3.

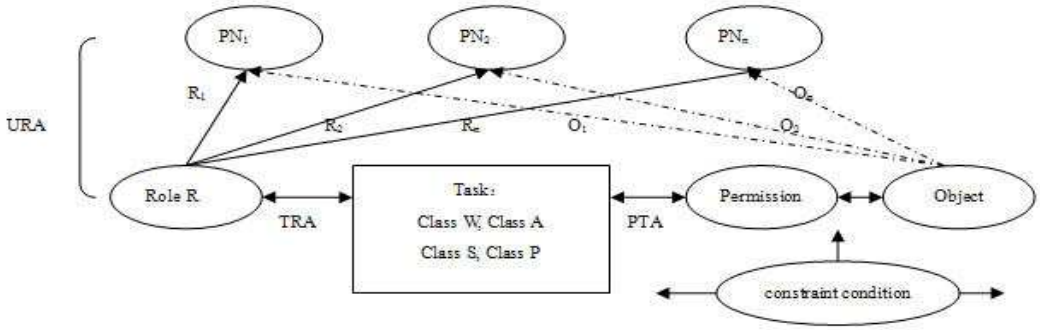

Figure 3 Access Control Model of PN Coalition Environment

Internal Security Structure of PN Members. To achieve each independent member to unify a PN federation model, PN_T-RBAC required each member introduced SMN-service management node in the local security structure. In PN coalition, each PN had its own address, while SMN had its own unique name, they were visible for other league members. Fig 4 indicated the local security structures of members *I* in PN, each member should have such local security structures, and it could be uniquely identified which PN belonged by SMN name. Thus SMN among each PN could negotiate, clarified the rights and obligations of PN in the league, and jointly safeguarded PN_T-RBAC model system. Wherein the specific content that SMN negotiated included a trust

mechanism was established between SMN, the goals or plans of PN Union were determined, the targets were refined number of tasks, the specific content of roles, permissions, and object mapping coalition environment were determined.

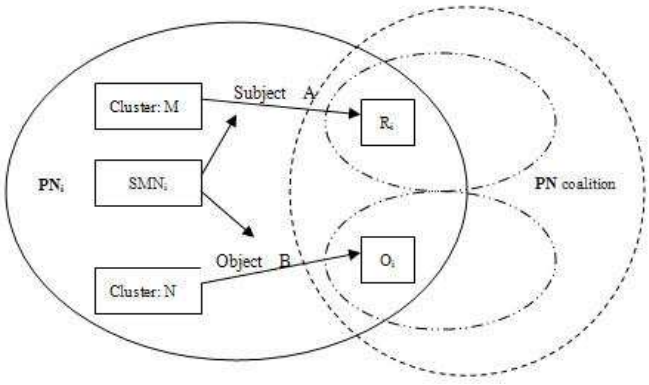

Figure 4 Local Security Structures of Members in PN Coalition

Summary

Personal networks had the potential which communicated with anyone any time, any place, with any form, it must have broad application prospects. This article focused on thesecurity access controlproblems in PN coalition, a viable model programwas proposed on the basis of theprior art. Personal networkwas more complex, as atheoretical model, improved model didn't make practical model system. There were many problems needed to be solved, especially in an environment containing a dynamic cluster.

References

[1] H. B. Shen and F. Hong, *Review of access control model*, Application Research of Computers, Vol. 17(2007), p. 9

[2] R. F. Han and H.X. Wang, *Research of task-role-based access control modl* , Computer Engineering and Design, Vol.12(2007), p. 800

[3] F. Z. Chen and F. Hong, *Task-based access control (TBAC) Model*, Mini-micro Systems, Vol. 24(2008), p. 621

[4] Sejong Oh and Myong Park, Tasked-role-based Access Control Model, Information System, Vol.28(2008), p. 533

[5] S. S. Chen, The time frame of dynamic trust model based on DyTrust: for P2P system, science and techonoly information,vol.35(2011),p.123

Advanced Materials Research Vols. 989-994 (2014) pp 4755-4758
© (2014) Trans Tech Publications, Switzerland
doi:10.4028/www.scientific.net/AMR.989-994.4755

Research of Trust Model for File-Sharing System

Chunfeng Jiang[1,a], Wei Xu[1,b]

[1]Jilin Agricultural Science and Technology College, Jilin, China

[a]hero_jcf@126.com, [b]xuwei_jl@126.com

Keywords: P2P; RTBD; trust model; trust value

Abstract. In this paper, a trust model based on real-time behavior detection scheme was proposed in P2P file-sharing system. It solved the problems in computing trust value only by past performances and choosing service nodes improperly. It took real-time behavior detection both in trust computing and service choosing, improving the accuracy of the trust value and the rationality in service nodes choosing. The experimental results proved the advantage of this scheme.

Introduction

Peer to peer-abbreviation was P2P- networks had been rapid development recently. Applications based on P2P networks were increasingly abundant, the file sharing system for P2P networks had achieved great success on the internet. However, it was a big hidden danger of P2P networks' security when it provided favourable conditions for the spread of computer viruses, forgery, and garbage data owing to the dynamic, anonymity, autonomy and loose coupling between nodes and other characteristics of P2P networks.

It was a really social network environment for human communication provided by P2P networks. Because trust was the core of human relations, researcher introduced trust to file sharing system of P2P networks, and described the relations between nodes in P2P network with trust relationship.

Trust Models for P2P File-Sharing System

It was a really social network environment for human communication provided by P2P networks. Because trust was the core of human relations, researcher introduced trust model to file-sharing system of P2P networks, and described the relations between nodes in P2P network with trust relationship.

Trust model divided the trust content and the degree of trust, and proposed a mathematical model from a subjective measure of confidence to start trusting. In P2P networks, trust was reflected in the service capacity and quality of service. Service capabilities such as computing power, storage capacity, bandwidth, quality of service were reflected in the time-line nodes, friendliness, reliability, service delivery. Dued to the impact of nodes trust relationship factors varied, in practical applications, it was difficult to carry out all of the information fusion trust calculations. Therefore, in the P2P network, the trust between the nodes was identified by of the transaction satisfaction. Currently, the trust of P2P networks mainly established a reliable trust model in P2P networks to resolve.

There were two types of trust models for file-sharing system of P2P networks proposed. The first was structured trust model, its network structure was strictly controlled, and trust value stored in affirmatory location, it ensured the update and query of trust had high efficiency, it could collect trust information in the whole network, and gained global trust value. The structured trust model was often a great deal of overhead, if once the number of users increased, would form a great performance bottlenecks, scalability, relatively poor, and likely to cause a single point of failure. The second was non-structured trust model, its network topology was without any restriction, there wasn't relative between trust value and network structure, it was more suitable for strong dynamic P2P network.

In order to systematically understand the P2P network trust model, the non-structured trust model was divided into trust model based social network, trust model based on probability estimates, trust model based on fuzzy logic, trust model based on game theory. In recent years, dued to the continuous development of social networks, the research of trust model based on social network was endless. Relationships and trust in society and interpersonal relationships were very similar, they were the core of interpersonal trust relationships, and trust between individuals often depended on the recommendation of other individuals, which was based on third-party recommendations indirect trust. In fact, this interdependent relationship of trust form a so-called trusted network. In such a trust network, the credibility of any individual was not absolutely reliable, but could serve as an individual basis to determine their interactions. The trust model based on probability estimates proposed a trust evaluation was divided into both positive and negative, if the transaction was successful, the trust evaluation set 1, otherwise 0, and thus presented a probabilistic model based on the binomial distribution. The trusted computing problems into problem solving mean binomial probability density. Only based on Bayesian/Bayes network trust model focused on describing different aspects of trust, so that nodes could obtain different aspects of the performance of nodes according to different scenarios on demand. When a node could not determine the reliability of the file provided by using the recommendation information to the other nodes established a trust relationship, there was provided a method for the integration of different flexible trust information. The basic idea of trust model based on game theory was to model a system in which each member to achieve their own purposes through the interaction, included the maximization of their function in specific situations, to get the maximum benefit. Interactive game was a member between player and game. D. Houser proposed a framework for a trust model based on game theory to calculate the trust in limited trust environment. C. Dellarocas proposed a specific trust model based on game theory, and for such a trust system, made some enlightening questions, such as how to motivate nodes provide feedback, how to deal with the false feedback. But it required a trust center to collect all of the feedback. There was a big security risk.

Real-Time Behavior Detection Mechanism. The RTBD-real-time behavior detection-mechanism was proposed in this paper, it consisted of two parts. When trust computing, firstly, it obtained trust value of real-time behavior through target nodes, and then integrated with other trust value in the traditional trust model. When serviced for the destination nodes, it not only considered the nodes trust value, but also assessed the target node's service capacity and service quality with real-time behavior detection mechanism, integrated trust value and service quality to select the service. Real-time behavior detection mechanism avoided effectively overloading the nodes which had high trust value and others with good service were free as the same time.There were five symbols in RTBD, TV meant trust value, RTV was recommended trust value, RTBTV was real-time behavior trust value, DTV was direct trust value, PTV was past trust value.

Real-Time Behavior Detection of Trust Computing. The risk of P2P file sharing system which based on historical behavior was historical behavior could not represent current conduct, some nodes could be malicious behavior as slander, collusion after obtained a high trust value by providing good service. Although most of the trust models proposed appropriate punishment mechanism to curb the malicious behavior of nodes, the problem was not fundamental solution. The concept of observation period was introduced. System would observe the behavior of downloaded nodes before downloading and the observation would be the other basis for trust value calculating.

The traditional trust models were simply calculated trust value of target nodes based on their historical behavior. The trust value included two parts; they were direct trust value-DTV and recommended trust value-RTV as Fig. 1. In trust models which used real-time behavior detection mechanism, trust value comprised past behavior trust value-PTV and real-time behavior trust value–RTBTV as Fig. 2. The RTBTV was from evaluation of immediately dynamic data. The real-time behavior would be past behavior after real-time behavior finished, so RTBTV was a relative item to PTV. The direct trust value and the recommended trust value constructed PTV.

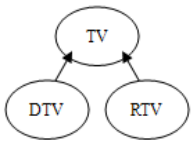

Figure 1 Traditional Trust Value Composition.

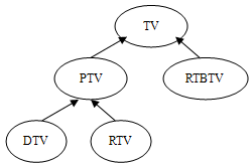

Figure 2 RTBD Trust Value Composition.

The traditional trust value could be expressed as in (1), in RTBD; the trust value could be expressed as in (2). α, β and γ were trust factors, their values would dynamically adjust according to actual networks. α, β would be reduced and γ would be increased when malicious nodes were more.

$$TV=\alpha\times DTV+\beta\times RTV,\ \alpha+\beta=1 \quad (1)$$

$$TV=\alpha\times DTV+\beta\times RTV+\gamma\times RTBTV,\ \alpha+\beta+\gamma=1 \quad (2)$$

The RT-response time and QOF-quality of files were standards of measure to the RTBTV. The response time defined as the time from user sent files requester to receive a response. The quality of file defined as the fit degree of file hash values between users gave and received from target node. So the *RTBTV* could be expressed as in (3).

$$RTBTV \propto QOF/RTV \quad (3)$$

Real-Time Behavior Detection of Select Services. The disadvantage of traditional trust model was that target nodes' service capacity could not be effectively since they selected node which trust value was highest as service node. On the one hand, it easily led to too overloading to cause single point failure of highest trust value node. On the other hand, the resources on some nodes which had higher trust value could not use fully, and it deprived them of the opportunity to enhance trust value. The RTBD mechanism selected service nodes based on trust value and CR-congestion rate, it selected node which had higher trust value and lower *CR* as service node. The congestion rate was defined as in (4).

$$CR \propto L/C \quad (4)$$

L was the load of nodes; *C* was load capacity of nodes. When *L*>*C*, the nodes were congested, otherwise, *L*<*C* meant they were non-blocking. RTBD policy was as table 1.

Table 1 RTBD Policy

Step	Description
1	Get a pool of service providers $S=\{S_1,S_2,...S_i...\}$

2	For each node S_i in pool S
	Request the attribute of node S_i <content_hash, L,S,C>
	Get the hash value of the content
	Content_hash=hash_fuction(pack.content);
	Calculate the congestion rate
	CR_i=cong_fuction($S_i.L$, $S_i.C$);
	Get required hash of pack.fileno;
	Evaluate the quality of file and response time;
	Eval_result=eval_fuction(content_hash,reply_hash, response_time);
	If (Eval_result) that meant receiving right packet then
	Add S_i into it local cache, store the content of packet into the
	Data buffer;
	Else remove S_i from local cache;
	Endif
	Output the result as <eval_result, CR_i>;
	Endfor;

3	Choose the provider with higher trust value and smaller congestion rate

Simulation Experiment

The performance of RTBD mechanism was tested in the classic trust model of file-sharing system in peer to peer network-Eigen Trust, through simulated experiment. There were three types of nodes in experiments, good nodes-which provided well files, normal nodes-which furnished well files as well as malicious files, malicious node-which supplied malicious files.

The number of file downloads from good nodes and malicious nodes were recorded in peer to peer network. In the same experimental condition, two hundred tests were simulated, there were one thousand downloads requests each test, the number of file downloads from good nodes was compared in Eigen Trust in system between which used RTBD mechanism and it without RTBD mechanism. The result was described as Fig. 3. In the experimental progresses, there was faster growth rate of document downloads from good nodes in Eigen Trust with RTBD mechanism, its file downloads was 100 more than the Eigen Trust which without RTBD in the same network condition, that meant RTBD mechanism was benefit to improve the trading volume level of system. Trust model was not only to encourage good behavior of the network good nodes, but also to suppress the malicious behavior of malicious nodes. There were one hundred tests in the same condition for file downloads from malicious nodes, one thousand download requests each test. As records, file downloads of test with RTBD mechanism decreased more rapidly than it without RTBD mechanism as Fig. 4.

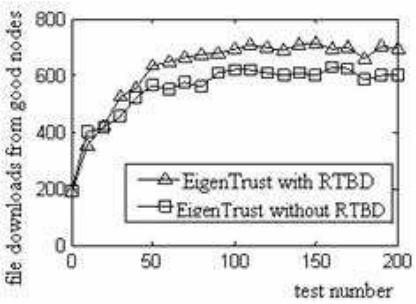

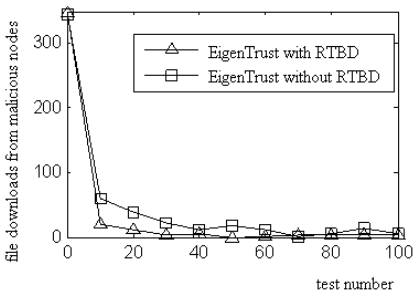

Figure 3 File Downloads from Good Nodes. Figure 4 File Downloads from Malicious Nodes

Summary

In the trust model of peer to peer network, a new real-time behavior detection mechanism-RTBD was proposed based on traditional trust models. It could achieve accurate trust value and choice reasonable service nodes used RTBD in trust value computing and service nodes selection. The follow-up work of RTBD mechanism was to apply it to more trust models.

References

[1] Y. Sun, Z. Han, and K.J.R, *Defense of trust management vulnerabilities in distributed networks Communications Magazine*, Communications Magazine, Vol. 46(2008), p. 112

[2] R.F. Zhou, K. Hang and M. Cai, *GossipTrust for Fast Reputation Aggregation in Peer-to-PeerNetworks*, IEEE Transactions on Knowledge and Data Engineering, Vol.20(2008), p. 1282

[3] J.G. Zhang and X. Guo, *Trust Model Based on Dynamic Recommendation in P2P Network*,Computer Engineering, Vol. 67(2010), p. 174

[4] J.S Chang, H.M. Wang and G. Yin, *DyTrust- a dynamic trust model based on time frame for P2P system*, Chinese Journal of Computers,Vol.08(2008), p. 1301

[5] Y. WANG, N. KAO, *A.Poisonedwater: An improved approach foraccurate reputation ranking in P2P networks*. Future GenerationComputer Systems(2010).

Advanced Materials Research Vols. 989-994 (2014) pp 4759-4762
© (2014) Trans Tech Publications, Switzerland
doi:10.4028/www.scientific.net/AMR.989-994.4759

Research and Implementation Of Image Transmission Key Technological Based On WSN

Zhongsheng Wang, Dongli Huang

College of Computer Science and Engineering, Xi'an Technological University, Xi'an 710021, P.R.China

Email: wzhsh1681@163.com

Keywords: ZigBee; CMOS camera; ARM processor; Compress.

Abstract. ZigBee technology is mainly used in short distance, low power consumption, low rate, low complexity of equipments for data transmission. When image has a large amount of data, it should be processed firstly, and then transmitted. This essay makes a research on healthy care system, using CMOS camera to get image and compress image. Then, the compressed image is transferred to ARM processor, and divided into data packets according to the requirement of the ZigBee network transmission. Finally, the image is transferred to control center and displayed. After the final test, this system can get images to meet the requirements, which has some practical values.

Introduction

At present, the wireless image transmission mostly uses the GPRS/CDMA technology, Within the scope of the GPRS/CDMA network coverage, the images can be transmitted steady. But in some specific cases, the transmitting base station appear problem, the whole networks would be paralyzed. But the ZigBee technology can solve the disadvantages well,just only one gateway node can organize a network, the other nodes can join the network directly or join the network by way of multiple hops.

ZigBee is a low power consumption, low cost, short time delay, network of large capacity, high security features two-way communication technology, wireless sensor network (WSN) has been widely used in embedded devices, automatic control, industrial control, medical monitoring, intelligent household and other fields. But because of its small bandwidth, low transmission rate, when the transmission data is large data files such as image, audio and video, it may met a bottleneck. To address this issue, this essay establishes a image collection and transmission system based on ZigBee under the research background of the community home endowment system. The system chooses a village as the ZigBee network coverage, and install cameras in the monitoring objects'rooms, the monitoring center can send photo instruction according to the need, to collect real-time image and get the real time status of monitoring objects.

The overall structure design

The system mainly includes two parts of upper computer and lower computer, the lower computer is mainly used to take and transmit image, the upper computer is mainly used to process and display image. The overall structure of the system is shown in figure 1.

The upper computer of system is mainly composed of CMOS camera installed in room, ARM processor and ZigBee module nodes, which called end device. It takes images and transmits the image from the ZigBee routing nodes to the ZigBee gateway node. The gateway node is connected to the PC and responsible for the establishment of the network, at the same time it receives data from multiple routing nodes, transmits the collected images to the monitoring center. The user interface software is developed based on Visual C++ 6.0 in Windows.

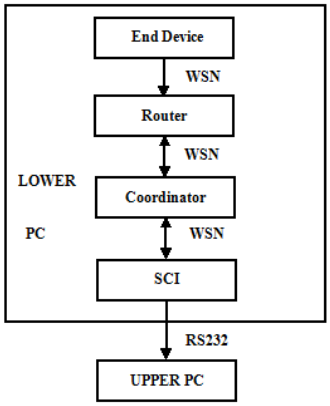

Figure 1. System structure Figure

The Hardware Design Of The System

There are three types of ZigBee protocol about the network topology structure: star structure, tree structure and mesh structure. Mesh topology structure has a high ability to adapt to the environment. Every node in the network is a small router, all have the ability to reroute choice, in order to ensure the reliability of the network to the greatest extent. In a mesh network , each node can communicate with at least one other node, this approach can achieve better than a tree or a star topology of network connectivity. So according to the characteristics of this system, a mesh network topology structure is more suitable for this system.

Routing nodes and gateway nodes of the system, adopted based on ZigBee CC2530 suite for development platform. CC2530 not only support 2.4GHz IEEE802.15.4 /ZigBee standards of practical application, but also have high cost performance, can be at a lower price to form a powerful network performance.It is a combination of standard enhanced 8051 CPU and the advantages of the RF, and own the larger programming space at the same time.

The end device is mainly composed of PTC08 serial camera based on VC0706, ARM processor of S3C44B0X, and CC2530 ZigBee modules.

PTC08 serial camera can be used for image acquisition, control, data compression, serial transmission. Its built-in high-performance digital signal processing chip implements to the high proportion of the original image compression. The output image through the camera is compressed standard JPEG format. At this time, the image data is still big, and do not conform to the requirements of the ZigBee network transmission byte size. So it need to transmit the image to the ARM processor, then according to a certain compression algorithm to the subcontract the image data,and at last traveled through the network transmission. The lower computer work process is shown in figure 2.

The software Design Of The System

The entire image transmission system can be divided into the following three modules: data transfer module, data processing module, image data storage and display module, as shown in figure 3.

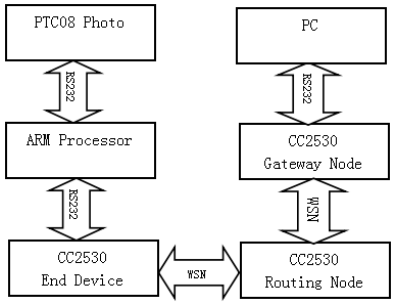

Figure 2. Lower computer flowchart Figure

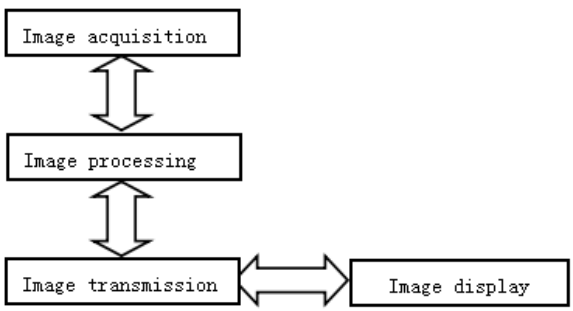

Figure 3. System function figure

The data transmission module programming

ZigBee network wireless transmission module mainly realizes the data transparent transmission, that is when the PC exchange data with the camera, only need to consider whether there is data to send, and don't need to consider the format of send instructions. When the image data the camera takes sent via routing nodes, it must be divided into a number of data packets according to the requirement of the ZigBee network , and then send each packet in order. In the gateway nodes receive the sent data in order and transmit the data to the PC software to decode, so as to complete the whole process of large amount of data transmission.

The data Processing module programming

The main task of this module is to receive the image information the serial port camera send, then the data were processed and sent out by ZigBee routing nodes. In the process of processing and data communications,it need ensure the integrity , safety and accuracy of the data. Because ZigBee network can only transmit data in low speed, so the most complicated problem is to realize function that the image data subcontract firstly and then to send.

The Image display module programming

When the image data subcontracted transmit via wireless network to the PC machine, PC software needs to extract the sequential packets according to certain decompression algorithm and then to display.

The system test

According to the above system hardware and software design, completed the development of this system. And the system was tested, the test results are shown in figure 4 and figure 5.

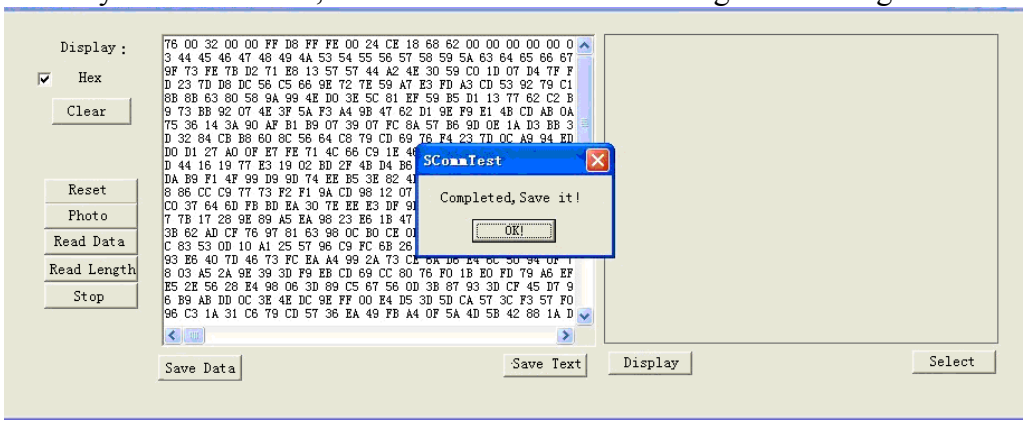

Figure 4. Image hexadecimal representation Figure

This study constructs the whole image transmission system, uses serial camera to collect information in the old man's living environment. This system gets through RS232 data processing module to transmit data to the ARM processor and then the ARM UART module pass the data to ZigBee routing nodes, eventually it reaches the ZigBee wireless transmission center through the ZigBee network nodes. It displays image data finally back into the original after processing, which transfers data to PC using the connection between the PC with the RS232 module. The image data of this study can dock with the existing home endowment system database for storage that can enrich the data. During the development process, this design completes the hypogyny machine program's design and the implementation of the PC software. The camera image information acquisition mainly use the serial port based on VC0706 chip during the development process about the Lower computer. Lower computer system uses serial camera based on VC0706 to collect image information, ARM development board based on S3C44B0X to divide image information into many

data packages, ZigBee modules based on CC2530 to construct wireless network for data transfer. Upper computer system uses VC6.0 and ADS1.2 to develop program, realizes serial communication and .original image display.

Figure 5. Image display Figure

When the upper computer software send photos command, the camera take images, send the image data back to the software. Figure 4 shows the sequence to reach the PC software hexadecimal data information of the image and click save data button, the image data file stored in JPG format. Then click the button, the image will display as JPG format. Set the size of the image resolution 320 * 240 when test, the image size returned is about 13 KB, which can be clearly seen from figure 5 captured image,and this realize the wireless transmission of images.

Conclusion

The paper introduces the design of image getting and transmission system based on ZigBee from two aspects of hardware and software. At last, the design of the system is realized. Pass the final test, it can get the real-time captured images clearly. In the healthy care system, it can well help doctor understand the patients' condition. At the same time, it also provide important design idea for the wireless sensor network (WSN) of large amount of data in the file transmission, and it have certain research significance and practical value.

References

[1] Liu Lijian, and Zhang Guangming, Smart home management system design based on ZigBee wireless technology[J], Computer Technology and Development , 2011,21 (12) :250-253.
[2] SAFARIC S, MALARIC K. ZigBee wireless standard[Z], IEEE, 2006: 259-262.
[3] Gao Shouwei and Wu Canyang, ZigBee technology practice tutorial --Solutions based wireless sensor networks CC2430/31 [M], Beijing: Bei HangUniversity Press, 2009.
[4] Xiong Maohua and Yang Zhenlun, ARM architecture program design [M] , Beijing:Tsinghua University Press, 2009.
[5] Zheng Dong. "ID-based Proxy Blind Signature[C]//Proc. Of AINA'04. [S. l.]: IEEE Press, 2004: 380-383.
[6] Zhang Fangguo. Efficient ID-based Blind Signature and Proxy Signature from Bilinear Parings[C]//Proc. of ACISP'03. [S. l.]: Springer-Verlag, 2003: 312-323.
[7] Gu Chunxiang. An Efficient ID-based Proxy Signature Scheme from Pairing[EB/OL]. (2006-10-02). http://eprint.iacr.org/2006/Pdf.
[8] Akyildiz I F, Su W, Sankarasubramaniam Y. Wireless sensor networks:a survey［J］. Computer Networks, 2002, 38(4) : 393-422.
[9] Baronti P, Pillai P, Chook V. Wireless sensor networks: A survey on the state of the art and the 802.15. 4 and ZigBee standards［J］, Computer Communications, 2007, 30(7) : 1655-1695.

Advanced Materials Research Vols. 989-994 (2014) pp 4763-4766
© (2014) Trans Tech Publications, Switzerland
doi:10.4028/www.scientific.net/AMR.989-994.4763

Research on user behavior analysis engine system

Shanhong Zhu[1] Pei Tang[2]

[1]School of Computer and Information Engineering ,Xinxiang university, Henan, China

[2] School of Art and design ,Xinxiang university, Henan, China

Email: zshazhu@163.com

Keywords: engine system; behavior analysis;

ABSTRACT: the user behavior analysis is the effective way to enhance the user viscosity, large Internet sites to maintain the flow. meanwhile efficient processing and storage, cloud database test showed that, the system can significantly improve the effect and efficiency of user behavior analysis.

0 Introduction

The dynamic behavior of user refers to the user (including login and not logged in two cases. The user login, registered account user identification by acquiring ID; for users who are not logged in, record visit their website SessionID logo) occurred in accessing the page a moment of behavior, the behavior includes the occurrence time, the page (contains the page title and page URL), related to the operation and behavior subject, real-time capture them and carry on the effective analysis, has an important significance for understanding user behavior characteristics[1].

From the client gets information including the user dynamic behavior and context information, the context, including: behavior occurrence time; the current user ID or SessionID; the current page title; the address URL of the current page; the current user search conditions; access to the same page number; page retention time; do you want to save the page; printed the page whether or not ;whether add to favorites ; copy or cut the page content and so on ; the environmental context information includes: the client machine configuration, current network condition, the server working condition etc..

1 The historical behavior mining

Analyzing the historical behavior mainly comes from on the WEB log mining[9], due to a surge in the number of Internet, the amount of data the WEB log and exponential growth, which makes the analysis platform of based on the single node has been unable to meet the needs of massive data analysis[2]. Therefore, the analysis engine user behavior based on cloud platform, the cloud storage technology will be the mass of WEB log is stored in the HDFS distributed file system, and the calculation model by using MapReduce, the log file cleared, denoising, protocol, finally, on a variety of data mining algorithms are parallelized modification, in the form of services to the users with mining analysis functions, including: analysis, research, user behavior improved matrix vector association rules method based on clustering algorithm based on user interest degree of user behavior query vector space model based on cloud environment, mining results, stored in the HBase user behavior information base, in order to combine with the dynamic behavior, reasoning user interest. In order to enhance the efficiency analysis of log file.

2 Study on the vector space model of retrieval based on user behavior

Vector space model (VSM:Vector Space Model) proposed by Salton and others in twentieth Century 70 years, it is the basic idea of each text and query contains some features independent properties reveal its content, and each feature attributes can be regarded as a dimension vector space, then the text can be expressed as a collection of these attributes, ignoring the complex relationship

between paragraphs, sentences and words in the text structure[3]. At the same time, given the feature weight vocabulary certain (weight), anti should vocabulary in the importance and the value of the contents of the file identification, this value is called the indexing vocabulary "significant value (Term Significances)" or "weight", by the lexical statistics calculate the document and to, such as: the feature words appear frequency (Term frequency, TF). Vector of each file is in fact all the document feature through a combination of computing, called "the document feature item vocabulary matrix". And then all of the document vector based on specific computing methods of similarity measure between each other.

Vector space retrieval model can be described as $I=(D,T,Q,F,R)$ Among them:

$D=\{d_1,d_2,...d_n\}$ As a collection of text, n text collection number;

$T=\{t_1,t_2,...t_n\}$ Set as a feature, m feature of all. A text m feature indexing can be represented as a vector space $d_i=\{w_{i1},w_{i2},...w_{im}\},i=1,2,...,n$, w_{ij} is characteristic t_j for the text d_i of the weight, if the weight value w_{ij} is 0, indicating t_j that it is not appeared in d_i

$Q=\{q_1,q_2,...q_m\}$ for the query set, a query q_r can be represented by vectors $q_r=\{q_{r1},q_{r2},...q_{rm}\}$, q_{rj} is a characteristic to t_j the query q_r weights, if the weight value q_r is 0, indicating that t_j is not appeared in q_r.

Further definition:

Frequency tf_{ij}: t_j is the feature for text d_i appear in the frequency;

Inverse document frequency word idf_i (inverse document frequency): the word in the quantitative distribution of document collection, the calculation $\log(N/n_k+0.5)$ is usually, where N is the total number of document centralized, n represents a number of documents containing K, called the document frequency of the term.

The normalization factor: in order to reduce the inhibitory effect of high frequency characteristics of individual word on other low-frequency feature words, the standardization of components.

Based on the above three factors to term weighting formula:

$$w_{ik}=\frac{tf_{ik}\log(N/n_k+0.5)}{\sqrt{\sum_{k=1}^{n}(tf_{ik})^2\times[\log(N/n_k+0.5)]^2}} \quad 3.1.$$

The similarity between the text and the query can be used to measure the distance between two vectors. There are many kinds of calculating method of similarity, commonly used methods of inner product, Dice coefficient, Jaccard coefficient and cosine coefficient, usually uses the cosine coefficient method, namely the cosine of the angle between two vectors to represent the similarity between the text and the query $Sim(d_i,q_j)$, see equation (3.2). Cosine similarity calculation method

is a normalization, the angle between the two vectors of the smaller, the greater the degree of correlation between documents, correspondence $\cos$ is higher. Two vector included angle cosine is equivalent to their standard vector inner product unit length, it reflects the similarity term component two vector of relative distribution.

$$Sim(d_i, q_j) = \cos\theta = \frac{\sum_{k=1}^{n} w_{ik} \times w_{jk}}{\sqrt{(\sum_{k=1}^{n} w_{ik}^{2}) \times (\sum_{k=1}^{n} w_{jk}^{2})}} \tag{3.2}$$

Algorithm design

Input: user access to key words each time the user query log in;

Output: the similarity with the query keywords vector existing values in the database is not paper and similarity of 0, and according to the similarity value from big to small order;

1）extracted from each Webpage keywords as the feature word, and these feature words and keywords query every time the user binding, rearrangement and according to a lexicographic order, combined together to form a standard feature set of words;

For example, there are Webpage document set (NDoc1, NDoc2, NDoc3, NDoc4), all the feature words together for (W1, W2, W3, W4, W5, W6), and when the query words (WQ1, WQ2), where wq1= W4, the standard set of words as features (W1, W2, W3, W4, W5, W6, WQ2), Webpage document feature item vocabulary matrix in table 1.

3 Application examples

Using the above research results, relying on the research project, the analysis engine system user behavior based on cloud computing is a design and development[4].

The analysis engine platform running on the Ubunt12.10 user behavior, the software mainly includes: jdk-1.7.0_11, Jena-2.6.4, Myeclipse-8.0, Hive-0.10.0, HBase-0.94.4, Hadoop-1.0.4, Tomcat-6.0, Jquery-1.6, Spring-3.0, Struts2-2.2.1, the browser is above IE8.0. The context aware behavior analysis as an example, system operation is as follows:

The system calculates the Markoff matrix intermediate important, as shown in figure 2.

chengli	www...	www...	www...	www...	www...	www...	www...	www...	www...	www...	www...
www...	0.196	0.176	0.078	0.176	0.196	0.0	0.176	0.0	0.0	0.0	0.0
www...	0.0	0.0	0.0	0.0	0.0	0.176	0.0	0.0	0.274	0.274	0.274
www...	0.0	0.0	0.0	0.0	0.0	0.0	0.0	1.0	0.0	0.0	0.0

lucky	www...	www...	www...	www...	www...	www...	www...	www...	www...	www...	www...	www...	www...
www...	0.258	0.258	0.0	0.0	0.0	0.241	0.0	0.0	0.241	0.0	0.0	0.0	0.0
www...	0.0	0.0	0.340	0.0	0.0	0.0	0.0	0.340	0.0	0.0	0.0	0.0	0.318
www...	0.0	0.0	0.0	0.378	0.378	0.0	0.0	0.243	0.0	0.0	0.0	0.0	0.0
www...	0.0	0.0	0.0	0.0	0.0	0.0	1.0	0.0	0.0	0.0	0.0	0.0	0.0
www...	0.0	0.0	0.0	0.0	0.0	0.0	0.0	0.0	0.0	0.5	0.5	0.0	0.0
www...	0.0	0.0	0.0	0.0	0.0	0.0	0.517	0.0	0.0	0.0	0.0	0.482	0.0

Figure 2 Markoff matrix

4 Research and Prospect

User behavior analysis engine through the WEB log, the user dynamic behavior and the context information, multi-channel, all-round, three-dimensional access to large-scale user behavior information increasing, the use of cloud environment MapReduce parallel computing model, HBase cloud storage capacity, and uses the relevant data mining algorithms, static analysis, dynamic monitoring of user behavior characteristics and synthesis reasoning, behavior of rich information content, comprehensive, complete, and can efficiently for the user to push their interested information and provide the basis for the site structure adjustment.

Because of the time and energy constraints, this work is currently only integrates three cloud platform of the data mining model, looking for more scene data mining model, and transformation, in the cloud platform integrated, make the system more universal, universal, is the next step of work to do.

References

[1]Joohee Kim, Chankyou Hwang, Eunkyoung Paik, Youngseok Lee.Analysis of IPTV User Behaviors with MapReduce [J].International Conference On Advanced Communication Technology.Feb. 19~22, 2012

[2] Bai Xiaoli, Chen Fei.The Prediction of Web User's Behavior Based on Web Usage Mining[J].2010 ETP/IITA Conference on Telecommunication and Information (TEIN 2010).2010,1：32-35.

[3] Song-Kyoo.K. Enhanced user experience design based on user behavior data by using theory of Inventive Problem Solving[J].in Industrial Engineering and Engineering Management (IEEM)，2010 IEEE International Conference on，2010,1(1)：16-23.

[4] Wen-Hung, L.,Yao and C. Chien-Pao. Analysis and Interpretation of e-Reader User Logs: A Case Study of High School Students' User Behaviors[J].in Advanced Learning Technologies (ICALT)，2011 11th IEEE International Conference on，2011,11(1)：106-112.

Advanced Materials Research Vols. 989-994 (2014) pp 4767-4770
© (2014) Trans Tech Publications, Switzerland
doi:10.4028/www.scientific.net/AMR.989-994.4767

Resource Sharing Between Social Network And UPnP Network

Haolin Jia[1, a], Yan He[2, b] , Chengcheng Zhang[3, c] , Lei Chen[4, d]

[1]School of Information and Engineering, Communication University, Beijing100000, China;

[2]School of Information and Engineering, Communication University, Beijing100000, China;

[3]School of Information and Engineering, Communication University, Beijing100000, China;

[4]School of Information and Engineering, Communication University, Beijing100000, China.

[a]jiahaolinmail@163.com, [b]hey4tc@163.com,[c]chchengzhang@126.com, [d]stifler12@126.com

Keywords: UPNP AV; OAuth; Media Server; Open Platform

Abstract. Universal Plug and Play (UPnP) is a technology for devices interconnection and resource sharing in the home network. However, the UPnP network has a construct. User can only access local resources within the UPnP network, but user is Unable to access the resources outside the home network such as the resources of the user on the Internet. Now social network is popular, the user has a lot of resources in their own social network. How can the user realize resource sharing on social network to the UPnP network? It can make user can easily access to the user's social resources on the network in their own UPnP home network. We found that most of the social network based on open platform OAuth authorization to third party that call the API to access the resources in social network. We now put forward a solution that is based on the architecture of UPnP AV, we can extend the media server's function that call the social network open platform API to realize the resources sharing between social network and the UPnP network.

I. Introduction

UPnP [1] is a network protocol that UPnP forum proposed and implemented to promote a set devices interconnection. It is also a uniform standard. UPnP technology defines the various kinds of intelligent electronic devices and household devices such as peer to peer connection of the network. This protocol's goal is to make home network device can be connected and realize resource sharing, but the UPnP network has a construct that user can only access local resources in the UPnP network. After various kinds of electronic devices' interconnection and resource sharing of the home network, People hope that the home internal network resources can be extended to the external network. In other words, people in the home network can access resources outside the home network. There is no regulation and the corresponding solutions in the UPnP technology. It also become a UPnP technology's research direction in the future .

In the paper, we put forward a solution that make the resource Sharing between social network and UPnP network. In Section II, we introduce the basic knowledge of UPnP AV [2] frame and OAuth [3] protocol for open platform authorization. In Section III, we introduce the model of our solution. In Section IV, we set up the experimental environment and analyze the simulation results. In Section V, we conclude this paper.

II. The UPnP AV And OAuth Protocol For Open Platform Authorization.

In the section, we make a brief introduce of UPnP AV frame and the OAuth protocol that used for open platform's authorization in social network.

A. UPnP AV frame

UPnP AV is an important framework of UPnP, it consists of control point, media server, and media renderer [4]. We can make the media renderer play the specified media resource on the media server through the control point's control.

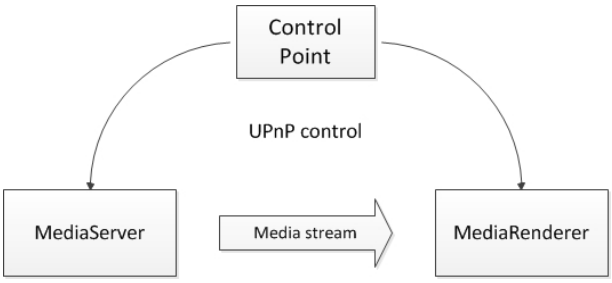

Fig. 1 The model of UPnP AV frame

- Media Server: It includes a lot of media resources. The main role of the media server is used to locate the media resources [5]. These resources are stored in the media server or other devices that media server can access to.
- Media Renderer: Media Renderer is used to play media source from the media server through the UPnP network's transmission.
- Control Point: It is used to coordinate and synchronize media server and media renderer. It makes the media server and media renderer establish connection and transfer media source from media server to the media renderer through the control of the control point. Noted that when the media server and media renderer establish connection and begin to transfer media resource, then control point is irrelevant [6]. The control points and media server or media renderer's interaction is independent.

In the UPnP network, control point found the media server and media renderer and get the devices description such as media resources' URL, transport protocol and data format supported by media server and media renderer. Then Control points call actions to make the media server and media renderer's connection established. At the time, control point can select the media resources in the media server and call the media renderer to play.

B. OAuth protocol

Each user has a lot of resources such as photos, video, music, and so on in their social network sites. Many social network sites are now provide a wide range of Open API for users calling to access their resources, but user must get the owner of the social network resources' authorization. If we get the authorization, we can access to the resources on the social network through third party applications. In other words, we design a scheme that can make our UPnP devices get the authorization of our social network [7]. So we can call the Open API of social network in our UPnP network.

Now, most social network sites are popular in using OAuth authorized technology. The OAuth workflow [8] is as shown in the figure.2.

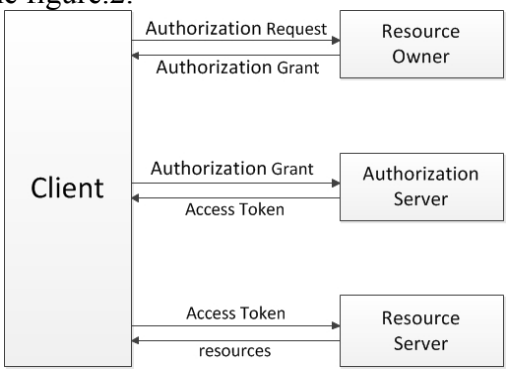

Fig. 2 The workflow of OAuth authorized technology

There are client, resource owner, authorization server and resource owner four parts in the OAuth authorized technology. The user send authorization request to resource owner through a third party. If the resource owner agree with this authorization, the resource owner send authorization grant to the client. Then the client send the authorization grant to the authorization server for getting the access token. When the client get the access token, it can access to the resources of the resource server.

III. The Model Of Our Solution.

In the section, we will introduce the model of our solution. The model of our solution is as shown in the figure.3.

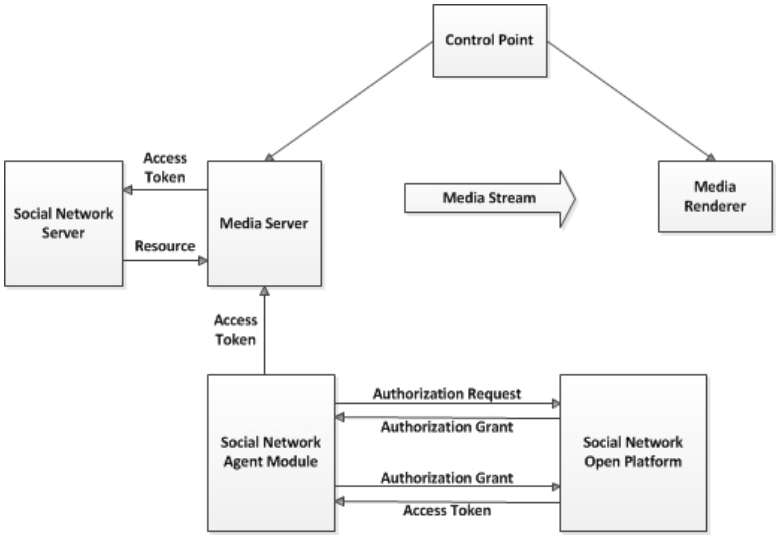

Fig. 3 The model of our solution

In our solution, we make the media server act as the third party client in the OAuth protocol. In the workflow of our solution, there is a social network agent module in the media server. We register a application through enter our account and password on the social network open platform. Then we get the AppKey and AppSecret. The AppKey and AppSecret represent our application. We send authorization request to the social network open platform to get the access token through the social network agent module. When the agent module get the access token, the media server get the access token through the agent module. The media server can call the open platform API to get the resource URL through the access token. So when the control point found the media server, it can get the social network resource URL and the UPnP network's local resources. The control point can call the media renderer to play the UPnP local resources or social network's resources selected by user.

IV. Performance Analysis.

In the section, we set up the experimental environment and analyze the simulation results.

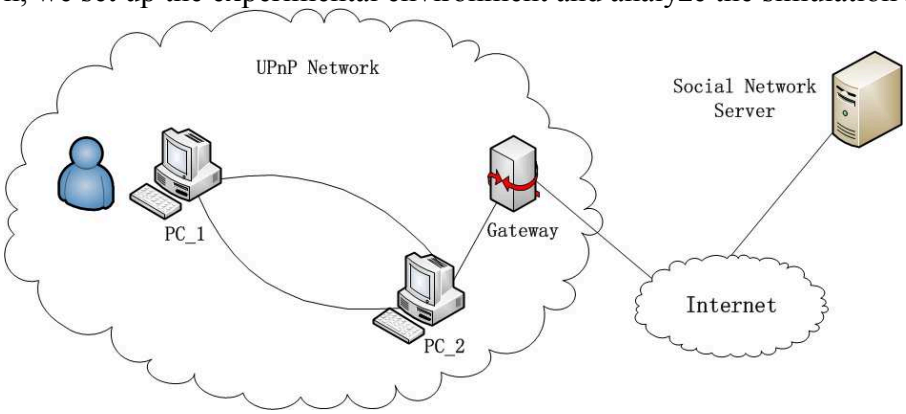

Fig. 4 The model of experimental environment

We use two computers to set up the environment. A computer will be act as the media server, the other act as the control point and media renderer. We use web browser act as our media renderer. In our UPnP network, we set up the http connection between the computers. On the two computers, we are all based on the Eclipse development platform to realize its function in the Java language on the Windows operating system. We use sina microblog act as our social network.

In our simulation experiment, we found the media server and get the local picture URL through the control point, then we call our browser to show it. We send the local picture to microblog through

calling the interface in the open platform. Now media server can get the picture URL in the sina microblog through calling the API. At last, we show the picture through the control point call the browser. The result as shown in the figure.5.

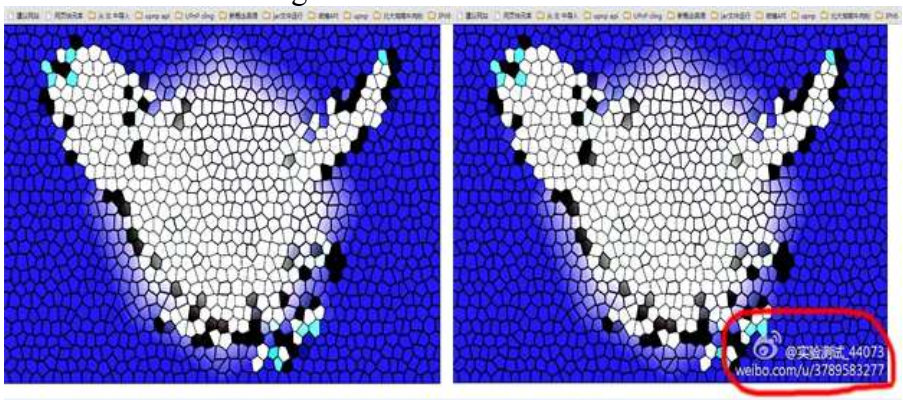

Fig. 5 Compare the picture in the UPnP network and social network

We found that the pictures on the microblog are signed by watermark logo. After we send the local picture to the microblog by media server calling the API, the picture will be the resources in the microblog and are signed by watermark logo.

V. Conclusion.

Based on our OAuth authorization, we make the media server can call social networks open platform API. We expand the media server's function and implement the resources sharing between social network and UPnP network. Through our experiment simulation and the picture demonstration, we proved that we can use the UPnP network's local resources and social network's resources in our UPnP network. Besides, we can interact with social network and make the local resources upload to the social network.

References

[1] Universal Plug and Play (UPnP) Forum，URL：www.upnp.org，Date 15 October 2008.

[2] UPnP Forum UPnP AV Architecture For UPnP™ Version 1.0, June 25, 2002.

[3] The OAuth 2.0 Authorization Protocol, http://tools.ietf.org/html/draft-ietf-oauth-v2-16, 2011.5

[4] Li Pingjun, Shen Jian. UPnP AV system structure design and implementation [J], Computer engineering and design, 2007, 28 (14): 3 521-3, 525.

[5] Peng Huan, Jiang Tianfa. Digital home UPnP and AV framework research [J], modern electronic technology, 2009, 32 (16) : 57-59.

[6] Zhang Li. Based on UPnP and UPnP AV multimedia synchronization and playback [J], computer science, 2008, 35 (5) : 92-93.

[7] Guo X, Li J. Extending SNS Media to DLNA Content Sharing Systems[C]//Intelligent Systems (GCIS), 2013 Fourth Global Congress on. IEEE, 2013: 219-223.

[8] Shi Ziqing, Liu Jinlan, Tan Xiaohua. Based on the OAuth2.0 certificate authority technology[J]. Computer system application, 2012 (3) : 260-264.

Advanced Materials Research Vols. 989-994 (2014) pp 4771-4774
© (2014) Trans Tech Publications, Switzerland
doi:10.4028/www.scientific.net/AMR.989-994.4771

Research and Design on P2P Business Process Execution Framework for Workflow Management Systems

Tao Wu[1, a]

[1]Department of Computer Science and Technology, Tsinghua University, Beijing 100086, China;

[a]violin2696@gmail.com

Keywords: Business workflow, distributed execution, process migration, load balance scheduling.

Abstract. Efficient business workflow management in large-scale areas is in great demand. However, current business workflow management systems are short of distributed workflow execution support. In our paper, we design and implement a distributed framework called PeerODE for Apache ODE (Orchestration Director Engine) [1], an open-sourced business workflow engine. PeerODE presents a scalable approach to P2P business process execution. The scheduling experiment on PeerODE shows that the framework handles the distributed business process execution effectively.

Introduction

Business workflow management is a rapidly growing research area. The technology has been widely used in enterprise management, manufacturing management, etc. As the scale of these organizations increases, workflow management in distributed areas is in great demand.

Current workflow systems include business workflow systems, scientific systems, etc. Most of their architectures fall into three categories: server/client, cluster-based and P2P. Their representatives are METUFlow [2], Pegasus [3] and SwinDeW [4], separately. Only the P2P architecture can offer us the ability of distributing workflow engines in wide areas. The server/client and cluster-based workflow systems have single point of failure problem while P2P systems don't. These metrics make P2P architecture an appropriate choice for distributed business workflow systems.

While business processes can execute normally in a single node, problems come when the processes execute from peer to peer. The business workflow's design focuses on process integrality, so distributed execution needs process slicing and migration support. Current research on process migration are mainly about process execution with different schemas [5, 6], with little attention on process slicing and migration [7]. The PeerODE framework proposes a process migration module to slice and migrate business processes from one peer to another. This module can help business processes execute on peers in wide areas.

PeerODE has peer management module to manage data and control requests between peers. The framework also supports human task since it's an essential part in business workflow. PeerODE chooses BPEL (Business Process Execution Language) as its business modeling language and Apache ODE as its execution kernel.

PeerODE adds a scheduling framework and implements a load balance algorithm. The algorithm migrate business processes from heavy-load peers to light-load peers. The scheduling results can verify the correctness of the process migration module and the function of the whole framework.

Design of the PeerODE Framework

Architecture. As shown in Fig.1, the PeerODE framework consists of five parts.

ODE Engine module is the BPEL process execution kernel. It can execute BPEL processes and communicate with outer web service. The control layer of ODE Engine can receive different kinds of operation requests, such as suspend and replay, on specified processes. The engine can also communicate with local modules through integration layer.

Peer Manager module communicates with other peers through JAVA NIO (New IO) interface to form a P2P network. The module is also responsible for processing data and control requests from remote peers and inner modules. For example, Peer Manager can tell other peers the number of processes in its own peer's ODE Engine module, and it can also help the Scheduling Framework module of its own peer to suspend a specified process in other peers.

Process Migration module implements the function of process slicing and migration. The process executing in the ODE Engine module can be suspended and migrated to other peers to continue its execution from the original suspending state.

Human Task module supports integrating manual work with abstract BPEL activities. The module uses message queue to map the start and end of manual work to the start and end of Invoke activity, a kind of abstract BPEL activity. In this way, the ODE Engine can execute manual work just the same way as executing an ordinary BPEL activity.

Scheduling Framework module is a peer state monitor. It can monitor different kinds of characteristics of the peer. In this paper we implement a load balance algorithm. The algorithm keeps an eye on the number of processes in the ODE Engine module. If the processes number exceeds the upper limit set by Peer Manager, the algorithm will ask Peer Manager to find light-load peers in its neighbor of P2P network and migrate over-loaded processes to the idle peers.

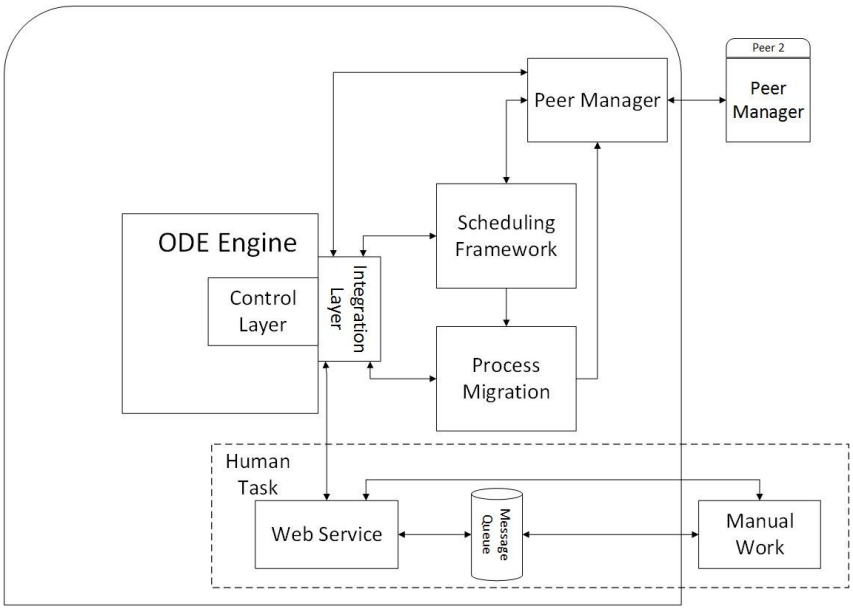

Fig. 1 PeerODE architecture

Execution Procedure. The business process distributed execution is mainly conducted in the PM (Process Migration) module. This module uses four functions of ODE Engine control layer: Suspend, GetCommunication, Replay and Terminate. Suspend helps suspend specified processes. GetCommunication can get process execution history. Replay helps quickly reproduce the process state from execution history. Terminate can delete specified processes from ODE Engine.

As shown in Fig.2, process migration begins when PM suspends and gets execution history of the specified process through ODE control layer, which is the process slicing procedure. If the ODE Engine is executing human tasks, the suspend function will not response until the manual work completes. Then PM sends the execution history to the remote peer. After receiving the execution history, the PM module in the remote peer can reproduce the process state and continue the execution. To this point, the business process migrates from one peer to another, which is indeed a successful distributed execution. The last step is to terminate the original process. It ensures that only one instance of the migrated process exists in the whole system at the same time.

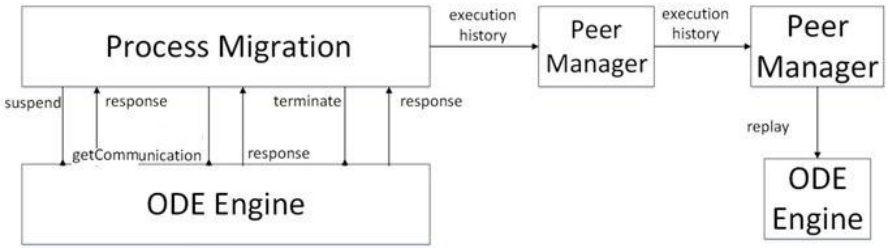

Fig. 2 Execution procedure

Principle Analysis. The two key points of process migration are obtaining business process execution history and reproducing execution state. Process execution history is the history of BPEL activities' messages. During the BPEL process execution, the ODE Engine records the input and output message of every executing activity. These messages can determine the unique execution history of current process, which guarantees the effectiveness of process slicing. The execution state reproduction is through the Replay function of ODE Engine control layer. The function is intended for failure recovery. We rewrite the function for general process state reproduction. The function analyzes the received message history to get the unique execution history. Then it quickly takes the ODE Engine through a mock execution to the process state before suspending. After the mock execution, it begins to invoke real new BPEL activity next to the suspending point and continues the distributed execution.

Scheduling Experiment

Experiment Design. As shown in Fig. 1, the scheduling framework is located in the middle of Peer Manager, Process Migration and ODE Engine. These three modules communicates with the algorithm in the framework, through which we can observe the execution state of the three modules. The scheduling algorithm in the experiment is a load balance algorithm.

In the experiment, 3 peers are launched to form a P2P network. Each peer has different number of processes executing concurrently in their ODE Engine module from the experiment begins. These processes are all the same. The upper limit of process number in each peer is 10. The experiments can verify the correctness of distributed process execution and the effectiveness of the scheduling algorithm.

Result and Discussion. The experimental result is shown in Table 1. We conduct 5 group of experiments. In each group, we have 2 experiments in comparison. Their initial load condition is same to each other. The only difference is that the experiment in the upper row has load balance algorithm monitoring itself while the experiment in the lower row has none algorithms.

The measured variables in the experiments are: average process execution time, load condition of 3 peers. The experimental result is shown in Table 1.

Table 1 Experimental result

Experiment Group	Initial peer load			Final peer load			Average process execution time (ms)
	Peer1 load	Peer2 load	Peer3 load	Peer1 load	Peer2 load	Peer3 load	
1	10	10	0	10	10	0	17277
	10	10	0	10	10	0	17283
2	20	0	0	7	3	10	28450
	20	0	0	20	0	0	30850
3	25	0	0	9	2	14	28795
	25	0	0	25	0	0	35101
4	30	0	0	8	6	16	36581
	30	0	0	30	0	0	45822
5	35	0	0	8	8	19	37654
	35	0	0	35	0	0	44214

From the experimental result, we can see that except for the first group, all the experiments with load balance algorithm monitoring successfully migrate processes from heavy-load peers to light-load peers. The result can not only prove the correctness of scheduling algorithm, but also convince us that distributed business process execution framework is effective. The reason why experiments in the first group do not execute process migration is that the load of their peers has not exceed their upper limit. Since process migration also need system resources, it's an appropriate choice not to migrate processes when all the peers are already light-load.

Meanwhile, the experiments also record the average process execution time. From the result we can see that the more activities the peers have, the longer the average execution time is, even when all the processes execute concurrently. It means the peer load has negative impact on process execution. In every group except for group 1, the average process execution time of experiment with load balance algorithm is shorter than the experiment with no algorithms. This status can convince us that the load balance algorithm can effectively improve the system performance.

Conclusion

This paper proposes a P2P business process execution framework for workflow management systems. After the survey on current workflow architectures, we choose P2P as our distributed architecture. The framework uses Process Migration module to handle the main work of process distributed execution. The Peer Manager and Human Task module are enhancement for process migration and execution. The scheduling experiments convince us that the distributed process execution is correct and the load balance algorithm is effective.

Our work on distributed business process execution is a first step for developing a scalable P2P workflow management system. Future work towards this object should include P2P management and scheduling framework enhancement. With these metrics the workflow system will perform better on peer management and overall execution.

References

[1] Information on http://ode.apache.org

[2] Dogac, Asuman, et al. Design and implementation of a distributed workflow management system: Metuflow, in: Workflow Management Systems and Interoperability, Springer Berlin Heidelberg, 1998, pp. 61-91.

[3] Deelman, Ewa, et al. Pegasus: A framework for mapping complex scientific workflows onto distributed systems, Scientific Programming 13.3 (2005): 219-237.

[4] Yan, Jun, Yun Yang, and Gitesh K. Raikundalia, SwinDeW-a p2p-based decentralized workflow management system, Systems, Man and Cybernetics, Part A: Systems and Humans, IEEE Transactions on 36.5 (2006): 922-935.

[5] Omar, MS Haji, P. W. H. Chung, and C. W. Dawson, A Novel Workflow Management System for Handling Process Adaptation and Compliance, Advanced Information Networking and Applications Workshops (WAINA), 2013 27th International Conference on. IEEE, 2013.

[6] Nowak, Alexander, Frank Leymann, David Schumm, and Branimir Wetzstein, An architecture and methodology for a four-phased approach to green business process reengineering, in: Information and Communication on Technology for the Fight against Global Warming, Springer Berlin Heidelberg, 2011, pp. 150-164.

[7] Long Hong, Xiang Yong, Design and implementation of scheduling framework for P2P workflow system (In Chinese), in: Computer Engineering and Design, 33.1 (2012): 138-146.

Advanced Materials Research Vols. 989-994 (2014) pp 4775-4779
© (2014) Trans Tech Publications, Switzerland
doi:10.4028/www.scientific.net/AMR.989-994.4775

Research on a Theatre Recommendation System

Yulong Li[1, a], Ying Li[1, b], Wei Jiang[2, c], Zhi Zhou[1, d]

[1]School of Computer, Communication University of China, Beijing 100024, China

[2]School of Information Engineering, Communication University of China, Beijing 100024, China

[a]lyl_fmyl@yeah.net, [b]liy@cuc.edu.cn, [c]jw@cuc.edu.cn,[d]zzsquarrel@163.com

Keywords: recommendation system, theatre, bipartite graph, standardization, similarity.

Abstract. Nowadays the recommendation system has been widely used, especially in the field of e-commerce, SNS, music, etc. On the basis of recommendation systems which are widely used, the paper puts forward a theatre recommendation algorithm which is more suitable in the field of theatre. In order to achieve the recommendation of theatre, the paper uses a series of steps, including weight, bipartite graph, data standardization, similarity calculation. After using this algorithm, some theatres will be recommended according to recommendation level. The results of recommendation are more reasonable, effective and satisfied.

Introduction

With the coming of internet time, a variety of data are increasing faster and faster, and thus information overload appears. It is very difficult for us to find out the thing we are interested in from a large amount of information, so the recommendation system was born. Recommendation system is to help users find some valuable information they need. Nowadays the recommendation system has been used in many fields, including e-commerce, movie, music, SNS, network, reading, ad, and e-mail.

Theatre is a place for stage performance. Due to the rising number of theatres, it is a urgent need to study how to pick out some suitable theatres from a large quantity of theatres for a specific play, however, predecessors in the field of theatre ignored it. The paper will apply the recommendation system to the field of theatre, and put forward a particular algorithm to solve the problem.

Traditional recommendation algorithms

Recommendation algorithm is the most important and key part in the recommendation system. It has a great influence on the performance of the recommendation system. At present, the traditional recommendation algorithms that are widely recognized include content-based recommendation algorithm, collaborative filtering, social network-based recommendation algorithm, and mixed methods [1].

Content-based recommendation is that, according to the objects selected by users, users get those characteristics of similar objects as recommended results. Collaborative filtering is that users get those objects some other users who share the same interests and hobbies like, or the users themselves like before. Social network-based recommendation is that users get recommended results by means of trust between interpersonal relationships.

The paper shows a theatre recommendation algorithm based on the information of the play. Because the content of the play is wide-ranging, the distinction of different plays is not obvious, content-based recommendation is not fit. Because different plays have no intersection, they don't have the same interests or the similar ones, collaborative filtering is not fit. Because the theatre has nothing to do with social network, social network-based recommendation is not fit, either. Above all, the paper puts forward a suitable theatre recommendation algorithm, combined with the traditional recommendation algorithm.

A theatre recommendation algorithm

Experimental environment. The paper mainly shows how to recommend the suitable theatres according to the information of play and something related. The information of play refers to the title of play, the type of play, the parameters of facilities about theatre (such as seating capacity, size, suspender, lighting, audio, etc.).

The paper uses the title of play, the type of play, the theatre seating capacity as three typical parameters. Through the following algorithm, in accordance with the recommendation level of the theatres, we get some suitable theatres.

Algorithm steps. Assuming the recommendation level of all theatres is 0.

Firstly, assuming the requirement of theatre seating capacity is M, Candidate quantity of the theatres is N, and the seating capacity respectively is N_i (i=1, 2, … , n). When N_i<M*0.9 (i=1, 2, … , n), the ith theatre is ruled out. When N_i>M*1.2 (i=1, 2, … , n), the recommendation level of the ith theatre adds 1, that is 0+1=1. When N_i>=M*0.9 and N_i<=M*1.2 (i=1, 2, … , n), the recommendation level of the ith theatre adds 2, that is 0+2=2.

Secondly, if the title and the type of play could be found from the historical data, the corresponding theatre recommendation level adds 1.

Thirdly, according to the historical data set, we respectively count the show number of this play type in each theatre. Assuming the show number of this play type is S, the number of theatres is N, and the show number of each theatre of this play type is T_i (i=1, 2, … , n). If F_i (i=1, 2, … , n) presents weight, we have the formula 1.

$$F_i = \frac{T_i}{S} \quad (i = 1,2,\dots,n \ \ and \ \ T_1 + T_2 + \cdots + T_n = S) \tag{1}$$

If the recommendation levels of theatres are same, the theatres rank from large to small, depending on F_i. If F_i>=0.2, the recommendation level of the ith theatre adds 1.

Fourthly, drawing a bipartite graph about the play types and the theatres to find out the professional theatres [2]. See the example Fig. 1.

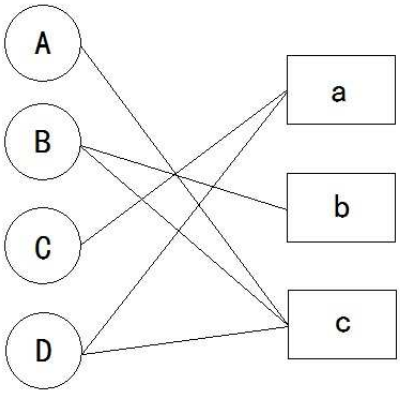

Fig. 1 An example of bipartite graph

Assuming A, B, C, D respectively represent 4 play types, and a, b, c respectively represent 3 theatres. Each link line refers that a play showed in a theatre before. Here, theatre a's in-degree is 2, theatre c's in-degree is 1, theatre c's in-degree is 3, so c is a professional theatre and c's recommendation level adds 1.

Finally, due to the show number of some big theatres is large, their ranks are relatively in the top, likewise, the show number of some small theatres is low and their ranks are relatively in the end. That is, these big theatres are likely to be recommended preferentially. In order to increase the coverage rate of the theatres, this paper uses z-score standardization [3, 4] and cosine similarity [5] to find out the suitable theatres whose historical show number is low.

Experiment and analysis

Data set. Here, the data set is from some theatre's official websites and the Internet. This experiment's data set has 500 data which include 7 theatres. The 7 theatres are *the Opera House of*

National Centre for the Performing Arts (OHNCPA), *the Concert Hall of National Centre for the Performing Arts(CHNCPA)*, *the Drama House of National Centre for the Performing Arts (DHNCPA)*, *the Opera Hall of Guangzhou Opera House（OHGOH）, the Experimental Theatre of Guangzhou Opera House (ETGOH)*, *the Opera Hall of Qingdao Theatre (OHQT)*, *the Concert Hall of Qingdao Theatre (CHQT)*. Table 1 shows the information of 7 theatres and their seating capacities.

Table 1 Seven theatres

Theatre	Seating Capacity
OHNCPA	2398
CHNCPA	2019
DHNCPA	1035
OHGOH	1804
ETGOH	443
OHQT	1600
CHQT	1200

Here, this experiment's data set include 5 play types. The 5 play types are *modern drama*, *opera*, *traditional opera*, *dance drama*, and *concert*. Table 2 shows the statistics of the show number of 7 theatres and 5 play types.

Table 2 Statistics of theatres and play types

	Modern Drama	Opera	Traditional Opera	Dance Drama	Concert
OHNCPA	0	27	0	32	5
CHNCPA	0	0	0	0	64
DHNCPA	20	12	43	9	0
OHGOH	18	30	15	61	50
ETGOH	27	0	0	0	36
OHQT	3	7	3	12	6
CHQT	0	0	0	0	20

Operation. Assuming the play title is *The Lady of the Camellias*, the play type is *opera*, the seating capacity is 1150.

Firstly, the requirement of seating capacity is 1150. We get two results through calculation: 1150*0.9=1035, 1150*1.2=1380. Compared with the 7 theatres' seating capacities, *ETGOH* whose seating capacity is 443 is ruled out. The recommendation level of *DHNCPA* whose seating capacity is 1035 adds 2, that is 0+2=2, because its seating capacity 1035>=1035 and 1035<=1380. In the same way, the recommendation level of *CHQT* whose seating capacity is 1200 adds 2. Because the seating capacities of the rest theatres are greater than 1380, their recommendation levels add 1.

Secondly, matching the play title *The Lady of the Camellias* with all the historical data, and we find out that *OHNCPA* showed this play before, so its recommendation level adds 1, that is 1+1=2.

Thirdly, calculating the weight of each theatre in accordance with the show number of *opera* in Table 2 and the formula 1, and getting the results. Table 3 shows the results of the calculation.

Table 3 Statistics of each theatre's weight in opera

	Show Number	Weight
OHNCPA	27	0.355
CHNCPA	0	0
DHNCPA	12	0.158
OHGOH	30	0.395
OHQT	7	0.092
CHQT	0	0
sum	76	1

If weight is greater than or equal to 0.2, the recommendation level adds 1. So the recommendation level of *OHNCPA* adds 1, that is 2+1=3, and the recommendation level of *OHGOH* adds 1, that is 1+1=2. The theatres order by recommendation level. If the recommendation levels are same, order by weight.

Fourthly, by calculating [2], see the following Fig. 2.

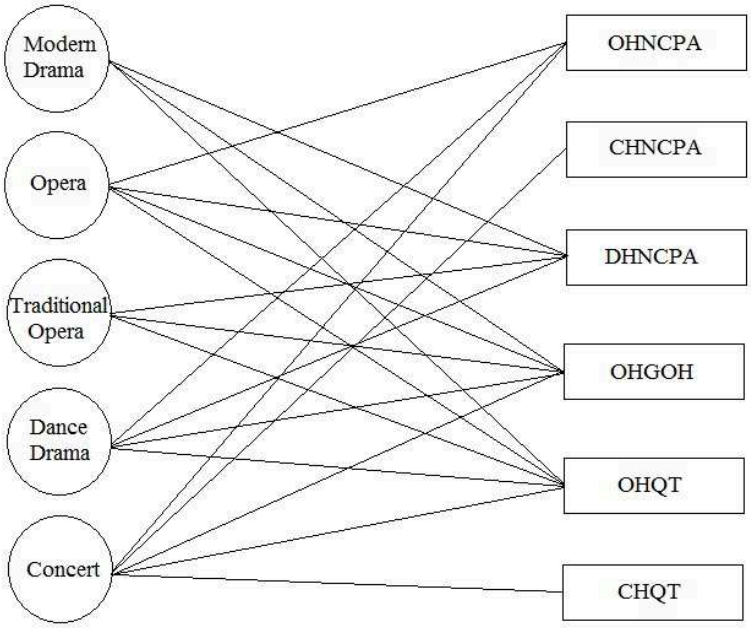

Fig. 2 Bipartite graph

Clearly, the in-degree of *CHNCPA* and *CHQT* is 1, so they are professional theatres in *concert*. However, the play type required is *opera*, so the recommendation level of this step has no changes.

Finally, finding out the suitable theatres whose historical show number is low. The theatres whose weights are greater than or equal to 0.2 are *OHNCPA* and *OHGOH*. The weights of the other four theatres are lesser than 0.2. And then calculate the similarity of the two theatres weights>=0.2 with the other theatres.

Before similarity calculation, the data standardization is needed. Because the maximum value and the minimum value of each theatre's show number are unknown, the most commonly used method of standardization min-max is not suitable. Here, z-score is used.

Z-score standardization is based on numerical mean value and stand deviation [3, 4].

See the mean formula 2.

$$\mu = \frac{1}{n}\sum_1^n x_i \quad (i = 1,2,\dots,n) \tag{2}$$

See the standard deviation formula 3.

$$\sigma = \sqrt{\frac{\sum_1^n (x_i-\mu)^2}{n-1}} \quad (i = 1,2,\dots,n) \tag{3}$$

See the z-score formula 4.

$$z(x_i) = \frac{x_i-\mu}{\sigma} \quad (i = 1,2,\dots,n) \tag{4}$$

Then use cosine similarity to calculate the similarity of theatres [5] and see formula 5 below.

$$sim(D_1, D_2) = \frac{\sum_1^n w_{1k}\cdot w_{2k}}{\sqrt{\sum_1^n w_{1k}^2 \cdot \sum_1^n w_{2k}^2}} \quad (k = 1,2,\dots,n) \tag{5}$$

Table 4 shows the results of cosine similarity calculation.

Table 4 Results of cosine similarity

	CHNCPA	DHNCPA	OHQT	CHQT
OHNCPA	-0.2816	-0.4589	0.8996	-0.2816
OHGOH	0.4229	0.7704	0.8814	0.4229

Here, assuming the threshold value of similarity is 0.8. If the similarity is greater than or equal to 0.8, it certifies the two theatres are exactly similar and two results fit which are 0.8996 and 0.8814. That is *OHQT* is exactly similar with *OHNCPA* and *OHGOH*, and the recommendation level of *the OHQT* adds 1.

Now all the operations have been finished. Table 5 shows the final results of theatres' sequence.

Table 5 Final sequence of theatres

Sequence Number	Theatre	Recommendation Level	Weight
1	OHNCPA	3	0.355
2	OHGOH	2	0.395
3	DHNCPA	2	0.158
4	OHQT	2	0.092
5	CHQT	2	0
6	CHNCPA	1	0

Evaluation. The calculation of the weights based on historical data ensures the accuracy of the forecast and users' satisfaction. The match of the play title and the seating capacity also improve users' satisfaction. The similarity calculation enhances the coverage for the suitable theatres whose historical show number is low [6].

Summary

By analyzing the theatre and play, the paper realizes a theatre recommendation system by a special recommendation algorithm in this special field, however, the paper also has some deficiencies, such as the quantity of experimental data set is few, and the effects of recommendation have no visualized digital evaluation. As a result, there are many problems needed to be solved.

Acknowledgment

The work is supported by National Key Technology R&D Program (2012BAH02F04), Engineering Planning Project for Communication University of China (3132013XNG1323).

References

[1] Guoxia Wang and Heping Liu: Computer Engineering and Applications, Vol. 48 (2012) No.7, p.66. (In Chinese)

[2] Yijin Wang and Yao Zhao: Software, Vol. 33 (2012) No.11, p.198. (In Chinese)

[3] Bing Liu: *Web Data Mining: Exploring Hyperlinks, Contents, and Usage Data* (Springer, Germany 2011), p.155.

[4] Arthur M.Glenberg and Matthew E.Andrzejewski: *Learning from Data: An Introduction to Statistical Reasoning* (Lawrence Erlbaum Associates, America 2008), p.69.

[5] Hongwei Ma, Guangwei Zhang and Peng Li: Journal of Chinese Computer Systems, Vol. 30 (2009) No.7, p.1282. (In Chinese)

[6] Yuxiao Zhu and Linyuan Lv: Journal of University of Electronic Science and Technology of China, Vol. 41 (2012) No.2, p.163. (In Chinese)

Advanced Materials Research Vols. 989-994 (2014) pp 4780-4784
© (2014) Trans Tech Publications, Switzerland
doi:10.4028/www.scientific.net/AMR.989-994.4780

The Analysis of Constructing Fully Homomorphic Encryption over Integers

Lei Jin[1, a],Xinxia Song[2, b]

[1]Xinjiang Medical University Affilliated Tumor Hospital,Urumuqi830000 ,China;
[2]College of Junior，Zhejiang Wanli University,NingBo 315100, China.
[a] ijinlei@gmail.com, [b] sxxx99@21cn.com

Keywords: Fully homomorphic encryption, encryption, approximate-GCD problem

Abstract: Fully homomorphic encryption has long been regarded as cryptography's prized "holy grail"–extremely useful yet rather elusive. At 2010 van Dijk et al. described a fully homomorphic encryption scheme over theintegers. The main appeal of this scheme is its conceptual simplicity. simplicity comes at the expense of a public key size in$\tilde{O}(\lambda^{10})$ which is too large for any practical system. The construction is based on the hardness of the approximate-GCD problem. At 2011 Coron et al. reduced the public key size to about $\tilde{O}(\lambda^{7})$ by encrypting with a quadratic form in the public key elements, instead of a linear form. This scheme is based on a stronger variant of the approximate-GCD problem. An implementation of the full scheme was obtained with a 802MB public key. At 2012 Coron et al. described a compression technique that reduces the public key size to about$\tilde{O}(\lambda^{5})$. This variant remains semantically secure, but in the random oracle model.A level of efficiency very similar to above scheme was obtained but with a 10.1MB public key instead of a 802MB one.Coron et al. also described a new modulus switching technique for the DGHV scheme that enables to use the new FHE framework without bootstrapping from Brakerski, Gentry and Vaikuntanathan with theDGHV scheme. At present asymptotics of FHE over integers are much better.

0 Introduction

Encryption has traditionally been viewed as a mechanism that enables secure communication[1].For someone who have the secret decryption key can learn the entire message, but without the decryption key, the ciphertext is completely useless. Can we do arbitrary computations on data while it remains encrypted, without ever decrypting it? This question from Rivest et al.and then become a open problem in cryptography[2]. In a breakthrough work Gentry described in 2009 the first construction of a fully homomorphic scheme[3]. At 2010 van Dijk et al. described a fully homomorphic encryption scheme over theintegers[4]. In recent years DGHV scheme was improved continuously by Coron et al.[5][6].Asymptotics of FHE over integers are much better now.

1.The idea of fully homomorphic encryption

The first step in framework of Gentry's scheme is to describe a somewhat homomorphic scheme that supports a limited number of additions and multiplications on ciphertexts rather than do arbitrarycomputation on ciphertexts[7]. This is because every ciphertext hasa noise component and any homomorphic operation applied to ciphertexts increases the noise in the resulting ciphertext. Once this noise reaches a certain bound the resulting ciphertext does not decrypt correctly anymore. For example, the bit-size of noise is$\rho$and the threshold of noise size is$k\cdot\rho$,then the bound is reached after only$\log_2 k$levels of multiplication.

If one wants to achieve fully homomorphic encryption, the problem of noise growth must be solved. The Gentry's idea of solving it is to decrypt ciphertext, but homomorphically!The decryption circuit is inputted in the bits of a secret key and the bits of a ciphertext,each encrypted under another public key.As long as the decryption circuit can be handle by this somewhat homomorphic scheme,the output is another ciphertext for the same plaintext.If the degree of the decryption polynomial is small enough, the new ciphertext's noise would less than the old cipertext's noise; this is called the "ciphertext refresh" procedure. One can refreshciphertexts before

every homomorphic operation. So, the decryption circuitis augmented by some gate- e.g., Add; call this augmented circuit.Since AND gate and XOR gate have the property of functional completeness[8]. That is, any other logic function can be implemented by combining AND gate and XOR gate. If the somewhat homomorphic scheme can handle augmented circuits, it means it do arbitrarycomputation on ciphertexts.This somewhat homomorphic scheme can obviously handle AND gate and XOR gate. So, it is critical whether the decryptioncircuit can be handled. If it can be, this calls"bootstrapping". Unfortunately, it is not. Hence one needs to squash the decryption circuit so that the degree of the decryption polynomial is small enough. Then the somewhat homomorphic scheme can do arbitrarycomputation on ciphertexts.It means we get fully homomorphic encryption scheme.This framework has been instantiated with a number of cryptographic assumptions, yielding progressively simpler and more efficient schemes[9,10,11,12,13,14].

2.The DGHV scheme

At 2010 van Dijk et al. described the first fully homomorphic encryption scheme over theintegers. The DGHV scheme was got from a symmetric encryption scheme. Encrypt: $c \leftarrow m+2r+pq$; Decrypt: $m \leftarrow (c \bmod p) \bmod 2 = (c - p \cdot * \lceil c/p \rfloor) \bmod 2 = \mathrm{Lsb}(c)\ \mathrm{XOR}\ \mathrm{Lsb}(\lceil c/p \rfloor)$. The key is a random odd integer p.Choosing at random large q and small r. A bit $m \in \{0,1\}$. The plaintext space is a set of binary, and theCiphertextspace is a set of integers.The system as described above is obviously a somewhat homomorphic encryption scheme. Ciphertexts from above scheme are near-multiples of p. We call (c mod p) the noise associated to the ciphertext c. It is the distance to the nearest multiple of p.In order to turn it into a public key system, we take advantage of the homomorphic nature of the system. That is zero and one are also valid encryptions of themselves.

The public key is $pk=\{ x_i ; x_i=r_i+pq_i \}$. Encryption of a plaintext m is then performed by selecting a random subset S from pk, a random noise r, and outputting the ciphertext c according to: $c \leftarrow m+2r+2\sum_{i \in s} x_i \bmod x_0$.Decryption is as same as above. This is a somewhat homomorphic encryption scheme in DGHV scheme. The security of the scheme reduces to the hardness of the approximate-GCD problem. The bound of noise is set to be p/8 in DGHV scheme. In fact, p/4 or p/16 is also correct, but p/2 is not.Because computing $\lceil c/p \rfloor$ is complicated,Ecannot handlethe function $f(p,c)=\lceil c/p \rfloor$ (Does it surprise you?).Hence it makesthe decryption circuit become shallow by squashing the decryption circuit.

The main idea of the transformation is to replace c/p, which multiplies two long numbers, with the summation of a fairly small set of numbers. In termsof the bits of the addends, this summation corresponds to a polynomial of fairly low degree that the somewhat homomorphic scheme can handle. Since c is ciphertext and shouldn't be changed, we only transfer p to the summation of a fairly small set of numbers. However, p is secret key and cannot be open; p can only be hide in the summation. Hence we need a trapdoor to ensure the security of the hidden p. This trapdoor is the sparse subset sum problem (SSSP).Generate a set $y = \langle y_1,\ldots\ldots,y_t \rangle$ of rational numbers in [0,2) such that there is a sparse subset S $\{1,\ldots\ldots,\ t\}$ of size$\alpha$with $\sum s_i \cdot y_i \approx 1/p \bmod 2$ ($i \in S$). Set sk* to be the sparse subset S, encoded as a vector s $\{0,1\}^t$ with Hamming weight α. Set $pk^* \leftarrow (pk, y)$. Since $\sum s_i \cdot c \cdot y_i \approx \sum s_i \cdot z_i \approx c/p \bmod 2$, we transfer $\lceil c/p \rfloor$ to $\lceil \sum s_i \cdot z_i \rfloor$. Now the decryption circuit is converted to$\mathrm{Lsb}(c)\ \mathrm{XOR}\ \mathrm{Lsb}(\lceil \sum s_i \cdot z_i \rfloor)$. The ciphertext c* consists of c and $\mathbf{z}=\langle z_1,\ldots\ldots,\ z_t \rangle$.To see that the somewhat homomorphic scheme can handle the decryption function plus an additional gate when$\alpha$is set small enough,let us consider the computation of the sum $\sum s_i \cdot z_i$. In this sum,we have numbers $\{a_i \mid 1<=i<=\alpha\}$, each ai expressed in binary$\{a_{i,j} \mid 1<=i<=\alpha,\ 0<=j<=-l\}$ with $l=(\log\alpha)$, where at most$\alpha$of the ai's are nonzero. We want to express each bit of the output as a polynomial of the input bits, while minimizing the degree of the polynomial and the number of monomials. It can be achieved by some calculating skills. Finally,the somewhat homomorphic become bootstrappable. Then we get a fully homomorphic encryption scheme over integers.

The public key size is $\tilde{O}(\lambda^{10})$. In practice the size of the x_i's should be at least 2^{23} bits to prevent lattice attacks. The public key size is then at least 2^{46} bits, which is too large for any practical

system. The somewhat-homomorphic scheme relies on hardness of approximate-GCD. Resulting scheme relies also on hardness of sparse-subset-sum and circular security. There are two types attacks. The first consider attacks on the approximate-gcd problem for two numbers including brute-forcing the remainders, continued fractions, and Howgrave-Graham's approximate gcdalgorithm[15]. The second consider attacks for arbitrarily large values of t including lattice-based algorithms for simultaneous Diophantine approximation[16], Nguyen and Stern's orthogonal lattice[17], and extensions of Coppersmith's method to multivariatepolynomials[18]. Since the sparse subset sum problem is not well study[19], it need to study deeply.

3.Variant of the DGHV Scheme—CMNT scheme

At 2011 Coron et al. proposed some techniques in [5] to reduce the public key size and increase the efficiency of the DGHV scheme, the most important of which is to use a quadratic form instead of a linear form for masking the message when computing a ciphertext. The idea consists in storing only a smaller subset of the public key and then generating the full public key on the fly by combining the elements in the small subset multiplicatively. More precisely, ciphertexts are computed as: $c \leftarrow m+2r+\sum (b_{i,j} \cdot x_{i,0} \cdot x_{j,0}) \bmod x_0$ for $1 \le i, j \le \beta$,where$\beta$is a new parameter.Then only 2βintegers need to be stored in the public key in order to generate theβ^2 integers used for encryption.Evaluate and decrypt is same as in the original scheme, except that ciphertexts are reduced modulo $x_0$after addition and multiplication. The idea of Squashing decryption circuit is same as DGHV scheme in order to get a fully homomorphic encryption scheme. However public key is be compressed in CMNT scheme by some techniques. Generate the y_i's using a pseudo-random generator f(se) instead of storing the y_i's in the public key as in [4]. Then only the seed se and y_1 need to be stored in the public key, and the other y_i's can be recovered during ciphertext expansion by applying f(se) again. In addition, encryptions of the secret key bits should also be made available publicly so that the Recrypt procedure is simply obtained by applying the decryption circuit to the ciphertext bits and the encrypted secret key bits. Therefore one uses two bit vectors$\mathbf{s}(0)$ and $\mathbf{s}(1)$ of length$\Theta^{1/2}$ Instead of generating the secret key as a single bit vector $s=(s_1,s_2,\ldots\ldots,s_\Theta)$ .Then s is recovered on the fly during decryption as the following matrix withΘentries:$s_{i,j} = s_i(0) \cdot s_j(1)$.The encryption of the bits of s(0) and s(1) is $\sigma(0)$ and $\sigma(1)$. Finally, the secret key as sk = (s(0) ,s（1）), and the public key as pk = (pk*,se,$u_{1,1}$, $\sigma(0)$, $\sigma(1)$) .This brings down public key size to about $\tilde{O}(\lambda^7)$.

CMNT scheme is still semantically secure, but under the (stronger) error-free approximate GCD assumption. The know attacks include brute force attack on the noise, approximate-GCD attack on the public key and lattice attack on the sparse subset-sum problem.Corresponding 72 bits of security,encryption and recryption take 3 minutes and 14 minutes respectively, with a public key size of 800 MBytes.

4.Variant of the DGHV Scheme—CNT scheme

At 2012 Coron et al. describe three technologies to improve DGHV schme.

The first is a technique to reduce the public key size of DGHV-like schemes [5] by several orders of magnitude. The technology is first to generate the secret-key p. Then, use a pseudo-random number generator f with public random seed se to generate a set of γbit integersχ_i(i.e. the χ_i's are of the same bit-size as the x_i's). Finally, compute small corrections δ_i to the χ_i'ssuch that $x_i=\chi_i-\delta_i$ is small modulo p, and store only the small corrections$\delta_i$in the public key, instead of the full x_i's.Knowing the PRNG seed se and the δ_i's is sufficient to recover the x_i's.Therefore instead of storing a set of largex_i's in the public key we only storethe muchsmallerδ_i's. The new public key for the somewhat homomorphic scheme has size about$\tilde{O}(\lambda^5)$.Corresponding 72 bits of security,encryption and recryption take 7 minutes and 12 minutes respectively, with a public key size of 10.1MBytes. This encryption schemeis still semantically secure under the error-free approximate GCD assumption, albeit in the random oracle model.The know attacksis same as CMNT scheme.

The second isCoron et al. prove that the natural extension of this quadratic encryption technique to to cubic forms, and more generally forms of arbitrary fixed degree d, remains secure, making it possible to further reduce the public key size. However,this quadratic encryption technique doesn't use in the implementation. This is because the "squashed decryption" procedure adds an incompressible additional term u1 of size$\gamma = \tilde{O}(\lambda^5)$ to the public-key, so it is unnecessary to reduce the number of public-key elements x_i or the number of encrypted secret-key bits.

The third is Coron et al. show how to adapt Brakerski, Gentry and Vaikuntanathan's (BGV) new FHE framework [20] to the DGHV scheme over the integers.The new BGV framework is described in [20] with Brakerski and Vaikuntanathan'sscheme [21], and the key technical tool is the modulus-switching technique of [21] that transformsa ciphertext c modulo p into a ciphertext c' modulo p' simply by scaling by p'/p and roundingappropriately. This allows to reduce the ciphertext noise by a factor close to p'/p without knowingthe secret-key and without bootstrapping. Under the BGV framework the noise ceiling increases only linearly with multiplicative depth, instead of exponentially.However the modulus switching technique cannot directly apply to DGHV since in DGHV the moduli p and p' are secret. However we cannot reveal s in clear, so instead we provide a DGHV encryption under p' of the secret-key bits si, as in the bootstrapped procedure. Then the expanded ciphertext can be collapsed into a new ciphertext $c''=2\langle\boldsymbol{\sigma},c'\rangle+[c]_2$ under p' instead of p, for the same underlying plaintext. Corresponding 72 bits of security, encryption and recryption take 3seconds and 2hours 27 minutes respectively, with a public key size of 18MBytes.The running time of the Recrypt operation is disappointing compared to the non-leveled implementation; however we think that there is room for improvement.A leveled fully homomorphic scheme include the bootstrapping operation; although not strictly necessary, this enables to get a FHE that canperform homomorphic evaluations indefinitely without needing to specify at setup time a bound on the multiplicative level.

5. Conclude

We describe the progress of fully homomorphic encryption over integers. The result shows fully homomorphic encryption over integers is not only conceptual simplicity but also asymptotics are much better now. We think the high efficientmethod is similar tothemodulus-switching technique should be to study in fully homomorphic scheme over integers. Moreover, we think, the running time of the Recrypt operation in the leveled implementation, there is room for improvement.

Acknowledgments

This research was supported in part by Funding of Jiangsu Innovation Program for Graduate Education (No.CXLX12_0162) and the Fundamental Research Funds for the Central Universities, and Ningbo Natural Science Foundation (No.2012A610067,No.2013A610071).
The second author is corresponding author.

Reference

[1] W. Diffieand M. Hellman, "New directions in cryptography,"IEEE Transactions on Information Theory, vol.IT-22, pp. 644–654, 1976.
[2] R. L. Rivest, A. Shamir, and L. M. Adleman, "A method for obtaining digital signatures and public-key cryptosystems(reprint)," Commun. ACM, vol. 26, no. 1, pp. 96–99,1983.
[3] C. Gentry.Fully homomorphic encryption using ideal lattices.STOC,2009,169–178.
[4] M. Dijk, C. Gentry, S. Halevi, and V. Vaikuntanathan,Fully homomorphic encryption over the integers, EUROCRYPT, 2010,24–43.
[5] J.S.Coron,A.Mandal,D.Naccache and M.Tibouchi,Fully Homomorphic Encryption
[6] Integers withShorter Public Keys.CRYPTO,2011,6841:487-504.
[7] J.S. Coron, D. Naccache and M. Tibouchi.Public key compression and modulus switching for fully homomorphic encryption over the integers.EUROCRYPT,2012,7237:446–464.

[8] C. Gentry, A fully homomorphic encryption scheme. Ph.D. thesis, Stanford University, 2009.
[9] Enderton, Herbert.A mathematical introduction to logic(2nded.),Boston,Academic Press,2001.
[10] N.P. Smart,F. Vercauteren,Fully homomorphic encryption with relatively small key and ciphertext sizes.PKC 2010, 6056:420-443.
[11] D.Stehle,R.Steinfeld,Faster fully homomorphic encryption. ASIACRYPT 2010, 2010, 6477:377-394.
[12] C. Gentry, S. Halevi,Implementing Gentry's fully homomorphic encryption scheme. EUROCRYPT 2011, 6632:129-148.
[13] Z. Brakerski,V. Vaikuntanathan.Fully Homomorphic Encryption from Ring-LWE and security for Key Dependent Messages, CRYPTO 2011,6841:505-524.
[14] C.Gentry,S.Halevi,N.P.Smart.Better Bootstrapping in Fully Homomorphic Encryption, Cryptology ePrint Archive, 2011, Report 2011/680.
[15] C.Gentry,S.Halevi.Fully Homomorphic Encryption without Squashing using depth-3 arithmetic circuits,FOCS 2011,107-109.
[16] N. Howgrave-Graham. Approximate integer common divisors.CaLC'01,2001, 2146:51–66.
[17] J. C. Lagarias. The computational complexity of simultaneous diophantine approximation problems. SIAM J. Comput.,1985,14(1):196–209.
[18] P. Q. Nguyen, J. Stern. The two faces of lattices in cryptology.Cryptography and Lattices,CaLC'01,2001, 2146:146–180.
[19] D. Coppersmith. Small solutions to polynomial equations, and low exponent RSA vulnerabilities.J. Cryptology,1997,10(4):233–260.
[20] V. Vaikuntanathan. Computing blindfolded: New developments in Fully Homomorphic Encryption, FOCS 2011,5-16,
[21] Z. Brakerski, C. Gentry and V. Vaikuntanathan, Fully Homomorphic Encryption without Bootstrapping. Cryptology ePrint Archive, Report 2011/277.

Advanced Materials Research Vols. 989-994 (2014) pp 4785-4788
© (2014) Trans Tech Publications, Switzerland
doi:10.4028/www.scientific.net/AMR.989-994.4785

Latent Semantic Index Applied in Question-Answering System about Agriculture Technology

Cao Li-ying[1], Zhang Xiaoxian[2], San Xiaohui[1], Chen Gui-fen[1],*

[1]College of Information and Technology Science, Jilin Agricultural University, Changchun,

[2]Software Institute, Changchun Institute of Technology, Changchun 130012, China.

* Correspondence author

Keywords: latent semantic indexing; agricultural knowledge; questions and answers system

Abstract: In this paper was proposed to use latent semantic indexing technology in agricultural knowledge questions and answers system in accordance with the current condition of agricultural knowledge resources in JILIN province and the problems existing in the agricultural knowledge questions and answers system and professional work process. This technology can enhance or reduce the influence on the semantic in the document and can more clear the semantic relationships, retrieve the natural language to some extent, eliminate the interference from identity and polysemantics and obtain better search results.

1. Introduction

With the rapid development of computer technology, agriculture as a basic industry, is an integral part of social information, so agriculture is bound to be a computer network technology, multimedia technology and intelligent features of the information technology wave of the baptism. Currently more and more variety of agricultural information network for agricultural scientists and farmers use, they often search using various search engines of agricultural information. Since search engines are not designed for the agricultural sector, most search results are often unable to meet their needs, Agriculture Question Answering System is in this case developed. Knowledge of the system of agriculture is agriculture-related field of agriculture user input natural language questions, it is able to give a concise, accurate and user-friendly answer. Is a comprehensive use of various natural language processing technology, new agricultural information retrieval system.

From a large number of agricultural information quickly and accurately obtain the information most needed is the development of agricultural knowledge question answering one of the difficulties. How to make existing information resources in Jilin Agricultural fully utilized effectively to improve the Jilin Province, the quality of agricultural information services, staff of agricultural research has become a hot spot. Latent semantic indexing, is the gradual rise in recent years, the search is different from the keyword search engine solution, the practical effect of its search results closer to the natural language, to a certain extent, improve the relevance of search results, has been gradually applied to the library, database and search engine algorithms were.

Latent semantic indexing is an extension of the vector space model, the concept of using statistical calculations to find out the index information retrieval, rather than the index of words, words. Latent semantic indexing based on the existence implied in the document library on the word, the word used in semantic structure, a portion of this semantics as the semantics of a document or masked by the diversity of form and not very obvious. Latent semantic indexing is through the words of the original document library - documents created by singular value decomposition of the matrix calculation, and then whichever is the former k largest singular value, then the corresponding singular vectors to form a new matrix, with its approximate expressed that the original word document libraries - document matrix. Because the new matrix reduced the semantic relations between words and documents ambiguity, so this method is more conducive to information retrieval.

2. The basic principles of latent semantic indexing

Between the text and vocabulary because there is a certain correlation, so the number of articles a number of words from the text and the correlation between them constitute the semantic model; use

mathematical algorithms and computer technology to analyze this model and its computing and processing, keep the main text and the correlation between words, remove the other redundant, secondary factors, such models have been optimized; the final form of the semantic structure and the original text, terms related to compare the structure and scale to much smaller, and also retains one of the major correlation with the model text and vocabulary mining implicit relations; in the upcoming search, the use of the semantic structure as a basis, the statistics of the implied terms and the correlation between the text .

In vector space, each document can be represented as a vector space vector word Di = (wi1, wi2, ..., wim) (T1, T2, ..., Tm) T, so that each entry documents also can be expressed as space vector Tj = (w1j, w2j, ..., wnj) (D1, D2, ..., Dn) T, between the entries and the entries using vector cosine similarity to calculate.

In the latent semantic indexing algorithm, a document library can be expressed as a m × n word, document large matrix A. Where n indicated the number of documents in the library, m that contains all of the library the number of different words. Each line of the matrix A corresponds to a different word, each column of matrix A corresponds to a document. A is expressed as:

$A = [aij], 1 \le i \le m; 1 \le j \le n$

Aij is the element in the feature item in the document Dj Ti or the frequency of emergence weight. Practical applications, because the number of words and documents may be very large, the word appears in a single document and very limited, so A is generally higher in the sparse matrix.

At this time the use of vector algebra proof that the relevant knowledge, matrix A can be decomposed into three matrices, namely:

$A = U\Sigma VT$ (1-1)

Where the diagonal matrix Σ that matrix, the matrix A is the diagonal singular value of the element. Matrices U and V are orthogonal column vectors normalized. U is the m × r "left singular vector matrix"; V is r × n of the "right singular vector matrix", r is the rank of matrix A and are:

U = VT V = In (In the n-order unit matrix)

A matrix decomposition [4] shown in Figure 1.

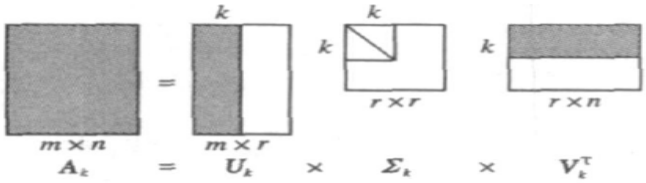

Figure 1 Schematic diagram of singular value decomposition

The diagonal matrix of singular values Σ descending order, the matrix of the first k diagonal elements were retained, the rest set to 0, while taking matrix U and matrix V in the front row constitutes a k-approximation matrix A Ak the rank K. So that you can get a new approximate decomposition matrix Ak:

Ak = Uk × Σk × VTk

Uk Vk matrix column vector and matrix are orthogonal vectors. So we can use Ak approximated the original term document matrix A, matrix and matrix Vk Uk row vector, respectively, in the words and documents, in this decomposition method, based on further knowledge related to agriculture or other document retrieval kinds of document processing. This is based on latent semantic indexing of Jilin Agricultural Knowledge Q & A basic idea of the system.

Although the latent semantic indexing is included in the document the words to express the semantic content of the document, but the latent semantic indexing algorithm, the concept of the reliability of the document with the document can not be fully expressed in words. Because of the diversity of words in the text, to a large extent overshadowed the relationship between words and documents, latent semantic index of the original document through the vector matrix of the singular value decomposition, taking the k-order approximation of the decomposed matrix This first cut of the original word document matrix contained in the "noise" such as synonyms, the words and semantic relations between documents is more protruding; the second is to make the word of the

document vector space dimension of greatly reduced, thereby can increase the efficiency of agricultural knowledge of the document retrieval.

3. Based on the Chinese text retrieval system LSI

Latent semantic indexing based question answering system of agricultural technology sub-five steps to retrieve the main steps, namely:

1) words, the establishment of the document vector matrix A;

Using non-dictionary word segmentation algorithm, the text of the library entries in the segmentation and word frequency statistics, the establishment of a word document library, document vector matrix A, and its normalized;

2) The singular value decomposition;

The establishment of the matrix A by the method described above singular value decomposition to obtain a matrix Vk, Vk matrix corresponding to each row in the library of all documents;

3) the query vector of the projection;

The query vector projection to get the equivalent transform k-word document matrix, the matrix Vk is the vector of the line;

4) similarity calculation and measurement;

Vector distance formula or the vector used cosine similarity formula, according to the degree of similarity between vectors, find the most similar with the query result set, ordered by descending value of similarity, and similarity greater than a value return document;

5) repeatedly to find, until satisfactory results

The satisfaction of the query results, and if not then spend time to transform the query results and re-locate the most similar document, this process can be recycled, until satisfied.

On latent semantic indexing techniques and classification techniques commonly used to compare the accuracy, experimental results show that the former is significantly better than the latter, because the latent semantic model to some extent, weakened or eliminated each class The noise in the vocabulary. However, latent semantic indexing technology is still not handle the full semantics of the text, so that the performance in some applications than commonly used classification algorithm, it requires a deeper semantic algorithm research. For the whole text classification, latent semantic indexing technology to overcome many shortcomings of traditional models, in many applications have achieved good results, shown in Figure 2.

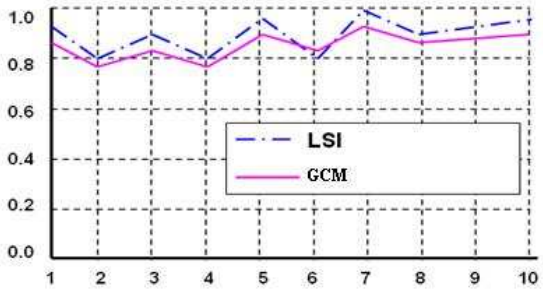

Figure 2 Classification accuracy comparison

4 Conclusion

Agricultural Knowledge Q & A system is a comprehensive, complex system that involves many technical aspects of information processing. As the complexity of agricultural knowledge and particularity of the past, information retrieval technology is difficult to solve the information in the synonymy and polysemy problems. In this paper, the new information retrieval method - LSI to introduce the system of agricultural knowledge quiz, question answering system for the retrieval of agricultural knowledge presents a new way of thinking and processes. Experiments show that this technique shows significant performance advantages, effective solution to the noise data on the classification of the negative impact brought about to raise a question and answer questions the accuracy of the system.

Acknowledgement

This work was funded by the National High-Tech Research and Development Plan of China under Grants Nos.2006AA10A309 and 2006AA10Z245; the National Spark Program Nos. 2008GA661003.

References:

[1] Qi Yong, XU Yong, Feng-Yu Liu. Based on latent semantic indexing WEB document automatic classification [J]. Computer Engineering and Applications, 2004,40 (22) :28-31.
[2] Yuzheng Tao, Xiao-Zhong Fan, Guo Jianyi, et al. Latent Semantic Analysis Based on Chinese Question Answering System answer extraction [J]. Computer, 2006,29 (10) :1890-1892.
[3] Zhou, Gong Li Ming, Jiang Lan. Latent semantic instance retrieval and analysis of samples in Chinese [J]. Computer Applications, 2004,24 (Z1) :273-276.
[4] FURNASGW. Information Retrieval Using a Singular Value D ecom-position Model of Latent Semantic Structure [A]. Proceedings of SIGIR 88 [C]. 1988. 36-40
[5] Wei Baozi, Wang Jing Ru. Latent semantic indexing technology in the agricultural question and answer system [J]. Microelectronics and Computer .2008 (7) .48-51.
[6] Wang Chunhong, Zhang Min. Latent Semantic Indexing Model for Analysis and Research [J]. Computer Applications .2007 (5) .1283-1288.

Advanced Materials Research Vols. 989-994 (2014) pp 4789-4793
© (2014) Trans Tech Publications, Switzerland
doi:10.4028/www.scientific.net/AMR.989-994.4789

Creating a new combined influence measure: an analysis of the citation network

Rui Deng

School of North China Electric Power University, Baoding, 07100, China

rui-yo@163.com

Keyword: Influence measure, network science, citation network

Abstract. This paper utilizes social network analysis to create a comprehensive evolution system to determine the significance of research papers. Citation network was analyzed from H-index, Impact factor and relative citation rate, which indicates the influence of the author, published journal and the paper on the field respectively. Influence citation network was built visually though transforming the 16 science network paper's citation multi-value matrix into two-value matrix in UCINET and by analyzing those influence measures, the scores of each paper were calculated and results maps through visualization. The results concern: the paper of Collective dynamics of `small-world' networks laid a foundation on network science. Besides, a general methodology is provided to determine the role or influence measure of academic journals.

Introduction

One of the techniques to determine influence of academic research is to build and measure properties of citation networks. Citation a manuscript usually connotes a strong influential connection between researchers. In order to measure such influence, there are network-based evaluation tools that use data to determine impact factor of researchers, publications, and journals. Some of these are Science Citation Index, H-index, Impact factor.

We want to further discuss the relation structure of research papers on network science, and take the citation relations of core paper on network science as a social network, to see which paper lay in the center, which lie in the margin of this network. This paper attempts to utilize social network analysis to disclose the relation of core papers. We will provide a general methodology to determine the role or influence measure of an individual network researcher.

Data and method

Data. Network science is a new, emerging, diverse, interdisciplinary field so there is no large, concentrated set of journals that are easy to use to find network papers even though several new journals were recently established and new academic programs in network science are beginning to be offered in universities throughout the world. I collected related paper data for those publications from the Science Citation Index (SCI) and the Social Sciences Citation Index (SSCI) compiled by the Institute for Scientific Information (ISI), because SCI and SSCI are two of the best sources of citation data. I used Web of Science, which is a Web-based user interface for ISI's citation databases, as well as Google Scholar Search. The table below is a listing of possible papers that could be included in a foundational set of influential publications in network science. I use these papers to analyze and develop a model to determine their relative influence.

Table 1 Set of research papers on Science Network

	Author	Paper Title	Journal
1	Erdös, P and Rényi, A	On Random Graphs,	Publications Mathematicae,
2	Albert, R. and Barabási, A-L.	Statistical mechanics of complex networks.	Reviews of Modern Physics,
3	Bonacich, P.F.	Power and Centrality: A family of measures,	American Journal of Sociology
4	Barabási, A-L and Albert, R.	Emergence of scaling in random networks.	Science,
5	Borgatti, S.	Identifying sets of key players in a network.	Computational and Mathematical Organization Theory,
6	Borgatti, S. Everett, M.	Models of core/periphery structures.	Social Networks,
7	Graham, R.	On properties of a well-known graph, or,What is your Ramseynumber?	Annals of the New York Academy of Sciences,
8	Kleinberg, J.	Navigation in a small world.	Nature,
9	Newman, M.	Scientific collaboration networks: II.Shortest paths, weighted networks, and centrality.	Physical Review E,
10	Newman, M.	The structure of scientific collaboration networks.	Proc. Natl.Acad. Sci. USA,
11	Newman, M.	The structure and function of complex networks.	SIAM Review,
12	Watts, D. and Dodds, P.	Networks, influence, and public opinion formation.	Journal of Consumer Research,
13	Watts, D., Dodds, P. and Newman, M.	Identity and search in social networks.	Science,
14	Watts, D. and Strogatz, S.	Collective dynamics of `small-world' networks.	Nature,
15	Snijders, T.	Statistical models for social networks.	Annual Review of Sociology,
16	Valente, T.	Social network thresholds in the diffusion of innovations,	Social Networks,

At first, I develop the citation network matrix which indicate the relationship among those papers and visualize the network by applying the UCINET, network analysis software. To make the network clear, we define:

paper node *v* cites node *i* paper node *i* cites node *v*

Figure 1 The Direction of Citation Relationship

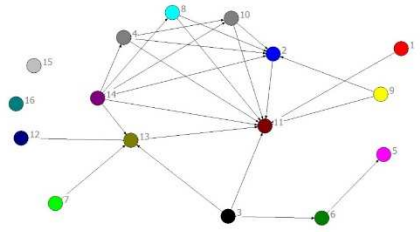

Figure 2 Citation Network

Method. In order to compare the significance of each research paper, firstly, three influence factors explored related to the research paper were and the data was collected respectively; then I develop an influence measure model of research paper and illustrate the analyzing procedure schematically in figure 3. At last, a general algorithm to determine the role or influence measure of academic journals is provided.

Influence factors

H-index (HI)

The H-index is an index that attempts to measure both the productivity and impact of the published work of a scholar. The index is based on the set of the scientist's most cited papers and the number of citations that they have received in other publications. From *Web of Science*

Impact Factor (IF)

The impact factor of an academic journal is a measure reflecting the average number of citations to recent articles published in the journal. It is frequently used as a proxy for the relative importance of a journal within its field, with journals with higher impact factors deemed to be more important than those with lower ones. From *http://www.medsci.cn/*

Citation Rate(CR)

The Citation Rate is the times of a paper being cite which reflect its influence directly in the field of academic. By exploring the references of each paper, we can list the citation rate in the set of paper. Specifically, after analysis the dataset, we determined the degree of network nodes to measure level of concern outside. From *http://scholar.google.com*

Model. Based on the previous analysis, the citation influence model is developed which illustrate the influential research paper form different parts. The method is below.

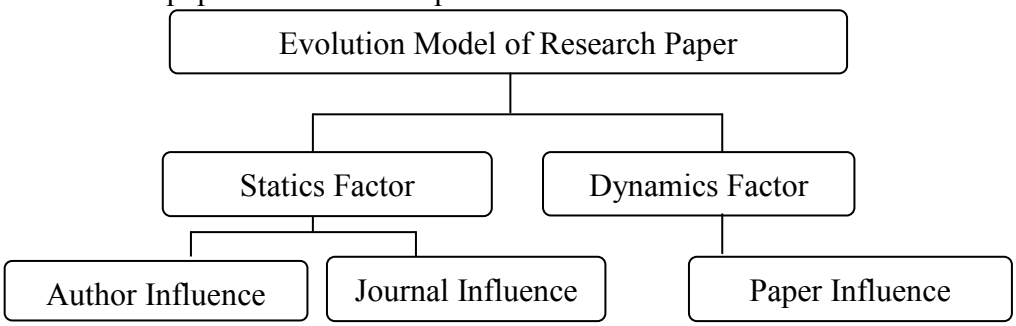

Figure 3 The evaluation influence model

Computation of Static Influence(SI). Considering that the size of the network might change, to compare the centrality
of different graph, normalized measure can be derived:

$$SF(i) = IF(j) + HI(i) \tag{1}$$

$$IF(i) = \frac{IF(i) - \min[IF(j)]}{\max[IF(j)] - \min[IF(j)]} \tag{2}$$

$$HI(i) = \frac{h(i) - \min[h(j)]}{\max[h(j)] - \min[h(j)]} \tag{3}$$

Where SF represents the inherent influence in the citation network, $IF(i)$ represents the impact factor which the paper i published in, $HI(i)$ represents the H-Index of the author.

Computation Dynamic Influence (DI). We choose the type of influence measure to compare the significance of a research paper by analyzing the important works that follow from its publication. In the citation network, we use the papers cited rate to weigh the relative importance of the paper. The measure can be written:

$$DF(i) = \sum_{i=1}^{16} d_{ij} \times f_i \tag{1}$$

$$f_i = \frac{\sum_{i=1}^{16} d_{ij}}{\sum_{i=1}^{16}\sum_{j=1}^{16} d_{ij}} \tag{2}$$

$$DF(j)=\frac{c(j)-\min[c(i)]}{\max[c(i)]-\min[c(i)]} \quad (6)$$

Computation Overall Influence (OI). Taking all kind of measures to be considered, we define the overall influence as the OI to compare the significance of a research paper. The measure can be written:

$$OI(i)=SF(i)+DF(i) \quad (3)$$

Results and discussion

Results. After the analysis of the citation network, we listed the inherence influence and dynamic influence score. Finally, we give the overall influence score of the 16 paper.

Table 2 Four Measure Scores

Paper Title	HI	IF	CF	**OI**
Collective dynamics of `small-world' networks.	0.33	0.74	1	**2.08**
Identity and search in social networks.	1	0.61	0	**1.61**
Statistical mechanics of complex networks.	0.37	1	0	**1.37**
Emergence of scaling in random networks.	0.37	0.61	0.3	**1.28**
Navigation in a small world.	0.19	0.74	0.1	**1.03**
The structure of scientific collaboration networks.	0.6	0.18	0.1	**0.88**
Scientific collaboration networks: II.Shortest paths, weighted networks, and centrality.	0.6	0.04	0.1	**0.74**
The structure and function of complex networks.	0.6	0.11	0	**0.71**
Power and Centrality: A family of measures,	0.19	0.11	0.3	**0.59**
On properties of a well-known graph, or,What is your Ramseynumber?	0.19	0.1	0.2	**0.48**
Networks, influence, and public opinion formation.	0.4	0.06	0	**0.46**
Models of core/periphery structures.	0.37	0.06	0	**0.43**
Identifying sets of key players in a network.	0.3	0	0	**0.3**
Statistical models for social networks.	0.19	0.09	0	**0.27**
On Random Graphs,	0.19	0.08	0	**0.26**
Social network thresholds in the diffusion of innovations,	0.19	0.06	0	**0.24**

Discussion. We compare our results in the table, we can easily find the paper named *Collective dynamics of `small-world' networks* is the most significant work. Besides, the author of this paper is the pioneer in the field of Science Network Analysis.

Conclusion

The influence of academic journals is based on the academic background and the creativity, the influence in society as well as the influence of the reflected recognition readers a comprehensive effect. To investigate the academic journals influence in the same field, we can also use the Evolution model. The calculation procedure is as follows:

Step1:Dataset Collection and Extraction

First, choose a set of journals and collect the number of literatures included in the journal respectively Then, search for the each journal retrieval system or database income data; At last, count the recitation rate inside and outside of the each journal.

Step2:Build the analysis network

Take the self-cited rate as the value of the correlation matrix diagonal from the journals and the links value as the rest of the matrix. Then, we will obtain the incidence matrices. At last, by the software UCINET6, draw the network of the journals citation network.

Step3：Comprehensive Assessment

Compute the inherent influence and dynamic influence by applying the network centrality. Then, calculate the overall influence sore and ranking journals. At last, we can obtain the most influential journal.

This paper represents a comparative study to investigate the performance of research paper for detecting emerging research fronts among citation networks. A case studies in a science network research domains with 16 important papers. After citation networks were constructed, papers were explored in three different aspects using those measures of Science Citation Index, H-index, and Impact factor. By using the weight based on the frequency of citations, the influence of the paper is detected. By using the weight based on the H-index, we can see the impact of the published work of a scholar. By using the weight based on impact factor shows the relative importance of a journal within its field. We develop the comprehensive evolution system and evaluated the visibility, defined as overall scores, determining the significance of the research paper or academic journals. This general methodology can applied into other academic field to compare their relative influence.

References

[1] Watts, D. and Strogatz, S. "*Collective dynamics of `small-world' networks*" Nature, Vol.393,pp.440-442, 1998.

[2]Barabasi, AL., and R. Albert, *"Emergence of scaling in random networks."* Science. Vol.286, no.5439, pp.509-512, 1999.

[3]Braam, R.R., H.F. Moed, and A.F.J. van Raan *"Mapping of science by combined co-citation and word analysis. i. structural aspects."*Journal of the American Society for Information Science, 42, pp.233–251, 1991.

[4]Derek J. de Solla Price *"Networks of scientific papers."*Science, 149, pp. 510–515, 1965

[5]Kessler, M.M., *"Bibliographic coupling between scientific papers."*American Documentation, 14, 10–25, 1963.

Advanced Materials Research Vols. 989-994 (2014) pp 4794-4798
© (2014) Trans Tech Publications, Switzerland
doi:10.4028/www.scientific.net/AMR.989-994.4794

OpenFlow-Based Global Load Balancing in Fat-Tree Networks

Yuwen Wu [1, a *], Wei Zhang [1, b]

[1] Computer Science and Technology Department, East China Normal University, Shanghai, China

[a] bearberni@gmail.com, [b] wzhang@cs.ecnu.edu.cn

Keywords: OpenFlow; Load balancing; Fat-tree; Mininet; POX

Abstract. Cloud services have been explosively popular over the last decade. And data centers play an essential role in providing cloud services. Inside a data center, any server instance has the chance to inject traffic of various applications into the network. Yet how to balance the enormous internal load to make the best of data center network is a highly prioritized problem to be solved. To provide balanced traffic in data centers, this paper proposes an OpenFlow-based GLB load balancing algorithm in data center fat-tree networks. GLB uses a path-related weight to select path. This weight indicates how balanced of a path. We implement GLB algorithm as a module in an openflow controller platform, POX. On the self-defined modified mininet emulation platform, we conduct experiments in a fat-tree topology environment running random traffic to generate performance data. Experiment results demonstrate that our proposed GLB algorithm outperforms DLB algorithm in terms of load balancing.

Introduction

With the spring of Cloud service, data centers have become the vital infrastructures that Cloud service providers focus on. Inside a data center, any server instance has the chance to inject traffic of various applications into the network. Therefore, how to balance the enormous internal load to make the best of data center network is a highly prioritized problem to be solved.

Fat-tree [2], a special instance of Clos topology is adopted in data center networks to lower the cost of building such a network and provide multiple paths between any two hosts. A k-ary fat-tree is consisted of k pods and each pod have two layers of k/2 switches. The k-port switches in the edge layer are directly connected to k/2 hosts and the other k/2 ports are connected to k/2 ports of the aggregation layer switch. The hierarchy has $(k/2)^2$ k-port core switches and each of them has one port connected to each of k pods.

Load balancing is to adjust the load of system dynamically, so as to make the load of each node closer. Load balancing in networks usually use dynamic algorithm to distribute traffic load between different links. Traditional load balance solution can be divided into two types:

Software-based solution is simple and cost lower and the configuration of software solution is flexible, but it needs more time to deal with the load. And the software may be the bottleneck of the system. Hardware-based approach is faster but it also cost more. And it also needs proprietary hardware without much flexibility, and may be the single point of failure in the network.

OpenFlow [6] derives from a research project in Stanford. It decouples control plane from legacy switches into a centralized controller, which instructs switches what to do with received packets by installing flow table entries. OpenFlow takes advantage of both software and hardware load balancing. With commodity OpenFlow switches, OpenFlow provides line-speed forwarding performance, improved security with SSL, flexibility and reusability with programmable hardware.

In this paper, we propose GLB (Global Load Balancing) algorithm. GLB generates a weight based on current available bandwidth of each link along the path. This weight represents how balanced of this path. When selecting path, simply pick up the path with highest weight. We implement GLB as a module in the POX [7] controller platform. On the self-defined modified mininet [8] emulation platform, we conduct experiments in a fat-tree topology environment running random traffic to generate performance data. We evaluate our algorithm by average bandwidth ratio, average packet delay and link load jitter. Experiment results demonstrate that our proposed GLB algorithm outperforms DLB algorithm in terms of load balancing.

Related Work

In this section, we introduce a typical data center network topology, that is, fat-tree topology. We also present other openflow-based load balancing research. Since the characteristics of openflow such as decoupled control plane and flexible network configuration are very suited for providing load balancing service, there already exists some research work that combines openflow technology with load balancing.

Plug-n-Serve system, presented in [3], tries to minimize response time by controlling the load on the network and the servers using customized flow routing. The system utilizes up-to-date status of the network and adapting to current load conditions to dynamically reschedule network requests. But this system is for campus network. It doesn't consider data center networks. [4] proposes an innovative openflow-based load balancing mechanism that supports multi-service. For each different service traffic in the network, there is a separate controller respectively.

For example, one controller handles the standard network trafffic between the server nodes, while another controller handles the load-balancing of the web-servers and another one the load-balancing of video streaming servers. Yet it's not specifically aimed at data center networks, which have different traffic distribution needed to be well handled. [1] introduces a DLB (Dynamic Load Balancing) algorithm aiming at data center networks. DLB is an openflow-based load balancing algorithm that fits into data center network topology . This algorithm exploits depth-first method, picking up the best link on every hop, trying to end up an overall best path. In [1], DLB is compared with other two load balancing algorithms: hash-based randomized path selection NLB (None Load Balancing) and location-based SLB (Static Load Balancing). The results show that in fat-tree topology networks DLB provides higher average bandwidth ratio and shorter average packet delay than the others. Still, this greedy path selecting policy doesn't count for overall link load distribution in the network and may leads to a local best path.

Algorithm Design and Implementation

In this section, we illustrate our GLB algorithm design and implementation.

Algorithm Design

In this paper, we propose an openflow-based load balancing algorithm, that is, GLB. GLB pre-stores all possible paths between every two hosts in the network into a path set $\{Paths\}$:

$$\{(Host_{src}, Host_{dst}): \{Path_1, Path_2, \cdots, Path_i\}\}$$

For each complete path in the Paths set, GLB calculates a path weight W_{path}:

$$W_{path} = \overline{linksBw}/\sigma_{linksBw} \quad \text{(Eq. 1)}$$

$\overline{linksBw}$ is the average current available bandwidth Bw_i of each $link_i (1 \le i \le n)$ in $Path_i = \{link_1, link_2, \cdots, link_n\}$:

$$\overline{linksBw} = \frac{\sum_{i=1}^{n} Bw_i}{n} \quad \text{(Eq. 2)}$$

The value of W_{path} is growing along with the increment of $\overline{linksBw}$, indicating that average available link bandwidth is higher than any other paths.

$\sigma_{linksBw}$ is the standard deviation of available bandwidth of every link along the path:

$$\sigma_{linksBw} = \sqrt{\frac{\sum_{i=1}^{n} (Bw_i - \overline{linksBw})^2}{n}} \quad \text{(Eq. 3)}$$

The decreased value of $\sigma_{linksBw}$ leads to the elevated value of W_{path}, meaning that difference between available bandwidth of every link is lower and that odds of certain link bottleneck caused congestion are smaller.

W_{path} will be updated as link statistics gets updated. So the real-time link quality could be reflected.

Instead of single-hop best link path selection policy, GLB chooses a complete path based on the path weight, which reflects load of every link along the corresponding path.

Given $Host_{src}$ and $Host_{dst}$, GLB algorithm process is presented in Fig.1:

Algorithm GLB Path Decision Algorithm

Require: Flow(srcHost, dstHost), paths

```
1: PathDecision(){
2: srcEdge = FindEdgeByHost(srcHost)
3: dstEdge = FindEdgeByHost(dstHost)
4: topLayer = GetTopLayer(srcEdge, srcEdge)
5: if topLayer == edgeLayer then
6:     return srcEdge
7: end if
8: candidatePaths = paths.Get(srcHost, dstHost)
9: return BestPath(candidatePaths)
10: }
```

Figure 1. Algorithm Process of GLB

GLB first calculates the highest level switch need to access, according to the source host and the destination host. If source and destination host connect to the same edge switch, algorithm directly return this edge switch as selected path. If the highest level reaches aggregation or core switch, GLB will look up all candidate paths by tuple key ($Host_{src}$ and $Host_{dst}$ in the path set {Paths}. Then GLB choose the path with highest W_{path} as the output of the algorithm.

Algorithm Implementation

Our proposed GLB algorithm is implemented as a module named LoadBalancer in POX [7] controller. This module contains two self-defined components, which are PortStatsMonitor and FlowDispatcher. A built-in topology discovery component is also loaded to provide nodes adjacency information.as reference.

As a module of POX, LoadBalancer is responsible for two main functions: monitor port traffic statistics and schedule flows with no matching flow entries.

1) PortStatsMonitor
   Our algorithm require latest available bandwidth of each link. Yet this information cannot be directly retrieved from both switches and controller. In our implementation, PortStatsMonitor component periodically inquires all the switches about ports statistics, calculates transmitted bytes on every port during this interval and consider incremented bytes as the measurement of link available bandwidth. We define a monitoring cycle T. Every start of T, component sends OFPT_STATS_REQUEST openflow message with type OFPST_PORT to all switches, demanding an OFPT_STATS_REPLY message. When receiving port statistics reply message, component calculates incremented bytes in the cycle T as the link load info. Then, component finds all links that this port participates and update link load info. After updating link load info, component should refresh W_{path} of each path in $\{Paths\}$.
2) FlowDispatcher
   An OpenFlow switch maintains a flow table. On receiving a packet, switch matches packet header and incoming port number with flow entries in the flow table. If match succeeds, packet will be handled according to the action field of the matched flow entry. Otherwise, switch buffers the packet with a buffer ID and send a Packet-In message with this ID to POX. As a component, FlowDispatcher would process this Packet-In message and then select the best appropriate path. It's a list of switches needed to traverse from source host to destination host. FlowDispatcher then converts determined path into a series of FlowMod message targeting on switches along the path. At last, component installs flow entry along the path by sending these FlowMod messages to build up the path.

Evaluation

In this section we define our measurement methods, specify our environment setup and reports our performance study for the proposed GLB load balancing algorithm and DLB load balancing algorithm.

Measurement Method

1) Average Bandwidth Ratio
A flow's designed bandwidth is the bandwidth at which Iperf client sends UDP flow. A flow's actual bandwidth is the bandwidth that Iperf server actually receives at. Due to network congestion caused packet loss or possible transmission error, a flow's actual bandwidth is less or equal to its designed bandwidth. Average bandwidth ratio φ is the average ratio of every flow's actual bandwidth and designed bandwidth, as in Eq. 4.

$$\varphi = \sum_{i=1}^{n} \frac{actual\ bandwidth\ of\ flow_i}{designed\ bandwidth\ of\ flow_i} \Big/ n \quad \text{(Eq. 4)}$$

Average bandwidth ratio relates to the extent of load balancing in the network, the higher Average bandwidth ratio, and the more balanced network gets.

2) Average Packet Delay
Packet delay μ is defined as the duration from the time packet sent out in the client to the time received by the server, as in Eq.5.

$$\mu = \frac{\sum_{i=1}^{n} t_{i-server} - t_{i-client}}{n} \quad \text{(Eq. 5)}$$

3) Link Load Jitter
Link load jitter Δ is defined as follows: in unit interval T, the standard deviation of load of all links in the network, as in Eq.6.

$$\Delta = \sigma(linkload) = \sqrt{\frac{\sum_{i=1}^{n} (load_{linki} - \overline{load_{links}})^2}{n}} \quad \text{(Eq. 6)}$$

$\overline{load_{links}}$ is the average load of all links.
For all the links in a network, higher link load jitter indicates that link load distribution deviates more from the average link load and that traffic loads are more unbalanced, vice versa.

Traffic load, serving as the variable in the experiment, is defined as the ratio of occupied bandwidth and total bandwidth on links between hosts and edge switches. We tested 9 groups with traffic load ranging from 0.1 to 0.9.

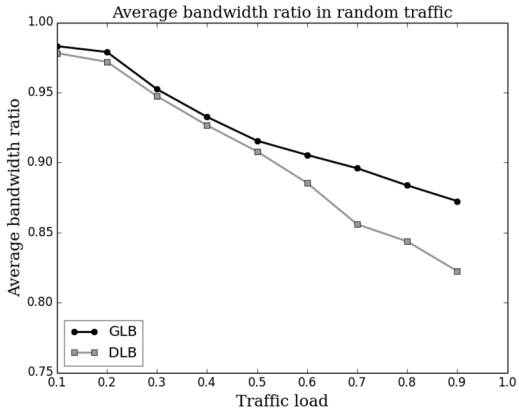

Figure 2. Average bandwidth ratio in random traffic

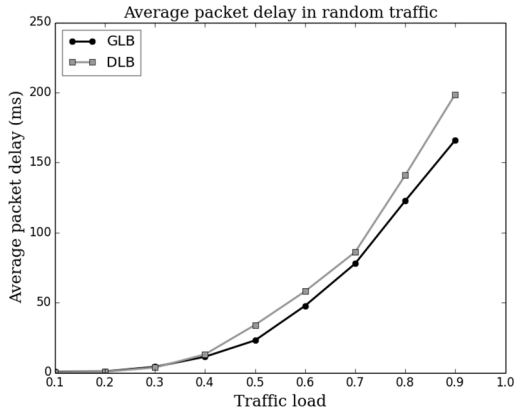

Figure 3. Average packet delay in random traffic

Environment Setup

We build a self-defined 8-ary fat-tree topology environment on Mininet emulation platform. POX controller runs with our implemented LoadBalancer module. Mininet and POX get running on different PCs so as to reduce the CPU usage. We use Iperf tool to generate random traffic pattern [5] between any two hosts in the fat-tree topology.

Results

After running experiment, we analyze reports generated by Iperf servers. Results are as follows:

From fig.2, we can see that average bandwidth ratio of both algorithms decrease as the traffic load rises. GLB has a better performance in terms of average bandwidth ratio than DLB, especially after traffic load reaches 0.6. This is probably because under heavy load circumstances DLB is more likely to cause network congestion by choosing local best link, raise packet loss rate and lower average bandwidth ratio. While GLB bases global load information to select path, making it less possible to cause congestion.

Fig.3, shows average packet delay in random traffic. Generally average delay changes more radically than average bandwidth ratio. GLB outperforms DLB on packet delay attributed to global path choice, which lower the probability of congestion. When the load reaches 0.9, packet delay of both algorithms exceeds 150ms. This fact implies that when hosts send flows at nearly its maximum bandwidth, most links in the network are busy, packets have to wait longer in the queue of switches.

Conclusion

This paper focuses on the load balance issues in data center fat-tree topology networks. It analyzes the existing studies of OpenFlow-based load balance, and points out the defects of single hop greedy routing policy that is from the DLB algorithm proposed [1]. Based on the aforementioned analyses, this paper present the GLB algorithm that overall considers the current available bandwidth of each link in the whole path and selects the links with respect to their weights. Then, the proposed GLB algorithm and its load balancing module are both realized on the POX controller platform. In addition, the user-defined fat-tree topology environment is established on the Mininet simulator and the random traffic scenario is adopted in the experiments. The experimental results have shown that the proposed GLB algorithm achieves better performance in load balancing of data centers using fat-tree topology as compared to the benchmarking DLB algorithm.

In future work, we plan to re-evaluate the effectiveness of the proposed algorithms by using more precise data center traffic patterns generated by [9].

References

[1] Li Y, Pan D. OpenFlow based Load Balancing for Fat-Tree Networks with Multipath Support[C]//IEEE International Conference on Communications (ICC), 2013

[2] Leiserson C E. Fat-trees: universal networks for hardware-efficient supercomputing[J]. Computers, IEEE Transactions on, 1985, 100(10): 892-901.

[3] Handigol N, Seetharaman S, Flajslik M, et al. Plug-n-Serve: Load-balancing web traffic using OpenFlow[J]. ACM SIGCOMM Demo, 2009.

[4] Koerner M, Kao O. Multiple service load-balancing with OpenFlow[C]//High Performance Switching and Routing (HPSR), 2012 IEEE 13th International Conference on. IEEE, 2012: 210-214.

[5] Al-Fares M, Loukissas A, Vahdat A. A scalable, commodity data center network architecture[C]//ACM SIGCOMM Computer Communication Review. ACM, 2008, 38(4): 63-74.

[6] McKeown N, Anderson T, Balakrishnan H, et al. OpenFlow: enabling innovation in campus networks[J]. ACM SIGCOMM Computer Communication Review, 2008, 38(2): 69-74.

[7] Information on https://openflow.stanford.edu/display/ONL/POX+Wiki/.

[8] Lantz B, Heller B, McKeown N. A network in a laptop: rapid prototyping for software-defined networks[C]//Proceedings of the 9th ACM SIGCOMM Workshop on Hot Topics in Networks. ACM, 2010: 19.

[9] Kandula S, Sengupta S, Greenberg A, et al. The nature of data center traffic: measurements & analysis[C]//Proceedings of the 9th ACM SIGCOMM conference on Internet measurement conference. ACM, 2009: 202-208.

Advanced Materials Research Vols. 989-994 (2014) pp 4799-4801
© (2014) Trans Tech Publications, Switzerland
doi:10.4028/www.scientific.net/AMR.989-994.4799

Research on the Cloud Services Plat form Architecture of Digital Library Based on Cloud Computing Technology

Shanhong Zhu[1,2] TAO Kuang[1]

[1]School of Computer and Information Engineering ,Xinxiang university, Henan, China

[2]International School of Software, Wuhan University, Wuhan, China

Email: zshazhu@163.com

Keywords: cloud computing; digital library; cloud services platform

Abstract: The Digital Library has begun to enter the cloud computing era after experienced the Internet era, This paper constructed a cloud services plat form of digital library based on cloud computing technology, then described the service processes and the operating mechanism of the digital library cloud services plat form.

With the development and progress of various computer, network, and information technology, the concept of networks, digital and virtual libraries have appeared, and their substance have no difference, just the perspective of observing and understanding is different. For digital libraries, there is no uniform definition, but it can be described as that digital library is a service system through combining computer and communication technology under the network environment, that organize, integrate and manage effectively for the user. Essentially, digital library is still an information resource system, but it is different with the traditional library, for example, digital libraries are used to save some of the country's rare and precious books and other valuable data in digital form; Facilitating saving and difficult to wear the information resources; Facilitating information resources sharing; Facilitating information retrieval for the information users. But digital library also facing difficulties, first is that digital libraries are faced with the dilemma of technology, which makes information resources stored issues become the biggest problem. So the technology of image retrieval, multi-language retrieval, data exchange between different data standards, human-computer interaction technology, then software and tools which needed by digital libraries, all of these have to be improved and further developed. Besides that massive resources lead to the limited data management, backup, and storage capacity also presents a challenge to the digital library. Secondly, the digital library is facing a dilemma with the growing information needs of information users. Although Digital Library makes Library Services breaking the original space constraints, and the traditional library services can be extended, the information users' increasing demand for continuity, personalization, diversity and timeliness of the information service require digital library to provide with better information services[1].

2. Construction of the Digital Library Service Model

The framework of the design of libraries cloud service centers, presented by this paper, is based on the support of infrastructure layer , which providing an open platform(developmental environment) as well as software services.

2.1 IaaS Layer (Infrastructure Layer)

Infrastructure layer is the foundation of the entire cloud service center to support the operation, it consists of a cluster of servers, storage devices,network communications facilities. There are two major sources of these resources: First is the local library resources , the second is the resources bought from the cloud computing service providers. The physical location of these resources are scattered, we only need to use virtualization technology to change physical resources into logical resource which can be managed, that kind of technology can virtual these sources into a pool of resources, and then make the resources in the resource pool for unified deployment.. Virtualization

technology enables the deployment environment and the physical platform independent, which makes the local library's resources can be well integrated with the newly purchased resources of cloud computing service providers , then managed through the virtual platform and continue to expand, migrate and copy based on changes in demand. Resource pool will form multiple isolated virtual private servers , where each virtual server can run independently with separate root access , IP addresses , memory, files, system libraries function and configuration files. With this technology, cloud service center provide users with more and more competitive services, and safe, stable environment. The function of resource pool is to provide computing and storage resources needed for the various applications. Managing the computer processor and memory virtually by the way of resource pool can greatly improve the resource utilization. The aim of infrastructure layer, which use a virtual storage to formed a unified management of a variety of storage devices in a storage pool, is to provide users with the storage system of high data transmission capacity [2]. Further, the virtual storage can also reduce the cost and complexity, and to achieve unprecedented flexibility and choice, so that the efficient flow of information can be extended to the outer boundary of cloud services, improving horizontal collaboration and communication in order to promote efficient growth of computing services.

2.2 PAAS Layer (Platform as a Service)

Through solving the problem of storage capacity and computing efficiency virtually of cloud service centers, infrastructure layer become a support for the center of cloud services, just like a giant supercomputer floating in the clouds. PAAS layer is a system built on the infrastructure layer, managing, monitoring, applying to infrastructure, which called as “huge super computer”. PAAS layer provides management and services through serving for middleware to communicate with the infrastructure layer. The basic function of the PAAS layer is to standardize and operate the identify, authentication, authorization, directories, security and other services by hiding the underlying hardware, operating systems and network heterogeneity, which provides a unified standardization program interface and protocol for application, in order to achieve a unified management of the network resources. Its user management covers user authentication, user license, and user customization. And resource management covers load balancing, resource monitoring, failure detection, etc. Security management covers authentication, access authorization, security audit, comprehensive protection, etc. Image management covers image creation, deployment and management [3]. In addition, the PAAS layer will build a open platform for application. The realization of this platform is to open the application programming interface or function through the software system of the PAAS layer, which in order to increase the function of the software system of the PAAS layer and use the resources of the system. Open application platform will not only provide open interfaces for the providers of third-party computing software services, but also for the native libraries and end-users. Through this open interface, first for a authentication, only the local libraries of the alliance and their users, as well as the third-party cloud computing software service provider can be tested and verified. After verification, third-party service provider can add their own application software systems embedded in the platform, and these software systems will be rent by users’ payment. After authenticated, users are able to query the required services in the service catalog, and have the access to these services, that is to say, it is a way by using a variety of software systems to meet their service needs, which users have to pay or share the platform layer. What’s worth mentioning is that open with sharing is the features of the open application. As long as the role is authenticated (users, third-party service providers, local libraries), can embed software developed by their own., this will allow an open platform for better sharing, and cloud service center will be based on the quality and the condition of using to filter out the reliable and popular software, which will become the basis for the collection of services software layer.

2.3 SAS (Software Air Serves)

Software Air Serves are based on PAAS Layer, which contains all of the applications needed by library users. These applications come from two major sources. First is the application open

platform. Cloud software service provider rent the right of software use, and users are able to rent software as required, not the way of payment. Secondly, the application software developed by cloud service center. The software engineer of cloud service center will independently develop a part of core application software based on the system of PAAS layer, which including the series software of personal digital library service, online office system software and database service software, etc. Cloud service center preserve ownership and use right on the software developed independently and only participate in profit-sharing through rental software, but it does not have the ownership for the third-party developed software, which take responsibility for software management and maintenance. The application software of service layer is not exclusive, but has a super sharing [4].Those software are arranged in a "cloud" side, and different users can use these software service online. The reason is that the virtual resource pool of IAAS layer have a good flexibility, it can support the computing of application software and changes of storage capabilities to ensure the service. When the needs of users surge on the same software, the underlying elasticity can provide reliable communication, computing capability and storage space. While the user log off or reduce the use of resources, the occupied resource of this software will decreases with it, and the space computing capability will be used to support other software systems running. Users will be able to use the high-performance software services through the cloud and pay the appropriate fee based on time, without concern for software maintenance and management. As for cloud service center and the third-party software providers, the paid sharing of any piece of software can bring service value and profit sharing. Since the operation of open platform of the PAAS layer, SAS layer will inherit its openness. Cloud computing concept is supplied on demand, but the change needs of users is infinite. So the professional third-party software service providers offer thousands of software services and ensure the software updates and maintenance, but this is not able to fully keep up with the changing needs of users.Web2.0 era let each network user of us become a "weaving man", it is opening of Web2.0. Similarly, the opening of SAS layer is that the user can also add independent and opening software [5].

Conclusions

In addition, cloud computing provides a convenient and coordinating information sharing for information users. Wherever the users are, as long as they access to the "cloud" side, they can not only take advantage of a unified virtual platform, provided by cloud computing, and continue their work, but can also share their data on multiple devices.

References

[1] Adomavicius G, Tuzhilin A. Multidimensional recommender system: a data warehousing approach[C].In: Proceedings of the 2th International Workshop on Electronic Commerce, Lecture Notes in Computer Science, Springer-Verlag,2001:180-192.
[2] Adomavicius G, Sankaranarayanan R, Sen S, Tuzhilin A. Incorporating contextual information in recommender system using a multidimensional approach [J]. ACM Transactions on Information Systems,2005,23(1):103-145.
[3] Lee B-H, Kim H-N, Jung J-G,et al. Location-based service with context data for a restaurant recommendation[C].In: DEXA, Lecture Notes in Computer Science, Springer, 2006: 430-438.
[4] Yap G-E, Tan A-H, Pang H-H. Discovering and exploiting causal dependencies for robust mobile context-aware recommenders [J].IEEE Transactions on Knowledge Data Engineering, 2007,19(7):977-992.
[5] Baltrunas L, Ricci F. Context-dependent terms generation in collaborative filtering[C]. In:Proceedings of the 2009 Work

Advanced Materials Research Vols. 989-994 (2014) pp 4802-4805
© (2014) Trans Tech Publications, Switzerland
doi:10.4028/www.scientific.net/AMR.989-994.4802

Data Integration in B2B E-Commerce

Yan Zhang

School of economics and management ,Xinxiang university, Henan, China

zshazhu@163.com

Keywords: E-commerce;B2B market; communicate

Abstract: the dramatically increased flexibility afforded by the Internet in business-to-business transactions also presents steep challenges in merging information coming from so many sources. B2B marketplaces, which function as an intermediate communications layer, reduce the number of mappings needed .

1 Introduction

A successful marketplace must integrate various hardware and software platforms and provide a common protocol for information exchange. However, the real problem is the exchanged content's heterogeneity and openness. This heterogeneity arises in at least three levels: the content, product catalog structure, and document structure[1].

The content of the exchanged information must be modeled. Historically, many different ways to categorize and describe products have evolved. Often, vendors have their own private way to describe their products. Structuring and standardizing the product descriptions is a significant task in B2B e-commerce, ensuring that the different actors can communicate with each other so that their customers can find the products they want. Here, content management solution providers can offer added value by helping their vendors build and instantiate an ontology for certain product domains.

E-commerce is about electronically exchanging business information—of which product descriptions are just one element. The product descriptions are an electronic catalog's building blocks, together with information about the vendor, the manufacturer, the lead time required, and numerous other business-related considerations. Furthermore, a catalog provider should include quality control information, such as catalog version, date, and identification number. The total composition of these building blocks is called the *catalog structure*. Where there are two electronic catalogs involved—for example, when two vendors in one marketplace have different catalog providers, or when two different marketplaces want to communicate—the structure of these catalogs must be aligned as well.

Going one step further into the content-management process, we come upon the catalog's actual use. In a marketplace, a buyer will want to send a purchase order after picking up the necessary information from the catalog. The vendor must reply with a confirmation, which starts the buying process. For the buyer and the vendor to read and process each other's business documents again requires a common language. Marketplace software developers such as Commerce One, which developed its structures based on the xCBL language, provide a large collection of document structures that reflect different aspects of a trading process. Aligning these document structures with other document definitions such as those from Ariba (cXML) is far from a trivial task[2].

Consequently, three types of mismatches can arise. The first type, in content, mainly concerns the real-world semantics of the exchanged information: people describe the same products in different ways. The second and third types, in product catalogs and business documents, more generally concern the exchanged information's syntactical structure.

The overall information integration process must tackle a number of serious problems. In particular, product descriptions must be structured; classified; (re)classified and (re)described in various dimensions because no standard product classification exists; and personalized to let customers find the products they seek. Figure 1 provides a snapshot of the overall process.

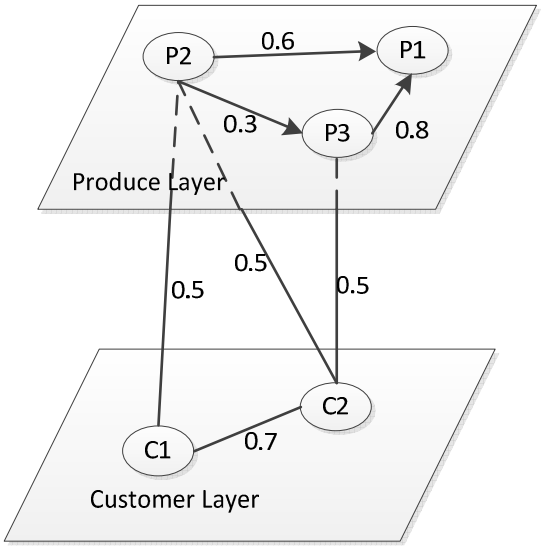

Fig1 Overall process.

2 Information integration in B2B e-commerce

With the progress of human science and technology, the renewal speed of knowledge is increasing, if the person just rely on the traditional teaching mode and teaching method to learn the knowledge of books, that when the learning process is ended，knowledge what learners are learning may already outdate, it is undoubtedly a great irony, also unnecessary waste of education resources in short supply conditions，knowledge is processed by using the digital information technology, and transfer and share in various learning equipment[3]. Learners can use the internet to visit education resources of universities, libraries, education institutions, without restriction by the lectures and books. Thus education of knowledge application value is in the maximum. The application of digital information technology, not only improve the education resource sharing rate and utilization rate, but also cause the transfer of teaching ideas. It is well-known that "the science and technology are the first productivity", Productivity means that the social demand for high-quality talents are also ascending simultaneously, the simple of talent training mode in the past is out of date in fierce competitive society already, only full of knowledge, skilled, strong learning ability, creative thinking people can be available and become the most outstanding person in the society. In recent years, educational experts point out that the new way of education in which the traditional way of learning activities the teacher is the center transfer to the learners as the center, and the digital information education resources provide enough solid technical support to the new mode of education practice.

Suppliers have product catalogs that describe their products to potential clients. They want to make this information available online through a B2B marketplace. Because so many product catalogs already exist electronically, you might think this would be a simple task. However, these product catalogs are designed for the human reader. Thus, extracting the actual product information, classifying it, normalizing it, and storing it in a structured format is primarily a series of manual tasks. Content management solution providers often have several hundred employees working in content factories to manually perform this information processing, often starting with only printed catalogs.

3 The characteristics of electronic commerce

（1）Trading virtualization Through represented by the internet computer internet network in the trade, trade both sides from trade negotiations to pay was done through the Internet, such as the transaction virtualization.

（2）Low transaction cost No intermediary participation, reduce the intermediate links to deal, paperless trade reduces file handling charges, the seller can undertake product propaganda through the Internet, reduce the advertising expenses. No store, save the rent.

（3）High efficiency Companies use the internet to transfer information, improve the information transmission rate. Computers can store large amounts of information, query generation consumers,

can transmit information quantity and accuracy, far more than other media, and can meet the market demand, update the product or adjust the price, so can effectively understand and meet the needs of customers in a timely manner.

（4）Hyalinization Buyers and sellers trade negotiation, signing and pay to the delivery notice of payment, the entire transaction process in a network to ensure the all kinds of information query and check it.

（5）Worldwide The characteristics of the Internet is under the condition of the network popularization, the information can be radiation to the world, and Shared by people, under the condition of the electronic commerce globalization, globalization shopping.

（6）Harmony In the e-commerce environment, it requires more various merchants, payment, logistics and distribution center, communications department, technical services, and other departments ability of cooperation.

Taobao, founded in 2003 on May 10th, founded by alibaba group investment at present, taobao is Asia's largest network retail business circle, the goal is committed to create a global network retail business circle. By combining community, river's lake, gang to increase the viscosity online population, and using the latest online mode, make online shopping the crowd very happy. The emergence of taobao for the entire network shopping market to create a transparent, the good faith, fair and open trading platform, whitch will affect people's shopping habits. Promote offline market transparent, integrity, as well as the production and circulation. Thus derived a "open and transparent, sharing, and responsibility" of the new commercial civilization[4]

Profit model

（1）Direct sales Make purchase price and sale price difference between the online sales, more than 30000 kinds of product varieties, product 10% cheaper than offline stores - 20%.Inventory turnover rate for 12 days, the spot with suppliers now, had a 7% lower rate than gome, sunning, gross margins around 5%, the industry chain of suppliers and end customers to provide more value. Implementation of jingdong "low stress scale" of the business model.

（2）Virtual store rents Store rent, products of landing fees, transaction fees.

（3）Precipitation money income Using the received customer payment for goods and pay the supplier time lag of money precipitation reinvested in order to gain profit. Jingdong mall on the third-party payment platform have Tenpay, Bill and Alipay.

（4）Advertising expense At present, the network advertisement gradually accepted by people, for some large media websites, online advertising has become one of the important source of business income.

4 Classified product descriptions

At this stage of the content-management process, we can assume that our product information is structured in a tabular way. Each supplier might use different structures and vocabularies to describe its products, but that might not cause a problem for a one-toone relationship where the buyer could well get used to the supplier’s private terminology. B2B marketplaces that enable *n–m* commerce cannot rely on such an assumption. They must classify all products according to a standard classification schema that helps buyers and suppliers communicate their product information. The Universal Standard Products and Services Classification is a widely used classification schema in the US [5].

UNSPSC was created when the United Nations Development Program and Dun & Bradstreet merged their separate commodity classification codes into a single open system. Currently maintained by the Electronic Commerce Code Management Association (http:// eccma.org), a not-for-profit membership organization, the UNSPSC is a hierarchical classification with four levels: segment, family, class, and commodity. Each level contains a two-character numerical value and a textual description.

Again, classifying the products according to a classification schema like UNSPSC is a difficult and largely manual task. It requires domain expertise and knowledge about the product domain,

which makes the process costly. High quality is important for ensuring maintainability and visibility of product information [6].

References:

[1] Soto-A costa P, M erono-Cerdan A L. Analyzing e-business value creation from a resource-base d perspective[J]. International Journal o f Information Management, 2008, 28(1): 49- 60.
[2]Malho traA, Gosain S, E Saw O A. Absorptive capacity con figurations in supply cha ins: Gear in g for partner-enabled market know ledge creation[J]. M IS Quarterly, 2005, 29(1): 145- 187.
[3] Chae B S, Yen H J R, Sheu C. Information technology and supply cha in collaboration:Moderati ng effects of existing relationships between partners[J]. IEEE Transactions on Engineering Manage men t, 2005, 52(4): 440- 448.
[4] Goode S, G regor S. Rethinking organizational size in research: Meaning, measurement and rede velopment[J]. European Journal of Information Systems, 2009, 18(1): 4- 25.
[5] Molla A, L icker P S. E-Commerce adoption in developing countries: A model and instrument[J] . Information & Management, 2005, 42(6): 877- 899.
[6]W right P, Dun fo rd B, Snell S. H um an resource and the resource-based view o f the firm [J]. J ournal of Management Information System s, 2001, 6: 701- 721.

Advanced Materials Research Vols. 989-994 (2014) pp 4806-4810
© (2014) Trans Tech Publications, Switzerland
doi:10.4028/www.scientific.net/AMR.989-994.4806

Election System Based on Prior Knowledge

Wu Guodong[a], Liu Zhengyi[b]

College of Computer Science and Technology, Anhui University, Hefei, 230601, China

[a]email:wookwoktung@gmail.com, [b]email: liuzywen@ahu.edu.cn

Keywords: Election system; prior knowledge; Ballot input direction; Efficiency; Multiple election options

Abstract. In order to optimize the election system, we present a vote counting system based on prior knowledge, which makes the ballot style more flexible. The system processes votes by using prior knowledge presetted after obtaining images from the scanner. And it can effectively determine ballots' side to solve the problem of direction uncertainty. The speed of processing each ballot is improved so the problem of limited efficiency can be solved. In addition, the system identifies the position of each option on the ballot to solve the multiple options problems. Experimental results show that the method of the system development is reasonable, effective, and it has high practical value.

Introduction

With the rapid social development, electoral system becomes the main democratic system of our country. People select suitable candidates for specific positions in accordance with certain procedures. Currently, several methods have been widely used. The method of processing ballots manually is very primitive and time consuming. Using Optical Mark Reader (OMR) to process ballots [1-3] needs special ballots. Electronic voting [4-7] is easy to operate but can hardly be accepted by voters because there are no ticket stubs. The method based on layout understanding and Optical Character Recognition (OCR) [8-12] is proposed to compensate for disadvantages of previous methods. This method uses the technology of OCR to recognize the election results after acquiring scanning images of ballots. We compare these four kinds of election methods and the results are shown in Table 1. Apparently, we can see the election system based on layout understanding has superior advantages. However, it still has some disadvantages. The speed of processing ballots is limited because we need to correct some skewed ballots. Meanwhile, it cannot effectively deal with the multiple options problems. In order to improve the election efficiency, Chan et al. [10] proposed a recognition algorithm based on the run-length of table line, which omits the step of tilt correction. The idea of the algorithm is to put all the election information in a table at first, then find out all of the horizontal and vertical lines in the scanned images, finally define each cell based on the intersection. In order to solve the multiple options problem, Zhang et al. [12] proposed a recognition algorithm based on hierarchical division. The main idea is to put the entire election in a table, each subtable represents an electoral item, then search for cells step by step according to the four sides of border. In this paper, we propose a prior knowledge based election system on the foundation of the two approaches. We first scan the ballots, then use the preset information to identify the votes and the voters' intention and eventually count the election results.

Table 1. Comparisons of several election methods

Election Method	Manual	OMR	Electronic Voting	OCR
Accuracy Rate	General	High	High	Relatively high
Speed	Slow	Relatively Fast	Fast	Relatively Fast
Flexibility	High	Poor	High	High
Paper Ballot	Yes	Yes	No	Yes
Security	General	High	Poor	High
Cost	Low	Relatively High	High	Relatively Low
Acceptance	High	General	Low	High

Election Settings

Ballots setup. When more than one position needs to be elected in an election, each position will form an election option. But the election may contains more than one election option and too many candidates that can't be displayed on one ballot, normally, we solve this problem by putting one election option in one ballot and use different colored ballots to represent different election options. But then voters are required to fill in multiple ballots, so sometimes, some ballots are omitted to be filled. In this paper, we design an election system based on prior knowledge, which can process both sides of the ballot to solve such problem, at the same time, the number of ballots is reduced.

The ballots we use in the system contain several election options which can be arranged in both sides. Every election option is composed of several parts: name of election, the electoral requirements, names of candidates and other candidates. We can set the bar code to identify different ballots, election options, and the side of the ballot. Fig 1 shows a simple election ballot. Voters need to fill in the symbol like "√,O,×,\,—, / " under the columns of candidates to express their intention. The system uses the technology of OCR, which is a good method to identify various ballots and symbols. One simplest way is to fill "√" to express yes, use "×" to express no, and use "—" to express abstention. At present, the technology of OMR is widely used in electoral system, but the ballots have two columns that represent support and abstention respectively. As shown in Fig 1. So the system we proposed also needs to process such kind of ballots.

List of Candidates

(elect one from the following two)

Candidate	Opposition	Abstention
Tom		
Jim		

Choose Another

Figure 1. One simple election option

Prior knowledge of the election. The prior knowledge required in the system includes the following three categories:

(1) Ballots layout information

The information includes: (a) whether the ballot has two sides. (b) the maximum number of candidates, the maximum number of other candidates, the number of bar code and the location of its horizontal lines. (c) the way to distinguish the ballot's directions.

(2) Election options information

The information of one selection option include: the storage location of election options information, the name of the election options, and the side of the ballot. As well as the information about ballot's layout, the meaning of each symbol, the list of candidates, the information about voters.

(3) Election information

The information of one election may contain multiple election options which include the name of each election option, the storage location of election options information, the serial number of the ballot, election rules, the devices used.

The method of ballots processing

To be able to recognize the information of the ballots, we process images according to the flow shown in Fig 2 after getting the scanned image of ballots.

(1) Find all horizontal lines

Traverse both side of the image we scanned, to capture all the horizontal lines of an image. However, images may be skewed and the lines may be intermittent. We solve this problem as follows: Firstly, find out black pixels around a black pixel we found in advance. Secondly, use the

"two points determine a line" axiom to determine the direction of the line. Then along this direction looking for other black pixels nearby. Finally, referring to the proximity relation of their ordinate values, we link two pixels where they have nearest abscissa values. If we find that the length of a line is different with the lines we preset in the layout, then we will ignore it. After finding out all horizontal lines, examine if the number is consistent with the number of lines presetted. If so, continue the following steps, otherwise this ballot is invalid.

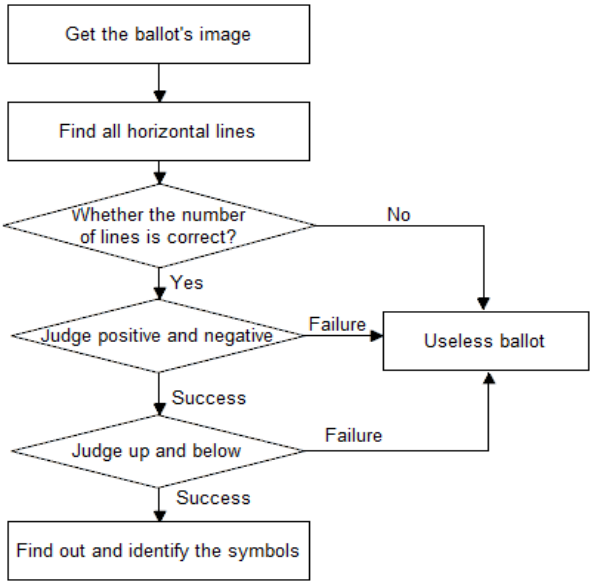

Figure 2.The flow of ballot's processing

(2) Judge the side of ballots

If the election information is only displayed on one side of the ballot, then we can judge the positive side of the ballot by examining whether there are lines or not. If both sides of the ballot have election information, then we use the presetted prior information to identify the ballot's positive and negative side in three ways: (a) horizontal lines: If the number of lines is different in two sides, then the number can be used to judge the side of the ballot. (b) the margin of the ballot: If the sum of top margin and bottom margin is different in two sides, then this feature can be used to represent different sides. (c) Bar code[13]: we can judge the side of the ballot by checking whether there is a bar code. If we successfully judge the side of the ballot in this step, then continue the following steps, otherwise the ballot is invalid.

(3) Determine whether the ballot is upside-down

We use three kinds of methods to judge whether the ballot is upside-down: (a) the margin of the ballot: if the top margin is different with the bottom margin, we can determine the direction by comparing the margin. (b) special regions: if there are two centrosymmetric regions, they have different pattern, for example, one region has black lines or word marks and another region is empty, then this feature can be used to determine the direction. (c)bar code: If two regions are centrosymmetric with each other, and one of them have a bar code, then the feature can also be used. If we find a ballot is upside down, we rotate the image 180 degrees.

(4) Find out and identify the symbols

According to the correspondence between lines in the ballot image we scanned and lines presetted, along with the information about the location of fill-in columns, we predict the location of rectangle boxes in the ballot's image. Though the image may be skewed and the location of rectangle boxes we predicted may not be right, the center of the rectangle box is in the practical fill-in column. So we can use this center point to find out the rectangle box's four vertexes, then use these four points to get the rectangle's real location. At last, according to the symbols in the fill-in columns that we scanned, we count voters' intention about the election. The judge criteria towards symbols "√,O,×,\,—,/" are shown as follows[14]: (a)"√": scan the image pixels from top to down, in the upper part, each row is filled by a single point, in the lower part, each row is filled by two

non-adjacent points. (b) “O”: each row has two non-adjacent points. The distance between the two non-adjacent points becomes bigger at first and becomes shorter later. (c)“×”: each row has two non-adjacent points, and the distance between the two points becomes shorter at first and becomes bigger at later. (d)“\ ,—, /”: each row has a single point.

(5)Statistics

When we get the symbols written by voters in previous steps, then we can count the final results by calculate symbols’ location and meanings.

Experiments

The election system based on prior knowledge is developed by using C# language in VS2010 environment. The operating environment is Intel (R) Celeron (R) CPU E3400@2.60GHz, 2GB of memory. We evaluate the system by testing ballots in different direction. In each direction we detect 100 ballots. Detection results are demonstrated in Table 2.

Table 2. Experimental results

Direction	Upward Positive	Downward Positive	Upward negative	Downward negative
Average processing time	265.6 Ms	312.5 Ms	353.1 Ms	412.1 Ms

Experimental results show that the average processing time is shortest when the ballot is right side up, if we change the ballot from up to down and front to back, the average processing time is longest. That’s because the system needs time to correct the ballot’s direction.

Conclusions

In this paper, we proposed a method to solve the problem of multiple election options and it had a high efficiency. Once voters fill the ballots with standardized symbols, the system can process the ballots faster and better. But in the case of processing non-standard symbol, the result was not ideal. Therefore, we need to focus on how to improve the technology of character recognition in future studies.

Acknowledgments

We would like to express our gratitude for financial support from the 211 Project of Anhui University, Anhui Provincial Science and Technology Development (Grant No.1301b042020) and Joint Specialized Research Fund for the Doctoral Program of Higher Education (Grant No.20133401110009).

References

[1] WANG Qingsheng, ZHANG Jian, XIE lei.Computer Vote System with OMR[J].Application Research of Computers，2002(12):88-92.

[2] QIN Sheng, LIU Xiaoming.Realization of OMR Based on Image[J].Journal of Computer Applications,2003(10):17-19.

[3] ZHANG Ting.Research and Application of OMR Based on Image Recognition Technology[D].An Hui:Anhui University,2007.

[4] David L. Chaum. Untraceable Electronic Mail, Return Addresses, and Digital Pseudonyms[J].Communications of the ACM,1981,24(2):84-88.

[5] Horng-Twu Liaw.A Secure Electronic Voting Protocol for General Elections[J].Computers and Security,2004,23:107-119.

[6] WANG Sijia, HAN Wei, CHEN Kefei.Challenges and Development of Electronic Voting Research[J].Computer Engineering,2006,32(15):7-9.
[7] ZHONG Hong, HUANG Liusheng, LUO Yonglong.A Multi-Candidate Electronic Voting Scheme Based on Secure Sum Protocol[J]. Journal of Computer Research and Development ,2006,43(8):1045-1410.
[8] LIU Haiping.Research on Ballot Recognition Algorithm Based on Layout Understanding[D].Zhe Jiang:Zhejiang University of Technology,2007.
[9] XIAO Gang, LIU Haiping, CHEN Jiujun, GAO Fei.Understanding Algorithm of Ballot Layout Structure Based on Undirected Graph [J].Computer Engineering,2008,34(18):223-225.
[10] SHEN Junqiang.Research on Layout Understanding and fast Recognition of Ballot Image[D].Zhe Jiang:Zhejiang University of Technology,2009.
[11] Xiao Gang, Shen Jun-qiang, Chen Jiu-jun, Gao Fei. Analyze and understand the layout characteristics of ballot image[A].International Symposium on Computer Science and Computation Technology[C],Shang hai: IEEE society,2008,414-417.
[12] ZHANG Jingjing.Research on several Key Technologies of Ballot Recognition Based on Layout Understanding[D].Zhe Jiang:Zhejiang University of Technology,20012.
[13] ZHONG Ruodan.Barcode Recognition Method that Based on Digital Image Processing[D].Xi’an:Xi'an Technological University，2010.
[14] HU Lirui,Wu Jianguo,Guo Xing.Speedy Method of Ballot Image Recognition[J]Computer Engineering and Design,2012,33[12]：4629-4633.

Advanced Materials Research Vols. 989-994 (2014) pp 4811-4814
© (2014) Trans Tech Publications, Switzerland
doi:10.4028/www.scientific.net/AMR.989-994.4811

Audio and Video Media Asset Management System Based On Cloud Storage

Cong Li[1, a], Sanxing Cao[1, b] and Lingjun Yang[1, c]

[1,2,3]School of Communication University of China, Beijing 100024, China;

[a]licongcuc@163.com, [b] caosx_cuc@126.com, [c] yanglj@cuc.edu.cn

Keywords: Media resource, cloud storage, massive data

Abstract. Cloud storage has become increasingly widespread application and deep into various fields of radio and television industry. In this paper, we researched the approach to store media resources of video on demand based on the network and of televisions, in the context of tri-play network convergence. We presented media resource management in conjunction with cloud storage to manage massive data, and build a resource sharing platform types of content without limits, instance participation. Thus information providers and information recipients become an integral relying on the Internet.

Introduction

Cloud storage is based on the development of cloud computing, which results from Distributed Computing, Parallel Computing and Grid Computing. The massive data in the cloud is divided into many small parts to be computed in large system consisting of multiple servers. And the system returns the calculated data to the users. Network service providers can deal with tens of millions of information in a few seconds with cloud computing. Cloud storage provides data storage and service access by a large number of various types of storage devices with the application of cluster application, network technology and distributed file system.

To put it simply, users connected to the cloud through the Internet and transmit storage resources to the cloud. The system provide guarantee to protect the data safe at the same time to save the storage space.

Cloud Storage Architecture

Users enjoy a variety of services such as upload or download files, read files, classified files, backups and so on with cloud storage system.

The system model is shown in Fig.1.

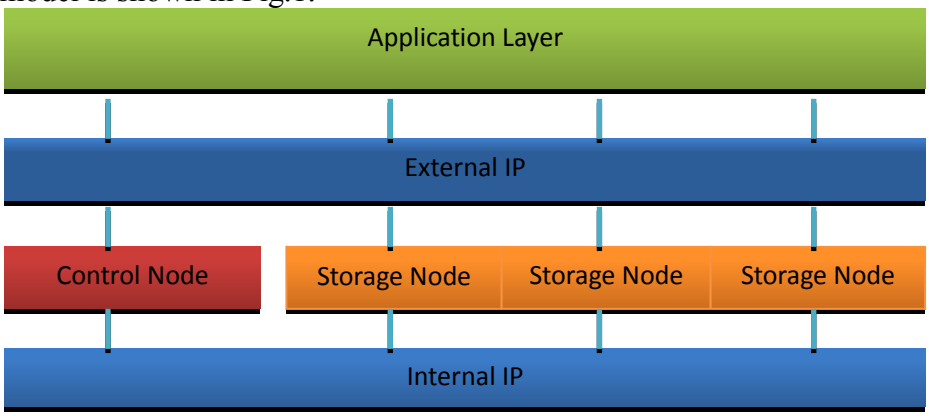

Fig.1. Cloud storage architecture

The storage nodes are marked as orange, they are used to file all documents which uploaded by users. And in red is called Control Node and used to monitor the orange parts' storage capacity, at the same time control loads balancing. The red part and orange parts constitute a cloud storage. Control node and storage nodes are all servers, and more hard disk in a storage node server than control node server. This is determined by the characteristics of a storage nodes server. Each storage node and control node needs at least two network cards, one piece is used for communicating with storage node or control node and transmitting data; the other piece is used for interacting with external application terminal data.

Application terminal needs a PC is used for the storage nodes management in cloud storage. Cloud storage is a file management system for the application side, supporting many network protocols such as NFS, HTTP, FTP, WebDav and so on. This characteristic makes the old system is easy to combine with the new system.

An Overview of Media Assets Management

Media asset contains two parts: media content includes digital media audio and video files and other information beyond media content which are called as metadata. The two parts are respectively stored in different database. The metadata does not have a separate existence value, it is the description of the media file information, including basic information file name, category, edit information etc. Storage management and metadata management of media content is combined with a set of digital media assets for the user, data storage, management, retrieval catalog browsing in a complete solution.

The Media Asset Management System Based On Cloud Storage

In this paper, cloud storage and existing media resources management system are combined, established special cloud storage for audio and video programs. Some equipment and cloud system are connected, these devices are storage devices, the streaming media server, communication server. These devices are arranged in cloud, integrated upload, cataloging, storage, query audit of media resources. A simple architecture is shown in figure 2.

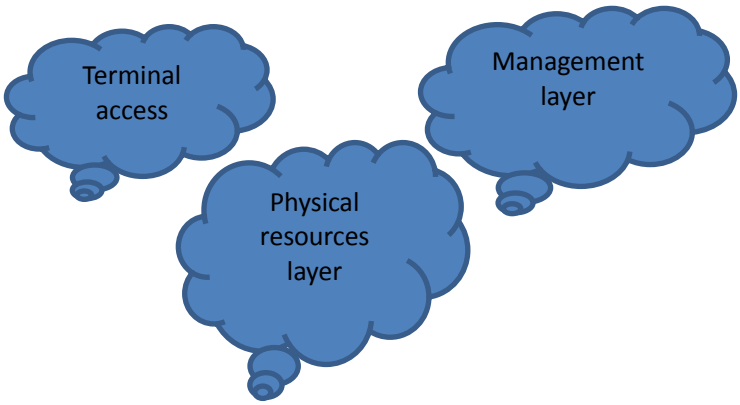

Fig .2 Architecture of media assert management

Storage devices, transport servers, transcoding servers, import and export workstations and other physical equipment are stored in the material resources layer. Terminal access layer upload, cataloging, searching, audit and management operating by using several of internet terminals. Management layer is used to management the operation of configuration, storage and content processing. Processing these operations in the clouds, reduce the pressure of local server. Resources are storage in the type of tape or disk is converted to digital resources.

DESIGN OF AUDIO AND VIDEO ASSET MANAGEMENT SYSTEM BASED ON CLOUD STORAGE

The platform adopts the streaming media server as a storage of audio and video media asset hardware platform, This system includes injection module, content editing module, content audit module, content packaging and classification module and the content query module, to complete the injection and edit the content information, playback and review the video, packaging and content of the classification, the content query function. The structural diagram of the structure has shown in Fig3.

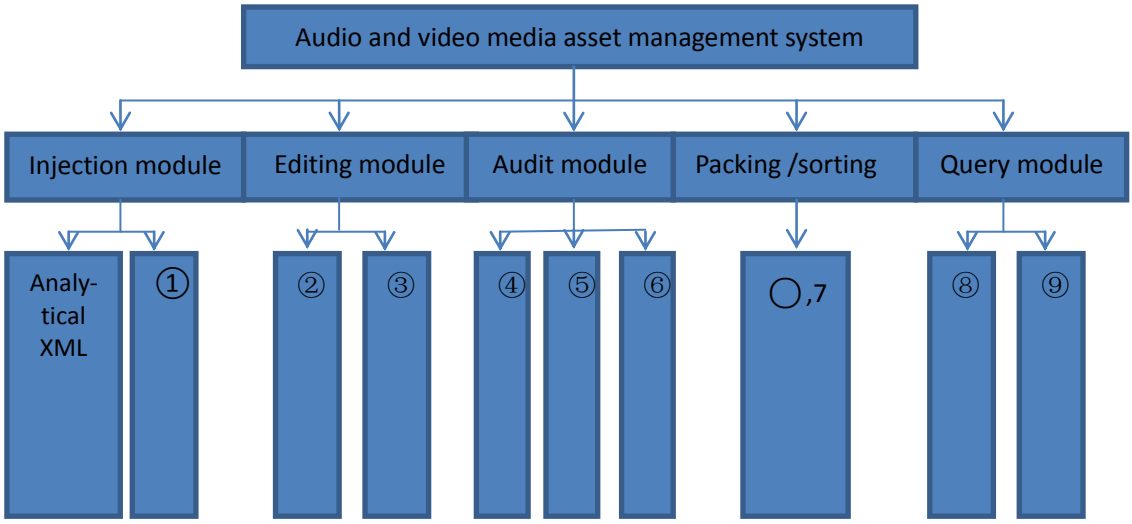

Fig .3 Audio and video media asset management system structure diagram

No.1 representatives content injection module which mainly supported formats for on-demand content metadata information like MP3, MOV, flv, RMVB, mpg.

No.2 representatives modify the content information. No.3 representatives delete the content information. Content editing module can edit information which has been injected into the content .

No.4 representatives video playback. No.5 representatives add audit reasons. No.6 representatives video injection. The content of audit module mainly realizes the video information successfully injected into the content playback and review, by calling the streaming media server interface, the content which has passed audit injected into the streaming media server.

No.7 representatives add the content packaging and classification. Content packaging and classification module realize content business packing and sorting function.

No.8 representatives the query input. No.9 representatives contents of fuzzy retrieval. The content query module can provide function which according to the query condition, return the content list in accordance with the terms of the query.

The system can be deployed separately, independent processing complete content injection, editing, audit, packaging and classification and query functions. System information processing process is shown in figure 4.

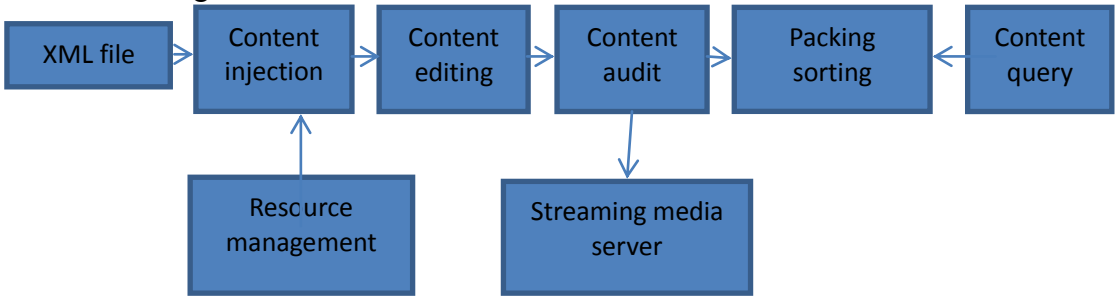

Fig. 4 Information processing system

The code shown in the following which used to inject the content information of the source data into the database management after treatment:

```
<?php foreach($result as $key => $item): ?>
<tr><td align="center"><img src="<?php echo $config['root']; ?>admin/mms/poster/<?php echo $item->logo; ?>" width="60" height="60"/></td><td align="center"><?php echo $item->guid; ?></td>
<td align="center"><?php echo $item->name; ?></td><td align="center"><?php echo $item->streamtype; ?></td> <td align="center"><?php echo $item->resolution; ?></td>
<td align="center"><?php echo $item->type; ?></td> <td align="center"><?php echo $item->live_url; ?></td> <td align="center"><?php if($item->insert_complete == '0')
```

SUMMARY

Cloud technology has the characteristics of flexible, efficient, real-time etc. Various industries put these characteristics to good use not only promote the rapid development of the cloud but also contribute a lot to its development. The combinations of radio and television system and cloud technology improve the efficiency of resources storage and offer convenient services for audio and video resources play and transmission. These combinations enrich the form of the radio and television industry, improves efficiency, reduce cost, provide greater development space for the radio and television industry.

REFERENCE

[1] Yuanyuan Zhang. The media resource management system based on cloud technology [J]. video production, 2013,19,(4)

[2] Yunru Wen. Feasibility analysis of the media resources management system [J]. This media, 2013,3

[3]Liying Hu. The discussions on the necessity of media resource management in TV media industry [J]. China Media Technology, 2012,8

[4]E-books. The media asset management system [OL].http://baike.soso.com/v58743431.htm

Advanced Materials Research Vols. 989-994 (2014) pp 4815-4818
© (2014) Trans Tech Publications, Switzerland
doi:10.4028/www.scientific.net/AMR.989-994.4815

Resource query mechanism research of Structured P2P network based on node interest community

Jingli Jiao [1,a] , Mingzhu Zhang [2,b]

[1]School of Communication and Information Engineering, Chongqing University of Posts and Telecommunications , Chongqing 400065 , China;
[2]School of Electronic and Information Engineering, Lanzhou Jiaotong University, Lanzhou Gansu 730070 , China .

[a] Jiaojingli000@126.com , [b] 925453324@qq.com

Keywords: Interest community; P2P; Chord; piecewise hash

Abstract. Through utilizing node interest community in P2P network, put forward a new method on how to combine node interest community and traditional Chord algorithm. By using piecewise hash, making nodes in the same interest community adjacent to each other in the Chord algorithm, forming a virtual double Chord ring structure. Simulation tests show that this method is superior to the original Chord algorithm at path length and routing latency, improving the scalability of system.

Introduction

With the rapid popularization of P2P network, resource search performance of P2P network has attract the user's attention. Studies has shown that in P2P networks ,there has been the existence of interest community between nodes as in the social network .Because the network community can bring a good user experience , such as Shared resources.When the nodes want to look up resources, first of all ,it will look up the resource in the community that it owns to, due to the nodes with similar interests are more likely to find the resources each other. if the query can be met in the community , then it can narrow the search scope, shorten the query path length,the community has become Repeated communication object.

In unstructured P2P networks, existing methods are mainly concentrated in the use of the formation standards of the community for the choice of routing nodes [1-4], in unstructured P2P networks ,it is relatively simple to use the ideas of community , because the standard of nodes forwarding the query message is based on community relations between nodes thus reducing the number of invalid forward, to a certain extent, improve the efficiency of resource search.In structured P2P (refer to as DHT (Distributed hash table) network) network, each node has a unique identifier, every resource also has a unique resource identifier.According to some kind of mapping rules, the resource identifier is mapped to a node identifier.Resources are mapped to the corresponding node, thus formed a lot of (Key, Value) pairs, all of the (Key, Value) pairs constitute a large hash table, each node is responsible for part of the hash table.If we want to apply the idea of community to the unstructured P2P network to improve the efficiency of resource search ,that will be a challenge.In [5] ,considering the interest of nodes, when forwarding query message ,first select nodes with similar interest with itself for forwarding.The basic idea is that if a node is able to meet query request of another node , that means the two nodes are likely to have the same interest , the next query will forward to the nodes in the first place.However, the measurement criteria of node interest is not accurate.Therefore,in[6],the author put forward a classification method of node interest ,and in turn,the nodes can be classified. This method can measure the interest of nodes more accurately,but it need to traverse all the text in nodes,thus limit the size of the system.In [5],the query request is forward to only one node,in order to using community relations between nodes,the method of establishing a interest community is put forward[7] .

All these above methods are based on to save the interest nodes list for each node,With the expanding of network size,the size of interest nodes list will become larger ,the system has poor scalability.This article is based on the former method ,proposing a new method on how to combining node interest community and DHT(for example: Chord[8])network.

1 .The discovery method of network interest community

Community structure is an important feature of peer-to-peer networks. The current community discovery methods mainly include the method based on edge betweenness [9], the method based on spectral clustering and the method based on random walk [10,11].

In this paper, the creation of the interest community algorithm derives from the past research of network community, mapping the interest community to the network maximum flow problems. Node interest community reflects the range of node interest, including the nodes that have similar interests. In order to build node interest community,we should make sure which nodes made of the community. One of the methods is based on the historical data, namely, whether node X can satisfy the request from the node Y in the past period of time. The method of this article is utilizing the current sharing content of two nodes to determine the similarity between nodes .

Node interest communities can be seen as a undirected graph, with the vertex as node.when two nodes share a common interest such as the same document,then establish an arc between the two vertex.Each arc can set an weight according to the different measurement criteria , this article uses the number of same keywords between two nodes as the weight of the arc.The node that create community called seed node , at first place, seed node try to find the nodes that have shared the same document with it in the network.The specific method can be seen as follows :Seed nodes randomly selects a subset of keywords and send the request to some nodes in the network, check to see if these nodes stores these documents; the nodes that processing the request is selected from node set known by the node which send the request . The nodes that share at least one keyword with the seed node are added to the graph , the depth of this nodes is 1, that is, they attached directly to the seed node.when it comes to the second step, for the nodes (named p)that added to the graph in the first step repeat the action of seed nodes ,some new nodes (can be named as q) will be added to the graph with the depth of 2.Then a arc can be produced between p and q with the shared number of keywords as the weight .Third step,add a point as the collect point and make connections with all the nodes in the graph.Deciding the friend nodes of seed node by determining maximum flow between the seed node and collect point and then build the interest community of seed node.The select standard of seed nodes is in the light of the number of the documents stored in the nodes.When a node belong to multiple interest community ,then it joins the community with the biggest similarity .

2.Resource query mechanism based on the interest community of nodes

Chord uses consistent hash function to compute nodes and keyword identifiers.By hashing the IP address and the keywords of document can obtain the identifier of node and keywords. Then the identifier of keywords is mapped to the identifier of nodes.In Chord , all nodes are organized into a single ring with the size of 2^m.The keyword identifiers is stored in its successive nodes.In traditional Chord ring, the query request is based on the hash value of query keywords.The key problem of query is looking up the successive nodes of keyword.

When taking the node interest community into consideration ,by adopting the idea of piecewise hash,allocate a community identifier for each interest community .In Chord,nodes is represented by the correspond node identifier with m bits,in order to making the nodes in the same interest community can be adjacent in the logical space,we adopt piecewise hash and divide the m into two parts:m1 and m2,with m=m1+m2. Assuming X and Y is correspond to the community identifier and IP address of node,so node identifier can be divided into two parts ,Xid andYid,expressed as N(Xid,Yid).N.Xid=Hash（X）mod 2^{m1} and N.Yid=Hash（Y）mod 2^{m2} ,N=Xid* 2^{m2} +Yid.Xid is made of the former m1 bits of node identifier and determined by the community identifier,Yid is made of the m2 bits of node identifier determined by the IP address of node. Because all nodes in the same community have the same community identifier,bringing about that nodes in a community is adjacent in the logical space ,resulting in the virtual double layer structure(as shown in figure 1).Selecting a node with good processing ability as the leader node to be responsible for the query request between communities.When the search request of the nodes have not been met in the community that it own to ,then the leader node will forward the request to the other communities in

accordance with the traditional resources localization algorithm of Chord.This method have superiority not only in the lookup time delay but also in the scalability.

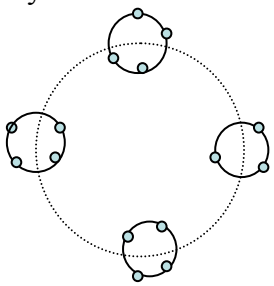

Figure 1 Virtual double layer structure

3. Performance Evaluation

We have conducted simulation experiments to evaluate routing performance of our model .In this paper, the testing standard is the average search path length and the average routing latency.we use Test1 as the test result of our model and Test2 as the test result of the traditional Chord search algorithm .

Experimental parameters is mainly include the number of nodes , the number of documents and the number of resource requests with the proportion 1:1:10.In our simulation ,we vary the number of system nodes from 200 to 3200.

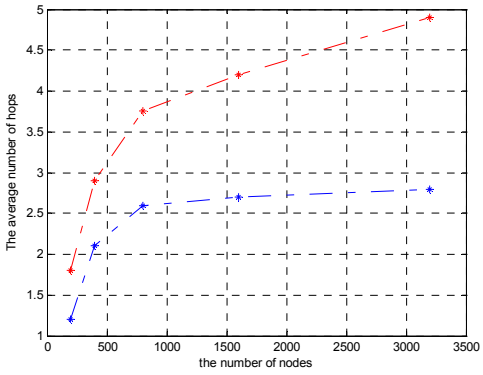

Figure 2

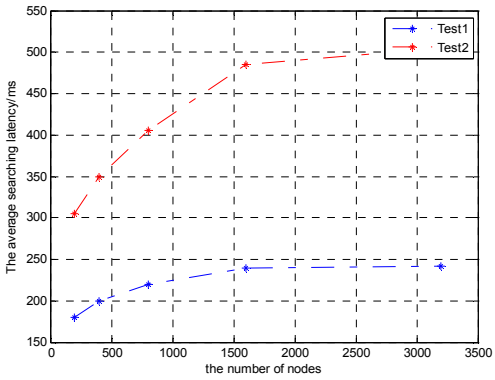

Figure 3

(1)The average search path length

Path length refers to the logical network hops the node that issues a query request has passed until find the resource. Figures 2 shows the comparison results measured by metric of “Search path length .Assuming that each community contains m nodes and there are N nodes in the network .The complexity of looking up is 0（log N）in the traditional Chord. When it comes to the model in this article ,then the complexity of looking up will only be 0（log m）if the query request can be met in the local community.

(2)the average routing latency

When users want to find resource ,it will first look up in the community that it own to and also the success rate is relatively high .Therefore ,the average routing latency becomes shorter on account of the shorter in the Search path length ,as is shown in the figure 3.

4. Summary

In this paper ,we propose a new model for the resource query in the structured P2P network and make explanation in detail for the resource search mechanism.By analysising the simulation result we conclude that the model that we proposed is superior compared to the traditional Chord algorithm.However ,this paper does not take the forward among interest communities into consideration .The interest correlation among communities also affect the efficiency of resource

search to a certain extent .In the next step ,we will study the message forwarding mechanism among communities.

Literature References

[1]Chen G, Low C P, Yang Z. Enhancing search performance in unstructured P2P networks based on users' common interest[J]. Parallel and Distributed Systems, IEEE Transactions on, 2008, 19(6): 821-836.
[2]SUN Li,CHEN Lan,YUAN Yuan. Non-structural P2P Search Mechanism Based on Peer Interest[J].computer engineering,2009.
[3] Chen W T, Chao C H, Chiang J L. An interested-based architecture for peer-to-peer network systems[C]//Advanced Information Networking and Applications, 2006. AINA 2006. 20th International Conference on. IEEE, 2006, 1: 707-712.
[4] Khambatti M, Ryu K D, Dasgupta P. Structuring peer-to-peer networks using interest-based communities[M]//Databases Information Systems and Peer-to-Peer Computing. Springer Berlin Heidelberg, 2004: 48-63.
[5] Sripanidkulchai K, Maggs B, Zhang H. Efficient content location using interest-based locality in peer-to-peer systems[C]//INFOCOM 2003. Twenty-Second Annual Joint Conference of the IEEE Computer and Communications. IEEE Societies. IEEE, 2003, 3: 2166-2176.
[6] TAN Yihong,CHEN Zhiping,LIN Yaping. Research and implementation on searching mechanism based on interest mining in unstructured P2P systems. Computer Application,2006,26(5):1164-1166.
[7] WANG Fang.Efficient resource search technology and application research of Peer-to-Peer network[D].Shandong Normal University ,2006.
[8] I. Stoica, et al., “Chord: A Scalable Peer-to-Peer Lookup Service for Internet Applications,” in Proc. of ACM SIGCOMM , San Diego, CA, 2001, pp.149-160.
[9] Girvan M, Newman M E J. Community Structure in Social and Biological Networks[J]. Proceedings of the National Academy of Sciences of the United States of America, 2002, 99(12): 7821- 7826.
[10] Ramaswamy L , Gedik B. A Distributed Approach to Node Clustering in Decentralized Peer-to-Peer Networks[J]. Parallel and Distributed System s, 2005, 16(9) : 814- 829.
[11] Tang Y, Zhang Z, Chen S, et al. A distributed hybrid scheme for unstructured peer-to-peer networks[C]//Communications, 2006. ICC'06. IEEE International Conference on. IEEE, 2006, 1: 30-35.

Advanced Materials Research Vols. 989-994 (2014) pp 4819-4822
© (2014) Trans Tech Publications, Switzerland
doi:10.4028/www.scientific.net/AMR.989-994.4819

Research on Accounting Decision Support System Based on Data Warehouse and Data Mining

Li Zhiwei[1,a] , Bai Dong [1, a]
[1]China Satellite Maritime Tracking and Control Department, China
[a]348237548@sina.com

Keywords: Data Mining, Accounting Decision Support System, Data Warehouse

Abstract. With the intensification of market competition and the demand of information society development, extracted from large amounts of data (retrieval and query, etc.) used for decision making and analysis of information becomes more and more important. Through the accounting data warehouse design, data extraction, data maintenance, accounting decision-making needs design, mining algorithm is designed, and the mining operation, the expression and interpretation, etc, can discover useful from vast amounts of financial data, important information, etc. Provide scientific decision-making for the enterprise development, leading technical support.

Introduction

DSS (Decision Support System), Decision Support System, is in the process of semi-structured and unstructured decision-making activities, through the man-machine dialogue, provide information to Decision makers, to help Decision makers find and analyze problems, to explore the decision-making plan, evaluation, prediction and options, in order to improve the decision-making efficiency of a by means of computer information systems. The accounting Decision Support System (ADSS) is the application of Decision Support System in the field of accounting, is on the basis of accounting management information System.

At present, the market of all kinds of financial management software, and decision support system to a large extent is the manifestation of quantitative technical decisions. Mathematical model is set up is their common characteristics significantly. However, not all influence business decisions in the practical work of information can be completely quantified. Especially in the complicated environment enterprise facing many decision problems, tend to be goal vague and multiple targets conflict each other, scheme comparison and selection of no fixed rules or procedures, required information is not complete or vague, this kind of decision problem, based on the relational database of ADSS couldn't solve. Based on data warehouse and data mining technology to construct the accounting decision support system solutions can effectively solve the unstructured accounting decision problem.

1 Data warehouse and Data Mining

With the intensification of market competition and the demand of information society development, extracted from large amounts of data (retrieval and query, etc.) used for decision making and analysis of information becomes more and more important. This demand requires both online services, also involves a large amount of data for decision making, and the traditional database system has been unable to meet this need. It embodies in three aspects: history data volume is very big; Auxiliary decision-making information data involves many departments, and different system data integration; Due to lack of the ability to access data on a large amount of data access performance decreases obviously.

With the maturity of C/S technology and the development of the parallel database, the development trend of information processing technology to extract Data from a large number of transactional database, and clean up into a new storage format, it is the decision goal the Data aggregation in a special format. With the development of the process and improvement of the support decision making, special Data storage that is referred to as a Data Warehouse (Data Warehouse).

Data warehouse technology was applied to build the accounting decision support system, can realize centralized storage and management of accounting data, which can reduce the time of I/O and computing time, reduces the data redundancy, and solved the DSS system is inconsistent with the data in the database.

The key technology of data warehouse including data extraction, cleaning, conversion, load, and maintenance. The basic framework of data warehouse is shown in figure 1.

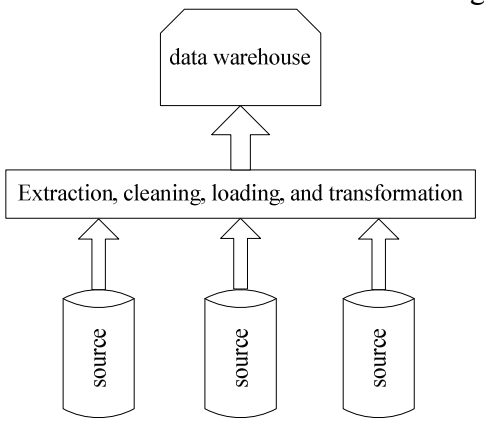

Fig1 Data warehouse framework

Accounting information system running after years of accumulated mass, in various forms of storage data. But when faced with more and more rapid expansion of the database, but people don't begin to understand the information contained in the data, more difficult to gain valuable knowledge, the original decision support system (DSS) can not meet needs. Concept of data mining is to make people have the ability to overcome the difficulties, to discover the contained in the data information and knowledge. Data mining is the international one of forefront research direction in the field of database and information decision, caused the wide attention of academia and industry.

Using the data mining technology to the accounting decision support system, will benefit from a large amount of data found potential, valuable, and unknown relationships, patterns and trends, and represented in the form of easy to be understood. Through data mining in ADDS to found the complex relation between data and the effect of the contact of decisions.

Data warehouse is a to better support the enterprise or the organization's decision analysis process of data collection, data warehouse technology to complete the enterprise internal work, all kinds of business data integration for enterprises laid a solid foundation for subsequent business application; Data mining from huge amounts of data, extract implicit in it, people don't know in advance, but potentially useful information and knowledge. The process of data mining analysis on the data warehouse, can find many cannot find information manually, can want to come to the conclusion that. So can say: data mining is a data warehouse on value-added technology.

The data mining based on data warehouse, on the one hand, can improve the ability of the decision support of data warehouse system; On the other hand, due to the completed data cleaning, data warehouse ETL (extract, transform, load), data mining is facing through preliminary processing of data, more conducive to data mining function.

2 Data warehouse and data mining based accounting decision support system

In order to effectively accounting decision, solve the traditional ADSS can't solve the problem of unstructured decision making, based on the data warehouse and data mining technology to build the accounting decision support system is feasible, the basic framework is shown in figure 3. The system, remote data mainly comes from internal and external accounting and management system and its related systems; Data model USES the set up time, business dimensions, such as user geographical and multidimensional data model; The function of the system structure can be used C/S architecture, by the client, application server and data warehouse server.

Accounting should be clear at the beginning of building the data warehouse theme, according to the analysis of the theme target integrated all the relevant data and information, integration, the

greater the amount of data, the more comprehensive, the more accurate decision analysis conclusion more objective. The construction of data warehouse is a spiral development process, with the passage of time, can adapt to different needs. The theme of the major accounting data warehouse contains are: the theme of the economic forecasting, pricing decisions, investment decisions, corporate sustainable development forecast, product marginal profit forecasts, etc.

Build a data warehouse of accounting requires the following process:

1, accounting data warehouse design. According to the accounting decision subject design data warehouse structure, general star model and snowflake model was adopted to design the data model (model), in the design process shall ensure that the accounting data warehouse system of standardization and necessary contact. Each element has the following three steps: first, define the subject needed for details of each data source, including the computer platform, the owner, data structure, using the data processing, warehouse updated plan, etc. Second, define the data extraction principle, in order to extract the required data from each source. Define how the data transformation, loaded into the theme of which data table. In the end, will be a theme refining for multiple business theme, form the subject table, choose multiple data subset from the data warehouse accordingly.

These data definition direct input in the system, as metadata (metadata) storage, used for data management module and analysis. The metadata stored in the metadata repository, it is not only the documentation of the data warehouse, used for management, maintenance staff, and also for the user query, make it a better understanding of the data warehouse structure, raise the level of their use.

2, the accounting data extraction. Topics within the accounting data extraction is based on the metadata database table definition, data definition, data extraction rules defined for different heterogeneous data sources (including the database of different platforms, text files, HTML files, knowledge base, etc.) for cleaning, conversion, and the data again organization and processing, loaded into the data warehouse target in the library. In the process of organizing data from different sources, to transform data into an intermediate model first, and then move it to a temporary workspace. Processing data is to ensure that the target data in the database for completeness and consistency.

3, the accounting data maintenance. Accounting data maintenance is divided into two aspects of the target data maintenance and metadata maintenance. Target data maintenance is defined according to the metadata database update frequency and update data item update project task to refresh the accounting data warehouse, to reflect the change of the data sources, and to deal with time correlation. There are two kinds of update operation situation, the original data in the table is in the warehouse for some of the data update and create a new time interval data, because many of summary data and the data warehouse information elements, must complete summary, so as to ensure the consistency of all information.

Accounting data warehouse size is compared commonly big, from the beginning of the established shall ensure that its manageability, an enterprise may establish several data warehouse, but they can share a meta database on it management. First of all, from the yuan required metadata database query, then update the data warehouse operations, after the update, RMB will update records in the database. When running environment, structure of data source and the target data maintenance plan changes, need to modify the metadata. Metadata is an important part of data warehouse, metadata quality determines the quality of the data warehouse.

Data mining in the ADSS system including accounting decision-making needs, a large amount of data mining algorithm and 3 parts. Accounting decision demand is the early stage of the real data mining of work to clear, the clear goal of decision-making; A large amount of data is the accounting information system and related system operation after years of accumulated mass, in various forms of storage of data; Mining algorithm is one of the hot spot of current research, mainly around the new mining algorithms to solve specific problems and the improvement of mining algorithm. By the mining algorithm can form mining tools.

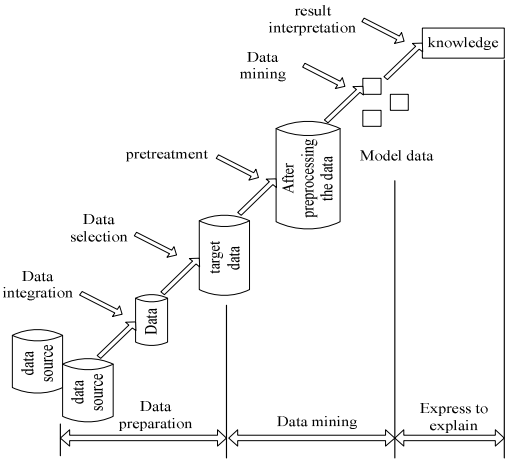

Fig2 Data mining

Knowledge discovery process may consist of three main stages: data preparation, mining operation, the expression and explanation, knowledge discovery is the three stages of repeated. As shown in figure 2.

Data preparation, data integration will be more data in a file or database runtime environment merge processing, solve the omission of semantic fuzziness, processing data and clean the dirty data. Data selection to determine the need analysis of the data collection, improve the quality of data mining. Pretreatment is in order to overcome the limitations of the current data mining tools.

Data mining:

1) to determine how to produce first assumptions. Is that the data mining system for users to produce hypothesis, or the users themselves may contain knowledge hypothesized reference database. The former is called found type (discovery-driven), data mining, the latter is called authentication type (verification-driven) of data mining.
2) select the appropriate tool.
3) data mining operations.
4) confirmed that find knowledge.

Results expression and explanation: the extraction of information analysis, through decision support tools presented to decision makers. This stage is not only give expression to the result, and knowledge discovery system will adopt interpretation and reasoning mechanism, the knowledge directly provided to decision makers, can also be provided to the domain experts, revision had been Shared knowledge base for the system. If not satisfied, need to repeat the process of knowledge discovery.

Summary

Data warehouse and data mining technology to provide decision support for the development of a set of systematic effective feasible solutions, it is a process of problem solving, rather than a software product can be obtained. Through the accounting data warehouse design, data extraction, data maintenance, accounting decision-making needs design, mining algorithm is designed, and the mining operation, the expression and interpretation, etc., can discover useful from vast amounts of financial data, important information, will push the further development of accounting decision support system, and continuously improve the decision quality and efficiency of the enterprise, for enterprise development, and leadership decision-making, etc. To provide scientific support.

References

[1] Yang Xiaoling. Data analysis system based on data warehouse[J]. Shanxi Electronic Technology, 2008(7):65-67.
[2] Zhang Suping. Introduction to decision support system based on data warehouse[J]. Com puter Application Research,2009(5):22-25.

Advanced Materials Research Vols. 989-994 (2014) pp 4823-4826
© (2014) Trans Tech Publications, Switzerland
doi:10.4028/www.scientific.net/AMR.989-994.4823

Design of mobile police store system based on the technology of information security

ZHANG Xue-yuan[a], JI Hua zhen[b] and LI Min[c]

Information Security Technology Department, the Third Research Institute of Ministry of Public Security, Shanghai, 201204, China

[a]13482130378@139.com, [b]lim@crgs.com, [c]jihz@crgs.com

Keywords: mobile police terminal, application warehouse system,application background, application front, information security

Abstract. In order to enrich the mobile police application and enhancing mobile police application security,analysis of current situation and requirement of the mobile police application,to put forward a kind of police mobile application store system based on information safety technology.Specific depicts system overall design,background design,front design,the use of information security technology,and the test results of the system are described.The design and development of the police mobile application warehouse system,have certain reference siginficance.

0 Introduction

With the development of science and technology,mobile police terminal function is becoming more and more powerful,mobile application more bearing,and due to the convenient and practical,mobile police terminal will be popularized in the police on duty.But how to make the application software of various new and useful rapid push to the arranged around the police,and realization application populated use the minimum cost and the fastest speed,and achieve rapid construction of information system,all of these have become subject to the information construction of police security system.Therefore the development of a system of policing in various kinds of application software for the authorization,unified management,flexible configuration,block push,makes the mobile police terminal can be convenient,safe to install application sofeware is urgently needed.Application warehouse system is designed in this background.

1 The design of the whole system

Application warehouse system is to provide secure signature authorization application software management and service platform based on ANDROID operating system of a mobile police terminal.From the application to create ,apply,examine,test run,release and off the shelf and other procedures to ensure application of the normal release.Application can be applied through users and user groups.The client can conveniently realize view application software introduction,application download,search application,evaluation application,application management,application unloading etc. function.The specific product diagram as Fig1 :

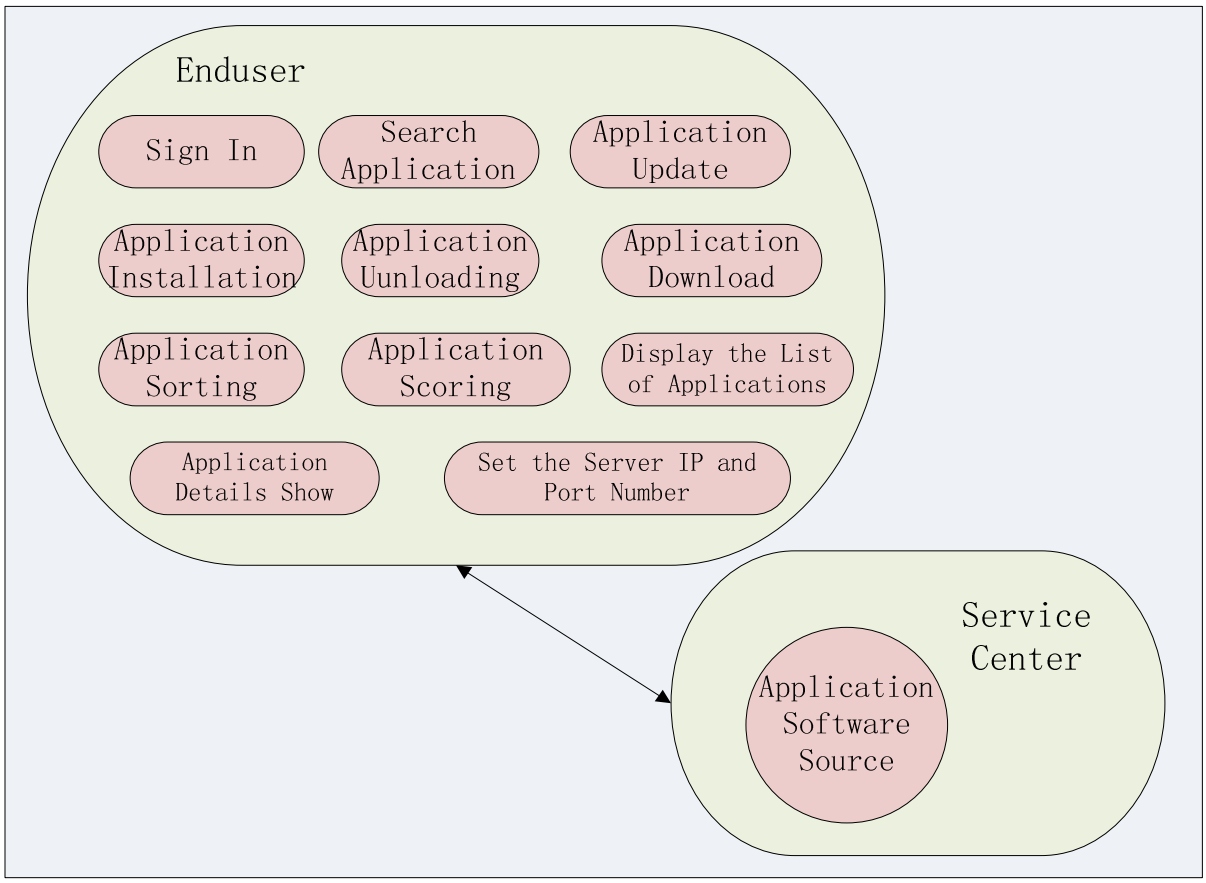

Fig-1

Application warehouse is designed with client/server structure,it's background is designed with SSH architecture,use JAVA programming language.The front-end client for any ANDROID operating system terminal,the APK file form.Now,client software can only support different versions of ANDROID operating system terminal.It's background software is composed of WEB interfacr,database and terminal event handing etc. function components,commom deployment on a single server,can also own distribution deployment,provide the performance of the system.The request of the system is initiated by the terminal application repository client software launched by HTTP,access the data of background,can be well compatible with the mobile access platform,system architecture specific as shown in Fig-2:

2 The design of the system background

The background is the core of application warehouse system,The design contains the following seven modules:

Processing the service request from the mobile terminal:the acceptance of mobile terminal upload application by request,accept the mobile terminal uploads the terminal application status request,acceptance of mobile terminal upload update application strategy of terminal request,accept the mobile terminal uploads the emergency service processing request application function.

Treatment of mobile terminal sends service request:to achieve remote control of mobile terminal equipment directive,the server of high security level message notifications.

User management:including the administrator application and business supplier business.

Develop application strategy:including the development of mobile terminal application offline strategy,strategy for mobile terminal application online.

DB:the use of ORACLE database,can not cluster.

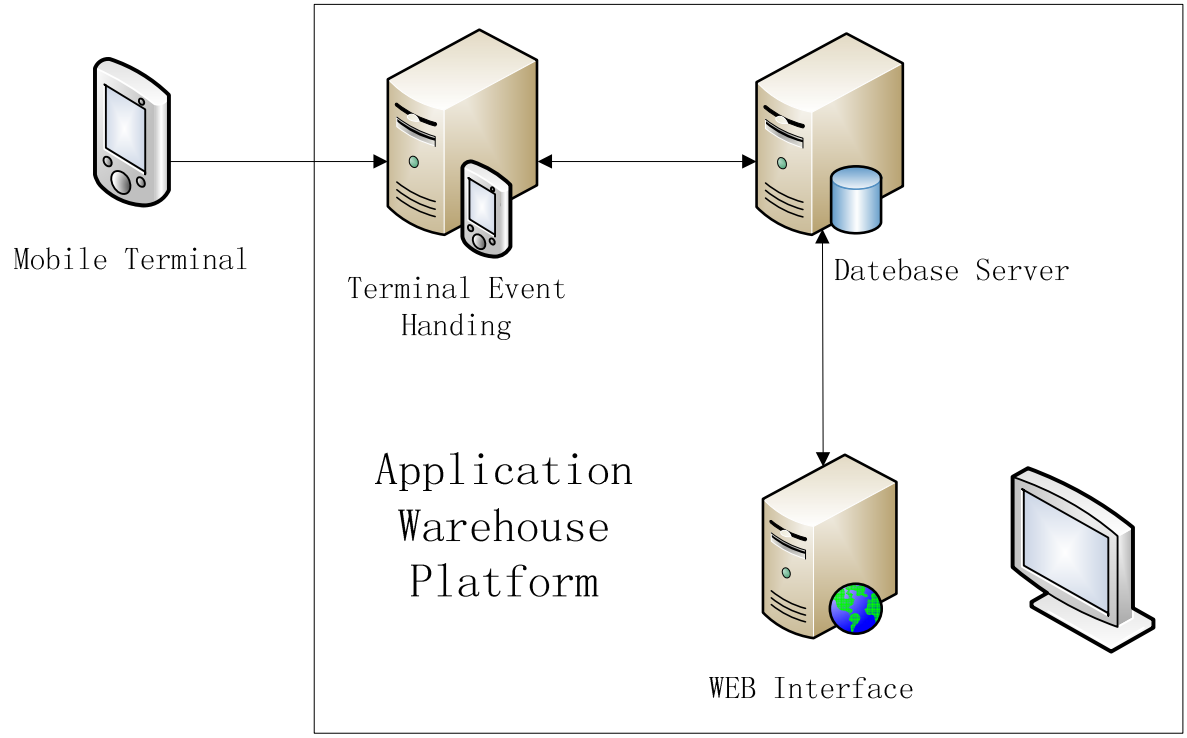

Fig-2

Analysis of application security access mobile and display:according to the input to the application of the warehouse information,analysis and applicaiton of safety state,according to the security filter condition display,display application security status,according to the application of security analysis,provides the application strategies or methods.

surveilance audit client:application log and data acquisition application warehouse,report and use data to the supervision and examination of cascade system,log and data warehouse application.

3 The design of the front-end of system

Application of the client in the ANDROID terminal in the form of APK,designed to contain such as several modules:view application recommendation,search application,charts,classfication,trial operation,management,application management,application setting,dowload details,scoring and evaluation version of history.

4 Information security technology used in system

1). Terminal Security Reinforcement

Through the terminal operating system and terminal OS reinforcement work along both lines,set up by the business layer until the kernel Stereo omni-directional integration layer of reinforcement.

2)Authentication of Application Signature

System uses proprietary tool needed to install the application for signature verification,to ensure that the appliction can be trusted,the validation does not pass refused to install the application.

3)Hierarchical Control of Application

Application of the warehouse system for unified management of the application of all operation,according to the operation needs and system safety.Requirements will be applied into mutiple levels,set up different security control measures according to different level.

5 Test Results

In this police application warehouse system,2 servers were used as the database server and application server,use the general ANDROID mobile phone,through the security reinforcement as

mobile police terminal and tested using remote security assessment system of green alliance.The test result is as follows:
1)Function test:The background and the front end of the functions is to basic achieve simple version of APPSTORE requirements.
2)Performance test:Through structure optimization and hardware performance improvement,number of concurrent users,online user number,terminal response time can meet the demand of actual combat.
3)Safety evaluation index test:The products have no high vulnerability through remote security assessment system of green alliance scanning mainly port.

6 Summary

This article from the current situation and demand of police mobile application,in-depth analysis of the overall design and application of warehouse system and the security technology.According to the design,application warehouse system of public security work put forward a set of terminal user management,application release,distribution,statistics,application system security audit in one,can solve the application fatigue and application security risk at present mobile police terminal face,has the importment practical significance.

References

[1] WAN Ping,MCGUIRE M,DONG Xiao-dai: Near-optimal channel estimation for OFDM in fast-fading channels Vol. 82-87 (2011), p. 13.

[2] Hu Weijian:Network security and confidentiality,Xi'an;Xi'an Electronic and Science University,2003.

[3] Wang Yu,Yan Hui:Information security technology,Beijing:National Defence Industry Press,2010.

[4] Wang Lina:Introduction to information security,Wuhan:Wuhan University press,2008.

[5] Zhao Lei,Fu Xiao,Liu Jin:Network of information security risks and preventive strategy of 2011.

[6] Liu SuFen:Current status and protection strategy of network information security,Electromechanical product development and innovation of 2012.

[7] Liu Yangfu.The computer network security and virus prevention,Hainan Province Institute of Communications Conference papaers,2008.

Advanced Materials Research Vols. 989-994 (2014) pp 4827-4831
© (2014) Trans Tech Publications, Switzerland
doi:10.4028/www.scientific.net/AMR.989-994.4827

A Study on Security Mechanism for Resource Identifiers in Ubiquitous Network

Minglang Jiang, Fang Cheng, Peng Zhang

Key Laboratory on Communication Networks and Testing Technology, Chongqing University of Posts and Telecommunications, Chongqing 400065, P. R. China

jiangminglang@qq.com

Keywords: UNRI; Resource Identifier; Security Mechanism; Ubiquitous Network

Abstract. Due to the openness of Ubiquitous Network, there is high risk for sensitive information leaked by users if any misuse of the resource identifier exists, regarding quantity, usage, storage, and content, which leads to a variety of security concerns. This article puts forward a means of protection against URI attacks in UNRI which is based on authentication, MD5 encryption and redirected URI. Through these methods, latent security threats can be guarded against effectively. Compared with other methods, the mechanism proposed by the author features shorter encryption time, yet more encryption parameters, which guarantees its wider application in ubiquitous business environment.

Introduction

As Ubiquitous Network implements information interaction through networks, resource identification becomes the author's first concern. For simplicity, "ubiquitous network resource identifier" is shortened to "UNRI" in this article. UNRI is mainly in the use of identifying logical and physical resources like data and services etc. in a unique way, and then managing ubiquitous network resources.

Related researches show that physical and virtual resources in trillion level interconnect to have formed a huge pool of resources, but scattered in a relatively independent state from each other. The independence of each system is caused by the lack of clear and interoperable standards for the classification and identification of key resources, coupled with a variety of heterogeneous networks, heterogeneous terminals and heterogeneous access. As a result, the situation brings significant barriers to UNRI, hindering interoperability between different networks and systems.

Web technology is an excellent example [1], anyway, Ubiquitous Network can take advantage of this for the basic interaction between systems, and data and power are taken as abstract resources, then identify resources in way of RESTful URI. Users can access to and manage resources with the proper permissions over the Web.

Related Work

As Ubiquitous Network is a huge network with variant degrees of openness, attacks against UNRI are endless.

In recent years, E. Du mentioned semantic URL attacks in the access links [2]. When users verify permissions, attackers can illegally obtain login password as well as other information by tampering request parameters. In 2011, G. Liu proposed that it is likely that other similar resources to be found and carried out illegal operations by attackers if the end of the identifiers allotted by resource management center cohere with the naming rules of resources themselves [3]. Meanwhile, G. Qin noted that URL attacks aiming at Web are mainly SQL injection and cross-site scripting (XSS) attacks [4]. SQL injection describes the problem that attackers can avoid oversight of systems and thus illegally access and manipulate resources in ubiquitous network by entering pre-designed SQL statements in identifier validation phase. While XSS could catch hold of the inaccuracy of program code, and embed illegal scripts into users' browser with maliciously structure resources URI included.

Moreover, R. Moskowitz. noted that ID and secret key are bound in Host Identity Protocol (HIP) scheme [6]. Thus it inevitably causes key expiration as well as other problems. Since the security of UNRI depends on the key and ID, expiration would bring great security risks, it is necessary to introduce effective mechanisms to manage its lifetime.

Considering the security issues pointed out in the previous studies, we shall introduce a new security mechanism based on lightweight considerations for UNRI. The author of this article presents a kind of security mechanism in UNRI which is based on authentication and MD5 encryption. By the protection of URI redirection, this method prevents attacks from many aspects, leading to a greatly enhancement upon the security of UNRI.

Security Mechanism for UNRI

REST defines the application standards of Web. Design based on RESTful for UNRI would make full use of the merits of Web-based architecture, and meet demands of integration and mashup of various identifiers. It also provides standardized and formative UNRI for different applications.

User Authentication and UNRI Redirection. Usually, UNRI applicants may choose whether to open to all or partially. If a user does not get access to the appropriate resources or UNRI is considered not credible by management center, resources can't be accessed or operated. Authorized users could use redirected URI which is distributed by Front Server (hereinafter referred to as FS) to access real resources, which to some extent, enhances the security of UNRI.

As for the security mechanism designed in this article, firstly the identification system servers are divided into FS that users can directly access to Resource Server (hereinafter referred to as RS) where resources are located. As shown in Figure 1, to access real resources, users need to visit one of the Front Servers for user authentication.

All user information is saved by FS. And users would obtain the redirected URI after passing certification. Then they could get real resource information from RS in accordance with the redirected URI.

In the process of generating each URI, FS would take advantage of account (FSId), assigned key (FSKey) and timestamp (FSTime) which records the generating time of redirected URI.

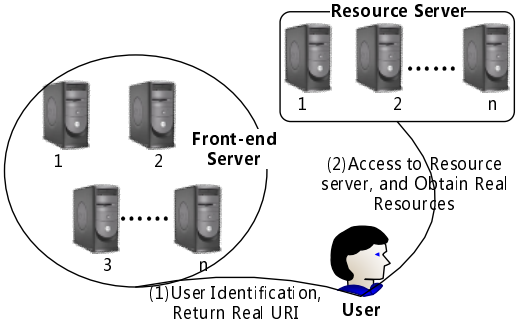

Fig. 1 UNRI System Access Diagram

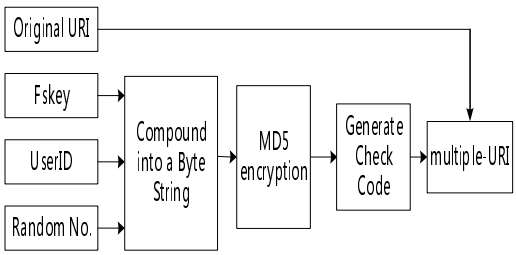

Fig. 2 Identity-based Redirected Resource URI

To ensure that ubiquitous network resource server receives a credible redirected URI, 3 ways are recommended here. Prevention of fake URI by public network users. Redirected URIs must be credible and returned by a FS. Prevention of accessing of expired URI. To prevent hotlinking, redirected URIs should have timeliness. It can be achieved by adding timestamp on URI request.

Prevention of fake URI by untrusted FS. Sometimes when a redirected URI or a certain FS is considered untrusted, system need to make a timely response to prevent accessing.

Since RS allows all authorized users to access and generally does not communicate with FS directly, thus authentication could be recommended. According to our proposed mechanism, we should first use MD5 algorithm to encrypt the URI request. Then we need take the synthetized URI with cryptography information to FS for verification.

If verified, FS will provide real resource URI to user and ensure that no same URI is available. The following part will elaborate the security mechanism in detail.

Generation of Redirected URI through Customized Encryption Function. We intend FSKey, FSId and some random number as parameters, and synthetize them in accordance with certain rules. Then we need to encrypt the compound string using a customized encryption function (MD5) and generate check code. Finally, as shown in Figure 2, we obtain real identity-based redirected resource URI after combining the check code with original resource URI.

Each user will get a unique ID in UNRI system, and different ID have different permissions. In practical applications, some of the resources must be accessed by authorized users.

To ensure the safety of UNRI, we add permission-auditing process in the mechanism and periodically change the FSKey.

In view of this, the redirected URI generated by customized encryption function is as follows:

…/FSId=***&uri=***&signmsg=md5(encode(uri,FSId,FSKey))

Upon receipt of the URI request, RS would determine whether the certain FS is credible or not on the basis of FSId. If FS is credible, then RS gains the FSKey from FS in line with FSId. Afterwards, RS will generate signature string in the same way as cryptographic signature process of parameters. Finally, compare the signature of redirected URI (signmsg) with a locally generated signature. If they are the same, the URI could be considered to be credible, otherwise illegal.

Implementation of Security Mechanism. As clearly illustrated in Figure 3, the implementing process of the security mechanism is elaborated as follows:

Step 1 Identify user in FS after the user login.

Step 2 Type in URI request to check existing permissions set to resources.

Step 3 Move to step 5 if there is no permission settings; examine the user's authority if there is any.

Step 4 Move to next procedure if user is permitted to access the resources, otherwise empty links will be achieved.

Step 5 Combine FSKey, random numbers, URI requests and user ID into redirected URI through a customized encryption function (here MD5 is in application).

The design and implementation of the mechanism, to some extent, have ensured the safety of UNRI. In fact, users can only access to real resources from the redirected URI. And furthermore, we shall make evaluations respectively after comparing this method with several other commonly used ones in the next section.

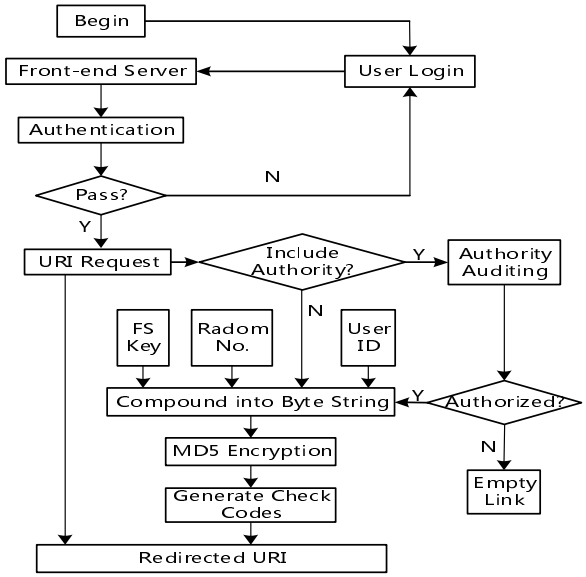

Fig. 3 Implementing Procedure of Security Mechanism

Evaluation of Security Mechanism for UNRI

As mentioned above, the security of UNRI has been heightened with a new security mechanism achieved by identity verification, customized encryption function and redirected URI. The other two

available methods for secure encryption are introduced below. A comparison between them and the previous one will be conducted in terms of encrypting time, parameters, etc.

Acquisition by Symmetric Encryption. In this method, RS firstly distributes different DES keys (FSKey) for different FS. Then des(params) will be acquired after FS encrypting the combined transmission parameters (including user URI request) in way of DES (a kind of symmetric encryption algorithm).

The redirected URI acquired by symmetric encryption is as follows:

…/FSId=***&desmsg= des(params)

Upon receipt of the URI request, RS would check whether the certain FS is credible or not on the basis of FSId. If FS is credible, then the DES key from FS (FSKey) would be achieved in line with FSId. Afterwards we need to decrypt the information of desmsg by means of FSKey. And we can't access to real resources if it ends in failure.

Acquisition by Asymmetric and Symmetric Composite Encryption. A key (des(params|FSKey)) is generated randomly by FS as the public key of the symmetric encryption algorithm. And rsa(key) would be achieved after RSA asymmetric encryption using the public key provided by RS.

The redirected URI acquired by asymmetric and symmetric encryption is as follows:

…/FSId=***&rsamsg=rsa(key)&desmsg=des(params|FSKey)

Upon receipt of the URI request, RS will check whether the certain FS is credible or not on the basis of FSId. If FS is credible, then rsa(key) will be decrypted in accordance with the private key from RS. Afterwards, according to the key gained above, des(params|FSKey) will be decrypted. Finally, RS will get FSKey from FS in line with FSId. Comparing the FSKey with encrypted FSKey, if they are not the same, the URI request would be considered to be a fake one.

Comparison and Evaluation. The public key of DES (a kind of symmetric encryption algorithms) is allocated in advance and may keep invariant for a long time. Thus the encrypted data may be cracked and fake request URI will arise once FSKey is available.

Comparing with single symmetric encryption, the use of asymmetric and symmetric composite encryption prevented key from being intercepted because public key should have been open to the public. Problem lies that receivers of public keys are not able to make sure whether the keys have been imitated or not.

Genuine and secret information has been concealed by the mechanism proposed in this article, which requires corresponding authority from users if they intend to access to the resources. Furthermore, MD5 has been very mature in encrypting which cannot be cracked so far.

Table 1 presents the comparison between MD5, DES and RSA in their encrypting process after which URI is redirected for UNRI. It draws the conclusion that redirected URI with MD5 is better than the other two methods in terms of performance. In addition, changing FSKey periodically will ensure the credibility of user's requests to a larger extent and guard against latent threats in a further step.

Table 1 Evaluation of Security Mechanism for UNRI

Method / Merit	Redirect URI with Symmetric Encryption	Redirect URI with Asymmetric and Symmetric Composite Encryption	Redirect URI with Customized Encryption
Features	Shorter key/lifecycle/ packet; Slower arithmetic speed	Secure; yet inefficient	Low-cost; Efficient
Encryption Times/s	30,000	17,000	62,000
Encryption Params	Less	General	More
Overall Merit	1. Long-term unchanged public key: possible to be cracked. 2. No guarantee against pass key not being intercepted.	1. Compound Encryption:avoid a single encryption intercepted. 2. RSA:no guarantee of the accuracy of the public key's sources.	1. MD5:most widely used Hash functions, uncrackable. 2. Redirected URI: Hide real information of resources, only authorize users can access to resources.

Conclusion

Being ubiquitous, capable, and inclusive consists of the 3 key features of Ubiquitous Network, with the intent of barrier-free communication by anyone, any objects at anytime, anywhere.
The security of UNRI is under threat as other heterogeneous networks join in. To solve this problem, a security mechanism is put forward by the author to prevent latent threats and illegal acquisition of UNRI. The author also conducted a comparison among the three means of encryption, after which URI is redirected, and proved the validity and practicability of the Security Mechanism.

Acknowledgments

This work is financially supported by " National Science and Technology Major Project (Next-generation Broadband Wireless Mobile Communication Network, Grant No. 2012ZX03005008", "the 863 Project (Research of the General Technology of 5G Mobile Communication System, Grant No. 2014AA01A706)", and "Chongqing University Innovation Team Support Plan(Grant No. KJTD201312)".

References

[1] M. Zhou, "The Research and Implementation of Key Technologies of Telecommunication Protocol between Gateway and Platform in Ubiquitous Network Based on Web", M.S. degree thesis, Beijing University of Posts and Telecommunications, Beijing, (2013).
[2] E. Du, "Secure Link Method for Preventing URL Attack and Fine Granularity Rights Management", Journal of Computer Applications, 2009(8): 2230-2232.
[3] G. Liu, "The Algorithm Design for Preventing URL Modified Based on MD5", Journal of Science & Technology Information, 2011 (3): 88-89.
[4] G. Qin, T. He, J. Chen, "Model of preventing URL attacks based on artificial immunity", Journal of Computer Applications, 2012, 32(5): 1400-1403.
[5] S. Liu, X. Li, Improvements of Network Security for IPv6, Video Engineering, 2007, 31(2): 58-59.
[6] R. Moskowitz, P.Nikander, IETF Internet Standard, RFC4423—2006. Host Identity Protocol (HIP)Architecture[S].

Advanced Materials Research Vols. 989-994 (2014) pp 4832-4836
© (2014) Trans Tech Publications, Switzerland
doi:10.4028/www.scientific.net/AMR.989-994.4832

Research of Wireless Sensor Network Intrusion Detection Based on Ant-Miner

Tao Liu[1, a], Shaoyu Liu[1, b], Dan Wei[1, c] and Jie Cui[2, d]

[1]North China Electric Power University, Baoding 071000, China.
[a]taoliu@ncepu.edu.cn, [b]liushaoyu520@126.com, [c]weidan999@126.com, [d]cui_jie456@163.com

Keywords: wireless sensor networks, intrusion detection, Ant-Miner algorithm, network simulation

Abstract. In this paper, we propose an intrusion detection program based on improved Ant-Miner (AM). The proposal needs to collecting out the node data, using intrusion detection module to test, compared with other wireless sensor network intrusion detection scheme, this scheme saves energy consumption of the sensor node effectively. Through the network simulation, this scheme proposed has a lower false positive rate and a higher true positive rate comparing with the current typical wireless sensor network testing program.

Introduction

With the rapid development and increasing sophistication of microelectronics technology, computing technology, wireless communication and sensor technology, Miniature Sensor, having the ability of perception, computing and communication, appears in the world. Wireless sensor network (WSN) [1,2] is a network which is formed by MANET manner by laying large numbers of low-cost sensor nodes to monitor and then through a wireless to connect. Perceive the cooperation between nodes, and monitor the status information of the target region, then transmit them to the users via the network. Wireless sensor networks are developed based on the basic technically of wireless communications technology, embedded technology and sensor technology, with the characteristics of low power consumption, low cost, distributed and self-organization, etc.[3,4].

Wireless sensor network has the characteristics of large-scale, self-organizing, multi-hop routing, dynamic, resource-constrained, data-centric and application-related, so it has been widely used in the fields of military, environmental monitoring, medical, industrial control, etc. [5], is the focus and the high ground in current international technological competition, has become a hot research at home and abroad. For the wireless sensor networks is more widely used in many fields in recent years, especially in some very sensitive areas, such as in military field, where the security issue becomes a very critical issue restricting its development [6], so the study of its security issues becomes more important.

Currently, the technologies solving wireless sensor security problem include encryption, authentication, secure routing, and secure data transmission, intrusion detection and trust mechanisms etc.. This paper studies an intrusion detection scheme based on improved Ant-Miner algorithm. Experimental results show that this algorithm has a lower false positive rate and higher true positive rate compared with the original testing program.

Ant-Miner Algorithm and its Improvement

Ant-Miner Algorithm Introduction. Parpimelli and his colleagues proposed Ant-Miner algorithm in 2002, the first time to solve classification problems using ant colony algorithm. The classification rules can be broadly described as: IF <conditions> THEN <class>. The Ant-Miner algorithm pseudo code is as follows:

```
Initialize: Training Set=all training samples;
    While (NO.of uncovered cases in the Training Set>Max_Uncovered_Cases)
  i=0;
Repeat
    i=i+1;
```

Ant_i constructs a classification rule incrementally;
Prune the just_constructed rule;
Update the pheromone of the trail followed by Ant_i;
Until (i≥No_of_Ants) OR (Ant_i constructed the same rule as the previous NO_Rules_Converge-1 Ants)
Select the best rule among all constructed rules;
Remove the cases correctly covered by the selected rule from the Training Set;
End while
End

In Ant-Miner algorithm, the information of all nodes is initialized to the same value:

$$\tau_{ij}(t=0)=\frac{1}{\sum_{i=1}^{a} b_i} \tag{1}$$

Where a is the number of attributes, i is the property label, b_i is the number of attribute value belongs to i-th attribute.

Each ant start with a blank rule, and then to construct rules, the probability of being selected for these attributes which have not been selected can be calculated by the following formula:

$$P_{ij}(t)=\frac{\tau_{ij}(t)\times\eta_{ij}}{\sum_{i}^{a}\sum_{j}^{b_i}\tau_{ij}(t)\times\eta_{ij}},\forall i\in I \tag{2}$$

Where η_{ij} is heuristic function of $term_{ij}$; I is the attribute set which have not been selected by the ants.

In Ant-Miner algorithm, the heuristic function is calculated based on information entropy, as following formula:

$$\eta_{ij}=\frac{\log_2 k-\inf oT_{ij}}{\sum_{i}^{a}\sum_{j}^{b_i}(\log_2 k-\inf oT_{ij})} \tag{3}$$

Where $\inf oT_{ij}=-\sum_{w=1}^{k}(\frac{freqT_{ij}^{w}}{|T_{ij}|})\times\log_2(\frac{freqT_{ij}^{w}}{|T_{ij}|})$, k is the number of classes, $\inf oT_{ij}$ is $term_{ij}$'s information entropy, $|T_{ij}|$ is the number of samples satisfying $term_{ij}$, $freqT_{ij}^{w}$ is the number of samples meeting $term_{ij}$ and its type is w.

In order to avoid over-fitting of the sample, we need to prune them after the rules generates. The idea for pruning rule: Repeat judge whether it increases the quality of the rule after delete a $term_{ij}$, if YES remove the condition, otherwise retain the condition until only one attribute node is left or it can not increase the quality after delete any attribute node, then the pruning rule ends. The quality of the rule is given by the following formula:

$$Q=(\frac{TP}{TP+FN})\times(\frac{TN}{FP+TN}) \tag{4}$$

Where Q is the quality of the rule; TP is the number of samples satisfying the rule antecedent and consistent with the type of prediction rule; TN is the number of samples dissatisfying the rule antecedent and inconsistent with the type of prediction rule; FP is the number of samples satisfying the rule antecedent, but inconsistent with the type of prediction rule; FN is the number of samples dissatisfying the rule antecedent, but consistent with the type of prediction rule.

After an ant completes the construction of a rule, the information of the attribute node appearing in the rule is updated as follows:

$$\tau_{ij}(t)=\tau_{ij}(t-1)+\tau_{ij}(t-1)*Q,\forall term_{ij}\in rule \tag{5}$$

In Ant-Miner algorithm, the volatilization of the information is achieved by dividing the pheromone worth of all conditions with the pheromone of the condition.

Improved Ant-Miner Algorithm. While Ant-Miner algorithm tests have proven to achieve better classification results, there are also some undesirable places in the pheromone update and the path selection. Aiming at these problems, we proposed optimized solutions about the pheromone update strategy and its deadlock problems.

This Ant-miner algorithm achieves a positive feedback mechanism and accelerate the convergence speed using pheromones, but it make the algorithm easy to appear premature stagnation. From the pheromone update formula, we can see that the increasing of pheromone τ_{ij}'s which are in the elected attribute node $term_{ij}$ is over-reliance on the feedback information of rules quality Q, while the pheromones, which are not in the elected attribute node, volatilize too fast. This mechanism is easy to make the algorithm converges to a rule prematurely, resulting in reduced prediction accuracy of the rules. In order to make a closer behavior between the update pheromone and ant foraging, In this article, we learn from predecessors who introduce pheromone evaporation rate ρ [7], volatilizing the pheromone in the selected attribute nodes, initializing the attribute node which are not selected.

$$\tau_{ij}(t) = (1-\rho) * \tau_{ij}(t-1) + \tau_{ij}(t-1) * Q, \forall term_{ij} \in rule \quad (6)$$

And after the completion of a rule construction, regardless of the pros and cons of it (quality), all the attribute node pheromone will increases included in the rule, then these attribute node is certainly more likely to be selected in the process of construction. But in fact, if the rules quality is poor, it should reduce all attribute node pheromone appearing in the rule to avoid these attribute nodes appear in the next one rule. Therefore, we modify the pheromone update method, after construct three rules continuously, compare the quality of these three rules, make pheromone feedback for the highest quality, give up the other two rules. The modified algorithm stress the rules of quality; and the quality of the build rules will determine whether the attribute nodes pheromone appearing in the rule increase, and whether the optimization is reasonable and effective.

Anther risk appearing in Ant-Miner algorithm is a deadlock. Through trial we can find that if there are a few records belong to the same class, and the value of their corresponding certain characteristics attributes values are more consistent, and different with other record eigenvalues, that is these records in this category have extremely strong correlation, so the heuristic function value calculated will surely bigger, they are more likely to be selected into the rules to be constructed in the next. But if the number of these few records cannot achieve Min_Class_Per_Rule, they cannot be elected to construct the rule, then it will appear the condition of only electing several properties, but not constructing, in the end the algorithm gets into an infinite loop.

In this paper, we use a method which deletes these attribute nodes, make the construction of rules skip these attribute nodes.

Simulation results

One of the key issues of intrusion detection systems is feature selection. It is not the fact that if we have more characteristic parameters, we may not get higher rate of intrusion detection, the number of extracting and processing characteristics parameters is not a linear relationship with the performance of classifier. To select the eigenvectors reflecting the state of the system is an effective method of improving intrusion detection efficiency. The most influential traditional data network intrusion detection system evaluation is DAPRA1998 which selected 41 properties. Because the sensor nodes have limited resources, we can only select a small number of features for intrusion detection. Literature [8] studied the relationship between the attacks and network traffic, selected the appropriate flow indicators representing various attacks. For DoS attacks, we select the number features to receive packets; for Hell flooding attack, we select energy features for packets sent; for selective forwarding attacks, we select two characteristics of the number of packets sent by routing error and the number of packets received by routing error. In this paper we select the WSN node

throughput, node packet loss rate, the energy consumption rate, the number of request packet, the packet average delay as the characteristic parameters of the intrusion detection system.

In this simulation, we use NS2, deploy 100 nodes in 1000m*1000m rectangular area. The MAC layer protocol applies IEEE802.15.4, which is designed for low-complexity, low power, low data rate short-range network; the network layer uses the LEACH protocol, the radio propagation model is two-ray ground model, the carrier frequency is 2.4GHz, the initial energy of each node is 2J, simulation time 300s. Considering the probability of node moving is small in wireless sensor networks, so the node movement is not considered in the simulation.

First, through the simulation of various attacks and normal conditions, we obtain the sample data, then train the intrusion detection module based on improved Ant-Miner algorithm.

There are mainly two performance indicators of WSN intrusion detection systems: detection rate, false detection rate. True positive rate (TPR) is defined as the number of sample attacks which are correctly detected divided by the total number of sample attacks; false positive rate (FPR) is defined as the number of sample attacks which are incorrectly detected divided by the total number of sample attacks. By analyzing the performance of WSN intrusion detection, we compare it with literature [8], in this literature the TPR is obtained by attack detection scheme based on traffic prediction (TPDD). Replay rate increases from 10% to 50%. Comparative results are shown below:

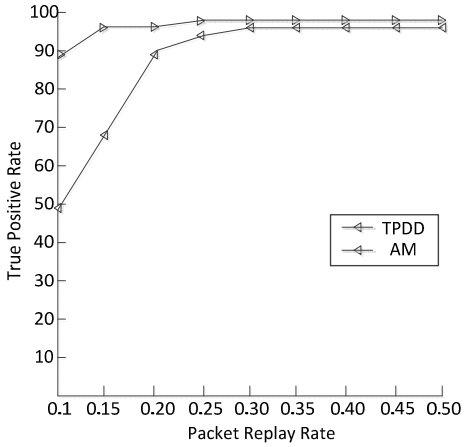

Fig. 1 Comparison of WSN true positive rate

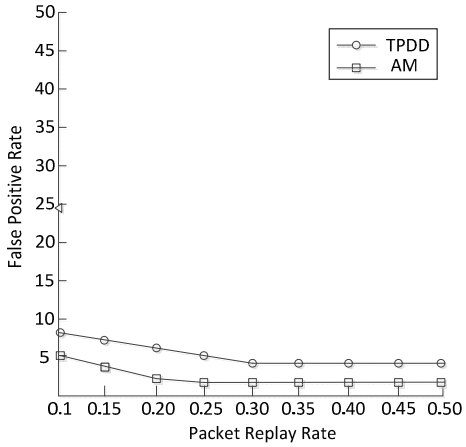

Fig. 2 Comparison of WSN false positive rate

From Fig.1 we can see that using the method in literature [8], when the attack strength is weak, the true positive rate is low. When we use the AM, we can obtain a high detection rate, thus this algorithm overcomes this disadvantage effectively. This is mainly due to our new intrusion detection scheme, in this scheme, we use five parameters which can effectively reflect the characteristics of the sensor network parameters, and establish the corresponding detection rules, rather than just detect the change of WSN-flow.

For another important evaluation criterion of false positive rate concern the performance of intrusion detection, we compare with literature [8], the result is shown above.

From Fig.2 we can see that our program has a low false positive rate than literature [8]. This is mainly because we have chosen more characteristic parameters, even if one characteristic parameter is mistaken for the attack characteristic parameter, the other four have not been mistaken for attack parameters, and you can still make the right judgments.

Conclusion

This paper analyzes the characteristics of wireless sensor networks, for attacks of the wireless sensor networks, we propose an intrusion detection scheme based on improved Ant-Miner algorithm. The program uses an improved Ant-Miner algorithm to detect algorithm, use NS2 simulation tool to model intrusion detection rules, and compare with the intrusion detection scheme based on typical traffic in WSN. The results show that the improved Ant-Miner algorithm based on for intrusion detection scheme has a lower false positive rate and higher true positive rate.

References

[1] L.L. Du, X.D. Zhang and D. Tu. A Survey of Wireless Sensor Network. J. Shanxi Electronic Technology. (2007) 4, p.74-76.
[2] A. Perrig, R. Szewczyk, J.D. Tygar, V. Wen, D.E. Culler. SPINS: Security Protocols for Sensor Networks. J. Wireless Networks. 8(2002)5, p.78-82.
[3] F.Y. Ren, H.N. Huang, C. Lin. Wireless Sensor Networks. J.Journal of Software. (2003)7, p.1282-1291.
[4] Z.C. Ma, Y.N. Sun, T. Mei, Survey on wireless sensors network J. Journal of China Institute of Communication. 25(2004)4, p.231-236.
[5] M.Y. Liu, Y. Wu, W.G. Wu, Wireless Sensor Nerwork, J. Microelectronics & Computer, 22(2005)7, p.56-60.
[6] X.W. Zhou, B.P. Tan, F.H XU. Wireless sensor network and security [M]. Beijing: National Defence Industry Press. (2007)6, p.185.
[7] J. Xiao, Y.H.Liang. Classification Rule Mining Based on Improved Ant-miner Algorithm. J.Computer Engineering. 38(2012)9, p.162-165.
[8] X.M. Cao，Z.J. Han and G.H.Chen. DoS Attack Detection Scheme for Sensor Networks Based on Traffic Prediction. J.Chinese Journal of Computer. 30(2007)10, p.1798-1802.

Advanced Materials Research Vols. 989-994 (2014) pp 4837-4840
© (2014) Trans Tech Publications, Switzerland
doi:10.4028/www.scientific.net/AMR.989-994.4837

A Fuzzy Trust Model for Public Key Distribution in Body Area Networks

Guowei Wu[1,a], Zuosong Liu[1,b], Poria Pirozmand[1,c]

[1]School of Software, Dalian University of Technology, Dalian, 116023, China

[a]wgwdut@dlut.edu.cn, [b]sandyliu1988@163.com, [c]compirozmand@mail.dlut.edu.cn

Keywords: Body area networks. Trust model. Key distribution.

Abstract. It is now possible to implant a network of sensors inside the human body for monitoring the human body functions and the surrounding environment. In a body area network (BAN), the confidentiality and integrity of the sensitive health information are particularly important. The key establishment is thus a fundamental security service in BANs. To guarantee validity of the key and avoid misbehavior of selfish nodes, we propose a fuzzy trust model for public key queries in BANs. Every user accesses the public keys of other nodes from those trusted neighbors rather than all of its neighbors. The proposed trust model uses fuzzy sets to calculate every node's trust value. Our trust model exploits multiple metrics rather than a single metric, and converts them into a single numerical ranking. We perform an extensive evaluation of the proposed approach. The results indicate that our trust model can not only identify abnormal nodes' behaviors, but can also reduce query traffic while improving the reliability of the returned public keys.

Introduction

The use of wireless sensors in health care makes it possible to monitor physiological vital signs, physical activities, as well as environmental parameters for human. They are used to cooperatively monitor physical or environmental conditions, which forms a body area network (BAN) [1]. What's more, a BAN has distinct features such as the mobility of sensors, and the sensitive nature of the data and the proximity to potential attackers [2]. These distinct features make it easily exposed to a variety of attacks such as eavesdropping, node compromising and physical disruption. In this paper, we design a light weight and flexible public key distribution scheme, which is based on a series of recent works in distributed key caching. For example, in [3], each node caches the public keys of a mix of local and remote nodes. If one node's public key is unknown, it is possible to obtain it from some chains of trusted nodes. Our scheme even takes into the consideration of selfish nodes in the network when they refuse to forward packets. In our trust model, every node can calculate the trust values of their neighbors. Selfish nodes will be given a small trust value. Key request messages are only transmitted to the trusted neighbors rather than to all of its neighbors. The benefits are two-fold: not only it reduces the number of control messages transmitted in the network, but also it improves the reliability of the returned public key.

A Fuzzy Trust Model for Public Key Distribution

In our fuzzy trust model, every node can calculate the trust values of its neighbors based on the neighbors' trust information. Some neighbors with higher trust values will be chosen to forward key queries. Our scheme can be divided into three stages: trust information observations, trust calculation and trust ranking.

Trust information observations. In this phase, nodes collect first and second hand information according to different trust metrics. We adopt four trust metrics: the probability of successful interactions, the success rate of exchanging, packet loss rate and battery energy.

The probability of successful interactions: The probability of successful interactions is chosen as the basic metric in many existing trust models and used to collect information about the packet forwarding behaviors of the neighbors. Every node, such as n_i, maintains two records for every

neighbor n_j, Ns_{ij} (the total number of packets sent to n_j by n_i) and Nf_{ji} (the total number of packets forwarded for ni by n_j). Then the probability of successful interactions between n_i and n_j, Psi_{ij}, evaluating whether n_j is honest enough to forward packets for n_i, can be calculated as follows:

$$Psi_{ij} = \frac{Nf_{ji}}{Nf_{ji} + \lambda(\mathrm{Ns}_{ij} - \mathrm{Nf}_{ji})}. \tag{1}$$

Success rate of exchanging: We use F_{ij} to denote the number of successful data exchange between n_i and n_j. If n_i receives a message from n_j, the value of F_{ij} will be added by one. Then F_{ij} is used as a metric to represent the trust attitude of n_i towards n_j.

Packet loss rate: A node is capable of overhearing its neighbors' transmissions in the promiscuous mode. It is assumed that n_j is overhearing a neighbor of n_i. Nin_i and Nou_i represent the total number of packets received and forwarded by n_i. Then the packet loss rate can be calculated.

Energy: In BANs, it is a very important issue to use energy efficiently, so the energy information of every neighbor can serve as a metric to determine the ranking order of the neighbors. In our scheme, we adopt the method proposed in [4] to detect a neighbor's energy.

Trust calculation. Based on the trust information from the first phase, we can adopt the method of fuzzy mathematics to calculate the trust values or trust levels.

To assign trust level to every node, four remark levels are defined, that is, $V = \{\mathrm{v}_1, \mathrm{v}_2, \mathrm{v}_3, \mathrm{v}_4\}$. v_1 means "full trust". v_2 means "relatively trust". v_3 means "general trust". v_4 means "not trust". Based on the trust degree of each metric, n_i can generate a matrix DT for every destination based on the first hand trust information, where DT_{ij} represents the membership degree of metrics i to comprehensive evaluation level j.

$$DT = \begin{pmatrix} DT_{11} & DT_{12} & DT_{13} & DT_{14} \\ DT_{21} & DT_{22} & DT_{23} & DT_{24} \\ DT_{31} & DT_{32} & DT_{33} & DT_{34} \end{pmatrix}. \tag{2}$$

Then, n_i can generate a matrix IT for every destination based on the second hand trust information. When nodes meet each other, they will exchange their DT matrixes. Then, n_i can combine other nodes' DT to generate a second hand matrix (IT) for every destination. Combining with DT and IT, n_i can get the fuzzy evaluation matrix R. Here, ω represents the weight of the direct information. Because the direct information is relatively important, we can increase the proportion of subjective judgment by increasing the value of ω.

$$T = \omega_{dt} \cdot DT + IT. \tag{3}$$

Finally, we can get the comprehensive evaluations as follows:

$$\begin{aligned} S &= W \times T = (\mathrm{s}_k)_{1*n} \\ &= (\omega_1, \omega_2, \omega_3) \times \begin{pmatrix} T_{11} & T_{12} & T_{13} & T_{14} \\ T_{21} & T_{22} & T_{23} & T_{24} \\ T_{31} & T_{32} & T_{33} & T_{34} \end{pmatrix}. \end{aligned} \tag{4}$$

In the formula, the weight matrix W represents weights of different metrics. Here we set W = {0.3,0.3,0.4}. T is fuzzy matrix and t_{ij} means the membership degree of metrics i to comprehensive evaluation level j. By calculating S, we can get a remark set of membership values for different nodes. Finally the trust level can be assigned to a node according to the following formula.

$$Vso_{ij} = \frac{\sum_{i=1}^{n} u(v_i) \cdot \mathrm{s}_i^k}{\sum_{i=1}^{n} s_i^k}, \quad U = \{4,3,2,1\}. \tag{5}$$

In the formula, $u(v_i)$ represents the remark of the four trust levels, meaning 4 represents v_1 and 1 represents the last trust level v_4. For example, if the final trust value is 3.1, then the trust level of the node is closing to v_2 which means it is relatively trusted.

Trust ranking. We use the trust levels calculated in Trust calculation and E_{ij} (the battery energy information) to determine the ranking order of all alternatives of neighbors. The trust ranking phase takes place when the node wants to forward a key request message.

$$F_{in} = \omega_1 * Vso_{ij} + \omega_2 * Energy\,. \tag{6}$$

Then according to the ranking order, the sender chooses the more trusted neighbors to forward the key request messages. The percentage of nodes may vary as the application changes.

Performance Evaluation

We use NS2 simulator in our simulations. We simulate a body wireless sensor network to evaluate our Fuzzy Trust Model for Public Key Query. We focus on the returned number of public key copies for the destination within a limited number of hops and the number of control messages for obtaining them. In our scheme, a balance between control messages overhead and public key copies is maintained by the control message forwarding rate.

We compare our designed scheme with two related schemes in overhead (in terms of number of control messages) and the number of key copies found. The two schemes include a caching scheme with no trust consideration [3] and a scheme with basic trust consideration [5]. In [3], all nodes are trusted. In [5], however, a basic trust model is used. Instead, our scheme considers all four metrics and uses a fuzzy model to combine them into numerical ranks.

Figure 1 shows the number of control messages transmitted in each key query. In the no-trust scheme, all nodes are trusted. Therefore, all neighbors are utilized to forward the queries, resulting in a large overhead. The basic trust scheme reduces the overhead significantly with the help of some trust relationship developed among neighbors. Our fuzzy trust model further reduces the overhead compared to the basic trust model as well as the no-trust model, demonstrating the benefits of its accurate trust relationship. When there are more and more selfish nodes in the network, the overhead increases because of the negative effect caused by the selfish nodes' dropped packets.

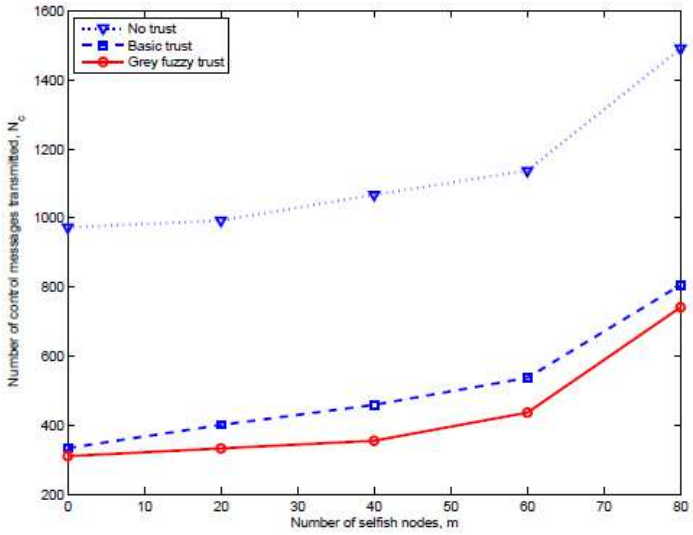

Fig. 1 Overhead in networks with different numbers of selfish nodes, m..

We show the copies of public keys found, K, in networks with different numbers of selfish nodes, m, in Figure 2. The trend of smaller number of copies found as m increases can be clearly seen from all three curves. As more and more nodes in the network become selfish, they refuse to forward key queries, reducing the chance of finding public keys. Another clear observation from Figure 2 is that the basic trust model returns fewer key copies than the other two, but the fuzzy trust model is able to

return roughly the same number of key copies as the no-trust model does. The sometimes slightly higher numbers might have been caused by the randomness of simulations.

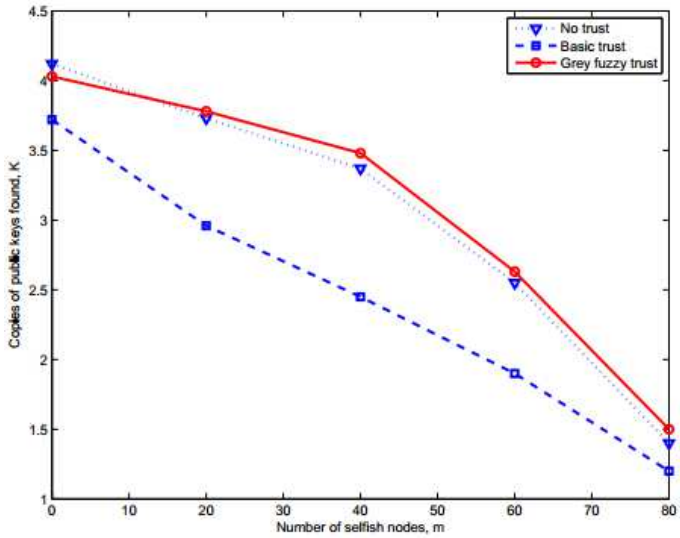

Fig.2 Copies of public keys found, K, under different selfish nodes, m

Summary

In this paper, we have investigated crucial trust issues in BANs, with the aim of guaranteeing validity of the key and avoiding misbehavior of selfish nodes. We have proposed a fuzzy trust model to allow nodes to rank their neighbors, based on the first-hand and second-hand information obtained from other nodes. Instead of using only one metric for trust evaluation, our technique takes advantage of four metrics: the probability of successful interactions, packet dropping rate, success rate of message exchange, and battery energy level. We have also exploited a novel approach of fuzzy to combine all four metrics into a numerical ranking for each node to choose a subset of neighbors to trust.

References

[1] Y. S. Li M, G. J. D, Secure ad hoc trust initialization and key management in wireless body area networks, ACM Transactions on Sensor Networks (TOSN) 9 (2) (2013) 18.

[2] M. Mana, M. Feham, Trust key management scheme for wireless body area networks, IJ Network Security 12 (2) (2011) 75–83.

[3] Y. Kong, J. Deng, S. R. Tate, A distributed public key caching scheme in large wireless networks, in: Proc. of IEEE Global Telecommunications Conference on Communication and Information System Security, Miami, FL, USA, 2010, pp. 1–5.

[4] R. Vidhyapriya, P. Vanathi, Energy aware routing for wireless sensor networks, in: International Conference on Signal Processing, Communications and Networking, IEEE, 2007, pp. 545–550.

[5] S. Marti, T. J. Giuli, K. Lai, M. Baker, Mitigating routing misbehavior in mobile ad hoc networks, in: Proceedings of the 6th annual international conference on Mobile computing and networking, Vol. 6, 2000, pp. 255–265.

Advanced Materials Research Vols. 989-994 (2014) pp 4841-4844
© (2014) Trans Tech Publications, Switzerland
doi:10.4028/www.scientific.net/AMR.989-994.4841

Exploration and Implementation of Electronic lottery Distribution System Based on Struts framework

Renjie ZHANG[1,a], Ying XIAO[1, b]

[1] College of Information and Communication Engineering, Dalian Nationalities University, Dalian, 116600, P.R.China

[a]email: 123275786@qq.com, [b]email:xiaoying@126.com

Keywords: The Browser/Server; Struts Framework. Fixed-line Lottery Ticket Sales System; Unified Payment

Abstract. The amount of fixed telephone service usage is becoming much bigger, and the using of the fixed-line to buy lottery tickets is more convenient. So exports have achieved a management platform of fixed-line ticket sale system branch in the Struts framework implements. The system based on B/S architecture and uses MVC (model-view-controller) design pattern. The system can realize the user for personal lottery ticket purchase information query and management. It's helpful for the administrator to unified payment platform of integrated information management. Under B/S architecture, the system uses the Struts framework design technology, which makes the system have good scalability, portability and maintainability. Users can use fixed-line ticket sale system in a more convenient and safe environment.

Introduction

Fixed line usage amount is decreasing, but the usage of the fixed line business is growing, so on this basis, we have added an electronic lottery sale business. That is using fixed line to buy lottery tickets[1]. A perfect function, it is easy to use and extensible fixed-line's Lottery sale system can greatly facilitate the users to use the system as well as Lottery betting station costs, but because of fixed-line has instability and poor visualization, so the sale management platform system is particularly important, for the information of the fixed-line's lottery system and payment platform management can improve the system availability.

The management platform of fixed-line's Lottery sale system can facilitates users to manage and query the lottery information, as well as provide a plan for each sale system's payment and management. System can be used in a number of marketing systems such as: ticket sale system, food sale system, and a variety of electronic ticket sale systems. Using b/s structure of the system so that users do not need to consider the client's hardware requirements, and using JSP+Struts+JavaBean framework make it easy to maintenance and upgrades of software in the future, to meet higher requirements may emerge in the future of the system's management. The system can provide perfect and humanized management services for managers .At the same time it offers for all types of sale systems with a user commonly used business services, so it makes the management platform system in all kinds of sale system which has a certain competitiveness. This paper introduces the management platform of fixed-line's Lottery sale system main techniques, design and realization methods.

MVC design pattern used in the development of the management platform

MVC's full name is the Model View Controller[2], a model - view - Controller acronym,and a software design paradigm for organizing code in a method of separating business logic and data, thereby so that the same program can use different forms of expression. The purpose is to ensure the existence of C M and V sync, once M change, V should be synchronized. This design pattern helps to enhance the program's scalability, reusability, maintainability, reducing development time.

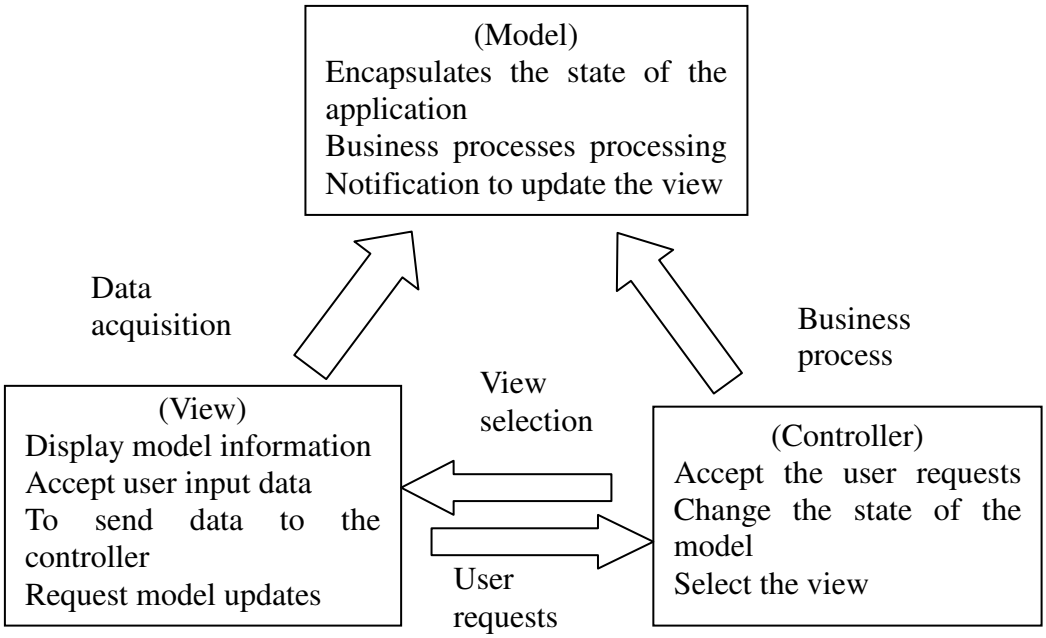

Fig.1. The flow chart of MVC pattern work

View: Display data (database records), the view is the user interface to interact with the terminal.

Model: representing the core applications (such as database records list), the model is the main part of the application, including business logic and data modules. Model objects are usually responsible for accessing data in the database.

Controller: process input (record into the database), typically read the data from the view controller is responsible to control user's input, and send the data model.

Specific process: the user enters data in the view screen, make a request, the controller receives user requests for processing and returns the data model, the controller calls the appropriate view output data, the user interface to view the output data through the view.

Design Management Platform of Landline lottery sales system

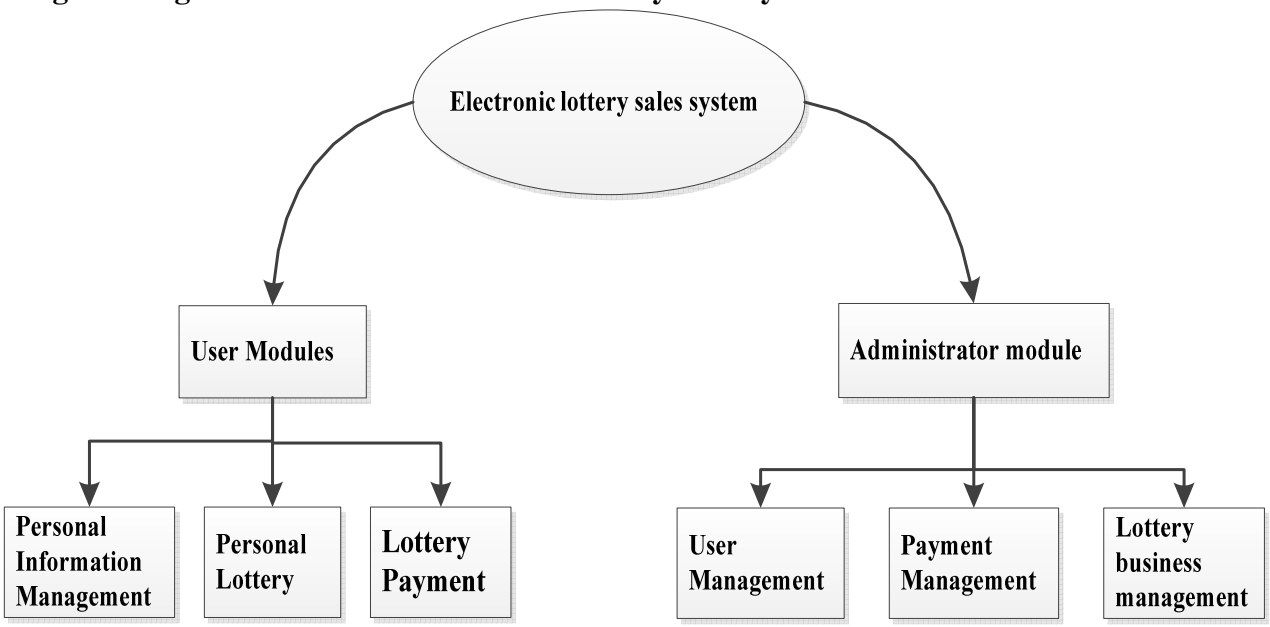

Fig.2. Pattern of the Electronic lottery Distribution System

The requirement and analysis of system. According to preliminary analysis of the situation of the lottery sale system,to meet the needs of users and managers,the system is mainly to achieve the following functions:

Login. For improving the comprehensive management ability, there are three types of people use the system, ordinary users, general administrator and super administrator, that will login the system according to the assigned user name and initial password.

The information management. Users can change their login password and other basic information.

Lottery ticket purchase information. Users can check to see the lottery whether they have purchased and drawn case of the day according to the their own lottery. And they can also check to see the payments and canceled unpaid lottery bet.

Business management of users lottery. Users can choose to subscribe to or apply for cancellation of the state of their business, the administrator or super administrator can handle the application that the users want to change the status of the business.

The management of unified fixed payment. Administrators can manage unified payment platform that is under the connection of the Fixed lottery sales system, to ensure proper payment.

Administrators to manage. Super administrators can perform account,cancel the account management to common administrators.

The management platform of fixed-line lottery slaes system allows this system can manage the purchase cases of fixed-line lottery better.Also provides users with accessing to personal information of lottery and to open new lottery business.

The design of user and administrator features modular

The super administrator has rights to manage common administrator, and to add or remove common administrator. The user modules added the individual fixed-line business management and ring tones' management, improving the utilization of the fixed telephone.

Database design. Demand for fixed lottery sale system through the contents of the fixed lottery sales management, data flow and analysis of basic information, as well as standardization of design requirements, The main database tables of this system include: user data table (cx_user), lottery business table (cx_phoneservice), lottery information table (cx_phonecalllog), lottery pay bills table (cx_addlog), fixed information table (cx_ring), the operation log table (cx_log), operating package table (cx_mealtype), Bureau of the user table (cx_device_cfg), fixed management table (cx_servicebill).

Each table in the database is connected to each other and provides valid data for the system, the final completion of the design of the database tables based on the relationship between each individual and the primary key of the table.

The implementation of fixed telephone cluster management system based on Struts framework

The workflow of Struts in system development. Struts is an open source project sponsored by the Apache Software Foundation.It is a classic MVC design pattern to achieve the application pattern of MVC design pattern,which uses the Java Servlet[3] and JSP technology.Struts is an object-oriented design, MVC design pattern "separate display logic and business logic" advantage to play the most.[4]Beacause of its powerful tag library,the efficiency of development has effectively improved.The adventages of its development framework is clear structure and stable performance,simplifying application development.In Struts, the controller achieved by the ActionServlet or Action; view constituted by the JSP page; model consists JavaBean or EJB components.Struts processing flow is as follows:

Users submit requests information and transmitted to the server by HTTP.ActionServlet,the central controller to the next step through the configuration file struts-config.xml,users fill out the form data to the corresponding ActionForm.According to the received request, the request is distributed to the appropriate processing Action.Action class called Model components to business logic processing.Finally, the controller forwards HTTP requests, call the appropriate view component to format the data returned by the model, the view component corresponding information presented to the user.

Build the platform environment. The system selected mysql[5] database as database applications, using tomcat6 as a Web application server,and using MyEclipse as a development tool, which integrates Struts components.

Deployment of the system. The role of system development model can handle data received form, based on business logic to process the request, and the output data to the view.The same model can be reused multiple views to improve the reusability of the application.In login module as an example, a user fixed cluster management system is divided into three categories: user, general manager, super administrator.In accordance with the user's login will be different privileges, enter a different window interface.Page displays using JSP technology, which is inserted into the Java program segment (Scriptlet) and JSP tag (tag) in a traditional web page HTML file.WEB application development with JSP can run cross-platform, regardless of the operating system restrictions.Since the MVC design pattern view layer and the business layer separation, thus allowing to change the view layer code without recompiling the model and controller code.The controller receives the user's request, and then decide which one model to process the request and configured jump page for displaying the output data.

After the project is completed, the next step for the deployment, use MyEclipse development tool or manually deploy the project on tomcat.On the server host, the appropriate configuration database data and the path is ready, users can access the system through a browser client in the end.

Conclusion

This system utilized popular Struts framework in the development of WEB applications, providi ng some design ideas and solutions for Fixed buy lottery tickets, and ultimately. Since the Struts has the advantages in web application development ,as the software upgrades and extensions are more convenient, it can be applied to different enterprises and institutions after slightly modified. Compre hensive traffic information management and business service are a great convenience to fixed-line u sers and managers to improve office efficiency. With the further development of fixed-line business and further tapping of the potential of fixed, fixed management system has a wider range of applica tions.

Acknowledgement

In this paper, the research was sponsored by The Students' Innovation and Entrepreneurship Training Program (Project No. 201112400450401).

References

[1] Steve Souders. High Performance Web Sites[M].USA, 2009.

[2] Malcolm Davis. Struts -- an open-source MVC implementation[M]. 2006.

[3] Craig Walls, Ryan Breidenbach. Walls: Spring in Action[M]. Craig Manning Publications,2007.

[4] LI Shao-hui,BIE Hong-xia. A New Web Development Technology and Online Paper Publishing System Based on the Struts Framework [J]. Computer Engineering&Science, 2009, (8):130-132.

[5] Baron Scbwartz Peter Zaitsev,Vadim Tkacbenko. High Performance MySQL[M]. USA, 2012.

Advanced Materials Research Vols. 989-994 (2014) pp 4845-4850
© (2014) Trans Tech Publications, Switzerland
doi:10.4028/www.scientific.net/AMR.989-994.4845

Topic-oriented Information Retrieval

Li Li[1, a], Li Weijiang[2,b,*] and Fan Yuanyuan[2,c]

[1]School of Law, Kunming University of Science and Technology, Kunming, 650500,CHINA

[2]Yunnan Key Laboratory of Computer Technology Applications, Kunming University of Science and Technology, Kunming, 650500,CHINA

[a]79845978@qq.com, [b]hrbrichard@gmail.com

*Cresoponding author: Li Weijiang E-mail:hrbrichard@gmail.com

Keywords: Information retrieval, Crawler, topic

Abstract. With the rapid development of Internet, more and more information has been displayed to people. More and more researcher pay more attention to how to find useful information from this huge information ocean. We design the topic-oriented information retrieval system in order to overcome the drawback of generic crawler. The system retrieves topic information efficiently and helps user get useful information rapidly and exactly.

Introduction

Undoubtedly, it is the best way for people to get information from WWW. The current information retrieval (IR) systems, however, which aim at covering whole web pages has a challenge because web information growth rapidly and information environment is becoming more and more complicated. Firstly, magnitude of web pages expands too rapidly to index all of pages for IR systems, even Google which is the biggest search engine in the whole world presently, it only index 40% proportion of total web pages[1]. On the other hand, web information resource is change dynamically, so search engine, like Google, its average replacement cycle is extend as long as a month in order to maintain vast databases, this resulted in a certain web pages in pages retrieved by search engine are out of date or even cannot be displayed. Secondly, information services provided by traditional search engine cannot be satisfied with the increasing demand for personalization [2]. Therefore, research on topic-oriented crawler is becoming a hot spot in next generation of information retrieval.

Subject-oriented is only for a theme, a web page, such as literature, medicine, sports, music, MP3, software, etc., to collect. In other words is only collecting the subset of the network. It collects the web pages related to the theme of the pre-determined on the network selectively.

Topic, in other words is the type definition of user retrieval. It can be determined by a series of Webpage specified by the users, also can be confirmed by a series of feature words. Generally speaking, the user determines a series of samples collected Webpage firstly, determines the theme; then, analyzes samples Webpage, extracts feature information; Later in the process of collecting, according to the characteristics of information, for each collection of Webpage, a certain degree of correlation are given. The higher the correlation, means that the more similar to the topic.

Subject-oriented crawling technology is the core of the system to search the theme structure. Specific topics which study how to use crawlers have the option of access on the Internet, subject those and predefined related pages to download only in Web. These predefined topics are not only using some keywords, but also need to provide the sample document. Different from those who search for all Web pages, general search engine answers all the questions, crawler analyses of each link and determine which links to pages may be predetermined theme related to these links which will be crawled firstly and discard irrelevant links. Its goal is to collect as much as possible with a specific topic and Webpage, utmost ground avoids irrelevant Webpage download, to save hardware and cyber source are obvious meaning.

Focused crawling was proposed by De.Bra[3], the method of keyword matching to determine the relationship between simple Webpage through dual classification system. On this basis, M.Hersovici et al. [4] extended this method, considering the Webpage link anchor text relevance to Webpage in URLs according to the priority order, the relativity on the last page of the attenuation factor to succeed his father. Different methods of De.Bra, the method in the vector space model and can be arbitrary in 0 and 1 between the real values, and the anchor text and context to compute the similarity. J.Cho et al. [5] also improved the breadth first approach, improvement is not big, but the method by using the PageRank[6] method in the calculation of URLs priority weights. As the network information retrieval tools, topic crawling technology in recent years has been more and more attention of researchers [7-9].

SUBJECT-ORIENTED CRAWLER

Theme Confirm

The biggest difference is the qualified theme between network crawler subject oriented and general web crawler. How to define the theme is how a complete specification of the needs of users, if only the superficial told crawling to the Web page to find out about basketball, crawler may not know the one about Yao Ming whether the page should belong to this category; understand the crawler for the field of "Basketball" only the word "basketball" itself. When more complex, may the user need to find Web on the "Beijing" and "SARS", but does not include the "bird flu" page, this needs a good way to define the subject, to understand the user's interest.

The theme of the user input (a sentence or a paragraph text describing theme) input as a query to Baidu (http://www.baidu.com), then crawl down the first twenty Webpage given in Baidu, as a typical Webpage and related theme (training set). Then for the theme user input and training set grab obtained respectively, we do the participles, to stop words and word frequency statistics processing. After the extraction of high frequency words, delete of common words and meaningless words, use them as the relevant characteristics in this theme. This formed the two set, the corresponding subject content input by the user is the main key phrases, grab get training sector responding is the key phrase, which constitutes the foundation behind the judgment.

The Retrieval Algorithm of Topic Oriented

After the index has been established, preprocessing is complete. The inverted index and other related documents to the query node retrieval. For mass document retrieval, need a lot of server coordination calculation. At present the basic use of distributed computing to complete the calculation. When the user submits a Query to the server, the server will do some initialization work is transmitted to the computer to calculate the node, each node computer through calculation to find the most relevant K documents, back to the server, the server on all nodes of the returned documents ordered by Rank value, part of the ranking result is returned to the user.

The above is the basic approach of general search engine at present, so the back too many results, users find useful results into a dilemma. In fact, in general, from the understanding of Query point of view, if the Query is not strict enough ambiguity returns results may be closer to the needs of users, if Query is too loose may have many kinds of understanding, the understanding is returned will contain a variety of, then the user will take some time to find myself the desired results. If Query is "Andy Lau", the others in addition to the users are very difficult to judge what the user looking for information about Andy Lau, what about Andy Lau's film, or a song, or personal life. So if the retrieval system made the subject classification about Andy Lau information, then returns the results will show the Query related what theme, and the system will do the sort of theme in the relevant subject, recommended to the user which topics more relevant. So that the user can quickly find needed information by selecting the theme. Because after the users choose the theme, the returned results on the whole is the theme of the document. Of course, there may be a user looking for information relating to a theme, so that the user can respectively on the multiple themes do choose to find out useful information. So the topic information, can allow the user to find needed information quickly.

```
The algorithm of retrieval
Input: query
output: result of retrieval
procedures:
1. analyzing query;
2. segmenting for Chinese and stemming for English;
3. getting TermID after analyzing;
4.  allocating resource for every Term;
5. set int nResNum=0;
6. finding reverse list of every Term in reverse index
7. While (nResNum< the number of the retrieved result)
   {
        scanning reverse list;
        if (finding a relevant  document)
        {
          computing related values of the document;
          nResNum++=1;
        }
    }
8.  if  (nResNum< the number of the retrieved result)
    {
        finding reverse list of every Term in reverse indexing;
        While (nResNum< the number of the retrieved result)
        {
              scanning reverse list;
               if (finding a relevant  document)
              {
                    computing related values of the document;
                    nResNum++=1;
               }
         }
    }
9. if (the current is general retrieval)
   {
      finding the top N documents of the best weight in retrieved result;
      finding the DocID of  the N documents;
      return;
   }
   else
   {
       finding topic documents user demanded from retrieval results;
       finding the top M topic documents;
       return;
   }
```

Test Results and Analysis

In information retrieval evaluation on the retrieval effect standard accuracy, recall and average precision rate. But in the massive search engine by using approximate algorithm to search, so the evaluation standard is not the best estimate, questionable. And in information retrieval for standard text library evaluation, and for the search engines do not have standard Webpage database open for

evaluation. Therefore, for the evaluation of this system, we can make comparison with Baidu. Input Query and let Baidu do the search, the first 50 pages to download the Baidu results returned as a list of the system Webpage retrieval, then compare this system with Baidu's top10 or top20, see which one have a higher accuracy. Because here is the experimental analysis, the results showed that URL expressed in Webpage DocID.

In fact, the user using the search engines to look up information, in most cases, only view the content of the first two pages. So a search engine wants to retain customers, accuracy in front of him several items must be high. Therefore, in this sense, with the Top K index in the evaluation of search engine may be more meaningful.

Input "life career family" in Baidu, and extract the first 50 Webpage in the return results as the system data. The first 20 results of Baidu as shown in Figure 1, the retrieval time is June 4, 2007. The retrieval results of this system are shown in Figure 2 and Figure 3.

1. A new career, a new family, a new life Yang Yunqing shows a helmet
2. How to Balance Career and Family. If you are a working mom or dad
3. Use these simple tips to ensure a balance between the two most important things in your life
4. How to Balance Career and Family
5. Japanese work customs make it almost impossible for women to have both a family and a career
6. will not understand the value of the family. ? No career our life is blank
7. I used to be radical and thought one could not be a success in career
8. Career or Family: which is more important
9. career, family, and life satisfaction in three cohortsCatherine
10. Getting It Right: How Working Mothers Successfully Take Up the Challenge of Life, Family
11. family should be the number one in one's life
12. Have Breast Cancer!: Regain Control of Your Life
13. deem it more important to pursue their career
14. Life, Career, Family, Sexuality, and Faith
15. I am so grateful for the team and the opportunity to be there for my family
16. career can provide us with a means to live on. On the other hand
17. making their future retirement planning even more challenging than it already is
18. Career Advice for Life Scientists Women in Cell Biology
19. the family through marriage conferences
20. such as family and career Life

Figure 1 Baidu retrieval "life career family" top 20 results

For the retrieval results of Baidu, here to see more intuitive, listed only the title of the result documents. However the results of this system are shown as the retrieval result figure. From the lower left of Figure 6 shows that the retrieval time is 16 milliseconds. Here only to retrieve 48 documents because there are two documents not download, so only 48. The first 10 results in Baidu fourth and sixth little relevance. Because add the topic information in this system, so the foregoing documents in the search results are the high correlation.

The results show that the proposed algorithm compared with the general web crawler can be more significantly increase the number of the relevant Web pages, and improve the efficiency of the subject-oriented searching.

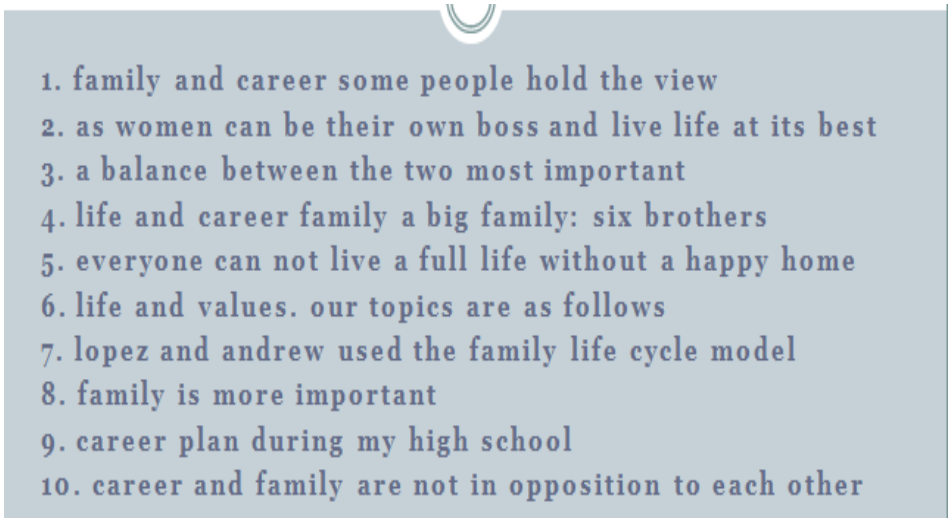

Figure 2 The retrieval system of "life and career family" top 10 results

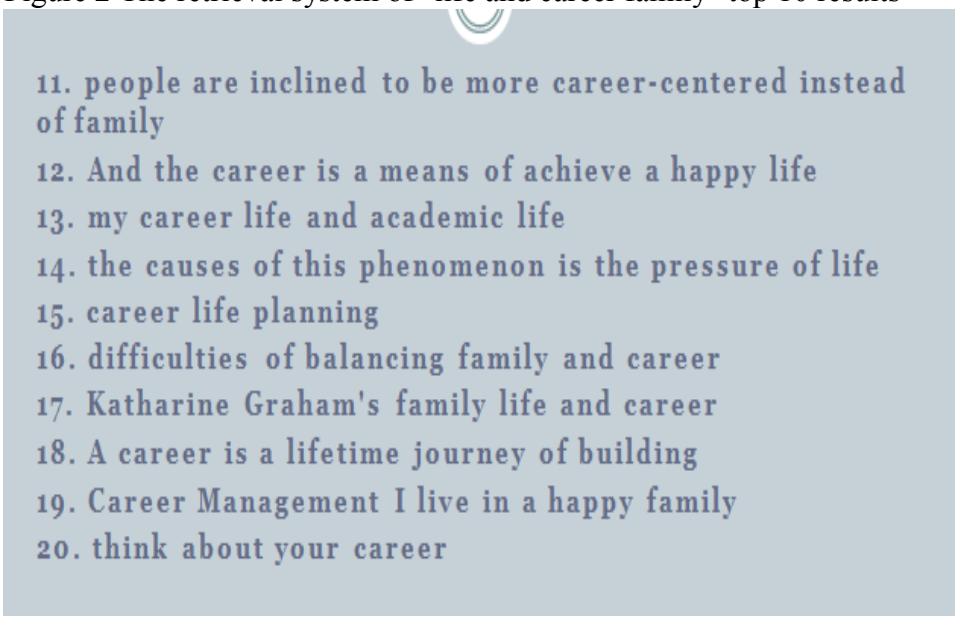

Figure 3 The system retrieval "life career family" eleventh to twentieth results

Acknowledgements

This work was financially supported by the project of the national natural science foundation of china (61363045).

References

[1] L. S, G. L. Accessibility and Distribution of Information the Web[j]. Nature. 1999, 400:107-109

[2] M. Ester, M. Gross, H. Kriegel. Focused Web Crawling: A Generic Framwork for Specifying the User Interest and for Adaptive Crawling Stratrgies[c]. In: Proc of the International Conference on Very Large Database (VLDB'O1). 2001

[3] P. D. Bra, G. Houben, Y. Kornatzky, et al. Information Retrieval in Distributed Hypertexts. In Procs. of the 4th RIAO Conference. New York, 1994:481-491

[4] M. Hersovici, M. Jacovi, Y. S.Maarek, et al. The Shark-search Algorithm. an Application: Tailored Web Site Mapping. Proceedings of the 7th International World-wide Web Conference. 1998:317-326

[5] J. Cho. Efficient Crawling Through URL Ordering. Computer Networks and ISDN Systems. 1998, 30(1-7):161-172

[6] L. Page, S.Brin, R. Motwani, et al. The Pagerank Citation Ranking:bringing Order to the Web. Stanford digital library technologies project, 1998

[7] F. Menczer, G. Pant, P. Srinivasan, et al. Evaluating Topic-driven Web Crawlers. Proceedings of the 24th annual international ACM SIGIR conference on Research and development in information retrieval. 2001:241-249

[8] F. Menczer, G. Gant, P. Srinivasan. Topic-driven Crawlers: Machine Learning Issues. ACM TOIT. 2002

[9] M. Ehrig, A. Maedche. Ontology-focused Crawling of Web Documents. In Proceedings of the 2003 ACM symposium on Applied computing. 2003

Advanced Materials Research Vols. 989-994 (2014) pp 4851-4854
© (2014) Trans Tech Publications, Switzerland
doi:10.4028/www.scientific.net/AMR.989-994.4851

Representing and Preparing for Resources in EPM's Execution Model

Qian Yu[a], Tong Li, Xuan Zhang, Ying Lin, Yong Yu and Na Zhao

School of Software, Yunnan University, Kun Ming, 650091, China

Key Laboratory in Software Engineering of Yunnan Province

[a]yuqian2001cn@163.com

Keywords: Resource Representation, Resource structure, Software Evolution Process Model, Execution Model, Preparation for Resource, Knowledge Base.

Abstract. Software evolution process model (EPM) is a knowledge-intensive process which is described in EPDL(Software Evolution Process Description Language) and modelled by semi-formal approach based on EPMM(Software Evolution Process Meta-Model). In order to support process improvement and process automation, the execution model is represented by logic programming. Activity in EEM (EPM's execution model) is not implemented until its needing all kinds of resources are satisfied by system execution environment. The paper discussed the representations of all kinds of resources in EEM and their structures are proposed. The preparation resources method is presented in order to execute the EEM automatically. The converter program is realized and the correct results have presented to prove the correctness of the method.

Introduction

Resources are essential element in software evolution processes. Software evolution processes are very sensitive to the scarcity or abundance of resources. All data, cost, time, human resources, software, hardware, and other objects supporting software evolution can be regarded as resources [1]. Methods of resources' representations and managements are various with different application domain. Methodology of knowledge representation based on OWL is put forward to meet the requirement of integration management of enterprise resource [2]. Semantic converter which converts knowledge representation in Conceptual Graphs into representation in Resource Description Framework is designed to overcome the barriers in knowledge sharing and reuse due to lack of consensus of knowledge representation formats between these two knowledge representation models [3]. Instantiation policies as a compact formalism proposes are proposed and integrated to a process modeling language to allow user-defined reusable management strategies for resource instantiation [4]. Applying multiparadigm simulation modeling in the scope of two process areas with the aim of supporting decision making and determining the optimal values of cost and schedule according to the management needs [5]. Resources are encapsulated in components [6].Approaches above not mentioned the method of representing and preparing for the resources during executing software process.The paper proposes the method of representing and preparing for the resources in EEM. The preparation method of resources at process level, activity level and task level are respectively proposed. According, the paper is organized as follows. Section 2 review the relative research work about EPDL and modeling approach of EPM in [1]. Section 3 presents representation methods of all kinds of resources in any EPM. Section 4 presents the representation results of the resources in EPM's execution model using empirical data in case. Finally, Section 5 draws some conclusions.

Relative Research Work about Resources in EPDL and EPMM-based Modeling Approach

The structure of resources in EPM is represented with three levels in EPDL and EPMM-based Modeling approach.

(1) The first level resources are resources at process level which describe the partial order relations among activities. These resources are control information resources of activities in EPM. If an activity

has been provided with needing control information which is called precondition resources, the activity has the execution authority. The post-condition resources will be produced after the activity has been done.

(2) Activity can be a set of tasks. Any activity is defined as an abstract data structure which includes data structures and operations on these structures. The second level resources are input resources and output resources which respectively are described by imports data structure and exports data structure. Output resources of activity are generated by activity after its execution.

(3)The third level resources are local resources demanded by the tasks in activity of EPM at task level. Roles resources described local data structures are responsible for executing task(s).

The paper only considered the local resources such as roles resources. The activity can be executed only have three level resources been satisfied which are respectively the control information resources at process level, the input resources at activity level and local resources at task level.

Representation methods of all kinds of resources in EEM

Each type resource in three-tier resources in EPM can be described using a duality predicate "resource/2", which is resource(resourcetype, resourcetypevariable). The 'resourcetype' is used to denote type of resource, moreover the 'resourcetypevariable' is used to show variable of resource type, which is instantiated during running the execution model. Resource representation at three levels are respectively discussed below.

Resource representation at process level. There are two kinds of control resources that are precondition resources and post-condition resources. Each control resource has its name. These resources are expressed by the duality predicate 'resource(msg, resource's name)'. Using 'resource(msg, resource's name)' expresses the existence of this resource in execution system, while using 'not(resource(msg, resource's name))' shows this resource does not exist in execution system.

Resource representation at activity level. There are two kinds of resource which are respective system type and structure type used to express the import resources and export resources. System type are string type, enum type, et al. Structure type is defined by '*TYPE*' keyword in EPDL using system type and other defined structure type.

For import resources, each system type variable is expressed with 'resource(system type name, type variable(uppervariable))' and structure type variable is expressed with 'resource (strtype, littstruVar(X_1, … , X_m))', of which strtype and littstruVar are respectively used to express the structure type and structure variable with lowercase and X_j ($1 \le j \le m$) is name of the J-th domain of the structure variable with uppercase.

For export resources produced by activity, necessary information is provided by the role executing the activity. So Firstly, each string system type variable 'strVar' needs three sub-goals separated by comma in clause of Prolog. The first sub-goal is "write('Please input the value of lowstrVar')" prompting for the role information of input, where lowstrVar is variable name in lowercase. The second sub-goal is "read(uppstrVar)" receiving the input information by the role of executing the activity. The third sub-goal is "asserta(resource(string , lowstrVari(uppstrVar)))" adding the resource to the knowledge base. Secondly, each enum system type variable 'enumVar' also needs three sub-goals separated by comma in clause of Prolog. The first sub-goal is "write('Please input the value of enumVar，has $enumValue_1$,… , $enumValue_n$ for selecting')" prompting for the role selecting the value from set of enum. The second sub-goal is "read(uppeenumVar)" receiving the enum value selected by the role of executing the activity. The third sub-goal is "asserta(resource(enum , littenumVar(uppeenumVar)))" expressing adding the resource to the knowledge base. Lastly, each variable of structure type defined by user in EPDL need sub-goals which respective is hinting information, receiving the input information from the environment by the role executing the activity and adding the resource to the knowledge base.

Resource representation at task level. The important role resource indicating a person or software or hardware is described at this level in EPDL. For each role having a role name denoted by

RName, a sub-goal is needed which is "resource(role, lowRName (uppRName))" meaning to add the resource to the knowledge base.

The Method of Preparing for Resources in EEM

Resources Needing to Preparing for. There are two kinds of resources needing to preparing in execution model of EPM. The first are input resources which are not export resources of other activities. The second is each role needed by each activity for executing, but duplicate role only needs to be instantiated once.

Method of Preparing for resources. Those supported by the environment when resources are prepared are realized by informing the environment during running the execution model. In order to realize to prepare for the resources at activity level, the EPDL file is scanned twice based on the model transformation. The four kinds of information must be reserved during scanning first which are all STRUCTURE types and all domain names and types of those domain names defined in EPM and denoted by 'TypeSet', input resources of all activities denoted by 'IRSet', export resources of all activities denoted by 'ESet', role resources of all tasks denoted by 'RSet'. The resources of set denoted by 'InitIRS' which is determined by the formula (1) are prepared.

$$InitIRS = IRset - ESet. \quad (1)$$

Presenting the Resulting of representation and preparing for resources in EEM

ISO/IEC 12207 standard [7] describes the maintenance process model in software life cycle. Tong creates the EPM of this process in EPDL[1]. By method above, resources prepared for this EEM are described in prolog and listed in Table 1.

Table 1: Resources prepared for this EEM

```
resource(msg,start).
resource(requirements_type,requirements(proreports,modifireque)).
resource(string,problem(problema)).
resource(string,problem_report(probreportfile)).
resource(string,modification_request(modifreqfile)).
resource(string, original_requirements(origrequirmentfl)).
resource(string, contract(contractfile)).
resource(string,migration_request(migrrequfile)).
resource(string,iso_iec12207_standard(iso12207file)).
resource(system_type,old_system(docfiles,datafiles,progfiles)).
resource(string,retirement_request(retirereqfile)).
resource(system_type,new_system(docfiles,datafiles,progfiles)).
resource(role,pm(alice)).
resource(role,prm(michale)).
resource(role,dr(michy)).
resource(role,ma(alice)).
```

Conclusions

In this paper, representation methods of all kinds of resources in any EEM are proposed. The preparation method of resources at process level, activity level and task level are respectively

proposed. The converter program has been realized and the correct results have presented to prove the correctness of the method.

Acknowledgements

This work is financially supported by the National Natural Science Foundation of China under Grant No. 61379032, No. 61262024 and No. 61262025; Scientific Research Fund of Yunnan Provincial Department of Education under Grant No.2012C108, No. 2010Y250 and No. 2011Y120; Education Innovation Fund of Software School of Yunnan University under Grant No.2010EI13 and No.2010EI14; Scientific Research Key Fund of Yunnan Provincial Department of Education under Grant No.2013Z057, Science Foundation of Yunnan Province under Grant No. 2010CD026, No.2012FB118, No. 2012FB119; Science Foundation of Yunnan Education Department under Grant No. 2012Y257; Science Foundation of Key Laboratory of Software Engineering of Yunnan Province under Grant No. 2011SE09 and No.2012SE305.

References

[1] Tong Li. An Approach to Modelling software Evolution Processes[M].Tsinghua University Press, Beijing,2008.

[2] Du, Laihong.Research of Enterprise Resource Knowledge Representation Based on OWL. The 7TH International Conference on System of Systems Engineering(SOSE), IEEE. 2012 : 943-946.

[3] Yao, Haining; Etzkorn, Letha. Automated conversion between different knowledge representation formats. Knowledge-Based Systems. Vol. 19. No. 5. (2006), p. 404.

[4] Lima Reis C A, Reis R Q, Schlebbe H, et al. A policy-based resource instantiation mechanism to automate software process management. Proceedings of the 14th international conference on Software engineering and knowledge engineering. ACM, 2002: 795-802.

[5] Crespo D, Ruiz M. Decision making support in CMMI process areas using multiparadigm simulation modeling. Simulation Conference (WSC), Proceedings of the 2012 Winter. IEEE, 2012: 1-12.

[6] Jian Wang, Na Zhao, Wei Du, Peng Li, Jinzhuo Liu, and Zhongwen Xie. Dynamic-Competition Based Architecture for Component Library Under the Software Evolution Model of SDDM[J]. ADVANCED SCIENCE LETTERS, Volume 7,March 2012 , pp. 618-621(4).

[7] The International Organization for Standardization (ISO) and the International Electrotechnical Commission (IEC), (ISO/IEC 12207) Standard for Information Technology—Software Life Cycle Processes, 1998.

Advanced Materials Research Vols. 989-994 (2014) pp 4855-4860
© (2014) Trans Tech Publications, Switzerland
doi:10.4028/www.scientific.net/AMR.989-994.4855

Application Of Gis in Environmental Impact Assessment

Dongqin Chen [1.2]

[1]School of Environmental Studies China University of Geosciences(Wuhan), Wuhan 430074,China

[2]Hubei Urban Construction Vocational and Technical College, Wuhan 430205, China

Keywords: EIA, GIS, Application.

Abstract. This paper Based on the composition, types, functions and applications in the field of geographic information systems, analyzes the advantages of GIS technology in environmental impact assessment. From the project environmental impact assessment (EIA) of the limitations of departure, outlining the current status of the EIA study, while an overview of the geographic information system (GIS) functionality and applications, focusing on the status of the application of environmental impact assessment in the field of geographic information systems Necessity and Prospect. And use some of the existing management and analysis of environmental monitoring information system based on GIS examples further illustrate the application of GIS in Environmental Monitoring Data Management Analysis, give full play to the advantages of GIS spatial information processing and comprehensive analysis of expression, making the environmental monitoring data more effective.

Introduction

Environmental assessment is a commentary on the pros and cons of Environmental Quality is based on certain evaluation criteria and evaluation methods to determine the scope of a regional environmental quality, forecasting trends and evaluate the impact of changes in environmental quality of human actions on the environment. Environmental assessment is an important branch of the scientific basis for environmental science disciplines, new developments; environmental management is an important means to achieve a comprehensive environmental management.

With the wide application of environmental assessment EIA development and computers, computerized EIA standardization is to improve the overall level of environmental assessment requirements, but also the inevitable trend of development of the EIA. Computer Applications in EIA also from the simple to the complex process of continuous development. In the EIA computer technology can be used to store and process the basic data, EIA management, environmental monitoring and management. GIS data processing, analysis, powerful computing, recognized by our users. GIS analysis using powerful three-dimensional and three-dimensional display capabilities for environmental quality monitoring data obtained various evaluation methods to select a single element of a comprehensive evaluation of regional and automatically complete analysis and evaluation of factors to calculate the output results of evaluation and assessment, and application-specific analytical procedures, the spatial distribution of the contaminants in the image contours visually displayed, help to understand the spatial distribution of pollutants regularity; their data can generate pie charts, bar charts and other manifestations. Resources and Environmental Asessment as one of the major areas of GIS application, the application can greatly reduce the workload, speed up the evaluation process and to facilitate the evaluation of the results of dynamic management, updating and applications.

Research Status

Since the 1970s, the United States Tennessee Valley Authority using GIS technology to process and analyze a variety of watershed data, provide decision services for watershed management and planning, GIS had been used in hydrology and water resources management. Colorado's some agencies jointly developed the Colorado River Decision Support Systems, GIS is used to store basin space, retrieval, analysis and display. A research team of the University of Utah using GIS

technology to areas bordering Mexico and the United States carried out an environmental impact assessment, the establishment of surface water and groundwater pollution path model, and has resulted in the economic development of the region by GIS spatial analysis functions (such as buffer analysis) environmental impact analyzes; HECHANSHENG comprehensive evaluation of the impact of non-point source pollution of river water quality MICHIGAN CASS State GRASS software in support of the next; VENTURA, such as the use of GIS for urban non-point source pollution were analyzed and evaluated, combined with land use distribution type of control measures to provide basis for decision making. United States national, state environmental agencies and pollution control department developed the BASINS program. BASINS full advantage of recent developments in software, database technology and computer functions, and using Arc View GIS software as integrated watershed data to the entire United States, watershed analysis and water analysis software to unify, to provide users with an easy-to-understand , the point source and non-point source watershed management tool to unify. [1]

Institutions in some European countries to jointly develop a decision support system for watershed planning process simulation with hydrology, water pollution control, water resources planning and other functions / WATERWARE0, the system utilization of GIS, database, simulation, optimization procedures and expert systems function. GIS is mainly used for storage basin for all spatial information, providing data for the simulation system is also used to display the results of analysis and simulation.[2][3]

The Feasibility of the Application of GIS in EIA

GIS spatial database, spatial data and spatial expression analysis of three aspects of GIS may be widely used in environmental monitoring.

GIS Spatial Database to Achieve Effective Management of Environmental Monitoring Data

The main results of the environmental monitoring of environmental data , environmental monitoring continuity features make environmental monitoring data of tens of thousands each year , so the vast amounts of data is difficult to rely solely on manual management to ensure consistency and accuracy of the data . Establish an environmental monitoring database. The traditional structure of the database is not well expressed, storage information, can not be achieved and spatial information analysis and management of spatial data. Solving environmental problems must be combined with the reality of geospatial information. GIS database is a collection of some characteristics with certain geographic features are stored together in the area of organization of the relevant data. As the GIS database with large amount of data , spatial data and attribute data are inextricably linked , and has a significant spatial data between topology and other characteristics , so GIS database management features to environmental monitoring, in addition to the monitoring point attribute data related outside the DBMS functionality also includes management techniques for monitoring point spatial data. For example, the spatial location of monitoring sites and monitoring information retrieval environmental factors, such as retrieving and location monitoring points from the environmental quality control conditions.[4]

GIS Vivid Image Representation

GIS has very powerful graphical display and map making capabilities. But by no means just a mapping tool, it is geographic information about the environmental pollution monitoring, environmental management, and environmental factors such as geographical features combined analysis system. Data visualization of expression and maps, tables and graphs, and also the implementation of dynamic coupling between them, manage, and query, so a lot of abstract, boring data becomes vivid, intuitive and easy to understand. Electronic map visually interact with the user, the user can rely on the inherent human understanding and logic operations data for the natural world. Especially in recent years GIS application and development of virtual reality technology for the study of the spatial distribution of environmental pollution dispersion law provides an accurate, intuitive visual display, as well as real-time, dynamic display changes in environmental conditions.[5]

Integrated GIS Analysis Functions

This technology was developed by computer technology GIS and spatial data generated by the combination, which includes a variety of advanced spatial information processing capabilities, but its basic function is to collect data management processing, analysis and output. Rely on these basic GIS functionality through the use of spatial analysis, model analysis technology, network technology and database and data integration technologies, such as the interpretation of the secondary development of a variety of applications. It is precisely because GIS has such a powerful spatial data management capabilities and comprehensive analysis of spatial data, while 85% of the above-mentioned space-related environmental information, making it the management to analyze and solve environmental problems environmental monitoring data more superiority. Another combination of GIS and environmental models provide a more efficient and professional handling capabilities. Therefore, the analysis techniques to achieve comprehensive information processing environment is also necessary and reasonable use of powerful GIS space.[6]

The Main Application GIS in Environmental Monitoring Data Management Analysis

GIS biggest feature is the ability of the whole or part of the Earth's surface (including the atmosphere) the geographic distribution of the data space for the collection , storage, processing and management of information management, computation , analysis and visualization , spatial and attribute information has been able to for reprocessing , draw scientific conclusions. It is these features make it possible to combine with environmental monitoring, another angle GIS intervention makes a variety of environmental issues and environmental processes described in more realistic, interactive and friendly interface, easy spatial analysis, intuitive and vivid results display so undoubtedly promote the development of environmental monitoring technologies.

Environmental monitoring is accurate, timely and comprehensive picture of the status and trends of environmental quality, provide a scientific basis for environmental management, pollution control, environmental planning. Specific environmental monitoring purposes can be summarized as follows:

(1) According to the environmental quality standards, evaluation of environmental quality.

(2) According to the distribution of pollution, track looking for sources to provide the basis for the realization of supervision and management, pollution control.

(3) To collect background data, the accumulation of long-term monitoring data for the study of environmental capacity, the implementation of total control, goal management, forecasting environmental quality to provide data.

(4) to protect human health , environmental protection, rational use of natural resources , the development of environmental regulations, standards , planning and other services. Articles based on environmental monitoring purposes, divided into environmental quality monitoring, pollution supervision and monitoring, emergency monitoring three aspects to further illustrate the application of GIS in Environmental Monitoring Data Management Analysis. GIS spatial data storage and visualization of expression is a basic GIS functions , for any purpose in the form of environmental monitoring data will be used in all of the following three aspects will not bore you tired , mainly from the following GIS angle and comprehensive analysis of spatial analysis capabilities to illustrate the application of GIS.

Environmental Quality Monitoring

Environmental quality monitoring is the core monitoring. It is the pollution of the environmental elements of the situation and trend monitoring of pollutants, was evaluated to determine the effect of control measures and improvement of environmental standards implemented environmental progress achieved, the accumulation of quality monitoring data to determine the status of a certain area and the development of environmental pollution trend.

Environmental quality monitoring in general is for areas (such as basins, urban, etc.), and the region's air, water, noise, solid waste and other sentinel, long-term, long-term monitoring to determine the sources of the status quo in the region objectively comprehensive evaluation of the contaminated area to reflect the extent and spatial distribution. Environmental monitoring data are

usually obtained data on the number of discrete points in space, how to use these discrete monitoring data quality of responses to the real environment. Here you can use the interpolation method of GIS spatial data. Spatial interpolation of data can simply be described as follows: a set of spatial data set, they can be in the form of discrete points, the partition may also be in the form of data, these data are found from a function formula that changed the relationship The best approximation of these known spatial data, and can infer the value of any point within the region, or any other partition change function according to the relationship. [7]

Pollution Monitoring

Pollution monitoring is routinely monitored in order to grasp pollution monitoring, surveillance and monitoring of major sources of variation in space and time taken regularly sentinel. It is mainly the concentration of pollutants, the total emissions and pollution trends monitoring, pollution monitoring network to take advantage of trends and conditions of a region predict, forecast. Impact assessment of pollution on the environment, in addition to the concentration and amount of access to sources of emissions data, but also must rely on space background information sources where the geographical environment, the same pollutant emissions, because they are in a different location (including meteorological, terrain conditions, etc.), the degree of pollution and scope will vary. This is characteristic of geospatial sources. Geospatial characteristics determine the effect on pollution sources must be integrated geographic analysis of quantitative thinking and spatial analysis tools combine - Geographic Information System (GIS). Not only to conduct quantitative analysis of sources, such as the calculation of the size of emissions, but also to perform spatial analysis, such as calculating the relationship between emissions and ambient concentrations.

GIS spatial analysis of sources of pollution dispersion buffer impact analysis provides a powerful tool. Buffer space is analyzed based on analysis of the object point, line, and plane entity created automatically ribbon area around them at a distance, to identify these entities or subject scope or impact of the radiation on near objects. Here the application mainly in accordance with the position of sources (weather conditions, terrain conditions) model combined with the environment, such as calculating the degree of impact on near objects, draw a buffer zone to the performance impact of changes in scope and concentration of pollution sources, total control of pollutants, reduction program developed to provide decision support. For example, buffer analysis and path analysis can be used for a variety of elements that contains the figure and close analysis, analysis of pollution discharge destination, showing sources of influence, combined with pollution monitoring data, analysis and evaluation of emissions which contribute to the pollution of rivers rate (see Figure 1).

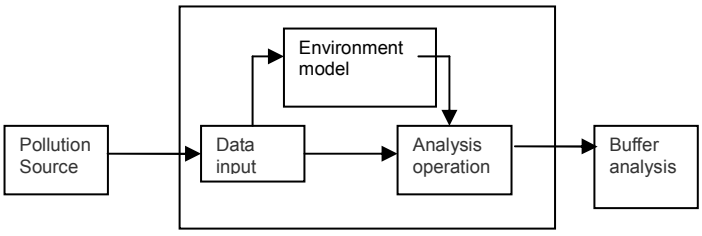

Fig.1, Buffer analysis of pollution sources

Emergency Monitoring

Emergency Monitoring is also known as monitoring a particular purpose, according to a specific purpose and can be divided into the following four categories: pollution incident monitoring, emergency monitoring carried out in the event of pollution incidents in order to determine the type and extent of contamination hazards, diffusion direction, the diffusion rate and endanger the range, provide the basis for the control of pollution; arbitration monitoring: mainly for pollution accidents disputes, conflicts in the implementation of environmental law arising monitoring; assessment verification monitoring, including environmental appraisal staff assessment, method validation and new projects and pollution Acceptance Monitoring governance projects when completed; consulting

services monitoring: government departments, research institutions and production units monitoring the services provided.

Pollutant monitoring and emergency pollution accidents are a variety of on-site monitoring to track, find out the degree of contamination and the scope of its accidents, damage caused by size. Environmental pollution dynamic continuous monitoring of major pollution incidents and respond quickly, Environmental monitoring is an important direction of development in order to implement effective pollution accidents have emergency requires the use of geographic information system technology to conduct a comprehensive analysis of relevant data and methods to first determine the location of the accident, and then use a combination of GIS and environmental models range forecast affected area to provide sensitive units within the contaminated area through GIS visualization, rescue units, population, and the best path from the accident site to the designated location and other information for emergency monitoring, carry out emergency rescue work to provide basis for decision making . , GIS spatial analysis used here as shown in Figure 2 the main buffer analysis, spatial data analysis and queries, and a collection of network analysis.

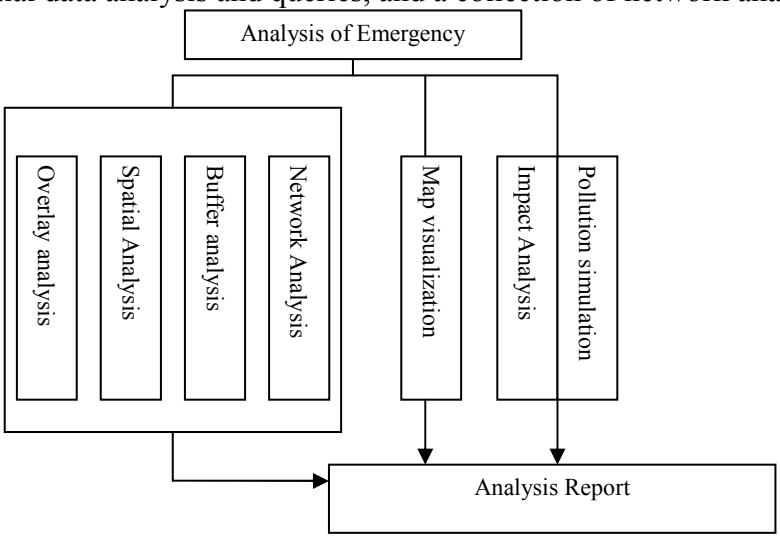

Fig. 2, Pollution Accident Analysis

Buffer Analysis

Buffer Analysis former already mentioned, the use of buffer diffusion and impact analysis and environmental pollution accident prediction models affected by a combination of regional and range, but can also affect the results of the analysis of the diffusion of rendering to visualize the concentration of contaminants or degree of impact.[8]

Query Spatial Data

Database query spatial data areas are generally defined as to identify all the properties to meet space constraints and the constraints from the database of geographic objects. Property constraints and traditional database query is similar. Space constraints with space for expression described by the predicate logic, spatial predicate by the spatial relationships between objects evolved geography , such as contain , intersect, separate , overlapping, distance and direction . Therefore, the role of spatial query function on the library body, returns the contents of the user's request, also belong consultative analysis.[9]

Conclusion

Temporal GIS, such as three-dimensional GIS and WebGIS from these new GIS technology and development not only extends the GIS own connotations, and no doubt it will also promote innovation in the field of environmental monitoring technology. Such as three-dimensional dynamic time series studies demonstrate GIS spatial data, which has the same area or a particular object change over time at different phases of geographic data to study the spatial variation, and in the form of three-dimensional animation on display. The results of environmental monitoring will bring a qualitative leap, not only that, if combined with a professional environment model in

environmental pollution forecasting, simulation, and emergency and other aspects will also improve the performance of the three-dimensional form of the model, improve operational efficiency model, making management analysis of environmental monitoring data more quickly, real and effective. With the development of GIS technology, GIS application in environmental monitoring data management analysis will also get an endless supply of the driving force.

References

[1] Gontier, Mikael, Comparing GIS-based habitat models for applications in EIA and SEA, Environmental Impact Assessment Review,V.30(1）(2010),p. 8-18.

[2] Ivo, Basting, EIA approach with application of spatial multi-criteria analysis, 30th Asian Conference on Remote Sensing 2009, ACRS 2009, V.2, p.842-849.

[3] Erikstad, Lars , Environmental value assessment in a multidisciplinary EIA setting, Environmental Impact Assessment Review, V.28(2-3), p.131-143.

[4] Myrtho Joseph, Fahui Wang， Lei Wang，GIS-based assessment of urban environmental quality in Port-au-Prince, Haiti， Habitat International，2014, V.41, p.33–40.

[5] Xueqin Liao, Wei Li, Jinxiang Hou，Application of GIS Based Ecological Vulnerability Evaluation in Environmental Impact Assessment of Master Plan of Coal Mining Area. Procedia Environmental Sciences, V.18, 2013, P.271-276

[6] Sören Gebbert, Edzer Pebesma, A temporal GIS for field based environmental modeling. Environmental Modelling & Software, V.53, 2014, P.1-12

[7] Thomas Kistemann, Friederike Dangendorf, Jürgen Schweikart, New perspectives on the use of Geographical Information Systems (GIS) in environmental health sciences . International Journal of Hygiene and Environmental Health, V.2005(3), 2002, P.169-181

[8] Zhou Qun, Yuan Yujin, Kang Yuena,GIS Application System Design Applied to Information Monitoring Physics Procedia, V.25, 2012, P.2235-2241

[9] Xueqin Liao, Wei Li, Jinxiang Hou, Application of GIS Based Ecological Vulnerability Evaluation in Environmental Impact Assessment of Master Plan of Coal Mining Area .Procedia Environmental Sciences, V.18, 2013, P.271-276

Advanced Materials Research Vols. 989-994 (2014) pp 4861-4864
© (2014) Trans Tech Publications, Switzerland
doi:10.4028/www.scientific.net/AMR.989-994.4861

Remote Maintenance System Based on Browser\Server and VIRTOOLS

Tao Yuan[1, a], Cheng-De Yang[1, b] and Bin Shen[1, c]

[1]Wuhan mechanical College, Wuhan, China

[a]ytzw7981@163.com, [b]ychd1962@163.com, [c]tcaixs@163.com

Keywords: Remote maintenance; Equipment; Common platform; Browser \ Server; VIRTOOLS;

Abstract. In the analysis of the development and the functional requirement of the network-based maintenance training system, combining the long-distance maintenance service and virtual reality technology, the long-distance maintenance service based on Browser\Server has been founded, and the system architecture, key technologies and implementation methods have also been researched and discussed. The system will provide a powerful technical support platform for carrying out long-distance maintenance service.

Overview

With the development of science and technology, the contradiction between the increasing trend of high-tech equipment and the inadequate maintenance force which adapts has become more prominent. Interactive device remote maintenance system based on network being used to guide the remote user's equipment maintenance can maximize authoritative technical experts to share and off-site training of personnel. It will play a unique role in major equipment repairs, reducing maintenance costs and maintenance and technical personnel training. This is an urgent research topic in the actual maintenance of equipment.

Remote maintenance is the electronic transmission of data or information between the maintenance personnel and remote staff or sources of information. It can make the field service personnel prepair spare parts and tools timely before the return of equipment to perform tasks according to real-time transmission of equipment information, or get maintenance training and guidance in the field. And then ,when the equipment is returned ,it can be repaired immediately. Through the transmission system, the maintenance personnel in the field can get technical guidance and maintenance information from the rear base. Remote maintenance can not only ensure maintenance of high quality in the first time, but also within the effective time, improve the level of skilled maintenance personnel by sharing experiences. It can reduce training requirements, and there will be a significant reduction in the time of on-site repair and disable time .So it is very helpful to improve equipment readiness and reduce the costs of use and protection.

Build a remote diagnostic system based on Browser / Server Mode

B/S model includes three layers, the presentation layer, functional layers and data layers. The presentation layer is the user interface portion of the application which charged with the function of dialogue between the user and the applications. The functional layer is the body of the application which it compiles the specific business processing to one program logically. The data layer is a database management system, which it defines and manages the contact of the database and the application and it is responsible for the management of read and write data in the database. Accepting user requests through the network, executing corresponding processing, and then sending the response back to the browser, B/S mode further simplifies the client software. Because of the browser as a unified client, just modifying the server-side software, the system can be upgraded which it is helpful to system maintenance and management.

Remote fault diagnosis center should be built in research institutions, maintenance factories and office functions and connected with the troops through military communications network. The fault

diagnosis and maintenance of dynamic alliance which is composed of relevant experts who come from the institute, repair factories and manufacturing plants will provide remote troubleshooting and repair services for the system. All troops (client) establish a real-time fault detection system. When the local fault diagnosis system can not solved the problems, the troops can access the remote fault diagnosis center through military communications network. The remote system provides technical support, repairs the damaged equipment timely. So that technical resources can be effectively shared.

This remote fault diagnosis and maintenance system is divided into three layers. The first layer is the user diagnostic layer that it is “client” in the figure1. When equipment fails, fault is detected and diagnosed firstly by the fault diagnosis system resided in the user's own, and then the equipment is repaired. When they can not find out the reason, they apply for technical assistance to the center through military information network. That is the second layer-the center of the diagnostic layer. After the diagnostic center has received customers’ requests, it diagnoses and gives maintenance recommendations. The third layer is a group consultation.

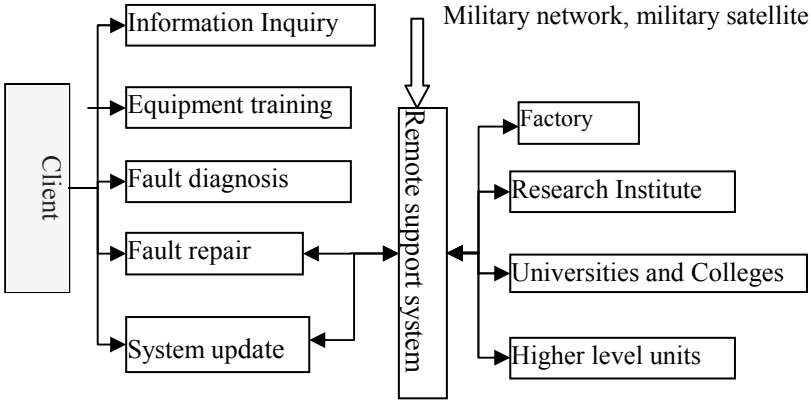

Fig1. The structure of the remote maintenance service

The remote fault diagnosis system has the following features: experts from all sides can achieve offsite "consultation" of many difficult problems through the network. The diagnostic knowledge and databases within the scope of the military will be shared and then it can provide reference and basis for solving similar problems of army. It also can achieve full life-cycle management of weaponry which is from the production, reserves to use and provide a reliable guarantee for improving equipment performance and combat effectiveness. With open system architecture, the new network’s forces can share all the resources online and it facilitates technology popularization and promotion.

Create Query System

VIRTOOLS production can get immersive virtual environment. It generates participants various sensory information such as vision, hearing, touch, taste, etc and gives participants an immersive feeling. So it is a new development, with the meaning of a new human-computer interaction system. The automata visual simulation of a certain type of equipment has achieved the maintenance of automatic systems in virtual conditions by the simulation of repair process of the systems. Visual simulation of the entire process with high fidelity can display the entire system all-round, and response real-time during operation with three-dimensional gesture.

Virtual Training

Users can take advantage of virtual operating platform and make equipment put into use as soon as possible with automatic machine virtual operating model which it is based on VC and VIRTOOLS using 3dmax modeling. At the same time, the model increases the virtual presentation capabilities by showing capabilities need to be operated by virtual reality or video mode. Among them, video presentation is strongly realistic so users can learn from the global. Virtual presentation has dual function of global and local and users can observe by cross-sectional and multi-angle.

Virtual Assembly

An important part of removable equipment maintenance is decomposition and combination of the equipment, but the complex structure always hampers the process of user operations. Virtual Assembly may well solve this problem. The key of virtual assembly is founding a reliable three-dimensional modeling of the new equipment. The specific technical route is: determining the serial number of the part by the order of assembly parts, curing the assembly sequence of equipment with the rules set by VC programming and judging that the parts of the assembly is qualified or not according the distance of separate parts and whole parts. In this process, whether the user's using dedicated tools is correct is judged by VC program, and the different perspective switch is completed by the use of the camera lens' conversion which it is convenient for locating the assembly quickly.

Virtual Maintenance

Virtual maintenance includes local and remote maintenance service. The local repair uses animation to reflect the failure phenomenon in VIRTOOLS and feedbacks to the user with the effect of auditory and visual. Animations mainly reproduce the fax machine's function of the original send and the copy, join judgment point in the phenomenon of simulation, and determine whether the object is faulty maintenance. If the object fails, the feature presentation will stop and present the symptom. Wave Player BB controls voice broadcast, Show BB and Hide BB real-time controls the display screen and warning lights texture, Cheek for Message BB is the failure to determine the point. Scripts of the symptom presentation can be written by the above combination of BB. The basis of fault diagnosis in virtual maintenance is judgment for collision. When users take virtual maintenance, there will be a collision, and the VC program will determine maintenance tasks and repair processes.

As new weapons being equipped, even if the troops have the virtual training system, they are still unable to combine virtual reality with actual equipment perfectly. Remote service just can complete this combination. This is reflected in the following two aspects: first, during the virtual maintenance training, users can interact with the remote expert through the system to seek remote support for solving difficult problems timely. Secondly, when users are maintaining new equipment, remote experts can guide the operation of the local virtual system to help local users directly by the platform.

Self-learning of the Fault Diagnosis System

Knowledge base Of new equipment maintenance system needs to update constantly by exchanges of manufacturers, research institutes and the users. Knowledge base of remote diagnosis expert system can be based on open architecture Web database. It consists of two systems: local knowledge and remote repository. Local knowledge is maintained by the users. With the operation and use of the system, the local knowledge will be enriched constantly. But, whether or not the samples of local repository are reliable lies on information exchange between users and remote experts. When remote repository receives the users' information, it is analyzed and summarized by full-time staff. And then it is updated and sent to all users knowledge base with the new version of the form. In this way, the user's response time of treatment failure is assured, but also the knowledge base has a wide coverage and a faster update rate. Diagnostic database established by the framework standard achieve a shared of diagnostic data formats and specifications. As long as the data comply with the standard, the system can identify. Thereby the open of the database is greatly enhanced. The management of system knowledge base is classified by failure characteristics of different devices. Each fault can be set or sets of solutions.

Information module based on fault diagnosis module. In fault diagnosis diagnostic database, history table has been created simultaneously. After the users inquiry fault diagnosis module, the "Symptom" of high frequency fault and maintenance difficulty coefficient, they can storage "Device Name", "Defective parts", "the best solution", etc. fields in history diagnostic library. In the next similar failure, having input "Access time", "Device Name", "Defective parts" selectively in Information module, users can get history record of the "best solution" directly which it is stored in maintenance program. Thus, it saves time that the client accesses to the server and improves the efficiency of the network.

Because access permissions of data maintenance module has high-level requirements for user roles, the system improves the encryption to this module in the application development process. The data maintenance module is used by a modular structure of B/S mode, and developed by the VC language. Only the client has installed data maintenance module subroutine and the users have been authenticated, they have permission to access the data maintenance module. It greatly improved the security of the system. In addition to managing the system users, data maintenance module mainly can extend the equipment of system remote technical support. As long as failure analysis of the device is made, fault tree model or troubleshooting hierarchical model is established, and equipment indicators such as introduction of equipment, technical parameters, methods of operation, maintenance guidance, are given, the model can expand the device to the remote diagnosis system maintenance database, and then it can expand maintenance equipment types of the system for remote diagnosis.

Summary

The remote maintenance system based on VIRTOOLS is mainly used in the field of equipment maintenance. It is a new maintenance program breaking the constraints of time and space. Network diagnosis and maintenance decision associate the design, manufacture, installation, use, maintenance and management organically by the data for the goal that the equipment runs safely and reliably. The system has accurate judgment in cause, nature, location of equipment failure and possible consequences, and it is significant for reducing the accident rate, shorting the maintenance time and improving the quality of maintenance. The network remote maintenance system based on VIRTOOLS will become the key technology during the army equipment management modernization.

References

[1] Jun Yang,Yushui Gao, Enxiang Du. Over Technology of Virtual Testing and Maintenance Trainning System for a Type of Gun-Launched Missile. Journal of Ordanance Engimeering College. 2007;19(6):20-24

[2] Hao Lu, Quansheng Liu, Shuaishuai Wang. Assessment on a new type of tank fire simulation training system performance based on AHP. Journal of Sichuan Ordnance, 2011.32 (5):146-148

[3] Jinling Liu, Fanming Zeng, Development of Virtual Maintenance Training Software for Marine Power Plant. Computer Simulation. 2009.26(5):324-327

[4] Tianshui Li, Fanming Zeng, Huiling Liu, Study on Virtual Maintenance Training Technology Based on CATIA for Marine Power Plant. 2007.20(6):49-51

[5] Songyang Du, Xiancheng Wang, Manqing Chen. Study on Key Technology of Virtual Maintenance Training for a Military Equipment Based on VIRTOOLS 4.0.2009.30(9):41-43

[6] Jianbing He, Qunxing Su, Pengyuan Liu. Computer Equipment Virtual Maintenance Training Simulation Based on Process Modeling. Journal of Ordanance Engimeering College. 2009;21(4):6-9

[7] Jianping Hao, Keyi Jiang, Songshan Wang. Virtual Maintenance Simulation Theory and Technology. Bei Jing: National Defence Industry Press. 2008: 19.

Advanced Materials Research Vols. 989-994 (2014) pp 4865-4868
© (2014) Trans Tech Publications, Switzerland
doi:10.4028/www.scientific.net/AMR.989-994.4865

Improved XFBT: A Low-power Topology of Network-on-Chip

Hongbing Chen[1, a], Chao Li[1,b]

[1]School of Computers, Guangdong University of Technology, 510006, China

[a]hongbchen@163.com, [b]771781910@qq.com

Keywords: NoC; topology; low-power; improved XFBT

Abstract. The article discusses the issues related to the on-chip network topology, analyzes the XBFT topology, improves its structure in power consumption. Authors designed a simulation program that by analyzing the topology routing hops to roughly determine the power consumption of routing topology and for the preparation of modified XBFT roughly determine the topology of the routing topology by analyzing the power consumption topology routing hops the simulation program, Finally, the results from the running of 6 simulation program that extracted and these results were analyzed. The result shows that the improved topology saved about 20% of the number of routing hops.

Introduction

According to Moore's Law , integrated circuit performance approximately doubled every 18 months . Before SoC, Integrated circuits primarily by increasing the number of transistors that Integrated circuits accommodated to achieve improved performance, but with the IC into the ultra-deep submicron technology and IP core reuse dominated era , doubling the number of transistors again in a certain area on the chip has become very difficult, doubling the number of transistors again in a certain area on the chip has become difficult, the limited address space bus architecture, time communication, global synchronization caused by poor scalability, low communication efficiency, high power consumption and other issues severely limits the MPSoC development.

To solve the problems facing the development of complex MPSoC , learn computer network communications-centric thinking, presents a number of research institutions MPSoC Solutions - From the architecture to solve the communication bottleneck of MPSoC, Use this method to Solve problems of bus architectures.Compared with the bus architecture MPSoC, on-chip network (NOC) has good scalability, reusability, flexibility and parallelism [1-3] and so on.

NoC mainly concern is the problem of communication between multiple processing units, in the chip design process, bisection width and other aspects select the appropriate topology is one of the important research focus NoC. MPSoC development , especially the wide application of mobile intelligent terminals , power endurance of systemsis one of the main measure of performance parameters , prompting chip design increasingly take into account the power factor , low power consumption -oriented topology designed to be hot chip design research questions .

NOC topology description

NOC topology can be described using graph theory . In the on-chip network ,topology can be expressed as a mathematical model linkages between the IP core collection and a collection of discrete IP cores in concrete , which is defined as described in Definition 2.1 .

Definition 2.1 A network topology (Topology) is an ordered pair <N,L>, denoted by T = <N,L>, where:

N = {n1, n2, ..., nn} is a finite non- empty set , ni called nodes (node), N is called the set of nodes (node set).

L is a finite set , called the link set (link set). Each element in the L N in the corresponding node , called a link .

Each nodes exchange information through links,such a figure is a communication network. NOC topology directly affect the routing of IP core network node and the network map and

determine the diameter of the network chip , Thus the chip average network latency, area, network throughput, power consumption and other performance parameters plays a critical influence the NOC topology features fully reflected in the topology itself parameters. From graph theory and computer network -related knowledge, the mainly parameters of the topology of the nodes , the network diameter , the width of the points of the sub- bandwidth connectivity and so on.

Common NOC topology

NoC topology divided into regular and irregular types. Topology rules with the rules of network parameters, has good reusability, scalability and versatility, and simple. Regular topology can be divided into direct network and indirect network according to whether each communicate node of network has computing nodes directly connected, Unlike regular topology as regularity, Irregular network topology parameters mostly are based upon the specific application customization or combination other characteristics,can be optimized in in power, latency, area, and throughput, etc.Currently, a common NoC topologies are mainly 2D Mesh[4], 2D Torus[5], Octagon[6], Spidergon, CLOS, SPIN and so on. Some common NoC topology is shown in Figure 1.

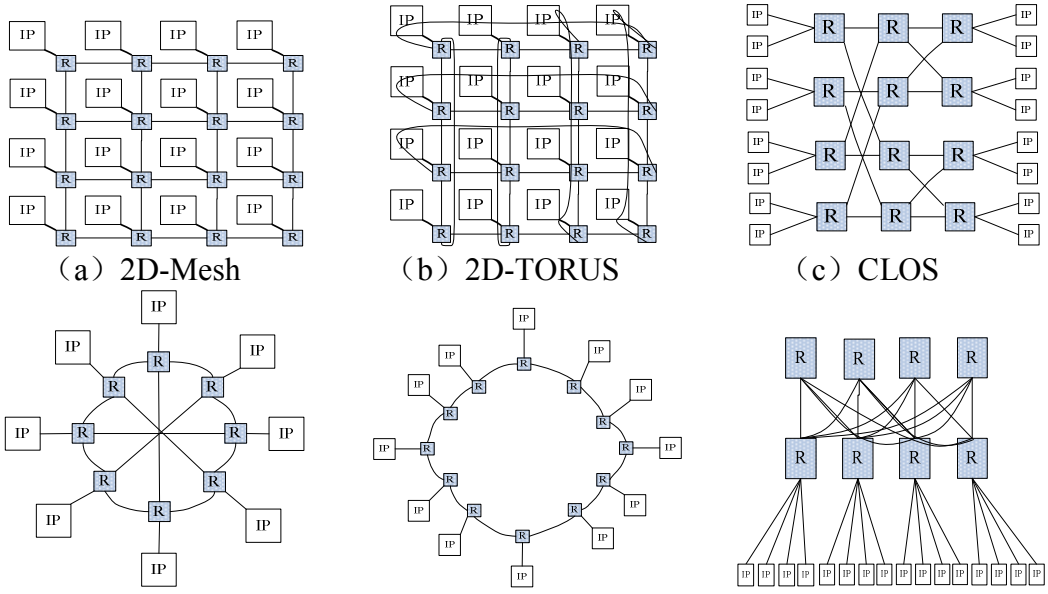

Figure 1 Some topology of NoC

Improved XBFT topology

XBFT topology is described by Zhou liberal arts degree thesis in his study of network topology and routing algorithm on an improved type of film BFT proposed [7] . Figure 2 is a schematic XBFT 64 when this topology calculating means to the IP core. Can be seen from the figure , routing hops required for its communication procedure up to 6. Each computing node 4 is connected to a routing node , and only connected to the routing node on the first layer. The first layer is connected to the routing node twenty-two form a link pair, then the routing node and the second layer connections . Each routing node of the second layer and the following pair of two adjacent links , respectively, to select and connect the two routing node , the network component 16 comprises a computing node , which is required for the communication process through the hops The maximum number is 3. In other words, XBFT tree almost from the beginning than the information routing hops torus structure is less that XBFT tree topology to be less than the power consumption torus structure. Each sub-network in the same layer as the second layer next to the routing node connected between the additional connection to a node is the less.

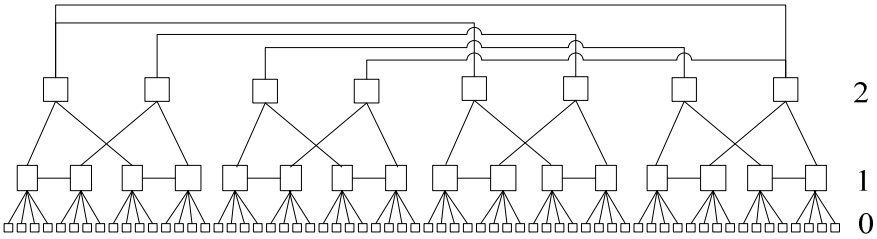

Figure 2 XFBT topology

XBFT structure of an improved structure shown in Figure 3, the base structure of high XBFT improved to some extent on the path router, the number of nodes such that each routing node can be connected to a relatively large saving on the cost of the mountain road the integrated circuit device. At the same time, Unlike regular topology as regularity, Irregular network topology parameters mostly are based upon the specific application customization or combination and modifications of topology rules, has specificity and efficiency and other characteristics,can be optimized in in power, latency, area, and throughput, etc. In connectivity, improved XBFT structure let the first layer routing node sequentially divided into four groups, each group has four routing nodes; The second layer routing node is according to their order of appearance in the second layer routing node to link position corresponding routing node of lower routing group A connector as in each group of the first router, B is connected in each group of the second router. Through this connection, you can reduce routing hops message in the communication process through which that reduce the distance between the two compute nodes, while increasing the connectivity of the network.

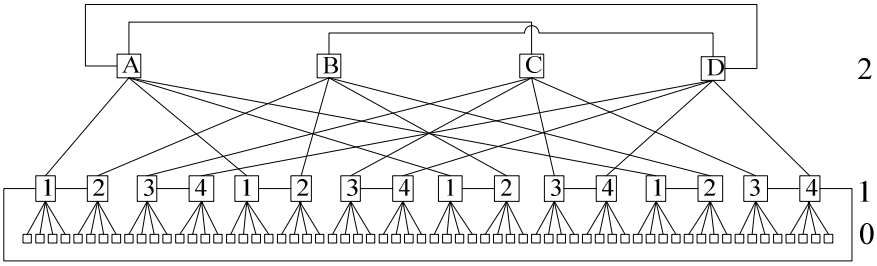

Figure 3 Improved XFBT topology

The simulation results and Summary

This article uses the C language simulation program on REHLL5. The simulation program to simulate the topology of the communication process to measure performance and power topology, you can configure the router and the power consumption of each link must be used to determine the shortest path routing communication process data transmission path, the simulation only consider routing hops, the main consideration by reducing the number of router hops to measure power performance. So by getting any two nodes in the route calculation the average number of hops, to compare the power consumption of the two topologies are feasible and more intuitive.

This made a total of six groups of six test data obtained, respectively, the input number of communications computing node 100 times, 500 times and 1000 times. As shown in Table 1, improved topology routing hops are significantly reduced.

Table 1 Router routing hop number

	XBFT topology routing hops	Improved XBFT topology routing hops
6400	26875	19984
32000	131604	103814
64000	263112	208915

As shown in Table 2, the average number hops of improved topology roughly about 25 percent to 80 percent for the improved topology.

Table 2 Router average routing hop number

	XBFT topology average routing hops	Improved XBFT topology average routing hops
6400	4.20	3.12
32000	4.13	3.24
64000	4.11	3.26

Combined with the above data analysis, improved power consumption without considering the topology of the crossbar and distribution circuits and connections, such as specific logic circuits and routing algorithms and topology-independent factor F. Improved power topology is not improved 80 percent of the mountain road topology XBFT.

Acknowledgement

The work described in this paper was supported by Funds from National Natural Science Foundation of China (61106019), Guangzhou Science and Information Bureau(No. 201300000021) and Yuexiu District Science, Technology and Information Bureau, Guangzhou (No. 2013-CY-006).

References

[1] D. Heckerman, C. Meek, and G. Cooper. A Bayesian approach to causal discovery. In C. Glymour and G. F. Cooper, editors, Computation, Causation, and Discovery, pages 141–166. MIT Press, 1999.

[2] T. Richardson and P. Spirtes. Automated discovery of linear feedback models. In C. Glymour and G. F.Cooper, editors, Computation, Causation, and Discovery, pages 253–304. MIT Press, 1999.

[3] R. Silva, R. Scheines, C. Glymour, and P. Spirtes. Learning the structure of linear latent variable models.Journal of Machine Learning Research, 7:191–246, 2006.

[4] S. Kumar et al., A Network on Chip Architecture and esign Methodology, Proc.Int'1 Symp.VLSI(ISVLSI), pp.117-124, 2002.

[5] W.J. Dally and B. Towles, Route Packets, Not Wires: On-Chip Interconnection Networks, Proc. Design Automation Conf. (DAC), pp. 683-689, 2001.

[6] F. Karim et a1,An Interconnect Architecture for Networking Systems on Chips[C].IEEE Micro，vo1.22，no.5，pp.36-45，Oct,2002.

[7] WANG Ji-He, GUO Bing,etc..Analysis and Modeling of Directory Protocol Energy Consumption in NoC[J].Chinese Journal of Computers,,2011,34(9): 1603-1610.

Advanced Materials Research Vols. 989-994 (2014) pp 4869-4872
© (2014) Trans Tech Publications, Switzerland
doi:10.4028/www.scientific.net/AMR.989-994.4869

A Database Grid Service with A Novel Mutation Operator

Jian Cao[a], Yanbin Li[b], Cong Yan[c]

Air Force Engineering University, Xi'an, Shaanxi Province 710051, P.R. China

[a]cao_jian1972@163.com, [b]Lyanbing@163.com, [c]yancong192@qq.com

Keywords: Grid; Mutation; Service; Optimization

Abstract. Database grid service provides users with a unified interface to access to distributed heterogeneous databases resources. To overcome the weakness of collaborative services ability in different grid portal, a new grid portal architecture based on CSGPA (Collaborative Services Grid Portal Architecture), is proposed. This paper aims to enhance the performance of PSO in complex optimization problems and proposes an improved PSO variant by incorporating a novel mutation operator. Experimental studies on some well-known benchmark problems show that our approach achieves promising results.

Introduction

PSO is a recently proposed intelligent search technique, which was inspired by the social and cognitive behavior of swarm. As mentioned before, PSO as well as EAs are population-based random search algorithms, which usually start from a set of initial members or particles (called initial population) and towards the global optimum by executing iterative operations. In PSO, each particle has two features: velocity and position. The velocity determines the step size of movement every generation, and the position represents a candidate solution in the search space. Every generation, PSO utilizes a velocity and a position updating equation to recalculate the new velocity and position of each particle. When a particle moves in the search space, it remembers its previous best position (called pbest) and the global best position (called gbest) found so far. PSO's social and cognitive behavior is based on these two particular particles. The grid is a giant supercomputer of high efficiency, which integrates the distribution system and heterogeneous computing resources, and it provide the full sharing of computing resources, storage resources, data resources, information resources, knowledge resources, expert resources, and equipment resources [1]. Grid Service is the use of grid services for users. In this paper, GDT is used to establish the database grid service for handling and processing the distributed, heterogeneous database.

In the grid environment of grid system architecture based on OGSA, each grid resource is seemed as a grid service. These grid services are provided to grid users to sharing use [2]. Grid portal is to provide a way of users accessing the grid resources, and each single grid portal can provide a subset that users can access these grid resources, therefore, grid users need to access different grid resources via independent and different grid portal, and the situation of the current existing grid portal is also like this. How can we make the single grid portal connect better, make the different grid portal collaborate services for users needs. The paper puts forward a new grid portal, which can make the single grid portal share the information, share the grid resources and a strong scalability system architecture to build new grid portal. We named Collaborative Services Grid Portal. Because of the formulation of the WSRP (Web Services for Remote Port lets) standard, making use of WSRP, users can standardize the single grid portal architecture of all the organization [3]. In the portal architecture, many small portal share the content, and needn't deploy the single portal any more, each IT service only deploy once, and then it can achieve to use all IT service consistently. Therefore, WSRP provides the strong support for collaborative services grid portal [4].

At present, data of each application fields is increasing at an amazing speed. In the real application environment, most of massive databases exist in the form of distribution. If the distributed data was concentrated into a data warehouse for mining deal, it will pose a threat to the distributed data's security and privacy, and further reduce the efficiency of mining, but also make a

higher requirement of network communication bandwidth. It becomes an urgent requirement to achieve sharing among the distributed and heterogeneous database resources.

Database grid service can support high-performance needs and data distribution well, and store, manage huge amounts of data more effectively, and analysis and handle a large number of heterogeneous distributed database resources more efficiently. Database grid service has many applications features, such as data-intensive, data resource diversity and heterogeneity, large-scale collaboration with the local control rather than global control, data security, load balancing of data resource access, etc. Clients interact through the appropriate database grid services and data service resources. The database grid encapsulates the function that need to use Web Service interface to open data services resources.

Database Grid Service Introduction

According to practical requirements on site, the online computer five-anti system based on multi-layer network architecture is designed with the help of current advanced communication technology and embedded technology. The system architecture is shown as Fig.1. The intelligent lock is the important components of online computer five-anti system. Different electrical equipments have their special requirements for lock method due to their different structures and operation principles. So different latch locks should be installed based on site conditions.

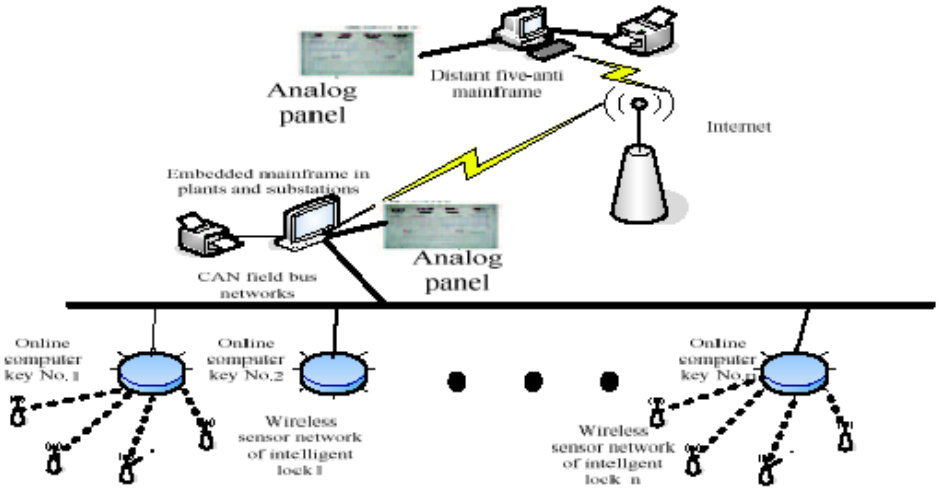

Fig.1 System framework based on multi-layer network architecture

Architecture and Operating Mechanism of Collaborative Services Grid Portal

The architecture of collaborative services grid portal is shown in Fig.2. Its operating mechanism is as follows.

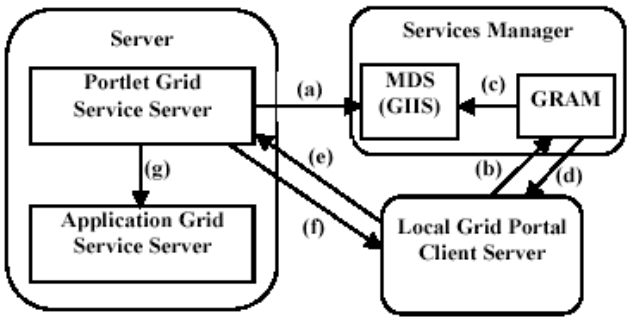

Fig.2 Architecture of CSGP

Hardware Circuit Design

The Central Processing Unit (CPU) applies the industrial chips of MC9S08 AC16, which are industrial eight-digit single-chip microprocessors with ultra-low power consumption. This type of chips internally integrate a 16K-byte FLASH and a1k-byte RAM memory with SPI interface, A/D conversion circuit.

CC2430 has small number of external components. It employs an unbalanced antenna to connect the unbalanced transformer so as to make the antenna have better function.

The parts of hardware in detail are designed as Fig.3.

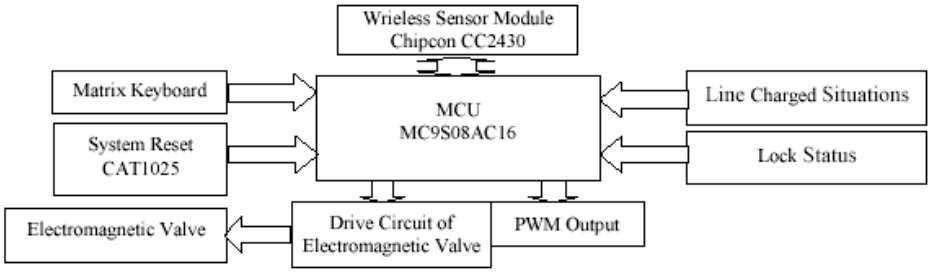

Fig.3 Hardware system framework

In the collaborative services grid portal architecture, a server can allow running many Port let grid services, and of course, the whole architecture also allow existing many Port let grid services which provide the same function, some Port let grid service can access the corresponding one or more application grid service. By this means, Port let grid service can mainly process the display logical. Port let grid service provide an interface service to the terminal users of the grid portal, while the gird resource that terminal users need to access and use, is provided by the application grid service running on the other server. In this way, we can separate the display logic from the application logic in grid portal better. In the whole grid portal system based on collaborative services grid portal architecture, the amount of the servers of running Port let grid service can be dynamic change, but they don't have the close connection between the each Port let grid service server, so any one server goes wrong, it will not influence the normal operation of the whole architecture. To the requestors, because of each Port let grid service is developed based on the standard, so the requestors are very convenient to plug Port let grid service in grid portal itself by configuration, and don't need to add other program code.

In allusion to the network topology and application distribution of grid system, combining with the collaborative services grid portal architecture above, we provide the application system architecture based on CSGPA, as shown in Fig.4.

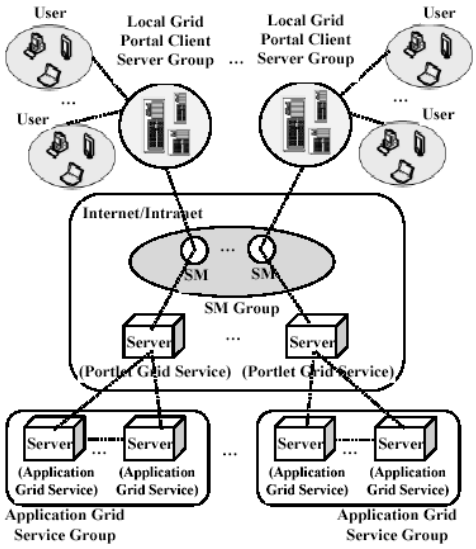

Fig.4 Application system architecture based on CSGPA

Conclusion

It is to hope this improvement can help trapped particles jump to better positions. Simulation results on ten problems show that CSGPA not only achieves more accurate solutions than PSO, but also converges faster. Collaborative services grid portal architecture is presented in this paper. Through our study, analyze and evaluation contrast to the architecture, we can find that the architecture is clearer than some current grid portal architectures, and it improves the scalability and reusability of the grid portal. The emphases of next step work are to solve the dispatching problem in the case of the large number of concurrent and the many-to-many relationships problem of grid service.

References

[1] Fernando Bellas, “Standards for Second-Generation Portals,” IEEE Internet Computing, vol.8, pp. 54-60, February 2004.

[2] Chen Xiao-wu, “A multilayer portal model for information Grid,” China Grid Annual Conference, China Grid'08, Gansu,vol1, pp.78-85, August 2008.

[3] Zhang Feng-juan, “Research and design of grid portal based on hibernate,” Computer Engineering and Design,vol.30, pp.71-79, January 2009.

[4] I.Foster, C.kesselman, J.Nick, S.Tueck, “Grid Services for Distributed System Integration,” Computer, vol. 35, pp. 37–47, June 2012.

[5] D. C. Chu. “Polyphase codes with good periodic correlation properties,” IEEE Transactions on Information Theory (Corresp.), vol. 18, no. 4, pp. 531-532, July 1992.

Advanced Materials Research Vols. 989-994 (2014) pp 4873-4876
© (2014) Trans Tech Publications, Switzerland
doi:10.4028/www.scientific.net/AMR.989-994.4873

Research on Algorithm to improve performance of Wireless-Optical Broadband Access Network

Jian Cao[a], Yanbin Li[b], Cong Yan[c]

Air Force Engineering University, Xi'an, Shaanxi Province 710051, P.R. China

[a]cao_jian1972@163.com, [b]Lyanbing@163.com, [c]yancong192@qq.com

Keywords: Capacity Utilization; Improving; Failure Detection; Algorithm

Abstract. There are many factors that can affect network performance, such as delay, packet loss and capacity utilization. A Wireless-Optical Broadband Access Network (WOBAN) is gaining more attention because its good performance and merits such as reliability, robustness and high capacity as well as flexibility. In this paper, we proposed the Flow Limited and Risk Aware Routing Algorithm (FLRAR), which takes capacity utilization and link failure into account. And we also used Link Success Rate (LSR) to detect the link failure and redirect the related packets. The research results show that the process of information fusion has abilities of adapting and self-learning.

Introduction

A Wireless-Optical Broadband Access Network (WOBAN) is a hybrid of wireless networks and optical networks with passive optical networks (PON) in its backend and wireless mesh networks (WMN) to supply end users with the access[1]. The head terminal of PON resides at Central Office (CO) which is driven by Optical Line Terminal (OLT), while the tail end consists of Optical Network Units (ONU). ONUs connects to wireless Base Stations (BS) which form a multi-hop wireless mesh networks. Some BSs are called gateway routers, of which the location is critical. The end user sends packets or messages to one of neighborhood BS (or called routers). This BS then sends the packet into wireless mesh of WOBAN. The packet will reach the optical backbone through OLT/OC in the manner of multiple hops. The upstream of WOBAN in the wireless end is any cast while the downstream of WOBAN in the wireless end is uncast. This architecture can heal and organize itself with help of wireless mesh networks. The architecture is shown as Fig.1[2].

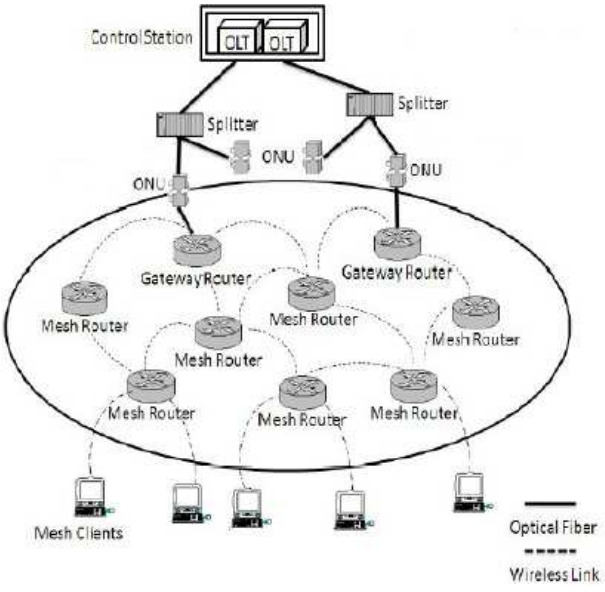

Fig.1 Architecture of WOBAN network

Performance Analysis

In this part, we will discuss the network performance based on FLRAR in four parts: load balance, number of hops, bandwidth utilization and self healing.

A. Load balance

If we only consider one aspect of the network constraints, other aspects of the network performance pay affect the whole performance. Take delay for example. If delay is the only factors for the algorithm, proposed in [3], congestion will occur if most packets select one single link whose link weight is minimum for transfer. We call this load congestion. In our algorithm, we set the link capacity and LSR for each link, which ensures that the load on one link cannot cause the load congestion and also ensures that the network can detect the link failure on time. So FLRAR helps to achieve the load balancing in the network[4]. We show this in Fig.2.

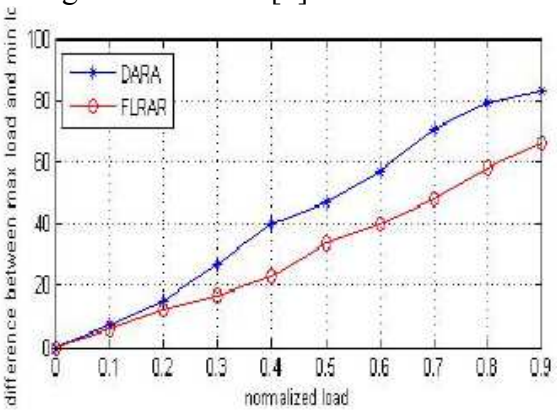

Fig.2 Comparison for load balance

B. Number of hops

Although the algorithms such as SPRA and DARA can effectively reduce the hops of the data link, lack of considering capacity and link failure cause the whole hop number increases as the load in the network increases. Our algorithm, FLRAR, effectively take capacity and link failure into account, which means that the hops will decline to an ideal level.

C. Bandwidth utilization

According to the previously proposed algorithms, such as DARA, the link with minimum weight will be assigned much more lead than other links. This will cause the bandwidth of this link is over utilized, which will cause congestion in the network. While other link bandwidths are underutilized. In FLRAR, the load is dynamically allocated according to the link condition. Thus FLRAR can increase the bandwidth utilization.

D. Self healing

In our algorithm, if one link gets failure, the LSR will decrease and the LWA will increase, which will cause tags added to the packet in this link. As a result, the network will redirect the packet to backup links. So FLRAR can achieve self healing effectively. To sum up, FLRAR can optimize the network performance in load balance, number of hops, bandwidth utilization and self healing.

Simulation Model

From the performance analysis, we can find that FLRAR can significantly improve the network performance in load balancing, number of hops, bandwidth utilization and self healing[5][6]. In this section, we choose bandwidth utilization and packet loss to simulate the model. The simulation model generates 1500 data packets and the repeating time is 10 times. For the bandwidth utilization, we compare the FLRAR and DARA; for packet loss, we compare FLRAR and CaDAR.

Fig.3 shows the capacity utilization of FLRAR and DARA. We can find that DARA maintain the capacity utilization at 50 percent as it select the data link only based on the LWA. On the other hand, with the increase of the load, FLRAR gain more and more advantage on capacity utilization. When the curve becomes flattened, the value can reach 70 percent. This shows that FLRAR have

advantage on capacity utilization. If we take one step further, we can get that FLRAR is suit for the extension of the network, as the load increases, the data link can be allocated dynamically, thus reduce the congestion.

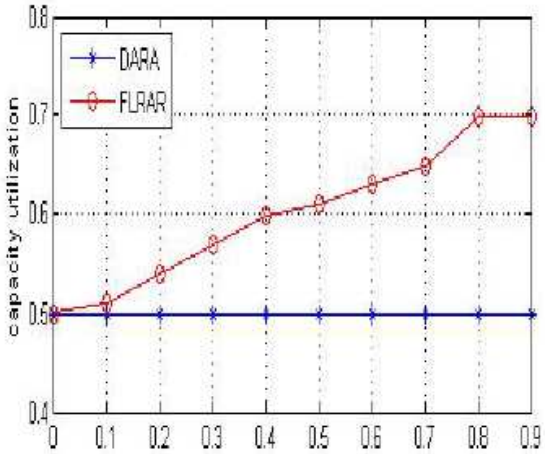

Fig.3 Capacity utilization of FLRAR and DARA

Fig.4 shows the comparison of packet loss number of FLRAR and CaDAR. The result shows that the tendency of two algorithms is the same. However, FLRAR can effectively reduce the packet loss number in order not to reach the threshold. On the other hand, CaDAR may cause too many packet loss, thus LSR is less than the threshold. The result is uniform with the performance analysis. So we can get that FLRAR can effectively reduce the packet loss.

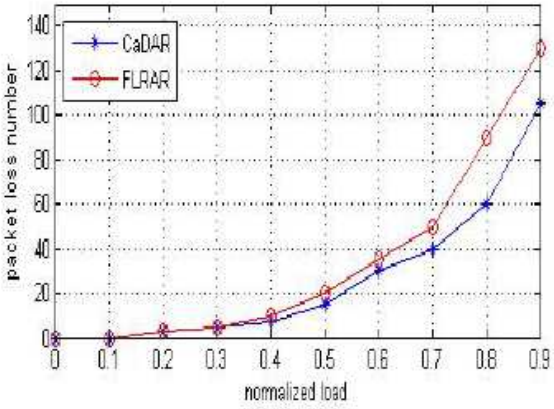

Fig.4 Packet loss of FLRAR and CaDAR

Conclusion

WOBAN is an effective architecture as it combines the merit of both wired and wireless network: reliability, robustness and high capacity as well as flexibility. However, ineffective routing algorithm can cause the declination of the network performance.

Flow Limited and Risk Aware Routing (FLRAR) algorithm take many factors into account, such as flow in each data link and link failure. It improves the network performance in load balance, number of hops, bandwidth utilization and self healing. The advantage of FLRAR is significant when the network load increases, so it is good to improve the scalability of the network.

References

[1] Suman Sarkar, Hong-Hsu Yen, Sudhir Dixit, Biswanath Mukherjee, "A novel delay-aware routing algorithm (DARA) for a hybrid wireless-optical broadband access network (WOBAN)", IEEE International Conference on Communications (ICC) 2009

[2] Abu (Sayeem) Reaz, Vishwanath Ramamurthi, Suman Sarkar,Dipak Ghosal, Sudhir Dixit, Biswanath Mukherjee, "CaDAR: an efficient routing algorithm for wireless-optical broadband access network", ICC, Beijing, China, May. 2010.

[3] Abu (Sayeem) Reaz, Vishwanath Ramamurthi and Suman Sarkar, "Flow-aware channel assignment for multi-radio wireless optical broadband access network", IEEE ANTS, Bombay, India, Dec. 2012.

[4] Abu (Sayeem) Reaz, Vishwanath Ramamurthi, Suman Sarkar, Dipak Ghosal and Biswanath Mukherjee, "Hybrid wireless optical broadband access network (WOBAN): capacity enhancement for wireless access", IEEE Globecom, New Orleans, LA, USA, Nov-Dec. 2009

[5] J. Li, X. Ba, S. Anjum and J. Chen, "Adaptive PLL Based Carrier Tracking Algorithm for GPS Signals IN High Dynamic Environment," Chinese Journal Of Electron Devices, vol. 30, no. 4, pp.1440-1443, August 2007.

[6] S. K. Shanmugam, "New Enhanced Sensitivity Detection Techniques for GPS L1 C/A and Modernized Signal Acquisition," Ph. D. Thesis of University of Calgary, Calgary, Alberta, 2010.

Advanced Materials Research Vols. 989-994 (2014) pp 4877-4880
© (2014) Trans Tech Publications, Switzerland
doi:10.4028/www.scientific.net/AMR.989-994.4877

Research on Image Vectorization Based on Fuzzy Neural Network and Expert System

Shaosong Wan[1,a], Jian Cao[2,b], Qunsong Zhu[2,c]

[1]XiJing University, Xi'an, Shaanxi Province 710123, P.R. China

[2]Air Force Engineering University, Xi'an, Shaanxi Province 710051, P.R. China

[a]12156555@qq.com, [b]cao_jian1972@163.com, [c]yancong192@qq.com

Keywords: Algorithm; Image; Fuzzy NN; Expert System

Abstract. Because the traditional linear vectorization methods have some shortcomings including processing data slowly, being sensitive to noises and being easy to be distorted. Fuzzy rules and its inference mechanism are the assurance of achieving feature fusion. However, the self-learning function of FNN could train its weights; it is difficult to optimize fuzzy rules. Besides, the common FNN training algorithms have low constringency speed and are liable to run into the local optimization.PSO algorithm has high convergence speed and it is simpler on the operation and is more potential on optimizing FNN. Thus, PSO algorithm could be adapted to train FNN weights, and prune the redundancy links, optimize fuzzy rules base. In the paper we present an improving immune genetic algorithm based on chaos theory. The over-spread character and randomness of chaos can be used to initialize population and improve the searching speed, and the initial value sensitivity of chaos can be used to enlarge the searching space. To avoid the local optimization, the algorithm renews population and enhances the diversity of population by using density calculation of immune theory and adjusting new chaos sequence.

Introduction

Genetic algorithm (GA) is an effective probability searching algorithm based on the natural selection and the genetics principle, and it carries on the search and the optimization through the simulation organic evolution, and it automatically gains and accumulates the related knowledge of searching space in the searching process, and it controls the searching process to obtain the optimal solution of the question.

The genetic algorithm has many merits such as the good overall search ability and easy realization and so on, but it also has some insufficiencies such as the slow convergence speed and the bad partial searching ability and easy precocious and so on, and it cannot obtain the unsatisfied solution frequently when it solves the optimal question of continuously differentiable complex multi-peak function. The expanded population scale and the improvable heredity operator can improve the partial searching ability, but it can reduce the operating efficiency of algorithm too. The immunity evolution algorithm is an emerging algorithm which develops by the immunity concept and theory in the life sciences[1][2]. This algorithm has many characteristics such as automatic identification of antigen, feature extraction, the diversity of immune body, distributional examination, learn and memory, self-plan etc, and it is also parallel distributional self-adaptive system which has the great potential in the application of intelligent computation. In recent years the immunity genetic algorithm has obtained the widespread application in many domains because it can effectively maintain the diversity of population and eliminate not mature astringency and the oscillatory occurrences. The reference presented an immunity genetic algorithm which extracts vaccine from the system knowledge and vaccinates to the evolution process, thus, it can fully use the system message, but the algorithm has not considered the diversity of population which influences the evolution process.

Feature-Level Fusion of Detection Information Based on Fuzzy Neural Network and Expert System

The feature-level fusion algorithm could be proposed by integrating FNN and ES. The fuzzy rules and its inference mechanism are the assurance of achieving feature fusion. However, the self-learning function of FNN could train its weights; it is difficult to optimize fuzzy rules. Besides, the common FNN training algorithms have low constringency speed and are liable to run into the local optimization.PSO algorithm has high convergence speed and it is simpler on the operation and is more potential on optimizing FNN. Thus, PSO algorithm could be adapted to train FNN weights, and prune the redundancy links, optimize fuzzy rules base.

The structure of fuzzy neural network is shown as Fig.1.

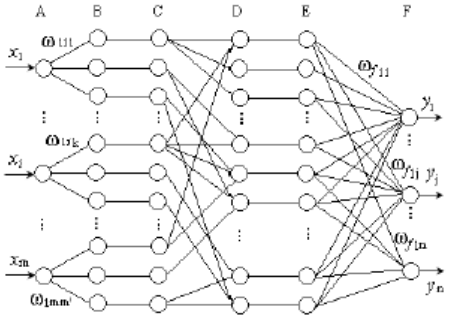

Fig.1 Structure of fuzzy neural network

For ease of comparison and visualization, the discriminator gains were normalized. The discriminating performance curves of the three algorithms with the correlator placing d = 0.25 (chip) and d = 0.5 (chip) are presented respectively in Fig.2.

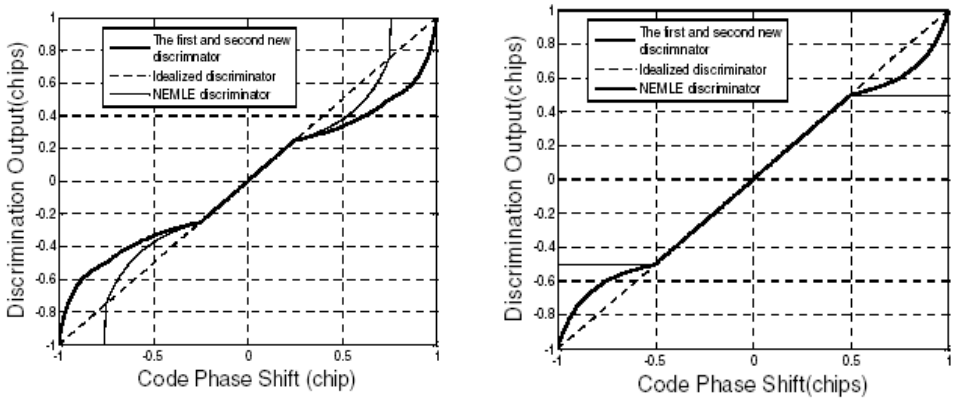

Fig.2 Discriminating performance curves with the correlator placing *d=0.25*(*chip*) and *d=0.5*(*chip*)

The analysis of the comparison obtained from Fig.2 is that, discriminator is better when d=0.25(chip), and the two new discriminators are better when d=0.5(chip).

Basic Theory in Mathematic Morphology

With the extensive application of digital images, vectorization of the original paper images has become an important task [3]. There are some shortcomings in the traditional method used in the image vectorization, such as the slower processing rate, sensitive to noises and easy to be distorted. Mathematical morphology, a nonlinear methodology, describes the characteristic of each image researched and the relationship between them by studying the geometry characteristic of objects in the image researched [4].

The mathematical morphology of binary images is the most basic morphological theory. The so-called binary image is the image whose gray value is either "0" or "1". Applying the basic binary morphology operations and combinations of them, we can analyze and process the shape and structure of the image. Supposing A is the original image to be processed (also called the target point set) and B (coordinates (I, J)) is a structural element, we introduce these types of binary morphological operations.

The original scanning image and the linear feature extraction results of the scanning images attained by this method are shown in Fig.3.

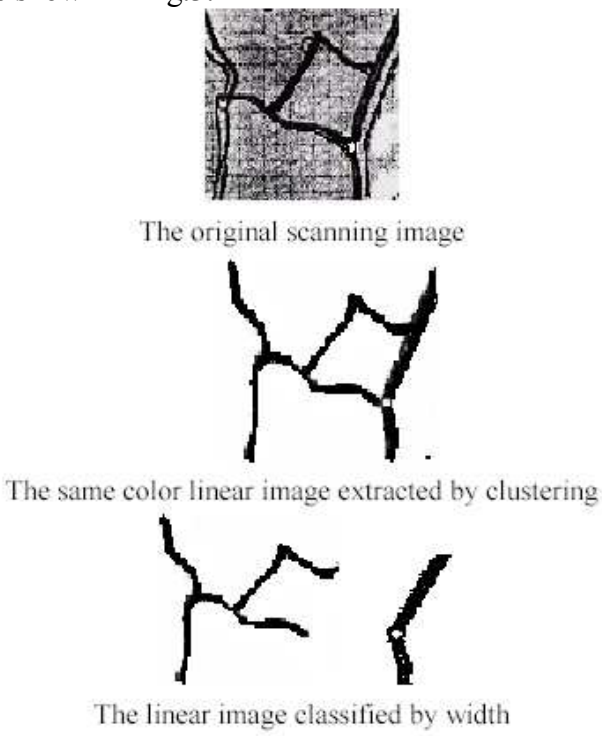

Fig.3 Results of edge detection algorithm based on the four structural elements

The noises and edges in the image are the places of the mutation of gradient, but the edge has different form from the noise. So during the edge detecting, we should confirm the pixels firstly and then distinguish the pixels to confirm they are the edge or the noise according to several structural elements. Filter them out if they are noise, otherwise retain them. Because we needn't take a mathematical morphology operation for each pixel of the image, large numbers of unnecessary operations are reduced. This operation can be carried out as following three steps:

(a) Select pixels of the mutation of gradient by taking use of the difference of adjacent pixels;

(b) Take the several structural elements binary morphology erosion operation for pixels of the mutation of gradient, so that we can filter out the noise and extract the edges;

(c) Attain the edge image.

Experimental Analysis of Performance of Two New Algorithms in Tracking Loop

The digital IF signal data with the sampling frequency 8.184MHz and the fixed Doppler frequency shift -600Hz, is generated by using simulation method. Supposed that, after signal acquisition, the carrier Doppler frequency estimation value is 590Hz, and the code phase estimation values are respectively 199.5(chip) and 199.2(chip). In the carrier tracking loop the sentenced cross-type FLL discriminator was used, and the correlator placing d is set to be 0.5(chip). Under these conditions, the signal tracking process can be presented respectively by Fig.4.

This algorithm combines the genetic algorithm, the immune algorithm and the chaos theory, it regards the question as the antigen, and it regards the solution of the question as the immune body. The affinity through the antigen and the immune body describes the approachable degree of the feasible solution and the optimal solution. To the outside antigen's invasion, the system produces the immune body through the chaos, and the system realizes to environment auto-adapted through the immune body density's judgment and adjustment. To enhance the precision of the solution and improve the convergent speed, the chaos is used to carry on the partial optimization nearby the optimal solution. The immune body density calculation is one of essential methods which retain the diversity of population.

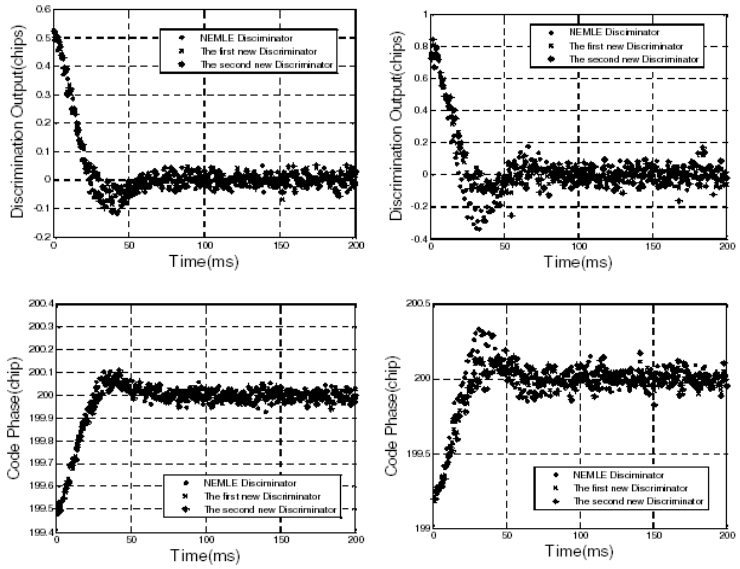

Fig.4 Tracking performance with the code phase estimation 199.2(chip) and 199.5(chip).

Conclusion

PSO algorithm could be adapted to train FNN weights, and prune the redundancy links, optimize fuzzy rules base. In the paper we present an improving immune genetic algorithm based on chaos theory. The over-spread character and randomness of chaos can be used to initialize population and improve the searching speed, and the initial value sensitivity of chaos can be used to enlarge the searching space. The algorithm applies in the function optimization question. The improved algorithm brings the question space and the corresponding solution space into correspondence with the antigen and the immune body, and it controls the reproduction of the partial optimal solution through the density. The algorithm can improve the search speed because chaos is introduced in the initial population and diversity adjustment. The algorithm can carry on the local optimization and increase precision nearby the optimal solution. The result of experiment shows the algorithm validity. We can draw a conclusion from experiment comparison, the paper's algorithm makes average movement algebra small, and the algorithm overcomes the shortcoming of slow convergent speed which generic algorithm has, and the algorithm is superior to convergent speed of immune genetic algorithm. Through the optimal value, we come to the conclusion that the paper's algorithm can avoid the local optimization and overcome precocious phenomenon of the genetic algorithm. Through the average optimum value, we may see the paper's algorithm has the good stability.

References

[1] Olfa Nasaroui, Fabio Gonzdez, Dipankar Dasgupta.The Fuzzv Artificial Immune Svstem: Motivations, basic Concepts and Application to Clustering and Web Profiling [J].Fuzzy Systerm 2012, 1(2):711-716.

[2] LEANDRO N, CASTRO DE TIMMIS J Artificial immune system: a novel computational intelligence approach [M]. Springe–Verlag 2010.

[3] S. Wang, D. Yang, Z. Liu and D. LUO, "Simulation Study on High Dynamic GPS Software Receiver," The international journal for computation and mathematics in electrical and electronic engineering, vol. 28,iss. 6, pp.1386- 1401, 2009.

[4] J. Li, X. Ba, S. Anjum and J. Chen, "Adaptive PLL Based Carrier Tracking Algorithm for GPS Signals IN High Dynamic Environment," Chinese Journal Of Electron Devices, vol. 30, no. 4, pp.1440-1443, August 2007.

[5] Abu (Sayeem) Reaz, Vishwanath Ramamurthi, Suman Sarkar, Dipak Ghosal and Biswanath Mukherjee, "Hybrid wireless optical broadband access network (WOBAN): capacity enhancement for wireless access", IEEE Globecom, New Orleans, LA, USA, Nov-Dec. 2009

Advanced Materials Research Vols. 989-994 (2014) pp 4881-4884
© (2014) Trans Tech Publications, Switzerland
doi:10.4028/www.scientific.net/AMR.989-994.4881

Research on Social Engineering in Network Security

Gang CHEN[1, a], Jun YANG[1, b], JunPing CAI[1, a]

[1]Academy of National Defense Informaiton, WuHan, 430010, China

[a]email: cg0916_cn@sina.com, [b]email:yangjun_gfxx@sina.com

Keywords: Social Engineering; Network Security; Complex Network; Deception

Abstract. The social engineering techniques such as flattery, persuade, induce, disguise, threat, obedience and infiltration was summarized. The main methods and steps of social engineering research and the main six aspects contents such as social engineering technology analysis, social engineering case survey were also put forward. Finally, a model of social engineering attack based on complex network is built and some prevention methods aiming to social engineering attack were presented.

Introduction

Vulnerability of network security is ubiquitous and any system has potential security risk. As taking more advanced and rigorous system security protection measures, exploits are becoming more and more difficult in technology [1]. Considering higher cost of attack and big technical difficulty, network attacker has to seek human vulnerability, which is called social engineering. The incident breaking through network security protection with social engineering method presents the obviously up-trend in recent years and it has been the most vulnerable link. It will be an important network security countermeasure field of information invasion in future.

Summary of Social Engineering

Social engineering originally means studying social problems with engineering method. In network security, it especially means the skillful use of some peculiarities in human nature including curiosity, greedy, trust, obedience and instinct by attacker for stealing valuable information. It combined multiple subject knowledge and skills including psychology, human relations, praxiology and so on [2]. Such attack involves every aspect and they influence one another and it has been seen as a very complicated systematic engineering. So this attack method is named by social engineering.

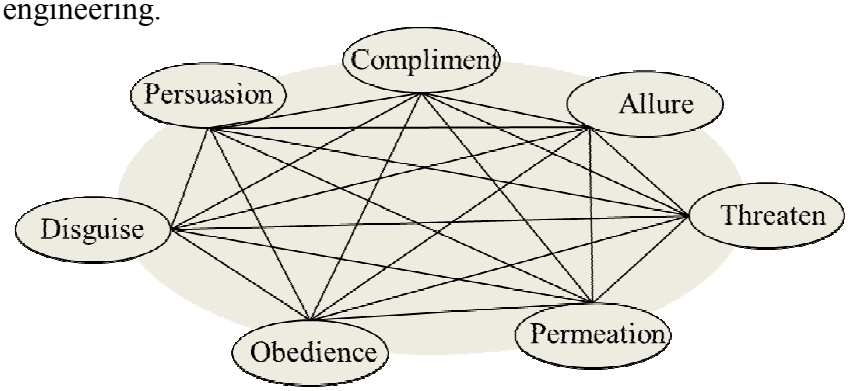

Fig.1. The relationship of multiple social engineering attack means

Differences between social engineering and other attack method are combined application of psychical attack and behavioral attack. As it is shown in Figure 1, the psychical attack was given even more weight and main means covers compliment, persuasion, allure, disguise, threaten, obedience, permeation, and so on. A wise network attacker of social engineering will never dwell on single means during the process of attack and they will be instinctive to perform attacking with one or more methods based on practical situation. They can easily jump from one method to anthoer method and make attack impossible to protect.

Research Precedure and Method of Social Engineering

Socail engineering can be reserarched as follow steps. Firstly, main components of social engineering method will be extracted to perform mental analyzing and technology analyzing according to investigation statistics. Secondly, the whole process of attack should be abstraction modeled and be described with XML format, which can provide model driven for subsequent simulation [3]. Thirdly, all attack means of social engineering is reproduced in order to provide research objects and samples protecting network attack of social engineering. Finally, traceback aiming at attacker will be performed to help analyzing mental activity locus and behavior pattern. The research precedure is shown as Figure 2.

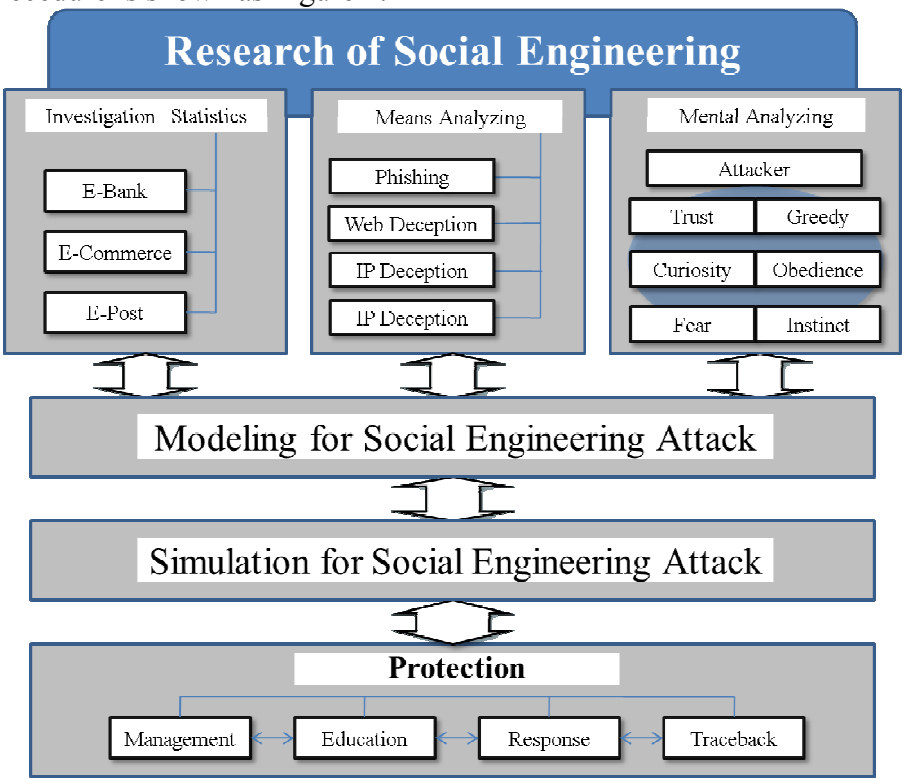

Fig.2. The research precedure of social engineering

Research methods are mainly consistes of five different kinds. First is comparing with various technology methods of social engineering. Second is investigating to massive network user extensively. Third is analyzing to mental activity and attack process, which will finds its features and laws. Fourth is building mathematical modeling for social engineering attack. Fifth is simulating attack means and performing actual attack with special respondents.

Studies of Social Engineering

Case Study. Social engineering attacks aiming at E-bank, E-commerce, etc will be investigated as a case sample. Cases can be collected by discussion and questionnaire with numerous sample workers. So first-hand materials and samples will be gained by analyzing with attack results in investigation case.

Means Analysis. All kinds of attack means including network phishing, Web deception, IP deception, DNS deception must be analyzed. Social engineering attacks mianly directs at mind habit and mind set, its behaviour rules and feartures are traceable. There is association between technology and attack tool. Rules can be summarized by analyzing process, method and means.

Mental Analysis. It analyzes mental of attackers and objects. Both attack object and protection object are persons, whose network behaviours are easily influenced in mental including greedy, fear, trust, curiousity, obedience, instict, etc. Aiming at different targets, attacker can apply comprehensive with multiple means. So it can help protect network attack by reproduced thought processes of attackers.

Attack Model. A complete social engineering model should be built with case study, means analysis and mental analysis. It covers most of the aattack methods and means. Attack and protection can be studied mathematically, and probabilities of success can also be calculated in allusion to each attack.

Simulation. That is simulation for social engineering scene and attack. Real experience will be provided to investigation object in simulation and it can also protection awareness aginst social engineering attack.

Protection. It is not only passive protection for social engineering attack. Besiding security management, educaiton and emergency response, it can find out physical adress and IP adress of attacker by traceing source and back. So attackers will be investigated and revenged even they successed.

Attack Model

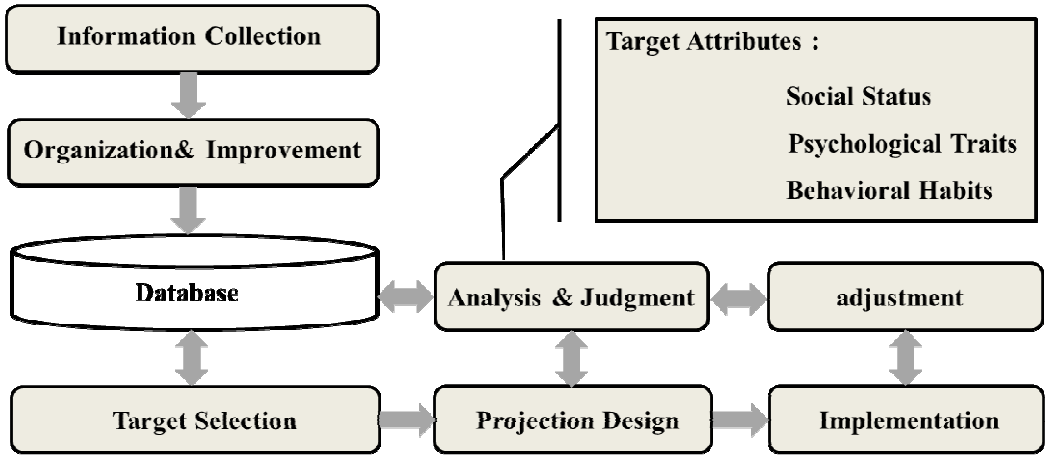

Fig.3. The model of social engineering attack

Social engineering attacker usually collects all kinds of information preparing for subsequent attack action. As it is shown in Figure 3, analysis and judgment will be the most difficult and complicated steps in social engineering attack model together with projection design. Human being is the world's most complex organisms owning nature and social attributes. Social engineering attackers can't success even they have further studied sociology, psychology, human relations, praxiology, economics, politics, and so on. Basing on viewpoint of complex network, relationship of creatures in nature and social life forms a very complex network [4]. It is shown in Figure 4.

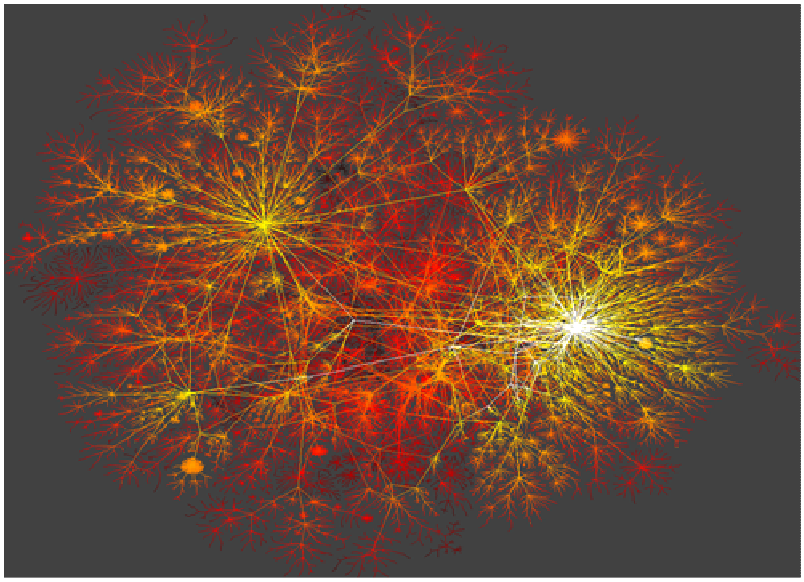

Fig4. The complex network of relationship

Security Protection

Social engineering attack isn't simple deception and it involves complicated psychology elements. It is hard to protect user from attack for it is difference to attack with technology methods [5]. It is critical that two operations including checking identity and authorization of requester must be acted. In general, protection can be started with security awareness, educational training, security management, strategy making, security technology, and so on.

Correct Security Awareness. Protecting personal information should be paid more attention and learned. Security concept must be clutivated to enhance protection awareness and form rational analysis habit. Knowledges need to be mastered and it can be realized with education, training and propaganda.

Educaitonal Training. The basic protection quality for trainees can be built by educational training. They can query anyone who posts request no mater anybody he claimed. They will check identity and authorization of anyone requesting information or operation. They will protect sensitive information and acquaint with data classificaiton system.

Strategy Making. Information security management strategy is about security problem in system adopted corresponding principles, requirement for security products, data protection methods and security running of important system. Responsibility of system management should be separated as far as possible and authority owning by system manager should be distributed reasonably.

Security Technology. Some simple network security technologies should be teached to user and security risk will be lowered effectively. So network security technologies will be applied actively and attack difficulty will be increased.

Conclusion

The scientific methods of mathematical statistics were put forward to study social engineering and its attack case. Each attack method and mean is analyzed comprehensively with its technology characteristics. It has application value in the practice no matter at operation or theory research and it will help to perform effective security protection measures aiming at social engineering attack.

References

[1] Shi Mingyu, Chen Shaojun. Discrimination of Sociology on Engineering Project and Social Engineering [J]. Academics. 2011 3 57-63.

[2] Jiang Yu. Social Engineering Research of Computer Network Attack [J]. Journal of Hunan Economic Management College. 2006 17(6) 279-280.

[3] Gao XiaoYan. Deceiving Technology Research of Attack and Defence in Network Security [J]. Journal of ZhengZhou Economics & Management Institute. 2006 21(1) 84-86.

[4] Sun LiJuan. Discuss of Social Engineering [J] Journal of Kaifeng Institute of Education. 2009 29(4) 48-49.

[5] Zhao QingQiang. Social Engineering Attack and Defence Countermeasure for Online Bank User [J]. Journal of ABC Wuhan Training College. 2011 147 78-79.

Advanced Materials Research Vols. 989-994 (2014) pp 4885-4888
© (2014) Trans Tech Publications, Switzerland
doi:10.4028/www.scientific.net/AMR.989-994.4885

Network Security Situation Awareness Based on Multi-source Data Fusion

Gang CHEN[1, a], JunPing CAI[1, a], Jun YANG[1, b]

[1]Academy of National Defense Information, WuHan, 430010, China

[a]email: cg0916_cn@sina.com, [b]email:yangjun_gfxx@sina.com

Keywords: Situational Awareness; Network Security; Information Fusion

Abstract. Network security situation awareness is an effective way to analysis security situation of complex network.The concept and model of network security situational awareness was introduced.A new model of network security situation awareness was proposed. Considering the characteristics of multi-source information in network security research, a security situation awareness algorithm based on information fusion was adopted. This algorithm advanced modified D-S evidence theory, gets the values of security situation awareness of network by data source level fusion, host-level fusion and system-level fusion. The results can reflect the general security state of network.

Introduction

With network going deep into social life, malicious activities aiming at network are growing and attacks such as Dos/DDos are becoming a growing threat. The traditional network security management is usually dependent on discrete deploying network security devices involving firewall, anti-virus and intrusion detection. So many problems including single function, larger warning information and too much irrelevant warning information will appear. Network security manager is hard to control being confronted with security situation of total network due to facing too much warning information. This would cause effective responses can't be taken in time.

Research of network security situation awareness is a hot field developing in recent years and it fuse warining information coming from security detection tools. It can also provides the foundation for network security managers with decision by analysing current network security situation and predicting attack behavior which will happen in next step. It is of great importance to imporving monitoring capability of network, emergency response capbility and predicting development tendency of network security.

Network Security Situation Awareness

Definition of situation awareness was firstly proposed by Endsley in 1988 [1]. It means precepting and comprehending environmental factor in a certain time and space. After that, future trends will be projected. The concept model ot the definition is shown as Figure 1.

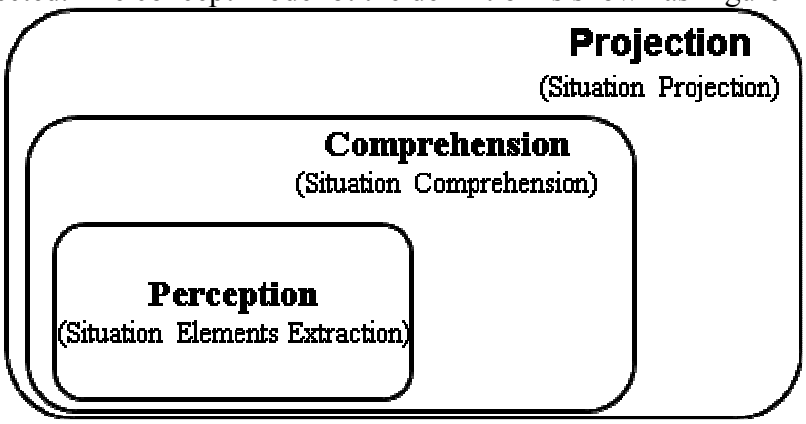

Fig.1. The concept model of situation awareness

The concept named network situation awareness was firstly proposed by Bass in 1999. The function model of network situation awareness based on multi-sensor data fusion based upon data fusion with joint directors of laboratories [2]. The function model is shown as Figure 2.

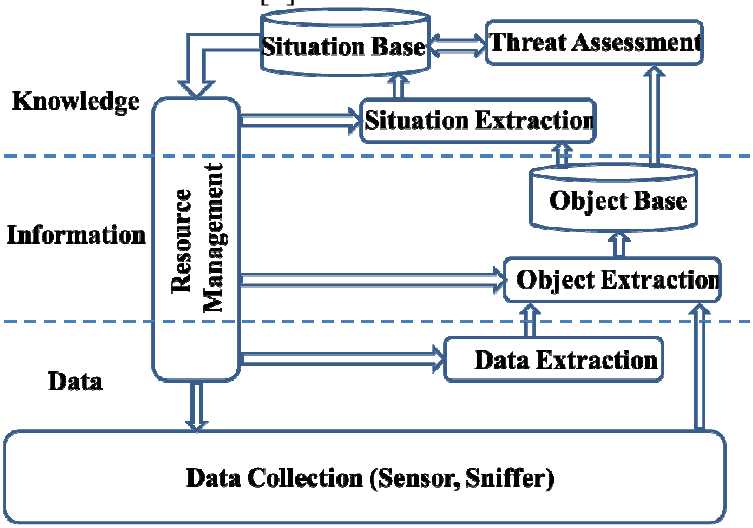

Fig.2. The function model of network situation awareness

Basing on different application fields, network situation can be divided into security situation, topology situation, transmission situation, and so on. But the current research of network situation is all about networksecurity situation [3].

In fields of network security, preception is extration process of network security situation element data. That is extracting data generated by all network security tools such as sensor and sniffer deploying in network. Comprehension is analytic processing process with extraction data. That is comprehending inner meaning of data by object extraction. Projection is predicting future trends of network security by threat assessment and knowledge reasoning process based on current and history information. Total situation of network security will be formed eventually by extracting and abstracting with data, information and knowledge.

Network Security Situation Awareness Model Based on Multi-source Data Fusion

In large and complex network, extraction data by situaion awareness are characteristics of multi-source, heterogeneous, big data, etc. Fusion processing with the data mentioned above is a difficult problem for situation awareness of large-scale complex network [4]. Combined with the concept model and function model shown as Figure 1 and Figure 2, a three layed model of network security situation awareness based on multi-resource data fusion is presented, which is shown as Figure 3.

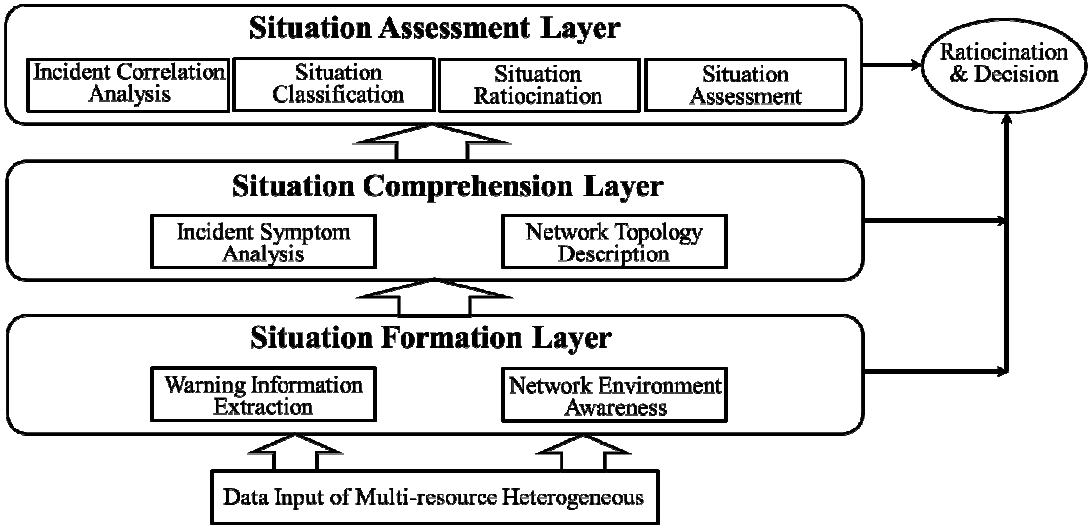

Fig.3. The network security situation awareness model based on multi-source data fusion

As it is shown in Figure 3, the first layer is network security situation formation layer, which performs physics collectting original data or signal. The environment scene can be described with current network topological structure and running state by correlation and processing. Then the data collection required by network security situation assessment will be formed.

As it is shown in Figure 3, the second layer is network security situation comprehension layer, which accepts data input forming in situation formation layer and completes refinement of target data. That is performing correlation analysis of target position, state, characteristic parameter and identity attributive information collected by multiple detectors with some criterion or algorithm. So precise expression of single entity target can be gained and the primary description and assumption of current network security situation can be performed.

As it is shown in Figure 3, the third layer is network security situation assessment layer, which determines current network security situation condition. Rational analysis and explanation will be performed combined with knowledge of field expert on the basis of network security incident symptom generating in situation comprehension layer and correlation analysis result of security incident. The network security situation condition is intention recognition of attack event, threat analysis and trend analysis of security situation.

Based on the model mentioned above, perception index of network security situatin can be reduced to two kinds called system structure information N and attack information I. The formal desciption of them are expressed as follow.

$N=(H,T)$, The H expresses collection of host node in system including server, terminal, all kinds of routers and switches. For some host node $h\in H$, it can be expressed as a four group $(id,wh,svhn,vulsh)$. The id is the unique identifier of host node and the wh is weight of host node. The $svhn$ is application server running in host node and the $vulsh$ is existing vulnerability in host node, which includes hardware vulnerability, wrong configuration, and so on. The T expresses network topological information which is collection of all physical connection relationship. It is expresses as $T\subseteq H\times H$.

$I=(I_p,I_d)$, The I_p expresses known attack information. For any known attack information $i_p\in I_p$ in system, it can be expressed as a four group $(id,vulsl,\log p,v)$. The id is the unique identifier of attack information and the $vulsl$ is needed by attack. The $\log p$ is log collection of known attack in detection device and the v is value of attack threaten limiting by $[0,1]$. The I_d expresses attack information detected. For anyone attack information $i_d\in I_d$ in system, it can be expressed as a dualistic group $(id,\log d)$ and the id is the unique identifier of detection device. The $\log d$ is log collection actually detected by detection device.

$SA=(N,I)$ is expressed as security situation value of system, which is formed by system structure information N and attack information I.

Data Fusion Algorithm

Data fusion is a data processing characteristic by multi-level and multi-layer, which mainly completes processing with data of automatic monitoring, interaction, correlation, estimation and combination coming from multiple information sources. Through integrated usage of multiple-source information, data fusion can get more objective and intrinsic knowledge of certain object or target.

A kind of three-level data fusion algorithm is adopted. The first level is data source level fusion, which is mainly solving fusion of multi-source warning information. It computes support rate $m(A)$ of some attack event happening by data source fusion based on detection log and host configuration information of multiple related detection devices. The second level is host level fusion, which computes security situation of host node with attack event happening support rate $m(A)$, attack successful support rate $S(A)$ and attack threaten. The third level is system level

fusion, which computes system security situation value with security situation of host node and weight of each node, and system security situation can be traced out.

Data Source Level Fusion. Fault and fail rate are higher on account of uncertainty of detection device. For judging a true attack event with some warning, support rate of some attack behaviour happening is needed to compute with fusion of these warning information. D-S evidence theory provides a synthetic method of related evidence and it can fuse evidence supplied by multiple evidence sources [5][6]. The D-S evidence theory is based on nonempty sets Θ, which is named as recognization framework. Each situation element comes form recognization framework $\Theta = \{N, A\}$. The N expresses normal behavior, the A expresses attack behavior and $NA = \phi$.

Host Level Fusion. Detection result indicates happening probablity of external attack and influence to host node is combined action with external attack information, interior fragility information of host node and threaten information of attack. So computing security situation of host node is need to fuse host situation elements with attack happening support rate $m(A)$, successful attack support rate $s(A)$ and attack threaten V.

System Level Fusion. The system security situation value will be gained by fusing security situation and weight of each host node in system level fusion.

The system security situation value SA will be computed by data resource level fusion, host level fusion and system level fusion. This value reflected total condition of system security and values of multiple time intervals can be used to drawing situation curve graph, with which system security condition can be mastered intuitively by security manager. Finally, system security trend can be predicted on the basis of the situation curve graph.

Conclusion

Based on provided network security situation awareness model, a multi-soure data fusion method adopting “data source level fusion-host level fusion-system level fusion” is presented to precept and assess security situation of network. It affords effective method for developing visual situation awareness system. In future work, multi-source data fusion algorithm needs to be optimized and the model should be proved by simulation examples [7].

References

[1] Endsley M R. Design and evaluation for situation awareness enhancement. Proceeding of the Human Factors Society 32nd annual meeting [C]. 1988.97-101.

[2] Bass T, Arbor A. Multisensor data fusion for next generation distributed intrusion detection systems. Proceeding of IRIS National Symposium on Sensor and Data Fusion [C].1999.24-27.

[3] XI Rong-rong, YUN Xiao-chun, JIN Shu-yuan, ZHANG Yong-zheng. Research survey of network security situation awareness [J]. Journal of Computer Applications, 2012 32(01) 1-4,59.

[4] HU Hua-ping, ZHANG Yi, CHEN Hai-tao, XUAN Lei, SUN Peng. The study of large scale networks intrusion detection and warning system [J]. Journal of National University of Defense Technology, 2003 25(1) 21-25.

[5] Li Bicheng, Wang Bo, Wei Jun, et al. An efficient combination rule of evidencet heory [J]. Journal of Data Acquisition & Processing, 2002 17 (1).34-36.

[6] Feng Chuan, Network security situation awareness system key technologies [J]. Network Security Technology & Application, 2013 (9) 119-120.

[7] Yang Jia-xing, Simulation analysis of complex network security situation assessment model [J]. Computer Simulation, 2013 30(8) 289-292.

Advanced Materials Research Vols. 989-994 (2014) pp 4889-4892
© (2014) Trans Tech Publications, Switzerland
doi:10.4028/www.scientific.net/AMR.989-994.4889

Research on Mobile E-commerce in 3G Environment

Ying Luo[1, a] , Bin Gui[2,b]

[1]TVET Research Institute, Jiangxi Science & Technology Normal University, Nanchang, China

[2]Education School ,Jiangxi Science & Technology Normal University, Nanchang, China

[a]mooonly@126.com, [b]154296945<guivipbin@qq.com

Keywords: mobile e-commerce, 3G era ,strategy

Abstract. With increasing integration of mobile communication and internet technology, mobile e-commerce is begining to becomet useful supplement of traditonal e-commerce and shows strong vitality and development potential, relying on superiority in technology and application. The paper presents current situation of mobile e-commerce in 3G era, analyzes the problems, and puts forward corresponding strategies and rational suggestion.

Introduction

With the coming of 3G network, e-commerce mode is facing new revolution, the rising of mobile electronic business. The so-called 3G, the abbreviation of 3rd generation, shorted of the third generation mobile communication technology, refers to the cellular mobile communication technology for high speed data transmission. The 3G service can transmit sound at the same time(call) and data information(e-mail, instant messaging and so on), which characteristic is providing high-speed data service.

Mobile commerce (M-Commerce) refers to the electronic commerce of B2B, B2C or C2C through mobile phone, PDA, handled computer and other wireless terminals. It perfect combines the internet, mobile communication technology, the short distance communication and other technology, so that people can carry out a variety of business activities at any time and any place, realize online and offline shopping and transaction, electronic payment and various business activities, financial activities and related service activities whenever and wherever.

Advantages of mobile e-commerce

Mobility. The traditional electronic commerce is limited by network linear and terminal equipment fixed, but mobile e-commerce with wide wireless network and mobile communication equipment can effectively eliminate the distance obstacle. Mobile e-commerce can create more efficient interactive information, and use mobile communication and real-time communication directly oriented to users to breakthrough the limitation of online communication efficiency, so as to provide unlimited mobile service for users.

"4A" effect. The mobility of mobile e-commerce, the most significant feature, should be reflected in that anyone has access to information communication and realizes any service at any place and anytime. "4A" effect develop greater free scale business environment for mobile e-commerce, reduce the requirement of traditional electronic commerce to equipment and network environment, and reduce the threshold of users' participation.

Commercial value changes. Investigation report of development situation of China mobile internet shows that in Chinese 356000000 mobile phone users, intelligent mobile phone users reach 190000000. It makes development space of mobile e-commerce further increased. Because the characteristic of mobile communication equipment make each mobile terminal represent a certain consumer, it reflects its special business resource and value. In the modern business environment cored as the customers, the concern to internet uses turns more to mobile communication consumers of doubling population, which is the effective transformation of commercial value.

Problems existing in the development of mobile e-commerce

The consumption concept is too traditional. Influenced by traditional ideas, some people still hold wait-and-see attitude. Developing mobile e-commerce is not only a major change, but also a revolution of commodity trading idea. The traditional shopping way, selling cash-and-carry, has been ingrained in the thought of most consumers, but online electronic payment cannot be accepted. Therefore, consumption habits formed long term and inherent payment mode is the threshold in the growth process of fast service.

Laws and regulations are not perfect. Mobile e-commerce, as a new business mode, will inevitable bring a series of legal issues. But the relevant law is electronic signature law promulgated in April, 2005. Compared with foreign countries, the existing laws and regulations are far. The development of mobile e-commerce in our country is still in initial stage, so the relevant laws and regulations have not been introduced, which makes problems about mobile e-commerce trade, tax and security issues inextricability. Therefore, there is certain difficulty in protecting basic rights and interest of participant in mobile e-commerce.

Safe risks are still the key. Safe problem is the core and key restricting the development of mobile e-commerce, which is a universal phenomenon. Due to security concern, some consumers step back to mobile e-commerce. The wireless channel, an open channel, gives wireless users communication freedom and flexibility, and also brings many unsafe factors. Personnel information registered in the network may be stolen and tampered, which is security problem of mobile network; account number and password of bank card input at the time of payment may be stolen, which is security problem of payment system; the mobile phone may be installed software stealing users' information, which is security problem of mobile terminal. So how to establish efficient and uniform safety standards has become the problem of mobile e-commerce development needing to be solved.

Awareness of using mobile means is not high. Investigation report of China mobile internet development shows that application permeability of overall mobile internet in 2011 increased, communication application and information obtaining lead the development while the entertainment and business application developed relatively slow. Mobile phone instant communication and micro-blog, the representative of communication application, is the mainstream application to promote the development of mobile internet at this stage. The traditional consumption idea is difficult to change in the short term, and few consumers support mobile e-commerce development project, such as online payment, online banking, mobile phone booking, network group purchasing. The awareness of using mobile means is not high.

Value application of mobile e-commerce is not complete. Although the scale of mobile internet users is growing fast as well as mobile phone users, the development of mobile e-commerce market is only depends on the increasing number of users, but the developing and mining of mobile e-commerce application value. If the mobile service only focuses on the information inquire entertainment and so on, the industry chain of mobile e-commerce can not be further improved, and users' service demand and the business profit demand can not be satisfied, which reflects the value application of the mobile e-commerce is not complete and mobile operators should develop large-scale mobile service.

Mobile application development lack attractiveness. With the appearance of new mobile technology, telecom operators join the application field of e-commerce, and mobile e-commerce mode also emerges as the times. Mobile e-commerce lead by telecom operators is in its infancy, technology development of mobile communication is far less powerful than software development ability of Network Company. Operators don't have experience in e-commerce operation and lack deep analysis to the market and user need. With the continuous introduction of 3G service implementation, it is difficult to develop the application service of mobile e-commerce targeted to customer demand, so mobile service application development lack attractiveness.

High data fees reduce the willingness to pay. Investigation report of China mobile internet development shows that mobile phone users' demand for wireless network traffic is not large. Most users use mobile phone to hang QQ and brush micro-blog, while mobile users are very sensitive to the

wireless network traffic and the corresponding price. The mobile phone lack Software tool types and contents of the corresponding version, leading to that users are unwilling to pay for internet products. More than 80% mobile phone users haven't bought mobile phone application service in the past six years, the higher fees of mobile internet tariff influence the development speed of mobile e-commerce.

Development strategies of mobile e-commerce

Strengthen the construction of correlation laws and regulations, and create harmonious legal industry environment. At present, there are no targeted laws and regulations to guide 3G mobile e-commerce industry, so the competition in mobile e-commerce industry will be so hot that trade disputes will increase under the background of financial crisis. Once trade disputes and industry problems occur, there is no uniform standard to handle with and all the participants' rights will be in the unprotected state. What's more, the economic crisis lash, e-commerce industry develops too rapidly, industry competition increase, external shocks strengthen, which all call for related laws and regulations. Creating harmonious legal industry environment is extremely urgent.

Improve the industrial chain and promote the development of correlation industry. First, improve the industry chain to seek common development. 3G mobile e-commerce is proposed on the basis of traditional e-commerce and depends on the new 3G network. So it should carry out depth cooperation from the level of industry, for example, jointly establish and perfect 3G network, expand e-commerce market using industry, expand online good, build brand protection and credit improvement, carry out joint promotional activities, enhance consumption experience of user terminal, etc.

Improve the customer terminal service and enhance the directional effective communication. Compared with the traditional e-commerce terminal equipment, terminal equipment function of 3G mobile e-commerce is more powerful. Mobile phone users and other targeted consumers use these equipments to make personal touch and customize information according to personal characteristics and interests. According to database containing a large number of active customers and potential customer information, Mobile business can make full use of the advantages of 3G network to carry out more targeted information advertising through personalized SMS, MMS and other service activities, and improve the directional effective dissemination of advertising information. Second, cooperate with mobile phone manufacturers to joint research mobile e-commerce trading platform software. From the view of users, develop private, timeless, convenient and efficient terminal software to improve consumption experience of user terminal and perfect customer terminal service.

Establish the network security strategy and enhance customer trust. How to guarantee the security of e-commerce activities is the core problem of e-commerce development. After the outbreak of the financial crisis, consumer behavior and enterprises' investment behavior are becoming cautious. So the development of 3G mobile e-commerce must first solve the problem of network security and thoroughly remove the future problem of the consumers. The characteristic of e-commerce, virtual trade platform, determines that it should carry out business activities through network. Mobile e-commerce mainly relies on mobile phone, panel computer and other terminal devices to transmit information by wireless channel. The wireless channel is an open channel, which makes communication flexible, mobile, vulnerable and instable. Although the birth of 3G network greatly alleviate this situation, however, protecting consumers' personal information and commercial secret is still the problem we should pay attention to. We could solve the network security fundamentality through technological innovation, and also can promote network security of e-commerce through technological innovation.

Strengthen industry self-regulation and jointly cope with external force. Compared with foreign 3G mobile e-commerce industry, our 3G mobile e-commerce industry is still in the primary stage of development. The outbreak of financial crisis makes all the countries focus on China and hope to get rid of the economic crisis by China, a consumption power with 1.3 billion populations. Facing the

impact of external force, the e-commerce industry of our country should unite as one, jointly cope with, create industry standards, strengthen self-discipline, upgrade the industry level and deal with foreign competition. Specifically speaking, we should spur with long accumulation, strictly control speculation and develop in the steady.

Improve the correlation industry. Virtual 3G mobile e-commerce extremely relies on the logistics distribution system. Over the years, logistics and distribution network system in China is not perfect, which is a bottleneck restricting the development of mobile e-commerce. If 3G mobile e-commerce wants to have new breakthrough and development in the long run, we should develop and improve the logistics distribution network system. Provide the most convenient and safest delivery service to the minimum inventory level; choose the nearest distribution outlets and the most convenient transportation means from the nearest delivery route to make the goods reach the hands of consumers completely.

Improve the personnel training system and promote industry soft power. In 21the century, talents are the most important. Mobile e-commerce, as an emerging industry, should pay attention to the training of professional talents for rapid development. Mobile e-commerce, the multiple of business management and information technology, needs business talents with professional business knowledge in terms of market application. But the induction of 3G mobile network urgently requires practitioners to have technical knowledge. Many factors make the choosing and training of 3G mobile e-commerce practitioners become the priority among priorities. Specifically speaking, fist, cultivate by school. Set up courses related to the network technology in the e-commerce subject and related subjects of all universities, solving the problem of talent lack from the source. Second, in view of the current 3G mobile e-commerce practitioners, enhance the quality of employees through short-term professional training. Third, enterprises and school cooperate with each other to cultivate 3G e-commerce talents directly.

Conclusions

In 2003, SARS brought development opportunity to traditional electronic commerce. We have reason to believe that in the post financial crisis period, 3G mobile e-commerce will rely on favorable environment of economy, politic and industry to cope with the challenge positively and effectively to realize the leap development of e-commerce industry.

References

[1] F．Robins.The marketing of 3G．Marketing Intelligence 21. 2003(6)：370～378.

[2] Willimn Grawford.Jonathan Kaplan. J2EE Design Patterns. 0'Reilly Media. Inc. 2003.

[3] Lianying Wang. Development prospects of mobile e-commerce in 3G communication era[J]. China technology expo, 2009(14).

[4] Yiqiang Li. Effect of 3G on the mobile e-commerce in Chia[J]. Business review, 2011(11).

[5] Haobo Sun. Development of electronic commerce under financial crisis. National business(theory), 2010(12).

Advanced Materials Research Vols. 989-994 (2014) pp 4893-4896
© (2014) Trans Tech Publications, Switzerland
doi:10.4028/www.scientific.net/AMR.989-994.4893

Research And Analysis Process Of Android Communication Platform In AIDL Model

AnMing Hu

Tianhe College of Guangdong Polytechnical Normal University

GuangZhou 510540 E-mail: anminghu@hotmail.com

Key words: Android, AIDL, interprocess communication

Abstract. AIDL is a android platform to describe the inter process communication interface description language, can simplify the process of data exchange between the format and data code.Research on AIDL communication mechanism has an important significance to the realization of the Android platform interprocess communication. This paper analyzed the AIDL model and the communication mechanism and gives examples to discuss.

Introduction

Android is a mobile platform Google development based on Linux operating system,The platform is open source, the advantages of stable, easy development etc,Affected by the developers, users and developers alike, has become the most widely used mobile intelligent platform. With the wide use of Android platform, all under the platform of Android application system based on also emerge as the times require, HoweverAndroid platform application development with the traditional Windows and Liunx, Interprocess communication is used as the underlying technology is very important in the operating system, to understand and grasp the inter process communication, is very important for the development of application system under Android platform.

In the traditional operating system, communication, realize the function of the system platform of resource sharing among multiple processes, is a very basic and important function of the application, At the same time, The important function of interprocess communication is the operating system kernel part。Android operating system is based on Linux, in the Linux process communication generally use the traditional IPC (Inter-Process Communication, IPC) model，And the IPC model to achieve the shared memory, pipes, message queues and socket etc., Although widely used IPC model, but the UID/PID data in IPC mode is filled by an application, the existence of poor reliability, easy to be tampered with, difficult to maintenance. In order to solve the problem of Android platform, the interface description language (AIDL). Implementation of interprocess communication through the interface and the proxy class methods, solve this problem.

AIDL (Android Interface Definition Language) is a Android system custom interface description language IDL, Is one of the common ways of implementation of interprocess communication in Android platform, AIDL grammar rules and similar Java language, without written by C++ interface, no mixed C++ compiler, simplifies the process of communication development. Belong to lightweight communication mechanism, with high efficiency, simple implementation.

The Principle And Process Of AIDL Implementation

AIDL language is a system level primitives, but the syntax structure and Java language is very similar, AIDL is mainly used to define access interface, no implementation process.

Table 1. The grammar characteristics.

Type	Explain	Need to introduce
The basic types of Java language	Including Boolean, byte, short, int, float and double etc.	FALSE
String	java.lang.String	FALSE
CharSequence	java.lang.CharSequence	FALSE
List	Among all elements must be supported AIDL data types	FALSE
Map	All the bond and element must be AIDL supported data types	TRUE
Other AIDL interface	Any other use of the interface type AIDL language generation	TRUE
The Parcelable object	An object that implements the Parcelable interface	TRUE

Unlike Java, AIDL allows you to define the direction of transfer function parameters, support three kinds of direction in AIDL: in, out, inout.

Identification of in parameters will be passed from the caller to the remote service;

Identified as out parameters from the remote service delivery to the caller;

Identified as inout parameters will be passed from the caller to the remote service, and from the remote service is returned to the caller.

The process of ADIL implementation according to the following steps:

to create the AIDL interface description file;

Through the Java interface to realize the remote service AIDL interface android.os.Iinterface interface;

And use the remote service binding;

The client calls;

In the case of AIDL communications, server generally consists of a AIDL file and a IService interface and the Service class, The IService interface is used to access method defined in AIDL, and IService must be a android.os.Iinterface interface, Service is the AIDL interface implementation class.

1) AIDL files are defined as follows:

```
package com.TestAIDL;
  interface IService {      int getAccountBalance();
     int getCustomerList(in String branch, out String[] customerList);       }
```

2) Implementation of the Iservice interface

Consisting of three parts in the Service interface AIDL interface to achieve its internal structure, The internal static abstract class Stub, Stub class and its subclasses are very important in the whole AIDL communication, is used to implement the AIDL interface implementation class, Stub must be implemented subclasses of Android.os.Binder and Iservice; Static inner classes Proxy, Proxy belongs to a class is provided to the remote service invocation interface class; Is the IService to achieve AIDL access interface method. The Iservice interface part of the code is shown as follows:

```
public interface IService extends android.os.IInterface
{public static abstract class Stub extends android.os.Binder implements com.lifeblood.ITestService
{private static final java.lang.String DESCRIPTOR = com.TestAIDL .ITestService";
public Stub(){this.attachInterface(this, DESCRIPTOR);}
private static class Proxy implements com.lifeblood.ITestService
{private android.os.IBinder mRemote;
…….
int getAccountBalance();
int getCustomerList(in String branch, out String[] customerList);
```

/Static inner classesProxy /……..
public int getAccountBalance();
public int getCustomerList(in String branch, out String[] customerList);

3）Implementation of the TestService class

The TestService implementation class, is a common Service class Android.os.Service class Android, Is an important implementation class implements the AIDL interface, but the process is a bit special, is defined by the ItestService.Stub type member variables, The method of calling Iservice interface, which is defined in the AIDL interface method. Following this kind of mechanism:

public class TestService extends Service {private Context mContext = null;
private IService.Stub binder = new Stub(){ private String name = null;
public int getAccountBalance() throws RemoteException { return 1000;}
public int getCustomerList(String branch, String[] customerList)
throws RemoteException { customerList[0] = name;
System.out.println("Name:"+branch);return 0;} };

4）Start the Service service in the Activity class

In this case the Service is to provide remote services, without the need for access to the local Activity, so Service can be activated using the Intent class, the code is structured as follows:

Intent service = new Intent(this, TestService.class);startService(service);

5) The AndroidManifest.XML Configuration

The AndroidManifest.XML file configuration is very important, the remote service access by other processes to service, is using the AndroidManifest file name for the configuration of positioning, the Service configuration is as follows:

<service android:name="TestService" android:process=":remote"> <intent-filter>
<! -- AIDL full path name. Must specify the class name, the client can pass the AIDL to find the implementation class -- >
<action android:name=" com.TestAIDL.TestService" /></intent-filter></service>

6) The Client Process Calls

The client process calls and similar to JNDI method, by implementing the ServiceConnection interface of remote service binding, get the Service object, so as to realize the call, the client instance also need to copy the AIDL interface file. The following ServiceConnection structure:

public void onServiceConnected(ComponentName name, IBinder service) {
tService =TestService.Stub.asInterface(service);
System.out.println("Bind Succeed:"+tService); }
public void onServiceDisconnected(ComponentName name) {tService = null; } };

7) The Test Run

The procedure of the program are as follows:
The first running TestService server
Then run the AIDLClient client
Click AIDL to get Service service connection binding, and display call information.

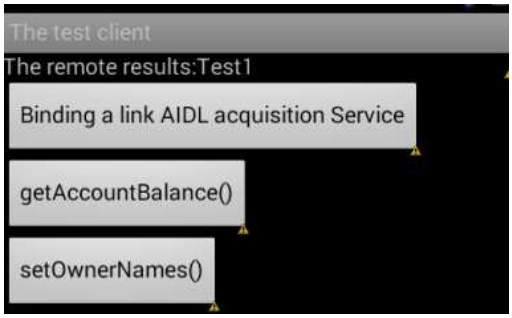

Fig.1 To obtain Service effect

Conclusion

The AIDL interface description language grammar structure and Realization principle, And the implementation process of AIDL in remote call process,Configuration method and correlation are analyzed and discussed.

AIDL is based on object-oriented design implementation of interprocess communication, and AIDL language with primitives rule system in Android platform, Android system development process, inter process communication provides a more simple and convenient access model.

References

[1]Ruyan Wang. Analysis and Research on communication mechanism of Binder process under Android. Computer technology and development 9:108-11. (2012).

[2]Jing Li. Research and application of Binder mechanism in Android. The industrial control computer.4:66-68(2012).

[3]Ping Chen Bo Wu. Research and improvement of LinuxIPC security mechanism. Journal of PLA University of Science and Technology. 5:78-82. (2004)

[4]Jingxin Guan, Yongquan Li. Android Activity life cycle[J] Computer knowledge and technology.5:27-29. (2013)

[5]Frederic, Translated by Xiaodong Yang. Intelligent mobile phone standard Web programming [J] Tsinghua University press5:27-36. (2010)

[6](United States) Li Weimeng, Chenguang He. Android 4 programming classic entry -- development of intelligent mobile phone and tablet computer application .Tsinghua University press6: 13-27. (2012)

Advanced Materials Research Vols. 989-994 (2014) pp 4897-4901
© (2014) Trans Tech Publications, Switzerland
doi:10.4028/www.scientific.net/AMR.989-994.4897

Push Technology Based on Analytic Hierarchy Process

Liu Zhi[1, a], Xia Xincheng[1] and Li Yue[1]

[1]Nanjing Research Institute of Electronics Engineering, Nanjing 210017, China

[a]liuzhi271692225@163.com

Keywords: server push mode; analytic hierarchy process; server performance; server load

Abstract. First of all, three current server push modes are elaborated in this paper, including a detailed analysis and comparison. Due to a single server push mode is used by the current push frame, most application requirements can not be meet. Push techniques based on analytic hierarchy process is proposed in this paper, which selects optimal push mode in different situations by theory of operations research. This method not only improves server performance but also reduces server load. Finally, experimental results show that the proposed method is superior to other single mode.

Introduction

With the rapid development of internet network technology, internet technology has entered a mature stage. In recent years, internet has come to be the primary method for people to get information. In web technology, the real-time information transmission has a wide range of application, which including device monitor, network conference, collaborative work and so on. In order to realize these applications, the server must push change message to client [1, 2].

As a new message push technology, web-based push technology can push change message to the client asynchronously. At present, appropriate browser plug-in are generally required to be installed in client with these techniques, so deployment, maintenance and security issues will bring a series of problems. According to different client request types, this paper propose a real-time message push model based on Http, which can select optimal push technology in different situations by theory of operations research.

Three Http-based Push Modes

A. Ajax-based Polling Mode

Http is stateless and one-way protocol, so users can only send request to the server though the client, and the server returns response message after processing by the server. Ajax-based polling regularly refers to set timer in the client, and periodically send asynchronous request to the server from a web page. After the request is processed by the server, the client will parse the returned XML and refresh partial page [4].

In order to ensure real-time of data acquisition, most invalid and redundant responses send to the client frequently. This mode is not only a waste of server computing resources, but also occupies the network bandwidth and the invalid net flow. If we choose to adjust the polling frequency, which means increasing time intervals to reduce the load on the server, real-time of data can not be guaranteed and the server pushes requirements can not be achieved.

B. Ajax-based Long-polling Mode

Ajax-based long polling mode means when a request sends to a server asynchronously by Ajax in the background will not be return immediately, but maintain the original HTTP link in the server for some time until events arise or connection timeout. The process flow is shown in Fig. 1.

The main advantage of this mode is to maintain a long connection between the client and server, but server thread and memory resource consumption will increase after requests are blocked. When the number of connections increases, the response speed of the server will be affected. This mode not

only makes full use of the request processing time in the server, but also makes the very short stay as long as possible by blocking mechanism. This mode reduces the average number of requests, so it is better push technology presently.

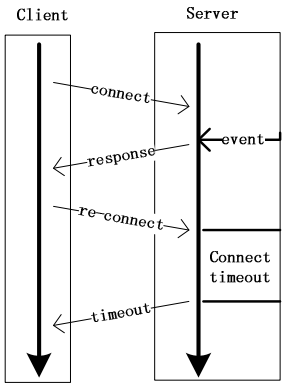

Fig. 1 Ajax-based long-polling mode

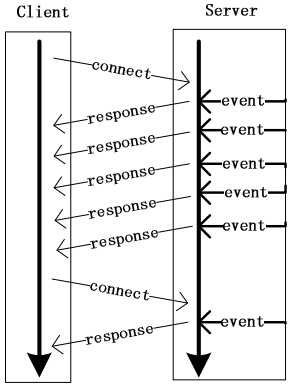

Fig. 2 Iframe-based Streaming Mode

C. Iframe-based Streaming Mode

Iframe-based streaming mode is a technology which hides the iframe in web page and sets its src attribute as the never closed connection request. The server continuously sends data to the hidden iframe of the client, and the client will refresh partial page according to the received data. From Fig. 2, the server and the client always remain connect. When events are generated from the server, the client can receive data from the server directly without re-establishing the link. This mode can save more setup link time and network bandwidth compared to the two modes above.

D. Comparison of Three Modes

From Table 1 of push technology in the three modes we can see, each kind of push technology has its own advantages and applicable scene. Ajax-based polling mode is applicable to scenes of server events with a fixed interval; Ajax-based long polling mode is applicable to scenes of server events with short interval and high real-time requirements; Iframe-based streaming mode is applicable to scenes of server events with frequent interval and high real-time requirements.

Table 1 Comparison of polling, long-polling and streaming

Mode	Polling	Long-polling	Streaming
Memory consumption	low	high	relatively high
Real-time	worse	good	very good
Request frequency	high	normal	low

AHP-based Push Mode

A. Analytic Hierarchy Process

AHP (Analytic Hierarchy Process) was put forward by the operational research experts of USA, which is an effective multi-target decision method combining qualitative analysis with quantitative analysis [5, 6]. The problem is divided into the target layer, criterion layer and decision layer. To avoid multiple factors confusing decision-making, AHP makes the decision process more clear and reasonable by hierarchical analysis of problems [7]. Steps of the weights of attributes calculated by AHP are as follows:

(1) The establishment of evaluation system hierarchy structure. Make clear of the problems to be analyzed, divide the factors contained into different layers to establish a hierarchical structure.

(2) Structure of comparison matrix. Judgment matrix means the relative importance of a factor in this level compare with last level.

$$A=\left[\frac{\beta_n}{\beta_m}\right]_{m,n},\ B^{CPU}=\left[\frac{C_i^{CPU}}{C_j^{CPU}}\right]_{i,j},\ B^{Mem}=\left[\frac{C_i^{Mem}}{C_j^{Mem}}\right]_{i,j},\ B^{Time-Delay}=\left[\frac{C_i^{Time-Delay}}{C_j^{Time-Delay}}\right]_{i,j},\ B^{Event-frequent}=\left[\frac{C_i^{Event-frequent}}{C_j^{Event-frequent}}\right]_{i,j},$$
$$B^{Connect-count}=\left[\frac{C_i^{Connect-count}}{C_j^{Connect-count}}\right]_{i,j} \quad (1)$$

We can describe the elements $(\beta_m^*,\beta_n^*)\in\{\beta_{CPU}^*,\beta_{Mem}^*,\beta_{Time-Delay}^*,\beta_{Event-frenquent}^*,\beta_{Connect-count}^*\}$ and thus $(C_i^*,C_j^*)\in\{C_{Polling}^*,C_{Long-Polling}^*,C_{Streamin\,g}^*\}$

(3) The calculation of the weights. The weights calculation means the calculation of the maximum largest eigenvalue and eigenvector of the judgment matrix. Though the eigenvalue method $A\tilde{\omega}=\tilde{\lambda}_{\max}\tilde{\omega}$ to calculate eigenvector $\tilde{\omega}$, and $B\omega=\lambda_{\max}\omega$ to gain eigenvectors ω. Then the eigenvalue and eigenvector in three Http-based push modes can be described as $\lambda_{\max}$, $\lambda_{\max}^{CPU}$, $\lambda_{\max}^{Mem}$, $\lambda_{\max}^{Time-Delay}$, $\lambda_{\max}^{Event-frenquent}$, $\lambda_{\max}^{Connect-count}$ and $\tilde{\omega},\omega^{CPU}$, ω^{Mem}, $\omega^{Time-Delay}$, $\omega^{Event-frenquent}$, $\omega^{Connect-count}$.

(4) Consistency of judgment matrix. In order to maintain the consistency of judgment thinking, consistency of judgment matrix is required when AHP method is used. The calculation of the consistency is as follows:

$$C\cdot I=\frac{\lambda_{\max}-n}{n-1} \quad (2)$$

The coefficient C can be used to check the consistency of judgment matrix as shown in the following Eq. 3：

$$C\cdot R=\frac{C\cdot I}{R\cdot I} \quad (3)$$

Where $C\cdot R$ is consistency index, when $C\cdot R<0.1$, we accept the judgment matrix.

(5) So the hierarchy weight can be finally calculated as:

$$\mu=\left[\omega^{CPU}\quad\omega^{Mem}\quad\omega^{Time-Delay}\quad\omega^{Event-frenquent}\quad\omega^{Connect-count}\right]_{5\times5}\tilde{\omega}_{5\times1} \quad (4)$$

B. AHP-based Push Frame

Server push technology is based on the browser platform, which can push abundant information to the client browser server actively and meet the needs of the real-time required information for client. With the continuous improvement of server push technology, the mature server push technology framework appears. These technical frameworks focus on issues of server performance, and use a single server push mode for all service requests without paying attention to the specific application needs and ignoring the differences between different application requirements.

In this paper, the differences in the different application requirements are considered. In order to optimize the performance of the overall application and make full use of system resources, we can perceive the change of application status and adjust server push mode dynamically by AHP method. The main considerations in AHP analysis layer include event frequency, CPU resource, memory consumption, the number of user connections, network bandwidth and so on. The AHP-based push frame in this paper is shown as in Fig. 3.

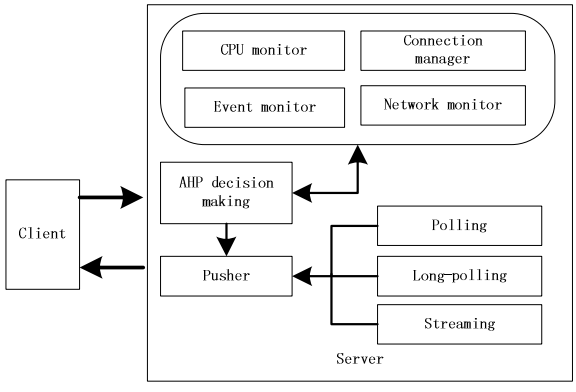

Fig. 3 The structure of AHP-based Push Frame

Experimental results

In the same LAN environment, the three modes in above section and the mode proposed by the paper are simulated respectively. In order to simulate a high number of clients, we use open source tool Grinder, which is an open source load generation and data collection tool, providing an internal TCP Proxy, allowing to record events sent by the browser and later replay them. CPU usage and triptime is two major quality indexes of service concerned by us. We define triptime as follows:

$$\text{Triptime} = |\text{Data Creation Date} - \text{Data Receipt Date}| \tag{3}$$

Mean triptime and server CPU usage results are presented in Fig. 4 and Fig. 5：

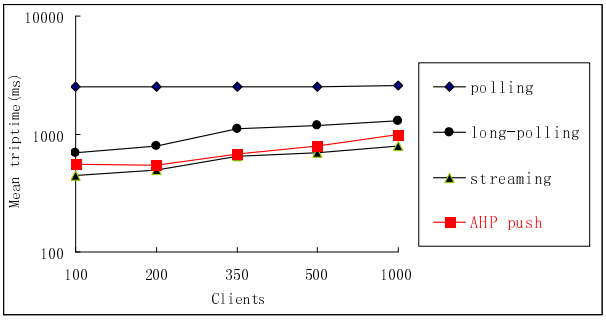

Fig. 4 Mean triptime result

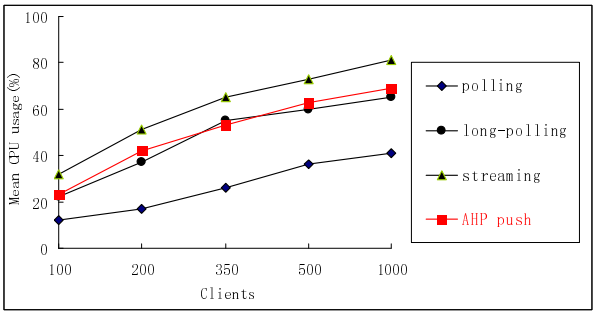

Fig. 5 Mean CPU usage result

From the results it can be found, triptime of streaming and long-polling method are shorter than that of polling method if there is fewer number of client. This is because in the streaming and long-polling mode, the server can send message to the client immediately after the change event, while the polling mode is bad real-time capability. We also find that long-polling mode produce data flow more than streaming mode in our experiment, because client will be forced to send request after receiving data in long-polling mode. Triptime of streaming mode is the shortest in three modes, the flow can be controlled at a minimum in this mode. With the increase of the number of clients, the difference between streaming mode and other two modes will become more obvious.

The AHP push mode proposed in this paper realize the fusion of three modes in an application, so that each request is applied to be push in an appropriate way and the precious resource of the server will able to be used effectively. In ensuring the overall quality of service at the same time, the application of different allocation strategies can improve server performance and reduce the server load in a certain extent.

Summary

AHP-based Push Mode by this paper orders appropriate server push technology for different types of requests, which can improve quality of application service and server performance more effectively than single push mode.

References

[1] M. Ammar, K. Almeroth, R. Clark, and Z. Fei. Multicast delivery of web pages or how to make web servers pushy. Workshop on Internet Server Performance, 1998.

[2] M. Bhide, P. Deolasee, A. Katkar, A. Panchbudhe, K. Ramamritham, and P. Shenoy. Adaptive push-pull: Disseminating dynamic web data. IEEE Trans. Comput., 51(6):652–668, 2002.

[3] R. Srinivasan, C. Liang, and K. Ramamritham. Maintaining temporal coherency of virtual data warehouses. In RTSS' 98: Proceedings of the IEEE Real-Time Systems Symposium, page 60. IEEE Computer Society, 1998.

[4] A. Mesbah and A. van Deursen. Migrating multi-page web applications to single-page Ajax interfaces. In CSMR' 07: Proceedings of the 11th European Conference on Software Maintenance and Reengineering, pages 181–190. IEEE Computer Society, 2007.

[5] Golnam. The integration of an RE method and AHP: A pilot study in a large Swiss bank.2013.

[6] Mason. Obtaining fuzzy membership functions and rule sets in fuzzy expert systems with AHP. [M].Systems, Man, and Cybernetics, 1998. 1998 IEEE International Conference on,1998.

[7] Newman. Evaluating risks of new substances in electronic products: using an abridged lifecycle assessment-analytic hierarchy process (ALCA/AHP) computer-based tool. [M].Electronics and the Environment, 1998. ISEE-1998. Proceedings of the 1998 IEEE International Symposium on,1998.

[8] V. Trecordi and G. Verticale. An architecture for effective push/pull web surfing. In 2000 IEEE International Conference on Communications, volume 2, pages 1159–1163, 2000.

Advanced Materials Research Vols. 989-994 (2014) pp 4902-4904
© (2014) Trans Tech Publications, Switzerland
doi:10.4028/www.scientific.net/AMR.989-994.4902

Information Management of Digtal Libirary Based on Data Mining

HUANG Suyu[1, a]

[1]Wuhan Donghu University, Wuhan 430063，China

[a]huangsuyu425@126.com

Keywords: Data mining, digital libirary, Internet, research, Web data, information management;

Abstract. With the development and maturity of digital libirary, the Internet has become more and more intelligent, humane and social. It began gradually infiltrated into every aspect of people's lives, influence and change people's way of life. digital libirary era as representative products -- information management has been the suddenness of a thunderbolt swept the interaction information user global information managementing platforms began showing explosive growth trend however, and people are facing information explosion but the core concept of wisdom barren embarrassing situation. [1]

Introduction

Digital libirary era is to take the customer as the center, pay attention to the user experience and user interaction, therefore, how to effectively collect and use information management platform of Shanghai amount of user mutual information, and dig out valuable knowledge from the information management, in order to improve the user experience, become the hot topic of Internet industry research and discussion in order to improve the use of information managementing users interactive data rate, the paper tries to apply the Web data mining technology into information management applications to the mining information management characteristics and in-depth study of relevant theories of personal tag cloud and exploration of Web data Cable, putting forward the innovative concept of information management platform based on individual tag clouds, and the design and implementation of the main information management personal tag cloud system in this paper includes the following two aspects: the first part of theoretical research, firstly, a detailed analysis of the related theory of data mining and Web mining, and summarizes the main techniques the classification of data source function process and key problems.

The use of Web data mining laying the related characteristics of the technology with a good theoretical basis and detailed summary analyzes the main content and structure elements of information management expression characteristics and function etc. [5]

It also helps us to fully understand the development status of information management architecture model of user demand and facing major problems for the development of information managements based on individual tag cloud to provide a good platform second theoretical basis for the practical research, mainly reflected in the design and implementation of personal tag cloud system information management based on the first in-depth research and design of the pretreatment method of information management data, mainly divided into the log preprocessing And the text pretreatment two parts to elaborate, for the text mining provides high quality data sources next step detailed introduces the design and implementation of personal tag cloud, and summarizes the practical significance of creating information managements based on individual tag clouds, pointed out the direction for the future research. [4]

Web data mining

(1) The concept of Web data mining

Data mining is a process to reveal the implicit, previously unknown from large amounts of data in the database and the potential value of information. [2]Web data mining is the application of data mining technology in the Web environment is to discover the potential, useful model or information

from Web documents and Web activity. It is a comprehensive technology, involves many fields of Internet, artificial intelligence, computational linguistics, information science, statistics etc.

(2) The type of Web data mining

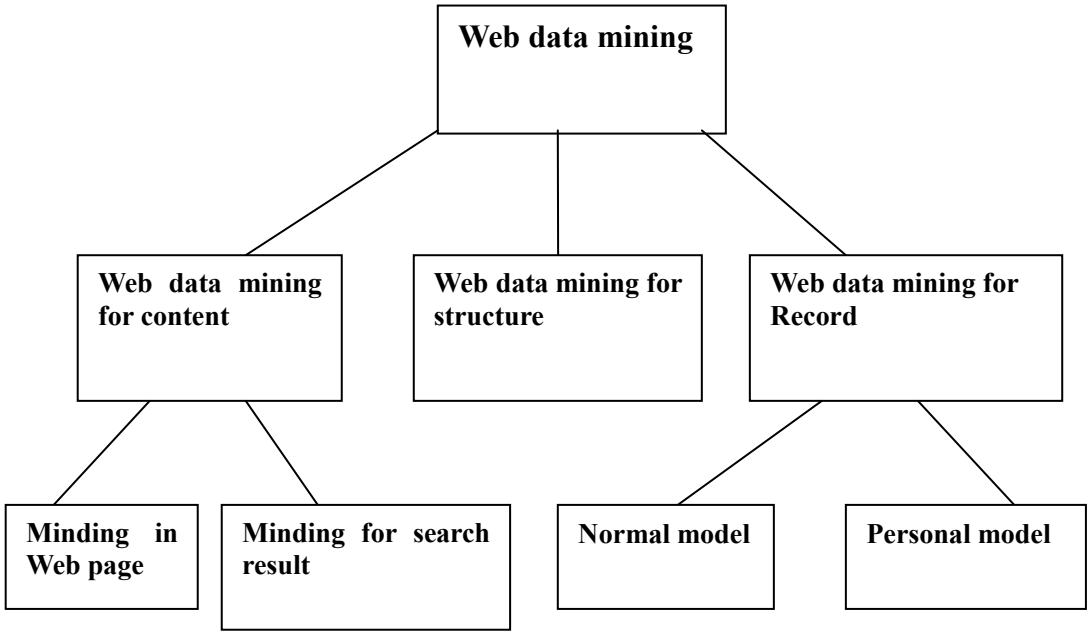

Support (F- I) =P (F∪I) (formula 1)

Confidence (F- I) =P (FBI) (formula 2)

For example, association rules: (X. "20... 29) "^income X. 20K"... 29K ") buys (X." HR_PLAYER "[Support=2%, confidence=60%]) Where X is the variable, representing the tourists, the rule analysis database instance 2% (support) in 20-29 years, the annual income of 20k-29k. There are 60% possibilities of this age and income groups of customers to buy the HR player (the degree). [1]

Diversity of Web information in electronic commerce determines the diversity of the data mining tasks. According to the Web treatment of different objects, Web data mining can be divided into the following three types [1]:

a. Web content mining (Web Content Mining): can be divided into the Web search results page content mining and mining. The former refers to mine the data on Web. The latter refers to a search engine based on mining, search results, and to get more accurate and useful information. Web content mining methods commonly used are Web OQL and Ahoy.

b. Web structure mining (Web Structure Mining): can be divided into a hyperlink mining, URL content mining and mining. The whole Web space, useful knowledge not only included in the Web page content, and included in the structure of the page. Web structure mining is the mining structure mode link potential Web, is a mining structure of Web page directory path hyperlink relationship, document structure, document in the URL. The Page2Rank method is the use of inter document links to find related pages Web, the algorithm is flowed:

Split_Infox(X) = -SUM ((|T|/|Ti|)*LOG (|Ti|/|T|))

Gain ratio(X) = Gain(X)/Split_Infox(X)

WTX-W0 >0 X∈ω1 -WTX-W0 <0 X∈ω2

P(Y | X) = P(X | Y)P(Y) / P(X)（1-1）

P (Xi | Yi) = (nc + mp) / (n + m)

c. The Web usage mining (Web Usage Mining): can be divided into general access pattern mining and personalized service pattern mining. It is from Web access logs extraction interest

pattern. Each server in the WWW has retained the access log, recording user access and interaction information. Analysis of these data can help understand user behavior, improve the structure of the site, or to provide personalized service to users [1].

Application of Web data mining technology in electronic commerce

(1) To retain the old customers, and tap potential customers

Through Web mining, electronic commerce operator can learn each visitor personal interests, to fully understand customer needs, providing customized products according to the unique needs of each customer, and according to the dynamic demand to customers to do page recommendation, adjust the Web page, increase customer satisfaction, customer retention time prolonged, reach retain customers to. By mining the Web log records, can be the first to classify existing visitors from its classification, and then determine whether a new client is a potential customers.

(2) Product marketing strategy formulation, optimization of promotional activities

Mining and sales through access to goods, enterprises can gain access to regular customers, identify customer life cycle, according to the change of the market, develop appropriate marketing strategies for different products [4].

(3) To reduce operating costs, improve the competitiveness of enterprises

The owner of the electronic commerce through Web data mining, can obtain reliable market feedback information, careful analysis of customer behavior in the future, for e-commerce marketing activity; can be decided according to the pattern of advertising a product of the visitor's browsing interest position, increase advertising targeted advertising, improve the rate of return on investment, thereby reducing operating costs, improve the competitiveness of enterprises.

Conclusion

Information management has become the most popular application of the digital libirary era; this paper focuses on how to apply Web mining technology to the analysis of online information managements. Meanwhile, it also introduces the Web mining and information management technology and concepts, and shows how the Web mining technology used in information management analysis. The analysis process of Web mining information management, and analyzes the future research direction in this field and trend are also involved in this paper.

References

[1] BingLiu.Webdata Miding [M].Beijing: Beijing Tsinghua University Publishing House, 2011, PP34-37.

[2] Agrawal, R., Rajagopalan, "Mining Newsgroup Using Digital Libirary Arising From Social Behavior" In Proceedings of World Wide Web 2003 Conference [M]. Budapest, Hungary, pp. 529-535.

[3] Chen, D., Shao, Z.,"Mining Hidden Community in Heterogeneous Information managements" In Proceedings of LinkKDD 2005 Conference [Z]. August 21, 2005, Chicago, IL, USA, pp. 58-65.

[4] Cooley, R. Mobasher, B. and Srivastave, J. "Web Mining:. Information and Pattern Discovery on the World Wide Web" [C].In Proceedings of the 9th IEEE International Conference on Tool with Artificial Intelligence, 1997, pp. 558-567, Newport Beach, CA, USA

[5] Pierrakos, D., Paliouras, G., Papatheodorou, C., Spyropoulos C. D. "Web Usage Mining as a Tool for Personalization: A Survey", User Modelling and User Adapted Interaction [J].Vol.13, Issue 4, pp. 311-372, 2003.

Advanced Materials Research Vols. 989-994 (2014) pp 4905-4908
© (2014) Trans Tech Publications, Switzerland
doi:10.4028/www.scientific.net/AMR.989-994.4905

Research on E-government Model Based on Big Data

Yiqing Lu[a]

School of Information Management, Beijing Information Science and Technology University, Beijing, 100192, China

[a]email: luyiqing@126.com

Keywords: E-government; Big data; Cloud computing; Public management

Abstract. The rapid development of big data will greatly change the government's management mode. Each country in the world has issued various policies to deal with the development of big data, and our government also attaches great importance to the industry of big data. The e-government model based on big data proposed in the paper raises new ideas for the innovation of e-government affairs.

Introduction

Big data, a general term for the massive amount of digital data being collected from all sorts of sources, is too large, raw, or unstructured for analysis through conventional relational database techniques. Almost 90% of the world's data today was generated during the past two years, with 2.5 quintillion bytes of data added each day. Moreover, approximately 90% of it is unstructured. Still, the overwhelming amount of big data from the Web and the cloud offers new opportunities for discovery, value creation, and rich business intelligence for decision support in any organization. Big data also means new challenges involving complexity, security, and risks to privacy, as well as a need for new technology and human skills. Big data is redefining the landscape of data management, from extract, transform, and load, or ETL, processes to new technologies (such as Hadoop) for cleansing and organizing unstructured data in big-data applications.

Although the business sector is leading big-data-application development, the public sector has begun to derive insight to help support decision making in real time from fast-growing in-motion data from multiple sources, including the Web, biological and industrial sensors, video, email, and social communications. Many white papers, journal articles, and business reports have proposed ways governments can use big data to help them serve their citizens and overcome national challenges (such as rising health care costs, job creation, natural disasters, and terrorism).There is also some skepticism as to whether it can actually improve government operations, as governments must develop new capabilities and adopt new technologies (such as Hadoop and NoSQL) to transform it into information through data organization and analytics[1].

Introducing of Big Data

Big data is the term for a collection of data sets so large and complex that it becomes difficult to process using on-hand database management tools or traditional data processing applications. The challenges include capture, curation, storage, search, sharing, transfer, analysis and visualization. The trend to larger data sets is due to the additional information derivable from analysis of a single large set of related data, as compared to separate smaller sets with the same total amount of data, allowing correlations to be found to "spot business trends, determine quality of research, prevent diseases, link legal citations, combat crime, and determine real-time roadway traffic conditions."

As of 2012, limits on the size of data sets that are feasible to process in a reasonable amount of time were on the order of exabytes of data. Scientists regularly encounter limitations due to large data sets in many areas, including meteorology, genomics, connectomics, complex physics simulations, and biological and environmental research. The limitations also affect Internet search,

finance and business informatics. Data sets grow in size in part because they are increasingly being gathered by ubiquitous information-sensing mobile devices, aerial sensory technologies (remote sensing), software logs, cameras, microphones, radio-frequency identification readers, and wireless sensor networks. The world's technological per-capita capacity to store information has roughly doubled every 40 months since the 1980s; as of 2012, every day 2.5 exabytes (2.5×10^{18}) of data were created. The challenge for large enterprises is determining who should own big data initiatives that straddle the entire organization.

Big data is difficult to work with using most relational database management systems and desktop statistics and visualization packages, requiring instead "massively parallel software running on tens, hundreds, or even thousands of servers". What is considered "big data" varies depending on the capabilities of the organization managing the set, and on the capabilities of the applications that are traditionally used to process and analyze the data set in its domain. "For some organizations, facing hundreds of gigabytes of data for the first time may trigger a need to reconsider data management options. For others, it may take tens or hundreds of terabytes before data size becomes a significant consideration." [2]

Big data is becoming the new power to promote the social innovation in the 21st century. Meanwhile, the reform caused by the big data also promotes the development of e-government in each country in the world [3-5]. In May, 2010, Australian government issued "open government declaration" to increase the transparency of the government. Currently, over 30 countries in the world have joined the rank of open data. Under the promotion of global open data, in November 2011, EU clearly proposed the strategy of open data. On March 29, 2012, US Obama government proposed "big data research and development plan", thus improving the understanding on the big data to the national development strategy level, proposing to breakthrough the core technology in the big data processing field, quickening the innovation of science and engineering fields, and strengthening US' national competitive development plan in the information age. In July 2012, the United States issued the big data government white paper "Big Data Promotes the Development: Challenge and Opportunity", pointed out that the big data is a historical challenge for the United Nations and each government, discussed how to use the big data resource including the social network for the benefit of mankind. The United Nations points out that the big data era has arrived, people can use the great wealth of data resources including old data and new data to conduct the unprecedented real-time analysis on the social population. With the example that the social network activity growth in Ireland and US as the early warning signs of the rising unemployment, the report shows that if the government can reasonably analyze the grasped data resource, it will rapidly respond with the data. The report also explains how does the big data help the government better respond to the social and economic indicators, such as income, unemployment, food price, etc.

At present, our country has issued a series of policies to promote the development of big data industry, including "the 12th five-year plan" national strategic emerging industry development plan, Internet of Things "the 12th five-year" development industry planning and NDRC's opinion on strengthening and improving the national e-government project, etc. In December 2012, Guangdong Province firstly started the big data strategy in the country, and issued "Program to Implement Big Data Strategy Working in Guangdong Province". The launch of the policies and plans indicate that our government attaches great importance to the big data industry, and the development strategy objective is clear. The situation makes our independent innovation leading enterprise usher in a great development opportunity. Therefore, how to make the big data play greater value in the government information project becomes the hot topic at present.

Influence of big data on e-government

The Obama Administration recently unveiled its Big Data Research and Development Initiative to "improve [American] capability to extract knowledge and insights from large and complex

collections of digital data; harness these technologies to accelerate the pace of discovery in science and engineering; strengthen national security and transform teaching and learning."

Big Data processing enables governments to make choices based on large-scale analysis. Goals include allowances for greater policy transparency, and identification of high social and economic value. Most broadly, data mining aids decision-making through the discovery of patterns in large data sets based on facts or observations. Data mining tools can process structured numeric data in traditional databases or extract relevance from semi-structured and unstructured data, such as text, graphics, images, and web data. Leveraging Big Data can enable breakthroughs in e-Government management, where, like the many industries using Big Data to identify opportunities for innovation, governments are able to act on the best available information.

Big Data processing is not simply waiting for automatic results; it is necessary to master the tools and skills to transform raw data into information, knowledge, and wisdom. Skills and techniques to be mastered include data warehouse integration, business intelligence, and data visualization, as well as business analysis and forecast modeling. In addition, organizations must develop appropriate work processes and policies; find talent for drawing sound conclusions to meet ever-changing citizen needs[6-8].

E-government Model Based on Big Data

The e-government model based on big data can be established, as shown in Figure 1. Firstly, the big data from the government website, forum, social network, microblogging are collected, including the structured relational data and semi-structured and unstructured data. Secondly, the data source is extracted and integrated for the relationship and entity. After the relevance and polymerization, these data are stored with the structure with unified definition. When integrating and extracting the data, the data shall be cleaned to ensure the data quality and credibility. The finished big data are analyzed with the quantitative statistics, data mining and machine learning to used for the social population analysis, economic data analysis and other usages, and it can be submitted to the government user through the browser. The government can formulate the related policies according to the result of big data analysis.

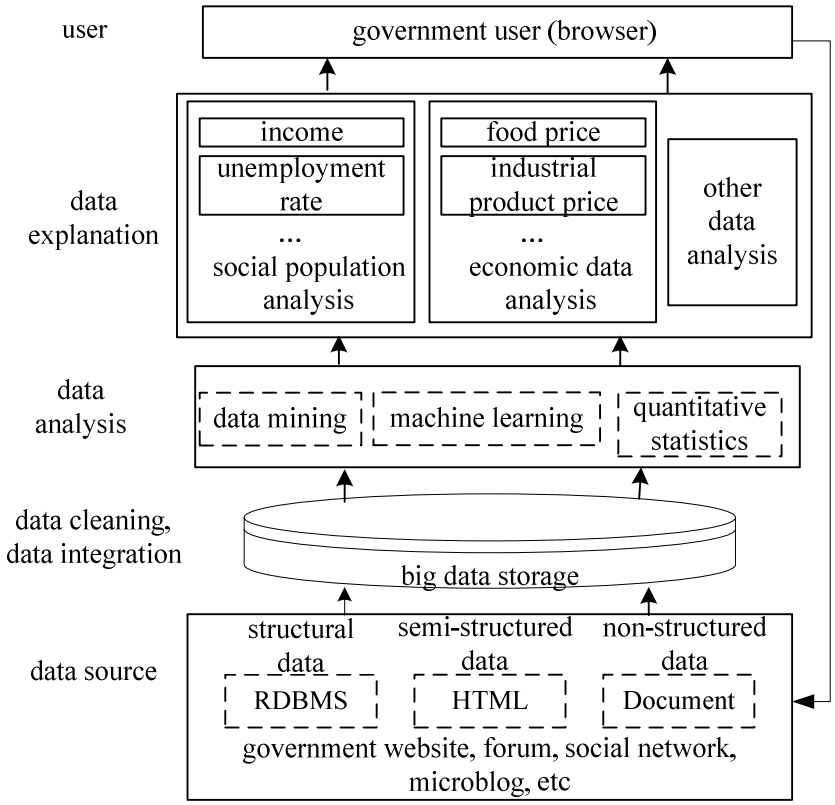

Figure1 E-government model based on big data

In summary, we must extract knowledge from massive data collections to build core capabilities in the development of e-Government services.

Acknowledgement

This work was supported by the National Natural Science Foundation of China under Grant (No. 61272513), Funding Project for Academic Human Resources Development in Institutions of Higher Learning Under the Jurisdiction of Beijing Municipality (No. PHR201106133), and and the Projects in the National Science & Technology Pillar Program (No.2012BAH08B02).

References

[1] Kim G H, Trimi S, Chung J H. Big-data applications in the government sector[J]. Communications of the ACM, 2014, 57(3): 78-85.

[2] Wikipedia. Big data. http://en.wikipedia.org/wiki/Big_data.

[3] Meng Xiaofeng, Ci Xiang. Big data management: concepts, techniques and challenges [J]. Journal of computer research and development, 2013, 50(1): 146-169.

[4] Bughin J, Chui M, Manyika J. Clouds, big data, and smart assets: Ten tech-enabled business trends to watch[J]. McKinsey Quarterly, 2010, 56(1): 75-86.

[5] Chen H, Chiang R H L, Storey V C. Business Intelligence and Analytics: From Big Data to Big Impact[J]. MIS Quarterly, 2012, 36(4).

[6] Three Development Trends in e-Government: Cloud, Collaboration, and Big Data. http://enterprise.huawei.com/en/about/e-journal/ict/detail/hw-275536.htm

[7] West D M. E‐Government and the Transformation of Service Delivery and Citizen Attitudes[J]. Public administration review, 2004, 64(1): 15-27.

[8] Metaxiotis K, Psarras J. E-government: new concept, big challenge, success stories[J]. Electronic Government, an International Journal, 2004, 1(2): 141-151.

Advanced Materials Research Vols. 989-994 (2014) pp 4909-4912
© (2014) Trans Tech Publications, Switzerland
doi:10.4028/www.scientific.net/AMR.989-994.4909

Internet Public Opinion Recognition and Tracking Based on Web Mining

Huailiang Shen, Feixia Bao

Zhejiang Business Technology Institute, Ningbo 315012, China

huailiang_shen@163.com

Keywords: internet public opinion, web mining, recognition, tracking.

Abstract. Recent years have observed the frequent occurrences of grave negative events. Along with the application and evolvement of Internet and new media, enthusiasms in distribution and discussing public opinion events have heightened. Internet public opinion research has thus become one of the research priorities of scholars in recent years. Internet public opinion research places heavy premium upon the emergence, evolvement, influencing factors and other aspects of public opinion. With rapid development and deepen evolution of internet public opinion in the internet, a variety of new methods occur on network. As the internet public opinion possesses the features of various topic, complex content and large amount data, the paper constructs an internet public opinion recognition and tracking based on web mining. Then the framework of the internet public opinion recognition and tracking system is presented. At last, it puts forward the whole workflow of the system to process the internet public opinion.

Introduction

The characteristics of the network public opinion has spread fast, wide audience, interactive ability, in the current political, economic, life has a great influence. Spontaneous, non rational and emotional characteristics of Internet users, the network public opinion and the rumor is difficult to distinguish, the authenticity of public opinion face huge challenges, become an important source of social instability. Therefore, to enhance the real-time monitoring of network public opinion, accurately grasp the impact of Internet public opinion trends and identification of public opinion, to give full play to the positive role of network public opinion in the social management and political democracy, has important significance.

Information society and network society further change the traditional values and social structure at the same time, also increased the instability and risk. Characteristics of various emergencies worldwide present normalization, diversified and systematic. Public crisis is no longer in society, and become the internal elements in the social structure. In the public crisis event occurrence, development and variation in the process, the network media and the internet groups active or randomly to the network as a platform, through the news, forum transmitted by means of information collection, analysis and exchange, forming a network of public opinion events or variation based on the characteristics of distributed, multiple etc. network public opinion has formed spontaneously storm, content complex of magnanimity and argument. The existing rigid intervention as the main means, in the traditional authority of the organization for the management level of passive response mode, it is difficult to adapt to the network supervision of the pressure, often in the management of a "one to many", "slow fast", "opposite" predicament. The dynamic and complex network environment information society puts forward new challenges to the emergency management of public opinion of the organizations at all levels, not only makes the information to transmit large range in a relatively short period of time, also broke the traditional government as the main body of the "single level" information communication control mode. How to realize the network public opinion effectively prevent and respond to emergencies in the multi polarization information communication mode of multimedia interactive participation, is a hot topic and a difficult problem in practice at present. In the transmission of emergency information and communication, various information trigger, coupling,

concurrent, conversion between the media presence, formed a reticular structure has a particular network topological properties between the emergency organization and individual.

According to the Internet public opinion main sources and distribution characteristics in the hot, information acquisition, information acquisition for the timeliness of the mainstream media websites and search engines, sources of information, high reliability, and good real-time performance, small amount of information collection, analysis and processing speed. Key words representative, simplicity, efficiency, information a large amount of Related words, correlation degree higher characteristic, to the maximum to minimum the amount of information covering the theme and intension of hot topic. This paper extraction as a hot topic tracking clues to the keywords, from the collection of the pages in the collection to extract a keyword set, and then taking these keywords clustering, is hot topic mining. Keyword based clustering to calculate minimum, high efficiency. To get the keywords set, the first keyword extraction of a single document set.

Web Mining

Web mining is not an unattended automatic discovering knowledge from the data of the algorithm, but is divided into a plurality of steps in the mining process. The workflow of the web mining is shown in figure 1.

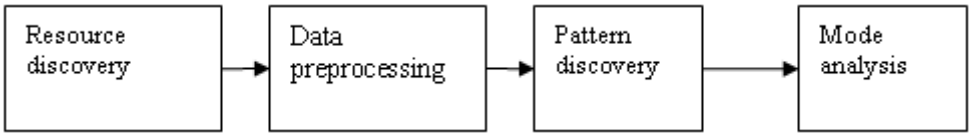

Figure 1 Web mining workflow

Resource discovery: needed to retrieve the text block, to obtain the required data from.

Data preprocessing: due to the local cache, proxy server, firewall, the Web log data are not precise, direct mining there may be erroneous results. Data cleaning is mainly whether the records, delete and algorithm independent judgment is an important access is not recorded; the user session is all a user request in a certain period of the web page; transaction identification is mainly the page should ask logic unit sequence as the representative of web transaction or user session.

Pattern discovery: pattern discovery is the use of statistics, machine learning methods such as mature technology, knowledge from Web usage mining. Method is found to be related with the electronic commerce mode with statistical analysis, cluster planning and dependency modeling. By using the statistical method, can choose the method to analyze the Webpage use characteristic, can analyze a character Webpage of click stream number, adjust the Webpage content and link structure according to the obtained results.

Analysis of the model: model analysis is mainly using appropriate techniques and tools, model analysis to assist the analysis understanding. Analysis of the most commonly used method is analyzed using the SQL query. Another analysis method is to import the data into multidimensional data cube, and then analysis and visualization of the results output by using the OLAP tool.

The Internet Public Opinion Recognition and Tracking Based on Web Mining

The network media information makes people in the acquisition of information often confused and meaningless, or to produce one generation, all Overgeneralization error. Network public opinion constantly, both published in well-known portal sites, famous newspaper website, also have somewhere deep in other forums, BBS and so on. Obviously, these tasks rely on limited manpower is not complete or not complete, objective. A desirable approach is: combining the data web crawler technology, mining technology, statistical theory and TDT technology together to complete, the automatic discovery and intelligent public opinion hotspot tracking process. The framework is shown in figure 2.

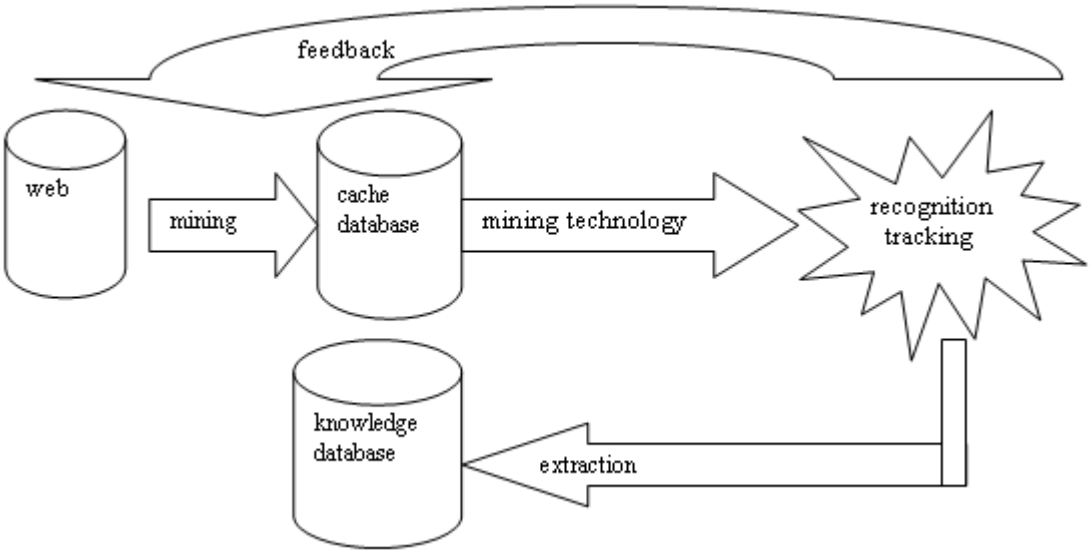

Figure 2 Internet public opinion recognition and tracking

Data preprocessing in Web mining

Pretreatment of Web using data is including data cleaning, session identification, page recognition and transaction identification. Because of the existence of the client cache and proxy server caching requirements, personalized service high need for improved path.

The use of Web data preprocessing, eventually get all page set appears in the transaction file and all user transaction set. All pages appear in the transaction file in the set P, where each page through its URL address uniquely identifies user transaction set T is expressed as T = {T1, T2,., TM}, transaction set in each transaction ti is a subset of the set P page. In order to facilitate subsequent data mining work (such as clustering), transaction set in each transaction t can convert to browse the n dimensional page space to quantity, i.e.:

t = < w (, t) , w (, t) , ··· , w (, t) >

(W, t) for t ∈ T weight affairs in page ∈ P

Many, a method to determine the weight size for example, if the transaction accesses the page, the weight is 1, otherwise the weight is 0 can also be a transaction in the browse page of retention time as its weight, which can be expressed on the transaction page interest degree. In order to deal with simple, using the above 0 - 1 weight representation methods.

The contents of Web data preprocessing includes from the text data and metadata extracting relevant features. If the page is based on the product page, or does not contain the text content, the page metadata extraction is very important. This paper mainly content extraction to the text content includes Meta tag contains XML or HTML and browse page. In order to calculate the similarity between different page content, content feature extraction must be given appropriate weight. The metadata, its weight is provided by the commercial website designers; the text features, its weight is widely used by information retrieval field term frequency inverse document frequency (TFIDF) decision, that is a particular word appeared on a page are of high frequency, while other pages appear in the frequency is very low, the words on the page of the weight is higher.

Content feature mining

In order to reference to recommendation engines, said method features should be and general use feature representation methods remain the same, also need to vector form. Unlike the general feature is, in the content feature mining, clustering process as far as possible will compare the contents of similar pages were clustered into the same cluster. Due to the same clustering browse page content is similar, but different user groups may be different part of the same page browsing interest, so the content features can reflect user overlapping interests and information needs

Page clustering is obtained by standard clustering algorithm is not suitable for representing the content characteristics. In order to use the characteristics and general representation consistent, can not be directly used to cluster web page clustering, but content feature extraction, data preprocessing

phase of browse page content feature matrix transpose, and every a content features can be regarded as browsing the n dimension vector space on the page, each dimension representing the content in the page weight. By clustering the clustering algorithm using a variety of standard features mentioned above, the result of clustering can be used in a clustering ensemble FC said, FC = { }, each content feature clustering CI consists of a series of content features

And the overall feature mining similar, need to browse page weight in the content features in CG are consistent processing, all the pages and filter out the significance threshold r weight less than specified

Given a feature clustering G and significant threshold R, the following methods to construct the content feature CG

$$C_G = \{ < p , \text{weight} (p , C_G) > | p \in P , \text{weight} (p , C_G \geq r \}.$$

Weight (P, P) for the page in the content feature weights, calculated as follows

$$\text{weight} (p , C_G) = \sum_{f \in G} \text{fw} (p , f) \Big/ \sum_{i=1}^{n} \sum_{f \in \theta} \text{fw} (p_i , f)$$

Summary

In this paper, we construct an internet public opinion recognition and tracking based on web mining. Then the framework of the internet public opinion recognition and tracking system is presented. At last, it puts forward the whole workflow of the system to process the internet public opinion.

Acknowledgment

This research is supported by University Students' Scientific and Technological Innovation Project of Zhejiang Business Technology Institute.

References

[1] Zeng J, Zhang S, Wu C, et al. Predictive model for internet public opinion[C]//Fuzzy Systems and Knowledge Discovery, 2007. FSKD 2007. Fourth International Conference on. IEEE, 2007, 3: 7-11.

[2] Songjie Gong, Learning User Interest Model for Content-based Filtering in Personalized Recommendation System, International Journal of Digital Content Technology and its Applications, Vol. 6, No. 11, pp. 155 ~ 162, 2012.

[3] Guan Q, Ye S, Yao G, et al. Research and design of internet public opinion analysis system[C]//Services Science, Management and Engineering, 2009. SSME'09. IITA International Conference on. IEEE, 2009: 173-177.

[4] Songjie Gong, A Collaborative Filtering Recommendation Algorithm Based on Trust Network and Trust Factor, Journal of Convergence Information Technology, Vol. 8, No. 5, pp. 1111 ~ 1118, 2013.03.

[5] CUI W, ZENG R, WANG G. Bibliometric Analysis of Internet Public Opinion in China [J][J]. Information Science, 2011, 1: 131-135.

[6] Songjie Gong, Research on Attack on Collaborative Filtering Recommendation Systems, AISS: Advances in Information Sciences and Service Sciences, Vol. 5, No. 10, pp. 938 ~ 946, 2013.05

[7] Mingyi G, Renwei Z. A Research on Social Network Information Distribution Pattern With Internet Public Opinion Formation [J][J]. Journalism & Communication, 2009, 5(4): 72-78.

Advanced Materials Research Vols. 989-994 (2014) pp 4913-4916
© (2014) Trans Tech Publications, Switzerland
doi:10.4028/www.scientific.net/AMR.989-994.4913

Data Redundancy Replication Strategy based on Relevant Failure in Cloud Environment

Liu Lei, Li Dan, Shen Chun*,Zhou WenBo

College of Computer Science and Technology, Jilin University, Changchun 130012, China

*shenchun@jlu.edu.cn

Corresponding author: shenchun@jlu.edu.cn

Keywords: Cloud Storage; Relevant Failure; reliability; Replication Strategy

Abstract Cloud storage is an active research domain currently, and how to secure the reliability of data is an important research issue. For the moment, most systems apply the static data replication strategy, which causes a serious waste of storage resources. Considering the user requirements and the factors influenced on data reliability, i.e., the node reliability and Relevant Failure Degree, Data Replication Strategy based on Relevant Failure is provided in this paper. According to the results of the experiments, our strategy reduces the number of data replicas and meets the user requirement of reliability at the same time. Besides, the strategy has a better performance on increasing the utilization of storage resources.

Introduction

Cloud storage provides data storage and access service to the outside by collecting the different types of storage devices in the network through the clustered applications, the network technology, the distributed file system and so on. There are many companies have its own data storage systems, for example, Google File System[1], Hadoop Distributed File System[2] and Amazon S3.

An outstanding feature of Cloud storage system is that its underlying hardware facilities are constructed by inexpensive commerce servers. The system may be failure due to the interference of program, hard disk, memory, network, power supply and so on. These factors usually lead to the failure in two aspects, single-point failure and multi-point failure, i.e., Relevant Failure. Therefore, fault-tolerant technology is necessary in cloud storage. With duplication technology, it is recoverable by accessing the replicas of data resource when the data is failed or lost. However, duplication technology also results in serious dissipation of storage resources while improving fault tolerance of the system. GFS adopt a typical 3-replicas data replication strategy by default, i.e. store 3 data copies at one time, to meet the requirement of data reliability. Literature [3] proposed a novel dynamic data replication strategy which facilitates an incremental replication method to reduce the storage cost, but this strategy only consider the reliability of node without considering the effects of the relevant failure between nodes.

To tackle this issue, in this paper we propose an effective dynamic data replication strategy named Data Redundancy Replication (DRR). According to the results of the experiments, DRR can reduce the number of data replicas and meet the user requirement of reliability at the same time. Besides, the strategy has a better performance on increasing the utilization of storage resources.

Cloud Storage Environment Modeling

In this subsection, we model cloud storage environment and formalize it as follow.

Definition 1. The cloud storage environment is defined as a collection of many storage nodes, and it can be represented as the following formula:

$$Storage_System = \bigcup_{i=1,2,3,\ldots,m} \{n_i\} \quad (1)$$

where n_i is the number of the node i.

Definition 2. Relevant Failure Degree is defined as the possibility of relevance failure between two storage nodes, denoted by σ. All of relevance failure degrees can be represented as a matrix:

$$Relevance = \begin{bmatrix} 0 & \sigma_{12} & \sigma_{13} & \dots & \sigma_{1m} \\ \sigma_{21} & 0 & \sigma_{23} & \dots & \sigma_{2m} \\ \sigma_{31} & \sigma_{32} & 0 & \dots & \dots \\ \dots & \dots & \dots & 0 & \sigma_{(m-1)m} \\ \sigma_{m1} & \sigma_{m2} & \dots & \sigma_{m(m-1)} & 0 \end{bmatrix}$$

where σ_{ij} is the possibility of the node n_i and n_j are failure simultaneously. For each $i, j \in \{1,..,m\}$, we can conclude that:

1) $\sigma_{ij} = \sigma_{ji}$, if $i=j$, then $\sigma_{ij}=0$;

2) The bigger σ_{ij}, the weaker the relevance between n_i and n_j, and vice versa.

Definition 3. $\forall i, j = 1,2,3,\ldots,m$ and $i \neq j$, the distance between n_i and n_j is S+1, where S is the number of network switching devices from n_i to n_j. We represent the distance as the following matrix:

$$Distance = \begin{bmatrix} & d_{12} & d_{13} & \dots & d_{1m} \\ d_{21} & & d_{23} & \dots & d_{2m} \\ d_{31} & d_{32} & & \dots & \dots \\ \dots & \dots & \dots & & d_{(m-1)m} \\ d_{m1} & d_{m2} & \dots & d_{m(m-1)} & \end{bmatrix}$$

Definiton 4. $\forall i, j = 1,2,3,\ldots,\mathrm{m}$ and $i \neq j$, the Relevance Failure Degree σ_{ij} between n_i and n_j is represented as:

$$\sigma_{ij} = \frac{1}{d_{ij}} \tag{2}$$

Reliability Modeling

Tian[4] proposed a method for calculating the failure rate based on Weibull(scale, shape) distribution:

$$\lambda(t) = \left[\frac{shape}{scale}\right] \times \left[\frac{t}{scale}\right]^{shape-1} \tag{3}$$

where scale is the lifetime parameter, which measures the average life of the node.

Definition 5. $\forall i, j = 1,2,3,\ldots,\mathrm{m}$, the reliability of node is represented as:

$$R(n_i) = 1 - \lambda(t_i) \tag{4}$$

where t_i is the run time of node i.

Definition 6. Assume that data is randomly saved in the set of nodes $\bigcup_{i=1,2,3,\ldots,m} \{n_i\}$. The reliability of node $R(n_i)$ and the relevance failure matrix Relevance are given, then the reliability of data can be defined as follow:

$$\theta = \begin{cases} R(n_1), k = 1, \\ 1 - (1 - R(n_1)) \times \prod_{i=2}^{k} \left[1 - \frac{1}{i-1} \sum_{j=1}^{i-1} \left(\frac{1}{1+\sigma_{ij}}\right) \times R(n_i) \right], k > 1 \end{cases} \tag{5}$$

Where k is the number of replicas.

Data Redundancy Replication（DRR）Strategy based on the Associated Failure

The idea of DRR is to use the minimum number of replicas while meeting the data reliability requirement. By solving data reliability function (3), (4), (5) separately, the reliability of the data can be determined, which indicate when the current number of replicas cannot meet the user requirement any longer and a new replica should be created.

The pseudo code of DR is shown in Figure 1.：

Algorithm Data_Copy_Strategy(C_need, $\bigcup_{i=1,2,3,...,m}\{n_i\}$)

{//input：user requirement and the set of storage nodes

//output：the number of data replica

① n_{chose} = rand（ $\bigcup_{i=1,2,3,...,m}\{n_i\}$ ）；//chose one node n_{chose} in $\bigcup_{i=1,2,3,...,m}\{n_i\}$

②Chose_Set= Ø

③k←0;

④k=k+1；

⑤Chose_Set=Chose_Set∪ $\{n_{chose}\}$；

⑥Data_Reliability (Chose_Set , θ)； // solve the function of data reliability

⑦if($\theta \geq C_need$) then return k；

⑧else loop ①//create one more replica for the data if current data reliability is lower than

Fig 1. The pseudo code of DR strategy

Experimental Evaluation

This paper simulates a cloud platform through building a trilaminar network switch model of twelve storage nodes. The model is shown in Figure 2. With the platform, we made a test on the data replication strategy proposed by this paper.

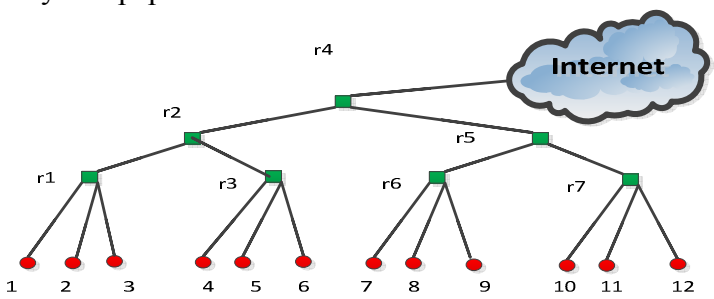

Fig 2. The simulation platform

Under the model, a relevance failure matrix Relevance is created, $\sigma_{1,2}$=1/2 , $\sigma_{1,4}$=1/4 , $\sigma_{1,7}$=1/6 ...

A parameter value of shape in formula (3) is assigned by a value of [0.7, 0.8] at random when nodes start to run. After a period of one day, the shape is fixed by a value of [2, 3] randomly[4]. We set the value of scale 120 based on the research to Google cluster[5].

Reliability of storage data, represented by parameter C_need, can be set by users. It is based on an analysis of many users that while the value of C_need is 99.00%, it is sufficient to meet the need of reliability of a majority of users. So we make C_need not less than 0.99, and C_ need ∈ {0.99, 0.999, 0.9999} in this paper.

Assume that all storage nodes are isostructural and launch simultaneously, so they have identical failure rates at the same time. At different time points, extract several users at random and combine the users with different storage nodes randomly. By the data replication strategy proposed by this paper, figure out the number of redundancy storage without losing user demands. A portion of experimental results is listed in Table 1.

Table 1. The Experimental Results

Customer	C_need	T/[day]	Data Reliability	The number of replicas
1	0.99	0.1	0.9939	2
2	0.999	2.5	0.9999	1
3	0.99	10.8	0.9998	1
4	0.999	10.8	0.9999	2
5	0.99	34.2	0.9996	2
6	0.99	65.4	0.9926	1
7	0.999	80.0	0.9994	3
8	0.99	80.0	0.9977	2
9	0.999	95.9	0.9996	2
10	0.9999	118.7	0.9999	3

From the result of Table 1, we can claim that only 1*3+2*5+3*2=19 storage cells are needed in our strategy but 10*3=30 storage cells in a typical 3-replica strategy. The simulation shows that our data replication strategy for reliability can significantly reduce the number of replicas.

Conclusions

This paper presents a data redundancy replication strategy based on relevant failure. The strategy takes into account the user requirements and the factors influenced on data reliability, i.e., the node reliability and Relevant Failure Degree. Experiments show that the strategy can improve the utilization of storage resources while meeting user requirement of reliability. However, there are still some works not well studied in this paper. First, how to model the storage node failure process is very critical for the implement of DRR in real system. Second, when choosing the storage node, we do not consider the load balance between the nodes. These issues will be done in the near future.

Acknowledgments

This work was supported by National Natural Science Foundation of China under Grant No. 61300049; the Program for New Century Excellent Talents in University of China under Grant No. NCET-10-0436; the Specialized Research Fund for the Doctoral Program of Higher Education of China under Grant No. 20120061120059; the Key Program for Science and Technology Development of Jilin Province of China under Grant Nos. 20130206052GX, 20140520069JH.

References

[1] Shvachko K, Kuang H, Radia S, et al. The hadoop distributed file system[C]//Mass Storage Systems and Technologies (MSST), 2010 IEEE 26th Symposium on. IEEE, 2010: 1-10.

[2] Ghemawat S, Gobioff H, Leung S T. The Google file system[C]//ACM SIGOPS Operating Systems Review. ACM, 2003, 37(5): 29-43.

[3] Li W, Yang Y, Yuan D. A novel cost-effective dynamic data replication strategy for reliability in cloud data centres[C]//Dependable, Autonomic and Secure Computing (DASC), 2011 IEEE Ninth International Conference on. IEEE, 2011: 496-502.

[4] Tian G H, Meng D, Zhan J F. Reliable resource provision policy for cloud computing[J]. Chinese Journal of Computers, 2010, 33(10): 1859-1872.

[5] Ford D, Labelle F, Popovici F I, et al. Availability in Globally Distributed Storage Systems[C]//OSDI. 2010: 61-74.

Advanced Materials Research Vols. 989-994 (2014) pp 4917-4919
© (2014) Trans Tech Publications, Switzerland
doi:10.4028/www.scientific.net/AMR.989-994.4917

Research and Implementation of Oracle Database Synchronization Timing

JinfengWang[1, a], ZhenfengShi[2,b] ,ZheQu[3,c] and ShanShanLi[4,d]

[1] Institute of disaster prevention,china

[2] The people's Bank of Changzhi Center branch in china

[3] Institute of disaster prevention,china

[4] Institute of disaster prevention,china

[a]darkbus001@gmail.com, [b]szf1212@126.com, [c]quzhe@cidp.edu.cn, [d] lishanshan@cidp.edu.cn

Keywords: Oracle Synchronization; Timing; Export; Import

Abstract. In the practical application of developmental internet, often synchronizing Oracle database tables, the establishment of a reliable remote database synchronization scheme is necessary. The paper uses the EXP/IMP logical backup tool of oracle, tuning of EXP/IMP, and combined with shell command, to implement a remote database synchronization scheme. In addition, this program implements the timing of the Oracle database synchronization.

Introduction

EXP/IMP is a logical backup tool provided by Oracle and a logical backup start to work in case of the database is started. The essence of exporting is reading a set of database record (even it's a data dictionary) and write the record to a file. There is no relation between exporting the records and their physical location. The essence of importing is reading the dump file and executing the commands. This approach is backed by Oracle's export and import utilities to implement. 'Export' is to export the data, and 'import' is to import the uninstalled data, exported by 'export', into the database. This tool can be derived from a variety of functions, for instance, the whole database backup, table structure reconstruction, data transmission, etc.

Oracle Export/Import tools provide a flexible functionality and export/import models, the three most commonly used mode is User, table and full Database. In addition, the tools can decide to export/import whether the object contains information about the data dictionary, for instance, index, constraints, authority etc. However, using EXP/IMP has a flaw. Using the Export tool is a logical backup of the database, which can only be used in logical data. If the database is physically damaged, leading to not start, logical backup data does not help to restore the database.

Export and Import of key technologies

The key technologies of Export and Import.The Oracle exp command is used to implement the export operation on the database. This command import dmp files to local Oracle server. Three kinds of importing table modes: table recovery, user recovery, complete recovery.

1.1 Exporting table mode

Backup mode specified under a user object (table). Business databases often use this backup method. If backing up to a local file, use the following command:

exp myName/myPassword rows=y indexes=n compress=n buffer=65536 feedback=100000 volsi ze=0 file=exp.dmp log=exp.log tables=tab1,tab2,tab3

1.2 **User mode**

Backup all objects under a user mode. Business databases often use this backup method. If backing up to a local file, use the following command:

Exp myName/myPassword owner=youWantOutUser rows=y indexes=n compress=n buffer=65536 feedback=100000 file=exp.dmp log=exp.log

1.3 **Complete mode**

Backup the entire database. A business database doesn't use this backup method. The command of backup: exp myName/myPassword rows=y indexes=n compress=n buffer=65536 feedback=100000 full=y file=exp_.dmp log=exp.log

Three modes of importing and exporting are identical. The only difference is changing EXP to IMP.

Achieve timing backup software

2.1 **the flow chart of software design**

Flow chart of the software as shown in Figure 1.

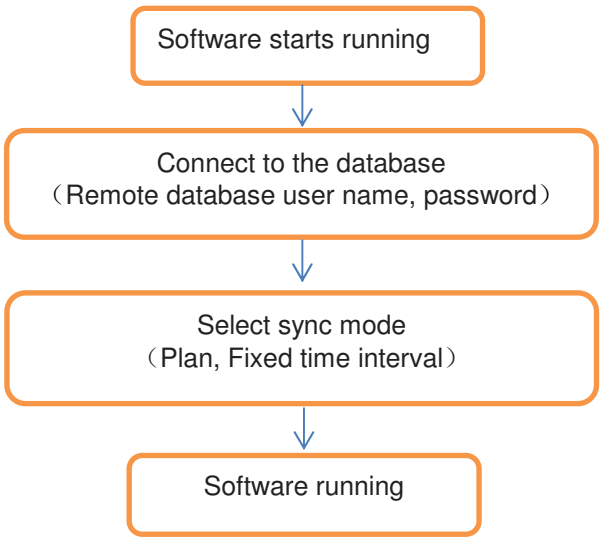

Fig.1 Software process design

2.2 **Oracle timing synchronization interface and operation**

The Microsoft Foundation Class Library (also Microsoft Foundation Classes or MFC) is a library that wraps portions of the Windows API in C++ classes, including functionality that enables them to use a default application framework. Classes are defined for many of the handle-managed Windows objects and also for predefined windows and common controls.

The software using MFC Library. The software interface shown in Figure 2.

The key code is as follows:

Key backup code： exp myname/mypassword@192.168.100.152/orcl file = d:\my.dmp tables=(test1,test2);

Key synchronization code：imp myname/mypassword@192.168.100.152/orcl file = d:\my.dmp tables=(test1) ;

Set the timer：Creates a timer with the specified time-out value.

```
UINT_PTR WINAPI SetTimer(
  _In_opt_  HWND hWnd,
  _In_      UINT_PTR nIDEvent,
  _In_      UINT uElapse,
  _In_opt_  TIMERPROC lpTimerFunc
);
```

The specific operation as follows:

(1) Fill the database connection information, and test the connection.

(2) Select the synchronous mode. There are three ways to synchronize the situation: You can choose to perform once; Can be synchronized according to plan；Can be synchronized at fixed intervals.

(3) Determine and run the software.

Summary

To prevent data loss caused by a failure, which cannot be recovered, backup the data. How to reduce the complexity of database management. Establishing a Centralized, online, real-time synchronization system has a very important significance. This paper describes the strategy of timing backup Oracle database, after a lot of practical application, for improving efficiency in the use of the Oracle database synchronization has a great role and certain advantages in the security, economy and reliability.

Acknowledgements

Three of Authors (JinfengWang) thank the financial support from Special Fund of Fundamental Scientific Research Business Expense for Higher School of Central Government (Projects for young teachers) (ZY20130209)

References

[1] B. Carr, J. Garmany, S. Karam, L. Hartmann and V.J. Jain, Oracle 1 Ig New Features, Ed. RampantTechPress, USA,（2008）.

[2] J. Garmany, S Karam, L. Hartmann and V.J. Jain, Oracle llg SQL performance analyzer concepts, Oracle Tips by Burleson Consulting January 16th, 2008, USA,（2008）.

[3] D.K. Burleson, Oracle Tuning: The Definitive Reference, Ed. Library of Congress, USA, (2006).

[4] J.Lewis, Cost Based Oracle: Fundamentals, Ed. Apress, USA, (2006).

[5] Information on http://www.oracle.com/technology/products/database/oraclellg/index.html

[6] Information on http://9host.cn/oracle/200742218400613143.html

Advanced Materials Research Vols. 989-994 (2014) pp 4920-4925
© (2014) Trans Tech Publications, Switzerland
doi:10.4028/www.scientific.net/AMR.989-994.4920

User Behavior Prediction Analysis based on Time Context

Wei Gu[1, a], Lianjun Chen[1, b]

[1]College of Information Technicology, Shanghai Jianqiao University, Shanghai, 201319, China

[a]email: guwdx@126.com, [b]email:lianjun94@126.com

Keywords: Time Context; User Behavior; Clustering

Abstract. Analysis of user behavior management control has important significance for network users. This paper uses the clustering algorithm to cluster the user behavior for clicking certain software or Website in different times, through the time context of user behavior to analyze user behavior rules. Additionally, this paper analyzes the clustering result in detail, then, divides user behavior into different types. Finally, according to the clustering result, more targeted pages and applications are recommended to the network users to create huge business value.

Introduction

With the rapid increase of network users, how to utilize the rich contextual information and user behavior information to obtain the user's preferences, to provide users with personalized services, is an important issue each Website needs to focus on currently.

Context is the description of environment related information, the information can be any kind of environmental information related to a user or device, including time, place, people around, emotions and etc. This paper is to analyze network user behavior patterns based on the time context, namely according to the records of accessing various Websites every day, knows what users, in what time, do what things, and do how many times, then, the user's behavior patterns can be applied to many scenarios. For example, personalized Website display according to different user behavior patterns, user behavior patterns can also assist e-commerce sites to do market segmentation. Furthermore, user behavior pattern can also help advertising push, according to their behavior in a particular time to push the corresponding advertising.

Data sources and pretreatment

The data used in this paper is provided by the CNNIC which provides 5000 randomly selected sample users. The data includes the behavior log these users access to the software and Website in 4 weeks, and the corresponding sample population attribute information. A log file is created every time a sample user turns on the computer. The first 2 lines in the log file record the following 2 values:

Last: the number of seconds when the last updated time of log subtracts the boot time. L_Start: The boot time of sample user (Year-Month-Day Hour-Minute-Second)

Next, the data collection procedures will scan the focus window on sample users' computer in a frequency of 2 seconds. If the focus window changes, a new record will be appended into the log file. See Figure 1 for the appended record information.

According to the sample data statistics, the computers of these 5000 users are turned on about 20% of the time in 28 days on average (about 5 hours a day). These data records an important part of entertainment and work in daily life for each user, so the user behavior patterns mining is very meaningful. The purpose of this article is to observe the behavior of each user every day, that is the user does what things in what time. For example, a user spent half time to deal with business related work on computer and the other half time on entertainment in the morning. Then, the user behavior can be included into "work and play" in the morning.

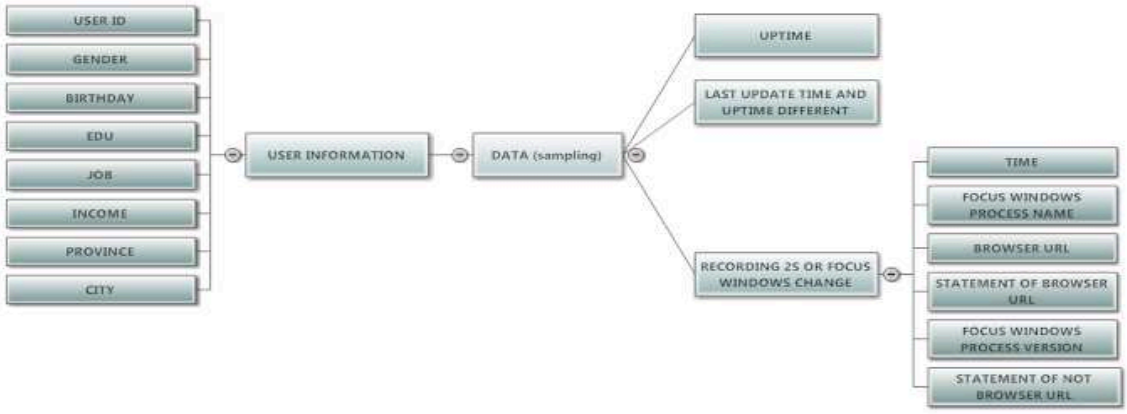

Figure 1 Data collection for sample user

Specific data processing architecture as shown in figure 2. First of all, pre-treat the data, then, import data to the Sql Server to generate the required reports and intermediate data, and then labels the data to generate the correct file format required by the following data mining. This article uses weka as the analysis engine generates the required schema information, and use mahout for data mining, then, generate the final behavior classification mode.

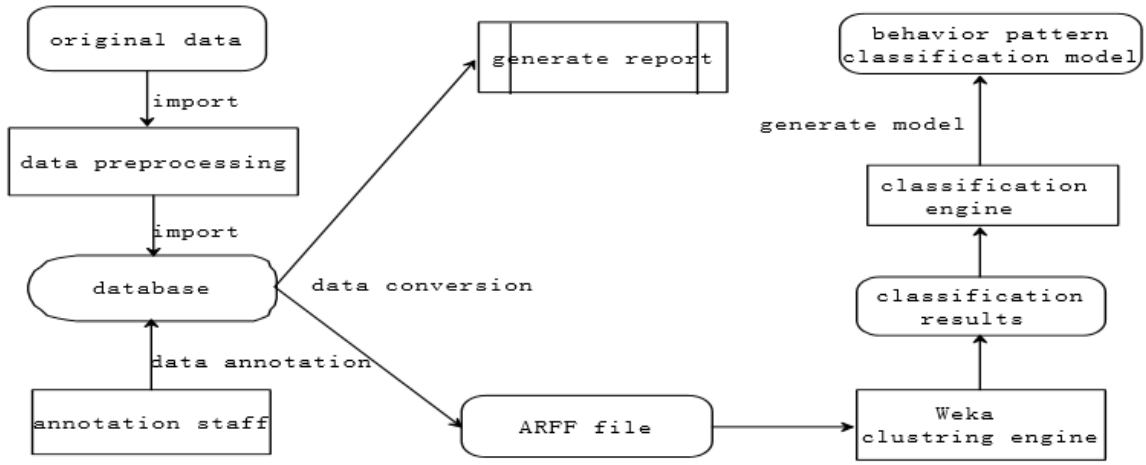

Figure 2 Data Processing Architecture

K-means clustering technology

Clustering analysis is to divide a set of objects into clusters, similarity degree is high within the cluster, while similarity degree is low between the clusters. Clustering is an unsupervised learning, namely, the division is reasonable according to the respective characteristics of the objects, no model for reference or to follow. Clustering analysis is an important technology in data mining, and are widely used in every field of the database. In 1967, McQueen proposed k-means clustering algorithm, the algorithm is described below[2][3]:

Input: Dataset D which contains n objects and cluster numbers K

Output: Collection of K clusters.

Steps:

(1) Choose K objects from the dataset D as initial center of K clusters.

(2) Repeat.

(3) Categorize each object to similar cluster according to the average value of the objects in the cluster

(4) Re-calculate the average value of cluster.

(5) Until the average value of cluster does not change.

The algorithm complexity is 0 (NKT), n represents the total number of objects, k represents the number of clusters, t represents the number of iterations.

Data Processing

1 Data Label

Firstly, turn on the related data labeling process, extract most common 1000 software and 1000 URLs out of the existing data behavior log, and then label these software and Website URL. For more information, see table 1 and table 2. From the following tables, we can see, in the process of software use, the proportion of chat, games, and the working software is relatively high. In the URL visit, the proportion of news, social, and shopping sites is relatively heavy.

Table 1 Software Labeling

Business Class		Life Class		Entertainment Class	
Label	Statistic	Label	Statistic	Label	Statistic
Office	2325963	Shopping	1026192	Chat	7197165
Financial	215098	Digital	105998	Game	2344107
Stock	81168	Travel	62959	Video	1146866
Reading	31629	Life	59022	Music	435519
Calculator	25698			Picture	418738
Study	25433			Online Game	370157
Working	22236			Download	305884
Programming development	17732			Social Website	138864
Programming	7625			News	35447
E-Mail	4456				
Summary	2757038	Summary	1254171	Summary	12392747

Table 2 Website Labeling

Business Class		Life Class		Entertainment Class	
Label	Statistic	Label	Statistic	Label	Statistic
Information Retrieval	1879894	Shopping	2857628	Social Website	1726251
Blog	395896	Life	150416	News	1443780
E-Mail	342209	Digital	99348	Video	758507
Office	259055	IT	64527	Navigation	716571
Financial	146140	Car	59825	Game	456789
Working	36986	Sports	41396	Picture	244776
Economics	20058	Travel	30194	Chat	153956
Recruitment	3773	Real estate	1127	Novel	92577
…	…	…	…	…	
Summary	3084011	Summary	3305409	Summary	5741607

2 Data Feature Extraction

According to the characteristics of the data label, we divide software and Website into three categories: work related software, life related software and entertainment software. Additionally, user access time is divided into morning and afternoon, and measurement choice is the frequency ratio a user in a certain period of time access to certain Websites or software. Then, we give each user a feature vector to his every day statistical behavior by use this data modeling, and then cluster these eigenvectors. For more information, see Table 3 and Table 4.

Table 3 Clustering Statistic

Clustering Goal	Statistic user each day behavior
Time Division	morning & afternoon
Behavior Categeory	Work, life, entertainment
Characteristic value choice	Clicking frequency for different software or Website

Table 4 User Behavior Statistic

ID	Morning Work	Morning Life	Morning Entertainment	Afternoon Work	Afternoon Life	Afternoon Entertainment
User A 08/01	30	21	24	12	3	10
User B 08/01	11	12	75	0	0	3
User A 08/02	5	3	41	4	3	44
……	……	……	……	……	……	……

According to the clustering analysis and calculation, the user behavior is divided into five categories, respectively class 0, class 1, class 2, class 3 and class 4, specific data for each class is shown in Table 5.

The characteristics of users in Class 0 is using computer for a long time every day for work, life, and entertainment. These users are highly dependent on computer;

The characteristics of users in Class 1 mainly use computer for work and entertainment for a long time every day. While, their life rarely uses the computer. These users are highly dependent on computer for the work and entertainment;

The characteristics of users in Class 2 mainly use the computer to work and play for appropriate time, they use more in the afternoon. These users belong to modest dependence of the computer user group;

The characteristics of users in Class 3 mainly using the computer to work and play for moderate time, they use more in the morning. These users belong to the morning play computer users group;

The characteristics of users in Class 4 mainly using the computer to entertainment for a short time, , they use more in the afternoon. These users belong to play for a while computer user group.

Table 5 User Behavior Clustering Category Table

Cate-gory ID	Morning Work	Morning Life	Morning Entertainment	Afternoon Work	Afternoon Life	Afternoon Entertainment	Category Proportion
0	57.3	152.8	128.4	58.5	148.8	147.0	9%
1	95.4	19.0	178.2	94.8	10.6	201.6	12%
2	0.1	0.0	10.0	3.2	1.3	52.2	31%
3	10.9	2.4	41.3	29.2	20.1	114.1	26%
4	20.5	12.0	95.5	0.8	0.0	11.4	22%

According to the category classification and statistics, we can get the user behavior model, as shown in Figure 3.

According to the proportion of categories and user behavior model, we can see that, 9% of the behavior belongs to the class 0, the characteristic of this kind of behavior is active both in the morning and afternoon, while life or entertainment occupies more time in the morning, such users extremely dependent on computer.

12% of the behavior belongs to class 1, the characteristic of this kind of behavior is more active in the morning, and proportion of visiting working class software or Website is high.31% of the behavior belongs to class 2, the characteristic of this kind of behavior is the proportion of morning & afternoon software visit is balanced, and most of the time is on a visit to the entertainment related software.

The characteristic of Class 3 behavior is active in the morning, and most of the time is on a visit to the entertainment related software.

The characteristic of Class 4 behavior is only active in the afternoon, the main content of the activity is for fun.

According to this clustering of category, the effect from homogeneous degree and the interpretability of each class is very good.

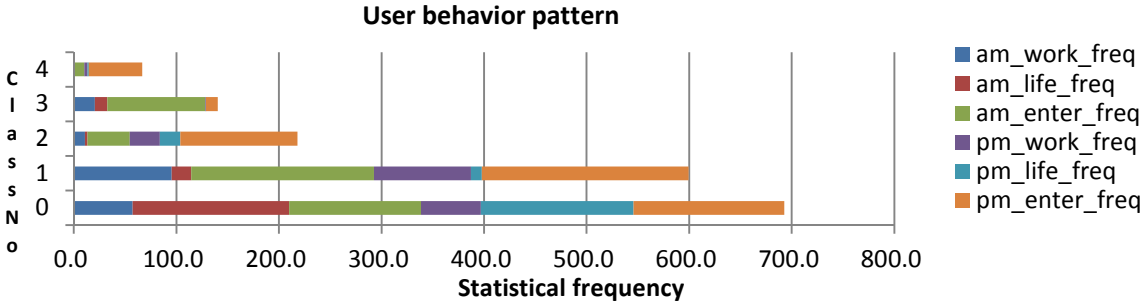

Figure 3 Each Day User Behavior Schema

According to the clustering results, it can be predicted to each user behavior, then, calculate the user behavior category. In order to verify the user behavior prediction accuracy, the author respectively cluster the user behavior for four weeks with the same time period, behavior category and characteristic value as daily behavior. Figure 4 get user behavior model for four weeks through clustering classification.

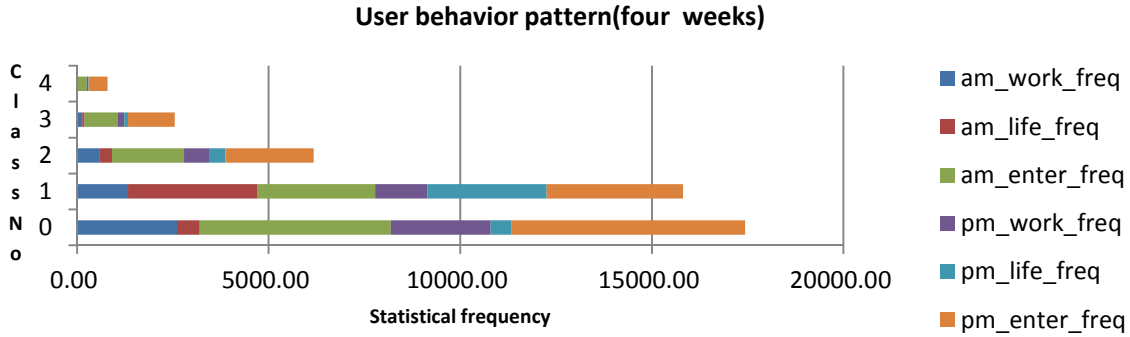

Figure 4 Four weeks User Behavior Schema

Through all the eigenvalues of users on a daily basis to forecast classification, the result accuracy was 97.58%, using user behavior patterns for four weeks to predict classification, the result accuracy was 91.54%, the daily prediction accuracy is higher than four weeks behavior prediction accuracy.

In order to verify the accuracy, we predict behavior model through the user basic, its accuracy is only 26.81%. However, predict the user daily behavior characteristic of the accuracy is 67.52%. Meanwhile, predict the user four week behavior characteristic of the accuracy is 62.40%.

To prove the result of the experiment is not accidental, the author conducted a series of eight experiments. Firstly, we divide clustering goals into two kinds, namely daily the user statistic behavior and four week user behavior. In time aspect, in addition to adopt the way of dividing morning & afternoon, also adopted the way of the division of work and non-work time. Through

experiments, the result accuracy is over 95%, the average is 97.53% for users all the daily eigenvalues prediction classification. And result accuracy is over 80%, the average is 89.58% for four week prediction. The experimental data shows that the accuracy of user behavior prediction is rather high.

Conclusion

In this experiment, according to the different clustering goals, different ways of time division, the different approach to deal with eigenvalues, different clustering algorithm parameters, we get a total of 16 groups of experimental results. The clustering result is clear and easy to explain.

Use all user behavior information proves the rationality of the classification, the accuracy is between 85% and 100%. Additionally, use part of the user behavior information to predict the user's behavior model is feasible and accuracy between 50% and 70%. However, it cannot correctly predict the user's behavior pattern only from the user basic information (age, education, geographic area), because the accuracy is only between 10% and 30%. By the experimental results, we can also see that daily statistics action as target clustering is superior to the four week statistical behavior as clustering around the target.

Therefore, it has great research significance and application value to apply predicted user behavior model to a variety of situations through time context user behavior patterns prediction model, to provide information, personalized service and etc.

References

[1] Qianglin Zhang. Research of context aware system based on Semantic Web[D]. Beijing Jiaotong University 2010.

[2] TAL l, MUNTEAN G. User-oriented cluster-based solution formultimedia content delivery over VANETs [C]//2012 IEEE International Symposium on Broadband Multimedia Systems and Broadcasting(BMSB). Seoul, 2012: 1 - 5.

[3] Song S, Chen L,Yu P S. On data dependencies in data spaces[C] / /IEEE 27th International Conference on Data Engineering(ICDE). Hannover, 2011: 470 － 481.

[4] Dong Y, Shen D, Nie T. Discovering relationships among data resources in data excavate［C］/ /6th Web Information Systems and Applications Conference． Xuzhou, 2009: 76 － 81.

[5] GATTAL A, CHIBANI Y. Segmentation and recognition strategy of hand written connected digits based on the oriented sliding window [C]//2012 International Conference on Frontiers in Handwriting Recognition(ICFHR), Bari, 2012: 297 - 301.

[6] JohnC, Duchi, Lester W, Mackey, Michael, Jordan. On the Consistency of Ranking Algorithms, Proceedings of the27thIntemational Conference on Machine Learning[J], 2010, l—8.

Advanced Materials Research Vols. 989-994 (2014) pp 4926-4929
© (2014) Trans Tech Publications, Switzerland
doi:10.4028/www.scientific.net/AMR.989-994.4926

Research of the minimum vertex-cover solutions on the tree and lattice structures

Yunjia ZHANG[1, a], Wei WEI[2, b], Ting WANG[3,c]

[1,2,3] LMIB and School of Mathematics and Systems Science,

Beihang University, Beijing, 100191, China

[a]email: zhangyunjia22@gmail.com, [b]email: weiw@buaa.edu.cn, [c]email: wangting33@gmail.com

Keywords: Minimum Vertex-Cover Problem; Computational Complexity; Solution Space Organization

Abstract. We focus the solution space of a most fundamental problem - Minimum Vertex-Cover problem - in theoretical computer science. After some rigorous analysis, we provide the formation mechanism of minimum vertex-cover solutions on the tree and give the organization of these solutions on arbitrary lattice structure. By the results, we can easily calculate the solution numbers on these structures and have better understanding of the hardness of Minimum Vertex-Cover problem. The proposed study and algorithm can make a new way on detecting the essential difficulty of NP-complete problems and designing efficient algorithms on solving them.

Introduction

Minimum Vertex-Cover problem is one of the most important NP-complete problems [1], which has wide applications in immunization strategies in networks [2] and monitoring of internet traffic [3]. As a basic problem in mathematics and theoretical computer science, how to understand the complexity of solving Minimum Vertex-Cover is a hot topic attracting many attentions from mathematicians, physicists and computer scientists.

The computational complexity of Minimum Vertex-Cover problem is attributed to the complicated organization of it solution space, especially some structures, such as frozen nodes [4], mutual-determinations [5] and clustering [6]. Unfortunately, few rigorous results on the structures are obtained and most analysis is based on some empirical assumptions. In the viewpoint of computational complexity, the corresponding analysis of these structures belongs to the #P class [7], the complexity of which is considered much harder than that of NP-complete.

As a simple case, we can easily find a solution of Minimum Vertex-Cover when the given graph is a tree or a forest. Besides, for the graphs with no leaf-removal core, finding a minimum vertex-cover can also be finished in polynomial time complexity [8]. However, when the graph becomes denser with hard core after the leaf-removal, solving the minimum vertex-cover generally needs exponential time complexity [8].

In this paper, we focus on the Minimum Vertex-Cover solutions of trees and lattices, and make analysis on finding different solutions of them. Besides, based on the organization of different solutions, we study the information dissemination process on the nodes by vertex-cover and give strategy on calculating the solution numbers. The investigation of the information dissemination on the minimum vertex-covers will provide scientific directions on solving the NP-complete problems and help make further understanding on their solution space structures.

The minimum vertex-covers on a tree

A vertex-cover on an undirected graph G(V,E) with the node set V and the edge set E is a subset S = {i1,i2, . . . ,ik} of its nodes such that every edge has at least one end node in S. The Minimum Vertex-Cover problem is an optimization problem to find the minimum size of a vertex-cover on a given graph.

In mathematics, and more specifically in graph theory, a tree is an undirected graph in which any two nodes are connected by exactly one simple path.

If the graph is just a tree, the leaf removal [9] should be mentioned .Given a graph G, a leaf is a couple of nodes {v, w} in which the first one has degree 1 and the second one is the only neighbor of it. Here, node v is a pendant node in the graph, node w acts as a petiole, and for the same petiole there may be more than one pendant nodes connecting it. For each leaf has at least one node to be covered, we can set the petiole nodes covered. To define the leaf removal, if the nodes pair {v, w} is a leaf in graph G, remove the two nodes with the edges touching them. It is very interesting that the leaf removal process can destroy all the leaves in graph G and can produce new leaves for the rest of the graph. By this process, the following facts can be determined: a) covering a petiole provides a local optimum; b) The tree can be solved by step by step leaf removal process; c) the local optimum can help to obtain the global optimum. Evidently, covering all the petioles on a tree can obtain a minimum vertex-cover. In FIG.1, the process of obtaining minimum vertex-cover by leaf removal for a simple graph is shown.

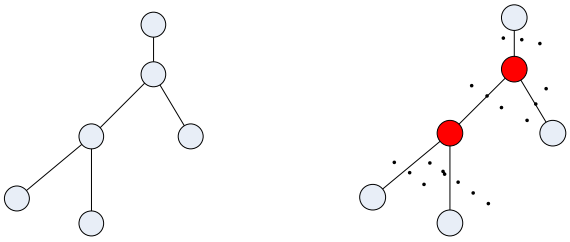

FIG.1 A simple graph with two leaves and two petioles covered

Obviously, we get a minimum vertex-cover of the tree, and also get the size |Vc| of it. Based on it, we can extend this rigorous result and find all the minimum vertex-cover, and provide strategy on calculating the total number of all the minimum vertex-cover solutions of a tree. The whole process of leaf removal can be seen as an information dissemination process from the leaves to the roots. When a node is determined to be uncovered, it will force its adjacent nodes to be covered. There is no effect of information dissemination to the neighborhood of the covered nodes. Besides, it is an important fact that the petiole must be covered when there are more than one pendant nodes in the leaf.

So, if a tree is concerned to calculate the number of all its minimum vertex-cover solutions, we can find its solution space by a branch-and-bound algorithm in the following:

We can treat the tree as a series of leaves in the viewpoint of leaf-removal process:

a) If the current petiole is connected with more than one pendant, cover it and delete the leaf with edges connected to it. Result a sub-graph.

b) If the current petiole only has one pendant, the two nodes can be covered either, so

1) Cover the petiole, and delete the leaf with edges connected to it. Result a sub-graph.

2) Cover the pendant, and consider the information dissemination process. Result a sub-graph.

3) Add up the number of solutions in the above two cases.

c) For the sub-graphs obtained, repeat step a)-b) until there is no leaf left.

b) The total number of all its minimum vertex-cover solutions is obtained.

Evidently, the above algorithmic strategy is polynomial in computational complexity. In FIG.2, a simple example is shown. Its number of minimum vertex-cover solutions is four, and the minimum vertex-cover has seven nodes.

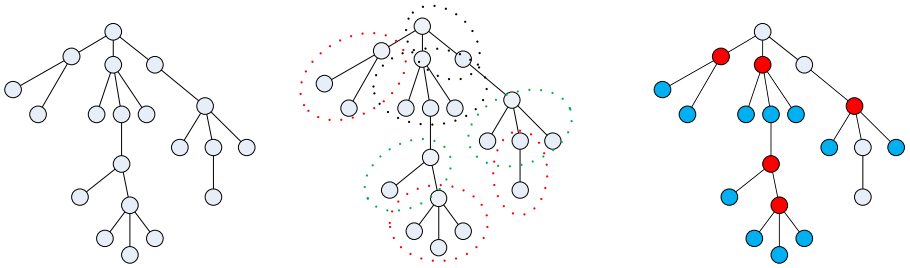

Original tree graph different leaves on the tree resulted graph

Fig.2 An example for the branch-and-bound algorithm: the red nodes must be covered in the minimum vertex-cover, the blue nodes must be uncovered and the rest two white leaves are free to cover the petiole or the pendant

The minimum vertex-covers on a lattice

Lattice is a graph that can be drawn within a repeating arrangement of nodes. Typically, no clear distinction is made between such a graph in the more abstract sense of graph theory and its drawing in plane or 3D space.

In the plane lattice, we divide the node set into two distinct subsets M, N by the diagonal relationship. For example, in a lattice G, we use (i, j) to mark each node, $M = \{(i, j) \mid i + j = 2n, n \in N+\}$, $N = \{(i , j) \mid i + j = 2n +1, n \in N+\}$. The nodes in set M only connect the nodes in set N, and so do the nodes in N. In left graph of FIG.3, we have $|M| = 13$ and $|N| = 12$ in lattice G, and based on this partition, covering all the nodes of N can obtain a vertex-cover of G. Similarly, M can also form a vertex-cover of G, but the scale of N is smaller. Obviously, the coverage of nodes in N is a minimum vertex-cover of G. To prove it, we delete some edges of the lattice to obtain a sub-graph G', which is shown in the middle graph FIG.3. The structure of G' is very simple, it is one-dimensional. In this figure, it is clear that M, N are both vertex-covers of G'. According to leaf removal algorithm [9], N is the minimum coverage of G' and is the only coverage, which is shown in the right graph of FIG.3. As is known to all, if the only minimum vertex-cover of sub-graph G' can still cover graph G, it is also the minimum vertex-cover of G.

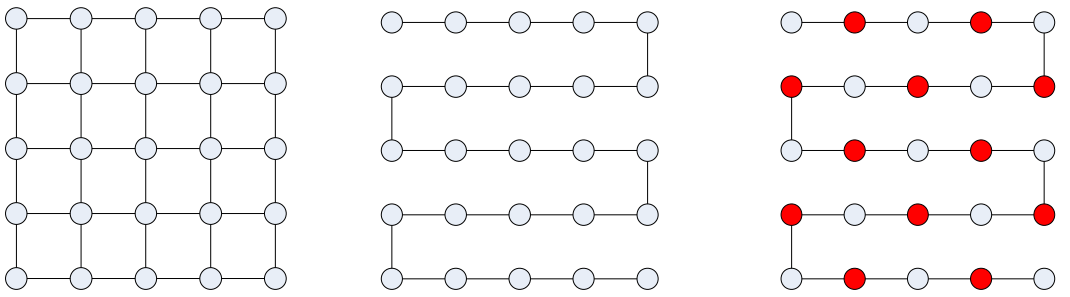

G *G'* minimum vertex-cover *N*

FIG.3 An example to calculate the minimum vertex-cover of plane lattice

Thus, we get a conclusion on the plane lattice that if the sizes of set M and set N are not equal, the set with smaller size will be the only minimum vertex-cover of plane lattice G.

If the partitions M, N have the same size, then the sub-graph G' has several minimum vertex-cover including M, N. As a special case, the node sets M, N are certainly minimum vertex-covers. However, the above analysis process in figure may lead to mistakes. For example, in the following G1' of FIG.4, the red dots are shown as the coverage S. Obviously it is a solution of the minimum vertex-cover of graph G1'. We can see that in the middle of this one-dimensional lattice, the coverage strategy is changed, in which node a is covered and b is not. In graph G1, the nodes b, c are connected and this edge is not covered by S, i.e., S is not a vertex-cover of the original graph. Then, minimum vertex-covers of the sub-graph G1', except M and N, cannot be

easily generalized to minimum vertex-covers of the original graph G1. After simple deduction, we can get the second conclusion: when the partitions of M, N have the same size, M, N are the only two minimum vertex-cover solutions of G1.

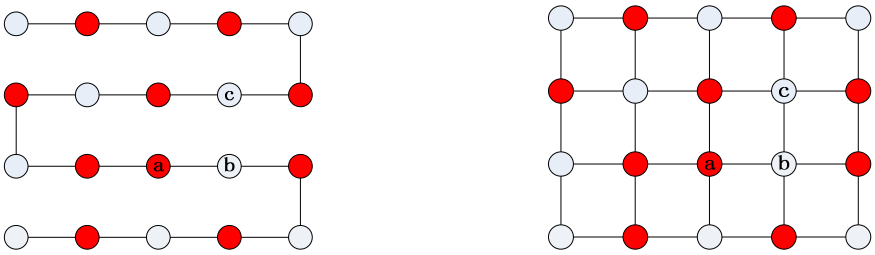

G_1' with coverage S G_1 with S

FIG.4 An example to verify the invalidity of the analysis process in FIG.1

In summary, if G is a lattice with 2n +1 nodes, the minimum vertex-cover of G has one and only one solution N, and the size of N is n; If there are 2n nodes in G, then the minimum vertex-cover solution space of G is {M, N}, where the size of M or N is n. All the above conclusions can be extended to high dimensional lattices.

Conclusion

Some basic characteristics of the minimum vertex-covers on the lattice and tree structures are investigated in this paper, and rigorous results or algorithm are proposed on calculating the solution numbers. Certainly, all these two cases belong to the easy-solving case in Minimum Vertex-Cover Problem, and how to generalize the idea to solving other complicated cases, such as random graphs [10] or scale-free graphs [11], is still quite difficult. We hope more efficient algorithms can be proposed based on the results in this paper, and it will be an interesting research direction.

Acknowledgement

This work was supported by the Natural Science Foundation of China (Grant No. 11201019) and the Fundamental Research Funds for the Central Universities.

References

[1] R.M. Karp, in Proc. Sympos. IBM Thomas J. Watson Res. Center (Plenum, New York, 1972), pp. 85–103.

[2] J. Gomez-Gardenes, P. Echenique, and Y. Moreno, Eur. Phys. J.B 49, 259 (2006).

[3] Y. Breitbart, C. Y. Chan, M. Garofalakis, R. Rastogi, and A. Silverschatz, in Proc. IEEE INFOCOM (IEEE Communication Society, Anchorage, Alaska, 2001), pp. 933–942.

[4] P. Kilby, J. Slaney, S. Thiebaux, and T. Walsh, in Proc. of the 20th Ntl. Conf. on Artificial Intelligence and the 17th Innovative Applications of Artificial Intelligence Conf. (AAAI/MIT Press, Menlo Park, 2005).

[5] W.Wei, R. Zhang, B. Guo, and Z. Zheng, Phys. Rev. E 86, 016112 (2012).

[6] A. Braunstein, M. Mezard, and R. Zecchina, Random. Struct. Algor. 27(2), 201 (2005).

[7] L.G. Valiant, Theor. Comp. Sci. 8(2) (1979) 189-201.

[8] M.Weigt and A. K. Hartmann, Phys. Rev. Lett. 84, 6118 (2000).

[9] M. Bauer and O. Golinelli, Eur. Phys. J. B 24, 339 (2001).

[10] B. Bollobas, Random Graphs (Academic Press, New York, 1985).

[11] A. Vazquez1 and M. Weigt, Phys. Rev. E 67 ,027101 (2003).

Advanced Materials Research Vols. 989-994 (2014) pp 4930-4933
© (2014) Trans Tech Publications, Switzerland
doi:10.4028/www.scientific.net/AMR.989-994.4930

Research on multi-channel network information interactive technology

Xiao-Hua Wang[1,a], Jia-Qing Zhang[2,b,*] and Chao-Chun Ou[3,c]

[1] China Nuclear Power Technology Research Institute

Shenzhen, China

[2] China Nuclear Power Technology Research Institute

Shenzhen, China

[3] China Nuclear Power Technology Research Institute

Shenzhen, China

[a] wangxiahua@cgnpc.com.cn, [b] zhangjiaqing@cgnpc.com.cn, [c] ouchaochun@cgnpc.com.cn

* Corresponding author Jia-Qing Zhang

Keywords: Ubiquitous computing, Multimodal human-computer interaction, Information integration

Abstract. Changes in the development of computing technology and calculation model of a profound impact on the development of human society, the popularity of networks and portable devices today and in the future, desktop computing mode has not been able to adapt to the changes in the development of the computer man-machine relationship changes and user computer method. Pervasive computing is in this context is proposed. The new model emphasizes the computer into people's daily life and working environment, to form a "at any time, everywhere and invisible" computing environment. In such a computing environment, user can calculate the services and information resources through the handheld, wearable devices used or other conventional, unconventional computing devices without obstacles. The innovation from the desktop computing to ubiquitous computing can be seen, human-computer interaction is an important index for pervasive computing.

Introduction

Pervasive computing refers to the ubiquitous, anytime, anywhere can be a way of computing. Users in this computing environment, wherever and whenever. As long as necessary, you can have access to the information the90s, Dr. Weiser United States proposed "ubiquitous computing" This new concept began to future human exploration of the process of the computer age [1] In the era of ubiquitous computing, there will be a lot of computing devices with computing and networking capabilities will provide services for us, a wide variety of computing devices are embedded in the walls, chairs, clothing, light switches, etc. all things automotive. Everything has the computing power of the devic y need by some devices. The present era, the computer has been entered in all areas of human life. The actual status of the computer in people's daily life, had earlier is no longer a simple tool for human use. With the advent of the development of computer-related technology, communications technology and a variety of new sensors, computer equipment to access the Internet, people more insight into the calculations everywhere. The early 19e will be fully utilized, making today's expensive "thin client" while a "thin server." An important sign of pervasive computing is a natural and efficient human-computer interaction. In recent decades, with the rapid development of computers, human-computer interaction has also undergone a major change, we can say history is the history of the development of the man-machine interface of a computer. From the initial input to the panel switches and tape devices to interact characterized today's graphical user interface, HMI has undergone enormous changes.

Many people through road desk alternately technology background

Research on human-computer interaction technology is a problem when people use the computer to complete a task, the mutual exchange of information between the computer and the ways and means. Can abstract a dialogue between human and computer-level interface, called interactive interface. It is an important part of a computer system, through which the user and the computer information exchange [2].

With the popularization of computers, more and more ordinary users started using the computer in contact, on the other hand also contributed to the development of computer hardware and software it has become the way people work, learn and important tool life. It is in this process, the status of human-computer interaction is becoming increasingly important, and it is the people know it is inseparable. Importance of the human-machine interface is that it is the interface between the user and the computer, which greatly affects the use of end-users. Today, a measure of the success of an application, the user interface is easy to become an increasingly important operational indicators.

Currently, thanks to other relevant computer technology such as the development of speech recognition, natural language understanding, gesture recognition, computer vision, and many other technologies, human-computer interaction research entered a new area of human-computer interaction more than one channel. The so-called channels, meaning people in this exchange of information with the computer the way, is the classification from the user's point of view in this way information exchange carried out.

Multi-channel human-computer interaction is developed in the traditional man-machine interface of an emerging technology, but also human-computer interaction techniques developed to a certain stage of historical trends inevitably arise. Direct manipulation of today's popular graphical user interface (GUI) there are still insufficient, mainly due to inconvenience users, even if it is difficult to integrate multimedia technology to change the fundamental problem [3].This is because although the GUI and direct mode of operation allows the use of computers has become intuitive, simple, integrated multimedia technology have greatly enriched the computer feedback manifestations , but the operation mode of the computer still does not change , the operator is still restricted next to the computer . Users can use according to their own habits and have to adapt to the computer, which is used as a tool for the computer itself, it is far from reaching its objectives. Because the instruments of its own starting point is to facilitate the use of human. Multi -channel technology, human-computer interaction is generated in this context. Multi-channel interaction through a variety of interactive features designed to use an integrated way that people feel the effect channels and channels in parallel and collaborative manner to interact with the computer task. It is the biggest difference with the traditional place interactive graphical user interface that simultaneously use a variety of interactive devices and the integration of information from multiple interaction channels. It is designed in the context of ergonomics , the exchange of information through research into the habits and behavior patterns , the integrated use of sight , speech , gestures and other new interactive channels , devices and interactive technology that enables multiple users can natural channel , parallel , collaborative approach to human-computer dialogue , integration of accurate and inaccurate input from different channels to capture user interaction intent to improve the efficiency of natural and human-computer interaction , and ultimately achieving people-centered interaction.

With the popularization of computers and more intelligent, the popular interactive mode cannot meet the needs of people interact. Especially under the concept of ubiquitous computing, human-computer interaction is needed breakthrough improvement, the need to develop a more user-friendly interactive methods and techniques. Multi-channel technology is a hot topic nowadays human-computer interaction technology. It is against this background, this article will present theoretical results at home and abroad, for the multi-channel technology research.

Enter the concept of multi-channel information fusion

In order to achieve the purpose of mutual understanding and the computer must be understood in different ways for people to do something about computers. Expression and understanding of the way

people are multi-channel, non-precise, descriptive, and understandable manner on rigid computer a lot, need to understand the precise input. For as long as the person concerned in the particular occasion communicators need to express the idea of fully demonstrated, the understanding of people take into account many factors, such as background knowledge, specific field units, communicators background knowledge to understand the user wants to express the precise meaning. And can finally understand. Understanding of computers is not the same, requires the user to enter accurate information, but also in accordance with very strict chronological order.

The way people communicate is a multi-channel, such as when people communicate using both languages, there are gestures, as well as the eyes, facial expressions and the way of drawing and so forth. The purpose of the multi-channel computer interaction is the customary way people try to manipulate the computer. The key question is which one is converted into a multi-channel computer can understand how the form of the process. We called multi-channel integration. In dealing with this problem have been proposed different models and algorithms.

(1) Layered fusion model

Stratified according to ideological convergence, the integration process into the lexical, syntactic and semantic layers. In the lexical level, there are multiple channels to express the same information. In other words lexical layer that unifies the different forms of input channels, at this level, the process of handling two or more channels though not the same. However, they express the content is the same, i.e., the contents thereof can be expressed by the same word. In the syntax layer, the layer primitives according to information from the lexical grammar specification into human-computer interaction, said command primitives, which means that primitive objects representing primitive object properties. In the semantic layer. The use of task-driven mechanism, combined into a primitive primitives various specific tasks. In the semantic layer, using task-driven mechanism, the original language combined into a variety of specific tasks.

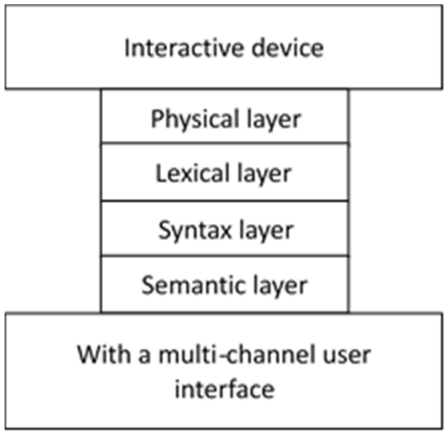

Figure: Hierarchical structure of multi-channel interaction

(2) Fusion model based on the probability of the alleged

Probability theory has a long history, it has successfully addressed many of the uncertainties related issues. There are abundant theories and systems. Probability fusion model is the main feature of the input event handling. In the probabilistic fusion mechanism, the event from any one channel are simultaneously sent to the action extractor, object extractor and various parameter extractor analysis and the results of each extractor and related parameters, including the results of the fusion probability, was sent to command fusion for further analysis, interactive commands and associated probability of formation of fusion. Fusion success probability depends on the input size.

(3) Multi-channel model of task-oriented interface structure

Multi-channel interface structure model ATOM-oriented tasks proposed by the domestic. The basic process of handling multi-channel interface is the input to block the flow of information, and make a proper understanding of the perceptual process. From the viewpoint of the task, the process is to capture user input, considering the passage of factors, contextual factors, interaction history information, to obtain the user's interaction with intent, the final

process of the formation of a task [4]. This process, the syntax constraint information input by the user becomes task configuration information, user information fusion process task is the formation of human computer interaction intention understanding.

Summary

The main topic of this paper is the pervasive computing environment, structure and method of program design of multimodal interaction. With the development of a variety of interactive technology, multi-channel technology will be put into practical application is more and more widely, according to the characteristics of multi-channel system, to study the module has a greater practical significance. Through the analysis of multi-channel system of semantic representation. A package model and algorithm more efficient template for multi-channel system developers call, is conducive to focus on design and function of the user interface and application related. At the same time, with the idea of modularization, improvement of multi-channel fusion model based on other multi - channel technology research results can only reflect to the template, then no need to change for multi-channel system using it.

References

[1]M.Weiser，The computer for the twenty2first century Scientific American，1991，265(3)

[2]M．Johnston，S．Bangalore。Finite—state Multimodal Parsing and Understanding．AT&T Labs-Research Shannon Laboratory．

[3]M．Tormanen，R．Myllyla，Pulp consistency determined by a combination of optical and acoustical measurement techniques Measurement Science and Technology，2010(1)

[4]R．S．Jason，J．L．Hill，A compassable framework for secure multi-modal access to internet services from Post—PC devices．Mobile Networks and Applications，2012，7(5)：389-406

[5] W3C Multimodal Interaction Framework，http：//www.w3.org/TR/mmi-framework/，2013, 5

[6]A．K．Dey，D．Salber，G．D．Abowd，A Concenptual Framework and n Toolkit for Supporting the Rapid Prototyping of Context-Aware Applications Anchor．Human-Computer Interaction(HCI)Journal，2011，16(2—4)：97-166

Advanced Materials Research Vols. 989-994 (2014) pp 4934-4939
© (2014) Trans Tech Publications, Switzerland
doi:10.4028/www.scientific.net/AMR.989-994.4934

Collective Communication Optimization for Solving Linear Algebraic Equations

Xiaoguang Ren, Wenhao Zhou, Juan Chen

State Key Laboratory of High Performance Computing

National University of Defense Technology

Changsha, Hunan 410073

hbszrxg@gmail.com

Keywords: Optimization, Linear Algebraic Equations, MPI, Collective communication

Abstract. With the development of the electronic technology, the processors count in a supercomputer reaches million scales. However, the processes scale of a application is limited to several thousands, and the scalability face a bottle neck from several aspects, including I/O, communication, cache access .etc. In this paper, we focus on the communication bottleneck to the scalability of linear algebraic equation solve. We take preconditioned conjugate gradient (PCG) as an example, and analysis the feathers of the communication operations in the process of PCG solver. We find that reduce communication is the most critical issue for the scalability of the parallel iterative method for linear algebraic equation solve. We propose a local residual error optimization scheme to eliminate part of the reduce communication operations in the parallel iterative method, and improve the scalability of the parallel iterative method. Experimental results on the **Tianhe-2** supercomputer demonstrate that our optimization scheme can achieve a much signally effect for the scalability of the linear algebraic equation solve.

Introduction

The performance of High Performance Computing (HPC}) had been greatly developed, and extended to E-scalar. However, the HPC applications cannot fully take the advantages of HPC performance as the scalability problem. The scalability problem means that the application performance cannot extend with the processors count, even show up a negative speedup when the application takes massive processors. There are various bottlenecks cause the scalability problem, including I/O problems, memory access, load balance, and communication, among which communication is the focus of this paper.

Linear algebraic equations solving is the core module of most scientific computing, especially the partial differential equations (**PDE**) solving. According the researchers' work, linear algebraic equations solving accounts for up to nearly 70% of the whole scientific application execution time, whose performance plays a critical role in the scientific computing.

Linear algebraic equations solving also faces the scalability problem, which concentrates on the communication bottleneck. Message Passing Interface(**MPI**) is a defacto standard for HPC communication, and the communication operations can be classified into point-to-point communication and collective communication. Collective communications essentially are synchronization operations, and heavily limit the performance of linear algebraic equations solving.

In this paper, we try to optimize the communication in the linear algebraic equations solving through reducing the collective communication operations. Iterative methods are the mainstream method for linear algebraic equations solving. Our work is on the base of the analysis of the iterative methods, and we try to eliminate some collective communications operations in the iterations, which will greatly enhance the scalability of the computing of linear algebraic equations.

The main contributions of this paper are summarized below:

- We analysis the feature of the linear algebraic equations, find that the collective communication operations are the main bottlenecks for the applications' scalability problem.
- We optimize the iterations method for linear algebraic equations through eliminating the collective communications, which will greatly enhance the scalability of the HPC scientific computing.
- We show by experiments on Tianhe-2 supercomputer with a typical iterations method for linear algebraic equations that our strategies have greatly improved the scalability of the linear algebraic equations solving.

Background

Linear algebraic equations. Solving linear algebraic equations is the core of most problems in computational mathematics. Most of the scientific computing problem is to solve the Partial Differential Equation (**PDE**), which is discrete into linear algebraic equations by various discrete methods like Finite Volume Method (FVM) and Finite Difference Method (FEM). Linear algebraic equation has the form shown as Eq.1:

$$Ax = b \tag{1}$$

Where A is a matrix, and b is a vector, x is the vector to be solved. Depends on the features of the PDE and the discrete mesh, the matrix A is tense or sparse, and the density of the non-zero elements in the matrix A is critical for the performance of the linear algebraic equations.

There are several algorithms for solving a system of linear equations: direct method and iterative method. In the problems of finding the root of an equation (or a solution of a system of equations), an iterative method uses an initial guess to generate successive approximations to a solution. In contrast, direct methods attempt to solve the problem by a finite sequence of operations. In the absence of rounding errors, direct methods would deliver an exact solution (like solving a linear system of equations Ax = b by Gaussian elimination). Iterative methods are often the only choice for nonlinear equations. However, iterative methods are often useful even for linear problems involving a large number of variables (sometimes of the order of millions), where direct methods would be prohibitively expensive (and in some cases impossible) even with the best available computing power[1].

In this paper, we mainly focus on the iterative method, and take the Preconditioned Conjugate Gradient (PCG) method as an example to demonstrate our propose. The preconditioned conjugate gradient method takes the following form:

Algorithm 1 Preconditioned Conjugate Gradient Method

1: $r_0 = b - Ax_0$
2: $z_0 = M^{-1}r_0$
3: $p_0 = z_0$
4: $k = 0$
5: **while** $|r_k| < tol$ **do**
6: $\quad \alpha_k = \frac{r_k^T z_k}{p_k^T A p_k}$
7: $\quad x_{k+1} = x_k + \alpha_k p_k$
8: $\quad r_{k+1} = r_k - \alpha_k A p_k$
9: $\quad z_{k+1} = M^{-1} r_{k+1}$
10: $\quad \beta_k = \frac{z_{k+1}^T r_{k+1}}{z_k^T r_k}$
11: $\quad p_{k+1} = z_{k+1} + \beta_k p_k$
12: $\quad k = k + 1$
13: **end while**

Where *tol* is the floor of the residual error, and x_{k+1} is the solution result. The whole algorithm do the iterations until$|r_k|$ is smaller than *tol*.

Parallel scalability of iterative method. We still take PCG method as an example to demonstrate the parallel scalability of iterative method, the parallel implementation of PCG has been described in many papers[2-4]. The parallel implementation of PCG mainly on the base of block partition, i.e. decompose the matrix A and vector b into several parts, and each part is computed by a

process. The block matrices is shown in Fig.1, where the matrix A is divided by row as well as the vector b, and each process computes a matrix block and a subset of b.

The scalability of a parallel application on a parallel system is a measure of its capability to effectively utilize an increasing number of processors[5]. However, the scalability of the iterative method is so poor that the speedup can't expand with the processors number. We test the performance of PCG with processors from 2 to 2048, the result of which is shown in Fig.2. We can find from the result that when the processors number is greater than 512, the speed up become negative.

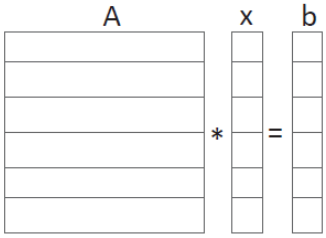

Fig.1 Parallel implementation of iterative method

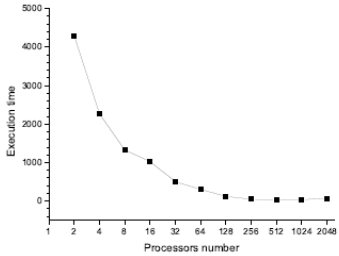

Fig.2 Performance of PCG with different processors number

There are several bottlenecks causes the poor scalability, including the cache block, I/O, communication, .etc, among of which, communication cost is the mainly reason for it. According to our experimental data, we test the communication cost in the iterative method for PCG method, as shown in Fig.3, the percentage of the communication cost increases with the processors number. When the processors number is greater than 1024, the communication cost will become the main cost of the whole execution time, and become the bottleneck of the parallel execution.

Communication bottleneck analysis for iterative method

In this section, we still take PCG method as an example to analyse the communication bottleneck for the parallel iteration method.

The parallel implementation is based on Message Passing Interface (MPI), which the d'fact standard for parallel is programming. There are two kinds of communication operations in the PCG method: point-to-point communication operations and collective communication operations. Taking PCG method as an example, as shown in Alg.1.

The point-to-point communication operations are mainly occurs in the matrix-vector multiply operation. When one row of the matrix multiplies a vector, the process just holds a subset of the whole vector, and a point-to-point communication operation has to be performed to exchange data between different processes.

As shown in Alg.1, there are three matrix-vector multiply operations in PCG method, respectively in line 6,8,9 of Alg.1. These matrix-vector multiply operations involves two point-to-point communication operations, and the data size of these point-to-point communication depends on the vector data to be exchange with other process.

As shown in Alg.1, there are two collective communication operations in PCG method, respectively in line 5, 6, 10 of Alg.1, which are respectively to calculate the scalar variables $|r_k|$, α_k, β_k. Take the calculation of β_k as an example, the collective communication operation is reduce sum operations, each process send its local variable β_k to the master process, and the sum of all the local variables value is calculated, and the sum result is broadcast to all the processes.

Although collective communication operation involves just a scalar data, it is a synchronization operation and a very time-consuming process. Because the collective operation in each process will not finish until all the processes done the collective operations, and the performance of the collective communication operation will be limited by the slowest process.

Through other researchers' work, the cost of various communication operations in PCG solver is tested, and the results are shown in Fig.4[6]. We can find from the results that collective

communication operations are the most time-consuming operations. Although the point-to-point communication operations (send and receive) occur most, the time cost of them are far smaller than the collective communication operations (reduce).

So, in the following sections, we will try to optimization the collective communication operations by reducing the number of collective communication operations.

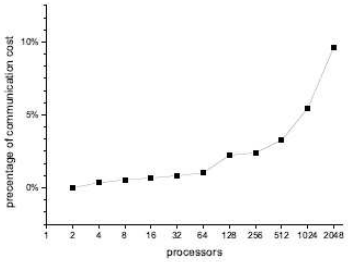

Fig.3 The percentage of the reduce cost increases with the processors number

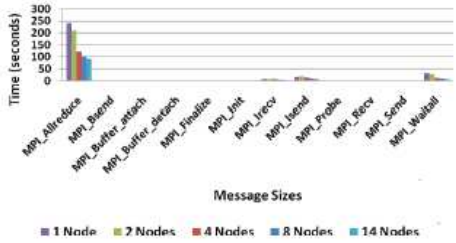

Fig.4 The time cost of different communication operations in PCG

Collective communication optimization for iterative method

In this section, we will demonstrate our collective communication optimization method for iterative method by taking PCG as an example. The core of our optimization method is to reducing the number of the collective communication operations as much as possible, especially the reduce operation.

The feather of PCG solver provides opportunity for our optimization. As the analysis in the former sections, there are three reduce communication operations, and the core of our optimization is to combine the reduce communication operations or eliminate it. So there mainly two optimization schemes for the reduce communication operations.

reduce elimination. The scalar variable $|r_{k+1}|$, the resid error has to be calculated for every iteration method for linear algebraic equations, which is used to check whether the iteration has reach to the convergence value. The compare between the variable $|r_{k+1}|$ and \$tol\$ is performed at the end of every iteration, if $|r_{k+1}|<tol$, the solution can be considered to be convergence and the iteration will be stopped. Otherwise, the iteration has to be continued until the condition $|r_{k+1}|<tol$ is met.

However, each calculation of the resid error $|\boldsymbol{r_{k+1}}|$ has to perform a reduce communication operation. As the roll of the compare between the variable $|\boldsymbol{r_{k+1}}|$ and tol is just to check whether the iteration should be continued, the compare can be cancelled at some condition. If the compare is cancelled, there will be no need to perform the calculation of $|\boldsymbol{r_{k+1}}|$, and the corresponding reduce communication operation will be also cancelled.

However, if the compare is cancelled, the iterations cannot judge when to stop. In this paper, we propose three schemes to solve this problems: Fixed iteration number, coarse check, and local resid error, and we will introduce them respectively.

Fixed iterations number: Instead of check the residual error for each iteration, we can set a fixed iterations number, and the iterations will continued without check until all the fixed iterations number had been finished. The reduce communication operations will be eliminated with the fixed iterations number scheme. In fact, most of the iteration number in traditional iterative method is dynamic. The disadvantage of the fixed iteration number is that the iterations number may be less or more than the actual value, so this scheme just valid for the iterative method with known iterations number.

Coarse granularity check: Instead of check the residual in the end of every iteration, coarse granularity check performs the residual error check in a coarse granularity, i.e. the check interval is more than one iteration, may be two or more. As the check interval last for longer time, the number of the residual error checks will sharply decrease, and the reduce communication operations also decrease with the residual error check number. Coarse granularity check can greatly reduce the

number of residual error checks as well as the reduce communication operations. However, if the residual error check interval consist too many interations, the total iteration number may be greater than the predetermined iterations number, and import external performance overhead. So the residual error check interval is very critical for this coarse granularity check scheme, and we will discuss this problem in the next section.

Local residual error: The root of the reduce communication operation in the calculation of residual error $|r_{k+1}|$ is that all the processes have to contribute to the final residual error value and get the final value from the root process. In our local residual error scheme, every process tries to calculate its own local residual error value without data exchange with other processes, and check it locally.

However, as the original residual error is the sum of the local residual error from all the processes, the local residual error will be less than the global residual error. To approximately keep the residual error check effect, the condition $|r_{k+1}| <$tol has to be met, here $|r_{k+1}|$ is the global residual error. We assume that $|r_{k+1}|^{i}$ is the local residual error in process *i*, and then we can get the following condition should be met Eq.2:

$$\sum_{i=0}^{n-1} | r_{k+1}^{i} | < tol \tag{2}$$

For a single process *i* out of *n* processes, we take a conservative scheme, i.e. the local residual error just had to meet the following equation:

$$| r_{k+1}^{i} | < tol / n \tag{2}$$

If every process meets the condition Eq.2, the condition Eq.3 will be also met.

In this local residual error scheme, all the processes will carry forward without synchronization with other processes, so all the processes will not reach the convergence point at the same time. If one process reach the convergence point firstly, it had to continue the iterations until all the processes reach the convergence point.

In a word, the three schemes above are suitable for different application background, but the most practical one is the local residual error scheme. We will check its performance in the experiment section.

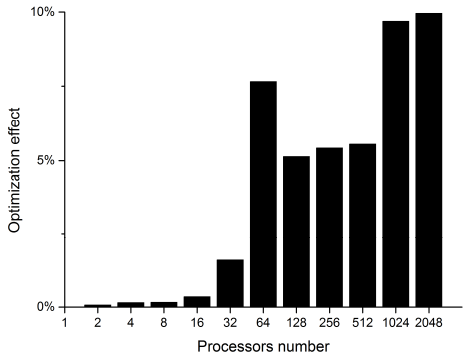

Fig.5 Optimization effect of local residual error scheme

Experiment

We demonstrate our scheme on the Tianhe-2 supercomputer with PCG solver in OpenFOAM framework. Subsection 5.1 discusses the OpenFOAM selected. Subsection 5.2 introduces the computer platform Tianhe-2 used in the experiments. Subsection 5.3 describes the methodology used for compare work. Subsection 5.4 presents and analyzes our results.

OpenFOAM. OpenFOAM is a open source Computational Fluid Dynamics (CFD}) software platform, which is based on Finite Volume Method (FVM}). There are multiple iterative methods for linear algebraic equation solving, including PCG method. We test the PCG method through a dambreak benchmark. dambreak is a simulation of dam break based on the volume of fluid (VOF) method. The two phase flow solver interFoam in OpenFOAM is used.

platform. The Tianhe-2 supercomputer was built by China's National University of Defense Technology (NUDT}), which is currently the world's fastest supercomputer with a 33.86 PFLOPS peak performance according to the TOP500 list in June 2013[7]. Our experiments use a subsystem of Tianhe-2 with 128 compute nodes as the test platform, and each computing node comprises two Intel Ivy Bridge Xeon processors, three Xeon Phi chips (accelerator card), and 64GB DRAM. It should be pointed out that our experiments only use the processors, rather than the accelerator card.

Evaluation methodology and result analysis. We tested our local residual error scheme in PCG method on OpenFOAM platform. The experiment mainly compare the performance of the original PCG solver and the PCG solver with local residual error optimization, especially the time cost of the reduce communication operations. As shown in Fig.5, it is the optimization effect of our optimization scheme, which is thetoltal execution time in the original PCG solver compared to the total execution time in the PCG solver with local residual error optimization. We can find that our optimization scheme can optimize about 9% of the total execution time.

Conclusion

In this paper, we analysis the bottleneck of the iterative method for linear algebraic equations solving, and find that reduce communication operations are the main reason for the parallel scalability problem. On the base of taking PCG method as an example, we propose three optimization schemes to reduce or eliminate the reduce communication operations. our experiment demonstrates that our optimization can significantly improve the performance of the iterative method.

Acknowledgment

This work is supported by National Natural Science Foundation of China (Grant No.61221491, No.61303071, and No.61120106005), and Fund (No.134200026) from Guangzhou Science and Information Technology Bureau, Fund of State Key Laboratory of High Performance Computing (No.201303-01)

References

[1]I. Jacques and C. Judd, “Linear algebraic equations,” in Numerical Analysis. Springer, 1987, pp. 8–42.
[2] A. Gupta, V. Kumar, and A. Sameh, “Performance and scalability of preconditioned conjugate gradient methods on parallel computers,” Parallel and
Distributed Systems, IEEE Transactions on, vol. 6, no. 5, pp. 455–469, 1995.
[3] A. Meyer, “A parallel preconditioned conjugate gradient method using domain decomposition and inexact solvers on each subdomain,” Computing, vol. 45, no. 3, pp. 217–234, 1990.
[4] G. Meurant, “Multitasking the conjugate gradient method on the cray x-mp/48,” Parallel Computing, vol. 5, no. 3, pp. 267–280, 1987.
[5] V. P. Kumar and A. Gupta, “Analyzing scalability of parallel algorithms and architectures,” Journal of parallel and distributed computing, vol. 22, no. 3, pp. 379–391, 1994.
[6] H. A. Council, “Openfoam performance benchmark and profiling,” 2010.
[7] [Online]. Available: http://www.top500.org/

Advanced Materials Research Vols. 989-994 (2014) pp 4940-4944
© (2014) Trans Tech Publications, Switzerland
doi:10.4028/www.scientific.net/AMR.989-994.4940

Trusted Software Architecture Evolution Based on Graph Transformation Rule

Jiang Huowen[1, a], Wang Runliu[1, b]

[1]Collage of Mathematics & Computer Science, Jiangxi Science & Technology Normal University, Nanchang 330038, China

[a]jhw_604@163.com , [b]sjxywork@163.com

Keywords: evolution rule, software architecture, trusted attributes, graph transformation

Abstract. In current software architecture evolution community, Trusted attributes of component are less considered; and the concept of trusted software architecture evolution has not generally agreed. Focused on above shortages, This paper propose the idea of trusted software architecture evolution, it helps to increase the trustworthiness of evolution; on the basis of graph transformation rule, establish some basic evolution rules, Evolution operations are implemented according to these evolution rules. It can ensure the exactness of evolution process. The paper also introduce E-R diagram to represent trusted software architecture evolution; and finally through an evolution case, exactly and visually describes the sophisticated evolution process of trusted software architecture evolution.

1 Introduction

With the rapid development of modern computer technology, especially mobile internet and internet of things, the complexity of external environment and software system itself is increasing, so software evolution is becoming more and more complex. Software Architecture(SA),which is considered as the foundation of software system, provides an effective way and basis for people to generally grasp software evolution. How to specify and analyze the evolution process in the architecture level has also been the key problem of the software evolution research[1].

SA evolution mainly relates to addition,deletion,replacement of components or connectors,and components relation and the change of its topology structure[2,3]. The literature [4,5,6] used graph to represent SA.The research effort in the literature [4] ,representing component using edge,representing communication port using vertex, focused on build of SA style and SA dynamic evolution; The literature [5] ,representing the superposition relationship of program using edge,representing program using vertex, depicted SA reconfiguration process by using graph rewriting rule. on build of SA style and SA dynamic evolution; The research effort in the literature [6] ,representing communication connection using edge,representing component using vertex, focused on describing SA style by using graph grammer. So each graph used in the literature[4-6] was endowed with different meaning. But these literatures did not focus on the research of SA evolution process defined on the basis of graph transition rule and based on some basic evolution operations as adding component,deleting component,etc.,also did not involve the trusted attributes of software system. The literature [1,4] made research on SA dynamic evolution based on hypergraph grammar,but did not involve the trusted attributes of component.The literature [7] proposed a kind of component model of supporting trusted software evolution, focused on improving the environmental perception and adaption ability of component to ensure trusted SA evolution, but did not specially consider trusted attributes of system, also did not involve SA evolution process on the premise of verifying trusted attributes of component.

So we can see that Although the investigator at home and abroad have launched much research on SA evolution, However, the concept of trusted SA evolution was rarely mentioned, the study on trusted SA evolution based on graph transformation rule was also rarely seen. This paper make the study on the conceptual ideas and evolutionary mechanism of trusted SA evolution, apply graph transformation rule to the SA change, describe the operations like addition,deletion and replacement

of trusted component through the change of the analogy diagram of representing SA, thus represent and specify the SA evolution process with some credible guarantee

2 The corresponding concepts

2.1 Graph transformation rule and SA evolution

Def.1 (graph transformation rule). A graph transformation rule P:L→R, it refers to a graph mapping relationship, let L be sub graph before transformation, R denotes the sub graph after one transformation.

Def.2 (Software Architecture,SA).SA of one software system includes the component,which is operating unit of system,the connector which connects components and specifys interactive behavior between components,and the configuration which formulates how to combine components and connectors together. SA can be expressed as a 3 tuple, $SA=(C_p,C_n,C_r)$,here,C_p represents the set of components ;C_n represents the set of connectors;C_r represents the set of constraints.

Def.3 (SA evolution). It refers to SA transformation such as addition,deletion,replacement,etc. of component or connector, and the corresponding change of interaction relationship between components and its topology structure due to some change, in which user requirements,running environments,software faults are , and other influences related to software system.

Def.4 (SA evolution rule). Let the corresponding graph of one SA be G, given a graph transformation rule P:L→R, if we have G' by using the rule to carry out one transformation to G, and the G' denotes the other SA, then P is called a SA evolution rule.

SA evolution rules can be applied to carry out SA evolution. given the graph G, which denotes one SA, and a SA evolution rule P:L→R, we can define the evolution process of applying P to G as the following:

1.Searching for the sub graph L' which is isomorphic to the graph L in the graph G, if successful then go on to step 2, else the rule P cannot be applied to carry out the evolution;

2.Deleting all the nodes and edges which are in the sub graph L', but not in the sub graph R, from the graph G;

3.adding all the nodes and edges which are in R, but not in L', into the graph G;

4.retaining the common nodes and edges of L' and R, meanwhile connecting the rest parts and newly added parts with the common parts of L' and R, and keeping the other parts of G unchanged, then we have the other graph G', the G' is the new graph denoting the SA after evolution.

Def.5 (SA evolution operation). It refers to some detailed evolution steps such as adding, deleting and replacing component, etc., for the graph representing SA by applying SA evolution rule to carry out.

SA evolution operation reflects SA evolution process, appears to a sequence of operations including addition, deletion,replacement,etc.of component or connector due to some reasons,e.g.,software function change,running environments change. The essence of SA evolution can be come down to modify the relationship between components.for example,when the functions of software system need to be expanded,it is ususaly to be needed to add new components;when some functions to be cut, to delete relative components needed.

2.2 Trusted SA evolution.

Trusted attributes are important elements of measuring software quality. software trusted attributes mainly include completeness for functions(Completeness), consistency for actions(Consistency), reliability for quality(Reliability) and security for program(Security). Completeness reflect to what extent software can realize its pre-design functions and satisfy users demands; Consistency refers to the capacity of maintaining no contradiction in the process of software running; Reliability reflects the system robustness to maintain functional properties confronted with special applications or unexpected errors; Security refers to the system capacity of preventing being used or refusing to services to unauthorized users in the meanwhile providing services to authorized users. The four attributes above comprehensively reflect software trusted characteristic, constitute the space of

trusted attributes, in which each attribute is composed of a vector of trust evidence, for instance, Reliability includes some trust evidences as the mean up time, the MTBF and the MTTR.

Def.6 (trusted attributes of component). It refers to attributes set of reflecting trusted characteristics like components quality and performance, including Completeness, Consistency, Reliability and Security.

The component is software function unit, is major portion of constituting SA and describing its evolution process. Trusted attributes of component can be analyzed and estimated by using state automation based on observation logic, protocol state machine and other techniques. According to several vector values of trust evidence, the integrated trusted degree of components can be obtained. When the value of trusted degree is greater than or equal to setting threshold value, the component could be seen as to be trusted. Only Trusted components are allowed to be evolved. The evolution of non trusted components is prohibited because it may conceal risks, for example, it may results in spreading errors if the components which are not available in one or several functions are evolved.

Def.7 (trusted SA evolution). It refers to SA evolution on the premise that the value of trusted degree is not less than threshold value when trusted attributes of components like Completness,Consistency, Reliability and Security were verified.

3. Basic operation of trusted SA evolution

3.1 **Analogy E-R diagram representation of SA**

In the design of database, we often use E-R diagram(Entity Relationship diagram). Here we introduce it to represent SA with trusted attributes to specify trusted SA evolution, each of its parts is separately given new representation meaning: rectangular box represents component; diamond box represents relationship; oval box represents trusted attribute of component.Connecting line with mark represents connection and interaction relationship between component and connector. It is called analogy E-R diagram, which is applied to represent software architecture with trusted attributes (SA-T). Fig.1 shows one SA-T represented with analogy E-R diagram. it includes 3 components:Client,WebServer and OracleS,each component is attached to four trusted attributes, such as Completeness, Consistency, Reliability and Security; 2 connectors:C-W connector and W-O connector; 4 edges, which are labeled with marks(named labeled edge):connecting the corresponding component to connector, showing the connection relationship between them, and reflecting interaction of each other,the mark on the edge indicate the news conveyed from component to connector,while the mark under the edge indicate the news from connector to component. for example: R_{Client}, $R_{webServer}$, $A_{oracleS}$, independently represents client request, webserver request, OracleS response.

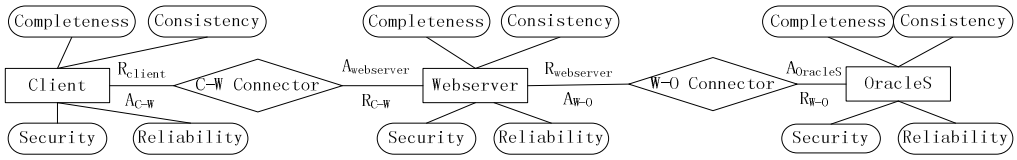

Fig.1 SA of Client/WebServer system represented with analogy E-R diagram

Def.8 (SA-T diagram). It refers to a SA diagram with trusted attributes represented by using analogy E-R diagram, it can be described as a 5-tuple $G_{SA}=(V_{SA},E_{SA},e_{cp},e_{cn},AR_{SA})$

For example, the fig.1 is a SA-T diagram. In G_{SA},V_{SA} is the nodes set, indicating all components and connectors in SA-T diagram, namely $V_{SA}=(C_p,C_n)$, C_p is the set of components, C_n is the set of connectors; E_{SA} is the set of labeled edges, indicating connecting relationship between component and connector(namely can indicate the communication ports between two sides); Both e_{cp} and e_{cn} are the set of mark on labeled edges, indicating the interaction relationship of each other, e.g., e_{cp}:$C_p \rightarrow C_n$,indicating message input from components to connectors, is marked on labeled edges; e_{cn}:$C_n \rightarrow C_p$, indicating message input from connectors to components, is marked under labeled edges. AR_{SA} is the set of trusted attributes of component, including four trusted attributes such as Completeness, Consistency, Reliability and Security.

In SA-T diagram, the component c_i, connector cn_i can be described with unary relation $C_p(c_i)$ and $C_n(cn_i)$; The connecting relation between component c_i and connector cn_i, namely connecting edge e_i between them, can be described with binary relation $e_i(c_i,cn_i)$; The interaction relationship between component and connector, namely e_{cp} and e_{cn}, which indicates the relationship of message passing ,can be separately described with unary relation $cp(e_i)$ and $cn(e_i)$, $cp(e_i)$ represents the input message from component c_i to connector cn_i on the edge of e_i, while $cn(e_i)$ represents the input message from connector cn_i to component c_i; Four trusted attributes of component c_i can be separately described with AR_{ci}(Completeness),AR_{ci}(Consistency), AR_{ci}(Reliability) and AR_{ci}(Security). Since each component is with above-mentioned four trusted attributes attached, in the process of evolution, they are added or deleted together. In order to express succinctly, the formalized description of four trusted attributes is be omitted when we give evolution rules in section 3.2.

3.2 SA evolution rule and evolution operation

One SA-T diagram represents a SA with trusted attributes. However, SA-T diagram can be considered as a kind of graph, graph transformation rule can be applied to SA-T diagram transformation. For example, Both rectangle box representing component and diamond box representing connector can be seen as the nodes in graph. The labeled edge connecting component to connector can be seen as the edge in graph. According to the formalized relation description before and after SA diagram change, we can define evolution rules for trusted SA evolution. Trusted SA evolution is based on these evolution rules, consists of a sequence of basic evolution operations. Basic SA evolution operations have addition, deletion, and replacement of the component or connector, the other complex evolution operations like splitting, recombining the component or connector, parallel evolution, etc., can be compounded of some basic evolution operations. To facilitate expression, we only give four basic evolution rules below, including adding component, adding connector, deleting component and replacing component. Meanwhile, we give the figures that show the corresponding SA-T diagram transformation to exemplify the trusted SA evolution process.

3.2.1 Adding a component or connector

Assuming G be the current SA-T diagram, the following formula (1) gives the evolution rule of adding a component c_i ; and the formula (2) gives the evolution rule of deleting a connector cn_i

$$G \rightarrow G \cup \{C_p(c_i),e_i(c_i\text{-}G(cn_i)),cp(e_i),cn(e_i),\ldots\} \quad (1);$$

$$G \rightarrow G \cup \{C_n(cn_i),e_i(G(c_i)\text{-}cn_i),cp(e_i),cn(e_i),\ldots\} \quad (2);$$

In formula (1), $C_p(c_i)$ denotes the component c_i; $e_i(c_i\text{-}G(cn_i))$ denotes the edge connecting the component c_i to the connector cn_i in the SA-T diagram; $cp(e_i)$, $cn(e_i)$ indicating the interaction between the component and the connector on the edge e_i, respectively denote input message and output message of the component c_i. Maybe the newly adding component has connecting and interaction relationship with multiple connectors, more than one newly labeled edges need to be added accordingly, so "…" is used to denote omission, like this, the "…" is used in the other evolution rules to be given below. In formula (2), $C_n(cn_i)$ denotes the connector cn_i; $e_i(G(c_i)\text{-}cn_i)$ denotes edge connecting the component c_i in the SA-T diagram G to the connector cn_i; $cp(e_i),cn(e_i)$ respectively denote their interaction relation; The fig.2 describes the SA evolution process of adding component c_i and connector cn_i.

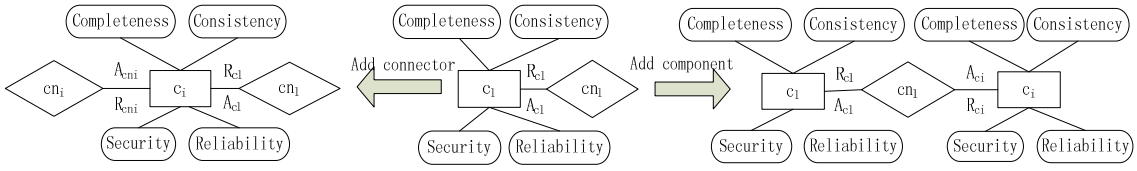

Fig.2 Adding a component/connector

3.2.2 Deleting and replacing a component

Assuming G be the current SA-T diagram, the following formula (3) gives the evolution rule of deleting component c_i ; and formula (4) gives the evolution rule of replacing component c_i with component c_k.

$$G \rightarrow G\text{-}\{C_p(c_i),e_i(c_i\text{-}G(cn_i)),cp(e_i),cn(e_i),\ldots\} \quad (3);$$

$G \rightarrow G-\{C_p(c_i),e_i(c_i-G(cn_i)),cp(e_i),cn(e_i),\ldots\} \cup \{C_p(c_k),e_k(c_k-G(cn_i)),cp(e_k),cn(e_k),\ldots\}$ (4);

When a component is out of use, formula (3) can be applied to delete it from its SA-T diagram;when the system need to replace a component, rule (4) can be applied to carrying out the corresponding SA evolution operations. The fig.3 describes the SA evolution process of deleting a component and replacing a component.

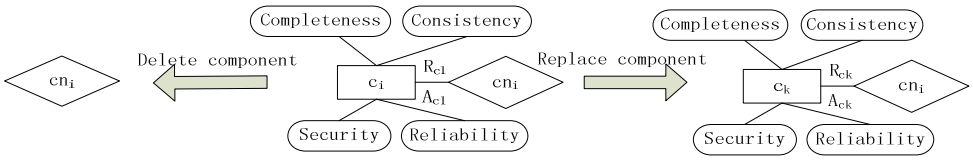

Fig.3 Deleting a component and replacing a component

4. Conclusions

Software evolution has become a existing form of software, is indispensable in the software life cycle. Architecture evolution reflects software evolution from a higher abstraction level, is an important means to study and implement software evolution. Focused on some problems in trusted SA evolution research, like its concept confused, modeling theory deficient, this paper proposes the concept of trusted SA evolution; establish some basic evolution rules based on graph transformation; introduces E-R diagram to represent SA with trusted attributes, carrying out evolution operations according to evolution rules, specify basic evolution process of trusted SA evolution. The approach presented in this charter has formalized basis of graph, and also has graphical concision.On the foundation of this paper, further, we will investigate the perception and verification of trusted attributes of component before SA evolution, the description of behavioral semantics evolution for SA, and so on.

Acknowledgements

This work was supported by the Project of Science & Technology Plan by Education Department of Jiangxi Province under grant No.GJJ13569. the Research Subjects of Jiangxi Science & Technology Normal University under grant No. Ky2012zy11.

References

[1] Xu HZ, Zeng GS, Chen B. Conditional Hypergraph Grammars and Its Analysis of Dynamic Evolution of Software Architectures. Journal of Software, 2011, 22(6): 1210-1223.

[2] Cheng XY,Zeng GS,Xu HZ. Description of Software Architecture Evolution Based on Delta-Grammar. Computer Science，2010，37(9): 127-130, 150.

[3] Xu HZ, Zeng GS, Dynamic Evolution of Software Architectures Based on Hypergraph Grammars. Journal of Tongji university(natural science),2011, 39(5): 745-750.

[4] Hirsch D, Inverardi P, Montanari U. Graph grammars and constraint solving for software architecture styles. In: Proc. of the Int'l Workshop on Software Architecture. New York: ACM Press, 1998. 69–72.

[5] M. Wermelinger, J. L. Fiadeiro. A graph transformation approach to software architecture reconfiguration. Science of Computer Programming, 2002, 44(2): 133-155.

[6] D. L. Métayer. Describing software architecture styles using graph grammars. IEEE Transactions on Software Engineering, 1998, 24(7): 521-533.

[7] Ding B,Wang HM,Shi DX,etc,.Component Model Supporting Trustworthiness-Oriented Software Evolution. Journal of Software [J],2011,22(1):17-27.

Advanced Materials Research Vols. 989-994 (2014) pp 4945-4948
© (2014) Trans Tech Publications, Switzerland
doi:10.4028/www.scientific.net/AMR.989-994.4945

The Method Research of Environmental Noise 3D Graphic Expression based on CityEngine

Xianglou LIU[1,2, a], Xiyue YANG[1,2, b], Tong ZHU[1,2, c]

[1]Northeast Petroleum University, Daqing, 163318, China

[2]The University-enterprise R & D Center of Measuring and Testing Technology & Instrument and Meter Engineering in Heilongjiang Province, Daqing, 163318, China

[a]email: liuxianglou@163.com, [b]email:yangxiyue0108@163.com, [c]email: 45232655 @qq.com

Keywords: CityEngine; Environmental Noise; 3D Graphic Expression; CSG; B-Rep

Abstract. Based on CityEngine as software platform, this paper put forward 3D graphic expression of environment noise, and establishes the environmental noise monitoring model of 3D space by CSG and B-Rep hybrid algorithm. Then, according to the noise data and the legend of the color grade, we render the surface area of the 3D monitoring geometric model with the expression of grid method. Finally, the simulation shows that this method can be applied to 3D graphical expression of environmental noise.

Introduction

Now, the study on the environmental noise map model and city environment evaluation system is mostly based on 2D plane, but there is not too much research on modeling and data analysis of the vertical dimension. With the development of the virtual city area, city construction tends to 3D. The research on distribution law of the environmental noise pollution of 3D city space can help to use the space resources of city more reasonably. Situation of noise pollution in 3D space can be showed intuitively by expression of 3D graphical environment noise which can be used in city planning, transportation and environmental protection. Therefore, the study of 3D graphical expression of environmental noise has practical value.

Esri CityEngine, a new member of the GIS system modeling software [1], can be used for digital cities, urban planning and other aspects of 3D simulation [2]. Because Esri CityEngine supports geographic information data types of Shapefile and Geodatabase which makes the basis of existing GIS data can be used directly without any conversion, and also shortens the construction period of the 3D GIS system [3]. The rules based on CGA (Computer Generated Architecture) in CityEngine can be used to analyze the component of 3D model [4], the release of CityEngine makes 3D solution of ArcGIS more perfect. The applications of CityEngine based on the above characteristics are now increasingly used in various fields, such as urban parametric modeling [5], batch modeling, rapid prototyping, virtual reality [6], city planning [7] and other areas. In the environmental noise evaluation of the past, 2D environment noise graphical expression is the mainly research content, but compared with the 2D graphical expression of environmental noise, 3D can be more close to the real noise distribution. So the 3D graphical expression of environmental noise will become the development trend. By consulting the CityEngine literature, has not found its application in the field of environmental noise assessment. Combined with 3D modeling algorithm and the environmental noise related method, the author puts forward the application of CityEngine in 3D graphical expression of environmental noise and does some research in the establishment of monitoring model and space environment noise expression method.

Establishment of 3D Space Environmental Noise Monitoring Model

In order to reflect the distribution of the environmental noise in 3D space entities, when we set up the 3D model of environmental noise monitoring we must base on the model of the 3D space geometric entities. We put the noise monitoring points in the place of buildings' sound point to get

the value of the noise data. There are two ways to set up the model of the 3D geometry. First is CSG(construction solid geometry), it is set up by Boolean operations, the other one is B-Rep (boundary representation), it structures the entity by describing the characteristics of the entity (point, line, surface) boundary. If we use the structure of CSG, first, we should do the geometric decomposition description of the entity, divide it into simple geometries based on the decomposition rule, and then we can get a group of CSG geometry voxels [8]. Geometric primitives can be divided into basic and expanded CSG voxels. The process of this decomposition to 3D geometric building shows in Figure 1, divide a single building into parts of A, B, C, and D. The CSG modeling algorithm has the characteristic of simply method, simply data structure, small amount of data and so on. But the CSG has local to empress the entity and it is hard to change any part of the entity after finish it, that all because of limiting of types of voxels. The describing objects of the B-Rep model is the boundary of the space, it is the pyramid structure of point, line, surface, volume. The describe information includes the geometrical information and topological information. B-Rep model pays the most important of the external details of 3D space goals. The geometrical information and topological information of the 3D space are recorded by correlation chart of the point, line, surface and the 3D attribute table, thus can spatial analysis functions easily. The Figure 2 is the representation of the 3D geometric entity by B-Rep. The characteristic of the B-Rep algorithm is the relation information of the point, line and surface. And the B-Rep algorithm also has limitation, such as the poor ability to describe the entirety of geometric objects, can not record the original data and the large need of information when describing the entity.

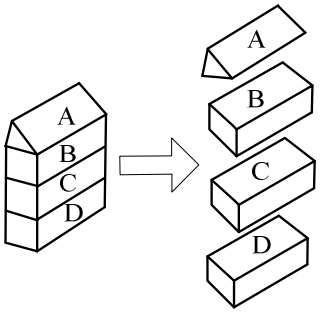

Fig.1. The process of CGS decomposition

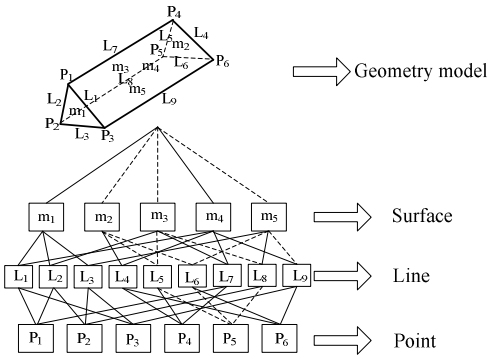

Fig.2. The process of B-Rep decomposition

It is need to layout noise monitoring points in 3D space the environmental noise monitoring model, and also need visual analysis which is based on the noise data. The CSG algorithm is able to express the basic building blocks of geometry, but lack of the expression of the surface, in this aspect; it can be supplemented with the B-Rep algorithm [9]. So the method of combining two algorithms could be used to build 3D monitoring of environmental noise model. Then the model is closer to reality, and also in favor of setting environment noise monitoring points and the expression of the surface of geometrical model. Figure 3 is a flowchart which is based on CSG and B-Rep mixed algorithm to achieve environmental noise 3D monitoring model.

The Process of Environmental Noise 3D Graphic Expression

Apply CSG and B-Rep hybrid algorithm, 3D model texture and CGA rules to constitute the environmental noise 3D space monitoring model, and grid the geometric model. According to the environmental noise data and its corresponding noise legend to render geometric model, to realize 3D graphical expression of environmental noise. The whole process is shown in Figure 4.

The Method of Environmental Noise 3D Graphic Expression

In this paper, taking a single building as an example and using a-weighted sound pressure level as the measurement unit of environmental noise. We consult the noise emission standards of social life environment [10] which divided the acoustic environment areas into 5 types according to the

function, each of these standards are corresponding to maximum limits values of the noise pollution in daytime and nighttime. For example, class 1 standards are applied to residential areas, cultural and educational areas as well as institutions concentrated area, standard formulates the noise emission values shall not exceed 55dB (A) in the daytime and shall not exceed 45dB (A) in the nighttime. By analyzing the noise limit values in five regions, we design gradient color with graded levels to show environmental noise value, the color and noise corresponding value as shown in table 1.

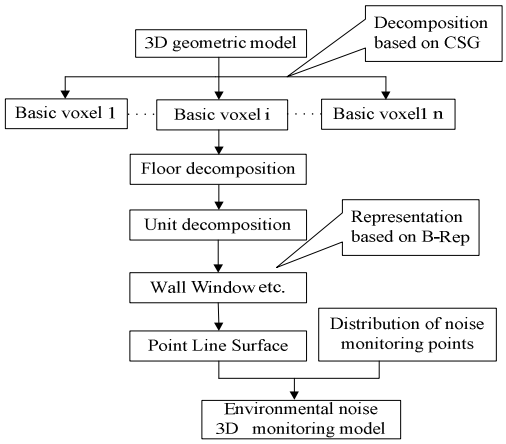

Fig.3. Flowchart based on CSG and B-Rep mixed

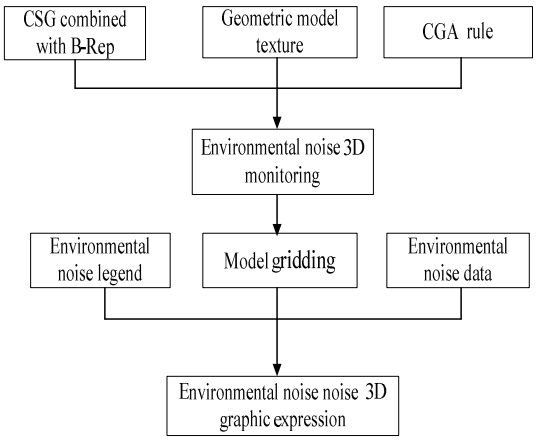

Fig.4. The whole flowchart

a-weighted sound pressure level dB（A）	Color Legend
>=70	
65—70	
60—65	
55—60	
50—55	
45—50	
40—45	
<=40	

Table.1. Grade legend table

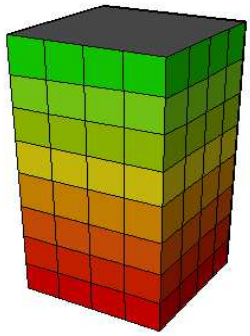

Fig.5. Example of the single building 3D environmental noise graphic expression

According to the grid design thought，the surface of each single building is divided into many grids the size of which is set according to the required accuracy environmental. Noise data can be derived from the manual measurement, but the manual measurement is not only time consuming, and the precision is also affected by human factors and a variety of geographic environmental factors. With the progress of science and technology, environmental noise automatic monitoring technology will become a trend. So distribution with the application of noise automatic monitoring technology can automatically obtain environmental noise data by sound region, as well as obtain environmental noise data by existing environmental noise prediction model combining related algorithms and rules. Then under the legend style as shown in Table 1 to determine the range of noise data belongs, each grid of 3D building are rendered with legend. The shown in Figure 5 is the single building 3D graphic example of environmental noise pattern. From the figure we can understand environmental noise pollution of each grid area, thus providing a three-dimensional environmental noise pollution conditions for residents, schools and commercial location.

In actual application process, the surface of single building is divided into grids with the grid design idea, the size of the grid is set according to the required accuracy environmental noise data can be derived from the manual measurement, but the manual measurement is not only time consuming, and the precision is also affected by human factors and a variety of geographic

environmental factors. With the progress of science and technology, environmental noise automatic monitoring technology will become a trend. So distribution with the application of noise automatic monitoring technology can automatically obtain environmental noise data by sound region, as well as obtain environmental noise data by existing environmental noise prediction model combining related algorithms and rules. Then follow the legend style as shown in Table 1 to determine the range of noise data belongs, each grid of 3D model are rendered with legend. As shown in Figure 5 for the single building 3D graphic example of environmental noise pattern. From the figure people can understand environmental noise pollution of each grid area, thus providing a 3D environmental noise pollution conditions for residents, schools and commercial location.

Conclusion

Taking CityEngine as software platform of 3D graphic expression of environment noise, combined with CSG and B-Rep hybrid algorithm, we establish 3D space model for environmental noise monitoring which not only can express the information of 3D geometrical model completely, but also has significance for the distribution of noise monitoring point on 3D model. Grid thought can be used to realize the 3D graphics expression of environment noise. The simulation results show that this method can be used as a 3D graphic expression method of environmental noise.

Acknowledgement

In this paper, the research was sponsored by the Nature Science Foundation of Heilongjiang Province (Project No. F201227).

References

[1] Esri (China) Information Technology Co., Ltd.. CityEngine Chinese Course [Z]. BeiJing,2012.

[2] Shi Tianyue. The preliminary study of the application of Esri CityEngine in Urban Design [J]. Architecture & Culture. 2013(7)98-99.

[3] Hua Li-zhong, Wang Zhao-bing and so on. XMUT:A Use-Case Realization of a Digital Campus WebGIS on CityEngine and ArcGIS Flex API[J]. Journal of Xiamen University of Technology.2013(12):57-61.

[4] Lv Yong-lai Li Xiao-li. Reserch on 3D Architectural Modeling Based on CityEngine CGA[J]. Surveying and Mapping of Sichuan. 2013(4):91-94.

[5] Juan Li, Jieyu Han, Lijiao Hao. The Discussion of Appling Parametric 3D Modeling in Urban Design Based on CityEngine[J]. Advanced Materials Research Vols. 2013(9)774-776.

[6] Liang Shiwen and so on. Application of CityEngine in city construction[J]. Applied Technology. 2014(3)168-170.

[7] Lv Yong-lai Li Xiao-li. Exploration and Realization of 3D Modeling Method Based on CityEngine for High-speed Railway[J]. Surveying and Mapping of Sichuan. 2013(2):19-22.

[8] Yang Jing, Ji Xuemin, Chen Lizhong, Sun Changsong. Object-Oriented Based CSG Modeling[J] Journal of Harbin Engineering University. Vol.23, No.3 Jun. 2002.

[9] Qi Xiangqian. 3D Model realization of single building in digital city[J]. ShangXi Architecture. Vol.30 No.7 Apr.2004.

[10] Department of Environmental Protection. HJ2.4-2010 Technical Guidelines for Noise Impact Assessment [S]. Beijing: China Environmental Science Press, 2010.

Advanced Materials Research Vols. 989-994 (2014) pp 4949-4952
© (2014) Trans Tech Publications, Switzerland
doi:10.4028/www.scientific.net/AMR.989-994.4949

Study on CDIO Talents Training system based on the Internet of Things and Cloud Computing in Big Data era

Hui Yan [1, a], Haiyan Hu [1,b]

[1] Department of Information Engineering,Jilin Business and Technology College,Changchun,China

[a] yanhui7125@126.com, [b] hhy1979_711@sina.com

Keywords: Resource Scheduling Mechanism, CDIO, QoS, Big Data

Abstract. Since CDIO talents training informatization system is employed in Big Data era, this paper shows some studies on the application of the internet of things , cloud computing, Big Data service and other advanced technologies in CDIO talents training informatization system, an informatization framework for the internet of things and cloud computing is constructed based on CDIO talents training, in order to solve the difficulties in managing and monitoring the fully distributed architecture, a distributed resource scheduling mechanism with QoS is proposed.

Introduction

Big data has been widely used in various fields and is becoming increasingly mature because of its distributed computation, virtualization, cloud storage and other features. Similarly, big data platform will provide a large internet environment for knowledge application and innovation and thus lays a foundation for top notch talents training. The application of the internet of things and cloud computing to the field of CDIO talents training can meet the requirements for the collection, transmission, storage, management, processing, sharing and analysis of the data of various teaching links, and effectively improves the informatization level of CDIO talents training. It is a challenge as well as an opportunity to accelerate the establishment of such a CDIO Talents training system that is dominated by colleges and universities, guided by market, supported by enterprises and combines production with education and research.

Informatization framework for CDIO talents training based on the internet of things and cloud computing

(1) The conceptual model of the informatization framework for CDIO talents training

Fig. 1 shows the conceptual model of CDIO talents training informatization system based on the internet of things and cloud computing. This conceptual model preliminarily represents the following relationship. The data collected and processed by the equipment are first transmitted to the data center, and then managed, processed, computed and published by the cloud computing platform, and the final data resources and computing resources are accessed by clients through the application interfaces.

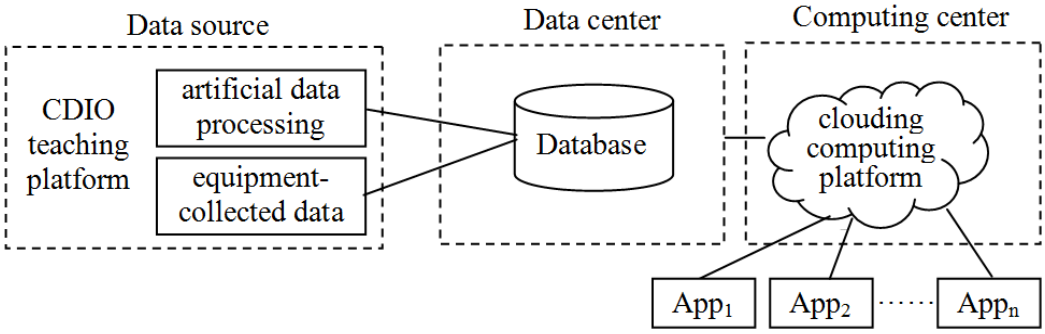

Fig. 1. Conceptual model of CDIO informatization system based on the internet of things- and cloud computing

(2) The framework model of CDIO talents training informatization

Fig. 2 displays the framework of CDIO talents training informatization system based on the internet of things and cloud computing (from the bottom to the top: internet of things of teaching, Big Data center, cloud computing platform of teaching, application). This framework is a complete architecture composed of data generation, organization, storage, query, analysis and service, and can provide reference for intelligence teaching.

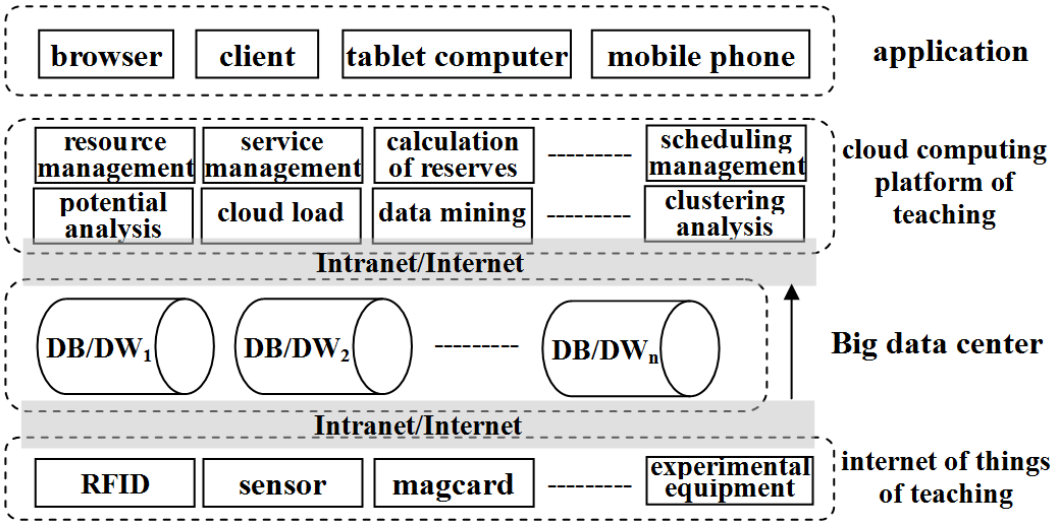

Fig. 2 Framework of the internet of things- and cloud computing-based CDIO talents training informatization system

The cloud computing-based distributed resource scheduling mechanism with QoS guarantee

The cloud computing architecture is usually centralized because of the requirements of business models, feasibility and maintainability. This paper proposes a distributed resource scheduling mechanism with QoS guarantee to solve the difficulties in managing and monitoring the fully distributed architecture.

(1) System model

Priority P1 and P2 are allocated to two kinds of users, and P1 is higher than P2. That is to say, the users with priority P1 has higher requirement for service response time than the users with priority P2. Higher priority is more likely to acquire high quality system resources, which will be discussed in detail in the following section. Similarly, this method can be used to easily extend the priority to n to meet the requirements of different business. Here, U1 refers to the users with priority P1, U1={U11, U12, …, U1(x-1), U1x}; U2 represents the users with priority P2, U2={U21, U22, …, U2(y-l), U2y}. When Priority=l, it means that the request is sent by the user from U1, and when Priority=2, it means that the request is sent by the user from U2.

Va is the average transmission rate of the network, Tr1 refers to the execution time cost by the user from U1 in reading the standard file under the experimental design environment, Tsa is the average addressing time of the hard disk, Tr2 is the the execution time cost by the user from U2 in reading the standard file under the experimental design environment, Tra refers to the average time cost by reading the data per unit, Tc1 refers to the execution time cost by the user from U1 in performing the computing task under the experimental design environment, W is the standard weight. If this standard weight is lower than the weight of the fragment resource combination allocated by the system to the user from U2, the request fails. Tc2 refers to the execution time cost by the user from U2 in performing the computing task under the experimental design environment. The time of storage-oriented business is as follows:

$T_{r1} = T_{sa} + n \cdot \delta \cdot T_{ra}$, $T_{r2} = n\delta / V_a + n \cdot (T_{sa} + \delta \cdot T_{ra})$

For the compute-intensive business:

$T_{c1} = T_{sa} + n \cdot \delta \cdot T_{ra} + \varepsilon$, $T_{c2} = n\delta / V_a + n \cdot (T_{sa} + \delta \cdot T_{ra} + \varepsilon)$

The QoS constraint of the system:

$T_{r2} \le T_r$, $T_{c2} \le T_c$ or $W_s \le W$, $W_c \le W$ 。

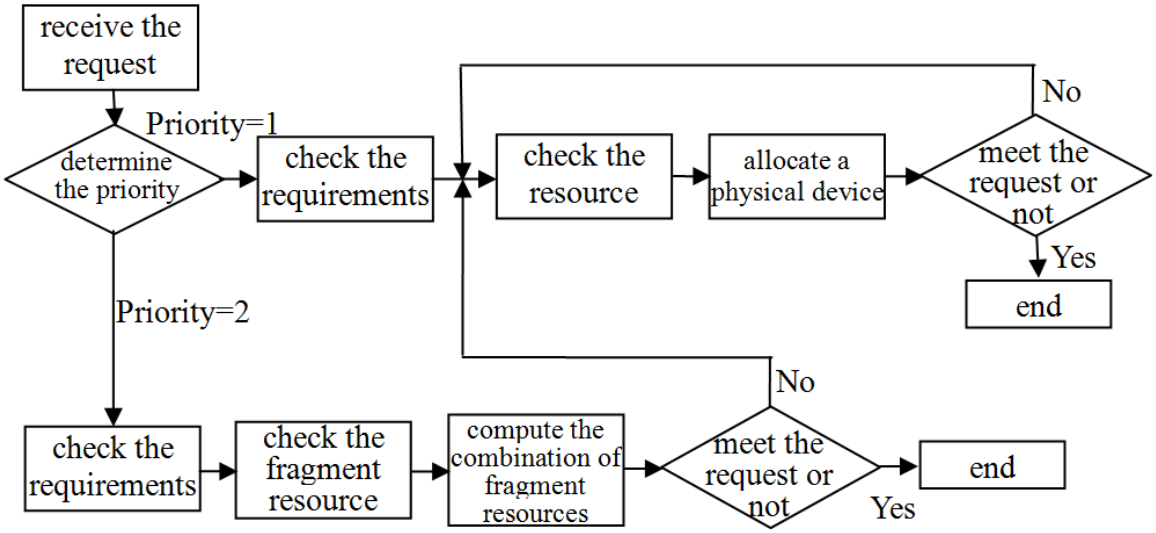

Fig. 3 Chart of the resource scheduling.

(2) A distributed, triple, resource search algorithm with QoS guarantee

It optimizes Chord algorithm and puts forward a distributed task scheduling algorithm with QoS guarantee to share the pressure of centralized schedulers. DQCRS simplifies the clouding computing system itself as well as the application design based on this system, and thus greatly reduces the adjustment and optimization workload of the system in this course.

Firstly, the system determines which type of operation is wanted according to the request R (CPU, Mem, Disk, type, Priority) submitted by the user. Secondly, the system uses the innermost Chord ring to look up and locate the hard disk storage resource that meets the requirements of the user, and then with the location of this storage resource as the fulcrum, the system uses the middle Chord ring to look up and locate the appropriate memory resource; finally the system looks up the appropriate CPU resource according to the location of the memory. The outmost Chord ring is first used to look up and locate the CPU resource that meets the requirements of the user, and then with the location of this resource as the fulcrum, the middle Chord ring is used to look up and locate the appropriate memory resource, and finally the location of the memory is used to look up the appropriate hard disk storage resource. The complexity of this algorithm is O (N *logn).

This search algorithm is located in “look up the fragment resource pool” and “compute the combination of fragment resources” of the flow chart as shown in Fig. 3. It optimizes the chord search process in the second and third rounds of the resource location.

(3) Simulation

The simulation result mainly shows the utilization rate of system resources when DQCRS is applied. In this experiment, the CloudSim simulation software is used to simulate the experiment environment. The experiment results indicate that DQCRS makes full use of the fragment resources in the cloud computing system, and certainly has higher utilization rate, about 13% higher than those systems which ignore the utilization of fragment resources.

Conclusions

Against the background of the age of big data and with the combination of the internet of things and cloud computing technology, this paper conducts an in-depth applied research on CDIO talents training informatization, builds the informatization framework for the internet of things- and cloud computing-based CDIO talents training and proposes a distributed resource scheduling mechanism

with QoS guarantee based on the improved Chord query algorithm. The simulation result shows that this mechanism can effectively improve the utilization rate of fragment resources of the system.

Acknowledgements

The authors gratefully acknowledge the fund of this study by Jilin province science and technology department soft science research project（20130420026FG）"Study of Jilin province engineering and technology talent support for strategy emerging industry" and the Jilin province talent development project in 2013 (20131079) and the Jilin Province Department of Education research project (2012366).

References

[1] Bing Li. The Research of Dynamic Resource Management key technologies in Cloud Computing [D]. Beijing University of Posts and Telecommunications.2012.5.

[2]Hui Yan,Haiyan Hu. Design and Realization of Innovation and entrepreneurship Service Platform for Undergraduates Based on Big Data[J]. ITMI2013. 2013.7: 394~397.

[3] Sun Qi-bo,Liu Jie,Li Shan,Fan Chun-xiao,Sun juan-juan.Internet of Things:Summarize on Concepts,Architecture and Key Technology Problem[J],Journal of Beijing University of Posts and Telecommunication.2010,33(3):1~9.

[4] Liu Qiang,Cui Li,Chen Hai-ming. Key Techonologies ane Application of Internet of Thing [J]. Computer Science. 2010,37(6):1~4,10.

[5] Hong Wen,Zhao Yong. Cloud computing resource scheduling management [M]. Chinese Journal of Computers .2011.7. National Defence Industry Press.

Advanced Materials Research Vols. 989-994 (2014) pp 4953-4956
© (2014) Trans Tech Publications, Switzerland
doi:10.4028/www.scientific.net/AMR.989-994.4953

Research on Setting Strategy of Area Router Based on Scale-free Internet

SONG Junqiang [1, a]

[1]Wuxi Professional college of science and technology, Wuxi 214028, China

[a] SongJunqiang09@yeah.net

Keywords: interaction network; internet; scale-free; transmission structure; setting strategy; area router;

Abstract. Due to the large communication network, represented by the Internet such as: biological cell protein interaction networks, collaboration networks, air transport network, many real-world networks are proved to have the characteristics of small world network and scale-free (scale-free) connection properties, research on complex networks and dynamics mechanism has increasingly aroused people's attention.[1] For to the network, people are most concerned about is how to realize the information interaction without congestion, so in scale-free the basic connection problems of information flow transmission structure on the network is becoming a hot research.

Introduction

For the transmission of information to achieve efficient, there have been many studies have been devoted to the routing strategy is proposed to better. Some articles are proposed according to the topological connection information for routing selection judgment. This may apply to the nature of the test in small networks, but for changing wireless network connection structure similar to Internet scale network or high dynamic character, required for this routing strategy of large calculation and energy consumption is not satisfied. [3]So people begin to pay attention to the local routing strategy. Random walk strategy is the local routing strategy of the most primitive, but due to the random walk approach is too simple, the actual effect is very poor in the network. Wang Wenxu et al proposed a local routing strategy, the sending node is calculated according to the index specified neighbor node connectivity and Strategies of the forwarding probability, makes the routing, the routing of the fixed preference factor, so called static preference local routing strategy.[3]

The local routing strategy in this setting the neighbor nodes according to load the dynamic relationships and the ability to send fixed, preference factor adaptively adjust each neighbor node. First of all, the network information flow moderately concentrated to the node degree is large, increasing the utilization of high rate of the node, so as to effectively reduce the average transmission delay of packets in the network; secondly, shunt in the business increases, avoid some degree node supersaturated bring congestion of the whole network, as far as possible make full use of the ability to send all the nodes, improve the network capacity.

The model and definition

In order to losing the general B - A model proposed by Barabdsi and Albert as the basic structure of network, model generation method is similar to the reference, the node degree distribution has a power-law characteristics, namely P (k) ~ K-Y, y=3. [2]

The node degree with high betweenness large in a scale-free network, is the key node in the shortest path connecting nodes in concentrated on, so we should try to use the node degree in communication, making it easy to find the destination quickly (the call node scale-free network medium large as hub node); [4] when business intensified, it should be appropriate to shunt in order to avoid congestion in the hub node. Therefore in the packet generation rate is not high and all nodes are not saturated, it should make the node degree be greatly packet reception probability

preference; while in the node degree of saturation, the node traffic transfer to load light transmitting capability according to its load condition to reduce the probability of acceptance.

The transmission process is defined as follows:

(1) Every moment with R packets generated in the network, and then the packet generation rate is R, which selects packet source and destination nodes for each new generation randomly.

(2) Each node has the storage space of infinite hold packets, packet queue to obey the FIFO principle, transmission capacity of the node i fixed node connectivity ki. [4]

(3) All the nodes in the network at the same time as the cache will be sent to each packet of the next hop destination search and send. If the destination node information packet is the neighbor nodes of the current node, is directly put the packet to the destination node, and to eliminate the packet from the network. Otherwise, by preference in all the neighbor nodes, send packets to the neighbor node are the probability of i.

$$\mathbf{II_i = K_i^a / (\sqrt{K_j^{ai}})} \quad \textbf{(formula (1))} \qquad (1)$$

In the formula (1), ki is the node of I; AI is an adaptive node i adjustable selection index (later called the preference factor), in the initial time of all nodes preference factor is 0. The denominator is the sum of all the neighbor points. [4]

(4) Preference factor all nodes are updated in the network. The adaptive process is as follows: when a node i time stored information packet queue length is less than the transmission ability of Ki, the preference factor AI is increased by one step length; on the contrary, when the queue length of node i moment exceeds the transmitting ability of Ki, the preference factor AI can reduce a step length. At the same time as the preference factor set upper and lower Amax (>0), Amin (0 '). [5]

It is sequential steps of (1) ~ (4) completed service transmission at each time.

Set boundaries Amax, Amin reason is taken into account when preference factor growth is too large, the node preference probability of node will be far greater than the degree of smaller, packets will all try to large degree nodes, probability transfer to small node is very low, is not conducive to search the destination node in the network. To set an upper limit, so the Amax is AI; and the preference factor if the variable is lesser negative, means that the information will try to choose a small degree of ending point as the transfer object, completely avoid the hub node will cause the packet transmission delay greatly increased, so also to set the lower limit for AI amin. It should be noted in the adaptive transmission mechanism under the definition of this strategy, the length of l (KI) increased gradually from 0, when l (KI) ≤ Ki, the completion of each transmission will not have packets stranded at the nodes, so nodes in unsaturated steady state; on the contrary, if l (>ki, Ki). [1] Message packet will accumulate continuously in the node, the node in the supersaturated congestion state. So called l (k) =k as the node is not saturated phase boundary and the saturated.

Setting strategy

In the adaptive strategy, the selecting of any non-negative preference factor limit Amax can get the maximum network capacity Rc_max the same. This is because the adaptive strategies according to the relationship of load and the ability to send the changing preference factor AI, and then adjust the flow of information into the rate, continuously to the node unsaturated shunting packets so that the packets, not in the saturated nodes continue to accumulate, avoiding the node reaches saturation caused global congestion. Unsaturated node, because the queue length has been meet L (KI) ≤ Ki, the preference factor AI will increase with time, until it is equal to its upper limit Amax. In the feedback adaptive preference factor under saturated nodes, packet into the rate will be substantially equal to the transmission capacity, namely, the average queue length stable at the phase boundary L (KI) =ki, because of the phase boundary slope of 1, a reference type (1), preference factor to obtain saturated nodes close to 0. At the same time, taking into account, when all nodes are saturated,

preference factor AI is close to 0, the network to achieve the maximum capacity. So in any preference factor limits under Amax, network has only the maximum capacity of the same Rc_max. [3]

Below picture (2) is the reflection of the different transmission rate, an average queue length of node changes. The phase boundary is represented in the thick line graph. Nodes are not saturated, reflected in the diagram is the L (KI) does not contact the dividing line, then l (KI) subject type (1). With the increase of R, part of the node contact boundary began to enter saturated state, l (KI) also is divided into two sections. The average queue length is part of a larger saturated nodes and phase boundaries coincide, the average queue length is l (KI) =ki; another part of the node does not reach the saturated state, the average queue length keeping the original slope. [5]

$$L(K_i) \sim K_i^{1+\alpha max} \quad (2)$$

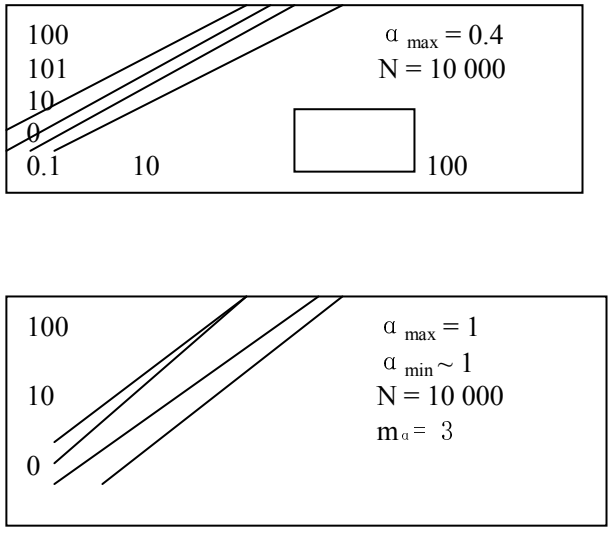

Figure 1. The reflection of the different transmission rate

Conclusion

Each node forwards probability by the node degree of K and a together determine the preference factor. Preference factor is regarded as a value of every node in the cache according to the average queue length adaptive changes. When the node cache average queue length is greater than the ability to send (equal to the node degree k), it will decrease a lot. Upper and lower limit of Amax a, Amin adjustable, and opposite number. When all the nodes in the network are not saturated, preference factor of different degree of nodes are basically reached the upper limit of Amax; when some nodes reaches saturation, the node preference factor shows that the statistical properties of a=0, the node preference factors still remain as amax. It makes the hand regardless of network business degree, which can guarantee the network information flow preferentially to the hub node, connected node degree is fully utilized; on the other hand can make the nodes transmit ability properly use and not to "saturated" state, adaptive to avoid the occurrence of congestion.

References

[1] Tang furong, Li zhaohui, The Scale-free Network Embedding-delete-compensation Model Establishment and Analysis [J], Journal of China University of Mining and Technology Pres s, 2005, 03.

[2] Zhu haiyan, Wei zhongshan, Small World Networks and the Scale-free Network the Sa me Evolution Model [J], Journal of Qingzhou College, 2006, 06.

[3] Zhangli, Liu yun, Study on the Evolution Process of Virtual Community Networks [J],J ournal of Physics, 2008, 09.

[4] Guo jinli, Statistical Mechanics of Complex Network Differential Equation Method [J],A pplied Mathematics and Mechanics, 2008, 09.

[5] Wang yan, Zhen zhigang, No Cmmunication Dnamic Saling on the Ntwork [J], Journal of Physics, 2008, 07.

Advanced Materials Research Vols. 989-994 (2014) pp 4957-4961
© (2014) Trans Tech Publications, Switzerland
doi:10.4028/www.scientific.net/AMR.989-994.4957

Information Construction of Chinese Local Government in the Era of Big Bata

Hua Yanhui[1,2,a], Wang zhijian[1,b],Geng Meili [1,c], Liu Bangfan[2,d]
[1]Qinhuangdao Vocational and Technical College，Qinhuangdao China 066004
[2]Humanities-law College Yanshan University，Qinhuangdao China 066004
[a]email:ysdxwenfa@126.com, [b]email:ysu888@yeah.net,
[c]email :ysdxwenfa@163.com , [D]email :liubangfan@sina.com

Keywords:Big Data; Information Technology; Local Government

Abstract：The era of big data is an inevitable trend of world development, environmental changes poses severe challenges around the local government of information construction in China. On the basis of the full analysis of the content and features of the era of big data, clarify the urgent need of the local government to further deepen the Information Construction in the era of big data, analysis the challenges for local governments of building big data era. On this basis, we propose a solution in the angle of the user, government resource integration, demand forecast and the government's responsibility.

1.The Meaning of the Era of Big Data

In modern society, although big data is a specialized vocabulary, yet it is closely related to each person's life: social networking tools and e-commerce platform in our daily life are both important part of the era of big data. Today, the network is becoming increasingly popular, whether the local government, which is close tied with the public life, can grasp the pulse of the construction of government information is not only related to its application and promotion of the work in local government, but also relate to achieve a successful transition of the government which is about to adapt the requirements of the current economic and social development. It is a key to judge whether government can complete the administrative and service functions or not.

Technological innovations is brought about by the information revolution. In the past, we have always put emphasis on "technology" of the information technology innovation, however, with the continuous development of information technology, the "Information" should be the basis of supporting the development of information technology. Therefore, when the technology reaches a certain level, we should give the "information" more attention. "Big Data" is a phenomenon and results that the development of the information age has reached to a certain level and the information shows explosive trends and accumulate to trigger the revolution. Vast amounts of information and data growth not only posed a serious challenge to the information and data storage, but also require for changing existing ideas and method of information and data processing. As a result, "big data" came into being.

Administrative activities of government, is largely an information processing activities. The level of government Informatization and information processing capabilities is not only the index of measuring the strength of the government, but also an important factor of efficiency. "Big Data" era is a major change for the way we live, work and think: it changes the previous surveys and statistical methods so that we can use all the data and not just a random sample; it changed our obsession with the pursuit of accuracy and allow Imprecision appeared as well as accept the existence of hybridity; it changed our stubborn pursuit of "causal relationship" and let us to focus on the "relationship" of discovery and use. Because of these changes, the information construction of local government is urgent and necessary in the era of big data.

2. Meaning and Necessity of the Government Information in Era of Big Data

2.1 Basic Meaning of Local Government Information

The government information is the use of modern information technology and related equipment, through a variety of information services, to develope and manage the information resources which the government needs.

The era of big data is an inevitable trend of future social development, and will promote the use of open data, and strengthen the open and transparent public information. At the same time, open data is bound to affect the work of government management innovation, local government behavior in the network society and real society interaction management will be greatly enhanced, thereby giving the local government new meaning and requirements.

2.2 The Necessity of Information of Local Government Information in Era of Big Data

In recent years, information technology has made significant progress in the development of China, information network and the intelligent terminals rapidly popularize, by the end of 2012, China's Internet users reached 564 million, Internet penetration rate of 42.1% for the 420 million mobile phone users, 309 million microblog users. Government network public service system has gradually formed, the central and provincial government websites penetration rate has reached 100 %, and the municipal government websites penetration rate reached 99.1%, more than 85% at district level. Although China is not treating big data strategy as a national strategy currently as the Western developed countries, but the relevant departments also showed the importance of big data will be presented at the National Science and Technology as National Basic Research and Development Plan, in February 2013 the basic research should focus on supporting large data calculated in the information sciences. In the era of big data, greater emphasis on transparency and sharing of information, local governments have become increasingly frequent interaction with the public, the extent and level of information technology directly affects the public impression and understanding of the ability that government administration; local government informatization of service-oriented government is also a window of public, it need to be paid more attention.

3.The Challenge of the Local Government Faced in the Era of Big Data

3.1 The Needs of Construction of the Information is More Urgent

In the era of big data, in order to better build a service-oriented government which give full play in communicating with the public, local government should expand channels of communication with people, improve the government portal platform through information technology, to strengthen communication and interaction between government and the public. At present, China has basically completed the establishment of local governments portals, but the efficiency of information integration and use is still relatively low, poor communication between the government and fragmented severely restricts the communication and sharing of information; addition, there are considerable number of local government portal merely hanging introduction on the line, and there is no link with the service information, the public demand for information on official line is difficult. It is not only stray far from the job which the government should do, even in mind different to the construction of informatization.

3.2 Lack of Information and Follow the Trend of Building Construction

Big Data era raise higher requirement of government information collection and storage of workers. However, for the government at all levels , to achieve the government 's information technology resources will face limitations and conditions which the objective conditions and resource shortages faced by local governments tend to be more prominent. Local Government preparedness capacity building in information technology, construction of the objective environment in which the information relative to the challenges facing more serious, far less can be done overnight. For example, compared to higher levels of government or government-developed regions, local governments do not usually have sufficient financial support , in addition to the quality of the civil service and general users can adapt the information reaches all need a process that requires a huge investment.

In addition, in local government information construction process, there are one-sided emphasis on common government information technology , the tendency to underestimate or even ignore the particularity of government information technology throughout its development stages; prevalence of one-sided emphasis on information technology capacity building, despise or ignore government defects environmental differences and environmental construction , there is a certain disregard its own special environment and conditions, blindly copy others' development model of information technology issues.

3.4 Local Government Needs to be Improved Utilization of Information Technology Facilities

In the quite a long time past, China's information infrastructure has been severely constrained economic and social development, accelerate the construction of information capacity, increase the supply of information and communication technology, information technology became a major task. But with the huge investment of resources in recent years, China's information infrastructure has made great progress in many places even a serious communication resources idle phenomenon. Again, a number of local governments disregard the local environment and user needs, the use of the funds is not sufficient to build a more powerful website online functionality, but not many users. In addition there is duplication of grass-roots government building information existing in the process, which will inevitably lead to unnecessary idle capacity and a waste of resources. While local governments directly to the public, in information technology should be more oriented to the needs of the masses, in order to facilitate the people as the goal, efforts to increase public acceptance of local government public information construction.

3.5 the Era of Big Data Related to Increased Risk of Data Misuse

In the era of big data to provide a lot of convenience to local governments and the public but also threaten our freedom and privacy. In the era of big data to make almost lost the ability to forget the whole society, the value of the data is not just based on its basic purpose, which is more secondary use, including forecasts. While the large data emphasize the correlation rather than causality between things, so local governments can organize relevant information to predict future events that may occur, such as grass-roots government through the analysis of relevant data to predict future events may occur in groups and take certain mandatory measures to prevent. However, the public should have done something for him to be responsible, rather than the data predicted by his behavior and responsible. However, current technology still can not analyze the authenticity of the data, we can not guarantee that the data is completely reliable, it is likely to make big data predict to some extent become a "punishment."

4. Strategies Big Data Era of Basic Government Information Technology

4.1 User-Oriented, Moderate Information Technology

The era of big data is released so that the government is no longer the sole source of information, the public enjoys a large degree of freedom of access to information and publishing rights , the traditional small data era is the era of government -led information sources lopsided , information dissemination and public become propagating body . The purpose of government information technology and administrative activities in principle the construction of a " citizen- centered, results-oriented and market- based" computer and network to carry out, to provide more efficient services to the public, so its operation becomes more rational and efficient virtual electronic government. Especially local governments , directly undertake the implementation of administrative work , the most contact with the public , so how can we meet the public demand for government information , how can the rational use of the information infrastructure owned by the Government to better serve the public , local government information technology must think about.

Here, the "User " refers to the actual use of government information resources of people, including public and government , including public servants . User-centric , information capacity builders and information service providers should listen to the views of users more fully consider the needs of users , in the case of resource constraints , the heavier users think business priority the actual utilization of the status of deployment , to create conditions to improve these business improvement services to improve user satisfaction with these services, and strive to achieve the relative

importance of services in the information technology , the reference uniform rate and service satisfaction. To avoid grass-roots government information construction process "information island " phenomenon and idle resources , should develop a unified planning and design of information technology of local government , we must have a long-term strategic vision to make investment in the construction of the current information technology facilities can adapt to the future of e-government development process , but also the construction of information based on the level of economic and social development of the region. Local Government final evaluation criteria and application of information technology should be controlled by the user 's hand.

4.2 Robust Relational Database, Integrating Government Resources

With the development of the process of government information, various local governments have their own portals basically established the level of government resources database, but not have integrated data resources within the library, which information mostly in scattered, isolated and quiet state. In the era of big data there is no longer limits to the use of the data for the first time, the use of data is more secondary or even multiple. Integrate the resources of the database can give full play to the relationship between the data through the use of correlation, we can draw a lot of new information.

Local governments should further collected in a database on the basis of the original information, rich library of data types, and data collected for classification. Meanwhile, governments and departments at all levels must break the monopoly and sealed of information to achieve the integration of government information resources, emphasis on the continuous development of information resources, updating and maintenance; construction of the repository of government information should be in accordance with national governing bodies of unified leadership, standardization of organizations in order to reduce the lack of standardization and regulation and a waste of resources , enhance sharing between government departments.

4.3 Predict Public Demand,Improve the Quality of Government Decision-making

Prediction is the core of large data. In the era of big data, due to the amount of data and more miscellaneous contents, the cost of government when collecting less information in decision-making and public policy feedback is more convenient. Because we can analyze more data, and sometimes we can process a particular phenomenon, without relying on random sampling. With the development of big data, a variety of social networking, instant messaging platforms will become tools for public comment in the media. Therefore, local governments can collect, mining and analysis big data through mobile phones, the Internet and other tools to response to the public opinion in time. Using of big data technologies, local governments may be have full consideration of public views and comments in early time, timely collection and processing of public feedback on the policy decision making process executed, to increase public acceptance and satisfaction of policy, thereby enhancing the quality of decision making.

4.4 Responsibility and Freedom of Both the Local Government Information Management

In the era of traditional small data, and the use of informed consent or fuzzy processing anonymized data can better protect user’s privacy, but in the era of big data, either because these traditional methods can confirm the correlation with each other, either too vague and cannot really protect privacy, or to be too narrow thus limiting the potential value of using big data, so there’s a very high risk of loss the privacy and the data protection is extremely difficult. There is no doubt that local government will face greater difficulties and risks because of financial or technology cause; also there are identifying difficulties and a higher risk when dealing with large data’s "prediction” function.

Therefore, local governments should emphasize principles of responsibility and freedom of information technology construction. The meaning of "freedom" is that local government allow free speech in the public network platform within the legal framework , local governments can use the portal to get the information needed; "responsibility" refers to the government 's obligation to protect its local public information data safety, the obligation to protect the rights of citizens equal access to relevant non-classified government information , the obligation to develop data antitrust-related policies and regulations and assist the legislature to introduce and implement the relevant laws.

References

[1](Britain)Viktor Mayer-Schonberger, &Kenneth Cukier. *Big Data*.Hangzhou,Zhejiang People Press,2013：13.

[2]Jiang Xiangdong & Wang Qiping.*The Theory, Method and Application of the Electronic Government Administration Ecology.E-Government,*2007(11).

[3]Wang Zhiqiang. *Study on Information Construction of Basic Government in Our Country*. Shandong University,2009.

[4]Liu Yeting & Wang Chunxiao. *Big Data,New Behaviour -- Analysis of the Transformation of Government's Mode under Big Data*. *Leadership Science,*2012,35:4-6.

[5]Huag Huahuan & Xue Lifang.*Big Government, Big Data, New Network - the Direction of E-government network in the Era of Big Data*. *E-Government,*2013,05:104-109.

[6]Zhan Xiaoyang. *Study on Public Service Oriented to Information Vulnerable Groups of Basic Government*. Wuhan University,2010.

Advanced Materials Research Vols. 989-994 (2014) pp 4962-4965
© (2014) Trans Tech Publications, Switzerland
doi:10.4028/www.scientific.net/AMR.989-994.4962

Realization of RIP module on GPON OLT system

Wenhui KANG [a], Xiaohang HUANG, Shicai ZHANG, Xiaoyuan ZHANG [b]

Tianjin Normal University, Tianjin, 300387,China

[a]email: 1316675905@qq.com, [b]email: zh_xiao_yuan@126.com

Keywords: GPON; OLT; RIP

Abstract. As networks to be flattened, a direction has been put forward clearly by Telecom operators that Optical Line Terminals (OLT) of Gigabit Passive Optical Network (GPON) should become aggregation[1] OLTs, which makes them to work as both aggregation switches and edge access devices. According to this requirement, a scheme that realizes Routing[2] Information Protocol (RIP) on GPON OLT is put forward after deep analysis of GPON system[3] [4] [5] and RIP. Results shows that IP routing on GPON OLT is realized, which allows OLTs to work on the network layer, at the same time simplifies the broadband network levels and increases the reliability of the network.

Introduction

Recently，flattened network construction has attracted attention of operators, convergent optical line terminal (OLT) with large capacity, small office and high reliability gains more favor because of its contribution to the network construction cost. After a multi service transport platform (MSTP) of SDH, convergent OLT can access to backbone network, this simplifies the network level and saves the cost of operation and maintenance. Traditional GPON OLT works in the, so it needs switch in the convergence layer to access to the transmission network. If three layer routing function has been developed on the GPON OLT, it can work not only in the data link layer but also in the network layer, this conform to the development trend of flat network construction, and bring new challenges and competition for the development of GPON OLT. So, RIP routing protocol implemented in GPON OLT is becoming the focus of our attention.

GPON OLT system framework

Figure 1 is a block diagram of the GPON OLT system. From the chart we can see clearly the RIP module in the OLT system in place. Before the traditional two layer OLTs are all two layer interfaces, have no L3 interface model, so to realize RIP protocol on OLT, the primary work is to create three layer interface.

Realization of three layer interface and three layer driven

In order to realize the creation of three layer interface, we adopt supervlan technology, namely supervlan aggregation technology, Its principle is a supervlan contains one or more sub-vlans, each sub-vlan is a broadcast domain, two layers between different sub-vlan are isolated. A supervlan corresponds to a end driver, which contains two key points: the state of the supervlan and the IP address. These two key points determines supervlan can provide IP interface configuration and perceive the change of the state, thus users between sub-vlans can achieve three layer communication and RIP module can achieve three layer routing function.

In addition, we need to achieve some driving function in the exchange chip. First, there is a ACL module, the RIP module registers some protocol message dispatching rules to ACL module, then the ACL module send these rules to the exchange chip, so the exchange chip will only send the packets conformming to the rules to CPU to deal with, the packets not conformming to the rules are discarded. There is a three layer forwarding table, which contains three tables: the host routing table, network routing table and three layer interface table. Routing management module (RTM) manage RIP routing table, the exchange chip driver application program interface (API), RTM module calls these APIs to write the corresponding table into the three forwarding table of the exchange chip, ultimately to achieve hardware forwarding of three packets.

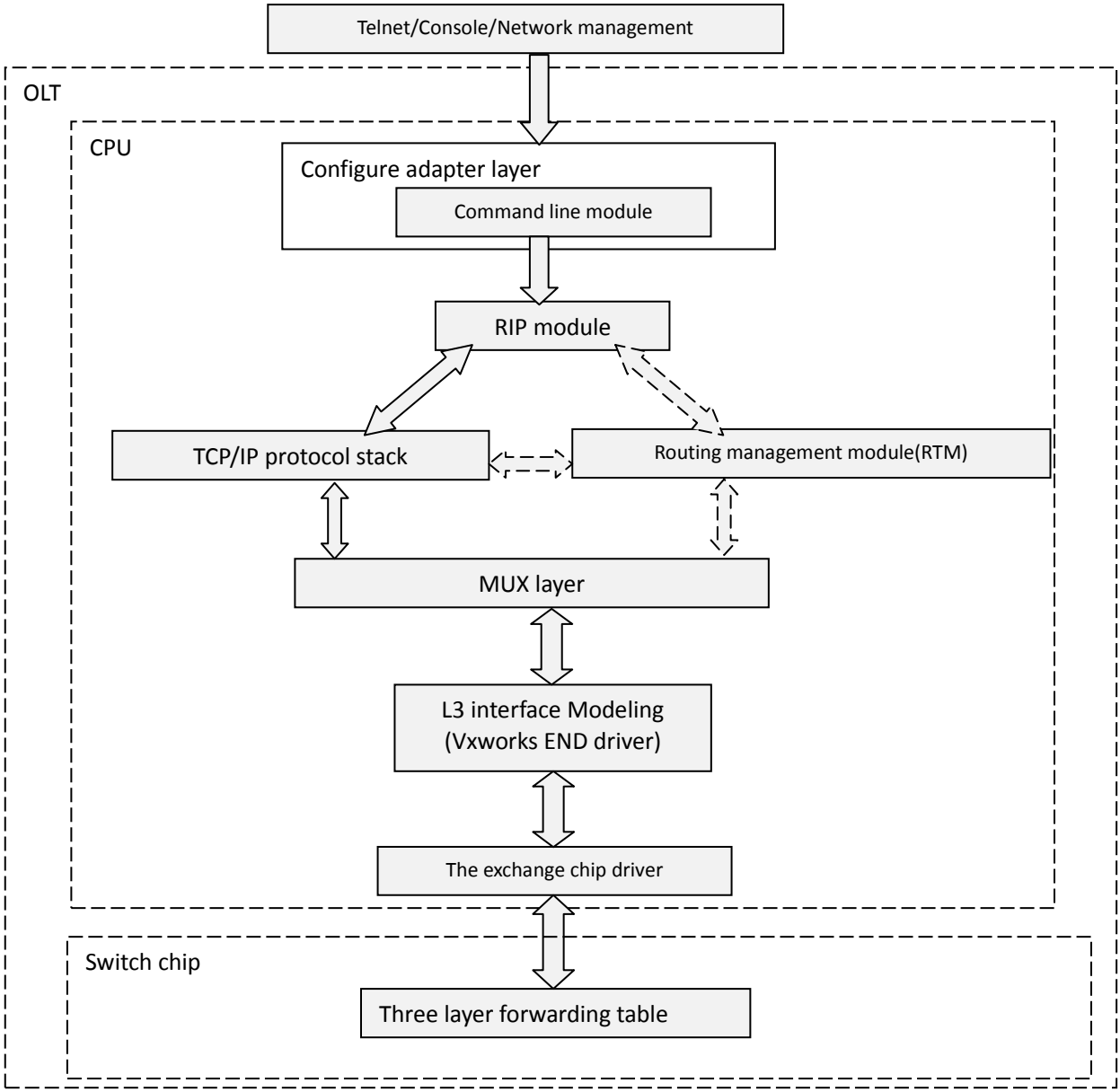

Figure 1 Diagram of the GPON OLT system

Implementation of RIP module

The overall structure of the RIP module as shown in Figure 2 can be separated into several sub module to achieve its function: the protocol module, network management interface module, input processing module, output processing module, Interface management module and RIP routing management module. Except the protocol module, the other modules are all responsible for communication with external module.

If network management interface module communicates with external network configuration module, external network configuration not only can be achieved through the graphical interface of network management but also can be achieved through the command line. But no matter which kind of form, that is needed to send related parameters configuration to the network management module, and then call the API of the network management module to achieve the control and management of RIP.

Input and output processing module communicate with TCP/IP protocol stack through the socket. TCP/IP protocol stack enables server socket. Because RIP is based on UDP, it is needed to create a SOCK-ET-DGRAM type socket to communicate with TCP/IP protocol stack. When we start an instance of RIP, the RIP messaging will be achieved through this created socket. The main function of input processing module is to obtain the protocol data packet received from interface, thus obtain routing information and peer information, and to give the response correspondingly according to the

type of data packet. The output processing module is to send interface function of a response message to the neighbor, form the response protocol, and through the RIP socket send the appropriate message to the adjacent router.

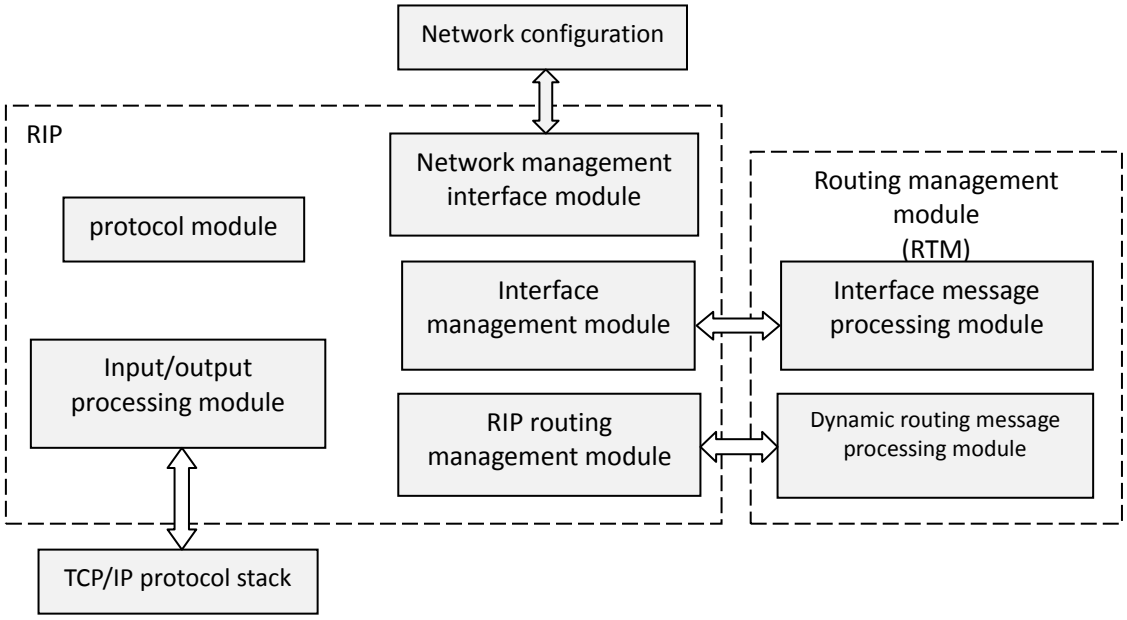

Figure 2 Structure of the RIP module

Interface management module is responsible for communication with interface message processing module of RTM module, they communicate mainly by sending messages with each other. In the RIP initialization interface management module register callback function to the RTM, when the underlying hardware changes, the bottom will notify the RTM, and RTM send corresponding status messages to interface management module of the RIP, then interface management module call corresponding callback function to change the port information saved in RIP system.

RIP routing management module is responsible for communication with routing the message processing module of RTM, it not only can send a message of receiving the routing to the RTM, but also can send a message of adding or deleting destination routing. If RIP want to redistribute a class of routing, such as redistribution of OSPF routing or static routing, it will send a message of adding redistribution to RTM module, and RTM will send the redistributed routing message back. Similarly, when a certain redistribution routing changes, RIP can send this message to RTM, and RTM carry out corresponding processing according to the message.

The protocol module does not communicate with any external module, it mainly process messages received from the input processing module or will sent out from the output processing module, and provide some interface functions for other module to get and set related information of the protocol entities, and directly call these interface functions.

Application of RIP protocol on GPON OLT system

After developing RIP routing software in GPON OLT, we apply it to a small network with voice services, network structure as shown in Figure 3.

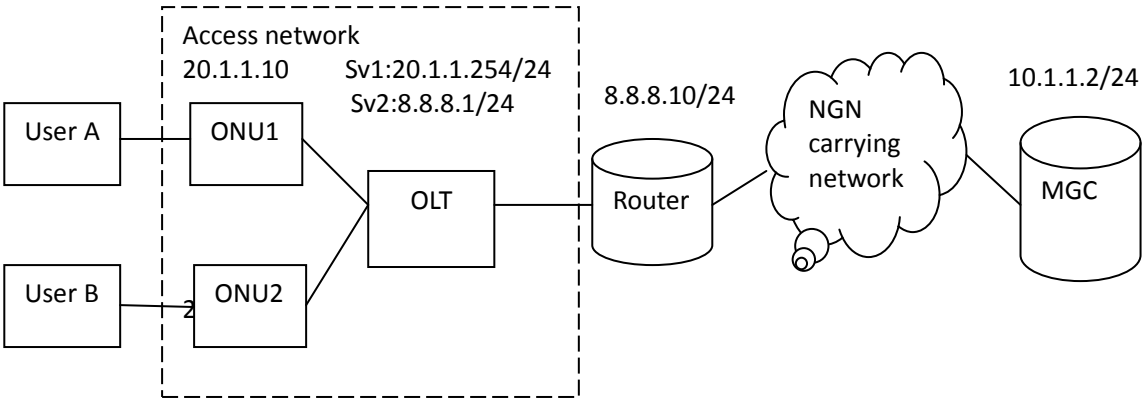

Figure 3 Network NGN voice service under three layer network

We will create two interface with three layers in OLT, as follows:

(1) Create Supervlan1 and Supervlan2.
(2) Create user side and network side Sub-vlan, two layer VLAN traditional.
(3) Join the user side Sub-vlan into Supervlan1, and join the network side Sub–vlan into Supervlan2.
(4) Configure IP address for Supervlan1 and Supervlan2, as shown Sv1 and Sv2 in Figure 3.

Open the RIP protocol in OLT and declared Sv1 and Sv2 corresponding network. If the user A under ONU1 want to phone with user B under ONU2, first of all they must be registered to the MGC (media gateway controller), through the MGC to establish a two-way channel between the user A to the user B and realize a normal conversation between them. To register with the MGC, they must send corresponding control signaling which is transmitted based on IP. Traditional two layer OLT must be externally connected with a three layer switch as the OLT gateway to forward the message. After implementation of the RIP protocol in the OLT, there is no need to pick the three layer switch in access layer of the OLT, we can directly open the RIP dynamic routing protocol in the OLT, and dock with the local side network which is planned well.

Conclusion

The characteristics of this scheme lies in that RIP protocol is introduced into the traditional OLT with two layers, this integrate the function of the aggregation switch and the edge router with no the need for construction of two layer convergence network, so it meets the need of the development of network operators, reduces the number of levels of broadband network and network nodes, saves network construction and operation the cost and greatly enhance the network reliability.

The scheme has been tested in the laboratory by scene. Of course, RIP has its limitation, the agreement provided that a valid routing information for metric cannot be more than 15, which makes the agreement not applied to large network.

Acknowledgement

In this paper, the research was sponsored by the College students' innovative training program (Project No. 2013046).

References

[1] Cheng Chuanqing, Huang Qiugen, Wang Li. A Study of VLAN Aggregation Implementation. Journal of Wuhan University of Technology, 2005,Vo l. 29(1):141-146.

[2] Guo Li , WU Jun-ping, LI Yue-zheng.Interface design of routing in EPON system.optical communication technology,2010,34（12）:5-8.

[3] ITU-T Recommendation G.984.4,Gigabit- capable Passive Optical Net-works(G-PON): ONT management and control interface specification[S].

[4] Zhou Yu. GPON used in traffic information management system research [D]. Beijing university of posts and telecommunications, 2007:18-20.

[5] Liu Yuan-ming. Comparative study of several key technologies of EPON and GPON [D]. Beijing university of posts and telecommunications, 2008:8-21.

Advanced Materials Research Vols. 989-994 (2014) pp 4966-4969
© (2014) Trans Tech Publications, Switzerland
doi:10.4028/www.scientific.net/AMR.989-994.4966

The Study of iPark Cloud Platform Construction and Application Modes

Tian Xu[1,a], Zhigang Zhang [2,b], Yi Wu[3,c], Qun Pan[4,d], Shu-hai Fan[5,e,*]

[1,2,4,5] Department of Industrial Engineering, Nanjing Tech University, Nanjing 210009, China

[3] Wuxi software industry development co., LTD, Wuxi, 214000, China

[a]xutian107107@126.com, [b] 285487987@qq.com, [c]yi.wu@263.net, [d]1027856210@qq.com, [e]fanshuhai@tsinghua.org.cn

Keywords: cloud platform, cloud computing, application mode

Abstract. Based on the background of Wuxi Software Park, building cloud platform system was proposed. The concept of cloud computing and cloud platform functionality was outlined. This paper studied the cloud platform application framework. Discoursing Park Intelligent Property Services cloud platform subsystem, park integrated services cloud platform subsystem and Park enterprise IT services cloud platform subsystem. The system can take advantage of cloud platform mobile terminal to provide application modes for companies, employees, park agencies, Software Park, operators and so on.

1. Introduction

Wuxi Software Park (iPark) is a scientific practice window of the new district to promote the optimization and upgrading of industrial structure. Its build-up area is 1.5 million square meters, including 0.55 million square meters which has been completed. It mainly includes the innovation and creative industry park, Jiangsu software outsourcing industrial park, sensor network information service park and so on.

Cloud computing is based on the addition of internet-related service and delivery mode used. It's always concerned about providing dynamically scalable resources by internet, which is always virtualized [1-3].

The establishing of cloud computing is to improve efficiency so that we can reduce the cost of enterprises. Physical separation can be achieved with logic together. In addition, efficiency can be significantly improved by virtualization, Thus operation cost, hardware cost and software cost will be reduced greatly. But in current trend of cloud computing development, the park is urgent to solve some problems in the process of setting up public service platform such as scattered resource, multiple managements.

2. Construction of cloud platform

IPark cloud platform will be mainly made up of cloud platform portal, park intelligent property, service cloud platform sub-system, park comprehensive service cloud platform sub-system, park enterprise IT service cloud platform sub-system and relevant public supporting infrastructure. It's planned on the whole and carried out step by step. Among them, main work contents of iPark's cloud platform construction includes park property and infrastructure's transformation, construction and integration; enterprises' online service for portals; individual self-help service system; IT service products supermarket's planning, designing, construction and operation.

2.1 Application system of intelligent property service cloud platform

Property systems concerning intelligent park management are security system, public management sub-system and apartment / building management sub-system. The wisdom park's four-staged intelligent property system of iPark is as shown in figure 1.

Construction and operation purposes of intelligent property service cloud platform in cloud portal mainly include: (1) parking and food consumption, bus ride, access control attendance card [4-5]. (2) releasing the park's public information(words, images, speech sound) , displaying unified resources management, providing channels such as image display and activities promotion for enterprises and sellers. (3) intelligent management of parking space and traffic [6-7].(4) introduction and practice of wireless park idea.

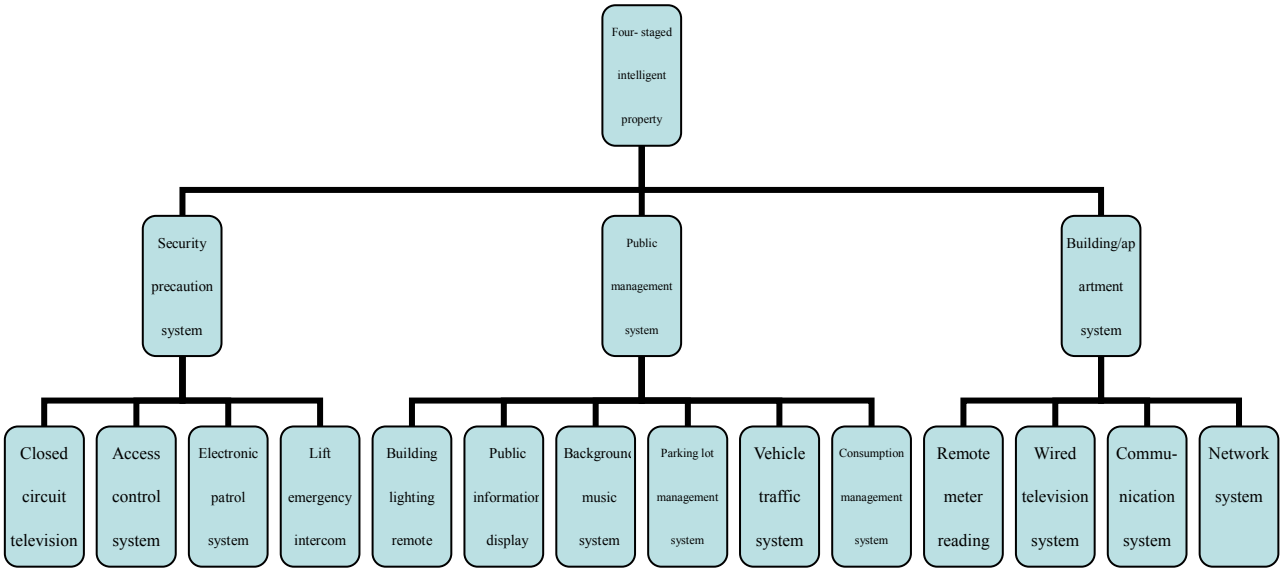

Fig.1: Four-staged intelligent property system of iPark

2.2 Application system of enterprise's IT cloud platform

IT service cloud platform is a generalized and open enterprise application service center, which needs to bring in and operate mature service business models and virtualized universal products from the industry. IT service cloud is orientated as operator of public service platform, which is more inclined to provide SaaS platform level service and serve online service suppliers [8-10].

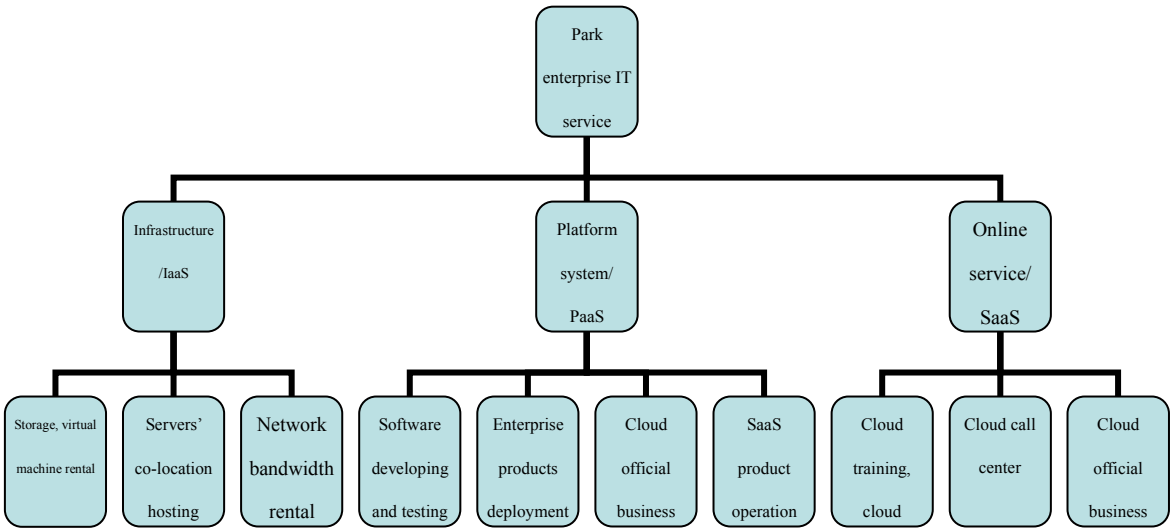

Fig.2: IT service cloud of enterprises in iPark

3. System application mode

3.1 Application of enterprises and staff members in park

Cloud platform will allocate automatically exclusive enterprise user ID for it from the time an enterprise is sure to settle in the park to its departure. The services as follows can be enjoyed by enterprise portals: (1)property services: housing rental, business handling, property repair handling, payment notice, enterprise online payment, query of expenses details and so on. (2) notice: information push, information subscription, complaints proposals and feedback. (3) image display: enterprises' dynamic information releasing in iPark web portals, recruitment releasing, enterprise information's updating. (4) industrial services: statistical investigation, form downloading, material uploading.(5) resource application: rental application of convention and exhibition center as well as public areas.

The park's staff members can register in cloud portals to apply for accounts, real-name registration in principle. They can enjoy the services: (1) property services: housing rental service handling, triple nets service handling and property repair service handling, notice of payment, personal payment, query of expenses details and so on. (2) announcement: information push, information subscription, complaints proposals and feedback. (3) resource application: rental application of convention and exhibition center, sports venues and public areas.

3.2 park institutions, business merchant application

After service agencies/merchants sign a cooperation agreement, the cloud platform will allocate and open exclusive platform provider user ID as "passage key" to interact information with their customers and software park management center in the process of carrying out business activities. Services provided for suppliers are: (1) property service: house rental service handling, property repairing service handling, notice of payment, enterprise online payment, query of expenses details and so on. (2) notice: information push, information subscription, complaints proposals and feedback. (3) image display: enterprises' dynamic information releasing in iPark web portals, promotion information updating and so on. (4) resource application: rental application of convention and exhibition center as well as public areas. (5) cooperative accounting: cooperative accounting agreement with the park, reconciliation, settlement of accounts, distribution and so on.

3.3 Application and Operation of Software park,

The software park is manager and operator by default, while some business operations of the service cloud platform(such as IT service cloud platform, operation and clearing business of the park's one-in-all cards, wireless network services and so on) could be packaged to operate by professional teams from the third party. As service center of park, it provides: (1) business handling and charging: housing resources (flat) leasing transaction service handling, property repairing service handling, public resources rental service handling, charging for call, online payment handling (well versed in both inside and outside with the software park inside business OA system); (2) all-in-one card business: card management, online recharging, query of expenses details and so on; (3) releasing and pushing of all sorts of information, enterprises/sellers releasing information audit, statistical investigation and so on; (4) complaints proposals acceptance and feedbacks; (5)

monitoring center: park entrance intelligent monitoring system with traffic guidance inside park, remote meter control, electronic patrol, closed-circuit television and so on.

4. Conclusion

The construction of iPark cloud platform system has realistic significance in these aspects. It will contribute to the development of Wuxi software park and science and technology industry inside the park and in the surroundings. It can improve customer service efficiency and specialization as well as fine management work efficiency and enhance the satisfaction of enterprises and loyalty of practitioners inside park. Also it could help establish iPark high-end brand image so that investment and construction, canvassing and settling, enterprise service can head towards a virtuous-circle direction. Each part of it has direct and indirect economic benefits and significant social benefits. It's economically viable, according with actual situation of the park's orientation and industry characteristics.

Acknowledgements

The research work was supported by National Natural Science Foundation of China under Grant No. 71171110 and No. 71371097.

References

[1] Yong liang, Panxiang Zhang, Qiuhua Chen, Construction and maintenance program of enterprise-level database cloud platform, Telecommunications Science Vol.28(2012), p. 146-155

[2] Wuxue Jiang, Jing Zhang, Zhiming Wang, Cloud computing and its framework mode, Journal of Liaoning Technical University (JCR-SCI) Vol. 4(2011), p.25

[3] Yin K, Cloud Computing: Concept, Model, and Key Technologies, ZTE Communications Vol. 8(2010)

[4] Fengming Liu, Kejian Tan, Ren Huang, Property management and information service systems of intelligent district, Journal of Chongqing Jianzhu University Vol. 23(2001), p. 95-97

[5] Shellhammer S J, Goren D P, Pavlidis T, Novel signal-processing techniques in barcode scanning, Robotics & Automation Magazine, IEEE Vol. 6(1999), p.57-65

[6] Linyuan Dong, Application of modern electronic technique in intelligent district, Journal of Beijing Institute of Petrochemical Technology Vol. 12(2004), p.61-64

[7] Meifeng Wang, Chao Han, Fang Zhao, Design of property management information system in WEB intelligent residential district (IPMIS), Intelligence Building Vol.8(2006), p.40-43

[8] Yang Zhou, Building e-government service cloud platform of SaaS mode, China Management Informationization Vol. 4(2012), p.25

[9] Xiaoqin Wang, Gang Zhao, Study of enterprise IT service management center framework, Information Construction Vol.5(2006), p.53-54

[10] Zhen Zeng, The future IT serves, CEOCIO China Vol. 17(2009), p.78-79

Advanced Materials Research Vols. 989-994 (2014) pp 4970-4973
© (2014) Trans Tech Publications, Switzerland
doi:10.4028/www.scientific.net/AMR.989-994.4970

Research on APT and Its Secrutiy Protection

Gang CHEN[1, a], ChuLe YANG[2, b], Jun YANG[1, c], JunPing CAI[1, c]

[1]Academy of National Defense Information, Wuhan, 430010, China

[2]Wuhan University, Wuhan, 430072, China

[a]email: cg0916_cn@sina.com, [b]email: 297526831@qq.com, [c]email: yangjun_gfxx@sina.com

Keywords: APT; Network Attack; Social Engineering; Security Protection

Abstract. Advanced persistent threat (APT) has become a serious chanllenge to network security in recent yeas. Characteristics of this kind of network attack involve purposiveness，concealment，sustainability and variability, and it is hard to protect for critical infrastructure, financial systems, elements of national power, etc. These threats range from unwitting hackers to nation-states, each at various levels of competence. For performing security protection, five typical cases of APT including Night Dragon attack, Google Operation Aurora, RSA SecurID attack, Stuxnet attack and Shady Rat attack were analyzed. Its commonly attack process and technology characteristics are summarized. Finally, some suggestions and opinions on secrutiy protection were presented.

Introduction

With the development of Internet, network security is faced with the flinty challenge and the main security threatens are from new attacks which are characteristic of organization, aiming at special target, sustainability, etc [1][2]. This kind of threaten is usually called APT (Advanced Persistent Threat) attack and its specific connotation can be shown in Figure 1.

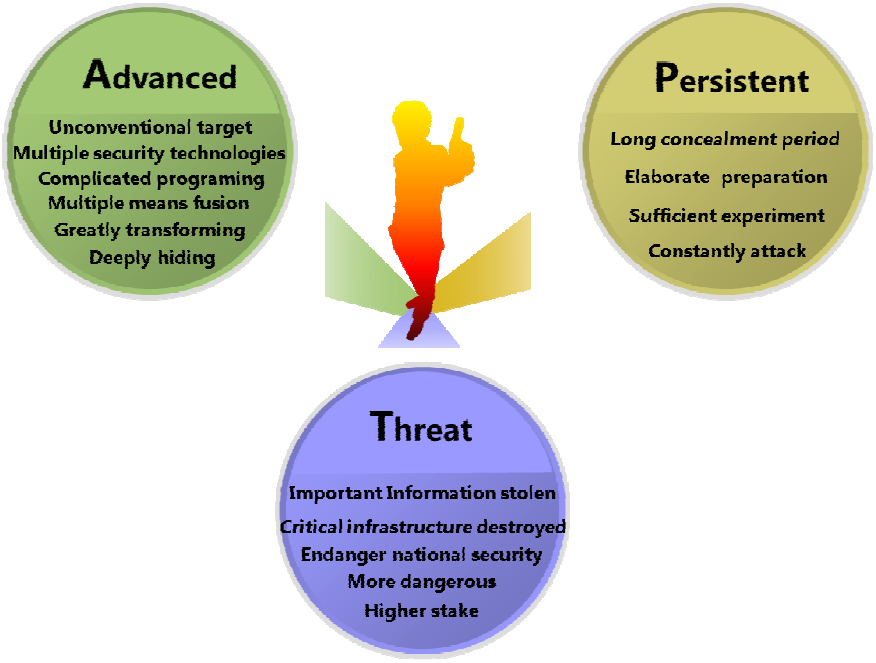

Fig.1. The specific connotation of APT

Since nucleus facilities of Iran waw attacked by Stunex worm virus in July 2010, a lot of APT attacks including Night Dragon, Google Operaion Aurora, RSA SecurID and Shady Rat have happened. The global nerwork warfare on behalf of APT attack weapons has begun a new stage until the Flame virus swept over the Middle East in May 2012 [3]. Considering attack targets of APT are mainly focusing on network infrastructure and key department such as energy, power, finance and national defense, it can endanger security of country politics and economy. It will be meaningful analyzing with typical APT cased and performing pertinence precautionary measures for maintaining security of core cecret information and important industry control system.

Typical APT Attack Cases

Night Dragon Attack. It was found attacking global major energy companies by McAfee in Feb 2011 and its specific attack process is described as follow. Firstly, attacker broke Web server of external network by SQL injection. Secondly, terminals and servers in internal network were scanned with broken Web server. Thirdly, password of terminals and servers in internal network was cracked with brute force. Fourthly, malware including trojans and backdoors were planted, and plenty of secret sensitive files were sent back to attacker. Fifthly, Emial with malware attachment was sent as a top executive and more terminals in internal network would be invaded by inducing emplyee to click the Email.

Google Operation Aurora Attack. Network was permeated for months due to clicking a malicious link in instant message by a Google employee and all kinds of secret system data were stolen. Its specific process is described as follow. Firstly, attacker collected personal information of Google emplyee by social engineering method. Secondly, a Web server hosting photo website was faked by a dynamic DNS provider. So Google employee would be induced dowloading and running malware when he clicked web link receiving from one person he belive. Thirdly, the account password accessing Google server would be stolen by continuous listening after establing connection with terminal of victim within a SSL security tunnel. Fourthly, the Email content information of special Gmail account was stolen continually when attacker succeed in permeating Google Email server taking advantage of account password of the google employee.

RSA SecurID Attack. RSA company affiliating with EMC company was intruded in Mar 2011. As a rusult, part of SecurID technology and customer information were stolen. Several American defense contractors including Lockheed Martin Corporation and Northrop Corporation were attacked leading to important data stolten. Its specific process is described as follow. Firstly, attacker sent two groups of malicious Email to four employees of RSA, and its attachment was excel named 2011 Recruitment plan.xls. Secondly, one employee read this Email and its excel attachment containing new 0Day vulnerability of Adobe Flash. Thirdly, the termial of this employee was panted remote control tool named Poison Ivy and perform task by download instructs from BotNet. Fourthly, attackers left immediately and transformed all data compressed with encrytion by FTP when they were found by RSA. Fifthly, attackers began intruding companies using SecurID after stealing SecurID information.

Shady Rat Attack. It lasted for years and was found by McAfee/Symantec in Aug 2011. It permeated and attack network of global corporations and groups including American government, the United Nations, Red Cross, weapons manufacturers, energy company, financial company, and its number is up to seventy. Its specific process is described as follow. Firstly, attacker collected information of target by social engineering method. Secondly, attackers sent some temptatious Email containing attachment to some typical person of target company. Thirdly, trojan would be planted when victim opened Email and saw the attachment. Fourthly, trojan would connected with remote server and download malicious code. Fifthly, attacker would control terminal of victim by building remote shell connection.

Process of APT Attcak

Tab.1. The comparsions of typical APT permeated methods

Typical APT Cases	Permeating Methods
Night Dragon Attack	SQL Injection, Oday Vulnerability, Password Crack, Malicious Email
Google Operation Aurora	Oday Vulnerability, Malicious Email, Social Engineering
RSA SecurID	Oday Vulnerability, Malicious Email, Social Engineering
Shady Rat	Malicious Email, Social Engineering, Vulnerability Aiming at Excel
Stuxnet	U Disk Ferry, Oday Vulnerability, Social Engineering, Vulnerability Aiming at PLC

Targets of APT attack are usually protected closely and attacked difficultly. The typical target is internal network which has no physical connection with Internet and is protected closely by DMZ isolation. Its representative process is generally permeating outside-in and diverse attack methods, which involves U disk ferry, SQL injection, malicious Email, etc. Oday vulnerability and social engineering are principal methods, which plays a vital role in attack process [4]. Comparsions of typical APT permeated methods are shown as Table 1.

The main process of APT attack consists of three phases such as attack preparation, external penetration and insider attack. It can be shown as Figure 2.

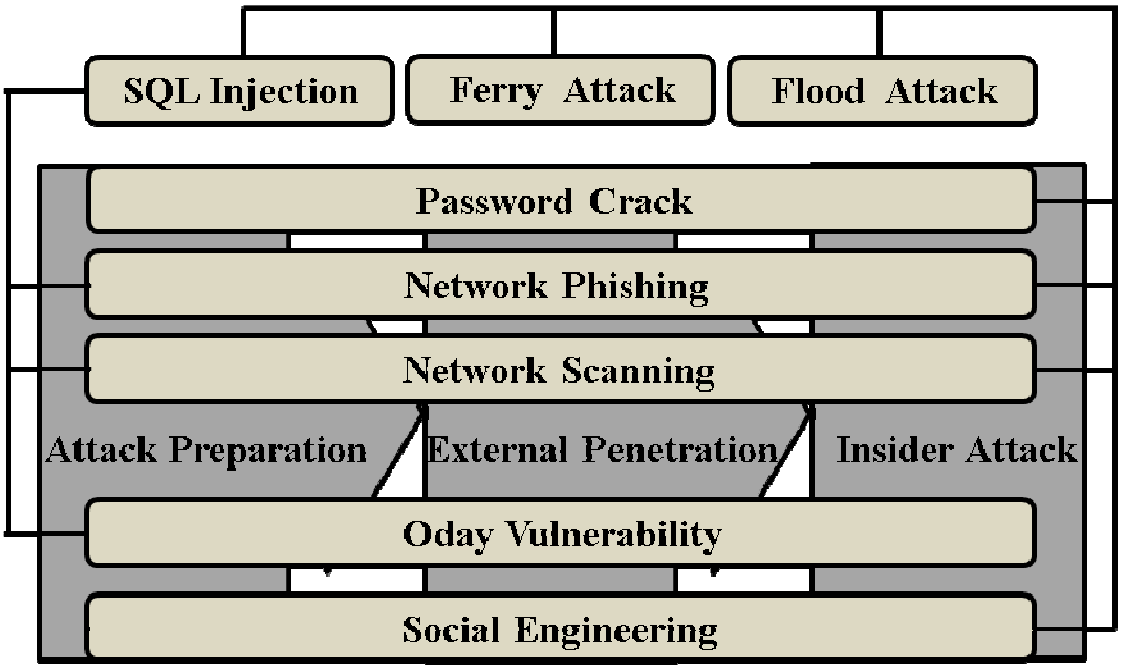

Fig.2. The main process of APT attack

Attack preparation need collect plenty of preparation work in the early after selecting target by attacker. Informaiton of target will be collected and sorted utilizing various technology means including social engineering methods and network phishing. External penetration means permeating and intruding into internal network utilizing various means including remote flood attack, SQL injection and U disk Ferry.

Security Protection of APT attack

As advanced and persistent permeating attack, security danger can't be eliminated by preventing one attack action. Security protection of APT attack must be a long-term and persistent process. Security manager must be on the alert and raise security awareness [5]. The specific security protection measures of APT attack are listed as follow.

Detection of APT Attack. Effective detection is premise for blocking and stopping of APT attack. Multiple dimensional security protection model involved test of technology and analysis-tracing of management should be built in detecting APT attack. It must be able to recognize and analyz unnatural conditions of network and server. So that key actions of APT attack may be captured and overall solution of APT action monitoring could be deduced. Intrusion tracks including network penetration, trojaner plantation and data duplication will be detected no matter how carefully the plan was put forward. Then security action should be put into effect and operation site should be saved. Those suspected infectious terminals should be isolated immediately and inspected in detail.

Response on APT Attack. It depends on effective detection means. More effective countermeasures and higher success rates will be obtained when more information of infected terminals, APT attack means and target information has been collected [6]. Security protection

actions can be put according to predefined protection strategy if APT attack response has been included in emergency plans of information system. Facing with unkown APT attack mans, response methods covering disconnecting with infected terminals, blocking network areas, reconfiguring IDS, locating intrusion and permeating reversely should be adopted.

Prevention of APT Attack. Firstly, prevention should start from users and terminals. Poor security consciousness is important reason for breaking security defence by hacker. As the last defence, terminal must has a certain degree of security protectin capability. Secondly, Control of system operations and network flow must be strengthened. Operations should be allowed in line with security stragegy and malicious operations should be stoped. Finally, system manager should master new security threat and answer unknown security risk actively.

Conclusion

As a new category of network attack method, APT has constituted a huge menace to information security of enterprise and government [7]. Given that APT attack adopted various new technologies and presented some new characteristics including purposiveness，concealment，sustainability and variability, it is hard to protect for personnel of technology and management. The general attack process and technology characteristics are summarized. Some suggestions and opinions on secrutiy protection were also presented. It will provide beneficial reference for protection various unknown APT attack means.

References

[1] Li Zhan-bao. The Perspective of Stuxnet Virus [C]. National Conference of Computer Security Science. 2011 26(9) 230-232.

[2] Gao XiaoYan. Deceiving Technology Research of Attack and Defence in Network Security [J]. Journal of ZhengZhou Economics & Management Institute. 2006 21(1) 84-86.

[3] Liu Xing, Zhao Min. Offense and Defense Technology in Cyberwar — Analysis on Project Suter [J]. Command Information System and Technology. 2011 2(4) 1-9.

[4] Report on the Worm Stuxnet's Attack, Published by Antiy CERT, V3.1 2010-09.29.

[5] Wu Mo-ping. Challenge of military information security and its countereasure [J]. Journal of Daliam Naval Academy. 2004 27(1) 9-11.

[6] CHEN Jian-feng, WANG Qiang, WU Miao. Network-based APT Attack and Defense Strategies [J]. Information Security and Communications Privacy. 2012 (7) 24-27.

[7] XU Ting. A Hierarchical-centralized Network Security Architecture Effectively Preventing APT attacks [J]. Academic Research. 2013 (6) 65-67.

Advanced Materials Research Vols. 989-994 (2014) pp 4974-4979
© (2014) Trans Tech Publications, Switzerland
doi:10.4028/www.scientific.net/AMR.989-994.4974

Data Mining Technology Applied in Network Security

Zhiyan Wang [1, a], Beizhan Wang [2,b] and Yidong Wang [3,c]

[1,2,3] Software School of Xiamen University Xiamen, China

[a] ilovexmu@foxmail.com, [b] wangbeizhan@gmail.com, [c] dong0v0er@126.com

Keywords: data mining, network security, high dimensional data, text clustering.

Abstract. As the Internet is developing fast, network security issues are rising. Data mining technology is applied to the analysis and understanding data, revealing hidden data secret inside knowledge. Especially high dimensional data mining can be used in information security data analyze, making the study of high-dimensional data mining very important. In this paper, traditional data mining is introduced; the concept and core ideas of high dimensional data mining are described, as well as its applications in network security.

Introduction

The rapid development of the Internet brings in a whole bunch of changes to people's life, especially in entertainment and working life, but the openness and security of the Internet is a contradiction. For the sake of a lot of convenience and fun that the Internet brings to us, we have to face the fact that things that are harmful to us are being uncontrolled transmitted, network security issues become increasingly prominent.

For example, users are being spammed, business websites have been hacked by malicious computer programs etc., resulting losses to businesses and users. How to improve network security has become a hot spot of current research.

As an emerging field, many disciplines and methods are involved in data mining[1] .Its core technology has experienced several decades of development, including statistic, nearest neighbors, clustering, decision trees, neural network etc.

Today, these advanced technologies have been put in use in network security, and have achieved good results. For example, network intrusion detection systems based on data mining technology have many advantages over traditional ones.

However, in practice there are still many unresolved issues. One of the most difficult problems is to make the decisions when to use what kind of data mining techniques. In order to be wiser when choosing which data mining technology to use, this paper introduces data mining technology in network security and a variety of data mining techniques applicable occasions.

Data Mining Technology

In recent years, researchers have paid more and more attention to data mining technology in the field of information security. Capable of handling massive amounts of data and easily discovering the hidden information and patterns independently which are subjectively neglected by people are the advantages of data mining technology.

Traditional Data Mining. In the process of information security analysis, we can take advantage of data mining technology to effectively analyze the information, and automatically generate accurate detection model from massive data[2]. Of course, data mining is not simply to build a detection model only, it is a process of knowledge discovery. Knowledge Discovery is iteration consists of the following sequences, including data cleaning, eliminating noise and inconsistent data; data integration, putting together a variety of data sources; data selection, data extraction from data sources which are related to analysis tasks. Data transformation is the process that the data converted into a form suitable for unified mining. Data mining is data mode extraction using intelligent method.

Assessment model is a technique according to certain measure, to identify really meaningful patterns of knowledge. Knowledge representation shows users the mined knowledge in an appropriate way.

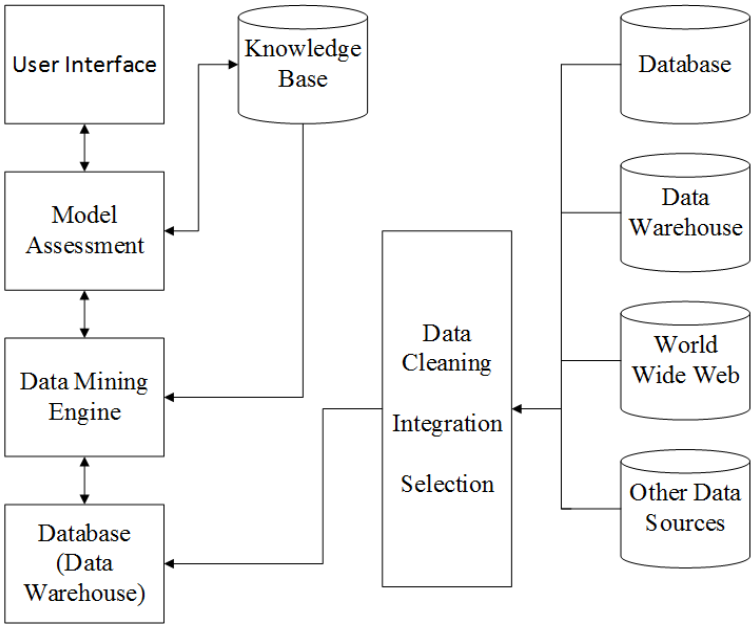

Fig. 1. A typical data mining system components

In the process of knowledge discovery above, data mining is one of the most important steps, and the broader point of view is that: Data mining is the process of discovery of interesting knowledge from large amounts of data which is stored in databases, data warehouses, or other repository. For the reasons above, the typical data mining system has the following main components shown in Fig.1.

Databases, data warehouses, World Wide Web or other information library is a complex set of data sources, which can contain multiple types of repository, where data can be cleaned and integrated.

Database or data warehouse server is used for containing the processed data according to the mining demands of users.

Knowledge base is the domain knowledge from and experts and the users' beliefs, can be used to guide the search mode degree of interest or the assessment of the results. Degree of interest may include additional constraints and thresholds, and meta data.

Data mining engine is a fundamental part of the process, ideally by a set of functional modules for performing characterization, association and correlation analysis, classification, prediction, cluster analysis, outlier analysis and evolution analysis and other tasks. It is capable to describe and predict the two major types of mining according to different needs of users. The so-called descriptive mining refers to the general description of the data; predictive mining is to analyze the existing data inference, predicting future behavior. Specifically, the concept can be divided into descriptions, association rule mining, clustering analysis, classification, anomaly detection and evolutionary analysis. And based on the need to guide the learning process can be divided into data mining methods in: supervised learning and unsupervised learning, the main method of the former is classification, the main method of the latter is cluster analysis method.

Model assessment is the module that interacts with the data mining module, it can be used to filter patterns which have been found, the metrics is the interest threshold. Model assessment can usually be connected together with the data mining module for effective data mining.

User Interface is the module completes the communication between the user and the data mining system , which allows users to interact with the system , to better illustrate the key data mining tasks or queries , and give the user a platform to submit information to help focus. Intermediate results can dig exploratory data mining based on the data. In addition, this component also allows the user to

browse the database, a data warehouse or a data structure model to assess the mining model, to achieve visualization of the model from different angles.

High Dimensional Data Mining. In many application fields of data mining, data is becoming increasingly complex[3]. In fact, various types of transaction data, document data, gene expression data, network communications data can reach dozens, hundreds or thousands of dimensions. If we represent these data into a high dimensional point, the objective world of things can be represented by a collection of high-dimensional data, data mining for that is the high-dimensional data mining problems.

Typical high-dimensional data includes the following:

(l) Shopping basket data: shopping basket data records customer buying behavior for customer relationship management.

Consider using a table to record the customer's once purchase behavior, each row of the table represents a transaction record, in addition to some basic information about the customer , the columns of the table need to record the transaction time, location, transaction method, payment information and promotional information and other items; in addition, you can also breed every kind of goods or services as a column, if customers purchase certain goods or services, then the corresponding columns can be marked or record the quantity or amount of purchase, so that the "shopping basket" of data is a high-dimensional data.

(2) Document data: types of documents typically use vector space model (VSM) to represent. In VSM, each document is represented by a space vector of words.

A typical text mining systems need to process thousands of words, therefore the document data actually have very high dimension. Document data mining specifically includes document classification, text clustering, etc.

(3) Program file data: Program file data is a set of program files to reflect the characteristics of program behavior data, which is the base of data mining computer virus or malware detection system. For example, in Microsoft Windows operating system, the files that records the program API function name calls or a string containing the program files can be used to describe a program, such data typically has thousands of dimensions.

Text Clustering. Text clustering is the most typical application in automatic data classification with high-dimensional data clustering method. A text clustering system is shown in Fig. 2.

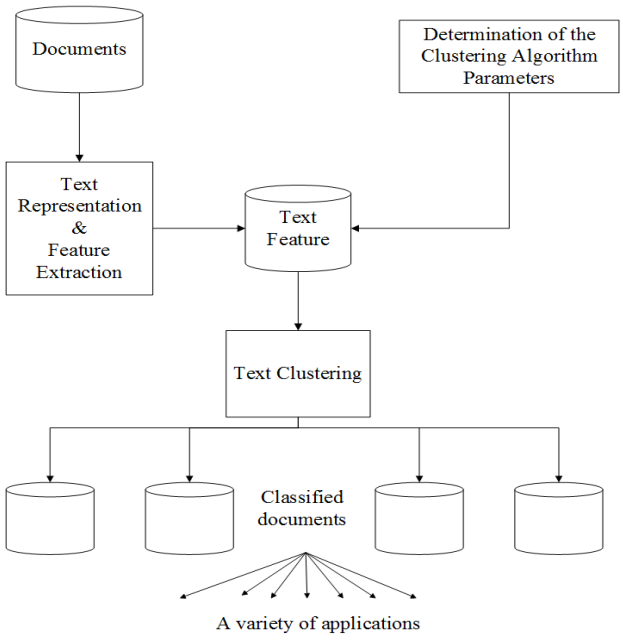

Fig. 2. Structure of a text clustering System

As shown, because the document is unstructured, before text clustering various types of documents need to be converted into structured data. Commonly we use vector space model (VSM)[4] to convert this structured data.

The documents need to be preprocessed when it is represented in VSM (eg: stemming English text, word and POS tagging Chinese texts, stop words filtration, etc.) each document is represented as a vector in word space, which is a high-dimensional sparse space.

VSM-based document clustering also has the typical characteristics of subspace clustering. Clearly, a different set of keywords is different categories of documents, the text subspace clustering subspace clustering features, using local feature weighting method to classify documents at the same time, you can also extract the different document categories there are differences set of keywords.

Network Security

In recent years, with the development of the Internet, network security problems have become more serious[5], and the virus as one of the main issues of information security has become an issue of concern to many researchers.

The Internet is a mixed bag of the world, at the same time a lot of important information, irrelevant information is spread on the Internet, so build information security system is particularly important, including security protocols, computer security operating system security mechanisms (message authentication, data encryption, digital signatures), and the security system, any security vulnerabilities can be a threat to global security. Information is of great significance for specific individuals or group, as a resource, it is universal, shared, and even value-added. Protection of information system or network information resources from various threats is the essence of information security. The typical data mining techniques can be applied to network security projects are anti-spam, intrusion detection and malware detection. .

Some Applications of Data Mining Technology in Network Security

Currently, high-dimensional data mining analysis has been applied in many fields, such as face recognition, voice recognition, the paper recommendation, customer relationship management and web search engines. Following is some application of high-dimensional data mining.

Anti-Spam. A famous anti-spam organization once gave a definition of spam, that junk e-mail should have the following two characteristics: First, uninvited, meaning the user don't request or agree to receive e-mail before; Second, batch , meaning a copy of the e-mail is sent may times in a short period of time to one or more users.

Content-based spam filtering[6] is one of the specific applications of text mining in network security field. Currently, there are two types of spam filtering techniques: content-based and rule-based approach. Rule-based methods include the white list and black list technology, rules -based filtering and content scanning, keyword matching, etc. The downside is that the rules need to manually continue to discover, review and update. It also needs to be considered spam features may change over time and we have to change the rules.

Text content based spam filters get a lot of attention, the basic starting point is regardless of the spam address or other structural part of the change, spam the text content is always different from ordinary email.

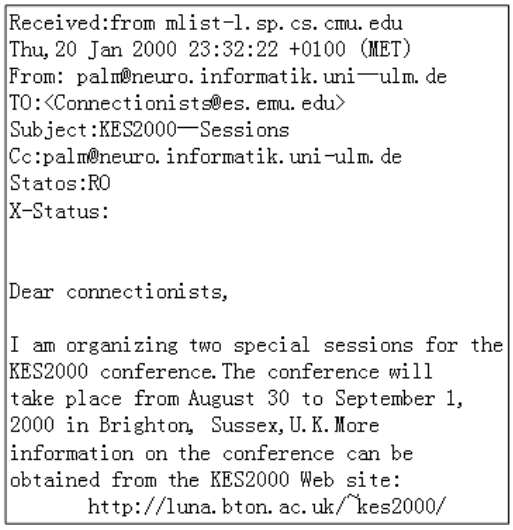

```
Received:from mlist-1.sp.cs.cmu.edu
Thu,20 Jan 2000 23:32:22 +0100 (MET)
From: palm@neuro.informatik.uni—ulm.de
TO:<Connectionists@es.emu.edu>
Subject:KES2000—Sessions
Cc:palm@neuro.informatik.uni-ulm.de
Statos:RO
X-Status:

Dear connectionists,

I am organizing two special sessions for the
KES2000 conference.The conference will
take place from August 30 to September 1,
2000 in Brighton, Sussex,U.K.More
information on the conference can be
obtained from the KES2000 Web site:
       http://luna.bton.ac.uk/~kes2000/
```

Fig. 3. Illustration of conference email

```
Received:from hP01.thaen.eom
Sun,15 Nov 1998 05:49:41+0100(MET)
From:JWPEASE@logiesouth.com
To:fnielsen@eivind.imm.dtu.dk
Subject:testing
StatUS:RO
X-Statos:

Dear Future Associate,

You Can Work At Home & Set Your Own
Hours.Start eaning Big Money in a short
time.
  NO Newspaper Advertising!
Your job will be to stuff and mail
envelopes.You will receive $.25 for each
and every envelope you stuff and mail out.
For example stuff and mail 1000 envelopes
```

Fig. 4. Illustration of spam

There are two kinds of email above. Obviously, Fig. 3 is an email notification of some conference, there is a great difference between the message content of Fig. 4, the message content of Fig. 4 would normally be viewed as spam filters.

Similar to the general text mining system, content-based spam filters typically use VSM Model to structure mail files.

The VSM Model is consisted of the glossary of the mail text, each element of the table is the frequency of words appeared in the corresponding text (which is the simplest form of VSM model) .Various classification methods based on that kind of text representation method, such as decision trees, SVM, etc., are applied to the text-based spam

However, text classification need guidance, it is hard to classify spam with unclear subject. But now application text clustering and subspace clustering technology without guidance based spam classification method has been proven to effectively improve the recognition rate of spam.

Intrusion Detection. Internet is an open environment and sharing of information, security issues is always a severe challenge.

Because the system security vulnerability exists objectively, operating systems, application software, hardware, equipment, etc. security vulnerabilities inevitably exist. Some of the network protocols design exist a number of security risks, which are easily used in hacking web applications.

How to protect network security, prevent network intrusion become an issue of concern. The thought of applying data mining techniques to intrusion detection system is due to increasing amount of network security data issues. The most important feature of clustering based intrusion detection method is no guidance, it can be marked on the audit data were not found new or unknown types of intrusions.

The basic idea of intrusion detection algorithm based on cluster analysis with a different number is from the thought that the difference between invasions and normal behaviors and abnormal behavior patterns should be much larger than the number of acts of intrusion ones[7], so the data set can be divided into different categories, which distinguish between normal and abnormal behavior to detect intrusions. Portnoy first proposed intrusion detection technique based on cluster analysis. Network intrusion detection data is of high dimensional features, we need to use some high-dimensional cluster analysis, for example, using subspace clustering literature to detect hostile access. In Intrusion detection based clustering, outlier is often seen as representative of intrusions which are quite different from normal behavior.

Identification of malware. Computer viruses have serious implications for the normal operation of the computer system and people's daily work and life. With the development of Internet and software technology, the number of computer viruses and attacks is hidden and difficult to prevent. In recent

years, there are about 30 to 100 kinds computer viruses being produced a day, the total number of all types of the virus has reached 100,000 kinds.

At the same time, the concept "computer virus" is also slowly changed, various forms of trojan horses, worms, spyware and backdoor behavior has been difficult to distinguish form "computer virus", we will collectively name the software above as malware.

Currently, in detection and prevention of malware, signature detection is still the main technique. In order to improve the ability of identifying malware, it is crucial to quickly analyze and judge suspected malware or the variant of the malware known, this is malware identification problems.

Using data mining methods for malware auxiliary identification is a good method. Like text clustering, before that we need to convert files into structured data, which is the characteristic of the program file. Through the PE program (Microsoft Windows operating system executable program, including .EXE, .DLL files, etc.) static analysis, using the API function calls to represent their program characteristic is a commonly used method in recent research. Clustering analysis methods can be used to achieve the auxiliary identification of malware.

We can use clustering analysis based on the data files for automatic classification. On the basis of the extracted API call, analyze the program's behavior .Using cluster analysis algorithm for automatic analysis of malware. However, due to frequent variants of malware, and the behavior of the normal software program with "fuzziness" and other factors inherent in these automated analysis tools. There are some false positives and false negatives are to be improved.

Summary

If you Protecting Network information security from damaging is a large, complex work, which need to be fully take into account the diverse data sources. However, if we can excellently make use of data mining techniques in dealing with massive data, the data mining algorithm can automatically dig out effective rules, and can update the rules to improve the system of automation Degrees. But for a perfect system, there are many works to be done, such as: improving data mining algorithms, improving the system's adaptability, improving the timeliness and accuracy of detection systems, etc.

References

[1] Maimon, O., Rokach, L.: Data Mining and Knowledge Discovery Handbook, pp. 803–808. Springer (2010)

[2] Muazzam Ahmed Siddiqui. Data Mining Methods for Malware Detection[D]. University of Central Florida, 2008

[3] L.Parsons, E.Haque and H.Liu. Subspace Clustering for High Dimensional Data:A Review[J].ACM SIGKDD Explorations Newsletter, 2004,6(l):90•105.

[4] F.Sebastiani. Text Categorization [J].ACM Computing surveys, 2002, 34(1): 1-47.

[5] Julisch K. Data mining for intrusion detection: A critical review. IBM Research, Zurich Research Laboratory.

[6] Cai Y, Clutter D, Pape G, et al. MAID: mining alarming incidents from Data Streams. ACM-SIGMOD Int Conf Management of Data (SIGMOD04), New York: ACM Press, 2004, 919-920.

[7] N.Wu, L.Shi and Q.Jiang. An Outlier Mining-Based Method for Anomaly Detection [C]. Proceeding of 2007 IEEE Intenational workshop on anti-counterfeiting Security, Identification, 2007, PP.52-156.

Advanced Materials Research Vols. 989-994 (2014) pp 4980-4984
© (2014) Trans Tech Publications, Switzerland
doi:10.4028/www.scientific.net/AMR.989-994.4980

The Optimized Evaluating Model and Method of Transaction Credit for E-commerce

Xikun LIANG[1, a], Limin TAO[2, b]

[1]Hangzhou Institute of Service Engineering, Hangzhou Normal University, Hangzhou, 311121, China

[2]Hangzhou Institute of Service Engineering, Hangzhou Normal University, Hangzhou, 311121, China

[a]email: schenken@163.com, [b]email: tlm5460@163.com

Keywords: E-commerce; Credit Evaluation; Model and Method; Seller Credit; Customer Credit

Abstract. Based on the brief introduction of the credit evaluation system for the primary e-commerce platforms, the advantages and disadvantages of the existing systems were analyzed in details. Moreover, some important problems of e-commerce credit evaluation were systematically discussed, which include the uniform standard of rating scales and marks, the pattern of product rating, the evaluating model and algorithm of sellers and customers credit, etc. A complete credit evaluating model was constructed and an effective credit evaluating method was given. They can be selected as the reference for the practice of credit evaluation for e-commerce.

Introduction

Since there are many characteristics such as the remoteness, the changeability of the trading record, the complexity of the subjects, etc in e-commerce, network transaction maybe faces greater risk than the physical market trading. Usually, objective and accurate credit data can provide strong support for the trading decision and reduce the transacting risk to a certain extent. So both the reliability of the credit model and the practicality of the rating method have an important influence on e-commerce activities [1-4].

In order to overcome the shortcomings in the current systems, a model called SMA (Standard-Model-Algorithm) is established as an effective and objective tool of e-commerce transaction credit evaluation. The following contents are included in SMA: the rating scales and marks, the product rating, the evaluating method of sellers and customers credit, etc.

The Main features of current E-commerce Credit Evaluation System

After a comprehensive analysis of the representative e-commerce service platforms including Amazon, Epinions, BizRate, CNet, eBay, Yahoo and Alibaba, some features of the current transaction credit rating system can be summarized as follows [5-8].

- All of the rating system provides credit information of the trading partners.
- Most of the rating system holds the detailed record of product evaluation results.
- The rating system can timely respond to the request of buyers and quickly generate a list of recommended products for them.
- All the credit information is open and real-time updated. While the computational method of the evaluating indexes is relatively fixed.

On the other hand, there are some limitations in the existing systems in different ways to a certain extent [9-12].

- The credit rating scales are not uniform and the rating marks are not standardized. The credit is divided into five levels in most of the rating systems, but three levels or seven ones are used in other systems. On the other hand, either ‘the pentacle’ or ‘the tick’ or ‘the smiley’ may be selected as the rating marks in different systems.

- The semantics of the rating is vague or ambiguous. In different systems, there are great differences in the corresponding relationship between the semantics, the grade and the mark of the same credit rating. Obviously, this situation is not convenient for credit data sharing
- As one of the most important factors of credit evaluation, the definition of 'Quality of Service' is usually neglected in most system, let alone its measurement method.
- The function relation between credit and time is constructed in a few systems, but other index as the clustering weighted method of the review or the reviewer grade is rarely considered in the system design.
- Overall, qualitative analysis methods are adopted by most systems. While the quantitative analysis ones based on objective data are ignored

The Optimized Model and Method of Credit Evaluation for E-commerce

• Rating Scales and Marks

According to the international practice, the credit is divided into five levels from the 1st to the 5th grade. The grade scores are set in reverse order form, which vary from five points to one point. And also, the corresponding semantics of the classifications can be expressed as excellent, good, moderate, limited and bad respectively. Finally, the related logos are selected from five pentacles to one pentacle. The above contents can be summarized in table 1.

Table1. Five rating scales and its marks

Credit rating	Grade score	Credit semantics	Level logo
1st	5points	Excellent	★★★★★
2nd	4 points	Good	★★★★☆
3rd	3 points	Moderate	★★★☆☆
4th	2 points	Limited	★★☆☆☆
5th	1 point	Bad	★☆☆☆☆

• Rating Model of the Products

Usually, the quantitative calculation is mainly adopted in product rating. A unique first grade index called the overall rating and some secondary indexes are included in this rating scheme. The rating scores of secondary indexes are obtained according to the various attributes of the product, which vary from five points to one point. And also, the overall rating value is drawn by weighted sum of the secondary scores. Moreover, this value can be converted into semantics grade or pentacle logo. This course is detailed shown in table 2.

Table 2.Quantitative rating of the product

<table>
<tr><th colspan="2">Indexes</th><th>Score</th><th>Weight</th><th colspan="2">Grade</th></tr>
<tr><td>First order</td><td>Overall rating</td><td>$y=\sum_{i=1}^{n} w_i x_i$
$0 \le y \le 5$</td><td></td><td>Semantics</td><td>Logo</td></tr>
<tr><td rowspan="3">Second order</td><td>Index 1</td><td>x_1</td><td>w_1</td><td rowspan="3">Semantics</td><td rowspan="3">Logo</td></tr>
<tr><td>……</td><td>……</td><td>……</td></tr>
<tr><td>Index n</td><td>x_n</td><td>w_n</td></tr>
<tr><td colspan="2">Notes</td><td>$x_i \in \{1,2,3,4,5\}$</td><td>$0 \le w_i \le 1$
$\sum_{i=1}^{n} w_i = 1$</td><td colspan="2">The grade is rounded up by the value of the variable y</td></tr>
</table>

As an example, the rating course of 'Furniture Product' is given in table 3. (Equal weight is selected in this example. On the other hand, it is obviously that non-equal weight may be adopted according to the different importance of the secondary indexes)

In a period of time, the cumulative overall rating score of a commodity can be calculated by the formula $\bar{y} = \sum_{j=1}^{m} y_j \big/ m$. Where, the variable m represents the times of product rating. And, y_i stand for each rating scores.

In addition, a qualitative rating for product can be given by the buyers in the form of 'Product Review'. It can be regarded as a necessary complement of the overall rating. Usually, the product review focus on the content does not involve in the quantitative evaluation.

Table 3.The rating course of 'Furniture product'

Indexes		**Score**	**Weight**	**Grade**	**Logo**
First order	Overall rating	4.2		2nd	★★★★☆
Second order	Price	5	0.2	1st	★★★★★
	Function	4	0.2	2nd	★★★★☆
	Material	3	0.2	3rd	★★★☆☆
	Appearance	5	0.2	1st	★★★★★
	Firmness	4	0.2	2nd	★★★★☆

Table 4.The evaluating method of the seller credit

Indexes		**Sub-variables**	**Score**	Weight
First class	Overall rating		$y=\sum_{i=1}^{4} w_i x_i$	
Second class	*Product*	g_1, g_2, g_3	$x_1 = g_1 w_{11} + g_2 w_{12} + g_3 w_{13}$	w_1
	Price	p_1, p_2	$x_2 = p_1 w_{21} + p_2 w_{22}$	w_2
	Delivery	d_1, d_2	$x_3 = d_1 w_{31} + d_2 w_{32}$	w_3
	Quality of service	s_1, s_2, s_3	$x_4 = s_1 w_{41} + s_2 w_{42} + s_3 w_{43}$	w_4

Table 5.The illustrations to sub-variables

Sub-variables	**Semantics**
g_1	The quality of the product
g_2	The integrity of the product
g3	The consistent degree of the produce to the description
p_1	The comparative advantage of the price
p_2	The performance-price ratio
d_1	The delivery of the seller
d_1	The delivery of the logistics company
s_1	The quality of service for the seller
s_2	The quality of service for the logistics company
s_3	The quality of after-sale service

- **The Credit Evaluating Model and Algorithm for the Seller**

1. A single transaction credit evaluation

Generally, the evaluating system is made up of three levels indexes. The first class index is called overall rating of the seller. It is set as the variable T. This variable is regarded as the weighted sum of the four second class indexes. Which include the rating results of the four aspects: the product, the price, the delivery and the quality of service. Moreover, the value of every second class index is supported by several sub-variables. The calculating method of the seller credit is detailed shown in table 4 and the illustrations to sub-variables are listed in table 5.

2. The cumulative transaction credit evaluation

Normally, the reliability of credit scoring can be considered as a decreasing function of the variable for time. So the cumulative credit of the seller will be calculated by the method of weighted average based on all the credit scores in the past time.

In a certain cycle, the evaluating period is usually divided into four categories: x_1, x_2, x_3 and x_4. Where the variables $x_i, i = 1, 2, 3, 4$ are set as the distance from the evaluation time to today. Let the time unit is one day, then the value ranges of x_i can be selected as [0, 30], [30, 90], [90, 180] and [180, +∞] respectively.

Corresponding with the variable x_i, the weighted factors $w_i, i=1,2,3,4$ are taken for 0.50, 0.25, 0.15 and 0.10 respectively. Suppose the credit average of every period is written as $\overline{y}_i, i=1,2,3,4$, then the cumulative transaction credit evaluation of the seller can be drawn by the following formula.

$$\tilde{y}=\sum_{i=1}^{4} w_i \overline{y_i}$$

- **The Credit Evaluating Method of the buyer**

Similarly, a first class index called overall rating of the buyer is set in the evaluating system. It is usually expressed as the function of the five second class indexes including the date of payment, the quality of evaluation, the ratio of evaluation, the quality of review and the ratio of review respectively. The calculating method of the buyer credit is detailed shown in table 6.

Table 6.The rating method of the buyer

Indexes		**Score**	**Weight**
The first class	The overall rating	$y=\sum_{i=1}^{n} w_i x_i$ $0 \le y \le 5$	
The second class	The date of payment	x_1	w_1
	The quality of evaluation	x_2	w_2
	The ratio of evaluation	x_3	w_3
	The quality of review	x_4	w_4
	The ratio of review	x_5	w_5

SMA system of transacting credit evaluation for e-commerce

The model and method of credit evaluation constructed in this paper can be summarized as a schematic diagram in Fig.1.

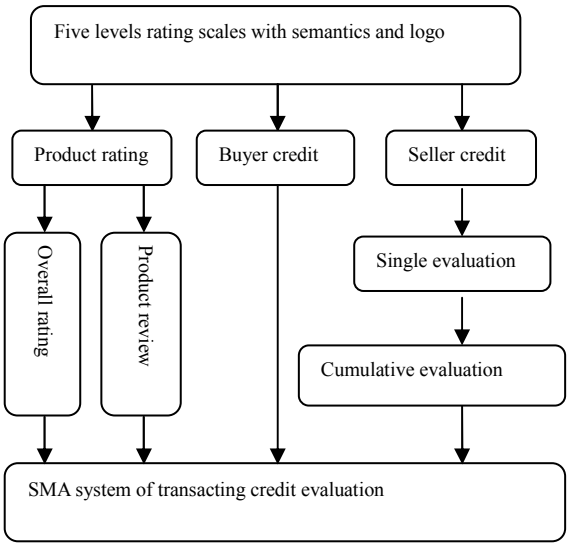

Fig.1. Schematic diagram of SMA

Conclusion

In this paper, some problems of credit evaluation for e-commerce are discussed and a rating system called SMA is designed to improve the traditional credit evaluating methods. Both the quantitative and the qualitative scheme are adopted in this system. It is hoped that SMA can be

selected as a means of credit evaluation in current e-commerce transacting platforms. It should be emphasized that the weighting method may have a great influence on the credit Data. Which method is more suitable for e-business practice will be detailed discussed in another paper.

Acknowledgement

This work was financially supported by the Natural Science Foundation of Zhejiang Province (Y6110178) and the Science and Technology Planning Project of Zhejiang Province (2012C21031). We would like to express our gratitude to all those who helped us during the writing of this thesis.

References

[1]Chang,Elizabeth.Dillon, Tharam.Hussain, Farookh.K. Trust and Reputation for Service-Oriented Environments: Technologies for Building Business Intelligence and Consumer Confidence[M], John Wiley & Sons Inc, 2006.160-210.

[2] Manchala, D.W. E-commerce trust metrics and models, IEEE Internet computing [C], 2000 4(2) 36-44.

[3] Florian Skopik, Daniel Schall, Schahram Dustdar. Modeling and mining of dynamic trust in complex service-oriented systems. Information Systems, 2010 35(7) 735-757.

[4] Zaki Malik, Athman Bouguettaya. RATEWeb: Reputation assessment for trust establishment among web services. The VLDB Journal, 2009 18(4).

[5] WU Jian-bin1, Lü Gang. Trust and reputation evaluation for Web services based on user experience. Journal of Computer Applications, 2009(4).

[6] Yuan Haiyan. Reform of the Credit Evaluation System in the View of Credit Speculation in the C2C Trade of China. Science Mosaic, 2009(10).

[7] Guan Xiaoyong. The logics of technology development for the credit evaluation between China and Occident with its comparative research. Science Research Management, 2009 (4).

[8] Wang, Zhi-Bing Li, Chang-Yun. Research on credit assessment based on trade behavior for e-commerce. Application Research of Computers. 2010 27(3) 945-947.

[9] Yu-Chung Tsao, Lu-Wen Liao. An Algorithm for Joint Multi-item Replenishment Problem under Trade Credits. 2010 Second International Conference on Computer and Network Technology. Bangkok, Thailand.

[10] Fatoki Olawale and A. Van Aardt Smit. The impact of the business environment on the availability of trade credit to new SMEs in South Africa. African Journal of Business Management, 2010 4(9) 1790-1799.

[11] Guofu Zhang, Jitian Wang. The Analysis on Credit of State-Owned Enterprises Based on BP Neural Network. 2010 International Conference on Intelligent Computing and Cognitive Informatics. Kuala Lumpur, Malaysia.

[12] Yi-Hui Chiang and Chih-Young Hung. Trade credit evaluation for Taiwan's broadband communications equipment manufacturers. International Journal of Management and Decision Making. 2010 11(1) 37 – 54.

Advanced Materials Research Vols. 989-994 (2014) pp 4985-4989
© (2014) Trans Tech Publications, Switzerland
doi:10.4028/www.scientific.net/AMR.989-994.4985

Research and Implement of Micro-Blog Social Network System Based On Users'Association Analysis

ChenHao

Computer School of Shenzhen Polytechnic, Shenzhen, Guangdong,518055, China

Keywords: Users' association; Micro-blog; Social network system;

Abstract. With the widespread application of web2.0 technology, micro-blog has become an important part of life for many people. A well-designed micro-blog system has the better users' experience and allows users to get the information what they want with high efficiency in the shortest time. After analyzing each of the existing micro-blog systems, we found that the most information of micro-blog is sorted by time. With the users' attention gradually increased, the frequency of message update, its contents appeared homogeneity and repetition, and thus leaded information overload. To solve this problem, this article puts forward a method based on users' association analysis and implements a micro-blog system which presents its contents in priority based on users' interest by way of users' association analysis. It can sort the contents of the micro-blog and show the contents which the user interest in priority.

Introduction

In 2010, the fastest growing of web2.0 application of internet was the micro-blog service in China. After the following SMS, instant messaging, blog, SNS, communication tools and so on, micro-blog relied on its good user experience, and quickly entered the global Internet users' view. Web, which is a small blog can be available for releasing news, its biggest feature is the length of a short post, the diverse ways of post [1]. Micro-blog is so popular, because it is more casual, convenient and instant than other media. There is no need to consider logical rigor. It can use here and here. In addition, user can express their ideas to the public everywhere in any time [2].

Micro-blog system is a platform that we can share, disseminate and obtain information based on users' association. With the fast transmission of information and the strong fidelity, it can achieve the point transmission and show information [3]. A good micro-blog can be widely disseminated in a similar property circles, at the same people's social needs have been greatly satisfied.

In micro-blog network, users have established close relationship (attention and is concerned) than the forums and other social networks the between the users. Not only established a dynamic relationship between users by forum posts. Dynamic can be understood as information flow. Information can treat the static users' relationship as a track and flow to various users [4]. Therefore, when the micro-blog develops to a certain extent that users' relationship is at the beginning and the information flow is at the back, the relationship shown in Figure 1.

The article combines with the current mainstream micro-blog site, in depth study of the basis of its design and architecture, through the analysis of access to information among users, mining association between the users that designs a user-based association relation and meets social network system key requirements. It is a micro-blog social network system that may show the information which the users interest in priority.

Related work

The first prototype of micro-blog was proposed by Evan Williams in March 2006 in America. It meant the birds' twitter and was extended to the idea for everyone to express their wish and share their desire. The core of the first prototype of micro-blog is in short and random, which is not more than 140 words and tell the others what were you doing [5]. Twitter was fame when it was invented firstly. The annual growth rate of it was reached to 1382％ and its users was over ten million. Moreover, Obama is its loyal users, too.

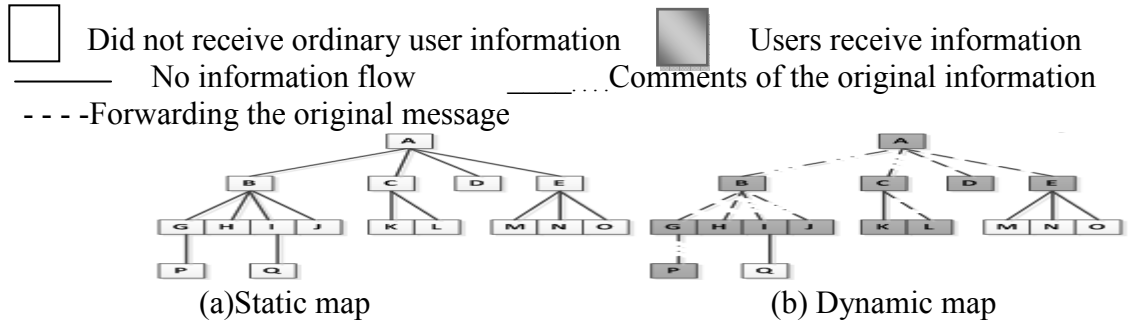

(a)Static map (b) Dynamic map

Figure 1 Users diagram

In May 2007, Chinas' domestic micro-blog service providers began to appear. From February 2009, the domestic micro-blog has been full of new vitality. Micro-blog sites have on-line continuously and the number of users increases sharply. Micro-blog has become a new feature of the development of internet. In August 2009, Sina micro-blog was on-line and became China's most influential micro-blog. Driven by Sina micro-blog, integrated portal micro-blog, vertical portal micro-blog, news site micro-blog, E-commerce micro-blog, SNS micro-blog, independent micro-blog sites have been established one after another. Even the TV station telecom operators have begun to get involved to micro-blog service [6]. China has really entered into the micro-blog era.

Micro-blog information can spread by means of users' relationship net. Users have their own property, such as stars, media, or grassroots. Users' relationship refers to the micro-blog system that depends on it. And it can excavate the concerned users and the published contents. We can extract the users' property, interest, hobbies and so on. Before the new information arrived, it can sort out the contents combined with the users' property. It can show the micro-blog information that we interest in priority.

Micro-blog user association analysis

Using the correlation theories focus on the number of users, the number of micro-text and are concerned about the number three information analysis, based on the analysis results, the user can calculate the number of targets to increase attention to the behavior of the trend. The correlation coefficient used to indicate the degree of linear relationship between two variables, the Pearson correlation coefficient of the main, Spearman correlation coefficient and correlation coefficient of three kinds of Kendall. Usually Spearman correlation coefficient is calculated as follows:

$$r_s = 1 - \frac{6\sum_{j=1}^{n}(R_j - Q_j)^2}{n(n^2-1)} \quad (1)$$

Where, R_j and Q_j are the j-th rank values of two variables. Believed, | r | closer to 1, the higher the degree of linear correlation; | r | the closer to 0, the lower the degree of linear correlation. $r > 0$, which means that two variables correlated; $r < 0$, which means that negative correlation of two variables; $r = 0$, which means that two uncorrelated variables.

The number of micro-text and concerned are an important factor to measure activity level of micro-blog. While the number of being concerned is an important factor to measure users in the micro-blog. Users are usually most concerned about the factor. Learn the relationship between them, it is good to understand users' behavior and determine the level of activity of the user. In order to eliminate the impact of celebrity, we should remove the celebrity and the user to be concerned about the number, concerned about the number and the number of any one of the micro-text which has no user. Then use SPSS software to the number of micro-text and concern as the control variable number of partial correlation analysis, the specific results as shown in Table 1 and Table 2.

The number of concerned (NOC) is used to a person who pays attention to others' Micro-blog. The number of being concerned (NOBC) is used to a person who is followed by others.

Table 1 The number of micro-text for the control variables and correlation coefficients of the NOC and the NOBC

Control variables	Variable	Parameter category	NOBC	NOC
The number of micro-text	NOBC	The correlation coefficient	1.000	-0.017
		Associated probabilities	0.000	0.376
		Quantity	0.000	2854
	NOC	The correlation coefficient	-0.017	1.000
		Associated probabilities	0.376	0.000
		Quantity	2836	0.000

Table 2 The NOC for the control variables and correlation coefficients of the NOBC and the number of micro-text.

Control variables	Variable	Parameter category	NOBC	NOC
NOC	NOBC	The correlation coefficient	1.000	0.074
		Associated probabilities	0.000	0.000
		Quantity	0.000	2854
	The number of micro-text	The correlation coefficient	0.074	1.000
		Associated probabilities	0.000	0.000
		Quantity	2836	0.000

As can be seen from Table 1,removing the effect of the micro-text, the correlation coefficient concerned about the number and the number of attention is - .017, 376, related to the probability is 0.376, indicating that there is no relations between the two. As can be seen from Table 2, in the removal of several concerns, the correlation coefficient concerned about the number of micro-text and numbers becomes into 0.074, indicating that there is no relations between the two basic.

Using SPSS software calculates Spearman correlation analysis of relations between any two, the results are shown in Table 3.

Table 3 Correlation coefficients of the NOBC, the NOC and the number of micro-text

The correlation coefficient	Variable	Parameter Type	NOBC	NOC	The number of micro-text
Spearman	NOBC	The correlation coefficient	1.000	0.309	0.569
		Associated probabilities	0.000	0.000	0.000
		Quantity	2785	2785	2785
		The correlation coefficient	0.309	1.000	0.437
	NOC	Associated probabilities	0.000	0.000	0.000

		Quantity	2785	2785	2785
		The correlation coefficient	0.569	0.437	1.000
		Associated probabilities	0.000	0.000	0.000
	The number of micro-text	Quantity	2785	2785	2785

As can be seen from Table 3, the correlation coefficient concerned about the number of concerns with the number is 0.309, the relevant probability is 0.000, indicating that there is a certain correlation between the two. Combined analysis Table1 shows that when the number of affected by the micro-text, it is concerned about the existence of relations between the number and the number of attention. If the users release micro-text frequently, there will be more people to concern him. Thus increase the number to be concerned about. With the increasing number of fans, it is easy to make the users to concern others. Otherwise, it is on the contrary. Is concerned about the number and the number of micro-text correlation coefficient is 0.596, the relevant probability is 0.000, showing a moderate positive correlation. Table 2 combined analysis shows that when the number of affected concern, there is a relationship between the number of attention and concern number. That is, if the user paid little attention to other people, even if slightly more users to publish text, others pay attention to him nor the General Assembly.

Users realize the associated

In micro-blog system, each user has two roles there, followers and those who are concerned. It is important how to deal with the relationship between users and let users′information effectively circulate between the two roles.

In Figure 2, it is a conceptual model including users (in the conceptual model entity name for Users) micro-blog information (in the conceptual model entity name for Messages) and customer relationship (in the conceptual model entity name for Relations). For example, user A add the concerned operation to user B. Then it can conduct a piece of corresponding data from A to B, which indicates that A concerns to B. When A gets the new information, then we can find out the corresponding relation with A. Then we can connect to the micro-blog information through a database table relations and get their message queue.

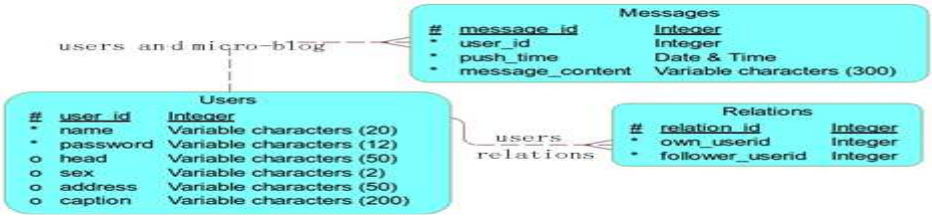

Figure 2 Users, micro-blog conceptual model diagrams and relationships

A user association model is important for users association. We can generalize the user′s module by the user's interests and behavior information. Firstly, we should obtain all the published micro-blog of the users, then analysis the features of the information and describe it in the form of natural language. We can conduct word processing, removing the word and forming the keyword list. We should give appropriate weight to each keyword to form micro-blog feature table. Micro-blog features reflect the characteristics of each user's interests, hobbies, habits and behavior. On the basis of the relationship between the users, through micro-blog characteristics associated table, we can get the user association model. It can reflect the common point of interest between the users. The system is the basis for this analysis of the new micro-blog messages, allowing users to more timely access to the message might be interested.

System Design and Implementation

The system server is designed mainly for using ASP.NET technology. ASP.NET is built on HTTP protocol. It is full of using HTTP commands and strategies to establish bi-directional communication and collaboration browser to server (B / S). It is the biggest difference with other Web development technologies that made it an abstract programming model (Abstract Programming Model), that is, the Web Forms model [7]. Therefore, we can easily use rich controls on the server side development.

Open the website system, users enter the login screen and import a nickname and a password and then click on the login. Otherwise you cannot get in it. When entering the home page, the users concerned people have micro-blog updated and presented at this time. On home page, people can check the concerned people or un-follow. People can also check who concern me. If not, he can concerns them. We can publish the micro-blog or delete the micro-blog. Setting basic personal information, saved to the database, if not saved directly back home; logout login, delete the user's login status, back to the login page.

Conclusion

This system can excavate associations between users and predict new Twitter users ' level of interest and reorder the new micro-blog through the Twitter data for analysis. Interface is simple and clear navigation buttons improve the system efficiency data lookup and data updates, so micro-blog home is more convenient to use and has a strong fault tolerance and security.

We need to further improve the place in the system development, such as the complexity of the algorithm which will lead to lower home micro-blog update efficiency. In the next study, the manner contemplated by calling interface realizes the system with the current mainstream micro-blog system (Sina micro-blog etc.) and achieve information sharing of data. Meanwhile, micro-blog system can also be ported to mobile devices user at any time through the use of smart mobile terminals micro-blog system.

References

[1]Wang Shuhua. "Micro-blog era" Media Response [J]. Journalism practice 2009 (10) .
[2]Kai-fu Lee. "micro-blog: change everything" [M].Shanghai University of Finance and Economics Press, 2011(2).
[3]Zeng shiqi ,Liu xinyu etc. Progress Analysis micro-blog system [J]. Ecommerce 2012 (4).
[4]Yin Yanteng, Li Xueming etc. Based on micro-blog user relationships with opinion leaders attribute mining method [J]. Computer Engineering 2013 (4).
[5]Wang Lu,spread social micro-blog new media analysis 2011
[6]YuanYi, the mechanism Chengming Yang micro blog user communication, structure and characteristics [J]. Library Forum 2010 (6).
[7]Li Zhanbo eds. Development [M] ASP.NET-based Web applications. Tinghua University Press 2012 (9).

Advanced Materials Research Vols. 989-994 (2014) pp 4990-4995
© (2014) Trans Tech Publications, Switzerland
doi:10.4028/www.scientific.net/AMR.989-994.4990

Chinese-Uyghur Sentences Alignment Using Multiple Clues

Saimaiti MAIMAITIMIN[1, a], Min HOU[2]

[1]Postdoctoral Station of Computer Science and Technology, Xinjiang University, Urumqi 830046, China

[2]Communication University of China, Beijing 100024, China

[a]Email: tilchin@sohu.com

Keywords: Sentence Alignment; Chinese; Uyghur

Abstract. This paper introduces a new method to Chinese-Uyghur sentence alignment, in which a two-step procedure is applied. In the first step, multiple clues such as proper names, technical terms, numbers, punctuation marks, location information and length information are used to generate anchor sentences that satisfy some conditions. In the second step, texts are divided into several segments by using the anchor sentences as boundaries, and then the sentences in each segment are aligned by using a length-based approach. By applying the segmentation technique, the method avoids complex computation and error spreading. Experimental result shows that the accuracy of the method is 95.2% on the average for multi-domain texts.

Introduction

For parallel corpora, the most important annotation is alignment, especially sentence alignment, which is a minimal and essential requirement for a parallel corpus. Aligning Chinese-Uyghur parallel texts at the sentence level, however, is already very difficult because of the considerable differences in writing systems and syntactic structures of the two languages. Chinese uses Chinese characters as its writing system while Uyghur uses alphabetic character. Chinese is an analytic language that has SVO word order. In contrast, Uyghur is a suffixing and agglutinative language that has SOV word order.

A number of alignment techniques have been proposed for other language pairs, varying from statistical methods to lexical methods. There are basically three kinds of approaches on sentence alignment: the length-based approach [1][2], the lexical approach [3], and the combination of the two [4]. However, the method does not capture enough word correspondences for structurally different languages such as Chinese and Uyghur.

This paper introduces a new method to Chinese-Uyghur sentence alignment, in which a two-step procedure is applied. In the first step, multiple clues such as proper names, technical terms, numbers, punctuation marks, location information and length information are used to generate anchor sentences that satisfy some conditions. In the second step, texts are divided into several segments by using the anchor sentences as boundaries, and then the sentences in each segment are aligned by using a length-based approach.

An Overview of the Alignment Method

Our method is similar to Wu's [5] in that it uses both sentence length and lexical information. But in our method, some clues such as proper names, technical terms, numbers, and punctuation marks are used to find anchor sentences. Our method is similar to Simard's [7] in that it uses cognates or anchors for sentence alignment. But in our method, length information and anchors are used at different stages of sentence alignment. Our method is similar to Melamed's [6] in that it uses a bi-text mapping technique to locate anchor points, but in our method, sentences are used as anchor points instead of words or characters. A segmentation technique that splits the text into several sections is also introduced to improve the length-based approach.

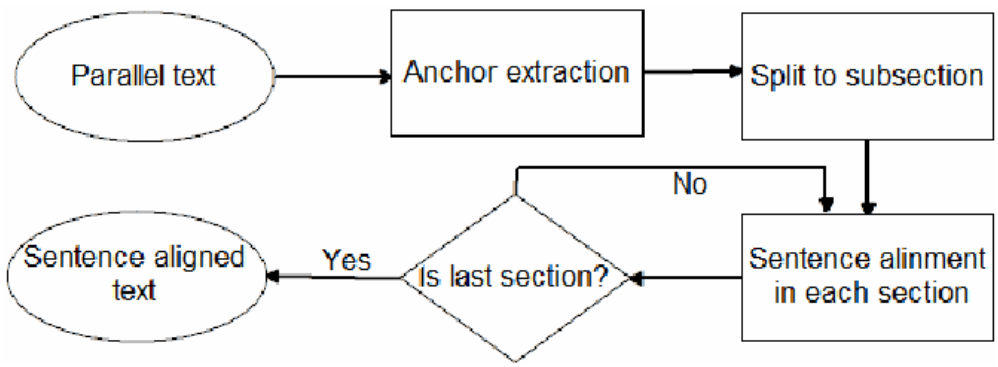

Fig.1. Flowchart of Chinese-Uyghur sentence alignment

As we can see from Fig.1, a two-step procedure is applied to sentence alignment. In the first step, some (1:1) sentence pairs, called anchor sentences, are extracted by using multiple clues. The anchor sentence extraction procedure, as a key part of whole method, will be explained in the following section. In the second step, texts are divided into several segments (subsections) by using these anchors sentences as separator, and then all sentences in each segment are aligned by using a length-based approach.

Anchor Sentence Extractions

3.1 Anchor Sentence

In a parallel corpus, the anchor sentences are specific (1:1) sentence pairs that are strongly correlated and that satisfy some conditions. All such sentence pairs which were extracted from bilingual texts during the first step are seen as anchor sentences. The goal of anchor sentence extraction is to divide the source text and the target text into one-to-one smaller segments. And using the segmentation technique, we attempt to improve the length-based sentence alignment procedure. Sentence alignment tends to be better with shorter segments and, consequently, better sentence alignments are obtained.

For anchor sentence extraction, we applied a bitext mapping technique. A bitext map is a set of pairs (x, y), where x and y refer to precise locations in the first and second texts respectively, with the intention of denoting portions of the texts that correspond to one another [7]. However, we used a bitext map of sentence pairs instead of words or characters to point out the correspondences between these anchor sentences.

In the bitext map, the horizontal axis denotes the sentence number in the Uyghur text, and the vertical axis denotes the sentence number in the Chinese text. The anchor sentences, which are shown as anchor points in the bitext map, can be characterized by three properties:

- **Injectivity:** No two anchor points in a bitext map can have the same x or y coordinates.
- **Linearity:** Anchor points tend to line up straight. In other words, all anchor points are to appear around a straight line.
- **Low variance of slope**: The slope of the anchor points is rarely much different from the bitext slope.

3.2 Algorithm Description

In our anchor sentence extraction algorithm, a three-step process is applied to extract anchor sentences. In other words, the search for each anchor sentence pairs alternates between the following three steps: generation, correction and recognition.

1) Generation

In this step, the search for an anchor sentence begins in a small search rectangle in the bitext map, its diagonal is parallel to the main diagonal. The algorithm generates candidate anchor sentence points within a search rectangle. We define a search rectangle as follows: Rectangle($x,y; x+3, y+3$) in which x is last anchor point(x) in Uyghur and y is last anchor point(y)in Chinese. The first search rectangle is anchored at the origin of the bitext map where x=0, y=0.Subsequent search rectangles are anchored at the previously found points. If no candidate points are found, the search rectangle is

proportionally expanded by the minimum possible amount, and the generation cycle is repeated. The rectangle keeps expanding until at least one acceptable point is found. Three kinds of information such as sentence length, location information and lexical information are used to generate anchor points. Sentence pairs that satisfy the following three conditions are added to the candidate anchor sentence array.

(1)Sentence length ratio

The sentence length ratio is also a very good indication of the alignment of a sentence pair. In our method, sentence pair *P(C,U)* would be candidate anchor sentences, if

$$LenRatio(C,U) \in [MinLenRatio,\ MaxLenRatio] \quad (1)$$

In Eq.1, *MinLenRatio* and *MaxLenRatio* are calculated by using Eq.2

$$MaxLenRatio = TC + A/(L_c + B),\ MinLenRatio = TC - A(L_c + B) \quad (2)$$

$$TC = (C + Len(C)/Len(U))/2 \quad (3)$$

The constant *C* is the expected number of Chinese characters per Uyghur word and *C =2.01*. *TC* is the weighted value when taking whole text size into account, the constants *A=10, B=14*.

(2) Matching score

The matching score is calculated according to the matching degree of clues that explained in subsection 3.3. If the matching score of a sentence pair is above the threshold (we set the threshold = 1.1), it is considered as a candidate anchor sentence. By applying this condition, we reject some sentence pairs with a matching score smaller than the threshold.

(3) Maximum angle deviation (MAD)

According to the properties of the anchor sentences, the slope of the anchor points should not be much different from the bitext slope. So some sentence pairs are rejected by setting a maximum angle deviation. The angle of each anchor point's least-squares line is compared to the arc tangent of the bitext slope. The anchor point is rejected if the difference exceeds the maximum angle deviation threshold (MAD=3). The angle between the least-squares line and the bitext slope is calculated according to the Eq.4

$$\theta = \arctan\left(\frac{|A - B|}{1 + A * B}\right) \quad (4)$$

In Eq.4, A is the slope of the least-squares line, B is the bitext map slope. This filtering process generates anchor sentences with higher accuracy; however, it causes errors in some cases. So, we introduced another correction procedure in order to reject some wrongly aligned sentence pairs.

2) Correction

In this step, some candidate sentences that shouldn't be anchor sentences are eliminated according to characteristics of anchor sentences. Firstly, the algorithm checks if there are any conflicts between anchor points. The injective property of anchor sentences implies that whenever two anchor points overlap in the x or y axis, but are not identical in the region of overlap, then one of the points must be wrong. To resolve such conflicts, we employed a lookup method to eliminate conflicting points. Secondly, length ratios of corresponding segments divided by candidate anchor sentences are calculated according to a similar formula in Eq.2 in order to reject wrongly aligned anchor points.

3) Recognition

A number of candidate anchor sentences can be obtained in a certain search region during application of the above two steps. For anchor sentence alignment, accuracy is more important than recall rate. So it is essential to introduce a recognition step in order to achieve higher accuracy by eliminating some unlikely anchor sentences. In the recognition step, one best anchor sentence pair is selected from candidate anchor sentences according to two parameters: matching score and length similarity. The anchor selection algorithm gives a score to each proposed sentence pair during the recognition phase, and finds the alignment with the largest sum of scores. A parameter estimation method is described in the following section.

3.3 Parameter Estimation

(1)Matching Score

As previous works suggest [4][5], lexical information is critical for sentence alignment, especially for finding anchor points. It is well known that some proper names and technical terms have transliteration or literal translation in many languages; numbers and punctuations appear in the same or similar forms in both source text and translated text. In a parallel text, for instance, if a sentence contains a question mark, it is likely to be aligned to a sentence that also contains this mark, which can be a strong clue for sentence alignment. This is also true for Chinese-Uyghur translations. However, in our method, these clues are not used to align all sentences, but to estimate matching scores and to find the best anchor sentences. We used multiple clues such as proper names, technical terms, punctuation marks and numbers. In most cases, proper names, including person names, location names, organization names, and technical terms have unique translations that will be matched easily. But, the problem is that person names and technical terms are often unknown words. How to identify them is a difficult problem. In our case, we first collected some popular proper names and some most frequent technical terms into a small lexicon that we call key lexicon. More than 6000 words are included in the key lexicon at present. Then, a very simple searching method is applied to match corresponding words (items).

In addition, punctuation marks, including other symbols (e.g. #$%&), are the most obvious clues in Chinese and Uyghur translation. The correlation between Chinese and Uyghur punctuations is extremely high. For punctuation and numbers, no external resources but some rules are applied to estimate the matching degree of these clues.

$$MatchScore(i,j) = 1 - \frac{(x-y)^2}{(x+y)^2} \tag{5}$$

In Eq.5, x is the total number of words (symbols), and y is the matched number of x. The matching scores are calculated according to the average number of matched clues. In other words, the more the matched proper names, technical terms, punctuation and numbers, the higher the matching score.

(2)Length Similarity

Length similarity is a score that reflects the similarity between the length ratio of the current sentence pair and the expected length ratio. The following formula is applied to calculate the length similarity of a proposed sentence pair (C_i, U_j):

$$LenSimilar(C_i,U_j) = \frac{\left|Len(C_i)/Len(U_j) - TC\right|}{TC} * WL \tag{6}$$

TC is the value weighted by the whole text size that is obtained from Eq.3. The sentence length ratio is not stable when a Chinese sentence is shorter than 10 characters. So it is necessary to add WF to obtain more accurate result. Hereby $StableLen=10$, $a=0.5$ and WF is calculated as following:

If $Len(C_i) \le StableLen$, then $WF = a * Len(C_i)/StableLen$, else $WF = 1$.

Length Based Sentence Alignment

According to previous work [1][2], length-based approaches are simple and can achieve good performance for different language pairs. Because of the simplicity, many later researchers integrated this method to their sentence alignment methods. We also applied the length-based approach to the second step of sentence alignment.

4.1 Measuring Length in Words and Characters

Uyghur is an alphabetic language while Chinese is a non-alphabetic language. Therefore, it is a difficult problem to select the best length measuring model. In general, a Chinese sentence does not have word boundary information, so one way to define Chinese sentence length is to count the number of characters in a sentence. Another way is to count how many words are in a sentence after word segmentation. For Uyghur sentences, we can similarly define the length by the number of characters or words. In our case, we examined three possible length models described in the following Table 1.

The mean sentence length ratios, variances and correlation coefficients for each of the length models are calculated from a Chinese-Uyghur corpus of 988 sentence pairs. Statistics of the three sentence length models are shown in Table 1.

Table 1: Statistics on three different length models

Method	Description	Mean	Variance	Correlation
L1	Chinese character to Uygur character	3.99	0.71	0.976
L2	Chinese word to Uyghur word	1.07	0.23	0.953
L3	Chinese character to Uyghur word	2.01	0.21	0.978

In general, the smaller the variance, the better the sentence length model should be. From Table 1, we can see that the character-based length ratio model (*L1*) has significantly larger variance (0.71) than the other two models (*L2: 0.23, L3: 0.21*). This means L1 is not as reliable as *L2* and *L3*. Both *L2* and *L3* have similar variance, but *L3* is better than *L2* with regard to the correlation coefficient, which indicates that sentence lengths have higher correlation if the lengths of Chinese and Uyghur texts are measured in characters and words, respectively. A regression analysis of the three models also proved this result. So we applied the *L3* model to the length ratio examination and length based sentence alignment.

4.2 Preliminary Statistics for the Length-based Method

A length-based sentence alignment program is based on a very simple statistical model of sentence lengths. The model makes use of the fact that longer sentences in one language tend to be translated into longer sentences in the other language, and that shorter sentences tend to be translated into shorter sentences. A probabilistic score is assigned to each pair of proposed sentence pairs, based on the ratio of lengths of the two sentences and the variance of this ratio. This probabilistic score is used in a dynamic programming framework in order to find the maximum likelihood alignment of sentences. The parameters C and S^2 are used for likelihood estimation. C is the expected number of Chinese characters per Uyghur words. The parameters C and S^2 are determined empirically from a hand aligned parallel corpus of multi-domain texts. According to our statistical results, we have $C=2.01$ and $S^2=3.24$.

From the above statistical results, it is clear that the correlation between the length of a Chinese sentence in characters and the length of its Uyghur translation sentence in words is extremely high. This high correlation suggests that length might be a strong clue for sentence alignment. In our cases, we applied the length-based approach to in each segments divided by anchor sentence.

Experimental Results

5.1 Test Corpus

In our experiment, we randomly selected ten texts (total 1483 sentence pairs) from Xinjiang University's Chinese-Uyghur Parallel Corpus as our testing corpus. The texts are come from five domains: fiction, law (legal) texts, official documents, scientific texts and news.

5.2 Results

Firstly, we aligned sentences by using two approaches: a length-based algorithm and our method that using multiple clues. Then we manually checked the alignment results for errors and calculated precision and recall rate.

Table 3: Experimental results

Method	Fiction	Law	Official	science	News	Average
Length- based(Accuracy)	88.5	98.6	97.6	88	89.3	92.5
Length- based(Recall Rate)	87.2	98.1	96.8	88.9	87.6	92.0
Our method(Accuracy)	92.5	100	99.2	90.3	93.5	95.2
Our method (Recall Rate)	92.5	100	98.4	91.3	95.3	95.1

As we can see from Table3, Experimental results show that our method yields higher accuracy than the purely length based approach. The precision of the method is 95.2% on the average for Chinese-Uyghur sentence alignment in multi-domain texts. This is 2.7% higher than that of a purely

length-based approach. We also analyzed all errors of sentence alignment in order to find reasons and solutions.

Conclusions

We have developed a very effective sentence alignment method based on multiple clues. In our method, firstly, anchor sentences are extracted from parallel texts to sentence align by using proper names, technical terms, numbers, punctuation marks, location information and length information; secondly, whole texts are divided into small segments by using anchor sentence points; finally, sentences in each small segment are aligned by using a length-based approach. We have implemented the method on the parallel Chinese-Uyghur corpus. Experimental results show that the precision rate of the method is 2.7% higher than that of a purely length-based approach.

Acknowledgement

The research was supported by the Natural Science Foundation of Xinjiang, China (No.2012211B08).

References

[1] Peter F. Brown, Jennifer C. Lai, and Robert L. Mercer. 1991. Aligning sentences in parallel corpora.In Proceedings of the 29th annual meeting on Association for Computational Linguistics (ACL'91). Association for Computational Linguistics, Stroudsburg, PA, USA, 169-176.
[2] William A. Gale and Kenneth W. Church. 1993. A program for aligning sentences in bilingual corpora. Computational Linguistics. 19, 1 (1993), 75-102.
[3] Martin Kay and Martin Ro¨scheisen. 1993. Text-translation alignment. Computational Linguistics. 19, 1 (1993), 121-142.
[4] Stanley F. Chen. 1993. Aligning sentences in bilingual corpora using lexical information. In Proceedings of the 31st annual meeting on Association for Computational Linguistics (ACL '93).Association for Computational Linguistics, Stroudsburg, PA, USA, 9-16.
[5] Dekai Wu. 1994. Aligning a parallel English-Chinese corpus statistically with lexical criteria. In Proceedings of the 32nd annual meeting on Association for Computational Linguistics (ACL '94). Association for Computational Linguistics, Stroudsburg, PA, USA, 80-87.
[6] I. Dan Melamed. 1999. Bitext maps and alignment via pattern recognition. Computational Linguistics. 25, 1 (1999), 107-130.
[7] Michel Simard and Pierre Plamondon.1998. Bilingual Sentence Alignment: Balancing Robustness and Accuracy. Machine Translation, 13(1), 59-80.

Advanced Materials Research Vols. 989-994 (2014) pp 4996-4999
© (2014) Trans Tech Publications, Switzerland
doi:10.4028/www.scientific.net/AMR.989-994.4996

E-commerce personalized recommendation

Yan Zhang

School of economics and management ,Xinxiang university, Henan, China

Email: 837457026@qq.com

Keywords: E-commerce; recommendation; personalized system

Abstract: With the rapid development of electronic commerce, the problem of "information overload" leads to the difficulty that user can't search the required goods effectively , personalized recommendation technology has been applied in e-commerce and popularization. By using the method of qualitative analysis of the current e-commerce site, the paper compare the information retrieval, association rule, content-based filtering and collaborative filtering four main recommendation technologies and analysis the advantages and disadvantages in the application layer, the recommendation technologies are introduced to review e-commerce research hot topic in the field of personalized recommendation, and analysis the current domestic e-commerce personalized recommendation theory research and application status, finally propose the challenges faced by e-commerce personalized recommendation domain.

1 Introduction

The rapid development of e-commerce not only makes the enterprise to save the traditional mana gement mode of the necessary physical investment costs, but also eliminates the traditional store dis play space constraints, gives shoppers a huge counter (also is infinite) goods[1].But because the cust omer can't skim all of the goods through the small computer screen in a short time, and lacking sale s promotion personnel guide carefully, so that users face "information overload". Information overlo ad refers to the commodity information web site to provide users with too much, cause it is difficult to quickly find needed goods, so a user could get tired until losing interest in shopping and leave. Th ee-commerce sites is facing a serious problem: How the user browsing the web site will be suitable f or the users of the goods to him or her, to overcome the adverse effects of information overload, ther eby contributing to more deals in order to increase enterprise sales. At present, information retrieval, association rules, based on the content filtering, and collaborative filtering has been widely used in t he electronic commerce recommendation system. The four kinds of technologies have achieved a ce rtain degree of user oriented personalized recommendation, but it also has some deficiencies. In this context, recommendation system came into being which is according to the user's interests, recomme nd in line with the object of user interests, also known as the personalized recommendation system.

According to the characteristics of the recommended object, at present there are two main types of recommendation system, an object is recommended Web search system, mainly USES the metho d and technology of Web data mining, for users to recommend conforms to the interests of Web pag e, such as Google, etc. Another is online shopping environment for recommended products personal ized recommendation system, referring users to conform to the interests of commodities, such as boo ks, audio and video, etc. Says the recommend system for e-commerce personalized recommender sy stems, hereinafter referred to as e-commerce recommendation system[2].

2 Introduction to e-commerce recommendation system

In this research, we considered only content-based, collaborative filtering, and hybrid approaches that can be implemented by automatic techniques(but not knowledge engineering). By choosing different types of links to use in a recommendation generation process, content-based, collaborative, and

hybrid approaches can be performed using our model. If only product information is used, which means only links in the product layer are activated, it is a content-based approach. If customer-layer and interlayer links are activated, it is a collaborative approach. If all links are activated, it becomes a hybrid approach. The model is flexible because different combinations of links can be activated at run time. For example, we can choose to use product description and price to form product similarity, use demographic data to form customer similarity, and use customers' ratings and purchase history to form interlayer links. The representation can even be personalized for each customer by using a customized weighting scheme. For example, if a customer relies more on the collaborative recommendation, we can assign higher weights to interlayer links and customer-layer links. If the customer is more price-driven, we can assign higher weights to the price information of the product when computing the similarity between products [3].

Recommendation Methods for the Graph Model

Different recommendation methods can be developed based on our model. By viewing the recommendation process as a graph search, we use our model to generate recommendations by finding nodes that have high associations with the starting nodes. Many recommendation methods can be developed based on this graph view. We developed three recommendation methods that covered a wide range of methods being used in the field. For each method, we also describe how collaborative, content-based, and hybrid recommendation approaches can be performed. The direct retrieval method generates recommendations by retrieving products similar to the target customer's previous purchases and products purchased by customers similar to the target customer. It covers most of the recommendation methods that form neighborhoods of customers or products. For content-based recommendation, products that are similar to the target customer's previous purchases are retrieved as recommendations. This situation is similar to document retrieval, in which documents similar to the input queries are retrieved. For collaborative recommendation, a list of customers similar to the target customer is first obtained. Then, similarities can be traced through customer-layer links or through interlayer links from the target customer's previous purchases. In other words, similar customers are those who are demographically similar to the target customer or those who bought the same books as the target customer. The products that are linked to this set of similar customers are retrieved as the collaborative recommendation for the target customer. The hybrid recommendation is obtained by combining the recommendation results from the two approaches described above as shown in Fig1

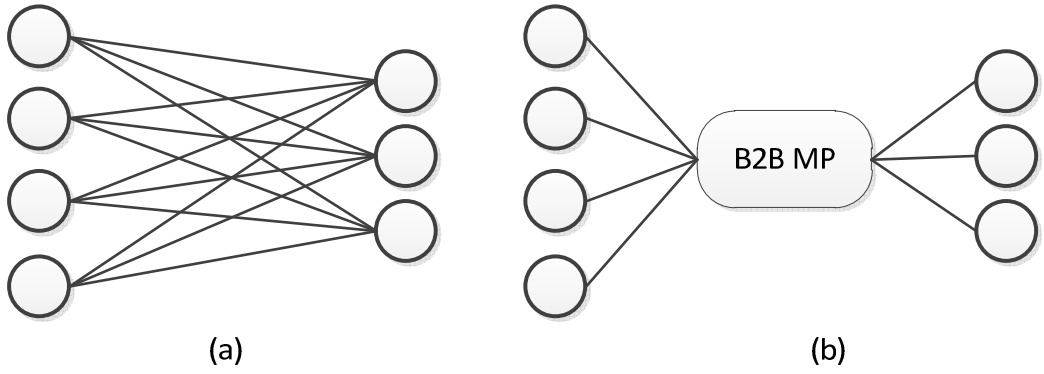

Fig .1 Recommendation system

Recommendation technology

(1)Content- based recommendation It is the continuation and development of the information filtering technology, features related to the project or object by attribute to define. System based on the characteristics of the evaluation objects to learn the user's interest, and to predict the degree of match project according to the user data to recommend, such as newsgroups filtration system[4].

(2)Demographic based recommendation Recommendation system based on users' personal attributes to the user classification, based on class again to recommend classes of users, users are not required to have a history data, and the collaborative filtering and content-based recommendation technology needs to be.
(3) Utility- based recommendation It is calculated according to the utility of users to use the project, the core problem is how to create the utility function for each user, and consider the product attributes, such as providers of reliability and availability of the product and so on.
(4)Know ledge- based recommendation To some extent may be regarded as a kind of reasoning technology, the method has the obvious difference due to different knowledge used in.
(5)Association rule based recommendation Based on association rules, already bought goods as the rules header, recommend object as rules. The association rules are the bottleneck of the algorithm, which are found the key and most time consuming. But can be done offline, name of commodity synonymity problem is also a difficulty of association rules.
(6)Content-based filtering Content-based filtering have many similarities in terms of technology and information retrieval, the difference is that it meets the user's information needs for a long time. Based on content filter for each user to establish a user description , record the contents of the user's likes and dislikes. Then comparing with the content of the project(such as goods, Web page, movies, music, etc.)The similarity of higher project recommended to the user, thus improve the scalability of recommend, and can better explain the recommendation results. Users can describe through the system to the user likes to machine learning to get the content of the project, or by the user's query, questionnaire feedback, etc. Based on the content filtering system such as LIBRA [5].
(7)Collaborative filtering recommendation Collaborative filtering recommendation is one of the most studied the personalized recommendation technology, it based on the recommendations from the neighbor user data to get the target users, recommended by the high degree of personalized collaborative filtering is based on the content to overcome the disadvantages of filters, such as Gold - berg is called collaborative filtering is proposed. The working mechanisms of content-based filtering and collaborative filtering is shown in figure 1.Collaborative filtering according to the target users with similar interests and preferences of other users of certain information to determine whether the information on the target user value, and then decide whether to recommend this information to target users, so as to relieve the information overload. The advantage of the collaborative filtering is to do not need to consider the recommended content of the project, so will not only filter object expanded to all types of resources, and realize the novelty is recommended. To be widely used in the electronic commerce recommendation systems, one of the most successful recommendation algorithm[6].

Recommendation Comments

Recommendation is also recommended, an important problem in the field of overall recommendation can have two kinds of methods: One is the on-line evaluation, another is the line evaluation. Online evaluation is online survey the user evaluation of recommendation system. K.Sw earing enthe recommendation system of evaluation and to recommend your friends compared the experimental results show that the friend's recommendation is often better than recommended recommendation system, recommendation system gives recommendations than friends recommended updates, and identify the key factors for several of the recommended design. Offline evaluation with a set of known data to evaluate the performance of the recommendation system, now generally adopt the digital equipment corporation system research center to provide a special experiment database, the library is a collection of 1996 ~ 2013, a total of 72916 users to 1628 films of 245667618 projects value assessment information, and evaluation analysis using discrete (0, 2, 4, 6, 8, 10),which can be downloaded from the company. Measure generally USES predictive value and the actual and estimated values of the average absolute error, Top - N recommend quality measure generally USES the standard, the evaluation system of information retrieval with accuracy, precision and recall rate (recall), measured accuracy and recall rate to a certain extent, is a pair of contradictory indicators, relatively high accuracy low recall rate. In order to balance the two, usually adopts the comprehensive evaluation index F- measure, in order to control the accuracy and recall rate of preference, E -

measurer index is introduced. A typical experiment database offline Each Movie evaluate all recommendation algorithm is not necessarily correct, especially when considering the date and time, use offline evaluation is not very good for starting from customer satisfaction to evaluate the efficacy of the recommendation.

3 Conclusion

Recommender systems have been applied in different applications to deal with product information overload and to help locate useful information. Their data representations usually are tailored for their specific problems and hence are not flexible enough for use in other applications. In this article, we have described a generic graph model for product recommendation. Customers, products, and transactions were modeled in an extended two-layer graph. To demonstrate the comprehensiveness and flexibility of this model, we experimented with three methods (direct retrieval, association mining, high-degree association retrieval) of making recommendations using three approaches (content-based, collaborative, hybrid). Evaluation results showed that a hybrid recommendation approach achieved better performance than the collaborative approach or the content-based approach. However, the high-degree association method did not perform significantly better than the association mining method or the direct retrieval method because of the high density of the data set we used. We believe that our model is flexible because it can represent different combinations of product, customer, and transaction information and it has the potential to accommodate many graph search techniques for making recommendations. To further validate the current experimental results, we will extend the evaluation study to include frequently used recommendation data sets and directly compare our proposed graph-model-based approaches with approaches employed in previous studies.Other future work includes the use of other graph search algorithms as well as other data mining techniques, the use of a sparse data set to further test the strength of the high-degree association retrieval method and a completesubject evaluation on the usability of our system.

References

[1] MICHAEL O, NEIL H, NICHOLAS K, et al. Collaborative recommendation: a robustness analy sis [A] . ACM Transactions on Internet Technology, Special Issue of Machine Learning for the Inter net [C].2002.

[2]ADOMAVICIUS G, T UZHILIN A. Extending recommender systems: a multidimensional appro ach [A] . Proceedings of the Fifth ACM Conference on Digital Libraries [C].2001. 115 -123.

[3]RAYID G, ANDRES F. Building recommender systems using a knowledge based of product sem antics [R] . Chicago: Accenture Technology Labs, 2001.

[4] Soto-A costa P, A L. Analyzing e-business value creation from a resource-based perspective[J]. International Journal o f Information Management, 2008, 28(1): 49- 60.

[5]MalhotraA, Gosain S, E Saw O A. Absorptive capacity con figurations in supply cha ins: Gear in g for partner-enabled market know ledge creation[J]. M IS Quarterly, 2005, 29(1): 145- 187.

[6] Chae B S, Yen H J R, Sheu C. Information technology and supply cha in collaboration:Moderati ng effects of existing relationships between partners[J]. IEEE Transactions on Engineering Manage ment, 2005, 52(4): 440- 448.

Advanced Materials Research Vols. 989-994 (2014) pp 5000-5003
© (2014) Trans Tech Publications, Switzerland
doi:10.4028/www.scientific.net/AMR.989-994.5000

Research of the Issues based on Trusted Cloud Security

Huang Yi[1,2,3,a] , Ma Xinqiang[1,2,b], Liu Youyuan[1]and Li Danning[2,c*]

[1] Key Laboratory of Machine Vision and Intelligent Information System, Chongqing University of Arts and Sciences, Chongqing, 402160, P.R China

[2]Guizhou Academy of Science, Guiyang 550001, P.R China

[3]School of Computer Science and Technology, Guizhou University, Guiyang 550025, P.R China

[a]cqhy@21cn.com, *Corresponding author: [c] lidn121@hotmail.com, [b]mxq345@sohu.com

Keywords: Cloud Security; Access Control; Information Security; Trusted Computing Platforms

Abstract. Cloud computing represents one of the most significant shifts in information technology many of us are likely to see in our lifetimes. It offers an innovative business model for organizations to adopt IT services without upfront investment. Cloud computing moves the application software and databases to large data centers, where the management of the data and services may not be fully trustworthy. Security is one of the major issues which hamper the growth of cloud. The security for cloud computing is emerging area for study and this paper provide technical components of cloud computing and security idea in terms of cloud computing based on analysis of cloud security treats.

Introduction

According to the NIST definition, key characteristics of cloud computing include on-demand self service, broad network access, resource pooling, rapid elasticity, and metered service similar to a utility [1]. There are also three main service models—software as a service (SaaS), in which the cloud user controls only application configurations; platform as a service (PaaS), in which the cloud user also controls the hosting environments; and infrastructure as a service (IaaS), in which the cloud user controls everything except the datacenter infrastructure. Amazon EC2 is a well known example of IaaS, Google App engine is an example of PaaS and salesforce.com is an example of SaaS. Further, there are four main deployment models: public clouds, accessible to the general public or a large industry group; community clouds, serving several organizations; private clouds, limited to a single organization; and hybrid clouds, a mix of the others.

It extends Information Technology's (IT) existing capabilities. In the last few years, cloud computing has grown from being a promising business concept to one of the fast growing segments of the IT industry. But as more and more information on individuals and companies are placed in the cloud, concerns are beginning to grow about just how safe an environment it is. Security issues in cloud computing has played a major role in slowing down its acceptance, in fact security ranked first as the greatest challenge issue of cloud computing. After several years of focusing on cloud as a delivery model for their solutions, security vendor strategists are finally turning their attention to securing broader IT application and data workloads as these migrate from corporate data centers into managed cloud services. This shift, from security in the cloud to security of the cloud, marks the beginning of a significant and sustained transformation for the IT security market. This work is a survey more specific to the different security issues and the associated challenges that has emanated in the cloud computing system [2].Cloud security is a complex issue, involving the different levels of the cloud, external and internal threats, and responsibilities that are divided between the user, the provider and even a third party. This paper provides technical components of cloud computing and security idea in terms of cloud computing based on analysis of cloud security controls and threats. In the same time, it proposes a trusted cloud computing platform (TCCP) for ensuring the confidentiality and integrity of computations that are outsourced to IaaS services.

Components of Cloud Computing

As shown in the Fig. 1, key functions of a cloud management system is divided into four layers, respectively the Resources and Network Layer, Services Layer, Access Layer, and User Layer. Each layer includes a set of functions [3]:

1. The Resources and Network Layer manages the physical and virtual resources.
2. The Services Layer includes the main categories of cloud services, namely, NaaS, IaaS, PaaS, SaaS/CaaS, the service orchestration function and the cloud operational function.
3. The Access Layer includes API termination function, and Inter-Cloud peering and federation function.
4. The User Layer includes End-user function, Partner function and Administration function.

Other functions like Management, Security and Privacy, etc. are considered as cross-layer functions that covers all the layers. The main principle of this architecture is that all these layers are supposed to be optional. This means that a cloud provider who wants to use the reference architecture may select and implement only a subset of these layers. However, from the security perspective, the principal of separation requires each layer to take charge of certain responsibilities. In event the security controls of one layer are by passed (e.g. access layer), other security functions could compensate and thus should be implemented either in other layers or as cross-layer functions.

Cloud Security Controls and Threats

Security threats on cloud users are both external and internal. Many of the external threats are similar to the threats that large data centers have already faced. This security concern responsibility is divided among the cloud users, the cloud vendors and the third party vendor involved in ensuring secure sensitive software or configurations. Cloud security architecture is effective only if the correct defensive implementations are in place. Efficient cloud security architecture should recognize the issues that will arise with security management. The security management addresses these issues with security controls. These controls are put in place to safeguard any weaknesses in the system and reduce the effect of an attack. While there are many types of controls behind cloud security architecture, they can usually be found in one of the following categories [4]: **Deterrent controls**: These controls are set in place to prevent any purposeful attack on a cloud system. Much like a warning sign on a fence or a property, these controls do not reduce the actual vulnerability of a system. **Preventative controls**: These controls upgrade the strength of the system by managing the vulnerabilities. The preventative control will safeguard vulnerabilities of the system. If an attack were to occur, the preventative controls are in place to cover the attack and reduce the damage and violation to the system's security. **Corrective controls**: Corrective controls are used to reduce the effect of an attack. Unlike the preventative controls, the corrective controls take action as an attack is occurring. **Detective controls**: Detective controls are used to detect any attacks that may be occurring to the system. In the event of an attack, the detective control will signal the preventative or corrective controls to address the issue.

Threats for Cloud Computing Users are as follows[5]: first generation biosensor, loss of governance, loss of trust, service provider lock-in, unsecured cloud service user access, lack of information/asset management, data loss and leakage. Threats for cloud service providers are as follows[5]:responsibility ambiguity, protection inconsistency, evolutional risks, business discontinuity, supplier lock-in, license risks, bylaw conflict, bad integration, unsecured administration API, shared environment, hyper visor isolation failure, service unavailability, data unreliability, abuse right of cloud service provider.

Cloud Security and Privacy

Identity management: every enterprise will have its own identity management system to control access to information and computing resources. Cloud providers either integrate the customer’s

identity management system into their own infrastructure, using federation or SSO technology, or provide an identity management solution of their own. **Physical and personnel security**: Providers ensure that physical machines are adequately secure and that access to these machines as well as all relevant customer data is not only restricted but that access is documented. **Availability**: Cloud providers assure customers that they will have regular and predictable access to their data and applications. **Application security**: Cloud providers ensure that applications available as a service via the cloud are secure by implementing testing and acceptance procedures for outsourced or packaged application code. It also requires application security measures are in place in the production environment. **Privacy**: Finally, providers ensure that all critical data (credit card numbers, for example) are masked or encrypted (even better) and that only authorized users have access to data in its entirety. Moreover, digital identities and credentials must be protected as should any data that the provider collects or produces about customer activity in the cloud. **Legal issues**: In addition, providers and customers must consider legal issues, such as Contracts and E-Discovery, and the related laws, which may vary by country.

Trusted Computing Platforms

Traditional trusted computing platforms like Terra take a compelling approach to this problem [5]. For example, Terra is able to prevent the owner of a physical host from inspecting and interfering with a computation. Terra also provides a remote attestation capability that enables a remote party to determine upfront whether the host can securely run the computation. This mechanism reliably detects whether or not the host is running a platform implementation that the remote party trusts. These platforms can effectively secure a virtual machines (VM) running in a single host. However, many providers run data centers comprising several hundreds of machines, and a customer's VM can be dynamically scheduled to run on any one of them. This complexity and the opaqueness of the provider backend create vulnerabilities that traditional trusted platforms cannot address.

The Trusted Computing Group (TCG) [6] proposed a set of hardware and software technologies to enable the construction of trusted platforms. In particular, the TCG proposed a standard for the design of the trusted platform module (TPM) chip that is now bundled with commodity hardware. The TPM contains an endorsement private key (EK) that uniquely identifies the TPM (thus, the physical host), and some cryptographic functions that cannot be modified. The respective manufacturers sign the corresponding public key to guarantee the correctness of the chip and validity of the key.

In a computer and service systems, access is a specific type of interaction between a subject and an object that results in the flow of information from one to the other. Exactly what the subject does when it accesses the object is further defined by introducing access modes such as read, read-write, write, and execute. Access control deals with the limits on the interactions between subjects and objects [7].

Trusted Cloud Computing Platform

We present the trusted cloud computing platform (TCCP) that provides a closed box execution environment by extending the concept of trusted platform to an entire IaaS backend. The TCCP guarantees the confidentiality and the integrity of a user's VM, and allows a user to determine up front whether or not the IaaS enforces these properties. TCCP enhances today's IaaS backbends to enable closed box semantics without substantially changing the architecture as shown in Fig. 2. The components of the trusted cloud computing platform include a set of trusted nodes (N) and the trusted coordinator (TC). The untrusted cloud manager (CM) makes a set of services available to users. The TC is maintained by an external trusted entity (ETE). The trusted computing base of the TCCP includes two components: a trusted virtual machine monitor (TVMM), and a trusted coordinator (TC). The TCCP must guarantee that the node's configuration remains trusted; otherwise the node could compromise the security of the TCCP.

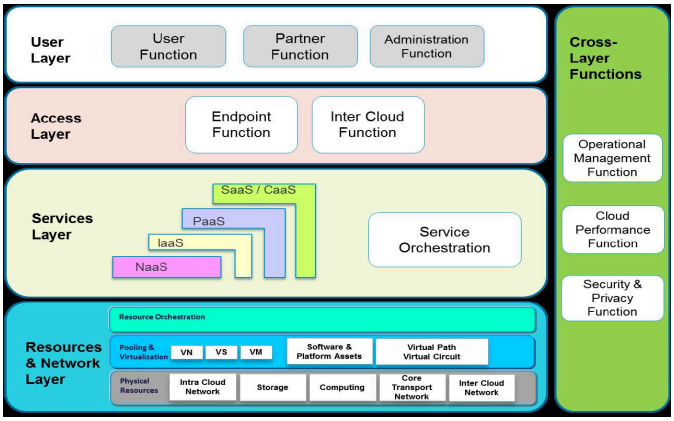

Fig. 1 Key functions of a cloud management system

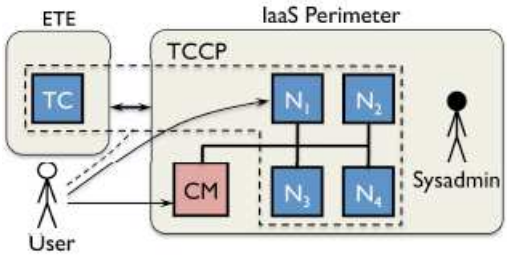

Fig. 2 Changing the architecture of TCCP

Conclusions

In this paper, we argue that concerns about technical components of cloud computing and security idea in terms of cloud computing based on analysis of cloud security controls and threats. In the same time, it proposes a trusted cloud computing platform (TCCP) for ensuring the confidentiality and integrity of computations that are outsourced to IaaS services. We plan to implement a fully functional prototype based on TCCP design and evaluate its performance in the near future.

Acknowledgments

This work is supported by the Science and Technology Foundation of Guizhou Province (20112205, 20122185) and the Natural Science Foundation Project of CQ CSTC (cstc2013jcyjA40053) and the Scientific and Technological Research Program of Chongqing Municipal Education Commission (KJ121219, KJ131218, and KJ111217) and the Natural Science Foundation Project of Ycstc (2013nb8001, 2013ad2002, and 2011AD2001).

References

[1] P. Mell and T. Grance. NIST definition of cloud computing. National Institute of Standards and Technology. October 7, (2009).

[2] Kuyoro S. O., Ibikunle F. , and Awodele O. Cloud Computing Security Issues and Challenges, International Journal of Computer Networks, Volume (3) : Issue (5) : (2011) : p. 247-255.

[3] Rahul Bhatnagar, Suyash Raizada, and Pramod Saxena. Security in Cloud Computing, International Journal for Technological Research in Engineering, Volume 1, Issue 4, December (2013): p. 2347-4718.

[4] Krutz, Ronald L., and Russell Dean Vines. "Cloud Computing Security Architecture." Cloud Security: A Comprehensive Guide to Secure Cloud Computing. Indianapolis, IN: Wiley, 2010. 179-80.

[5] T. Garfinkel, B. Pfaff, J. Chow, M. Rosenblum, and D. Boneh. Terra: A Virtual Machine-Based Platform for Trusted Computing. In Proc. of SOSP'03, (2003).

[6] TCG. https://www.trustedcomputinggroup.org, (2014).

[7] Yi. Huang and Xinqiang Ma. An access control model based on Trusted Computing (In Chinese), Journal of Chongqing University of Arts and Sciences, (2010), 29(3): p. 54-57.

[8] Nuno Santos, Krishna P. Gummadi, and Rodrigo Rodrigues, Towards Trusted Cloud Computing, MPI-SWS, (2013).

Advanced Materials Research Vols. 989-994 (2014) pp 5004-5006
© (2014) Trans Tech Publications, Switzerland
doi:10.4028/www.scientific.net/AMR.989-994.5004

The Application based on the Internet of Things and Cloud Computing

Liao Zineng[a], Hu Yanrong[b]

Wuhan Bioengineering Institute, Hubei Wuhan China

[a]36955655@qq.com, [b]391640622@qq.com

Keywords：Internet of Things;RFID; Cloud Computing

Abstract. With the rapid development of information technology and network technology， especially the RFID technology, the development of internet of things has been greatly promoted. Meanwhile, the integration of the technology of internet of things and the Cloud Computing products the increasing number of information goods based on the RFID technology. This paper mainly expounds the application of the integration of the technology of internet of things and the Cloud Computing by analysing bar code which are extensively applied in the RFID technology, and interprets the application research of orientation tracing, remote control and information security products based on the RFID technology.

Internet of Things

Since the concept of Internet of Things was proposed in 1999, it has been gotten more and more attention, which was called the third wave of the world information industry after the computer, internet. Recently, with the constantly improvement and widely application of the core technologies, such as RFID, sensor technology, global standard of Internet of Things, the Internet of Things has been a hot topic that was gotten board attention at home and abroad.

The concept of "networking" was developed on the basis of the concept of "internet", it extends and expands its client to the between of any goods, which is the concept of network of conducting information exchange and communication, and it could also be named "internet of goods attached". Specifically speaking, Internet of things refers to as IOF, which is the network that through the sensing equipment information, such as radio frequency identification (RFID) device, infrared sensors, global positioning system, laser scanner, according to the agreement, it connects any goods and Internet, conducting exchange of information and communication, in order to realize intelligent identification, location, tracking and monitoring and management. Its purpose is to let all goods can remote perception and control, and combine with internet to a more wisdom production system of life.

The concept of "Internet of Things" evolves continuously, which named from "the wisdom of earth" of American to "the perception of China" of China, M2M is the specific pattern that the internet of things are using now. M2M represents the connection and communication of Machine to Machine, Man to Machine, Machine to Man, Mobile to Machine, which covers the technologies and methods that realized among all the people, Machine, systems' communication connection.

The blockage of the network development

With the internet of things gradually applied, its unprecedented function are slowly thorough popular feeling, everybody was very forward with a change of meaning that the arrival of the era of internet of things. But, as a new product, the road of internet of things will be difficult and long, currently ,we are facing the five big bottleneck .

A. the industry standard is lacking

This is the biggest constraining bottleneck. At present, the development of internet of things in all countries is different, countries all over the world have different standards, and mutual compatibility. Different industry related technology and product also have each difference, the uniform standard won't achieve real interworking.

B. Security problems

Security is the most pressing of the internet of things, which will greatly influence the development and application of this technology. The sensing technology content networking is mainly RFID,implant the chip, the products, could be perceived by anybody, it can be convenient to carry on the management by this system. But it also has a huge problem, other people are able to perceive, so how to do in perception, transmission, application process, these valuable information can be adopted by us, but not used by others. This needs the safety fluctuation and formed a strong security system. Now, what should be said that security problems, how to deal with these problems, how to screen is some very complex problems, even is not clear.

C. Unified agreement

The internet of things is the extension of the Internet thing, the former's core level based on TCP/IP protocol, it would also involve various types of agreement, GPRS/CDMA, text messaging, sensors, cable, etc channels, The internet of things need a uniform protocol stack.

D. Expansion and compatible with IP address problems

To ensure that each item in the content can be looking for to, networking must assigne a unique address to everyone. Because of the internet of things related to hundreds of thousands of items, so many things to the IP address of the network, it will lead to the current use of IPv4 resource exhaustion, it needs the support for IPv6. Transition form IPv4 to IPv6 is a long process, so the internet of things once use IPv6 address, which will inevitable result of the compatibility issue of existence and IPv4.

E. The ecological system (Eco-system)

Stability problem ,for the internet of things, it needs many fields, such as hardware with the coordination, firmware, software, (firmware) interface, etc. This is a big industry chain, only put a complete set up the ecological system, the internet of things can truly networking the sustainable development.

The strategies of the development of the Logistics Network

The development of the Logistics Network is still in the primary stage in the whole world, which will face variety problems. How to promote the development the Logistics Network ? How to solve the problem in the course of the development, due to the cooperation of the whole world. In my opinion, we can start with following invention at present.

A. Establish the standard system

The standard is the unified specification to any technology, the whole industry and the market will become confusion if there is no unified standard, the users can not choose and apply in more situations. The development of the Logistics Network is still in the primary stage in the world, there are no uniform standards, and the missing of the standard will restrict the development greatly. The basic problem which will be solved in the primary stage is to reinforce the international cooperation, draw up the related international standard.

B．Breakthrough the core technology of the sovereign intellectual property rights

The core technology of the sovereign intellectual property rights are the fundamental driving force of the sustainable development of the Logistics Network. As the emerging technologies of the national strategy, it will face more and more problems in the future development in the international competition, if we have no crucial core technology. Therefore, the most important in the development of the Logistics Network is to establish national and area research center, and then, grasp the core technology of the sovereign intellectual property rights.

C．Formulate the active and feasible policies

The Logistics Network is the strategic and emerging technology, which play more and more important role in the national strategy and sustainable development. According to the different characteristics of the application, the country consort to offer the dedicated or shared frequency resources. The country also provide related preferential policy in the industry of the Logistics Network, which similar to the software industry, IC industry. The administration, the production sector, the teaching institutions and the research institute should be responsible for the affairs which belongs to themselves, and committed to the cultivate demand, applied research and core technology research, carry out standard strategy and promote the industrial distribution, in order to promote the form and the development of the Logistics Network industry chain.

D．Actively coordination and cooperation among authorities in different area

The application area of the Logistics Network is very wide, there is so much overlapping in many industries, which belongs to different government function department. In order to guarantee the smooth development of the Logistics Network effectively, we should strengthen the coordination and cooperation in the course of the industry. For example: strengthen the cooperation of the radio and TV, telecommunications and the traffic, in order to establish the information and intelligent traffic system.

E．Take precedence the major special industry in the implement application area

We also have to establish some major application special to promote the development of the Logistics Network industry, promote the key technology research and application demonstration, according to the industry development mode that experimental partly and focus on demonstration, to promote the sustained orderly development in the whole industry.

The prospect of the Logistics Network is very optimistic, the value of the Logistics Network was forecasted to as 30 times as the internet. Though, the development of the Logistics Network will face many resistances, which need verities support from the government, the enterprise, the association of the industry , the media ,even the public, only in this way we can realize a new and transformational period.

References

[1] The Internet of Things[EB/OL].<http://www.itu.int,2009-9-6.>
[2] Internet of Things in 2020:Roadmap for the future[EB/OL].<http://ec.europa.eu/,2009-11-16.>
[3] U-Japan Policy[EB/OL].<http://www.soumu.go.jp,2009-10-22.>
[4] U IT.ITU Internet Reports 2005:The Internet of Things[R].2005
[5] Floerkemeier C，Langheinrich M，Fleisch E，Mattern F，Sarma SE.2008.The Internet of Things.Berlin：Heidelberg.p378.
[6] Weber R H.Internet of things New security and privacy chal-lenges.Computer Law&Securety Review，2010，26(1):23 30.

Advanced Materials Research Vols. 989-994 (2014) pp 5007-5009
© (2014) Trans Tech Publications, Switzerland
doi:10.4028/www.scientific.net/AMR.989-994.5007

Research on the security of the digital learning resources library based on cloud storage

Hui Cao

Henan Radio and Television University, Zhengzhou 450008, China

402793927@qq.com

Keywords: cloud storage, digital learning resources library, cloud system, hidden danger, safe storage.

Abstract. This paper mainly analysis the hidden dangers exist in the process of the construction and application of cloud system, and presents new strategies of safe storage for the digital learning resources library based on cloud storage to realize the protection of data transition and storage.

Introduction

The digital learning resources library based on cloud storage is a cloud system, that is used to solve the Integration, integration and sharing of the lifelong learning resources which is distributed, heterogeneous, massive and multi mode; and that offers the public services of digital learning resources. The digital learning resources library based on cloud storage is the specific application of storage management of the digital learning resources, through the cluster applications, grid technology and distributed file system and other functions, this system adapts the application software to organize the devices, that are distributed in different regions of the network and in a large variety of different types, to load balancing and work together to offer data storage and business visits for the users of the digital learning resources library.

With the increase in the number of users of cloud storage, the data storied in cloud increase, whether these data are security has become a hot issue. These years, data leakage incidents occurred frequently, for example, in 2009, 30000 customers' credit cards information of Japanese life-insurance company Aliko leaked[1]; in 2011, 6000000 users' information of the largest programmer community in China were stolen[2]; in 2013, the secrete file about American National Security Agency (NSA) stole data was exposed[3]. These events indicate that the data is lack of strict protection and the systems still exist security flaws in the network world.

Whether the cloud storage services how powerful, the cloud storage can solve the security problem is always the determining element of the cloud storage life. Only the safe cloud storage can stimulate the user enthusiasm. Therefore, cloud storage security must get people's attention. This paper mainly analysis the hidden dangers exist in the process of the construction and application of cloud system, and presents new strategies of safe storage for the digital learning resources library based on cloud storage to realize the protection of data transition and storage.

The hidden danger of the digital learning resources library based on cloud storage

User access control: User access control is mainly refers to the identity authentication. Rapid and effective user authentication determines the safety and efficiency of cloud service. The system should realize single sign on, Strengthen the identity authentication system, take a unified way to authenticate users of different levels, the users can have a unique identity authentication to access system data to ensure legal users accessing safe and reliable data at any time.

Data transmission security: The system data story in the cloud, data management and maintenance is carried out through the network. The Internet environment is very complex, the system data face the hacker's attack at any time and have the risk of interception. If the data is not encrypted or the encrypted data are easy to crack, the accident of Leakage of

information, data destruction and service interruption will happen. To protect the data cloud storage system security must enhance the password technology and platform reinforcement technology so that ensure the integrity of the system and identity authentication based on PKI, as well as the security server.

Storage virtualization: The most popular understanding of the storage virtualization technology is the abstract expression on storage hardware resources. They provide comprehensive and useful function service uniformity through integrating one (or more) target service or function with other additional functions. Typical virtualization includes the following situations: shield the complexity of system, increase or integrate new functions, simulate, integrate or disintegrate available service etc. Virtualization is in one or more entities and these entities are used to provide storage resources or other services. Users do not have to care about their data through which path to which a specific storage device.[4] Storage virtualization contribute to improve the storage efficiency and reduce the storage cost, at the same time, bring some security risks. Since the physical location of data storage can not be clearly defined, the difficulty of protection measures about data storage increases. The system have to adapt effective strategies of spatial separation and effective division of physical storage space to ensure the security of user data and data switching and transmission security between the virtual platforms.

Data audit: Data audit can record real time data activities on the network, manage data operation with fine grained auditing, give an alarm of the risk data suffer from and block attacks. Through recoding, analyzing and reporting behaviors that users visit database, it helps users to produce compliance report, trace accident, enhance recording network behavior of Internal and external database, improve data assets security.[5]

Cloud service provider: The digital learning resources library based on cloud storage to be deployed on a commercial cloud, must choose a cloud service provider. How to ensure data security of infrastructure, the key application and sensitive data, it is important to choose the cloud service provider. Cloud service providers must have the technical strength to ensure the security of data, and provide third party audit to prove that they have this ability.

Countermeasures of safe hidden danger of the digital learning resources library based on cloud storage

Strengthen the management and monitoring: The digital learning resources library based on cloud storage must strengthen the monitoring capacity of user access behavior, take authority verification and control measures to monitor and limit users' behavior and permissions. Measures to protect the resource base for the core data can be from two aspects, one is to adopt the perfect encryption algorithm to encrypt core data, on the other hand is that the core data is arranged in the private cloud and the non sensitive data is arranged in a public cloud. The resource base needs to detect and protect base threat from the client, adopts monitoring technology to guard against unknown threats. When the suspicious flow appears, cloud monitoring center will analyze data by the powerful computation ability and send the analysis results to all the clients and security gateway to improve the control ability of the resource base for security threats.

Enhance the robustness of the system: The system adopts advanced password technology to realize security encryption of data. During the transfer, the data can not be decrypted even if stolen. Through the reinforcement on the server, operating system, database and application system, timely patch the application and system, reduce the number of vulnerabilities, ensure the security of the server and programs and prevent illegal tampering.

Safety measures based on virtual technology: System memory safety includes the authentication service, data encryption storage, safety management, safety log and audit. According to the identity of the user, the system grants different levels of permissions. The user can only operate on the authorization data so as to protect users' private data and space. When the resource library and other application sharing server, the system should ensure users of different applications have separated operating system and application software, isolate storage data fully in logic and realize resource database communication security during virtual machine system, software and platform to ensure the security of data switching, data transmission, data synchronization between multiple virtual platforms.[6]

Data backup strategy: The system adopts cloud backup service to storage data remotely. The data will be stored on the local and cloud after data backup. The clouds can be one or more private data center or a virtual data center. Local backup save recent data and the clouds storage all data. Local backup can be used to quickly restore data to the nearest backup node. Backup data in cloud is used to recovery data to prior backup node, that can be used for disaster recovery scenarios or restore data to a different site.

Conclusion

With the construction and application continually deepening and expanding, the safety issues of operation, maintenance and customer service of resource database will be more prominent. The system should be analyzed comprehensively for system security threats in design phase and use advanced security technology, not only that, but also follow the latest development in security field continually to make sure the system can respond to network environment varied from minute to minute.

References

[1] K. Hu: *Security and confidentiality of data in the cloud* (China, 2012).
[2] Information on http://www.d1net.com/cloud/security/84577.html.
[3] Information on http://sec.chinabyte.com/127/12828127.shtml.
[4] Information on http://baike.baidu.com/link?url= 5nJIW2QNZS2v1CCVkp2EoI4feHi_6ZaPwS_ dKLEe4kD2MZdt6WVibxQjzxHNesSr.
[5] Information on http://baike.baidu.com/link?url=0gW3JLjhcS36TM_qcvBgHxPjj0XquoQJ KxiL rSP9lGs5pe9ZbwjYpjiydbA6jT_ QCDl8B3EK92YA09URuUqWD_.
[6] W. Jin: *Research on construction and data security and backup scheme of university library storage system* (China, 2009)

Advanced Materials Research Vols. 989-994 (2014) pp 5010-5013
© (2014) Trans Tech Publications, Switzerland
doi:10.4028/www.scientific.net/AMR.989-994.5010

Coaches Ranking: a Time-irrelevant Data Mining Solution with Flexibility and Objectivity

Yongyu Chen[1, a], Mengjiao Zhang[2], Zhou Shen[3, b], Jianxin Chen[4, c]

[1]Department of Telecommunication and Information Engineering, NJUPT, Nanjing 210003, China

[2]Department of Automation, NJUPT, Nanjing 210046, China

[3]Video Engineer of Department of Technology, JSBC, Nanjing 210000, China

[4]Department of Telecommunication and Information Engineering, NJUPT, Nanjing 210003, China

[a]13010634@njupt.edu.cn, [b]jsxssz@163.com, [c]chenjx@njupt.edu.cn

Key words: Data mining; AHP; Elo rating system

Abstract. The ranking of coaches is of great significance for sports teams to find talented coaches. Traditional ranking mechanism is relatively subjective which is usually accomplished by voting. In this paper, we establish a ranking mechanism based on both subjective and objective factors. We use data mining method to classify and analyze the data. The regression tree and the decision tree (CART) are used to narrow down the number of coaches to a reasonable scale. We put forward our AHP model to rank the "candidates" and propose a coach rating analysis system (CRAS) for evaluating the accuracy of system. We verify our ranking system more comprehensive in terms of the evaluation of the coaches through analyzing the result. The proposed mechanism is also significant to find potential coaches.

Introduction

The ranking of coaches is of great significance for sports teams to find talented coaches. The traditional ranking mechanism is relatively subjective and it is usually accomplished by voting, therefore sometimes the result is not that convincing. According to the final goal of coaches ranking, we collect the related data on the internet [1, 2] and use them to improve the objectivity. To find out the top 5 coaches we firstly use data mining [3] (the analysis step of the "Knowledge Discovery and Data Mining" process, or KDD) methods to classify and analyze the data. Then we introduce CART [4] to narrow down the number of the candidates according to the features we have. After the filtering we change the evaluation features to accomplish further ranking. The reasonability of every chosen feature is verified by the correlation coefficient analysis [3] on SPSS. After the analysis we found the relative features for the AHP model [5] we build to find out the result that suits our goal of coaches ranking best [6]. Then we introduce Elo rating system [7], which is a method for calculating the relative skill levels of players, and propose our CRAS model to achieve our ranking goal. Finally we analyze the result and find out our ranking mechanism as time-irrelevant with flexibility and objectivity. It can be applied into other fields such as qualitative comparison or other related fields.

Problem formulation

Suppose our goal is to find out the top 5 college coaches in the last century and we take the sport of American football as an example. Then we should collect the data we need and analyze it. We have thousands of candidates, therefore it is reasonable to narrow down the range to a reasonable scale [8].

In this section data filtering model is mainly designed according to the ideology of CART. We use this model to process data, which can be divided into two major phases[9]:

Phase1: Primary filtering. According to the ideology of recursively dividing the independent features' space. We use the median of *OG*, *NC* and the mean value of *OP*, *SRS* one by one to narrow down the range of the candidates to a reasonable scale of 3%-5%.

Phase2: Limited filtering. According to the ideology of cutting the data with the validation features, we choose the top 5 candidates according to *OG*, *OP*, *NC* and *SRS* respectively and then collect them together. It is reasonable that if there is no feature ranking top 5(Suppose our goal is to acquire the top 5 coaches), then the candidate have no reason to stay in the candidate list.

We want to analyze a coach from 5 main aspects: professionalism; ability; achievement; psychological control on major matches; support rate. Each of the candidate has 6 main features:

1. *OG*: game number that the coach directing in NCAA data record -Stands for professionalism.
2. *OP*: win-lost percentage in NCAA data record -Stands for ability.
3. *NC*: NCAA championship winning time -Stands for achievement.
4. *FP/FFP*: winning percentage of NCAA final/final four -Stands for psychological control on major matches.
5. *Ye*: year of the coaches' career in college -Stands for professionalism.
6. *SRS*: a rating system proposed by the NCAA official -Stands for Support rate.

In primary filtering model, we choose *OG*, *OP*, *YE* and *NC* as our main features considering their integrity, comprehensive and generic. After the primary filtering, we need to change the evaluation features. In order to determine the main features during the evaluation of the coach, we have done correlation analysis for all the features. The result is listed in Table.1.

Table. 1 Correlation Coefficient (CC)

Spearman		*YE*	*OG*	*OP*	*NC*	*SRS*
YE	CC	1.000	0.979	0.036	0.438	0.165
	Sig	0.000	0.000	0.775	0.000	0.186
OG	CC	0.979	1.000	0.031	0.547	0.156
	Sig	0.000	0.000	0.804	0.000	0.210
OP	CC	0.036	0.031	1.000	0.130	0.561
	Sig	0.775	0.804	0.000	0.298	0.000
NC	CC	0.438	0.547	0.130	1.000	0.216
	Sig	0.000	0.000	0.298	0.000	0.082
SRS	CC	0.165	0.156	0.561	0.216	1.000
	Sig	0.186	0.210	0.000	0.082	0.000

If correlation coefficient ranks high and sig ranks low, the corresponding parameters are more likely to be correlated. Table.1 shows that *YE* and *OG* are significantly correlated, while others are not. Therefore, we choose one of the features between *YE* and *OG* to represent the professionalism. *NC* can reflect coaches' achievement of high level. *SRS* reflects the support rate of coaches. Finally, we decided to adopt the following features in the limited filtering model: *OG*, *OP*, *NC* and *SRS*. After the limited filtering, the data are reduced to less than 15. We can see *FP/FFP* is a generic factor for these coaches. Then, *OG*, *OP*, *NC*, *FP/FFP* and *SRS* are selected for the AHP model.

AHP model

Our AHP model aims at generating the top 5 according to the parameters: *OG*, *OP*, *NC*, *FP/FFP* and *SRS*. The Structure of the AHP model consists of 3 different layers: goal; criteria; alternatives. The relationship is shown in fig.1.

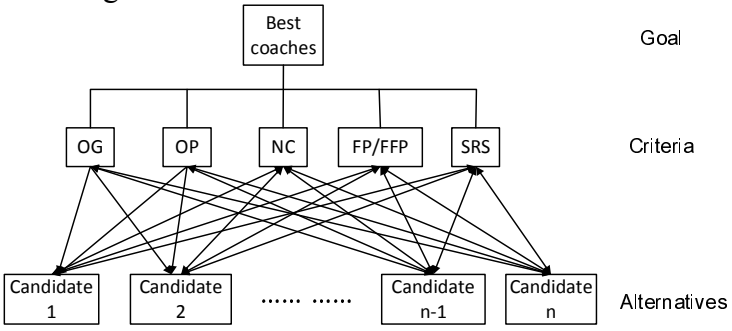

Fig. 1 AHP model hierarchy

The criteria was achieved by the analysis of the data and the target. The alternatives refer to the candidate list and it is achieved by the data filtering. The relative strength of rating scale 'a_{ij}' is achieved by the analysis against the value of the 5 features listed on the criteria. A rating scale is shown on table.2, where C_i refers to the absolute strength. Through the AHP model we got the preliminary relative strength 'R_{ij}'.

Table. 2 Rating scale

scale a_{ij}	meaning
1	$C_i = C_j$
3	$C_i > C_j$ and R_{ij} is tiny
5	$C_i > C_j$ and R_{ij} is small
7	$C_i > C_j$ and R_{ij} is moderate
9	$C_i > C_j$ and R_{ij} is
2,4,6,8	$C_i > C_j$ and R_{ij} is between the adjacent R that mentioned above
1,1/2,...,1/9	$C_i < C_j$ and R_{ij} is the reciprocal of the R that mentioned above

The 5 features may be impacted by time. For example the number of matches taking place 100 years ago is definitely less than that of today. Inspiration: considering that it is impossible to take everything into consideration and the data we got have its limitation. We introduce the Elo rating system to combat it. If we want to compare two different coaches A and D, whose careers were located in the different timespans. We may have to introduce B and C who have competence records enough to build a relation diagram. It is shown in Fig.2.

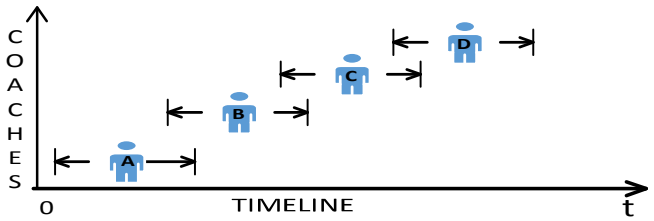

Fig.2 Relation schema

Assume coach i and j represent two coaches. $i = j$ means two same coaches. $i \neq j$ means two different coaches. E_i and E_j represent the expected score for coach i and coach j. There is 3 different results of a match: win; lose; tie. Each ot them have its percentage. Assuming that each coach's base score is 100, we change the base value according to the AP poll to get the initial rating R_i of coach i. Then we use equations to get the final R_i. With the introduction of K-factor we, we not only consider the competition information but also consider the potentiality of a coach. We compare the AP post of two different coaches and limit the range of it from1 to 25. Table.3. show the divide 5 levels we divided for the strength of coaches.

Table. 3 Strength of coaches

Difference of AP post	Sacle coach ij	Meaning
[-25,-20)	1	Preceding large stronger
[-20,-15)	3	Preceding moderate stronger
[-15,-10)	5	Preceding small stronger
[-10,-5)	7	Preceding tiny stronger
[-5,0)	9	Equal
(0,5]	-1	Equal
(5,10]	-3	Behind tiny stronger
(10,15]	-5	Behind small stronger
(15,20]	-7	Behind moderate stronger
(20,25]	-9	Behind large stronger

The expected score E_i of coach i follows the formula:

$$E_i = 1/(1+10^{(R_j - R_i)/40}), \quad (1)$$

Where R_j is the coaches' rating of coach j. The CRAS model is a linear enhancement proportional to the amount by which a coach over-performed or underperformed his expected score. The maximum

possible per game called the *K*-factor, was set to $K = 16$ for the stronger coaches and $K = 32$ for the weaker coaches. *K*-factor may reflect the potentility of a coach. Supposing coach *i* was expected to score E_i points but actually scored S_i points. The formula for updating his rating is:

$$R_i^{'} = R_i + K(S_i - E_i) \quad (2)$$

Table.4 listed part of the results compared with the result on the NCAA official website[10].

Table. 4 Results

scale a_{ij}	AHP model	Weight(AHP)	CRAS model	Final Ri	NCAA list
1	Joe Paterno	0.1568	Bear Bryant	92.45	Bear Bryant
2	Tom Osborne	0.1511	Woody Hayes	86.42	Nick Saban
3	Bobby Bowden	0.1455	Bud Wilkinson	73.6	Bobby Bowden
4	Bear Bryant	0.1236	Joe Paterno	67.16	Eddie Robinson
5	Barry Swither	0.1116	Bobby Bowden	62.86	Woody Hayes

Conclusions

According to the NCAA list, the CRAS model performs better than the AHP model. Supported by the data, we consider our system more reliable and objective than the traditional methods. The proposed system is not limited by the time line horizon, the gender and the different sports field. With the development of computer technology and data technologies, our ranking system will be greatly expanded and applied into other fields such as qualitative comparison or other related fields. For sports team, the proposed system has a huge advantage to find the talent coaches.

Acknowledgement

This work is partly supported by the State Key Development Program of Basic Research of China (2013CB329005), National Natural Science Foundation of China (Grant No. 61201165 and No. 61271240), Priority Academic Program Development of Jiangsu Higher Education Institutions, Wireless Broad Communication and Wireless Sensor network Department of Education Key lab Open Program(Grant No. NYKL201306), Education Natural Science Foundation of Jiangsu Province (13KJB510026), and Nanjing University of Posts and Telecommunications Foundation (Grant No. NY211032).

References

[1] Data of the coaches on http://www.sports-reference.com
[2] Data of the coaches on http://en.wikipedia.org/wiki/College_football
[3] U. Fayyad, G. Piatetsky-Shapiro, and P. Smyth: From data mining to knowledge discovery in databases, AI magazine, vol. 17 (1996), pp. 37.
[4] R. R. Vempada and K. S. Rao: *National Conference on Communications (NCC)* (IIT Kharagpur, India, Feb 3-5, 2012), pp. 1-5.
[5] T. L. Saaty: *Fundamentals of decision making and priority theory with the analytic hierarchy process* vol. 6 (Rws Publications, American 2000).
[6] A. SIGKDD, "Data mining curriculum," ed, 2012.
[7] Information on http://en.wikipedia.org/wiki/Elo_rating_system#Mathematical_details
[8] A. Halevy, P. Norvig, and F. Pereira: The unreasonable effectiveness of data: *Intelligent Systems, IEEE,* vol. 24 (2009), pp. 8-12.
[9] M. Bramer: *Principles of data mining* (Springer, Germany 2013).
[10] Top 10 coaches list on http://www.ncaa.com/

Advanced Materials Research Vols. 989-994 (2014) pp 5014-5020
© (2014) Trans Tech Publications, Switzerland
doi:10.4028/www.scientific.net/AMR.989-994.5014

Ontology of Aircraft Carrier Geographic Information

Zonglin Shi[1] , Daquan Tang[1], Zhen Tan[1], Guifang Wang[2]

[1]Science and Technology on Information Systems Engineering Laboratory, National University of Defense Technology, Changsha 410073, China;

[2]Shaanxi University of Technology, Hanzhong 723000, China.

997860224@qq.com

Keywords: Ontology, Aircraft Carrier, Geographic Information

Abstract. This paper aimed to build an ontology of aircraft carrier geographic information, defined ontology's constants, predicates, functions about aircraft carrier geographic information, and proposed a series of competency questions which could be solved by this ontology. Paper presented disjoint axioms, simple axioms and complex axioms of this ontology around these competency questions, and proved the consistency of the carrier ontology by examples. Finally, paper gave the answers for competency questions.

Introduction

An ontology is a declaration of terminology together with a specification of the meaning (semantics) of the terms, just likes a particular conceptual model. Ontology of aircraft carrier can help us understand the information of carrier easily and infer the actions of the carrier during the next period of time. Geographic information is an important part of aircraft carrier ontology, regardless of the carrier itself, or people related to carrier, things, facilities, events ..... they are closely associated with geographic information. Geographic information including aircraft carrier, people, ports and other's locations and coordinate information, you can get this information to analyze the aircraft carrier state, route, and even the tasks being performed. Such as through the port to get the docked state of aircraft carrier; Based on the location of boatyard that build aircraft carrier to get the country which this aircraft carrier belong to; Based on the sail track of aircraft carrier at sea to get its route and then analyze the task being performed ..... So reasoning geographic information of carrier by ontology can provide more information, and that is necessary for reasoning of the country's military action in sea.

Related Work

Recently, ontology was emerging as a new hotspot of research in computer science [1]. Contents of those researches involved all aspects of ontology, including the theory concept; application of information system; semantic Web etc [2]. Many domestic scholars have done research about geographic information ontology. Li Hongwei [3] elucidated the exact meaning of geographic ontology and the function and the sense of ontology in the geographic information science domain, presented a three-layer ontology framework by acting the basic concept design for geographic ontology, and showed the ontology's research potential and value in geographic information science domain. Huang Yong-qi [4] discussed how to adopt three theories to build geo-ontology, and prove its solution was feasible by experiment. Liu Wei and Gu He-he [5] proposed a solution for spatial data retrieval, took Dalian Bay land utilization ontology as the example, and showed the availability of its method by experiment. Foreign scholars have done many studies on ontology of geographic information. Agustina Buccella [6] proposed a novel system to integrate geographic sources by formalizing the information as normalized ontologies and provided a consistent and complete integration of their sources by testing in the context of projects of the Italian Institute for Environmental Protection and Research.

Although there were many researches of geographic information ontology, few scholars did research on building the ontology of aircraft carrier geographic information. There was no related literature in the result by searching in all the literatures with “aircraft carrier ontology” as keyword. This paper aimed to build an ontology of aircraft carrier geographic information, provided a detailed description of all the objects of aircraft carrier geographic information. It was important for the construction of ontology of aircraft carrier.

Competency Questions

Before building this ontology, we should find out what the ontology’s goals are，in other words, we should make it clear that what the requirements of using ontology to complete task are. Competency questions are these requirements which can be specified a set of queries that the ontology should be able to answer. We propose the following competency questions for the ontology of aircraft carrier geographic information. Note that x and t represent unknown quantities.

- Which country doses the aircraft carrier x belong to?
- Which port does the aircraft carrier x stay at?
- Which ocean is the aircraft carrier x shipping in?
- What is the longitude of the aircraft carrier x?
- Which aircraft carrier is at the position x?
- What are the positions of the route points when carrier x carry out task t?
- What is the northernmost latitude of area x?

Intuition

Aircraft carrier geographic information mainly concerns the area related to carrier. Figure 1 shows the basic elements of our ontology which is build by intuition.

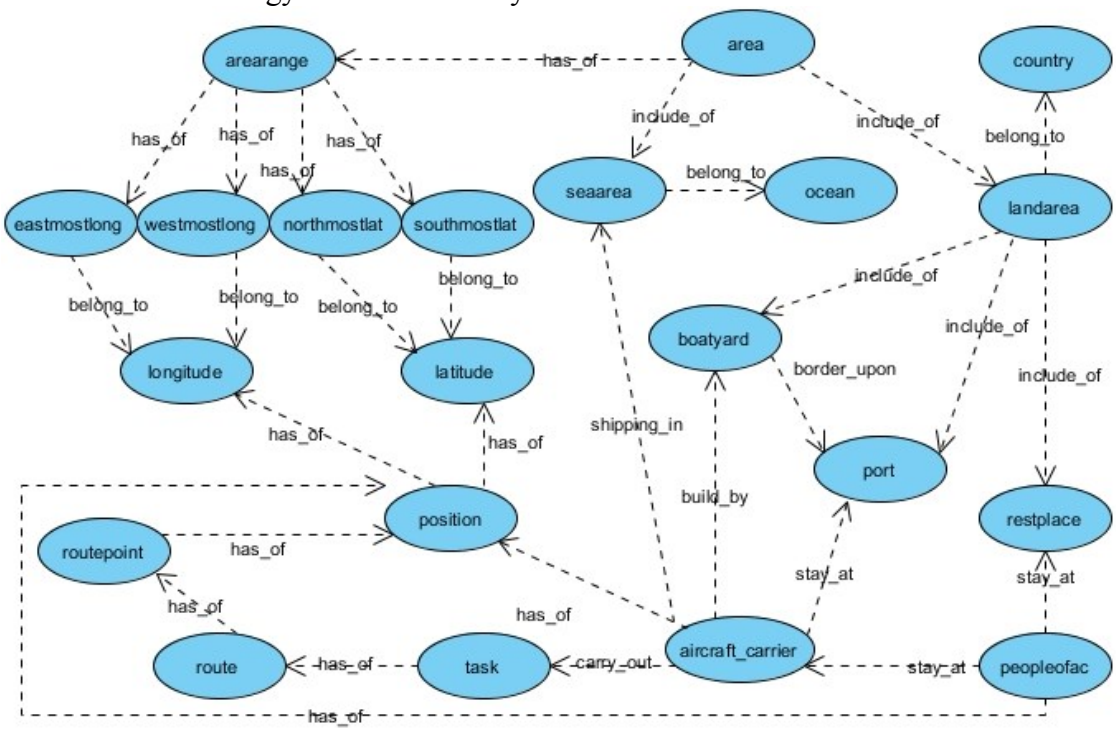

Figure 1: Structure of the aircraft carrier geographic information ontology

Through the understanding of the aircraft carrier, we can get following intuition.

Intuition 1: Areas related to aircraft carrier include the sea and land. The sea area belongs to one ocean and the land area belongs to one country. The land areas are mainly ports, boatyards and rest place where the people related to carrier live in.

Intuition 2: Each area has its range. The range of area has four attributes: easternmost longitude, westernmost longitude, northernmost latitude, southernmost latitude. The area range can be expressed by these four attributes.

Intuition 3: Aircraft carrier is built by boatyard and it sails in sea or stays at port. Aircraft carrier performs task, each task has its route. Aircraft carrier must pass through the route points given by the performing task.

Intuition 4: Route points and aircraft carriers, people have these positions. And each position has the exclusive longitude and latitude.

Nonlogical Lexicon

After giving the structure of ontology, we should get the nonlogical lexicon about aircraft carrier geographic information. The lexicon likes vocabulary that is one part of expressing knowledge. The lexicon contains the set of named individuals, types of objects, the set of attributes, relationships etc. Those lexicons are expressed by predicates, functions and constants. The following is our design of the nonlogical lexicon in our ontology.

Unary predicate

- aircraft_carrier(x) denotes object x is aircraft carrier.
- area(x) denotes x is a region.
- seaarea(x) is subclass of area(x) and denotes x is sea area.
- landarea(x) is subclass of area(x) and denotes x is land area.
- ocean(x) denotes x is an ocean.
- country(x) denotes x is a country.
- arearange(x) denotes x is the range of area.
- eastmostlong(x) denotes x is the easternmost longitude of an area.
- westmostlong(x) denotes x is the westernmost longitude of an area.
- northmostlat(x) denotes x is the northernmost latitude of an area.
- southmostlat(x) denotes x is the northernmost latitude of an area.
- boatyard(x) is subclass of landarea(x) and denotes x is a boatyard.
- port(x) is subclass of landarea(x) and denotes x is a port.
- restplace(x) is subclass of landarea(x) and denotes x is a rest place.
- position(x) denotes x is a position of an object.
- longitude(x) denotes x is longitude. West longitude is represented by negative
- latitude(x) denotes x is latitude. South latitude is represented by negative
- peopleofac(x) denotes x is people about aircraft carrier.
- task(x) denotes x is a task.
- route(x) denotes x is a route.
- routepoint(x) denotes x is a route point.

Binary predicate

- has_of(x,y) denotes the relation in which x has the property y.
- include_of(x,y) denotes the relation in which x include y.
- belong_to(x,y) denotes the relation in which x belongs to y.
- stay_at(x,y) denotes the relation in which x stay at y.
- build_by(x,y) denotes that aircraft carrier x is built by y.
- border_upon(x,y) denotes the relation in which x border upon y.
- carry_out(x,y) denotes that aircraft carrier x carry out task y.
- shipping_in(x,y) denotes that aircraft carrier x is shipping in sea area y.

Functions

- getlongitude(x). This function can get the longitude of position x.
- getlatitude(x). This function can get the latitude of position x.

Constants

There are many constants, and they will be presented in the practical application.

Axiom

According to the ontology, the axioms are based on the intuitions above. The building of axioms is in order to answer and solve the competency questions, and through axioms our ontology can express the competency questions necessary and sufficient. We just show the following examples of all kinds of axioms in our ontology.

Disjoint Axioms

- Sea area and land area are disjoint sets; Boatyard, port and rest place are disjoint sets.
  $(\forall x)seaarea(x) \supset \neg landarea(x)$ $(\forall x)boatyard(x) \supset \neg(port(x) \vee restplace(x))$
- At same area range, easternmost longitude and westernmost longitude are disjoint sets. Northernmost latitude and southernmost latitude are the same.
  $(\forall x)eastmostlong(x) \wedge has_of(y,x) \wedge arearange(y) \supset \neg westmostlong(x)$
  $(\forall x)northmostlat(x) \wedge has_of(y,x) \wedge arearange(y) \supset \neg southmostlat(x)$
- Longitude and latitude are disjoint sets.
  $(\forall x)longitude(x) \supset \neg latitude(x)$

General Axioms

1) Has_of:

- Axiom 1.1: One area must have one and only one area range.
  $(\forall x)area(x) \supset ((\exists y)arearange(y) \wedge has_of(x,y)) \wedge (\forall z)arearange(z) \wedge has_of(x,z) \wedge (y = z)$
- Axiom 1.2: One area range must have one and only one easternmost longitude. The same to westernmost longitude, northernmost latitude, southernmost latitude. We don't repeat them here.
  $(\forall x)arearange(x) \supset ((\exists y)eastmostlong(y) \wedge has_of(x,y)) \wedge (\forall z)eastmostlong(z) \wedge has_of(x,z) \wedge (y = z)$
- Axiom 1.3: One position must have one and only one longitude. The same to latitude.
  $(\forall x)position(x) \supset ((\exists y)longitude(y) \wedge has_of(x,y)) \wedge (\forall z)longitude(z) \wedge has_of(x,z) \wedge (y = z)$
- Axiom 1.4: Aircraft carrier must have one and only one position. The same to carrier-related people.
  $(\forall x)aircraft_carrier(x) \supset ((\exists y)position(y) \wedge has_of(x,y)) \wedge (\forall z)position(z) \wedge has_of(x,z) \wedge (y = z)$
- Axiom 1.5: Route point has one position, and there is only one position correspondence with this route point.
  $(\forall x)routepo\,\mathrm{int}(x) \supset ((\exists y)position(y) \wedge has_of(x,y)) \wedge (\forall z)position(z) \wedge has_of(x,z) \wedge (y = z)$
- Axiom 1.6: Agreed in our ontology, one task must have one route.
  $(\forall x)task(x) \supset ((\exists y)route(y) \wedge has_of(x,y)) \wedge (\forall z)route(z) \wedge has_of(x,z) \wedge (y = z)$
- Axiom 1.7: Route has some route points.
  $(\forall x)route(x) \supset (\exists y)has_of(x,y) \wedge routepo\,\mathrm{int}(y)$

2) Include_of:

- Axiom 2.1: The area includes sea area and land area.
  $(\forall x)area(x) \supset seaarea(x) \vee landarea(x)$
- Axiom 2.2: Boatyards belong to land area. Ports and rest place also belong to the land area. We also don't repeat them.
  $(\forall x)boatyard(x) \supset landarea(x)$

3) Belong_to:

- Axiom 3.1: Each one sea area belongs to only one ocean.
  $(\forall x)seaarea(x) \supset ((\exists y)ocean(y) \wedge belong_to(x,y)) \wedge (\forall z)ocean(z) \wedge belong_to(x,z) \wedge (y = z)$
- Axiom 3.2: Each one land area belongs to only one country.
  $(\forall x)landarea(x) \supset ((\exists y)country(y) \wedge belong_to(x,y)) \wedge (\forall z)country(z) \wedge belong_to(x,z) \wedge (y = z)$
- Axiom3.3: Easternmost longitude belongs to longitude. The same to westernmost longitude.
  $(\forall x)eastmostlong(x) \supset longitude(x)$

- Axiom 3.4: Northernmost latitude belongs to latitude. The same to southernmost latitude.
  $(\forall x)northmostlong(x) \supset latitude(x)$

4) Stay_at:

- Axiom 4.1: Either aircraft carrier ships in sea area or stays at port.
  $(\forall x)aircraft_carrier(x) \supset (\exists y)port(y) \wedge stay_at(x,y) \vee (\exists z)seaarea(z) \wedge shipping_in(x,z)$

5) Build_by:

- Axiom 5.1: Aircraft carrier was built by boatyard.
  $(\forall x,y)build_by(x,y) \supset aircraft_carrier(x) \wedge boatyard(y)$
- Axiom 5.2: Agreed in our ontology, there is only one boatyard built this aircraft carrier.
  $(\forall x)aircraft_carrier(x) \supset ((\exists y)boatyard(y) \wedge build_by(x,y)) \wedge (\forall z)boatyard(z) \wedge build_by(x,z) \wedge (y=z)$

6) Border_upon:

- Axiom 6.1: The two units are border upon to each other is port and boatyard.
  $(\forall x,y)border_upon(x,y) \supset (boatyard(x) \wedge port(y)) \vee (boatyard(y) \wedge port(x))$
- Axiom 6.2: A port border upon the boatyard so that the boatyard border upon the port.
  $\text{border_upon}(x,y) \supset \text{border_upon}(y,x)$
- Axiom 6.3: Each boatyard has only one port border upon.
  $(\forall x)boatyard(x) \supset ((\exists y)port(y) \wedge border_upon(x,y)) \wedge (\forall z)port(z) \wedge border_upon(x,z) \wedge (y=z)$

7) Carry_out:

- Axiom 7: Aircraft carrier carries out its task.
  $(\forall x,y)carry_out(x,y) \supset aircraft_carrier(x) \wedge task(y)$

8) Shipping_in:

- Axiom 8.1: Aircraft carrier ships in sea area.
  $(\forall x,y)shipping_in(x,y) \supset aircraft_carrier(x) \wedge seaarea(y)$
- Axiom 8.2: Every aircraft carrier only ships in one sea area.
  $(\forall x)(\exists y)aircraft_carrier(x) \wedge seaarea(y) \wedge shipping_in(x,y) \supset$
  $(\forall z)seaarea(z) \wedge shipping_in(x,z) \wedge (y=z)$

Complex axioms

- Axiom 9: Different aircraft carriers have different position.
  $(\forall x,y)aircraft_carrier(x) \wedge aircraft_carrier(y) \wedge (x \neq y) \supset$
  $(\exists xp,yp)position(xp) \wedge position(yp) \wedge has_of(x,xp) \wedge has_of(y,yp) \wedge (xp \neq yp)$
- Axiom 10: Aircraft carrier is shipping at sea area. The position of aircraft carrier is in the sea area range. That is to say its longitude will not exceed the scope of the longitude range of sea area. Its latitude will not exceed the scope of the latitude range of sea area too, we also don't give it. By the same token, when carrier is staying at port, its position is in the port.
  $(\forall x)aircraft_carrier(x) \wedge seaarea(y) \wedge shipping_in(x,y) \wedge position(xp) \wedge has_of(x,xp)$
  $\wedge arearange(yr) \wedge has_of(y,yr) \wedge eastmostlong(ye) \wedge has_of(yr,ye)$
  $\wedge westmostlong(yw) \wedge has_of(yr,yw) \supset (yw < getlongitude(xp) < ye)$
- Axiom 11: Aircraft carrier performing task and its position is same as the position of route point of the task.
  $(\forall x)aircraft_carrier(x) \wedge carry_out(x,k) \wedge task(k) \wedge has_of(k,r) \wedge route(r)$
  $\wedge has_of(r,pt) \wedge routepo\text{int}(pt) \wedge has_of(pt,p) \wedge position(p) \supset has_of(x,p)$

Consistency Proofs

After the building of ontology, we should test and verify its consistency. The following example can prove the above axioms are consistent.

Example

"Kitty Hawk" aircraft carrier (USS Kitty Hawk CV-63) is the U.S. Navy Kitty Hawk-class aircraft carrier of the first ship, "Kitty Hawk" aircraft carrier built by the boatyard in New York, watered in New York sea area in 1960, first entered service in 1961. New York sea area is in Atlantic.

After shakedown from Atlantic waters, the USS Kitty Hawk left Norfolk in August 11, 1961.Then USS Kitty Hawk carried out a task that joint exercise with the Brazilian Navy. The requirement of the task was that USS Kitty Hawk should pass Cape Horn in the October 1, pulled into Chile 's Valparaiso Harbor in October 13.

Then USS Kitty Hawk entered the Peruvian waters (easternmost longitude -76.87' , westernmost longitude -77.35', northernmost latitude -11.60', southernmost latitude -12.40') two days later. According to satellite monitoring the position of USS Kitty Hawk was (-77.50',-12.22') at that time.

Proof

1) By analyzing the first paragraph, we can get a series of constants:

aircraft_carrier(KittyHawk) seaarea(NewYorkSeaArea)
country(USA) boatyard(NewYorkBoatyard)
landarea(NewYork) port(NewYorkHarbor)
ocean(Atlantic)

These constants have some relationship between each other, expressed by the following formulas.

include_of(NewYork, NewYorkBoatyard) belong_to(NewYork, USA)
build_by(KittyHawk, NewYorkBoatyard) belong_to(NewYorkSeaArea, Atlantic)
border(NewYorkBoatyard, NewYorkHarbor)

Through axiom 2.2, axiom 5.1, axiom 5.2, axiom 3.1, axiom 3.2, we can get the facts:

belong_to(NewYorkBoatyard,USA) belong_to(NewYorkHarbor,USA)

Through axiom 6.1, axiom 6.2, axiom 6.3, we can get the fact:

border(NewYorkHarbor, NewYorkBoatyard)

2) By analyzing the second paragraph, we can get a series of constants:

country(Chile) routepoint(CapeHorn)
port(ValparaisoHarbor) position(CapeHornPosition)
task(JointExercise) latitude(-55.59')
route(JERoute) longitude(-67.16')
belong_to(ValparaisoHarbor, Chile)

The relationship between them is following:

carry_out(KittyHawk ,JointExercise) has_of(JERoute, CapeHorn)
has_of(JointExercise, JERoute) has_of(CapeHorn, CapeHornPosition)
has_of(CapeHornPosition, -55.59') $\wedge$ latitude(-55.59')
has_of(CapeHornPosition, -67.16') $\wedge$ longitude(-67.16')
getlongitude(CapeHornPosition)= -67.16' getlatitude(CapeHornPosition)= -55.59'

Through axiom 1.3, axiom 1.5, axiom 1.6, axiom 1.7, axiom 7, axiom 12, we can get the fact: has_of(KittyHawk ,CapeHornPosition) when Kitty Hawk carried out the JointExercise task in October 1.

Through axiom 8.1, axiom 4.1, we can get the fact:

stay_at(KittyHawk, ValparaisoHarbor) $\vee$ shipping_in(KittyHawk, ?seaarea) $\wedge$ belong_to(?seaarea, Atlantic), "?" express unknown.

3) By analyzing the third paragraph, we can get a series of constants and the relationship:

seaarea(PeruvianWaters) arearange(PeruvianWatersRange)
has_of(PeruvianWaters, PeruvianWatersRange)
has_of(PeruvianWatersRange, -76.87') $\wedge$ eastmostlong (-76.87')
has_of(PeruvianWatersRange, -77.35') $\wedge$ westmostlong (-77.35')
has_of(PeruvianWatersRange, -11.60') $\wedge$ northmostlat(-11.60')
has_of(PeruvianWatersRange, -12.40') $\wedge$ southmostlat(-12.40')
position(KHPosition) has_of(KittyHawk, KHPosition)
has_of(KHPosition, -12.22') $\wedge$ latitude(-12.22')
has_of(KHPosition, -77.50') $\wedge$ longitude(-77.50')
getlongitude(KHPosition)= -77.50' getlatitude(KHPosition)= -12.22'

Through axiom 3.3, axiom 3.4, axiom 1.1, axiom 1.2, axiom 1.3, axiom 1.4, axiom 10, we can get the fact:

-76.87'<-77.50'<-77.35' -12.40'<-12.22'<-11.60'

It is proved that these axioms are realistic. Some axioms don't write here. Obviously they can be proven because of the above proof.

Competency Revisited

In this section we repeat the competency and follow each with the query that would provide the answer. Note that parameters that are preceded with a "?" are variables. We also leave out the situational calculus predicates since all of the logical statements refer to the current situation.

- Which country doses the aircraft carrier x belong to (?c is the answer)?
  $build_by(x,?b) \wedge belong_to(?b,?c)$
- Which port does the aircraft carrier x stay at (?p is the answer)?
  $stay_at(x,?p)$
- Which ocean is the aircraft carrier x shipping in (?s is the answer)?
  $shipping_in(x,?s)$
- What is the longitude of the aircraft carrier x (?l is the answer)?
  $has_of(x,?pn) \wedge has_of(?pn,?l) \wedge longitude(?l)$
- Which aircraft carrier is at the position pn (?x is the answer)?
  $has_of(?x,pn)$
- What are the positions of the route points when carrier x carry out task t (?pn is the answer)?
  $carry_out(x,t) \wedge has_of(t,?r) \wedge has_of(?r,?rp) \wedge has_of(?r,?pn)$
- What is the northernmost latitude of area x (?nmlat is the answer)?
  $has_of(x,?ar) \wedge has_of(?ar,?nmlat) \wedge northmostlat(?nmlat)$

Conclusions

Ontologies are shared views of domains. They provide conceptualizations that are agreed upon by participants in collaborative action and decision making. The explicit existence of such shared perspectives makes it possible for people to communicate and cooperate.

The paper presents ontology for geographic information of aircraft carrier. With the help of this ontology, people will know more clearly about aircraft carrier. And reasoning geographic information of carrier by ontology can provide information about war. It helps leader analysis and decision.

References

[1] Du XY, Li M, Wang S. A survey on ontology learning research [J].Journal of Software, 2006, 17(9):1837−1847.

[2] DENG Zhihong, TANG Shiwei, ZHANG Ming, YANG Dongqing CHEN Jie. Overview of Ontology [J]. Acta Scientiarum Naturalium Universitatis Pekinensis, Vol. 38 , No. 5 (Sep ,2002)

[3] Li Hongwei. The Research on Geo-information Services Based on Ontology[D]. Information Engineering University of the People's Liberation Army, 2007

[4] Huang Yong-qi, Cui Wei-hong, Zhang Yang-jian, Deng Gao-yan. Research on Development of Agricultural Geographic Information Ontology[J]. Journal of Integrative Agriculture, 2012, 11(5):865-877

[5] Liu Wei, Gu He-he. Geo-information spatial relationships retrieval based on semantic [J]. Science of Surveying and Mapping, 2013,38(5)

[6] Agustina Buccella, Alejandra Cechich, Domenico Gendarmi, Filippo Lanubile, Giovanni Semeraro, Attilio Colagrossi. Building a global normalized ontology for integrating geographic data sources[J]. Computers and Geosciences , 2011, Vol.37 (7), pp.893-916

[7] Xianghui Wang. Query and reasoning ontology and its application in the military domain[J]. Chongqing University, 2012

CHAPTER 9:

Advanced Information and Innovative Technologies for Management, Logistics, Economics, Education, Assessment

Advanced Materials Research Vols. 989-994 (2014) pp 5023-5028
© (2014) Trans Tech Publications, Switzerland
doi:10.4028/www.scientific.net/AMR.989-994.5023

Study on Utilizing Foreign Direct Investment in Underdeveloped Areas

Jianbo HU

Guizhou University of Finance and Economics, Guiyang 550025 China

email:hjbbo@126.com

Keywords: Underdeveloped Areas; Foreign Direct Investment; Performance Index

Abstract. The use of foreign investment is an important engine of developing inland opening economy. In 2012, in face of weak external demand, insufficient domestic effective demand and other serious and complex economic situation, the introduce of foreign investment in Guizhou keeps high growth , the actual use of foreign capital breakthrough $1 billion for the first time, up to $1.046 billion, growing by 55.35% year on year. The total amount ranked the sixth and the growth ranked the third in western regions. The utilization of foreign investment has realized the improvement of speed, quality and efficiency. The economic contribution of foreign investment to Guizhou has improved continuously, laying a solid foundation to accelerating the speed of economic development for Guizhou. But we also found many problems existing in the process of attracting foreign investment in Guizhou. And we need to seek reasonable countermeasures to further strengthen the role of foreign investment in promoting the economy of Guizhou and improve the core competitiveness of Guizhou to realize sustainable development of the economy.

Introduction

With the continuous development of economic globalization, International Investment is playing a more important historic role than any other time. As an important part of international investment, International Direct Investment (IDI) has an essential effect on promoting global economy. Since reform and opening up, China's foreign direct investment (FDI) has made great progress on both quantity items and amount in total, which has been driving GDP growth in China.Western regions where economic development are relatively backward in China, are also trying to attract FDI in various ways, trying to solve the "funding gap" and control the bottlenecks of slow growth of capital effectively. Therefore, introducing FDI has always being a strategic guidance for all levels of government in western regions to improve the level of local economic growth and the structure of the industrial development.Guizhou as less developed western region, is later than other provinces in China on introducing FDI. But in recent years, with national policies tilting to the western regions and expanding and improving opening to the outside world and the strategy of introducing FDI in Guizhou, introducing of FDI in Guizhou has advanced unprecedentedly both in the scale and quality.

The development status of FDI in Guizhou

1) Scale of FDI.There were total 53 industrial items from FDI enterprise in 2012, falling by 19.7% year on year. Thereinto:11 items of primary industry accounted for 20.75%, increasing by 83.33% year on year; 27 items of secondary industry remained the same year on year, accounting for 50.94%;15 items of tertiary industry fell by 54.55% year on year, accounting for 28.3%. Contracted foreign capital of FDI enterprise by industry was $573.83 million, falling by 66.4% year on year. Thereinto: contracted foreign capital of primary industry was $57.83 million, accounting for 10.08% of contracted foreign capital, falling by 33.27% year on year; contracted foreign capital of secondary industry was $306.66 million, accounting for 53.44%, falling by 63.81% year on year; Contracted foreign capital of tertiary industry was $209.34 million, accounting for 36.48%, falling by72.95% year on year. Foreign investment in actual use of FDI enterprise by industry was $1045.82 million in 2012, increasing by 55.35% year on year, and it ranked sixth in western areas, placed behind Chongqing, Sichuan, Inner Mongolia, Shanxi and Gansu. Its speedup ranked front

three in western areas. Contracted foreign capital which has been actually used of FDI enterprise was $491.16 million, accounting for 46.96%, falling by 4.70% year on year. According to statistics of department of foreign exchange control, foreign loan of the difference between investment and registered investment which has been actually used of FDI enterprise in Guizhou was $173.83 million, accounting for 16.62%; Domestic investment which has been actually used of FDI enterprise accumulated to $380.84 million,accounting for 36.42%. Thereinto; foreign investment which has been actually used of primary industry was $12.36 million, accounting for1.18%; Foreign investment which has been actually used of secondary industry was $688.25 million, accounting for 65.81%, among which foreign investment which has been actually used of manufacturing was $107.92 million, accounting for 15.68%; foreign investment which has been actually used of tertiary industry was $345.22 million, accounting for 33.01%. The industries of scale of foreign investment which has been actually used of tertiary industry ranked front five respectively; real estate, $224.84 million, wholesale and retail sale, $63.98 million, scientific research, technical service and geological exploration, $29.91million, leasing and business service industry, $15.08 million, information transmission, computer service and software industry,$5 million. Foreign investment which has been actually used of these five industries accounted for 65.13%, 18.53%, 8.66%, 4.37%, 1.45% respectively.

2) Means and structure of FDI.After reform and opening-up, every industry opened up to the outside world moderately and with measured strokes. Entering of foreign investment into every industry was somewhat limited at first, but with the deepening of reform and opening, the limitation was less and less. Foreign investment is allowed to enter into for most industries except for a few industries. At initial stage of reform and opening-up, foreign investment did not have enough faith in China because of little understanding. Foreign investment generally entered into Chinese market in the way of joint venture or cooperation for the sake of sharing risk. Although sole proprietorship can work on own and enjoy the benefit exclusively, but its risk was higher. Foreign businessmen would not choose singleproprietorship. Through more than 30-years' reform and opening-up, the growth miracle of Chinese economy is obvious to all. With the continuous enhancing faith of foreign businessmen to Chinese economy, single proprietorship has become the main way for foreign businessmen in China. As to Gui zhou, the transferring process of FDI ways is basically similar to the whole situation of our country. The items of Sino-foreign joint venture decreased from 18 to 4 from 2007 to 2010, and increased to 22 in 2012; FDI actual use is rising all the time, increasing from $42.88 million to $178.54 million from 2007 to 2012; The numbers of items of Sino-foreign joint venture is less than wholly foreign-owned enterprises all along. The items of wholly foreign-owned enterprises reached up to 31, FDI which has been actually used rises to $309.51 million, which is 1.73 multiples of foreign investment that has been actually used of Sino-foreign joint venture; Scale of Chinese-foreign cooperative enterprise is at a low situation. There were 7 items in 2010, even none left in 2012. The investment was only $3.2 million, which was far below other two investment ways.

3) Countries (regions) of origin structure of FDI.In view of the foreign investment by countries and by areas, we could find some facts. There were 42 enterprises in Asian countries (regions) invested Guizhou in 2012, downed 8.7% year on year; The value of contractual foreign investment were $384.84 million, downed 70.02% year on year; The actual use of foreign accounted $316.88 million, downed 21.89% year on year. There are 1 enterprise in European countries (regions) invest Guizhou in 2012, downed 75.00% year on year; The value of contractual foreign investment were $4.06 million, downed88.02% year on year; The actual use of foreign accounted $4 million, increased 41.84% year on year. There are 1 enterprise in South American countries (regions) invest Guizhou in 2012, downed 50% year on year; The value of contractual foreign investment were $1.58 million, downed 97.54%year on year; The actual use of foreign accounted $16.31 million, increased35.35% year on year. There are 1 enterprise in North American countries (regions) invest Guizhou in 2012, downed 75% year on year; The value of contractual foreign investment decreased $27.31 million, downed 122.47%year on year; The actual use of foreign accounted $58.26 million, increased 5.93% year on year. There were 1 enterprise in Oceania countries (regions)

invest Guizhou in 2012, downed 50% year on year; The value of contractual foreign investment were $0.63 million, downed 96.10% year on year; The actual use of foreign accounted $6.5 million, downed 30.11% year on year.

4) Industry structure of FDI.According to the FDI by industry, we could find some facts. There were 11 companies invest the agriculture animal husbandry and fishery in 2012, increased 83.33% year on year; The value of contractual foreign investment were $57.83 million, downed 33.27%year on year; The actual use of foreign accounted $7.55 million, downed 90.79% year on year. There were 3 companies invest The mining industry enterprise in 2012, increased 50% year on year; The value of contractual foreign investment were$36.77 million, increased 96.11%year on year; The actual use of foreign accounted $4.5 million, downed 38.94% year on year. There were 20 companies invest Manufacture in 2012, increased 25% year on year; The value of contractual foreign investment were $237.79 million, downed 56.99%year on year; The actual use of foreign accounted $51.79 million, downed 74.21%year on year. There were 3 companies invest electricity, gas and water production and supply industry in 2012, downed 57.14% year on year; The value of contractual foreign investment were $30.68 million, downed 80.20%year on year; The actual use of foreign accounted $81.88 million, increased 11.71%year on year. There was 1 company invest construction industry in 2012, downed 50% year on year; The value of contractual foreign investment were $1.42 million, downed 98.82%year on year; The actual use of foreign accounted $53.28 million, increased 25271.43%year on year. There was 1 company invest Transportation, warehousing and postal service in 2012, the value of contractual foreign investment were $80.53 million. There were 3 companies invest wholesale and retail sales in 2012, downed 57.14% year on year; The value of contractual foreign investment decreased $11.6 million; The actual use of foreign accounted $25.26 million, increased 115.53% year on year. There was 1 company invest real estate in 2012, downed 80%year on year; The value of contractual foreign investment were $4.83 million, downed 98.03%year on year; The actual use of foreign accounted $224.84 million, increased 889.61%year on year. There were 6 companies invest leasing and commercial service in 2012, downed 40%year on year; The value of contractual foreign investment were $123.14 million, downed 55.88%year on year; The actual use of foreign accounted $5.48 million, downed 91.34%year on year. The actual use of foreign of scientific research, technical service and geological prospecting industry accounted $29.91 million, increased 50.86%year on year. There was 1 company invest water conservancy, environment and administration of public facilities in 2012, downed 66.67% year on year; The value of contractual foreign investment were $640000, downed 98.40%year on year; The actual use of foreign accounted $640000.

Problems in the Process of Guizhou's FDI development

1) Small investment scale and inferior quality.As we can see from the absolute number, the ranking that amount and the number of enterprises of Guizhou's FDI is lower in 31 provinces. For example, in 2012, number of entry and contract amount that Guizhou used were reductive. Number of entry only accounted for 0.21%, and actual foreign capital Guizhou used only accounted for 0.44% over the country. Although the actual foreign capital increased a little, the total amount only accounted for the sixth in western region. As we can see from the relative number, maybe we can show with a Inward FDI Performance Index (IND) of foreign capital that a district attracted. (IND) means that in a certain period, the proportion that a region's FDI inflow accounted for the country's was divided by the proportion that the region's GDP accounted for the country's, which can be showed with mathematical formula as in (1):

$$IND_i = \frac{FDI_i / FDI_n}{GDP_i / GDP_n} \tag{1}$$

Thereinto, i represents a certain province , n represents all provinces of the country, That is n=1,2,...,31; if the greater a region's economic scale is, the more FDI that a province attracts is, so

the more close to 1 IND is, on the contrary, the more close to 0. According to the above formula and the relative dates of Guizhou's FDI, we can solve IND of Guizhou in recent years, the details are shown in table 1. In the table, all IND are below 1, and the most of IND is lower than 0.2, which shows that the promote force of FDI to Guizhou's economic development needs to be improved, and further shows that the proportion Guizhou using FDI is on the low side, so Guizhou still needs to further increase the intensity of introduction of foreign capital.

Table.1 Inward FDI performance index in Guizhou from 2007 to 2012

	2007	2008	2009	2010	2011	2012
Actual use of FDI in Guizhou ($0.1 billion)	1.27	1.49	1.34	2.95	5.15	4.91
Actual use of FDI in Chia ($0.1 billion)	747.7	924	900.3	1057	1160	1117
proportion that FDI in Guizhou accounting for China （%）	0.17	0.16	0.15	0.28	0.44	0.44
GDP in Guizhou (0.1 billion yuan)	2884	3562	3913	4602	5702	6852
GDP in China (10 billion yuan)	2658	3141	3409	4015	4731	5189
The proportion that GDP in Guizhou accounting for China（%）	1.08	1.13	1.15	1.15	1.21	1.32
IND of FDI in Guizhou	0.16	0.14	0.13	0.24	0.36	0.33

Data sources: the information is calculated and sorted according to the relative data of China Statistical Yearbook in 2013 and Guizhou Statistical Yearbook .

2) Higher utilization of foreign capital in individual industries and regions, and unbalanced distribution of development.One is that the distribution of FDI industry is unbalanced. In addition to the individual year, investment proportion of FDI in the primary industry was larger, the other years' was less, and it showed no continuity, which indicates that investment of FDI in agriculture is less and no obvious endurance; For a long time, the FDI investment mainly concentrated in the second industry, and especially in the manufacturing industry. The average capital investment of FDI in the third industry accounts for about 30%, but since 1992, the amount of investment to the third industry presents the obvious increasing trend, by 2012, which has been more than the second industry, mainly concentrated in the real estate, scientific and technical services, geological prospecting industry, finance, insurance and so on; in 2012, the ratio between the number of three times industry and the actual investment of foreign capital was 20.75: 50.94: 28.30 and 1.54: 38.98: 59.48. The Second is that the regional distribution of FDI is not unbalanced. FDI exists in every city in Guizhou, but it is not uniformity. Guiyang accounts for the highest proportion, for example in 2012, the number of new signing projects, the actual use of foreign capital and the investment amount of foreign merchant's agreement respectively accounted for 23%, 31.5% and 39.4% of the whole Guizhou. And in the 9 cities and states, the actual investment of foreign capital in Guiyang was more than one third, which played a leading role; the amplification of actual use of foreign capital in Tongren and other cities and states was larger, but the gap between Guiyang and the other cities and states did not shrink, and the actual use of foreign capital scale in mountainous and hilly region was smaller, and such imbalanced situation was bad for comprehensive and balanced development of Guizhou's economy.

3) Foreign capital of country of origin comparative intensively, Euramerican foreign businessmen investment on the low side.FDI enter into Guizhou on a large scale, which has become one of the important sources of capital accumulation, promoting rapid growth of stock of agent of production effectively, and then pushing Guizhou economic sustainable growth to a large degree. However, highly centralized source of FDI make Guizhou be influenced easily by international economic cycles and bear higher risk. Since affected by original industry base, Guizhou competitive industries concentrate on resource-integrated industry, labor-integrated industry, resource processing and so on. High processing industries develop deficiently, and added value of industry products is one the low side. Comparing to eastern province, tertiary industry develops evident laggingly. For example, in 2010, tertiary industry accounts for 36.4% in Chongqing, 46.1% in Tianjin,57.3%in Shanghai, 75.1% in Beijing, but only 26.4% in Guizhou. Modern service industry

in Guizhou. Develops laggingly, financial environment is not perfect, research and development ability is weak, new high-tech industry develops slowly, causing Hong Kong to become the main source district of foreign capital in Guizhou, and European and the United States foreign capital is short for it requests environment higher. Taking 2010 as an example, a new body of foreign-investment enterprise in Guizhou mainly concentrates in Hong Kong, Taiwan,Malaysia, items of which are 29, 4, 3 respectively, accounting for 67.92% of total items; Contracted foreign capital concentrates in Hong Kong, reaching up to $334.56 million, accounting for 58.3% and surpassing half; Contracted foreign capital which has been actual used mainly concentrated in such as Hong Kong, Bermuda, British Virgin Islands, Singapore, capital which has been actually used is $296.28 million, $56.45million, $13.61 million and $9.99 million respectively, the total capital that above-mentioned capital plus accounts for 76.62%.

Measures of accelerating the utilization of FDI in Guizhou

1) Try to perfect the policy on industry development and strengthen support and guidance on accelerating development of foreign capital.According to the Catalogue for the guidance of foreign investment industries and catalogue of priority industries for foreign investment in central and western regions promulgated by the state council and the file spirit of the western development and acceptance the industry transfer, we should consider about the actual of Guizhou, enlarge the support of attracting foreign capital policy and strengthen the 12th five-year development strategy planning in order to lead the foreign investment into modern agriculture in Guizhou and promote the industrialization of agricultural effectively. Encouraging foreign investment into native, advantageous and capital and technology intensive industries of Guizhou, and setting up production bases and research and development centers should also be done. Perfecting foreign participation in the high-tech industrialization and establishing open type autonomous innovation system of policy measures is also necessary. We should pay attention to increase state enterprise restructuring intensity and boot foreign investment into Guizhou state enterprise of technology and assets restructuring and optimize state enterprise capital structure. Try to research and develop the policy measures of improve zone competitiveness, achieve transformation upgrade and sustainable development. Perfect foreign investment established venture investment enterprise and equity investment enterprise of policy and control effectively "three high" (high energy, and high pollution, and high emissions) industries of blind investment; vigilance based facilities of repeat construction and the ahead construction; strictly according to national industry policy and the acts about foreign investment , we cannot blind mention some unrealistic of "leap" type of slogan blindly or act in incessant movements to deal with the investment and construction, then promote economic prosperity in Guizhou’s cities and states.

2) Try to guide foreign investment into cities and states and promote regionally balanced development of foreign capital.As the seat of the capital of Guizhou, Guiyang whose economy is more developed and investment environment is superior, with strong appeal to foreign investment has always been the preferred destination of foreign investment while investing in southwestern, the southeast and the south areas in Guizhou has less foreign investments. Continued to maintain the advantages of absorbing foreign capital, Guiyang, should also optimize the expanding foreign investment actively. Foreign investment in Guizhou in a long period of key industries including: agriculture, infrastructure construction, high-tech industry, energy, environmental protection and raw material industries, urban facilities upgrading and tertiary industry. Introduction of the high-tech industry, basic raw materials industries and service work should be combined with the adjustment of industrial structure in Guizhou and modern enterprise system reform. Relevant government departments should gradually reduce the introduction of labor-intensive capital, with a focus on developing high-tech industries such as electronic information, bio-pharmaceuticals. While, government sector should effort to improve traffic, and communications, and water, based facilities conditions in Guizhou southwest, southeast, and the south areas and constantly perfect investment environment, adjust industry structure, improve industrialized level, increase publicity intensively in order to create good conditions to attract foreign capital , boot foreign investment from center

city to around areas actively and promote the balance development of foreign capital in each city in Guizhou.

3) Optimizing the industrial structure of investment attraction and accelerating the development of service outsourcing.It is supposed to actively undertake industrial transfer, and promote a further opening-up and optimization and upgrading of industrial structure together, besides, Taking the initiative to undertake industrial transfer abroad is beneficial. Apart from that, it is seizing the opportunities of global industrial restructuring, relying Guizhou resources, comparative advantage and industrial base markets that can put various development zones carrier and platforms into full play and can optimize the conditions of the business environment and supporting industries. Also, focusing on undertaking modern agriculture, high-end manufacturing, high-tech industries, modern service industry, new energy and energy-saving environmental protection industry transfer are firmly important. Moreover, it is a must to boost the related service institution and the innovation of government regulation, to make special economic function areas (such as Guiyang Comprehensive Bonded Zone) become a big platform facing the international market to develop service outsourcing industry so that government can enhance their own capacity in Guizhou service outsourcing industry and strengthen the service outsourcing talents education and training. Both taking every effort to train local service providers and undertake location services are equally essential. And actively guide the medium-sized state-owned enterprises and private enterprises with strength to participate in this process in order to deepen the division of labor, and strengthen self-service subcontracting as its starting point, and then will be able to constantly improve the level of participation in domestic and international division of labor services. Through enhancing the level of cooperation by multinational corporations, promoting the core competitiveness of local service levels, ultimately, it can facilitate a number of local outsourcing providers to success.

Acknowledgments

We thank Project Supported by MOE (Ministry of Education in China) Project of Humanities and Social Sciences (Grant No.13YJC790045) , National Statistical Science Project of National Bureau of Statistics in China (Grant No.2013LY104), Project of Science & Technology Department of Guizhou Provice(Grant No. QiankeheJ[2013]2090), Education Department of Guizhou Provice Project of Humanities and Social Sciences (Grant No.12QN035).

References

[1] Hansen H, Rand J. On the causal links between FDI and growth in developing countries[J].The World Economy,2006(01):21-41.

[2] Agosin, M.R.,Machado, R. Foreign investment in developing countries: does it crowd in domestic investment?[J].Oxford Development Studies,2005, 33(2):149-162.

[3] Allee, T.,Peinhardt, C. Contingent credibility: the impact of investment treaty violations on FDI [J].International Organization, 2011, 65(3):401-432.

[4] Moosa,I.A.,Cardak,B.A.The determinants of FDI: an extreme bounds analysis [J].Journal of Multinational Financial Management, 2006(16): 199-211.

[5] Girma S,Gorg H,Pisu M.ExPorting,linkages and productivity spillovers from FDI[J].Canadian Journal of Eeonomies,2008,41(l):320-340.

[6] Basu &Guariglia.FDI,inequality,and growth[J].Journal of Macroeconomics,2007,29(4): 824-839.

Advanced Materials Research Vols. 989-994 (2014) pp 5029-5032
© (2014) Trans Tech Publications, Switzerland
doi:10.4028/www.scientific.net/AMR.989-994.5029

Analysis of Reliability and Validity in Computer Assisted English Teaching Test

ZOU Xiaowei[1, a], WANG Xiaoli[2] and WANG Yan[3]

[1,2,3]College of Humanities & Social Sciences, Heilongjiang Bayi Agricultural University, Daqing city 163319,China

[a]ZouXiaowei425@yeah.net

Keywords: English test, computer, reliability, validity

Abstract. With the rapid development of computer technology, the computer has rapidly entered our daily life. People begin to use the computer for scientific research, production, entertainment, and information consulting and other activities widely, which brings about the Computer Aided Designing, Computer Aided Manufacturing, Computer Aided Instruction in order to improve the efficiency and quality of life. Using computer technology in language testing has become the trend of language testing both at home and abroad. Communicative language teaching becomes the guiding ideology and theoretical basis of modern language testing. The reliability and validity in computerized language assessments have become the two important criteria of evaluation of test quality. Computer Assisted English test with its unique advantages has opened up a new heaven and earth for English test.

Reliability and validity

Reliability of language testing refers to the reliability of the results, which means whether the test results is relatively stable or not. If the results of a set of questions tested today compared to a few days later are consistent, the reliability of the questions is high. The scale of the reliability of language testing mainly reflects the actual language behavior. There are many factors which can affect the reliability; they exist in every link of language testing.

Validity is a kind of correlation, indicating the connection degree of the test and objectives of the test. Generally speaking, if a set of questions measures what the designers want to measure or test about content or ability, then this is a test with high reliability and validity. According to the traditional explanation of structuralism, validity of language testing refers to whether it takes an examination of the test.

The reliability of language testing explains the relationship between examination results and language behavior. No reliability means that the test results are not credible and are not the real reflection of the examinees' language behavior, according to which is difficult for us to measure anything. With no validity but only the reliability of the test is meaningless, because it accurately measured the not related or unrelated things with language ability. In this case, we can't speculate the true language ability of these examinees from the test results also. To achieve the purpose of a language testing, reliability and validity are both required, which are the unity of the two relations.

The guiding ideology of computer aided English testing.

To design a good Computer Aided English Testing System and to improve its reliability and validity, we must have a basic understanding of the development of its guiding ideology and theory. The US education testing service put forward to establish a new English Testing System based on cultivating communicative ability. Obviously, this sets CLT (communicative language teaching) as the basic guiding ideology and theoretical basis, a new test model of communication skills to test candidates. CLI was brought about in 1960 ~ 1970 s by the British linguistics, it greatly improves the efficiency of language teaching and the learners' learning because it completely abandoned the previous thoughts that were putting emphasis on the mastery of language knowledge, and focusing

on calculation and improvement of the communicative competence, and thus has been widely accepted and promoted.

Communicative language testing includes communication ability such as grammar, discourse and social language ability and strategy ability and by the truth to make the candidates clearly handles language information and the implied meaning or function at the same time. Computer Assisted Language Testing is a new exam system based on the communicative competence, which is a kind of examination setting Communicative Language Teaching as the basic guiding ideology and theoretical basis, and its main purpose is to test actual communication skills of the recipients.

Testing models assisted by computer.

Use computer technology to test is a supplement to traditional language testing means. It can make up for the defect of system model and improve working efficiency to some extent and can achieve paperless test.

3.1Online testing model.

Online examination is suitable for large-scale network. After designing the test, the tester will compile the questions into database and put in the Data Server as stipulated. When examined, examinees enter personal information first, and then answer questions. When time arrived, it will automatically end the exam. Some tests just have objective questions, it can show examinee's score immediately, and print statements and the related certificate according to their need. In the future, examinee may use the form of dial-up in their own home to take the examination. If there is a large enough database and the questions have been dealt with certain difficulty processing, every time the examinee takes a test, computer can automatically generate a set of questions. So, the test can open all the year round, examinee can be flexible to arrange the time according to their own conditions.This will greatly improve the processing speed of the examination paper, save time and energy for reading; lower the error rate to zero. if the detailed performance statistics are not issued on the spot, it can also be sent to students via email quickly.

3.2PC testing model.

For the usual class test, phase test and homework test, the most feasible way is standalone software test. Questions are designed by the teacher on the special software. Students take the disk to attend the exam in a unified computer classroom or to test at home or at friend's on computer easily. Due to the same time that the software gives each student to answer, test is fair on the whole. Then, students hand the disk back to teachers, who read through the test software which actually done by computers and gives teachers the statistical report of the results. Stand-alone software test can reduce teachers' workload, increase students' interest in subjects, and can also greatly reduce the cost of printing papers. It has a very practical effec for all levels of the teaching unit.

3.3Unique advantages of the computer aided English testing.

With the development of English teaching reform, the use of multimedia network source to strengthen students' listening and speaking skills has become a important task in English teaching. Computerized test has gone through many forms, is born with the characteristics of dynamic, intuitive, image.

Problems can use words, pictures, voice or video or other forms to let the examinee maximum show their language skills and interpersonal skills within the given time. The computer aided test can not only check the basic language such as grammar, voice quality of the candidates, but also can test the examinees' speculative ability, understanding ability, personal skills and the understanding of the culture both at home and abroad, the grasp of the English idioms and interpersonal communication in foreign language etc. All in all, realizing the modernization of language testing and pick up with the world are the trend of the Times, are also the only way to our English test reformation in the future and improvement of the quality of foreign language teaching. Computer aided teaching may make students understand easily, especially difficult math. For example, some functions can be drawn to pictures and set math model such as **$y=a+bx$, $1/y=a+b/x$, $y=(x^b)$, and $y=a(e^{b/x})$ est.**

FFT and CAT.

FFT is face-to-face test, which examinees take test when the teachers are present and monitoring. CAT is computer aided test, which examinees take test on the computer.

Chart 1

	Average	Mode	Twin Tail	Minimum	Maximum
FFT	78.755	81	0.312	39	98
CAT	77.675	80	0.312	33	96

We see from chart 1 that the average grade of the FFT is higher than CAT. And chart 1, chart 2 and chart 3 show that CAT has higher discreteness while FFT has a trend to centre, among which the grade of 70-89 accounts for 85%, while 60-69 only accounts for 5% and more than 90 accounts for 8%. Compare to FFT, CAT is more reasonable. CAT system helps reduce the judge for scoring reliability of subjective factors, therefore, the result is more scientific and reliable.

Chart 2

Scores	<40	40-59	60-69	70-79	80-89	>90
FFT	2	1	6	51	62	12
CAT	1	1	23	40	46	23

Chart 3

	Reading	Question 1	Question 2	Discussion
FFT	0.65	0.72	0.77	0.75
CAT	0.70	0.69	0.75	0.71

Improving the reliability validity of computer-assisted English test.

Training the examiner before the test is a useful way to guarantee the reliability and validity. Examination is a kind of education measurement. For the so-called measurement, the first thing to have is a standardized measuring tool; then people who use the measuring tool should be able to maintain the consistent standards. If computer-assisted language testing examiner want to achieve this, the examiner must have a consistent view on the measured language ability, have a consistent understanding on scoring criteria, and grasp the scoring criteria consistently. Language testing is not only a performance test, but also a proficiency test, because the fundamental purpose of the test is that student learn through specific textbook content finally learned the content and form a kind of ability, both language ability and auxiliary language understanding and expression of language ability. This kind of reliability is indispensable to any kind of exams and is an important feature in any exam, otherwise the examination results will not be able to accurately reflect the real examinee's true ability.

Summary

Facing the trend of computer aided language testing at home and abroad, to design good Computer Aided English Testing System, improve its reliability and validity need designers and managers of the Computer Aided English Testing System to understand and grasp the guiding ideology and theoretical basis of modern language testing, at the same time, do more research and exploration in the examiner training and the quality monitoring of computer aided testing marks. Only with the validity and reliability of test, will the exam reflect the real level of the examinee and promote the development of English teaching.

Acknowledgements

Supported by Philosophy and Social Science Research Program in Heilongjiang Province (Grant No. 13E046) and Higher Education teaching reform Program in Heilongjiang Province (Grant No. [2013]351:371)

References

[1]Anna Taddio,Mary-Ellen Hogan,Paul Moyer,Angela Girgis,Sandra Gerges,Linda Wang,Moshe Ipp. Evaluation of the reliability, validity and practicality of 3 measures of acute pain in infants undergoing immunization injections[J]. Vaccine,2010,297:.

[2]Lisa Hartling,Andrea Milne,Michele P. Hamm,Ben Vandermeer,Mohammed Ansari,Alexander Tsertsvadze,Donna M. Dryden. Testing the Newcastle Ottawa Scale showed low reliability between individual reviewers[J]. Journal of Clinical Epidemiology,2013,:.

[3]Jeffrey J. Hebert,Shane L. Koppenhaver,Deydre S. Teyhen,Bruce F. Walker,Julie M. Fritz. The evaluation of lumbar multifidus muscle function via palpation: reliability and validity of a new clinical test[J]. The Spine Journal,2013,:.

[4]Jun-Young Jeon,Won-Seob Shin. Reliability and validity of the Korean version of the Trunk Control Measurement Scale (TCMS-K) for children with cerebral palsy[J]. Research in Developmental Disabilities,2014,:.

Advanced Materials Research Vols. 989-994 (2014) pp 5033-5036
© (2014) Trans Tech Publications, Switzerland
doi:10.4028/www.scientific.net/AMR.989-994.5033

Comparative Analysis of the Professional Situations and System of Television Basketball Commentator in China and America

Fan Yanwei, Fan Xiao

Physical Education Department of Ji'nan University, Guangzhou, 510632

Keywords: television basketball commentators; China; America; comparative analysis

Abstract. As unique scenery when the fans are appreciating high-level basketball matches through television signals, the television basketball commentators stand as an excellent channel for the fans to better and carefully appreciate the matches and to learn the information in and off the court. By means of document and data and comparative analysis, this thesis makes an analysis of the professional situations and system of television basketball commentator in China and America. Finally, it arrives at a conclusion that compared with those in America, Chinese television basketball commentators have huge gaps in many aspects, especially that the professionalization of working system urgently requires improvement and enhancement.

Basketball matches in China are growing energetically. Every year, hundreds of high-level basketball matches from China Basketball Association and China University Basketball Association are held significantly. In the meantime, on the other coast of the Pacific Ocean, countless high-level matches are held in America, and the so-called "the kingdom of basketball" and NBA (National Basketball Association) have been universally recognized as the professional sports event with the highest competitive level and appreciation values. It is the basketball matches of the highest level all over the world, including Olympic Games and the World Basketball Tournament that become the necessities for Chinese basketball fans. In order to satisfy the large demands from fans, every year, live broadcasting of numerous basketball matches prove to be materialized by CCTV-5. Different local stations and online channels enable the Chinese fans to watch high-level basketball matches closely, learn match process and characteristics in time and cheer for their own favorite teams, in all of which the television commentators play a crucial role. A qualified commentator requires the ability to allow the fans to learn information in and off the court at all aspects more comprehensively, watch the matches more intensely and enjoy an on-site experience and a long aftertaste of the matches.

The current era in which the electronic media constitute the mainstream is replete with internet information. The basketball matches are becoming more and more worth appreciating, in that the spectators include basketball fans as well as experts in basketball teaching, training and researching. They collect information by all means, conduct further researches in sports and athletes and possess rich first-hand materials comparable with those possessed by television commentators. Meanwhile, along with the results of the matches no longer as the single focus, it proves to be the major content to analyze matches from all perspectives and track the latest life information and details of teams, player and caches, all of whom gradually bring basketball matches back to their complex and diverse ontology plane and the diversification edge of the entertainment. Therefore, the traditional "know-all" television sports commentators fail to meet higher requirements from audiences and it will be a mainstream for the professional basketball commentators to commentate matches. Compared with the professionalized and specialized American basketball commentators who enjoy profound professional basis and commentating capacity, the Chinese basketball commentators encounter gaps at the following major aspects.

To Compare Chinese And American Basketball Commentators From The Perspective Of Composition

Most commentators in China come from the channel of CCTV, different local television stations and network channels. Most of them prove to be broadcasters or prove to major in sports news, including Yang Yi, Su Qun and Sun Zhengping. In the meantime, a minority of commentators

possess professional sports background, including Zhang Weiping (former main power forward of Chinese National Basketball Team) and Xu Jicheng (former player of Beijing Military Area Basketball Team). From time to time, some high-level professional athletes or coaches are invited as the commentary guests, for instance, Yao Ming and Wang Shipeng were invited as the commentary guests in the 2011 Wuhan Asia Championship for Men and some domestic famous basketball characters including Li Nan and Zhang Jinsong. Two former players of Rockets, Wang Fei, the chief coach of Zhejiang Guangsha, were invited as the commentary guests during the broadcasting of CBA matches; however, few commentators who have commentated basketball matches with rich professional basketball experience are available, due to which some conspicuous basketball tactic mistakes during commendation would occur and mislead the basketball fans.

A large number of NBA commentators turn out to be former prestigious NBA stars, coaches or team accompanying staff, including "Evil Bird" Charles Barkley, former player of Phoenix Suns, Reggie Wayne Miller, former player of Indiana Pacers and "the Glide" Clyde Drexler, former player of Huston Rockets. After their player career in NBA, they gradually became well-known NBA basketball commentators and Barkley had been laughed at by the fans across the world since kissing the ass of a donkey due to losing the bet that Yao Ming would never score over 19 points in his first year in NBA. Van Gundy, former chief coach of Huston Rockets, the team Yao Ming once played for, becomes an outstanding NBA commentator after his coach career.

Thanks to energies required in professional basketball matches and their own tolerable language talents, with professional systematic trainings, these players or coaches prove to be commentators of the basketball matches at will. What's more, some "professional" basketball commentators would drop some comments on their own sporting experience at intervals, which turns out to be fans' favorite thing.

To Compare Chinese And American Basketball Commentators From The Perspective Of Commentating Style

Excellent commentations would allow the adrenal hormone of fans and players to soar in a short time. On the contrary, however, monotonous ones would devitalize the exhilarating matches. Therefore, it is not uncommon for us to notice that some fans would like to watch a match for a specific commentator while some would turn off the sound of the TV when they are watching the matches. With every commentator characterized with his or her own personalities, Chinese and American commentators bear huge differences in commentating styles. As for American television commentators, individuality is encouraged so that some incredible actions would be presented during the commentations; nonetheless, most Chinese commentators prove to be modest and prudent, and they could always provide their audiences with soul-stirring feelings at the vital moments.

Local television stations in America are characterized by typical American style and the resonant American pronunciation accords with the court atmosphere perfectly; nevertheless, it can be easily found out that most commentations broadcast by local stations prove to be descriptions for the matches. Some commentators are used to commentating energetically. For instance, once they are invited as the commentators of ESPN, Bill Walton looks like an extremist and feels like employing a series of words to express one opinion powerfully and vigorously. By comparison, in American commentating field, Charles Barkley from TNT turns out to be more explosive in that he frequently displays some unbelievable actions. Apart from the coexistence of steady and profound academism styles, for example, Hubie Brown from ABC television station seems to pay more attentions to "rationalness". With unparalleled understanding of basketball, old Brown would endow anyone sitting beside with basketball knacks within a short period of time. During the prudent and humorous commentating, Van Gundy successfully gets himself "vampire eyes" with his pervious experience as a basketball coach.

Chinese television commentators tend to attach more attentions to the style of a team, the backgrounds of the players, as well as the tactics. Unique styles have been formed in Chinese commentations which can be exemplified by CCTV. Among all CCTV-5 commentators, Sun

Zhengping might be taken as a has-been while Yu Jia and Yang Jian present outstanding commentations; with regard to the commentary guests, with plain languages, Xu Jicheng is as kind as a senior who watches the matches over drinking tea; humorous and exhilarating, Yang Yi is quite familiar with the overall information of NBA and presents audiences with well-organized and logic commentations or bombing words and expressions. Home at the basketball knowledge, Su Qun, the chief editor of *Basketball Pioneers*, has conducted numerous highly professional interviews in NBA All-stars and finals; at the time when it comes to the professional level of domestic men's basketball commentations, Zhang Weiping turns out to be second to none, due to which he has been entitled to "rational tutor" by his fans out of the good will. During the commentations, Chinese commentators apparently tend to give emphasis on the explanations of tactics, as well as the analysis of players' actions.

Differences Between Chinese And American Working System Of Television Basketball Commentators

China has witnessed an immature selection and evaluation system for television basketball commentators, most of who suffer from the low professionalization due to undertaking commentations for other sports. Professional basketball commentators prove to be peculiar to CCTV in that all CBA teams possess no television basketball commentators and there are only three local television stations, including Beijing, Shanghai and Guangdong Province that are equipped with their own professional television sports commentators. All of them have to be commentators of other sports at the same time and sometimes invite the assistant coaches or retired players as the commentary guests. With profound basketball knowledge, these guests can not become qualified television basketball commentators without systematic knowledge and professional training of being commentators.

Each team in NBA employs its own professional basketball commentators to commentate matches at local television stations. For instance, Clyde Drexler, former player of Huston Rockets became a basketball commentator for Huston Rockets after his retirement and he made commentations of numerous matches of Yao Ming. Having been working for his team for 27 years, Brad Davis, commentator of Dallas Mavericks, is quite familiar with the players and coaches and from time to time blurts out some novel punch lines. In America, all local television stations possess their own professional basketball commentators. Once establishing Bulk Dynasty together with Micheal Jordan, Steve Kerr used to be a commentator at TNT television station to offer on-site feelings for the audiences with his rich court experience. Thanks to the long-term company with the teams, their professional experience in NBA as players and constant commentating, they enjoy a high level of professional commentations.

Differences In Payments For Television Basketball Commentators In China And America

There exist huge gaps when it comes to the payments for television basketball commentators between China and America. While being invited as commentary guests in Wuhan Asia Basketball Championship for Men, Yao Ming and Wang Shipeng received 500RMB, which proved to be incomparable with the payments of CBA professional players. As the commentary guests for CCTV in CBA matches in 2008, Wang Fei was paid over 3000RMB in total after a half of the season, which even proved to be lower than the salaries of workers in some private enterprises in south China. Therefore, it turns out to be rather difficult for them to attract the domestic basketball elites to commentate matches with such low payments.

The author came across Josh Brown, a consultant invited by China's Basketball Association and former television basketball commentator for a certain NBA team at a CUBA summer camp, who revealed to the author that in America commentation payment for one match was 5,000 dollars and as for NBA celebrities, the payment could be higher. For instance, Van Gundy, mentor of Yao Ming signed a five-year contract with ESPN, with the annual salary as 1.2 million dollars (nearly 7.6 million RMB) which required CCTV commentary guests to commentate 15,320 matches. Charles Barkley, a TNT commentator and NBA celebrity obtained an annual salary of 1 million dollars

(nearly 6.4 million RMB) while those with narrow reputations, including Mark Jackson and Jon Barry, could receive an annual salary of 600,000 to 800,000 dollars. Compared with 50,000 dollars, Americans' average annual salary, proved to be much higher, though far lower than that of the NBA stars. Therefore, plentiful payments attract more stars and celebrities to commentate, due to which more fans would like to watch live broadcastings.

Conclusions and Suggestions

A. Conclusions

Compared with television basketball commentators in America, Chinese television basketball commentators possess their own job category and commentation characteristics, both of which play a vital role in enabling the basketball fans to better appreciate the basketball matches. Here are the specific conclusions as follows:

• China and America differ greatly in the sources of television basketball commentators. Speaking it more concretely, Chinese commentators are mainly engaged in professional news media, and few of them have possessed professional experience; however, most American commentators are retired players or accompanying staffs from NBA teams, who constitute the majority of American commentators. Their professional level in basketball and professionalization of commentation are absolutely higher than those in China.

• Both Chinese and American television basketball commentators enjoy their respective commentating styles. The commentators China are relatively more prudent and serious, while those in America are alive with their characteristic individuality, which can be mainly explained by their differences in the cultural landscape.

• The working system of China's television basketball commentators proves to be partially professionalized than that of America in that as professional commentators. Most commentators in America are professional, who engage themselves into basketball commentating all year round; however, in China, and the vast majority of the commentators are temporary or part-time commentators who are players or coaches invited from CBA teams. This is quite common phenomenon in China.

• Compared with that in America, the payment of Chinese basketball commentators proves to be rather low, which differs greatly from that in America. It is really difficult to employ the retired players or coaches from CBA or other high-level basketball leagues. It is directly influencing the professional grade of commentators.

B. Suggestions

• It requires Chinese television basketball commentators to fulfill their own commentating personalities on the condition that the modesty and prudence are maintained so that more basketball fans can be attracted by their unique styles. They should give full play to their individuality in being a commentator so as to attract more and more fans.

• China should further specialize and professionalize the working system of television basketball commentators. In the meantime, all local television stations should also employ the corresponding professional commentators, in order to satisfy the infinite demands from all of the fans of basketball.

• The payment of professional television basketball commentators in China must be increased to a higher level, so as to attract all kinds of elites with professional basketball experience to apply for commentating. In this way, the overall level of China's basketball commentating can be further improved and enhanced to a higher level to better serve the fans.

References

[1]. http://baike.baidu.com/.
[2]. http://sports.qq.com/a/20080621/000406.htm.
[3]. Zhang xiaodan, Professionalization of Television Sportscast Commentators, Journalism Lover, 2010 (24).
[4]. Cai Jiabao: Research in Nourishment of Sports Commentators for 2008 Beijing Olympic Games, Journal of Wuhan Institute of Physical Education, 2006 (8).
[5]. Jin Beiping: Differences between Sports Commentators of Old and New Generation, Modern Communication, 2008 (2)
[6]. http://www.tudou.com/groups/posts1876636p1.html.

Advanced Materials Research Vols. 989-994 (2014) pp 5037-5040
© (2014) Trans Tech Publications, Switzerland
doi:10.4028/www.scientific.net/AMR.989-994.5037

The impact of RMB appreciation on the sporting goods industry and Countermeasures

Fan Wei Yan , Fan Xiao

Sports Ministry, Jinan University, Kaifeng 475001

Keywords: domestic currency appreciation; sporting goods industry; effects and countermeasures

Abstract. This paper uses literature survey and online survey to analyze the reasons for the appreciation of the currencies and its impact on the sporting goods business in China. It proposes a few strategies for the companies to deal with the appreciation such as: Restructure the finance and manage the foreign currency debt effectively; utilize the oversea resources to reduce the production cost; improve the added value to the products, increase the investment in the research and development, follow the brand and sales strategy and become more competitive.

Objective

Exchange rate is an important international financial issue closely related to national economy. The fluctuation can have significant impact on the international trade. Since China adopted the reform policy, the rapid development of China's foreign trade surplus

Has accumulated a large reserve and exert unprecedented pressure on RMB appreciation. As Chinese sporting goods industry heavily rely on exports for its growth, the RMB exchange rate is critical. They need to comprehensively understand the impact of the RMB appreciation and make timely changes in terms of resource allocation and sales, restructure the business.

Research Methods

2.1 Literature survey

Through journals, newspapers and other books, we gained more information about the RMB appreciation and investigated on both the positive and negative impact of currency appreciation on the sporting goods industry.

2.2 Field survey

We visited Zhejiang, Fujian, Guangdong and other sporting goods manufacturing centers and sent out questionnaires to 80 companies, among which 74 were recovered (the effective recovery rate of 92.5 %).

2.3 Online information query

The reference material we found online include State Sports Information Institute's "foreign sports information database", China Sporting Goods Association's "Sports Information Network China". From them we can better understand the sporting goods industry, changes in operating conditions and the impact of the exchange rate.

Results and Analysis

3.1 The reasons behind RMB appreciation

As U.S. still dominates the world economy, the fluctuation of the U.S. dollar exchange is a top news for the world finance. From the historical peak of 0.8 euros, the dollar decline against the euro has accumulated more than 60%. As a result of pegging the foreign exchange rate to the dollar, the yuan against other major currencies depreciated indirectly[1]. For a time, from their own interests, the United States, Europe, Japan, all advocated to revalue Yuan. And the rumors on the new exchange policy for the RMB kept on coming, while the non-deliverable forward contract (NDF) discount rate reached record highs. China exchange rate policy became the world top attention.

3.1.1 RMB appreciation is due to decreased U.S. dollar value

The depreciation of U.S. dollar is caused by the market worries of the large US debt and the rapidly deteriorating current account deficit. America has always been a high consumption, low savings country. Therefore, the current account deficit inevitably accompanied the huge budget deficit. When Bush took office in 2001, there were $127.3 billion federal fiscal surplus, but after the large-scale tax cuts, the economic recession led to revenue decreases, and the war on terror further increased the financial expenses dramatically. The financial situation deteriorated rapidly. In fiscal year 2004 , the federal deficit reached $ 413 billion. In addition to these two points, the U.S. dollar was also affected by the impact of direct investment. In 1999 and 2000, foreign direct investment in the United States reached $ 283.4 billion and $ 314 billion; but then the world's direct investment went to a low ebb, and the amount was significantly reduced, by 44.9% from 2002 to 2003. As U.S. current account imbalance becomes more severe, the pressure on a cheaper dollar has increased.

3.1.2 The inflation pressure

Recently a large number of speculative capital flew into China's financial markets, betting on RMB’s appreciation. The rapid increase can be seen from China’s foreign exchange reserves since 2003,. Over a long period of time, China's capital flight had been a problem. Although there were huge trade surplus, the amount of foreign exchange reserves did not reflect the growth of these "surplus". Since 2003, even if the surplus did not increase as much, foreign exchange reserves climbed up really fast. Customs statistics showed that in the first eight months of 2004 China's total trade surplus was $8.86 billion only, but according to the Bank of China’s statistics, September 2004 alone saw China's foreign exchange reserves increasing by $183.69 billion. As of end of March 2005, China's foreign exchange reserves reached $659.1 billion and broke a new record. Under the mandatory sale of foreign exchange, large amount of dollars were sold to the central bank, and the central bank had to pay 8.28RMB to each dollar. As RMB were circulated, inflationary pressure followed.

3.1.3 The internal dynamics within the economic system

The major internal factors for Chinese economy include foreign exchange reserves, inflation, price levels, balance of payments, interest rates and economic growth conditions [2]. The RMB appreciation would help alleviate the “overheating" of the economy. In certain circumstances the currency appreciation pressure can be converted to inflationary pressure and help get rid of the fixed currency model, preparing for yuan to become the world's hard currency. It is also an opportunity to narrow the difference between the RMB and the Hong Kong dollar for the gradual transition to 1:1, and in due course, the yuan, the Hong Kong dollar, the Macao dollar can be integrated to form a single currency.

3.1.4 Historical Reasons and External Pressure

Between1994 and 2004, the RMB exchange rate had not been adjusted for 10 years. Since then, China began to implement a managed floating exchange rate system and officially ended the pegging system. China resumed the pegging during the recession but eventually let it flow again. In the last ten years China's economy has undergone profound changes. The trade surplus got too large, and foreign exchange reserves got excessive due to the payment imbalances. RMB appreciation is unavoidable. In addition, since 2001 currencies in all major Southeast Asia countries have been greatly appreciated against dollar, and RMB was devalued as it pegged to the dollar. After joining the WTO, the trade surplus further increased as China exported a large number of cheap goods all over the world and affected the domestic labor markets. For example, US government has elevated the currency issue to a key political issue, hoping to use RMB appreciation to limit Chinese imports.

3.2 The Impact of the exchange rate fluctuation on the sporting goods business

3.2.1 RMB appreciation affected the export significantly

China's sporting goods companies are mostly focused on production only, in the processing trade, and in the middle of the smile curve, playing the production role in the global value chain [3]. Currency appreciation brings into less domestic currency. Coupled with price increases and high

inflation, exports almost have no profit and even have to suffer losses. Many companies are not willing to accept orders and having hard time to continue with their productions.

3.2.2 RMB appreciation can help the companies to repay the foreign debt

Since the exchange rate reform, the RMB against the U.S. dollar dropped from 1:8.7 to 1:6.34 (December 2011), which is very beneficial for companies bearing foreign debts. they should delay the repayment time, to increase the amount of foreign debt purchases, to reduce debt costs. Data shows that RMB appreciation can inhibit the inflow of foreign capital, which includes foreign direct investment and foreign borrowing to debt.

3.3 RMB appreciation is conducive for direct trade to foreign partners

3.3.1 RMB appreciation will help lower purchasing cost of overseas material and reduce production cost RMB appreciation means the devaluation of the foreign currency.

Companies can use an equal amount of yuan to buy more raw materials from overseas market, and therefore reduce the final cost and hedge the impact of the domestic inflation. Along with the RMB appreciation, the domestic price level rises rapidly for raw materials and labor costs and harms the export competitiveness of enterprises. Companies should seize the opportunity to take advantage of the high currency, increase the purchase of foreign low-cost factors of production, reduce production costs to rise.

3.3.2 Able companies should increase the direct overseas investment

In the 1990s, the sharp appreciation of the yen forced many Japanese enterprises to develop new technologies and new products to improve value-added products and reduce production costs, but the magnitude of the appreciation of the yen was too large to offset the yen's appreciation [4]. To increase the competitiveness, the majority of enterprises adjusted the business strategy and adopted approach of the direct investment. They built local factories, purchased and sold locally and thus maintained the share of exports business. Therefore, Chinese companies should learn from their experiences and set up factories overseas. This is not only to seize the foreign market but also to bypass the barriers and reduce the increasing trade friction.

Suggestions and strategies

4.1 Speed up the product innovation and promote the development of industrial clusters

Most of the sporting goods industry are labor-intensive, low value-added. They are likely to get hit first during market turmoil due to the lack of product innovation and brands. The sporting goods industry cluster development can promote the product specialization, increase the economies of scale, reduce transaction costs, and help share information, technology, brand and sales network channels and thus increase the ability of resisting the risks.

4.2 Adjust the industrial structure and speed up the industrial upgrading

RMB appreciation can reduce the raw material cost and can be used to adjust the product structure and accelerate new product development and research. With increased usage of imported parts and raw materials, companies can further increase their export shares, China's sports goods exports was mainly targeted at the United States, Japan and Hong Kong. RMB appreciation would weaken the competitive advantage of these companies. They are forced to speed up the restructuring and upgrade their products [5] and move from the low value-added processing to high value-added products. During this value chain upgrade, companies can enhance their international competitiveness and reduce the exposure to the risks of price competition.

4.3 Use "going out" strategy to reduce trade friction and avoid trade barriers

After thirty years of development, there emerged a number of listed Chinese sporting goods companies who own their own brands and R & D capabilities. They have the capital, technology and marketing channels and the ability to expand overseas. They should take advantage of the RMB appreciation to invest in foreign markets directly, use local production and local sales to bypass trade barriers and reduce trade friction. On the other hand, they should actively explore new markets and focus on Africa, Eastern Europe, Central Asia and other emerging markets to avoid the adverse trade situation due to over-concentration on developed markets.

4.4 Actively participate in the export credit insurance

Export credit insurance is the insurance policy offered from the Chinese insurance companies and banks to encourage enterprises to export and protect their income stability. Under the circumstance of large fluctuation of RMB, sporting goods export enterprises should participate in these insurance programs, using limited insurance costs to lock down the currency benefit of the coming period and have the insurance company to share the losses caused by appreciation. This will help enterprises to maintain more stable operation.

4.5 Improve the business training and increase the enterprise's risk awareness

Chinese enterprises have been accustomed to a fixed exchange rate and relying on the currency devaluation and low cost to stimulate exports instead of strengthening the management, reducing costs, improving the efficiency to enhance export competitiveness. A considerable number of domestic companies are still not aware of the potential impact and risk of rising exchange rate. Government should reach out and do more research to educate these companies. 5. Conclusion. In summary, RMB appreciation has become unavoidable and the sporting goods export enterprises bear the brunt of its impact. It is not so meaningful to discuss the pros and cons at this moment and it is more important for companies to find coping strategies, such as increasing the purchase of foreign raw materials and other parts, more direct investment in local markets to get around the trade barriers, and upgrading the products and more innovations.

References

[1] Zhang Qing. Strategic innovation of China's sports goods industry[j]. Journal of Xi'an Sports Institute. 2003-3

[2] Bao Ming-xiao. Sports industry a new economic growth point [N]. People's Sports Publishing House. 2002-6

[3] Bai Zheng. Examination of the Sporting industry based on global value chain [D]. Henan University doctoral dissertation, 2008.

[4] Bai Zheng. Upgrade China's sporting goods industry in the global value chain [J]. Wuhan Institute of Technology 2010, (7) :18-20.

[5] Zhou Yuntao, Bai Zheng, etc. Upgrade China's sporting goods industry in the global value chain [J], Journal of Beijing institute, 2009 8.

[6] Li Hongwei, Bai Zheng, etc. Opportunities and challenges for China's sporting goods companies facing the ASEAN Free Trade Area [J], Beijing University of Physical Education, 2010, (11) :12-14

Advanced Materials Research Vols. 989-994 (2014) pp 5041-5044
© (2014) Trans Tech Publications, Switzerland
doi:10.4028/www.scientific.net/AMR.989-994.5041

Analysis of Things technology to promote the dynamic alliance virtual performance evaluation

Hongxia Zhang[1, a], Qiang Zhang[2,b]

[1] Shenyang University of Chemical Technology, Shenyang, China

[2] Shenyang University of Chemical Technology, Shenyang, China

[a] hhsyln@126.com, [b] sy24365@126.com

Keywords: virtual performance evaluation; Internet of Things; dynamic alliance performance

Abstract. With the development of modern information and communication technology and network technology, modern enterprises choose to build virtual dynamic alliance to achieve business development goals. There are many uncertain relationships between the participating companies in the virtual dynamic alliance. These companies join together to accomplish a particular goal, but also has their own unique individual needs. Internet of Things is an important part of a new generation of information technology. Things technology is an extension and expansion of the network based on the Internet. Basis for building virtual dynamic alliance is the Internet. The enterprises participating in a virtual dynamic alliance communicate with each other relying on information communication technology. Internet of Things technology provides real-time performance evaluation data to the participating enterprises. This will ensure real-time performance data communication between the dynamic alliance enterprises relatively loose.

Introduction

Dynamic alliance is a virtual dynamic structure, which incorporates many enterprises management realistic goals and expectations of future developments. Dynamic alliance is a common mode of operation and management of the project. Many enterprises will participate in the dynamic alliance in order to complete specific core projects. These participating enterprises of dynamic alliance have their own management entity.

In order to better achieve the specific project objectives, the dynamic alliance need to establish an effective of real-time performance evaluation system. Such evaluations system will be beneficial to each participating enterprise for the real-time regulation and management. If each participating enterprises can achieve real-time performance communication, performance evaluation of dynamic alliance can be achieved on the participating enterprises real-time evaluation. Meanwhile each participating enterprises can also get rectification dynamic alliance performance evaluation system in the first time.

The dependency between the participating companies of dynamic alliance is a dynamic process of change. Performance evaluation system of the dynamic alliance will collect the daily performance effects of the participating enterprises real-time. Virtual combination architecture of dynamic alliance requires a dynamic real-time data communication platform. Things technology can take full satisfy the real-time data communication needs of virtual performance evaluation in dynamic alliance. Things technology can efficiently complete the communication and sharing of data, combined with the actual implementation of the core projects in the dynamic alliance virtual performance evaluation process.

Performance evaluation of the dynamic alliance

Virtual dynamic alliance is an external optimization and integration based on the core competencies of the core business. Alliance's core businesses will focus their own investment and

management attention on their core capabilities. They make other dynamic alliance enterprises to accomplish the non-core capabilities and the ability that they could not master in a short time.

The more common performance evaluation process will use mathematical statistics, operations research principles and specific indicators. In the performance evaluation, the organization will reference to a uniform standard, accordance with certain procedures. Generally, the organization's performance evaluation will rely on quantitative and qualitative comparative analysis method. Within a certain period of operation of each project, the normal performance evaluation process will make an objective, fair and accurate operational efficiency and comprehensive evaluation results of operations for these projects.

Dynamic business alliances is an integrated enterprises combination based on the core needs of the project. The enterprises themselves are individual independent body. All enterprises in their business activities have established a performance evaluation system in line with their own development needs. Each enterprise in a dynamic alliance enterprises need to adapt to other collaborative enterprises according to the actual operation of the core project. These enterprises will continuously adjust their own management process in compatible with the overall performance of dynamic alliance in order to meet the requirements of the overall dynamic alliance performance evaluation system.

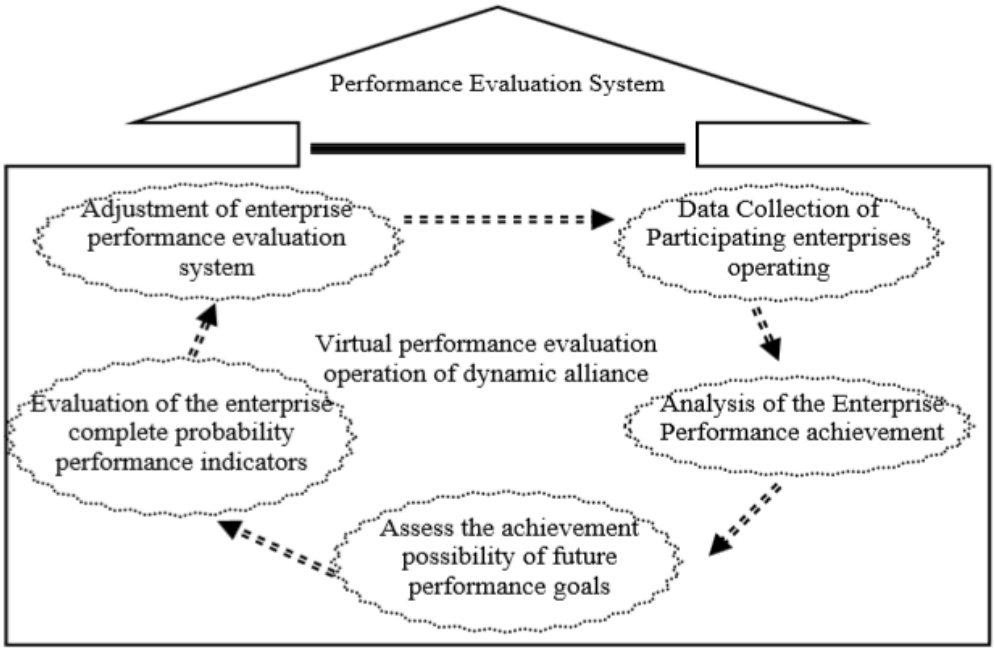

Figure 1. Virtual Performance Evaluation of Dynamic Alliance

Performance evaluation of dynamic alliance is different from the ordinary business of the daily performance evaluation process. Dynamic Alliance of each enterprise will be subject supervision and evaluation of real-time, based on performance evaluation system dynamic alliance. Guided by real-time performance evaluation indicators, the participating enterprises can conduct business management and operations to meet the overall goal of dynamic alliance. Performance evaluation of dynamic alliance will no longer be directly linked to the expected evaluation of specific participants. The foundation of the dynamic alliance is based on the expected return of the core projects. Each participating businesses will organize their own business enterprises in accordance with their understanding of the expected benefits of the project. Therefore, the participating enterprises are possible to adjust their position in the dynamic alliance at any time, even with dynamic alliance relationship, according to the needs of their own survival and development. Performance evaluation of dynamic alliance should always be in the form of a dynamic evaluation system. Such performance evaluation will play a supervisory role for the alliance participating enterprises in the process of realization of dynamic alliance's overall performance goals.

About Internet of Things

Internet of Things is an important part of a new generation of information technology. Internet of Things is a model which is based interconnection, grand Integration and based SaaS operations on cloud computing, etc. Internet of Things will connect the ubiquitous of terminal equipment and facilities, using a variety of wireless or wire line long-distance or short-distance communications network.

Internet of Things technology is widely used in the integration of network resources through intelligent perception, recognition technology and pervasive computing, etc. The clients can already extend and expand the process of information exchange and communication between any goods and goods. Internet of Things is an extension and expansion of the network based on the Internet. Core and foundation of Internet of things is still the application about the Internet.

Internet of Things is an extension of the Internet technology in modern information communication and processing technologies. It will meet the needs of the actual resources sharing between customers at a deeper level and extent of broader. Internet of Things includes all resources on the Internet and the Internet. Internet of Things is compatible with all Internet applications. But at the same time all the elements in Internet of Things have the characteristics of personalization and privatization. So, Internet of Things will be able to provide basic networking platform to ensure the integration of the personalized resources and the common network applications.

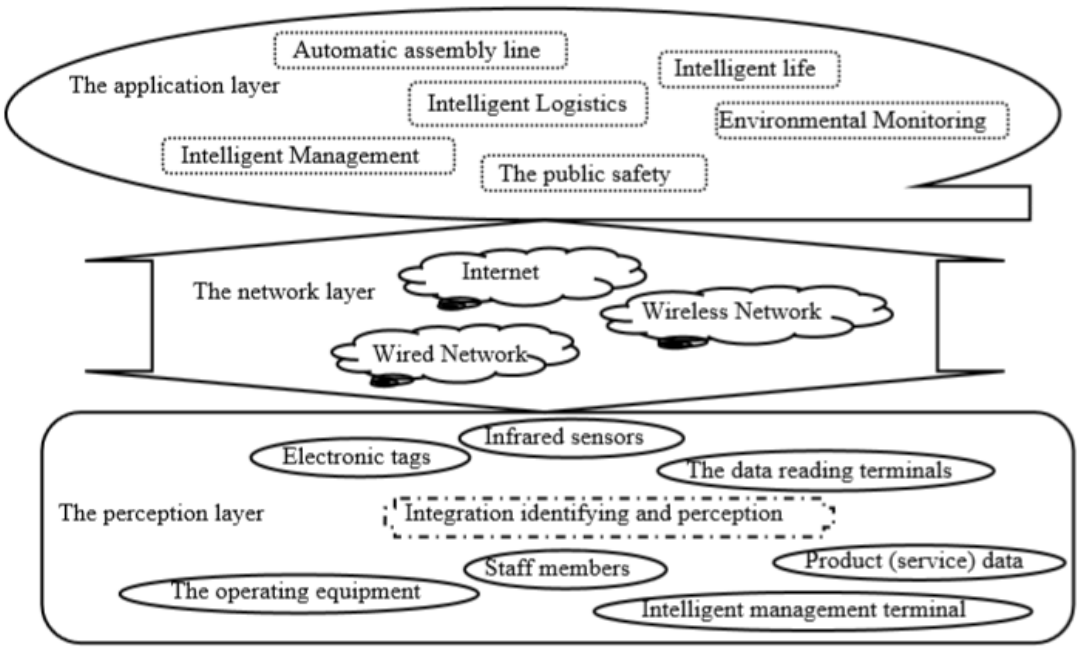

Figure 2. Internet of Things constitution

Internet of Things will provide a real-time open, smooth communication customer communication space as a new the application Internet technology. Internet of Things will be able to ensure timely obtain the relevant information and make the appropriate feedback based on certain criteria. Various services provided by Internet of Things are based on all types resource sharing and instant communication needs between users.

Things technology impact on the dynamic alliance virtual performance evaluation

Basis for the establishment of a dynamic alliance is dynamic random integration purposeful for each of the participating enterprises. In the implementation process of the project, these companies can maintain instant communication and information sharing fully. In order to achieve the common goal, the dynamic alliance will build up a performance evaluation index system focus on the project implementation process.

With operation of dynamic alliance, the virtual performance evaluation index system will conduct performance evaluation in real time for each of the participating enterprises. Virtual Dynamic Alliance is a loose organizational structure. There are no fixed mutual restraint mechanisms within the Alliance between the various participating companies. In order to ensure the efficient implementation of the dynamic alliance project, the participating enterprises need ensure the smooth realization of the overall performance objectives by developing and implementing effective performance evaluation system. The excellent performance evaluation system requires a practical implementation system. The participating companies of dynamic alliance can guarantee real-time communication with each other through the implementation demand of specific projects.

Internet of Things widely used provides an effective support for real time communication and information shared between the companies of dynamic alliance. So each participating companies can play a unique role in the dynamic alliance while ensuring their own development. Performance evaluation system the dynamic alliance requires all participants to ensure timely adjustments in project implementation process. Application of Internet of Things technology can provide maximum support to meet this demand. Internet of Things will play an important role in constituting in the dynamic alliance.

Dynamic Alliance need to ensure that the status of each participating enterprises revolve around the overall objectives of the Alliance. The various enterprises in the loose alliance need maintain close mutual communication to reflect and observe through the actual business indicators. Internet of Things can provide timely the reaction current status of business execution of each participating enterprise data.

Summary

Dynamic Alliance has a strong adaptability and vitality in adapting to the changing needs of the market process. Enterprises involved in the dynamic alliance work efficiently with other participating companies in the process of achieving their own development. Highly efficient collaborative work among the participating companies needs an effective performance evaluation system. Virtual Performance evaluation of dynamic alliance requires keep abreast of the participating company's performance implementation.

Internet of Things technology stands ready to provide communication and information sharing effective protection for various enterprises in organizations operation process of the dynamic alliance. Internet of Things technology will facilitate the effective operation and favorable development of dynamic alliance virtual performance evaluation system.

References

[1]Daniel D. Giusto, Antonio Lera, Giacomo Morabito , Luigi Atzori: *The Internet of Things*, edtied by Springer-Verlag New York Inc (2010)

[2]Judith Hale: Performance-Based Evaluation: *Tools and Techniques to Measure the Impact of Training*, edtied by Jossey-Bass San Francisco (2002)

[3]Olivier Hersent, David Boswarthick, Omar Elloumi: *The Internet of Things*, edtied by Key Applications and Protocols (2012)

[4]T. Ihde: Dynamic Alliance Auctions: *A Mechanism for Internet-based Transportation Markets*, edtied by Physica-Verlag GmbH & Co (2003)

[5] Information on http://zh.wikipedia.org

Advanced Materials Research Vols. 989-994 (2014) pp 5045-5048
© (2014) Trans Tech Publications, Switzerland
doi:10.4028/www.scientific.net/AMR.989-994.5045

Research on dynamic relation model of LOGINK service innovation

Tingting Huang[1, a], Shouwen Ji[2,b], Linshuai Wang[3,c]

[1] Center of Cooperative Innovation for Beijing Metropolitan Transportation, China
[2] Center of Cooperative Innovation for Beijing Metropolitan Transportation, China
[3] Center of Cooperative Innovation for Beijing Metropolitan Transportation, China
[a]2292647124@qq.com, [b]jishouwen@126.com, [c]13120852@ bjtu.edu.cn

Keywords: Service innovation; Logistics public information platform; LOGINK

Abstract. By taking the national transport logistics public information platform as the research object, the differences between the logistics public information platform and service enterprises in organizational structure, operational management, information flow, etc., are analyzed in this article. On the basis of four dimensional model of service innovation, three dimensional multi-dynamic model of LOGINK service innovation is proposed. Besides, the connotation and the mechanism of each innovative factor in the model are analyzed.

Introduction

Currently, the research on service innovation targets mainly companies and four dimension model, driver model and other conceptual models of service innovation are studied in China. Regional logistics information platform, the dimension and driving force of service innovation of which are greatly different from those of service enterprise, is one part of the service industry. Because of the less study on service innovation of regional logistics information platform ,the dynamic relational model of service innovation for Regional logistics information platform is analyzed, taking the national transport logistics public information platform (LOGINK) as an example.

Logistics exchange code, logistics information exchange sharing and logistics common software are provided freely for logistics industries in LOGINK platform. LOGINK platform user objects include government regulators, industry associations, logistics providers, logistics demanders and other logistics activity participants.

Four dimension model and basic dynamic model of service innovation

Basic dynamic model of service innovation. Sundbo and Gallouj take a single enterprise as the interface to identify the driving force and divide the driving forces into internal driving force, which includes corporate strategy and management, staff, innovation departments and R&D departments, and external driving force, which contains track and behavior [1].

Guangming Zhang(1998) puts forward a service innovation universally applicable model——four dimensions of service innovation model, which shows that service innovation outside the innovation technology triggers occur more often. What' more, it more involves the following factors, such as changes of service feature itself, sales way, way of "customer – producers", service production process and so on. Generally speaking, service innovation contains the effects of a variety of factors, which are intertwined through a complex process to generate innovation. While four dimensional model uses a structured way to describe, analyze and integrate the multiple factors influencing service innovation[2].

The four dimensions in four dimensional model are respectively referred to new service concept, new customer interface, new service delivery system and technology. Figure 1 shows the relationship of the four dimensions.[1]

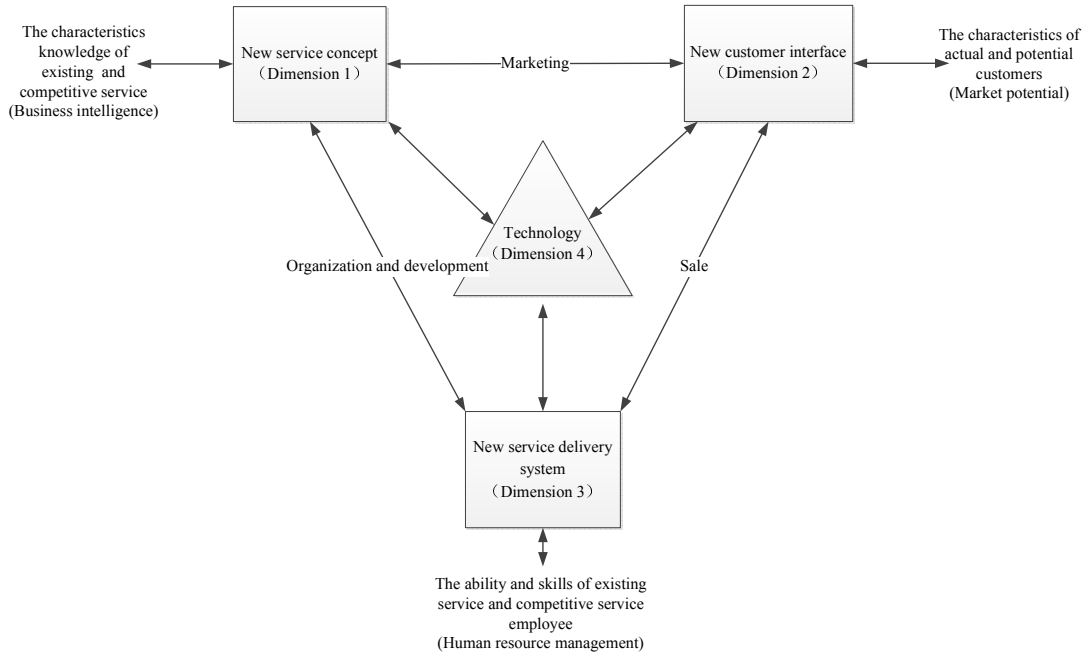

Fig.1 Four dimensions of service innovation model

Three dimensional multi-dynamic model of LOGINK service innovation

The application objects of basic dynamic model of service innovation are service enterprises. However, There are significant differences between service companies and logistics information platform in the organizational structure, operations management, information flow, etc. LOGINK is analyzed as follows.

LOGINK employees includes operation and maintenance personnel and customer service staff of the platform. Operation and maintenance personnel is mainly responsible for the general website and server routine maintenance, less contacting with the users. While customer service staff on the one hand helps the unit of data exchange construction to complete the server deployment and access. On the other hand, the staff completes the recommendation and certification of logistics management software, a certain contacting with the users.

（2）LOGINK strategy, which is determined before the platform development, in order to guide the platform development and construction, but difficult to guide the platform operation is provided by knowledge and technology suppliers. There are no special marketing departments and innovation sectors during LOGINK operations. Hence the platform innovation is more from construction planning and strategy formulation.

（3）LOGINK customer interface for one thing exists between customer service staff and users, for another thing among general website, logistics management software, public application service and users. This requires specialized tools to get information of the actual users and potential users.

（4）The particularity of LOGINK customer interface and organization structure makes the service delivery system and customer interface work together to the users, which affects the user's perception of service products.

Based on the above various factors, considering the difference between the characteristics of logistics information platform service production process and the problem angles which four dimensional model describes, three dimensional multi-dynamic model of service innovation of transportation logistics public information platform is proposed. This model is showed in Figure 2.

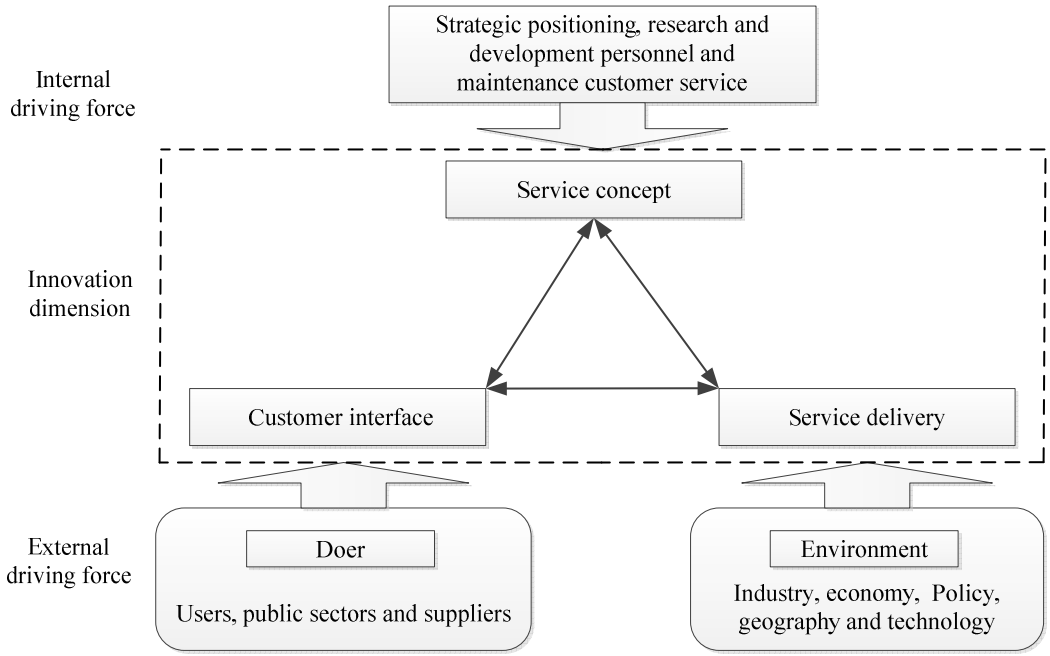

Fig.2 Three dimension multi-dynamic model diagram

Service innovation driving force. Three dimension multi-dynamic model consists of external driving force, internal driving force and innovation dimensions. Among them, the driving force module is characterized by that what forces logistics information platform in reality to drive all kinds of innovations. If a logistics information platform is used as the interface of driving force identification, the driving forces can be divided into internal driving force and external driving force.

For internal driving force of logistics information platform, strategic positioning, research and development personnel and maintenance customer service are included and the strategic positioning is the main internal driving force. The strategic positioning determines the core functions of logistics information platform, customer interface and business model, namely the core service, service delivery method and expanded service supply in the dynamic model of Gronroos expanded service supply. Setting a good strategic positioning provide an excellent innovative and competitive environment， where logistics information platform should make full use of its internal driving force, through the strategic positioning to promote the emergence of innovation.

External driving force of logistics information platform contains doers and environment. Doer is an important external driving force of logistics information platform service innovation, which generally includes users, public sectors and suppliers. The users, which can be a person, a department, an enterprise or even another logistics information platform, create demand for logistics information platform and are also the most important source of innovative ideas in the service package production, service delivery and expanding service supply. For logistics information platform, public sectors are also the important driving force of service innovation, some public sectors are demand service sectors, which use their own needs to drive service innovation of logistics information platform. While some are control departments of logistics information platform, which increase or decrease constraint conditions to cause a variety of innovation. Obviously, Logistics information platform service provider, which refers to technology and knowledge supplier, is also an important driving force of service innovation. The suppliers are an important source of innovation thought and important enabler of innovation activities and have the ability to promote the implementation of service innovation.

Environment is the other external driving force of logistics information platform service innovation, which contains industry environment, economic environment, policy environment, geographical environment and technology environment. Here, the industry environment is divided into logistics industry environment, which comprises logistics industry scale, the logistics industry development speed, the total cost of logistics industry influence factors of logistics industry scale,

logistics industry development speed and total logistics industry cost, and logistics information environment, which includes influence factors of logistics information platform and logistics software. Besides, the economic environment contains GDP, scientific research investment, research and development (R&D) spending and so on. The policy environment mainly refers to the geographical location of logistics information platform service object, for example, whether is located at the border port, and whether there is water transport demand, etc. The technology environment mainly devotes the application maturity of technology related to logistics industry and information technology, for example, whether there is application of new technologies, etc.

Service innovation dimensions. Innovation dimension can be understood as degrees of innovation achieving, including service concept, customer interface, service delivery. The service logistics information platform provides is high invisible, thus the innovation is conceptual. For example, the core functions of the platform and additional functions are part of the innovation of service concept, the core problem of which is that what kind of function products the logistics information platform targets to provide for users. Customer interface refers to what kind of windows the logistics information platform shows the customer. The layouts, beautiful and convenient degrees of general sites, and even the memorability of the domain name are important points of service innovation to producing. Besides, service delivery devotes the mechanism operating which makes the logistics information platform healthy for long-term, including the mechanism how to build and how to operate.

Summary

Regional logistics information platform is one of the important categories of service sector and the service innovation usually occurs in three dimensions of service concept, customer interface, transmission mode. The driving force which impulses the generating of driving service includes two aspects, one is internal driving force, which contains strategic positioning, R & D personnel, customer service maintaining and so on, and the other is external driving force, which contains actors and environment. Users, public sectors and suppliers are involved in actors. And Environment refers to industry environment, policy environment, economic environment, technology environment and geographical environment, etc.

[1] This paper is funded by national science and technology support plan project 2014BAH24F02.

References

[1] Sundbo J., Gallouj F. Innovation as a loosely coupled system in services[J]. International Journal of Services Technology and Management, 2000, 1(1):15-36.
[2] Guangming Zhang. Research in logistics service innovation model[J]. Economic management,2006 (18):57-61.

Advanced Materials Research Vols. 989-994 (2014) pp 5049-5052
© (2014) Trans Tech Publications, Switzerland
doi:10.4028/www.scientific.net/AMR.989-994.5049

The Research on Visual Simulation Technology Applied in College English Teaching

ZHAO Ming[1, a], ZHANG Wang[2,b*]

[1] Foreign Language Department ,Harbin University of Science and Technology, Harbin 150001,China

[2] School of Astronautics ,Harbin Institute of Technology, Harbin 150001,China

[a]ZhaoMing08@yeah.net

Corresponding author: [b]zhangwang@126.com

Key words: visual simulation technology; college English

Abstract. With the rapid development of modern information technology, visual simulation technology is widely used popularized in the construction of college English. Therefore, this paper tries to have a further research on visual simulation technology into college English. Results show that the visual simulation is very important to improve students' recognition, understanding of tourism English training courses.

1. Introduction

Visual simulation technology is a new branch based on computer simulation technology, computer graphics, image generation technology and information synthesis technology, display technology. Its aim is to realize the simulation of realistic effect in the real environment through the visual graphics representation, image representation, structure information and visual characteristics. As the key presentation form of Virtual reality (VR for short), visual simulation technology has more perceptual (multi-sensory), immersion, interaction and vision (imagination) and other typical characteristics. At present, the visual simulation technology has been widely used in military drills, city planning, film and television production, simulation, driving simulation, interactive entertainment, virtual tourism scenic spots and historical sites and other fields. Relevant scholars attempt to study different levels, but the research associated with college English is little. In this research, the author tries to explore the application of visual simulation technology in the college English.

2. Research design

Based on visual simulation environment software Vega technical requirements, the school creates simulation practice interactive visual simulation platform combining with Photoshop software technology. Combining scholars like Luo Yu's research results and experience, such as building "human-computer interaction platform to create a visual simulation technology practice job evaluation scenario a" in the integration of training higher vocational tourism English teaching framework (see figure 1)

3. Training class

This part will introduce the procedures of the class training.

3.1 Task assignment

Learn to use the interactive platform through human-computer interaction platform with the visual simulation, training students to use English and improve language communication skills in the 3d imaging business scene matching workplace. For example, when virtual scene of festival activities appears the human-computer interaction platform, students use headphones to hear several groups of slogan to clearly distinguish the most suitable English festival activities propaganda and click action through the mouse and make the right decision

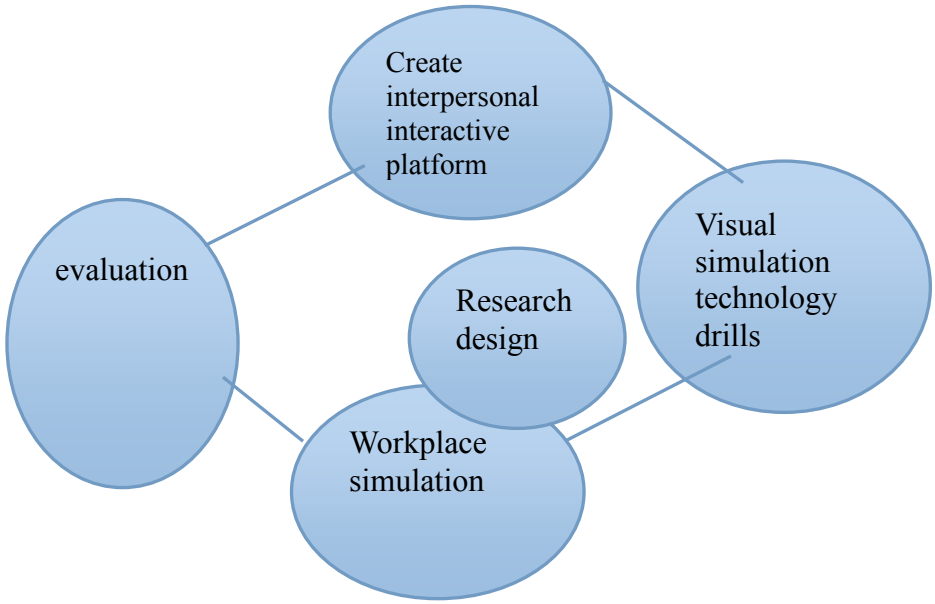

Figure 1 Activities framework

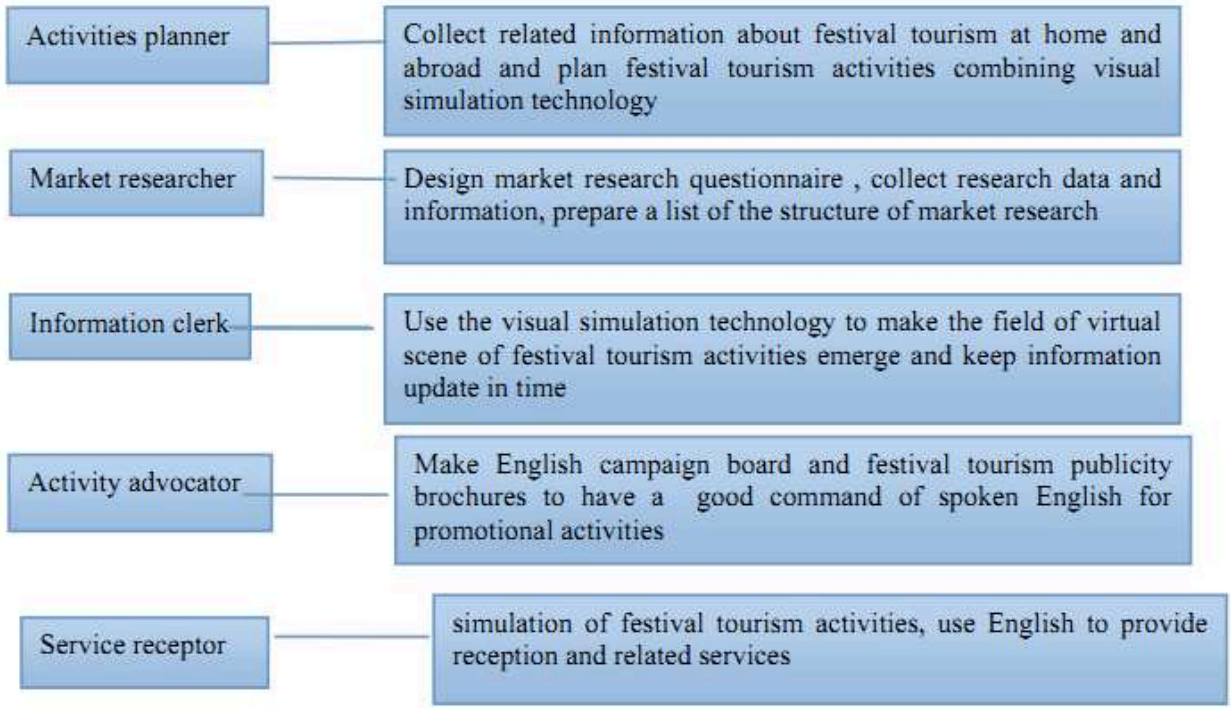

Figure 2 Task assignment

2.2 Form a good workplace communication English expression.

Through standard English demonstration function in human-computer interaction platform , correct the mistakes of English pronunciation, word spelling error and non-standard use habit, gradually form correct and authentic English behavior. For example, some students use Chinese English expression, conduct market research in the early time, ask privacy issues such as gender and age. Then the visual simulation of virtual workplace environment will give the prompt to help correct the language and give correct demonstration.

The role played respectively and the practice According to three dimension visual simulation of festival tourism planning and publicity virtual work scene, the students play a variety of different

roles and receive training, and do different jobs of typical tasks (see figure 2), to motivate students' learning initiative, develop students' ability of creative thinking and practical application.

4. Evaluation of learning results

Teachers give real-time monitoring to students in the whole training, give instant solutions to the problems of students, and meanwhile give a comprehensive assessment and evaluation of typical tasks from different levels.

Assessment program	Content
Human-computer interaction platform control ability	Application ability of visual simulation technology
	Graphics auxiliary processing skills
	Three dimensional simulation and human-computer docking ability of virtual workplace situations
Comprehensive use of English	Accuracy of English pronunciation
	English listening
	Simulating English dialogue
	English normative exhibition planning, and writing accuracy
	The match between workplace and working language
The implementing ability of tasks	The accuracy of completing the task
	Timeliness of completing the task
	The flexibility of coping with emergency
	Cater for the standard of the field
Professional quality	Awareness of work role
	Responsibility
	Awareness of team work
	Communication ability

Summary

The application of the visual simulation technology into the classroom teaching of college English, on the one hand, gives the workplace through the three dimensional simulation where the student can practice and have a clear cognition of the concrete work, lays a good foundation for the future career. On the other hand, it provides the human-computer interaction platform where students can have access to information and create a more efficient, convenient and information sharing of the English language learning atmosphere, stimulate the students' interest in learning tourism English and passion. In fact, based on the visual simulation research, the research on the the modern technology has been broaden and more importantly, students work by simulating the real scene, enhance its typical tasks to specific jobs and cognition and improve the professional quality of personal and professional dedication through it. This research only focuses on one aspect, in the future study more aspects can be studied.

In the college English class, it is evident that visual simulation technology is useful so that it can an aid to English teaching. It not only stimulates the interest of English learning but also improve the efficiency of English.

Acknowledgements

Project supported by the Social Science Research Project of Heilongjiang Province (Grant No. 12E131); Education Science "Twelfth Five-year" Plan Project from Heilongjiang province,2011(Grant No. GBC1211057); Universities Educational Reform Project in Heilongjiang province, China (Grant No. JG2012010208).

References

[1] Suchman L. Plans and Situated Actions: The Problem of Human-machine Communication[M]. New York: Cambridge University Press, 1987.
[2] Jerome Seymour Bruner. The culture of education[M]. MA: Harvard University Press, 1996.234
[3] Brown.H.D. Teaching by Principles-An Interactive Approach to Language Pedagogy[M]. Englewood Cliffs: Prentice Hall Regents,1994.159
[4] Spolsky,B. Conditions for Second Language Learning: Introduction to a General Theory[M]. Oxford: Oxford University Press,1989.166
[5] Ellis,R.Task-based Language Learning and teaching[M]. Cambridge: Oxford University Press, 2003.125

Advanced Materials Research Vols. 989-994 (2014) pp 5053-5056
© (2014) Trans Tech Publications, Switzerland
doi:10.4028/www.scientific.net/AMR.989-994.5053

The Application of Modern Information Technology in Competitive Sports

XIAO Bo[1, a]

[1]Department of physical education, Sichuan University For Nationalities, Kang Ding 626001, China

[a]XiaoBo509@yeah.net

Keywords: modern Information Technology, competitive sports, modern Science

Abstract. Science and technology is the first productive force. The development of the society and the rapid development of science and technology have brought great push to the economy and social development. By means of computer and the Internet for information transmission, high and new technology and the emergence of a multidisciplinary scientific research such as modern science and technology become our milestones of the contemporary social modernization. Current new revolution of science and technology will further accelerate the process of modernization of competitive sports and have great influence on the development of sports skills. Modernization of competitive sports has become the inexorable historical trend. Therefore, modern science and technology plays a very important role in sports.

1. A general introduction of Modern Information Technology.

Chart 1 we know that information technology is the study of information acquisition, transmission and processing technology, which consists of the computer technology, communication technology, the combination of microelectronics technology, sometimes called "modern information technology". That is, information technology is the use of computers for information processing, the use of modern electronic communication technology in information collection, storage, processing, utilization and related products manufacturing, technology development and new subject of information service. Information technology mainly includes the sensor technology, communication technology, computer technology, micrographics etc.

Task of sensing technology is to extend the function of sensory organs to collect information. Communication technology's mission is to extend the human nervous system function of passing information. The development speed communication technology is amazing. Computer technology to extend the human's organ function of dealing with information and decision-making. Computer technology and modern communication technology together constitute the core content of the information technology. Microfilm technology to extend the function of the memory organs to store information.

2.Modern Information Technology and sports.

Sports, is a integrated discipline refers to natural, social and psychological and technology. It produces with the production of the society, also develops with the development of society. In the transformation from traditional sports to modern sports, its connotation and structure have been changed. As the trend of sports socialization, modernization and globalization, information technology plays a more and more magical effect in competitive sports.

Chart 1 we see sports needs information technology, and in turn, information technology also needs sports. The development of sports and information technology together has become not only an important part of sports development, but also the objective request of modernization of sports and the inevitable trend in the development of sports.

The 21st century is the century full of information and technology. In Chart 1, Information as a subject is known as the four important subjects, including life sciences, materials science, information science and environmental science. The development of competitive sports and the improvement of athletes performance to a large extent depend on the information technology.

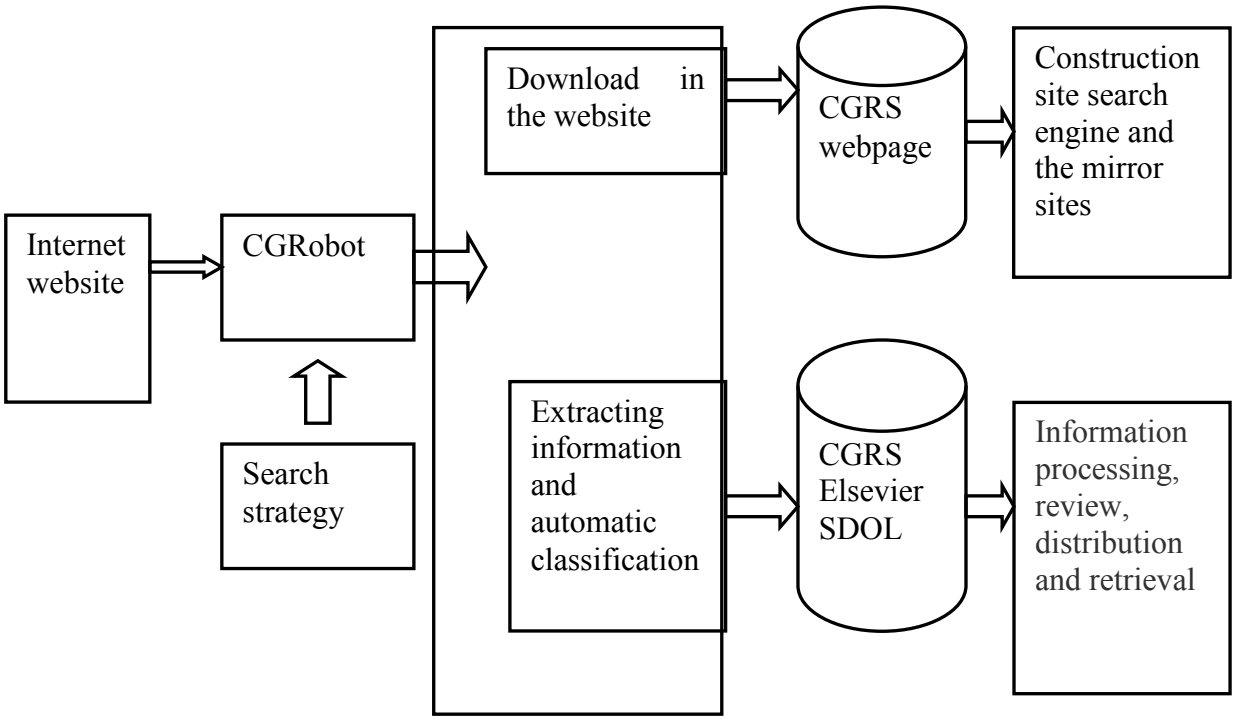

Chart 1: Structure of internet information collection

3.The necessity of information technology in the research of competitive sports.

With the development of competitive sports, the sports performance has been more and more close to the limit of human physical, so creating new records bacomes more and more difficult for human beings. In order to creat new records and good scores close to limited range, countries around the world, especially developed countries, spare no effort to developf information technology and applly in sports, which becomes one of the focuses on the information technology and sports scientific research. Application of information technology provides a reliable basis for improving competitive sports and training method.

Currently, application of information technology in competitive sports mainly includes: to diagnose the sports training, which provides a new way and new method for scientific diagnosis such as: using infrared light spot to measure the position of human space; using two-dimensional human body center plate machine to test the stability of the shooter and to establish data quick feedback system of the sports technical characteristics.; using high-speed photography, camera machine, quantitative analytical technique movement, electronic telemetry technology developed by heart rate meter, remote sensing telemetering heart muscle, to measure the heart rate of all the athletes in the movement and scientifically diagnose the athletes' functional status.

4.Application of information technology in competitive sports.

Modern athletic sports gradually developed from natural and simple activities to the degree of standardization and normalization by using modern information technology. It is based on scientification and standardization of sports; it relys on the development of modern information technology. It plays the decisive role in raising the level of competitive sports.

4.1 Application of information technology in the diagnosis.

Computer is widely used in technical analysis of athletic sports, as human eyes can nethier distinguish whether the player swivels shoulders more or less nor determine that some athletes' foot landing forward 1 cm , but the internet can measure these diny differences. Through the use of advanced video technology, multidimensional camera, photography and parsing technology we can diagnose the defects of techniques, and compare with the correct and advanced technology gap to provide the means and key to improving technology.

From chart 2 we know that computer has the characteristic of fast and efficient feedback, making use of this characteristic can greatly improve the training effect. Because the computer has the function of storing information, and can store all kinds of training and function index data for the comparative analysis later. And using computer to know your opponent's skill and tactics, feedback to their coaches and athletes in time in order to adopt targeted training methods, thereby improving their performance.

	2001	2002	2003
Archery	A	A	A
Athletics	A	B	A
Badminton	A	D	A
Baseball	B	D	B
Softball	C	A	A
Basketball	C	A	A
Boxing	A	A	A
Canoeing	B	A	A
Bicycle	A	A	A
Horsemanship	C	B	C
Fencing	A	A	A
Football	A	A	A
Handball	A	A	A
Gymnastics	B	D	A
Gymnastics Rhythmic	D	D	B
Trampoline	A	A	A
Hockey ball	A	A	A
Triathlon	A	B	A
Judo	D	B	A
Est.			

Chart 2: Capacity analysis of the score statistics from 2001 to 2003

A means World Cricket Championship pro; B means World Cup; C means World Ranking; D means other international contests.

4.2 Application of information technology in learning new skills and doping control.

The modern athletic sports competition is not only the competition of physical strength and skill, but also the competition of high-tech information intelligence. Shoot the process of aopeitio and make it digital to use computer to transform into line diagram, to analyze every movement, to identify every action, speed, strength and acquisition and other important factors of the body.

Before the 60s, each country focused on the research of all kinds of cholesterol drugs. Under the same conditions, whose drug research level is high, who can get the more gold medals. Untill the early 90 s, the number of illicit drugs limited by the world anti-doping commission has been more than 120. People are looking forward to the development of information science, biology, genetic engineering and molecular biology and other high-tech development to make greater contributions to the development of competitive sports for the 21st century.

Summary

Modern science and technology plays an important role in sports, the emergence and development of a series of sports are important embodient. The process of sports scientification promotes the reform of sports training system and management system. Experts have undertake training task load and administrative tasks. The traditional experience type of training system and

management system have been replaced by scientific training system and management system. The application of computer, electronics, laser, space and other modern technology is another important symbol of modernization of competitive sports.The constantly emerging of new records and superior performance in the field are connected with the development of science and technology.

References

[1] D. Douglas and so on. Introduction to Sociology of Deviance. Shijiazhuang: Hebei People's Publishing House.1997.
[2] Durkheim. Sociological Methodology. Beijing: China Press.1998.
[3] F. D. Wolinski [United States]: Health Sociology. Beijing: Social Sciences Academic Press, 1999.
[4] Jacques Temprado, M. Della-Grasta, M. Farrell, M. Laurent, A novice-expert comparison of (intra-limb) coordination subserving the volleyball serve Human Movement Science, Volume 16, Issue 5, October 1997.

Advanced Materials Research Vols. 989-994 (2014) pp 5057-5061
© (2014) Trans Tech Publications, Switzerland
doi:10.4028/www.scientific.net/AMR.989-994.5057

Based on project-driven ASP.NET Teaching Research and Exploration

Wendong Zhao [1, a], Haiyan Zhou [1,b]

[1] Huaiyin Institute of Technology, china

[a] zwd_139@163.com, [c] zhy_5703@163.com

Keywords: project driven, asp.net, teaching reform program

Abstract. With the popularization and promotion of the Internet, ASP.NET has gradually become the mainstream of development platform for WEB application. At present, most colleges and universities have opened the door for students majoring in computer courses. Because of the complex of ASP.Net teaching and the teaching target key requirement to cultivate the students' ability of practice, the traditional mode is not applicable to the teaching of Theory of teaching. So, this article made based on the project - driven ASP.Net Teaching. By teachers in selecting suitable project topics, the teacher according to the project needs to explain the knowledge of ASP.NET and ultimately by the students to complete the design and development of the entire project in teaching. Practice has proved that the project-based driving teaching method for students' active learning teaching content and improve students' ability to analyze and solve problems.

Introduction

With the popularization and promotion of Internet, Web programming and Web applications has been an unprecedented development. WEB-based programming has become one of information technicians that must master and the social demand for Web application developers is growing. Current mainstream WEB-based programming languages-among ASP, PHP, ASP.NET and JSP, ASP.NET is for next generation enterprise network computing Web platform, Microsoft.Net is an important part of the strategy, in which new technical architecture will make programming easier for everyone, based on this, an increasing number of colleges of science and engineering to open a course of ASP.NET as a computer science course. And they are in a very important position in the teaching plan.

As an integrated high professional class, prior to student learning ASP.NET, generally fragmented learning principles and application of Internet technology, data structures and database courses, learning through ASP.NET and use theoretical knowledge in practice, a process that I learned, emphasis is on action, so the course is practical. If we still use a single, traditional teachers teaching, students' practice teaching mode, cannot effectively improve students' practical ability, also fail to cultivate the students' ability to independently develop a small and medium sized Web project. Exploration team went more than two years of research and teaching, teaching teams set up a WEB-based program development, develop a practical teaching plan and an effective teaching method.

Set up a team, pre-ordered courses teaching

ASP.NET programming knowledge involved much, page layout of the HTML markup language, classes and objects, database operations, XML files and JavaScript scripting language to use. Due to limited class and the difficult of course settings, and cannot arrange the content of lessons. So organization has WEB program development of practice of teacher composed teaching team, again by members of teams, Division completed static page of produced, C# programming, database, XML language and JAVA program design. Finally, ASP.NET, integrating all knowledge, in the design and development of a student familiar with the project, such a teaching plan, through a semester learning ASP.NET, teaching is notable.

Based on project-driven curriculum teaching

Students learn a computer course, whose main aim is not just to learn some basic information on this subject and, more importantly, is to acquire the knowledge and flexibility to use. In other words, students learn the basic concepts and key technical points, to can learn to apply his knowledge to practical application of the skills. For computer science students, inspired by using a variety of modes, independent learning, strengthening practical training and foster innovation, build up the team spirit is very important. Past, we just according to this and textbooks of order to teach ASP.NET knowledge points, to knows existing of about ASP.NET of textbook, each chapter of knowledge points is not coherent of, After students complete, run into practical problems, still won't work, so learn active enough. There are some students began to study seriously, but with the subjective teaching, many students have given up on ASP.NET learning initiatives, teaching was not satisfactory. To end this, we use the method that based on teaching practice, the development of practice and project-driven teaching method is used in the long term. It is the interaction between teaching and learning mode, the basic idea is: through the whole teaching process to a complete software development project from beginning to end, to build the project as a clue to arrange the teaching steps, the teaching process is driven by the project's tasks. Students in the learning process for a complete project, the whole process of analysis, design and implementation, which combine theoretical and practical education in the classroom teaching organic combination.

In project-driven teaching, the students under the teacher's guidance, specialized theoretical learning, while actual project development. Needs of teachers according to the project design and teaching expertise, which is a combination of theory and knowledge into skills teaching method and fully mobilize the students' interest in learning. It can encourage students to collaborate on the project for the purpose so that students in active and independent learning environment can mutual learning and practice in the learning environment. Students during the teaching process will no longer be a passive recipient, but rather active participants, such openness, innovation of educational thoughts and patterns conducive to overcoming the disadvantages of teaching pattern in the past, more conducive to students' level in the development of the computer information management system to improve.

1) Program selection and grouping

Based on project-driven teaching methods, the key issue is to select an appropriate project and select a project should have the following characteristics:

(1) Projects should have a certain level of representativeness, while a project may not have all the features of a class.

(2) Projects should have a certain degree of practicality. Project comes from actual job requirements, selection and actual needs of the project as much as possible. Combining with scientific research tasks, technological development, needs of the construction and practical application of selection is required.

(3) The size of the project you should moderate. Big-scale projects are difficult to complete a course contact hours and students are elusive. Small-scale projects are difficult to cover the major points and lacks integrity and challenging.

(4) Instructor for the selected projects should be very familiar with and preferably teacher personal development projects.

(5) Project echo students living close to enhance the students' interest on the one hand, but more importantly is to facilitate students' understanding and acceptance so that students focus on the technical aspects of the project, and can't waste too much time on the investigation.

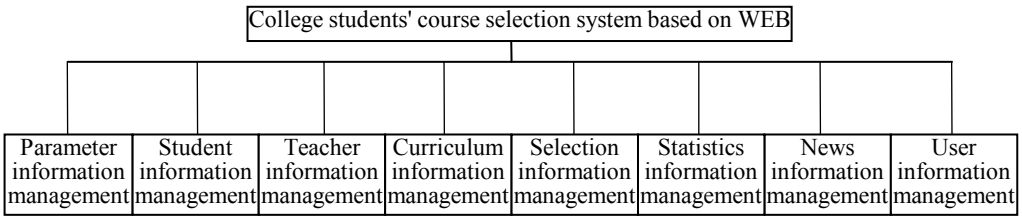

Fig. 1 College students' course selection system functional block diagram

Based on the above factors, in our teaching practice of ASP.NET, we use "University students' course selection system based on B/S mode" as a case study. Main modules of the system as shown in Fig. 1. After you decide the project, focused teaching classmates, based on four people in a group, each group to identify a group, each group in the Division of personnel, then the leader, according to the software engineering mind to organize and coordinate. Ask each group at the end of the term, it submit a software design and software user manual assessment of each student as semester basis.

2) According to the required, adequate, strengthening the relevance and applicability of principle of reforming teaching contents.

If single, sequentially teach that content also makes students feel teaching is not practical, nor can stimulate students ' learning activeness. To standardize the teaching content and our ability to course objectives the course modules are divided, projects combined with select, refines each unit of competency requirements according to the required, adequate, strengthening the relevance and applicability of principle of reforming teaching contents, this section requires students to learn by themselves accomplish. Specific teaching contents as shown in table 1.

Table 1 ASP.NET academic content

Chapter	Project content	Practice of project
Basic controls	validation controls, Html controls, navigation controls.	1 Data entry page; 2 Shows output page; 3 Member registration; 4Information.
ASP.NET programming	ASP.NET built-in object and file processing.	1 page access control; 2 site visit statistics.
Database operations	ADO.NET, basic database operations, and controls such as Gridview.	1 student information management; 2 course registration information management; 3 various access database operations.
Integrated project	ASP.NET application design.	College students' course selection system.

3) Based on the implementation of project-driven teaching

In the teaching of teaching content, take the spiral model is similar to software engineering, not once finished the entire contents of a cell, but according to needs of the project, take the spiral strategy, along with a project to use the knowledge gradually increased , naturally joined gradual learning content. This is the "project-driven" strategy.

User information management, information management and student three modules based course management throughout the entire process of teaching. Through the project down into a typical case, using succinctly and training, teachers operate, then students practice understanding, in order to achieve the main line tasks. Deepen students' understanding of the importance of professional courses, specific teaching process is shown in Fig. 2. Through each lesson task to achieve, students completed the project tasks, but also mastered the new knowledge in ASP.NET. Teachers completed the task of teaching, but also allow students to practice and theory of organic integration, but also improve the students' independent analysis of issues and problem-solving skills.

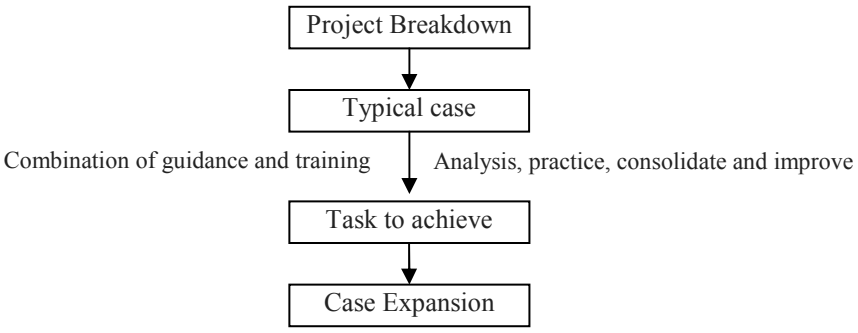

Fig. 2 Project-driven teaching processes

4) Strengthen secondary education

Since the reduction of teaching content, much content requires students to complete self-study after school. To this end we produced a dynamic Web Design Course Website, including multimedia courseware, curricula, teaching materials, online solutions, online testing and instructional video. Excellent use of network resources and guidance to help students after school to learn, but also saves time for the students to find information when self-learning, but also to break through the restrictions of time and space, in a timely manner to solve problems by answering online learning experience, and ultimately train the students independent problem-solving skills to analyze problems. Also contribute to the ultimate realization of the project, so as to complete the task of teaching ASP.NET.

5) Reform the examination pattern, the transition from knowledge assessment for capacity assessment

Traditional "paper-based assessment" approach has not achieved the "test and promote learning," the purpose, basic does not reflect the student's skill level and ability. Therefore, in the evaluation, to achieve diversification and diversification evaluation evaluation topics. Developed a comprehensive evaluation of teaching rated quantization table based on ASP.NET projects, from the overall layout of the site before and after the station management, the learning process, analyze problems and problem-solving skills, active learning and teamwork skills, etc.

6) Teaching Achievement

More than two years, we have adopted the project approach, received remarkable results. Whether the student exams pass rate, or vocational skills certification and graduation rates by more than the proportion of well-designed, has a markedly improved. Of particular importance is due to the students' practical software development capability has been significantly improved, greatly enhancing their employability and competitiveness

Conclusion

ASP.NET-based project-driven teaching computer courses in a strong practical teaching, has incomparable advantages. It enables students to grasp the essence of the mastery of a course at the same time, strengthen the student's computer application software development capabilities, improve their computer software engineering principles to the development of the project analysis, architecture, design, management, documentation, such as the ability to write, to students after graduating in computer technology continues to self-development has laid a good foundation, but also train the students working in cooperation and teamwork spirit.

The rapid development of computer technology and applications, we must promote the reform of the traditional mode of teaching computer courses, constantly updated teaching concept, teaching content, teaching methods and teaching methods. Based on project-driven approach, as we explore in the teaching reform, and achieved some results, we will summarize the experience and lessons learned, the project will be extended to other software development pedagogy teaching practice.

References

[1] Ye Hong-wei. Design of Web Application Based on ASP.NET MVC Frame work. Journal of Hebei North University, 2009, 25 (6): 61- 65.

[2] Wen Ji-quan1, Dong Liang. Applied of task-driving teaching method in Asp.net curriculum teaching. Journal of Science of Teachers′ College and University, 2013, 33(3):88- 90.

[3] Wei Guo-biao. The teaching research of ASP.NET course based on CDIO model. Journal of Anqing teachers college, 2014, 20(1): 115- 118.

[4] Ma Lingling. An Empirical Study on Developing Students' Autonomy Learning Ability through Project- Based Learning. Journal of Shanxiadio & TV University, 2010, 75(2): 53- 55.

[5] Liu Chun-xi. Application and practice of the project-driven teaching method in Java Language teaching. Journal of Binzhou University, 2013, 29(3):102-106.

[6] Zhao Xiang-hui, Wang Xu-sheng. Study on Applying Project and Task- Based Method in Teaching ASP.NET in Higher Vocational School. Journal of Langfang Teachers College, 2011, 11(6): 135-137.

Advanced Materials Research Vols. 989-994 (2014) pp 5062-5065
© (2014) Trans Tech Publications, Switzerland
doi:10.4028/www.scientific.net/AMR.989-994.5062

Application Development of Student Score Analysis System for Secondary School Based on Standard Score

Wendong Zhao [1, a], Youdong Zhang [1, b]

[1] Huaiyin Institute of Technology, china
[a] zwd_139@163.com, [b] zyd@163.com

Keywords: Standard score, Secondary school, Score analysis system, MVC

Abstract. They rarely involve deep-seated score analysis in the existing teaching management software, Therefore, we can not evaluate science teaching, Based on this, This article uses the Struts framework and Hibernate framework to design Student Performance Analysis System based on MVC pattern, it Proposed optimization algorithm based on standard score, We can achieve student achievement statistics and analysis with it, This algorithm can better reflects relative position that the individual is in groups, and has a certain scientific. Experimental results show that the system has a good safety and openness, and provides support information for academic departments to promote better teaching work, and finally improve the quality of teaching.

Introduction

With the development of computer technology and Engineering construction that all schools links Internet, the important task of school principals is that achieve educational and teaching quality information management. At present, not only do we want to achieve paperless management computer in the research of score Analysis System, and development a new Student Performance Analysis System Under the existing conditions based on openness and real-time of network. At the same time this system improves the management level, and Document student score, reporting and statistical analysis, assurance student achievement information can be quickly and accurately communicated to students and parents. We carefully study and analysis of existing performance analysis system based on previous research, we adopt standard score as the mathematical model, design and implement analysis and management system of student score using Struts framework and Hibernate framework based on browse/ server mode and J2EE platform, Solve problems of using JDBC technology connection to the database under struts framework model, high coupling between layers and difficult to maintain.

Struts and Hibernate

1) Struts

Struts framework is an open source project of the Apache Software Foundation organized, it provides the underlying support for the development of MVC system [1]. The Core of Struts is a MVC-style controller; source can not contain business processes by using the configuration files of struts controller, this makes maintenance and flexibility greatly strengthened. Although there is no requirement in view, but it offers a lot of classes for developers to use, but struts merely provides an action Class in the model section, let this class to implement all of the back-end business, so Struts support for model section is also lacking.

2) Hibernate

Hibernate is a persistence layer development framework by using ORM mechanism, It is a bridge between Java applications and relational databases, and is responsible for mapping between Java objects and relational databases. It encapsulates operations of JDBC access database that is an independent object persistence framework; It provides API for database access based on OOP to upper class [2]. Programmers can avoid manually write method of access to the data persistence layer; they only need to focus on the development of business logic. Hibernate simplifies the development of difficulty, accelerate the development of the project. However, Hibernate provides only partial support for the model, if we only use the Hibernate framework to develop applications;

System can only be improved in the business model section, logic processing, process control, and views of the system have not been effectively separated, so coupling of the system is not too high, and it is not easy in the latter part of system maintenance.

3) Web application development based on struts and hibernate

We compare the advantages and deficiency of struts and hibernate, if we develop the project by using Struts and Hibernate, By Struts technology to reduce the coupling between the layers of MVC, reduce development effort of the business model by using Hibernate framework, it is a fast and effective solution for Web applications, you can refer the article [3] about their application methods.

The Analysis algorithm of scores based on standard score

In recent years, we assess student test scores with hundred mark system, if a student scores less than 60 points, and then he is a failure in this course. This method is unscientific, it does not accurately reflect the true student learning, because of the difficulty, number and focus of each exam questions are likely to be different, so, it is not science reflect actual student learning situation by using with absolutely scores. So how so you solve this problem? We propose a method to measure student achievement based on standard score [4].

When the computer standard scores, through calculating the value of one score minus the Average of all student scores by using formula (1), then calculated the value of the expression, the value divided by standard deviation, it can better reflects relative position that the individual is in groups.

$$score_i = \frac{x_i - E(x)}{\delta(x)} \quad (1)$$

In the formula (1), $score_i$ represents standard scores for a student, x_i is the original score, $E(x)$ is the average of all student scores, $\delta(x)$ is standard deviation of the original group scores. This evaluation system by calculating standard score certainly has some scientific, but the calculation of standard scores are still relatively complex, we also designed a special optimization algorithms.

The design of Student score Analysis System for secondary school

Through the early research and Qingjiang secondary design requirements, we design Analysis System of Student score for secondary school shown in Fig. 1. The system set up administrators, teachers and students of different types of users. Teachers can input student achievement into system within a specified time, and analysis about class scores, etc. Students can browse the results at any time and place. Administrators can base on the analysis results to adjust teaching methods and teaching ideas.

Administrators are principally engaged in the management of academic information, them main function is to statistics and analysis student scores. Academic Information management is composed of several modules, but the method of each module are similar, in order to facilitate the description of the methods and means of the module, combined with the pre-design requirements, we main explanation class management module, design a timing diagram of class information management In the Senate subsystem shown in Fig. 2.

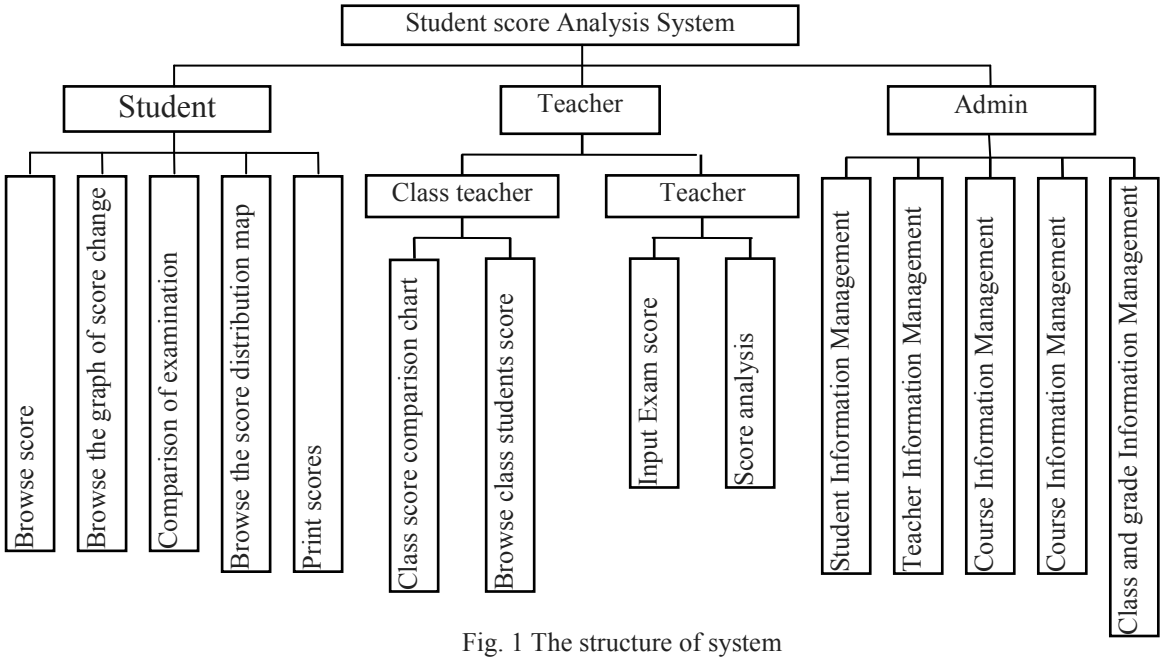

Fig. 1 The structure of system

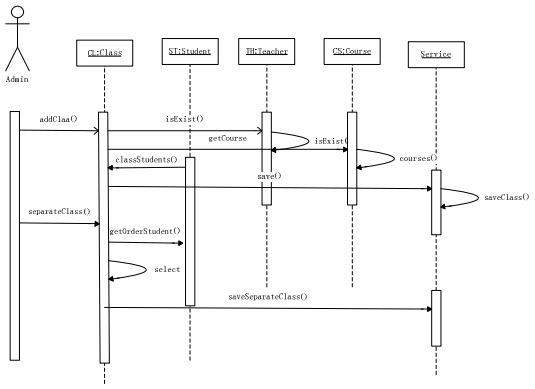

Fig. 2 Timing diagram about class

We can see that management class information is primarily to add new classes, modify class information, Delete class information, show class information and re-division classes according to test scores, for this reason we can abstract the relationship between various types of educational subsystems, shown in Fig. 3.

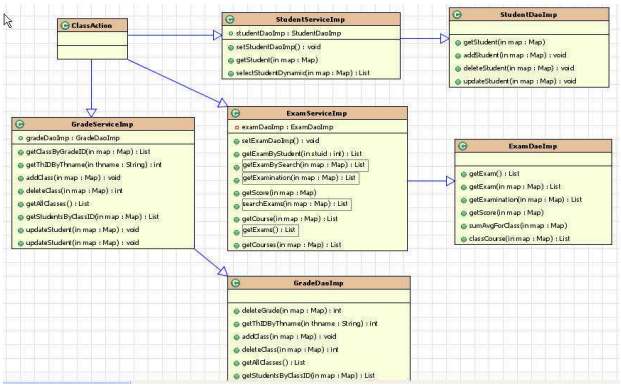

Fig. 3 The class diagram of class

The development of Student score Analysis System for secondary school

When we develop system, design Patterns in strict accordance with the MVC, first adopt JSP to achieve the display of the page, Achieve pages and data steering control by using Struts, Data processing and business logic to be achieved by the corresponding Java Bean, and access the database operations to be done Ibatise, Student score sorted graph is shown in Fig. 4.

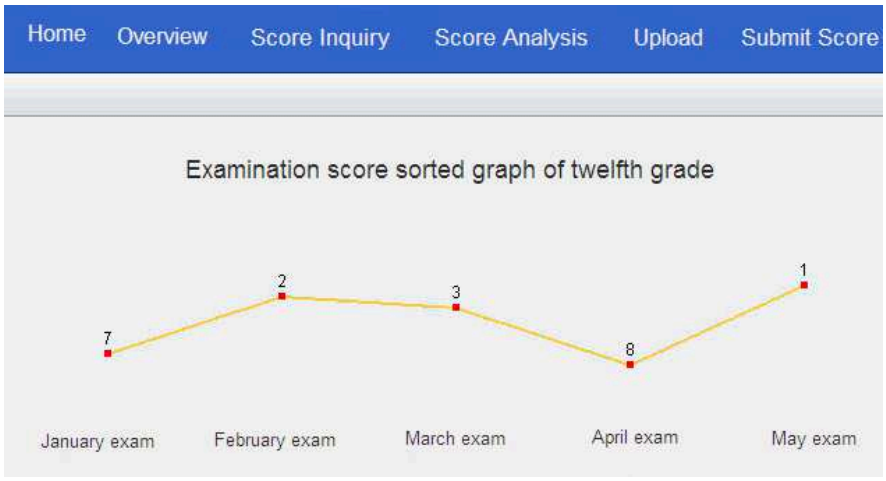

Fig. 4 Examination score sorted graph of grade

Conclusion

This article uses the Struts framework and Hibernate framework to design Student Performance Analysis System based on MVC pattern, after a period of application of the feedback, the results show that the system has good security and openness, the optimization algorithm based on standard score can better reflects relative position that the individual is in groups, and has a certain scientific, and provides support information for academic departments to promote better teaching work, and finally improve the quality of teaching.

References

[1] Andreas Spillner, Tilo Linz. Software Testing Foundations: A Study Guide for the Certified Tester Exam, 2004.

[2] Du Ming, Li Chao-chun. Design and Implementation of Struts+EJB on J2EE Platform. Application Research of Computers, 2009, 17(5): 223-228.

[3] Wang Hai-tao, Jia Zong-pu. Web Application Development Based on Struts and Hibernate. Computer Engineering, 2011, 37(9):112-114.

[4] Hao Shang-fu, WANG Zhi-hui. The Study of Score Analysis for Secondary School Based on Data Mining Technology. Computer Knowledge and Technology, 2010, 6(29): 8164-8165.

[5] G. Erieh, H. Richard. Design Patterns Elements of Reusable Object-Oriented SoftWare, 2008.

[6] Duan Bin, Li Guang-hui. Public Administration Performance Evaluation System Based on MVC Framework. Computer Engineering, 2009, 35(6): 263-268.

Advanced Materials Research Vols. 989-994 (2014) pp 5066-5069
© (2014) Trans Tech Publications, Switzerland
doi:10.4028/www.scientific.net/AMR.989-994.5066

Research of Current Situation and Risk of Bitcoin

Yiqing Lu[a]

School of Information Management, Beijing Information Science and Technology University, Beijing, 100192, China

[a]email: luyiqing@126.com

Keywords: Bitcoin; Peer-to-peer; Electronic currency; Digital money; Virtual currency

Abstract. Bitcoin is a pure electronic money based on cryptographic proof instead of trust. The principle of Bitcoin can allow any two willing parties to transact directly with each other without the need for a trusted third party. Bitcoin can represent a totally new anarchy virtual currency and an innovation of digital currency. But its development also needs to face to the security of national policy risk, technology risk and trading risks.

Introduction

Bitcoin is a peer-to-peer payment system introduced as open source software in 2009, proposed by Satoshi Nakamoto[1]. The digital currency created and used in the system is alternatively referred to as a virtual currency, electronic money, or acryptocurrency because cryptography is used to control its creation and transfer. Conventionally, the capitalized word "Bitcoin" refers to the technology and network, whereas lowercase "bitcoin" refers to the digital currency. The Bitcoin system is not controlled by a single entity, like a central, and this has led the US Treasury to call bitcoin a decentralized currency.

The Principle of Bitcoin

Bitcoins are created by a process called mining, in which computer network participants, i.e. users who provide their computing power, verify and record payments into a public ledger in exchange for transaction fees and newly minted bitcoins. Users send and receive bitcoins using wallet software on a personal computer, mobile device, or a web application. Bitcoins can be obtained by mining or in exchange for products, services, or other currencies.

An electronic coin is defined as a chain of digital signatures, as shown in figure 1. Each owner transfers the coin to the next by digitally signing a hash of the previous transaction and the public key of the next owner and adding these to the end of the coin. A payee can verify the signatures to verify the chain of ownership[2].

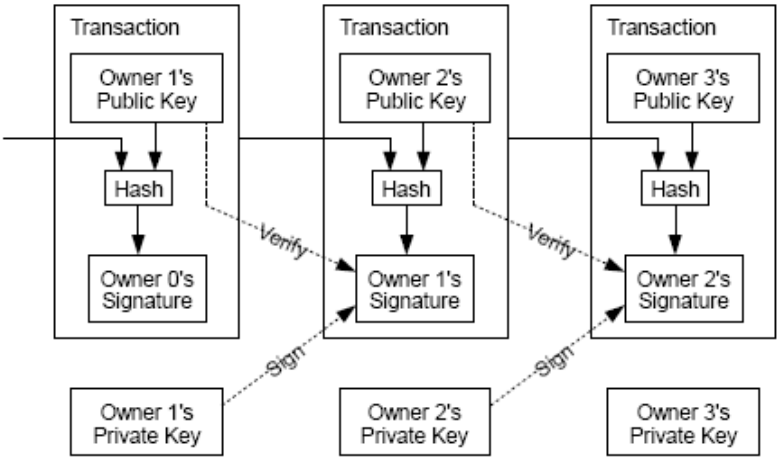

Figure1. Transactions of electronic coin

In the process, to the recipient's inspection，a common solution is to introduce a trusted central authority, or mint, that checks every transaction for double spending. After each transaction, the coin must be returned to the mint to issue a new coin, and only coins issued directly from the mint are trusted not to be double-spent. Bitcoin introduces a timestamp server. A timestamp server works by taking a hash of a block of items to be timestamped and widely publishing the hash, such as in a newspaper or Usenet post, as shown in figure 2[2].

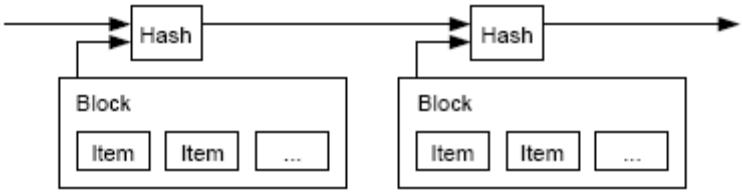

Figure2. A timestamp server

The proof-of-work involves scanning for a value that when hashed, such as with SHA-256, the hash begins with a number of zero bits. The average work required is exponential in the number of zero bits required and can be verified by executing a single hash.

For the timestamp network, the proof-of-work is implemented by incrementing a nonce in the block until a value is found that gives the block's hash the required zero bits, which is shown in figure 3. Once the CPU effort has been expended to make it satisfy the proof-of-work, the block cannot be changed without redoing the work. As later blocks are chained after it, the work to change the block would include redoing all the blocks after it[2,3].

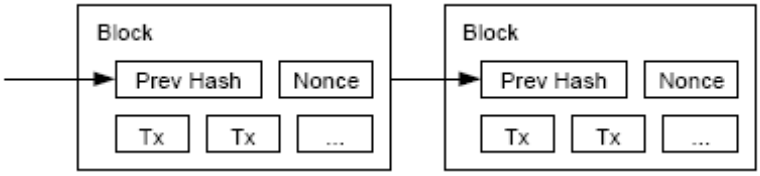

Figure3. The proof-of-work

Therefore, the nature of the Bitcoin can be as a pile of the special solution generated by the complex algorithm. Special solution is refers to the system of equations which can be an infinite number of (in fact, the currency is limited) solution in a group. And every special solution can solve equation and is the only one. Mining process is through a large amount of calculation to seek solutions of the equations. The equation is only 21 million special solutions by design. So the upper limit of bitcoin is 21 million.

The Bitcoin algorithm can ensure all mining and everyone store the results obtained with a mining - Bitcoin trading records. Their manufacture fake doesn't count as a result; still have to must be cut in the recognition of others. Such a design as a result, a person can't forge their wealth, and his wealth will be cut in all people to prove, not easily be deprived.

Bitcoin network has fault-tolerant mechanism. It can ensure even have the deceiver (false information has been released) and troublemakers (has refused to acknowledge others' trade) also won't affect the whole network operation[2, 4].

The Development Status of the Bitcoin

Bitcoin was first mentioned in a 2008 paper published under the name Satoshi Nakamoto. In early 2009, the first open source client (or wallet software), called Bitcoin-Qt, was released and the first bitcoins were issued. In 2009, a feature in the Bitcoin-Qt software was exploited and large numbers of bitcoins were created. This was due, in large part, because Bitcoin-Qt was the only software that facilitated bitcoin transactions and mining. This feature was later removed because specialized mining software turned out to be more efficient. Since then, the bitcoin open-source software has been maintained and enhanced by a group of core developers and other contributors.

By May 2011, interest in Bitcoin was growing as were concerns. The price of bitcoins has fluctuated wildly since its inception, going through various cycles of appreciation and depreciation, which have been referred to by some as bubbles and busts. In 2011, the value of one bitcoin rapidly rose from about US$0.30 to US$32 before returning to US$2. In the latter half of 2012 and during the 2012-2013 Cypriot Financial Crisis, the bitcoin price began to rise, reaching a peak of US$266 on 10 April 2013, before crashing to around US$50.

In March 2013, a technical glitch caused a fork in the block chain, with one half of the network adding blocks to one version of the chain and the other half adding to another. For six hours two Bitcoin networks operated at the same time, each with its own version of the transaction history. The core developers called for a temporary halt to transactions, sparking a sharp sell-off. Normality was restored only when the majority of the network downgraded to version 0.7 of the Bitcoin software from the flawed version 0.8.

Mainstream services began accepting bitcoins as a form of payment as well as certain non-profit or advocacy groups such as the Electronic Frontier Foundation. The first law enforcement events occurred in May 2013: Assets belonging to the Mt. Gox exchange were seized by Department of Homeland Security and the Silk Road drug market website was shut down by the FBI.

In October 2013, Chinese internet giant Baidu had allowed clients of website security services to pay with bitcoins. During November 2013, the China-based bitcoin exchange BTC China overtook the Japan-based Mt. Gox and the Europe-based Bitstamp to become the largest bitcoin trading exchange by trade volume. On 19 November 2013, the value of a bitcoin on the Mt. Gox exchange soared to a peak of US$900 after a United States Senate committee hearing was told that virtual currencies were a legitimate financial service. On the same day, one bitcoin traded for over RMB¥6780 (US$1100) in China. On 5 December 2013, the People's Bank of China prohibited Chinese financial institutions from using bitcoins. After the announcement, the value of bitcoins dropped and Baidu no longer accepted bitcoins for certain services. Buying real-world goods with any virtual currency had been illegal in China since at least 2009.

The first bitcoin ATM was installed in October 2013 in Vancouver, British Columbia, Canada.

With roughly 12 million existing bitcoins as of November 2013, the new price increased the market cap for Bitcoin to at least US$7.2 billion. By 23 November 2013, the total market capitalization of Bitcoin exceeded US$10 billion for the first time.

Commercial use of Bitcoin, illicit or otherwise, is currently small compared to its use by speculators, which has fueled price volatility. Bitcoin as a form of payment for products and services has seen growth, and merchants have an incentive to accept the currency because transaction fees are lower than the 2–3% typically imposed by credit card processors. The largest purchase using Bitcoin as of March 20, 2014 was payment for buying a villa in Bali, worth over $500,000 [1, 5-7].

The Future of the Bitcoin

The future development of Bitcoin needs to face three major risks, namely the national policy, technical security risk and transaction risk.

National policy directly influences the development of the Bigcion in the country. At present some countries recognize Bigcion as legal currency, some countries take a wait-an-see attitude, and some countries have banned directly.

The Bigcion is also facing the development of technical security risk. On the one hand, as the growth of the Bigcion users, circulation scale is more and more large, which will slow down the speed of the system and endanger their own development. On the other hand, hackers, site failure and difficulty for network monitoring of middlemen and other issues may also affect the development of the Bigcion.

And the volume of the Bitcoin market is small, which is very vulnerable to a banker manipulation and exploded slump. The transaction risk is very large.

In a brief, Bitcoin is a virtual currency, with a limited number, non-credit guarantees, decentralization, trading anonymity, globalization and hedging transaction characteristics. Besides, there are also many risks such as difficulties for Bitcoin to be compatible with the existing statutory monetary and financial system, value instability，supervision difficulties, distribution and allocation unequal et al. Let's wait and see the development of the currency.

Acknowledgement

This work was supported by the National Natural Science Foundation of China under Grant (No. 61272513), Funding Project for Academic Human Resources Development in Institutions of Higher Learning Under the Jurisdiction of Beijing Municipality (No. PHR201106133), and and the Projects in the National Science & Technology Pillar Program (No.2012BAH08B02).

References

[1] Wikipedia. Bitcoin. http://en.wikipedia.org/.

[2] Nakamoto S. Bitcoin: A peer-to-peer electronic cash system[J]. Consulted, 2008, 1: 2012.

[3] Babaioff M, Dobzinski S, Oren S, et al. On bitcoin and red balloons[C]//Proceedings of the 13th ACM Conference on Electronic Commerce. ACM, 2012: 56-73.

[4] Barber S, Boyen X, Shi E, et al. Bitter to better—how to make bitcoin a better currency[M]//Financial Cryptography and Data Security. Springer Berlin Heidelberg, 2012: 399-414.

[5] Reid F, Harrigan M. An analysis of anonymity in the bitcoin system[C]//Privacy, security, risk and trust (passat), 2011 ieee third international conference on and 2011 ieee third international conference on social computing (socialcom). IEEE, 2011: 1318-1326.

[6] Androulaki E, Karame G O, Roeschlin M, et al. Evaluating user privacy in bitcoin[M]//Financial Cryptography and Data Security. Springer Berlin Heidelberg, 2013: 34-51.

[7] Grinberg R. Bitcoin: an innovative alternative digital currency[J]. 2012.

Advanced Materials Research Vols. 989-994 (2014) pp 5070-5074
© (2014) Trans Tech Publications, Switzerland
doi:10.4028/www.scientific.net/AMR.989-994.5070

Risk Analysis of a Large-scale Construction Project

Wenjie Dai[1, a]

[1] Business School, Jiujiang University, Jiujiang, Jiangxi, China

[a]email:68344816@qq.com

Keywords: Risk Factors, AHP, Fuzzy Synthesis Evaluation, Risk Grade

Abstract. Huge investment, long construction period, many risk factors are existed in large-scale construction project. They are faced with various risks intervened with each other. this study using analytic hierarchy process and fuzzy evaluation method, conducts the comprehensive analysis of project risk level, and by combining list sorting method with subjective evaluation method grade the risk factors according to their likelihood of occurrence, the degree of serious consequences, and the controllability of occurrence, so that by the multiplication of three scores, the level of risks can be obtained and corresponding strategies can be established according to these different risks.

Introduction

A. Research Background. The large-scale construction project not only has huge investment, but also has a long implementation cycle, involving a wide range of uncertain elements, economic and technical risks and high quality requirements. Apart from the external political, economic and natural risks, it also meets the technical and non-technical risks in the decision-making and implementation. From the setting-up and complement, the running of the large engineering project must be given great attention to risk management during its entire lifecycle. Taking full advantage of all information gathered in the project management and personnel's management experience, the investor will depend on the assessment of the overall level of project risk as well as its analysis of the results and its circumstances to make investment. And such investment must be ensured to achieve its project goal by developing strategies for dealing with risks.

B. Research Contents. Therefore, investors need to investigate the actual situations of a large engineering project from the external environment, technical and non-technical aspects, by combining qualitative analysis with quantitative analysis formulate the corresponding measures to different risks according to the influence degree of various risk factors. And try to reduce the possibility of occurrence of a risk and its negative effect on the project to ensure the achievement of the goal of construction.

C. Research Methods. The object of the study is a domestic large-scale construction project, which has been put into operation completely. Through the survey and audit of engineering project risk events and technical and economic analysis and combining with project managerial staff‘s ideas. this study using analytic hierarchy process and fuzzy evaluation method, conducts the comprehensive analysis of project risk level, and by combining list sorting method with subjective evaluation method grade the risk factors according to their likelihood of occurrence, the degree of serious consequences, and the controllability of occurrence, so that by the multiplication of three scores, the level of risks can be obtained and corresponding strategies can be established according to these different risks.

Risk Analysis of a Large-scale Construction Project

A. Analytic Hierarchy Process. The main risk in the project management can be summarized as: external environment, non-technical and technical risk three categories. Political risk, economic risk and natural risk are the main external environment risk. Technical risk refers to the loss caused by the uncertainty technical conditions. Including design and construction works. Main risk in project selection, project design, project construction process, to determine technical standard selection,

analysis of the calculation model, the safety factor of the deviation. Non-technical risk refers to the project planning, organization, management, coordination and other non-technical conditions caused the project goals cannot achieve, including purchase, progress schedule, project organizational management, etc. After analysis, establish the AHP model (Fig.1).

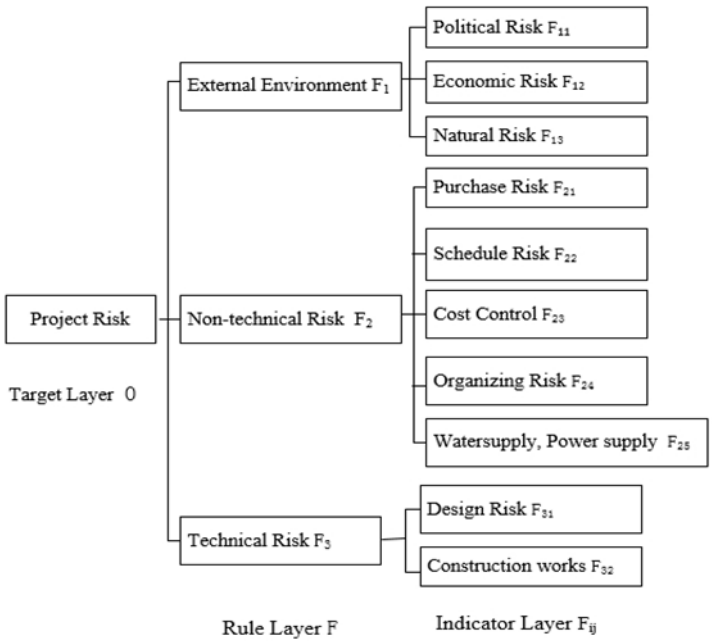

Fig.1 AHP model

The evaluation index system can be divided into three layers: target layer, rule layer and indicator layer. Based on inspecting and studying, a number of experts judge the importance of n indicators on the same layer by Delphi method, then to establish the judgment matrix, and check the consistency. Consistency index is CI=(λ_{max}-n)/(n-1)， according the mean random consistency index RI, obtains relative consistency index CR, CR=CI/RI. If CI<0.1, the weight order meets the requirements, the results are satisfied, or to adjust the judgment matrix, and to obtain the weights again by the above steps [1].

Judgment matrix O－F : $A=\begin{pmatrix} 1 & 1/8 & 1/2 \\ 8 & 1 & 7 \\ 2 & 1/7 & 1 \end{pmatrix}$, λ_{max}=3.035,CI=0.0175, CR=0.03<0.1, the judgment matrix O-F has consistency. W=（0.081, 0.784, 0.135）^{T}

Similarly calculate F_1-F_{1j}, F_2-F_{2j}, F_3-F_{3j}:

w_1=（0.297, 0.163, 0.54）^{T}, w_2=（0.456, 0.056, 0.305, 0.092, 0.092）^{T}, w_3=（0.875, 0.125）^{T}.

Table 1 Weight of the Indicators

Rule Layer	Weight	Indicator layer	Weight	Weight
F_1	0.081	F_{11}	0.297	0.024
		F_{12}	0.163	0.013
		F_{13}	0.540	0.044
F_2	0.784	F_{21}	0.456	0.358
		F_{22}	0.056	0.044
		F_{23}	0.305	0.238
		F_{24}	0.092	0.072
		F_{25}	0.092	0.072
F_3	0.135	F_{31}	0.875	0.118
		F_{32}	0.125	0.017

B. Fuzzy Synthesis Evaluation. Establishing evaluation set V = (V_1, V_2, V_3) = (high risk, medium risk, low risk), Experienced engineering managers analyses different risk factors. calculate membership degree (A_{ij}). Such as the political factor, there are 1 people think is high risk, 1 people think is medium risk, 8 people think is low risk, obtain membership degree A_{11}=（0.1/ high risk, 0.1/ medium risk,0.8/ low risk）,then obtained the results of comprehensive evaluation(Table 4), finally to build the total evaluation[2, 3, 4].

Table 2 Evaluation Results of Various Indicators

Rule Layer	Indicator layer	Membership Degree (A_{ij})	Weight	Evaluation Set V		
				High Risk	Medium Risk	Low Risk
F_1	F_{11}	A_{11}	0.024	0.1	0.1	0.8
	F_{12}	A_{12}	0.013	0.1	0.2	0.7
	F_{13}	A_{13}	0.044	0.2	0.4	0.4
F_2	F_{21}	A_{21}	0.358	0.1	0.7	0.2
	F_{22}	A_{22}	0.044	0.2	0.2	0.6
	F_{23}	A_{23}	0.238	0.7	0.2	0.1
	F_{24}	A_{24}	0.072	0.4	0.4	0.2
	F_{25}	A_{25}	0.072	0.1	0.1	0.8
F_3	F_{31}	A_{31}	0.118	0.5	0.4	0.1
	F_{32}	A_{32}	0.017	0.3	0.4	0.3

$$C = WS \tag{1}$$

$$c_{ij} = \bigcup_k (w_{ij} \cap s_{ij}) \tag{2}$$

w and *s* intersection calculation take the minimum value, *w* and *s* union operation take the maximum value, then

C= [0.238，0.358，0.2]

Grade calculation result is as follows:

B= [1.0，0.5，0.2], $D=BC^T=0.457$

The project belongs to low risk, can invest construction.

C. Risk Grade and Risk Ranking. By combining list sorting method with subjective evaluation method grade the risk factors, from possibility, severity and controllability. Experienced managers with subjective evaluate risk grade from three aspects. 0 represents not risk, 10 represents the greatest risk, by the multiplication of three scores said risk grade. It is concluded risk grade of the risk factors, calculating the correlation degree (r_{ij}) for risk grade in weight.

Table 3 Risk Grade

Rule Layer	Indicator layer	Weight	Risk Evaluation			Risk Grade	r_{ij}
			Possibility	Severity	Controllability		
F_1	F_{11}	0.024	1	1	6	6	0.14
	F_{12}	0.013	0	0	4	0	0
	F_{13}	0.044	1	1	10	10	0.44
F_2	F_{21}	0.358	3	5	5	75	26.85
	F_{22}	0.044	2	1	4	8	0.36
	F_{23}	0.238	10	5	3	150	35.70
	F_{24}	0.072	7	6	4	168	12.10
	F_{25}	0.072	1	8	3	24	1.73
F_3	F_{31}	0.118	8	10	6	480	56.64
	F_{32}	0.017	10	8	5	400	6.80

Risk ranking is r_{31}> r_{23}> r_{21}> r_{24}> r_{32} > r_{25} > r_{13}> r_{22} > r_{11} > r_{12}.

The Construction Project Risk Control Strategies

Investment must be ensured to achieve its project goal by developing strategies for dealing with risks through risk evasion, risk control, risk transfer and risk retention in the construction project.

A. Risk Evasion .When the project's possibility of potential risk is too big and adverse consequence is very serious, in the case of no other strategies to reduce, the initiative to abandon the project or change the project objective and action plan is a strategy to avoid risks.

B. Risk Control. Reducing the facing risk is a kind of positive management means, and project managers who are reluctant to give up or transfer the risks, by minimizing the possibility of loss and adverse influence, can also achieve the goal of controlling. When there is a rainy day, for example, it is impossible to carry on outdoor construction, but to arrange as many as possible personnel and equipment to be engaged in the indoor work is a kind of engineering project risk reduction measure.

C. Risk Transfer. To transfer the risk of loss of the project to other individuals or units doesn't reduce the risk of harm, for it is only to make another party to bear the transferred risk. This kind of risk control measure is mostly used for dealing with such situations that the risk probability is small, but the loss is big, or engineering project organization is difficult to control the engineering project risk. The realization of the transfer of risk, to great extent, depends upon agreement or contract to transfer the loss of legal responsibility or financial consequences to others to take.

D. Risk Retention. Bearing the losses caused by risk accidents and taking the risk retention mainly depend on investors' own management and financing ability. Risk retention and risk control are not the same, because the former is the post-processing of its financial loss after the happening of risk accident, while the latter is the pre-processing before the risk accident so as to change the possibility of risk occurring and the severity of losses when it happens.

In this paper，project manager used risk control Strategies for the construction project.

Table 4 Construction Project Risk Control Strategies

Indicator	Risk Factors	Risk Management Strategy	Risk Counter-measure
F_{11}	Political Risk	Risk Transfer, Risk Retention	Insurance , Claim
F_{12}	Economic Risk	Risk Retention, Risk Transfer, Risk Evasion	Strict contract Clause, Subcontract, Arbitrage transaction
F_{13}	Natural Risk	Risk Transfer	Insurance
F_{21}	Purchase Risk	Risk Transfer, Risk Evasion	Bid guarantee, Prequalification
F_{22}	Schedule Risk	Risk Retention, Risk Control	Claim, Preventive Measures
F_{23}	Cost Control	Risk Retention, Risk Control	Contract Management, Subcontract
F_{24}	Organizing Risk	Risk Retention, Risk Control	Rigorously enforce rules and regulations, Preventive Measures,
F_{25}	Water supply, Power supply	Risk Transfer	Claim, Insurance
F_{31}	Design Risk	Risk Evasion, Risk Transfer	Claim ,Distinguish Responsibility in Contract
F_{32}	Construction works	Risk Retention, Risk Control, Risk Control	Claim, Preventive Measures, Insurance, Rigorously enforce rules and regulations

Summary

In this paper, investors investigate the actual situations of large-scale construction project, through the survey of construction project risk events combining with internal and overseas current information. By combining qualitative analysis with quantitative analysis formulate the

corresponding measures to different risks according to the influence degree of various risk factors, and try to reduce the possibility of occurrence of a risk and reduce its negative effect on the project to ensure the achievement of the goal of construction.

References

[1] Morash E A: *Supply chain strategies, capabilities, and performance*, Transportation vol. 3(4) (2001), p.124-126.

[2] Miao Zhiguo, Zheng Quancheng: *Grey comprehensive evaluation for customer satisfaction index in pachaging*, Packaging and Food Machinery vol. 28(1) (2010), p. 22-24.

[3] Niu Huiyong: *Study on safety evaluation of urban road traffic based on gray theory*, China Safety Science Journal vol.15(9)(2005), p. 92-95.

[4] Dai Yi, Huo Jiazhen, and Zhang Qian: *Fuzzy comprehensive evaluation of enterprise internal risk*, Journal of Tongji University(Natural Science) vol36(6) (2008), p.864-868.

[5] Li Li: *Fuzzy AHP - Based Quality Evaluation of Health Examination Service*, Chinese Health Quality Management, vol 19(1) (2012), p. 53-55.

[6] Wang Zhuopu: *Engineering Project Risk Management - Theory, Method and Application*, Chinese Water Conservancy and Hydropower (2003), p.123-134

[7] Zhu Deng-hua, Zhang jian-she, Cao guang-ping: *Engineering project risk analysis method based on AHP*, Journal of Tianjin University,(2002).3

Advanced Materials Research Vols. 989-994 (2014) pp 5075-5077
© (2014) Trans Tech Publications, Switzerland
doi:10.4028/www.scientific.net/AMR.989-994.5075

Internet Financial Credit Evaluation for the Small and Medium Enterprises

Yiqing Lu[a]

School of Information Management, Beijing Information Science and Technology University, Beijing, 100192, China

[a]email: luyiqing@126.com

Keywords: Internet financial; Credit Evaluation; Big data;

Abstract. In this paper, a credit evaluation system based big-data is designed to change the information asymmetry between the finance institutions and enterprises, reduce the credit risk of internet financial institutions and investors, by utilizing the information and technology advantages. The research objective of this project have important theoretical and application value to the development of small and medium-sized enterprises (SME) credit evaluation system.

Introduction

In short, in many developing Asian economies, it is not easy for SMEs to do business, and one element of that is that getting credit is quite difficult in many countries.

There are many reasons why access to finance is difficult in developing Asia:

- Large numbers of SMEs are in the informal sector. They are not registered, they do not have all the necessary documentation. It can be difficult for potential lenders to distinguish the financial situation of the company from that of its owners. They are less able to provide collateral.
- Financial markets are underdeveloped in many Asia countries. They do not offer a complete range of financial products and services. They may also suffer from regulatory rigidities.
- The fixed costs of all the paperwork mean that it is easier for banks to make bigger loans to larger enterprises.
- In many countries, large enterprises enjoy privileged access to finance from banks. Many of these banks are state-owned or have close links with the government which uses bank lending as an instrument of industrial policy to develop specific sectors. Banks may also have ownership and other ties to industrial interests and will tend to favor affiliated companies. This means that it is difficult for SMEs to obtain finance.

So, even in normal economic conditions governments have recognized that, to survive and grow, SMEs need specific policies and programs especially to facilitate their access to finance.

Let's move on to the crisis. SMEs and their financing have been especially hard hit by the global crisis leading to massive job losses. For example, Lim reports that over 100,000 factories in southern China alone have closed.

This has occurred as revenues have fallen, and the credit crunch has reduced access to finance for SMEs, which are perceived as riskier, more than for large enterprises. [1-3]

Internet Financial

Different from the indirect financing among commercial banks and the direct financing of stock and bond markets, the internet finance is a new thing generated from the combination of internet and finance in recent years, and is a new financial service mode which realizes funds allocation, payment and information intermediary depending on internet technology and mobile communication technology.

In recent years, new internet finance institutions have been emerging continuously in many regions of China and the market scale has been growing increasingly.

Under such new financial mode, internet and relevant software technology have replaced the professional services of financial and security institutions, complicated transactions such as risk pricing and immunization hypothesis are not only simplified greatly but are also easy to operate. Loans, issuance and transactions of stocks and bonds, and delivery versus payment can be done online directly.

Currently people are lack of investment channels. Being a financing service platform with low risk and high return and easy to participate and operate, internet finance can be easily accepted by the public. Common people can make financial transactions through the internet, the market participants are more popular and the huge benefits brought by the transactions can bring more benefits to the public[4-5].

Internet Financial Credit Evaluation based on Big Data

Concerning the traditional financial institution, there is no difference on the operational cost between the large loan and small loan[6]. For the financial information in the small and medium enterprise tends to be imperfect, it is hard for the bank to accurately evaluate the credit condition of the small and medium enterprise, thus causing the bad debt of small loan is higher and the non-performing loan ratio with the good governance maintaining 3%. Due to the high cost and high bad debt rate, the bank does not pay attention to the small loan for a long term. However, under the Internet finance, using the technical means of big data, cloud computing, data mining and social network can integrate various related data and set a more accurate credit ranking indicator to evaluate the enterprise's credit condition. On the basis, the credit evaluation model based on the big data can be established, as shown in figure 1.

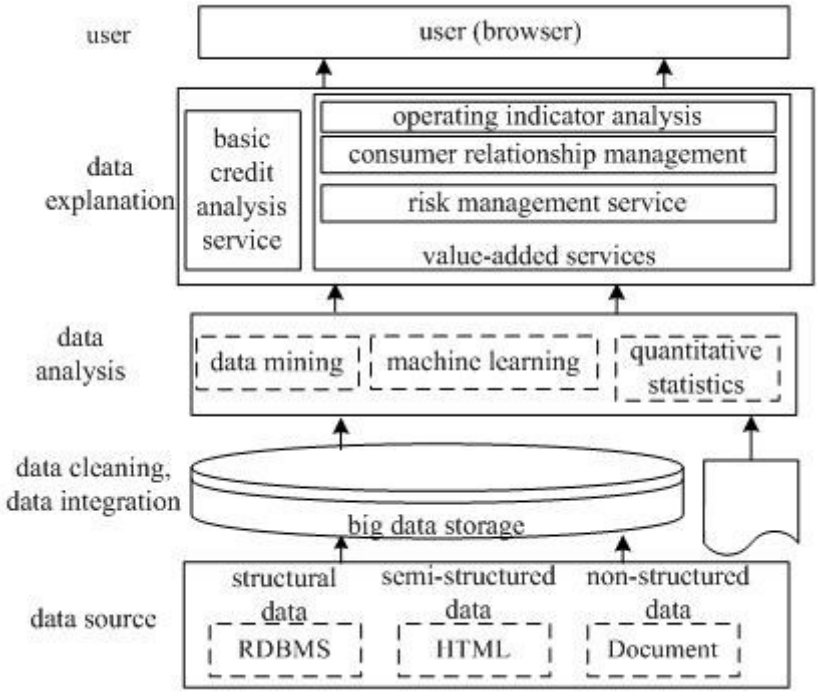

Figure 1 Internet financial credit evaluation

- Large data collection

Under the traditional financial model, the credit institution can obtain limited data, and the accuracy to evaluate the credit of the small and medium enterprise is insufficient. However, under the Internet financial model, the credit institution can collect large amounts of data through the technical means to comprehensively judge the credit condition of the credit object and make a more accurate credit evaluation. There are three main means for the source of big data: 1) When submitting the loan application, the demand side shall perfect the data, submit the information including the company,

family, spouse, education and housing. 2) In order to further improve the data, enhance the data dimension, and improve the risk control level, the external data shall be introduced, such as customs, taxation, electricity, water, telecommunication, central bank credit system and other data, the Internet information of the loan enterprise can be collected and integrated, such as the consumer interaction data and search data in the social platform, etc. 3) Concerning the enterprise developing e-commerce, the e-commerce data can be collected, such as upstream and downstream transaction, consumer data, logistics data, reputation evaluation, certification information, recent trading dynamic, real-time operating condition, platform tool usage status, etc., the data can be integrated and processed.

- Design credit evaluation indicator

The small and medium enterprise's credit evaluation indicator under the Internet financial environment can be established according to the collected big data. Concerning the small and medium enterprise developing the e-commerce, in addition to consider the indicators reflecting the enterprise operating capacity, profitability, solvency and development capacity, the indicators reflecting the enterprise network marketing, network service capacity and network management capacity shall be considered. The credit data shall be analyzed and calculated with the data mining, machine learning, metering statistics and other mathematical methods and models to finally form the credit report of the enterprise.

According to the credit evaluation indicator, the collected big data shall be analyzed with credit evaluation algorithm. In addition to provide the basic credit analysis service, the result can be used for the operating indicator analysis, consumer relationship management, risk management service and historical data management and other value-added services.

Acknowledgement

This work was supported by the National Natural Science Foundation of China under Grant (No. 61272513), Funding Project for Academic Human Resources Development in Institutions of Higher Learning Under the Jurisdiction of Beijing Municipality (No. PHR201106133), and and the Projects in the National Science & Technology Pillar Program (No.2012BAH08B02).

References

[1] SME financing and the crisis. http://www.mrglobalization.com /finance/329-sme-financing-and-the-crisis

[2] Cosh A, Hughes A, Bullock A, et al. SME finance and innovation in the current economic crisis[J]. Centre for Business Research (http://www. cbr. cam. ac. uk/pdf/crcr_econcrisis. pdf), 2009.

[3] Taketa K, Udell G F. Lending channels and financial shocks: The case of small and medium-sized enterprise trade credit and the Japanese banking crisis[J]. Monetary and Economic Studies, 2007, 25(2): 1-44.

[4] China embracing Internet finance boom. http://en.ce.cn/Insight/201311/14 /t20131114_ 1752466.shtml.

[5] Narayanasamy K, Rasiah D, Tan T M. The adoption and concerns of e-finance in Malaysia[J]. Electronic Commerce Research, 2011, 11(4): 383-400.

[6] Yan G. Contents and Measures for Supervision on Internet Finance[J]. Advanced Science Letters, 2013, 19(4): 1197-1201.

Advanced Materials Research Vols. 989-994 (2014) pp 5078-5081
© (2014) Trans Tech Publications, Switzerland
doi:10.4028/www.scientific.net/AMR.989-994.5078

College Aerobics Curriculum System Construction in Perspective of Systems Theory

Ying Zhang

School of Education and Sports, Bohai University, Jinzhou, P.R. China

47086132@qq.com

Keywords: systems theory; colleges; aerobics; curriculum system; construct

Abstract. The physical education curriculum is an important part of the school curriculum system, is to achieve the goal of school physical education, quality education, promoting students to adapt to society, students complete an effective way to cultivate individuality. In this study, aerobics as the college physical education curriculum reform and the practice object, on the base of the comprehensive analysis the development status, according to "National College of Physical Education Curriculum Guidelines" spirit, combining with the college aerobics teaching characteristics and rules, system theory is curriculum ideas, from the target system of aerobics courses, teaching content, teaching form, teaching methods, curriculum evaluation, and other aspects, to construct the aerobics curriculum system of higher education. Effectively cultivate student's sports consciousness, physical ability and innovation capabilities, to meet the needs of the student physical and mental health, and lay a solid foundation for lifelong physical reserves.

Introduction

Aerobics in the late 1970s into China, in the 1980s gradually been adopted by the physical education curriculum of college. Aerobics as an emerging sports project, financial gymnastics, music, dance, martial arts as a whole, to physiology, psychology, aesthetics, music and other disciplines theory as the instruction, with its energetic and progressive youthful vitality and aesthetic appreciation, attracting more and more people, the majority of young students like [1]. However, after investigation, many schools are still no clear teaching syllabus and supporting materials, there is no complete teaching system in aerobics curriculum of some schools, the teaching goal is not clear, single teaching content, teaching in the form is boring, Teaching evaluation using a simple technology scoring system, Too dependent on teachers' subjective judgments, not fully checked, assessed the quality of student learning. Based on this, we propose to form and establish a comprehensive system of college aerobics courses, to achieve the teaching content, teaching evaluation and other aspects of the deepening reform measures, to be closer to the actual students and teachers, to meet the needs of the market and the situation, adapt curriculum content needs, to provide a reference for college aerobics teaching reform and promote the construction of college aerobics courses. Construction of College Aerobics Curriculum System is based on training colleges personnel specification requirements, lifelong physical education requirements and spirit of the "Outline" [2], the introduction of the system theory on the college aerobics teaching, it can not only motivate their students directly participate in aerobics teaching enthusiasm, but also significantly improve the aerobics teaching quality.

Construct the Theory Basis of Aerobics Curriculum System

Systems theory is an intermediary theory between science and philosophy. According to the research method of system theory, the research object as a system to consider analysis, in-depth study, can not only focus on the whole and the part (main system and subsystem) research, but also focus on the relationship between the system and the external and the environment, the study of interaction, can fully demonstrate its dynamic, comprehensive, holistic, optimal performance characteristics [3]. The article using system theory on college aerobics teaching research, the entire college aerobics courses as a complicated system engineering, also as a main system, thus the four

subsystems-teaching goal, teaching content, teaching methods, teaching evaluation were to be discussed (Fig. 1).

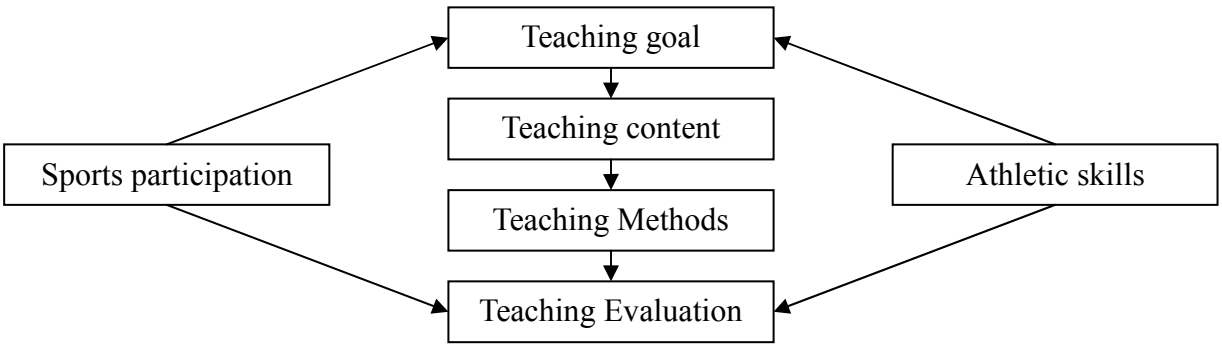

Fig. 1. Aerobics course system structure diagram

Aerobics Curriculum Goal System

The curriculum goal is the reflect of certain educational values in curriculum field [4]. In the 2001, "curriculum standards" explicitly pointed out the sports classroom learning goal is "to participate in sports, sports skills, physical health, mental health, social adaptation" (Table 1). Aerobics curriculum teaching goal is in a short period of time to allow students to acquire the skills and knowledge, to enhance students' interest in aerobics sports, to cultivate students' consciously exercise habits, laying the foundation for lifelong sports.

Table 1. Aerobics course goal system

Content	The basic goal
Sports participation goal	To actively participate in aerobics exercise and form the habit of conscious exercise Understanding the designing principles and methods of aerobics, learn to complete aerobics choreography, and can make personal fitness program Understand aerobics competition rules, has a certain ability to appreciate the aerobics performances or competitions
Athletic skills goal	Develop athletic ability of students to participate in the aerobics Master the basic method of aerobics, the teaching method and the physical quality training method Master several sets of aerobics or popular gymnastics Master disposal method of common sports injuries
Physical health goal	To develop good habits, to form a healthy lifestyle Self-evaluation on fitness effects Can reasonably choose the personal food of health and nutrition
Mental health goal	To develop good habits, to form a healthy lifestyle Self-evaluation on fitness effects Can reasonably choose the personal food of health and nutrition
Social adaptation goal	Exhibiting good sportsmanship and teamwork spirit Correctly handle the relationship between competition and cooperation To enable students to have the courage to perform, good performance, with modern consciousness

Aerobics Teaching Content System

Aerobics teaching content system is a subsystem of physical education teaching, according to author's own teaching practice, put forward the aerobics college teaching content system of fit fact: Select informative content, select the skill content, and select operability content. Meanwhile, the establishment of "hierarchical teaching" (primary, intermediate, senior) teaching model, According to the number of students and the different of basic level, to carry on the hierarchical teaching,

primary open “basic course”, intermediate open “improving lesson”, senior class open “selective course” and “ popular project additional lesson”.

Basic Course (primary) teaching settings: students master basic skills of aerobics and related theoretical knowledge. Improve lesson (Intermediate) teaching content settings: the students' favorite hip-hop, Latin aerobics, prosodic fighting, physical training and other content introduced into the classroom, using the “segmented” teaching, teaching content is segmented to arrange. Any selective course (advanced course) teaching content settings: Latin aerobics, hip-hop, rhythm fighting, physical fitness training and other fashion content introduced into the classroom. In the implementation process of the new aerobics teaching model, to fully reflect the leading role of teachers and the main role of students. So that different levels of students to fully enjoy every aerobics class, and get a good emotional experience in aerobics teaching

Aerobics Teaching Method System

Teaching methods include teaching means and organizational forms, is to achieve teaching goal and improve the teaching quality to service [5], the scientific teaching method could promote the rapid formation of student proficiency and rational use of skills, to achieve effective teaching results, so as to inspire and cultivate the students' interest in learning, and enhance the confidence to learn aerobics, achieve the purpose of lifelong physical education. In aerobics teaching, just by changing the traditional teacher lectures and demonstrations to teach students basic skills teaching methods and action routines, and more use of multimedia teaching, the abstract transform into concrete, so that improving the students' consciousness of participation and learning initiative [6]. Meanwhile, in the process of teaching, give full play to students' dominant role, based on mastering certain actions, according to the law of creation of action, inspire students to create sets of aerobics. In addition, in order to promote examination by competition, in order to promote competition by examination, is also a bright spot in process of college aerobics classes teaching. This not only gives students the opportunity to test their aerobics technical level in aerobics course learned, to improve their capabilities, also can cultivate the students' competition consciousness, make the students have confidence to show themselves, and have the team spirit of unity and cooperation.

Aerobics Curriculum Evaluation System

With the development of modern science and sports science education, more and more fields have begun to use control theory, information theory to study the evaluation system [7]. Because of individual differences in evaluation objects, evaluated from the perspective of a single evaluation steering multi angle and more comprehensive quality assessment method, implemented at different levels of hierarchical assessment, and establish the combination between student end and the process evaluation, combining the multiple evaluation, qualitative and quantitative evaluation of the combination, have been a major evaluation system of aerobics courses (Fig. 2). Thus having the comprehensive evaluation to learning process and learning effect, to form a evaluation system that not only pay attention to process evaluation and focus on the effect evaluation, dilute the evaluation of the selection function, strengthen comprehensive education, testing, feedback, encouragement integrated functions.

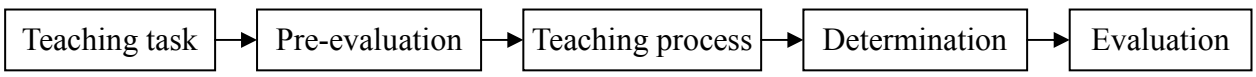

Fig. 2. Aerobics courses evaluation system

(1) Combined with the end and the process evaluation. Pay attention to the result evaluation. At the same time, is more attention to process evaluation, evaluation of learning attitude, active participation and innovative evaluation. Emphasis on the development and progress of the student's own magnitude, so that every student can give full play to their strengths, make up for their

shortcomings, encouraging progress, especially pay attention to the special situation of the individual differences and weak students, so that every student has the progress of confidence.

(2) Multiple evaluation. From the multi angle, multi method, multi form to do a comprehensive evaluation, fully enhanced guidance, education, experience, feedback, identification, specification, deepen and incentive comprehensive functions. On examination content, to highlight the capacity and quality assessment on the basis of theoretical knowledge assessment; in the examination ways and means, to strengthen the functions of the various ways and means, advantages and disadvantages the reasonable combination, and form scientific and reasonable evaluation mechanisms.

(3) Combined with the quantitative and qualitative evaluation. The physical shape, physiological functions and exercise capacity, which can be measured data to determine the human body development. The student sports attitude, morality, psychology, exercise capacity and other indicators, there is a lot of humanities factors, with a significant qualitative characteristics, it is difficult to quantify, can take a qualitative evaluation or fuzzy comprehensive evaluation method.

Conclusion

This study were from five aspects of sports participation, sports skills, physical health, mental health, social adaptation to do the detailed description of aerobics curriculum content. Recommended that future seriously learn the advanced experience of foreign countries, insist integration and optimization of the overall curriculum system, construct with a reasonable, flexible curriculum areas and course modules, courses for schools and students to enhance the adaptability , so as to promote the reform and development aerobics curriculum system.

Acknowledgment

This work is supported by 2013 Bohai university research of teaching reform project (JG13QN017).

References

[1] Y. H. Zhang, "Research on System of Aerobic Exercise Elective Course in Colleges and Universities," Journal of Beijing University of Physical Education, vol. 25, no. 3, pp. 373-375, 2012.

[2] H. M. SUN, "Consideration on the Construction of Aerobics Curriculum System in Higher Education," Journal of Beijing Sport University, vol. 29, no. 1, pp. 107-109, 2006.

[3] W. W. Jia, "The Construction on the College Tennis Curriculum System under the Perspective of Systems theory," Journal of Bohai University (Philosophy & Social Science Edition), vol. 46, no. 1, pp. 155-157, 2012.

[4] L. H. WANG, "The Innovation of the Course Mode of Aerobics in Common Universities and the Diversification of P.E.Value," Journal of Beijing University of Physical Education, vol. 30, no. 3, pp. 395-397, 2007.

[5] Baidu Library, "Application of occurrence statistic iterative method to the index weighting," http://wenku.baidu.com/view/d73dd4c308a1284ac85043eb.html, 2013-11-24.

[6] J. L. WANG, "Cultivation of student's teaching and curriculum development capacities via the aerobics course from the perspective of the theory of multi-area intelligence," Journal of Physical Education, vol. 16, no.11, pp. 45-48, 2009.

[7] Q. Li, X. J. Dong, "Construction and Implementation of the Curriculum Teaching Pattern of Aerobics in University," Journal of Guangzhou Sport University, vol. 27, no.1, pp. 124-126, 2008.

Advanced Materials Research Vols. 989-994 (2014) pp 5082-5085
© (2014) Trans Tech Publications, Switzerland
doi:10.4028/www.scientific.net/AMR.989-994.5082

Development of Logistics Bases in China- A Case Study of Jiangxi Yinyan Logistics Base

Xiong Wei[1, a], Zhang Man[2,b]

[1] Headmaster's Office, Jiangxi Science & Technology Normal University, Nanchang, Jiangxi,China

[2]School of Information Engineering, Nanchang University, Nanchang, Jiangxi, China

[a]572383070@qq.com, [b]manzhang201010@163.com

Keywords: Logistics; Yinyan Logistics Base; Development; Case Study

Abstract. Logistics in China is on its rapid development stage as more and more distribution centers and logistics bases were established. However, due to China's specific national conditions, there are some problems existed in logistics compared with the international logistics. Research on the problems existed in logistics bases will help to find solutions to the logistic problem in China. Therefore, the paper analyzed the status and development measures of China's logistic bases taking Yinyan logistic base in Jiangxi as an example to do an primary research on the development strategies of logistics bases in China.

Introduction

With the development of logistics in China, logistics bases are beginning established in China. In fact, logistics base in a new form of logistics with its development to a certain degree[1], also it's a result of logistics developing[2] . To response the requirement of modernization in China, the government formulated policies on the construction of logistics bases to promote the development of logistics in China. Many provinces began their constriction of logistics bases[3]. As more and more logistics bases are built, researches on its status and efficiency is important so as to examine the real condition of logistics in China. Jiangxi Yinyan logistics base is a logistics base with freight, display and storage functions which achieves the third-party logistics requires while using modern electronic systems for the majority of enterprises to provide a good trading platform. The base is divided into four sections as display area, storage area, LTL(less than carload) distribution area, and information trading center. The purpose of Yinyan logistics base is service the nation based on the central region, and truly achieving the goal of smooth flow of goods through the world.

The paper analyzed the status and development measures of Yinyan logistics base in Jiangxi to find out the real situation of logistics base and to provide advices for the development of logistics bases in China.

Status of Yinyan logistics base

Yinyan logistics base is located in the east of Shengmi Brige of Nanchang, Jiangxi province. It is near to Nanchang University and has a convenient transportation, and it's one of the biggest logistics bases in Jiangxi province which has a 320,000 square meters covering and 270,000 square meters total construction area. It is invested by Beijing Cheng Yi Co. Ltd with a funds of 20 million Yuan, is one of the key investment projects in Jiangxi Province. The total investment to Jiangxi Yinyan logistics base is 300 million Yuan with a covers of 477 acres located in the Xihu District of Nanchang Chaoyang farm in order to build the largest logistics base in Jiangxi Province.

The strategic orientation of Yinyan logistics base is: make Yinyan logistics base be one of the mainland's transit station for Yangtze River Delta, Pearl River Delta and Fujian Delta to enter the inner land based on Nanchang as the foundation. It can pull the construction of Nanchang city from the establishing of Yinyan logistics base to build a domestic and international logistics hub nodes with a system constitute of road, water and air transport while making the road system as the main transportation means. The corporation vision of Yinyan logistics base is: Jiangxi Yinyan Company

Limited will accelerate the construction of logistics infrastructure and high-tech logistics technology and equipment, improve the base supporting aspects, introduce professional management personnel, and establish a logistics system relatively synchronized with advanced international logistics industry to provide a platform and a logistics base with high quality services for enterprises. What's more, Yinyan will expand exchanges and cooperation with their counterparts in the international logistics companies to achieve multinational operations, will stream into the international market and promote the international development of the logistics industry and will improve the development of logistics in China from all aspects after it is established.

In fact, the real statuses of Jiangxi Yinyan logistics base are shown as following:

(1)The logistics base in Jiangxi Yinyan is made up of numerous small-scale logistics companies, each company operates on its own rules, and the chances of information exchange and cooperation between them are few.

(2)Each company's logistics facilities is outdated, small-scale and scattered. The management is traditional and relies on manpower with low specialization degree. There is no high-tech operation and information management system.

(3)The socialization and organization level of each logistics company is low, and the convergence on various aspects of logistics and distribution is poor. Few companies among Yinyan logistics base can provide one-stop services.

(4)Most companies use logistics information mainly stay in the level of collecting and transmitting information, few of them know about the operation and its significance of analysis and data mining for logistics information.

As it can be seen from the above real status of Yinyan logistics base, it's more like goods transfer station than a real logistics base for it has a big gap with the real logistics distribution center especially with the developed distribution center. The utilization of logistics technology and logistics systems in Yinyan logistic base is beyond the average level. With the lack of special information management system, the base has a low informatization level. Of course, this has a great relationship with the status of China's logistics development. The real statuses of China's logistics development are: low operation level; low economic benefit[4]; uneven development[5], the east has a better logistics performance than the west and Midwest; rarely exchanges of logistics technologies and information between different regions. As logistics is on its development stages in China, it need time and experience to improve the status of logistics development in China.

Development Measures for Yinyan Logistics Base

To improve the status of Yinyan logistics base in Jiangxi, there are many works need to be done to make it a effective logistics base in China even in international logistics field. For logistics distribution center of Yinyan logistics base, it should learn from the experience of developed countries and take use of modern facilities[6], starting from the consideration of national, region and business situation for it, to develop a logistics base with its own characteristics.

Establish a comprehensive information exchange processing center. Yinyan logistics base should rectify all enterprises within it, unite all business information among its sub-centers to create an integrated information processing center (as shown in figure 1). It can use some computer software and systems, such as information management systems and decision support systems to strengthen exchanges between enterprises[7], and to improve the delivery and utilization of logistics information management effectiveness. If there is information that will benefit to the development of the company or information about collaborative works needs to work together, each sub-company can find collaborators by using the internal information management system to seek common development with its collaborators. From this way, the utilization of resources this can be enhanced, and it will promote the development to the logistics base.

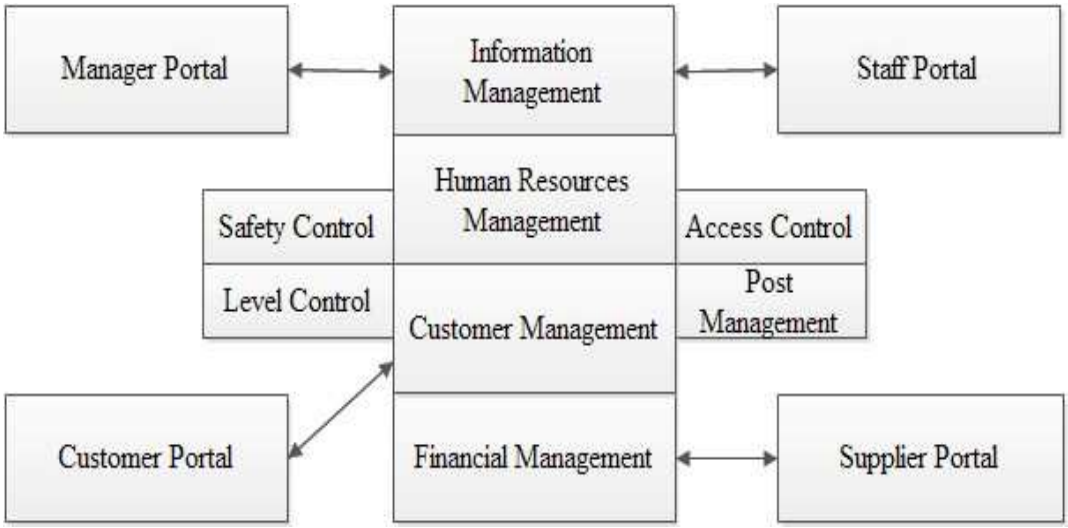

Fig.1 Information exchange processing center for Yinyan logistics base

Introduce technology and equipment to improve the technological level of Yinyan logistics base. From the construction of an automatic three-dimensional warehouse, the purchase of advanced logistics and material handling vehicles, and the introduction of information technology to make up of an advanced information technology system for logistics base; Of course, to make up an advanced information technology system, the initial investment is huge which may need the support of national policy or foreign investment. The specific introduction and establishment of appropriate advanced technology and equipment should also combine with the real conditions of Yinyan to improve its information management level in a feasible way. For example, what kind of information management system to be introduced or what kind of information should be collected and how man new professionals on information management should be employed, and son on, all these questions related to the real effectiveness of the new introduced information technology system. With the help of the new information management system, Yinyan will improve operational effectiveness greatly. There are automatic identification technologies, EDI technology, geographic information technologies in physical information systems will help to effectively improve the work efficiency for Yinyan logistics base.

Improve the quality of its staff. Yinyan logistics base has an advantage that near major colleges and universities of Nanchang which will benefit it to abort high-tech talents with a relative less economic cost. With rapid economic and technical development in this era[8], a professional of a filed is playing a more and more important role on the development of the economy and society. As to Yinyan, it should make efforts on improve its personal quality by to attract high-tech talents or tanning on its original staff to fit with the development needs of it. With the reasonable use of its advantages, the status of Yinyan Logistics base will be improved to a great extent with a certain investment on this part.

Summary

From the current development situation of Jiangxi Yinyan, we can see that it has a long way to achieve its goal to be a domestic and international logistics hub node. Also,, we can see that though many provinces are engaged in building its logistics bases to response to the call of the national policy, the development situation of these logistics bases is uneven and not optimistic, there are still many problems of logistics bases in undeveloped cities like Jiangxi, as Yinyan logistics base is its biggest logistics base. With the rapid development of information technology today, logistics bases should pay their attention on the investment and application of high-technology and information management system. As to Jiangxi Yinyan logistics base, the managers should seize the opportunity to absorb the advanced technology and experience to have a steady progress, and be vigilant at all times on the major problems of its own during the rapid development of it. Yinyan logistics base seize

the opportunity to develop, it is reasonable to believe that the development prospects of Yinyan logistics base is very optimistic.

References

[1] Rommert Dekker,el at. On the use of installed base information for spare parts logistics: A review of ideas and industry practice. International Journal of Production Economics,vol.143, no. 2, p.536-545, 2013

[2] Cimen Karatas-Cetin, Gul Denktas-Sakar.Logistics Research beyond 2000: Theory, Method and Relevance. The Asian Journal of Shipping and Logistics,vol.29, no. 2, p.125-144, 2013

[3] Abduwali Mahpula, DeGang Yang, Alishir Kurban, el at. An overview of 20 years of Chinese logistics research using a content-based analysis. Journal of Transport Geography,vol.31, p.30-34, 2013

[4] Chen Xianglian,Lin Hua.Research on e-Commerce Logistics System Informationization in Chain. Procedia - Social and Behavioral Sciences, vol.96, no.6, p.838-843, 2013

[5] Hooi Hooi Lean, Wei Huang, Junjie Hong.Logistics and economic development: Experience from China.Transport Policy,vol.32, p. 96-104, 2014

[6] Fei Ye, Xiande Zhao, Carol Prahinski,el at.The impact of institutional pressures, top managers' posture and reverse logistics on performance—Evidence from China.International Journal of Production Economics,vol.143, no. 1, p.132-143, 2013

[7] Hanna Grzybowska,Jaume Barceló.Decision Support System for Real-Time Urban Freight Management. Procedia - Social and Behavioral Sciences,vol.39, p.712-725, 2012

[8] Jose Tongzon, Hong-Oanh (Owen) Nguyen.China's economic rise and its implications for logistics: The Australian case. Transport Policy,vol.16, no.52, p.224-231, 2009

Advanced Materials Research Vols. 989-994 (2014) pp 5086-5089
© (2014) Trans Tech Publications, Switzerland
doi:10.4028/www.scientific.net/AMR.989-994.5086

Discussion of Chinese industry information service transformation

Mao Shujuan[1, a], Zhang Lingyu [2,b]

[1] School of Education, Jiangxi Science & Technology Normal University, Nanchang, Jiangxi,China

[2]School of Information Engineering, Nanchang University, Nanchang, Jiangxi, China

[a]cnliu2010@163.com, [b]1145163178@163.com

Keywords: .Industry Information; service; transformation; Discussion

Abstract. In the context of building an innovative country, innovation and development-oriented enterprise transformation and restructuring of industry information services, creation and innovation for our country to adapt to national construction industry information service system has a theoretical guidance.

Introduction

In January 2006, the CPC Central Committee and the State Council's decide to build an innovative country. Building an innovative country, the core is to enhance the capability of independent innovation as the strategic basis for the development of science and technology [1], out of the path of independent innovation with Chinese characteristics, promote leapfrog development of science and technology. The Core is to enhance the capability of independent innovation as the adjustment of industrial structure and changing the growth mode of the central link, building a resource-saving and environment-friendly society, promote rapid and healthy development of national economy. Core is to enhance the capability of independent innovation as a national strategy, through to all aspects of modernization and inspire the whole ethos of innovation. And train high-level innovative talents, to create favorable institutional mechanisms for independent innovation, and vigorously promote theoretical innovation, institutional innovation, and technological innovation, continuously consolidate and develop the great cause of socialism with Chinese characteristics. Based on our background of building an innovative country, the development of innovation-oriented enterprise transformation and restructuring of industry information services[2], require the creation of nation-building and innovative information services industry to adapt to the system. As of 2013, China-based telecommunications industry presents the following basic features:

First, industry revenue grew steadily. Near the first half of 2013, China-based telecom services revenue grew by 8.9%[3], the growth rate dropped 0.3 percentage points over the same period last year, higher than the same period GDP growth of 1.3 percentage points.

Second, the data traffic class outstanding contributions to business income, and the proportion of non-voice revenue increased gradually. Non-voice revenues in the telecom business income accounted for more than 50 percent of telecom services revenue contribution of over 90%, basic telecom industry gradually transition to an integrated information service operator.

Third, 3G mobile phone users exceed 300 million firstly and fusion class of business to take shape. As the industry continues to transition and information services industry continues to promote cross-border integration, industry converged business has begun to take shape.

Fourth, broadband Chinese special action and proved to significantly increase broadband consumption.

Fifth, the traditional mobile business spending fell significantly, and the business gradually becomes saturated.

Sixth, the rapid development of mobile Internet traffic operations gradually forms a new model. Gradually saturated with traditional business is relatively rapid development of mobile Internet-related businesses. Mobile Internet data traffic related to rapid growth in business spending [4], promote the rapid development of mobile Internet applications store this rapid development of

traffic management based on new business models, new business operating model based on data flow is gradually advancing exploration.

Seventh, the Internet industry is flourishing, growing industrial scale.

Eighth, the effect is obvious investment-led, coordinated development of information and communication industry chain. In the context of the rapid development of mobile Internet, the various operating companies are closely cooperation with the upstream and downstream industry chain manufacturers.

Questions and Problems

Our national innovation-oriented information services industry restructuring and development compared with developed countries, which have their own advantages; there are problems to be solved. Transformation of industry information services major problem exists in five areas:

First, the main trade association for the information service system failed to establish industry, industry associations' mechanism needs to be established. Also need to rationalize the relationship between trade associations and government functions of management, the establishment of government-led trade association system under the supervision of planning and information services.

Second, the role of industry information services to protect innovation and development in the industry is not clear; especially in the industry sector organization information service system is decentralized, disorderly development of the state. Multiple centers in an industry often overlapping construction, operation and service efficiency is not high.

Third, after the successful implementation of the institutional reform of the State Council, the reform of the information service industry innovation and development of the system to be further deepened, industry information service under the auspices of the State can not guarantee institutionally. Meanwhile, the relationship between technology and economic information services, industry bodies and government services to be further rationalized.

Fourth, international trade information service, open technology needs to be strengthened. EU countries and the EU in order to promote the common development of economic globalization, the information real common market plan, promote regional cooperation, so as to enhance the capacity of countries to enterprises and service levels. This experience can be used in the restructuring of industry information services.

Fifth, information services and developed into comparative industry, there is a gap. Especially the reform of government institutions has led the industry into the relationship between changes in information services, information services industry, there are mechanisms to adjust and change into question[5], the key to solving the problem is to seek diverse and innovative development of enterprise investment system to adapt.

Sixth, macroeconomic uncertainty poses serious challenges to the industry. World economic situation is still complex and deeper impact of the financial crisis and the debt crisis continues to appear. Worldwide rise of trade protectionism, trade frictions spread from the previous labor-intensive industries to technology-intensive industries, China's enterprises raise security question, etc., that will have a profound impact on the development of the industry.

Seventh, the New Deal and taxation of business changed to increase bring challenges to the development of the industry. The original intention of this program is to address double taxation[6], but in the beginning of the implementation, as telecom companies' current difficulties in obtaining tax-deductible invoice operations, may cause periodic increasing rather than reducing the tax burden, resulting in industry revenues and profits decline. Meanwhile, the new tax reform is bound to drive the way the telecommunications companies to adjust financial systems and business processes, changing its inherent sales model.

To build an innovative country, industry information service organizations should be based on information technology and economic globalization, in order to enhance the capability of independent innovation of China's industry, the core competencies and capabilities for the purpose of international development. The authors therefore believe that it should be explored from reorganization under five in the transition process: First, give full play to the advantages of our

system, strengthen the government's management of industry information services[7]. Second, industry information service system reform, specifically the role of government, industry associations and other subjects, in order to build government-led trade association as the main form of socialized industry information service system. Third, the government department in the information industry and industry associations belongs to realize two-track operation, emphasizing the public service, while actively explore the market-oriented services. Fourth, the development of the industry information service, rationalize the relationship between the relevant industry[8], to co-organized way, construction industry group information network, while achieving national and regional trade information network linkage. Fifth, concern legal construction industry information services, communication services industry institutionalized and standardized.

Development measures

For innovation and development of organizational change and restructuring industry information service, the basic structure shown in Figure 1.

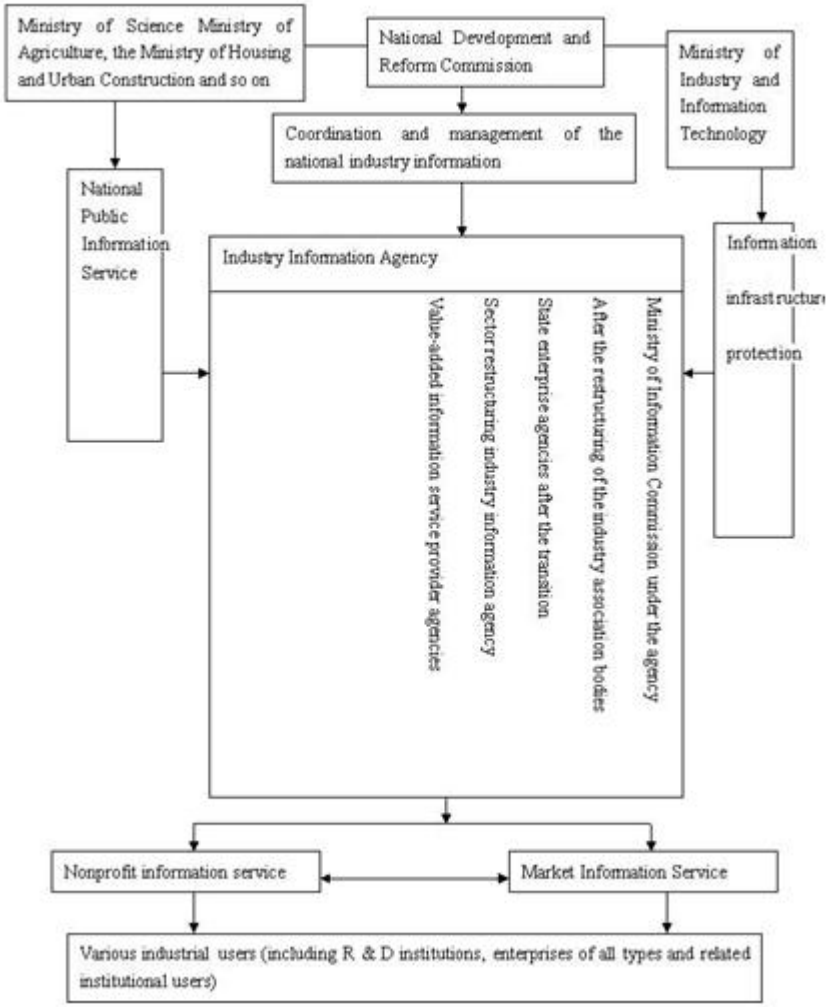

Fig.1 China's information services industry restructuring and reorganization Structure

The figure shows two meanings: First layer: the management do accountability and each perform their duties. First, the National Development and Reform Commission undertake overall planning tasks, its establishment of a national agency coordination and management information services industry specific information agency coordinating the operation of the various sectors; Second, the competent authorities undertake a national public information service only straight pipe tasks and achieve public agency sharing of information and industry information; Third, the Ministry of Industry and Information Technology bears only the information technology infrastructure in charge of the responsibility to protect, and provide support for industry information agency. Second layer: do the paid services and free services to run dual track parallel form interaction for government, industry

and the public welfare services, will form part of the service paid into the implementation of market-oriented operations.

Summary

China is building an innovative country in 2006 the National Conference on the development goals. To build an innovative country information services industry restructuring and development as the starting point, in the context of building an innovative country, from strategic positioning information services industry starting prominent strategic position in the information services industry innovation and development in the country, based on our industry Status information services, analyzes the advantages and problems of industry information service system, the proposed development of the industry information service transformation and reform and restructuring of countermeasures.

Of course, the information center for the Chinese industry innovation and development network backbone over 120, belonging to the State Council ministries (Commission, Council), industry associations, state-owned enterprises, research institutes and universities, such as, in fact, China's various industries for different scale National and local industry information service network of different affiliations and different management system has reached thousands. With the rapid development of digital, networked, the new industry-oriented information services have mushroomed in the fore, in this context, the Chinese construction industry information service transformation and development of innovation-oriented country, not just involve a small number of key Information Center network, considering the information services industry restructuring process should be more co-ordination of new information services network into account, this can only be more comprehensive.

References

[1] Martin Kenney, Dan Breznitz, Michael Murphree. Coming back home after the sun rises: Returnee entrepreneurs and growth of high tech industries. Research Policy, vol.42, no.2, p. 391-407, 2013

[2] PagesA.J.J. , Braaksma, W., el at. A review of the use of asset information standards for collaboration in the process industry. Computers in Industry,vol.62, no.3, p. 337-350, 2011

[3] Tian-Jian Yang, Yue-Jun Zhang,el at.Estimating the energy saving potential of telecom operators in China. Energy Policy, vol.61, p. 448-459, 2013

[4] Jeffrey L. Funk. Standards, critical mass, and the formation of complex industries: A case study of the mobile Internet.Journal of Engineering and Technology Management, vol.26, no.4, p. 232-248, 2011

[5] Mohamed M. Mostafa, Ahmed A. El-Masry. Citizens as consumers: Profiling e-government services' users in Egypt via data mining techniques. International Journal of Information Management,vol.33, p. 627-641, 2013

[6] Patrick Besson, Frantz Rowe. Strategizing information systems-enabled organizational transformation: A transdisciplinary review and new directions. The Journal of Strategic Information Systems,vol.21, no.2, p. 103-124, 2012

[7] M.K. Chen, Shih-Ching Wang. The critical factors of success for information service industry in developing international market: Using analytic hierarchy process (AHP) approach. Expert Systems with Applications,vol.37, no.1, p.694-704, 2010

[8] Yuanqiong He, Kin Keung Lai. Supply chain integration and service oriented transformation: Evidence from Chinese equipment manufacturers. International Journal of Production Economics,vol.135, no.2, p. 791-799, 2012

Advanced Materials Research Vols. 989-994 (2014) pp 5090-5093
© (2014) Trans Tech Publications, Switzerland
doi:10.4028/www.scientific.net/AMR.989-994.5090

Distribution Research of Survival Road for Local Retail Businesses in Relatively Backward Areas - A Case Study on Luoyang Dazhang

Xiong Wei[1, a], Zhang Man[2,b]

[1] Headmaster's Office, Jiangxi Science & Technology Normal University, Nanchang, Jiangxi,China

[2]School of Information Engineering, Nanchang University, Nanchang, Jiangxi, China

[a]572383070@qq.com, [b]manzhang201010@163.com

Keywords: Retail Business; Risk; Distribution; Management

Abstract. Distribution of logistics plays an important role in the modern market, and the distribution of retail has its own unique characteristics and needs. The economy market of China has been developed with an amazing speed. But there are weakness and risks in the market compared with the developed countries, thus it need time and practice to increase the management level of economy market in China. Since the development of the market will bring risks and anti-changes to business, enterprises should prepared for the challenge. The paper analyzed successful cases of retail business to provide advices for retail business in backward areas to prepared for market challenge and risks in order to promote the development of local retail business in backward areas in China.

Introduction

The development of Chinese retail business has followings characteristics: early beginning, slow-growing and small-scale. Under the impact of a global internalization, retail business of China is weak and small with few market shares in the vast market of China. Coastal area cities have an international level of economy market which has a clear market structure influence by modern economic mode, while market in the middle and west of China is under developed which is still exploring its development mode. The difference is caused by the management level of these two groups. The coastal areas begin its modernization in the early 90s in 20th century while the development of middle and west of China is later than coastal area. As China continues to accelerate international integration process, the Chinese market will inevitably meet the full impact of the world economic tide. Thus, research on market of inner land is very important as to increase its competition power.

Retail business has following characteristics :(1) Small order quantity, numerous retail chain stores[1], high order frequency, and time requirements. In order to meet with the consumer demands and product quality, products which difficult to preserve and have intensive needs will have to deliver three times a day. (2) Wide range of goods and diverse forms of transport and storage needs. Faced with numerous types of goods distribution and different goods have different characteristics, it requires different storage forms and transport forms[2], such as frozen, fragile and so on. (3) High frequency of price changes. That is the purchase price of the products has a quick price changes, usually the price of fast moving consumer goods in supermarket chain operating changes rapidly according to the supply and demand in market have also frequently manufacturers or retailers often change due to promotional prices. (4) Returned goods. The distribution center needs to cope with gifts, return goods and other issues. (5) Open stock. Distribution center need to unbundled and sort the bundled goods provided by suppliers according customer orders. (6) Replacement. As the obsolete frequency of goods in retail business is high[3], it need increase new products timely and obsolete dead stock. The paper takes Dazhang distribution as an example and analyzes its status and distribution characteristics to explore survival road for local retail businesses in relatively backward areas and to provide advices for retail business to face with fierce competition in the future.

Distribution Status of Dazhang

The distribution centers of Dazhang locate in Wuhan road, covering nearly 100 acres which provides an important support to the development of Dazhang. Its distribution center played an important role in against the SARS and the snow disaster in 2008, and provided an important safeguard to protect people's lives which benefit its performance increasing in recent years. According to its business needs, Dazhang built its second distribution center with higher information management level in 2009, covering 300 acres, which provide perfect fresh sorting, safety testing, refrigeration and wholesale distribution for the company. Currently the merchandise, food, fresh, clothing and many other basic commodities of Dazhang achieve its purchasing in the original manufacturers or origin all over the country.

The dense shop setting and convenient information network of Dazhang facilitate the implementation of efficient distribution, which make it has advantages like convenient transportation, safe, high-quality, low price, good service,and so on, and set a good image for Dazhang among consumers. The paper analyzed the general framework of Dazhang distribution centers with its three sub-centers instead of its detailed distribution centers setting. That is we analyze the information system network which make up of three sub-centers,that is, fresh, clothing,and general merchandise and food departments. Fresh and cooked food implement a delivery principle of distribute it three times a day among the urban distribution, while other goods distribute according to its sales. The distribution methods for distant areas are different.

Characteristics Analysis of Dazhang Distribution

By analyzing the development process and store location of Dazhang, we summarize several key features of its distribution combined with the analysis of its management strategies:

(1) Distribution methods combine joint distribution and refining distribution. Joint Distribution is suitable for the distribution of high frequency, multi-species and small units goods to save the overall time and cost savings on goods and improve its efficiency greatly.

(2) Clear label division and best route choosing of distribution management. With years operation of Dazhang, it has been quite familiarity with the local geography,the road transport and the community location which make it have their own perception and management strategies on distribution management, and make resources distribution much more effective. By the distribution advantages, the distribution punctuality is guaranteed.

(3) The earlier introduction of information systems than other retail companies. This makes Luoyang Dazhang has formed their own competitiveness before international giants settled in Luoyang. Especially in the supply of fresh food, it has l much more effective distribution operations as Dazhangs' information system terminal has been extended to the major local fresh food manufacturers systems which is commendable in undeveloped area.

(4) The appropriate location and scale of distribution center. The distribution center of Dazhang located in Wuhan road, and it is near to Longhai Line in its left and near to Lin-Ning-luo high-road in its right while it's close to raw market but not overcrowd. Built in 2003, the year before the full liberalization of the domestic retail industry, the high starting point and functional clear of the construction Dazhang's distribution center bring a rare opportunity to it.

(5) Close relationship with suppliers and responsibility of inventory and distribution departments upwards transfer. Dazhang focuses on fresh food supply, and its supply side is mainly concentrated in the vicinity of several large suppliers or supply areas. Dazhang makes its ordering plans with risk analysis and demanding analysis in future market based on data analysis through its information systems. By this distribution method, the inventory and distribution tasks of considerable amount of goods or special goods can be transferred to the suppliers ,and ensure the freshness of the product.

Disadvantages of Dazhang distribution

The main disadvantages of Dazhang's distribution are:(1)Distribution management is not standardized in some distribution processes. Some distribution process is mess and repetition which reduced the distribution efficiency; on the other hand, personnel arrangements are casual and responsibility is not clear.(2) High distribution costs. Vehicles return empty wasted vehicle resources; the mixed using of human resources and equipment resources in distribution center is not conducive to take advantages of their own strengths which will resulting to a double waste of the resources, and is not conducive to reducing costs.(3) Limited distribution capacity. Dazhangs only has two distribution centers, the single scale level of each center is limited and its distribution capacity and automation level is much lower than that of international enterprises.

New Features of Distribution in Retail Business Development

The new features of distribution in retail business development are shown as followings:

(1)Distribution center of retail business will increase or strengthen the distribution function [4]of freezing or fresh food.With the increasing competition in the retail market and the improvement of peoples' living standards, there is a increasing demand for fast food, semi-finished products of fresh and frozen food, and it's a logistics trend for large retail enterprises to set up food processing centers and distribution centers[5]. For example, specializing logistics and distribution companies for meat, eggs, milk, bread and other fresh foods distribution will be formed as a multifunctional logistics center with functions like logistics, refrigeration, packaging, distribution processing, distribution as the living standards of people improved and their requirements on product quality increased

(2) The introduction of third-party logistics. In Japan, about 30 percent chain enterprises rely on the professional distribution companies in a large extent. With the the rise and mature of professional logistics companies in society, retail chain logistics and distribution work transfer to a professional logistics company will become an option for chain enterprises.

(3)Standardization of Distribution center operational processes. Retail vitality lies in its strong normative and normative. Chain operations achieve its scale economies through principles of standardization, simplification while standardization is also an important means of logistics management and it plays an important role on logistics costs and benefits .

(4)Re-construct of logistics information systems. Logistics systems of Chain enterprises related to information systems including internal information management systems and data exchange Systems with suppliers or an electronic ordering system[6]. With the popularization and promotion of e-commerce, retail enterprises, especially retail chain enterprises begin data transfer and ordering online by using of Internet and logistics distribution center, and selling and inventory information of shared goods by upstream suppliers to provide collaborative support for electronic order, commodity inspection, returns, promotion, price change, settlement, payment and other sectors.

Proposals for Distribution of Retail Business in Inland of China

The work of retail business is complex, and the functional of information system is highly integrated[7], thus it requires personal with high quality to be qualified for the work. It need employers of retail business take personal quality into consideration when make strategy project for their enterprises. As the development of retail business is highly dependent on information transmission, the more strategies on attracting professionals or training their staff, the longer running of the enterprise.

Improve distribution efficiency according to the adjusted position of the supplier under the enterprise status will benefit the retail enterprises. As the scale of company expanded, and the changing of distribution range, companies should re-evaluate its supplier according to its distribution demand and suppliers' distance with the market which will reduce distribution costs by reduce the frequency of vehicle empty return.

The redesign and standardization of distribution process can help retail enterprises reduce its costs . Regularly evaluate the efficiency of each distribution business conduct. From product damage, punctuality, operating costs, the degree of satisfaction with various aspects of the evaluation branch distribution, and analysis of each distribution chain efficiency one by one to optimize distribution processes and reduce operating costs. Strengthen the standardization and specialization construction of distribution centers to improve the handling capacity of distribution center.

Flexible management of retail enterprises will help to increase human creativity. Information management is not a simple computerized manual operation[8], but a to new business model by using information technology to build a new information platform. Human resources play an important role during information management as the system running dependent on human-being.

Implement information integration to form a chain operation net and accelerate demand response speed can improve service quality of retail enterprises. The golden rule to the retail industry is to provide high quality services. The golden rule to the retail industry is to provide high quality services. High degree of information integration can accelerate response speed of demand and improve demand forecasting accuracy to enhance the competitiveness of enterprises.

Summary

High degree of information integration can accelerate response speed of demand and improve demand forecasting accuracy to enhance the competitiveness of enterprises.

The economic development of China inland is uneven which provides a basis for the development of small and medium enterprises with Chinese-style. The retail model need subject to market demand. On one hand, it need to find the market characteristics to choose their own way of running business; on the other hand, it need to improve the ability of predicting the market and scientific management according to the international market trends. This paper argues that relatively backward areas need to cultivate powerful medium-sized enterprises to develop its retail business, and to cultivate more local targeted core competitiveness. Distribution is the core of the retail chain, and efficient distribution center is the premise of protecting the supermarket chain to achieve efficient operation. We need retail operations as a whole from the perspective of integration while combined the distribution software and hardware facilities, staff quality and operational characteristics of local market with each other to improve its service quality and competitiveness with scientific information management of retail enterprises. The retail business can survive from exploring and developing its own local advantages to away from the advantages of international retail business when faced with fierce competition in the future.

References

[1] Chen Xianglian, Lin Hua. Research on e-Commerce Logistics System Informationization in Chain. Procedia - Social and Behavioral Sciences,vol.96, no.6, p. 838-843, 2013

[2] Mohammed A. Quddus, Michael G.H. Bell,el at.The impact of the congestion charge on the retail business in London: An econometric analysis. Transport Policy, , vol.14,no.5, p.433-444, 2007

[3] Alina Sorescu Ruud T. Frambach Jagdip Singh,el at. Innovations in Retail Business Models. Journal of Retailing, , vol.87, p.S3-S16, 2011

[4] Kathleen Keeling, Debbie Keeling, Peter McGoldrick.Retail relationships in a digital age.Journal of Business Research, , vol.66,no.7, p. 847-855, 2013

[5] Barbara Dinter. Success factors for information logistics strategy — An empirical investigation. Decision Support Systems, vol.54, no.3, p.1207-1218, 2013

[6] Michel Zaffran, Jos Vandelaer,el at.The imperative for stronger vaccine supply and logistics systems.Vaccine,vol.31, p. B73-B80, 2013

[7] Shih-Che Lo, Randolph W. Hall. The design of real-time logistics information system for trucking industry. Computers & Operations Research, vol.35, no.11, p. 3439-3451,2008

[8] Techane Bosona, Girma Gebresenbet. Food traceability as an integral part of logistics management in food and agricultural supply chain. Food Control, vol.33, no.1, p. 32-48,2013

Advanced Materials Research Vols. 989-994 (2014) pp 5094-5097
© (2014) Trans Tech Publications, Switzerland
doi:10.4028/www.scientific.net/AMR.989-994.5094

Statistical Analysis on Primary and Secondary School Digital Disaster Education in China

Mao Shujuan[1, a]

[1] School of Education, Jiangxi Science & Technology Normal University, Nanchang, Jiangxi,China

[a]cnliu2010@163.com

Keywords: . Statistical Analysis; Primary and Secondary School; Digital Disaster Education

Abstract. Along with the progress of human society, the disasters in human society are becoming more frequent and more serious but the situation of primary and secondary school on disaster education in China is not ideal. The paper verified the viewpoint from the analysis of surveys on the theme retrieved through the first data. The paper included some main problems on digital disaster education and proposed an improvement strategies model to improve the situation.

Introduction

Along with the progress of human society, the disasters in human society are becoming more frequent and more serious. Increasingly prominent disasters continue to cause great concern of social sectors. In the current context, Digital Disaster Education has increasingly become an important research topic in this age, and it is urgent to increase the awareness of disaster prevention and mitigation among the whole people including primary and secondary students. To enhance Digital Disaster Education in the whole society and to improve the nation's disaster awareness and the level of scientific and technological knowledge have become the strong tone of the era. Frequent disasters happen in China. And the teachers and students more or less lack the disaster literacy to a certain degree, casualties are most concentrated and most serious disasters in the schools when a disaster occurs. Therefore, in order to reduce the losses brought about by the disaster to the school, investigating the digital disaster emergency education in primary and secondary schools and understanding the status of Digital Disaster Education and finding the perfect strategy for the situation is required and it is the trend.

Exploring the digital disaster emergency education status and problems in primary and secondary schools, and seeking effective measures can enhance disaster literacy of teachers and students in primary and secondary schools and reduce the disaster damage to a certain extent. And primary and secondary students are the hope for the future, their knowledge and comprehensive literacy is directly related to the future of the national quality and the national spirit. The nation's hope lies in young people, in order to improve the national disaster prevention and mitigation ability and enhance the civic disaster literacy, it must be started from the primary school students. Therefore, digital disaster emergency education in primary and secondary schools also contribute to improving the comprehensive national strength and quality of the nation.

The Key Points of Primary and Secondary School Digital Disaster Emergency Education

Digital disaster emergency education in primary and secondary schools has a great realistic significance, it responds to the realistic needs. It plays an important role in the growth and development of young people, as well as in improving the future quality and development of society.The teachers and students in primary and secondary schools to varying degrees lack the necessary knowledge for disaster prevention, self-help and mutual aid. Thus, the primary and secondary digital disaster emergency education is the necessary way to solve practical problems. It encourages schools to pay much attention to the digital disaster emergency education and enable students to understand the national disaster status. Ultimately, the educational outcomes should satisfy the practical needs and reach the effect of disaster prevention and mitigation.

Based on the characteristics of physical and mental development of primary and secondary students, we can know that this stage of their growth is with high plasticity and great volatility, and their future thinking and behavior patterns more depends on the shape of this period, this growth period has an essential impact on the development of their whole life. Education is to last for generations. Since primary and secondary students are the future of the country, we must pay attention to their education. Digital disaster emergency education is an essential part of education, and it should not be ignored.

Effective Digital Disaster Education enable us to recognize the reason, law and countermeasures of disasters, it can help to alleviate the extent of human losses brought by the disasters, and it fully mobilize the people's consciousness and passion to understand the nature and society and optimize the living environment. Schools are the specialized agencies engaged in educational activities, they are the main bearer of knowledge. Therefore, we must attach great importance to the school Digital Disaster Education, especially Digital Disaster Education in primary and secondary schools. To carry out Digital Disaster Education among primary and secondary students can help them to deepen their understanding of disasters. They represent the future of our country, and their disaster literacy to a certain extent determines the rise and fall of the nation and the state. At the same time, Digital Disaster Education is the important part of the quality education in schools, it can effectively improve the students' knowledge and ability to prevent disaster, and it can also improve the sense of crisis and awareness of sustainable development as well as their moral feelings.

Digital Disaster Education starts from the people's ethics, it eliminates the unsafe behavior of people in disasters. The aim is to improve people's ideology and the practical ability. Through Digital Disaster Education and training, people can master a certain number and types of disaster information. For this reason, many researchers have studied what the Digital Disaster Education should contain and propose their respective insights from multiple perspectives. These provide valuable advices to schools for Digital Disaster Education.

From the purpose of Digital Disaster Education, it is not difficult to think that the contents of the most basic of Digital Disaster Education should include disaster-related knowledge, awareness, capacity and skills. Knowledge is not only the basis of awareness creation, but also the prerequisite for a good disaster emergency response capability.Of course, every researcher has a different opinion. The author believes that Digital Disaster Education consists of knowledge teaching, practical exercises and other aspects from the macro level. Thus, the core contents of primary and secondary Digital Disaster Education first should include the following aspects: primary and secondary disaster emergency knowledge education, primary and secondary disaster awareness education, primary and secondary disaster emergency capability education, primary and secondary disaster emergency psychology education, primary and secondary disaster ethics education, primary and secondary environment protection education.

A Survey on the Remedy for the Present Secondary and Primary Schools

We prepare totally 30 questions for the secondary and primary students. This questionnaire tests the basic understanding on the knowledge towards the problem, to examine on their capability of survive towards the problem, their awareness on the problem on daily life, and the schools' response on dealing with the problem. The questionnaire for secondary and primary students on their remedy towards the problem.

The 114 effective questionnaires, 80.5% think they are closely related, 3.5% think they are not related and 15.9% of them are not sure. From the statistics, most of the students can realized the natural disaster is closely related to human behavior, just a small percentage of them hold the opposite view. There are still a certain percentage of students who do not have the above concept. This warns us that education have to be improved with the relationship between natural disaster and human behavior, leading the students realizing the hidden disaster in their daily life.

88.5% of the students choose A. this shows the students' tendency on knowing more about the disaster. 0.9% chooses B and C, and even a small percentage of the students think that it is fine unless it does not affect their academic. Students who choose this may be affected by the

examination-oriented education, where examination is necessary and important in study where knowing more about disasters is complementary. Enlightening these students can impress them with the significance and the urgency on acquainting with the disaster. Predominating over the technique on remedy for the disaster can make sure people will not get sucks when they face the disasters.

Emergency readiness is a key experience to the awareness on disaster emergency. It will be easier to handle the disaster when you have the awareness on how to deal with it in advance. From the above table, more than half of the participants have a little preparation, 17.7% of them are ready while 15.8% are quite ready, and even 14.2% are not ready. This shows that secondary and primary students have a low degree in their intention on the remedy of the disaster. This reflects the awareness on getting ready for the disaster is not high. Moreover, it is warning the methods of education and the educational administrators to emphasis on this aspect. The focuses of the schools arouse the students' interest to think about it. This can successfully strengthen students' awareness.

This survey is from the aspect of students' initiative on the information about the disaster. Whether the students pay attention to the study and the information about the prevention of the disaster reflects students' standard in the study of it. The multiple choice question shows the students' cognition is not enough, 75.3% of them will seldom realize and only 16.8% always realize and even 9.7% of them never realize. How can students' initiative towards the disaster be improved? This is the problem faced by the educators.

Understanding of the shelter nearby can directly improve the capacity and effectiveness of emergency refuge, but also a reflection of the awareness. When a person initiatory understands the refuge areas, this awareness has risen to a certain level. Certainly, this consciousness is the result of a combination of daily life and social education, family education, school. The table shows that the vast majority of people do not know the shelter in their area where only 34.5% of people know.

This survey is on learning the need for disaster prevention knowledge. The result shows the problem is still relatively optimistic, 88.5 percent of the students feel the need and those who think it is unnecessary only occupies 4.4%, 7.1% of them say they don't know and this either relates to their contact in this respect knowledge, or they don't know much about the time of the disaster, or they lack of the understanding of disaster prevention-related knowledge.

Publicity and educational content to the image, radio, print materials on disaster prevention and mitigation will arouse people's interest to them. 32.7% of them will pay attention to them and look forward to learn some skills, and their respective 8% of people do not look or do not care, watching from afar. Primary and secondary schools still plays a emotional thinking predominant role in the development stage, so they usually pay attention to what they are interested in, so the publicity disaster education time should be used in a proper manner which made the educational content colorful to attract students, as well as enhancing the publicity and the effect of promoting education. This can greatly improve the education quality and efficiency of knowledge towards disasters

From the survey, more than one-fifth of the household have first aid supplies, a third of them have some, 17.7% of people do not know whether they have first aid supplies, 26.5% do not have first aid supplies at home. This reflects the level of preparedness of the emergency first aid supplies of the primary and secondary household is not high. A considerable part of primary and secondary students are not familiar with first aid supplies at home.

This question is to check the students' understanding of the disaster, the debris flow of the original forest should be considered as natural disasters. The result of the survey showed that 51.8% of the students consider it as natural disaster, 36.3 % choose uncertainty, and the remaining 11.5% of people do not think it is. This reflects more students do not have a deep understanding about the natural disasters.

Summary

With the frequent occurrence of disasters in China in recent years, as well as in the face of risk of severe losses, it is generally able to recognize the importance of disaster emergency knowledge. Although the primary and secondary school students, teachers, educational administrators consciously agree with the need for disaster emergency response education, recognition of disaster emergency power of knowledge. However, this awareness of putting it into practice has not translated into guidelines for action.

Weighing theory heavier than practice is the common problem of China's traditional education. Digital disaster emergency education is no exception. Survey found that students, teachers or administrators, share their response on the school digital disaster emergency education and re-known light training. Schools are more or less involved in the learning of the disaster-related emergency knowledge, but very little or almost no drill, resulting in the knowledge learned cannot be applied. They do not know how to use the emergency equipment available. The result is the study of knowledge does not translate into the ability, whether school teachers or students. Disaster emergency response capacity, as well as disaster literacy, has always been high.

Passive digital disaster emergency education are what teachers granted students. Teachers are passively follow instructions in accordance with the requirements of the school leadership education for students, and school administrators need to convey a higher level of notice. All these coupled with heavy education theory and practice of light. The entire process, in addition to going through the motions of the traditional core guidelines, are for giving and receiving knowledge, without any generated nor an innovative and forward-thinking leadership to schools in line with local conditions and individual condition. Combined with the point of national policy, the educational resources of the region are fully exploited to join forces to make the school digital disaster emergency education really play effectiveness, causing the digital disaster emergency education of the school to close in.

Organizational disaster drill or developing Digital Disaster Education resources, it is not only the matter of time or manpower, but the certain of financial capital. Practise need places, drill equipment. Supplies are needed to purchase, but require more development resources technical needs financial support. Primary and secondary schools, especially schools of remote areas, are having funding difficulties. Thus, they can only eliminate the need for this project, or in a simple way. This is why many schools found it difficult to implement the education needs of disaster emergency.

References

[1] Yifeng Dong. Research on Disaster Education in the Geography Teaching in MiddleSchools,Northeast Normal University of China,2008

[2] anru Wei,Mingyin Zhu. empirical research on disaster education of primary schools,Journal of Southwest University(Social Sciences Edition),2012.

[3] Trey Menefee, Bjorn Harald Nordtveit. Disaster, civil society and education in China: A case study of an independent non-government organization working in the aftermath of the Wenchuan earthquake, International Journal of Educational Development, Vol. 32, p.600-607, July 2012.

[4] Ying Zhang, Min Wang. Preliminary Thought on Research of Disaster Education Theory andPractice, Journal of Catastrophology, 2011

[5] Karen S. Hammad, Paul Arbon, Kristine M. Gebbie. Emergency nurses and disaster response: An exploration of South Australian emergency nurses' knowledge and perceptions of their roles in disaster response, Australasian Emergency Nursing Journal, Vol. 14, p.87-94,.May 2011.

[6] Patrick Besson, Frantz Rowe. Strategizing information systems-enabled organizational transformation: A transdisciplinary review and new directions. The Journal of Strategic Information Systems,vol.21, no.2, p. 103-124, 2012

[7] M.K. Chen, Shih-Ching Wang. The critical factors of success for information service industry in developing international market: Using analytic hierarchy process (AHP) approach. Expert Systems with Applications,vol.37, no.1, p.694-704, 2010

Advanced Materials Research Vols. 989-994 (2014) pp 5098-5101
© (2014) Trans Tech Publications, Switzerland
doi:10.4028/www.scientific.net/AMR.989-994.5098

Fashion Design Professional Basis Based on Design Process

Guo Tao[1, a]

[1]School of Mathematics and Science, Shijiazhuang University of Economics, Shijiazhuang 050031, China

[a]sjzueguotao@163.com

Keywords: Fashion Design, Design Process, Professional Basis

Abstract. In the process of fashion design, design process is very important, and it can be implemented by the computer assistant design software using the 2D&3D modeling technique. Virtual fashion design and simulation involves a combination of a large range of techniques, involving mechanical simulation, collision detection, and user interface techniques for creating garments. In this paper, we study the computer assistant fashion design based on the 2D&3D modeling technique by the design process. We perform an extensive review of the fashion design and its design process, and studied computer assistant fashion design based on the 2D&3D modeling technique.

Introduction

Fashion design is the art of the application of design and aesthetics or natural beauty to clothing and accessories. Fashion design is influenced by cultural and social latitudes, and has varied over time and place. Fashion designers work in a number of ways in designing clothing and accessories. Some work alone or as part of a team. They attempt to satisfy consumer desire for aesthetically designed clothing; and, because of the time required to bring a garment onto the market, must at times anticipate changing consumer tastes.

Computer Assistant Fashion Design

The garment industry is still attached to the traditional way of designing garments, which is based on designing patterns (shapes of fabric) which are then seamed together on a mannequin. While CAD tools (Lectra, Gerber, Investronica) are now highly involved in the 2D design process of the patterns, the actual prototyping is still performed using real cloth pieces and mannequins. Some attempts were made to bring this validation phase in the virtual world as well, using cloth simulation techniques. This approach is still quite inefficient because of the lack of integration between the 2D pattern design process and the 3D simulation. Interactivity between design and simulation is the key idea for solving this bottleneck. While current systems require the re-assembly and draping of the garment over the body for any design change on the garment patterns, we propose a new approach offer a smart integration of the 2D pattern shape editor along with the 3D garment shape view to assess interactively the effect of any pattern shape edit or posture and measurement change on the mannequin.

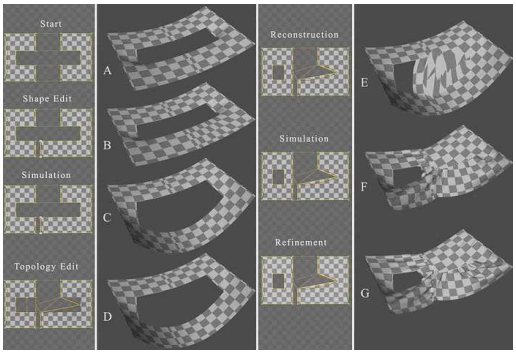

Figure 1. Interactive garment design: from an initial draped pattern (A), editing the 2D contour of a pattern while keeping its 3D shape constant (B) allows mechanical simulation to smoothly drape the pattern to its new 3D shape (C). If pattern editing involves topology or seaming changes (D), the pattern surface is automatically reconstructed in the same position (E) using interpolation if necessary, and simulation performs the draping (F). The surface may be refined at any time (G) for more accuracy.

2.1. Interactive design of patterns

Using patterns imported from industry CAD tools, the proposed framework obviously addresses the issues of placing the patterns around a mannequin, seaming the patterns together, and performing the draping using mechanical simulation. However, the main interest of the framework is rather related to the possibility of refining and altering the design of the patterns in real-time, with interactive preview of the effects on the garment draped on the mannequin. These edit possibilities include resizing, reshaping, adding darts, holes, seams, pleats, attachments (zips, buttons), changing the fabric material (mechanical properties and texture). The mannequin can be interactively changed as well, both for measurements and for postures and motion sequences.

The system reacts immediately to these changes by updating the draped garment interactively. The new garment shape is automatically recomputed using accurate mechanical properties in order to exhibit the features that have been altered by the edits. Geometrical accuracy of the simulation may be changed at any time to provide the optimal compromise between accuracy and interactivity at any stage of the design process. Advanced visualization tools can also display at any time the local mechanical properties of cloth (mechanical deformations, contact forces) for a good evaluation of the fitting and the comfortability, for any chosen size and posture of the mannequin which can also be customized (measurements, posture and appearance) and animated interactively.

Using an innovative design tool for garment design and simulation (in Figure 1), we intend to bring new advances not only in the field of garment simulation for computer graphics characters, but also as a valuable design and prototyping tool for the actual needs of the garment industry.

2.2. The mechanical model

This mechanical model is based on an accurate representation of the surface deformation of a triangular surface element equivalent to a first-order finite element description. Weft, warp and shear deformation and deformation speed are accurately measured on each element and translated into forces using the strain-stress curves defined by the mechanical properties. These forces are then propagated onto the mesh vertices, and any kind of integration scheme traditionally used for particle systems may then be used. Bending viscoelasticity is modeled as forces between adjacent mesh elements derived from the bending measured between them.

At the crossroad of particle systems and first-order finite elements, this model offers a very good compromise between speed and accuracy. Weft, warp, shear and Poisson viscoelasticity behavior is accurately represented by this scheme and, unlike representations based on spring-mass models, and the accuracy is quite well maintained with large deformations.

Another benefit of this model is that it does not rely on regular particle arrays, but satisfies itself from any triangle mesh for describing the cloth surface. This allows complete freedom in the design of the pattern shape, as well as optimal surface representations using adapted or dynamic local mesh refinements.

2.3. Collision detection and response

While much emphasis is put the efficiency and accuracy of the mechanical simulation, processing the collisions which occur between the cloth and the body, as well as between two different parts of the cloth, remains a compulsory issue to address efficiently. This problem relates both to detection (how to find out efficiently the geometrical contacts between complex moving surfaces) and response (how these geometric contacts alter the mechanical behavior of the cloth realistically, and how this integrates efficiently to the simulation scheme). The main issue is to master the complexity of the problem due to the discretization. The cloth surface, as well as the body surface, are represented by polygonal meshes that can have several thousands polygons each. Testing each couple of polygons for potential collisions is an unrealistic task. Many optimized algorithms have been developed for that purpose, either based on space subdivision or hierarchisation (voxelisation, octree), object hierarchisation (volume-box hierarchies), spatial projection and ordering. As soon as the distance separating two objects is small enough to consider that they are interacting, a 'feedback' should be performed on their behavior. Collision response aims to reproduce this interaction in an accurate way, primarily to avoid unrealistic interpenetration of the objects, and secondary to simulate realistic bouncing and friction effects.

2.4. Simulation of dynamic meshes

An interactive design framework obviously needs efficient mechanical simulation and collision techniques for animating mechanical objects quickly enough for an immediate feedback of the design actions. However, user interaction will only be useful if an adequate management of the pattern design give immediate feedback of the changes to the mechanical simulation system.

The key idea of the system is to take advantage of a dynamically constructed mesh that automatically adapts to the shape and feature changes of the garment patterns during their design. Hence, any action altering the 2D shape of the patterns would have a direct mechanical effect on the 3D shape of the garment surface.

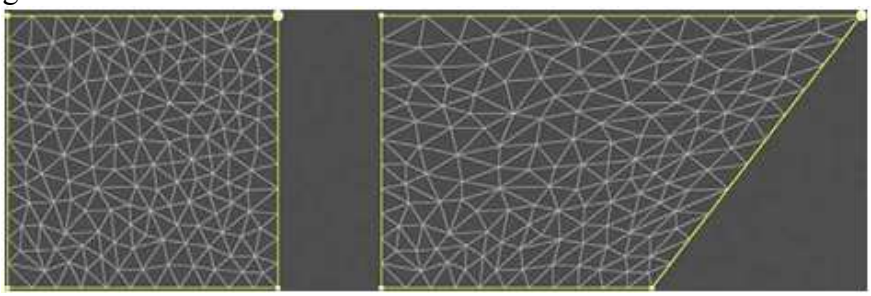

Figure 2. Interactive edition of patterns: each mesh vertex of the pattern surface is displaced by a weighted amount of the displacement of the pattern contour point.

2.5. Real-time animation of garments

The real-time animation has been integrated to the garment design tool to provide a preview of the clothes. Given an animated body and a garment whose rest shape has been computed with the garment design tool, this module provides the real-time visualization of the garments on the animated body. This module can be used at any time during the making of the clothes helping the designers to judge the quality of their clothes. Simulating garments in real-time requires drastic simplifications of the simulation process to be carried out, possibly at the expense of mechanical and geometrical accuracy. Our approach is based on a hybrid method where the cloth is segmented into various sections where different algorithms are applied. When observing a garment worn on a moving character, we notice that the movement of the garment can be classified into several categories depending on how the garment is laid on, whether it sticks to, or flows on, the body surface. For instance, a tight pair of trousers will mainly follow the movement of the legs, whilst a skirt will flow around the legs.

Conclusion

In the process of fashion design, design process is very important, and it can be implemented by the computer assistant design software using the 2D&3D modeling technique.

However, virtual prototyping still cannot pretend being a complete substitution to manual prototyping for a matter of accuracy, and it nevertheless allows speeding up the design cycle of garments by allowing the garment designer to address quickly the issues related to draping and fitting. Computer assistant fashion design can enhance these features by drastically shortening the cycle between pattern edition and visualization of the changes on the garment, skipping the process of reconstruction of new virtual garment models for each step of the design, and the measurements and the posture of the mannequin can also be changed interactively.

References

[1] Graphicpush. Graphicpush, In Praise of In-House Designers, Retrieved 13 May 2012.

[2] Steven Snell, 17 Tips for Designers on Starting a Freelance Business, Design Mag (in English). DesignMag. Retrieved 13 May 2012.

[3] Meng-Dar Shieh, Chih-Lung Huang, Chih-Chieh Yang, "A Rough Set Approach to Elicit Customer Preferences for Fashion Design", JCIT: Journal of Convergence Information Technology, Vol. 8, No. 3, pp. 338 ~ 349, 2013.

[4] Pauline Weston Thomas, Haute Couture Fashion History, Fashion-Era.com, Retrieved 13 May 2012.

[5] http://fashion.telegraph.co.uk/news-features/TMG7883236/Haute-couture-Making-a-loss-is-the-height-of-fashion.html.

Advanced Materials Research Vols. 989-994 (2014) pp 5102-5105
© (2014) Trans Tech Publications, Switzerland
doi:10.4028/www.scientific.net/AMR.989-994.5102

Research on Development and Application of Computer Supplementary Software in PE Teaching of Higher Education

Yuhua QIU [1, a], Yingming WANG[2, b], Kai HU [1, a]

[1]Department of Sports China University of Geosciences (Wuhan), Wuhan, 430000, China

[2]Department of Sports Central China Normal University, Wuhan, 430000, China

[a]email: honeyqyh@163.com

Keywords: Higher Education; PE Teaching; Computer Supplementary Software; Development and Application Research

Abstract. Based on the scientific design, development, application, evaluation and management of study processes and teaching resources in PE teaching in higher education, centered by the educational ideas of human centered and health first, this study explored the development and application of computer supplementary software of CAI, CAT, CMI in PE teaching, widened the new study channel of students! development and research study mode, cultivate students! Creativity and practical ability, improve thoroughly students basic sport knowledge, basic techniques, physical fitness and the level of health, therefore enhance the modernization of PE teaching, measurement, educational management methods in PE teaching of higher education.

Introduction

Exploring the development and application of computer aided software in the sports teaching is of very important practical significance in broadening the channels of learning, improve the quality of physical education, cultivating the students' innovation spirit and practice ability, promoting the scientific and modernized level of teaching management in college physical education, physical curriculum test and teaching management.

Research objects and methods

Guided under the modern education technology theory, this paper took the software applying in the physical education teaching in colleges and universities such as CAI, CAT and CMI as the research object. By using the methods of literature review, software and its application and statistical analysis, this paper tried to explore the universities sports teaching (or learning) process, teaching (or learning) resources' design, development, utilization, evaluation and the rules and characteristics of management.

The results and analysis

Results

Software of Sports Online Course Selection System

By combing the Dream weaver MX web software and Microsoft ASP.NET technology with the reality of sports teaching in colleges and universities, the software of sports online course selection system was developed independently.

Through the sports online course selection system, students can get the teachers' basic information and their relative curriculum. At same time, students can also query the questions through an online real-time problems solving between teachers and students to avoid the passive or blindly curriculum choosing. Students can get much more detailed and more comprehensive understanding of the teachers, much more deep understand of sports and more information on the relative course such as opening weeks of the course, teaching plan, teaching content and etc. In this

case, the problem for students how to choose their favorite sports curriculum can be solved. Furthermore, teachers can also use "sports online course selection system" software to get a comprehensive understanding on the information of their courses choosing including the number of students and their basic information timely in order to improve their sports teaching.

Sports courseware

By using Macromedia Authorware and combing with the Flash and Poser, a variety of sports teaching courseware have been developed. In the process of developing the sports teaching courseware, the aim of the courseware is always insisted to translate the teacher's demonstration tools into the students' cognitive tools, the transition from the traditional teaching process logic analysis to the process of students to discover problems, explore the problems. By using the sports courseware, the students' sports skills and their ability to body health care can be cultivated.

Fabrication of the human animation using Poser The software of Poser provides a rich and colorful human body 3D models for the developing the sports courseware. By using those models, the shape and the movement of the body can be constructed easily and quickly. The human body model provided by the software can be customized a variety of types and posture according to the requirement which can be used in the design of the courseware directly. The exquisite realistic human action produced by the software can be saved for the sports courseware material. The import function of the Poser allows the scene control by the 3Dstudio Max and Light Wave which largely enriched the creation of the human body modeling and motion design. And the Export function of the Poser allows characters designed to convert into other 3D design software. The Export function can also make it work with the Flash software and the output into 2 d Flash animation which can be exported through Viewpoint Media Player to realize three dimensional animation of human body model demonstration on the Internet.

Sports teaching technology animation developed using Flash Flash software is one of the most popular animation software. By using this software, the human body model developed by Poser can be exported and deal wit photoshop software to produce colorful human body movement which can be exported again into Flash to demonstrate very lifelike technique movement by setting key frames of movement.

Development of synthetic sports teaching courseware using Macromedia Author ware Although there are many tools can edit synthetic sports courseware, the best interactive sports courseware developed tools is still Macromedia Authorware. It not only can synthesize human technique movement produced by a variety of software, but also can utilize the word, voice, picture, video and animation edited by using other software. In this case, the interaction between teachers and students can be realized in physical education teaching.

Finally, the sports teaching courseware suitable for colleges and universities characteristic can be developed. This courseware should be used on trial in the teaching both for teachers and students after its preliminary revision completed to test whether the courseware is suitable for. Through their using, the modification can be made based on their suggestions for revision, and at same time, the teachers with rich experience can be invited to make evaluation on the courseware and the further revision can then be completed. After full consideration, the courseware can be packaged and burned into a CD to make it directly run on the other computer.

Sports online examination system

During the process of sports teaching, the summative evaluation and formative evaluation are always paid much more attention of the teaching process. At same time, the main measurement of physical education teaching quality monitoring is developed by taking the codes as the reference for the quantitative measurement and comparison. the sports online examination system can achieve interactive tests, assignments and exams, automatic statistics scores.

Sports teaching evaluation system

The correct and fair evaluation of teachers' teaching level and teaching ability is the guarantee of improving teaching quality. According to the practical situation of sports teaching in colleges and universities, five aspects such as preparation before class, teachers' basic skills, teaching contents, teaching methods and ability cultivation are adopted for the comprehensive evaluation of teachers.

Based on this, by adopting the method of mathematical statistics and combining with the web page creation software Dreamweaver MX and Microsoft ASP. NET technologies, the evaluation content are produced into an interactive web pages. The system calculate automatically the teaching evaluation level of average score based on the teachers online self and mutual evaluation, student evaluation according to each item A, B, C, D.

Sports teaching integrated management system

By using Visual FoxPro6.0 database, the development of the sports integrated management system software can realize the assessment of school physical education teachers and the management of the teaching file and teaching materials, students, standard test of student physique healthy, extracurricular sports activities, extracurricular sports training, sports competition, sports funds, sports venues and equipment, sports information and etc, which making the school sports management and sports teaching scientific and standardized. Besides this, the quality of physical education teaching depends on the processing capability of all kinds of information which is also the sign of a school sports teaching management level. This sports integrated management system software can handle well the teaching file and teaching equipment in physical education teaching, student achievement, ability of teacher's professional level of data. Furthermore, based on these data, the software can finish the comprehensive statistics, analysis and evaluation of various data.

Analysis

Computer aided software development

Based on the general law of sports teaching including the preparation before class, the process of physical teaching, summary after class, the management system meeting the demand of physical education teaching and testing are designed by using the survey method to collect the basic information of students need and with scientific data analysis.

To deal with the problem in the process of teaching and learning, the computer aided software are designed and developed including the clarify of content analysis, object analysis, specific goals, strategies, design, media selection and production, etc. by applying the modern education theory and technology. After trial using, Modification are made on the basis of formative assessment and the teaching effect. After all, the summative evaluation are made based on the actual situation of teaching.

Establishment of the ASP technology and database

By using Web page creation and ASP technology, the sports online course selection system, the sports online examination system and the sports teaching integrated management system are developed. The detail process are as follows:

At first, a new folder is created with a name. Then open the Access or Visual Fox Pro6. 0 database software to create a new database db1 and set up two tables. The relationship field between the two tables and table field is category name. After that, open the Dreamweaver MX web page for a new web page and choose the Dynamic page and Asp VBScript to expand the Application panel to enter the ODBC Data Source manager. Finally, a home page is established which can link the student id link to the database .ASP.

CAI analysis

Based on the knowledge of computer operation and good command of software, such as image processing software (photoshop, coreldraw and freehand), voice processing software (Ulead media studio, sound forge, cool edit, wave edit), animation processing software (Auto Desk Animator Pro, 3DS MAX, Maya and Flash) and other common courseware developing software (PowerPoint, Author ware, Director, Tool Book and Flash), the physical teachers can develop teaching courseware suitable for college physical education by integrating the collective wisdom and studying diligently the teaching material, teaching methods, carefully designed and writing scripts.

CAT analysis

Currently, the application of CAT in the sports teaching is realized mainly through operation of the background database by using ASP, Php technology to make modification in time and reflect those modifications on the user's browser side to realize the dynamic and personalized online sports

computer aided teaching test page. Through internet, students can input sports terminology and basic concepts of hot word to complete query and browse the relative knowledge point including difficult point and important point. Besides this, students can get the knowledge through the instance analysis, problem analysis and recommendations to master the knowledge and skills needed on the internet.

CMT analysis

CMT is applied to the university sports teaching management to relive the heavy burden of PE teachers on the student performance statistics and attendance statistics. It can print all kinds of report conveniently. With CMT, student's sports qualified standard statistical elements including physical education, the year total score, national physical exercise standard scores and grades and morning fuck action classes course of absenteeism can be provided easily. And the sports qualified standard form can be filled very conveniently.

Conclusions and suggestions

Conclusions

The development and application of CAI in sports teaching. This application can stimulate students interest in learning to mobilize the enthusiasm of students' active participation and expand students' knowledge and can provide students with a variety of learning sports basic knowledge, basic technology and skills.

The application of CAT in physical education teaching can improve the efficiency in a series of links such as storage, test paper generation, implementation, testing, scoring, the results of statistical analysis and score query. All this can relive the labor burden on the teachers and education administrators.

CMI application in physical education can improve the management level of physical education and improve the efficiency of sports teaching and the degree of specification to a large extent.

Suggestions

The computer and network hardware and technical support should be strengthened.

The teaching practice innovation and theory research of computer aided sports should be improved.

the application and development of CAI, the CAT and the CMI software in sports teaching should be broadened.

The ability of teachers developing the CAI, the CAT and the CMI software should be improved.

Acknowledgement

This work was financially supported by the Special Fund (No: CUGW120244) for Basic Scientific Research of Central Colleges, China University of Geosciences (Wuhan).

References

[1] Zhu Zhiting, The modern education technology to education informalization [M]; Education science press, 2003. 3.

[2] Peng Lixiao, The human body 3D animation; Beijing, Aviation industry press, 2000.

[3] Li Xuelong, Ding Pinqing, Wen Lin; Multimedia teaching optimization design[M]; Guangzhou, Guangdong higher education press, 1996. 12.

[4] Wang Mingfei, Shao Yong, ASP. NET application debugging; Beijing, China electric power press, 2002. 5.

[5] Wang Yulin, Liu Jinqing, The modern teaching evaluation theory; Harbing, Heilongjiang people's press [M].

Advanced Materials Research Vols. 989-994 (2014) pp 5106-5111
© (2014) Trans Tech Publications, Switzerland
doi:10.4028/www.scientific.net/AMR.989-994.5106

Constructing Micro-teaching Experimental Environment with Information Technology

Jian-xin Wang [1, a]& Sheng-quan Ma[2, b]

[1]Educational Technology Institute of Hainan Normal University, Information Technology, 571158, China

[2]Educational Technology Institute of Hainan Normal University, Information Technology, 571158, China

[a]Email:81665146@qq.com; [b]Email:554749578@qq.com

Keywords: information technology; construction principles; multimedia classroom; micro-classrooms; teaching environment integration, Educational Technology

Abstract. By using the Information Technology, the paper sets out to start a systematical design and exploration of micro-teaching and E-learning resources adopted in a public experiment teaching course named "Educational Technology" in some advanced normal universities. Besides, by examining the constructive principles of the experimental teaching environment, it has transformed the single experiment learning model which took place in traditional classes, improved the teaching efficiency and quality. And lastly, it discusses such items as learning resources on the internet, the integration of multimedia and micro-teaching as well as the micro-grid classroom construction principles, and puts forward the present college media environment building program, which meanwhile promotes the integration between technology and curriculum.

Multimedia teaching involves texts, graphics, animation, video, sound, special effects, and also includes unlimited imagination. It not only changed the way we learn and the method to solve problems, but also changed the way through which information is spread. It is a technique combining many subjects such as computer graphics, image processing, video art, music, fine arts, education, psychology, artificial intelligence, information science and electronic science and one that brings words, graphics, images, sound, video images, 2-D and 3-D animation together, which fully mobilize the visual and auditory processing.

Microteaching is actually a practice environment that enables everyday classroom teaching to become simple by decomposing it, which, at the same time, will help the learners get lots of feedback. Being a controlled practicing system, it makes normal students or in-service teachers focus on certain teaching behaviors and learn under controlled conditions. It is also a method of training teachers which bases on the teaching theory, visual theory as well as technology.

The principles of constructing multimedia and micro-teaching environment

1. A multimedia classroom construction principle

(1) Utility, which is the main goal of building an effective classroom, because the highest profits can only be guaranteed by the best effects. It is easy and free enough to operate for learners of different majors.

(2) Reliability. Reliability is the first principle when thinking about constructing a program, because human safety, machine reliability and long-term stable operation of the equipment will ensure that the users are provided with the relevant guidance when the system is under processing, which will help to reduce the cost of labor and capital during the operational process.

(3) Compatibility. The device has similar equipment compatibility with different manufacturers and different models.

(4) Advancement. The selection of equipment, especially the central control software must adapt to the direction of technological development, and fully reflect the advancement of the entire system.

(5) Expansibility. A primary principle for a multimedia classroom is whether it can be associated with Internet and whether it can call the outdoor classroom teaching resources.

(6) Security. Considering the security of multi-media classrooms during the non-instructional time, the console should be customized according to equipment specifications and take into account the factors such as security and fire.

(7) Convenience. The device makes it easier for teachers to operate the device by getting rid of the process of switching the equipment in and after class. That is, the power will be cut off with a remote control or by locking the device.

(8) Economy. System design and equipment selection should focus on the practical function, aim at reducing the overall investment, and seek a perfect unity between advancement and economy. In term of this, we should consider the actual demand of school teaching management and try to get rid of all that are not needed.

2. The micro-classroom construction principle.

(1) Being easy to control. The micro-teaching system is an intelligent and digital system and it should be designed to meet the authenticity, validity and convenience principle. Being easy to control helps to satisfy the needs of teaching, and simplify the process in which students as well as teachers are trying to improve their teaching skills.

(2) Scientific. The construction of intelligent micro-teaching system should meet the whole idea of micro-teaching and follow the trainers ' psychological needs. Meanwhile, it should keep in pace with times in the choice of equipment, make scientific predictions of the development trend of micro-teaching, and then manage to achieve it.

(3) Utility. While ensuring the usefulness of teaching and training needs of micro-teaching system construction, one should also consider an appropriate price. According to the Value Analysis, the overall value can be obtained (V) through a functional analysis of its value and the actual value of the investment ratio. In this case, one can make the appropriate analysis based on the engineering analysis for selection.

The constructing of multimedia and micro-teaching environment

1. Multimedia classrooms construction

Multimedia classrooms should be constructed according to the constructive principle, and make a scientific and rational selection of the equipment. In the paper, a multimedia console is designed, and then multimedia classrooms are constructed relatively concentrated according to the discipline needed in the course, which also takes into account their location, shapes, size as well as seats. The construction of the classroom is made up of two parts, i.e., the design of laboratory and the teaching equipment. The teaching system will keep the digital and intelligent development.

(1)The construction of multimedia classrooms under the network managing environment. These classrooms are suitable for the areas where multimedia classrooms are relatively concentrated. And they will be different in function according to the needs of different subjects. The specific equipment program is shown in Table 1.

Table 1 Multimedia classroom network management solutions:

Equipment Name	Amount	Remarks
Multimedia computer	1	Requires a DVD drive P4 2. 6 above configuration
The central control system	1	Network control and management
Projector	1	Configure the projector and screen brightness based on classroom size
Electronic screen writing	1	Not only for writing but also as a computer monitor screen
Console (custom)	1	According to the actual needs of customization, in line with security, safe, aesthetics, practice
Amplifier (lavaliere wireless microphone)	2	Equipped according to PA, have a line input function
Monitoring on-demand system	1	Master the dynamic teaching, play on time when there is a demand.
Intercom System	1	Helpful for real-time communication and solving problems
Multimedia network classroom software		Realize broadcasting, monitoring, voice teaching of teachers to students, help students complete the learning and use of computer software.

The configuration applies the central control system of a network, and the network operator can either use a remote control or a local control, which increases the control system. The correlation function is as following.

(1) Central control system. Network managing multimedia classrooms uses a network central control system, including classroom network control and total control software. The system is highly integrated, rich in interfaces and very powerful. It is embedded with network interface. By using TCP / IP technology, and through the campus network interconnection, a remote centralized control can be achieved. Besides, 3 controlling ways are to be chosen, i.e. network, software and manual control panel. Lastly, it owns the delay function to prevent damage to the equipment when electricity is off.

(2) Console. Similar to the stand-alone multimedia classrooms, the console is also based on rational design to make it easy to use (such as the required teaching device interface installation) and meet the security demand. Console door opening can be controlled remotely through the network, which can be realized through local operation too. In other words, the controlling lock linked with central control system also acts as a console lock. Thus a lock is of great use and convenience lying in that the opening and closing of computers are all controlled by it with the assistance of the Various Linkage System.

(3) Demand monitoring systems. The adoption of the system is better for the managers to master the remote teaching dynamic. The associated control software allows teachers to use the contents on the screen to get the synchronization audio or video records, which could get to instant on-demand and broadcast capabilities through the system.

(4) Intercom systems. The application of intercom system can help to discover and solve problems immediately. Currently intercom is found in different ways, such as duplex, half-duplex intercom systems, telephone intercom systems, IP telephone network methods, etc.

(5) Extensive practical function. This includes screen broadcasting, video broadcasting, voice broadcasting, programme distributing, homework gathering, mass discussion, division sign, and so on.

2. Intelligent micro-classrooms construction

Smart micro-classrooms should be constructed according to the constructing principles, and the equipment selection is designed according to the teaching content. The choice of equipment should also be designed along with the two factors. Similarly, teaching systems should keep the digital and intelligent development. Apart from this, it requires to make scientific predictions to the micro-teaching trends from time to time. Intelligent micro-classrooms teaching include the teaching equipment and laboratory design (shown in table 2).

Table 2 Smart micro classrooms program:

Name of the Equipment	Amount	Remarks
Multimedia computer	1	Responsible for the overall control, management and production of power equipment systems
Microphone, camera	2	Completion of the acquisition for video and audio signals
Video and audio Presenter	1	Depending on the completion of control playback of audio files,
Network File Server	1	Micro-teaching resource library, installed in the control center of the campus network.
Smart micro-grid network classroom software	1	The core of the whole system.
Console (custom)	1	According to the actual needs of customization, in line with security, safe, aesthetics, practical

The configuration applies the central control system of a network, and the network operator can either use a remote control or a local control, which increases the control system. The correlation function is as following.

(1).Video intercom call box. The simulated classroom is equipped with video intercom call boxes, through which the trainer can call the control center via a button on the call box. The camera has visualization functions, so that the control room staff can keep abreast of the different simulation classroom training situations and conduct the timely processing and feedbacks. What's more, video intercom equipment can be installed among classrooms, making communication of different simulation scenarios possible.

(2).Remote control. The intelligent management could finally be achieved as the network administrators can control and manage the relevant device system and data remotely via loading the campus network management system.

(3).Sub-control system. The controlling function of the control chamber, on the one hand, could be achieved through a multimedia computer with controlling function. And it can also decentralize the control functions. For example, one can control the corresponding devices respectively by setting the camera remote control and the audio console. On the other hand, it integrates the device control system and controls by a controlling system. What's more important, it brings the sub-control advantages of micro control equipment systems of previous generations of system and has complementary advantages.

(4) Multicast video play. In terms of video play, smart micro-grid equipment system can effectively control the digital signals, as well as transmit data regularly within the campus network. It can control the time and place of the file to play, which is not only helpful for the same video files spreading to different classrooms, but also for different files spreading to different classrooms by regulating the computer software.

(5) Evaluating lessons. Evaluation function is important in micro-teaching. In addition to record, produce and play the trainers' live training process, it has also the function of giving an objective

evaluation of the training results. Observation and evaluation work can be conducted in the observation rooms. At the same time, comments can be given by sending the relevant reviews through the campus network or by the use of video conference.

(6) Demonstration. Teachers could make a demonstration of the fine courses in the simulated classroom. And the courses, of course, will be broadcast to classrooms installed with a TV or video player via multicast broadcast, which serve as good examples.

(7) System monitoring and scanning. There is dedicated monitoring software in the intelligent multimedia micro-teaching system. It can start to scan the files and data in the entire system, measure the transforming speed as well as efficiency, and the transmission errors are thus effectively controlled.

(8) Remote transmission. The system enables people to transmit the live teaching process to other places through the campus network, and it also has remote teaching management and evaluation functions, makes up for the micro teaching equipment of previous generation where live broadcast was confined in a small areas.

(9) Standby interface. In order to meet the needs of users to upgrade, smart micro-teaching system reserves the stand by interface. Users can optimize and upgrade the system according to actual need.

The Integration of Multimedia and Micro-teaching System.

It changed the unity of the original experimental teaching methods, overcomes the objective limitations of the experimental lessons and equipment. It is a traditional laboratory extension in time and space, which can promote the integrating process of technology and curriculum.

(1) The similarity between multimedia and micro-teaching system by the discussion above, there is a great similarity in the functions of the multimedia and micro-teaching system (shown in Table 3).

Table 3 The similarities in the function of multimedia and micro-teaching system

Similarity	Remarks
Central control system	Includes classroom network control and total control software.
Monitoring on-demand system	Associated control software allows teachers to choose the demanded contents.
Multicast function	transmit data regularly
Network management functions classroom teaching	Corresponding teaching management functions to assist.
Alternate interface functions,	Requires the user to upgrade
Remote transmission function,	Remote teaching management, remote teaching evaluation
Sub-control functions	Integrated control device, the control system controlled by software
Classroom management and maintenance。	Easy maintenance

(2) The design of a micro-media device system

Multimedia and micro-teaching system equipment is the core of the whole system. The overall structural design of the device system is shown in the following FIG.

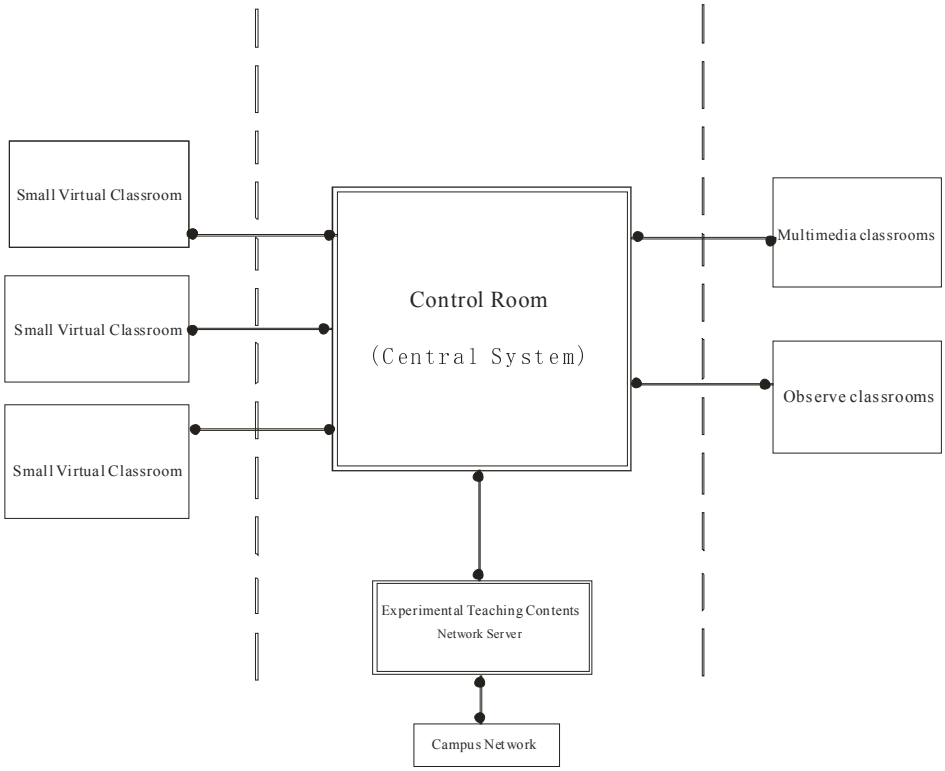

Media Control Center microteaching

References

[1] Jiang Ling. Design and construction of micro-teaching system [J]. Sichuan Teachers College, 1999, (9) :286-289

[2] Chen Xingyao like. Microteaching and remote management system [J]. Application of Electronic Technique, 2000, (12) :11-15

[3] Like Dong. New educational technology base [M]. Shanghai: East China Normal University Press, 2001, (9)

[4] Zhang Jian Wei. The new IT-based curriculum model curriculum integration [J]. Zhejiang teaching and research, 2000,2 P36-38

[5] Like Dong. Digital Learning - information technology and curriculum integration of core History Shu people, Zhang Jingsheng county and township building and problem analysis of primary and secondary multimedia classroom

[6] [J] Education Research, 2004 (1): 76280.

[7] Yangquan Nan returned to Australia to talk about the construction and management of Multimedia Classroom [J] Chinese education technology and equipment, 2003 (9): 61264.

[8] Zhang Wuwei choice about multimedia classroom equipment configuration scheme [J] Modern Educational Technology, 2003 (3): 73248.

[9] Zhu Guanghui, Shao Hong, Ma Tao of network-based multimedia classroom Application of [J] Experimental Technology and Management, 2004, 21 (5): 61263.

Advanced Materials Research Vols. 989-994 (2014) pp 5112-5115
© (2014) Trans Tech Publications, Switzerland
doi:10.4028/www.scientific.net/AMR.989-994.5112

The Study of Risk Management of Government IT Service Outsourcing

Bo Liang[1,a], Haifeng Liu[1, b], Guining Geng[2, c],Guang Yang[3,d]

[1]Beijing Information Security Test and Evaluation Center, Beijing, 100101, China

[2]China Information Security Research Institute, Beijing, 100191, China

[3]China Information Technology Security Evaluation Center

[a]email: liangbo@bjeit.gov.cn, [b]email: liuhf@bjeit.gov.cn, [c]email: gengguining@cecr.ac.cn, [d]sunwina@126.com

Keywords: Government IT service outsourcing, security and risk management

Abstract. There are potential risks and uncertainties in each phase of IT service outsourcing, which will pose a huge threat on governmental and national security. In order to benefit the outsourcing of government IT service, this paper will study the security and risk management strategies for government IT service outsourcing.

Government IT Service Outsourcing Risk Management

1.1 The Overall Process of Government IT Service Outsourcing

As presented in Fig.1, the overall process of government IT service outsourcing is divided into four stages: planning, acquisition, implementation and termination [1]. In the planning stage, the government needs to analyze needs, conduct market research, develop action plans, and conduct staffing. The primary task of IT service outsourcing acquisition is to choose the right outsourcing service providers. Implementation phase needs to manage the safety, schedule, quality of IT service outsourcing. Termination phase can propose improvements [2] [3] [4].

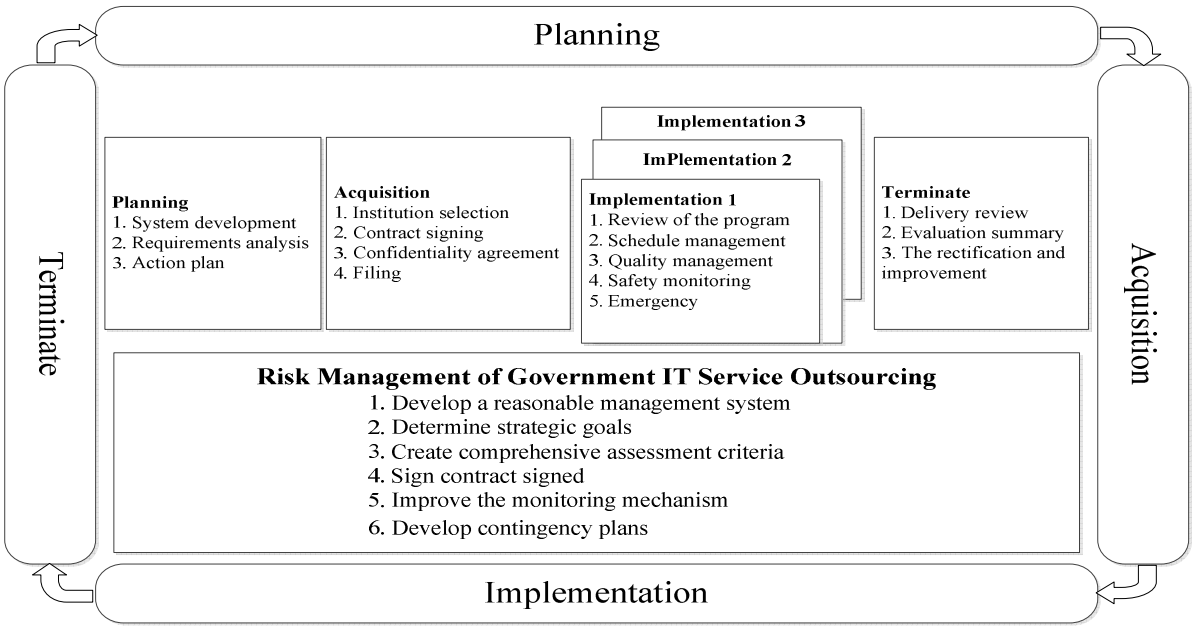

Fig.1. The main frame of IT service outsourcing

1.2 Control Measures Against the Risks of Government IT Service Outsourcing

To address these risks, the government must establish a scientific and reasonable resource management system and develop a sound management system in IT service outsourcing. The government should strictly supervise and manage the entire process of IT service outsourcing, and continue to explore new business development form, and tap new business needs.

Against risks from the government IT service outsourcing, and with reference to China Information Technology Service Standards (ITSS), this paper offers measures which the

government should take in each stage as presented in Fig.2. The followings describe the measures which are specifically addressed these risks in accordance with the order to achieve the IT service outsourcing:

(1) Establish a scientific and rational management system

In the activities of IT service outsourcing, the establishment of rational resource management system is very important, it directly determines the success and safety of the entire outsource activities [5].

Fig.3 shows the framework of the relationship between government and enterprises in IT service outsourcing. Relevant government organizations and enterprises form an alliance which rely on contractual agreements as a link and provide quality services or products. Its structure is composed of three levels: the business layer, management and coordination layer, and outsourcing enterprise level. Among them, the management and coordination layer is composed by three expert groups: development strategy group, Legal Unit and implementation monitoring group, or other departmental structure which perform similar functions. Table 1 gives the detailed composition of the expert group and the various business functions.

(2) Define a clear strategic objective and determine the technical requirements.

With the help of development strategy group, the governmental organizations which intend to implement IT service outsourcing need to plan the development of information systems and information technology, study and explore the technology needs, determine to implement the technological development programs. Generally includes four aspects:

(a) Understand and seek new approaches and channels to apply IT in government business applications and explore new opportunities for the development of government information systems;

(b) Find the existing and ongoing information technology, the actual needs of government business, the gap between the current status of IT application and development objectives. Then survey the needs of application department and decide which projects will be outsourced and which projects need to wait. At last, determine the specific program of IT application;

(c) Evaluate the new developed and popular information technology, forecast the development prospects of the application of new technologies in the government, develop IT development strategy planning and implementation strategies for governmental organizations; and

(d) Collect, classify and analysis the IT development.

The development strategy group should draft scientific information systems development strategy, and determine the proper technical requirements. It should not blindly pursue new technologies to avoid the unnecessary risks of information technology applications, or the excessive financial burden.

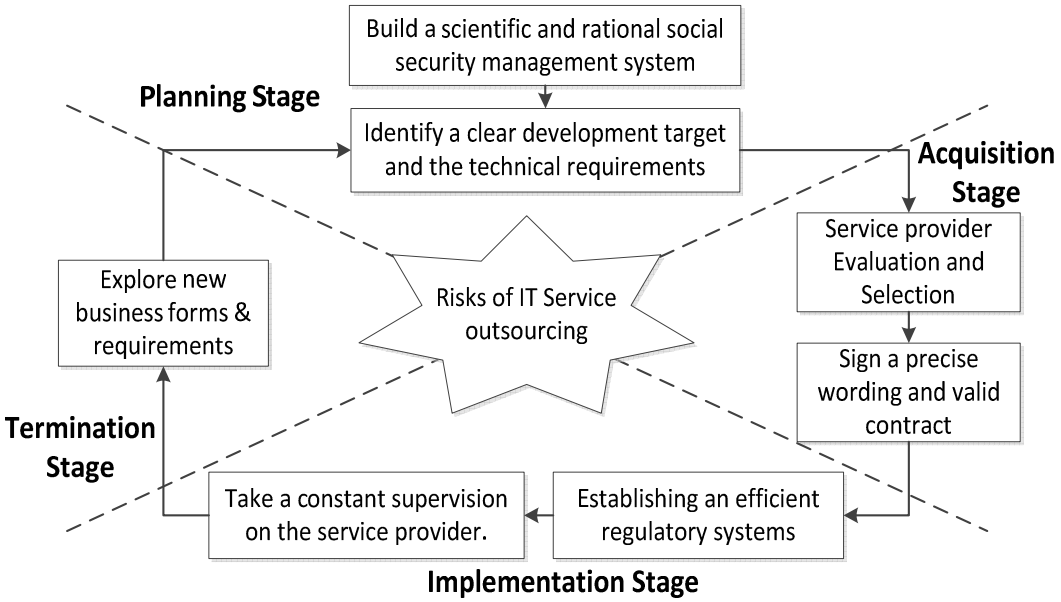

Fig.2 Countermeasures against risks of government IT service outsourcing

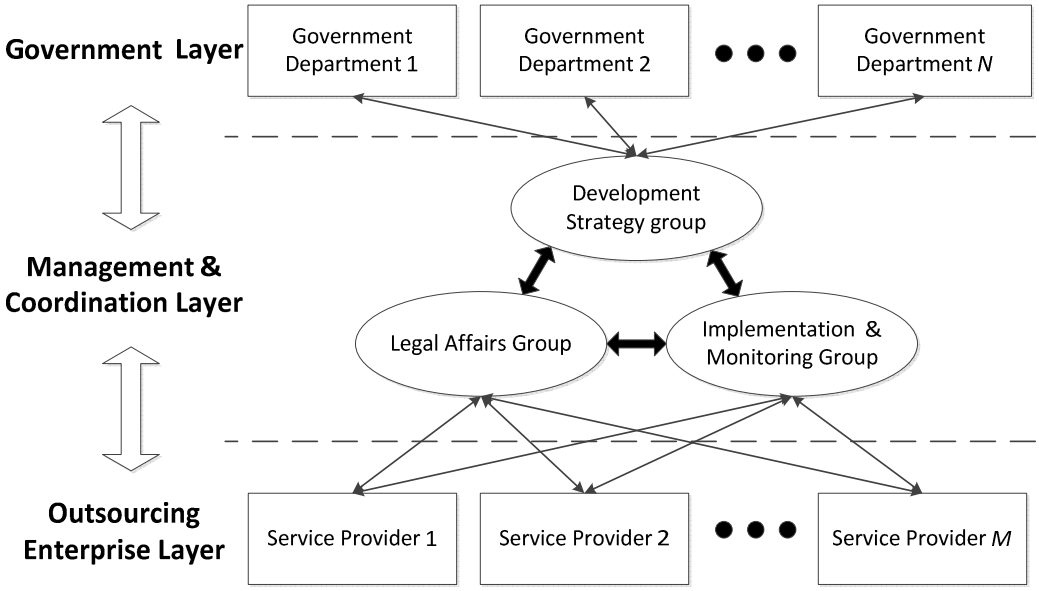

Fig.3 The framework of the relationship between government and enterprises

Tab.1 The detailed composition of the expert group

	Staffs	Functions
Development Strategy Group (DSG, Leaded by the senior fellow of the government)	1.Representatives of the government business department. 2. Experts on information technology; 3. IT outsourcing consulting company; 4. Experts on industry strategy planning.	1. Explore applications of the new information technologies in government IT system. 2. Planning and implementing IT strategy; 3. Explore the requirement of the IT departments, and determine the requirement level; 4. IT application evaluation, determine outsourcing project, implementation scheme, service provider selection etc. 5. Information collection and feedback.
Legal Affairs Group (LAG, Leaded by the Representatives of the DSG)	1.Representatives of DSG; 2. Representatives of IMG; 3. Legal experts on information technology.	1. Negotiation and signing IT outsourcing contracts & agreements; 2. Assisting IMG in resolving the disputes during implementation, and dealing with the corresponding legal affairs; 3. Information collection and feedback etc.
Implementation and Monitoring Group (IMG, Leaded by the delegate of the DSG)	1. IT professionals; 2. Staffs of contracts and agreements management; 3. Coordinators.	1. Reconcile the disputes between government departments and service providers, and the disputes between the service provider; 2 Monitoring the process of the project and participate in project acceptance; 3. Collect materials for possible legal cases; 4. Information collection and feedback etc.

(3) Comprehensively assess and select the service providers.

After the development strategy group study and explore the technology needs of government business sector, they need to evaluate the service providers to determine if their financial and operational capacity can meet needs or not. It mainly includes the following three aspects.

(a) Assess professional skills of service providers and capabilities of professionals.

(b) Assess the level of service provider's understanding of relevant laws and regulations, as well as outsourcing professional knowledge.

(c) Investigate the financial condition and credit worthiness.

(4) Sign a stringent and effective outsourcing contract.

(a) Set a clear outsourcing service boundary and a flexible agreement contract.

(b) Give a reasonable description of service level and measurement.

(c) Build clear liability and dispute settlement procedures.

(d) Limit cost increment and define the right to terminate the contract.

(5) Develop a sound regulatory system

(a) Information security management system. It includes the required information application process in the implementation of the project and authorization method for secret information, to ensure that these measures conduct comprehensive protection for government information confidentiality, integrity and effectiveness.

(b) Business management system. The system includes the specific approaches for government departments to carry out the progress management, to exchange and communicate between the government and service providers or among the service providers, as well as to assess the service quality of the service providers.

(c) Resource management system. The system should guarantee the government resources will not be stolen, misused under the institutional norms.

(6) Conduct strict and constant supervision of service providers.

(7) Explore the new forms of information technology service outsourcing, and tap new business needs.

In addition to taking risk management strategies, and in order to reduce and control the risk of weakening internal learning and innovation, development strategy group should be responsible for exploring new forms of outsourcing. New forms may include partnerships with IT service providers, introducing a shareholding system, to co-invest in new areas of technology and share risks and proceeds. The government shall appoint specific members to research the long-term changes in the business environment, and continue to tap new business needs. The advantages of IT service outsourcing can be fully realized without jeopardizing the internal leaning ability and innovation capacity.

References

[1] ISO/IEC 20000-1:2005, IT Service Management, The first part: Specification.

[2] ISO/IEC 20000-2:2005，IT Service Management, The second part: Rules of Practice.

[3] Information Technology Service Standards (ITSS), 2010.

[4] Federal Procurement Regulations, 2005.

[5] Li X. M., Li M.Q., Kou J.S., Study on Management Model of IT Outsourcing. System Engineering-Theory & Practice [J], Issue (9), page(s):10-15, 1999.

Advanced Materials Research Vols. 989-994 (2014) pp 5116-5119
© (2014) Trans Tech Publications, Switzerland
doi:10.4028/www.scientific.net/AMR.989-994.5116

A Spectrum of Findings: Mechanisms for Third-party Evaluation of the Quality on the Application-oriented Undergraduate Teaching

Liang Lei [a], Jun Peng[b*]

College of Electrical and Information Engineering,
Chongqing University of Science and Technology, Chongqing, 401331, China

[a]email: cqlei.l@163.com, [b]email: pengjun70@126.com, *Corresponding author

Keywords: teaching quality; teaching assessment; social evaluation

Abstract. The evaluation on the students' vocational skills and teaching quality is more often unilaterally performed by the school side. The results are not recognized by business, industry and other employers, and further to affect the students' employment rate and quality. This work team carried out a series of research subjects on how to establish a mechanism for third-party evaluation of teaching, where businesses were invited to join the teaching management, with their views on graduates being collected for the initial establishment of an effective evaluation mechanism. This played a very important role in exercising and improving the overall quality of students.

Introduction

Along the universities are undergoing the conversion from elite education to mass education, the mechanism for evaluation on the quality of undergraduate teaching has been explored and gradually become one of the research focus of all universities and enterprises and institutions[1][2].

For teaching quality, an objective and impartial evaluation is an important means to guide teachers on improving their teaching methods and quality. The evaluation on the quality of undergraduate teaching may cover three areas: self-evaluation of teachers, internal evaluation from students, supervisors, university leaders and peers plus the third-party evaluation of any one sector in independent institutions, also known as social evaluation [3].

Teacher's self-evaluation is taken to improve the quality of teaching and promoting the personal development of teachers as the ultimate goal. Meanwhile, the teacher's self-evaluation is largely manifested in the evaluation of students. Currently, most colleges and universities still tend to evaluate the students in the traditional way for general education, which is based on assessment at the end of the semester. Assessment methods are divided into two categories: test and examination. Generally, tests mainly include the written exams, practical operation and usual practice, with attendance as an important indicator to examine student motivation and learning attitude; and examination is mainly based on the usual motivation and learning attitude. These seemingly well-functioning evaluation mechanism actually failed to let the students truly know themselves objectively, nor really inspire the internal driving force from students, much less provide a scientific and rational reference to further enhancement of students. This evaluation method does not recognize the potential that may be found inside students, nor the difference and emphasizes commonality, only counting on the uniform criteria to measure differences in intelligence, behavior, knowledge, background, family environment, hobbies and other aspects of individual students [4]. In addition, the evaluation mechanism cannot play a good role as to improve the quality of teaching.

Internal evaluation given by students, supervisors, college leaders and peers is now widely used in higher education [3]. Student evaluation of teaching quality mainly refers to the teaching evaluation before the end of the course undertaken. The evaluation by supervisors, college leaders and peers are mainly completed through lectures and in the form of questionnaires.

The school side evaluates the students on their professional competence and the teaching quality, where teachers and educational administration act as a major subject. The evaluation on the students' professional competence is mainly implemented through exams organized by schools themselves. Basically, the whole evaluation process is conducted in line with the wishes of the

school, lack of participation and supervision by business, industry and employers, making it difficult to fully consider the requirements by industry for skilled competence and professional quality. This can be a failure to develop a scientific content, criteria and methods for evaluation based on professional competence required for business tasks, resulting in a mere formality throughout the evaluation. The evaluation results are not recognized by businesses, industry and other employers, further to affect the students' employment rate and quality [3].

Focused on this topic, the work team has visited part of the application oriented universities and enterprises located in Shenzhen, Guangzhou, Beijing, Shenyang, Xi'an, Chengdu and Chongqing, also including the visit to University of Michigan. Graduates were given an anonymous questionnaire, where the social assessment served as an important indicator of teaching quality, which played an important role to improve the teaching quality and study atmosphere.

Necessity of Companies Fully Involved in the Evaluation on the Undergraduate Teaching Quality

Business recognition to graduates is the biggest certain for teaching quality. In fact, all along, all colleges and universities in teaching educational administration attach great importance to the evaluation from employers on the quality of teaching. But most college students may wait until the graduates begin to work after graduation, and organize the relevant functional departments or the department personnel to conduct research in enterprises and institutions, carrying out follow-up survey of graduates in the forms of inquiries, questionnaires and seminars to listen the advice from business on the teaching quality of graduates Evaluation of [5]. In this way, views collected on the existing training programs could have a pivotal role in training students. Nonetheless, this sort of assessment is passive with a strong one-sidedness and hysteresis. For this reason, these employers may be part of the planning process and teaching management, and the organizational aspects of teaching, which have a very important significance to improve the quality of teaching.

Companies Fully Involved in Building a Mechanism for the Evaluation on Teaching Quality of Comprehensive Undergraduate

Targeted at the problem that may be present in the system to evaluate the teaching quality, the evaluation of the quality of teaching cannot be limited to the teachers and schools alone as the evaluating subject. Rather, an independent third party with the school should be entrusted for teaching quality evaluation, which is commonly used abroad as a model. That is, industry management experts and technical personnel are combined with institutional experts as a third-party to evaluate the subject, so as to fundamentally raise the level of professional competence of students to improve students' employability and competitiveness [3].

Construction of a third-party evaluation mechanism, the idea is designed based on the "industry-led" concept, according to "***Who***, ***What***, ***How*** and ***What***" regarding evaluation results [3]. In this paper, " ***How*** and ***What*** is the research focus.

Enterprises being part of school teaching management

Making the training plan. When institutions are developing a personnel training plan, enterprises should be invited to participate in the discussion on the adequacy of the social research personnel training program, the accuracy of the market and social positioning, whether the plan is able to meet the future needs of community, whether the implementation plan is in line with corporate standards, whether the personnel evaluation criteria are to meet the enterprise's requirements for job training.

Curriculum setting. Curriculum system is the important support to reflect a personnel training program. Enterprises to participate in the discussion on course content as to whether meeting business needs, whether covering job requirements for knowledge and ability and quality, whether curriculum meets the certification standards of professional engineering education.

Evaluation of the steps of practical training. Enterprises can get involved in the evaluation training segment which should be derived from real projects of enterprises, whether to adopt corporate training methods, whether training course meets the corporate governance norms and standards, whether to be able to achieve the required level of corporate career.

Evaluation of teaching quality. Enterprise is to evaluate whether the content of textbook has an appropriate theory depth and breadth, whether the experimental guide book is modeled on business practices, and whether the forward-looking textbooks are chosen.

Evaluation of the quality of teachers. Enterprises involved in the evaluation of teachers' familiarity on the business process, software development process and development tools, that is, practical ability. Also, the proportion of being "double" teachers and that of enterprises to participate in class are considered.

Enterprise evaluation of graduate students

Enterprise evaluation on the students is designed for graduates with at least three years of working experience, mainly regarding the student's professional and ethical standards, professional attitude, quality and skills and so on. Data collection methods and Enterprise feedback will be described in the section.

Work team has visited the enterprises located in Chongqing, Shenzhen, Guangzhou, Beijing and Shenyang, in the form of questionnaires, feedback from graduates and field survey, collecting a lot of comments from employers on their students. This provides an important basis for us to amend our talent training plan.

Questionnaires. According to the time arrangements by employers, our computer department used the questionnaire to conduct a follow-up survey on the graduates that already had been employed for some time, allowing the employers to give a comprehensive evaluation of the graduates, providing recommendations on our computer professional talent training.

Internships feedback form. Since graduation practice and design sessions are jointly undertaken by companies and universities in teaching tasks, where companies can understand the aspects of the school situation in the computer professional practice teaching. Therefore, an internships feedback system is established. After each end of the internship, the relevant personnel with employers is about to fill an internships feedback proposal form, in order for professional quality evaluation on our computer science teaching.

Field survey. The work team took issues with the personnel training program and visited a number of enterprises, seeking their comments so as to make a training plan to meet the real needs of enterprises.

The work team collected data for analysis, where computer science students are divided into three categories: (a) IT institutions; (b) software development; (c) computer research. And the work team got many enterprise feedbacks.

IT Institutions. Enterprise is focused primarily on students' knowledge and ability in computer networks and hardware, as well as common statistics and analysis capabilities. Common evaluation criteria are shown in Table 1. Evaluation of content includes Attitude, Discipline, Quality, Professionalism, Skills, Teamwork, Innovation, Results, Hardworking, Self-learning, Dedication, Friendliness, Honesty, Impetuous, Respect, Consideration, Complacent, Money Worship, Self-reflection, Communication, Sense of Ownership, Responsibility, Legal Awareness, Hardware Maintenance, Network Maintenance, Office Software, Image Processing.

Software Development. Enterprise is focused primarily on student teamwork and the familiarity with software tools. Common evaluation criteria are shown in Table 1. Evaluation of content includes Attitude, Discipline, Quality, Professionalism, Skills, Teamwork, Innovation, Results, Hardworking, Self-learning, Dedication, Friendliness, Honesty, Impetuous, Respect, Consideration, Complacent, Money Worship, Self-reflection, Communication, Sense of Ownership, Responsibility, Legal Awareness, Algorithm Design, Embedded Programming, Mathematical Foundation, . net or Java, Reading Comprehension, Hardware and , Interface Technology, Data Structure.

Table 1 Assessment by Enterprises on Students

Evaluation of Content	Evaluation Factors	Evaluation Criteria				
		Excellent（90~100）	Good（80~89）	Moderate（70~79）	Qualified（60~69）	Unqualified（0~59）
Test results: A-Excellent B-Good C-Moderate D-Qualified E-Unqualified						

Computer Research. The employers are focused primarily on student math, English and professional theoretical basis. Common evaluation criteria are shown in Table 1. Evaluation of content includes Attitude, Discipline, Quality, Professionalism, Skills, Teamwork, Innovation, Results, Hardworking, Self-learning, Dedication, Friendliness, Honesty, Impetuous, Respect, Consideration, Complacent, Money Worship, Self-reflection, Communication, Sense of Ownership, Responsibility, Legal Awareness, Algorithm Design, English Proficiency, Professional Basis, Programming Capability, Mathematical Foundation, Computer Hardware Foundation.

Different employers may vary on the weight for each of the quality requirements, that is, they may counting on different "evaluation factors". Nevertheless, the above evaluation criteria presents that all employers tend to pay more attention to unity among students, and their innovation, hard-working and self learning abilities.

Conclusion

To establish a third-party evaluation of the quality of teaching mechanisms for application-oriented undergraduates, the work team made a lot field surveys on enterprises and institutions, concluded by establishing a set of methods initially regarding a third party being involved in the community with their teaching management and evaluation of the overall quality of the graduates. This set of mechanisms, when applied to the personnel training mode, has been proven to play a pivotal role in the comprehensive training of our computer science students.

Acknowledgement

The work described in this paper was supported by Higher Education Research Project of Chongqing University of Science and Technology (No. GJ201205), Teaching Reform Projects of Chongqing Education Committee (No. 102123), Eleventh-Five-Year State-Level Projects by the Ministry of Education (No. FIB070335-A8-02), and Data Structure and Algorithm project in the national bilingual education model curriculum in 2009. The authors are grateful for the anonymous reviewers who made constructive comments.

References

[1] Zhang, Aijun,Ge, Yujia, Li, Biwei.Pulse-based analysis on teaching quality evaluation[C], Lecture Notes in Electrical Engineering,107 LNEE,2012,729-737

[2] Plumbridge, Bill,Teaching quality assessment - an inside view[J],Materials World, 1996, 4(5): 276-278

[3] Wu Shuang. A Preliminary Study on the Third-Party Evaluation Mechanisms for the Teaching Quality of Vocational Colleges[J], China Education Innovation Herald, 2012, 20:230

[4] Li Jie. Establishment of the Enterprise-oriented Evaluation System for Students in Vocational Schools[J], Education & Teaching Practice, 2013, 3 (3) :37-38

[5] Zhang Yi. Analysis on the Connotation of Enterprise Evaluation in Personnel Training Quality Evaluation in the Mode of "School-Enterprise Cooperation"[J], Journal of Bayin Vocational and Technical College, 2012, 2:11-13

Advanced Materials Research Vols. 989-994 (2014) pp 5120-5123
© (2014) Trans Tech Publications, Switzerland
doi:10.4028/www.scientific.net/AMR.989-994.5120

Research on Design & Application of Multimedia CAI Courseware for Technique Teaching in Physical Education Courses

Yuhua QIU[1, a], Gaozhi OU[1, a], Jing HUANG[1, a]

[1]Department of Sports China University of Geosciences (Wuhan), Wuhan, 430000, China

[a]email: honeyqyh@163.com

Keywords: Technique teaching in physical education courses ; multimedia CAI technique ; courseware ; design ; application method

Abstract. With the help of modern learning theory, educational media theory, systematic science theory and modern teaching design theory, the mode of making multimedia CAI courseware for technique teaching in physical education courses was designed. Based on this mode, the Multimedia CAI Courseware for Back Layout Teaching has also been made. By application in teaching, a conclusion that there are five advantages of using the Multimedia CAI Courseware for technique teaching in physical education courseware was reached, and three different levels of software and hardware should be prepared for the multimedia CAI courseware teaching. Thus, the three-chain teaching mode for using the multimedia CAI courseware in technique teaching was constructed.

Introduction

As the most notable achievement and human wisdom for education in the 20th century, CAI (Computer Aided Instruction) has become a major part of the educational science and modern educational technology. Meanwhile, it also has become the direction of strategic issue and teaching innovations in scientific research. In this paper, Multimedia CAI Courseware in Back Layout is made and applied in teaching to explore production methods for Technique Teaching in Physical Education Courses with the rules and characteristics of using multimedia CAI technology. The early popularity of multimedia CAI technology in physical education, so as to improve the quality of Physical Education and provide services for training compound sports talents to meet the needs of the 21st century.

Design Process of courseware

Overall Design of Courseware

Making mode of multimedia CAI courseware According to the basic principles of CAI and teaching software development, as with the professional characteristics and the actual situation of courseware development, a mode of CAI courseware that is suitable for Technique Teaching in Physical Education Courses is made.

Teaching target of courseware By the application of courseware in teaching or self-learning process, it can provide a vivid and intuitive learning environment for students. Taking advantage of computer graphics, image, animation, audio, video and other functions, students can develop positive technical concepts and master the project (such as the Back Layout) technology. Besides, they can master mission, action specification, technology essentials and teaching methods of different technical phases in theory with identification, causes analysis and corrective methods of common mistaken actions.

Teaching content of courseware The courseware should be based on the syllabus and the new materials to prepare teaching content. Moreover, it need teachers who work permanently in the front line with extensive experience in the teaching project to check, also a special forum should be held and the courseware content is identified after several revisions.

Teaching media selection and information presented in the form The selection of instructional media is mainly based on the teaching objectives and teaching contents. Because the computer can deal with sound, images, video, text, which makes the choice of media is more

convenient, flexible and economic, but the media must choose the right combination in order to achieve the best effect.

Script Design of Courseware

Manuscript writing Manuscript is a text form of courseware content, which includes all of the text content of designable courseware and can be written separately.

Script card design Script card has a very important role in making courseware. Script card design is mainly based on the content of the manuscript with teaching ideas, teaching strategies, teaching media and forms of information presented designed to each page. It specifically includes text, images, graphics, video, sound, music, and other specific content and forms of presentation. Therefore, script card has a direct impact on the accurate accomplishment of the teaching content, vividness of teaching style and the mix combination of media properly. Script card design is usually done by professionals together with CAI production experts, so that it can ensure CAI experts can better understand the course requirements.

Courseware Making

Structural design of multimedia CAI courseware In order to strengthen interactive learning and convenience of teaching use, courseware usually adopts hypertext (Hypertext) link and every page owns different buttons and hot words.

Multimedia material preparation

Production of text material In the courseware, there are three kinds of commonly used text: 1) ordinary static text; 2) animated text; 3) WordArt. These three words are produced by different software. In summary, the production of text adopts different forms according to different themes and contents.

Image production The image is mainly the pictures, photos and graphics that are used by courseware interface. This section has three main sources: 1) Generating an image file through the scanner, and then use Photoshop and Impactbulm to deal with; 2) For some downloading images, they are put into clipboard through the Print screen and saved for using; 3) To grab some representative pictures in the video by Video Snip and be saved as an image file, and then they are applied to the courseware.

Production of animation material The courseware mainly uses 3Dmax StutioR3 to produce. We make a complete technique demonstration , venues, background about Back Layout from different angles. To make full techniques, the complete technical essentials of Back Layout, action diagrams of elite athletes and teaching illustrations are adopted to abstract an idealized model of three-dimensional animation.

Production of audio material Three kinds of sound are usually used in the courseware: 1) The sound of explanation is recorded based on the text script;2) MIDI music which is as a background;3) The sound is collected from the videotape by acquisition card. The sound of explanation is required to be accurate, clear and reasonable.

Production of video material Sports technology courseware is to help students develop the right, intuitive and clear demonstration actions. In the process of making video material, the major outstanding audio-visual materials should be chose. In the collection, sound, no sound, slow motion and normal speed action are collected according to the different needs of courseware. Meanwhile, a number of important teaching methods and typical errors are recorded with a Panasonic video camera by athletes and student.

Overall production of courseware The overall production of courseware is began after the text, images, video, animation, audio, and other materials are ready. The overall preparation of courseware is mainly based on the script cards and CAI courseware hierarchy diagram. Courseware production is mainly done by Authorware. This part is not just to move the contents of the script card, it also includes modification of forms about information presented, background, re-election of music, text size, color, font changes, etc. The overall production is made through page after page, with hypertext links to achieve its strong interaction, forming a three-dimensional network structure between the various pages.

Courseware Trial

After completion of the overall synthesis and preliminary modifications, courseware should normally be in the teaching of trial by teachers and students for testing the applicability of courseware, and then amendments are proposed to make further modifications.

Sorting and Packing of Software

According to comments on the courseware for further revision, then it is burned to a CD, so you can run directly on other computers.

Application and Evaluation of Courseware

In order to explore the law and teaching mode of using multimedia CAI courseware, a questionnaire for the Multimedia CAI Courseware for Back Layout Teaching is adopted from 35 students of 2010,2011 grade in Sports Institute of Henan University .From the results of the questionnaire, students basically give full recognition evaluation. In addition, eight experts who are long engaged in teaching and training of back layout and six specialists who are engaged in production of CAI courseware are invited to evaluate. Finally, they agree that the courseware has great innovation and reach the advanced level of similar products.

Analysis and discussion

Ideas of Courseware Design

Guiding ideology of courseware system Multimedia CAI proposes a new teaching mode that emphasizes the initiative of students in the process of teaching and creates an environment where students' interest in learning and desire for knowledge is stimulated with providing an electronic teacher that is ready to give guidance and correct errors. Therefore, the thought of combining the teaching design with advantages of computer software is as the guiding ideology of making Multimedia CAI Courseware for Technique Teaching in Physical Education.

Theoretical basis of courseware design Courseware is often developed for certain objects and should be determined first in part of courseware design.

Basic Principles of Courseware Design

General principle; control principle; scientific principle; optimum principle of media selection and combination; friendly interface and simple operation principle.

Superiority of Multimedia CAI Courseware of Physical Lessons Using Technology

1) the difference in favor of teaching, individualized;2) conducive to the excellent teaching experience and promote outcomes;3) There are factors beneficial to students' intellectual and non-intellectual factors;4) will help save teachers' strength and energy to ensure that teachers have a good mental state to creatively preparation, teaching.

Conditions of Track and Field Teaching Multimedia CAI Courseware

Hardware facilities The simplest condition is that track and field surrounded by one or more CAI classrooms, so teachers can meet the multimedia presentation of CAI. The best conditions is that the student dormitory is equipped with a computer or open to students at any time multimedia CAI classrooms, students in school can also use multimedia CAI courseware preview or review and consolidate. With the development of technology standards and the improving of people's living standards, computer prices have also dropped dramatically, which has achieved the CAI teaching sports technology provides a viable condition.

Software environments The software should keep up with the basic hardware facilities. It mainly consists of two meanings: First, the basic requirements for teachers and students, teachers and students should have basic computer knowledge and use of modern media and cameras and other basic skills, the second is to have a good multimedia CAI courseware, this is a "source "problem, if there is no good multimedia courseware, no matter how good the hardware can't also play a role.

The Usage of Sports Technology Teaching Multimedia CAI Courseware

In order to achieve good teaching effect in the teaching process we usually require students to preview before class, conscientiously study in the classroom, consolidate and improve after-school .Using multimedia CAI courseware for teaching, should also teach these three main teaching.

Conclusion and recommendations

Conclusion

1) Based on the optimization of teaching courseware design ideas and teaching objectives and content, design, writing scripts and script courseware to create multimedia CAI courseware card is the key link;2) for text, images, animation, audio, video and other media material collection and skillful editing is a important prerequisite of multimedia CAI courseware ;3) "Physical Technology Course Multimedia CAI Courseware" development and application of teaching provides advanced and visual teaching methods. Make up for the deficiencies of conventional teaching and have improved the students' sense of participation and enthusiasm for learning. It has deepened students' understanding of knowledge, the abstract becomes concrete, revealing the nature of the problem, students can promptly correcting, review, strengthen and consolidate the knowledge, help to optimize the teaching process.

Proposal

1) Updating of education, teaching ideas, attaches great importance to the significance of CAI technology in education and teaching reform.2) The higher education departments should strengthen the teaching of multimedia hardware construction, pay attention to cultivating teachers to use modern media awareness and to provide teachers with good learning opportunities.3) the higher authorities should be system teachers, will be included in a multimedia CAI courseware condition teacher induction, and get its appraising the linked.4) Teachers themselves should be a sense of urgency, and should take the initiative to accept new things, and introduced it into teaching, to improve the teaching effectiveness and the quality of classroom teaching.

Acknowledgement

This work was financially supported by the Special Fund (No: CUGW120244) for Basic Scientific Research of Central Colleges, China University of Geosciences (Wuhan).

References

[1] Yongsheng Wang. The feasibility study of Action sports competition of the use of computer-aided design[J].Physical University of Technology of Beijing,1998 (1) : 90 - 94.

[2] Rulin Qian, Xiaoping Huang. How to use technology of audio-visual media in teaching [J] .Track and field,1998(12) : 32 - 33.

[3] Wan Yang, Zhangchang Feng. The Preliminary Study of Development of technology for teaching gymnastics of CAI[J] .Beijing: PE Teachers College in Beijing, 1999 (1) : 62 - 69.

[4] Xuenong Li, Pingqing Ding, Ling Wen. Optimal Design of of multimedia teaching[M] .Guangzhou: High Education Press in Guangdong,Guangzhou:1996. 12.

[5] Qiu Bao. World trends in education and Chinese educational reform[M] .Beijing: People's Education Press.Beijing:1998. 6.

[6] Department of Higher Education. Deepening teaching reform, requires training to adapt to the 21st century, high-quality talents——The first meeting of the National College teaching documents and information Material compilation[M] .Beijing：High Education Press，Beijing:1998. 10.

Advanced Materials Research Vols. 989-994 (2014) pp 5124-5127
© (2014) Trans Tech Publications, Switzerland
doi:10.4028/www.scientific.net/AMR.989-994.5124

Economic Analysis and Governance Countermeasure of Overload and Out-of-Gauge on the Highway

Lijun Zhou

School of Economy and Management, Nanjing Institute of Industry Technology, Nanjing, 210023, China

email: zhoulj@niit.edu.cn

Keywords: Highway transport; overloading; governance countermeasures

Abstract. With the development of highway transport, the social harms caused by overload and out-of-gauge on the highway become prominent. Though it is banned for a long time, it continues to exist. The article conducts the research that the most fundamental reason for the overload and out-of-gauge is that the transport operators pursue to maximize benefits from the perspective of economy. Then such five countermeasures for solving the overload and out-of-gauge transport shall be put forward: changing the punishment mode of overload, reforming multi-sectoral administration pattern, taking the road of intensive development, strengthening transport vehicles market management and making full use of modern science and technology.

Introduction

Highway transportation is one of five modes of transportation. For a long time, highway transportation plays an important role in our national economy and daily life. Especially in this twenty years, with the rapid economic development and under the support through national policies, the road infrastructure improve constantly with the increase of service stations and expansion of the scope, and a wide range of flexibility in space, time, batch, transporting conditions and services. So, highway transportation gives full play to the "door to door" transportation advantage. However, in recent years, the problems relating to overload and out-of-gauge intensify, which has hindered the economic development of transportation. With the widespread of overload and out-of-gauge, the roads are badly damaged because of the long-term overloading rolling, resulting in the great reduction of traffic efficiency and serious impact on the lives and property of the people, which is dubbed highway killer" and "accident culprit". Therefore, study on the overload and out-of-gauge in the highway transportation has a great practical significance.

Definition

The so-called overload transport indicates that transporting vehicles on the highway are loaded with excessive weight (beyond the approved load). Public security traffic management department shall review whether the net weight, total weight and axle load, which are stamped on the vehicles by their manufacturers, conform to the requirement in accordance with national standard. And the vehicles in conformity with the standard shall be registers and granted operation.

The so-called out-of-gauge transport indicates that for the vehicles on the highway, their total weight, axle load or dimension exceeds the specified standard.

Analysis of Overload and Out-of-gauge of Highway Transportation from the Perspective of Economy

As an economic activity, highway transport carriers lay emphasis on the profits in transportation activities process. If R represents transport profits, S represents transport revenue and C represents transport cost, the transport profits may be expressed as follows,

$$R = S-C \quad (1)$$

Transport revenue is mainly defined by freight load, transport price and transport distance so you can use S = f (m, p, l), where:

m represents cargo load with ton as unit

p represents transport price with ton and km as unit

l said transport distance with km as unit.

Then, $R = S-C = f(m, p, l) - C$ (2)

As transport revenue is proportional to the transport price, freight load and transport distance, the f (m, p, l) in (2) can be expressed as:

$f(m, p, l) = p \times m \times l$

According to whether transport costs vary with the transport mileage, transport costs can be classified into fixed costs C_f and variable costs C_v. Fixed costs are composed of the depreciation of the vehicles C_1, the salaries of administrative staff C_2, driver wages C_3, employee benefits C_4, transportation management fee C_5 and insurance C_6 while variable costs include fuel C_7, repairs C_8, tire fees C_9, tolls C_{10}, freight surcharges C_{11} and other penalties C_{12}.

Given that variable costs are proportional to the distance and freight load, they can be expressed as:

$C_v=k\times m\times l$ （3）

Here, k consists of such variable items as fuel C_7, repairs C_8, tire fees C_9, tolls C_{10}, freight surcharges C_{11} and other penalties C_{12}. That is, $k = f(C_7, C_8, C_9, C_{10}, C_{11}, C_{12})$, which means the necessary variable cost per unit of transport mileage. Then formula (2) can be expressed as:

$R=S-C= f(m, p, l) - C=p\times m\times l-k\times m\times l-C_f=(p-k)\times m\times l-C_f$ （4）

As can be seen from the above expression, when p> k, the transport carrier is qualified for transportation. Though the profit is negative, the variable costs and part of fixed costs can be made up. When $(p-k)\times m\times l>C_f$, , the transport carrier obtains profits. When transport distance is specified, in order to maximize profit, one way is to increase freight, which is not feasible under current fierce market competition because the transport carrier tends to gain a competitive advantage through reducing price while the other way is to improve the freight load, which is feasible under the current circumstance. Correspondingly, the carriers may obtain higher profits though tolls increase and possible fines occur for overload and out-of-gauge.

Solutions to Overload and Out-of-gauge of Transportation

1. Learning from foreign experience and changing the mode of penalty for overload

In Germany, more than 700 checkpoints are set along the national highway of a total of 11,000 km to test the overload of the vehicles and the driver timeouts. If the driver is judged for overload for the first time, the case will be registered and the driver will receive a verbal warning. The driver will be imprisoned for three months for the second time. If the driver is judged for overload more than three times, he/she will be deprived of his/her driving license and on the blacklist who may not work at driving all his/her life, thus enabling him/her not to drive overloaded vehicles.

In Japan, if the driver is judged for overload, penalty will be claimed on the driver, owner of the goods and the transport enterprise. According to the regulation of Japanese laws, the driver will be given punishment of stop driving for overload for the first time. If the driver commits it again, the duration of stop driving as punishment shall be lengthened, even the driver may be deprived of his/her driving license. Among them, 1 point shall be deducted from the driver if he/she is given the punishment of stop driving for ten days. If 20 points accumulated in three years are deducted from the transport enterprise, it shall be published in the list of violators; if 50 points accumulated in three years are deducted from the transport enterprise, it shall be ordered to suspend business to bring up to standard; if 80 points accumulated in three years are deducted from the transport enterprise, its business license shall be withdrawn. If the owner of the goods knows its overload, he/she shall be fined not to sell the goods or distribute them to the vending companies otherwise the owner shall be sentenced to less than six months in prison or a fine of 100,000 yen.

To learn from the operation in Germany and Japan, our traffic management departments shall establish the credit files of the transport enterprises and business vehicle driver and network with the highway information systems in different provinces. Once the vehicle is specified for overload, the related information about the transport enterprise and ownership shall be defined so the corresponding penalty shall be claimed on driver, transport enterprise and owner. For driver, the violating behavior shall be registered and published. And for a vehicle, if the notice is published less than 2 times, the driver shall be fined; if the notice is published more than 3 times, his/her driver qualification shall be withdrawn. For transport enterprise, if the vehicles with the notices published for overload exceed a certain proportion, its qualification shall be reduced.

2. Reforming multi-sectoral co-administration pattern and forming specific law enforcement agency

At present, there are many units who are involved in administering overload and out-of-gauge, such as Ministry of Communications, Ministry of Public Security, the National Development and Reform Commission, the State Administration of Quality Supervision, State Administration for Industry and Commerce, the State Administration of Work Safety. However, it is difficult to define their responsibilities respectively resulting in duplicate law enforcement: if they can benefit from the enforcement, they will struggle to handle it while if they have to burden the responsibility, they will put it aside. On the other hand, Enforcement standards in the enforcement process are not unified so the duplicate penalties may occur for the same overload and out-of-gauge. For the improvement, centralized management is a general way, which lack long-term, unified and coordinated supervision. Once the centralized management period is over, the overload and out-of-gauge will re-occur. Indeed it is hard to achieve the purpose to eradicate the overload and out-of-gauge in highway transport. Therefore, the current governance mechanism should be changed to form a specialized law enforcement agency so as to clarify their responsibilities, ensure the fairness and avoid duplicate law enforcement.

3. Changing the traditional management model and keeping to networking, intensive and large-scale development path

At present, the number of enterprises in the highway transport market is large, scale small and competition intensive. The main reason is that the barriers for entry to freight transport market are set very lowly, which is affected by economic theory of traditional transport. Before the reform and opening up, highway transport had been considered as an industry short of the benefits of economies of scale and its scale is confined to a smaller scope. After the reform and opening up, state-owned transport enterprises generally carry out vehicle-contracted policy so self-empolyed transport increases with an annual rate of 20%, further exacerbating the decentralized management.

To change this situation, the relevant administrative departments, industry associations, transportation companies can take the following measures:

1) They should adjust the existing vehicle tax policy, set the high-standard entry to the freight market, encourage the transport enterprises to make mutual acquisition and merger so as to establish a number of large transport conglomerate according to modern enterprise system, encourage self-employed persons to affiliate to large-scale transport enterprises and limit new micro transport enterprises to gradually die a natural death.

2) They should develop society-oriented transportation system, encourage the existing enterprises to outsource self transport so as to form specialized transport market with the result that highway freight industry develops towards the healthy and orderly direction and promote its comprehensive, coordinated, sequent and sustainable development.

4. Strengthening transport vehicles market management and eliminating violating and illegal action in the vehicle production

Transport vehicle production chain management should be strengthened so as to prohibit illegal modification of vehicles and the production of illegal overloaded vehicles. Freight vehicle production management directory should be put in order and straightened and relevant accountability system should be set so as to eliminate "big tons marked with small tons" on the vehicle and resell product certification. Efforts should be made to investigate illegal enterprises. For

the vehicle with "big tons marked with small tons", public security vehicles management department should order them to correct its permitted weight or renew its driving license. Transport departments should press the owner for the payment of its extra load in the stipulation.

Traffic police should also strengthen the source management of vehicle registration so as to check its registration. Once the technical data on driving license are inconsistent with actual technical ones, its registration is not approved. Related departments shall ban vehicles of unauthorized modification and self-employed persons from driving according to law so as to prohibit vehicles of illegal modification from running on the road.

5. Making full use of modern technology to increase the tracking and monitoring of transport vehicles

At present, in China, related departments of traffic management and road administration enforce the law to check on the highway. Because of manual check, there are some disadvantages of high cost, inefficiency, unable to conduct long-term continuous supervision for a whole day and all the time, and it is possible for law enforcement officers to make arbitrary decisions. The supervisory practice for ten years shows that the supervisors can't effectively administer overload and out-of-gauge but cause a variety of arbitrary fines with the result that the phenomena of the overload and out-of-gauge on the highway intensify.

To effectively solve this problem, it is necessary to make use of modern technology to build a modern, all-the-time highway monitoring system. The system includes the following features: Firstly, vehicle identification system shall be established. The information interaction through the system can be achieved. If necessary, vehicle information, goods information and owner information will be automatically transmitted to the monitoring station of transportation management department.

Secondly, the supervision system of road transport management departments shall be established including automatic weighing system in the charge station and all-levels controlling centers connected through network. Through such modern technology as the Internet, Internet of Things and GPS systems, transport vehicle can be connected with the supervisory system of transport management departments so as to form the highway supervision system automatically through computers to handle the vehicle information. Through the system, the related departments can conduct all-sections, all-weather and all-time real-time supervision for transport vehicles.

In short, the governance of overload and out-of-gauge transport is a long and arduous task. In the process of governance, if we can introduce the practice from mature markets, use new science and technology and innovate management patterns with the collaboration and perseverance of different departments, we can guarantee the smooth flow of the vehicles on the highway in good condition so as to promote the healthy and rapid development of the economy.

Acknowledgement

In this paper, the research was sponsored by 2012 Year University Philosophy Social Science Foundation of The Education Department in Jiangsu Province (Project No. 2012SJD630027).

References

[1] Jiang Zai-wen. Governance Mechanisms and Countermeasures of Overload and Out-of-Gauge Transport on the Highway[D]. Xi'an: Chang'an University, 2010:61

[2] Wang Zhenqing. Introduction to Out-of-Gauge Transport on the Highway [M]. Beijing: China Communications Press, 1997:112-114.

[3] Zhou bing, Wei Wen-ke. Systematic Reason and Governance of Overload on the Highway [J]. Journal of Shandong University (Philosophy and Social Sciences), 2013(1):146-147.

[4] Li Zhong-kui. Market and System Analysis of Freight Industry [M]. Beijing: Economic Science Press, 2009:43-44

[5] Guo Wei. Analysis and Solutions to Overload and Out-of-Gauge in Hei Longjiang Province [J]. Communications Science and Technology Heilongjiang， 2011（8）：279-280.

Advanced Materials Research Vols. 989-994 (2014) pp 5128-5131
© (2014) Trans Tech Publications, Switzerland
doi:10.4028/www.scientific.net/AMR.989-994.5128

Governance Mechanism of Rural Population Hollowing under the Background of Balancing Urban and Rural Development

Fan-jin Song[1, a], Dong-qiang Wang [2, b], Shu-qin Tian[3 ,c]

[1]Public Management College, Chongqing University of Arts and Sciences, 402160, Chongqing, China

[2]Public Management College, Chongqing University of Arts and Sciences, 402160, Chongqing, China

[3]Public Management College, Chongqing University of Arts and Sciences, 402160, Chongqing, China

[a]E-mail: ketizu6002@126.com [b]E-mail: cqwdq2011@163.com（Corresponding author）, [b]E-mail:tianshuqin99@126.com

[2,b]（Corresponding author）

Keywords: balancing urban and rural development; rural population hollowing; governance mechanism; development anthropology

Abstract: Under the process of balancing urban and rural development, many villages appeared the phenomenon of rural population hollowing. The number of rural population reduction and demographic imbalance greatly influenced the process of building new socialist village. From the perspective of development anthropology, to solve the problem of rural population hollowing fundamentally, we must reflect the existing ways to governance rural population hollowing and propose the political, economic, social and cultural governance mechanism to governance rural population hollowing under the process of balancing urban and rural development from the perspective of system correction mechanisms and multi-center levels of governance according to the paradigm of urban-rural dual system analysis.

1. Introduction

Under the background of the central attaching importance to three agriculture-based issues, the phenomenon of rural population hollowing is the important difficulty of balancing urban and rural development. About agriculture-based issues, the eighteen reports of the Party point out “the problem of farmers is the priority to other problems, the integration of urban and rural development is the fundamental way to solve three agriculture-based issues" [1]. Balancing urban and rural development and adhering to the new urbanization road of Chinese feature is the inevitable choice and effective way to solve the three agriculture-based issues. Since twenty-first Century, China has entered the stage of rapid urbanization. With the rural population of non-agricultural employment and income increasing, many villages appeared the population hollowing phenomenon, which greatly affects the process of building new socialist countryside. In fact, the problem accumulation and of contradictions intensification under the background the long two structures of urban and rural areas, especially the current rural hollowing problems in China because of some deviation of urban and rural system are far more complicated and more serious than other countries. The sixth national census data show that the Chinese population geographical distribution is undergoing profound changes; the central province of hollowing trend is higher than the eastern and western provinces. Therefore, to solve the three agriculture-based issues fundamentally, we must realize the coordinated development of urban and rural, and reflect on the rural hollowing governance ways and put forwards the following suggestions to realize the rural population hollowing governance.

2. Local Cultural Demand Realization Mechanism

The development of anthropology emphasizes respect for diversity of local culture, respect for history that only a specific area formed the social and cultural knowledge, sustainable development can be achieved in rural areas. Just as Agrawal said: "the local knowledge is independent, has obvious geographical characteristics, in its holder, life, so try to summarize the essence, isolation, archiving, conversion will be a very difficult thing" [2]. In the process of governance in rural population of hollow, we must improve the local cultural appeal mechanism, because it reflects the local requirements, and exists in the local people's life. One is to establish respect for local culture consciousness. In the face of rural urbanization in the process of local culture edge trend, we must reassess the role and status of local culture in the maintenance of natural ecological balance and sustainable development. The second is a flexible mechanism to realize the growth of rural population. For example, in the course of urbanization, poverty area in remote mountainous areas, ethnic minority areas, a large number of rural labor transfer makes the lack of care for elderly population, at the same time, implementation of the family planning policy of rural population, the child will be unable to take good care of the elderly left behind. Therefore, respect for these regions fertility culture growth, fertility policy of rural population local adjusted to "promote a tire, allowing a second child, put an end to the three fetal", so as to solve the rural population and reduce the left behind elderly care problem. The third is to perfect the mechanism of migrant workers returning home for business. In order to realize the migrant workers pining for home feelings, we can encourage migrant workers to return home business, improve migrant workers' entrepreneurship ability of returning home, from the aspects of policy support mechanism, the human capital investment mechanism, three-dimensional training mechanism, resources integration mechanism. Which not only can solve the rural surplus labor employment problem, solve the left behind elderly, rural left-behind children and other issues, to provide the necessary talent support for new rural construction, but also promote the coordinated development of urban and rural areas to the adjustment of rural industrial structure?

3. The Bottom-up Participatory Social Development Mechanism

In the view of developing anthropology, the development of urbanization of rural land resources is not intended to plunder or occupation of the market the vast rural areas, but in order to help people in rural areas get rid of poverty, improving the living standards of rural residents. It therefore, in the course of urbanization, especially in the urban and rural power resources, land resources, human resources and the process of rural urbanization mode, local employment transfer mode and rural community model, must fully consider their own resources of local and traditional culture, advocate the bottom-up participatory social development mechanism.

3.1 The empowerment and participation mechanism

Empowerment is an important theory and anthropological research methods development, rural population hollow governance is to achieve the rural transfer of rights and the transfer through the design of the system and, at the same time by rural residents to participate in power and supervision power, eventually return to and in the service of the rights of rural residents. Empowerment is connected with the concept of community participation in, the real community participation in practice to have at least the following characteristics: with transparent decision-making process; a high proportion of community residents participation rate; high degree of meaningful local participation; fair and effective procedures; high levels of local ownership and management of [3]. Practice has proved that the development of urban and rural development, rural itself must be fully carried out the social mobilization through a bottom-up approach to rural residents to actively participate in. For example, the planning of small towns, the village center planning and community planning, should be vigorously publicity, respect the people's right to know and the right to participate in the mobilization of the rural residents, local participation in regional transportation,

housing, tourism, education, medical and other planning and decision making process, on the basis of fair and reasonable process, widely listen to their ideas and for planning and construction of the attitude, do demonstration and feedback, good constructive ideas reflected in the plan. At the same time in the planning and decision-making and implementation process, to fully absorb the rural residents to participate in, so they have real decision-making power and supervision power, thereby reducing them to the planning of the resentment, correcting and smoothing implementation of the plan.

3.2 Rural hollowing mechanism of multi center governance

Hollowing out of rural population is a complex issue, involving government, enterprise, community residents, multi stakeholder relations, the government cannot do without the various stakeholders in the overall participation. The rural population hollow governance mechanism of multi center has the following four characteristics: management is not a set of rules, is not an event, but a process; the basis of governance process is not controlled, but coordination; governance not only relates to the public sector, or including private sector; governance is not a formal system, but continues interactive [4]. In combination with the specific practice in the process of urbanization of the rural population, hollow governance should start from the relationship between government, enterprises, residents, community organizations and other social organizations, to explore the rural population hollow governance mechanism of multi center, thus the effectiveness of rural population hollow governance to ensure, to improve the overall level of urban and rural economic and social development.

4. Balancing urban and rural political and economic system error correction mechanism

Anthropology of development history so far, has been stressed that human is in the center position in the development, including the development goal is to realize the all-around development of human development, the way to pay more attention to people to participate fully in. Cultural diversity and development practice and advocated to respect area, the opposition in the development of practice and the common people and their cultural marginalization of local. In the course of urbanization, the household registration system reform is an important breakthrough dualistic structure change of urban and rural areas, it is not only a relates to land adjustment, allocation of resources economic problem, but also a political issue involving the identity transformation and social stability. But in the urban and rural practice, we have had the force transfer, jump on the bandwagon, a turn of, copy and many other deviations in the process of the reform of household registration system, the rural population is becoming more and more serious problem of hollow. So learn from the development of theories and methods of anthropology, must carry out rectification to the reform of the household registration system.

4.1 Promote the reform of household registration system

The general office of the State Council in 2012 issued the "Office of the State Council on actively and steadily push forward the reform of household registration system notice" clearly pointed out that some local household registration reform chaos, "in some places, regardless of local economic and social development of the actual situation, the one-sided pursuit of rapid urbanization; in some places is not divided city category regardless of the city's comprehensive carrying capacity, a located in the city of taste to relax the conditions; in some places to break through the national policy, the damage to the vital interests of" [5]. Therefore, the reform of the household registration system must be based on the actual situation around, fully consider the city scale and structure of local public resources, the reasonable measure of the city's comprehensive carrying capacity; fully respect the farmer himself, not a mandatory or compulsory reclaim land and contracted arable land, woodland, grassland; gradual reform of the household registration system, and gradually open the

residence permit system and the relaxation of the settled standard in towns, farmers clear after achieving the right content and sequence.

4.2 Overall the household registration system matching reform measures

Fundamental reform of the household registration system is the need to register on stripping the interests of attachment, the household registration system to return to its social function, so it should be the reform of household registration system orientation transformation of household register management to identity management. At the same time, the household registration system reform measures in the national legislation should be introduced to the household registration law and related legislation as soon as possible, to guarantee citizens' freedom of movement and clear registration transformation procedure, rights, obligations and specific content. The second is to improve the government performance evaluation mechanism to reduce green, the proportion of economic construction in achievement assessment, strengthening social justice, environmental protection, people's livelihood security index. Second is to improve the social security system in urban and rural areas. Increasing the intensity of the central financial transfer payment, the farmers, migrant workers, urban workers and city resident’s social security policy objects into the construction of unified financial payment system, to promote the social security system effective cohesion among regions.

5. Inclusion

According to the core thought and main views of the development of anthropology, the innovation of the rural population hollow governance model can indeed provide feasible path selection to solve the "three rural problems". But to truly realize the coordinated development of urban and rural must be in the perspective of developing anthropology to urban and rural two element analysis paradigm to investigate the rural population hollow governance in the process of urbanization in the political, economic, social and cultural system realization mechanism from system error correction mechanism and multi center governance.

Acknowledgements

The article is sponsored by the annual research project of humanities and social science of ministry of education（number: 13YJA630075）（the head of the project: Song Fan-jin）

References

[1] Hu Jin tao. Firmly march on the path of socialism with Chinese characteristics, and strive to complete the building of a moderately prosperous society in all respects-- Report to the Eighteenth National Congress of the Communist Party of China[Z]. Xinhua news agency reports, 2012-11-08. (In Chinese).

[2] Liu Jin long. Traditional knowledge and its Enlightenment on practice from the view of development anthropology [J]. Journal of China Agricultural University (SOCIAL SCIENCE EDITION), 2007 (02).138. (In Chinese).

[3] Quoted from Chen Gang. Tourism ecology development from the perspective of development anthropology [J]. Guangxi nation studies, 2009 (03).163-171. (In Chinese).

[4]Yue Chun yu. How to understand the theory of global governance in the "governance" [J]. Journal of Hebei Institute of socialism, 2008 (01):85-86. (In Chinese).

[5] Office of the State Council. Notice issued pushing forward the reform of household registration system actively and steadily [EB/OL].,http://www.gov.cn/zwgk/2012-02/23/content_2075082.htm, 2012-2-23.

Advanced Materials Research Vols. 989-994 (2014) pp 5132-5135
© (2014) Trans Tech Publications, Switzerland
doi:10.4028/www.scientific.net/AMR.989-994.5132

The Application of Factor Analysis in the Study on Cultural Industry Competitiveness Evaluation Index System

Sun Ping

Department of Management Tianjin University of Technology, Tianjin, China

wy_sp@126.com

Keywords: competitiveness of cultural industries; ANP; factor analysis; SPSS

Abstract. Based on the premise of an existing condition data, using factor analysis methods to build a cultural industry competitiveness evaluation index system and evaluation model, the corresponding indicators in the model will be evaluated at the final evaluation results. Statistical analysis using SPSS software, score differences in various parts of, analyses the major gaps.

1. Introduction

Cultural industries are accompanied by cultural restructuring and emerging new industries, reform of cultural system began in 2003; The Sate Council has released "Cultural industry revitalization plan" in 2009, rising to promote the development of cultural industry of national strategic level. In recent ten years, Development of China's cultural industries have made great strides, rendering out of healthy, good momentum of vigorous development. Value added of national cultural industries annual average prices rising faster than23% in 2004-2010. Chinese culture and value added of industry corporate units achieve 11052 hundred millions in 2010, GDP share of 2.75%. In 2010 the emerging cultural industry has rapidly development. Strategic emerging cultural industries are growing faster than 50%. Cultural industry has become a pillar industry of local economic development. But at the same time China's cultural industry development level is not high, dynamic strong enough. With increasing spiritual and cultural needs of the people are not fit. And even better adapted to the Socialist market economic system is not.

Competitiveness of cultural industries is a barometer of the development of cultural industries. Cultural industries ' competitiveness has a variety of forms. From the point of view of input-output, its largest gains with minimal investment; from the internal structure of the cultural industries, it expresses for the cultural industries of various rational and effective combination of factors of production. From the spirit of the cultural industry, it provides the public with a growing wealth of cultural products to meet the spiritual needs of the public. In the regional context of increasingly fierce competition, the importance of enhancing the competitiveness has particularly cultural industries. It is crucial that a province has a complete and accurate evaluation of cultural industry competitiveness.

A provincial cultural industry competitiveness situation, depending on the overall environment in the province, is that provincial and municipal productivity development level, various production factors, cultural needs and cultural market development, corporate governance, government policies and the legal situation, cultural traditions of a variety of factors, such as a combination of results. The intention of this article is trying to create a culture of covered carrier, cultural content, cultural, spiritual and cultural value of the comprehensive evaluation index system and the system on the basis of comprehensive analysis of the competitiveness of cultural industries in other provinces, thus contributing to the competitiveness of cultural industries in different provinces can be integrated sorting and evaluation.

2. Construction of index system

2.1 Principles of construction of index system

Establishment of the index system has the following basic principles: focused representation, the system of comprehensive principles, stable principles of comparability, concise scientific principles,

principles of combining quantitative and qualitative indicators, indicators of accessibility principles. In addition, the indicators system should not only describe the combined static and dynamic characterization. Not only has the evaluation function, but should also develop early warning of potential, future role.

2.2 Choose of index system

Based on the above setting principles, we will be integrated system analysis and reasonable factors, presents a comprehensive evaluation index system of three levels (see table 1):

(1) Cultural industry strength, which includes: talent of cultural industry; financial inputs to the culture industry; the attraction of foreign capital.

(2) Cultural values, which includes: per capita GDP; GDP proportion of the tertiary industry; proportion of residents ' cultural consumption.

(3) Carriers of culture, which includes: engine of the tourist industry to the cultural industries; education industry to the cultural industries of engine; engine for cultural industries of the information industry.

(4) Cultural resources and infrastructure, which includes: resource abundance; cultural quality of creative and business talent; corporate management standards in culture; the creative industries.

Table 1. Cultural industry competitiveness evaluation system

objective	standard	target
Cultural industry competitiveness evaluation	Cultural industry strength	talent of cultural industry
		financial inputs to the culture industry
		The attraction of foreign capital.
	Cultural values	per capita GDP
		GDP proportion of the tertiary industry
		proportion of residents ' cultural consumption
	Carriers of culture	engine of the tourist industry to the cultural industries
		education industry to the cultural industries of engine
		engine for cultural industries of the information industry
	Cultural resources and infrastructure	resource abundance
		cultural quality of creative and business talent
		corporate management standards in culture
		the creative industries

This indicator system, industrial-strength, cultural values and cultural carrier of culture, cultural resources and infrastructure and so on, basically includes the impact on the competitiveness of China's cultural industry has a relatively important factor. From a horizontal view, these factors and its indicators covers the main developments in the industrial sector of the cultural industries and production capacity and production of cultural products and services, cultural consumers ' spending power and intentions, cultural level of market development, human resources and research capacities in the industry, industrial raw material for the development of resources and facilities. From the vertical view, these factors also constitute a "manufacturer + carrier + → → cultural products and cultural resources and facilities services culture consumption markets", the complete production and consumption of products and services in the industry.

3.Factor analysis model[1]

Basic idea of the factor analysis is based on the correlation between variables grouped the original size, with dependencies between variables in a group higher, but lower variable correlation between the different groups. Factor analysis model as follows:

(1) $X=(X_1,X_2,....,X_p)$ is the observed random vector, and its expect vector is 0, covariance and correlation matrices are equal.

(2) $F=(F_1,F_2,....,F_m)$ (m< p) is an observation vector, and its expect vector is 0, covariance Cov (f) =I, that is, the components of a vector are independent of each other.

(3) $\varepsilon=(\varepsilon_1,\varepsilon_2,....,\varepsilon_p)$ and F are independent of each other; and its expect vector is 0. Covariance matrix is a diagonal matrix, that is, between the components are independent of each other, so model:

$$\begin{cases} x_1=a_{11}f_1+a_{12}f_2+a_{13}f_3+...+a_{1k}f_k+\varepsilon_1 \\ x_2=a_{21}f_1+a_{22}f_2+a_{23}f_3+...+a_{2k}f_k+\varepsilon_2 \\ x_3=a_{31}f_1+a_{32}f_2+a_{33}f_3+...+a_{3k}f_k+\varepsilon_3 \\ ..... \\ x_p=a_{p1}f_1+a_{p2}f_2+a_{p3}f_3+...+a_{pk}f_k+\varepsilon_p \end{cases} \quad (1)$$

Because the models are for the variables, various factors are orthogonal, therefore, also known as r-type orthogonal factor model, Its matrix form as: X = AF+ε。 F is called the public factor of X, the matrix A is called the factor load matrix, the factor load a_{ij} is the correlation coefficient of the i variable and j factor, it is reflected the importance of the I variable on the J factor. There are two statistics is very important in the factor load matrix A, is Variable common variance and common factors contribution; ε is called the special factor of X. The larger of the element absolute of a_{ij} in matrix A, the more of X_i and F_j dependent. it is one of the purposes of the factor analysis that to find the value of each factor loading. If the all a_{ij} (j = 1, 2,…., m)of factor loading matrix A is calculated , sorting according to size, it can be extracted from the most influential public factor。When the factor analysis model is established, an important role is the application of factors analysis model to evaluate each sample position in the model as a whole, that a comprehensive evaluation.

4.Evaluate consequence analysis

This paper empirical analysis of Beijing, Shanghai, Tianjin, Nanjing, Dalian and other, all quantitative indicators from the 2011 Statistical Yearbook and the Government Statistical Web site exposed data, qualitative indicators for listening to the views of relevant experts, in accordance with the Delphi technique eventually formed. The analysis results on factor analysis model.

(1) In the SPSS software runs on data, came to the correlation matrix. Select using principal component analysis and extraction of common factors. The first three factors explained variance total variances of more than 93%, while the former two factors would explain the two, essentially full response of many indicators information.

(2)Maximum orthogonal rotation method has been used variance factor rotation, after orthogonal rotation, the Comparability of indicators variables (common) did not change, but the common variance contribution factor is no longer the same as original, marked reduction in contribution of factor 1 and factor 2 contributions increased significantly. Bartlett estimates worked out a sample of the comprehensive index score, factor scores and ranking of cities as shown in table 2.

Table 2 The factor scores and rankings of Bartlett Estimation

City	F_1	ranking	F_2	ranking	scores	ranking
Tianjin	- 0.223	3	-0.48	4	- 0.0491	4
Beijing	0.853	2	1.22	1	0.928	2
Shanghai	0.977	1	1.15	2	0.931	1
Nanjing	- 0.479	4	0.101	3	0.067	3
Dalian	- 0.827	5	- 0.742	5	- 0.786	5

The analysis conclusion Comparative of Factor Analysis is almost identical. The competitiveness of urban cultural industry development level of overall branch 3 tier: first echelon represented by Shanghai, Beijing, Tianjin, Nanjing, as the representative of the second Echelon, to Dalian as the representative of the third Echelon. Due to the strength in the index system and indicators per capita, thus the comparability between provinces and cities. Judging from the results, in Shanghai to a higher value in the first place, visible in recent years in Shanghai, along with the economic development of the cultural industry is continuing to grow. Economically more developed and people's living standards higher areas on the development of cultural industries, also have some advantages. Dalian with strength and per capita indicators of good performance overcomes the lack of total followed suit.

5. Conclusion

Studies on the basis of this article at home and abroad, scientifically selected representative cross section of 5 targets, the establishment of a comprehensive evaluation index system for regional competitiveness of cultural industries, innovation is the establishment of an independent evaluation system, analysis of the model of factor analysis method.

Due to limitations in time and article space, only 5 cities were selected based on this article, selection of indicator system should be further improved. Further, we can also through the analysis of time series data to study areas where credit conditions change over time. In addition, during factor analysis, orthogonal rotation method for maximum variance (Varimax), the factor score regression estimation method using “Bartlett” estimate of the consequences of this law and “Thomson” estimate method is slightly different, could have some impact on results. Causes also need further analysis.

Acknowledgements

This work is supported by Tianjin art scientific research planning project “Cultural products comprehensive index system research”(C12034).

References

[1] He X.Q, Multielement Statistics Analyse [M]. China Renmin University Press, Beijing，2004 .

[2] Sun P. The study of the evaluation index of cultural product’s Business value based on cloud model[J]Commercial Times. 2014(11):14-15

[3] P.Sun. The application of cloud model in teaching quality monitoring and evaluation, Applied Mechanics and Materials, Vol.519-520,Part2 p.1686-1689.

[4] Song Jian. The Empirical Study on Establishing Regional Credit Evaluation System based on AHP & Factor Analysis[J] China Soft Science 2006(6):111-119

[5] Zhao Y.Y. Evaluation and analysis of competitiveness of China's cultural industry[J] Journal of Renmin University 2006(4):72-82

Advanced Materials Research Vols. 989-994 (2014) pp 5136-5139
© (2014) Trans Tech Publications, Switzerland
doi:10.4028/www.scientific.net/AMR.989-994.5136

Research on rapid bidding of forgings

Gu Feng

School of Mechanical Engineering, Nantong Vocational University, Nantong, China

465819860@qq.com

Keywords: forging enterprise, rapid bidding, Activity-Based Costing (ABC), cost composition, enterprise business process

Abstract. Forging, as a traditional machining, plays an important role in Chinese economics construction and equipment production. It is essential to enhance the level of management for forging enterprises. This study aims to reveal the cost composition of forgings and the law of bidding, and thereby make an integrated and intelligent bidding for forgings with reduction of bidding the difficulty and improvements of accuracy. Activity-based costing bidding for forging is studied in depth after analysis of forgings cost composition and enterprise business process. The research promotes the integration and intelligence of forging bidding as well as the accuracy and reasonableness.

Introduction

Forging, as a traditional machining, plays an important role in Chinese economics construction and equipment production. Forging production provides the necessary parts for industries of automotive, agricultural machinery, iron and steel smelting and so on [1]. The importance of forging industry to national equipment manufacturing industry is self-evident. Thus, it is essential to enhance the level of management for forging enterprises [2]. However, with the development and expansion of the forging industry, some problems forging enterprises facing also slowly emerged: increased competition and diversities of customer requirements for forging quality as well as delivery and after-sales service [3].

Bidding is an important link between forging enterprise and customers. Also, it is critical for customers to make supplier selection decision and for forging enterprise to make order acceptance decision. The price of forgings is essential for the survival of forging enterprises. With the increased competition due to the open market, customers are increasingly sensitive to the price of forgings. Empirical bidding by sales staff and managers in the past cannot satisfy market competition and customer needs because of slow response, imprecise bidding and other factors in actual business [4].

This study aims to reveal the cost composition of forgings and the law of bidding, and thereby make an integrated and intelligent bidding for forgings with reduction of bidding the difficulty and improvements of accuracy.

Principle of cost accounting based on ABC

Activity costs are generally composed of direct material cost, direct labor cost and manufacturing cost. The first two can be directly obtained by statistics of finance department, and manufacturing cost is required for detailed decomposition and calculated by multiplying each activity cost ratio and the number of activity costs. As for forging enterprise, direct material costs include forging materials and packaging materials, and direct labor costs are denoted by employee benefits. Manufacturing costs need to conduct a detailed investigation of each project to analyze each activity as well as corresponding cost ratio. The price based on ABC can be calculated as [5]:

$$P = \sum_{i=1}^{19} (\alpha i \times \beta i) + \lambda + \gamma \tag{1}$$

P : Bidding price; αi : The number of activity drivers; βi : Activity cost ratio;

λ : Direct material costs; γ : Direct labor costs.

Production cost accounting based on ABC

(1) Manufacturing costs calculation

Items of manufacturing cost and cost drivers are listed in the first two rows of Table 1. After investigations and analysis of forging enterprise, it can be concluded:

1) Products are generally produced and delivered in batches according to customer requirements, so the number of production planning times is the same as of delivery.

2) The number of process analysis times is the same as the number of product types.

3) When process planning, work hour is given directly by the craft.

4) Heat treatment times are determined directly by production department.

5) Free forging products are inspected one by one, so inspection times equal to the number of production as well as cutting and packaging.

6) Equivalent procurement weight is calculated as weight of the blank sourcing.

7) Storage amounts are considered as 10% of WIP (work in product).

8) Since forgings are distributed by forklifts with usually one forging once, so delivery times consistent with the number of productions.

9) Times of after-sales service are considered as 2% of monthly production capacity.

After statistics, the details of activity drivers within a month for A and B, two types of forgings, are as shown in the 3rd and 4th row of Table 1.

Table 1 Items of manufacturing cost and cost drivers

Activity	Cost driver	A	B
Inquiry activity	Number of product types	1	1
Process analysis	Times of analysis	1	1
Delivery assessment	Number of product types	1	1
Production planning	Times of production planning	2	4
Purchasing	Weights of procurement	2820	20000
Cutting	Times of production planning	15	250
Stacking	Numbers of products	15	250
Forging and machining	Work hour	40	120
Heat treatment	Times of heat treatment	3	10
Quality control	Times of quality inspection	15	250
Package	Numberso f packaged products	15	250
Delivery	Times of delivery	2	4
Storge	Storage amounts	1.5	25
Distribution	Times of distribution	15	250
Order	Order times	1	1
After-sales service	Times of after-sales service	0.3	5
Equipment depreciation management	Work hour	76	156
Plants depreciation management	Numbers of products	15	250
Fuel and water consumption	Numbers of products	15	250

According to ABC approach and production costs statistics over a period of time, actual activity costs ratio of each cost drivers can be obtained as shown in the first three rows of Table 2. Furthermore, according to the above analysis, details of activity cost of A&B are listed in row 4th and 5th of Table 2.

(2) Direct material cost calculation

Direct material cost is the amount spent on purchases of rough forging. According to the product of each blank price (RMB / kg), weight (kg) and the yield of production, it can be obtained:

Direct material costs of A = 8.5 × 190 × 15 = 24225 RMB.

Direct material costs of B = 8.5 × 80 × 250 = 170000 RMB.

(3) Direct labor costs calculation

Total labor costs of A and B can be obtained by monthly statistics from financial department, which will be shared by A and B respectively according to the ratio of processing time they occupied. For certain month, total labor cost 12480 RMB. Then,

direct labor costs of A are: 12480 × [76 ÷ (76 +156)] = 4088 RMB
and direct labor costs of B are: 12480 × [156 ÷ (76 +156)] = 8392 RMB
After the above calculations, the details of costs for A and B are obtained as listed in Table 3.

Table 2 Activity cost of A & B

Activity	Cost driver	Cost ratio /RMB	Number of driver	
Inquiry activity	Number of product types	100	A	B
Process analysis	Times of analysis	300	1	1
Delivery assessment	Number of product types	100	1	1
Production planning	Times of production planning	200	1	1
Purchasing	Weights of procurement	0.1	2	4
Cutting	Times of production planning	3	2820	20000
Stacking	Numbers of products	1	15	250
Forging and machining	Work hour	32	15	250
Heat treatment	Times of heat treatment	330	40	120
Quality control	Times of quality inspection	20	3	10
Package	Numberso f packaged products	3	15	250
Delivery	Times of delivery	200	15	250
Storge	Storage amounts	200	2	4
Distribution	Times of distribution	20	1.5	25
Order	Order times	200	15	250
After-sales service	Times of after-sales service	500	1	1
Equipment depreciation management	Work hour	8	0.3	5
Plants depreciation management	Numbers of products	10	76	156
Fuel and water consumption	Numbers of products	20	15	250

Table 3 Cost details of A & B

Products		A	B
direct material	forgings	24225	170000
	packaging	75	750
direct labor		4088	8392
Inquiry activity		100	100
Process analysis		300	300
Delivery assessment		100	100
Production planning		400	800
Purchasing		282	2000
Cutting		45	750
Stacking		15	250
Forging and machining		1280	3840
Heat treatment		990	3300
Quality control		300	5000
Package		45	750
Delivery		400	800
Storge		300	5000
Distribution		300	5000
Order		200	200
After-sales service		150	2500
Equipment depreciation management		608	1248
Plants depreciation management		150	2500
Fuel and water consumption		300	5000
Total		34653	218580

Determination of margin

Under ever-changing market, customer needs tend to be dynamically diverse. Therefore, pricing decisions need to consider a variety of factors. In addition to production costs discussed in the

previous section, delivery capability, ease of forgings, game between business and markets as well as business and customers, etc. are also included.

(1) Delivery

In such a high degree of information technology today, rapid response is an important indicator to evaluate enterprise capabilities. Faster response of business to market and to customers, can account for the initiative in the competition. So delivery has become a major factor affecting bidding. Customer's demand for shorter delivery time will result in more profits of enterprises.

(2) Difficulty machining facing for forgings

For forging enterprises, machining difficulty often depends on the geometrical characteristics of the product as well as internal quality characteristics needs. Facing complex shape (which means higher forging process capability) and higher heat treatment technology demand from customers, highly profitable pricing strategy can be developed.

(3) Market competition

Market competition is also an important factor to consider for product pricing. Whether competitions are intense or not, depends on the threshold of the industry, the number of enterprises in the industry as well as the balance degree of enterprises' capacity in the industry [6]. Overall, more competitive, smaller profits. Conversely, enterprises receive more profits.

Combined with the calculated production cost previously, the final bidding price based on cost-plus pricing method can be obtained. Cost-plus is by far one of the most widely bidding method. According to the above study, final pricing can be decided as follows:

$$P = p_1 \bullet (1+\delta) \tag{2}$$

P - Final bidding price; p_1 - Production costs; δ - Margin

Conclusions

According to the current enterprise's production capacity and market share, expected profit is decided between 5-18%. Those orders from non-VIP cooperative enterprises or profit less than 5% will not be accepted by forging enterprise. Thus, according to experiences from experts and marketing managers, profit margin is set as8%.

Bidding price of A = 34653 × (1 +8%) = 37425.24 RMB.

Bidding price of B = 218580 × (1 +8%) = 236066.4 RMB.

This study focuses on the quick bidding for a forging enterprise combined with ABC and cost-plus method. The presented research can help to reduce the forging cost of forgings, to improve the competitiveness of forging enterprise, and to enhance the management of forging enterprise.

References

[1] Santangelo A., Blanke P., Hadifi T., Wolter F. E., and Behrens, B. A: Production Engineering Vol. 7(2013), p. 409.

[2] LIU L, ZUO X, and TONG Y: Forging & Stamping Technology Vol. 6(2010), p.46.

[3] Liu G Z.: Applied Mechanics and Materials Vol.521 (2014), p.476.

[4] Fayard D., Lee L. S., Leitch R. A., and Kettinger W. J.: Accounting, Organizations and Society Vol. 37(2012), p.168.

[5] Liu Yan Hong, and Shu Lin Gong: Applied Mechanics and Materials Vol. 120 (2012) , p.432.

[6] Damanpour F.: British Journal of Management Vol.21(2010), p.996.

Advanced Materials Research Vols. 989-994 (2014) pp 5140-5143
© (2014) Trans Tech Publications, Switzerland
doi:10.4028/www.scientific.net/AMR.989-994.5140

Study on Evaluation Index System and Methods of Vendor Selection

Congjun Rao[1,2], Jinhui Dong[1]

[1] College of Mathematics and Computer Science, Huanggang Normal University, Huanggang 438000, China

[2] Institute of Systems Engineering, Huazhong University of Science and Technology, Wuhan 430074, P. R. China

cjrao@163.com

Keywords: Vendor selection; Evaluation index system; Supply chain management; multi-objective decision

Abstract. The quality of the vendor effects on the market competitiveness of enterprises and the whole supply chain, and the vendor selection decision is the key to supply chain management. Focusing on the problem of selecting vendors, this paper introduces the research history and the newest research trends of the design of index system of vendor evaluation and the methods of vendor selection, and presents many widespread theoretical and applications problems. Moreover, assumptions, main ideas, and conclusions of literature related to vendor selection are reviewed and commented.

Introduction

In supply chain management, vendors are the manufacturing center, service quality assurance center and cost control center of the supply chain. Vendor selection has always been considered a key one within purchasing and supply management [1]. Indeed, some considerit to be the most important of all the responsibilities of thefunction, as the choice of vendor has a significant impact on the optimisation of the quality, quantity, timeliness and price of purchased goods and services [2]. Furthermore, vendors have a direct and significant impact on the quality, cost and lead time of new products and technologies needed to meet new market demands. In short, the vendor is the foundation of supply chain operation, and is the key to gain the core competitiveness of the supply chain for the enterprises [3].

With the growing scale of the supply chain, the structure of supply chain is becoming more complicated, which brings more and more supply chain risks [3-4]. Therefore, in the risk management of supply chain, in order to share the supply chain information for all members, improve the response rate and overall flexibility of the supply chain, and enhance the competitiveness of supply chain, we must make prediction, evaluation, control and decision-making for various possible potential risks in internal and external supply chain. In particular, the evaluation and selection of vendors is the foundation and the key in supply chain management, and is the emphasis in risk control of supply chain. Through scientific vendor evaluation and selection, we can effectively reduce supply chain operational risks and improve continued appreciation ability, and provide strong support to establish a strategic partnership among enterprises. However, selection is complicated by the fact that different potential vendors may have different performance characteristics for different attributes. Therefore, vendor selection is an inherently multi-objective decision, which seeks to minimise some evaluation criteria whilst and, at the same time, maximising others. It might be expected that purchasing and supply managers would look to use quantitative methods to help inform their decision-making. However, until recently quantita-tive methods have typically been found to be inadequate and limited [1].

Scholars have focused on two hot issues about the vendor evaluation and selection, i.e., the design of index system of vendor evaluation, and study on methods and models of vendor selection. In the following sections, we present the widespread theoretical and applications problems for the study on the design of index system of vendor evaluation and the methods of vendor selection, in order to

introduce the research history and the newest research trends of vendor selection in the supply chain management.

The Design of Index System of Vendor Evaluation

For the study of vendor evaluation index system, Dickson is one pioneer research scholar. His study was based on a questioneer sent to 273 purchasing agents and managers selected from the membership list of the National Association of Purchasing Managers, and then he proposed 23 criteria as the evaluation indexes for vendor selection[5]. In 1990, another pioneer research scholar Weber reviewed 74 related articles published since Dickson (1966) in order to provide a comprehensive view of the criteria that academicians and practitioners have found to be important in vendor selection. Specific attention is given to the criteria and analytical methods used in vendor selection process [6].

Following these two pioneer research scholars, Dickson and Weber, many scholars have joined the ranks of research on index system of vendor evaluation. The representative outcomes are as follows. Wilson [7] examined the relative importance of supplier selection criteria longitudinally by reviewing the findings of studies published during the past two decades. Those results are then compared with the findings of this study to gain insight about the relative importances of decision criteria used by purchasing professionals in selecting suppliers. Choy and Lee [8] presented an intelligent generic supplier management tool (GSMT) using the case-based reasoning (CBR) technique for outsourcing to suppliers and automating the decision making process when selecting them. The development of GSMT and how the CBR technique is applied is then given, followed by an application of GSMT in Honeywell Consumer Products (Hong Kong) Limited, and 13 evaluation attributes are given to select manufacturing outsourcing vendors. Willis and Huston et al [9] was to aid just-in-time (JIT) manufacturers in selecting the most appropriate suppliers and in evaluating supplier performance, and presented neural network based supplier selection and supplier performance evaluation systems.The proposed neural network based systems are tested with data taken from an automotive factory, and the results show that the proposed systems can be used effectively.

Later, Patton [10] proposed a similar index system of vendor evaluation with Willis. And then Yahya and Kingsman [11] and proposed a similar evaluation system with the literature Patton and Willis by investigating many experienced business managers and executives. But the difference with Patton and Willis is that they further gave the weights of all attributes by using the method of AHP. Petroni and Bragha [12] used the method of Principal Component Analysis to construct a index system of vendor evaluation from the point of supply chain. The composition of his index system is similar to the index system in [10], but they deleted the attributes of the sales support and financial condition, and added the attribute of management capacity. Menon and MoGini [13] studied the vendor selection of the third-party logistics services, and used empirical research methods to prove the effectiveness of the index system for the vendor selection and evaluation of the third-party logistics service.

Recently, Shemshadi et al. [14] treated supplier selection as a group multiple criteria decision making (GMCDM) problem by considering the evaluation index system including the products quality, effort to establish cooperation, vendor's technical level, vendor's delay on delivery and price/cost, and obtained decision makers' opinions in the form of linguistic terms. Then, these linguistic terms are converted to trapezoidal fuzzy numbers. Similarly, Chen and Wu [15] proposed a modified failure mode and effects analysis (MFMEA) method to select new suppliers from the supply chain risk's perspective and applies the analytic hierarchy process (AHP) method to determine the weight of each criterion and sub-criterion for supplier selection such as cost, quality, deliverability, technology, productivity, service, and so on. Especially, they showed that in the emerging supply chain environment, supply chain risk management plays a more important role than ever, so the companies must focus not only on the efficiency of supply chain, but also on its risks. That is to say,

when design the vendor evaluation index system, we needs to consider not only the commercial factors such as quality, price and delivery time, but also the risk factors in a supply chain.

Methods and Models of Vendor Selection

On the methods and models of vendor evaluation, many scholars proposed a number of different evaluation methods and models. To sum up, it is mainly divided into three categories. The first one is the qualitative selection methods [3], for example, the judgment method based on direct experience, the consultations choice method, and so on. The qualitative selection methods are simple and practicable, but they are too subjective and lack of science and rationality, and the most make choices based on experience or some certainty attributes. Therefore, the qualitative methods are gradually replaced by the second method, i.e., quantitative selection methods. Many scholars studied the quantitative selection methods, for example, the benefit-cost analysis method propoed by Federgruen et al. and Hammami et al. , new normalized goal programming model given by Jadidi et al., locally linear neuro-fuzzy model established by Vahdani et al., fuzzy integral-based model established by Liou et al., believable rough set approach presented by Chai et al., integrated data envelopment analysis model established by Toloo et al., Green DEA given by Kumar et al., multi-objective integer linear programming model established by Choudhary et al., two-level Genetic algorithm presented by Aliabadi et al., and so on. The quantitative selection methods have more obvious advantages than the qualitative selection methods, and can solve specific problems under the deterministic environment, but the quantitative selection methods are generally based on deterministic evaluation attributes, and are difficult to quantify some qualitative attributes, and then unable to meet all requirements of processing uncertain information in supply chain environment.

The last one is the combination of quantitative and qualitative methods. For example, Deng et al. proposed a D-AHP method is for the supplier selection problem, which extends the classical analytic hierarchy process (AHP); Shawa et al. used fuzzy AHP and fuzzy multi-objective linear programming in supplier selection for developing low carbon supply chain; Liao et al. presented an integrated fuzzy TOPSIS and MCGP approach to supplier selection in supply chain management; a weighted max–min fuzzy model is developed to handle effectively the vagueness of input data and different weights of criteria in this problem. To handle the subjectivity of decision makers' assessments, a new ranking method on the basis of fuzzy inference system (FIS) is proposed for supplier selection problem. Moreover, a new approach based on Adaptive Neuro-Fuzzy Inference System (ANFIS) is presented to overcome the supplier selection problem. And an integrated approach including fuzzy Technique for Order Preference by Similarity to Ideal Solution (TOPSIS) and a mixed integer linear programming model is developed to select the best supplier in a multi-item/multi-supplier environment. The combination of quantitative and qualitative methods can solve more problems by more scientific and rational way. But how to deal with the uncertainty under the complex and changeable situation in the vendor selection process is further valuable study direction.

Reviews and Perspectives

From the above literature review, we can see that the study of vendor evaluation and selection has been a hot research direction of supply chain management, and the recent research has the following characteristics. Firstly, the evaluation attributes and index system gradually become systematic, diverse and comprehensive. The original single evaluation which only considers the production factors such as quality, price and cost is gradually replaced by the comprehensive evaluation by considering many aspects such as production, service, cooperation, and environmental. So the evaluation index system is more comprehensive, and the evaluation results are more scientific. Secondly, the evaluation methods and models tended to more and more reasonable from the original mainly qualitative judgment, gradually to develop in the direction of the combination of qualitative and quantitative methods. On model applications, it is from using a single model to evaluate, gradually to develop in the direction of the combination evaluation with multiple models. Thirdly, the

evaluation object gradually refined from the original general studies to steer specific industries and specific vendor evaluation. And some studies have proposed different evaluation index systems for different industries and vendors.

However, there are also some disadvantages for existing studies. Firstly, no clear evaluation measurement standards are given for some evaluation attributes. And these attribute data are rarely combined with enterprise's actual demand, so it is difficult to apply in practice. Secondly, the weight determination of evaluation attribute and the evaluation results are over-dependent on mathematical models, so the limitations of the model itself may affect on the accuracy of the evaluation results. Thirdly, in the vendor evaluation, most of the literature does not consider the risk factors in the supply chain environment. Even a few literatures studied on the vendor selection problem in risk management of supply chain, but most still remain in the qualitative analysis. They did not really quantify the risk factors and not consider the quantified risk in the overall level of vendor evaluation. Fourthly, for the quantitative evaluation of vendors in many literatures, the evaluation attributes values are generally given by accurate values.

But in the practical data statistics, due to the complexity of the decision-making system and decision-making environment, and the ambiguity of the human mind, many attribute values are difficult to count by using the accurate numbers such as the reputation of vendors, vendor service level, etc. The evaluation results of these qualitative attributes are given often only in the form of linguistic fuzzy variable (such as better, good, bad or very high, high, low). Also, for instance, in the evaluation of technology risk and management risk for the vendors, the results of risk evaluation are generally given by high risk, low risk, and so on. For the problem of vendor evaluation and selection under mixed data information environment (the real numbers and linguistic fuzzy variable are coexisting), there are few literatures discussed. In addition, the existing procurement mechanisms and evaluation index system are proposed mostly by considering a unique good or multiple indivisible goods. The research on a kind of divisible goods with the characteristic of homogeneousness and continuity is few.

Acknowledgments

This work is supported by the 2014 Key Project of Hubei Provincial Department of Education (No. D20142903).

References

[1] X. Luo and C. Wu: Journal of Purchasing & Supply Management Vol. 15 (2009), p. 249-262.
[2] E. Adida and V. DeMiguel: Operations Research Vol. 59 (2011), p. 156-172.
[3] S.H. Ma and Y. Lin: Supply Chain Management (China Machine Press, Beijing, 2000).
[4] A. Federgruen and N. Yang: Operations Research Vol. 56 (2008), p. 916-936.
[5] G. Dickson: Journal of Purchasing Vol. 2 (1966), p. 5-17.
[6] C.A. Weber: European Journal of Operational Research Vol. 50 (1991), p. 2-18.
[7] E. Wilson: International Journal of Purchasing & Materials Management Vol. 25 (2006), p.35-41.
[8] K.L. Choy and W.B. Lee: The Journal of Supply Chain Management Vol. 8 (2003), p. 140-154.
[9] T. H. Willis and R. Huston: Production and inventory management Journal Vol. 34 (2005), l-5.
[10] W.E. Patton: Industrial Marketing Management Vol. 25 (2008), p. 135-149.
[11] S. Yahya and B. Kingsman: Journal of Operational Research Society Vol. 50 (2009), p. 916-930.
[12] A. Petroni and M. Braglia: The Journal of Supply Chain Management Vol. 36 (2010), p. 63-69.
[13] M. K. Menon and M. A. McGinnis: Journal of Business Logistics Vol. 19 (2008), p. 121-137.
[14] A. Shemshadi and H. Shirazi: Expert Systems with Applications Vol. 38 (2011), p. 12160-12167.
[15] P. S. Chen and M.T. Wu: Computers & Industrial Engineering Vol. 66 (2013), 634-642.

Advanced Materials Research Vols. 989-994 (2014) pp 5144-5147
© (2014) Trans Tech Publications, Switzerland
doi:10.4028/www.scientific.net/AMR.989-994.5144

Analyze the combination of national symbols and design aesthetics

Yingyan Chen

School of Arts and Communications ,

Wuhan Polytechnic University, Wuhan, Hubei, 430023, China
252687081@qq.com

Keywords: National symbol; Design aesthetic; Visual form; Change.

Abstract. Current product forms are quietly changing. Duc to the change of consumer personal aesthetic needs, thus causing products need more "non-necessary" functions. Through renovating design concepts by consumer demands, to promote contemporary design pay more attention to the content of visual aesthetics and spiritual cultures. Therefore, contemporary design methods must cater to era development trend, in order to strengthen consumers' experience and emotion recognition for products. In view of this situation, this article from the perspective of national symbolic languages and aesthetic forms to study design methods and innovation concepts, and draw a conclusion.

The situation of contemporary design

China modern design originated from the reform and opening up. Along with the improvement of materials and living standards, Chinese visions and aesthetic also followed developments. Therefore, In this situation, the change of thoughts made contemporary design trend toward User-friendly design.Combining sense and sensibility to meet the functional and aesthetic needs. By product forms, to reflect the organic unity of their internal functions and external visions. Foreign design develop earlier than China. They pay more attention to the design of enterprise culture. And they are to guarantee the basic function of products, but also concern into the products through design culture, which reflects the national languages and aesthetic values.

In the tide of global economic integration, the competitiveness of enterprises are particularly prominent,which reflects in the design is not only the considerations of technical measures, but also the cultural competition.Therefore, some enterprises lack competitiveness in China, in addition to technical reasons, also lack of obvious corporate cultures. Fortunately, there are some enterprises do relatively far sighted, they invite professional design companies to develop the culture of products, or by supporting design competitions, to launch more groups for design service,The benefits of this is to deeper in the inherent culture of products through public power，which makes enterprise to obtain the good development space.

The nationalization of design forms

A kind of cultural form reflected in the product is the reproduction of cultural symbols. Human have been experienced thousands of years of practical activities, dissemination and development of all human civilization have to rely on culture to achieve. The application of cultural symbols is based on nation's cultural systems. Through refining and summarizing the form of nation culture symbols, to have the intrinsic extension in the contemporary design,whichshows a combination of cultural accumulation and technological prowess.

To implement the design form of nationalization, it must reflect ethnic characteristics and style, it has to rely on religious customs, art, genetic characteristics, and other cultural contents. Due to different cultural backgrounds, different districts and nations must have differences in customs, beliefs, hobbies, taboos, color and values, etc. There is such a word to describe the cultural differences of products: Japanese car is a tool, and German car is a machine, while the United Kingdom is art. It shows a national culture form completely reflected by products.Germans is famous for rigorous practical, its products style is simple, precise and machine, which is an objective reflection of national culture; In United Kingdom, its style exudes an elegant and sophisticated,

long-term. It originated from the British people are keen on adhering to traditional culture art. They pay attention to the protection and inheritance of technology and pursuit of perfect quality,which refracts the British national characteristics; Look at Japanese products, Japan is good at learning foreign advanced technology and combining them with national culture, and emphasizing the primacy of practical principles. Their products have a strong sense of national identity and contemporary styles.

Also the other design powers have their own national characteristics,such as Italian design, its products are extremely concise colors and assertive personality, which shows strong Italian style; French design style is often luxury and avant-garde, lead the trend of fashion development. While the five Nordic countries advocate a simple and plain life view , their Scandinavia design styles show the flexible functionalism. It makes national internal spirit and concept into modern design,this is the inevitable result of design nationalization.

In visual forms, a country or nation should combine indigenous aesthetics with modern design style to form an independent design system, which is the development trend of current design.Modern design tends to agree with the national cultures which may derive inspiration from symbols and graphics.Exploring the connotation of national cultures, to find a intersection of national culture and design object, this is the realization of design nationalization.

Famous designer Alan Chan，who is a typical representative of Hong Kong,China. He is good at expressing Oriental culture concept by western design forms, achieve mastery through a comprehensive study. Based on the understanding of national cultures, to borrow western design concept and technique of expression into national languages. It need to achieve a profound understanding and dialectic relationships between cultures.These excellent national cultures are in an open and inclusive environment,which neither blind anti-foreignism, inherits constantly,nor worship foreign countries curries favor with foreign powers.They need to be inherited and innovation, and assimilate the best of foreign culturals into their own national languages. The ultimate goal is to achieve national design, enable national design to have more formidable power and space for development,(as shown in Fig 1).

Fig.1 CocaCola logo in both English

The aesthetic values of national design

National symbols are the legacy of cultural properties after changings of the times, which can express and refer to national cultures' connotations, features, spirits .They have two aspects of value Performances: From intrinsic says, national symbols originated in the life, which contain a wealth emotional life and living state.And nation's spiritual values concentrated in the symbol, have a profound foundation of the people; externally,some outstanding national symbols reflect human universals,and contain the cognitive basis of human.In other words, it is a universal visual language with no national boundaries, any country or nation can through symbols to feel the power of spiritual culture, form a common and shared ideological realm, become a communication link of human consciousness.

Based on the national symbols, to implement design nationalization is actually to grasp national culture symbols, by simplifying language forms to show national emotions, become a window of understanding national customs and aesthetic psychologies. In terms of product culture, we see the external aesthetic forms of products are always the extension of national sentiments, such as German automotive and industrial products which give person a mechanization and solemn feeling, this is the embodiment of national character and express an aesthetic orientation of the German nation. Its products make a profound impression to person. I'm afraid this's the reason of national aesthetic

diversities. Excellent technology makes the public form an awareness of German design through external appearances, which just fill in the blank of other national aesthetics. Therefore, the aesthetic values and spiritual concepts of products can be conveyed through their external images.

China national culture emphasizs “a bad compromise is better than a good lawsuit”. In fact it is a middle course that pursuits natural, humble and suitable styles, while pursuing the spiritual realm of self-reliance. This kind of life aesthetics has positive enlightenment significance to society. In modern materialistic era, people face more and more temptations. If make oriental life aesthetics into design language, it can communicate correct value guidances through products .This is not only to realize the nationalization of material objects, but also a powerful dissemination and promotion of national cultural heritages. And let more people understand national cultures. As shown in Fig 2, this is called a contentment tea-sets. It uses Chinese bamboo as design elements, besides reflecting insulation function, also Cleverly reflects the cultural essence of bamboo. With calm, peaceful and perennial meaning to guide modern people's life attitude, emphasizing ascetic and open-minded spirit. Using oriental philosophy to interpret modern lifestyle and to achieve the perfect unity of both styles and practices.

Fig.2 Contentment tea-sets

Implementing design nationalization, is seeking "to change". There is a word "Any circumstance hitting a limit will begin to change. Change will in turn lead to an unimpeded state, and then lead to continuity". The modern design concept is "to change" in essence. The combination of national symbol and modern design is the conversion mechanism between content and form.This combination is not only to grasp the law of national culture, but is the best representation of aesthetic characteristics. Reconstruction of national symbols is the focus of modern design aesthetics.therefor, symbolic forms must reflect modern people's spiritual pursuit. It is deeply rooted in peoples’ lifestyles and aesthetic practices, which constitutes potential aesthetic qualities and psychological accumulations of the public(as shown in figure 3).

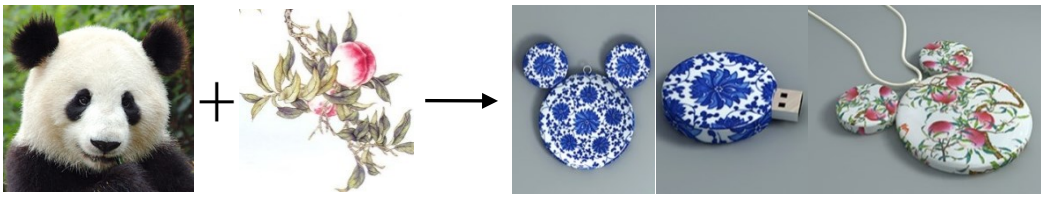

Fig.3 Chinese style U disk

In modern society, symbolic forms are affected and changed by cultural diversities. Only grasping the cultural characteristics of national design accurately and understanding the connotation of design elements correctly, may create a modern aesthetic design (as shown in fig 4). The diversities of design forms, with a different aesthetic consciousness. Whether look at Chinese culture with western values, or on the contrary, our national design should keep its own liberation and beyond. Of course, we can use foreign design forms to disseminate our national aesthetics. With design form to reflect national emotion, is the rea sense of national design internationalization.

Fig.4 Orient Landscape logo

Conclusion

At present, China design industries develop very rapid, but to reach the standard of "designed in China" is still a very long way. So-called "designed in China" is not a formal national design. The key is to figure out what is the cores of China national cultures,and to dig those hidden in the signs which can really reflect the essence of national culture spirits. While grasping the development law of design culture and integrating subtle elements into modern design forms and languages. So it can make national culture spirits and globa design languages together into the mainstream of modern design, this will lead China design has more extensive culturality and nationality.

References

[1] Li Chaode Guoxin, design aesthetics. Anhui Art Press.2004.

[2] Xu Hengchun, design semiotics, Tsinghua University Press,2008(1).

[3] Chen Hanqing,Cao Yali,to read design symbol language and its native culture,decorazione,2005(12).

[4] Suke,the aesthetic character of design, art observation,2003(12).

[5] YangwWei,analysis of Alan Chan design thinking,business forum,2013(13).

[6] Zhang Yaohui,the design aesthetics in contemporary art,art observation,2013(10).

[7] Zhang Yanxin ,The contemporary value of design aesthetics,decorazione,2006(11).

Advanced Materials Research Vols. 989-994 (2014) pp 5148-5151
© (2014) Trans Tech Publications, Switzerland
doi:10.4028/www.scientific.net/AMR.989-994.5148

Application of Game Theory in Mode Selection of Combined Training of the Postgraduate

Tongying GUO, Jiejia LI, Bin MA, Jinxiang PIAN, Haichen WANG, Fengyan HAN

Shenyang Jianzhu University, Shenyang, Liaoning, 110168, China
tyhchguo@126.com

Keywords: Combined Training; Postgraduate; Game Theory; Mode Selection

Abstract. In this paper, the necessity and significance of combined training of Postgraduate is analyzed. Game rules, strategies and payoffs is introduced about the combined training of Postgraduate. The application problem is researched based on game theory about the mode selection of combined postgraduate.

Introduction

In 2010, the Ministry of Education issued file which is the guiding ideology changed in educational philosophy, training model, reforming the management system, improving training quality, through various forms of cooperation such as schools and enterprises, or industry organizations, in order to actively explore and innovative training model. The Ministry of Education proposed to establish and explore personnel training new mechanism with in personnel training project of serving the special needs of the state in 2011[1].

Combined training of Postgraduate is very important to integrate educational resources of enterprises, universities, and research institutions, which have important practical value to train the innovative talents with founding the problem, solving the questions and independently engaging in research, and to promote technological progress and enhance the competitiveness of enterprises. In recent years, a number of practice researches have explored in aspects of combined training Postgraduate, but it is still in the exploratory stage in the whole. It should be in-depth researched how to create a win-win, sustainable mode of combined training of Postgraduate [2].

This paper will use game theory to analyze the selection problem of combined training mode of Postgraduate , and provide some policy recommendations.

The Basic Concepts of Game Theory

Game theory is how to achieve a set of interdependent strategies and actions interaction between the decision bodies with interest conflict. The basic elements of the game theory include actors, behavior, information, strategies, pay (utility), which are collectively known as the rules of the game. Through all elements of the game theory, the basic model of game theory can be expressed as: G = {P, A, S, I, U}.

(1) Player: refers to the process of the game by choosing their own behavior (or strategy), to maximize their own utility can independently undertake the result of individual decisions. Usually player is represented with i = 1,2, ..., K.

(2) Action: refers to the players in the game during a moment of decision variables. Ai represented by the general behavior of the player for a particular i, with the set of Ai = {ai} which means that all of the activity may be employed.

(3) Information: refers to the knowledge obtained during in the game, such as the characteristics and behavior of the other players. The amount of information of players will have a direct impact on its decision accuracy which is related to the overall success of the game.

(4) Strategy: refers to the players choose their own behavior rules which should take actions during the selection of behavior. Si represents a specific decision by the players of i, Si = {si} represents a collection of all the policy of No. i player. Strategy combination S = (S1, ... Si, ... Sk) is an ordered set of policy of the K game players.

(5) Payoff: also known as Utility, refers to the utility obtained players in a particular combination game strategy. Payoff is the fundamental basis of individual decisions of all players, which is the content really cared by each player. The payoff of No.i player is expressed by ui, u = {u1, u2, ..., un} expressed payoff obtained in a particular game player.

Research on Game Theory of Combined Training of Postgraduate Student

The cooperation bodies of combined training of Postgraduate have businesses, schools and research institutes. Enterprises are market-oriented, the most fundamental purpose is the pursuit of economic interests, so companies will focus on maximizing the economic benefits of cooperation mode selected. Generally, companies are in favor of co-development, so that they can participate in the whole research to improve their Research & Develop capabilities, improving the status of information asymmetry. Schools and research institutes to pursue not only the pursuit of economic interests, also some non-economic benefits, such as academic reputation, etc., schools and scientific research institutes prefer to maintain independence, and therefore schools and research institutes generally biased technology in a collaborative manner, so the choice of the cooperation model is a product of the game between parties of combined training of Postgraduate. Here are some game rules of combined training of postgraduate student, policies and payments

1. Game rules of the combined training of postgraduate student

To clear the Postgraduate in the rules of the game, we need to know the game's players, player action, and these actions will eventually get what kind of results. Companies, universities and research institutions are main bodies in the process of combined training of Postgraduate . In study, in order to simplify the process of game analysis, the two people often are regarded which enterprise is as one game, universities and other research institutions are seen as another game. Action players are to participate in the game at some point of decision variables, in general, ia represents a specific action of the i-th player, iA = {ia} express all actions can be chosen for the collection for No.i player. Action of players may be discrete, or continuous. For example, the mode of choice of combined training of postgraduate student e, action is discrete, the distribution of benefits of action is continuous.

2. Game strategy of the combined training of postgraduate student

The game strategy is the action rules of player in the case of a given set of information, which provides players choose what actions. In general, we use “is” to represent a specific strategy of the No.i player, all strategic collection of the No.i player is a strategic set of the No.i player, denoted iS = {is}, i ∈ N. Each player chose a strategy, all strategies constitute the vector s = (1s, 2s, ..., ns) called a strategy mix, which “is” is a strategic choice of the i-th individual. Strategies and actions described above are talking about here is the same only in a static game model, in other cases they are not the same.

3. Combined training of Postgraduate in game party payoff

Game payoff refers to the utility level obtained by player under the combination of a specific strategy, or the expected utility level obtained by player. Payoff is something that people really care by the game of player. Generally, the payment is a function, and therefore can be said that players pay function “i” is defined in the strategies of combination sets S, the value of a function in the real space R, denoted iU (s). In game theory model, the player's benefit is mutual restraint. The benefit consists two parts in the process of combined training of Postgraduate, one is the overall benefit of cooperation, as well as a member of their own part of benefit between the cooperation the parties, if it is a non-cooperative game, the first consideration between the game is their own party individual benefit, rather than considering the overall benefit. If it is a cooperative game, the first consideration is to maximize the overall benefits of cooperation, and then is allocated to maximize their individual benefit.

Game Analysis of Combined Training Mode of Postgraduate

In recent years, some universities explore the combined training models of postgraduate, which are summarized in the following modes:

1. Training model based on the different stages of cooperation. One is the whole process of cooperation. Business experts are awarded doctoral and master instructor certificate by university, the universities and enterprises participate the whole training process of postgraduate. Another is stage of cooperation. College and business cooperate in aspects of the training postgraduate, mainly in the stage of postgraduate studies and practices stage.

2. Training model depending on the subject of cooperation. One is school-enterprise cooperation model. Another is schools and research institutions cooperation. No matter what form, it has a certain basis.

3. The two models of technology transfer and cooperative development in the model of school-enterprise cooperation.

In this game we have constructed two models: a model of cooperation innovation of school-enterprise player and another model of technology transfer. If technology transfer, assuming that the company pays to the transferee technical university technology transfer fee is D If cooperation innovation, the corporate commitment to technology after the successful development of paid pro rata k commission to universities, colleges upfront technology supply side is I, under normal circumstances (excluding capital costs), after deduction of the subsequent technical development fee income is X, universities do not the relative probability of a successful case under technical development cooperation (willing to technology transfer) of p. Corporate uncooperative (willing to technology transfer), the non-payment of royalties to the university. In this model, we follow the general principles of school-enterprise cooperation: namely, whether to participate in the co-innovation or pure technical trading, technology transfer, colleges and universities as the supply side of technological innovation, companies demand side as the emergence of technological innovations.

Considering the transfer of the latter, university cooperation needed to pay the costs of resources converted into Y, get the game payoff matrix shown in Figure.1.

	Cooperation development	Technology transfer
Cooperation development	(D-I+XK-Y, X-XK-D)	(D-I-S，X-D)
Technology transfer	(D-I+Xpk, Xp-Xkp-D)	(D-I, Xp-D)

Fig.1 Cooperation development and technology transfer game model

Through the above analysis, on the one hand we can motivate a constraint angle design technology transfer mode of R & D compensation, financial external oversight mechanisms to maximize conversion mode, but the general conditions under which the two sides can not achieve the goal; But on the other hand for this article discusses the conversion mode selection, we can choose to co-innovation model, that is, through the development of effective cooperation contract design, the game will be a one-time shift of technology transfer mode multi-stage repeated game, build credibility conversion mechanism between the two sides, which could achieve Pareto improvement.

Conclusion

By studying postgraduate training model, the theoretical knowledge learned in postgraduate has been further consolidated and strengthened, and solving engineering problems by finding corporate laws of science, the practical ability of postgraduate training, pragmatic style and teamwork, in addition to work closely with research technical exchanges institutes, research institutes and

enterprises to follow the mentor and expert learning exchanges and discussion, and further increase their knowledge of Postgraduate, Postgraduate broaden their horizons. Greatly enhance the ability of innovation and academic postgraduate, truly all-round development. Meanwhile, in order to provide Postgraduate in training mode similar reference reform, promote the development of postgraduate education.

REFERENCES

[1] Cheng Aijie, Research on model and problems of combined training of postgraduate, Research and education development, 2008.13

[2] Liu Jinsong, Research on model and explore of combined training of postgraduate, Culture, 2012.2

[3] Liu Wencui, Research on mode selection of Xinjiang combined training of postgraduate, Xinjiang Finance and Economics University, 2012.4

[4] Niu Wanxia, Research on innovation technology of school-enterprise cooperation based game, Xi'an Technology University, 2005.3

[5] Shi Yuexiang, Research on questions of innovation ability combined training of postgraduate, Industry and Information Technology, 2013.10

Advanced Materials Research Vols. 989-994 (2014) pp 5152-5156
© (2014) Trans Tech Publications, Switzerland
doi:10.4028/www.scientific.net/AMR.989-994.5152

The Revelation from MOOCs on Our Country's Remote Education

Wang Junfeng

Distance Education Research Center of Shaanxi Province

Shaanxi Province, Xi'an ,China

wangjynfeng@sina.com

Keywords: MOOCs; Challenges; countermeasure .

Abstract. Since 2012, known as the first year of "massive open online Courses (MOOCs)", its development speed beyond our imagination, only Courses one company registered online learners reached more than 4.1million people (up to July 21, 2013). MOOCs will be bring what challenge for distance education development in China, how to deal with these challenges, is our reality problem need to concerned. We hope through the above question discussion to accelerate the change of distance education in our country, to adapt to the trend of the internationalization of higher education, promoting its healthy development..

Introduction

In 2012 , MOOCs（Massive Online Open Courses）As a new type of higher education online mode gradually entered people's horizons. And formed three online courses teaching website by Coursera，Udacity and edX represented, the resources of website are provided by the world first-class university, offering free online teaching service for global learners, and make the registration at any time, any place can enjoy the best education resources. Coursera, Udacity and edX these three company are called MOOCs "The big three".

MOOCs into China, no doubt that is a big impact to for our existing remote education, we need seriously face it. Such as: Which impact and influence that the rapid rise of the MOOCs brings to our country's higher education, especially in remote education? How the Distance Education should be deal with the challenge of MOOCs? And so on Problems need to think deeply and parsing.

I. The challenge from MOOCs for our remote education

A. The challenges of higher education thoughts

(a) Globalization education thoughts

The impact of MOOCs to China's remote education on the first embodied is globalization education thoughts. In today's information technology changes, MOOCs broke the limitation of national, ethnic, regional, national, provided free Stanford, Harvard, MIT, Cambridge, Oxford and other world-class university's online courses to the entire world, even provided certificate of these courses , the learners in learning knowledge at the same time, also can practice English hearing, improve their English, why not to do it?

And look back on behalf of our country's first-class higher education curriculum standard of national fine course construction, on the one hand, the resource acquisition is difficult, utilization rate is not high, nearly all require registration to browse the resources, is a barrier, compared with countries and about the huge investment in curriculum development, utilization and investment performance is low, contrary to the purpose of the fine course construction; On the other hand even high quality teaching resources, also does not implement free and promote throughout the country, let alone in the global promotion, lack of strategic thinking of the globalization, make our high-quality curriculum "unknown" . [1]

(b) The concept of free learning

In an age of course certificate can be provided free, we still charge according to professional education mode is somewhat outdated? Higher education is training qualified workers and qualified citizen for society, it is a public welfare undertakings, but constantly improve the amount of fees for many families feel difficult. MOOCs appear, it is our hope, she will bring a challenge for the higher education existing "registration fee system of charge before they are learning".[2]

(c) The people-oriented education thought

The curriculum design of MOOCs is learners-centered embody the people-oriented thoughts. And our country's higher education still basically following teachers' leading teaching mode - "teachers speak, the students listen to" very little interaction between teachers and students, teacher leave the classroom in a hurry after class, pay little attention of how much can students mastered. Remote education generally used video lectures, less interactive, learners often study after work, even can't get help from teacher because commuting time limit when they meet difficulties in learning, feel learning is difficult to continue, and finally had to drop out of school.

(d) The education thought of paying equal attention to knowledge and ability

Compared with domestic focus on knowledge learning, MOOCs pay attention to the dual cultivation of student’s knowledge and ability. By setting learning program, make students themselves to form a team, search data, conduct field research, and statistical analysis of survey data and come to the conclusion. This kind of teaching method, not only change the monotony traditional teaching process ,also make the students experience the process of knowledge acquisition, thus cultivating students' ability to obtain information, processing information ability, communication cooperation ability with people, etc., through the learning process all kinds of social practice ability has improved. Review of our higher education, still in imparting knowledge as the main focus.

B. The influence of the way of education

(a) Social learning environment

MOOCs provide social teaching environment, on the one hand, through assignments of some course , learners need in-depth society to carry out the actual research; On the other hand the same region of learners can form a study group, and regularly or aperiodically use cafes, schools and other venues to discuss learning. Our students have to make up for all the "social" lesions after graduation.

(b) The change of teaching means

One is through the virtual experiment and actual practice of research, discussion and other forms of "knowledge" to “acquire knowledge "; Second it is course video clips control within 15 minutes, to achieve fragmentation learning; Third, use depth of education technology, to realize intelligent and personalized management of teaching process.

(c) The High demand of Teacher's role and the professional ability

Teachers embodied in the following: on the one hand, each course teaching tasks are assumed by a teaching team, contains the master teacher, teaching assistant, courseware, etc.; The second is in general the master teachers are outstanding person of the subject, has a high academic reputation, erudite is their common; Third, teachers' teaching design is under a lot of work, for the wonderful

course lay a solid foundation. Compared to our teachers, there is a big gap with MOOCs in breadth and depth in the field of professional knowledge and teaching.

(d) The changes of students learning style

For college students, MOOCs undoubtedly provide a new opportunity and choice, they can accept the teacher's teaching in the school, also can register and login MOOCs. What they faced is no longer the school teachers to teach "unify the whole country", they use MOOCs learning at the same time, also sought to change the traditional learning style they formed over the years.

C. Management

(a) Depend on for-profit and nonprofit company to carry out the network education

MOOCs use the company's operations, Coursera and Udacity is a for-profit company, edX is a for-profit company. The education industry with low barriers to entry, conducive to more companies to join MOOCs camp, compete, and make the learners have more choice, better learning resources and learning support services, namely the learner are the ultimate beneficiaries.

(b) Use course authentication, easy for learner to autonomy and self-control

Course authentication way, require learners to registered in a certain period of time to study, schedule time every week, to spend 2-3 hours to participate in the study. This is equivalent to the learners and the site signed a teaching agreement , the implementation of the agreement, need learners constraints themselves, manage themselves and restrained himself, namely from the traditional learning "heteronomy" into "self-discipline".

(c) The application of technology in the management

MOOCs using information technology to record, store, analysis and processing learner’s data, give corresponding hint for learner's present learning status, and through the analysis of large data on learners' learning behavior, provide empirical support for the teaching reform. MOOCs also use information technology build virtual laboratory, especially pay attention to the interactive courseware, and solves the influence of the "emotional island" phenomenon in network education.

III, The strategy of deal with MOOCs

A. Set up the globalization education thought

To deal with he challenges of global education, can start from the following several aspects: One is to go out. Training excellent teachers Can fluently teaching in English are short of college in our country, through send domestic university outstanding teachers to do high-end visiting scholar at Harvard and Oxford University, in one aspect mastering English teaching at the same time also learn from foreign counterparts in the good teaching ways and methods, improve their teaching level unceasingly.

Second are output courses for free. Output our students like good teacher’s course through MOOCs abroad, we emphasize output courses must teaching and interact in English. The process as seem as our understanding of the first-rate university: at the beginning we known the status of the top universities abroad in Chinese, when require communication after we known, and then began to learn English, in order to facilitate better communication. Both to attract more international students to understand China's universities, understand Chinese culture, it is also a kind of potential recruitment of students propaganda.

Third it is change the passive to active, abandon the narrow intercollegiate ideas, and open the existing teaching resources. Make up our mind to give up the artificial barriers between high quality network courses and universities, remove the password, registration and other restrictions for off-campus learners, open the existing teaching resources, truly free, serving the domestic learners; At the same time also provide English version as much as possible, to facilitate the international learners of non Chinese language learning.

Forth is Introduce a corresponding system, encourage domestic university to participate in international education competition. Through formulate the related policies, encourage universities approved course credits similar to the MOOCs, use course internationalization to promote the pace of internationalization of higher education in our country, through the internationalization of higher education to promote reform in the field of higher education in China. [3]

B. Change the way of teaching

We have been saying for a long time to change the way of teaching, but the effect is difficult to satisfactory, MOOCs give us inspirations are the following:

Change the way of teaching, the first is return to the origin of education, namely the activities of "cultivate people's , teachers should focus on the educates - class students, by building a classroom and extracurricular social learning environment to make student exchange experience for process of" knowledge capture ", instead of the current popular class time "feed in".

Second is put big strength training "masters", promoting "masters" effect ", to carry out other teachers teaching way transformation by carry out bilingual teaching "masters". Globalization of education, requirements "teacher" have the strategic vision of globalization, globalization of teaching ability and professional quality, to cultivate the talents of globalization.

Three is change the existing teaching mode, change personal teaching to team collaboration, set the wisdom of the collective to carry out course teaching research, guide students to change learning style at the same time, improve the teaching results. [4]

C From knowledge-transference to ability training

For a long time, we accepted the education of students from kindergarten to university is the students listen to the teacher "the knowledge feed in" mode, and the evaluation is focused on the master degree of knowledge, less attention to the formation of student ability, lots of "high score low-energy" phenomenon. In MOOCs era learner’s ability training should focus on the following aspects:

One is the cultivation of learners' learning ability. In reality we often found there are many of students at ordinary times very hard, but learning result is bad. Much of these student is not master the suitable learning method for their own, namely the ability to learn, usually wasted effort. Such as English learning through more than 10 years in primary school to university study, we still can't communicate with foreigners freely, of cause there are problems such as culture, teaching methods, but one of the main reasons is teacher didn't pay enough attention focus on students' English learning ability training. [5]

The second is the cultivation of the learners' self-control and self-discipline. Learning is learner’s personal things. But we have stressed discipline education from primary school to university, and not pay enough attention on learners' self-awareness, self-management and self-discipline level; we pay too much attention to external factors, while neglecting the learners' initiative. Use learner's self responsibility consciousness education to cultivate their autonomous self-discipline, and self management.

Three is the cultivation of the learners' communication ability. Communication ability has always been a "short board" in our education. In traditional classroom teachers' teaching and students have no chance to express their opinions, the interaction between teachers and students is extremely limited, cause lack of communication ability. Create conditions to carry out the discussion-based

teaching, make each learner to actively participate in class interaction, improve their communication ability in learning.

D. Simplified management, pay attention to technology application

Simplify the management of higher education, to relax the admittance threshold of higher education, attract the foreign high-quality education resources into China, and then promote the development of higher education in China.

Compared with MOOCs, remote education technology is not backward in our country, but for the depth of the technical application we still has the very big gap, such as through to the learners' big data processing and analysis, put forward the corresponding countermeasures and Suggestions for teaching, etc., we're in the shallow of data processing application, lack of mining and analysis. Our reality choice is pay attention to the depth of the education technology application, introduction of large data statistics and analysis talents to join the teaching team, improving the teaching performance.

References

[1][2]Prashant K Nanda(2013). Learn anytime, anywhere and largely for free: Anant Agarwal.[EB/OL]:http://www.livemint.com/Politics/TFqJqM6l4K39Q2gq8JNg5O/Learn-anytime-anywhere-and-largely-for-free-Anant-Agarwal.html.(2013.8.8)

[3] [4] [5]Research shows that young unmarried men love selfstuday with public class learning. [DB/OD]:http://tech.163.com/13/0712/12/93J6ITVG000915BF.html(2013.7.21)

Advanced Materials Research Vols. 989-994 (2014) pp 5157-5164
© (2014) Trans Tech Publications, Switzerland
doi:10.4028/www.scientific.net/AMR.989-994.5157

The Coupling Relationship between Information Technology Level and Public Transportation: a case study of cities in Guangdong

Miaoxi Zhao[1, a], Qin Gu[2, b], Yang Duan[3, c] and Jingyu Liang[4, d]

[1]School of Architecture, South China University of Technology; National key laboratory of subtropical architectural science, 510640, P.Guangdong, P.R.China
[2\3\4]Department of Urban Planning, School of Architecture, South China University of Technology, 510640, P. Guangdong, P.R. China
[a]zmx0207@163.com,[b]312109700@qq.com, [c]dychestnut@foxmail.com, dastro.gary@hotmail.com

Corresponding Author: Dr. Miaoxi Zhao, zmx0207@163.com

Keywords: information technology, transportation, passenger flow, coupling relationship.

Abstract. During the rapid development of information technology, the global widespread information wave has come. Exploring the intelligent information technology on the mechanism of the urban space helps to drive targeted policy-making about city planning. In this paper, taking cities in Guangdong as samples , we firstly discuss about the relationship between the level of information technology and personal travel. Primarily, analysis the fitting relationship between information flow and public traffic flow of the 21 cities at a certain time. Secondly, investigate how information technology influences the residents' travel at the micro level by means of questionnaire surveys. The study shows that internet information has a significant promoting effect on the residents' travel of general cities, but a substitution effect in a few large cities which has highly developed service sector.

1. Introduction

Traffic is the main artery to promote urban function in modern times, which has been put forward by Athens Charter. The rise of information technology undoubtedly has great significance in urban traffic development. Transportation and information has become topics in recent years, and are often classified into the same category. They have closet contacts and influence to each other, and play common role in social and economic development at the same time.

Many scholars have carried out considerable research on how information technology affects the city traffic, Graham, Marvin (1996) summed it up in four effects - *physical developmental effects*, *substitution effects*, *generation effects* and *enhancement effects*.[1] The substitution effect refers to the development of communication technology that can overcome the obstacles of interpersonal communication. Gaspar, Glaeser (1998) thought information technology is not only a supplementary for face-to-face communication but also a substitution.[2] Generally, it weakens the urban agglomeration.[3,4](Negroponte, 1995; Sridhar, Sridhar 2003) In other similar empirical study, Gothoskar, Sharma (2000), Ng, Jin (2000) and other scholars found that due to the development of information, technology switching of information space increases the possibility of multi-location work, and then information technology leads to spatial dispersion and reduces the demand of travel.[5,6]

Other scholars focused on the impact of information technology on different traffic streams. Typically, Golob and Regan (2001)argued that personal travel behavior which impacted by electronic information could reduce to *consumer electronic commerce*, *other telesevices*, *flexible working arrangements*, *self-employment*, *contingent*, *part-time working arrangements*, *mobile working* and *ATIS for vehicles*.[7]They also reduce the commercial activities under the influence of travel information flow to *business-to-business e-commerce*, *structural changes in the freight transportation*, *logistics industry* and *ATIS for commercial vehicles*.[7]

In this respect, there are many studies about the impact of Electronic Commerce on traffic (Mokhtarian, 2002, Visser, Lanzendorf, 2004).[8,9] For instance, Weltevreden, Rotem-Mindali (2008) pointed out that, the informatization in B2C (businesses-to-consumer e-commerce) will reduce the

traffic demand while the informatization in C2C(consumer-to-consumer e-commerce) may make the travel behavior more likely to occur.[10] Similarly, face – to - face communication will still play an irreplaceable role in the advanced producer service sector due to the demand of tacit knowledge. IT substantially stimulated this kind of traffic demand and has improved intercity traffic and the demand of informational linkage. Thereby, the management and control of division of global industry can be realized. This is also the objective basis of the formation of global cities network.[11,12](Sasssen，2001；Taylor, Ni and Derudder, 2009)

Some scholars believe that although the electronic communication has greatly expanded the frequency and intensity of non-local connection, it did not lead the local communication to be meaningless. Instead, it greatly enhances the diversified contact of local people (Zook, 2004).[13] In these years, some scholars such as Axhausen (2008), Carrasco, Hogan (2008), have focused on the social activities and travel, which provides a new perspective for different types of traffic flow research under IT.[13,14,15]

In the related research in China, meanwhile, Hong Zhen(2000) and other scholars have already done research about the relation between information technology and transportation thoroughly in an early time.[16]Zi Lu and Huiqiao Zhang(2003) analyzed the positive impacts on the urban spatial structure through the organization of traffic flow, that caused by the approved traffic directing system in Shijiazhuang.[17] Referring to the web services statistics, Shifeng Wu and ZiLu(2007) created the criteria of realistic traffic flow, and calculated the substitution impacts which the internet information movement has exerted on realistic traffic flow.[18]After studying the intelligent community in Hangzhou, Ruiling Han, Qiuluan Zhang and Zi Lu(2010) discovered that the virtual community does affect the resident behaviors in reality; the intelligence of internet plays the greatest leading role. The homogenization of affected population is a prominent feature when virtual community's information flow guides the choices of residents.[19]Based on these summary of relationship between information technology and transportation, Miaoxi Zhao (2014) puts forward his expectation about the use of intelligent transportation in the situation of smart cities.[20]

According to the evidence discussed above, some studies have not come to a clear conclusion. What's more, comparison between different cities is inadequate in existing studies; No study was done about relation between information technology and travel behavior from both macro and micro aspects. Therefore, in order to have a further study about the spatial mechanism of information technology, it is important to choose representative region, and to compare the relationship between information technology level and prohibition of commuting.

2. Research Design

2.1research object

In the 21st century, the process of Chinese urbanization and mechanization is continually accelerating. From 2000 to 2013, Chinese urbanization rate increased from 36.2% up to 53.7% and the average annual growth was about 1.15%. The urban population grew from 460 million to 730 million, making a net growth of 270 million. Nevertheless, the possessing capacity of vehicles in first-tier cities like Beijing, Shanghai, Guangzhou, Chengdu, Hangzhou, Shenzhen, has exceeded one million. To regional economy, it becomes a core issue that how to allocate the limited resources properly to make urban traffic function efficiently when lacking public hardware facilities. However, how information technology affects urban resident trip remains to be further investigated. Therefore, 21 cities in Guangdong province are chosen as survey targets.

In China, Guangdong province is the most prosperous one in economy. However, the socioeconomic discrepancy between the different internal regions still exists. Guangzhou and Shenzhen have developed into very significant node cities in the global economy, and some peripheral regions underdeveloped still exist there.

Thus the uneven urban development helps to compare the causality of IT and passenger transport better, and we can achieve the purpose of this research, clarifying the spatial mechanism of information technology by exploring residents-travel characteristics for different cities in

Guangdong Province, and analyzing the specific impact on residents travel caused by ITC more deeply.

2.2 research methods

The empirical study consists of a regional comparison at macro level and a questionnaire survey at micro level. Firstly, we use 21 prefecture-level of Guangdong as targets for comparison to explore the fitting function relationship between information technology level and transportation; secondly, through questionnaire study on how IT influences transportation, and discusses how information technology influences the decision of residents travel from a microscopic angle.

3. The overall level of regional comparison

This study first compares the relationship between internet technology level and traffic volume among different cities by using analysis of variance.

For a polynomial fitting, known set of points with n（i_a， $f_1(i_a)$），a=1,2,3…, find m times （$m<n$） polynomial $f_m(i)$:

$$f_m(a)=k_0+k_1 i+k_2 i^2+\ldots k_m i^m \quad (1)$$

And figure out the Residual sum of squares and select polynomial. And Q_m is the minimum value for the residual sum. Make significant test on polynomialf_m.

In the process of quantifying the indicators of informatization, LiuyuLu(2002) pointed out that the application of internet technology is an important mark to measure the degree of information, but he didn't have the exact statistics, so we replace it with other related indicators.[21] The total number of mails, the number of newspapers and periodicals, the total number of the total number of mobile phone users, the total number of expressage as well as the total number of telephone users have been selected in this article.

Arranging the trips, people will get the information in advance to make travel more effective. However, the level of information technology varies in different cities of Guangdong province, with the Pearl River Delta region occupying a geographic advantage, while access and use of information in developed cities such as Guangzhou, Shenzhen are more fully. These cities have a higher level of information technology; while western northern region economy is relatively backward, experiencing serious brain drain, which results in generally low level of information.

At the same time, levels of economic development and the impact of geographic location varies in different regions of Guangdong Province. The urban traffic as the Guangzhou-Shenzhen regional transport get a good head, while that in remote areas develops still slowly. Taking account of the practical problems, select the amount of municipal public transport as a measure of urban transport. Let's take 2012 Guangdong Statistical Yearbook tables 14-19 steam tram and public taxi data to calculate the per capita amount of public transportation as a measure of traffic travel. Organizing the data above, evaluate the logarithm of the amount of information technology level standards and per capita amount of public transportation to get data in Table 1.

Table1: Standard date of 21 cities of Guangdong Province in 2012

City	Information Technology Level	Per Capita Amount of Public Transportation
Shanwei	*4.22*	*5.85*
Yunfu	*5.07*	*11.14*
Yangjiang	*6.05*	*8.52*
Chaozhou	*7.12*	*8.66*
Heyuan	*7.17*	*19.33*
Shaoguan	*7.89*	*33.61*
Jieyang	*8.39*	*4.27*
Zhaoqin	*8.59*	*30.08*
Meizhou	*8.73*	*8.28*
Qingyuan	*8.98*	*26.32*
Maoming	*10.42*	*7.39*

Zhanjiang	*11.14*	*31.00*
Zhuhai	*12.48*	*229.49*
Shantou	*15.12*	*27.19*
Huizhou	*15.36*	*58.60*
Zhongshan	*15.91*	*90.21*
Jiangmen	*19.57*	*39.27*
Fuoshan	*40.17*	*87.57*
Donguan	*45.34*	*89.13*
Shenzhen	*79.35*	*255.13*
Guangzhou	*99.21*	*266.99*

Table 1 presents observable liner relationship between information technology level and traffic volume. resident population in Zhuhai remains only 1.58 million, less than 1/6 of Guangzhou . It gives an abnormal high level to public traffic of per capita of Zhuhai, affecting the overall results of the analysis of data, so we delete the sample of Zhuhai in the end.

Based on the table fitting function $T(i)$ at different polynomial variance analysis as shown in Table 2.

Table 2：Analysis of variance under different number of polynomial

n	*T(i')*	R^2
1	$y = 2.8284i - 4.5062$	*0.933*
2	$y = 0.0051i^2 + 2.3506i + 0.1313$	*0.935*
3	$y = -0.0002i^3 + 0.0399i^2 + 1.099i + 8.6715$	*0.937*

As in Table 2, the cubic polynomial $y= -0.0002i^3 + 0.0399i^2 + 1.099i + 8.6715$ fits the facts most. At this time $T(i)$ basically reflects the relationship between Per Capita Amount of Public Transportation and Information Technology Level. Study also uses the coupling relationship between the development of urban transportation and information technology development, as showed in Fig.1.

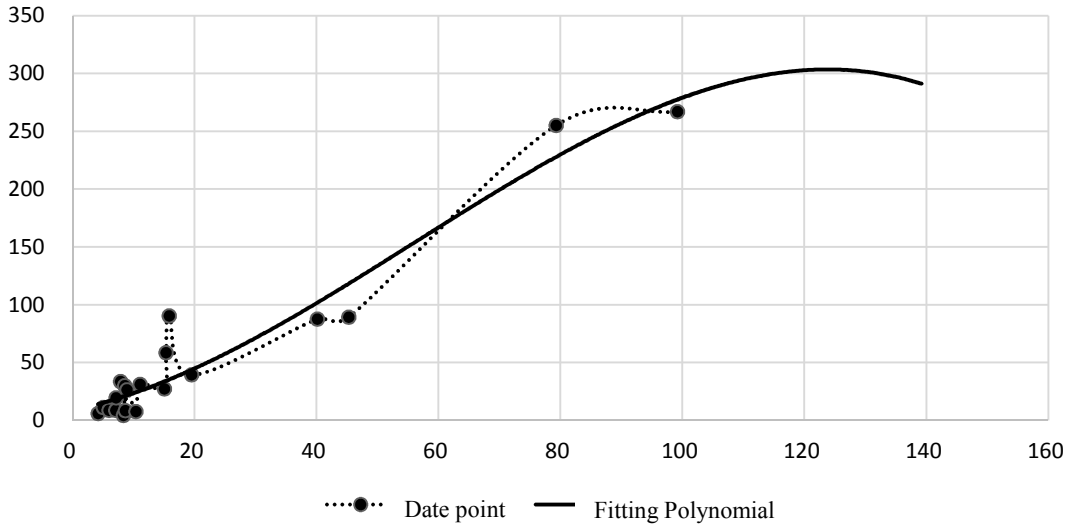

Figure 1: The Impact of Information Technology on Regional Traffic Travel Trends

Table 2 illustrates that traffic in the cities such as Shanwei, Jieyang are at very low levels.With the lower level of ITC consuming, their transport trips are still increasing. Obviously, in the early stages of urban development, information technology facilitates communication among residents. Individuals using the obtained information for more efficient travel, increases travel efficiency since the communication time is reduced and the cost is greatly increased.

However, when the level of IT reaching a certain level this marginal benefit will be reduced, resulting in a substitution effect proposed by Graham, Marvin (1996).[1]In the developed cities such as Guangzhou, Shenzhen, with wider use of information technology, internet mobile devices, and

social networks allow people to talk without meeting face to face. "Web conferencing", "e-learning" and "home office" and other way of e-life have been more accepted by people, meanwhile the rise of online shopping meets the needs of contemporary society "home" life crowd.

Nowadays, people can stay at Homes to complete the work or study at the same time without losing contact with the outside world life. As a result, people will greatly reduce travel. With more advanced information technology used in residents' daily life, people will choose the way to get non- travel resources they need, thus greatly reducing the amount of traffic. But as the study has reviewed, differences on the degree of information region, education level and those of individuals can be seen visually different a lot.

To summer up, in a city there exists promoting and substitution effects between information technology and transport. With the restricts of local factors such as the level of development in different regions, these two effects trades off and takes turns., and ultimately show the total effects of promoting or substitution.

4. Exploration of micro-level mechanism

4.1Travel distance under the impact of Information Technology

To explore the mechanism on the relationship between information consuming and traveling, respondents in the questionnaire study are classified into groups by the difference of the time using Internet every day. And a random survey was carried out in suitable areas. The data of the answers on the Internet, electronic equipment and transportation are organized to analysis in quantity and nature, which verifies whether the impact of the level of information technology on urban traffic flow meets the aforementioned mathematical models. Shunde District of Foshan city is selected as the study area, which has a resident population of 195.53million.

The questionnaire distributed in 2012, mainly related to the Internet using, commuting time, transportation modes, transportation costs, traffic destination, leisure travel time at weekend, content of traffic information accessing and other issues. According to the feedback, information technology level is characterized by the time they surf the net each day. Traveling behavior includes many factors such as traffic time, traffic consumption, travel distance etc. Four variables characterizing personal trip, include home time in weekdays, monthly travel costs, luxury shopping places, and leisure trip time at weekends. By studying the relationship between variables of IT and transportation to explore the impact of information technology on the traffic flow in the region.

The quantitative relationship was studied by Binary Logistic regression analysis.

Logistic regression model is often used to study the relationships between response variables and other independent variables. The two results of binary response variables Y are denoted by 1 and 2. Four independent variables affect the response variable Y is denoted by X_1, X_2, X_3, X_4. The conditional probability of "Case 1" under the influence of the 4 independent variables is donated by$p = P(Y = 1|X_1,\ X_2,\ X_3,\ X_4)$. The Logistic regression model is denoted as

$$p = \frac{\exp(\beta_0 + \beta_1 X_1 + \beta_2 X_2 + \beta_3 X_3 + \beta_4 X_4)}{1 + \exp(\beta_0 + \beta_1 X_1 + \beta_2 X_2 + \beta_3 X_3 + \beta_4 X_4)} \quad (2)$$

In the formula above, β_0 is the constant term, and $\beta_1, \beta_2, \beta_3, \beta_4$ are called regression coefficients in Logistic regression model. Home time in weekdays, the monthly cost of personal trip, distance to luxury shopping places and single-trip time of leisure travel at weekends are selected as independent variables. Whether surfing the net more than two hours a day sever as dependent variable. "1" represents surfing the net less than or equal to two hours, "2" represents surfing the internet more than two hours.

Table 3. The letters of corresponding variables

Variable	Whether surfing the net more than two hours	Monthly transportation costs	Home time	Luxury shopping places	Leisure trip time at weekends	Constant
Corresponding letters	Y	X_1	X_2	X_3	X_4	β_0

Table 4. Output of binary Logistic regression analysis

		Coefficient	Sig.
Step 1	X_1	0.162	0.000
	X_2	-0.12 0	0.000
	X_3	0.193	0.000
	X_4	0.001	0.785
	β_0	-0.532	0.010
Step 2	X_1	0.164	0.000
	X_2	-0.12 0	0.000
	X_3	0.194	0.000
	β_0	-0.52 0	0.010

From the table above, single-trip time of leisure travel at weekends is excluded from the regression equation. Home time on weekdays, the monthly cost of personal trip and distance to luxury shopping place are retained, moreover their values of P is less than 0.05. The coefficient of transport costs, distance to luxury shopping places is positive, while the coefficient of home time is negative, which indicates that increasing of the time for surfing the net, monthly transport costs and the distance to luxury shopping place will increase, while home time will decrease (it means commuting time will rise).

Comparing with the group of less Internet time, people with more Internet time would spend more time and expense on commuting, and incline more to travel to faraway places as luxury shopping places. A conclusion can be drew that information technology will enhance the probability of travelling in various aspects (travel time, travel costs, travel distance, etc.)

4.2 Information technology embodied in the transportation

The aforementioned analysis indicates that level of information technology will promote transportation. The following part will explore the inner reason of this situation from acquiring traffic information. Traffic information will directly affect the transportation modes and willingness to travel. The reason why IT can promote transportation to a certain extent, may be that IT provides a relatively adequate information for people to travel, increasing the willingness and feasibility of people to travel. To determine this assumption, the Internet time of respondents (≤2hs/per day, >2hs/ per day) characterize the frequency of using IT, when " traffic information hope to obtain before traveling " sever as the test variables, to study the relationship between the frequency of using information technologies and ways to obtain traffic information as well as content. First the T-test is used to test the significant of Internet time and seven variables about traffic information obtaining.

Table 5. Output of T-test

		Levene test of variance equation	T-test of mean equation
		Sig.	Sig. (Bilateral)
Travel time to destinations	Equal variances assumed	0.000	0.000
	Equal variances not assumed		0.000
Road toll	Equal variances assumed	0.001	0.095
	Equal variances not assumed		0.096
Map and guidance	Equal variances assumed	0.000	0.000
	Equal variances not assumed		0.000
Weather	Equal variances assumed	0.921	0.128
	Equal variances not assumed		0.128
Real-time traffic situation	Equal variances assumed	0.261	0.575
	Equal variances not assumed		0.575
Parking lots	Equal variances assumed	0.001	0.084

information	Equal variances not assumed		0.086
Others traffic	Equal variances assumed	0.000	0.023
information	Equal variances not assumed		0.021

From the t-test results: there is a significant between characterization of traffic information and Internet time, consistent with the standard allowing a 5% chance of errors (except for the weather and road conditions in real time travel).

The respondents are also divided into two groups "two hours or less online" and "more than two hours online", to calculate the percentage of five variables in the two groups. Study the difference of percentage of the same variable in two groups, to find the impact of using IT on acquiring traffic information.

Table 6. Percentages of traffic information hope to acquire before travel in two groups

Information hope to get		Two hours or less online (%)	When the Internet grew up in two hours (%)
Weather	No	48.2	51.9
	Yes	51.8	48.1
Real-time traffic	No	63.2	64.5
	Yes	36.8	35.5
The time to reach destinations	No	49.5	38.6
	Yes	50.5	61.4
Road toll	No	76.0	72.5
	Yes	24.0	27.5
Map and guidance	No	50.1	37.9
	Yes	49.9	62.1
Parking Information	No	88.0	85.2
	Yes	12.0	14.8
Other Information	No	88.4	91.8
	Yes	11.6	8.2

From the table above, people who spend more time on the net have a stronger willingness to require traffic information than those spend less time on the net, such as time to reach destinations, road toll, map and guidance, parking information and other information. According to T-test, it is known that how long one spends on the internet is not obviously relative to willingness of requiring information about weather and real-time traffic. It is because such two kinds of information can be obtained easily and adequately form traditional media, such as television, newspaper and radio, instead of Internet. However, acquiring other four kinds of traffic information depends on the Internet instead of traditional media.

From the analysis of the relationship between IT using and traffic time, cost, distance, it is known that one of the reason why IT is able to promote transportation is that IT can bring the traffic information which can't be required from traditional media easily or adequately. It increases the willingness of searching traffic information and improves the feasibility of travel.

Shunde area belongs to the typical area of "IT level promotes traffic flow" in the aforementioned mathematical model. Therefore, the mathematical model of the coupling relationship between information technology level and the probability of travelling accords with the empirical results.

5. Summary

This paper uses statistical methods for data processing to obtain the level of information consuming and urban transport travel metrics, least squares polynomial fitting and analysis of variance for the two mathematical models were fitted to explore these the relationship in the cities

of Guangdong Province. By analyzing the functional relation, the role of the information for the residents of the city's traffic travel in general plays a significant role in promoting, but in a small number of highly developed cites with advance service sector there are certain metropolitan substitution effect. The followed data based on survey reveals the mechanism of relationship between information technologies and prohibit of travel choices.

To illustrate, in the mathematical model of the process, we set a pre-condition of the hypothesis, the traffic travel decisions and IT assumes a single linear causality, but it can be further explored in future studies of the process of decision-making mechanism to travel under the influence of multiple factors, which will provide specific policy recommendations for transportation planning practices.

Acknowledgement

Supported by National Natural Science Foundation of China (51108184), National Social Science Foundation of China (11&ZD154), State Key Laboratory of Subtropical Building Science of China (2013KB20), the Fundamental Research Funds for the Central Universities (2013ZZ0022).

References

[1] Graham, S. and Marvin, S. (1996), Telecommunications and the City: electronicSpaces, Urban Places, London: Routledge.
[2] Gaspar J, Glaeser E L. Information technology and the future of cities[J]. Journal of urban economics, 1998, 43(1): 136-156.
[3] Negroponte N. Being digital[M]. Random House LLC, 1995.
[4] Sridhar K S, Sridhar V. The effect of telecommuting on suburbanization: empirical evidence[J]. Journal of Regional Analysis and Policy, 2003, 33(1): 1-26.
[5] Irani A, Gothoskar S, Sharma J C. Potential and prevalence of teleworking in Mumbai[J]. Economic and Political Weekly, 2000: 2269-2276.
[6] Ng C, Jin K K. Teleworking in Malaysia: issues and prospects[J]. Economic and Political Weekly, 2000: 2308-2313.
[7] Golob, Regan. Impacts of information technology on personal travel and commercial vehicle operations: research challenges and opportunities. Transportastion research-part C. 2001,4(9):87-121.
[8] Mokhtarian P, Telecommunications and travel: the case for complementarity. Journal of industrial ecology. 2002, 2(6):43–57.
[9] Visser E, Lanzendorf M. Mobility and accessibility effects of B2C e-commerce: a literature review. Tijdschriftvooreconomische en socialegeografie. 2004,2(95):189–205.
[10] Jesse W.J. Weltevreden, Orit Rotem-Mindali, Mobility effects of B2C and C2C e-ommerce: A literature review and assessment. 2008
[11] Sassen S. Global cities and developmentalist states: how to derail what could be an interesting debate: a response to Hill and Kim[J]. Urban Studies, 2001, 38(13): 2537-2540.
[12] Taylor P J, Ni P,Derudder B, et al. The way we were: command-and-control centres in the global space-economy on the eve of the 2008 geo-economic transition[J]. Environment and Planning A, 2009, 41(1): 7-12.

Advanced Materials Research Vols. 989-994 (2014) pp 5165-5168
© (2014) Trans Tech Publications, Switzerland
doi:10.4028/www.scientific.net/AMR.989-994.5165

The research of building CAI table tennis teaching system

Zhang Baowei

Lixin University of Commerce, West Zhongshan Road.2230, 200235 Shanghai, China
zhangbaowei.66@163.com

Keywords: CAI multimedia courseware table tennis

Abstract: The CAI technology and Multimedia technology applied in physical teaching can improve the teaching efficiency, arouse the students' interest in learning, improve teachers' teaching ability, promote students' learning enthusiasm and accelerate the update speed of knowledge. The basic program of multimedia courseware development is the courseware topic .design, writing and operation. In education of sports theory teaching, PE teachers using the image and video or other functions of computers to create a variety of situations, improve the theoretical knowledge of visual in practical application. Students can understand theory on the courses more deeply.

1 Preface

Table tennis is a project which mainly requires skills. It includes speed, rotation, arc, placement, rhythm and adjustment. Table tennis has the characteristics of speed and rotation .As a representative of modern information technology of multimedia---CAI (Computer Assisted Instruction). Its novelty and diversity is vital to stimulate interest in learning. CAI courseware set text image, animation, voice and video as a whole to form teaching system through processing. In table tennis teaching, teachers take students' attention to the teaching content through visual and hearing. Create pleasant situation and motivate the students to learn. It has important significant to efficiently complete the study task.

2 The research method

2.1 The literature method: Access to literature and books about computer technology. Access to literature and books about table tennis.

2.2 Multimedia production method. Collect text, picture and video information about the rules of table tennis match PP widely and process it .Use Word, Photoshop, Movie Maker, Author ware etc. for the production of multimedia courseware.

2.3 Expert evaluation method: Interview and communicate with other institute table tennis teachers and computer science experts before making courseware .Consult experts as the reform of the teaching method and the understanding of table tennis' concept and the difficult of the research and application of the courseware. Provide advice and guidance to the research of this text. The course focuses on training to seeking problems in the real world and knowing how to solve problems.

2.4 Questionnaire survey method

Project questionnaire about classified the mistake in table tennis teaching .Investigate the national table tennis teaching experts and professors.

3 Design and analysis of courseware

3.1 Analysis of the courseware requirements.

Multimedia courseware mainly used for the students in table tennis general class auxiliary teaching .Teachers can make multimedia courseware presentation in class while students can learn by themselves through the courseware .In a questionnaire on students learn., students have access to media teaching method. The main teaching method is by slide and videos mainly in theory class. Students feel more vivid after watch it, willing to accept multimedia CAI courseware in sports technology.

3.2 The guiding ideology of courseware design.

Changing the teaching method is for the purpose to improve the quality of teaching. This courseware guided by the modern education thought. This courseware based on teaching book <the rules of table tennis match>. This courseware combined with modern education technology and traditional teaching methods. Build a new teaching type about the rules of table tennis. Give students a learning environment combined with vivid and visual through the application of courseware. Achieve the goal of reforming and improving the teaching method and objective .Improving the teaching efficiency and quality. What teachers teaching (to students) and how teachers teaching (through what way to teach) is the mainly problem in multimedia teaching. The category, number and the intension of information and the transmission media all affect the process of teaching and development in learning. Different learning stages are based on the basis of previous learning phase. It is not a simple repeat process, but a development of the sublimation for students. So, it is our basic guiding ideology that how to make difficult textbook to be suitable for mental ability development. Transmitting and speeding the process to students effectively through a variety of media

3.3The goal of design courseware

Teaching goal is the basis of all teaching activities. Grasping the teaching goal influence the choice of teaching media and the design of teaching unit. CAI courseware in design should pay attention to the teaching goal of guiding role. According to the content and requirement of <the table tennis match rules>, the CAI courseware 'goal is: Give students a learning environment combined with vivid and visual through the application of courseware. Make full use of the courseware guidance, demonstration and the interactive practice function. In order to make students master the content and the connotation of <the table tennis match rules>.Improving students' learning interest, efficiency and the practical ability.

3.4 The principle of courseware design

The general principle: This courseware produced by Macromedia Authorware7.0 platform. After completed, files are packaged to generate in the form of an application suffixed by '.exe', and it can be used in any computer without the software, which is fully based on the general principle.

The scientific principle: It mainly displays in the scientific description of the concept, the accurate statement of the problem and the correctness of the reference data. This courseware ensures that the rules of the original content remains the same in the production process .And to explain the rules by texts and graphics, through access to various data, it makes every effort to make the courseware more normative and accurate.

The principle of elicitation: The CIA courseware in the design and production should focus on the teaching objectives, and is teacher-led, student-centered. Through the multimedia CAI courseware provides vivid, intuitive materials, to stimulate students' association, arouse learners' knowledge in long-term memory, their experience so as to assimilate new knowledge, to cultivate learners' innovation consciousness. Therefore, the design of CAI courseware on the choice of content and form also follows the principle of inspiration innovation.

3.5 Courseware platform

PE teacher's choice of tools to make courseware are various, such as PowerPoint, Authorware7.0, Director Flash. This courseware is based on Authorware7.0 as platform. Macromedia Authorware7.0 is an interactive multimedia authoring tool based on flow charts. With its advanced, rich visual media production solution, elements like pictures, animations, text and films can be fused into the field of multimedia applications. Furthermore, some pictures will use Photoshop for partial treatment, to produce more professional multimedia courseware.

3.6 The script writing of a courseware

Before making a courseware the primary task is to write a script that is the core and main basis of a courseware, and will have a direct impact on production quality of the courseware. The courseware based primarily on "(2006)," Table Tennis Competition Rules "compiled by Chinese Ping Pong Association, and also it keeps an eye on the latest version of other rules and some constantly

updated, revised books about tennis rules .I also collected some teaching experience from table tennis experts in our college, to strive to make writing scripts with strong authority and persuasive.

4 The analysis of basic structure of teaching material

Bruner subject structure points out that no matter what we teach it is important to make students understand the basic structure of the subject. Once students understand that and they can extrapolate. Therefore, when we study the teaching method, the key is to study the content, structure, logical relationship of the teaching material and students' learning methods. Through various media means, in order to be able to fully reflect the teaching material content in the limited teaching space, on the media design, first of all, not according to the order and structures of teaching materials to produce on a variety of media, but in the study, on the basis of the teaching material content, set up the logical structure of knowledge, in order to certain the key knowledge and learning levels of each chapter, and then we can choose the media. Second, based on the teaching material content and the logic structure of knowledge, we can increase the vivid picture, different angles of animations, etc., to rich the knowledge of classroom teaching, to build a good atmosphere of learning, and to increase understanding of the teaching material content.

5 Courseware development ideas

5.1 Basic principles of courseware design:

1) scientific2) universality 3) controllability 4) practicality

5.2 Courseware teaching objectives:

Give students a learning environment combined with vivid and visual through the application of courseware. Full use of computer graphics, images, animations and other features that enables students to develop the right concept of the action of Tennis Forehand Fast Break, to master the main points of the teaching content, to improve students' learning efficiency and to broaden their knowledge.

5.3The production of the courseware materials

5.3.1The production of the text:

Making the text includes two aspects. The first is WordArt production in interface part. It is achieved through Word and Photoshop, The second is the production of context, which is use Word for production.

5.3.2 Image production:

Most images in the courseware are formed by the scanner, and then processed by Photoshop. But some images are produced by "Brush" software and then processed according to Photoshop.

5.3.3Animation production:

Animation production is the most important and most difficult step in the process of making a CAI courseware about Tennis Forehand Fast-Break. In this case, the animation means using POSER4.0 animation software imitate the movement on computer. Because most of the courseware demonstrations are done by the animation, its quality will directly affect the quality of the courseware. The overall courseware production is achieved by Authorware7.0.

6 Conclusions

6.1 The design and manufacture of multimedia teaching should highlight the characteristics of the teaching material content, and to solve the difficulty in the routine teaching as the development of multimedia.

6.2 Multimedia table tennis teaching highlights the importance of feedbacks, enlarges the way of teaching information’s transmission, enriches the students' learning activities, and makes students learn independently.

References

[1]Tianming Sun, Ping Li. Introduction the forehand attack method in sports college table tennis ordinary class [J] Liaoning sports technology 1995 5

[2]Yanling Sun, The research and analysis of develop table tennis forehand attack method by CAI courseware [J] Guangzhou Sport University academic journal 2004 7

[3]Bei Hu, Development and application of left push and right attack of table tennis by multimedia CAI courseware Guangzhou university sports institute Masters thesis 2011 7

[4] ChaiWanglin, the construction of campus culture and quality-oriented Education, School management, 2008.9

[5] Fu Derong, education informatization and educational information competence, China Audio-Visual Education, 2003(2)

Advanced Materials Research Vols. 989-994 (2014) pp 5169-5172
© (2014) Trans Tech Publications, Switzerland
doi:10.4028/www.scientific.net/AMR.989-994.5169

Construction the Bottleneck and Countermeasures of BIM High-end Talent Cultivation in Colleges and Universities

Baoku Qi[1, a], Hong Xue[2,b]

[1,2] Shenyang Jianzhu University Room 9， Hunnan east Road，Hunnan New District, Shenyang City， Liaoning Province , China.
[a]1633818090@qq.com, [b] 573412980@qq.com

Keywords: BIM;BIM high-end talent;Colleges and universities;Communication platform

Abstract: With the construction of "The 12th Five-year Plan" put BIM (building information model)On the agenda,the development of construction industry is more and more inseparable from the BIM high-end talent.Based on the analysis of the development of BIM at home and abroad and applications in the construction industry and the present situation of fostering BIM high-end talent, on the basis of the fuzzy comprehensive evaluation model based on AHP is established. Discuss the bottleneck of BIM high-end talent cultivation, and find out the key factors ,meanwhile put forward countermeasures,which provides scientific basis for fostering BIM high-end talents.

Introduction

What BIM will cause a technology revolution in the construction industry has been unstoppable trend.At present, in our country, to vigorously promote BIM technology is very timely and necessary.But based on the development of BIM in China at an early stage, technology and theory is not yet mature, which extreme lack of high-end talent plus construction industry.High-end talent fostering BIM is vigorously carry out the ministry of education on deepening the reform of personnel training mode, and improve the systems and mechanisms to improve the quality of teaching.In-depth implementation of the teaching quality and teaching reform project in colleges and universities, the employment as the guidance of the support of the reform and construction of colleges and universities.BIM construction and practice of teaching idea at the same time, to carry out the training curriculum system, cultivating both conform to the requirements of the construction industry development and talents of integrating with social practice, for the BIM high-end talent shortage and college students difficult employment problem put forward an effective solution.

The current situation of the development of BIM and it's application in the construction industry

The foreign current situation of the development of BIM
Abroad, development of BIM technology is already very mature.At present, the study of the theory of the BIM technology is ripe.It is rich practical experience in developed countries and wide application range.Such as the United States, Japan, Singapore and other developed countries It's worth noting that the government agencies, private enterprises in various fields such as construction industry and academia is widely involved in research of BIM technology.
Domestic development status of BIM
In our country, the development of BIM is still in the primary exploring stage.BIM technology in our country's construction industry is mainly used in engineering design, consultancy and training institutions.With the popularity of BIM technology application, the department of housing and urban-rural development put forward, in the "twelfth five-year" period, the basic elements of a construction enterprise information systems, to popularize and apply to speed up the building information model (BIM),and web-based collaborative work, etc. New technology application in the engineering, promote the construction of the information standard, carry out the research and application of BIM technology, and promote the BIM technology application extends from the design phase to construction phase.

The application of BIM in construction industry
The rapid development of BIM and its own technical advantages, which determines its will be applied to all aspects of the construction industry, including the owners and developers to design, construction, cost, purchasing, marketing, management scope;Design unit building, structure, water supply and drainage, HVAC, electrical, fire protection, design of the technical and economic activity;Construction enterprise project management, engineering cost, construction plan, construction technology, operational property agency operations, maintenance, and all kinds of activities will involve the application of BIM technology.

The current situation of talents fostering BIM

BIM began to be China's colleges and universities focus on research in 2006 , but in this short eight years has also made gratifying achievements.
First of all, in the early period of the colleges and universities to establish associated with BIM software courses.According to the latest statistics in 2013, 85% of colleges and universities have courses in CAD.With the development of BIM, most colleges and universities for engineering construction (especially to the characteristics of colleges and universities) has set up a 3 d software similar to that of the BIM course, such as Revit software.Some universities have courses in BIM software.

Secondly, colleges and universities set up scientific research institutions.Some universities have established BIM research and research centers. A growing number of doctor, master choose BIM technology as a research direction, which promote the development of BIM technology in our country.
Third, colleges and universities actively take part in the national colleges and universities BIM software building information model contest.With the development of BIM technology, colleges and universities participate in this contest in the constantly expanding.The number form 70 universities to the 147 universities .The fifth session of the national colleges and universities , cup contest of BIM software modeling start-up and format the workshop ended successfully.According to statistics, there are 248 colleges and universities to participate in the competition.

The bottleneck of BIM high-end talent in college education

Analyze the bottleneck of BIM high-end talent
With gradually promotion of BIM technology and further to speed up the pace of construction industry fields as well as the society and the construction industry for BIM talent demand is increasing, the BIM high-end talent cultivation reforms in colleges is inevitable.But there exists a series of obstacles in the process of the implementation of the promotion.This article selects the BIM technology experts to hinder the implementation of BIM factors discussed analysis of high-end talent training.After discussion experts divided it into four categories: technical factors, economic factors, operational factors, motivation factors.
The college education of BIM bottleneck of high-end talent evaluation index is established
Through implementation of BIM high-end talent cultivation in colleges and universities ,it established the evaluation index system of high-end talent cultivation in colleges and universities implement BIM bottleneck.The system includes four indicators: technical factors, economic factors, operational factors, motivation factors.4 first-level indicators have 15 secondary indexes.
Based on the AHP ,it hinder the implementation of BIM high-end talent training the weight of each factor

College education of BIM high-end talent countermeasures

Satisfy the demands of high-end talent fostering BIM technology
At present, the domestic BIM database development work is not perfect, and the existence of such problems as IT forces are relatively weak in the process of BIM high-end talent cultivation in colleges and universities .In order to solve this problem, the country can focus on cultivating talents

on BIM standards (put BIM standard research talent) and BIM tools (make BIM software tools development and research of talent).Government established the BIM software and tools, for example, research and development team, and with BIM technology developed countries (the United States, Singapore, etc.) on BIM technology exchange meeting, cultivating a understand information professional knowledge of sexual talents.Software development companies and research institutions can be committed to the development of BIM related software, can provide operating software for the society.

Solve the problem of talents fostering BIM funding

According to this article ,evaluation of high-end talent fostering BIM bottleneck analysis is derived from the funds of the issues hampering the more facing colleges and universities.To solve this problem, from the state, universities and enterprises can take measures three aspects.The government should appropriately increase the fiscal expenditure of high-end talent fostering BIM.It regularly organize BIM technology expert lectures and guidance for colleges and universities, also it can create BIM communication society, which provide a platform for fostering BIM high-end talents.University management personnel shall adjust the BIM high-end talent training of education funds to purchase BIM software to provide teachers and students to learn hardware facilities.Teachers and students are encouraged to attend BIM technical training.Construction companies and BIM training institutions can make the corresponding contribution.The construction enterprise investment for colleges and universities, for example, cooperation to develop high-end talent plus;Training institutions and universities alliance, to lower the cost of both teachers and students study BIM software, etc.

Improve the operating environment of BIM high-end talent cultivation

In the process of BIM high-end talent cultivation in colleges and universities ,it faced with relevant experts, less teaching platform not perfect, and low software developer support.To solve these problems should be from the state, colleges and universities, and software developers.Countries introduced corresponding policy, perfecting the BIM database, and establish a system of BIM education system, as well as the development of China's construction industry to promote application of BIM technology is obtained and concrete goal, to various colleges and universities put forward operable, which helps for research;Colleges and universities can provide operating BIM software platform (e.g., colleges and universities established BIM training center), cooperating with BIM training institutions to establish a good interaction system.Software developers BIM software develope more adapt to China's development, the cultivation of the colleges and universities support policy, which will prepare for the implementation of BIM software development work.

Promote the fostering BIM high-end talent policies

Government can encourage eligible university priority to implement of BIM high-end talent training scheme.Found the problem from the university of training scheme and timely solve, sorting, summed up a set of feasible reform education plan, which is introduced in the universities.University management should not just be satisfied with their current mode of education.They should organize relevant personnel of colleges and universities hold seminars dealing with BIM technology revolution education mode reform policy.Recruiters (mainly refers to the enterprises related to construction) should realize that there exits storm by the BIM transition from 2 d to multidimensional , and the storm will bring change to the future development of the enterprise direction.For construction enterprises in the recruitment, it consciously choose BIM high-end talent for encouraging universities to develop high-end talent plus, and paying attention to the acceptance of BIM talent.

Conclusions

Currently, what BIM will cause a new round of revolution in the construction industry after CAD has no doubt because government had to write BIM clear into the development of construction industry "Twelfth five-year" plan and it will be phased in and go deep into the construction of various fields.BIM is expected to become the theme of China's construction industry information in the next decade.It analyzes the bottleneck of BIM high-end talent cultivation, and find out the key

factor affecting college education of BIM high-end talent.From the perspective of countries, colleges and building enterprise it put forward countermeasures, receiving in the process of promoting talents fostering BIM always adhere to the "national guide, industry forward".Providing effective BIM high-end talent cultivation in colleges and universities of the platform, We look forward to the smooth implementation of colleges and universities to develop high-end talent plus plan just around the corner.

References

[1]Jianxin Zhang,he building information model applied in the engineering design industry in our country barriers to study [J]. Journal of engineering management, 2010, 8 (4) : 387-392.
[2]Chuang Qiu based on the architecture model (BIM) project management revolution [J]. Journal of construction and management of joint pioneer, 1).
[3]Qinghua He,BIM application at home and abroad, the status and obstacles to study [J]. Journal of engineering management, 2012, 11 (26) : 012-016.
[4] Yabin Huang, enterprise-level BIM application implementation steps [J]. Journal of information technology in civil engineering and construction, and 2013.3 (2) : 56-61.
[5] Guanpei He, BIM in China development strategy and pattern to explore (1). Information technology in civil engineering and construction, 2011.3 (2) : 114-118.

Advanced Materials Research Vols. 989-994 (2014) pp 5173-5177
© (2014) Trans Tech Publications, Switzerland
doi:10.4028/www.scientific.net/AMR.989-994.5173

Purchase cost control in Electronics Manufacturing Service(EMS) corporations

Daixi Lin [a], Zhouyang Lu [b*], Li Ma [c]

Business School, Hohai University, Nanjing, Jiangsu Province, China, 211100
[a]daixilinhohai@163.com, [b]lzyseu@hhu.edu.cn, [c]mary_mali_99@sina.com
*corresponding author

Keywords EMS; Purchase cost; Cost control

Abstract The rapid development of electronic technology has produced numerous demands, which have generated a new-born industry--EMS. In EMS corporations, purchase cost is a large proportion of total costs, so purchase cost control is one of the key competitiveness for EMS. Analytic Hierarchy Process (AHP) help EMS solve the problem of purchase cost control.

Introduction: The Analysis of Purchase Cost of EMS Corporations

EMS offer a service chain to OEM (Original Equipment Manufacturing). Chinese EMS industry is rapidly developing. iSuppli estimated that 75 percent of industry increases were made by Chinese EMS industry. But the average rate of net profits in EMS industry is only 2 to 5 percent. Purchase cost of EMS includes material costs, ordering costs, maintenance costs and shortage costs.[1]

Definition of Purchase Costs Control of EMS Corporations and their Limitations.

1. The definition of purchase costs control of EMS corporations.

1st parity purchasing. 2nd : centralized purchasing. 3rd : the third-party logistics . 4th : avoid import risks by localized procurement.

2. Limitations on purchase costs control of EMS corporations.

1st : ineffective purchase cost control: in the BOM of EMS, more than 80 percent of materials are appointed by OEM. 2nd : External market is unpredictable. 3rd orders uncertainties. EMS have to buy already-made products. 4th : some suppliers show incongruous when negotiating.

3. Using The Analytic Hierarchy Process (AHP) to Control Purchase Costs of EMS.

AHP[2] separates problems into factors then arrays hierarchies by comparing importance.

(1) The Establishment of hierarchical analysis model

① 1st "the best purchase costs control of EMS ". 2nd principal hierarchy: purchase costs projects controlled by customers. 3rd : the subprincipal hierarchy made by every factor.

② Take factor of principal hierarchy having downward affiliation as the first factor to make a judgment matrix.

Then fill in the judgment matrix by importance comparison as Table 1:

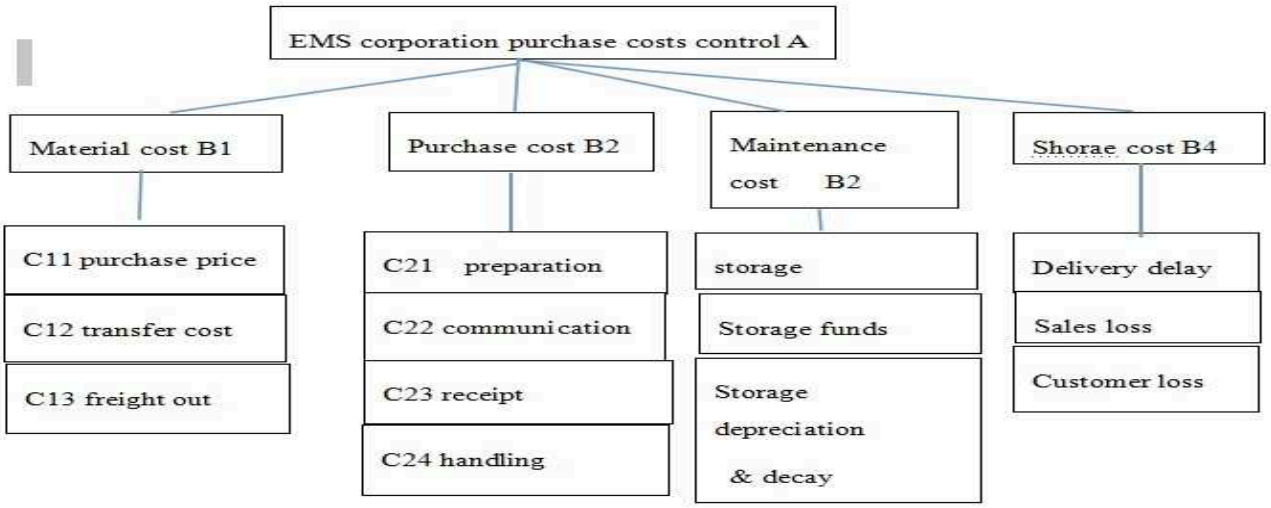

Fig 1. EMS Purchase Cost AHP chart

Table 1: Scale exponents to Evaluate Matrix Factor B_{ij}

Scale exponents	Meanings
1	The two factor weigh same after comparison
3,5,7,9	Factor i weighs more than factor j after comparison
2,4,6,8	The mid-value of exponents above
Reciprocal	Judgment of factor j and factor i is $B_{ij}=1/B_{ji}$

a. Invite S employees of EMS corporations and experts in related fields to participate.

b. Assign experts weights λ_k : high-grade experts weight 1.2, others weight 1, $\sum_{k=1}^{s}\lambda_k=1$.

c. Send the hierarchical analysis model, the blank judgment matrix and the table 2 to experts.

$$\overline{b_{ij}}=\sum_{k=1}^{s}\lambda_k b_{ijk} \tag{1}$$

$$\sigma_{ij}=\sqrt{\frac{1}{s-1}\sum_{s-1}^{s}(b_{ijk}-\overline{b_{ij}})^2} \tag{2}$$

b_{ijk} : given by K experts judging the factor in the i row and the j column of matrix.

a. Feedback the result and rejudge factor whose $\delta>\varepsilon$ =1, then establish the second cycle.

e. Factors whose standard deviation $\delta<\varepsilon$ =1, can be used as the values, Such as Table 3:

Table 2: $A \leftarrow \{B_1, B_2, B_3, B_4\}$

A	B_1	B_2	B_3	B_4
B_1	1	7	5	8
B_2	1/7	1	1/3	1/2
B_3	1/5	3	1	3
B_4	1/8	2	1/3	1

③ Compute the eigenvectors by "root method":

$$A=\begin{bmatrix} B_{11} & B_{12} & B_{13} & B_{14} \\ B_{21} & B_{22} & B_{23} & B_{24} \\ B_{31} & B_{32} & B_{33} & B_{34} \\ B_{41} & B_{42} & B_{43} & B_{44} \end{bmatrix} = \begin{bmatrix} 1 & 7 & 5 & 8 \\ 1/7 & 1 & 1/3 & 1/2 \\ 1/5 & 3 & 1 & 3 \\ 1/8 & 2 & 1/3 & 1 \end{bmatrix}$$

a. Compute the product M_i of factors in each row of judgment matrix A;

b. Compute the fourth power $\overline{W_i}$ of M_i;

c. Normalize $\overline{W} = (\overline{W_1}, \overline{W_2}, \overline{W_3}, \overline{W_4})$ and get the result:（0.6620, 0.0636, 0.1875, 0.0869).

④ Consistency check:

a. compute the eigenvalue of maximum $\lambda_{\max}$;

$\lambda_{\max} = \sum_{i-4}^{4} \frac{(PW)_i}{n\, W_i} = \frac{1}{n} \sum_{i-4}^{4} \frac{(PW)_i}{W_i}$, $(PW)_i$ is the i factor of PW, $i=4$.

$$PW=\begin{bmatrix} (PW)_1 \\ (PW)_2 \\ (PW)_3 \\ (PW)_4 \end{bmatrix} = \begin{bmatrix} B_{11} & B_{12} & B_{13} & B_{14} \\ B_{21} & B_{22} & B_{23} & B_{24} \\ B_{31} & B_{32} & B_{33} & B_{34} \\ B_{41} & B_{42} & B_{43} & B_{44} \end{bmatrix} \begin{bmatrix} W_1 \\ W_2 \\ W_3 \\ W_4 \end{bmatrix}$$

Plug the given values into it, we can get that $\lambda_{\max} = 4.4353.$

b. compute CI (Consistency Index);

$$CI = \frac{\lambda_{\max} - n}{n - 1}$$

c. Find corresponding RI (Random Index), shown in Table 4-8:

Tab. 3-8, Random Index

n	1	2	3	4	5	6	7	8	9	10	11
RI	0	0	0.58	0.90	1.12	1.24	1.32	1.41	1.45	1.49	1.51

Get RI from Table 3-8. A is a matrix with fourth order, and its RI =0.90.

d. Compute CR (Consistency Ratio);

$$CR = \frac{\text{CI}}{\text{RI}}$$

$A = \{B_1, B_2, B_3, B_4\}$=（0.6620, 0.0636, 0.1875, 0.0869）

CR =0.0501 <0.1, this judgment matrix is consistent. So, $A = \{B_1, B_2, B_3, B_4\}$=（0.6620, 0.0636, 0.1875, 0.0869)

e. Compute the weights set; Take *B1* as an example:

$B_1 = \{C_{11}, C_{12}, C_{13}\} = (0.7334 \ , \ 0.1990 \ , \ 0.0676 \ )$

Consistency check: $\lambda_{\max} = 3.0940$, $CI = 0.0470$, $CR = 0.0810$ <0.1

⑤ Results analysis:

EMS should pay more attention to cost with higher weight.

Table 3-9 Weight and rank of each item in total purchasing costs(Take A and B1 as examples)

Code	Item	Weight	Subcode	subitem	weight	Average Weight	rank
A	Purchase cost	1.000					
B1	Material cost	0.6620	C11	Purchase price	0.7334	0.4855	1
			C12	Transfer cost	0.1990	0.1317	3
			C13	Freight out	0.0676	0.0448	5

How to control purchase cost of EMS corporations

① Purchase price control

a. Use Target Cost Management, since what EMS presuming for is PPV (Purchase Price Variance).

b. Use Target Cost Management to control purchase price: compare standard one and real one.

c. If the price is predicted to be stable, long-tern cooperation can avoid purchase risk.

② Storage cost control

a. Establish effective information channels , combining bar code, POS systems and EDI.

b. Build rapid response system to set up a common cooperative goal.

References

[1] rongguang Huang, meixue Du: *The Analysis of Purchase Costs Control of Manufacturer Industry*[J]. Shanghai Management Science, 2006, 28 (6): 52-55)

[2] Zhao, Lindu: *The Management of Supply Chain and Logistics*[M]. China Machine Press, Beijing, 2007, 7

[3] Coyle, J: *The Management of Logistics of Corporations：From The Viewing Angle of Supply Chain* [M], China Machine Press, 2007.7, Beijing

[4] Coyle, J: *The Management of Logistics of Corporations：From The Viewing Angle of Supply Chain* [M], China Machine Press, 2007.7, Beijing

[5] Zhu, Jianjun. *The Research and Practice of Problems of AHP* [D] (Northeast University, Shenyang, 2005)

[6] Zhou, yun. *The Management of Purchase Costs and Suppliers* [M]. China Machine Press , 2009

[7] xinhui Lei, taoyong Su: *The Research of Strategic Cost Control Management* [J]. Journal of Fudan University (Natural Science), 2007(4): 457-459)
[8] Martin Christopher. Logistics and Supply Chain Management: *Strategies for Reducing Cost and Improving Service* [M]. Financial Times Prentice Hall, 2003.
[9] Wenzek, Hagen. Rewiring Electronics: *Discovering Strategies for Sustainable Growth from a Business Ecosystem Perspective* [J]. IBM Business Consulting Services, 2005(5):16-19.
[10] Michael A. Hitt, R. Duane Ireland, Robert E. Hoskisson: *Strategy management--competition and globalization*

Advanced Materials Research Vols. 989-994 (2014) pp 5178-5181
© (2014) Trans Tech Publications, Switzerland
doi:10.4028/www.scientific.net/AMR.989-994.5178

The Application of The Multimedia Technology in College Physical Teaching Reform

Shi Jian-hua

School of Science, Communication University of China Beijing 100024,China
shijh@cuc.edu.cn

Keywords: Multimedia Technology; College Physics Reform；Teaching Effect

Abstract. This paper aims to effective combination between college physics and multimedia to optimize the teaching procedure of physics as a serious basic course in college. Through combining multimedia technology with the teachers' subjective initiative, perfecting multimedia course system based on the network, multimedia simulation laboratory organic coupling with real experimenting, we discusses how the actual teaching use of multimedia technology，explore the application of the rules and characteristics of multimedia technology. we are able to develop the advantages of multimedia and explore its potential so that we make it better service in physics teaching and enhance teaching effect .

Introduction

Physics is a natural science based on experiments. The knowledge, understanding and master of physics concept by students relies on the perception of physical phenomena. The content for teaching of university physics covers mechanical, thermal, electromagnetics, optics and modern physics with less relationship between them, and similar with that for high school physics curriculum, reducing students' interest. However, for traditional teaching of college physics, only certain physics experiments can be present to the students in the classroom, and the students can not access to dynamic and intuitive perceptual knowledge and clear physical pictures. Most students think it difficult to learn university physics. Although multi-media teaching method has been applied, it is still insufficient. The usage and method needs to be improved, and the means need further improvement and exploration.

Effective application of multimedia technology in university physics teaching can change the form of information, integrating graph, text, sound and image on PC, improving the expressive force of the teaching content, so that the students can actively participate in multi-media activities via multi senses, mastering the knowledge actively instead of passive acceptance. At the same time, it also provides a powerful tool for teaching and research, as well as reliable and technical support for smooth and efficient teaching. In addition to improvement of knowledge, application of multimedia can make the single straight teaching content intuitive, so as to inspire the enthusiasm of students, improving learning efficiency. Integrating graph, text, sound and images, the multimedia courseware can not only reproduce or simulate various physical experiments and phenomena, but also simulate the physical process, presenting physical laws more intuitively, so as to increase expression of the teaching content, mobilize students to participate in multi-media activities via multi senses, improve classroom atmosphere, attract the attention of students to better stimulate learning interest, while contribute to clarifying the physical ideas, processes and methods. Application of multimedia technology can provide students with vivid, clear, realistic emotional material in the classroom, so that students can perceive complete, clear and image physical phenomena which is difficult to observe or achieve, feel many scene which is impossible in traditional teaching in classroom, building physical model with initiative. Moreover, the students

can understand physical concepts, laws and theorems more easily; at the same time, the teaching is easy and the efficiency is increased.

By effective application of multimedia courseware in university physics teaching, the writing and drawing amount of teachers on the blackboard will be reduced greatly. The teachers can spend more time for lectures, delivery more quality information in the classroom with same teaching hours compared with traditional means. Therefore, it is necessary to use multimedia courseware effectively in the university physics teaching, and significant to improve college physics teaching effectiveness and level.

Effective Usage of Multimedia Technology in University Physics Teaching

Effective Combination of Multimedia Technology and Teacher's Initiative. Most concepts and laws in common university physics textbooks are derived via abstract theories and complex mathematical formulas. For the students, it is very difficult to master and understand the physical concepts and laws via complex mathematical formulas in a short period. As a classroom teaching aid, the advantage of multimedia courseware in the physical classroom is dynamic simulation, which can simulate visual experiments via unique analog animation, creating good physical scenarios to stimulate students' interest. So the students can achieve distinct impression, grasp and understand physical concepts and laws quickly.

In practice, the multimedia courseware for university physics must be fine and simple, demonstrating critical contents. The multimedia should mainly solve important and difficult points for classroom teaching, explain and deal with physical theories, processes and phenomena which are difficult to clear via traditional methods and media.

Application of multimedia courseware in university physics to make up traditional teaching not only saves the time, meeting teaching requirements, but makes abstract physical content more visual and intuitive via combination of video and audio means. In addition to shorter teaching time and higher teaching density, the teaching efficiency and quality is greatly improved, so as to accommodate and promote combination of university students with their ability.

There are two sides to everything, including multimedia teaching as a new form of teaching means. The teachers must not weaken their dominance in the classroom just for using of multimedia courseware. To avoid using of multimedia lesson as another blackboard and teaching the students just via the video, the teachers should focus on guiding students to analyze physical phenomena and principles, inspire and coach students to think, deepening understanding of physical concepts, processes, laws and theorems, teaching students to analyze and solve problems.

Improving of Web-based Multimedia Courses. University physics covers mechanical, thermal and electromagnetic contents etc. Generally due to less class, the students’ questions can not be resolved in time, and difficult to review, weakening the enthusiasm of students to a certain extent. Qualified teachers can provide college physics multimedia course system, including complete teaching files, clear requirements and rich materials, covering course, submission and correction of homework, analysis of samples, simulation of exams and real-time Q&A etc.

Online University Physics Multimedia Paper Evaluation System is a new model of teaching management. This system provides the students with a set of university physics simulation exams for the students to simulate test on PCs and prepare for formal exams. Through the system, the students can test mastering of university physics by themselves in order to consolidate learning results. University physics examination mainly tests mastering of basic physics knowledge by the student, covering multiple choice, true-false, fill-in-blank, short answer, calculation and proofs. After the student submits the test, the scoring system gives the score immediately, so as to stimulate student's motivation for learning. At the same time, the system must be able to collect and store student's number, name, profession, class, scores and other information, to provide raw data for analysis of the paper and mutual assessment between different courses, so as to provide the basis for teaching management, feedback of teaching information and improvement of the quality.

Combination of University Physics Multimedia Simulation Lab with Real Experiment. Physics experiment is the basis of physics, an integral part of physical education, promoting teaching of physical theories. Real experimental demonstration is an irreplaceable part of university physics teaching, playing a complementary role. Demonstration experiment is set to compensate the teaching content in class, which is mainly operated by teachers. A well-designed experimental demonstration will show the basic physical quantities in a simple form, helpful for students to establish a physical image of abstract concepts, contributing to understanding and mastering of the concept and laws, breaking through difficulties, broadening view of students, stimulating imagination, increasing interest of learning, and bringing up of students' ability.

The simulation laboratory is an innovative model of physics experiment teaching, integrating lab equipment, teaching content, teachers' guidance and thinking/operations of learners organically via PCs, forming a lab system to simulate virtual experimental environment. The system provides a powerful tool for physics experiment teaching, while overcoming the long-term class/time limitation of experimental teaching, extending the content concerning time and space, effectively improving the quality of preview, review and the experiment, comprehensively improving the actual ability, helpful for training of innovation and exploring spirit, so that the students can obtain systematical experimental theoretical techniques and complete skills.

Almost all physical process, phenomena and experiments can be reproduced vividly via multimedia means. Thus some teachers tend to use multimedia courseware instead of the real demonstration experiments in the class, completely dependent on the multimedia courseware. This teaching idea and method shall be corrected. The teachers must carry out real demonstration experiment in the classroom for students instead of multimedia tools as possible to demonstrate physical processes and phenomena. On one hand, this will train students to observe and analyze the real physical processes and phenomena, guide students to master the physical nature, understand and grasp the real nature; on the other hand, it will train the students to respect scientific idea and spirit of exploring for truth.

Conclusion

High-quality university physics multimedia courseware is the best means to provide a variety of audio-visual images, which can show a lot of physical processes and phenomena vividly which is difficult by common means. Especially, it combines the advantages of multimedia courseware for

university physics and that of traditional teaching of physics, greatly improving teaching results of college physics. Therefore, it is very important to strengthen and improve research of university physical multimedia technology, focusing and strengthening combination of advantages of multimedia technology and traditional teaching, so as to improve the quality of university physics teaching.

References

[1] Zhang Xiao-zhen. Curriculum Reform and computer aided instruction [J]. Curriculum, teaching materials, teaching methods, 2002

[2] Li Hui-zhang. Physical design and development of multimedia courseware [J]. Tianjin Vocational Technical Teachers College, 2004, 14 (2)

[3] Chen Jian,Qian Wei-ying,Zhu Chun. The implementation of modern teaching physics program profiles [J]. Wuxi Institute of Education, 2004, 24 (2)

[4] Xia Hong-wei. Advantages of Using Multimedia Technology in Physics Teaching [J]. Journal of Inner Mongolia University for Nationalities,2003,8(4)

[5] Fu Jing.Discussion on teaching reform of University Physics[N]. Global Market Information Guide, 2013,24

Advanced Materials Research Vols. 989-994 (2014) pp 5182-5185
© (2014) Trans Tech Publications, Switzerland
doi:10.4028/www.scientific.net/AMR.989-994.5182

Prediction of Cigarette Sales Amount and Average Price based on Lunar Calendar

Yang Xiao

School of Management Science and Engineering, Shandong University of Finance and Economics, Erhuan East Road 7366, Jinan, China

Email: yangxiao@sdufe.edu.cn

Keywords: Cigarette Sales Prediction; ARIMA; Lunar Calendar

Abstract. Prediction of cigarette sales amount and average price is important for anomaly detection of orders, customers and cigarette brands. Besides this, prediction can be support of storing and production arrangement. By analyzing large amount historical sales records, a cigarette sales amount and average price foresting model is built to predict the weekly sales based on ARIMA model which using lunar time as the calendar. Result on the five years sales data from a Chinese city indicate that sales prediction based on ARIMA using lunar time can be an effective way to improve forecasting accuracy.

Introduction

In Chinese, tobacco sales are monopolized by the tobacco companies, so the prediction of sales volume and average price of all kinds of cigarette, and sales of each tobacco band are very important for the tobacco companies to analyze user preferences in each region. Prediction of cigarette sales can be used to guide the cigarette company to stock and develop sales policies according to smokers' preferences [1, 2].

There are a large number of orders and customer information during several years' accumulation in cigarette companies, which contains a wealth of information. We can use these data to predict the sales amount and average price using machine learning method.

Sales of cigarettes showed obvious seasonal fluctuations [3]. For instance, people will present gifts to each other in traditional holidays, and cigarette is one of welcomed gifts as a means of people interaction. Thus, cigarette sales increase much more influenced by the impact of holidays. Sales amount from years 2008 to 2012 of a municipal cigarette corporation is shown as an example in Fig.1. Meanwhile, the average price of the cigarettes is also showed obvious seasonal fluctuations, where Fig. 2 is shown as an example.

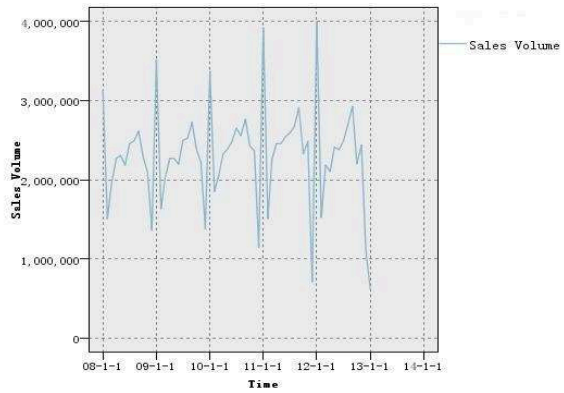

Fig. 1 Sales amount of a city in years from 2008 to 2012.

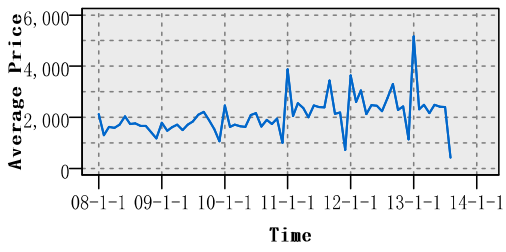

Fig. 2 Average price of a city in years from 2008 to 2012.

As can be seen from the cigarette sales amount and average price as Fig. 1 and Fig. 2, we can find cigarette sales meet the obvious characteristics of time series, and the time series of cigarette monthly sales showing seasonal fluctuations trend, therefore it often consistent with the typical characteristics

of double trend, and the predicted value tends to have a high correlation with the history of cigarette sales. For such complex nonlinear system, the classic stochastic models such as moving average and regression are unable to get satisfactory results, so we choose the ARIMA (Auto Regression Integrated Moving Average) model, which is a parametric stochastic model to detect the cigarette sales anomaly.

ARIMA Model

The ARMA model, which is a very suitable for predicting a stationary time series, is widely used in forecasting random phenomena of physical science, economics, weather etc.

Optimized from the ARMA model by an extra operation of difference on a non-stationary time series, ARIMA model [4] is used to forecast non-stationary time series. Non-seasonal ARIMA processes are defined by:

$$\theta_p(B)(1-B)^d y_t = w_q(B)a_t \tag{1}$$

where B is the backward shift operator, and for a non-stationary time series y_t, $(1-B)^d y_t$ could come to a stationary series by using the difference operator $1-B$. B satisfies $By_t=y_{t-1}$ and $B^k y_t=y_{t-k}$. Additionally, p, d and q are integers. The equations

$$w_q(B) = 1 - w_1 B - w_2 B^2 - w_3 B^3 - \cdots - w_q B^q \tag{2}$$

$$\theta_p(B) = 1 - \theta_1 B - \theta_2 B^2 - \theta_3 B^3 - \cdots - \theta_p B^p \tag{3}$$

are polynomials in B of degrees q and p. The integer d is the number of regular differences, p is the order of $\theta_p(B)$, q is the order of $w_q(B)$, and a_t is a current interference with mean = 0 and variance σ^2. Typically, we consider a_t as the estimated residual at time t. Meanwhile, a_t is also an independent and identically distributed normal random variable. The roots of $w_q(y) = 0$ and $\theta_p(y) = 0$ should all lie outside the unit circle.

The ARIMA model can get a reliable predictive result to short-term forecasting which have stable and seasonal characteristics, and can achieve the desired confidence interval. In addition, ARIMA model has strong flexibility, and it can express the various properties of time series of the data. So, ARIMA model is a widely applied time series model has been analyzed extensively by researchers and used widely by forecasting practitioners due to its attractive theoretical properties and empirical evidence.

Prediction on ARIMA Using Lunar Calendar

In some traditional lunar festivals, especially Autumn Festival and Spring Festival, which are the most important traditional festivals to Chinese, people have custom to send each other gifts [5]. High-grade cigarettes and wines are one of the important gift-giving items. Therefore, the sales of cigarettes will surge in these traditional festivals. This trend can be reflected in consumer sales fluctuations in Fig.1 and Fig. 2. Therefore, we are modeling ARIMA on lunar time to forecast sales when encounter the Chinese traditional festival, while forecasting based on solar time in other time.

Since the ordering is arranged by week, that is to say, customers have only one chance to order cigarette in a week, we predict the weekly sales amount and average price. Using the weekly sales data between years 2008 to the first half of 2013, we forecast the sales amount and average price of the next 4 weeks. The prediction is done on solar and lunar calendar separately. After deleting the null record, prediction based on ARIMA model is carried on in Clementine which is widely used data mining software. Prediction on the solar calendar and lunar calendar are carried through respectively to test the effectiveness of time-series analysis model established on lunar time. After differencing, the Clementine choose automatically ARIMA(1,0,2) for average price and ARIMA(2,0,7) for sales amount on solar time, and choose ARIMA (0,1,2) for average price and ARIMA(1,0,7) for sales amount on lunar time. The prediction results are shown in Fig. 3 to Fig. 6. From the figures, we can see intuitively that the ARIMA model can fit the data well.

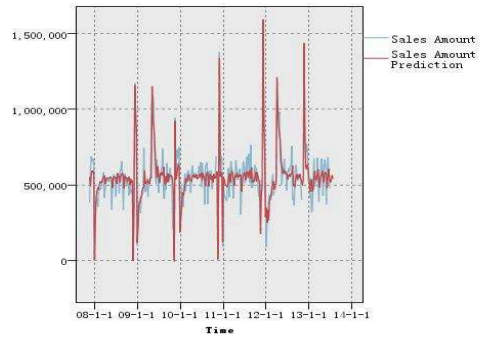

Fig. 3 Prediction of Average Price on lunar Calendar

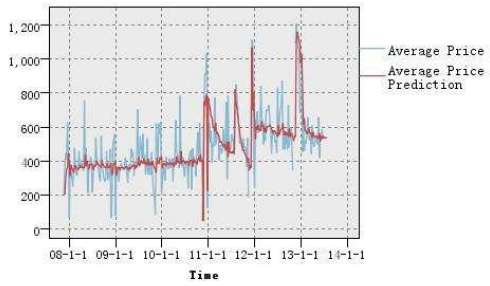

Fig. 4 Prediction of Sales Amount on lunar Calendar

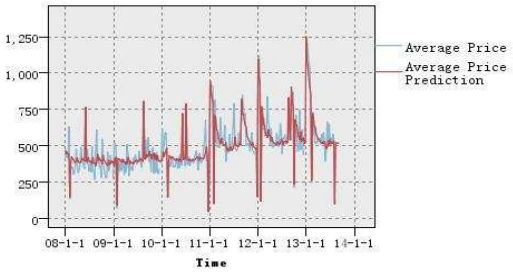

Fig. 5 Prediction of Average Price on Solar Calendar

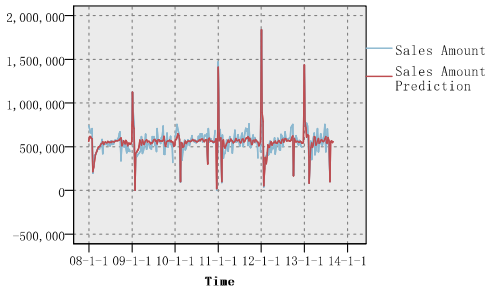

Fig.6 Prediction of Sales Amount on Solar Calendar

To compare the predictive effect of weekly sales volume and average price on solar calendar and lunar calendar, the metrics R2, RMSE, MAPE and MAE are given in Table 1 and Table 2.

Table 1. Weekly prediction accuracy of sales volume on solar and lunar calendar.

	on solar calendar	on lunar calendar
R2	0.8663	0.9307
RMSE	137055.1	176713.4
MAPE	4.945791	5.846084
MAE	96897.58	123969.8

Table 2. Weekly prediction accuracy of average price on solar and lunar calendar.

	on solar calendar	on lunar calendar
R2	0.7760	0.9613
RMSE	420409.7	269789.5
MAPE	8.9541	5.1877
MAE	276129.8	176978.4

Assume a data set has values y_i, and each of which has a predicted value $\hat{y}_i$, the four metrics are defined as follows:

$$R^2 = 1 - \frac{\sum_i (y_i - \hat{y}_i)^2}{\sum_i (y_i - \bar{y})^2}, \quad \text{where } \bar{y} = \frac{1}{n}\sum_{i=1}^{n} y_i \tag{4}$$

$$MAE = \frac{1}{n}\sum_{i=1}^{n} |\hat{y}_i - y_i| \tag{5}$$

$$RMSE = \sqrt{\frac{1}{n}\sum_{i=1}^{n} (\hat{y}_i - y_i)^2} \tag{6}$$

$$MAE = \frac{1}{n}\sum_{i=1}^{n} \left| \frac{\hat{y}_i - y_i}{y_i} \right| \tag{7}$$

The MAPE of four models are all under 10, which illustrate the predictive accuracy on both lunar and solar calendar is relatively high. From the tables, we can see that the predictive accuracy based on lunar is better than on solar in general. Especially R2, which is a metric to measure the fitting degree of model, model on lunar is much better than the one on solar. And the RMSE, MAE and MAPE of sales volume on lunar calendar are lower than the solar calendar, which show the superiority of the

model. But the RMSE, MAE and MAPE of sales volume on lunar calendar are higher than the solar calendar. Through analyzing the data, we found that the lunar time is cannot be used directly in the model. For example, the month April and May in year 2012 is both convert to April, because April in lunar year 2012 is an intercalary month in the lunar calendar. Then the sales volume in April of year 2012 is summed by April and May in solar calendar, so it is extremely high. But the average price is not affected by the intercalary month in the lunar calendar, so all of the metrics is better than the solar time. Based on the above discussion, the prediction on lunar time is used only when encounter lunar festival, and prediction on solar calendar is used for other data.

Conclusion

ARIMA model consider trend variation, periodic variation and random disturbance comprehensively, and the model parameters can be quantified to remove people's subjective judgment to a certain extent, so it is widely used in prediction.

This paper used five years data to predict the sales amount and average price of the cigarette, this work can help officers to specify cigarette market.

The conversion from solar time to lunar time is not much accurate, manual correction should be done to improve the predictive accuracy. The sales amount and average price can be affected by other factors, such as policy. The future work should include these factors.

Acknowledgements

The work presented in this article was supported in part by the research grant from National Science foundation of China (No.61201269), the Foundation of the Ministry of Education, Humanities and Social Sciences (No.10YJC630017), Shandong Doctor Foundation (No.BS2011DX026), Shandong Social Science Planning Fund Program (No.13CGLZ02), Shandong Provincial Natural Science Foundation, China (No.ZR2013GQ011) and Humanities and Social Sciences Project of Shandong Provincial Education Department (No.J13WG19).

References

[1] B Luo, L Wan, WW Yan, JJ Yu, A New Type of Combination Forecasting Method Based on PLS - The Application of It in Cigarette Sales Forecasting, American Journal of Operations Research, 2012, 2, pp. 408-416.

[2] Lan LV, Yuesong TONG, Hongmei ZHANG, Application of Seasonal Decomposition on Short-Term Forecast of Cigarette Sales in Xifeng, 2012 International Conference on Engineering and Business Management, pp. 792- 796.

[3] Aiyun Zheng, Weimin Liu, Fanggeng Zhao, Double trends time series forecasting using a combined ARIMA and GMDH model, Control and Decision Conference (CCDC), 2010 Chinese ,pp.1820-1824, 26-28 May 2010.

[4] Asteriou, Dimitros; Hall, Stephen G. (2011). "ARIMA Models and the Box–Jenkins Methodology". Applied Econometrics (Second ed.). Palgrave MacMillan. pp. 265–286.

[5] Zou yimin, Research on lunar-based time sequence forecasting model and its applications on tabacco sale forecasting, Master's degree thesis, University of Inner Mongolia, 2008.

Advanced Materials Research Vols. 989-994 (2014) pp 5186-5188
© (2014) Trans Tech Publications, Switzerland
doi:10.4028/www.scientific.net/AMR.989-994.5186

The study of SWOT analysis and countermeasures on developing tourism resources in Xinxiang City

Xiuxia LI

School of Art and Design，Xinxiang University,Henan,China,453000

14878670@qq.com

Keywords: SWOT analysis ; tourism resources; Xinxiang City

Abstract: In the course of developing regional tourism resources, there are certain strength, weakness, opportunity and treat, which can be exchanged each other. To analyze SWOT factors scientifically and suit measures to local conditions serve to change disadvantages into advantages and challenges into opportunities. The paper analyses SWOT in Xinxiang city and realizes that Xinxiang should establish itself both in resources and market. Xinxiang should develop from all directions and depth.

0.Introduction

Andrews SWOT analysis is a strategic analysis framework proposed by the American scholars in the 1970s which is a method to the development direction for the research object with the comprehensive consideration of SW (internal strengths and weaknesses) and OT (external opportunity and threat), With the deepening of tourism and related disciplines, the tourism development mode based on the SWOT which is more and more mature, has become an important tourism development process analysis method.

1. Advantage in developing Xinxiang tourism resource

Richness in natural, excellent cultural resources.

Xinxiang is rich in natural tourism resources, famous TaiHang mountains is located in the south of Xinxiang[1].Due to the Taihang mountains in the geography of the second and third stage joint, natural formed unique cliffs, cliffs, waterfalls, temperature Spring, is the first choice for people of the north travel for an outing. Xinxiang's tourism as the pillar of the henan tourism area, within its borders Thousands of taihang mountain scenic spot has a beautiful town, baligou's water scene, guanshan's lofty mountain, huilong's jun, male of baoquan, as well as the king of qi village and paomaling amorous feelings. Xinxiang, relying on the unique natural scenery has become a henan tourism Card, every year attracts millions of tourists at home and abroad to visit and sightseeing. In addition, xinxiang is rich in water resource, is located in Two main river of the Yellow River, the haihe river. Xinxiang Yellow River communist-held existing a large number of lakes, swamps and wetlands, a national forest Park, wetland nature reserves and other precious natural resources.In addition, xinxiang has a long history and profound culture Background, Xinxiang is the activity center from xia-shang-zhou dynasties, the shang dynasty were reincarnated. In the long history of xinxiang Its unique historical and cultural background for human left behind the precious wealth and rich historical relics，familiar King zhou period's story coring of bigan. Chow time's makino war, Spring and Autumn Period's relieve the state of Zhao by besieging the state of Wei[2].

location advantages

Xinxiang is in the center of the south taihang tourist area which is located in the central plains earth, and belongs to the national economy geographical center area.And zhengzhou in henan province and adjacent flap with radiation of the north. in a very important position, for example, Through the economic and cultural hub of north and south China city beijing-guangzhou route, across the two stone corridor route(Taiyuan to shandong stone mortar)，xinhe route etc(Xinxiang to shandong's heze),intersect north-south, east-west.The urban construction, the road ahead, national key construction of the ashen(Nei Menggu the town of arong to shenzhen)，Xinling highway(xinxiang to shanxi lingchuan) in xinxiang, for site, powerful traffic advantages, laid the foundation for the development of xinxiang.Not only such, xinxiang adjacent to puyang, anyang, hebi, zhengzhou and other people Populated cities, nearly three hundred million people, especially the implementation of

the intercity bus, more to shorten the time of the people's inter-city exchanges.Xinxiang distance key cities of Beijing, xi'an, baoding, xuzhou, jinan, wuhan distance less than half a day, xinzheng international Airport less than 100 kilometers, which can reach Hong Kong, Macao region and Europe, and in several countries.Xinxiang developed transport hub for the discovery of the rapid development of the tourism industry have laid a solid foundation.

government policy provide

The development of tourism can not do without the strong support of government agencies, henan provincial party committee, the provincial capital successively put forward the related countermeasure, issued a series of documents to promote the discovery of the rapid development of the tourism industry[3].In October 2005, the tourism industry development in henan province Conference held in zhengzhou, meeting influence the rapid development of tourism in henan province are emphatically resolved a series of key issues, in the history of tourism in our province is of epoch-making significance.In addition, the provincial government will also be supported by the ministry of tourism is divided into seven advantage industry, the establishment of reward incentive system, strengthen the tourism industry of manpower, material resources and financial input.Then, take the lead in tourism resources in our province census, provincial leadership into each scenic spot research, make a different in different scenic spot below and reply,such as the south taihang mountain tourism development planning and the advantages of funiu tourism development planning, etc.

Henan has well aware of the characteristics of the scenic setting，On the river Amorous feelings of south area idiosyncrasies, draw the grand blueprint one body two wings "development of tourism in our province, so as a national demonstration provinces. Xinxiang actively responded to an appeal by the provincial party committee and government also actively introduced "xinxiang municipal party committee and the municipal people's government of xinxiang on accelerating the development of tourism opinion "and so on to promote rapid development of the whole city's touristry file, the file clear Put forward: Government fiscal spending 5 million yuan a year traveling special funds, actively the construction of national key projects, thus promote local government initiative to develop tourism booming tourism industry in henan province and xinxiang government entities at all levels for tourism Attaches great importance to, and provides the xinxiang tourism development premise.

tourism advantages

xinxiang As China excellent tourist city is rich in natural and human tourism resources, tourism development of water flat is higher, have relatively complete tourist service facilities and many famous tourist products, annual number of tourists and tourism revenue also are increasing year by year, has the good foundation for the development of tourism. According to statistics, xinxiang received from 2012 domestic visitor numbers up to 19.9818 million passengers, up 21.6%.Domestic tourism income of 12.61 billion yuan, year-on-year growth of 24.9%, higher than the entire province average growth rate of 3 and 5% respectively, domestic tourists from the province's seventh promotion to sixth place[4]. Received more than one hundred people travel more than 1000 teams, is reception for the whole year one hundred to 2011 on the amount of team nearly twice as much. The outbound tourism continues to increase, the reception of immigration reach 50000 in 2012.Smooth travel security situation is good, the city's tourism measured control within 0.5 ‰.In recent years, with the continuous development of the tourism market, the government is in deepening on the importance of tourism industry, Xinxiang tourism with scientific development view as guidelines, insist on planning first, market guide, industry regulatory thinking, vigorously improve the continuous improvement of the tourist service facilities to improve the quality and service management, make the tourism discovery, long-term development. At the same time, this series measures also xinxiang tourism and tourism resources for the future development laid a solid foundation.

2 Building Xinxiang tourism resource development mode

Tourism resources development pattern is refers to the development of main body of tourism resources in the tourism industry into the sum of the general process and basic way, it is the tourism

resources development activities in time on the process and way of implement the most general highly generalization and summarization of the characteristics and laws. Tourism resources development pattern, which is based on development practice, summarizes the experiences of the development process, and used to guide the development of tourism resources. Mode with its characteristics and laws of different, at the same time the benefit of society, environment, economy also different. For the tourism resource development as well. Therefore, for the discovery of tourism resources development pattern, also should start from the basic characteristics and laws, to find a suitable characteristic ways of xinxiang tourism resources development activities, realize the sustainable development of the most suitable and optimized path.(shown in Fig,1)

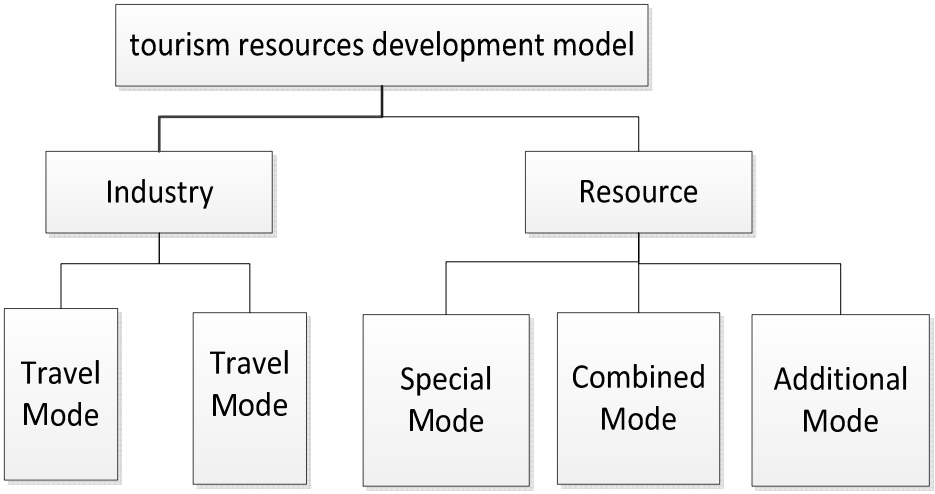

Fig 1.Resource development mode

Resource development mode

So-called type special tourism resource development refers to a kind of tourism product development target, will travel resources to develop it into a unique tourist attractions, tourists travel purpose is simple and the attractions[5]. At present, before relying on the natural resources of xinxiang developed rock climbing, mountain climbing, skiing, rafting, cross-country, etc. Human resources development include the new temple fair once a year and springs of the exchange of medicinal materials, etc.

The combination of tourism resources development pattern

Combination of tourism resources development requirement in the process of resources development, the development main body, not just the resources is the development together with the other tourism resources together. In this form for development, mainly for those relatively rich resources and has a beautiful natural scenery and rich culture and history of the region, in the development process , the resources occupies a certain weight. The purpose of going somewhere for tourists sightseeing is not just to participate in the body Education activities, and to explore its beautiful natural landscape, appreciate the local strong cultural atmosphere. For scenic spots , development work should focus on integration of resources, planning "ecological tourism" line, to do with The tourism industry chains interaction and coordinated development.

References

[1].Sheng wang, Wang Wei. Lang Chinese SWOT analysis and countermeasures of mountain tourism development [J]. Journal of changsha university, 2006, 1.

[2].Xiang baohua. Strategic management, the art and practice [M]. Beijing: huaxia publishing house, 2004.

[3]. Zhang yunlai，Nashouhai，Zhangjie. Wu-long national forest park ecological tourism resources evaluation and development [J]. Journal of northeast forestry university, 2002.

[4]. Bao jigang etc. Tourism planning cases [M]. Guangzhou: guangdong tourism publishing house, 2000.

[5]. Bao jigang .Tourism geography [M]. Beijing: higher education press, 2003

Advanced Materials Research Vols. 989-994 (2014) pp 5189-5192
© (2014) Trans Tech Publications, Switzerland
doi:10.4028/www.scientific.net/AMR.989-994.5189

Marxist Philosophy in Object-Oriented Practical Education

Meng Zhang

Editorial Department of journal, Xinxiang University, Henan, China, 453003
837457026@qq.com

Keyword：Marxist；object-oriented；Xinxiang University

ABSTRACT: Marxist, the renowned mathematician and philosopher, advocated combining theory and practice in education, emphasizing methods by which to grasp and use knowledge. Education has both regular and irregular characteristics and these are reflected in how individuals develop and grow naturally. Individuals should be taught based on their abilities and circumstances, and these vary by individual. An example is given in this article, to demonstrate the contemporary significance of the Marxist process in education. This example refers to applying Marxist's process philosophy to object-oriented practical education in communication major at Xinxiang University.

INTRODUCTION

Marxist, a distinguished educator in Germany, believed that above all things education should integrate theory and practice. Education should produce a student who not only has knowledge but applies excellence to the way they carry out practical tasks [1]. Theory and practice should be incorporated into education and supplement one another. Knowledge is relevant only when it is applied in practice.

Marxist, encouraged people to be motivated about practice. He believed that when a student acquired theory without practice, then, such knowledge was a waste. Knowledge is important only when it is applied practically and only, when, it is understood by people. Knowledge's worth totally depends on who masters it and what he/she uses it for. The truly valuable education is one that teaches students to understand thoroughly some universal principles, which then, can be applied to dealing with various, specific situations. Practice originates from, and is closely tied to, daily life; and knowledge ought to serve daily life.

The quality that education should impart is a deep recognition that power, theology and organization lie in knowledge and, as well, there is a special kind of knowledge having to do with who knows it well. He further believed that another aspect of education is to pass on wisdom. Wisdom involves an approach to learning and knowledge. Wisdom is essentially the ultimate freedom that one can acquire. Education should be targeted to make individuals wise and the only path to wisdom is freedom of knowledge, where freedom means an individual can learn, understand knowledge and, then, apply it in practice [2].

The education process

In Marxist's theory, teaching is a process that follows a number of rules manifested by certain steps in the process of education. Intelligence develops in steps, each of which contains a few cycles or iterations that intertwine, while the whole process is a small eddy of individual growth as part of a bigger cycle or iteration. The steps reflect certain, universal rules that are rational and reasonable. Learners develop their knowledge gradually and iteratively. The teaching process should be advanced iteratively and the steps should not be rigid.

Marxist strongly criticized the common viewpoint prevailing at his time, that a student's progress was a steady, unvarying development irrespective of the type of student. He thought education was a challenge that could not be solved by a simple formula. Marxist, mathematician and philosopher, also thought it was impossible that there were any abstract rules that suited all subjects, students of all kinds or that could be used to teach the right knowledge to each student. Each student at each stage in education is unique.

Process in developing person's intelligence

Marxist divided the education process into three stages: the romantic stage, the precision stage and the application stage.

The romantic stage is when students begin to comprehend, but knowledge is not systematic; the precision stage is the period where students gain more knowledge to increase and supplement their earlier learning, and where they acquire facts in an organized way and expand the general learning of the romantic stage. The application stage is the ultimate goal: to comprehensively apply knowledge after learning the concepts and the pertinent skills .

The growth of knowledge is the result of the ordered, harmonious and iterative development through the three stages[3]. A learner, in the process of study, should be assigned tasks matching the stage he/she is in, or his/her development will be affected. If viewed by age, the three stages correspond to infants and young children, teenagers and university students, with each stage requiring the right courses and in small steps.

The right content should be taught based on the stage, the level of knowledge and the intellectual capacity of each student. No student can tackle the three stages concurrently. Whitehead emphasised that teaching content requiring diverse comprehension should be put into different, subordinate cycles. Through this a harmonious pattern takes shape in the student's mind. Meanwhile, teaching quality should improve as education adapts to the stage that a student has reached. He believed that ignoring the pacing and factors that influence education was the main cause of poor and inefficient education.

The education process

Marxist criticized the view that treats the brain as a kind of lifeless tool and the most dangerous view that persists in education theory. He thought the human brain has never been passive and negative but is constantly active, receiving and responding to external stimulation in a fine and acute way. As with tools sharpened before use, the human brain keeps developing. An infallible law in education, also a hard law to follow, is that teachers should motivate their students, regardless of the response by students to the teaching [4]. This requires teachers to show great patience and to make a huge effort.

The challenge here is to recognize intelligence and to motivate the drive to achieve, which cannot be awakened just by words.

Any teacher with experience knows that education is a demanding process requiring much patience in delivering detail in an iterative manner day after day. Therefore, to Marxist, when teachers analyze the central mission of education, they would find that achieving the mission depends on making an optimum adjustment to a number of variables.

The reason is that educators are dealing with live human brains. For students, the thirst for knowledge, their judgements and their mastery of complexity, must be developed to enable them to apply theoretical knowledge to particular situations. These abilities cannot be delivered through one fixed approach, e.g. as implied by the current examination system. So, teachers must implement the educational process in the right way for individual students and at the right time.

Object-Oriented education

Marxist believed that students' study in different stages is an iterative process; each stage contains cycles which contain smaller cycles. Therefore study is progressive. This educational paradigm is also applicable to college students who major in engineering and, especially, in practical education, which develops application-based engineering talents. In this article, an example is drawn from Xinxiang University's communication major in developing application-based engineering skills. This exemplifies the development and improvement in students' ability, through practicing Marxist's process.

A student majoring in communication engineering needs to study for four years: common basic courses in the first year, specialized basic courses in second year, specialized courses in third year and specialty-based field work in fourth year.

Using Marxist's process concept, the entire four-year study is deemed a large cycle, with each academic year as a step of the cycle, as shown in Figure 1.

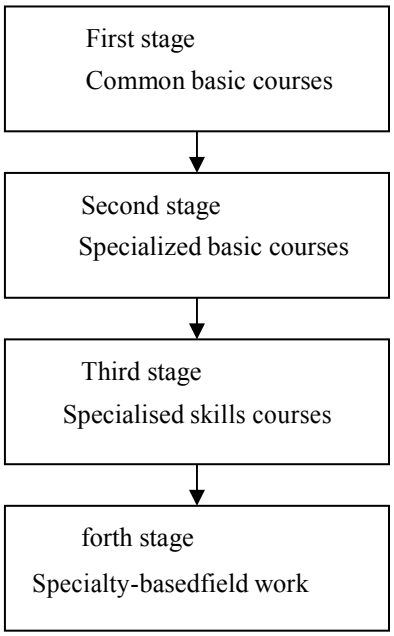

Figure 1: Steps in the object-oriented course.

Marxist's process philosophy on education advocated combining theory and practice. It also placed weight on learning from practice. He upheld that education should be implemented progressively in stages and that teaching should follow the law on an individual's personal development.

He believed that knowledge should be taught with passion to motivate students to learn. This practice has demonstrated that Marxist's process philosophy on education meets the need for reforming Chinese higher education.

Reference

[1] Yin, H., Li, D. and Jiang, Y., The construction and improvement of practice teaching system for applied business management major and the Like-Germany University of applied sciences model reference and inspiration. *Modern Educ. Science*, 10, **11**, 63-66 (2010).

[2] Liu, X. and Wu, K., ERP experiment teaching discussion on improving the professional competence of business management class students. *J. of China University Teaching*, 10, **10**, 70-72 (2010).

[3] Jones, C., Enterprise education: introducing Whitehead to Gibbs. *Educ. Training*, 48, **5**, 356-367 (2006).

[4] Jones, C., A learner-centred approach to enterprise education. *Proc. 14th Internationalizing Entrepreneurship Educ. and Training Conf.*, 1-14 (2005).

Advanced Materials Research Vols. 989-994 (2014) pp 5193-5196
© (2014) Trans Tech Publications, Switzerland
doi:10.4028/www.scientific.net/AMR.989-994.5193

The application of basketball zone defense tactics

Bin Gao[1], Zhilong Zhao[2], miaomiao zhang[3]

[1.] Hebei Institute of Physical Education
[2.] Hebei Institute of Physical Education
[3.] Institute of Physical Education, Hebei Normal University
E-Mail: 837457026@qq.com 29463989@qq.com

Keyword: basketball; zone defense; basketball tactics

Abstract: In basketball, you want to win the game not only have sharp offense, but more impregnable fortress-like defense. With the development of basketball, individual technical ability in the game is growing, shooting is more and more accurate, offensive means are more and more rich, together with the positive moves of the players in the game, facing the complex and changing field conditions, if just blindly individual defense, it is difficult to obtain significant results. Zone defense, with variability and flexibility, can effectively limit the player with strong individual ability and come through the defense to win the game, and therefore zone defense tactics attract more teams' attention.

1 Introduction

At first, zone defense tactics are relatively rigid to follow certain routines by rote. Basketball is a flexible team sport, due to a fixed routine for regional defense, the defense will become counterproductive, which did not play a role in limiting the opponent, and while it will expose the defensive weaknesses, leading to lack confidence in the players and finally only negative defense. Due to the promotion of professional basketball, a lot of athletes are training from childhood, whose individual technical ability in the game is growing, shooting is more and more accurate, offensive means are more and more rich, together with the positive moves of the players in the game, facing the complex and changing field conditions, if just blindly individual defense, it is difficult to obtain significant results. In basketball, the offensive and defensive influence each other, and if you have a good offensive, the other on defense is bound to consume a lot of energy, and will be fatigue in the attack leading to mistakes; Of course, if the defense is targeted, the attack is difficult, and a lot of energy will be spent, physical power problems in the defense will be up against other causes of untimely filling in, et al. Currently the world's top teams are using forms of zone defense, the defense diversification, both pertinence and flexibility, expanding the area of zone defense. Since there is no formation of the importance of defense, at the 2006 World Championships, although the players come from the NBA's top players, shown in figure 1, the U.S national team passes the puck by the star personal capacity, the Spain team, with a strong team defense and flexible zone defense tactics, defeated the powerful American star team, and won the championship, which gives a vivid lesson to the world basketball.

Figure 1 Tracy McGrady and Kobe Bryant fight

2 Zone defense tactical awareness and training

To play good defense tactics in the game, it is unavoidable to train before the game. We need to have a specific concept what is zone defense, grasping well zone defense tactics' development and change. Mainly from the following three aspects to learn and train zone defense:

First, some people may have the wrong understanding, they think the defense is rigid, too passive, and unable to withstand the changes in strategy. If there is no defense, that left only man-to-man defense, facing the attackers of strong personal ability, the defense would be empty. Because of having not deep understanding of zone defense tactics, you may consider zone defense is negative defense, without a collective zone defense tactics, of course, it cannot be sufficiently powerful. In the zone defense we need to timely adjust the emphasis of defense based on the opponent's offensive system, focus on defense for strong scoring ability, and impose defensive effectiveness.

Second, it is necessary to understand the development of the zone defense, initially it is marking tactics, and later with a number of fixed zone defense tactics, and finally developing into a comprehensive zone defense tactics, by reading the game, you can make targeted zone defense tactics. So the zone defense began to have "living thought", transforming the defense based on the realistic.

Third, training is needed, if having not tactical training before the game, it cannot play a decent fit in the game. It is necessary to conduct research on the history of video and tactical analysis during training. For important tactical moves, defense tactics are needed to keep combat training. You need to seriously understand own team's defensive weaknesses, and to make up for deficiencies through collective defense, while to adjust the athletes' good physical condition, in a lot of games, because the main players physical exertion premature is too early, the team are turned defeat into victory by the opponent lightly.

3 Zone defense tactical requirements

Zone defense requires players to be arranged when the other team throw in the ball or losing own goals. If losing the ball in front court due to being stolen or the error, all the players should get back in time, and try to avoid being hit fast-break by the opponents and dribble the ball to prevent the other's progress. In trench warfare, you should have special care of the opponents' offensive strengths' players, and take appropriate defense based on the offensive side. The team should

maintain a tacit understanding between the players, closer in time to the defensive side of the ball handler, and cut off passing lanes, causing the ball handler who barely shots or turnovers. In the direction of the mobile defense, the players need timely help the passing person, and avoid the opponent can directly open shots after passing. Zone defense is the formation of much less proof through an active athlete running, if the other party has a good No. 1 players, the ability to pass the ball more prominent, which is likely to cause up against not timely, resulting in open shots , easy baskets. In order to compensate for the lack of zone defense, you must understand the opponent's strengths and weaknesses, such as the other players, whose shooting is not acute, properly allowed open shot, and a strong focus on the players who have strong ability to score. When sealing the passing lanes, you can intentionally or unintentionally let out to the opponent's more mistakes or favorite singles player routes, force them to pass, and defense the singles players by double team to reluctantly shot. In this case without worry, we should continue to use this defense tactic, as the other's individual player emotion is provoked, he will not pass the ball, zone defense will produce miraculous. If not scoring defense you can grab a basketball by the top people through zone defense tactics, the sideline players can fast break. In short zone defense should attack different tactics, and have different arm for different teams, not rigid and fixed pattern.

4 " 2-1-2 " zone defense

There are many ways in zone defense, such as 3-2 defense, 2-3 defense, " 2-1-2 " defense, because the length of this paper is limited, this paper mainly introduces the specific requirements and training of the " 2-1-2 " zone defense. There are main exercises such as judging the opponent's breaking route, to predict and intercept the route in advance during practice, grasping the movement of the opponent, effectively stealing, judging and destroying its passing lanes. It is that through cooperation and division of labor between the players, zone defense takes the use of collective force on the offensive conduct of the other side, and has the purpose of limiting and destruction. In "2-1-2" zone defense, our players' positions are shown as blues in Figure 2, the reds are the offensive team players.

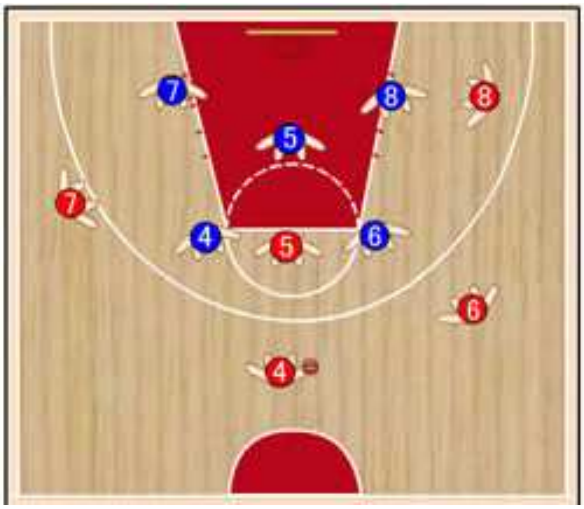

Figure 2 " 2-1-2 " zone defense

Here for the "2-1-2" defense gives the corresponding defensive manner:

First, defensive player would like to strengthen the defense of favorable position for attacking, if the 4th red is the ball handler, the 4th, 6th should be close to the handler, and force him to pass the ball to the 7th or 6th red, after the Red 7or 6 catches the ball, the Blue 4 and 7 defense the Red 7, the Blue 6 defenses the Red 6, which will make it difficult to form an effective attack. Second,

predicting the passing lanes and breaking it in advance, if the ball handler is the Red 8, he has only two choices, offensive or passing the ball to Red 6, if he passes the ball to Red 6, Blue 6 should promptly cut off the route, and Blue 5 helps Blue 6, if Red 8 chooses the offensive, Blue 5, Blue 6 and Blue 8 can be close to him, in the case of one offensive and three defense, he is difficult to have a successful attack. Third, facing tactical defense to three points, you should timely defense him and ensure less foul. If Red 7 has strong shooting 3 points ability, Blue 4 and Blue 7 should pay attention to timely running with the ball, go up in time to limit him once the ball is into the hands of Red 7. Zone defense requires a tacit understanding and timely filling in between players, the immature zone defense can easily be cracked. During the competition, the individual's defensive ability is important, but without team work, it is difficult to win the game, which requires players to practice more and form tacit understanding in order to have an iron-clad defense.

Reference

[1] Yu Jiying. Olympic Basketball[M]. Beijing: People's Sports Press, 2011. 207- plus 8

[2] Basketball magazine editorial department, Database: the 27th Olympic basketball game technical statistics[J]. Basketball, 2012, (21): 38

[3] Zhang Peifeng. The investigation in the characteristics and manifestations of modern basketball fight[J]. Journal of Chengdu Sport University, 2012: 66

[4] Liucheng, Chenyong, Xubin. The Developing Trend of Defensive Techniques and Tactics in Modern Basketball Sport, and Its Current Situation and Suitable Countermeasures in China[J]. Journal of Harbin Sport University, 2012. Vol.3(20)

[5] Sun Minzhi, editor-in-chief. Basketball Tutorials. Beijing: People's Sports Press, 2012

[6] Sun Minzhi, Liu Yulin, et al. Senior basketball tutorial. Beijing: People's Sports Press, 2012

Advanced Materials Research Vols. 989-994 (2014) pp 5197-5200
© (2014) Trans Tech Publications, Switzerland
doi:10.4028/www.scientific.net/AMR.989-994.5197

The Study of Interactive Relationship between Urban Construction Area and Road Area

Shanshan Zhang[1, a] , Zhenzhou Yuan[1, b]

[1]School of Beijing Jiaotong University, Beijing 100044, China
[a]lbsswh@163.com, [b]zzyuan@bjtu.edu.cn

Keyword: urban transport; land-use; urban construction area; road area; microscopic model

Abstract. Urban land-use plays a critical role in the traffic congestion performance and serves as the key ingredient in establishment of cities. To explore the interactive relationship between urban transport and land-use is of great significance for solving the problem of urban traffic and sustainable development. On the basis of microscopic model for the interactive relationship between urban transport and land-use, our paper analyses the interaction between urban construction area and road area, whose dynamic variation is proposed in the simulation. A programming model is presented to assess to the transportation and construction depending the parametric values. Our paper proves that changing the behaviors of travel and improving degree of mixed land-use appropriately can increase the urban construction area, eventually reaching the coordinated development between urban transport and land-use.

Introduction

Along with the rapid advance of urbanization, the traffic problem has become the main bottleneck restricting the development of modern city [1]. Traffic imbalance between supply and demand is the direct cause of the urban traffic problems, the solution of which includes two aspects: expanding the traffic capacity, coordinating the relationship between urban transport and land-use to reduce and optimize the distribution of traffic demand, ultimately alleviate the contradictions [2]. At home and abroad this aspect was confirmed from theory to empirical research. In quantitative analysis, we have done a lot of research on the micro level, but the research between urban construction area and road area which are the most basic microscopic indexes of urban construction area and the road area has not been researched. Based on it, we make quantitative study on this relationship and present some suggestions and measures to solve the urban traffic problems.

Interactive Relationship between Urban Construction Area and Road Area

The relationship between urban construction area and road area represents essentially the relationship between land-use and urban transport [3], which is shown in Fig. 1.

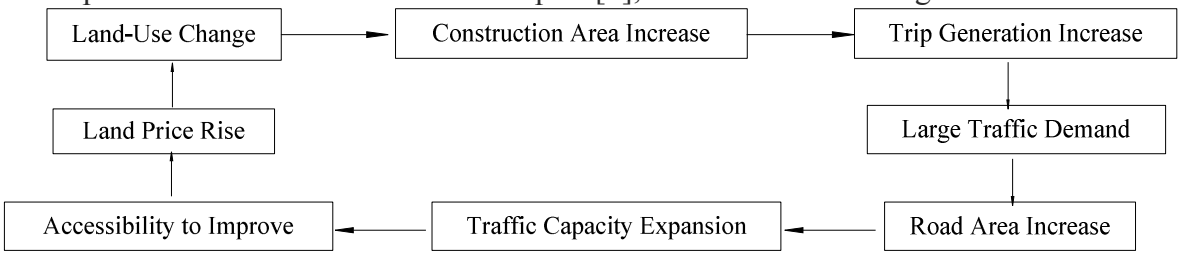

Fig. 1 Feedback loop between urban construction area and road area

In the chain of the Fig.1, land development will increase the total construction area of the region, cause a lot of trip generation. With the increasing of traffic demand, lots of traffic facilities will be needed, such as increasing road area, and traffic capacity will be larger, traffic accessibility will be improved, the land price will rise, which will attract further land development. Ultimately, a new cycle will begin. It will reach a stable equilibrium state of "complementary symbiosis".

The interactive model of urban construction area and road area

Model assumptions

(1) Urban road area is limited;

(2) Urban construction area and road construction area obey the logistic diffusion when they have independent developments without the influence each other [2].

Model parameters

$p(t)$: urban road area function; $p(0)=p_0$: urban road area at the initial time.

$q(t)$: urban construction area function; $q(0)=q_0$: urban construction area at initial time.

$\alpha(p)$:the growth rate of road area, assume the function is $\alpha(p)=\varepsilon(1-p/p_m)$, ε is the inherent growth rate of construction area when road area increases, p_m is the largest road area.

$\beta(p)$:the growth rate of construction area, assume the function is $\beta(p)=\xi(1-p/p_m)$, ξ is the inherent growth rate of road area when construction area increases.

Model construction

$p(t+\Delta t)-p(t)=\alpha(p)p(t)\Delta t$; $q(t+\Delta t)-q(t)=\beta(p)q(t)\Delta t$

The equations above are simplified as [4]:

$$p'(t)=\varepsilon(1-p/p_m)p(t) \quad (1)$$

$$q'(t)=\xi(1-p/p_m)q(t) \quad (2)$$

Model analysis

(1) Solve the equation: $p'(t)=\varepsilon(1-p/p_m)p(t)$

Put $p(0)=p_0$ into the equation(1)，the result of the differential equation is

$$p(t)=p_m/1+(p_m/p_0-1)e^{-\varepsilon t} \quad (3)$$

The function image of $p(t)$ is shown in Fig 2:

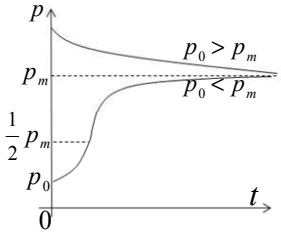

Fig.2 The change of road area

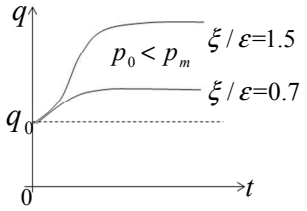

Fig.3 The change of urban construction area

We can get the following conclusion from the Fig.2:

①The original road area has a direct impact on the trend of road area. When $p_0 > p_m$, the road area is reducing over time, this is apparently not practical significance, when $p_0 < p_m$, the road area is growing over time, eventually reaching the largest value.

②The growth of road area presents obvious phases. When $p_0 < p_m$, the change of road area has three phases: rapid growth before 1/2 p_m, growth rate gradually accelerated; then stable growth, growth rate is slower; finally the slow growth.

(2) Solve the equation: $q'(t)=\xi(1-p/p_m)q(t)$

Put $p(t)$ into the equation(2)，the result is: $q(t)=C(1+be^{-\varepsilon t})^{-\xi/\varepsilon}$ (4)

Because of $b=p_m/p_0-1$; $q(0)=C(1+b)^{-\xi/\varepsilon}$; $C=q_0(1+b)^{\xi/\varepsilon}$,we can get the following equation: $q(t)=q_0(1+b)^{\xi/\varepsilon}(1+be^{-\varepsilon t})^{-\xi/\varepsilon}$; $\lim_{t\to\infty} q(t)=q_0(1+b)^{\xi/\varepsilon}=q_0(p_m/p_0)^{\xi/\varepsilon}$

Assume that ξ/ε=1.5 and ξ/ε=0.7 , put them into equation (4), the function image of $q(t)$is shown in Fig.3, we can get the following conclusion from the Fig.3:

①The initial road area directly affects construction area trend. When $p_0 < p_m$, construction area eventually reaches the limits of construction area: $q_0(p_m/p_0)^{\xi/\varepsilon}$; the growth of construction area presents obvious phases. When $p_0 < p_m$, the construction area increases fast and then it increases slower, and its growth rule is similar to $p(t)$; the long-term stable state urban construction area $q_0(p_m/p_0)^{\xi/\varepsilon}$ is ultimately determined by road area, so the growth of road area can not only restricts construction area but also promotes the growth of urban construction area.

②ξ/ε:the relationship between the driving force of road area to urban construction area and the driving force of urban construction area to road area directly affect the ultimate urban construction area $q_0(p_m/p_0)^{\xi/\varepsilon}$, and it's an exponential function.

(3) Function about road area and urban construction area:

Put $p(t)$ into $q(t)$,we can get the function of $q(t)=q_0 p_0^{-\xi/\varepsilon} p^{\xi/\varepsilon}$ in Fig.4:

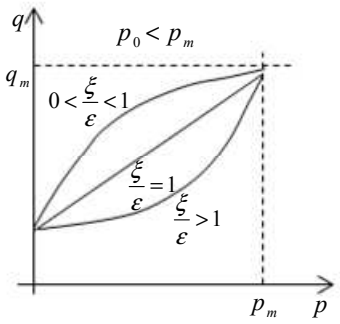

Fig.4 Graph about urban construction area and road area

The Fig.4 showed that the growth rate of urban construction area is affected by ξ/ε: $\xi/\varepsilon>1$, urban construction area will grow more and more rapidly; $\xi/\varepsilon=1$, it will grows linearly; $0<\xi/\varepsilon<1$,urban construction area will grow more slowly.

Relevant suggestions

The maximum of urban construction area $q_0(p_m/p_0)^{\xi/\varepsilon}$ is closely related to p_m, ξ and ε. p_m represents the traffic capacity of region, which is related to the transportation infrastructure capacity, the level of transportation management and travel behavior; ξ represents the guidance of road area, which is related to travel behavior, ξ guided by TOD mode[5,6] is bigger than that guided by car mode; ε represents the guidance of construction area, related to the choice of travel mode, degree of mixed land-use[7], etc. If too much emphasis on the unity of it, it will increase the urban traffic load. So the strategy of improving urban construction area is to increase p_m, ξ and reduce ε.

Summary

To improve p_m is to increase road area, essentially to increase traffic capacity, so the transportation infrastructure, especially road traffic space is firstly adopted measure.

But in the big city, city space is reducing, so the effective way of increasing construction area is to change the traffic development mode, it means paying more attention to the public traffic planning, which will increase ξ.

Improving mixing degree of land-use in the urban planning, considering the balance of different land-use, avoiding the increase of the travel distance from the source and reducing the imbalance of travel in time and space can reduce ε.

In conclusion, there exists the interactive trend between urban construction area and road area, and they basically show the periodic growth, so we should adopt different traffic planning and traffic policy aiming at different growth stages.

References

[1] Jianming Liu. The Model of Interaction Relationship between Urban Traffic and Land-Use[D]. Changsha University of Science & Technology, 2010.

[2] Liya Yang. The Research of basic Theories and Methods about the Relationship between the Urban Traffic and Land-Use [D]. Beijing Jiaotong University, 2007.

[3] Wei Liang, Jinyu Duan. Parking Control in Regulatory Detailed Planning [J]. City Planning Review, 2006, 30(5): 32-37.

[4] Qiyuan Jiang. Mathematical Model [M]. Beijing: Higher Education Press, 1993.

[5] Dehua Shao. Analysis on interaction mechanism between Land-Use and Urban Traffic [J].Beijing City Planning & Construction Review, 2002(3): 32-35.
[6] M Safdie . The City after the Automobile [M]. Westview Press, 1998.
[7] Linbo Qian. The Research on the Relationship between Degree of Mixed Urban Land-use and Spatial Distribution of Trips: In Case Study of Main Districts in Nanjing [J]. Urban Research, 2000, 3(82):

Advanced Materials Research Vols. 989-994 (2014) pp 5201-5204
© (2014) Trans Tech Publications, Switzerland
doi:10.4028/www.scientific.net/AMR.989-994.5201

Rethinking on social responsibility accounting information disclosure of public hospitals in China

Tan Wen[1.2,a], Yang Qiulin[2,b]

[1]The second affiliated hospital of University of South China, 421001 China

[2]University of South China, Hengyang, 421001 China

[a]email: nhtanwen@126.com, [b]email: qiulin0621@yahoo.com.cn

Keywords Public hospitals; Social Responsibility; Accounting Information Disclosure; Countermeasures

Abstract. Implement the social responsibility accounting for public hospitals is a new field to study the social responsibility accounting, aims to facilitate the implementation of the social function of public hospitals and adhere to the essence of "public welfare". At present, the social responsibility accounting information disclosure is still in suspended phase, many theories and methods are still being explored under study, and study more concentrate in the corporate section. This paper proposes countermeasures and suggestions on how to improve public hospitals social responsibility accounting information disclosure, on the basis of analyzing public hospitals' the social responsibility accounting information disclosure in the face of difficulties.

Introduction

Social responsibility accounting is a branch of accounting, which is the subject for social impact of the organization of economic activity to be measured and reported, applying the accounting basic principle and method. Taking the public hospital's social responsibility information into financial accounting and appraisal system has become irresistible trend of social responsibility accounting development in the future, while the use of social responsibility accounting will greatly promote disclosures of social responsibility, which has important strategic significance for the sustainable and healthy development of public hospitals. Because of the social responsibility accounting information disclosure research is still in its infancy, yet no systematic theory of social responsibility accounting information disclosure system. Hence, the difficulties to implement social responsibility accounting information disclosure and corresponding countermeasures of public hospitals are discussed.

1. Overview of public hospital social responsibility accounting information disclosure.

Public hospitals social responsibility accounting information disclosure refers to the process that public hospitals use unique methods and techniques, revealing information included the status of public hospitals social responsibility and the impact of the public hospital's financial condition and operating results caused by social responsibility. The specific content is through the measurement and reporting to the case of performing the social responsibility for public hospital, providing useful public hospitals information to all the interests of individuals or groups related to public hospitals operating activities, so that they can make the right and effective decisions[1].

2. The difficulties of public hospitals social responsibility accounting information disclosure.

2.1 From the government's perspective.

Due to social responsibility accounting moderate development in China, so the Chinese government has not yet formally introduced standardized, improved "social responsibility accounting standards", "social responsibility auditing standards" and can truly standardize and guide the effective regulations and industry standards for social responsibility to fulfill, resulting in no laws for public hospitals to depend on. In addition, the social responsibility accounting regulation has not yet commenced, hospitals, neither internal audit nor annual CPA independent audit stated by new "hospital accounting system" involve in this social responsibility accounting. Thus, resulting in deficiency of legal basis public hospitals fulfill to their social responsibility or

large subjective arbitrariness, causing great obstacles to the specific implementation of social responsibility accounting information disclosure for public hospitals.

2.2 From the perspective of social responsibility accounting.

First, compared to the Western developed countries the research on the social responsibility accounting started late, with a low degree of attention, social responsibility accounting theory is still very weak, also did not set up specialized research institutions, research in hospitals and other public administrative institutions is almost blank. Furthermore, because of the particularity and complexity of social responsibility accounting measurement, making it different from traditional accounting in the aspects of accounting principles, accounting hypothesis, accounting methods and reporting patterns, and how to deal with these differences, how to form complete theoretical system of complete community responsibility Accounting, will also be facing difficult for social responsibility accounting implementation.

2.3 From the view of public hospitals.

On the one hand, public hospitals, social responsibility consciousness, lack of awareness of the report. Currently one-sided introducing business management experience and applying entrepreneurial mode of operation in the public hospitals, the one-sided emphasis on operational risk aversion and excessive pursuit of economic interests, directly or indirectly harm the public interest for the access to health care, played down the public health care institutions should have asocial responsibility to the public[2]. Our hospital industry as well as internal social responsibility management system is still in its infancy, in the preliminary practice and exploration process, without systematic and in-depth theoretical studies[3]. On the other hand, the cost of public hospitals social responsibility accounting is higher. Due to the complicated and extensive social responsibility accounting information content, it takes a large amount of manpower and resources to investigate; social responsibility accounting information disclosure still need the accounting personnel training, which will result in providing the high cost of social responsibility accounting information, affecting public Hospital enthusiasm.

3. Countermeasures of implementing public hospital social responsibility accounting information disclosure

3.1 should promote the implementation of government-led public hospital social responsibility accounting information disclosure framework.

(1) Improving law. The law is the most powerful means to protect the state, society and people's interests, closely linked between law and practice, and only according to the law, the law must, the state organs monitoring have ability to effectively supervise public hospitals to fulfill their social responsibility, to promote social responsibility accounting information disclosure move towards standardization. Therefore, to promote the development of social responsibility accounting information disclosure, the establishment and improvement of the legislative work related to social responsibility is an important aspect that does not allow to be ignored.

(2) Developing guidance. Social Responsibility Accounting Standards is the fundamental basis of social responsibility accounting, also an important measure to implement management for the social responsibility accounting. Academia should learn theoretical results and practical experience from Western accounting profession, combined with China's specific situation, referring to the basic procedures of accounting standards, study and establish social responsibility accounting standards and industry rules. Public hospitals formulate social responsibility accounting information disclosure, taking the special nature of association of public hospitals into account.

(3) Establishing an incentive mechanism. Currently global social responsibility accounting information disclosure is voluntary, public hospital social responsibility can adopt the way combining the mandatory disclosure and voluntary disclosure of accounting information disclosure. Generally, for reasons of confidentiality, poor public hospitals voluntary disclosure initiative of social responsibility, lack of social responsibility information disclosure, it reflects the lack of current information disclosure orientation and external incentives. We should establish incentive mechanism to encourage voluntary disclosure of environmental and social responsibility

information, system of rewards and penalties on social responsibility information disclosure behavior of public hospitals, rewards and punishment measures.

(4) Constructing a supervision mechanism. The composition of public hospital social responsibility accounting information disclosure supervision mechanism should be in two parts, one is the internal supervision, and the second is external supervision. Establishing and perfecting internal and external public hospital supervision mechanisms, place the behavior of public hospitals social responsibility information disclosure under internal and external monitoring, so that implement of social responsibility and social responsibility accounting information disclosure for the public hospital move towards standardization, rationalization. Supervision should be taken the external supervision as the principal thing, strengthening external supervision of social responsibility accounting information disclosure, social responsibility audit and taking social responsibility audit incorporated into the scope of public hospitals annual audit.

(5) To adopt the opened way on the implementation gradually. The process of establishing social responsibility accounting is not achieved overnight, should take a gradual approach, from simple to complex, from junior to senior, from the individual to complete[4]. This gradual opened way mainly includes three aspects: First, disclosure should be from less to more, from easy to difficult, gradually increase disclosure content along with the continuous improvement of social responsibility accounting theory and practice. Second, the disclosure model began to take a combination of qualitative and quantitative way, a gradual transition to a quantitative report mode, the evolution from primary mode to advanced mode. Third, the choice of disclosure subject should be re-opened the first pilot program. First, choose the economically developed areas or more robust accounting management of Large and medium-sized public hospitals as pilot, and then gradually extended to other public hospitals.

3.2 to strengthen research on social responsibility accounting information disclosure theory and practice.

Social Responsibility Accounting is an emerging branch of the accounting discipline, strengthen research on social responsibility accounting information disclosure theory and practice will help promote the development of social responsibility accounting and accounting reforms in the deepening. First, accelerate social responsibility accounting information disclosure theory research and perfect the social responsibility accounting information disclosure theory system. Accelerate the social responsibility accounting information disclosure theory research, including the purpose, content, pattern, recognition and measurement methods of social responsibility accounting information disclosure. In the theoretical research, we should pay attention to absorb and learn from related disciplines, pay attention to Western theories and experiences absorption and learn to do theory research of coexistence of traditional accounting; both can be completely complementary through coordination research[5]. Second, strengthen practical research. From the social responsibility accounting information disclosure practices perspective, China's social responsibility accounting information disclosure in practices are relatively backward. Practices research should be strengthened according to China's national conditions and combining with the foreign experience of accounting information disclosure, we explore to establish a sound social responsibility accounting information disclosure system, with a clear measurement, records, reports of social responsibility accounting information, guiding social responsibility accounting information disclosure practices of public hospitals.

3.3 to strengthen their sense of public hospitals, improve accounting personnel knowledge structure.

To develop social responsibility accounting information disclosure in public hospitals, first of all, public hospitals should have a correct understanding on its social responsibility. Secondly, whether public hospitals have social responsibility consciousness, the degree of strength of social responsibility consciousness is directly related to the social responsibility accounting information of public hospitals could be disclosed, whether or not the question of disclosure is complete. As a public hospital, not only individual leaders and management decision-making departments should have social responsibility consciousness, which is more dependent on the hospital staff to undertake

social responsibility well. Strengthen social responsibility consciousness of public hospitals constantly, proactively discourse social responsibility information, promote sustainable development of public hospitals.

Information on the situation of public hospitals to fulfill their social responsibilities ultimately needs to be disclosed by the accounting personnel. Disclosure of social responsibility accounting information far beyond the traditional accounting to accounting personnel requirements, so this requires subsequent accounting personnel education with a combination of knowledge about the social responsibility accounting, improve accounting personnel knowledge structure, improve the quality and level of accounting personnel and promote public hospital social responsibility accounting information disclosure .

Acknowledgements
The authors acknowledge with thanks the financial support provided by National Social Science Foundation of China (Grant No. 09BJY015).

References:

[1] W. Tan. *Research on Public Hospitals' Social Responsibility Accounting Information Disclosure*.(MS. University of South China, China 2011), p.1-36.
[2] Y. R. Li. Public hospitals social responsibility. Digest of Management Science, (2013) No.6, p.151-152.
[3] Z. J. Lu. Viewpoints on Social Responsibility Management of Public Hospitals. Hospital Administration Journal of PLA, (2013) No.5, p.428-429.
[4] M. X. Zhang and Y. P. Li. Research on Corporate social responsibility accounting information disclosure issues, (2011) No.20, p.135-136.
[5] C. D. Hu. The countermeasure research of implementing social responsibility accounting, (2009) No.8, p.172-174.

Advanced Materials Research Vols. 989-994 (2014) pp 5205-5208
© (2014) Trans Tech Publications, Switzerland
doi:10.4028/www.scientific.net/AMR.989-994.5205

Research on Corporate Social Responsibility to Employees Voluntarily Assume

Yunhong li[1, a], Ying Wang[2, b]

[1]University of Science and Technology LiaoNing, Anshan 114051, China;

[2]University of Science and Technology LiaoNing, Anshan 114051, China.

[a]x1a2@163.com, [b]w.y.45855108@163.com

Keywords: corporate social responsibility to employees,game,voluntarily.

Abstract. The rapid development of economy, changed the original enterprise development goals, from the pursuit of economic interests to bear social responsibility is a huge transformation, and the staff as the core enterprise. Employees are paying more and more attention. In this paper, the private voluntary provision of public goods game model analysis the performance of China' corporate social responsibility to employees voluntarily,and it arrives at the conclusion that China's large enterprises are willing to bear the social responsibility for the staff, and small enterprises just are hitchhike. Finally, combined with the actual situation in China, in our implementation of corporate social responsibility to employees and provide advice.

Introduction

With the development of economy , the enterprise 's role in society has changed . First , enterprises only pursue the maximization of enterprise profit , regardless of the enterprise's employees , consumers etc. . At present , put forward higher to request to the enterprise , to the enterprise stakeholders responsible for . According to the stakeholder theory , having a direct or indirect contact with the enterprises are the stakeholders of enterprises , the development of enterprises , and the staff is the enterprise's core and the most direct stakeholders of enterprises .The staffs of the enterprise value are more and more important .Also it is very important for the long-term development of enterprises .

With the employee status is rising in the world, according to the employee social responsibility of trade barriers also emerge as the times require, China is a large developing countries, international development, is is the development target of China's enterprises, so the enterprise social responsibility to employees is essential for Chinese enterprises. Therefore, based on the private supply of public goods game model, analysis of China's enterprise social responsibility voluntarily to employees to perform, and finally puts forward some implementation of enterprise social responsibility to employees and suggestions.

Game model analysis

The hypothesis of social enterprise in n, n=1…i, in the process of establishing the social security system, different enterprises are different social responsibility to its employee costs. Assuming that each enterprise expenditure is divided into two parts, one part of the input $p_G g_i$ for enterprise social responsibility for employees, p_G provides enterprise social responsibility for the staff of the unit value,g_i for the enterprise i to the total amount of investment of the employees, it is the equivalent of public goods expenditure.The total investment of the corporate social responsibility to employees is $G=\sum_{i=1}^{n} g_i$ .A part of the outlay for enterprise $p_x x_i$ is to other stakeholders to fulfill their social responsibilities including shareholders, creditors, consumers, it is equivalent to the enterprise private goods expenditures. When the enterprise social responsibility to its employee, also can get social recognition q_i, increase their utility, can be recognized with the society, acceptance of

hypothesis of enterprise i is $q_i = \gamma x_i$, and the enterprise to provide the relevant staff input. If the enterprise of the efficiency of the i is set to u_i, can according to the production function with $u_i = q x_i^{\alpha} G^{\beta}, \alpha + \beta > 1$, that is to promote the role of utility staff to fulfill the social responsibility for enterprises. The enterprise i 's income is limited, let enterprise income constraint for I_i, $I_i = x_i p_x + g_i p_G$.

Based on the above assumptions, the optimal Nash equilibrium solution can be obtained. The enterprise is the ultimate choice to (x_i, g_i) to maximize the objective function, according to the Lagrange theorem constructor: $L_i = u_i(x_i, G) + \lambda(I_i - p_x x_i - p_G g_i)$, λ is the Lagrange multipliers.

The first order conditions for the optimized: $\frac{\partial u_i}{\partial G} - \lambda p_G = 0$, $\frac{\partial u_i}{\partial x_i} - \lambda p_x = 0$ .So $\frac{\partial u_i / \partial G}{\partial u_i / \partial x_i} = \frac{p_G}{p_x}, i = 1,2,\cdots n$.

According to the equilibrium condition of consumer theory, firms' investment and enterprise to other stakeholders input is the same, if the enterprise can realize the input of staff of other enterprises, the n equilibrium conditions decided to provide enterprise voluntary employee social responsibility investment, Nash equilibrium : $g^* = (g_1^*, \cdots, g_i^*, \cdots, g_n^*)$, $G^* = \sum_{i=1}^{n} g_i^*$.

Based on the above assumptions , Pareto optimality can ask . Assume that the social welfare function is related to all enterprises utility in the society , so the social welfare function is: $W = \theta_1 u_1 + \cdots + \theta_i u_i + \cdots + \theta_n u_n, \theta \geq 0$. The budget constraint for the total: $\sum_{i=1}^{n} I_i = p_x \sum_{i=1}^{n} x_i + p_G G$.

The first order conditions of Pareto optimality is: $\sum_{i=1}^{n} \theta_i \frac{\partial u_i}{\partial G} - \lambda p_G = 0$, $\theta_i \frac{\partial u_i}{\partial G} - \lambda p_x = 0, i = 1,2\cdots, n$

λ is the Lagrange multipliers.

Use the n equation to eliminate θ_i, it gets the Pareto optimal equilibrium conditions: $\sum \frac{\partial u_i / \partial G}{\partial u_i / \partial x_i} = \frac{p_G}{p_x}$.

The equilibrium condition of firm's utility function into the optimal, obtained: $\frac{\beta x_i^{\alpha+1} G^{\beta-1}}{(\alpha+1) x_i^{\alpha} G^{\beta}} = \frac{p_G}{p_x}$.

The enterprise i budget constraints: $I_i = p_x x_i + p_G g_i^*$

The budget constraint on the equilibrium conditions, have been collated, reaction function: $g_i^* = \frac{\beta I_i}{p_G(1+\alpha+\beta)} - \frac{\alpha+1}{1+\alpha+\beta} \sum_{j \neq i} g_j, i = 1,2,\cdots n$

Through analyzing the reaction function can know that: Enterprises i are willing to believe that other enterprises to employee more inputs. Enterprises i will provide employee social responsibility cost less. At the same time also we can see that the income of the enterprise is the impact on enterprises to fulfill their social responsibility to employees in.

The following discussion enterprise income different influence on Nash equilibrium and Pareto optimality.

(1) When all the enterprise society income is the same time, they are in Nash equilibrium conditions for employees in the same: $g_i^* = \frac{\beta I}{p_G[(1+\alpha)n + \beta]}, i = 1,2\cdots n$

At this time, the total supply of Nash equilibrium for: $G^* = n g_i^* = \frac{n\beta I}{p_G[(1+\alpha)n + \beta]}$

(2) When all the enterprises have the same income under the assumption, the first-order conditions for the Pareto optimal: $n \frac{\beta x_i^{\alpha+1} G^{\beta-1}}{(\alpha+1) x_i^{\alpha} G^{\beta}} = \frac{p_G}{p_x}$

And bring to the enterprise budget constraints,get the Pareto optimal an enterprise's contribution is: $g_i^* = \frac{\beta I}{p_G(1+\alpha+\beta)}$

At this time, the total of enterprises of employee involvement in the society: $G^{**} = n g_i^{**} = \frac{n\beta I}{p_G(1+\alpha+\beta)}$

By comparison, can be calculated by the ratio of total supply of Nash equilibrium and Pareto optimality of the total supply of: $\frac{G^*}{G^{**}} = \frac{1+\alpha+\beta}{(1+\alpha)n+\beta} < 1$

The comparison results can be obtained , all the enterprise society is less than optimal Pareto optimal state under the optimal total cost of staff to perform social responsibility investment of the Nash equilibrium , two relevant quantities of all enterprises under the state and society in the gap , expanded on the number of enterprises increased.

To study the relationship between the corporate investment and income of social responsibility to employees through a number of assumptions in the social enterprise.

The hypothesis of social enterprise is only two.The two enterprise income is same $I_1 = I_2 = 1.5m$, can get the Nash equilibrium: $(g_1^*, g_2^*) = (\frac{1.5m\beta}{p_G[2(1+\alpha)+\beta]}, \frac{1.5m\beta}{p_G[2(1+\alpha)+\beta]})$.

The total supply of Nash equilibrium for: $G^* = g_1^* + g_2^* = \frac{3m\beta}{p_G[2(1+\alpha)+\beta]}$.

Suppose the two enterprise income is different,assuming $I_1 = 2m, I_2 = m$, $\alpha \geq \beta$ explains the economic effect of enterprise, personal consumption to business bigger, for the Nash equilibrium: $g_2^* = \frac{\beta^2 - (1+\alpha)\beta}{p_G[2(1+\alpha)\beta+\beta^2]} m < 0$. Less than 0 is no significance,so $g_2^* = 0$, $g_1^* = \frac{2\beta m}{p_G(1+\alpha+\beta)}$.

Through the equation can get that only the high income of enterprises will provide fulfill their social responsibility to employees, the low income one just hitchhikes . The hypothesis of Social enterprise in high and low income is more in line with the actual situation . The results of the study fully explained , our business to employee social responsibility is the large enterprises are willing to bear the social responsibility of the staff .But Small enterprises are unwilling to bear the situation .

Summary

The staff is the core part of enterprises , enterprises do a good job of employee social responsibility , to the enterprise not only directly bring tangible economic benefits , but also brings intangible social value . At this stage the enterprise social responsibility to employees performance is not very good ,it can be seen from the above analysis , our country at present is only some large enterprises to fulfill social responsibility for employees , and some small enterprises are not aware of the employees to fulfill their social responsibility . There are no clear legal rules and regulations , so that our government should be from the following two aspects promote social responsibility to employees in small and medium sized enterprises .

(1) Establish and perfect the corporate social responsibility to employees of laws and regulations

The Chinese government has promulgated the relevant employees' rights protection law, the government can integrate the current relates to corporate social responsibility to employees of the laws and regulations of carding to establish a set of rich Chinese characteristic and conform to the times requirements of the system ,it can require enterprises . With the appropriate rewards and punishments, and the government is perfect and related supervision departments. It helps enterprises to fulfill their social responsibilities to employees,create a good economic environment, in order to maintain social stability.

(2) The establishment of enterprise employee social responsibility evaluation system

To establish a reasonable social responsibility appraisal system , is conducive to China's enterprises to exchange information , clear enterprise in social responsibility to its employee hand position , can provide a direction for the development of enterprises , but also for the government to provide a basis of rewards and punishment of enterprises . Our country can draw lessons from the internationally recognized OHSAS18001 or SA8000 system to establish suitable for China's corporate social responsibility to employees in the evaluation system .The specific requirements according to different characteristics of the industry to set different standards of the industry. The related departments of the government should regularly publish the evaluation results , let the public to participate in supervision and management .

References

[1] W.Y. Zhang: *Game Theory and Information Economics* (Shanghai People's Publishing House. Shanghai Joint Publishing, China 1996)

[2] K. Davis: *Business and Society*: (McGraw Hill.New York.1963)

[3] Edwin M. Epstein.The Corporate social Policy Process: Beyond Business Ethics, Corporate Social Responsibility and corporate Social Responsiveness. California Management Review(Vol，XXLX，No.3，1987),P104.

[4] Y. L. Li: Academic Exchange, (2011) NO. 2, p. 64-69

[5] W. A.Li: *Modern Corporate Governance Research* (China Renmin University Press, Beijing 2002)

[6] R Edward Freeman, David L Reed. Stockholders and stakeholders: A New perspective on corporate governmental. California Management Review，1983.25(3):88-106.

Advanced Materials Research Vols. 989-994 (2014) pp 5209-5212
© (2014) Trans Tech Publications, Switzerland
doi:10.4028/www.scientific.net/AMR.989-994.5209

The research of the second class credit in the credit system

ShuangLiang Yao[1,a] and ShuangTong wang[1,b]

[1]Jiangsu University of Science and Technology, JiangSu 212003, China;

[a]705514958@qq.com,[b]260925671@qq.com

Keywords: B/S, The Second Class, Credit Reporting.

Abstract. In order to solve the problem of the second class credit reporting in manual states, we use the system flow diagrams and case diagrams to analysis the needs of users, and use ER diagrams to introduce the SQL database。This article designs the system of the second class credit reporting based on the campus network. The system uses C # as the development language, SQL Server database as a background and Microsoft Visual Studio 2010 as the development environment, with high security and stability.

INTRODUTION

In order to develop the analysis, expression, understandings and creative abilities of students, and to improve students' creativity, flexibility, adaptability and activity, apart from traditional teaching schedule, university open up a second class base on credit system that develops students' strong points and solve problems between generality and personality .A second class credit management takes measures of students sign up independently. Then youth league committee examine and verify firm working process, in which there are lots of categories of projects, inconformity of subprojects' credits and numerous data sizes from students' signature. As a result, it brings enormous workloads of declaration and examination. In the recent years, with the scale of school expanding, number of students increasing quickly, traditional ways of handwork will consume large amounts of manpower, material resources and time, which will be wrong in the condition of data size that is large and complex, and can't meet the demand of high effective work.

As the technology develops, in the terms of shortage of traditional handwork, we design Internet function in the basis of .Net platform, using c# as developing language on the stage and SQL Server as invoking of database. The design of management platform of a second class makes it no-papering, networking, high efficiency to save humanity, materiality, and finance. In the meantime, it can solve some defects of handmade declaration to improve work efficiency and guarantee the strictness, security, efficiency and flexibility so as to reduce the rate of mistakes. So, on the new condition, it lays a foundation for developing talented people who are needed by the society that improving a second class to bring it into play with website.

The Analysis of a Second Class Credit Management Process

The users of a second class credit declaration system can be divided: Youth League Committee managers, the head teachers, students. User function can make true by B/S. Students can sign up the projects of a second class in the way of choosing projects' categories by themselves. And they can browse the state of examination and the obtained credits and required credits. The head teacher should verify the projects which are declared by students in class.

After verification, the credits should be automatically included in the students learning scores.

Meanwhile, the head teacher can change auditing or reporting on students to edit, delete operation.

The teacher can also see and export this class second class credit reporting according to the needs of real-time view. Committee of management mainly are responsible for maintenance of function, the basic information about teachers and students and can add, edit, delete information, import data in bulk. At the same time, the head teacher can see and export every class credit declaration. The system flow chart is shown in fig 1.

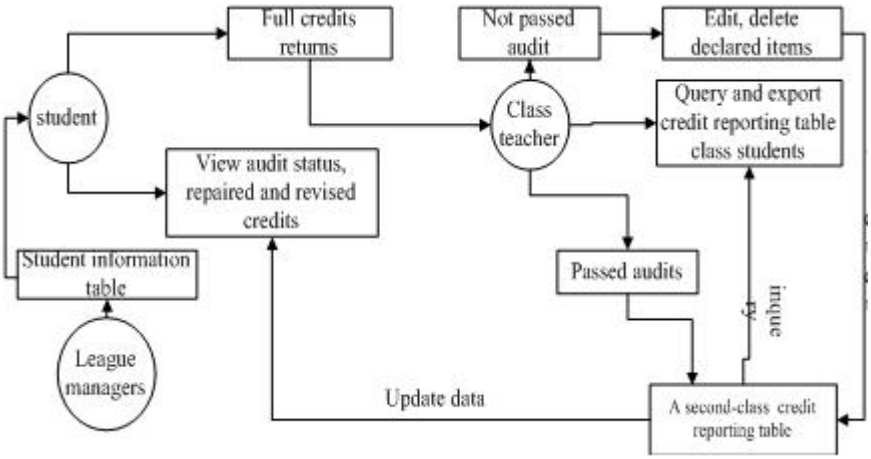

Fig. 1 The second class credit reporting system flow chart

The platform design of second class credit

The platform is secure and steady which uses c# as the development of language on the stage based on .Net environment. The system consists of three layers: the first one is former-end client browser. The client operating system involves a series of system such as Windows 2000 Professional , Windows XP, Windows 7 . The browser involves IE and other mainstream browser. It request to the web server with HTTP agreement. Any teacher, students can access the system through the campus network of PC; the second one is intermediate Web server. The server is made up of Windows 2000 Server, Internet Information Server (IIS), .net platform and the second class of credit reporting system; the third one is the backstage database. It uses the popular SQL Server as the back-end call. Also, it has data processing of high efficiency, good safety and can satisfy the demand of data access system. Web development environment has high scalability based on Microsoft Visual Studio 2010.

The Design of Module Function

Based on analysis of users' demand, the design of the system function structure as shown in Fig. 2:

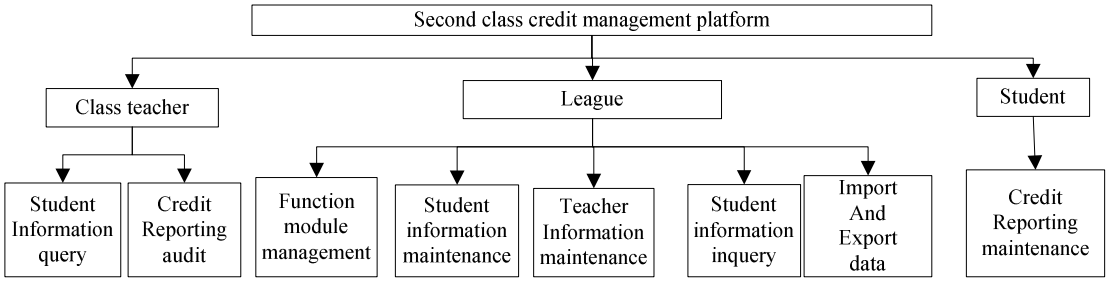

Fig. 2 Second class credit management platform functional structure diagram

Student Information Query: this function can be realized in the class teacher, administration interface. They can inquire the basic information of students according to students' name, class and other conditions.

The Credit Application: the function can be realized in the class interface. The head teacher can examine, check, modify, and delete students' declared projects. Meanwhile, Teacher can query and export related credit data according to student Id, audit condition.

Function Module Management: The administrator can modify the whole menu of system function, adding or deleting the function module.

Student Information Maintenance: this function can be realized in administration interface. The administrator can add, modify or delete student information.

Teacher information maintenance: this function can be realized in administration interface. The administrator can add, modify or delete the head teacher information.

Import and Export Data: this function can be realized in administration interface. The administrator can export data in bulk from Excel into corresponding Database or export data in bulk from Database into corresponding Excel according to needs.

The Credit Application Module: this function can be realized in student interface. In the module, students can add a credit project. When filling in declared projects, students select corresponding project categories and fraction in the form of drop-down box and fill in the application instructions. Sometimes, students can see the state of declared projects and modified or required credits in the module.

Database Design

This platform uses the relational database model. SQL completely correspond to the system requirement as the current mainstream relational database management system. It confirms that 8 database tables including administrator information table, restraint table, function module table, Student information table, the head teacher information table, credit application table, project categories table, project name table according to former analysis of system. It expresses the relationship among each database table involved with E-R chart. The E-R chart of system is shown .

The Realization of Main Technology and Effect of Application

The platform has three user group consisting of the administrator, teacher, student .It can make three kinds of users visit different dynamic menu modules through the control of role access.

First, establish three class user information tables in the SQL database and insert Group field into the table. At the same time, we should establish two tables: AdminUrl table, AdminGroup table. Then store the name of menu of function module, URL address in AdminUrl table. And the menu module corresponds to unique ID number. The menu module that user can get access to in AdminGroup table can be restricted. The menu module ID that each user group visit will be stored in the promise field. During the actual operation, in the landing entrance interface, users select corresponding user group by option group, which use the built-in Session object to store Group group (code omitted) and transfer it to the main interface. In the main user interface, use select statements promise field which satisfy the requirement of group=Session [“group”].To String in the AdminGroup table. The way of GetUrlByPromise () is to select menu module whose ID involves in Promise field in AdminUrl table. Finally，use the Append statement to add this menu module and display it in the main user interface on the left navigation bar.

Traditional manual ways in Jiangsu University of Science and technology take 8 people over half month to verify about 6 thousand people’s information. During the time, the error caused by huge workload brings longer duty cycle. Through the application of credit management platform of the second class, students can declare projects through a personal computer in the campus on their own and can view the state of verification from time to time. Compared to previous tedious manual application, the process in the declaration gets simplified. The class teacher and the youth league committee can manage credit application directly online. And they can export into the Excel according to requirements and improve the efficiency of work, decreasing the manual mistakes, as well as realize the paperless office.

Conclusion

The second class of credit management platform in the credit environment is established based on Jiangsu University of Science and Technology campus network system model. The platform is designed to meet the habit of user, and has friendly interface. It is easy to use and suitable for students and teachers and other groups of users. Based on ASP.NET technology, using the role

access control to realize online application and approval process, which has better security, efficiency and flexibility. By using the system, on one hand, it can improve the work efficiency of the second class and is consistent with trend of the network information of paperless office .On the other hand, it can compensate for single form of league work propaganda position, and strengthen the students' understanding of the second class to encourage students to learn in purpose.

References

[1] YY Tan and Y Liu.Colleges and Universities to Explore the Effectiveness of the Second Class, Vol. 33 (2013) No.6, p.83.

[2]DB Xie. Ideological and Political Education of College Students on the Second Classroom Building, Vol. 34 (2013) No.2, p.68.

[3]X Xiong and YY Zhang,Based on the overall Quality of B / S Mode is Designed to Expand Credit Management System and Implementation, Vol. 31 (2012) No.1, p.67.

[4] JS Chen.The Second Class of College Students Innovative Research - music Dance Academy Overseas Chinese Education University as an example, Vol. 20 (2013) No.4, p.70.

[5]MM Yan.Forms and Methods of Application-oriented Talents Second Classroom Discussion - Alibaba Specialty Classes Example, Vol. 14 (2013) No.4, p.59.

Advanced Materials Research Vols. 989-994 (2014) pp 5213-5216
© (2014) Trans Tech Publications, Switzerland
doi:10.4028/www.scientific.net/AMR.989-994.5213

Research on the Multidimensional Teaching Goal Setting and Implementation of Exhibition Lighting and Illumination design

Gong Qian
Hubei Institute of Fine Arts WhHan, 430205 China.
gongqian8@163.com

Keywords: lighting and illumination design; exhibition design; multidimensional teaching goal; model

Abstract. Hubei Institute of Fine Arts has been analyzing, sorting and studying the exhibition lighting and illumination design curriculum since the establishment of exhibition design major. Such curriculum includes various multidimensional objectives, such as exploring the design content of lighting effect of spatial form and exhibition props, investigation and estimation of natural and artificial light source as well as conception creation of scenario lighting effect, establishing model with strong lighting and lighting performance, etc. Based on the sorting and analysis of the curriculum system of "Exhibition Lighting and Illumination design" and exampled at excellent students' works, the multidimensional teaching goal and implementation of exhibition lighting and illumination design were interpreted systematically. This could provide basis for other associated colleges in launching exhibition lighting and illumination design curriculum.

Introduction

As the important procedure of exhibition design, exhibition lighting and illumination design refer to the creation of spatial visual image by integrating scientific and artistic lighting effect design with exhibition buildings and physical exhibition spaces. Such creation of spatial visual image not only provides comfortable visual presentation of exhibition goods and space and displays the real exhibition goods to improve their quality, but also includes the implication and guidance of visual psychology.

After taught theories of exhibition lighting and illumination design, students have to deeply analyze and sort the spatial lighting and illumination design requirements according to different exhibition space types, functional partitioning of spaces and scale demands, calculate and set natural light and artificial light, select the comprehensive lighting approach, conduct software simulation as well as final lighting effect design control in considering of the properties of exhibition goods and scale demand of exhibition props, create conceptive scenario lighting effect according to design style and visual presentation mode, and finally establish a model entity with stronger lighting effect representation capacity.

Status and analysis of exhibition lighting and illumination design

Viewed from design approaches, the lighting and illumination design procedures in the past are often based on established exhibition building spaces, and lacks early considerations to the design and plan of one important organic component of light, thus often resulting in the waste of energy lighting, inconsistency between exhibition contents and lighting effects, etc. Early cooperation between lighting designer and the exhibition building architect in design goal, space presentation and behavior shaping can develop a good interaction, in which the exhibition building architect is responsible for planning and designing of spatial organization and layout, while lighting designer is responsible for proposing specific requirements on light control, lighting illumination, image refracting visual effect and psychological effect and cooperating with the exhibition building architect to perfect the architectural design. Such two-way interaction seems more reasonable and easier to create appropriate exhibition design scenario comparing with the passive lighting design solutions.

Viewed from design process, lighting and illumination of traditional buildings are often designed after the completion of building construction. Such design model often gives architect a false sense that lighting design is secondary work. It is the "strawberry on the cake", which is the lastly considered but firstly gave up (when the budget is reduced). Furthermore, the clever application of natural light, visual adaptation, light glare problem, coloration and spiritual conception creation in the lighting and illumination often are viewed only as the selection of lamps and lanterns modeling. Such misunderstandings are caused by our ambiguous understandings on light concept.

Viewed from the design goal, the core goal of exhibition design is the information delivery, the core characteristic of exhibition design different from architecture space design. Museum spaces are used for culture and knowledge communication. Store spaces are used for the co-marketing of brands and products. Large world exposition is used for cultural exchange as well as reflection on science and technology. These space-based information transmissions can be concluded into the exhibition space design. This analysis revealed that exhibition space design and lighting and illumination design can achieve same goal: effective information transmission.

Viewed from design requirement, lighting and illumination design is the comprehensive design under the multidimensional requirement, including lighting equipment entities, lighting equipment amount and illumination quality standard. Meanwhile, it also implies the limitation and requirement of energy conservation and environmental protection. Different from material, shape and color requirements, lighting designers shall have clear aesthetic and functional goals on their design, understand the final diversified and complicated visual presentation effects, structure and construction requirements, and calculate energy consumption under the limitation of budget and technical parameters during the initial lighting and illumination design.

Teaching goal of exhibition lighting and illumination design

The primary curriculum content of "Exhibition Lighting and Illumination Design" includes introduction to light, natural light and basic principle of artificial illumination, relationship between light and vision and color, optical characteristics, and other theoretical knowledge. It transits from the basic principle of natural lighting in exhibition environment to the analysis of design approach, technical requirement and aesthetic significance gradually. It emphasizes on the deep analysis of artificial illumination, detailed introduction to the classification of common artificial illuminations as well as performance and characteristics comparison of different artificial illuminations. Furthermore, based on the disciplinary characteristics of exhibition design, it puts forward and analyzes the specific requirement and design procedure of lighting and illumination design in considering of exhibition contents of different natures, such as business show, museum, exhibition, etc. It aims to create teaching contents with deeper intrinsic logicality and sequentiality.

Based on the integrative interaction between lighting and illumination design and exhibition space, the design philosophy not only includes the natural lighting and artificial illumination design into design process at the very beginning, but also accomplish a series of design work in proper sequence from design consideration to design deepening and then to natural lighting and artificial illumination design. This, in return, give architects opportunities to revise, deepen and facilitate the exhibition architectural space design. The exhibition building, daylight opening as well as the illumination lamps and lanterns are designed and selected according to various contents in natural lighting design, such as light reflection, light direction and exhibition goods' requirement on light. In other words, lighting effect design is accomplished gradually with the exhibition architectural space design and the physical exhibition architectural space design, in return, will be deepened by the progressing of lighting effect design, thus achieving good interaction and virtuous cycle. This finally leads to the integration of aesthetics, functions and technologies in thinking.

During design process, students shall carry out a detailed analysis on different lighting and illumination design requirements of exhibition public space, information space, space for communication and reception, flow space, aesthetic and emotional space, and other different types of spaces. Based on the illumination requirements (e.g. universal lighting, spot lighting and situational lighting) of different areas, the natural lighting is controlled and applied, and artificial illumination is set and integrated according to the basic composition principle of optical system and professional

lighting design approach, thus finally achieving the goal of independent exhibition design by students.

Market research part requires students to survey the lamps market to understand the types and parameters of artificial lighting as well as their differences. They will begin to know various different types of lamps, such as filament lamp, halogen tungsten lamp, fluorescent lamp, low pressure sodium lamp (LPSL), high intensity discharge (HID) lamp, etc. They will know the luminescence principle, luminous efficiency, color rendering, color temperature, average service life, characteristics and other parameters of different types of lamps as well as their applicable space types. Meanwhile, students are required to making deep survey on local museum space, business space and exhibition space. Furthermore, they also have to study some excellent design cases and make detailed reports on their selection and application of artificial lighting systems for different exhibition spaces.

The software part requires students to master drawing techniques of real luminous efficiency simulation and output the design sketch through the cooperation of 3dmax and vary. They shall be able to simulate the real luminous efficiency by selecting corresponding lamps with delax lighting design software and output complete lamp report as well as power consumption. Besides, they shall be able to output a series of complete drawings through CAD software, including construction drawing of lamp circuits and electric circuit diagram, which are used for matching engineering exhibition design with practical construction.

To make a physical model with true exhibition lighting and illumination design, model making requires students to know the basic circuit access way and select proper circuit materials (e.g. equipments, wires, switches and converters) according to the practical requirement of luminous efficiency.

Curriculum practice of exhibition lighting and illumination design

Market survey

During the teaching of "Market Survey", the author led students to visit the Shanghai New Liuying Lamps Market and surveyed lamp types that are highly welcomed by customers. In addition, professional industrial experts were invited to offer a detailed explanation on the types, application ranges and prices of artificial illumination lamps. On this basis, the author led students to Shanghai Science & Technology Museum, Shanghai Museum, Suzhou Museum as well as other domestic excellent museums and exhibition halls in order to investigate and make a deep analysis on the practical application of lamps as well as various lighting approaches. The survey and analysis results were reported and represented through display panel.

Design basis

The initial curriculum design of "Exhibition Lighting and Illumination Design" accomplishes site planning, architectural modeling, traffic route, entrance and exit setting, function division, scale requirement, fire protection and water drainage. Students are asked to perfect the draft to architectural appearance molding, internal plane layout planning and simple design sketch drawing. This curriculum requires students to determine the overall lighting and illumination design idea according to their theme comprehension.

Design development

It requires students to think how to improve the architectural design through the illumination design development to enhance the visual effect of indoor exhibition and how to integrate the illumination equipments into the built environment through the optimal way. Additionally, it emphasizes on the design creativity. Finally, the teacher-student discussion enables students to have a clear understanding on the concept of lighting and illumination design. Students are required to analyzing the illumination requirement differences among different functional areas. For example, students have to analyze whether it is necessary to introduce natural light into the public space and how to control the natural lighting effectively through various techniques; whether the information space has satisfying illumination of key areas and appropriate space-environment luminance ratio. In addition, students have to design key and subordinate luminous efficiency in the flow space based on the comprehensive consideration of illumination control and security. In artistic conception design, students have to analyze various visual presentation factors like color temperature and illumination and think how to create appropriate harmonious exhibition space environment.

Lighting and illumination analysis and design

The design development pays superior attentions on students' effective representation of their designs. The design representation requires students to communicate with teachers through drafts firstly, emphasizing on the artistry of designed shape as well as illumination efficiency requirements of different areas. Furthermore, students have to analyze lighting systems according to different requirements through plane and three-dimensional drafts and accomplish initial lamp selection. Teachers will teach in accordance of their design content, focusing on analyzing the artistry of their designed shapes, evaluating whether the selected lamps are appropriate and helping students to enrich weak knowledge of artificial illumination lamps and deepen their designs.

The communication based on design draft requires students to draw visual design sketch with stronger luminous efficiency expression by using 3dmax and vary. This not only trains students' independent design and sketch drawing ability, but also evaluates their design style, construction structure, security, color matching and other comprehensive requirements according to their design sketches. After finishing the design sketch drawing, students are asked to output complete circuit diagram and lamps arrangement plan through CAD software. During this period, teachers will be mainly responsible for helping students in solving some technical problems, such as lamps circuit layout and electric circuit arrangement. Furthermore, students have to select lamps practically and output complete lamps report through delax software.

Model making and representation

Model making procedure: make the bottom light box of model according to determined size and then punch holes at the base for connection. Connect the small LED lamps in series connection to the base and then connect to the main switch after the power supply is installed. Finally, arrange the outdoor scene and indoor furniture. The bottom lamp tube is responsible for the theme illumination of the whole exhibition hall. Meanwhile, showcase models in the exhibition hall are made and connected with lamps with every component fixed well. Finally, all models are perfected.

conclusion

The exhibition lighting and illumination design curriculum targets at the achievement of multidimensional goals. In design platform, the exhibition space design and lighting and illumination design interaction mode enable students to connect the initial luminous efficiency design with achievements of previous curriculum, and further develop and deepen these achievements. In design idea, it enables students to have a clear idea on the design theme, luminance, lighting and expected lighting effect of the exhibition content at the very beginning. In technical requirements, it requires students to investigate the lamps market, including lighting types, parameters, differences, etc. In software, students can use software to simulate real lighting and luminous effect and make practical lamps report. Finally, the achievement is represented through a model entity with lighting and illuminating devices.

The Exhibition Lighting and Illumination Design curriculum for the Exhibition Design Major of Department of Industrial Design of Hubei Institute of Fine Arts requires to be established in "weekly" curriculum system. Teachers emphasize on different aspects in different teaching weeks. The teaching is supplemented and design is facilitated by theory, design, representation and implementation. It not only guides students to establish the two-way interaction design idea of exhibition space design and exhibition lighting and illumination design, but also trains their comprehensive analysis and problem solving ability in exhibition lighting and illumination design field, aiming to lay a solid foundation for exhibition design discipline, improve the exhibition design talent quality, facilitate the design quality of exhibition industry and strive to develop wide-scope and interdisciplinary exhibition design talents.

References

[1]Li Liangjun et al. "Exhibition Lighting and Illumination Design". Hubei Fine Arts Publishing House, October, 2012.

Advanced Materials Research Vols. 989-994 (2014) pp 5217-5220
© (2014) Trans Tech Publications, Switzerland
doi:10.4028/www.scientific.net/AMR.989-994.5217

A Discussion about Economic Theory Used in Safety Investment of Petrochemical Enterprises

Dong Xu[1, a] and Su Hu[2, b]

[1]College of Management and Economics, Tianjin University, Tianjin 300280, China;

[2]Department of Safety Technology and Engineering, China University of Petroleum (East China), Qingdao 266580, China.

[a]grammarxudong@aliyun.com, [b]globalhusu@163.com

Keywords: Petrochemical enterprises, economics, safety investment, safety benefits.

Abstract. Petrochemical industry plays a vital role in the world's economic development. However, companies are still faced with a great number of economic loss and a lot of safety investment activities, thus, it needs to study and discuss the theories and methods of safety economics so as to guide economic activities and make enterprises gain the greatest safety benefits. This article is in the view of economics and from the perspective of safety investment, which analyzed the importance, characteristics, categories of safety investment and establish a safety investment model. Companies should seek a way to make full use of economic resources and carry out different safety investment policies according to different production methods.

Introduction

With the emergence of the first oil well in the United States on August 29th, 1859, it lifted the curtain on the world oil industry and became the beginning of modern oil industry. The oil industry is a high-risk and technology intensive industry. It has an extremely important role in the process of the development of the global economy. However, the oil industry is a dangerous industry which is easy to have accidents, such as poisoning, fire and explosion. Once the accidents happen, there will be a large number of deaths and injuries and huge property losses.

Safety means a stable and relatively predictable environment. People and groups won't be interrupted or injured and don't need to worry about interference or damage when they chase for their goals in this kind of environment [1].

According to the 'The annual report on the Boao Forum for Asia in 2012', China National Petroleum Corporation was still at the top of the list and Sinopec was the fourth. From that we can draw a conclusion that China's petroleum and petrochemical industry is developing rapidly. However, safety needs to be paid special attention on the back of the rapid economic development without ignorance. A case study of hazardous chemicals of Chinese petrochemical enterprises, there were 813 accidents and 1360 people were killed between 2004 and 2010 (Fig. 1). The number of dangerous chemicals accidents and deaths was on a declining line, which was linked closely with safety investment.

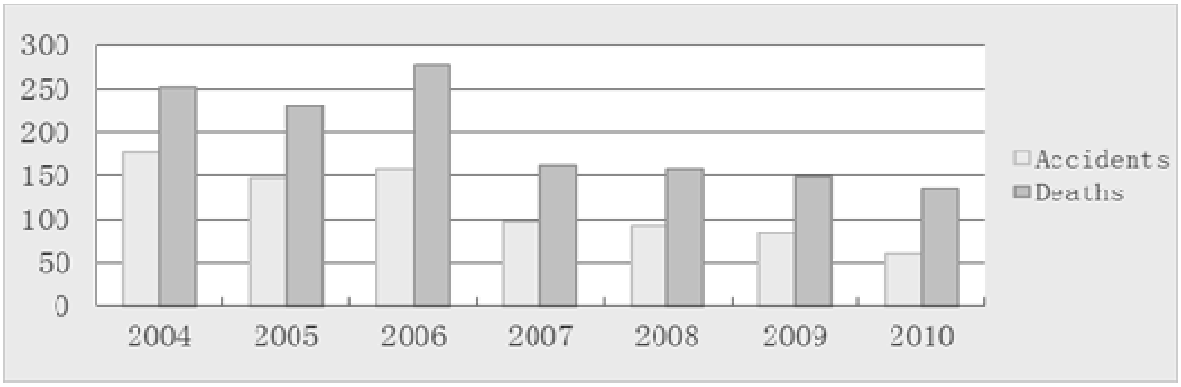

Fig. 1 Accidents and deaths of dangerous accidents

Overview of safety investment

Safety investment is the sum of all human, material and financial resources. The benefit of safety investment is different from common investment, which can't be directly reflected in the improvement of the production and quality. There are not obvious incomes, but in the process of production and business operation and it is reflected in the safety investment which can guarantee the normal and continuous production. Safety investment does not directly increase the product value, only to avoid the value loss caused by unsafe conditions [2].

From the perspective of economics, safety has the function and role of avoiding, reducing the consumption and loss of accidents, maintaining the productivity and guaranteeing the social and economic wealth [3]. Also, from the perspective of economic development, if the safety in production is good, then the performance of enterprises will be better, employees' working and living conditions and the order of production will be normal so as to give play to social and economic benefits.

Model of the safety benefits

The relationship between benefits and safety investment is a monotonically increasing function. With the increase of safety investment, the benefits of companies increase accordingly [4]. Through the analysis of companies' production and operation data, we can get the relationship between safety investment and safety benefits (Fig. 2).

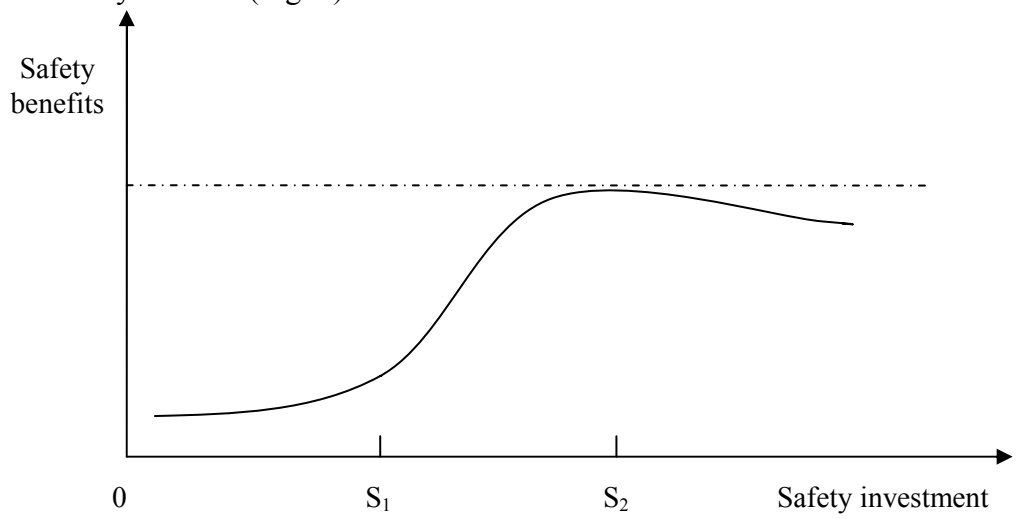

Fig. 2 Relationship between safety investment and safety benefits

From the safety investment and safety benefits curve, the influence of safety investment can be divided into three regions.

(1) $(0, S_1)$ is in the name of safety instability area. Though there is some safety investment, but the safety condition and benefits of companies can't be guaranteed. S_1 is called safety instability point.

(2) (S_1, S_2) is in the name of safety improvement area. If safety investment is increased in this region, the improvement of the safety state will improve the companies' benefits obviously. S_2 is called best safety point.

(3) $(S_2, +\infty)$ is in the name of overflow area. If companies increase the safety investment without limit, though the safety condition is very good, the benefits of the enterprises will decrease.

Thus, there is a limit to how much of the safety investment [5]. When the safety cost and the accidents losses achieve the minimum, the investment is the best point at this time in theory. But in some cases, even though there is a lot of safety investment, it won't ensure that no accidents may happen. As soon as the safety level reaches an acceptable level, the safety investment should be combined with economic benefits. The safety investment is not the bigger the better and different safety investment plans will generate different effects. The effectiveness of the safety investment can be determined according to the benefit-cost ratio of economics (Eq. 1, 2).

$$V=B/I \tag{1}$$

$$E = E_1 + E_2 + E_3 + E_4 - E_5 \quad (2)$$

V: Effectiveness of safety investment;
B: Safety benefits;
I: Safety investment;
E: Economic benefits of the safety investment;
E_1: Direct economic benefits which are created by reducing accidents;
E_2: Indirect economic benefits which are created by reducing accidents;
E_3: Economic benefits which are created by reducing the safety investment;
E_4: Potential economic benefits;
E_5: Safety investment.

Characteristics of the safety benefits

Hysteresis. The function of safety in reducing the casualties and property losses can't be reflected at the time of the security operations, but shows its value and function at the time of the accidents. Safety investment can't be done when accidents occur. Instead, safety investment should be done before in case of accidents, so safety has the characteristic of hysteresis.

Indirectness. The economic benefits' value of safety is reflected by reducing the casualties and property losses. On the one hand, the losses of society, enterprises or individuals can be eased which realize the indirect value. On the other hand, due to the protection of the production technology or equipment, the production can be added value. Most of the safety investment is to realize its use value, such as the measures to reduce the casualties and losses. However, the investment of safety education, health care and labor protection, environmental protection and other aspects can reflect the social benefits of society, so this kind of investment belongs to consumption. Its role is indirect relative to the safety investment.

Potential. The economic benefits of safety measures are not the direct performance from their functions, but behind the potential in the process of the safety [6]. One of the main goals of safety is to ensure people's safety and health, but the value of people's safety and health is hard to be measured by currency. Safety can make people safer and protect the economic conditions and resources of human beings.

Categories of safety investment

Safety investment refers to the cost which is related to safety, and it is the general term of the economic activities and resources which are used to guarantee the business operation in peace [7]. It may include human resources, material resources, financial resources, space and time, etc. In the implementation process of safety investment, Fig. 3 shows the steps of safety investment.

Categories of safety investment include engineering project investment, labor protection investment, safety education investment, safety management investment, emergency rescue investment, insurance investment, accident investment and other necessary investment.

Summary

The realization of safety needs the economic supports and safety is the product of people's economic development in essence. Specific economic level determines the specific safety level. Safety is not a direct substance production. The value of safety is reflected by reducing the casualties, property damage, environmental damage and social impact. Safety shows its value and function at the time of accidents. The characteristics of safety investment result in the petrochemical industry for safety investment is not paid enough attention.

From the point of safety economics, this article analyzed the safety investment of petrochemical enterprises. The safety investment needs to meet the objective requirement of the production

technology and the most effective use of safe resources should be sought. Different safety investment policies are carried out according to different production technology.

National government and regional government should strengthen the legal system, establish the regulatory system and urge the safety investment of petrochemical enterprises. Companies which ignore safety investment and cause casualties should impose economic sanctions. The amount of pensions paid for employees should be raised to urge petrochemical enterprises to increase investment in safety. Safety investment can guarantee the personal security, decrease the accident rate and raise the international image and social image of countries, governments, enterprises and organizations. It also adapts to the needs of the national economy and social development, reveals the safety investment of companies and promotes the development of labor protection utilities, security, science and technology.

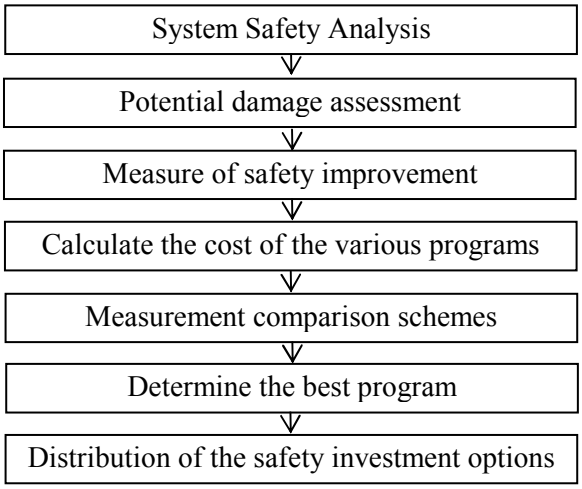

Fig. 3 Steps of safety investment

References

[1] J. van der Geer, J.A.J. Hanraads, R.A. Lupton, The art of writing a scientific article, J. Sci. Commun. 163 (2000) 51-59.

[2] Stephenson J. System safety 2000: A practical guide for planning, managing, and conducting system safety programs[J]. 1991.

[3] Soby B A, Ball D J, Ives D P. Safety investment and the value of life and injury[J]. Risk Analysis, 1993, 13(3): 365-370.

[4] Xian Zhang. Safety—benefit curve[J]. MODERN OCCUPATIONAL SAFETY, 2003 (2): 42-43.

[5] Rune E. How would setting policy priorities according to cost-benefit analysis affect the provision of road safety[J].Accident Analysis&Prevention, 2002, (868), l~14.

[6] Blair, E H. Achieving a Total Safety Paradigm through Authentic Caring and Quality[J]. Journal of American Society of Safety Engineers.

[7] Andreoni D. The cost of occupational accidents and diseases[M]. Geneva, Switzerland: International labour office, 1986.

Advanced Materials Research Vols. 989-994 (2014) pp 5221-5223
© (2014) Trans Tech Publications, Switzerland
doi:10.4028/www.scientific.net/AMR.989-994.5221

Analysis of Digital Electronic Teaching in Higher Vocational Colleges ——Cultivating and Stimulating Learning Motivation

Yanhong Li
Shandong Water Polytechnic, Shandong 276826,China.
liyanhong_2008@126.com

Keywords: Digital Electronic, Teaching, Learning Motivation.

Abstract. Digital Electronic Technology is a very important professional foundation course in higher vocational college, especially those majors in mechanical or electrical engineer. How to arouse students' enthusiasm and initiative in every possible way, and make them pleased to acquire knowledge, it is the major research topic. So the key to success in teaching is the cultivation and simulation of learning motivation.

Introduction

With the development of digital circuits, digital technology has penetrated into every field of our daily life. Digital electronic technology is a kind of computer, communication and electronic information, such as basic required courses for professional public technology. The main purpose of this course is to enable students to learn the basic principle of digital logic circuit and the basic circuit, which is helpful to grasp system analysis method, the design method of digital logic circuit and its application. It is necessary to learn and master the modern electronic technology. Therefore, how to arouse student's enthusiasm and initiative, make students master the knowledge happily, cultivate and stimulate their learning motivation is a key factor to the success or failure of the teaching.

1 The Importance and Necessity of Cultivation and Simulation of Learning Motivation

Learning refers to stimulate students individual learning activities, maintain the learning activity which has been caused, and behavior towards a certain learning objective of a process or internal inner psychological state. If students want to study hard, learning enthusiasm, initiative has a lot to do. Once students have developed an interest in digital electronic technology course, they will show a strong desire for knowledge and concentration and classroom efficiency naturally in the classroom. Therefore, the teacher should pay attention to digging depth from the attach importance to cultivate and stimulate students learning motivation, let the students change from passive learning to active learning.

2 Cultivating and simulating learning motivation in Digital Electronic Technology Teaching

2.1 Stimulating Interest and Maintaining Curiosity

Interest and curiosity are the most core part of the learning motivation. Cultivating the students learning interest is the first task of teaching no matter in what stage of learning. Where there is a possible, to prove to students that the learned information is useful. Creating problem situations to inspire students thirst for knowledge and curiosity is a kind of very effective method. Creating problem situations refer to provide an opportunity for students to question and engage in activities, to explore the answers to questions, certain efforts are conducive to successfully solve the problem of learning materials, conditions, and practice. Effective teaching is the key principle to form a kind of atomosphere to make the students understand a little knowledge, uncertain problem situation resulting conflicts, doubts, surprises and then arouse the greatest intellectual curiosity and interest in learning, in this way, a desire and intention of learning are brought out.

In order to arouse their interest in learning and maintain curiosity for content, a teacher wants to import teaching meticulously and stimulate students thirst for knowledge. There are many import methods of teaching, but the most common and obvious effect is the instance of import design method. When they talk about the sequential logic circuit, for example, triggers section, using PPT for presentation quiz answer after the video program, putting forward the problem which is similar to a few players seem to be press the buzzer at the same time , but why only one contestant vies to answer the first success? Let them think about the problem, and then draw out the main content of the lecture. Such imports can not only stimulate the students curiosity and thirst for knowledge, but also make students believe that the importance of content and interesting, so as to cultivate the students learning motivation.

2.2 Setting the right goals

The law of learning motivation is important. When the target is set by yourself, rather than when it is set by others, oneself often pay more efforts. Such as, before digital electronic technology experiment, let students expect the length of time for myself under the situation of guaranteed accurate every time. When the goal is set, teachers can discuss with students the targets set by the implementation situation, the probability of success or failure, respectively, so that they set suitable goals for themselves. Finally, the teacher wants to praise students in goal setting and its implementation in the experiment summary. Throughout the semester, the teacher will be surprised, it can not only makes students learn digital electronic technology actively, but also cultivates their ability to innovate in the course and to achieve the purpose of fostering a good learning motivation.

2.3 Developing Appropriate Self-efficacy

After the students have the corresponding knowledge skills, self-efficacy has become the decisive factor of their behavior. Self-efficacy is put forward by bandura in the 80s, who makes a subjective judgment of behavior success or not by oneself. It is the individual of their ability to perform a behavior of speculation and judging. The factors influencing self-efficacy are personal behaviors of success or failure experience, substitute experience, verbal persuasion,etc.Many students especially students whose learning results are bad, they are skeptical about their ability to learn, so they often show the low self-efficacy level. In this part of the students, such as, when the teacher asks questions of kano logic function graph reduction problem in class, she can give some hints. Try to construct the interpretation of each chapter, each problem, pay attention to guide students to summarize the rules. For example, in digital electronic technology on karnaugh map reduction, this content in addition to the book of methods, teachers can guide students to summarize some effective laws.

For example: in the four variables f (A, B, C, D) in the karnaugh map, m0, two minimum sum of ml can get rid of one variable. Using the method in the book are two algebraic method according to the sum of the smallest reduction, may guide the students to observe karnaugh map m0 and ml minimum two items of the small squares in A, B,C three variables constant, only the variable D in the corresponding box as the variables, m0 in ml box corresponding to the original variables, that is to say, in A, B, C, D four variables only D variable has changed, so D variable elimination in two minimum operation.

For some more complex expressions, in the reduction or even require students to use some skills, if using this method is more helpful to show its unique superiority. Such as expression for reduction，$\overline{F = AC+\bar{A}BC+\bar{B}C + AB\bar{C}}$，using the concept of collection, we can still according to fill out directly by the expression method of karnaugh map. Due to logic is equivalent to complement operation, the corresponding collection of the first item $\overline{AC+\bar{A}BC+\bar{B}C}$ is the type of complement for the collection of the item $AC+\bar{A}BC+\bar{B}C$. So the item can be found out $AC+\bar{A}BC+\bar{B}C$ place in the karnaugh map, fill in its complement position 1. And with the second

set, to get the same result. , due to not be involved in the concept of fill 0 here is only related to the use of collection, the students are familiar with the knowledge, easy to grasp.

So it is convinced that everyone has the ability to learn, let them gain continuously successful experience, and improve the level of self-efficacy. At the same time, teachers can also be used to change students attribution and train their ability to learn the wrong judgment, judge the right self-efficacy formation and learn motivation stimulated the nature.

2.4 Attribution Training

Attribution is named after behavior, refering to the relevant information: the causes for the clues to the behavior of individuals are according to speculate and judging process. Attribution is a universal thing that human need. Everyone has a behavior from its own experience summing up out the connection between the reason and its behavior of views and ideas. To change students' incorrect attribution and improve learning motivation can be listed from the two aspects: the first one is "effort attribution", no matter success or failure is due to to hard or not. The second is "reality attribution ", which guides the student to do a reality for some specific problems of attribution.

As they talk about the shift register, teachers can let the students design a loop control of neon lights, such as the "elixir of love" four word cycle light, get different combinations, or "good moon flowers, take a full moon, for good month circle". With real life together, the design of the students enthusiasm is very high. Finally, according to the design of the students, teachers guide all students to analysize, thus receiving the recognition from the students. Students like this way, from which they can not only can feel real mastery of book knowledge, but also find out the problem of cultivating their independent thinking ability at the same time. At the same time, students see their successful product design, which can produce a strong sense of achievement.

In the process of teaching, the author once met a student, she thought she had low intelligence. However, after communicating with her, it is as a result of her learning method which is not correct. Before this attribution training can change students' error of judgment and its advantage, find out the problem and point out the ways to solve these problems. The students can not only get knowledge, but also gain confidence. This will better suit the remedy to the case, to stimulate students' learning motivation from the aspects.

3 Conclusion

Digital electronic technology is a professional foundation course which is abstract and difficult to understand. In order to improve the classroom efficiency, the author explores actively from the aspects such as the cultivation and stimulation of learning motivation in the last three years of the digital electronic technology teaching practice, all these have got some achievements, but it’s only a preliminary attempt, there are still many problems that need to be further explored.

References

[1] Yu Meng-chang, Digital electronic technology basic introductory tutorial (second edition), higher education press,Beijing,1999.

[2] Liu Mengxiong, Qin Yilin. Mouth behavior guide item teaching method in the application of PLC application technology course teaching J. Journal of changzhou institute of information technology, 2008, 7 (1) : 31-33.

[3] Yang Na, Integration of digital electronic technology teaching, J. Journal of changzhou institute of information technology, 1 (2009) 55-57.

[4] Yang Zhizhong. Digital electronic technology M. higher education press, Beijing,2005.

[5] Deng Zhiyong,Hou Qing. To develop the innovative ability of students’ try in computer teaching ,J. Journal of vocational and technical education, 2006, 17 (27) : 59-60.

[6] Liu Yuanchao. Digital circuit teaching reform exploration, J. Journal of Yangtze university (natural science edition), 2009 (6).

Advanced Materials Research Vols. 989-994 (2014) pp 5224-5227
© (2014) Trans Tech Publications, Switzerland
doi:10.4028/www.scientific.net/AMR.989-994.5224

The Application of Project Driven Teaching Method In Win Server 2008

Chengbo Yin[1, a,] Deli Lin[1, b] and Pen Ren[1, c]

[1]College of telecom and business, huanghai University, Shandong 266427, China;

[a]ycb1004@126.com, [b]459797867@qq.com, [c]renppc@sohu.com

Keywords: project-driven, course assessment, network operating system

Abstract: Project driven and course designed teaching and examination mode is a kind of brand-new teaching and examination mode, it is a student oriented mode which focus on how to train highly skilled people in practice courses. Combined with course《Win server 2008 network operation system》,below paper give a more detailed and comprehensive introduction for this teaching mode, based on which writer would like to popularize this teaching method with specific demonstration.

Introduction

"Project driven and course designed" teaching and examination mode is a new mode for both teaching and examination which is combined with traditional project teaching mode, case study teaching mode and the new course design criterion. The core for this mode is "student oriented, attach importance to students' proactive knowledge exploring, and also the initiative to find the relationship between the project and knowledge"[1]. Meanwhile, the mode also advanced new assessment method for practice course, which is not purely written examination but is assessed via the quality of course designed by student or the task finished by student, which can reflect the degree how student grasp the knowledge, through all above this mode well achieves the aim to train high quality talent with "qualification, flexibility and being user-friendly" [2].《Win server 2008 network operation system》can well apply this mode, thus can well combine the strongpoints for course and teaching.

The link between the course and actual enterprise commercial activities

The technique《Win server 2008 network operation system》covered can well can be applied to many areas, such as computer network project design, management and maintenance, guide for MCSE, network management, server installation, configuration, management, local area network management, network maintenance, etc. Thus the knowledge point for this course can be further divided from the actual enterprise business needs, which means enterprise project oriented course design.

Specific project conclusion and division

Taking the network building and management as starting point, the project as carrier, living the project oriented thinking, focusing on project design, we combine all the knowledge point of 《Win server 2008 network operation system》 with practice, with the theory knowledge being the fundamental for practice, to avoid long term boring theory teaching that may hurt the student's learning interest, we develop simple practice to attract the spontaneous question from students, then

explain main theory and properly analyze. This helps students deeply understand the theory after interesting practice.

Project division. We divide the theory and practice mentioned in《Win server 2008 network operation system》to 13 items listed in below table(Table 1：Project division example):

Table 1：Project division example

Item	Item description
Item 1	Installation and Planning for Windows Server 2008
Item 2	Hyper-V server installation and set up
Item 3	Deploy and manage Active Directory domain service environment
Item 4	Manage user account and group
Item 5	Manage file system and shared resource
Item 6	Set up and manage basic disk and dynamic disk
Item 7	Set up and manage printers
Item 8	Set up and manage DNS server
Item 9	Set up and manage DHCP server
Item 10	Set up and manage Web and FTP server

Task analysis for each item. Below please find the specific tasks for each item:

- Item 1:Installation and Planning for Windows Server 2008
  Task 1: Install Windows Server 2008 R2 with CD.
  Task 2: Set up Windows Server 2008 R2
  Task 3: Add and manage administrator role
  Task 4: Use the management and control platform for Windows Server 2008
- Item 2:Hyper-V server installation and set up
  Task 1: Install Hyper-V role
  Task 2: Uninstall Hyper-V role 2
  Task 3: Establish visual machine
  Task 4: Config the property for visual machine
  Task 5: Install operating system for visual machine
- Item 3:Deploy and manage Active Directory domain service environment
  Task 1: Create the first domain
  Task 2: Install additional domain controller
  Task 3: Transformation service role
  Task 4: Backup and resume activity directory
- Item 4:Manage user account and group
  Task 1: Create local user account
  Task 2: Set up the property for local user account
  Task 3: Remove local user account
  Task 4: Manage the group account in domain
- Item 5:Manage file system and shared resource
  Task 1: Set up resource sharing
  Task 2: Visit network shared resource
  Task 3: Use Volume Shadow Copy
  Task 4: Succeed to and stop NTFS authority

Task 5: Copy and move file and file folder

- Item 6:Set up and manage basic disk and dynamic disk
  Task 1: Manage basic disk
  Task 2: Get to know dynamic disk
  Task 3: Create dynamic disk volumes
  Task 4: Maintain dynamic disk volumes
- Item 7:Set up and manage printers
  Task 1: Install printer server
  Task 2: Connect to shared printer
  Task 3: Manage printer server
- Item 8:Set up and manage DNS server
  Task 1: Understand the concept and theory for DNS
  Task 2: Add DNS server
    Sub task 1：Establish the DNS server needs and environment
    Sub task 2: Install DNS server
  Task 3: Deploy DNS zone for main DNS server
    Sub task 1：Create a forward main zone
    Sub task 2: Create a reverse main zone
  Task 4: Config the DNS client and test the primary DNS server
    Sub task 1：Config the DNS client
    Sub task 2: Test DNS server
    Sub task 3: Manage DNS client cache
  Task 5: Deploy the assistant DNS server
    Sub task 1：Establish the assistant DNS server needs and environment
    Sub task 2: Establish zone transfer function on primary DNS server
    Sub task 3: Install DNS service on assistant DNS server and create assistant area
    Sub task 4: Config DNS client test on assistant DNS server
  Task 6: Deploy subdomain and delegation
    Sub task 1：Establish the subdomain and appointment needs and environment
    Sub task 2: Create subdomain and its resource directory
    Sub task 3: Zone delegation
- Item9:Set up and manage DHCP server
  Task 1: Get to know DHCP
  Task 2: Set up and manage DHCP server
  Task 3: Set up DHCP relay agent server
- Item 10:Set up and manage Web and FTP server
  Task 1: Get to know the service provided by IIS 7.0
  Task 2: Set up and manage FTP server
  Task 3: Set the AD isolation user FTP server

Team division and Project implementation

Teachers must ensure they well know every student in terms of both life and leaning, and must make sure to make good balance among teams in terms of team member's learning ability and interest. Teachers must assign 1 to 2 foals for each team, the foals need to monitor and reflect the learning status of his/her team and also communicate duly with teachers for the issue they encountered.

In this mode, teachers is not the one who is instructing everything and explaining everything, teachers need to know clearly about the plan, progress, issues for each team and give support to assist student to find solutions for the issues they encountered. Teachers must ensure to be well prepared for all kinds of issues for each team he/she can foresee, this is to avoid the embarrassing situation that even teacher do not know how to deal with the issue. Besides, the students' lacking initiative and creative which was resulted in by traditional education mode is also a barrier for the new mode, in order to avoid this, students must be required to establish detail project plan independently, meanwhile organize both life and learning all by themselves in a specific period, and most important is that to present the project achievement clearly and specifically [3].

Establish course assessment criterion

Teachers need to keep close monitor the completion status, the degree that student grasped knowledge, the interest, adjust the project task details and difficulty. For the difficult knowledge, teachers need to add practice explanation and demo session, this is to avoid teaching stopped due to knowledge is too difficult.

As to <Win server 2008 network operation system>, it is difficult to establish overall assessment criterion. The assessment is mainly referred to periodical project report and usual performance of individual student.

Summary

With the new mode applying to course《Win server 2008 network operation system》, student's learning interest and thinking eager is greatly inspired, meanwhile student's learning confidence is also improved significantly, all these really reflect the characteristics for vocational education. Students can be very efficient, have strong learning ability and also great adaptability to different environment.

Through this new mode, purely classroom course is transferred to on site training and practice which can gain real experience and ability, students grasped the solutions for the possible issues they may encounter in future work, meanwhile, teaching quality and comprehensive professional quality can be fully improved. And the new mode also inspires teachers to explore for new knowledge and enrich teachers with actual enterprise experience.

References

[1] P.Li: On The Project Teaching Method, Cuide to Business, (2011)NO.10, p235-236

[2]Q.Wang: Application of Task Driven Teaching Method in "VB programming", Journal of Hubei Radio& Televisonuniversity,Vol.32(2012).No.8, p.144

[3] M.H.Zhou and M.L. Wang: Analysis of the Implementation of the Project Driven Teaching Method and Case Study, CHINA MODERN EDUCATINOAL EQUIPMENT, (2010), p6-8

[4] J.H. Xiong and F.M. Zhang: Application of Project Teaching Method in The Occupation Technology Education, 2011 Wuxi Vocational Education Teachers in the Forum, (2012)

[5] Yong Gil Lee:The Teaching Method of Creative Education, Creative Education,Vol.04(2013) NO.08, pp.25-30

[6] Adriana Maria Procópio de Araujo and Vilma Geni Slomski: Active Learning Methods-An Analysis of Applications and Experiences in Brazilian Accounting Teaching, Creative Education, Vol.04 (2013),pp.20-27

Advanced Materials Research Vols. 989-994 (2014) pp 5228-5231
© (2014) Trans Tech Publications, Switzerland
doi:10.4028/www.scientific.net/AMR.989-994.5228

Application of the Multi-level Fuzzy Comprehensive Evaluation Method to Software Companies' Choice of Competitive Strategies

Wendan Zhang[1,a], Zhixia Jiang[1,b] ,Yanzhong Li[1,c,*] and Su Zhang[2,d]

[1.]School of Science,Changchun University of Science and Technology,Changchun130022,China;
[2.] School of Economics and Management,Changchun University of Science and Technology, Changchun130022
[a]custzwd@126.com,[b]zhixia_jiang@126.com,[c,*]lyz@cust.edu.cn,[d]zhangsu1972@163.com

Keywords: fuzzy comprehensive evaluation method, Analytic Hierarchy Process, SWOT analysis, competitive strategy

Abstract: This paper attempts to employ the matrix of Strengths, Weaknesses, Opportunities, Threats(SWOT) to establish an evaluative index system for software enterprises in Jilin Province. The SWOT analysis is performed in combination with the Analytic Hierarchy Process (AHP) to determine the relative weights of various criteria in the analytic hierarchy as they are related to the overarching goal. The ultimate assessment of the developmental status of those provincial IT enterprises from the local (departmental/segmental) to the global (corporate/industrial) level will then be derived by applying a fuzzy comprehensive evaluation matrix in accordance with the principle of maximum associations. This approach promises to overcome drawbacks commonly found in conventional hierarchical analyses, where frequent adjustments and tests are often required to make results from judgmental matrix consistent. Examples with concrete analytic results have shown that this innovative, synthetic method is of promising guiding significance to corporate strategic formulations.

Introduction

The competitive strategy of a corporation involves processes through which a firm rationally allocates and matches its internal and external resources to develop and implement business plans in order to obtain a competitive edge. Typically, formulators of such strategies use the SWOT analysis to obtain qualitative assessment of strengths and weaknesses as well as opportunities and threats coming from both within and without the firm in quest for a best-fitting developmental strategy. However, a vague description of the competitive position, in fact, can be finally formed based on this method, so that the conclusion from such analyses tends to have some differences from the reality[1]. In recent years, many researchers seek to add quantitative rigor to such qualitative evaluations by applying fuzzy mathematics to analyses of multi-variate things or objects for overall assessment, which has solved certain analytical problems traditionally deemed as being vague. However, it is difficult to quantify [2,3]. In this paper, we attempt to establish an evaluative index system as it pertains to software companies in Jilin Province based on the SWOT analysis, which is carried out in combination with a multi-level fuzzy decision-making method to solve the problem of their strategic choice.

1. Formulate the Evaluation System

The SWOT analysis is carried out on the provincial software enterprises in Jilin to examine their internal and external environment, in order to construct an evaluation index system to facilitate choices in corporate competitive strategies.

(1) Construct an SWOT analytical matrix [4]

In this paper, the results of the SWOT analysis of the software enterprises in Jilin from the lens of the regional economic development are summarized in the matrix shown in Table 1.

Table 1 The matrix of the SWOT analysis for the development of the software enterprises in Jilin

Strength（S）	Weakness（W）
1.the advantage of the region (S_1) 2.the advantage of the talents (S_2) 3.the advantage of the industry (S_3) 4.the advantage of the base (S_4)	1.optimization required for the industry environment (W_1) 2.the scale is so small for the whole software industry (W_2) 3.weakness in the creative ability for the software company(W_3) 4.it is incomplete for the support of the oversea's market (W_4)
Opportunity（O）	Threat（T）
1.Strategy for the Pilot Changchun-Jilin-Tumen Open-up & development zone (O_1) 2.Enhancing the support of the government(O_2) 3.Embedded software as the represent of the automotive electronics (O_3) 4.Wide prospect of outsourcing market in export for software(O_4)	1.Internalization of international competition (T_1) 2.Existing problems in the construction of the software park(T_2) 3.Serious brain-drain，the structural contradiction of industry is prominent(T_3)

(2) Establish the indexing system

In light of the specific circumstances concerning software development in Jilin, the developmental strategy for the provincial software companies (G) is defined as the overarching goal, and S , W , O , T are referred to as the first-level (parent) indicators, whereas specific factors S_1 , S_2 , S_3 , S_4 , W_1 , W_2 , W_3 , W_4 , O_1 , O_2 , O_3 , O_4 , T_1 , T_2 , T_3 represent secondary (child) indicators respectively.

2. Determine the Relative Weights of Respective Indicators

In this paper, we use AHP to determine the relative weights of the differentially leveled indicators, where the pairwise comparisons are undertaken on the same-level indicators for their relative importance to the parent indicator at the upper level to form a judgmental matrix. A characteristic vector will then be identified for each group of indicators, and its consistency will be tested accordingly.

(1)Construct the judgmental matrix

Based on the index system, the Delphi method is taken to form the judgmental matrix - each for factors S , W , O , and T respectively - following steps outlined below:

$$S=\begin{pmatrix} 1 & 1/3 & 1/3 & 1/2 \\ 3 & 1 & 1/4 & 2 \\ 3 & 4 & 1 & 4 \\ 2 & 1/2 & 1/4 & 1 \end{pmatrix},\quad W=\begin{pmatrix} 1 & 1/2 & 1/3 & 1/3 \\ 2 & 1 & 1/2 & 1/2 \\ 3 & 2 & 1 & 3 \\ 3 & 2 & 1/3 & 1 \end{pmatrix}$$

$$O=\begin{pmatrix} 1 & 1/2 & 1/5 & 1/3 \\ 2 & 1 & 1/3 & 1/2 \\ 5 & 3 & 1 & 5 \\ 3 & 2 & 1/5 & 1 \end{pmatrix},\quad T=\begin{pmatrix} 1 & 1/3 & 1/3 \\ 3 & 1 & 1/2 \\ 3 & 2 & 1 \end{pmatrix}$$

(2)Calculate the weight for each indicator

The characteristic vector of the matrix is obtained through the square root method, which is then normalized for consistency check, as shown in Table 2.

Table 2 The weight of all model and the result of the consistency check

Strength		Weakness		Opportunity		Threat	
Weight W_1	Consistency check	Weight W_2	Consistency check	Weight W_3	Consistency check	Weight W_4	Consistency check
0.1003 0.2212 0.5400 0.1385	$\lambda_{max}=4.2216$ $CI=0.0739$ $CR=0.0830$	0.1038 0.1789 0.4576 0.259	$\lambda_{max}=4.1649$ $CI=0.0550$ $CR=0.0618$	0.0798 0.1424 0.5766 0.2012	$\lambda_{max}=4.1777$ $CI=0.0592$ $CR=0.0666$	0.1396 0.3325 0.5278	$\lambda_{max}=3.0536$ $CI=0.0268$ $CR=0.0515$

3. Construct the Evaluation Model

(1)Determine the field of characteristic factors influencing the evaluation

Based on the literature review, we divide the collection of comments on qualitative indicators (V) into five grades in terms of importance, namely: {not important at all, not important, general, fairly important, very important}, with their corresponding value to be assigned according to Table 2, as shown in Ref. 5. The set of factors is obtained by synthesizing expert opinions both at home and abroad. The four fuzzy relational matrix for the factorial modules represented by S, W, O, T are denoted as U_1, U_2, U_3, U_4 respectively , with their specific forms as follows:

$$U_1=\begin{pmatrix}0.04 & 0.09 & 0.43 & 0.26 & 0.18\\ 0.08 & 0.11 & 0.24 & 0.37 & 0.20\\ 0.07 & 0.10 & 0.14 & 0.37 & 0.32\\ 0.03 & 0.08 & 0.19 & 0.41 & 0.29\end{pmatrix} \quad U_2=\begin{pmatrix}0.03 & 0.05 & 0.12 & 0.46 & 0.34\\ 0.10 & 0.16 & 0.23 & 0.30 & 0.21\\ 0.05 & 0.10 & 0.30 & 0.42 & 0.13\\ 0.06 & 0.18 & 0.34 & 0.27 & 0.15\end{pmatrix}$$

$$U_3=\begin{pmatrix}0.05 & 0.12 & 0.41 & 0.24 & 0.18\\ 0.20 & 0.35 & 0.19 & 0.17 & 0.09\\ 0.08 & 0.12 & 0.18 & 0.34 & 0.28\\ 0.06 & 0.18 & 0.34 & 0.27 & 0.15\end{pmatrix} \quad U_4=\begin{pmatrix}0.07 & 0.09 & 0.13 & 0.20 & 0.51\\ 0.06 & 0.10 & 0.15 & 0.41 & 0.28\\ 0.05 & 0.09 & 0.14 & 0.19 & 0.53\end{pmatrix}$$

(2)Determine the degree of index memberships

To multiply the relative weights $W_i(i=1,2,3,4)$ assigned to the four factorial modules used in the SWOT analysis by $U_i(i=1,2,3,4)$ according to the formula $B_i=W_i\cdot U_i(i=1,2,3,4)$, we get the comprehensive evaluation results for the software enterprises in Jilin, as shown in Table 3.

Table 3 The subordinated level of one grade indicator

One grade indicator	not important at all	not important	General	fairly important	very important
S	0.0637	0.0984	0.1981	0.3645	0.2753
W	0.0595	0.1263	0.2792	0.3637	0.1713
O	0.0907	0.1648	0.2320	0.2937	0.2188
T	0.0561	0.0933	0.1419	0.2645	0.4440

(3)Get the comprehensive evaluation results

The final results of the modular evaluations as they pertain to software enterprises in Jilin Province are computed with the assistance of the fuzzy comprehensive evaluation rating method by assigning values to the above-mentioned five grades of importance based on the formula $G_i=B_i\cdot V_i^T$: i.e., V_i ={not important at all, not important, somehow important, fairly important, very important}, where (i=1,2,3,4). The calculation also takes into consideration the actual situation of those enterprises. The final results are presented as follows:

(4)Select strategic options for business development for Jilin software enterprises

In this paper, we use the coordinate graph to present the SWOT analysis[6], where a total of four alternative strategies are plotted, namely the Pioneering Strategy, the Reversing Strategy, the

Defensive Strategy and the Stabilization Strategy. Based on the coordinate data, the area defined by the combination of Advantages and Opportunities is calculated to be 12.4890, which represents the largest area. Therefore, the option represented by the first quadrant should be selected as the strategic objective, namely the Pioneering Strategy. Meanwhile, the software companies in Jilin must pay attention to the Stabilization Strategy represented by the combination of Opportunities and Disadvantages, in order to seize opportunities like implementing the strategy for the Pilot Changchun-Jilin-Tumen Open-up & Development Zone, so as to avoid internal industrial weaknesses, and to achieve the sustainable development of the software enterprises in Jilin.

4.Conclusion

This paper reports on an objectively-and-faithfully-conducted SWOT analysis of the development of the software enterprises in Jilin Province. The analysis has been carried out in combination with AHP and the fuzzy comprehensive evaluation method to assess strengths, weaknesses, opportunities and threats confronted by the software enterprises in Jilin. Based on the final results of the evaluation, it is recommended that the Pioneering Development Strategy is taken by the provincial software companies to pursue their business development.

References

[1] Ru Guo and H.Z. Yang: Roadmap of renewable Energy Industry Development in Chongming Ecoisland[J]. Journal of Tongji University (Natural Science),vol. 40 (2012) No.8,p.1204-1209.

[2]Y.Z. Li and Y.Sh. Yang: *Application of fuzzy mathematics*(Jilin Peoples Publishing House,China,2001),p.35.

[3]J. Zhang and J.J. Yang: Research on the practical production scheduling decision based on fuzzy synthetic evaluation, Journal of Hunan University(Natural Sciences),vol. 41(2014) No.2,p.79.

[4]the Ministry of Industry and Information Technology Operation Monitoring and Coordination Bureau: *Chinese Electronic Information Industry Statistical Yearbook(Software)2012*, (Publishing House of Electronics Industry, China, 2013), p.59-61.

[5]S.J. Liu, H. Li and T. Wang: Study on selection of agricultural material supplier based on SWOT analysis and fuzzy AHP[J], Logistics Technology, Vol. 31(2012)No.11,p.195-198.

[6]Y.Q Ti: Study on the Development Countermeasure of Newenergy in Hebei Province based on Comprehensive Evaluation and SWOT(Ph.D., North China Electric Power University, 2012), p.35.

Advanced Materials Research Vols. 989-994 (2014) pp 5232-5236
© (2014) Trans Tech Publications, Switzerland
doi:10.4028/www.scientific.net/AMR.989-994.5232

Analysis of Low Carbon Development Path for Coal Industry of Multiagent Network Structure under Carbon Tax Background

Lihua Wang [a], Xin Li [b], Yingju Yuan, Qingxiang Cai

School of Mineral Engineering, China University of Mining and Technology

[a]WANGHL1979@163.com, [b]LIXIN.B@163.com

Keywords: Low carbon development path; Multiagent network structure; Carbon tax; Coal industry chain

Abstract. Based on coal industry chain features and decision-making behavior features, considering the marketing environment changes caused by the carbon tax, models are separately set up specific to the whole industry chain and different individuals' optimized decision-making differences, and the individual decision-making target is taken as a connecting link between the preceding and the following for the variable to integrate the model into a double-layer programming model. The results show that the model can reflect the influence of the individual selection of the industry chain on the overall interests and direct the decision-making.

Introduction

In related studies at present, only a few researches have been made into the influence of self-management from different individuals on the whole coal industry chain .Under the operating mechanism of large coal enterprises in China at present, different levels of the industry chain show a behavioral tendency ---longitudinally, they are mutually related to each other and supposed to provide uniform services for the overall interests of the enterprises, while in the internal management of the enterprises, separate settlement is always required in each level to pursue maximum individual benefits. All of these reflect the "two-sideness" of each level in the industry chain which not only represent the benefits of the industry, but also pursue the individual benefits; the whole industry chain represents the features of multiagent collection. Especially under the background of low carbon development required by the present society, the whole industry chain always needs product adjustment by individual enterprise, and they even have to give up part of the high-profit products in order to meet the carbon discharge requirements, which further deepens the contradiction between the whole industry chain and the individuals. Therefore, seeking the relationship between the enterprise individual development of each level in the coal industry chain and the overall development of the industry chain helps the industry adjustment and industry structure optimization, so as to realize the overall upgrading of the coal industry.

Modeling and analysis

Modeling assumptions. Before modeling, the complex real world should be firstly simplified to be convenient for building the mathematical description language, so as to realize the reflection of practical problems in a real way. For this reason, the following assumptions are carried out:

Assumption 1: The decision-making behavior of each procedure in the coal industry chain complies with the "economic and rational" assumption. Deep consideration has been carried out to its decision-making process, and the decision-making selection authentically reflected the practical benefits. This assumption is set for eliminating data deviation produced from some radical selection, and eliminating mutation of data set.

Assumption 2: Each procedure of the coal industry chain is in the same environment, and the environmental factor produces the same influence on different decision-making bodies in the same turn.

This assumption is designed for avoiding the inestimable deviation of decision-making behaviors generated from sudden change of the environment.

Individual decision-making model of coal industry chain. As for the operating individuals in the industry chain, there is:

$$MaxZ_n = \sum f(B) - \sum f(C)$$

s.t.

$$\begin{cases} B, C \in N \\ f(B) \geq 0, f(C) \geq 0 \end{cases}$$

That is, as for the n^{th} industry chain, the maximum difference between the total revenue and the total cost is the goal to be pursued.

It can be obtained from the analysis of the function of the above equations,

$$f(B) = \overline{B} \cdot Q$$

$$f(C) = \overline{C} \cdot Q + C_Q + f(C_E)$$

i.e., the revenue of the industry chain and the average product benefits are directly related to the output; while the costs of the industry chain can be divided into three parts, which respectively are variable cost which is directly proportional with the output, fixed cost and upstream transferred cost. In this way, the individual decision-making model of the industry chain can be transferred into:

$$MaxZ_n = Q\sum(\overline{B} - \overline{C}) - C_Q - f(C_E)$$

Network path model of coal industry chain. As for the whole industry chain, the interrelation of different operating individuals forms the operating network, which enables the industry chain to form product cluster in the market to obtain different additional benefits. Considering the network properties of the industry chain, its value transfer and the increment process are accompanying the extending of the value chain, which reflects the chain path extending in the network, therefore, it can be discussed via transferring it into the network model.

Network model is built for the industry chain, and different modes and link names are endowed, which is shown as Figure 1. This network is composed of some nodes of different levels of O, A, B, C, D and their connecting chain path.

The figure is analyzed, combined with the production features of the coal industry chain, and the following results can be obtained:

A. Due to the irreversibility of production and processing, the connection from the upper level nodes to the lower level nodes is smooth; conversely, they cannot be connected.

B. Due to the overlying existence effect of the industry chain and value chain in the industry chain, the one-way arcs in the diagram possess the arc lengths which can be calculated, which shows the cost paid from the upper level procedure to the lower level procedure in the economic significance. Considering the less social labor change of the industry chain in certain period, in order to be convenient for discussion, large change cost can be adopted for the arc length.

C. Each point in the diagram represents different operating individual: who seek profit tendency in decision making, i.e.: economic rationality, therefore, in the environment with different variable costs, more or less path distributary will occur to the network flow.

Decision-making model of coal industry chain. Based on the analysis above, the production and operating behavior of the coal industry chain falls into two parts: individual operating decision-making process and network routing process. In order to integrate them into a system for systematic discussion, confluence analysis should be carried for the two parts.

It can be seen from the analysis of the network diagram of the industry chain that the directed arc parameters in the structure diagram of the industry chain can independently and visually reflect the relation between upstream and downstream individuals.

Therefore, the individuals of the industry chain and the path models can be transferred. The consequences generated from the decision-making behavior of the individual operating in the industry chain is $f(Z_n)$, and those consequences are considered to directly act on the downstream individuals,

and the influence generated from this action possesses uniqueness and the reversible feature. Therefore, the decision-making consequence $f(Z_n)$ can be taken as the path parameter to be combined into the path of the downstream.

The network structure diagram of the industry chain can be transferred as Figure 2.

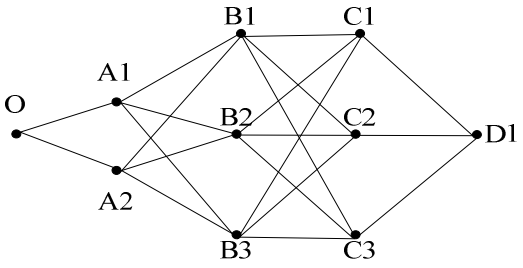

Figure 1. Industry chain network diagram

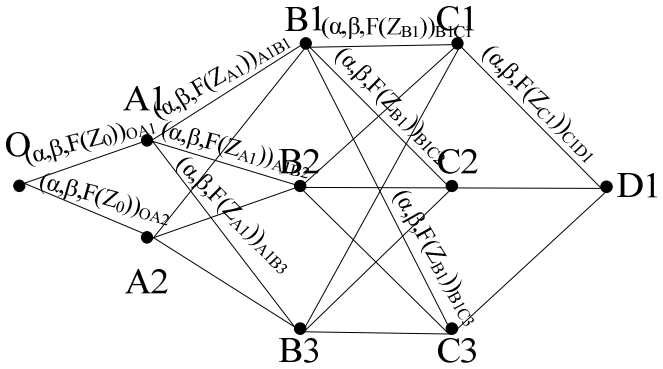

Figure 2. Diagram of industry chain network structure transfer

For the convenience of drawing, only part of the parameter change conditions of industry chain connection is indicated in Figure 2.

As the graphical representation, the individual operating decision function $f(Z_n)$ of the industry chain is taken as a sub-parameter of the directed arc, which is paralleled to the other parameters α and β. While the points in the industry chain network are deemed as smooth knuckles with limitless capacity, i.e.: the directed arcs change direction at the points, which are connected via the points, they are not limited by these points. Being transferred, the parameters of the points in the network diagram are transformed into the arc parameters, which makes it possible to build the model for the whole network structure of the industry chain.

α and β are taken as the cost parameters for influencing the delivery of the industry chain, and C_{ind} as the overall cost of the industry chain, then, the overall decision-making model of the industry chain is:

$$MinC_{ind} = \sum_{i=1}^{n}\sum_{j=1}^{m}(f(\alpha)_{ij} + f(\beta)_{ij} + f(Z)_{ij})$$

Decision-making model of the development of multi-individual coal industry chain. Based on the models with various levels derived from the above deduction, it can be seen that the decision-making model of the development of multi-individual coal industry chain is a group of multi-level programming models, among which: the upper level model reflects the overall benefit demand of the industry chain; the middle level model reflects the benefit demand of each operating individual of the industry chain; while the bottom level model reflects the transfer willingness of the individual cost increment with different levels. The specific mathematic expression equations are as follows:

(M):

$$\begin{cases} \text{(U):} \\ MinC_{ind} = \sum_{i=1}^{n}\sum_{j=1}^{m}(f(\alpha)_{ij} + f(\beta)_{ij} + f(Z)_{ij}) \\ \text{(L1):} \\ MaxZ_n = Q\sum(\overline{B} - \overline{C}) - C_Q - f(C_E) \\ \text{(L2):} \\ f(C_E) = f(R_n, I) \end{cases}$$

Wherein: α and β are the cost parameters for influencing the transfer of the industry chain; C_{ind} is the overall cost of the industry chain; Z is the individual benefit of the industry chain; $\overline{B}$、$\overline{C}$ are the

average benefit and average cost of the individual product of the industry chain; C_Q is the fixed cost; C_E is the upstream delivery cost of the industry chain; R_n is the cost conditions for delivering from different levels of the industry chain to the downstream; and I is the acceptance level of the final consumers.

Model solving algorithm

The solving process of the existing multi-level programming model generally is calculated via transferring it to be the repeatedly nested bi-level programming model[57]. It can be seen from the analysis of the built model that the upper level programming of the model limits the middle level and the lower level, and the middle level also limits the lower level. The upper level programming of the model is connected with the middle level via the variable Z, while the middle level programming and the lower level programming are connected via the variable C_E. Therefore, this model can be transferred to be several bi-level programming problems for solving. The specific model is as follows:

(M1):

(U):

$$MinC_{ind} = \sum_{i=1}^{n}\sum_{j=1}^{m}(f(\alpha)_{ij} + f(\beta)_{ij} + f(Z)_{ij})$$

(L):

$$MaxZ_n = Q\sum(\overline{B} - \overline{C}) - C_Q - f(C_E)$$

(M2):

(U):

$$MinC_{ind} = \sum_{i=1}^{n}\sum_{j=1}^{m}(f(\alpha)_{ij} + f(\beta)_{ij} + f(Z)_{ij})$$

(L):

$$f(C_E) = f(R_n, I)$$

(M3):

(U):

$$MaxZ_n = Q\sum(\overline{B} - \overline{C}) - C_Q - f(C_E)$$

(L):

$$f(C_E) = f(R_n, I)$$

Large difficulties generally exist for solving the bi-level programming problems. On one hand, even the very simple bi-level programming has NP-hard problems, which generally does not have polynomial solving algorithm; another important reason that the lower level programming of this kind of bi-level programming model is essentially a nonlinear constrained problem, therefore, this kind of problem is non-convex programming problem. The locally optimal solution exists, but the globally optimal solution can hardly be found. Please refer to Table 1 for the general solutions of the bi-level programming problems:

Table 1. Table of general solutions of the bi-level programming problems

S.N.	1	2	3	4	5
Method	Simulated annealing algorithm	Tabu search algorithm	Trust region algorithm	Descent algorithm	Genetic algorithm
S.N.	6	7	8	9	
Method	Neural network algorithm	Penalty function algorithm	Great quantity algorithm	Chaos optimization algorithm	

Conclusions

In conclusion, each procedure in the network structure industry chain is deemed to be independent individual, and its choice behavior is included into the overall model for investigation, which can effectively reflect the connection between the overall operation of the industry chain and the individual production.

References

[1] Qiao Aijun. Research about Coal Industry Risk Management Tool in China. Shanxi: SHANXI UNIVERSITY OF FINANCE & ECONOMICS, 2008: 6-9.

[2] Li Xiao-ge，Ma Xing-bin，Gong Shu-yan. The Research on coal chemical industry chain development in china based on value-added Model. SMART MATERIALS AND INTELLIGENT SYSTEMS，2011: 222-226.

[3] Liu Yong, Deng Shuping, Jiang Yunfeng, Xiong Zhijian. Extension and Risk Control of Coal-Chemistry Industry Chain. 2010 THE SECOND CHINA ENERGY SCIENTIST FORUM,2010:1-3.

[4] Qiao Bin, Zhang Bao-zhi, Zhao Xiao-liang, Han Zheng-rong. An empirical analysis based on the industry chain of China coal industry cluster. 2009 INTERNATIONAL CONFERENCE ON INFORMATION MANAGEMENT, INNOVATION MANAGEMENT AND INDUSTRIAL ENGINEERING,2009: 136-140.

[5] Chen Hong, Han Zhe-ying. Sample Study on Heilongjiang Coal Industry for Local Government Behavior in Green Supply Chain Formation. 2009 INTERNATIONAL CONFERENCE ON MANAGEMENT SCIENCE & ENGINEERING (16TH), 2009: 2171-2178.

[6] Wang Jun, Liu Xi-lin. Study on the Stability of Circular Economy Industry Chain of Coal Enterprise. 2009 GEOLOGY RESOURCE MANAGEMENT AND SUSTAINABLE DEVELOPMENT,2009: 3-11.

[7] CHEN Li-min. Rational Analysis and Countermeasures on Coal Industrial Chain Extension. Shanxi Coal,2012(6): 61-64.

[8] WANG Zhi-hong, LIU Qiang, WANG Chong. Regional efficiency evaluation and development strategy of coal industry chain. Journal of China Coal Society,2012(4): 705-710.

[9] WANG Bang-jun, YANG Dong-tao. Evolutional Process and Simulation on Coal Industry Chain Based on System Dynamics:Taking Huaibei Coal Group as an Example. Journal of Wuhan University of Technology (Social Sciences Edition),2011(5): 680-687.

[10]Zhan Yanling. Study on Evolution Mechanism & Integration Path of Industrial Chain of Coal. Jiangsu:China University of Mining and Technology,2009: 32-34.

[11]PENG Hong-jun, ZHOU Mei-hua, LIU Man-zhi, ZHANG Yu, HUANG Yan-bo. A dynamic optimization model of an integrated coal supply chain system and its application. Mining Science and Technology,2009(11): 842-846.

Advanced Materials Research Vols. 989-994 (2014) pp 5237-5240
© (2014) Trans Tech Publications, Switzerland
doi:10.4028/www.scientific.net/AMR.989-994.5237

The enterprise oriented computer graphic design courses construction of practice teaching system

Erjing Bai[1, a], Deli Lin[1, b]

[1]College of Telecom and Business, huanghai University, Shandong 266427, China;
[a]Baierjing0620@163.com, [b]459797867@qq.com

Keywords: graphic design courses, practice teaching, teaching system

Abstract. Nowadays, the computer graphics technology is widely used in the area of design. The author puts forward the enterprise oriented computer graphic design courses construction of practice teaching system, which is for improving the employment rate of the computer students and making the students can directly blend in the enterprise after graduation. This system includes four big modules. They are the construction of teaching staff, the construction of practical condition and cooperation with enterprise, practice teaching system, teaching quality supervision and feedback system[1]. Each module is decomposed into several small modules.

Introduction

Computers are used in all walks of life, in the rapid development of computer technology today. Computer graphics technology is increasingly mature and development. Computer is widely used in the field of design, so it is to form the computer aided design —CAD. Designers use computer design software such as Photoshop, CorelDRAW etc. to express customer's design thinking, and we can see that the computer is the designers' "hand" and "eye" etc. Nowadays computer graphic design industry is vigorous development in the countries all over the world, especially the country is like Japan. Nowadays, the value which is generated by computer graphic design industry is a significant role in Japan's gross domestic product (GDP). In the world, many countries use relevant preferential policies to promote the development of the computer graphic design industry. Such as in South Korea, the government has set up a special fund to support its development. Comparing with other countries, the development of computer graphic design in our country has a long way to go. In our country, many big cities such as Beijing, Shanghai etc. are very lack of designers. So the author that is based on several years teaching experience proposes the enterprise oriented computer graphic design courses construction of practice teaching system. Through the application of this system in practical teaching situation, it can relieve the lack of designers in surrounding environment and can reduce the investment of the enterprise for the staff and can reassure the parents of students and can make the students find a satisfactory job and can improve our employment and so on.

This system includes four parts: teaching staff, the construction of practical condition and cooperation with enterprise, practice teaching system, teaching quality supervision and feedback system.

The construction of teaching staff

A strong teaching staff is the basic guarantee for completing the teaching process. A strong teaching staff does not mean that the teachers' number is huge; it is double type teacher in theoretical teaching and practical teaching for computer professional graphic design classes. Especially the teachers' practical teaching ability is very important in graphic design courses. In order to develop teachers' practical teaching ability, we can do it from the following aspects:

First, we can organize teachers to participate the enterprise training. By taking part in the enterprise training, that can raise the teachers' practical ability, can cultivate double type teachers, can make teachers zero contact with enterprise and can know what's talent that the enterprise is needed.

Second, we can organize students to take part in skills competition and skills tests. The teachers' practical teaching ability will be improved soon in the process of tutoring for students in skills competition and skills tests.

Third, teachers can improve practical teaching ability through learning himself. As an old saying goes, "it's never too old to learn". It's very necessary to guide the teachers to learn in their spare time. Making all teachers realize that only learning new knowledge constantly won't be eliminated by the society.

The construction of practical condition and cooperation with enterprise

Complete experiment equipment is the basic guarantee for teaching process. For computer graphic courses, complete experiment equipment only need several computers which are installed teaching software. Special instructions, installing teaching control software is very important in addition to install the necessary teaching software in a computer. Through the teaching control software, teachers can broadcast teaching, receive and send a student's work, monitor the student machine, etc. Such auxiliary teaching software is very helpful for practical lesson. Constructing university-enterprise cooperation can prompt the student to zero distance contact with the enterprise, and can reduce the impact for graduate students from training institutions. It's very useful to adopt the training institutions experience in teaching. The teaching methods and teaching means which our college is used should be merged with training institutions, and we should apply flexible. Ultimately it can make the students suit community and market.

Practice teaching system[2]

Course objective. Course objective is the direction of teaching, it is teaching purposes. If it is without direction and purposes in teaching process it can not be called a qualified teaching. We should clear the course objective before teaching, and it should be different for different levels of students. It's not the same course objective for undergraduate students and college students ,For the same course 《Photoshop》. If we want to clear the course objective, we should understand it from three dimensions. The three dimensions are knowledge and skills, processes and methods, emotional attitudes and values. Knowledge and skills are the most basic requirements, they are the most basic knowledge and the most basic skills in the course. For these, the vast majority of teachers can complete. For example, the course《Photoshop》is to teach students how to matting and how to apply filters and other basic skills. Its purpose is to enable students to learn the basic skills of this course. The process and method is to allow students to explore knowledge. It let students themselves identify problems, analyze problems, solve problems. Through this can cultivate the students' innovative spirit and practical ability. For computer graphic design curriculum, teachers can allow students to do curriculum design to achieve this goal. The third dimension is to develop students' emotions, attitudes and values. It is to allow students to have a correct outlook on life, values and world views, so students can have a correct learning attitude, etc. As teachers we should not only teach students knowledge, but also answer students' puzzled. The author believes that "teaching" is to teach basic knowledge, basic skills for course. "Answering puzzle" is to answer all confusion (including outside of the course) for students. Through "answering puzzle" can guide students to the right direction about outlook on life, values and world views. For computer graphic design courses, in this goal, teachers can find some healthy and beautiful life works to guide students' correct emotion, attitude and values.

Course content. If we want to arrange course content, we must first to choose good teaching material. The selection of teaching materials is very important for teaching. For computer graphic design courses, the teaching materials include theory and practice.

Theory is the summary and method of practice, and practice is the embodiment of the theory. They are very important, and both them can't be short of. In order to unify theory and practice, it is feasible to choose a few books as reference. For example the graphic course 《CorelDRAW》, the

author chose two textbook as reference. One course is《CorelDRAW X4 Chinese standard tutorial》of Tsinghua university press, the other course is 《CorelDRAW X3 Computer instruction and practice》of Posts and Telecom Press. 《CorelDRAW X4 Chinese standard tutorial》 is much theoretical content and knowledge system but less instance; 《CorelDRAW X3 Computer instruction and practice》is Based on examples, but knowledge is a bit messy. In the process of teaching, combining with two books will make the teaching process very systemic, and will make students both learn theory and practice at the same time. Of course, for Course content we should omit or add content according to Course objective, should not accept the whole book content.

Curriculum implementation. Curriculum implementation is to implement Course objective and course content. Through curriculum implementation, we can realize course content and achieve course objective. The curriculum implementation must be achieved through teaching activities. In order to implemented better for graphic design courses，teachers must pay attention to the selection of teaching mode, teaching methods and teaching methods. For computer graphic design courses, the author used "issue – found" teaching mode. For example in the "CorelDraw X4" course the author gives the students the work first, and then allows students to check textbooks and to try to do it himself. The last the author explains it. Through practice, the author found that this teaching model is very suitable for teaching practical courses. Teaching method is also very important in the teaching process. The author generally uses the lecture method, practice method, experiment method, practice operating method. Experiment method is particularly important. Traditional teaching methods (a book, a piece of chalk and a blackboard, etc.) can not meet the teaching of computer graphic design courses. In such teaching, the author uses both computers and multimedia.

Course assessment. Course examination includes unit skills, integrated design, vocational skills certification, vocational skills competition four parts, and it isn't a paper to give students the score of a semester or even an academic year. First, unit skills is the usually score, is to check the students' knowledge points of each chapter. Through this, teachers can understand students' understanding of the knowledge points. Then it is integrated design. Grasping every knowledge good isn't necessarily to achieve better results in the integrated design. Because in this design, it is not only check students' knowledge, it is more important to check students' the ability of innovate and the teamwork skills. Finally, vocational skills certification and vocational skills contest can add scores for participating students. By adding scores can encourage students to participate in vocational skills test or vocational skills competition and it can culture student interests.

Teaching quality supervision and feedback system

In order to protect the quality of teaching, the system includes teaching quality supervision and feedback system modules. This module contains four sub-modules: evaluation system, peer assessment system, real-time evaluation mechanisms[3].

Evaluation system. Evaluation System has two parts: Process evaluation and outcome evaluation. In the teaching process，in order to get a good teaching results, you must strictly control the teaching process. So both teaching process and teaching results are important, they need to grasp strictly. Process evaluation has two main objectives: and the quality of student learning. Teaching quality is mainly through college expert evaluation and student evaluation. The quality of student learning is through the evaluation of the employer, of course, also includes the evaluating of the students' parents.

Peer assessment system. Peer assessment system is mainly through listening to each other, learning together for the teachers that teach the same course. For the same course, every teacher has different method, for students which one is the most willing to accept? Through listening to each other, teachers can achieve the purpose of studying together. Thus peer assessment system is a tool for mutual learning and mutual progress for teachers.

Real-time evaluation mechanism. Real-time evaluation mechanism refers experts, parents, employers, peer teachers, students through network or letters to evaluate students learning and to evaluate teachers teaching at any time and any place. The Advantage of real-time evaluation

mechanism for teachers is to know his shortcomings at once, and for students is to receive feedback immediately.

Conclusion

Practice has proved that the implementation of the teaching system is very useful, it can regulate our computer graphic design course of practical teaching, it can enhance teachers' practical teaching ability, and it can improve students' practical ability, innovation ability, etc. Of course, the teaching system is not set in stone, it need to adjust according to actual teaching situation.

References

[1] B.Fang: Journal Of Huaihua University, Vol. 32 (2013) No. 3. (In Chinese).

[2] D.X.Zhang, X.W.Yang and J.Li: Journal Of Shiyan Technical Institute, Vol.23 (2010) No.1. (In Chinese).

[3] L.Chen, Y.Y. Dong,etc. :Experimental Technology And Management , Vol.26(2009) No.11.(In Chinese).

Advanced Materials Research Vols. 989-994 (2014) pp 5241-5244
© (2014) Trans Tech Publications, Switzerland
doi:10.4028/www.scientific.net/AMR.989-994.5241

Quasiconvex Cash Subadditivity Risk Measure for Portfolios

Hongwei Liu[1,2,a] and Caibo Xiao[3,b]

[1]School of Science, Tibet University, Lhasa, Tibet 85000, China;

[2]school of Mathematics and Statistics, Wuhan University, Wuhan 430072 ,China;

[3]School of Economics and Management, Tibet University, Lhasa, Tibet 85000, China.

[a]email:lhw_28@163.com,[b]email: caibo20020703@163.com

Keywords: Cash subadditivity, Risk measures, Product space, Quasiconvexity

Abstract. In this paper, quasiconvex cash subadditivity risk measures for portflios is studied. We propose the concept of quasiconvex cash subadditivity risk measures for portflios and provide a dual representation.Which is more flexible than the one introduced by Cerreia-Vioglio and Maccheroni and Marinacci(2011).

Introduction

Risk measure is one of the most important facets of risk management as capital requirement and principles of premium calculation for the regulator and supervisor. Artzner et al. (1999) firstly introduced the concept of coherent risk measure, by proposing four basic properties to be satisfied by every sound financial risk measure. Föllmer and Schied (2002b) and, independently, Frittelli and Rosazza Gianin (2002)introduced the broader class, named convex risk measure. However, the cash additive axiom has been criticized from an economic viewpoint.Cash additivity fails as soon as there is any form of uncertainty about interest rates.For this reason EL Karoui and Ravanelli (2009) suggest to replace cash additivity with cash subadditivity. But in the situation, the equivalence between convexity and diversification principle no longer holds, in fact,it is implied by quasiconvexity, Cerreia-Vioglio and Maccheroni and Marinacci (2011) proposed quasiconvex risk measure.

Recently,multidimensional risk measures for portfolio vectors have been studied. The multivariate analogue of the Value-at-Risk discussed by Embrechts and Puccetti (2006) is based on set-valued quantiles of the multivariate cumulative distribution function.Jouini et al.(2004) and Kulikov (2008) defined multidimensional risk measures as set-valued functional,and they proved the corresponding representation results. For set-valued measures of risk, see also Cascos and Molchanov (2007), Hamel and Heyde (2010) and Hamel (2006). Burtert and Ruschendorf (2006) defined multidimensional risk measure and proved representation results for convex and coherent risk measures for portfolio vectors.

In the present paper,we will propose a framework of multidimensional quasicovex cash subadditivity risk measures.We will define quasicovex cash subadditivity the multidimensional risk measure and provide the representation results.

Preliminaries

Notations. Let $L^{\infty}(\Omega,\mathcal{F},P)$ be the space of bounded random variables.Its topological dual is denoted by $\mathcal{M}_{1,f}(\mathcal{F})$ and coincide with the set of finitely additive probabilities that are absolutely continuous with respect to P , $\mathcal{M}_1(\mathcal{F})$ is the subset of $\mathcal{M}_{1,f}(\mathcal{F})$ consisting of all its countably additive elements.For this reason,given $X \in L^{\infty}(\Omega,\mathcal{F},P)$ and $\mu \in \mathcal{M}_1(\mathcal{F})$,we indifferently write: $\mu(X)$, $E_{\mu}(X)$ .The specification of the probability space $(\Omega,\mathcal{F},P)$ is often omitted and we just write L^{∞} , $\mathcal{M}_{1,f}$ .From now on, let $N \geq 1$ be a fixed positive integer.For $1 \leq i \leq N$,we denoted by g_i the

space $L^{\infty}(\Omega_i, \mathcal{F}_i, P_i)$ .Let g^N be the product space $g_1 \times \ldots \times g_N$, $I = (1, \cdots, 1)$, $aM = (aX_1, \cdots, aX_N)$, $a \in R$,if $a = (a_1, \cdots, a_N) \in R^N$,the $aM = (a_1 X_1, \cdots, a_N X_N)$ .For $M_1 = (X_1, \cdots, X_N) \in g^N$, $M_2 = (Y_1, \cdots, Y_N) \in g^N$, $M_1 \le M_2$ means $X_1 \le Y_1, \cdots, X_N \le Y_N$, $M_1 + M_2$ stands for $(X_1 + Y_1, \cdots, X_N + Y_N)$, $M = (X_1, \cdots, X_N) \in g^N$,define $\|M\| = \|X_1\| + \cdots + \|X_N\|$, $I = (1, \cdots, 1)$,where $\|X_i\| = \sup_{\omega \in \Omega} |X_i(\omega)|$,

then $(g^N, \|\cdot\|)$ is a Banach space. We can interpret $(g^N, \|\cdot\|)$ in two distinct but related ways:

(1) For $M = (X_1, \cdots, X_N) \in g^N$, M can be understood as a portfolio held by a firm with its subportfolios $X_1, \cdots, X_N$. X_k can be interpreted as the payoff an asset of type $k \in \{1, \cdots, N\}$. Under this interpretation, g^N stands for all the portfolios held by the firm.

(2) We can represent a firm by an element $M = (X_1, \cdots, X_N) \in g^N$, $1 \le i \le N$ where X_k is referred to the k^{th} portfolio of the firm M , and can be interpreted as the payoff a business of type $k \in \{1, \cdots, N\}$ .In this case, g^N stands for all the firms. This interpretation can be adopted in the capital allocations.

Quasiconvex cash subadditivity risk measure. EL Karoui and Ravanelli (2009) replaced cash additivity with cash subadditivity, named cash subadditivity risk measure.

Definition 2.1 A cash subadditivity risk measure is a function $\rho : L^{\infty} \to R$ monotonicity,convex and satisfying the following cash subadditivity.

$$\rho(X + m) \ge \rho(X) - m, m \in R^+$$

Remak: The meaning of this condition is" when m dollars are injected into a future position the present capital requirement is reduced by less than m dollars ".This is a much more compelling assumption than cash additivity since it just relies on the fact that an additional reserve of m dollars surely cover the additional loss of the same amount.

Cerreia-Vioglio and Maccheroni and Marinacci(2011) relaxed the convexity into quasiconvexity and draw quasiconvex cash suadditivity risk measure.

Definition 2.2 If a map $\rho : L^{\infty} \to R$ satisfies with monotonicity,cash subadditivity and the following quasiconvex property

$$\rho(\lambda X + \lambda Y) \le \max(\rho(X), \rho(Y)) \quad X, Y \in L^{\infty}, \lambda \in (0,1)$$

Then ρ called quasiconvex cash subadditivity risk measure.

Theorem2.1(Cerreia-Vioglio and Maccheroni and Marinacc) A function $\rho : L^{\infty} \to R$ is a quasiconvex cash subadditivity risk measure if and only if there exists $F \in F_1(R \times \mathcal{M}_{1,f})$ such that

$$\rho(X) = \max_{\mu \in \mathcal{M}_{1,f}} F(E_{\mu}(-X), \mu) \text{ ,for any } X \in L^{\infty}, \mu \in \mathcal{M}_{1,f} . \quad (1)$$

The function $F \in F_1(R \times \mathcal{M}_{1,f})$ for which (1) holds is unique and

satisfies $F(t, \mu) = \inf\{\rho(X), E_{\mu}(-X) = t\}$,for any $(t, \mu) \in (R \times \mathcal{M}_{1,f})$

Main results

In this section,we shall define quasiconvex cash subadditivity risk measure for portfolios, and provide the corresponding representation result.

Definition 3.1 A risk measure $\rho : g^N \to R$ is called a quasiconvex cash subadditivity risk measure for portfolios,if it satisfies the following three axioms:

(a)Monotonicity: $M_1 \le M_2$ implies $\rho(M_1) \ge \rho(M_2)$ for any $M_1, M_2 \in g^N$.

(b)Cash subadditivity: $\rho(M + (a_1 + \cdots + a_N)) \ge \rho(M) - (a_1 + \cdots + a_N)$ for any $M \in g^N, a_i \in R^+$.

(c)Quasiconvexity: $\rho(\lambda M_1 + (1 - \lambda) M_2) \le \max(\rho(M_1), \rho(M_2))$ for any $\lambda \in (0,1)$ $M_1, M_2 \in g^N$.

Remark Let $\rho : g^N \to R$ be a quasiconvex cash subadditivity risk measure for portfolio vectors. ρ is normalized,when $\rho(0)=0$,Define $\rho_i : g_i \to R$ as $\rho_i(X_i) := \rho(Me_i)$ .Then ρ_i is a quasiconvex cash subadditivity risk measure for portfolios on g_i .Conversely ρ_i is quasiconvex cash subadditivity risk measure for portfolios on g_i .Then define $\rho(M)=\rho_1(X_1)+\cdots+\rho(X_N)$ is also a quasiconvex cash subadditivity risk measure for portfolios. Let $\mu=(\mu_1,\cdots,\mu_N)\in \mathcal{M}_{1,f}^N$, $\mathcal{M}_{1,f}^N := \mathcal{M}_{1,f}(g_1)\times\cdots\times\mathcal{M}_{1,f}(g_N)$, $E_\mu(M)=E_{\mu_1}(X_1)+\cdots E_{\mu_N}(X_N)$ for any $M\in g^N$.

Proposition 3.1 let ρ_i be a quasiconvex cash subadditivity risk measure if and only if ρ_i is quasiconvexity and Lipschitz continuous with constant 1.

Proof: if ρ_i is Lipschitz continuous with constant 1,then $\rho_i(X_i)\le\rho_i(X_i+a_i)+\|X_i-(X_i+a_i)\|$ for any $X_i\in g_i$, $a_i\in R^+$, that is, $\rho_i(X_i+a_i)\ge\rho_i(X_i)-a_i$ .Conversely, $X_1,X_2\in g_i, X_1-X_2\le\|X_1-X_2\|$,the $X_1-\|X_1-X_2\|\le X_2$,monotonicity and cash subadditivity imply $\rho_i(X_2)\le\rho_i(X_1-\|X_1-X_2\|)\le\rho_i(X_1)+\|X_1-X_2\|$,as wanted.

Theorem 3.1. Any quasiconvex cash subadditivity risk measure for portfolios ρ on g^N is of the form $\rho(M)=\max\limits_{(\mu_1\cdots\mu_N)\in\mathcal{M}_{1,f}(g_1)\times\cdots\mathcal{M}_{1,f}(g_N)} F(E_{\mu_1}(X_1)+\cdots E_{\mu_N}(X_N),(\mu_1\cdots\mu_N))$ for any $M\in g^N$ .The function is unique and satisfies $F(t,\mu)=\inf\{\rho(M):E_\mu(-M)=t\}$ for any $(tI,\mu)\in R^N\times\mathcal{M}_{1,f}^N$.

Proof: It only remains to show that ρ is qusiconvex cash subadditivity risk measure for portfolios if and only of F is Lipschitz continuous with constant 1 in the first component.

suppose ρ is cash subadditivity,then for $(tI,\mu)\in R^N\times\mathcal{M}_{1,f}^N$ and $m\in R^+$

$$F(t+m,\mu)=\inf\{\rho(M):E_\mu(-M)=t+m\}=\inf\{\rho(M):E_\mu(-M-mI)=t\}$$
$$=\inf\{\rho(H-mI):E_\mu(-H)=t\}\le\inf\{\rho(H)+m:E_\mu(-H)=t\}=F(t,\mu)+m$$

Therefore,monotonicity of F we can get the following inequality

$F(t',\mu)\le F(t+|t-t'|,\mu)\le F(t,\mu)+|t-t'|$, $t,t'\in R$, $\mu\in\mathcal{M}_{1,f}^N$

Conversely,if F is quasiconvex and Lipschitz continuous with constant 1 in the first component,then,for all $(tI,\mu)\in R^N\times\mathcal{M}_{1,f}^N$ and $m\in R^+$,

$$F(t+m,\mu)\le F(t,\mu)-|t-(t+m)|=F(t,\mu)+m$$

Moreover,for all $M\in g^N$,There is $\mu'\in\mathcal{M}_{1,f}^N$,such that

$$\rho(M-mI)=F(E_{\mu'}(-(M-m)),\mu')\text{ .Therefore}$$
$$\rho(M-mI)=F(E_{\mu'}(-(M-mI)),\mu')\le F(E_{\mu'}(-M),\mu')+m$$
$$\le\max_{\mu\in\mathcal{M}_{1,f}^N}F(E_\mu(-M),\mu)+m=\rho(M)+m$$

Proposition. Let $\rho : g^N\to R$ can be an upper semicontinuous and quasiconvex risk measure for portfolios.Then ρ is positively homogeneous if and only if $F(\cdot,\mu)$ is positively homogeneous for any $\mu\in\mathcal{M}_{1,f}^N$.

Proof:Let $t\in R$, $\lambda\in(0,\infty)$ and $\mu=(\mu_1\cdots\mu_N)\in\mathcal{M}_{1,f}^N$, $M\in g^N$ then

$$F(\lambda t,\mu)=\inf\{\rho(M):E_{\mu_1}(-X_1)+\cdots+E_{\mu_N}(-X_N)=\lambda t\}=\inf\{\rho(M):E_{\mu_1}(\frac{-X_1}{\lambda})+\cdots+E_{\mu_N}(\frac{-X_N}{\lambda})=t\}$$
$$=\inf\{\rho(\lambda H):E_{\mu_1}(-H_1)+\cdots+E_{\mu_N}(-H_N)=t\}=\inf\{\lambda\rho(H):E_{\mu_1}(-H_1)+\cdots+E_{\mu_N}(-H_N)=t\}$$
$$=\lambda\inf\{\rho(H):E_\mu(-H)=t\}=\lambda F(t,\mu)\text{ .}$$

Conversely,assume that $F(t,\mu)$ is positive homogeneous for all $\mu=(\mu_1\cdots\mu_N)\in\mathcal{M}_{1,f}^N$ and let $M\in g^N$ and $\lambda\in(0,\infty)$ .Then

$$\rho(\lambda M)=\max_{\mu\in\mathcal{M}_{1,f}^{N}} F(E_{\mu_1}(-\lambda X_1)+\cdots+E_{\mu_N}(-\lambda X_N),(\mu_1\cdots\mu_N))=\lambda\max_{\mu\in\mathcal{M}_{1,f}^{N}} F(E_{\mu_1}(-X_1)+\cdots+E_{\mu_N}(-X_N),(\mu_1\cdots\mu_N))$$
$$=\lambda\max_{\mu\in\mathcal{M}_{1,f}^{N}} F(E_{\mu}(-M),\mu)=\lambda\rho(M).$$

Conclutions

We have introduced the concept for quasiconvex cash subadditivity risk measure for portfolios and provided its representation theorem,which is more flexible than the one introduced by Cerreia-Vioglio and Maccheroni and Marinacci(2011).

References

[1]Artzner, P., Delbaen, F., Eber, J. M. and Heath, D., Coherent measures of risk, Mathematical Finance ,Vol.9 (1999) No3, p.203-228.

[2]Artzner, P., Delbaen, F., Eber, J.M. and Heath, D., Coherent multiperiod risk adjusted values and Bellman's principle, Annals of Operations Research,Vol.152 (2007) No.1, p.5-22, 2007.

[3]Burgert, C., Ruschendorf, L., consistent risk measures for portfolio vectors, Insurance: Mathematics and Economics,Vol.38 (2006) No.2,p.289-297.

[4]EL Karoui N, Ravanelli C. Cash subadditive risk measures and Interest rate ambiguity.Mathematical Finance,Vol.19 (2009) No.4, p.561-90.

[5]Cerreia-Vioglio.S.,Maccheroni.F. and Marinacci.M.,Risk measures:rationality and diversification, Mathematical Finance,Vol.21(2011) No.4, p.743-774.

[6] Kratschmer V. Robust representation of convex risk measures by probability measures. Finance Stochastics ,Vol.9 (2005) No.4,p.597-608.

[7]Burgert, C., Ruschendorf, L., consistent risk measures for portfolio vectors, Insurance: Mathematics and Economics,Vol.38 (2006) No.2, p.289-297.

[8]Cascos, I., Molchanov, I., Multivariate risks and depth-trimmed regions, Finance Stochastics Vol.11(2007) No.3,p. 373-397.

[9] Föllmer, H. and Schied, A., Robust preferences and convex measures of risk ,(Advances in Finance and Stochastic), pp. 39-56. Berlin Heidelberg New York: Springer 2002a.

[10]Föllmer, H. and Schied, A., Convex measures of risk and trading constraints, Finance and Stochastics,Vol. 6(2002b), p.429-447.

[11] Föllmer, H. and Schied, A., Stochastic Finance: An introduction in discrete time, 2nd ed,De Gruyter Studies in Mathematics 27, 2004.

[12] Frittelli, M. and Rosazza Gianin, E., Putting order in risk measures, Journal of Banking and Finance,Vol.26(2002) No.7, p.1473-1486.

[13]Frittelli,M.,and G.Scandolo,Risk measures and capital requirement for processes,Mathematics Finance,Vol.16(2005) No.4,p.589-612.

[14] Kulikov A.V., Multidimensional coherent and convex risk measures, Theory Probab. Appl, Vol.52 (2008) No.4,p.614-635.

[15] Hamel, A.H., Heyde, F., Duality for set-valued measures of risk, SIAM J. Finan.Math, Vol.1 (2010) No.1, p.66-95.

[16] Ludger Ruschendorf, Mathematical Risk Analysis, Springer, 2013.

[17] Deprez, O., Gerber, Hans U., On convex principles of premium calculation, Insurance: Mathematics and Economics,Vol. 4 (1985) No.3,p. 179-189.

[18] Acciaio B, Follmer H, Penner I. Risk assessment for uncertain cash flows: model ambiguity, discounting ambiguity, and the role of bubbles. Financ Stoch,Vol.16 (2012) No.4,p.669-709.

Advanced Materials Research Vols. 989-994 (2014) pp 5245-5249
© (2014) Trans Tech Publications, Switzerland
doi:10.4028/www.scientific.net/AMR.989-994.5245

An Analysis of Characteristics and Purchase Predisposition of Consumer of Urban Community Commercial Service

Qingfeng GENG[1, a]

[1] School of Management, Fuzhou University, Fuzhou 350108, China

[a]fgengqing@126.com

Keywords: Community service; Urban community; Community net store; Characteristic; Purchase predisposition

Abstract. This article is primarily for the research and analysis of demand for commercial service of urban community. First of all, it suggests the urgency and importance by redefining community's connotation and function from the views of the development of society. Then through questionnaires we visited community residents in 18 districts of Tianjin, and finally sum up the essential characteristics and purchase predisposition of consumer of community commercial service.

Introduction

Currently, most urban living environment is mostly developing as community, today electronization is becoming more and more often stressed, community should not only provide the safe living environment, but be functional for business use as well. The electronization of community provides communication channels among residents, it control and ensure the digitization and internetization in the community and community availability of community information.[1] Although community residents can do shopping at the nearby department stores, the purchase costs will be relatively raised. If we can integrate their demand for commodities and develop the chain-store model, we'll be able to do large bulk purchases so as to provide cheaper goods and more convenient service for community residents. Thus it can be seen that the rapid development of modern community, perfect pattern of community management and community electronization are the foundation of modern community. To community service provider and other outside businesses, community means commercial opportunity. And what they call community commerce is defined as a business different from regional business center, huge shopping centers and featured pedestrian shopping streets, it is strongly regional and mainly for residents in region.[2] So we must research the purchase characteristics of community residents, their purchase tend to diversification, topicalization and individuation. And the demand is transforming from subsistence to a comfortable life. What the community service system we're establishing need to do is to draw this "community commercial map", building the information bridges between commercial tenant and resident, helping residents find the goods or service they need rapidly. [3] This passage assessed Tianjin, and analyzes characteristics and purchase predisposition of consumer of urban community commercial service through sending questionnaires to residents in 18 districts.

Empirical research of community commercial service in Tianjin

Questionnaire design and sample selection. The purpose of this research is as following: before building the logistics system, we should know exactly what residents want to community. So we can set up a community service system that meets the residents' demand. This investigation is for studying residents' demand to community commerce, especially to community net store, the new business model. [4, 5] The samples of this research are residents of 18 districts in Tianjin. The questionnaire contains four sections: the first part is about the buying situation of community store, there are 8 questions, including their buying reason, types of goods, purchasing frequency, consumption amount, the important factors and pointless factors, products they want to add, etc. The

second part is the research about networking situation, there are 13 questions, including the buying reason, the type of goods, purchasing frequency, consumption amount, payment method, unpleasant experience, what they want to be improved and why they don't choose online shopping, etc. The third part is about how they think about community online supermarket, there are 14 questions, including whether they accept this new way to shop or not, why they like the networking supermarket or why don't, what kind of goods they want to buy, what service they want to be provided, factors they think important as well as that they think pointless and what they think about the development prospect of this new shopping way, etc. The last section is about the respondents' basic information, there are 6 questions, including their district, age, family structure, educational status, profession and monthly income.

Questionnaire recovery and general situation. The questionnaires are mainly distributing to residents from 18 districts including 6 areas, 4 suburbs, 5 counties and Binhai New Area in Tianjin. The qualities is as following: 100 to 6 areas in the city, 150 to Xiqing (where the school is located) and 50 to every other area. Totally 1300 questionnaires have been given out, and the recovery rate is 100%. After screening, we got 544 effective questionnaires which account for 42.62 percent among it.

The 554 effective questionnaires show: First, from the aspect of areal distribution, it is not balanced in 18 districts, Xiqing (24%) and Nankai (17%) rate is much higher, because more questionnaires have been given out there, and respondents are serious about this for their high educational status. Second, from the aspect of age, it is also not balanced because most respondents are from 15 to 55, as well as most questionnaires from the young or the old are not available. Effective questionnaires are mainly from people ages 15 to 35, which account for 85%, for there are much more people of this age are our respondents and their questionnaires are more normative. Third, As the hand of family structure, 64% respondents are unmarried, this is because their ages are mainly from 15 to 35, they care more about fashion, personality and Less quantitative, so it's easier for them to accept new business model. Married people account for 35%, their families are mainly of three people, and their shopping is focus on babies, they pay more attention to the benefits and convenience. Fourth, on the hand of educational status, respondents are from sorts of background. Most are undergraduate students (57%), because more respondents are from them and most of their questionnaires are effective. Sixth, seen from the family incomes, most are between 2000 and 6000 Yuan, which accounts for 60%, the income reflects purchasing-power terms.

Demographic characteristics of the target customers. The research makes the group who do frequent community store shopping and always do online shopping. The so-called frequent community store shopping is consumers who go to community store at least once.

After the analysis of 554 effective questionnaires, 338 people are selected as the target consumers. The demographic characteristics of these 338 people are described as the following Fig.1.

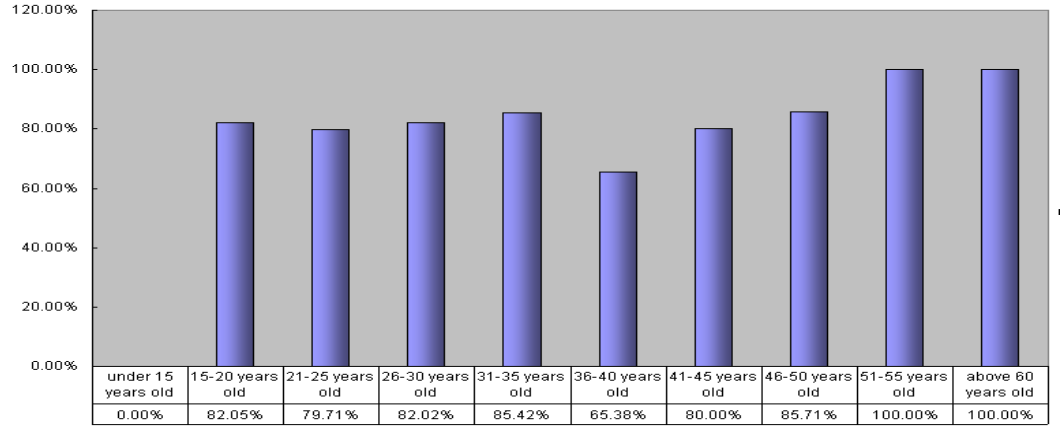

Figure1. The proportion of target of all ages

First, from the geographical point of view, the target consumers concentrated in the more affluent and higher maturity areas, the proportion of target consumers exceeds 50 percent in most areas expect Hebei District, Jinan District, Ninghe Contry, Baodi Contry and Dagang District. And the proportions

of Jinnan District, Ninghe contry, Baodi Contry are lower than 40 percent .This data shows that Tianjin has high potential demand of the community services.

Second, judging from the age structure, the target consumers of all ages account for more than 60 percent, except the group under 15 year-age (for the respondents are too less), and the needs of the elderly of the community services are greater than that of the young.

Third, from the marital status, the proportion of the married and unmarried groups are both more than 80 percent.

Fourth, from the educational background, target customers of the crowd who do not enter high school makes up the lowest proportion, the PhD group accounts for a little more proportion. While the target consumers of university student are the most. The proportion of target customers increases as qualifications increase when educational background from junior high school to university level, while it is the opposite when it comes to the situation from the university to PhD. The data shows that the crowds of university undergraduate are relatively most easy to accept new things, and low degree group might do not accept so much because of the difficulties caused by the application of new things, while the high degree group might do not accept so much because they have more questions and concerns to new things.

Fifth, from the professional vie, the proportion of target customers from financial officers and auditors is the lowest, the proportion of customer service staff is a little higher, the target customers of the independent entrepreneurs accounted for a greater proportion, while the target customers from the rest of the occupational background is more than 75 percent.

Sixth, When it comes to the purchasing power, the target customers of high-income groups exceed 50 percent, thought it declines.

Target customers purchase tendency analysis. This research will analysis the purchasing preference, to provide a basis for the determination of the business scope, product selection, service content choice and service level choice of the new business model.

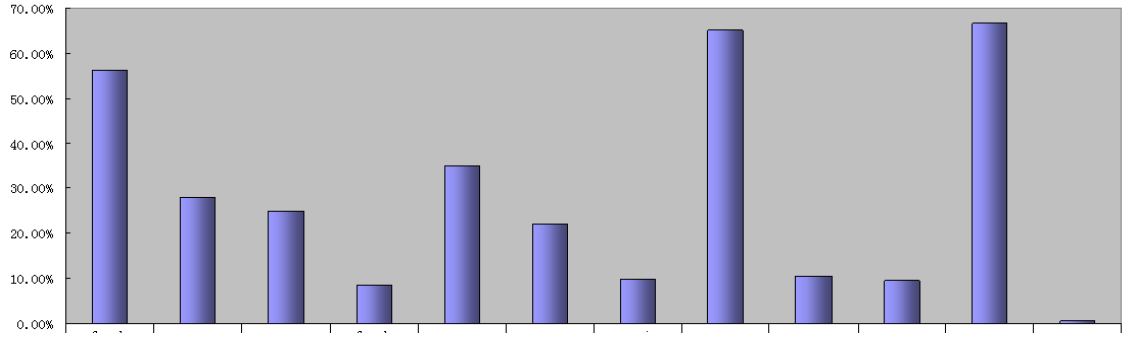

Figure2. The commodity type purchased by the target customers in the community stores

First, from a commodity type of view, On the one hand, community residents major buy daily necessities, snacks , fresh fruits and vegetables, things like milk, rice, meat, eggs and so on are not considered so much, just as shown in Fig.2. At present, the fresh local aquatic products, semi-finished products, breakfast and dinner do not sell that well, which was caused by the lack of providing a wide variety of these goods. While the supply of these goods becomes essential as people working rhythm speeding up, there is potential requirement of these kinds of goods.

One the other hand, the commodity types which the target consumers want to get more mainly are medicine, book, CDs and metal tools. The next is the demand of the cosmetic, maternal and infant supplies, health care products, and cars, just as what was shown in Fig.3. So the amount of these goods can be increased in the community net stores.

Second, we analyzed the point of consumption amount. Above all, we find that the quantity of the target consumers who expend twenty Yuan to fifty Yuan one time accounted for the largest proportion, which reaches 38.76 percent. The quantity who's a single consumption under 20 Yuan or more than 100 Yuan is fewer, which are 11.24 percent and 11.83 percent respectively. This shows that community store commodity whose unit price is higher is not easy to be selected. In the next place, we need to analysis the shopping frequency of the target customers go to community store, which help us

grasp better the spending power of the community store. The data shows that most people go to community store every two or three days, the proportion reaches 51.78 percent, which explain that consumers always solve temporary needs or emergency required in the community store.

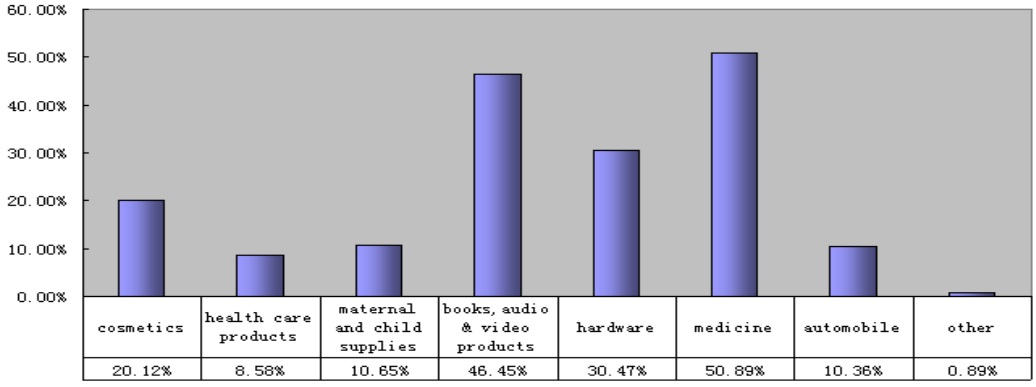

Figure3. The commodity types the target consumers want to increase

Third, by analyzing the demand points, we find that: First of all, the most attractive place of the community net store is its characteristic of shopping convenient, low prices and home delivery. Unlike online shopping, the consumers see the time-saving and home delivery more important when they surf the community net store. In addition, the consumers like the community net store of its temporary emergency, fashion and fun; they can easily get a lot of goods information and shop around. Specific data is shown in Fig.4.

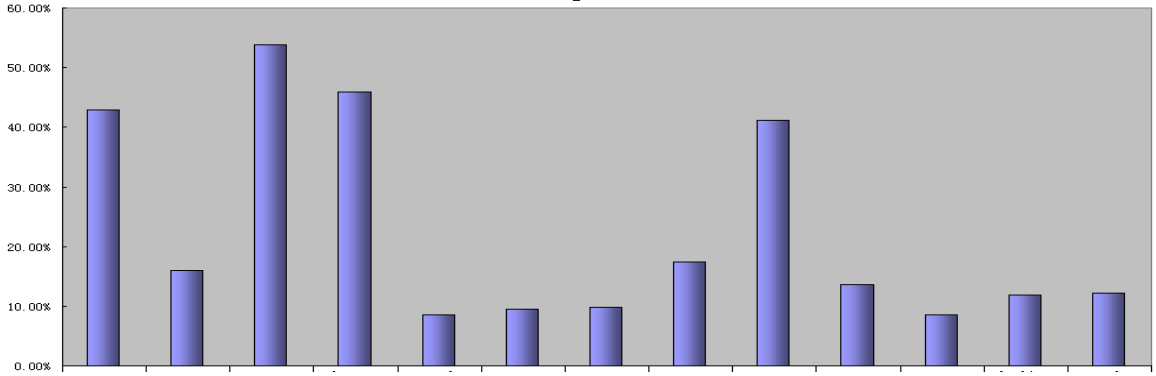

Figure4. The most attractive of the community net store

In the next place, the quality of goods is the most important one, the proportion of people who hold this idea is 81.66 percent. Others think that timeliness, prices and integrity management are also important. Moreover, the full range of products, after-sales service, network security, service attitude, real information and legal protection also matter. Fig.5 shows these messages.

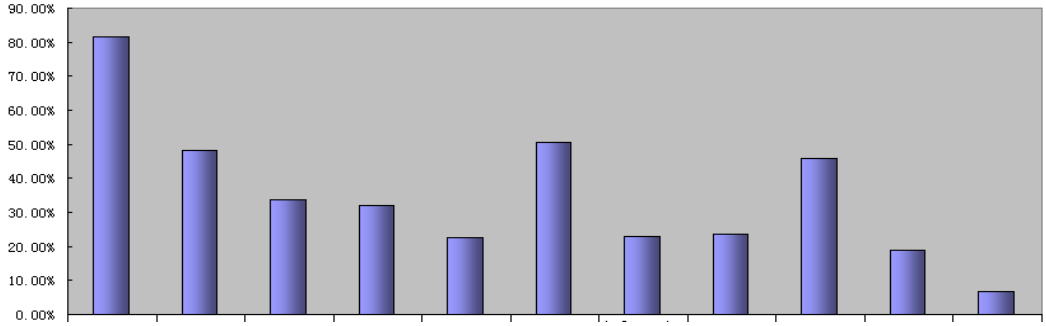

Figure5.Which characteristics of the community net store is important

Furthermore, we should do point analysis for the target consumers, because we have to get not only what he cares most about, but also what does not matters. We should better maximize the limited resources to improve consumer satisfaction for we do not own so endless resources. The majority of people believe shopping atmosphere, after-sales service is not important to the community store. In addition, traffic convenience does not play an important role as supermarket for it mainly addresses the needs of local residents. One the other hand, a lot of people think that personalized service is not

important, because everyone do this shopping mainly for temporary and emergency needs which do not involve too much customization needs.

Conclusions

The paper focuses on Tianjin, make research of residents from 18 districts and counties of community.

On the one hand, we can describe the basic characteristics of the target customers through data analysis. Large potential demand for community services exists in the more affluent and higher maturity areas. The needs of the elderly of the community services are greater than that of the young. The choice of whether to accept a community service does not be affected by the family structure; it only affects the demand point. The proportion of target customers increases as qualifications increase when educational background from junior high school to university level, while it is the opposite when it comes to the situation from the university to PhD. The highest proportion 0f target customers are the Bachelor. The proportion of target customers from financial officers and auditors is the lowest, the proportion of customer service staff is a little higher, the target customers of the independent entrepreneurs accounted for a greater proportion, while the target customers from the rest of the occupational background is more than 75 percent. When it comes to the purchasing power, the target customers of high-income groups exceed 50 percent, thought it declines.

On the other hand, we can draw the purchasing preference of the target customers through data analysis. From a commodity type of view, community residents major buy daily necessities, snacks, fresh fruits and vegetables, things like milk, rice, meat; eggs and so on are not considered so much. The type of goods they want to increase mainly are medicine, book, CDs and metal tools, then the cosmetic, maternal and infant supplies, health care products, and cars. Judging from the amount and proportion of the expense, the quantity of the target consumers who expend twenty Yuan to fifty Yuan one time accounted for the largest proportion, which reaches 38.76 percent. A number of people go shopping every two or three days, the proportion reaches 51.78 percent. When it comes to the demand points, the most attractive pace of community net-supermarket are shopping convenient, low prices and home delivery. In addition, the consumers like the community net store of its temporary emergency, fashion and fun. They also consider the shopping atmosphere, after-sales service and traffic convenience not so important.

References

[1]Y.Zhang: Analysis on the Community-based Service Industry Based on the Electronic Commerce, Journal of Sichuan Engineering Technical College, Vol.9 (2006) No.9, p.21-23.

[2]H.T.Yang, Z.H.Wu and H.P.Shen: *Study on the System Reform and Construction of Legal System in Urban Community* (Shanghai Jiao Tong University Press, China 2004).

[3]B.Y.Lu, L.He and B.Y.Cheng: Research on Intelligent Logistics Information Platform with Pickup-delivery for Urban Communities, Journal of Intelligent, Vol.7 (2011) No.7, p.145-149.

[4]Information on http://www.hlgnet.com.

[5]Y.Wang: the Creation and Development of Community Democracy and Starfish Community Network: Analysis on Beijing Huilongguan Community Network Operation Mode, Dang Dai She Ke Shi Ye, Vol.8 (2010) No.7, p.42-45.

Advanced Materials Research Vols. 989-994 (2014) pp 5250-5253
© (2014) Trans Tech Publications, Switzerland
doi:10.4028/www.scientific.net/AMR.989-994.5250

An evaluation index system of physical education quality based on analytic hierarchy process model (AHP)

Wenying Chen[1], Jianbo Hu[2]

[1]Department of Sports, Guizhou University of Finance and Economics, Guiyang, China
[2]School of International Economics, Guizhou University of Finance and Economics, Guiyang, China

Keywords: physical education; evaluation system; AHP

Abstract. In today's competitive educational environment, the quality of physical education is ever more recognized as a fundamental factor in gaining competitive advantage. The evaluation and improvement of the quality of physical education in higher education is an important issue of on-going concern. The aim of this article is to focus on an automated management and evaluation system to efficiently control the administration of physical education. Reported in this article is an evaluation index of the quality of undergraduate education, and an analytic hierarchy process (AHP) model that is both practical and has proven to be successful. The results of the presented case study demonstrate the practicability and effectiveness of this model in physical education quality evaluation.

Introduction

In today's highly competitive marketplace, college students demand that education be of high quality, of reasonable cost, and with good support services. The evaluation of physical education quality has become a feature of the higher education landscape [1]. On the one hand, physical education quality assessments are being carried out by the new national funding bodies in response to the needs of society in the present age. On the other hand, the major stakeholders in higher education increasingly want to be assured of the quality of physical education.

In fact, the evaluation of education quality can be planned and implemented by small, i ndependent task groups. Heads of schools and evaluation departments have been encouraged to monitor the operation of their evaluation assessment schemes in order to improve educa tional quality. Much experience in the higher education system has led to the conclusion th at high quality is one of the keys to improve physical education [5].

The content of this article touches upon the construction of an evaluation index system for physical education quality. No attempt has been made to establish an absolute evaluatio n index system, because it is felt this would be not only impractical but also restrictive [6]. The present quality assessment systems for physical education can be conveniently used in developing a new system. The first step was to set up an evaluation index system involvi ng the formal appraisal of staff performance and the effectiveness of the education process. The second step was to set up a more effective evaluation model based on the analytic hi erarchy process (AHP) method. The evaluation index system for physical education quality i s extremely varied。

After the literature review, the author introduces a new model for administrative management to strengthen the existing evaluation index system. In this article, the author attempts to provide a finished model for physical education evaluation by using the AHP method. There are different qualitative and quantitative indicators for physical education quality. The aim of this study is to provide a tool to facilitate this. The effective assessment of the quality of physical education is one of the keys for education administrators in implementing university education.

Research discussed in this article is logically ordered into various sections. First, the eva luation index system for physical education quality based on the AHP method is presented. In the next section, the application of this evaluation index system is explained through a case study. Finally, conclusions are drawn.

Evaluation index system for physical education quality

In such a diverse environment, there are a number of methods that can be applied. In the study outlined in this article, an evaluation index system of physical education quality, based on an analytic hierarchy process model, was applied. A novel model is presented in this article for a college evaluation index system for physical education quality. The proposed model and its evaluation index system would enable a physical education quality evaluation.

The Ahp Method

The analytic hierarchy process or AHP method, which was established in 1977, is a popular way to solve multiple criteria decision problems. The AHP method provides a comprehensive structure by which to combine both quantitative and qualitative criteria in the decision-making process. Practice has proven that the method is easy, comprehensive and logical. Based on AHP, the factors involved in undergraduate education can be varied and a unified evaluation index system can be created.

In the AHP method, the problem is structured hierarchically in different levels. Any complex problem can be decomposed into several sub-problems using AHP, and hierarchical levels, where each level represents a set of criteria relative to each sub-problem. As AHP is a very powerful method by which to solve complex decision problems, it was selected as the major tool in this study. Next, the simulation methods are described in detail.

The AHP method is based on the use of pair-wise comparisons, which lead to the elab oration of a ratio scale. In the AHP method, multiplicative preference relations are called ju dgment matrices, and are adopted to express the decision makers' preferences. The pair-wise comparisons constitute square matrices, as shown in the matrix (1), the values of which ar e between 1/9 and 9.

$$\begin{bmatrix} 1 & x_{12} & \cdots & x_{1i} & \cdots & x_{1j} & \cdots & x_{1n} \\ 1/x_{12} & 1 & \cdots & x_{2i} & \cdots & x_{2j} & \cdots & x_{2n} \\ \cdots & \cdots & \cdots & \cdots & \cdots & \cdots & \cdots & \cdots \\ 1/x_{1i} & 1/x_{2i} & \cdots & 1 & \cdots & x_{ij} & \cdots & x_{in} \\ \cdots & \cdots & \cdots & \cdots & \cdots & \cdots & \cdots & \cdots \\ 1/x_{1j} & 1/x_{2j} & \cdots & 1/x_{ij} & \cdots & 1 & \cdots & x_{jn} \\ \cdots & \cdots & \cdots & \cdots & \cdots & \cdots & \cdots & \cdots \\ 1/x_{1n} & 1/x_{2n} & \cdots & 1/x_{in} & \cdots & 1/x_{jn} & \cdots & 1 \end{bmatrix} \quad (1)$$

As mentioned before, in this study, the AHP method was applied to evaluate the quality of physical education. The AHP method searches and evaluates the cause and effect relatio nship between a goal and alternatives by breaking down the structure of the problem. Finall y, the AHP method was used to measure education quality by utilizing the evaluation index system.

Proposed evaluation index system based on the ahp method

As the pace of market globalization quickens, the number of potential evaluation indices of physical education quality assessment increases; and the aim of this study was to develop an evaluation index system of physical education quality that would be effective and efficient. A large attribute set has been reduced and transformed into a lesser number of sub-targets to facilitate the evaluation of education quality.

This study introduced the AHP method to establish an integrated evaluation model. The physical quality education problem involves analyzing and measuring the performance of a s et of candidate indicators.

Case study of physical education quality evaluation

During the case study, the AHP method was applied to solve the problem of physical education quality evaluation. The proposed evaluation index was used by an independent college in China's Hubei province. The staff implemented a physical evaluation in their departments as part of a quality assurance process. It included a total of 17 criteria, divided into five cognate groups covering all the basic aspects of the college course. The evaluation index system of physical education quality is shown in Figure 1. The criteria were based on the overall aims and objectives of the physical course.

In the study, the AHP method was applied to screen indexes and the weight coefficients were defined. According to the proposed model, the estimation of an evaluation index system of physical education quality involves the following phases. First, an investigation was carried out of current physical education quality. Second, an analysis was made of the legitimacy of the evaluation index system. Third, the evaluation process was transformed into concrete operational procedures and standards. At the same time, the evaluation indexes to evaluate physical education quality were selected. However, when the data are collected, it will be necessary for respondents to determine the complicated network of the state-education relationships.

Table 1: Evaluation index system and index weights

First class index		Second class index	
Index name	Index weights	Index name	Index weights
A: Talent development	0.285	A_1: Course content	0.137
		A_2: Course proportion	0.284
		A_3: Course construction	0.193
		A_4: Textbook compilation	0.386
B: Teaching methods	0.207	B_1: Teaching approach	0.364
		B_2: Teaching means	0.245
		B_3: Teaching technique	0.391
C: Teaching staff	0.116	C_1: Construction and training	0.216
		C_2: Full-time teacher	0.183
		C_3: Scientific research	0.327
		C_4: Practical education	0.274

Thus, it was found that these proposals are not only very effective in helping AHP deci sion makers to reach consensus, but they also provide convincing alternatives for physical e ducation quality. Based on the findings from the preceding literature reviews, an AHP mode l was formulated to evaluate physical education quality, as shown in Table 1, the models o f AHP were studied, and the AHP algorithm was analyzed. Then, the AHP method was us ed to determine the weights of the evaluation index system for physical education quality. The basic information with respect to index weights is shown in Table 1.

Conclusions

The overall purpose of this article was to explore and contribute to an evaluative process for physical education quality. Automated evaluation makes the difficult task of evaluating physical education quality, simple and easy. The feedback received from the various institutions indicated that the evaluation index system has proved successful in achieving its various aims.

The evaluation results also provided a great deal of useful information about the effectiveness of the approved AHP model used in the education quality assessment process. At the same time, this work should prove its value as an empirical reference for other evaluation index systems for physical education quality for other nations or states. It is also hoped that it will be of interest to colleagues, and the author would be pleased to provide further information about the evaluation of physical education quality.

Acknowledgments

We thank financial Supported by education and reformation key program of graduated students of Educational Commission of Guizhou Province in China (Project No. JG [2013]017)

References

[1] Siddiqui, A.T. and Masud, M., An e-learning system for quality education. *Inter. J. of Computer Science Issues*, 9, 4, 375-380 (2012).
[2] Kukulska-Hulme, A., How should the higher education workforce adapt to advancements in technology for teaching and learning? *Internet and Higher Educ.*, 15, 4, 247-254 (2012).
[3] Doloswala, K.N., Thompson, D. and Toner, P., Digital based media design: the innovative contribution of design graduates from vocational and higher education sectors. *Inter. J. of Technol. and Design Educ.*, 23, 2, 409-423 (2013).
[4] Pears, A.N., Does quality assurance enhance the quality of computing education? *Proc. Conf. on Research and Practice in Infor. Technol. Series*, Brisbane, Australia, 9-14 (2010).
[5] Pires, A., Chang, N-B. and Martinho, G., An AHP-based fuzzy interval TOPSIS assessment for sustainable expansion of the solid waste management system in Setubal Peninsula, Portugal. *Resources, Conservation and Recycling*, 56, 1, 7-21 (2011).
[6] Kirkwood, A. and Price, L., Examining some assumptions and limitations of research on the effects of emerging technologies for teaching and learning in higher education. *British J. of Educational Technol.*, 44, 4, 536-543 (2013).

Advanced Materials Research Vols. 989-994 (2014) pp 5254-5257
© (2014) Trans Tech Publications, Switzerland
doi:10.4028/www.scientific.net/AMR.989-994.5254

Experience and Enlightenment of American Internet Finance Supervision

Jianbo Hu

Guizhou University of Finance and Economics, Guiyang 550025, China

hjbbo@126.com

Keywords: Internet Finance; American Supervision Experience;Enlightenment

Abstract. Emerging internet finance is a general term that based on the internet and formation of financing activities.Internet finance promotes national economic development and at the same time also increases the instability of financial markets. The internet finane except with traditional financial risk types, also brings new risks, such as technical risk, special law and system risk,information security risk, etc. In our country, there are no special laws and supervision to regulate and govern on internet finance, and also have no special department plan and support its development.The United States's finance is more developed, and the internet finance concept is widely popular and traditional bank network degree is more perfect. Based on this, the experience of the internet finance development and supervision of USA,which will undoubtedly have important strategic significance and practical application value to promote the internet finance healthy and orderly development in China.

Introduction

As to the internet finance, at present the theoretical and practice cycles have not yet formed a widely accepted concept of authority. Xie P, Zou C W (2012) and other scholars believe that the internet finance refers to an emerging financial that relying on internet financial tools such as payment, big data, cloud computing, social networking and search engines to realize financing, payment and information intermediary business[1]. In essence, the internet finance is the combination of internet technology and financial function, relying on big data and cloud computing, forming an open and functional financial forms o and its service system on the internet platform, including but not limited to the financial organization system, financial market system, financial products and services system, financial consumer groups and internet financial regulatory framework which based on network platform. In the United States financial where finance is more developed, the concept of internet finance is widely popularized, the network degree of traditional bank is relatively perfect, using the experience of its regulation of the internet finance will undoubtedly has important strategic significance and practical application value to the healthy and orderly development of our country.

Internet finance development and regulation of the American experience

1)The practice of American network micro credit supervision.The United States bring network micro loans into securities regulatory perspective, focusing on market access and information disclosure. Firstly, the federal Securities and Exchange Commission (SEC) requires internet credit platform registered as securities brokers, identifying that vouchers sold by internet credit platform are securities; Secondly, it is the high cost of registering with the SEC that prevented other potential market participants. For example, the registration cost of network platform Lending loan Club is up to $4 million, so the British largest net credit platform Zopa gave up entering into the American market; thirdly, the SEC focused on the fact that whether the net credit platform discloses information according to requirement. Once appear funding risk, as long as the investors can prove there are omissions or errors of the key information in the prospectus, then the investors can recover

the loss through legal means; Fourthly, in addition to the SEC registration, net credit platform also needs to be registered in the corresponding state securities regulator. The requirement of state securities regulator is similar to the SEC, but some states added some related standards of personal finance to investors, including a minimum income, the upper limit of the securities investment proportion of assets, etc[2].

2)The practice of American P2P industry regulations.The main practices of the US to P2P industry specific regulation include: Firstly, the United States did not formulate special laws for P2P regulation, and mainly by looking for existing P2P related legal content, through which find useful regulatory measures; Secondly, it is subject to the state and federal dual control; Thirdly, the Securities and Exchange Commission (SEC) monitor P2P lending in the way of information disclosure, mainly through mandatory disclosure, anti-fraud and other related responsibility to protect lenders; Fourthly, although the federal trade commission is not regulators, but it can take enforcement actions to P2P lending company which is beyond the scope of its power and involved in debt-collection of the third party. That is to say, the federal trade commission have law enforcement responsibility for P2P lending; Fifth, strengthen protection and supervision to financial consumer rights and interests, and the Consumer Financial Protection Bureau(CFPB)that established after the crisis is responsible for protection and regulation of financial consumer rights and interests of the P2P platform [3]. The savings institutions operating P2P platform involves residents mortgage lending, private student education loan, and working loan, or in accordance with the "other consumer financial products and the large participants in the service market ", or as a service provider in some cases, the P2P platform needs to accept a consumer financial protection agency regulation (Huang Zheng, 2013).At the same time, the consumer financial protection bureau accepts consumer complaints on P2P platform, in order to protect the borrowers.

3)The practice of American third party payment regulation.On the third party payment regulation problems, the United States mainly adopts the following five aspects practices: one is In the identification of nature of institutions, that will treat the third party payment companies and other types of banking deposit institutions differently, and list it as a "currency services" in the concrete regulation, identifying it as general enterprise which only engaged in money transfer or money services business, not a real deposit institutions, and not need to apply for and obtain the general banking business license in the law; Two is manage and regulate monetary service agencies in the form of licensing, specifying the content of initial capital, the free flow of capital, investment scope limit, recording and reporting system, anti-money laundering, etc; Three is regarding retention money of the third-party payment platform as debt, which under the supervision of U.S. Federal Deposit Insurance Corporation (FDIC). Platform retention money need to be put in ginseng protect commercial bank interest-free account, and the capital insurance limit of each account is 100000 dollars; Four is that stipulate all monetary service agencies need to register on the Treasury's financial crimes enforcement network FinCEN, and should be maintained through related identification before opening; Five is that monetary services accept federal and state governments' two-stage control. States formulate regulatory standards and scope under the federal law, undertaking corresponding regulatory responsibilities [4].

4)The practice of American crowd funding regulation.On April 5, 2012, the United States went through the Jumpstart Our Business Act (JOBS Act), which allow small firms acquire equity capital through crowdfunding on the premise of meet the requirements of the securities laws and regulations, and the United States become the first country which really change the articles of association of the relevant regulation and make citizens freely participate in crowdfunding[3]. The JOBS Act released the raise equity financing, and made detailed provision in protecting the interests of the investors. One is that letting go of all the raise equity financing appropriately. The JOBS Act clarifies crowdfunding platforms satisfied the following conditions don't have to go to the federal securities and exchange commission (SEC) registered to conduct equity financing: agent registered

by the SEC acts as an intermediary; Who raise no more than $1 million every year through the network platform; Investors' annual income or net worth is less than $100000, and the total funds shall not be more than $2000, or 5% of the total income; more than $100000, 10% of its income is available for such investment, but up to $100000. The second is to protect the interests of the investors. The JOBS Act puts forward the corresponding requirements for borrowers and financing platform provided services, in order to protect the interests of the investors. For borrowers, the JOBS Act cleared about four requirements. That requires complete the file in the SEC , and disclose information to investors and intermediary institutions regulations; using advertising to promote the issue is not allowed; Limit how to raise compensation promotion; Borrowers must submit the annual report of enterprise operation and financial situation to the SEC and the investors[2].

5)The practice of American internet financial regulation.In view of American regulatory practice for internet fund (The American version Yu E bao PayPal), as the PayPal money market funds is an independent entity which is not affiliated with PayPal entities and operate independently, strictly operate according to the federal Securities and Exchange Commission (SEC) rules and subject to its daily supervision, and the money market funds did not reflect in PayPal balance sheets, therefore, the authorities take status quo and relatively prudent countermeasures and have not yet taken it as a new special legislation to regulate[2].

The enlightenment of American internet financial regulatory experience for our country

1)Legal and regulatory framework of perfecting internet financial regulation.Legal risk mainly embodied in the lack and blank of internet finance law, legal documents. China's regulation of financial laws and regulations of object mainly is the traditional financial sector, because it could not cover many aspects of the internet finance, still further can't fit unique characteristics of the internet finance, which is bound to cause a certain number of legal conflicts. Specialized legal and regulatory files is still a blank, for example there is no clear legal norms in detail on the aspects of internet financial market access standards, the legitimacy of the works, traders' identity authentication, the electronic contract and the effectiveness of electronic signature confirmation, etc. Internet users will face a lack of law and the risk of conflict of laws in the process of using the internet to provide or to enjoy the process of financial services, easily getting into the dispute of the legal blind area, this will not only increase the transaction costs but also affect the healthy development of the internet finance[3]. Based on this, the relevant functional departments of our country should formulate the internet financial related laws and regulations as soon as possible, to protect the internet financial healthy and orderly development of our country.

2)Information technology to improve the internet financial regulation.Technical risk is the common fault of the almost all internet business, mainly reflected in two aspects of operation risk and security risk[5]. Operation risk is the possibility of potential losses caused by system reliability, stability and safety of major defects, mainly comes from investors or improper operation of staff[3]. The security of the internet financial risk is caused by the system reliability, obvious defects of integrity, specific performance are that hackers illegally invade system to steal customer information and cause customer losses, or internet companies design, operate and maintain the internet platform of system improperly, leading to the phenomenon that customer information is stolen and customer rights and interests is damaged. Internet companies should, therefore, prevent the customer information and customer money being stolen and other security issues, by modifying or deleting service program, on the certain defects existed in computer facilities (hardware and software), compatibility, and malicious attacks from internal network and external network. At the same time, we should also develop advanced, independent intellectual property rights of information technology facilities (including hardware and software), improve the level of the key technology of the computer system and key equipment security defense capabilities [5].

3)The mechanism of improving the internet financial regulatory system.One is that the internet companies strengthen the construction of internal control system, for example, establishing internal control system of audit to prevent internal personnel violating compasses operation and stealing and selling customer information[5]; Two is that we should build up a "firewall" between the traditional finance the internet finance, gradually establishing grading warning mechanism of internet finance market, innovating digital and off-site regulatory means, to improve the effectiveness of the internet finance regulation; Three is to build up a joint supervision main body system which give priority to “one bank and three commissions” and give auxiliary to Ministry of Science and Technology, Ministry of Industry and Information Technology, Ministry of Commerce, and State Administration for Industry and Commerce, Administration of Taxation and other departments, to realize the comprehensive supervision of internet banking business; Four is to strengthen international regulatory cooperation, promoting the coordination of the multinational network financial risk events, promoting financial international internet governance mechanism[6].

4)Strengthening the education and protection of financial consumers.Firstly, we should attach great importance to the education of financial consumers and investors, strengthening the consciousness of risk prevention[2]; Secondly, clear regulation subject as soon as possible, make protection methods of internet financial consumers' rights and interests, make specific provision on internet financial transaction security, risk taking and responsibility Liability exemption, information disclosure, privacy and data protection[6];Three is to found a dedicated internet consumer financial protection agency, responsible for coordinating with the internet financial related service complaints and dispute resolution; Four is to make regulatory measures and corresponding punishment measures to protect the rights and interests of consumers to the maximum extent[7].

Acknowledgments

We thank Project Supported by MOE (Ministry of Education in China) Project of Humanities and Social Sciences (Grant No.13YJC790045) , National Statistical Science Project of National Bureau of Statistics in China (Grant No.2013LY104), Project of Science & Technology Department of Guizhou Provice(Grant No. QiankeheJ[2013]2090).

References

[1] Xie P, Zhou C W. Internet financial model research[J].Journal of Financial Research,2012(12):11-22.

[2] Zhang F, Wu J.Foreign Internet financial regulatory experience and enlightenment to our country[J]. Finance and Economics,2013(11):53-56.

[3] Rui X W, Liu L H.China's Internet financial development report[M].Beijing:Social Sciences Academic Press,2014.

[4] Zhao R J. The European and American experience’s enlightenment to perfect our country third party payment regulation[J].Financial Computerizing, 2008(11):86-87.

[5] Gao H. Development and legal regulation of internet finance[J]. Journal of Zhongzhou, 2014(02):57-61.

[6] Wang S G,Zhang C X.Chinese modes of financial innovation and financial development in the internet[J]. Changbai Journal,2014(01):80-87.

[7] Peng H Q,Long W. Innovative research on internet financial model-- taking financial companies in emerging network as an example[J]. Hunan Social Sciences,2014(01):100-103.

Advanced Materials Research Vols. 989-994 (2014) pp 5258-5262
© (2014) Trans Tech Publications, Switzerland
doi:10.4028/www.scientific.net/AMR.989-994.5258

Influential factors of college students' mobile phone recycling behaviors

WANG You-ying[1, a], MA Bu-qing[2, b]

[1]SHU-UTS SILC Business School Shanghai University, Shanghai 201800, China

[a]chenyoudy@126.com, [b]seahorse@126.com

Keywords: telephone recycle; Theory of planned behavior; structural equation model; regression model.

Abstract. As China's rapid development in economy and technology, people's consumption concept transforms fast. Thus, the mobile phone replacement cycle becomes shorter and shorter. Recycling wasted mobile phone is beneficial to reuse of resource and decline in environmental pollution. Researches show that, college students, whose consumption concept is between adult and teenager, have both rational and irrational behavior trend and have largest probability of changing mobile phones. This article analyzes characteristics of college students' recycling behavior and its influencing factors. Then, relevant suggestions are provided to enhance recycling efficiency.

1. Introduction

As the development of economy and the improvement of people's life standard, demand for electronic products increases. According to **s**tatistics from Ministry of Information Industry, users of mobile phones in China reached to one billion at the end of 2012 [1]. It has also been found, the number of annual wasted telephone has risen to over 5 thousands, which keeps increasing at the rate of 20% [2]. However, the current situation of mobile phone recycling is not optimistic in China. According to Nokia's survey report in 13 countries, the recycling rate in China is rarely 1%, which is far below than western countries. Researches show that college students are most activist users who change mobile phones. Therefore, based on the situation of mobile phone recycling, this article will study college students' features in recycling behavior, related influential factors and related mechanism. And then some improvement advices for recycling will be provided.

2. Literature Review

Some researchers have classified the recycling modes and treatment methods of mobile phone in China. Xia and Wang [3] found that wasted mobile phones were often given away to others or standing idle or selling to recyclers. Some useless parts of mobile phone were abandoned directly. Mu and Yang [4] considered the recycling process based on Life Cycle Analysis (LCA) of technical product, and concluded that the recycling mode of mobile phone in China was marquise-shaped. The causes of problems can be summarized as follow. Firstly, consumers usually have low awareness of recycling. Secondly, normal and effective recycling channels have not been established yet. Thirdly, the procedures and policies to motivate the manufactures are absent [5-7]. To address this issue, researchers have designed various recycling system for China's mobile phone market. Sun [8] came up with a reconstruction model after studying some factors about products, e.g., cost, quantity and price. Ma [9] also designed a model to describe industry chain of reconstruction system for wasted electronic products. Some scholars put forwards Extended Producer Responsibility based on experiences of western countries. However, there are few researches that pay attention to consumers' recycling behavior.

3. Questionnaires

A. Research Design

In order to explore customers' attitude and behavior tendency towards recycling, the questionnaire based on Theory of Planned Behavior (TPB) is divided into three sections. First part considers demographic factors, such as age, revenue, gender and education level. Second section contains

rational components, such as recycling awareness, attitude, and cost, etc. Third part has included some irrational factors like affection. Reading published articles is the main method to find basic factors, while interviewing and expert-consulting are used in probing affection factors.

After collecting factors, a small program named implicit association test (IAT) is operated to verify accuracy, in case that the process of probing influential factors would have errors. Until all factors have been tested, the questionnaire designing completes. Finally, the researched factors (i.e., independent variables) are attitude (A), subjective norm (SN), cognitive behavioral control (CBC), personal affection (PA), safety, past experience (PE), behavioral cost (BC), self-awareness (SA), orthodox recycle channel (ORC) , recycling awareness (RA) and bandwagon effect (BE). SPSS is the data processing tool used in this article.

B. Data Resource

As Shanghai is a prosperous metropolis where living standard is at the top of China and has higher possibility to suffer huge amount of wasting telephones, this article chooses some typical universities in Shanghai as the main data sources. Colleges in other provinces (e.g., Anhui, Jiangsu) are also considered. Then, unvalued data is removed to ensure data quality. Overall, the sample contains 94 females and 100 males, ranging from freshman to second grade of graduate students. 45% of them are Economy Management students, and nearly 25% of them come from Shanghai.

4. Data Analysis

A. Describing and Deducing of Independent Variables

Structural equation modeling (SEM) is introduced to classify questions and match them with independent variables reasonably. According to result of confirmatory test, comparison of goodness of fit index (CFI) has reached to 0.919, which gets close to 1. Therefore, the match model between questions and independent variables should be received.

After initially analyzing the researched data, it can be found that 42.6% of female and 55% of male who have changed mobile phones at least once. The main reason is the failure of the old telephone. Based on TPB, other descriptive statistics are conducted. In terms of attitude, 56.9% of participants believe that it is worthwhile to recycle wasted telephones and 56.4% of them are worrying about pollution caused by wasting. As for subjective norms, 53.8% of them will recycle if recycling has become a good social atmosphere. When it comes to behavioral cost, 64.8% of colleges will participate in recycling if the recycling process is standardized enough.

B. Analysis of Dependent Variables

1) Descriptive Analysis of Dependent Variables

According to statistics, there are mainly six disposing channels for wasted mobile phones. SPSS is used to calculate the percentage of male and female participants who choose each dissolving method. The results are shown in table 1. The two main treatments are standing idle (80.5%) and giving to others (14.9%). Furthermore, two genders also behave differently in choosing disposing methods. In detail, male prefers these three options: to stand telephone idle, to give others and second-hand sale; however, female often choose to stand idle, to give away and to throw away.

TABLE1 Percentage of Current Disposing Methods for Wasted Mobile Phone

		Recycling site	Sell to waste collection	Give to others	Throw away	Second-hand sale	Stand idle	Total
women	Amount	1	1	16	6	4	79	95
	% in women	1.1%	1.1%	16.8%	6.3%	4.2%	83.2%	
	% in men and women	50.0%	50.0%	55.2%	50.0%	36.4%	50.3%	
	% in Total	0.5%	0.5%	8.2%	3.1%	2.1%	40.5%	48.7%
men	Amount	1	1	13	6	7	78	100
	% in men	1.0%	1.0%	13.0%	6.0%	7.0%	78.0%	
	% in men and women	50.0%	50.0%	44.8%	50.0%	63.6%	49.7%	
	% in Total	0.5%	0.5%	6.7%	3.1%	3.6%	40.0%	51.3%
Total	Amount	2	2	29	12	11	157	195
	% in Total	1.0%	1.0%	14.9%	6.2%	5.6%	80.5%	100.0%

2) Difference Test of Dependent Variables

In order to estimate whether there is any difference between above disposing methods, based on data from sample, percentage U Test is applied. Take throwing away and second-hand sale as an example, if p_1 and p_2 represent percentage of people who respectively choose to throw away and choose second-hand sale, then

(1) Give null hypothesis and alternative hypothesis:

H_0: $p_1=p_2$; H_1: $p_1 \neq p_2$

(2) Calculate the value of u and uc, the equations are as follow:

$u= (p_1-p_2)/S_{p1-p2}$, $u_c = (|p_1-p_2|-0.5/n_1-0.5/n_2)/ S_{p1-p2}$,

$S_{p1-p2} = [p' (1-p') (1/n_1 + 1/n_2)]^{1/2}$, $P' = (n_1*p_1 +n_2*p_2)/ (n_1+n_2)$

After calculating, the absolute value of u or u_c will be compared with 1.96 and 2.58, only under the circumstance that |u| is less than 1.96 can null hypothesis (H_0) be received. Here, because u is 10.94 (> 1.96), it can be concluded that there is a significant difference between various recycling alternatives, on the premise of 5% significance level.

C. Regression Analysis of Variables

In order to reduce the subject errors caused by deducing independent variables from reading published articles, correlation analysis of independent variables is conducted. Table 2 presents that, there is strong correlation between behavioral cost and orthodox recycle channel, bandwagon effect and subjective. Furthermore, recycle awareness is tightly related to cognitive behavioral control and personal affection. It also shows that personal awareness and bandwagon effect have high correlation with each other.

TABLE 2 Pearson Correlations

	A	PE	CBC	BC	RA	ORC	BE	PA	SN	SA
A	1	-0.049	-0.059	0.039	-0.043	0.002	-0.007	-0.019	0.02	0.005
PE	-0.049	1	-0.044	-0.022	0.106	-0.091	-0.017	-0.01	-0.046	-0.044
CBC	-0.059	-0.044	1	-0.052	0.153*	-0.035	-0.068	0.057	-0.002	-0.109
BC	0.039	-0.022	-0.052	1	.-0.022	0.764**	0.634**	0.008	0.601**	0.026
RA	-0.043	0.106	0.153*	-0.022	1	-0.123	-0.001	0.226**	-0.129	-0.054
ORC	0.002	-0.091	-0.035	0.764**.	-0.123.	1	0.542**	-0.105	0.494**	-0.023
BE	-0.007	-0.017	-0.068	0.634*	-0.001	0.542**	1	0.075	0.483**	0.184*
PA	-0.019	-0.01	0.057	0.008	0.226*	-0.105	0.075	1	-0.086	-0.034
SN	0.02	-0.046	-0.002	0.601*	-0.129	0.494**	0.483**	-0.086	1	0.012
SA	0.005	-0.044	-0.109	0.026	-0.054	-0.023	0.184*	-0.034	0.012	1

*at the level of 95% significance

**at the level of 99% significance

To merge independent variables that have high correlation with one another and to simplify variables, we calculate and compare the value of CFI to create the fittest model. The process completes until each variable has low or no correlation with each other while the value of CFI is still high. After that, another correlation analysis will be conducted using independent variables being merged. The details are shown in Fig.1, and BC, RA and PC stand for behavioral cost, recycling attitude and personal affection, respectively. The CFI value of modified model (0.921) is larger than that of original model (0.919), which proves the modified one has higher accuracy. Eventually, above seven variables (will be regarded as regression variables.

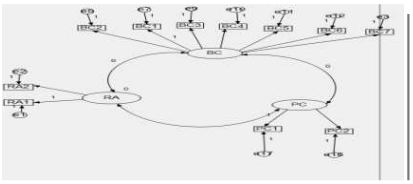

Baseline Comparisons

Model	NFI Delta1	RFI rho1	IFI Delta2	TLI rho2	CFI
Default model	.860	.825	.922	.901	.921
Saturated model	1.000		1.000		1.000
Independence model	.000	.000	.000	.000	.000

Fig. 1 Modified and Tested structual equation model

1) Regression Model

This part focuses on establishing regression models and equations to numerically describe the relationship between dependent and independent variables. Take standing idle as an example, after SPSS standardizes the data, regression analysis reveals a regression equation (1) about dependent variables (standing idle) and seven independent variables:

$$Y_1 = -0.204 * X_4 - 0.147 * X_5 \quad (1)$$

In (1), X4 and X5 respectively stand for standardized value of past experience and cognitive behavioral control. It can be deduced that higher value of cognitive behavioral control and past experience of recycling will lead to less possibility to stand wasted telephone idle. The procedures of regression analysis about other dependent variables are similar to above-mentioned process, other dependent variables and relative main influential factors are listed in table 3.

TABLE3 Recycling Behavior and Major Influential Factors

Recycling behavior	Throw as rubbish			recycle	Giving to others	
Main influential factor	Cognitive behavioral control	Behavioral cost	Subjective norm	Behavioral cost	Cognitive behavioral control	Self-awareness

For the purpose of improving exploring accuracy, based on results of simple regression analysis, square data prediction is conducted. In detail, for each disposing option of wasted mobile phone, we calculate square of excluded variables and deal with regression analysis again. Table 4 shows the relationship between disposing decisions and square of factors. According to it, although both option of standing idle and throwing away are closely related to personal affection, they have positive and negative relationship with personal affection factor respectively.

TABLE 4 Quadratics Equation of Recycling Behavior and Factors

Options of disposing methods	Standing idle	Throwing away	Recycling
Quadratics factors	Personal affection	Personal affection	Subjective norm

4. Conclusions and Advices

This article briefly describes recycling situation of mobile phone and analyzes related problems and causes. Then based on Theory of Planned Behavior (TPB) and Implicit Association Test (IAT), a survey is applied to collect data about mobile phone users. According to analysis results, different recycling methods are decided by different factors. The option of standing idle is related to past experience, cognitive behavioral control and personal affection. The behavior of giving away to others is decided by cognitive behavioral control and personal awareness. The option of throw away is linearly dependent on cognitive behavioral control, behavioral cost and subjective norm, while has binary linear relation with personal affection. The behavior of recycling mobile phone is linearly related to behavioral cost, but has binary linear relation with subjective norm.

Some advice is put forward to improve recycling rate. Firstly, more attention should be paid to recycling convenience for users. Secondly, normal and professional recycling pricing system should be established. Thirdly, more announcements and education about benefits of recycling should be conducted among users. Last but not least, the information security of users when participating in recycling must be protected. The survey in this article still has some limitations in questionnaire designing and sampling, it is worth expecting richer researches to emerge in future.

Acknowledgment

This research is financially supported by National Creative Activity Plan for College Students, named “Research on management system for mobile phone recycling based on analyses about consumption behaviors of college students”.).

Reference

[1] The promising market of mobile phone recycling in 2012. http://www.huishouq.com/news_detail.asp?id=1492

[2] Y. La, A study on consumer participation and take-back models of waste household electronic appliances management, *Dalian University of Technology: a dissertation for doctoral degree*, (2009) pp.1-124.

[3] X Q. Xia and D P. Wang, A study on present recycling model of discarded mobile phones in China, *Journal of Beijing Jiaotong University (Social Science Edition)*, vol.10 (2011), no.4, pp.39-44.

[4] H S. Mu and J. Yang, Analysis on structure of mobile phone recycling and related technological policies, *Science & Technology Progress and Policy*, vol.26 (2009), no.7, pp.101-105.

[5] X L.Hu and X Z. Wang, Construction of protection mechanism for recycling network of electronic waste lead by government, *Social Scientist*, (2009) no.142, pp.73-76.

[6] S T. Zou and J T. Wuli, Analysis on reverse logistic for recycling of urban electronic waste, *Economic and Management Research*, (2009) no.4, pp.102-105.

[7] Y N. Gao and H. Xu, Distribution of economic responsibility for recycling of wasted mobile phone in China, *Environmental Pollution and Control*, vol.33 (2011), no.9, pp.104-107.

[8] J. Sun and X Q. Ge, A study on pricing strategy for recycling of wasted electronic product, *Journal of Beijing University of Science and Technology Information,* vol.24 (2009), no.3, pp.13-16

[9] H. Ma, et al, A study on price construction mechanism for recreate and reuse industry chain of wasted electronic product, *Journal of Xi'an University of Electronic Science and Technology*, (2009) pp.34-40.

Advanced Materials Research Vols. 989-994 (2014) pp 5263-5266
© (2014) Trans Tech Publications, Switzerland
doi:10.4028/www.scientific.net/AMR.989-994.5263

Application of Cooperative Project Teaching Method in the Program Design Teaching

Shouqiang Sun [1, a], Chengbo Yin [2,b], Yumei Su [3,c]

[1] Qingdao Huanghai University, Shandong266427, China;

[2] Qingdao Huanghai University, Shandong266427, China;

[3] Qingdao Huanghai University, Shandong266427, China;

[a]ssq.vss@163.com, [b]ycb1004@126.com, [c]576792490@qq.com

Keywords: Teamwork; Project Teaching; Role Orientation; Contribution Rate

Abstract: At present, students' education is still in an independent, passive and closed learning environment in university: students still passively accept knowledge and study what teachers teach, that leads to a state that the study is passive and closed. Therefore, teachers should guide students to emphasis on teamwork and overall, active and open teaching, to attach importance to team work, to actively explore the issue and try to apply a variety of ways and resources both within and outside the school to solve the problem, not confine to knowledge in textbooks.

1. Preface

At present, university education in our country is still in the state of training the students' ability to solve problems, in stead of cultivating the students' ability of problem mining, solving, and then creating. This is our country long-term formed disadvantage under the entrance examination system for many years. Once students leave school, go out of the classroom, go into the community and go into the enterprises, they are lack of the adaptability and future creativity.

This teaching method used in programming courses has been implemented for three years. Under this teaching method, students can completely study themselves and experience the mode of operation in the simulated real environment after leaving school and then don't have any regrets for the disconnection between theory and reality. Of course, whether this teaching method can be integrated into other disciplines has been required to further verify.

2. Teamwork

2.1 Team size

5-7 students per team (this can be adjusted according to the number of students in the class).

2.2 Role orientation (the duties and powers: according to the nature of curriculum, teachers can consider role types by themselves)

(1) Project Manager (1 student)

He must co-ordinate the overall situation, be responsible for the team project planning, the project schedule control and so on; he is the team's supreme executive and has the exercise right and the right to a veto vote, etc.

(2) Systems Analysts, System Architects (1-2 students)

They are responsible for client interface, acquiring requirements, selecting the development process, tools and methods, global system architecture design and so on.

(3) Database Engineer (1 student)

He is responsible for system data format specification, the choice of data persistence method, design of data access class and so on.

(4) Software Designer, Test Engineer (1-2 students)

They are responsible for the design and coding of software module, perform unit testing, integration testing, system testing, and organizing clients to conduct validation testing and so on, then finally complete the system implementation.

(5) System Artist (1 student)

He is responsible for image design of system identification, human-computer interface and so on.

2.3 The team culture logo

Each team must design identification and culture concept.

2.4 Team meeting

Each team must have regular team meetings, build up the common vision, draw up the team planning, arrange team task of the near future, talk about team work plan, in order to exercise debate eloquence, learn communication skills, and gather more team centripetal force.

3. Project Teaching

In order to improve the teaching schedule of program design course, cut the grammar explanation time, increase the intensity of work development explained, this teaching method is based on project teaching method and looks for software development case to explain, to improve the students' level of software development, and expand the students' knowledge.

4. Team division

The first wrong solution: only establishing outstanding students' team

Once leading to the consequences: maximum potential for outstanding students will give up most of the students as the sacrifice. Most of the students lose interest in learning the course, and it is easy to let the students have a sense of inferiority (they feel not as good as the outstanding students), jealousy (students can easily be leaded to estrangement), and this is not conducive to the harmonious of class collective.

The second wrong solution: allowing students to set up team freely

Once leading to the consequences: outstanding students freely combine themselves into only one team, so that the teams' competition is not fair, the teams' rankings has been established without no assessment and this solution is not competitive.

The third defective solution: establishing the team through the teacher and class representative's participation.

Once leading to the defect: higher vocational students' foundation is generally too low, with high level, high understanding students in a minority. Most students have great dependence, inert because of the boring program design and teamwork cannot get sufficient play. With few members working, project progress is slow and most developed works seem to be some insufficiency, lower-tech because of limited manpower and knowledge limitations.

The fourth optimized solution: based on the third solution, we will set up a teaching assistant team alone (outstanding students in each team) that will carry out the following work:

(1) For the teaching assistant team, teacher will train them to master the basic knowledge and basic skills after school or computer-experiment, then these small sirs shall provide guidance to team members and let the students master the knowledge and the practical skills through classroom randomly testing ways (test scores are included in team scores).

(2) For the teaching assistant team, teacher will train them to master the advanced knowledge and extended skills after school or computer-experiment. They will be composed of technological development team to develop the big projects, so as to realize the focused training of top students.

5. Testing ways

So-called "no pressure, no power", closed education only is unreasonable, and opening education simply is not practical. When the education is only paid attention to the form and is forgotten its purpose, this will become a misunderstanding. We always say students' burden. If we

cut the length of the school hours, reduce the difficulty of the course examination, reduce the pressure of studying, what will happen? Some students have entered the game room, cinema, played cards, chatted on QQ, picked up internet addiction and it has interfered with the normal school education. Opening education is not a liberal education. If the school gives students opening education with free style, the students will relax to own request. That is because now college students' self-control ability has not yet reached the degree of conscious learning without a reminder. So adopting various testing ways which make the students highly focused, such as quizzes, homework or training report, mid-term exam or research report, attendance, curriculum design and the final exam, will let more students feel learn something.

6. The role orientation between teachers and students

At the end of the semester, the works published will be raised. At the scene simulation product launch, all students can perform on the stage according to their own role in the team, setting up the assessment group, carrying out the comments and letting the audience of students speak freely, in order to exercise the stage students' eloquence of the debate, expanding the audience students' vision and knowledge.

At the moment, teacher is a listener, an adviser and an inspirator. Students become very easy to communicate with each other, because they consider it is their work and responsibility. The classroom is not only the classroom bus also has been transformed into a performing venue. This adjustment of the team learning and the roles of teachers and students is a rare experience and enjoy for us who are accustomed to the traditional roles of teachers and students.

7. The contribution rate

In team learning, in order to inspire students to unite in a concerted effort, go to all lengths, to avoid the previous too strong dependence and inertia of some members of the team, and to avoid the regret for the unfair results of each team member's with same score, teachers should prearrange on the score calculation. The basic practice is: at the end of the semester, each member in the same team will be separated to check and evaluate each other in secret. the rating method is that Si Li, Wu Wang, Liu Zhao will be evaluated by San Zhang, the total score is three hundred points; in the same way, the others will be evaluated by Si Li, and then each team member's scores will be added up by teachers after class; the scores will be divided by 300 and the contribution rate will be worked out. As in the example, San Zhang gets 110%, Si Li gets 86.7%. The rating data shall be kept by the teachers for a period of time, in order to prepare students for asking for review.

Table 1 The calculation example of contribution rate

Name	Score 1	Score 2	Score 3	Score 4	Total
San Zhang		100	120	110	330
Si Li	90		80	90	260
Wu Wang	110	100		100	310
Liu Zhao	100	100	100		300

San Zhang's contribution rate：330/300=110%

Si Li's contribution rate：260/300=86.7%

8. The score conversion

Using the team PK (competition) mode in order to improve the practicability of this mode. The score conversion method is as follows:

- 5-7 students per team (this can be adjusted according to the number of students in the class).
- The team PK scores= Quizzes (20%) + Curriculum design (80%).
- Calculating every member's contribution rate by the way of grading each other in the same team.

- Personal PK scores=team PK scores*personal contribution rate.
- Personal final scores= Homework scores (10%) + midterm exam scores (20%) + attendance scores (10%) + personal PK scores (60%)

The reason why the author doesn't put homework scores, midterm exam scores and attendance scores into the team PK scores is in order to avoid the too many dependence and inertia of some members of the team and avoid the entire team scores being very low because of someone's poor scores

9. Summary

Above all, you can understand the design conception, the principle, and the implementation process of the teaching method. This teaching mode has cultivated students' sense of teamwork through certain team cooperation, has improved students' practical ability, has made the students take the initiative to study spontaneously, has made the students enjoy the classroom performance like competition of places, has letted the education go out of the classroom, into the community, into the enterprises and has provised a good platform for practice to make students quickly adapt to the job and get into work units.

10. References

[1] D.Y. Zhan: *The two sides of the Taiwan Straits' Vocational Education Conference* (Qingdao, China, October 30-31, 2008). Vol. 1, p.5. (In Chinese)

[2] WattsS.Humphrey: *The TSP training team* (People's Posts and Telecommunications Press, China 2008). (In Chinese)

[3] P.Shen: SILICON VALLEY, Vol.2008 No.14, p.137. (In Chinese)

Advanced Materials Research Vols. 989-994 (2014) pp 5267-5272
© (2014) Trans Tech Publications, Switzerland
doi:10.4028/www.scientific.net/AMR.989-994.5267

A discussion on the Construction of Information Integration Based on the Integrated Development and Management of International River

Sizhe Guo[1,a],Qingping Wang [2,b *] ,Mingming Hou[1]

[1]Faculty of Environmental Science and Engineering, Kunming University of Science and Technology, Kunming, China, 650093;
[2]City college, Kunming University of Science and Technology, Kunming, China, 650051.
[a]gszkmust@163.com,[b]wqpkmust@163.com.

Keywords: international river；information integration；integrated development and management.

Abstract: Integrated development and management of international rivers requires objectively international river's information integration.Based on the analysis of the connotation and requirement of integrated development and management of international rivers, the article point out that the information integration is the basis and means of the of integrated development and management of international rivers. And then analyze how to utilize modern information technology to build information management system of international river to achieve international river's information sharing and scientific decision-making. Finally, analyze the factors affecting international river information integration.

0 Introduction

International rivers have the features of water body flowing, integrity of hydrology and geography and being politically divided into different parts and belong to different countries, which made basin countries influence and interdepend each other in exploiting and utilizing the international rivers. And the ecological and environmental problem caused by exploiting and utilizing international rivers will spread to the whole basin countries. All above increase the possibility of conflicts and disputes among or between watershed countries for exploiting and utilizing international rivers which seriously threaten to the regional peace and stability and the security of water resource. Since 1990s, along with the development and infiltration of the concept of sustainable development and the idea of integrated river basin management, the theory of integrated development and management of international rivers began to formed and initially piloted in a number of rivers. The theory emphasizes the integrity of the system and the relevance of the elements of the international rivers and requires to implement integrated multi-objective overall watershed planning and water resource management. The theory also require embodying protection in the planning and to realize protection during exploiting and utilizing the international rivers, in order to ensure the regional security and stability of international society and the sustainable utilization of water resources.

Integrated development and management of international river basin is built on information integration of international rivers. Information integration of the international river can help to achieve information sharing among the river basin countries and enhance their mutual understanding and trust, and make decision-making based on scientific and fair basis, which can promote a large process of the integrated development and management of international rivers.

1 The Theoretical Connotation of Integrated Development and Management of International Rivers Require Objectively the Information Integration of International Rivers

The theory of integrated development and management of international Rivers which is based on system theory, sustainable development theory and the coastal community of interests theory, during the 20 years of development of theory and practice, has formed the following connotation and requirements:

(1) Because of system wholeness and regional linkage of international river basin, development and management of international rivers requires cooperation between or among basin countries. International river basin boundary and the boundaries of countries are not consistent, but itself is a system.There is inevitable connection between regions in basin and between upstream and downstream counties.So a single country cannot resolve problems such as soil erosion, salinization, river cleaning,water wasting, pollution and

other cross-border issues. Because the interests and goals of different countries in developing and using water resource are disaccord, it is easy to cause the contradiction and conflict. For example, the upstream countries' irrigation utilizing and hydropower development will decrease water level of downstream and bring affect to downstream ecology, so downstream countries is bound to oppose. Therefore they are objective requirements to look the international river basin as a whole, strengthen the cooperation between riparian countries, coordinate with each other in the target of using, compensation benefits, to reduce conflict.

(2)The relevance between the various elements within the catchment basin require overall planning and coordinated development in basin. The development and utilization of any resource should consider the effect to other related resources. Land using (such as cropping, grazing, deforestation, road construction, mining, urbanization, etc.) usually cause a series of changes in the water quantity and water quality (such as runoff, runoff velocity and sediment), and cause generation, migration and transformation of pollutants through water. In addition, the basin's land planning and layout of the economy and social culture all exert important effect on the spatial and temporal distribution of water resources and water environment and ecology. Therefore, the international river resource management cannot be separated from other resource management and must conduct a overall planning and integrated management.

(3)The coastal states' relationship of the interests of the community requires joint management. As a geographical and economic unit, international river basin is the community of interests, just like that all basin countries take "a leakage world boat", because ecology, water quality problems are related to the survival of all river basin countries. So they should share resources and share the future. The integrated management is the direction of development. Basin countries jointly established watershed management international institutions to formulate and implement of integrated river basin management and development policies and to achieve the best overall development objectives and the entire watershed.

(4)The scientific and openness of decision-making of integrated development and management requires information sharing and joint participation requirements. The development of international river is changing from separate development of a single country to joint development of basin countries. Participants in international river development include not only very basin country but also non-governmental organizations, associations, private investors and etc. Developing programs and policies that multiple subjects involve in must base on comprehensive and objective information sharing basis ,to ensure decision-making scientific and acceptability.

The theoretical connotation of integrated development and management of international rivers require objectively the information integration of international rivers. First,international rivers' basic geographic and hydrological information should be integrated.For a long time,basin countries of many international rivers lack of the basic informational exchange platform due to geographical, linguistic, political barrier, resulting the basic data of international river deficient and lack of uniform standards. Joint research results based on watershed overall is little, which hindered basin countries to cooperate on the integrated development and management of international river. Furthermore,consensus and common decision-making of the integrated development and management of international river must be based on information sharing, strengthening mutual understanding and trust, in which the information integration play a key role.Finally, the water resources development, utilization, management, configuration,flood control and disaster mitigation, water conservancy construction and benefit distribution cannot do without the support of modern information technology. Therefore the international river information integration is the foundation of the integrated development and management of international rivers, only to achieve information integration to promote the implementation of integrated development and management of international rivers.

International river information integration is to build a integrated information system platform between watershed countries, through which it can achieve integrated management of international river basin information data collection, processing, storage, analysis,simulation, and the output. Aim of doing this is to achieve watershed information sharing and to form consensus and scientific decision of the integrated development and management of international river. Therefore, the river information integration is not objective,but the means to implement integrated development and management of international rivers.

2 The Way to Information Integration of International River—Constructing Jointly the Integrated Information Management System of International River Using Modern Information Technology

2.1 A Brief Introduction of Modern information technology

Modern information technology is combined of computer technology and electronic communication technology which both are based on microelectronics. And it is a general term of the technology of acquisition, processing, handling, storage, dissemination and using information such as voice, image, text, numbers and various sensing signals. The core of modern information technology is the information science. Modern information technology is a very extensive technology group,which includes micro electronics technology,electronic technology, communication technology, network technology, sensor technology, control technology and display technology. Enter in 21th century, the modern information technology is rapidly developing as the speed that other technologies never have and is involving in all aspects of society in the depth and breadth that other technologies never have. Especially with the development, mixing and integration of three space technology- remote sensing (RS), global positioning system (GPS)and geographical information system(GIS)and modern communication technology,especially wireless communication technology ,a strong technology system has formed, which can realize to collect, process and update the spatial information and environmental information rapidly, flexibly ,accurately and reliably. Modern information technology shows a broad application prospect,especially the "3S" technology has been widely used in city planning, land use, investigation and management of resources, ecological investigation of watershed planning and management, and recovery, environmental monitoring and protection, disaster prevention and mitigation.

2.2 The application of modern information technology in the integrated information management system of international river

The construction of the integrated information management system of international river, which based on the integrated development and management, aims at building a technology system through application modern information technology, which can realize collection, management, operation, analysis, simulation, display and output of international river basin spatial, non spatial data (text, digital).Through the information transmission and sharing, the system can achieve a comprehensive, accurate, timely grasp of the information of international river, it can help to made the international river basin planning,allocation of water resources,ecological environment management and project construction on the basis of the jointly and scientific decision.The integrated joint decision of the basin countries based the information sharing can enhance the cooperation of the riparian countries and benefit sharing, realize the principles of international law of fair and reasonable utilization of international rivers and not causing significant damage, reduce the disputes and conflicts in the development and utilization and the ecological environment protection of international rivers .

In order to realize the system functions, the integrated information management system based on the integrated development and management of international river is made fo three subsystems which Closely contact with each other and support each other.

(1) Data acquisition subsystem.Data acquisition subsystem is mainly distributed in the river basin management agency of basin member countries of international river,which are responsible for collecting and providing the relevant basic information of the domestic part of international river basins,including hydrology, water quality,biology,land use, the quantity of water using,sewage, the forest coverage, soil erosion,meteorological phenomena and so on, which relates to all aspects and are updated.The technologies used are mainly 3S technologies in addition to the environmental monitoring equipment, on-site investigation and other traditional methods.

(2) Information integration, processing, management and maintenance center system.The system is the key part of information system of the integrated development and management of international river basin. It has two functions.The one is classification , numbering, saving, adding and updating to the information in the data library that is ready at any time to be called by each application subsystem.The two is information processing,analysis and summary, generating charts and at last forms watershed integrated information,such as the total annual flow,sediment,Biological community distribution,pollution discharge,the rate of pollution

discharge,etc.This system provide information and data for decisions of international river water resource basin planning,allocation,Comprehensive development and utilization,ecological and environmental protection and management.And it is the foundation to solve international disputes on water.

(3) Application of decision subsystem.The subsystem is the system to realize the aim of the integrated development and management of international river basin information system,which apply the information and data to the specific decision of development and utilization, protection and management of international river to ensure decision-making being scientific. The subsystem can provide support for decision-making through constructing various mathematical models that have forecasting,analysis,simulation and evaluation function.For example, the water distribution and scheduling model, hydrology stimulation model,river eco-environmental water requirement water model, conservancy and hydropower project environmental impact assessment model, watershed ecological planning model, flood disaster prediction and flood control decision model,etc. The main technology applied in this subsystem is computer information processing technology.

The structure of the international river integrated information management system based on the integrated development and management of international rivers see Figure 1:

2.3 Information Sharing and Security Control

The information collection subsystem that distribute in every basin member countries and the information integration,processing, management and maintenance center system and the application of decision subsystem achieve the interconnection and resource sharing through internet technologies.The information center of Comprehensive Management and Coordination Committee of the international rivers is central platform of information connected which provides the unified software and hardware environment for development and operation of each subsystem and complete the information collection and transmission.

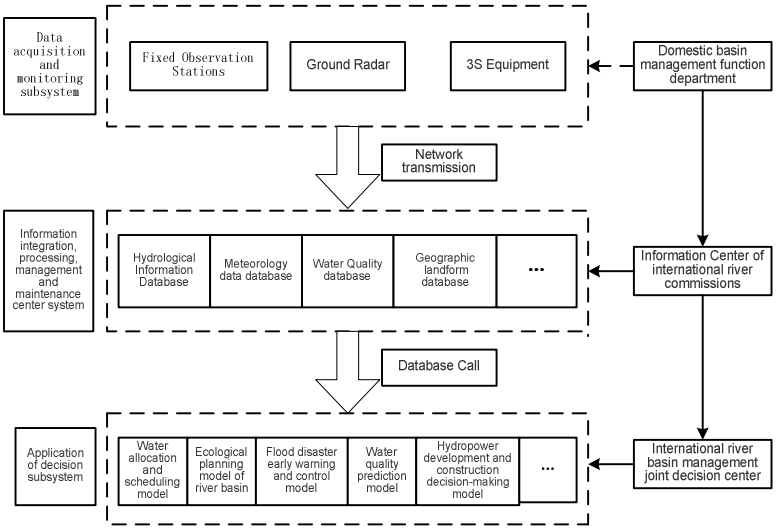

Figure1 The structure of the international river integrated information management system based on the integrated development and management of international rivers

In addition, the system can set the public information platform that realize the connection through the network and external network,let basin public participate and understand of international river's information and development and management decision-making , protect the public's right to know and participate.

The information of integrated development and management information system of international river may involve state secrets that is at stake sovereignty security and political stability.In order to ensure the information security, it is necessary to control of information system security. Applying authorization management of the access to and use of database and encryption technology,the system can prevent the information leak to unauthorized individuals or entities,and protect information are not modified, damaged and lost in exchanging, transmission, storage and processing, keep information intact and complete.

3 The Analysis of Factors that Influence on International River Information Integration Advancement and Implementation

Information integration is the basis and means for promoting the integrated development and management of international river.In turn, the degree of the impact and acceptance of the idea of integrated development and management of international river will also affect the promotion and implementation of information integration of international rivers.The two complement each other.Because the international river problems relate to water resources sovereignty of different countries and and are affected by complex geopolitical and economic factors,to promote and implement the international river information integration in a international river basin will be influenced by mang factors.

(1)The political will of cooperation of the integrated development and management of international river

The integrated development and management of international river emphasis the overall interest of basin.When the overall interests of the basin conflict with national self-interests and difficult to co-ordinate, if basin countries are unwilling cooperated and take unilateral development and management,the integrated development and management of international rivers would be difficult to implement.In this case the basin countries will not support the information integration of international river basin. At the same time, based on political mistrust, the watershed countries are not willing to share information, and even to protect information of international rivers as state secrets.

(2)Regional cooperation system and mechanism.

The political, economic, technological, cultural exchanges and cooperation between countries of the region,including the system and mechanism of cooperation, can strengthen their relation of mutual trust and mutual dependence, which can create positive and effective conditions for the establishment and development of the mode of the integrated development and management of international river. The higher the degree of international regional economic integration, information exchange and sharing of between countries will strengthen.So it will be easy to promote the implement of the integrated development and management of international river.The development of the North American Free Trade Area and the European integration has played an important role in promoting integrated management of international river basin,in which information integration plays an important role.

(3) Organization guarantee of International river information integration.

In recent years, with the deepening of the international river basin integrated management idea,it has become a trend for coastal states to establish international river joint management organization according to the agreement or treaty to coordinate the international river development and management.Many international rivers have established a similar international river commission.Management of international river information integration function should become one of the important functions of International River Commission, responsible for the operation of integrated information management system of international river, coordinate the domestic river basin management agencies or departments, to promote the construction of river information integration.Domestic river basin management agencies and departments of is specifical department involved in information management, including the collection and provide real-time hydrological, geographical, river water quality dynamic information, to participate in international river agreement negotiation and decision process.

(4)Talent and funds to support the information integration of international rivers.

The construction of the international river information integration needs the support of capital. On the one hand for the purchase of equipment, software development, Internet information maintenance and other costs, on the other hand for the funds of the introduction of the talent and research expenses. Operation and management of international river information system need numerous and technical experts and jurists to

bend themselves into the information system development, maintenance,management, and use the information to carry out applied research, making integrated development and management scheme, rules and communication and coordination, participation in contract negotiations and settling disputes and disputes.

4 Conclusion

With the development of the crisis of the world's water resource, the problems of the development and utilization and income distribution and environmental and ecological protection of international rivers water resource become the focus of regional conflicts. The integrated Development and management model of international river is the right development direction to solve the conflicts between protection and utilization of international rivers,which has put into practice in the economically developed regions in Europe and America.International river development and management based on the information integration of international rivers and rely on information integration implementation. Using the modern information technology to construct the information system of the integrated development and management of international rivers, will greatly promote implement of the integrated development and management in international river basins, and realize the balanced and sustainable development of the economic developing, social justice and ecological protection in the international river basin.

References

[1] HongXia Peng, ChanGan Li,The Progress of Science and Technology, 2003(8),p26-27.

[2] LiHui Chen, ZunGu Zeng,Resource and Environment of ChangJang river basin,2001(4),p305-319.

[3] Kenedy.Volz,International Political Theory.Shanghai Century Pulishing Group, Shanghai,2003,p284.

[4] KLIOT N,SHMUELI D, SHAMIRU,Water Policy, 2001(3),p229.

[5] MCINTYRE O,Sweden International Development Agency? International Trans boundary Water Resources Management Course, 2006.

[6] Yu ZhaoTian,DaXin, International academic dynamic.2008(5)p43-45.

[7] Minghua Bai,The comment of Diplomacy,2013(5):p102-112.

[8] Wenjun Hu ,Heqing Huang .Resource Science,2011(11),p2099-2105.

[9] DengWei Liu,Ge Li.International outlook,2010(5),p69-74

[10] Heng Liu,JiWei Chen , China water Conservancy,2006(7),p55-58.

[11] Information on http://www.yrec.cn/HotSubj/shzhh/dynamic-01.htm.

Advanced Materials Research Vols. 989-994 (2014) pp 5273-5277
© (2014) Trans Tech Publications, Switzerland
doi:10.4028/www.scientific.net/AMR.989-994.5273

The Research on Site Selection of Urban Infrastructure towards the Major Function Zoning

Shuping Zhang[1, a], Hairong Li[2, b]

[1] Faculty of Geosciences and Environmental Engineering, Southwest Jiaotong University, Chengdu 610031, China

[2] Institute of Geophysics, Chengdu University of Technology, Chengdu, Sichuan 610000, China

[a]shuping-1985@163.com, [b] lihairong_lc@yahoo.com.cn

Keywords: Planning and site selection, functional zoning, indicator system, Analytic Hierarchy Process, Panzhihua City

Abstract. In order to standardize the patterns of land use for urban infrastructure construction, and improve the scientific and rational nature of site selection for urban infrastructures, a method of site selection and function zoning for urban infrastructures, which is oriented to the main function zones, is proposed. Based on the planning concept of main function zones, the indicator system for site selection and function zoning is established according to the conditions of areas for site selection, and the areas for site selection and function zoning for urban infrastructures are divided into various function zones. The practical application with Panzhihua City as an example indicates that the main function zones-oriented method of site selection and function zoning for urban infrastructures both embodies and takes into account the radiation of urban infrastructure functions, and rationalizes the layout of site selection for infrastructures and also optimizes the urban spatial pattern. The proposal and application of this method provides guidance on the decision-making for urban infrastructure planning.

Introduction

Site of urban infrastructure planning area is an important part of city infrastructure planning. With the continuous progress of urbanization, urban infrastructure problems caused by unreasonable siting become increasingly prominent, mainly in waste of resources caused by blind siting a lot of land, irrational facilities lead to duplication facility or facilities in short supply, and environmental damage caused by ignorance impact of facilities on the environment[1-2]. In order to improve the scientific nature and rationality of facility location, some cities plan site suitability evaluation. in facility location. Suitability assessment for a single project site you improve facilities siting unreasonable conditions, but due to lack of macro-regulation and co-ordination on the site of space, facility location still has arbitrary, and is not conducive to the conservation and space pattern optimization of land resources.In view of this, we propose a method of urban infrastructure site planning oriented MFOZ. Based on division thinking of the main functional areas, urban infrastructure siting space is divided into different functional areas due to the location of regional conditions, to improve urban infrastructure siting science and rationality,optimize urban spatial structure, and improve land utilization.

The principle of the main functional area planning method

The main functional area planning is a macro planning methods to optimize the spatial structure, mainly used in large space planning such as country, province, city etc. The main idea is based on different regional conditions, considering population distribution, economic layout, land use and urbanization patterns, identifying the main functions of different regions and a clear development direction, controlling the strength of development, and regulating the development order [3-4]. City Infrastructure Planning Division is also partition of large scale regional land space. Based on regional

environmental characteristics , optimize the allocation of resources through function, rational space layout of city infrastructure, improve the scientific planning, reduce the ecological environment destruction of the blindness location. In this paper, by learning from the district planning methods of main function, define facilities planning area for different functional areas, combined with the city basic facilities location conditions, construct facilities location function area dividing index system to realize the function division. Take Panzhihua City, Sichuan Province as an example, to prove the division of functional areas location of city facilities based on the of main functional area planning.

The location area planning method

Facility location function classification. In this paper, reference to define and classify of the main functional areas, combined the characteristics and requirements of urban infrastructure planning siting , considering various towns in Panzhihua City as planning unit, the infrastructure planning siting area is divided into key planning areas, encouraged planning area, and restricted planning area three types of functional areas. Among them, the key planning areas means the area whose infrastructure siting area conditions meet safety requirements, the region needs large urban infrastructure, and the region exists clear traffic dominance. Through infrastructure planning in that region will help to improve regional economic development, and improve the living standards of local residents. Encouraged planning area means the area whose infrastructure siting area conditions meet safety requirements, is more appropriate for the construction of infrastructure projects, and fewer existing urban infrastructure. Through infrastructure planning in that region will help to meet regional economic development, and satisfy the living standards of local residents. regional restricted planning area means the area has existence of the certain geological disaster risks, and needs small urban infrastructure, whose infrastructure impact on the regional environment is greater than the benefits of play.

Index system of facilities planning siting function zoning. Indicators facilities planning siting function zoning main used to measure the ability of regional planning conditions, and evaluation the suitability of facilities planning and construction. In order to assess the analyzed region planning condition objectively and accurately, facilities planning siting function zoning indicators must be true reflection of the regional site security, building needs of regional planning and regional planning construction of existing conditions. Therefore, selection the indicators should follow the scientific, systematic, comparable, easy to get and streamlining principles [4-5]. Based on urban infrastructure planning siting requirements, combined with urban characteristics and development status of the study area, this paper intends to determine the distribution of geological disasters in the region, regional population density, type of regional planning and regional transport dominance as a function of zoning index. Index system is shown in Table 1.

Table 1 Index system of planning siting function zoning

	Constrained Layer	Index layer	Quantitative Methods
Index	Regional site security	Distribution of geological disasters	Landslides, mudslides, avalanches hidden spots and dangerous trend level
	Regional planning construction needs	Population distribution	The population density
		Type of urban planning	Level and type of urban functions
	Existing regional planning conditions	Transportation Advantage	Various types of road network density

Index weight calculation. Weights indicate the importance of each evaluation index, which means that each of the different roles the evaluation in overall plays. After building planning siting function zoning index system, we use The analytic hierarchy process to determine the weight of each index. The analytic hierarchy process (The analytic hierarchy process, AHP) is the analysis method for multiple attribute decision making system put forward by America University of Pittsburgh professor T.L.Saaty in the mid 70's, which combines qualitative and quantitative analysis and is simple and effective, making the experience to quantify, as the utility in condition of the complex

factor structure and lack of data case [6]. The algorithm idea is to arranged complex evaluate objects in an whole of orderly hierarchical structure, and make pairwise comparisons and judgment between the various evaluation, and calculate the relative importance of evaluation projects, namely the weights.

Division practices of urban infrastructure siting functional areas in Panzhihua

Status of the study area. Panzhihua City, a municipality directly under the central government in Sichuan Province, is a typical mountain resource type city of our country. Due to the construction principle: "Patron, dispersed, hidden" and into the hole taken to build the city under the particular circumstances, the city's urban development structure is mainly in the line of industrial layout, causing the city's irrational industrial structure and spatial issues [7]. At present, Panzhihua city is in the industry transition, through scientific planning of city space is conducive to change the spatial structure problems left over by history, and rationalization city space layout. While the city infrastructure planning is an important factor to decide the city space layout, therefore, through the functional division to the city infrastructure planning site area, it's conducive to the promotion of industrial economic development of Panzhihua city and the adjustment of industrial structure. Based on increased space utilization, protection of ecological environment and resources is very important to improve the regional development capacity.

Process analysis.

(1) Index system analysis

1) Regional site safety. Panzhihua city is in geological disaster-prone areas, the main types of geological hazards are landslide, debris flow, collapse, in addition, crack, surface collapse, and unstable slope is more. In general, geological disaster has a wide distribution, large-scale disasters and other features. There're a lot of mudslides, landslides, avalanches and other geological disasters occur every year the city, causing huge losses to the city [8]. According to the scale and risk trend of geological disaster, disaster grade were assigned (Table 2).

Tab.2 Exponential assignment of geological disasters

Scale and risk trend of geological disaster	Serious	Heavy	No trouble
Large	0	1	-
Medium	1	2	-
Miniature	2	3	-
None	-	-	5

Tab.3 Exponential assignment of population density

population density	value
≥135	4
85~135	3
45~85	2
＜45	1

Note: The degree of hazard and disaster-scale trend data derived from the "geological disaster prevention planning regulations in Panzhihua City"

2) Regional planning needs. A. Population density distribution. According to the sixth census data in Panzhihua City, population density distribution is divided into four grades, and assigned in Table 3.

B. Town planning type. According to "Panzhihua City Master Plan" (2010-2025) [9], Panzhihua urban system is divided into four towns based on the size of the town and the urban population. Various types of urban planning and development efforts may be in descending order of Industry and Trade, comprehensive, tourism and farmer-type. Towns type assignment is shown in Table 4.

Tab.4 Exponential assignment of town type

Urban grade Urban type	Industry and trade	Comprehensive type	Tourism	farmer
Level 1	8	7	6	5
Level 2	7	6	5	4
Level 3	6	5	4	3
Level 4	5	4	3	2

Tab.5 Exponential assignment of road network density

Range	Value
≥0.45	4
0.3~0.45	3
0.2~0.3	2
＜0.2	1

3) regional transport superiority degree. Considering the 5 counties 44 towns of Panzhihua City as the research unit, calculate the road network density analysis of regional transport superiority degree. According to the road network density formula the township transit network density was calculated. According to the road network density, assignment of the regional road network is shown (Table 5).

the index weight calculation. Calculated function area dividing index weight values were: regional site safety weight 0.52, regional planning and construction demand weight 0.33, regional planning both conditions weight 0.15.

Analysis of the results

Through a comprehensive analysis of Panzhihua City, the landslides, mudslides, landslides and other geological disasters hidden point, population density distribution, urban planning level and planning and construction type for functions of demand regional, as well as traffic dominance cases based on the regional road network density, index weights determined in accordance with AHP, 44 towns of Panzhihua City, will be divided into three different types of site planning functions area. Combined with the types and characteristics of functional areas, various types of planning proposals were given.

Tab.5 Analysis on the various types of functional zones

Types	Region Features	Planning proposals
key planning area	Mainly in towns with industry and trade functions, a small regional geological disaster risks, no large-scale disaster, low degree of geological disasters dangerous trend, facility in siting meet safety; Meanwhile, great regional population density, high level of urban planning, main functions in urban industry and trade; significantly regional transport dominance, improved existing road network structure.	This type of regional planning area should be the focus, to bring the service efficient facilities, and improve facility utilization.
Encouraged planning area	less existed urban infrastructure; no serious risks of geological disasters, low trend of geological disasters dangerous; moderate population density and level of TPB planning, facilities construction demand weaker than key planning areas, main in integrated urban planning types.	Planning and construction of urban infrastructure will promote regional economic growth, and promote regional development. To meet the needs of the premise of the construction of infrastructure, these areas can be priority.
Restricted Planning Area	more geological disaster prone point, major geological disaster; relatively small regional population density, low level of urban planning. Such areas' planning functions are main in farmers and tourism, small infrastructure needs of urban planning and construction; both limited in area construction and conditions, urban infrastructure construction revenue less than the extent of the damage to the ecology.	Only suitable for small-scale of urban infrastructure planning area, but not suitable for large-scale of development and construction, and in small-scale of facilities planning process, it should be priority to followed the principle of protecting and moderately developing.

According to the results of urban infrastructure siting division of functional areas, Panzhihua City space planning site is divided into three different regions, through recommendations for planning of different areas, here provided decision support for the city's urban infrastructure planning. Meanwhile, staggered distribution area in urban infrastructure siting, optimized the pattern of urban space and improved the urban land utilization.

Conclusion

Urban infrastructure siting division planning area is planning method adhering to the concept of the division of main functional areas. This planning method, not only realized the full demonstration of its own characteristics of proposed regional conditions and facility , but also achieved maximum utilization of land resources, optimized the spatial pattern of the city, achieve regional development according to local conditions, has a positive effect of improvement of rationality of urban infrastructure facility siting and enhancement of land space utilization. In this paper, the function area dividing index is based on the study of regional conditions. Taking into account of the regional city planning, it still has some limitations. Various factors should be considered in the next step of the study, it's necessary to further refine for various indicators, improve the rationality and preparation of functional division. This study is to deepen the division of main function region further, and have a meaning of draw lessons of similar research in related fields.

Acknowledgements

World Bank loans Urban Environment in Sichuan Management Project (Project ID: P083322).

References

[1] Wan Bo.Study on the Public Service Facility Location Problem (Huazhong University of Science and Technology, China 2012)
[2] CAO Wei-dong, CAO You-hui, WU Wei, LIANG Shuang-bo: Bulletin of Soil and Water Conservation. Vol. 22 (2010) no. 2, p. 136-138
[3] Y.G. Zong: Spatial planning decision support technology and its application (Science Press, China 2011).
[4] Wang Dan, Ge Da-bing, Wu xiao-ling, Zhou Yan, Ge Lei, Zhao Wei: Acta Agriculture Jiangxi, vol. 22 (2010) no. 2, p. 136-138.
[5] MA Ren-feng, SHEN Yu-fang, Wang Xiao-chun, LIU Xiu-tong: World Regional Study, vol. 18 (2009) no. 3, p. 53-59.
[6] Y. Long: Planning Support Systems Principles and Applications (Chemical Industry Press, China 2007).
[7] Panzhihua City Planning and Construction Bureau, Geological disaster prevention planning, Panzhihua City, (2010).
[8] Panzhihua City Planning and Construction Bureau, Panzhihua City Master Plan, Panzhihua City, (2010).
[9] Panzhihua Municipal People's Government, Panzhihua City Land Use Master Plan, Panzhihua City, (2010).

Advanced Materials Research Vols. 989-994 (2014) pp 5278-5281
© (2014) Trans Tech Publications, Switzerland
doi:10.4028/www.scientific.net/AMR.989-994.5278

Comparative Study of R&D Spillover Effect for High Technology Industry and Traditional Industry

Fan-jun MENG

(school of management, Tianjin University of Technology , Tianjin 300384,china)
Mfj416@163.com

Keywords: R&D spillover; spatial econometric model; high technological industries; traditional industries

Abstract. Based on economic distance weights matrix, using the R&D input-output panel data sets of high technological industry and traditional industry in 29 provinces in China from 2001 to 2010 and spatial econometric method，this paper analyzes their R&D spillover effects respectively between provinces. The results indicate: Even though R&D in the high technology industry in China are active, the R&D spillover in this industry is lower than that in the traditional industries; R＆D capital contributes to R&D output more than R＆D labor for high technological industry, while the traditional industry is just the opposite.

1 Introduction

New economic growth theory and a large number of empirical studies indicate that R&D is the source of scientific and technological innovation, R&D not only can drive the regional innovation output, and can pass the spillover effects in other parts of the innovation output.

As early as in 1962, Arrow studied on the R&D spillover effect, and thinks that enterprise creates an knowledge is easy obtained by other enterprise, and innovators can't get any compensation [1]. Arrow's description of phenomenon, in fact, is a kind of R&D spillovers,then many scholars analyzing R&D spillover from multiple levels, Griliches (1979) set up R&D spillover effect model measuring technology of distance between the enterprise and the industry on the R&D spillover effect [2], on the basis of the production function created by Griliches,Jaffe introduced the overflow effect, and apply the model to study the regional R&D spillovers, emphasized the geographic space of industry, college and the importance of similar technology[3]. Huang Zhiqi (2013) use the system of generalized moment estimation method to study the research and development and knowledge spillover effect and discrepancy in the high-tech industrial clusters [4], Wang Qingxi (2013) through establish different spatial weight matrix investigated china provincial knowledge spillover effect under different proximity of high technology industry [5].

Through the sorting of literature ,we found that scholars of high technology industry R&D spillover effect using a variety of methods, from the perspective of a variety of research, but ignored the traditional industry R&D spillover effect. We do not deny that the high-tech industry R&D spillover effects on the importance of economic growth, but the traditional industry as the main part of modern industrial economy, it is important for the innovative development of our country and the economic transformation.

2, Model Implications and Interpretation

2.1 spatial panel model

Based on spatial panel data model are mainly the spatial lag model (SLM) the spatial error model (SEM) and spatial Dubin model (SDM). Combining the reality of the article, We establish the following spatial lag model (SLM), the spatial error model (SEM) and space doberman model (SDM)

$$SLM:\ \ln A_{ij} = \xi\sum_{j=1}^{n} w_{ij}A_{it} + \beta_1 \ln L_{it} + \beta_2 \ln K_{it} + \mu_i + \lambda_t + \varepsilon_{it} \quad (1)$$

$$SEM:\ \ln A_{it} = \beta_1 \ln L_{it} + \beta_2 \ln K_{it} + \rho\sum_{j=1}^{n} w_{ij}\Phi_{it} + \mu_i + \lambda_t + \varepsilon_{it} \quad (2)$$

$$SDM:\ \ln A_{it} = \xi\sum_{j=1}^{n} w_{ij}A_{it} + \beta_1 \ln L_{it} + \beta_2 \ln K_{IT} + \theta_1\sum_{j=1}^{n} w_{ij}\ln L_{it} + \theta_2\sum_{j=1}^{n} w_{ij}\ln K_{it} + \mu_i + \lambda_t + \varepsilon_{it} \quad (3)$$

A_{it} represents the output of R&D, L_{it} represents the R&D personnel input, K_{it} represents the capital stock; i represents the space the number of units; T represents the time; α represents intercept, w represents weights matrix; ξ represents the spatial autoregressive coefficients; ρ represents the spatial autocorrelation coefficient; μ represents the area effect, λrepresents the time effect. For the recognition of the above model, Anselin and Florax（1995）put forward the judgment standard of the model: If found in the spatial dependence of inspection, LMLAG than LMERR statistically more significant, and R- LMLAG significant but LMERR was not significant, you can conclude that spatial lag model is the suitable model; On the contrary, if LMERR than LMLAG statistically more significant, and R -LMERR significant but R - LMLAG was not significant, it can be concluded that the spatial error model is appropriate model.[6]

2.2 Spatial weight matrix

Spatial weight matrix represent the interdependencies between the space unit and associated degree, it is essential reasonably choose correct spatial weight matrix measurement[7]. In this paper, we adopted the economic distance weighting matrix .It generally according to the reciprocal of two provinces in per capita GDP gap setting, The greater the GDP gap between the two provinces, the smaller the weight, on the other hand, the greater the weight. Defines as follows $W_{ij} = \begin{cases} \dfrac{1}{|Y_i - Y_j|}, & i \neq j \\ 0, & i = j \end{cases}$

Y represents the i province level of real per capita GDP

3, Data Sources

This article selects the 29 provinces in China during 2001-2010 (Tibet, xinjiang data lack of serious, slightly) on high technology industry and traditional industry R&D input and output data. consider the data availability, the traditional industry data we use data instead of large and medium-sized industrial enterprises in our country.

R&D activities have a variety of output, we use the patent number as the index of R&D output. The R&D activities personnel full-time equivalent as labor input of R&D activities; We choose the capital stock on behalf of R&D capital investment, and we use perpetual inventory method to accounting R&D capital stock.

4, Results

firstly, We should check whether the spatial correlation exists, then research the R&D spillover between different areas. Moran's I index is the most commonly used indicators. After examination, the Moran's I in different space all above 0.2, indicating a spatial correlation. Below we will analyze the different matrix estimation results.

Table 1. Two kinds of industry R - squared

paramete	High-tech industry			traditional industry		
	SLM	SEM	SDM	SLM	SEM	SDM
$\ln L$	0.134 (1.347)	0.073 (0.695)	0.051 (0.505)	0.292*** (4.594)	-0.001 (-0.010)	0.004 (0.045)
$\ln K$	0.694*** (4.521)	0.592*** (3.318)	0.499*** (2.829)	-0.042 (-0.277)	0.118 (0.597)	0.246 (1.140)
$W \times \ln L$	/	/	0.860*** (2.992)	/	/	1.264*** (7.448)
$W \times \ln K$	/	/	0.106 (0.301)	/	/	-0.309 (-1.166)
ξ	0.541*** (9.909)	/	0.246*** (2.684)	0.775*** (22.964)	/	0.314*** (3.911)
ρ	/	0.742*** (17.344)	/	/	0.880*** (42.447)	/
R-squared	0.907	0.813	0.911	0.95	0.724	0.953
sigma^2	0.079	0.083	0.076	0.027	0.028	0.025
LOG-L	-35.58	-49.271	-24.856	109.52	101.145	134.114

* , **, *** *significance at 1%.5%,10%

The table 1shows that under the different models, two kinds of industry R - squared all above 0.7, Model fitting is good, spatial correlation coefficient remarkable, and highly significant under 1% level. Indicates that china economic level similarity between provinces and cities regional R&D has strong space complementary and dependence. it shows that the economic factors on the R&D spillover has an important influence. With the growth of economy, distance barriers for the R&D spillover will smaller and smaller. Even though R&D in the high technology industry in China are active, the R&D spillover in this industry is lower than that in the traditional industries; R＆D capital contributes to R&D output more than R＆D labor for high technological industry, while the traditional industry is just the opposite. Two kinds of industry labor in SDM model spatial lag were significantly positive, shows that labor in similar economic level has positive spillover effect between regions

5, Conclusions

This paper based on Chinese 29 provinces in 2001-2010 high technology industry and traditional industry data, the analysis of the weighting matrix in the space of R&D spillover. The study found that:

High-tech industry R&D activities, the influence of the capital investment on R&D output significantly, it has to do with Wang Qingxi etc. (2013) results consistent, show that R&D output of high-tech industry in China is still mainly depends on capital investment; Input of R&D output has a positive influence on R&D personnel, but much smaller than the capital investment; Unlike high technology industry, the traditional industry R&D activities, labor input coefficient significantly, spillover effect is better than high technology industry. This shows that although the high technology industry's R&D activities more active, but the high technology industry is lower than that of the traditional industry in terms of R&D spillover of R&D spillovers. To sum up, the traditional industry with high technology industry R&D activities is the core of the national innovation system development momentum. Although the influence factors of R&D activity output

both is different, but all have significant spatial spillover effects of R&D, and the traditional industry spillover effect is stronger, if consider absorption capacity and other factors is not easy to measure, the traditional industry spillover is likely to be higher, so we in the emphasis on high technology industry R&D spillovers can't ignore traditional industries at the same time.

References

[1] Kenneth Arrow. Economic welfare and the allocation of resources for invention. In the rate and direction of inventive activity: Economic and Social Factors, NBER: 609-626.

[2] Griliches Z. Issues in assessing the contribution of research and development to productivity growth[J]. The Bell Journal of Economics, 1979,(10): 92-116.

[3] Adam B. Jaffe. Real effects of academic research[J]. American Economic Review,1989，79 (5)：957-970.

[4] Huang zhiqi The model and empirical analysis of knowledge spillover effects in hi-tech industry clusters [J] Science Research Management, January,2013:154-162.

[5]WANG Qing-xi. Inter-provincial knowledge spillovers under multiple dimensions of proximity :an empirical examination by spatial panel data analysis(1995-2010)[J].
Studies in Science of Science.Jul.2013:1068-1076.

[6] Anselin L, Varga A, and Acs Z J. Local geographic spillovers between university research and high Technology innovations [J].Journal of Urban Economies, 1997, 42(3):422-448.

[7] Anselin L, Varga A, and Acs Z J. Local geographic spillovers between university research and high Technology innovations [J].Journal of Urban Economies, 1997, 42(3):422-448.

Advanced Materials Research Vols. 989-994 (2014) pp 5282-5285
© (2014) Trans Tech Publications, Switzerland
doi:10.4028/www.scientific.net/AMR.989-994.5282

A Study on Web-based EVP Teaching Platform

Wenjun ZHANG

Jinhua Polytechnic, Jinhua, 321017, China

email: zhangwenjun.1976@163.com

Keywords: web-based; EVP; platform; the ecological teaching model

Abstract. The current EVP program in China is facing many challenges such as the incomplete teaching reform, misconceptions in the use of network technologies and the lack of in-depth scientific research into English courses and teaching. To address these problems, an ecological teaching model that consists of classroom teaching and teaching in virtual environments by developing a web-based EVP teaching platform is constructed. The teaching platform, designed in accordance with higher vocational college students' characteristics, adopts the course structure of "basic college English +industry-specific English", which is effective to stimulate the students' learning motivation and enhance the teaching quality.

Introduction

Higher vocational education is an important part of higher education in China. It has already accounted for about half of the total higher education in terms of the number of vocational colleges and that of students enrolled [1]. However, higher vocational education in China still has a long way to go in such perspectives as the teaching philosophy, the school system, the teaching contents and the methods. In recent years, EVP (English for vocational purposes) teaching has undergone some reforms in teaching models, shifting from the traditional teacher-centered model to the current student-centered multimedia model [2]. This field has been a focus of concern among college English teachers and researchers and has yielded many research fruits [3][4][5][6]. EVP teaching, however, has not developed relatively sound theories and research so far. There still existed many problems such as the incomplete teaching reform, misconceptions about the use of multimedia network technologies, and the lack of in-depth exploration and research on curriculum and teaching etc. The EVP program needs some breakthroughs before it achieves a leaping development.

Design of the ecological teaching model

EVP teaching reform can be viewed from the "ecological" perspective [2]. When computer and Internet are integrated into EVP teaching program, many traditional elements (teaching materials, contents, methods, etc.) are replaced by new elements (multimedia, web content, technology and methods, etc.). Thus, the original ecosystem of EVP teaching is broken. To maintain the dynamic harmony and balance of the teaching system, it is essential to stabilize the teaching structure and make teaching elements compatible to each other. It is equally important to timely build ecological teaching model, monitor healthy functioning of teaching, balance the elements of the niche, and promote individual development.

Structure of the model

The structure of the ecological teaching model is as followed in Figure 1. Overall, this teaching model consists of two parts: classroom teaching and teaching in virtual environment. Virtual environment refers to the web-based EVP teaching platform, which is composed of three systems: online autonomous learning system, the teaching system and management system. This model is student-centered as students are the body of learning process and active constructors of knowledge while the instructor is the organizer and mentor, helping and promoting students' construction of meaning. The new model sets up an information-based teaching and learning environment. The

teacher, students, teaching media and teaching contents are the major elements. The teacher fulfills his job of guiding students' learning, teaching and assessing through classroom teaching and virtual platform, and interacts flexibly with students in suitable niche to maintain a balance.

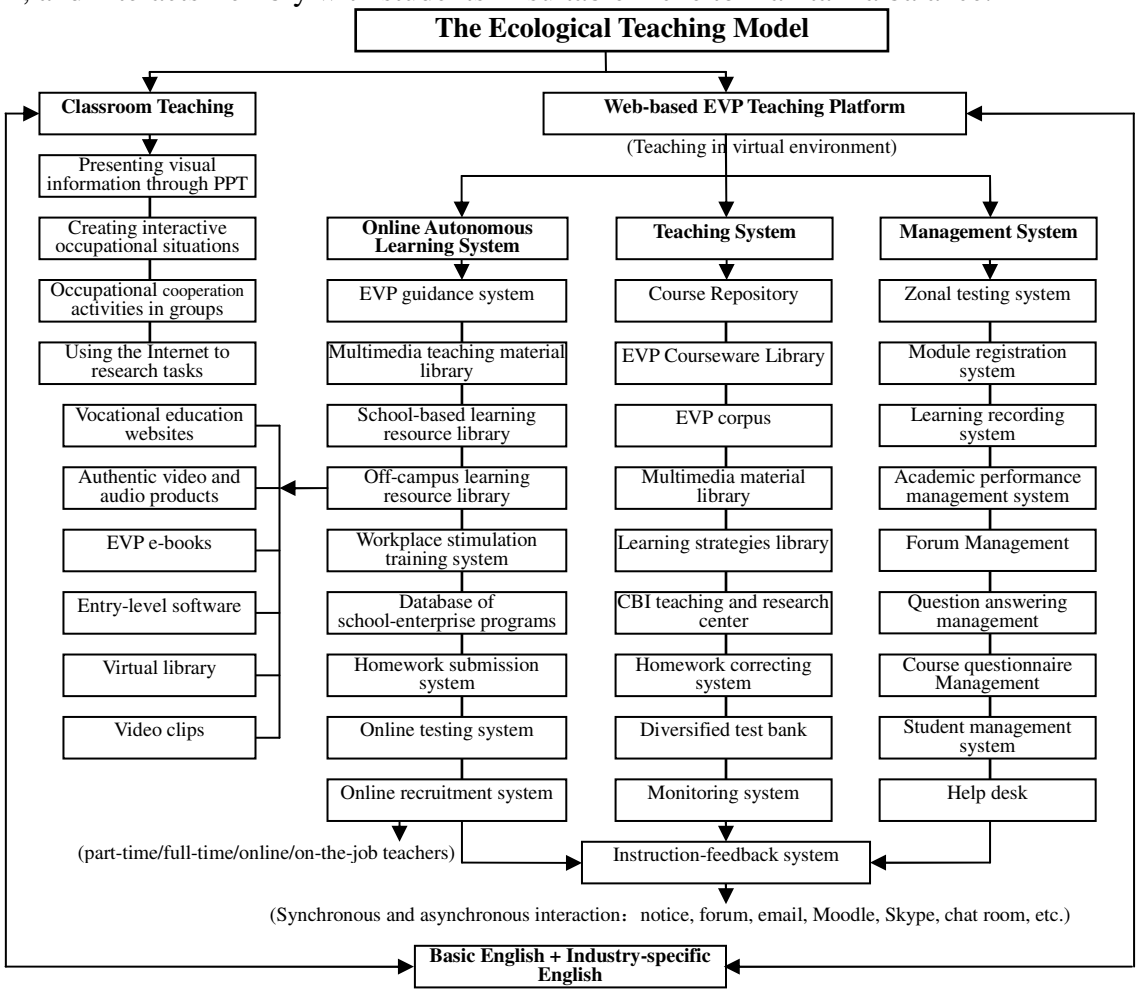

Basic English refers to Integrated English courses, College English Test Band Three, and Practical English Test for Colleges (Level B).
Industry-specific English includes vocational spoken English, Listening for workplace situations, Workplace reading, Vocational practical writing.

Figure 1: Structure of the ecological teaching model

The first interface of network self-learning system is EVP guidance system. This system is, in essence, the unique objectives and plans of each student' vocational English learning at different phases, which are made after the full communication with the instructor based on his own academic achievements in the entrance examination as well as his learning style and learning characteristics. This system emphasizes students' step-by-step process as well as their individual differences. It provides navigation for the learning platform. In the teaching system, the teacher (or teacher team) constructs course repository and EVP courseware library. He can prepare lessons, design and upload assignments, or set up a diversified test bank. He can also make a notice through the feedback system which is shared by the autonomous learning system and management system. Additionally, he can initiate discussions and interactions in the forum, and give synchronous feedback to students through Skype, Moodle or chat rooms. In the CBI teaching and research center, the teacher can publish teaching experiences, share teaching achievements as well as discuss research projects through sharewares like Alfresco, Wiki or teacher blogs. In this way the teacher can promote interactions with his peers and thereby enhance his own teaching and research capabilities. Through the monitoring system, the teacher can observe students' online learning, identify their problems, and guide or help them accordingly.

The management system is a support system for the teaching system and learning system. It enables students to record, monitor, assess and manage their learning process. It is also a help desk.

Course structure

The first step to reform teaching model is to change the course structure. The focus of the reform is to fully incorporate the element of modern information technology into the current structure of English courses (Basic English + industry-specific English) so that multimedia information technology can be utilized in every step of higher vocational English teaching. From the perspective of ecology, such reform aims to put all the elements of the ecological environment in right niche so as to stabilizing the teaching structure and maintaining the ecological balance of the teaching system. It can be seen from Figure 1 that in the new model, the course structure of "Basic English + vocational English" goes throughout the whole teaching process. Basic English, on one hand, enables students to make a link with high school English and improve their comprehensive ability of listening, speaking, reading and writing and get prepared for vocational English learning in the next stage. On the other hand, it prepares students for College English Test Band Three or Practical English Test for Colleges (Level B) required by the syllabus.

Teaching process

The teaching process consists of five parts.

(1) Zonal test of English proficiency. In the orientation week, all vocational students will take a hierarchical test of English proficiency on line. After they submit their answers, the system automatically gives feedback and evaluation. It also makes suggestions on levels and modules that each student should choose.

(2) Register for classes on line. Students complete the registration by choosing the level, modules, and the instructor. The system generates students' ID and password and establishes their e-learning archives.

(3) Study in appropriate level. Students preview the texts on the autonomous learning system and do other extra-curriculum learning according to their own needs.

(4) Study in the classroom. The instructor presents course information through PPT (powerpoint), and encourages students to blend into workplace stimulation learning context, actively engaged in various classroom activities as well as research tasks on the net. The network-based classroom interaction involves six procedures (see Figure 2).

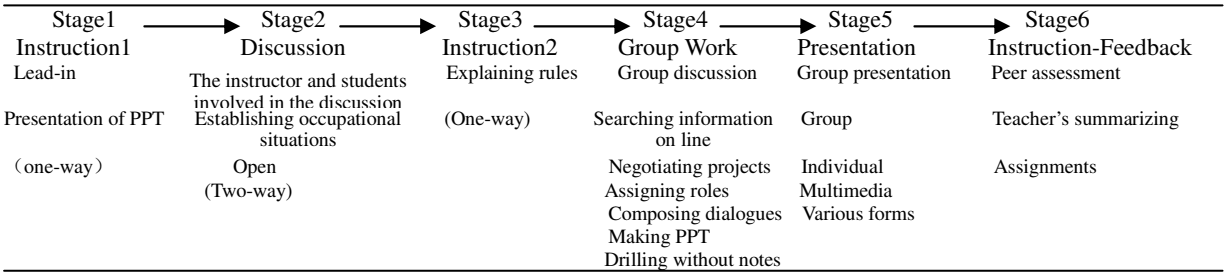

Figure 2: Flow chart for interactive classroom activities

In stage 1, the teacher gives instructions. This is usually a one-way process. In stage 2, the teacher invites and guides students to discuss by posing enlightening questions. This is an open, two-way discussion. Stage 3 is a one-way instruction. The teacher explains rules guiding group activities. Stage 4 is a process of group discussions. By taking the group discussion, students independently complete their tasks. In stage 5, students make group presentation based on the discussion. Stage 6 is a process for the instruction-feedback and peer assessments.

(5) Assessment and testing. Formative assessment is made based on the frequency and quality of students' participation in online discussions, classroom performance, homework, feedback from the firm where students work as interns, and the record of learning process as well. Summative assessment is a comprehensive assessment of language skills, mainly in the form of practical assessment in the end of the semester.

Learning process

Students' learning process consists of four steps. (1) Preview before class. Students' learning material includes those available in EVP multimedia teaching material library, school-based as well as off-campus learning resources library. (2) Classroom learning. (3) Consolidating what they have learned by means of assignments, consulting online library or testing. (4) Training in occupational situation and job interview. Students can use workplace stimulation training system, data-base of school-enterprise programs and online recruitment systems. In the learning process, students can communicate with the teacher, classmates and network administrators and receive feedback from them as well through the communication-feedback system. Students can either communicate with others through such non-real-time interaction ways as messages, emails or BBS, or make synchronous video communication through Skype or Moodle in agreed office hours. Students have access to a very rich source of vocational English knowledge, including vocational education website, the original audio and video products, and EVP e-books.

Conclusion

The ecological teaching model is employment-oriented. Through the web-based teaching platform, computer and network technologies are integrated into the whole process of EVP teaching, and become an indispensible organic part of the teaching model. The philosophy of ecological education permeates every link of English teaching. The model shows respect for individual difference and diversity of life. It attaches importance to personalized learning process and diversified evaluation methods. It is an open and comprehensive foreign language teaching system combining learning and practicing. It updates the concepts of traditional teaching model and inherits some advantages at the same time, and it is helpful to solve the problems existed. Of course, teaching reform is by no means easy. As English teachers, we must strive to foster strengths and circumvent weaknesses and constantly make exploration and improvement. With the rapid development of computer and network technologies, the potential for the development of web-based foreign language teaching is immeasurable.

Acknowledgement

The paper is supported by a research grant from the "Qianjiang Talent" programs of Zhejiang Province of China. The fund project is "On the Design and Construction of 'Multilateral Interaction' Autonomous Foreign Language Learning Platform," Grant No: 2011R10056.

References

[1] Liu Dailin, Zhang Jianyu. The Current Teaching Situations and Reforms in General English Teaching in Vocational Higher Education: Analysis and Prospects[J]. Foreign Languages in China, (6):77-83, 2009.

[2] Chen Jianlin, Gu Zhizhong. More Reasonable and Precise Requirements with Realizing Directions——Interpreting the 2007 College English Curriculum Requirements[J]. Computer-Assisted Foreign Language Education:6, 2008.

[3] Chen Jianlin. On the Integration of Computer and Internet into Foreign Language Teaching Program——From an Ecological Point of View[J]. Computer-Assisted Foreign Language Education:3-10, 2006.

[4] Zhang Jiachen. Reform Course of College English Teaching Mode of China Since Reform and Opening-up[D]. Fujian Normal University:9, 2008.

[5] Wang Zhe,Xia Ji-mei. The Effects of College English Teaching-Learning by the Combination of Network and Classroom[J]. Computer-Assisted Foreign Language Education: 13-20, 2010.

[6] Shi Lin. A Study of the Ecological Web-based College English Teaching Environment from the Constructive Perspective[J]. Computer-Assisted Foreign Language Education: 62-65, 2012.

Advanced Materials Research Vols. 989-994 (2014) pp 5286-5289
© (2014) Trans Tech Publications, Switzerland
doi:10.4028/www.scientific.net/AMR.989-994.5286

Research on Evaluation Index System of Risk Management Capacities of Private Banks in China

YANG Liu[1,a], WU Feng-ping[1,b]

[1] Business school, Hohai University, Nanjing211100, China

[a]18751963515@163.com, [b]wu_feng_ping@163.com

Keywords: private bank; risk management capacities; evaluation index system

Abstract. With the gradual deepening of financial reform in China, the development prospect of private banks is bright. However, the fierce competition in the banking sector and the nature of the private banks themselves make them face complex and diverse risk. Thus, it's particularly important to construct a reasonable evaluation index system of risk management capacities of private banks to reach an objective and clear evaluation of risk management level.

Introduction

In 2013, China's financial sector reform has achieved a new level. The 3rd Plenum of the 18th CPC pointed out relaxing private bank entry threshold and promoting the reform of RMB exchange rate formation mechanism. The establishment of China (Shanghai) Pilot FTZ aims to explore the new path and model of China's opening to the outside world, and to deepen the open innovation in the financial sector. In recent years, China's private economic grows stronger continuously; private capital markets gradually become active. CBRC offers proposals on encouraging and guiding private capital to banking. The State Council points out let private capital launch private banks, financial leasing companies and consumer finance companies or other financial institutions at their own risk. These new policies above provide opportunity to the establishment and development of private banks.

However, private bank in China is still a new thing which is inexperienced in many aspects; what's more, a series of financial opening policies make the sources and types of risks become more complex. Therefore, it's particularly important that private banks could understand their own risk management capabilities objectively and clearly.

Literature Review

In the study of private banks, many scholars make a study of the feasibility and future strategies. Ma Yuanyue[1](2004) pointed out moral hazard was prominent in all risks of private bank and gave the financial regulation initiatives. Xia Biying[2](2011) analyzed risk control mode of several private banks in Taizhou, put forward the private banks in China should perfect the governance structure, improve business strategy, and transform growth mode to strengthen the credit risk management.

In the study of risk management capacities of private banks, Liang Lijun[3](2010)pointed out that the evaluation of the bank's operational risk management ability can be divided into head office management level, department level, staff level and environment level. Ni Biao[4](2013) considered innovative companies need manage scientifically significant risk to maintain continuous innovation.

Different aspects and methods were used in private bank and risk management capabilities. However, few scholars combine private bank with risk management capability to build quantifiable evaluation index system and the corresponding evaluation method.

Connotation of Private Bank Risk Management Capabilities

Particularity of private bank risks.

Public trust risk. Private bank is different from state-owned commercial bank; it has no national prestige support, which means it has a greater risk of public trust than general commercial bank.

Industry competition risk. The competition covers deposit-taking business, management talent, financial services and technological innovation. Private bank must keep constant innovation, improve service quality, and increase public trust to have a larger space for development.

Capital shortage risk. Whether capital is adequacy determines whether the banks have strong economic strength and solvency. Private bank just has a single capital source at its inception, economic strength is limited. It must expand the various channels to boost capital, as soon as possible to promote business.

Insufficient funds risk. Since private bank has weak financial strength and low public trust at its inception, deposit business performance is not optimistic. The constant deepening of financial reform in our country, the increasing of financial institutions and the limited deposit resources lead to the greater risk of insufficient funds.

Associated loans risk. Most private enterprises set up private bank for providing financing channels and facilities to the enterprise. However these enterprises which are small and fund-limited have weak anti-risk capabilities, and they cannot repay the loan with a bit careless.

Connotation of risk management capabilities. Private bank risk management capabilities mean that private bank possess the knowledge and skills for risk management goal. Private bank reduce the probability of loss and enhance competitiveness by its general and specific risks management. To enhance the efficiency of risk management for private bank is good to establish a good reputation and to gain a larger market.

Private Bank Risk Management Capability Evaluation Index System

According to the index selection principle and characteristics of private bank, the paper builds three layers of evaluation index system.

Table 1 Private bank risk management capability evaluation index system

target	element	index
private bank risk management capability	risk assessment C_1	assessment method C_{11}
		assessment index system C_{12}
		assessment criteria C_{13}
		assessment process C_{14}
	risk monitoring C_2	:internal audit C_{21}
		monitoring mechanisms C_{22}
		risk tracking C_{23}
		department supervision C_{24}
	risk prevention C_3	NPL coverage C_{31}
		diversification rate C_{32}
		capital adequacy ratio C_{33}
		short-term loans ratio C_{34}
	risk response C_4	emergency level C_{41}
		company scale C_{42}
		profit margin C_{43}
		risk aversion C_{44}
		risk transfer C_{45}
		risk compensation mechanism C_{46}
	managerial	risk management concept C_{51}

communicationC_5	risk management system C_{52}
	risk management information system C_{53}
	risk management organizational structure C_{54}
	staff's quality C_{55}
	communication efficiency C_{56}

Risk assessment. Private bank takes certain risk criteria and method to evaluate measure for risk size and risk occurrence probability and the relative importance in order to identify risk factors and consequences.

Risk monitoring. Internal audit is an independent inspection, supervision and evaluation activities. The establishment of the monitoring mechanism is to supervise and control the risk management process. Risk tracking management can improve the force of recognizing the old and new risk. Private bank need to be limited and monitored by CBRC and other specific institutions. This regulation can promote private banks managing risk more effectively.

Risk prevention. NPL coverage mainly reflects the private bank's ability to compensate for loan losses and prevent the loan risk. Enterprises need as much as possible to avoid risk concentration in the process of business, appropriately disperses risk to other institutions. Capital adequacy ratio reflects the ability of private bank to make up for the loss of creditors with their own capital.

Risk response. Private bank should have emergency management system, including recognition, early warning, monitoring, treatment, prediction, etc. Scale of private bank directly reflect its overall strength, the larger the scale, the stronger the strength of its ability to cope with risk. Profit is the basis of the banks to survive. In order to reduce or avoid loss caused by risks, private bank usually takes certain measures of prevention and post-processing to avoid risk. Risk transfer means that the private bank takes some measures to make other organizations or individuals to undertake its original part or all of the risks and losses. At the beginning of establishment of the bank, related departments should establish some compensation mechanism.

Managerial communication. This part mainly involves management hardware and communication software.

For quantitative index, the data can be got from bank annual report or related institutions; for qualitative index, the data can be got by the expert scoring method.

Private Bank Risk Management Capability Evaluation Method

The influence factors of private bank risk management ability are numerous; the factors interact with each other. The paper use extension synthetic evaluation method to evaluate the private bank risk management capability. “Things, index, value” is the main content of the extension synthetic evaluation method. Assume T represent evaluation object name, C represent characteristic index, and V represent the value of C. Q= (T, C, V) constitutes the basic unit of describing things. The steps of extension model as follows:

Step 1: Determine the classical domain and joint domain of the model

According to the evaluation index C, the private bank risk management capability indexes are divided into m standard classes.

$$Q_p=(T_p,C_i,V_{pi})=\begin{bmatrix} T_p & c_1 & v_{p1} \\ & c_2 & v_{p2} \\ & \vdots & \vdots \\ & c_n & v_{pn} \end{bmatrix}=\begin{bmatrix} T_p & c_1 & (a_{p1},b_{p1}) \\ & c_2 & (a_{p2},b_{p2}) \\ & \vdots & \vdots \\ & c_n & (a_{pn},b_{pn}) \end{bmatrix} \quad (i=1,\,2,\,\cdots,\,n) \tag{1}$$

T_p is for private Banks risk management capability, V_{pi} is for value range of C_i, namely $\langle a_{pi},b_{pi}\rangle$. Q_j is for j level risk management capability of matter-element extension evaluation model. T_j is for lower than j level risk management capability. $(i=1,\,2,\cdots,n\,;\ j=1,\,2,\cdots,m)$

Step 2: Establish correlation functions

$$\pi(v_i, v_{ji}) = \left| v_i - \frac{a_{ji} + b_{ji}}{2} \right| - \frac{1}{2}(b_{ji} - a_{ji}) \quad (i = 1, 2, \cdots, n;\ j = 1, 2, \cdots, m) \tag{2}$$

$$\pi(v_i, v_{pi}) = \left| v_i - \frac{a_{ji} + b_{ji}}{2} \right| - \frac{1}{2}(b_{pi} - a_{pi}) \quad (i = 1, 2, \cdots, n;\ j = 1, 2, \cdots, m) \tag{3}$$

$\pi(v_i, v_{ji})$ is for the proximity of v_i and v_{ji}, $\pi(v_i, v_{pi})$ is for the proximity of v_i and v_{pi}. If $\pi(v_i, v_{ji}) \geq 0$, v_i is outside of v_{ji}, if $\pi(v_i, v_{ji}) \leq 0$, v_i is inside of v_{ji}.

$$K_j(c_i) = \begin{cases} \dfrac{\pi(v_i, v_{ji})}{\pi(v_i, v_{pi}) - \pi(v_i, v_{ji})} & v_i \notin v_{ji} \text{ and } \pi(v_i, v_{pi}) \neq 0 \\ \dfrac{-\pi(v_i, v_{ji})}{|v_{ji}|} & v_i \in v_{ji} \\ -\pi(v_i, v_{ji}) - 1 & v_i \notin v_{ji} \text{ and } \pi(v_i, v_{pi}) = 0 \end{cases} \tag{4}$$

$K_j(c_i)$ is the correlation of c_i and level j.

Step 3: Determine the index weight

The paper uses fuzzy chromatography analysis to determine the index weight. The experts with their understanding of the evaluation objects give the evaluation opinion; the index weight is calculated on the basis.

Structure judgment matrix between elements layer and target layer and index layer and element layer. Sort for each layer; calculate the element weight of each layer. Sort for total layers; calculate the weight of each index compared with the evaluation target.

Step 4: Layer calculation

Assume $w_i (\sum_{i=1}^{n} w_i = 1)$ is the index weight coefficient, the correlation function of private bank capability is: $K_j(M) = \sum_{i=1}^{n} w_i K_j(v_i)$; $j = 1, 2, \cdots, m$.

Total correlation function of risk management capability is: $K(M) = \max_{1 \leq j \leq m} K_j(M)$.

Conclusion

Based on the new policies and measures and general and special risk analyses faced by private bank, the paper builds the evaluation index system of private bank risk management capacity, and selects the corresponding evaluation method. The paper can provide evaluation and decision-making basis to private bank and the relevant departments, provide reference to similar financial institutions, also make the commercial bank risk management theory and evaluation system more rich and perfect.

References

[1] Ma Yuanyue: Economic problems(2004).

[2] Xia Biying: Taizhou university journal(2011).

[3] Liang Lijun, Li Zhixiang: Management review(2010).

[4] Ni Biao, Xiang Gang: Scientific and technological progress and countermeasures(2013).

Advanced Materials Research Vols. 989-994 (2014) pp 5290-5293
© (2014) Trans Tech Publications, Switzerland
doi:10.4028/www.scientific.net/AMR.989-994.5290

The research and practice of Network Teaching Pattern

Zhao Lingling[1,a], Sun Qiaoyun[1,b], Liu Xiaoxiao[1,c] and Gao Qinghua[1,d]

[1]Beijing city University, Beijing, 100083, China

[a]zhaolingling@bcu.edu.cn, [b]sunqy@bcu.edu.cn, [c]lxx535@163.com,

[d]qhuag@bcu.edu.cn

Keywords: Network Teaching Pattern, Module Division, Vocational Qualification Certificate

Abstract. The network teaching creates new education and teaching idea and brings huge impact and challenges to the traditional education pattern. This paper studies the webpage making courses under the network teaching pattern, proposes modular and phase teaching idea, inspires learning interests of students, exercises innovative ideas of students and improves teaching quality with student as the guide.

Introduction

With increasing development of network technology, the network applications are becoming extensive and extensive and the websites have become one important platform for information demonstration of the companies, enterprises or individuals. For college students majoring in the computer, it is very practicable and important to grasp webpage making method and website concurrency technology, which can extensively expand their employment areas and improve their employment competition capability. As one foundational course for occupational skill of the computer specialty, the webpage making courses can cultivate the webpage design, webpage making and website management capability of the students and is a very practicable and comprehensive course.

Problems in teaching of webpage making course

The webpage making course is a very technical, applicable and practicable course, but now traditional class teaching pattern is used in many colleges, namely teachers instruct by the steps in the teaching material and then students practice them on the computer. The traditional teaching pattern can play the dominant role of teachers and monitor the whole teaching process, but it ignores the main role of students, reduces learning interests of students, and is unfavorable to cultivation of the innovation thinking and capability of students.

With increasing development of information technology, the teaching plans of colleges are experiencing continuous reforms. The computer specialties are developing to the high-end and front technology area. The webpage making courses are cut down in the computer specialties due to limited course class hours, so students have not opportunities to learn webpage making knowledge and skills, so they are lack of webpage making capabilities.

Teaching reform scheme of webpage making course under network teaching pattern

For the above cases, the authors propose the teaching reform scheme of the webpage making courses under the network teaching pattern. This scheme mainly explores the teaching pattern under the network teaching pattern in which the students mainly learn by self via the network teaching platform and the teachers instruct students in 6-8 class hours in the classroom as the auxiliary means. Finally students learn the basic knowledge and operation skills on webpage making and make the medium-size websites. This scheme not only offsets the insufficient teaching periods of the webpage

making source, but also improve self-learning capability, actual practice capability and webpage making skills much.

Reform of teaching contents. The webpage making course is a comprehensive course and involves many aspects such as webpage making, image art and code programming. The teaching contents of webpage making course are divided into different modules, so teaching contents are simple and specific, are clear in thinking, reduce self-learning difficulties of students and assist students to arrange learning keys. The webpage making courses are divided into eight modules, shown as the figure 1.

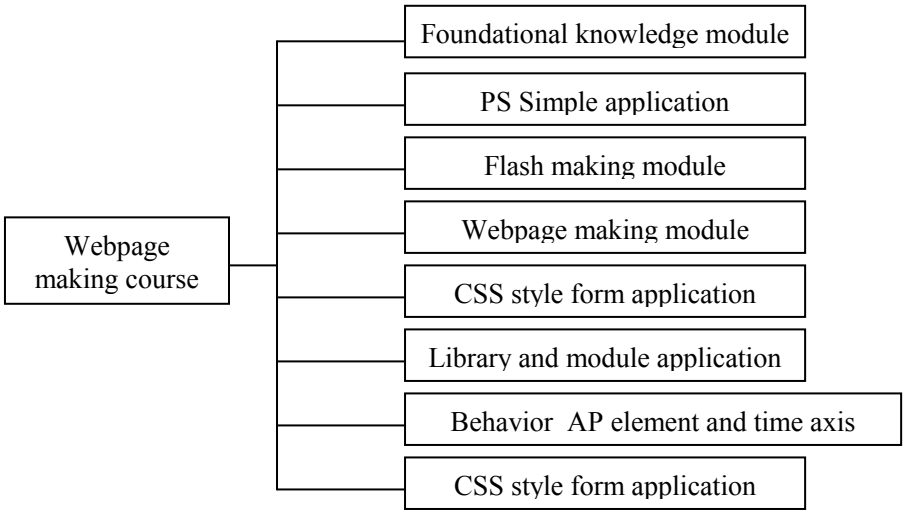

Figure 1 Eight module diagram

All modules are independent of each other and associated with each other. Independence indicates that each module is a complete key and includes independent module ppt and teaching case. An individual module job is designed for each module. Association indicates mutual relation among modules. All knowledge keys are arranged from shallow to deep. All modules coordinate with each other to complete final teaching target.

Each module is taught with the task-driven method. After a student completes self-learning task of each module, he should complete the "tasks" specified by the teacher, namely module jobs. Self-learning capability, practice operation capability and independent exploration spirit of students is cultivated in "task" completion process. Teachers deploy modular jobs via the network teaching platform. Students submit "task" achievement via the network teaching platform. Teachers inspect "task" achievements from students and feed back to students in time to urge students to complete necessary learning of necessary teaching contents and improve network teaching quality.

Reform of teaching form. The network teaching pattern mainly utilizes openness and interactivity of network teaching and richness of network reaching resources, offsets the weakness "students learn what teachers teach" under the traditional teaching pattern, inspires learning interests of students and exercises innovative thinking of students.

（1）Openness of network teaching: The network teaching makes student be free of time and location restriction and students can flexibly and independently learn and repeatedly learn the difficult knowledge keys.

（2）Interactivity of network teaching: the network teaching platform features a better interactivity and can be used for exchange and learning between teachers and students and between students.

（3）Richness of network teaching resources: the network teaching platform not only includes courseware made by the teachers in our college, but also links fine course website of many key colleges, technology forum website, excellent enterprise website and material websites for students to learn.

Reform of assessment pattern. The assessment of the network teaching of the webpage making course focuses on and emphasizes whole-process examination of students. Student learning is tracked

and managed via modular jobs. After students learn all modules, the modular jobs can be combined into a comprehensive website as the examination work. Students can also participate in webpage designer examination organized by Ministry of Industry and Information. Flexibly assessment regulation alleviates examination load of students and implements the idea of "quality education and capability cultivation".

Implementation process of teaching reform

The network teaching pattern of webpage making course is divided into pre-course preparation, student self-learning phase, teacher face-to-face teaching phase and student assessment phase.

Pre-course preparation. The pre-course preparation phase is mainly completed by teachers. Teachers propose course teaching reform scheme, make teaching plan, prepare teaching materials, perfect network teaching platform and organize students to register and select courses.

（1）Make network teaching reform scheme: make network teaching outline and teaching progress, and make teachers know teaching target and teaching contents and grasp teaching progress and make students know teaching form and teaching requirements by making teaching scheme.

（2）Prepare teaching documents: prepare modular teaching ppt and each modular job, collect teaching instances via network resources and prepare the teaching question database.

（3）Perfect network teaching platform: perfect the network teaching platform, store the teaching documents, teaching requirements and teaching progress on the network teaching platform and guide students to learn by self via the network platform according to the teaching progress.

（4）Organize students to register voluntarily: organize students to join voluntarily and propose requirements.

Student self-learning phase. Self-learning phase of students is completed by students. Students learn by self via the network platform, complete modular jobs, participate in interaction between teachers and students, read the network teaching instances and know theory knowledge on webpage making course via the question database.

Teacher face-to-face teaching phase. After students complete all courses, teachers can provide face-to-face teaching during 6-8 class hours. The face-to-face teaching mainly explains problems in the student modular jobs. Teachers will instruct students to make a real website with a comprehensive website as one example.

Student assessment phase. After students complete all learning tasks, they should submit a complete website job for term examination. Students can also participate in webpage designer examination organized by Ministry of Industry and Information.

Conclusions

The network teaching pattern is a new teaching pattern, overcomes the weaknesses in the traditional face-to-face classroom teaching, fully utilizes the network teaching resources, solves urgent campus resources and insufficient course class hours in the colleges, improves comprehensive development of learning proactivity, thinking capability and personality of students, and enhances self-learning capability of students.

Acknowledgements

This Project is supported by "The Research of Students Autonomous Learning Ability under Network Teaching Mode" of Beijing City University Education Science Research Subject in 2014 and Major Project of BCU JYB201120.

References

[1] Fu Feng. Discussion on Network Teaching of Public Computer Course in Colleges [C]. Henan: Journal of Tianzhong, 2003:101-103

[2] Yu Limei, Jiang Wenfeng, Gao Zhanxian. Exploration on "Organic Chemistry" Network Teaching Practices [C].Beijing: Education in China Universities, 2007:88-89

[3] Zhong Daijun, Gao Feng. Discussion on Public Computer Zero-Period Teaching Based on Campus Network [C]. Anhui: Computer Knowledge and Technology, 2008:777-779

[4] Chen Mo, Wu Tao. Dreamweaver CS3 Standard Textbook [M]. Beijing: Beijing Kehai Electronic Press, 2008

[5] Information on http://www.edu.cn

Advanced Materials Research Vols. 989-994 (2014) pp 5294-5299
© (2014) Trans Tech Publications, Switzerland
doi:10.4028/www.scientific.net/AMR.989-994.5294

Technical Risk Assessment of Large-scale Construction Project Based on Triangle Whitening Weight Function

Ma Wei[1]

Department of economics and management from Tianjin university of science and technology, Tianjin

maweilwtg@126.com

Keywords: large-scale construction project, technical risk assessment, triangle whitening weight function

Abstract. Technical risk assessment model of large-scale construction project has been established by using triangle whitening weight function of grey theory against the problems of technical risk assessment of large-scale construction project. In the end, through example verification, this model is approved to be feasible and have certain value of reference and utilization in similar problems.

Along with the development of scientific technology and the demand of urban modernization, more and more high and new technologies have been applied to large-scale construction project. However, while pursuing for multiple functions and high compatibility, the high and new technologies also have brought higher risk to construction of large-scale construction projects. More complicated engineering and newer technology will lead to higher technical risks. The insufficient estimation to technical risk often leads to great influence on final utilization, maintenance, cost and progress of large-scale construction project.

During construction of large-scale construction project, the technical risk assessment is often lack of necessary historical data and faces the problem of "inadequate and deficient information": technology is neither clear nor certain in itself, it has a portion of known information and a portion of unknown information; the solution of technical risk assessment is featured by differentiation and non-uniqueness and the experience, identification ability and cognitive level of human being are also limited. All these fully demonstrate the "grey" [1] nature of technical risk assessment. Therefore, on qualitative basis, this article uses grey system theory and methods to make quantitative analysis on technical risk assessment of large-scale construction project.

Grey assessment method based on triangle whitening weight function [2]

Suppose there are n objects, m assessment indexes and s grey clusters, then the sample observation about index j of object i is $a_{ij}\ (i=1,2,\ldots,n;\ j=1,2,\ldots,m)$.

Main procedures of grey assessment method based on triangle whitening weight function are as follows:

1) Divide the value range of each index into s grey clusters based on the number of grey clusters required by assessment. For instance, the value range of index j $[a_1, a_{s+1}]$ can be divided into $[a_1,a_2],\cdots,[a_{k-1},a_k],\cdots,[a_{s-1},a_s],[a_s,a_{s+1}]$, among which, the value of $a_k\ (k=1,2,\cdots,s,s+1)$ can be generally determined by requirements of actual situations.

2) Suppose the whitening weight function value of $\lambda_j^k=\left(a_j^k+a_j^{k+1}\right)/2$ of cluster K is 1, connect $\left(\lambda_j^k,1\right)$ with a_j^{k-1}, the start of grey cluster k-1, and a_j^{k+2}, the end of grey cluster k+1 (see in Figure 1) to get the triangle whitening weight function on grey cluster k of index j $f_j^k(x)\left(j=1,2,\cdots,m;k=1,2,\cdots,s\right)$.

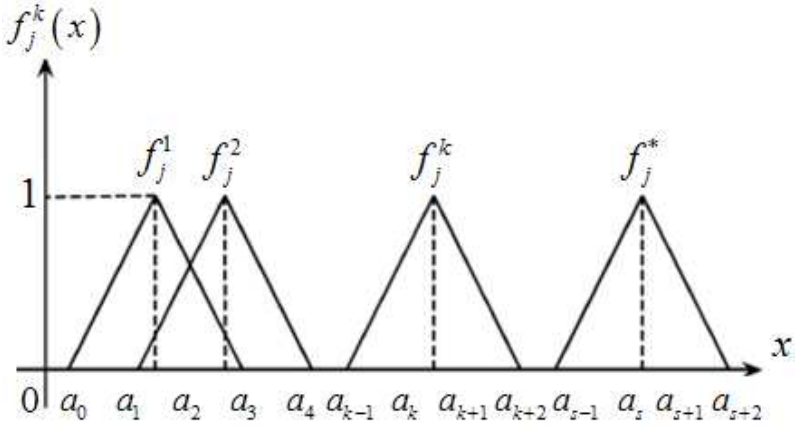

Figure 1 Triangle Whitening Weight Function

3) As to $f_j^1(x)$ and $f_j^s(x)$, the range of index value can be extended to the left and right till a_j^0 and a_j^{s+2} respectively; while for the index observation value x_j, based on the following formula, we can get the whitening weight function value $f_j^k(x)$ of grey cluster k.

$$f_j^k(x)=\begin{cases} 0 & x\notin\left[a_j^{k-1},a_j^{k+2}\right] \\ \dfrac{x_j-a_j^{k-1}}{\lambda_j^k-a_j^{k-1}} & x\in\left[a_j^{k-1},\lambda_j^k\right] \\ \dfrac{a_j^{k+2}-x_j}{a_j^{k+2}-\lambda_j^k} & x\in\left[\lambda_j^k,a_j^{k+2}\right] \end{cases} \tag{1}$$

4) Calculate the comprehensive cluster coefficient σ_j^k of object $i(i=1,2,\ldots,n)$ in grey cluster k:

$$\sigma_j^k=\sum_{j-1}^{m}f_j^k\left(x_{ij}\right)\cdot\eta_j \tag{2}$$

Among which, $f_j^k\left(x_{ij}\right)$ is the whitening weight function of object i in grey cluster k of index; η_j is the weight of index j in comprehensive cluster and can be estimated by experts with fuzzy analysis.

5) With $\max\limits_{1\le k\le s}\left\{\sigma_j^k\right\}=\sigma_j^{k^*}$, we can determine that object i belongs to grey cluster k^*. If there are many objects in grey cluster k^*, then we should confirm the position of each object according to the value of comprehensive cluster coefficients.

Technical risk assessment of large-scale construction project based on triangle whitening weight function

Now, taking technical implementation of a large-sale construction project as the example, we make assessment on technical risk of this project by triangle whitening weight function.

1）Through consulting, statistics and collection of information, in reference to opinions of experts, we set up the index set of the analyzed system [3-4] as shown in Table 1.

Table 1 Index System of Technical Risk Assessment of Large-scale Construction Project

	Structural index	Analysis index
Index system of technical risk assessment of large-scale construction project	Technical maturity (x_1)	Maturity of key technology (x_{11})
		Reserve of related technology and materials (x_{12})
	Technical complexity (x_2)	Breadth of related technologies that have been mastered (x_{21})
		Compatibility of technical integration (x_{22})
		Whether the technology can be easily mastered by construction personnel or not (x_{23})
	Technical reliability (x_3)	Service life (x_{31})
		Maintainability (x_{32})
	Technical foresight (x_4)	Very conform to development tendency (x_{41})
		Whether it has further development potential or not (x_{42})
		Can it be protected by strict intellectual property right? (x_{43})

2）According to the requirements of assessment, this index can be classified into 4 grey clusters: low risk V_1, medium risk V_2, high risk V_3 and rather high risk V_4.

In technical risk assessment, many indexes are qualitatively determined[5]. Since they cannot be calculated directly with quantitative indexes, a certain conversion rule is required. Psychologist G. A. Miller proved by experiment that when judging a program in terms of a certain feature, the number of level that can be correctly identified by ordinary people is from 5 levels to 9 levels, so, the index in word is usually described as the judging index from 5 levels to 9 levels subjecting to specific requirements. So, 1-9 scaling method is introduced to define the qualitative analysis by quantitative numbers. See the meaning of each level in Table 2.

Table 2 1-9 Scaling Method

Definition	Very bad	Bad	Ordinary	High	Very high	Between adjacent definitions
Scale	1	3	5	7	9	2,4,6,8

According to technical integration information owned by the construction group about this large-scale construction project, in reference to the opinions of experts, we grade each index and get a set of realizations of all indexes: index x_{11}, x_{12}, x_{21}, x_{22}, x_{23}, x_{24}, x_{31}, x_{32}, x_{41}, x_{42} and x_{43}, respectively corresponding to 5.9, 8.1, 6.5, 4.3, 6.8, 7.0, 7.2, 8.0, 6.8 and 6.0.

Based on the above, according to the index system of technical risk assessment of large-scale construction project listed in Table1 and by discussion of experts, the analysis value index system of technical risk assessment of this large-scale construction project has been set up as shown in Table 3.

Table 3 Analysis Value of Technical Risk Assessment of Large-scale Construction Project

Index x		Weight η	Rather high risk V_4	High risk V_3	Medium risk V_2	Low risk V_1
Technical maturity (x_1)	x_{11}	7	[1, 2.5]	[2.5, 4]	[4, 6]	[6, 8]
	x_{12}	8	[1, 3]	[3, 5]	[5, 7]	[7, 9]
Technical complexity (x_2)	x_{21}	7	[1, 3]	[3, 5]	[5, 7]	[7, 9]
	x_{22}	6	[1, 4]	[4, 6]	[6, 8]	[8, 9]
	x_{23}	6	[1, 4]	[4, 6]	[6, 8]	[8, 9]
Technical reliability (x_3)	x_{31}	7	[1, 4]	[4, 6]	[6, 8]	[8, 9]
	x_{32}	6	[1, 3]	[3, 5.5]	[5.5, 8]	[8, 9]
Technical foresight (x_4)	x_{41}	5	[1, 3]	[3, 5]	[5, 7]	[7, 9]
	x_{42}	4	[1, 4]	[4, 6]	[6, 8]	[8, 9]
	x_{43}	2	[1, 4]	[4, 6]	[6, 8]	[8, 9]

According to the value index system shown in Table 3, the calculation of triangle whitening weight function is the same as formula (1). If j=1, we can extend the value range of x_{11} to $a_{11}^0 = 0.5$ and $a_{11}^6 = 8.5$, and respectively get four threshold values: rather high risk V_4, high risk V_3, medium risk V_2 and low risk V_1, namely,

$a_{11}^1 = 1$, $a_{11}^2 = 2.5$, $a_{11}^3 = 4$, $a_{11}^4 = 6$, $a_{11}^5 = 8$.

Take the average value of a_1^k and a_1^{k+1} as λ_1^k,

$\lambda_1^1 = 1.75$, $\lambda_1^2 = 3.25$, $\lambda_1^3 = 5$, $\lambda_1^4 = 7$

Put the number into formula (1) and get the whitening weight function $f_1^1(x)$.

$$f_1^1(x) = \begin{cases} 0 & x \notin [0.5, 4] \\ \dfrac{x_1 - 0.5}{1.75 - 0.5} & x \in [0.5, 1.75] \\ \dfrac{4 - x_1}{4 - 1.75} & x \in [1.75, 4] \end{cases}$$

Similarly, we can get the function of $f_1^2(x)$, $f_1^3(x)$ and $f_1^4(x)$.

Respectively put the value of key technical maturity $x_{11} = 5.9$ to the above four whitening weight functions to get the value of whitening weight function of key technical maturity index x_{11} against the 4 grey clusters, “rather high risk”, ” high risk”, “medium risk” and “low risk”:

$f_1^1(5.9) = 0$; $f_1^2(5.9) = 0.036$; $f_1^3(5.9) = 0.7$; $f_1^4(5.9) = 0.63$

From the result of index x_{11}, we can see that the risk of key technical maturity is in “medium” level.

Take the value extension of various indexes in the whole index system and calculate their whitening weight functions against the four different grey clusters, as shown in Table 4.

Table 4 Value of Whitening Weight Function

Index	x_j^0	x_j^6	f_j^1	f_j^2	f_j^3	f_j^4
x_{11}	0.5	8.5	0.000	0.036	0.700	0.630
x_{12}	0.5	9.5	0.000	0.000	0.300	0.930
x_{21}	0.5	9.5	0.000	0.167	0.830	0.000
x_{22}	0.5	9.5	0.486	0.825	0.900	0.000
x_{23}	0.5	9.5	0.000	0.600	0.930	0.320
x_{31}	0.5	9.5	0.000	0.667	1.000	0.400
x_{32}	0.5	9.5	0.000	0.730	0.111	0.500
x_{41}	0.5	9.5	0.000	0.000	0.330	1.000
x_{42}	0.5	9.5	0.000	0.600	0.930	0.320
x_{43}	0.5	9.5	0.000	0.667	0.667	0.000

With formula (2), we can get the comprehensive cluster coefficient of grey cluster K of this large-scale construction project, as stated below:

$$\sigma_j^1 = \sum_{j=1}^{10} f_j^1\left(x_{ij}\right) \bullet \eta_j = 2.916$$

$$\sigma_j^2 = \sum_{j=1}^{10} f_j^2\left(x_{ij}\right) \bullet \eta_j = 22.754$$

$$\sigma_j^3 = \sum_{j=1}^{10} f_j^3\left(x_{ij}\right) \bullet \eta_j = 38.460$$

$$\sigma_j^4 = \sum_{j=1}^{10} f_j^4\left(x_{ij}\right) \bullet \eta_j = 25.850$$

By virtue of $\max\left\{\sigma_j^k\right\} = \sigma_j^3 = 38.460$, we can know that the comprehensive technical risk of this large-scale construction project is in “medium risk” level. Seen from the data in Table 4, the maintainability, technical compatibility and intellectual property right protection of technical risk of this large-scale construction project are in or on the verge of the “high risk” grey cluster, so these aspects still need close follow-up and it is necessary to pay close attention to them during construction for further reduction of technical risk.

Conclusion

This article discusses the feasibility to carry out technical risk assessment of a large-scale construction project by triangle whitening weight function, so as to provide an effective approach and solution for technical risk assessment of large-scale construction project. However, triangle whitening weight function theory still needs further improvement in itself, e.g. the intersection of two grey clusters or above. The reference [2] has brought up a method for improvement called center-point triangle whitening weight function and it is worth learning. Besides, since this method is featured by simple principle, easy operation and high practicability, it is worth promotion in the area of project management and decision-making analysis etc.

[1] Ma Wei, Male, Born in 1979, from Hebei Langfang, Han nationality, PhD student from Tianjin university of science and technology, Research orientation: Technical economy on constructional engineering.

References

[1] Deng Julong: *The Primary Methods of Grey System Theory* (Huazhong University of Science and Technology Press, Wuhan 1990).

[2] Liu Sifeng, Xie Naiming:*Grey System Theory and Its Application* (Science Press, Beijing 2008).

[3] Chi Baoshan, Li Yongtai: Study on the R&D Technology Risk Assessment Based on the Uncertainty Theory. Journal of Academy of Armored Force Engineering. Vol. 19(2005), p.65

[4] Dai Ran: Application of Grey Triangle Whitening Weight Function in Assessment of Hydraulic Projects. ZHI HUAI. Vol.34(2009) , p.37

[5] Zhang Xinli: *Project Risk Management* (China Machine Press, Beijing 2007).

Advanced Materials Research Vols. 989-994 (2014) pp 5300-5303
© (2014) Trans Tech Publications, Switzerland
doi:10.4028/www.scientific.net/AMR.989-994.5300

Design of Expressway Construction Safety Evaluation System Based on AHP[1]

Hai-lin Guo[1,a], Zhi-ning Wang[1,b], Li-xin Zhang[1,c], Liu Xiao[1,d]

[1]China University of Geosciences, Wuhan 430074, China

[a]hl_guo2004@163.com,[b]1321662628@qq.com,[c]lx_zhang1989@qq.com,[d]2577155946@qq.com

Keywords: Analytic Hierarchy Process; Safety Evaluation; System Design

Abstract. Chinese expressway construction security situation is grim at present. Based on the index system, determining the importance of every factor on each level by the experts scoring method and 1-9 scale law. A expressway construction security evaluation system is designed and developed using Analytic Hierarchy Process(AHP) and the modern computer-aided technology, and finally validated. The results show that this system accurately indicated the safety situation of expressway construction, and realize systematism, standardization and automatization of safety evaluation.

Introduction

Along with the large scale construction of expressway in china, the construction security situation is grim, and accidents happen so frequently. To prevent and reduce accidents, safety evaluation of the construction process must be incorporated into the safety evaluation of Highway Engineering [1]. Especially expressway construction project in the mountainous area with bad geological conditions, extra-long tunnels, long-span bridges, steep slopes and other hazardous factors. Through designing and developing the expressway construction safety evaluation system, it can evaluate the risks of construction process, and adopt the corresponding countermeasure to avoid safety accidents. It proved to be effective, and can reduce the engineering risk, prevent and control accidents, ensure the life and property safety of working staff.

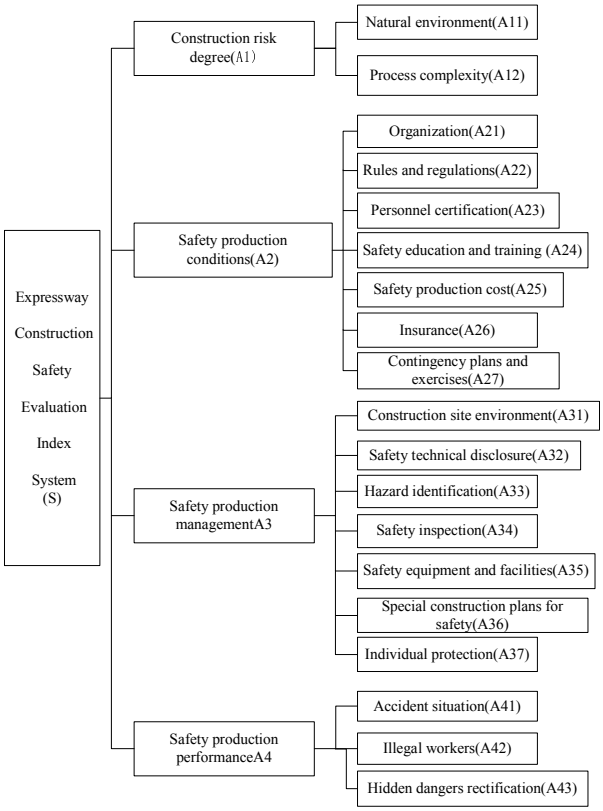

Fig 1.Index system

Establishing evaluation system and Modeling

Establishing evaluation system

Construction objects, construction environment, equipment, personnel, facilities and operations are considered as the main criteria in highway construction. With construction progress, some factors are static, but more dynamic, which is a complex system [2]. In order to evaluate the security situation in the production, it is important to establish a comprehensive, scientific, rational and typical evaluation system for highway construction.It is shown as Fig 1.

Modeling

It is can be seen the evaluation index evaluation system is divided into three layers.In order to improve the evaluation system reliability and quantitate, based on Analytic Hierarchy Process with 1-9 scoring scale and expert-scoring way, the evaluation system, which evaluate risk factors in the highway construction site, is established.

(1) Dividing the hierarchy

The model has a two-step approach. First, the main attributes (construction risk degree, safety production conditions, safety production management and safety production performance) are identified. Second, 19 alternative for each criterion, shown as Fig 1..

(2) Determining the matrix structure

In order to reduce human and other subjective factors on the weights, the evaluation model by constructing judgment matrix approach for each index weights are constructed. The basic assumption of AHP is the reciprocity of the pairwise comparisons:

$$\sum_{i=1}^{n}\sum_{i=1}^{n} a_{ij} = 1, \quad a_{ij} \geq 0, \quad a_{ij} = 1/a_{ji}, \quad (i, j=1,2,3,....n) \qquad (1)$$

1) 1-9 scale assignment. Using Professor Thomas L. Saaty 1-9 scale proposed method [3]for the assignment, a number of experts are invited to assess the relative importance of each index score to eliminate errors further. Finally, all levels of judgment matrix are acquired. Assignment method scaling are shown in Table 1:

Table 1 The linguistic description of the numerical scale in AHP

Scale	Definition	Explanation
1	Equal importance	Two activities considered equally important
3	Moderate importance of one over another	One activity is marginally favoured over another
5	Essential or strong importance	One activity is strongly favoured over another
7	Very strong importance	One activity is very strongly favoured and its dominance is demonstrated in practice
9	Extreme importance	The evidence favouring one activity over another is of the highest possible order
2,4,6,8		Intermediate values between two adjacent judgments

provides an estimation of the weight vector. The reliability of this estimation can be measured by the Consistency Ratio (CR): this measure indicates how consistent the comparisons are relative to large number of purely random judgements. Perfectly consistent judgments result in a consistency ratio of 0; CR=1 indicates that judgments were made randomly. As a general rule, a consistency ratio which does not exceed (0.10) is considered acceptable

2) Consistency test. In order to avoid the influence of other factors on the matrix, consistency test must be determined and the results can be analyzed. The calculation method on consistency for the judgment matrix is as follows:

$$CR = CI/CR \qquad (2)$$

The reliability of this estimation can be measured by the Consistency Ratio (CR). As a general rule, a consistency ratio which does not exceed (0.10) is considered acceptable,or we need to adjust the Elements of determine matrix.. *CI* is called Consistency Index. $CI=(\lambda_{max}-n)/(n-1)$, *Where λmax is the largest eigenvalue, n is the order of the matrix. RI is called* Random Index [4], shown as Table 2.

Table 2 Random Index

n	1	2	3	4	5	6	7
RI	0.00	0.00	0.58	0.90	1.12	1.24	1.32

After doing consistency test, based on the maximum eigenvalue λmax, the corresponding feature vector W is solved and W is normalized. Then the weights of alternatives, which reflect the relative importance of the attributes, are acquired.

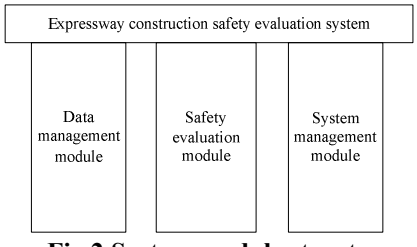

Fig 2 System module structure

Design of the evaluation system

Evaluation system function analysis

The expressway construction safety evaluation system adopts B/S structure and based on the database application system.The modular structure is shown in Fig 2.

The expressway construction safety evaluation system including data management module, safety evaluation module and system management module three modules.

(1)Data management module

The data include: system role authorization data, project attribute information, the construction unit, etc. The main function of this module is to complete a variety of data input, editing, storage, query, export, backup, etc.To prepare data for further safety evaluation, and complete the basic function such as output.

(2)Safety evaluation module

This module is the core module of the system, and can complete the safety evaluation on the selected object in human-computer interaction.Through analyzing the factors of safety performance, the evaluation units on-site status to get the production safety level and find the problems existing in the various units of production safety.Meanwhile, Sort the results of the safety evaluation and comparative analysis of the security situation of the construction unit. Provide scientific basis for safety management and decision-making.

(3)System management module

System management module provides the user rights management capabilities to ensure the security of the system data.

Evaluation system function design

The expressway construction safety evaluation system is an effective means to realize automation, construction site safety evaluation standardization, systematization [5]. Its main function is divided into two kinds: one kind is the data management, another kind is data analysis,as shown in Fig 3.

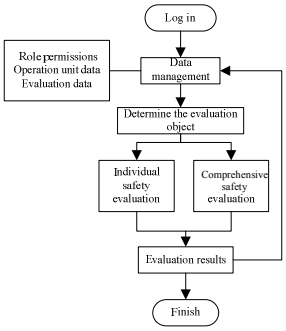

Fig 3 System function structure diagram

(1)Log in

In order to ensure the security of the system, the system implementation role to log in.The role is divided into seven categories, shown in table 3.

Table 3 Role Permissions

Attribution	Classification	Permissions
construction unit	System administrator	With full privileges
	Safety manager	Managing,inputting,editting,deleting and outputting the data of the construction unit; querying, statistics,and outputing the data of the operation units and supervision units.
	general staff	Browsing the data of the construction units
operation unit	Safety Manager	Managing,inputting,editting,deleting and outputting the data of operation unit;querying, statistics,and outputing the data of the operation units.
	general staff	Browsing the data of the operation units.
supervision unit	Safety manager	Managing,inputting,editting,deleting and outputting the data of supervision unit;querying, statistics,and outputing the data of the operation units.
	general staff	Browsing the data of the operation units.

(2) Data management

The data is the basis of the safety evaluation.The primary function of the system is to manage and maintain these data, including data input / output, storage, query, modify, and delete etc.

(3) Safety evaluation

Safety evaluation function of the system, including the individual safety evaluation and comprehensive safety evaluation of the operation unit.Rick evaluation is the core function of this system which is to analyze all the data, the calculation process.The system through the evaluation wizards in the project manager to guide step by step to complete the evaluation task.Its features include:

Create or query evaluation project.The system can create a new project evaluation and according to evaluation project name, evaluator or evaluation time to refer to the previous evaluation.

Defined scope of the evaluation, which means determine which construction units including the and evaluation content.

Get the evaluation result. The system can provide the evaluation object the level of safety and production safety problems, sort of production safety level of each evaluation object and comparative analysis of its security situation. Analysis results can be graphically intuitive description.

Instance apply

To verify the practicability of this evaluation system, we select a certain section of under construction expressway to study. First of all, through the expert evaluation, the security levels correspongding with the evaluation scores from 0 to 100. Specific corresponding standards as shown in table 4.

Table 4 Security levels corresponding table

Evaluation criteria	Security level	Actual situation
A≥90	V1 Very well	Construction safety situation is very well, the possibility of accident tends to zero
80≤A＜90	V2 Well	Construction safety situation is well, the possibility of accident is relatively small
70≤A＜80	V3 In general	Construction safety situation is ordinary,accidents may happen
60≤A＜70	V4 Bad	Construction safety situation is bad，the possibility of accident is great
A＜60	V5 Very bad	Construction safety situation is very bad, the possibility of accident is considerable

Using the Safety Check List and expert evaluation method to score for the all factors, score results as shown in table 5.

Table 5 Each evaluation index score table

Index	*A11*	*A12*	*A21*	*A22*	*A23*	*A24*	*A25*	*A26*	*A27*	*A31*
score	80	80	80	85	90	75	80	80	75	80
Index	*A32*	*A33*	*A34*	*A35*	*A36*	*A37*	*A41*	*A42*	*A43*	
score	75	85	70	80	80	85	80	70	75	

For the relative importance of each factor, there use the 1-9 scaling method to assign each index and at the same time structure Judgment Matrix at all levels. After passing through the consistency test, the weights of each index values as shown in table 6.

Table 6 All levels of index weight

Primary index / weight	*A1*/0.123			*A4*/0.101			
Secondary index / weight	*A11/0.753*		*A12/0.247*	*A41/0.176*		*A42/0.361*	*A43/0.463*
Primary index / weight	*A2/0.358*						
Secondary index / weight	*A21/0.253*	*A22/0.132*	*A23/0.127*	*A24/0.151*	*A25/0.154*	*A26/0.053*	*A27/0.130*
Primary index / weight	*A3/0.418*						
Secondary index/ weight	*A31/0.068*	*A32/0.085*	*A33/0.256*	*A34/0.266*	*A35/0.142*	*A36/0.088*	*A37/0.095*

After calculate the index weight of each secondary index can calculate the primary index scores,and then can calculate the score of the certain section of under construction expressway. After calculating, we can get the A1=80,A2=80.525,A3=78.67,A4 =74.075; the score of the certain section S=79.03. As the table 3 shows, the construction safety situation in this section is ordinary and accidents may happen. But through this data we know that the construction safety situation tends to be good.

[1]Fund project:Supported by“the Fundamental Research Funds for the Central Universities”(2013059010).

References

[1] MA Hai-tao,YANG Run-lin,REN Zhi-gang,ZHANG Zhi-zeng. *Study and application on safety pre-assessment of free way construction project*[J].Journal of Safety Science and Technology,2006,05:71-75.

[2] Pan Fengming.*Study on Construction Projects Safety Condition Evaluate of FengYun highway in ChongQing*[D].Chang’an University,2012.

[3] Huang Shi-guo.*The Safety Comprehensive Assessment System Study on Construction Field*[D]Chongqing University,2007.

[4] Jiao Shufeng.*The Algorithm of Mean Random Consistency Index in AHP and its Implementation*[J].Journal of TAiYUAN NORMALl UNIVERSIT (Natural Science Edition),2006,04:45-47.

[5] Yang Wentao. *Safety evaluation information system design and development*[D].China university of geosciences (Beijing),2005.

Advanced Materials Research Vols. 989-994 (2014) pp 5304-5310
© (2014) Trans Tech Publications, Switzerland
doi:10.4028/www.scientific.net/AMR.989-994.5304

Design and Implementation of Teacher-Student Interactive Platforms in the Campus Network Based on UML

Cheng Yunli[1,a], Zhang Yanhong[2,b]

[1.] Department of Electronic Information Engineering,Guangzhou Nanyang Polytechnic, Conghua,China

[2.] Department of Computer,Tianhe College of Guangdong Polytechnic Normal University, Guangzhou,China

[a]22002840@qq.com, [b]zyhldy2010@163.com

Keywords: UML, Network Teaching, Interactive Platform

Abstract. Open network teaching is an important way of reforming and the trend of future development in the area of teaching, network interactive teaching platform is the key. This platform system is supported by network technology, relying on the campus network, effectively build an interactive learning environment with professional teachers, specialized courses and self-learning students. This paper mainly discussed the issues that how to use RUP and its iterative incremental development methods to carry out the object-oriented analysis, design and implementation; the detailed modeling techniques problems, such as how to use UML language to make the demand analysis and structural design for the platform system were also studied in this paper.

Introduction

UML (Unified Modeling Language) is a standard graphical Modeling Language, is also the third generation mechanism of industry standard, used for visualization, specification, construction and documentation of software system. UML can be put into use with all the development methods, life stages, application fields and media together, making the exchange of information in the software development process become more easily and convenient. Model (model) is purposive simplification for things, and provides a blueprint of the system. The basic reason for modeling is: because people can't understand a complex system completely, modeling is to make people have a better understanding of the system being developed.

This topic carries on researches aiming at a practical teaching reform project, and according to the law of education teaching, based on the discipline and specialty construction, giving full considerations to the characteristics of subject knowledge and the specific requirements of the teaching, it has studied how to use UML frame scientific and reasonable professional course network teaching system, design and build a common professional courses teaching website. The research and development not only has certain advancement in theory, at the same time has also reached the practical stage in the practical application. After some modification, it can get comprehensive promotion in each department and each professional as a general course teaching website.

Demand Analysis

Iterative incremental software development method. Object-oriented software development generally adopts the iterative incremental development process, this method is not disposable software submission at the end of the project, but block successive development and submission. Each iteration contains all of the stages of software life cycle, namely: analysis, design, implementation and testing phase [1]. As shown in Figure 2-1:

RUP development process. RUP defines requirements for "(under construction) the conditions system must conform to or the functions it must possess ". RUP is a test-driven, architecture-centric, iterative and incremental development process. The core characteristics of RUP is test-driven. The process of constructing test-model and user interface prototypes is an repeatedly iterative process,

which constantly interacts with the user in the iteration, and modifies the model and interface prototype according to the user's feedback information.

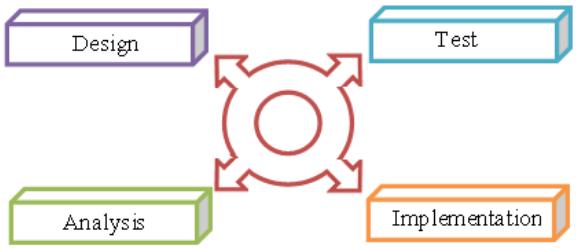

Figure 2-1 Iterative software development method

System Requirements.

1) Functional Requirements

The aim of teacher-student interaction platform system model, is to build a network teaching interaction platform for professional course teaching. The teaching platform construction should consider the characteristics of subject knowledge and the specific requirements of the subject teaching, based on subject construction. Therefore, the function requirements of the system mainly includes the following aspects:

Students can log platform modify personal information, ask questions online, online viewing and online testing.

- Students can login the platform to modify personal information, asking questions, viewing and testing on the Internet.
- Teachers can login the platform modify to personal information, answering questions, managing tests and courses on the Internet.
- System administrator can maintain pages, managing classes, teachers and curriculum provision.

2) Performance requirements

System model should have openness, high reliability, strong security and confidentiality [2].

Campus network platform for teachers and students mainly have three kinds of users: students, teachers and administrators, and different categories of users have different requirements on the function, efficiency, security and so on of the system. Platform system provides the following services:

1) Students and teachers access and use the system through the Web

2) Administrators can access and manage the system through the Web

The system should proceed the permissions distribution, the separation of land management and application for different roles, realizing the user registration, user login, user information changes, course management, test management and test, and other functions.

System Design

Any software design task can be shown as figure 3-1:

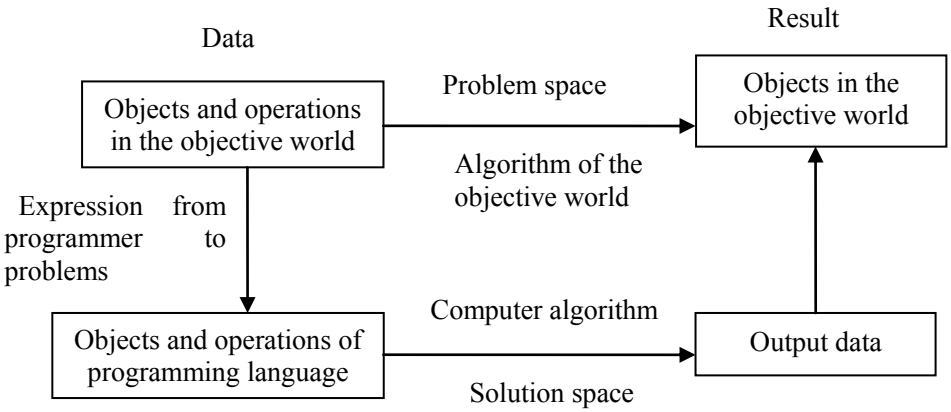

Figure 3-1 Typical model of system design task

In the problem space, problems are usually characterized by a set of objects of the objective world and operations on the object, and the task of the design is to transform these objects and operations of the objective world into an acceptable form for computer, namely in the solution space using programming language to express.The main task of object-oriented approach design phase is main parts design, user interface design, task management component design and data management component design. In software design phase, it needs further refinement for the demand, from the perspective of system implementation, with a model established in the requirements analysis stage as the input, which means to achieve all the requirements.

System function description.

1)System architecture

The core part of the site is a communication platform between teachers and students. According to functional requirements of the case and the definition of the system structure, functional architecture divided by professional courses teaching website is shown in figure 3-2 below:

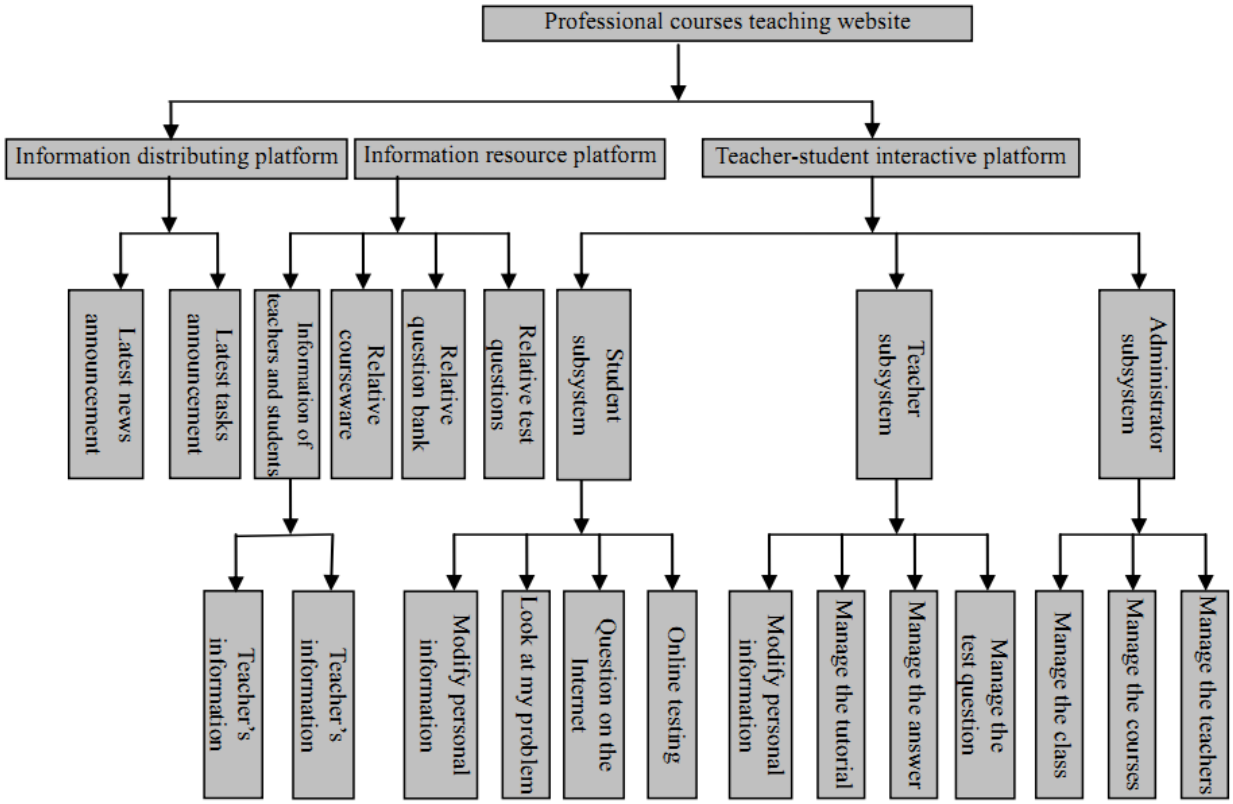

Figure 3-2 Site architecture diagram

2)User interface prototype design

The user interface is window of the system, and interface shapes the feeling of users on the system. Therefore, the design of the interface is in the primary position of human-computer interaction. The design of the interface follows the three important principles:

(1) under the control of the user

(2) reduce the user's memory load

(3) keep the consistency of the interface

System dynamic behavior model. State diagram is a model for the behavior of a single object, mainly observes state changes in the life cycle of the single object, including all of the states. The state diagram of the system is shown in Figure 3-3.

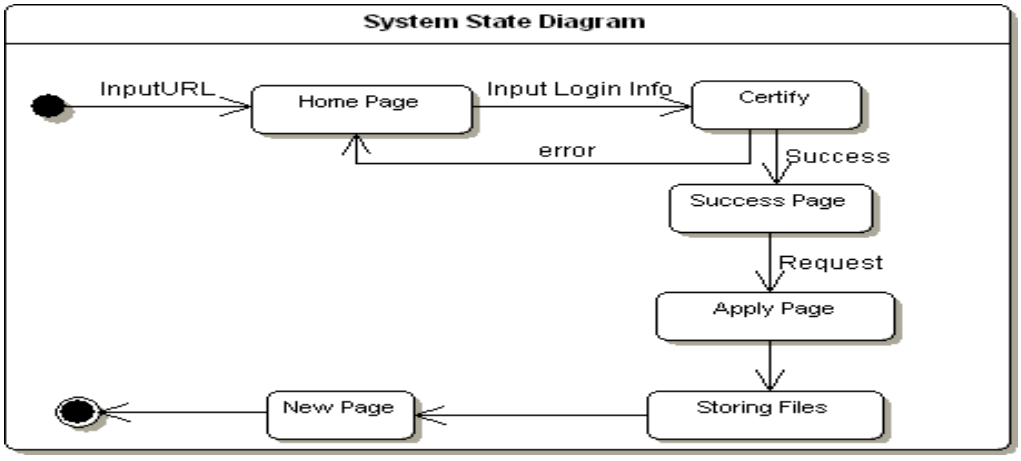

Figure 3-3System state figure

System static structure model. RUP is based on the object-oriented method, and in the requirements analysis phase its main task is to refine the demand requirements elicitation phase capturing. Firstly, extract each use case analysis classes, including boundary, control and entity classes; Then proceed implementation analysis for each use case according to the analysis classes, and analyzes the relationship between the classes, determine the class's attributes and methods; Finally, synthesize the analysis classes individual cases extracting to get the analysis class structure diagram of the whole system, so as to establish the static structure model[3].

System key technology.

1) Using ASP and its components technologies

2) Using software testing technology

3) Using UML modeling technology and RUP development technology

4) Using Web technology, and combining with ADO database programming interface and RDBMS technology

System implementation

System implementation.

1) System calculation mode

B/S mode client application software will be transplanted into the server, so the client will no longer need application program, through the browser to perform the application program. Its structure is shown in the following figure 4-1 [4].

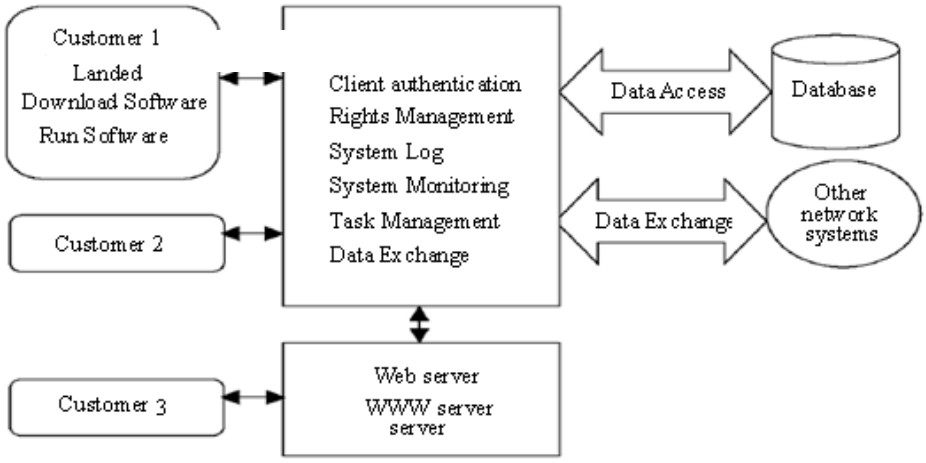

Figure 4-1 B/S structure mode

Logically, it is divided into four levels: client, Web server, application server and data server. The client is mainly responsible for human-computer interaction; The Web server is mainly responsible for the centralized management of the client application program. The application server is mainly responsible for centralized management of the application logic, namely transaction processing. In

the B/S structure, the size of the client has been compressed, and it becomes a simple browser. The application logic is centralized, located in one or more servers (application server).

2) Platform system logic model and component diagrams

a)Three-tier structure of teacher-student interaction platform system

According to the three-level structure theory, draw up system three-tier structure diagram, shown in Fig.4:

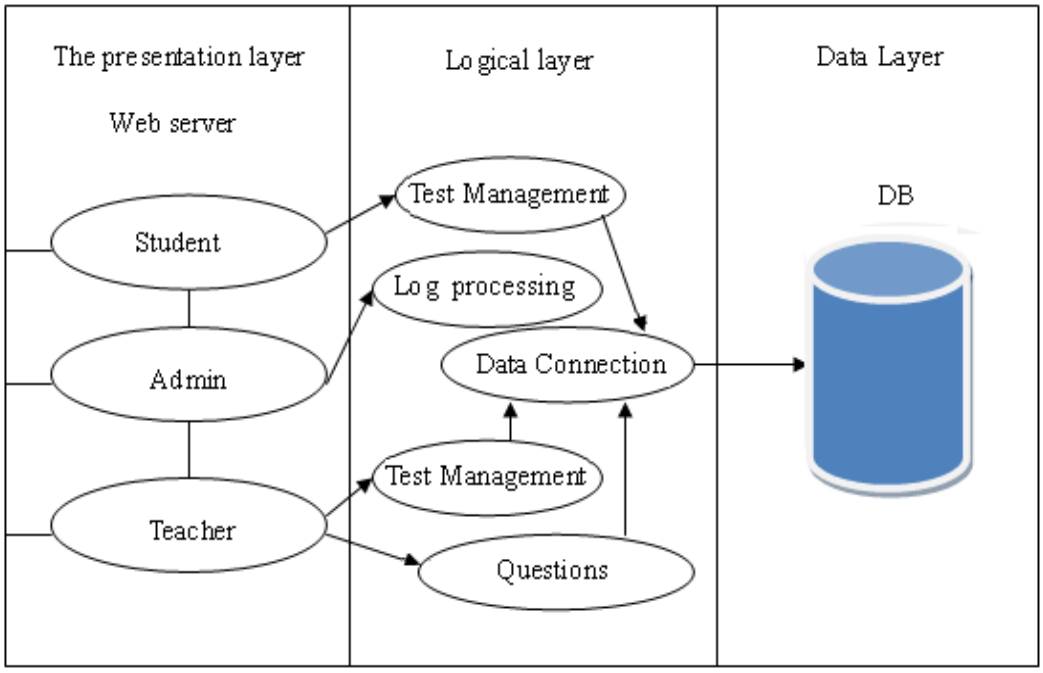

Figure 4-2 Three-tier structure of the system

(1) Presentation layer

System consists of three modules: the administrator module, students modules and teachers modules.

(2) Business layer

Business layer specifically defines the logic how to access information, namely how to define the SQL commands to access information.

(3) Data layer

Using ACCESS database as a backstage server, storing and managing persistent objects.

b) System component block diagram

The component diagram of the platform system is shown in figure 4-3.

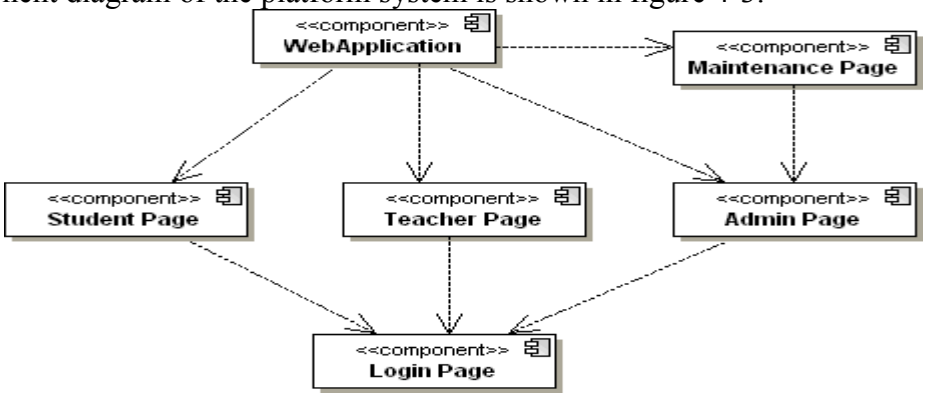

Figure 4-3 System component diagram

3) Physical model diagram and deployment diagram of the platform systems.

Deployment diagram is used to model for the physical aspects of object-oriented, establishing a visual model for physical nodes in the system model and static aspects of the relationship between the nodes[5].

From the three-tier structure model diagram, we can get the deployment diagram of the system model, as shown in figure 4-4: it has three nodes, "Web Server" and "DB Server" and "PC", peripherals "Printer".

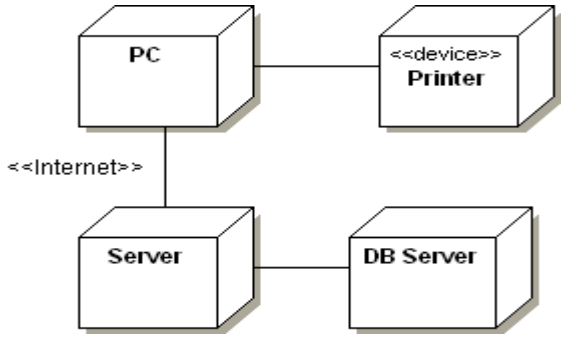

Figure 4-4System deployment

The system adopts B/S structure, using the Microsoft's 11 S architecture Web server, with the ACCESS as the database platform, and by using ASP technology, Web technology and database technology, has developed and designed the teacher-student interactive platform. Basic physical structure is shown in figure 4-5:

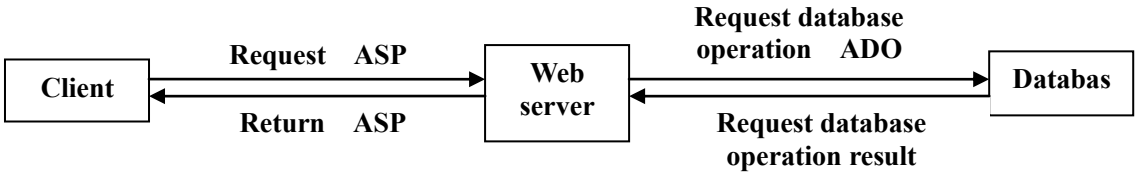

Figure 4-5 Basic structure of system

4)Platform system database implementation

The system uses Windows Access 2000 as the background database, and database is named CSTUDY.mdb. Database design refers to entity class diagram of the system design stage, the basic data collection of database, data structure and data processing flow should constitute a detailed data dictionary.

1) The design results of main tabular in the system database are shown in the figure below.

- Teacher table structure is shown in figure 4-6.

The Teacher table records the basic information of teachers registering, run by the administrator, and the teachers can modify the personal information.

teacher : 表

字段名称	数据类型
ID	自动编号
name	文本
age	文本
position	文本
photo	OLE 对象
or	数字
introduction	备注
IDname	文本
passwd	文本
email	文本
amount	数字
enroltime	日期/时间

Figure 4-6 Teacher table structure chart

tutorial : 表

字段名称	数据类型
ID	自动编号
rule	文本
title	文本
路径	文本
describe	文本
teacher	数字
refer	日期/时间

Figure 4-7 Tutorialtable structure chart

- Tutorial table structure is shown in figure 4-7.

The curriculum schedule records course name, path, the course description and the basic information of the course teachers, updated by the administrator.

2) Database connection

Using ADO database programming interface technology to connect.

System testing. Software testing is important for software quality assurance. After the discovery of errors by testing, diagnosis and correcting mistakes, to develop high quality software fully meeting the requirements of users. After the completion of the teacher-student interaction platform development, it need to review and test the designed webpage. On the one hand, through the establishment of a large number of test cases to test software. On the other hand, in the actual teaching, through constant interaction with students to verify and modify, thus ensuring the quality of the whole system.

Conclusion

Teacher-student interaction platform is a Web-based networked learning environment, which provides a networking platform of learning and working for teachers, students and administrators. Platform system adopts a hierarchical design structure, with Internet as the technical support, and the curriculum teaching for business support, realized the teaching interaction between professional teachers, curriculum and students on the true meaning. Due to the production work of the system is a system engineering and a long-term work, now it just build an online interactive system framework, establish and complete partial interaction function, compared with the teaching practice, its functions are relatively less and imperfect, which still need to be supplemented and improved in the future according to the actual teaching.

References

[1] McDermid,J,P. Rook.”Software Development Process Models,”in Software Engineer’s Reference Book.CRC Press

[2] Zhenjun Fan. The Design and Implementation of Online Exam System based on ASP.NET

[3] Feng Ding, Weitai Liang. The Research and Application of RUP Software Engineering Process. Computer Engineering

[4] Sheguang Zhang. The Design and Implementation of Online Teaching System- Study on the Management Mechanism and Security Mechanism of Online Teaching System in Beijing University of Technology

[5] Zhenyan Ji. Analysis Design and Application Case of UML System. The 1st Edition. Beijing: People's Posts and Telecommunications Press

Advanced Materials Research Vols. 989-994 (2014) pp 5311-5314
© (2014) Trans Tech Publications, Switzerland
doi:10.4028/www.scientific.net/AMR.989-994.5311

Research on Distribution Issues of Book Chain Taking Xinhua Bookstore As An Example

Xiong Wei[1, a], Zhang Man[2,b]

[1] Headmaster's Office, Jiangxi Science & Technology Normal University, Nanchang, Jiangxi,China

[2]School of Information Engineering, Nanchang University, Nanchang, Jiangxi, China

[a]572383070@qq.com, [b]manzhang201010@163.com

Keywords: Distribution Center; Distribution Model; Book Chain; Problems

Abstract. Coordinated and efficient distribution center is important for the standardization and modernization construction of chain operation for chain enterprise. As to book chain enterprises in China, it's a common issue for them as lacking of efficient distribution center and it's essential that every book chain enterprise have a scientific and rational managed distribution center. Therefore, the paper analyzed the status and problems of book chain enterprises in China while taking Xinhua Bookstore as an example, and proposed solving methods for them.

Introduction

As the bookstores owners often need to prepare a lot of book reserves to meet with the various needs of different groups [1], and they need to buy new books for the previous books will have few buyer after they have sold over a certain period of time, it's important for bookstores to have a high quality and speed of turnover. The distribution center combined of coordinated and efficient distribution system and information exchange systems is useful to ensure the quality and speed of resources turnover, and plays an important role in standardization and modernization construction of chain operation. Therefore, the ability to adapt to the establishment of distribution centers will determine the development of chain enterprises as well as its rise and decline.

Distribution center refers institutions and their facilities which receive and process ordering information from terminal users, sort various goods from upstream, fulfill picking, processing, distribution and other works according to user requirements, and deliver goods based on completed works[2]. That is they are organizations which get resources from its supplier with reasonable prices, require flip, classification, storage, distribution processing, information processing and other operations, and distribute required goods according to requires orders with their facilities and a satisfactory level of service.

Consumers have great differences in preferences for books and their selling time. To meet with the great differences, book stores often need to own many different books. As some books will have few buyers after they were sold some time later [3], its an important issue for bookstore to balance book varieties and book selling limitation. Thus, it requires bookstore owners to make right decision and make new books on selling as soon as they were published to meet with readers' requirement and requirement of high turnover of books. Also the outdated need to remove from the bookshelves as soon as possible and return to book publisher to decrease inventory costs [4], otherwise it will cause great increase in inventory costs. From the analysis above, we can see that distribution center is important for book sells, especially for book chain enterprises. The paper analyzed status, issues and solving methods of China book chain enterprises while taking Xinhua Bookstore as an example.

Status of Xinhua Bookstore Distribution Center

After a long specification and development, Xinhua Bookstore has been a book chain enterprise with many entity bookstores distributed in many cities from provinces to counties level allover China. Also, Xinhua Bookstore has been a worth choosing and trustworthy bookstore brand for its books reserves, involving disciplines, book quality and reader facing books, and so on.

For example, Wang is a purchaser of Xinhua Bookstore United Company Limited (Xinhua Bookstore Co. Ltd.). His daily works process is simple: first, login in Jiangxi Xinhua Bookstore website after input his user name and password; second, check the latest bibliographic of that day and the sales and inventory situation of various types books of its working bookstore and the headquarters; determine the book list of new books needed to buy and fill and confirm online orders; last, write down orders need to be confirmed. The headquarters will pick and distribute books required by orders from its sub-institution within 24 hours. Sometimes, Wang also drove four kilometers to exhibition hall of Chain Logistics Information Center in Nanchang Jingdong development Zone to pick sample books according to selling situation of his company, and input his requirement to ordering system which will send the information to the halls computer center and send books to Wang's working place within 24 hours.

This new distribution access is benefited from chain logistic distribution system of Jiangxi Xinhua Bookstore Co. Ltd (shorted as Jiangxi Xinhua Bookstore). running from September, 2003. Ordering information will be data exchanged through network video recorder screen software and logistics system software, and generate picking list automatically, and then be finished as picking and distribution operation completed under the conducted of electronic tag. This kind modern logistics distribution system makes Jiangxi Xinhua Bookstore has advantages facing to the new competition in the market.

The case above is only a better bookstore than other Xinhua Bookstores. In fact, there are Xinhua Bookstores still work under their traditional distribution system which can not meet with requirements of readers and the market, such as, selling books on the market demand can not be supplied timely and replenished; outdated can not be returned timely resulting sharp increase in the cost of inventory. The disadvantages of traditional distribution system of Xinhua Bookstores lead to little profit and bankrupting risk. Thus, a profitable distribution system is essential to Xinhua Bookstores to solve its market demand control problems and get profit from reasonable distribution system.

Distribution Model of Xinhua Bookstore

Concept of self-distribution model. Self-distribution model refers to a model that enterprises themselves build, organize, and manage all aspects of logistics and distribution business[5] to distribute internal and external goods for them. This model is conducive for enterprise to integrate its supply, production and sales operations. This model has a relatively high degree of systematization which can meet with the distribution needs of internal raw materials, semi-finished and finished products of the enterprise, also it meet the business needs to expand foreign markets. But, the distribution model will increase investment cost when establishing the distribution system, and will enhance distribution costs and expenses when the distribution scale of the enterprise is relatively smaller. Xinhua Bookstores chose this distribution model to distribute books by establish its own distribution system to complete enterprise distribution business, including the distribution and delivery of productions to enterprise internal and external customers for each sub-bookstore.

Xinhua Bookstore advantages under the self-distribution model. First, Xinhua Bookstore has a strong ability to control all aspects of its distribution. By using this model, it can plan reasonable management processes, improve the efficiency of logistics operations, reducing circulation costs. Self-logistics can make logistics and cash flow, information flow and business flow combine with each other closely, thereby improving logistics operations as well as a full range of work efficiency greatly. Second, it can make book purchasing, distribution, and production support the integration strategy to achieve timely book purchases, thus to increase purchases books batches, reduce its volumes, regulate inventory, reduce funds and reduce costs. Third, it can make the distribution of Xinhua Bookstore react fast and flexible by meet with time, space requirements in the logistics business and the more quickly and flexibly market requirements.

Disadvantages of Xinhua Bookstore with self-distribution model. First, the cost of investment to establish its own distribution system is high and the investment on it will increase operation cost.Second, the scale of self-distribution model often limited, and has lower specialization degree of

logistics and distribution compared with the distribution capacity of logistic enterprises, resulting to low distribution efficiency and increasing the difficulty of management control. Except that, the high logistics cost deduce the product competitiveness in the market and the limited scale of distribution system and low degree of logistics specialization can not meet with the increasing market needs.

Related Problems and Countermeasures for Book Distribution

Book distribution is a complex logistics process which similar to apparel industry in many respects. When new books launch, books may be on selling and short of supplying, but it can also become outdated goods within months as people turn their attention to update the books. For example, books write by some famous younger writer in China may short of supply in a month but date-out in a few months later which can illustrate this problem. Therefore, it's important to have enough reserves when a book on selling and return outdate books to suppliers to avoid inventory costs rise dramatically, giving a negative impact on corporate profits.

The main problems and resolution strategies to book chain distribution are shown as follows:

(1) The construction of distribution system for bookstore chain is lagging behind. The outstanding performance of this problem including three areas: the distribution scale is small; asymmetry information of many bookstore chains; backward technology and low distribution efficiency.

The solving strategies are: first, raise funds to build a logistics and distribution system with economies scale. With introduce of the advanced logistics technology and equipment, it can build modern warehouse, modern warehouse processes and automatic access and picking system.Second, strengthen the logistics infrastructure construction to form a scientific logistics network and to improve organization and networking degree of the construction of book chain distribution system which will perfect distribution information and improve the utilization of logistics resources.Third, promote the standardization of logistics technology, equipment and appliances. With the improving of logistic and distribution technologies, the operation efficiency of logistics and distribution will be improved. It can learn successful experience from distribution of chain enterprises at home and abroad to achieve scientific and rationalization construction of book chain logistics and distribution systems.By using a complete computer network system, distribution centers can achieve the integration of procurement[6], distribution and order processing, and can improve the accuracy of orders, efficient distribution and exchange of information to achieve scale management.

(2) Unreasonable site layout of distribution center. Faced with increasing global competition, companies have to increase its product quality, service levels and response speed to survive and develop in the market. Generally, logistics costs of a company is about 30 percent of its sales[7], thus, supply chain management is an effective way to reduce enterprise costs and an effective way to improve its efficiency. As the key component of the supply chain, distribution center determines the flow costs and supply chain efficiency [8]. Therefore, the location problem of distribution center is particularly important.

The solution is to design a rational distribution plan. The objectives of rational distribution includes: efficiently use space, equipment, personnel and energy resources ; minimize material handling; simplify processes; shorten the production cycle; seek investment minimum; provide convenient, comfortable, safe and healthy working environment for workers. Unscientific, irrational and unstandardized planning of logistics and distribution centers will result to low distribution efficiency, and result to increasing in waste and cost. Scientific and rational logistics center location and layout is very important.

Most chain bookstores still need to expand their scale; the outlets layout of these bookstores has not been locked. Thus, the site distribution center should be changeable to meet with changes of bookstore network, and the scale of distribution center should change according to the development of chain operation in order to have a rational planning of distribution centers construction, to reduce distribution costs and to improve chain efficiency.

(3) Lack of professionals on distribution management. To establish a logistics centers is to meet with the need of enterprises development, and the need of product to quick enter the market. But business executives is significant deficiencies in the experience and standardized management of

logistics and distribution, their basic concept of distribution has not changed, and their operations on logistics management and logistics technology is basically still stuck in the traditional job. What are worse, bookstores are unwilling to contribute to hire experts and practical aspects of logistics personnel to guide the construction and conduct training and education their staff. This may cause a problem that bookstores have modern distribution related facilities, but delivery and distribution management personnel is still under the traditional way of thinking which lead to the bookstore chains are lack of scientific distribution management.

To make modern bookstore chain have normal operation, modern logistics management software and professionals who use these logistics software. However, professionals in China's logistics industry are beyond the need. Therefore, we must make effort on the introduction of talent professionals; organize training programs to ensure the normal operation of the logistics center.

Summary

The unique diversified services of distribution center can relieve the burden on the business inventory adjustment, maintenance and other commodities of bookstore chain, which can improve the professional level of the retail book chain, to achieve the optimal combination of resources. Distribution center with high mechanization, high automation and advanced technical experience can protect the quality and distribution of goods to a great extent and effectively improve the efficiency of logistics, in order to achieve chain operation efficiency, conservation and high quality service. In short, the scientific rationalization distribution centers help to promote the development of book chain, increase its profits, and reduce inventory costs.

References

[1] Lieve Doucé, Karolien Poels, Wim Janssens,el at. Smelling the books: The effect of chocolate scent on purchase-related behavior in a bookstore. Journal of Environmental Psychology, vol.36, p.65-69, 2013

[2] Milan Andrejić, Nebojša Bojović, Milorad Kilibarda. Benchmarking distribution centres using Principal Component Analysis and Data Envelopment Analysis: A case study of Serbia. Expert Systems with Applications, vol. 40, no.10, p. 3926-3933, 2013

[3] Ting-Peng Liang, Hung-Jen Lai.Effect of store design on consumer purchases: an empirical study of on-line bookstores. Information & Management,vol.39, no. 6,p.431-444,2002

[4] Pietro Romano, Marco Formentini. Designing and implementing open book accounting in buyer–supplier dyads: A framework for supplier selection and motivation. International Journal of Production Economics, vol. 137,no.1,p.68-83, 2012

[5] Maike Tietjens, Philipp Alexander Freund, el at. Using mixture distribution models to test the construct validity of the Physical Self-Description Questionnaire. Psychology of Sport and Exercise, vol. 13, no.5,p. 598-605, 2012

[6] Yingfeng Ji, Hualong Yang, el at. Location Optimization Model of Regional Express Distribution Center. Procedia - Social and Behavioral Sciences, vol. 96, no.6,p. 1008-1013, 2013

[7] Santoso Wibowo, Hepu Deng. A fuzzy rule-based approach for screening international distribution centres. Computers & Mathematics with Applications, vol. 64,no.5,p. 1084-1092, 2012

[8] Nurgül Demirtaş, Umut R. Tuzkaya. Strategic Planning of Layout of the Distribution Center: an Approach for Fruits and Vegetables Hall. Procedia - Social and Behavioral Sciences, vol. 58, no.12,p. 159-168, 2012

Advanced Materials Research Vols. 989-994 (2014) pp 5315-5318
© (2014) Trans Tech Publications, Switzerland
doi:10.4028/www.scientific.net/AMR.989-994.5315

Research on Methods of Distribution Center Facility Siting

Xiong Wei[1, a], Zhang Lingyu [2,b]

[1] Headmaster's Office, Jiangxi Science & Technology Normal University, Nanchang, Jiangxi,China

[2]School of Information Engineering, Nanchang University, Nanchang, Jiangxi, China

[a]572383070@qq.com, [b]1145163178@163.com

Keywords: Factors Breakeven analysis; Center of gravity method; Facility Location

Abstract. The so-called facility location means how to use scientific methods to determine the facility's location, so that the overall business operations and enterprise systems combine to effectively and economically achieve corporate business objectives. This paper introduces the Fuzhou Municipal Bureau of distribution center location tobacco case to be analyzed on the basis of this issue describes the significance of facility location, facility siting factors and principles are analyzed and siting of facilities the methods are summarized proposed general facility siting process steps, facility sitting decisions provide some guidance.

Introduction

A factory or service facilities should be set up where important decisions for the company is the design of business strategy. Especially in a large industrial facility siting, layout of the national economy of a country has a significant impact [1]. For an enterprise, facility location is the first step in the establishment and management of the enterprise is also the first step in expanding the business. The importance of facility siting is obvious importance mainly due to: facilities election after detachment facilities layout and production after the completion of the production and operation costs, and the cost of product and service quality has a great and lasting impact. Therefore, during the facility location must be fully taken into account many factors, careful decisions. Secondly, in addition to the new corporate facility location problem, with the development of differences in economic development, urban expansion, as well as between regions, many enterprises are facing the problem of relocation[2]. Thus, the facility location is a lot of companies are facing the modern enterprise management is an important issue.

In recent years, with the construction of the logistics industry to accelerate the pace to achieve low cost, high efficiency, excellent service distribution center is the target of the tobacco industry urgently front row. Thus, the location of distribution centers is essential.

Factors affecting the distribution center facility siting

This mainly refers to the stability of the regime of a country, whether legal sound, the existence of the trade embargo policy, as well as policies and regulations, finance, taxes and so on. China's economic development zones and industrial parks have policies.

Market conditions. Whether it is manufacturing or service location, facilities and customer must close and is the closer the better. Also, considering the demand for products and services area, the consumption level to adapt products and services and, if sales of the two close, transport costs will be reduced.

Resource conditions. Choose region should be considered the main raw materials, fuel, power, water and other resource conditions. In addition to material resources, but also give full consideration to human resources, the quality of workers of different products has different requirements.

Infrastructure. Trafficroads, telecommunications, and other infrastructure investments also have an impact on the establishment of the factory. Different sites have different costs spent. For my country, should try to use the land for farming is not suitable for siting of industrial facilities, not to take up agricultural land.

Competitors. In corporate location decisions must take into account the layout of competitors. Enterprises should be based on characteristics of the product or service itself, and to decide whether near or far away from rival competitors.

During facility siting, enterprises have influence factors are to be considered. In considering these factors, the needs to pay attention to are: first, we must carefully weigh these factors are listed, determine which is closely related with the facility location, though what the business or results of operations related. But the relationship with the facility location is not large, so that the decision is prioritizing, grab the key. Otherwise, too many factors listed sometimes easy to prioritize specific decisions could not tell at the time, can not make the best decisions. Second, under different circumstances, the same type of factors has influence. Therefore, any policy provision must not be applied mechanically, nor imitate copy existing experience. Finally, it should be noted that, for the manufacturing and non-manufacturing businesses, the impact and importance of the factors to be considered the same factors may be very different.

Distribution Center Location principles

Lot of success stories prove, on the siting, qualitative analysis is more important. Qualitative analysis is a prerequisite for quantitative analysis. In qualitative analysis, it is necessary to determine several principles.

Specific siting principles are as follows:

Cost principle. The first is the economic entity enterprise, economic benefits for business whenever and wherever they are important. Construction of the initial fixed costs, after running into variable expenses, product revenue after the sale, is related with the site.

The principle of aggregation of talent. Talent is the most valuable resource[3]; business address election was conducive to attracting the right talent. Conversely, due to corporate relocation inconvenience caused by the staff of life, the facts that staff turnover often occur.

Close to the user principle. For the service sector, almost without exception, are required to follow this principle, such as savings banks, post offices, cinemas, hospitals, schools, retail stores, etc. all. Many manufacturing companies have built their factories near the consumer market, in order to reduce shipping costs and losses.

The principle of long-term development. Business location is a strategic management activities with, so to have strategic awareness. Site work should take into account the rational distribution of productive enterprise, to consider the market development; access to new technologies should be conducive to new ideas. In the current world economic integration become more and more background, to consider how conducive to participate in international competition.

Locating

Factor score. Common factors in the siting scoring method is perhaps the most widely used one[4], because it will be easy to understand patterns of different factors together. Specific steps factor scoring method is as follows: Determine a set of factors related to siting decisions; for each assigned a weighting factor to reflect the importance of this factor in the ownership of weight. Value of each factor is determined according to the weight, and the weight will have a cost according to the determined standard deviation, rather than the cost value is determined; scoring of all the factors of a common set ranges, usually 1-10 or 1-100; for each alternative addresses for all of the factors set range by scoring; Score multiplied by the corresponding weight of the weight of each factor, and the value of all the weighting factors are added to obtain the address of each alternative final score. Select the address with the highest total score as the best location.

Using this method should be noted: The use of factor score in the calculation process can be found, because the right to determine the number and grade score relies entirely on people's subjective judgment, as long as the error of judgment will affect the numerical score, the final impact on the likelihood of decisions. There are a lot number to determine the right approach is more objective and accurate method the Analytic Hierarchy Process(AHP) [5].The method is not complicated, there is a

more rigorous scientific basis, we recommend the program to do more when using AHP as multi-factor evaluation.

Breakeven analysis.Profit and loss analysis is a basic method of plant siting, also known quantity-benefit analysis [6]. This method is based on the following assumptions: Various options available can meet the basic requirements of site selection, but the amount of investment for each program is different, different changes in raw material costs, fuel, power and other future production. Then, you can use the principles of breakeven analysis to the level of production costs as compared to the production standards. The basic steps are as follows: Determine the fixed and variable costs of each option; make different programs cost income curve; determined at a predetermined production or sales, the lowest cost or profit in accordance with the highest principles select a best solution.

Center of gravity method. Center of gravity method is a method of individual facilities layout [7]; this approach should consider the distance between the existing facilities and the amount of cargo to be transported. It is often used for the intermediate storage of the selection. In the simplest case, this method assumes that the incoming and the costs are equal, it is not considered in the full load condition without increasing the cost of special transportation.

Center of gravity method first bid at the location coordinates of each site; the purpose is to determine the relative distance between each point. Coordinate system can easily be established. Then, the value of the transport position is obtained at the lowest cost according to the coordinates X and Y in the horizontal and vertical coordinates of each point in the coordinate system.

Comprehensive evaluation method. Gravity method and breakeven analysis is a quantitative method. But in real life, there are some non-facility locations factors beyond quantitative analysis with quantitative model area, various factors must be taken into account in order to make the right decisions.

Delphi analysis model. Some location analysis involving multiple facilities and multiple targets, its decision-making is relatively vague goals, and even emotionally. One way to solve this problem is to use the Delphi site analysis model. The model takes into account various factors in the decision-making process. Use Delphi analysis model involves three groups, namely coordination group, team and strategic forecasting group[8]. Each team plays a different role in decision-making. To use this model as follows:

(1) The establishment of two groups. Internal and external personnel consultant closed, acting as coordinator, responsible for designing the questionnaire and guidance Delphi survey. Some of the people elected advisory group set up two groups. A team responsible for forecasting and social trends and the factors that affect the organization of the external environment test. Another group determines the organization's strategic objectives and priorities (Strategy Group). Members of the team from the company strategy in the selection of senior managers

(2) Identify threats and opportunities exist. After several rounds of questionnaires, coordinating group should be asked to forecast the development trend of social groups, market opportunities and threats facing the organization. This stage, should listen to the views of the majority as far as possible.

(3) Identify strategic objectives and strategic direction of the organization. The coordination group findings back to the group's strategic forecasting group. Strategy team used this information to determine the strategic direction and strategic objectives of the organization.

(4) Make alternative. Once the team identified long-term strategic objectives, it should focus on the various options proposed. (Alternative party is the expansion of the existing plant facilities or compression and for all or part of the plant's location change).

(5) Optimization options. Step 4 alternatives proposed in the strategy group should be submitted to the relevant personnel to get their subjective evaluation of programs.

(6) In considering the strengths and weaknesses of the organization on the basis of the model can identify trends and opportunities in the organization. In addition, the model also takes into account the company's strategic objectives, in the modern corporation as a typical comprehensive group decision making method is widely used.

Summary

Facility location is an issue of economic politics, culture and technology intersect, with the advance wave of economic globalization to the globalization of production; capital is characterized by globalization and the globalization of markets. Site occupies the entire logistics system is very important for the low, are research questions of logistics management strategic level, it is a single enterprise, which determines the level of the entire logistics system, and other structures, plays an important role in enterprise management, effectively do site work, far-reaching impact on the development of enterprises.

References

[1] Nicolas Raimbault, Dina Andriankaja, Elsa Paffoni. Understanding the Diversity of Logistics Facilities in the Paris Region. Procedia - Social and Behavioral Sciences,vol.39, p.543-555, 2012

[2] Laetitia Dablanc, Catherine Ross. Atlanta: a mega logistics center in the Piedmont Atlantic Megaregion (PAM). Journal of Transport Geography, vol.24, p. 432-442, 2012

[3] D.N.P Murthy, O Solem, T Roren. Product warranty logistics: Issues and challenges. European Journal of Operational Research,vol.156, no.1, p. 110-126, 2004

[4] Arifa Sultana, Amit Kumar.Optimal siting and size of bioenergy facilities using geographic information system. Applied Energy, vol.94, p.192-201, 2013

[5] Manja K. Kuzman, Petra Grošelj, el at. Comparison of passive house construction types using analytic hierarchy process. Energy and Buildings,vol.64, p. 258-263, 2013

[6] Zuca Marilena, Tînţă Alice. The Profit and Loss Account–Major Tool for the Analysis of the Company's Performance.Procedia-Social and Behavioral Sciences,vol.62, no.6, p.382-387, 2012

[7] Jill Boughen, Kylie Dunn, Jennifer Nitz,el at. A new method of interpreting the centre of gravity location using the modified Clinical Test of Sensory Interaction on Balance: A reliability study. Hong Kong Physiotherapy Journal,vol.31, no.2, p. 64-68, 2013

[8]Christoph Markmann, Inga-Lena Darkow, Heiko von der Gracht.A Delphi-based risk analysis — Identifying and assessing future challenges for supply chain security in a multi-stakeholder environment. Technological Forecasting and Social Change,vol.80, no.9, p.1815-1833, 2013

Advanced Materials Research Vols. 989-994 (2014) pp 5319-5322
© (2014) Trans Tech Publications, Switzerland
doi:10.4028/www.scientific.net/AMR.989-994.5319

Study on Classification of body shape and Size Grading on Young Women of Quanzhou District

Can-yi Huang[1,a]

[1]Deparment of Business and Information, Quanzhou Normal University, Quanzhou, Fujian, 362000, P.R. China;

[a]email:yidyj126@sina.com

Keywords: young women; classification of body shape; size standard; data grading

Abstract. Body measurement was carried out on 500 young women, who come from Quanzhou district, and we also utilized SPSS software to carry on statistic analysis to the samples, 13 measuring body variables were chosen and 11derived variables were calculated. Then classification analysis was used to classify the body shape .Then this paper subdivided the upper body of young woman's body shape into 4 kinds, the lower body into 4 kinds also .Finally, values of intermediate of every type and stepping number values of every measurement are calculated through regression analysis.So the database of classification of body shape and data of young woman was obtained.

Introduction

Nowadays, apparel's fitness has been widely considered as an important indicator affecting clothing's appearance and comfort. The intention of body shape classification is providing the basis for the clothing's style and structure design, and it will greatly affect the fitness of clothing products [1]. Our country is still using the old national standard of garment size; body data of this standard come from last century 90's anthropometric data. However, the standard now can not truly reflect the characteristics of somatotype in china. Therefore, it is necessary to improve the standard of garment size by using more reasonable shape classification method [2].

Body measurement experiment

In the experiment, 500 Quanzhou female university students at the age of 18~ 22 are measured. This study uses the manual measurement method, in order to make the scale unified and data accurate, special groups of measurers are designated to take the measurement experiment. Testees all wore thin underwear, remain stationary and natural upright when measuring. Martin measuring instrument s and measuring reels are used in the manual measurement.

This study selected 13 human representative measurement parts, which can cover all main control parts of the whole body. They were: height, chest circumference, waist circumference, hip circumference, shoulder width, neck circumference, front waist length, back waist length, upper body length, lower body length, chest horizontal length, hip horizontal length and hip height.

Analysis of body shape clustering

In current national standard of apparel size, the human body shapes are divided into 4 categories. And the standard can not really reflect the size differences between human bodies[3]. Meanwhile we try to divide human shape more in detail, so this study attempts to classify the upper and lower human body separately. This research takes derived variables which can reflect human body's horizontal and vertical changes and other relevant variables as the reference index for body shape's classification. These derived variables are calculated through important controlling parts of the body. These derived variables are shown in table 1.

Tab. 1 Each derived variable and definition

derived variables	definition	derived variables	definition
R1	chest circumference - waist circumference	R7	hip circumference - waist circumference
R2	chest circumference / waist circumference	R8	hip circumference / waist circumference
R3	upper body length / chest horizontal length	R9	lower body length / hip horizontal length
R4	front waist length – back waist length	R10	lower body length / hip circumference
R5	upper body length / chest circumference	R11	lower body length / waist circumference
R6	upper body length / waist circumference		

3.1 The body shape cluster analysis

Using single factor variance analysis through SPSS statistical software, each derived variables of the upper body is inspected and analyzed separately with the key parts of upper body，upper body length, chest circumference and waist circumference. Table 2 shows F value and significance level of the single factor analysis of variance. Synthesis results show that: the variable R3 is significant with chest circumference and waist circumference [4], and close to be significant with upper body length, significant effect is better than the other four indicators; the variable R5 is significant with the upper body and waist circumference, and close to be significant with chest circumference. So this research takes these 2 variables as indicators to cluster analysis. Table 3 gives the K-MEANS cluster analysis, the index terminate clustering center and sample proportion when samples are divided into 3, 4, 5, 6 kinds. After comparing the results when samples are divided into different categories, we find out that the result that samples are divided into 4 categories, difference between each two categories show adjacent to clear and uniform. So the young female body shape is divided into 4 categories. They are indicated with A, B, C, D.

By using the same method with upper body, the synthesis results show the significant effect of R9 and R8 are better than the other four indicators, so take these 2 variables as indicators for clustering analysis. And the young female lower body shape is divided into 4 categories. They are indicated with W, X, Y, Z, and the classification results are in table 4.

Tab. 2 Onaway anova between each derived variable and the key part of upper body

	parts	R3	R4	R1	R2	R6	R5
F value	upper body length	1.295	2.020	0.995	1.116	1.992	3.068
	chest circumference	3.573	0.782	1.449	3.972	3.416	1.369
	waist circumference	2.827	0.862	1.005	4.977	1.069	3.865
significance level	upper body length	0.058	0.001	0.506	0.549	0.002	0.000
	chest circumference	0.002	0.846	0.055	0.001	0.003	0.019
	waist circumference	0.004	0.730	0.490	0.000	0.386	0.000

Tab. 3 Final cluster center of K-MEANS and sample ratio (upper body)

Category	R3/R5	Ratio	Category	R3/R5	Ratio	Category	R3/R5	Ratio	Category	R3/R5	Ratio
1	1.05/0.53	34.0%	1	1.03/0.52	17.4%	1	0.9/0.42	0.60%	1	0.89/0.41	0.50%
2	1.18/0.57	46.7%	2	1.11/0.56	26.4%	2	1.04/0.52	25.3%	2	1.04/0.52	22.1%
3	1.26/0.63	19.3%	3	1.19/0.59	37.6%	3	1.11/0.57	24.6%	3	1.16/0.56	23.3%
			4	1.27/0.63	18.6%	4	1.18/0.59	32.7%	4	1.09/0.57	20.0%
						5	1.27/0.63	16.7%	5	1.19/0.62	22.0%
									6	1.28/0.62	12.1%

Tab. 4 Cluster result of body type

Category	R3	R5	Sample number	Category	R9	R8	Sample number
A	1.03	0.52	87	W	2.78	1.31	106
B	1.11	0.56	132	X	2.92	1.33	150
C	1.19	0.59	188	Y	3.03	1.36	167
D	1.27	0.63	93	Z	3.21	1.38	77

Determination of intermediate type values and stepping values of each measurement parts

4.1 Determination of intermediate type values of each measurement parts

Filtering out sample body with each figure types of the upper and lower body, we can obtain 7 data files. Take the mean values of anthropometric data as the final values intermediates body type, for the consideration of the convenience of data application, some simplifications were done to the data, the results are in Table 5 and table 6.

Tab. 5 Reduced measurement data of intermediate type of upper body cm

categaory	Upper body length	Chest circumference	Waist circumference	Shoulder width	Neck circumference	Chest horizontal length
A	37.5	84.0	68.5	39.0	33.5	34.5
B	38.0	82.0	66.0	38.5	33.0	33.5
C	39	81.5	65.0	38.0	32.5	32.5
D	39.5	80.0	63.0	37.5	32.0	31.0

Tab. 6 Reduced measurement data of intermediate type of lower body cm

categaory	Lower body length	Waist cicumference	Hip cicumference	Hip horizontal length	hip height
W	96.5	69.5	93.0	35	20.5
X	98.5	67.0	90.5	34	21.5
Y	101.0	64.5	88.0	33	22.5
Z	103.0	62.0	85.0	32	23.5

4. 2 Determination of stepping values of each body shape

In this research, the stepping number of the three basic control of parts of the body (body height, chest and waist) will be smaller than the current standard of 5 • 4 series, we consider 2.5• 2 series. So, values of each measurement parts can be calculated by simple or duality linear regression with body height and chest circumference, mathematical model of regression is: $y = \alpha x1 + \beta x2 + \gamma$. So as long as we get the stepping values of basic parts of human body,we can calculate each measurement parts' stepping values [5].So, the stepping values of each part= α *stepping values of height+ β *stepping value of chest。Results are simplified as shown in table 7.

Tab. 7 Stepping values of measured parts of upper and lower body cm

measured parts	Stepping value				measured parts	Stepping value			
	A	B	C	D		W	X	Y	Z
Upper body length	0.60	0.50	0.50	0.60	Lower body length	1.7	1.8	1.9	2.0
Chest circumference	2.0	2.0	2.0	2.0	Waist circumference	2.0	2.0	2.0	2.0

Waist circumference	2.0	2.0	2.0	2.0	Hip cicumference	2.0	1.9	1.8	1.7
Shoulder width	0.7	0.8	0.8	0.7	Hip horizontal length	0.8	0.8	0.7	0.7
Neck cicumference	1.1	1.0	1.1	1.0	Hip height	0.4	0.4	0.4	0.5
Chest horizontal length	0.50	0.50	0.50	0.60					

Conclusion

Using SPSS statistical analysis software to analyze the measuring data, through the single factor analysis of variance, upper and lower body indexes were obtained, and further through K-MEANS quick cluster, the youth female upper and lower body are divided into 4 categories respectively, Finally, the stepping value and intermediate type values can provide a powerful data support for young woman's clothing production enterprises whose target customer group is Quanzhou area.

Reference:

[1] L.H Bai, WB. Zhang, Classification methods of figure type in the female garment size standards: Journal of Textile Research, 2006, (7):113-116.

[2] S.G.Wu, Discussion on Body Figure Division and Classif ication System of Boys of 6～9 Years old in Liaoning Province of China:Journal of Beijing Institute of Clothing Technology [J]. 2007.27(3): 116-119.

[3] H.Dai, Apparel size standard and applications:Edition 2, Beijing: China textile press, 2001:38-45.

[4] P.Zou. S.G.Wu, Amendment of f igure types and grading values of youngwomen in China Northeast area :Journal of Textile Research, 2009, 30(11):115-119.

[5] C.Y.Huang . X.Zhang, Analysis on neck clustering of young men and size specifications of shirts : Journal of Textile Research, 2007(1):91-93

Advanced Materials Research Vols. 989-994 (2014) pp 5323-5326
© (2014) Trans Tech Publications, Switzerland
doi:10.4028/www.scientific.net/AMR.989-994.5323

City Waterfront Landscape Post Assessment Based on System Dynamics

Zhao Lei[1,2,a]; Gui Chao[1,b]

[1]College Civil engineering and architecture, Xinxiang University, Xinxiang, Henan, 453000, China

[2]Wuhan University of Technology, Wuhan, Hubei, 430070, China

[a]1164068609@qq.com, [b]guichao0714@163.com

Key word: the waterfront, post evaluation, system dynamics

Abstract. City waterfront landscape project post assessment research is still at the starting stage in our country, the related system research is very few. There are still many shortcomings of the original evaluation, it need to improve, the system dynamics makes up the deficiency in many respects. We can evaluate and analyse the city waterfront landscape by using hybrid evaluation method of the method of system dynamics. Construct the post assessment of waterfront landscape suit to the situation of our country.

Introduction

Water gives birth to life, waterfront gave birth to the city and city culture, is an important part of city development. Waterfront landscape occupies an important position in the city landscape. With the rapid development of the city today, People on all aspects of the requirements in gradually enhancement. The better Waterfront landscape not only has its aesthetic value, but also develop its ecological function, To promote the development of the city. Therefore, according to the relationship between the city and the waterfront landscape development as a starting point for research, discussion and evaluation on the waterfront landscape, In the future, it is good for us to contribute to the planning of waterfront landscape.

Post Assessment has many methods can evaluate city waterfront landscape

Contrast method. Evaluate the waterfront landscape by using contrast method. First of all, starting from the change before and after a waterfront landscape construction, find out the reasons for the changes, comparison of the effect of the waterfront landscape of city, people, environment effectively. In addition, from the point of view of with and without, judge City waterfront landscape has effect to the city development, and evaluate the waterfront landscape.

Statistical forecast method. Evaluate the waterfront landscape with the statistical forecast method, before the construction of waterfront landscape，based on statistics，using the quantitative prediction methods, evaluate the project. This method needs to collect some information, including the area's ecological environment, traffic conditions, flow of people, and the people hold the construction of waterfront landscape attitude etc. Test prediction method is applicable, and determine the predictive value ultimately.

Logical framework approach. Evaluate the waterfront landscape by using logical framework approach, this is a method of discuss project, use this method to evaluate the waterfront landscape, the project must be given a clear definition. Through establish logical framework, evaluate the city waterfront landscape.

The analytic hierarchy process. We can use the analytic hierarchy process to evaluate thewaterfront landscape, construct of a city waterfront landscape，there are N targets，Each target analyse independently, and each target can influence other targets through any factor. Through hierarchy analysis, evaluate the city waterfront landscape.

Causal analysis. We can use the causal analysis to evaluate the waterfront landscape, After the completion of the construction is still having the funds to maintain its stability, it can be considered

as a long-term project. Analysing the engineering before and after construction. We can analyse the largest influence of the waterfront landscape, and find the crux of the problems, through the in-depth research and drawing the causality diagram, analyse the causality diagram, and evaluate the city waterfront landscape.

Comprehensive evaluation. We can use the comprehensive evaluation to evaluate the waterfront landscape, the Post evaluation needs to analyze the project economic effect, environment effect, social effect, evaluate the project synthetically.

Success assessment. We can use the success assessment to evaluate the waterfront landscape, rely on the rich experience of experts and expert groups, evaluate the project objective synthetically. According to the degree of success criteria, evaluate the project. Evaluate the waterfront landscape base on the evaluation method of grey theory, relate to the degree of a number of different indicators and projects based on many experts, establish the mathematical relationships and analysis, evaluate the project synthetically.

Research Status

The Research of city waterfront landscape post assessment is still at an early stage, the Research of complete system are very few. Yue Liang used the fuzzy comprehensive analysis method to evaluate the city waterfront landscape, it contained landscape, ecological evaluation, social evaluation, economic evaluation et, the landscape evaluation involves many elements, the secondary factor has no clear boundary, according to the two levels of evaluation elements and factors in the system, present two level fuzzy comprehensive evaluation. Zhu Jianhong used the method of fuzzy mathematics to establish a mathematical evaluation model, evaluate the city waterfront landscape, provide decision basis for the design and construction of the waterfront landscape[1]. Zhu Runyu use the simulate evaluative method as a guide, take Nanjing Mochou Lake as an example evaluate the landscape, and get the important factors which influence the quality of the waterfront landscape, it is help for the future planning and design. Huang Guoping use the fuzzy mathematics to establish the matrix model, solve the fuzzy matrix and obtain all the factors weight coefficient of the waterfront landscape, it can guide the planning and design of the city water landscape.

System dynamics is used in various types of system

System dynamics is used in assessment of tourism planning. Xu Honggang used the theory and principle of the **sys**tem dynamics to plan tourism. Usd the principle and method of the **sys**tem dynamics in the tourism planning, make analysis of tourism planning of Guilim. Its contents include the determination of the reference mode, a lot of feedback analysis and process analysis, establish the relevant feedback and planning graph, and discuss the significance of system dynamics in tourism planning[2].

System dynamics is used in the agricultural ecological environment evaluation. Tang Jie make Jilin Daan as an example, according to various characteristics of agricultural ecological environment, usd the principle and method of the **sys**tem dynamics to establish the simulation model of the system dynamics, Studied on the ecological environment planning simulation, and find out the best scheme suitable for economic development[3].

System dynamics is used in evaluation of sustainable development. Zhang Aisheng presented the system dynamics was applied to regional sustainable development research, presented the regional resources development and ecological balance as the core to plan and research, pointed out the key directions for future research on Sustainable Development[4].

System dynamics is used in the health evaluation of water system. Huang Guoru Researched on the evaluation index system of water system health. First of all, used AHP to get the weight of each index, according to the method of system dynamics to build water system health evaluative model, collected some related materials, used the system dynamics to simulate the health water system next few years, through feedback regulation of each index, Can promote the stable, healthy development of water-based system[5].

System dynamics is used in city waterfront landscape post assessment.

The post assessment system of the city waterfront landscape sustainable development is an important part of the system of the city waterfront landscape post assessment. The system of the city waterfront landscape post assessment is showed on figure 1, the effect of post evaluation system contains several main indexes. It includs the water ecological environment sustainable index, construction and maintenance of sustainable index, social and economic development policies and sustainable management index, each indicator consists of a number of factors, each factor is divided into several secondary influence factors. The multiple effect factors can be used to analyze and evaluate rely on the system dynamics.

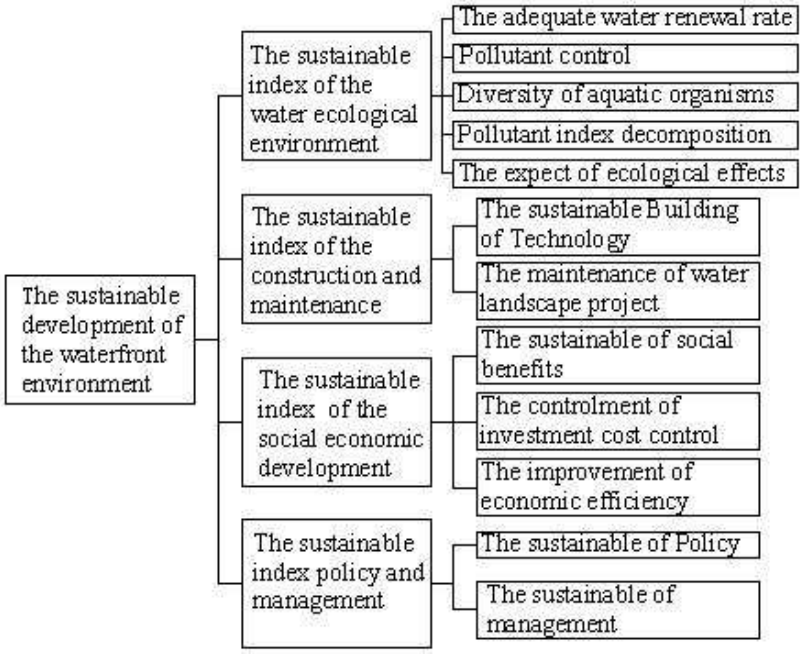

Figure 1

The system dynamics is a discipline which includes study and analysis of information feedback system, according to the feedback among the various factors affecting the waterfront ecological function, aesthetic value, economic benefit, evaluate the waterfront environment synthetically.

The ecological environment of causal feedback diagram is showed on figure 2, it can reflect the relationship between the waterfront ecological system of sustainable development and the influence factors simply. According to the feedback causality diagram, evaluate waterfront environment ecosystem sustainable development.

The figure present The relationship between the waterfront ecological system of sustainable development and the influence factors, according to the feedback causality diagram evaluate waterfront environment ecosystem sustainable development. The typical positive feedback and negative feedback loop is shown as follows.

(1)The ecological environment of the waters $\xrightarrow{+}$ The quality of the landscape $\xrightarrow{+}$ The flowrate of people $\xrightarrow{+}$ Landscape visibility $\xrightarrow{+}$ Capital investment $\xrightarrow{+}$ The ecological environment of the waters.

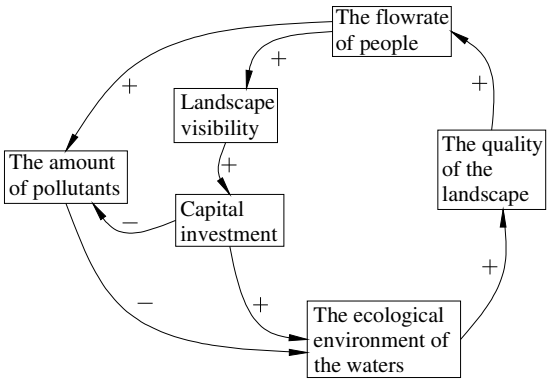

Figure 2

(2) The ecological environment of the waters $\xrightarrow{+}$ The quality of the landscape $\xrightarrow{+}$ The flowrate of people $\xrightarrow{+}$ The amount of pollutants $\xrightarrow{-}$ The ecological environment of the waters.

Rely on analysis on causal loop system, establish the system dynamics model of the city waterfront landscape to analysis the whole system.

Summary

At present, many method rely on establish the fuzzy mathematical model to Analyse and evaluate the city waterfront landscape, and guide the design of waterfront landscape. Used hybrid evaluation method which includes system dynamics, combined with computer simulation technology, detection and repair technology of environmental engineering, Outstanding landscape user participation, accessibility and fairness. Present the effect post assessment of the city waterfront landscape, the effect post assessment of the landscape, the post assessment of the sustainable development, guide the waterfront landscape design well. System dynamics is suitable for the study of complex systems, it is suitable for processing some problem which require long period and insufficient data. Although the history of its development is relatively short, but its method system is continuously improved, the correct guidance system design, represent the full range of value.

References

[1]ZHU Jian-hong, TANG Xian-li, GUO Zong-lou, Appraisal of the Urban Waterfront Landscape Environment on the Basis of Fuzzy Mathematic[J], Journal of Agricultural Mechanization Research, 2008, (3)197-200.

[2]XU Hong-gang, BAO Ji-gang, Theory and Method of te Application of System Dynamics in Tourism Planning[J], Economic Geography, 2003, 23(5)705-709.

[3]TANG Jie, SHE Xiao-yun, LIN Nian-Feng, A Study on System Dynamics Model in Eco-environment Planning for Da'an of Jilin Provience[J], Acta Ecologica Sinica, 2005, 25(5)1178-1183

[4]Zhang Ai-sheng, LI Feng-rui, KANG Ling-fen, System Dynamics and Its Applications in Regional Sustainable Development Research: A Review[J], Arid Meteorology, 2005, 23(2)70-74.

[5]HUANG Guoru, XIANG Biwei, FENG Jie, Health State Assessment of Base-system of Dongjiang Basin Based on System Dynamics Method[J], Water Resources and Power, 2012, 30(7)1-5.

Advanced Materials Research Vols. 989-994 (2014) pp 5327-5330
© (2014) Trans Tech Publications, Switzerland
doi:10.4028/www.scientific.net/AMR.989-994.5327

The modeling of buildings cost assessment expert system with differences

Yin haiwen

Pingxiang University, Pingxiang Jiangxi 337000, China

Keywords: hybrid construction; costs assessment model; multi-cost information constrains

Abstract: It's difficult to estimate the costs of hybrid constructions with great differentiations. This paper proposes a hybrid construction costs optimization model by reasonably selecting the feature attributes during costs estimation. SVR prediction model is established and it's trained to shape the analog hybrid construction cost information estimation model. The experimental results show that the proposed model can accurately predicate the hybrid construction costs with higher efficiency.

1 Introduction

It's important for the construction management personnel effectively estimates and controls the construction costs which will allow them provide optimal construction costs schemes to reduce the costs and maximize the profits. Each building has its own characteristics and there are common characteristics associated with different buildings. The analysis of the similarity of these characteristics can effectively estimate the costs of the hybrid constructions [1,2]. It's difficult to estimate specific costs of the hybrid construction due to the impact factors are variable and complicated. Only the probability of the costs in some specific range can be estimated. Therefore, it's important to search effective construction costs estimation method [3,4]. It's research focus for accurately estimate hybrid construction costs in current construction cost analysis area. With the increase of the constrains for the construction costs, the amounts and characteristics of the building are diversified. The traditional BP neural network estimation method cannot be used for the cost-oriented hybrid construction cost estimation issue because it cannot build the effective convergence assessment model and cannot get accurate costs estimation results.

2 The project cost assessment model

2.1 The selection of the feature attributes

In the project establishment phases, the project features refer to the characteristics that mostly impact the project costs. Therefore, it's important to select the project features while using SVR to estimate the project costs. There are two main principles in this paper for selecting the project features- "fine" and "difference." "Fine" refers to the selected project features must have a greater impact on the costs. Obviously, there is no practical significance for selecting the features with little impacts on the project costs; "difference" refers to that the selected features should show the differences because if all the features are the same they cannot be distinguished by SVR model and have no contributions for the prediction results.

Because the above reasons and the brick structure residual buildings are considered, 6 attributes-building area, basic form, layers, structure types, maximum opening, and amounts of windows and doors, are used as the project estimation features.

2.2 The establishment of SVR prediction model

This paper applies Libsvem-3.1 toolbox to build SVR predication model and the detailed steps are as follows.

1）Data normalization

In order to make the attributes comparable, they are normalized by equation (1).

$$y = (x - x_{\min}) / (x_{\max} - x_{\min}) \quad (1)$$

In the equation, x,y$\in R^n$, n denotes the amount of attributes, x_{min}=min(x), x_{max}=max(x). The purpose of the data normalization is to map the original data to the range of [0,1] to make them comparable.

2）The selection of core functions

The types of the core functions in the Support Vector Machine are directly related with the regression results. The performance of SVR based on Radial Basic Functions (RBF) is much better that those with other core functions. Therefore, RBF in the proposed SVR model should be carefully selected.

3）The determination of optimal parameters

SVR has two parameters which are regularization parameters *c* in objective function and the parameter *g* in the core function. Because they impact the predication performance of SVR to large extent, the parameters should be optimized.

The K-fold Cross Validation (K-CV）method is used to search the optimal parameters whose principles are gradually adjusting the parameters of c and g to minimize the predication Mean Squared Errors (MSE). Finally, the optimal value is c=256，g=0.0068012 and MSE=0.023229.

2.3 The training and predication of the model

This paper selects the data from 14 residential buildings as the training samples. Artificial Neural Network (ANN) and SVR are used to build the prediction models respectively. The data of A15 is used to testify the correctness of the two models and the experimental results are shown in Table 1.

Table 1 The predication results based on SVR and ANN project cost assessment models

No. of the building	The actual cost	SVR predication value	SVR relative errors	ANN predication value	ANN relative error
A15	1.08125	1.08442	0.0029	0.94674	-0.1244

In the Table 1, the fitting results of SVR model is very satisfactory and the relative error is 0.29% which is less than 1%. Compared with ANN model, the relative errors of SVR is 0.29% which is obviously less than those of 12.44% in ANN model. The results illustrate the predication performance of SVR model is better than ANN model.

In this case, it's reasonable that the predication effects of SVR model are better than ANN model. For one aspect, the design of SVR model considers the fitting and generalization of the test samples, while ANN model only considers the fitting of the data; for another aspect, ANN model is usually applied in large scale of data and SVR model focuses on small scale of data. There are only 14 training samples in this experiments which is typical small scale of data. In summary, SVR model is better for project assessment model than ANN model.

3 Experiments and simulations

3.1 The source of the experimental data

The experiments are used to test the proposed hybrid construction costs assessment model based on multi-cost information reasonable constrains. The experiment selects 10 groups of data of different types of hybrid residential constructions from the *hybrid construction costs* of some city from 2008 to 2011.

These data are preprocessed and 8 features of the average construction areas, average number of floors, average height of each floor, flat shape, structure type, base type, bearing capacity, and depth from different types of hybrid constructions are selected as the relative hybrid construction costs features and the specific data are described in Table 1.

3.2 The hybrid construction cost assessment

In order to verify the validity of the proposed model for hybrid construction costs assessment, the proposed model and traditional BP neural network model are used to evaluate the costs of different types of hybrid construction in Table 2. The structure of BP neural network is 10*22*2. The detailed hybrid construction costs are described in Table 2.

Table 2 The assessment results of the proposed model and the traditional BP neural network model

	The hybrid construction costs（yuan·m^{-2}）				
Models	18	19	20	21	22
Actual cost	1476.6	1409.8	1424.6	1378.9	1349.0
Proposed model	1469.7	1488.7	1419.5	1367.4	1336.8
BP neural network model	1587.9	1577.9	1564.9	1451.6	1400.8

In order to prove the advantages of the proposed model, The Mean Squared Errors (MSE) and Mean Absolute Percentage Errors (MAPE) of the proposed model and BP neural network model are compared by combining Table 2. MSE and MAPE are expressed by

$$MSE = \frac{\sum (y_i - \hat{y}_i)^2}{p}$$
$$MAPE = \frac{\sum |y_i - \hat{y}_i| / y_i}{p} \times 100 \tag{2}$$

In the equations, y_i denotes the actual value, $\hat{y}_i$ denotes the assessment value, p denotes the amount of assessment samples. In Table 1, MSE in the proposed model is 18.16 and MAPE is 0.53 with equation (10) while MSE and MAPE are 76.54 and 0.79 respectively in BP neural network model, which illustrate the accuracy of the proposed model for hybrid construction costs assessment is higher than that in traditional BP neural network model. The assessment results of the proposed model can well match the actual results which demonstrate the proposed model has advantages and practical values.

The assessment errors comparison between the proposed model and BP neural network model for the hybrid construction costs are described in Fig. 1 in which the errors of the proposed model are less than those in BP neural network model and the assessment errors of the proposed model remain around 0.12 while those in BP neural network model have obvious fluctuations.

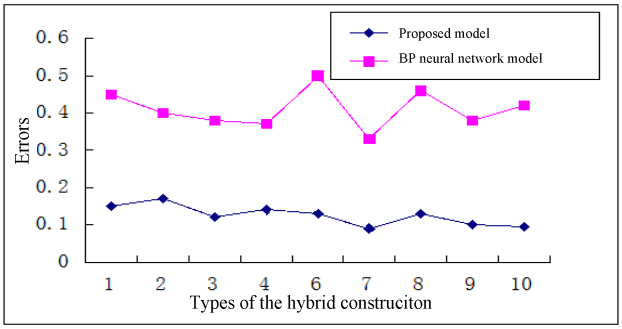

Fig. 1 The error analysis of different hybrid construction cost assessment models

4 Conclusions

This paper presents a hybrid construction optimization model based on multi-cost information reasonable constrains which can effectively increase the predication accuracy for the hybrid construction cost assessment models. The experimental results show that the proposed model can accurately evaluate the costs for different types of hybrid construction costs with higher efficiency.

References

[1]. NiuDongXiao, begging, make great contribution to cotton xing. Construction project cost estimation model based on variable structure neural network study [J]. Journal of north China electric power university journal of north China electric power university, 2001, 28 (4) : 1-4.
[2]. Xu Ning. Construction project cost estimation method based on fuzzy neural network [J]. Journal of jianghan petroleum institute, 2000, 22 (1) : 87-88.
[3]. NiuDongXiao, cotton. Xing time sequence estimation model of wavelet neural network study [J]. Journal of systems engineering theory and practice, 1999, 12 (5) : 89-92.
[4]. Beam section people talk about construction project management and project cost control [J]. The relationship between construction of Shanxi Province, 2005, 31 (1) : 144-145.

Advanced Materials Research Vols. 989-994 (2014) pp 5331-5335
© (2014) Trans Tech Publications, Switzerland
doi:10.4028/www.scientific.net/AMR.989-994.5331

Research on the Organization Operation Mode of the Hong Kong-Zhuhai-Macao Bridge Based on VSM

SHENG Gang[1, a], YU Jia-qing[2,b]

[1] Chang An University, Xi'an Shanxi 710064, China

[2] Research Institute of Highway Ministry of Transport, Beijing 100088, China

[a]g.sheng@rioh.cn, [b]jq.yu@rioh.cn

Keywords: organization design; VSM; HZMB.

Abstract. Based on describing the status of the organization structure of the related projects at home and abroad, the construction scheme and the project management features of the Hong Kong-Zhuhai-Macao Bridge (HZMB) are discussed, and the main operation and maintenance business after the opening of the HZMB is analyzed. Learning from the advanced organization design model-the Viable System Model (VSM), the organization operation mode of the HZMB is built, and at last a suggested solution to the organizational structure of the HZMB is proposed.

Introduction

Following the closer economic ties among Hong Kong, Macao, and the mainland as well as the increasingly mature integration of the Pearl River Delta, the demand to construct the large cross-border infrastructure and change the investment environment is becoming urgent. Therefore, the construction of the Hong Kong-Zhuhai-Macao Bridge (HZMB) formally began on 2009.

The in-construction HZMB which consists of a series of bridges and tunnels will connect Hong Kong, Macau and Zhuhai, three major cities on the Pearl River Delta in East Asia [1]. The proposed 50 km link, with an estimated investment of 72.94 billion yuan and a designed service life of 120 years, consists three parts: Offshore Bridge-cum-Tunnel, Boundary Crossing Facilities (BCF) at Hong Kong, Zhuhai and Macao, and Link Roads in these three regions [2]. When completed, it'll become the longest six-lane immersed tube tunnel, and the longest cross-sea bridge and tunnel combined highway in the world.

The Nobel Prize winner Herbert Simon once said " that the first condition of developing effectively social resources is to establish effectively organization structure" [3]. While a study by Harvard Business School and McKinsey & Company concluded that organizational structure is one of the key points of project management. Mintzberg has written extensively and significantly on the importance of organizational structure [4]. Moreover, organizational structure and design are closely entwined [5] with many aspects of human resource management.

This paper is organized as follows: In Section 1, the related projects and the project features of HZMB are investigated and summarized. Requirement analysis is taken into account in Section 2. Section 3 proposes the organizational structure of HZMB. Section 4 summarizes the paper.

Related projects

A. The Storebælt link

As a proud monument, The Storebælt link connects the islands of Zealand and Funen and is a crucial traffic artery between East and West. The 18 km long fixed link across Storebælt between East and West Denmark comprises two bridges and a tunnel. The organization of A/S Storebælt is shown in the Fig. 1:

B. Hong Kong-Shenzhen Western Corridor (HK-SWC)

HK-SWC (also known as the Shenzhen Bay Bridge) is a 5.5-kilometre long dual 3-lane carriageway of which the Hong Kong section is 3.5-kilometre. Spanning across Deep Bay, HK-SWC links up the northern end of Deep Bay Link at Ngau Hom Shek of Hong Kong with Shekou of Shenzhen [7].

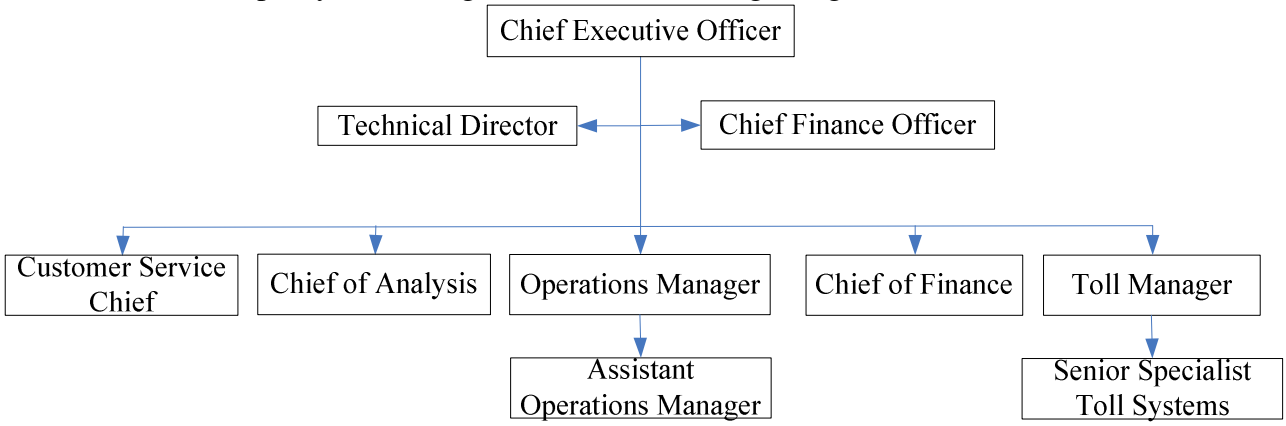

Fig. 1. Organizational Structure of the Storebælt link.

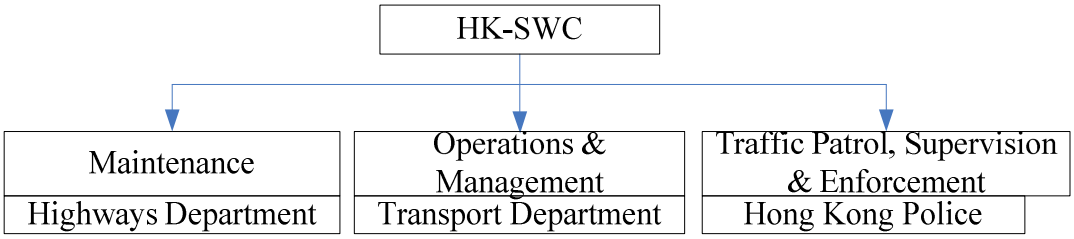

Fig. 2. Organizational Structure of HK-SWC.

REQUIREMENT ANALYSIS

The main business of the HZMB Authority is understood to fall into three categories: operation management, maintenance management and administrative management.

(1) Operation Management

The main contents of operation management include: toll, traffic management, highway law enforcement, emergency rescue, safety and environment protection, auxiliary business, etc.

(2) Maintenance Management

The main contents of maintenance management include: the main structure and infrastructure, Electro-mechanical system and equipments, roadside facilities, house-building engineering and facilities, landscape engineering, etc.

(3) Administrative Management

The main contents of administration management include: human resource, project planning, finance, logistics, party-masses, etc.

Organization Operation Mode of the HZMB based on VSM

A. Basic concepts

The Viable Systems Model, or VSM is a model of the organisational structure of any viable or autonomous system, seen in Fig.3. It has been used extensively as a conceptual tool for understanding organizations, redesigning them (where appropriate) and supporting the management of change.

Any organization needs to include two systems in place if it is to operate effectively in its environment: operation system and management system [8]. The operation system (system 1) implements all the basic work of the organization and contains several separate autonomous units, which keep contact with the external environment to adapt its change and are controlled by the management system to ensure the effective operation among these autonomous units. While the

management system, providing service for the operation system, has four systemic functions in order to make the whole organization integrally and cooperatively work. These four systemic functions are: Co-ordination (system 2), Control (system 3), Intelligence (system 4) and Policy (system 5).

All the sub-systems are interrelated and interact on each other, whose relationship can be shown from the Fig. 3.

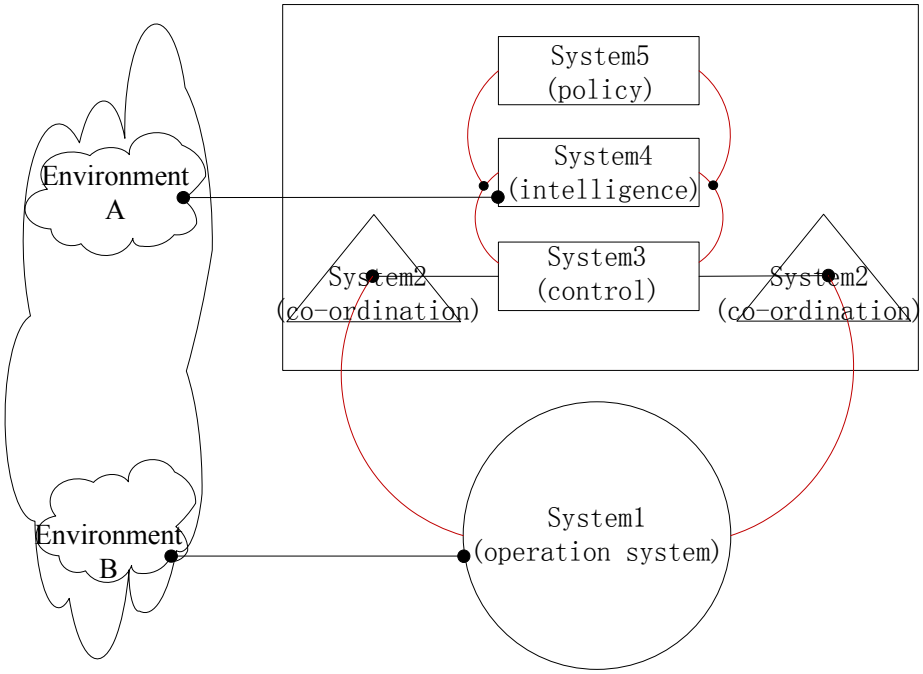

Fig.3 Viable System Model

B. Organization Operation Mode of the HZMB based on VSM

The organization operation mode of the HZMB contains five modules, which carry and build naturally upon each other, as shown in Fig. 4.

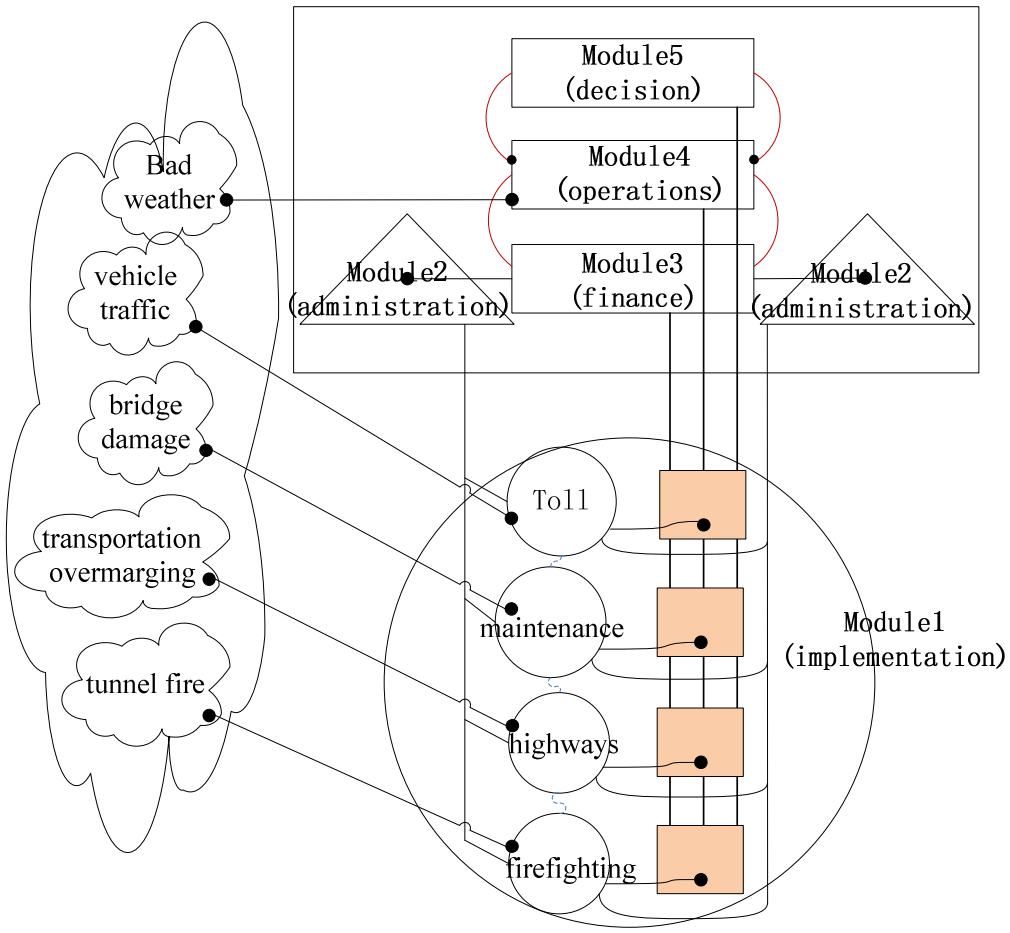

Fig.4 The organization operation mode of the HZMB

(1) module 1: implementation
This module is composed of four units: toll, maintenance, highways and firefighting.
(2) Module 2: administration
This module is responsable for the human resource, office secretary and assets management.
(3) Module 3: finance
This module not only provides finance plan and management service for the module 1, but also provides the related information about the operating situation of all the other modules.
(4) Module 4: operations
This module is in charge of acquisition of the regular operation and maintenance information of HZMB, monitoring the operating condition of the HZMB, and provide support for module 5.
(5) Module 5: decision
In this module, policy-makers make the development goals and the future of the HZMB to ensure the safe and efficient operation.

Summary

In this paper, the organizational structure design of HZMB is studied to achieve the construction and management goals. Because of the unique feature that project engages three regional governments administered under the policy of “One Country, Two Systems”, this paper could give a novel perspective for the organization design.

Acknowledgements

This work was financially supported by No.3 Special Subject Study in the sub-topic 2 of the Key Technologies Research and Development Program of China (2011BAG07B05-2) and Preparation of the Operation and Maintenance Manual (Traffic Engineering).

References

[1] N. Hussain, Carlos Wong, Matt Carter, Samuel Kwan, Tak-Wah Mak. Hong Kong Zhuhai Macao Link. Procedia Engineering, 2011, 14, pp. 1485-1492.

[2] Yu Lie. Crossing the Lingdingyang, HONG KONG-ZHUHAI-MACAO BRIDGE, 2011, (1), pp. 10-17.

[3] REN Hao, Liu Shilan. Design Organizational Structures on the Basis of Strategy. SCIENCE OF SCIENCE AND MANAGEMENT OF S. & T., 2005, 26(8): 123-126.

[4] Goold, M., Campbell, A. Do you have a well-designed organizatio. Harvard Business Review, 2002(R0203K): 5-11.

[5] GONG Hangjun，WEI Xianwei. Study on Comprehensive Evaluation of Operation Safety of Expressway Tunnel. Journal of Highway and Transportation Research and Development, 2010, 27(8): 127-130.

[6] Lars Møller. Increasing Traffic and Revenue through Marketing at the Great Belt Bridge. Proceedings of the 2006 IBTTA organization management workshop, pp. 1-11.

[7] Lee, Joseph; Kong, Alex; Chan, Eric. Hong Kong-Shenzhen Western Corridor and Deep Bay Link: Design Development and Environmental Challenges. Proceedings of IABSE Symposium Shanghai 2004, Metropolitan Habitats and Infrastructure, pp. 25-30(6).

[8] Schwaninger Markus. Design for viable organizations: The diagnostic power of the viable system model. The International Journal of Systems & Cybernetics, 2006, 35(7-8): 955-966.

Advanced Materials Research Vols. 989-994 (2014) pp 5336-5340
© (2014) Trans Tech Publications, Switzerland
doi:10.4028/www.scientific.net/AMR.989-994.5336

Physiological Mandarin Speech Corpus for the International Preparatory Students in China: Design and Initial Application

Xiuping DU[1, a], Wenping ZHANG[2, b], Yufen HOU[2], and Jianguo WEI[3,c*]

[1]School of International Education, Tianjin University, Tianjin, 300072, China

[2]School of Education, Tianjin University, Tianjin, 300072, China

[3]Tianjin key Laboratory of Cognitive Computing and Application, Tianjin University, Tianjin, 300072, China

[a]email: duxiuping@tju.edu.cn, [b]email: zwp084510@sina.com, [c*]email: jianguo.fr@gmail.com

Keywords: Preparatory Students; Physiological; Mandarin; Speech Corpus

Abstract. In order to visualize pronunciation teaching and explore the law of articulation evolution in TCFL (Teaching Chinese as a Foreign Language), we proposed an approach to design a physiology Mandarin speech corpus for the international preparatory students in China. Preparatory students are usually beginners to learn Mandarin, so they are selected as testers to gain the most real law of Mandarin articulation evolution. The corpus was different from an ordinary speech corpus. It consisted of not only text information (such as age, gender, nationality, mother language, Mandarin learning experience, etc.) and audio information, but also the physiological data (such as speech organs' moving morphology). When the corpus was constructed, data were gathered by a supersonic collecting system because of its safety and low cost. In the initial experiment, 21 initial consonants, 36 simple or compound vowels and tones were tested. The results showed the corpus was significant in Mandarin teaching.

Introduction

The reason why human beings can speak, in physical way, is that the phoneme is pushed out by airflow, via the adjustment of tongue and the resonance of vocal tract. So the shape of vocal tract, especially movement of the tongue is significant in language teaching. As we all known, Mandarin has its own characteristic. There are 21 initial pronunciation, 36 simple or compound vowels, and four tones in Mandarin pronunciation which usually confuse foreign learners. The most special, different from other languages, is that the Mandarin speakers use the front of mouth to speak, voice is difficult to identify its hidden features through the sense of hearing only[1].Thus, research on Mandarin articulation could reveal the secret to speak Mandarin well and make great sense for Mandarin teaching. In TCFL, it's most important for foreign students to have pure pronunciation followed by fluent expression and communication. At the same time, teachers often let students imitate their intonation with the help of pronunciation sketch map in the phonetic teaching. As the phonetic is often accompanied with complex movement of speech organs and manner of articulation, the pronunciation sketch map can do a little work, the students can only rely on their feelings to adjust their articulatory state. That's why foreign students and teachers can get the meaning of each other, but it doesn't work when communicating with the ordinary Chinese people[2].It is inefficient to meet the demand of TCFL.

Design of the Physiological Mandarin Speech Corpus

Corpus in modern linguistics refers to finite collection of machine-readable texts, sampled to be maximally representative of language variety [3]. In this paper, we design and construct the Mandarin speech corpus for the international preparatory students in China based on the physiological features of pronunciation to help students learn Mandarin pronunciation accurately and successfully. By the corpus, students recognize intellectually what kind of errors they may have and researchers can get abundant and accurate data useful in TCFL research field.

The corpus consisted of not only text information (such as age, gender, nationality, mother language, Mandarin learning experience, etc.) and audio information, but also the physiological data (such as speech organs' moving morphology).

Data Gathering

1) Testers Selecting

As the first batch of preparatory education Demonstration University for foreign students studying in China under Chinese government scholarship program, there are many preparatory students every year who are usually beginners to learn Mandarin in School of International Education, Tianjin University. To gain the most real law of Mandarin articulation evolution and take advantage of the stable and abundant human resources, we choose them as testers.

Preparatory students leave away form their own countries to China at first time. Everything is brand and new for them. Good care and protection from teachers and classmates is really needed. Therefore, they need more humanistic concern than Chinese students. We need explain the meaning of experiment and how to do it so that the participants can support the experiment and does it well. The experimental equipments must be harmless and test itself mustn't hurt participants. To avoid psychological stress, participants should be in good psychological quality and adapt to the life in China. During the test, experimenters should enhance the participants' sense of responsibility to make sure the reliability of the result.

2) Instrument

According to professor Wei jianguo's research (School of Computer Science and Technology in Tianjin University), there are many methods to observe and record the motion of interior speech organs such as ultrasound equipment, EMA or MRI(Magnetic Resonance Imaging). Particularly, the ultrasound can acquire the images in the speed of 60 frames per second [4]. In this paper, we choose a ultrasound system to gather data. Hence, compared with EMA and MRI, the ultrasound equipment is cheaper, more portable, more comfortable, and high frame frequency. The ultrasound system is designed and developed by School of Computer Science and Technology in Tianjin University based on the portable TERASON T3000. Audio information is recorded via high-quality microphone and then saved as audio files. The information of speech organs' motion morphology observed by ultrasound equipment will be saved as high resolution image.

a. Function

The system is able to collect both ultrasound and audio information. The portable TERASON T3000 can display the current motion of tongue in the max speed of 85 frames per seconds (steadily，60 frames per seconds and below), and every frame of picture will be directly saved as BMP in the local disk. The default size(maximum) is 640×480(can lower). The bit depth 8 and the size of every picture is 302KB. High-quality microphone and sound recording program is used in the system to handle the audio files. The format of audio files is wav. The default parameters are shown as follows: mono, 44.1 KHz (sampling frequency), 16bit (quantization bit). The parameters can be set to meet the actual demand.

Data acquisition system using multi-threading technology makes synchronize data collection available and it records the systematic time to ensure synchronization among the data steams. While collecting the data, the system automatically generates the text files to record the basic information of each picture such as systematic time, serial number and the time of "every frame" in audio streams. With the serial number, experimenters can get the situation of image collection: they can know if there is a picture missing or time losing. When collecting the audio information, the audio files are saved in hard disks frame by frame. When each frame of audio is save successfully, the system will access the image acquisition threads to get and record the serial number of the image so that experimenters can verify the synchronization of each data stream.

b. Modules

Based on categories of data, there are two main functional modules: audio acquisition module and ultrasound data acquisition module. The audio acquisition module can be divided into different parts: real-time display of audio files, data acquisition, parameter setting, and parameter status

display, naming and saving. Ultrasound data acquisition module also can be divided into some different parts: real-time display of ultrasound data, parameter status display, parameter setting, naming, saving, and setting and display of ultrasound's parameters.

Data Processing

1) Original image

Ultrasound display the motion of tongue in the max speed of 85 per frame, and at the same time, each frame image is saved as BMP into hard disk. We should make sure that files are named well in detail. Images' default size(max) is 640×480(can lower) . The bit depth is 8 and the size of each image is 302KB.

2) Profile of tongue

Professionals analyze, compare and synthesize pictures that are taken before and after a steady speech, and finally the shape of tongue is drawn as a curve. Then the image is saved.

Via these equipments both voice features and the motion of speech organs can be analyzed. Hence, the corpus has abundant content such as text information, audio information, and speech organ's motion morphology.

Initial Applications

Technology Roadmap

The corpus can be used in TCFL, the technology roadmap is shown in Figure 1. Firstly, we collect text and audio information by the advanced instrument of observation like ultrasound equipment or high-quality microphone. Preparatory students' speech data, physiological form of speech organs and motion data can be well collected, and then be inserted to the database. Secondly, the bias error of Mandarin pronunciation is analyzed with concluding and analyzing the data we got. The pronunciation will be repeatedly examined and adjusted continually when teaching and learning.

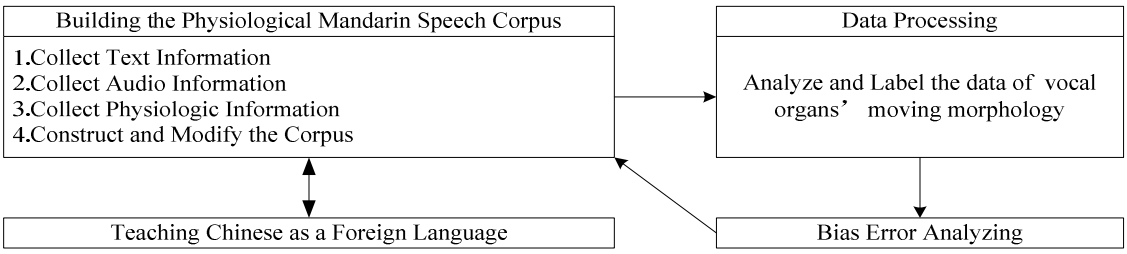

Fig.1. Technology roadmap

Experiment

At the beginning, 21 initial consonants, 36 simple or compound vowels and Mandarin tone should be tested. This time, we choose four preparatory students who start to learn Mandarin from the very beginning as testers, and then we choose three different periods in a term to do the test. The test content is the same: initial consonant, simple or compound vowel and the Mandarin tone.

Firstly, the original pictures were gathered by the ultrasound audio data collection system, as show in Figure 2.

Secondly, the professional described a curve of the tongue after analyzing, comparing and synthesizing many pictures of a stable pronunciation, as shown in Figure 3.

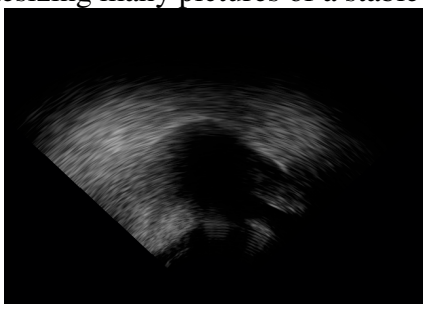

Fig.2. Original image of a certain frame by ultrasound

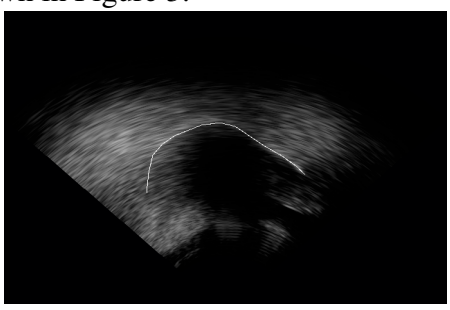

Fig.3. Final shape of the tongue

We import the corresponding audio files to the Praat, find the image that formant is steady. Ultimately, a final tongue position image was formed after comparing and compositing those two pictures, as shown in Figure 4.

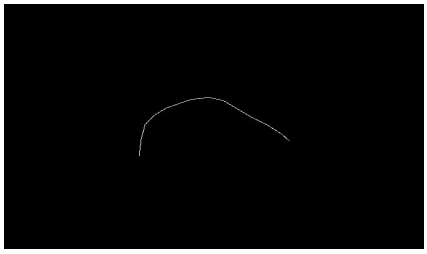

Fig.4. The final position of tongue

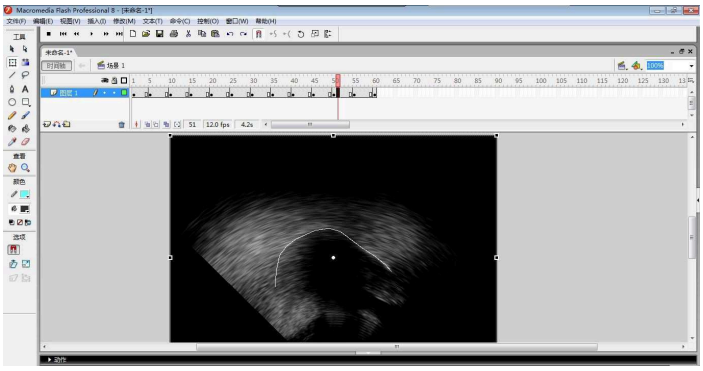

Fig.5. Animation of the tongue's movement

The system uses a high-quality microphone and recording program to acquire and process audio files in WAV format. Using the Praat software, we can observe other language features and acquire data in need. This process needs cooperate with research on experiment results and applications. To make the best of the experiment results, we will continuously analyze and mine the data deep.

The tongue is one of the most significant speech organs which can distinguish phoneme. The tongue position control is basic condition, but it's difficult to position the tongue with ears only [5].After comparing test results acquired in three times, the progress and changes become obvious. In this experiment, verifying and comparing the results in experiment with teaching rules, we can summarize all kinds of mistakes that can be made by foreign students in different phases. The images we get can show difference between right tongue position and tongue position of foreign students.

Application

1) Learning curve of phonetic learning

The acquisition of experimental data consists of horizontal and vertical features. Vertical feature is that experimental test should have phases and traceable properties. It has been widely accepted by the teachers that the foreign students who learn Mandarin as beginners have terrible bias errors in the first two weeks. Influenced by their mother tongue, students make kinds of mistakes from pronunciation to the Mandarin tone. It makes great difficult and obstacle in Mandarin learning. With in-depth study, some foreign students can comprehend the way of Mandarin pronunciation and tone so that they make a great progress, but others are not. Some students even can't have access to the way of learning Mandarin in a long time. They can't get language sense, often memorize tone and the word mechanically without understanding, or always find it's difficult to learn Mandarin and don't know what to do.

2) Finding out the systematic error pattern

With vertical comparison, we can observe the process of participants' study, the problem they are faced with and situation of promotion. The horizontal feature is capturing the prime vocal feature in different phases, especially for the wrong vocal feature and the habitual mistakes. Even the common problem encountered by the learners from different countries or different language background is analyzed so that we can develop targeted method to improve the situation. The corpus can show the characteristics of native speakers and the systematic error pattern of foreigners. Getting the error pattern of a specific learner group is of great importance in improving teaching method of Mandarin disyllables.

3) Pronunciation demonstration animation and the computer-assisted language learning (CALL)

We can develop some animations and video games to show how speech organs motion or make some models or toys to simulate the motion of speech organs. We had make a simple animation (as shown in figure 5) which can show clearly the movement of the tongue when pronounce a specific pronunciation. We can also compare this with the standard mandarin pronunciation and find the differences. So it is easily for the foreigner students to learn Mandarin by themselves through the

computer-assisted language learning (CALL).The literature on CALL mentions a number of its potential advantages: elimination of time limitations and dependence on the teacher, possibility to work at the user's own tempo and to store his/her profile in order to monitor the progress, constant access to a number of additional materials such as visualizations, recordings and animations as well as elimination of stress related to the fact that the learner is being listened to by his/her classmates, the last of which is particularly important while acquiring L2 (second language) pronunciation and prosody.[6]

Summary

The Mandarin speech teaching for foreign students has its own peculiarities, which is always a big problem for TCFL. Due to the complexity of Mandarin speech, different students from different countries are often faced with many bias errors. The corpus could be used as a basic database to visualize pronunciation teaching and explore the law of articulation evolution in TCFL. This corpus is a meaningful attempt. We expect it can provide support and inspiration to the future work.

Acknowledgement

This research was financially supported by 2013 Tianjin University Independent Innovation Projects.

References

[1] Zhuang mu-qi, Bu You-hong. Research of phonetic teaching and visualization [J]. E-Education Research, 2011, (2): 92-98.

[2] Lv Jun, Cao Xiao-ying, Design and Implementation of Automatic Chinese Speech Scoring System Based on Speech Recognition [J]. Computer Engineering and Design,2007,(5): 1232-1235.

[3] A. Kilgarriff and G. Grefenstette, "Introduction to the Special Issue on the Web as Corpus, " Comput. Linguist. , vol. 29, no. 3, pp. 333-347,Sep. 2003.

[4] Wei Jian-guo, "A model-based learning process for modeling coarticulation of human speech", IEICE Transactions on Information and Systems IEICE Trans. Inf. & Syst. No.10, pp.1581-1591, 2007.

[5] Hu A-xu, CHEN Gui-ping, YU Hong-zhi. Application of Multimodal Phonetics Lab in Language Studies [J]. Journal of Northwest University for Nationalities(Natural Science),2012,(3): 12-17

[6] Demenko,G. (Dept. of Phonetics, Adam Mickiewicz Univ,Poznan, Poland); Wagner,A.; Cylwik, N. The Use of Speech Technology in Foreign Language Pronunciation. Training Archives of Acoustics, v 35, n 3, p 309-29, 2010

Advanced Materials Research Vols. 989-994 (2014) pp 5341-5344
© (2014) Trans Tech Publications, Switzerland
doi:10.4028/www.scientific.net/AMR.989-994.5341

Construction and Implementation of the Network Teaching System of Mechanical Design Basic Course based on Web

RAN MengChun [1, a], XIA Ming [2]

[1,2]Chongqing Vocational Institute of safety & technology, Chongqing 404020，China

[a] RanMengChun@yeah.net

Keywords: Machine Design; CAI; Web

Abstract. With the development of network education, the importance of the research network teaching system is more and more prominent. The network teaching system an autonomous, distributed teaching environment based on Web by using the network as the carrier of information, construct. Along with the network popularization, the network teaching based on Web will become one of the most important teaching modes of education in the future. Computer assisted instruction (CAI for short) is one of the most advanced means of modern education technology. This paper mainly discusses the application of computer network technology in auxiliary mechanical design course teaching. The advanced network technology in computer aided instruction is introduced in the auxiliary mechanical design course teaching, which is one of the most significant reform teaching systems facing in the 21st century.

Related technology review

1.1 JSP technology

The emergence of the Java language lays the foundation for Web application and provides sufficient technical support and implementation mechanism to establish a safe, reliable and compatible, open, distributed application system, it is on a par and the Web to promote each other, hand in hand. Web technology based on Java has deepened into every aspect in people's lives, areas covered including e-government, telemedicine, distance learning, etc. [1]The role of Java technology in the Web makes remote performance of the network teaching system greatly enhance. Java language is a kind of very good language; its good features are below:

(1) Platform neutrality. The most important feature of the Java language is that it can be run in any operating system. Using the Java virtual machine is to make support has nothing to do with the operating system and can run in any system.

(2) Security. Java takes three kinds of measures to ensure safety. First of all, Java itself in design is to eliminate the illegal operations. [2] Cancelled the pointer hackers are good at although lost flexibility fundamentally put an end to one of the most powerful damage safety hidden trouble. Good encapsulation of Java can in the program purposely prevent some object related to the system resource modified by other objects.

(3) Multithreading. To do multiple tasks at the same time within a process, a number of different threads can be designed to work separately. [3] Java does almost all the thread mechanism well and multi-thread mechanism has been implemented in the base class library. Better is that it has completed data synchronization process many other languages is difficult to implement or poor implementation of.

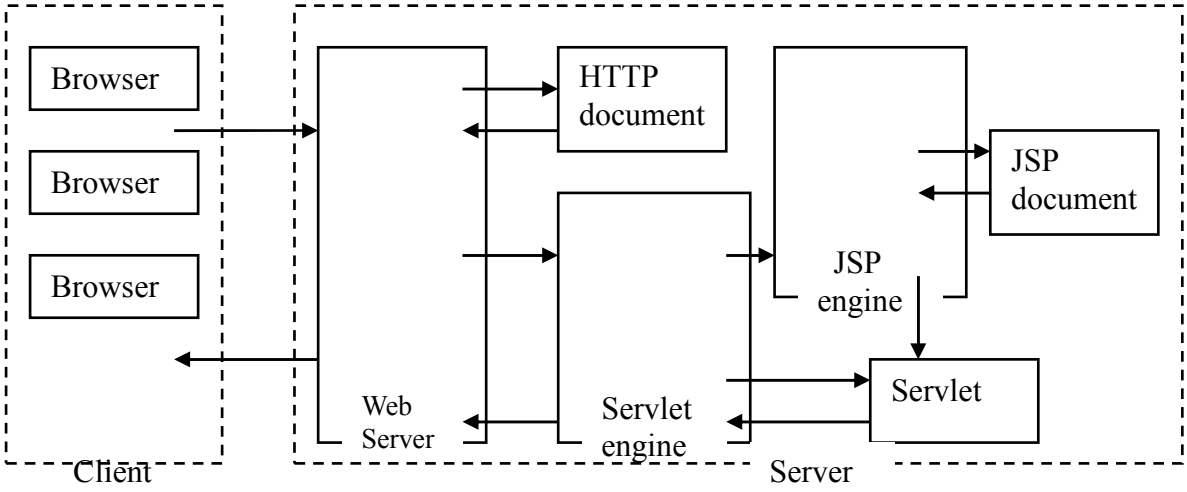

Figure1. Basic Principle of JSP

1.2 JDBC technology

Web page calls the background data in the database, so JSP and database's connection is involved, which is a very important subject. In order to manage the database, you have no choice but to use the JDBC technology.

JDBC is a kind of Java API (Application Programming Interface) that can be used to execute SQL statements. [4]It consists of a number of Java language classes and interfaces.

JDBC provide a standard application programming interface for database application developer, database front desk tools developing personnel to allow developers to write complete database application in pure Java language.

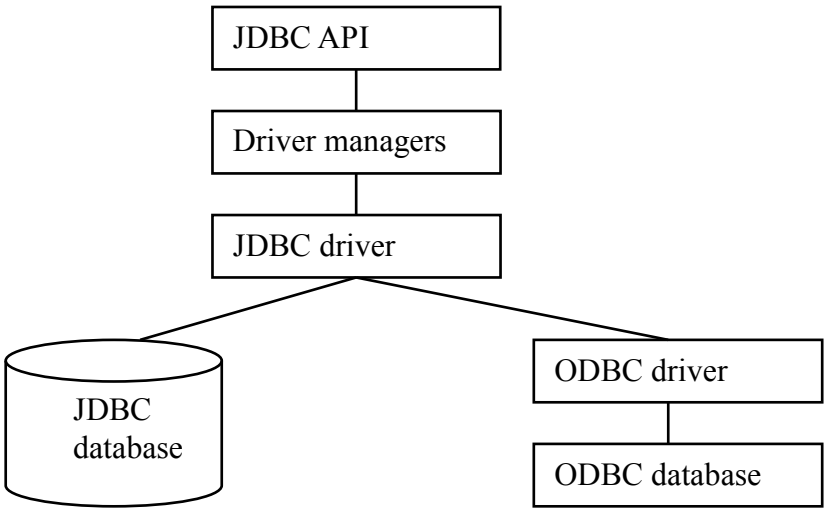

Figure2. JDBC relational chat

JDBC API (Application Programming Interface) has two different layers: the application layer is for the database Application developers; driver layer is for driver manufacturer. Figure 3 shows the application's connection to the driver.

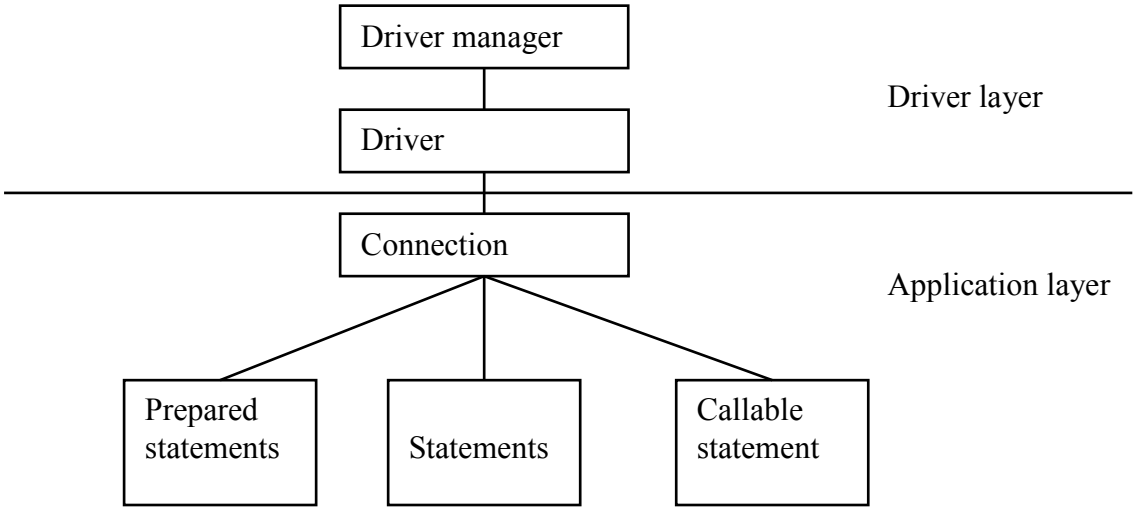

Figure3. Connection of application and driver

Adaptive testing

With the progress of society and the popularization of computer network technology, the requirements of society for workers and the technical personnel's knowledge and ability is becoming more and higher. As a measure of the ability of an important means, exam occupies further higher position in the modern life, and goes deep into the all aspects of the society. With the development of computer technology, the test methods and media is in the event of a revolutionary change, from the traditional paper and pencil test to the computer aided test, and then to the latest Web-based test.

2.1 Classical test theory

Since this century, the classical test theory has been the basis of education and psychological measurement work. The theory is also called True score theory. Its basic idea is: every individual has a certain amount of psychology that cannot be directly observed, they are called "true score" (T), we can use the “observed score"(or called "ack scores") (X) actually received, of a certain measurement error (E) as the estimated value of the true score, its mathematical model is:

Observed score = true score + error, namely X = T + E

This is a linear model; it said that the linear relationship exists between the observation points and true score. Although the classical test theory has been widely used in various types of test preparation and analysis of the test score interpretation, has a long history and has obtained many recognized achievements, it still has many insurmountable technical problems.

2.2 Item response theory

Linear model is used in classical test theory, but with the progress of mathematical research, measurer’s attention has turned to nonlinear model, and the result in the item response theory.

Item response theory model

Bright characteristic differs item response theory from the classical test theory is the ability and the difficulty on the same scale, the examinee scores (ability) related to the title number and the right number. If L is the number of subjects, r is right rate, the capacity can be represented as:

$$Ln(\frac{r}{L-r}) \quad (1)$$

Difficult degree of questions is related to the examinee number and the correct rate. If N is total number of candidates, s is for the examinee answer on the topic, the topic the difficulty can be represented as:

$$Ln(\frac{N-s}{s}) \quad (2)$$

In this way, one measuring unit unifying the ability and the difficulty came into birth, called logarithmic unit in IRT, remember answer wrong rate as O, then for probability for is right:

$$P = \frac{O}{1+O} \tag{3}$$

The item response theory of single parameter logistic model:

$$P_i(\theta) = \frac{e^{(\theta - b_1)D}}{1+e^{(\theta - b_1)D}} \tag{4}$$

Double parameters model for:

$$P_i(\theta) = \frac{e^{Da_i(\theta - b)}}{1+e^{Da(\theta - b_i)}} \tag{5}$$

Three parameters model for:

$$P_i(\theta) = c_1 + \frac{(1-c_i)e^{Da_1(\theta - b_i)}}{1+e^{Da_1(\theta - b_i)}} \tag{6}$$

Summary

Starting from the mechanical design course teaching actual requirements this paper carries out preliminary research for the mechanic design assisting auxiliary teaching system based on Web combined with the most advanced network technology. Mechanical design auxiliary teaching system software can run independently on the campus network, or wan, and students in schools and correspondence learners can learn about the course and test work by combining with their actual students. The auxiliary teaching system based on Web can greatly stimulate students' interest in learning to fully grasp the requirements of the curriculum knowledge, and at the same time also reduce the financial burden on the teachers.

References

[1] Caballe Santi, Xhafa Fatos, Barolli Leonard. Using mobile devices to support online collaborative learning [J]. Mobile Information Systems, 2010, 6(1):27-47.
[2] Francis Y Chin, Gultekin Ozsoyoglu. Statistical database design [J]. ACM Transactions on Database Systems (TODS), 1981, 6(01): 113-139.
[3] Shari L Pfleeger. Software Engineering: Theory and Practice, Second Edition [M], United States: Pearson Education, 2001, 1-84.
[4] Nada D, Brenda B. Online learning: Concepts, strategies and application [J].New Jersey: Prentice Hall, 2004.

Advanced Materials Research Vols. 989-994 (2014) pp 5345-5348
© (2014) Trans Tech Publications, Switzerland
doi:10.4028/www.scientific.net/AMR.989-994.5345

The Application of Multimedia Technology in Medical Information Management

NIU Jing[1, a], GUO Qiong[2]

[1,2]Nanyang Medical College, Nanyang 473000,China

[a] nyniujing@126.com

Keywords: Multimedia; Image processing; Database; Information management

Abstract. The development of science and technology has entered the information age. Information rapidly grow which need be accessed by the advanced technology, the development of computer multimedia transmission provides the most intuitive the most powerful support for today's information processing. Combining health care information management and computer multimedia technology, multimedia information system design is introduced in this paper, emphatically from the technical methods to discuss the requirements of the system hardware and software environment, and put forward some design methods from the universal database to tackle multimedia database and its data model. In system design, according to the characteristics of multimedia database, much data, unstructured information, information not fixed, sensitive characteristics of voice, video, and the timeline, the corresponding solutions are put forward.

Characteristics of multimedia database

1.1 Differences between media data and relational data

Relational data is data of a certain structure and can be interpreted. Multimedia data is composed of a variety of different types of media general, known as text, graphics, images, audio, video, animation, and other different types of media. Data collection, storage, processing and transmission of these media information are through different media, and the processing of each type of media has its own theory and proprietary technology. Even if the same type of media can often have different expression.

Relational data and non-relational data are used in multimedia database to express the various types of combination of multimedia data. [1]The non-relational data is multimedia content itself, the form of binary information flow; Relational data is an explanation of all aspects of multimedia data. Because of the characteristics of multimedia data, the multimedia data is difficult to be managed by using common data management methods.

1.2 OLE (Object Linking and Embedding) control

Multimedia data use relational and non-relational data combining ways to express. As it is easy to store relational data into a relational database, the storage of multimedia data is focused on how to make the relationship between the multimedia content stored in to the database. Every kind of multimedia has its own characteristics, structure and expression; we could not provide for each multimedia a way of storage and expression. So divide the three types according to the pictures, audio and video for multimedia. So you need to set up three database tables, each table used to store each type of multimedia data.[2] As long as all three to achieve storage, all multimedia can be stored and expressed. In relational database, data cannot be divided from the structure like in a storage database, as the division of the data structure, different structure of the data stored in the database can be different in the table column, but need to have a container that can receive a lot of binary information flow. At this moment OLE controls are introduced to store multimedia data.

The realization of the function of OLE controls: OLE control properties contains being able to share data and multimedia database application software. So you just need to carry out attribute set based on OLE controls so as to realize the multimedia database and Shared data between media editing software.

Design of multimedia data model and multimedia database

Multimedia database is a comprehensive technology, combing database technology and multimedia technology; it can carry out efficient organization, storage and management for the multimedia information. But in the specific design for multimedia database, many factors need to be considered, should be able to handle a single media as well as process composite media. At the same time, also need to consider the system efficiency, practical usage, easy expand, and so on in terms of human nature.

2.1 Multimedia data model

Being the same as the traditional database, data model is the core of the multimedia database system. It make the user and the structural details of the management and storage device isolated, and abstracts the static and dynamic properties of the data, in order to provide the basis of the formal to establish the use tools of multimedia data. [3] Static attributes include multimedia data object, relationship between objects and attributes of the object, and the dynamic properties include interactions between objects, object operation and user interaction, etc.

The basic task of the multimedia data model is:

1. Support structured data (such as numerical characters) and unstructured data (such as video, sound, image, etc.) and said U attribute description.

2. Support Prescntation of multimedia modeling, namely multimedia data model can express the semantic relationship the temporal and spatial relations between media objects.

2.2 Multimedia database retrieval

The multimedia data query can be divided into different types, mainly as follows:

1. Query based on the multimedia information. Content of multimedia information has been described by media data related to media objects, so these queries are based on direct access to metadata and media object.

2. Query based one example (QBE). QBE query is by looking for an example similar to the object. User's processor must correctly specify the characteristics of the object matching examples of user's request. When conduct the similarity matching, require the user to specify or systematic analysis of the texture, color, space characteristics or provide the image of the shape of the object, and can match in whole or in part. For partial matches, the query processor must match the degree of fault tolerance.

3. Time index search. These queries are used to dealing with the media time characteristic of the object, the time features can be stored by segment tree. [4]Query processor process time indexing query by accessing with segment tree storage index information or other similar methods.

4. The spatial query. These queries can be used for processing space features associated with object, these features can be generated as the media information. The query processor can access these media data information and respond.

5. Application specific query. Application specific description can be used as metadata information storage; query processor can access this information and respond.

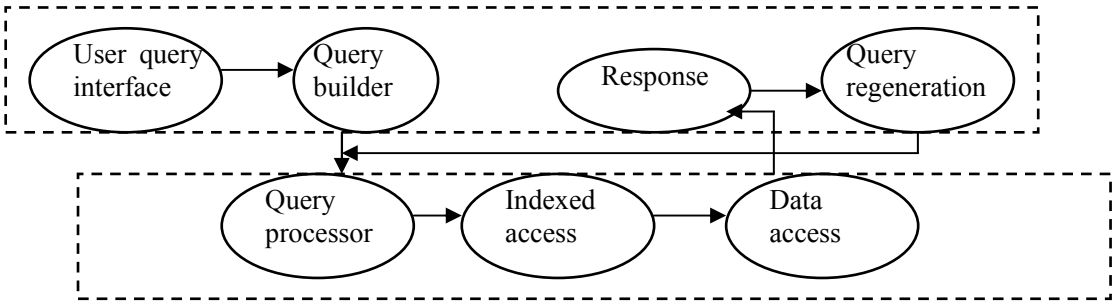

Figure1. Query management

Electronic medical record system design

3.1 Analysis of function requirement

The aim of electronic medical record system development is to record the information of the patient in an instant electronic way in order to satisfy the demands of the patient's daily diagnosis and treatment in hospital. Through the analysis it is determined that this system is mainly to achieve two roles of functional requirements, system management and medical personnel (here mainly for the doctor).

(1) System management cases

System management personnel are the runner of the system who maintains normal operation of the system. The permissions are for the entire system configuration settings and user management; such as modify the other user privileges to add or delete users, reset password, etc.

(2) Doctor cases

Doctor is the main users of electronic medical record system. The doctor may login to write case, refer to and modify the medical records, print it, add the doctor's advice, management advice, and actual operation such as printing orders.

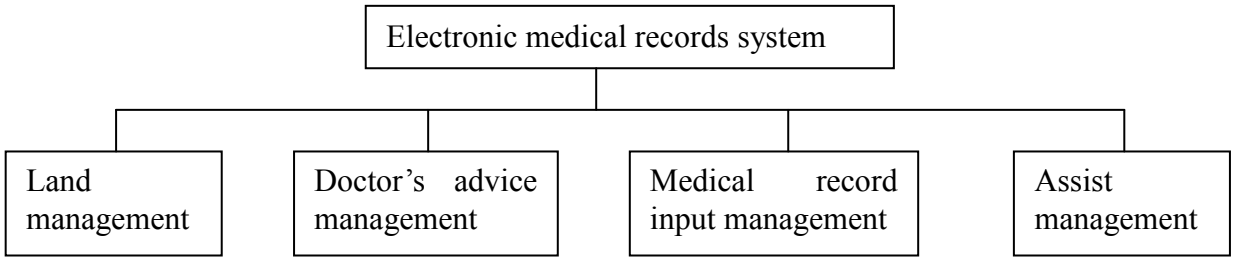

Figure2. Electronic medical record system function structure

3.2 Basic flow

The usage of basic process of electronic medical record system to is as shown in the figure below, after landing system the doctor, obtain the patient list through the HIS system, and offer the doctor's advice timely and medical records in a quick manner. As shown in figure3.

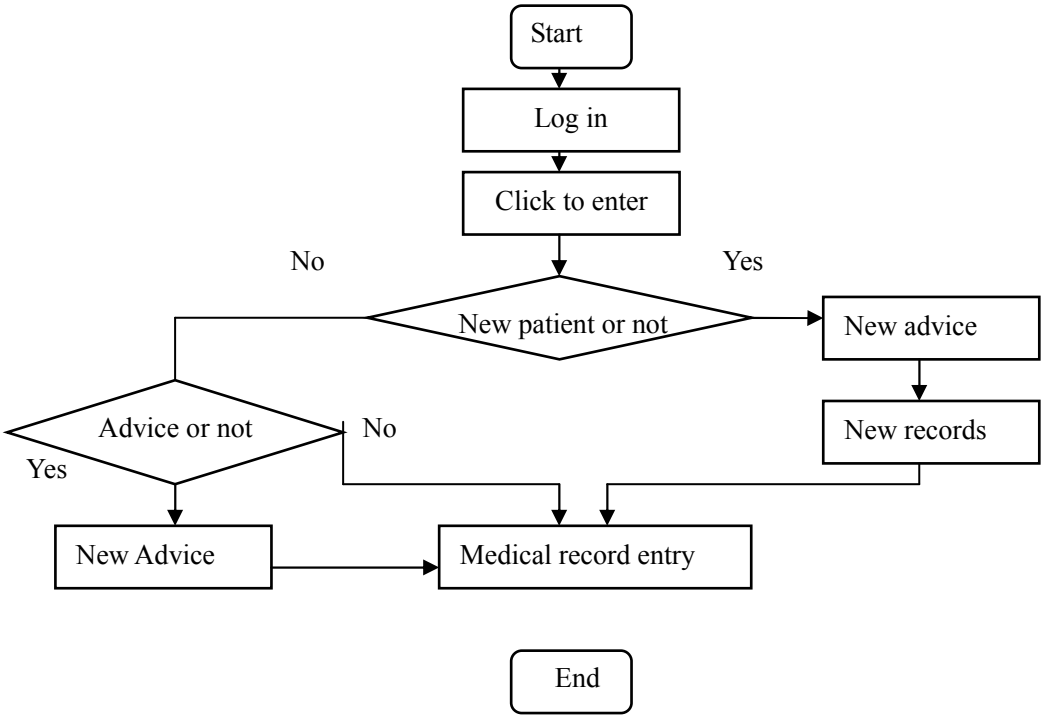

Figure 3 Basic flows of electronic medical records

Summary

Digital regional health is the inevitable trend of China's economic and social development and it is also a specific instance of the new medical health system reform. Construction of regional health information platform is an important means of promoting national health care reform, as well as to regulate information construction of medical and health industry, promote the socialization of the electronic medical records and personal health records so as to form a unified platform for the health service and health information publishing platform and health macro management support platform. Regional health information platform construction is complicated system engineering, which need the top-level design, distributed implementation. The hospital information construction is an important part of regional health information platform construction, and clinical information system construction is the main task of the hospital information construction at the present stage.

References

[1] Vijay VARMA. Structured Data System for a Breast Cancer Medical Record. in: Studies in health technology and informatics, 2009,143.
[2] Patricia SULLIVAN-TAYLOR. Development of Electronic Medical Record Content Standards to Collect Pan-Canadian Primary Health Care Indicator Data. Studies in health technology and informatics, 2009,143.
[3] S.Abiteboul, On Views and XML, InProc. ACMSIGMOD/SIGACT Conf. On Prine of Database Syst. (PODS), Philadelphia, PA, May-June1999.
[4] E.Ozkarahan, Multimedia document retrieval, Information processing & Management, Vol.13, N0.1, 1995, 113-131.

Advanced Materials Research Vols. 989-994 (2014) pp 5349-5352
© (2014) Trans Tech Publications, Switzerland
doi:10.4028/www.scientific.net/AMR.989-994.5349

Cultivating college students' information literacy under network environment

An Wang[1, a], Xiangqing Zhang[2, b]

[1]Education School, Jiangxi Science & Technology Normal University, Nanchang, China

[2] Jiangxi Science & Technology Normal University, Nanchang, China

[a]wanganwangmenghua@163.com；[b]z_xiangqing@foxmail.com

Keywords: network environment, university students, information literacy, training measures

Abstract. information literacy is not only the basic quality of college students in information age, but also a extremely important part of college students' comprehensive quality. With rapid development of computer technology, communication technology, network technology and other modern information technology, the way of acquiring information has occurred fundamental reform, so in order to survive, college students must have basic knowledge of information technology, certain information literacy and innovative thinking ability. The paper presents the current situation of college students' information literacy education, and puts forward relevant countermeasures.

Introduction

The concept of information literacy evolutes from the concept of library literacy and was first proposed by American information industry association chainman Paul Zerkowski in 1974. He defines information literacy as techniques and skills using information tools. With deepening study, the understanding of information literacy is deepening. In 1998, American library association and education communication and technology association jointly designated 9 information literary standards that students should study. In 2001, American higher education association passed through the "information literacy competency standards for higher education", which includes 5 standards, divided into 22 executive standards and several sub items. Information literacy training is extremely important and is the basic quality of lifelong learning for students.

Present situation of college students' information literacy training

University students' information literacy influences the success of quality education, and is of great help to upgrade college students' comprehensive ability. However, there are many problems existing in information literacy education.

School infrastructure investment is not enough. University information construction has direct impact on students' information literacy training. Good information construction is conductive for students to touch a variety of media and information tools, and to enhance the ability of using the information tool and information consciousness. However, informatization construction in universities can not keep up with the development of school, which leads to that the opportunity of contacting with media and various information tools reduce and hinders the development of students' information literacy.

Teachers' information literacy needs to be improved. College teachers lack the consciousness of information technology application in teaching, and most are limited to use multimedia to display teaching content while ignoring that effective use of information technology is important to college students' physical and mental development. In addition, in the process of evaluating teachers, universities always pay more attention to scientific research achievement, which cause teachers only to emphasize scientific research achievement and ignore teaching. Most teachers give students echo what the books say, and ignore the mining of information resources, thus affecting the development of students' comprehensive ability.

College students lack the sense of information. Most students in primary and secondary schools accept the "spoon feeding" education. They used to passively receive information rather that take the initiative to obtain information, which makes college students' main information resources from traditional classroom teaching and textbook. And because lacking teachers' effective guidance, quite a few students cannot acquire information through computer network, TV, or media, and underestimate the importance of information literacy.

Information ability is not enough. College computer teaching evaluation emphasizes on basic knowledge while neglecting students' comprehensive ability. Therefore, a considerable number of college students' computer operation level is limited to webpage browsing, simple software using, information collection, which causes the waste of information resources and the lack of comprehensive application ability.

Information ethics is incomplete. With the development of science and technology, information becomes easier to acquire. Quite a part of college students insist on "ism" attitude. In recent years, students' plagiarism events and network events occur more, which shows college students' information morality and concept exists problems.

Computer application courses lack effective integration with document retrieval course. The course of computer application has become the basic course of college students. Its key is to make students to have certain computer operating ability. Document retrieval and application course emphasizes that how to let students acquire and use information by using information tool effectively. In actual teaching process, the two are often disconnected and have no relation with each other. Technical course don't attach importance to the application, and the ability course learning neglect the importance of operation skills. So it causes students' technology and ability separated.

The main factors influencing the information literacy of university students

College students' information technology ability is not enough. College students possess the ability of information retrieval, but they are poor in how to use the internet to obtain information, analyze and evaluate information, integrate information into the existing knowledge structure. The initiative, consciousness and self-discipline of using information technology of college students cannot meet the need of lifelong learning and autonomous learning.

The effect of information environment. First of all, resources about special education seem to be all in a mess, and teachers and students hardly can find resources suitable to teaching and learning. Some network educational resources are not suitable to school students, which make many students embody low learning efficiency and get poor learning effect. Secondly, the network disorder also become one of the important factors hindering the people's behavior, which mainly display as slow speed, network virus, hacker intrusion, and so on. Thirdly, variety of network information is easy to disturb students' study, especially the students with poor self-control.

Information literacy education is lagging. The rapid development of information technology makes the hardware and software update quickly. However, about how to use information technology and the effect research of information technology on education, education theory and school is obviously insufficient in theory and practice. Education itself has a lot of inert, so it is not accomplished at one stroke to prompt educators and society to change education concept, let teachers use new technology correctly and adapt to new teaching method and mode in new technology environment. At the same time, software and hardware configuration was not enough to support the new teaching and learning mode. Although the network infrastructure and bandwidth has been greatly improved, from the view of computer terminal configuration and quantity, there is big distance to let all the students and teachers comprehensively use cyber source. Software and hardware configuration can not fully meet the need of the reform of education and teaching in information technology environment.

Tactics of strengthening the information literacy of university students

Increase propaganda of information quality to train students' information consciousness, and create social environment of cultivating information literacy. College students are in such a complex social environment, in which the flow of information is throughout the network. University students' information literacy training cannot separate with the effect of society. The popularization of social information culture directly relate to the training of university students' information literacy. We should strengthen the propaganda and improve the status of information literacy. Then on the basis of enhancing understanding, put the information literacy education and training on an important position.

Further improve the public network hardware facilities. The internet is the platform for students to acquire network information. The information technology, cored as the computer and network, play positive role in promoting students' subjective cognition and information emotion. The popularity of network culture, information technology also plays an important role in training college students' information literacy. If there is no the support of information technology, it is difficult to imagine the students how to get good information literacy. In order to improve college students' information literacy, the public network hardware facilities should be established to let students smoothly in the process. Powerful hardware facilities is helpful to provide information technology basis for cultivating students' information literacy, improve students' information utilization rate, and cultivate students' enthusiasm of information acquisition.

Improve college teachers' information literacy consciousness and level. To a certain extent, the focus of a new round of competition in education is talents with rich science and technology competitiveness and high cultural quality. Training specialized teachers with high information literacy has become an important way of deepening curriculum reform, promoting information quality education, and improving education comprehensive competitiveness. Teachers are the organizers and implementers of teaching activities. A teacher with higher information literacy will subliminally cultivate students' information literacy while imparting professional knowledge at the same time, For example, teachers' information behavior. So improving college teachers' information literacy consciousness and level is the key to carry out the information literacy education. Organizing information technology training for special teachers according to a certain way, let teachers integrate information technology into various elements of the curriculum teaching system. Information technology should be internal part of the classroom like all the other teaching aids.

Innovate information technology and information retrieval course and integrate information technology and curriculum. The teaching of information technology and information retrieval is the main means of information literacy training in current countries and regions. Universities should systemically arrange teaching contents and complete learning materials, set up information literacy evaluation methods and standards by the way of public courses, compulsory courses, or elective course in the university curriculum system. At the same time, the information literacy education needs to penetrate into the teaching of course. Take the cultivation of information literacy into education goal and evaluation system of all the courses. Using the method of integrating information technology and curriculum, connect information technology with curriculum content in teaching process to complete the teaching task. Integrate the information technology, the channel of teaching means and cognitive tools and multi-discipline permeation, into course to improve teaching efficiency, improve teaching effect, and change the traditional teaching form.

Strengthen college students' network moral education. We should strengthen students' information ethics, especially the network moral education. At the same time, it should avoid that students give up thinking and tracing back to nature, and should keep the depth and thickness of traditional culture. In technology, intelligence and other aspects, students have more advantages in the network world than the ordinary citizen, and have greater influence on network society and culture. Cultivate students' social responsibility in information literacy is necessary to improve their sense of mission in network society or in virtual society, the healthy development of the real society and network society, lead the progress of network and society, and establish the order of network society.

Conclusion

Information literacy has become an indispensable ability in information age. Universities should pay attention to the information literacy education, and combine with the practice to carry out information literacy education through various means to enhance students' ability of adapting to society and social competence.

References

[1] Yi Li, Baichang Zhong. Detailed explanation of information literacy[J]. The course teaching materials, 2003(10).

[2] Fang Lu, Xuechao Luo. Research and practice of approaches to cultivate university students' information literacy[J]. China medical education technology, 2006(5).

[3] Zhiyue Li. Training mechanism and methods of college students' network information literacy[J]. Information science, 2005(5).

[4] Tingting Zhou. The methods of college students' information literacy education[J]. Agriculture network information, 2010(4).

[5] Fei Wang. The way and mode of college students' information literacy education[J]. Education exploration, 2006(5).

Advanced Materials Research Vols. 989-994 (2014) pp 5353-5356
© (2014) Trans Tech Publications, Switzerland
doi:10.4028/www.scientific.net/AMR.989-994.5353

Application of Virtual Technology in Medical College

Lirong Shen[1,2]

[1]Department of Medical Electronics and Information Engineering,Shanghai Medical Instrumentation College,Shanghai 200093,China

[2]School of Optical-Electrical and Computer Engineering,University of Shanghai for Science and Technology,Shanghai 200093,China

E-mail:shenlr@smic.edu.cn

Keywords: Virtual Laborary; Teaching Reform; Resources Sharing

Abstract. Electrical and electronics laborary is the important institutions of basic practical teaching in medical colleges for the students majoring in electronics, which is the bridge to professional knowledge. Due to that the mode of traditional teaching has many disadvantages ,the introduction of virtual electrical and electronics laborary become one of the researchs in many colleges. Based on the teaching reform on electrical and electronics laborary in our college, this paper analyzes deficiency of current laboratory, determining design goals of virtual laboratory, describing its some technologies, and illustrates success of new laborary. After the lab was set up, the students' ability of practice have been improved by the teaching method—combination of virtual and actual train. Furthermore, it makes school resources sharing. The laborary has very broad prospect of application for its benefits.

Introduction

With the change from superior education to general education in colleges, the number of graduates is increasing year by year. How to cultivate students' practical and innovative ability to meet the needs of society and companies, is an urgent problem.Therefore, reform of practice teaching become a key part of school's development.The conventional mode of electrical and electronics experiment teaching do not fully meet development level of science and technology as well as market's demand.And it has several outstanding problems as follows:

- Student's scale expands continually, building a new laboratory needs a large amount of capital investment. That involves purchase of many equipments, employing lab management and maintenance of lab.
- Experimental teaching is restricted by time and place, then usage of laboratory is low.
- The traditional experiments are always simplex confimative, and they are boring. Then it do not stimulate students' learning interest and enthusiasm.
- Because of long-term heavy management and teaching, laboratory teachers gradually are out of the vanguard of modern techniques,and degradate ability of scientific research .Then they can not provide better service to college and students[1,2,3].

In view of above situation, our college begin to try a virtual network platform in the electrical and electronics laborary, which enriched contents and forms of experimental teaching to help students better understand and grasp knowledge.

Design Goals of Virtual Laboratory

For establishing the virtual electrical and electronics laboratory, our college collected suggestions and opinions from teachers and students after a long- term investigation. Finally, we determined the design goals, combining with the actual situation.The design goals are as follows:

- The student can open the webpage of virtual electrical and electronics laboratory through internet, enter the name and password of a user into individual account, then make an appointment for the experiments.

- The relevant experiment handout can be downloaded. They should preview the contents before experiment. After mastering the knowledge, students can start the experiment in virtual platform. During that time, if encountering problems which can not be solved by themselves,they can watch online teaching video for inspire or discuss with students and teachers in online communication platform.
- After completing the experiments, they should record and analysis the data, updown the experiment reports.
- For students' different levels of learning and understanding, our college use multi-level method in experiment teaching .Each project is defined as 1 point, 3 points, 5 points according to different difficulty. The students can choose validation or innovation project. Before finishing all experiments on internet,there are 10 credits left to be gained.
- Meanwhile, the students must also participate in the actual experiment in order to acquire perceptual knowledge of components and instrumentation, and learn practical and trouble shooting skills.
- The laboratory can provide some off-line simulation software and relevant tutorial downloading, such as Matlab and Multisim for their self-study.
- At the beginning of the term, the teacher can visit the virtual laboratory as a local administrator, update the experiments, import lists of students in table form and set passwords.
- During the time when students are doing experiments, the teachers answer questions online patiently and provide services. After students complete the experiments, the teachers review experiment reports and provide achievements.
- According to the professional needs of students, experimental projects can be modified and developed.

Technology Related to Virtual Laboratory

A. Architecture of virtual experiment platform

Two kinds of system structure used in the current virtual laboratory are compared, the structure of C/S (client/server) and structure of B/S (browser/server) respectively. Compared with C/S structure, B/S structure is an improved structure composed of three layers. Furthermore, it has such features as standard, low cost of creating and maintaining, providing user-friendly and flexible systems, low requirement on client, mutually independent module and high safety performance. According to the analysis, this system uses B/S structure. It is the architecture of virtual platform shown in Figure1.The whole is divided into three layers: presentation layer, function layer and data layer[4].

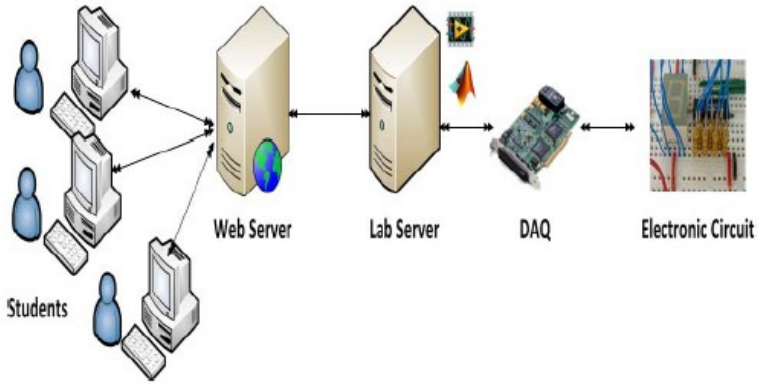

Fig.1 Structure of virtual electrical and electronics laborary

B. Development of virtual experimental environment

The virtual experiment environment is developed by Labview. Laboratory Virtual Instrument Engineering Workbenck is Labview for short. It is innovative software product developed by

American National Instruments Corporation, similar to C and BASIC development environment. The significant difference between Labview and other computer language is: Other computer languages are the code generated by text-based languages ,but Labview is the program that is writed by graphical editing language G. Its program is in form of block diagram ,and the panel and function of it is very similar with the actual instrument. It has all functions, such as the hardware that meet GPIB, VXI, RS-232 and RS-485 protocols, and the communication of data acquisition card.The standard library functions is installed internally,such as TCP/IP, ActiveX. So it is currently the most widely used, fastest and most powerful virtual instrument software. Labview development environment integrates all the tools , by which scientists and engineers can quickly build all kinds of application to solve problem and improve productivity and innovation[5,6].

C. Data acquisition system

The data acquisition system consists of sensor, transducer , singnal adjustment circuit, data acquisition card driver, hardware configuration management software, application software and computer. Its main working process is:

The physical signals is converted into electrical signals through sensor. Electrical signals becomes the data that acquisition card can store by amplification, isolation, filtering, gain, linearity etc. Then the data is processed and analysised by computer[7,8].

Success of new laborary

Since the establishment of virtual electrical and electronics laboratory in our college, it has been used for some time and get affection from students and teachers. It achieved remarkable success, and the web page of lab is as shown Fig2.Summarized as follows:

- The mulitifunctional and opening laboratory is really achieved, changing traditional experiment mode and making experiment service anytime. A new experiment environment is advocated.
- Online multimedia teaching video have rich pictures,texts and sounds, which not only provide more forms of learning ,but also effectively help students to memorize , understand and think.
- By the new experiment teaching means, the students have a solid foundation for professional knowledge and participating in Design Competition of Electronics.
- The students' enthusiasm for experiments of circuit, digital circuit and analog circuit, is increased. It demonstrates their subject status. Then many students also form interest groups, their work is as shown Fig3.
- The lab teachers decrease some work of experiment preparations and guiding experiments,and have more time to devote themselve to new experiment items. Then they can improve the scientific research and teaching ability.
- The cost of experiment teaching is lower. The problem of lack of laboratory space is solved. Usage of commodities and damage of instruments are inevitable in actual experiments, which can be replaced by the virtual experiment platform, so the money is saved effectively.
- It is safe. Failure to follow experimental instructions could result in electrical shock causing death or injury ,due to that 220V or 380V AC voltage source is used in some experiments . Nevertheless, the virtual experiment platform can avoid such problems.

Conclusion

Virtual electrical and electronics laboratory can not only solve the problem of shortage of teaching resources, but also help students give an active role in study. And the teachers' professional skills increase by it. This laboratory has a lot of advantages and is worth of generalizing. But it is still in its infancy because of some shortcomings , such as higher construction costs, not sharing resources between universities and so on. With the development of network and virtual technology, the virtual laboratory platform will be more perfect and innovative continuously and help universities foster high level talented students .

References

[1] Cheng Mei, Dai Chengjian. Design and Realization of Electrical and Electronic Network Virtual Laborary Based on LabVIEW [J].Research and Exploration in Laboratory.2011:30 (2):74-81.

[2] Song Xiangjun. Prospects of the Applicationon Vitual Laboratory Experimental Teaching in Colleges [J]. Experimental Technology and Management.2005:22(1):35-47.

[3] Zhao Xiaoqiang. Exploration and Practice of New Mode of Laboratory Management [J].Research and Exploration in Laboratory. 2010:29(11):138-139.

[4] Song Haojie. Research of the Net-based Virtual Laboratory Laboratory (D).Nanjing.Naning University of Aeronautics and Astronautics.2014. 12-17.

[5] Gu Xiaoyan ,Zhang Xiaodon, Chen Xi. A Virtual Laboratory for Electrical and Electronics Teaching [C].IEEE International Symposium on Microwave,Antenna,Propagation and EMC Technologies for Wireless Communications Proceeding. 2005.491-494.

[6] He Zhenlei ,Zhu Shan'an. Design and Implementation of An Internet-based Electrical Engineering Laboratory [C].IEEE International Conference on Control and Automation. HangZhou:China,2013.176-179.

[7] Zhang Huan ,Zhu Shanan. Internet-based Electrical Engineering Lab Integrates Real and Virtual Experiments [C].The 8th International Conference on Computer Science&Eucation. Colombo: Sri Lanka,2013.11-15.

[8] Ou Qizhong ,Tang Yingzi. Research on Network Virtual Electrical and Electronic Laboratory [C]. 2010 Asia-Pacific Conference on Power Electronics and Design.2010.20-22.

Advanced Materials Research Vols. 989-994 (2014) pp 5357-5360
© (2014) Trans Tech Publications, Switzerland
doi:10.4028/www.scientific.net/AMR.989-994.5357

Research on Cloud Computing-based virtual logistics enterprise performance management

Hongxia Zhang[1, a], Xiaodan Zhang[2,b]

[1] Shenyang University of Chemical Technology, Shenyang, China

[2] Shenyang University of Chemical Technology, Shenyang, China

[a] hhsyln@126.com, [b]zhang_024@126.com

Keywords: virtual logistics enterprise, performance management, Cloud Computing

Abstract. Virtual Logistics Enterprise is a joint collaboration between multiple companies to adapt to changing market demands. These member companies have complementary resources and technologies. Cloud computing can provide dynamic resource for each member of virtual logistics enterprises mainly based on Internet-related services. Virtual Logistics Enterprise performance management can efficient and timely acquire the implementation of various companies performance objectives relying on cloud computing platform. Through cloud computing, corporate members can obtain real-time information on the implementation of the overall performance objectives virtual logistics enterprise. Virtual Logistics Enterprise Performance Management can also help member companies to improve their internal performance management. Cloud computing is efficient contact these dynamic virtual logistics enterprise members together. Virtual Logistics Enterprise member companies will be integrated in accordance with pre-set performance management objectives with the cloud computing.

Introduction

Virtual Logistics Enterprises can realize the logistics operation and management of the whole organization relying on modern computer network technology. The participating companies can work together to achieve inter-enterprise logistics resource sharing and optimal allocation. Virtual Logistics Enterprise's strategic goal is to achieve resource sharing, risk sharing, complementary advantages and other characteristics. Under the conditions of maintaining its independence, each member enterprises established more stable partnerships with other member companies.

The member companies of virtual logistics enterprise are many independent individual in nature. Virtual Logistics Enterprise performance management can effectively integrate and regulate each member enterprise resource advantages. Simultaneously each member companies will adjust their internal performance management process around the target virtual logistics enterprise performance management.

Cloud computing is a computing model that provides virtualized resources dynamically scalable by way of Internet services. The cloud computing model provides users multiple types of resources with virtualization technology. Cloud computing will promote the member companies of the virtual logistics enterprise to remain concerned about the overall performance management and actively play its positive role

Virtual Logistics Enterprises

With the trend of economic globalization, the logistics process gradually formed a trend of internationalization. Large logistics systems with international and long-range characteristics have been impossible to build by an established business. Large modern logistics system is a virtual logistics enterprise that relies on information technology and network technology support.

The virtual logistics enterprise is not an independent enterprise in fact. But the virtual logistics enterprise can put the whole system works very effective like a very large scale of independent

business. In the case of the rapid development of the information technology and the rapid development of the logistics concepts, the service process of modern logistics industry will become a new service area which involved many links, a wide range and dispersion of businesses. The object and scope of services provided by the real logistics enterprises have significant limitations. A separate logistics enterprise could not easily face large-scale international logistics needs of users across time, across regions independently. The logistics service market is facing a large number of cross-industry, cross-regional supply and demand of customers. And also the logistics service market is facing a huge number of logistics business activities occur at any time. Large number of logistics demand side need a logistics service provider that can provide comprehensive, all-weather, the whole process of logistics services.

Logistics supply and demand sides will quickly and easily reach the needs of logistics services. Modern new logistics services necessarily have electronics, networking, automation and integration features. Virtual Logistics Enterprise quickly and easily perform the flow business activities to achieve the logistics of speed, security, reliability, low cost of aim, through a virtual network of logistics organization, trade, service, management.

Virtual logistics enterprise performance management

The foundation of virtual logistics enterprise is the reality of logistics services demand side cross-regional, cross-industry. All involved in the virtual enterprise logistics service providers will focus on the formation of a logistics business with a dynamic organization. This organization will continue to change along with the reality of cross-regional, cross-industry logistics needs. Each company involved in providing services, especially logistics enterprises will closely linked. So the virtual logistics enterprise performance management must also be improved revolved around discrete organizational structure.

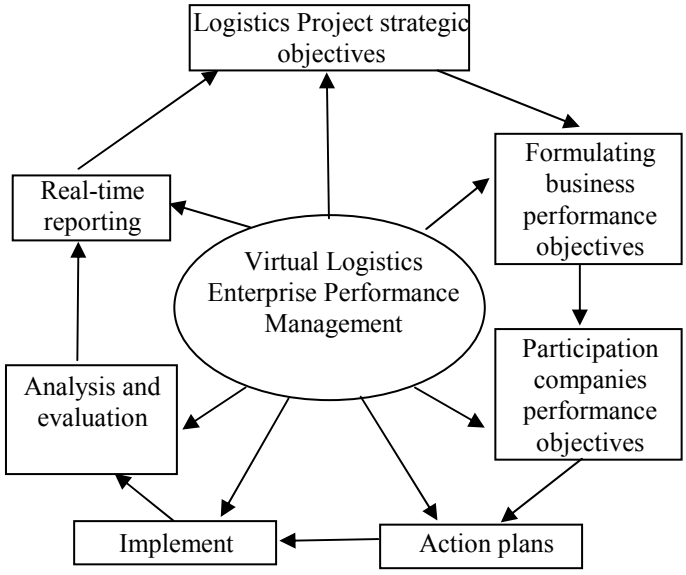

Figure 1. Virtual Logistics Enterprise Performance Management

Virtual Logistics Enterprise Performance Management is an application with interactive features across multiple industries and characteristics. The formation basis of virtual logistics enterprise has the characteristics of certain realistic needs. So the performance management for virtual logistics enterprise will also revolves around those concrete reality demand for logistics services. In this process, the actual business of the participating companies will be expanded along with the actual business of logistics. The performance management for each participating enterprise will be subsequently commenced. This set of performance management rules is the basis of performance

measurement and analysis for virtual logistics enterprises to complete the actual process of logistics services in the future.

Cloud computing and virtual logistics enterprises

Cloud computing is an Internet-based computing approach. Through cloud computing, hardware and software resources and information sharing can be provided to computers and other devices on demand. Cloud computing can provide a dynamic and scalable resources based on Internet-related services. For economic management practical activities, the spread resources are often virtualization. Virtual Logistics Enterprise member companies are involved in this dynamic organization for a logistics project. The essence closely to promote these enterprises is a virtual integration of performance management objectives.

The basis of virtual logistics enterprise is a specific inter-regional and cross-industry complex logistics project. All enterprises involved in this complex project are independent entities. Their close ties need an open platform as a basis. Currently the cloud computing can provide maximum help to them. Cloud computing provides services a unified resource space for various member companies through management, scheduling and integration of the various resources of each virtual logistics enterprises member.

The resources provided by cloud computing derived from virtual logistics enterprise virtual space. Integration of these virtual space resources is based on established performance management objectives. Each member companies are sharing their competitive advantages and the resources in the cloud space based on jointly performance management objectives identified.

Influence of cloud computing on virtual logistics enterprises performance management

In most cases, the basis for measurement and assessment of virtual logistics enterprise performance management is a pre-established performance evaluation index. The performance management and evaluation for all member alliance's dynamic are required to establish under a stable, common evaluation standards. Logistics Services objects and logistics projects environmental and other factors will generate some random variation.

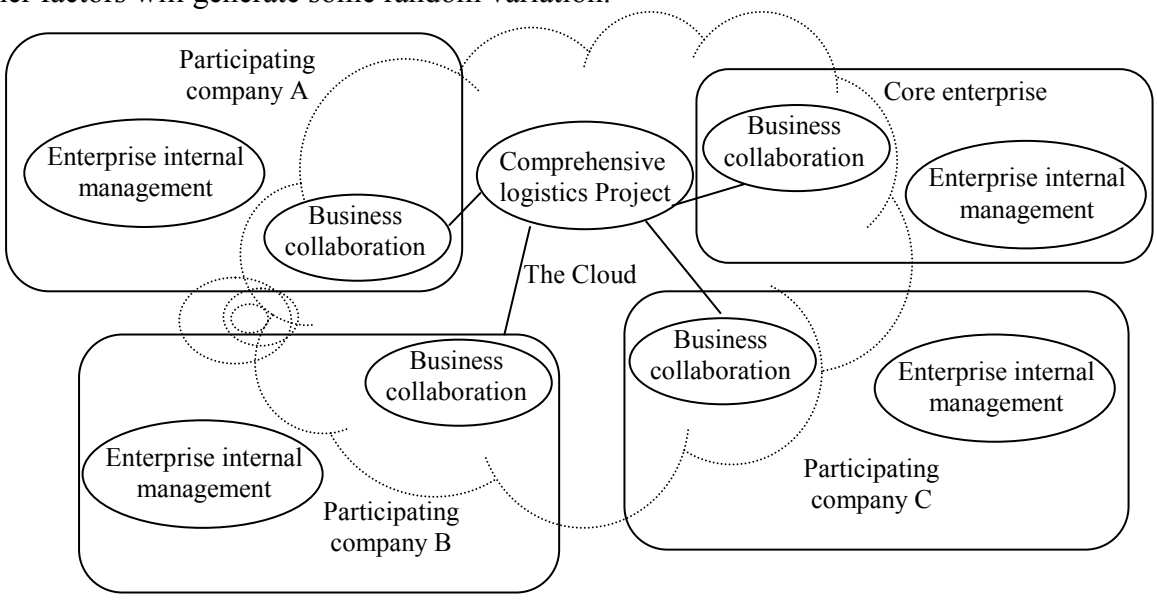

Figure 2. Virtual Logistics Enterprises Performance Management base on Cloud Computing

The virtual logistics enterprise performance management needs to establish a real-time performance evaluation and restraint mechanisms for dynamic alliance members to complete the real-time performance in order to adapt the impact of these changes. In the united underlying network

structure inherent in the companies, the cloud computing can give full play features, such as real-time, multi-faceted, multi-angle, multi-agent communication, to promote real-time virtual logistics enterprise performance management objectives.

When the performance management target system is established, virtual logistics enterprises not only pay attention to the performance of member companies, but also concern about the performance of the entire dynamic organization to adapt to the environment. Cloud computing will effectively integrate various types of information such as performance information for each member enterprise of the virtual logistics enterprise, external environmental benefits information, related industries benefit information, and benefit information related areas for the logistics projects. Virtual Logistics Enterprise performance management can be timely performance evaluation and supervision of the members enterprises based on this information. With various applications provided by cloud computing, virtual logistics enterprises can improve long-term performance management system of virtual logistics enterprise focus on specific logistics project led by the core enterprises.

Summary

Virtual Logistics Enterprise Performance Management is a comprehensive activity. Guiding role of the core business and active participation of the member companies will affect the performance management effectiveness of virtual logistics enterprise. Therefore, the effective communication platform between the participating enterprises is particularly important. With cloud computing, virtual logistics enterprise performance management can maximize the collection of each member enterprises.

Cloud computing provides possibilities of the real-time communication and sufficient information sharing for Virtual Logistics Enterprise Performance Management. Virtual Logistics Enterprise performance management is different from the traditional enterprise performance management. Virtual Logistics Enterprise Performance Management cannot periodically evaluate and assess. In most cases Virtual Logistics Enterprise Performance Management need to ensure real-time communication. The various enterprises will also actively complete the Virtual Performance Management combined with their own internal performance management by means of cloud computing information sharing.

References

[1] Robert Bacal in: *Performance Management*, edtied by McGraw-Hill Professional; 2nd Revised edition (2012)

[2] Jill Nemiro, Michael M. Beyerlein, Lori Bradley, Susan Beyerlein in: *The Handbook of High Performance Virtual Teams: A Toolkit for Collaborating Across Boundaries*, edtied by Jossey-Bass (2008).

[3] Syed Tauhid Zuhor in: *Cloud Computing*, edtied by LAP Lambert Academic Publishing (2012).

[4] Harish Vepuri in: *Cloud Computing*, edtied by LAP Lambert Academic Publishing (2012)

[5] Information on http://zh.wikipedia.org/wiki

[6] Information on http://www.mbalib.com/

Advanced Materials Research Vols. 989-994 (2014) pp 5361-5363
© (2014) Trans Tech Publications, Switzerland
doi:10.4028/www.scientific.net/AMR.989-994.5361

Design and Implementation of Real Estate Sales System Based on B/S

Xiaoyan ZHU[1, a]

[1] Engineering school of economics ,Hunan communication polytechnic, Hunan Changsha,410132,China

[a]Xiaoyanzhu0427@yeah.net

Keywords: real estate sales system, B/S, design and implementation

Abstract. As the housing system reform and the rapid development of real estate sales business, people put forward higher requirements on housing sales management. In the modern information society, people who buy houses just want to get the real estate sales and selling information as soon as possible. Real estate sales agent needs to communicate with buyers quickly. Real estate sales information management system is different from general management Information System in theory and real practice, which attach more information to the timeliness of issued information.

With the development of our society and the increasing competition, real estate businessman pay more and more attention to information technology, and more real estate developers realize the importance of improving efficiency, decreasing cost and expanding business through information technology. Therefore, to develop a real estate sales system suiting the current market, and to solve problems that they meet in the housing market have practical significance.

Brief introduction of B/S.

1.1Introduction of B/S network mode

B/S mode, that is browser or server mode. It is a new network structure model developed from the traditional two-floor C/S mode, its essence is a three layers structure C/S mode. In B/S mode, clients use browser software, which asks Web server to have access to the database in the form of hypertext.[1]

Web server accepts the request, then convertes the request to SQL syntax and passes to the database server to verify its legitimacy, carry on data processing and then processed results back to the Web server. The Web server dwill receive the reverted results again, change the results to HTML form, forward to client browser and show in the form of a friendly Web page.

1.2Characteristics of B/S network mode.

(1) Economics of the development, maintenance and upgrade of the system. For large software, the cost of its development, maintenance and upgrade is very high, while the frame structure of B/S model can mostly save the cost, and at the same time, the B/S mode puts forward low request to the front desk client to avoid the tremendous blind cost on hardware upgrade.[2]

(2) It can be cross-platform operatied. The client only need a WWW browser as the applicated software in B/S mode is based on a Web browser. Some browser interface are similar which can reduce the training fee of the software.

(3) B/S mode has good openness and scalable. In B/S mode, the external users can also visit through the browser.

(4) B/S model has stronger information system integration. B/S mode integrates different kinds of services instead of scattered a single problem, which can provide higher working efficiency.

(5) B/S mode provides flexible exchange of information and the service of releasing information. B/S model can effectively solve the problem of a large number of irregular information exchange inside the company with the help of the Internet information release and transmition.

6) B/S mode provides the most realistic basis of online, network openness, unified service of heterogeneous machines, heterogeneous network, heterogeneous application service.

1.3Reason for adopting B/S network mode.

The traditional information system based on client/server mode need to install application programon the client and configure database.Every time when using it, the work is quite tedious. As

the prosses have been on the client in advance, security has also been a problem. While Web technology is based on browser/server mode, program is actually in the client, do not need to the client to install any program, so it can solve the problems of the existing client/server mod e well.[3]

The system based on Web technology is with the aid of the Internet around the world to make the job be done at local or can also be carried out in another place, which greatly expand the flexibility.

Design of the B/S real estate sales system.

2.1Aim of the real estate sales system.

System adopts B/S mode commonly used in the mainstream operation system platform, which uses ASP as the main development instrument. Backstage database adopts SQL Server 2000, HTML, ASP technology to edit web pages, and uses ASP technolog to associate SQL Server 2000 database with dynamic web pages, so the building information can be preserved and updated timely in order to realize the functions of the real estate sales system and be more dynamic.[4]

2.2Design of the real estate sales system.

System adopts dynamic development based on Web database, and associates the Web with database system closely, which is built according to the Browser /

Server structure, visiting the database through the Browser and can realize the dynamic interaction of Internet information service technology. Its function includes online data query and data processing etc. The dynamic Web development of online database is increasingly becoming the core problem in Web application. How to create building intelligent interactive Web applications, how to connect the Web server with backstage database and how to have access to the database for the users are the very hot topics in the study of the current development of Web application. To understand and master the technology as a kind of Web construction technology and technical reserves have great positive and realistic significance.[5]

From chart 1 we see that Web database system basically consists Web server, database, middleware, and network protocol software, among which the middleware si responsible for managing the communication between the Web server and database, and provides the application service program. It can directly or invorke external programs or scripts to visit the database. So it can provide dynamic HTML pages related to the database and accept the users' query, shift the results to HTML page and reture back to the browser through the Web server.

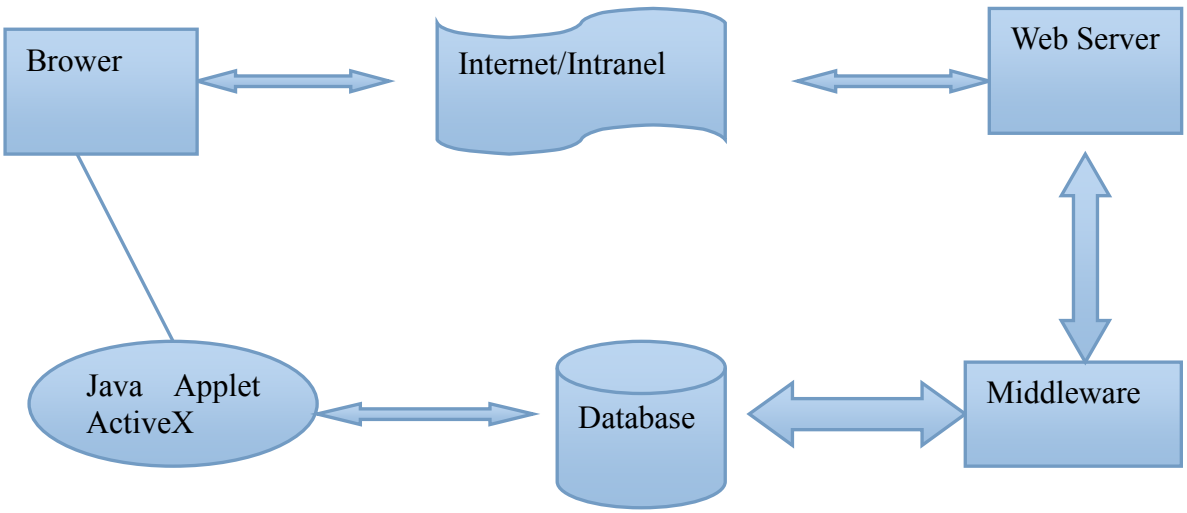

Chart 1: The Basic Structure of Web Server and database to achieve connection

2.2Process design of the system database.

The final step about data analysis is the analysis of data flow, namely to independent the flow of data within the organization abstractly, abandon the specific organization, information carrier, supplies, materials, and test data processing mode in actual business.

Chart 2 of the process shows us the fuction of the system. Information management and fow of the whole system is mainly housing dources and client information. According to the main fuction if the system, DFD at the top of the system reflects the data flow of the system on the macro aspect.

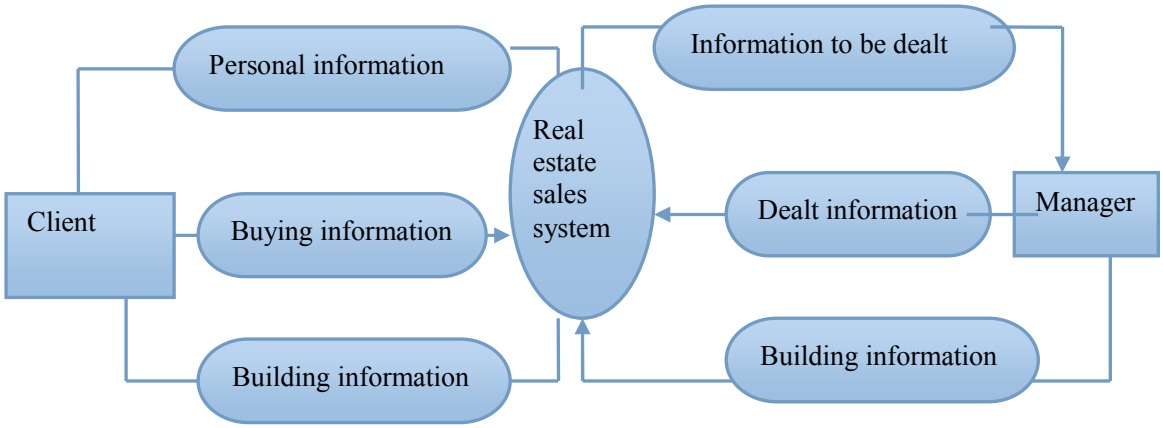

Chart 2: Chart of database processing on the top lever of the system

Implementation of the real estate sales system.

System has realized functions of the management of buildings and sales, such as users' registration, message leaving function. System also has the news reading fuction which makes clients know more about the current real estate news and common sense, which can save many time and human resources for the company.

The website of the system mainly provides the clients resources of the real estate including sales, need, renting information. The main functions of the system includes management of the real estate, management of the clients, management of the building sales, maintaining of the system, management of the system and the management of the news.

Characteristics of the system are as follows: the first one is updating the sales and renting information at any time; the second one is convenient, simple and flexible operation; the last one is friendly IOS and easy query.

Summary

At present, most of the real estate sales management system is still in the database management stage in our country, the management level is still in the level of completing some simple table printing jobs, can not adapt to the demand of the modern real estate sales. According to these situation, The system developes several main function modes from the real estate sales in the process of buying and selling.

The goal are convenient management, simple operation obvious pictures. It is of extremely important significance fo the real estate sales management and customer information management.

References

[1]Chen Hong, Design And Implementation of The Real Estate Sales Management Base on B/S, 2000.
[2]Chu Tiansi, Pang Yajuan, Technological Development of ASP, 2007.
[3]David C Hay, Requirements Analysis, 2004.
[4]Jiang Lihua, Xiang Yunzhu, Design of the Sales Management System Based On C/S,2005.
[5]Xue Huacheng, System of the Information Management,2007.

Advanced Materials Research Vols. 989-994 (2014) pp 5364-5368
© (2014) Trans Tech Publications, Switzerland
doi:10.4028/www.scientific.net/AMR.989-994.5364

The design of finance assistant management system for the modern enterprise management by using computer

Ge Liu [1, a], Hai-bing Zhang [2,b]

[1] Tangshan Industrial Vocational Technical College,Tangshan,063000.China

[2] Modern technology and education center , Hebei United University, Tangshan, 063009.Hebei,China

[a] liuge_lg@sina.com, [b] seaman_zhb@163.com

Keywords: computer,management system,modern enterprises.

Abstract. With the deepening reform of the management system of modern enterprises, the effective use of new technology and science has become increasingly important to every enterprise in order to make themselves in an invincible position in the competition must establish their own set of efficient operation of information management systems, the company embarked on a road of healthy development. Based on this, the paper mainly discusses the use of computer management information systems in the modern enterprises.

Introduction

Compared with the international modern enterprises business , the development of China's modern enterprises started late, so the computer management in modern enterprises also cause behind many countries and regions. Before 2000, the use of computer technology in the management of modern enterprises to manage a handful of units . Until after the country 's computer technology to develop after 2000, only a little application , but on the management level with developed countries , there are still some gaps . On current usage , although compared to the past has been a big improvement and development of the overall situation, new management techniques and measures computer just some of the bigger state-owned modern enterprises and public institutions were application , and the application and the amount of those small and medium private enterprises in less than in application mode , the application of integrated management capabilities of the computer are ignored , and only some of the individual management practices are widespread popularity and use. On the system and means in terms of the whole operation , because of the lack of uniform standards and management practices standardized , making the management of modern enterprises in the computer application is still in the lowest level stage , you can not achieve information sharing and quick delivery.

The necessity of a management information system

Development of each enterprise are never mature maturing process , the development of modern enterprises are also the same. As a result of the traditional modern enterprises using traditional management methods , making a lot of manpower and material resources and financial waste in place may not be wasted , resulting in low efficiency of traditional modern enterprises . The rapid development of modern science and technology in the modern society , a variety of high technology and equipment continue to be applied to a variety of business management process, so inevitably we need to introduce new equipment and management techniques in the management of modern enterprises to change the drawbacks of traditional modern enterprises . Then the computer management technology as an efficient and practical means of management was introduced , because the computer management techniques using a variety of complex information can be systematically analyzed and processed further in a quantitative way to express our a variety of basic information and data needed , greatly reducing the repetitive and mechanical work , the more management personnel freed from the workplace .

Development of computer information management system is an emphasis on human-machine closely systematic individualized engineering development projects. It just requires timely development and application of innovative technologies , more emphasis is kind of old management regime change. Computer information management system in modern enterprise management emphasized that the use of high technology and new equipment will change the traditional management model into computer management model , which requires the introduction of a number of specialized kinds of talent management and learning computer applications make them play their professional knowledge and skills to a variety of modern enterprise management work place .

Key in the development of management information system

Rational development principles. Many companies in the development process management system only requires software development management personnel management information system developed in line with the corporate management system to adapt now , which makes the development of management information systems in the management and application of technology are behind the times the pace of development . So, we just want to change the information management system of the computer, but to develop a reasonable development principles , emphasizing the development of a new information management system must be in a certain extent, the current management system is a technology and innovation and on measures change, rather than the previous management system duplication and imitation. Modern enterprise managers to develop appropriate policies to manage and support the establishment of a new management structure of the system.

Decisive leadership. Implementation of the success or failure of a unit can not do without a wise decision led initiatives . But individual leaders in modern modern enterprise is also a serious lack of such careful observation and close attention , mainly in the following aspects :(1)lack of awareness of information management , there is no advance information management to predict advantages and good prospects ; (20work management information system can not belong to the effectiveness of the high-income projects, but have to invest a lot of money and human resources, leadership in the face of this problem had to take a perfunctory attitude decision-making, which makes information management work carried out extremely difficult.

The key role of talent. Competition in a variety of high-tech focus to the last performance in the competition above all talent , so leading modern enterprises should pay attention to the training of professionals and computer management, a variety of operating systems and management practices of their skilled operation units , continuously updated techniques and methods for the management and planning advice unit .

Development and application of three management information system

Overall planning scheme. The total planning scheme is proposed in a variety of professionals in the theory and practice of research on the basis of details on the use of various management measures and technical computer management information systems on a variety of projects modern enterprise management information system planning and design of overall design.

The overall development of ideas. Modern enterprises is an organic unity of the whole , in the management of modern enterprises in horizontal linkages between the various projects is very important . To improve the overall efficiency of modern enterprises must then develop ideas for the future and direction of enterprises particularly clear understanding. During the construction of modern enterprise information management system, must develop a standardized overall development of ideas, projects and projects will be carried out every reasonable arrangement and layout , starting from the establishment of a database information system must be on all the items from which organic unity link chain under the management of the modern companies do a good job .

Factors affecting the development. For modern enterprises systematic management information systems planning and design must take into account the various factors affecting their development : for example, efforts to support the leadership , resources and facilities to improve the degree of near-term business development plan objectives, each a series of old species work management system and the traditional system of established standards and so on. This must be taken into account are the impact factor , because the combined effect of these factors constitute the modern enterprises standardized operation mode.

Use of Software. Modern enterprises to establish a standardized management information system is inseparable from the software using a variety of computer systems , information management system managers need to buy their own management software, but also consider it consistent with the company's other software fitness , the best use of the principle of the trial after the first purchase , and gradually establish a standardized information system suitable for their own enterprises want to use the software . We can build a team of specialized software minorities constitute a team of management personnel in the modern enterprise information management system for software testing and adaptation of Use . So not only can ensure that when we choose to external software quality assurance and software functionality they provide is that we need these personnel , can have the leisure to develop and manage a variety of small software , these developed among the software used to create the modern enterprise information management systems go . Currently , there is a certain degree of fit between accommodate a large variety of domestic and international software development , but how to choose the right and be compatible with the modern enterprise management system software is really a huge amount of work tasks. So we have specialized personnel to conduct regular training and learning , so that they better make efforts for the application to work in the modern enterprise software.

Examples of Application

Example Overview. According to wave through soft "631X" business model , management of enterprise software applications in the course of about sixty percent probability by universal test the software , the rest of the remaining forty percent , and a quarter of I belong to personalize the needs of various business units , and three-quarters of the functions belonging to various industry needs . In view of this , a variety of technical and management personnel to develop software must select the function will be added generic products in development management process throughout the software. For example: modern enterprises using computer aided management of the financial system (referred MECMFS) custom software development , including financial indicators data acquisition system, the transformation of financial software custom development and units of special requirements. Financial Indicators data acquisition system uses an incremental replication technology, financial data for each subordinate units through the " mastery " of financial analysis required for the formation of financial indicators .

The design on MECMFS.(1) questions , with all kinds of modern enterprises expanding business scale , the current management can not meet the development needs of the situation , decided to assist the development and application MECMFS financial management system . (2)System development environment. MECMFS developed on a computer , computer configuration requires good (conventional software configuration and data management language , capacity, speed and other parameters can be determined depending on the circumstances) , and with laser printers and scanners and other advanced equipment . (3)The main task . The main task is to use computer MECMFS modern enterprise financial information data query, modify, delete , and storage ; using a computer to quickly carry out this task , and can be made personalized programs and reports, to provide each kind of information to contribute. (4)systematic design ideas. System uses computer management information system development software engineering design approach to design . In this way

technical documentation is complete, create favorable conditions for future repairs, modifications. System development documentation there : MECMFS project plan ; MECMFS test mission statement ; MECMFS user manual.

The role of functional modules. (1)leading module. Module controls the entire system , built with the right port user password with select menu prompts , the operator explains how to use the system. By function selection , adjusting the various functional sub- blocks. When the operation is completed the required operating personnel , and then return to its sub-function control module ; (2)establish accounts module. Is divided into two sub-modules , database and update modules ; (3)Input Module . According to evidence a single input data, financial data content can be changed directly , you can enter the query module for viewing when they encounter problems ; (4)query module . Tip 5 function selection module , the implementation of human-computer dialogue conducted on the contents of the database have chosen to view ; (5)modify the module . Module in accordance with the financial database lateral , vertical content changes and logical addition to measuring the physical delete function.

System effects. Changed the previous system, the smaller the screen during the setup of the system , the operability is not strong and other drawbacks and disadvantages. In the course of various modern enterprise management information systems need to operate simple , powerful operating system. Use of this system was in line with the various requirements of modern modern enterprise management information system , of course , it is not without its shortcomings when dealing with issues such as finance-related , it will deal with inadequate performance , so even further improved .

Conclusion

Use a high level of enterprise information management systems is critical in today's businesses to succeed in the fierce market competition. Therefore, we must be combined with the current situation of various innovative technologies and measures , positive computer management information systems used in modern enterprise management.

Acknowledgements

This work was financially supported by the 2013 Science Foundation of Hebei United University (Project No. Z201302) and .the 2013 scientific research on higher education of Hebei Association of Higher Education(Project No. GJXHZ2013-321).

References

[1] Ariza-Villaverde, A.B,Gutie´rrez de Rave´, E.; Jime´nez-Hornero, F.J.; Pavo´n-Domi´nguez, P.; Muñoz-Bermejo, F.: Computer Applications in Engineering Education, v 21, n 4, p 573-80, 2013

[2] Bhattacharjee, Sudipta,Roy, Pramit; Ghosh, Soumalya; Misra, Sudip; Obaidat, Mohammad S.: Journal of Systems and Software, v 85, n 3, p 571-581, 2012

[3] Taler, Jan,Trojan, Marcin; Taler, Dawid Source: Archives of Thermodynamics, v 30, n 2, p 59-76, 2009

[4] British Coal Corportion in: Management Information Syste, European Commission (1991).

[5] R.L. Grayson in: Use Computers in Coal Industry, Taylor & Francis (1990)

[6] Jie Zheng,Ng, T.S.E.; Sripanidkulchai, K.; Zhaolei Liu IEEE Transactions on Network and Service Management, v 10, n 4, p 369-82, 2013

[7] Saeedi, A, Doolen, T.L: International Journal of Data Analysis Techniques and Strategies, v 4, n 1, p 1-20, 2012
[8] Chen, Shih-Ming ,Griffis, F.H.; Chen, Po-Han; Chang, Luh-Maan: Automation in Construction, v 35, p 89-110, 2013
[9] Sunderman, C.,Waynert, J. source: 2012 IEEE Industry Applications Society Annual Meeting, p 5 pp., 2012
[10] Huang, Hui,Source: WIT Transactions on Engineering Sciences, v 80, p 735-743, 2013, Advances in Industrial Engineering, Information and Water Resources

Advanced Materials Research Vols. 989-994 (2014) pp 5369-5372
© (2014) Trans Tech Publications, Switzerland
doi:10.4028/www.scientific.net/AMR.989-994.5369

Design and Realization of Computer Teaching Room Based on VMware Visualization Technology

SHAO Hongcheng[1, a]

[1]Basic Computer Center, School of Information Engineering, Yancheng Institute of Technology, Yancheng 224003,China

[a]ShaoHongcheng08@yeah.net

Keywords: Computer teaching room, VMware, Visualization technology

Abstract. As information technology is developing at an unprecedented speed, computers are widely applied in the process of teaching in colleges. A large number of universities and colleges purchase computers for practical teaching such as experiment, course design as well as visual simulation.

Due to the diversity of software versions and their differences, all teaching softwares are repeatedly installed, updated and uninstalled with the changes of courses. In such a circumstance, staff who take charge of computer teaching rooms will take on a great amount of working pressure. How to effectively meet the practical needs of all courses, release computer teaching rooms' burdens and increase the comprehensive efficiency will be a tough problem and challenge.

1. Problems in computer teaching rooms.

In order to meet diverse needs for various courses in teaching processes, computer teaching rooms in universities and colleges have to install various systematic softwares such as Windows XP, Vista, Windows 7, Windows 8 and Linux or operational softwares including Windows Office, Photoshop, AutoCAD, Visual Basic, Java and SQL Server. All of the above softwares are required to be installed in distinct operational environments and with discrepant configurations. However, in terms of computer hardwares, purchasing time as well as hardware type must be taken into consideration.

Meanwhile, in daily management of computer teaching rooms, some problems wait to be figured out. Installation of various softwares with multi-path boot in a single computer will result in systematic conflicts and compatibility problems. In addition, the large number of softwares installed will also cause prolonged starting time, dull running and worse property. What's more, the lack of safety patches and virus softwares arouses potential risks.

Therefore, how to effectively meet the practical needs of all courses, release computer teaching rooms' burdens and increase the comprehensive efficiency will be a tough problem and challenge. All of the above problems are also incomparably difficult and each of us are faced with great challenges in the near future. Design and realization of computer teaching rooms is a long way for all of us.

2. VMware.

VMware , as a pioneer and leader of present x86 platform visualization, is one of the most developed software companies in the whole world. VMware's Ballon Driver Theory, Shadow Page Table Theory and Visual Device Driving Programs have been widely applied. Besides, it is in possession of three major visualization production line, including data center visualization products, desktop visualization products, application visualization products as well as some assistance products.

VMware ThinApp is a visualization product of application program produced by VMware whose desktop visualization products cover VMware Workstation, VMware Fusion and VMware View. Data center production line is mainly server-oriented for enterprises, producing VMware vSphere, VMware GSX Server and VMware vCloud.

VMware Server is a visualization product for free and a visualization machine counting on visualization models, which can be installed in Windows and Linux. As the visiting of physical hardwares must be finished through bottom operational systems, part property consumption will occur. However, VMware Server is a perfect choice for enterprises with small size.

VMware vSphere is a visualization software set with abundant functions, being able to provide basic frames of visualization as well as application programs and management, mainly covering ESX Server, vCenter Server, Virtual Machine File System, Symmetric Multiple Processor, Distributed Resource Schedule, VMotion, Storage VMotion, Fault Tolerance, High Availability and Consolidated Backup. The following figure1 indicates the basic frame of vSphere.

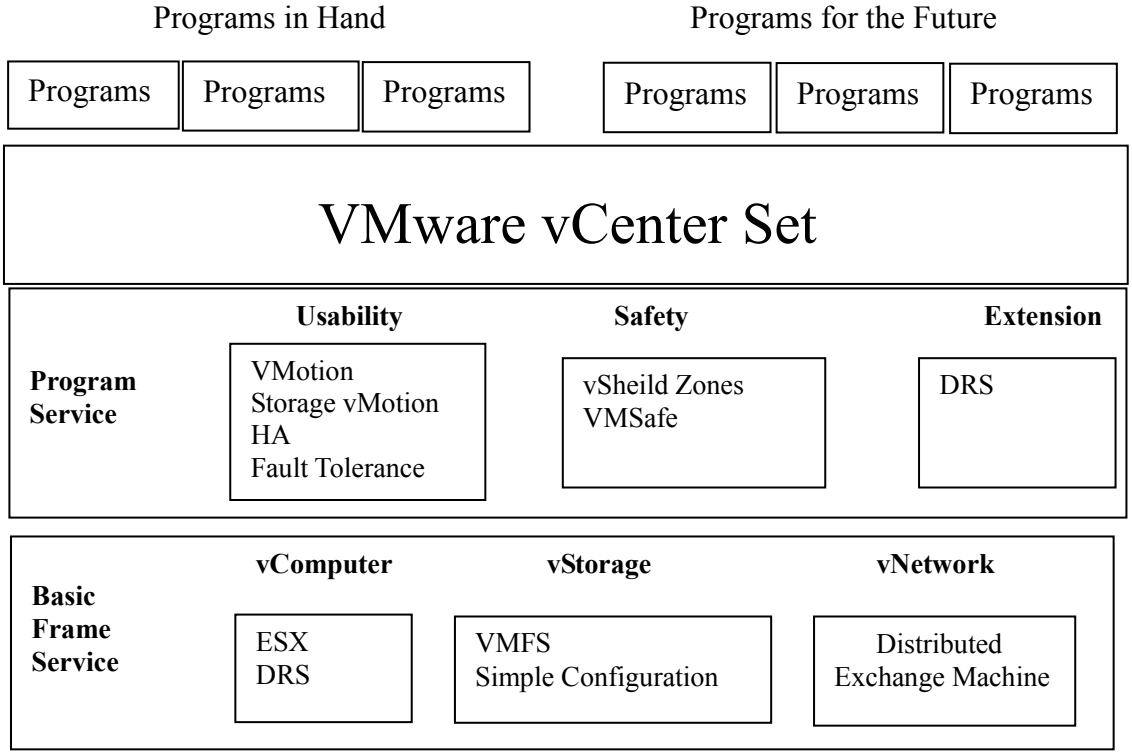

Figure 1. Basic Frame of VMware vSphere

3. Advantages of VMware visualization technology.

VMware visualization technology, as a heated topic researched by both educational and industrial circles, is in possession of some prominent advantages.

3.1 High utilization efficiency of resource.

In present enterprise data centers, for reasons of convenient management, safety and high property, the majority of x86 servers only run a single application, which results in low utilization efficiency of CPU, on average ranging from 5%~20%.

VMware visualization technology is able to integrate several servers into a single physical server to increase utilization efficiency of the physical server. In the mean time, segregation and capsulation offered by VMware visualization technology is able to make sure of safety and good property of the former server.

3.2 Low power consumption.

Power consumption in data centers mainly lies in the IT devices such as refrigeration and ventilation, but power consumption of computers only accounts for the minority. How to increase the proportion of computers' power consumption in the total consumption will be a vital problem.

Switching off the servers with low use ratio is the most visual way to save power. However, in traditional patterns, it will switch off the application when it is running in a sever if the server is switched off. In such a circumstance, VMware visualization technology is able to integrate all of the applications running in servers into few servers so that vacant physical servers can be turned off.

3.3 Rise of compatibility and acceleration of applications.

Segregation and capsulation offered by VMware visualization technology is able to segregate the platform in which applications run from the bottom servers. Thus, administrators no longer need to frequently adjust the applications according to bottom environments. A single application version keeps everything in control.

Deploying a application equals to capsulation of a operational system and a applied program's visualization machine, usually taking several minutes. Compared with traditional deploying ways, it saves manual labor, shortens deploying time and reduces deploying cost.

3.4 Reduction of cost.

Data centers are in need of constant fund to update and maintain IT infrastructures, including purchasing cost of softwares as well as operation and maintenance cost.

VMware visualization technology is able to reduce the number of physical servers so as to decrease the investment in servers and power consumption. In addition, VMware visualization technology is also able to let IT administrators get rid of a large amount of spare work which is related with physical server, operational system and compatibility problem and pay more attention to application management. In the mean time, management instruments provided by VMware companies obviously reduce administrators' working pressures, increase working efficiency and also drop IT running and maintenance cost. VMware visualization technology is definitely a good selection for reduction of cost.

4. Property data calculation in computer teaching rooms.

4.1 Use ratio of CPU.

The use ratio of CPU mentioned in this paragraph refers to average use ratio and its calculation method can be concluded as follows.

1) Extract the number of CPU and mark it as N.

2) Extract the present systematic time(the number of Ticks), subtract the systematic time kept before and finally get a systematic time gap marked as S.

3) Extract the present systematic vacant time, substract the vacant time kept before and finally get a vacant time gap marked as I.

Below formula indicates how average use ratio of CPU is calculated.

$$AverageRatio = 100 - I / S / N * 100 \quad (1)$$

4.2 Use ratio of internal memory.

Calculation of use ratio of internal memory should count on WIN32 API function and its calculation can be finished through below formula.

$$dwMemoryLoad\ (\%) = \frac{dwTotalPhys - dwAaiPhys}{dwTotalPhys} * 100 \quad (2)$$

4.3 Storage utilization.

In Windows, storage utilization refers to the utilization of all logic drivers and its calculation conforms to below formula.

$$DriverUtilization(\%) = \frac{driverTotalPhy - driverAailPhy}{driverTotalPhy} * 100 \quad (3)$$

Summary.

Application of VMware visualization technology tremendously changes traditional computer teaching room pattens, realizes central management and flexible control of teaching softwares and figures out the common problems existing in different operational system versions as well as compatibility problems in various application softwares. Besides, VMware visualization releases administrators' working volume, increases working efficiency, prolong the lifetime of hardware devices, reduces the cost invested in computer room construction, maintenance and management. Finally, comprehensive use ratio is largely boosted.

References

[1] Wu Ronglong, Design and Implementation of Data Collection and Control System based on VMware Visualization, 2008.
[2] Lei Wanfang, Samples of Cloud Calculation, Platform and Application[M], 2012.
[3]Bao Jinghai, Zhou Xiaozhu, Fan Donghong, Research on Construction of Virtual Network Lab Based on VMware[J], 2010.
[4] Wang Qiang, Zhang Jianglu, He Caihui, Construction of Open Computer Laboratory Through Resource Integration[J], 2011.

Advanced Materials Research Vols. 989-994 (2014) pp 5373-5377
© (2014) Trans Tech Publications, Switzerland
doi:10.4028/www.scientific.net/AMR.989-994.5373

Construction of evaluation index system for Finnish design policy

Chaojie Chen[1, a], Fang Hai[1, b] and Dongjiu YU[1, c]

[1]School of Art and Design, Guangdong University of Technology, Guangzhou 510000, China;

[a]Chen-chaojie@QQ.com, [b] fanghaimail@163.com, [c]yu9design@foxmail.com

Keywords: Finnish design policy; evaluation index system; industrial design .

Abstract: Finland is the first country that formulates the design policy, and these successful experience and lessons are deserved to be focused and studied. This paper has a research on the Finnish policy index with the factor analysis approach and Delphi Method, and sorts out the opinions of policy planners, building the index system of design policy which is used to evaluate the effectiveness and result of Finnish design policy, and then studies the exterior policy environment where design innovation drives the development of country, and provides important reference for the system summary, the effectiveness, problem and tendency of the Finnish design policy.

Introduction

Nowadays, as an advanced research field of design management science, design policy has become the important part of the strategic choice and the policy setting of countries in the world in the innovation economic age. Finland is the most successful design founded nation after the World War II, as well as the first country that formulates the design policy. It can be clearly seen that Finnish government regards design as the national policy, developing design industries by investing money and making policy, which help the country strengthen national power and enhance the international competitive capability.

In China, the research and practice of how to add the value of design creation to develop the economy at the national level are still insufficient, which is obviously different from that Finnish regards the industrial policy as a part of national development strategies to make the national revitalization policy of design. The experience of making and implementing design policy is worthy learning from and taking as reference. However, how to evaluate the effectiveness of Finnish design policy effectively and objectively needs to research and build the index system of design policy, which provides important reference for the system summary, the effectiveness, problem and tendency of the Finnish design policy.

1. Finnish Design Policy and the Development of Finnish Design Industry

1.1 Definition of Design Policy

As for the definitions of the design policy, most of them focus on the three levels, namely design national policy, industrial policy and cultural policy, which can be found from the books, Internet and documents[1]. “Design policy” in this paper refers to the public policy which is implemented nationwide, and it aims to promote the development of the nation. As a part of the national policy, aside from under the unified leadership of the central government, the design policy also needs to promote close cooperation among the departments which are related with the design industry, such as the government, the marketing intermediaries, professional association, design enterprise and other departments. These relevant departments should implement the policy from the design promotion, design education, and design support dimensions, developing this comprehensive and crossing field.

1.2 Finnish Design Policy and the Development of Finnish Design Industry

Finland is located in the Arctic, a special geographical position with forested mountains and numerous lakes which has a great influence on Finnish design tradition and culture. Finns learn about

the world through the nature and integrate the plainness of the nature and the affection of the natural resources into the design culture, which forms the character that the Finnish design pays more attention on people-oriented and natural and plain environment. Therefore, it can say that “Finland is the real hometown of the modern ecological functionalism design ”.

The support of the development of design industry from the Finnish government has entered a mature period, covering all the design promotion types at every stage of the evolution of design innovation policy among EU countries, and releasing policy to promote and assure the implementation of these activities[3]. The Finnish government made the policy of “design founded nation” in 1950s, which helps Finland overtake other Nordic countries in design. From the year of 1990 to 1998, Finland government made the “outline of leading design”. In this outline, design, engineering and marketing are integrated into the system of IDBM[4]. In the late 1990s, greatly promoted by SITRA, national commission on arts and crafts and design council, the deciders of Finland education, research, industry and politics stared to prepare and make a five-year plan of the Finnish design policy, putting forward that the design should be the main factor of the competitive power and be a part of national innovation systems. In June 2000, Finnish government released the design policy of “Design 2005”, and it was formally approved by the Finland’s parliament. Design has been integrated into the national innovation system which aims to improve the competitive power of industry in this plan. And it is a sign that “design has become a part of national innovation system”, and design formally enters into the nation’s highest level, becoming the national strategy that design innovation drives the development of country.

1.3 Main Contents of the Finnish Design Policy

As the world’s first policy outline which is advocated by the government, “Design 2005!” “is not limited itself to explain the design in the cultural dimension, at the same time, it also analyzes the design from the aspects of industry and economy”, which is a major breakthrough[4]. “Design 2005”focuses on the long-lasting impact of government’s investing in design, therefore, the government’s impact can be seen in the outline everywhere which consists of 73 measures. The outline expresses that “the executive body is the Ministry of Education of Finland and Department of Trade and Industry”, and the two departments provide the main sources of capital finance to the design industry as well as call on the the international monetary funds, professional associations and educational institutions to support the design industry, besides, they also release policy to guide the development of design industry[5].

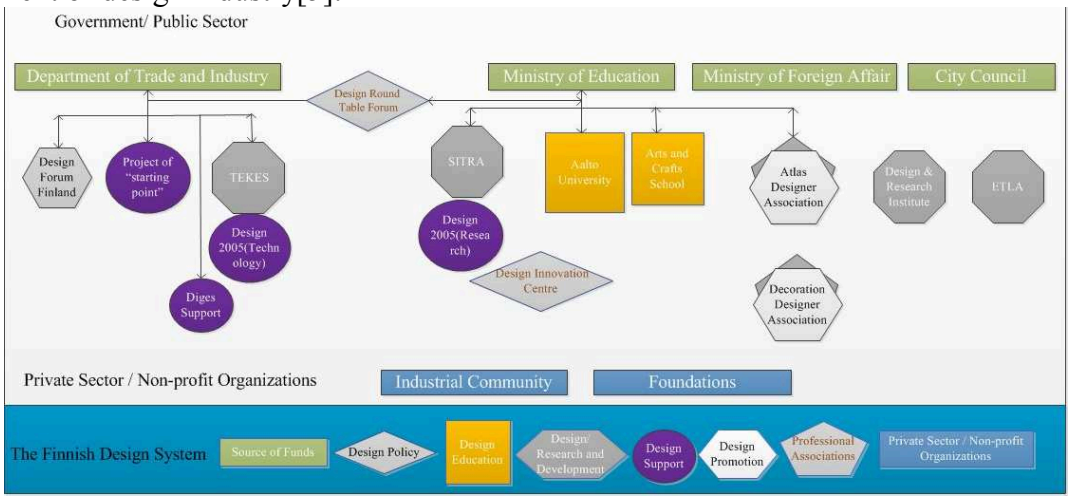

Fig. 1 Index System of Finnish Design Policy’s Assessment

Based on the actual national condition, the Finnish government enhances the direct support for research activities of design through a lot of means, for example, the Finnish government funds the technical research of design trough the Tekes and Academy of Finland. These measures include: supporting for formulating the design research standards; encouraging the enterprise to research and develop the design in the enterprise’s management stratagem; supporting the development of local

design enterprise and strengthening their operational capacity; requiring the educational and research associations to add the design speciality to their fields, and dividing up the goals of talent cultivation of various design colleges. The execution architecture of Finnish design policy is shown in figure 1.

"Design 2005" makes a tremendous splash in the world, for "the mode of combining the design with industry, national policy, culture and education" is a extraordinary accomplishment, which shows that design has been regarded as a national innovation policy, "having the right to make decision, while there was no voice for design previously "[6] .

2. Establishment of Index System of Finnish Design Policy's Assessment

The difficulty of study on Finnish design policy lies that how to evaluate the executive effectiveness of it objectively. Thus, it requires to formulate the assessment tool of "policy indicator" of the system, aiming to measure and monitor the changing industrial environment caused by executing the Finnish design policy.

2.1 Design -policy Indicators

Design-policy indicators aim to develop a set of new statistical series to evaluate the the development of design industry and its influence on social life changes. And the design-policy indicators can also observe the development trend of design industry. Therefore, the basic definition of the policy indicators should include two levels of analysis of goal and statistic. The design-policy indicators should evaluate and measure the current situation and trend of Finnish design industry and related social phenomenon after implementing the design policy through objective scientific text and data, and turn the credible economy power and social statistic into the statistic that can evaluate the development situation of Finnish design industry.

2.2 Construction Idea of Index System of Finnish Design Policy's Assessment

The goal of establishing the index system of Finnish design policy's assessment is to simplify the complicated relation among the fields which are related to performance structural systems of Finnish design policy, and to obtain more assess information by using appropriate assessment indicators. Construction approaches and procedure of index system of Finnish design policy's assessment is shown in the figure2.

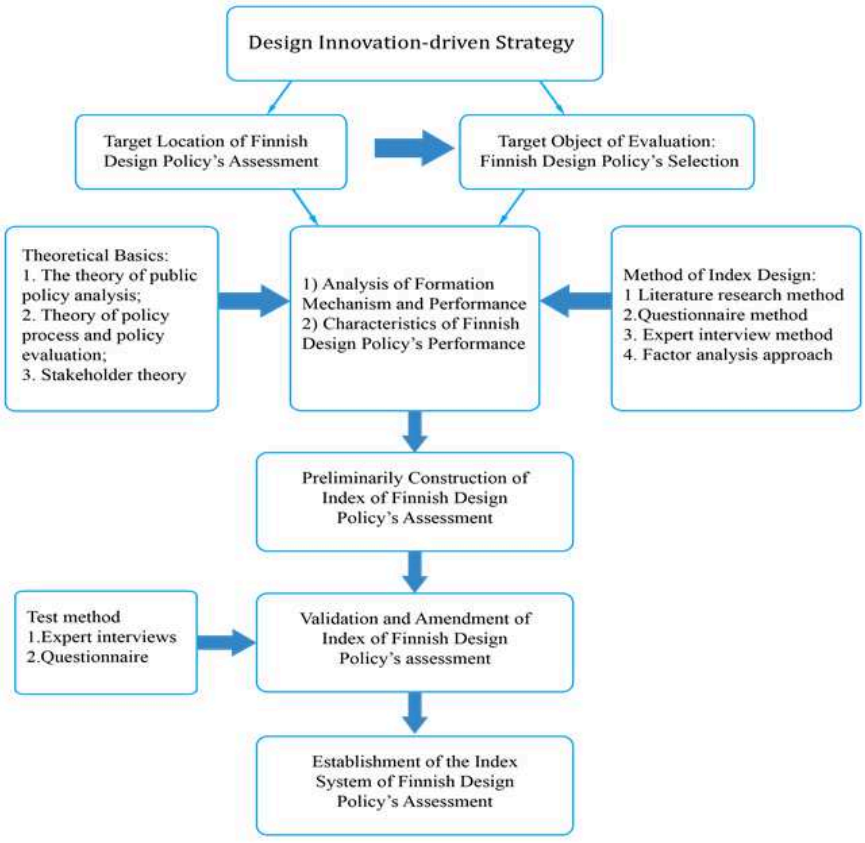

Fig2. Construction Method and Procedure of the Index System of Finnish Design Policy's Assessment

Firstly, with the guidance of Finnish design system, definite the connotation, goal and object of Finnish design policy. Secondly, based on the overseas and domestic policy assessments, the relevant theories of design industry, and other theoretical basis such as the theory of design industry development, theory of policy process and policy assessment and stakeholder theory, make a probing analysis of process of design process, the formation mechanism and performance characteristics of Finnish design policy's performance. And analyze the related fields and components of these fields which have influence on the index of design policy by applying the factor analysis approach and Delphi Method, and then design the index system. According to the index design principle and logical framework, design the hierarchical structure of index system and preliminary secondary index system and apply the expert interviews to correct. And refine the second class indicator into the third class indictor when the former is certain. At last, establish the index system of Finnish design policy's assessment. It is shown in Table 1.

Table 1 Index System of Finnish Design Policy's Assessment

First Class Indicator	Second Class Indicator	Third Class Indicator
Indicator group of industry policy	**Government funding**	1)annual growth rate of government's investment on design industry (%)
	Research personnel	2）the number of graduate of design-related colleges 3）the percentage of PhD researchers in the researchers of universities (%) 4）the percentage of researchers with master degree or higher level in enterprises 5）the number of researchers with bachelor degree or higher level per 10，000 persons
	Industry Development	6）ratio of design industry revenues to GDP 7）annual revenues of design industry 8）yearly revenues growth rate of design industry(%) 9)Quarterly fixed asset investments of design industry(billion Yuan) 10) annual growth of fixed asset investments of design industry(%)
Indicator group of cultural policy	**Culture Creative Policy**	12)ratio of the number of design entrepreneurship to the number of national total entrepreneurship (%) 13)employment rate of manpower of design industry（%） 14)ratio of manpower with bachelor degree of design-related universities in the category of cultural creativity (%) 15)the number of national work's being awarded in design in the international competition (/year) 16)the number of passing the design patent application (/year) 17)ratio of cultural consumption to household expenditure (%)
	Cultural Services	18)popularity rate of gallery and museum (/ thousand people) 19)utilization rate of gallery and museum (person-time/ thousand people) 20)times of design exhibition activities (Time/Year) 21)times of every citizen's taking part in the cultural activities of design(Time/Year)
Indicator group of Education policy	**Vocational Education**	22)ratio of population of vocational education to total population of education (%) 23)ratio of vocational education budget to total education budget(%)
	University Education	24) ratio of university education budget to total education budget(%)

		25) ratio of investment into university education equipment (%) 26) student-faculty ratios in university(%) 27) the number of college teacher's publishing papers(/year)
Indicator group of communication policy	**Information Dissemination of Design**	28) ratio of annual investment into design performance by government(%) 29) hours of government's using media to publicize the design-related issues (Hour/Month) 30) hours of per thousand citizens' attending the design-related cultural issues publicized by media per month (Hour/Month) 31) the annual average number of holding nationwide design-related seminars(/year) 32)the annual average publication number of design-related research papers (/year) 33) annual average publication number of design-related books (/year) 34) average visits of the design-related websites (Time/Day)
Indicator group of sustainable design policy	**Sustainable Design Policy**	35)ratio of achieving the goal of energy conservation design of enterprise product(%) 36)ratio of achieving the goal of resource recycling design of enterprise product(%) 37)ratio of achieving the goal of simplified packaging design of enterprise product（%）

IV Conclusion

This paper, for the progressive contents, is based on the general idea of comparative study and general domain of policy research, progressing in the way of "policy background - policy formation process - policy objective and content - policy implementation - policy evaluation". This paper analyzes the background and the evolution of Finnish design policy and clarifies the process that the Finnish design policy plays a role during the nation development; and on this basis, from the perspective of policy objective, the paper establishes the index system, and explores the index system of Finnish design policy by using the factor analysis approach and Delphi Method.

References

[1] liu Shuang.*The design council of UK bring to UK design Public Policy influence*(MS. The central academy of fine arts，China2008)，P.2.

[2] Hugo Thenint. *Design as a tool for innovation，A PRO INNO Europe project: Global Review of Innovation Intelligence and Policy studies*, (2008),P. 12.

[3] Wang Xiaohong. Experiences and Enlightenments of the Development of Industrial Design at Home and Abroad .Design，2011（04）,P.56.

[4] Pekka korvenmaa. *Finnish design — a concise history*(China Architecture & Building Press,China 2012).p.53.

[5] Guo Wen， Zhang Hongyun . Comparative analysis on national design system and its implications. Scientific research management[J]2012(10),P.56-63.

[6] Pekka korvenmaa. *Finnish design — a concise history*(China Architecture & Building Press,China 2012),p.125.

Advanced Materials Research Vols. 989-994 (2014) pp 5378-5381
© (2014) Trans Tech Publications, Switzerland
doi:10.4028/www.scientific.net/AMR.989-994.5378

Process and Technology Research on Information Management of Agricultural Disaster Prevention and Reduction

Yinghuan Wu [1,a], Wenlong Liu[2,b]

[1] School of Economic Management, Nanchang Institute of Technology, Nanchang, Jiangxi, P.R.China

[2]School of Economic Management, Nanchang Institute of Technology, Nanchang, Jiangxi, P.R.China

[a] cnliu2010@163.com, [b]1772493063@qq.com

Keywords: Process; Technology; Information management; disaster prevention and reduction

Abstract. This paper analyzed research status of agricultural prevention and reduction, and summarized the three information management process stages: preparedness, response and recovery of agricultural disaster prevention and reduction. Finally, the paper analyzed information management technology model of agricultural disaster prevention and reduction.

Introduction

Crisis information management research mainly focused on the nature of crisis management and crisis to illustrate the significance of the crisis information in crisis management, thus to reveal the crisis management from information viewpoint so as to draw peoples attention on the crisis information management. As Mitroff and Pearson believes in his book Crisis Management, the gathering, analysis and dissemination of crisis information is the primary task of crisis management [1]; W.A. Wagenaar analyzed crisis information management issues and revealed the importance of information management in crisis management in Profiling Crisis Management[2]; Robert Heath proposed crisis management framework and divided information management department into information organization department, the public and media sector, consulting image management department[3];R.L.Chartrand systematically studied the application of crisis emergency communication systems and IT crisis in crisis management[4] ; Nick Collin studied the importance of crisis information management and information technology management; Sherif Kame systematically expounded the important role of decision support systems in crisis management[5]. There are also many other scholars researched on crisis management mechanisms, processes, rules and method from many aspects.

Research status of agricultural disaster prevention and reduction information management

Due to the special nature and vulnerability of agriculture, it makes agriculture often susceptible to the external environment. As the complexity of agriculture, research on agricultural public crisis early warning is difficult than other crisis warning studies. With the economic development of China, the importance of agriculture are constantly increasing and attracting more researcher research on crisis management. As BOND studied disaster losses in agriculture, and found out that if we can make the public know about early disaster information and make them take the appropriate preventive or escape behavior, it will reduce the impact of disasters effectively. Fiona Duggan and Linda Banwell built crisis information dissemination model [6]. There is studied on information processing mechanisms of early warning system for agriculture, and proposed many constructive comments [7]. However, we can find out that agricultural disaster information management researches in China is on its infancy stage through analysis of crisis information management research documents all over the world. At the same time, although China has increased investment in the construction of crisis information management [8], but the overall effect of the crisis information management is still

weaker than developed countries. In modern society, public crisis is a major social problem all countries have to face with, and is a issue related to a country's stability, security, social and economic development, and its citizen's life and property. Agriculture is one of a country's ancient core industries, therefore the study of public disaster information management in agriculture is significant, and there is a great research expansion space of the field.

Basic processes of information management of agricultural disaster prevention and reduction

Agricultural disaster prevention and reduction is a matter of the government, disaster management organizations, rescue workers, the executive branch and the general public that is high flexible collaborative decision-making process which needs continued support and rapid response capability [9]. In the course of this ongoing collaboration, the organization and dissemination of information and data play a key role. In other words, at the right time, the right place to pass the correct amount of the right information to the right people is very important. The whole disaster management process can be divided into preparation, response, recovery and reconstruction three stages. Depending on the time point of each stage, they have different tasks to be solved (as shown in Table 1). During the preparation stage, it mainly focused on monitoring: recognition and mitigation supply needs, threats and possible consequences, and further action also includes the development of new tools and technologies. Response stage directly related to the primary objective of mitigation - to save people, including victims who need psychological and physiological treatment. Therefore, action at this time including information gathering, rescue teams, health personnel and resources (such as food, medicines) transport. As the rescue operations are likely to be affected by the disaster emergency situations, new potential threats and available resources should be considered. If necessary, the decision maker should ask the country and even internationally rescue teams for help timely to provide direct security support timely. Reconstruction stage is to explore new solutions, construct and reconstruct destroyed infrastructure to build resistance capacity for any future stronger disaster.

Table 1. Tasks in various stages of disaster emergency information management

Preparation Stage	Response Stage	Reconstruction Stage
Survey	Warnings	Disaster detection
Train	Data management	Data management
Raise public awareness	Allocation of rescue tasks	Archiving, backup
Integration of information and communication technology	Rescue	Information dissemination
Cooperation of stakeholders	Cooperation of stakeholders	Cooperation of stakeholders

At the process of agricultural disaster prevention and reduction, there are interaction between people and people, people and computers. Interpersonal communication includes face to face communication, wired and wireless phones, and computers. People and computer interaction including databases, modeling and simulation technology, computer-aided, alarm and security systems, and monitoring technology, such as cameras, satellite systems, robotics and broadcast media, among them, there are three main forms of collaboration: collaboration detection tools; collaborative decision-making process; cooperation in the implementation of the resource. Collaboration often occurs among the local, regional, and national organizations. Department ready response, to be called as the reconstruction stage shown in Table 2, among them, public utility services includes local and regional level administrative departments: power, gas, sewage and water. The transport department includes local or regional administrative airways, highways, railways, waterways services. In addition, government departments, all other institutions of national and regional as well as administrative agencies all of them should incorporate into the local disaster management plan and prepare and support the work.

Table2. Agricultural Disaster prevention and reduction information management departments of various stages

Stages	Related Depatments
Preparation Stage	Designer/Planner, Mobile Communication Service Providers (Such As China Mobile, China Telecom, China Unicom,Etc.), Project Managers, Public Health Departments, Engineers, Experts, Health And Safety Executive, Security Control Center, Material Manufacturers, Media Focal Point, Propaganda Department, The Meteorological Department, Disaster Agencies, Water Sector
Response Stage	Stage Ambulances, Mobile Communication Service Providers (Such As China Mobile, China Telecom, Etc.), Casualty Centers, National Disaster Relief Headquarters, The Fire Department, The State Council, Hospitals, Security Control Centers, Medical Personnel, Media Focal Point, The Foreign Ministry, The Police Survivors Reception Center, Department Of Transportation, TV/Radio, Utility Services, People's Liberation Army, The Chinese People's Armed Police Force And The Militia
Reconstruction Stage	Stage designer/planner, project managers, engineers, experts, the State Council, materials manufacturers, the publicity department of the PLA, the Chinese People's Armed Police Force and the militia, TV/radio, public utility services sector

Information Technology model of Agricultural disaster prevention and reduction

In the agricultural disaster prevention and reduction process, information quality is the most important issue, and effective flow of information will help to promote and strengthen cooperation between the various departments rescue. It needs to identify and overcome the collaborators and technical problems due to the failure of disaster management of the process. In a disaster, there are generally four transmission channels of information flow: the internal organization of the participants (such as agriculture bureau), from people to the organization and to the people from the organization. The reliability of information gotten by decision-makers must be checked. Therefore, it is necessary to introduce data filtering function during the transmission of information flow between the various departments. Data filtering network (DFN) can minimize information overload, spreading of misinformation, releasing of incomplete information, changing information and conflicting information problems. It has three main functions: (1) collect related data and information of disaster from the public, media and specific experts; (2) organize useful data; (3) send the necessary final filtered metadata, data and information to its subordinate. Thus, the information and communication technologies play an important role in the process of agricultural disaster prevention and reduction. It facilitates the flow of information and collaboration between organizations to improve disaster planning, mitigation and management level. Information and communication technology systems should be adapted to the needs of users. However, as the number of users of the system increase, it is difficult to ensure adequate flow of information (particularly in large-scale natural disasters). Therefore, the amount of information users have to make the system fault, the risk of information loss and delay minimize.

Information and communication technology (ICT) framework used in agricultural disaster prevention and reduction is a combination of a series of orderly composition of ICT, it refers to the completion of a systematic reconstruction of ICT in certain environments interact with each other in disaster collaborative model being used by various organizations, thus forming the network to help achieve effective two-way communication in disaster management process, in order to improve the efficiency of cooperation. Figure1 is information technology model of agricultural disaster prevention and reduction. In all stages of the disaster management process, the applied information and communication technologies includes the internet, information security, computer databases, integrated data management, intelligent data management, audit tools, multi-agent systems,

multi-language support, data filtering, mobile communication technology, wired communication technologies, and wireless communication technologies. Some of these techniques can be applied to all stages of the disaster management process; others can only apply to a specific stage.

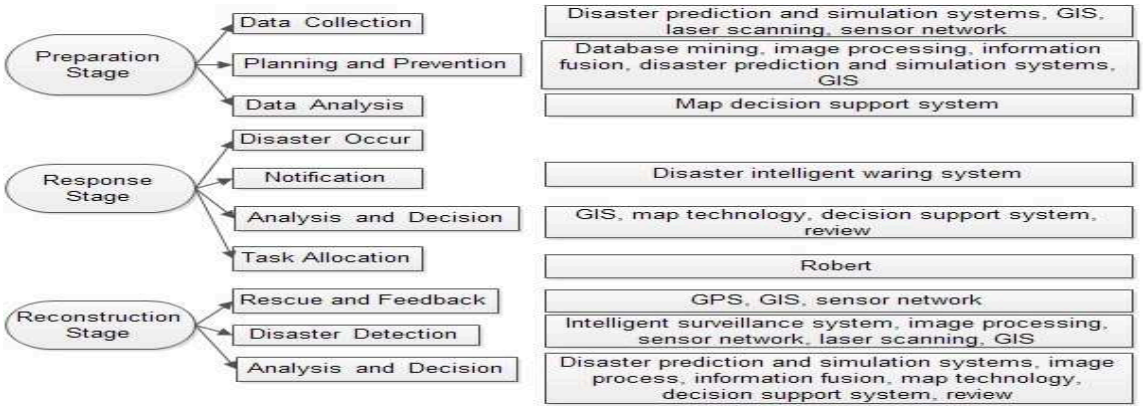

Fig.1 Information technology model of agricultural disaster prevention and reduction

Summary

The purpose of disaster prevention and reduction of agricultural information management is to facilitate the exchange of information in disaster management process, and to achieve effective cooperation among the participating departments. Information management processes of agricultural disaster prevention and reduction make agricultural disaster prevention and reduction management more effective and the work of rescue and relief timely. The information technology model of agricultural disaster prevention and reduction provide technologies basis to the construction of agricultural disaster prevention and reduction system which needed deep researches and developed system functions.

Acknowledgement

This work was supported in part by Science and Technology Plan Projects of Jiangxi, China (Grant No. 20132BBA10007).

References

[1] WangLi. Research of enterprise networks dissemination based on crisis management. Wuhan: Huazhong Normal University, 2009.
[2] Wagenaar W A. Profiling Crisis Management, Journal of Contingencies and Crisis Management, vol.4, no.3, pp.169-173, 1996.
[3] Robert Heath. Crisis Management version 2, Zhongxion Publishing House, 2003.
[4] Liu Tuo. Research on Fake Information Chaos Theory of Public Crisis , Intelligence Theory and Practice, vol.6, pp.825-828, 2008.
[5] Zhang Gang, XieYangqun. Review research of information management. Journal of Information, vol.8, pp.22-25,2008.
[6] Lu Tijia. Internet Crisis information research on its propagation rules and problem solving model University of Science and Technology of China, 2010.
[7] Bo Fengxian. Research on information resources exploration and utilization of agricultural disaster , Meteorology and Disaster Reduction Research, vol.4, pp.57-61, 2011.
[8] Liuyao Long, Xu Shiyuan, Wang Jun, el at. Research on sharing of international disaster data and information, Disaster, vol.3, pp.109-113, 2008.
[9] Khaled Zamoum. Teaching crisis management in Arab universities: A critical assessment, Public Relations Review, vol. 39, no. 1, pp 47-54, 2013.

Advanced Materials Research Vols. 989-994 (2014) pp 5382-5385
© (2014) Trans Tech Publications, Switzerland
doi:10.4028/www.scientific.net/AMR.989-994.5382

Research on Information Management Frameworks of Agricultural Disaster Prevention and Reduction

Ruren Deng [1,a], Yinghuan Wu[2,b]
[1]Party Committee Organization Department, Jiangxi Science & Technology Normal University, Nanchang, Jiangxi, P.R.China
[2]School of Economic Management, Nanchang Institute of Technology, Nanchang, Jiangxi, P.R.China
[a] 572383070@qq.com, [b]cnliu2010@163.com

Keywords: Agricultural; Disaster prevention and reduction; framework; Information management

Abstract. The paper analyzed agricultural prevention and reduction framework research status, and summarized its design and implementation principles. Finally, the paper proposed the framework of agricultural disaster prevention and reduction information management based on the analysis above .

Introduction

With the increasing levels of agricultural information, in the form and number of agricultural disaster information is rapidly increasing. With the development of information and communication technology, it brings more opportunities and challenges to the agricultural disaster management, information sharing and information exchanging. Agricultural disaster prevention and reduction is a long-term process that need to consider the lasting mitigation of disaster impact and effective communication between all stakeholders[1]. Therefore, it's necessary to apply information and communication technology to agriculture disaster management in order to ensure successful coordination and orderly communication of decision-makers, resource providers, and victim rescue teams. From the economic point of view, to provide efficient coordination and communication is also beneficial because it time saving and supports the sharing of resources and views [2]. However, in disaster prevention and reduction of agriculture, it's not enough if there only have information and communication technology applications [3], all information and communication technologies should provide support for the implementation of specific operations, such as personnel training and infrastructure improvements.

Research status on information management framework of agricultural disaster prevention and reduction

Designing and implementation of disaster emergency information management systems provide an advanced and effective decision support software tools for mining and discovering periodic potential rules and inherent properties of disaster risks. However, the current disaster information management systems are often used disaster data warehouse product as its center and developed based on different architecture environment which meet with different needs and under different operating environment. Thus, the application architecture and extension of these systems are not unified. As environmental changes, service changes, function needs increase of disaster risk analysis [4], the original disaster information management system is difficult to adapt the changes [5]. In the past few years, with the gradual maturity of software and systems engineering, there is a growing need to view disaster information service system from structure viewpoint. As the interaction of disaster information platform and application systems becoming more complex and government agencies reduce investment on IT which bringing increasing benefits reliable pressure, all these changes need deep thinking on how can disaster information engineering and application system support disaster risk management. Meanwhile, with the rapid development of Internet technology, people are faced with massive, heterogeneous, geographically disaster information which make access and analyze of these data user difficult. To get effective disaster risk decision-making

knowledge from such a large number of geographically dispersed disaster information is an extremely difficult task which facing enormous challenges. To solve this massive problem of distributed heterogeneous data analysis, an disaster risk information resources and services integrated, open and flexible framework is needed.

The existing disaster information management systems mainly build based on available technology [6] when the event occurs which can not meet the needs of full collaborative information management. Most of them assume that the disaster management network system is built to ensure stakeholder collaboration through local city control center [7]. And disaster management network has no data filtering function which can facilitate collaboration of stakeholders and collect all of the information flow, and only has information and communication technologies which artificially manipulate data management, information flow, and as a communication tool.

Information management framework of agricultural disaster prevention and reduction is an process of integrating information and communication technology into agricultural disaster prevention and reduction processes to facilitate all participant involved in the conceptual model. It an authentication system with high degree of information security and speed, and it has data interoperability, system interoperability, automatic data conversion of two-dimensional (2D) and three-dimensional (3D)[8] , audio and text, multi- language support, automatic text summary and other features to help achieve effective communication and cooperation in disaster management process of organizations.

Information management framework of agricultural disaster prevention and reduction

The preparedness, response, recovery and reconstruction stages of agricultural disaster prevention and reduction can use various information and communication technologies to achieve specific functions so as to achieve disaster cooperative management technical support. The information management framework of agricultural disaster prevention and reduction is based on communication and collaboration difficulties and suggestion reports of relevant departments. It is designed to support and strengthen coordination and information flow in disaster management process and introduced an intelligent ICT for disaster management system involving data filtering network. Agricultural disaster prevention information management framework is shown in figure 1. In this model, Disaster Collaborative Emergency Information Management Systems (DCEIMS) have three different systems at local, regional and national level which are called local DCEIMS, regional and national DCEIMS. Compared with the existing disaster emergency information management system, the framework applies coordinate emergency information management system to the collaborative process to replace human operator of data filtering and data distribution.

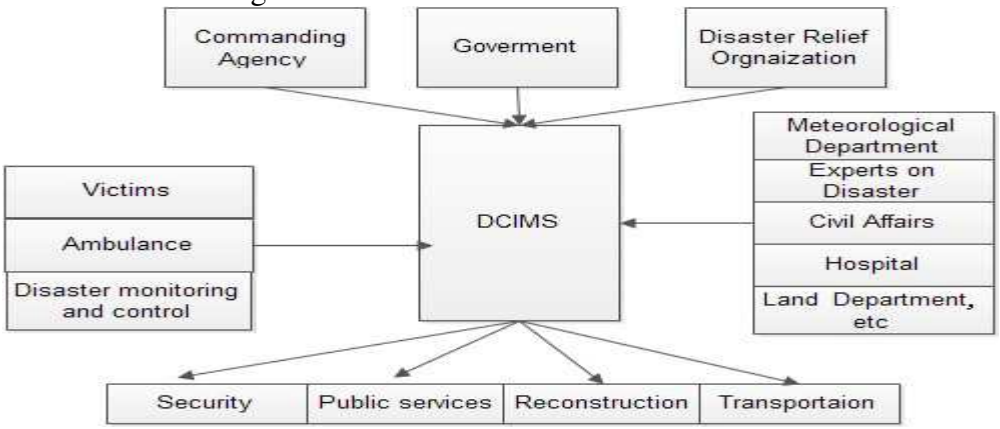

Fig.1 Information management framework of agricultural disaster prevention and reduction

Principle analysis of agricultural disaster prevention information management framework

Agricultural disaster prevention information management process has three stages: preparation stage, response stage and reconstruction stage.

At preparation stage, the local DCEIMS, as the control center, responsible for disaster management and to provide a local database, it's far from high-risk areas. Local DCEIMS system like a bridge that make cities, the public, environment building experts , regional and national DCEIMS cooperate with each other much more fast and effective. Local DCEIMS is responsible for disaster preparedness stage on the following works:

(1) Disseminate disaster information, alarm systems, preventive measures, and other information, through the media, newspapers, magazines, electronic billboards, local DCEIMS website, disaster-related sites, well-known sites, and automated messaging system to establish public awareness.

(2)Build a network database based DCEIMS training systems, and connect with all domestic local DCEIMS system to provide support of training personnel who will participate in disaster response and reconstruction. Everyone will be notified training schedule, rules changes, technological developments and changes, with permission of the information about the nature and impact of disasters through the system necessary to access, and accesses to training notes via e-mail and text messages as well as the necessary inter- discipline data. In addition, the training is to improve disaster response exercises, including simulation technology and physical exercise.

(3)Establish volunteer relief groups, and train on them by simulating specific relief activities (such as rescue and medical supplies). Analog recording will be announced and open to the public. Experts and volunteers support by synchronous and asynchronous activities based on computer, and should enable them to access certain privileges by DCEIMS training systems.

(4)Integrate available information and communication technologies to the system and to help monitor the efficiency of disaster information management. These systems inherit data filtering network (DFN), automatic data interpretation, advanced CCTV camera, intelligent early warning system. They are self-healing system, in the event of a system failure can be reconfigured, and can be specific interoperability. Each system is equipped with alternative power sources.

(5)When systems, tools or communication channels have troubles that can not be solved, the control rights should pass to the previous level.

At Response stage, disaster monitoring experts (such as meteorological bureau) provide warning information to the State Department, and analyzed information gathered from closed circuit television cameras should send to the local DCEIMS.

Local DCEIMS alerts the relevant authorities through DCEIMS systems, such as the local ambulance, police and other emergency response agencies, as well as health, transportation and utilities suppliers, etc., and activates public warning system. Citizens can know about disaster information through radio, television, Internet, mobile phone text messages, e-mails, websites, and cable broadcasting systems installed in different locations (such as the railway station). Local DCEIMS requests all parties concerned departments to take action after receiving information filtered through information filtering network. In addition, all partners are communicating with each other through DCEIMS. Mobile health services dispatched to the appropriate location, and communicate with hospitals and local DCEIMS through wireless network. Rescue teams, fire brigade and police at the disaster site with their respective departments through L-DCEIMS and portable wireless devices. Local DCEIMS using GPS and installation of closed circuit television cameras to monitor key locations affected areas in order to support rescue operations and further confirmation response action. Satellite maps of the affected areas and generates a 3D model with advanced tools to display a visual representation, and try to support the decision-making process. Predictive model is used to predict disaster affected areas and disaster relevant events occurrence probability. Web GIS is used to collect, display and share information on the disaster websites. Collecting photos of disaster areas through visual communication tools and closed circuit television cameras carried by rescuers, and these photos can be used for rescue operations in the decision-making process. Local DCEIMS have spare power supply equipment which can operate automatically after a power off. If the local DCEIMS is damaged during the response stage, the response will be automatically passed to the regional DCEIMS.

At repair and reconstruction stages: information of casualties, missing persons can be obtained from local hospitals and police stations in DCEIMS. All data confirmed in the local DCEIMS will be provide to victims' families and the media. Information from architecture and disaster experts also input to local DCEIMS database. Web GIS, aerial photographs and laser scanning technology are also used in disaster detection. Data collected by disaster specialists from disaster site will help to developed 3D simulation system to help analyze more details in disaster in to confirm the failure factors. Backup system is used to store data. Data from various data sources filtered through filter network share to all DCEIMS systems, education institutions and research centers through internet.

Summary

Agricultural Disaster prevention and reduction information management is to improving information management effectiveness to cope with agricultural disasters, and to improve cooperation effectiveness of related subjects who coped with agricultural disasters. Agricultural disaster prevention information management framework presents challenges to the construction of information and communication technology, and will promote changes and innovation to information and communication technology framework. That is to say, it is no longer the era of the simple exchange of information and people, but the form of human communication with machines, and the machine communications with equipment. However, it needs to be implemented and tested through further research on the full realization of disaster prevention and reduction of agricultural information management, especially on the development of collaborative emergency disaster information management system.

Acknowledgement

This work was supported in part by Science and Technology Plan Projects of Jiangxi, China (Grant No. 20132BBA10007).

References

[1] Bo Fengxian. Development and utilization research on Information resources of agricultural disaster. Meteorology and Disaster Reduction Research, vol.4, pp.57-61,2011.

[2] WangLi. Research of enterprise networks dissemination based on crisis management. Wuhan: Huazhong Normal University, 2009.

[3] Cai Naiao, Leye. Disaster information resource management research for government decision making . Sichuan University (Philosophy and Social Sciences) , vol.6, pp.116-123, 2012.

[4] Liuyao Long, Xu Shiyuan, Wang Jun, el at. Research on sharing of international disaster data and information, Disaster, vol.3, pp.109-113, 2008.

[5] Tian Fengbin. Design Strategies for agricultural disaster warning information platform based on Web GIS- take Jilin Agricultural disaster warning information platform as an example. Agricultural Technology and Equipment, vol.6 , pp.39-40, 2008.

[6] Akbar Badpa, Bijan Yavar, el at. Effects of Knowledge Management System in Disaster Management through RFID Technology Realization, Procedia Technology, vol.11, pp. 785-793,2013.

[7] Xingpeng Liu, Jiquan Zhang,el at. Information diffusion theory based spatio-temporal risk analysis of grassland fire in northern China. Knowledge-Based Systems, vol.23, no.1,pp. 53-60,2010,

[8] Siti Hajar Othman, Ghassan Beydoun. Model-driven Disaster Management, Information and Management , vol. 50, no.5, pp.218-228, 2013.

Advanced Materials Research Vols. 989-994 (2014) pp 5386-5389
© (2014) Trans Tech Publications, Switzerland
doi:10.4028/www.scientific.net/AMR.989-994.5386

Internet Financial Innovation based on Enterprise Growth Cycle for the Small and Medium Enterprises

Yiqing Lu[a]

School of Information Management, Beijing Information Science and Technology University, Beijing, 100192, China

[a]email: luyiqing@126.com

Keywords: Internet financial; Financial innovation; Enterprise growth cycle; The small and medium enterprises

Abstract. Financing is always a big problem in the development of small and medium-sized enterprises (SME) in our country. It's necessary to develop Internet financial to support the development of real economy and improve SME's financing situation. In this paper, an analysis of the SME's financing innovation is described and then an internet financing innovation which is oriented to growth phase SME is proposed, in order to better meet SME's financing requirement in different growth phases.

Introduction

Since China implemented its reform and opening up policies, there is a rapid development in China's SMEs, which plays a more and more important role in the whole national economy and has made great contributions to China's rapid economic growth. In recent years, with increasingly fierce competition among enterprises, constraints and factors that affect the development of enterprises are gradually increasing, making enterprises facing great difficulties in further development. Among which, the financing problem of SMEs is a major obstacle to its development[1-3].

Enterprise Growth Cycle

Firms progress through four stages of a developmental life cycle, each with their own funding needs.

In the first stage, a new company begins with the seed of an idea. Its external financing needs (EFN) are high, since it needs money to develop but lacks retained earnings. These young firms are frequently financed through debt, acquiring loans from banks and acquaintances. They may also acquire seed money, a form of securities offering in which an investor (usually friends, family, or angel investors) purchases part of a business. The source of the financing may depend on the perceived riskiness and growth of the business.

After the firm is able to acquire external funding and develop its product/service, it enters the growth phase. Once a company has a successful strategy, it attempts to offer its products or services to potential customers--expanding first to other states and regions and then often internationally and globally. Successful companies can turn in increasing earnings year after year, evidenced by the increasingly steep slope in the diagram. Firms may face an increase in competitors. In the growth stage, a firm's initial EFN is high relative to its current value; it needs significant funds for growth. If it fits the specifications for venture capital (high growth potential, innovative product) a VC firm may agree to finance the firm. It may also raise capital through equity financing. As it progresses through the growth stage, earnings begin to increase less rapidly. At some point, the company may decide to go public, offering its stock to the general public on a security exchange as a means of equity financing.

Eventually, all possible customers have the product or service. They may still buy parts or replace their product with newer models, etc, but growth slows. This is the mature stage of a company's

development. If the firm has no new projects in the works, their EFN is quite low and internal funding is high. In fact, the firm may have so much in retained earnings that they cannot put all of it to productive use. They can choose to finance operations by issuing bonds and equity [4-6].

Internet Financial Innovation based on Enterprise Growth Cycle

Compared with the commercial banks in China, the Internet financial institution has more advantages to develop the financial innovation from the thinking model, cost or mechanism. The financial products shall be designed targeted to better dock the financial demands in different growth stages for the small and medium enterprises [7-8]. According to the enterprise's financing demand at different stages of the growth cycle, the financial products with different loan life and amount shall be designed; According to the enterprise's different transformation and upgrading paths, the financial innovative models of mortgage pattern innovation, financial innovation and supply chain finance shall be adopted flexibly, as shown in Figure 1.

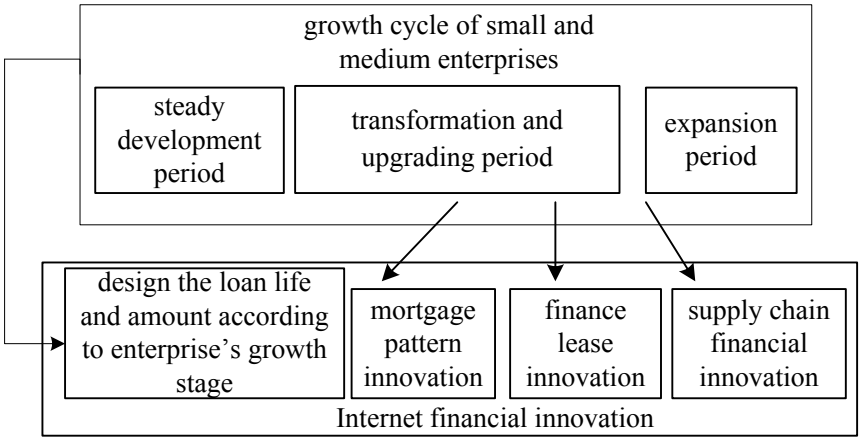

Figure1 Internet financial innovation based on enterprise growth cycle

- Design the loan life and amount according to enterprise's growth stage.

Generally, the financial aim for the small and medium enterprise is mainly to obtain the circulating fund, therefore, the small-amount and short-term loan accounts for the largest proportion in the capital structure for the small and medium enterprise with stable operation. However, in the transformation and upgrading process, the small and medium enterprise needs the fund support with a longer term and larger amount. Firstly, no matter to transform the technology or update the equipment, even including the typical cross-industry restructuring mode- exiting from the labor-intensive industry and entering into the capital-intensive industry, it needs large sums of money to support, and the usual fund supply scale with the aim to supply the liquidity in the small and medium enterprise is overstaffing. Secondly, in the product upgrading process, it is a long process from the initial increase of research and development investment to the production of new product to the channel expansion to the final sales obtaining the income, therefore, the loan with a longer term is needed to match with the process; Moreover, the industrial conversion and production base transfer and other strategies also need a stable, long-term and large-amount credit fund.

- Mortgage pattern innovation

The Internet financial institution can design the innovative mortgage pattern to solve the problems confronted in the transformation and upgrading process in the small and medium enterprise. In the process to transform from the export to the domestic sales in the foreign-based small and medium enterprise, due to different sales method, it may occur the situation of ballast product and increasing inventory, thus tightening the enterprise fund. The inventory loan can be considered, which can not only help the enterprise solve the problem of huge fund occupation pressure brought by the overstock, obtain the liquidity, but also provide the powerful fund aid for the enterprise to quickly open the domestic market. In addition to the inventory mortgage, the intangible asset mortgage can play an

important role. Most small and medium enterprises may select to improve the technical capacity and improve the product quality as the path for transformation and upgrading, while some enterprises may choose to transfer to the high-tech enterprise with small fund. The core asset grasped by these enterprises is the intellectual property, technology patent and other intangible assets. Therefore, innovating the intangible asset financing product on the technology and scientific achievements formed in the transformation and upgrading process in the small and medium enterprise can not only break the traditional fixed asset mortgage mode, open a new financing source for the enterprise, but also promote the industrialization of patented technology and promote the enterprise's rapid and healthy growth.

- Internet financing lease innovation

In the upgrading process of machinery and equipment, in order to avoid the pressure brought by the one-time amount expenses needed to buy the equipment, the Internet financial institution shall consider to adopt the financing lease form to use the fixed asset, then halve the buying expense within a longer period in the future, thus smoothing the enterprise expenditure and avoiding the large fluctuation of the enterprise's operation condition.

- Supply chain finance innovation method

If the small and medium enterprise selects to extend along the upstream and downstream supply chain, the Internet financial institution can consider to select the supply chain financing mode to provide the fund support for the process. Adopting the supply chain financing product can extend the good credit qualification in the core enterprise in the supply chain to the upstream and downstream of the supply chain, strengthen the dominant power and control of the upstream and downstream enterprise, and improve the competitiveness of the whole supply chain, thus laying a favorable condition to adopt the acquisition mode to enter into the upstream and downstream. With the supply chain finance's comprehensive financing service on the upstream and downstream enterprise, the supply chain core enterprise selecting the transformation will be more smooth to extend the industry.

Acknowledgement

This work was supported by the National Natural Science Foundation of China under Grant (No. 61272513), Funding Project for Academic Human Resources Development in Institutions of Higher Learning Under the Jurisdiction of Beijing Municipality (No. PHR201106133), and and the Projects in the National Science & Technology Pillar Program (No.2012BAH08B02).

References

[1] Guanghua X, Ming L. Analysis on financing problems for small and medium-sized enterprises[C]//Communication Software and Networks (ICCSN), 2011 IEEE 3rd International Conference on. IEEE, 2011: 232-235.

[2] Fraser S. Finance for small and medium-sized enterprises[J]. Report on the, 2004.

[3] Ballantine J, Levy M, Powell P. Evaluating information systems in small and medium-sized enterprises: issues and evidence[J]. European Journal of Information Systems, 1998, 7(4): 241-251.

[4] Lumpkin G T, Dess G G. Linking two dimensions of entrepreneurial orientation to firm performance: The moderating role of environment and industry life cycle[J]. Journal of business venturing, 2001, 16(5): 429-451.

[5] Chittenden F, Hall G, Hutchinson P. Small firm growth, access to capital markets and financial structure: Review of issues and an empirical investigation[J]. Small Business Economics, 1996, 8(1): 59-67.

[6] Mueller D C. A life cycle theory of the firm[J]. The Journal of Industrial Economics, 1972: 199-219.

[7] Anthony J H, Ramesh K. Association between accounting performance measures and stock prices: A test of the life cycle hypothesis[J]. Journal of Accounting and Economics, 1992, 15(2): 203-227.

[8] Bernanke B S, Gertler M, Gilchrist S. The financial accelerator in a quantitative business cycle framework[J]. Handbook of macroeconomics, 1999, 1: 1341-1393.

Advanced Materials Research Vols. 989-994 (2014) pp 5390-5393
© (2014) Trans Tech Publications, Switzerland
doi:10.4028/www.scientific.net/AMR.989-994.5390

Impact of digital technology on Architectural Design Teaching

Fangda Yu

Hubei Engineering University, Xiaogan 432000, China

Key words: Digital architecture; digital technology; sketch thought; architectural design

Abstract. Modern education is dominated by the " rational technology "and pursuit the education of" rational technology ". Digital technology with hitherto unknown speed penetrated into many aspects of higher education, the formation of some cross fields, "digital architecture" is a typical representative. But the national universities course construction is relatively backward which is the cross course of architectural design and digital technology. The article analysis on the status of "digital building" and to discuss the innovation and integration of digital technology and construction courses.

Introduction

Modern education is dominated by the "rational technology "and pursuit the education of" rational technology" [1]. The architecture is an interdisciplinary science model, which relates to computer science, geography, environmental science, information technology, sociology, culture , arts, engineering, law, political science and even disciplines. With the development of information technology and learning theory, a theory and method can not simply rely on the classroom,but also can not simply use the traditional media, and should integrate different theories and methods.

Background of Research

With the development of digital technology, which occupy a certain position in the development of national economy, digital technology has penetrated into all walks of life, and become a kind of important means to capture the benefits of all walks of life. Building industry as a modern industrial, under the influence of digital technology has changed its use, especially in the architectural design, has been widely applied. It is self-evident, digital technology has become the main method of large modern architectural design, the organic combination of architectural design with digital technology, can make the architectural design of digital realization of great leap forward. At present, the application of digital technology in architecture design, so that the efficiency of architectural design has been greatly improved, and enhances the four-dimensional analysis (Fig. 1, Fig. 2). Moreover the design cycle and cost has improved, in this case, the interest is improved, but also more in line with the trend of socialization.

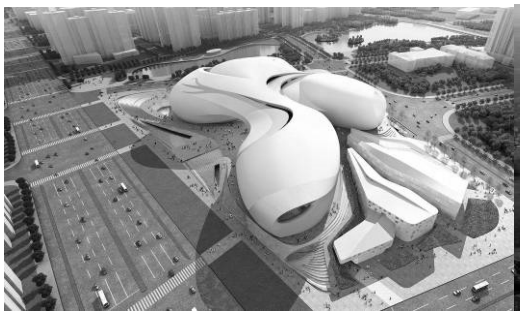

Fig.1

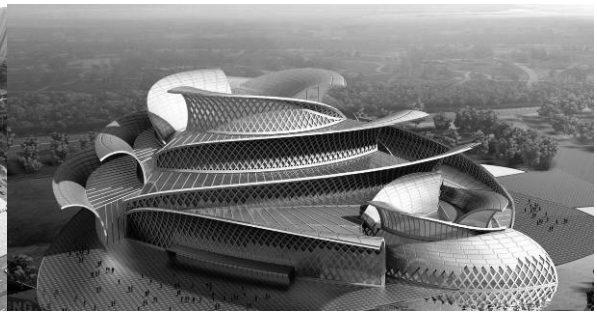

Fig.2

The status of digital technology integrating into Teaching

Digital technology integrating into the school teaching,which close the contaction of the education and the external world ,Improve educational efficiency .At the same time, the digital technology support on innovation teaching methods, speed up the implementation of teaching and learning in the way and idea innovation, so as to improve the traditional teaching mode is important significance.

In recent years, The modernization of education was promoted by the education informatization has become an important strategic measures for the development of education in china. Basic education is a development trend in the application of the integration of information technology and curriculum characteristics. At present, only about 10% of teachers into the advanced stage of the application of information technology to create a stage, most of the teachers still in primary technology application stage, the effectiveness of educational informatization should be further improved. Have a significant impact attitude, self-confidence, informatization teachers school environmental factors on Teachers' information technology into teaching behavior and different stages of integration.

From the practical experience, the digital technology is to Architectural design a lot of help, but the rise of digital technology for a short time, and there are not mature, so there are still shortcomings when used in architectural design. For example, digital technology is the lack of a unified standard, and the lack of qualified technical personnel, in addition to intelligent digital technology is very low. Therefore, the application of digital in industry and in architectural design should carry on the innovation based on the use.

The status of Digital Architectural Design Course

At present ,Most of the colleges in Architectural Education, still work digital technology as a tool for CAD tools or design, the real distance use digital technology into the architectural design, or use digital technology to integrate the whole design process is still a certain gap.

The teaching content of building digital technology including the use of methods, drawing, performance statistics, analysis, word processing, Internet softwares and programming knowledge, these knowledge in teaching from different courses. How to put the teaching and research of these knowledge around the building design together, to form a set of digital architectural design teaching system. [2]

In some colleges, the basic training of traditional design method has been greatly weakened because the advantages of digital technology in the construction aspect, ,design principle and design method of teaching weakened, premature low grade students to make the design and performance of digital tools, produced is not conducive to learning the basic theory and improve the negative effects of culture art accomplishment and professional quality. [3] Some design department is also reflected that some architecture graduates lack of knowledge and ability to solve practical problems, only with the computer now.

In the situation of the Digital technology rapid development , in the face of these problems, teaching need the method in the light of its general trend to solve the problem, the teaching reform of architectural design need to stand in the height of the information age, and gradually find out a way to adapt to digital architectural design teaching and the development of digital technology .

Curriculum integration of digital technology and architectural design

Architecture students must have high sensitivity to the graphics, image, color, lighting changes, building space and other factors, it is often the traditional teaching method was more difficult places, and multimedia technology can greatly enhance the students ability of thinking in images.

For beginners, the shape and the spatial construction is a difficult course of architectural design. In order to improve and cultivate the students' space thinking ability, at the same time the basic method can be focused on the elements, space design approach, combining the traditional teaching method, Introduce the three-dimensional computer and network technology. Namely, using a variety of media: textbooks, blackboard, teaching aids, video (VCD), slide, projection, CAI courseware, GIS technology, network media and other means to the storage, transmission and processing of information. Scientific arrangement of teaching processes and factors, to provide a good learning conditions for students, develop students' space thinking ability, drawing and interpret the images ability, improve the architectural design teaching effect. [4]

How to realize the benign transition from space elements to the teaching of architectural design, how to understand the design thinking and methods of the architectural design, which requires the reasonable architectural design teaching organization. Course design requires students to design a material form must be established on the basis of investigation and analysis, architecture design object should involve building elements and city elements, also should be the size and scale of the students can grasp in a short period of time. Design thinking should inherit architectural design training to obtain the logic thinking, image thinking and microcosmic thinking, rational thinking, but also expand the digital design of the comprehensive thinking and macro thinking.

The teaching of architectural design course requires students to form scheme based on elaboration of 3D model, the students can inspire the deep function of various software, after the spatial ability to set up is more complex, spatial thinking to the students can get rid of beam, to play the greatest degree. Such as the undulating slope or the base which in need of care or protection of surrounding retained buildings. The base simulation is established through the integration of transformation from field data, to balance and minimize earthwork. The sketch is to combine the objective and accurate digital perfect intuitive sense and the computer in a way. Although some sketches may not be accurate control in the figures, some design such as the master architect Frank Gehry, but is very helpful to direct architects creativity and the subjective intention, reflect the liquidity and other architectural characteristics, which itself has no digital limit accurate. [5] teaching can choose the computer design of the basic knowledge and various design system, arrange the computer drawing software design method of digital design, subjective and objective three attribute three attribute and the design of the physiological and psychological factor theory. And with"grasshopper" plugin of rhinoceros software, through changing the parameters, precise control of physical form. From simple method of traditional sketch thought hand-painted, extended to the surface and plane collocation and complex combination, focus on mastering their mutual complex configuration aspects (Fig.3, Fig. 4), describes a set of scientific, practical building design method, both rich emotional elements of architectural design the architectural design, and improve the scientific work efficiency, innovation for the modern education technology drives the course structure and teaching content.

Conclusions

Architectural design is also faced with hitherto unknown challenge Under push of digital technology, "digital architecture" is rebuilding the new ethics system FOR the architectural design in the process of immaterial and material. The teaching should be keen to adjust teaching strategies and the architectural concept, so to follow the trend of development.

Fig.3

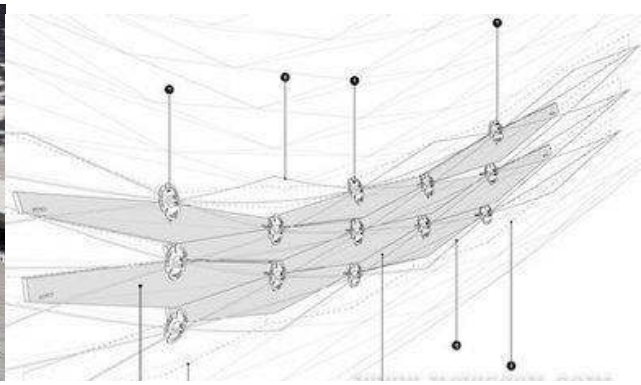

Fig. 4

Acknowledgments

This work was financially supported by the provincial teaching research project of Hubei province, the number of project is [2012368].

References

[1] Hua Zhang. Integration of curriculum and teaching theory, volume 2 of education research(2000). (In Chinese).
[2] Jiancheng Li, Shuo Wang, Haiying Yang. Discussion on Digital Architectural Design Teaching. volume 2 of The south building(2009). (In Chinese).
[3] Deqian Li. The negative effect of digital architectural education. volume 2 of Southern Building (2002). (In Chinese).
[4] Ni Li,.Thinking about basic teaching of urban planning . volume 9of Research on the development of city (2010). (In Chinese).
[5] Peng Pen. The Reflection on Architectural education in digital age. volume 9 of Journal of Shijiazhuang Railway University Press (2010). (In Chinese)

Advanced Materials Research Vols. 989-994 (2014) pp 5394-5397
© (2014) Trans Tech Publications, Switzerland
doi:10.4028/www.scientific.net/AMR.989-994.5394

Study on the landscape pattern change of Haikou City based on GIS

Fengxia WANG[1, a], Weihong LIU[2, b, *]

[1] College of Tourism in Hainan University, Haikou, 570028, China

[2] InformationCneter of Land and Resources Department of Zhejiang Province, Hangzhou, 310000, China

[a]email: summer_wangfx@126.com, [b]email:1413195789@qq.com

* Correspondance Author：Weihong LIU，1413195789@qq.com

Keywords: Landscape pattern; Haikou City; landscape index; land transfer matrix

Abstract. The article is studying on the Haikou city, using Remote Sensing technique and GIS technology, with ArcGIS, ERDAS, FRAGSTAS, analyzing the temporal and spatial variation of landscape in Haikou City from 2000 to 2010, drawing the conclusion: residents, construction, farmland and forest land is the main part of landscape pattern and increased rapidly. Besides the decrease of unused land and water area, it also reflects that not only the landscape fragmentation degree of the integral sight in Haikou City in relatively high, but the landscape fragmentation degree of the residents, construction, farmland and forest land, which are the main part of Haikou City , is also relatively high.. Besides, the data also shows that each landscape didn't connect well and the exchange of material energy among landscapes is not smoothly, which go against the mutual development between the landscape. However, the distribution of landscape in Haikou City is fairly balanced. There is no particularly advantaged type, which contributes to the balanced development of the landscape.

Introduction

Landscape pattern is landscape elements arrange and combine in the space. It also shows the landscape heterogeneity. The study of landscape pattern is the most important part of the research of landscape ecology. We can study the mechanism between land-use and landscape pattern change through the progress of landscape pattern change. By the research result, we can offer the basic research for the optimization in landscape pattern and sustainable land use.

Landscape pattern is one of the three core elements of the study in landscape ecology. It's also the base of the progress of studying landscape and landscape function. Landscape pattern usually means the distribution and combination rule of the landscape spatial unit (plaque) in different size, shape and nature reflected in the space. It is the specific performance of the landscape heterogeneity and the results of various ecological progress in various scales effects..

Landscape pattern index is a short of simple quantitative index that can highly concentrate landscape information and reflect the structure and characteristic. By the landscape pattern index, we can quantitative study landscape's characteristics, spatial arrangement and dynamic change. This article specifically selects some landscape pattern indexes as follows: NP, CA/TA, %LAND, LPI, IJI, PR, SHDI, SHEI and CONTAG.

This article used the remote sensing image date of Haikou City in 2000 and 2010. The data images are disposed by image geometric correction, mosaic, projection transform, clipping and fusion by using ArcGIS10.0 and ERDAS IMAGINE9.2 software. Based on it, we used ERDAS IMAGINE 9.2 to radiate the image and enhance the space, improving the quality of the image. And then, we used the method of supervised classification to sampling, establishing classification modules, interpreting images and evaluating the accuracy. Then we concluded two phase current land landscape pattern in Haikou City by analyzing. After that, we calculated the landscape pattern index by using ArcGIS10.0 and FRAGSTATS4. We analyzed the change of the landscape pattern in Haikou city by analyzing two phases of image data and calculating the landscape index.

Study Area

Haikou city is located in north latitude 19 ° 32 ′ -20 ° 05 ′, longitude 110 ° 10 ′ -110 ° 41 ′, located in the northern part of Hainan Island, Flat terrain, slightly heart-shaped.landscape basic is divided into the northern coastal plain, central order along the Yangtze river region, eastern, southern tableland, lava in western region; East from DaZhiPo old town village, west to west township south village, 60.6 kilometers distance, South from Dapo Town five car Village, north to the sea, 62.5 km distance, the city's land area of 2304.84 square kilometers. Haikou city is located in the low latitude tropical edge, belongs to the tropical maritime monsoon climate, annual sunshine time is long, the radiation energy is large, the average annual sunshine hours 2000 hours, solar radiation can be up to 11 to 120000 Card, annual average temperature 24.2 ℃, annual average rainfall of 1684 mm, the average annual evaporation is 1834 mm, the average relative humidity is around 85%, southeast and northeast wind is given priority to all the year round, the annual average wind speed 3.4m/s;north Linhai, sea area of 830 square kilometers,a coastline of 131 kilometers , sea water average temperature 25 ℃

The Research of Landscape Pattern Change of Haikou city from 2000 to 2010

We analyzed the land-use transfer matrix of Haikou city in 2000 and 2010 by using ArcGIS10, obtaining the data of two phase of land-use transfer matrix of Haikou city in 2000 and 2010, follow the table 1.

Table 1 Land use transfer matrix of Haikou city in 2000 and 2010 unit: Ha

2010 / 2000	Settlement and construction land	Unused land	Arable land	waters	forest land	in total
Settlement and construction land	-	16.44	123.38	7.44	66.85	214.11
Unused land	263.44	-	385.6	2.15	211.61	862.80
Arable land	237.7	59.96	-	5.85	221.26	524.77
waters	103.08	10.37	47.25	-	28.66	189.36
forest land	221.63	32.67	388.54	0.82	-	643.66

From table 1,it can be seen, in 2000,the land use type of Haikou city, the transformation of unused land area is the most, followed by the cultivated land and forest land, and transformation of water area at least. Among them, the unused mainly converted into residential areas, cultivated land and forest land and construction land, be transferred to the water area is less; Cultivated land mainly transferred to cultivated land, forest land and settlement and construction land; Woodland mainly transferred to cultivated land, forest land and settlement and construction land, which can also explain in 2000 the cultivated land, forest land and residential areas and the construction land area changes in Haikou city large, and growth tendency. From the perspective of the land use type of 2010, settlement and construction land mainly come from the unused cultivated land and forest land from the 2000 years, cultivated land mainly comes from the forest land and unused land and farmland from the 2000 years, forest land mainly comes from the cultivated land, forest land and unused land..

First, by using ArcGIS10.0, we transferred the two raster data classification results of Haikou city in 2000 and 2010 into GRID raster data. Then we calculated the landscape pattern index which has selected by using FRAGSTATS4.0. Calculation results are shown in table 2 and table 3.

Table 2 Calculation result of landscape pattern index of Haikou city in 2000 and 2010

Index / Land type	NP		CA		%LAND		LPI	
	2000	2010	2000	2010	2000	2010	2000	2010
Settlement and construction	240932	50456	17258.74	76872.06	7.65	34.07	0.44	13.31
Unused land	234320	22523	28503.32	7799.67	12.63	3.46	0.54	0.05
Farmland	86253	35167	126958.39	85085.01	56.27	37.71	42.91	11.44
Water	71090	7501	19258.40	6130.98	8.54	2.72	4.27	0.28
Forest	249092	52009	33635.39	49724.73	14.91	22.04	2.92	0.62

Table3 Calculation result of landscape pattern index of Haikou city in 2000 and 2010

Index / Year	NP	TA	LPI	IJI	PR	SHDI	SHEI	CONTAG
2000	881687	225614	42.91	74.13	5	1.275	0.792	30.59
2010	167656	225612	13.31	60.87	5	1.282	0.797	29.55

Through two transverse comparisons of data in Table 2, it can be seen that residents, construction, forest land and farmland is increasing rapidly, whereas unused land and water area is decreasing rapidly. In addition, residents and construction's increase speed is the largest. In the proportion of the whole landscape, it increased from 7.6497% in 2000 to 34.0726% in 2010. And unused land's decrease speed is the fastest. In the proportion of the whole landscape, it decreased from 12.6337% in 2000 to 3.4571%in 2010. What's more, by the LPI of various landscape, it can be seen that except the maximal plaque of resident and construction's proportion of the whole landscape increased rapidly, LPI of other kinds of landscape are all seem to decrease, which indicates that due to the development of the city, Haikou city's land area of residents and construction increased rapidly from 2000 to 2010.

Table3 shows the whole landscape pattern of Haikou city to calculate the landscape pattern index of Haikou city and analyze the change of landscape. As for NP, the number of 2000 is much larger than the number of 2010, which indicates the fragmentation index of the whole landscape pattern of Haikou city in 2000 is fairly large and the landscape is more fragmentized than 2010's. From the CA of two periods of data, it can indicate that the area change of Haikou city from 2000 to 2010 is not large. Compare the LPI to table 2, it indicates the advantaged type of Haikou city in 2000 and 2010 is farmland, residents and construction. What's more, the future social and economic activities in Haikou city are mainly based on residents and construction. IJI can be used to show the overall spread and tied in plagues. In 2000, IJI is 74.1287 and in 2010 IJI is 60.873, which shows that the connected and approaches conditions among each plague in 2000 is better than 2010's. However, both data are not large, which means on the whole, the connection among the landscape of Haikou city is not well. The connection and communication among the landscape are not well smooth. What's more, the number of CONTAG indicates that there is no well connection among the landscape, and the degree of fragmentation of the landscape is still rather high. Both SHEI and SHDI are used to compare the index of diversity change in different landscapes or the same landscape in different times. From the data in table 3, it can be seen that various landscape types in Haikou city distribute equally and there is no landscape has apparent advantage type.

Conclusion and Prospect

From the analysis above, it can be seen that Haikou city from 2000 to 2010, with the rapid development of economy and the improvement of people's living standard, especially the boom in the tourism of Hainan province and Haikou city and the construction of Hainan international tourism island in recent years, it made the landscape pattern in Haikou city changed apparently. From 2000 to 2010, in the land utilization type of Haikou city, the area that unused land transferred into other land type is the most, the next is farmland and forest land, the smallest area is water area.

In the land utilization type transferred from unused land, there is mainly residents, construction, forest land and farmland. Besides, in the land utilization type of Haikou city in 2010, the area in residents, construction, forest land and farmland increased relatively large. It also indicates, from 2000 to 2010, there are mainly the increase area in residents and construction and the decrease area in unused land. In the landscape, residents, construction, farmland and forest land are the main part of landscape and increased rapidly. Besides, unused land and water area decreased rapidly. It also shows that not only the landscape fragmentation degree of the integral sight in Haikou City in relatively high, but the landscape fragmentation degree of the residents, construction, farmland and forest land, which are the main part of Haikou City , is also relatively high. What's more, the data also indicates that there is no well connection among each landscape and the communication of material energy among landscape is not smooth enough, which go against the mutual development between each landscape. Nevertheless, we can also see that various landscape types in Haikou city distribute equally and there is no landscape has apparent advantage type, which help the harmonious development between each landscape.

Acknowledgement

In this paper, the research was sponsored by the Hainan Province Nature Science Project（Project No. 413122）and National Soft Science Project (Project No. 2013GXS4D140).

References

[1] Turner IIBL. Land use and Land cover change (LUCC) : Science/Research plan [R]. IGBP Reports, N035, 1995-6-9.
[2] Chen Youqi, Yang Peng. The land use / land cover change research progress [J]. Journal of economic geography, 2001,21 (1): 0095-0100.
[3]Shi Mingle. International LUCC research present situation,problems and future prospect [J]. Journal of Shangrao Normal University,2004,24 (3): 0089-0094.
[4] Shili Li, Tang Guotao, Dong Xiansheng, Wang Sijie. The domestic and foreign land use / land cover change research [J]. Guangxi Agricultural Sciences, 2008,23 (3): 0042-0044.
[5] Ni Shaoxiang. In recent years our country land use / Cover Change Research Progress -- land cover change and its environmental effects [M]. planet publishing house, 2002:7-8.
[6] Xiao Duning Li Xiuzhen. The progress and outlook of contemporary landscape ecology [J]. Journal of geographical science, 1997 (4) : 356-364.
[7] Guo Jinping. discipline integration of landscape ecology and Chinese landscape ecology outlook [J]. geographical Science, 2003,23 (6): 277-281.
[8] Liu Delin, Li Bicheng. The Loess Plateau on the yellow small watershed land-use landscape pattern analysis [J]. journal of Surveying and mapping, 2014,39 (01): 0078-0082.
[9] Zheng Xinqi, Fu Mei Chen. Landscape pattern spatial analysis technology and its application [M]. Beijing: Science Press, 2010:92-146.

Advanced Materials Research Vols. 989-994 (2014) pp 5398-5402
© (2014) Trans Tech Publications, Switzerland
doi:10.4028/www.scientific.net/AMR.989-994.5398

Design of Information disclosure platform in Engineering based on Reliability model

Qingfeng Meng[1,a], Zhengqian Feng[2,b], Li zhao[3,b], Hao Shengyan[4,d]

[1] Shandong Computer Science Center, Shan Dong E-cloud Information Technology Co., Ltd., Jinan, 250000, China

[2]Department of Shandong Provincial Key Laboratory of computer Network, Shandong Computer Science Center, Jinan, 250000, China

[3]Shan Dong E-cloud Information Technology Co., Ltd., Shandong Computer Science Center, Jinan, 250000, China

[4]Shan Dong E-cloud Information Technology Co., Ltd., Shandong Computer Science Center, Jinan, 250000, China

[a]email: fengzhengqianf@126.com, [b]email:fengzhengqianf@126.com

Keywords: Information Disclosure; Reliability Model; Workflow

Abstract. This paper presents a public information platform based on reliability coefficient for information disclosure process in construction field. In this platform, we constructed a model of enterprise reliability coefficient and enterprise credit evaluation system, unified credit standards of Shandong Province in the construction industry sectors. Meanwhile, we adopt flexible workflow to definite workflow model of public information platform and using SOA architecture which is service-oriented and object-oriented programming ideas to realize the entire system. Finally, the article analyzes the public information platform in the field of engineering construction in Shandong province, and after the test run, the results show that the system has better scalability, stability and high security.

Introduction

Project information and the construction of credit system in the construction field are major decisions made by the central on the basis of reality. In recent years, construction field are prone to corruption mostly associated with the project decision-making, the approval authority and capital management is not open and transparent. Establishment of project information disclosure system and the integrity of our security mechanism in the construction field is an important way to solve the construction information is not open, transparent, market entry and exit mechanism is not perfect from the system, and which is an important part of controlling corruption from the source. Promoting the construction project information disclosure, is to promote the construction field projects to accept supervision under the sun, and is an important measure to prevent the occurrence of corruption, Which is an important measure to ensure implementing the "Regulations on Open Government Information", protecting the people's right to know, to participate and to supervise, and the construction of socialist democratic politics.

According to the requirement of central commission and Shandong province for discipline inspection, information disclosure and credit system construction work in Shandong Province construction field projects has already started. It requires all levels of departments to adjust measures to local conditions and make full use of the internet and all levels of government websites focus on disclosure of information to avoid redundant construction and waste of resources. Making information disclosure and credit system construction can be combined with commercial bribery governance, social credit system construction and other work to promote mutual.

Shandong province puts forward the development and construction of project information and credit information sharing service platform in Shandong construction field. Combined with the basic project information and basic credit information guiding catalogue, and depending on business workflow, it further refinement of project information and credit information collection,

publication, management and use, reached to strengthen the industry regulator and gradually achieve full coverage of all kinds of information on construction engineering and establish credit files for businesses and individuals. Insist on the principle of openness, fairness and justice, honesty and credit, it can promptly publish all kinds of specification information related to the construction field.

This paper takes information sharing service platform in Shandong province construction field for example, analyzed the information publicity business process and system architecture in the construction field, and accordingly proposed a model based on the reliability coefficient. The research in this paper has certain academic significance and application value.

Credit reliability model definition

(1) Engineering credit status

Currently, the engineering involves transportation, water, construction and other industries. All levels of the industry departments are responsible for detecting credit behavior of the main local area parties involved in the construction and collect, audit, record the credit information of the business units and personnel in the construction activities according to the unified credit information management measures in the industry. Employees with a different unit or qualification of employees in different sectors identified, which resulted in the inter-industry mutual recognition of credit information sharing difficult. The paper puts forward the innovation of using the reliability coefficient model, construction field credit system, unified trade credit standards, credit information sharing among industries.

(2) Credit reliability model definition

To quantitatively describe enterprise credit in the engineering field and definite enterprise credit reliability calculation model, the calculation steps of the model is just as follows: 1) Obtaining the main factors affecting the enterprise credit through principal component analysis method and noting for S^1, S^2, …, S^n. 2) Random inviting m groups of experts to rate these factors, scores were recorded as d^{11}, d^{12}, …, d^{1n}; d^{21}, d^{22}, …, d^{2n}; …; d^{m1}, d^{m2}, …, d^{mn}. 3) Because each factor has different dimensions, so the results of each factor score was normalized, and then calculate each factor of the arithmetic mean value, the calculation results denoted as: X^1, X^2, …, X^n. 4) Calculate the product of each factors and the corresponding weights according to the weight set, the result is marked Y^1, Y^2, …, Y^n. 5) Taking into account the experts may have uncertainties subjective or objective factors in the process of scoring, in order to reduce the influence of uncertain factors. First of all, equivalent normalization processing results of Y^1, Y^2, …, Y^n to make Y^1, Y^2, …, Y^n obey the standard normal distribution asymptotic. Secondly, set the same confidence level a of enterprise credibility, and then obtain business confidence interval according to the theory of confidence in Statistics. Finally, complete the quantitative analysis and grading of enterprise reliability according to this confidence interval.

Design of Information disclosure process

(1) Information disclosure process introduction

Taking the project as center and approval process as the main line, accordance with the principle of "who is in charge, who released", project management units need to do a good job of information collection, release and maintenance, etc. Project approval authorities collect, review and publish project approval, filing and other related information. The project construction units provide project management and key staff behavior information and the department in charge of the project review and issue this information according to the management authority. Land and resources departments collect, review and release the information of land use rights, mining rights approval and transfer. Basic information of related companies is disclosed by the competent authorities in accordance with the enterprise registration functions. Basic information of related enterprise qualification and personal qualifications is disclosed by construction quality management according to the functions.

(2) Workflow engine design

The workflow engine is responsible for the interpretation of the process definition and controls the operation of the process instance. Information release process using the simplified workflow engine takes each workflow execution engines package into a Web Service interface. These interfaces include: 1) Process Definition: responsible for the interpretation and instantiate a detection workflow; 2) Monitoring Tools: responsible for status monitoring of active and inactive process flow, version management, process management and business process statistics; 3) Workflow client applications: responsible for receiving and feedback the client application requests; 4) other related services interface: the interface includes a document printing, view, data summary printing and other related services.

In the workflow management platform, a plurality of workflow engine cooperative work to promote the execution of a workflow instance. Each workflow engine is responsible for part of the active control and management in a process and calls the relevant resources and application tools to complete the implementation of these activities. Between each workflow engine and workflow engine and user interface using SOAP messages for interactive. Information disclosure process adopts simplified workflow engine, and the design is shown in Figure 1.

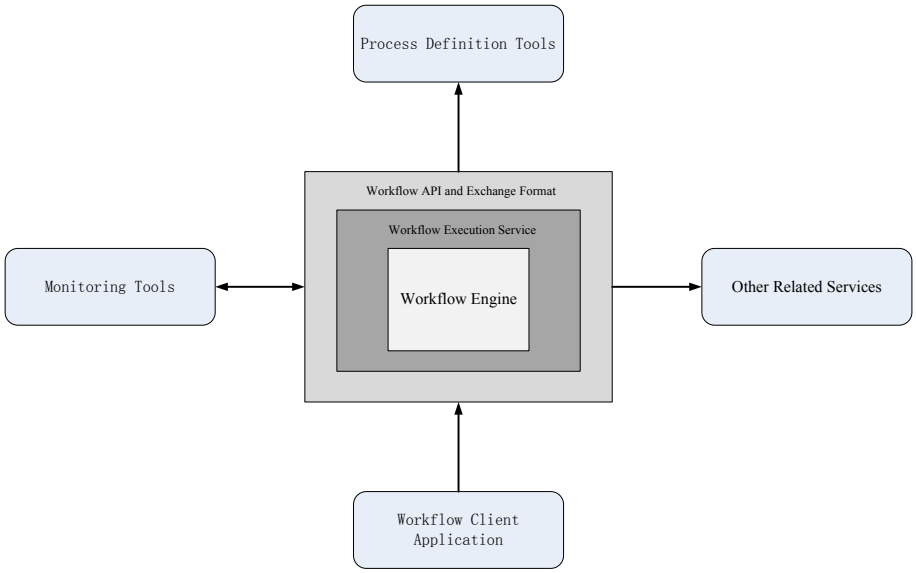

Fig.1. Workflow engine design

Design and implementation of system architecture

The design, development, deployment and testing of project information, credit information sharing and information exchange platform in Shandong province construction field are all in cloud platform of Shandong province cloud computing center. This platform is based on B/S technology architecture, using .NET framework coding, and application server uses authorized by Microsoft Windows 2003 Server, the database used SQL Server 2005 above which is authorized by Microsoft. Our goal is aimed at building a secure and reliable large-scale integrated management information system adopting a unified data exchange, unified interface standard and unified security.

The entire platform system architecture is based on advanced multi-tier architecture model and the MVC (Model-View-Controller) pattern. Some applications can be built by multi-tier architecture which has features such as loose coupling, easy to reuse, scalability. In addition to facilitate the organization and implementation of software development, it can also facilitate system maintenance and expansion in the future. In the MVC pattern, Model component encapsulates the kernel data and functionality, so that the core functions are independently of the output representation and input, and view component obtains information from the model displaying to the users. Through the mutual separation of model, view and controller, which makes the development of frame can be flexibly adapt to changing requirements of the function of user interface.

System from the bottom to the main frame is divided into three layers: the data tier, business tier (divided into application support tier and application tier) and the presentation tier (divided into client tier and presentation tier). The overall architecture of the system is shown below in figure 2.

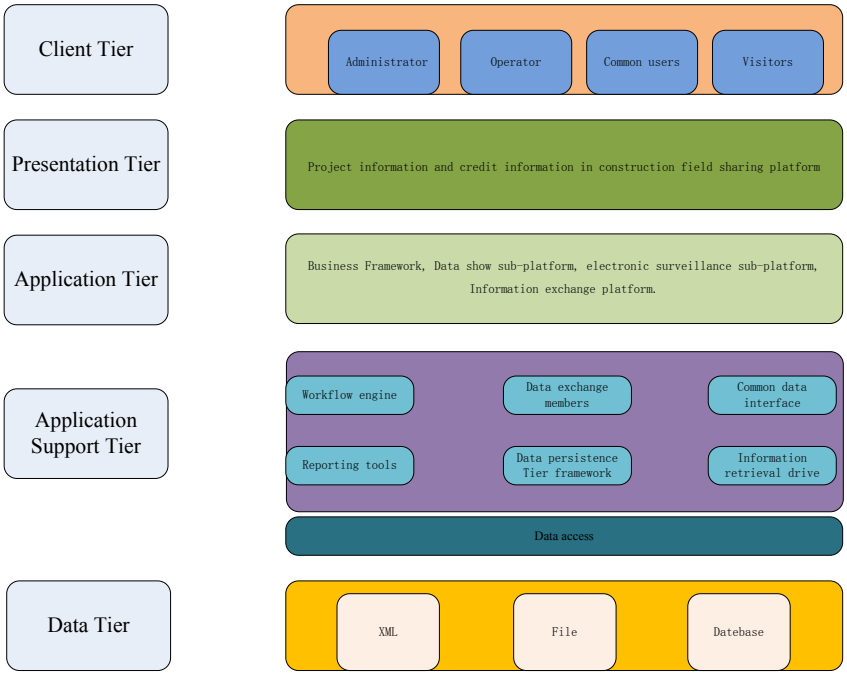

Fig.2. System Architecture of Information disclosure platform

Instance analysis

Project information and information sharing service platform of Shandong province engineering construction field has started to run in December 2013. The information platform in accordance with the requirements of Shandong province commission for discipline inspection and project information disclosure and credit system construction work coordination group in Shandong province construction field. The information platform in accordance with the commission for discipline inspection of Shandong province and the provincial engineering construction project information and the requirements of good faith system construction work coordination group, further combed information disclosure processes in Shandong construction field and improve the standards of information released. All business functions are running on the line, and the program runs very stable. In particular, this paper innovatively proposed the use of reliability coefficient model and building engineering credit system, unifying industry credit standard. This is also the major initiatives in the anti-corruption which focus on the prominent problems in the field of construction management in Shandong province.

Conclusion

Based on information disclosure in engineering construction field as the breakthrough point, this paper presented a designing scheme of public information platform in the field of engineering construction based on reliability model and innovatively proposed the use of reliability coefficient model and building engineering credit system, unifying industry credit standard, sharing industry credit information. Using a simplified workflow engine makes the system easy to build and using service-oriented architecture SOA and object-oriented programming ideas for system implementation solves the construction field of information disclosure shared problems. From the design example of Shandong province engineering construction field of information disclosure, we got satisfactory results after test run. Next, we will further optimization in the design of reliability model.

References

[1] Hang Zhengnan. Reliability analysis of expert judgment [J]. Chinese Journal of Health Statistics. 2000(6):47-49.

[2] Xu Linsheng,Wang Zhiquan, Dai Yuewei. Expert's Credibility Model and Evaluation Method. Journal of Nanjing University of Science and Technology [J]. 2010(34):30-34.

[3]Cheng Haijin, Liao Linqing. Analysis on Evaluation Reliability of A Single Expert During Process of Approach Evaluation [J]. Journal of Chongqing Institute of Technology. 2009(23):41-43.

[4] Li Jingjie, Wang Weiping. Review on approaches of flexible workflow. Computer Integrated Manufacturing Systems [J]. 2010,8(6):1570-1574.

[5] Zhu Jianping,Lu Hailong. Research and Application of Flexible Technology for Workflow Management System [J]. China CIO News. 2013, 5:63-64.

[6] Wang Yinghui, Wang Dongbo. Study on bionic flexible workflow modeling and adaptation algorithm[J]. Application Research of Computers. 2011,5(28): 1692-1695.

[7] Shi Yinxue, Sun Ruizhi. Flexible workflow based on dynamic planning [J]. JOURNANL OF SOUTHEAST UNIVERSITY. 2010,A02(40):258-262.

[8] Guan Hongjie, Wang Ke. Research and application of workflow management system based on SOA [J]. Computer Engineering and Design. 2011, 5(32):1655-1657.

[9]Zhu Shengli. A Workflow Model to Improve System Flexibility [J]. Computer and Modernization. 2012,3:71-73.

[10] Fan Yushun. Foundation of Workflow Management Technology [M]. 2001.

[11] W.M.P.van der Aalst.The Application of Petri Nets to Workflow Management [J].The Journal of Circuits, Systems and Computers.1998,8(1):21-66.

[12] Duan Huiying,Chen Deyun. Workflow Management System Based on SOA [J]. JOURNAL OF HARBIN UNIVERSITY OF SCIENCE AND TECHNOLOGY. 2009,5(14):72-75.

Advanced Materials Research Vols. 989-994 (2014) pp 5403-5406
© (2014) Trans Tech Publications, Switzerland
doi:10.4028/www.scientific.net/AMR.989-994.5403

The Research on Statistical Characteristics of China Civil Aviation Network

Hongguang YAO[1]

[1]School of Air Transportation Shanghai University of Engineering and Science

Shanghai, 201620,P.R. China

email:Yhg1yhg@sina.com

Keywords: Statistical Characteristics, China Civil Aviation Network, complex networks

Abstract. Aviation network as an important infrastructure, play a huge role in social and economic development. There is a close relationship between the efficiency and its network structure. In this paper, navigation of the 163 cities and 2198 air routes network composed of analysis the statistical characteristics of the empirical analysis, the basic structure of our aviation network properties.

An overview of China's aviation network

The number of routes and the coverage is often used as a measure of a national air transport network an important indicator of the level of development. In recent years, China's rapid economic development has greatly driven the development of the domestic air transport, navigation and route number of cities are growing rapidly. By 2010, China's domestic routes 2198 (not including Hong Kong, Macao), shipping more than 163 cities, covering the initial formation of the major cities in the domestic air transportation network. However, the uneven distribution of the density domestic routes, the East Mississippi condition sparse and not with the number of shipping routes to increase the airport has changed.

Been expanding at the same time, the efficiency of the existence of low air network, the network had no obvious effect of economies of scale and other issues. The main reason is, whether airlines or the CAA during the route planning is usually only one route open route the demand analysis as the main index, but not on the new route synergies with existing networks for analysis, ignoring the air Network integrity. Overseas experience shows that with the constant expansion of aviation network, the potential economic advantages of scale increasingly huge. Through the analysis of airline network structure, help to optimize the aviation network structure, improving the efficiency of air transport.

China Civil Aviation Network data acquisition

The Tourism Net boat class timetable as the main source of data, by the end of May 16, 2011, a total acquisition navigable City 163, 2198 domestic routes, flight 9611.In 163 a navigable city respectively as a matrix of rows and columns, with two flights between city as weight, forming a 163 * 163 weighted aviation network adjacency matrix. Using the matrix, to be navigable city in aviation network important degree as the standard, obtains the Chinese aviation network navigation city social structure. More important is the closer to the center position, indicating that the navigable city in aviation of the importance of the network more and more strong.

Chinese aviation network statistical analysis

①Degree and strength

Degree of node and node is defined as the total number of border. In the aviation network, a node of the city of greater means connected with the city number, it has few routes are also more. The flight number is a measure of the importance of node city key factors, only through the "degree" of value is not enough to reflect the importance of node city[1]. Therefore, the node degrees

corresponding to evolve into another parameter, strength, in order to reflect the city node in the aviation network status, defined as:

$$s_i = \sum_{j \in N_i} w_{ij} \quad (1)$$

Wherein N_i represents a node i neighbor sets ; W_{ij} said node i and node j arc weights that nodes i and j city node between JAL class number.

In this paper the application of the University of California at Erwin (Irvine) scholars prepared free of large scale network analysis software Ucinet calculation of the Chinese 163 navigable city degree and the point of the right, the top 20 spots in the city as shown in Table 1.

As you can see from table 1 degree and strength before the 20 city with a high degree of overlap, shown in China has the most course of 20 city is as JAL class number 20 city. China's aviation network point intensity distribution is obviously divided into two parts, in the point strength = 57 bend, obeys a power-law distribution. At present, China has 2198 domestic routes and flights of 9611, ranking the top 20 City flights accounted for the proportion of the total number of the flight reached 52% and 68%, China air transport resources distribution not balanced, large and flight routes are concentrated in a small city. [2]

Table 1 The navigable City moderate top 20 city summary table

Rank of Degree	city	Degree	strength	Rank of strength
1	BJS	118	809	1
2	CAN	96	498	3
3	SHA	95	676	2
4	CTU	68	390	7
5	KMG	67	400	6
6	SZX	66	455	5
7	CKG	63	307	8
8	XIY	62	479	4
9	XMN	52	281	9
10	CSX	46	208	16
11	DLC	44	191	17
12	NKG	43	212	14
13	HGH	41	272	12
14	WUH	40	211	15
15	TAO	40	260	13
16	TNA	40	221	14
17	URC	39	183	18
18	KWE	39	154	22
19	SHE	37	156	20
20	CGO	36	153	23
Total		1132	6516	

②Aviation network average shortest path

The shortest path is defined in the network two the distance between nodes, which connected the two nodes of the shortest path contains the number of edges ; the average path length refers to all nodes in the network between the average shortest distance, it can be used to measure the transmission efficiency of the network[3]. In the aviation network, city of between the average shortest path, can reflect the passengers from one city to another city to average at least the number of transit, reflect the aviation two nodes in the network city travel convenience. The whole network average shortest path is calculated by the following formula type (2). [4]

$$L = \frac{\sum l_{ij}}{\frac{1}{2}N(N+1)} \quad (2)$$

The application of Ucinet software and data matrix, the calculation of Chinese aviation network average shortest path 2.16.From our country an arbitrary navigation based on average only need a transit can reach other navigable city.

In Chinese aviation network all possible travel routes, direct route accounted for only 8%, while the longest path is 4, namely the need to transfer 3 times. Need many transit navigation city are mainly distributed in the periphery of Figure 1, in the whole air network is relatively important

position, for example, if the program from Xinjiang Akesu to Guangxi white, subject to Urumqi and transit of Chongqing, after the 3 transfer to reach the destination of Baise.

Dielectric and dielectric number distribution

Betweenness refers to all nodes in the network of the shortest path through the point ratio, a node betweenness can reflect the nodes in the network's influence. In the aviation network, a navigable City referred to a number of larger shows the city transit of ability is more strong, the aviation network plays more and more important. The application of Ucinet software and data matrix, calculated 163 navigable City dielectric numerical, referred to the number of top 20 city are shown in Table 2.

Table 2 Betweenness to the number of top 20 city summary table

City	BJS	CAN	SHA	URC	XIY	KMG	CTU
Betweenness	7411	3460	3430	2417	2391	1909	1478
City	CKG	KWE	CZX	HRB	HET	XMN	CSX
Betweenness	1395	1113	917	541	389	368	349
City	KRL	DLC	CGO	WUH	SJW	TAO	
Betweenness	322	257	227	208	198	183	

Through the calculation shows that the current Chinese 163 navigable City referred to the number of differences and disparities, Beijing referred to the number 7410.88 ranked the first, and 79 navigation City referred to the number of 0, as shown in Figure 1.Show all navigable city in China in nearly half of the city is still cannot play the transfer function.

As aviation network two key statistical indicators, referred to the number and strength are closely linked.163 navigation City referred to the number and strength of relationships as shown in Figure 2 below, whole betweenness basically with the level increases, but there are many little deviation from the straight line, fall on the line below. This referred to the number and strength has a certain connection, but not strictly obey the known power-law function relationship. Some high strength city are mainly distributed in the municipality directly under the central government, provincial capital (capital) and some important province city, such as Xiamen, Qing Dao ; and referred to the number of high city in addition to the city, also includes a number of important regional transport hub such as Urumqi, Korla and so on. The above suggests that in Chinese aviation network has more routes, a multi-day flight navigation city often is a network of important transit hub ; in addition some navigation city routes and flights although the amount is more limited, but still in transit network plays an important role. Has a high strength and referred to the number of navigation city is Chinese aviation network key nodes in the network communication plays an important role. [5]

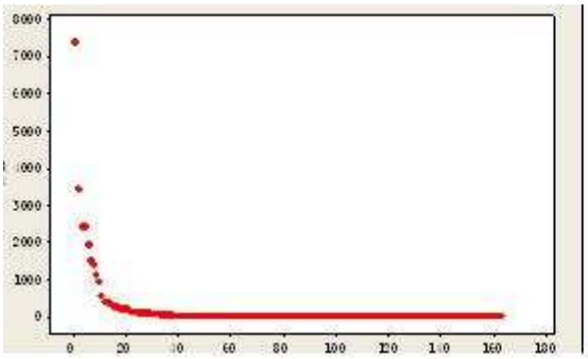

Fig 1 Navigable City betweenness distribution map

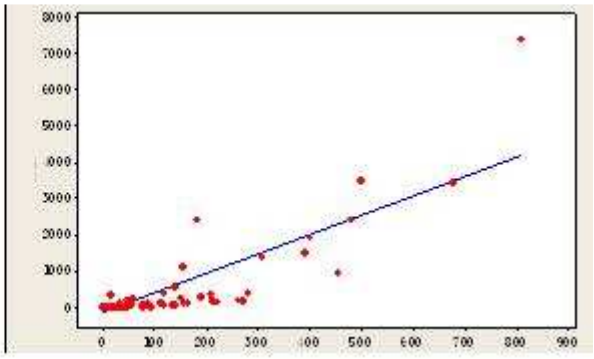

Fig 2 Navigable City referred to the number and intensity of scattered diagram

Conclusion

aviation network has the following properties:

(1) With the increase of flights, passenger throughput does not increase linearly, but rather to increase exponentially. This can be used in economics to understand the network externalities, the more the route connecting the airport, people are more willing to go the airport, because in this airport, either direct or transit is more convenient, there are enough Flights to choose from, can save the transit waiting time.

(2) from any airport in China, to any other airport, the average require only one transfer. Direct flights can be accounted for only about 9% of flights. The longest path is 5, that requires transit 4.

(3) between the nodes can find a shorter path connection from the network as a whole, the small-world network polymer layer also has large coefficients and small average path length of the statistical characteristics of the two. China's aviation network from the high polymer layer coefficient and the relatively short average path length of the term, it can be concluded, China's aviation network is a small world network.

Note: This paper supported by the 2013 annual Shanghai City Board of education research and innovation key project (13ZS127).

References

[1] Liu HK, Zhou T. Topological properties of Chinese city airline network[J]. Dynamics of Continuous, Discrete and Impulsive Systems B, 2009(14): 135-138.

[2] Chunhua Gao.Airline Integrated Planning and Operations [D].Georgia Institute of Technology, 2007.

[3] Porta S, Crucitti P, Latora V. The network analysis of urban streets: A dual approach[J]. Physica A, 2008(369): 853—866.

[4] GuimeràR, Mossa S, Turtschi A, et al. The world-wide air transportation network: Anomalous centrality, community structure, and cities'global roles. Proc Natl Acad Sci USA, 2005, 102(22): 7794-7799.

[5]Zhou T,Wang B H,Hui P M,et al.Topological properties of integer networks[J].Physica A,2006,367:613-618.

Advanced Materials Research Vols. 989-994 (2014) pp 5407-5410
© (2014) Trans Tech Publications, Switzerland
doi:10.4028/www.scientific.net/AMR.989-994.5407

Application of digital media technology in exhibition design for the geological museum

Kaifeng Zhou[1, a], Jianshe Wang[2, b]

[1]City College, Kunming University of Science and Technology, Kunming, China 650093

[2]Faculty of Land Resource Engineering, Kunming University of Science and Technology, Kunming, China 650093

[a]Corresponding Author & email: 806673714@qq.com, [b]email: kmlgdxhaveme@163.com

Keywords: Digital exhibition-design;Henan Province, Virtual reality;Geological museum

Abstract. The digital technology has been brought a profound social change to human, especially in the digital display technology. In order to explore the application of Digital exhibition in geological museum field, the author applies by the "building roaming + picture + text" way to the audience on the Architectural layout and displayed content of Henan Geological Museum, not the traditional construction roaming form, according to the "Henan Provincial Geological Museum exhibition design" case.

Introduction

In recent years, with the development of computer technology, digital media technology have made a spurt of progress, especially digital exhibition combining with computer technology has gradually become the new subject field of display design. Nowadays, digital exhibition hall has broken through the traditional exhibition wall, showcase, making it more interactive, comprehensive and strong sense of the scene. Existed display mode of Henan Province Geological Museum: Exhibiting through the floor structure, caused by too tight space layout, make the geological nature mood lost. In order to make the Geological Museum of Henan province reached the level with harmony, high-tech, unique to Henan, and to explore how does the Digital Media technology apply more effective in exhibition design museum of geology. The author uses the following creative ideas in this work.

1. Scattering with original hall. The original ore forest and mineral hall merge into ore mineral hall. The dinosaur hall, ancient elephant's hall and ancient life evolution hall merge into paleontology Hall. The original lobby becomes into entrance gate of the geological museum, Mineral resources hall, geological environment hall and earth hall are unchanged, Cinema 4D dispersed in all inside. It is convenient for reasonable arrangement of all exhibition halls, expanding the exhibition's area, achieving grinding, strong attraction and integration of the natural effect.

2. Designed separately each exhibition hall, making its architectural style independently. This can prevent phenomenon of "the crow black".

3. Applies by the "building roaming + picture + text" way to the audience on the Architectural layout and displayed content of Henan Geological Museum.

Animation continuity design

Table 1 Animation continuity design

number	Lens / description	Caption	Time	description
1	Dolly shot		15s	Film leader
2	The logo fades in and appeases zooming in the mode of light layer	Title 1	5s	Perform museum

3	Translation lens in middle shot, Cameral pan		15s	building layout and surrounding environment
4	Shake lens		5s	
5	Aeroview shot		5s	
6	South-north central road roaming lens		15s	Central avenue
7	East-west central road roaming lens		15s	
8	Background appeases zooming and text description	Title 2	17s	
9	The design introduces by the captions	Title 3	6s	Perform the doors
10	The door roaming		10s	
11	The text introduction	Title 4	2s	mineral resources hall
	The hall roaming		10s	
	Animation in the excitation		8s	
12	The text introduction	Title 5	4s	Perform ore mineral hall
	The hall roaming		10s	
	Animation in the excitation		8s	
13	The text introduction	Title 6	4s	Perform paleontology Hall
	The hall roaming		10s	
	Animation in the excitation		8s	
14	The text introduction	Title 7	4s	Geological environment hall
	The hall roaming		10s	
	Animation in the excitation		8s	
15	The text introduction	Title 8	4s	Perform the earth hall
	The hall roaming		10s	
	Animation in the excitation		8s	
16	Walking-caption animation	Title 9	25s	Trailer

Caption 1 -- "Henan Provincial Museum of geology"

Caption 2 -- Geological Museum of Henan province is located in the Jinshui District of Zhengzhou City, the museum consists of five exhibition halls, including: the earth hall, paleontology Hall (ancient dinosaur hall, hall, the evolution of life hall), Ore mineral Hall (ore hall, minerals hall), mineral resources department, geological environment Hall.

Caption 3 -- " Henan geological Museum -- touch the history of the earth, staring at the essence of nature. As is shown below the hall's design of Henan geological Museum , roughly the shape using the arc, the column top designed 'Globe' appearance, in front of the small garden around the 'geological Hammer' sculpture, permeated with the subject of 'geo'.

Caption 4 -- mineral resources hall, it shows mainly the main mineral resources and the mineral resources economic Henan province

Caption 5 -- ore mineral hall, including ore hall and minerals hall, mineral hall main display hundreds of mineral crystal, jade specimen, enjoy the nature spirit; ore hall mainly display typical ore in Henan province found.

Caption 6 -- paleontology hall includes dinosaur hall, ancient elephant's hall and ancient life evolution hall. Dinosaur hall main display Mesozoic overlord -- dinosaur; Ancient hall mainly display the characteristics of Henan Province -- the Yellow River basin is Kingdom of the ancient Elephant ; The evolution of life hall adopts a double helix structure, describes the earth life growing out of nothing, from low to high evolutionary process to everybody.

Caption 7 -- geological environment hall, the halls area is smaller, but which still would be enjoy the rich geological resources remains in the Central Plains of China, understudied the function of geological environment for human survival and health, social development and progress of civilization; known geological environment and mass, and thus learned to live in harmony with nature or the geological environment

Caption 8 -- the earth hall, mainly introduced relevant knowledge of the universe and the earth to everybody. It includes eight planets of the solar system; various rock from the geological formation; influence of weathering, Karsts landform and glacial on human beings; the characteristics of Henan -- the Yellow River, loess, the Yellow River culture.

Caption 9 -- "looking forward to your visit Henan Geological Museum", "producer: Jianshe Wang", "end".

Product steps

3.1 previous preparation Collect Geological Museum exhibition design related on materials, such as works, documents, materials, textures, background music, picture and so on. Be familiar with the geological museum exhibits typical case. Sort and deal with materials in the "Adobe Photoshop cs4", such as three-dimensional materials and textures, seamless textures etc..

3.2Make 3D model Hall According to the pre-collected material and the demand analysis, then make 3D model of Henan Province geological Museum. It includes that a door, paleontology hall, ore minerals hall, mineral resources hall, geological environment hall, earth hall and the overall layout. Concrete steps will not go into here.

3.3Make 3D animation of exhibition hall According toTable2.1,and then make 3D Animation of museum displayed hall. Because concrete steps of making roaming animation are basically similar to each displayed hall of Geological Museum, making concrete steps to "make and render the whole animation" as an example. The other part of those is not much.

No.1 Make and render the whole roaming animation

Part 1 Product and render browsing animation of the overall layout

1) Using 3ds max 2010 to open the scene file named "overall layout.max".
2) Set the time arrangement for the 500 frame, PAL format. Parameters of time configuration are shown in Figure 3.1.

Fig. 1 Time configuration

3) Create three target cameras, used as making camera animation and key frame animation.
4) Choose a camera, then adjust the camera so that the screen at the door of geological museum in accordance with the animation overhauling script.
5) Set key point, moving camera overall and make image alignment to Central Avenue intersection.
6) Rotate camera, then move the focus of lens, and align inside the gate of the geological museum, set key frames at last.
7) Change focal length of the camera, set animation.
8) Turn off the key frame, browse the whole animation, and adjust little according to the animation effect.

9) The animation rendering settings.

Part 2 Product and render animation of the bird's eye view.

1) Make the translational animation of the camera along Central Avenue by choosing a target camera in accordance with the animation overhauling script.
2) Make the path animation of bird's eye view by choosing a target camera in accordance with the animation overhauling script.
3) Render three camera animations as image frame sequence form, namely the file as “bird’s eye view.tga”.
4) Save the source file.

3.4Post digital compositing and editing we can carry out later digital synthesis and nonlinear editing after completing previous preparation and middle of the production. We should be strictly in accordance with the animation overhauling script in the process of digital synthesis and the final video editing at this stage. First of all, rendered image sequence frame file in the “3DsMax” import in “After Effects” and sub layer. Then make titles and joined the lens appropriate transition effects. Make and render output the final transition and transition effects in Premiere.

3.5The test run Make sample and timely be communication with customers after rendering the works, at last system testing. Animation effects as shown in Fig.

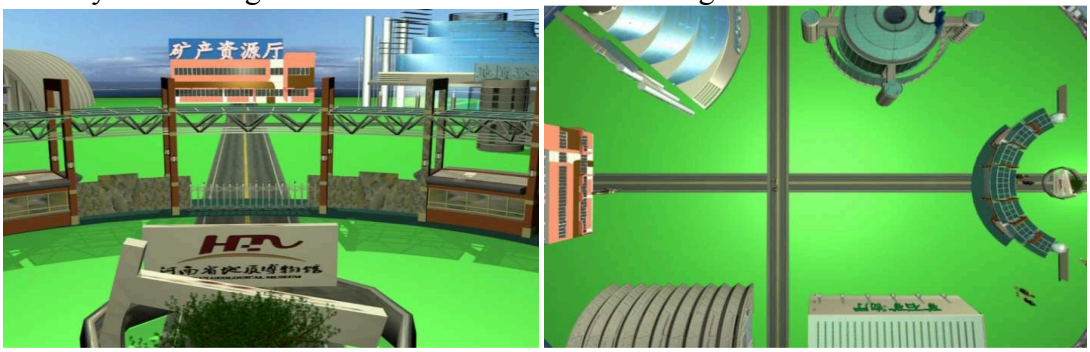

(a) Museum foyer (b) The overall layout

Fig. 2 Key frame of animation

Conclusion

We display successfully on Henan Geological Museum hall by 3D animation in the case. We combine with the use of "3DsMax + After Effects + Premiere" three kinds of digital media mainstream software in the process of production. However, the application of digital exhibition design in geological museum display field is just unfolding. We not only need to master the technology of computer software, but also understand geology; it said by composite talent. So it needs those people to explore and unremitted efforts.

References

[1] Guangran Liu. Virtual Reality Technology, 2011.

[2] Mingtan Tang. Small towns planning--research standard, method, example, 2008.

[3] HaichaoQiao. Research and implementation of digital virtual museum based on VRML [D]. Xi an: 2010.8-12.

[4] Jingling Yang. Research and application of digital technology in modern display design [D]. Shanghai: 2009.1-5.

[5] Jinshan Hu, Jianrong Kang, Qingzhong Wu. 3 dimensional map of the campus roaming implementation based on 3DSMAX [J]. Geomantic And Spatial Information Technology, 200831(5)5-8.

Advanced Materials Research Vols. 989-994 (2014) pp 5411-5414
© (2014) Trans Tech Publications, Switzerland
doi:10.4028/www.scientific.net/AMR.989-994.5411

Application of Information Visualization in Museums' Display and Design

Jieming HU [1, a]

[1] Donghua University, Shanghai 200051,China

[a] edu163819@163.com

Keywords: Museums, Exhibition and design, Information visualization

Abstract. Information visualization is more inclined to two-dimension design in traditional design field. As known to us all, it is unable to be applied in three-dimension. However, with the rapid development of design science, a growing number of people who are engaged in design have found that the application of information visualization can't be only restricted to graphic design as graphic design is gradually crossing with space design.

Museums' display and design is part of display design. And long time of exhibition is the main character differing from the temporary exhibitions. As the chief carrier of mankind's cultural heritage, museums are visited and browsed by people and finally realize information's expression, acceptance and cognition. In this process, information is visualized.

Background of this subject

Museums are the main carriers of culture and thoughts, sites of collecting, demonstrating and protecting mankind heritage as well as diary notes recording the development of human civilization. In addition, museums also shoulder responsibilities of popularizing public culture and providing visitors a relaxing and vivid atmosphere. Most importantly, display and design of museums have been a vital symbol measuring national economic and civil level.

With the rapid development of economy, people's material life standards have been largely increased. Therefore, museums have been the most favorable sites for people to entertain and meet their spiritual needs.

Museum display is an art of well connecting visual language with display space. People's needs for museums are never restricted to information but more about visual enjoyment.

Museum display and design is a comprehensive subject in the field of art of design, involving the crossing of a great many other subjects such as museum study, literature, aesthetics, optics and psychology. As far as I am concerned, based on such a background, research on the application of museum display and design will be pragmatic and promising in the near future.

Concept of information visualization

Just like mankind's language, information visualization, a kind of visual language, must abide by some special grammars and their own laws. In museum display and design, the visual language is indicated through some detailed media such as exhibition plates, light boxes, slides and simulation models. Whether the visual language is used properly and accurately decides the efficiency of information's spreading.

In addition to visual elements and visual grammars, the features of visual language ought to be focused at the same time. In display and design, visual language will work better than any other language and six requirements including visual cognition, legibility, accuracy, nationality, and contemporary characters must be satisfied.

Another important concept in information visualization is opaque setting. Below is a formula calculating the density of the distance from the items displayed from the visitors.

$$\rho_i = (N_{il} + N_{ir}) / (N_{/\max} + N_{r\max}) \qquad (1)$$

ρ_i is the density, N_{il} is the number of all points in the left space and N_{ir} is the number of all points in the right space. $N_{l/\max}$ and $N_{r/\max}$ are respectively the amount of data in both left and right spaces. Moreover, formula (2) will also help calculate the density.

$$\rho_i = n_i / \sum_{k=0}^{m} n_k \quad (2)$$

Obviously, calculation of density will help shorten the distance between visitors and the item displayed, giving full play to information visualization.

Influence of museum's environment on information visualization

Information visualization is an indispensible part in the display space. However, information visualization is impacted by space area and building height.

3.1 Spatial scale on information visualization

Visual language's existence depends on spatial interface which directly affects the corresponding tempo. The larger the spatial scale is, the longer visitors' observing distance will be. Therefore, spatial scale must be taken into consideration while designing the visual language.

The size of space to some extent decides the size of words. The bigger the size of space is, the bigger words should be set in bold. To take unit specification for example, based on the normal spatial distance 1000mm to 1500mm, the smallest specification words in the layout should be no smaller than 36pt as smaller words will make it more difficult for readers in the process of reading. If the spatial distance is added to 2000mm, the smallest words should not be lower than 48pt. However, in the small specification plates which should be read in close distance, it is acceptable to restricted the size of words within approximately 24pt.

To draw a conclusion from what has been claimed above that the size of words is supposed to be in proportion to visitors' observing distance. According to daily working experience, the relationship between observing distance and suitable size of words can be concluded through figure 1.

Observing Distance	The Smallest Word Size of Headline's Words	The Smallest Word Size of Explanatory Words
1000mm	72pt	36pt
2000mm	110pt	48pt
3000mm	150pt	72pt
4000mm	200pt	90pt

Figure 1. Relationship between observing distance and word size

3.2 Influence of light on information visualization

Light plays a vital role in museum's display and design. The majority of museums' light made in an artificial way. However, currently, a growing number of modern museums are in favor of natural light in view of energy conservation.

Most of the natural light in museums' display and design space is brought in only in the public places, but the light for items in display is supplied artificially. Compared with natural light, artificial light is more stable with stronger expressive force. Besides, artificial light is able to effectively control the tempo and color of the whole display space, letting the visual language provide better service for the display.

What's more, perception of the words, background pictures and colors in museums' display space are closely related with brightness. The stronger brightness is, the longer observing distance is.

The observing distance for brightness and colors conform to the following rules: white plus black, yellow plus black, green plus black, white plus green, white plus red, yellow plus red, white plus blue, black plus orange are feebly influenced by brightness, but orange plus black, blue plus black, red plus black, black plus white, blue plus white, red plus white, gray plus white, black plus gray, red plus gray, black plus green, black plus red, yellow plus black are obviously influenced by brightness.

Based on different brightness, figure 2 recommends the right chars and colors.

Strong Brightness		Medium Brightness		Weak Brightness	
Chars	**Background**	**Chars**	**Background**	**Chars**	**Background**
Black	Yellow	Black	Yellow	Orange	Black
Red	White	Orange	Black	White	Black
Orange	Black	Red	White	Black	Yellow
White	Black	White	Black	White	Blue
Yellow	Black	Blue	White	Yellow	Black
White	Blue	White	Blue	Yellow	Red
Black	Gray	White	Red	Red	White
Black	Red	Yellow	Black	Blue	White
Blue	White	Yellow	Red	White	Red
Black	Green	Black	Gray	Black	Gray

Figure 2. Character table for different brightness

Expression ways in museum display and design

4.1 Exhibition plates

Most of the information in museum display is spread through exhibition plates. As a spreading medium, plates are in possession of a great number of pragmatic characteristics such as low cost, convenient installation as well as stability. Therefore, a great many carriers of visual language are made through plates. In museum exhibitions, the selection of plate materials is obviously different from that of temporary expositions. The plate materials used in museum exhibitions mainly include aluminum alloy plate, PVC plate and wooden plate. Plates of different materials differ according to the distinct requirements of exhibitions.

4.2 Light boxes

Application of light boxes are quite common as they mainly count on the brightness of background lights to make the exhibitions are attractive in the public. Light boxes are fixed with some steel bones or model frames with lamp pipes shining behind.

Generally speaking, the information which needs to be illustrated through light boxes is significant part in the entire exhibition. It is sometimes concluded with brief words, pictures or words plus pictures.

Summary

Like human language, visual language is a major medium of mankind's civilization and historic heritage. As the main body displayed in museum space, the role it plays is indispensible and vital. The combination of visual language with museum display means that union of traditional two-dimension design and spatial will be a must in the field of design in the near future.

References

[1]Shen Haijun, The Application Research of Visual Language in Museum Display and Space,2009.

[2]Dong Chunxin, Exposition Space and Art Design, 2007.

[3]ZhuXiang, Display and Design of Commercial Space, 2007.

[4]Li Yanzu, Lu Ying, History and Aesthetics of Visual Expression Design[M], 2000.

Advanced Materials Research Vols. 989-994 (2014) pp 5415-5418
© (2014) Trans Tech Publications, Switzerland
doi:10.4028/www.scientific.net/AMR.989-994.5415

Based on computer network security in financial informationization construction of colleges and universities

Shizong Wu[1, a]

[1]China West Normal University,Nanchong City,Sichuang Province,China

[a]jccwsz@163.com

Keywords: computer network security,financial,informationization construction,colleges

Abstract: The computer network bring great benefits to the financial information and daily management of university. At the same time, we should pay attention to the potential safety hazard and threats brought by the network finance. We can security network financial information from two aspects of technology and management, technology mainly focus on the configuration and set with the computer application software and hardware; And management is the information security management. According to the situation and conditions of the university itself, considering safety factors, the establishment of a stable security network financial information management system, it is the important foundation of financial management in colleges and universities, is also the important prerequisite for healthy and stable development in colleges and universities.

Introduction

In the information age, widely used in modern computer network technology will become the inevitable developing trend of financial management and accounting,because the financial accounting demand timely, accurate and complete information.But under the network environment of financial management and accounting system in an open platform, it will inevitably face many risks such as hacking, virus infection. Solve the problem of financial network security and data security is the premise to realize network financial management and accounting.

As a new financial management mode,Financial network truly achieve the financial work of mobile, it brings a change of financial management science, develops the network fastly. Network financial security is not only a technical problem, but also the safety management problems, we must considering safety factors according to their own actual situation, setting reasonable goals, technical case and related supporting regulations, etc., to establish a secure network financial system, to bring financial management to a new level.

Financial network security problem of universities.

The inappropriate use of financial software.In colleges and universities, many sort of financial software are used, the software vendors have different technical ability, part of the software in the design when there is a loophole, most likely by criminals or hacker attacks, and even the whole system paralysis, leading to loss of data.At present,The colleges and universities lack of strict financial software on the user privileges division: refer to history of financial information and financial data revision history record is too general, didn't do the strict records of user level, when a financial accident will not work by looking at the history of illness.

A computer virus spread and attack.Computer virus spread fast, financial personnel download network information freely, use mobile hard disk, usb flash drive, and so on and so forth. Combined with some computer did not install a firewall, and even not installed antivirus software or no update virus, can cause computer network virus, not only cause serious damage to the users' personal computer security, but also affect college financial network users. Even may ruined the database, data is damaged, a serious threat to the network information security.Some illegal users through legal user password theft, illegal user identity, into the network to tamper with or damage of the data, the illegal invasion behavior put forward great challenge to college network information security. With the rapid

development of Internet, network attack form is more sophisticated, may make it harder for users to notice. Everywhere on the network of trojans, virus software, such as in Mass under the flexible use of attackers easily achieve the goal of the attack, causing a system crash or run, lead to the database is destroyed, a serious threat to the network information security[1].

Defects in the financial networks configuration.Configuration is incomplete or improper configuration will affect network information flow, even will cause the network paralysis, make the processing of financial data cannot be correct, complete, caused serious data leaks and lost. Reality has the following a few questions. Such as network back door failed to timely plugging, server Administrator account no password or the password is too simple, the database link with SA supreme authority account and provide WEB services account no independent, WEB directory permissions without segmentation, no effective firewall configuration scheme, and so on[2].

There are risks in internal management.In the era of financial network, Some units emphasis on computer hardware and software aspects of risk, ignore the internal staff operational risks, strengthen internal management is important for the financial network.The lack of financial file backup mechanism[3]. At present, the college financial information has become increasingly complex, the information level is higher and higher. In colleges and universities, financial electronic statements inconsistent with corresponding accounting voucher filing. Financial network monitoring and protection mechanism is also weak. Under the Internet environment, electronic symbol is accounting data, magnetic medium is the transmission medium of accounting data and saving way, therefore, under the informationization of financial data, in theory, can be accessed at any time any place. In terms of financial data in colleges and universities, the network protection consciousness is still very weak.Financial personnel in colleges and universities lack of knowledge of computer and network information knowledge, They pay more attention to the normal operation of the financial system than the quality of financial security. In addition, the financial personnel understanding of computer safety management is not clear, understanding of the dangers of the virus and Trojan software insufficiency, the attention is not enough to download the network information, in the department of internal use mobile hard disk, usb flash drive, and so on and so forth. This infection may cause the financial system on the one hand, on the other hand can also cause financial personnel user information being stolen, and financial personnel protection of users' information consciousness is not enough.

College financial network security.

Standardize the use of financial software, improving access to financial software standards. College financial software is different, the software vendors should draw lessons from other institutions and government departments in our country, standardize the accounting software standards, improve financial software of barriers to entry, implemented under the unified financial system architecture universities personality optimization. Lack of specification standard is difficult to effectively upgrade the software, it is difficult to effectively regulate the financial operation process. Colleges and universities can draw on its unique ability of organization, seek common ground while putting aside differences, establish a unified, standard of university financial software. Abroad, can improve the leverage of the financial software provider, regulate the behavior of the software vendors and software quality. Internally, to optimize the financial management, but also helps to improve the financial software upgrade speed, reduce maintenance costs[4].

Upgrade hardware and software , prevent virus attacks.Using hardware firewall. Using hardware firewall through the definition of safety rules, open port and protocol, less as far as possible can effectively improve the protection system of time; The analysis of the firewall log system, reduces the cost of testing safety problems; Graphical interface can effectively reduce the response of the concise countermeasure of the implementation of the time. , therefore, have a hardware firewall system is convenient management system in colleges and universities financial network infrastructure, is indispensable.Install the server version of antivirus software. Install server version of antivirus software is to protect the network security of the other a effective way to improve the protection time, rapid processing of viruses to further improve the responding ability and speed of students.To

strengthen the preventive measures against the virus. First of all, using multi-level multistage other enterprise anti-virus system, the virus to achieve full protection. Second, the firewall technology is adopted to across the border from network information filtering, will visit against illegal intrusion, including virus, in the internal network, thus play a role to protect the internal information.

Strengthen the management of financial network Settings.The configuration directory permissions management. Detailed configuration directory permissions are for the implementation of the access control, user isolation can strengthen the protection ability of the system. Based on the principle of a web site a separate directory, allocation of independent accounts belong to the GUESTS group, don't use the system default account, to web directory, if only run asp, the administrators group is only required to assign all rights; IIS_WPG assigned reading, operation rights; Assignment of anonymous access account read permissions operation.Strengthening the management of database link bank account and computer users. In order to strengthen protection, improve the strength of access control, database link account will not be able to use SA, can separate in the database server to establish an account, follow the principles of a database to limit an account, this account is only available to the general library, read and write access, or even just read permissions. In this way, even if the injection, also can't through the bank account set up system, while SA privileged accounts can be. For other relevant account password must conform to the requirements of the complexity, it is best to common combination of letters, Numbers and symbols. Use the user name password system security technology method, it can be in the boot password, network user name password and application system password used on three levels. A user level, database level control and network system level control system of multilevel access control mechanism. User level can rational division of rights of network users, is now operating authority centralized management, strong chemical system administrators on each mold piece of software operation of unified authorization, guarding against the illegal users gain access; Database level can prevent the unincorporated member of financial data leakage, reigned change and delete; Network system level to prevent accidents due to power outages, communication line fault caused by the electronic accounting files are damaged or missing. The type, the user's identity, the operation of the system operation, system parameters and the state, as well as between real-time monitoring system of sensitive data and records, the necessary permissions, so that you can for a variety of different permissions for user identification.

Strengthen technical safety measures.Using the data encryption technology, the public network transmission of IP packet is encrypted and encapsulation[5], only the specified user or network equipment to decrypt data, so as to realize the confidentiality and integrity of data transmission. Using vulnerability scanning technology, can to local area network (LAN), a WEB site, the host operating system, system services, and firewall security vulnerability scanning system, the system administrator can check out of the running unsafe network services that exist in the network system, and exist in the operating system may lead to a buffer overflow attack or denial of service attack security vulnerabilities, can also check whether there is a firewall system security vulnerabilities and configuration errors. Intrusion detection technology for suspicious intrusion behavior on the network to make policy response, and cut off the invasion of the source, record and timely notify the system administrator, by all means help system administrators to deal with network attacks, enhance the capacity of the system's security administrator, is considered to be boundary firewall after the name of the second gate. It can also detect an open to the public service of illegal access, is the reasonable supplement of firewall. Using authentication technologies[6], including technology, such as identity authentication, information integrity check to prevent illegal users of the financial system of network attack, information theft and tampering, guarantee the authenticity of the data, integrity, confidentiality, and non-repudiation.

Strengthen internal management.Establish a perfect network system of internal control. Perfect internal control system can effectively reduce the risk of moral hazard due to internal personnel, risk of system resources and computer fault caused by the damage. Under the network environment of financial management system should be established to adapt to the network system of internal control system and control system. Should control range from single financial sector into a common control

and computer management departments. Control mode should be organized by pure manual control into control, manual control and process control with the combination of internal control.To establish the necessary management system. Strengthen the awareness of information security, perfect the rules and regulations. Strengthen the network users to the correct understanding of information security, improve found the network information security problem representation and influence of information security behavior of sharpness, and maintenance of the network information security initiative. At the same time, according to the characteristic of the complex network shares, from the system application, network security, data privacy, information security, etc, to establish information security applications technical standards and specifications. The rules and regulations to establish and improve not just, more important is, must strictly abide by, strong execution, supervision, pay equal attention to. More to manage in place at the same time, the power and responsibility clear, clear responsibility, strengthen the consciousness of society and sense of responsibility. In addition, increase capital investment, improve the management expertise, expand the network construction, personnel real construction of a high quality managerial talent team, improve the security, maintenance and emergency response capacity.Build a network security incidents emergency response mechanism[7]. In the enterprise, the network financial information set of emergency measures, can make the enterprise for a rainy day, in an emergency situation, such as major natural disasters, information system for computer virus in paralysis, able to timely and orderly response to deal with the crisis, as soon as possible to restore enterprise daily production and business operation activities, to reduce the losses to a minimum, the enhancement enterprise's competitiveness and vitality. For emergency mechanism set, first of all, should set up the corresponding contingency plans, for the main direction of crisis management and policy, clear responsibilities in effect at the time of the emergency distribution and personnel changes, etc. Second, is the establishment of emergency department, in terms of network financial information, the focus of the emergency mechanism is set, is in the enterprise information system for related emergency software configuration, including important financial information backup, of the viral attack area of the information or system Isolation and treatment etc.Optimization and attaches great importance to the network monitoring and build a perfect defense measures. Due to the limitations of funds, and other hardware conditions, college financial network monitoring closely enough, hard to prevent vicious attacks. By purchasing a commercial software to achieve effective monitoring defense cost is too high, the uniqueness of the university financial information available to set up a "limit non-isolating" within the control combined with external interface mode, colleges and universities to strengthen the internal financial restrictions island - external interface mode. Its characteristic is the main financial information and financial work distribution in far Internet network, and needs to be released via the Internet or transfer financial timing and financial system has been connected to the Internet connection, and update the data load.

References

[1] Ni Zhao. Net Friend World (In Chinese). Vol. 4(2014).

[2] Wenjie He. Theory and Practice of Contemporary Education(In Chinese). Vol.6 No.3 (2014).

[3] Lei Cong. Friends of Account(In Chinese). No. 11(2014) .

[4] Xiongping Li. China Economist(In Chinese). No. 4(2014).

[5] Ke Zhang. Science & Technology Information (In Chinese). No. 8(2014).

[6] Haiyi He. Special Zone Economy (In Chinese). No. 6(2010).

[7] Qi Lu. Business Economy (In Chinese). No. 4(2013).

Advanced Materials Research Vols. 989-994 (2014) pp 5419-5422
© (2014) Trans Tech Publications, Switzerland
doi:10.4028/www.scientific.net/AMR.989-994.5419

Study on Application of Database Synchronization Technology in the CDIO Teaching System based on Android

Haiyan Hu [1, a], Hui Yan [1,b]

[1] Department of Information Engineering,Jilin Business and Technology College,Changchun,China

[a] hhy1979_711@sina.com, [b]yanhui7125@126.com

Keywords: Android;CDIO; Synchronization Management ;Hash Digest Algorithm

Abstract. As a breakthrough in teaching methods, the teaching system for CDIO talents training is extended to the Android mobile phone platform for engineering talents training better. This paper focuses on constructing the teaching system for CDIO talents training on the Android mobile platform, Hash digest algorithm is applied to the synchronization management of Android platform-based CDIO teaching system databases, significantly reduces the data traffic on the wireless network, and greatly enhances the data interaction between the embedded devices and servers. This application also dramatically reduces the number of write operations on the memory stack and improves the performance of the I/O read-write efficiency of the memory stack.

Introduction

In the age of rapidly-developing wireless internet, mobile phones and other mobile devices have become an essential part of people's lives. Under the circumstances, mobile learning develops as a new style of digital learning. This paper put forwards the Android mobile technology combination with the CDIO teaching model to change the traditional, single teaching methods. This combination realizes the deep integration of relevant technologies from the interdisciplinary fields, applies the "anytime and anywhere" information exchange and means of services to teaching to adapt to students' mobile, effective, synchronic, individualized open learning and, thus provides a teaching platform for training comprehensive talents with CDIO qualities. Students can learn from the teaching system through Android mobile phones, store and process such learning records as learning time, self-testing scores and number of questions, and obtain the updated teaching information from the sever.

Construction of the learning system for Android-based CDIO talents training

The presentation layer is the interface where the system interacts with the user through mobile phones, PDA, UMPC and other mobile terminal devices. This layer also provides different interfaces for different identities (learner, teacher and administrator) to login. The user can access WAP platform through the client to browse the resources on the internet. For the mobile learning system, the internet layer mainly includes the internet and the mobile wireless communication network, and mobile phones and PC can access the uniform resources through the server. The business logic layer is used to package the business services of the system, and is responsible for the application requests of the presentation layer. Here it is mainly in charge of the three kinds of users' business service request for the three function modules: student module, teacher module and administrator module.

The architecture of the system is shown in Fig1:

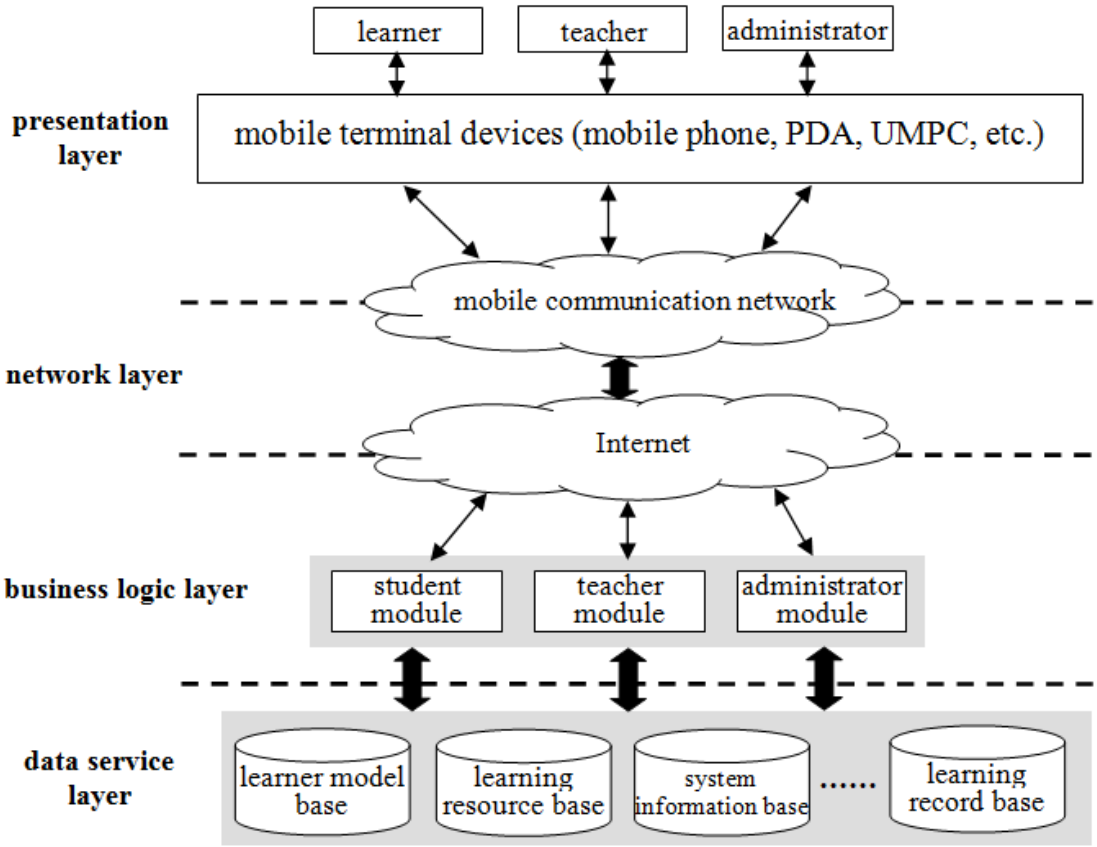

Fig 1. The architecture of the system

Synchronization technology of Hash-based Android system

The process of the synchronization model of Hash-based Android system is described as the Fig.2.The system performs a query operation; the system acquires query information from its local database, and uses Hash algorithm to digest its query data results; the system submits the digest information and query statement to the server database through the wireless network; after receiving the query request, the server database receives a set of data results, and uses the same Hash algorithm to acquire the digital "signature" of this set of data;then the server compares the two signatures; the server only returns the inconsistent data results to the Android system through the wireless network; after receiving those inconsistent data, the system updates its local database and writes them on the memory stack.

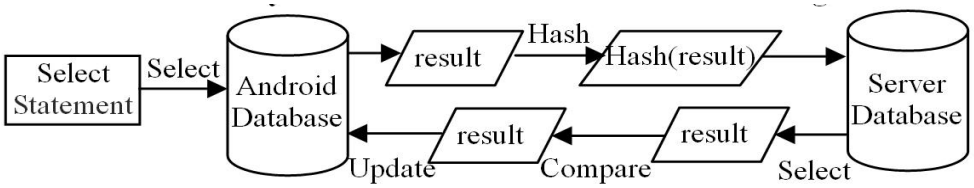

Fig. 2 The process of the synchronization model of hash-based android system

Synchronization of the client database management system in the Android system

After the Select query, N rows of results can be obtained in the storage database of the Android system, which are assumed to be (R1,R2,…,Rn), and the data length of each row is m;N Hash digests are obtained: (H1,H2,…,Hn) ,after Hash algorithm is applied to each row of results, and the length of each Hash digest is n;HE with the length of n is obtained after Hash algorithm is applied to the N rows of results;HL, (H1,H2,…,Hn) and the query statement are sent to the server through the wireless network.

Synchronization of the database management system in the server

The client sends the latest data to the server from time to time to update the data of the server; and it is also responsible for making timely response to the query of the client database service system.

After receiving the request of the client, including HL, (H_1,H_2,…,H_n) and the query statement, the server performs the following operations.It uses the query statement to query the server database, and obtains T rows of data results: (R_1' , R_2' , …,R_n'), and the data length of each row is m;It processes this set of data results with the same Hash digest algorithm, and obtains T rows of results: (H_1' ,H_2' ,…,H_n'), and the length of each digest is r;it applies Hash algorithm to all N rows of results and obtains HE′ with the length of n; it compares HL and HL′ ;if they are the same, according to the features of Hash digest function, it can be certain that the data results received by the client are consistent with the data results received by the server database, and the server database need not return all query results to the client, but informs the client that the data on it are the latest data and the current data on all of its embedded devices are valid.If HL and HL′ are different. The server will compare (H_1,H_2,…,H_n) got from client-side and (R_1' , R_2' , …,R_n') from server-side one by one and all different results will be updated or added. The original data results corresponding to different Hash should all be transmitted back to client-side by network.

The client will update the received different data results to its local database to maintain data consistency with the server.

Experiments show

Given: the system has K records in total, and requires the Hash digest with the length n=32.

It can be computed that the Hash digest results of the two different data have the same collision efficiency: when n=32, K=10000, the collision efficiency equals P. Since the collision efficiency is small enough, the digest can solely represent an original data without conflict. Therefore, this Hash digest algorithm can be used to realize the synchronization of databases. After the use of Hash algorithm, the statistic B of the data volume of the uplink and downlink can be obtained:

The data volume of the uplink:

$$q+n\times(N+1) \tag{1}$$

The data volume of the downlink:

$$(P+N\times z\%)\times m \tag{2}$$

Given: there are 2000 records of query results (N=2000), 10000 records in total. Each original result has 100 bytes (m=100), and the Hash algorithm which produces digests with the fixed length of 32 bytes is applied. There are 200 additional records in the server database (P=200), and the length of the query statement is also 32. There is 10% “dirty” data in the memory stack of the Android system.

The following result can be obtained after these data are substituted into the above formula (1)(2). Comparision of the data volume of the uplink and downlink is shown in Table 1.

Table 1. Comparision of the data volume of the uplink and downlink

Using Hash algorithm or not	The data volume of the uplink	The data volume of the downlink
Without using Hash algorithm	32	100×(2000+200)=220000
Using Hash algorithm	32+32×(2000+1)=64064	(200+2000×10%)×100=40000

It can be seen from the above test that Hash digest algorithm significantly reduces the data traffic on the wireless network and thus greatly improves the data interaction between the Android system and the server.

Conclusions

This paper introduces the CDIO teaching system into the Android mobile platform to meet the requirements of CDIO talents training and make students have individualized learning at “anytime and anywhere”, hence making a breakthrough in the teaching methods. In addition, it applies Hash digest algorithm to the database management of the Android system, which significantly reduces the

data traffic on the wireless network and greatly improves the data interaction between the Android system and the server. This application also sharply reduces the number of write operations on the memory stack and enhances the performance of the I/O read-write efficiency of the memory stack.

Acknowledgements

The authors gratefully acknowledge the fund of this study by the “12th Five-Year-Plan” Planning issues of Educational Science in Jilin Province (GH12335); and Education Department of Jilin Province “The 12th Five-year Plan” Science and Technology Research Project “A Research and Implementation of the Mobile Learning Platform in Personnel Training System of CDIO Project Based on Android” (2013-404); Jilin province science and technology department soft science research project（20130420026FG）; Jilin Province Department of Education research project (2012366).

References

[1] Cai Jing. Research and application of Android mobile terminal data synchronization technology[J] .Guangdong Communication Techology. 2011,31(1).

[2] Tao Tao: Synchronization and Strategy of Optimization for Embedded Database based on Android Platform, Dissertation of Master’s Degree in Nankai University,(2010).

[3] Xie Panke.Design and Implementation of a M-Learning System Based on Android[D]. Central China Normal University.(2011).

[4] Bing Li. The Research of Dynamic Resource Management key technologies in Cloud Computing [D]. Beijing University of Posts and Telecommunications.2012.5.

[5] Zhu Li.Embedded Database Synchronization Case Based on Android System [J].Value Engineering, Vol.30 No.16 pp.177 (2011) .

Advanced Materials Research Vols. 989-994 (2014) pp 5423-5426
© (2014) Trans Tech Publications, Switzerland
doi:10.4028/www.scientific.net/AMR.989-994.5423

A Comprehensive Experimental Practice for Ship Bridge Resource Management Training Based on Ship Handling Simulator

Yufeng YANG[1, a], Mingkui FENG[2, b]

[1]Department of Ship Command, China Maritime Police Academy, Ningbo, 315801, China

[2]Department of Ship Command, China Maritime Police Academy, Ningbo, 315801, China

[a]email: yyf41212@sohu.com, [b]email:fmkjg@sohu.com

Keywords: Ship Handling Simulator; Bridge Resource Management (BRM); Reform of Teaching

Abstract. There is short in the number of large ship handling simulator and it has high failure in BRM training. They could not remain for a long time in the laboratory for teachers qualified with captain and highly educated full-time laboratory personnel. Marine institutions begin to carry out practical teaching reform for these problems, which make people to work hand with policy support and scientific and rational evaluation mechanisms, innovative training teaching methods and establish an objective assessment criteria. By BRM training students enhance the ship's emergency response, role awareness and situational awareness, which have important practical significance to enhance navigational safety and strengthen risk awareness.

Introduction

Bridge Resource Management Course is one of the seamanship professional courses which have been carried out for some time in some institutions. The training purpose is to improve ship management skills on board to ensure the navigation safe, reducing the occurrence of man-made accidents. Entered into force in accordance with the 2012 Manila amendments, most of the crew and students need to undergo mandatory training BRM[1-4]. Therefore, the need to explore new models of a comprehensive experimental practice for ship bridge resource management training based on ship handling simulator to cultivate innovative ability of students.

There Are Some Problems in the BRM Experimental Process

Firstly, it is insufficient number of instruments and equipment which is failure to carry out the experimental of BRM. In order to construct a realistic marine environment and improve practical skills of crew trainees, all maritime colleges and training institutions have developed or introduced large ship handling simulator which is very expensive. BRM training has three of the ship that can accommodate up to 12-15 people at ship handling simulator, however, a maritime training college has only a ship handling simulator, which is in urgent need of 280,000 officers are not trained.

Secondly, ship simulators have different types which are different unstable, such as single-channel fault or visual or radar charts machine crashes and machine image disappears non-normal. Three ships require to see each other at the same time in BRM experiments, one of the ship fails, the other ships will be affected, or even need to exit the system and restart the experiment, the effect of experimental scenarios was greatly reduced.

BRM is a simulation comprehensive experiment at sea about ship bridge resources, which is innovative experiment subjects and higher guidance teacher requirements. Currently, treatment and status of teachers major in marine technology often are neglected, a licensed captain's income far exceeds income in colleges or training institutions. Therefore, it is very great difficult to introduce a practical experience captain at sea as a full-time laboratory assistant. On the other hand, ship handling simulator is a large equipment, it’s operation and maintenance need specialized knowledge of higher laboratory assistant. And higher education faculty reluctant to stay long in the laboratory because of treatment assessment, so personnel mobility is greater.

Comprehensive Experiments Conducted Design and Practice

Integrated design experiment project design. Change the traditional single confirmatory test project based teaching philosophy, conscious design experiments conducted comprehensive project design. In the design process, we can use a variety of methods, for example, in actual operation, the development of several typical operating regions, namely the development of the reference card title. Title card contains experimental time, scoring criteria, specified experimental waters, vessel name and other basic information. The process of navigating the scene is set, a comprehensive experiment is shown in Figure 1.

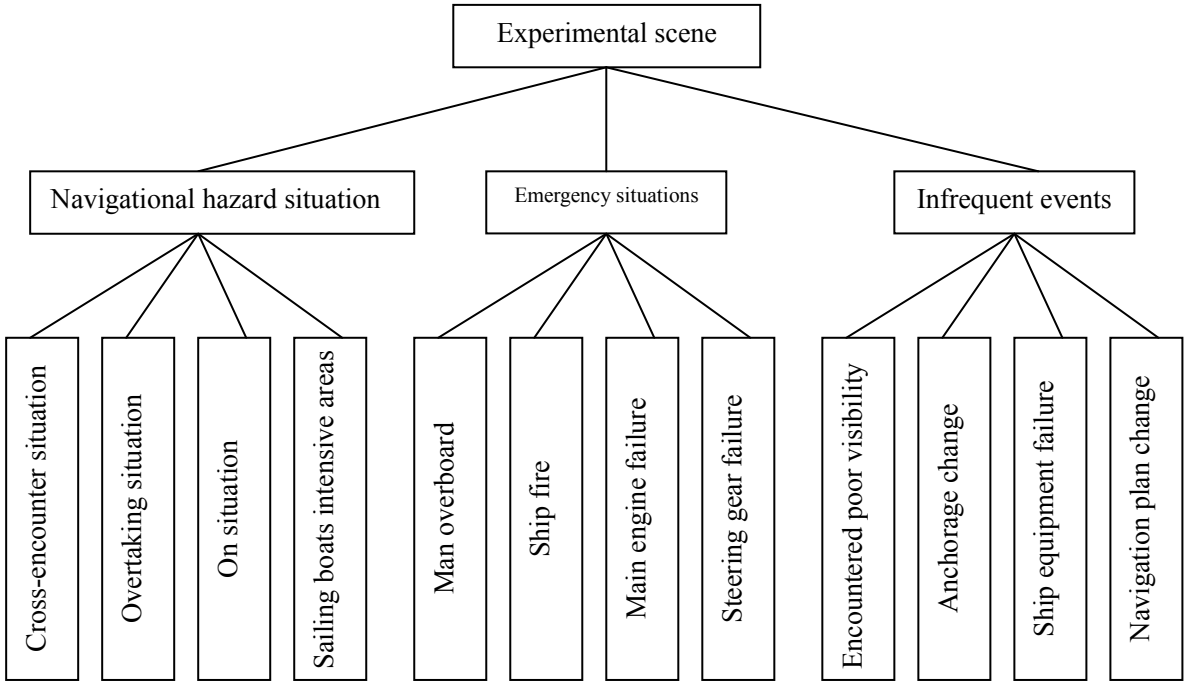

Fig.1. A comprehensive experimental scene

In a comprehensive experiment, we can select one navigational hazard situation, two emergency situation, an infrequent events as the experimental scene for each group.

In the process of integrated design experiment project implementation, the role of transformation experiments make learner's enthusiastic participants increased

A 15-person group, same experiment can be divided into three experimental groups, each group of five people randomly assigned to play the role of each person, who respectively play the role of captain, first mate, two mate, three mate and sailor. After an end of the project in each personnel were summed assume the role of experience. When the next project various roles rotation, so that each different maritime role transformation, participants experiment enthusiasm and enthusiasm, the experimental results are very clear, the role of awareness and situational awareness were trained.

By discussions and interactive teaching, students can think independently and initiative to mobilize the enthusiasm of the experiment. Before the simulator experiments, each voyage plan based on faculty members to develop a given experimental project, team members discussed jointly develop solutions needed to find the voyage sailing books, and emergencies that may arise in practice do good plan. In the experiment, the crucial role of captain, he was commander of the team. When he was in command and the negligence of the details, the team members should remind each other, which was reflecting the sense of team. At this time, the role of guidance teachers was to become auxiliary. The role of each team member responses recorded at the end of the project the collective sum up the discussion. Team experiment can spend 2 hours, one hour to focus discussion. In each group, the captain, first mate, two mate, three mate and sailors take on the role of role are summarized in this group, such as advantages and disadvantages and experiences.

The role of teacher is the key to a comprehensive experimental design successfully implemented. Experimental teaching process and the experimental station instructor trainer's role is also crucial.

In order to ensure the pilot project sporadic and sudden, three teams need constantly to create trouble, such as setting poor visibility suddenly, speed boat as a suspected pirate ship, oil spills, ship fault, man overboard, etc. In order to examine each team 's emergency measures maximize the simulated emergencies at sea. Meanwhile, the two guiding teachers bear the cabin, VTS attendant , ship company roles and timely communication and exchanges with each team. Three ships run at the same time, we must set the order of the items in turn and continue to prevent a failure of the ship and the ship is no other emergency situations occur. In an experiments, we can make the ship's three project settings and communication exchange table. In the 1st of the ship as shown in Table 1, Table 1 is set in the corresponding action on the 1st of each reaction vessel for the cabin, VTS and ship companies have done. If there is no response, the corresponding location in the table count is 0. Recovery column under each action corresponds to 0 means that the ship made the engine room, VTS and the company and the end of the reaction one has counted as a response, no response count is 0. The reaction experiments can record the degree of communication and team communication consciousness. Records from Table 1, the action on the 1st of each boat timely exchange and communication to the company, the key positions with the cabin failed to timely communication and exchange.

Table.1. Set up emergency scenarios and communications records on coach station

Ship 1	Stand by	Poor visibility		Main engine failure		Man overboard		Steering gear failure		Radar Failure	
Set/recovery	Set	Set	Recovery	Set	Recovery	Set	Recovery	Set	Recovery	Set	Recovery
Engine room	1	0	1	1	1	0	0	1	0	0	0
VTS	1	1	1	1	0	1	1	1	1	0	0
Ship company	1	1	1	0	1	1	1	1	1	1	1

Ship 1	Suspected pirates		Compass failure		Anchor		Oil Spill		Others	
Set/recovery	Set	Recovery	Set	Recovery	Set	Recovery	Set	Recovery	Set	Recovery
Engine room	0	1	0	0	1	0	1	1	1	1
VTS	1	1	0	0	1	1	1	0	1	1
Ship company	1	1	1	1	1	1	1	1	1	1

Experimental Evaluation

Its timely assessment to the experiment effects to test the student experiments to form a closed loop of BRM experimental teaching. According to the maritime sector suggested assessment form[5] and the actual situation of the experimental teaching, we make an evaluation criteria and assessment elements which contained in the mission analysis and planning, through the designated waters practical, work attitude and situational awareness. In each elements, simulation experiment accounted for 40%, 60% of experimental evaluation. The overall evaluation have two levels which are qualified and unqualified. Real-time simulation of the case by the transfer of coaches stop playback function, the details of the experiment in the three groups of the ship two hours playback trajectory control assessment criteria, given the objective results. Figure 2 shows that the three cases is the ship track playback experiment teaching after the 1st boat anchor job in progress, the 2nd man overboard boat project has been completed emergency response, emergency steering gear failure being manipulated under the 3rd ship is conduct man overboard emergency operation.

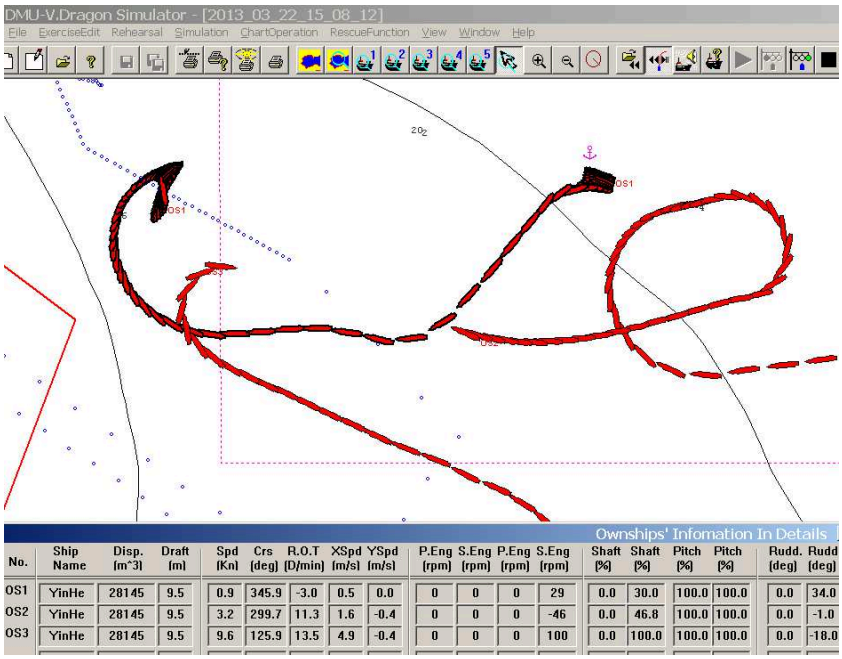

Fig.2. Three ships track playback experiment

Conclusion

In order to make up BRM experimental teaching for few instruments and equipment and high failure rates, we make some effective methods to improve the utilization of experimental teaching equipment. For educated laboratory personnel greater mobility in common, trying to create a bolt from the heart to keep people in a lab environment policy, job evaluation and other aspects. On the experimental teaching methods, by innovative teaching model, the student is able to change the passive learning independent thinking, active learning, interactive learning. Validation experiments to change the traditional teaching based concept, the design of advanced integrated BRM concept design experiments to the complex projects to the environment, can improve their safety awareness and emergency response, in order to minimize the the risk of an accident occurs to a ship .

Acknowledgement

In this paper, the research was sponsored by the Zhejiang Provence Higher Education Classroom Teaching Reform Project (Project No. kg2013494).

References

[1] Quangen Fang. Ship bridge resource management [M] Beijing: People's traffic Press, 2006.

[2] Junzhong Bao, Mingqiang Xu. Faced main problem of China 's maritime education and training[J]. Maritime education research. 2007, (1) :23- 24.

[3] Jie Wang. Reflections on the ship resource management training [J]. Maritime education research.2002, (1):46- 50.

[4] Enhong Li. Manila amendments to the STCW Convention interpretation[J]. World seaborne.2011, (1):14 -15 .

[5] Shun Liu, Jiangqiang Hu. Seamen certificate to update their knowledge [M] Beijing: People's traffic Press,2012:277-278 .

Advanced Materials Research Vols. 989-994 (2014) pp 5427-5430
© (2014) Trans Tech Publications, Switzerland
doi:10.4028/www.scientific.net/AMR.989-994.5427

Research on the Platform of 3D Information Management for the Ordnance Maintenance Equipment

Zhiyong Cheng [1, a], Rongyue Xie [1, b], Qiu lei [1, c], Zhou xiao [1, d],Chaofa Yu [1, e]

[1] Wuhan Mechanical Technology College, Wuhan, 430075, China

[a]email: zycheng72@sina.com, [b]email: ryxie@126.com, [c]email: hnnhlxy@163.com,

[d]email: leopzhx@sohu.com, [e]email:chaofa_y@163.com,

Keywords: Maintenance Equipment; three-dimensional Information; Synchronous display

Abstract. Based on the current situation that the current ordnance equipment maintenance information management system is not intuitive, a new information system was designed and realized, which could display the two-dimensional Information and three-dimensional information synchronously. This system can well compatible with the existing one. Through studying the analysis of the original data structure, importing way for the 3D model of equipment, synchronous display for the 2D information and 3d model, the 3D information management system was realized, which provides a new digital method for equipment management person.

Introduction

With the development of military information construction, maintenance equipment information management work faces the development of the new challenges, which as the basis for army ordnance equipment finance, storage, supply and management. The original information management system, excel as the main form, can't meet the requirement of information management. Developed with digital visual characteristic of ordnance equipment maintenance information management system becomes real demand.

In this paper, we study the technology of the three-dimensional model combined with 2 d information for the maintenance equipment. Then the digital visual means for maintenance equipment data is realized, which provides correct, complete and intuitive maintenance equipment information for the units at the grass-roots level operators and maintenance persons. The new system can adapt to the ordnance equipment rapid development, realize the general requirements of the ordnance equipment management.

General scheme of the system

A. System Composition

According to the requirements for digital platform, the system can feet needs for different hierarchy and level of equipment management persons. Considering the different users, we explored the system by modular design method. There are three basic function modules, importing and exporting for equipment catalog data module, loading and maintenance for model module, equipment inventory management module. The system can be packaged distributed for different users. The block diagram of the 3D information management system is shown as Fig. 1.

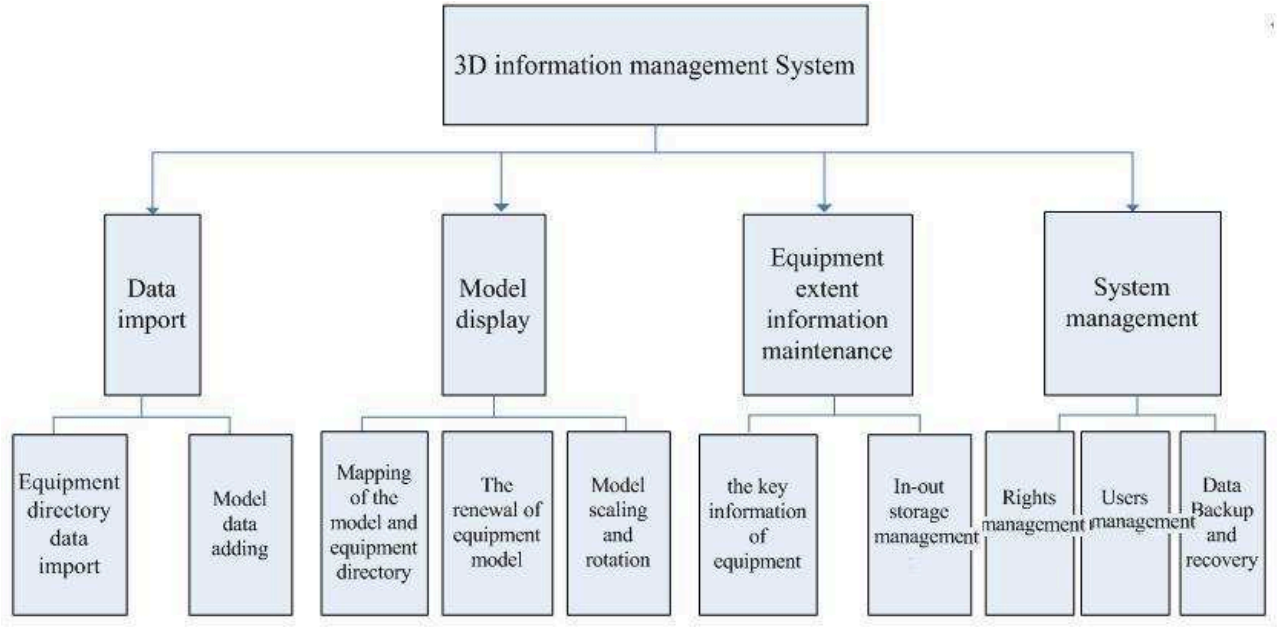

Figure.1 Block Diagram of the 3D information management System

B. Approaches of General Scheme

Visual Studio 2010 is adopt as system integrated development environment in this paper. The maintenance equipment models are built in Solidworks, rendering by the OSG as 3D graphics engine, using access database as data engine. A 3d visual information management platform is provided for user. The diagram of the framework is shown as Fig. 2.

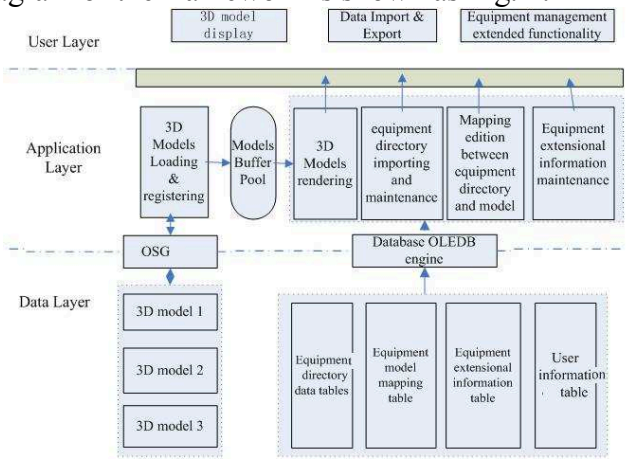

Figure.2 Diagram of the Framework

The Specific Contents of the System Research

A. The construction of digital management platform

Showing the 3D model and its effectiveness is the core content of the digital management platform. Importing the equipment model to the equipment catalog information system, it can provide equipment management persons with intuitive and visual information, can provide the equipment management persons to obtain rapidly the detail information of equipment with short way. For the organic integration of the equipment directory and model data, it need to get the original model data into the appropriate data format, at the same time we need make some new part model of the equipment. The flow chart of building platform is shown as Fig. 3.

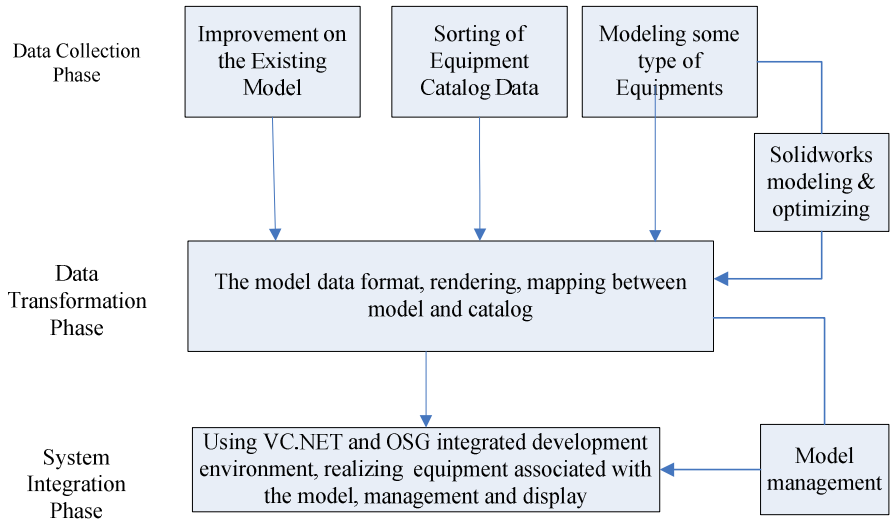

Figure.3 Chart Of building platform

B.Structure Optimization and Data Reorganization for the Existing Equipment Management System Test results

To studying the function, system and the data structure of the existing equipment information management system, it lay the foundation for the new system to compatible with the old one. This new system can be compatible with the equipment data in the old system, can realizing to the existing equipment directory data importing, editing, and exporting.

C. Flexible Query and Association between the Equipment Directory Data and Model Data

Equipment maintenance material catalogs and multi-channel digital visualization query system should be built firstly by systematic and modular design method. According to the equipment code, name, figure number and so on many kinds of ways , the system realize the complex query for equipment catalog data. By setting the part library module, it can realize the general equipment model data query and reuse, and it greatly improve the efficiency on the use of the model data. People can set and edit equipment directory data and model data flexibly, and can realize data query on multi-condition.

D. Equipment 3D Model of Equipment Displaying

By the management platform we can show the 3D model and edit the model attribute easily. The system provides two types of model display function, such as importing the whole model of the equipment and Import folder consisting of many single equipment models. For the first one, the each node of the whole equipment model can be list in the platform, but it doesn't destroy the relationship and structure of mechanical connection in the whole equipment model. It provides the technical foundation for showing the position relationship among equipments.

Key Techniques of the System

A. Equipment directory data import function designing

Firstly the database operation module is designed in order to realize building links with the underlying database. It can recognize the table header of the EXCELL file which user wants to import into the platform. At the same time, it provides the modifying and adding field function.

B. Model import function designing

Import the model file directory is the premise of the model corresponds to the equipment have been imported into the system. The premise condition on importing model is that the corresponding equipment directory has been imported into the system. Importing the model file Performs two ways, which are importing the whole equipment model and importing the model folder. Importing model process is divided into the following three basic process. Firstly, equipment list that has not yet been imported model should be obtained. Then it should traversing all models in folder. Lastly, Finally, the model of file should be copied to the system folder.

C. Model display function designing

This function module mainly aims at synchronous display of the equipment directory and the 3D model. It includes three basic process. Firstly, the specified equipment directory and equipment node should be opened. Secondly, correlation between equipment directory and correspond model should be built. Loading for the first time, the system will automatically build the corresponding relation between model equipment directory according to the of equipment name. The corresponding relationship need to be manually set which system cannot match. The last process is displaying models. The system main interface is shown as Fig. 4.

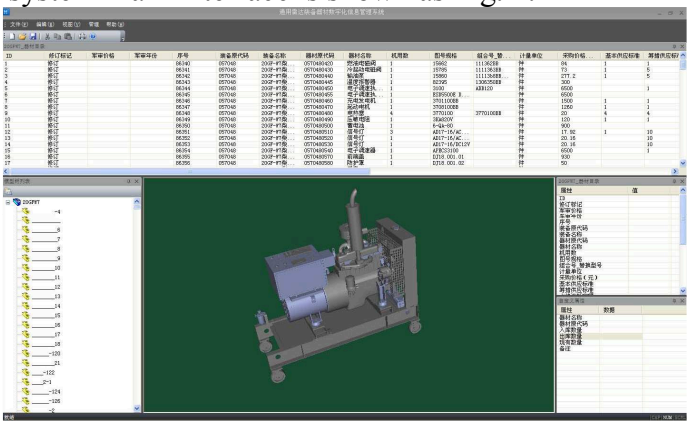

Figure.4 Main interface of system

Summary

By using solidworks, visual studio dot net and OSG graphics engine, we built 3D information management platform of ordnance equipment maintenance in this paper. It well meet the demand of related management persons of the new information demand. It improved the efficiency and level of equipment management informatization. At the same time, as the general platform for the 3D information management of maintenance equipment, this system had portability, expandability, and upgradability. This system could be reference for other weapon equipment management persons or use directly. This platform was of great significance for the management work on the ordnance equipment maintenance equipment informatization.

References

[[1] Cheng Hongfang,Zhang Dengfeng, Li Gaomin. Research on Effectiveness of Visual System Based on Flight Engineering Simulator[J]. Journal of System Simulation, 2006.18(2):441~443(in Chinese)

[2] Li Jun, Wang Shaodi,Chang Jiangang, Sun Zhixin,Wang Ruchuan.Analysis and Design of Rendering Software Based on Vega[J]. Journal of System Simulation.2003,15(3):397~400(in Chinese)

[3] Xu Dongping, Zhong Tao, Zhou Shisheng. Research on Framwork for Real-Time Interactive Scene Simulation System[J]. Journal of Wuhan University of Technology,2004,28(6):930~932(in Chinese)

[4] Linyi, A Novel Software Architecture for Visualization Simulation[J], JOURNAL OF NORTHWESTERN POLYTECHNICAL UNIVERSITY, 2008 26(2):184~188

[5] Shuchang. Research on an Equipment Visual Emluator Based on 3Dmax and OGRE[J], Command Control & Simulation, 2009.31(5):78~80.

[6] G Antonino, Zachmann Gabriel. Virtural reality as a tool for verification of assembly and maintenance process [J]. Computer and Graphics ,1999, 23(3):389~403.

Advanced Materials Research Vols. 989-994 (2014) pp 5431-5434
© (2014) Trans Tech Publications, Switzerland
doi:10.4028/www.scientific.net/AMR.989-994.5431

Study on Fire Safety of Building External Thermal Insulation Materials

Liang Yang

No.2 fuxing road, jinlai road, xiqing District, Tianjin, China

korne@126.com

Keywords: External insulation material, PU, PF, fire performance, heat release

Abstract. Energy-saving and emission-reducing must be achieved based on the reliable performance of fire safety. External thermal insulation material is the main component of external thermal insulation system, and also the main combustion participants when a fire occurs; the combustion performance is an important factor affecting the fire scale of external thermal insulation system. The main material and heat release principle was introduced in this paper, tests were carried out, and fire hazard was analyzed based on large amount of test data. The research will provide theoretical support for external insulation material choice, system construction, fire prevention and rescue.

Introduction

The external insulation system refers to the non load bearing construction built on the building facades, to reduce heat exchange between building and the natural environment. The main component of external thermal insulation is thermal insulation material, other accessories such as, mortar, alkali Mesh, anchor bolts, are all inorganic or metal components, the fire risk is small. although the construction technology will impact on the safety of external thermal insulation system, once fire occurs, which involved in combustion is the huge amount of external thermal material, so the scale of external thermal insulation system fire is mainly depends on the material burning characteristic. So for reducing the fire risk of thermal insulation system, in addition to a reasonable improvement on system structure design and construction process management, reducing the fire risk of external insulation material is also particularly important

Therefore, more information about burning performance and fire risk of external thermal material will do great benefit to improve the external thermal insulation system safety level, optimize structure design, and even improve the fire alarm and fire ability of external thermal insulation system. In this paper, burning performance of external insulation materials were compared, in order to improve the fire performance of external thermal insulation system, guarantee the safety of people's lives and property, and ensure the healthy development of building energy saving in China.

Categories and characteristic of common external insulation material

The basic requirements of thermal insulation material for building includes: thermal conductivity is not more than 0.17W/ (m.K), apparent density should be less than 1000kg/m^3, compressive strength should be greater than 0.3MPa. Thermal insulation material can be divided into three categories according to the material texture； inorganic insulation materials, organic materials and composite insulation material. The main characteristics of common insulation materials comparison is presented in Table 1.

It can be seen from the comparison in the table 1, the inorganic thermal insulation material has significant advantages on fire performance compared with organic insulation materials, but because weather resistance ability and bulk density varies greatly, the application situation and the construction environment are obviously different. Though organic insulation materials have low density, convenient construction requirements generally, fire risk must be considered.

So for the thermal insulation material selection, we should take all of application environment, fire safety, energy efficiency into account, with a full and accurate understanding of the burning performance of various types of thermal insulation materials. In this paper, several representative

thermal insulation material are selected, tests are carried out according GB8624-2012, burning performance is analyzed based on a large number of test data, and further fire safety assessments of external thermal insulation material are given.

Table 1: Main characteristics of common insulation materials comparison

Category	advantages	disadvantages	examples
Inorganic material	High thermal conductivity High compressive strength Easy to Construct	Poor weather resistance Damaging effect on the environment during production process High water absorption rate	Rock wool Foam glass Aerated concrete
Organic insulation material	Low water absorption rate Low thermal conductivity Better compressive strength Easy to construct Steady dimension scale Tolerance in a wide temperature range	Lower usage temperature limit, normally below 80℃ Great heat release Easy to drop when burning Great smoke generation Serious smoke toxicity High price	EPS XPS PIR PUR PF
Composite insulation material	Better insulation performance than inorganic material Good anti condensation performance High compressive strength Strong adhesion	Construction difficulty Long construction period Lower Strength than ordinary EPS	Polystyrene particles Modified polyphenylene

Burning performance of common thermal insulation material

Inorganic material. The representative inorganic foaming material includes foaming cement and foaming glass. The foam cement refers to the light insulation material with a large number of closed stoma foamed by foaming system after intensive mixing of inorganic component and foam agent, the main components of which are silicate. In table 2 noncombustible and combustion heat of the above two kinds of inorganic foaming material are listed.

Table 2 Characteristic of inorganic foaming material

Test sample	Density, kg/m³	Non combustible test			Combustion heat, MJ/kg
		Furnace temperature rise, ℃	Flame time, s	Mass loss, %	
Foaming cement	203.7	2	0	25.3	0.2
Foaming glass	315.6	1	0	19.6	0.0

The inorganic foaming material in table2 have wide application range in thermal insulation field, and fire performance level A1 can be achieved according to GB8624-2012《Classification for burning behavior of building materials and products》. But there are difficulties during construction process because of high bulk density and heavy insulation blocks, so great Bearing weight is required on the building surface. Thermal conductivity of these kind of materials are about 0.06-0.28W/(M.K), so the new energy-saving requirements must be achieved by increasing the thickness of the insulating layer, it will inevitably leads to great thermal insulation material consuming amount . In addition, rock wool products are also be regarded as inorganic thermal insulation material. Rock wool is a kind of Inorganic fiber produced by high speed centrifugal equipment with melting Xuan Wuyan and Dolomite. Rock wool material has the same burning performance with foaming cement. But because of the poor water resistance ability, intensity of Rock

wool will decrease greatly after Water absorption , even fall from the building surface. To improve the water resistance of rock wool products, rock wool is usually be compressed with adhesive added. But the organic adhesive may cause greater heat of combustion, thereby reducing the fire safety.

Organic insulation material. Thermoplastic organic insulation materials. Polystyrene board is a kind of thermoplastic organic insulation materials commonly used in exterior thermal insulation, such material is easy to melt and drop when heated. Polystyrene plate generally includes EPS and XPS, between the two kinds, XPS has the greater strength and higher density. Polystyrene plate is foamed by mixed polystyrene resin and foaming agent while heating at the same time, then continuous obturator structure is formed, so the thermal conductivity of EPS and XPS is very low, usually between 0.02-0.03W/(M.K）.

Table 3 Fire performance of thermoplastic organic insulation materials

Samples	thickness, mm	FIGRA, W/s	THR, MJ	Classification	OI,%
EPS 1#	30	$FIGRA_{0.2MJ}$=67.5	4.5	B1(B)	35
EPS 2#	30	$FIGRA_{0.4MJ}$=79.8	5.9	B1(C)	34
EPS 3#	50	$FIGRA_{0.4MJ}$ =198.5	12.7	B1(C)	37
EPS 4#	80	$FIGRA_{0.4MJ}$=147.6	19.6	B2(D)	32
XPS 1#	50	$FIGRA_{0.4MJ}$ =83.2	7.5	B1(C)	32
XPS 2#	50	$FIGRA_{0.4MJ}$ =149.5	12.8	B1(C)	28
XPS 3#	50	$FIGRA_{0.4MJ}$ =498.5	12.7	B2(D)	29
XPS 4#	100	$FIGRA_{0.4MJ}$ =856.1	48.4	B2(E)	31

Polystyrene board is very suitable for building external thermal insulation also because of its good mechanical and weather resistance. However, due to its main components are all organic polymers, when fire occurs, polystyrene boards are easy to shrinkage, drop, even burn seriously.

Using polystyrene board as insulation materials usually leads to a fast developing extension on a burning building. The fire continues to spread to the top rapidly, and a empty space can be formed from bottom to the top of the building between the outer protective layer and the main structure surface, making it possible for much fresh air coming into the burning location. Such process promotes the development of combustion process significantly. In addition, rolling polystyrene material droplets along the thermal insulation surface leads to a pool fire on the ground, which also contributed greatly to the fire development.

Thermosetting insulation material

Typical thermosetting insulation material includes polyurethane(PU) and phenol formaldehyde(PF), which will keep their original shape unchanged without any melt droplet on fire. The fire only spread upward on the building surface when such kind insulation materials are applied, generally the lower material will not be ignited, and these also stop the fire to spread to some extent.

Table 4 Fire performance of thermosetting insulation material

samples	Thickness, mm	FIGRA, W/s	THR, MJ	Classification	OI,%
PU 1#	30	$FIGRA_{0.4MJ}$=315.6	5.0	B2(D)	35
PU 2#	40	$FIGRA_{0.4MJ}$ =895.2	4.5	B2(E)	32
PU 3#	50	$FIGRA_{0.4MJ}$=1002.8	6.3	B2(E)	28
PF 1#	30	$FIGRA_{0.4MJ}$ =56.3	3.6	B1(B)	43
PF 2#	50	$FIGRA_{0.4MJ}$ =104.6	4.5	B1(B)	50
PF 3#	50	$FIGRA_{0.4MJ}$ =98.6	5.1	B1(B)	49

PU and PF board has good flame retardant performance, this is because carbonized layer on the burning surface will be formed quickly, preventing the contact between fresh oxygen and the combustible material. On the other hand the carbonized layer also played a role in cooling. But this

does not mean the thermosetting insulating material can certainly obtain high combustion performance level, As we can see from the table, the FIGRA data of PU material is not ideal.This is because, though there is only a short period before carbonized layer on the surface is formed, but the violent burning release lots of heat, so heat release rate(HRR)is very high. While the combustion rate of growth index FIGRA focuses on the heat release rate of growth, so those kind of materials with greater HRR growth rate usually have greater FIGRA, like PU. Also because the carbonized layer only appeared on the outermost surface, Interior materials and back fire surface generally do not participate in combustion, so obvious relationship cannot be found between size and thickness of PU board to FIGRA and THR. But PU is still a kind of thermal insulation material in the construction field, its extremely low thermal conductivity, weather resistance and excellent mechanical properties usually make PU as the main force of external thermal insulation materials field, especially the foam construction capacity which can not be achieved by any other materials, greatly enhance the bonding strength of the insulation base layer and substrate.

On the other hand, GB/T29416-2012《building exterior insulation system of combustion performance test methods》 has been taken into practice in 2013.10, system method was adopted when evaluating the fire performance of exterior thermal insulation system. In fact, the fire risk of PU can be reduced greatly by good external protection and reliable construction process supervision.

Phenol formaldehyde board is another kind of thermosetting material. PF has the similar combustion process as PU, carbonized layer is formed on the sample surface to avoid internal material to contact with flame. Because of better formula composition of PF than PU, most of PF board can reach B1 (B) level, and THR is relatively low. Another advantage of PF is its higher oxygen index. In addition, PF and PU materials burn without any melting droplet, avoiding the formation of flow fire on the building surface and pool fire on ground.

Composite insulation material

Composite insulation material refers to the insulation material interposed between inorganic and organic material. Polystyrene particles are a typical kind of composite insulation material. This kind of material has the advantages of thermal insulation and fire, burning performance A2 can be achieved generally.

However, along with the increasing requirements of building insulation in our country, better insulation performance must be realized by organic materials composited or thickness increasing in polystyrene particles exterior insulation system, these inevitably increase construction difficulty and building load-bearing requirements.

Conclusions

With the development of building energy-saving requirements and industry level, building insulation materials also develop towards the goal of diversification, high efficiency, safety and durability. As the main components of building insulation system, thermal insulation material must play an important role in it. In this paper thermal insulation material is divided into three categories, several kinds of external thermal insulation materials are selected as typical representative of organic, inorganic and composite insulation material, fire performances are introduced and comparatively analyzed. The research of this paper has important significance on research, development and selection of thermal insulation materials and insulation system construction.

Reference:

[1] The Building Regulations 2000 (2006 edition, amended 2007), Approved Document B(Fire safety)[S], the United Kingdom.
[2] MBO 2002 - Musterbauordnung[S], ARGE Bau, Germany.
[3] EN 13501-1: 2007, Fire classification of construction products and building elements——Part 1: Classification using data from reaction to fire tests[S]
[4] ASTM E 84, Standard Test Method for Surface Burning Characteristics of Building Materials[S].
[5] ASTM E 119, Standard test methods for fire tests of building construction and materials[S].

Advanced Materials Research Vols. 989-994 (2014) pp 5435-5438
© (2014) Trans Tech Publications, Switzerland
doi:10.4028/www.scientific.net/AMR.989-994.5435

Analysis and Control of the Pollution Problem in the Process of Wheat Anther Culture

Yang Xue, Wang Ding, Zhang Li-qin*,Chang Hui-ping, Liu Chun-lei, Han Hong-peng, Xing Wen-hui, Wang Shi-jie

Department of Life Sciences, Henan Institute of Education, Zhengzhou Henan, 450046

Sws211@163.com

Keywords: Wheat anther culture; Pollution; control

Abstract. The prevention and control of pollution is an important technical link in haploid breeding of wheat. From the pollution types,causes and prevention methods in the process of wheat anther culture to analyze how to reduce pollution problems appeared in the tissue culture,so as to achieve the purpose of decreasing the cost of wheat breeding,and improving the efficiency of breeding purposes.

In recent years, plant tissue culture technique (PTCT) has become one of the most extensively used biotechnologies, which is inseparable from agriculture, gardens and medicine etc. wheat anther culture technique is to go on wheat breeding with the PTCT to get the haplobiont, which is very meaningful for shortening wheat breeding time, enlarging breeding scope as well as increasing breeding efficiency. In the cultivating progress of wheat anther, that contamination rate is usually as high as 10%, even to 30%, has become the first problem, which increases the breeding cost, influencing breeding efficiency.

1 Types of contamination

Contamination is the phenomenon of abnormal growth and development of culture material because of microorganism breeding on the culture medium or culture material, such as bacteria and fungus. Common contamination etiologies included bacteria and fungus. Therefore, the contaminations in breeding progress can be divided into two types: bacterial contamination and bacterium contamination. Surface bacteria contamination will show after 1~2 days. Surface of the culture medium will show mucus shape dental plaques. But contamination caused by endophytic bacteria is not obvious at beginning. With the increase of times of culture connection, the quantities of bacteria accumulate, and the contamination occurred [1]. Fungus contamination usually occurred 3 days later, the manifestation of which is the appearance of villiform hypha at beginning then turned to colorful spore layers.

2 Reason analysis (way) of contamination

Reasons of contamination in wheat breeding progress are various, which are as follows: improper explant or halfway disinfect; halfway sterilization on culture media or appliances; nonstandard operation when inoculating; unclean environment of inoculation and culture; break of culture container.

2.1 Explant

2.1.1 Drawing materials

The season and the time of drawing explant influenced the contamination rate of culture material. Generally, spring material has fewer bacteria than summer and winter ones. Material survival rate is relatively high in spring. Materials of wheat anther culture are drawn in mid-end of April and first 10 days of May. Sunny days should be selected and rainy days and severe lowery days should be avoided. Keep in mind that material with water is undesirable. Dew in the morning and rainwater will increase the amount of bacteria in culture material. Then the bacteria will contaminate wheat anther along the water. There will be great trouble to deal with the material. Contamination rate will improve invisibly.

2.1.2 Treatment

The treatments of explant include pretreatment and disinfection.

Wheat material taken from growing field should be packed by plastic wrap and be pretreated for 3~7 days. There are 3 advantages. Firstly, preserve moisture of the material; secondly, be isolated with the outside; thirdly, passivate the bacteria with low temperature. The pretreatment of the material will decrease the contamination rate.

Halfway disinfection of explant is one of the main reasons of contamination. For wheat anther culture, inoculate material is anther, which is very tender, so disinfection progress should be undertaken on the wheatear. Therefore, the selected disinfector should not only has good disinfectant effect to kill all microorganism of the material surface but also do little harm on organization of the material without affecting its growth. Generally, liquor with 75% alcohol and 0.1%mercuric chloride was used as disinfector. In addition, sodium hypochlorite, calcium hypochlorite, bleaching powder, hydrogen peroxide and silver nitrate can also be used as disinfectors. The types of disinfector and the disinfection time depend on the tender degree, the amount of bacteria of the material, which will be decided by the experience of the handlers. Because the alcohol has stronger penetrating power, 75% alcohol is commonly used as disinfection in the progress of wheat anther culture. 20~30 seconds will be OK for disinfection. If the disinfector isn't strong enough, 0.1% mercuric chloride liquor can be used. Because it is hard to wipe off and very harmful to plants, the disinfect time shouldn't be long.

2.2 Culture medium and various appliance

Culture medium and all appliance used in the inoculation process should be disinfected strictly. Halfway disinfection will lead to high contamination rate.

Autoclaving is usually used to contaminate bacteria on culture media. With autoclaving, contamination should be lasted for about 20 minutes, so as to get better contamination results. Be attention that the cover of the autoclaving pot should be tight to get better sealing condition, or contamination temperature can't meet the demand, which leads to halfway contamination on the culture media. Besides, the components, which can't be contaminated with autoclaving method on the medium, such as some certain hormone, should be contaminated with bacteria proof filter. Then add them to the culture medium on the super-clean bench. The contaminated medium should be preincubate for 3 days. If the contamination isn't thorough, the microorganisms will occur during preincubation.

Generally, before the entry to the vaccination room, all kinds of appliances used in the vaccination progress should be autoclaved. Without thorough contamination of these appliances, contamination rate will be very high. Culture dishes and ironware should be packed with multilayer paper when going on autoclaving. Make sure the integrity of papers to avoid secondary pollution when touching air.

2.3 Inoculations

A lot of material and goods will be used in inoculation link. Labile factors of environment and human increase the possibility of microbial contamination on the culture medium. Only every step was treated strictly in the inoculation progress that the contamination rate would be lowest.

2.3.1 Disinfection of the inoculation room

Fungus exist in the air of inoculation room, so regular disinfection is needed. In common, mixture steam of formaldehyde and potassium permanganate (or 70% ethyl alcohol and 0.5% phenol) is used to disinfect [2]. Research of Yiting Wang [3] shows that formaldehyde fumigation can decrease the fungus by 87%~100%, and regular disinfection restrain bacteria in the culture environment effectively. Before inoculation, the room should be contaminated by ultraviolet ray for 20 minutes to decrease the amount of bacteria.

The ground should be often swept with disinfectant. Except conventional clean, before and after inoculation the ground should be swept once to make sure the low content of microorganism.

2.3.2 Use of super-clean bench

Classify and identification of tissue cultured seedling contaminant did by Zhou Junhui [4] showed that most microorganism came from air of inoculation room and exhaust of super-clean bench air blower. Proper usage of super-clean bench is helpful to lower the contamination rate of wheat anther culture. Before inoculation, the super-clean bench should be ventilated for 30minutes firstly. Then the board should be disinfected for 15minutes with UV lamp. Before operation, the operator need to sweep the board with 75% alcohol wipes to kill the bacteria and fungus.

2.3.3 Human factor (inoculation process specification)

In the inoculation progress, irregular operation of people is one of the main reasons of contamination, especially fungous contamination. To reduce the contamination rate, standard operation is necessary in the inoculation progress. The follows need to pay attention to.

(1) Hygiene of operators. Before the entrance of inoculation, operators should wash their hands carefully, especially the nails. In buffer room, they should change their cloth to lab-gowns, slippers, lab-caps and respirators. Besides, their hands and arms should be scrubbed with 75% alcohol wipes as well as the ectotheca of the culture bottle.

(2) The use of metal utensils especially tweezers should be standard. The anther was inoculated on culture medium in the process of wheat anther culture. Anther need to be taken out by tweezers from the florets, and then put them on the medium. In the process of taking anther, glumes should be wiped off firstly, then use a disinfected tweezers to take the anther. Tweezers can't be mixed. So operators should contaminate the tweezers in time.

(3) Avoiding petty action. In preliminary stage, operators aren't familiar with the operation procedure. Some petty actions occurred, such as play their phones or touch other place. If return to the super-clean bench without disinfection, materials on the bench will be contaminated. Therefore, for beginner the contamination rate is relatively high, even to 100%.

(4) The anther from the touched material by hands can't be used.

(5) On the premise of standardized operation, inoculation speed should be as fast as possible. the less the time, the lower the contamination rate.

2.4 The management of the culture room

Unclean environment or culture container damage will increase the contamination rate. So pay attention to the management of culture room constantly. Specially-assigned person is necessary to manage the culture room.

Wheat anther culture should go on in specific culture room. Air and the ground will breed bacteria if the culture room was free for a long time. Therefore, before using the room should be disinfected with mixture steam of formaldehyde and potassium permanganate. As for busy room, it is necessary to be disinfected constantly with mixture steam or 75% alcohol mist spray. The culture room should adjust temperature and humidity a few days earlier because wheat anther culture needs proper condition. In mid-end of April, indoor temperature is about 15~20℃. it can't meet the requirement of anther inoculation on the differential medium. So the culture room should rise the temperature 1~3 days earlier as well as the humidity.

In the culture process, ultraviolet sterilization for 10~15 minutes is needed. And sweeping the floor with disinfectant is also necessary to keep the environment clean. Observe the growth of culture material and take note carefully. Contaminated culture bottle should be isolated in time. Besides, culture containers may be broken or the sealing material may be loose. If these phenomenon haven't been found on time, culture material may be contaminated.

3 Prevention, government and control of contamination

3.1 Prevention and control of contamination

Reasons of contamination have been discussed above. So we can take some specific measures to prevent contamination.

(1) Draw materials at 9~10 o'clock AM and 3~4 o'clock FM of sunny day to avoid rain, haze, smog and dew.

(2) Do better pretreatment, and contaminate explant thoroughly.

(3) Contaminate culture media and appliances used in inoculation process thoroughly.

(4) Do standard operation in inoculation link, follow the Aseptic operating procedures strictly.

(5) Better management of inoculation rooms and culture rooms, and keep them clean.

(6) Observe the culture material carefully to find and change the broken culture containers in time.

3.2 Government and control of contamination

As for the government of contaminated tissue seeding, antibiotic was widely used. But is has bad stability. Classify and density depend on the experiment data. So in the culture of wheat anther, antibiotic is not used. In order to prevent cross contamination, the whole contaminated bottles with material should be disinfected with autoclaving, then to wash them.

References

[1] Kritzinger EM, Vuuren RJ van, Woodward B,et al.Elimination of external and internal contaminants inrhizomes of Zantedeschia aethiopica with commercial fungicides and antibiotics. Plant Cell, Tissue and Organ Culture, 1998, 52(2): 61-65.

[2] D.X. Wu, F.R. Hu: Plant tissue culture (second edition) (Shanghai Jiaotong University Press, China 2009).

[3] Y.T. Wang, L.P. Wang, H.J. Mu, et al: Anhui Agricultural Sciences, vol. 33 (2005) no. 12, p. 2357- 2358

[4] J.H. Zhou, H.B. Li, Y.Q. Yang, et al: Journal of Microbiology, vol. 22 (2002) no. 2, p. 53-55

Advanced Materials Research Vols. 989-994 (2014) pp 5439-5443
© (2014) Trans Tech Publications, Switzerland
doi:10.4028/www.scientific.net/AMR.989-994.5439

The Research of Wisdom Campus Construction and Development Based on Internet of Things

Wang Yipeng

Shandong College of Tourism & Hospitality, 250200

embird@126.com

Keywords: Internet of things, wisdom campus, construction development, student teachers

Abstract. With the continuous development of science and technology, new information technologies such as Internet of Things, Mobile Internet quickly get into various industries. The vast majority of colleges and universities are actively constructing wisdom campus based on Internet of Things to effectively integrate campus personnel identification, library management, campus id and other information, and to ensure digital resources integration and sharing. This article mainly aims at further exploration of the construction and development of wisdom campus based on the characteristics of Internet of Things.

The Internet of Things and wisdom campus

A. The concept of Internet of Things

The Internet of Things is physical Internet which can achieve global objects'real-time share information. It takes Internet, RFID technology, and EPC coding technology as foundation, and makes use of computer Internet to share information. The Internet of Things is very common in our life, which only need to embed one transceiver of middle or short distances in all kinds of daily necessities, and can provide people with a new communication dimension in communication and information world, and expand traditional human communication interconnection of any place, any time, any people to the category of physical interconnection, and the interconnection of things and people.

The Internet of Things system is structured, including comprehensive perception layer, reliable transmission, and intelligent processing layer. Comprehensive perception layer makes use of various means of perception, acquires real-time object dynamic information, such as two dimensional code, sensors, blue-tooth devices, which can get real time information of objects, and they can get instant recognition like sensory organs, and gather data information. Reliable delivery layer can use all sorts of information networks, Internet perception information in a timely, real-time, accurate and reliable manner. Intelligent processing layer can analyze and handle huge amounts of information data, control object through intelligent technology, and help make right decisions, and connect people and things.

B. Wisdom campus concept

Internet of Things technology helps people obtain, transmit, and use intelligent information. It gradually promotes the construction and development of wisdom campus at the same time of changing people's life, work, and study. The acceleration development of Internet technology achieves highly sharing of digital campus internal resources, and information flow, internal teaching environment, education resources and teaching activities are gradually tends to be digital. Wisdom campus has three distinctive features: first, wisdom campus can provide comprehensive and systematic intelligent perception teaching environment for teachers and students and a comprehensive information service platform, promote the roles'personality development of teachers and students; Second, wisdom campus can fuse information service on the basis of computer network technology into various application service areas, and ensure the interactive collaboration of resources mutual connection and related personnel in the university; Third, wisdom campus can use intelligent sense environment and comprehensive information service platform to let the school be connected with the outside world, and perceive each other.

C. Wisdom campus based on the Internet of Things

Wisdom campus is on the basis of digitalization, which takes data information network as the connection, and use digital networking of things technology to comprehensively manage campus environment, resources and activities. Wisdom campus based on Internet of Things can not only provide a more convenient, efficient, and intelligent campus environment for teachers and students, it can also integrate the currently most fashionable popular intelligent transportation systems, energy conservation and emissions reduction system, security monitoring systems, and mobile application system into wisdom campus construction, and get it into education informationized, scientific decision-making, management standardized high quality teaching environment, and improve the quality of teaching. The details are as follows:

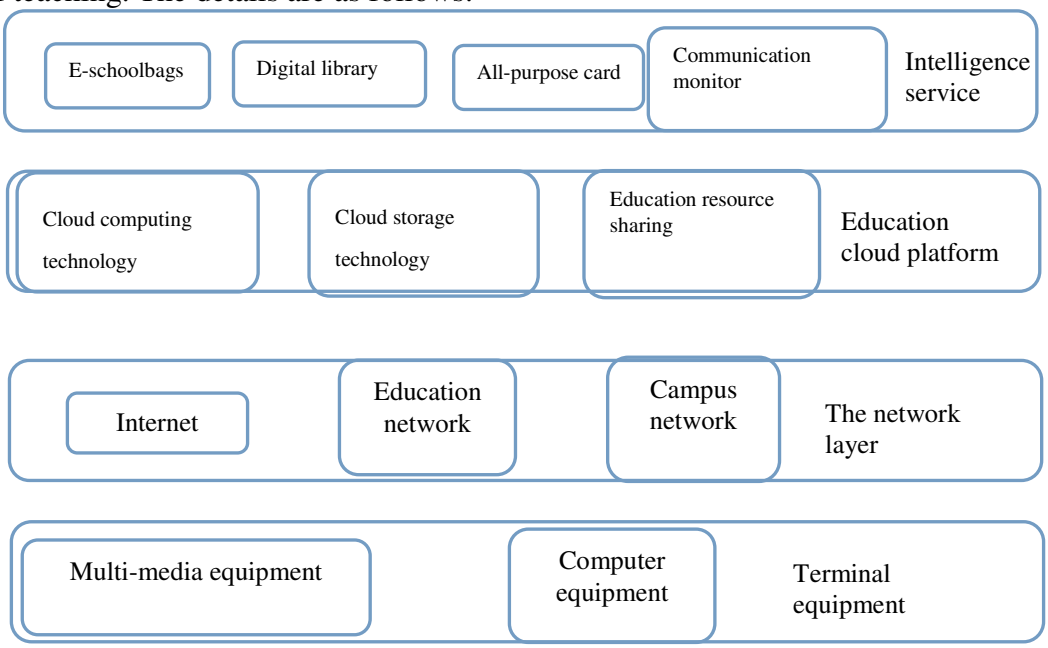

Figure 1 Wisdom campus structure based on Internet of Things

Effective Measures of Wisdom Campus Construction Based on The Internet of Things

Effective construction of wisdom campus based on Internet of Things should be on the premise of campus network, and at the same time take teaching resources as the core, and establish a management platform with fused information to ensure that campus internal becomes digital and intelligent integrated management network platform.

A. Build a unified teaching platform

Wisdom campus should actively build a unified teaching platform, vigorously introduce domestic and foreign high-quality digital teaching resources, give all kinds of high quality network courses at the same time, establish a comprehensive network teaching cloud database; At the same time, also construct digital library and virtual laboratory and truly unify teaching resources ‘flexible open of public service platform.

Network teaching platform and teaching database are important platforms to ensure school education informationization, which can realize the integrated management of teaching resources, effective help teacher prepare lessons, online teaching, students training, really carry out students' autonomous learning, provide a good chance of communication for teachers and students, and co-construct and share teaching resources. School administrators can understand teachers and students ‘teaching status and evaluate teaching quality through unified teaching platform in a timely manner; Parents can understand students' learning in school through this platform; while companies can help guide students practice teaching through the platform. In short, the establishment of unified content couplet teaching platform not only can promote scientific utilization of teaching resources, bring more high quality resources sharing service for teachers and students, also can improve the students' learning quality, enrich students' knowledge, and strengthen students' various skills.

In addition, colleges and universities should actively build cloud computing service platform. Through the establishment of teaching cloud database, develop network teaching course, including continuous integration of the existing teaching resources to achieve the sharing and application of teaching resources. And cloud computing service platform can integrate large purchase high quality resources to eliminate the limitation of heterogeneous systems, avoid internal barriers of resource sharing technology, improve the whole service level of library, effectively display teaching resources, and provide teaching resources to the users through the directory joint, retrieval unification, document delivery, and other functions.

B. Construct unified data platform

Due to long-term lack of unified and effective planning and leadership department of traditional colleges and universities information construction, colleges and universities departments form independent college information application system and information isolated island, and gradually form stable data repository, but resources data are unable to achieve full sharing between subsystems, which is no good to the uniform data query in colleges and universities, and data applications.

Wisdom campus basic task based on the Internet of Things is to make full use of the campus existing application system and information data to construct a unified data reception. And the key of wisdom campus construction is to establish a unified platform for data fusion, accomplish campus data resources integration and sharing of information management, and provide users with high-quality service data fusion. Wisdom campus data come from other entities related to learning teaching in addition to information relating data from school business administration. Due to different entities have different heterogeneous data sources and management mechanism, the lack of unified platform data sharing will not provide good data fusion for campus user services. To sum up, only when university actively build unified perfect data integration platform, can the construction of wisdom campus based on Internet of Things be built smoothly.

C. Construct unified information publishing platform

The unity of wisdom campus development information publishing platform can provide users with efficient and fast information terminal content management. When the content play, style management, material management, task distribution of each terminal are through campus center control point, they can get unified management, comprehensive distribution, and comprehensive monitoring by all terminal equipment's.

D. Construct unified identity authentication platform

Building a unified identity authentication platform is an important content of contemporary new wisdom campus construction. Unified identity authentication platform not only can provide the user with a centralized user authentication management and business integration environment, also can solve many problems of the traditional college certification model such as too complicated to use, slow, poor portability and safety concerns. It provides comprehensive unified user identity authentication service to wisdom campus every application systems, and can also manage the users'digital identity information in information system. As a result, the user simply needs a user name and password belonging to him to use the entire application system authorized by wisdom campus, which effectively avoids repeated logging bad situation. And, in wisdom campus, some important documents and goods are to be labeled qr code and GPS, perception and track function effectively, guarantee the safety management of items, positioning monitor vehicles entering the campus, and ensure traffic safety campus order. In some special area of the campus, set intelligent sensor to implement safety monitoring. Once suspicious, perception will alert management center and begin in-depth analysis of events.

Wisdom Campus Outlook Based on Internet of Things

A. Efficient visualization intelligent management

Wisdom campus based on the Internet of Things can directly connect each physical object in campus environment, at the same time, perceive campus information, gain comprehensive and collated campus latest data information, and do data processing analysis, find out problems and put forward relevant basis for managers to solve the problem. This wisdom campus visualization

environment on the one hand can provide efficient service for campus management, on the other hand it can also implement campus humane, scientific and intelligent management, and control real time campus object data and feedback information in time.

In the wisdom campus environment based on the Internet of Things, teachers and students can not only conveniently complete the identity recognition and attendance record, also can visually monitor campus environment and security system, connect each network, and control intelligent network through variously installed perception of human body movement, sound, temperature, light sensors on the campus, effectively implement the wisdom management of internal campus teaching environment, and safety environment.

B. Build teaching environment of wisdom

The development of network technology provides a more convenient way for people to get a lot of teaching resources and learning materials, but the network's virtual learning environment is always lack of authenticity and touch, still cannot restore the real scene of teaching experiment. Internet technology can effectively connect the real world objects, fully integrate real learning space and virtual learning environment, and achieve the good purpose of physical space and digital information space interconnection. Above all, the Internet of Things can realize the digitalization, visualization and networking of each object on wisdom campus. The teachers and students can have real perception teaching scenario, operate and learn the laboratory research object of experimental equipment, experimental site, also have close observation of experiment, effectively promote human-machine interconnected, entry interaction, and provide more opportunities to communication between teachers and students. In addition, the Internet of Things can also integrate the existing campus teaching platform. Students complete the learning activities by remote control experimental equipment, which provides more broad space for development and quality management services for remote teaching activities. Internet of Things, therefore, provides strong support for teaching activities in wisdom campus, eliminates sharing obstacles in teaching equipment, breaks the limitations of traditional teaching, strengthens students' practical operation ability and inspires the ability of thinking.

C. Implementation of regional resource sharing

To realize fair education, effective means are used to solve major issues of co-construction and sharing of education resources in education career area. At present, the colleges and universities deepen reforms, and gradually implement key school system, which results in a certain gap among different schools in the area. This is mainly embodied in the difference high quality education resources of colleges and universities. Colleges and universities use the Internet of Things technology to make the resource equilibrium among institutions of education. Such as some large high quality laboratory equipment, library resources can be shared to achieve the co-construction and sharing of regional colleges and universities teaching resources through the Internet of Things technology. The teachers and students of different areas can have the same and equal education resources to achieve "low cost, high quality service". On the other hand, students can also choose the appropriate content according to their own hobby, meet the demand of their own learning, improve the liquidity of learning information, deepen students' understanding of knowledge and understanding, and help learners establish collaborative innovation partnership. Wisdom campus based on the Internet of Things, therefore, has a good development potential. It can effectively improve the level of teachers' level of colleges and universities, eliminate the difference of regional colleges and universities teaching resources, and improve the utilization of teaching resources.

D. Broaden learning space

The Internet of Things technology has extended learning space, provides development potential of service, which can help students combine the theoretical knowledge and teaching examples they learned in class, eliminate the problem of theory breakaway from teaching practice. And, Internet technology connects college education resources and related closely with the company, the enterprise resource effectively, which truly achieves the bidirectional interaction between campuses and enterprises. Only by establishing a good strategic partnership with complementary advantages between enterprises and companies, on the premise of improving teaching quality, can students'

innovation ability and practice ability be strengthened. Besides, university education management mode can extend through the Internet to all areas, and implement intelligence service of multidisciplinary and cross area, truly meet the needs of mobile learning, and provide users with ubiquitous resource management services.

Conclusion

To sum up, the emergence of the Internet of Things effectively promotes the development of college education informatization process, brings more innovative services and innovative applications for colleges and universities education, which greatly promotes the transformation of traditional teaching mode, and management mode. Wisdom campus construction based on Internet of Things not only gradually optimizes the environment of teaching, but is an important way to deepen teaching reform, and an important direction of future education. Wisdom campus construction based on Internet of Things aims to effectively implement teaching wisdom, management wisdom and scientific wisdom, wisdom of life and service, and to make teachers gradually update teaching ideas, innovative teaching mode, and provide more high quality teaching service and technical support for students.

Acknowledgment

Fund project: college humanities and social science research project in Shandong province in 2014: wisdom tourism and its impact analysis based on user experience

References

[1] Hai Dayong. Analyses on how to apply the Internet of Things in wisdom campus construction [J]. Journal of Modern Distance Education Research. 2013 (19)

[2] Ming Junlin. Explore the Internet of Things role in the construction of wisdom campus [M]. Beijing: Science Press, Beijing. 2012.4

[3] Tian Suying. Advantages and development of the Internet of Things [J]. Chinese Education Analysis. 2013 (9)

Advanced Materials Research Vols. 989-994 (2014) pp 5444-5447
© (2014) Trans Tech Publications, Switzerland
doi:10.4028/www.scientific.net/AMR.989-994.5444

Review of the Integrated Researches on Internet of Things and GIS in Fire Emergency Plan

Linjun Yu [1, a], Huan Wei[1,2, b], Zezhong Zheng [2, c], Yalan Liu*[1, d], Tianhe Chi[1, e] and Ling Peng[1, f]

[1] Institute of Remote Sensing and Digital Earth, Chinese Academy of Sciences, Beijing, China

[2] University of Electronic Science and Technology, Chengdu, China

*corresponding author: [d]liuyl@irsa.ac.cn

[a]yulinjun81@gmail.com, [b]18201615329@163.com,
[c]zezhongzheng@uestc.edu.cn ,[e]chith@irsa.ac.cn,[f]plqiqi@126.com

Keywords: Internet of things, fire emergency plan, VR animation, GIS

Abstract. Emergency plan is crucial to efficient fire recuse. Facing with the existing problem of China's fire fighting and fire emergency plans' status, this article firstly describes the progress in emergency plan and a variety of emerging Internet of Things technologies in fire rescue, then proposes a new form of fire rescue emergency plan which integrates the techniques of Internet of things, VR (virtual reality) animation, GIS and indoor positioning technology. The integration is an innovative way to enhance fire supervision, to improve fire-fighting and rescue capabilities, and to achieve the fire management efficiently, powerfully and more intelligently.

1 Introduction

With urban development, the buildings are built much higher and their area is getting much larger, also more and more staff -intensive. Also a variety of underground space, as the underground street, underground shopping malls, underground parking, underground buildings, etc. link together , as if they form into a small underground city. This particular space is crowded, narrow export, beneath the ground, rapid and effective rescue is very difficult. Once emergency occurs, whether from internal or external, it's very difficult to implement the rescue [1].

When Meng Jianzhu reported the work on Fire Rescue to Chinese State Council, he summarized the main issues in current firefighting: fire safety infrastructure suited to the economic and social development situation has not fundamentally changed ,fire rescue and security capability not meets the social needs situation has not fundamentally changed, public fire safety awareness not suites the social requirement situation has not fundamentally changed ,so we are still in the fire-prone, fire-much period. About the next step , Meng Jianzhu proposed "it needs to further enhance fire professional team construction and to build a sound fire emergency rescue command platform and social linkage mechanism, to improve rescue emergency plan , to strengthen the special fire-fighting and tactical research and professional training, and to enhance the combat effectiveness of the fire emergency rescue".

2 Progress on fire emergency plan

There are two kinds of fire emergency plans. One is paper-based, and the other is digital emergency plan.

(1) Paper-based emergency plan

The fire police prepares a paper fire emergency plan for each fire safety key unit, and divides plans into level-one, level-two, level-three and several cases of different fire area. On one hand, the capacity of this plan is large, and storage is difficult due to the fire units' quantity; on the other hand, when a unit is on fire, it is difficult to find the suit plan from a large paper emergency plan. Emergency plans still have some other problems, like complexity of preparation, difficulty of deduction and amendment, low utilization, poor practical applicability.

(2) Digital emergency plan

The research of digital plan technology is emerging in recent years, it has gone through several stages as follows from concept proposed to now:

The first stage: the electronization of fire emergency plan. Built on the basis of the information management system, some functions have been achieved: emergency plans text editing, classification search, add, delete, as well as the organization and management of the sub-text. However, the digital plan is simply digitized store in text, only providing a number of conveniences on the information finding.

The second stage: the visualization of fire emergency plan. It is built on a comprehensive digital software platform, and has functions of risk analysis, comprehensive judgments, decision support, can automatically generates digital plans. Therefore, it can be used to address the problem of less information, accessing to information inconvenient and not intuitive. It can combine the graphic, text, audio, video and other elements to achieve the plan execution process visualization. The emergency plan has some features that strong visibility, high maneuverability, intuitive information. Meanwhile, it can also be used in portable and flexible command system, such as laptops, PDAs and other forms of portable equipment [2,3] .FIS (Fire Information System) based on GIS by Zhang Juanxia makes full use of confined manpower and material resources to finish the fire control tasks efficiently [4]. The Fig. 1 below shows its functional framework.

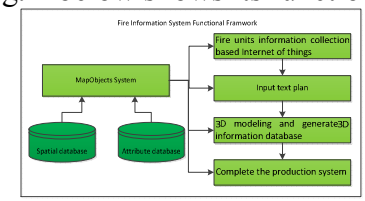

Fig. 1 FIS functional framework

FIS can achieve the management of 119 receiving and responding to the alarm, fire information protection, fire emergency plan making, data maintaining and the disaster prediction. It can efficiently solve the problems of fire control by using all kinds of data from Internet of Things.

Afterwards, researches about emergency plan based on Internet of Things developed rapidly in the field of firefighting. Beijing has established Internet of Things fire-fighting monitoring system and realized the visualization and automation of data thoroughly. The Fig. 2 below shows the Internet of Things constitution about the firefighting.

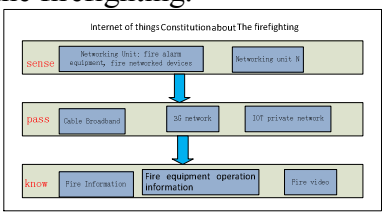

Fig. 2 Internet of Things constitution about the firefighting

By using the detection results of video surveillance and all kinds of sensor such as smoke detector, light detector and temperature detector, also the new technology arranging server and managing data like cloud computing and cloud storage on cloud infrastructure, it can achieve receiving the alarm, transporting the video, collecting the vehicles' running state, automatically monitoring online, searching and counting, publishing the information etc.

The third stage: the intelligentization of the emergency plan. Recently, most of the emergency plans display in paper forms or 2D electronic forms, which have less information than 3D and needs firemen know well of the fire places. Through the 3D way can we make swift and right decision to find out the road, water source, distribution of buildings and escape routes in the rescue scene [5].

Using the advanced computer technology, CONECT, VR(have advantages of making interactive virtual environment and reappearing the real city) technology to research 3D GIS is applied to the fire-fighting and fire drill .It provides the fire forces an easy-operating and intuitive interface of 3D digital fire emergency plan and vivid training course, boosting the Fire Station's rescue ability greatly. Therefore, we utilize the new technology to train, assess, and develop firemen to formulate sound emergency plan.

3 Current problems in fire emergency plan

The limitations of digital emergency plans influence its large-scale promotion and application. It mainly shows in the following aspects [3]:

(1) High production costs. Digital plans are usually made by digital multimedia technology, which is strong technical that non-professionals generally find it difficult to make independence, and expensive that usually cost thousands or ten thousands RMB.

(2) Long production cycle. Digital fire emergency plans need to have text, live pictures, various deployment diagrams of different stages, power calculation ability, and even 3D figures, a key unit's emergency plan usually takes at least two weeks or a month.

(3) Difficult to make. Due to technical reasons, the digital fire emergency plan requires several types of 3D software, graphics, programming, it is difficult for the basic staff to make. Making this kind of emergency plan is only products of a few patents or software companies.

4 Future trends and prospects for Fire emergency plan

The emerging network technology provides an important way to solve the contradiction between the present situation of fire management and the application requirements. Supposing to combine GIS and future indoor positioning technologies, then it can provide strong technical support for the innovation of fire supervision and management, also the rapid and effective fire rescue; additional adding the Internet of things ,then we can build an intelligent 3D fire emergency plan based on remote monitoring system. For some sites, particularly crowded places where it's vulnerable to fires, explosive agencies, higher buildings, and other fire risk agencies, we can monitor fire facilities' running status, unblocked fire exits, and the fire control room, also combine the fire events with real-time video to achieve remote real-time monitoring. Also using VR animation to dynamically simulate the fire occurrence and development of fire agencies, allowing firefighters immersive experience the building environment of the agencies, to be familiar with fire-prone places and know how to act correctly; while achieving Fire training and assessment . Adding 3D structures of the building's external environment and indoor electronic map, can achieve the finding and positioning of outdoor fire vehicles, fire water, etc... Indoor positioning technology can locate the people trapped in fire, thus shortening the rescue time and help solve the search and rescue difficulty. Comprehensive analysis, we can establish 3D fire rescue system based on the above technologies, it should have features showed in Fig. 3:

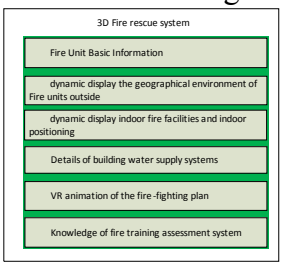

Fig. 3 3D Fire rescue system

The 3D emergency plan based on the system has some features: strong visibility (widely monitoring system), high reliability (truly present the building structure and fire facilities), highly targeted (strictly in accordance with the system requirements to design).

5 Conclusions

With the aid of Internet of things to monitor the fire facilities' status and possible fire disaster, so that all the useful information can be easily acquired. While taking advantage of the 3D GIS to simulate fire occurrence, development and people's response in VR to achieve training, assessment and improving the ability of firefighters, it can also generate an auxiliary emergency plan to analyze the fire, make action plans and real-timely get fire equipment, vehicles' status, firefighter's action tracks etc. By making the indoor electronic maps, further more using indoor positioning technology

to get real-time location information of indoor personnel, thus greatly facilitates Fire Rescue. Based on this, to formulate the digital emergency plan for all types of enterprises is very important, and it helps to make the fire rescue and fire training more scientific , intelligent , virtual .

6 ACKNOWLEGEMENT

This work is jointly funded by the projects No. 2011FU125Z24 from Chinese Ministry of Science and Technology and the project of Special Industrial Development and Application of Satellite (Fire Emergency Rescue Application Platform Based on High-Precision Positioning Seamless Indoor and Outdoor) from National Development and Reform Commission.

References

[1] Liu Wenjie: Study on sudden accident and emergency rescue of Urban Underground Space [D] Harbin: Harbin Institute of Technology, 2012.

[2] Xu Jianying: Design and implementation of emergency plans for hazardous chemicals workplace's emergency plan management system [D], Chengdu, China: University of Electronic Science and Technology, 2012.

[3] Zou Xiang: *Preliminary Application of digital fire and rescue emergency plan platform* (Technological innovation, 2011).

[4] Zhang Juanxia: *Research and Implementation of Fire Information System Based GIS* (Guangdong Science and Technology, 2013).

[5] Xue Li: *Discussion about fire safety remote monitoring system based Internet of things* (POLICE FORCE ACADEMY, 2012).

Advanced Materials Research Vols. 989-994 (2014) pp 5448-5452
© (2014) Trans Tech Publications, Switzerland
doi:10.4028/www.scientific.net/AMR.989-994.5448

Analyses of the Model Design of Urban Emergency Management System

[1,a] Wang Xiaoming, [2,b] Lv Ying

[1,2] Jiangsu Academy of Safety Science and Technology, Nanjing, JiangSu, China, 210042

[A,b]wxmtalk@163.com

Keywords: Urban Emergency Management System; Framework Model; Crisis Evaluation; Policies.

Abstract. In order to tackle the insufficiency of policies of urban crisis management and conform to the ability to deal with urban crisis, it asks to establish a comprehensive emergency management system. Under this circumstance, this paper puts forward a general framework of urban crisis, analyzing the corresponding key technologies of the system and founding a risk rating evaluation model of urban natural calamities based on the improvement of projection pursuit so as to offer scientific basis to the effective establishment and application of the evaluation system and the enhancement of the abilities to urban disaster emergency.

Introduction

To build an efficient and unified urban emergency management system is an inevitable choice for a city to enter the modern management. The possible influences of unexpected public events on a city with a larger scale are great, so it needs a more sensitive and efficient emergency management system. In many a city in developed countries, urban emergency management system has become an integral part of people's daily life, even having been the symbol of urban management level. Therefore, how to establish an efficient urban emergency management system has become an urgent task for urban managers. The paper focuses on the establishment of urban emergency system, has proposed a general framework model of urban emergency management system based on three dimensional cube structures, and effectively controls urban emergency management taking into account the risk rating evaluation model of urban natural calamities based on the improvement of projection pursuit.

Analysis of the Construction Model of Urban Emergency Management System

Urban emergency management system is a multi-level, multi-sectoral and multi-functional complicated giant system with dynamic changes. Essential factors within the system generate multiple feedbacks and constitute compound system with some structure and function by interaction, interplay, interdependence and mutual constraint during the circulation and exchange of materials, information and energy. Urban emergency management information system adopts advanced network technology, computer technology and multimedia technology. The system performs functions such as aided policies of emergency command and scientific mobilization of emergency resources through the collection, transmission, storage, settlement and analysis of all kinds of data on unexpected public events. According to the general framework model of urban emergency management system and the features of urban emergency management, the general technology framework model of urban emergency management system is put forward.

General Frame Diagram of Construction Model of Urban Emergency Management System

Technology framework model of urban emergency management system consists of five layers: network communication layer, information resource center, application supporting platform, business application platform and integrated information gateway. Before the sudden public events occur, the system can assist the emergency management personnel in the preparation of emergency work and exert the functions of real-time monitoring and warning; when the unexpected public events happen, the system can swiftly provide emergency commanders and decision makers accurate and detailed resource information and status of events. It also can assist decision makers in making emergency decision by the application of intelligent decision-making technology so as to execute scientific

commanding mobilization. After the unanticipated public events, the system is able to aid the emergency management personnel to return to the emergency works.

Analysis of Key Technology of Urban Emergency Management System

The Establishment and Renewal of Plan Library of Urban Emergency Management System: Experts formulate a series of reasonable emergency plans by means of some forming process and methods of plan, including plans made under stimulated situation and past successful cases. Then they build plan library in virtue of computer information system. Plan library engages in the storage and organization of plans formulated under stimulated circumstance and past successful cases. Each plan includes complete description of related issues and solutions. The addition of a new plan accompanies the establishment of index of its main features. Based on that, the establishment and renewal of plan library are realized by the management system of plan library. The management system of plan library is mainly composed by five sections, shown on the Figure1. The whole system is based on the comprehensive information bank, it will exert sort management on plans within plan library according to the characteristics of emergencies and offer functions such as the unload, download, inquiry and renewal of plans.

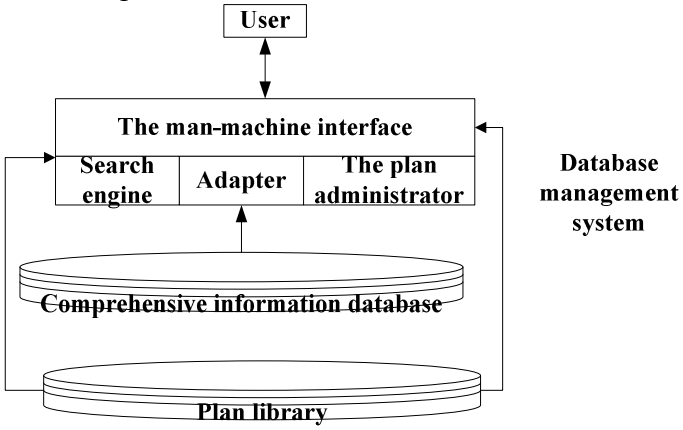

Figure1 Working Diagram of Management System of Plan Library

Risk Rating Evaluation Model of Urban Natural Calamities Based on the Improvement of Projection Pursuit: The basic principle of projection pursuit is to project high-dimensional (namely m dimension) data on the subspace of low dimension. The projection space that can reflect features of high-dimensional data should be the rank dimension of high-dimensional matrix, set as K dimension ($1 \leq k \leq m$), that is to say, when high-dimensional data is projected on its space of rank dimension, the space is the one that losses the least original data information. Furthermore, when the dimension of projection space is below k, the amount of information reflected original data gradually decreases with the reduce of dimension. Immune Clonal Selection Algorithm (ICSA) optimizes the projection .direction in order to have access to divisible low-dimensional data. Details are shown in document [5].

Assuming the sample set of each index value within the evaluation rating table as {x*(i, j)/i=1, 2, 3, …, n;j=1, 2, …, m}, where x*(i, j) means the i-th sample and the j-th index value while n and m refer to the number of sample city and the amount of evaluating indicators respectively. To eliminate dimension of each index value and unify change range of each index value requires non-dimensional treatment. Projection index is founded by combining the projection pursuit model built by Firedman-Tukey:

$$Q(a) = S(a) * d(a) \quad (1)$$

Compared to the three-dimensional space, the amount of the lost information on the one-dimensional space is less in the course of lowering dimension. Under that situation, the paper selects to lower to the three-dimensional space due to the clustering algorithm of projection pursuit of ICSA. Class separation distance and class density of projection index are referred to S(a) and d(a) respectively while three projection directions of three-dimensional space are indicated as x, y and z, so we have:

$$S(a)=\{\sum_{i=1}^{n}[1-\frac{dx_i\times d\bar{x}+dy_i\times d\bar{y}+z_i\times d\bar{z}}{\sqrt{(dx^2{}_i+dy^2{}_i+dz^2{}_i)\times(d\overline{x^2}_i+d\overline{y^2}_i+d\overline{z^2}_i)}}]/n\}^{\frac{1}{2}} \quad (2)$$

dx, dy, dz refer to the projection characteristic value of x, y, z on three-dimensional space. $d\bar{x},d\bar{y},dz$ are the mean value of dx, dy, dz. If S(a) is bigger, distances between classes are bigger, that is to say, on-class degree of association of original data is smaller. Just like Formula (3), correlation coefficient of any two in-class data is taken as rrk. The bigger rrk is, the denser in-class distribution is. S(rrk-R) is unit speed function. R<rrk,S(rrk-R)=1. Under other situation, values are 0.

$$d(a)=\sum_{i=1}^{n}\sum_{k=1}^{n}r_{rk}s(r_{ik}-R)$$
$$r_{rk}=\frac{dx_i\times d\bar{x}+dy_i\times d\bar{y}+z_i\times d\bar{z}}{\sqrt{(dx^2{}_i+dy^2{}_i+dz^2{}_i)\times(d\overline{x^2}_i+d\overline{y^2}_i+d\overline{z^2}_i)}} \quad (3)$$

The theory of projection index proposed by Friedman-Tukey is the same as the clustering measurement criteria, which means class separation distance and class density are inspected under no supervision. In ICSA, projection index will be the object function counting the antibody affinity. The computational process is displayed below:

$$f=\max Q(a)$$
$$||(a)||=1 \quad (4)$$

In the one-dimensional to three-dimensional projection space of pp algorithm, the paper chooses three-dimensional space so it has three projection directions: ax, ay, az. Hence, ICSA has to successively optimize three groups of initial population generated randomly, that is, ax(k), ay(k), az(k). Individual of each population locates in the same place combines a group, able to describe a group of projection direction. Detailed process of operator is shown as follow:

(1) Clonal Operator. Firstly, it is to set clonal scale---q and then take the projection individual of population as antibody and begin cloning. Hence any individual of the population can be cloned for q times. It is shown in Formula (5):

$$\begin{cases}a_x^c=\{a_x,a_{x1},a_{x2},\ldots,a_{xq}\}\\ a_y^c=\{a_y,a_{y1},a_{y2},\ldots,a_{yq}\}\\ a_z^c=\{a_z,a_{z1},a_{z2},\ldots,a_{zq}\}\end{cases} \quad (5)$$

(2) Mutation Operator. The key step of ICSA is mutation. The mutation of ICSA only affects clonal population and save the original population as antibody. In Formula (6), a_x^m,a_y^m,a_z^m means the individual needing mutation among clonal population. The paper selects three projection direction so the mutation way is to choose a direction for hyper-mutation randomly, where α,β,γ are situated among the random number [0, 1].

$$a_x^m=a_x+\alpha,a_y^m=a_y+\beta,a_z^m=a_z+\gamma \quad (6)$$

(3) Selecting operator, calculating the affinity of population and comparing the differences of affinity of the individual after mutation and the original one. If f(axm)>f(ax), then choose axm;; otherwise, it is ax.

Based on the projection pursuit clustering model of Immune Clonal Selection Algorithm, the flow is shown below:

Normalizing high-dimensional data;

Initializing algorithm parameters, ensuring projection direction randomly and forming initial antibody population;

Exerting linear projection on normalized high-dimensional data;

Optimizing projection index by the application of Immune Clonal Selection Algorithm, achieving the most optimal projection direction;

Linearly projecting high-dimensional data on the most optimal direction, gaining three-dimensional space;
Exerting K-Means clustering on three-dimensional space;
Getting the distance between each point of three-dimensional space and the clustering centre point regarded as the evaluation value.

Experimental Verification

The paper selects IRIS data set and SONAR data set for the test. IRIS data set is four-dimension and has 150 samples while SONAR is sixty-dimension and has 208 samples. One of the data set belongs to high-dimensional data and the other is low-dimensional data. Moreover, the gap of the capability of samples is rather small; hence it applies to the verification of the effect of two kinds of clustering algorithm on high-dimension and low-dimension. After testing, results we have are shown on Figure2 and Figure3:

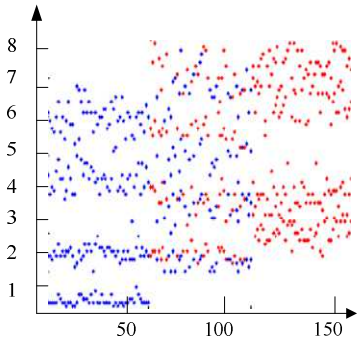

Figure2 PP Clustering of IRIS Data Set

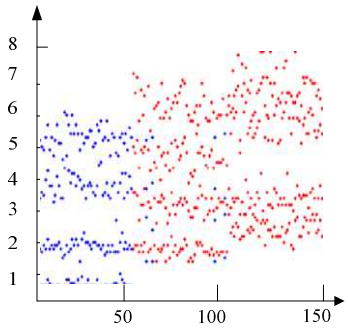

Figure3 K-Means Clustering of IRIS Data Set

The abscissa of clustering diagram represents the types of sample while the ordinate is the value of each dimension of the sample, red and blue being the types of clustering. It is shown that the accuracy of the PP clustering of high-dimension is rather high. So is low-dimension. Compared to the accuracy of data of UCI data set derived from the direct use of K-Means clustering algorithm, the accuracy will become higher by the application of K-Means clustering algorithm after having lowered its dimension.

Conclusion

To build an efficient and unified urban emergency management system is an inevitable choice for a city to enter the modern management. The possible influences of unexpected public events on a city with a larger scale are great, so it needs a more sensitive and efficient emergency management system. The paper studies framework model of urban emergency management system, building a risk rating evaluation model of urban natural disasters. It lowers high-dimension to three-dimension by projection pursuit and during that optimization procedure, it replaces Genetic Algorithm with Immune Clonal Selection Algorithm, accelerating the convergence speed and avoiding local optimization and finally proves the validity of the model been improved.

References

[1] Tang Chengpei. Emergency System and Methods of Unexpected Public Events of Middle-sized and Small Cities[D]. Shanghai: Tongji University, 2007: 111-132.
[2] Tong Zhijun. Study on Integration of Emergency Management and Decision Support of Grassland Fire Disaster[D]. Changchun: Northeast Normal University, 2009: 67-91.
[3] Chen Limei. Perfection Countermeasure of Performance Evaluation on Emergency Management[J]. Journal of Zhengzhou Institute of Aeronautical Industry Management, 2007, 26(3): 195-197.

[4] Wilson J, Yemaiel A O. The evolution of emergency management and the advancement towards a profession in the United States and Florida[J]. Safety Science, 2011（39）：117-131.
[5] Jiao Licheng, Du haifeng. Development and Prospect of the Artificial Immune System[J]. Acta Electronica Sinica, 2003, 31(10): 540-548.
[6] Yin Zhane. Study on Risk Assessment and Demonstration of Urban Natural Hazards[D]. Shanghai: East China Normal University, 2009: 15-67.
[7] Wang Hongwei. Introduction of Emergency Management[M]. China Renmin University Press, 2011.
[8] Chen Wentao. Study on Community Based Emergency Capacity Assessment Indicators System[J]. Chinese Journal of Management Science, 2007: 733-736.
[9] Yang Qing. Comprehensive Capacity Evaluation System of the Urban Disaster Emergency Management Based on Process Management[J]. Chinese Public Administration, 2007, 3(261): 103-104.
[10] Lulu. Comprehensive Evaluation on Fire Prevention Capacity of Urban Public Buildings[J]. Journal of Safety Science and Technology, 2012, 8(12): 68-73.

Advanced Materials Research Vols. 989-994 (2014) pp 5453-5456
© (2014) Trans Tech Publications, Switzerland
doi:10.4028/www.scientific.net/AMR.989-994.5453

Inventory Information Management of Logistics Supply Chain

ZHUANG Zhijie[1,a]

[1]Department of Computer Science and Technology, Tangshan College, Tangshan Hehbei 063000, China

[a]zhuang9889@126.com

Keywords: grey clustering, logistics supply chain, inventory information management

Abstract. The supply chain information management of logistics has become an important method to enhance its competitiveness. The inventory information management and application of the logistics supply is researched based on grey clustering decision-making methods. The inventory theory and methods are studied firstly, and the fuzzy mathematics and grey system theory are used to solve the classification problem. The electronic industry logistics supply chain is taken as the example, the inventory information management problem is solved. The inventory information management theory is improved in this paper, and it can more accurately reflect the market situation, it provides the reference for the classification of inventory information management in logistics supply chain.

Introduction

With the rapid development of logistics industry, the supply chain has played an increasingly important role. The information management of supply chain is becoming as the focus of research in the logistics industry. The complete process of supply chain is the raw material management to the products after each link in the production chain. Through distributors, retailers and transport business process, the products are sent to the customer finally[1]. In the electronic industry, the logistics supply chain research has attracted more and more attention today. The inventory information management is an important part of the whole electronic industry supply chain, and it has an important function in various activities of security and smooth management[2]. Especially, the electronic industry is a special industry with special characteristics, a certain amount of goods should meet the customers with nice goods quality and services, and it can greatly shorten the delivery time for meeting the needs of customers. However, inventory goods need to take great risks, the risks mainly contain the payments and inventory costs risk, as well as the risk of backlog of goods. So the study of inventory classification and the implementation process of chain information management have great theoretical and practical significance. Based on the above analysis, this paper takes the electronic industry logistics supply chain as the research object, the inventory information management of logistics supply chain is researched, and the relative algorithm is designed. The customer satisfaction is taken as the basis, and the fuzzy mathematics and grey system theory are used for solving the classification problem of inventory information management[4,5]. The research result has good application value in supply chain optimization and inventory information management.

Problem description

The electronic industry is special industry, which makes the inventory is becoming more and more important in logistics and supply chain management. In the supply chain, logistics transport process changes the state space of goods, and inventory is changed the goods time state. It plays an important role in modulating every link of the production, and the relationship between production and marketing is adjusted. In addition, it also can greatly shorten the delivery time, reduce costs and increase profits. However, in the electronic industry, different departments have the different attitudes, and transportation procurement can reduce cost and increase inventory levels, inventory information management departments tend to reduce inventory levels. The cost of inventory goods amount is reduced. It shows that inventory information management departments and other

departments have the conflict. There is contradiction between investment of inventory levels and customer satisfaction. With the development of logistics information management technology, the enterprises can solve this problem, and the coordination between the various departments and clients is implemented.

So far, ABC classification method is often used in the inventory information management technology, the method can limit the enterprise resources with biggest effect, at the same time, the goods classification is obtained, and the information management system is designed. Specifically, more and more human and material resources can be put into the relatively expensive items, and the information management is taken. Therefore, the goal is to reduce costs, ensure that the inventory of goods can be managed automatically. However, its defect is obvious, such as a good may itself is not precious materials, we pay no attention to the inventory quantity, but the goods are indispensable parts of the production process. So it is possible result in interruption of production chain and sales chain. It causes greater losses. In addition, this method is subjective without taking into consideration the quality, the inadequate supply and many practical situations are missed.

Model construction

A.Model assumption

The significant characteristics of logistics supply chain is to realize the combination of logistics and human beings, therefore, in the classification of goods inventory information management, how to divide the product, how the allocate the resources, these problems have very important meaning. In the classification of products, involving many different kinds of evaluation index, such as the shortage of supply, customer satisfaction, these indicators are vague and grey, in order to exact these indicators as features, the feature extraction algorithm is researched, and the inventory management of the fuzzy classification is obtained. The gray system theory is introduced in the storage management of goods, if there is a new storage, and the inventory information is counted according to the classification.

In the logistics supply chain, there are many concepts is difficult to define, especially in the electronics service industry, the satisfaction degree of customer is difficult to quantify, and the evaluation of products is difficult to quantify, the indicators are difficult to quantify, they are vague, so the grey clustering decision method is used to analyze the data.

B. Construction of grey clustering decision model

Grey clustering analysis methods can be divided into two types as grey clustering and grey whitening weight function clustering. In the logistics supply chain, mainly using grey clustering method is to simplify the classification system, similar factors is classified. The whitening weight function clustering method is studied to check the goods category according to the standard set before, and the scientific and reasonable classification of the inventory of goods logistics in supply chain is studied.

a.Establishment of the evaluation matrix

First, we need to determine the decision object of supply chain, decision criteria and decision grey. In this paper, assumed that the decision-making object is $i \in I = \{1,2,3,.....m\}$, the decision index is $j \in J = \{1,2,3,.....n\}$, the decision grey classification is $k \in K = \{1,2,3,....w\}$, when the gray is $k = 1$, it means that the supply chain is good, when the decision grey $k = w$, it is bad. According to the decision criteria and decision object, establish the sample matrix $A = \left(x_{ij}, i \in I, j \in J\right)$, where, the sample data.

Because the data sample has different indicators with different dimension, the difference is big, in order to evaluate sample data further, the evaluation matrix is standardized, the formula is:

$$x_{ij}=\begin{cases}\left(d_{ij}-\min\limits_{i}d_{ij}\right)\Big/\left(\max\limits_{i}d_{ij}-\min\limits_{i}d_{ij}\right)\\ \left(\max\limits_{i}d_{ij}-d_{ij}\right)\Big/\left(\max\limits_{i}d_{ij}-\min\limits_{i}d_{ij}\right)\\ 1-\left|d_{ij}-f_i\right/\left|\max\limits_{i}\left|d_{ij}-f_i\right/\right|\end{cases} \tag{1}$$

b. Establish the model

According to the grey decision $k\in K=\{1,2,3,....w\}$, assumed $f_j^k(*)$ is the whitening weight function of clustering index j about k gray class. If the clustering index j is independent on k grey clustering weight, namely clustering weight of clustering index j is $\eta_j(j=1,2,,,,,n)$, and $\sum_{j=1}^{n}\eta_j=1$,then:

$$\eta_j^k=\frac{\lambda_j^k}{\sum_{j=1}^{3}\lambda_j^h},\ \sigma_i^k=\sum_{j=1}^{m}f_j^k(x_{ij})\bullet\eta_j^k \tag{2}$$

The formula as above represents clustering weight of *k* gray about the clustering index *j*, the formula σ_i^k is the clustering coefficient of clustering object *i* belongs to the *k* gray class, after normalization process, the clustering coefficient vector is: σ_3^1, σ_3^2, σ_3^3 ,When $\max\limits_{1\le k\le w}\{\sigma_i^k\}=\sigma_i^{k*}$, it means that the object *i* belongs to the gray *k*.

Example and experiment of the model

In this paper, the electronic industry supply chain is taken as an example for study, the inventory states are taken scientific classification of three kinds of product, the classification of the goal is to reduce the cost, increase profit, and it can be classified from the importance of inventory information management and the cost of products. Based on the data collecting and collating information, the index sample value X_{ij} (i=1.2.3; j=1.2.3;) of i th product is obtained. Therefore, according to the matrix A , we can get the indexes such as price of the products, shortage condition, and customer satisfaction etc, the of can get the, the whitening weight function is shown as follows:

$$A=(1-\lambda t)(1-t)^3,\ A=B_{40}+\tfrac{1-\lambda}{4}B_{41},\ B=\tfrac{3+\lambda}{4}B_{41}+B_{42}+\tfrac{3+\lambda}{4}B_{43},\ C=\tfrac{1-\lambda}{4}B_{43}+B_{44} \tag{3}$$

Analysis as above, we can get: $\sum_{i=0}^{2}b_{2i}=A+B+C=\sum_{i=0}^{4}B_{4i}=1$

Because $\sigma_i^k=\sum_{j=1}^{m}f_j^k(x_{ij})\bullet\eta_j^k$, while $i=1$, we can get:

$$\sigma_1^1=\sum_{j=1}^{3}f_j^1(x_{ij})\bullet\eta_j^1=f_1^1(x_{11})\bullet\eta_1^1+f_2^1(x_{12})\bullet\eta_2^1+f_3^1(x_{13})\bullet\eta_3^1=0.74$$

When $\max\limits_{1\le k\le 3}\{\sigma_1^k\}=\sigma_1^1$=0.74, the results are: $\max\limits_{1\le k\le 3}\{\sigma_2^k\}=\sigma_2^2$=0.74, $\max\limits_{1\le k\le 3}\{\sigma_3^k\}=\sigma_3^1$=0.59

Result analysis

From the above results, with the analysis of the first and third products, it shows that it is a very important grey, while the second product is an important grey. In addition, according to the clustering coefficient, even it belongs to the uniform grey, first products and third products also have the difference, if the segmentation of grey is taken, we will obtain different results. This shows that the grey clustering decision method can improve the efficiency of the inventory information management in supply chain.

Conclusions

In this paper, inventory information management of logistics supply chain is taken as the research object, the inventory theory and related methods are discussed, and the fuzzy mathematics and grey system theory are used to solve the classification problem. The inventory information management theory is improved, and it can reflect the field situation comprehensively. The factors of the customer satisfaction degree and shortage of goods are obtained, and the corresponding improvement measures are proposed. The research result has good application value in practice.

References

[1] GUO Qiu-xia, DENG Xiang-ming, OU Yang-jiang. Evaluation of Value Chain Risks Based on BP Artificial Neural Network[J]. Logistics Technology, 2011; 30(7): 120-122.
[2] JIA An- chao, ZHOU Gang. Study on Selection of Suppliers Based on Rough Set and BP Neural Network[J]. Logistics Technology, 2012, 31(12): 229-232.
[3] LUO Hai-chi, LI Yue-Yang, SUN Jun. Filtering Method for Images Based on Adaptive Neuro-fuzzy Interference System[J]. Computer Science., 2013, 40(7): 302-306.
[4] Zhu Zhen. A Support Vector Machine Algorithm Based on Pretreatment of Neural Network Ensemble[J]. Bulletin of Science and Technology, 2013, 29(4): 26-30.
[5] CHEN Xiu-feng, XU Hongguo, NI An-ning. Dynamic Load Balancing Mechanism and Algorithms in Parallel Microscopic Traffic Simulation[J]. Computer Simulation, 2013, 30(8): 164-168.

Advanced Materials Research Vols. 989-994 (2014) pp 5457-5460
© (2014) Trans Tech Publications, Switzerland
doi:10.4028/www.scientific.net/AMR.989-994.5457

The design of transaction condition expert evaluation system for the logistics online retailers

Geng jihua

ShanDong labor vocational and techncal college, Shandong jinan 250022

Keywords: Electronic-commerce; online retailer; evaluation system

Abstract: With the rapid development of Electronic-commerce, the traditional logistics industry is gradually combined with Electronic-commerce which fully opens the era of logistics online retailer. The basic network platform is the basis of the logistics online retailers. This paper focuses on the establishment of the Electronic-commerce platform with architecture and design techniques. The platform can ensure the stability, efficiency, security, redundancy and scalability of the evaluation system for the logistics industry and economic conditions of the online retailers.

1 Introduction

The logistics industry, integrating the complex new industries such as warehousing industry, freight forwarding industry, has played a crucial role in China's economic development, which also illustrates the national level of comprehensive modernization of a country[1~2]. At present, the development of China's Electronic-commerce logistics information platform stay at the initial stage[3~5]. The logistics online retailers build the logistics Electronic-commerce platform which automatically identify and communicate between human and machine or machine and machine. It can also provide comprehensive awareness, online trading and intelligent recognition which promotes the rapid development of logistics Electronic-commerce[6]. This paper focuses on the establishment of Electronic-commerce platform through architecture design techniques which can ensure the stability, efficiency, safety, redundancy and scalability of the valuation system for the logistics industry and economic conditions of the online retailers.

2 The expert evaluation system model for logistics online retailers

2.1 The online retailer platform model design based on Internet of Things

The logistics Electronic-commerce platform based on Internet technology is faced to the logistics companies, suppliers, manufacturers, retailers, partners, customers, governments and banks. With the Internet technology, the platform can integrate the logistics resources based on logistics market and operation main bodies, optimize the social logistics resource configuration, reduce social logistics costs and provide professional online logistics throughout all aspects of the logistics operation and other value-added online services. The platform is based on the SOA structure and three-tier structure of Internet of Things including six layers of logistics resource layer, data acquisition layer, the network communication layer, data layer, application layer, and user layer.

2.2 The function module analysis for logistics online retailer information service platform

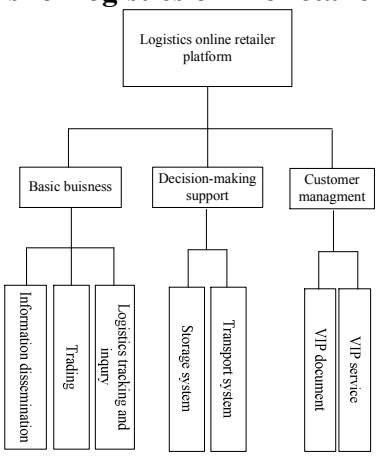

Fig. 1 The function modules for the logistic online retailer service platform

The logistics online retailer information service system mainly consists of three functional subsystems-basic business system, decision support system and customer management system. The basic business system is mainly to maintain the basic business for the logistics online retailer information service system including information dissemination, trading, logistics tracking and inquiry functions. The decision support system provides decision-making support for the logistics online retailer information service system and optimization for many aspects of the logistic service, such as warehouse management and transportation management. The customer management system is a bridge between the system and customers and customer including VIP file management and VIP services. The specific function modules of the system are shown in Fig. 1.

2.3 Evaluation computation equation

The classification super surfaces of the risk transaction potential factors in the Support Vector Machine optimization problem are normalized. Let $\Delta = 1$ and the corresponding compress coefficients are u and k respectively. The corresponding support vectors are expressed by

u·x+k=1, if y=1

u·x+k=-1, if y=-1 （1）

The distances between the support vectors to the classification super surfaces of the potential factors are denoted by 1/||u||. The linear programing function with some constrains is used to classify the potential factors as the equation (2).

$$\min_{u,\ k} \frac{1}{2}\| u \|^2$$

$$z.p.y_i(u \bullet x_i + k) \geq 1,\ \ i = 1,\ \ \ldots,\ \ h. \qquad (2)$$

Based on the optimal principles, the optimal solutions of the objective function with constrains can be obtained. The Lagrange function is described with equation (3).

$$H = \frac{1}{2}\| u \|^2 + \sum_{i=1}^{h} \beta_i [1 - y_i(e \bullet x_i + k)] \qquad (3)$$

In the equation, $y_i(u \bullet x_i + k) \geq 1$ denotes the constrain, $\beta_i \geq 0$ denotes the Lagrange product factor with constrains. With KKT norms, there are:

$$\frac{\partial}{\partial u} H = u - \sum_{i=1}^{h} \beta_i y_i x_i = 0 \Rightarrow u = \sum_{i=1}^{h} \beta_i y_i x_i$$

$$\frac{\partial}{\partial u} H = \sum_{i=1}^{h} \beta y_i = 0 \qquad (4)$$

With Wolf couple principles, the Wolf couple problem with optimization can be expressed by

$$\max_{a} u(\beta) = \sum_{i=1}^{h} \beta_i - \frac{1}{2} \sum_{i,j=1}^{h} \beta_i \beta_j y_i y_j x_i \bullet x_j$$

$$z.p. \sum_{i=1}^{h} \beta y_i = 0. \beta_i \geq 0, i = 1,\ \ \ldots,\ \ h.. \qquad (5)$$

The optimal solutions of the previous equation can be obtained in order to obtain the corresponding super surfaces. If β^{Δ} denotes the optimal solution, β^{Δ} is usually 0; If β^{Δ} is not 0, the corresponding vector x_i is support vector and the linear set for training sample vectors is $u^{\Delta} = \sum_{i=1}^{h} \beta^{\Delta}{}_i y_i x_i$. The support vector of x_ii is randomly selected in order to determine k^{Δ} which is $k^{\Delta} = y_i - u^{\Delta} \cdot x_i$. Finally, the obtained evaluation function is described in equation (6).

$$g(x) = \log al(u^{\Delta} \bullet x + k^{\Delta}) = \log al(\sum_{i=1}^{h} \beta^{\Delta}{}_i y_i x_i \bullet x + k^{\Delta}) \qquad (6)$$

In the equation, log al（·） denotes the sign function with

$$\log al(p) = \begin{cases} 0 & p < 0 \\ 1 & p \geq 0 \end{cases} \qquad (7)$$

By the equation (6), the potential factors can be classified and the classes are used to evaluate corresponding risk conditions.

3 Simulation experiments and results analysis

Take some large scale logistic Electronic-commerce trading platform as an example. The local classification for the logistic Electronic-commerce trading with volume larger than 300,000 is described in Table 1.

Table 1 The classification of main risk factors for a local logistics enterprises

Score	Rank	Transaction volume	Number of transaction	Feedback
0-0.5	Risk out of control	30-50	800-500	0.8-1
0.5-1.2	Major risk	50-60	500-400	0.8-0.9
1.2-1.5	Medium risk	60-70	400-300	0.8-0.6
1.5-2.6	Normal risk	70-50	300-200	0.6-0.7
2.6-3.4	Credit pass	50-80	200-100	0.4-0.6
3.4-4.0	Credit medium	100-150	100-80	0.6-0.5
4.0-4.5	Credit good	150-200	80-50	0.1-0.12
4.5-5.0	Credit excellent	Above 200	50-20	Below 0.1

These factors reflect the area level segmentation of the main relative factors in the logistic online retailers' transaction processes in which the segmentation approaches are random. Therefore, the proportional weights in the overall logistic risk assessment model can describe the fluctuation conditions in the main body. The objective factors have strong operational capabilities and the risks caused by the relative constrain factors are strongly objective which can be quantitatively analyzed to ensure the stability of the overall environment of the E-commerce transactions as shown in Fig. 2.

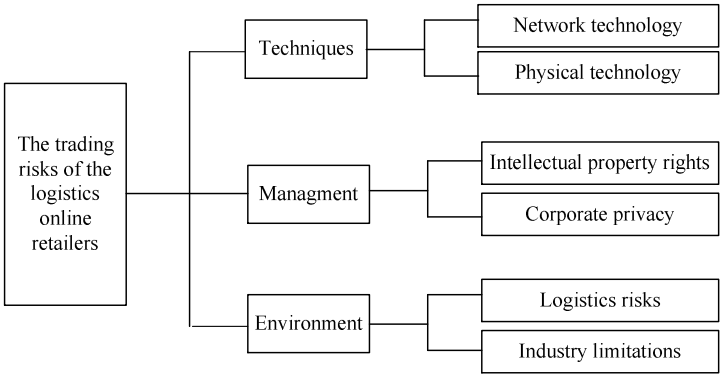

Fig. 2 The trade risks for the logistic online retailers

The comparison experiments evaluate the advantages of the proposed method. The traditional neural network algorithm is used as comparison object. The mean relative errors are used as the experimental evaluation index and results are described as follows.

Table 2 The comparison of prediction performance with different algorithms

Prediction model	MSE	MAE
BP neural network	8.656	0.353
RBF neural network	6.665	0.445
Proposed method	2.433	0.035

The predication results in Table 2 illustrate the proposed algorithm has advantages in the computation speeds and predication accuracy compared with the traditional algorithms because the proposed method can judge the classification penalty factors which can classify different penalty factors with categories. This overcomes the defects of traditional methods which prevent the defects of local minimum and slow convergence speeds in the traditional Support Vector Machine methods.

4 Conclusions

In the Internet era, the online retail platform for the model logistic enterprise is imperative which is beneficial to maximize efficiency and profits. The trading condition expert evaluation for the electronic trading platform is a new technology that can detect potential malicious transactions and reduce harmful transaction. In this paper, the accumulative data during the Electronic-commerce is effectively used to predict future data and evaluate the transaction risks for different level of customers in the future trading. The experiments illustrate the proposed Electronic-commerce risk predication method can predict the security conditions in different online trading with high accuracy which overcomes the shortcomings of traditional methods and it is more suitable for the current network transactions.

References

[1] XiaodongWbng, DavidC.Yen, XiangFang.E-CommereeDeveloPmentinChinaandits ImPlieationforBusiness[J].AsiaPacifieJoumalofMarketingandLogisties, 2004:1011—1015.

[2]Jay Joong-Kun Cho, John Ozment, Harry Sink. Logisties caPability, logisties outsoureing and firm Performanee in an e-eommerce market [J]. International Joumal of Physieal Distribution & Logisties Management, 2008:1034—1038.

[3]Olsen R A. Trust as Risk and the Foundation of Investment Value[J]. The Journal of Socio-economics, 2008, 37(6): 2189-2200.

[4] Jsang A, Ismail R, Boyd C. A Survey of Trust and Reputation Systems for Online Service Provision[J]. Decision Support Systems, 2007, 43(2): 618-644.

[5] Salton G, Yang C S. On the Specification of Term Values in Automatic Indexing[J]. Journal of Documentation, 1973, 29(4): 351-372.

[6] T Bass. Intrusion detection systems and multi-sensor data fusion: Creating cyberspace situational awareness[J]. Communications of the ACM, 2000,43(4):99-105.

Advanced Materials Research Vols. 989-994 (2014) pp 5461-5463
© (2014) Trans Tech Publications, Switzerland
doi:10.4028/www.scientific.net/AMR.989-994.5461

Application of visual correction on physical training

Zhai Qiang

Physical Education College of Luoyang Normal University Henan Luoyang 471022 China

Keywords: irregular; single frame; moving images; dimensional posture; correction

Abstract: A method is presented for three-dimensional motion posture correction employing Fuzzy kernel estimation and affine transformation. As selecting human moving node by a visual sensor and smoothing single frame image with irregular motion, noise interference is reduced. Based on principles of perspective and affine transformation, adjustment strategy of three-dimensional posture is deduced for irregular single-frame motion picture. In addition to determination of motion picture rotation, accurate correction of irregular single-frame motion picture is proposed. Experimental results show that, under different noise conditions, the algorithm corrects posture of a three-dimensional moving image accurately and presents strong anti-noise performance.

1 Introduction

With gradual development of machine vision principle and direction of high-speed, high-precision, high sensitivity sensors, application of monocular vision technology continues to expand, which is hot issues in aerospace, industrial automation, artificial intelligence and other fields[1,2]. Traditional three-dimensional posture correction method[3] is mainly based on analyzing different characteristics of frames. As confusing with noise on non-significant edge, characteristics of irregular single-frame motion image is interfered by noise factors to reduce quality of image characteristic. For this reason, it is impossible to correct posture effectively, there is big drawbacks for tradition method[4,5].

2 Correction of three-dimensional posture

2.1 Selection of physical node

In process of three-dimensional human motion, the most important matter is to collect human characteristics of key nodes. Typically, it is need to divide physical body for motion analysis into several subareas, and set the subareas as a child node of the tree structure. Based on these child nodes, virtual physical body is established to surround tree hierarchy. The hierarchy is searched from a child node of the top; according to top-bottom sequence, all the child nodes constructs a linear collection and calculates bounding box of the linear sets, until root node is obtained. These results are described in Figure1:

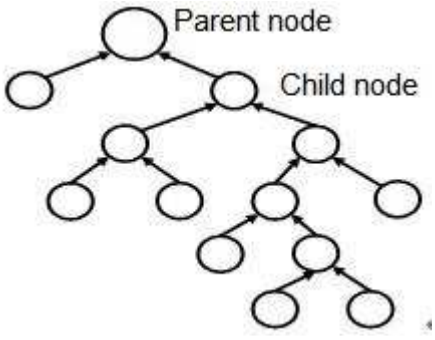

Figure 1 Physical motion characteristics of hierarchical bounding tree

Since it is prone to come into various non-normal contacts between different parts of torso section, independent analysis of these portions are needed. Using the following Figure2, tree hierarchy is described by building all the joints in the body of each tree as a child node:

It is capable of collecting human motion data and capturing body movement, by image-sensing instruments and trajectory tracking device. In data collection, miniature sensors are installed on joints of physical body, which transfers the case of joint motions to control terminal. However, due

to spatial sensor can not capture position of body motion, trajectory tracking device is installed to obtain trajectory of each joint.

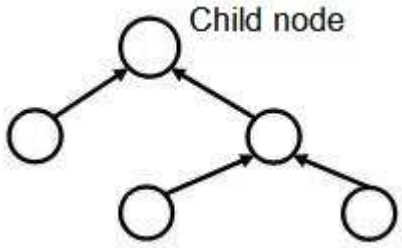

Figure 2 Tree hierarchy of torso section

The relationship between bending movement of physical body and data collected of image sensor can be described by the following equation:

$$b = \frac{\max_b - \min_b}{W_p} * W_d \quad (1)$$

Where b is bending motion of the joint in the body, $\max_b$ is the maximum bending of joint, $\min_b$ is the minimum bending of joints, W_p is the data collected by joint sensor, W_p' is correction factor of data collected by sensor joint. As can be represented by the following formula,

$$W_d = \frac{W_p - U_{\min}}{U_{\max} - U_{\min} \times g} \quad (2)$$

Where $U_{\max}$ is used to describe as upper limit of flexion degree, $U_{\min}$ as lower limit, g is magnification of image data corresponding to sensor acquisition.

2.2 Three-dimensional posture correction method based on affine transformation

When the midpoint of image starts rotated transformation, the transformation matrix can be used to rotate the tilting movement of the image to adjust new three-dimensional posture. As the rotational transformation matrix for adjusting the tilt of the motion picture, the data is summarized into two cases as follows:

（1）If three-dimensional motion posture of the image is tilted to the left, adjust the formula as：

$$\begin{bmatrix} x' \\ y' \\ 1 \end{bmatrix} = \begin{bmatrix} \cos(\theta_1) & -\sin(\theta_1) & 0 \\ \sin(\theta_1) & \cos(\theta_1) & 0 \\ 0 & 0 & 1 \end{bmatrix} \begin{bmatrix} x \\ y \\ 1 \end{bmatrix} \quad (3)$$

Wherein, x, y respectively represent the two-dimensional coordinates of the original image pixel, x', y' respectively represent the two-dimensional coordinates of the adjusted pixel. Corresponding to the adjustment coordinate x', y' and x, y coordinates of the pixel, a new motion picture is reformed as adjusted three-dimensional image.

（2）If three-dimensional motion posture of the image is tilted to the right, adjust the formula as：

$$\begin{bmatrix} x' \\ y' \\ 1 \end{bmatrix} = \begin{bmatrix} \cos(-\theta_1) & -\sin(-\theta_1) & 0 \\ \sin(-\theta_1) & \cos(-\theta_1) & 0 \\ 0 & 0 & 1 \end{bmatrix} \begin{bmatrix} x \\ y \\ 1 \end{bmatrix} \quad (4)$$

In the above formula, θ_1 means angle of image rotation transformation. Depending on the angle deviation, correction is completed.

3 Experimental Analysis

In order to verify effectiveness of this method, relevant experimental analysis is needed. Experimental analysis of traditional methods and corrected method is proposed under different experimental conditions. The three-dimensional motion posture assessment is standard evaluation criteria of image correction method as this paper describes: root mean square error (RMSE), which will assess error between corrected image and original image, the mathematical model is:

$$RMSE = \sqrt{\frac{\sum_{i}^{n} (x_i - y_i)^2}{n}} \tag{5}$$

Where, x, y represent the original image and the corrected image. As the corrected image is similar to the original image, RMSE value is small. In experiment, random noise is added to motion blurred image. As noise gain is defined as the maximum of noise, noise value is [0, noise gain]. When correcting image, set decay rate of the threshold t as 0.1, set regularization parameter γ=10 , λ=0.002 , the image block size as $[6\times6]$.

Figure 3 depicts the effect of noise magnitude on correction results. As the noise intensity increases, RMSE for correction of the image increases slightly. RMSE increase of this method obtained from corrected image, is slower than the conventional image. The method described herein significantly reduces the noise effect.

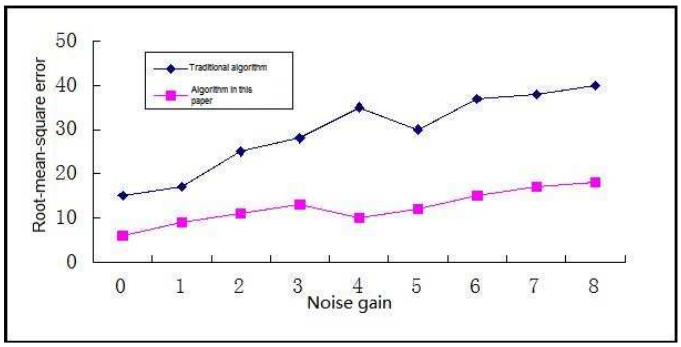

Figure 3 Image correction between methods in different noise gains

4 Conclusions

This paper presents an application of three-dimensional posture correction method based on fuzzy kernel estimation and affine transformations. Combining with the determination of the motion picture rotation, 3D pose of the moving image is adjusted to achieve an accurate three-dimensional motion correction of irregular posture. Experimental results show that, under different noise conditions, the algorithm corrects posture of a three-dimensional moving image accurately and presents strong anti-noise performance.

References

[1] Jiang Guangwen, Huang Zhichao, Fu Sihua, et al. Study on deformation measurement of position and attitude based on monocular vision[J]. Journal of Optoelectronics # Laser. 2009(6):775-775.

[2] Zhao Minghua, You Zhisheng, Liu Zhenfang, et al. Novel face recognition based on 3D model projection[J]. Opto-Electronic Engineering. 2007,34(12): 77-81.

[3] Chen Jiashi, Zhuang Yueting, Zhu Qiang, et al. 3D motion reconstruction from perspective projection[J]. Journal of Computer Aided Design & Computer Graphics. 2002,14(11):1041-1046.

[4] Cai Weike, Wen Gongjian, Xi Fei. A method for pose estimation based on single camera and object model[J]. Journal of image and graphics. 2008(3):513-51.

[5]Zhang Shijie, Cao Xibin, Zhang Fan et al. monocular vision determined algorithm for three-dimensional position and orientation of space target based on feature points [J].Science China: information science.2010(4):591—604.

Advanced Materials Research Vols. 989-994 (2014) pp 5464-5467
© (2014) Trans Tech Publications, Switzerland
doi:10.4028/www.scientific.net/AMR.989-994.5464

Monitoring system of High-power project control network data storm under non-uniform format

LIU Jin[1,a], Dai Yu[1,a], CHEN Jia-jia[1,a]
[1]College of Economics and Management, ChongqingUniversity of Posts and Telecommunications, Chongqing 400065

[a]Liujin@cqupt.edu.cn

Keywords: project control system; network data; monitoring system

Abstract. By analyzing the structure of high-power data project control monitoring system under non-uniform format, the control model and status of the system are introduced. Direct at the requirements of data acquisition machine information exchange and the complete deployment for project control system, medium flow and pressure control, it not only improves the performance of the system, but also makes the system reliable, flexible and easy to expand. Running results show that the proposed system for the realization of high-power project control system data monitoring is valid, the data transmission efficiency significantly higher than traditional serial communications.

Introduction

Project control system is the core part in most large equipment and with complex technical. But because many causes of failures cannot be diagnosed through the device running after the unit shut down [1]. Fault diagnosis at equipment downtime can increase the difficulty of fault detection, fault diagnosis and determination, which delays fault finding, diagnosis and treatment, seriously affects the normal use of the device, and may cause significant economic losses [2]. Establishment of project control system diagnostic system will be very necessary, it can provide a digital signal processor for fault diagnosis of project control system, is a network processing unit which can make high-speed real-time processing when the analog signal transfers into a digital signal [3]. Chip is a high-speed dedicated microprocessor which developed based on ultra large scale integrated circuit technology and computer technology, with powerful computing capabilities and high-speed data transfer capability, can easily handle real-time signal which is main based on computing and not allowed to delay. It can achieve the signal acquisition, conversion, filtering, valuation, enhancement, compression, recognition and other treatments [4, 5].

This paper presents a study design for data monitoring system of the project control system under non-uniform format which is aim at real-time monitoring to power temperature and other parameters of high-power project control system, as well as on-site environment. And it can be transmitted through existing communication networks. All of these can lay a good foundation for fault diagnosis of equipment [6].

Data Monitoring Principles

A.Traditional data monitoring system

MWp standard sub-square building program is used in traditional data monitoring system which is convenient for the construction of project control systems and operations management. Data monitoring system is achieved by making a single configuration data acquisition cabinet in the center control system. The center control system includes data acquisition unit, the ring network switches and other devices. Weakness of the traditional approach is that: 1) Communication Manager is easy to damage, it will cause serious crashes of data monitoring system, affect the reliability of the overall operation of the system; 2) the amount of transfer equipment is too much, communication structure is more complex, direct resulting high failure rate of the data monitoring system, longer time costing of faults troubleshooting and resolution as well as more labor-intensive. All of these will impact the intelligent management, and increase the operating and maintenance costs.

B.The new data monitoring system

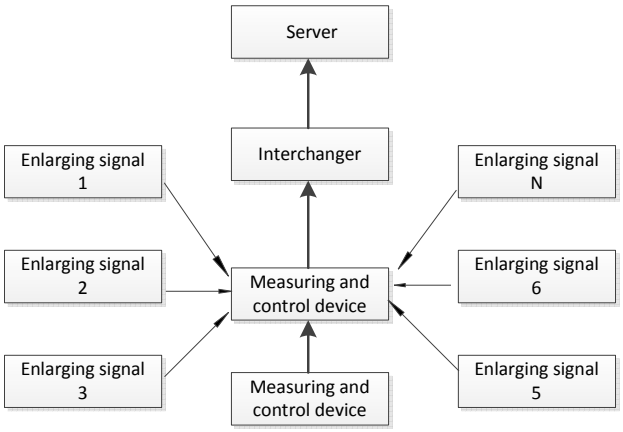

Figure 1 The structure drawing of project control network data monitoring system

With the development of project control networks, it has developed the monitoring and control devices which can make data acquisition, conversion and upload to one. The volume of such devices is small and full-featured. It can achieve the acquisition upload and protection of their own signals, and provide with an integrated data acquisition and expansion interface, which can access a large number of signals and is convenient for all functions such as ring networking, data acquisition, conversion and uploading. Figure 1 shows the structure drawing of project control data monitoring system under non-uniform format based on monitoring and control device constitution.

C.The validation rules of new data Monitoring System

Data validation rules of high-power project control data monitoring system is divided into two categories: 1) correlation validation of single data; 2) the complex correlation verification of multiple data.

For time-continuous data, high-power project control data monitoring platform also uses a more complex but more reliable data verification method, namely the Kalman filtering technique. The state equation and observation equations are:

$$X_k=F_{k,k-1}X_{k-1}+T_{k,k-1}U_{k-1} \quad (1)$$

$$Y_k=H_KX_k+N_k \quad (2)$$

Wherein, X_k and Y_k are the state vector and the observation vector at time k; $F_{k,\,k-1}$ is a state transition matrix; Uk is the dynamic noise at time k; $T_{k,\,k-1}$ is the system control matrix, H_k is the observation matrix at time k; N_k is the observation noise at time k. Pre-estimated by calculating the covariance matrix and the gain matrix and covariance can be applied to detect data mutations. Multi-data complex correlation validation is depended on the management relationship detection between multi-data to test the reasonable of data. Kalman filtering technique is also used to monitor the changes situation of variance in data monitoring platform, which can more accurately judge the bad data.

Simulation and Analysis

the data monitoring platform of a mechanical and electrical equipment is applied as the example. It can be shown in Figure 2 that the design consists of five sub-modules, namely: 1) parameter management module, is responsible for monitoring the parameters setting and managing which is needed for platform; 2) data validation module, is responsible for the verification and screening data to record the check results to log database and provide application calling interface; 3) information monitoring module, is responsible for monitoring the data transfer and calling the interface for data validation check; 4) information notification module, is responsible for sending message according to the monitoring situation; 5) log management module, is responsible for recording the related results of the operation and calibration.

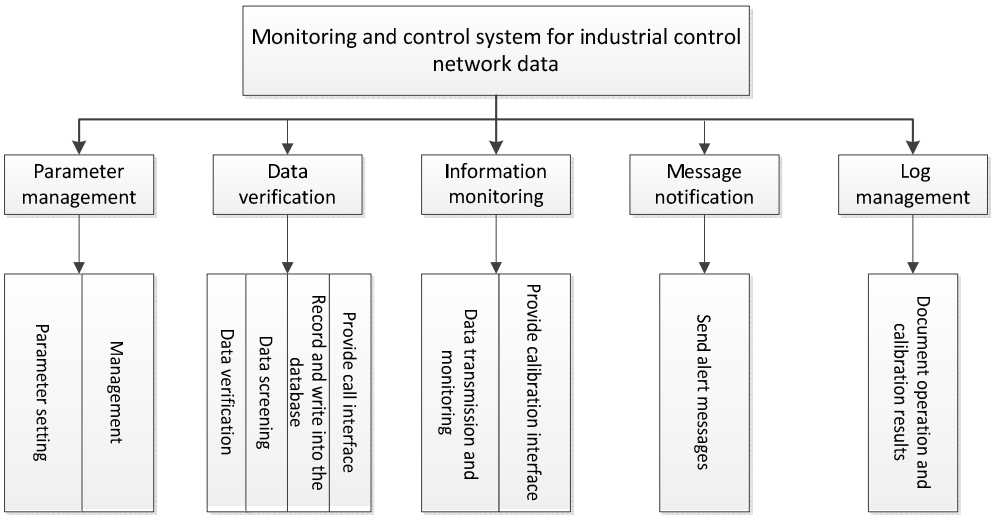

Figure 2 Data monitoring system constitution of project control network

It can be seen from the following three aspects to make conclusion:

(1) construction cost savings

the dimensions of Non-uniform data format project control monitoring device (width × depth × height) is about 200mm × 200mm × 200mm. Compared with the original equipment layout, it can at least reduce 3.2m^2 construction area, and the construction cost of per square meter is about 3,000 Yuan, a total construction costs of 19.2 million of 20 sub-matrices can be reduced.

(2) equipment cost saving

in traditional scenario, data acquisition system is 31,000 Yuan/set, and control devices is about 8000 Yuan/set, rather than the 20,000 Yuan/set of a monitoring device under uniform format project control data monitoring system. That means the equipment cost savings of 380,000 Yuan. As can be seen from the above analysis, the non-uniform data format project control monitoring system can save about 57 million in construction and equipment costs.

(3) The measured frequency, temperature and voltage from a unit will be described as an example in Table 1:

Table 1 The data of frequency, temperature, and voltage in a unit

	frequency	Temperature of generator bearing	Temperature of engine bearing	Enclosure temperature of unit	line voltage AB	line voltage BC	line voltage AC
standard value	200	43.2	41.9	29.8	230	230	230
test value	200	42.8	41.3	29.7	230	229	230
standard value	200	52.6	50.6	28.5	220	220	220
test value	200	51.9	49.8	28.5	221	220	220

From the above data, it can reflect the changes of a unit voltage and other parameters in a process of operation, and we can see that the frequency error is zero, voltage accuracy is 1V, the temperature accuracy degree is 0.1 ℃. All of these can basically meet the resources needs of electrical and mechanical equipment monitoring system.

Conclusions

Data storm monitoring system of High-power project control network under non-uniform format is the basic platforms part of the project control network data monitoring systems. Through a unified management of data validation and alert of all aspects of data processing, it can control and ensure data accuracy and reliability.

To solve the complex data screening and verification problems of project control network data monitoring system through the high-power project control network data storm monitoring system platform under non-uniform format can make effective management for network data. It can ensure the stable and efficient operation of multi-level project control network system, and promote the practical work of project control network data monitoring system. It is also the foundation and

important part of successful construction and efficient coordination operation of multi-level industrial control network.

Acknowledgement
The Teaching Reformation Key Project of Chongqing Education Commission（132004，1201004）

References

[1] Hadoush A and Boogaard A H V D. Efficient implicit simulation of incremental sheet forming[J]. International Journal for Numerical Methods in Engineering， 2012， 90（5）:597–612.

[2] Kim J， Kang S-J， and Kang B-S. A comparative study of implicit and explicit FEM for the wrinkling prediction in the hydroforming process[J]. The International Journal of Advanced Manufacturing Technology， 2003， 22（7–8）:547–552.

[3] Oliver J， Huespe A E， and Cante J C. An implicit/explicit integration scheme to increase computability of non-linear material and contact/friction problems[J]. Computer Methods in Applied Mechanics and Engineering， 2008， 197（21–24）: 1865–1889.

[4] Noels L， Stainier L， and Ponthot J-P. Energy conserving balance of explicit time steps to combine implicit and explicit algorithms in structural dynamics[J]. Computer Methods in Applied Mechanics and Engineering， 2006， 195（19–22）:2169–2192.

[5]Rao Yutai,Yang fan. Network Intrusion Stir the Network Instability Control Methods of the Research[J]. Bulletin of Science and Technology, 2014, 30(1):185-188.

Advanced Materials Research Vols. 989-994 (2014) pp 5468-5471
© (2014) Trans Tech Publications, Switzerland
doi:10.4028/www.scientific.net/AMR.989-994.5468

The Research on the Six Sigma Management Integrated System Design Based on Minitab/DDE

Ting-Hua Huang[a], Shu-Hai Fan[b,*] and Lan-Juan Dong[c]

Nanjing University of Technology (Jiangpu Campus, P. O. Box No. 184), Jiangsu Province, China

[a]huangtinghua90@126.com, [b,*]sf507@cam.ac.uk, [c]donglanjuan618@163.com

Keywords: Six Sigma Management; Minitab; DDE; Integrated System.

Abstract: As a systematic and quantitative mode of continuous improvement, six sigma management can thoroughly analyze the problem and solve it based on the data. This article proposed a framework of six sigma management integrated system based on Minitab/DDE and applied it in the practical problem. This system supports us to access the daily production data through the DDE link dynamically and interactively, ensuring the timeliness and validity of project analysis to achieve continuous improvement.

Introduction

Six sigma management is an improving philosophy and method invented by Motorola Inc [1]. The detail implementation mode is DMAIC, which refers to Define, Measure, Analyze, Improve and Control [2]. As a systematic and quantitative mode of continuous improvement, six sigma management can analyze the problem quantitatively based on the data, to identify the process defects and then solve it practically [3-5].

However, the daily production data of enterprise is not only enormous, but it also updates fast. The simple process analysis by statistical software can not ensure the timeliness of data and validity of result. Therefore, the six sigma management integrated system is proposed to create the DDE (Dynamic Data Exchange) link between statistical software Minitab and database, supporting the project analysis by effective real-time data sharing, thus to enhance the competitive advantage in delivery time and multiple varieties of enterprise.

The overall framework of integrated system

Six sigma management integrated system based on Minitab/DDE takes the five stages DMAIC of six sigma improvement mode as the core. The bottom of the system is that Minitab creates DDE link to support the process analysis by the real-time access of production data. And it is applied to the practical project at the top level. Through these, a continuous improved system based on six sigma management is formed as Fig. 1.

(1) By creating a DDE link, Minitab can share the information with any external program which also has DDE function. Click *Edit>Worksheet Links>Manage Links* in Minitab to create a new link and then input *application, topic, item* and some other terms in the popup dialog. The rule of each term is shown in Table 1. Then the real-time and dynamic data transmission between Minitab and DDE containers such as Excel can be realized to support the process analysis of six sigma management.

(2) Unlike the traditional solution “define - improve”, six sigma management has a whole set of improving system, that is, defining the key issue, ensuring the effectiveness of measurement system, analyzing the causes of defects, determining the improving plan, and verifying and maintaining the improvement. Therefore, the application of six sigma management in the practical project can effectively identify the problem thoroughly and achieve continuous improvement.

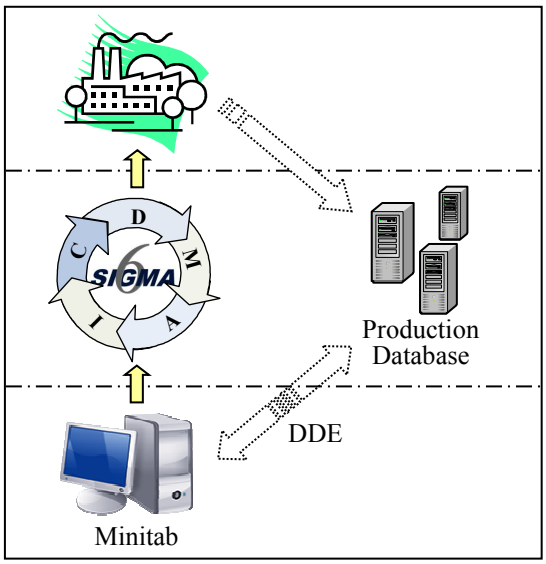

Fig. 1: The overall framework of integrated system

Table 1: Inputting rules of Minitab creating the DDE link

Term	*Explanation*	*Example*
Application	Application name	Excel
Topic	File name (if the file contains several windows, use brackets)	C:\ [Book1.xls]Sheet1
Item	Rows/columns or matrix area imported	R1C1:R8C10
Status	Status of the links	Active/Inactive
Priority	Priority of the worksheets	1~32 (high-low)
Update method	Way of the data transmitting to the worksheet in Minitab	Replace/Append
Anchor Column	Beginning column of the data	1
Action	Anticipated operations after the data transmitting to the Minitab	Update data and execute commands/ Update data only/Execute commands only
Commands	Anticipated commands after the data transmitting to the Minitab	(Action is: Update data and execute commands/Execute commands only)

Application example

Integrated system based on Minitab/DDE is proposed to design the six sigma management system for the quick changeover project of a key line in a motor manufacturing plant. Through the DDE function of Minitab accessing the production data, the process analysis can be supported to shorten the changeover time and lower the production cost.

Define Create the Minitab/DDE link (Fig. 2) to access the daily production report to collect the changeover data of each line in the first half of year 2013. Average changeover time of each line in the first half of year 2013 is as: (1) Turning, 108.2min; (2) Rotor Winding, 46.2min; (3) Stator Winding, 41.0min; (4) Rotor Assembly, 36.8min; (5) Motor Assembly, 34.4min; (6) BS shield Assembly, 25.1min; (7) Oven, 9.8min. Among them, changeover time of turning machine is the longest. So we choose the turning machine as the research object in the six sigma project.

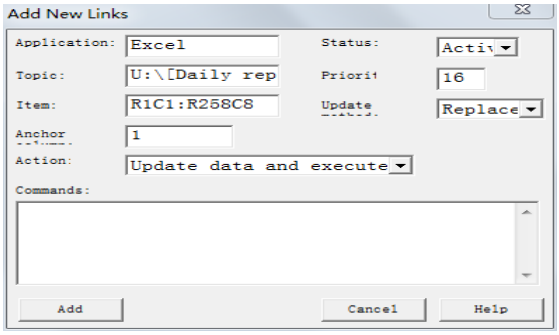

Fig. 2: DDE link of Minitab accessing the changeover data

Measure In the motor manufacturing process, turning machine is used to lathe the bearing hole in the middle and four location holes on the diagonal of AS (top) shield and BS (bottom) shield. And the usual measurement is completed by Coordinate Measuring Machine.

Select the CTQ (Critical to Quality) "Cutting depth from bearing hole to the diagonal" of AS shield as the measuring object. Let three quality checkers measure the 20 different shields twice respectively to do the Repeatability & Reproducibility analysis of gage.

According to the R&R analysis from Minitab, Coordinate Measuring Machine can be accepted.

Analyze According to the changeover process of AS shield, which is Preparation, Changeover, Checking/Debugging and Measuring, the project members analyze the possible causes from 5M1E (Man, Machine, Material, Method, Measurement, Environment) through brainstorming.

The problems mainly focus on the Changeover and Checking/Debugging:

(1) Changeover. ①The improper cooperation of two changeover workers led to the long changeover waiting and we should reallocate the actions of workers; ②It is difficult for workers to distinguish the various types of wrenches, so we take multifunctional wrench into consideration.

(2) Checking/Debugging. The Poor positioning calibration and low pass rate of "bounce from the bearing hole to the bearing turning surface" make workers to debug repeatedly and produce several pieces of scrap. To this, we may improve the craft equipment and use MAHR meter to check the locating seat of bearing hole respectively.

Improve Do the DOE (Design of Experiment) for the problems above to confirm the feasibility of the recommendations. Levels of each factor are as Table 2.

Table 2: Levels of each factor

	Lever 1	*Lever 2*
Factor A: Changeover actions	A1	A2
Factor B: Wrench	B1: Multifunctional wrench	B2:Various types of wrenches
Factor C: Craft equipment	C1: Position by MAHR meter	C2: Keep the original craft equipment

In the Table above, *A1* refers to: Dismantle and install two clamping jaws (worker X), dismantle and install one clamping jaw (worker Y), dismantle the base of UM (Y), install the base of BLDC (X), dismantle the tool rest of UM (X), install the tool rest of BLDC (X); *A2*: Dismantle and install two clamping jaws (X), dismantle the tool rest of UM (Y), install the tool rest of BLDC (X), dismantle and install one clamping jaw (worker Y), dismantle the base of UM (Y), install the base of BLDC (Y).

Besides, if the improvement of Factor C works, the problem of poor positioning can be solved and the quality of the shield also can be improved.

Create the Taguchi Design by Minitab to do the experiments. As the response variables are smaller-the-better, the SN ratios are larger-the-better and the Means are smaller-the-better. The best match is A2B1C1, that is, using the second changeover process, adding the multifunctional wrench and positioning calibration with the aid of MAHR meter.

Control The maintenance of the improvement is crucial for the project in the control stage. Not only should it standardize and document the improving process, but it also needs to build a long-term process control system to achieve continuous improvement. To this, DDE function of Minitab is more useful to realize the real-time track, identifying and guiding the secondary improvement.

Create the DDE link by adding a new link. The session command is shown as Fig. 3.

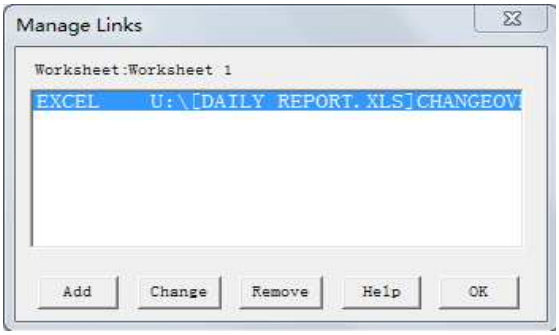

Fig. 3: DDE link command of Minitab accessing the changeover record

Access 40 changeover records in the last month and draw the Mean-Standard Deviation control chart. The points in the chart arrange randomly and are all in the limits. The mean value is 47.89min. It can be believed that changeover records are in the state of statistical control. The changeover time has reduced and stays stable. Further improvement can be achieved by the technical progress. If the points are out of limits or arrange non-randomly, abnormal causes should be analyzed. And control chart should be drawn after the improvement to determine whether the process is in control or not.

Conclusions

This paper designed the six sigma management system for the practical project based on the Minitab/DDE integrated system. This system supports the real-time interactive access to the production data to analyze the process, thus to achieve the continuous improvement of six sigma management and enhance the competitiveness of enterprises.

Acknowledgements

This work was supported by National Natural Science Foundation of China (Grant No. 71171110 and No. 71371097).

References

[1] Lin Ma and Zhen He: Six Sigma Management (Chinese People's University Press, Beijing 2007).
[2] Pyzdek T: The Six Sigma Handbook (McGraw-Hill, New York 2003).
[3] Biao Xiang and Tongjun Chen: The Combination and Practice of Lean Production and Six Sigma Management. Shanghai Quality. Vol. 1 (2012), p. 66~69.
[4] Yuqian Wang, Shuhai Fan and Mimi Pan: Application of process quality improvement in assembly of magnetic system based on Minitab. Machinery Design and Manufacture. Vol. 1 (2012), p. 62~64.
[5] Zhihao Du and Hui Li: The improvement of spot-welding process quality based on DMAIC and orthogonal experiment. Machinery. Vol. 6 (2013), p. 13~17.
[6] Werner A J. Schippers: An integrated approach to process control. International Journal of Production Economics. Vol. 1 (2001), p. 93~105.
[7] Jeroen de Mast and Joran Lokkerbol: An analysis of the six sigma DMAIC method from the perspective of problem solving. International Journal of Production Economics. Vol. 2 (2012), p. 604~614.

Advanced Materials Research Vols. 989-994 (2014) pp 5472-5475
© (2014) Trans Tech Publications, Switzerland
doi:10.4028/www.scientific.net/AMR.989-994.5472

Research on the Specialization and Theory of Building Engineering

Zhijun Zhang[*1,a]

[1]Harbin University, Harbin 150086, People's Republic of China

[*a]zzj-zy@vip.sina.com

Keywords: Building Engineering; Specialization; Theory

Abstract. Architectural engineering, also known as building engineering, is the application of engineering principles and technology to building design and construction. Definitions of an architectural engineer may refer to an engineer in the structural, mechanical, electrical, construction or other engineering fields of building design and construction; a licensed engineering professional in parts of the United States; in informal contexts, and formally in some places, a professional synonymous with or similar to an architect. Structural engineering involves the analysis and design of physical objects (buildings, bridges, equipment supports, towers and walls). Those concentrating on buildings are responsible for the structural performance of a large part of the built environment and are, sometimes, informally referred to as "building engineers".

Introduction

Structural engineering is a field of engineering dealing with the analysis and design of structures that support or resist loads. Structural engineering is usually considered a specialty within civil engineering, but it can also be studied in its own right.

Structural engineers are most commonly involved in the design of buildings and large no building structures but they can also be involved in the design of machinery, medical equipment, vehicles or any item where structural integrity affects the item's function or safety. Structural engineers must ensure their designs satisfy given design criteria, predicated on safety (e.g. structures must not collapse without due warning) or serviceability and performance (e.g. building sway must not cause discomfort to the occupants).

Structural engineering theory is based upon physical laws and empirical knowledge of the structural performance of different materials and geometries. Structural engineering design utilizes a number of simple structural elements to build complex structural systems. Structural engineers are responsible for making creative and efficient use of funds, structural elements and materials to achieve these goals [1].

Structural Engineers

Structural engineers are responsible for engineering design and analysis. Entry-level structural engineers may design the individual structural elements of a structure, for example the beams, columns, and floors of a building. More experienced engineers may be responsible for the structural design and integrity of an entire system, such as a building.

Structural engineers often specialize in particular fields, such as bridge engineering, building engineering, pipeline engineering, industrial structures, or special mechanical structures such as vehicles, ships or aircraft [2].

Structural engineering has existed since humans first started to construct their own structures. It became a more defined and formalized profession with the emergence of the architecture profession as distinct from the engineering profession during the industrial revolution in the late 19th century. Until then, the architect and the structural engineer were usually one and the same - the master builder. Only with the development of specialized knowledge of structural theories that emerged during the 19th and early 20th centuries did the professional structural engineer come into existence.

The role of a structural engineer today involves a significant understanding of both static and dynamic loading, and the structures that are available to resist them. The complexity of modern structures often requires a great deal of creativity from the engineer in order to ensure the structures support and resist the loads they are subjected to. A structural engineer will typically have a four or five year undergraduate degree, followed by a minimum of three years of professional practice before being considered fully qualified. Structural engineers are licensed or accredited by different learned societies and regulatory bodies around the world (for example, the Institution of Structural Engineers in the UK). Depending on the degree course they have studied and/or the jurisdiction they are seeking licensure in, they may be accredited (or licensed) as just structural engineers, or as civil engineers, or as both civil and structural engineers. Another international organisation is IABSE (International Association for Bridge and Structural Engineering). The aim of that association is to exchange knowledge and to advance the practice of structural engineering worldwide in the service of the profession and society [3].

History of Structural Engineering

Structural engineering dates back to 2700 B.C.E. when the step pyramid for Pharaoh Djoser was built by Imhotep, the first engineer in history known by name. Pyramids were the most common major structures built by ancient civilizations because the structural form of a pyramid is inherently stable and can be almost infinitely scaled (as opposed to most other structural forms, which cannot be linearly increased in size in proportion to increased loads).

However, it is important to note that the structural stability of the pyramid is not primarily a result of its shape. The integrity of the pyramid is intact as long as each of the stones is able to support the weight of the stone above it. The limestone blocks were taken from a quarry near the build site. Since the compressive strength of limestone is anywhere from 30 to 250 MPa, the blocks will not fail under compression. Therefore the structural strength of the pyramid stems from the material properties of the stones from which it was built rather than the pyramid's geometry.

Throughout ancient and medieval history most architectural design and construction was carried out by artisans, such as stone masons and carpenters, rising to the role of master builder. No theory of structures existed, and understanding of how structures stood up was extremely limited, and based almost entirely on empirical evidence of 'what had worked before'. Knowledge was retained by guilds and seldom supplanted by advances. Structures were repetitive, and increases in scale were incremental.

No record exists of the first calculations of the strength of structural members or the behavior of structural material, but the profession of structural engineer only really took shape with the Industrial Revolution and the re-invention of concrete. The physical sciences underlying structural engineering began to be understood in the Renaissance and have since developed into computer-based applications pioneered in the 1970s.

Structural Failure

The history of structural engineering contains many collapses and failures. Sometimes this is due to obvious negligence, as in the case of the Pétionville school collapse, in which Rev. Fortin Augustin said that “he constructed the building all by himself, saying he didn’t need an engineer as he had good knowledge of construction” following a partial collapse of the three-story schoolhouse that sent neighbors fleeing. The final collapse killed 94 people, mostly children.

In other cases structural failures require careful study, and the results of these inquiries have resulted in improved practices and greater understanding of the science of structural engineering. Some such studies are the result of forensic engineering investigations where the original engineer seems to have done everything in accordance with the state of the profession and acceptable practice yet a failure still eventuated. A famous case of structural knowledge and practice being advanced in this manner can be found in a series of failures involving box girders which collapsed in Australia during the 1970s.

Specialization

Building Structures

Structural building engineering includes all structural engineering related to the design of buildings. It is the branch of structural engineering that is close to architecture. Structural building engineering is primarily driven by the creative manipulation of materials and forms and the underlying mathematical and scientific ideas to achieve an end which fulfills its functional requirements and is structurally safe when subjected to all the loads it could reasonably be expected to experience. This is subtly different from architectural design, which is driven by the creative manipulation of materials and forms, mass, space, volume, texture and light to achieve an end which is aesthetic, functional and often artistic.

The architect is usually the lead designer on buildings, with a structural engineer employed as a sub-consultant. The degree to which each discipline actually leads the design depends heavily on the type of structure. Many structures are structurally simple and led by architecture, such as multi-storey office buildings and housing, while other structures, such as tensile structures, shells and grid shells are heavily dependent on their form for their strength, and the engineer may have a more significant influence on the form, and hence much of the aesthetic, than the architect.

The structural design for a building must ensure that the building is able to stand up safely, able to function without excessive deflections or movements which may cause fatigue of structural elements, cracking or failure of fixtures, fittings or partitions, or discomfort for occupants. It must account for movements and forces due to temperature, creep, cracking and imposed loads. It must also ensure that the design is practically buildable within acceptable manufacturing tolerances of the materials. It must allow the architecture to work, and the building services to fit within the building and function (air conditioning, ventilation, smoke extract, electrics, lighting etc.). The structural design of a modern building can be extremely complex, and often requires a large team to complete.

Earthquake Engineering Structures

Earthquake engineering structures are those engineered to withstand earthquakes. The main objectives of earthquake engineering are to understand the interaction of structures with the shaking ground, foresee the consequences of possible earthquakes, and design and construct the structures to perform during an earthquake. Earthquake-proof structures are not necessarily extremely strong like the El Castillo pyramid at Chichen Itza shown above. In fact, many structures considered strong may in fact be stiff, which can result in poor seismic performance. One important tool of earthquake engineering is base isolation, which allows the base of a structure to move freely with the ground.

Civil Engineering Structures

The structural engineer is the lead designer on these structures, and often the sole designer. In the design of structures such as these, structural safety is of paramount importance (in the UK, designs for dams, nuclear power stations and bridges must be signed off by a chartered engineer).

Civil engineering structures are often subjected to very extreme forces, such as large variations in temperature, dynamic loads such as waves or traffic, or high pressures from water or compressed gases. They are also often constructed in corrosive environments, such as at sea, in industrial facilities or below ground.

Mechanical Structures

Principles of structural engineering are applied to variety of mechanical (moveable) structures. The design of static structures assumes they always have the same geometry (in fact, so-called static structures can move significantly, and structural engineering design must take this into account where necessary), but the design of moveable or moving structures must account for fatigue, variation in the method in which load is resisted and significant deflections of structures.

The force which is parts of a machine is subjected to can vary significantly, and can do so at a great rate. The force loaded on a boat or aircraft are subjected to vary enormously and will do so thousands of times over the structure's lifetime. The structural design must ensure that such structures are able to endure such loading for their entire design life without failing.

Aerospace Structures

Aerospace structure types include launch vehicles, (Atlas, Delta, Titan), missiles (ALCM, Harpoon), Hypersonic vehicles (Space Shuttle), military aircraft (F-16, F-18) and commercial aircraft (Boeing 777, MD-11). Aerospace structures typically consist of thin plates with stiffeners for the external surfaces, bulkheads and frames to support the shape and fasteners such as welds, rivets, screws and bolts to hold the components together.

Nanoscale Structures

A nanostructure is an object of intermediate size between molecular and microscopic (micrometer-sized) structures. In describing nanostructures it is necessary to differentiate between the numbers of dimensions on the nanoscale. Nanotextured surfaces have one dimension on the nanoscale, i.e., only the thickness of the surface of an object is between 0.1 and 100 nm. Nanotubes have two dimensions on the nanoscale, i.e., the diameter of the tube is between 0.1 and 100 nm; its length could be much greater. Finally, spherical nanoparticles have three dimensions on the nanoscale, i.e., the particle is between 0.1 and 100 nm in each spatial dimension. The terms nanoparticles and ultrafine particles (UFP) often are used synonymously although UFP can reach into the micrometer range. The term 'nanostructure' is often used when referring to magnetic technology.

Structural Engineering Theory

Structural engineering depends upon a detailed knowledge of applied mechanics, materials science and applied mathematics to understand and predict how structures support and resist self-weight and imposed loads. To apply the knowledge successfully a structural engineer generally requires detailed knowledge of relevant empirical and theoretical design codes, the techniques of structural analysis, as well as some knowledge of the corrosion resistance of the materials and structures, especially when those structures are exposed to the external environment. Since the 1990s, specialist software has become available to aid in the design of structures, with the functionality to assist in the drawing, analyzing and designing of structures with maximum precision; examples include AutoCAD, StaadPro, ETABS, Prokon, Revit Structure etc. Such software may also take into consideration environmental loads, such as from earthquakes and winds.

References

[1] G. D. Shaffer: J Fiel Archaeol. Vol. 20 (1993), p. 59

[2] W. Sandermann, R. Kohler: Holzforschung. Vol. 18 (1964), p. 53

[3] R. C. Weatherwax, H. Tarkow: For Prod J. Vol. 14 (1964), p. 567

[4] M. Hachmi, A. A. Moslemi and A. G. Campbell: Wood Sci Technol. Vol. 24 (1990), p. 345

[5] Z. Hong, A. W. C. Lee: For Prod J. Vol. 36 (1986), p. 87

[6] A. Demirbas, A. Aslan: Cement Concrete Res. Vol. 28 (1998), p. 1001

[7] W. Y. Ahn, A. A. Moslemi: Wood Sci. Vol. 13 (1990), p. 77

[8] S. Pushkar, R. Becker and A. Katz: Build Environ. Vol. 40 (2005), p. 1126

[9] Y. S. Lee, D. A. Guerin: Build Environ. Vol. 45 (2010), p. 1104

Advanced Materials Research Vols. 989-994 (2014) pp 5476-5480
© (2014) Trans Tech Publications, Switzerland
doi:10.4028/www.scientific.net/AMR.989-994.5476

The Construction of the Agricultural Products Traceablity Code System Based on a Type of Barcode Technology

ZHAO YAN[1, a], ZHENG GUANG [2,b]

[1] International Education College of Henan Agricultural University, No 63, Nongye Road, ZHENGZHOU City, Henan Province, China

[2]College of Information and Management Science, Henan Agricultural University, No 63,Nongye Road, ZHENGZHOU City, Henan Province, China

[a]suzannezhao@163.com, [b]ggzan0215@sina.cn,

Keywords: PDF417, two-dimensional barcode, agricultural products, Traceability code system

Abstract. Using Visual Basic as the development platform, the agricultural products traceability code system was constructed based on the PDF417 two-dimensional bar code technology through the embedded c++ dynamic link library (DLL) in the paper. The system implemented the expression of the related information for agricultural products origin, agricultural products, certification types, agricultural products processing enterprises, production date, shelf life of agricultural products and so on. Through the effective traceability of agricultural products, the requirements of the consumers to agricultural product quality were satisfied by the system.

Introduction

Currently, the problem of food safety increasingly aroused people's concern[1]. The establishment of the agricultural products quality safety traceability system and the realization of the "from farm to table" whole process of tracking management and quality control provided the possibility of solving the problem of food safety from the sources[2-3].Applying the modern information technology in agricultural product traceability system, the efficient agricultural products traceability information platform was established using the two-dimensional bar code PDF417 bar code technology. The establishment of the complete traceability system of agricultural product quality safety in the process of agricultural production and processing could solve the problem of food safety fundamentally and further improve the quality of agricultural products in China.

PDF417 two-dimensional barcode

The development of PDF417 barcode. The PDF (Portable Data File) 417 invented by the Doctor WangYinjing was a type of layered, continuous and length variable 2 dimensional barcode. In the barcode, each symbol character is made up of four vertical bars and four spacing. If the narrowest vertical bar or spacing of barcode was called a module, the total number of the modules of the above four vertical bars and four spacing must be 17. Therefore, the barcode was called “417” code or PDF417 code. The top and bottom of the barcode were both blank area. The multilayer structure was located between the upper and lower blank area. Each layer was right and left justified and connected directly. The minimum number of the layers was 3. The largest number of layers was 90. The number of data characters in each row was same. The well-determined start character and terminate character were expressed by the 81111113 and 71111121 separately and not included in the scope of coding.

The characters of the PDF417 barcode. As a portable data files, the PDF417 barcode was widely used in logistics, manufacturing, postal service, library management, and other industries. The features of the barcode as follow:

Large capacity of information: In addition to letters, Numbers and ASCII characters, PDF417 code could also express a binary number. To make the code more compact and improve the information density, the PDF417 bar code can be used three formats in the coding: extensional alphanumeric

compressed format (can hold 1850 bytes), binary/ASCII format (can hold 1108 bytes) and digital compression format (can accommodate 2710 figures).
Strong error correction ability and confidentiality: PDF417 barcode which adopted the world's most advanced RS error correction technology could not only prevent the wrong reading and improve decoding reliability effectively, but also retrieval the missed information due to the bar code damage and pollution in a large extent.
Wide scope of coded information: PDF417 barcode could be used for coding for a variety of text, images, and biometric information such as fingerprint, palmprint and voice coding and had extensive application scope.
Easy printing and durable: PDF417 barcode was easy to manufacture and had low costing. The printing requirement of it was also not high. It could be printed on paper, CARDS and various kinds of commonly used barcode carrier employing ordinary printing devices. Moreover, the barcode should not be restricted to the number of times of read card.
The flexible methods of read: The PDF417 barcode could be identified through software after collecting data by the devices such as general camera or scanner.
Public code system: The PDF417 barcode had formed the international standard. In China, the national standard (GB/T 17172-17172) of the PDF417 barcode had formulated.

The coding design of agricultural products

The Characteristics of the agricultural product coding. To realize detailed traceability of the key information of the agricultural products, the formulating of the trace code set was the one of the most important step. To meet the constantly updated needs and practical requirements of the Chinese agricultural product traceability, the agricultural product traceability system must have the following features:
The unity of the traceability information: Unique coding was a basic principle of coding. It meant that the same objects should be assigned the same identification code and the different objects should to share the identity of the code. Once the identification code was distributed, it should try to remain the same as long as the basic characteristics of the identified object had not changed
The universality and maturity of the traceability technology: The universality generally referred to the coding can be applied and identified in the national and even global scope. The implementation of the encoding, especially for the coding used in the trade between the two parties, should adopt international standards as far as possible and follow the international standards in order to improve the commonality of the coding in the world.
The stability and maintainability of the traceability system: The condition that the code resources would not be run out in the future for a long time must be ensured. Even though the code resource was exhausted in some applications, it was must facilitate the expansion for the developers. In the case of must changing the coding, the recoding must to be realized under the condition that changed the original code as less as possible.

The composition of the agricultural products code. To achieve the traceability of the agricultural products, the agricultural products code should contain related information such as the source area, products, certification types, processing enterprises, manufacturing date, and shelf life.
The construction of agricultural products traceability code: As shown in Table 1, the agricultural products traceability code was constructed by the source area code, the processing enterprise code, the product code, the product certification type code, the manufacturing date code and the expiration date code and represented by the 31 digital code and 2 Chinese characters in this paper.
Products source area code designing: Products source area referred to the location of the agricultural planting and breeding. The source area code should be able to identify the comprehensive and detailed information of the planting plots or aquaculture area of the agricultural products. In the “encoding rules of source area of Chinese agricultural products” (the standard number: NY/T 1430-2007) which issued and implemented by the ministry of agriculture, the source area code was expressed by 20 digits. However, in this system, the source area code was designed as follow: The code for the county or higher level administrative division was expressed by the first 6 digits of the

administrative area code. The code for the street agency, town, township and village was represented by the Chinese characters.

Table 1 Construction of agricultural products traceability code

Code	*Digits*	**Chinese characters**
Products source area	6 digital codes for county or city	Geographical Names
Processing enterprises	6 digital codes for position of enterprises	Enterprise name
Products	5 digital codes	
Certification type	1 digital code	
Manufacturing date	6 digital codes	
Expiration date	6 digital codes	
Eerror correction	1 digital code	

Product processing enterprises code designing: The enterprises which process the agricultural products were identified employing product processing enterprises code. Due to the name of the enterprise which registered within the same administrative division could not be repeated, the location code of the products processing enterprises were indicated by the administrative division codes. The enterprise names were represented in Chinese characters.

Products code designing: The products code identified the agricultural products themselves based on the basic properties information of them including the types, names, varieties and so on. In this paper, the product code coded the agricultural products depending on the classes (using 1 digit), categories (using 2 digits) and product names (using 2 digits) of the agricultural products according to the basic characteristics of agricultural information. The varied and complex classes of the agricultural products referred to the primary products or processed products of various kinds of animals and plants produced by planting, breeding, aquaculture, animal husbandry, forestry and so on. According to the traditional customs, the agricultural products could be divided into seven major classes which were grain, vegetables, fruits, flowers, forest products, animal products, aquatic products and other sideline products and represented using 1 digital code. There were different corresponding categories in each class of the agricultural products. For example, according to the characteristics of agricultural biology, the vegetable class could be further divided into: cabbage, Chinese cabbage, melons, beans, edible fungus, mustard, tap root, tuber, solanaceous fruit, onion garlic, green leafy vegetables, perennial vegetables, aquatic vegetables and so on. Moreover, each category also had corresponding different genus or varieties. The genus or varieties of each category of agricultural products could be expressed as commodity name or product name. For instance, the cabbage category of the vegetable class also included cabbage, cauliflower, broccoli, turnip cabbage and so on. Therefore, during encoding the classification of agricultural products, the commodity name of the agricultural products could be used as coding object directly and uniformly and coded by 2-digital code in the agricultural product code. The 2-digital code had 99 kinds of coding set totally which was enough for further extending and reserving.

Date code designing: Date code was used to identify the production date and keeping date of the agricultural products. In the "general principles for prepackaged food labels" (GB7718-2004, mandatory national standards), the production date was clearly defined as the date of the food was processed to final product [9]. In this system, the data code was coded adopting the traditional data presentation and recorded as YYMMDD. In this 6-digital data code, YY, MM and DD expressed the year, month and date respectively. The range of MM code was 01 to 12 and denoted January to December of one year. The range of DD code was 01 to 31 and denoted each day of one mouth.

Certification type code designing: At present, the agricultural product certification types in China mainly included 3 types: the pollution-free agricultural products certification, the green agricultural product certification and the organic agricultural products certification. The other types of the

agricultural products certification which was not included in above three types could be classified as "other agricultural product certification" and represented using 1 digital code.

System implementation

The design of agricultural products traceability code system. Employing the VB as development platform, the system was established through embedded Access database and VC DLL. The flow chart of the system was shown as Figure 1:

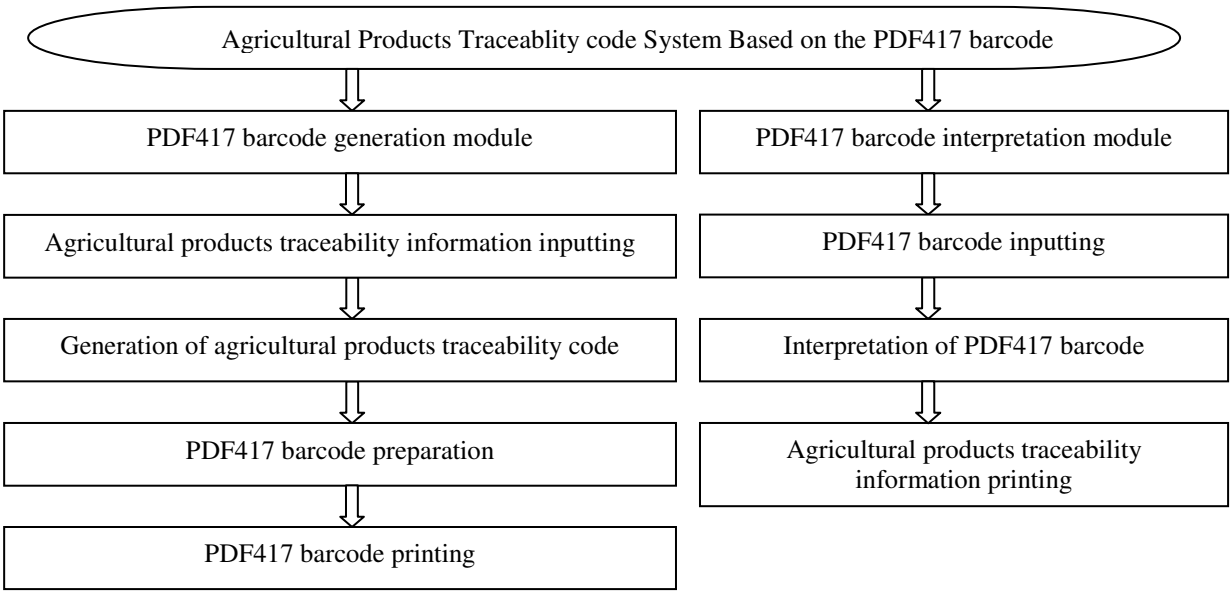

Figure 1 The flow chart of system structure

Database design: Using Access, the related database of the agricultural products traceablity code system was established. The database which consisted of the products source area code table, products code table, certification type code table, administrative district and division code table was implemented to code the agricultural products data. Under the environment of VC, the PDF417 encoding and decoding application programs were written based on PDF417 two-dimensional barcode coding principle and the coding scheme of the agricultural products traceability code described in this paper. After that, the dynamic link library (DLL) also was generated to encode the organized coding information of the agricultural products to the PDF417 barcode.

Agricultural products information inputting: The information of agricultural products such as source area, manufacturing enterprise location, enterprise name, types of product certification, product category, product name, production date and expiration date was entered in the textbox of the main interface of the system. At the same time, this information of agricultural products was produced into a text file and stored in the current folder. The text file would be loaded in the text box of the main interface of the system during the system operating.

Agricultural products code generation: Click on the code generation button on the main interface, the system would classify the data on the basis of the agricultural products information in the textbox and further form a code generation interface. On the interface, the agricultural products information could be altered. After confirmation, press the save button, the agricultural products information code would be generated.

PDF417 barcode generation: Press the barcode generation button, the PDF417 barcode of the agricultural products would be generated call the coding program of dynamic link library (DLL) and displayed in the picture box of the system main interface.

Barcode analysis: Press the graphics file button on the main interface, the PDF417 barcode image saved as the bitmap (BMP) file would be imported in the picture box of the system main interface. Press the barcode analysis button next, the system would call the decoding program of the dynamic link library (DLL) and resolve the PDF417 barcode. The analytical would be shown in the text box at top right-hand corner of the system main interface.

Summary

The agricultural products traceablity code system based on the PDF417 barcode was constructed in this paper. The system standardized the coding and decoding process of the PDF417 barcode of the agricultural products. The operation interface of the system was simple and easy to use. At the same time of satisfying the general requirements of enterprises, the system also considered of the features of the corresponding enterprise and would be widely used and popularized.

References

[1] Shuo WAN, Xifeng ZHANG, Ping XIA and Dong FENG. The research and application of agricultural product quality safety traceability system[J]. Liaoning Agricultural Sciences, 2011, (5): 68-71.

[2] Fangquan MEI. The development and analysis about the concept of the food security control[J]. Food and Nutrition in China, 2002, (5): 4-6.

[3] Yanqing CHENG. The characteristics of the America's food recall system[J]. World Agriculture, 2002, (10): 16-18.

[4] Qinying DOU, Qing YAO. The development and application of the barcode technology[J]. Computer Engineering and Science, 2003, (5): 50.

[5] Xing ZHOU, Xinting YANG, Shanqin WANG, Jianping QIAN and Chuanheng SUN. The Design and Implementation of the Information Management System of the Standardized Production Base for the Agricultural Products based on MapObjects in Beijing [J]. Chinese Journal of Agricultural Resources and Regional, 2008, (1): 36-40.

[6] Xuexin LIU, Xinting YANG, Jianping QIAN, Zengtao JI and Chuanheng SUN. The Construction of the Coding System of the Aquatic Product Quality Traceability System Based on Breeding Process [J]. Agriculture Network Information, 2008, (1): 18-21.

[7] Xinting YANG, Jianping QIAN and Zheng ZHANG. The Coding Design of the Agricultural Products Traceablity Code Based on the Geographic Coordinates and Multiple Encryption[J]. Transactions of the Chinese Society of Agricultural Engineering, 2009, 52(7):131-135.

[8] Hua YU, Zhenhua WU. The coding research of the Agricultural Products Traceablity Code [J]. Agricultural Sciences in China, 2011, 44(23):4801-4806.

Advanced Materials Research Vols. 989-994 (2014) pp 5481-5485
© (2014) Trans Tech Publications, Switzerland
doi:10.4028/www.scientific.net/AMR.989-994.5481

Research on Designing the Information Management Platform of Physical Education based on B/S Model

Guoying Wang

Sports Department, Henan University of TCM, Zhengzhou, 450008, China

Keywords: B/S framework; VB programming; PE; Management platform; Communication port; Editor; LED display

Abstract: This paper, by using multi-layer B/S framework model, combines with VB programming to carry out innovative design of physical education (PE) platform, which has got the B/S framework platform of PE management. PE information management platform mainly comprises the teacher end, the central processor unit (CPU) and the student end, where the communication interface mainly comprises the editor and the computer, and the input of teacher end includes the computer buttons, sensors, and so on. While for the core parts of the system, they are the CPU and the memory demonstrated by PE. Student end through the I/O expansion function analyzes and displays the teaching sound and video signal displayed by using LED or LCD. Finally, the paper designs the data analysis and transfer function of PE information platform, and obtains the curve of information throughput with time changing, which provides a new computer method for the research of PE.

Introduction

The principle of B/S framework-based data mining algorithm is mainly with the membership function to search for the correlation of data[1,2]. In the design of PE information platform, the management and analysis of student performance data is one of the most important parts to be designed. Using the data mining theory can realize the layering and sorting of data. For the sorted data, it can use B/S framework model to make information statistics, then it can eventually obtain the correlation between local data and the overall data, so as to provide theoretical guidance for the PE [3,4]. It can use the membership function to analyze student performance data, where the expression form of the membership function is as shown in formula (1).

$$P(y)=\frac{y-m}{M-m}. \tag{1}$$

Where M denotes the maximum value of student performance, and m denotes the minimum value of student performance. The calculation expressions of the output performance data processing are as shown in formula (2).

$$\begin{aligned} x_{m,\frac{n}{2}} &= \sum_{i=-M+n}^{n} b_{i-n}, d_{m+1,i} \\ y_{m,\frac{n}{2}} &= \sum_{i=-M+n}^{n} u_{i-n}, d_{m+1,i} \end{aligned}. \tag{2}$$

The sorting formula of student performance can be expressed as the formula (3).

$$f_{o,p}{}^{(n)} = f_{o,p}{}^{(n-1)} - [\sum_{o} u_{o,p+1}{}^{(n)} G_p{}^{(n)} + \frac{1}{2}]. \tag{3}$$

Where G_p denotes the sorting coefficient of B/S framework-based data algorithm, it can eventually obtain student performance of multi-level B/S framework-based data structure model, and the equation is as shown in formula (4).

$$\begin{array}{l} G_{p1}^{\ i} \quad \ldots \quad G_{p}^{\ i}{}_{n/2i} \\ \quad \ldots \\ G_{p1}^{\ 2} \quad \ldots \quad \ldots \quad G_{p}^{\ 2}{}_{n/2i} \\ G_{p1}^{\ 2} \quad G_{p2}^{\ 2} \quad \ldots\ldots\ldots \quad G_{pn}^{\ 1} \\ \Rightarrow \quad \Rightarrow \quad \Rightarrow\Rightarrow\Rightarrow\Rightarrow\Rightarrow\Rightarrow\Rightarrow\Rightarrow\Rightarrow . \\ S1 \quad S2 \quad \ldots\ldots \quad \ldots \quad \ldots\ldots \quad \ldots\ldots \quad S_n \end{array} \tag{4}$$

Where S denotes the level and the number of calculation of the algorithm. The student performance is carried out the data analysis by using VB program in this paper, and the used main program algorithm is shown as follows.

```
#include <stdio.h>
void main()
{float x,y(float c),a,b;
  a=-10;
  b=10;
  do
  {x=(a+b)/2;
       if (y(a)*y(x)<1e-10) b=x;
       else a=x;}
  while (a-b>0.00001);
  printf("x=%f,\n\n",x);}
float y(float c)
{float z;
  z=2*c*c*c-4*c*c+3*c-6;
  return(z);}
```

Application Research of Computer in the Design of PE Management Platform

In order to verify the validity and reliability of the mathematical model and the algorithm for performance management designed in the second part in this paper. The algorithm is debugged by using VB programming software, and it finally obtains the applicability of the B/S framework model by using the correlation of multiple groups of user's mode debugging data[5,6].

	A	B	C	D
1	**User name**			
2	2013010151			
3	2013010152			
4	2013010153			
5	2013010154			
6	2013010155			
7	2013010156			
8	2013010157			
9				

Fig. 2 Design of student user management

As shown in Figure 2, the student ID without blank lines in the student course selecting list is saved, and the saved path is on the "username" that is in the "imp_stutolesson_demo" file [7]. It can quickly upload student course list by using the function, finally, the course list of Excel file can be imported to the corresponding network teaching course.

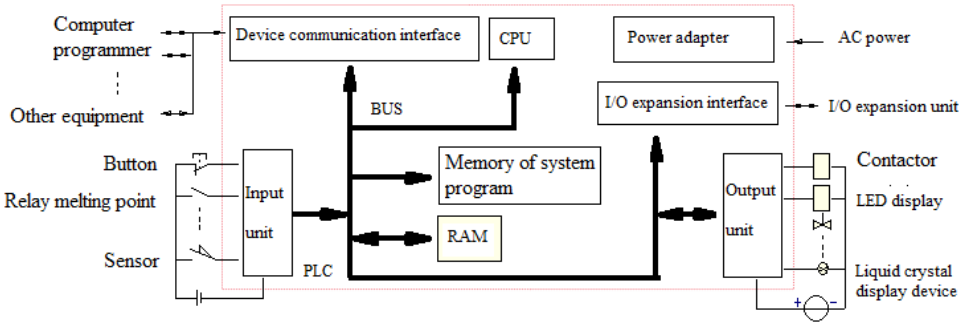

Fig. 3 Schematic diagram of computer and circuit port

Figure 3 shows the schematic diagram of computer and data interface of circuit. The communication interface mainly comprises the editor and computer. The input unit includes computer buttons, sensors, and so on. The core parts of the system include the central processing unit and the memory demonstrated by PE [8]. With the expansion function of I/O, teaching management information platform transmits the teaching sound and video signals through the device, and after the signals are delivered to the student end, that are displayed by using LED or LCD.

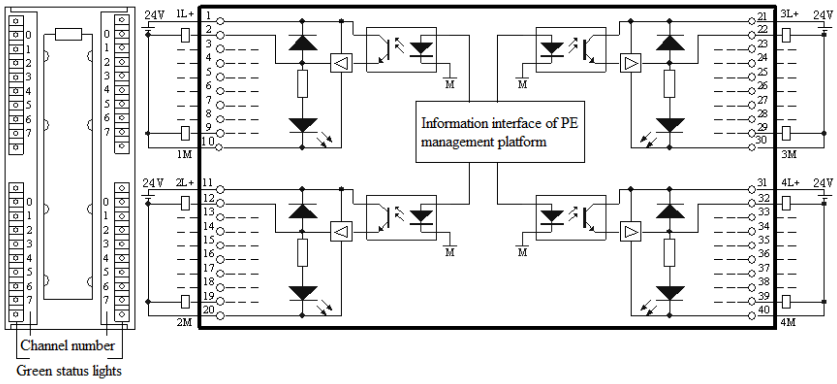

Fig. 4 The internal circuit and external terminal wiring diagram of the output module from digital transistors

Figure 4 shows the internal circuit and external terminal wiring form of the output module from digital transistors. With the use of this circuit connection, it can realize processing of mass data, at the same time, teacher end can realize teaching information upload, and student end can realize the save function of student information.

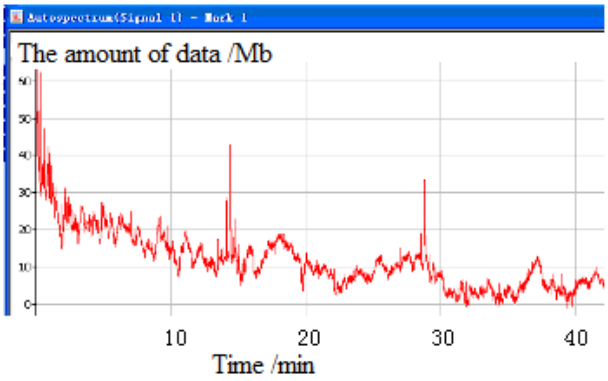

Fig. 5 The process of data transmission

Figure 5 shows the process of data transmission. It can be seen from the chart, the amount of data transmission is obviously different at different time, which shows that the used function and the number of users are different at different times, when the users use the teaching information management platform [9]. It can be seen from Figure 5 that the system function is in normal operation, and there is no amount of data overflow or negative.

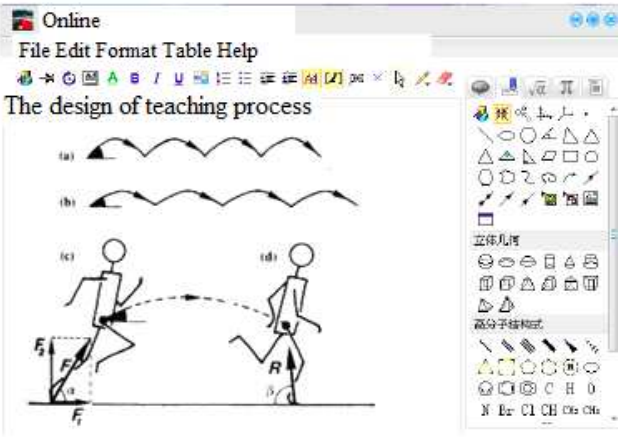

Fig. 6 Visual function of teaching system interface

As shown in Figure 6, visual function of teaching interface mainly includes the drawing, data transmission and redrawing . In the process of image drawing, the user can draw graphs of various forms by using the brush function, and the image can be presented to students in real time by using the information transmitting device.

Table 1. Association membership table

Performance level	Range	Value
Fail	Min-B1	B1
Good	B1-B4	B2
		B3
		B4
Excellent	B3-max	B4

Table 1 shows the association membership table of student performance designed by using PE information management platform. With the use of B/S framework model, it can make classification statistics on student performance, and with the correlation function, it can study the correlation of student performance data, so as to find the influence of student partial performance on the overall performance, which can provide a theoretical reference for the PE process.

Conclusion

This paper established B/S framework mathematical model of data mining algorithm and combined with VB programming algorithm to carry on the design of PE information platform. Finally, it obtained a new sorting method of PE performance, and the algorithm realized the correlation analysis of student performance. The teacher end, the central processor and the student end of PE information management platform were respectively designed, and the function of platform was design by using the central processing unit, the memory and I/O expansion functions. Based on these, it obtained multifunctional PE management platform. The paper carried out the design of correlation for teaching performance by using PE information management platform, which had provided technical support for the research of PE.

Reference

[1] Qian Yue, Shan Feng. Systematically analysis of calculation performance for genetic algorithm [J]. Chinese Journal of computers, 2011, 32(12): 2389-2392.

[2] Junhua Li, Ming Li, Lihua Yuan. The pseudo parallel genetic algorithm based on clustering [J]. Pattern recognition and artificial intelligence, 2012, 22(2): 188-194.

[3] Jian Zhuang, Qingyu Yang, Haifeng Du, Dehong Yu. High efficient complex system genetic algorithm [J]. Journal of software, 2010, 21(11): 2790-2801.

[4] Shouwen Chen, Mingdong Li. An improved genetic algorithm and its simulation [J]. Computer Applications and Software, 2010, 27(9): 100-102.
[5] Kang Wang, Xuesong Yan, Jian Jin, Zhigang Zhan. An improved genetic K-means clustering algorithm [J]. Computer & Digital Engineering, 2010, 38(1): 18-20.
[6] Biao Wang, Chanlun Duan, Hao Wu, Yonggang Song. Research and application of rough sets and fuzzy sets [M]. Beijing: Publishing House of electronics industry, 2012: 1-8.
[7] Guohui Li, Hui Chen, Bing Yang. Prediction query algorithm for data flow based on probabilistic model [J]. Computer science, 2011, 35 (4): 66-69.
[8] Anlong Chen, Changjie Tang, Chang'an Yuan, Mingfang Zhu. Compression algorithm for multi-data stream based on Wavelet and coupling characteristics [J]. Journal of software, 2011, 18(2): 177-184.
[9] Xueling Zhu, Jun Lan, Shouqi Li, Yan Jia. Anomaly detection for data stream based on tensor decomposition [J]. Computer engineering and science, 2013, 31(6): 75-78.

Advanced Materials Research Vols. 989-994 (2014) pp 5486-5490
© (2014) Trans Tech Publications, Switzerland
doi:10.4028/www.scientific.net/AMR.989-994.5486

Study on the Construction of Linguistics Examination Database based on Computer Network Technology

Yuan Zhang

School of Foreign Languages, Jiangsu University of Science and Technology, Zhenjiang, 212003, China

Keywords: VB software; English linguistics; Network examination database; Feedback system; Distortion; Network teaching

Abstract. In this paper we use the VB software to programming the group program of tests, combined with neural network residual training principle, establish optimization design model of network examination database. We improve the English linguistics question bank based on computer network technology by using the program and the model, and set up the feedback system of students' suggestion and Corporate Data Stores system of examination paper, and establish optimization model of network examination database. In order to verify effectiveness and reliability of network test optimization system, we optimize the network examination database of English Linguistics for three times, obtain the optimal distortion curve of test, and analyze optimized test scale. It provides technical support for the research of network English teaching.

Introduction

In recent years, with the extension of network application, the computer is getting close with educational fields. Paperless electronic paper is a new method to deepen the reform of education and promote innovation teaching. The computer network examination database greatly improves the efficiency of examination, saving a lot of teaching resources, but the construction of network examination database is still at primary stage, many problems still remain to be perfect [1, 2]. Combined with the neural network residual training method, we use the VB software technology to design the optimization system of computer network technology English examination database, and use three optimizations to optimize the network examination database. It provides a new method for application of computer in English teaching and network education.

Application of Computer Network Technology in the Construction of English Examination database

With the development of Internet and information technology, network examination database is widely used in English teaching. The question bank not only can save a lot of resources, but also make the teachers and students to make full use of network source, improving efficiency of teaching and learning, enhance the students' self-study ability [3, 4]. In this paper, we use the VB software to optimize the design of English network examination database, and apply the computer in the English linguistics examination. The design process of examination database is as shown in Figure 1.

Figure 1 shows the network examination database optimization flow chart of English linguistics. From it we can see, by VB software it can realize several optimizations of English network examination database, and the optimization is t tree distribution [5]. After one optimization we can get $ST1, ST2, \cdots, STn$; after two optimizations we can get $ST11, ST12, \cdots, ST1n$; after n optimizations we can get the optimal model of examination database, the convergence residual of examination database is the lowest, distortion of test is lowest, and the effect of network test is the best.

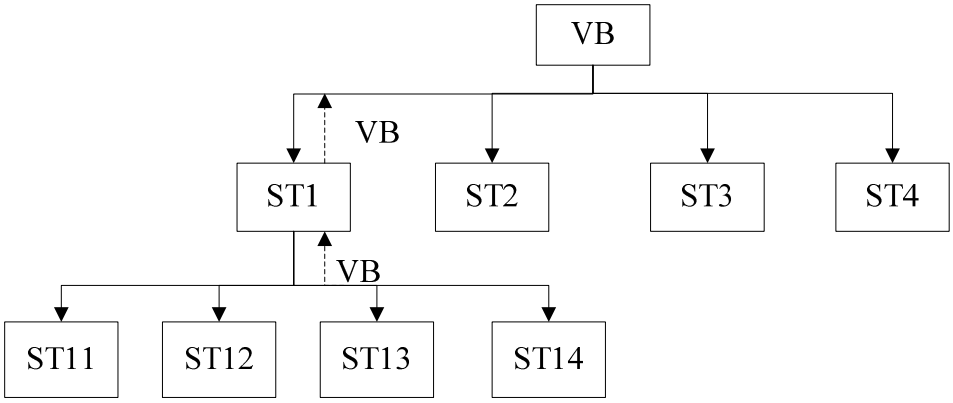

Fig. 1 Network examination database optimization process

The Mathematical Model and Algorithm Design of English Linguistics Examination database

In order to optimize the English linguistics examination database and accelerate the convergence speed, we improve the calculation model using the first order difference quotient. First defining the parameters of initialization examination database x_0, after modifying parameter of examination database is x_1 [6, 7]. So, one order difference quotient can be written as shown in formula (1).

$$P(x_0, x_1) = \frac{P(x_1) - P(x_0)}{x_1 - x_0}. \tag{1}$$

The two order training difference quotient is defined as:

$$P(x_0, x_1, x_2) = \frac{P(x_0, x_2) - P(x_0, x_1)}{x_2 - x_1}. \tag{2}$$

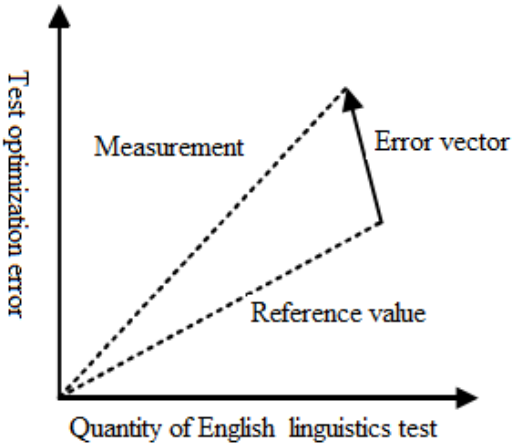

Fig. 2 Optimization model of English linguistics test

As shown in Figure 2 it represents optimization model of English linguistics test. According to the reference quantity and test quantity, we can do two order difference quotients training on English linguistics examination database [8]. The deviation table in computer is as shown in formula (3).

$$\begin{cases} F_{i0} \Leftarrow P(x_i) \quad , \qquad i = 0,1,...,n \\ F_{ij} \Leftarrow (F_{ij-1} - F_{i-1\,j-1})/(x_i - x_{i-j}), \quad j = 1,2,...,n. \quad i = j, j+1,...,n \end{cases}. \tag{3}$$

According to the definition of difference quotient, data x can be seen the point between $[a,b]$ in English linguistics examination database, so we can get:

$$P(x_0,x) = P(x_0,x_1) + P(x_0,x_1,x)(x-x_1),$$
$$\cdots$$
$$P(x) = P(x_0) + P(x_0,x\ )(x-x_0) \quad . \tag{4}$$
$$P(x_0,\ldots x_{n-1},x) = P(x_0,x_1,\ldots,x_n) + P(x_0,\ldots,x_n,x)(x-x_n)$$

Based on the neural network model of English linguistics examination database, we use the VB software to design the examination database. The main program of VB is as shown follows:

```
#include <stdio.h>
void main()
{void average(float *p,int n);
    void search(float (*p)[4],int n);
    float score[3][4]={{65,67,70,60},{80,87,90,81},{90,99,100,98}};
    average(*score,12);
    search(score,2);}
void average(float *p,int n)
{float *p_end;
    float sum=0,aver;
    p_end=p+n-1;
    for (;p<=p_end;p++)
        sum=sum+(*p);
    aver=sum/n;
    printf("average=%5.2f\n",aver);}
oid search(float (*p)[4],int n)
{int i;
    printf("the score of NO.%d are:\n",n);
    for (i=0;i<4;i++)
        printf("%5.2f",*(*(p+n)+i));}
```

Research on Examination Database Design of English Linguistics based on Computer Network

In order to verify the effectiveness and reliability of the English linguistics network examination database optimization model and VB program, we use the design of network linguistics examination database as an example to analyze the optimization effect of network examination database [9]. Before the examination database optimization we need to set the variable environment of ActiveX control, as shown in Figure 3.

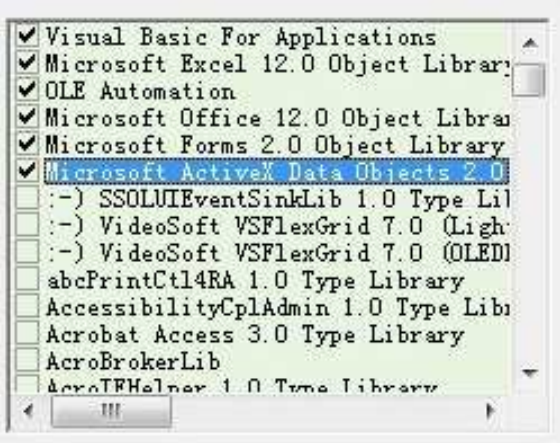

Fig. 3 Variable settings of ActiveX control

As shown in Figure 3 it represents variable setting of ActiveX control. Using Microsoft ActiveX Data Objects2.0, we design the space variable environment, and connect it with Web Server, and establish the optimization platform of English linguistics examination database as shown in Figure 4.

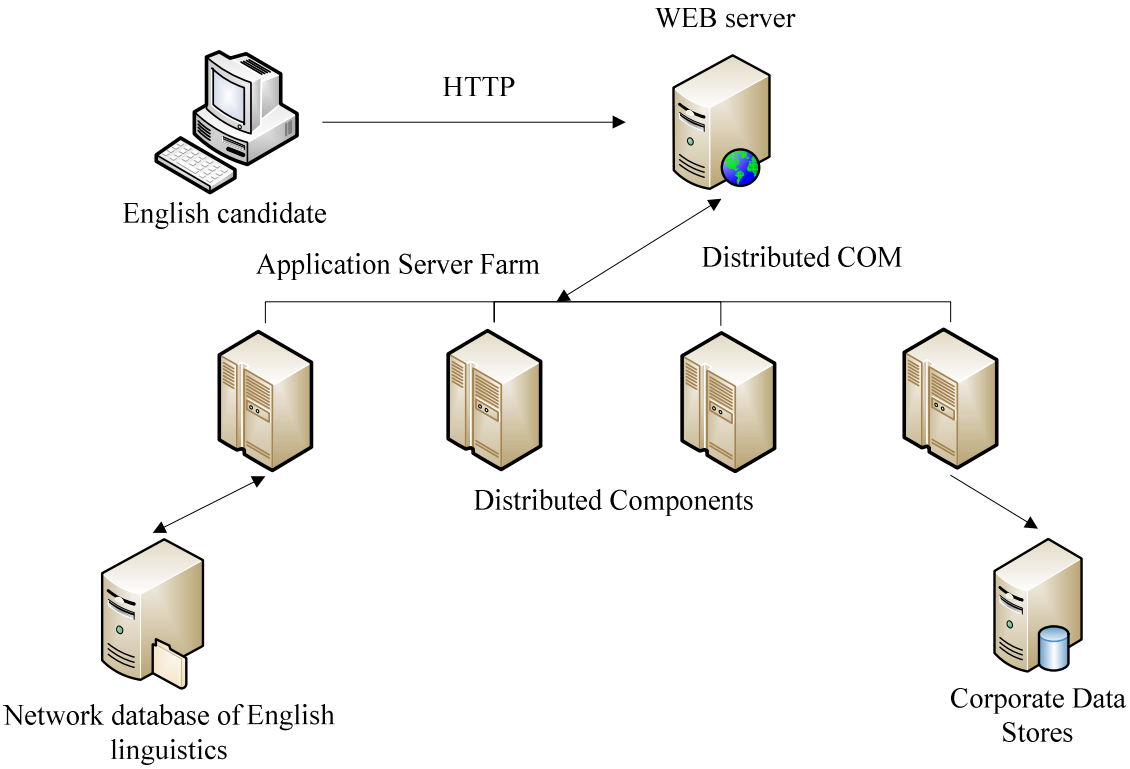

Fig. 4 Network examination database optimization platform of English linguistics

Figure 4 shows the Network examination database optimization platform of English linguistics designed in this paper. Students can use the platform to select questions and finish the test paper. Test paper distribution uses distributed allocations of Web Server and Disrtibuted COM, and uses different Disrtibuted Components to optimize the test papers [10]. Students can also feedback the examination information timely, and use Corporate Data Stores to collect data, finally forming network examination database of English linguistics.

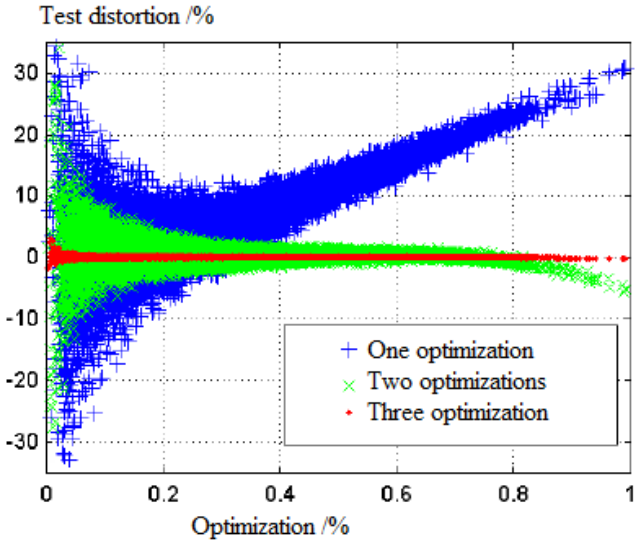

Fig. 5 Three optimizations of English network examination database

Figure 5 shows the three optimizations of English network examination database using VB program. The abscissa represents the optimal percentage, the ordinate represents distortion rate of test. From the figure we can see, distortion rate of one optimization and two optimizations is significantly larger than three optimizations. After three optimizations the distortion rate is close to *0*, which achieves the optimization effect of network examination database. We list the test quantity of three optimizations as shown in Table 1.

Table 1. Three optimizations results of English network examination database

Project	One optimization	Two optimizations	Three optimizations
Listening	201213	198651	185672
Speaking	101325	98256	88926
Reading	8592	7986	6931
Writing	7983	6526	5308

Table 1 shows the three optimizations results of English network examination database using VB [11]. In order to verify the effectiveness of the system, we use the method of three optimizations to optimize the listening, speaking, reading and writing in English examination database, and finally get the quantity of the optimized test.

Summary

In this paper we use the principle of neural network two order difference quotients training to establish optimization mathematic model of network examination database, and use VB software to program the algorithm to obtain the paper packet program. We use VB software and Microsoft ActiveX Data Objects2.0 to design optimization platform of network examination database, and introduce the paper feedback system and the Corporate Data Stores system on the platform, and perfect the optimization function of network examination database. In order to verify effectiveness and reliability of network test optimization system, we optimize the network examination database of English Linguistics for three times, obtain the optimal distortion curve of test and the quantity of optimization examination database. It provides technical support for the research of network English teaching

References

[1] Li Na. Overview of data mining software products [J]. The popular science, 2010(1): 22-24.

[2] Deng Qianni, Chen Quan. Cloud computing and its key technology [J]. Application and development of high performance computing, 2012, 26(1): 2-6.

[3] Zhu Qiandong, Pang Hongshen. Review of personalization search of search Engine [J]. Journal of library, 2011(6): 14-17.

[4] Li Yanling. Application of artificial neural network in remote sensing image analysis and processing [J]. Heilongjiang science and technology information, 2011(23): 23-26.

[5] Wang Huajin. Review of visualization technology in data mining [J]. Science Plaza, 2011(1): 235-237.

[6] Zhang Yanhong. Study on writing strategy for non English majors [J]. Social science, 2011, 24(8): 172-173.

[7] Zhang Yanhong. Dynamic evaluation system construction of university English writing teaching [J]. Journal of PLA Foreign Languages Institute, 2010, 33(1): 46-52.

[8] Zou Shen. Writing test validity based on corpus - using "English writing teaching corpus" as an example [J]. Foreign language electricity teaching, 2012(1): 16-21.

[9] Cai Chun. Dynamic assessment of teachers' professional development [J]. Education and teaching research, 2010, 24(8): 27-28.

[10] Chen Dezhi. Dynamic assessment study on the pattern reasoning ability of primary school children based on cognitive diagnosis [D]. Jiangxi Normal University, 2011: 2-16.

[11] Han Baocheng. Application of dynamic evaluation theory, mode in foreign language education [J]. Foreign language teaching and research, 2012, 41(6): 452-458.

Advanced Materials Research Vols. 989-994 (2014) pp 5491-5494
© (2014) Trans Tech Publications, Switzerland
doi:10.4028/www.scientific.net/AMR.989-994.5491

Research and Implementation of Groundwater Management Information System Based on J2EE

Dongmei Ma[1, a], Haiping Zhang[1, b], Hongdan Xue[1, c] and Ting Zhang[2, d]

[1] Hebei Institute of Architecture Civil Engineering, Zhangjiakou, Hebei, 075000, China

[2] China Institute of Water Resources and Hydropower Research, Beijing 100048, China

[a]mdm916@163.coml, [b]274874553@qq.com, [c]1970294452@qq.com, [d]21812003@qq.com

Keywords: Groundwater; J2EE; management information system.

Abstract. The design of groundwater management information system: using Struts Spring and Hibernate framework for system design and application development, according to the three layer design of J2EE，the key technology of every layer of the groundwater management information system was designed. The system functions include the basic data maintenance, data analysis, modeling and integrated management. The system provides management personnel with system level support in the analysis of historical data, daily monitoring and groundwater utilization.

Introduction

With the rapid development of Internet, it is becoming the mainstream of management information system basing on the browser to access WEB. J2EE architecture is suitable for application characteristics and the trend of Internet. The architecture provides standard model for the development and deployment of enterprise applications. The J2EE is adopt for the design thought which is the different layers of components .It makes business logic independent of the traditional client and the server. It is adapted to the changing needs of the business and the complex logic .It is convenience for the development, maintenance and use of the system [1]. Groundwater management information system is based on J2EE architecture to design and develop. The information system, according to the principle of high cohesion and low coupling, has the characteristics of scalable, cross-platform, easy maintenance. It provides a convenient, reliable and efficient information service about groundwater for staff, managers and decision makers.

System architecture design

J2EE is a multi-layer architecture based on component and application service [2].It is the technology architecture for the WEB system development. It is divided into the presentation layer (UI), business logic layer (BLL), and data access layer (DAL) from the business application level. It is the standard platform for the enterprise to provide a platform independent, portable, multi-user, safety and to simplify development, management, and deployment for the application system. The architecture design of groundwater management information system based on J2EE layered is shown in Fig.1.

SYSTEM FUNCTION FRAME

The function of groundwater management information system mainly includes basic data maintenance, data analysis, modeling information analysis, comprehensive management, and interacting with the GMS modeling platform for data. This system offers a variety of charts of the groundwater data analysis .These charts include histogram, pie charts, trend charts, radar map, geographic information as well as the output image from GMS modeling.

In the rights management aspect, this system designs multi-layer rights such as researchers, roles, functions and data access and so on. The rules are according to the different personnel distribution of different roles, and according to the different role assignment of open function permission and data

permission. The system could provide Announcement, industry news and simple OA office functions. The frame diagram frame of the system is shown in Fig.2.

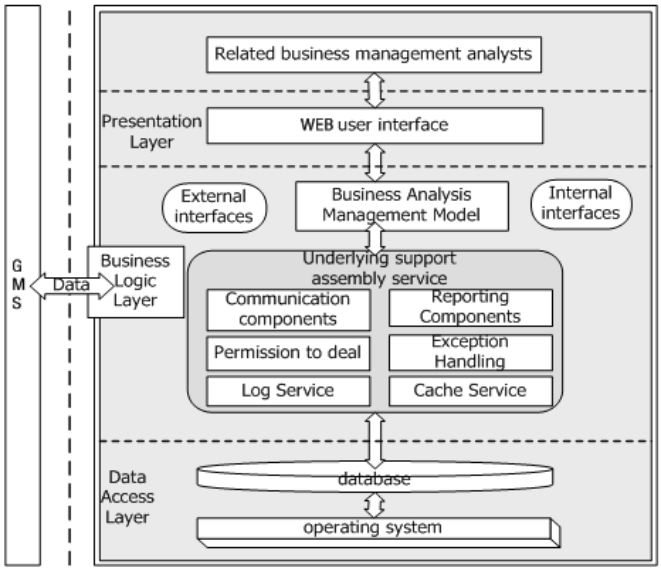

Fig.1: The architecture design of groundwater management information system

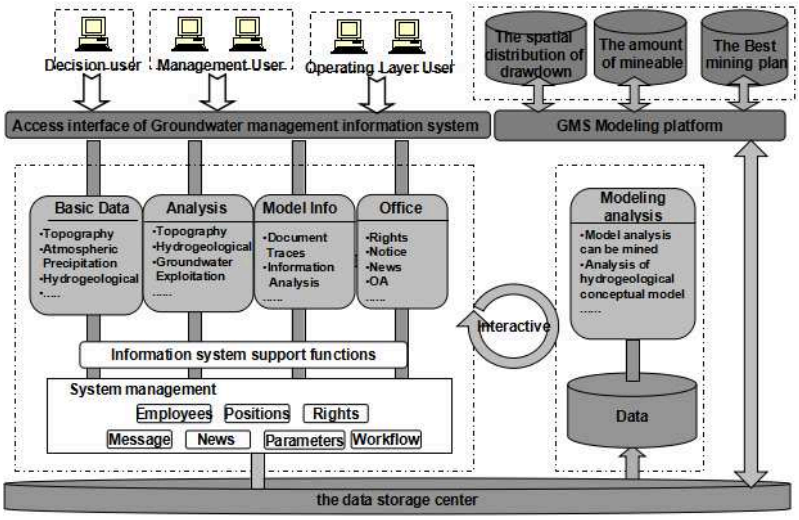

Fig.2: The frame diagram frame of the system

Maintenance functions to basic data. The maintenance function of basic data is the basis of groundwater management system function. Groundwater basic information is given preferentially with the batch information import, and other system interface is complementary. artificial acquisition entry for supplementary manner. This manner is as far as possible to reduce artificial workload, and to improve the accuracy and timeliness of information input.

Data analysis and modeling information analysis function. The function of data analysis and modeling information analysis is the core of the groundwater management system. This part is made logic operations and analysis of data and batch calculation of database through the study of basic data and GMS modeling results. This part gives various indicators of groundwater by means of statistical analysis, trend analysis and forecasting analysis. The purpose is to provide technical support and assurance for groundwater management system.

Comprehensive management function Comprehensive management function is the auxiliary function of groundwater management system. This feature can promote system security, convenience and industry development.it is the necessary basic function to the daily office.

System design and development

Performance layer----the Struts framework Struts is widely used in the JSP Web application field. This technique is an application framework which is based on the MVC (Model View Controller) pattern. The Struts controller component is integrated to achieve the model and the view [3]. The level of the Struts framework structure is clear, high reusability. The characteristic of struts enhances the scalability of system development, and provides a method of central treatment for a single page verification, access control and log processing, internationalization and so on.

Relevant jar package of the Struts is put under the WEB_INF file, at the same time, and introduced in the web.xml. The introducing corresponding configuration content is as follows:

The core part of the Struts is Action Servlet which is a part of controller. When JSP page submits request, the Action Servlet controls the traffic flow and jumps page through the configuration file struts-xx-config. This configuration file is defined on the web.xml at the same time.

Business logic layer----the Spring framework Spring is a lightweight framework of container .It could realize control inversion and aspect oriented programming, so that to solve the complexity and redundancy of enterprise application development .This technique provides a consistent management business object method. By means to control inversion, it achieves loose coupling between the system modules. Spring also provides the only access to data abstraction, including JDBC framework which is simple and efficient. This way greatly improves the efficiency and reduces the possible errors. Spring provides support for the framework of Struts and Hibernate [4], it is in favor of integration of other excellent open source framework as well.

Groundwater management information system uses the Injection method of setter and getter which exists in the Spring framework. It is made a following statement in the corresponding configuration file --applicationContext-xx.xml.

Data access layer-----Hibernate framework Hibernate framework is used in the data access layer. It is easy to use and efficient greatly which is based on O-R-Mapping (object-relational Mapping) framework. It improves the convenience and performance of database operations. Hibernate makes lightweight object encapsulation for JDBC (Java database connectivity).It may manipulate the database by way of object-oriented programming. It encapsulates database operations and shields code difference from different system .That systems are produced by the different database products (such as Oracle, Sybase, SqlServer etc).The advantage of Hibernate is improving the applicability and extensibility of the data access layer code.

Groundwater management information system integrates Hibernate framework by the Spring framework. The configuration file is in application-context.xml.

GMS modeling results output Groundwater numerical simulation model is an important tool for evaluation and management of groundwater resources. The hydrogeological conceptual model of the numerical simulation is established by using the GMS （Groundwater Modeling System）. GMS is a comprehensive groundwater numerical simulation software including model pre-processing, the numerical calculation and model after-processing [5].Groundwater management information system obtains the data analysis of GMS software and the corresponding multi-dimensional graphic data through Interface and stores these into the system. These files are maintained and associated binding information through the management interface. Other people can see the intuitive modeling and analysis results through system.

Charts and data analysis Data analysis charts are showed by the HighCharts plug-in. HighCharts is the chart written in pure JavaScript library. Its interface is aesthetics. It could be interactive charts. The realization of HighCharts does not need to use any client plug-in, and also does not need server in the background generated in advance [6]. It can take a variety of different types of charts such as histogram, trend chart to integrate a multi-dimensional analysis shows in the same chart. This system imports related highcharts.js, exporting.js into HighCharts. The data obtained is displayed in figures.

Conclusions

Groundwater management information system was designed based on J2EE architecture combined with the GMS groundwater modeling software, the system provides function s including information sorting, analysis, calculation and integration, and improves the groundwater historical information data usage and utilization. The system provides groundwater researchers and managers with the data analysis, modeling information analysis function and a good basis for scientific management of groundwater. Through the construction of groundwater information management system, unified management，planning and analysis are promoted.

Acknowledgements

This work was financially supported by Zhangjiakou science technology research and development program (1101004B)

References

[1] Ming Cai, Yongyun. Chen, Computer Applications and Software: Vol. 21(2004), p.42-44

[2] Ke Tian, Shibo Xie and Ma Fang. Computer Engineering: Vol. 29(2003), p.93-95

[3] Xianglong Yu, Jingzhong Zhao, Transactions of Beijing Institute of Technology, 2003, 23(3), p.337-339

[4] Xiaofeng Xi, Liangshuang Lv and Peng Lu, Computer Engineering and Applicationgs, 2005, 41(29) p.208-210

[5] Xiaodong Guo, Hui Tian, Meigui Zhang, et al. Urban Geology, Vol. 32(2010),p.5-7

[6] Shaobo Wang, Jiancang Xie and Xiaoli Sun, Journal of Information, Vol. 25(2006) p.77-79

Advanced Materials Research Vols. 989-994 (2014) pp 5495-5497
© (2014) Trans Tech Publications, Switzerland
doi:10.4028/www.scientific.net/AMR.989-994.5495

Research of the Multimodal English Teaching in the Cloud Computing Environment

Su Han [1,a], Xindai Zhang [2,b]

[1,2] Department of Basic Courses, Shandong University of Science and Technology, Tai'an, 271000, China
[a]email:hs56923@163.com, [b]email:1561750710@qq.com

Keywords: multimodal teaching; English; cloud computing

Abstract: With the rapid development of computers and the Internet, information technology has brought about great changes to our educational field. At present the ubiquitous "cloud service" has brought education into "the cloud era". Cloud computing has found more applications in our English teaching. Integrating the technology of "cloud computing" with the theory of "multimodal discourse analysis", this paper researches how to carry out multimodal English teaching in the cloud computing environment.

I. Introduction

The 21st century is an information age. Now information technology has been widely used in our educational field. The ubiquitous "cloud service" has brought education into the "cloud era". In our college English teaching, by integrating the technology of "cloud computing" with the theory of "multimodal discourse analysis", we can establish the new multimodal English teaching mode based on cloud computing, which can construct the open learning platform and implement "individualized" teaching program so as to foster more new practical talent for our country.

II. The Necessity of Multimodal English Teaching in Information Age

With the wide application of digital, network and multimedia technologies, multimodal communication has become an important part of social communication. On the basis of such a social background, the research of multimodal theory came into being. "Multimode" generally refers to the five communicative modes: casual mode, auditory mode, tactile modality, olfactory modality and taste mode, which come from the five perceptual channels. Visual mode and auditory modality are most closely linked with foreign language teaching.

The British scholar Halide once pointed out "language is a social symbol"[1]. Language is to express meaning. The famous Chinese scholar Zhuanglin Hu also pointed out "all kinds of modes have the potential to express meanings"[2]. Another British scholar Kress thought "Halide's theory of social semiotics promoted the research of multimodal expressions"[3].

Education is a key on which the multimodal research focuses. The modern foreign language teaching is an activity in which teachers and students interact and communicate with each other by means of many kinds of media. We think that the English teaching mode can be chosen from the following three angles: 1.Providing teaching situations and convenient conditions for English teaching so as to improve teaching efficiency. 2. Providing auxiliary conditions for English teaching so as to improve teaching efficiency. 3. Providing multichannel expressions of discourse for multimodal communication of discourse [4]. In addition, we should pay attention to the training of "multiliteracy ability" when we entered the new century. Our era has changed from the era of "pen and paper" to the "information era". "Multiliteracy ability" denotes that one can read all the educational and modal information that he can get in touch with [5]. We think that developing students' "multiliteracy ability" should be carried out in the following ways:

A. Classroom Teaching

Classroom teaching is a process of multimodal discourse, which involves teacher's speech and actions, the interaction between teachers and students, PPT demonstrations, the words and pictures of the textbook, interactive whiteboard, audio frequency and visual frequency, etc. Sometimes one

mode depends on the other modes to finish passing information, for example, pictures must be accompanied with oral explanations and PPT courseware must be accompanied with teacher's verbal explanations and body language. In addition, classroom teaching resources should also be multimodal. PPT courseware should include cartoons, audio frequency, visual frequency and other meaningful expressions. The teachers should flexibly use multimodal materials to present teaching contents in the network environment.

B. Extracurricular Autonomous Learning

In information age, college students' extracurricular learning is based on the network, which differs greatly from the traditional extracurricular learning. The network environment supported by cloud computing will further promote the multimodal learning, for example, teachers can put a lot of multimodal learning materials on the "cloud". Students can search the Internet for the needed materials, finish the learning tasks online, submit their homework and communicate with their teachers. Online reading and writing provide multimodal requirements for designers, guiders and learners. The dynamic nature and hyper connectivity of online reading and writing demand learners to possess cognitive flexibility of crossing disciplines, modes, languages and cultures. In this sense, carrying out "multimodal teaching" is not only an inspiration but also a great challenge. In the multimodal environment, teachers should first possess strong "multiliteracy", then they can gradually guide students to develop the corresponding ability.

C. The Research of Teaching Materials

The teaching material is the basic element of the English teaching, the main base of teachers' teaching and the central content of students learning. In order to adapt to the needs of advanced information technology and students' multimodal learning, compiling multimodal English teaching materials has become an important task. Multimodal English teaching materials refer to the English teaching materials which are formed by multimode, including written language, pictures, forms recording and videotapes, in which written language plays an important role, but many modes vie for attention [5]. Multimodal English teaching materials include paper teaching materials, electronic teaching materials and demonstrative teaching materials. Cooperation, multidimension, network and intelligence characterize the teaching materials. But there was little such research at home and abroad in the past.

Guided by the theories of multimode and the language teaching in the cloud computing environment, we can use the experience of compiling the corresponding teaching materials for reference to further study how to compile multimodal English teaching materials.

III. The Multimodal English Teaching in the Cloud Computing Environment.

We think that the multimodal English teaching in the cloud computing environment should include the following contents:

A. Developing the Multimodal English Teaching Resources in the Cloud Computing Environment

One of the basic elements of carrying out multimodal English teaching is multimodal teaching resources which are very important for both teachers' teaching activities and students' extracurricular autonomous learning activities. The central content of developing teaching resources is the construction of multimodal corpus. In addition, it includes compiling teaching materials with excellent pictures and texts, hypertext PPT courseware and network teaching materials, etc. We should extensively collect multimodal oral and written English materials by means of all kinds of modern information means, classify them according to their uses and modes such as text, recording, visual frequency, etc. We should do a good job of numbering and keyword search, gradually set up the multimodal corpus and constantly perfect it in the teaching practice so as to make it effectively serve classroom teaching and extracurricular autonomous learning in the cloud computing environment.

B. The Design of Multimodal English Classroom Teaching Supported by Cloud Service

Cloud service includes the service of network cooperative platform provided by network operator and the service of interpersonal communicative platform which people often get in touch with in their daily life. Classroom design includes teaching objectives, teaching contents, modal transfers, teaching methods and steps, etc. The theoretical guidance of the design is the theory of multimodal discourse analysis. We should utilize the advanced technology of multimodal discourse analysis such as the cooperative cloud computing platform and text visualization software to analyze the schematic structure of the text and language features, select the suitable materials from the cloud service platform and integrate all kinds of multimodal teaching resources so as to make students efficiently master the corresponding English knowledge and quickly improve their English level.

C. The Establishment of the Multimodal English Network Learning Environment Based on Cloud Computing

First, we should put all kinds of multimodal learning resources on the cloud. The search engine of the cloud should be connected with corpus and electronic teaching materials. We should present FAQ, the search of keywords, the analysis of the language points and the themes of the texts in the website. In addition, we should create blogs, micro messages and real-time dialogue programs to let teachers and students communicate with each other after class, and establish the platforms of teaching plans and homework displays. By means of different ways, the students can comprehensively experience the advantages of network learning in the cloud environment, which can fully demonstrate the effective supplement of extracurricular learning for classroom teaching. Based on the university's website and sound laboratories, we can set up a language learning laboratory of cloud computing. In class, we can extract materials from the public server to coordinate teaching. After class, students can log on to the network platform to review the materials learned in class and download more learning materials.

In the multimodal English teaching based on cloud computing, classroom teaching must be combined with the extracurricular autonomous learning. They must supplement each other to cooperatively improve students' English level.

IV. Summary

The multimodal English teaching in the cloud computing environment integrates cloud computing with multimodal English teaching. The combination of the information technology with the advanced educational theory facilitates teachers' teaching and students' learning in the information age. This innovative English teaching mode also provides a new research perspective for us English teachers. We should make good use of the new teaching mode and try hard to improve our English teaching level so as to train more useful talent for our country and society.

References

[1]Halliday, M.A.K: Language as Social Semiotic: The Social Interpretation of Language and Meaning (Eduard Arnold, London 1978)
[2]Zhuanglin Hu: submitted to Foreign Language Teaching and Research (2007)
[3]Kress, G..R: submitted to the International Literacy Conference (2001)
[4]Delu Zhang: submitted to Foreign Language Education (2009)
[5]Delu Zhang: submitted to Foreign Language World (2010)

Advanced Materials Research Vols. 989-994 (2014) pp 5498-5503
© (2014) Trans Tech Publications, Switzerland
doi:10.4028/www.scientific.net/AMR.989-994.5498

Research of Public Service Platform Based on Cloud Computing for Middle Size Enterprises

Chunxiao Wang[1, a], Ying Guo[1, b], Xiugang Guo[2, c]

[1]Shandong Provincial Key Laboratory of Computer Network, Shandong Computer Science Center, Jinan 250014, China

[2]Weifang University of Science and Technology, Weifang 262700, China

[a]wangchx@sdas.org, [b]guoying@sdas.org, [c]guoxiugang5111@163.com

Keywords: middle size enterprise; cloud computing; public service platform;

Abstract. Based on the research in cross-regional resource scheduling and massive data storage, the article built public service platform including IaaS, PaaS and SaaS. It provided all kinds of management software and business software for middle size enterprise users, and provided the development, testing, deployment platform for software vendors, and provided unified resource management, monitoring and maintenance for platform operators which finally become cloud service platform to support enterprise management and software development lifecycle. This helps to form a self-loop and self-development cloud computing ecosystem, to form the linkage of cloud services production, cloud services consumption and cloud service management, and to provide comprehensive information support for the growth and development of middle size enterprise.

Introduction

Middle size enterprise is important component in the development of our national economy, which plays an important role in the expansion of the total economy, alleviating employment pressure, promoting technological innovation and maintaining the social stability. With the progress of economic globalization, middle size enterprises pay more attention to the use of information technology to improve enterprise profitability and competitiveness. But due to their small scale and low capital investment, middle size enterprises invest little in Informatization. These formed the following contradiction. The demand for IT resources is increasing year by year, the demand for various kinds of software is increasing day by day, the demand for rapid construction of information system and service portal is growing [2]. The emergence of cloud computing provides a new way to solve the difficult information problem, its technical characteristics and business model has to promote and support function that can improve the management level, production efficiency and market competitiveness. Firstly, enterprise user can use high-quality service and don't need to invest a lot of money, which can relieve the pressure on funds shortage and reduce the risk of system implementation. Secondly, software vendors can reduce operating investment and maintenance costs, and gain huge business opportunities. Finally, platform operators can realize unified management, unified control and unified backup etc.

Foreign cloud computing platform is relatively mature. Amazon's Elastic Compute Cloud (EC2) and simple storage service (S3), dedicate to the task of calculating and storing process for small software enterprises; Google cloud computing platform provide the application hosting, enterprise search and Internet application services to users. America Apps.gov website, providing commercial, social media, productivity applications such as SaaS service, realizes e-government collaboration. In our country, the cloud platform construction has made great progress, Beijing "auspicious clouds" project form technology, products and services integration. Shanghai's "sea of clouds" plan forms cloud computing demonstration platform for city management, e-government, and middle size enterprise.

Platform Design

In the overall architecture, public service platform can support open, flexible, collaborative IT technology system, to support enterprise management and services and to provide IT new value model for enterprise Informatization construction. Platform apply cloud services as the core design idea, build a unified business engine, information resources, management tools on the basis of the hardware equipment, and provide all kinds of services for enterprise users. Logically, platform service system is composed by the infrastructure layer, support layer and service layer. In addition, it provides uniform access interface, uniform standard specification, unified safety management measures for enterprise users ,and builds a full range of cloud computing services platform in one set of infrastructure service (IaaS), platform services (PaaS), software service (SaaS). The three services form the ecological chain of sustainable development. The overall architecture diagram is shown in Fig. 1.

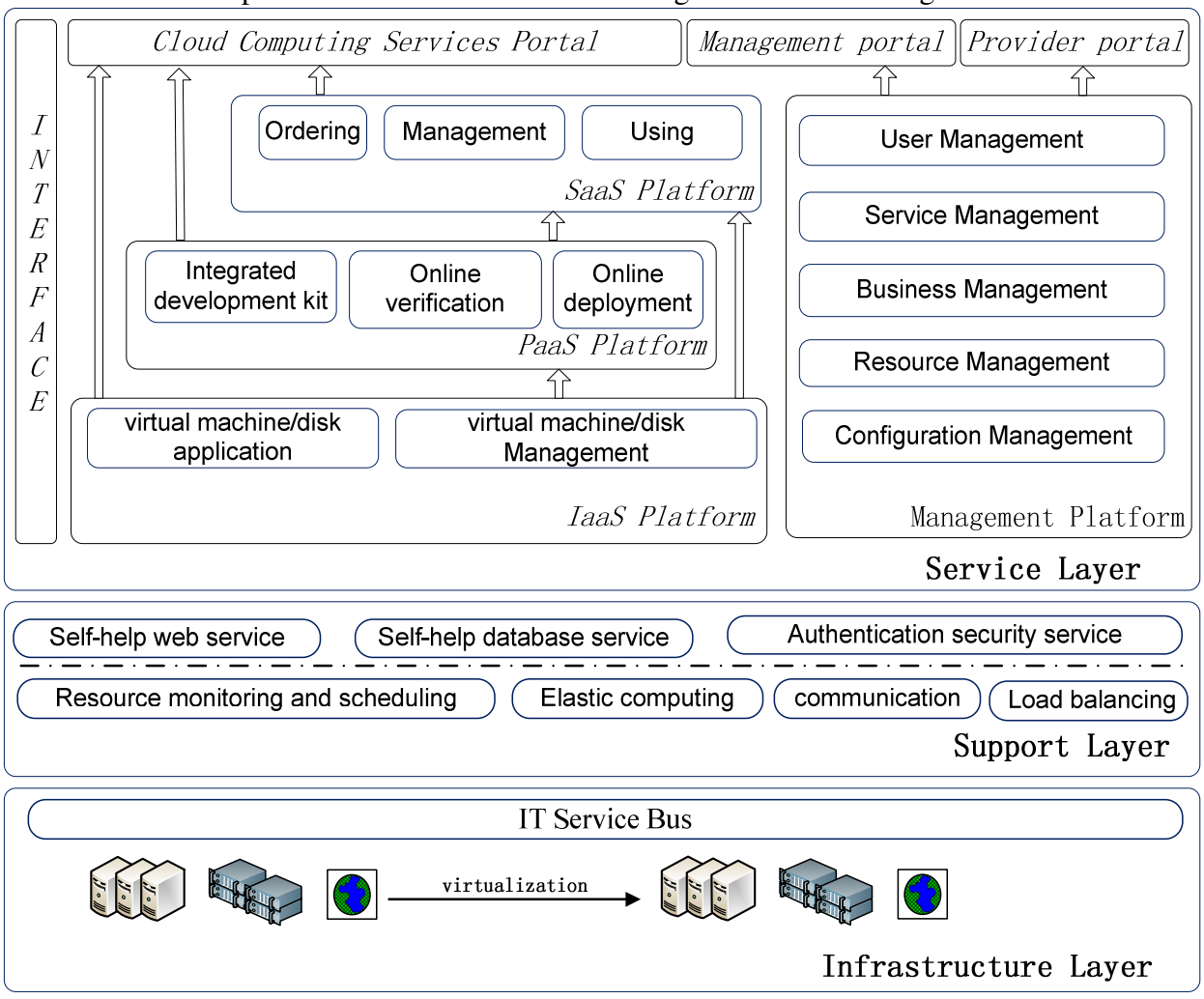

Fig.1 Cloud platform architecture

Infrastructure Layer. The infrastructure layer includes servers, storage, network, other physical equipment and virtual machine, virtual disk, virtual network, and so on. Using IT service bus, resource scheduling, application engine, data storage is packaged to service, through message communication realizing service invocation and interoperability; it provides not only registered operating environment, but also the technical support for upper layer.

Support Layer. Support layer mainly provides technical support for IaaS, PaaS, SaaS services, which can be divided into IaaS support platform, PaaS support platform and SaaS support platform, and is the bridge to infrastructure layer and the Foreign Service. It can call infrastructure service bus, managing virtual machine, and also can provide the universal interface such as self-service web services, self-help database services, and mass data processing services to service layer.

Service Layer. Service layer opens three different portal to users, including public services portal, management portal, and software vendor portal. Three portals are supported by four service platform, providing the corresponding services for different users. As the window of Foreign Service, the layer also provides uniform access interface, for authentication and data interaction between the software and platform.

IaaS Service Platform. IaaS service platform provides virtual hardware resources for enterprise users, including online applications and management of virtual machine and disk. Users do not need to buy hardware equipment, only build their own development environment through the internet.

PaaS Service Platform. PaaS services platform provides integrated development components and verification environment, which is a one-stop application platform covering the software life cycle. Using the platform, software developers can get integrated development component and unified access interface to quickly complete and release the project.

SaaS Service Platform. SaaS service platform provides a wide range of software services to users, including ordering, opening, managing, using and so on, users does not have to buy the software and hardware equipment, but to rent them by web browser.

Management Platform. Management platform is divided into IaaS management platform, PaaS management platform and SaaS management platform. It provides user management, service management, business management, resource management, and other functions for the cloud platform operators, and provides product management, business management, sandbox management, and other functions for software vendors. It establishes a unified information management, product management and resource management to improve public service ability specifically for middle size enterprises.

Public Service Interface. Public service platform provide a unified external access interface for software development companies and software vendors, including SSO authentication interface, SSO heartbeat interface, the client login interface, product access authentication interface, information interface, enterprise employees interface, and so on.

Key Technology

Rapid Deployment of Infrastructure Cluster. At present, the virtualization technology has basically realized the elastic expansion of resources that is increasing or decreasing the resources according to the variation of the load, in order to solve the conflict between resource supply and demand [6]. However, application system are usually not deployed in a virtual machine, but running in the virtual machine cluster, such as a typical Web system is made up of application server, database server, the cache server, load balance server. With the increase in business, the number of servers requires a corresponding increase. If only using virtualization technology, the server creation and deployment can be automatically implemented in minutes, but virtual networking and cluster configuration need take a couple of hours manually. Based on virtualization technology, the research realized the automatic virtual networking and cluster configuration, the time of resource adjustment shorted to minute level, and realized the scheduling of virtual clusters. The implementation method is shown in Fig.2.

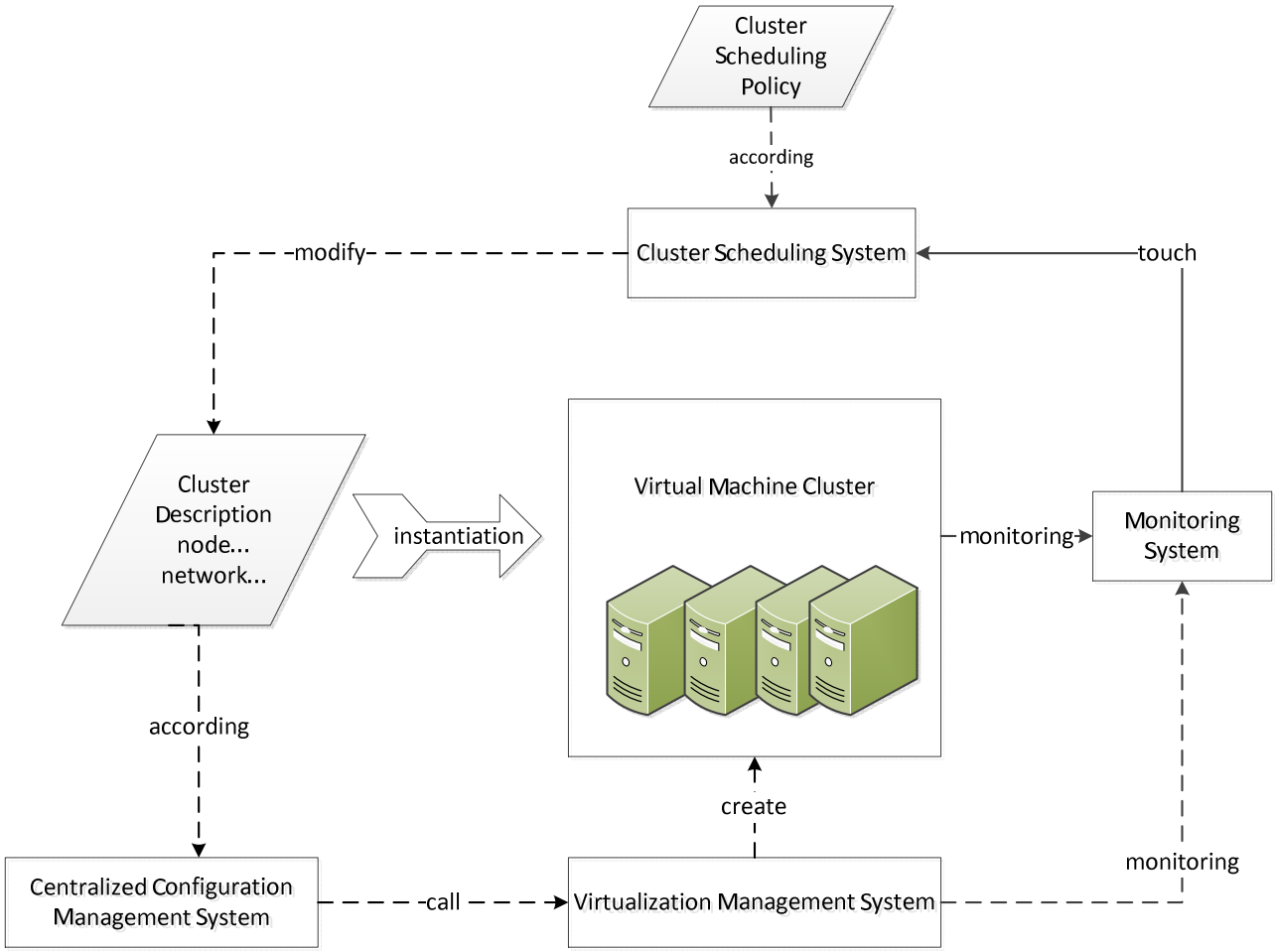

Fig.2 Rapid deployment of cluster

Practical steps are as follows:

- To describing the virtual cluster nodes and network using formal methods;
- To configure management system and create virtual cluster which according to the virtual cluster description and calling virtual management system or IaaS system
- To establish a unified monitoring system for hardware, virtual cluster and application;
- To make a cluster adjustment strategy by the monitoring indicators, cluster adjustment system modifies the description information based on the strategy, and thus triggers the cluster adjustment.

Online Deployment Technology. Online deployment system includes service system, management system and support system. Service system has unified entrance in the public services portal, which provides one-stop services such as product development, testing, and release for software development enterprises [9]. Management system extends corresponding module in the management portal, handles the work of component management, interface management, service application management, and release management and so on; Support system as a part of general support platform provides a common interface for service platform. Platform architecture diagram is shown in Fig. 3.

Service system. Service system provides a series of online service for software development enterprises. Integrated development kit includes a set of development component, the SDK, frameworks and access interface supporting C#.Net language and Java language, it allows users to quickly build locally software application. Online verification contains sandbox environment and debugging log. Online deployment support online operation of Web services and database service.

Management system. Management system contains the maintenance and information audit. Component information is development tools such as the SaaS model of product components, the SDK and product framework. Interface information is a series of operations including interface deployment, release interface, and monitoring.

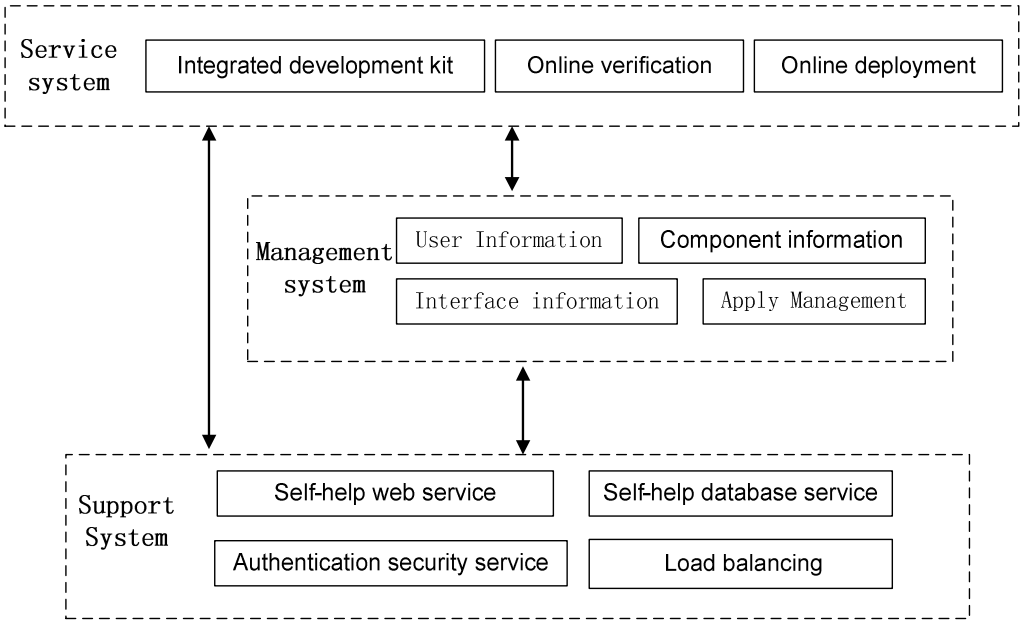

Fig.3 PaaS platform design

Support system. Support system consists of four parts. Self-help web service provides an interface which can automatically create the web service and is called by PaaS management system, it supports IIS and Tomcat Web server. Self-help database service provides a management interface which can automatically create the database, tables, views and stored procedures and is called by PaaS management system; Authentication security service support login authentication , single sign-on authentication and the client login authentication. Load balancing can make virtual resources extend according to application needs.

Software Service Integration Technology. Software service integration is the transformation of the application software in SaaS mode, so as to adapt to the demand of the cloud computing platform.

Traditional software transformation. The traditional software is generally a single tenant, and SaaS service requires multi tenant, therefore, multi tenant transformation is the key of software transformation. Among them, achieving data isolation among different users is the key link, which can be divided into database isolation, Schema isolation and Schema share.

Software Integration. After the cloud model transformation, software interface need be implemented in accordance with the standards, the interfaces include customer service interface and customer staff service interface to realize unified management, unified operation, unified single sign on service.

Conclusions

Based on the cloud computing service platform, we can enhance the rate of software and hardware resources, use enterprise management and business software online, and rapidly deploy product of its own. These effectively improve enterprise informatization level and expand sales channels.

Acknowledgements

This work was supported by the Information Industry Development Special Fund Project of Shandong Province of China under Grant No. 2013R2201 and the Science-Technology Development plan Project of Jinan City of China under Grant No. 201218009.

References

[1] Lei Wan-yun. Cloud Computing: strategy and practice of enterprise informatization. Beijing: Tsinghua University Press, 2010, 12.

[2] Hong Chao,Wang Jing,Xia Yong-quan. Design of public information service platform for small and medium enterprises. Software Guide, 2013,05. (In Chinese)

[3] Meng Fan-sheng, Yin Peng. Risk Total Cost of Ownership of Supply Chain Management System with SaaS Mode. Nanjing: Journal of Nanjing University of Science and Technology (Natural Science), 2011, 01. (In Chinese)

[4] W.Huang, R Li, C. Maple, H. J. Yang, D. Foskett, V. Cleaver. Web applications development lifecycle for small and medium enterprises (SMEs). In Proceedings of the 8th International Conference on Quality Software, Oxford,UK,pp.247-252,2008.

[5] D. Breitgand, E. Henis, O. Shehory, and J. Lake, Derivation of response time service level objectives for business services, Proceedings of the 2nd IEEE/IFIP International Workshop on Business-Driven IT Management BDIM, pp. 29–38, May 2007.

[6] Fang Bing-Yi Zhang Yun-Yong Chen Qing-Jin, etc. Network virtualization technology of cloud computing [J]. Information and Communications Technologies，2011，(1):50-53. (In Chinese)

[7] Thom as Rings, Jens Grabowski, Stephan Schulz. Grid and cloud computing: opportunities for integration with the next generation network. Journal of Grid Computing, 2009, 07.

[8] Wang De-Shuai, Zhang Yi-Chuan, Zhang Bin, Liu Ying. Load Balancing Strategy for Multi-tenancy SaaS Applications Supporting Service on Demand. Journal of Northeastern University (Natural Science), 2011,03. (In Chinese)

[9] Ding Li-Li. Research on PaaS Supply chain structure model. electronic commerce,2013.02:2. (In Chinese)

[10] Poladian V，Arlan A，Shaw M，et al.Leveraging resource prediction for anticipatory dynamic configuration[C]. First International Confe- rence on Self-Adaptive and Self-Organizing Systems ，2007：214-223.

[11] Liu Pengcheng, Yang Ziye, Song Xiang, et al. Heterogeneous Live Migration of Virtual Machines[C]. Proc. of the Int'l Workshop on Virtualization Technology. Beijing, China: [s. n.], 2008.

[12] Hyun Jung La, Soo Dong Kim. A systematic process for developing high quality SaaS cloud services. Proceedings of the 1st International Conference on Cloud Computing, LNCS 5931, Heidelberg: Springer Berlin, 2009.

Advanced Materials Research Vols. 989-994 (2014) pp 5504-5507
© (2014) Trans Tech Publications, Switzerland
doi:10.4028/www.scientific.net/AMR.989-994.5504

Design and Implementation of Agricultural Logistics Distribution Vehicle Scheduling System Based on LBS

Rui Ma[1, a], Guozhen Xie[1*, b] and Chi Zhang[2, c]

[1] School of Software, Beijing Institute of Technology, Beijing, China

[2]National Engineering Research Center for Information Technology in Agriculture, Beijing, China

[a]mary@bit.edu.cn, [b]xieguozhen1990@hotmail.com, [c]zhangc@nercita.org.cn

Keywords: LBS, agriculture, logistics distribution, route planning, mobile clients.

Abstract: Lack of effective and real-time information in agricultural logistics distribution, which will cause the vehicle cannot accurately obtain the current location and cannot select the best distribution route, results in serious vehicle load and resource waste. Aiming at the problems, this paper proposes an logistics distribution vehicle scheduling system based on LBS. Using three-tier system architecture including application layer, logic layer and data layer, the system provides services of location, navigation, route planning, surrounding location query and agricultural news. Mobile clients can not only receive the latest news about agriculture, but also receive real-time vehicle location and query distribution route planning, which will help the delivery staff complete distribution tasks efficiently, consequently reduce logistics distribution costs and the waste of resources.

Introduction

Information services based on LBS have attracted more and more attention of society sectors. Today a variety of industries, especially in logistics, distribution and transportation, has put forward higher requirements on location-related services. On the basis of obtaining real-time vehicle location, users can further improve operational efficiency, reduce operating costs, improve service quality, reduce unnecessary waste and achieve real time monitor and management of the whole transportation links[1,2]. Moreover, with the popularity of smart phones and the rapid development of 3G networks, mobile application could provide users with more convenient information services.

Agricultural logistics distribution is a very important part throughout the supply chain of agricultural products. Its efficiency has a great impact on reducing logistics costs and improving customer service quality. Advanced information technologies, such as location-based services, could be used to agricultural logistics distribution enterprise. And this will optimize agricultural distribution paths, provide the shortest path for transportation staffs to travel, and minimize transportation costs. It will have a great significance on improving the efficiency of logistics enterprise resource consumption and the entire agricultural products supply chain.

System Design

Architecture. The system architecture consists of three-layer: application layer, logic layer and data layer. It is shown in Fig. 1.

1) The application layer is the portal of system. Users could access the system via the mobile client, PAD clients, laptops and other mobile devices.

2) The logic layer is the core layer of system. It consists of communication networks, mobile positioning gateways, web servers and GIS application servers.

The communication network connects users and service centers. It should be real-time response and accurately transmit users' requests and the response of service center. GSM, CDMA, GPRS and CDPD are common means of wireless communication. In addition, there are a number of optional communication links, such as wireless communication private network, or even wired telephone, paging and satellite communications networks, wireless LAN, and Bluetooth technology.

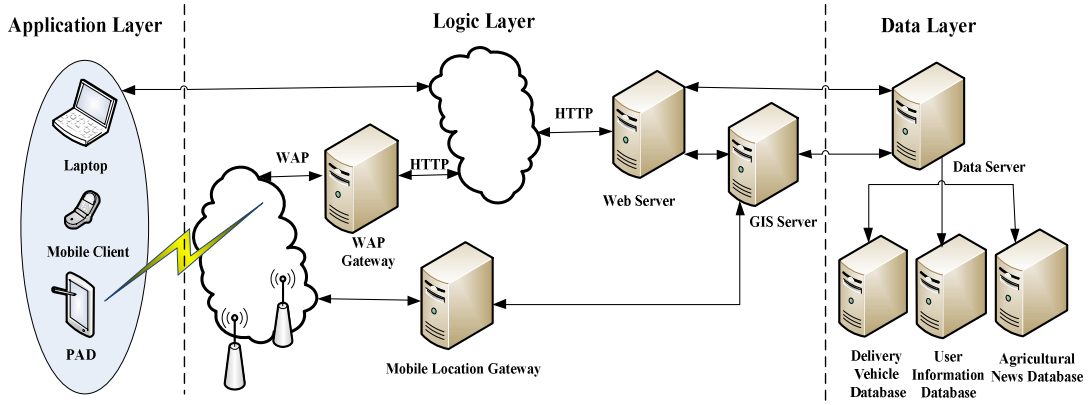

Fig.1 System Architecture

The mobile positioning gateway, web server and GIS application server are the core of location-based services. They are responsible not only for information exchange between servers and terminals, but also network interconnection between servers and the various sub-centers which includes location server and content providers[3,4]. Then they are in charge of completing the classification, record and forwarding of various kinds of information as well as monitoring the entire network.

3) The data layer is used for the unified management of all kinds of database and the flexible information exchange. It consists of databases which store all kinds of basic traffic information and related information, including the delivery vehicle information database, user information database and agricultural news database.

Positioning. Spatial positioning technology is the core of LBS. The main work flow of positioning is shown in Fig. 2.

Firstly, the user sends a location service request through a mobile terminal. Then the request, which should be forwarded through various communication gateways of mobile operators, is accepted by mobile location service center. After the certification, the mobile location service center invokes the positioning system to obtain the user's location information[5,6]. On the other hand, when the user has devices to automatically positioning, the mobile location service center could also obtain the user's location information through wireless networks. According to the location information, the mobile location service center could respond to the contents of services and forward them to the user through communication gateways. Finally, the user could obtain the respond to its service, such as displaying roadmap.

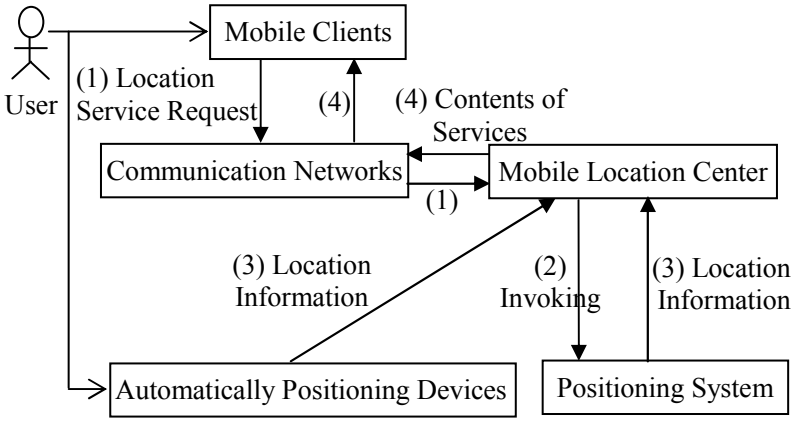

Fig.2 Work flow of Positioning

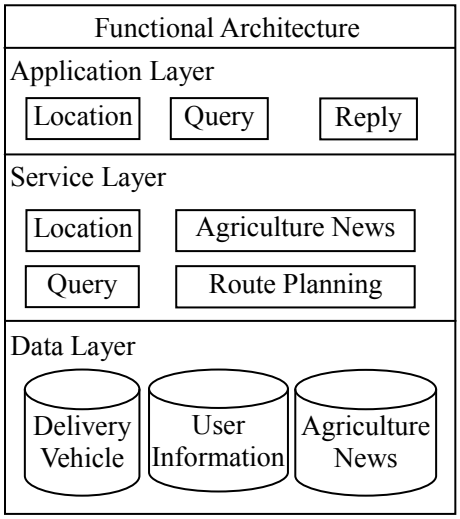

Fig.3 System Functional Architecture

Functions. As shown in Fig. 3, the functional architecture corresponds to the system architecture and consists of application layer, system service layer and data layer.

1) The application layer is used for the interaction between users and the system. This layer collects user location information, receives service requests and other user data, calls related services provided by the system, and then returns the result to the users.

2) The system service layer is the hub layer in the realization of the system. In addition to providing an answering service, this layer also provides traffic information services to the application layer, and manages the data layer simultaneously.

The system service layer is the core of the whole system. Information services provided by the layer include:

Agricultural information services. By using the service, users would obtain latest agricultural news on the mobile terminal. The news is pushed by the system.

Positioning services. By using the service, users could obtain themselves current location. This is done by positioning technology of location-based services.

Route planning services. When users need to query paths from the start to the destination, the system will return to three route planning schemes: public transport, walking and car. The result will be sent to the user through the application layer.

Location query services. By using the service, users could obtain a positional distribution map of nearby restaurants, hotels, gas stations, car parks and so on, as well as a convenient route to a specific location.

3) Data layer is used to store and provide traffic information. Data stored in this layer includes: delivery vehicle information data, agricultural news data and user information data.

System Implementation

The location-based service is the most important part of the system. The system uses map controls to locating and the Android SDK of AutoNavi to display map, and then further provides related services.

Location Service. Location-based service is the key of system. However, the traditional GPS technology has the following disadvantages: (1) it takes longer time to get navigation message; (2) it could not detect satellite signals in indoor; (3) it consumes more power. These shortcomings greatly limit the application of GPS technology in LBS. Therefore, the system uses a hybrid GPS positioning technology which is combined GPS with network positioning. The basic idea of this technology is to create a mobile communication network connected to a GPS reference network. This communication network monitors satellite status continuously. Then the auxiliary data from the GPS reference network is sent to the phone with built-in GPS receiver so as to speed up the startup process of the receiver[7]. Auxiliary data is used to improve the positioning accuracy and reduce the time of obtaining a signal. Furthermore, it is compatible with different positioning solutions.

Location function is custom implemented based on AutoNavi map. For cities which have better information network services, the positioning accuracy could achieve 100 meters and the shortest positioning cycle is 10 seconds.

Surrounding Location Query Services. This function mainly helps users query the surrounding location information. Through surveys on the user needs, the system provides four kinds of surrounding location services including gas stations, car parks, banks and service stations. It is faster and more convenient for users to directly select different service type by pop-up dialog box. For example, assuming that the user's location is currently positioned "weigongqiao". If the user selects "bank" mode, the map will display blue balloon icon to show all banks distribution around the "weigongqiao". Then you can click on the map to zoom in so as to see the details of specific location.

Route Planning. Route planning of the system is divided into three ways including walking, bus, and car. Firstly a user provides the starting address and the destination address to query as well as selects the positioning mode. Then the system will present the best route in the map with

different icons. For example, if the user selects "BIT" as the starting address and "Beijing Agricultural Building" as the destination address, and then selects "bus" mode, the map will present the shortest route with different icons.

Conclusions

As an important part of the development of agricultural logistics, agricultural logistics distribution has great significance on promoting the healthy development of modern agriculture. This paper addresses an agricultural logistics distribution vehicle system. Using three-tier system architecture including application layer, logic layer and data layer, the system provides services of location, navigation, route planning, surrounding location query and agricultural news. Mobile clients can not only receive the latest news about agriculture, but also receive real-time vehicle location and query distribution route planning, which will help the delivery staff complete distribution tasks efficiently, consequently reduce logistics distribution costs and the waste of resources. The system is easy to use. With the growing popularity of smart phones, the system has broad application prospects, not only in agricultural logistics distribution but also throughout the logistics industry.

Acknowledgements

This work was financially supported by the Beijing Municipal Commission of Science and Technology under Grant No. D131100000813002.

References

[1] X. Chen, J. Li, F. Yang, et al: Design and implementation of vehicle routing optimization system based on toll-by-weight. Manufacture Information Engineering of China, 17 (2007), p. 69-72

[2] C A. Marentakis, M. Bourlakis, I. Vlachos, et al: Telematics for efficient transportation and distribution of agrifood products. Intelligent Agrifood Chains and Networks, John Wiley & Sons (2011), p. 87

[3] L. W. Tang, and J. B. Yuwen: The study on digital traffic service system and key technologies of location based service. 2013 the International Conference on Remote Sensing, Environment and Transportation Engineering (2013), p. 613-616

[4] K. Petrova, and B. Wang: Location-based services deployment and demand: a roadmap model. Electronic Commerce Research, Vol. 11-1 (2011), p. 5-29

[5] D. C. Huang: Location Based Service combining Closed Range Photogrammetry and Assisted-GPS Technologies. Master Thesis, National Taiwan University of Science and Technology (2006)

[6] W. Gibson: Implementing a Personalized and Location Based Service for Delivering Advertisements to Android Mobile Users. European Journal of Innovation and Business, Vol. 10-1 (2013), p. 1-5

[7] S. Merrill, N. Basalp, et al: Privacy through uncertainty in location-based services. IEEE 14th International Conference on Mobile Data Management, Vol. 2 (2013), p. 67-72

Advanced Materials Research Vols. 989-994 (2014) pp 5508-5511
© (2014) Trans Tech Publications, Switzerland
doi:10.4028/www.scientific.net/AMR.989-994.5508

Spatial Characteristic Indicator of Pedestrian Facilities for Evacuation

Mei Li [a], Hao Yue[a], Binya Zhang[a], Xueyu Mi [b]

[a]MOE Key Laboratory for Urban Transportation Complex Systems Theory and Technology, Beijing, 100044, China

[b]He Bei United University College of Civil and Architectural Engineering, Hebei, 063009，China

[a]email: 13120953@bjtu.edu.cn, [b]email: pengto_2007@sina.com

Keywords: Public safety, Pedestrian facilities, Evacuation network, Spatial characteristics

Abstract. The spatial characteristic indicators of pedestrian facilities for evacuation are presented in order to contribute to the organization and management of pedestrian evacuation flow. An evacuation network is constructed based on the spatial layout of pedestrian facilities, in which the nodes represent moving sub-areas and two-way arc is on behalf of moving bottlenecks. Spatial characteristic indicators are built based on Multiple Origins Single Destination (MOSD) evacuation network including movement distance, movement amount, evacuation bottleneck, and evacuation aggregation extent. Through a case, the computation and application of the spatial characteristic indicators are presented in the layout analysis of pedestrian facilities, in which relevant improvement measures of spatial layout are advised.

Introduction

With a rapid expansion of the urban size and population, the large-scale activities of pedestrian became very frequent. In order to meet the demand of the city dweller for group activities and trips, the building size of pedestrian facilities is increasingly enlarged such as transportation hubs, stadiums, theatres, shopping center. The large pedestrian facilities have some characteristics, such as complex spatial layout, large-term construction cycle, organization difficulty of emergency evacuation and so on. Therefore, the spatial layout of large pedestrian facilities seriously affects pedestrian's normal or emergency evacuation. A reasonable spatial layout is conducive to improve the organization and management of pedestrian evacuation. The study on spatial characteristics of pedestrian facilities is a significant topic in pedestrian facilities construction.

In the research field of evacuation from a large pedestrian facilities, the work mainly include the evacuation sign[1], evacuation path or exit choice[2], evacuation design and evaluation[3], evacuation simulation[4], evacuation dynamics [5], etc… The theory and method about rational spatial layout or characteristics of large pedestrian facilities are relatively less researched.

In this paper, in order to form a reasonable spatial layout of the large pedestrian facilities, the physical space of pedestrian facilities is transform into an evacuation network based on evacuation bottleneck. And the space characteristics are analyzed based on evacuation network and evacuation path.

Spatial Layout of Pedestrian Facilities

The physical space of pedestrian facilities can be divided into moving space and obstacle space. Moving space can be occupied by pedestrians such as walkways, corridor, stair, room, in which pedestrian can move to door and evacuate from room. Obstacle space is occupied by internal obstacles, which cannot be used for pedestrian movement, such as columns, walls, table, no-go room. When internal obstacle affected pedestrian movement, there will form a moving bottleneck. Fig.1(a) shows the moving space, obstacle space and moving bottleneck in pedestrian facilities.

The width of moving bottleneck is the shortest distance between two obstacles, through which pedestrian can walk in evacuation. To calculate the width of moving bottleneck, the outlines of the obstacle spaces are simplified to arc and line segment, as shown in Fig.1 (a).

Evacuation Network of Pedestrian Facilities

In pedestrian facilities, moving space can be divided into different and non-overlapped moving sub-areas by moving bottleneck (See Fig.1(a)). Evacuation network can be constructed based on moving space (See Fig.1(a)). Evacuation network is composed of two parts: nodes and two-way arc. The nodes represent moving sub-areas and two-way arc is on behalf of moving bottlenecks. In evacuation network, nodes are classified into three types: origin node, destination node and intermediate node, which respectively represents pedestrian moving sub-area of initial site, aim site and passing area.

In emergency or normal evacuation of pedestrian, pedestrian facilities can be defined as a Multiple Origins Single Destination (MOSD) evacuation network based on pedestrian evacuation flow, as shown in Fig.1(c).

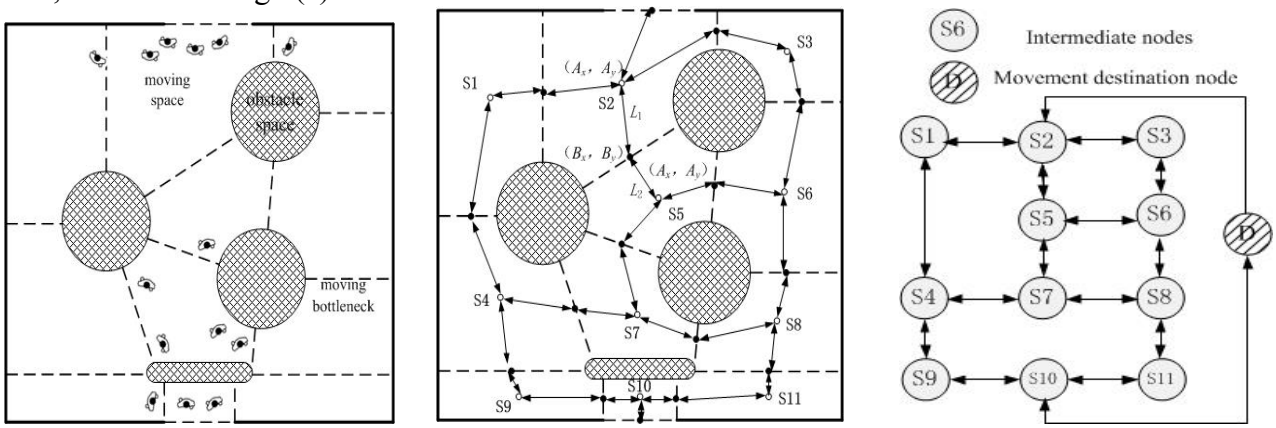

(a) pedestrian facilities (b) evacuation network (c) MOSD network

Fig.1. The illustration of pedestrian facilities and evacuation and MOSD network

Spatial Characteristics of Pedestrian Facilities

Spatial characteristics of pedestrian facilities for evacuation are analyzed from the view of spatial layout, in which it is assumed that the shortest path with spatial distance is adopted in pedestrian evacuation.

Based on MOSD evacuation network, the characteristic indicators of pedestrian facilities for evacuation are presented as shown in table.1.

Table.1. The Characteristics Indicators of Pedestrian Facilities for Evacuation

Indicator category	Characterization
Evacuation distance	The distance from moving sub-areas to exit
Evacuation amount	The total amount of pedestrians movement distance
Evacuation bottleneck	The width of the moving bottleneck in pedestrians evacuation
Evacuation aggregation extent	The extent of pedestrians gathering in evacuation process

Examples

A shopping center is selected as an example to analysis the spatial characteristic indicators of pedestrian facilities for evacuation. The size of the facilities space is 20m × 20m, with two exits. It has 6 rectangular section counters and a circular section counters. The layout of internal obstacles in shopping center was shown in Fig.2. It is assumed that there are 346 people in the shopping center, and evenly distributed in moving space. In order to compute the characteristic indicators, the evacuation tree is constructed based on evacuation network and the shortest path with spatial distance. The evacuation networks and evacuation tree was shown in Fig.3.

The spatial characteristics indicators of shopping center are calculated as shown in table 2.

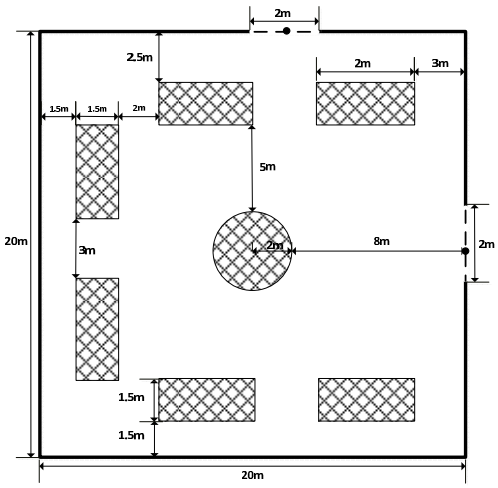

Fig.2. The illustration of the layout and size of obstacles in shopping center

From table 2, it is can be found that there is a large difference between the maximum and average evacuation distance. So in order to shorten the pedestrian movement distance, it is advised to increase the number of safety exit or balance the relative position between the exit and obstacles. It is also found that there is a big difference between the maximum and minimum evacuation amount, which indicate that the spatial layout of the facility is unreasonable. It is advised that the counters that can attract more shoppers should be put to the location that nearest to the exit, so as to achieve the purpose of the reasonable layout of the pedestrian.

From Figure.3 and table 2, there are most people through the moving sub-area S2 to evacuate from shopping center, so it is advised to increase the size of sub-area S2.

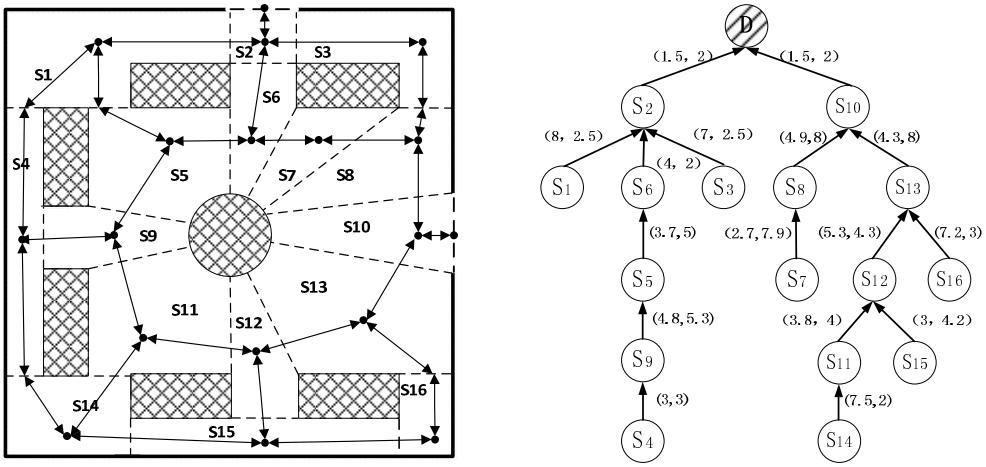

(a) evacuation network (b) evacuation tree

Fig.3 The illustration evacuation networks and evacuation tree in shopping center

Conclusion

In the paper, the spatial characteristic indicators of pedestrian facilities for evacuation are presented based on an evacuation network. The physical space of pedestrian facilities can be divided into moving space and obstacle space, and the width of moving bottleneck is computed by the outlines of the obstacle spaces. The MOSD evacuation network is constructed based on the spatial layout of pedestrian facilities. Through an example, the spatial characteristic indicators of pedestrian facilities for evacuation are computed, based on the assumption that pedestrians evacuate from walking facilities along the shortest path with spatial distance. Simultaneously, an improvement in special layout of pedestrian facilities is advised.

Table .2. The characteristic indicators of pedestrian evacuation in shopping center

Indicators category	The name of indicators	Indicators value
Evacuation distance	Maximum distance	22.4m
	Average distance	9.64m
	Weighted average distance	10.2m
Evacuation amount	Total evacuation amount	3536.9m
	Maximum evacuation amount	536.4m
	Average evacuation amount	208.1m
	Minimum evacuation amount	7.5m
Evacuation bottleneck	Minimum bottleneck width	2m
	Maximum bottleneck width	16m
	Average bottleneck width	3.7m
	Weighted bottleneck width	21m
Evacuation aggregation extent	Maximum aggregation coefficient	3
	Average aggregation coefficient	0.94

Acknowledgment

Project supported by the National Basic Research Program of China (973 Program, 2012CB725400), the National Natural Science Foundation of China (11172035, 51338008), the Fundamental Research Funds for the Central Universities (2013JBM046) and the China Postdoctoral Science Foundation (201003036).

References

[1] Chunxiao C, Qiang L, Shinji K, et al. Location optimization algorithm for emergency signs in public facilities and its application to a single-floor supermarket[J]. Fire Safety Journal 2009, 44(1): 113-120.

[2] Kobes M，Helsloot I，Vries B，et al. Way finding during fire evacuation； an analysis of unannounced fire drills in a hotel at night[J].Building and Environment， 2010，45(3)：537-548.

[3] Fang Z，Li Q，Li Q，et al. A proposed pedestrian waiting-time model for improving space-time use efficiency in stadium evacuation scenarios[J].Building and Environment，2011，46 (9)：1774-1784.

[4] Guan-Yuan Wu，Shen-Wen Chien，Yuan-Ting Huang. Modeling the occupant evacuation of the mass rapid transit station using the control volume model[J]. Building and Environment，2010 ，45 (10) ：2280-2288.

[5] Hu Qing-mei, Fang Wei-ning, Li Guang-yan, et al. Review on Pedestrian Behavior Characteristics and Crowding Mechanism in Public Buildings[J]. China Safety Science Journal, 2008,18(8):68-73.

Advanced Materials Research Vols. 989-994 (2014) pp 5512-5515
© (2014) Trans Tech Publications, Switzerland
doi:10.4028/www.scientific.net/AMR.989-994.5512

Frame Research of the Building Information Model in Project Management Information System

Xiangshuo He[1, a],Xiaona Yu[2,b] Xuezeng Ma[3,c]

[1]Department of Economic Management, North China Electric Power University ,Baoding, China

[2]Environmental Design, China University Of Geosciences Great Wall college, Baoding, China

[3]Engineering Management, China University Of Geosciences Great Wall college, Baoding, China

[a]hexiangshuo@126.com, [b]yuxiaona@126.com, [c]174035205@qq.com

Keywords: Project management information system; Building information model; BPS framework; Life cycle; Integrated Management

Abstract. According to the definition of building information model (BIM), authors compare the merits of traditional project management information system (PMIS) with the one based on the BIM model and BPS framework. Then authors approximately analyze the functions of the PMIS of this framework construction and discuss how this system will interpretably operate in life cycle. Finally authors give some advices on the issues in designing process.

Introduction

In the theoretical study of information systems, the vast majority of domestic research article will focus on the entire system architecture theory, but for the understanding of this architecture is still stuck in a pile of simple module level, or just based on project different construction period, the number of separate functional modules level combinations. Yet to propose a theory-based project management system, some of the theoretical framework advanced life-cycle management, integrated management systems integration to build the model. This article will focus on the establishment of such a model, and the model operation mechanism in the system.

Building Information Model Definition and Development Status

The so-called building information modeling (referred to as BIM) is the physical and functional characteristics of open industry standards in facilities, and projects related to the life cycle can be calculated or manifestations operation information. All information related to the organization and building information modeling in a continuous application, and allows access to, modify, and other operations. In a nutshell is, through a common standard (currently mainly IFC) and the integration of all relevant project information model.

From 2002, the company presented Autodesk BIM concept beginning, more and more software development companies have begun competing to design the model -based design software. There are Autodesk's Revit software, Bently company namesake software, Nemetschek Allplan software and Graphisoft 's ArchiCAD software company. The software has a dynamic process, 3D models and integrated document reporting. BIM 's core technology is a database of three-dimensional computer model of the formation, including in the design drawings (3D graphics, supplemented by various 2D sketch plane) is based, integrated from design to building construction until the end of the whole life cycle All works during the project information. Various kinds of information is always integrated in a three-dimensional model database. With BIM -based projects as building the system can continue to provide a variety of real-time data items in real time, complete and reliable information in real time and fully coordinated. BIM -based project system can be in a network environment, keep the information instantly refresh, and provide access, add, change, or delete operation, architects, engineers, construction workers, owners, end users and all users can be clearly related to the project system comprehensive understanding of the status of the project at this time. The information in building design, construction and operational management processes, accelerate

decision-making to promote and improve the quality of decision making, reduce project costs, so that the project to improve the quality and increase revenue.

Characteristics Compared with Traditional Built BIM Based Project Management Information System

Shortcomings of traditional construction project management information system

1) Due to the many aspects of the information transmission project management units and departments involved, the information entered can only stay in the engineering department or monomer interface, there are often lag, difficult to transmit to each other the whole project in a timely manner, of course, also hindered the entire project summary of the information, will inevitably lead to information island phenomenon.

2) Information about the progress of the project processing, investment, quality, contracts and other data, the number of large and dynamic changes, the traditional input information is difficult to timely summary, the parties involved often makes it difficult to grasp the feeling. Engineering drawings, documents, data and other documents, the number of large and generally stored in paper form, can not be random access to any time, affecting the efficient use of management information. Thus, information on all aspects of the construction has not formed a unified interface, can not form a whole.

3) Information on the use of building construction and management process will inevitably produce a large amount of information, and information for each array produces island situation, so that the information can not be shared and inefficient. More information can not be combined screening, meet the owners, contractors, subcontractors demand providers, contractors and other parties in each phase of the project.

Based BIM Construction Project Management Information System Benefits

According to the characteristic features of modern projects and project management theory, project management information system based on BIM features built in addition to the advantages of traditional management information systems, but also meet the following requirements:

1) Integrated management requirements in modern project management, there is a growing emphasis on integrated management, project management, integrated project management requires a higher level of systematic. Similarly, the integrated management information system is for the management requirements as well. For example: The goal of the project design, feasibility studies, decision-making, design and planning, supply, implement control, operation and management together to form an integrated management process; The objectives of the project, subsystems, resources, information, activities and organizations together, according to the plan so as to form a coordination complex operation; various project management functions, such as cost management, schedule management, quality management, contract management, information management, together, form an organic overall; integration and integration ¼ owners, contractors, design institutes, project management of all aspects of the management company.

2) Life cycle management requirements of modern construction projects required could be like other industrial sectors, in order to be able to provide end-use features as the main service. Life-cycle management philosophy is to ask the construction and management of projects to be considered for the platform in the project life-cycle process, the whole life of the project considering the various issues construction projects, making the overall goal of the project reach optimal. Reflected in the management information system construction, construction management information system is not just for the project implementation process, taking into account the management of information systems in business after completion of the works included in the operational phase of the application, so that both meet the needs of the owners actually work but also for the owners, end users, contractors, subcontractors, supervision agencies, such as the construction side provided some late summary data, which is currently lacking in many domestic research institute.

BPS System Architecture BIM Based Project Management Information System

BPS is also namely the browser server architecture. In this structure, the user through a Web browser, access the wide area network to achieve. Most of affairs to be achieved through the server side, between the terminal and the terminal server and the network connection, you can get real-time data transfer and integration process. Like system architecture that is the so-called three-layer structure of the network system, project management information system architecture shown in Figure 1.

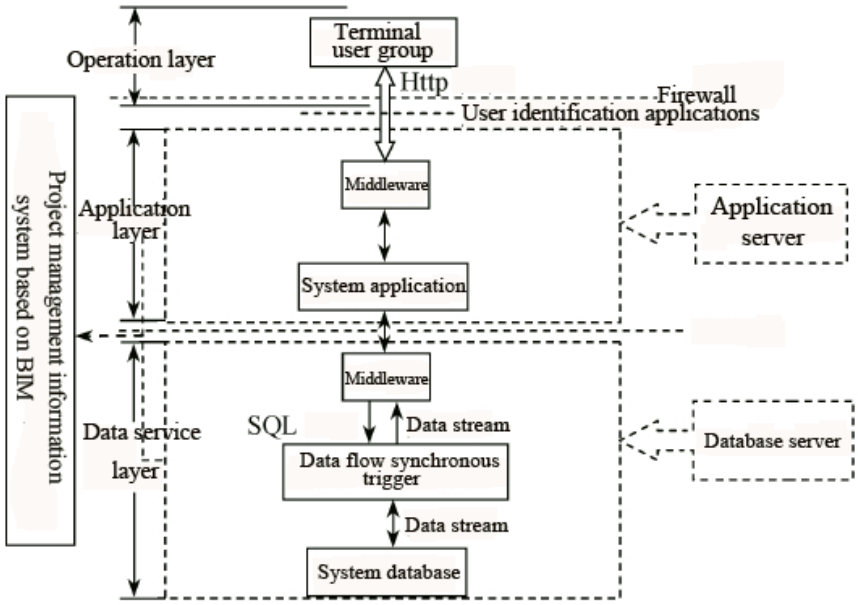

Fig.1. Network Architecture Project Management Information System

The first layer is the operating layer, also called user interface for end-user group (mean all people may operate the system, including the owner, design units, general contractor, subcontractors, construction side, end users, etc.) through a network provides browser, currently mainly Internet Explorer, users within the network permissible range (Line, VPN and even entire WAN), network protocols via Http, after identification, and make the appropriate operating authority empowered to enter the system, the associated operation; layer 2 is the application layer, the management information system applications loaded on the application server, the user receives access commands through middle ware, and then the results back to the user; layer 3 is a data services layer, middle ware connectivity through responsible for data processing instruction involves translation and processing, such as read, query, delete, add other operations.

Special attention is needed to load in the data between the database and middle ware is an important component stream synchronization trigger an implementation of BIM. Be achieved when the system database, which triggers an application is loaded all the data on the database table space. With this component, the current client application to issue any operating instructions (especially data-related operations, such as search, add, delete, etc.), you can synchronize each database triggers (eg: project planning document databases, contracts database, etc.) after integration, user feedback to the appropriate action. But in order to facilitate the understanding of the mechanism of the trigger, which was independent from the database table space. Information management systems in general, because there is no use of the data for all the components of the integrated database, so the system can not provide integrated data for each database, or that can not provide the data of each part of an integrated project management functions.

Architecture built using the BPS system because such system architecture also has the following advantages:

1) Low maintenance costs of the system architecture based on BPS basically just need major maintenance for the server, a single client even if the operating system is abnormal, it will not affect the server with other clients to run.

2) Upgrade costs and reduce development enterprises in the system upgrade, only the server applications and databases can be upgraded without the need for each client to upgrade the operating software and databases.

3) The server can run cross-platform server and client browsers on different platforms browser does not mutually exclusive, as is the Linux server browser, the client uses Windows IE browser still can exchange data and information.

4) The client runs the client load that is greatly reduced simply to exchange information with each other, and all operations are borne by the server, just to ensure fast processing speed of the server is running faster to complete the exchange of information with each other. Enable enterprises to reduce the use of client configuration requirements, us reducing the cost.

Conclusions

BIM-based project management information system through parametric simulation modeling technology that enables a computer to express all the information possessed by the project, the architectural design of information technology can be truly realized. With the development of BIM, not just the current advances in technology and upgrading of production will also be reflected in the transformation of organizational models and management, and long-term impact on people's thinking for the project. Although the system has not yet been devised, but with the deepening of theoretical discussion, practical work progressing, and such software for the entire construction industry will have a profound impact.

References

[1] ISOPTC 184PSC4.Industry automation systems and integration Pindustry data[S]. International Organization for Standardization, Geneva, 1994.

[2] Art K. Requirements management interface to building product models [D].Stanford University,2005.

[3] Edward H G.Is BIM the future for AEC design? [EBPOL]. http: PP aec. cadalyst. Com Paec Particle ParticleDetail.jsp id=133495,2004.

[4] Wagn Tingxi. BIM-The revolution of construction [EBPOL]. http: PP www.yuedadc. ComPeditu PUploadFileP2007210152649597.pd.

[5] Sailed kartam.Introducing a new concept and approach to modeling construction[J].Journal of Construction Engineering and Management, ASCE,2003,(1).

Advanced Materials Research Vols. 989-994 (2014) pp 5516-5519
© (2014) Trans Tech Publications, Switzerland
doi:10.4028/www.scientific.net/AMR.989-994.5516

Study on Architecture of Power Marketing Management Information System based on Web Service

Qing Zhang

Department of Economic Management, North China Electric Power University,Baoding, China

23571581@qq.com

Keywords: web service; power marketing; management information system; architecture; system integration

Abstract. A multilayer distributed structure based on web service is put forward. The layer structure of power marketing business is described, based on the layer structure. The paper deduces that every business can be encapsulated by web service and each of them can communicate easily. The connection between the power marketing management information system and other systems is analyzed, and then the use of web service is presented to realize the integration between this system and the related systems. In the end, with the real example of a power marketing management information system, the solution for web service and the corresponding codes are presented.

Introduction

In recent years, the theoretical study of power marketing management information system has achieved some results, mainly into two categories, one is the study of software development from the perspective of the system structure and key technology system implementation; the other is from the management functional module business perspective on research system. Power Marketing Management Information System on the country has been put into operation, the application of the effect is not ideal, its main deficiencies as follows: First, marketing data or the provincial, city, county, four units of the power of decentralized management, failure to achieve full sharing of data; second, failed to properly resolve system compatibility and scalability, it is difficult to implement multiple power management modules organic integration of information services; third, it is difficult to achieve power marketing management information systems and other enterprise integration between information systems, such as integration with scheduling systems, production systems, substation operation system, line GIS, ERP, etc.. Some of these deficiencies in the due administration level, but is largely determined by the software development technology, the traditional two-tier C / S structure of the system communication applications on the Internet, CORBA, DCOM, etc., can not be achieved because of its own dedicated agreement difficult to achieve integration between heterogeneous systems.

XML Web Service is based on open standards and protocols, cross- platform, regardless of the development language, can cross the firewall, easy deployment and maintenance features, have become an ideal application integration technology. Therefore, we propose the use of Web Service technology to build power marketing management information system and related systems integration and resolve between.

Web Service Description

Web Service definitions

Currently Web Service is not a strict definition. Generally, Web Service component technology is an extension on the Internet, using a service-oriented architecture (SOA), which defines a set of standard protocol for the interface definition, method calls, registered Internet-based component and a variety of applications. Web Service with a cross-platform, regardless of the development language, can cross the firewall, easy deployment and maintenance features. Web Service function can be achieved with a simple response to user's requesting, it can be a more complex applications.

Once a Web Service published on the web, or other Web Service other applications can discover and invoke the services it provides.

Web Service Architecture

Web Service the architecture includes three kinds of entities and the three kinds of operation, the structure shown in Figure 1. Of which three kinds of entities are service providers, service requesters, service registry; 3 kinds of operations are publish, find, bind.

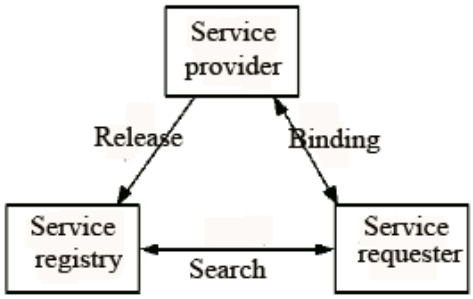

Fig.1. Web Service Architecture

(1) Web Service in the three kinds of entities: 1) Service Provider: the owner of the service, you can publish the services provided, and the use of their services to respond to the request; 2) Service requester: consumer services, in Find service registry services needed, and then call the service; 3) Service registry: also known as service agent, is used to register the service description. Service providers publish their services here; service requestor here to find the services they need to obtain binding information services.

(2) Web Service operation of three kinds: 1) Release: service providers to register their service registry provides functionality and access interface; 2) Find: Find a service requestor services needed to service registry, and receive calls service relevant information required; 3) Binding: service requester and service provider binding, which can use the services provided by the service provider.

Based on Web Service Power Marketing Management Information System Architecture

Software Architecture

Web Service based power marketing management information system using multi-tier distributed architecture, as shown in Table 1, including its four levels: the presentation layer, Web services layer, application service layer, the database service layer.

Table.1. Software Architecture

The presentation layer	Web browser.XML / HTML page. Applet. DCOM Clinet. CORRA Client
Web services layer	IIS. Apache. Web Logic
Application service layer	Web Services (business expanding, energy metering, electricity inspection, electricity tariffs, comprehensive analysis, reporting, icons statistics)
Data services layer	Oracle.SQL Server.Sysbasc.DB2 etc

(1) Presentation layer: mainly man-machine interface, responsible for inputting information display.

(2) Web services layer: mainly responsible for grant management and information presentation layer SOAP requests coming release.

(3) The application service layer: mainly responsible for handling transaction processing and logic operations to the Web Service package of services, depending on the power marketing business provides multiple Web Service.

(4) Data Services Layer: storage, and a variety of database management organization primarily responsible for the data.

System Hierarchy

According to the National Power Corporation "Power Marketing Management Information System Design Specification (Trial)" requirements, power marketing management information system is divided into layers of customer service, marketing, business layer, the quality of

management and marketing management decision support layer 4 levels. The relationship between the layers is shown in Figure 2.

Fig.2. System Hierarchy

(1) Customer Service Layer: The goal is to provide customers with efficient, convenient and high-quality service, establish a good corporate image of the service of power, for the power companies to win competitive advantage. The main contents include the operating room by means of a variety of services, call centers, Internet and customer site, etc., to provide customers with electricity regulations, electricity policy, knowledge of electricity, electricity technology and information services, such as electricity consumption, real acceptance by customers Newly submitted in a variety of ways, Capacity and electricity and other information queries and complaints and reports and consulting services and other services.

(2) Marketing business layer: the goal is to follow the flow of information marketing business standardized, scientific management principles for power marketing business to achieve fast, accurate processing. The main contents include processing new clothes, Capacity and power changes, contract management, electricity tariffs, fees and account management, energy management and metering and load management and other business processes.

(3) Marketing Quality Management: The objective is marketing business layer by layer, and customer service business process standards, business processing time, customer service assessment to monitor specific indicators of management functions, etc., to find problems quickly be reflected, urge relevant departments to rectify. The main contents include workflow optimization and supervision; marketing business auditing, contract management and implementation of complaint management.

(4) Marketing Management Decision Support layer: the goal is to develop a marketing strategy, marketing operations and development, customer information analysis, performance evaluation, public relations and corporate image design, management practices, and to provide a scientific basis for marketing decisions. The main contents include marketing business layer through the customer service level, quality management and other marketing information flow analysis applications, providing market operations and development, customer demand information, market forecasts and dynamic decision support information such research.

Integration with related systems

Power marketing management information system is not closed and isolated, but with other information systems are linked, there is a certain amount of information exchange and sharing. If you need to transfer the receivables electricity generation marketing and management information systems to financial management information system to establish accounts receivable, collection of data need to be passed after the recovery of funds to finance the tariff system and receive funds from the financial system to complete the arrival information manage cash flow; conducting marketing and management analysis, you can use the line carried GIS substations, lines, integrated query variable sets of statistics and analysis and forecasting; production MIS need to adjust the load from the relevant power marketing management information system information. In addition, there are some on the information exchange between the lower power supply companies, such as higher-level units need to subordinate units to check the quality of marketing efforts, the provincial power supply enterprise management decision analysis requires all cities within the province 's electricity

supply enterprise marketing relevant business data for statistical analysis. Therefore, power marketing management information system must achieve two major integrations: vertical integration and horizontal integration. Horizontal integration is mainly between the power marketing management information systems and other related subsystems integration of the unit, such as the production of MIS, line GIS, SCADA systems, financial MIS, ERP, CRM, OA, supplies MIS, MIS personnel, etc. integration; vertical integration is the integration between the major subordinate units power Marketing Management information System and superiors. Each subsystem does not require new development in the integration scenario, simply some functions can be called Web Service package into power marketing management information system, because power marketing management information system is constituted by a large number of Web Service, and they can also be other the system calls, thus achieving effective integration between systems.

Conclusions

In Web applications, dynamic web pages to achieve a lot of static functions can not be achieved, static web pages can also be part of the dynamic features, in appropriate circumstances, to achieve a certain dynamic web functions transferred to the more static pages to implementation, in order to get the system performance greatly improved, with storage exchange rate, feasible space for time, the growing emphasis on the user experience in the network, more user-centric today, this conversion has a wide range of practical value.

References

[1] Sebastian E, Gregg R, Srikanth K. Leveraging user-session data to support web application testing[J].IEEE Transactions on Software Engineering, 2005,31(3):187-195.

[2] Stefania G, Diego L, Mieke M. Formal test-case generation for UML state charts[C]. IEEE Proceedings of the Ninth IEEE International Conference on Engineering Complex Computer Systems Navigating Complexity in the E-Engineering Age. Washington: IEEE Computer Society, 2004:75-84.

[3] Ancient music, Shi Jiulin Introduction to software testing technology [M] Beijing: Tsinghua University Press,2004:152-158.

[4] Ding Yuehua, Wangfang Li. Performance testing Web-based software [J]. Computer and Digital Engineering, 2006,34 (1):47-48.

[5] Lu Xiaoli, Ge Wei, Chen Xinli, etc. to build Web Application Test Model [J]. Computer Applications and Software, 2006,23 (11):22-23.

Advanced Materials Research Vols. 989-994 (2014) pp 5520-5523
© (2014) Trans Tech Publications, Switzerland
doi:10.4028/www.scientific.net/AMR.989-994.5520

Analysis and Design of Supply Chain Inventory Management System under Internet of Things Environment

Zhi-Ping Peng

Department of Basic Education,Hebei Vocational College of Rail Transportation, ShiJiaZhuang, China

vicacer@163.com

Keywords: Supply Chain Inventory Management; Internet of Things

Abstract. The networking technology in warehouse management can be automated cargo management, operations and real-time access to inventory. Application networking technology greatly reduces the workload of warehouse management and unnecessary losses. Through the intelligent management of the goods, but also improve the utilization of warehouse space, to enable enterprises to understand the real-time inventory, thereby reducing inventory costs, improve the accuracy of inventory management.

Introduction

Warehouse Management, referring to the effective control of the transceiver, balances and other activities warehousing of goods, and its purpose is to ensure that the enterprise intact warehousing of goods, to ensure normal production and business activities, and activities on the basis of various types of goods status classification records to chart a clear way of expressing the quantity, quality aspects of the situation warehousing of goods, and general management in the form of the current geographic location, department, vesting orders and warehousing degree of dispersion conditions.

Internet of Things is an important part of a new generation of information technology. As the name suggests, things are material objects connected to the Internet. This has two meanings: First, the core and foundation of the Internet of Things is still, in the Internet based on the extension and expansion of the network; Second, the extension and expansion of its client to any goods and items of information exchange and communication. Things are "connected to the Internet." Things through IntelliSense, identification technology and pervasive computing, widely used in converged networks, and has therefore been called following the computer, the Internet world information industry development Third Wave. Things are applied to expand the internet, things are not so much the network, as it is a business and networking applications. Therefore, the application of innovation is the development of the core things to the user experience as the core of the development of innovative 2.0 is the soul of things.

Analysis of System Requirements

Things technology-based warehouse management system is the introduction of RFID technology in warehouse management, warehouse receiving inspection, storage, a library, transfer, shift library shift, inventory and other operational aspects of the data, automated data collection, ensure that all aspects of warehouse management data entry speed and accuracy to ensure timely and accurate grasp of corporate real inventory data, reasonable maintain and control inventory. Meanwhile, through scientific coding, also easily batch items on shelf life, such as management.

The new warehouse management system should meet the following aspects: a warehouse management information system usually rights management, data query, statistics and management functions; through the introduction of RFID technology can improve the accuracy of the goods query; through the introduction of RFID technology can improve the efficiency and quality of the library inventory operations; help companies reduce the cost of inventory management; operation of the system can accelerate the speed of goods out of stock, thereby increasing throughput inventory centers; able to give managers and decision-makers to provide timely and accurate inventory

information; able to automate the collection of inventory information, in order to achieve paperless inventory management.

According to the above requirements, based networking technologies warehouse management system should have the whole process automated warehouse operations; warehousing information instantly and effective feedback; update RFID tag collection and storage of data, ease of integration with other enterprise systems, ease of maintenance and scalability and other five basic functions.

System Architecture Analysis

At present, the common system architecture that there are two major: C/S architecture and B/S architecture. Advantages of C/S structure lies: in the data processing speed B/S fast that C/S is more conducive to handling large amounts of data. C/S technology is to design a flexible user interface, in order to fully meet the customer's own individual requirements. C/S has a strong interaction technique. In C/S, the client has a comprehensive application that has powerful features in an error message, online help, etc., and can switch between the subroutine. C/S mode provides a more secure access mode.

B/S structure also has its own advantages: B/S structure of information dissemination, data gathering speed faster; data sharing easy. B/S structure of the foreground client requirements low, avoid blindly caused a huge waste of hardware upgrades. Structure B/S mode is easy to expand and have a stronger information systems integration.

According to the actual needs of the system, combined with advanced maturity and B C/S structure / S structure, the system uses the architecture of C/S structure and B/S structure combining.

In the warehousing business internally, it takes into account the complex and onerous business client computing, the use of C/S structure of the transmission and processing of information within the system. In addition, the client can install the client software to improve data confidentiality, to prevent outside intrusion. B/S mode is mainly used to enhance the interactive warehouse management systems with external information systems, as well as publish and query public information, thereby improving the supply chain data sharing.

In the C/S structure section, networking technology into the warehouse management system to achieve automatic collection and processing of data. In order to achieve seamless RFID systems and warehouse management systems to achieve business process management and automation of the entire process of tracking and monitoring, the system will be C/S structure is divided into three layers.

The first layer is the data collection layer, mainly via RFID devices automatically collect data, including location RFID tags, electronic goods label, wireless RFID data collection terminals, automated guided vehicles.

The second layer is a data conversion layer, i.e., by wireless communication technology, to transfer the collected data after conversion to the server, including wireless access equipment and RFID middleware.

The third layer is the data management, data collection management, including database servers, network servers and other equipment and warehouse management system software.

System Functional Design

By utilizing the advantages of RFID technology, networking technology can strengthen warehouse management information system based on the enterprise storage features, optimize process, flexible configuration items, to provide customers with better management and data analysis basis. Through analysis, the RFID technology and enterprise storage processes combined into the new system features six modules: system management, basic data management, warehouse management, RFID dynamic management, statistical analysis, and financial management.

Systems Management: including contract management, role management, early warning management of the three functions. Contract management contract can query, add, modify, and void management. Role management can be associated with the operating system privileges to different

roles, and the roles assigned to specific operators realize the operator rights management. Warning is mainly about warehouse capacity management, inventory of goods and product shelf life for early warning. Depending on the type of storage, warehouse inventory warning conditions set and monitored. Warehouse capacity warning is the level of spare capacity on the warehouse early warning. Inventory Cargo warning, the number of goods in stock inventory customers early warning management, mainly for cargo minimum and maximum inventory value inventory value in inventory management for early warning. Shelf life warning is the shelf life of the goods on the early warning management.

Basic data management: including customer information management, employee information management, warehouse management, location management, cargo management, equipment management six functions. Customer information management can add, modify and delete customer information. Employee information management can add, modify and delete employee information. Warehouse Management can name for the warehouse, load-bearing capacity, volume, type, cost and other information processing to add, modify and void functions. Location management, including the type of management location, location and location rules governing appointment. Warehousing and cargo information can be managed to increase by location type, save, modify, and void function processing. Warehousing and cargo management can assign rules to increase by location rule, save, modify, and void function processing. By location booking appointments can add, modify and delete management. Cargo management including maintenance and cargo goods category archives management. By commodity maintenance can create, save, and delete categories of goods. File management via cargo can add, modify and delete details of the goods, the goods file management. Device Management

Including the consumption class device management, the device management and electronic machinery and equipment are management. Information storage devices need to add, modify and delete processing.

Inventory Management: The main system management module is responsible for the entire warehouse process control, its function modules include: storage management. The main function of this module are: procurement contracts signed by the purchasing department will convert pre Receipt; according to the pre- storage lists, check the spare location, identify a sufficient location and arrange location; storage of the goods when the goods Receipt itemized statement with the pre-check, check for input errors or omissions, goods name, quantity, etc. are the same. The agreement is permitted storage.

Goods inventory management. Including inventory planning, inventory -production, production and other capabilities inventory report card. With this feature you can add, audit, check inventory operations and other operations.

Transaction data management. Transaction data refers to data during the library carrying a tray Changes the number of items, mainly for the items in the library discontent whole tray needs to be adjusted some data related to the change. The main changes in the number of items handled tray, the tray to update data in the electronic tag items, while updating the corresponding data.

Database management. The most important function of this module is to audit the goods out of the library. Goods for the library system needs to be carefully audited, controlled goods information on the library notice and cargo container by the breakdown and handheld RFID reader to read electronic tags inside to see whether the input errors or omissions, cargo the name, quantity, etc., etc. are the same, if the same, then the use of facilities and equipment and warehouse regional planning system to determine the library platforms, completed by truck loading operations, the actual progress of jobs and other correction data input standby database as a repository add item database, a reduction of inventory database and print out the voucher documents and all kinds of practical library work report.

Reported loss management. Damaged goods can be generated by this single function, query, modify its operating status is processed. RFID dynamic is management. This module includes treating logistics management Basic information security

Equipment, implants, while taking advantage of reading and writing device for the collection of information across space stored within the RFID tag of its circulation, and then passed through the entire logistics information system database data conversion layer. This module is the cornerstone of the entire run RFID logistics information systems, while carrying the carrier of information flow and transfer function for the good functioning of the follow-up of each module plays maintain function.

Statistical Analysis. Statistical analysis module mainly pooled analysis of daily business, including: cost statistics, business statistics, product statistics, and customer statistics.

Financial management: including product account management, inventory management accounts of two functions. Account management products can query a product over a period of time out of storage conditions. Inventory account management can query a product over time inventory changes.

Conclusions

Use networking technology, companies can optimize the supply chain management system management processes and structure, improving the speed and accuracy of information transmission and physical match, improving the supply chain works. In this paper, the connotation of things, things key technology and supply chain management systems and many other aspects of analysis and discussion, completed the design, application and implementation of integrated design optimization system based on Internet of Things technology enterprise supply chain business processes.

References

[1] Ronald H. Ballou .Business Logistics Management. [J]. ACI Materials Journal 1988, 85 (6): 583-593.

[2] Abolhassan Astaneh-As. Comprehensive Transportation [R/OL]. 2002 [2006-09-20]. http: //www. ce.berkeley. edu /~astaneh /1-Research /blast/

[3] JCI-SF4 Method of test for flexural strength and flexural toughness of fiber reinforced concrete (Standard SF4) [S]. JCI Standards for Test Methods of Fiber Reinforced Concrete, Japan Concrete Institute, 1983: 45-51.

[4] ASTM C1018 Standard test method for flexural toughness and first crack strength of fiber reinforced concrete [S]. ASTM Standards for Concrete and Mineral Aggregates, V. 04.02, Standard Designation C1018, 1989.

[5] Guo Wenjun, Ramon Gilsanz. Nonlinear static analysis procedure) Progressive collapse evaluation [R]. Design Engineers of GilsanzMurray Steficek, LLP., 2003:1-11.

[6] Corley W G. Applicability of seismic design in mitigating progressive collapse [R/OL]. [2006-09-20]. http: //www.nibs. org M/ MC /

Advanced Materials Research Vols. 989-994 (2014) pp 5524-5527
© (2014) Trans Tech Publications, Switzerland
doi:10.4028/www.scientific.net/AMR.989-994.5524

A study on the data design of residents electronic health records system

Liu Ning

Jining Medical University, Jining, Shandong, 272067, China

yideyou9@163.com

Key words: residents electronic health records; Health records system; Database design

Abstract. Residents' health records is different from general hospital medical records, because it is not just about people receive medical service records, or a continuous, sustained, long-term, comprehensive, more extensive information about health information. This article according to the actual situation to the residents of electronic health records system database design are analyzed, and the residents' information table, the doctor information table, a medical information table, health file information table, travel information table and announcement information table 6 design of basic data table made a specific description.

Introduction

Both in developed and developing countries, health is the focus of attention, health for all human beings are trying to target, the basis for achieving this goal is to establish and implement a comprehensive health records, the health of all residents are unified into management. Residents' health records is different from general hospital medical records, because it is not just about people receive medical service records, or a continuous, sustained, long-term, comprehensive, more extensive information about health information. It has a high value in clinical practice, and more important to scientific research and medical education with valuable information. But each country's health records still exist many problems, for example, many countries and regions are still using paper files, most convenient also focused on the clinical medical purpose, the application range is not wide. Of course, this development with the basic national conditions of each country, the situation is closely related to social and medical conditions, and in the specific implementation process, also will have a lot of big hospital business management complex, hospital information there is no universal norms, standards and legal basis of the difficult problems such as lack of necessary data exchange. This article according to the actual situation to the residents of electronic health records system database design is analyzed, to provide the reference for related work.

The database design principles

In order to ensure the database of the clear and strong, as far as possible to maintain data integrity and cleanliness, custom database tables and fields demand as succinct as possible, redundant data should be as little as possible, which means that duplicate data should be reduced to a minimum. For example, the residents can't each table has a contact, or it will causing problems for data maintenance and consistency check. When a resident's contact details change, you need to update multiple tables to implement the action, if you have a table was unfortunately ignored, then it may lead to data inconsistency.

Database Concept Structure Design

After demand analysis, operation of the user's public electronic health records system has three roles; these are residents, doctors and administrators. System functions mainly include news announcement management, personnel management, hospital management, system management and so on four modules. Database concept structure design is to get the user demand for abstract information structure; typically with e-r diagram is described. ER diagram is a problem-oriented conceptual

model, which describes the representation does not involve data in the database and access methods. ER diagram of the basic elements that constitute the entity type (Entity) attributes (Attribute) and contact (Relationship), in this system, there are six major entities, that residents, doctors, administrators, archival records, bulletin information, medical records, travel information. Due to space limitations, this article is no longer listed ER diagram of the system.

The design of the database logic structure

According to the actual demand, general residents' database of electronic health records system mainly contains information table, the doctor information table, a medical information table, health file information table, travel information table and announcement information table 6 basic data tables.

The residents' information table. Residents information table including residents number, name, password, gender, date of birth, telephone number, home address, and notes and other basic information about the residents, their fields, type, length, etc. Specific requirements are shown in Table 1, residents' number that uniquely identifies the field as the residents, asking them to main keyword, and not be empty. In addition, it is only store the basic information such as date of birth, gender, don't store residents' age, height, weight and other information changes at any time.

Table 1 Residentss' information data table design

Field name	Instructions	Type	Length	Can be empty	Primary key
UserID	residents' Number	int	18	N	Y
xm	name	varchar	10	Y	N
mm	Password	varchar	20	Y	N
xb	gender	char	2	Y	N
sfzh	ID number	varchar	18	Y	N
phone	Phone	int	11	Y	N
birthdate	Date of birth	datatime	8	Y	N
adrress	Home address	varchar	50	Y	N
bz	Remark	varchar	100	Y	N

The doctors' information table. Residents' information table including Doctor No., name, password, gender and departments, where hospitals, job title, whether administrators, and notes and other information, specific requirements field, type, length, etc. As shown in Table 2. Residents of electronic health records system should be universal in all hospitals in a region, Therefore, doctors attribute not only to set the home department, but also indicate from which the hospital.

Table 2 The doctor information data table design

Field name	Instructions	Type	Length	Can be empty	Primary key
DocID	residents' Number	int	8	N	Y
xm	name	varchar	10	Y	N
mm	Password	varchar	20	Y	N
xb	gender	char	2	Y	N
ks	Subordinate departments	varchar	10	Y	N
hospital	The hospital	varchar	50	Y	N
zc	Title	varchar	10	Y	N
isAdmin	Whether the administrator	bit	1	Y	N
bz	Remark	varchar	100	Y	N

Medical Information Sheet. A medical information table including medical number, number, age, height, weight, family history of genetic, primary physicians and medical check-up date and other

information, generally will increase if there is a field of common diseases gastritis, tuberculosis, hepatitis, heart disease, etc. It is used to record whether the residents have similar medical history, specific requirements field, type, length, etc. As shown in Table 3. The table with the residents by resident ID information table associated, doctors and physicians through the main inspection information table associated with it. Residents of each physical examination in this table have a corresponding to a record, all the medical information can be retrieved by the resident population numbers.

Table 3 Medical information data table design

Field name	Instructions	Type	Length	Can be empty	Primary key
tjID	Medical ID	int	12	N	Y
userID	residents' Number	varchar	18	N	N
nl	Age	int	3	Y	N
tall	Height	int	4	Y	N
weight	Weight	int	3	Y	N
jbby	Gastritis	bit	1	Y	N
jbfjh	Tuberculosis	bit	1	Y	N
jbgy	Hepatitis	bit	1	Y	N
jbxzb	Heart disease	bit	1	Y	N
jzs	Family genetic history	varchar	2000	Y	N
tjDate	Examination date	datetime	8	N	N
docID	The main check doctor	int	8	N	N
bz	Remark	varchar	100	Y	N

Health Records Information Table. Health record information table includes the file number, the residents' number, age, treatment concluded, filing date, filing and physician notes and other information, its fields, type, length, etc. Specific requirements are shown in Table 4. The table with the residents by resident ID information table associated, doctors and physicians through the main inspection information table associated with it. Residents of visits or medical records in this table have corresponding a record, by residents' number can query to all the residents' health records.

Table 4 Health Record Information Data Table Design

Field name	Instructions	Type	Length	Can be empty	Primary key
recordID	File number	int	18	N	Y
userID	Residents' number	varchar	10	N	N
nl	Age	int	3	Y	N
jzjl	Conclusion visits	varchar	50	Y	N
recordDate	Filing date	datetime	8	N	N
docID	Filing Physician	int	8	N	N
bz	Remark	varchar	100	Y	N

Itinerary. The itinerary is the doctor's visits arrangements to facilitate medical appointments or medical residents, including stroke number, time, location, and other subjects and Memo fields are checked.

Table 5 The itinerary table

Field name	Instructions	Type	Length	Can be empty	Primary key
xcID	Tour Code	int	10	N	Y
xcDate	Time	datatime	8	Y	N
addr	Location	varchar	20	Y	N
km	Account	varchar	10	Y	N
bz	Remark	varchar	100	Y	N

Announcement Table. Announcement table used to store the system information announcement issued, including the number, title, content, authors and time and other fields.

Table 6 The Announcement Table

Field name	Instructions	Type	Length	Can be empty	Primary key
annID	Notice No.	int	10	N	Y
title	Title	varchar	30	N	N
content	Content	varchar	500	Y	N
author	Author	varchar	10	Y	N
addTime	Time	datatime	8	Y	N

Summary

Residents' electronic health records system is the core of human health throughout their entire life stages, the correct approach is "one filing, lifetime use", therefore, in the construction process, it should be possible to standardization, specialization, particularly in the design of the database requires a unified standard, so that different regions and hospital data can be generic, and so as to realize the co-construction and sharing, avoid detours, rework.

Source: A Project of Shandong Province Higher Educational Science and Technology Program, Project No. J14LN77

References

[1] Daniel J. Friedman, R. Gibson Parrish, and David A. Ross. Electronic Health Records and US Public Health: Current Realities and Future Promise. American Journal of Public Health,2013,103(9):1560-1567.

[2] Wu Sijing, Guo Qing. The application status and development dilemma of domestic and foreign electronic health record. Chinese general medicine, 2011, 14 (2): 226 – 228.

[3] Shabestari O,Roudsari A.Challenges in data quality assurance for electronic health records. Stud Health Technol Inform. 2013,183:37-41

[4] Yang Jian, Hu Xinping, Dong Jiancheng. Cloud based regional electronic health records storage and exchange framework. Journal of medical information, 2010,31 (3): 54-57.

[5] Tate AR, Beloff N, et al. Exploiting the potential of large databases of electronic health records for research using rapid search algorithms and an intuitive query interface. J Am Med Inform Assoc. 2014,21(2):292-298.

[6] Liu Xiaofang. Management and application of electronic health records of urban and rural residents. Journal of community medicine 2013,11(23):28-29.

[7] Heisey-Grove D, Danehy LN, et al. A national study of challenges to electronic health record adoption and meaningful use.Med Care.2014,52(2):144-148.

[8] Francis T. Electronic health records: where we are and where we're going. Physician Exec. 2013,39(4):82-84.

[9] Dong Jiancheng, Yang Jian, et al. Cloud computing based electronic health records system construction conception and practice. Chinese Journal of health information management, 2010,7(6):43-46.

[10] Rodrigues JJ, de la Torre I, et al. Analysis of the security and privacy requirements of cloud-based electronic health records systems. J Med Internet Res.2013,15(8):e186.

Advanced Materials Research Vols. 989-994 (2014) pp 5528-5531
© (2014) Trans Tech Publications, Switzerland
doi:10.4028/www.scientific.net/AMR.989-994.5528

Research on emotional interaction design of mobile terminal application

Xiaomeng Mao

Shanghai JianQiao University, Shanghai 201319, China

25575355@qq.com

Keywords: emotional interaction design; interaction design; mobile terminal

Abstract. Discusses the realization of the path of the mobile terminal application software emotional interaction design. Analyzed design features of mobile terminal application software with combined hardware and software features. Analysis of the current features of emotional interaction design software applications. People's basic functional requirements of the mobile terminal application software for rising to the emotional and reflective user experience. Realize the emotional user experience needs improvements of interactive mode; interface design patterns; human-computer interaction applications feedback and deep-rooted experience of the target software features.

Introduction

In the rapid development of mobile terminals today, people's smart phones, tablet PCs have been a growing number of applications APP, APP and its people have noticed the interaction design of mobile terminals. More and more manufacturers are on this emerging platform for their own place. And how to make the APP in can meet the demand of the user experience of deeper more and more attention by people.

The characteristics of the mobile terminal application software interaction design

With the continuous development of mobile terminals, mobile terminal positioning of software are also constantly changing. From the initial PC-side software to be ported to the current mobile terminal centric software group, such as microblogging, letters and so on. Software mobile terminal relative to the desktop PC platform is unique in its development.

The use of the mobile terminal characteristics. The current mobile equipment has obtained huge development. Smart phones have greatly popularized the handset software applications. At present most of the software are developed a version of the mobile terminal, people can use these software using handheld devices anytime and anywhere.

The characteristic of mobile devices has decided the application on this platform has its features: First of all, as a result of the mobile terminal screen is limited by the size, and mobile terminal integrates many sensors, makes the application software are free to call these sensors for interaction design. And the use of the touch screen has been accepted by most users, accelerometer and gyroscope sensor such as there are a lot of potential.

The second is that people in the use of mobile device environment is more complex, probably on public transportation, the light of the road, is more likely to be in dim the pillow and so on. Most of the current application software design is more concise appearance and contrast the stronger or darker flexible interface design.

Finally, and using the characteristics of the important feature of mobile terminals, is that the current mobile terminal is highly personal and general use are relatively private. In today's software emphasized user, on the basis of the concept, everyone in a more intimate used for mobile terminal software. Each software is to some extent represents a personal login account on behalf of a piece of software added to a person with this software-centric social network.

Interaction characteristics of mobile terminal

Interaction design characteristics of the current mobile terminal platform software is given priority to with interaction of multiple sensor technology based on touch screen, touch with finger along with voice, accelerometer, gyroscope and light sensors and other operation mode of mobile terminals to interact.

An emotional interaction design

Emotional designs. Norman at three different levels of cognitive and emotional "Emotional Design" a book made of the process, namely visceral, behavioral and reflective. Among them, which is designed instinct-based design, which is a direct response to people usually easy to notice the parts, such as visual and other senses. The most direct can feel the change in the design to bring. For the behavior level design is perfect for the user's behavior. In Norman's theory, behavioral-level processing in three levels directly affect the other two levels of processing, because users use the product as the ultimate goal is to complete the goal. If it is not centered on behavior level, a product is likely to lose its real value. Rethinking design are the three levels of one of the most not intuitive, but reflect on design for product build long-term relationship with users. To match the instinct to design, to reflecting the emotional design, user will establish emotional bond with the product [1-3].

The realization of interaction design goal. Norman has not proposed method in the "emotional design" in the three-level theory in design practice and user studies. Alan cooper in the "About face 3" will correspond to the three levels of the three target user. Alan cooper mentioned three objectives were: experience goals; ultimate goal and purpose in life. At this time of everyone is talking about the user experience, user experience seems to be beyond some of the important indicators into the highest goal of interaction design. Because human beings are emotional animals, people in the use of the product, can really influenced by product design, if the experience is not good, people feel stupid or uncomfortable, will naturally cause changes leading to the user of the product to disgust.

Users in the use of a product are the fundamental motivation for the product they need to help them complete a basic goal that is the ultimate goal. Users before using this product will have a desired result, satisfied the user of this is become one of the most important goals determine product overall experience.

People in the use of products, there will be a situation of the vision, it is beyond the product design, and life goals expressed the user's personal desire. This is why the user to complete the final goal of drive and motivation, or is the real purpose behind the final goal. This can be embodied in, users expect a better life, to work in some way, achieving ideal and so on.

In interaction design, the current mainstream direction is to achieve continuously improve people's interaction experience. This is in interactive design experience goals.

Emotional interaction designs. Emotional interaction design is before two characteristics after interaction design to satisfy the need to achieve a new goal. The purpose is to let users to human-computer interaction feel more human, and not just the interaction with machines. At the same time, the emotional interaction design is through the different form to the user to create a comprehensive experience, the experience may through a humanized interface design can reflect, may need a whole set of the man-machine interaction pattern can reflect. In the mobile terminal platform, can use a variety of integrated equipment, emotional interaction design goal becomes more likely to be fully realized.

The main form of the mobile terminal design reflects the emotional interaction

Reflect the main form of emotional interaction. Product main forms including reflect emotional interaction: the application software of main interaction patterns; interface design pattern; application of human-computer interaction feedback; software functions of deep experience goals.

First, the interaction patterns reflected in the main interactively products. Most current software interaction patterns with touch screen click, sliding. There is also some frontier software using the

touch screen gestures. To clear the software, for example, which is a wholly gestures notepad software, it does not have a dedicated button controls. Users only need to be on a touch screen to sign all the operation can complete the software. This concerned in the interaction design of mobile terminal software has caused many discussions in the crowd.

The second, the interface design pattern is embodied in the basic set up to meet the viewing habits of people and the interaction of people used to give priority to. After the multi-touch screen is widely used, people mainly use finger interactions; it is the interface controls such as buttons on the new requirements are put forward. So much of the current mobile terminal software to meet people mainly controls the size of a finger, fully embodies the design concept for the center with itself characteristic.

Third, feedback, people in the use of mobile terminal the easiest question is that how the machine feedback has been done to the people. In a traditional PC, due to equipment limited, only through sound and image to feedback to the user. The mobile terminal has its advantages, such as vibration. Android platform of smart phones generally set with a touch of micro vibration, to make up for the touch screen brings feedback problem.

Fourth, behind the function of the software to provide people, how to make software for a long time remain in the user's mobile terminal in a matter of great concern to all manufacturers. Such as gaming companies, how to make the game with a viscous, let the user as long as possible to maintain interest in the game; Functional software such as notepad, to remind the software, how to enable users to focus on software, and so on for a long time. This requires the function of software and content ideas can satisfy the user's deep emotional needs.

Emotional interaction design application analysis. Currently it has been a part of the application software has been used emotional interaction design concept. Because the target user experience is different, the use of application software for mobile terminal characteristics has done many improvements.

In Netease news, for example, as a web page to mobile client transplantation, the user carrying the expanded scope of the availability of the user is enhanced several tasks. Netease news has chosen the people most concerned about a few big news classification, and by as much as possible on a mobile device within the limited screen size to display the need of news content. Netease news compared with several other client differences is interactive. In each of the news, the user can press carried a message to this thread, which has played a significant use of the characteristics of mobile devices. To the people to the discussion of some hot news created platform, it in people's emotional have a way of the communication. At the same time, netease news mobile client for individual users in the use of background characteristics joined the night mode, fully consider the use environment of the iPhone and other mobile devices, by lowering the brightness contrast and color Settings interface, let people browse news experience more comfortable in bed. For users in different, netease news using GPS module to set the automatic location of the device and display the local news and weather patterns. This module Settings with around characteristics to people's emotional also brought a lot of help, people like to communicate with a local press officer. In pieces give full play to the user time, netease news list of news column was optimized [5-7]. Netease news under the headline in one sentence: sum up the main content of the news, let users can browse the news list roughly to master the main content of the news, when I was greatly save the user's valuable time.

A current hot game software called "you draw I guess," the game comes from a very common game. But be transplanted into represented by touch screen mobile terminal platform, after the game, not only has realized the inherited the interaction of the real game experience, more to extend people's emotional interaction.

In real life, "I guess you must be a few people at the same time in one place. Speculation and the game process and graffiti has occupied the people a lot of time. In the mobile client version you draw I guess, users can easily use the networking of the mobile devices and any people all over the world. Greatly enhance the space range over the game. On the game time, as a result of simultaneous set the game, the user can at any time to open the game playing with other users. Thus caused a total of time and space, in this time, there is no time difference between people, there is no distance [8]. For people

of the quickening pace of life today, this is a very good with your family, friends of communication space.

Emotional interaction design

In the latest release iPhone5s, integrates let a person feel strange and familiar with the equipment - the fingerprint sensor. Although fingerprint sensor has been applied in early on the PC, but for the mobile terminals equipped with this device has a deeper meaning. Because it can reflect the characteristics of mobile terminal - more personal, the role of the mobile terminal from ordinary personal electronic devices gradually turned into an interface of a natural person in the online world. With the fingerprint sensor, after people get rid of the login user and password in the various application software process, greatly improving the user experience.

Now, more and more applications to focus on the comprehensive utilization that various sensors on mobile devices. It's including the gravity sensor, gyroscope, and touch screen, GPS positioning module and a microphone and camera. So behind in providing people with good software interaction, are actually in the direct indirect emotionally to people to support, make people in reducing the consumption of emotion in human-computer interaction. And some social, interpersonal communication for the application of the ultimate goal is to meet the emotional needs of the people higher [9].

Interaction design is still considered the most current whole our common humanity, in the optimization of user experience on most are based on human cognitive or universal human common psychological basis. When interaction design to continue developing the most common user experience are basically completed, the user experience should be more on the basis of the different culture background and experience background, the optimization of users to make more detailed close [10]. Let people feel when using application software is not only complete the task, but in a way of life experience, feel closer to his ideal.

Conclusion

At present, mobile devices have greatly changed people's life, way of communication; at the same time also become an important part of people life. It is the need for interaction has not only stayed on the user experience, but by the higher spiritual and cultural needs. With the help of the current the most advanced personal communications terminal, set up a full range of communication through the network. Not only on the exchange of information, but also on the emotional culture communication. In the future mobile terminal application design, the product will be more people to consider cultural differences, national identity, using the background and personalized interaction design experience.

Acknowledgments
This work was financially supported by: private colleges backbone teachers' scientific research project of Shanghai (AAM12005). Author introduction: Xiaomeng Mao(1983-), male, lecturer, main research direction for interaction design, three-dimensional design. E-mail: maomxm@163.com

References

[1] Donald A. Norman emotional design. Qiong Mei, Beijing: CITIC Publishing House, 2003.
[2] (U.S.) Cooper, Arimidex, etc. About Face3 essence of interaction design. Songtao LIU Beijing: Electronic Industry Press, 2012.
[3] Jing Li, Shiguo Li from the perspective of human emotional interaction design exploration and product communication. Packaging Engineering 2008, 29 (9) :151-153.
[4] Xinqin Peng. Construction of emotional interaction and the design value. Journal of Chongqing institute of technology (social science edition), 2013.6:165-167.

Advanced Materials Research Vols. 989-994 (2014) pp 5532-5535
© (2014) Trans Tech Publications, Switzerland
doi:10.4028/www.scientific.net/AMR.989-994.5532

Intelligent classroom attendance checking system based on RFID and GSM

Hao Chen[1,a]

[1] (College of Chemistry and Chemical Engineering, Xuzhou Institute of Technology, China)
[a]chh_email@126.com

Keywords: RFID technology; GSM system; intelligent attendance checking

Abstract: Nowadays many colleges use galaxy network technology as well as computer and Internet technology, give full play to various technical means of information network and make good use of various kinds of various education, scientific research and information resources, develop all kinds of application system and management system, realize network interaction management, and thus fully promote the development of higher education informatization. An intelligent classroom attendance checking system is introduced in this paper. As an important part of campus management system, this system can intelligently complete examining students' attendance. In addition, this system can automatically collect data information in real time, automatically analyze and process the collected data, report these data using visual interface, and thus intelligently implement SMS notification at the same time. The traditional way is to assess, record and manage the attendance of students by roll call or magnetic card, which not only consumes the time, but also interferes with each other; while RFID student attendance application system is applied to manage the attendance of students using RFID technology, which not only completes the attendance checking conveniently and quickly, but also saves resources.

Preface

In recent years, RFID technology has been applied in many fields, including logistics, retail industry, manufacturing industry, clothing industry, medical care, identification, anti-counterfeiting, asset management, food, animal identification, libraries, automobile industry as well as aerospace and military affairs. It has had a significant impact on improving people's quality of life, enhancing the economic efficiency of enterprises, strengthening public safety and improving the level of social information.

1. Overall design scheme of the system

When using this system, students with RFID chip student card can complete auto-induction attendance checking when entering the classroom door without the need for touching clocking-in machine, and many people can achieve attendance checking when entering the door of school buildings simultaneously without the need for queuing; meanwhile, the reader can be controlled to upload the received information to computer terminal for processing, thus accurately recording the entering and leaving time of students as well as other information. The information of students who failed to attend the class punctually will be sent to the relevant person in charge of the attendance affairs through GSM system in the form of text messages. The block diagram is shown in Figure 1.

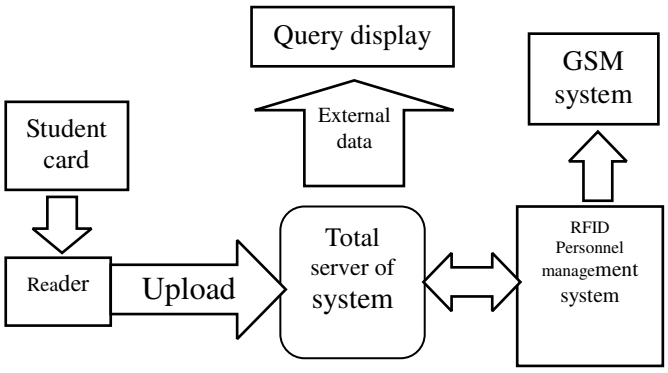

Figure 1 Block diagram of classroom attendance system

2. **RFID chip**

RFID chip is manufactured with CY-14443A series RF reader module. Using the chip dedicated for contactless reader based on ISO14443 standard, this module adopts 0.6 micron CMOS EEPROM technology, supports ISO14443typeA protocol, and also supports MIFARE standard encryption algorithm. An analog modulation and demodulation circuit is highly integrated in the chip, so the chip can work using a minimal amount of peripheral circuits, support UART interface (-C), I2C interface (-U) or SPI interface (-P); in addition, a digital circuit has two voltage working modes, namely TTL and CMOS. The chip is especially suitable for the reader application of billing system or identification system under ISO14443 standard, including water and electricity meter, vending machine, access control and telephone.

CY-14443A Series support Mifare One S50, S70, Ultra Light & Mifare Pro, FM11RF08 and other compatible cards. The cards can be detected automatically, and automatic card detection is the default state. CY-14443A series are all equipped with onboard built-in antenna, and external antennal can be connected. The advantages of built-in antenna are to improve the integration, read the card with a size of less than 6cm, basically meet most of the design needs without the need for externally connecting large antenna, and connect to the external antenna without the need for replacing the circuit, so as to improve the reusability of the system and significantly reduce the costs. In addition, the reading head of built-in antenna can be used as an active antenna. This module also adds 4kBits EEPROM, EEPROM byte addresses from 0x00 to 0x1FF to read PN and SN of PCD.

Single-chip microcomputer and RF module conduct communication using SC2 interface, with simple communication interface, as shown in Figure 2:

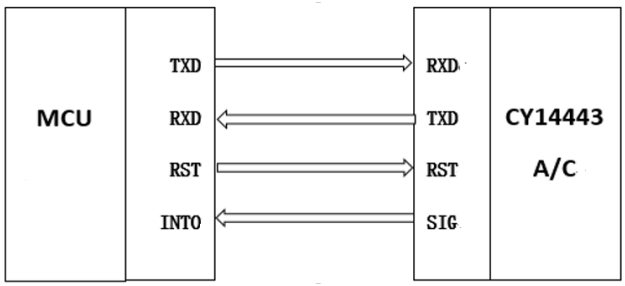

Figure 2 Serial connection mode of CY-14443A series RF reading and writing module

3. Software part

The central management and control software is the center of classroom attendance system. It is used to control the operating state of reader and RFID card as well as conduct statistical processing for the data of students when going into or leaving the classroom. The main features are as follows: it is easy to operate and control this software; the reader can be controlled and the data

can be transmitted through serial communication protocols; it is easy and convenient to input student information, with good maintenance and confidentiality; the statistical processing can be conducted for data quickly; this software has perfect data query functions.

The functional modules of system software mainly includes: user login module, real-time report and classroom leaving display module, reader control module, database management module and statistical processing module of data, as shown in Figure 3:

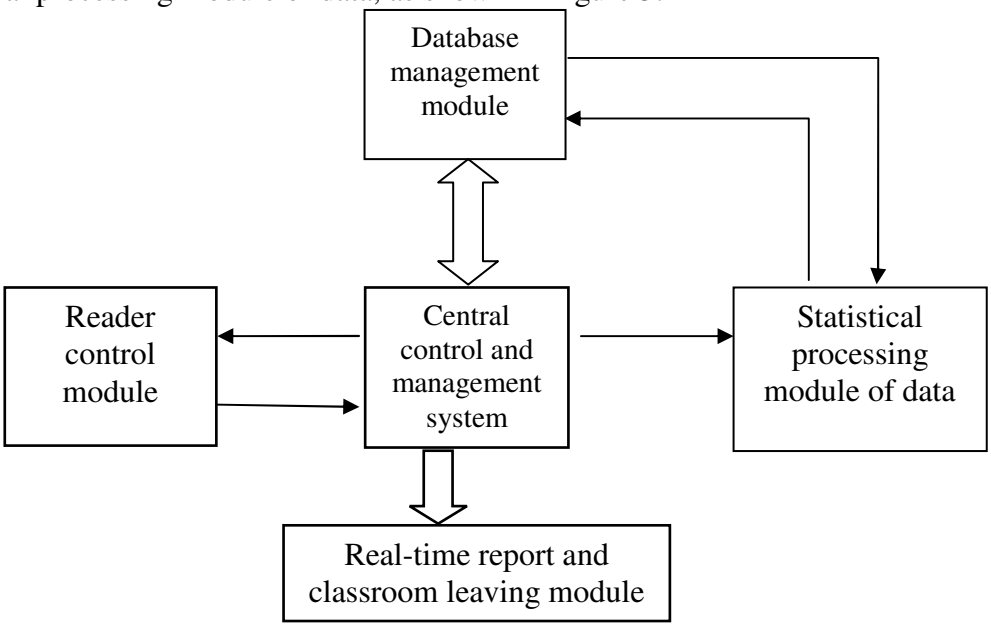

Figure 3 Software system display module

4. Part of relevant codes

```
private void btnrfido_close_Click(object sender, EventArgs e)
        {
            int i = int.Parse(comboBox1name.Text);
          //    int i =( int)comboBox1name.SelectedItem      ;
            // int j = int.Parse(comboBox2.Text);
              int j = 19200;
              //Read the card regularly
            timer1xunka.Enabled = true;
            // timer1xunka.Enabled = false ;
              timer1xunka.Interval = 1100;
              //Send short messages regularly
              timer1duanxin.Enabled = true;
            // timer1duanxin.Enabled = false ;
              timer1duanxin.Interval = 1000;
              if (btnrfido_close.Text == "Connect RFID")
              {
                    if (setupcom(i, j) == 0)
                    {
                          MessageBox.Show("Failed!");
                    }
                    else
                    {
                          btnrfido_close.Text = "disconnect RFID";
                          MessageBox.Show("Open success!");
```

```
                }
            }
            else
            {
                closecom();
                btnrfido_close.Text = "Connect RFID";
            }
        }
private void button3send_Click(object sender, EventArgs e)
        {
            if (sp.IsOpen)
            {
                SendSMS(textBox2duanxinzhongxin.Text, textBox1receivedhaoma.Text,
textBox3duanxinneirong.Text);
                MessageBox.Show("Sent successfully");
            }
            else
            {
                MessageBox.Show("Please open the serial port");
            }
        }
```

5. Conclusion

This paper studies the intelligent check-in of students through RFID system. The relevant data are displayed and processed at computer terminal, and intelligent SMS notification is conducted via GSM system. In the entire study and experiment process, good results have been achieved. The system can be installed in many places of the campus, and teachers and instructors can realize the real-time monitoring of student distribution in the campus only after logging in computer terminal system, thus greatly improving the efficiency of student management by colleges and universities. Moreover, this system can be used as an intelligent teacher conference report system, and it can be specifically used for relevant applications in governments, enterprises and other departments as an intelligent teacher conference report system, thus greatly improving the efficiency of conference management. It is believed that with the rapid development of RFID technology, this system will be continuously improved and widely used.

References

[1] Zhou Xiaoguang, Wang Xiaohua. RFID technology principles and application examples [M]. Beijing: Posts and Telecom Press. 2006,pp:12-26.

[2] Horng SJ, Chen YH, Run RS, Lai JL, Chen RJ, Chen WC. A novel anti-collision algorithm in RFID systems for identifying passive tags (J). IEEE Trans and Inform, 2010, 6 (1)， pp: 105 - 21

[3] He Hongjiang, Ding Xiaoye, Zhai Yaoxu. A study on the [J]. Computer application method to estimate the impact factor based on RFID tags, 2011, 11 (11), pp: 4131-4133

[4] Kong Lingzhong, Tang Dingjia. Application of RFID in electronic tag[J]. Information research, 2011, 2(4), pp: 17-22.

Advanced Materials Research Vols. 989-994 (2014) pp 5536-5539
© (2014) Trans Tech Publications, Switzerland
doi:10.4028/www.scientific.net/AMR.989-994.5536

Inflation Forecast Based on BP Neural Network Model

Yuechun Wen[a], Lina Tan[b*] Hailong Wu[c]

School of Economics & Management Tongji University Shanghai, China

[a]wenyc1965@126.com, [b]candytln@163.com, [c]hailongwoo@gmail.com

Keywords: BP Neural Network Model; Inflation Forecast; CPI

Abstract. This paper analyzes inflation forecast based on BP neural network model. Firstly, it reviews some references about BP neural network and finds that it is a nonlinear adaptive data-driven model with induction ability and a wide range of function approximation ability so that BP neural network could be applied into forecast research. Secondly, it builds up the BP neural network model to predict CPI, selecting the four indicators, which are excess liquidity, exchange rates, inflation expectation and macro-economic leading index. Then it carries out empirical experiment and takes advantage of the monthly data of the above four indicators from March 2005 to December 2012 to forecast CPI. The results show that when prediction period is 3 months, the maximum absolute error between forecast value and real value is 0.0139, and the minimum absolute error is 0.0005. When prediction period is 6 months, the maximum absolute error is not more than 0.02. It proves that BP neural network model can predict coming CPI trend at least 6 months according to the existing data and it means it is suitable for the study of inflation forecast.

Introduction

Since the 1990s last century, inflation has gradually become one of the world's core economic issues of common concern. Inflation can distort price, erode of savings and inhibit investment, hindering the healthy development of the economy. Therefore, how to effectively control inflation is the focus of monetary policy in a national central bank. Because there exists a time lag of monetary policy in the implementation process, how to accurately predict inflation is particularly important, in order to better achieve the goal of monetary policy. In this context, inflation forecast is of great practical significance.

Literature References

BP Neural Network (Back Propagation Network) was created by Rumelhart and McClell [1] in 1985, which is a kind of multilayer feed-forward network structure. It takes advantages of error back propagation algorithm to train network output and the outputs are commonly between 0 and 1. Neural network has the following four advantages which make it suitable for time variables forecast research.

First of all, compared with traditional theoretical model, neural network is an adaptive data-driven model and it only needs a few assumptions to build a model for the problem. So even if time variables' internal formation pattern is unknown or hard to describe, neural network can also learn from the training samples and the form a stable function relationship. Based on this characteristic, Han [2], Kuo & Sheng-Feng [3] pointed out that neural network can be seen as a multivariable, nonlinear and nonparametric statistical model.

Secondly, neural network has induction ability, and even if the training sample has a large amount of noise information, it can also correctly infer the trend of time variable through study. This point is very important, because forecast itself is to predict the future behavior based on the past and present through observation data.

Thirdly, the neural network has a wide range of function approximation ability. Hong[4], Huang[5] found that neural network could approximate any continuous function with arbitrary precision. Any prediction model assumes that time series have internal relationship between its past, other related variables (input variables) and future variables (target variable).

Last but not the least, neural network is nonlinear. Traditional forecast models such as ARIMA hypothesize inner forming process of time variables is linear, but Barra[6] pointed out that real economic system is generally nonlinear. So it is inappropriate to build linear models to estimate nonlinear time variable, which would easily lead to a larger prediction error. The nonlinear characteristics of neural network make it suitable for the nonlinear part of the time series and improve the forecast precision.

BP neural network model analysis

In order to facilitate the research, this model selects monthly data of the four indicators, which are excess liquidity, exchange rates, inflation expectation and macro- economic leading index from March 2005 to December 2012 to do forecast. The data is classified in the first place and generally 80% of input and target data are used to train the network and the remaining 20% are used to test the network. In this paper, the prediction period of neural network is classified into 3 months and 6 months, respectively, thus there are two different data sets and specific data classification is shown in the table below:

The network layer. Wang and Jianjun[7] have proved that a feed forward neural network containing only one hidden layer can approximate any continuous function, so this paper uses a three layers BP neural network structure that contains only one hidden layer.

Number of neurons in hidden layer. Determining the number of hidden layer's neurons has always been a very complex problem, because the number directly affects the nonlinear performance of the network. According to the experience, there are two reference formulas to determine the optimal number of hidden layer's neurons:

(1)$m = 2n + 1$, m is the number of hidden layer's neurons and n is the number of input layer's neurons.

(2)$m = \sqrt{\mathrm{n} + \mathrm{n}_1} + \alpha$, n_1 is the number of output layer's neurons and α is a constant between 1to10.

In this paper, the input layer has four input variables and the output layer has one variable. According to the above formula, the optimal number of hidden layer's neurons is 4 ~ 13, but the specific number would be determined by the network training error.

Transfer and training function. At present, there are three kinds of neural network transfer function: Log-sigmoid, Purelin and Tan-sigmoid. Log-sigmoid and Tan-sigmoid are s-shaped function while Purelin is linear function. Tan-sigmoid is suitable for input and output between -1 to 1, in line with the characteristics of input and output's normalized vector, therefore, it is taken as the transfer function of hidden and output layer. Traingdx is taken as training function, and this function's learning algorithm uses gradient descent momentum method. Moreover, the learning rate does not need to set additionally, which can automatically adjust according to the training process.

Steps training. Some related research pointed out that the accuracy of network had a great influence on the prediction: if it has low accuracy, forecast ability of the network is poor while high accuracy would easily lead to cause over fitting and the network's generalization ability is weak as

well. To avoid this phenomenon, this paper sets network's training to 1000 steps, and accuracy of training to 0.01. Other parameter values of the network are shown as follows:

Experiment and analysis

According to the above set of BP neural network parameters (programs are written using MatlabR2009b), and then specific network training can be carried out.

Determination of hidden layer neurons' number. In the process of BP neural network training, it needs to determine the optimal number of hidden layer's neurons, and in the former part of the paper, the number of neurons is temporarily determined as 4 to 13. Therefore, experiments were performed with different number of neurons. The selection criterion is the minimum value of network's error and the evaluation index is the mean absolute error (MAE).

There are 2 different prediction periods in the paper and both need to determine the optimal number of hidden layer's neurons. To make it simplified, Table 1 only gives neural network training results for prediction period as 3 months.

Table 1 Performance of different neurons table (prediction period is 3 months)

Number of neurons in hidden layer	Training error	Training steps	Number of neurons in hidden layer	Training error	Training steps
4	0.0097	298	9	0.0070	246
5	0.0048	145	10	0.0079	329
6	0.0061	234	11	0.0075	332
7	0.0053	228	12	0.0085	224
8	0.0039	131	13	0.0064	244

The experimental results in the table show that when the number of neurons is 8, it could get minimum training error, and only after 131 times it reaches the target error set by the network. As a consequence, the optimal number of hidden layer's neurons is 8. Although when the number of neurons is 5 and 7, the training error is also small, they need more training steps, increasing the network's training time. In addition, with the number of hidden layer's neurons becoming larger and larger, the network training error is not smaller. For instance, when the number is over eight, the training errors increase obviously. However, too few neurons would also reduce network's classification capacity and this would also make the network lack of efficiency, such as when the number of neurons is 4, the training error gets to the maximum.

Forecast and analysis. This paper selects the former 20% of training data set as a confirmation group to verify. As to network, confirmation group is a set of known data and the specific results are shown in the Fig. 2.As we can see that structure of the well trained network is stable. The neural network's maximum absolute error of prediction period for 3 months and 6 months is 0.0047, 0.0064, respectively. Basically it is a satisfactory network structure and the network testing can go to the next step.

From Fig. 3, we can get that prediction effect is good for the three months static forecast. The CPI trend for future direction is basically consistent with the actual trend, and as to the specific month's CPI point forecast, the estimate accuracy is also high. The maximum absolute error is 0.0139, and the minimum absolute error is 0.0005. As for six months forecast, the forecast and the real value is relatively very close with the maximum absolute error not more than 0.02.

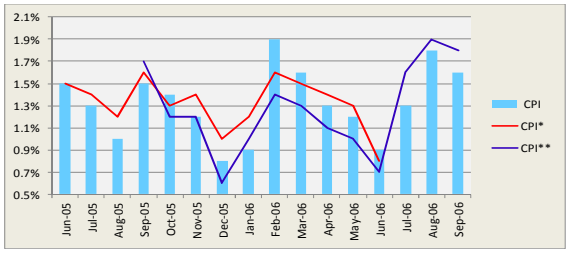

Fig. 2 Test results of BP neural network model*

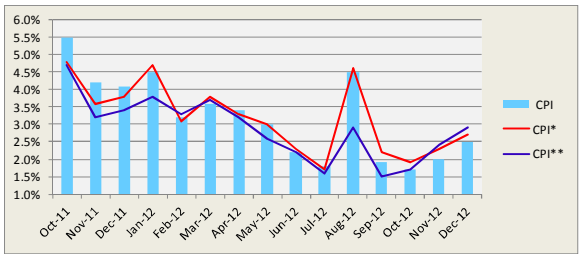

Fig. 3 Forecast value and real value trend chart *

Summary

The BP neural network as a new prediction method begins to get applied in the field of inflation forecast more and more often in recent years. This paper takes four factors into consideration, which are excess liquidity, exchange rate, inflation expectations, and macroeconomic leading index to forecast CPI and then carries out empirical test based on BP neural network model, using monthly data from March 2005 to December 2012. The model has two different forecast periods, including 3 months and 6 months, respectively. The empirical results show that forecast effect of the neural network is good and it also proves that BP neural network model is suitable for inflation forecast research.

ACKNOWLEDGMENT

This research was supported in part by NSFC projects (71273190) and The Major Projects of National Social Science Fund(11&ZD139).

References

[1]. Rumelhart, David E., and James L. McClelland. On learning the past tenses of English verbs. Institute for Cognitive Science, University of California, San Diego, 1985.

[2]. Han, Chang-Wook. Fuzzy Neural Network-based Time Delay Prediction for Networked Control Systems. Appl. Math 8.1 (2014): 407-413.

[3]. Kuo, Sheng-Feng, et al. A comparative study on the estimation of evapotranspiration using back propagation neural network: Penman–Monteith method versus pan evaporation method. Paddy and Water Environment 9.4 (2011): 413-424.

[4]. Hong, Ying-Yi, Huei-Lin Chang, and Ching-Sheng Chiu. Hour-ahead wind power and speed forecasting using simultaneous perturbation stochastic approximation (SPSA) algorithm and neural network with fuzzy inputs. Energy 35.9 (2010): 3870-3876.

[5]. Huang, Sunan, and Kok Kiong Tan. Intelligent friction modeling and compensation using neural network approximations. Industrial Electronics, IEEE Transactions on 59.8 (2012): 3342-3349.

[6]. Barra, Adriano, Giuseppe Genovese, and Francesco Guerra. The replica symmetric approximation of the analogical neural network. Journal of Statistical Physics 140.4 (2010): 784-796.

[7]. Wang, Jianjun, and Zongben Xu. New study on neural networks: the essential order of approximation. Neural Networks 23.5 (2010): 618-624.

* CPI: Real CPI value; CPI*:Prediction period is 3 months; CPI**:Prediction period is 6 months

Advanced Materials Research Vols. 989-994 (2014) pp 5540-5543
© (2014) Trans Tech Publications, Switzerland
doi:10.4028/www.scientific.net/AMR.989-994.5540

Research on Related Model for Urban Public Crisis Handle Mechanism

Yongchang Ren

College of Information Science and Technology, Bohai University, Jinzhou, P.R. China

1213552916@qq.com

Keywords: urban management; public crisis; handle mechanism; evaluation model; prediction model; stakeholders

Abstract. China is in a critical period of urbanization, and various social contradictions continue to be accumulated, emerged and enlarged, so public crisis management mechanism has been highly valued by governments at all levels with the public crisis events are occurred frequently. The paper conducts study for the problems in the current urban public crisis handle mechanism. First, the evaluation model of crisis management can be researched, and crisis management can be divided into four stages to evaluate respectively, they are Reduction, Readiness, Response and Recovery; then, we should research crisis prediction model to strengthen prediction, prevention and monitoring of the crisis before the crisis happened; finally, stakeholders analysis model should be studied, and scientific analyzing the interests of the various stakeholders and the relationship among them. From the theoretical point of view, the paper carries on a study for crisis handle mechanism to provide support for improving the crisis handle level.

Introduction

"Public Crisis" is an abnormal state and event with high uncertainty, instability and threatening, and it can cause serious damage to lives and properties, cause widespread panic in the public psychology, disrupt normal social orders and public relations and destroy the basic social values and norms. Public crisis handle is an important area of public administration, is an organized, planned, ongoing dynamic management process, and the government must take a series of control behaviors at different stages of crisis development to effective prevent, treat and eliminate crisis for the potential or current crisis [1,2].

Our country urban public crisis handle management is still in its infancy. There are many problems in China's public crisis handle work, so it still has a long way to go, compared to the western developed countries which have a perfect crisis handle management system and mature crisis handle mechanism such as United States, Japan and Russia. The majority of our local governments' contingency response system is very immature because it just amends and supplies the original disaster management system. In addition, there are many problems in China's urban public crisis management, and there is a considerable distance between our urban public crisis management and its theoretical assumption, so the research efforts of China's urban public crisis management still need to be strengthened. The relevant model of urban public crisis handle studied in this research provides support for the management of public crisis handle and decision-making.

Crisis Management Evaluation Model

The evaluation of crisis management is an important aspect of crisis management. Evaluating the crisis events and approaches can help us identify crisis events, and it also can look for ways to prevent the crisis from happening again and improve treatment measures of response and rebuild action. Scholars at home and abroad focus on evaluation method of crisis management performance, establishment of evaluation index system, institutional construction of crisis management evaluation, crisis handle process evaluation and other aspects in crisis management evaluation.

Crisis management evaluation model studied in the paper bases on the famous 4R model which proposed by America crisis management expert Robrt Heath. Public crisis management is

composed of reduction, readiness, response, recovery, so we can take the first letter in English to become 4R model, and the structure shows in Fig. 1 [3,4]. Transverse is the four stages of the crisis evolved, and lengthwise divides the evaluation content of crisis into three factors and the evaluation content at each stage can be evaluated from these three factors.

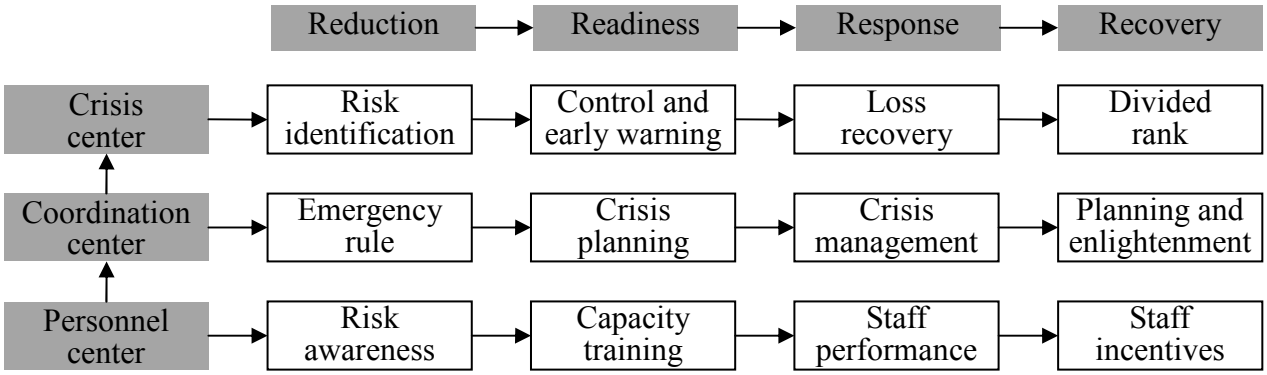

Fig. 1. Crisis management evaluation model

Four stages of the crisis evolved are illustrated as follows: Reduction is the core content of crisis management. The occurrence and impact of the crisis can be reduced by reducing risk, avoiding wasting time and diluting poor resource management; Readiness mainly conducts crisis prevention, and the relevant government departments can choose various experts, so a crisis management team is consisted to develop crisis management plans and conduct daily work of crisis management; Response, which emphasizes crisis comes, is that the relevant departments should make what kind of reaction to resolve the crisis strategically; Recovery includes two aspects, it can provide experience and support for future crisis management to avoid repeating the mistakes of history.

Three elements of evaluation content are explained as follows: Crisis center: the source of the crisis, the control of crisis and precaution system, the partition of crisis level and restoration from losses caused by the crisis belong to the scope of the crisis center; coordination center is a process which the managers make great effort to when they manage activities, deal with crisis and communicate with people; personnel center is all the personnel involved in crisis management, it includes managers, victims, bystanders and so on.

Crisis Event Prediction Model

This paper selects GM(1,1) prediction model that is based on the theory of gray, and the model is expressed as follows [5,6]:

Leting the original series is $x^{(0)}$, and the series generated by 1-AGO is $x^{(1)}$, and the differential equation model is established according to the cumulative created series as follows:

$$\frac{dx^{(1)}}{dk}+ax^{(1)}=u \tag{1}$$

The discrete form of solution is described as follows:

$$x^{(1)}(k+1)=\left(x^{(0)}(1)-\frac{u}{a}\right)e^{-ak}+\frac{u}{a} \tag{2}$$

You can get the predicted cumulative sequence according to this model to analogy when you determined the parameters *a* and *u*, and when it passed the examination, then cumulating it to get predictive value. Modeling steps are as follows:

(1) The original sequence of $x^{(0)}$ can be cumulative generated series of $x^{(1)}$ according to the following formula to calculate;

$$x^{(r)}(k)=x^{(r-1)}(1)+x^{(r-1)}(2)+\cdots+x^{(r-1)}(k)=\sum_{i=1}^{k}x^{(r-1)}(i)=x^{(r)}(k-1)+x^{(r-1)}(k) \tag{3}$$

(2) Using the least square method according to the following formula to determine the model parameters for $x^{(1)}$;

$$\hat{a} = [a \quad u]^T = \left(B^T B\right)^{-1} B^T y_N \tag{4}$$

(3) Building prediction model and calculating cumulative sequence;

$$\hat{x}^{(1)}(k+1) = \left(x^{(0)}(1) - \frac{u}{a}\right)e^{-ak} + \frac{u}{a} \tag{5}$$

(4) Conducting residual test for prediction model;

(5) The upper and the lower bounds of the predictive value should be determined according to future changes in the system, namely the gray plane can be determined according to the following formula;

upper bound: $x^{(1)}_{\max}(n+k) = x^{(1)}(n) + k\sigma_{\max}$; lower bound: $x^{(1)}_{\min}(n+k) = x^{(1)}(n) + k\sigma_{\min}$.

In the formula, it is an increased upper bound of $x^{(0)}$ when the $\sigma_{\max}$ in behind of n point; it is an increased lower bound of $x^{(0)}$ when the $\sigma_{\min}$ in behind of n point.

(6) Using the model to predict. Using accumulation to generate predictive value of series $x^{(1)}$, and using regression to restore it, so that you can get the predictive value of the original series $x^{(0)}$, such as the prediction can be completed once meet the condition of gray factor.

Stakeholders Analysis Model

At present, China's public crisis management is a critical transformation period from the traditional "vertical management" to multiple collaborative governance. This requires us to form networked multi-management structure of "transverse to the edge, vertical to the end, the layers of contact, interlocking" objectively. Elements of the structure are extremely complex, and the complexity determined its operation mechanism, at the same time, it corresponding means that it inevitably involves in governing relationship between the government and society, between citizens, between communities, between behavioral relationship of interest groups and interest relationship. Therefore it is necessary to build stakeholders analysis model of multiple interests in public crisis, and it shows in Fig. 2 [7-9].

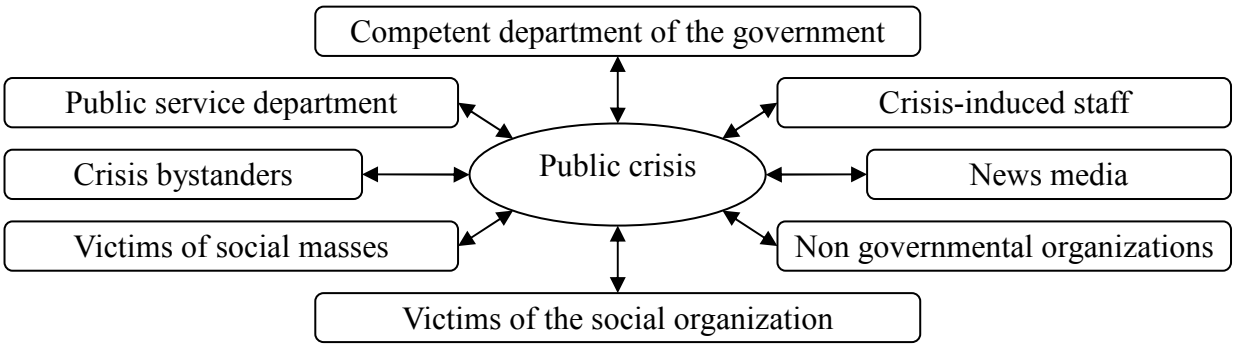

Fig. 2. Stakeholder on public crisis

As can be seen from Fig. 2, stakeholders include eight categories. Drawing on the thinking of "Mitchell score", stakeholders are classified as follows according to the relevancy, impact and urgency of stakeholders in the public crisis:

(1) Strong core stakeholders are the urgent organizations which have high relevancy and large influence in the occurrence and treatment process of public crises, and they have the responsibility and obligation to manage crisis. This kind of stakeholders mainly refer to competent government departments related to crisis and those induced by the crisis in the public crisis.

(2) Vulnerable core stakeholders are organizations or individuals with weak influence but have the urgency, and its the occurrence of the crisis is correlated to influence height, and they include

both public victims and victims of social organization. They expect to get proper rescue and remedy and recovery of interest in a public crisis.

(3) Fringe stakeholders refer to the organizations which can participate in crisis handle on account of responsibility or moral after crisis happened, and they have some relevance and influence with crisis, but the urgency is weak. They mainly include Non governmental organizations, News media and Public service department and so on.

(4) Potential stakeholders refer to some organizations and individuals with weak relevancy, urgency and impact in terms of public crisis. This type of stakeholders can grow into core stakeholders, fringe stakeholders and non stakeholders with the development trend of the public crisis, and the major potential stakeholders are bystanders of crisis in the crisis.

Conclusion

The frequent occurrence of all types of emergencies, group events, safety accidents and others have become a factor serious affecting China's urban harmony and stability, so building an effective urban public crisis handle mechanism suited for our country's condition becomes arduous task as soon as possible without delay. This paper aims to study and explore new theories and new ways of urban public crisis handle management to address the key issues of urban public crisis emergency management, so we can reduce the risk of decision-making, improve the government's ability to govern particular the ability to manage complex situations and the ability to deal with crises events. The paper can theoretically further enrich and complement existing theories and methods of urban crisis management, and it can provide scientific reference for the decision-making behavior in government crisis management in practice.

Acknowledgment

This work is supported by social science fund project of Liaoning province (L12BZZ009).

References

[1] Naim Kapucu, "Disaster and emergency management systems in urban areas," Cities, vol. 29, no. 1, pp. 41-49, 2012.

[2] L. Feng, M. H. Zhang, "Construction of model for public crisis management mechanism in China: analysis based on theory of organizational integration," Journal of Wuhan University of Science and Technology(Social Science Edition), vol. 9, no. 1, pp. 56-60, 2007.

[3] Z. Wang, S. M. Yan, "Construction of public crisis management assessment and discussion of the conceptual model," Economic Forum, vol. 23, no. 18, pp. 112-114, 2009.

[4] Baidu Encyclopedias, "4R crisis management theory," http://baike.baidu.com/link?url=HRzzeCZP6r1_1yM_GbgiEvw7U9BgRrxc9be9k31OdlJ_ly8mM48_X6Ri2n244kUsfF1yR0YeWIMGvp2-eGp7lq, 2014-4-5.

[5] Q.Z. Wu, "System Engineering," Beijing Institute of Technology Press, 2006.

[6] X. M. Liu, "Research on Prediction Model of Public Crisis Events and Its Application," Master's degree of Lanzhou University, 2013.

[7] Y. Z. Sha, H. Q. Liu, "Stakeholders Analysis Model of Public Crisis," Science Economy Society, vol. 27, no. 1, pp. 58-61, 2009.

[8] S. Lin, "Standards system theory and process theory of public crisis management -- Based on the stakeholder analysis with Swarm," Seeker, vol. 30, no. 10, pp. 119-121, 2010.

[9] X. M. Hu, B. Y. Tang, "Standards system theory and process theory of public crisis management -- Based on the stakeholder analysis with Swarm," Wuhan University Journal (Philosophy & Social Sciences), vol. 30, no. 10, pp. 119-121, 2010.

Advanced Materials Research Vols. 989-994 (2014) pp 5544-5546
© (2014) Trans Tech Publications, Switzerland
doi:10.4028/www.scientific.net/AMR.989-994.5544

Study on the Effectiveness Evaluation of Missile and Artillery Air Defense Group

Peichao Zhang[1], Yuanzeng Cheng[1], Wei Mei[1], Binqian Cao[2]

[1] Ordnance Engineering College, Shijiazhuang, 050003 Email: 553406497@qq.com

[2] PLA 77,618 troops in Lhasa, 850000

Keywords: network-centric warfare; missile and artillery air defense group; damage effectiveness

Abstract. Currently, missile and artillery air defense system under the conditions of the network has become a very important air defense weapon system, and play an unprecedented role in modern warfare process. To develop high damage performance missile and artillery air defense system has become common goal. It is necessary to study the impact of missile and artillery air defense system damage performance for improving damage probability of missile and artillery air defense system.

Introduction

In modern warfare, threats are changing constantly, destructiveness, threatening and universality of the war have constantly increased, and it makes the need for joint defense weapons systems on combat tactics, the war needed to cover the range of low, a diverse range of low altitude and high-altitude regions such as operational requirements. Currently, missile and artillery air defense system under the conditions of the network has become a very important air defense weapon system, and play an unprecedented role in modern warfare process. To develop high damage performance missile and artillery air defense system has become common goal. It is necessary to study the impact of missile and artillery air defense system damage performance for improving damage probability of missile and artillery air defense system.

Research Statuses

2.1 Network Centric Operation System Effectiveness Evaluation

"Network Centric Warfare" is a new concept of operations for the U.S. Navy to develop and adapt to the IT revolution, the new military requirements consequent proposed. It is defined as follows: through the Global Information Grid, the scattered distribution of combat elements integrated into networked battle command systems, combat forces and combat system, security system, between the various operational elements shared situational awareness, to maximize the information advantage into the decision-making and action advantages, give full play to the overall combat effectiveness [1].

With the continuous development of the U.S. Navy weaponry and combat theory, "Network Centric Warfare" goes from vision to reality. Compared with the traditional "platform-centric warfare" in the NCW C^4ISR system "combat multiplier" effect is more prominent, the impact on operations is also greater. Meanwhile, the C^4ISR system performance and operational impact assessment has become an increasingly important issue, and has important theoretical and practical significance [2].

Traditional system performance and operational effectiveness are still focused on the definition of weapons and equipment systems, which obviously do not meet information warfare or combat systems against requirements. Therefore, it is necessary to extend the concept of weapon system performance, and put forward the concept of system performance.

System performance evaluation is the highest level of effectiveness of the performance evaluation. Network Centric Operation System Effectiveness Evaluation refers to the network-centric warfare environment, assess the main measure of network-centric warfare systems carry out combat operations troops reached the actual extent of the process. It is

believed that network-centric warfare system performance assessment is to combat system to measure and evaluate the level of play.

2.2 Network Centric Operation System Effectiveness Evaluation Method

2.2.1 Analytical Method

Analytical method [3] is used to describe and solve mathematical analytical expressions number of relationships in the real world, the analytic expression results in an accurate value indicates the number of solution results. As the process of applying combat weapon system is a random process, so the mathematical basis of the analytical method used in this regard is mainly probability theory and stochastic process theory, the corresponding modeling probabilistic methods are usually resolved. Its essence is to use analytic analysis of the effects of the war, the method of random factors such functions by random factors known to calculate the probability characteristics. Specific methods are: WSEIAC (Weapon System Advisory Committee) model, queuing network theory, information theory methods and objective planning methods. Queuing network theory and information theory methods have been applied to evaluate the performance of network-centric warfare systems.

Advantage of the analytical method is the formula transparent, and easy to understand, simple to calculate, application flexibility. For some of the potential problems, such as the system of "bottleneck" subsystem performance impact of certain parameters, such as changes in the whole system, analytical method can draw a clear understanding of the law. The disadvantage is that the analytical method to establish the difficulty of mathematical models, mainly in: Category combat effectiveness evaluation system objects more widely, from the strategic to the tactical level, there are performance assessment of the different levels of the system, the mathematical application of analytical method Difficulty model is different, the higher the level the system, the more complex the system, the more complex the relationship between the index, the more difficult to establish the mathematical model; restricted even for the same system, the performance is also affected by the environment, tasks and other factors, by analytical Mathematical models have created a different method.

2.2.2 Statistical Experimental Method

Statistical experimental method [4] is known as Monte Carlo method or a computer simulation method, and it is a computer simulation of random phenomena as a tool for mathematical method. Its main features are: distributed random variables in order to obtain the number of known probability distribution of the decision of unknown random variables, generates a random number with every random variable with a known distribution of mathematical methods (that is, one of the random variable The possible values), and entered into a mathematical model of these random variables determine the unknown random variables, the calculated random number of random variables is unknown. Such independent enough times calculated the unknown random variables can be a random number; this group is called the random collection of a sample of the random variable.

Using statistical experimental method is the basic premise: You must be able to construct a specific weapon system in line with the course of affairs characterized by physical and mathematical model and has a high resolution. In addition, you must also know the known distribution pattern of random variables, the distribution density and distribution functions. Through statistical experimental method to compare the dynamic response of the actual situation realistically, and with high reliability, but there are difficulties in the accuracy of modeling complexity and model.

2.2.3 Analysis Hierarchy Process

AHP (Analytic Hierarchy Process) is proposed by T.L.Satie in 1970s [5].

AHP is a practical method for multi-criteria decision making, which embodies the basic characteristics of the analysis process decision-thinking people, that decomposition, judgment, synthesis. This method of combining its qualitative and quantitative factors to deal with the characteristics of various decision-making, as well as systems, flexible, simple and advantages in the field of complex systems to assess attention and has been widely applied. Advantages AHP is

available on a variety of weapon systems programs and mission analysis tasks, the disadvantage is difficult to describe the interactions and nonlinear relationships weapon systems and combat concepts.

Summaries

There are many ways to assess the effectiveness of Network-centric warfare system, but in this study, because of the limited equipment and related technology, only some simple, intuitive and effective methods are used for effectiveness evaluation of the missile and artillery air defense system.

Damage assessment for a single weapon platform effectiveness can be the first analytical method for detecting ability, shooting ability and the ability to damage a single weapon platform system were analyzed to obtain a single weapon combat effectiveness evaluation of the results of a comprehensive platform after; then develop simulation system using statistical experimental method for damage efficiency single weapon platform for analysis and verification.

For multi-weapon platform effectiveness of cooperative damage assessment can be integrated using the analytical method, AHP and fuzzy analysis method for multi-platform systems ability to detect weapons, shooting ability, and ultimately damage the ability to model and analyze the effectiveness of combat; then develop simulation system, in two steps, the use of experimental methods and exploratory statistical analysis methods to verify the multiple weapons platforms cooperative combat performance gain.

References

[1] Zhiping Dai.Network CentricWarfare under Conditions of Informatization [M]. Beijing: Military Yiwen Press, 2010.

[2] Xiaotong Jiao, Yuguang Wang, Jinxu Yuan. "Network centric warfare" in the United States Navy C^4ISR System Effectiveness Evaluation [J]. Shipboard Electronic Warfare, 2006, 29 (1):7-12.

[3] Zhenlei Wang, Xueshan Luo. Preliminary Network Centric Operation System Effectiveness Evaluation Method [J]. Command Control & Simulation, 2006, 28 (3), 20-24.

[4] Zhenlei Wang, Xueshan Luo. Network Centric Operation System Effectiveness Assessment [J]. Fire Control and Command Control, 2007, 32 (9), 5-9.

[5] Sunan Zeng, Yinnian Li. Silver Case Studies in Integrated Joint Operations [M] Beijing: Military Science Press, 2004.

Advanced Materials Research Vols. 989-994 (2014) pp 5547-5550
© (2014) Trans Tech Publications, Switzerland
doi:10.4028/www.scientific.net/AMR.989-994.5547

Optimal Design for the Manufacturing/Remanufacturing Integrated Logistics Network under Fuzzy Environment

Ligang Sun [1,a], Zheng Zhang [2,b]

[1] Shanghai Dianji University, Shanghai 2001306, China

[2] Shanghai Dianji University, Shanghai 2001306, China

[a] sunlg@sdju.edu.cn, [b] zhang65176393@163.com

Keywords: integrated logistics; manufacturing; remanufacturing; fuzzy chance constrained; confidence level

Abstract: Considering the uncertainty of waste products recovery quantity in consumption areas, a fuzzy optimization model for manufacturing/remanufacturing integrated logistics network with capacity constraints was constructed to determine the number and location of the facilities, the flows between each facility. A numerical example was provided to demonstrate the feasibility of the model.

Introduction

Remanufacturing is a process that transforming the waste products into new products. The raw material is the old machinery equipment. It is a new manufacturing process using specialized technology. Due to reusing the scrap value of waste products, it can help save natural resources, reduce pollution and promote the development of circular economy. Now, it has drawn more and more countries' attention, especially the industrialized countries. For the successful implementation of remanufacturing, improving efficiency and effectiveness of logistics systems operations, many scholars studied the optimization design problem of remanufacturing logistics network[1,2,3,4,5,6,7]. And most of these studies have focused on independent construction of remanufacturing logistics network and new construction of manufacturing/remanufacturing integrated logistics network. But constructing manufacturing/remanufacturing integrated logistics network based on the original logistics network contributes to reduce the total construction cost. In addition, most remanufacturing logistics network optimization model is deterministic, stochastic programming model and fuzzy programming model are less. Based on the above studies, this paper uses fuzzy parameter to describe the uncertain recovery quantity, and constructs a fuzzy programming model for the manufacturing/remanufacturing integrated logistics network. A numerical example is provided to demonstrate the feasibility of the model.

Model Formulation

Problem Description. The manufacturing/remanufacturing integrated logistics network is composed by the consumption areas, recycling centers, remanufacturing centers, manufacturing centers, distribution centers and waste disposal points and the transportation routes between them. The integrated logistics network optimization design is to determine the quantity and location of recycling centers, remanufacturing centers, and find the suitable flows between various facilities to minimize the total cost.

Model Assumption. In order to facilitate analysis, we give the following assumptions:

(1)The recovery quantity in consumption areas is a fuzzy number;

(2)The quantities and locations of distribution centers, manufacturing centers and waste disposal points are certain;

(3)New facilities only can be established in the known candidate locations;

(4)The fixed cost, operating cost and transportation cost are certain;

(5)The recycling centers and remanufacturing centers have capacity limitation;

(6)There is a linear relationship between the transportation cost and distance.

Formulation of the Model. The notation can be represented as follows:

Indices:i: consumption area ($i = 1,2,\dots,I$);j:distribution center($j = 1,2,\dots,J$);k: manufacturing center($k = 1,2,\dots,K$);l:recycling center candidate ($l = 1,2,\dots,J,J+1,\dots,L$); m; remanufacturing center candidate($m = 1,2,\dots,K,K+1,\dots,M$); n: waste disposal points($n = 1,2,\dots,N$).

Parameters:Q_i: recovery quantity of waste products in consumption area;F_l,E_l,W_l: fixed cost, operating cost and maximum capacity of l;F_m,E_m,W_m: fixed cost, operating cost and maximum capacity of k;p:unit cost of waste products; d_{il},TC_{il}: the distance and transportation cost between i and l;d_{lm},TC_{lm}: the distance and transportation cost between l and m;d_{ln},TC_{ln}: the distance and transportation cost between l and n;d_{mj},TC_{mj}: the distance and transportation cost between m and j;d_{mn},TC_{mn}: the distance and transportation cost between $m$and n;d_{ji},TC_{ji}: the distance and transportation cost between j and i;α,β: the discard rate of waste products in distribution centers and remanufacturing centers;p: the unit cost of waste products.

Decision variables: Y_l: 1,if distribution center is opened at location l,0,otherwise;Z_m: 1,if remanufacturing center is opened at location m,0,otherwise;x_{il}: quantity of waste products shipped from i to l;x_{lm}: quantity of waste products shipped from l to m;x_{ln}: quantity of solid wastes shipped from l to n;x_{mj}: quantity of waste products shipped from m to j; x_{mn}: quantity of solid wastes shipped from m to n;x_{ji}: quantity of waste products shipped from j to i.

The problem can be formulated as follows:

$$\min Z = \sum_{l\in L} F_l Y_l + \sum_{m\in M} F_m Z_m + \sum_{i\in I}\sum_{l\in L} x_{il} TC_{il} d_{il} + \sum_{l\in L}\sum_{m\in M} x_{lm} TC_{lm} d_{lm} + \sum_{l\in L}\sum_{n\in N} x_{ln} TC_{ln} d_{ln} + \sum_{m\in M}\sum_{j\in J} x_{mj} TC_{mj} d_{mj} + \sum_{m\in M}\sum_{n\in N} x_{mn} TC_{mn} d_{mn} + \sum_{j\in J}\sum_{i\in I} x_{ji} TC_{ji} d_{ji} + E_l \sum_{i\in I}\sum_{l\in L} x_{il} + E_m \sum_{l\in l}\sum_{m\in M} x_{km} + OT\left(\sum_{l\in L}\sum_{n\in N} x_{ln} + \sum_{m\in M}\sum_{n\in N} x_{mn}\right) + p\sum_{i\in I}\widetilde{Q}_i \quad (1)$$

$$\sum_{l\in l} x_{il} = \widetilde{Q}_i \qquad \forall i \quad (2)$$

$$(1-\alpha)\times\sum_{i\in I} x_{il} = \sum_{m\in M} x_{lm} \qquad \forall l \quad (3)$$

$$\alpha\times\sum_{i\in I} x_{il} = \sum_{n\in N} x_{ln} \qquad \forall l \quad (4)$$

$$(1-\beta)\times\sum_{l\in L} x_{lm} = \sum_{m\in M} x_{mj} \qquad \forall m \quad (5)$$

$$\beta\times\sum_{l\in L} x_{lm} = \sum_{n\in N} x_{mn} \qquad \forall m \quad (6)$$

$$\sum_{m\in M} x_{mj} = \sum_{i\in I} x_{ji} \qquad \forall j \quad (7)$$

$$\sum_{i\in I} x_{il} \le Y_l W_l \qquad \forall l \quad (8)$$

$$\sum_{l\in L} x_{lm} \le Z_m W_m \qquad \forall m \quad (9)$$

$$Y_l, Z_m \in \{0,1\} \qquad \forall l,m \quad (10)$$

$$x_{il}, x_{lm}, x_{ln}, x_{mj}, x_{mn}, x_{ji} \ge 0 \qquad \forall i,j,k,l,m \quad (11)$$

The objective function (1) tries to maximize the profit after removing the total cost. Constraint (2) requires the total outgoing flows from each consumption area should be the same as the waste products recovery quantity. Constraints (3) and (4) are the balance equations to ensure the quantities that enter to recycling centers must be equal to the quantities that leave them. Constraint (5) and (6) ensure reusable components would be shipped to remanufacturing centers, and the rest would be transported to waste disposal points. Constraint (7) ensures the total outgoing flows from

remanufacturing center should be equal to the quantities that leave them. Constraint (8) and (9) are the maximum capacity limitation for recycling centers, remanufacturing centers, respectively. Constraint (10) represents the binary variables. Lastly constraint (11) enforces the non-negativity restriction on the decision variables.

Solution method for the model

In order to solve the model, the fuzzy parameter should be clarified. Based on the study of Liu and Iwamura [6,7], the model can be transformed to the following mixed integer programming model.

$$\min f \tag{12}$$

$$\sum_{l\in L} F_l Y_l + \sum_{m\in M} F_m Z_m + \sum_{i\in I}\sum_{l\in L} x_{il} TC_{il} d_{il} + \sum_{l\in L}\sum_{m\in M} x_{lm} TC_{lm} d_{lm} + \sum_{l\in L}\sum_{n\in N} x_{ln} TC_{ln} d_{ln} + \sum_{m\in M}\sum_{j\in J} x_{mj} TC_{mj} d_{mj} + \sum_{m\in M}\sum_{n\in N} x_{mn} TC_{mn} d_{mn} + \sum_{j\in J}\sum_{i\in I} x_{ji} TC_{ji} d_{ji} + E_l \sum_{i\in I}\sum_{l\in L} x_{il} + E_m \sum_{l\in l}\sum_{m\in M} x_{km} + OT\left(\sum_{l\in L}\sum_{n\in N} x_{ln} + \sum_{m\in M}\sum_{n\in N} x_{mn}\right) + p\sum_{i\in I}(1-\theta)Q_{i3} + \theta Q_{i2} \le f \tag{13}$$

$$\sum_{l\in l} x_{il} \ge (1-\theta)Q_{i1} + \theta Q_{i2} \qquad \forall i \tag{14}$$

$$\sum_{l\in l} x_{il} \le (1-\theta)Q_{i3} + \theta Q_{i2} \qquad \forall i \tag{15}$$

Other constraints are the same as the constraints from (3) to (11), where $\theta(0 \le \theta \le 1)$ is a given confidence level. So the model has been converted to a deterministic model. And it can be solved by commercial software CPLEX, LINDO, LINGO, and so on.

Numerical Example

A manufacturing/remanufacturing integrated logistics network needs to be constructed. The recovery quantity is fuzzy parameter. p=800RMB/t, $TC_{ij}=TC_{jk}=TC_{kl}=TC_{km}$=6RMB/(t·km), θ=0.9. Other parameters are shown from table 1 to table 5.

Tab.1 Recovery quantity in consumption areas (t)

	Quantity		Quantity		Quantity		Quantity
I1	(25,27,37)	I2	(31,34,36)	I3	(42,45,49)	I4	(18,19,22)
I5	(22,24,27)	I6	(19,22,24)	I7	(27,29,33)	I8	(33,34,38)
I9	(22,26,31)	I10	(17,21,25)				

Tab.2 Distance between potential recycling centers and consumption areas, potential remanufacturing centers (km)

		Consumption areas										Remanufacturing centers					
		1	2	3	4	5	6	7	8	9	10	1	2	3	4	5	6
Recycling centers	1	22	14	18	25	19	12	25	31	19	12	31	23	28	21	14	19
	2	23	30	16	19	24	15	9	17	24	15	23	14	17	31	22	18
	3	37	29	31	16	22	35	17	18	22	35	22	13	17	25	27	26
	4	21	14	19	36	25	30	13	21	25	30	33	24	27	19	20	31
	5	22	15	23	32	19	15	19	22	21	22	17	14	31	22	25	18
	6	34	27	18	27	23	23	17	25	27	28	22	27	16	41	29	33

Tab.3 Distance between potential recycling centers, potential remanufacturing centers and waste disposal point (km)

	Recycling centers						Remanufacturing centers					
	1	2	3	4	5	6	1	2	3	4	5	6
Waste disposal point	44	35	26	31	19	37	32	27	52	29	44	37

Tab.4 Distance between potential remanufacturing centers and distribution centers (km)

		Remanufacturing centers					
		1	2	3	4	5	6
Distribution centers	1	31	22	17	22	35	17
	2	24	19	14	29	32	42
	3	27	34	25	31	16	18

Tab.5 Maximum capacity, fixed cost and operating cost of potential recycling centers and remanufacturing centers

	Storage centers						Dismantling centers					
	1	2	3	4	5	6	1	2	3	4	5	6
Maximum capacity (t)	100	100	100	100	100	100	100	100	100	100	100	100
Fixed cost (RMB)	650000	650000	650000	900000	900000	900000	3250000	3250000	4760000	4760000	4760000	4760000
Operating cost	1750	1750	1750	1750	1750	1750	5500	5500	5500	5500	5500	5500

Having the above parameters, the model can be solved by LINGO11.0. The optimal solution of structure variables is given in table 6. The optimal total cost is 17513210 RMB. We build recycling center at $L1$, $L2$ and $L3$, remanufacturing center at $M1$, $M2$ and $M5$.

Tab.6 Optimal solution of structure variables

Y_1	Y_2	Y_3	Z_1	Z_2	Z_5	Others
1	1	1	1	1	1	0

Conclusions

This paper studies the optimal strategy of manufacturing/remanufacturing integrated logistics network when the recovery quantity is fuzzy number, and constructs a fuzzy programming model for it. Finally, an example is given to demonstrate the feasibility of the model. And the multi-objective situation should be studied further in the future.

References

[1] Zujun Ma, Dianye Zhang, Ying Dai: Journal of Transportation Engineering and Information Vol. 2(2004), p. 53, In Chinese

[2] Ying Dai , Zujun Ma , Fei Liu: Computer Integrated Manufacturing Systems Vol. 11(2005), p. 1151, In Chinese

[3] Ying Dai, Zujun Ma, Fei Liu: China Mechanical Engineering Vol. 8(2006), p. 809, In Chinese

[4] Ying Dai , Zujun Ma , Fei Liu: Computer Integrated Manufacturing Systems Vol. 12(2006), p. 1853, In Chinese

[5] Weimin Di, Pei Hu, Zujun Ma, Ying Dai: Journal of System Simulation Vol. 20(2008), p. 2368, In Chinese

[6] Ying Dai, Zujun Ma: Journal of Southwest Jiaotong University Vol. 42(2007), p. 249, In Chinese

[7] Xinghua Wu, Xu Wang, Yun Lin: Computer Engineering and Applications Vol. 15(2010), p. 201, In Chinese

[8] Baoding Liu, Reiqing Zhao: Stochastic Programming and Fuzzy Programming (Tsinghua University Press, Beijing 1998).

[9] Baoding Liu, Iwamura K: Fuzzy Sets and Systems Vol. 94(1998), p. 227

Advanced Materials Research Vols. 989-994 (2014) pp 5551-5554
© (2014) Trans Tech Publications, Switzerland
doi:10.4028/www.scientific.net/AMR.989-994.5551

Application Research of Growth Management Model of Crop

Junfeng LIANG[1,a], Yanqing WANG [1,a], Linli AN [1,a], Xuning LIU [1,a]

[1]Department of Economic Management, Shijiazhuang University, Shijiazhuang, 050035,China

[a]email:sjzhei@163.com

Keywords: Crop, Growth, Management, Model

Abstract. In order to explore the growth mechanism of crop, further improve the level of crop growth management, the simulation research technology for management model of the crop growth is proposed, meanwhile ontology and visual model technology are used in the establishment process of crop growth model, so all kinds of states of crop growth at different stages can be predicted, then efficiency of crop growth management is greatly improved. The research on the crop growth model has important theory and practical significance in understanding the yield of the various parts of the crop, and help the manager understand the growth discipline of crop.

Introduction

The development of crop growth management model will make full use of information management, dynamic simulation, virtual reality, knowledge engineering, precise control and other modern information technologies[1], and the information and digital technology in production factors and production process of crop are regarded as main research targets, and we develop information management of crop growth and resources management, the digital simulation of crop growth management process, crop growth management knowledge expression modeling, visual design of key technologies in crop growth management and so on, further study the hardware and software technology of crop growth management development, then achieve digital control, high precision, visualization, and network of prediction of crop growth management model[2].

Key Technologies

Agricultural Ontology. Agricultural ontology is to use the computer language to regulate the concept expression of agricultural knowledge, which is the scientific methodology that implements knowledge services and agricultural origination. The exchange, reusing and sharing of information and knowledge have become an urgent task of computer technology. For knowledge engineer, natural language processing, information retrieval system, intelligent information integration and knowledge management, information exchange and software technology and other fields, the ontology is more than the database of information that can enrich in the lexical and semantic, and it is not just structure of data storage, but can provide a wealth of rigorous theory and describe moving and changing of things or concepts, so the ontology is the foundation of description of entities, attributes, processing and relationship. This formal description can become the sharing and reusable components of software system, which can achieve interoperability and inheritance between different systems, so basic structure is provided for the construction of knowledge base.

Classification and relation of characteristic words that are formed in the agricultural ontology are used to carry on the confirmation of uneven husband law, and form relatively discipline branch data dictionary which is composed of the finite character words, namely is the optimization of data dictionary. The retrieval word that is provided by user is used to match data dictionary, and strategy is used to analyze the results of matching to determine the subject of the information and index. The classification system of agricultural information network is made, indexing information is used to classify information. Computer programming is used to realize automatic classification and indexing of agricultural information network.

Growth Model. Virtual reality technology is the second generation of multimedia technology which is after the man-machine system interface technology, which combines a variety of the latest achievements of science and technology such as computer graphics technology, computer simulation technology, sensor technology, display technology, the three-dimensional graphical environment and their interactions are created as a true reflection of the simulation. The main characters of virtual reality technology system are as shown: a perception of visual, hearing, touch, smell, taste and other information; and allows users to temporarily escape from the external environment and integrated with virtual world. Visualization in scientific computing is to explore computing and data, and gain understanding and insight into the data. The goal is to test the numerical or large amounts of data obtained in accordance with its own combination of physical background, and show the relationship between the content and performance with the way the image data, so it is easy to grasp the overall evolution of the process and find its inherent laws, improve rich scientific way and shorten the research cycle.

Three-dimensional digital technology regards the computer as the core, and achieves accurate collection object space coordinates based on acoustic, optical, magnetic and other principles of development. The crops that can describe the morphology of the feature points are selected, then obtain three-dimensional coordinate system in the coordinates, so we can easily calculate the branching angle and azimuth, blade geometry and so on. Three-dimensional digital technology can achieve the continuous, accurate monitoring for the process of crop growth morphology, then determine its own rules. Now three-dimensional digital technologies based on laser, micro-radar technology have also been made, if these methods become mature, it will be able to achieve more rapid plant morphology, accurate, non-contact monitoring.

Database of Crop Growth Management Resource. The crop growth management resource database supports the query from the crop growth model and connects with the existing data to calculate the new data, which are used to predict or update data. The crop growth management resources database management system includes the management and maintenance functions of the resource base of crop growth management, then including crop growth and management of resources survey data searching, data management, system maintenance and so on. In order to meet the growth of agricultural crops, the management parameters of various crops growth not only timely understand and grasp, but also summarize the laws of crop growth and the requirements of the various parameters[5], the crop growth management resource database can give crops growth and management of resources real-time and the display of historical data table and the curve of real-time trend curves and historical trends, which can ensure that users can look at real-time resource parameters of the crop growth of the current value and trend curve[6].

Knowledge Ontology of Crop Growth Management. Ontology provides the shared conceptualization specification for crop growth model, this specification is described based on a kind of formal way, so that users and computers can share and reuse domain knowledge in a structured way. The ontology can clarify the structure of knowledge, the ontology elements such as concept, properties, functions, axioms and instances of domain-specific are used to describe knowledge and framework, ontology reuse can avoid repetitive domain knowledge, and unified terminology and concepts make it possible for knowledge sharing.

According to the definition of the ontology, the resources information ontology of crop growth management are defined as the conceptual models which the crop growth management resource domain involve, and consensus can be made in resource management of crop growth management field, and are expressed in computer, and provides resource decision domain sharing of crop growth management. The crop growth management resource information ontology consists of the concept, properties, axioms, instances, the crop growth management resource decision-making concept refers to the collection of involved nouns in the process of crop growth management resources business, the domains are for crop growth management resource areas, including the collection of the crop growth management resources and operational decision making.

Establishment of Crop Growth Model

The establishment of crop growth model requires the following steps:

The conditions of crop growth are shown at the different stages of crop growth and under different environmental factors, we can judge growth mode of branch, the type of scores, then determine the overall framework to describe the crop morphology.

The combination of the morphogenetic model and specific physiological and ecological model are made, which are based on biomass production and distribution in different organs at each stage, and calculate the growth and development state of crops in various stages of growth.

Based on the geometric dimensions and spatial position of the various growth stages which are calculated for each crop organs, the visual model structure is used to build three-dimensional crop graphics; The computer graphics technology such as texture mapping and light calculation, the depth of blanking anti-aliasing, projection and so on are used to deal with crops in three-dimensional geometric structure to generate a realistic image of the crops graphics.

Implementation and Test of Model

Composition of Module. The model system consists of the model management module, knowledge management module, inference engine, database management module, and model base, knowledge base, and human-computer interaction interface.Growth model of plant uses Visual C++ and three-dimensional drawing tool OpenGL. OpenGL is three-dimensional computer graphics software interface which is suitable for a variety of hardware platforms and operating systems. Currently it has become internationally recognized as the industry standard and open three-dimensional graphics, and is widely used. In order to verify the validity and correctness of the system, several modules of the system are tested. The results show that the comprehensive integration of expert system knowledge model and virtual growth model achieve complement of different levels of knowledge granularity reasoning of expert system. The cultivation management recommendations which quantitative analysis is based on model and expert heuristic knowledge are not only more scientific, but also are close to reality, which can guide the production.

Data Acquisition and Management of Crop. Data acquisition is the beginning of growth models of crops. Simulation of crops need large amount of data to determine the parameters. Data collection in building knowledge of crop is particularly important. In the methods of data collection, three-dimensional digital technology is developed to combine the traditional method of measuring crop with the information processing method, the use of computer graphics, image processing, pattern recognition and stereo vision and other methods quickly and accurately obtain the required information, such as access to the crops in three-dimensional coordinates of each component in the coordinate values, and further analysis of branching angle and azimuth, blade geometry and so on, on the other hand, the current system data of different types and formats vary widely, and the integration of these data management is very important to us, and the full share and application are important issues. These standards are made to establish the sharing mechanism of data.

Data Test. The test of model is to verify the suitable degree of simulation results and actual results, and check whether the model is applied in different environments by root mean square deviation between the observations and simulation values, the statistical agreement between simulation results and observations analysis and the relationship between the histogram are used to visually show agreement and reliability of analog respectively, it is said that the number of samples, the analog value, the value of the observations are much less, the prediction accuracy of the higher values and observed values of the average error are very good, then the consistency of simulation and actual values are very good, which indicate that the simulation results are generally greater than the analog value, and the actual deviation of simulated poor model will run in a simulated environment and is validated. After validation we can understand the simulation results are close to the real approximation of the model, thus confirming the correctness of the tolerance range.

Conclusion

Crop growth management simulation models have strong functions of system integration and dynamic prediction, the parameters of the model are required for high precision, poor operation, but also are difficult to direct the production system management decisions. System analysis methods and crop modeling techniques are used in knowledge expression system for crop growth, and it is expected to have both the advantages of crop simulation models and expert systems, and achieve the integration and coordination of dynamic prediction and management decision-making, so as to lay the foundation for the accurate and digitization of growth management of crop.

Acknowledgement

In this paper, the research was sponsored by the Nature Science Foundation of Shijiazhuang University.

References

[1]Lei Xiangdong,Chang,Lu Yuanchang,Zhang Tian,zhong Min. A Review on Growth Model and Visualization for Virtual Crops, Scientia Silvae Sinicae,2006(11)23-25.

[2]Qiu Jianjun, Xiao Yingyu, Cotton Production Management System Based on the Cotton Plus Model for Xinjiang and Huang-Hua-Hai Regions in China, Transactions of the Chinese Society of Agricultural Engineering, 2002(11)18-26.

[3]Barnsley M F, Demko S. Iterated Function Systems and Global Construction of Fractals . R Soc London Ser, 1985 (A399), 243-275.

[4]BrakeD. Lost in cyberspace. New Scientist, 2005(12)12-13.

[5]GuarinoN, MasoloC, VetereG. OntoSeek: Content Based Access to the Web. IEEE Intelligent Systems,2003(4)70-80.

[6]GehmeyrA,MüllerJ,Schappert, A.Mobile Information Agents on the Web. In:KluschM, WeB Geds. Lecture Notesin Artificial Intelligence,Berlin,Heidelberg, NewYork:SpringerVerlag, 2008(14)262-277.

Advanced Materials Research Vols. 989-994 (2014) pp 5555-5558
© (2014) Trans Tech Publications, Switzerland
doi:10.4028/www.scientific.net/AMR.989-994.5555

Fuzzy mathematics theory in logistics center address selection of application

Yu Hang[1,a] Zhang Kai[2,b]
[1]Jilin Agricultural University Changchun , Jilin

[2]Information and Economy College of JiLin of Finance and Economics Changchun , Jilin
[a] zhangkai_2001@sina.com
[b]4135356@qq.com

Keywords: logistics center location; fuzzy comprehensive evaluation ;factors

Abstract. Logistics center address selection is logistics system of strategic investment decision-making problem, the whole site whether reasonable logistic system has important implications. According to the principle of modern logistics center location affect the location of the factor analysis, through the system of fuzzy comprehensive evaluation method of center location mathematical model, and taking a regional logistics center location for example was introduced in detail.

Introduction

Fuzzy mathematics is a new branch of the fuzzy mathematics using the method of mathematics research and treatment of the phenomenon. Fuzzy mathematics the mainstream of development is in its application. Due to the concept of fuzzy have found a fuzzy sets, people use the description of the way the concept, evaluation, reasoning, and judge the process of decision-making and control can also use the fuzzy mathematics method to describe. For example the fuzzy clustering analysis and fuzzy comprehensive evaluation, fuzzy decision, fuzzy control, etc. These methods constitute a kind of fuzziness system theory, constitute a kind of speculative the prototype of the mathematics, it has in medical, weather, psychological and economic management, oil, geology, environment, biology, agriculture, forestry, chemical industry, language, control, remote sensing, education, sports and has a specific research results. This article utilizes the fuzzy mathematical evaluation method, the impact of the location of the logistics center the various factors on the overall system analysis, the method of qualitative and quantitative methods, organic combine for logistics center to provide the theoretical basis for siting. In this, combined with a region logistics center address selected cases, introduces fuzzy comprehensive evaluation method in logistics center location of application.

Logistics center location

Combined with a regional logistics center address selected case, the comparative method of logistics center location. Details of the alternatively, factors according to the logistics center location are rough screening, in the city's primary 4 optionally, respectively for 1 to 4. The comprehensive assessment of the optionally. In view of many factors to consider the project selection process, the application of the relevant theory of fuzzy evaluation method, qualitative analysis quantitative comparison method. According to the actual situation of logistics centers in the region, public facilities, social benefits, traffic condition, natural environment, several factors considered in selection scheme evaluation, establish the criteria, then determine the weight, expert scoring, the higher the score, the higher degree of satisfaction (near, the score may be the same), the proposed scheme according to the total number. To effectively divide the factors to influence the location of logistics center, the main influence factors can be divided into factors influencing the next level. Specific details are shown in table 1:

Table1 Logistics center location index system

The first level index	Second level index
The natural environment factor (U1)	Meteorological conditions (U11) Geological conditions (U12) Hydrological conditions (U13) Terrain conditions (U14)
Social benefits (U2)	Influence on city planning (U21) Influence of environmental protection (U22) The impact on regional economic development (U23)
Traffic conditions (U3)	Cohesion and the degree of city traffic network (U31) Relationship with the main flow of goods (U32)
Public facilities (U4)	The power and energy supply (U41) The communication status (U42)

Logistics center site selection index system is established

In combination with an area of the logistics center address selection case, this paper introduces the location of the logistics center comparison method. The optional to detailed introduction of the above logistics center, the location of the influence factors of the rough screening, the city's primary in four pieces of optional, make up respectively for 1 to 4. According to the actual situation of the regional logistics center, in for locating plan into consideration on evaluation of public facilities condition, social benefits, traffic condition, natural environment, set up several factors of each factors evaluation standard, respectively, determining the weight again, the expert scoring score the most high, the higher the level of satisfaction with the approaching, the same), and the last score can be made according to put forward the suggestion that plan. Through the influence factors on the location of the logistics center, and the effective divided the main influence factors and fine as the next level factors. One class index including：the natural environment factors (U1); Social benefits (U2); Traffic conditions (U3); Public facilities condition (U4), Secondary indexes including: Weather conditions (U11)
Geological conditions (U12),Hydrological conditions (U13),Terrain conditions (U14),The influence of the layout of the city planning (U21),The influence of environmental protection (U22),The influence on the region economy development (U23),And urban transportation network connection degree (U31),And the main flow of goods relations (U32),Power and energy supply (U41),Communication status (U42).
A region that are ready to build a logistics center, there are four candidates address to choose from, the evaluation index factor set to collect U, can be divided into the second floor. The first layer: U ={U1，U2，U3，U4}；The second floor: U1 ={U11，U12，U13，U14}；U2 ={U21，U22，U23}；U3 ={U31，U32}；U4 ={U41，U42}，Four candidates address that is prepared to choose sets V；V =(V1,V2,V3,V4)。

The fuzzy comprehensive evaluation in the logistics center location of application

In the multi-level fuzzy comprehensive evaluation model, due to the low level of factor is the level of fine factors on a stroke, weight coefficient of the size of the corresponding targets representatives in multi objective optimization of the importance of the problem, said in the important, conversely, the smaller the less important. Through the investigation and analysis of various factors, the corresponding evaluation 4 candidate address value, after data processing by fuzzy comprehensive evaluation are shown in table 2:

Table2 The Fuzzy Comprehensive Gudgement of some area

Influencing factors	1	2	3	4
Meteorological conditions	0.2	0.5	0.3	0.0
Address terms	0.1	0.3	0.5	0.1
Hydrological conditions	0.0	0.4	0.5	0.1
Topographic condition	0.0	0.1	0.6	0.3
Influence on city planning layout	0.5	0.3	0.2	0.0
Impact on environment protection	0.6	0.2	0.1	0.1

The impact on regional economic development	0.2	0. 2	0.3	0.3
Cohesion and the degree of city traffic network	0.1	0.4	0.3	0.2
Relationship with the mainflow of goods	0.3	0.4	0.1	0.2
The power and energy supply	0.1	0. 1	0.5	0. 3
Communication status	0.3	0.0	0.5	0. 2

Through the investigation and analysis of the four candidates address the various factors, the corresponding evaluation value will be after data processing by fuzzy comprehensive evaluation. In this article, the assumption experts consultation method to determine the weight, please 10 professionals to influence the logistics center respectively the location of the various factors of evaluation, take again average, the results are as follows: A1 ={0.3，0.1，0.4，0.2 }；A2 ={0.4, 0.1, 0.5}；A3 ={0.4, 0.6}；A4 ={0.3, 0.7}；A ={0.2，0.25，0.15，0.1 }；Through the fuzzy evaluation for comprehensive evaluation matrix R, composite operation B = A o R can get comprehensive evaluation result, secondary factors to judge: Ui (I =1,2,3,4), U1 ={ U11，U12，U13，U14}；The weight is：A1 ={0.3，0.1，0.4，0.2 }。To U11, U12, U13 U14, the fuzzy evaluation of a single factor judgment matrix: $R_1=\begin{bmatrix}0.2 & 0.5 & 0.3 & 0.0\\0.1 & 0.3 & 0.5 & 0.1\\0.0 & 0.4 & 0.5 & 0.1\\0.0 & 0.1 & 0.6 & 0.3\end{bmatrix}$ With operator M (∧, ∨), calculated the following level comprehensive evaluation:

$B_1=A_1 \circ R_1=\{0.3,0.4,0.1,0.2\} \circ \begin{bmatrix}0.2 & 0.5 & 0.3 & 0.0\\0.1 & 0.3 & 0.5 & 0.1\\0.0 & 0.4 & 0.5 & 0.1\\0.0 & 0.1 & 0.6 & 0.3\end{bmatrix}=\{0.2，0.4，0.4，0.2\}$；Similarly, U2 = {U21, U22, U23}, the weight is: A2 = {0.4, 0.1, 0.5} To U22 U23, the U21 international, a fuzzy evaluation of single factor judgment matrix: $R_2=\begin{bmatrix}0.5 & 0.3 & 0.2 & 0.0\\0.6 & 0.2 & 0.1 & 0.1\\0.2 & 0.2 & 0.3 & 0.3\end{bmatrix}$ Make level 1 comprehensive evaluation: $B_2=A_2 \circ R_2=\{0.4,0.1,0.5\} \circ \begin{bmatrix}0.5 & 0.3 & 0.2 & 0.0\\0.6 & 0.2 & 0.1 & 0.1\\0.2 & 0.2 & 0.3 & 0.3\end{bmatrix}=\{0.4，0.3，0.3，0.3\}$；

$U_3=\{ U_{31}, U_{32}\}$， The weight is: the A3 = {0.4, 0.6}, To U31 U32, the fuzzy evaluation of a single factor judgment matrix: $R_3=\begin{bmatrix}0.1 & 0.4 & 0.3 & 0.2\\0.3 & 0.4 & 0.1 & 0.2\end{bmatrix}$， Make level 1 comprehensive evaluation: $B_3=A_3 \circ R_3 =\{0.4，0.6\} \circ \begin{bmatrix}0.1 & 0.4 & 0.3 & 0.2\\0.3 & 0.4 & 0.1 & 0.2\end{bmatrix}=\{0.3，0.4，0.3，0.2\}$；

$U_4=\{ U_{41}, U_{42}\}$， The weight is: $A_4=\{0.3, 0.7\}$， To U41 U42, the fuzzy evaluation of a single factor judgment matrix: $R_4=\begin{bmatrix}0.1 & 0.1 & 0.5 & 0.3\\0.3 & 0.0 & 0.5 & 0.2\end{bmatrix}$ Make level 1 comprehensive evaluation: $B_4=A_4 \circ R_4 =\{0.3，0.7\} \circ \begin{bmatrix}0.1 & 0.1 & 0.5 & 0.3\\0.3 & 0.0 & 0.5 & 0.2\end{bmatrix}=\{0.3，0.1，0.5，0.3\}$

In primary factors of the comprehensive evaluation The known U = {U1, U2, U3, U4}, the weight A = {0.2, 0.25, 0.15, 0.1}, Total factor judgment matrix for: $R=\begin{bmatrix}B_1\\B_2\\B_3\\B_4\end{bmatrix}=\begin{bmatrix}0.2 & 0.4 & 0.4 & 0.2\\0.4 & 0.3 & 0.3 & 0.3\\0.3 & 0.4 & 0.3 & 0.2\\0.3 & 0.1 & 0.5 & 0.3\end{bmatrix}$,
Make level 2 comprehensive evaluation:

$$B = A \circ R = \{0.2,\ 0.25,\ 0.15,\ 0.1\} \circ \begin{bmatrix} 0.2 & 0.4 & 0.4 & 0.2 \\ 0.4 & 0.3 & 0.3 & 0.3 \\ 0.3 & 0.4 & 0.3 & 0.2 \\ 0.3 & 0.1 & 0.5 & 0.3 \end{bmatrix} = \{0.25,\ 0.4,\ 0.4,\ 0.25\}$$

To sum up, optional ground of the comparison results, was the result does not show very significant difference, so 4 piece all the region logistics center as the optional. But according to the high score, the satisfaction degree is higher (approximates to the same score, can be the principle of first selection, the project team suggest no. 2, 3 (2, 3), and then tied for land is no. 1, no. 4 (1, 4 and tied for).

Conclusion

The article introduces fuzzy comprehensive evaluation method, based on the modern logistics location principle, to affect the location of the center of each factors in comprehensive evaluation, and finally determined the optimal program, this method to make up for the rely on quantitative analysis and qualitative analysis of the shortcomings, to simple and effective help policymakers to choose the most suitable location, at the same time, the fuzzy comprehensive evaluation method also has certain inadequacies, such as logistics center of the location of the influence factors, including a score some uncertainty factors, and fuzzy mathematics this quite new mathematical method and thought method, remains to be perfect, but its application prospect but are very wide.

Acknowledgement

This paper comes from jilin agricultural university research fund project start, the project Numbers for 201134 .

References

[1] MaXiaoYan. Theory of modem logistics center the general idea of specific countermeasures and [J]. Reform and strategy, 2008, (24) : 80-82

[2] ChenSiYun, LiuXinBin influence logistics center. The location of the factors and a location method [J]. These college news, 2006, (2) : 20-23

[3] XuJie, ZhengKai, the latest RuYiGong. Logistics center, the location of the impact factor analysis and case [J].sweden, 2010, 25 (5) : 80-82

[4] XuJie, the latest RuYiGong. Logistics center, the location of the influence factors and case analysis [J]. Logistics technology, 2012, (2) : 28-31

[5] SongHan. Traffic network of balance city logistics distribution center layout model of reconciliation [D]. Xian: chang-an university, 2010,.

[6] FanBiXia. The set covering model in the logistics center location of the application [J] decision-making and information (financial observation), 2011,9:49-50

Advanced Materials Research Vols. 989-994 (2014) pp 5559-5564
© (2014) Trans Tech Publications, Switzerland
doi:10.4028/www.scientific.net/AMR.989-994.5559

Merging Unit Performance Evaluation of Intelligent Substation Based on the Triangular Fuzzy Number

Haitao Liu[1], Mingyu Huang [1] and Yonghao Zhang [2]

[1] Ningxia Electric Power Research Institute，Yinchuan 750002，China;

[2] Beijing Join Bright Digital Power Technology Co., Ltd., Beijing 100096, China.

hetton@126.com

Keywords: merging unit, performance evaluation, triangular fuzzy number, weight, fuzzy comprehensive evaluation.

Abstract. According to the deficient situation of study in merging unit performance evaluation, this paper set up a comprehensive evaluation model for merging unit performance evaluation. Introduced triangular fuzzy number and determined the index weight through certain processing conversion, and set up a scientific system of performance indicators, and then selected normal distribution as the membership function. On this basis, this paper established a hierarchical and sub-aims comprehensive evaluation model. Finally, the model was applied for evaluating a merging unit performance. The evaluation result showed that the weight was effective and the fuzzy comprehensive evaluation model was simple and reliable.

Introduction

Intelligent substation is an important part of smart grid, and can be divided into process layer, spacer layer and Stand accused layer. The typical protecting device within process layer are intelligent terminal and merging units, which mainly collect switch and analog variables from primary equipment, then send control command, and has other functions. With the application of electronic transformer, merging unit as part of the electronic transformer takes on the important work for digital transmission of intelligent substation model, and also takes some corresponding work, such as synchronization and integral algorithm [1-2]. In the process of advancing intelligent substation, merging unit often cooperates with the traditional transformer in the form of independent equipment, merging and syncing the three-phase electric parameters from sensor module, then providing the digital signals processed for spacer layer devices.

The key mission of merging unit is to keep multiple inputs time synchronization in a short time, and forward organized data to protection and control devices. Due to the high delay and synchronization requirements of protection device in data processing, the time performance and other related performance indicators of merging unit also get attention accordingly. The performance of merging unit has been studied by many scholars [3-7], which provides a guidance for improving the performance of merging unit. But these studies mainly focused on the performance test methods and project, and the research of merging unit overall performance comprehensive evaluation method is less. Establishing a comprehensive evaluation model to evaluate the merging unit performance, can provide a scientific reference and basis for equipment selection, grasping the equipment operation condition and equipment failure analysis, and has a great significance for further construction and operation of intelligent substation.

In this paper, according to the research of the comprehensive evaluation theory, model and related technologies and methods, we introduce the triangular fuzzy number to determine index weight aiming at the index weight, at the same time set up a scientific system of merging unit performance index, which is used to realize the fuzzy comprehensive evaluation of merging unit and make the evaluation results more reasonable and scientific.

Triangular Fuzzy Number

Make fuzzy number $a=(l,\ m,\ u)$ as the triangular fuzzy number. Among them, *I*, *m* and *u* are real numbers, and meet $0\le l\le m\le u$; *m* is the principal value of triangular fuzzy number *a*; *I* is the lower bound and *u* is the upper bound; $(u-l)$ is ambiguity, showing the possible scope of values the experts giving. The fuzzy being greater, *a* is more ambiguous. When $l=m=u$, *a* become a real number in the common sense.

For any two fuzzy numbers $a_1=\ (l_1,\ m_1,\ u_1)$ and $a_2=\ (l_2,\ m_2,\ u_2)$, they has the following algorithm:

$$(1)\ a_1\oplus a_2=(l_1+l_2,\ \ m_1+m_2,\ \ u_1+u_2)$$

$$(2)\ a_1\otimes a_2=(l_1\times l_2,\ \ m_1\times m_2,\ \ u_1\times u_2)$$

$$(3)\ \lambda\otimes a_1=(\lambda\times l_1,\ \ \lambda\times m_1,\ \ \lambda\times u_1)$$

$$(4)\ (a_1)^{-1}=(1/u_1,\ \ 1/m_1,\ \ 1/l_1)$$

The Weight Based on the Triangular Fuzzy Number

If there are too many evaluation indexes in the same level, experts' judgment on the relative weights for each indicator will be difficult. The importance of merging unit performance indexes is estimated roughly by the expert, so it has a certain ambiguity. The triangular fuzzy number [9] can convert this uncertainty expression to the form of numerical value, which will be a good solution to solve the problem that it's difficult to accurately measure the relative importance degree of evaluation indexs. This article selects triangular fuzzy Analytic Hierarchy Process(AHP) [10] to calculate the weight of indicators. The concrete application steps are as follows.

1) Construct the fuzzy judgment matrix. All evaluation indexes are compared in pairs by experts, and construct fuzzy judgment matrix by using triangular fuzzy number. Note it as:

$$A=\left(a_{ij}\right)_{n\times n},\quad a_{ji}=a_{ij}^{-1} \tag{1}$$

where $a_{ij}=\left(l_{ij},\ m_{ij},\ u_{ij}\right)$, which is the degree of importance of the ith evaluation index compared with the *jth* index; m_{ij} is scale value when comparing in pairs with Analytic Hierarchy Process (AHP). The five scale is shown in Table 1.

Table 1. Scale

Comparison of importance	a_{ij}
u_i is as important as u_j	(1, 1, 1)
u_i is slightly more important than u_j	(1, 1.5, 2)
u_i is more important than u_j	(1.25, 1.5, 2)
u_i is much more important than u_j	(1.25, 1.5, 2.5)
u_i is extremely important than u_j	(1.5, 2, 2.5)

Make $m_{ij}-l_{ij}=u_{ij}-m_{ij}=\delta$, where δ is constant, and take $1/2<\delta<1$. When there are *K* experts to evaluate, a_{ij} is the comprehensive triangular fuzzy number and the computation formula is following.

$$a_{ij}=\frac{a_{ij}^1+a_{ij}^2+\cdots+a_{ij}^k}{K} \tag{2}$$

where $k = 1, 2,\ldots,K$; a_{ij}^k is the triangular fuzzy function given by the kth experts.

2）Calculate the comprehensive importance degree of every evaluation index

$$S_i=\sum_{j=1}^{n}a_{ij}\otimes\left[\sum_{i=1}^{n}\sum_{j=1}^{n}a_{ij}\right]^{-1}=\left(\sum_{j=1}^{n}l_{ij},\sum_{j=1}^{n}m_{ij},\sum_{j=1}^{n}u_{ij}\right)\otimes\left(\sum_{i=1}^{n}\sum_{j=1}^{n}l_{ij},\sum_{i=1}^{n}\sum_{j=1}^{n}m_{ij},\sum_{i=1}^{n}\sum_{j=1}^{n}u_{ij}\right)^{-1}$$

$$\approx\left(\frac{\sum_{j=1}^{n}l_{ij}}{\sum_{i=1}^{n}\sum_{j=1}^{n}u_{ij}},\frac{\sum_{j=1}^{n}m_{ij}}{\sum_{i=1}^{n}\sum_{j=1}^{n}m_{ij}},\frac{\sum_{j=1}^{n}u_{ij}}{\sum_{i=1}^{n}\sum_{j=1}^{n}l_{ij}}\right) \tag{3}$$

where S_i is the degree of comprehensive importance of the *iith* evaluation index compared with the other indexes within the fuzzy judgment matrix.

3）Calculate the possibility of being more important than , calculation formula is as follows.

$$V(S_i \geq S_j) = \begin{cases} 1 & (m_i \geq m_j) \\ \dfrac{l_j - u_i}{(m_i - u_i) - (m_j - l_j)} & (m_i < m_j, l_j < u_i) \\ 0 & \text{others} \end{cases} \quad (4)$$

where $j = 1, 2, \ldots, n; j \neq i$.

4）Calculate the weight of every index

$$W' = (d_1, d_2, \cdots, d_n);\ d_i = \min_{j=1,2,\ldots,n;\ j \neq i} V(S_i \geq S_j) \quad (5)$$

Get the weight W after unitary:

$$W = (w_1, w_2, \cdots, w_n)$$

The Fuzzy Comprehensive Evaluation Method

Merging unit performance evaluation is a multi-index comprehensive evaluation problem. For qualitative indexes through quantifying or some quantitative indexes, it is uncertain that the evaluatation result belongs to a certain hierarchy. The fuzzy comprehensive evaluation method makes full use of the fuzzy relation between evaluation index and membership grade, and makes comprehensive evaluation from various angles, so it is a kind of comprehensive decision method matching people's critical thinking. This method divides the change interval of the merging unit performance index, and makes analysis about merging unit performance indexes more deeply and objectively. Figure 1 is shown the evaluating process of fuzzy comprehensive evaluation method.

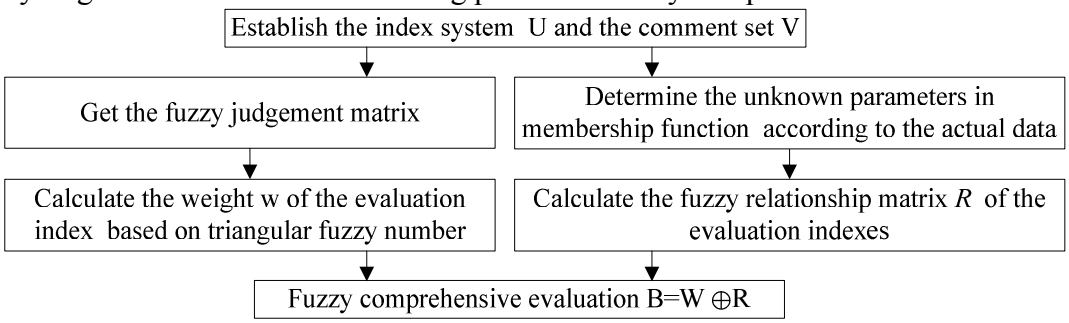

Figure 1. Fuzzy comprehensive evaluation method based on the triangular fuzzy number

Evaluation Index

Data information used by protection principle should be at the same time. When the data information from different merging units converges to one protection, it will cause protect out and even endanger grid security if the delay between each data is too big. So we must accurately grasp the merging unit performance in terms of time. With Intelligent substation being more networked, merging unit should be able to adapt to correspond through the network, and ensure data integrity in the communication. Data collection is an important function of merging unit, and it is very important for the grasp of the data accuracy. Not only accurately grasp the normal data, but also monitor the changes of emergency data in time. So we shall have corresponding indexes to measure the steady-state performance and dynamic performance.

In order to achieve the goal of intelligent substation merging unit performance evaluation, the target is divided into four points to evaluate, as shown in Figure 2.

According to the experiences and opinions of experts, merging unit performance evaluation result should be divided into three kinds of levels: optimal, good and general. So the comment set of comprehensive evaluation is $V = (v_1, v_2, v_3)$.

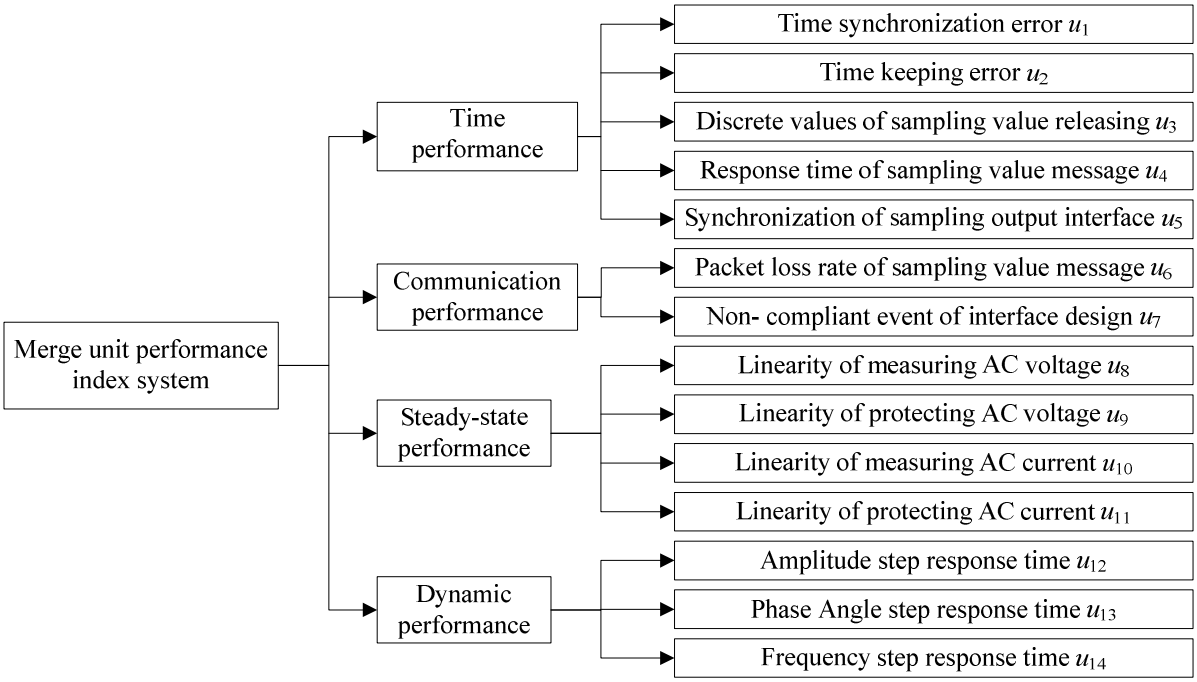

Fig.2 Performance indicators system of merging unit

Determine Membership Function

One another key of using fuzzy mathematics method to establish mathematical model is to build a practical membership function. At present, fuzzy distribution applied on engineering are matrix distribution, trapezoid distribution, parabolic distribution, normal distribution, triangular distribution, etc. According to the continuity characteristics of merging unit performance and the advantage which membership function of normal distribution can gather more information, we intend to apply fuzzy normal distribution membership function of domain for 6σ in the evaluation. The expression is as follows.

$$r_1(u)=\begin{cases}1 & ,u\le\mu_1\\ e^{-\frac{(u-\mu_1)^2}{2\sigma_1^2}} & ,\mu_1<u\le\mu_2\quad ,\sigma_1=\dfrac{\mu_2-\mu_1}{3}\end{cases}$$

$$r_2(u)=\begin{cases}e^{-\frac{(\mu_2-u)^2}{2\sigma_{21}^2}} & ,\mu_1<u\le\mu_2\quad ,\sigma_{21}=\dfrac{\mu_2-\mu_1}{3}\\ e^{-\frac{(u-\mu_2)^2}{2\sigma_{22}^2}} & ,\mu_2<u\le\mu_3\quad ,\sigma_{22}=\dfrac{\mu_3-\mu_2}{3}\end{cases} \tag{6}$$

$$r_3(u)=\begin{cases}e^{-\frac{(\mu_3-u)^2}{2\sigma_3^2}} & ,\mu_1\le u<\mu_3\quad ,\sigma_3=\dfrac{\mu_3-\mu_2}{3}\\ 1 & ,u>\mu_3\end{cases}$$

where, μ_1 is the given expectation value of "optimal", μ_2 is the given expectation value of "good" and μ_3 is the given expectation value of "general".

According to the standard for the merging unit and the practical engineering experience of relevant operation personnel, each parameter value of the membership function can be determined, as shown in Table 2.

Table 2. Parameters of the membership function

	u_1 (μs)	u_2 (μs)	u_3 (μs)	u_4 (ms)	u_5 (μs)	u_6 (%)	u_7 (%)	u_8 (%)	u_9 (%)	u_{10} (%)	u_{11} (%)	u_{12} (ms)	u_{13} (ms)	u_{14} (ms)
μ_1	0	0	0	0	0	0	0	0	0	0	0	0	0	0
μ_2	0.5	2	5	0.5	0.5	0.05	5	0.1	3	0.1	0.5	20	20	20
μ_3	1	4	10	1	1	0.1	10	0.2	6	0.2	1	34	34	34

Example Application

Taking a type of merging unit as an example, this paper evaluates its performance with the use of fuzzy comprehensive evaluation method based on the triangular fuzzy number in Figure 1. According to the test statistics, the value of each evaluation index is U = [0.6, 1.5, 7, 0.6, 0.3, 0.04, 2, 0.17, 1, 0.13, 0.2, 10, 23, 26].

According to the hierarchical theory, the importance of each index in the evaluation index system are compared based on three experts' judgment, and the fuzzy judgement matrix is generated after taking an average. Taking the time performance as an example, the weight of each time performance index is calculated, as shown in Table 3.

Table 3. Fuzzy judgement matrix

	u_1	u_2	u_3	u_4	u_5
u_1	(1, 1, 1)	(1, 1.5, 2)	(1.25, 1.5, 2)	(1, 1.5, 2)	(1, 1, 1)
u_2	(1/2, 2/3, 1)	(1, 1, 1)	(1.25, 1.5, 2)	(1/2, 2/3, 1)	(1/2, 2/3, 1)
u_3	(1/2, 2/3, 4/5)	(1/2, 2/3, 4/5)	(1, 1, 1)	(1/2, 2/3, 1)	(1/2, 2/3, 1)
u_4	(1/2, 2/3, 1)	(1, 1.5, 2)	(1, 1.5, 2)	(1, 1, 1)	(1, 1, 1)
u_5	(1, 1, 1)	(1, 1.5, 2)	(1, 1.5, 2)	(1, 1, 1)	(1, 1, 1)

Calculate the comprehensive importance degree of every evaluation index according to the Formula (3), and the results are as follows: S1 = (0.1610, 0.2468, 0.3721), S2 = (0.1150, 0.1709, 0.2791), S3 = (0.0920, 0.1392, 0.2140), S4 = (0.1380, 0.2152, 0.3256), S5=(0.1534, 0.2278, 0.3256).

And then calculate the possibility of being more important than according to the Formula (4):

$V(S_2 \geq S_1)=0.6085$, $V(S_2 \geq S_4)=0.7610$, $V(S_2 \geq S_5)=0.6881$, $V(S_3 \geq S_1)=0.3296$, $V(S_3 \geq S_2)=0.7576$, $V(S_3 \geq S_4)=0.4999$, $V(S_3 \geq S_5)=0.4061$, $V(S_4 \geq S_1)=0.8387$, $V(S_4 \geq S_5)=0.9315$, $V(S_5 \geq S_1)=0.8965$, $V(S_1 \geq S_2)=V(S_1 \geq S_3)=V(S_1 \geq S_4)=V(S_1 \geq S_5)=V(S_2 \geq S_3)=V(S_4 \geq S_2)=V(S_4 \geq S_3)=V(S_5 \geq S_2)=V(S_5 \geq S_3)=V(S_5 \geq S_4)=1$

Plug the above results into Formula (5), and then calculate the weight: $d_1 = 1$, $d_2 = 0.6085$, $d_3 = 0.3296$, $d_4 = 0.8387$, $d_5 = 0.8965$. Get the weight after unitary: W = (0.2722, 0.1656, 0.0897, 0.2283, 0.2441).

Calculate the membership value of every index, then get the fuzzy relationship matrix R:

$$R=\begin{bmatrix} 0.0015 & 0.8353 & 0.0561 \\ 0.0796 & 0.7548 & 0.0009 \\ 0.0001 & 0.4868 & 0.1979 \\ 0.0015 & 0.8353 & 0.0561 \\ 0.1979 & 0.4868 & 0.0001 \end{bmatrix}$$

Get the comprehensive evaluation of the time performance after weighting:

$$B_1 = (0.0623, 0.7056, 0.0460)$$

Similarly, the weight of the communication performance can be obtained: W = (0.6842, 0.3158), and the comprehensive evaluation is B_2 = (0.1921, 0.6340, 0.0011).

The weight of the steady-state performance can be obtained: W = (0.3142, 0.2914, 0.2464, 0.1480), and the comprehensive evaluation is B_3 = (0.2489, 0.2677, 0.2367).

The weight of the dynamic performance can be obtained: W = (0.5375, 0.2647, 0.1978), and the comprehensive evaluation is B_4 = (0.1753, 0.4763, 0.0620).

Due to the time performance, communication performance, steady-state performance and dynamic performance being the same importance, their weight is: W = (0.25, 0.25, 0.25, 0.25), then get final comprehensive evaluation of merging unit: B = (0.1696, 0.5209, 0.0864).

According to the maximum membership principle and fuzzy comprehensive evaluation results, we can know that the comprehensive performance of the merging unit is good. In the secondary performance index, the membership degree of the time performance, communication performance and dynamic performance is bigger. In the first-level index, the situation of minority performance indexes such as Non- compliant event of interface design is excellent, the situation of linearity of

measuring AC current being general, and most of the rest of the performance index is in good condition. If the evaluation score is needed, we can set a corresponding score for each grade, and calculate the score of the merging unit performance evaluation. By evaluating score, performance can be compared between different types of merging unit, and then find out the better product in equipment selection work.

The index weight of merging unit performance calculated by the triangle fuzzy number is in accordance with the fuzziness of people's subjective thinking about relative important degree. It retains the advantage of the subjective understanding and experience to judge, and guarantees the weight objective and reliable on the algorithm.

Summary

The index weight of merging unit performance is obtained by mathematical processing with triangular fuzzy number, and can improve the defects of traditional subjective weight in a certain extent. On the above basis, a merging unit performance evaluation index system and a fuzzy comprehensive evaluation model are established, providing a systematic model and basis for the merging unit performance evaluation. The instance shows the effectiveness of using the triangle fuzzy number to calculate the index weight, and the reliability of the fuzzy comprehensive evaluation model established.

References

[1] CAO Nan, LI Gang, WANG Dong-qing. Key technologies and construction methods of smart substation. Power System Protection and Control, 2011, 39(5): 63-68.

[2] LIU Hao-yu, ZUO Qun-ye, ZHANG Bao-shan. Process level network performance testing and analysis in smart substation. Power System Protection and Control, 2012, 40(12): 112-116.

[3] HU Guo, TANG Cheng-hong, XU Zi-an, et al. Development of a new MU for digital substations. Automation of Electric Power Systems, 2010, 34(24): 51-54.

[4] HAN Ying, MU Long-hua, ZHOU Wei. Application and Realization of IEEE1588 Protocol in Merging Unit. Proceedings of the Chinese Society of Universities for Electric Power System and its Automation, 2012, 24(3): 16-21.

[5] FAN Chen, NI Yi-min, SHEN Jian, et al. Research of the application of IEEE1588 in the merging unit based on IEC61850-9-2. Automation of Electric Power Systems, 2011, 35(6): 55-59.

[6] LIU Hai-tao, HUANG Ming-yu, ZHAO Xu-yang. Time Measurement for Merging Units of Intelligent Substation. East China Electric Power, 2013, 41(1): 0119-0121.

[7] HUANG Bai-lin, CUI Xin-you, LIU Li-bin, et al. Research and Implementation of Resistance to Electrical Fast Transient of Merging Unit. Low Voltage Apparatus, 2013, 4:9-13.

[8] WU Cheng-guo, WANG Yi-min, JIN Ju-liang, et al. Comprehensive risk analysis based on triangular fuzzy number for reservoir flood control operation. Journal of Hydroelectric Engineering, 2011, 30(4): 30-35.

[9] YANG Lun-biao, GAO Ying-yi. Principle and application of fuzzy mathematics. Guangzhou: South China University of Technology Press, 2005.

[10] MING Jiao, LIU Dai-yong. Alarm in formation classification model of AVC system for district power network based on improved analytic hierarchy process and fuzzy synthetic evaluation. Power System Protection and Control, 2011, 39(2): 50-54.

Advanced Materials Research Vols. 989-994 (2014) pp 5565-5570
© (2014) Trans Tech Publications, Switzerland
doi:10.4028/www.scientific.net/AMR.989-994.5565

Research on Travel Time Prediction under the Condition of Urban Rainstorm in Overpass Area

Song Bi[a], Zhongcheng Zhao[b], Guan Wang[c], Lin Kong[d], Qi Diao[5, e], Cunwu Han[f], Dehui Sun[g]

Beijing Key Laboratory of Fieldbus Technology and Automation North China University of Technology, Beijing 100144, China

[a]email: bisongo@163.com, [b]email: zhaocheng900118@163.com, [c]email: wangguan@163.com, [d]email: houaihua1969@163.com, [e]email: diaoqi@163.com, [f]email: han_cunwu@126.com, [g]email: sundehui@ncut.edu.cn

Keywords: urban road network; overpass area; ponding depth detection; travel time prediction; traffic guidance

Abstract. Overpass is an important hub for urban road network facility, its traffic capacity severely restricts that of the entire road network. Since overpass area is easy to gather water in urban road network, rain water under the overpass is an important incentive for traffic jams. In this paper, a reliable and easily maintainable method is discussed to detect the depth of the road surface water, which designs and implements a monitoring system of urban road network ponding depth. Based on this, technique of predicting travel time has been researched about overpass area under water-logging condition. Through a real example, the technique discussed in this paper has been proved to be highly effective and veracious, and can be used to provide basic data for traffic guidance to plan out sound routes.

Introduction

With the development of social economy and urbanization, the number of the population and that of the vehicles in the city is increasing. Therefore, the problem of the traffic jam becomes more serious, and meanwhile, the economic and environmental cost further restrains the development of the city. How to relieve the traffic congestion has become an important problem for all big and medium-sized cities in the world to face and to solve. To solve the problem, limiting the traffic participants, increasing the traffic network capacity and raising the traffic efficiency could be considered. However, the service function of the city requires that the city can't endlessly limit the number of the traffic participants or the time of using the traffic facilities, or the space in the city requires that the city can't endlessly increase the traffic network capacity. Moreover, it has been proved that merely depending on the increasing of the traffic network capacity can not solve but aggravate the problem of the traffic jam [1]. Under the present traffic condition, improving the operating efficiency of the traffic network is a practical way to solve the problem of the traffic jam [2]. Traffic guidance, according to the cost of a traveler driving from the starting point to the destination, provides an optimal route for the traveler to link the starting point and the destination. The traffic guidance system has been proved to be a significant method to improving the operating efficiency of the traffic network in the city. Travelling route planning is a core element of the traffic guidance, which could be attributed to a problem of looking for the shortest route of weighted directed graph. The weight of the directed graph is the link travel cost, directly influencing the accuracy of the travelling route planning.

The link travel time is conditioned by many factors due to the complexity of urban road network. Therefore, this problem has received serious attention from many researchers. The communication system between road infrastructure and vehicles, collecting the data of the roads and time of vehicle traffic at regular intervals, is used to infer vehicles' travel speed in large numbers of roads [3]. Under the premise of a license plate as vehicle identification, the travel time of urban main road is predicted by analyzing the time vehicles appeared in urban main road in the multiple surveillance

videos [4]. The detection method of road traffic flow data which is based on the signal matching method of upstream and downstream vehicle detector is studied and the prediction method on the link travel time is designed based on it. The method has good robustness for situations of traffic congestion and signal leak [5]. The prediction method on cycle and time of traffic light signal based on the road travel time is studied to predict queue length and the travel time of traffic intersection [6]. The travel time estimation model, based on the methods of step function, linear interpolation and so on, is studied in accordance with the principles of that accumulative flow can be segmented linearization [7]. The data analysis method of upstream and downstream vehicle running speed and direction is studied based on space-time queue model, then the travel time prediction method on rapid fluctuations is described based on the extracted parameters [8]. Affected by the traffic control signal, the traffic data of the downstream coil can not be used to predict travel time, so the modified method on data detected by downstream coils and the prediction method of the link travel time are proposed by studying the dynamics of the vehicle near the stop line [9]. The present studies are mainly focused on the characteristic extraction methods on the state of traffic flow states and the prediction methods of the link travel time in conventional weather conditions. However, there has been a lack of effective means of prediction in the conditions of disasters.

In recent years with the constant advancement of China's urbanization, the scale and complexity of the city road network has been also increasing. Meanwhile, as an important way to build complex road network, overpass achieves a rapid growth in number [10]. The overpass is a multilayer complex structure, so constraints of the existing city planning, traffic facilities, the surrounding buildings and other factors lead to ponding in overpass area [11]. As the hub of urban road network, the ponding in the overpass area which there have intensive vehicles and large traffic flow, will seriously affect the road network traffic capacity to cause traffic congestion [12]. Therefore, how to monitor the depth of water covering the city overpass area and how to predict the travel time are of important practical significance to ease traffic congestion and improve operation efficiency of road network under rainfall condition [13]. In this paper, the detection system based on depth of the water in overpass areas covering the entire road network is put forward and the travel time prediction model based on the characteristics of ponding existing in the overpass area is built.

Design of the Urban Water-logging Monitoring System

Overpass water points have the characteristics of a local focus and global dispersion characteristics. For example, multiple water points in overpass area are distributed in the scope of one square kilometer, but different overpasses have greater distance. Zigbee communication technology has the characteristics of low cost, high reliability and multiple ad-hoc networks. The communication technologies with mobile communications network makes wider access coverage and channel bandwidth. Therefore, the combination of the two networks to obtain the hybrid communication network has characteristics of wide coverage, high communication efficiency and low operating costs. Urban water-logging monitoring system has data interfaces with departments of traffic guidance, fire fighting and fight floods and has the ability to send short messages directionally and provide directional web services. The design of urban water-logging network monitoring system structure is shown in Figure 1.

Currently, ultrasonic ranging is the basic method of measuring surface gathered water. But the water waves caused by moving person or vehicle will significantly impact water depth measurement accuracy, and the personnel and vehicles moving under the ultrasonic sensor also decrease measurement accuracy, resulting in malfunction. To overcome these disturbances, we can use the external protective pipe to limit the movement of objects into the detection region of the ultrasonic sensor. However, because surface water contains more sediment to plug the pipe easily, there will be high maintenance costs. Based on an optical liquid level sensor, an easy maintainable urban ponding detection method is designed in this paper. The optical liquid level sensor can react to whether being submerged. Therefore the detector exposed to water avoids the problem of difficult maintenance in ultrasonic detection methods. The structure of the water depth measurement device is shown in Figure 2 based on optical liquid level sensors. The data acquisition

and transmission board based on the single-chip microcomputer to realize to measure water depth and transfer data among nodes in shown in Figure 3.

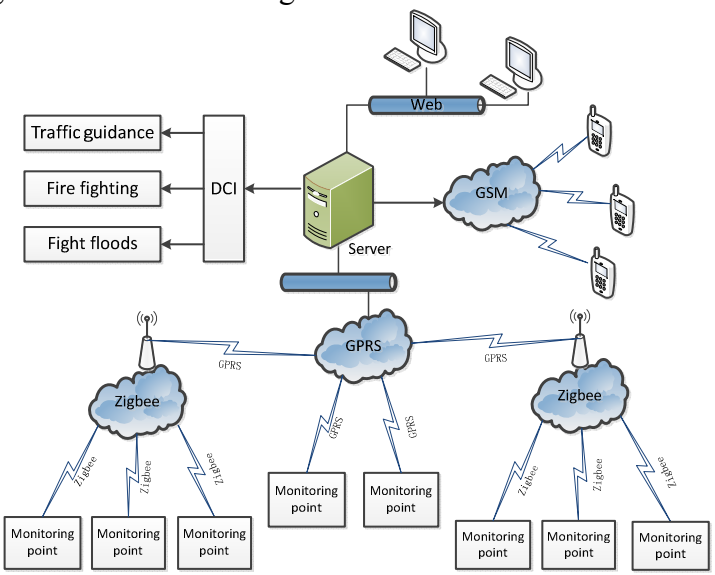

Fig.1. The structure of urban water-logging monitoring system

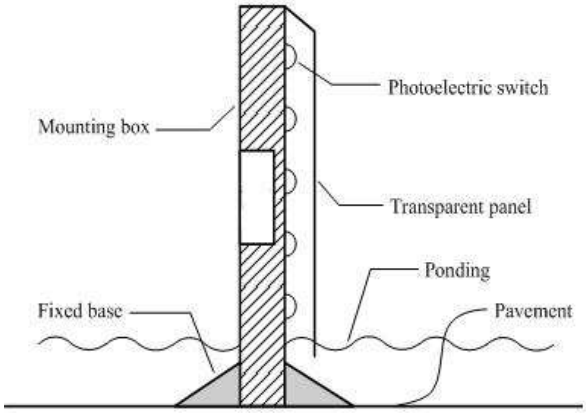

Fig.2. The structure of ponding depth detection device based on photoelectric switch

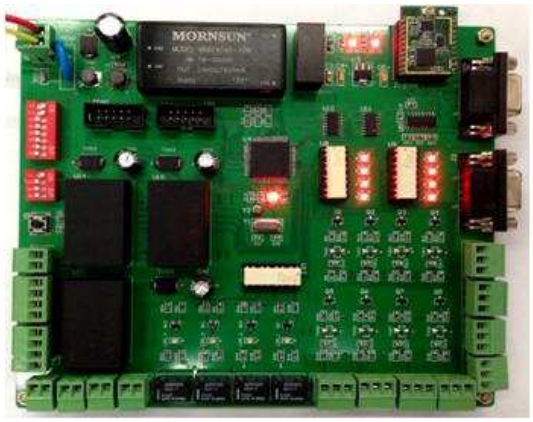

Fig.3. The device of ponding depth data acquisition and transmission

Travel Time Prediction in the Overpass Area under Water-logging Conditions

Prediction Model Design

Many factors affect travel time in overpasses area, which includes transport factors such as traffic flow, traffic state, vehicle types and road system factors such as green ratio and section length and environmental factors such as weather conditions and the surrounding public buildings. Among many factors, traffic state, traffic flow and weather conditions on the overpass area have a relatively large impact on travel time. Urban transport system is a large complex of randomness and uncertainty system. With the increase of complexity of the system, the accurate prediction of the link travel time is meaningless, and the results of a qualitative description of the link travel time accords to actual situations. Fuzzy approach is an effective method to describe uncertain problems, and therefore to process traffic-related parameters fuzzily accords to urban traffic characteristics. Assuming the link travel time is T, traffic flow F, traffic state S, water depth H, using the Self-Organized Map (SOM) method to calculate the cluster centers of the characteristics.

To assume the cluster centers corresponding to traffic flow of small, medium and large as C_{f1}, C_{f2} and C_{f3}, to traffic state of smooth, amble and congestion as C_{s1}, C_{s2} and C_{s3}, to water depth of small, medium and large as C_{h1}, C_{h2} and C_{h3}, and to traffic time of short, medium and long as C_{t1}, C_{t2} *and* C_{t3},. To assume the membership corresponding to traffic flow of small, medium and large as μ_{h1}, μ_{h2} and μ_{h3}, to traffic state of smooth, amble and congestion as μ_{s1}, μ_{s2} and μ_{s3}, to water depth of small,

medium and large as μ_{h1}, μ_{h2} and μ_{h3},, and to traffic time of short, medium and long as μ_{t1}, μ_{t2} and μ_{t3}. So L_{h1}, L_{h2} and L_{h3} is the Euclidean distance between water depth and the cluster center of that, and set the current water depth as h, then the calculation rules are:

1) If $h < C_{h1}$, then $\mu_{h1} = 1$, $\mu_{h2} = 0$, $\mu_{h3} = 0$.

2) If $h > C_{h3}$, then $\mu_{h1} = 0$, $\mu_{h2} = 0$, $\mu_{h3} = 1$.

3) If $C_{h1} < h < C_{h3}$, then memberships to three categories is $\mu_{h1} = L_{h2} / (L_{h1}+L_{h2})$, $\mu_{h2} = 1- \mu_{h1}$, $\mu_{h3} = 0$, when $L_{h1} < L_{h2} < L_{h3}$.

For other situations, the degree of membership is calculated as above. Similarly, the degrees of memberships of traffic state, traffic flow, and travel time can be obtained according to the above method. In this paper, the degree of memberships, as input parameters, are used to predict the link travel time by BP network.

Verification of an Example

Extraction of 50 samples tested under Jinyuan bridge in Shijingshan District of Beijing from May 20, 2013 to August 20, 2013 is used to verify the proposed method after normalization. The location of the sample data collected and verified is shown in Figure 4.

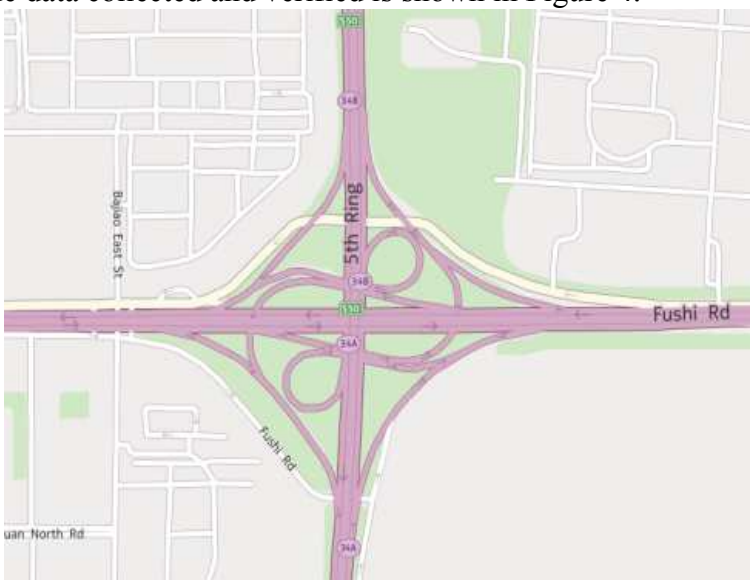

Fig.4. The location map of sample data collected

The clustering centre data computed by SOM is shown in Table 1.

Tab.1. The clustering centre data

C_{f1}	C_{f2}	C_{f3}	C_{s1}	C_{s2}	C_{s3}	C_{h1}	C_{h2}	C_{h3}	C_{t1}	C_{t2}	C_{t3}
0.389	0.672	0.831	0.152	0.328	0.456	0.217	0.587	0.652	0.028	0.439	0.842

The normalized data of test samples is shown in Table 2.

Tab.2. The normalized data of test samples

Sample ID	F	S	H	T
1	0.764	0.166	0.191	0.019
2	0.583	0.281	0.389	0.406
3	0.368	0.373	0.556	0.593
4	0.184	0.491	0.611	0.764
5	0.105	0.438	0.713	0.912

The degree of membership calculated out by putting normalized data respectively into the corresponding membership function is shown in Table 3.

Tab.3. The membership data of test samples

Sample ID	μ_{f1}	μ_{f2}	μ_{f3}	μ_{s1}	μ_{s2}	μ_{s3}	μ_{h1}	μ_{h2}	μ_{h3}	μ_{t1}	μ_{t2}	μ_{t3}
1	0.000	0.421	0.579	0.920	0.080	0.000	1.000	0.000	0.000	1.000	0.000	0.000
2	0.314	0.686	0.000	0.267	0.733	0.000	0.535	0.465	0.000	0.080	0.920	0.000
3	1.000	0.000	0.000	0.000	0.648	0.352	0.084	0.916	0.000	0.000	0.618	0.382
4	1.000	0.000	0.000	0.000	0.000	1.000	0.000	0.631	0.369	0.000	0.194	0.806
5	1.000	0.000	0.000	0.000	0.141	0.859	0.000	0.000	1.000	0.000	0.000	1.000

Put the membership data of test samples into estimating model of the travel cost of traffic overpass area which is trained by Back Propagation under the condition of rainstorm, and calculate out the estimation results of the degree of membership. The data of actual results and estimation results are shown in Table 4. The deviation is the distance value between actual value and estimated value. The calculation method on deviation value is:

$$\varepsilon = \sqrt{\sum_{i=1}^{3} (C_i - \hat{C}_i)^2} \tag{1}$$

In the type: C_i stands for the actual value of the degree of membership of the travel cost; $\hat{C}_i$ stands for the estimated value of the degree of membership of the travel cost.

Tab.4. The comparison between estimated simulation results and actual results of traffic capacity in overpass area under water-logging condition

Sample ID	Actual Value	Estimated Value	Deviation
1	0.792	1.000	0.293
	0.191	0.000	
	0.017	0.000	
2	0.035	0.080	0.114
	0.872	0.920	
	0.093	0.000	
3	0.018	0.000	0.108
	0.534	0.618	
	0.448	0.382	
4	0.014	0.000	0.224
	0.029	0.194	
	0.957	0.806	
5	0.006	0.000	0.026
	0.015	0.000	
	0.979	1.000	

Conclusion

In this paper, a detection method on the depth of the road surface water is discussed under the condition of urban water-logging, which designs and implements a monitoring system of urban road network ponding depth. In the meantime, a prediction model of the link travel time has been set up

by Back Propagation, which is based on traffic flow, traffic state and the depth of the road surface water. Through a real example, the technique discussed in this paper has been proved to be highly feasible and effective to predict the link travel cost under the condition of urban rainstorm.

Acknowledgement

In this paper, the research was sponsored by the Natural Science Foundation of China (Project No. 61174116), the Natural Science Foundation of Beijing (Project No. 4142014) and Graduate Education called the Training Base in Combination with Production, Teaching and Research for Graduates (Project No. PXM2013_014212_000028).

References

[1] Xinmei Sun. The countermeasures to solve the problem of urban traffic Jams [J]. Economist, 2010 (9) 62-63.
[2] Shiquan Zhong, Shoufeng Ma, Guoguang He. Description and simulation of dynamic route guidance system road network [J]. JOURNAL of Systems Engineering, 2009 24 (2) 25-38.
[3] Meng Li, Zhijun Zou, Fanping Bu. Arterial Travel Time Estimation Using VII Probe Data and Point-based Detection Data [C]. 13th International IEEE Annual Conference on Intelligent Transportation Systems, 2010.1764-1769.
[4] Dewang Chen, Kun Zhang, Tao Liao. Practical Travel Time Prediction Algorithms Based on Neural Network and Data Fusion for Urban Expressway [C]. Sixth International Conference on Natural Computation, 2010.1754-1758.
[5] Mandoye Ndoye, Virgil F. Totten, James V. Krogmeier, et.al. Sensing and Signal Processing for Vehicle Reidentification and Travel Time Estimation. IEEE Transactions on Intelligent Transportation Systems, 2011 12 (1) 119-131.
[6] Peng Hao, Xuegang Ban, Kristin P. Bennett, et.al. Signal Timing Estimation Using Sample Intersection Travel Times. IEEE Transactions on Intelligent Transportation System, 2012 13 (2) 792-804.
[7] Jiancheng Long, Ziyou Gao, W.Y.Szeto. Discretised link travel time models based on cumulative flows: Formulations and properties [J]. Transportation Research Part B: Methodological, 2013 45 (1) 232-254.
[8] Li Li, Xiqun Chen, Zhiheng Li, et.al. Freeway Travel-Time Estimation Based on Temporal–Spatial Queueing Mode [J]. IEEE Transactions on Intelligent Transportation Systems, 2013 14 (1) 1536-1541.
[9] Zhaosheng Yang, Xueying Gao, Ciyun Lin, et.al. The link travel time estimation based on the detecting coil downstream sections [J]. Journal of Beijing University of Technology, 2010 36 (6) 790-795.
[10] Wei Zhang, Simin Li, Guangyin Sun. Effect mechanism of urban rainstorm water-logging formation in China [J]. Urban Development Studies. 2013 20 (1) 120-122.
[11] Yun Zhang, Ou Huang, Xiangrui Chen, et.al. Water accumulation causes caused by the urban water-logging of the recessed overpass in Beijing and control measures [J]. China Municipal Engineering. 2013 168 62-64.
[12] Shihong Chen, Saiqiong Peng. Application of ArcGIS on the problem of transportation route selection in urban water-logging [J]. Computer Knowledge and Technology. 2013 9 (1) 205-206.
[13] Yongbo Wang, Guohui Tao, Xueyi Jing, et,al. Research of urban rainstorm water-logging monitoring and early warning system in Harbin [C]. The 26th annual meeting at the Chinese academy of meteorological disaster and weather event early warning, forecasting and disaster prevention and mitigation at the venue. 2009.1192-1197.

Advanced Materials Research Vols. 989-994 (2014) pp 5571-5574
© (2014) Trans Tech Publications, Switzerland
doi:10.4028/www.scientific.net/AMR.989-994.5571

Application of Information Technology in Engineering Thermodynamics

Ji LI[1, a], Xiuyan WANG[2, b]

[1]School of Energy, Power and Mechanical Engineering, North China Electric Power University, Beijing 102206, China

[2]School of Energy, Power and Mechanical Engineering, North China Electric Power University, Beijing 102206, China

[a]email: jli@ncepu.edu.cn, [b]email: wxy@ncepu.edu.cn

Keywords: Information Technology; Engineering Thermodynamics; Blending Teaching

Abstract. Information technology has been greatly developed in recent years and brings opportunities as well as challenges for engineering courses. This paper surveys the development and characteristics of information technology. Then different methods of information technology are analyzed and applied. The new teaching mode based on information technology – blending teaching as well as detailed teaching case is proposed in the course of Engineering Thermodynamics.

Introduction

The booming development of information technology has greatly influenced higher education. Information technology brings opportunity as well as great impact on education industry especially higher education industry. Governments from different countries pay great attention on information technology in the last decade. In 2010, U.S. Department of Education announced national education technology plan [1]. Technology, especially information technology is proposed to transform and motivate the American future education in this plan. Chinese government also thinks highly of information technology and has proposed a series of steps to improve education development by information technology. In 2012, Ministry of Education announced "Ten-year development plan for education informatization from 2011 to 2020". In this plan, how to discover the comprehensive and deep integration of modern information technology with education to guide the innovation of modern education concept and education mode is proposed [2]. How to effectively make use of information technology in higher education field, especially for engineering courses are intensively focused in universities in recent years.

This paper first surveys the development and characteristics of information technology. Then, combined with course of Engineering Thermodynamics, different methods of information technology are analyzed and applied for this course. In the last part of this paper, the new teaching mode based on information technology – blending teaching in Engineering Thermodynamics as well as detailed teaching case is proposed. The main purpose of teaching and research in information technology is to carry out teaching reform and promote teaching effect of Engineering Thermodynamics in universities.

Characteristics of Information Technology for Higher Education

Traditional classes in universities have been applied for centuries. However, traditional classes also have the disadvantages of one-way teaching, passive accepting, and "duck-stuffing" teaching mode, etc. How to change traditional education, activate the creativity of students, improve the quality and ability of students, and pursue the development of individualized students, is the new teaching research topics we faced.

The development of teaching mode in universities has experienced four main steps: the first step is traditional classes, this mode is teacher-centered teaching mode which means teachers are the center of classes while students are in the passive role; the second step is apply information technology to support teaching processes which means teachers use some digitized resources such as electronic teaching plan, PowerPoint presentation, network teaching platform to assist the

teaching processes; the third step is the application of network-assisted teaching, which means network teaching accounts for a large proportion of the classes contrast to face to face teaching; the fourth step is online courses which means most classes or entire classes are taught by website online processes. Table 1 shows the development of information technology and their relationships in recent years in both USA and China [3].

	Face-to-face class process	IT support teaching process	Network assist teaching process	Online course process
Characteristics	Traditional teaching mode, no network teaching hours	Less than 30% network teaching hours	About 30% to 70% network teaching hours	More than 70% network teaching hours
USA progress	Before 1999	1999-2004 Risk investment on business corporations such as Blackboard and WebCT	2005 to now About 3000 universities use Blackboard	2012 to now edX, Coursea, Udicity MOOCs platform are constructed and applied widely
China progress	Before 2003	2003 to now Digital resources platform, course website, qualified course construction	2007 and 2008 Some universities discover teaching reform and innovation for some courses	2013 to now First year of MOOCs in China, and some famous universities issued MOOCs

Application of Information Technology in Engineering Thermodynamics

Information technology brings opportunities as well as challenges for engineering courses. The following part of this paper studies construction and application of Information Technology in Engineering Thermodynamics.

1. Application of digital resources in Engineering Thermodynamics

Digital university campus has been universal in China in recent years. Construction of digital resources for university courses may be regarded as part of digital campus. How to popularize and improve the digital resources for engineering courses should be focused by all the teachers and educators.

Digital resources for Engineering Thermodynamics include electronic teaching resources: course introduction, course specification, teaching plan, key and difficult problems, exercises in the class, exercised after class, references, PowerPoint presentation, exercise library, example library, lecture library, material library, academic paper library, further reading library, micro teaching voice library, micro teaching video library, etc.

All the digital resources should cover the fundamental knowledge, basic concepts, basic principles, typical cases, advanced topics, and hot issues in Thermodynamics field. For examples, hot issues can involve renewable energy issue, new energy issue, high-capacity power unit issue. During the construction process of digital resources, to actualize systemic and entire course resources as basic requirement, to actualize rich resources and open resources as basic goal, to make good service for the teaching and learning process as key point, to fulfill and improve actual reaching requirements as ultimate goal.

2. Application of network resources in Engineering Thermodynamics

As the products of information technology, micro courses and MOOCs (Massive Open Online Courses) is popular all around the world in recent years. Micro courses and MOOCs have the characteristics of online, open, transparent courses, which provide easy and friendly studying mode for students. With the increase of widely distributed students in the whole world of micro courses and MOOCs, new requirements including course content, knowledge structure, knowledge

classification, studying arrangement are proposed for the network courses. For engineering courses, the key step of course design is to tease out knowledge points and rebuild the knowledge structure in the proper form of MOOCs. According to the characteristics of Engineering Thermodynamics, how to classify the course content and knowledge structure reasonably to ensure each course unit is one complete knowledge point and close relations and fusions among these units, is the most important step to build network course. Besides course design module, other modules such as discussion unit, class instruction unit, interaction unit, Q&A unit, exercise unit, examination unit are also need to be designed reasonably and interspersed rationally in the whole network course [4]. At the same time, diversity and personality should be considered to attract the students' learning interest.

3. Blending teaching exploration in Engineering Thermodynamics

One new teaching mode based on information technology – blending teaching is carried out in the course of Engineering Thermodynamics. Blending teaching is different from traditional teaching mode, which employs a large proportion network teaching as well as face-to-face classes. There are three steps to perform the course teaching: face-to-face class, video course online, discussion class. Students can learn the important course contents through self-study in the course website online by video course. While in the classes, teachers solve problems which students can not deal with online and discuss with students for further study of the course. Discussion is also carried out online by teachers and students or even students and students. This kind of teaching mode can utilize fully of the advantages of modern information technology and make up the disadvantages of traditional teaching. To mobilize the interest of students, teacher organizes students to discuss interested issues or difficult issues in classes, no need to teach course contents in the classroom, and which can be called as flipped classroom. That means teacher can focus on the guided education to improve the thinking ability and creativity ability of students. Meantime, students' interest is improved since students can utilize their spare time and their best status to study the online course. Blending teaching and flipped classroom transform the teacher-centered teaching mode to student-centered teaching mode. Teaching case for moist air in Engineering is designed according to the concept of blending teaching and flipped classroom. Figure 1 shows the teaching case based on blending teaching in Engineering Thermodynamics [5].

Conclusion

In this paper, different information technology, such as digital resources, micro course, MOOCs, blending teaching, flipped classroom is analyzed and applied. Detailed teaching case for the knowledge of moist air is also proposed and applied in the course of Engineering Thermodynamics.

Acknowledgement

The research was sponsored by Beijing Teaching Reform Project (Project No. GJJG201404) and Beijing Teaching Co-construction Project.

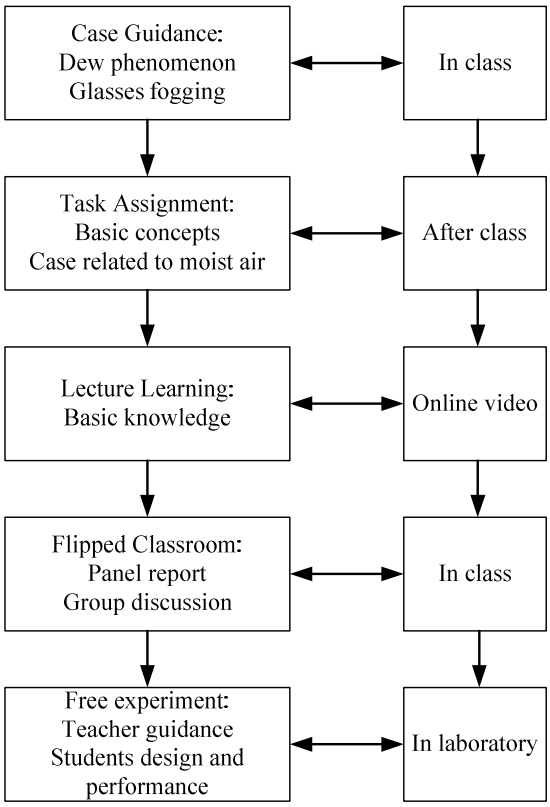

Fig.1. Teaching case based on blending teaching in Engineering Thermodynamics

References

[1] Office of Educational Technology, U.S. Department of Education. Transforming American education: learning powered by technology, national education technology plan 2010. http://www.ed.gov/technology/netp-2010, 2010

[2] Ministry of Education. Ten-year development plan for education informatization from 2011 to 2020. http://www.moe.gov.cn/publicfiles/business/htmlfiles/moe/s3342/201203/133322.html, 2012

[3] Yonghong Chen. From network assistance teaching to MOOCs. Workshop by China Association for Educational Technology [C]. Beijing, 2014.3

[4] Qi Wang, Long Li, Qiuju Xie. Research on the teaching mode of blending learning under the deep integration between information technology and higher education [J]. Electronic Test, 2014, (3): 146-147

[5] Ji Li, Xiuyan Wang. Course construction and teaching reform for Engineering Thermodynamics. Teaching reform conference for energy and power specialty in China. Zhenjiang, 2014.

Advanced Materials Research Vols. 989-994 (2014) pp 5575-5579
© (2014) Trans Tech Publications, Switzerland
doi:10.4028/www.scientific.net/AMR.989-994.5575

Wastewater Management in Shanghai

Jiancheng KANG[1, a], Hai LIN[1, b], Jiong ZHU[1, c], Guodong YAN[1, d]

[1]Shanghai Normal University, Shanghai 200234, China

[2]Shanghai University of Engineering Science, Shanghai 200234, China

[a]email: kangjc@126.com, [b]email: linhai@shnu.edu.cn, [c]email: zhujiong@shnu.edu.cn, [d]email: yanguodong@163.com

Keywords: Shanghai; Wastewater; Environment; City; Management

Abstract. In 1981~2012, the general urban wastewater in Shanghai was between 1.775~2.420 billion tons. Among the urban wastewater, the industrial wastewater emissions before 1988 was more than 1.4 billion tons, then, it was declining to about 649 million tons at 2002, a low value in the past 30 years, less than 50% of the 1980s. The percentage of industrial wastewater in the total urban wastewater discharge is falling from 76.9% in 1981 to under 30% in recent years. The living wastewater emissions increased from 424 million tons in 1981 to 1.697 billion tons in 2012. There is a relationship between the living wastewater increasing and the increase of the permanent residents in Shanghai. At the same time, the living wastewater emissions per capita per day were significantly increased from 100 kg (liter) around 1980s to around 190 kg (liter) in recent years. From 1995, the treatment and management of urban wastewater was continuing to intensify in Shanghai. The ratio of wastewater treating has increasing from 6.35% in 1995 to 85.62% of the total urban wastewater in 2012. Comparing the social-economic development and management of wastewater discharge in Shanghai, it can be seen, the wastewater emissions increasing amplitude was far less than the sizes of population growth and economic growth in the past 30 years

Introduction

Shanghai is located at the west bank of Pacific Ocean, the east frontier of the Asian continent, the center of the China coast. She faces to the East China Sea, bounds by Hangzhou Bay at the south, and neighbors with the Yangtze River at the north, is situated in the Yangtze River estuary. The area of Shanghai is 6340.5 square kilometers, the geographic coordinates is between latitude 30º40'N to 31º53'N, longitude 120º52'E to 122º12'E. She is part of the alluvial plain of the Yangtze River Delta, belongs to a subtropical monsoon climate.

Shanghai is China's largest municipality, a prosperous international metropolis, and an economic and financial center. Shanghai's GDP in 2012 was 2.018 trillion Chinese Yuan. The imports in Shanghai accounted for 17.1% and exports accounted for 24% of the whole nation. The population of permanent residents in Shanghai is more than 25 million; the resident's foreign population is more than 170 thousand people.

Water environment is related to the city's survival and the sustainable development of society and economy. Water environment management is one of the main missions of the Shanghai municipal government, the management of urban wastewater is the key work. There are the Shanghai Water Bureau and the Environmental Protection Bureau to take charge the work. In recent years, with the improvement of living standards of Shanghai and the rapid increasing in population, the pressure on water resources and environment is increasing rapidly. The water pollution incident has been reported from time to tome, the status of water environment is being more and more social attention.

Here by collecting data, analyzing the wastewater discharge and treatment, and comparing with relevant data of economic and social development of Shanghai since 1981, to discuss quantitatively the annual variability of urban wastewater management and the relationship with economic and social development; to reveal the trend of wastewater management at environment protection; to make society understanding the relationship between wastewater management and the public, for further improving urban wastewater management system.

Data Source

To ensure the reliability of the analysis, the data are only chosen from the Water Environmental Quality Communiques, Water Resource Bulletins, Newsletters, Year Books, which were published by government administrations at different years, such as the Shanghai Environmental Protection Bureau, Water Bureau, Shanghai Statistical Yearbook, etc. and the research reports and data collections from the staff in the institutes and departments of government management; to extract the relevant data. The data used to see references[1-7].

When meeting the deviation in the data for the same year, the original of the data from the management departments and the report from collecting staff would be considered firstly, and refer to the tendency of the data before and after a few years.

Analysis and Results

The change of the wastewater emissions in Shanghai from 1981 to 2012

1). From 1981 to 2012, the total amount of wastewater discharge in Shanghai was between 1.775- 2.420 billion tons. During the years, the wastewater emissions became minimum at 1982 and maximum at 1996. The emissions decreased after 1996 and increased again since 2003 (Figure 1).

2). The discharge of industrial wastewater (IW) was higher before 1988, more than 1.4 billion tons; the discharge was declining to about 649 million tons at 2002, a low value over the past 30 years, less than 50% in the 1980s. For last decade, the industrial wastewater emission has been maintained between 647 to 759 million tons per year (figure 1).

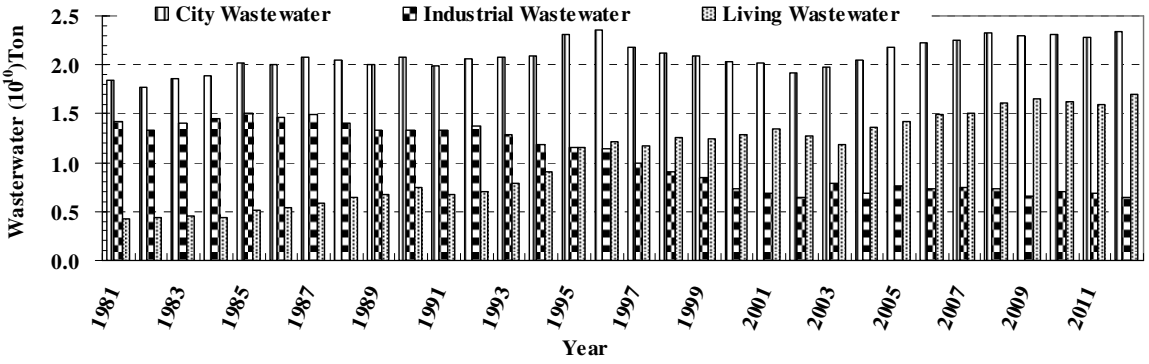

Fig. 1 The Shanghai city wastewater discharge during 1981-2012

The ratio of the industrial wastewater discharge in total city wastewater has continued to decline, from 76.9% in 1981 to less than 30% in recent years.

The Chemical Oxygen Demand (COD) emission by the industrial wastewater has been descended from 250 thousand tons at the year of 1990, to 26.2 thousand tons at 2012, about ten percent of the COD emission in 1990 (figure 2). The drop rate can be divided into two stages, before the year of 2000, the falling rate was up to 17 thousand tons per year; slowed decline rate, at about 2.45 thousand tons per year after 2000.

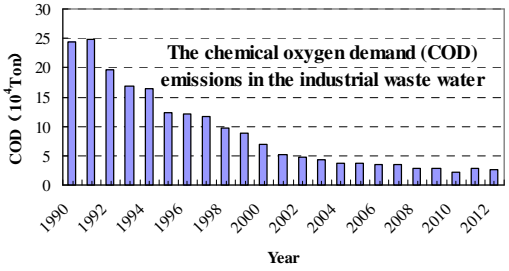

Figure 2 Annual variability of the chemical oxygen demand (cod) emission in the industrial waste water

The amount of industrial wastewater emission for the second industry output value per ten thousand Chinese Yuan, has fallen from 577.51 tons in 1981, to 8.24 tons in 2012 (figure 3). The

annual declining rate of wastewater discharge, reached 33.6 tons for the second industrial output value per ten thousand Chinese Yuan from 1983 to 1999, the annual declining rate of wastewater discharge, reached 2 tons in 2000-2012.

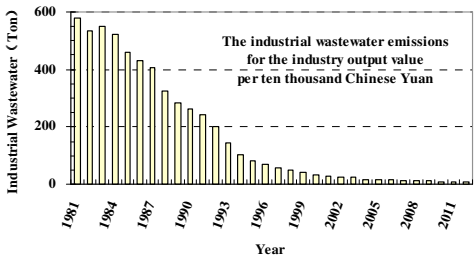

Figure 3 The annual variability of industrial wastewater emission for the second industry output value per ten thousand Chinese Yuan

3). The life wastewater discharge in Shanghai, showed a fluctuant increasing trend since 1981 generally, with some short-term negative growth in 1990-1991, 1996-1997, 2001-2003 and 2009-2010 (Figure 1).

There is a relationship between the life wastewater emission and the population of permanent residents in Shanghai. Comparing the data, it showed, with the increasing of the population, the wastewater emission was increasing. But it was not a simple linear relationship between the two (Figure 4a left), when the population was around 15 million, the increasing rate of wastewater was in turn; more than 15 million people, the growth rate of life wastewater emission was decreasing.

At the same time, the life wastewater emission per person per day were also greatly increased since 1981. It was around 100 liters emission per capita per day at the early 1980s, increased to 150 liters at 1990, up to a peak of 228.74 liters on 1996. During 1996-2001, the value was around 220 liters. In recent years, the average wastewater discharge per capita per day was falling under 200 liters (Fig 4 b, right).

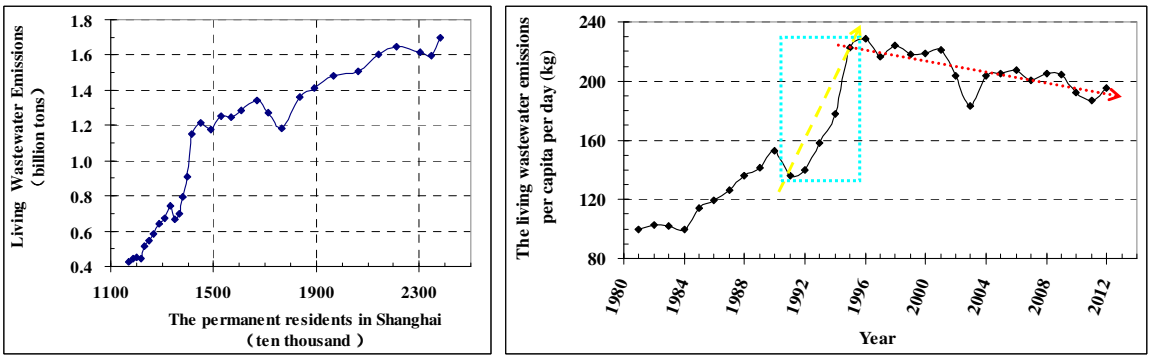

Figure 4a (left). The relationship between the life wastewater emission and the population of permanent residents in Shanghai

4b (right). The annual variability of the life wastewater emission per person per day in Shanghai

The wastewater management in Shanghai

Since 1995, Shanghai was continuing to increase the intensity of urban wastewater treatment. In 1995, the city has 17 sewage treatment plants, the wastewater treatment was 146.65 million tons, accounting for 6.35% of the total urban wastewater; to 2012, the sewage treatment plants has increased to 53, the treating capacity can be 2.01 billion tons, accounting for 85.62% of the total urban wastewater. From 1995 to 2012, with averaging, 2.1 new wastewater treatment plants were annually built, the treating capacity increased 135.73 million tons each year, and the increasing rate for wastewater treatment has 5.86% per year.

The process of wastewater management presented in the three phases by the inter-annual variability of wastewater treatment capacity and treatment rate. The first phase from 1995 to 2003, an average annual increase of wastewater treatment capacity was 31.84 million tons, an average annual increase of treatment rate was 1.77%. The second stage was between 2003-2006, the average annual increase in the amount of wastewater treatment was 370.04 million tons, an average annual increase of treatment rate was 15.81%, increasing about 10 times compared with the first stage. The years of 2006-2012 are the third stage, the wastewater treatment capacity increased by 81.56 million tons annually, the average annual treatment rate increased 3%.

The economic and social development and wastewater management in Shanghai

Shanghai's gross domestic product (GDP) increased with year since 1978. The growth rate can be divided into the three stages, turning points were at 1990 and 2002 respectively. From 1978-1990，annual growth rate was 0.4567 ten billion Chinese Yuan. The growth rate reached 4.587 ten billion Chinese Yuan per year from 1991 to 2002, about ten times is that of the previous stage. The growth rate was further increased in 2002-2012, reached to an annual 14.962 ten billion Chinese Yuan, 3.26 times compared with the stage between 1991 and 2002. The economy began rapid growth since 1991, and has continued to accelerate from 2002.

The population of permanent residents in Shanghai has continued to increase since 1978. The increasing amplitude could be divided into two stages, the turning point was in 1997. From 1978-1997, the population increased from 11 million to 15 million, the increasing rate was 192.77 thousand person annually. To 2012, the resident population increased to 23.8 million; the increasing amplitude was 653.66 thousand persons per year during 1997-2012, it is 3.39 times of the previous stage.

The GDP per capita in Shanghai was around 1500 us$ during 1978-1994. From 1994, it continued to grow. The growth could be divided into two phases, with a turning point at 2002. Between 1994 and 2002, the annual GDP per capita increased from 1,662 to 4,103 us$, with an increasing rate of 304 us$ per year. Since 2002, the growth of GDP per capita has accelerated, the annual increase was 1,021 us$, is 3.36 times of the previous stage; the GDP per capita reached 13,524 us$ at 2012.

For the annual variability of the total wastewater emission in Shanghai, three stages can be divided, the turning points are at 1996 and 2002. In 1981-1996, the wastewater emissions were annually increasing, the increasing rate was 28.4 million tons per year. The total wastewater emissions showed a downward trend during 1996 to 2002, the decrease was 59.9 million tons per year. From 2002, the total wastewater discharge again showed an increasing trend, the increasing rate was 40.6 million tons per year.

Contrast the social and economic development and wastewater management in Shanghai, it can be seen, since 1981, the Shanghai population has increased 2.04 times, the total economic output grew 62.14 times; but the total urban wastewater discharges increased only 1.28 times; the increasing amount of the wastewater discharge is far less than the magnitudes of the growth of population and economic. Since the year of 2000, Shanghai resident population has increased by 650,000 annually, per capita GDP has increased by nearly 1,000 us$ per year, the amount of the industrial wastewater discharge has maintained a low level in past 30 years, the life wastewater emission per capita has appeared a downward trend.

Conclusion

1) From 1981 to 2012, the total amount of wastewater discharged in Shanghai is between 1.775 - 2.420 billion tons.

2) The industrial wastewater emission in Shanghai before 1988 was higher, at more than 1.4 billion tons; to 2002, decreased to about 649 million tons, a low value in the past 30 years. The ratio of the industrial wastewater in the total city wastewater continued declining from 76.9% in 1981 to less than 30% in recent years. The amount of industrial wastewater emission for the second industry output value per ten thousand Chinese Yuan, has fallen from 577.51 tons in 1981, to 8.24 tons in 2012.

3) The life wastewater emissions have an increasing trend with volatility, from 424 million tons in 1981, up to 1.697 billion tons in 2012. Compared with 1981, the life wastewater emission per capita was also a substantial increase, from 100 kg for per capita daily at the early 1980s, to around 220 kg in the year of 2000, but dropped to about 190 kg in recent years.

4) Since 1995, Shanghai has continued to intensity urban wastewater treatment. From 1995-2012, an average 2.1 new wastewater treatment plants have been built annually in Shanghai, with an annual increasing capacity of 135.73 million tons, and annual increasing rate of 5.86% on wastewater treatment. By 2012, sewage treatment has reached 85.62% of the total urban wastewater discharge.

5) Compared the social-economic development and wastewater management in Shanghai, for past 30 years, the population has increased 2.04 times, the total economic output grew 62.14 times; but the city wastewater emissions increased only 1.28 times in Shanghai; the increasing amount of the wastewater discharge is far less than the magnitudes of the growth of population and economic.

Acknowledgement

This work was supported by Leading Academic Discipline Project of Shanghai Municipal Education Commission, Project Number: J50402.

References

[1]《Shanghai Environmental Bulletin》(1990-2005) [EB/OL]. 2007-12-25：
http://www.envir.gov.cn / law/ bulletin.asp.
[2]《Shanghai Water Environment Protection Statistics Data》(2000-2012) [EB/OL].
http://www.sepb.gov.cn/fa/ cms/shhj/shhj2072/shhj2074/index.shtml# 2014-02-25
[3]《Shanghai Water Resources Bulletin》(1998-2009) [EB/OL].
http://www.shanghaiwater.gov.cn/sw. 2010-9-30
[4]《Shanghai Water Resources Bulletin》(1998-2012) [EB/OL].
http://222.66.79.122/BMXX/default.htm?GroupName= 2014-02-25
[5] Cheng Xi, Zhang Mingxu, 2006: Shanghai wastewater trend analysis [J]. Shanghai Environmental Sciences. 25(2), 82-88
[6] 《Shanghai Municipal Population and Family Planning Commission》[EB/OL].
http://www.popinfo.gov. cn /stat/. 2010-9-30.
[7] 《Shanghai Statistical Yearbook》(2000-2013) [EB/OL].
http://www.stats-sh.gov.cn /data/release.xhtml, 2014-02-25

Advanced Materials Research Vols. 989-994 (2014) pp 5580-5583
© (2014) Trans Tech Publications, Switzerland
doi:10.4028/www.scientific.net/AMR.989-994.5580

The Implementation Of Network Teaching Resources Sharing Center Based On Google Cloud

Hui e Chen

Tianhe College of Guangdong Polytechnical Normal

University GuangZhou 510540

E-mail: yifanchenchen@163.com

Key words: Resources Sharing;Google Cloud

Abstract. The traditional network mode of resource sharing Easily lead to "information island", The link between information not unimpeded,With the development of information technology in education, The Google cloud network will break caused by geographical environment restricted resource barrier, Let the school quality curriculum and teaching resources sharing,Fully guarantee the fairness of education.

Introduction

This paper presents research program of teaching resources sharing based on google cloud network,A collection of cloud computing technology,The development technology of Web development platform,Using the advantages of cloud computing,To eliminate the "information island",Teaching can solve the uneven distribution of resources.

Google App Engine System

Google App Engine is a web application developed by google, In general, the online application service Google App Engine for developers to provide application development, application maintenance, operation and application of the host server and automatic upgrade.

As the network application service platform, App Engine architecture can be divided into three levels: The first layer is a data storage layer at the bottom of all the core technology, relying on the GFS Chunk Server and BigTable to construct the google infrastructure, Provides storage for Google cloud computing; The second layer is the web server layer. App Engine applications through CGI protocol and server communication;The third layer is the application layer. With the code repository and the module, designed for operating environment for the Python programming language.At present, App Engine using Python 2.5.2 version as the runtime environment.

Design Ideas

1） System Structure

The traditional network teaching resources sharing platform, is the university courses and resources sharing curriculum resources for unified management,Implementation of all the teachers and students of the sharing of resources, but in the process of teaching teachers and students will produce all kinds of teaching resources is the lack of flexible management document,

At the same time, also has the higher cost of repeated construction and maintenance. Cyber source sharing platform based on cloud computing, can realize the flexible management and good response is good, soft hardware also has high sharing and lower the cost of management and maintenance.

2）Function Module

Google cloud network teaching platform based on resource sharing, from the functions are divided into 6 functional modules, namely: Sharing center , My cloud space, Resource upload, Resource search and download, Resource management, System management.

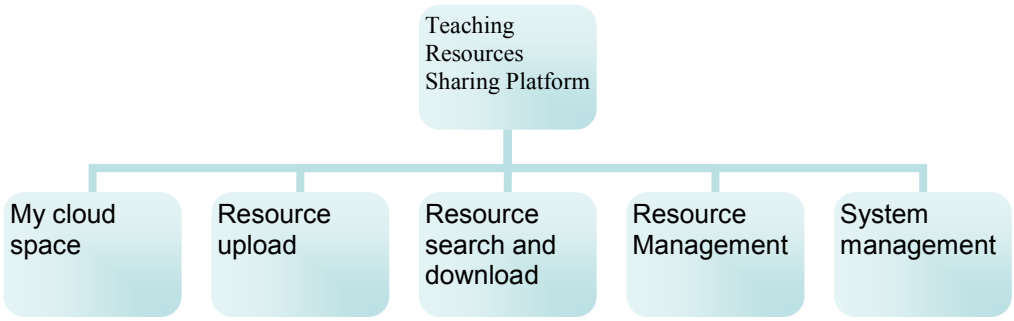

Fig.1 The structure is shown below:

Google cloud network teaching platform based on resource sharing, technology scheme using JavaEE+Google App Engine mixed development, development platform for the eclipse. The system uses the B/S structure, The Google App Engine for the development of the python language, before using the google website to register to download jar package, JSP ActionServlet page by submission, In the ActionServlet and Google App Engine, DataStore and Memcache processing all kinds of access request data, call the Google cloud services.

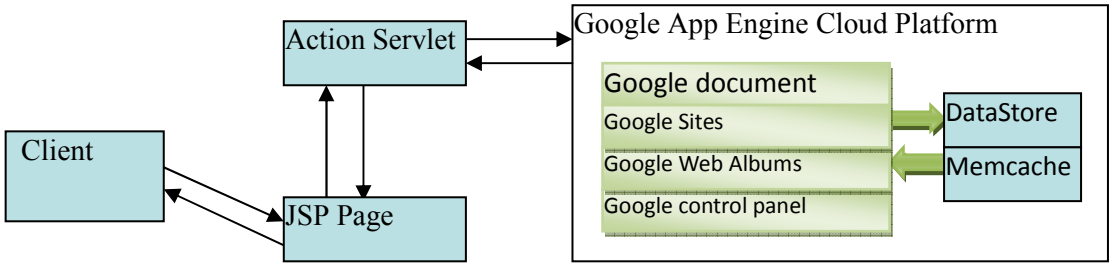

Fig.2 The structure is shown below:

In the development of JavaEE+Google App Engine hybrid,Servlet cannot use the thread, Struts start to start the manual mode, can be added to the project a set Servlet starting level of following the Web service startup,Add a Servlet listener or to the project, Struts is initialized in the listener to initialize the event, to achieve the following:

```
public class StrutsStartAdapter implements ServletContextListener {
    public void contextInitialized(ServletContextEvent servletContextEvent) {
        OgnlRuntime.setSecurityManager(null);
    } }
```

At the same time of the configuration of Struts in the Spring applicationContext.XML file modification, need to configure the stmts.objectFactory attribute value integration development process.Set the value of the struts.objectFactory property in the stmts.properties<constant name="struts.objectFactory"value="spring"/>.Then the configuration of Spring listener. Add the following content in the web.xml file <listener><listener-class> org.springframework.web.context.

ContextLoaderListener</listener-class></listener>

3）Database Table Structure

The network teaching resources sharing platform system, the database consists of 6 tables, respectively is the user information table, resource information table, resource category table, resource evaluation table, on the message list, department table.

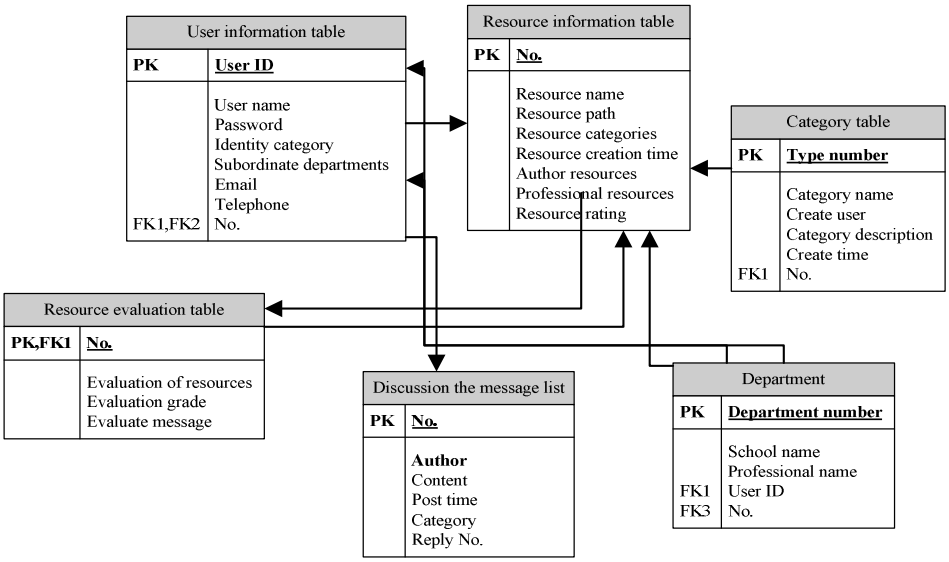

Fig.3 The structure is shown below:

4）Implementation Process

Google App Engine platform,did not provide database such persistence solutions,Instead of using a similar Bigtable technology and database persistence solutions, The Bigtable data is stored in a data storage area,And SQL is similar to GQL query language. Fig.3 table and any data logic relationship using JDO standard implemented in java,At the same time should create a JDOConfig.XML in the Web-INF configuration file when using JDO,The database table is shown to achieve the following code persistence:

```
public class User { @PrimaryKey
@Persistent(valueStrategy = GeneratorStrategy. IDENTITY)
private Key key;
@Persistent
private String usemame;
@Persistent
private String password;
@Persistent
…….
```

The data store using each Google App Engine platform in the request for a new instance of the PersistenceManager class.Examples of the use of PersistenceManagerFactory to complete the database crud operations.

For example, write to the database:

```
PersistenceManager pm = PMF.get().getPersistenceManager();
        try {                pm.makePersistent(accBean);        }
 finally {                pm.close();        }
```

Implementation Effect

The system uses Google App Engine cloud platform, The use of eclipse development tools. Give full play to the advantages of Engine platform Google App.

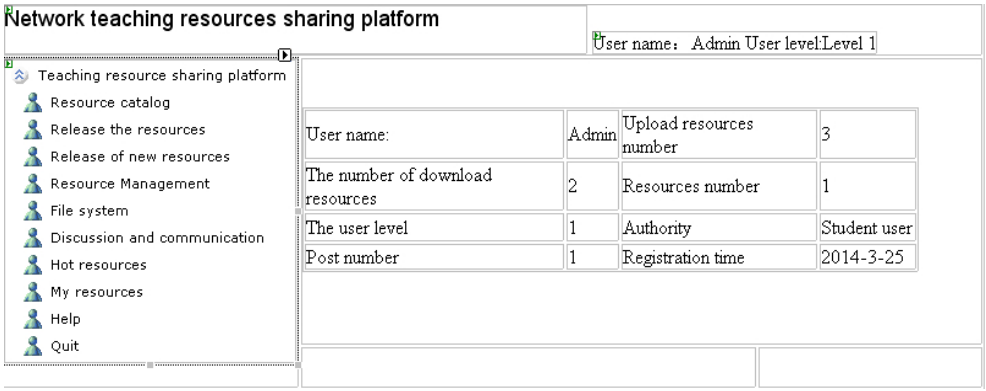

Fig.4 The effect of network teaching resources sharing platform:

Summary

This paper introduces the realization of network teaching resources sharing platform Google App Engine platform cloud technology,Google App Engine cloud platform technology compared with the traditional development technology has great advantage, summed up in the following points:

1) Good computational ability, Google App Engine using distributed technology, resources can be distributed to multiple server unified management, the service ability is not a single server can match.

2) Security is good, because Google App Engine using distributed technology, the distributed storage resources, good fault-tolerant performance, realizes the data a server will not damage the system data damage.

3) It is easy to develop and expand.

References

[1] Qiao Chen. Regional colleges and universities teaching resources sharing based on Cloud Computing[J]. China Education Informationization,2011.15:53~56

[2] Peng Wang. The key technology and application of cloud computing[M]. Beijing: People's Posts and Telecommunications Press,2010:35~63

[3]]Peter Fingar,Lingjun Wang Translation. Cloud computing -21 century business platform[M]. Beijing: Publishing House of electronics industry,2009:28.

[4]George Reese,hua Chen Translation. The application of cloud computing architecture[M]. Beijing: Publishing House of electronics industry,2010:98.

[5]Hai bo Wang. implementation of key problems of database in the cloud computing[D].Jilin: Jilin Science,2011:92.

Advanced Materials Research Vols. 989-994 (2014) pp 5584-5587
© (2014) Trans Tech Publications, Switzerland
doi:10.4028/www.scientific.net/AMR.989-994.5584

Study on the Environment tax realize ecological compensation in China

Liyuan Xu [1, a]

[1] Jiangxi University Of Finance and Economics, NanChang, 330013, China

[a]email:xly1912@163.com

Keywords: Environment Tax; Ecological Compensation; tax differentiation system

Abstract. The environment tax provide capital source for ecological compensation, Although the environment tax legal system give a guarantee for the environment and conservation of resources, The current environment tax legislation is lack of ecological compensation concept, lack of the preferential tax policy for different areas, and the funds of ecological compensation is limited. But the environment tax has irreplaceable function for realize ecological compensation, We should establish a set of environment tax law system, establish environment tax differentiation system and improving existing environment tax redistribution system.

Introduction

The ultimate goal of environmental taxes and ecological compensation is sustainable development. The environment tax provide capital source for ecological compensation.

Environmental taxes and ecological compensation through design and implement a series of systems, play a role to regulating human behavior and protect the environment, to some extent alleviate the contradictions between environmental protection and economic and social development.

The Relationship between Environment Tax and Ecological Compensation

The common theoretical basis

The economic base of environmental taxes and ecological compensation is externality theory. Due to the integrity and regional features, ecological environment have typical externalities. The behavior that somebody use natural resources result in ecological environment destruction or pollution, it inevitably influence others to use natural resources, cause external diseconomy (negative externalities); somebody pay a huge cost to protect the natural resources, he will get profits, and others are also get the benefits, the external economy (positive externalities) is produced. Environment tax system mainly solves the problem of negative externalities, the government levy tax on these external diseconomy behavior of pollution and damage to the environment, let the impairer get the damage cost, thus make the internalization of external costs; Ecological compensation mainly to promote the sustainable development of positive externalities, government design and realize secondary benefit distribution for the environmentalist and beneficiary by means of the compensation (subsidy) system, it can make the environmental beneficiary pay the reasonable cost benefit, so ,all people can enjoy the sustainable ecological benefits.

Environmental taxes and ecological compensation all reflect ecological justice value. What is the ecological justice? It is a complex problem. From Rawls's justice view, through design the reasonable system, it make all the social basic value -- the freedom and opportunity, income and wealth, self-esteem, get the equal distribution, unless one or all of the value of an unequal distribution are conform to everyone's interests.[1] So, in the field of environmental protection, it should comply with the essence of the ecological justice when seek the balance of different interests and development opportunities and coordination. A large number of external effects of environmental are huge ecological injustice, pollution, damage to the environment, but do not bear the corresponding cost, protection, construction of ecological environment has not been returned. The purpose of levy environment tax and the implementation of ecological compensation is to make the related bodies assume the responsibility, restore fair environment, realize ecological justice.

Environment tax provide stable sustainable sources of finance for ecological compensation

Ecological compensation is one of effective environmental economic means for environment protection and utilization, it has been widely used in the world, include China. The methods of ecological compensation in China is still the government investment or government transfer payment system, the government pay is doubtless true, but in the long run, the subsidies can lead to low efficiency, lead to a new "policy failure", such as economic undeveloped areas become dependent, lose endogenous support capacity, etc. Some local governments in China are exploring the market mechanism for ecological compensation measures (such as water rights trade), but the market mechanism and the area between voluntary consultation mechanism is not yet fully established, lack of funds is still the key obstacle for ecological compensation. Environmental tax can make the tax earmark a fund for its specified purpose only. Provide the continuous steady capital source for ecological compensation. Foreign environment tax law practice, the environment tax revenue as compensation for sacrifice development opportunities for ecological environment protection and construction, or used as a special fund, only dedicated to control environmental pollution and improve the environment, and so on, it is generally not allowed to move for him.

The Practice and the Existing Problems of Environment Tax Realize Ecological Compensation in China

In China, the environment tax play a role ecological compensation mainly include resource tax, consumption tax, urban maintenance and construction tax, cultivated land usage tax, urban land use tax and vehicle and vessel tax. Although the original intention of these taxes is not to environmental protection, but they have certain ecological characteristics, and have played an important role in saving resources, protecting the environment. In accordance with the law, the resource tax on crude oil, natural gas, coal, other non-metal ores, ferrous metal ores and non-ferrous metal ores and salt. Consumption tax in our country at the beginning of the set up is not considered taxable products produced by the external environmental cost, but the most of taxation scope have the characteristics of the environmental protection, such as covering the firecrackers and fireworks, motorcycles, cars, golf balls and ball, wooden disposable chopsticks, real wood floor and other 10 kinds of consumer goods. Urban maintenance and construction tax earmark a fund for its specified purpose only, guarantee for urban public utilities and public facilities maintenance and construction, in practice, it has become a important source of funding for flood control and drainage, afforestation, environmental health and other, as a "special tax" for environmental protection and ecological compensation. Cultivated land usage tax protect the cultivated land, forest land, grassland, water and fishery waters of the tidal flats, and other scarce resources. Urban land use tax promotes the rational use of urban land resources; improve the efficiency of land use. The article 4 of vehicle tax law stipulated in, "for saving energy, the vehicle that using new energy can be exempted or reduced tax", it embodies the national "friendly" attitude for energy.

The other tax about ecological compensation, for example, added- value tax, income tax, fixed assets investment adjustment tax, all directly or indirectly contains tax preference for environmental protection, they have played a certain role in ecological protection. Such as the regulation of "interim regulations on value-added tax" (2008), taxpayers selling or importing water, heating, air conditioning, hot water, coal gas, liquefied petroleum gas, natural gas, methane gas, household use coal, chemical fertilizers, pesticides, agricultural films, such as apply to the low rate of 13%; the ecological degree of income tax law is higher, have a number of environmental protection terms,and so on.

In practice, these ways play an important role to reduce environmental pollution, promote the comprehensive utilization of resources. But there are still the following problems:

First, the concept about ecological compensation in environmental tax law is deficient. There are common theoretical basis, such as the environmental externalities, sustainable development and maintaining ecological justice, in environment tax and ecological compensation, but it is difficult to find the "resonance" in the reality legislation. The purpose of related environment tax legislation in our country are mainly economic development and people's livelihood security, such as the

consumption tax, aims to regulate the consumption structure, guide consumption direction, suppress premature consumption and increase revenues. The effect of environmental protection is derived. The ecological compensation, derived from the environment tax legislation, reflect compensation indirectly for environment, it does not refer to the compensation for those people who make contributions or get sacrifice because protect environment and construct ecological environment, in addition, with the insufficient funds, it may deepen the plight of the ecological compensation. Because of the awareness on ecological compensation for the contributors and the victims is confused in practice, some people about Dongjiang River compensation consider, the water resources are owned by the state, the protection of water resources is everyone's responsibility. To some extent, Guangdong province is the owner and the beneficiary of Dongjiang river basin water resources, but at the same time, Guangdong province not only get own economic development, but also made due contributions to the nation. Therefore, our country should establish ecological compensation, the transverse compensation between local governments is not realistic.[2]

Second, it is very limited that the environment taxes realize ecological compensation. The ecological compensation fund quantity is very limited. For example, the national resources tax in 2010 are 417.55 billion yuan, only accounted for 0.54% of national total tax revenue, urban maintenance and construction tax 1887.09 billion yuan, accounting for 2.4% of the national total tax.[3] so, our country environment tax is too scattered, too small, accounted for the proportion of tax revenue is too low. It is difficult to play the role of regulation and guidance of environmental protection effectively. The more important thing is the lack of regional preferential tax. Our country set up regional preferential tax system in view of the special economic zones, coastal economic development zone, economic and technological development zone, hi-tech industry development zone, in the west areas and poor areas. But from the perspective of the content of system, they are based on preferential productive enterprises with foreign investment as the main object, the main favorable means for enterprise is that the income tax shall be levied at the reduced tax rate of 15% or 24% discount directly,without considering the resources endowment of the upper Midwest, natural conditions, location advantages and differences in the different region, it is difficult to promote the region economy coordinated development.

The Legal Thinking about Environment Tax to Realize Ecological Compensation in China

Propos establish “environment compensation tax” instead of “urban maintenance and construction tax”

First, China should set up the ecological compensation tax by legislation, the tax with the natural protection resources, pollution tax, and other related tax, build the environment tax law system for China. Natural resource tax mainly includes the existing resource tax, consumption tax, cultivated land usage tax, urban land use tax and vehicle tax, and other tax with the function of environmental protection; Pollution tax mainly include air pollution tax, water pollution tax, solid waste tax and noise pollution tax, discourage the behavior of the pollution of the environment; Other taxes, such as value-added tax, income tax from the design of the preferential tax system to protect ecological environment. The purposes of ecological compensation are ecological environment protection and promote the harmonious development between human and nature, based on the ecosystem service value, ecological protection development cost, opportunity cost, by means of government and market, regulating the interests relationship between ecological protection stakeholders.[4]

Ecological compensation adjusts the interests between the beneficiary and impaired people, so, the beneficiaries should be the taxpayer. From a legal perspective, the beneficiaries of ecological compensation include country, the enterprises and institutions and individuals. These beneficiaries who get the development and utilization of ecological environment and the negative externality of the environment, this section can be achieved by reform and perfect the existing resource tax, consumption tax, cultivated land usage tax, urban land use tax and so on to achieve the purpose of gathering ecological compensation; For those beneficiaries enjoy the good ecological environment, because of others (especially in poor areas) sacrifice development opportunity to protect the

ecological environment, we can achieve the purpose of gathering ecological compensation by establishing ecological compensation tax .

Second, we should replace urban maintenance and construction tax with ecological compensation tax. Specifically, we should replace the urban maintenance and construction tax ecological compensation tax in China. Urban maintenance and construction tax is closely related to environmental protection tax, it is imposed in 1985, although a large part of the tax revenues for environmental protection of urban area, but from the point in time, they have a long history and not conform to the current economic development, it need to reform and serve the value added tax, consumption tax and business tax as the tax basis, it will expand the subject of tax scope, accords with the special nature of the ecological compensation tax. Based on tax revenue legal doctrine principle, China should formulate “interim regulations on ecological compensation tax”, make the detailed rules about the subject of tax, tax calculation basis, tax rate, tax collection and administration and so on. The current urban construction tax only levy tax on domestic enterprises and individuals, but exclude foreign-invested enterprise, foreign enterprises and foreigners. It cause the unfair tax burden of domestic and foreign enterprises, the tax subject should include ecological compensation, unit of domestic and foreign enterprises and individuals. The urban construction tax is a kind of additional tax, it has very strong dependent. Because of the small scale urban construction tax revenues and income instability, it weaken the function that urban construction tax in raising funds and protecting the environment. [5] it is a good idea that serve value added tax, consumption tax, business tax and income tax as the tax calculation basis for ecological compensation tax for, at the same time, we should increase tax rate, to ensure its function. Ecological compensation tax should be the central and local shared tax, earmark a fund for its specified purpose only. Central tax is responsible for involving two or more than two provincial-level administrative region ecological compensation, local tax responsible for provincial administrative region ecological compensation.

Setting up the tax differentiation system of ecological compensation

Tax preference is an important policy tool, it is also a kind of effective means of ecological compensation. The central and western regions in China are often the rich resources and environment areas, they play “ecological security”, “resource reserves” and “landscape construction” role in the national development, but at the same time, it is lagging economic development and poverty area, they need compensation from benefit region or rich crowd, in order to balance the interests of all parties. Therefore, we should establish a conducive to ecological compensation tax differentiation system, especially set up the different preferential tax policy from the eastern region. In order to promote the effective implementation of the regional ecological compensation, we can take preferential tax levy measures to these areas；water conservation area, flood storage area, soil conservation area, windbreak and sand-fixation and biodiversity conservation area，the measures include tax reduction, duty free, tax reimbursement, tax credit. It can increase financing ability of regional ecological compensation from tax incentives, and guarantee the sustainable supply of good ecological environment.

References

[1] John Rawls,A Theory of Justice,The Belknap Press of Harvard University Press,1971,303.

[2] May guo: research on ecological compensation and ecological compensation about legislation river basin. sciences academic press, 2011), pp. 151-156.

[3] Data from: according to the Chinese tax yearbook 2011

[4] China's ecological compensation mechanism and policy research team, China's ecological compensation mechanism and policy research, science press, 2007. pp. 2-4.

[5] Li Xin. Study on construct a framework of environmental tax in China [J], The tax research 2005(6)47-50.

Advanced Materials Research Vols. 989-994 (2014) pp 5588-5591
© (2014) Trans Tech Publications, Switzerland
doi:10.4028/www.scientific.net/AMR.989-994.5588

Analysis and Design on Sports Meeting Information System

Lihua Chen[a], Tiezhu Niu[b]

Department of Physical Education, Dalian Nationalities University, Dalian, P.R. China

[a]lc@dlnu.edu.cn, [b]33512982@qq.com

Keywords: sports meeting; information system; SSH framework; workflow analysis; functional requirements analysis; framework structure design

Abstract. In the course of sports meeting, managing large amounts of data by hand is very difficult, the computer will be used in sports meeting management, accuracy and efficiency of data processing provides an important safeguard, in this paper, the sports meeting information system analysis and design. First, workflow analysis, pointed out the modern sports meeting work flow, as the basis for the next software development work; Then, functional requirements analysis, modeling example through interaction with each participant to clarify the main functions of the system implementation; Finally, the framework structure design, design the SSH three layer frame structure based on J2EE, for the presentation layer, business logic, data access layer is described in detail. To study the content of this article is based, easy to construct, easy maintenance, good reusability Web systems.

Introduction

The sports as the basis of various sports, occupy the important position in competitive sports, has a wide range of mass. Various schools usually have to be held annually, is to improve and test the health of students and teachers, to carry out an effective way to national fitness campaign. Organization of sports would be a complex and careful management, in particular arrangement, recording, announcements, many things to attend to, workload is big,]input of manpower, material resources, financial, and low efficiency, error prone [1]. Large amounts of data by hand are very difficult to manage, easy to go wrong. The computer will be used in sports meeting management, accuracy and efficiency of data processing provides an important safeguard. Currently, most universities have constructed a fast, advanced and applicable campus network, to achieve a collaborative management of internal campus teaching, research, communication and office, to enhance the overall level of the school information technology, to improve the school research, teaching efficiency. Sports meeting as an important part of school work, should also give full play to the role of the campus network. Therefore, will build sports meeting information system, to service in the whole process of the sports meetings, to achieve efficient, convenient, fast handling in the Sports information, is the future development trend.

Workflow Analysis

Sports meeting work is divided into three stages, namely the organization before, during, and after the data management and statistical analysis [2,3]. Workflow is shown in Fig. 1.

(1) The management before sports games. The School Sports Organizing Committee to develop competition rules, including the date, venue, race project, faculties and departments participated grouping, enrollment and limit the number of items reported faculties, admission ranking and awards, extra points; Organizing Committee among the departments issued sports meeting notice and competition rules; departments race project registration; The organizing committee according to the enrollment of each department, make the game schedule; The organizing committee print order book and various forms such as race schedule, team player information table, items grouped tables and others; The school issued the order book to each department.

(2) The management during sports games. The contest judges according to the competition situation truthfully record score; determine whether there is need for the final project, if necessary,

in accordance with the competition rules to screen out the final list, according to preliminary results are allocated the runway by the rules, and print the final notice; For the final project, after recording results, in accordance with competition rules to determined the obtain ranking athletes, and according to the project integral rules, the corresponding integration accumulated will add its units, print transcripts of the project contest for publicity.

(3) The management after sports games. All entry competition results carrying on the statistics, summary, calculate each class and each unit of the total scores (including athletes score, score, score of spiritual civilization score, manuscript scores and other extra points) and announce the results; athletes to the sports meeting with the previous sports meeting results and other sports scores compared to see whether the record-breaking situation. If there is, and the timely report to the chief judge and approved; finishing print out all the achievements and the sports meeting -related information, to facilitate the Organizing Committee announced at the closing ceremony. And data archiving and backup.

Fig. 1. Workflow analysis on sports meeting

Functional Requirements Analysis

The use case model is used to describe the designated system use cases, actors, portfolio cases — relationship with the participants. Use case modeling using the Unified Modeling Language (UML), UML is the beginning of an OMG standard in 1997, is a software system to support the development of modeling and graphical languages, providing modeling of all stages of software development and visualization support, including from the requirements analysis to the specifications, the structure and configuration. The use case model of the system is shown in Fig. 2, the interaction process of each participant is described as follows:

(1) Organizer: The main work includes the information release, venues and equipment management, data statistics and analysis. Information published by the website, including competition rules, game schedule, race project, registration, grouping and distribution runway conditions, individual performance, group performance, and others; venues and equipment on site for unified planning, unified distribution, unified management, in order to keep the competitions running smoothly; according to game data generated various reports, report data will be distributed to the relevant athletes and personnel, the relevant data for analysis and comparison, drawn sports meeting organizing successful experience.

(2) Staff [4]: The main work include registration management, grouping and distribution runway, performance management. Each participating units reported statements after checking into the computer system; according to registration, race project and game schedule, for track and field competition events grouped, for race project distribute runway, organized competitions official program, and in accordance with the actual situation, the order of the game be adjusted accordingly; The race results and names entry the system, provide timely results and ranking and other relevant information to the organizers.

(3) Athletes, referees and the public: do not have the data input, modify, delete function, can only query relevant information. Can query the sports rules, competition rules, the competition arrangement, organization, equipment space, registration, grouping and distribution runway, competitions official program, individual performance, group performance, individual nominations, ranking, and others.

(4) Administrator: The main work is to maintain the system, including network systems management and software system maintenance. Network systems management is mainly to design, installation, configuration, management and maintenance the network equipment and server systems on the whole network. To do technical guarantee for the safe operation of the internal network [5]. Software system maintenance task is to correct software systems in the course of discover the hidden errors, expand the new function and performance requirement by the user in the course of the use, its purpose is to maintain the normal operation of the software system.

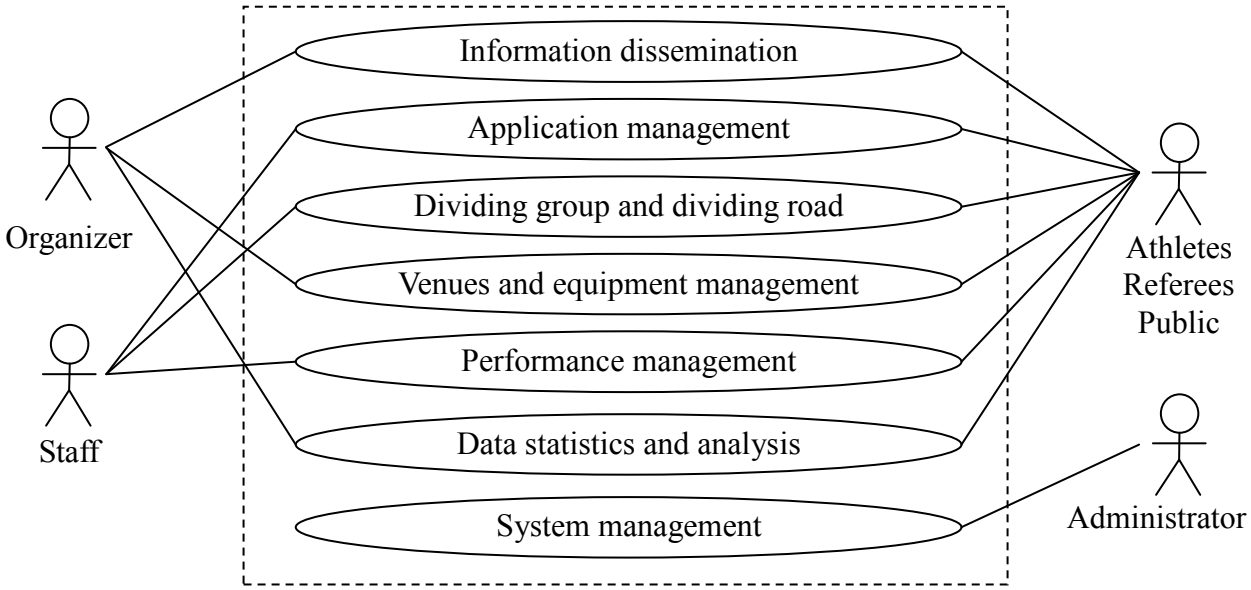

Fig. 2. Use case model on sports meeting information system

Framework Structure Design

Software framework is a set of related abstract model, used to guide large-scale software systems in all aspects of design. Software framework is a systematic sketch, is based on certain principles, from a different perspective on the various parts of the component systems to match and arrange, the formation of the system which consists of a number of structural framework, including the various components of the system, externally visible properties of components and relationships between components. From a business oriented software framework to transformation oriented technology, with shorter development cycles, improve software quality, reduce software costs, easy to modify and maintain. SSH is an integrated framework of Struts+Spring+Hibernate, is currently one of the more popular open-source Web application framework that helps developers build a clear structure in the short term, can be a good reusability and easy maintenance of Web applications [6-8].

SSH framework of basic business processes are: the presentation layer, first through the JSP page to implement interface, is responsible for receiving the request and send a response, then the Struts according to the configuration file (struts-config.xml) and to ActionServlet received Request delegate to the corresponding Action deal. In the business layer, Spring IoC container of managed service components is responsible for Action providing business model components and collaborative object data processing components to complete business logic, and provides transaction processing, buffer pools and other container components to improve system performance and ensure data integrity. In the persistence layer, depending on the object of the Hibernate mapping and database interaction, processing the requested data of DAO component, and returns the processing results.

Conclusion

The purpose of this system analysis and design is to develop a set of suitable for athletics information management system, and services in the sports meeting organizers, staff, athletes and referees, To facilitate the exchange of information between the audience and the manager, is conducive to improve the sports quality, efficiency and the management level. Workflow analysis pointed out the modern sports meeting organizing workflow, which is based on the demand analysis, pointed out the main function of the system; design the SSH three layer frame structure based on J2EE, easy to construct, convenient maintenance, good reusability the Web system. In the development and use of the process should pay attention to the following questions [9]: The sports meeting in repetitive and complex work is processing the standardized management of system; adapt to the development of today's information age, improve work efficiency; ensure the fairness of the sports meeting, fairness for athletes; reduce the work intensity of the sports meeting staff, save the sports meeting holding cost.

References

[1] M. H. Cao, F. Y. Li, J. P. Chu, "Design and Implementation of Sports Meeting Management Information System," Journal of Shandong Jiaotong University, vol. 15, no. 4, pp. 77-81, 2007.

[2] Y. L. Zhang, "Research and application for Sports Meeting decision support system," Master's degree of Jilin University, 2007.

[3] J. L. Xi, D. Meng, "On the Web-based Management System of General Sports Meet," Journal of Capital Institute of Physical Education, vol. 22, no. 1, pp. 91-93, 2010.

[4] J. K. Zhang, "The Computer Management System of Small and Medium-sized Track Meeting," Journal of Hebei Normal University(Natural Science Edition), vol. 36, no. 2, pp. 213-216, 2012.

[5] Baidu encyclopedia, "System administrator," http://baike.baidu.com /link?url=2oCxTcI1NR0L2aGiPJp-30QHewgIEcvafuNMvxnIV2KD3RscwtMDGDPhmwb_pJfJ, 2014-1-5.

[6] B. Song, "Design and Implementation of Sports Meeting Management System Based on J2EE," Master's degree of Fudan Universit, 2011.

[7] Liu F, Guo HX, Qi Q, Wang Q, "The Applied Research of E HR System Based on SSH," Journal Of Wuhan University Of Technology, vol. 31, no. 3, pp. 98-100, 2009.

[8] Cheng Y, Li S, Zhao YN, "Research and application of Web framework based on SSH+DWR," Journal of Nanjing University of Information Science and Technology: Natural Science Edition, vol. 2, no. 5, pp. 455-460, 2010.

[9] Y. L. Zhang, "Design and Implementation of Sports Meeting Management System," Master's degree of University of Electronic Science and Technology of China, 2010.

Advanced Materials Research Vols. 989-994 (2014) pp 5592-5595
© (2014) Trans Tech Publications, Switzerland
doi:10.4028/www.scientific.net/AMR.989-994.5592

Green Management of Tourist Attractions region under the Background of Circular Economy

Feilong Liu

School of Economics and Management Hunan Institute of Science and Technology, 414006,Yueyang, Hunan, China

E-mail:07302982@163.com

Keywords: circular economy; Tourist Attractions region; green management

Abstract. Circular economy is a new theory to realize the win-win of economic development and environment protection in the mid- to late 19th century ,and is a basic way to achieve the sustainable development of economic and social. Circular economy of tourism should be strictly follow the 3R principle of"Reduction, recycle and reuse"of circular economy .For the management of traveling scenic areas, it must carry out the green management effectively , so as to achieve the purpose of low consumption, low emissions and high efficiency.Therefore,we must establish firmly the new concept that to develop circular economy in tourism areas;to full carry on the management of green tourism ;and to strengthen the joint efforts that have traveler to participate in.

The basic concept of tourism circular economy

Circular economy is a new theory to realize the win-win of economic development and environment protection in the mid- to late 19th century ,and is a basic way to achieve the sustainable development of economic and social.This paper try to introduce the theory and method of circular economy to the tourism industry, not to study the six big elements that eating, living, traffic, travel, shopping and entertainment, but to study the concept and development pattern that develop the circular economy tourism.During the study, we mainly studied and discussed the basic path of circular economy carried on tourism scenic areas,In the view of the tourism industry, circular economy tourism should be mainly refers to creating value by carrying on the standard of services,that is to say,to realize the sustainable development of tourism,we should consider to eliminate or reduce the direct and indirect negative effect that the tourism enterprises and tourists on the tourism environment as much as possible, from designing product and development of tourism service to the whole traveling. Circular economy of tourism should be strictly follow the 3R principle--"reduction, recycle and reuse"-- of circular economy. Following the law of ecological development for all tourism economic activity,to realize feedback cycle process between resources and renewable sources(products)in the tourism resource development and tourism activities, in order to achieve the purpose of reasonable development, efficient utilization and minimum pollution, the clean production, comprehensive utilization of tourism resources, tourism, ecological design of tourism products and tourists the sustainable consumption,and to make the tourism economy system can harmoniously incorporate into the material circulation process of the tourism system in the end.[1]

The basic ideas of building circular economy in Tourist Attractions region

Under the guidance of the circular economy theory , the minor cycle of tourism enterprise demand we should establish a best link in the most economic objectives and the best environmental objectives, according to the concept of eco-efficiency,and by the common behavior that support the sustainable development.And scenic spots as a individual tourism management unit,which is engaged in the operation and management activities, is the core products of the tourism destination , also is the main research object and the important part of tourism circular economy .According to the concept of circular economy tourism, circular economy in the tourism scenic areas can be understood as the minor cycle in the level of tourism enterprises .Therefore, it’s necessary that

managers of traveling scenic areas should consider the development of tourism enterprise in the long run.they must adopt cleaner production technologies, reduce the use amount of tourism resources as much as possible, minimize or avoid human activities causing the abuse and destruction of tourism resources,and environmental pollution and ecological disturbance and destruction to the traveling scenic areas ,so that not only can ensure the ecosystem and attractive of the scenic spots, but also can constantly improve their ability for the development of circular economy,to realize the sustainable development of tourism scenic areas .circular economy in scenic spots included the usage of tourist resources in the stage of development and planning of the scenic area, control and governing the environmental pollution in the phase of tour, and waste recycling.In tourism scenic areas development process, bringing much joy to the tourists ,and bringing economic benefits to the local, negative impact should be reduced to a minimum in the development of local tourism ,that's to say, carrying the effective green management in the tourism scenic spots, so as to achieve the purpose of low consumption, low emissions and high efficiency.[2]

The basic path of carrying out green management in Tourist Attractions region under the background of circular economy

Firmly establish new ideas of circular economy in Tourist Attractions region

Ideas guide behaviors.Circular economy developed in the tourism scenic areas set up the new system, new resource outlook, new consumption and benefit must be based on the basic theory of circular economy and tourism, and combined with the actual situation of tourism scenic spots.For example,the beneficial outlook of the traveling scenic areas require to balance the relationships between the good social benefits and ecological benefits in the development of tourism resource.In terms of economic benefits, both the development of tourism resources and a tourism investment project, must study its feasibility at the first,carefully analysis investment benefit and constantly promote the development of tourism resource and add the economic benefits of tourism project investment, which is material conditions to ensure the sustainable development of the tourism industry.In terms of social benefit,it should be consider the level of local economic development when developing tourism resources and designing tourism products,and considering people's psychology to bear.In terms of the ecological environment benefit,it should be guided by the principle of reasonable use of tourism resources and meet the requirements of environmental supporting capacity,to promote environmental protection by development,and to improve the comprehensive benefits of development by environmental protection, so as to form the virtuous circle of the protection and development,and create harmonious ecological environment benefits.[3]

Full implementation of green tourism management

It is no doubt that promote and implement is first to develop circular economy in the tourism scenic areas.Government is the main power to of promote circulation economy in the tourism scenic areas.it is hard to imagine that the circular economy of the scenic areas can develop without government's leading and participation .Only by the government to formulate the scenic area in the development of circular economy development plan and policies, can effectively guide and promote green management of tourism enterprises.So,there are some work should be follow:

(1) Do well the plan and follow-up soft management.According to the characteristics, the first thing need to do is planning well of tourism scenic spots.Tourism development must adhere to the principle of "planning before the development, protection premier and careful development" , and emphasize the importance of ecological environment evaluation, planning, protection and construction management, strict enforcement of the environmental impact assessment system, strengthen evaluation and analysis to the impact on the environment, ecological and tourism carrying capacity.After the plan, the soft management to the management of the tourism industry should highlight .So-called soft management is refers to the government create a social environment to create conditions to support enterprise, or by means of administrative legislation and decrease the negative effects of development,and make the enterprise complying with the consumer trends, making environmental production, promoting sustainable development of business in the market system rather than by administrative means to intervene in the tourism business activity.Soft

management must first to pollution-free new energy, saving energy resources to replace non-renewable or harmful to the environment resources.

Second, the government should give policy on environmental protection product development, production.On the fiscal taxation and credit to give discount.Advocate green, the protection of resources, environment quality and human health, and meet the demand of green consumption and services.

Finally, construct the environmental protection enterprise culture construction.Environmental protection enterprise culture system requirements specification staff daily behavior, coordinate the enterprise benefit, social benefit and tourists benefit relationship, to balance the social ecology.[4]

(2) Developing green technologies and establishing green evaluation system. Developing circular economy in tourism scenic areas should follow the technical ideas to reduce the tourism consumption in the process of resource consumption and pollutants and emissions by the analysis of the logistics of tourism system .Building tourism green technology system is the precondition and key of developing circular economy in the tourism scenic spots .The green technology system including pollution control technology to eliminate the pollutants, recycling technology for recycling waste,clean production technology that is no wastes or less wastes to make green products,which can realize the waste minimization in production process by he implementation of the green technology.In the development process of scenic areas, it also need to actively promote the usage of clean energy, the development of energy-saving facilities,the standard implementation of the green hotels,the sewage treatment of hotels and scenic areas , and adopting gray water recycle technology , the construction of ecological trails, the construction of anhydrous ecological toilet, the protection of the natural river scenic spots, the control of air pollution in scenic areas,the restoration of vegetation and the engineering implementation of wildlife conservation, etc.On the basis of the traditional tourism, applying the principles of ecology,design the structure and function coordination, system optimization, benign operation of ecological tourism system.Working out relevant technical standards and specifications,constructing the evaluation system of development of circular economy in scenic spots.Circular economy in tourism scenic areas is a part of circular economy, cycle tourism economic development not only pursue the tourism economic benefits and the growth of benefits,but also more to highlight the protection and construction of tourism environment, showing the ecological implication, bringing higher spiritual enjoyment to tourists.Thus, to promote the development of circular tourism economy in scenic areas, must change the current tourism economic development level of the inspection way, that's to say , emphasizing on economic benefits, at the same time, strengthening the resources development and utilization of per unit of GDP, the level of recycling resources, tourists evaluation indicators such as pollution, tourism environmental bearing capacity, thus to develop circular tourism economy index into the tourism economic development appraisal system.Of course,formulating appropriate evaluation system according to the different tourism scenic spots resources characteristics and development status, index to reflect economy and green.[5]

(3)Actively guiding green consumption. Tourism consumption occupies an important position in the social and economic development, tourism products or services only after being final consumption can realize its value.Therefore, the most important link is advocating green consumption policy is to build a tourist scenic spots of circular economy .the concept of green consumption is generalized, it has three meanings: one is to advocate consumption not contaminated nor green tourism products to help the public health.Second, paying attention to in the process of consumption of garbage disposal will cause no tourism environment pollution;third is to guide consumers to shift consumption concept and pay attention to save tourism resources and energy and change the unfavorable way the public consumption of the environment .

(4) Try to develop green ecological education and promote development of circular economy in tourism scenic spots by ecological education.Ecological education is especially important in the circulation economy development of tourism scenic areas , is a major part in ecological tourism software operation, also the differences with the traditional tourism.It mainly includes: setting up the environment education infrastructures in tourist areas, such as to establish a scientific

explanation boards beside the landscape ecological environment ,signs remind passengers pay attention to the clean environment and environment waste boxes , etc.;using multimedia technology to make tourists accept of environmental education through various channels, such as add ecological knowledge and points on tickets, tourist map for attention, etc.;adopting the appropriate means of punishment, guide tourist to green habits and behaviors;distribute waste collection bags printed with "ecological tourism "must return the recycling of in the scenic spots for tourists ;advocating visitors to plant trees or memorial trees for conference in the appropriate place , and improving awareness of the participation of tourists.Tourism colleges and universities should open or strengthen courses about ecological tourism and protection of tourism environment, to strengthen the students' environmental knowledge and environmental awareness.Green consumption is the locomotive of promoting circulation economy in tourism scenic areas, it is only through ecological education, could better guide the public to actively participate in the green consumption, the concept of circular economy in the traveling scenic areas is deeply rooted in the mind of the people.[6]

(5) Strict implementation of government regulations and local laws. Nowadays,China is lack of relevant legal norms about circular economy of tourism scenic areas.Therefore, to promote the development of circulation economy in the tourism scenic areas should should quicken the pace of making the law and system.Developing circular economy of tourism scenic areas involves various aspects such as society, economy and environment, and need to establish an effective administration system and mechanism, and make the necessary laws and regulations, so that to immobilize the positive results .

Strengthening continuously the joint efforts participated by travelers

Implementation of circular economy in tourism scenic areas not only needs the advocacy of government and the self-discipline of enterprises, but also need to improve the social public participation awareness and participation ability.Tourism organizations and tourism enterprises at all levels have to widely publicize and guide to tourists so that they can actively support the local resources and environmental protection activities in the tourism activities, and to understand and respect as far as possible the local cultural and natural heritage, to prevent and stop the adverse effects on the tourism destination by taking some necessary measures ,to prevent and stop effectively the misconduct destruction of the ecological environment , and actively support green management activity of the scenic spots and the effective implementation of the sustainable development countermeasures.

Reference

[1] Jian-zhong Lv, Yan-li Yan.Green Management: Hotel Management New Topic[J].Commercial Research. 2003 (5)134-136.

[2] Liu Yong. The low-carbon economy times Green management reform path of enterprise[J]. Value Engineering.2010 (34)7-8.

[3] Lu Hong.Ethnic Village Green Management in Yunnan - Village of large bath[J].Journal of Kunming University of Science and Technology(Social Sciences). 2007 (6)82-87.

[4] Guang-hui Tang, Ming-yi Feng, Qiao-yi Li, Yong-jian Lin , Xiao-lan Deng. Based on the green management of four-management mode tof he regional eco-tourism[J].Resource Development & Market.2007 (12)1136-1138.

[5] Zou Jian.Based on the energy consumption of China green star hotel to create a study[J]. Science & Technology Information. 2012 (3)69-71.

[6] Shaoying Mo.Green Management - a source of sustained competitive of enterprise 21st Century[J].Ecological Economy.2010 (7)134-137.

Advanced Materials Research Vols. 989-994 (2014) pp 5596-5600
© (2014) Trans Tech Publications, Switzerland
doi:10.4028/www.scientific.net/AMR.989-994.5596

Research on Health Risk Assessment Methodologies of Municipal Solid Waste Landfill

Hongjian Zhang, Xinhua Liu, Shijun Wang, Lan Fang, Lihui Zhang*

Nuclear and Radiation Safety Center, MEP, Beijing 100082, China

*email: dyzhlh@126.com

Keywords: landfill gas, health risk assessment, exposure pathway, chemical contaminants

Abstract. Health risk assessment (HRA) methodologies of three stages of Municipal Solid Waste Landfill (MSWL), including operation period, maintenance and management period after closure, and usage period without any restricted limits were built in this paper. The major exposure pathways to environmental contaminants were considered: inhalation of gas and dust during operation period, and ingestion of four food pathways categories (plant foods, meat, milk, and fish), groundwater and dust during usage period without any limits. The endpoints of HRA of MSWL are individual lifetime carcinogenic risk for all the carcinogenic chemical contaminants, and hazard index (HI) for all the non-carcinogenic chemical contaminants to the landfill worker (only at the operation period), and to the public near to the landfill (at all the three stages) respectively. The parameter values of calculation model are conservatively chosen. This is the first time in China that an integrated risk assessment methodology for landfill gas and leachate is attempted to develop. HRA methodologies will facilitate rapid estimation of the risk level of MSWL.

Introduction

Health risk assessment is an important method of quantitatively assessing the risk for human health from contaminants released to or contained in the environment in which humans live. Gaseous and leachate are generated in the Municipal Solid Waste Landfill (MSWL). Gaseous contaminants can enter ambient atmosphere, and leachate can leach into groundwater, so the human health and the environment safety will be affected. The technical requirements of liner systems, monitor rules, and management guidance during closure period of the MSWL are determined in the Chinese Standard (Standard of Pollution Control on the Landfill Site of Municipal Solid Waste, GB16889-2008). The first stage, operation period, is concerned with air pollution. After operation period, the landfill site will not be released for usage until the contaminants concentrations in the leachate for the two successional years after closure period are below the concentration limits for the sampling and monitoring values of the leachate(e.g. 0.001mg/l for Mercury Contaminants; 0.05mg/l for Hexavalent Chrome; 0.1mg/l for Arsenic; and so on)[1][2].

The primary purpose of the Health risk assessment methodologies(HRA-MSWL) is to assist in the comparison of design alternatives for landfill, and to assess health risk from MSWL. Three parts of main contents are contained in HRA-MSWL: (1) Engineered barrier characteristics of MSWL. (2) Exposure Scenarios and pathway of HRA. (3) Health Risk Assessment.

Engineered barrier characteristics of MSWL

Landfill systems including various combinations of vegetation, cover soils, waste cells, lateral drain layers, low permeability barrier soils, and synthetic geomembrane liners may be modeled. The design of typical engineered barrier in China is monolayer impermeable synthetic membranes systems chose by HRA-MSWL. HRA-MSWL permits two or more barrier liners to be adjacent to each other. If a design has two or more soil layers adjacent to each other, All the layers would be expected to act as a single liner, and will remain nearly saturated and contribute significantly to the head loss and restriction of vertical drainage, then the depth of the two layers should be summed up and an equivalent saturated hydraulic conductivity should be computed for the combined liner.

The scalar parameters of the different liners, such as porosity, thickness, that is completely specified by its magnitude and has no direction, need to be summed up. Equivalent scalar parameters should be computed as the example of equivalent porosity of total barrier liners[3].

$$n = (n_1 d_1 + n_2 d_2) / (d_1 + d_2) \quad (1)$$

In the type: d_i(i=1,2)=the depth of i barrier liners, m. n_1, n_2 represents equivalent porosity of barrier liners 1, 2 respectively.

The vector parameters of the different barrier liners, completely specified by a magnitude and a direction, such as the equivalent saturated hydraulic conductivity, should be calculated in connection with direction. When the vector velocity of the water flow is vertical to the direction of the saturated hydraulic conductivity, the equivalent saturated hydraulic conductivity should be calculated as follows

$$K = \sum d_i / \sum (d_i / k_i) \quad (2)$$

In the type: K= equivalent saturated hydraulic conductivity, m/s. d_i=the depth of i barrier liners, m. K_i= the saturated hydraulic conductivity of i barrier liners, m/s.

When the vector velocity of the water flow is horizontal to the direction of the saturated hydraulic conductivity, the calculation method of the equivalent saturated hydraulic conductivity is the same as one of equivalent scalar parameters. The synthetic membrane liners are layers of nearly impermeable material that restricts significant leakage to small areas around defects. Leakage is computed to be the result from two sources: manufacturing flaws (pinholes) and installation defects (punctures, cracks, tears). Leakage rate of impermeable synthetic membranes can be determined by choosing experimental values. Before unlimited usage period of landfill sites, the volume of the seepage through the contaminated zone, Q_L, can be calculated by[4]

$$Q_L = A \times K_s \times \frac{d + h_{max}}{d} \quad (3)$$

In the type: K_s = equivalent saturated hydraulic conductivity, m/s. d = the equivalent depth of all barrier liners, m. A = bottom areas of landfill, m^2. h_{max} = hydraulic head above the barrier liners, m.

After unlimited usage period of landfill sites, the volume of the seepage through the contaminated zone, U^s is given by

$$U^s = I \times A \quad (4)$$

In the type: I = the infiltration rate of the seepage, m/a. A= the surface area of the contaminated zone, m^2.

The exposure assessment assumes a private well downstream of the source. This well is conservatively assumed to be so close to the source that no dilution with groundwater that has not been impacted by the source takes place. The transport modeling of the contaminants in the aquifer does not consider dispersion or diffusion effects. This is also a conservative assumption. The contaminants concentration(C_i^w) in the well water is given by the dilution with the groundwater volume (U^{gw}) flowing underneath the area of the contaminated zone:

$$C_i^w = \frac{U^s \times C_i^s}{U^{gw} + U^s} \quad (5)$$

$$U^{gw} = z^{gw} w^{gw} v^{gw} p^{gw} \quad (6)$$

In the type: U^s =the volume of the seepage through the contaminated zone, m^3. U^{gw} =the groundwater volume flowing underneath the area of the contaminated zone, m^3. C_i^w = the i contaminants concentration in the well water. C_i^s = the i contaminants concentration in the seepage, mg/m^3. z^{gw}= the thickness of the aquifer, m. w^{gw}= the width of the contaminated zone perpendicular to the flow of the aquifer, m. v^{gw}= the pore water velocity of the groundwater, m/a. p^{gw}= the effective porosity of the aquifer.

Exposure Scenarios and pathways of HRA

Exposure pathways

During the three stages of MSWL, there are some exposure scenarios and pathways by which contaminants can migrate from the source to a human exposure location. An inhalation pathway consists of two segments: (1) an airborne exposure segment linking the source (contaminated zone) with the airborne contaminants and (2) an inhalation segment linking the contaminants with the exposed individual. The inhalation segment is characterized as follows:

$$CDI = \frac{C_a \times I_a \times EF \times ED \times BA}{BW \times AT} \tag{7}$$

In the type: *CDI*=the average daily contaminants intake by inhalation, per unit body weight mg $kg^{-1}day^{-1}$. C_a=the pollution concentration in the inhaled air mg/m^3. I_a=inhaled gas rate m^3/h. *EF*=the exposure frequency h/d. *ED*=the exposure duration during lifetime a. *BW*=body weight kg. *AT*=the average time affected by contaminants d. *BA*=biological available factor, usually equal to 1.

When reference concentration (RfC) or Unit risk factor(URF) is in existence, the risk can directly be assessed by the product of the pollution concentration in the air and RfC/ URF.

The ingestion pathway categories include food pathways (plant foods, meat, milk, and aquatic foods), soil ingested, and drinking water. The plant food pathways category only choose the plant which can take in contaminants by root uptake from crops grown in the contaminated zone, and simultaneously by foliar uptake from contaminated irrigation water. The aquatic food pathway is for ingestion of fish. The average daily contaminants intake CDI is

$$CDI = \frac{C_{food} \times I_f \times EF \times ED}{BW \times AT} \tag{8}$$

In the type: C_{food}= the contaminant concentration in the plant food(mg/L), soil(mg/L), or drinking water(mg/m^3). I_f= ingestion rate of food (I_f, kg/a), soil (I_s, g/a)or drinking water (m^3/a). The other parameters are similar to the formula 7.

Dermal intake of contaminated soil or water: body surface can take in some contaminants when contaminated soil or water is contacted. The average daily contaminants intake CDI is soil:

$$CDI = \frac{C_{as} \times SA \times AF \times ABS \times EF \times ED \times BA}{BW \times AT} \tag{9}$$

water:

$$CDI = \frac{C_w \times SA \times PC \times ET \times EF \times ED \times BA}{BW \times AT} \tag{10}$$

In the type: C_{as}= contaminant concentration in the soil mg/m^3. C_w= contaminant concentration in the water mg/L. *SA*= body surface areas contacted with soil or water cm^2. *ABS*= dermal absorption factor, conservatively equal to 1. *AF*= dermal retardative factor mg/cm^2. *PC*= dermal penetrating factor, conservatively equal to 1. The other parameters are similar to the formula 7.

Air concentration calculations

Air concentration calculations are performed for area source for annual average meteorological conditions (D stability class, 1.5m/s average wind speed) using the formula 11[5].

$$C = \frac{Q}{\pi U \sigma_y \sigma_z} \exp\left(-\frac{H_e^2}{2\sigma_z^2}\right) \tag{11}$$

In the type: *C*=ground contaminants concentration at the downwind distance x(m), mg/m^3. *Q*=release rate of gas contaminants, mg/s. *U*=wind speed at the release height, m/s. σ_y=horizontal diffusion coefficient, m. Applicable to the leeward distance of 0~1000m, σ_z=vertical diffusion coefficient, m, Applicable to the leeward distance of 0~2000m. H_e=average height of the release of the area sources, m.

Horizontal and vertical diffusion coefficient σ_y, σ_z are estimated using the formula12 and formula 13 respectively. Horizontal diffusion coefficients, σ_y, are affected by sampling time span, especially when the sampling time span is more than 10mins, so need be corrected by formula14. Usually the calculated concentration is in connection with the sample time span of 30mins to the air pollutions. So the contaminants concentrations of the instantaneous landfill gas will be corrected by formula 15.

Wind speed at the release height U is calculated by formula 16.

$$\sigma_y = 0.143940x^{0.926849} + \frac{a_y}{4.3} \tag{12}$$

$$\sigma_z = 0.126152x^{0.838628} + \frac{H_e}{2.15} \tag{13}$$

$$\frac{\sigma_{y,30}}{\sigma_{y,t}} = \left(\frac{30}{t}\right)^q \tag{14}$$

$$\frac{C_t}{C_{30}} = \frac{\sigma_{y,30}\sigma_{z,30}}{\sigma_{y,t}\sigma_{z,t}} \tag{15}$$

$$U = U_{10}\left(\frac{\mathrm{H_e}}{10}\right)^{0.15} \tag{16}$$

In the type: a_y=the length of the area source on the ordinate(y-axis), m. U_{10}=wind speed on the height of 10m, m/s. U=wind speed at the release height, m/s. H_e=average height of the release of the area sources, m. x=the distance from the centre of the area source to the potential receptor location, m. C_t=ground contaminants concentration at the receptor location for the sampling time t, mg/m^3. C_{30}=ground contaminants concentration at the receptor location for the sampling time 30mins, mg/m^3. $\sigma_{y,t}$,$\sigma_{y,30}$=horizontal diffusion coefficient for the sampling time t, 30mins respectively, m. $\sigma_{z,t}$,$\sigma_{z,30}$=vertical diffusion coefficient for the sampling time t, 30mins respectively, m. q= time dilution factor, for 0.17~0.5, usually equal to 0.2. t= the sampling time span of MSWL, 10mins.

Finally, ground contaminants concentration at the receptor location for the sampling time span 10mins, C_{10}, is corrected by formula C_{10}=1.25C, C=ground contaminants concentration at the downwind distance x (m), mg/m^3.

Landfill gas output, Q_m

The major components during natural decomposition of materials deposited in landfills are CO_2 and CH_4. CH_4 is considered over 20 times more detrimental to the atmosphere than CO_2. There are many trace components in the landfill gas, including volatile organic components(VOCs).

$$Q_m = \sum_{i=1}^{n} 2kL_0M_i \cdot e^{-kt_i} \tag{17}$$

In the type: Q_m=Maximum output of landfill gas, m^3/a. L_0= biological methane potential (BMP), m^3/t. k=rate constant of methane production, 1/a. M_i= waste amounts in the unit i landfill, tonne. t_i= time span from beginning of gas production to assessment point, a.

Health Risk Assessment

For substances presenting risks other than cancer, a Hazard Quotient (HQ; analogous terms include “exposure ratio” and “hazard ratio”) will be derived as the ratio of the estimated exposure (for each critical receptor) to the toxicological reference values for risk characterization (RfD) or tolerable reference concentration (RfC), as follows[6]:

$$HQ = \frac{CDI}{RfD} \tag{18}$$

$$HQ = \frac{C}{RfC} \tag{19}$$

In the type: HQ= the comparison of the levels of chemical contamination at the site to levels that are known to cause harm, dimensionless. CDI= average estimated exposure per kg body weight per day, mg/kg/day. RfD= the toxicological reference values for risk characterization, mg/kg/day. C= chemical contamination concentrations in the ambient medium, mg/m^3. RfC= the tolerable reference concentration, mg/m^3.

HQ for individual exposure pathways should be presented where there are pathway-specific toxicological reference values. Where exposures via multiple pathways are being summed for comparison to a single RfD (for example, it is common to sum oral and dermal exposures for comparison to the oral RfD), it is necessary only to display the HQ for the summed exposure.

For substances deemed to be carcinogenic, the estimated exposure will be multiplied by the appropriate slope factor (SF) or unit risk (URF) to derive a conservative estimate of the potential incremental lifetime cancer risk (R) associated with that exposure. R is derived as[6],

$$R = CDI \times SF \tag{20}$$

$$R = C \times URF \tag{21}$$

In the type: *CDI*= average estimated exposure per kg body weight per day, mg/kg/d. *SF*=the appropriate carcinogenic slope factor, $(mg/m^3)^{-1}$. *C*= the concentrations of air-borne contaminants, mg/m^3. *URF*= unit risk value of air-borne contaminants, $(\mu g/m^3)^{-1}$.

Where pathway-specific slope factors or unit risks exist, the risks via inhalation and the risks via oral plus dermal exposure should be estimated separately. In other cases, the cancer risks posed by simultaneous inhalation/dermal/oral exposure will be estimated.

Conclusion

An integrated risk assessment methodology for landfill gas and leachate is attempted to develop for the first time in China, and conservatively facilitates rapid estimation of the risk level of MSWL. Health risk assessment (HRA) for landfill gas combines gas output with air concentration calculations by simplifying program and choosing parameter values. HRA for landfill seepage connected landfill engineered barriers with water and pollutants migration during the whole life span of landfill by simplifying program and choosing parameter values conservatively. The major exposure pathways to environmental contaminants were considered: inhalation of gas and dust during operation period, and ingestion of four food pathways categories (plant foods, meat, milk, and fish), groundwater and dust during usage period without any limits. The endpoints of HRA of MSWL are individual lifetime carcinogenic risk for all the carcinogenic chemical contaminants, and hazard index (HI) for all the non-carcinogenic chemical contaminants to the landfill worker (only at the operation period), and to the public near to the landfill (at the all the three stages) respectively.

The primary purpose of the model is to assist in the comparison of design alternatives for site selection and landfill engineered barriers, and to assess health risk of the different design alternatives. At the same time, the model will improve environmental impact assessment methodology having been universally used nowadays.

References

[1] Chinese Research Academy of Environmental Sciences, Tongji University, Tsinghua University, et al. Pollution control standard of municipal domestic refuse sanitary landfill[S]. GB16889-2008 Beijing: China Environment Science Press, 2008.

[2] Housing and urban-rural development of the People's Republic of China. Technical specification for operation and maintenance of municipal domestic refuse sanitary landfill [S]. CJJ 93-2011.

[3] Wang Hongtao. Porous medium dynamics of pollutant migration[M]. Beijing: Higher education press, 2008.

[4] International Atomic Energy Agency. Derivation of activity concentration values for exclusion, exemption and clearance. Safety reports series, No. 44, Vienna: 2005.

[5] Carlsen T M, Efroymson R A. Current Directions in Screening-Level Ecological Risk Assessments[G]. Society of Plastics Engineers/Environmental Protection Agency/Department of Energy Exploration and Production Environmental Conference. San Antonio: Society of Petroleum Engineers Inc., 2001(2) 26-28. https://e-reports-ext.llnl.gov/pdf/245234.pdf

[6] Safe Environments Programme, Environmental Health Assessment Services. Federal Contaminated Site Risk Assessment in Canada, Part I: Guidance on Human Health Preliminary Quantitative Risk Assessment (PQRA)[R], 2004(9).

Advanced Materials Research Vols. 989-994 (2014) pp 5601-5604
© (2014) Trans Tech Publications, Switzerland
doi:10.4028/www.scientific.net/AMR.989-994.5601

Effect of Hg in Jiaozhou Bay waters-the vertical variation of the Hg content

Dongfang Yang[1, 2, 3, a], Sixi Zhu[1, 2], Fengyou Wang[1,2], Xiuqin Yang[1,2] and Yunjie Wu[1, 2]

[1]Research Center for Karst Wetland Ecology, Guizhou Minzu University, Guiyang 550025, China;

[2]College of Chemistry and Environmental Science, Guizhou Minzu University, Guiyang 550025, China;

[3]North China Sea Environmental Monitoring Center, SOA, Qingdao 266033, China

[a]dfyang@shou.edu.cn

Keywords: Mercury (Hg), Content, Variation, Vertical, Jiaozhou bay.

Abstract. Based on the investigation data of mercury (Hg) in both surface and bottom waters in Jiaozhou bay in 1979 to 1981, this paper tried to analysis the vertical variations of Hg contents, and to reveal the transfer processes of Hg in the bay. Results showed that, Hg pollution in the bay is mainly discharged from the major rivers, the seasonal variations of Hg content in surface waters showed a similar trend in different years, with an order of spring (or summer) > autumn. The Hg contents in bottom waters were mainly determined by the sedimentation of Hg from surface waters. There were major three transfer processes of Hg as, 1) Hg from various pollution sources was transported to streams by rainfall, 2) Hg in streamflows was discharged to surface waters of the bay, and 3) Hg in surface waters was sedimented to the bottom of the bay.

Introduction

With the rapid development of social economic, atmosphere, lands and waters have been polluted by various pollutions. Jiaozhou Bay is located in south of Shandong Peninsula, which is one of the "frontier" of Chinese Reform and Opening, as well as an economic development region, has long been suffering from environmental pollution problems. Previous studies showed that this bay had long been suffering from both point and non-point sources pollution, and pollutants such as benzene hexachloride, petroleum hydrocarbon, and heavy metals had reach certain levels [1-11].

Hg is one of the one of the most critical environmental pollutants, with characteristics of high toxicity, bioaccumulation, and persistence. In previous several decades, Hg has been widely used in chloro-alkaline industry, plastic industry, electronic industry, metallurgical industry etc., as well as agricultural pesticide [12-13]. Based on the investigation data of Hg in waters in both surface and bottom Jiaozhou bay during time periods of 1979 to 1981, this paper tried to analysis the vertical variation of Hg in Jiaozhou Bay, to reveal the transfer processes of Hg, and to provide basis for pollution control.

Material and method

Study area. Jiaozhou Bay is located in the south of Shandong province (35°55′-36°18′ N, 120°04′-120°23′ E), and is around by economic developed cities such as Qingdao, Jiaozhou and Jiaonan etc. (Fig. 1). The total area and average water depth the bay is 390 km^2 and 7 m, respectively. This bay is typically a closed bay, whose bay mouth is only 3 km width. The main rivers are Haibo River, Licun River, Baisha River, Dagu River, Yanghe River, and Loushan River, all of which have seasonal hydrological features, and are transfer cannels for pollutants into the bay [1- 3].

Data source. The data was provided by North China Sea Environmental Monitoring Center. The measurement methods of Hg in water samples was follow by The Chinese National

Specification for Marine Monitoring (1991) [14]. The survey as conducted in May, August and November 1979, June, July and October 1980, April, August and November 1981, respectively. We defined April, May and June as spring, July, August and September as summer, and October, November and December as autumn, respectively.

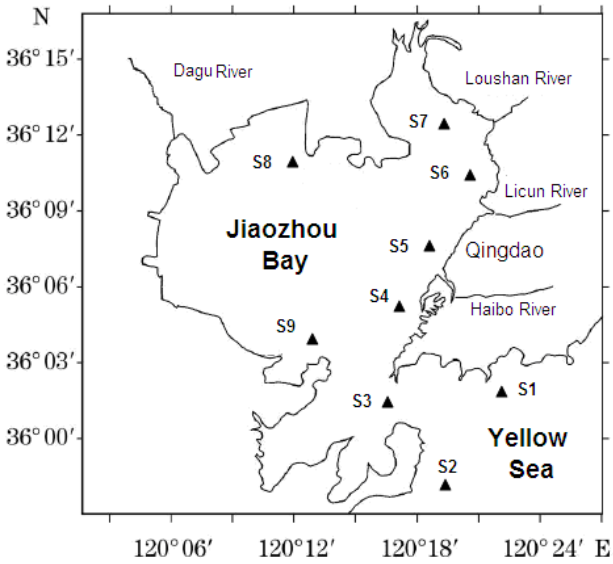

Fig. 1 Geographical location and sampling sites of Jiaozhou Bay

Results and discussion

Hg content. The Hg contents in surface and bottom waters in spring, summer and autumn in Jiaozhou bay were listed in Table 1[4-5, 8]. The seasonal variations of Hg content in surface waters showed a similar trend in 1979, 1980 and 1981, with an order of spring (or summer) > autumn. The reason is that the Hg pollution to the bay is mainly discharged from the major rivers, whose streamflows are mainly impacted by precipitation, which is concentrating in spring and summer. By comparison, the Hg contents in bottom waters had no significant seasonal variations, but increased with the increase of Hg content in surface waters in the same season. That's because Hg in bottom waters are mainly determined by the sedimentation of Hg from surface waters. However, in case of large input of Hg in spring (or summer), as in year of 1981 (Table 1), Hg content in bottom waters also showed an order of spring (or summer) > autumn. This trend indicated that Hg contents from surface waters to bottom waters decreased with time within the year due to the sedimentation of Hg in waters.

Table 1 The Hg contents in surface and bottom waters in spring, summer and autumn in Jiaozhou bay/μg.L^{-1}

		1979	1980	1981
Spring	Surface water	0.110-0.460	0.003-0.030	0.028-2.086
	Bottom water	0.030-0.140	0.002-0.007	0.029-3.125
Summer	Surface water	0.030-0.040	0.011-0.045	0.001-0.040
	Bottom water	0.020	0.002-0.029	0.002-0.026
Autumn	Surface water	0.010-0.020	0.010-0.030	0.002-0.017
	Bottom water	0.010-0.050	0.013-0.090	0.003-0.005

Hg transfer processes. Based on the vertical variations of Hg, we could draw a framework map to demonstrate the transfer processes of Hg in Jiaozhou Bay (Fig. 2). Fig. 2 clearly revealed the major three transfer processes of Hg as, 1) Hg from various pollution sources was transported to streams by rainfall, 2) Hg in streamflows was discharged to surface waters of the bay, and 3) Hg in surface waters was sedimented to the bottom of the bay. Previous studied showed that, Hg content in surface water of this Bay were always very high in waters close to river mouths of the major rivers, and showed decreasing trends with the flow directions [4-5, 8]. However, having in mind that the bay is a closed bay, the horizontal diffusion of Hg in surface water could be considered as but not the major transfer process.

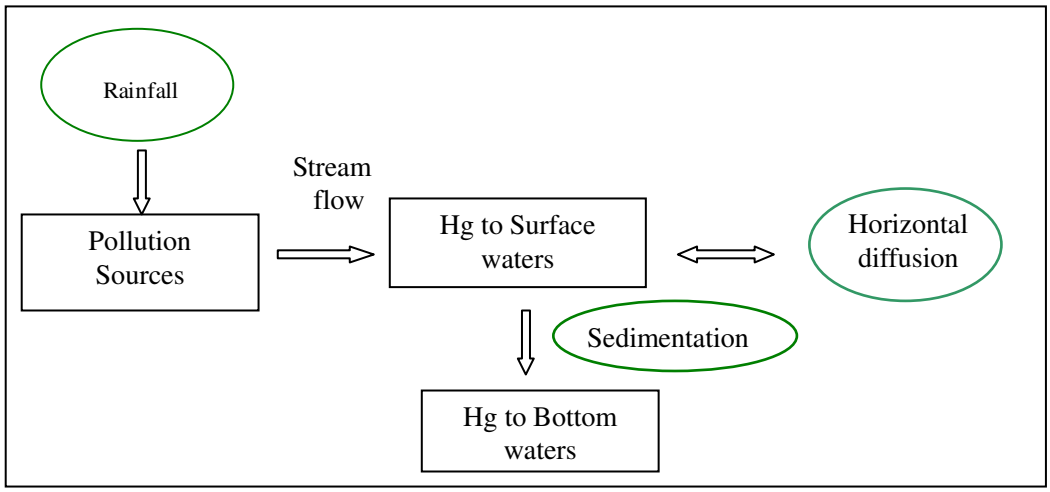

Fig. 2 The Schematic diagram of the waters transfer process of Hg.

Summary

Hg pollution to the bay is mainly discharged from the major rivers, the seasonal variations of Hg content in surface waters showed a similar trend in different years, with an order of spring (or summer) > autumn. The Hg contents in bottom waters were mainly determined by the sedimentation of Hg from surface waters. There major three transfer processes of Hg were, 1) Hg from various pollution sources was transported to streams by rainfall, 2) Hg in streamflows was discharged to surface waters of the bay, and 3) Hg in surface waters was sedimented to the bottom of the bay.

Acknowledgements

The work is supported by Education Ministry's New Century Excellent Talents Supporting Plan (NCET-12-0659), Project of Outstanding Technological Educators of Governor of Guizhou ([2012]71), Project of Low Carbon Technology Plan of Guiyang (2012205]), Project of Science and Technology Foundation of Guiyang (LKM[2012]05), and Special Research Projects of High Level Talents of Guizhou Province (TZJF-2011-44).

References

[1] S.M. Zhang, X.Z. Pang and S.Q. Zheng: Mar. Sci. Vol. 6(1987), p. 35-36. (in Chinese)

[2] X.Q. Lv, B.Y. Sum and Z.L. Shi: J. Ocean University of Qingdao. Vol.20 (1990), p. 107-114. (in Chinese)

[3] S.F. Chai: J.Oceanography of Huanghai & Bohai Seas. Vol. 16 (1998), p. 60-63. (in Chinese)

[4] Chen Yu, Gao Zhenhui , Qu Yanheng, Yang Dongfang and Tang Hongxia: Chin. J. Oceanol. Limnol. 2007, 25(4): 455-458. (in Chinese)

[5] D.F. Yang, H.R. Cao, Z.H. Gao, Q. Lu and Y.F. Qu: Mar. Environ. Sci. Vol. 27 (2008), p. 37-39. (in Chinese)

[6] D.F. Yang and Z.H. Gao: *Bay ecology (First Volume)* (Ocean Press, Beijiang 2010) , p.1-300. (in Chinese)

[7] D.F. Yang and Z.H. Gao: *Bay ecology (Second Volume)* (Ocean Press, Beijiang 2010) , p.1-300. (in Chinese)

[8] D.F. Yang, L.L. Wang, Z.H. Gao, Q. Lian and J.P. Zeng: Mar. Environ. Sci. Vol. 28 (2009), p. 501-505. (in Chinese)

[9] D.F. Yang and Z.Q. Miao: *Distrubution and seasonal variation of Jiaozhou Bay environment* (Ocean Press, Beijiang 2012) , p.1-115. (in Chinese)

[10] Y. Chen, Q.J. Zhang, J.H. Guo, Q. Shi and D.F Yang: Ocean Develop. Manag. Vol. 30 (2013), p. 81-83. (in Chinese)

[11] D.F. Yang, P.Y. Sun, L. Ju, Y.H. Zhao and Q.U. Feng: Coast. Engin. Vol. 32 (2013), p. 65-76. (in Chinese)

[12] O. Lindqvist: Tellus. Vol. 37B (1995), p. 136-159.

[13] D.O. Reimann: Water Air SoiL Pollut. Vol. 13 (1974), p. 179-193.

[14] China's State Oceanic Administration: The specification for marine monitoring (Ocean Press, Beijiang 1991), p.1-300. (in Chinese)

Advanced Materials Research Vols. 989-994 (2014) pp 5605-5608
© (2014) Trans Tech Publications, Switzerland
doi:10.4028/www.scientific.net/AMR.989-994.5605

Design and Implementation based on Java EE Student Attendance System

Zhihao Zhao[1, a], Yabing Chen[2, b]

[1]LG Inspur Digital Mobile Communications Co., LTD, Yantai,264006, China

[2]Yantai Engineering & Technology College,Yantai, 264006, China

[a]email: zhihao.zhao@lge.com, [b]email:chenyabing339@163.com

Keywords: Student Attendance System; Java EE; B/S Structure; Development of Mobile Terminal

Abstract. In this paper, according to the actual students management work in the school, and link to the student attendance work, we propose one design of the B/S structure system of student attendance management based on the Java EE framework. The system realizes performances such as request and approval leave online, students' attendance data summarize, and others which reduce the workload of student management and improve the working efficiency. With the rapid development of mobile network on campus, this system also has carried on the development of mobile terminal, to further expand the scope of application of the system with the desktop of the student management system transplantation.

Introduction

Student attendance work plays an important role in the student management. As well the attendance statistics are key reference data to undertake the student comprehensive assessment by employers or teachers. With the rapid expansion of network communication technology and the campus network engineering, the networkalization of student attendance system becomes a trend for better real-time performance, more convenient way of management to greatly reduce the workload of teachers and student management personnel, improve the work efficiency and save a lot of cost[1][2].

This paper fully carries on school student attendance system and researches the users type and operating scope of the system. According to the demand analysis, this paper designs the student attendance management system, and uses the Java EE framework to realize the system including performances of completing the background management, requesting for leave online by students, viewing hierarchically and level permission for student notes by teachers, as well statistical attendance rate of the whole term, and generate attendance reports, and so on[3][4][5].

As the development of the Internet technology and the computer technology, information technology is deeply affecting people's life. The development of mobile Internet, especially the third generation (3G) technology, it provides a powerful bearing channel and rich professional ability supports and makes the people's life more colorful. People also eagerly hope that they can browse the web to get information at anytime, anywhere and any place through the wireless network. But the mobile equipments have small screen, small memory, low bandwidth and other weakness that cannot compare with PC, so an abbreviated version of Student Attendance System is designed in the paper also.

Design of the Student Attendance System

According to system analysis, student attendance system is divided into four main kinds of users, students, teachers, students management, system administrator, as shown in Figure 1. Therefore, this system depending on the type of user will be divided into four modules, background management module and student module, teacher module and student management module.

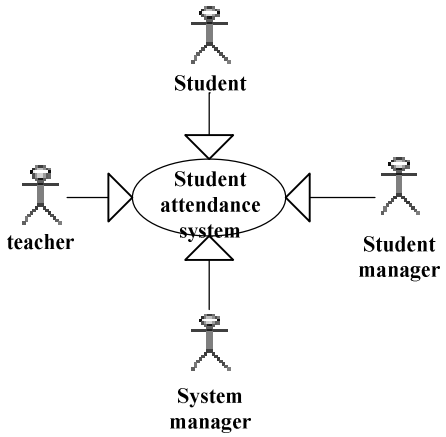

Fig.1. The Students Attendance System

For students, it is inevitable to ask for leave because of the various causes. For a long time leave request, it may even need the counselor of students submit for approval to the competent department. For general teachers, they need to checkroll of students, and assessment the final grades with average attendance. For the head teachers or counselors, besides the daily students' attendance situation, and leave approval, they also need make the final comprehensive evaluation reference attendance statistics of the students.

So, provided the specific function of this system mainly includes the following aspects:

1) Function to modify the personal information: all the system users can modify their personal information.

2) Query function: through the system, students, teachers, and administrators can query and related attendance information, and personal information. Such as the classroom teachers can just see they filled in, but can't query information filled by other teachers; while the head teacher can query a certain period attendance information of the class he charged.

3) Leave request functions: students can directly submit leave request online to the head teacher or counselor.

4) Checkroll function: mainly for logging in the system by classroom teachers, they can check who are absence in the class, and record the attendance for students.

5) leave approval function: the head teacher or counselor has approval right of one day's leave, in case of leave time out of one day, the superior manager’s approval right is needed.

6) data statistics function: teachers can get the absence of information of certain period or all time which include approved leave and truancy, and export the data to EXCEL table.

7) background management functions: each administrator can manage the background, such as add or delete information of students, class, teachers and others. But the general administrator has default access level 2, that means, he does not have permission to add, modify, delete the administrator. Only administrator with access level 1 can modify the administrator information.

The Framework of Student Attendance System

The implementation of this system, which is based on the field test of campus network and demand analysis for the function of the students attendance system, finally established the system goal. Depending on resources of campus network (see Figure 2), the system adopts B/S three layer structure of the data processing, in order to realize the workflow service and maintenance of all kinds of information query and permissions management, it integrates the attendance system and business system effectively[6][7]. The software framework of this system based on JAVA EE and database technology, combined Ajax technology, SQL Server 2000 as the backstage database, build a suitable school student attendance management system.

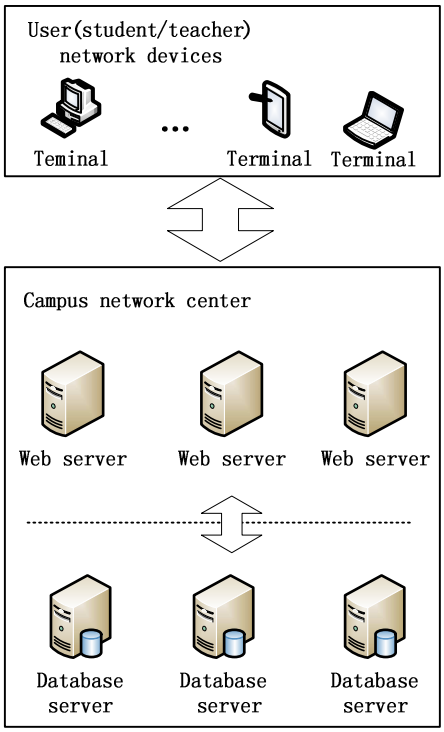

Fig.2. Campus's network resource

For students and faculty, this system is high frequency used so that it is requested simple interface and friendly operating. The class attendance statistics interface of this system is shown in Figure 3. The user just need simply click on the navigation bar on the left to switch each function.

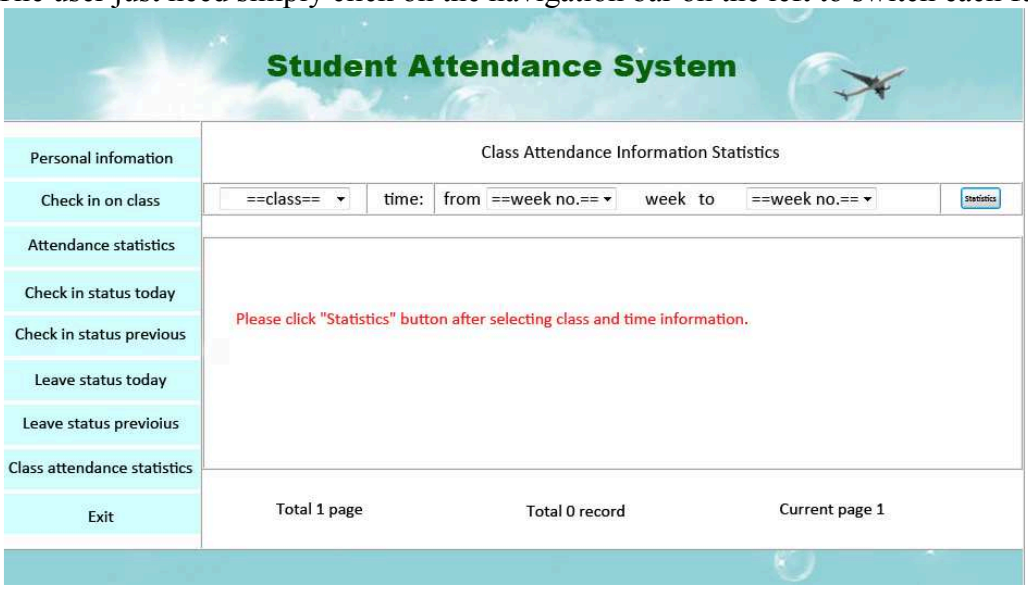

Fig.3. Interface of class attendance information statistics

Mobile client development

In recent years, with the rapid development of mobile communication technology and the expansion of smart mobile terminals, mobile Internet business steps into a golden period. Moreover, Campus life follows fashion trends tightly that almost all teachers and students own their smart phone. This provides the prerequisites for the student attendance system using in mobile terminal. But due to the mobile terminal screen is usually small, processing power is weak, so the functions of this system on the mobile end are selected.

This system mobile terminal classifies function according to user type as well:

1) students can login, write for leaving, check approval status;

2) teachers and staff can log in and view the leave request, approval and record attendance

And mass data requirement functions such as batch query, attendance statistics function are removed, which are only available in the desktop system.

Conclusion

The student attendance system was designed and implemented based on the campus attendance requirements. The system menu enabled different functions depending on the type of users to convenience for the user. For the same user with different levels of authority, provides the system data security. By the practical operation indicates that the system has high convenience, good fault-tolerance performance and certain economic practicality.

Although PC has been popular for teachers and students to deal with attendance process on campus, smart phone penetration is also reckoned because of small volume, easy to carry, more convenient for the teacher roll call at any time. So this system is applied to mobile client identification at the same time with reasonable cutting of the functions to make the design of a web page on the mobile device can be easily used.

References

[1] GE Fang-zhen,RAO Yun-tao,HE Bin,WEI Xiong. Design and Implementation of Check on Work Attendance anagement System Based on Three-tier B/S and C/S Architecture[J]. Computer and Modernization, 2005(1):88-90.

[2] Mark Weiser. The Computers for the Twenty-first Century. Scientific American, 1991 265(3): 94-104

[3] Jussi Myllymaki, Jared Jackson. Automatically extract information with HTML, XML, and Java[EB/OL]. http://www.ibm.com/developerworks/library/wa-wbdm/.

[4] Knapp A, Koch N, Zhang G. Modelling the behaviour of web applications with ArgoUWE [M] Web Engineering. Springer Berlin Heidelberg, 2005: 624-626.

[5] LV Guan Yan,LI Fen Hua. A model of requirements analysis based on UML in MIS. Microcomputer & Its Applications, 2010(20):8-10

[6] Liddle S, Embley D, Scott D, et al. Extracting data behind web forms. Advanced Conceptual Modeling Techniques, 2003: 402～413

[7] ZHANG Wei-hao. Current Situation and Development Trend of Campus Information Requirement Under Mobile Internet Information Environment[J]. Journal of Jianghan University (Natural Science Edition), 2013, 41:53-56.

Advanced Materials Research Vols. 989-994 (2014) pp 5609-5613
© (2014) Trans Tech Publications, Switzerland
doi:10.4028/www.scientific.net/AMR.989-994.5609

Research on Design of Modern Warship Networked Fighting Simulation System

Yan-Hui Wang, Jian-Zhou Mao, Zhi-Hong Xiu

Dept. of Operation and Command, Dalian Naval Academy, Dalian 116018, China

bagum908@sina.com

Keywords: Warship; Network; Fighting Simulation; Agent

Abstract. The simulation system of the overall system structure and function module are established, on the basis of the analysis of designment of modern warship's networked fighting simulation system, the solutions of network architecture and Agent construct are provided., some key problems are discussed for the realization of a simulation system. There is a certain reference value for the construction and research of warship network fighting simulation system.

Introduction

Modern warship is an integrated fighting system, which makes use of the network technology, shares combat information resources through coordination between units under the same mission control among each fighting unit of the warship. Its simulation system is an important tool for the study of warship combat system operation mode, information process, and the command process. The study of warship network fighting simulation system from the design concept, system structure, and key technology has important guiding significance for modernization of warships, organization and command for each unit of the cooperative engagement.

Summarize

The study of complex systems is the foundation of modern warship networked fighting simulation system design. At present, there are two main types of research methods in complex systems. The first method is trying to establish an individual from the individual behavior of the complex systems isomorphism of microscopic model[1], its basic idea is that the characteristics of the complex system are extracted according to the individual model of complex system, find out the relationship between the individual and the interaction; then, running system in the certain synthetic environment, observe the system of macroscopic overall behavior through individual interaction. The second method is trying to establish a complex system from macro level and to constitute complex system of the whole behavior model. Its basic idea is that the evolution process of the overall behavior system is studied and analyzed from the angle of macroscopic overall. This kind of situation does not need to establish a system model under the level of individual subsystems and their relationship, but, the basic ideas of feedback control theory and methods are introduced in the process of building some methods. The typical theory includes of system dynamics method, the influence graph model, neural network and integrated.

On the design concept, modern warship's networked fighting simulation system, should be especially emphasizes the complexity of network simulation object and the whole system compared with traditional warship combat simulation system. Networking of simulation objects bright the system unit problem such as the change of aggregation depolymerization and efficiency calculation [2]. Modern warship simulation has a finer granularity of networking combat simulation system. The degree of information of old warship combat system is relatively low, its basic fighting unit includes detecting equipment and weapon system, and the basic fighting unit of modern warship not only includes detection equipment, weapon system, but also C3I system, it makes the whole combat capability of the warship combat system greatly improved, and gives the restructuring ability between different units to strengthen. Therefore, the simulation design should consider fully the simulation

object granularity, aggregation restructuring ability. At the same time, the research calculation on warship combat efficiency of the system as a whole should be strengthened in terms of system effectiveness calculation, on the basis of single weapon efficiency is given priority to in the traditional calculation.

The complexity of the whole system mainly includes the complexity of the simulation object, the complexity of the system function and so on. As the simulation object of modern warship combat system, it is also a complex system, the bottom-up approach should be highlighted in the study of its collaborative, network architecture, design and implementation of agents.

According to the above design, modern warship networked fighting simulation system should have the following main features:

First, input and output driven by dialogue, use windows graphical user interface in the front desk, and allow opening multiple documents view;

Second, using object-oriented c++ source code library, facilitates the secondary development of end user or analyst;

Third, chart integration and decision-making based on the operational environment adaptability of dynamic;

Fourth, environmental associations and user defined Agent behavior;

Fifth, each unit has a communication link;

Sixth, having the department and the overall warship dynamic controllers;

Seventh, with data collection and visualization tools.

The overall structure of the system

To supporting different application requirements, the modern warship combat simulation systems adopts hierarchical service oriented architecture, the architecture of the simulation system is shown in figure 1.

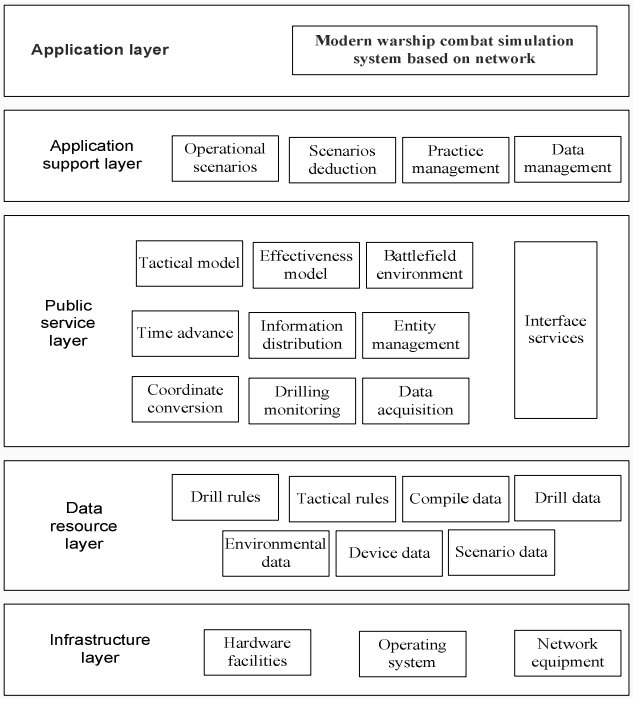

Fig.1The overall structure of the system block diagram

The infrastructure layer mainly includes computer and network devices for simulation, storage devices, input and output devices, and form a complete set of software, to provide the experimental environment support for completing the simulation task.

The data resource layer provides server and the mass storage device as the carrier, to store and manage the simulation experiments of all kinds of data resources, including the experimental plan, the test data, to set data, tactical rules, environmental data and equipment, etc.

The public service layer is the core of the framework, it provides a variety of public services for the system, mainly including the tactics model service, efficiency calculation service, time management, message distribution service, entity management service, coordinate transformation, the simulation monitoring service, data acquisition, and data interface services (to provide a wide range of standard data communication protocol interfaces).

The application support layer provides auxiliary tool module for performance analysis of combat simulation system of modern warship network, including test management module, scenario deduction module, scenario institution module, data record module, etc.

Function modules of the system

The realization of system function consists of seven sub modules, they are communication simulation module, environment simulation module, virtual force module, simulation management module, scenario compile module, scenario deduction module and record analysis module.

The communication simulation module is mainly to provide simulation system with high reliability of tactical communication system simulation support. In contrast to the old warships, one of the main characteristic of modern warship is its highly degreed information sharing network, its internal communication system including a digital network of combat system, video network, program-controlled telephones, etc. At the same time, information sources of warship combat are various, that also needs external communication system, including shortwave, ultra short wave communication system, satellite communication, data link, etc. Therefore, we should focus on its impact of communication simulation of difficult system network architecture and operation during the simulation, such as a result of damage caused by the topology structure of dynamic change. At the same time, factors of the complex electromagnetic environment of real time injection should be considered, and it should support receiving the interference of data from external module (such as the electromagnetic environment simulation module or control system), real-time calculate the influence of channel bit error rate by interference, which reflects the degree of communication interference[3].

Main function of the environment simulation module is to provide a consistent sea condition, weather condition, and electromagnetic environment conditions for simulation. Simulation object mainly is the modern warships and hostile forces, therefore in the environment simulation module, simulation environment factors, such as temperature, pressure, flow, wind, visibility, cloud and mist, all kinds of electromagnetic environment information, reef, drilling platforms and geographical environment and so on, should be outstandingly emphasized, which shows more influence on the warship than others entity.

The virtual force module mainly simulates detection equipment, command and control system, weapon systems, such as combat unit of the warship. Operations, such as information reconnoitering, auxiliary decision-making, arms controlling, weapons, electronic countermeasures, ship maneuvering, and so on, are driven by the combat mission. In a word , virtual force mainly include passive reconnaissance equipment, warning radar, tracking radar, all kinds of naval gun, the anti-ship missile, ship to air missile, torpedo, acoustic equipment, charge system, enemy's virtual force is mainly responsible for foreign warships, aircraft, missiles, etc.

The simulation management module is mainly responsible for experimental nodes, system parameters configuration, data acquisition planning, etc. It is also responsible for the test node time synchronization, to control and manage each operation node in the process of the simulation and estimate the ending conditions of the simulation, controls the test process according to the combat situation.

The scenarios compile module is a battle plan generating module. It is a supportively module used to determine the ship maneuvering under different operational conditions for command personnel and technical personnel on the basis of the battlefield environment and providing the initial conditions for man-machine confrontation simulation.

The scenarios inference module is mainly used for the dynamic deduction of scenarios, and tested the rationality of the battle determined elements, operational settings, etc.

The data recording module is mainly responsible for man-machine confrontation or the factor of forces in the process of deduction, such as the state, the location, the damage situation and interactive information recorded on both sides. It also could provide real-time both forces battle damage with curve, diagrams, tables, and so on.

Key technology of the system

The design of network architecture and Agent is the key technology of modern warship networked fighting simulation system, it is the critical factors of system structure and operation rules, and it is an important role to the system develop, it also is the foundation of the system overall design and key.

Network architecture

The network architecture of the system should not only solve the seamless link between elements, but also meet the end-to-end real-time transmission of information. In addition, the initial planning, network parameter settings and injecting should be more convenient, more shortcut. The network set up time is short, if the network structure changes, routing must adaptive dynamic adjustment, global topology does not have a significant impact when local network changes.

The establishment of the network architecture must accord with battle needs, adhere to the objective reality of modern warships, which requires the network structure should have a reasonable span and hierarchical structure. The span refers to the quantity of the domination unit of transverse department. The hierarchical structure is divided in longitudinal command level. Therefore, the studying of modern warship networked fighting simulation system should emphasize the benefits of span and hierarchical structure of modern naval combat system. Based on complex network theory, the WS network has the characteristics of the small path length (small-world features) and larger aggregation coefficient (polymerization features), as a result, network architecture of the modern warship networked systems can be conducted on the basis of the WS model[4]. Figure 2 is a modern warship combat system, the basic component of each unit in the network architecture symbols and coordinates are listed in table 1.

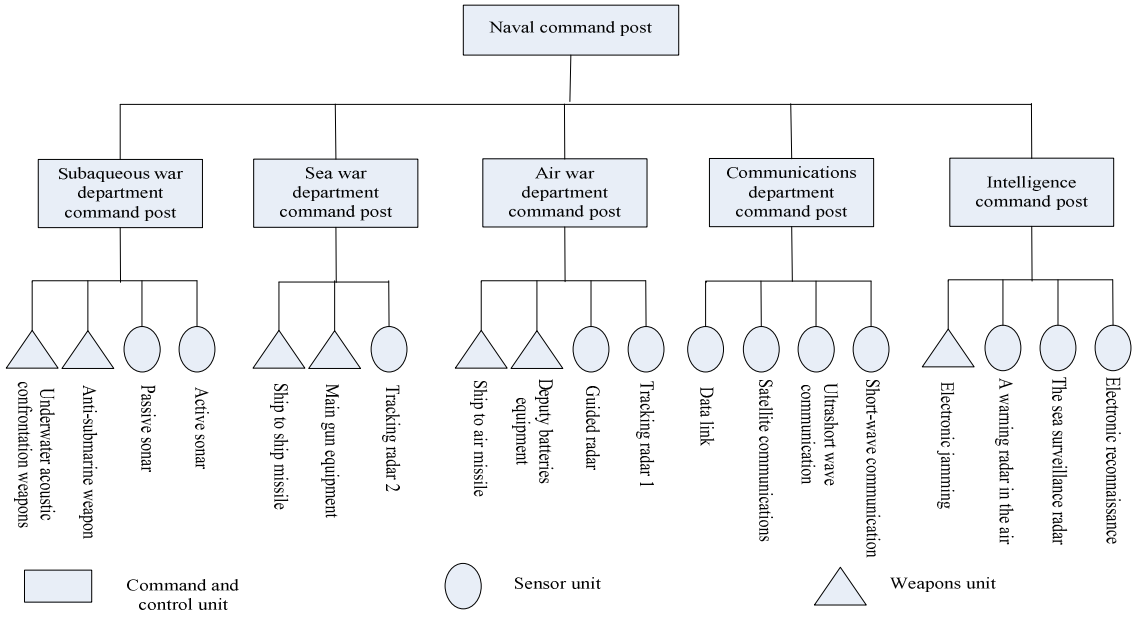

Fig. 2 The combat system of modern warship

Table 1 Each node code and coordinate

Node name	code	coordinate	Node name	code	coordinate	Node name	code	coordinate
Naval command post	JZ	(3.0, 3.0)	Electronic reconnaissance	GR	(1.0, 4.4)	Tracking radar 2	GL2	(5.2, 4.3)
Intelligence command post	QB	(2.2, 2.9)	Short-wave communication	DB	(2.4, 5.4)	Main gun equipment	ZP	(5.4, 3.5)
Communications department command post	TX	(2.7, 3.7)	Ultrashort wave communication	CDB	(3.1, 5.5)	Ship to ship missile	JJD	(5.5, 2.7)

Air war department command post	DK	(2.7, 2.2)	Satellite communications	WT	(3.9, 5.3)	Active sonar	ZSN	(5.2, 1.9)
Sea war department command post	DH	(3.6, 3.5)	Data link	SJL	(4.6, 4.8)	Passive sonar	BSN	(4.7, 1.2)
Subaqueous war department command post	DQ	(3.5, 2.5)	Tracking radar 1	GL1	(1.7, 0.8)	Anti-submarine weapon	FQ	(3.5, 0.5)
Electronic jamming	ZC	(1.6, 5.1)	Guided radar	YDR	(0.7, 2.1)	Underwater acoustic confrontation weapons	SK	(4.1, 0.7)
The sea surveillance radar	HJJ	(0.6, 3.6)	Deputy batteries	FP	(2.5, 0.5)			
A warning radar in the air	KJJ	(0.5, 2.9)	Ship to air missile	JKD	(1.1, 1.4)			

Design of Agent

Agent design is another key factor of the simulation system. Describing the agent need to establish entity model, behavior model and mathematical model. The entity model is mainly to describe each Agent levels, functions, components, equipment parameters, and to define the data type and scope, for the convenience of programmer's understanding; Behavior model is to define a set of the main Agent behavior rules, this need to list the action conditions, action termination conditions, structure and implementation process, action interactions, action data and structural description. Mathematical model is used to convert all kinds of behavior interaction to mathematical model, it is advantageous for the technical personnel to change the behavior of the structured rules into code execution. Among the three model, behavior model is the basis of Agent operation. Figure 3 is a naval gun unit behavior rules example, hence one can see that, clear Agent operating rules can be provided for developers from the figure description through rules, it solved the communication problem between military experts and technical experts.

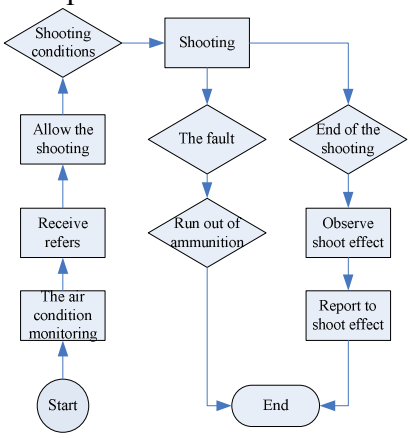

Fig. 3 The deputy artillery unit （Agent）fire behavior model

Conclusion

This paper analyzed the characteristics of modern warship networked fighting simulation system, system structure and function modules of the system are constructed, two key problems of the network architecture and the agent building are solved. The design of the simulation system is according to the development trend of modern warship networked fighting simulation system, it could well solve the problem of the construction of modern warship simulation system. This paper has a certain practical significance to deeply research warship network warfare and promote modern warship's operation ability based on information system.

References

[1] Tang Su-yan. *Agent-based simulation and analysis of networking air defense missile systems*. Systems engineering and electronics. 2012.12(12):2632-2637

[2] *Advanced technology for command and control system engineering*.Beijing, 2005

[3] Liu Wei-dong. *Simulation for networked torpedo control system*. Computer measurement control. 2008.16(11):1647-1649

[4] Zhang Qiang, Lei Hu-min. *Complexity of air defense and antimissile system based on small-world networks theor*y. Modern defense technology. 2010.12(6):1-5

Advanced Materials Research Vols. 989-994 (2014) pp 5614-5618
© (2014) Trans Tech Publications, Switzerland
doi:10.4028/www.scientific.net/AMR.989-994.5614

Application of Reusable Framework Technology on the Workflow System

Chunyan Xue

Xiamen University Tan Kah Kee College, Zhangzhou, Fujian Province, 363105

xuegirlxcy@sina.com

Keywords: Reusable Framework; Workflow System; Application

Abstract. Focus on workflow task duplication of information processing in the interface of the show, interact with applications and other complex technical difficulties, the paper design and implement tasking reusable framework technology, to enhance the flexibility of workflow system, while reducing the complexity of the task processing , in order to carry out the system development and maintenance. Establishing a common framework for the design task processing, to process basic tasks, task processing applications each parameterized configuration variable part, by explaining the configuration items, dynamically generated parameters interface and back-office services, so as to realize the application system and workflow platform universal interaction.

Introduction

Workflow system

Workflow is a model that is used to calculate the flow of work, which is a set of logic rules can organize works together, create an appropriate model and calculate the workflow. The main problem workflow solutions are: to achieve a business goal, among several participants, according to some predetermined rule using the computer automatically passed documents, information or tasks.

Core functionality of the workflow is routing functions. The ultimate goal of workflow is to simulate the real business in software products. Workflow routing can be divided in serial routing, parallel routing, dynamic routing, condition routing accordance with the actual situation[1].

Workflow Management System, WFMS is a system which can define, create, execute the workflow. WFMS can provide functionality to support the following three aspects:

1) Construction function: its components for workflow process definition and modeling activities;

2) Operational control functions: manage workflow processing and schedule the staff in the work flow.

3) Operation and interactive functions: interaction function among WFMS and the user (participants or controller of the operational work) and external application program tools.

Currently, workflow products can better solve the task scheduling, process control and other functions, and reduces the c technology complexity of the process control in the project development process. However, these products do not summarize, abstract and encapsulate task process,. The WFMS does not well to reduce the application complexity of the task process. Reusable framework technology to use in the workflow system can solve these problems.

Reusable framework technology

Reusable framework technology separated the process control logic of business from the business logic. Then business logic is further broken down into the core business logic and assistant business logic assist. The core business logic is divided into relatively independent business components which reduced the workload of the application development, thus speeding up the system building.

When the system is running and process logic changes, reusable framework technology can redefine the process in order to adapt to changing business processes, Reusable framework technology make application system managed unified the business process[2].

Reusable framework technology summarized reusable tasking based on business requirements analysis, designed and implemented in a common design patterns. Using reusable framework technology, workflow system need not additional design components when dealing the tasks which compliance with reuse applicable conditions, adjust the configuration items to complete with reusable tasking.

Operation Mechanism of the Reusable Framework Technology

The existence of the enterprise business process reflects the production and the business process, which necessarily involves division and collaboration of the staff that are multi departments, and multi-role. Some business processes are a complex process which is cross-level, cross-regional, cross-quarter and span widely in space and time. Therefore, it is necessary to improve and abstract the common features of the business[3].

Reusable framework determined the core technology solutions according to the difference of the roles, the division of labor and conditions, including information transfer, general-processing tasks, flexible configuration of the task element.

Reusable framework consists of definitions, interpretations and running, consisting of the following main components: page template, configuration items, task processing UCC (ITaskUCC); page element generate service (IPageElementGenerateService); specific task background processing (IFrameworkEmbededService / IFrameworkEmbededFactory).

Reusable framework consists of definitions, interpretations and running, consisting of the following main components: page template, configuration items, task processing UCC (ITaskUCC); page element generate service (IPageElementGenerateService); specific task background processing (IFrameworkEmbededService / IFrameworkEmbededFactory).

Figure 1 is a schematic diagram of the framework of the overall operation of the mechanism. Tasking reusable framework uses a JSF framework. Reusable framework through JSF framework when processing HTTP requests through reusable framework to generate service interface elements, reusable framework defines the interface configurations and interface templates to interpret and generate tasking interface that provides human-computer functional interaction. Behavior in the form of human-computer interaction interface events, by control of UCC processing framework through the JSF framework, the UCC processing logic and relationship process logic of tasks and processing.

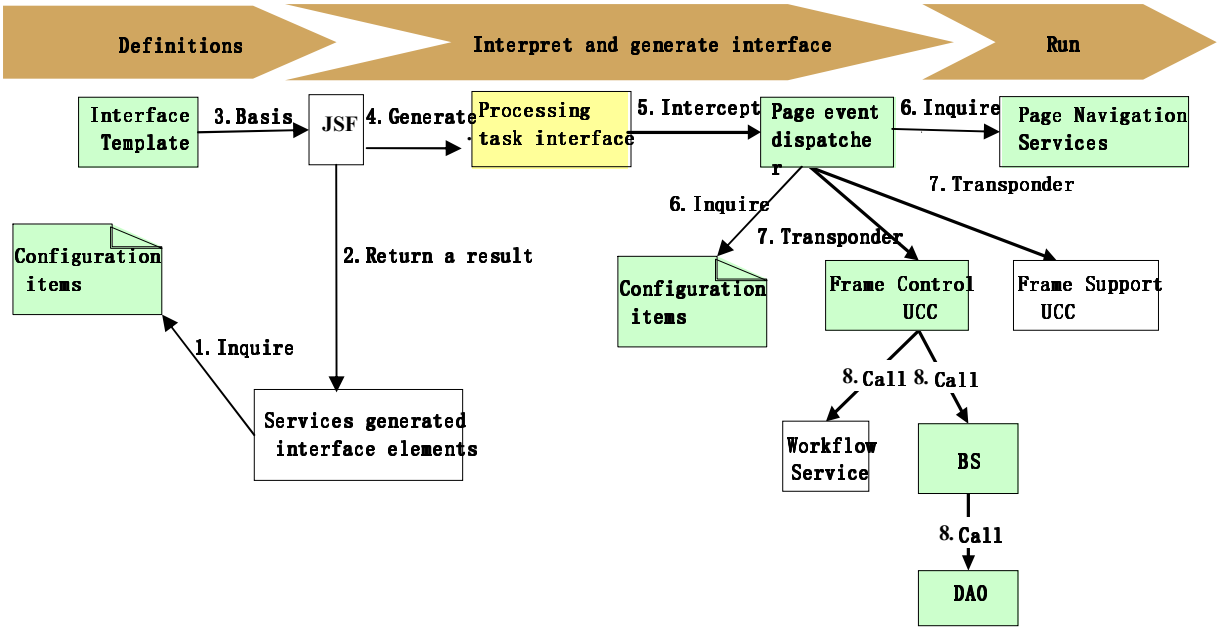

Fig.1 Framework operating mechanism

Page templates

Tasking need to define a page template for the realization of each frame, according to the page template definite the layout of the tasking page, the content of the page is divided into static definition section and dynamic generation section.

The static definition section refers to fixed and unchanging page elements that applied the scene of processing tasks in the framework

Dynamic part refers to that framework related services dynamically generated page elements. based on the contents of configuration items , status of the task and other elements.

Configuration item

Configuration item refers to the different parts due to the different attributes of tasks. The main role of the configuration item is achieved dynamically configurable portion by way of the parameters configuration in the page template and configurable information view. Reusable frame achieved configuration information based on the process tasking, the dynamic change portion is two-dimensional . Reusable frame show information's differences generated by attribute of each task. Reusable framework configured differences information content (elements of information) by way of configuration items. Reusable framework directly calls configuration items of information from the database.

Configuration items reusable framework can be divided into: critical data, supporting data, routing type, opinions conclusion specific task configuration items, business processing and document manipulation.

Critical data go to the process when the process starts, and may be modified in the process flow, so this type of data obtained during the execution of the process.

The items belong to a part of the property of the task that supporting data, the type of routing data, opinions conclusions identified in the course of the workflow definition. Data is obtained by querying the workflow definition in the course of process execution.

Read configuration items are responsible for the IConfig and as the base class for all configuration items tasking.

Tasks processing UCC（Use Case Controller）

Workflow system mainly consists of routing selection, personnel selection, job submission and other operations. Reusable framework abstracted a general-purpose processing from workflow tasks processing to form a tasks processing base class, All tasks processing inherited the base class can achieve task operation by way of the common application processing provided by the base class provides operations to greatly reducing duplication of development effort, and ensuring consistency of tasks processing.

ITaskUCC is the base class of all tasks processing UCC, It defines a set of common methods and properties of the task processing design. Each framework needs to define a tasking UCC and inherit the base class. UCC-tasking operation with processing tasks, such as pre-submit, submit, and other operations, in coordination with operation between IGeneralWorkFlowService and other background services.

ITaskUCCExtension is extension class of ITaskUCC, inherits ITaskUCC, is the base class for handling specific tasks.

Pretreatment specific task: needs to calibrate data or update flags before each task processing for a variety of business.

Page elements generation service

Configuration of the configuration items is reflected in the tasking interface, reusable framework provides page elements generated service class service as the base class for interface elements resolve to achieve configure page conversion.

Achieve Reusable Framework Technology in the Workflow System

Call workflow system applications

Workflow system applications are divided into "business units" and "Operation". Business units reflects what to do on an active node, the operation reflects the control authority in processing on this activity node, such as "approved", "rejected", "fight back" and so on. Business units and operations are certain types of applications, but to distinguish these two concepts that can help develop a application System which has smaller coupling and dependence on the process running . so that the development of the process is variable and easy to change. Formally, the business units can be called by the workflow engine, and the operating is called by system is he controlled method of the workflow engine by control to application system.

Task operations

The task operations in workflow system is operations of processing parts ,such as start the process, terminate the process, hangs the process, direct current, shunt (single handle) and combined flow (more than one person handling), joint trial, etc., in order to interference task processes freely, to achieve specific tasks independently.

Depending on difference of the task status, the persons who have different privileges of the tasks can perform the corresponding operation on the task, the state of the tasks changed accordingly after the operation. The relationship among of people, tasks and operations is not arbitrary. The relationship which are shown in Table 1 .

Table.1 Personnel Tasks Relational Table

Start	Operate	End	Permissions needed
Assigned	View	Assigned	Assigned Members List
Assigned	Claim	Claimed	Assigned Members List
Claimed	Complete	Completed	Claimant
Claimed and Assigned	Transmit	Assigned	Claimant
Claimed and Assigned	Cancel	Canceled	Administrator
Claimed and Assigned	Reassign	Assigned	Administrator
Claimed	Replace	Assigned	Claimant
Claimed and Assigned	Forced complete	Completed	Administrator

Processing tasks

The workflow system used of reusable framework technology is a real system of "man – machine", the user is the basic role of the system and the direct object of the task assignment. The operational staff can see the "task list" for themselves which the computer listed in and track the status of each task or continue a task . In order to the task processing of the reusable framework flow is able to implement in the organization "seamlessly", the project team must comply with the working methods which had already defined, practice identified and effectively, and must have measurable results at every stage. Task processing method as follows:

1) Create and assign tasks

When the users create a task, he must designate the owner to be the executor of the previous task executor unify. All task allocation algorithm is set to assign ToUsersAndGroups, all tasks must be claim and then perform. For general tasks, perform this task in my job list, the system automatically claim the task for the user when perform this task in my job list, complete the task only when the user submits tasks.

2) Task execution mode

Task execution mode decides the manner of the task which is performed during tasking operation. The three modes as follow:

First time: The first time you run the task in the process, you need to create and assign tasks;

Repeat: The task has been recreate and redistribute which had executed and completed previously, and the tasks are usually assigned again to the staff who had executed and completed the tasks;

Short: the tasks are no longer performed, and will be go to the next task directly.

3) Routing operation

Routing operation decide process execution path. The routing operations include: normal forward, return revision, return modify policy, wrong return, retrieve, supplementary materials, and so on.

Conclusion

Reusable framework technology of workflow system analyzes and abstracts the structure and composition of the actual business process, and divides the task processing into immutable part and a variable part. The technology achieves universal part of the task processing by building a generic model of reusable framework t. The reusable framework technology of tasking, reduced the complexity of application processing more quickly adapt to changing business requirements due to changes brought by the application processing of tasks.

References

[1] Wang Gang,Wenjuan He: Research of Computers Application Vol. 2 (2004), p. 19

[2] Longxiang Bao, Kangzhen Cao : Research of Computers Application Vol.3 (2003), p. 25

[3] Xiufang LI, Fuzeng Zhang: Science Technology and Engineering Vol.1 (2006), p. 87

Advanced Materials Research Vols. 989-994 (2014) pp 5619-5623
© (2014) Trans Tech Publications, Switzerland
doi:10.4028/www.scientific.net/AMR.989-994.5619

Research on the SWIM System and its Development

ZHANG Xian Hao[1, a], HUANG Jin[2,b] and XU Jia[3,c]

[1]Scientific Research Office, Civil Aviation Flight University of China

[2]School of Air Traffic Management, Civil Aviation Flight University of China

[a]cafczxh@126.com, [b]zyfcd@sina.com, [c]xujia1110@yeah.net

Keywords: SWIM; NextGen; SESAR; development

Abstract. This essay explains the concept of System-wide Information Management and discusses the merits of implementing SWIM in ATM systems. And the essay also introduces the current situation of the SWIM development worldwide, especially in USA and Europe. Additionally, it illustrates SWIM related programs which is carrying on in China, and the promising future for SWIM development in China.

1 SWIM Introduction

SWIM is an abbreviation form of System-Wide Information Management. SWIM provides flight information to airlines, aircrafts, airports, air traffic control centers and other apartments associated with flight. It acts as a "system of systems" [1] to serve for information sharing, exchanging and management among all parts of the civil aviation.

Currently, the aeronautical information exchange pattern is end-to-end; different systems transmit data through different data interfaces. This makes the data transmission links huge and complicated. The new concept of SWIM abandons the traditional end-to-end pattern, collects all kinds of aeronautical information to a single terminal and all information users acquire data through the terminal. SWIM simplifies the traditional information transfer method greatly as fig. 1 illustrates.

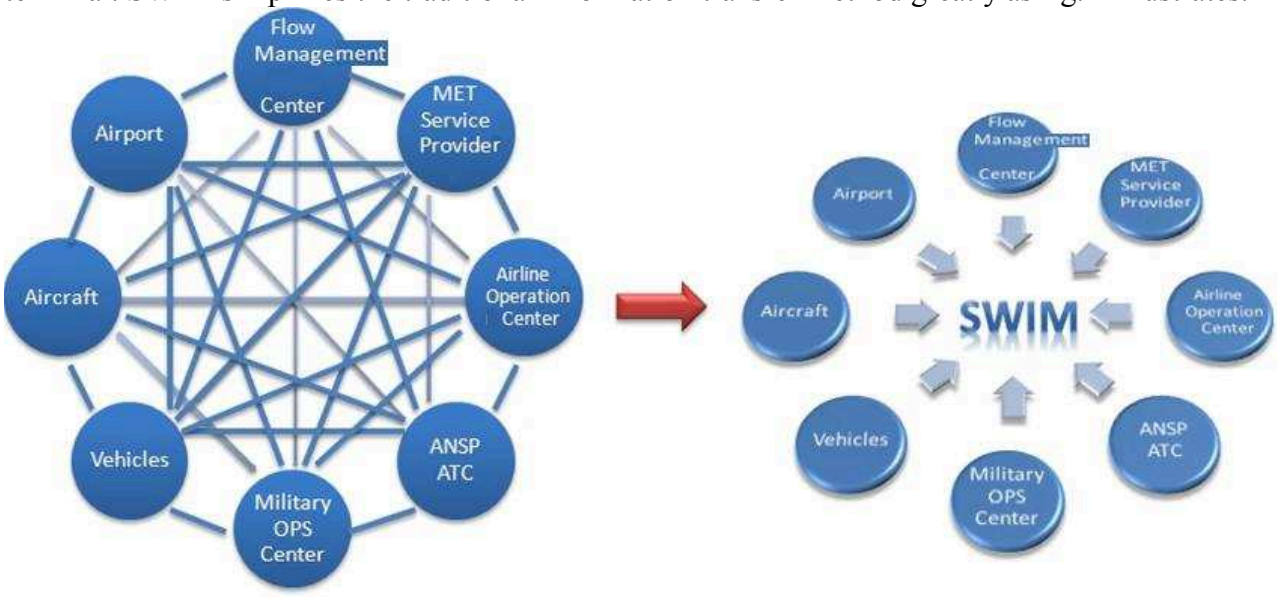

Fig. 1 The transition in exchanging aeronautical information

Implementing SWIM will bring various benefits. Initially, aeronautical information users like pilots, air traffic controllers and dispatchers can receive the same information to make appropriate decisions in order to improve the safety of civil aviation. Secondly, information sharing will enable the airspace users get information that may affect flight in time. In this case, it will enable better efficiency of airspace use. Moreover, SWIM will also improve the decision-making process and streamline information sharing for improved planning and execution. Ultimately, the information in SWIM concentrate in a common interactive terminal; it will save a large amount of constructing cost

of new interfaces and also save the maintaining fees of current interfaces connecting different systems.

2 SWIM Development Abroad

The concept of SWIM initially appeared in 1997, it was the concept of National Airspace System Wide Information Service (NWIS) which Federal Aviation Administration (FAA) presented. In 2001，Boeing Company put forward the concept of Common Information Network. Aeronautical Radio Technology Committee integrated NWIS into NAS concept in 2002. In the same year, FAA signed a contract with International Telephone and Telegraph Corporation (ITT) that ITT would design the functions and physical architecture for NAS. In 2003, ITT and FAA cooperated with each other and finished the basic function analysis and NAS-level requirement development. The work of study on the physical structure, transition selection and suggestion, structure simulation and acknowledgement were completed in 2004. Boeing Company and FAA worked together in 2004 and they defined the duty of SWIM under the framework of current and imagined NAS air traffic operation and communication system. In 2005, International Civil Aviation Organization (ICAO) also accepted SWIM concept in order to facilitate the information-based integration process of air traffic management. By far, Single European Sky ATM Research (SESAR) in Europe, Next Generation Air Transportation System (NextGen) in USA and Collaborative Actions for Renovation of Air Traffic Systems (CARATS) in Japan are all study on technologies related to SWIM.

2.1 SWIM in USA

NextGen is a concept which represents the American National Airspace System transferring from ground-based air traffic control to satellite-based air traffic management. It intends to develop programs and technologies which can operate more efficiently, SWIM included. SWIM provides authorized users with information to facilitate collaboration among different apartment in the NAS.

FAA develops SWIM in three segments. The first two segments are under development. On July 15, 2009 FAA Joint Resources Committee approved the development of SWIM segment 1. Segment 1 will last for 5 years and complete in 2015. The assignments are listed as follow [2]:

1. Implementation of a set of federated services in the NAS with SWIM-provided governance, standards, and software to support development of reusable SOA services;
2. SWIM provides requirements, schedule, and funding to seven SWIM Implementing Programs (SIPs);
3. Segment 1 results in services deployed to all Air Route Traffic Control Centers (ARTCCs), 39 Terminal Radar Approach Controls (TRACONs), the Air Traffic System Command Center, the William J. Hughes Technical Center (WJHTC), and NAS Enterprise Management Centers (NEMCs).

After the first segment accomplished, SWIM will equip with 9 capabilities which cover 3 areas including Aeronautical Information Management (AIM), weather, flight and flow management, as fig. 2 illustrates. The 9 capabilities are Special Use Airspace (SUA) Automated Data Exchange, Corridor Integrated Weather System (CIWS) Publication, Integrated Terminal Weather System (ITWS) Publication, Pilot Report (PIREP) Data Publication, Flight Data Publication Service (FDPS), SWIM Terminal Data Distribution System (STDDS), Flow Information Publication, Runway Visual Range (RVR) Publication, and Reroute Data Exchange. Up to March 2012, two capabilities, ITWS Data Publication and CIWS Data Publication, are complete and operational. Three capabilities are complete and waiting for installation, which are AIM SUA Automated Data Exchange, PIREP Data Publication, and Pre-Departure Reroute. And three other capabilities, STDDS, Flow Data Publication, RVR Data Publication, are on schedule and within budget allocation. FDPS has been replanned but is expected to be on schedule and within budget allocation.

In November 2010, FAA JRC approved to carry on the study on SWIM segment 2. This segment will last to the year of 2016 and the assignments are as follow [2]:

1. Continues provision of governance, standards, and software to additional NAS programs;

2. Implements enterprise messaging service (NEMS) for other NAS programs and facilitates transition by Segment 1 SIPs.

The core services in Segment 2 are messaging, interface management, security, and enterprise service management [3]. NEMS provides messaging service for SWIM Segment 2, and it is through Enterprise Service Bus that enable heterogeneous systems integrate together. There are 6 NEMS nodes which were already built till July, 2013. Interface management service includes interface specification, discovery, and schema management. Security service covers authentication, authorization, and audit services. And enterprise service management is service monitoring, service configuration, and system monitoring.

In 2012, SWIM enriched its concept level to four levels. The levels are FTI IP backbone, SWIM Messaging infrastructure, Standards for Data Exchange, and NextGen Application. The standards for data exchange are divided into three parts which are Aeronautical Information Exchange Model (AIXM), Weather Information exchange Model (WXXM) and Flight Information Exchange Model (FIXM). As three subprojects of SWIM, AIXM, WXXM and FIXM are all under development. The other key technologies of SWIM are aircraft access to SWIM (AAtS), cloud computing and so on.

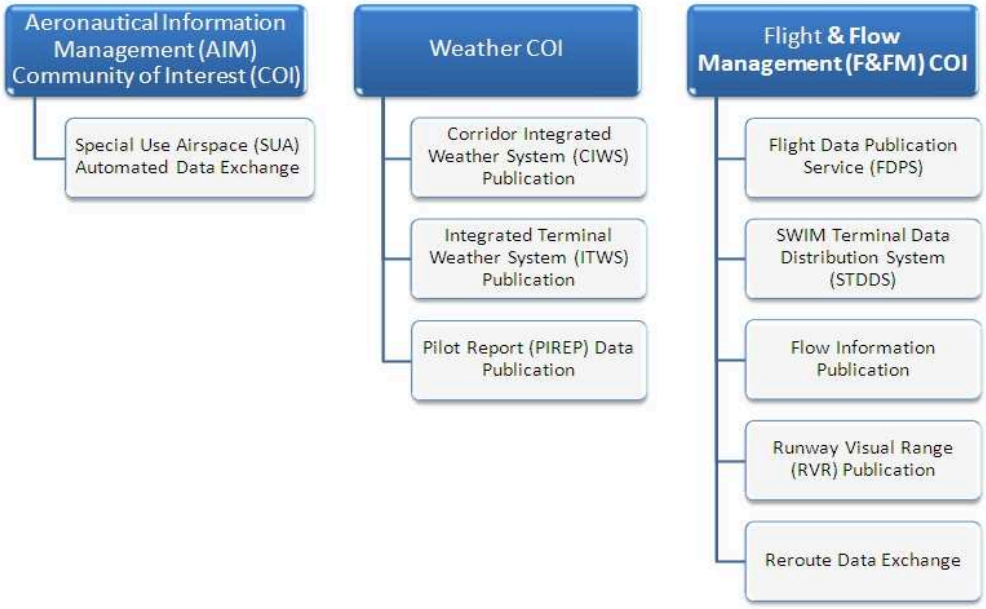

Fig. 2 The nine capabilities in implementing SWIM Segment 1

2.2 SWIM in Europe

From SWIM concept first appeared in Europe in1998, the following years SWIM was always mentioned in documents related to ATM. Considering lacking of systematic study on SWIM concept, there was no program aiming at SWIM. Not until March 2009, the overall ATM planning regard SWIM as a significant constraint in implementing SESAR that SWIM officially became a subproject of SESAR Joint Program which is commonly studied by departments related to ATM since then.

SESAR determined the operational concept of SWIM, which explains the definition, principles, the groundwork of transition, and the advantages in detail. Based on the principle of SWIM, SESAR will establish ATM Information Reference Model (AIRM) and Information Service Reference Model (ISRM), develop information management functions, put up SWIM infrastructure, and explore SWIM-based applications in the process of developing SWIM. AIRM offers consistent reference to other models so that the original meaning wouldn't change during information exchanging process and ensure the compatibility of semantic in ATM systems. Service-Oriented Architecture (SOA) is adopted when constructing the infrastructure of SWIM. In this way, newly built systems are connected with the old one. SESAR began to put the first step, prototype verification, into practice in 2012; the content of it are Flight Object (FO) allocation, publication and subscription of web services, and expanded NOP Business to Business web services [4].

SESAR work groups have two work packages concerning SWIM; one is information management (WP-IM) and another is SWIM infrastructure (WP-SI). WP-IM constructed the framework from information producers to information consumers, which is a management structure that includes all kinds of information management capabilities. WP-SI is in charge of the technical infrastructure of SWIM, which is used for dealing with data and services; it includes the common SWIM technical services which exchange information physically and adopts mainstream IT technologies.

2.3 Collaboration between USA and Europe

The Memorandum of Cooperation (MOC) between FAA and the European Organization for the Safety of Air Navigation (EUROCONTROL) for joint Research and Development (R&D) is in place for 26 years and work with each other will continue, especially between NextGen and SESAR R&D. In December 2009, FAA and SESAR JU had a discussion on the commonality, interoperability of SWIM. In November 2010, FAA and SESAR had another meeting discussing the roadmap and differences between each other in developing SWIM and figuring out the most suitable area for them to have a set of experiments. In April 2012, FAA and EUROCONTROL agreed a coordinated planning on SWIM interoperability. Currently, FAA-SESAR has 5 work groups. Work group 2 is focused on information management which includes SWIM interoperability, information management operability, and meteorological information exchange.

3 SWIM DEVELOPMENT IN CHINA

Given the fact that the air traffic grows rapidly in China and Asia/Pacific region [5], the emerging air traffic brings challenges to the current ATM systems. In China, we have launched several researches to cope with this situation, and hope to facilitate the informatization of our civil aviation.

In 2010, study on the SOA-based efficient mechanism of sharing ATM information, Guide of Science and Technology Project of Civil Aviation Administration of China (CAAC) [6], put forward the efficient information sharing and exchanging mechanism of SOA-based interoperable ATM data; it will allow all ATM systems connectively to each other and provide a synthesized information service. This program laid the foundation of SWIM construction in China. The contents of the program are SOA-based ATM information architecture, standardized interface management, messaging and security service, information sharing mechanism and prototype verification system.

In 2011, National Key Technology Support Program funded the project of Civil Aviation System-wide Information management technology and platform proposed by Beijing ATC Technology Corporation. The program designed the infrastructure of SWIM and analyzed the information sharing and exchanging technique. Moreover, this team cooperated with North China Air Administrative Bureau and built an experiment and assessment SWIM platform. In January 2013, during 2 years' study, requirement analysis, and development, Beijing ATC Technology Corporation successfully finished the initial construction of SWIM in North China Air Administrative Bureau Communication Network Center. The initial construction focused on installing the system server, network firewall, device end, connecting the network, and equipping the system with needed facilities. North China air traffic flow management system is the first system which accessed to SWIM system. In the future development, North China Air Administrative Bureau will construct connective platform with airlines' operation control center and airports to complete the SWIM system for information sharing and exchanging. In September 2013, North China Air Administrative Bureau held the new SWIM technique training class, it symbolized the SWIM system putting into use and test in China.

Regarding the twelfth national five-year planning as an opportunity, CAAC Air Administration Bureau applied for civil aviation integrated information service demonstration project. This project aims at popularizing the use of SWIM in the domain of civil aviation, so that the ATM, airlines' operation control center, airports and even military could share information with each other in order to realize collaborative decision-making and improve the air transportation capability and efficiency.

Because China hasn't study SWIM for that long, it develops SWIM with the help of international partners. During the year of 2010 and 2012, Chinese aviation specialists had five fruitful meetings

with FAA SWIM technician experts. Chinese professors learned a lot advanced experience in developing SWIM. And in June 2012, SESAR/SWIM international seminar was held in Civil Aviation University of China, it's a meaningful step for us to cooperate with SESAR. In December 2013, China Academy of Civil Aviation Science and Technology held EUCCAP-SESAR seminar. The Joint actuator governor of SESAR explained the up-to-date development of SWIM in SESAR.

Considering that SWIM concept is emerging in China and it is promoted all over the world, it is necessary for China to go further exploring this technique to make it operate in our ATM systems. And in order to act on international convention, there is a great possibility that China will also choose SOA to construct the whole SWIM system and use XML to transfer data across different interfaces. By far, SWIM has not been studied widespread, so SWIM (mainly its core models) will most probably act as a demonstration project in some local areas. Once the project makes any progress, it is promising for SWIM to develop in large-scale. The aim of developing SWIM is the same between China and abroad, but the situation of Chinese civil aviation facing is not alike. Firstly, the airspace is administrated by Air Force of PRC in China, and flight control is also supervised by Air Force of PRC; and the ATM in America is governed by government, it is an independent system. China has two systems of ATC, it is extremely important for us to coordinate the two systems at the same time in case to be safe. Additionally, the management structure of Chinese civil aviation is divided into three levels, the information system developed differently (web circumstances, hardware, and data standards are deviated), when developing SWIM the differences should be taken into consideration. Last but not the least, American and Europe all adopted web services to develop SWIM, but there still lies some room for improvement in operation efficiency. In terms of this, our SWIM developing teams should bring forth new ideas based on current mature technologies.

4 Conclusion

SWIM will provide ATM information sharing with flexible, safe and open information management architecture; it can address the isolation, repeated, inconsistent upgraded problems of current systems. Although China set up late in developing SWIM, the progress is fruitful in SWIM constructing. What's more, staying in contact with international advanced technologies will enable long-term growth of our civil aviation. In the future, China will still collaborates with USA and Europe in constructing SWIM, uses the mature experience to accelerate the informatization progress of Chinese civil aviation.

References

[1] Jere S. Meserole, John W. Moore, "What is System Wide Information Management (SWIM)," IEEE A&E SYSTEMS MAGAZINE, MAY 2007.

[2] Hoang Tran, System Wide Information Management (SWIM) Program Overview, http://www.icao.int/APAC/Meetings/2012_ATNICG_7/SP03_FAA - SWIM Program.ppt

[3] LUO Yi, XIN Quan, WANG Pei, CHEN Xuezhen, "System Wide Information Management Architecture Designing," Advanced Material Research Vols. 765-767 (2013) pp 1585-1588.

[4] SWIM Activities in Europe, http://www.icao.int/safety/acp/ACPWGF/ACP-WG-I-15/ACF5BB.pdf

[5] China SWIM INITIATIVES, http://www.icao.int/APAC/Meetings/2013_ATNICG_WG_8/IP11 - CHN AI.6 - China SWIM activities.pdf

[6] Information on http://blog.sina.com.cn/s/blog_a13ae32401013e89.html

Advanced Materials Research Vols. 989-994 (2014) pp 5624-5629
© (2014) Trans Tech Publications, Switzerland
doi:10.4028/www.scientific.net/AMR.989-994.5624

The Study of Bus Transit Network Design Methods for Different Sized Cities

Wenyuan Tu[1, a], Jihui Ma[1, b], Wei Guan[1, c], Xinjie Chen[1, d]

[1] School of Traffic and Transportation, Beijing Jiaotong University, Beijing 100044, China

[a]13120897@bjtu.edu.cn, [b]jhma@bjtu.edu.cn, [c]weig@bjtu.edu.cn, [d]13120779@bjtu.edu.cn

Keywords: Big Cities; Small-medium Cities; Bus Transit Network Design

Abstract. With the rapid development of the national economy, the construction of China's urban transportation is in the stage of rapid development. Both big cities and small-medium cities increasingly appear all kinds of issues such as traffic congestion. Priority to the development of public transport is the most effective way to solve the problem of urban traffic congestion, and urban bus transit network design is the first step in the planning of the public transport system, plays a vital role in the transportation system planning. Bus transit network generally consisted of rail transit, bus rapid transit and conventional bus in big cities, while it composed of conventional bus in small-medium cities. Therefore, this paper made research on the applicability of bus transit network design methods for different sized cities, analyzed the advantages and disadvantages of different methods, and explored a more excellent method for bus transit network design.

Introduction

With the development of economy, many cities in our country appeared the problem such as traffic congestion, traffic fairness and so on. The development of public transport is the most effective way to manage urban traffic congestion, through reasonable bus transit network design can take advantage of public transportation, improve bus service levels, facilitate urban trips, but also maximum ease road traffic pressure.

The early sixties of the last century, the main bus transit network design using qualitative methods, in general, it uses the formation that the authority of experts suggested forming line network layout, but the line program is rarely used quantitative analysis, it is likely to deviate from the actual situation. The late sixties to the early eighties of last century, bus transit network design based on the principle of combining related operations research and systems engineering, using the optimization of objective function lay line network. For example, in 1967, Lampkin [1] established a line network design model, which the comfort of passengers together with travel time as bus transit network service indicators. In 1968, Hirsch [2] tried to use fixed expenses to optimize bus network, the bus network optimization model has been designed as a fixed demand model. Since the late 1980 s, with the development of computer technology, heuristic algorithm was introduced to solve the bus transit optimization problem, such as artificial neural network and genetic algorithm. In 1998, Pattnaik [3] has proposed the use of genetic algorithm to design a bus transit network, the goal of the model is all bus passenger travel cost and operation cost minimum, generating circuit for selection first, and then optimized by genetic algorithm.

Starting from the bus transit network design development up to now, for the different size of the city's bus transit network approach has not been clear distinction. Public transport planning researchers have proposed all sorts of different method for the big cities characteristics, the bus transit network design in the big city is actual and applied. But the small-medium city's bus transit network is often in accordance with the big city's existing designed experience to implement, ignoring the small-medium city's road network is not mature, the proportion of bus travel is relatively low. It results problems that the bus transit attraction is inadequate and the utilization of bus transit network is not high, hindered the healthy development of the public transportation. As a result, depending on the city scale to divide the applicability of the different transit network design method, it plays a positive role in the development of urban public traffic. According to the different

traffic characteristics of the big cities and small-medium cities, the research that is suitable for different size of the city's bus transit network design method is very necessary.

The Division of Urban Size

At present, the theory of public transportation system planning has been preliminarily established, and gradually mature, so the distinctiveness of different scale of the city's public transportation system planning is very necessary. In this paper, in terms of the scale of urban development, road system, the size of the city has been divided.

"Green book of the small and medium-sized cities" promulgated in 2010 according to the present situation of China's urban population scale, put forward the new standard of city scale: The urban resident population below 1 million for the small-medium cities, more than 1 million for the big cities. The small-medium cities public transportation is composed of regular bus, public traffic in big cities usually consist of rail transit, bus rapid transit and conventional public. Small-medium city road network layout is a single chessboard, banded or radial, the general layout of road network in big cities by a mixture of a variety of forms, such as chessboard - ring - radiation hybrid and multicenter group, etc.

Either population size or road scale, the small-medium cities have different degrees of differences from the big cities. According to the above division of urban size, we can see that small-medium cities and big cities road traffic system differences mainly reflect in the following respects: Big cities road network system is relatively complete, forming a mature network system with expressway, arterial road, sub arterial road and branch, while small-medium cities arterial road network system is not formed or immature. Big cities road functional orientation is relatively clear, for example, the expressway plays a role of traffic rapid distribution, arterial road connects all major cities partitions, sub arterial road has both transport function and service function, the main function of the branch is service, while small cities road functional orientation is not clear.

Bus Transit Network Design Method for Small-medium Cities

Small-medium cities don’t pay attention to the problem of traffic planning in the early stages of urban development, compared with big cities, small-medium cities are relatively narrow, the arterial road network is not mature, traffic management condition is poor. Because residents travel distance is shorter, and bus transit design is not reasonable, leading the bus attraction is not enough, so it should start from the traffic characteristics and traffic demand of small-medium cities, using suitable for small-medium cities of bus transit network design method. The following summarizes several suitable for small-medium cities of bus transit network design method.

Manual Approach. Manual approach is a subjective experienced planning method at the early development stage of bus transit network design. Planners according to the line network planning and design principles or relevant specification of the bus transit planning manual listed, by virtue of their professional knowledge and technical experience to prepare bus transit network solutions. This method is suitable for small scale, simple road network in early urban development period, possesses the advantages of simple, convenient, low cost, but this kind of planning method is lack of scientific basis, the generated line network efficiency is not high.

System Analysis. System analysis is a bus transit network design method based on the evaluation. This method is based on the using of systems engineering and operations research relevant principles and methods, first preliminary design based on the experience of public transportation network planners, and then according to the passenger flow distribution theory and method to calculate the effect of each program line, and establish the evaluation model for comprehensive evaluation of bus transit network, if not satisfied with the evaluation results, we should adjust the bus transit network. This method is suitable for the complicated network, more lines of small-medium cities of recent or long-term strategic planning, with the advantages of systematic, simple, low cost, can be used for multi-objective optimization, suitable for comprehensive analysis, can objectively reaction of bus passenger flow demand. But it needs a large number of data, and manual participation more, less testing program.

Detailed Wiring Method [4]. Detailed wiring method namely "detailed layout, optimized network" method, it means of all the alternative routes, select direct passenger volume as the main target, find out the optimal bus lines, and according to the shortest route layout.

By the direct passengers to maximization as the objective function:

$$MaxS = \sum_{i=1}^{n} \sum_{j=1}^{n} z_{ij} x_{ij} \quad . \tag{1}$$

Among them: z_{ij} -- the line ij direct passenger volume;

x_{ij} -- 0-1variables, if the starting point i and end point j pairs, then $x_{ij} = 1$, otherwise $x_{ij} = 0$.

The method is based on the data support, in full consideration of the district bus OD traffic volume, correct the length of the line and non-linear coefficient, not only the model is put forward, but also easier to get the optimized bus routes. The idea is simple, intuitive, and practical, it is commonly used as a small-medium cities bus transit network design method. But it lacks reasonable feedback after this network, requires adjustment process repeated, and rework is too heavy.

Improved Detailed Wiring Method [5]. Since detailed wiring method only to direct passengers volume maximization as the goal, may ignore the influence of several other constraints, so with the idea that the main objective optimization first, and then the secondary objective optimization to make the improvement of detailed wiring method, to make up for the problem of insufficient for other constraint optimization. It proposed the line optimal coefficient Q, which is the minimum value of the sum of the coefficient on each section of alternate routes, find the minimum value of the sum of the coefficient on each road can determine the line with the optimal coefficient Q, then we can find the corresponding the biggest direct passenger volume's optimal routes.

The optimal coefficient Q calculation formula is as follows:

$$\begin{aligned} Q &= \min \sum_{O}^{D} Q_i \\ Q_i &= A_i + B_{ij} \\ A_i &= (L_i / L_0) \bullet 100 \\ A_0 &= A_{\max} - A_{\min} \\ B_{ij} &= A_{\min} + \lambda_j A_0 \end{aligned} \quad . \tag{2}$$

Among them: A_i--road length factor of section i;

B_{ij} --road grade value of section i;

λ_j -- weighting factor of road grade;

L_i --the length of section i;

L_0 -- the total length of all sections.

This method on the basis of the detailed wiring method, the original layout on the shortest path upgraded to layout in accordance with the minimum value of the sum of the coefficient on each section, more able to adapt the characteristics of small-medium cities bus transit network design. But the influence factors of sections coefficient use road length factor and road grade value, if they can make good choice to bus transit network design remains to be further research.

Flexible Bus Transit Network Design Method [6]. The flexible bus is a kind of dynamic bus service, bus lines don't have fixed sites and fixed lines, each bus line transports passengers within a particular service area, the vehicle's trajectory is related to the passengers trip distribution, according to the requirements of passengers pick up passengers. The flexible bus operating costs and user costs into the cost per unit time get the objective function is as follows:

$$\min Z = \lambda_Q Q + \lambda_M M + T + \delta e_T \quad . \tag{3}$$

Among them: Q --the total running distance of all vehicles unit hour;

M --all vehicles total operating time;

T --the time passengers in car;

e_T --transfer passengers heart punishment costs;

Flexible bus transit network design method can not only provide high quality service level for passengers, but also save the cost of operators, but the implementation of this method needs corresponding road system, vehicle positioning system, dispatching system and GIS to support and cooperation, and needs practice to verify analysis.

Bus Transit Network Design Method for Big Cities

Big cities have many features include frequent social economic activities, large population, large area, urban function zoning obvious and so on. With the great changes in urban social and economic structure, residents travel numbers grow in multiply, in order to solve the contradiction between bus supply and passengers travel demand, it provides big cities bus transit network design method as follows:

Interactive Auxiliary System Analysis Method Based on Computer. With the development of computer technology, geographic information system and the database management system, bus transit network design can directly do the interactive bus transit network optimization and evaluation with users by the help of computer arithmetic functions. Available computer can quickly process a large number of OD information and network information, and can output a variety of intuitive graphics, planners modification is also more convenient. But the cost is high, and it tends to improve the existing network, and is limited to the computer's capacity and processing power.

Mathematical Optimization Method [7]. Mathematical optimization method simplifies supply and demand relationship between bus transit network structure and passengers demand, establish a mathematical model to determine the optimal bus transit network solution. Issue of bus transit network design is a complicated multi-objective combinatorial optimization problem, its purpose is to make the balance of total travel cost at least, total operating cost minimum and most transport and traffic, making the maximal profit of the system. The objective function is as follows:

$$Max\varphi = \lambda_1(-W) + \lambda_2(-C) + \lambda_3 P \ . \tag{4}$$

Among them: W --travelers travel costs, including bus fares and travel time cost;

C --bus operating costs;

P --bus system fare revenue, equivalent to the transport of bus system;

λ_i --the weight factor of each objective function, and $\lambda_1 + \lambda_2 + \lambda_3 = 1$.

This method is a scientific and systematic method, using heuristic algorithm can get the optimal solution, but costs a lot, all candidates need to analyze, solving is more complex.

Hierarchical Planning Method [8]. Hierarchical planning method divides urban bus transit network into three levels of bus trunk, bus sub trunk, bus branch. First determine bus trunk network with the shortest travel time as the goal, and then determine bus sub trunk network with the goal of maximizing the direct passenger flow density, finally determine bus branch network with the goal of maximizing the line network coverage.

Bus trunk objective function:

$$\min T = \sum_i \sum_j Q_{ij} \bullet T_{ij} \ . \tag{5}$$

Among them: T -- line network total running time;

Q_{ij} -- OD volume from point i to point j;

Bus sub trunk objective function:

$$\max D = \max \sum D_{ij} = \max \sum \frac{\sum_{\forall i, j \in ij} q_{ij}}{l_{ij}} \ . \tag{6}$$

Among them: q_{ij} -- OD volume from the starting point i to the end of j of line ij;

l_{ij} -- the total length of line ij.

Bus branch objective function:

$$\max C = \max \sum C_{ij} \ . \tag{7}$$

Among them: C_{ij} -- the number of bus stops and travel centralized endpoints in line ij .

This method is simple, intuitive and feasible, it is suitable for big cities bus transit network design, but lack of reasonable feedback after forming network, needs to repeat the adjustment process, duplication of effort is more.

Rail Transit Feeder Bus Transit Network Design Method [9]. With the dominance of rail traffic in the big cities are becoming more evident, laid feeder bus lines to achieve efficient convergence with rail transportation has become research focus in big cities. This paper introduces a kind of feeder bus transit network design method with the goal of maximizing the efficiency of feeder lines, and discrete processing, building the objective function as follows:

$$\max E_i^F = \frac{\sum_{j=1}^{J} \left(q_{ij}^{FR} + q_{ji}^{RF} \right) \cdot l_{ij}^R}{\sum_{y=0}^{m} \sum_{x=0}^{n-1} A_{xy}^X w + \sum_{y=0}^{m-1} \sum_{x=0}^{n} A_{xy}^Y w} \ . \tag{8}$$

Among them: l_{ij}^R --the length from the track station i to j ;

q_{ij}^{FR} --passenger traffic volume that pick off the feeder line, from the track station i get on the car to the track station j ;

q_{ji}^{RF} -- passenger traffic volume that from the track station j get on the car to the track station i , and then take the feeder bus to destination;

Bus Rapid Transit Design Method [10]. In a variety of public transport vehicles, due to regular bus passenger traffic capacity is small, speed is slow, rail transport has large capacity, high speed, high service levels, but large investment, long construction period, slow return on investment, so there is bus rapid transit in big cities.

BRT mainly act as a “point to point” of the mass rapid transport tasks, bus lines should be laid in order to reach the largest amount of passengers as the goal. If the planning pivot point has n, the mathematical model is as follows:

$$\begin{aligned} &\max S = \sum_{i=1}^{n} \sum_{j=1}^{n} Z_{ij} \cdot X_{ij} \\ &\sum_{i=1}^{n} X_{ij} = 1 \qquad i = 1, 2, \cdots, n \\ &\sum_{j=1}^{n} X_{ij} = 1 \qquad j = 1, 2, \cdots, n \end{aligned} \ . \tag{9}$$

Among them: Z_{ij} -- when the starting point i and the end of j pairs, the amount of direct passengers the line can transport;

X_{ij} -- 0-1variables, if the starting point i and the end of j pairs1, then X_{ij} =1, otherwise X_{ij} =0.

Conclusion

Public transportation plays an important role in urban traffic network, for the convenience of the residents travel and ease congestion has an irreplaceable role. According to bus transit network design methods for different sized cities summarized above, bus transit network design methods should distinguish between big cities and small-medium cities will more conducive to the development of different sized cities public transportation, and find out a suitable bus transit network design method for different sized city.

Small-medium cities bus transit network design method can use the improved detailed wiring method, with the main objective of maximizing the direct passenger quantity, and then according to

the concrete practice of the city, with one or more other factors as the secondary goal for bus transit network design.

For passenger traffic in big cities should with rail transit as skeleton, bus rapid transit for assistance, regular bus as the main body, with full attention to rail and bus lines hubs planning, and make it progressively into a network to meet the travel needs of big cities. It should use the hierarchical planning method for different levels of bus transit with different objective functions in order to protect the applicability for various levels of bus transit network design method, combined with constraint conditions to heuristic solving, draw bus transit network layout solution.

Acknowledgement

This work was financially supported by National Natural Science Foundation of China (71131001-2), Fundamental Research Funds for the Central Universities (2011JBZ007), and Beijing Science and Technology Project (Z111109073511001).

References

[1] W. Lampkin and P.D. Saalmans: *The Design of Routes, Service Frequencies and Schedules for a Municipal Bus Undertaking: A Case Study*. Transportation Research, 1967, 18(4);

[2] Hirsch and Dantzig: *The Fixed Charge Problem*. Naval Research Logistics, 1968, 15(3);

[3] S.B. Pattnaik and S. Mohan: *Urban Bus Transit Route Network Design Using Genetic Algorithm*. Journal of Transportation, 1998, 24(4);

[4] Wei Wang, Xinmiao Yang and Xuewu Chen: *Urban public transport system planning methods and management techniques* (In Chinese). Science Press, 2002;

[5] Yubo Qiu: *Planning Methods of bus network in small and medium cities* (In Chinese). Beijing: Beijing Jiaotong University, 2012;

[6] Linyin Wang: *Research on Basic Methodology of Bus Transit Network Design* (In Chinese). Beijing: Beijing Jiaotong University, 2012;

[7] Xiang Luo: *Model and Algorithm of Public Transit Network Planning* (In Chinese). Chang Sha: Central South University, 2011;

[8] Yanyan Chen and Mingzheng Sun: *Multi-hierarchy Public Transit Route Network Planning and Evaluation Techniques* (In Chinese). China Communications Press, 2011;

[9] Xingjian Xue: *The Study on the Urban Rail Transit Feeder Bus Routes Optimization* (In Chinese). Changsha: Changsha University of Science and Technology, 2008;

[10] Quanyou Wei: *The Public Rapid Transportation Network Design of Large City* (In Chinese). Nanning: Guangxi University, 2005.

Advanced Materials Research Vols. 989-994 (2014) pp 5630-5633
© (2014) Trans Tech Publications, Switzerland
doi:10.4028/www.scientific.net/AMR.989-994.5630

Research of Agricultural Information Management and Retrieval

Junfeng LIANG[1,a], Chun JIN[1,a], Lei ZHANG[1,a], Xuning LIU[1,a]

[1]Department of Economic Management, Shijiazhuang University, Shijiazhuang, 050035,China

[a]email: sjzhei@163.com

Keywords: Ontology, Agricultural information, Management, Retrieval

Abstract. In order to improve the efficiency of agricultural information retrieval and provide the effect methods for the information retrieval of agricultural, the intelligent searching technology of agricultural information based on ontology is proposed. The paper firstly introduces the concept of ontology, analyzes the characters of agricultural knowledge, and constructs the related agricultural knowledge ontology and knowledge base, implementing the intelligent searching of the agricultural information. The results indicate that the research on agricultural ontology can contribute to organization and searching of agricultural scientific knowledge and provide methods for information organization and searching of agricultural knowledge.

Introduction

To search effective agricultural information from large and fast changing network requires that the user has to navigate the relevant information server without the help of tool, the large number of unnecessary information is surfing on the network, which not only increases the burden on the server, occupies the bandwidth of network and affects the speed of the network, but also increases data flow of network user[1], which enables users to pay unnecessary network cost and valuable time. The research and development of key technology on agricultural knowledge and semantic retrieve will provide knowledge retrieval technology based on agriculture domain ontology, and the single platform is used to access a variety of knowledge resources and to carry out the organization, mining[2], the retrieval and expression of agriculture, agricultural knowledge service which belongs to one or multiple is used to be made, which can greatly improve the accuracy and reliability of agricultural information retrieval.

Related Research

Agricultural Knowledge. Agriculture knowledge includes explicit knowledge and tacit knowledge, the explicit knowledge is easy to be saved and distributed by the information technology, and the tacit knowledge usually are the experience, skills and sixth sense of intuition, and sometimes only means that are not conveyed in words, which are dominant outsider, and which requires people make the formal code, the information technology is used to reach external storage and transmission, sharing and widely application of agricultural, the agricultural knowledge are different from the agricultural information, information and knowledge are interrelated and interdependent, but are very distinct[2].

Semantic Retrieval. The semantic retrieval of agricultural knowledge is not only single point urgent need of agricultural information service, but further is the premise and foundation of distributed knowledge grid environment semantic retrieval. Semantic retrieval of agricultural knowledge can not simply rely on semantic search technology literature resources, rapidly growing network of information resources and vast spatial information resource, meanwhile are also important information resources for semantic retrieval. In order to solve the current problems of information retrieval, the searching technology is more effective tool that is firstly applied to the network information searching. But there are some defects such as poor real-time information, searching technology in the database can not be changed with the network of dynamic documents, which is unable to provide timely updated information for the users, information seekers are poor and can not retrieve the corresponding areas of information according to the requirements of users,

leading to emergence of large number of irrelevant information, and frequently using searching technology every day for millions of users with services, even if such searching technology that uses high-performance server hardware systems is also difficult to provide such a range of rapid response[3].

Agricultural Ontology. Ontology is defined as the system description of objective world, and artificial intelligent regards ontology as basic terms and relation which made vocabulary of related fields, and the definition of extension of the rules that use relationships and these terms is made. As ontology is regarded as conceptual model tools which descript knowledge of information system in the semantic and knowledge level, since the introduction of domestic is made ,then foreign researchers pay great concern on it, and has been widely used in many areas of computer, which has good concept hierarchy structure and support of logical reasoning, and thus the ontology is used in semantic retrieve of information retrieve, it is intelligent search which is based on the conceptual understanding level and thinking searching[4]. The goal of ontology is to capture the relevant knowledge in the field, providing common understanding of knowledge of this area, determining the agreed-upon terms of areas and gives these words and the clear definition of terms of the interrelationship from different levels of formal model, through the relationship of concept the semantics of concept is described.

Application of Agricultural Ontology

Establishment of Agricultural Ontology. The ontology provides a set of terms and concepts to describe some field of agricultural information, the object library uses the ontology to express these terms in the field of facts and knowledge. The establishment of ontology knowledge base is to collect the information source data, with reference to the established ontology metadata model, all kinds of heterogeneous will be unified into a unified document format, and make restructuring and integration, which can solve the problems of heterogeneous nature.

Establishment of Distributed Data Collection Model. The establishment of universal applicability of the large multi-level distributed data acquisition model can help retrieval system to find data, which is one of the key of this study. In view of the proposes of data collection, providing protection for the source of information of the system can be effectively used for further information after the semantic reasoning and retrieval of information request.The issue to be resolved is to establish the page document vector space model and extract related topics from agricultural knowledge based on the relationship between learning algorithm model.

Document Classification. The ontology object library is a dynamic process, in order to keep pace with the ontology library and information resources, the system retrieves the introduction of intelligent agents in adaptive learning, when the retrieval agent in system service is small, the statistical user makes preference ontology library content, access user interest trends, and then take the initiative to build a searching query and submit to the search agent, then the searching agent can access the information resources, get new documents of related fields [5].

Establishment of Retrieval Reasoning Model. Reasoning model is the key of intelligent retrieval of knowledge, during the process of knowledge of agricultural products of intelligent searching, the retrieval system can obtain the access to the request from the user interface, then converters the request into the specified format, match data sets of requirement from the meta-database, further refer to enquiry goals and results is returned to users. The enquiries converter is achieved by calculating the similarity. This paper is to adopt the S-Match algorithm of calculating the similarity which includes the structure of shallow, middle and deep mapping mode. S-Match algorithm requires the input of two concepts c and c ', the concept of mapping patterns, combined mode. The output is the 'semantic similar to the comprehensive level of the concept c and c. Optional models includes the concept of mapping of shallow, middle and deep. Mapping of shallow-level language calculated only similarity, middle-class language, including mapping and structural similarity level, deep mapping addition, examples of calculation of similarity and the similarity of reasoning. Model portfolio, including the right to re-mix and Sigmoid function. If you

choose the former, you need to weight the array, if the latter is chosen, the requirements of the slope parameters[6-7].

Simulation Results and Discussion

Three Levels of System. The front of web browser is responsible for the display of classification tree and classification navigation information, the input, selection of searching criteria and performance of data enquiry results; The application of web server encapsulates all business logic, including the establishment of dynamic connection with database, enquiry and submission of sql, xql, parsing of xml, the traversal of dom tree and the expression which apply xslt and so on. Two database management systems of background database contain software tamino and MySQL. Tamino database stores category navigation information; And MySQL database stores information of forty thousand literature data. In fact forty thousand pieces of data information can be stored in Tamino database, so that navigation information and data information can be stored in database system, and simplify the complexity of development.

Simulation. The comparison of intelligent retrieval methods and the conventional methods are shown in Table 1:

TABLE I. THE COMPARISON

Traditional methods		Improved methods	
Accuracy	Recall	Accuracy	Recall
78	79	88	89
87	86	90	92
88	87	96	90
89	84	92	94
84	89	91	93
82	85	90	91
83	80	93	90
81	83	92	93
80	82	93	94
83	87	94	95
82	88	91	96
78	86	98	98
89	88	98	98

Discussion. It can seen from the simulation that the recall rate is higher than the conventional retrieval under the same conditions, and the precision rate of is more, which is also significantly better than the conventional retrieval precision. In short, the system fully considers the thinking way of people, reflects the level of structure in the organization of agricultural information, so the efficiency of user clicks is improved, and the relationship between the concepts which are described by ontology is applied to the retrieval of information, especially while the user is not certain for queries target, it can better reflect the intelligence analysis of user requirement and retrieval results effect.

Conclusion

This paper describes agricultural information retrieval model based on ontology, and the architecture, function and work flow are made. The research on agricultural ontology construction technology will contribute to the ontology establishment of different domains in agricultural information, and gradually build larger domain agricultural ontology which can develop from the senior or junior ontology to the heavy weight ontology, and lay the foundation for information resources of the network organization and construction of semantic web, making the organization of agricultural information resources, so the research on the ontology has general scientific significance and practical value.

References

[1] Y.Xue,D.Y. Ye,W.D Zhang, The Research on Saurus Construction of Domain Ontology China Classification. Journal of Intelligence, Vol.3(2007), p.16-18.

[2] BrakeD, Lost in cyberspace. New Scientist, Vol.129(2005),p.12-13.

[3] GuarinoN, MasoloC, VetereG, OntoSeek: Content Based Access to the Web. IEEE Intelligent Systems,Vol.14(2003),p.70-80.

[4] TheilmannW,RothermelK, Domain Experts for Information Retrieval in the World Wide Web, In:KluschM, Wei Geds Lecture Notes in Artificial Intelligence, Berlin, Heidelberg, NewYork:SpringerVerlag, Vol.23(2006),p.26-27.

[5] N.F.Xie,W.S.Wang, Construction Method of Agricultural Knowledge Ontology. Agricultural Network Information, Vol.28(2008), p.12-16.

[6] Theilmann W, Rothermel K, Domain Experts for Information Retrieval in the World Wide Web. In: KluschM, WeiBG eds, Lecture Notes in Artificial Intelligence, Berlin, Heidelberg, New York: SpringerVerlag, Vol.1435(1998),p.216-227.

[7] Xing Pingping,Shi Pengfei,Zhao Yi, Ontology-based Data Mining, Computer Engineering, Vol.5(27) (2001),p.25-27.

Advanced Materials Research Vols. 989-994 (2014) pp 5634-5637
© (2014) Trans Tech Publications, Switzerland
doi:10.4028/www.scientific.net/AMR.989-994.5634

Term Structure of Interest Rates with B-spline model during the Money–Shortage-Event in China

Peng Zheng[1], Lianqiang Yang[1],Zhenni Dai[2]

[1]School of Mathematical Sciences, Anhui University, Hefei 230601, China

[2] School of Economics, Anhui University, Hefei 230601, China

Email: ylqylq@aliyum.com

Keywords: bond; term structure of interest rate; yield curve; structural change

Abstract. Using the price data of bonds' transactions during June 2013, the discounting function is fitted by non-uniform cubic B-Splines and yield curves are modeled. Models' single parametric test and total test are both significant. Furthermore, the structural change's test shows that there is no significant structural change between adjacent transaction days, which means that the bonds' market is relatively steady during June 2013.

Introduction

In June 2013, Money-Shortage-Event broke out in China's financial market. From May, the interest rates had been soaring, on 19th June, Shanghai Interbank Offered Rate(Shibor) soared 578.4 basis points, reached 13.4440 points. After inter-bank interest rates hitted record, the interest rates dropped sharply almost 500 basis points on June 21 [1,2].Interest rate's term structure implied by bond market is functional relationship between risk-free rate of interest and duration. Interest rate's term structure plays a key role in economic and financial analysis and it is an important index for the research and the formulation of monetary policy[3].

Before the event, does the bond market predict the market's volatility? During the event, does the bond market fluctuate with the event? After the event, is the bond market affected by markets significantly? In this paper, with the Book-entry treasury bonds transaction price data throughout total, daily yield curves are constructed by non-uniform B-spline fitting. And structural changes of models between the adjacent transaction days are tested.

Model's Theoretical Analysis

Interest rate's term structure is illustrated by zero-coupon yield curve. Many spline models on the interest rate's term structure, such as polynomial spline model, exponential spline model, B-spline model are utilized[3,4,5,6]. In this paper, with the widely used non-uniform cubic B-spline, discounting function is fitted.

Note discount function as

$$\delta(t), \qquad t \in [0,T].$$

Where T is the maximum value of residual maturities for all the bonds. To the l*th* bond, whose cash paid at time t_j $(j=1,...,N_l)$ is $C_l(t_j)$, then the bond price P_l is

$$P_l = \sum_{j=0}^{N_l} C_l(t_j)\delta(t_j) \qquad (1)$$

where $l=1,...,M$. M is the number of bonds. Make the discounting function expressed in a linear combination of B-spline basis functions

$$\delta(t) = \sum_{i=0}^{n-k-1} a_i B_i^k(t_j), \quad t \in [t_k, t_{n-k}]. \qquad (2)$$

Where $B_i^k(t)$ is the i th basis function of k-degree B-spline on a given interval of knot[7], $n+1$ is the number of knots, and a_i is parameters. Let

$$knots = \{t_0, t_1, t_{2,}, ..., t_n\},\ \ n \geq k.\quad t_i \leq t_{i+1},\ \ i = 0, ..., n-1.$$

From（1）and（2), we can obtain

$$P_l = \sum_{i=0}^{n-k+1} a_i (\sum_{j=0}^{N_l} B_i^k(t_j) C_l(t_j)).$$

Denoted by:

$$\mathbf{P} = (P_1, P_2, ..., P_M)^T,\quad \boldsymbol{\alpha} = (a_1, a_2, ..., a_{n\text{-}k+1})^T, \mathbf{X} = (x_{l,i}),$$

$$where\ x_{l,i} = \sum_{j=0}^{N_l} B_i^k(t_j) C_l(t_j),\ l = 1, ..., M.\ i = 0, ..., n-k+1.$$

Thus, the model is

$$\mathbf{P} = \mathbf{X}\boldsymbol{\alpha} + \boldsymbol{\varepsilon}. \qquad (3)$$

Where $\boldsymbol{\varepsilon}$ is the random disturbance assumed to satisfy with hypotheses of classical linear regression model. Thus by OLS regression, we have :

$$\boldsymbol{\alpha} = (\mathbf{X}^T\mathbf{X})^{-1}\mathbf{X}^T\mathbf{P}.$$

Then the zero-coupon yield curve is

$$r(t) = -\frac{\ln \delta(t)}{t}. \qquad (4)$$

Model's Empirical Study

(1) The selection of sample data

Transacttion price data from Shanghai Stock Exchange in June 2013 is used, and the bonds of zero transaction amount and floating rate, as well as issue price is not equal to 100, are eliminated. The sample size of each transaction day is shown in Table 1.

(2) The selection of knots in B spline basis function

The selection of knots number follows the principle of Ruppert et.(2003,Chapter 5) [8]. In order to choose internal knots reasonably, we select the knot interval which satisfies with the requirement that the number of matured bonds in each knot interval is almost the same. Finally, with the additional knots ,the determined knot vector is: $knots = \{-3, -2, 0, 0, 3, 8, 12, 12, 13, 14\}$.

Therefore, $k = 3, n = 10$. The number of spline segments is 6 and the defined interval of fitting discounting function is [0,12].

(3) The fitting results of models

In the 17 fitting models, by the good flexibility of B-spline fitting, the single parameter test in each model is highly significant. Because of the coefficients are too much(17*6=102), we just show degree of freedom and F value in the F test of every model in Table 1 rather than the *t* values and *p* values of each parameter. Fitting yield curves are showed in Figure 1 and we also calculated the values of 17 fitting yield curve in 3, 5 and 10 years, as shown in Table 2.

Table1. The significance test of model in 17 transaction day

Model	1	2	3	4	5	6	7	8	9
Date	6.03	6.04	6.05	6.06	6.07	6.13	6.14	6.17	6.18
Number of Bonds	20	21	19	17	16	20	23	20	20
Degree of Freedom	(5, 14)	(5, 15)	(5, 13)	(5, 11)	(5, 10)	(5, 14)	(5, 17)	(5, 14)	(5, 14)
F value	169.30	81.24	165.42	150.54	60.92	149.41	111.91	71.20	79.49
Model	10	11	12	13	14	15	16	17	
Date	6.19	6.2	6.21	6.24	6.25	6.26	6.27	6.28	
Number of Bonds	21	20	19	19	23	23	19	9	
Degree of Freedom	(5, 15)	(5, 14)	(5, 13)	(5, 13)	(5, 17)	(5, 17)	(5, 13)	(5, 3)	
F value	95.39	125.51	195.84	167.89	177.08	99.83	74.50	152.62	

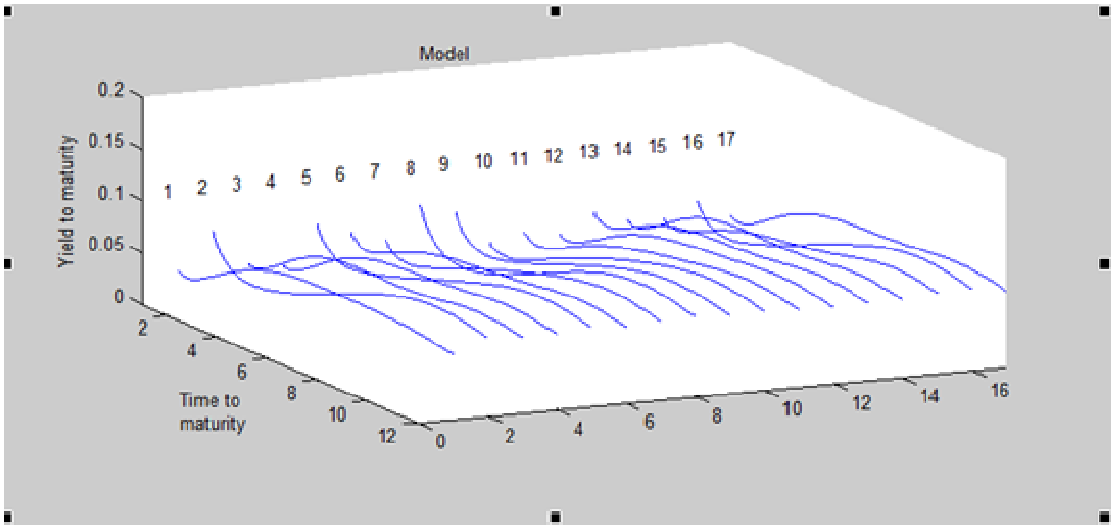

Figure 1. The yield curve of 17 transaction days

Table 2 The fitted yield on 3, 5 and 10 years

Date \ Maturity	3 years	5 years	10 years	Model
6.03	0.0421	0.0460	0.0716	1
6.04	0.0396	0.0451	0.0774	2
6.05	0.0464	0.0432	0.0724	3
6.06	0.0548	0.0644	0.0745	4
6.07	0.0430	0.0488	0.0788	5
6.13	0.0561	0.0612	0.0743	6
6.14	0.0444	0.0537	0.0798	7
6.17	0.0406	0.0454	0.0818	8
6.18	0.0426	0.0499	0.0783	9
6.19	0.0443	0.0534	0.0800	10
6.20	0.0482	0.0572	0.0757	11
6.21	0.0485	0.0638	0.0772	12
6.24	0.0601	0.0674	0.0753	13
6.25	0.0598	0.0663	0.0756	14
6.26	0.0552	0.0598	0.0776	15
6.27	0.0410	0.0492	0.0815	16
6.28	0.0573	0.0647	0.0751	17

(4)Structural change test in models

In order to test whether there is a structural change between adjacent transaction day in the model, structural change for *i*th model and (*i*+1)th *m*odel are tested.

Parameter vectors for *i*th model and (*i*+1)th *m*odel are denoted by $\boldsymbol{\alpha}_i, \boldsymbol{\alpha}_{i+1}$ and the hypothesis of test is

$$H_0 : \boldsymbol{\alpha}_i = \boldsymbol{\alpha}_{i+1} \quad , \quad H_1 : \boldsymbol{\alpha}_i \neq \boldsymbol{\alpha}_{i+1} \ .$$

Test statistics is

$$F = \frac{(RSS_{\mathrm{T}}\text{-}RSS_i\text{-}RSS_{i+1}) / k}{(RSS_i + RSS_{i+1}) / (T-2k)} \sim F(k, T-2k)$$

Where RSS_i, RSS_{i+1} represents residual sum of squares of *i*th model and (i+1)th model, RSS_{T}represents the residual sum of squares of model based on the total data from both models. k, T represent the number of parameters in regression model and the sum of sample size of *i*th model and(*i*+1)th model[13]. Testing results are shown in Table 3.

Table 3 Structural change test of models between adjacent transaction days in June 2013

Tested Model	1/2	2/3	3/4	4/5	5/6	6/7	7/8	8/9	9/10
Degree of Freedom	(6, 29)	(6, 28)	(6, 24)	(6, 21)	(6, 24)	(6, 31)	(6, 31)	(6, 28)	(6, 29)
F value	0.80	0.02	0.39	0.89	0.69	1.02	0.28	0.06	0.08
Tested Model	10/11	11/12	12/13	13/14	14/15	15/16	16/17		
Degree of Freedom	(6, 29)	(6, 27)	(6, 26)	(6, 30)	(6, 24)	(6, 30)	(6, 16)		
F value	1.33	1.60	2.19	1.90	1.64	1.62	1.02		

Economical Analysis of Model

According to the results of 17 models, 17 yield curves are smooth and almost monotonically increasing, that is consistent with the liquidity-preferred-hypothesis. As Table 3, 16 test results are not significant under significance level of 0.01, hence we cannot reject the null hypothesis, which means that there is no sufficient evidence to support that the term structure between adjacent transaction days changed structurally during June 2013. Two factors may contribute to the stability. Firstly, bond market regards that volatility of interest rate is one kind of short-term behavior. Secondly, separation between bond market and inter-bank market in China leads to ineffective transmit mechanism between the two markets.

On the other hand, from the F values in table 3 and the date of models in table 1, we find that before June 19, F value is small, but from June 19 to 20, F value increases up to 1.33, which indicates that bondmarket is affected by the changes of the inter-bank market's interest rates. Especially from June 21 to 24, F value reaches a maximum value 2.19 in this month which indicates that the impact were accumulated during the weekend and released on the next Monday.

Concluded, although China's bond market is affected by the inter-bank market during the Money-Shortage-Event, the yield is changing gradually but not suddenly. Maybe two reasons explain that phenomena, one is the bonds' market is confident in the stability of the risk-free interest rate, the other is the fact that transmitting channel between the inter-bank market and the bond market is not completely open in China.

Acknowledgement

This research is sponsored by the Natural Science Foundation of China (No. 11026076) and Undergraduate's research-training Project of Anhui University. (No. KYXL2012005).

References

[1]Maoqing zhou. Thoughts after the money shortage[J].Contemporary Economic Management, 2013(9):40-43.

[2]Yilin Pan. See Financial Innovation and Regulation from Money shortage event in June.[J]. Financial Economics (Theory), 2013(9):56-58.

[3]Gerong Tang. Static Fitting Empirical research in China's Term Structure of Interest Rate[D]. Xiamen University，2006

[4] McCulloch, J. H.. Measuring the Term Structure of Interest Rates[J]. Journal of Business, 1971(26):19-31.

[5] McCulloch, J.H. The Tax Adjusted Yield Curve[J]. Journal of Finance, 1975(30): 811-830.

[6]Rongxi Zhou, Meng Wu, Di Wang. Interest Term structure Model Based on PLS regression polynomial splines.[J]. Statistics and Decision, 2014(2):71-72.

[7] Piegl L., Tiller W.. The NURBS Book[M], 2nd ed, Berlin: Springer, 1997.

[8] Ruppert D.,Wand M.p.,Carroll R.J.. Semiparametric Regression[M].Cambridge Univeresity Press,2003.

[9] Yunhui Jin, Sainan Jin. Advanced Econometric[M].Beijing：Peking University Press，2007.

Keywords Index

^{40}K 1352
1-3 Piezocomposite 364
2-Acetylpyrazine 134
2-D Reconstruction Algorithm 3755
2-D Separable Sampling 3755
2Cr13 Martensite Stainless Steel 446
2D Numerical Simulation 2328
3-D Estimated Trajectory 2651
3-D Reconstruction 2651, 3844
3.5 G PAMAM 471
3D Data Acquisition 4161
3D Graphic Expression 4945
3D Motion Reconstruction 1997
3D Numerical Simulation 2332
3D Pipeline 4694
3D Pipeline's Application 4694
3D Reconstruction 1766
3D Rendering 3629
3G 4157
3G Base Station 4612
3G Era 4889
3G Technology 4608
4-4ID Model 2655
4-DOF Manipulator 3132
4-Morpholinothieno [3,2-*D*] Pyrimidine 568
4-SHS Parallel Robot 3105
4G 4152, 4157
6LoWPAN 4737

A

α-Stable Distribution 3710
AABB 2389
Abnormal Data Recognition 3814
Abnormal Sound Detection 3033
Abnormal Sound On-Vehicle 3319
Absorption Spectrum 467
Abstract Syntax Tree 1680
AC Motor 867
Accelerated Test 918
Access Authorization 4342
Access Control 4528, 4751, 5000
Access Control Protocol 4245
Accident 3443
Accounting Decision Support System 4819
Accounting Information Disclosure 5201
Accumulation 1313
Acetolactate Synthase (*ilv*BN) 997
Acid Inhibition 536
Acid Mine Drainage 966
Acidity 1428
Acoustic Attenuation Coefficient 638
Acquisition 2418
Action Mechanism 871
Action Recognition 2731
Action Skill 4367
Action Technology Structure 4362
Activated Carbon 803
Active 4466
Active Compensation 1173
Active Inverter 2886
Active Set 2398
Active Shape Model 2016
Activity-Based Costing (ABC) 5136
Actuator 3029
Ad Hoc Network 4482, 4633
Adaptive 288, 1173, 2161, 2965, 4187, 4269, 4556
Adaptive Code Length 1561
Adaptive Equalization 3702
Adaptive Filter 3934
Adaptive Learning Rate 3605
Adaptive Median Filter 3881
Adaptive Neighborhood 2381
Adaptive Parameters Adjustment 1185
Adaptive Radar 4009
Adaptive Sampling 1456
Adaptive Scale 3838
Additive White Gaussian Noise (AWGN) 4095
Adhesive-Bonded 943
Adjacent Construction 954
ADS1282 3274
ADS40/80 3534
Adsorbent 809
Adsorption 3, 312, 373, 441, 572, 827

Adsorption Conditions 841
Advanced High Strength Steel 238
Aerator Pipe 1364
Aero-Optics 863
Aerobic Granular Sludge 603
Aerobics 5078
Aerodynamics 2834
Aerosol Fire Extinguishing Agent 2629
Aerosols Hygroscopic 416
Aerospace Test 3379
Aerostatic Guideway 2807
Aerostatic Response 986
Aerostatic Stability 986
AES 1861, 4245
Affects of Partition 954
Affine Transformation 1602, 2555
AFM 387
Agenda Setting 4577
Agent 2033, 5609
Aggregate Function 2398
Agricultural 5382
Agricultural Information 5630
Agricultural Knowledge 4785
Agricultural Products 5476
Agriculture 5504
Agriculture Output Value 2723
Ahmed Model 3468
AHP 1522, 2314, 2580, 2588, 3212, 5010, 5070, 5250
Aid Decision Making 1704
AIDL 4893
Air Conditioning Fiber 771
Air-Conditioning Load 1150
Air-Conditioning System 2796
Air Pressure Signal 3667
Air Traffic Control 2671
Air Traffic Management 2671
Airborne 3497, 3683
Airborne MIMO Radar 3963
Airborne Three-Line Array CCD Sensor 3534
Aircraft 2829
Aircraft Carrier 5014
Aircraft Drag Parachute 3286
Aircraft Hydraulic Systems 2947
Aircraft Part 3153
Airflow 3667
AJAX 4452
Al-3.2Mg Alloys 325
Al Matrix Composites 515
Al_2O_3-Metal Coating 331
Al_3Ti 320
Al_4C_3 320
Alarm Association Rules Mining 2237
Alarm Management 4175
Alfresco Database 4643
Algebraic Degree 2599
Algebraic Immunity 2593, 2599
Algorithm 1770, 1798, 1924, 2024, 2499, 2621, 3177, 4427, 4873, 4877
Algorithm Complexity 4437
Algorithm Improvement 1985
Alkaline Earth 395
Alkalinity 1428
Allocation Problem 2580
Alloy Element 325
Alloy Properties 403
Alternate Heat 831
Aluminium Phosphide 845
Aluminum Alloy Truss 701
Aluminum Nitride 3509
America 5033
American Supervision Experience 5254
Amidation 233
Amplitude Weighting 3722
Analog Circuit Parameters 3041
Analysis 416, 1913
Analysis of Fluid Flowing Quality 3477
Analysis Platform 3667
Analysis Software 3567
Analytic Hierarchic Process (AHP) 1704
Analytic Hierarchical Model 2336
Analytic Hierarchy Process (AHP) 1464, 2410, 4461, 4897, 5228, 5273, 5300
Analytical Method 2768
Anchor Bit 2749
Android 4893, 5419
Angelica 1011
Annihilators 2593
Annotation 4069
Anode Material 316
Anonymity 4680
Anonymous Communications 4680

ANP 5132
ANSYS 2869
ANSYS Simulation 3189
ANSYS Software 407, 923
ANT Algorithm 1747
Ant Colony Algorithm 1833, 2192, 2196, 4294
Ant Colony Optimization 2675
Ant Colony Optimization Algorithm 2245
Ant-Miner Algorithm 4832
Antenna Array 3977
Anti-Counterfeiting Technology 3571
Anti-Oxidation 793
Anti-Plagiarism Technology 1594
Anti-Plane Crack 715, 1212
Anti-Ship Cruise Missile 1747
Anticancer Activity 568, 1048
Antimicrobial-Film 1052
Antioxidant 519
Anylogic Simulation 2283
AODV 4482
APDCDM 3583
APDL 2869
Application 23, 379, 552, 1097, 2709, 4223, 4229, 4358, 4855, 5614
Application Background 4823
Application Development Platform 4332
Application Front 4823
Application Method 5120
Application Mode 4966
Application Research 5102
Application Warehouse System 4823
Approximate GCD 4326
Approximate-GCD Problem 4780
Apriori Arithmetic 1586
APT 4970
Aqueous LiBr Absorption 831
Aqueous Lithium Batteries 316
AR Model 4019
Arbitrary Array 3693
Arch Steel Tower 3165
Architectural Design 5390
Architecture 1131, 1934, 5516
Archives Management 4219
Area Router 4953
Argon Ion Implantation 467
Argumentation 4617
ARIMA 5182
ARM Processor 4759
Arnold Cat Map 4183
Arresting 2829
Art E-Commerce 4533
Artemisia ordosica Community 975
Artificial Fish Swarm Algorithm 2467, 2555
Artificial Fish Swarm Searching Strategy (AFSSS) 1602
Artificial Gastric Juice 1020
Artificial Intestinal Juice 1020
Artificial Neural Network (ANN) 3505
Artillery Air Defense Group 5544
ASP.NET 4654, 5057
Asphalt 189
Aspheric Grinding Process 3110
Assembly Equipment 3323
Assembly Process 3153
Association Rule 1586, 1985, 3747
Astringency 2639
Astronomical Image 3827
Asymmetrical Thin-Wall Part with Variable Diameter 3306
Asymptotic Crack-Tip Displacement Fields 908
Asynchronous Motor 2807
AT Instruct 3054
Atmospheric Bulk Deposition 1286
Atmospheric Particulates 416
Atmospheric Pressure 1200
Atmospheric-Pressure Cold Plasma 340, 344
Atmospheric Scattering Model 2484
Atomic Force Microscopy (AFM) 739
Atrazine 853
Atropine 1007
Attack 4371
Attapulgite 160
Attendance Management System 4478
Attitude Control 3216
Attractor 1786
Attribute Importance 2029
Attribute Prediction 1526
Attribute Reduction 1536, 1775
Attribute Weight 2029
Attributes-Importanc 1736
Attributes Significance 1551
Au 344
Au Nanoparticles 471

Authentication 4514
Authentication Protocol Analysis 4698
Auto-Associative Neural Network (AANN) 3679
Auto-Rotated Precision of Gun Barrel 2849
Automated Code Generation 4488
Automatic 4069
Automatic Control 3228
Automatic Correction 2741
Automatic Film-Changing Mechanism 3294
Automatic Mapping 1891
Automation Process 2811
Automotive Wind Tunnel 2834
Average Gradient Angle 4205
AVR Kernel 3415
Axial Force 2845
Axis Calibration of Rotation Stage 3266
Azobenzene Moiety 494

B

β-Amino Ketone 134
β-CD 1052
B-Rep 4945
B/S 1841, 4452, 5209, 5361
B/S Framework 5481
B/S Structure 5605
B2B Market 4802
Back Noise 4019
Backfill Material 978
Background Modeling 2462
Background Subtraction 2605, 4107
Backsteeping 2965
Backup Frame 701
Bainite/Ferrite Two Phases 212
Balancing Urban Development 5128
Ballast Water Discharge 1161
Balling 39
Ballot Input Direction 4806
BAM Neural Network 1877
Band Structure 216
Bandgap Voltage Reference 1165
Bandwidth 3790
Barite 1408
Base-Level Cycles 1359
Based-Static Image Retrieval 3575
Basements 260
Basic Government 4713
Basketball 5193
Basketball Tactics 5193
Bat Algorithm 1646
Battery 3092
Battery Manage System 3092
Battlefield Damage 1141
Bauxite 1269, 1380, 1384, 1388, 1392, 1400, 1404, 1428
Bayesian Inference 4680
Bayesian Mdoel 4704
BayesShrink Threshold 3881
Bbig Datastyling 4704
Beam-Forming 3556, 3722
Beam Propagation 1909
Beaming Area 1135
Bearing Capacity 970
Bearings-Only Tracking 3526
Bed Pressure 256
Beddoes-Leishman Model 2258
Beef 1052
Behaivor 433
Behavior Analysis 4763
Beijing South Railway Station 2283
Benford's Law 2148
Benzene 55
BHA 519
BHT 519
Bidirectional Feedback 4082
Big Cities 5624
Big Data 1837, 2457, 4717, 4905, 4949, 4957, 5075
Big Data Internet 4594
Biginelli Reaction 83
Bilinear Parings 4409
BIM 5169
BIM High-End Talent 5169
Binarization 3865
Binary Analysis 1782
Binary Search Algorithm 1905
Binocular Stereo Vision 1766
Binocular Stereo Vision System 3007
Binocular Vision 3266
Bioceramic 775
Bioceramic Coating 767
Biochemical Composition 747
Biological Soil Crust 975
Biology Safety 1068

Biomass Material 138
Biomedical Automation 1077
Bipartite Graph 4775
Bipolar 3583
Bismuth Sulfide 11
Bistatic MIMO Radar 3710
Bit Allocation 2161
Bit Vector 3747
Bitcoin 5066
Bivariate Statistical Model 3734
Black-Box Testing 4542
Black Hole Attack 4482
Blast Furnace 3505
Blast Wave Signal 3956
Blending Teaching 5571
Blind Equalization 1865
Blind Extraction 1901
Blind Source Separation 1566, 3738
Block Adjustment 3534
Block Copolymer 102
Block Sampling 3856
Blocked Ratio 644
Blood Concentrations 2208
Bluetooth Control Technology 4215
Board-Level EMC 1977
Body Area Network (BAN) 4657, 4837
Body Measurement 4161
Body Scan 4161
Bohai Sea 2288
Bolt 943
Bond 5634
Book Chain 5311
Book Positioning Book Positioning by Radio Frequency Identification Technique in Mobile Phone Libraries 4140
Boolean Network 4417
Boost 4306
Border Router 4737
Borehole Camera 1396
Borehole Stability 903
Bottleneck 4115
Boundary 599
Boundary Data 1891
Boundary Element Method (BEM) 1825
Box-Constrained Program 2406
Box Girder 923
BP 2119
BP Neural Network (BPNN) 1814, 2629, 3382, 3968
BP Neural Network Model 5536
BPS Framework 5512
Brain Storm Optimization 1626
Brewer's Grains 841
Brick Cutting Machine 3228
Bridge in Construction 3165
Bridge Resource Management (BRM) 5423
Bridge Steel 883
Bridging Polysilsesquioxane 739
Bright Stray Light Suppressed 4107
Brilliant Cresyl Blue 841
Brine 540
Brominated Flame Retardants 506, 511
Browser 4841
Browser Server 4861
Browsing Behavior 4241
Brushless Dc Motor (BLDCM) 3172
Buffer Layer 65
Buffered Clock 3530
Building Engineering 5472
Building Information Model (BIM) 5512
Built-In Electric Spindle 2922
Bulk Modulus 216
Bulk Stockpile 823
Bus Transit Network Design 5624
Business Systems 4585
Business Workflow 4771
BYOD 4514

C

CA Authentication 4519
Cable-Stay Bridge 986
Cable-Stayed Bridge 3165
Cable Suspended Parallel Mechanism 3058
Cache 2414, 4447
CaF_2 Nanocrystals 305
CAI 5165, 5341
Calcium Hydroxide Concentration 19
Calculation Mental Image 1493
Calibration 3007
Calix [4] Arene Derivatives 523
Call Data Records 4200
Camera Model 3007
Camouflage 2882
Camouflage Design 4470
Campus E-Commerce 4388
Camshift 3587

Camshift Algorithm 2693
CAN Bus 3375
Canna 572
Canny Edge Detection 3973
Canny Operator 2088
Cantilever 3270
Capability Ratio 2268
Capacity Utilization 4873
Capillary Electrophoresis-Electrochemiluminescence (CE-ECL) 1007
Car 1150, 2796
Carbazole Unit 292
Carbon 146
Carbon Black 629
Carbon Coating 316
Carbon Dioxide 676
Carbon Emission (CE) 1248
Carbon Fiber 194, 587
Carbon Nanotube (CN) 789
Carbon Tax 5232
Carbonation 705
Carboxyl Density 151
Carboxymethyl Cellulose 697
Carrier Contribution 3806
Case-Based Reasoning 4625
Case Study 5082
Cash Subadditivity 5241
Castor Leaves 1029
Catalase 1292
Catalytic Combustion 671
Catalytic Hydrolyze 79
Catalytic Oxidation 490
Catalytic Ozonation 783
Catalytic Performance 1073
Cathode Material 462
CAZAC 2709
CBIR 4069
CBR 1704
CC2431 2999
CC2530 Chip 3419
Ccascaded Second Harmonic Generation 3790
CDIO 4949, 5419
CDMA 3540, 4290
Cell 4249
Cell Automata 4032
Cell Selection 1671
Cellular Automata 2340, 3050
Cellular Automaton 2385
Cellular Layout 2811
Cellular Neural Network 1473
Cement Coating 39
Cemented Carbide 871
Center of Gravity Method 5315
Centrality Analysis 2438
CeO_2 767
Ceramic Products' Information 4322
Ceramsite 572
Cervical Carcinoma 1044
CFD 2264
CGHAZ 576
Chain Drive 2890
Challenges 5152
CHAN Algorithm 2232
Change 5144
Changing Rate of energy. 3521
Channel 3730, 3823, 4590
Channel Capacity 1419
Channel Estimation 3521, 3786, 3902
Channel Impulse Response (CIR) 3786
Channel Model 3960
Channel Modeling 2576, 4111
Channel Reservation 3889
Channel Time-Coherence 4111
Chaos 2825
Chaos Optimization 2196
Chaotic Map 3561
Chaotic Series 1348
Chaotic System 1469
Character 2D Barcode 2135
Character Feature Extraction 2569
Characteristic 5245
Characterization 125, 301
Charge Density 2679
Chemical Contaminants 5596
Chemical Vapor Deposition Diamond Film 168
Chemistry Model 779
Chicken Cartilage 793
Children's Food 3262
Chimney 3485
China Civil Aviation Network 5403
Chinese 4990
Chinese Kang 3485
Chirality 1196
Chirp Signal 3934, 3942, 3977, 3989, 3993, 4046

Chirp Spread Spectrum (CSS) 4005
Chitosan 697, 1052
Chloroacetic Acid 399
Chlorobenzene 564
Chlorophyll Concentration 2184
Chlorothalonil 853
Chord 4815
Chromatographic Stationary Phase 626
Chromone 568
Churn Prediction 4200
Cigarette Sales Prediction 5182
CIP 4306
Circular Cutter 2908
Circular Degree 3730
Circular Economy 5592
Circular Slot Antenna 3497
Circulating Fluidized Bed 256
Circumcenter 2377
Citation Network 4789
Citral 1052
City Atmosphere 446
City Construction 1192
CityEngine 4945
Civil Unmanned Aerial Vehicle 3548
cl^- 458
Cladding 502
Classification 1509, 1692, 3617
Classification Decision 2080
Classification of Body Shape 5319
Clipping 4005
Close Degree 3689
Closed-Loop Control 3062
Closed-Loop Supply Chain Logistics Network 2519
Closed-Loop Vector Method 3683
Clothing Fit 4161
Cloud Computing 1513, 1930, 1934, 2115, 2192, 2349, 4314, 4396, 4717, 4799, 4905, 4966, 5004, 5357, 5495, 5498
Cloud Platform 4573, 4966
Cloud Security 5000
Cloud Services Platform 4799
Cloud Storage 2008, 2454, 4811, 4913, 5007
Cloud Storage Data 2200
Cloud Storage Security 2543
Cloud System 5007
Cloudstack 2297
Cluster 2245
Cluster Algorithm 3851
Cluster Analysis 2101, 3633
Cluster Based Routing Protocol 4281
Clustering 1570, 1942, 2051, 4920
Clustering Analysis 2047
Clustering Number 2431
Clutter Characteristics 3963
Clutter Modeling 3963
Clutter Reduction 2318
CMA 1865
CMOS Camera 4759
CNN Model 1621
Co-Doping 656
CO Oxidation 344
Co-Precipitation Method 462
Co-Simulation 3045
CO₂ 441
Coal 1415
Coal Industry Chain 5232
Coal Quality Analysis 3399
Coal Tar Pitch 194
Coastal Area 2328
Coastal Project 1240
COCOMO Model 1497, 1501
Code Template 4488
Cognitive Radio 3591
Cognitive Radio Networks 3889
Coherent Demodulation 4152
Coherent Detection 3806
Coherent Light 2024
Coil Transporters 2935
Coiler 3019
Cold Plasma Jet 1200
Collaborative Filtering (CF) 1445, 2188, 2241
Collapse Risk 947
Collective Communication 4934
College English 5049
College Female Students 1107
College Physics Reform 5178
Colleges 5078, 5169, 5415
Collision Detection 2057, 2389
Color Histogram 3552

Color Image 3798
Colorless ONU 3806
Column Study 966
Combination 4657
Combination Filter 3881
Combined Exposure 1319
Combined Training 5148
Combustion Adjustment 256
Combustion Performance 511
Comet Assay 1064
Command 3371
Common Platform 4861
Communicate 4802
Communication 3625
Communication as Planned 4570
Communication Module 3282
Communication Network 3814, 4179, 4474
Communication Platform 5169
Communication Port 5481
Community Net Store 5245
Community Service 5245
Comparative Analysis 5033
Comparison Results 1790
Compensation 2024, 3236
Competitive Sports 5053
Competitive Strategy 5228
Competitiveness of Cultural Industries 5132
Completed Bridge 3165
Complex Electromagnetic Environment 3212
Complex Frequency Shifted 1869
Complex Image Method 3777
Complex Network 1441, 2128, 4179, 4881, 5403
Complex Network Theory 4237
Complex-Step Differentiation 1938
Complex Structure 1918
Complexity 2659
Compliance Strategy 4514
Component 4660
Component Groups 1181
Composite 665, 943
Composite Element Method (CEM) 908
Composite Film 224, 412
Composite Material 337, 1073
Composite Polymers 556
Composite Slurry Valve Gate 3149
Comprehensive Scores 1821
Comprehensive Similarity 1680
Compress 4759
Compressed Sensing 3698, 3718, 3755
Compressed Video 1469
Compression Encoder 4100
Compressive Sensing 1610, 4187
Computation 2356
Computational Complexity 4926
Computer 5029, 5364
Computer Aided 2075
Computer-Aided Translation 4637
Computer Algebra Systems 1798
Computer Cluster 4269
Computer Digital Simulation 4362
Computer Forensics 2148
Computer Network Security 5415
Computer Network Topology 4237
Computer Numerical Simulation 4367
Computer Simulation 216, 220
Computer Supplementary Software 5102
Computer Teaching Room 5369
Computer Vision 1435, 3844
Concentrated Seawater 540
Concentrated Sludge 1252
Concept Drift 2101
Concept Extraction 2292
Concept Similarity 2179
Concrete 961
Concrete Durability 2688
Concrete Slump 228
Concrete Targets 982
Conductive Composites 181
Conductivity 859
Confidence Fusion Algorithm 2237
Confidence Level 5547
Conflict Prevention 4590
Confocal Arrangement 2761
Congestion Control 4427, 4493
Conjugate Gradient Method 2406
Consensus Problem 2639
Constraints 2020
Construct 5078
Constructing Algorithm 2106
Construction Development 5439
Construction Machinery 3323
Construction Method 1157
Construction Principles 5106

Consumption Reduction 1252
Contace Angle 267
Contaminated Sites 564
Content 1356, 5601
Context Learning 1610
Continued 1338
Continuous Attributes 2431
Continuous Function 1686
Contraction Capacity 1015
Contrast Test 2834
Contribution Rate 5263
Control 4747, 5435
Control Methods 2895
Control of AIDS 1097
Control Strategy 3282, 4650
Control System 2913, 3177, 3212
Controlled Cooling 475
Controller 2778, 4265
Converge Cast 4115
Convergence 2001, 2528, 2532, 2536
Convergence Speed 1728, 1732
Convex Hull Algorithm 3865
Conveying Part 2913
Cooling Capacity 2165
Cooling Tower Fan Gearbox 3302
Cooperative Diversity 3540
Coordinate Gap 2874
Coordinate Measurement 3266
Coordinated Beamforming 1671
Coordinated Control System 2839
Coordinative Optimization 1887
Copolymer 156
Copolymerization 560
Copper Ion 312
Copper-Nickle Ore 1411
Copper Phthalocyanine Film 680
Coprecipitation 383
Copy-Move Forgery 4127
Coral Reef 1396
CORBA 4175
Cordierite 671
Core Calibration Log Method 1372
Core Reservoirs 903
Corncob Hemicelluloses 412
Corporate Social Responsibility to Employees 5205
Correction 5461
Correction Factor 4082
Correlation 3633
Correlation Coefficient 2613
Correlation Coefficient Estimation 1883
Correlation Effect 3189
Correlation Immunity 2593, 2599
Corresponding Degree for Categorical Measures 2318
Corrosion Inhibitor 160
Corrosion Resistance 208, 308
Corrugated Cushion 3258
Corrugated Paperboard 3258
Corrugated Plates 831
Corrugated Thin-Walled Part 3306
Corrugated Waist Rail 425, 429
Cost Composition 5136
Cost Control 5173
Cost Estimation 1501
Cost Function 1464
Cost Sensitive 1756
Costs Assessment Model 5327
Counter 3029
Countermeasure 5037, 5152, 5201
Coupling 441
Coupling Mechanism 2065
Coupling Multivariate 1348
Coupling Relationship 5157
Course Assessment 5224
Course Selection 4358
Courseware 5120, 5165
CP800 238
CPI 5536
Cr 1415
Cr (VI) 1319
Cr Contaminated Soil 1313
Crack 502, 3185
Crack Tip Fields 719, 1212
Cracked Rotor-Active Magnetic Bearings 2825
Crankshaft 2745
Crashworthiness 898
Crassostrea gigas 1033
Crawler 4845
Creator 1981
Credit Evaluation 2931, 4980, 5075
Credit Reporting 5209
Creep Rupture Strength 264
Crew Scheduling 2523
Crisis Evaluation 5448

Critical Technology 2438
Crop 5551
Cross Compiler 3856
Cross-Correlation 3827
Cross-Correlation Processing 2278
Cross-Linked Polyethylene 1273
Cross Method 2135
Cross Power Spectrum 3877
Crossing-Selling 1586
Crosslinking 697
Crosstalk Noise 2647
Crowdsourcing 4708
Cryogenic Treatment 871
Cryptosystem 4183
Crystallinity 7
CS 199, 793
CSAMT 2278
CSCSA 83
CSG 4945
CTMV 3693
Cu-Based 652
Cu/Cu_2O 1073
CUDA 1664
Cue 3169
Cultural Archives 1779
Cultural Immune Algorithm 1887
Culture Industry 2070
CURE 1664
Currency Crisis 2560
Current Field 3460
Current Force 2332
Current State Map 2811
Current Waveform Control 3140
Curriculum System 5078
Curvature Constraint 1621
Customer Credit 4980
Customer Operation Center 1522
Cutter Contact 2908
Cutting Force 3248
Cutting Parameters 3331
CXF 4350
Cyber Topology 4233
Cycloaddition 676
Cylindrical Food 3513
CYP2D6 1041
Cyperus Alternifolius 1319

D

D9-intersection Model 2655
Dahlin Algorithm 3195
DALLTSA 2381
Damage Detection 3349
Damage Effectiveness 5544
Damping Force 3025
Danger Index 2340
Dark Channel Prior 3898
Dash 3371
Data 4452
Data Aggregation 3633
Data Analysis 3433
Data Center 1224
Data Cube 1657
Data Envelopment Analysis 1264, 3367
Data Fusion 3526, 3587
Data Glove 2057
Data Grading 5319
Data Management 1989, 4643
Data Mining (DM) 1453, 1578, 1586, 1837, 1985, 2047, 2070, 2080, 3747, 3802, 3814, 4383, 4538, 4594, 4608, 4819, 4902, 4974, 5010
Data Mining Methods 4474
Data Redundancy 2070
Data Sampling 3956
Data Security 2454
Data Sharing 2349
Data Storm 2970
Data Storm Monitoring 2970
Data Stream 3084
Data Warehouse 1657, 1955, 4383, 4819
Database 4447, 5345
Database Design 5524
Database Management 2075
Database Optimization 2020
DC-AC 3231
DC-DC 3231
DCT Coefficients 1469
DDA 2254
DDE 5468
De-Noising 3595
Debye Temperature 3509
Decaying Rate 3340
Deception 4881
Decision Level Fusion 4209

Decision Support System 1131
Decision Table 1536
Decision Tree 1692
Deep Open Pit 3070
Deep Structure of ELM (DS-ELM) 3679
DEFORM-3D 425, 429
Degradation 60, 1020
Degree Profile 4095
Dehazing 3898
Dehumidifier 3100
Dehydrochlorination 121
Delay Monitoring 3423
Delay Spread 3823
Delegate 4392
Demand Forecast 1485
Demodulation 2727, 3952, 3981, 4191
Dendronized Monomer 494
Denitrification 572
Denitrification Phosphorus Removal 603
Density 2169, 4273
Density Evolution 4095
Density Functional Theory (DFT) 688
Density of Carboxyl 228
Deobfuscation 1782
Derivative 2599
Design 1097, 2004, 2495, 2617, 2913, 2975, 4506, 5120, 5361, 5411
Design Aesthetic 5144
Design an Image Acquisition System 3861
Design Process 5098
Design Reasonableness of Transmissions 2955
Detail Enhancement 3893
Detecting 2764
Detection 146, 723, 1115
Determinants 1798
Development 23, 4223, 4229, 5082, 5619
Development Anthropology 5128
Development Mechanism 2065
Development of Mobile Terminal 5605
Development Platform 4302
Development Research 5102
Development Trend 4226
Device Clamp 69
DFIG 2980
DFT 3521
Di-Hydropyrimidin 83
Diabetes Mellitus 1015
Diagnosis 2735
Diaphragm 1015
Dictionary Learning 3885
Dielectric Barrier Discharge (DBD) 340, 344
Dielectric Constant 242
Dielectric Function 220
Diesel Generator 1224
Difference Degree 1551
Difference Frequency Generation 3790, 3794
Differential Evolution 1849, 4095
Differentiation-Integration Method 660
Diffusion 755
Digital 3851
Digital Architecture 5390
Digital Camouflage 4470
Digital Cultural Relics 1509
Digital Disaster Education 5094
Digital Electronic 5221
Digital Exhibition-Design 5407
Digital Forensics 1513, 4432
Digital Information Technology 4358
Digital Learning Resources Library 5007
Digital Libirary 4902
Digital Library 4799
Digital Media Arts 4223
Digital Money 5066
Digital Signal Processing 4195
Digital Technology 4226, 5390
Digital-to-Analog 2084
Digital Watermarking 1594, 4086
Diimine 731
Dimensional Posture 5461
Dimensional Wavelet Transform 3877
Dimensionality Reduction 2551
Dimethyl Diallyl Ammonium Chloride 348
Diode Array Detector 1060
Dioscorea bubifera L. 1044
Diploids 1033
Direct Geo-Positioning 3534
Direct Shipment 2519
Direct Torque Control (DTC) 2815

Direct Velocity Negative Feedback 2774
Direction Image 4209
Disassembly 3323
Disaster Prevention 5378, 5382
Disaster Reduction 5382
Disaster Rescue Robot 3298
Discernibility Matrix 1536
Discontinuity 2515
Discontinuous 908
Discrete Cosine Transforms (DCT) 4086
Discrete Fractional Fourier Transform (DFRFT) 4001
Discrete Logarithm 4310
Discrete Logarithm Problem 4409
Discriminant Analysis 1368
Discussion 5086
Disjunction Type 1607
Disk Spring 3224
Dislocation 387
Dispersing Ferric Oxide 156, 160
Dispersion Ability 151
Displacement Response 2904
Displacement Sensor 3029
Disputed 4223
Distance 1236, 1641, 4273
Distance Estimation 4547
Distortion 5486
Distributed 4594
Distributed Computing 1578, 2188
Distributed Execution 4771
Distributing Computing 1810
Distribution 1415, 1532, 5090
Distribution Center 5311
Distribution Model 5311
Distribution System 1181
Disturbance 2536
DLLTSA 2381
DNA Damages 1064
DO 603
DOA Estimation 1973
Document 4219
Document Image Process 3768
Domain Compound Concept 2292
Domestic Currency Appreciation 5037
Donor-Acceptor 292
Donor Unit 284
Doppler 2418
Double Buffer 3375
Double CPU 2886
Double Level 1364
Double Moving Average 1485
Double Negation 1720
Double-Spool 2845
Double Stations 1135
DPM 2D Barcode 3865
Drag Parachute Pneumatic Packing Machine 3286
Drag Transportation 1522
Dredger 2332
Drilling Fluid 1376
Drilling Mechanism 3136
Drilling Pump 2899
Drive Scheme 2955
Drive System 2899
Driving Amplitude 2926
Driving Rules of Freeway 2385
Drop Analysis 1802
Droplet Transfer Control 3140
Droplets 3354
Drug Analysis 993
Drug Interaction 1041
Drum Water Level 1449
DS 3868
DS/FH Hybrid Spread Spectrum Signal 4050
DSC 2791
DSP 3033, 3216, 3231
DSP Communication 3375
DSP Memory Allocation 1946
DSS 1131, 4383
DSTFT 3981
Dual-Feedforward Compensation 1169
Dual-Miller Compensation with Nulling-Resistor 1169
Dual-Mode 3127
Dual Threshold 3893
Dual Uncertainty Information 1845
Dust Emission 823
Dyadic Wavelets Transform 4127
Dyeing Properties 450
Dynamic 2254, 2536
Dynamic Alliance Performance 5041
Dynamic Binary Search Algorithm 1905
Dynamic Characteristic 3045, 3165
Dynamic Consolidation 2373
Dynamic DEA 2323

Dynamic Information Feedback 3447
Dynamic Management System 3379
Dynamic Mechanism 2782
Dynamic Model 2829
Dynamic Network 2639
Dynamic Programming 1547
Dynamic Response 74
Dynamic Simulation 3834
Dynamic Spatial Panel Model 1333
Dynamic Stall 2258
Dynamic Stress Intensity Factor 1825
Dynamic Systems 2515
Dynamic Update Rate 2310
Dynamical Analysis 4417
Dynamical Diffusion 3561
Dynamics Analysis 3079

E

E-Business 4318
E-Commerce 1887, 4538, 4617, 4802, 4980, 4996
E-Derivative 2593, 2599
E-Government 4302, 4717, 4905
E-Government 2.0 4713
E-Learning 1594
E.coli 997
Early-Warning Models 2625
Earthquake Emergency Drill 4551
Earthquake Prediction 1570
Earthworm 1313
ECOC 1895
Ecological City 1127
Ecological Civilization 1192
Ecological Compensation 5584
Ecological Destroy 1232
Ecological Engineering 1341
Ecological Environmental Quality 1228
Ecological Teaching Model 5282
ECOM 2288
Economical Manufacturing 3153
Economics 5217
ECU 3319
Edge-Coloring 4253
Edge Detection 1652, 2569, 2605
Edge Handling 4127
Edge Radius 2939
Editor 5481
Educational Technology 5106
EFDC 1240, 1244
Effect 4223
Effectiveness Evaluation 3212
Effects 5037
Efficiency 3025, 4806
Efficiency Index 1857
EIA 4855
Eigen-Expansion Method 715, 1212
Eigenvalue Buckling Analysis 2859
EIS 420
Elastic 2975
Elastic Constants 216
Elastic-Plastic Mechanics 2869
Election System 4806
Electric Bicycle Brake Force 3335
Electric Distribution Network 1204
Electric Inertia Simulation 3335
Electric Vehicle (EV) 3092
Electrical Power Equipment 1141
Electrical Resistivity 45
Electrical Simulation 599
Electrical Tree 1273
Electrocatalyst 340
Electrochemical Oxidation Process 591
Electrochemical Properties 462
Electrochemistry 446
Electrochemistry Transducer 615
Electrochromic 789
Electroless Plating 403
Electrolysis 308
Electromagnetic Compatibility 837
Electromagnetic Forming 2702
Electromagnetic Scattering 3777
Electronic Cash 4314
Electronic Commerce 2519, 4314, 5457
Electronic Currency 5066
Electronic Flight Bag (EFB) 1739
Electronic Government 4413
Electronic Reconnaissance 1135
Electronic Satellite 4062
Electronic Warfare Command 3212
Electrospinning 556
Element Distribution 331
Elliptic Curve 4183
Elo Rating System 5010
EMAS 2829
Embedded 4215

Embedded Linux Operating System 4447
Embedded Online Monitoring Unit 3278
Embedded Structure 1951
Embedded System 2173
EMD 3204, 3654
Emergency Management 1704
Emission Control 87
Emission Efficiency 3658
Emission Signal Current Waveform Recorder 2278
Emission Standards 1324
Emotional Interaction Design 5528
Empirical Mode Decomposition (EMD) 2713
EMS 5173
Emulsifier 189
Encoding 1509
Encryption 4780
Encryption Algorithm 2008
Encryption Strategy 2543
End-Bearing Ratio 970
Energy 1942
Energy Budget 1033
Energy Consumption 1248, 4294
Energy Efficiency 4169
Energy Efficient 4405
Energy Recycling 3025
Energy Saving 1252
Energy Storage 2820
Energy Storage Density 242
Engine System 4763
Engineering Thermodynamics 5571
English 2115, 5495
English Linguistics 5486
English Test 5029
Enhanced Bit-Plane 1473
Enhanced Coagulation 849, 853
Enhanced Fuzzy C-Means Clustering 1489
Enhanced Mixed Excitation Linear Prediction 1951
Enhanced Nitrogen Removal 1341
Enhancement 3798
Enlightenment 5254
Ensemble Empirical Mode Decomposition (EEMD) 3671
Enterprise Application Integration 4350
Enterprise Business Process 5136
Enterprise Growth Cycle 5386
Envelope Machining 2908
Envelope Material 3473
Environment 5575
Environment Tax 5584
Environmental Noise 4945
Environmental Rubber 407
Eosin 15
Epanechnikov Mixture Model 2719
Epipolar Geometry 1435
Epistasis 2426
EPON 4723
Equilibrium 4524
Equilibrium Point 2402
Equipment 4861
Equivalent Integral Equation 1712
Equivalent Model 2980
Erosion Resistance 270
Error Amplifier 3236
Error Conditions 3963
Error Diffusion 4082
Errors Compensation 3110
Escape-Time Algorithm 1806
Esterification 233
Estimation 1962, 2184
Estimation Error 1497
Estimation of Ecological Situation 1297
Estimation of Environmental Conditions 1301
Ethylene 727, 731
Ethylene Carbonate 79
Ethylene Glycol 79
Ethylene/Vinyl Acetate Copolymer 629
Eucheuma Gelatinae 1056
Euler Mapping 4119
Evacuation Network 5508
Evaluation 2323, 2488, 2688
Evaluation Flooding 638
Evaluation Index System 5140, 5286, 5373
Evaluation Model 5540
Evaluation System 5250, 5457
Event 4392
Event Driven 1541
Evolution 2033
Evolution Rule 4940
Evolutionary Algorithm 1955
EVP 5282
Excavation 3070
Execution Model 2144, 4851

Exhaust Purification 3456
Exhibition 5411
Exhibition Design 5213
Exp-Function Method 1716
Expand-Vector 2188
Expandable Graphite 814
Expanded Graphite 814
Expansion Model 814, 3649
Expected Convergence Time 1728
Experiment 961, 3177
Experimental Results 4452
Expert System 1770, 1841, 3181, 4877
Explosion-Proof Diesel 3456
Exponential Transform 3893
Export 4917
Exposure Pathway 5596
Extended Kalman Flter (EKF) 2555, 2705
External Ballistics 2849
External Flow Filed 3468
External Insulation Material 5431
Externalities 1324
Extraction 31, 1029, 3613
Extraction Rules 4322
Extre Water Level 2288
Extreme Learning Machine (ELM) 3679
Eye Movement Theory 4241

F

Fabric Image 3698
Face Modeling 2016
Face Recognition 2381, 2551, 4091, 4119, 4205, 4209
Facility Location 5315
Factor Analysis 2931, 5132
Factors 5555
Factors Breakeven Analysis 5315
Failure 3224
Failure Analysis 3302
Failure Detection 2495, 4873
Failure Mechanism Consistency 918
Failures 2947
Falling Film 831
FANUC 3290
Fashion Design 5098
Fast Median Filter 2273
FAST Project 701
Fasteners 3011
Fat-Tree 4794
Fatigue 3363
Fatigue Limit 879
Fatigue Strength 238
Fatigue Test 887
Fault Detection 3802
Fault-Diagnosis 1204, 2899, 3220, 3244, 3319, 3738
Fault Set 2735
Fault Signal 3802
Fault-Tolerant Model 1810
FCM 3743
Fe-Based 652
Feasible Sets of Shifts 2523
Feature Extraction 1260, 2016, 2043, 4187
Feature Points 1997
Feature Refining 3605
Feature Selection 4510
Feature Vector 3663
Feed Drive Vibration 3117
Feed-Forward Adjustment Amount 3386
Feed-Forward Control 3386
Feed-Forward Neural Network 1635, 1646
Feedback Mechanism 4524
Feedback System 5486
Feedforward 3464
FEM 352, 931, 2373
Femtocell 2051
Fermat Point 2377
Ferrate 15
FFCM 2047
FGPMs 1212
FH Communication 3693
Fiber Bundle 1700
Fiber Modification 450
Field 3851
Fighting Simulation 5609
File Analysis 2148
Film 4226
Filter Design 3718
Final Drive 3033
Finance Data 2457
Financial 5415
Financial Innovation 5386
Financial Risk 2625
Fine-Grained Access Control 4650
Finite-Difference Time-Domain 1869

Finite Differencing 1938
Finite Element (FE) 548, 986, 2922, 2939, 2995, 3185
Finite Element Analysis (FEA) 891, 2975, 3149, 3286
Finite Element Method (FEM) 970, 2702, 3248
Finite Element Modeling (FEM) 634
Finite State Markov Channel (FSMC) 2576
Finnish Design Policy 5373
Fire Emergency Plan 5444
Fire Performance 5431
Firefly Optimization (FA) 4074
Firewall 4690
Firing Table 2849
Fit Degree 3153
Fitness Function 2484
Fixed Assets Investment 2075
Fixed-Line Lottery Ticket Sales System 4841
Flame Retardance 607
Flanker Interference 1093
Flat Wheel 3110
Flatness Accuracy 2165
Flax 450
Flexible Manipulator 2774
Flexible Material 360
Flight Controller 2951
Flip-Frame 2890
Flooding Attack 2227
Flotation 1411
Flotation Reagent 1408
Flow Field 3456
Flow Meter 3270
Flow Stress 544
Flowing 3460
Fluctuation of Wind Power 1256
FLUENT Simulation 3477
Fluidity of Cement Paste 228
Fluorene 31
Fluorescence Spectra 121
Fluorescence Spectrometry 1352
Flywheel Energy Storage 2503
Foam Glass 260
FOC 867
FODA 1513
Fog-Degraded Images 2484
Food Packaging 3262
Food Thawing 3513
Football Coach 1821
Football Coach Selection 1821
Forecast 548
Foreground Enhancement 3872
Foreign Direct Investment 5023
Forging Enterprise 5136
Formal Solution 1969
Formaldehyde 615
Forming Quality 710
Fossils 1384
FPGA 3274, 4100
FPUF 511
Fractal Correlation Dimension 2507
Fractional Correlation 3706, 3710
Fractional Fourier Transform (FrFT) 3942, 3977, 3989, 3993, 4001, 4042, 4046
Fractional Lower Order Statistics 3706, 3710
Fracture 69, 576, 2356
Framework 1359, 4690, 5382
Framework Model 5448
Framework Structure Design 5588
Freakommendation 4538
Frequency 3497
Frequency Adjustment 887
Frequency Dactylogram 3349
Frequency Detection 2511
Frequency Estimator 3985
Frequency Hopping (FH) 4038
Frequency Selected Surface 837
Frequency Spectral Features 3671
Frequency Synthesizer 4058
Frequent Item Set 3747
FRFT 3934, 4005, 4009
Friction-Type Long Pile 970
Frieze Group 1786, 1806
Fructus Lycii 1368
FTU 3501
Full-Bridge Inverter 3231
Full-Wave Band CCD System 3782
Fully Homomorphic Encryption 4326, 4780
Fun Packaging 3262
Function Realization 4355
Functional 2070
Functional Framework 4302
Functional Requirements Analysis 5588
Functional Zoning 5273
Fundamental Matrix 1435, 3844

Furring Brick 260
Future State Map 2811
Fuyu Reservoir 1359
Fuzzy 2001, 3464
Fuzzy C-Means Clustering 3814
Fuzzy Chance Constrained 5547
Fuzzy Clustering 1641
Fuzzy Clustering Algorithm 2431
Fuzzy Comprehensive Evaluation 2438, 5555, 5559
Fuzzy Comprehensive Evaluation Method 5228
Fuzzy Control 3157, 3172
Fuzzy Enhancement 4136
Fuzzy Evaluation 1821, 2336
Fuzzy Grey Deviation Degree 1845
Fuzzy Grey Number 1845
Fuzzy Method 2488
Fuzzy Model 2719
Fuzzy Neural Network (FNN) 2684, 2815
Fuzzy NN 4877
Fuzzy PID Control 399, 3172
Fuzzy Set 1775, 2735
Fuzzy Synthesis Evaluation 5070
Fuzzy Theory 2314

G

G-Code 3290
γ-PGA 809
G-XML 4478
Gabor Filter 3644
Gabor Wavelet 3906
Gabor Wavelet Transform 4091
Gain 3497
GAMBIT Modeling 3477
Game 5205
Game Theory 2051, 5148
GaN 387
Gangue 939
GaNLED 623
Gantry Cranes 2995
Gaps Assessment 2268
Gas Distributor 2264
Gas Emission Quantity 3480
Gas Fractionation Unit 3493
Gate Processing 3786
Gateway 4447
Gauss 1489
Gaussian Noise 3881
GC-MS 506
GCL 433
Gear Coupling 2975
Gear Meshing Force 3037
Gear Modification 2917
Gearbox 2917
Gelatin 809
Gender Recognition 4187
Gene Index 1853
Generalized Ant Colony Algorithm 1732
Generalized J Sets 1806
Generation Engine 4488
Generator Matrix 2634
Genertic Algorithm 1853
Genetic Algorithm (GA) 1547, 1786, 1841, 1873, 2012, 2223, 2245, 2422, 2609, 2629, 3505, 3595, 3856, 3968
Genome Compression 1561
Genotoxicity 1064
Geographic Information 5014
Geological Museum 5407
Geological Significances 1400
Geomagnetic Matching 1602, 2555
Geomembrance 433, 1208
Geometric Modeling 1700
Geometry Design 3298
Geostress 3070
Ginkgo Biloba Extract 1015
GIS 4478, 4855, 5444
GIS Road Network 3639
Gl Studio 2951
Glass 369
Glass-Ceramics 305
GLCM 3906
Global Average Location 1582
Global Classifier 1762
Global Convergence 1802
Global Optimization 1626
Global Optimum 2377
Global Response 1161
Glow Discharge 60
Glow Discharge Electrolysis 55
Glutaraldehyde 697
Glycoprotein 96(gp96) 1037
GM (1, 1) Metabolism Model 3480

GM(1,1) 3443, 3480
GNS 4603
Goods Return 2519
Google Cloud 5580
Governance Countermeasures 5124
Governance Mechanism 5128
Government IT Service Outsourcing 5112
GPON 4962
GPRS 3419
GPT 1044
GPU 2169
Graft 676
Grain Growth 297
Grain Shape 297
Grain α-Phase 638
Graph 3747
Graph Based Learning 1088
Graph Model 1779
Graph-Oriented Model 1660
Graph Theory 2402
Graph Transformation 4940
Graphene 337, 373, 859
Graphene Oxide 125, 373
Graphic Design Courses 5237
Graphical Representation 3599
Grasp 3181
Gray Map 2634
Gray Theory 276
Grayscale Adjustment 3838
Grayscale Transform 3893
Greedy Algorithm 1946, 2161
Green Grinding 684
Green Light-Emitting 391
Green Management 5592
Grey Clustering 5453
Grey Correlation Analysis 2306
Grey Correlation Degree 2306
Grey Correlation Degree Method 2688
Grey Correlation Order 2306
Grey Forecasting Model 2723
Grey Histogram 2273
Grey System 2216
Grid 4869
Grid Environment 4379
Grid Method 2467
Grid Method Parameter Optimization 913
Grinding 3248
Grinding Fineness 1408
Grooved Nanofibers 556
Ground-Coupled Heat Pump 978
Ground Heat Exchanger 978
Ground Sense Coil 2511
Ground Simulation Test 3473
Groundwater 5491
Group Signature 4310
Group Sparse 3946
GrowCut Algorithm 4032
Growth 747, 5551
Growth Mechanism 552
GSM System 5532
Guide Groove 2874
Guide Pulley 2935
Guided Image Filter 3898
GWAS 2426

H

H Boolean Functions 2599
H-Matrix 1794
H22 Tumor Cells 1056
Haar-Like 1610
Hadamard Matrix 1895
Hadoope 4704
Haikou City 5394
Halcon 3007
Half-Life 2208
Halftone 4082
Halftone Screening Technology 3571
Halloysite 441
Handle Mechanism 5540
Handling Barred 4249
Handwritten Character 4742
Harmless Diposal 845
Harmonic Emission Level 3367
Harmony Search Algorithm 2528
HARQ 4132
Hash Digest Algorithm 5419
Haze 1338
HDFS 2450
Health Information Technology 1077
Health Records System 5524
Health Risk Assessment 5596
HEASoft Software 3489
Heat Capacity 3509
Heat Release 5431
Heat Transfer 3100
Heating 3485
Heating Rate 2679, 3399

Heavy Metal 454, 1208, 1305
Hedgehog Buckyball (HBB) 743
HEED 4405
Hemin 694
Henan Province 5407
Hepatocellular Carcinoma 1037
Heptadiagonal Matrices 1798
Herd Behavior 1993
Herd Consumption 1993
Herd Mentality 1993
Herringbone 2753
Heterogeneous Catalysts 83
Heterogeneous Multi-Agent System 2402
Heuristic Algorithm 4062
HF Channel 3702
HF Communication 3773
HFM Model 2655
Hidden Danger 5007
Hidden Markov Model (HMM) 2576, 3872
Hidden Terminal 4078
Hierarchical 4556
Hierarchical Division 1526
Hierarchical Optimization 4062
Hierarchy Analysis 4608
High Accuracy 3041
High-Carbon Steel 475
High Cycle Fatigue (HCF) 238
High Definition 1359
High Degree Seeking 1441
High Dimensional Data 4974
High Dynamic 3834
High-Efficiency Reverse Osmosis 108
High Energy Forming 1282
High Entropy Alloy Coating 246
High Gimbals 3195
High-Performance Computing Platform 1810
High Performance Liquid Chromatography 164
High Resolution Management 3447
High-Rise Building 947, 3075
High-Risk 4684
High Speed Milling 3331
High-Speed PCB 1977
High-Speed Railway (HSR) 3556
High-Speed Storage 2414
High Strength Gypsum 797
High Strength Steel (HSS) 379
High Technological Industries 5278
High-Voltage Cable 1273
High-Voltage DC Power Supply 1200
High-Voltage Transmission Line 3079
Higher Education 5102
Higher Order Fields 715
Highway 2675
Highway Transport 5124
Hilbert-Huang Transform 2713
Histogram 1489, 2693, 3689
Hole-Drilling Method 883
Home-Based Community Care for the Old 4501
Homogeneous Algorithms 1598
Homology Detection Software 1680
Homomorphic Filtering 3865, 4136
Homomorphism Decomposition 3798
Honeycomb Sandwich Panel 3349
Horizontal 1364
Horizontal Well 3096
Host Scanning 4286
Hot Corrosion 27
Hot Extrusion 515
Hot Metal 3505
Hot Water Extraction 412
House Plan 2588
Household Sub-Network 4215
Houttuynia Spray 723
HRXRD 387
HS1101 2962
HSV Color Space 4123
HTPB 172
Hub-and-Spoke Network Model 3861
Hub Centers 2811
Human Brain Functional Network 2037
Human-Computer Interaction 2057
Humidification Drying Cycles 705
Humidity Underground Coal Mine 2962
Huoyanshan Tectonic Belt 1376
HVS 2393
Hybrid 2-Population GA 2609
Hybrid Approach 2438
Hybrid Chaos 3621
Hybrid Cloud 2297
Hybrid Construction 5327
Hybrid Genetic – Particle Swarm Optimization Algorithm 1204
Hybrid Genetic Algorithm 2519

Hybrid Impact Hydroforming (IHF) Technology 1282
Hybrid Implicit-Explicit 1869
Hybrid Intelligent Diagnosis 3278
Hybrid Road Approach 3363
Hydraulic Cylinder 3323
Hydraulic Cylinder Clamping 2890
Hydraulic Pipe 2947
Hydraulic Press 3062
Hydraulic Support 2758
Hydraulic System 2802, 2904, 3323
Hydraulic Vibration Exciter 2904
Hydrazine Hydrate 181
Hydrogen Isotope 820
Hydrogen Plasma 779
Hydrophobic Property 739
Hydrothermal 11
Hydroxyapatite 312
Hydroxyl Radicals 55, 60
Hygrothermal Ageing 634
Hypergenesis 1297, 1301
Hyperspectral Image Classification 3885
Hyperspectral Remote Sensing 2184
Hyperthermia Resistance 595
HZMB 5331

I

I Evolutionary Programming 2084
IaaS 4396
IAGA 2609
IBE 2349
ICMP 4286
ICP-OES 480
Identification 1025
Identification Information 3675
Identify 1368
Identity Authentication 2543
IDS 4690
IEEE 802.11 MAC 4078
IEEE 802.15.4 MAC 4078
IFIR 4195
IIR 3985
Illumination Design 5213
Image 3181, 4877
Image Compression 3910
Image De-Noising 3973
Image Decomposition 4119
Image Denoising 4054
Image Edge 2393
Image Encryption 3561, 4183
Image Enhancement 3838, 4136
Image Extraction 3782
Image Features 2651
Image Fusion 1555, 3734, 3763
Image Index 3575
Image Matching 4104
Image Preprocessing 4205
Image Processing 3548, 3782, 3851, 3919, 5345
Image Quality 2368
Image Registration 3877
Image Retrieval 3552, 3579, 4069
Image Segmentation 1489, 1959, 2088, 2173, 3649, 3743, 3856, 4032, 4074
Image Sequence 2250
Imbalanced Data Set 1756
IMGS Iterative Method 1794
Immunocompetence 1056
Impact 1419
Implementation 5361
Import 4917
Impregnated Diamond Bits 3136
Improved Algorithm 2731
Improved Ant Colony Algorithm 1989
Improved Capacity Spectrum Method 3075
Improved Dynamic Binary Search Algorithm 1905
Improved Fast Marching Method 3544
Improved Local Tangent 4091
Improved PID Algorithm 3464
Improved XFBT 4865
Improvement Methods 450
Improvement of Design of Transmissions 2955
Improving 3177, 4873
Impulse Noise 3706, 3726, 3881, 4019
In-Place 1173
In Situ 320
In-Tree 2782
In Vitro Release 102
IN718 115
In718 Superalloy 27
Incidence Rule 2080

Inclined Pushing Rod 3127
Inclined Tube Sedimentation Tank 849
Incorporated Accelerated Corrosion 458
Increasing Yield 1146
Indentation 883
Independence 3609
Independent Component Analysis (ICA) 1901
Index Mechanism 1127
Indicator System 1157, 5273
Indium Oxide 35
Indoor Positioning 2232
Industrial Design 276, 5373
Industry Information 5086
Inertial Measurement Unit (IMU) 3216
Inertial Navigation 1602
Inertial Navigation System 2555
Inertial Unit 2985
Inflation Forecast 5536
Inflection Nonlinear 1582
Influence Analysis 4200
Influence Factors 2688
Influence Measure 4789
Information 3609
Information Acquisition 3452
Information Automation 1077
Information Classification 1989
Information Disclosure 5398
Information Encryption 3571
Information Entropy 1756, 2029, 4417
Information Fusion 4885
Information Hiding 2393
Information Industries 4456
Information Inquiry 2020
Information Integration 4930, 5267
Information Literacy 5349
Information Management 4902, 5345, 5378, 5382
Information Management Platform 1097
Information Pipe 4621
Information Recommendation 4625
Information Resources 4577
Information Retrieval 4845
Information Securities Investment 1541
Information Security 4261, 4342, 4823, 5000
Information Security Risk Management 4621
Information System 1551, 4621, 4650, 5588
Information Technology 4957, 5106, 5157, 5571
Information Technology Integration Service Platform 4383
Information Visualization 5411
Informationization Construction 5415
Infrared Absorption Method 115, 146, 2764
Infrared Image 3893
Inhibition of Return (IOR) 1093, 3169
Initial Atmospheric Corrosion 446
Initial Concentration 312
Initialization Method 3743
Inner-Lubricating Wheel 684
Inner Slider 3127
Innovation Experiment 599
Insect Repellant (Citral) 735
Inspection Controller 3114
Instruction Trace 1782
Instrument 3411
Insulin 1003
Intake Air System 3477
Integer Ambiguity 4014
Integrated Development 5267
Integrated Logistics 5547
Integrated Management 4573, 5267, 5512
Integrated System 5468
Integration Package 2515
Integrity Education 1594
Integrity Evaluation 1396
Intelligent Analysis 1841
Intelligent Attendance Checking 5532
Intelligent Cultivation Device 4298
Intelligent Home Furnishing 3419
Intelligent Materials 288
Intelligent Substation 3423
Intelligent System 4298
Intelligent Toilet 1077
IntelliJ IDEA 4585
Inter-Cell Classification 2001
Interaction 1909, 4421
Interaction Design 5528
Interaction Mode 4421
Interaction Network 4953
Interactive Image Segmentation 1088
Interactive Multiple Model 2212
Interactive Platform 5304
Interconnect 2647

Interest Community 4815
Interfacial Bonding Strength 177
Interfacial Crack 719
Interference 4050
Interference Suppression 4005
Intergranular Fracture 576
Interlayer 1388
Intermittent Load 2922
Internal Release 1286
International Competitiveness of Industries 1216
International River 5267
Internet 4902, 4953
Internet Finance 5254
Internet Financial 5075, 5386
Internet of Thing (IoT) 3415, 3419, 4261, 4290, 4298, 4447, 4598, 4657, 5004, 5041, 5439, 5444, 5520
Internet Public Opinion 4909
Internet QoS 1598
Interpolated Finite Impulse Response 4195
Interpolation 1739, 2503, 2617, 2709
Interpreted Languages 2097
Interprocess Communication 4893
Interval Data 1641
Interval Slope 1641
Interval System 3340
Intrinsic Mode Function (IMF) 3671
Intrusion Detection 4474, 4832
Intuitionistic Fuzzy 1751
Invasive Weed Optimization 1635, 1849
Inventory Information Management 5453
Inventory Model 1481
Inverse Emulsion Copolymerization 348
Inverse Kinematic Analysis 3105
Inverse Problems 958
Inverted Image 2393
Investor Selection 1845
Ion-Ion Interaction Energy 779
Ionic Liquid 498, 676
Ionic Liquid Crystal Polymer 626
iOS 1739
iPad 1103
IPv6 4346, 4519, 4737
Iron-Base Alloys 2768
Irregular 5461
IT Services 4573
Iterative Erosion 2173
Iterative Gradient 3702
Iterative Method 1857
Iterative Threshold Algorithm 2462

J

J-Integral 2356
J2EE 4298, 4332, 5491
Jacobi Iteration 1790
Java Ee 5605
Jess 4617
Jet 3460
JFreeChart 4452
Jiaozhou Bay 1356, 5601
Job Shop Scheduling 2609
Joint 943
Joint Time-Frequency Analysis 4009
jQuery Mobile 4501
JSP 4585
Jurassic 1415

K

K-Mean 1578, 2169, 2245
K-Means Algorithm 1664
K-Nearest Neighbor Classifier 1762
Kalman Filter 2985, 3587
Keep-Right-Except-to-Pass Rule 2470
Kerdock Codes 3556
Kernel Density Estimation 3689
Kernel Function 1873
Kernel Partial Least Squares (KPLS) 3671
Key 2008
Key Distribution 4837
Key Expansion 1861
Key Separation 2543
Kim Algorithm 3587
Kinetic Energy Projectile 982, 2787
Kinetic Model 827
Kinetic Monte Carlo Method 168
Kinetics 348
Kink-Type Solution 1716
Kirsch Masks Filter 4209
Kmeans 1837

$KMnO_4$ Solution 199
Knapsack Problem 1946
KNN 1541
KNN Algorithm 2123
Knowledge 4466
Knowledge Base 2144, 4851
Knowledge Fusion 1505
Knowledge Representation 1493
KOH-KNO_3 Fusion 480
Kurtosis 3609, 3738

L

L-Isoleucine 997
L/L Matrix 3599
l_1Minimizatio 1610
LabVIEW 2758, 3062
LabWindows/CVI 2951
Lake Taihu 1286
Laminar Flow 3354
Laminate 74
Land Transfer Matrix 5394
Land-Use 5197
Landfill Gas 5596
Landfill Leachate 591
Landscape Architecture 4229
Landscape Index 5394
Landscape Pattern 5394
Landscape Roaming Animation 4229
Landslide 2254
Lanthanum Nitrates 523
Lanzhou Reach of Yellow River 1236
Laplace Transform 1825
Laplacian Characteristic Polynomials 2643
Laplacian Integral Graphs 2643
Laplacian Spectra 2643
Large Complex Equipment Procurement Plan 2507
Large-Diameter 3149
Large Power Industrial Control Network 2970
Large-Scale Construction Project 5294
Large Strain Machining 352
Laser 2882
Laser Cladding 246, 767, 775
Laser Communication 3683
Laser Engraving 3919
Laser Induced Fluorescence 2761
Laser Metal Deposition Shaping 49
Laser Micro Shock Processing 45
Laser Optics 356
Laser Plasma 251
Laser Rapid Repair 502
Laser Shock Processing 27
Lasers 356
LASSO-Penalized 2426
Latent Semantic Indexing 4785
Laterite Nickel Slag 7
Lattice Boltzmann Method 619
Lattice Constant 220
Lattice Misfit 264
Launch Process 3379
Lavation 797
Layer-by-Layer 789
Layout of Integrated Freight Hub 1526
Layout Optimization 1192
LBS 5504
LDO 3236
LDPE 519
LEACH Protocol 4273
Leachate 783
Leading Eigenvalue 3599
Leakage 2959
Leaks 2874
Lean Management Techniques 2811
Leaning 2033
Learning Algorithm 2705
Learning Motivation 5221
Learning Rate 1566
Least Square (LS) 1962
Leave One out 2731
LED Display 5481
Leisure Agriculture 4298
Level Spacing 954
Lever Arm 1962
Lever Method 2955
Lexical Analysis 2097
LFM Pulse Signal 3706
LFM Signal 4001
$Li_{0.95}Na_{0.05}Ti_2(PO_4)_3/C$ 316
$Li_2SrSiO_4:Tb^{3+}$ 437
Liaobin New Town 1157
License Plate Color Information 2569
License Plate Location 1652
License Plate Recognition 2569
Life Cycle 5512
Life Prediction 648
Life Time 3224
Lifting Device 2935

Lifting Wavelet Transform 3910
Light 2778
Light-Emitting Material 284
Light Moisture Meter 3399
Lighting Design 5213
Lightning Protection Business 3437
Lightning Protection Devices (LPD) Inspection 3437
Lignite Combustion 256
Linear Algebraic Equations 4934
Linear Canonical Transform 1973
Linear Codes 2634
Linear Differential Equations 2208
Linear Discriminant Analysis 4119, 4209
Linear FGPMs 715
Linear Matrix 3382
Linear Regression 1497, 2220
Linearly Approximation Approach 4042
Liner System 433, 1208
$LiNi_{0.4}Co_{0.2}Mn_{0.4}O_2$ 462
Linux Operating System 3003
Liquid Crystal 185
Liquid-Phase Reduction 181
Lithium Ion Battery 3092
Littoral Wetland 1189
Liver 1044
$LnPO_4$ 391
Load Balance Scheduling 4771
Load Balancing 4269, 4794
Load Control Mode 2839
Load Transfer 1177
Local Binary Patterns 3885
Local Enrichment 908
Local Fuzzy Classifier 1762
Local Government 4957
Local Image 4577
Local Rubbing Fault 3244
Location 2999
Location Label 2292
Log 1924, 4432
Logger 3015
LOGINK 2782, 5045
Logistic 1861
Logistic Regression 1517, 2426
Logistics 1532, 5082
Logistics Center Location 5555
Logistics Distribution 5504
Logistics Engineering 2519
Logistics Optimization 3088
Logistics Public Information Platform 5045
Logistics Supply Chain 5453
Long-Term Tracking 1610
Longitudinal Wave 638
Loss of Customers 1517
Low-Carbon 1328
Low Carbon Development Path 5232
Low Carbon Ecology 1157
Low-Carbon Economy 1216
Low Consumption 3270
Low Contrast Road 3644
Low Damage Fracturing Fluid 3096
Low Density Parity Check (LDPC) Codes 4095
Low Gimbals 3195
Low-Grade 1408
Low Latency 4253
Low Power 3015, 4865
Low Power Consumption 3394
Low Rank Matrix Recovery 2462
Low-Velocity Impact 74
Lower Critical Solution Temperature (LCST) 494
LP Filter 3898
LSCCF Cathode 759
LTCC Technology 2895
LTE 3556, 4132
LTE-Advanced 1671
Lucene Search Engine 4643
Luminescence 369, 437
Luminescence Polymer 121
Lunar Calendar 5182

M

Machine Design 5341
Machine Learning 1743
Machine Tool 3117
Magnesium Alloy 246, 544, 548
Magnetic Memory Testing 3189
Magnetically Suspended Reaction Wheel 2865
Magnetron Sputtering 65
Mahalanobis Distance 4032
Main Disjunctive Normal Form 1607
Maintenance Equipment 5427
Major Depressive Disorder 2037
Majority Combining 3773
Malicious Nodes 2227

Management 5090, 5551, 5575, 5630
Management Information System (MIS) 5491, 5516
Management Platform 5481
Management System 5364
Mandarin 5336
Manifold-Based Learning 2551
Manifold Learning 3675
Manipulator 2802, 3079
Mannich 134
Mannich Reaction 233
Manufacturing 5547
MapReduce 1578, 2123, 2188
Marine Incinerator 4277
Marine Seismic Exploration 3274
Markov Chain 1728, 2474, 3889
Markov Models 1598
Markovian Parameter 1877
Martial Arts 4362
Marxist 5189
Masking Properties of Human Auditory System 2565
Mass Transfer 831, 3100
Massive Data 4811
Master Curve 172
MASW 958
Matched Points 4104
Material Supply 1481
Materialized View 1955
Mathematical Formula 2156
Mathematical Model 1127, 2001, 2216, 2220
Mathematical Morphology 2135, 3768, 4032
MathM 2156
MATLAB 1861, 2119, 2985, 3359, 3443, 3667
MATLAB Programming 3856
MATLAB Simulation 1574
MATLAB Software 2070, 3851, 4608
Matlab/Simulink Simulation 3172
Maxima-Order 4510
Maximum Differential Algorithm 1456
Maximum Likelihood 3938
Maximum Power Point Tracking (MPPT) 3427
Maximum PV Energy Tracking 1185
Maze 3371
Mcatalyst/Mcod 783
MCDM 2580, 2588
MCU 615, 2511
MD5 4603
MDE 2536
Mean Evolutionary Algorithm 1686
Measure 3613
Measurement 4585
Measurement Model 3526
Measurement Performance 4050
Measurement Range 3266
Measurement Ratio 2318
Measurement System 3041
Measuring Accuracy 2278
MEBN 2106
Mechanical Analysis 2943
Mechanical Behavior 939
Mechanical Property 515, 587, 961
Mechanism 814, 2890
Media Access Control 4727
Media Resource 4811
Media Server 4767
Median-Filter 1652
Median Filtering 3726
Medical Image Analysis 3827
Medical Image Fusion 1082
Medium Enterprises 5386
Medium-Sized Wastewater Plant 1252
Melting-Casting 331
Melting Temperature 320
Membership Matrix 3743
Memetic Algorithms 1849
Memory Management 4723
MEMS 2943
Mercury (Hg) 1356, 5601
Merging Unit 5559
Mesh Network 4629
Mesh Pecking 831
Mesosilicate 395
Meta-Analysis 1692
Meta-Model 4413
Metal Ions 966
Metal Magnetic Memory 891
Metal Matrix Composite (MMC) 270
Metal-Porphyrin 694
Meteoric Water 820
Method 125, 4980
Methylene Blue 531

Metrics 4680
Micro-Blog 4985
Micro-Blogging 4577
Micro-Channel 3354
Micro-Classrooms 5106
Micro Player 4355
Micro-Spring 2859
Microchip Laser 356
Microcontroller 3314
Micromouse 3371
Microorganism 1364
Microscopic Model 5197
Microstructure 267, 325, 331, 425, 515, 755, 763, 775
Microstructure Field 751
Microwave 1196
Microwave-Hydrothermal Method 35
Microwave Irradiation 471
Microwave NDE 3344
Middle Size Enterprise 5498
Migrant Group Incident 1704
Migration 433, 1208
Mild Steel 536
Military Camouflage 4470
Military Software 4684
MIMO Radar 3621
MIMO-SAR 1676
Mind Sports Games 2065
Mine 939
Mine Accident Risk 2306
Mine Internet of Things 4581
Mine Water Inflow 1814
Mineral Belt Image 4074
Mineral Element 1368
Mineralizaton Process 1269
Minimal Connected Components 2474
Minimum Arborescence 2156
Minimum Entropy Deconvolution 3220
Minimum Particle Diameter 611
Minimum Vertex-Cover Problem 4926
Mininet 4794
Mining Safety 3443
Minitab 5468
Misalignment 1962
Missile 5544
Mixed Characteristics 2731
Mixed Conductor 759
Mixing Layer 863
MJC4/3.0L 2962
MKdV Lattice Equation 1716
MMPI 1664
MMSE Channel Estimation 3759
Mn-Doped TiO_2 531
Mn-Mg-O_x Catalysts 490
MnO_x–ZnO/Cord Catalyst 671
Mo 264, 527
mO_3/mCOD 783
Mobile 3530
Mobile Clients 5504
Mobile Computing 4612
Mobile E-Commerce 4506, 4694, 4889
Mobile GIS Technology 3437
Mobile Learning 4157
Mobile Library 4608
Mobile Nurse Information System 1103
Mobile Phone Library 4140
Mobile Police Terminal 4823
Mobile Robot 4104
Mobile Terminal 2111, 3411, 5528
Mobile Web 4501
MobileCloudComputing 2111
MODBUS 3145
Mode Selection 5148
Model 1485, 2617, 3625, 4241, 4524, 4980, 5213, 5551
Model Analysis 4570
Model Checking 2474
Model Construction 2065
Model Parameters 2012
Model Validation 1517
Modeling 2037
Modern Enterprises 5364
Modern Information Technology 5053
Modern Science 5053
Modification 233
Modified 859
Modified Harmony Search 2528, 2532
Modified Staircase Method 879
Modifying 441
Modulation 4147
Module Division 5290
Moire Effect 3571
Molecular Weight 91, 151
Molecule 292
Monitor 3062
Monitoring 1220

Monitoring of Gas Concentration 2962
Monitoring Platform 4598
Monitoring System 3114, 5464
Monomer Conversion 91, 151
Monomolecular Layer 680
MOOCs 5152
Morphological 1240
Morphological Filtering 3220
Morpholoy 437, 462, 1652
Mosaicing 3548
Most Probable Mechanism Function 660
Motif 2128
Motion 3371
Motion Image Retrieval 3575
Motion Simulation Based on Pro/E 2741
Motion Simulation Platform 3683
Movement Video 3567
Moving Average Smoothing Filter 1489
Moving Feature 2540
Moving Images 5461
Moving Objects Detection 2310
Moving Target Detection 3122
Moving Target Tracking 3122
Moving Targets Transverse Direction 2787
MPI 4934
MR Image Reconstruction 3946
MSC2Promela 4698
MSD 2360, 2727, 3922, 3938, 3952, 3997
msp430f149 3394
Mu us Sandy Land 975
Multi-Agent 1505
Multi-Attribute Decision-Making 2547
Multi-Body Contact Dynamics 3037
Multi-Consumer 1887
Multi-Cost Information Constrains 5327
Multi-Deformations 352
Multi-Display 3411
Multi-Effect 203
Multi-Elements Doping 759
Multi-Feature Fusion 2693
Multi-Fractal Wavelet Model 4143
Multi-Frequency 3985
Multi Information Fusion 3278
Multi-Level Fuzzy Probability 947
Multi-Media Technology 3567
Multi-Objective 1732
Multi-Objective Comprehensive Evaluation 2507
Multi-Objective Decision 3447, 5140
Multi-Parameter Correction 3838
Multi-Path 4152
Multi-Peak Function 1626
Multi-Point Receiving 3773
Multi-Resolution Decomposition 3734
Multi-Resources-Constrain 2422
Multi-Sensor 3282
Multi-Signal Conflict 3818
Multi-Threshold 3649, 3856
Multi-View Video Coding 3714
Multi-Walled Carbon Nanotubes (MWCNT) 498
Multiagent Network Structure 5232
Multiblock Copolymers 142
Multicarrier 4290
Multicast Algorithms 2093
Multichannel 3274
Multichannel System 3629
Multidimensional Teaching Goal 5213
Multifactor 2723
Multifunction Gateway 4581
Multilayer Structure 837
Multilevel Filter 2292
Multimedia 5165, 5345
Multimedia CAI Technique 5120
Multimedia Classroom 5106
Multimedia Content 1660
Multimedia Technology 5178
Multimodal Human-Computer Interaction 4930
Multimodal Teaching 5495
Multipath 4669
Multipath Channel 3868
Multipath Interference 3960
Multiple Access Channel (MAC) 4095
Multiple Collaborative 1376
Multiple Election Options 4806
Multiple-Grain Cutting 3248
Multiple Mechanisms Coupling 360
Multiple Website 4241
Multiplexing Relationship 2004
Multiplexing Technique 3583
Multiplier 3041
Multiplier Method 2398
Multistage 3096
Multitasking 4684
Multivariate Data Visualization 2318

Multiwalled Carbon Nanotube 560
Municipal Sewage 603
Municipal Sewage Sludge 2791
Museums 5411
MUSIC Algorithm 1883
Mutation 2301, 2491, 2499, 2621, 4869
Mutation Operation 2528
Mutual Authentication 2349
Mutual Information (MI) 2029, 3671
MVC 4388, 5062

N

N-Gram Model 2062
N-Layer Framework Model 4388
Nacl 458
Namesake Task 1918
Nano Ag 242
Nano-TiO_2 Transparent Hydrosol 611
Nanofluid 619
Nanomelamine Phosphate 301
Nanometer Copper Film 45
Nanopowder 35, 280
Nanosilver-Nickel Alloy 181
Nanosized Magnesium Hydroxide 540
NAT 4346
National Symbol 5144
Natural Circulation (NC) 1348
Natural Clarifying agentsZTC1+1II 1011
Natural Gradient Algorithm 1566
Natural-Mining Industrial System 1305
Nature of the Pipeline 4694
NBI 4452
ND5 Protein Sequences 3599
Near Infrared Spectroscopy (NIRS) 4028
Near Space Airship 360, 3473
Negotiation 4617
Neighbor Authentication 4603
Neighborhood Average Filtering 4054
Neighborhood Correction 1997
Network 544, 3530, 4245, 4249, 4338, 4533, 5609
Network Apparatus 4249
Network Attack 4970
Network-Centric Warfare 5544
Network Control 4265
Network Data 5464
Network Diagram Method 3379
Network Environment 5349
Network Examination Database 5486
Network Hierarchical Structure 2004
Network Information Filtering 4400
Network Instruction 4421
Network Instruction Platform 4421
Network Intrusion 3810
Network Intrusion Detection 2012
Network Management 4338
Network Node 4612
Network Officing 4665
Network Operating System 5224
Network Science 4789
Network Security 2970, 4881, 4885, 4974
Network Simulation 4832
Network Teaching 5304, 5486
Network Teaching Pattern 5290
Network Technology 3567
Network Topology 4629
Network Traffic 4510
Network Traffic Classification 1895
Network Transmission Power Controller 1220
Networked Control Systems 3359, 3382
Neural Network 1424, 2080, 2119, 2569, 2659, 2663, 2667, 2671, 2675, 2705, 3386, 3427, 4100, 4143, 4437
Neutral Plane 3310
New Construction Land 2410
New Material 276, 407
New Nickel Inhibitor 1411
New Principle 3050
New Seawater Flocculants 203
News Gathering 4665
News Gathering Editing 4665
News Recommendation 4704
Newton Interpolation 2667
Newton's Method 1857
NextGen 5619
Ngn3 1003
Ni 1319
Ni (II) Complex 727
Ni Element 420
Ni-Sn-P Alloy 403

Ni(II) Complex 731
Niche Technology 1626
Nickel-Based Superalloy 927
Nitrification 572
NN 2503, 2709
NO 256, 490
NoC 4865
Node Localization 1574
Node Server 4338
Node's Dormancy 4566
Nodes Schedule Priority 2200
Noise 3199, 3810
Noise Point Detection 2273
Noisy Environments 3654
Non-Coal Mine Accident Cause 2306
Non-Isothermal Kinetics 660
Non-Linear 2926
Non-Linear Optimization 1435
Non-Parametric Statistics 2613
Non-Ranging 4169
Non-Stationary Signals 2713
Non-Thermal Plasma 490
Nonconfocal Arrangement 2761
Nonlinear Analysis 986
Nonlinear Equation 1857
Nonlinear Frequency Modulated Signal 4042
Nonlinear Shielding Layer 1273
Nonlocal Nonlinearity 1909
Nonnegative Matrix 4400
Nonsmooth Bifurcation 2825
Nonsubsampled Contourlet Transform (NSCT) 1082, 1901
Nonylphenol Polyoxyethylene Ether 189
Norfloxacin Lactate 993
Normal Load 918
NPD Database 3199
NPLS-Wt 863
NS2 4482
NSCT 3763, 4136
Nuclear Industry Level 2097
Numerical Control Transformation 3240
Numerical Modelling 3460
Numerical Simulation 49, 407, 751, 2254, 2470, 2679, 2697, 2787, 3070, 3456, 3485, 3513
Nutrient Loads 1286
Nutrition Prescription 1849

O

O-Dichlorobenzene 564
Oauth 4767
Object-Oriented 5189
Object-Oriented Programming 4392
Object Segmentation 3575
Object Tracking 2693, 3605
Objective Optimizationl Evolutionary Algorithms 3915
Oblique Penetration 982
Observer Pattern 4392
Ocean Sampling Platforms 1456
OCL 1513
Octree 2389
OFDM 2161, 3759, 3786, 3823, 3902, 4019
OFDM-PON 1695
OFDM-RoF 3521
OFDMA 3658
Office Automation 4219
Offshore Cargo Handling 3058
Offshore Drilling Platform Cleaning Robot 3282
Oil Pollution 2947
OLAP 1657
Oligomerization 727, 731
Oligomers 142
OLT 4962
On-Line Collection 4742
On-Orbit Modal Identification 1766
On-Site Data Process 3437
One-Card 3818
One-Lee Weight Codes 2634
Online FTIR 189
Online Learning 1610
Online Retailer 5457
Online Thematic Map 4466
Ontology 1505, 2179, 4413, 5014, 5630
Open Platform 4767
Open Source 4332
OPENCV 2173, 3973
OpenFlow 4794
Openness 3132
Operating Models 4318
Operating System Fingerprinting 4733
Operating System Scanning 4733

Operation Frequency 3344
Operational Deflection Shape 2899
Operational Training System 4277
Opportunistic Networks 4669
Opportunity Network 2227
Optical Beam 1909
Optical Emission 251
Optical Fiber Ethernet 4581
Optical Flow Algorithm 2540
Optical Flow Sensor 3216
Optical Flows 2731
Optimal Algorithm 2165
Optimal Arrangement 3433
Optimal Design 1849, 2917, 3818
Optimal Group 3689
Optimal Method 1177
Optimal Process 771
Optimal Sampling Path 1456
Optimization 591, 1532, 1873, 2344, 2398, 2450, 2802, 3344, 3379, 3639, 4869, 4934
Optimization Design 3208
Optimization Design System 2869
Optimization Model 2519
Optimized Analysis 4233
Optimizing 4566
Oracle Database 4585
Oracle Synchronization 4917
ORB 2651
Order of Convergence 1857
Ordered Dithering 4082
Organic Extracts 1064
Organic Light-Emitting 292
Organic Matter 603
Organic Molecule 284
Organic Pollution 1364
Organization Design 5331
Orientation 581
Oriented Identification 3968
Orthogonal 2659
Orthogonal Approximation 4437
Orthogonal Discrete Frequency-Poly Phase Coded 3621
Orthogonal Experiment 841
Orthogonal Semi-Supervised 2551
Orthogonal Test 898, 1029
Oscillating 4269
Oscillation Clock 3145
OSHMS 2314
OSPFv2 4603
Otsu 3751, 4074
Otsu Method 1959
Outlier 3367
Overheat Phenomenon 887
Overlap Extension PCR 1115
Overlapping Node 4400
Overloading 5124
Overpass Area 5565
Overtaking 2385
Oxidant 564
Oxidation 15
Oxidized Conditions 1404
Oxidized Starch 156
Oxygen Isotope 820
Ozone 803

P

P-Teredo 4346
P2P 1930, 4556, 4755, 4815
PAC Adsorption 853
Packages Flow 2811
Packaging Design 3262
Packet Delivery Ratio 4633
Packet Encryption 2454
Packet Loss 3382
Paclitaxel 102, 1060
Padé Approximation 2663
Padé Weight Function 2667
Painting Pattern 4470
Pairwise NQD 2491
Panzhihua City 5273
Paper Strengthening Agent 644
Parallel 2169, 2188, 2820
Parallel Flow 3100
Parallel Processing 3084
Parallel Sets 2318
Parallel Spring 2859
Parameter Estimation 1460, 3942, 3977, 4046
Parameters Design 2854
Paraphrase 1720
Parcel Sea Map 1891
Partial Discharge (PD) 1260
Partial Equilibrium 2377
Partial Least-Squares Regression 3367

Particle Filter 3161
Particle Swarm Optimization (PSO) 1566, 2301, 3579
Particle Swarm Optimization Algorithm 1570, 2192
Partitioning Strategy 2364
Passenger Flow 5157
Passive RDX 2679
Passivity-Based Control 2865
Path Loss 3625
Path Planning 1621, 2467
Pathway 199
Pattern Recognition 1260
Pb 1415
PBS 587
PC 3145
PCA 3617, 4510
PCI8602 3407
PCM/FM 2360, 2727, 3922, 3926, 3930, 3938, 3952, 3981, 3997, 4023
PCM/FSK 4191
PDC 2749
PDCA Cycle Model 1107
PDF417 5476
Pdx1 1003
PE 5481
PE Teaching 5102
Peak Point Detection 1489
Peak Searching 3942
Peak to Mean Ratio 3658
PED 1555
Pedestrian Facilities 5508
Pediatric Care 1111
Peer-to-Peer 5066
Penetration Performance 961
People Counting 2540
Peptide 727
Peracetic Acid 138
Perceptual Load 1093, 3169
Perceptual Model 2368
Perfectly Conducting Periodic Surfaces 3777
Perfectly Matched Layer 1869
Performance Analysis 3298
Performance Comparison 4547
Performance Evaluation 2314, 5559
Performance Index 5023
Performance Management 5357
Performance of Software 4497
Performing Environment 3473
Periodic Green's Function 3777
Periodically Pulsed Discharge 1200
Permanent Magnet Synchronous Motor (PMSM) 2815
Permanent Magnetic Brushless Dc Motor 2865
Permeability Estimation 1372
Personal Networks 4751
Personalization 1445
Personalized Operation 4650
Personalized Recommender Systems 4506
Personalized System 4996
Petrochemical Enterprises 5217
Petroleum Substances 803
PF 5431
pH 15
pH Value 97
Phase Behavior 185
Phase Correlation 3663
Phase Grouping 3644
Phase Locked Loop 2364, 4058
Phase Separation 619
Phase Space Reconstruction (PSR) 1348
Phase Transformation of Pearlite 475
Phase Transition Behavior 494
Phosphogypsum 39, 797
Phosphor 369, 623, 755
Phosphorus 827
Photocatalysis 611
Photocatalyst 1073
Photochromic Spiropyrans 523
Photodegradation 224, 527, 531
Photogrammetry 3844
Photoluminescence 623, 755
Photoswitches 523
Photovoltaic Cells 3427
Photovoltaic Inverter 1173
PHS 4478
Physical Chemistry 2679
Physical Driver 2414
Physical Education 5250
Physical Health Evaluation 1107
Physical Layer Network Coding 4147
Physical Sign 1120
Physicochemical Modeling 1297, 1301
Physiological 5336
Physiological Monitoring 1103

PI3K/mTOR Inhibitors 568
PID Control 1449, 3157
Piecewise Hash 4815
Piezoelectric 2774
Piezoelectric Effect 1120
Piezoelectric Impedance Sensor 1120
Piezoelectric Materials 719
Pigouvian Tax 1324
Pipe 3185
Piston Movement 2959
Pixel 1981
PKS 0537-441 3489
PLA 102
Plane 2480
Planetary Train 2753
Planning 4747
Planning Selection 5273
Plasma 55, 60, 2697
Plasma Polishing 308
Plasma Powder Spray Welding 763
Plasticity 212
Plasticizer 164
Platform 5282
PLC 2913
Plug-In Hybrid 2854
Pluronic F87 102
Ply Thickness 74
PM_{10} 1338
$PM_{2.5}$ 1338, 3294
PMAC 3132
PMAC Motion Controller 3290
Pneumatic Control System 3286
Point-Cloud 1555
Point Rupture 1829
Polarization 536, 1196
Policies 5448
Policy Simulations 1328
Pollution 454, 5435
Pollution Rate 2613
Pollution Treatment 1333
Poly Aluminium Chloride (PAC) 845
Poly(p-phenylene benzobisoxazole) (PBO) 560
Poly(p-phenylene vinylene) (PPV) 121
Polyaniline 181
Polycarboxylate Superplasticizer 228
Polymer Delivery System 735
Polymerization 164, 735
Polynomial Fit 2849
Polypropylene 581
Polysaccharide 1011, 1056
Ponding Depth Detection 5565
Poor Information 2723
Popularity Data 2152
Pore Size Distribution 705
Pore Solution 19
Porosity 1424
Porosity Calculation 1372
Porous Gels 373
Porphyrin 694
Porphyrin Film 680
Port Scanning 4286
Portable 3394, 4306
POS Analysis 2292
Pose Estimation 1615
Position Estimation Error 3252
Position Updating 2536
Positioning Technology 4169
Positive Position Feedback 2774
POSSs 743
Post Evaluation 5323
Post-Processing 4165
Post-Trigged 3956
Post-Weld Heat Treatment 576
Postgraduate 5148
Potential 458
Potential Energy 1555
Power Consumption 3015
Power Control 2051
Power Difference 2791
Power Distribution 4461
Power Distribution Network 1177
Power Line Communication 4019
Power Marketing 5516
Power Plant 108
Power Quality 2820
Power Smoothing 2820
Power Supply 2778
Power Supply Area 1278
Power Supply Rejection Ratio 1165, 3236
Power System 1224, 2854
Power System Communication Network 4175
POX 4794
Poyanghu Lake 820
ppp 1324
Practical Example 1204
Practice Teaching 5237
Pre-Oxidation Treatment 194
Precise Pose Control 3105

Precision 701, 1938
Prediction 544, 2152, 2684, 3443
Prediction Model 913, 1517, 1814, 5540
Preheating 11
Premature 1582
Preparation 125, 540, 723
Preparation for Resource 2144, 4851
Preparatory Students 5336
Preprocessing 797
Preservation 1052
Pressure Distribition 1282
Pressure Drop 3161
Pressure Index 1120
Pressure Monitoring 2758
Pressure Sensor 3029
Pressure Vessel Steel 879
Pretreatment 138, 771
Preventive Measures 1111, 3302
Primal-Dual Method 2462
Primary School 5094
Principal Component Analysis 2613, 4028
Principles of Dipartition 1278
Prior Knowledge 4806
Priority 2547
Privacy Protection 2008, 4261
Private Bank 5286
Privilege Separation 4675
Pro/E 3310
Probability Density Hypothesis 2212
Probability Model 1657
Problems 5311
Process 5378
Process Management 4441
Process Migration 4771
Process Mining 1918, 1924, 2101
Process Parameter 49, 763, 3919
Process Reengineering 2336
Process Simulation 3493
Process Variations 2204, 2647
Producer-Consumer Problem 2093
Product Data Quality 1631
Product Development 3208
Product Space 5241
Production Environment 3452
Professional Basis 5098
Prognosis 1037
Progress 1392
Progress Parameters 871
PROII 3493
Project Control System 5464
Project Driven 5057, 5224
Project Management Information System (PMIS) 4747, 5512
Project Teaching 5263
Promethazine 1041
Propagation Behavior 1590
Propagation Characteristic 484
Propellant 172
Property 65, 763
Proportion of the Common Edges of Two Networks 2037
Proposal Assessment 2588
Protection Failures 1181
Pseudomonas syringae 1025
PSNR 2368
PSO 3649
Pt/C 340
PU 5431
Public Crisis 1131, 5540
Public Greenbelt 1192
Public Hospitals 5201
Public Key Size 4326
Public Management 4905
Public Safety 5508
Public Sentiment 1590
Public Service 4713
Public Service Platform 5498
Publish/Subscribe 1660
Publishing 4452
PUCCH 4132
Pull 1522
Pull-Off Test 177
Pulley 2741
Pulse 3314
Pulse Coupled Neural Network (PCNN) 1082
Pulse Wave 1120
Pulsed MIG Welding 3140
Pumping 356
Purchase Cost 5173
Purchase Prediction 2241
Purchase Predisposition 5245
Pure Acrylic Coating 260
Pure Scale Efficiency 2323
Pure Technical Efficiency 2323
Purification 31, 1011
PUSCH 4132

Push System 4625
PVDF 242
PZT Volume Fraction 364
PZT/Epoxy 364

Q

QC-LDPC 3759
QCV Model 4708
QoS 3889, 4265, 4405, 4669, 4949
QoS Evaluation 1464
QR Code 4371
Quadratic Programming 2547
Quadric Surface 2480
Quadrotor 3216
Quality Evaluation 1228
Quality of Network Communication 4566
Quality of Service 4461
Quality Standard 723
Quantization 1743
Quantized Color Code 4123
Quasi-Newton Algorithm 1865
Quasi-Phase Matching 3790, 3794
Quasiconvexity 5241
Quasilinear Elliptic Equation 1829
Quenching 751
Query Information 1441
Questions Answers System 4785
Quota Decomposition in Rural Land 2410

R

R&D Spillover 5278
Radar Cross Section (RCS) 2878
Radar Imaging 3755
Radar-Scattering Characteristic 2878
Radar Stealth Technology 2878
Radial Basis Function 2705
Radial Solution 1829
Radio Frequency Identification (RFID) 4140
Radio Link 4249
Radioactive Concentration 1352
Radix Isatidis 1020
Radix Pseudostellariae 4028
Radon-Wigner Transform (RWT) 3989
Railway Transportation 2344
RAKE 4152
Rake Angle 352
RAKE Receiver 3868
Raman Spectroscopy 130
Random Noise 2278
Random Sets 2212
Random Variables Sequences 2491
Range Resolution 1676
RANS 3468
RANSAC 1615, 4104
Rapid Bidding 5136
Rapid Prototyping 3208
Rare-Earth 383, 775
Rare Earth Doping 391
Rare Earth Oxide La_2O_3 767
Rayleigh Fading Channel 2576
RBAC 4650
RBF 2671
RC-$\prod$ Model 2204
Re-Entry 1146
Reaction Diffusion 1969
Real Estate Enterprises 2625
Real Estate Sales System 5361
Real-Time Communication 4253
Real-Time Monitoring 3390
Real Velocity 2254
Received Signal Strength Index 4547
Receiving Power 1135
Recent Research Progress 379
Reclaimed Water Reuse 108
Reclamation 1305
Recognition 4909
Recognition of Isolated Words 2119
Recommend Mechanism 2188
Recommendation 4996
Recommendation Engines 1445
Recommendation System 4775
Recovery Strategy 1204
Recrystallization 429
Rectilinear Norm 2580
Recursive Least Squares Algorithm 1460
RED 4493
Reduced Conditions 1404
Reduction 5378
Redundant Recommendation Energy 4400
Reef 1424
Reentry Telemetry 3926
Reference 3613
Reference Car Models 2834

Reflectivity 220
Reflow Process 1252
Reflowing Technology 208
Reform of Teaching 5423
Regeneration Opportunity 3161
Region Analogy 1743
Region Growth Algorithm 2088
Region Spatial Frequency 1082
Regional Energy 3763
Regionalism Design 1150, 2796
Registration 3639
Regression Model 5258
Regularization 2250
Regulatory Agencies 3386
Related Processing 4014
Relation of Inter-Views 3714
Relative Speed 918
Relaxation 172
Relevance Feedback 3579
Relevant Failure 4913
Reliability 1181, 4913, 5029
Reliability Evaluation 4660
Reliability Model 5398
Reliable Node 4669
Reliable Restraint 4233
Reluctance Machine 2503
Remanufacturing 5547
Remote Control UAV 2951
Remote Maintenance 4861
Remote Sensing 3548, 3644
Remote Sensing Image 3617, 4100
Remote Sensing Image Denoising 3881
Repetitive-Element PCR 1025
Repetitive Task 1918
Replication Strategy 4913
Requirement Management Tools 4562
Requirement Process 4562
Research 4237, 4637, 4902
Residents Electronic Health Records 5524
Residents' Health Records 1097
Residual Energy 4273
Residual Height 2908
Residual Space 4161
Residual Stress 49
Resistance Change 595
Resonance Frequency 2926
Resource Identifier 4827
Resource Management 1930
Resource Representation 2144, 4851
Resource Scheduling 2192
Resource Scheduling Mechanism 4949
Resource Structure 2144, 4851
Resources Scheduling 4253
Resources Sharing 5353, 5580
REST 1934
REST-Style 1934
Restrooms 260
Retai 1532
Retail Business 5090
Retrieval 5630
Reusable Framework 5614
Revenue Management 2344
Reverse Engineering 1782
Review 4281
RF Wave Heating 2697
RFID 1905, 5004
RFID Technology 5532
RGB Color Space 4123
Rheological Property 629
Rhodamine B 60, 809
RIA 4466
Riccati Equation Approach 3340
Rice 2184
Rice Straw 665
Rift Valley Fever Virus 1115
Rigid Body Models 4367
Ring Singcryption 4409
RIP 4962
Risk 5090
Risk Factors 1111, 5070
Risk Grade 5070
Risk Management 5112
Risk Management Capacities 5286
Risk Measures 5241
River Runoff 1286
RLG 4195
RMDI 1396
RNG K-ε Turbulence Model 2264
Road Area 5197
Road Extraction 3644
Road Profile 3363
Robot 2467
Robot Hand 3181
Robust 4086
Robust Dissimilarity 4205
Robust Principal Component Analysis 2462

Robust Stability 1877
Robust Stabilization 3340
Robustness 2227, 4179
Role 4751
Role Orientation 5263
Rolling Bearing 3220
Rolling Element Bearing 3738
Rolling Force Fluctuations 3386
Rolling Motion 1348
Rolling Process Simulation 425, 429
Room Temperature 97
Root-MUSIC 1973
Rotary Valve 2845, 2874
Rotation Symmetric H Boolean Functions 2593
Rotor System 3244
Rough Set 1536, 1736, 1775
Rough Set Theory (RST) 1770, 2029
Roughness 308
Roulette 4062
Route Choice 2283
Route Planning 1747, 5504
Routing 1942, 4669
Routing Algorithm 2227
Routing Overhead 4629
Routing Protocol 1833
ROV 2965
RS-232 2962
RS-485 2962, 3145
RS485 Bus 3415
RSSI 1574, 2999, 4169
RT-PCR 1115
RTBD 4755
RTDS 1185
RTS/CTS 4078
Ruled Grating 2939
Rules Class 1631
Rules Set 1770
Running Mechanism 2935
Rural Development 5128
Rural Population Hollowing 5128
Rust 420
Ruthenium 480
RVM 1260

S

S-N Curve 238
S-V Model 2232
SaaS 4432
Safe Storage 5007
Safety 4314
Safety Assessment 2671
Safety Benefits 5217
Safety Evaluation 2340, 5300
Safety Facilities 2675
Safety Investment 5217
SAGA 2609
Saliency Map 3552
Salinity Changes 1244
Same-Beam Interferometry 4014
Sample Design 887
Sampler 3294
SAR 3639
Sargassum muticum 747
Saving-Energy 1150, 2796
SBN 2106
SBR 603
SC-FDMA 3658
Scale-Free 4953
Scale-Free Networks 4524
ScB_2 (0001) Surfaces 688
Scenario Editor 4551
Scenario System 4551
Scene Simulation 4277
Scheduling 4115
Scheduling Algorithm 2111, 4727
Scheduling Rule 3447
Scheduling Strategy 4062
Schrödinger Equation 1712
SCM 4058
Score Analysis System 5062
SCR 87
Scratch 502
Screw 69
Screw Separator 23
SDH Communication Network 2237
SDN 4690
Sea-Battlefield 1751
Sea Embankment 1244
Sea Surface Scattering 1135
Sealing 2959
Sealing Machine 2913
Search Steps 1441
Seat Allocation 2344
Seawater Environment 1161
Seawater Treatment 203
Second Class 5209

Secondary Development 407, 4562
Secondary School 5062, 5094
Secondary Watershed 4032
Security 4542, 4690
Security Communication 2349
Security Management 5112
Security Mechanism 4827
Security Model 4371
Security Multicast 4519
Security of Running Software 4497
Security Policy 4261
Security Protection 4970
Security Technology 4533
Sediment 1240
Sedimentation Tank 1309
Segmentation 3751
Seismic 379, 1359
Seismic Multiple Attributes 1424
Seismic Wave 484
Selection Operation 1686
Self-Adapt Distance Measure 3675
Self-Adapting Threshold Comparison 2273
Self-Adaptive 4191
Self-Calibration 3534
Self-Certified Public Key Cryptology 4409
Self-Diagnosis 288
Self-Learning Strategy 2532
Self-Organization Network 4633
Self-Organizing Network 4727
Seller Credit 4980
Semantic 4379
Semantic Expansion 2179
Semiconductive Shielding Composites 629
Sensing Sequence 3591
Sensitivity Analysis 3328
Sensor 288, 3415
Sensor Networks 2093
Sensor Node 3433
Sensorless Control 3252
Sensors 3452
Sentence Alignment 4990
Sentiment Classification 4375
Sentiment Dictionary 1913, 2444
Sentiment Tendency 1913
Separation 3613
Separation of CO_2/N_2 7
Sequence Stratigraphy 1424
Sequential Monte Carlo 2212
Sequential Spectrum Sensing 3591
Serial Communication 3390
Series 2820
Server 4841
Server Load 4897
Server Performance 4897
Server Push Mode 4897
Service 2491, 4869, 5086
Service Innovation 2782, 5045
SESAR 5619
Setting Strategy 4953
Settlement 2332
Settling Process 1356
Sewage 849
Sewage Sludge 138
Shanghai 5575
Shape Angle 2135
Shape from Shading 3544
Shape Memory Alloys (SMAs) 652
Shape Reconstruction 3544
Shape Technique 2878
Shear Wave 958
Sheet Metal Unfolding 3310
Shell 2869
Ship Handling Simulator 5423
Ship Loading Rate 1419
Shipboard Radio 3625
Shock Absorber 3011
Shock-Absorbing System 3298
Shock Wave 1282
Shortest Circuit for Three Villages 2377
Shortest Path 2474
Shrinkage 2895
Shuffled Frog-Leaping Algorithm 2245
Si4133 4058
Side Gate 3127
Side-Lobe Suppression 3722
SIFT 3663
Sign Set 2735
Signal 3609, 3613
Signal Constraint 2839
Signal Extraction 3810
Signal Optimization 3915
Signal Processing 2024, 2364
Signal Separation 3204
Signature Scheme 4310
Silane 441
Silhouette 2731

Silica/Phosphorus 607
Silicon-Based Composite 595
Silicon Content 3505
Silicon Microgyroscope 2926
Silicon Sealant 260
Silsesquioxane 735
Silt Brick-Making 3228
Similarity 3599, 4775
Similarity Calculation 1720
Similarity Measure 1779
Similarity Relation Matrix 1775
Simple Conjunction 1607
Simulated Annealing 2301, 3644
Simulation 168, 548, 867, 1141, 1240, 1244, 1724, 2043, 2084, 2515, 2839, 3019, 3359, 3625, 3960
Simulation Analysis 898, 2065, 2075, 2745, 2854
Simulation Experiment 2196
Simulation Optimization 1477
Simulink 3195
Simulink Toolbox 2070
Single Frame 5461
Single-Gaussian Background Modeling 2310
Single-Phase 3231
Single-Phase Motors 2511
Single-Spool 2845
Single Variable Cross-Section 923
Singular 1829
Singular Perturbation 1969
SINR 3693
Sintered Wall Material Products 710
Sintering 297, 2895
Sisal Fiber 581
Site Remediation 564
Site Selection 1522, 5273
Situation Assessment 1751
Situational Awareness 4885
Six Degrees of Freedom 2802
Six Sigma Management 5468
Size Standard 5319
Skeleton 3768
Sketch Thought 5390
Skid Steering 3045
SLAM 2651
Sliding Strategy 2360
Sliding Window 4427
Slope Stability 3070
Slow Release 665
SLP Algorithm 3088
SM-ESC 1185
Small Current Grounding Fault 3501
Small Enterprises 5386
Small Hollow Block 39
Small-Medium Cities 5624
Small Sample 1453
Small Sample Evaluation Methods 1453
Small Sample-Support 1453
Small-Sized Wastewater Plant 1252
Smart Car 3464
Smart Home 4598
Smith Predictive Control Algorithm 3195
Smith Predictor 3157
Smith Predictor Control 399
Smooth Effect 1256
Smooth Particle Hydrodynamics (SPH) 3248
Smoothness Constraint 1088
SMS 3054
$SnCl_4$ 403
SO_2 256
SOA 1103
Sobel-Operator 3730
Social Engineering 4881, 4970
Social Evaluation 5116
Social Network System 4985
Social Responsibility 5201
SOD 1044
Sodium Methylacrylsulfonate 91
Soft Demodulation 3926
Soft Soil Foundation 2373
Soft-Switching 2886
Softening Coefficient 39
Software 2418, 3084, 4637
Software Architecture 4940
Software Cost Estimation 1497
Software Crowdsourcing 4441
Software Evolution Process Model 2144, 4851
Software Failure Model 4684
Software Logical Model 4497
Software Platform 4501
Software Project 1501
Software Requirement 4562
Software Security 2128

Software Simulation 1477
Software Structural Stability 2128
Software System 3407
Soil 1189
Soil Invertase 1292
Soil-Water Coupled 484
Soildworks 2745
Sol-Gel 607
Sol-Gel Method 531
Solar Chillers 831
Solar Irradiation 527
Solid Sulfonic Acid 134
Solubility 859
Solution Space Organization 4926
Solvothermal Synthesis 301
Sorafenib 1048
Source 3609
Space Division 2389
Space Environment 360
Space Objects with Holes 2655
Space-Time Coding 3902
Spare Representation 3698
Sparse Representation 1610, 3885
Sparse Subset Sum Problem 4326
Spatial Characteristics 5508
Spatial Correlation 2204
Spatial Econometric Model 5278
Spatial Effect 1333
Spatial Scale 1256
Spatial-Spectra Features 3617
Spatial Statistics 4612
Special Group Line 2004
Special Structure 1400
Specialization 5472
Specific Energy 3136
Spectral Radius 1790, 1794
Spectrum Allocation 2051
Spectrum-Shaping 2565
Speech Coding Algorithm 1951
Speech Corpus 5336
Speech Enhancement 2565, 3654
Speech Signal 3667
Speed Mode 2865
SPH 1724
Spline Weight Function 2663
Spool Shaft 2874
Sporting Goods Industry 5037
Sports 4302
Sports Meeting 5588
Spray Pump 2745
Spring Security 4342
Sprocket 2890
SPSS 5132
SPWM 2807, 3231
$Sr(OH)_2$ 280
Sr_2FeMoO_6 130
$SrCO_3$ 280
SSH Framework 5588
Stability 688, 923, 2532, 2859
Stabilizability Criterion 3340
Stabilized Soils 19
Stable Cluster 4294
Stages Divided Method 1501
Stainless Steel 308
Staircase (SC) Test 238
Stakeholders 5540
Standard Particle Swarm Optimization Algorithm 1582
Standard Score 5062
Standardization 4775
Stannate 383
Starch 697
State-Space Equations 2258
Static Analysis 2829
Static Cushioning Property 3258
Static Prediction 3199
Static Pushover 3075
Static Stiffness 3328
Static Test 943
Statistic 1962
Statistical Analysis 5094
Statistical Characteristics 5403
Statistical Learning 2043
Steam Flow 1449
Steam Turbine Blade 2908
Steel 2764
Steel Fiber (SF) 177
Steel-Reinforced Concrete Structure 951
Steel Slag Filter Material 827
Steering-Wheel 3029
StelaLoma 2084
Step Change 1256
Stepped Cooling Control 2165
Stereo Matching 1555
STFT 3930, 4009, 4023
Stir Bar 164

Stitching 3663
Stock Index 2719
Stock Price Prediction 1635, 1646
Stone Processing 1309
Storage Control 1477
Storage Strategy 2450
Storm Surge 2288
Straightening Machine 2741
Strain Distribution 212
Strategy 4889
Stratigraphic Composition 484
Streaming Media 4556
Strength 19, 701, 943
Strength Properties 951
Strength Safety Coefficient 2753
Stress-Affected Zone 927
Stress Characterization 2943
Stress Concentration 3189
Stress Concentration Coefficient 931, 935
Stress Field 751
Stress Intensity Factor (SIF) 2356
Stress-Magnetization Effect 891
Stress Relaxation 3224
Stroke 4742
Strontium Titanate 467
Structural Change 5634
Structural Characterization 680
Structural Equation Model 2931, 5258
Structural Strength 2995
Structure 65, 2499, 2621
Structure of Protocol Analysis 4698
Structure of Software 4497
Struts Framework 4841
Student Attendance System 5605
Student Teachers 5439
Sub-Band Synthesis 1676
Sub-Sampling 3698
Sub-Synchronous Control Interaction 2980
Subspace Decomposition 1883
Subway Shock 3011
Success Rate 4346
Sucrose 134
Sulfate 966
Sulfonated Poly (Arylene Ether Sulfone) 142
Sulfonylurea 1048
Sulfur 146, 2764, 2768
Sulige Gas Field 1146
Sum-Modified Laplacian 1082
Summary 2768
Super Capacitor 2820
Super Gravity 280
Super-Pixel 3946
Super-Resolution 2250
Superabsorbent 665
Superalloy 264, 3306
Supercapacitor 337
Supercritical Carbon Dioxide Fluid Extraction 506
Superhydrophobicity 267
Superplasticizer 97, 233
Supply Chain Inventory Management 5520
Supply Chain Management 5140
Support Vector Machine (SVM) 1453, 1756, 1762, 1873, 1913, 2012, 2184, 2560, 4660
Support Vector Machine Regression 913
Supported Metal Catalyst 340
Surface Methodology 591
Surface Pretreatment 177
Surface Reconstruction 2908
Surface Roughness 3331
Surface Tension 3354
Surface Wave 958
Surge 2254
Surrogate Measures 3915
Sustainable Development 1232
SVG 1224
SVM 1895, 2043, 4375
SVM Classifier 2444, 3906
SVPWM 867, 2886
Swarm Intelligence 1570, 2499, 2621
Swift Satellite 3489
SWIM 5619
Switched Reluctance Motor 3252
Switching Function 1460
Switching Nodes 4338
SWOT Analysis 5186, 5228
SWOT Theory 4456
Symbol Synchronization 1695
Symmetric Positive Definite Matrix 1794
Synchronization 3952, 4023

Synchronization Management 5419
Synchronization Strategy 3629
Synchronous 3922, 3997, 4165
Synchronous Cutting Machine 710
Synchronous Display 5427
Syntax Analysis 2097
Synthesis 35, 185, 189, 731
Synthesis Method 552
Synthesize 233
Synthesized Weights 2268
Synthetic 626
System 4519
System Architecture 4538
System Design 4157, 5300
System Development 3240
System Dynamics 1248, 1328, 2782, 5323
System Integration 5516
System Model 1505
System Reconfiguration 1177
Systems Theory 5078

T

T Location-Scale Distribution 1256
T9 Input 2062
TA 519
Table Tennis 5165
Tabu Search 2523
Tag Anti-Collision 1905
Tailing Dump 1297, 1301
Tailings 1297, 1301
Takeoff Performance 1739
Tangent Line Angle 931
Tank Turret 2878
Target Integration 3169
Target Pixel Extraction 4107
Target Tracking 2212, 3587
Targets Submerge 4107
Task 4751
Task Management 4654
Task Oriented 2033
Task Scheduling Strategy 1810
Tax Differentiation System 5584
TBIR 4069
TCP 4286, 4427
TCP/IP Protocol Stack 4733
Tea Garden 1292
Tea Saponin 771
Teaching 5221
Teaching Assessment 5116
Teaching Effect 5178
Teaching Environment Integration 5106
Teaching Quality 2488, 5116
Teaching Reform 5353
Teaching Reform Program 5057
Teaching System 5237
Teager-Huang Transform 3244
Teamwork 5263
Tear Damage 360
Technical Framework 4302
Technical Risk Assessment 5294
Technique Teaching in Physical Education Courses 5120
Technogenic Pollution 1305
Technology 5378
Telecommunication 4200
Telemetry 3726
Telemetry Data 4165
Telemetry System 1068
Telephone Recycle 5258
Television Basketball Commentators 5033
Tellurite 305
Temper Embrittlement 576
Temperature 747, 1033, 2328
Temperature Coefficient 1165
Temperature Collection 3394
Temperature Control 3195
Temperature Controlled 498
Temperature Field 751, 2165
Temperature-Humidity Effect 1236
Temperature Measure 3015
Tensile Property 325
Tension Control 3019
Teredo 4346
Term Structure of Interest Rate 5634
Termal Dischage 2328
Terminal of Track 3851
Ternary-Tree 2156
Test 3062
Test Platform 3335
Test Signal Method 2980
Texel 1981
Text-Based 1680
Text Categorization 1541
Text Classification 2123
Text Clustering 1853, 4974

Text Extraction 3768
Text Orientation Analysis 2444
Text Pretreatment 2123
Texture 2393
Texture Feature 2693, 3605
Texture Mapping 1981
Texture Model 2016
Thawing Time 3513
Theatre 4775
Theoretical Calculations 2995
Theoretical Model 3331
Theory 5472
Theory of Planned Behavior 5258
Thermal Barrier Coating (TBC) 648, 3344
Thermal Conductivity 3509
Thermal Fatigue 648
Thermal Infrared Camouflage 2323
Thermal Load 595
Thermal Physical Simulation 475
Thermal Stability 437, 759
Thermal Structure Coupling 2922
Thermoresponsive 494
Thickness 387
Thin Film 656, 1829, 2882
Thin-Walled Part with Variable Diameters 3306
Thin-Walled Rectangular Beam 898
Thiophene 185
Three-Dimensional Information 5427
Three-Lane Cellular Automata 2470
Three-Line Coupling Model 1977
Three Networks Convergence 4456
Three-Stage Amplifier 1169
Three-Tier Architecture 4488
Three-View 3844
Threonine Dehydratasegene (*ilv*A) 997
Threshloding 1959
Threshold 3595, 3751, 4524
Through Nitrogen Drying 3399
Ti-6Al-4V Alloy 684
Ti-Ni Based 652
TiB2 270
Tibetan 4375
Tibetan Network 1590
TiC/Al Composite 320
Tight Sandstone Formation 1372
Time 1256
Time Complexity 2663, 2667
Time Context 4920
Time Delay 1877, 1969, 3340
Time Field 3204
Time Frequency Analysis 3810, 4001
Time Prediction 2101
Time Variant Channel Fading 4111
Timing 4917
Tinplate 208
TiO_2-Based 224
TiO_2 527
Titanium Alloy 502
TOA 2232
Token-Based 1680
Tool Path 2908
Tooth Profile Parameter 2753
Tooth Rake Angle 2749
Topic 4845
Topology 4865
Topology Discovery 4723
Topology Management 4723
Topology Relations 2655
TOPSIS 4062
Topsoil 454
Torque 2845
Torsion 923
Total Flavonoid 1029
Total Organic Carbon 1189
Tourism Resources 5186
Tourist Attractions Region 5592
Tourist Hotel 4318
Traceability Code System 5476
Tracking 4909
Tracking Accuracy 4038
Trade Barriers 1216
Trade Process 4533
Traditional Industries 5278
Traditional PID 3019
Traffic Flow 2340, 2684
Traffic Guidance 5565
Training 4358
Training Measures 5349
Training Sequence 1695
Training Set 2062
Trajectory 982
Trajectory Control 2965
Trajectory Profiles 3117
Tramadol 1041
Transdifferentiation 1003
Transfer Alignment 1962

Transfer Rate 2208
Transformation 5086
Transformation Parameters 3844
Transformation Relation 172
Transformer 1220
Transitive Closure 2474
Transmission 3423
Transmission Gear 3037
Transmission Line 69
Transmission Stability 1068
Transmission Structure 4953
Transportation 5157
Travel Time Prediction 5565
Traveling Controller 3114
Traveling Salesman Problem 2196
Treat Mechanisms 1141
Triangle Whitening Weight Function 5294
Triangular Fuzzy Number (TFN) 5559
Triploids 1033
Tris(2,2'-Bipyridyl)Ruthenium 1007
Tropical Crop 3452
Trust Model 4755, 4837
Trust Routing 4405
Trust Value 4755
Trusted Attributes 4940
Trusted Computing Platforms 5000
TT&C Signal 3834
Tufted Carpet Simulation 1700
Tungsten Carbide Nanorods 552
Turbo PMAC 3240
Turbulence Model 3468
Turnover Amounts 2713
Twin Screw Extruder 581
Two-Dimensional Barcode 5476
Two-Parameter P-NCD Conjugate Projection Gradient Method 1802
Two Steps 755
TWR 3363

U

UAVs 4147
Ubiquitous Computing 4930
Ubiquitous Learning 2115
Ubiquitous Network 4827
UDP 4286
UHMWPE Fiber 961
Ultimate Bearing Capacity 407
Ultra-Large-Scale System 4441
Ultra-Low-Bit-Rate 1951
Ultra Low Carbon 2764
Ultra-Low Output Buffer 3236
Ultra Low Sulfur 115
Ultra-Performance Convergence Chromatography 1060
Ultrasonic Frequency Spectrum 951
Ultrasonic Nondestructive 638
Ultraviolet/Optical Telescope 3489
UML 5304
Unbalance Vibration 3204
Uncertain Reasoning 1770
Unconstrained Optimization 2406
Under-Balanced Drilling 903
Underdeveloped Areas 5023
Underground 2999
Underlying Surface 1236
Underwater Acoustic Channel 1865
Uniaxial Compressive Strength 3136
Unidirectional Polymeric Composites 634
Unified Payment 4841
Uniform Circular Array 3722
Uniformity 2264
Universal Device Control Protocol 4215
University Students 5349
UNRI 4827
Unscented Filter 3526
Unsteady Aerodynamics 2258
Unsteady Heat Conduction 599
Unsteady Heat Transfer Analysis 1150
Uplink 3540, 3658
UPNP AV 4767
Upper Computer 2962
Upper Cover of Clamshell Phone 3127
UPS 1224
Urban Community 5245
Urban Construction Area 5197
Urban Emergency Management System 5448
Urban Management 1131, 5540
Urban Renewal 2580
Urban River 1341
Urban Road Network 5565
Urban Traffic 1248
Urban Transport 1328, 5197
Urea 87, 665
Urease 1292
USB Control Transfer 3861
User Behavior 4920

User Behavior Sequence 4432
Users' Association 4985
Users' Behavior 2241
USSOR Iteration 1790
USV 3407
Utility Harmonic Impedance 3367
Utilization Business 4461
UV-MALDI-TOF 743
UV-Spectrophotometry 993
UWB 2232, 3868
Uyghur 4742, 4990

V

V/Fe Co-Doped 611
Vacuum Countergravity Casting 927
Vague Set 2931
Validation Rules 1631
Validity 5029
Value Stream Mapping 2811
Vanadium Slag 3
Vanadium Titanium Catalyst 3
Vane Extruder 581
Variable Speed Limit 3050
Variable Step Length Synchronization 3938
Variable Step Size 3702
Variable Thresholds 3252
Variation 5601
Variation of Constants Method 1712
Variation Operation 1686
VB 3407
VB Programming 5481
Vb Software 5486
VBR Video Traffic Prediction 4143
VC Software 4608, 4612
Vector Control 2807
VEGFR2 Kinase Inhibitors 1048
Vehicle Classification 2043
Vehicle Dispatcher 2223
Vehicle Image 2605
Vehicle Management 2422
Velocity 638
Vendor Managed Inventory 1481
Vendor Selection 5140
Ventilation 3485
Verification 1297, 1301, 4708
Vertical 1364, 5601
Vertical Flow Constructed Wetland 572
Vertical Handoff 1464
Vertical Lift Machine 3105
Vertical Spacing 954
Vertical Zonation 1380
Vetiveria zizanioides 1313
VFD Filter 3834
Via Holes 1977
Vibration 958, 2904, 2959, 3025
Vibration Analysis 3058
Vibration Control 2774
Vicsek Model 2639
Video Correction 3714
Video Losing 3003
Video Monitoring 3003
View Scalability 3714
VIRTOOLS 4861
Virtual Currency 5066
Virtual Editing 4665
Virtual Laborary 5353
Virtual Logistics Enterprise 5357
Virtual Model 1615
Virtual Performance Evaluation 5041
Virtual Private Network 4245
Virtual Radio 3930
Virtual Reality (VR) 2057, 3629, 5407
Virtual Reality Technology 4229
Virtual Simulation 4551
Virtual Visual Servo 1615
Virtualization 4396
Virtualization Technology 2297
Viscous Pressure Forming (VPF) 3306
Visible 2882
Vision-Based 4104
Visual Data Mining 1692
Visual Form 5144
Visual Simulation Technology 5049
Visual Studio 2005 4654
Visualization 2457
Visualization Technology 5369
VLF Communication 4005
VMware 5369
Vocational Qualification Certificate 5290
VOCs 671
Voice Recognition 2119
Volatile Phenol 803
Volume 2480
Volume Resistivity 629

Voluntarily 5205
Voronoi Diagram 1278
Vortex-Grid Flocculation Reactor 849
Vortex-Grid Flocculation Tank 849
VR Animation 5444
VSM 1541, 5331

W

Wall Thickness Differences 927
Warehouse Layout 1547
Warning System 3319
Warship 5609
WASL 1934
Waste 2811
Waste Zirconium Dioxide Loaded Ruthenium-Zinc Catalysts 480
Wastes 1305
Wastewater 5575
Wastewater Treatment 1309
Water 939
Water Adsorption 705
Water Fluid 1724
Water Level Changes 1419
Water Purification 1341
Water Ratio 79
Water-Reducing Performance 97
Water Resources Carrying Capacity 1264
Water Use Efficiency 1264
Water-Washing Tank 3456
Waterborne Polyurethane 644
Waterfront 5323
Watermarking Capacity 2368
Wave 3460
Waveform Design 3621
Waveform Reconstruction 3993
Wavelength Conversion 3790, 3794
Wavelet 2560, 3595, 3973
Wavelet Decomposition 3798
Wavelet Kernel 4474
Wavelet Lifting 1469
Wavelet Reconstruction 4143
Wavelet Threshold 3654
Wavelet Transform 3726, 3910, 4054
Wavelet Transformation 3718
WC-Ni_3Al 297
WDM-PON 3806
Weak-Discontinuity 719
Weak Signal De-Noising 3718
Weak Signal Extraction 3278
Weapons System-of-Systems 2268
Wear 246, 918
Weathering Performance 3473
Weathering Steel 420
Web 4379, 5341
Web Application 4542
Web-Based 5282
Web Data 4902
Web Information Extraction 4322
Web Mining 4909
Web Network 4612
Web Public Opinion 4375
Web Service 4350, 4528, 5516
Web System 4660
Web Workers 4675
web3D Modeling 4277
Weight 1736, 2179, 2547, 4461, 5559
Weight Function 2659, 4437
Weight Loss 420, 536
Weight-Vector 3579
Weighted Centroid Localization 1574
Weighted Index 2431
Weighted Mean Square Error 3730
Weighted Modeling Context 1561
Weka 1837
Weld Edge Transition Arc Radius 935
Weld Toe Inclination Angle 935
Welded Butt Joints 935
Welded Cruciform Joints 931
Welding 3314
Welding Residual Stress 883
Wellbore Stability 1376
Wet Desulfurization Efficiency 913
Wettability 267
WEY 1598
Wheat Anther Culture 5435
Whisker 515
White-Box Testing 4542
White-Light-Emitting 369
White Light Emitting Diode 395
Wiener Filter 3881, 4038
Wiener-Filtering 2565
Wiener System 1460
WiFi 4581

Wigner-Ville Distribution (WVD) 3989, 3993, 4042
Wind 2778
Wind Speed 823
Wind Tunnel 3485
Wind Turbine (WT) 2917
Windbreak Wall 823
Winsock 3359
Wireless Body Area Network (WBAN) 4111
Wireless Communications 3530
Wireless Networks 4590
Wireless-Optical Broadband Access 2495
Wireless Power Transmission 1068
Wireless Sensor Network (WSN) 1833, 1942, 3390, 3633, 4169, 4281, 4294, 4405, 4493, 4547, 4570, 4737, 4832
Wisdom Campus 5439
Witness Simulation 3088
WLED 391
Wool 607
Work Breakdown Structure (WBS) 4747
Work Hardening 212
Workflow 4413, 5398
Workflow Analysis 5588
Workflow System 5614
Workpiece Deformation 2702
Workshop Layout 3088
Worm Geared Transmission 3328
WZD Area 1269, 1380, 1384, 1388, 1392, 1400, 1404, 1428

X

X-Ray Method 883
X-Ray Photography Image 3851
X80 Pipeline Steel 212
Xinxiang City 5186
Xinxiang University 5189

Y

Yangdachengzi Reservoir 1359
Yarn Modeling 1700
YCbCr 2605
Yield Curve 5634
Yinyan Logistics Base 5082
Young Women 5319
YS 1411

Z

Zadoff-Chu Sequence 2495, 2617
Zeolite 4A 3, 7
Zero Sequence Current 3501
Zero Watermarking 1473
Zhengzhou City 1228
ZigBee 3390, 3419, 4581, 4598, 4759
Zinc 480
Zipf Distribution 2152
Zirconium 480
Zn 1415
ZnCoO 656
ZnCuInS/ZnSe/ZnS Quantum Dots 623
ZnO:Al 65
Zone Defense 5193
Zoom 2457

Authors Index

A

An, C.Q. 208
An, L.L. 5551
An, T. 379
An, W.D. 2161
An, X.G. 4497
An, Y. 4456
An, Z.Y. 3195

B

Bai, D. 4819
Bai, E.J. 5237
Bai, J. 923, 3025
Bai, L. 4585
Bai, S. 2639
Bai, W. 727
Bai, Y. 498, 656
Bai, Y.C. 27, 45
Bai, Y.Y. 3683
Bai, Z. 4358
Bai, Z.L. 2474
Ban, L.Y. 3587
Bao, F.X. 4909
Bao, J.H. 3782
Bayati, M.R. 146, 2764, 2768
Ben, X.Y. 1626
Bi, D.Y. 3898
Bi, K. 623
Bi, S. 5565
Bi, X.M. 1517
Bi, Y. 91, 97, 151, 228, 233
Bian, S.H. 2288
Bian, W.L. 1220
Bie, F.F. 2899
Bo, Y. 4009
Bu, H.A. 2165, 3386

C

Cai, B. 1712, 1716
Cai, C.F. 966
Cai, C.G. 841, 1029
Cai, D.J. 3011
Cai, J.P. 4881, 4885, 4970
Cai, L.R. 684
Cai, Q. 1348
Cai, Q.X. 5232
Cai, S.Q. 4200
Cai, X.M. 1165, 1169, 3509
Cai, X.W. 2410
Cai, Y.M. 2356
Cai, Y.W. 2033
Cao, B.Q. 5544
Cao, C.C. 3290
Cao, C.G. 727, 731
Cao, C.L. 2349
Cao, C.Z. 4104
Cao, F. 1324
Cao, H. 2450, 2454, 5007
Cao, H.D. 125
Cao, J. 2491, 2495, 2499, 2503, 2617, 2621, 2709, 3177, 3181, 4869, 4873, 4877
Cao, J.D. 1460
Cao, J.L. 316
Cao, K. 1891, 2731
Cao, L.Y. 4785
Cao, P. 656
Cao, Q.Q. 4694
Cao, R.B. 831
Cao, S. 360, 3473
Cao, S.K. 3114
Cao, S.X. 4811
Cao, W.B. 2470
Cao, X. 1536
Cao, Y. 3868
Cen, K. 4551
Ceschi, R. 2985
Chang, C.G. 1192, 1887
Chang, F.J. 1173
Chang, H.P. 5435
Chang, Y.T. 3236
Che, H.C. 1324
Che, K. 3893
Che, Y.Y. 986, 3165

Chen, B. 3286
Chen, B.D. 3591
Chen, C. 568, 2679
Chen, C.B. 2212
Chen, C.J. 5373
Chen, C.Z. 1566, 2999
Chen, D. 216, 220
Chen, D.Q. 4855
Chen, F. 2043, 2975
Chen, G. 3639, 3644, 4881, 4885, 4970
Chen, G.F. 1700, 4785
Chen, G.H. 369
Chen, G.Q. 607
Chen, G.S. 3390
Chen, H. 4675, 4985, 5532
Chen, H.B. 4865
Chen, H.E. 4355, 5580
Chen, H.J. 1052
Chen, H.Y. 1901
Chen, J. 982, 2787, 4934
Chen, J.J. 2037, 5464
Chen, J.M. 4032
Chen, J.P. 3302, 3898
Chen, J.S. 3045
Chen, J.W. 3530, 4245
Chen, J.X. 5010
Chen, K.J. 4161
Chen, K.K. 2349
Chen, K.T. 1770
Chen, K.Y. 2173
Chen, L. 2634, 2745, 3070, 3132, 4082, 4767
Chen, L.H. 5588
Chen, L.J. 4183, 4920
Chen, L.L. 3698
Chen, L.Z. 3157
Chen, M. 1561
Chen, M.D. 671, 1913
Chen, M.S. 3526
Chen, M.Y. 3367
Chen, N.N. 1736
Chen, P. 387, 3274
Chen, P.Y. 599
Chen, Q. 1313
Chen, Q.D. 723
Chen, R. 1857, 4175
Chen, R.F. 27, 45
Chen, R.H. 2306, 3480
Chen, R.Y. 581
Chen, S. 1157
Chen, S.C. 172
Chen, S.M. 3062
Chen, S.W. 142
Chen, W.Y. 2250, 5250
Chen, W.Z. 2723
Chen, X. 1278, 1695
Chen, X.J. 5624
Chen, X.L. 11, 15
Chen, X.P. 420
Chen, X.Q. 3583, 3768
Chen, X.S. 3114
Chen, X.Y. 4306
Chen, X.Z. 3591
Chen, Y. 531, 560, 1252
Chen, Y.B. 5605
Chen, Y.H. 4310
Chen, Y.J. 506, 511, 4132
Chen, Y.P. 820, 831
Chen, Y.W. 467, 671, 4019, 4062
Chen, Y.Y. 1526, 5010, 5144
Chen, Z.C. 1048
Chen, Z.J. 1607, 2629
Chen, Z.Q. 1200, 3654
Chen, Z.S. 3140
Chen, Z.Y. 1657, 1692
Cheng, B. 918
Cheng, D.X. 1248, 3915
Cheng, F. 4827
Cheng, F.Y. 3838
Cheng, G. 3934, 3952
Cheng, L. 1704
Cheng, P. 2297
Cheng, P.Y. 1141, 3236
Cheng, Q. 3088
Cheng, R.J. 544, 548
Cheng, X. 898, 4488
Cheng, X.H. 1962
Cheng, Y.H. 3505
Cheng, Y.L. 5304
Cheng, Y.Q. 2761
Cheng, Y.Z. 5544
Cheng, Z.Y. 2024, 5427

Chi, T.H. 5444
Chiu, H.S. 4123
Chong, X. 715, 719, 1212
Chu, F.Q. 412
Chu, N. 1517
Cui, B.J. 1680
Cui, C. 1173
Cui, D.Q. 3394
Cui, F. 3889
Cui, G.W. 2065
Cui, H.F. 1802
Cui, H.N. 680
Cui, H.X. 69, 1044
Cui, J. 475, 4832
Cui, L.L. 789
Cui, M.T. 2208
Cui, P.Z. 3693
Cui, Q.L. 4452
Cui, Q.M. 747
Cui, T. 1269, 1380, 1384, 1388, 1392, 1400, 1404, 1428
Cui, W.J. 181
Cui, X.M. 4466
Cui, Y. 2227
Cui, Y.P. 3773
Cui, Z.J. 1829

D

Dai, C.H. 2318
Dai, D.M. 2373
Dai, H.L. 849
Dai, J. 2152
Dai, L. 19
Dai, P.G. 506, 511
Dai, W.B. 4082
Dai, W.J. 5070
Dai, X.W. 1873, 3718
Dai, Y. 715, 719, 1212, 5464
Dai, Y.P. 2569
Dai, Z.H. 3075
Dai, Z.J. 2569
Dai, Z.N. 5634
Dang, J.W. 1082
Dang, X.C. 3633
Deng, C.S. 1686
Deng, F.L. 2184
Deng, H.D. 2951, 3375
Deng, J.W. 3208
Deng, R. 4612, 4789
Deng, R.R. 5382
Deng, S.P. 3240, 3286, 3290, 3294, 3319
Deng, T. 4091
Deng, X. 3497
Deng, X.H. 751, 3037
Deng, X.X. 19
Deng, Y.J. 2675
Deng, Y.N. 2381
Deng, Z.B. 1411
Deng, Z.G. 3599
Di, J. 2565
Di, L.B. 340, 344
Di, S. 2655
Diao, Q. 5565
Dilmurat, H. 4742
Ding, W. 2834
Ding, X. 356
Ding, X.L. 2254
Ding, X.M. 2152
Ding, Y. 1747, 1751, 1853, 3019
Ding, Y.T. 515
Ding, Z.Y. 2444
Donelan, W. 1003
Dong, B. 1660
Dong, C.W. 3140
Dong, G.Y. 611
Dong, J.C. 3698
Dong, J.H. 1821, 5140
Dong, J.Y. 727, 731
Dong, J.Z. 2232
Dong, L. 3644
Dong, L.J. 5468
Dong, L.L. 1664
Dong, L.M. 383, 391, 395
Dong, Q.K. 4519
Dong, Q.Y. 684
Dong, R. 2393
Dong, T. 1077, 2943
Dong, T.L. 1135
Dong, W. 1664, 4229
Dong, X. 5217
Dong, Y.Q. 1762
Dong, Y.X. 1959, 3751
Dong, Z.H. 2254

Dou, Q. 1969
Du, C. 506
Du, F. 462, 2774
Du, H. 3062
Du, H.C. 3122
Du, L. 1770
Du, L.M. 1786, 1806
Du, M.L. 1415
Du, Q. 4396
Du, Q.L. 2913
Du, T. 3, 7
Du, W.Y. 4747
Du, X.P. 5336
Du, Y.F. 3786
Du, Y.L. 1341
Du, Z.B. 2406
Du, Z.H. 595
Duan, S.L. 845
Duan, W. 1756
Duan, X.W. 751
Duan, Y. 5157

E

E, Y.N. 1590, 4375
E, Y.S. 31

F

Fan, B. 2741
Fan, D.H. 3877, 3881
Fan, G.F. 2802
Fan, H.B. 4058
Fan, H.L. 312
Fan, J. 4542
Fan, J.J. 433, 1208
Fan, J.W. 3132
Fan, R.Y. 2462
Fan, S.H. 4573, 4966, 5468
Fan, S.P. 4273
Fan, T.L. 3786
Fan, X. 5033, 5037
Fan, X.Y. 3782
Fan, Y.H. 1946, 1951, 3534
Fan, Y.W. 5033, 5037
Fan, Y.Y. 4845
Fan, Z.H. 1093, 3169
Fan, Z.J. 4392
Fan, Z.L. 3898
Fang, H.H. 1048
Fang, J.G. 1037
Fang, J.H. 3452
Fang, J.J. 270
Fang, L. 1157, 1857, 5596
Fang, M.J. 4253
Fang, X. 3
Fang, X.L. 564
Fang, X.Z. 527
Fang, Y. 3759
Fang, Y.X. 4573
Fang, Z.G. 3033
Fang, Z.K. 3556
Feng, C.G. 242
Feng, J. 3946
Feng, J.J. 923
Feng, L. 1901
Feng, L.P. 2139
Feng, M. 3122
Feng, M.K. 5423
Feng, Q.H. 3919
Feng, R. 164
Feng, W.F. 3534
Feng, Y. 3922, 3930, 3997, 4547
Feng, Y.T. 69
Feng, Z.Q. 5398
Frolov, K. 1297
Fu, B. 1594
Fu, C.F. 91, 97, 151, 228
Fu, D.Q. 2156
Fu, G. 2360, 2364, 2414, 2418, 2693, 2727, 3084, 3844, 3922, 3926, 3930, 3934, 3938, 3942, 3952, 3977, 3981, 3985, 3989, 3993, 3997, 4001, 4005, 4023, 4165, 4191
Fu, H.Y. 4152
Fu, J. 759
Fu, J.W. 181
Fu, L. 615
Fu, L.P. 4625
Fu, M.Z. 4501
Fu, P. 1732

Fu, S. 626
Fu, X.W. 615
Fu, Y. 759
Fu, Y.Q. 3722, 3759
Fu, Z. 2241

G

Gai, K. 55, 60
Gan, X.S. 2671, 2705
Gang, Y.Z. 280
Gao, B. 1341, 5193
Gao, B.F. 2980
Gao, C.H. 2410
Gao, C.J. 540
Gao, C.X. 1441
Gao, F. 2569
Gao, H.L. 2705
Gao, H.S. 2237
Gao, J.B. 1766
Gao, J.J. 1341
Gao, L. 954
Gao, L.J. 194
Gao, L.L. 827
Gao, L.S. 527
Gao, M. 2273
Gao, M.H. 4362
Gao, M.Z. 2444
Gao, P. 4542
Gao, Q. 3633
Gao, Q.H. 4427, 5290
Gao, S. 2212
Gao, S.Q. 1236
Gao, W.H. 3258, 3262
Gao, W.Z. 4104
Gao, X.L. 1328
Gao, Y. 1007, 3314, 3838, 4723
Gao, Y.D. 467
Gao, Y.F. 1720
Gao, Y.P. 2499
Gao, Y.X. 399
Ge, B. 2457
Ge, J.H. 3571
Ge, S. 2106
Geng, G.N. 5112
Geng, J.H. 2741, 5457
Geng, M.K. 4409
Geng, M.L. 4957
Geng, P. 3798
Geng, Q.F. 5245
Geng, W.J. 2414, 4005
Georges, O.O. 4200
Gong, G.J. 3658, 4461
Gong, K.S. 2702
Gong, M.N. 644
Gong, Q. 2212, 5213
Gong, S.J. 4314
Gong, X. 1060
Gong, Y.C. 102
Gu, F. 5136
Gu, G.S. 3561
Gu, H.T. 2523
Gu, K. 2024
Gu, Q. 5157
Gu, S.P. 387
Gu, T. 2917
Gu, W. 4920
Gu, W.J. 4229
Gu, X.D. 701
Guan, H.N. 789, 809
Guan, R.F. 660
Guan, S.Q. 3698
Guan, T.H. 871
Guan, T.M. 3088
Guan, W. 2523, 5624
Guan, Y.T. 312
Gui, B. 4889
Gui, C. 5323
Gui, L.M. 238
Guo, B.H. 4417
Guo, B.Z. 1120
Guo, C.L. 2761
Guo, F. 3782, 4396
Guo, H. 2037
Guo, H.L. 2008, 5300
Guo, H.M. 680
Guo, J. 3015
Guo, J.S. 3790, 3794
Guo, J.Y. 723
Guo, L.D. 1877
Guo, L.Q. 1435
Guo, L.S. 779
Guo, M.H. 4306
Guo, M.M. 356
Guo, Q. 2080, 5345
Guo, R. 3910
Guo, R.C. 1041
Guo, S.J. 4107

Guo, S.L. 1695
Guo, S.S. 4617
Guo, S.Z. 5267
Guo, T. 5098
Guo, T.Y. 5148
Guo, W.W. 1309
Guo, W.X. 2697
Guo, X.G. 5498
Guo, X.H. 2859
Guo, X.R. 156, 160
Guo, X.W. 3204
Guo, X.X. 3195
Guo, Y. 5498
Guo, Y.C. 1252
Guo, Y.K. 356, 1938
Guo, Y.P. 373
Guo, Y.S. 502
Guo, Y.Z. 3025
Guo, Z.Z. 3423

H

Hai, F. 5373
Han, B. 2935
Han, B.Z. 629, 1273
Han, C.L. 2543
Han, C.W. 5565
Han, C.Y. 4514
Han, F.F. 3702
Han, F.Y. 5148
Han, H.C. 763
Han, H.P. 5435
Han, H.W. 1489
Han, L. 2426, 3328, 3331
Han, L.F. 1680
Han, P. 387
Han, Q. 688
Han, Q.B. 2713
Han, Q.T. 1477, 1481, 1485
Han, S. 797, 2115, 4637, 5495
Han, W. 3782
Han, Y.H. 1770, 3587
Han, Z.D. 383, 391, 395
Han, Z.Q. 1396
Han, Z.W. 560
Han, Z.Y. 1786, 1806
Hao, C.M. 1989
Hao, D.K. 3658, 4461
Hao, G.S. 1762
Hao, J.A. 203
Hao, J.H. 2488, 4019, 4461
Hao, L. 3963
Hao, Q.Y. 1946
Hao, S.G. 5398
Hao, Y. 648, 1891
Hao, Z.J. 3633
He, B. 2651, 3679, 3768
He, B.L. 931, 935
He, G.B. 3889
He, H.B. 2097, 2917
He, H.Z. 1356
He, J. 887
He, J.G. 803, 853
He, K.F. 803
He, L. 863, 3773
He, L.F. 4074
He, M.R. 2593
He, Q. 2360, 3926, 4038
He, Q.Y. 3407
He, W.J. 4650
He, X.F. 3427
He, X.S. 5512
He, Y. 2943, 4175, 4767
He, Y.J. 4175
He, Y.L. 3349
Hong, H.C. 2990
Hong, J.C. 4014
Hou, G.H. 665
Hou, G.Z. 4281
Hou, J.M. 4058
Hou, K.P. 3443
Hou, M. 4990
Hou, M.M. 5267
Hou, Y.F. 5336
Hou, Z.X. 305, 312, 337, 2895
Hsieh, T.M. 4123
Hu , Y. 1015
Hu, A.M. 4342, 4893
Hu, B.C. 694
Hu, C.D. 4452
Hu, C.Z. 2128
Hu, D.T. 2314
Hu, F.P. 849
Hu, G.C. 2258

Hu, G.J. 3075
Hu, H.Y. 4949, 5419
Hu, J.B. 1216, 5023, 5250, 5254
Hu, J.M. 5411
Hu, J.Q. 887
Hu, J.S. 185
Hu, J.W. 701
Hu, K. 4014, 5102
Hu, K.H. 727, 731
Hu, L.J. 735, 739, 743
Hu, M. 3041
Hu, M.Y. 1424
Hu, S. 5217
Hu, S.F. 519
Hu, T.J. 1328
Hu, W.B. 3003
Hu, X.D. 305, 312, 337, 3019
Hu, X.F. 595
Hu, X.J. 2495
Hu, X.P. 1264
Hu, Y. 1260, 2377
Hu, Y.J. 4147
Hu, Y.L. 1200
Hu, Y.N. 446
Hu, Y.P. 3058
Hu, Y.R. 5004
Hu, Y.W. 898
Hu, Y.Y. 35
Hu, Z.J. 2288
Hu, Z.X. 142
Hu, Z.Y. 3861
Hua, F. 3639
Hua, R. 4482
Hua, X.M. 387
Hua, Y.H. 4713, 4957
Hua, Y.Q. 27, 45
Huang, B. 3062
Huang, C. 4054
Huang, C.Y. 5319
Huang, D.L. 4759
Huang, F.F. 2101
Huang, G.M. 1135
Huang, H. 4383
Huang, J. 5120, 5619
Huang, J.E. 3231
Huang, J.L. 2593, 2599
Huang, J.Q. 879
Huang, K. 1934
Huang, K.J. 246
Huang, L. 2128, 4219
Huang, L.Q. 3521
Huang, L.X. 1333
Huang, M.Y. 3208, 5559
Huang, M.Z. 1157
Huang, P.H. 1869
Huang, Q. 671, 1578
Huang, Q.Q. 1700
Huang, S.W. 4074
Huang, S.Y. 4902
Huang, T.H. 5468
Huang, T.T. 5045
Huang, X. 3773
Huang, X.B. 1060
Huang, X.F. 3153
Huang, X.G. 3625
Huang, X.H. 4962
Huang, X.P. 540
Huang, X.T. 4326
Huang, Y. 891, 1236, 3189, 5000
Huang, Y.H. 2970
Huang, Y.S. 102
Huang, Y.X. 638
Huang, Z. 581
Huang, Z.J. 4621
Huang, Z.P. 3872
Hung, J.H. 4123
Huo, W.G. 684

I

Imran Shaban, B. 634
Itakura, K. 3136

J

Jhang, S.T. 2156
Ji, A.M. 3513
Ji, D. 2854
Ji, H.Z. 4823
Ji, L.X. 379
Ji, S.W. 2782, 5045
Ji, T.Z. 3427
Ji, Y.P. 11
Jia, C.Z. 2849
Jia, G.L. 2675
Jia, G.M. 1292
Jia, H.L. 2731, 4767
Jia, J.P. 3530, 4245

Jia, Q.L. 4551
Jia, X.D. 4152
Jia, X.F. 3045
Jia, X.M. 1561
Jia, X.W. 619
Jia, Z.F. 3252
Jia, Z.W. 1068
Jiang, A.M. 552
Jiang, A.N. 471
Jiang, B. 2943
Jiang, B.J. 783
Jiang, C.F. 3443, 4751, 4755
Jiang, D.D. 2745
Jiang, H.B. 767, 775
Jiang, H.D. 2625
Jiang, H.N. 3613
Jiang, H.W. 4940
Jiang, J. 2268, 2438
Jiang, J.F. 2697
Jiang, J.M. 783, 3433
Jiang, J.S. 1946
Jiang, L. 966
Jiang, M. 1517
Jiang, M.F. 3946
Jiang, M.L. 4827
Jiang, M.T. 1376
Jiang, M.Y. 1626
Jiang, P.Z. 767, 775
Jiang, S. 544, 548
Jiang, S.D. 2926
Jiang, T. 572, 727, 731, 2639
Jiang, T.T. 2318, 2457, 4269
Jiang, T.X. 203
Jiang, W. 4775
Jiang, W.W. 2016
Jiang, X.L. 841, 1029
Jiang, X.Q. 544, 548, 552
Jiang, X.W. 2377, 2398
Jiang, Y. 1695, 2208, 3889
Jiang, Y.F. 3354
Jiang, Y.H. 841, 1029
Jiang, Y.X. 2385, 3282
Jiang, Y.Y. 2839
Jiang, Z.H. 2697
Jiang, Z.T. 1555, 4326
Jiang, Z.X. 4409, 5228
Jiao, C.H. 3689
Jiao, J.L. 4815
Jiao, S.H. 1883, 3755
Jiao, X. 3437
Jiao, Y. 251
Jin, C. 5630
Jin, J. 2865
Jin, J.H. 280
Jin, L. 4780
Jin, N.S. 348
Jin, P.P. 515
Jin, X. 3946
Jin, X.C. 238
Jin, X.L. 1513
Jin, Y. 1641
Jin, Y.G. 599
Jin, Y.S. 3667
Jin, Z.Y. 189
Jing, F.B. 3088
Jing, L. 1756
Jing, Z.S. 1196
Ju, J.W. 2511

K

Kang, J. 4100
Kang, J.C. 5575
Kang, W.H. 4962
Kang, X.L. 369
Ke, D.P. 1204
Ke, H. 69
Keungputpong, N. 697
Kong, L. 5565
Kong, Z. 1056
Kostina, A. 1297
Kostina, A.M. 1301
Kou, J.B. 731
Kou, M.X. 3084, 3985
Krupskaya, L.T. 1305
Kuang, L.X. 887
Kuang, S.R. 1493
Kuang, T. 2422, 4799

L

Lai, D.R. 820
Lai, G.J. 3851
Lai, R.Y. 490
Lai, S.Q. 194
Lai, X.J. 644
Lai, X.Y. 441

Lang , L.H. 1282
Lee, C.H. 3340
Lei, J. 35
Lei, K. 4556
Lei, L. 1505, 1509, 5116
Lei, S.Y. 935
Lei, W.D. 2258
Lei, Y. 1652
Lei, Y.H. 993
Leng, Q.L. 2288
Li, B. 280, 1286, 4717
Li, B.Z. 2323
Li, C. 544, 548, 1165, 1169, 2753, 3844, 4811, 4865
Li, C.F. 3868
Li, C.G. 820
Li, C.H. 4447
Li, C.L. 1011
Li, C.M. 629, 1273
Li, C.Y. 629, 2438
Li, D. 845, 1146, 1150, 2796, 3096, 3663, 4913
Li, D.B. 845, 3906
Li, D.F. 2004, 3579
Li, D.H. 4143
Li, D.L. 511, 564
Li, D.N. 5000
Li, D.S. 15
Li, D.T. 3208
Li, F. 224
Li, F.C. 1551
Li, F.F. 2444
Li, F.L. 3513
Li, G. 267, 1025, 2491
Li, G.B. 337, 3423
Li, G.C. 660, 3349
Li, G.H. 3331
Li, G.L. 1115
Li, G.Q. 1165, 1169
Li, G.Y. 494
Li, G.Z. 3763
Li, H. 1918, 1924
Li, H.H. 849, 1973
Li, H.J. 1165, 1169, 4104
Li, H.P. 2671
Li, H.Q. 1260
Li, H.R. 5273
Li, H.T. 238
Li, H.X. 305
Li, H.Y. 2917, 2999
Li, J. 391, 837, 1352, 1372, 2555, 2599, 2834, 5571
Li, J.B. 4519
Li, J.C. 4062
Li, J.G. 3306, 3310
Li, J.H. 1700, 2955, 3477, 3526
Li, J.J. 2955, 3477, 5148
Li, J.Y. 498, 3354
Li, K. 490
Li, K.H. 536
Li, K.L. 151
Li, L. 519, 611, 1052, 2323, 3706, 3710, 3777, 3861, 4845
Li, L.F. 961
Li, L.H. 4556
Li, L.L. 2782
Li, L.N. 3240
Li, L.X. 2340
Li, L.Y. 446
Li, M. 1551, 1615, 1913, 2745, 4823, 5508
Li, M.C. 3460
Li, M.J. 2438
Li, M.X. 3571
Li, N. 189, 1861
Li, N.G. 4542
Li, P. 1359, 3493
Li, P.F. 4713
Li, Q. 383, 391, 395, 544, 548, 1165, 1169, 1739, 2381, 2519
Li, Q.J. 1341
Li, Q.R. 3493
Li, Q.W. 3070
Li, R.F. 879, 883

Li, R.L. 2364, 2414, 2418, 2727, 3084, 3930, 3938, 3981, 4046, 4165
Li, R.R. 759
Li, S.L. 7, 576
Li, S.M. 337, 715, 1212
Li, S.S. 4917
Li, S.W. 4501
Li, S.Y. 4577
Li, T. 2144, 2540, 4524, 4851
Li, T.F. 2406, 2499
Li, T.Q. 4684
Li, T.T. 1408
Li, W. 587, 1048, 1192, 1887, 3834
Li, W.B. 599, 2679
Li, W.J. 4845
Li, W.L. 4100
Li, W.W. 3278
Li, W.Y. 69, 2152
Li, X. 228, 1064, 1570, 1602, 1798, 3302, 3367, 5232
Li, X.B. 1913
Li, X.G. 2484
Li, X.H. 523, 4603
Li, X.K. 2735
Li, X.M. 1135
Li, X.P. 2323, 3157, 3489, 4519
Li, X.Q. 2065
Li, X.S. 1015
Li, X.T. 1313, 1368
Li, X.W. 611, 1969, 2084
Li, X.X. 454, 1228, 1232, 5186
Li, X.Y. 1033, 1161, 2995, 3427, 4269
Li, Y. 475, 1857, 1951, 2749, 3306, 3310, 3379, 4775, 4897
Li, Y.B. 1671, 2709, 4869, 4873
Li, Y.C. 1695, 3306, 3310
Li, Y.F. 3910
Li, Y.G. 387
Li, Y.H. 288, 652, 1376, 1901, 2995, 5205, 5221
Li, Y.L. 4533, 4775
Li, Y.M. 2237
Li, Y.P. 102
Li, Y.Q. 3349
Li, Y.S. 1165, 1169
Li, Y.W. 1469
Li, Y.X. 1590, 3768, 4375
Li, Y.Y. 2001
Li, Y.Z. 5228
Li, Z. 1574, 2101, 2935, 3963, 5398
Li, Z.F. 2975
Li, Z.G. 3110
Li, Z.H. 3140, 4241
Li, Z.K. 4119, 4205, 4209
Li, Z.L. 102
Li, Z.S. 576
Li, Z.T. 3136
Li, Z.W. 4819
Li, Z.X. 270
Lian, Z.S. 3456
Lian, Z.Z. 4143
Liang, B. 5112
Liang, E.X. 494
Liang, G.D. 3127
Liang, J.F. 5551, 5630
Liang, J.Y. 5157
Liang, J.Z. 809
Liang, L.J. 2723
Liang, S.J. 506
Liang, S.Y. 3015
Liang, X.K. 4980
Liang, X.Z. 2551
Liang, Y. 4581
Liang, Y.J. 2283
Liang, Z. 1671
Liao, H.C. 3540, 4290
Liao, J.B. 1435
Liao, L. 2970
Liao, P.S. 3340
Liao, X.H. 35
Liao, Z.N. 5004

Lin, C. 3605
Lin, D.L. 5224, 5237
Lin, D.Q. 4482
Lin, D.R. 735, 739, 743
Lin, D.X. 5173
Lin, D.Y. 4482
Lin, F. 125
Lin, G.M. 288, 652, 2947
Lin, H. 5575
Lin, H.P. 1037
Lin, H.Y. 4157
Lin, J.H. 2693, 3985
Lin, J.Z. 1165, 1169
Lin, L.J. 1060, 1282
Lin, S.H. 2791
Lin, X. 246, 1570
Lin, X.L. 966
Lin, X.Y. 1582
Lin, Y. 2144, 4851
Lin, Y.E. 2551
Lin, Y.F. 1720
Lin, Y.G. 4298
Lin, Y.L. 4452
Lin, Y.S. 908
Lin, Z.H. 3702
Lin, Z.P. 4643
Ling, J. 3561
Ling, P. 1762
Ling, S. 2336
Liu, A.G.D.M. 1338
Liu, A.J. 1056
Liu, B. 387
Liu, B.F. 4713, 4717, 4957
Liu, C. 2012, 3132, 3898, 4421, 4654, 4657
Liu, C.L. 1574, 5435
Liu, C.M. 208, 3270
Liu, C.Y. 399
Liu, C.Z. 1359
Liu, D. 883
Liu, D.F. 467, 4723
Liu, D.M. 4566, 4570
Liu, D.Y. 1056, 3872
Liu, F. 3216, 3910, 3993
Liu, F.G. 2264
Liu, F.H. 4338
Liu, F.L. 4318, 5592
Liu, F.Y. 115
Liu, G. 1348, 3889, 5364
Liu, G.C. 1236
Liu, G.F. 1930
Liu, G.H. 2859
Liu, G.Q. 3359, 3382
Liu, G.X. 2426
Liu, H. 1566, 1635, 1646
Liu, H.B. 125
Liu, H.F. 5112
Liu, H.M. 710, 871
Liu, H.Q. 2139
Liu, H.T. 5559
Liu, H.W. 5241
Liu, H.X. 45
Liu, J. 212, 803, 978, 1338, 1810, 2519, 2679, 2878, 2980, 4400, 5464
Liu, J.F. 308, 3282
Liu, J.G. 3411
Liu, J.H. 2922, 3127, 3806
Liu, J.J. 364
Liu, J.L. 2310, 2625
Liu, J.P. 3306
Liu, J.X. 1338
Liu, J.Y. 1704, 2349, 2511, 4091
Liu, J.Z. 576
Liu, K. 1368, 3427, 4028
Liu, L. 1278, 1561, 1924, 4913
Liu, L.B. 360, 1111, 3473
Liu, L.K. 3734, 3743
Liu, L.Y. 1861, 4086
Liu, L.Z. 4514, 4528
Liu, M. 1333, 4528
Liu, M.C. 1319
Liu, M.L. 3011
Liu, N. 1680, 2511, 5524
Liu, N.L. 3747
Liu, N.X. 4717
Liu, P. 1041
Liu, P.T. 3278
Liu, Q. 2258
Liu, Q.B. 767, 775

Liu, Q.X. 458
Liu, R. 420
Liu, R.X. 2111
Liu, S. 1161, 1551
Liu, S.G. 2389, 3973
Liu, S.K. 3220, 3244
Liu, S.P. 789, 809, 2075
Liu, S.Q. 1408, 3199
Liu, S.Y. 4832
Liu, T. 1419, 4832
Liu, T.B. 1541, 4332
Liu, T.X. 1526
Liu, W.H. 5394
Liu, W.J. 544, 548, 4562
Liu, W.L. 5378
Liu, W.Y. 623, 3868
Liu, X. 3722, 3755
Liu, X.B. 3105
Liu, X.D. 2895
Liu, X.F. 3726, 4657
Liu, X.H. 3045, 5596
Liu, X.J. 1020, 1093, 3169
Liu, X.L. 4945
Liu, X.N. 5551, 5630
Liu, X.Q. 3464
Liu, X.X. 2204, 2647, 5290
Liu, X.Y. 83, 134
Liu, Y. 1586, 1686, 1814, 2807, 3161, 4223, 4226
Liu, Y.F. 412
Liu, Y.G. 316
Liu, Y.H. 2565
Liu, Y.J. 276, 1607, 3132
Liu, Y.K. 4684
Liu, Y.L. 5444
Liu, Y.X. 2975
Liu, Y.Y. 1060, 2555, 5000
Liu, Z. 2135, 3671, 3865, 4897
Liu, Z.D. 450
Liu, Z.L. 87, 523, 3714
Liu, Z.Q. 823
Liu, Z.S. 4837
Liu, Z.Y. 2406, 4806
Long, B.L. 1680
Long, D. 364, 1833
Long, J.Z. 297
Long, R.S. 3456
Long, W. 2807
Long, X. 108
Long, Y.H. 2962
Lou, L. 4286, 4733
Lou, L.Y. 3314
Lu, B. 2254
Lu, C.F. 2815
Lu, F. 2878
Lu, G.C. 2917
Lu, H.L. 2097
Lu, H.Y. 4032
Lu, J. 23, 1739, 3658
Lu, K. 3452
Lu, R.H. 4322
Lu, S. 1003
Lu, S.F. 2643
Lu, S.Y. 540
Lu, W.W. 1352
Lu, X.L. 4470
Lu, X.Y. 1756
Lu, Y. 494, 1930, 1962
Lu, Y.F. 638
Lu, Y.L. 2398
Lu, Y.Q. 4905, 5066, 5075, 5386
Lu, Y.T. 3649
Lu, Z.L. 3485
Lu, Z.Y. 5173
Luan, T. 2377
Luo, B.J. 540
Luo, H.B. 1313
Luo, H.P. 3011
Luo, H.X. 3452
Luo, J. 4409
Luo, K. 958, 2245
Luo, L. 3117
Luo, S.Q. 544, 548
Luo, T.W. 3763
Luo, W.T. 3714
Luo, X.C. 74
Luo, X.L. 3730
Luo, X.Q. 1522
Luo, Y. 4889
Luo, Y.S. 2301

Luo, Z.W. 1189
Luo, Z.X. 4577
Lv, D.Y. 3872
Lv, F. 383
Lv, F.X. 2899
Lv, F.Y. 3579
Lv, H. 564
Lv, H.L. 3501
Lv, H.W. 2735
Lv, J. 2184, 3893, 3893
Lv, L.X. 1582
Lv, M.Y. 360, 3473
Lv, Q. 3216
Lv, S.L. 3667
Lv, X.F. 4737
Lv, X.L. 2323
Lv, X.Q. 3552
Lv, X.W. 1411
Lv, X.Y. 1635, 1646, 2344
Lv, Y. 871, 3228, 5448
Lv, Y.P. 3185
Lv, Y.X. 2381
Lysenko, A.I. 1301

M

Ma, B. 5148
Ma, B.Q. 5258
Ma, C.C. 603
Ma, C.R. 2491, 2495
Ma, D.M. 5491
Ma, D.P. 55, 60
Ma, G.J. 515
Ma, G.S. 2165
Ma, H. 2778
Ma, H.Q. 1173
Ma, J. 755, 3278
Ma, J.H. 425, 429, 1641, 2523, 5624
Ma, J.S. 2128, 2849
Ma, L. 1955, 5173
Ma, L.G. 1869
Ma, L.Y. 823
Ma, M.M. 3679
Ma, P.J. 1782
Ma, Q. 3544
Ma, Q.S. 1141
Ma, R. 5504
Ma, R.D. 4195
Ma, R.G. 2675
Ma, R.H. 3823
Ma, S.Q. 5106
Ma, T.B. 2774
Ma, W. 5294
Ma, W.B. 39
Ma, X.B. 918, 4669
Ma, X.C. 1853
Ma, X.F. 1946
Ma, X.J. 531
Ma, X.L. 3786
Ma, X.Q. 5000
Ma, X.Z. 4617, 5512
Ma, Y. 2878, 2882, 3050
Ma, Y.F. 2043, 3973
Ma, Y.P. 3806
Ma, Y.Z. 3136
Ma, Z.S. 1664
Maimaitimin, S. 4990
Mao, J.Z. 5609
Mao, S.J. 5086, 5094
Mao, W. 212
Mao, X.B. 3649
Mao, X.M. 3411, 5528
Mao, Y.F. 1869
Mao, Y.L. 2749
Matchariyakul, N. 697
Meheretu, E. 763
Mei, W. 5544
Mei, Y. 3294
Mei, Y.H. 3363
Men, Y. 1011
Meng, F.C. 4417
Meng, F.J. 5278
Meng, L.X. 3683
Meng, Q.F. 5398
Meng, Q.X. 1814
Meng, Q.Y. 1341
Meng, X. 4058
Meng, X.H. 556
Meng, X.J. 4482
Meng, X.Y. 2306, 3480
Meng, Y.H. 1260
Mi, P.P. 3473
Mi, X.Y. 5508
Miao, D.H. 3319
Miao, J.F. 4506

Miao, J.Q. 1489, 2088
Miao, L.P. 284, 292
Miao, W.L. 1905
Mu, S.L. 2016

N

Na, Z. 1359
Nakai, K. 484
Nan, N. 1020
Ni, H.J. 3208, 3228
Ni, L. 3114
Ni, P.P. 3216
Ni, W. 3105
Ni, Y.H. 3447
Ni, Y.X. 1460
Nie, F.M. 3110
Nie, J. 1877, 4603
Nie, P. 4660
Nie, S. 4223, 4226
Nie, S.H. 3810
Nie, S.Y. 4082
Nie, Y.H. 619
Nie, Y.M. 356, 1938
Niu, C.W. 3505
Niu, J. 2080, 5345
Niu, L.M. 2037
Niu, R.P. 3100
Niu, T.Z. 5588
Niu, X.C. 3513
Noda, T. 484

O

Okorie, S.O. 2890
Ou, C.C. 4930
Ou, G.Z. 5120
Ou, L.J. 519, 1052
Ou, Y.Y. 3561
Ouyang, L. 1150, 2796
Ouyang, L.B. 2292
Ouyang, Z.C. 4669

P

Pan, F.S. 544, 548
Pan, J. 3571
Pan, J.M. 480
Pan, L.A. 2913
Pan, Q. 4966
Pan, S.Y. 1993
Panfilov, O.O. 1305
Pang, B. 3220, 3244
Pang, Y. 1165, 1169
Pang, Y.L. 2373
Pang, Y.P. 1368, 4028
Peh, L.S. 3371
Pei, H.R. 4680
Pei, H.X. 727
Pei, J.F. 2899
Pei, P. 2985
Peng, C. 2702, 4556
Peng, D.H. 3689
Peng, J. 3906, 5116
Peng, J.J. 498
Peng, L. 5444
Peng, L.F. 462
Peng, L.Z. 506, 511
Peng, M. 727, 731, 3025
Peng, P. 1328, 4175
Peng, Q. 3889
Peng, S.Z. 1115
Peng, W. 297, 2381
Peng, W.J. 879, 883, 887
Peng, W.L. 1220
Peng, W.Q. 1341
Peng, X.Q. 2935
Peng, Y. 1775, 3773
Peng, Z.P. 5520
Pian, J.X. 5148
Ping, J. 1621
Pirozmand, P. 4837
Pu, G.L. 1445
Pun, C.M. 3605

Q

Qi, B.K. 5169
Qi, C.P. 1441
Qi, F.Z. 966
Qi, H. 3755
Qi, H.J. 3328
Qi, H.L. 55, 60
Qi, H.Y. 648
Qi, M.H. 1192, 1887
Qi, N.L. 1060
Qi, N.Z. 913
Qi, R.J. 1861
Qi, T. 194
Qi, X.L. 845

Qi, Y.M. 3258, 3262, 3298, 3319
Qi, Z.F. 3212
Qian, J. 560
Qian, J.X. 3617
Qian, L. 4215
Qian, Z. 970
Qiao, C.L. 3693
Qiao, L. 3070
Qiao, L.M. 2939
Qiao, P.Z. 2540
Qiao, S.D. 4169
Qiao, S.J. 3161
Qiao, Y. 471
Qin, G. 3394
Qin, G.W. 1196
Qin, H.S. 4409
Qin, J.F. 4470
Qin, L. 364
Qiu, A.P. 2926
Qiu, D. 4078
Qiu, F.X. 156, 160
Qiu, J. 1782
Qiu, L. 2702, 5427
Qiu, L.J. 2845
Qiu, W.Y. 1739
Qiu, X.R. 3675
Qiu, X.X. 4488
Qiu, Y.H. 5102, 5120
Qu, H. 2297
Qu, J.P. 581, 587
Qu, T. 1680
Qu, Z. 4917
Qu, Z.D. 751
Quan, H.D. 3693
Quan, H.W. 3526
Quan, S.C. 797

R

Rabreau, O. 2985
Ran, M.C. 5341
Rao, C.J. 1821, 1845, 5140
Ren, B.F. 595
Ren, F. 3045
Ren, H.L. 2273
Ren, H.R. 1068
Ren, J.X. 416
Ren, L. 3497
Ren, P. 5224
Ren, S.K. 891, 3189
Ren, S.R. 3806
Ren, X.G. 4934
Ren, Y.C. 1131, 5540
Ren, Y.M. 3885
Rong, X.S. 156, 160, 1762
Rong, Z. 27
Ruan, J.Y. 4161
Ruan, R. 1865
Rui, J. 3534

S

San, X.H. 4785
Sang, L. 1833
Sangirov, G. 3759
Sha, Z.Y. 1278
Shan, B. 3865
Shan, C. 2128, 4350
Shan, J.B. 2016
Shan, M.J. 2148
Shan, X.H. 2344
Shang, Q. 1011
Shang, X. 3390
Shang, Z.Y. 4510
Shao, A.J. 1814
Shao, H. 1770
Shao, H.C. 5369
Shao, H.Y. 2613
Shao, J. 331, 684
Shao, J.B. 2204, 2647
Shay, J. 2811
She, Y. 867, 2886
She, Y.Y. 134
Shen, A.D. 4183
Shen, B. 4861
Shen, C. 4913
Shen, D.Y. 4111
Shen, H.L. 4625, 4909
Shen, H.Y. 284
Shen, L.R. 5353
Shen, Q. 2179, 4727
Shen, R.D. 3248
Shen, S.B. 671
Shen, Z. 5010
Sheng, G. 5331
Sheng, P. 4452
Shi, B. 3092, 3433

Shi, C.C. 4542
Shi, F.M. 2878
Shi, H.L. 2713
Shi, H.Z. 1607
Shi, J. 2890
Shi, J.H. 108, 5178
Shi, J.S. 3838
Shi, J.Y. 1185
Shi, L. 1578
Shi, L.S. 189
Shi, M.J. 2634
Shi, Q. 2926
Shi, Q.N. 420
Shi, S.H. 1097
Shi, S.M. 260
Shi, W.Z. 1376
Shi, X. 3407
Shi, X.F. 1901
Shi, X.K. 4388
Shi, Y. 2381, 4091
Shi, Y.F. 2655
Shi, Y.Q. 1456, 3530
Shi, Z.F. 4917
Shi, Z.L. 5014
Shiau, Y.D. 3236
Shieh, P.I. 2811
Shou, J. 1107
Shu, C.Q. 2753
Shu, N. 3802
Si, Q. 3460
Si, W.J. 1883
Son, T.P. 705
Song, D.R. 1891
Song, F.J. 5128
Song, G.J. 1536, 4310
Song, G.L. 4461
Song, H. 1224
Song, H.Z. 1025
Song, J.P. 3675
Song, J.Q. 4953
Song, L.P. 3172
Song, L.Y. 903
Song, N. 224
Song, W.L. 4650
Song, W.Q. 3199
Song, X.H. 3423
Song, X.L. 399
Song, X.X. 4780
Song, Y. 2651
Song, Y.F. 2749
Song, Y.J. 270
Song, Y.Y. 4562
Song, Z.H. 4127
Su, C.H. 4123
Su, D. 3497
Su, D.G. 4466
Su, G.S. 731
Su, H.Y. 2169, 2188
Su, J. 2605
Su, L.T. 2426
Su, Q.Y. 1196
Su, S.Q. 927
Su, T.J. 536
Su, W. 2431
Su, X.H. 1782
Su, X.P. 2688
Su, Y. 2926, 2943
Su, Y.M. 5263
Su, Y.Q. 4581
Sui, H.G. 3639, 3644
Sui, L. 2859
Sun, B. 4136, 4566
Sun, B.S. 913
Sun, C. 233, 3902
Sun, C.Y. 568
Sun, D.H. 5565
Sun, F. 1938
Sun, F.P. 3893
Sun, F.S. 1586
Sun, G.Y. 177
Sun, H. 2639, 3644
Sun, H.C. 3240
Sun, H.F. 3443
Sun, H.Y. 2688
Sun, J. 1853, 3386
Sun, J.H. 4253, 4675
Sun, J.J. 3827
Sun, J.K. 997
Sun, J.L. 475
Sun, L. 1041, 1985, 3088, 4538
Sun, L.C. 2332
Sun, L.G. 5547
Sun, M.J. 189
Sun, N.W. 2318
Sun, P. 1779, 2939, 4132, 5132
Sun, Q.H. 3290
Sun, Q.Y. 4427, 5290

Sun, S.L. 1646
Sun, S.N. 3456
Sun, S.Q. 5263
Sun, S.Y. 3575
Sun, T.Y. 416
Sun, W.Y. 4405
Sun, X. 490
Sun, X.F. 2697
Sun, X.M. 1566
Sun, X.W. 2922
Sun, X.X. 284, 292
Sun, Y. 1810, 2410, 2935
Sun, Y.D. 1743, 4388
Sun, Y.J. 2402
Sun, Y.P. 2576, 4253
Sun, Y.Z. 1204

T

Tan, C. 809
Tan, F.L. 1938
Tan, G.L. 3319
Tan, H.F. 3763
Tan, L.N. 5536
Tan, W. 5201
Tan, X.L. 4629, 4633
Tan, Y.C. 1686
Tan, Z. 5014
Tan, Z.M. 1676
Tang, B.N. 3513
Tang, D.Q. 5014
Tang, G. 665
Tang, G.J. 3220, 3244
Tang, H.M. 1120
Tang, J. 1056, 3671
Tang, L. 3583, 3755
Tang, P. 2223, 4763
Tang, S.S. 2758
Tang, X.B. 803, 853, 1278
Tang, X.C. 395
Tang, X.G. 3956
Tang, X.L. 490
Tang, Y. 1453, 2111
Tang, Y.P. 3399
Tang, Z. 2245
Tang, Z.B. 284, 292
Tang, Z.M. 1513
Tao, B. 425, 429
Tao, H.T. 3977
Tao, J. 1435
Tao, L. 4100
Tao, L.M. 3058, 4980
Tao, M. 3926, 4042, 4191
Tao, X. 189
Tao, Y. 1464, 3552
Tian, J.Y. 2488
Tian, L. 576, 1489, 3029
Tian, L.F. 863
Tian, Q.Q. 316
Tian, R. 797
Tian, S.Q. 5128
Tian, X.R. 2625
Tian, Y. 2951
Tian, Z.J. 783
Tiptipakorn, S. 697
Tong, H.Z. 2825
Tong, X. 4074
Tong, Z.G. 849
Tu, W.Y. 5624
Tu, X.H. 1048

U

Ubul, K. 4742

W

Wa, D. 87
Wan, A. 2882
Wan, H.L. 4306, 4310
Wan, H.X. 1775
Wan, J.J. 820
Wan, L.J. 1248
Wan, S.S. 2503, 2617, 2621, 3177, 3181, 4877
Wan, X.F. 3208
Wang, A. 5349
Wang, A.D. 820
Wang, A.L. 3114
Wang, B. 1115, 1631
Wang, B.G. 4737
Wang, B.Z. 256, 4974
Wang, C. 1845
Wang, C.D. 2802
Wang, C.J. 4665
Wang, C.L. 4147
Wang, C.M. 3595

Wang, C.Q. 2188
Wang, C.X. 5498
Wang, C.Y. 1396, 1969, 2123
Wang, D. 1712, 5435
Wang, D.F. 676, 2839
Wang, D.H. 2310
Wang, D.J. 755, 2702
Wang, D.Q. 5128
Wang, D.S. 2368, 2393
Wang, D.Z. 3149
Wang, F. 2507, 4478
Wang, F.F. 242
Wang, F.J. 803, 853
Wang, F.W. 4654
Wang, F.X. 5394
Wang, F.Y. 1356, 1786, 1806, 5601
Wang, F.Z. 168, 2344
Wang, G. 5565
Wang, G.C. 3768
Wang, G.F. 5014
Wang, G.P. 1849
Wang, G.S. 3212, 3216
Wang, G.Y. 5481
Wang, H. 49, 208, 312, 1103, 1286, 1415, 3379, 4737
Wang, H.C. 5148
Wang, H.J. 1408
Wang, H.L. 3485, 4273
Wang, H.Q. 1857
Wang, H.S. 412, 680
Wang, H.W. 927, 2939
Wang, H.X. 2323, 2462
Wang, H.Y. 2389, 2410
Wang, H.Z. 1895, 4143, 4510
Wang, J. 203, 308, 997, 1025, 1513, 1704, 2139, 2467, 2523
Wang, J.C. 1396
Wang, J.F. 4917, 5152
Wang, J.J. 2908, 3621
Wang, J.K. 723
Wang, J.L. 3722
Wang, J.M. 3509
Wang, J.S. 5407
Wang, J.T. 827, 1064
Wang, J.W. 97, 903, 4405
Wang, J.X. 5106
Wang, K. 2029, 2735, 2908, 2922, 4009
Wang, K.H. 970
Wang, K.Y. 1115
Wang, L. 181, 185, 316, 595, 644, 3062, 3145, 3415, 3419, 4082, 4466
Wang, L.F. 2576, 4111
Wang, L.G. 3617
Wang, L.H. 5232
Wang, L.J. 3548, 3556
Wang, L.K. 364
Wang, L.L. 276, 3452
Wang, L.P. 1610, 2364, 2727, 3930, 3938
Wang, L.R. 4338
Wang, L.S. 2782, 5045
Wang, L.T. 4669
Wang, L.X. 4302
Wang, L.Y. 849
Wang, M. 1220, 2802, 4127, 4427
Wang, M.H. 305, 312, 337
Wang, P. 373, 1631, 2200, 2543, 3011, 4562
Wang, P.F. 467
Wang, Q. 69, 1177, 1181, 1200, 2935
Wang, Q.G. 2457
Wang, Q.L. 3456
Wang, Q.M. 701, 3045
Wang, Q.P. 5267
Wang, Q.S. 74
Wang, Q.Y. 416
Wang, Q.Z. 2528, 2532, 2536
Wang, R. 2609, 4590
Wang, R.L. 1942, 4940
Wang, S. 611, 986, 3165
Wang, S.B. 2306, 3480
Wang, S.F. 91, 97, 228
Wang, S.H. 305, 312, 337, 1282, 2895
Wang, S.J. 1621, 2959, 5435, 5596
Wang, S.M. 3407

Wang, S.S. 23, 1841
Wang, S.T. 5209
Wang, S.W. 1814
Wang, S.X. 4413
Wang, T. 3534, 4926
Wang, T.H. 2278
Wang, T.Y. 2807
Wang, W. 256, 789, 809, 4286, 4733
Wang, W.B. 4629, 4633
Wang, W.T. 403
Wang, X. 793, 1189, 1411, 3689, 4046, 4562
Wang, X.C. 845
Wang, X.F. 3675, 4261
Wang, X.H. 1997, 4930
Wang, X.J. 65
Wang, X.L. 5029
Wang, X.M. 3248, 5448
Wang, X.N. 348, 1615, 1621
Wang, X.P. 1037, 1598
Wang, X.R. 403
Wang, X.X. 2684
Wang, X.Y. 108, 1536, 4014
Wang, Y. 747, 1115, 1256, 1456, 2051, 3379, 3460, 4119, 4205, 4209, 4441, 4680, 4698, 4708, 5029, 5205
Wang, Y.C. 1341
Wang, Y.D. 2227, 4974
Wang, Y.F. 308, 3286
Wang, Y.H. 3371, 5609
Wang, Y.J. 242, 2047, 2062, 4157, 4603
Wang, Y.L. 3302, 4684
Wang, Y.M. 4524, 5102
Wang, Y.N. 4690
Wang, Y.P. 1082, 3468, 4140, 5439
Wang, Y.Q. 5551
Wang, Y.S. 172, 467
Wang, Y.W. 121, 2232, 4082
Wang, Y.X. 3041
Wang, Y.Y. 246, 1264, 5258
Wang, Y.Z. 2001
Wang, Z. 2593, 2599, 3818, 4107, 4161
Wang, Z.C. 3019
Wang, Z.F. 399
Wang, Z.G. 1873
Wang, Z.H. 320, 325, 331
Wang, Z.J. 1720, 1720, 3306, 4680, 4713, 4957
Wang, Z.K. 4237
Wang, Z.M. 763, 2609
Wang, Z.N. 5300
Wang, Z.Q. 4413
Wang, Z.R. 352
Wang, Z.S. 3390, 4759
Wang, Z.T. 1224
Wang, Z.X. 3790, 3794
Wang, Z.Y. 3100, 4974
Wang, Z.Z. 301
Wei , W. 4926
Wei, C.K. 2758
Wei, D. 4832
Wei, F. 2232
Wei, F.J. 2507
Wei, H. 5444
Wei, H.Y. 1376
Wei, J. 5571
Wei, J.G. 5336
Wei, J.X. 3054, 3902, 3960
Wei, M. 595
Wei, N. 138, 3153
Wei, P.Y. 146, 2764, 2768
Wei, W. 2161, 3885
Wei, X. 1700
Wei, X.F. 3105
Wei, X.J. 480
Wei, X.L. 1372, 2939
Wei, X.Y. 297, 4062, 4169
Wei, Y. 1918, 1924
Wei, Y.H. 1060
Wei, Z.J. 927
Wen, K. 4136
Wen, T. 1985
Wen, Y.C. 5536
Wen, Y.F. 194
Wu, A.L. 1590

Wu, A.Q. 2254
Wu, B. 2292, 4179
Wu, C. 3468
Wu, C.F. 3893
Wu, C.J. 568, 1048
Wu, C.L. 352
Wu, C.Q. 710, 871, 3228
Wu, C.S. 1456, 3530, 3575, 4245, 4249, 4338
Wu, D. 540
Wu, D.Q. 1841
Wu, D.Y. 4452
Wu, F. 1103
Wu, F.A. 1025
Wu, F.P. 5286
Wu, G.D. 4806
Wu, G.H. 638
Wu, G.K. 2922
Wu, G.W. 3595, 4837
Wu, G.Z. 2418, 3989, 4023, 4038, 4191
Wu, H.D. 3790, 3794
Wu, H.H. 540, 556
Wu, H.J. 441
Wu, H.L. 5536
Wu, H.W. 2519
Wu, J. 3149, 4281
Wu, J.F. 831, 3552
Wu, J.K. 3872
Wu, J.T. 3294
Wu, L.J. 511, 2467
Wu, L.X. 879, 4350
Wu, N. 1883
Wu, P. 4694
Wu, P.C. 3236
Wu, Q. 2908
Wu, Q.H. 3968
Wu, Q.T. 3110
Wu, R.W. 1704
Wu, R.Y. 1015
Wu, S.Z. 5415
Wu, T. 4771
Wu, W. 638, 4684
Wu, W.F. 4650
Wu, W.M. 3889
Wu, X.C. 4165
Wu, X.Y. 1473
Wu, X.Z. 1977
Wu, Y. 4573, 4966
Wu, Y.F. 1356
Wu, Y.H. 3587, 5378, 5382
Wu, Y.J. 2364, 2727, 3671, 3934, 3938, 3942, 3952, 3977, 3989, 3993, 3997, 4001, 4005, 4038, 4042, 4046, 4050, 5601
Wu, Y.L. 2913
Wu, Y.Q. 3270
Wu, Y.W. 3790, 3794, 4794
Wu, Z.J. 3734, 3743
Wu, Z.R. 779

X

Xi, D.D. 3485
Xi, S.Q. 680
Xi, X.W. 891, 3189
Xi, Y. 1292
Xia, F.Y. 4346
Xia, H.G. 2528, 2532, 2536
Xia, J. 4050
Xia, K. 1286
Xia, L.Y. 4028
Xia, M. 5341
Xia, S.S. 931
Xia, T. 723
Xia, X.C. 4897
Xia, X.Z. 2106
Xia, Z.Y. 4704
Xiang, Q. 1007
Xiang, T. 2540
Xiang, Y. 490
Xiao, B. 5053
Xiao, C.B. 5241
Xiao, F. 1739
Xiao, H.D. 360
Xiao, J.L. 4684
Xiao, K. 898
Xiao, L. 5300
Xiao, L.J. 903
Xiao, Q. 1309
Xiao, Q.J. 3599
Xiao, W.D. 2444, 2457
Xiao, W.J. 494, 498

Xiao, X. 3567, 3968
Xiao, Y. 1865, 4841
Xiao, Z. 2332
Xiao, Z.J. 3195
Xie, B.G. 1594
Xie, C. 1003
Xie, G.B. 3561
Xie, G.Z. 5504
Xie, H.B. 39
Xie, J. 3782
Xie, L. 3298
Xie, Q. 2250
Xie, Q.S. 3363
Xie, R.Y. 5427
Xie, T.T. 276
Xie, X. 1411
Xie, Y.A. 1676
Xie, Y.H. 2965, 3464
Xie, Y.J. 185, 2356
Xie, Y.N. 3621
Xie, Y.Z. 1873
Xie, Z.L. 387
Xie, Z.M. 172
Xie, Z.X. 4493
Xie, Z.Y. 2029
Xin, G. 1837
Xin, H.M. 4501
Xing, C.Z. 4594
Xing, L.N. 4062
Xing, Q. 4009
Xing, T.L. 607
Xing, W.H. 5435
Xing, Y. 2024, 2368
Xing, Z.H. 4654
Xiong, F. 4694
Xiong, L. 91, 151
Xiong, S.W. 1097
Xiong, T. 1411
Xiong, W. 1532, 5082, 5090, 5311, 5315
Xiong, W.Q. 35
Xiong, X.Y. 102
Xiu, X.Q. 387
Xiu, Z.H. 5609
Xu, B. 1037, 4019
Xu, B.B. 484
Xu, C. 216, 220, 1766, 3639
Xu, C.C. 2093
Xu, C.X. 1695
Xu, D.L. 837
Xu, G. 3658, 4461
Xu, G.F. 2033
Xu, J. 2745, 3963, 5619
Xu, J.C. 156, 160
Xu, J.J. 2431
Xu, L. 3629
Xu, L.B. 450
Xu, L.P. 793
Xu, L.Y. 1204, 1364, 2474, 5584
Xu, M.Y. 1829
Xu, N. 660, 665
Xu, Q.M. 1115
Xu, Q.Y. 997
Xu, R. 1372
Xu, S. 1048
Xu, S.H. 301
Xu, S.K. 3433
Xu, S.W. 4704
Xu, S.Y. 2845, 2874
Xu, T. 1240, 1244, 2328, 2332, 4573, 4966
Xu, T.Y. 623
Xu, W. 4755
Xu, W.D. 2878, 2882, 4470
Xu, X.H. 4675
Xu, X.J. 3029, 3033
Xu, X.L. 4441, 4708
Xu, X.M. 1946, 1951
Xu, X.X. 69
Xu, X.Y. 4091
Xu, Y. 1127, 2663, 4598
Xu, Y.B. 710, 871
Xu, Y.H. 3485
Xu, Y.L. 2753
Xu, Y.X. 2057
Xu, Z. 2609, 3407, 4581
Xu, Z.F. 130
Xu, Z.G. 3195
Xu, Z.H. 611
Xu, Z.W. 1115
Xue, C.Y. 5614
Xue, H. 879, 883, 887, 5169

Xue, H.D. 5491
Xue, H.W. 2070
Xue, J.F. 4350
Xue, J.X. 3140
Xue, Q. 27, 45
Xue, R.H. 3236
Xue, T. 142
Xue, X.F. 320, 325, 331
Xue, Y.F. 1146, 3096

Y

Yan, B. 2169, 2188
Yan, C. 2503, 2709, 3177, 3181, 4869, 4873
Yan, F. 1348
Yan, G.D. 5575
Yan, G.H. 3199
Yan, G.Z. 1068
Yan, H. 1837, 4233, 4949, 5419
Yan, H.W. 292
Yan, L. 2426
Yan, L.H. 961, 1895
Yan, Q. 1547
Yan, S.Q. 3798
Yan, T. 3714
Yan, W. 1578
Yan, X.Y. 4643
Yan, Y.M. 2029
Yan, Z. 3375
Yan, Z.B. 820
Yan, Z.C. 2301
Yan, Z.G. 2184
Yan, Z.W. 2165, 3386
Yang, A.M. 1011
Yang, B. 203, 403
Yang, B.F. 1473
Yang, C. 3489
Yang, C.A. 494, 498
Yang, C.D. 4861
Yang, C.H. 3248
Yang, C.L. 4970
Yang, D.F. 1356, 5601
Yang, F. 7, 4519
Yang, F.H. 2825
Yang, F.X. 519, 1052
Yang, G. 3521, 5112
Yang, G.L. 2555, 4195
Yang, H. 177, 519, 1497, 1501, 2192, 2196, 2208, 4294
Yang, H.T. 3489
Yang, J. 552, 1918, 1924, 2854, 2904, 2917, 4100, 4132, 4136, 4396, 4881, 4885, 4970
Yang, J.H. 3617
Yang, J.M. 256, 913
Yang, K. 3294
Yang, K.J. 4082
Yang, K.W. 2268
Yang, L. 1011, 1798, 2667, 2761, 2791, 3354, 3548, 4603, 5286, 5431
Yang, L.J. 1003, 4811
Yang, L.Q. 1547, 2895, 5634
Yang, M. 4111
Yang, P. 1338
Yang, Q. 3447
Yang, Q.L. 5201
Yang, Q.Y. 4603
Yang, R. 407
Yang, R.J. 552
Yang, S. 747, 3552
Yang, S.F. 1977
Yang, S.J. 2555, 2869
Yang, S.M. 2029
Yang, W. 1424, 2511, 4690
Yang, W.C. 4643
Yang, W.G. 3834
Yang, W.L. 3552
Yang, X. 3468, 5182, 5435
Yang, X.D. 1007
Yang, X.H. 3579
Yang, X.Q. 5601
Yang, X.Y. 1141, 4945
Yang, Y. 369, 564, 2152, 3548, 3806, 4350
Yang, Y.C. 1082
Yang, Y.D. 2849
Yang, Y.E. 3344
YANG, Y.F. 5423

Yang, Y.H. 2576, 4111
Yang, Y.P. 4524
Yang, Y.T. 2377, 2398
Yang, Y.X. 1037, 2507, 4078
Yang, Z. 1196
Yang, Z.F. 1909
Yang, Z.G. 83, 134, 4723
Yang, Z.H. 1861, 3556
Yang, Z.M. 3149, 4147
Yang, Z.S. 280
Yang, Z.X. 1115
Yao, H.G. 5403
Yao, L. 1177, 1181, 1419, 1586
Yao, M.M. 224
Yao, P. 3140
Yao, S.G. 619
Yao, S.J. 3625
Yao, S.L. 5209
Yao, S.W. 1918, 1924
Yao, W.L. 4277
Yao, X.H. 425, 429
Yao, X.L. 3981, 4050
Yao, X.P. 1115
Ye, C.T. 39
Ye, C.Y. 2336
Ye, F. 814, 1671, 3689
Ye, H.M. 4127
Ye, S.C. 2135
Ye, W.X. 35
Ye, X.H. 1918
Ye, X.J. 982, 2787
Yi Qin, S.G. 4367
Yi, B. 4547
Yi, H.H. 490
Yi, L. 4023
Yi, S.H. 863
Yi, Y.H. 1942
Yin, C.B. 5224, 5263
Yin, C.P. 1273
Yin, G.S. 923
Yin, H.W. 5327
Yin, J.B. 23
Yin, K. 1192, 1887
Yin, M. 2753
Yin, Q.L. 2480
Yin, S. 599
Yin, S.C. 2135
Yin, S.H. 1341
Yin, X.Y. 1522
Yin, Z.T. 3015
Ying, X.L. 4069
You, P.L. 437
You, X.R. 3915
Yu, A.L. 3856
Yu, B. 2741, 2820
Yu, C.F. 5427
Yu, C.M. 694, 4675
Yu, D.J. 5373
Yu, F.D. 5390
Yu, G. 412, 2227
Yu, H. 2173, 5555
Yu, H.B. 2815, 2829, 3335
Yu, H.J. 572, 591, 603
Yu, H.L. 2008
Yu, J. 2232
Yu, J.Q. 5331
Yu, K.L. 2959
Yu, L. 883, 986, 3165
Yu, L.J. 5444
Yu, L.L. 1861
Yu, L.Y. 4556
Yu, M. 853, 3075
Yu, M.D. 564
Yu, N.H. 3872
Yu, P. 3942
Yu, Q. 2144, 4851
Yu, Q.X. 412
Yu, R. 552
Yu, R.L. 2865
Yu, S.D. 1853
Yu, S.L. 4028
Yu, S.T. 665
Yu, S.X. 3306
Yu, T. 4694
Yu, W.X. 2605
Yu, X. 1435
Yu, X.N. 5512
Yu, Y. 572, 591, 603, 2144, 4690, 4851
Yu, Y.N. 3266
Yu, Y.T. 1747, 1751
Yu, Y.X. 931, 935
Yu, Y.Y. 4100
Yu, Y.Z. 827, 1064, 3224

Yu, Z.N. 523
Yu, Z.S. 2474
Yu, Z.X. 3335
Yuan , D.B. 4466
Yuan, C. 1348
Yuan, C.H. 1073
Yuan, C.Y. 747
Yuan, D.F. 2227
Yuan, D.L. 3654
Yuan, F. 288, 1951
Yuan, H.L. 320, 325, 331
Yuan, J.C. 1157
Yuan, L.H. 2084
Yuan, M.H. 228
Yuan, N.Q. 2639
Yuan, Q. 2515, 4200
Yuan, Q.S. 4147
Yuan, S.J. 130
Yuan, T. 4861
Yuan, X.D. 3105
Yuan, Y.F. 4514
Yuan, Y.J. 5232
Yuan, Y.X. 803, 853
Yuan, Z.Z. 2283, 5197
Yue, H. 5508
Yue, H.G. 1352
Yun, L.J. 3838

Z

Zalupski, P.R. 115
Zang, Y.J. 939
Zeng, G. 4432
Zeng, J. 723, 2402
Zeng, L.P. 4314
Zeng, P. 3045
Zeng, Q.F. 3437
Zeng, X.L. 4115
Zeng, X.P. 859
Zeng, Y.C. 556
Zeng, Y.S. 4069
Zeng, Z.Y. 2882
Zhai, J.W. 242
Zhai, Q. 5461
Zhan, J.H. 4437
Zhan, M.Q. 4322
Zhan, S.L. 458
Zhan, Y. 4474
Zhang , Y.H. 5304
Zhang, A.J. 203
Zhang, B. 364, 2268, 3806
Zhang, B.J. 2580, 2588
Zhang, B.W. 5165
Zhang, B.Y. 5508
Zhang, C. 1586, 1977, 2318, 2457, 4698, 5504
Zhang, C.C. 629, 4767
Zhang, C.F. 1766
Zhang, C.G. 1088
Zhang, C.H. 1981
Zhang, C.P. 680
Zhang, D.D. 3079
Zhang, D.H. 943, 1704, 2165, 3386
Zhang, D.M. 3919
Zhang, D.X. 3654
Zhang, D.Y. 1728, 1732, 2659, 2663, 2667, 4437
Zhang, F. 475, 665
Zhang, F.Y. 2356
Zhang, F.Z. 2543
Zhang, G.L. 2402
Zhang, G.M. 3344
Zhang, G.T. 1415
Zhang, G.X. 69
Zhang, H. 2273, 2462
Zhang, H.B. 5364
Zhang, H.C. 581
Zhang, H.F. 2854, 4650
Zhang, H.J. 5596
Zhang, H.K. 2318, 2457
Zhang, H.L. 441
Zhang, H.M. 3371
Zhang, H.N. 3675
Zhang, H.P. 2985, 5491
Zhang, H.X. 5041, 5357
Zhang, H.Y. 611
Zhang, J. 416, 626, 903, 1041, 1120, 1173, 1309, 2859, 3552
Zhang, J.G. 3306, 3310
Zhang, J.H. 177, 975
Zhang, J.M. 2655
Zhang, J.P. 4115, 4510
Zhang, J.Q. 4694, 4930
Zhang, J.S. 4566, 4570
Zhang, J.X. 3323, 4095

Zhang, K. 1185, 1313, 3868, 4195, 4478, 5555
Zhang, K.P. 1037
Zhang, K.X. 3675
Zhang, L. 475, 1141, 1248, 2024, 3915, 4187, 4379, 5630
Zhang, L.H. 5596
Zhang, L.L. 2655, 3286
Zhang, L.P. 1292, 1610
Zhang, L.Q. 2101, 5435
Zhang, L.X. 5300
Zhang, L.Y. 767, 775, 1532, 5086, 5315
Zhang, L.Z. 168, 3683
Zhang, M. 79, 238, 1505, 1509, 1849, 2179, 2216, 2220, 3427, 4383, 5082, 5090, 5189, 5311
Zhang, M.J. 467, 5010
Zhang, M.M. 5193
Zhang, M.N. 2152
Zhang, M.Z. 4815
Zhang, N. 312
Zhang, P. 1946, 3493, 3521, 4827
Zhang, P.C. 5544
Zhang, P.D. 3714
Zhang, Q. 130, 849, 947, 951, 1141, 4358, 5041, 5516
Zhang, Q.H. 607
Zhang, Q.L. 2560, 2719, 2869
Zhang, Q.X. 3763
Zhang, Q.Y. 450
Zhang, R. 387, 1829, 2349, 4452, 4456
Zhang, R.F. 4127
Zhang, R.H. 3100
Zhang, R.J. 4841
Zhang, R.L. 4603
Zhang, R.Z. 348
Zhang, S. 961, 1712, 1716, 3738, 5228
Zhang, S.C. 4962
Zhang, S.D. 208
Zhang, S.G. 1790, 1794, 4427
Zhang, S.H. 3204, 3266
Zhang, S.J. 1720
Zhang, S.P. 5273
Zhang, S.Q. 3919
Zhang, S.S. 5197
Zhang, S.X. 3354
Zhang, S.Y. 387, 2488
Zhang, T. 74, 3331, 5491
Zhang, T.Q. 623
Zhang, W. 352, 607, 751, 1825, 1981, 4617, 4794, 5049
Zhang, W.B. 297
Zhang, W.D. 5228
Zhang, W.G. 2947
Zhang, W.J. 2288, 5282
Zhang, W.M. 611, 3117
Zhang, W.P. 5336
Zhang, W.Y. 125, 2156
Zhang, X. 320, 325, 710, 1664, 2144, 2431, 3354, 4851
Zhang, X.D. 931, 935, 2115, 4273, 4452, 4637, 5357, 5495
Zhang, X.H. 576, 1088, 3282, 3323, 5619
Zhang, X.L. 676, 2807, 3140
Zhang, X.M. 4643
Zhang, X.P. 3
Zhang, X.Q. 203, 395, 5349
Zhang, X.W. 4082
Zhang, X.X. 185, 2268, 4785
Zhang, X.Y. 383, 684, 1570, 2939, 4823, 4962
Zhang, X.Z. 121, 203, 2540

Zhang, Y. 177, 450, 502, 623, 1088, 1248, 1652, 1981, 2169, 3274, 3534, 3658, 3915, 3968, 4427, 4528, 4802, 4996, 5078, 5486
Zhang, Y.B. 2820
Zhang, Y.C. 2834
Zhang, Y.D. 412, 5062
Zhang, Y.F. 3189, 4245
Zhang, Y.G. 1185
Zhang, Y.H. 1973, 2111, 3172, 3437, 5559
Zhang, Y.J. 755, 771, 4447, 4926
Zhang, Y.L. 1901, 3117, 4383
Zhang, Y.N. 3885, 4617
Zhang, Y.Q. 60, 2288
Zhang, Y.S. 203, 1877, 3963
Zhang, Y.W. 961
Zhang, Y.X. 1352, 3505, 3738
Zhang, Y.Y. 771
Zhang, Z. 767, 775, 2097, 2834, 3208, 3814, 5547
Zhang, Z.G. 3798, 4966
Zhang, Z.H. 814, 2629
Zhang, Z.J. 4493, 5472
Zhang, Z.L. 1177, 1181, 3270, 3274
Zhang, Z.M. 3204, 3266
Zhang, Z.X. 3007
Zhao, B. 2761
Zhao, B.B. 1739
Zhao, B.Q. 701
Zhao, C. 1419
Zhao, C.H. 1278
Zhao, C.J. 2970
Zhao, C.X. 2208, 3302
Zhao, D.A. 3252
Zhao, D.F. 2264
Zhao, D.X. 3683
Zhao, D.Y. 181
Zhao, F. 2119
Zhao, G.F. 898
Zhao, G.H. 986, 3165
Zhao, H. 688, 1728, 1973
Zhao, H.H. 2829
Zhao, H.R. 3844
Zhao, H.Y. 3019
Zhao, J. 755, 759, 1473, 3834, 4608
Zhao, J.M. 2639
Zhao, K. 264, 2820
Zhao, L. 23, 1273, 5323
Zhao, L.F. 2931
Zhao, L.G. 4302
Zhao, L.J. 3671
Zhao, L.L. 2204, 2647, 3718, 5290
Zhao, L.Q. 1977
Zhao, M. 1309, 1610, 3782, 4562, 5049
Zhao, M.X. 5157
Zhao, N. 2144, 2613, 4417, 4851
Zhao, Q. 701
Zhao, Q.Y. 1411
Zhao, R. 2659
Zhao, R.F. 3306
Zhao, S. 4388
Zhao, S.C. 4338
Zhao, S.N. 731
Zhao, S.Q. 2980, 4737
Zhao, T.X. 1657, 1692
Zhao, W.D. 5057, 5062
Zhao, W.L. 3649
Zhao, W.W. 1849
Zhao, X. 1724
Zhao, X.E. 199
Zhao, X.F. 194
Zhao, X.L. 2128
Zhao, X.Y. 823
Zhao, Y. 634, 1408, 1766, 5476
Zhao, Y.J. 3609, 3613
Zhao, Y.L. 3282, 4751
Zhao, Y.P. 591
Zhao, Y.R. 1905
Zhao, Y.X. 863
Zhao, Y.Y. 3252
Zhao, Y.Z. 4452
Zhao, Z.C. 5565

Zhao, Z.H. 5605
Zhao, Z.L. 1368, 5193
Zhao, Z.M. 797
Zheng, C.C. 3915
Zheng, G. 5476
Zheng, G.J. 91, 97, 151, 228, 233
Zheng, H. 2169, 2188, 2802
Zheng, H.R. 2135, 3865
Zheng, L.C. 4241
Zheng, P. 5634
Zheng, P.W. 568, 1048
Zheng, R.Y. 2020, 4585
Zheng, W. 954
Zheng, W.C. 3777
Zheng, W.Z. 4195
Zheng, X.K. 1680
Zheng, X.R. 779
Zheng, X.Y. 2173
Zheng, Y.D. 387
Zheng, Y.W. 3367
Zheng, Z.J. 4375
Zheng, Z.Z. 5444
Zhi, L.L. 1372
Zhong, C. 364
Zhong, F.P. 1435
Zhong, M.G. 2990
Zhong, Y.Q. 4161
Zhong, Z.J. 320, 325, 331
Zhou, B.J. 4551
Zhou, C. 3877, 3881, 4132
Zhou, C.J. 619
Zhou, D. 2895
Zhou, D.M. 2565
Zhou, D.X. 1052
Zhou, H. 233, 727, 731, 1566
Zhou, H.A. 2547
Zhou, H.D. 1341
Zhou, H.J. 1626
Zhou, H.M. 2314
Zhou, H.Q. 4219
Zhou, H.Y. 5057
Zhou, J. 1578, 3437, 4629, 4633
Zhou, J.C. 3437
Zhou, J.H. 3877, 3881
Zhou, J.J. 803, 853
Zhou, J.Z. 1093, 3169
Zhou, K. 1464, 2569
Zhou, K.F. 5407
Zhou, L. 1555, 1555, 2084, 3489
Zhou, L.F. 2241
Zhou, L.J. 5124
Zhou, L.W. 943
Zhou, M.Q. 4042
Zhou, N. 2995
Zhou, Q.N. 1165, 1169, 3509
Zhou, S.H. 2931
Zhou, S.L. 4409
Zhou, T. 1790, 1794
Zhou, W. 1319, 2684, 3354
Zhou, W.B. 4913
Zhou, W.F. 3294
Zhou, W.H. 4934
Zhou, X. 5427
Zhou, X.F. 2123
Zhou, X.H. 943
Zhou, X.N. 1204
Zhou, X.X. 3714
Zhou, X.Y. 3224
Zhou, Y. 337, 3290, 3893, 4265, 4286, 4733
Zhou, Y.Y. 519, 1286, 1716
Zhou, Z. 3228, 4775
Zhou, Z.B. 2745
Zhou, Z.H. 320, 325, 331, 2426
Zhou, Z.L. 1196
Zhou, Z.M. 1033, 1161
Zhou, Z.P. 2278
Zhou, Z.X. 3231
Zhu, A.M. 3625
Zhu, C. 4169
Zhu, C.G. 814, 2629
Zhu, C.R. 4152
Zhu, D.X. 2360, 3922
Zhu, F. 3153
Zhu, G. 212
Zhu, H.B. 3195
Zhu, H.J. 2004, 3818, 4590
Zhu, J. 316, 1615, 2488, 5575
Zhu, J.C. 4161
Zhu, J.F. 4478

Zhu, J.J. 3763
Zhu, J.P. 3738
Zhu, J.S. 4470
Zhu, L. 961, 1115, 1985, 4371, 4585
Zhu, L.Y. 2878, 2882
Zhu, M. 1449
Zhu, N.F. 4286, 4733
Zhu, Q. 108, 2051, 3140
Zhu, Q.S. 2503, 2617, 2621, 3177, 3181, 4877
Zhu, Q.X. 35
Zhu, S.H. 2223, 2422, 4763, 4799
Zhu, S.X. 1356, 5601
Zhu, T. 4945
Zhu, W.F. 568, 1048
Zhu, W.G. 4009
Zhu, X. 2057
Zhu, X.M. 3185
Zhu, X.Y. 5361
Zhu, Y. 2188, 2278, 2310
Zhu, Y.M. 4001
Zhu, Y.T. 2344
Zhu, Y.W. 3092
Zhu, Y.Z. 863, 3497
Zhu, Z.B. 2753
Zhu, Z.C. 2288
Zhu, Z.D. 3007
Zhu, Z.L. 1602, 2555
Zhu, Z.Y. 1146, 3096
Zhuang, H.Y. 2951
Zhuang, Q.X. 560
Zhuang, T.L. 903
Zhuang, Z.J. 5453
Zong, P. 2227
Zong, X.M. 308
Zou Qi, X.W. 280
Zou, C.M. 927
Zou, J.F. 803, 853
Zou, J.Y. 2643
Zou, W. 581
Zou, X.W. 5029
Zvereva, V. 1297
Zvereva, V.P. 1301, 1305